 © 1987 The Chemical Society of Japan Bull. Chem. Soc. Jpn., 60, 1—7 (1987)

Partial Molar Volumes in Aqueous Mixtures of Nonelectrolytes. I. *t*-Butyl Alcohol

Masao SAKURAI
Department of Polymer Science, Faculty of Science, Hokkaido University, Sapporo 060
(Received April 9, 1986)

The densities of mixtures of *t*-butyl alcohol (TBA) with water (W) have been measured at various temperatures over a wide range of concentrations. From these data the apparent ($V_{\phi,2}$) and partial (V_2) molar volumes as well as partial molar expansibilities (E_2) have been evaluated for both components. The limiting partial molar volumes, V^{∞}_{TBA} and V^{∞}_{W}, were smaller than the molar volume of TBA and water, respectively, at all temperatures studied. The values of E^{∞}_{TBA} was negative at temperatures below 15 °C and the value of E_W was also negative at all temperatures. Characteristic extrema were observed for the $V_{TBA}(X_{TBA})$ and $E_{TBA}(X_{TBA})$ curves in the water-rich region and for the $V_W(X_W)$ curve in the TBA-rich region. The unusual volumetric behavior found for the TBA-water mixtures at both ends of the composition may be attributed to the formation of strong hydrogen bonding between water and TBA molecules and to the unique properties of pure water, itself (i.e., the very small size of water molecules and the existence of a cluster structure).

There have been a number of studies on the volumetric behavior of mixtures of water with nonelectrolytes. Most of them have concerned water-rich solutions and have discussed structural changes of the solvent water caused by the introduction of nonpolar groups (i.e., so-called hydrophobic hydration or iceberg formation).

In 1959 Kauzmann turned his attention to data concerning negative volume changes during the transfer of hydrocarbons from nonpolar solvents to water and pointed out that iceberg formation results in a large decrease in volume.[1] He regarded this fact as a clear indication that the structures present in an iceberg are quite different from those in ordinary ice; in other words, an iceberg has a more dense structure than that of ordinary ice. On the other hand, Némethy and Scheraga,[2] Franks,[3] and Desnoyers and Arel[4] have postulated that an iceberg has a bulky structure like ordinary ice but that the increase in the volume due to iceberg formation can be largely overcome by the loss of free space due to the filling of solutes in the cavities of the iceberg. At present the latter interpretation appears to be generally accepted by many authors.

In any event, however, they have assumed *a priori* that the volume change accompanying iceberg formation can be estimated directly from measurements of the volume change during the transfer of nonpolar solutes from a nonpolar medium to water. This is apparently an oversimplified assumption. A volume change upon mixing two liquids can arise from a variety of origins. In their review article Handa and Benson[5] pointed out the following factors: (1) Differences in the sizes and shapes of the component molecules, (2) differences in the intermolecular interaction energy, (3) structural changes, and (4) the formation of new chemical species. In my opinion, many authors have overestimated factor (3) in order to interpret the unusual volumetric behavior of aqueous mixtures. It should be noted, furthermore, that the exact nature of icebergs has remained obscure; consequently, the volume change accompanying iceberg formation is still open to question. As has been claimed by Hvidt[6] and Nakajima et al.,[7] there is no explicit evidence as to whether iceberg formation results in an increase or decrease in volume.

It is well known that many unusual thermodynamic and spectroscopic properties have been observed for dilute aqueous solutions of *t*-butyl alcohol (TBA).[3,8,9] These have, in general, been interpreted in terms of an iceberg formed around the *t*-butyl group in water. Thus, TBA has been regarded as a typical hydrophobic structure-maker, although TBA is completely miscible with water in any proportion at room temperature (i.e., very hydrophilic in nature).

While many authors have reported the partial molar volumes of TBA in aqueous solutions,[10-18] precise studies of water dissolved in TBA (i.e., the partial molar volume of water in the TBA-rich region) are scare. It would be interesting to investigate the behavior of water in the absence of the characteristic structure of liquid water in order to clarify the interactions between water and TBA. The purpose of this study is to present precise density data regarding TBA-water mixtures at various temperatures over the whole concentration range, whenever possible, and to discuss the partial molar volume behavior at both ends of the concentration range.

Experimental

The solution densities, ρ, were measured using an oscillating-tube densimeter (DMA 60) that was described earlier.[19] In this study, two measuring cells (DMA 601) were used under the operation of a phase locked loop (PLL) mode in order to minimize the drift of period measurements. In most case the solutions were prepared by successive additions of a concentrated solution or a pure solute to a known quantity of solvent. The addition was carried out by

weight in a mixing chamber connected to the measuring cell with a teflon tube and a flow pump.

For very dilute solutions of water in TBA, the measurements were carried out as before.[20] The water concentration was determined with an automatic Karl-Fischer titration apparatus (Hiramuma, AQ 3) immediately after density measurements for each solution.

Water and TBA were purified as before,[20] the latter being further purified by fractional crystallization. No trace of impurities in the TBA was detected using gas chromatography.

Results and Discussion

In a mixture of components 1 and 2, the apparent molar volume of the component 2, $V_{\phi,2}$, is given by

$$V_{\phi,2} = X_1M_1(\rho_1^*-\rho)/X_2\rho_1^*\rho + M_2/\rho, \quad (1)$$

where X and M are the mole fraction and the molar mass of the component 1 or 2 and ρ_1^* is the density of component 1. The density of water, ρ_w^*, was taken from Kell.[21] The density of pure TBA, ρ_{TBA}^*, was determined by extrapolating the ρ values to infinite dilution. The estimated values of ρ_{TBA}^* are 0.77940, 0.77529, 0.77008, 0.76476, and 0.75937 g cm^{-3} at 26, 30, 35, 40, and 45 °C, respectively.

In Fig. 1 the apparent molar volumes of TBA, $V_{\phi,TBA}$, at 25 °C are compared with various values from the literature and generally show good agreement. In particular, the values in extremely dilute solutions given by Franks and Smith[12] are in excellent agreement with the present data within the experi-

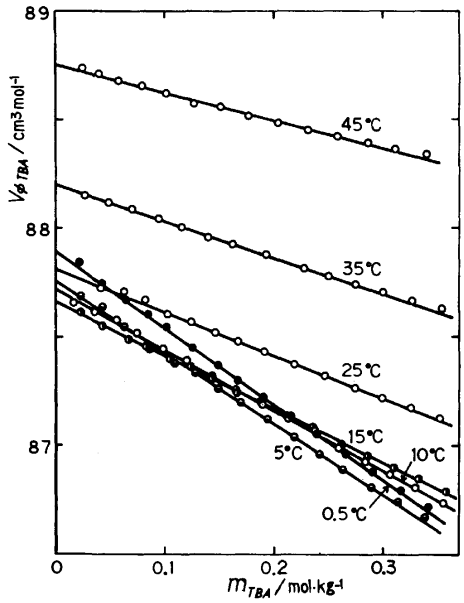

Fig. 2. Apparent molar volumes of TBA in very dilute aqueous solutions at various temperatures.

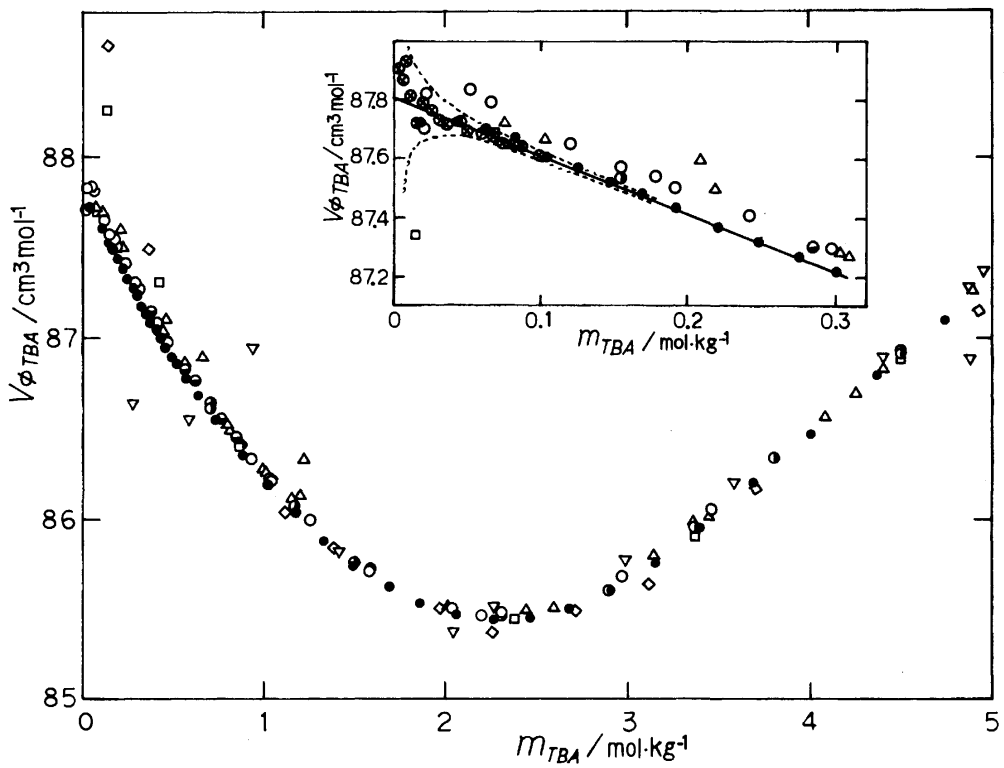

Fig. 1. Apparent molar volumes of TBA in the water-rich region at 25 °C as a function of molality. The dotted lines represent the uncertainties in $V_{\phi,TBA}$ corresponding to $\delta\rho = \pm 2 \times 10^{-6}$ g cm^{-3}.
●: This work, ○: Ref. 15, ◑: Ref. 13, ◒: Ref. 14, ⊗: Ref. 12, ◇: Ref. 11, □: Ref. 16, △: Ref. 17, ▽: Ref. 18.

mental uncertainty of the density measurement: $\delta\rho=\pm 2\times 10^{-6}$ g cm^{-3}.

Limiting Partial Molar Volume. For very dilute solutions, the apparent molar volume of solute 2 can be represented by a linear form:

$$V_{\phi,2} = V_2^\infty + A_2 m, \quad (2)$$

where V_2^∞ is the limiting partial molar volume of component 2, A_2 an empirical constant, and m the molality. The results for TBA in water and for water in TBA are plotted in Figs. 2 and 3, respectively, and the parameters of Eq. 2 are summarized in Table 1. The value of V_{TBA}^∞ at 25 °C is in good agreement with that from the literature: 87.82,[12] 87.90,[13] 87.73,[14] and 87.76 cm^3 mol^{-1}.[15] No precise V_W^∞ data were available with which the presented results could be compared.

The temperature dependence of V_{TBA}^∞ is shown in Fig. 4, including the results for *n*-butyl alcohol (NBA) solutions obtained by Nakajima et al.[7] The values of V_{BA}^∞ are smaller than the molar volumes of neat butyl alcohols, V_{BA}^*, at all temperatures. Figure 5 shows the temperature dependence of the excess limiting partial molar volume defined by

$$V_{BA}^E = V_{BA}^\infty - V_{BA}^*. \quad (3)$$

The values of V_{TBA}^* below 25 °C were evaluated from the temperature dependence of the densities of neat TBA. As described in the Introduction, a negative V_2^E has, in general, been regarded as a characteristic of iceberg formation.[1-4,8,9] If this is relevant the negative V_2^E would have to be reduced as the temperature is raised, since water structural effects become progressively reduced with increasing temperature. Thus, Kauzmann[1] has explained the larger negative values of V_2^E at lower temperatures for aliphatic hydrocarbon in water reported by

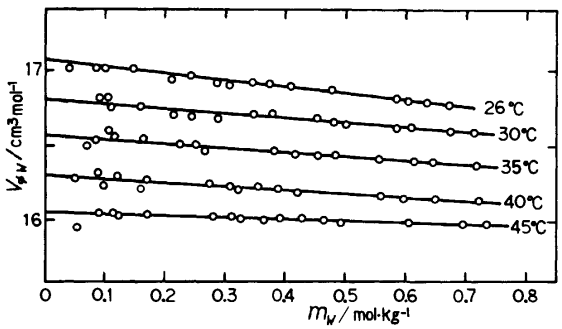

Fig. 3. Apparent molar volumes of water in dilute TBA solutions at various temperatures.

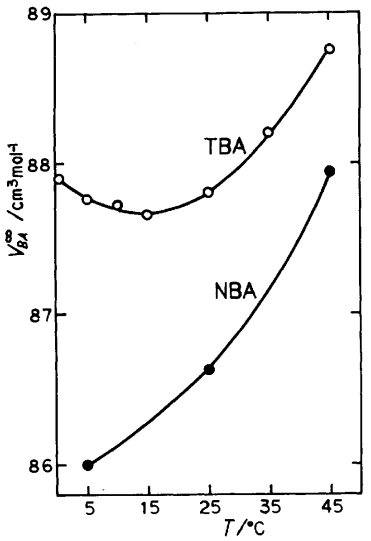

Fig. 4. Limiting partial molar volumes of TBA and NBA[7] in water as a function of temperature.

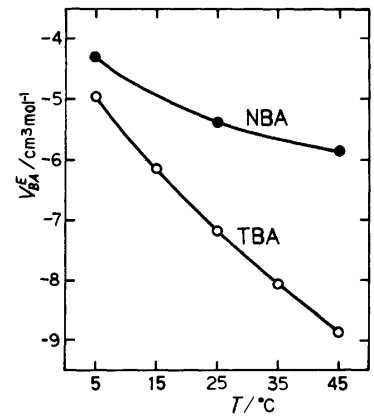

Fig. 5. Excess limiting partial molar volumes of TBA and NBA[7] in water as a function of temperature.

Table 1. Limiting Partial Molar Volumes and Deviation Constants for TBA-Water Mixtures

T/°C	V_{TBA}^∞/cm^3 mol^{-1}	A_{TBA}/cm^3 kg mol^{-2}	T/°C	V_W^∞/cm^3 mol^{-1}	A_W/cm^3 kg mol^{-2}
0.5	87.89	−3.52	26	17.07	−0.44
5	87.76	−3.29	30	16.80	−0.30
10	87.72	−2.82	35	16.56	−0.26
15	87.66	−2.47	40	16.30	−0.23
25	87.81	−2.01	45	16.05	−0.10
35	88.20	−1.68			
45	88.75	−1.26			

Masterton;[22] he had explained his results in terms of a break down of the water structure around hydrocarbons. On the contrary, Fig. 5 shows that the value of V^E_{BA}, as well as for many other alcohols, becomes very strongly negative as the temperature is increised. This is more significant for V^E_{TBA} than V^E_{NBA}.

Evidently, a complicated situation can take place through an assumption that the observed volume change in the transfer of nonpolar solutes from nonpolar medium to water is taken just as the volume change accompanying iceberg formation. Volume changes must arise from a number of factors, not only from iceberg formation even in aqueous systems.

The large negative V^E_2 observed for aqueous systems can be well explained in terms of the unique properties of solvent water itself, not the water-structural change caused by the introduction of solutes. Recently, Lee[23] investigated the partial molar volume based on a hard-sphere mixture model and clearly showed that the negative volume change is due to the small size of water molecules. This is the same conclusion that was postulated earlier by Assarsson and Eirich.[24] On the basis of the scaled particle theory, French and Criss[25] wrote: "The small V_2 values of nonelectrolytes in water are understandable in light of the low compressibility of water. Structural considerations are not neccessary." In addition, the linear correlation between the partial molar volumes of solutes and the compressibility coefficients of solvents has been illustrated by Hamilton and Stokes[26] and Dack.[27] That is to say, the volume of liquids is primarily given by the repulsive forces of hard spheres. Therefore, the greatest part of the negative V^E_2 observed for aqueous systems can be ascribed to the fact that the free volume in water or in dilute aqueous mixtures is considerably smaller than that in most organic systems, while the solute-solvent hydrogen bonding probably plays a role in the volume change for polar mixtures. Thus, the negative temperature dependence of V^E_{BA} (Fig. 5) can be interpreted in terms of the difference in the expansibilities of neat butyl alcohols and aqueous butyl alcohol solutions. The pronounced effect for TBA, compared to NBA, can also be explained by the fact that the expansivity of neat TBA (α=1.294 kk^{-1} at 25 °C) is much larger than that of neat NBA (α=0.948 kK^{-1} at 25 °C).

On the basis of the thermodynamic relation

$$(\partial C_p/\partial P)_T = -T(\partial^2 V/\partial T^2)_p, \quad (4)$$

Hepler[28] has postulated a criterion for discriminating between solutes in water as being "structure maker" or "structure breaker." It is well known that the limiting partial molar expansibility, $E^\infty_2(=\partial V^\infty_2/\partial T)$, of various alcohols in water greatly decreases with decreasing temperature (that is $\partial^2 V^\infty_2/\partial T^2>0$; therefore, alcohols have been regarded as structure makers), and it is in some cases negative at low temperatures.[7,15,29] In fact, Fig. 4 shows that the $V^\infty_{TBA}(T)$ curve passes through a minimum at about 15 °C. The results coincide with a prediction from the fact that the temperature of maximum density (TMD) of dilute TBA solutions is higher than that of pure water (3.98 °C).[30,31] The TMD of D_2O (11.23 °C) is higher than that of H_2O; this is one piece of evidence for supporting the idea that D_2O is more structured than H_2O at ordinary temperatures.[32] In analogy with this consideration, it is possible to consider that the introduction of TBA brings about a solvent water with more structure. Such a consideration leads us to the idea that iceberg formation is accompanied by a positive volume change;[6,7,33] this is in conflict with the generally accepted view.

However, structural considerations based on the sign of $\partial^2 V_2/\partial T^2$ or the shift in TMD also lead to the conclusion that benzene has little influence on the structure of water and that aliphatic hydrocarbon is a structure breaker.[28,30] This conclusion may be essentially in conflict with the definition of an iceberg. Furthermore, it should be noted that an anomalous negative expansibility has been observed even for the organic solvent systems described below.

The limiting partial molar volumes of water, V^∞_W, in TBA are plotted as a function of temperature in Fig. 6, together with V^∞_W in the other three isomeric butyl alcohols.[20,34] The values of V^∞_W are always smaller than the molar volume of water, V^*_W. This is probably due to a large V^*_W resulting from the water cluster, in addition to the factors operating in V^E_2 for aqueous solutions as pointed out before. It is of interest that for four butyl alcohol solvents the V^∞_W in TBA alone decreases monotonously as the temperature is increased. Such a negative E^∞_2 behavior in organic solvents has been also observed for urea in methanol[26]

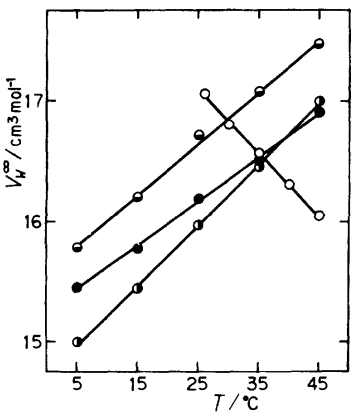

Fig. 6. Limiting partial molar volumes of water in four isomeric butanols.
○: TBA, ●: NBA,[20] ◑: isobutyl alcohol,[34] ◒: s-butyl alcohol.[34]

and water in methanol,[20] but is highly pronounced for the present system. Needless to say, in the absence of the water structure in the TBA-rich region, the volumetric behavior is not explicable by the structural change of water. Both the negative E^{∞}_{TBA} and E^{∞}_{W} may arise from a more effective packing due to a difference in the size and the strong hydrogen bonding between water and TBA molecules.

Concentration Dependence of Apparent and Partial Molar Volumes. The empirical constant A_2 of Eq. 2 is associated with solute-solute interactions. The values of A_{TBA} and A_W estimated from Figs. 2 and 3, respectively, are plotted in Fig. 7; this includes, for comparison, the values for NBA-water mixtures.[7,20] For dilute aqueous alcohol solutions the A_2 value is negative and becomes more negative with increasing the size of the hydrocarbon group and decreasing the temperature.[7,14] Therefore, such a negative A_2 value has, in general, been ascribed to iceberg formation.[4] As can be seen from Fig. 7, the A_{BA} values for aqueous TBA and NBA solutions are comparable with each other at all temperatures, while it has often been considered that the structural effect of TBA is much larger than that of NBA.[9] The absolute values of A_W are very small compared to those of A_{BA}. As will be described below, the variation of A_2 values with the size of solutes may mostly depend on the molar scale employed in Eq. 2. This problem is closely associated with the difference in the molality range in which Eq. 2 holds for an aqueous TBA solution (Fig. 2) and for a solution of water in TBA (Fig. 3).

From the $V_{\phi,2}$ values, the partial molar volume of component 2 at finite concentrations is given by

$$V_2 = V_{\phi,2} + X_1X_2(\partial V_{\phi,2}/\partial X_2)_{T,P} \quad (5)$$

The values of $(\partial V_{\phi,2}/\partial X_2)_{T,P}$ were evaluated by a local fitting procedure[35] in which five consecutive values of $V_{\phi,2}$ were represented by a quadratic equation in a certain mole fraction range.

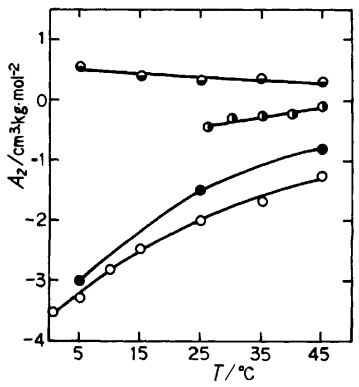

Fig. 7. Coefficient A_2 of Eq. 2 as a function of temperature.
○: TBA in water, ●: NBA in water,[7] ◑: water in TBA, ◒: water in NBA.[20]

Figure 8 shows the concentration dependences of the apparent and partial molar volumes of TBA and water over the whole mole fraction range at 35 °C. As is well known, the $V_{TBA}(X_{TBA})$ curve has a sharp minimum at a very low mole fraction. It is worth noting that the $V_W(X_W)$ curve also has a minimum, though not so outstanding compared to that for V_{TBA}. This obscure minimum in the $V_W(X_W)$ curve is apparently due to a comparison based on the molar scale. When the molar masses of the two components in binary mixtures differ significantly (M_{TBA} is about 4 times M_W), it may be better to compare the extent of the volume change based on the unit-mass scale rather than the molar scale. Figure 9 illustrates the apparent and partial specific volumes of TBA and water as a function of the weight fraction of TBA. The depth and the position of the two minima are comparable with each other. Thus, the volumetric behavior of the TBA-water mixture is unusual at both ends of the

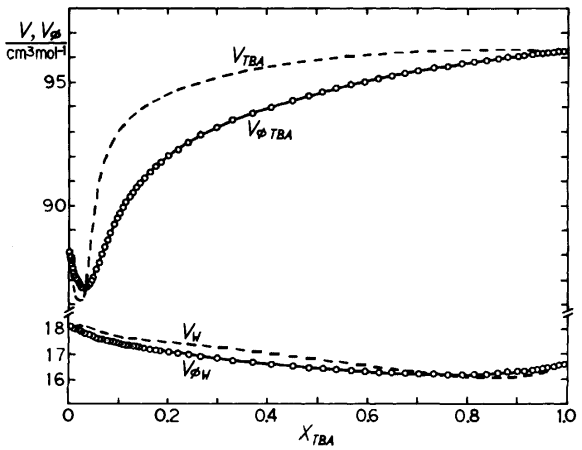

Fig. 8. Apparent and partial molar volumes of TBA and water in their mixtures as a function of mole fraction of TBA.

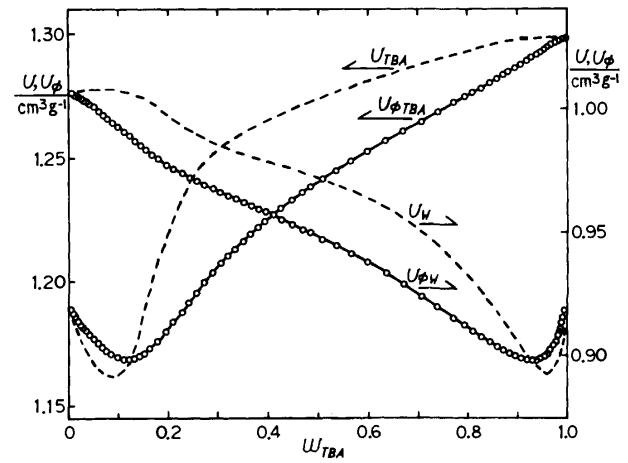

Fig. 9. Apparent and partial specific volumes of TBA and water in their mixtures as a function of weight fraction of TBA.

concentration range.

In Fig. 10 are shown the concentration dependences of V_{TBA} in the water-rich region at various temperatures. The appearance of the characteristic minimum in dilute aqueous solutions has also been associated with iceberg formation on the basis of the fact that it becomes more pronounced and shifts to a lower concentration as the alkyl group increases in size.[3,8] As can be seen from Fig. 10, the minimum is similarly more pronounced but occurs at a higher concentration as the temperature is lowered. On the other hand, Nakagawa et al.[36] have reported that the increase in the pressure also causes a more pronounced minimum and shifts it to a higher concentration. That is to say, such a minimum behavior is affected in a similar manner by a decrease in the temperature and by an increase in the pressure, both of which bring about a decrease in the volume in the usual way. The explanation of the minimum by using iceberg formation is, therefore, not consistent since iceberg formation may be less significant with both the increases in the temperature and the pressure.

It is worth noting that a similar behavior is found for the $V_W(X_W)$ curves in Fig. 11, where the minimum is also very pronounced and shifts to a higher concentration with decreasing temperature. A minimum in the $V_W(X_W)$ curve has been observed in tetrahydrofuran,[37] but not in *n*-alcohols.[20]

The appearance of a minimum in the $V_2(X_2)$ curve at a certain concentration means that the packing of the component molecules takes place more effectively up to this concentration. The exact nature of such a packing effect is not clear since the concentration dependence is a very complex phenomenon and is attributable to various types of solute-solvent and solute-solute interactions, which may include the destruction of self-associations in water and in TBA and the formation of hydrogen-bonded associations between water and TBA molecules.

Figure 12 shows the partial molar expansibilities, $E_2(=\partial V_2/\partial T)$, of TBA and water at 40 °C over the whole mole fraction range. The $E_{TBA}(X_{TBA})$ curve is characterized by a remarkable maximum and an

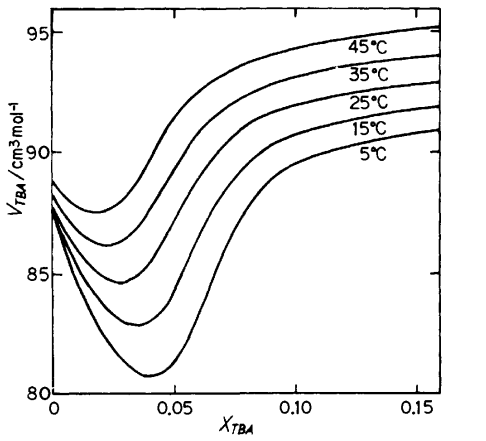

Fig. 10. Partial molar volumes of TBA in the water-rich region at various temperatures.

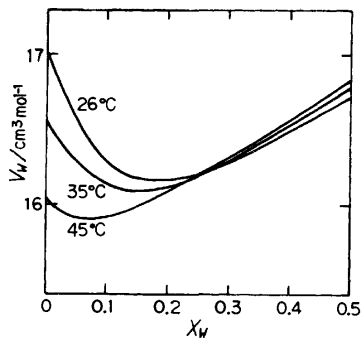

Fig. 11. Partial molar volumes of water in the TBA-rich region at various temperatures.

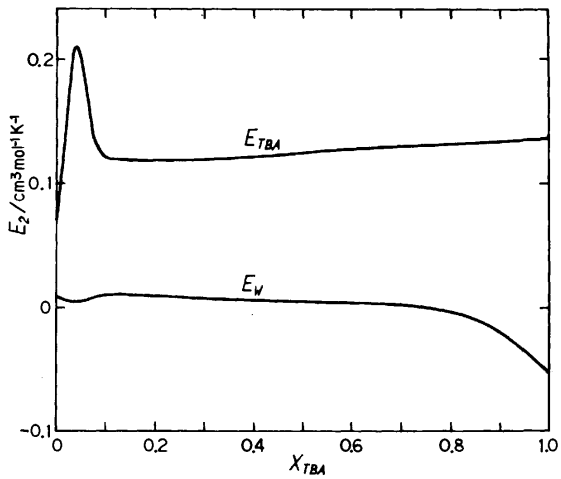

Fig. 12. Partial molar expansibilities of TBA and water as a function of mole fraction of TBA at 40 °C.

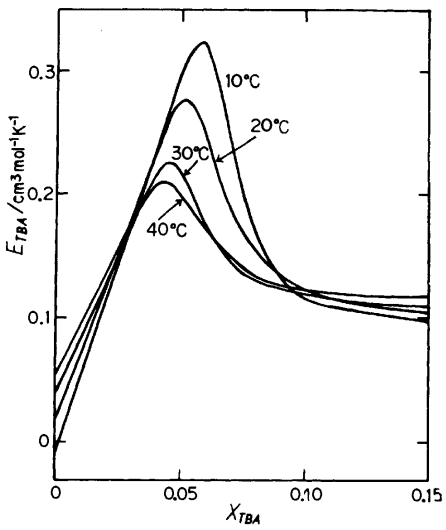

Fig. 13. Partial molar expansibilities of TBA in the water-rich region at various temperatures.

indistinct minimum at low X_{TBA}. The variation of the maximum with temperature is shown in Fig. 13. The maximum is more pronounced and occurs at higher concentration as the temperature is decreased. These are analogous to the minimum behavior in V_{TBA} (Fig. 10). However, it is noteworthy that the concentration of the maximum in E_{TBA} is higher than that for the minimum in V_{TBA}; i.e., the position of the E_{TBA} maximum coincides with that where V_{TBA} increases abruptly beyond the minimum with increasing concentration.

On the other hand, no extremum is found for the $E_W(X_W)$ curve in the TBA-rich regions. Consequently, the appearance of the E_{TBA} maximum may be associated with the destruction of the water structure. The expansibility of dilute aqueous TBA solutions is unusually small through the existence of the cluster structure of water initially present in solvent water. As the concentration is increased, the water cluster is progressively disrupted and the expansibility of the solution increases most steeply at the concentration referring to the E_{TBA} maximum. A further addition of TBA may extinguish most of the bulky water structure, and the volumetric behavior of the solution approximates more and more closely to that of neat TBA. In fact, Fig. 8 and 12 show that the values of V_{TBA} and E_{TBA} slightly depend on the mole fraction for $X_{TBA}>0.1$ and are comparable to those for neat TBA.

Conclusion

The characteristic volumetric behavior observed for dilute aqueous TBA solutions has been generally interpreted in terms of iceberg formation around the *t*-butyl group. The present study clearly shows that some anomalies can be found for the TBA–water mixture at both ends of the concentration. This fact confirms my suspicion that the volumetric behavior of aqueous TBA solutions may be irrelevant to iceberg formation. The peculiarity of the TBA–water mixture may be mainly attributed to the very small radius of water molecules, strong hydrogen-bonding between water and TBA molecules, and the cluster structure of pure water; not to iceberg formation by the introduction of TBA molecules.

The author wishes to thank Dr. Nobumichi Ohno, Akita National College of Technology, for drawing his attention to this problem. Financial support of this work which came from a Grant-in-Aid for Scientific Research by the Ministry of Education, Science and Culture is gratefully acknowledged.

References

1) W. Kauzmann, *Adv. Protein Chem.*, **14**, 1 (1959).
2) G. Némethy and H. A. Scheraga, *J. Chem. Phys.*, **36**, 3401 (1962).
3) F. Franks, *Ann. New York Acad. Sci.*, **125**, 277 (1965).
4) J. E. Desnoyers and M. Arel, *Can. J. Chem.*, **45**, 359 (1967).
5) Y. P. Handa and G. C. Benson, *Fluid Phase Equil.*, **3**, 185 (1979).
6) A. Hvidt, *Ann. Rev. Biophys. Bioeng.*, **12**, 1 (1983); *J. Chem. Thermodyn.*, **3**, 663 (1971).
7) T. Nakajima, T. Komatsu, and T. Nakagawa, *Bull. Chem. Soc. Jpn.*, **48**, 783 (1975).
8) F. Franks and D. J. G. Ives, *Quart. Rev.*, **20**, 1 (1966).
9) F. Franks and D. S. Reid, "Water, a Comprehensive Treatise," ed by F. Franks, Plenum Press, New York (1973), Vol. 2, p. 323.
10) K. Nakanishi, *Bull. Chem. Soc. Jpn.*, **33**, 793 (1960).
11) K. Nakanishi, N. Kato, and M. Maruyama, *J. Phys. Chem.*, **71**, 814 (1967).
12) F. Franks and H. T. Smith, *Trans. Faraday Soc.*, **64**, 2962 (1968); *J. Chem. Eng. Data*, **13**, 538 (1968).
13) L. Avėdikian, G. Perron, and J. E. Desnoyers, *J. Solution Chem.*, **4**, 331 (1975).
14) C. Jolicoeur and G. Lacroix, *Can. J. Chem.*, **54**, 624 (1976).
15) C. de Visser, G. Perron, and J. E. Desnoyers, *Can. J. Chem.*, **55**, 856 (1977).
16) A. Hvidt, R. Moss, and G. Nielsen, *Acta Chem. Scand.* **B32**, 274 (1978).
17) G. Perron and J. E. Desnoyers, *J. Chem. Thermodyn.*, **13**, 1105 (1981).
18) J. F. Alary, M. A. Simard, J. Dumont, and C. Jolicoeur, *J. Solution Chem.*, **11**, 755 (1982).
19) M. Sakurai and T. Nakagawa, *J. Chem. Thermodyn.*, **14**, 269 (1982).
20) M. Sakurai and T. Nakagawa, *J. Chem. Thermodyn.*, **16**, 171 (1984).
21) G. S. Kell, *J. Chem. Eng. Data*, **20**, 97 (1975).
22) W. L. Masterton, *J. Chem. Phys.*, **22**, 1830 (1954).
23) B. Lee, *J. Phys. Chem.*, **87**, 112 (1983).
24) P. Assarsson and F. R. Eirich, *J. Phys. Chem.*, **72**, 2710 (1968).
25) R. N. French and C. M. Criss, *J. Solution Chem.*, **10**, 713 (1981).
26) D. Hamilton and R. H. Stokes, *J. Solution Chem.*, **1**, 213 (1972).
27) M. R. J. Dack, *Aust. J. Chem.*, **29**, 779 (1976).
28) L. G. Hepler, *Can. J. Chem.*, **47**, 4613 (1969).
29) S. Cabani, G. Conti, and E. Matteoli, *J. Solution Chem.*, **5**, 751 (1976).
30) G. Wada and S. Umeda, *Bull. Chem. Soc. Jpn.*, **35**, 646 (1962).
31) M. Sakurai, T. Komatsu, and T. Nakagawa, *Bull. Chem. Soc. Jpn.*, **45**, 1038 (1972).
32) E. M. Arnett and D. R. McKelvey, "Solute-Solvent Interactions," ed by J. F. Coetzee and C. D. Ritchie, Marcel Dekker, New York (1969), p. 343.
33) D. M. Alexander and D. J. T. Hill, *Aust. J. Chem.*, **18**, 605 (1965).
34) M. Sakurai, unpublished results.
35) H. C. Zegers and G. Somsen, *J. Chem. Thermodyn.*, **16**, 225 (1984).
36) M. Nakagawa, H. Inubushi, and T. Moriyoshi, *J. Chem. Thermodyn.*, **13**, 171 (1981).
37) M. Sakurai and T. Nakagawa, *Bull. Chem. Soc. Jpn.*, **55**, 1641 (1982).

 © 1987 The Chemical Society of Japan Bull. Chem. Soc. Jpn., 60, 9—18 (1987)

Band Shape of Photoelectron Spectrum and Potential Energy Curve for Alkylamine

Masao TAKAHASHI,* Iwao WATANABE, and Shigero IKEDA

Department of Chemistry, Faculty of Science, Osaka University,
Toyonaka, Osaka 560
(Received May 6, 1986)

Accurate measurements of UPS and ab initio potential energy calculations have been carried out for ammonia and several alkylamines to interpret the band shape of the UPS. Theoretical photoelectron band shape was obtained by a simple Franck-Condon approach. The calculation predicted very well the alkyl substitution effects on the ionization potentials and on the band widths of the first bands in UPS for the alkylamines. The following conclusions were obtained by comparing these theoretical photoelectron bands with experimental ones. The threshold ionization potential observed in the UPS is not always thermodynamically adiabatic ionization energy, but it can be subject to hot bands. Adiabatic ionization potential I_{Pa} of ammonia is concluded to be 10.08 eV. And the values of I_{Pa} for a series of alkylamines are evaluated by taking account of molecular vibrational frequency for the neutral state.

Though numerous investigations on UV photoelectron spectra (UPS) for free molecules have been executed, most of them have been concerned only with their ionization energies. We have been interested in the information obtainable from the band shape of the UPS. Our attention has been paid to the first band of the UPS corresponding to the ionization of a HOMO electron which must play the most important role with respect to the chemical reactivity of the molecule. The band shape of the UPS is related to the degree of distortion in the molecular structure after the photoionization, viz., the larger the distortion, the wider the band width.[1] The distortion also occurs after one-electron oxidation in solution, so that the degree of distortion must affect kinetics of electrochemical oxidation reaction. We obtained accurate UPS for a series of alkylamines,[2] and found that the band width of the first band for amine molecule correlates with one of the kinetic parameters, transfer coefficient (symmetry factor), for electrochemical oxidation reaction in solution and qualitatively showed that both the band width and the transfer coefficient reflect the character of potential energy curves for neutral and cationic state.[3]

Nitrogen skeleton of amine of the neutral state is known to be pyramidal[4,5] and that of the cationic state planar.[6,7] Thus the equilibrium structure of the amine cation radical differs substantially from that of the neutral one. It results in a broad first band in the UPS with a long vibrational progression though the HOMO, from which an electron is removed, is a nonbonding orbital consisting mainly of nitrogen 2p orbital. In order to discuss the band feature of the UPS, the Franck-Condon factor for the transition from the neutral to cationic potential energy surface is necessary. The Franck-Condon factors were calculated and reported for simple molecules[8,9] by many workers. The calculations for ammonia were also performed and the first band of its UPS was theoretically obtained.[10] However the potential energy surfaces of neutral alkylamines and the corresponding cation radicals are far more complex and have not yet been calculated.

One must also pay attention to whether the adiabatic ionization potential, I_{Pa}, can be determined from the UPS for the molecule which undergoes large change in its geometry after the photoionization process. For ammonia it remains uncertain whether the first peak in the vibrational progression for the first band corresponds to I_{Pa} or not.[6b,11] It is known that the photoionization processes corresponding to I_{Pa} are intrinsically unobservable for water dimer molecule[12] and van der Waals molecules composed of inert gas atoms.[9]

We carried out ab initio MO calculations for ammonia, mono-, di-, and trimethylamine and mono-, di-, and triethylamine, with several different geometries both for the neutral and cationic states and obtained potential energy curves on the deformation coordinate of the bending vibration. Theoretical photoelectron band can be derived from the potential energy curves by using a simple Franck-Condon approach. The band shape of UPS theoretically obtained will be compared with the experimental UPS data to test the validity of the present approach. The effects of the alkyl substitution on the band shape and ionization potentials are also studied.

Experimental

The experimental setup for the UPS measurements has been presented elsewhere[2] and will be outlined here. The ionization energy scale was calibrated with either argon (I_P=15.759 eV) or xenon (I_P=12.130 eV) used as an internal reference. The instrumental resolution was 20—30 meV. The spectrometer was kept at about 300 K and the temperature of the ionization chamber was higher by about 20 K because of the heat of a helium discharge lamp. For a low vapor pressure sample of tripentylamine the spectrometer was heated to 307 K to obtain sufficient vapor pressure. The spectral data for the first bands corresponding

to the ionization of HOMO electron were accumulated more than 25 times. All the samples were commercial products and the samples obtained in the form of aqueous solutions were evaporated from the solution by adding sodium hydroxide.

Vertical ionization potential I_{Pv} was read at the maximum of the most intense vibrational component of the first band when vibrational progressions were well resolved. Threshold ionization potential I_{Pth} was read at the first vibrational peak of the band. For the molecule which displays no vibrational fine structure, I_{Pv} was read at the maximum of the band, and I_{Pth} was determined as follows. We took the point where the spectral intensity was 1% of the band maximum over the threshold region as the onset of the band. Then the I_{Pth} was obtained by adding 0.15 eV to the onset. 0.15 eV (0.148±0.017 eV) is the average distance between the onset and the first vibrational peak of the band for those molecules which display vibrational progressions. Bandwidth δ was determined from the full width at half-maximum (FWHM) of the first band. When the band displayed vibrational fine structure, the δ was read from the FWHM of the envelope connecting vibrational peaks. Though the accuracies of I_P and δ depend on the band shape, we believe that they are better than 0.02 eV.

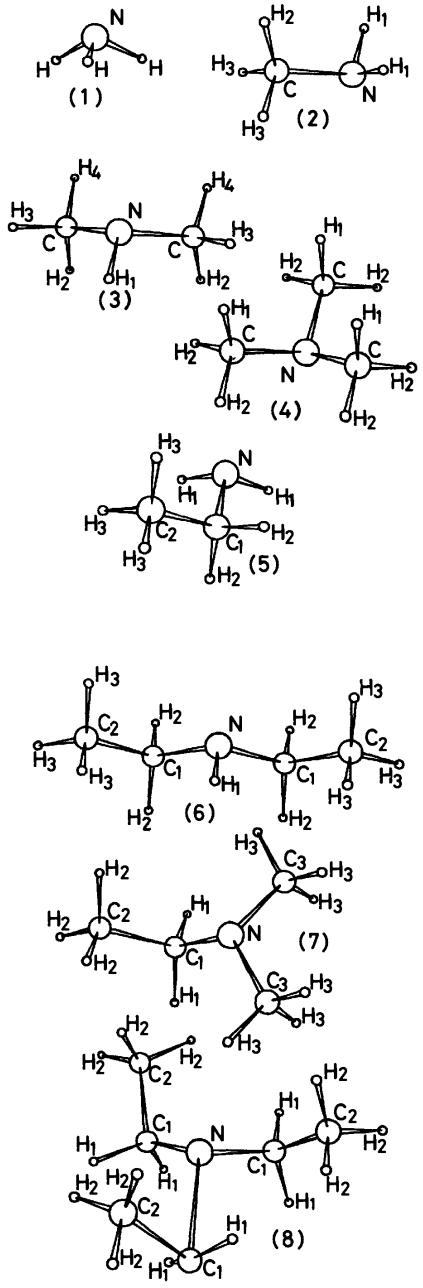

Fig. 1. Molecular geometries used for calculations for ammonia (1), methylamine (2), dimethylamine (3), trimethylamine (4), ethylamine (5), diethylamine (6), *N,N*-dimethylethylamine (7), and triethylamine (8).

Computational Procedure

In the present work, we performed ab initio MO calculations for ammonia, mono-, di-, and trimethylamine, *N,N*-dimethylethylamine and mono-, di-, and triethylamine. Calculations were carried out using the Gaussian 80 program and the IMSPACK program[13] with the minimal STO-3G basis set. For the cationic state, the open-shell calculations were performed with an unrestricted Hartree-Fock (UHF) procedure included in the programs.

The geometries for both neutral and cationic states were optimized by means of gradient method included in the Gaussian 80 program. The full-geometry optimizations were carried out except for diethylamine, *N,N*-dimethylethylamine and triethylamine, for which the structural parameters within ethyl group were fixed to the values optimized for ethylamine. The symmetries used for the calculations are; C_{3v} for ammonia and trimethylamine, C_3 for triethylamine, and C_s for all the others and also ammonia and trimethylamine. The optimized geometries are described in Fig. 1, and the structural parameters obtained are listed in Table 1. The bond lengths and angles are in good agreement with those obtained experimentally and calculated by others.[14]

As indicated in Table 1, the change in geometry of the cation radical from the neutral molecule is

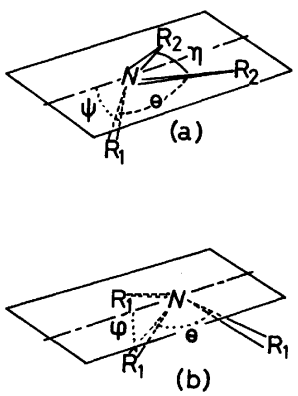

Fig. 2. Deformation angles and internal coordinates. R_1 and R_2 denote H, CH_3, or C_2H_5. (a) for C_s symmetry and (b) for C_3 and C_{3v}.

Table 1. Optimized Structural Parameters and Total Energy
(Bond length in nm, Bond angle in degree, and Energy in a.u.)

	Neutral state	Cationic state		Neutral state	Cationic state
Ammonia			Trimethylamine		
N-H	0.1033	0.1056	N-C	0.1485	0.1508
	(0.1006)			(0.1457)	
ϕ	24.4	0.0	C-H_1	0.1094	0.1094
	(0.0)			(0.1096)	
Total energy	−55.4554	−55.2070	C-H_2	0.1089	0.1091
	(−55.4377)			(0.1090)	
Methylamine			H_1-C-N	113.0	107.4
N-C	0.1486	0.1509		(113.1)	
	(0.1449)		H_2-C-N	109.3	108.6
N-H_1	0.1033	0.1054		(110.1)	
	(0.1009)		ϕ	18.6	2.7
C-H_2	0.1093	0.1098		(0.0)	
	(0.1096)		Total energy	−171.1919	−171.0214
C-H_3	0.1089	0.1093		(−171.1755)	
	(0.1091)		Ethylamine		
H_2-C-N	113.7	106.6	N-C_1	0.1490	0.1522
	(113.6)		C_1-C_2	0.1541	0.1544
H_3-C-N	109.1	107.9	N-H_1	0.1033	0.1053
	(110.2)		C_1-H_2	0.1093	0.1096
H_1-N-H_1 (η)	104.4	116.4	C_2-H_3	0.1086	0.1086
	(118.2)		C_2-C_1-N	110.5	109.1
ψ	60.9	0.0	H_2-C_1-N	110.1	105.6
	(0.0)		H_3-C_2-C_1	110.4	109.8
Total energy	−94.0329	−93.8167	H-N-H (η)	104.4	116.2
	(−94.0162)		ψ	61.5	0.0
Dimethylamine			Total energy	−132.6148	−132.4059
N-C	0.1485	0.1506	Diethylamine		
	(0.1452)		N-H_1	0.1033	0.1052
N-H_1	0.1034	0.1053	N-C_1	0.1488	0.1519
	(0.1011)		C_1-C_2	0.1542	0.1541
C-H_2	0.1091	0.1093	C_2-C_1-N	109.9	110.0
	(0.1095)		C_1-N-C_1 (η)	111.6	123.6
C-H_3	0.1089	0.1095	ψ	59.0	0.0
	(0.1089)		Total energy	−209.7757	−209.5970
C-H_4	0.1091	0.1093	*N,N*-Dimethylethylamine		
	(0.1095)		N-C_1	0.1498	0.1510
H_2-C-N	113.4	108.7	C_1-C_2	0.1547	0.1552
	(112.1)		N-C_3	0.1485	0.1500
H_3-C-N	109.0	107.4	C_2-C_1-N	110.6	108.0
	(109.4)		C_3-N-C_3 (η)	110.2	119.0
H_4-C-N	109.2	107.4	ψ	49.9	1.4
	(111.8)		Total energy	−209.7665	−209.6064
C-N-C (η)	111.2	125.8	Triethylamine		
	(121.2)		N-C_1	0.1494	0.1523
ψ	59.0	0.0	C_1-C_2	0.1545	0.1547
	(0.0)		C_2-C_1-N	111.1	111.6
Total energy	−132.6122	−132.4215	ϕ	18.4	2.1
	(−132.5968)		Total energy	−286.9283	−286.7754

ψ and ϕ are the angles defined in Fig. 2. Values in parenthesis are calculated for the planar form, i.e. ψ or $\phi=0°$. The following parameters are fixed for the neutral and the cationic state respectively, for diethylamine (H_2-C_1; 0.1093 and 0.1096, H_3-C_2; 0.1086 and 0.1087, H_2-C_1-N; 110.5 and 105.6, H_3-C_2-C_1; 110.5 and 110.0) and for triethylamine(C_1-H_1; 0.1093 and 0.1096, C_2-H_2; 0.1086 and 0.1087, H_1-C_1-N; 110.5 and 105.6, H_2-C_2-C_1; 110.5 and 110.0), and are fixed for both the neutral and the cationic states for *N,N*-dimethylethylamine (C_1-H_1; 0.1090, C_2-H_2; 0.1090, C_3-H_3; 0.1090, H_1-C_1-N; 110.0, H_2-C_2-C_1; 109.5, H_3-C_3-N; 110.0).

remarkable only in ψ or ϕ, which denotes the deformation angle as shown in Fig. 2. The first band of the UPS for the alkylamine has a very strong vibrational progression which corresponds to the deformation vibration. Thus we chose a potential energy curve on the coordinate of ψ or ϕ, for the calculation of theoretical band of the UPS. Potential energy curves were also calculated by using the angles HNH for methylamine and CNC for dimethylamine as the reaction coordinates. During the calculations other structural parameters were fixed at the optimized values for the neutral state.

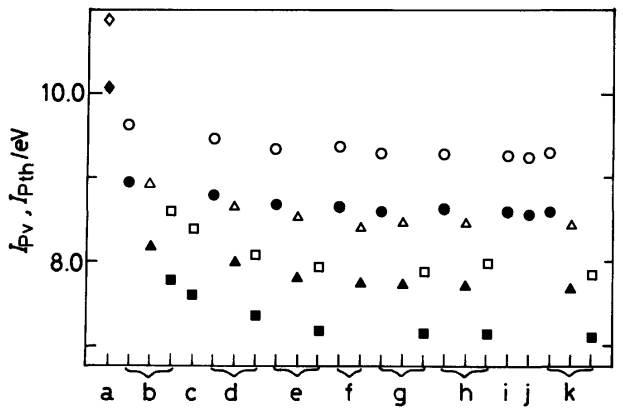

Fig. 3. Alkyl Substitution effect on I_{Pv} (open marks) and I_{Pth} (closed marks). Primary amines (○), secondary amines (△), tertiary amines (□), and ammonia (◇), (a) amomnia, (b) methyl-, (c) *N,N*-dimethylethylamine, (d) ethyl-, (e) propyl-, (f) isopropyl-, (g) butyl, (h) isobutyl-, (i) *s*-butyl,- (j) *t*-butyl-, and (k) pentyl-.

Results and Discussion

Observed Spectra. The He(I) photoelectron spectra of various alkylamines were previously reported.[2] The report includes their expanded first bands which are broad and are ascribable to the photoionization of a 2p non-bonding electron on nitrogen. Vibrational progressions are observed in the first bands for all the primary amines. The first bands for some of the secondary and tertiary amines also have vibrational structures. The vibrational frequencies listed in Table 2 are to be comparable to the ones for the neutral state and will be discussed in the following section. The vibrational structures are composed almost entirely of angle deformation mode and the other vibrational modes are only slightly observable, e.g., in the case of ammonia.[6b,11]

The I_{Pv} and the I_{Pth} for alkylamines decrease in the order of primary, secondary and tertiary amine as shown in Fig. 3. They also decrease with the length of alkyl group from methyl to propyl and level off. The successive decrease in ionization potential up to

Table 2. Vibrational Frequencies(cm^{-1}) and Populations(%) on Each Vibrational Level (Populations are in Parenthesis)

State	Experiment	Calculation
	Ammonia	
Neutral	933[a]	1450
	($v''=0$; 99), ($v''=1$; 1)	($v''=0$; 99), ($v''=1$; 1)
Cationic	900	1690
	Methylamine	
Neutral	780[b,c,d]	1370[e]
	($v''=0$; 97), ($v''=1$; 3)	($v''=0$; 100)
	875[f]	
	($v''=0$; 98), ($v''=1$; 2)	
	1623[b,c,d]	2740[g]
	($v''=0$; 100)	($v''=0$; 100)
Cationic	880	1330
	Dimethylamine	
Neutral	383[b,d]	670[g]
	($v''=0$; 84), ($v''=1$; 14), ($v''=2$; 2)	($v''=0$; 95), ($v''=1$; 5)
	735[b,d]	1130[e]
	($v''=0$; 96), ($v''=1$; 4)	($v''=0$; 99), ($v''=1$; 1)
Cationic	~520	1050
	Trimethylamine	
Neutral	366[b,d,h]	580
	($v''=0$; 88), ($v''=1$; 16), ($v''=2$; 2)	($v''=0$; 92), ($v''=1$; 7), ($v''=2$; 1)
Cationic	~400	660

Experimental values for the cationic state are collected in this work, see also Ref. 2. a) Refs. 4 and 15a. b) Ref. 33. c) Ref. 34. d) Ref. 35. e) Vibrational mode corresponding to ψ. f) Observed in Raman spectrum, taken from Ref. 36. g) Vibrational mode corresponding to η. h) Ref. 19.

propyl substitution indicates that for the amine with smaller alkyl groups, the cationic state is stabilized to a greater extent than the neutral state by the introduction of a longer alkyl group. It is a case for a series of aliphatic alcohols, in which the I_P values continue to decrease up to butyl substitution.[29] It seems that oxygen atom being more electronegative than nitrogen exhibits electron-attracting effect extending to longer range in alcohol than that in amine.

The half width δ of the first band decreases in the order of primary, secondary, and tertiary amine as shown in Fig. 4. The systematic decrease of δ with the length of alkyl group is also indicated. However there is unexpected behavior of I_P shown in the same figure that the value of $\Delta I_{Pv,th}$, the difference between I_{Pv} and I_{Pth}, does not exhibit such trend against the alkyl substitution. We will discuss the behavior of $\Delta I_{Pv,th}$ in the following section.

Potential Energy Curves. The potential energy curves calculated for the neutral and cationic state are shown in Figs. 5 and 6. The potential energy V used in this paper is referred to the minimum of the total energy for the neutral state. Potential energy curves shown in Fig. 5 are obtained by varying ψ under C_s symmetry and those in Fig. 6a by varying ϕ under symmetry of C_{3v} for ammonia and trimethylamine and C_3 for triethylamine.

Though the potential energy curves for neutral methylamine (2) and ethylamine (5) almost overlap as shown in Fig. 5, the curve for ethylamine cation radical is steeper than that for methylamine cation radical, and this is due to the fixed geometry within the ethyl group. Same trend is seen in the case of dimethylamine (3) or diethylamine (6).

As can be seen in Fig. 5, trimethylamine (4) and *N*,*N*-dimethylethylamine (7) have steeper curves at the larger $|\psi|$ for both the neutral and the cationic state. This is considered to be due to the steric hindrance of the bulky substituent group.

The geometries optimized for neutral ammonia and the methyl amines with planar nitrogen skeleton are included in Table 1. Obvious difference in CN and/or HN bond lengths exists between the molecules with the pyramidal and the planar nitrogen skeletons. These bonds are longer in the pyramidal form than in the planar form. The differences in total energy between the pyramidal and the planar form for the neutral state are 0.48, 0.45, 0.42, and 0.45 eV for am monia, methylamine, dimethylamine, and trimeth-

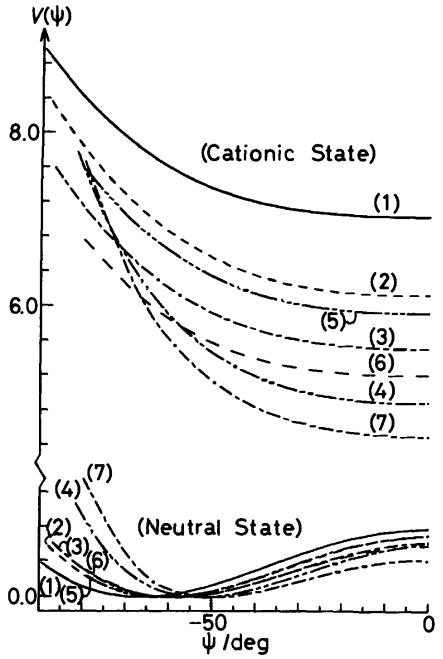

Fig. 5. Potential energy curves for ammonia and several alkylamines, against ψ under C_s symmetry. The notations 1 to 8 are the same as in Table 3. The molecular symmetry of (5) is C_1.

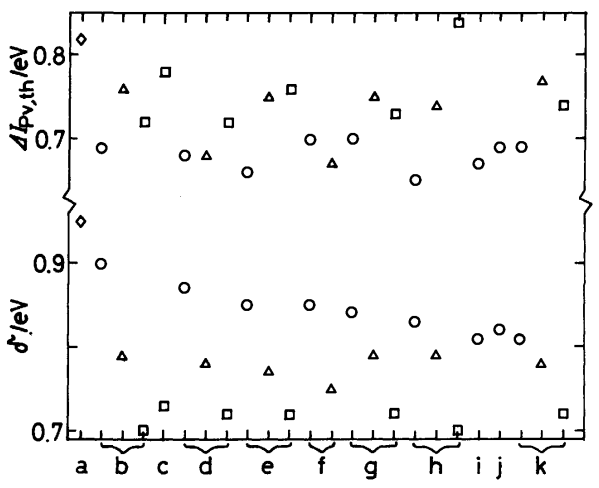

Fig. 4. Alkyl Substitution effect on $\Delta I_{Pv,th}$ and δ. Marks are the same as in Fig. 3.

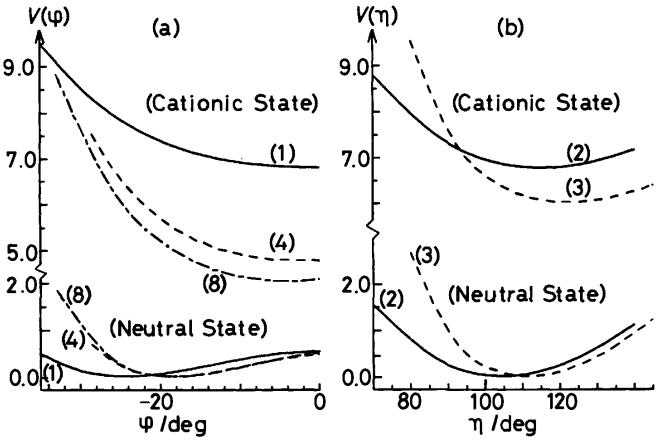

Fig. 6. Potential energy curves for several alkylamines, against ϕ under C_{3v} or C_3 symmetry (a), and against η under C_s symmetry (b). The notations are the same as in Table 3.

ylamine, respectivery. The differences corresponding to the amino inversion barrier are larger than those previously reported.[5a, 30] The barriers determined from Figs. 5 and 6a are even higher because the geometries at ψ or ϕ=0° are not energetically optimized.[31] Furthermore neglect of configuration interaction (CI) and lack of superior basis sets may well make the potential energy curves calculated here different from the actual ones. However, the fact that the MO calculations predict the drastic change on ψ or ϕ coordinate after the ionization suggests that the most important part of the intrinsic characters of the vibration induced by photoionization are describable with the present potential energy curves.

Potential energies as a function of the angle η were also calculated for methylamine and dimethylamine and are given in Fig. 6b. Although the value of η for each cation radical with the most stable geometry in the figure is different by about 10 degrees from that for the optimized geometry of neutral molecule, the curves for cation radical and neutral molecule are similar indicating that the deformation in η after the photoionization is small.

Band Shape of the Theoretical Photoelectron Spectrum. In order to obtain an envelope of a theoretical photoelectron band, we have carried out a following simple approach. First of all, we connected ψ or ϕ with an internal coordinate θ. A harmonic oscillator approximation on $V(\theta)$ gives a force constant and then a vibrational frequency is calculated by use of Willson's ***GF*** matrix method.[32] A wave function Ψ for the harmonic vibration is also calculated. Although it is well-known that an unharmonicity exists in the deformational vibration of amine at the large amplitude, we have neglected the unharmonic terms because of the simplicity of the calculation. Next, assuming a Boltzmann distribution at 320 K which is the temperature of the ionization chamber, the population p_i on each vibrational state i is obtained. The calculated frequencies and the populations are collected in Table 2 together with the experimental frequencies for ammonia and mono-, di-, and trimethylamine. Values of calculated frequencies are not in agreement with experimental ones. However, the following facts indicate that the essential property of molecular vibration in alkylamines concerned remains in the present potential energy curves; both experiment and calculation are in agreement on the point that the NH_2 wagging frequency is lower than the symmetric NH_2 deformational frequency for methylamine and that the CNC skeletal deformational frequency is lower than the a′ N–H deformational frequency for dimethylamine.

Now the theoretical photoelectron band *f* shown in Fig. 7 is obtained as follows. The curve *c*, Ψ_0^2, is projected on the potential energy curve *a* for cation radical and weighted with p_0 for the v''=0 state. This gives us the photoelectron spectrum intensity corresponding to the ionization from v''=0. Then the photoelectron spectrum *f* is obtained as the accumulation of all the ionizations from the vibrational states whose population is larger than 1%. In Fig. 8 are shown the theoretical photoelectron spectra for amines calculated in this work. In the figure, each spectrum is shifted in energy so that the maximum corresponding to I_{Pv} comes on the same position on abscissa. It is assumed for the simplicity of the

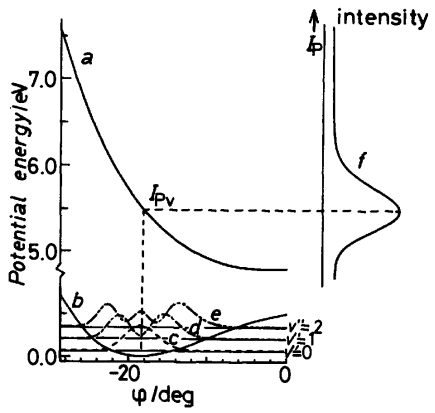

Fig. 7. Potential energy curves for the neutral (*b*) and the cationic (*a*) state of trimethylamine, the square of the wave function (Ψ_1^2) (*c*, *d* and *e*), and the photoelectron band (*f*) evaluated from them.

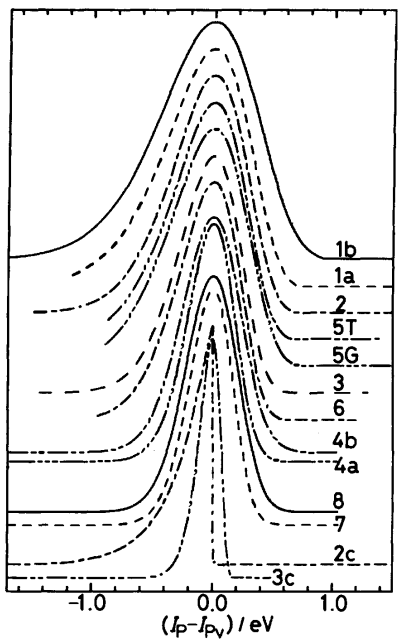

Fig. 8. Theoretical photoelectron band. The numerical notations are the same as in Table 3.
a; calculated under C_s symmetry and b; calculated under C_{3v} symmetry. T; trans conformation, G; gauche conformation. c; the curves noted with c are band shapes calculated under the assumption that only the coordinate of η vibrates.

theoretical treatment that the vibrational levels for the cationic state are continuous. This is not correct from the quantum chemical point of view. However because the vibrational symmetries for the neutral and cationic molecules are same, the curve obtained in this manner should be comparable to the envelope of the experimental photoelectron spectrum. In Fig. 8 are also shown the theoretical photoelectron bands arising from the vibration on η for methylamine and dimethylamine. Both of them are sharp and I_{Pth} is equal or close to I_{Pv}. This indicates that this kind of vibration less contributes to the band shape.

The band width δ and threshold energy I_{Pth} are determined from the theoretical photoelectron bands. The I_{Pth} is read at the onset whose intensity is 1% of the band maximum. Table 3 contains the theoretical values for δ, I_{Pth}, I_{Pa}, and I_{Pv}, together with experimental ones. The $I_{Pv}(\Delta SCF)$ is defined as a difference in total energy between the neutral and the cationic state with the same geometry which is the most stable for the neutral state. The I_{Pa} is defined as a difference in minimum total energy between the neutral and the cationic state each with the most stable geometry.

The calculated values of I_{Pth} are always larger than those of calculated I_{Pa}. This owes to the fact that the I_{Pa} is the difference in total energy between optimized geometries for the neutral and cationic state, while the I_{Pth} is evaluated by use of the potential energy curves as a function of only ψ or ϕ. That makes the total energy for cation radical at the minimum-energy point on the potential energy curve more unstable than that with the optimized geometry.[31] The theoretical values of I_{Pv}, I_{Pa}, and I_{Pth} are underestimated, and if a constant value of 3.1 eV is added to the theoretical values of I_{Pv}, they are in excellent agreement with the experimental ones. The calculations also predict the values of δ very well as shown in Fig. 9 in which the theoretical and experimental values are compared.

Band Width. The band width and the band shape depend on the following factors: (i) The difference in geometry between the neutral and cationic molecule each with the most stable geometry; (ii) the vibrational wave function for the neutral state which is based on the feature of the potential energy curve for the neutral state; (iii) the slope of the potential energy curve for the cationic state.

The calculated δ must be underestimated because the potential energy at minimum on the potential energy curve for cation radical is higher than that for the cation radical with the optimized geometry,[31] i.e., the potential energy curve for cation radical should be steeper. For ammonia and trimethylamine we have obtained the theoretical photoelectron band by two methods. One is the use of the potential energy curve for C_{3v} symmetry and the other is the use of C_s symmetry, i.e., the potential energy curve obtained as a function of ψ, while fixing the angle η to the value for the optimized geometry for the neutral state (1b and 4b in Fig. 8). δ's evaluated under the C_s symmetry have reproduced the experimental values more poorly

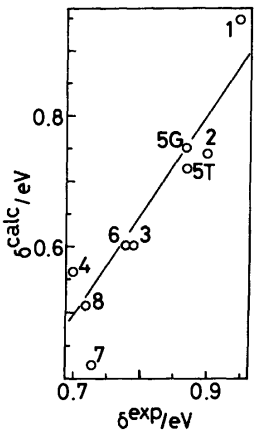

Fig. 9. Comparison between experimental and calculated δ. The notations are the same as in Table 3. G; gauche conformation. T; trans conformation.

Table 3. Experimental and Theoretical Ionization Potentials and Bandwidths (δ) (in eV)

	I_{Pv}		I_{Pa}[a]	I_{Pth}		δ		$\Delta I_{Pv,a}$	$\Delta I_{Pv,a}$[b]	I_{Pa}[c]	I_{Pa}[d]
	exp	calcd	calcd	exp	calcd	exp	calcd	calcd	corr	corr	corr
1) Ammonia	10.90	7.79	6.76	10.08	6.91	0.95	0.95	1.03	—	—	—
2) Methylamine	9.64	6.86	5.88	8.95	6.19	0.90	0.74	0.98	0.68	8.96	8.95
3) Dimethylamine	8.94	6.15	5.19	8.18	5.55	0.79	0.60	0.96	0.66	8.28	8.27
4) Trimethylamine	8.51	5.54	4.64	7.79	4.84	0.70	0.56	0.90	0.60	7.91	7.89
5) Ethylamine	9.46	6.67	5.68	8.78	5.98	0.87	0.75	0.99	0.69	8.77	8.78
6) Diethylamine	8.67	5.80	4.86	7.99	5.25	0.78	0.60	0.94	0.64	8.03	8.08
7) *N,N*-Dimethylethylamine	8.39	5.11	4.36	7.61	4.61	0.73	0.42	0.75	0.45	7.49	7.71
8) Triethylamine	8.09	5.02	4.16	7.37	4.42	0.72	0.51	0.86	0.56	7.53	7.47

a) The difference in total energies of the neutral molecule and the cation radical each with equilibrium geometry. b) Corrected $\Delta I_{Pv,a}$. c) $I_{Pv}{}^{exp} - \Delta I_{Pv,a}{}^{corr}$. d) Determined by adding the energy of a vibrational quanta to $I_{Pth}{}^{exp}$, see text.

than those under the C_{3v} symmetry. This is chiefly due to the fixed angle η.

As shown in Fig. 9 the deviation from the correlation line between experimental and calculated values is large for the case of *N,N*-dimethylethylamine. δ for this amine is quite underestimated because of the fixed CNC skeleton the same as the case of trimethylamine calculated under C_s symmetry. There is some limitation in the present method to estimate band width of the UPS, because the potential energy curve used is a cross section of potential energy hypersurface taken only on a single coordinate on which the change after the photoionization is greatest.

Threshold Ionization Potential and Potential Energy Curve. The I_{Pth} mainly depends on the next three factors: (I) The difference in the geometry between the neutral molecule and the cation radical each with the most stable structure; (II) the population on each vibrational level for the neutral state; (III) the value of vibrational probability density Ψ_0^2 for the neutral state with the geometry similar to the equilibrium geometry for the cationic state. When the difference for (I) is large, I_{Pa} may well be smaller than I_{Pth} and intrinsically undetectable in UPS. While the larger population on a higher vibrational level causes larger probability of hot band. When the value for (III) is large, I_{Pa} should be detectable. Note that even if the value for (I) is large, the large value for (III) makes I_{Pa} detectable.

It is interesting that although it is impossible to predict the values of $\Delta I_{Pv,th}$ accurately from the theoretical potential energy curves, the values of δ are predicted excellently from the curves as shown in Fig. 9 (except *N,N*-dimethylethylamine). This implies that the present potential energy curve for cation radical is distorted only around the equilibrium geometry for cation radical. With respect to *N,N*-dimethylethylamine, both δ and $\Delta I_{Pv,th}$ deviate from the correlation between experimental and calculated values. Thus the slope on the calculated curve for *N,N*-dimethylethylamine cation radical is gentler than the actual curve.

While I_P and δ systematically vary in the order of primary, secondary and tertiary amine, $\Delta I_{Pv,th}$ does not. This can be interpreted as follows. The populations on the higher vibrational levels for the neutral state increase in the order of primary, secondary and tertiary amine, since the vibrational frequency decreases in the same order. On the other hand the probability density Ψ_0^2 at the most stable geometry of cation radical decreases in the order of primary, secondary and tertiary amine. The two opposing factors result in the unsystematic order of $\Delta I_{Pv,th}$ as shown in Fig. 4.

Determination of Adiabatic Ionization Potential. The first ionization peak 10.075 eV in the UPS of ammonia, observed also by several other workers,[6b,7,11] has been regarded as the hot band.[6b,7] Population on $v''=1$ is, however, 1% as listed in Table 2, and the ratio of Ψ_1^2 to Ψ_0^2 at the equibrium geometry of ammonia cation radical is very small. Thus 0←1 ionization peak, i.e., hot band, should be indiscernible in the UPS. If the first peak were the 0←1 ionization peak, intensity of the first peak should be a few hundredth of that of the second peak according to Boltzmann distribution, since ionization cross section for the same vibrational mode is similar. The ratio of the first peak height to the second in the UPS is 0.24 and is too large to assign the first peak to 0←1 ionization peak. Then we conclude that the first peak is not the 0←1 but the 0←0 ionization peak, and that I_{Pa} is 10.08 eV. As for primary amines, the frequency of deformation vibration of ψ, viz., NH_2 wagging vibration, is in the range of 850—750 cm^{-1} from the infrared spectra of liquid phase,[36] so the population on $v''=1$ should be 2—4%. Peak height of the first peak in the vibrational progression in the first band for methylamine and ethylamine, compared to that of the second peak, however, is too large to assign the first peak to 0←1 ionization peak. Therefore the first peaks for methylamine and ethylamine pertain to the 0←0 ionization peak and the I_{Pa}'s are 8.95 and 8.78 eV, respectively.

Now we estimate I_{Pa}'s for mono-, di-, and trimethylamine and the ethylamines by use of I_{Pa}^{calcd} calculated here and experimental I_{Pth}^{exp}. I_{Pa}^{calcd} is largely underestimated because of the neglect of CI and the lack of superior basis set. So is I_{Pv}^{calcd}, but one expects that this is somewhat canceled out in the difference $\Delta I_{Pv,a}^{calcd}(=I_{Pv}^{calcd}-I_{Pa}^{calcd})$. $\Delta I_{Pv,a}^{corr}$ is obtained by adding 0.30 eV to $\Delta I_{Pv,a}^{calcd}$. The correction of 0.30 eV gives $\Delta I_{Pv,a}^{calcd}$ equal to $\Delta I_{Pv,th}^{exp}$ for methylamine and ethylamine. Finally I_{Pa} is estimated by subtracting $\Delta I_{Pv,a}^{corr}$ from I_{Pv}^{exp}. The values of I_{Pa} are included in Table 3 together with $\Delta I_{Pv,a}^{calcd}$ and $\Delta I_{Pv,a}^{corr}$. The difference between I_{Pa} and I_{Pth}^{exp} are 0.12 and 0.16 eV for trimethylamine and triethylamine, respectively. These values indicate that the hot band should be observable and that the hot band can be at least 0←2 ionization peak if considered that the frequency of the vibration of ϕ for neutral trimethylamine and triethylamine is about 0.05 eV.[36] For diethylamine the difference between I_{Pa} and I_{Pth}^{exp} is 0.05 eV, and this indicates that the hot band may be observable, or that the difference is only the error produced in the calculation because the frequency of the vibration of ψ is about 0.09 eV.[36] The difference for dimethylamine is 0.09 eV, and the hot band, 0←1 ionization peak, may exist. However, the hot band should not be observabvle, if the population p_1 and probability density Ψ_1^2 of the neutral state at the equilibrium geometry of the cation radical are considered. The hot band of dimethylamine may be due to the coupling of the vibration of ψ with other

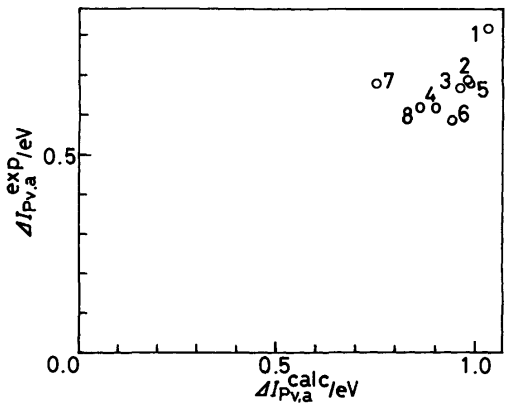

Fig. 10. Comparison between experimental and calculated $\Delta I_{Pv,a}$. The notations are the same as in Table 3.

vibrations.

According to the discussions one can estimate the thermodynamic I_{Pa} by combining photoelectron spectroscopic I_{Pth} and vibrational energy. Assuming that 0←1 and 0←2 ionizations are observable for the secondary and the tertiary amines, respectively, the values for I_{Pa} are obtained by adding 0.09 eV to I_{Pth} for the secondary and 0.10 eV for the tertiary amines and are listed in Table 3. By using the I_{Pa} obtained in this manner, we can obtain the values of $\Delta I_{Pv,a}^{exp}$, which are compared with the theoretical $\Delta I_{Pv,a}$'s in Fig. 10. The correlation indicates that 0.3 eV subtraction from the theoretical value predicts the experimental one excellently, except for ammonia, triethylamine and *N,N*-dimethylethylamine. This result also supports the present determination of the thermodynamic I_{Pa} for amines.

The authors wish to thank Professor Takayuki Fueno and Dr. Kizashi Yamaguchi, Department of Chemistry, Faculty of Engineering Science, Osaka University for the computer program of the IMSPACK revised for the computer in Osaka University. The calculations were carried out using HITAC M-200H at the computer center of IMS (Institute for Molecular Science) and ACOS NEAC 1000 at the computation center, Osaka University.

References

1) J. H. D. Eland, "Photoelectron Spectroscopy," Butterworth and Co., London (1974), Chap. 5.

2) M. Takahashi, I. Watanabe, and S. Ikeda, *J. Electron Spectrosc. Relat. Phenom.*, **37**, 275 (1985).

3) M. Takahashi, I. Watanabe, and S. Ikeda, *J. Phys. Chem.*, **87**, 5059 (1983).

4) G. Hertzberg, "Infrared and Raman Spectra of Polyatomic Molecules II. Infrared and Raman Spectra of Polyatomic Molecules," D. Van Nostrand Co., New York (1945).

5) a) R. A. Eades, D. A. Weil, D. A. Dixon, and C. H. Douglass, Jr., *J. Phys. Chem*, **85**, 976 (1981); b) S. Profeta, Jr. and N. L. Allinger, *J. Am. Chem. Soc.*, **107**, 1907 (1985).

6) a) A. D. Walsh and P. A Warsop, *Trans. Faraday Soc.*, **57**, 345 (1961); b) A. W. Potts and W. C. Price, *Proc. R. Soc. London, Ser. A*, **326**, 181 (1972).

7) D. H. Aue, H. M. Webb, and M. T. Bowers, *J. Am. Chem. Soc.*, **97**, 4136 (1975).

8) M. E. Wocks, *J. Chem. Phys.*, **41**, 930 (1964); b) T. E. Sharp and H. M. Rosenstock, *J. Chem. Phys.*, **41**, 3453 (1964); c) M. Halmann and I. Laulicht, *J. Chem. Phys.*, **43**, 1503 (1965).

9) a) P. M. Dehmer and J. L. Dehmer, *J. Chem. Phys.*, **69**, 125 (1978); b) P. M. Dehmer and J. L. Dehmer, *J. Chem. Phys.*, **68**, 3462 (1978).

10) a) W. R. Harshbarger, *J. Chem. Phys.*, **53**, 903 (1970); b) *ibid*, **56**, 177 (1972); c) P. Avouris, A. R. Rossi, and C. Albrecht, *J. Chem. Phys.*, **74**, 5516 (1981).

11) J. W. Rabalais, L. Karlsson, L. O. Werme, T Bergmerk, and K. Siegbahn, *J. Chem. Phys.*, **58**, 3370 (1973).

12) a) S Tomoda and K. Kimura, *Chem Phys.*, **82**, 215 (1983); b) S. Tomoda and K. Kimura, *Chem. Phys. Lett.*, **111**, 434 (1984); c) S. Tomoda and K. Kimura, *Chem. Phys. Lett.*, **121**, 159 (1985).

13) K. Morokuma, S. Kato, K. Kitaura, I. Ohmine, S. Sakai, and S. Obara, IMS Computer Center Library, Institute for Molecular Science, No. 0372 (1980).

14) The calculated bond lengths and angles for ammonia, and mono-, di-, and trimethylamine agree with the experimental values[4,15-19] within a few hundredths of an angstrom and within a few degrees. The structural parameters for ethylamine are similar to those used in Ref. 20b. For mono-, di-, and triethylamine, the calculated conformations of the neutral state are in agreement with the result of experiment as follows. Most stable conformation of ethylamine has been reported to be either G (gauche) conformation with respect to the lone pair of the nitrogen,[20] or T (trans) conformation.[21] We have found that the G conformation is the most stable. However, the energy difference between these two conformations is only 8 meV which is less than the noise level of the computational technique, which is also stated in Ref. 5b. Diethylamine takes TT (trans-trans) conformation, i.e., each ethyl group has a methyl group at trans position with respect to the other ethyl group.[22] Triethylamine takes G'G'G' conformation, i.e., each of the methyl group comes to the gauche position against the lone pair and other ethyl groups.[23] While another stable conformations were reported to be present,[23,24] we have taken the conformation of this molecule as G'G'G' which is the result of the present geometry optimization. The structural parameters for the neutral ammonia and mono-, di-, and trimethylamine are in good agreement with those calculated by others.[5,25-27] The conformations calculated by L. Radom et al.[28] for the neutral methylamine, dimethylamine and ethylamine are in reasonable agreement with the present results. For ethylamine cation radical the difference in total energy between T conformation and G conformation has been only 3 meV.

15) a) W. S. Benedict and E. K. Plyler, *Can. J. Phys.*, **35**, 1235 (1957); b) Y. Morino, K. Kuchitsu, and S. Yamamoto, *Spectrochim. Acta*, **24A**, 235 (1968); c) K. Kuchitsu, J. P.

Guillory, and L. S. Bartell, *J. Chem. Phys.*, **49**, 2488 (1968).

16) a) T. Nishikawa, T. Itoh, and K. Shimoda, *J. Chem. Phys.*, **23**, 1735 (1955); b) D. R. Lide, Jr., *J. Chem. Phys.*, **27**, 343 (1957); c) H. K. Higginbotham and L. S. Bartell, *J. Chem. Phys.*, **42**, 1131 (1964); d) K. Takagi and T. Kojima, *J. Phys. Soc. Jpn.*, **30**, 1145 (1971).

17) a) J. E. Wollrab and V. W. Laurie, *J. Chem. Phys.*, **48**, 5058 (1968); b) B. Beagley and T. G. Hewitt, *Trans. Faraday Soc.*, **65**, 2565 (1968).

18) a) D. R. Lide, Jr. and D. E. Mann, *J. Chem. Phys.*, **28**, 572 (1958); b) J. E. Wollrab and V. W. Laurie, *J. Chem. Phys.*, **51**, 1580 (1969).

19) J. N. Gayles, *Spectrochim. Acta.*, **23A**, 1521 (1967).

20) a) P. J. Krueger and J. Jan, *Can. J. Chem.*, **48**, 3229 (1970); b) A. S. Manocha, E. C. Tuazon, and W. G. Fateley, *J. Phys. Chem.*, **78**, 803 (1974).

21) a) J. R. Durig and Y. S. Li, *J. Chem. Phys.*, **63**, 4110 (1975); b) M. Tsuboi, K. Tamagake, A. Y. Hirakawa, J. Yamaguchi, H. Nakagawa, A. S. Manocha, E. C. Tuzan, and W. G. Fateley, *J. Chem. Phys.*, **63**, 5177 (1975).

22) A. L. Verma, *Spectrochim. Acta, Part A*, **27A**, 2433 (1971).

23) C. H. Bushweller, S. H. Fleischman, G. L. Grady, P. McGoff, C. D. Rithner, M. R. Whalon, J. G. Brennan, R. P. Marcantonio, and R. P. Domingye, *J. Am. Chem. Soc.*, **104**, 6224 (1982).

24) K. Kamur, *Chem. Phys. Lett.*, **9**, 504 (1971).

25) a) A. Rauk, L. C. Allen, and E. Clementi, *J. Chem. Phys.*, **52**, 4133 (1970); b) W. A. Lathan, W. J. Hehre, L. A. Curtiss, and J. A. Pople, *J. Am. Chem. Soc.*, **93**, 6377 (1971); c) D, J. Defrees, B. A. Levi, S. K. Pollack, W. J. Hehre, J. S. Binkley and J. A. Pople, *J. Am. Chem. Soc.*, **101**, 4085 (1979); d) W. R. Rodwell and L. Radom, *J. Chem. Phys.*, **72**, 2205 (1980); e) P. Puley, G. Forarasi, F. Pang, and J. E. Boggs, *J. Am. Chem. Soc.*, **101**, 2550 (1979).

26) a) P. Pulay and E. Török, *J. Mol. Struct.*, **29**, 239 (1975); b) E. Flood, P. Puley, and J. E. Boggs, *J. Am. Chem. Soc.*, **99**, 5570 (1977).

27) S. Skaarup, L. L. Griffin, and J. E. Boggs, *J. Am. Chem. Soc.*, **98**, 3140 (1976).

28) L. Radom, W. J. Hehre, and J. A. Pople, *J. Am. Chem. Soc.*, **94**, 2371 (1972).

29) A. D. Baker, D. Betteridge, N. R. Kemp, and R. E. Kirby, *Anal. Chem.*, **43**, 375 (1971).

30) J. M. Lehn, *Fortchr. Chem. Forsch.*, **15**, 311 (1970).

31) Because of the fixed structural parameters except ψ or ϕ, minimum total energies of the cation radicals on the present potential energy curves are higher than those with the optimized geometries by the following values; 0.04 eV for ammonia, 0.23 eV for methylamine, 0.29 eV for dimethylamine, 0.14 eV for trimethylamine, 0.22 eV for ethylamine both with G and T conformations, 0.32 eV for diethylamine, 0.12 eV for *N,N*-dimethylethylamine, and 0.18 eV for triethylamine.

32) E. B. Wilson, Jr., J. C. Decius, and P. C. Cross, "Molecular Vibrations," McGraw-Hill Inc., New York (1980).

33) G. Dellepine and G. Zerbi, *J. Chem. Phys.*, **48**, 3573 (1968).

34) A. Y. Hirakawa, M. Tsuboi, and T. Shimanouchi, *J. Chem. Phys.*, **57**, 1236 (1972).

35) From infrared spectra for mono-, di-, and trimethylamine, of Refs. 33 and 34, the bond angle deformation frequencies about nitrogen skeleton are as follows: for methylamine, 780 cm^{-1} corresponding to mainly θ and partly to η, and 1623 cm^{-1} corresponding to mainly η and partly to θ; for dimethylamine 383 cm^{-1} corresponding to mainly η and partly to θ and to torsional angle around C-N axis, and 735 cm^{-1} corresponding to mainly θ and partly to C-N bond length; for trimethylamine 366 cm^{-1} dominantly corresponding to θ. In Raman spectra similar vibrations have also been reported.[36]

36) F. R. Dollish, W. G. Fateley, and F. F. Bentley, "Characteristic Raman Frequencies of Organic Compounds," Wiley-Interscience, N. Y. (1973).

 © 1987 The Chemical Society of Japan Bull. Chem. Soc. Jpn., 60, 19—23 (1987)

Racemization of Mandelic Acid at the Surface of Talc Powder

Akiko IKEKAWA* and Sohachiro HAYAKAWA†
Faculty of Pharmaceutical Sciences, Showa University,
Hatanodai 1-5-8, Shinagawa-ku, Tokyo 142
†Laboratory of Applied Physics, Faculty of Engineering, Chiba University,
Yayoi-cho 1-33, Chiba 260
(Received May 10, 1986)

The addition of talc powder in an ethanolic solution of mandelic acid gave a large change of its optical rotation. It was confirmed by absorption spectrography, thin-layer chromatography, and gas chromatography that mandelic acid was racemized at the surface of the talc powder. The IR spectra showed that racemization took place when mandelate anions adsorved weakly at the surface of the talc. It was concluded that the H atom at the C atom in the second position of a mandelate anion was adsorbed at a basic site of the talc surface to deprotonate and also that the deprotonation was enhanced by the interaction between the carboxyl group and an acidic site.

Racemization of an optically active substance is of great interest with regard to the origin of life. Furthermore, racemization is of practical importance in pharmaceutical technology. In the case of such substances as amino acids, only one enantiomer is physiologically active. The inactive enantiomer can be converted into the active enantiomer by racemization.

Previously, the authors reported mechanochemical racemization of L-leucine in the presence of such an inorganic powder as talc.[1] This paper deals with the racemization of optically active mandelic acids in suspensions of talc.

Experimental

The materials used were *S*(+)-mandelic acid [*S*(+)-α-hydroxyphenylacetic acid] and *R*(−)-mandelic acid purchased from Aldrich Chemical Co. The samples of inorganic powder used were kaolin (acid washed, American standard) of Fisher Scientific Company, talc of Sanko Seiyaku Co., SiO_2 (precipitated) of Koso Chemicals Co., and γ-Al_2O_3 of Nishio Kogyo Co. The following samples were prepared:

$Talc_{AA}$: Talc was set aside in a vapor of acetic acid at a room temperature for more than 2 d, it was then washed with ethanol several times and dried at 60 °C.

$Talc_{TEA}$: Talc was set aside in a vapor of triethylamine at a room temperature for more than 2 d, it was then washed with ethanol several times and dried at 60 °C.

Inorganic Powder-M: After the suspension of the inorganic powder in an ethanol solution of mandelic acid had been set aside at 5 °C for more than 1 d, the supernatant was removed and the precipitation was dried at 60 °C. Ethanol, 2-propanol, 2-butanol, and formic acid were of guaranteed grade. Dioxane and cyclohexane, both of a guaranteed grade, were dried with molecular sieves 4A of Wako Pure Chemicals Industries, Ltd.

A certain amount of inorganic powder was added to the flask containing 30 ml of a mandelic acid solution, and the following processes were carried out at 5 °C or 20 °C; (i) the mixture was set aside after a vigorous shaking, (ii) it was stirred at 190 rpm., or (iii) it was stirred at 380 rpm. An aliquot of these suspensions was taken into a test tube at several intervals. (iv) Separately, 3—5 ml of an ethanol solution of mandelic acid were added to a test tube containing a certain amount of inorganic powder. The test tube was shaken vigorously, and then set aside at 5 °C for 1 h. The optical rotation of the supernatants obtained by centrifuging these suspensions were measured with a JASCO digital polarimeter (Model DIP-140). The absorption spectra of these supernatants were obtained using a Hitachi recording spectrophotometer (Model 340). The concentrated solutions of the supernatants were developed on thin layers of silica gel with a solvent system of 2-butanol-2-propanol-formic acid-water (15:15:4:10).[2] Gas chromatographic determination of the trimethylsilyl derivatives of mandelic acid in the supernatant was carried out at 170 °C with a Shimadzu gas chromatograph (Model 6A), using a column containing 10% SE 52 chromosorb W 60/80 mesh treated with AW-HMDS of Shimadzu Seisakusho.[3] IR spectra were measured with a JASCO diffraction granting infrared spectrophotometer (Model A-2). The Hammett's acidity function, H_0, and basicity function, H_0', for inorganic powder were obtained by the indicator method.[4]

Results and Discussion

Racemization of Mandelic Acid at the Surface of Talc Powder. In Figs. 1 and 2, α is the optical rotation of the supernatant obtained by centrifuging an ethanolic suspension of mandelic acid and talc. The value of $|\alpha|$ decreased immediately after adding talc to the solution of the optically active mandelic acid at 5 °C, though the value remained constant after the lapse of more than 10 min. Figure 3 shows the effect of talc on the absorption spectra of an ethanol solution of mandelic acid. The absorbance around 250—260 nm increased on addition of talc. According to many studies concerning the degradation of mandelic acid on oxidation or γ-irradiation, the main products are benzaldehyde, benzoic acid, and phenylglyoxylic acid.[5] On fractionating these solutions by thin-layer chromatography, benzoic acid was confirmed to be formed, but no spot corresponding to any product other than benzoic acid was observed. The areas of ΔABD, S_{252}, and ΔBCE, S_{257}, were not changed by adding talc. The concentrations of mandelic acid

in the solutions were determined using gas chromatography. The concentrations in the supernatants in Fig. 3 were identical with the concentration in the original solution. These results show that degradation and adsorption of mandelic acid at the surface of talc are negligible. It is also confirmed that optically active mandelic acids are racemized at the surface of talc, though the diastereomers of these active forms were not separated because of the difficulty in synthesis.

Effect of the Polarity of Solvents. In Table 1, α_0 is the optical rotation of the original mandelic acid solution, and $\Delta\alpha$ is equal to $\alpha_0-\alpha$. The value of $|\Delta\alpha|$ obtained by adding a mandelic acid solution to a suspension of talc, which had been stirred for more than 10 min, was smaller than the value obtained by adding talc to a mandelic acid solution. This fact shows that solvent molecules and mandelic acid molecules compete with each other for the surface of the talc. Bubbling nitrogen gas during stirring did not show any effect on $|\Delta\alpha|$; this fact shows that oxygen has little effect on racemization. The effect of the polarity of solvents on racemization was investigated, using the mixtures of various ratios of dioxane and cyclohexane at 20 °C. Here, $(\overline{S}/S_0)$ stands for $1/2\{(S_{252}/S_{252,0})+(S_{257}/S_{257,0})\}$, where $S_{252,0}$ and $S_{257,0}$ are S_{252} and S_{257} for original solutions, respectively. $(\overline{S}/S_0)$ was proportional to the concentration of mandelic acid determined by gas chromatography. As is shown in Table 1, $(\overline{S}/S_0)$ decreased on interaction with talc and this tendency became greater with decrease in the polarity of the solvent. Probably, the adsorption of mandelic acid on the surface of talc is greater in the solvent of lower polarity. The racemization percentage, R, is defined as $[\{(\overline{S}/S_0)-(\alpha/\alpha_0)\}/(\overline{S}/S_0)]\times100$. As is shown in Table 1, racemization does not take place in the suspension containing 5 v/v% of dioxane, though R is 4—15% in the suspension containing more than 10 v/v% of

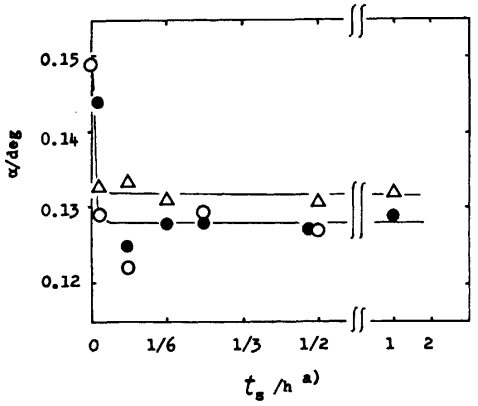

Fig. 1. Decrease in α of an ethanol solution of $S(+)$-mandelic acid at the surface of talc powder.
6.6×10^{-3} M of $S(+)$-mandelic acid solution: 30 ml, talc: 10 g, temperature: 5 °C.
Stirring velocity/rpm
△: 0, ●: 190, ○: 380
a) t_s is the stirring time.

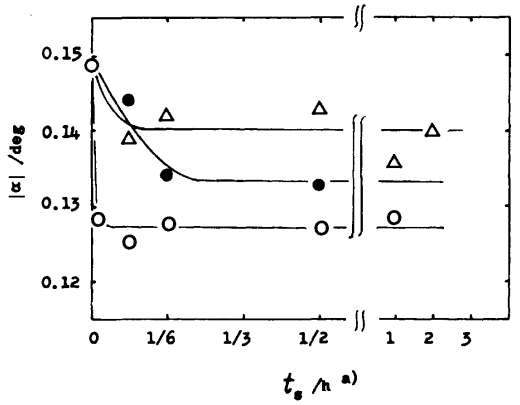

Fig. 2. Decrease in $|\alpha|$ of an ethanol solution of $R(-)$-mandelic acid at the surface of talc powder.
6.6×10^{-3} M of $R(-)$-mandelic acid solution: 30 ml, talc: 10 g, temperature: 5 °C.
Stirring velocity/rpm
△: 0, ●: 190, ○: 380
a) t_s is the stirring time.

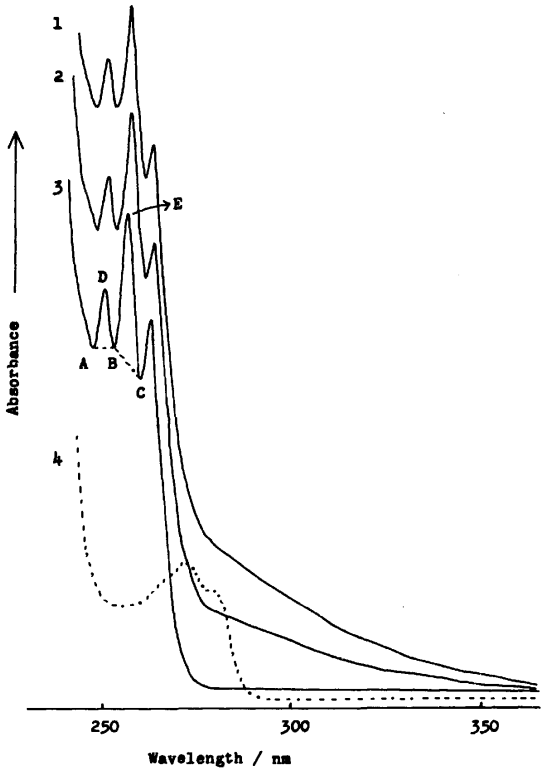

Fig. 3. Effect of talc on absorption spectra of an ethanol solution of mandelic acid.
1: The supernatant of the suspension of "3" and talc stirred for 30 min. 2: The supernatant of the suspension of "3" and talc stirred for 3 min. 3: An ethanol solution of 6.6×10^{-3} M of $S(+)$-madelic acid. 4: An ethanol solution of 4.6×10^{-4} M of benzoic acid.
Experimental conditions for "1" and "2"; "3" 30 ml, talc 10 g, temperature 5 °C, stirring velocity 190 rpm.

dioxane. This suggests that racemization is an ionic reaction.

Complex Formation. It is clear from Figs. 4 and 5 that Eq. 1 is applicable;

$$\Delta\alpha = K' W_T{}^n C^m, \quad 0<m, n<1, \tag{1}$$

where K' is a constant, W_T the amount of talc added to the suspension, and C the concentration of mandelic acid in the original solution. It is assumed that a complex M-T is formed between mandelic acid, M, and talc, T, as is shown in Eq. 2, and that Eq. 3 is applied;

$$\text{M+T} \rightleftarrows \text{M-T}, \quad K = [\text{M-T}]/[\text{M}][\text{T}], \tag{2}$$

$$\Delta\alpha \propto [\text{M-T}] \propto [\text{M}][\text{T}], \tag{3}$$

where [M] and [M-T] are the concentrations of M and M-T, respectively, [T] is the amount of T, and K a constant. In this case, Eqs. 4 and 5 are applied;

$$C = [\text{M}] + [\text{M-T}], \tag{4}$$

$$W_T = [\text{T}] + [\text{M-T}]. \tag{5}$$

Equation 6 is obtained from the above equations;

$$\Delta\alpha = K''\{C/(1+K[\text{M}])\}\{W_T/(1+K[\text{T}])\}, \tag{6}$$

where K'' is a constant. Equation 1 is similar to Eq. 6. This suggests that complex formation between mandelic acid and talc participates in racemization. As is shown in Table 1, the value of R in ethanol at 20 °C was lower than the value at 5 °C. Probably, dissociation of the complex is more remarkable at 20 °C than at 5 °C.

Active Sites at the Surface of Talc. Fukui et al. reported that both acidic and basic sites participated in dehydration of 2-propanol at the surface of talc.[6] Table 2 shows the values of Hammett's acidity function, H_0, and basicity function, H_0', for various talcs obtained by the indicator method.[4] Acidic sites with H_0 smaller than the pK_a value of mandelic acid (3.7 at 25 °C) are absent at the surface of $talc_{TEA}$. Basic sites are expected to be absent at the surface of $talc_{AA}$. On adding these talcs to an ethanolic solution of

Table 1. Racemization of $S(+)$-Mandelic Acid on Talc in Various Solvents
mandelic acid concentration; 6.6×10^{-3} M
experimental conditions; (iii)

T[a] °C	Solvent	t_s[b] min	$(\bar{S}/S_0)$	α/α_0	R[c] %
	Dioxane-Cyclohexane				
	1 : 0[d]	1	0.980	0.863	11.9
		3—15[e]	0.925	0.887	4.1
	1 : 9	1	0.890	0.760	14.6
20		15	0.713	0.655	8.1
	1 : 19	1	0.673	0.665	1.2
		7	0.434	0.446	—
		15	0.338	0.363	—
	Ethanol	1	0.984	0.895	9.1
		3—15[e]	0.972	0.926	4.7
5	Ethanol	1	1.00	0.865	13.5
		30	1.00	0.853	14.7

a) T is the temperature. b) t_s is the stirring time. c) $R=[\{(\bar{S}/S_0)-\alpha/\alpha_0\}/\bar{S}/S_0)]\times100$, R represents racemization percentage. d) These ratios are represented by volume. e) The data are the mean values for the stirring time between 3 min and 15 min, for $(\bar{S}/S_0)$ and α/α_0 remained nearly constant in these cases after a lapse of 3 min.

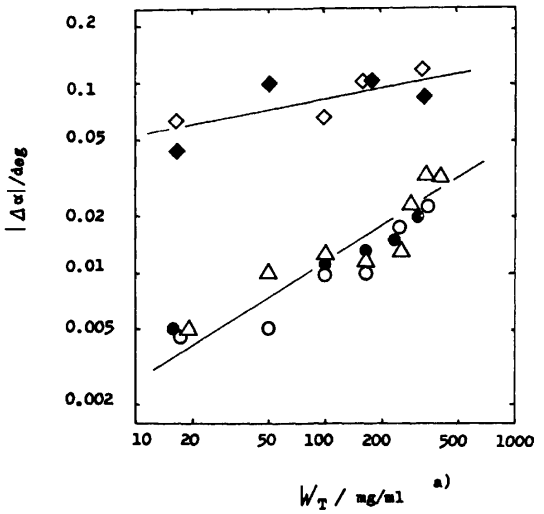

Fig. 4. Variation in α with the amount of talc

mandelic acid	concentration of mandelic acid / M	experimental conditions
◇ S	6.6×10^{-2}	(iv)
◆ R	6.6×10^{-2}	(iv)
△ S	6.6×10^{-3}	(iv)
○ S	6.6×10^{-3}	(iii)
● R	6.6×10^{-3}	(iii)

Solvent: ethanol, Temperature: 5 °C
a) W_T is the amount of talc.

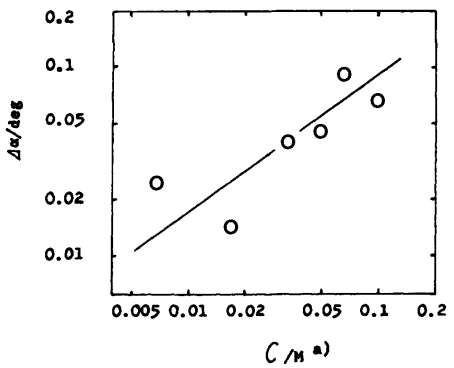

Fig. 5. Variation in α with the concentration of mandelic acid experimental conditions; (iv), solvent: ethanol, the amount of talc: 1 g/3 ml, temperature: 5 °C a) C is the concentration of $S(+)$-mandelic acid.

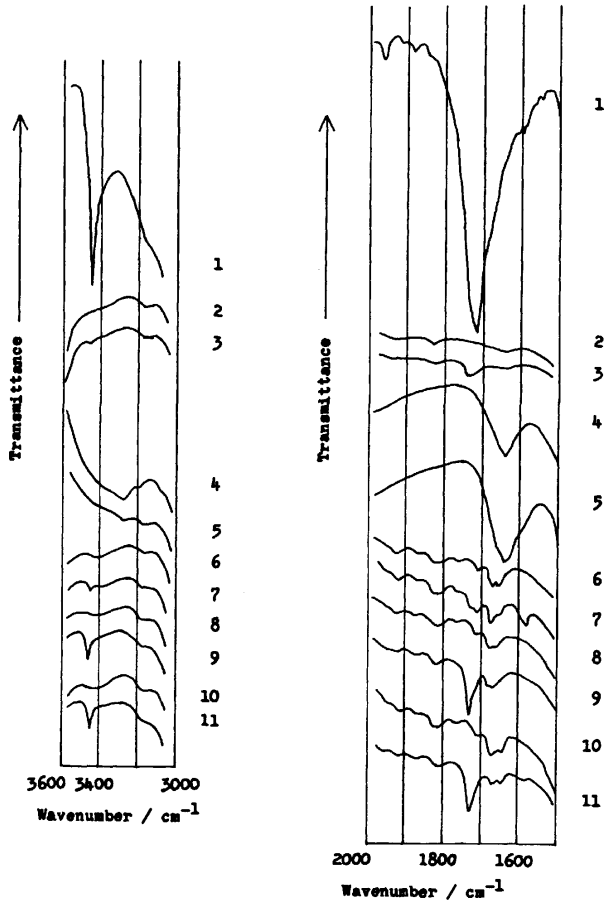

Fig. 6. IR spectra of mandelic acid and various inorganic powders by nujol method.
1: $R(-)$-mandelic acid, 2: kaolin, 3: kaolin-M, 4: γ-Al_2O_3, 5: γ-Al_2O_3-M, 6: talc, 7: talc-M, 8: $talc_{AA}$, 9: $talc_{AA}$-M, 10: $talc_{TEA}$, 11: $talc_{TEA}$-M.
Samples of No. 3, 5, 7, 9, and 11 were prepared using $R(-)$-mandelic acid.

mandelic acid at 5 °C, $|\alpha|$ and $(\bar{S}/S_0)$ decreased; this is considered to be due to the adsorption of mandelic acid at the surface of these talcs, as the shape of the absorption spectra was changed only slightly. Comparison between α/α_0 and $(\bar{S}/S_0)$ revealed that mandelic acid was not racemized at the surface of these talcs, as is shown in Table 2. It is judged from these results that both acidic and basic sites take part in racemization.

Addition of Various Inorganic Powders. On adding kaolin and γ-Al_2O_3 to an ethanolic solution of mandelic acid at 5 °C, $|\alpha|$ and $(\bar{S}/S_0)$ decreased; this is considered to be due to the adsorption of mandelic acid on these powders. Addition of SiO_2 had little influence on α. Comparison between α/α_0 and $(\bar{S}/S_0)$ revealed that racemization is slight at the surface of these powder. (Table 2) It is also clear from Table 2 that acidic sites, whose H_0 value is nearly equal to or smaller than the pK_a value of mandelic acid, exist at the surface of kaolin, talc and SiO_2. It is reported by many workers that basic sites exist at the surface of these powders.[6,7] It is also clarified in Table 2 that basic sites exist at the surface of γ-Al_2O_3.

Figure 6 shows the IR spectra of the various powders. In the spectra of kaolin-M, the band of the hydroxyl group at 3420 cm^{-1} was weak and the band of C=O was observed at 1730 cm^{-1}, though the band for mandelic acid was found at 1720 cm^{-1}. In the spectra of γ-Al_2O_3-M, no band was observed at 3420 cm^{-1} and a new band was found around 3200 cm^{-1}. No band was observed around 1720 cm^{-1} and the absorbance around 1600 cm^{-1} seemed to increase. In the spectra of $talc_{AA}$-M and $talc_{TEA}$-M, the band of C=O was at 1730 cm^{-1} and, in addition a new band was found at 1580 cm^{-1} in the spectra of talc-M, though the band of the hydroxyl group was at 3420 cm^{-1} in these spectra. In the spectra of SiO_2-M, the bands of mandelic acid in these regions were not

Table 2. Interaction of Mandelic Acid with Various Kinds of Inorganic Powders

Inorganic powders	H_0	H_0'	W_1[a] / g	V_m[b] / ml	Type of mandelic acid	$(\bar{S}/S_0)$	Racemization[c]
Kaolin	$0.8<H_0<3.3$	$H_0'<7.2$	1.5	5	*S*	0.773	−
					R	0.780	−
Talc	$0.8<H_0\leq3.3$	$H_0'<7.2$	1.0	3	*S*	1.00	+
					R	1.00	+
SiO_2	$0.8<H_0\leq3.3$	$H_0'<7.2$	1.5	5	*S*	1.00	−
					R	1.00	1/5
γ-Al_2O_3	$6.8<H_0$	$7.2<H_0'$	0.05	3	*S*	0.611	−
					R	0.597	4/7
$Talc_{AA}$	$0.8<H_0\leq3.3$	$H_0'<7.2$	1.0	3	*S*	0.900	−
$Talc_{TEA}$	$3.3<H_0<6.8$	$H_0<7.2$	1.0	3	*S*	0.892	−

a) W_1 is the amount of inorganic powder. b) V_m is the volume of an ethanol solution of 6.6×10^{-3} M of mandelic acid. c) +: Racemization of mandelic acid was observed. −: Racemization was not observed. *x*/*y*: Racemization was observed *x* times, when the experiment was repeated *y* times.

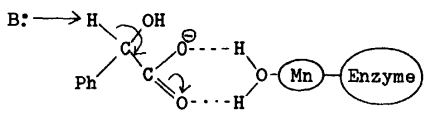

B ; Base

Scheme 1.

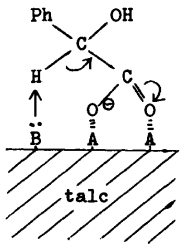

A ; acidic site, B ; basic site

Scheme 2.

distinguished clearly from broad and strong bands of the adsorbed water, though a small shoulder was observed around 1720 cm^{-1}.

Singurel[8] investigated the IR spectra of mandelic acid in carbon tetrachloride or in KBr pellets. He pointed out that the C=O vibrations at 1718 cm^{-1} and 1762 cm^{-1} belonged to the dimer and monomer, respectively. In the spectra of KBr pellets, a wide and intense absorption range between 2400 cm^{-1} and 3200 cm^{-1} was assigned to carboxylic OH groups of dimer molecules connected by hydrogen bonds and a band around 3400 cm^{-1} to the hydroxyl group. When a proton acceptor complexed with the COOH group of mandelic acid, the C=O band was observed between the monomer and dimer bands. Khadikar et al.[9] investigated the IR spectra of bivalent metal complexes of mandelic acid. The hydroxyl group frequency was observed around 3260 cm^{-1}, and the stretching frequency of the COO^- group occured around 1600 cm^{-1}. They concluded that chelation took place involving coordination of hydroxyl and carboxyl groups of mandelic acid.

The above facts suggest that the hydroxyl group of mandelic acid interacts readily with the surface of γ-Al_2O_3. It interacts only weakly with the surface of kaolin, and does not interact at all with the surface of the various talcs. The COOH group interacts with a proton acceptor at the surface of kaolin and the various talcs. The COO^- group of mandelate anions also interacts with the surface of talc. The COO^- group coordinates with the surface of γ-Al_2O_3. These results show that racemization takes place in the mandelate anion, whose hydroxyl groups are free; it weakly interacts with the surface of the inorganic powders.

Mechanism of Racemization. Maggio et al.[10] studied the mechanism of the action of mandelate racemase, using the EPR and NMR techniquss. They showed that this enzyme bonded with Mn^{2+} to which a water molecule liganded, and concluded that deprotonation from the C atom at the second position of a mandelate anion was enhanced by hydrogen bonding of COO^- with the ligand water, as is shown in Scheme 1. It is concluded from the above results that the H atom at the C atom in the second position of a mandelate anion interacts with the basic site at the surface of talc and that deprotonation is enhanced by interaction between the carboxyl group and the acidic site, as is shown in Scheme 2.

Difference between Racemization of *S*-Isomer and that of *R*-Isomer. The decrease in α for the solution of the *S*-isomer by adding talc powder was little influenced by the stirring velocity. On the contrary, the value of $|\Delta\alpha|$ decreased with the decrease in stirring velocity in the case of *R*-isomer, though the value at the stirring velocity at 380 rpm was identical with the value for *S*-isomer. (Figs. 1 and 2) The value of $|\alpha|$ for the solution containing 6.6×10^{-3} M of *R*-isomer did not decrease on adding talc by the process of (iv), though the value for the solution containing 6.6×10^{-2} M of *R*-isomer decreased. (Fig. 4) These results suggest that talc has a chiral surface.

References

1) A. Ikekawa and S. Hayakawa, *Bull. Chem. Soc. Jpn.*, **57**, 889 (1984).

2) A. Verweij, R. de Jong-de Vos, and H. G. J. Teisman, *J. Chromatogr.*, **69**, 407 (1972).

3) E. R. Blakley, *Anal. Biochem.*, **15**, 350 (1966).

4) K. Tanabe, "Shokubai no Hataraki," Kagaku Dojin, Tokyo (1974), Chap. 7.

5) T. J. Kemp and W. A. Walters, *J. Chem. Soc.*, **1964**, 1192; S. A. Baker, J. S. Brima Combe, and D. H. Spenee, *J. Chem. Soc. C*, **1966**, 511.

6) H. Fukui, T. Saito, M. Tanaka, and S. Ohta, *J. Soc. Cosmet. Chem. Jpn.*, **15**, 128 (1981).

7) O. Krilor and E. A. Fokina, *The Problems of Kinetics and Catalysis*, **8**, 248 (1955). K. Tanabe, T. Seiyama, and K. Fueki, "Kinzoku Sankabutsu to Fukugo Sankabutsu," Kodansha Scientific, Tokyo (1984) II, Chap. 1; K. Tanabe and T. Yamaguchi, *J. Res. Inst. Catal. Hokkaido Univ.*, **14**, 93 (1966).

8) Gh. Singurel, *Revue Roumaine do Chimie*, **25**, 1469 (1980).

9) P. V. Khadiker, R. L. Ameria, M. G. Kekre, and S. D. Chauhan, *J. Inorg. Nucl. Chem.*, **35**, 4301 (1973).

10) E. T. Maggio, G. L. Kenyon, A. S. Mildvan, and G. D. Hegeman, *Biochem.*, **14**, 1131 (1975).

 © 1987 The Chemical Society of Japan Bull. Chem. Soc. Jpn., 60, 25—30 (1987)

Partial Specific Compressibility and Its Relation to Solvation of Solute Based on Measurements of Suspension System

Hiroyasu NOMURA,* Fumio KAWAIZUMI, and Takeshi IIDA
Department of Chemical Engineering, School of Engineering, Nagoya University,
Chikusa-ku, Nagoya 464
(Received May 20, 1986)

The relation between limiting partial specific compressibility, $\bar{\kappa}_2^0$, and solvation of solute was reviewed and determination of $\bar{\kappa}_2^0$ was carried out in different types of solutions; ideal binary mixtures, such as benzene-toluene, and suspension systems of polystyrene latex and colloidal silica. In ideal mixture and polystyrene latex systems, the partial specific compressibility and limiting partial specific volume of each solute were equal to the corresponding value of the solute itself. The $\bar{\kappa}_2^0$ of the colloidal silica decreased from a positive to negative value with increasing pH of the media, showing strong hydration in alkaline solution.

In the last two decades compressibility measurement of solution has become quite familiar to many workers who are interested in solute-solvent interaction. Increase of attention to the compressibility in solution chemistry is ascribed to the appearance of commercial apparatus for ultrasonic velocity measurement and also to the development of molecular dynamical study of solution stimulated by computer simulation and various experimental techniques. As is well-known, the compressibility of solution is related to the radial distribution function of the molecules composing solutions.[1]

It goes without mentioning here the important role played by compressibility measurements in the estimation of amount of hydration of electrolytes which go back to the pioneering work of Passynski done as early as in 1938.[2] In his treatment, Passynski assumed that the compressibility of ionic solute and water molecules hydrated to the solute be incompressible. This hydration model, though simplified, is reasonable, since solvent molecules around ionic solute are subject to very strong electric field, namely they are electrostricted and their compressibility should be very small in comparison with that of bulk solvent.

On the other hand, for more general discussion of solute-solvent interaction from the point of solution compressibility, Nomura and Miyahara,[3] using a realistic model of solvated polymer molecule in solution, defined the limiting partial specific compressibility of solute, $\bar{\kappa}_2^0$, about twenty years ago. Since then, Miyahara and his coworkers determined the values of $\bar{\kappa}_2^0$ of many kinds of polymers in various conditions.[4] The solvation model proposed by them (abbreviated as N-M solvation model) can be extended to solutes other than polymers and amounts of solvent molecules bound to the solutes were determined for such systems as dextran in water[5] and in the mixed solvent of water-ethanol,[6] and cyclodextrin in the same mixed solvent.[7] Moreover, the N-M solvation model is useful in estimating the compressibility of certain kind of solute, for example polysaccharide, by means of ethanol-precipitation technique proposed originally by Shiio et al.[8]

As will be seen later in the present paper, the relation between $\bar{\kappa}_2^0$ and the amount of solvation is based basically on the assumption that the solvated or hydrated molecules make ideal solution with the solvent or water. This assumption is the same as that used in determination of the amount of hydrated water for electrolytes[9] and saccharides[10] from respective activity data. In spite of a number of papers dealing with the parameter $\bar{\kappa}_2^0$ reported by Miyahara's school,[3-7] direct experimental confirmation of the proposed relation of $\bar{\kappa}_2^0$ with the N-M solvation model using well-defined solute species is scare, except for one paper.[11] Considering recent increasing attention to the solution compressibility and importance of the information deduced therefrom, we found it appropriate to re-examine at this time the relation between the parameter $\bar{\kappa}_2^0$ and compressibility of solute in a more rigorous way. For this purpose we have undertaken the measurements of compressibility for the systems for which the compressibility of solute can be defined without any ambiguity.

The systems investigated are the ideal binary mixtures and the suspension systems. The formers are toluene-benzene, and -*m*-xylene, toluene being considered as solvent, while the latters are the solutions of monodisperse polystyrene latex and those of colloidal silica. As for the compressibility of suspension system, Urick[12] and Fukutomi and Wada[13] estimated the compressibility of a suspensoid from compressibility data for a dispersed phase and dispersion media.

Definition and Model

We briefly discuss compressibility of liquids and solutions and review the N-M solvation model.[3]

Definition of the Limiting Partial Specific Compressibility. The limiting partial specific compressibility of solute, $\bar{\kappa}_2^0$, is defined in the following equation:[3]

$$\bar{\kappa}_2^0 \equiv -\frac{1}{\bar{v}_2^0}\left(\frac{\partial \bar{v}_2}{\partial p}\right)_{s,0}, \qquad (1)$$

where $\bar{v}_2^0$ is the limiting partial specific volume of the solute. The subscripts zero and s refer respectively to the state at infinite dilution and the isentropic condition. An alternative definition of $\bar{\kappa}_2^0$ is

$$\bar{\kappa}_2^0 \equiv \frac{1}{\bar{v}_2^0}\left(\frac{\partial \kappa}{\partial x}\right)_0 + \kappa_1, \tag{2}$$

where κ is the compressibility and x is the concentration of solute expressed in g cm^{-3} of solution. In the present paper the subscripts 1 and 2 always refer to the solvent and solute, respectively. The quantity $\bar{\kappa}_2^0$ is evaluated from extrapolation of the data of compressibility κ and density d of solution in a following way;

$$\bar{\kappa}_2^0 = -\frac{\kappa_1}{\bar{v}_2^0}\lim_{x\to 0} K_x, \tag{3}$$

$$K_x = \left(\frac{d-x}{d_1} - \frac{\kappa}{\kappa_1}\right)\frac{1}{x},$$

Compressibility concerned here is that under adiabatic condition and is obtained from the well-known Laplace equation:

$$\kappa = \frac{1}{du^2}, \tag{4}$$

u being ultrasonic velocity in the solution. The parameter K_x is related to the apparent molar adiabatic compressibility $K_{s\phi}(=-(\partial\phi_v/\partial p)_s)$ by the equation,

$$K_x = -\frac{K_{s\phi}}{\kappa_1 M}, \tag{5}$$

where M is the molar mass of the solute.

Statistical Mechanical Expression of $\bar{\kappa}_2^0$. In order to have microscopic information on the solute-solvent interaction from the data of compressibility of solution, a statistical mechanical expression of $\bar{\kappa}_2^0$ is earnestly required. However, to derive statistical mechanical expression is a very hard task, since compressibility is directly related to the volume of the system under considerations. The only one theory available and based on the statistical mechanical treatment is the theory proposed by Kirkwood and Buff.[1] Using their theory, the limiting partial specific compressibility can be expressed as follows:

$$(\kappa_{2,T}^0 - \kappa_{1,T}) = \frac{1}{\bar{v}_2^0}[G_{112}^0 - G_{111}^0 + G_{11}^{0,2} - G_{12}^{0,2}] - \frac{v_1}{\bar{v}_2^0}[G_{11}^0 - G_{12}^0], \tag{6}$$

$$G_{1j}^0 = \int [g_{1j}^{(2)0}(r_{1j}) - 1]\mathrm{d}v, \tag{7}$$

$$G_{1jk}^0 = \iint [g_{1jk}^{(3)0}(r_{12}, r_{13}) - g_{1j}^{(2)0}(r_{12}) - g_{1k}^{(2)0}(r_{13}) - g_{jk}^{(2)0}(r_{23}) + 2]\mathrm{d}v_{12}\mathrm{d}v_{13}, \tag{8}$$

where the suffix T is used to refer to an isothermal condition and $g_{ij}^{(2)}(r_{ij})$ and $g_{ijk}^{(3)}(r_{ij}, r_{jk})$ are respectively the pair and triple distribution function in binary solution system. Comparison of Eqs. 6 and 2 shows what kind of information we can deduce from the values of $\bar{\kappa}_2^0$. The terms $[G_{112}^0 - G_{111}^0]$ and $[G_{11}^0 - G_{12}^0]$ are closely related to the solvation of solute and they can be estimated from the experimental data. Unfortunately, at present, we can not go any further into discussion of compressibility on molecular level starting from the values of the $[G_{112}^0 - G_{111}^0]$ and $[G_{11}^0 - G_{12}^0]$ terms. We, therefore, ought to rely upon a proper model in order to discuss the solute-solvent interaction in terms of compressibility data.

$\bar{\kappa}_2^0$ and the N-M Solvation Model. The proposed N-M solvation model is schematically represented in our previous paper.[3] In this model, we have assumed that the solvated or hydrated molecules make ideal solution with the solvent or water, and the so-called structure breaking region in the Frank-Wen model[14] is wholly ignored. If the volume additivity holds even after solvation for such solvated molecules in solution, then the total volume of solution V is given by

$$V = (n_1 - n_s n_2)v_1 + n_2(v_2 + n_s v_s), \tag{9}$$

where v_1, v_2, and v_s are the specific volume of the bulk solvent, solute and solvent in the solvation region, and n_s is the gram number of solvent in the solvation region per one gram of solute. In dilute solution, we may consider the n_s to be independent of the concentration of solute.

The partial specific volume of the solute is given by the differentiation of V with respect to solute concentration:

$$\bar{v}_2 = \left(\frac{\partial V}{\partial n_2}\right)_{n_1} = v_2 + n_s(v_s - v_1). \tag{10}$$

On taking the pressure derivative of Eq. 9 under the condition of constant entropy, we obtain the following relation according to the definition of $\bar{\kappa}_2^0$ shown in Eq. 1:

$$\bar{\kappa}_2^0 = \frac{v_2}{\bar{v}_2^0}\kappa_2 + \frac{n_s}{\bar{v}_2^0}(v_s\kappa_s - v_1\kappa_1). \tag{11}$$

If the solution concerned behaves non-ideally but so long as the volume contraction due to the solvation is negligible in order of magnitude, we can assume the relation below:

$$v_s \simeq v_1 \quad \text{and} \quad \bar{v}_2^0 \simeq v_2. \tag{12}$$

Equation 11 can then be written as

$$\bar{\kappa}_2^0 = \kappa_2 + \frac{n_s v_1}{\bar{v}_2^0}(\kappa_s - \kappa_1). \tag{13}$$

In case where no solvation occurs; i.e. $n_s=0$ and/or $\kappa_s=\kappa_1$. Equation 13 is reduced to an equation

$$\bar{\kappa}_2^0 = \kappa_2. \tag{14}$$

In more general cases in which the compressibility of solvation layer κ_s is taken into account, the amount of solvation can be calculated as follows:

$$v_1 n_s = \bar{v}_2^0 \frac{\bar{\kappa}_2^0 - \kappa_2}{\kappa_s - \kappa_1}. \quad (15)$$

For electrolytic solutes in solution, especially in aqueous solution, we can safely assume $\kappa_2=0$ and $\kappa_s=0$, as done by Passynski.[2] Then, we have from Eqs. 3 and 15

$$n_s = \frac{1}{v_1} \lim_{x \to 0} K_x. \quad (16)$$

If Eq. 9 is directly differentiated with respect to pressure and both quantities κ_2 and κ_s are assumed to be zero, as for the case of electrolytic solute, we have

$$n_s = \frac{n_1}{n_2}\left(1 - \frac{\kappa}{\kappa_1}\frac{V}{n_1 v_1}\right). \quad (17)$$

This equation is essentially the same as that proposed by Passynski.[2]

If the N-M solvation model is applied to the liquid-liquid mixtures where solute molecules interact negligibly with the surrounding solvent, the $\bar{\kappa}_2^0$ values should agree with the adiabatic compressibility of the solute itself in pure liquid state. Moreover, in ideal suspension system, the relation 14 should hold. As the adiabatic compressibility and specific volume of the suspensoid in solid state are defined and evaluated unequivocally, comparisons of the $\bar{\kappa}_2^0$ with κ_2 and $\bar{v}_2^0$ with v_2 are highly meaningful.

Experimental

Samples. Sample liquids *m*-xylene, benzene, and toluene used were all commercial products, spectral grade, of Nakarai Chemicals Co., Ltd. and they were used after purification by fractional distillation. Polystyrene latexes used were courteously supplied from Nippon Synthetic Rubber Co., Ltd. and their diameters were determined by the dynamic light scattering method using a spectrometer Coulter Model N4 as to be 246 (monodisperse), 123 (monodisperse), and 84±20 nm. The ζ-potentials, which serve as a measure of surface charge density, fall between −66 and −74 mV for the three latex samples mentioned above. The values were determined by a ζ-potentiometer Pen KEW 3000.

The colloidal silicas used in this work are commercial products Snowtex S, 20, and 20L supplied from Nissan Chemicals Co., Ltd. Particle size distribution was determined from the photographs taken by an electron microscope. The mean diameter of the sample Snowtexes are 8.1±2.9, 14.6±4.4, and 42.7±15.0 nm, respectively.

Measurements. The adiabatic compressibility of the sample solutions were determined from the measurements of ultrasonic velocities and densities of solutions. The former measurements were carried out using an ultrasonic interferometer operating at constant frequency of 5.000008 MHz, while the latters were done by means of a conventional Ostwald pycnometer of 20 cm^3. The procedure of sound velocity measurement and its accuracy is described in details elsewhere.[15]

Preparation of Sample Solutions. The original commercial products of colloidal silica Snowtex have the pH values about 10. Adjustment of the pH of colloidal silica solution was attained in two steps; first, making the colloidal silica pass through the ion-exchange resin (mixed bed, Amberlite IRA-400 and IR-120), then adding small quantity of solutions of HCl to raise the pH of colloidal silica solution to a desired pH value. The ion-exchanged colloidal solution has the pH values equal to 2—3 and this pH region corresponds to the isoelectric point of the colloidal silica.[16] Colloidal silica is unstable in the neutral pH region and if the solution is kept standing in the neutral pH region for one night, then the colloidal silica shows gelation. Therefore, measurements are difficult in the pH ranges 5—7.

Content of silica and polystyrene latexes in each colloidal solution and suspension was determined from the weight of solid residue left after drying the sample solution.

All measurements were carried out at 25 °C.

Results and Discussion

To illustrate the accuracy of extrapolation and also to confirm our assumptions, $(d-x)/d_1$, and κ/κ_1 are plotted against x for the typical examples of ideal

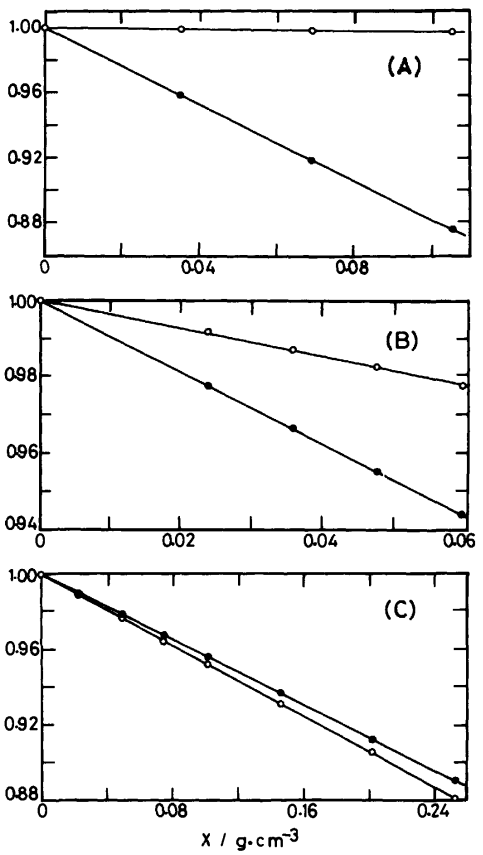

Fig. 1. $(d-x)/d_1$ and κ/κ_1 plotted against concentration X; ● $(d-x)/d_1$, ○ k/k_1.
A: *m*-xylene-toluene, B: polystyrene latex with diameter 84 nm, C: Snowtex S at pH 10.50.

binary mixtures of *m*-xylene-toluene, suspension of polystyrene latexes and silica sol, respectively in Fig. 1. As is seen in Fig. 1, linear relations were observed for both quantities in the concentration ranges investigated, that is, the value of K_x is independent of concentration. The limiting value of K_x was estimated from the slopes of these two lines. Values of $\bar{\kappa}_2^0$ are obtained by Eq. 3.

Values of $\bar{\kappa}_2^0$ in the Ideal Mixture. It is well-known that benzene, *m*-xylene, and styrene form ideal solution with toluene. In Table 1, the values of $\bar{\kappa}_2^0$ and $\bar{v}_2^0$ are compared respectively with κ_2 and v_2 for the solutes benzene, *m*-xylene, and styrene dissolved in toluene. As is seen Table 1, the relations $\bar{v}_2^0=v_2$ and $\bar{\kappa}_2^0=\kappa_2$ hold obviously, as predicted from Eqs. 12 and 14 for these systems. Consequently, in these mixtures no specific interactions are working between solute and solvent molecules.

Values of $\bar{\kappa}_2^0$ of Suspensoids. The results obtained from the ultrasonic velocity and density measurements of suspensions of various monodisperse polystyrene latexes are summarized in Table 2.

Although the values are scattering to some extent, the average values of $\bar{v}_2^0$ and $\bar{\kappa}_2^0$ are 0.941 $cm^3\,g^{-1}$ and 25.3×10^{-11} Pa^{-1}, respectively. The specific volume and compressibility of solid polystyrene are 0.953 and 24×10^{-11}, respectively at 20 °C in the same unit as above.[17] Therefore, the relation expressed as Eqs. 12 and 14 are retained in the suspension system in which particle diameters of suspensoid are ranging from 84 to 400 nm. It may be expressed that the smaller the diameter of suspensoid particle, the larger will be the surface effects in the values of $\bar{\kappa}_2^0$ which reflect the interaction between the surface of the particle and solvent molecules. However, down to the diameter 80 nm of the suspensoid, no appreciable surface effect was observed.

Values of $\bar{\kappa}_2^0$ and $\bar{v}_2^0$ of the Colloidal Silica Samples. The limiting partial specific compressibilities of electrolytes in aqueous solutions are mostly negative, for example, $\bar{\kappa}_2^0(KCl)=-162\times10^{-11}$ Pa^{-1} at 25 °C. This corresponds to hydration arising from very strong electrostrictive force. The colloidal silica is a sort of sols. It is stabilized by the electric repulsive force acting among colloidal particles and at the same time contributing to the formation of hydration layer around the particles. The colloidal silica can be taken as a model system of large hard sphere solute placed in a homogenious media.

The pH dependences of $\bar{\kappa}_2^0$ and $\bar{v}_2^0$ of colloidal silica sols are shown in Figs. 2 and 3, respectively. In these figures both quantities decrease with increasing pH value of the media. As will be seen below, these observations are interpreted in terms of the strong

Table 1. Comparison of the Values of $\bar{\kappa}_2^0$ and $\bar{v}_2^0$ in Toluene with the Compressibility Values in Pure State at 25 °C

	v_2 / $cm^3\,g^{-1}$	$\bar{v}_2^0$ / $cm^3\,g^{-1}$	κ_2 / Pa^{-1}	$\bar{\kappa}_2^0$ / Pa^{-1}
Benzene	1.150	1.145±0.001	67.69	68.70±0.06
m-Xylene	1.163	1.163±0.002	66.73	67.21±0.01
Styrene[a)]	1.120	1.119±0.001	61.30	58.94±0.05

a) Ref. 11 (at 34 °C).

Table 2. Values of $\bar{\kappa}_2^0$ and $\bar{v}_2^0$ for Various Polystyrene Latexes Dispersed in Water at 25 °C

Diameter / nm	$\bar{v}_2^\circ$ / $cm^3\,g^{-1}$	$\bar{\kappa}_2^\circ\times10^{11}$ / Pa^{-1}
400[a)]	0.961±0.07[a),b)]	26.8±0.6
246	0.919±0.006	21.4±0.7
123	0.941±0.008	25.2±1.7
84	0.941±0.001	27.6±0.6

a) Ref. 6. b) On p. 251 of Ref. 6, the value 0.691 is given as $\bar{v}_2^\circ$, which should be corrected as this value.

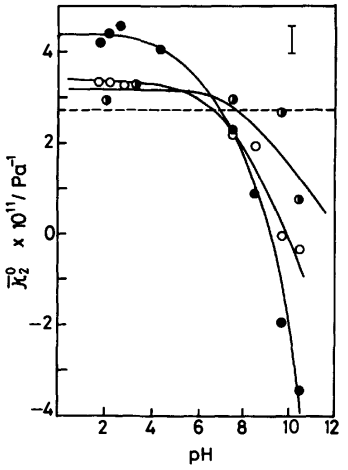

Fig. 2. Variation of $\bar{\kappa}_2^0$ of silica particle with pH of the media at 25 °C. The broken line refers to the κ_2 of quartz. The vertical bar indicates the preciseness of each measurement.
●: Snowtex S, ○: Snowtex 20, ◑: Snowtex 20L.

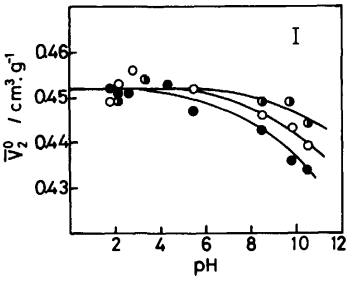

Fig. 3. Variation of $\bar{v}_2^0$ of silica particle with pH of the media at 25 °C. The vertical bar indicates the preciseness of each measurement.
●: Snowtex S, ○: Snowtex 20, ◑: Snowtex 20L.

hydration in alkaline region.

A number of silanol radicals -SiOH are distributed on the surface of colloidal silica particles and these silanol radicals are dissociated to a degree following the pH of the media. The silanol radical works similarly as an amphoteric electrolyte and its isoelectric point lies around pH 2. Therefore, in the higher pH region, the surface of the colloidal silica is charged positively like a cation. Somewhat different behaviors are observed in Figs. 2 and 3, depending on the particle size; in alkaline pH region the values of $\bar{\kappa}_2^0$ and $\bar{v}_2^0$ become smaller with decreasing particle size. However, in this work no examination was attempted to measure the surface charge density of each colloidal silica particle, as mentioned in the preceding chapter. At present it seems legitimate to postpone the detailed discussion concerning the particle size dependence until we have sufficient knowledge on this subject.

Following values[18] have been given for the values of κ_2 and v_2 of silica in bulk state at 25 °C.

$$\kappa_2 = 2.70 \times 10^{-11}\ \mathrm{Pa^{-1}} \text{ and } v_2 = 0.543\ \mathrm{cm^3\ g^{-1}}$$

In Fig. 3, the values of $\bar{v}_2^0$ in low pH region are close to the above mentioned specific volume of solid quartz. The fact that $\bar{v}_2^0 = v_2$ is equivalent to set $n_s = 0$ in Eq. 10.

This means that colloidal silica is not hydrated in acidic pH region. On the contrary, decrease of $\bar{v}_2^0$ with pH of the colloidal system suggests that $v_1 > v_s$ in Eq. 10 and that the term n_s increases with the pH value.

In correspondence to Fig. 3, the values of $\bar{\kappa}_2^0$ in acidic region are positive and a little larger than the compressibility of fused quartz as illustrated in Fig. 2, while they decrease to be negative in alkaline solutions. These variations correspond to $v_s\kappa_s < v_1\kappa_1$ in Eq. 11 or 13. As described just above, the relation $v_s < v_1$ holds. Therefore, the water molecules in hydration layer seem to be less compressible than those in bulk phase. In alkaline region where the relations $\bar{\kappa}_2^0 < \kappa_2$ and $\bar{v}_2^0 < v_2$ are observed, colloidal silica particles are doubtlessly hydrated. Evaluation of the parameters n_s and v_s is possible on solving simultaneously Eqs. 10 and 11. In doing so, a proper value must be assumed for the value of κ_s. The two cases were considered; $\kappa_s = 0$ and $\kappa_s = 11.1 \times 10^{-11}\ \mathrm{Pa^{-1}}$. The latter refers to the compressibility of hexagonal ice. The differences $\bar{v}_2^0 - v_2$ and $\bar{\kappa}_2^0 - \kappa_2$ used in this evaluation are significant to one or at most two figures and self-consistent, i.e. reasonable both for v_s and n_s, results were obtained only for the colloidal solutions with pH >8.5. Accuracy of the evaluation prevents detailed analysis of the results given in Table 3. However, the average values of v_s seems too small in view of the size of colloidal particles and the estimated electrostriction volume of ions in water.[19,20]

The authors are pleased to thank Nippon Synthetic Rubber Co., Ltd. and Nissan Chemicals Co., Ltd. for supplying them, respectively, polystyrene latex and colloidal silica with the data sheet of physicochemical analysis of these samples.

References

1) J. G. Kirkwood and F. P. Buff, *J. Chem. Phys.*, **19**, 774 (1951).

2) A. Passynski, *Acta Physicochim. U. R. R. S.*, **8**, 385 (1938).

3) H. Nomura and Y. Miyahara, *J. Appl. Polym. Sci.*, **8**, 1643 (1964). In this report, the notation $\bar{\kappa}_{20}$ is used. But at present time use of superscript ^{0} is recomended to refer to the property at infinite dilution.

4) For example, see the following papers and those cited therein. a) H. Nomura and Y. Miyahara, *Bull. Chem. Soc. Jpn.*, **39**, 1599 (1966); b) H. Nomura and Y. Miyahara, *Nippon Kagaku Zasshi*, **88**, 504 (1967).

5) H. Nomura, S. Yamaguchi, and Y. Miyahara, *J. Appl. Polym. Sci.*, **8**, 2731 (1964).

6) H. Nomura, M. Onoda, and Y. Miyahara, *Polym. J.*, **14**, 249 (1982).

7) H. Nomura, S. Koda, K. Matsumoto, and Y. Miyahara, *Stud. Phys. Theor. Chem.*, **27**, "Ions and Molecules

Table 3. Amount of Water Bound on the Colloidal Silica Surface and Specific Volume of Water in Hydration Layer in Higher pH Region of the Media

Sample	pH	$\kappa_s = 0$			$\kappa_s = \kappa_{ice}$		
		n_s / g g^{-1}	n_s' / g g^{-1} cm^{-2}	v_s / cm^3 g^{-1}	n_s / g g^{-1}	n_s' / g g^{-1} cm^{-2}	v_s / cm^3 g^{-1}
S	9.7	4.6×10^{-2}	4.6×10^{14}	0.64	5.6×10^{-2}	5.6×10^{14}	0.70
	10.5	6.1	6.0	0.70	7.5	7.4	0.75
20	9.7	2.7	5.0	0.65	3.4	6.0	0.72
	10.5	3.0	5.5	0.55	3.6	6.5	0.62
20L	10.5	2.0	10	0.56	2.3	12	0.63
				mean 0.62			mean 0.68

n_s' is amount of hydration per unit area of particle surface.

in Solution," ed by N. Tanaka, H. Ohtaki, and R. Tamamushi, Elsevier Scientific, Amsterdam (1983), p. 151.
8) H. Shiio, T. Ogawa, and H. Yoshihashi, *J. Am. Chem. Soc.*, **77**, 4980 (1956).
9) R. A. Robinson and R. H. Stokes, "Electrolyte Solutions," 2nd ed., Butterworth, London (1959), p. 238.
10) Y. Miyahara, *Kagaku*, **29**, 365 (1959).
11) H. Nomura and Y. Miyahara, *Nippon Kagaku Zasshi*, **89**, 145 (1968).
12) R. J. Urick, *J. Appl. Phys.*, **18**, 983 (1947).
13) K. Fukutomi and Y. Wada, *Onkyo Gakkaishi*, **15**, 22 (1959).
14) H. S. Frank and W.-Y. Wen, *Discuss. Faraday Soc.*, **24**, 133 (1957).
15) H. Nomura and R. E. Verrall, *J. Phys. Chem.*, **85**, 1042 (1981).
16) R. K. Iler, "The Chemistry of Silica," Wiley-Interscience, New York (1973).
17) Y. Wada, "Ko-bunshi no Bussei," Baifu-kan, Tokyo (1971).
18) "Cho-onpa Gijutsu Binran," ed by J. Saneyoshi, Y. Kikuchi, and O. Nomoto, Nikkan Kogyo Shinbunsha, Tokyo (1984).
19) J. Padova, *J. Chem. Phys.*, **39**, 1552 (1963).
20) F. Kawaizumi, H. Suzuki, H. Nomura, and Y. Miyahara, *Bull. Chem. Soc. Jpn.*, **55**, 2771 (1982).

 © 1987 The Chemical Society of Japan Bull. Chem. Soc. Jpn., 60, 31—35 (1987)

Phenomenological Relationship between the Fluidity and Tracer-Diffusion in Concentrated Electrolyte Solutions

Kazuko TANAKA* and Reita TAMAMUSHI†
The Institute of Physical and Chemical Research, Wako, Saitama 351-01
†Fukushima University, Matsukawa, Fukushima 960-12
(Received May 27, 1986)

An attempt has been made to correlate the mobility of component species with the fluidity of the solution over a wide range of concentration in aqueous solutions. A good linear correlation was observed between the relative fluidity and the relative tracer-diffusion coefficient of Cl^- in aqueous solutions of LiCl, NaCl, $MgCl_2$, $CaCl_2$, and $NiCl_2$, particularly at higher concentrations over 2 mol kg^{-1}. The correlation for the cations was very similar to that of water in aqueous solutions of such electrolytes. The feature of these plots presents that the structural properties of concentrated electrolyte solutions are reflected on these correlations.

In recent years, much attention has been paid to physicochemical properties of concentrated electrolyte solutions; a considerable amount of experimental data have been accumulated for transport processes in aqueous electrolyte solutions of varying compositions. However, many of the features of these experimental results still remain unexplained mainly because of a lack of appropriate theories and models which can be applied up to very high concentrations.

Since very early studies of transport phenomena in solution some simple correlations have been expected and examined between the velocity of a particle and the fluidity of the medium in which the particle moves, and the examination of so-called Stokes–Einstein equation[1] is still continuing.[2,3,4] Many of such correlations are empirical in nature, nevertheless they are expected to be useful to gain an insight into the nature of interactions among moving particles and the structure of the solution.

In electrolyte solutions the Stokes-Einstein equation is expected to be applicable to solutions at infinite dilution or very dilute solutions where the solution is assumed to be ideal, and have been examined by using limiting values of diffusion coefficients and molar ionic conductivities at infinite dilution.[5,6] Most of the previous studies have concerned the transport behaviour of only one component existing in the solution. In case of multicomponent solutions, however, it is important to study the transport properties of each component in the same solution. Among various transport properties only the tracer diffusion can provide the individual mobility data of each component.

In the present study, we have collected reliable tracer-diffusion data from the literature given in Table 1, and examined the correlation between the diffusion coefficients and fluidity of the solution for each individual component. Although no simple correlations may be expected between the mobility and fluidity in real solutions of finite concentrations, we have found that a substantial body of the experimental data reveals significant relationships between the mobility and fluidity in aqueous electrolyte solutions of very high concentrations.

Table 1. Sources of the Diffusion and Viscosity Data Used

Electrolyte	Tracer	Reference	
		Diffusion	Viscosity
LiCl	Li^+	(7), (8)	(29)
	Cl^-	(7), (8), (12)	
	H_2O	(8), (10)	
NaCl	Na^+	(9), (11)	(29)
	Cl^-	(12), (13)	
	H_2O	(14), (15)	
KCl	K^+	(7), (16)	(29)
	Cl^-, H_2O	(7), (12), (18)	
	H_2O	(17), (18)	
CsCl	Cs^+, Cl^-, H_2O	(18)	(29)
$MgCl_2$	Mg^{2+}, Cl^-	(19)	(29)
	H_2O	(15)	
$CaCl_2$	Ca^{2+}	(20)	(29)
	Cl^-	(20), (21)	
	H_2O	(17)	
$NiCl_2$	Ni^{2+}, Cl^-, H_2O	(22)	(26)
$CdCl_2$	Cd^{2+}, Cl^-, H_2O	(23)	(27)
CdI_2	Cd^{2+}, I^-, H_2O	(24)	(27)
R_4NBr	R_4N^+, Br^-, H_2O	(25)	(28)

The concentration dependence of tracer diffusion coefficients $D(Cl^-)$ of chloride ions in several aqueous electrolyte solutions is given in Fig. 1, in which relative diffusion coefficients as defined by $D_r(Cl^-)= D(Cl^-)/D^0(Cl^-)$ where $D^0(Cl^-)$ is the limiting diffusion coefficient calculated from the limiting ionic conductivity of Cl^- by the Nernst equation,[30] are plotted as a function of electrolyte concentration. This figure clearly demonstrates that the rate of diffusion of chloride ion is very much affected by the cations present in the solution. In KCl and CsCl solutions chloride ions diffuse faster than in LiCl and NaCl solutions, and the rate of diffusion decreases with increasing electrolyte concentration more rapidly in solutions of divalent cations than in solutions of

monovalent cations. The corresponding plot for relative fluidity $\phi_r=\phi/\phi^0$, (ϕ^0, the fluidity of pure solvent) is shown in Fig. 2. A comparison of Figs. 1 and 2 shows that the concentration dependence of tracer diffusion coefficients of Cl^- is very similar to that of fluidity of the solution, which gives us an indication that there seems to be some empirical correlation between relative tracer-diffusion coefficient of chloride ions and the relative fluidity of the solution.

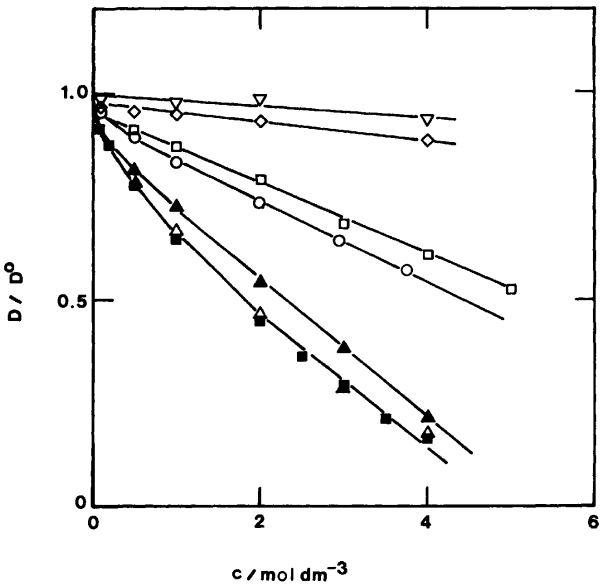

Fig. 1. Concentration dependence of the relative diffusion coefficients of Cl^- in aqueous solutions of LiCl (○), NaCl(□), KCl(◇), CsCl(▽), $MgCl_2$(△), $CaCl_2$ (▲) and $NiCl_2$(■) at 25 °C.

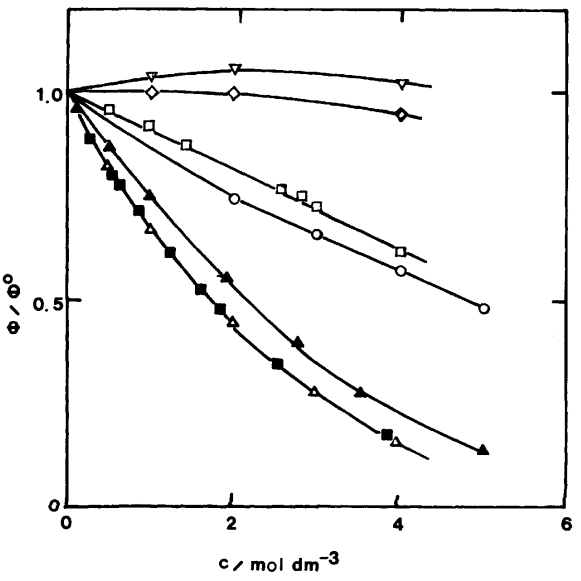

Fig. 2. Concentration dependence of relative fluidities of the aqueous electrolyte solutions (25 °C) given in Fig. 1; symbols are the same as those used in Fig. 1.

In Fig. 3, the relative tracer diffusion coefficients of chloride ion are plotted against the relative fluidity of the solutions, where the diagonal line represents the relation,

$$D(Cl^-)/D^0(Cl^-) = \phi/\phi^0. \quad (1)$$

A striking feature of this plot is that the experimental points for concentrated solutions (≥2 mol kg^{-1}) of LiCl, NaCl, $MgCl_2$, $CaCl_2$, and $NiCl_2$ (hereafter, these electrolytes will be called the LiCl-type for the sake of simplicity) are on or very close to the diagonal line, while those points for medium and low concentrations (0.5—2.0 mol kg^{-1}) lie slightly below the line.

The present empirical finding suggests that in concentrated solutions, the LiCl-type electrolytes affect the chloride ion diffusion and the fluidity of the solutions in a similar manner, which may be interpreted in terms of the structural aspect of chloride ions in the solution. In this respect, it seems worthwhile to note the neutron diffraction studies by Enderby's group which show that the geometric arrangement of water molecules around chloride ions is independent of concentration and also counter cations for a wide variety of electrolytes.[31]

Let us now examine the D_r vs. ϕ_r plot for the tracer-diffusion of cations and water (Figs. 4 and 5, respectively) in aqueous solutions of the LiCl-type electrolytes. As can be seen from Fig. 4, the experimental points for the cations at lower concentrations are close to the diagonal line, whereas most of the points at higher concentrations lie above the line, suggesting that the retardation of the diffusion rates of these cations is less than that expected from the decrease in fluidity of the solution.

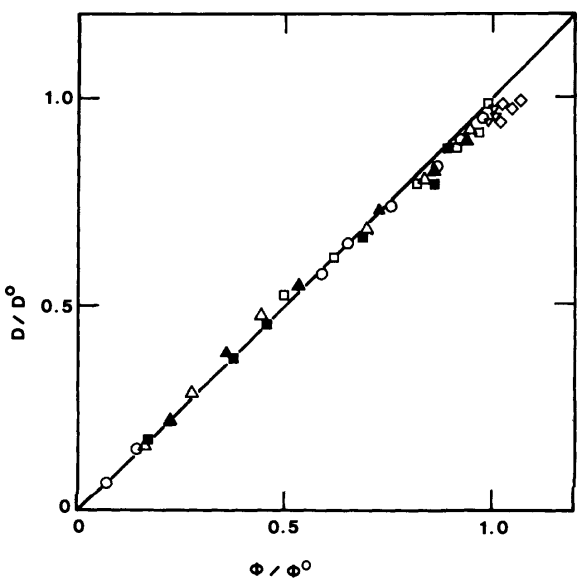

Fig. 3. D_r vs. ϕ_r plots for Cl^- in the solutions of LiCl (○), NaCl(□), KCl(▽), CsCl(◇), $MgCl_2$(△), $CaCl_2$ (▲) and $NiCl_2$(■) at 25 °C.

It should be noticed that most of the experimental points are on the same curve irrespective of the kind of cations.

The tracer diffusion of water in aqueous solutions of the LiCl-type electrolytes behaves very similarly to that of the cations (compare Figs. 4 and 5). This result may give a qualitative explanation that the above-mentioned behavior is associated with the strong interaction of water molecules with the cations in solutions of the LiCl-type electrolytes.

Relative diffusion coefficient vs. relative fluidity relationships for aqueous solutions of KCl and CsCl are different from those observed with the LiCl-type electrolytes. In the case of KCl and CsCl solutions, the fluidity and diffusion coefficient do not change very much with concentration; fluidity first increases and then decreases slightly with increasing concentration (see Fig. 2) and the increase in fluidity is more pronounced for CsCl at lower temperatures. The experimental points for these electrolyte solutions are located in the region corresponding to $\phi_r=1$ and $D_r=1$ of the D_r vs. ϕ_r diagram (see Figs. 3, 4, and 5). The points for the cations and chloride ion are always below the diagonal line. The observed transport behaviour of KCl and CsCl solutions may be related to the fact that K^+ and Cs^+ ions have large crystallographic radii and low charge densities so that

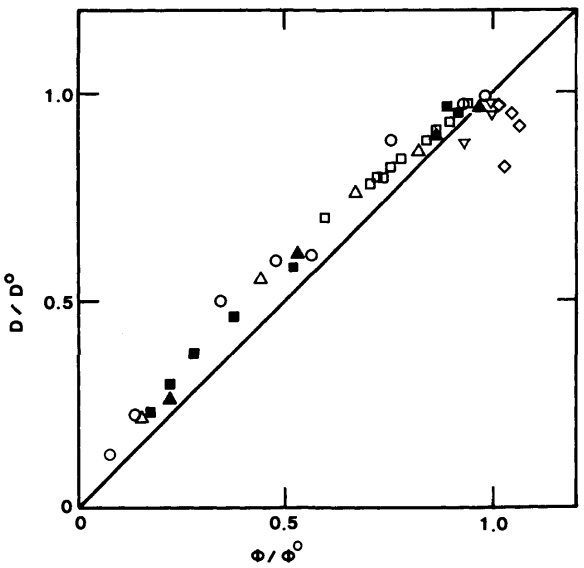

Fig. 4. D_r vs. ϕ_r plots for cations of the solutions given in Fig. 3.

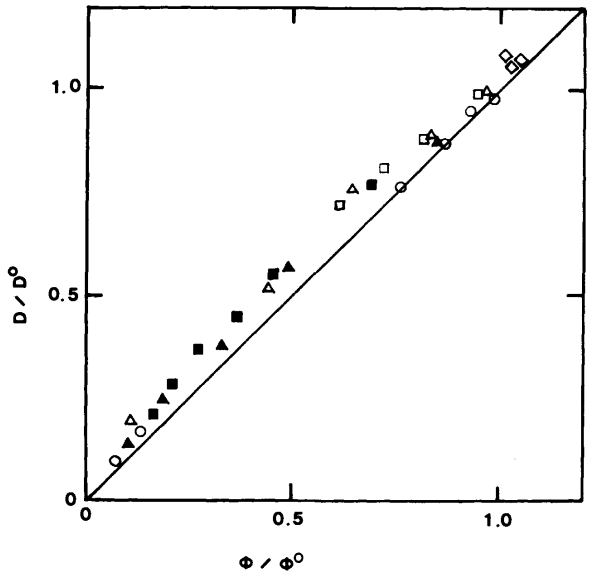

Fig. 5. D_r vs. ϕ_r plots for water of the solutions given in Fig. 3.

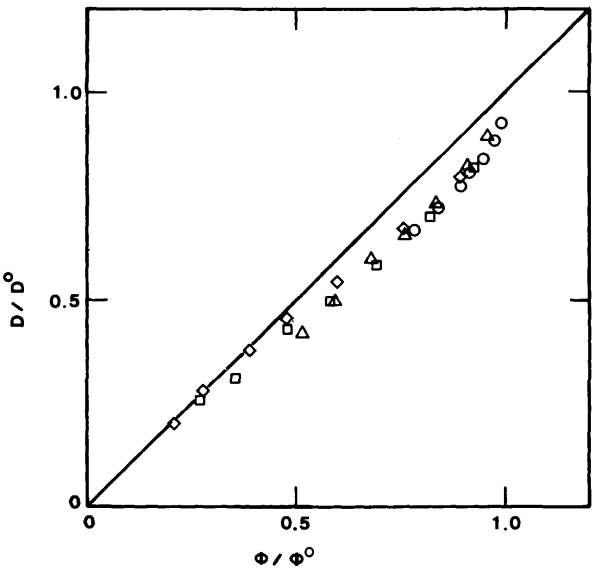

Fig. 6. D_r vs. ϕ_r plots for Br^- in aqueous solutions of Me_4NBr(○), Et_4NBr(△), n-Pr_4NBr(□) and n-Bu_4NBr (◇).

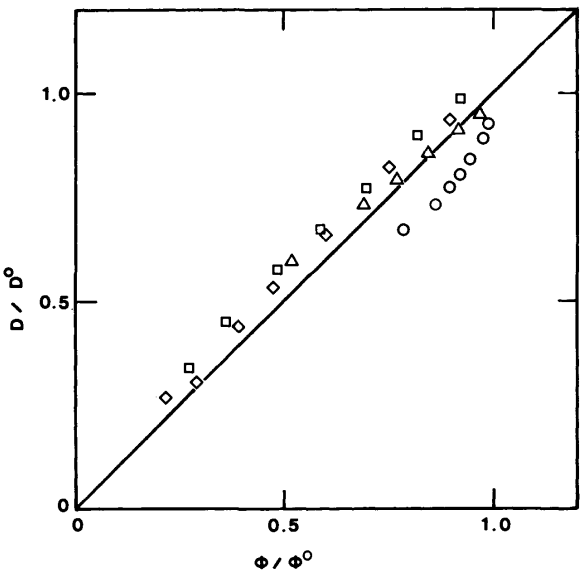

Fig. 7. D_r vs. ϕ_r plots for R_4N^+ of the solutions given in Fig. 6.

they cause weaker hydration.

Examples of the D_r vs. ϕ_r plots for aqueous solutions of tetraalkylammonium bromides which cause the so-called hydrophobic hydration, are given in Figs. 6, 7, and 8. For bromide ions all the experimental points lie on the same curve regardless of their counter tetraalkylammonium cations (Fig. 6); the correlation is similar to that observed for chloride ions in solutions of the LiCl-type electrolytes, although the linear relationship represented by Eq. 1 is satisfied at rather smaller relative fluidities ($\phi_r<0.5$) than in the case of the chloride ions of small electrolytes. Among the points for tetraalkylammonium cations, those for tetramethylammonium cation fall below the diagonal line, whereas those points for the other tetraalkylammonium cations are on or above the line (Fig. 7). The water diffusion in these solutions exhibits more complicated behavior (Fig. 8), and will not be discussed in detail until more experimental data have been available.

The D_r vs. ϕ_r relationships for aqueous solutions of cadmium chloride and iodides (Fig. 9) are examples where cations and anions have strong specific interactions such as complex formation. The most characteristic behavior of such systems can be seen on the correlation for the anions; all the points are far below the diagonal line, indicating that the anions in these solutions diffuse much slower than would be expected from the fluidity by Eq. 1. This transport behavior may be mainly ascribed to the specific ion-ion interaction, as a result of which the chloride and iodide ions are travelling together with cadmium ions whose diffusion coefficients are about one-third of the anions.

In this paper, we have demonstrated that different types of solute-solvent interactions exhibit different diffusion vs. fluidity correlations. The D_r vs. ϕ_r plots may not be adequate to study of validity of the Stokes-Einstein equation, and the correlations we found are entirely empirical. We believe, however, that the correlations will provide some fundamental information on the nature of ion-solvent interactions and structural properties of ions in concentrated electrolyte solutions. It is hoped that the empirical correlations presented in this paper could be explained by the future development of theories and models of concentrated electrolyte solutions.

References

1) R. A. Robinson and R. H. Stokes, "Electrolyte Solutions," Butterworths (1965), p. 44.
2) G. L. Pollack, *Phys. Rev.*, A **23**, 2660 (1981).
3) G. L. Pollack and J. J. Enyeart, *Phys. Rev.*, A **31**, 980 (1985).
4) R. Zwanzig and A. K. Harrison, *J. Chem. Phys.*, **83**, 5861 (1985).
5) R. L. Kay, "Water," ed by F. Franks, Plenum, (1973), Vol. 3, p. 173.
6) J. E. Desnoyers, *Phys. Chem. Liq.*, **7**, 63 (1977).
7) P. Turq, F. Lantelme, Y. Roumegous, and M. Chemla, *J. Chim. Phys.*, **68**, 528 (1971).
8) K. Tanaka, *J. Chem. Soc., Faraday Trans. 1*, in press.
9) R. Mills, *J. Am. Chem. Soc.*, **77**, 6116 (1955).
10) J. Tamas, S. Lengyel, and J. Giber, *Acta Chim. Acad. Sci. Hung.*, **38**, 225 (1963).
11) R. Mills and A. W. Adamson, *J. Am. Chem. Soc.*, **77**, 3454 (1955).
12) R. Mills, *J. Phys. Chem.*, **61**, 1631 (1957).
13) J. H. Wang, *J. Am. Chem. Soc.*, **74**, 1612 (1952).
14) K. Tanaka, *J. Chem. Soc., Faraday Trans. 1*, **71**, 1127 (1975).

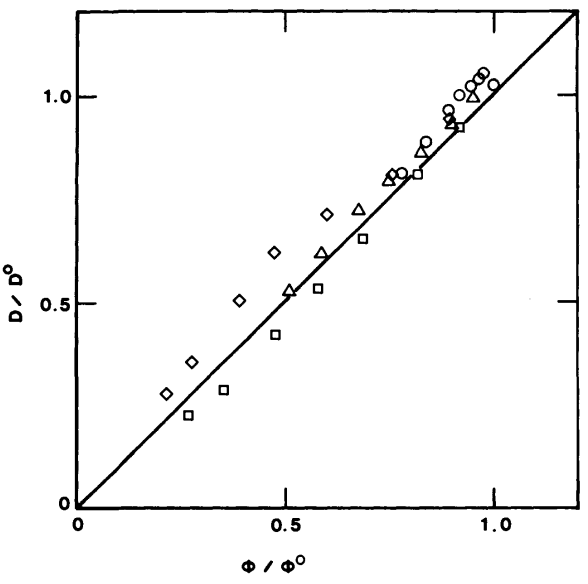

Fig. 8. D_r vs. ϕ_r plots for water of the solutions given in Fig. 6.

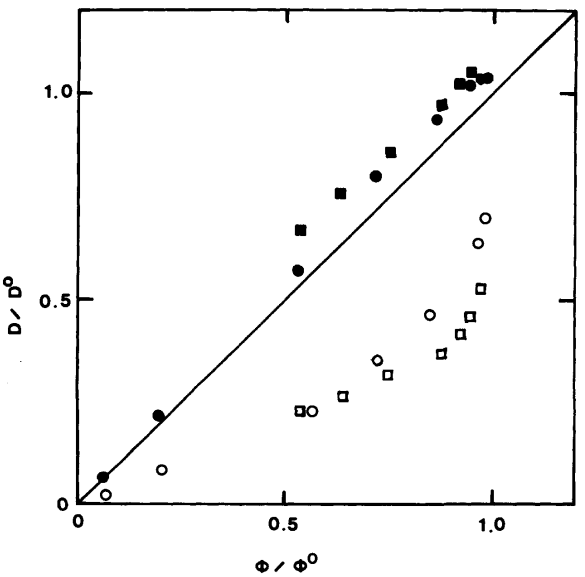

Fig. 9. D_r vs. ϕ_r plots for aqueous solutions of $CdCl_2$ and CdI_2 at 25 °C; Cd^{2+}(●) and Cl^-(○) in $CdCl_2$, and Cd^{2+}(■) and I^-(□) in CdI_2.

15) K. R. Harris, R. Mills, P. J. Back, and D. S. Webster, *J. Mag. Res.*, **29**, 473 (1978).
16) H. G. Hertz, M. Holtz, and R. Mills, *J. Chim. Phys.*, **17**, 1355 (1974).
17) J. Tamas and K. Ujszaszy, *Acta Chim. Acad. Sci. Hung.*, **49**, 377 (1966).
18) H. G. Hertz and R. Mills, *J. Chim. Phys.*, **73**,499 (1976).
19) K. R. Harris, H. G. Hertz, and R. Mills, *J. Chim. Phys.*, **75**, 391 (1978).
20) H. G. Hertz and R. Mills, *J. Phys. Chem.*, **82**, 952 (1978).
21) J. H. Wang, *J. Am. Chem. Soc.*, **75**, 1769 (1953).
22) R. H. Stokes, S. Phang, and R. Mills, *J. Soln. Chem.*, **8**, 489 (1979).
23) R. Mills and H. G. Hertz, *J. Chem. Soc., Faraday Trans. 1*, **78**, 3287 (1982).
24) H. G. Hertz, A. V. J. Edge, and R. Mills, *J. Chem. Soc., Faraday Trans. 1*, **79**, 1317 (1983).
25) L. A. Woolf and H. Weingartner, *Faraday Symp. Chem. Soc.*, **17**, 41 (1982).
26) S. Phang, *Aus. J. Chem.*, **32**, 1149 (1979).
27) Landolt Börnstein II Band, 5 Teil, Springer Verlag, (1969).
28) D. Eagland, and G. Pilling, *J. Phys. Chem.*, **76**, 1902 (1972).
29) T. Isono, *Rep. Inst. Phys. Chem. Res.*, **61**, 53 (1985).
30) R. A. Robinson and R. H. Stokes, "Electrolyte Solutions," Butterworths (1965), p. 317.
31) J. E. Enderby, *Pure Appl. Chem.*, **57**, 1025 (1985).

 © 1987 The Chemical Society of Japan Bull. Chem. Soc. Jpn., 60, 37—41 (1987)

The Effect of Phosphoric Acid Treatment on the Catalytic Property of Niobic Acid

Susumu Okazaki,* Masao Kurimata, Tokio Iizuka,† and Kozo Tanabe†
Department of Industrial Chemistry, Faculty of Engineering, Ibaraki University, Hitachi 316
†Department of Chemistry, Faculty of Science, Hokkaido University, Sapporo 060
(Received June 2, 1986)

The effects of the treatment of niobic acid with phosphoric acid, sulfuric acid, and hydrofluoric acid on its surface area, structure, acidic property, and catalytic activity have been studied. The treatment with phosphoric acid was found to be most effective for maintaining a large surface area and a large amount of strong acid sites and for preventing niobic acid from crystallizing even after the heat treatment at higher temperatures above 600 °C. The XPS study revealed that a large amount of phosphorous exists on niobic acid after high temperature heat treatment. In accordance with these results, niobic acid treated with phosphoric acid and heat-treated at higher temperatures exhibited high catalytic activities for methanol conversion and ethylene hydration, whereas the activities of niobic acid containing no phophoric acid were very low when heat-treated at high temperatures.

Recently, niobic acid ($Nb_2O_5 \cdot nH_2O$) is known to have a strong acidic property and catalytic activity towards acid-catalyzed reactions such as ethylene hydration,[1] esterification of acid with alcohols,[2] butene isomerization[3] etc. even on the heat treatment at lower temperatures (100—200 °C). However, on the heat treatment at higher temperatures (550 °C), niobic acid decomposes to become a crystalline niobium oxide and loses its acidic property and catalytic activity.[3]

On the other hand, it is known that the addition of SO_4^{2-} or F^- ions to a metal oxide such as Al_2O_3 or TiO_2 enhances the acidity of the metal oxide and that the addition of SO_4^{2-} prevents TiO_2 from changing to stable rutile crystals.[4]

Thus, in this study, the effect of the treatment of niobic acid with various acids, especially phosphoric acid, was examined for the purpose of strengthening the solid acidity of niobic acid even after the treatment at high temperatures. The conversion of methanol and the hydration of ethylene were tested to measure the effect of acid treatment on the catalytic activity of niobic acid.

Experimental

Catalyst Preparation. Niobic acid (AD-135) supplied by CBMM was dried in air at 120 °C for 6 h. For the preparations of acid-treated samples, niobic acid (10 g) was immersed in 30 ml of an acid solution prepared so as to have a given concentration (0.05, 0.25, 0.5, and 2.5 mol dm^{-3} of HF; 0.5 mol dm^{-3} of H_2SO_4; 0.25, 0.5, and 1 mol dm^{-3} of H_3PO_4). The suspension of niobic acid was allowed to stand for 48 h, then the sample was evaporated to dryness in air at 120 °C. The dried sample was calcined at various temperatures.

Surface Acidity and Specific Surface Area. The amount of surface acidic sites was measured by butylamine titration method, using various Hammett indicators. The BET method was used to measure the specific surface areas. Constant-volume adsorption of N_2 was carried out at 78 K for the sample having a particle size of 14—20 mesh.

TG-DTA, XRD, and XPS Measurements. For the measurement of TG-DTA, untreated and acid treated niobic acid, all dried at 120 °C, were used in an amount of 2.0 g each. The programmed temperature was raised at a rate of 10 °C min^{-1} up to 800 °C. The XRD experiments were done by using copper as the target and nickel as the filter. Some of the samples of untreated and acid treated niobic acid were subjected to XPS measurement for the surface composition after heat treatment at 400 °C or 600 °C. The Ar ion sputtering for 5 or 15 min was used to know the composition of several inner layers.

Methanol Conversion Reaction and Hydration of Ethylene. The methanol conversion was carried out at 400 °C, under normal pressure using a conventional flow reactor. One gram of catalyst, having a particle size of 14 to 20 mesh was fixed in the reactor and heat-treated in He stream at 400 °C for 1 h. The methanol feed was passed through a preheater at a constant rate of 1.8 ml h^{-1} by means of a microfeeder so that methanol was vaporized and led into the reactor by He carrier gas at a rate of 60 ml min^{-1}. The product gas was analyzed by gas chromatography. The reaction procedure of ethylene hydration was the same as reported previously.[3]

Results and Discussion

Surface Acidity. The acidity change of acid treated and untreated niobic acid after heating at various temperatures was summarized in Table 1. On the untreated niobic acid, strong acid sites of $H_o \leq -5.6$ appeared when samples were heat-treated at 200 or 300 °C. However, such strong acid sites were not found for the samples heat-treated at higher temperatures. In addition, the weaker acid sites of $1.5 \geq H_o > -5.6$ decreased with the rise of treatment temperature. The decrease of acid sites has been ascribed to the crystallization of Nb_2O_5.[3]

When niobic acid was treated with HF of concentration being 0.5 mol dm^{-3} or below, the amount of the weaker acid sites increased from 0.23 to 0.35—0.38 mmol dm^{-3}, whereas there was no change or somewhat decrease in the amount of the strong acid sites. However, the strong acid sites on HF treated sample remained after heat treatment at 400 °C in contrast with the case of untreated niobic acid. After

the treatment with HF of higher concentration, the acid sites on niobic acid decreased drastically.

If a niobic acid was treated with 0.5 mol dm^{-3} H_2SO_4, the acidity increased remarkably and the strong acid sites were retained even after the heat treatment at 400 °C. It is known that some metal oxides such as ZrO_2, TiO_2, and Fe_2O_3 show solid super acidity ($H_o \leq -12$) after the treatment with H_2SO_4 followed by the heat treatment at 500—600 °C.[5] However, on the surface of niobic acid, the strong acidity ($H_o \leq -5.6$) diminished after heating at 500—600 °C.

Figure 1 shows the surface acidity of niobic acid treated similarly with 1.0 mol dm^{-3} of phosphoric acid and then heat-treated at various temperatures. It is observed that the phosphoric acid treatment retains relatively large amount of strong acid sites. Surface treatment with 0.5 mol dm^{-3} of phosphoric acid enhances the surface acidity similarly to that with 1.0 mol dm^{-3} of phosphoric acid.

Figure 2 shows the relationship between the temperatures of heat treatment and the amounts of strong acid sites ($-5.6 \geq H_o > -8.2$) of niobic acid untreated or treated with acids. As obvious from this figure, the treatment with phosphoric acid differs from the treatment with other acids in that the strong acid amount is fairly retained at 600 °C and even 800 °C. As can be seen from a comparison of Fig. 1 with Fig. 2, the acid amount retained at 600 °C or higher temperature does not depend on the concentration of phosphoric acid.

As described above, the niobic acid treated with phosphoric acid does not lose strong acidity even after the heat treatment at high temperatures. This fact is considered to be due to the nonvolatile polyphosphate formed by the condensation of phosphoric acid on and near the surface of niobic acid. The ability of niobic acid to retain strong acidity at high temperature is not changed by the phosphoric acid concentration, and this fact indicates that a polyphosphate layer is formed in an amount enough to cover the full surface even when phosphoric acid is used at a relatively low concentration such as 0.5 mol dm^{-3}.

TG-DTA and XRD. TG-DTA was conducted to obtain an information about thermal stability of acid

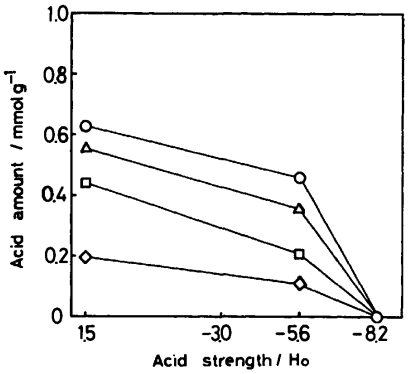

Fig. 1. Surface acidity of niobic acid treated with 1 mol dm^{-3} H_3PO_4.
Heat treatment temperature; ○: 200 °C, △: 400 °C, □: 600 °C, ◇: 800 °C.

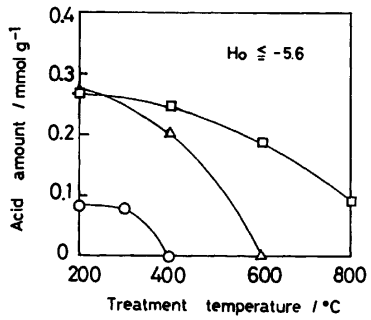

Fig. 2. Surface acidity of niobic acid before and after acid treatment.
○: Before treatment, △: after treatment with 0.5 mol dm^{-3} H_2SO_4, □: after treatment with 0.5 mol dm^{-3} H_3PO_4.

Table 1. Acid Amount on Niobic Acid Before and After Acid Treatment

Heat treatment temperature / °C	Acid amount on niobic acid/mmol dm^{-3}						
	Before acid treatment		Treated with HF of various concentration			Treated with H_2SO_4 of 0.5 mol dm^{-3}	
	LS[a]	S[a]	Concd / mol dm^{-3}	LS[a]	S[a]	LS[a]	S[a]
200			0.05	0.35	0.09		
	0.23	0.09	0.25	0.38	0.10	1.19	0.27
			0.5	0.38	0.04		
			2.5	0.10	0		
300	0.25	0.08					
400	0.13	0				0.42	0.20
500	0.10	0				0.35	0.05
600	0.03	0				0.15	0

a) LS: amount weaker acid ($1.5 \geq H_o > -5.6$) site. S: amount of strong acid ($-5.6 \geq H_o > -8.2$) site.

treated niobic acid. Figure 3 shows the TG-DTA patterns of the untreated niobic acid and phosphoric acid or sulfuric acid treated samples. At and near 200 °C, it shows a weak and dull endothermic peak. According to Sen et al., niobic acid has a composition of $3Nb_2O_5 \cdot 4H_2O$ at 150 °C and $3Nb_2O_5 \cdot H_2O$ at 300 °C.[6] Therefore, the peak around 200 °C is attributable to a partial elimination of water of crystallization. TG showed little change when untreated and H_3PO_4-treated samples were heated to temperatures ranging from 300 to 800 °C. However, DTA shows a sharp exothermic peak around 550 °C. This peak has been attributed to the transformation of niobic acid to crystalline niobium oxide.[3] The sharp exothermic peak near 550 °C is characteristic of niobium oxide. The crystallization of niobium oxide was prevented considerably by the addition of sulfuric acid or phosphoric acid. In DTA, the exothermic peak grew blunt and shifted to the higher temperature region. As found especially in H_3PO_4-treated samples, the effect becomes more remarkable with the increase in the treatment concentration. With a concentration of 1 mol dm^{-3} phosphoric acid, the exothermic peak is no longer observed. Sulfuric acid treatment also showed the similar effect, but TG showed the weight decrease at 600 °C or higher. This is probably due to the elimination of SO_3. Along with this elimination, the acidity of niobic acid rapidly decreased (See Fig. 2). In contrast, niobic acid treated with phosphoric acid did not show any weight loss due to the decomposition and retained the strong acid sites even after the heat treatment at high temperature.

In Fig. 4 are shown XRD patterns of untreated and acid treated niobic acid. After heating at 400 °C or below, samples showed only very broad peaks at about 30° (d=2.08 Å) and about 55° (1.67 Å). When heat-treated at higher temperatures, sharp peaks were observed on untreated niobic acid. The sample treated with sulfuric acid and heat-treated at 600 °C gave the peaks similar to those on untreated samples heated at 600 °C, but the peak strength was somewhat lower. At 800 °C, new peaks appear at 23.7° and 25.0°, but there is no change in main peaks. On the other hand, the diffraction peaks of the samples treated with phosphoric acid had quite low strength. Even after the heat treatment at 800 °C, the peaks were not so sharp. Thus, the treatment with phosphoric acid proves to be especially effective in preventing the crystallization of niobium oxide.

Surface Area. Samples untreated or treated with sulfuric or phosphoric acid were examined for the relationship between specific surface areas and heat treatment temperatures. As is shown in Fig. 5, the surface area of the untreated sample sharply drops between 400 and 600 °C. This decrease in surface area is due to the crystallization of niobium oxide occurring around 550 °C. Furthermore, the extremely small surface area observed at 800 °C suggests that the crystallization has been completed at this temperature. In the case of sulfuric acid treated niobic acid, the surface area was constant up to 600 °C, but drastically decreased after heating at 800 °C. The sample treated with phosphoric acid had lower surface area at 200 °C than that of the untreated niobic acid, but it showed the lowest extent of decrease with the rise of temperature. After heat treatment at 800 °C, the

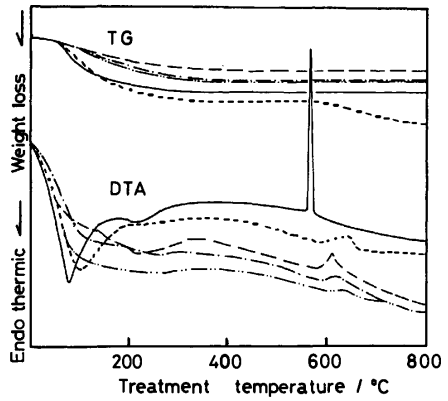

Fig. 3. TG-DTA patterns of niobic acid.
——: Before treatment, – – –: after treatment with 0.5 mol dm^{-3} H_2SO_4, — —: after treatment with 0.25 mol dm^{-3} H_3PO_4, —·—: after treatment with 0.5 mol dm^{-3} H_3PO_4, —··—: after treatment with 1.0 mol dm^{-3} H_3PO_4.

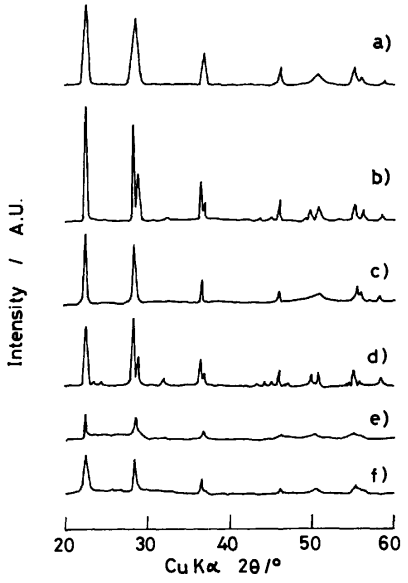

Fig. 4. XRD patterns.
a) Niobic acid heat-treated at 600 °C, b) niobic acid heat-treated at 800 °C, c) H_2SO_4-treated niobic acid, after heat-treated at 600 °C, d) H_2SO_4-treated niobic acid, after heat-treated at 800 °C, e) H_3PO_4-treated niobic acid, after heat-treated at 600 °C, f) H_3PO_4-treated niobic acid, after heat-treated at 800 °C. The concentrations of the H_2SO_4 and H_3PO_4 used for the treatment were 0.5 mol dm^{-3}.

sample retained a relatively large surface area of 33 $m^2 g^{-1}$. Thus, the effect of phosphoric acid treatment is remarkable to maintain the large surface area of niobic acid.

Surface Composition. The XPS study was made to obtain an information about surface composition of niobic acid. Surfaces of untreated and phosphoric acid treated samples were etched for 0, 5, and 15 min. In Table 2, the surface compositions determined by XPS are shown. The untreated sample gave a Nb/O atomic ratio of 27/73 regardless of heat treatment temperature. This ratio is roughly equal to the theoretical Nb/O value of Nb_2O_5 (29/71). After heating at 400 °C, the Nb/O ratio slightly increased as the time of Ar^+ etching became longer. After 15 min of etching, the observed value reached the theoretical value. On the other hand, after heating at 600 °C, the Nb/O ratio sharply increased along with the etching. This indicates that Nb atoms are regularly arranged on stable and strong grids and are difficult to eliminate on etching; therefore oxygen atoms are preferentially eliminated.

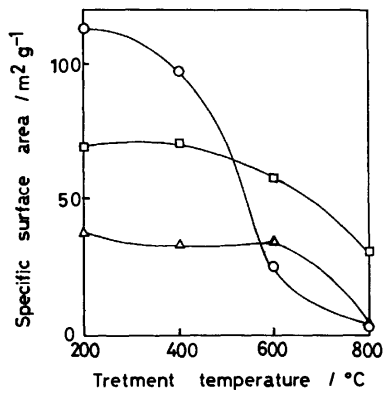

Fig. 5. Specific surface area of niobic acid.
○: Before acid treatment, △: after treatment with 0.5 mol dm^{-3} H_2SO_4, □: after treatment with 0.5 mol dm^{-3} H_3PO_4.

As regards the samples treated with phosphoric acid, the P/Nb ratio at 600 °C is slightly lower than that at 400 °C, indicating a possibility of the loss of P component and crystallization during the heat treatment at high temperatures. Even in this case, a P/Nb ratio close to 0.5 enables us to expect that a considerable part of surface layer will be covered with phosphoric acid (probably in the form of polyphosphate). Even when the sample was heat-treated at 600 °C, a relatively high P value of 6 atomic% is retained. This indicates that phosphoric acid penetrates to inner layers of niobic acid.

Catalytic Activity in Methanol Conversion. The product distribution of methanol conversion is shown in Table 3. Though the main product was dimethylether (DME), a considerable amount of methane formed over niobic acid heat-treated at 400 °C. After heating at 600 °C, which is higher than the crystallization temperature of niobium oxide, the activity decreased and especially methane formation was

Table 2. Surface Composition of Niobic Acid Before and After H_3PO_4-Treatment

Heat treatment temperature/°C	Ar^+ etching time/min	Composition/atomic/%		
		Nb	O	P
Before treatment				
400	0	27	73	
	5	28	72	
	15	29	71	
600	0	27	73	
	5	35	65	
	15	36	64	
After treatment with 0.5 mol dm^{-3} H_3PO_4				
400	0	11	19	70
	5	9	25	67
	15	8	25	68
600	0	9	20	70
	5	8	24	67
	15	6	30	63

Table 3. Results of Methanol Conversion Catalyzed by Niobic Acid Before and After Treatment with Phosphoric Acid

Heat treatment temperature/°C	Product distribution/mol/%[a]					
	CH_4	$CH_2{=}CH_2$	CH_3CH_3	$CH_3CH{=}CH_2$	DME[b]	CH_3OH
Before treatment						
400	32.4	0.8	0.7	0.4	45.6	20.1
600	8.1	0.1	0.1	0	65.8	25.9
After treatment with 0.5 mol dm^{-3} H_3PO_4						
400	8.1	0.3	0.2	trace	67.0	22.5
600	10.5	0.5	0.3	0.3	66.4	22.1

a) The reactions were carried out at 400 °C. The CH_3OH was fed to a conventional flow reactor containing 1 g of catalyst at a rate 1.8 ml h^{-1} through a preheater. b) DME denotes dimethyl ether.

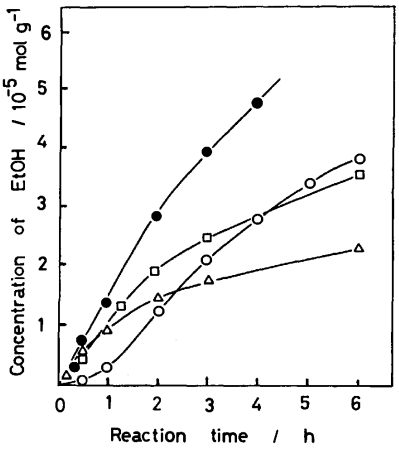

Fig. 6. Catalytic activity of niobic acid treated with 0.5 mol dm^{-3} H_3PO_4 for ethylene hydration.
○: Niobic acid, □: niobic acid treated with H_3PO_4, 1 st run, ●: niobic acid treated with H_3PO_4, 2 nd run (evacuated at 500 °C before the 2 nd run), △: solid phosphoric acid.
All these catalysts were heat-treated at 220 °C under evacuation for 1 h (for untreated or H_3PO_4-treated niobic acid) or about 5 min (for solid phosphoric acid) before use as a catalyst.

depressed.

On the other hand, the catalytic activity of niobic acid treated with phosphoric acid was not so sensitive to the heat-treatment temperature. Besides DME and methane, small amounts of olefin were formed in this reaction. The olefin formation was promoted more effectively by the niobic acid treated with phosphoric acid compared with the untreated sample after heat-treated at 600 °C. It is known that the olefin formation is promoted only by strong acid sites,[7] whereas the DME formation may be promoted by weak ones. So, the results described above suggest that strong acid sites should be formed and retained on niobic acid treated with phosphoric acid even after the heat treatment at higher temperature (600 °C).

Catalytic Activity in Ethylene Hydration. A gas-phase reaction was carried out in a circulation system at 220 °C to examine the catalytic activity of niobic acid treated with 0.5 mol dm^{-3} of phophoric acid in ethylene hydration reaction. The results obtained are shown in Fig. 6. For comparison, the previously reported results[1] obtained under the same reaction conditions for solid phosphoric acid and untreated niobic acid are also shown here. The untreated niobic acid has a higher catalytic activity than conventionally used solid phosphoric acid. It should be noted, however, that the activity is fairly low during the initial period of reaction. In contrast, niobic acid treated with phosphoric acid showed a high activity from the beginning. It is especially noted that, when the H_3PO_4-treated catalyst was heated at 500 °C in a vacuum, and then used in the reaction, the catalytic activity increased remarkably. This fact is in contrast to the case of untreated niobic acid which showed low activity when evacuated at 500 °C. Namely, the phosphoric acid treatment seems to be the reason for maintaining the catalytic activity even after the heat treatment at a high temperature such as 500 °C. In these ethylene hydration reactions, the heat treatments were carried out under evacuation, since they were attempted in the circulation system to use the niobic acid catalyst immediately after the treatment. However, it was confirmed that the heat treatment under atomospheric pressure affected the surface acidity and the catalytic activity of niobic acid, almost similarly to the heat treatment under evacuation. Thus, the H_3PO_4-treated catalyst has the advantage that the deactivated one can be recovered by heat treatment.

In the 1st-run reaction, the catalyst treated with 1 mol dm^{-3} phosphoric acid showed a higher activity than the sample treated with 0.5 mol dm^{-3} acid. However, in the second run reaction, the activity of the catalyst evacuated at 500 °C remained constant and independent of the concentration of phosphoric acid. As previously noted, the strong acid amount of niobic acid heat-treated at high temperatures remains roughly constant regardless of the concentration of phosphoric acid used for the treatment. Since the catalytic activity of H_3PO_4-treated catalyst is remarkably higher than that of solid phosphoric acid, it is speculated that phosphoric acid is not simply polymerized, but is condensed with niobium on the surface of niobium oxide and that for this reason, the H_3PO_4-treated catalyst works effectively to promote the reaction.

The authors are indebted to CBMM Ltd. for their providing the niobic acid samples and financial support on the present work.

References

1) K. Ogasawara, T. Iizuka, and K. Tanabe, *Chem. Lett.*, **1984**, 645.
2) Z. Chen, T. Iizuka, and K. Tanabe, *Chem. Lett.*, **1984**, 1085.
3) T. Iizuka, K. Ogasawara, and K. Tanabe, *Bull. Chem. Soc. Jpn.*, **56**, 2927 (1983).
4) S. Okazaki, *Senjosekkei*, No. 12, 46 (1981).
5) K. Tanabe, "Heterogeneous Catalysis," ed by B. L. Shapiro, Texas A & M Univ. Press, College Station, (1984), p. 71.
6) B. K. Sen, A. V. Saha, *Mat. Res. Bull.*, **17**, 161 (1981).
7) Y. Ono, *Petrotech*, **3**, 1039.

 © 1987 The Chemical Society of Japan Bull. Chem. Soc. Jpn., 60, 43—47 (1987)

Interaction between Dodecyltrimethylammonium Chloride and DNA

Keishiro SHIRAHAMA,* Koji TAKASHIMA, and Noboru TAKISAWA
Department of Chemistry, Faculty of Science and Engineering, Saga University, Saga 840
(Received June 12, 1986)

Binding of dodecyltrimethylammonium cation to calf thymus DNA was studied by using the surfactant-selective electrode as a function of added electrolyte concentration at various temperatures. Binding is highly cooperative and biphasic. An abruptly occurring binding attains a slight shoulder within a very narrow equilibrium concentration range followed by a further augmentation in binding, as the equilibrium concentration is increased. Temperature caused relatively small shift in binding isotherm, but a distinct inversion point was found around 27 °C. Above this temperature the isotherm shifts to the left and then to the right below it. Analogous binding studies as above were repeated with heat-denatured DNA, which binds the surfactant with higher intrinsic affinity but less cooperatively than the intact DNA. A fluorescent probe, pyrene, was employed to assess the microenvironmental polarity of pyrene in DNA before and after surfactant binding. The surfactant-DNA complex has a hydrophobic region akin to ordinary micelle.

Partition of a ligand molecule (ion) between a macromolecule and aqueous phase is very important and attractive phenomena. Actually a number of investigations on such molecular interactions have been published to cover synthetic as well as biological systems.[1-4] Binding isotherm among many others is a clear-cut evidence of interaction between ligand and macromolecule, and will allow not only qualitative but also quantitative interpretation of the phenomena by the help of statistical mechanics and other physical methods.

We also have studied some macromolecule-ligand systems in which ionic surfactants take part of the ligands.[5-12] Deoxyribonucleic acid (DNA) is viewed as a long cylinder with phosphate groups spirally arrayed on the surface, and thus has driven researchers to work on surfactant binding.[12-14] In a previous paper,[12] interaction between DNA and cationic surfactant, *N*-dodecylpyridinium halides, was reported. In the present work, dodecyltrimethylammonium chloride was used in place of the pyridinium analog to see if there is any difference in binding behavior. A fluorescence probe, pyrene was employed to assess the microenvironment of pyrene in DNA–surfactant complex. Binding studies were extended to thermally denatured DNA in the added electrolyte solutions of various concentrations at temperatures. These binding behaviors were semiquantitatively expressed in terms of one-dimensional Ising model.

Experimental

Materials. Dodecyltrimethylammonium chloride (Tokyo Kasei Co.) was recrystallized from acetone three times. The critical micelle concentration as measured by an electric conductivity method is 20.5 mM in water at 25 °C. Calf thymus DNA (Sigma, sodium salt) is the same sample as used before.[12] Thermal denaturation was carried out by heating DNA solution at 85 °C for 5 min.

Binding Isotherm. Propionyl-α-cyclodextrin electrode which had previously been used[11,12] responded also to dodecyltrimethylammonium cation as seen in Fig. 1, where a straight line has a slope of 59 mV per 10 fold concentration difference, or the Nernstian response. In the presence of DNA, however, there appeared a deviation from the linearity which was caused by a partial uptake of surfactant by DNA.

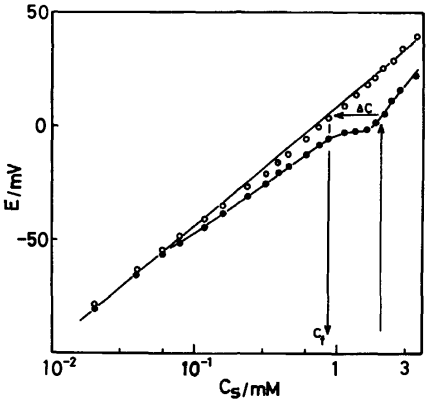

Fig. 1. Potentiometric titration of dodecyltrimethylammonium chloride in 20 mM NaCl at 25 °C. ○: without and ●: with DNA. See text for C_s, C_f, and ΔC.

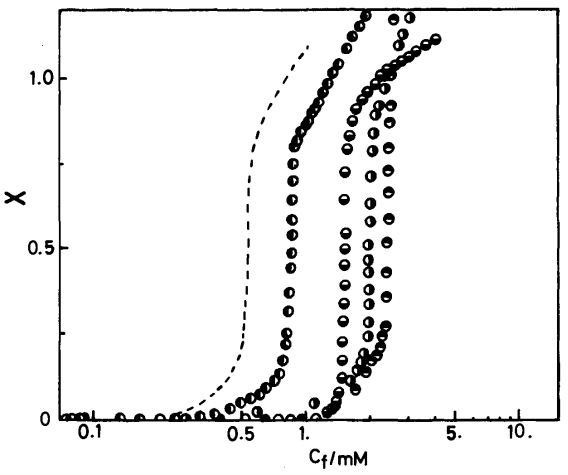

Fig. 2. Binding isotherms of dodecyltrimethylammonium chloride–DNA system at 25 °C. NaCl concentrations ◐: 20, ◒: 40, ◑: 80, and ◓: 160 mM, the dashed line for *N*-dodecylpyridinium chloride for comparison.

No hysterisis was observed when the potentiometric titration without DNA was repeated after the binding run. Following the arrows indicated in Fig. 1, an amount of binding, $\Delta C=C_s-C_f$, and an equilibrium concentration, C_f are easily obtained. A binding isotherm is built up by plotting a degree of binding, $X=\Delta C/$(total concentration of phosphate groups in DNA) vs. $\log C_f$ as shown in Fig. 2.

Fluorescent Probe Method. Emission spectrum from pyrene in the surfactant and/or DNA solution was recorded on a fluorescence spectrophotometer (Shimadzu RF-510).

We conveniently use the notation, 1 M=1 mol dm^{-3} throughout the paper.

Results and Discussion

Binding to Intact DNA. All the binding isotherms are characteristic of cooperative nature as well as biphasic. An abrupt appearance and completion of the first step binding is followed by the second step binding. It is clear that added NaCl causes the first binding shift to the right along the C_f axis as seen in Fig. 2. As for the second one, the effect of added electrolyte seems reversed. All these features are the same as observed previously with the DNA-*N*-dodecylpyridinium system and can be interpreted in the same manner. The first step binding is a process where DNA discharges and added electrolyte shields the electrostatic field attractive to surfactant cations leading to decreased binding affinity. On the other hand, in the second step binding, charge is built up on DNA on binding the surfactants with their hydrocarbon tails in contact with each other on DNA and with their charged head groups exposed toward the aqueous bulk phase. In Fig. 2, the binding isotherm of *N*-dodecylpyridinium Cl-DNA system (20 mM NaCl, 25 °C)[12] is shown by a dashed line for comparison. The equilibrium concentration at $X=0.5$ are 0.54 mM for *N*-dodecylpyridinium and 0.64 mM for dodecyltrimethylammonium, respectively. This difference, $RT\ln(0.64/0.54)=0.42$ kJ mol^{-1}, should be ascribed to the different structures of ionic head groups of the two kinds of surfactants. A positive charge delocalized throughout a flat pyridinium ring can approach a phosphate group on DNA much closer than that of trimethylammonio group gaining more electrostatic interaction energy.

Figure 3 shows binding isotherms at four temperatures. The temperature effect is small and even an inversion temperature is found around 27 °C, which is slightly higher than the one (23 °C) found with the pyridinium analog in the previous study.[12]

Binding to Thermally Denatured DNA. Figures 4 and 5 display binding isotherms for thermally denatured DNA. Binding begins at an equilibrium concentration lower than in intact DNA solution, and increases with less steep slope. This means that

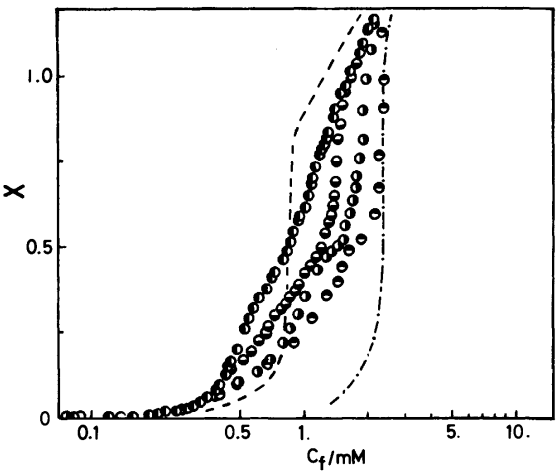

Fig. 4. Binding isotherms of dodecyltrimethylammonium chloride-heat denatured DNA system at 25 °C. NaCl concentrations: ◐: 20, ◒: 40, ◑: 80, and ◓: 160 mM. The dashed and chain lines for intact DNA in 20 and 160 mM NaCl at 25 °C, respectively.

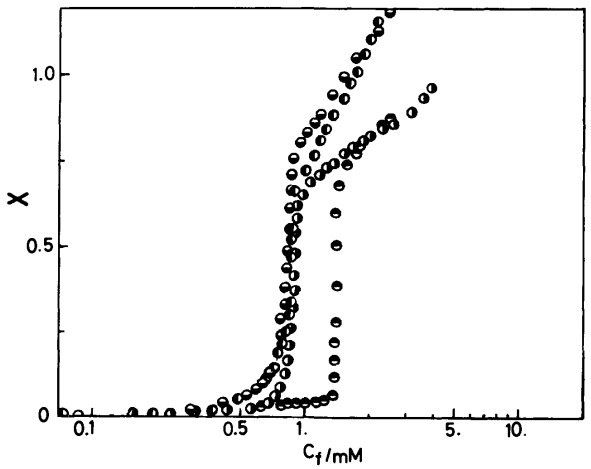

Fig. 3. Binding isotherms of dodecyltrimethylammonium chloride–DNA system in 20 mM NaCl at various temperatures(°C): ◓: 15, ◐: 25, ◒: 35, and ◑: 45.

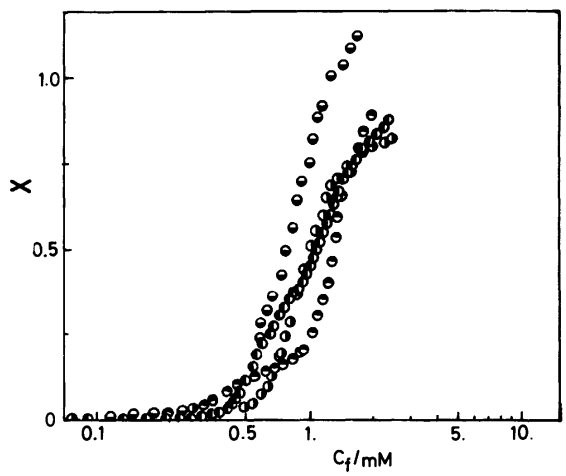

Fig. 5. Binding isotherms of dodecyltrimethylammonium chloride-heat denatured DNA system in 20 mM NaCl at various temperatures(°C); ◓: 15, ◐: 25, ◒: 35, and ◑: 45.

additional binding affinity is gained by contact between alkyl chains of bound surfactants and hydrophobic moiety of DNA which has been exposed to the aqueous phase by thermal denaturation. Randomized array of phosphate groups as a result of heat denaturation causes less effective interaction between alkyl chains of bound surfactants leading to a lower cooperativity, or a less steep growth of binding. It is to be noted that the binding isotherm overlaps that of not-heat-treated DNA (dashed and chained lines in Fig. 5) around $X=1$. This strongly indicates that the surfactant-DNA complex assumes the same dissolved state as the thermally denatured DNA does near the endpoint of surfactant titration, in other words, the cationic surfactant denaturates the DNA. Electrostatic shielding effect decreases the binding affinity in these systems, too.

In Fig. 5, the effect of temperature on the binding to the denatured DNA is shown. Here again an inversion temperature is observed around 27 °C: binding isotherm shifts to the left from 15 °C up to the inversion temperature, and moves back at 45 °C to the right. Regular structure of intact DNA may not be prerequisite for the inversion temperature phenomena, which is similar to a minimum found in a critical micelle concentration-temperature plot.[15-17]

Fluorescence from Pyrene. Fluorescence from pyrene provides significant information about microenvironment surrounding the molecule.[18] Figure 6 shows how relative fluorescence intensity at $\lambda=391$ nm, I_r, varies with the surfactant concentration. In the absence of DNA, and below cmc, I_r decreases. This means that fluorescence from pyrene molecules in aqueous environment is quenched on encounter with the cationic surfactant monomers. The pyrene molecules are, however, getting free from the quenching as soon as micelle formation begins. Pyrene molecules now find micelles where the quantum yield for fluorescence is enhanced. In the presence of DNA, I_r is much smaller than the one without DNA. When pyrene molecules are under the influence of DNA, they are probably intercalated between bases, and the quantum yield is very low.[19] However the fluorescence intensity is enhanced in parallel with the surfactant binding as seen in Fig. 6, where a dashed line shows the surfactant binding isotherm. That pyrene molecules are transferred to some hydrophobic micelle-like region in surfactant-DNA complex is suggested from comparison of curves (a) and (b).

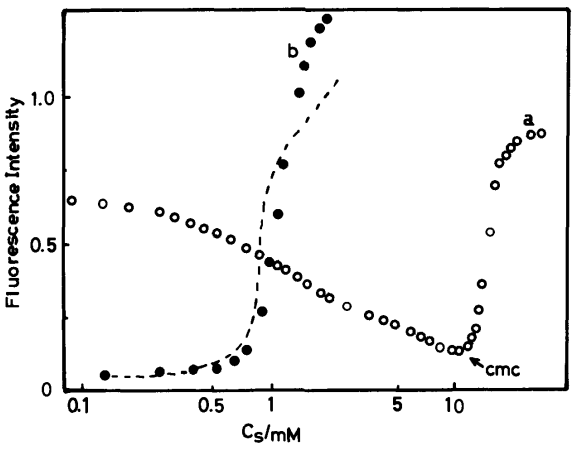

Fig. 6. Fluorescence intensity (in arbitrary unit) of pyrene ($\lambda=391$ nm) as a function of dodecyltrimethylammonium chloride concentration (in 20 mM NaCl at 25 °C). ○: Without and ●: with DNA. The dashed line shows a synchronized binding.

Ising Model. All these binding features will be semiquantitatively expressed in terms of statistical thermodynamics. Phosphate groups are taken as a one dimentional array of binding sites, on which the surfactant molecules are bound with their hydrocarbon chains in contact with each other. The partition function of the system is written as,

$$Z = aM^n a^* \tag{1}$$

with

$$M = \begin{pmatrix} 1 & 1 \\ s/u & s \end{pmatrix},\ a = (1,1),\ a^* = \begin{pmatrix} 1 \\ 0 \end{pmatrix},\ \text{and}\ s = KuC_f,$$

where K is equilibrium constant for a process that a surfactant is transferred from the aqueous bulk phase to an isolated binding site on DNA, and u an equilibrium constant of aggregation among bound surfactants, or cooperativity parameter.

When n is very large, Eq. 1 produces compact and useful expressions,[20] among which the following equations are convenient to extract thermodynamic informations,

$$X = \mathrm{dln}\, Z/\mathrm{dln}\, C_f = \{1-(1-s)/\sqrt{(1-s)^2+4s/u}\}/2 \tag{2}$$

$$K = 1/C_f(X=0.5)u, \tag{3}$$

where $C_f(X=0.5)$ is an equilibrium concentration assuring $X=0.5$. Lower halves of binding isotherms were fitted to Eq. 2 to calculate the value of u in conformity with the Manning's notion that electrostatic potential at polyelectrolyte surface remains relatively constant so long as the surface charge density is high enough.[21,22] The thermodynamic parameters thus obtained are shown in Figs. 7 and 8. It is noted in Fig. 7 that u increases, while K decreases with increasing the added electrolyte concentration. The value of u should be kept constant irrespective of added salt concentration, since it is an equilibrium constant for aggregation process of bound surfactants which are no longer charged. With increase in the amount of binding, electrostatic potential is reduced, although there may be a sort of compensation by the Manning's ion-condensation mechanism. This potential reduction brings about a negative cooperativity. The anticooperativity decreases with increase in added electrolyte concentration, as seen in Fig. 7,

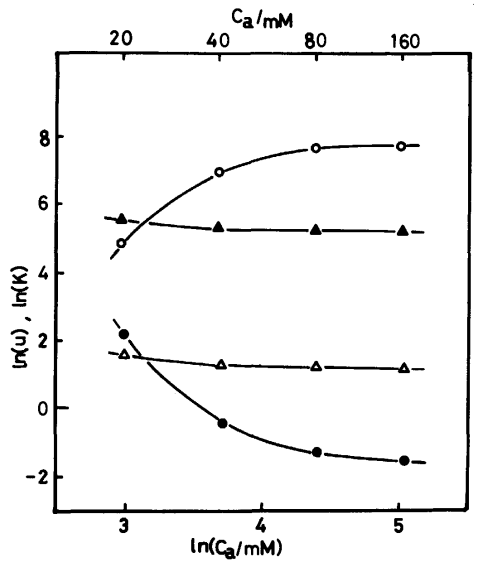

Fig. 7. ln u and ln K vs. ln C_a, where C_a is added NaCl concentration. ○: u and ●: K for intact DNA, and △: u and ▲: K for heat-denatured DNA.

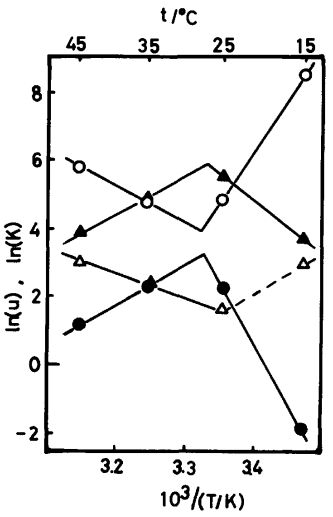

Fig. 8. ln u and ln K vs. $1/T$. ○: u and ●: K for intact DNA, and △: u and ▲: K for heat-denatured DNA.

where the effect of added electrolyte is almost saturated when C_a is as much as 160 mM. Figure 7 also shows the thermodynamic parameters for the thermally denatured DNA. Very low u and high K values may be responsible for the disordered phosphate array and exposed hydrophobic moieties of DNA as a result of heat denaturation as explained above.

Temperature dependence on the binding behavior is reflected on plots of ln u and ln K vs. $1/T$ in Fig. 8, where distinct reversal in the temperature dependence is observed around 26—27 °C, for both intact and heat-denatured DNA. Below the inversion temperature, K increases while u decreases with increasing temperature, and vice versa above it. Inversion in the temperature dependence in surfactant binding is also found for DNA[12] and dextran sulfate.[23] These phenomena are reminiscent of the similar minima found in cmc[15–17] as well as solubilities of some organic compounds in water.[24] Detailed studies on water structure and hydrophobic hydration are required before these inversion phenomena are fully understood.

Gross effect of added surfactant is to denature DNA which has ordinarily highly ordered structure. Proteins are also denatured by addition of surfactants, and the modes of action are very much complicated as well as diverse, reflecting the complexity of protein structures of primary, secondary, and higher orders.[25,26] In contrast, binding mode is simpler than that of proteins, and DNA behaves much like synthetic polyelectrolytes in binding surfactants.[8,11,23] However there is a distinct difference in DNA which undergoes an drastic order-disorder transition, while synthetic polymers will not show such a conformation change.

We thank Prof. Mitsuru Tanaka of Fukuoka University for providing the DNA sample.

References

1) A. J. Hopfinger, "Intermolecular Interactions and Biomolecular Organization," John Wiley and Sons, New York (1977).
2) J. Steinhardt and J. A. Reynolds, "Multiple Equilibria in Proteins," Academic Press, New York (1969).
3) "Microdomains in Polymer Solutions," ed by P. Dubin, Plenum, New York (1985).
4) I. D. Robb, "Anionic Surfactants, Surfactant Science Series," ed by E. H. Lucassen-Reynders, Vol. 11, (1981), p. 109.
5) K. Shirahama, *Colloid Polym. Sci.*, **252**, 978 (1974).
6) T. Takagi, K. Tsujii, and K. Shirahama, *J. Biochem. (Tokyo)*, **77**, 939 (1975).
7) K. Shirahama and N. Ide, *J. Colloid Interface Sci.*, **54**, 450 (1976).
8) K. Shirahama, H. Yuasa, and S. Sugimoto, *Bull. Chem. Soc. Jpn.*, **54**, 375 (1981).
9) K. Shirahama, M. Todoh, and M. Murahashi, *J. Colloid Interface Sci.*, **86**, 282 (1982).
10) K. Takeda, A. Iba, and K. Shirahama, *Bull. Chem. Soc. Jpn.*, **55**, 985 (1982).
11) K. Shirahama and M. Tashiro, *Bull. Chem. Soc. Jpn.*, **57**, 377 (1984).
12) K. Shirahama, T. Masaki, and K. Takashima, p. 299 in Ref. 3.
13) R. Chatterjee and D. K. Chattoraj, *Biopolymers*, **18**, 147 (1979).
14) K. Hayakawa, J. T. Santerre, and J. C. T. Kwak, *Biophys. Chem.*, **17**, 175 (1983).
15) B. D. Goddard and G. C. Benson, *Can. J. Chem.*, **35**, 986 (1957).
16) B. D. Flockhart, *J. Colloid Sci.*, **16**, 484 (1961).
17) Y. Moroi, N. Nishikido, H. Uehara, and R. Matuura,

J. Colloid Interface Sci., **50**, 254 (1975).
18) J. K. Thomas, *Chem. Rev.*, **80**, 283 (1980).
19) H. P. Nelson, Jr. and H. DeVoe, *Biopolymers*, **23**, 89 (1984).
20) G. Schwarz, *Eur. J. Biochem.*, **12**, 442 (1970).
21) G. S. Manning, *Acc. Chem. Res.*, **12**, 443 (1979).
22) G. S. Manning, *J. Phys. Chem.*, **85**, 870 (1981).
23) J. P. Santerre and J. C. T. Kwak, *Colloids Surf.*, **13**, 35 (1985).
24) A. Katayama, T. Takagishi, K. Konishi, and N. Kuroki, *Kolloid-Z. Z. Polym.*, **210**, 126 (1967).
25) W. L. Mattice, J. M. Riser, and D. S. Clark, *Biochemistry*, **15**, 4264 (1976).
26) B. Jirgensons, "Optical Activity of Proteins and Other Macromolecules," 2nd. Ed., Springer-Verlag, Berlin (1973).

 © 1987 The Chemical Society of Japan Bull. Chem. Soc. Jpn., 60, 49—54 (1987)

Time-Resolved Unimolecular Reactions of Pyridine Ions by Means of Trapped-Ion Mass Spectrometry

Ryuichi ARAKAWA* and Yozaburo YOSHIKAWA
Institute of Chemistry, College of General Education, Osaka University,
Toyonaka, Osaka 560
(Received June 16, 1986)

The electron-impact ionization-efficiency curves for the $C_5H_5N^{+\cdot} \rightarrow C_4H_4^{+\cdot} + HCN$ dissociation have been measured as a function of the ion-source-residence time by means of trapped-ion mass spectrometry (TIMS). The ionization-efficiency curves for residence times of 5 and 700 μs were fitted by QET calculation, assuming dissociation-rate models. A kinetic shift of 0.3 eV was observed from the time-dependent appearance energy measurements. The fragmentation of metastable ions was first sampled for the ion-source residence time of 0—100 μs. The preferable rate model was determined by the analysis of the ionization-efficiency curves and the metastable ion fragmentations. Time-resolved kinetic energy releases for pyridine and perdeuteriopyridine have been explained in terms of excess energy drop of metastable ions with their lifetime.

The $C_4H_4^+$ ion is one of the major fragments from benzene and pyridine in their mass spectra. The appearance energy of the pyridine reaction (Eq. 1) has been measured by a wide variety of experimental techniques.[1-5]

$$C_5H_5N^{+\cdot} \longrightarrow C_4H_4^{+\cdot} + HCN. \quad (1)$$

One of the main problems in these measurements is the so-called "kinetic shift," the excess energy required to produce a detectable dissociation of a polyatomic ion. Ion-trapping techniques are favored for clarifying this kind of problem. There have been two reports of experimental results for the dissociation of trapped pyridine ions. One was the study of Rosenstock et al.[6] by means of photoion-photoelectron coincidence (PIPECO) mass spectrometry, with a variable ion-source-residence time. The dissociation threshold energy at 0 K was determined by their detailed analysis of time-dependent breakdown curves obtained from the first derivative of photoionization curves with a microsecond ion-residence time. The other was studied by Lifshitz[7] using trapped ion mass spectrometry, with a millisecond ion-storage time. The second derivative of electron-impact ionization curves produced the breakdown curves.

In these two studies, a shift observed for time-resolved breakdown curves was used for evaluating the kinetic shift. The measurements of the breakdown curve shift give us less erroneous information about the kinetic shift than conventional appearance energy measurements for metastable ions, e. g., a semilog plot. This is because metastable ions usually have quite a low intensity relative to the normal ion intensity. Compared with the PIPECO experiment, the TIMS experiment can easily change the ion-residence time from zero to several milliseconds, so that unimolecular reactions of rate constants ranging from 10^2 to 10^5 s^{-1} can be observed. However, its energy definition for ionized precursors is rather uncertain because of electron-impact ionization.

Recently, the fragmentation of the bromobenzene ion to the phenyl cation has been studied by Lifshitz and her co-workers[8] using time-resolved photoionization mass spectrometry (TPIMS). Photoionization efficiency (PIE) curves at ion-residence times of 2 m s and 6 μs have been, for the first time, measured and compared with the calculated PIE curves near the threshold energy. A critical appearance energy was determined from the calculation of the quasi-equilibrium theory(QET). The TPIMS technique has employed a cylindrical ion-trap chamber to store ions over milliseconds, because the variable-time PIPECO technique limits ion-source-residence time to a microsecond time scale.

In the present work, electron-impact ionization efficiency (EIE) curves for the pyridine reaction (Eq. 1) have been measured as a function of the ion-source-residence time. Then, we observed a shift of time-resolved daughter EIE curves near the threshold energy, although the electron-impact energy had an spread of ≈1 eV. The EIE curves moved to a lower energy side with an increase in the ion-residence time. The time-resolved EIE curves will be analyzed by QET calculation using two available unimolecular rate models. The EIE curve can be expressed in the mathematical form of double integrations of breakdown curves, while the PIE calculation involves a single integration of breakdown curves with respect to energy. A difficulty in the EIE curve calculation is to estimate the internal energy distribution of parent ions ionized with a variable incident electron energy. Here, we estimated the internal energy distribution on the basis of the threshold behavior of the electron ionization. In addition, the energy spread of incident electrons should be convoluted for the EIE calculation.

The metastable peak intensity and the kinetic energy release have not been measured for a wide range of ion-source-residence times. Two rate models for the pyridine reaction (Eq. 1) have been reported using the PIPECO technique.[3,6] We will discuss the

validity of these rate models by analyzing the time-resolved metastable ion fragmentation, because its fragmentation depends greatly on the unimolecular rate constant. Moreover, the time-resolved kinetic-energy-release measurement can closely test an empirical relation between the kinetic energy release and the internal excess energy of precursor ions.

Experimental

The ion trapping technique employed has been described in detail by Herod and Harrison[9] and by Lifshitz.[10] Ions were produced when a negative pulse was applied to a Rhenium filament. A continuous 5-eV electron beam, forming a negative potential well, was used to trap the ions. The well-depth should be greater than the thermal kinetic energy of the trapped ions.[11] A small negative bias on a repeller plate is also necessary for effective trapping. At a known delay time after the ionizing pulse, a positive pulse, 6 μs in duration and 6 eV in height, was applied to a repeller electrode to remove ions for mass analysis. The ion-trapping efficiency was examined by the use of Kr or pyridine ions. These ions were stored up to several milliseconds without any serious decrease in the trapped-ion concentration. An ionizing pulse 2 μs in duration was applied to the filament at 1-ms intervals. The nominal electron energy was varied by changing the pulse height applied to the filament.

A home-built tandem mass spectrometer[12] was used to measure the fragment-ion abundance and the kinetic-energy release in the metastable ion dissociation. Fragment ions produced by unimolecular decomposition occurring in the second-field free region between two magnets were detected by means of a pulse-counting method. Their intensities were then analyzed by means of a microcomputer. The temperature of the ion source was 423 K. The ion-accelerating voltage was 1.5 kV. The ion-source pressure was kept at 2×10^{-6} Torr (1 Torr=133.32 Pa). The collisional induced reaction were negligible, because the pressure in the field-free region was always less than 1×10^{-6} Torr. The samples of pyridine and perdeuteriopyridine (99% atom D; MERCK) were commercially obtained.

Results and Discussion

Time-Resolved EIE Curves and Appearance Energies. Figure 1 displays the EIE curves of daughter-($C_4H_4^+$) and parent($C_5H_5N^+$) ions for the delay times of 5 and 700 μs. The EIE data have been accumulated for several hours because of low counting rates near the reaction onset. A kinetic shift of about 0.3 eV was observed near the onset. In the previous TIMS experiment,[7] the normalized second derivatives of the experimental EIE curves yielded the breakdown curves. A crossing point of daughter and parent fractions in the breakdown curve moved with the delay time, and its shift was compared with that of the QET calculation. The breakdown curves have a width of a few eV at the nominal electron energy. Thus, it should be emphasized that time-resolved EIE curves, as well as the PIE curves in the TPIMS analysis, should be analyzed in a narrow energy range above the onset.

The time-resolved EIE of the daughter ion at a nominal electron energy, V, can be written in this form:

$$\mathrm{EIE}(V,t) = c\int_0^\infty m(E_t-V) \times\left[\int_{AE_o}^{E_t} f(E_t,E)(1-\exp(-k(E)t))dE\right]dE_t. \quad (2)$$

Here, c is the constant; t is the ion residence time; $m(E_t-V)$ is the instrumental-electron energy distribution; E_t is the total electron energy, defined as V plus the energy of the electron emitted from the filament; $f(E_t,E)$ is the internal energy distribution at the electron-impact energy, E_t; E is the internal energy of the parent ion; $k(E)$ is the unimolecular rate constant, and AE_o is the appearance energy at 0 K.

Morrison has proposed that the EIE second derivatives for inert gases yield the electron-energy distribution, reversed with respect to the energy scale.[13] In the present case, the $m(E_t-V)$ distribution was obtained by differentiating the experimental helium EIE. The half-width of $m(E_t-V)$ was found to be 0.8 eV. From the threshold law of ionization,[14] the internal energy distribution is given by $f(E_t,E)=p(E)\cdot(E_t-E)^{K-1}$, where $p(E)$ is the energy deposition function; the exponent K gives the number of electrons that leave the collision complex; $K=1$ for

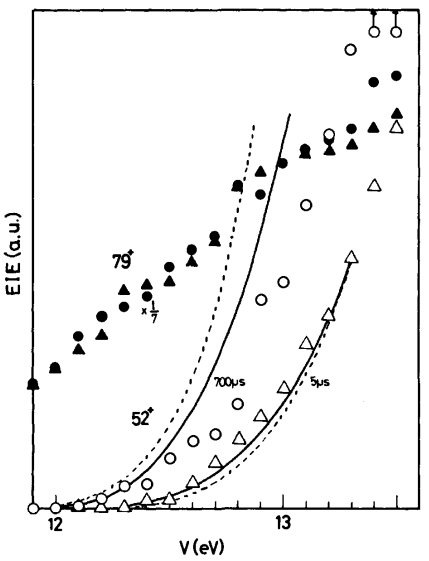

Fig. 1. Time-resolved electron ionization efficiency (EIE) curves measured with a 0.1 eV step of the nominal electron energy V. Experimental EIEs plotted on an arbitrary unit: ○, △, $C_4H_4^+$ fragment (52^+) for the delay times of $t=700$ and 5 μs, respectively; ●, ▲, parent ion (79^+). The EIE calculations based on the two available $k(E)$ models: ——, Eland et al.[3]; ----, Rosenstock et al.[6]. The calculated EIE curves were normalized at $V=13.3$ eV for the 5 μs curve.

photon impact, and $K=2$ for electron impact. The first derivative of the total PIE reported by Goffart et al.[15] was assumed to represent the $p(E)$ function upon ionization by electron impact. The mean vibrational energy of the pyridine molecules was 0.13 eV at 423 K. This thermal distribution was not considered in the EIE calculation, because the thermal effect was much less than the broad $m(E_i-V)$ distribution.

The experimental EIE curves were fitted using the two rate models proposed by Eland et al.,[3] $k_E(E)$, and by Rosenstock et al.,[6] $k_R(E)$. The $k_E(E)$ model has a tight transition state to fit their experimental $k(E)$ with the threshold energy of $AE_O=11.8$ eV. $k_R(E)$ is a loose model having $AE_O=12.15$ eV, which fits the measured crossover shift and the crossover energy of the breakdown curves. As a result, $k_R(E)$ has a somewhat steeper energy dependence than does $k_E(E)$.

The short delay time of 5 μs corresponds to the actual reaction time of 8 μs in the ion source. Figure 1 indicates that agreement with the experimental EIE curves is better for the $k_E(E)$ model than for the $k_R(E)$ model. This is consistent with the breakdown curve results[7] for fitting the experimental crossover shift for delay times of 5 and 1000 μs. From the time-resolved EIE calculation, the shift near the onset proved to depend only on the magnitude of $k(E)$ and to increase as the rate decreased. These results were actually due to the term of $1-\exp(-k(E)t)$ in Eq. 2. The $k_R(E)$ rate model, therefore, yielded a larger EIE shift than the $k_E(E)$ model, as is shown in Fig. 1; the rate constant near the threshold is smaller for $k_R(E)$ than for $k_E(E)$, because the $k_R(E)$ model has a higher reaction threshold. Thus, the amount of EIE shift is principally affected by the AE_O value.

The appearance energies, AE, of the $C_4X_4^+$ (X=H,D) ion, measured as a function of the delay time for pyridine and deuteriopyridine, are shown in Fig. 2. The convenient procedure for AE determination has been described by Burgers and Holmes[16] and by Gefen and Lifshitz.[17] On the basis of this procedure, we obtained the experimental AE value at a known delay time by comparing the EIE intensity of the fragment with that of a reference over a narrow range of ionizing-electron energies. The EIE comparison is usually made at the energy of ≈2 eV, far from the real onset, where the EIE intensity is statistically sufficient. The EIE curve for pyridine ions was employed as a reference. The ionization energy of pyridine (9.36 eV) was obtained by calibration with the ionization energies of benzene (9.24 eV)[18] and methyl acetate (10.27 eV).[2]

Lifshitz[7] has calculated the dependence of the delay time on the appearance energies using an equation for a minimum detectable ion signal developed by Gordon and Reid.[19] We recalculated the AE curve with the $k_E(E)$ rate model, as is shown in Fig. 2. The experimental AE of the $C_4H_4^+$ ion levels off at $AE=12.1\pm0.1$ eV. The kinetic shift of 0.3 eV for the $C_4H_4^+$ fragment was obtained from the AE gap between short and long reaction times. This AE gap agreed with the calculated one. In the present AE measurement, the EIE comparison was made at around $V=14$ eV. On the other hand, the time-resolved EIE measurement due to data accumulation produced an EIE shift of ≈0.3 eV at the lower energy of $V=12.5$ eV, as is shown in Fig. 1. Hence, it is worth

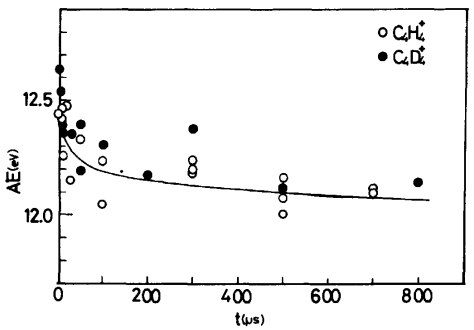

Fig. 2. Time dependent appearance energies AE for the reaction $C_5X_5N^{+\cdot}\rightarrow C_4X_4^{+\cdot}+XCN$(X=H, D). Experimental AEs at the ion source temperature of 423 K are indicated by open circles (X=H) and filled (X=D). The smooth line is the calculated AE for $C_4H_4^+$ using the rate model of Eland et al. Procedure for time-dependent AE calculation has in detail been described in Ref. 17. The minimum daughter concentration was calculated by setting $AE=12.5$ eV for $t=0$ μs. Since the detection sensitivity was independent of the delay time, AE for given delay time was then determined so as to produce the same concentration as calculated for $t=0$ μs.

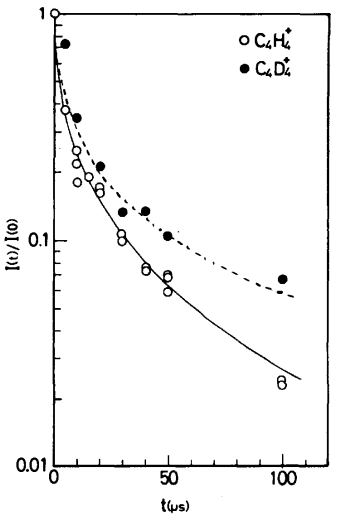

Fig. 3. The metastable ion abundances $I(t)$ for $C_4H_4^+$ (○) and $C_4D_4^+$ (●) measured as a function of delay times when $V=20$ eV. The data are nomalized at $t=0$ μs. The solid and dashed curves are the calculated $I(t)$ for $C_4H_4^+$ using the rate models of $k_E(E)$ and $k_R(E)$, respectively.

noting that the EIE shift measured is rather independent of the detection sensitivity of EIE. Finally, the rate model of Eland et al. is the preferable model for fitting the time-resolved EIE and AE curves. The AE values for the $C_4D_4^+$ fragment, as a whole, have a tendency to exceed those for the $C_4H_4^+$ fragment. The AE_0 value for perdeuteriopyridine was estimated by applying a zero-point vibrational energy correction[5]; at most, it proved 0.1 eV greater than that for pyridine.

Fragmentation of Metastable Ions. The relative abundance of the $C_4X_4^+$ resulting from the metastable transition of $C_5X_5N^+$ (X=H,D) was measured in the range of t=0—100 μs, as is shown in Fig. 3. For example, the $C_4H_4^+$ fraction relative to the parent ion was 3.1×10^{-2} at t=0 μs. The fragment abundance, $I(t)$, is given[20] by:

$$I(t) = c\int_0^\infty m(E_t-V) \times\left[\int_{AE_0}^{E_t} f(E_t-E)w(E)(k(E)/k_t(E))dE\right]dE_t, \quad (3)$$

where $k_t(E)=k(E)+k_n(E)$ is the total decay rate, $k_n(E)$ is a nondissociative rate such as the infrared radiative decay and the collisional relaxation in the ion source, and $w(E)=\exp(-k_t(E)t_1)-\exp(-k_t(E)t_2)$ is a fraction of the metastable-ion dissociation. (t_2-t_1) is the time ions spend in the second field-free region, where metastable ions are produced; $t_1=6.8+t$ and $t_2=11.8+t$ μs. The $I(t)$ curves for the $C_4H_4^+$ fragment were calculated with two $k(E)$ models in the case of $k_n(E)=0$. The calculated curve for the $k_E(E)$ model is in good agreement with the experimental curve, as is shown in Fig. 3. In this manner, the measurements of the time-resolved metastable peak abundances enable us to determine the $k(E)$ model, because the $I(t)$ curve is dependent on a rising steepness of $k(E)$. The rates corresponding to a peak of the $w(E)$ function when t=0 and 100 μs are $k(E)=1.1\times10^5$ and 9.1×10^3 s^{-1} respectively. These rates mainly contribute to the metastable fragmentation.

The approximate collisional relaxation rate is given by the Langevin ion-molecule reaction theory.[21] The relaxation rate of a bimolecular reaction is 80 s^{-1} at the present sample density if the polarizability of benzene, 10.3×10^{-24} cm^3, is taken as that of pyridine. Dunbar[22] has suggested that an upper limit on the lifetime of metastable-ion decomposition is determined by the competing relaxation of the infrared radiative cooling. This upper limit lies in the range of 15—60 s^{-1} for polyatomic molecules. The effects of the radiative decay on time-resolved PIE curves have been discussed in the case of a bromobenzene reaction.[8]

The nondissociative rate, $k_n(E)$, is, at most, 150 s^{-1}, as has been estimated above. This amount of $k_n(E)$ proved to have no effect on the quantity of metastable-ion fragmentation. For $k(E)\leq10^3$ s^{-1}, small values of $k_t(E)t_1$ and $k_t(E)t_2$ lead to $w(E)k(E)/k_t(E)\simeq(t_2-t_1)k(E)$ in Eq. 3. For $k(E)>10^3$ s^{-1}, $k_n(E)$ is negligible compared with $k(E)$. Thus, $I(t)$ is independent of $k_n(E)$.

Figure 4 represents the fragmentations of the metastable $C_4X_4^+$ ion by the loss of a hydrogen atom and a hydrogen molecule. The relative intensity of the two channels is nearly equal throughout the delay time.

Time-Resolved Kinetic Energy Release (KER). A metastable peak shape and its width are a very sensitive measure of the KER in unimolecular reactions.[23] In principle, a reaction with a large kinetic shift should show a large change in the KER with a increase in the metastable-ion lifetime. This has been demonstrated by Gefen and Lifshitz[17] in the case of iodobenzene. The KER value T, as determined by the peak analysis,[24] is given by:

$$T = m_1^2HV/(16m_2^3m_3)d^2 \quad (4)$$

Here, m_1 is the mass of the parent ion; m_2 and m_3 are the mass of the fragment ion and the neutral respectively; HV is the ion-accelerating voltage, and d is the peak width of the metastable ion, corrected by the normal peak width in units of the atomic mass. The experimental KER values at a half maximum, $T_{1/2}$, are listed in Tables 1 and 2. The error limits represent the standard deviation of several runs.

A simple method for the evaluation of the average KER $\langle T\rangle$ for a Gaussian-type metastable peak was described by Holmes and Osborne.[25] The $\langle T\rangle$ values were obtained from their relationship between the $\langle T\rangle/T_{1/2}$ ratio and the peak shape parameter n(=1.8 for the present case), which had itself been derived from width ratios at the given peak heights. Accord-

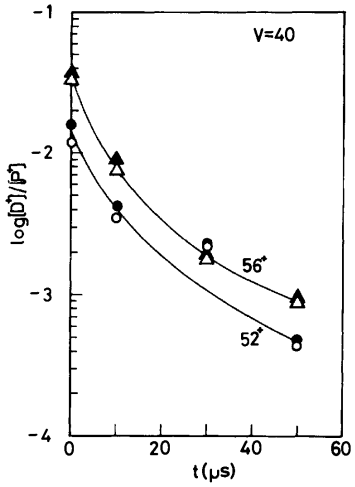

Fig. 4. Time-resolved abundances produced by two parallel fragmentations by X and X_2 loss from $C_4H_4^+$ (X=H, D) precursors. Symbols represent fragments by the H(○), H_2 (●), D (△), and D_2 (▲) loss. The abundances relative to the parent, $[D^+]/[P^+]$ at V= 40 eV are plotted on a logarithmic scale. The lines are for easy comparison.

Table 1. Time-Resolved Kinetic Energy Releases $T_{1/2}$ for the Pyridine Metastable Transition of $C_5X_5N^{+\cdot} \longrightarrow C_4X_4^{+\cdot} + XCN(X=H, D)$

$t/\mu s$	X=H			X=D		
	$T_{1/2}$/meV	E^*/eV[a]	E_p/eV[b]	$T_{1/2}$/meV	E^*/eV	E_p/eV[c]
0	49±10	1.5±0.3	0.90	53	1.6	1.2
5	41±8	1.3±0.3				
10	29	0.9	0.80	43	1.3	1.0
20	23	0.7				
30	29	0.9	0.70	36	1.1	0.90
40	8	0.3				
50	8	0.3	0.65	33	1.0	0.85
100	0		0.60	35	1.0	0.80

a) E^* represents the excess energy of metastable ions above the reaction threshold, which was obtained from the experimental $T_{1/2}$ values according to the relation of Haney and Franklin.[26] b) E_p is the peak energy for the $w(E)$ function above the threshold. It corresponds to the $k(E_p)=\ln(t_2/t_1)/(t_2-t_1)$ rate, where t_1 and t_2 are respectively, the entrance and the exit time in the second field-free region. The $k(E)$ model of Eland et al. was used for this calculation. c) The unimolecular rate constant for deuteriopyridine was obtained by directly computing the harmonic oscillator eigenstate sums and densities. The vibrational frequencies used were given in Ref. 5.

Table 2. Time-Resolved Kinetic Energy Releases $T_{1/2}$ for $C_4X_3^+$ and $C_4X_2^+$ Fragments from Metastable $C_4X_4^+$(X=H, D) Ions

$t/\mu s$	$T_{1/2}$/meV			
	$-H$[a]	$-H_2$	$-D$	$-D_2$
0	90±15	330±50	180	400
10	0	160	180	330
20	0	220	—	—
30	0	100	140	200
50	—	—	100	200

a) The notation of $-H$ represents the hydrogen atom loss.

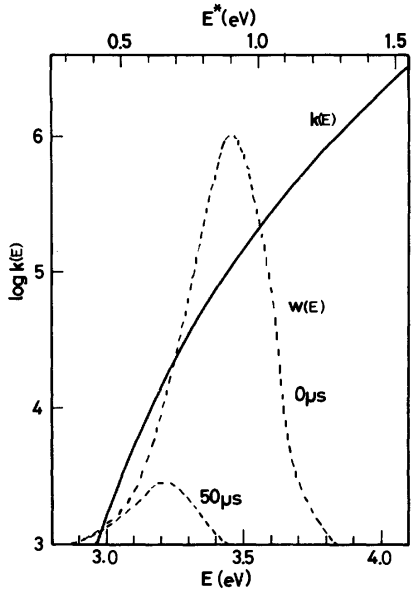

Fig. 5. The relationship of $k(E)$ and $w(E)$ for the pyridine reaction. $k(E)$ indicates the unimolecular rate constant of Eland et al. The $w(E)$ functions, as defined in Eq. 3, for delay times of $t=0$ and 50 μs are linearly plotted on an arbitrary unit vs. the internal energy E above ionization threshold. E^*(upper scale) represents the excess energy above reaction threshold.

ing to the empirical formula of Haney and Franklin,[26] $\langle T\rangle=E^*/(0.44N)$, the average KER $\langle T\rangle$ is related to the excess energy(E^*) of metastable ions above the threshold. Here, N is the number of vibrational degrees of freedom of the parent ion. $\langle T\rangle$ should approach zero as E^* approaches zero if there is no reverse activation energy. The excess energies estimated from the experimental $T_{1/2}$ values are given in Table 1.

Generally, the KER value decreases with the lifetime of metastable ions. The fragmentation takes place only for metastable ions with a limited range of excess energy, as defined by the $w(E)$ function in Eq. 3. The $w(E)$ curves for $t=0$ and 50 μs were calculated with the $k_E(E)$ model, as shown in Fig. 5. The increase in the delay time lowers the peak position of the $w(E)$ curve. A peak energy E_P of $w(E)$ above the threshold can be representative of the average internal energy, compared with E^*. The E^* values for every delay time in Table 1 are estimated to have the error limit of ≈0.3 eV. The experimental E^* values are roughly reproduced by the calculated E_P values, except at $t=0$ μs. The reaction of deuteriopyridine has slower rate constants than that of pyridine. This causes the larger KERs for deuteriopyridine than for pyridine; The excess energy of decomposing ions declines consistently with the increase in the rate constant. Strictly speaking, the metastable peak should be analyzed by taking the internal energy distribution into account. An sttempt to determine time-resolved KERs for pyridine has been made in a previous TIMS

study.[7] A rough estimate of the maximum KER ratio at delay times of 0 and 100 μs was $T_{max}(0\ \mu s)/T_{max}(100\ \mu s)=3.5$. The maximum KER, which reflects the internal excess energy, was obtained from the widths at the base of the peaks above the noise level. This KER ratio is far beyond the calculated E_P ratio of 1.5 between $t=0$ and 100 μs.

Table 2 represents time-resolved KERs by the X and X_2 loss of the metastable $C_4X_4^+$ ion. Our KER values of $T_{1/2}=90$ and 330 meV for $C_4H_4^+$ at $t=0$ μs are comparable to those of $T_{1/2}=49$ and 399 mV[27] respectively. As in the pyridine reaction, the $C_4D_4^+$ reaction always has a greater KER than the $C_4H_4^+$.

The present study has advanced understanding of the unimolecular decomposition of pyridine ions. The reaction rate model of Eland et al. proved to be best for time-resolved measurements of both the EIE curve and the metastable peak. In particular, the analysis of the EIE shift near onset permitted a determination of the AE_0 threshold energy, whereas the measurement of the metastable-ion fragmentation was effective for evaluating the rising steepness of $k(E)$. The empirical formula of Haney and Franklin was not ruled out by the present time-resolved KER measurements with the metastable-ion lifetime of 0—100 μs.

We wish to thank Professor C. Lifshitz, Department of Physical Chemistry, The Hebrew University of Jerusalem, for her helpful discussions and advice.

References

1) B-Ö. Jonssen, E. Lindehelm, and A. Skerbele, *Int. J. Mass Spectrom. Ion Phys.*, **3**, 385 (1969).
2) H. M. Rosenstock, K. Draxl, B. W. Steiner, and J. T. Herron, *J. Phys. Chem. Ref. Data*, **6**, Suppl. 1 (1977).
3) J. H. D. Eland, J. Berkowitz, H. Shulte, and R. Frey, *Int. J. Mass Spectrom. Ion Phys.*, **28**, 297 (1978).
4) H. M. Rosenstock and K. E. McCulloh, *Int. J. Mass Spectrom. Ion Phys.*, **25**, 327 (1977).
5) R. Arakawa, M. Arimura, and Y. Yoshikawa, *Int. J. Mass Spectrom. Ion Processes*, **64**, 227 (1985).
6) H. M. Rosenstock, R. Stockbauer, and A. Parr, *Int. J. Mass Spectrom. Ion Phys.*, **38**, 323 (1981).
7) C. Lifshitz, *J. Phys. Chem.*, **86**, 606 (1982).
8) Y. Malinovich, R. Arakawa, G. Haase, and C. Lifshitz, *J. Phys. Chem.*, **89**, 2253 (1985).
9) A. A. Herod and A. G. Harrison, *Int. J. Mass Spectrom. Ion Phys.*, **4**, 415 (1970).
10) C. Lifshitz, *Mass Spectrom. Rev.*, **1**, 309 (1982).
11) F. A. Baker and J. B. Hasted, *Philos. Trans. R. Soc. London*, **A261**, 33 (1966).
12) M. Arimura and Y. Yoshikawa *Mass Spectrom. (Jpn.)*, **30**, 183 (1982).
13) J. D. Morrison, *J. Chem. Phys.*, **21**, 1767 (1953).
14) M. R. H. Rudge, *Rev. Mod. Phys.*, **40**, 564 (1968); M. R. H. Rudge, and M. J. Seaton, *Proc. Phys. Soc.*, **83**, 183 (1982).
15) C. Goffart, J. Momigny, and P. Natalis, *Int. J. Mass Spectrom. Ion Phys.*, **3**, 371 (1969).
16) P. C. Burgers and J. L. Holmes, *Org. Mass Spectrom.*, **17**, 123 (1982).
17) S. Gefen and C. Lifshitz, *Int. J. Mass Spectrom Ion Phys.*, **58**, 251 (1984).
18) T. Baer, G. D. Willett, D. Smith, and J. S. Phillips, *J. Chem. Phys.*, **70**, 4076 (1979).
19) S. Gordon and N. W. Reid, *Int. J. Mass Spectrom. Ion Phys.*, **18**, 379 (1975).
20) A. N. H. Yeo and D. H. Williams, *J. Am. Chem. Soc.*, **93**, 395 (1971).
21) G. Gioumousis and D. P. Stevenson, *J. Chem. Phys.*, **29**, 294 (1958).
22) R. C. Dunbar, *Int. J. Mass Spectrom. Ion Phys.*, **54**, 109 (1983).
23) R. G. Cooks and J. H. Beynon, *J. Chem. Phys.*, **51**, 437 (1974).
24) S. T. Pratt and W. A. Chupka, *Chem. Phys.*, **62**, 153 (1981).
25) J. L. Holmes and A. D. Osborne, *Org. Mass Spectrom.*, **16**, 236 (1981); J. L. Holmes and J. K. Terlouw, *Org. Mass Spectrom.*, **15**, 383 (1980).
26) M. A. Haney and J. L. Franklin, *J. Chem. Phys.*, **48**, 4903 (1968); C. E. Klots, *J. Chem. Phys.*, **58**, 5364 (1973).
27) C. Lifshitz, D. Gibson, K. Levsen, and I. Dotan, *Int. J. Mass Spectrom. Ion Phys.*, **40**, 157 (1981).

Vapor-Phase Amination of Cyclohexanol over Silica-Supported Platinum Group Metal Catalysts

Hideaki HAMADA,* Yasushi KUWAHARA, Takahiro SATO,† and Katsuhiko WAKABAYASHI
National Chemical Laboratory for Industry, Higashi, Yatabe, Tsukuba-gun, Ibaraki 305
†Science University of Tokyo, Noda, Chiba 278
(Received June 24, 1986)

Vapor-phase amination of cyclohexanol with ammonia over silica-supported platinum and other platinum group metal (Ru, Rh, Pd, Ir) catalysts has been studied. Cyclohexylamine and aniline are the main products. Platinum is the most active metal, although there is not much difference in the activity between platinum and other metals. The reaction is suggested to proceed as follows. The first step, which is rate-determining, is the dehydrogenation of cyclohexanol to cyclohexanone intermediate, from which cyclohexylamine and aniline are formed in the parallel process via cyclohexylideneamine. From reaction-rate measurements on Pt/SiO_2 catalysts with different Pt particle size, the amination reaction has been found to be structure-insensitive. The catalytic activity decreases with time on stream probably because of the deposit of carbonacious or polymeric materials on the catalyst surface.

The amination of cyclohexanol to cyclohexylamine with ammonia has been carried out over various acidic catalysts such as ThO_2[1] and Al_2O_3.[2] In addition, supported or unsupported metal catalysts are also effective for this reaction. For example, Raney Ni, Co, Cu,[3,4] and Cu–Zn oxide catalysts[5] were used for the vapor-phase amination, and reduced Ni catalysts[6] for the liquid-phase amination.

Recently, it has been found that the reaction of cyclohexanol and ammonia over platinum group metal catalysts gives aniline by simultaneous amination and dehydrogenation. Baker[7] obtained aniline in high selectivity by vapor-phase reaction of cyclohexanol/NH_3/H_2 over Pt/C catalysts. Carrubba and Golden[8] used Pt/SiO_2 for the same reaction. Moreover, modified Pd/Al_2O_3 catalysts are also useful for aniline formation according to an European patent.[9] Richardson and Lu[10] studied dehydrogenation and amination of cyclohexanol over a commercial Pt/SiO_2 catalyst by changing contact time and reaction time and speculated a possible reaction pathway. However, no study has been made on the basic nature of cyclohexanol amination over platinum group metal catalysts, which is useful information to develop high-performance catalysts.

In this paper, the catalytic activity and selectivity of silica-supported platinum group metals for the vapor-phase cyclohexanol amination is first investigated. Then, the reaction mechanism is examined by changing reaction conditions or performing related reactions. Structure sensitivity of the reaction is also studied by changing metal particle size. Finally, catalyst deactivation is discussed.

Experimental

Preparation of Catalysts. All the catalyst samples used in this study were prepared by impregnation of silica (Davison #57) with an aqueous solution of metal chloride salts ($RuCl_3 \cdot H_2O$, $RhCl_3 \cdot 3H_2O$, $PdCl_2$, $IrCl_4 \cdot H_2O$, $H_2PtCl_6 \cdot 6H_2O$). The samples were then dried with a rotary evaporator (353 K 1 h, 383 K 1 h) and finally reduced in flowing hydrogen (773 K 3 h).

Characterization of Catalysts. In order to know the percentage metal exposed or dispersion (for fresh catalysts), hydrogen chemisorption measurements were performed at room temperature in the pressure range of 5—30 kPa with a conventional volumetric adsorption system. Catalyst samples reduced at 723 K were outgassed for 1 h at the same temperature before the measurements. The chemisorption values were determined by extrapolating the linear portion of adsorption isotherms to zero pressure except for Pd/SiO_2. In the case of Pd/SiO_2, the chemisorption value was taken as the difference between the first adsorption value and the backsorption value measured after evacuation at room temperature for 10 min, in order to eliminate the contribution of hydride formation.[11] Percentage metal exposed or dispersion was calculated from the chemisorption value on the assumption that one hydrogen atom is chemisorbed on each metal atom at the surface. Then, metal particle size was calculated by using the following equation, assuming a spherical shape.[12]

$$d = 6V/AD \quad (1)$$

where d is the metal particle size, D is the dispersion, V is the volume occupied by a metal atom in the bulk, and A is the effective average area occupied by a metal atom in the surface.

Reaction Procedures. The amination reactions were carried out with a continuous flow reactor at atmospheric pressure. Cyclohexanol was pumped by a motor-driven syringe to the preheating zone of the reactor. Ammonia from a cylinder was dried through a potassium hydroxide column and mixed with hydrogen before entering the reactor. The reactant gas flow was 24 mmol h^{-1} of cyclohexanol, 98 mmol h^{-1} of ammonia, and 98 mmol h^{-1} of hydrogen. The reaction products were trapped by bubbling into a ice-cold trap containing 2-propanol as the solvent and *N,N*-dimethylaniline as the internal standard for analysis.

Catalysts placed in the reactor were first reduced in flowing hydrogen at 723 K for 30 min and the temperature was lowered to the reaction temperature. Then, ammonia and cyclohexanol were fed. The products were analyzed by a gas chromatograph with a 3-m column of Silicone DC-

Table 1. Activity of Silica-Supported Platinum Group Metal Catalysts[a)]

Metal	Catalyst				Conversion	Turnover rate 10^{-3} s^{-1}			Selectivity %		
	L[b)] wt%	L[b)] mmol g^{-1}	D[c)] %	Weight g	%	Total	Cyclohexylamine	Aniline	Dicyclohexylamine	*N*-cyclohexylaniline	Cyclohexane +Benzene
Ru	0.51	0.050	17	1.01	7.9	63.62	61.17(96.1)	0.82(1.3)	1.36(2.1)	0.00(0.0)	0.28(0.4)
Rh	0.54	0.052	54	1.43	8.2	13.94	9.42(67.6)	2.51(18.0)	0.61(4.4)	0.33(2.4)	1.07(7.7)
Pd	0.50	0.047	35	1.45	6.7	19.01	11.44(60.2)	4.66(24.5)	0.82(4.3)	1.89(10.0)	0.20(1.0)
Ir	0.53	0.027	65	1.41	9.4	23.65	18.54(78.4)	1.13(4.8)	3.29(13.9)	0.19(0.8)	0.50(2.1)
Pt	0.50	0.026	64	0.25	7.3	114.87	77.23(67.2)	12.90(11.2)	1.89(1.6)	12.14(10.6)	10.72(9.3)

a) Reaction temperature: 493 K. b) L is the metal loading. c) D is the metal dispersion.

550 operating from 378 K to 468 K at a rate of 10 K min^{-1}. Product yield (Y), cyclohexanol conversion (C), product selectivity (S), and turnover rate of formation (TOR) were calculated on the cyclohexanol basis from the following equations.

$$Y/\% = \frac{\text{Product produced/mol}}{\text{Cyclohexanol fed/mol}} \times 100 \quad (2)$$

$$C = \text{Total product yields} \quad (3)$$

$$S/\% = \frac{\text{Product yield}}{\text{Cyclohexanol conversion}} \times 100 \quad (4)$$

$$TOR/\text{s}^{-1} = \frac{\text{Product produced/mol s}^{-1}}{\text{Amount of Surface catalyst metal atoms/mol}} \quad (5)$$

As carbon balance was fairly good, Eq. 3 is not a bad selection for the calculation of cyclohexanol conversion. The catalyst amount was controlled so that the conversion was less than 10% in most cases.

Results and Discussion

Catalytic Activity and Selectivity of Platinum Group Metals. Table 1 summarizes the reaction results on silica-supported platinum group metal catalysts. The loading of these metals was approximately fixed at 5 wt%. As catalyst deactivation was observed, initial activity values are taken in Table 1. The main products were cyclohexylamine and aniline. The by-products detected were cyclohexane, benzene, dicyclohexylamine, and *N*-cyclohexylaniline. As will be discussed later, the last two products are considered as the condensation products of two cyclohexylamine molecules, and one aniline and one cyclohexylamine molecule, respectively.

The most active catalyst is Pt/SiO_2 because the conversion per unit weight was the largest. It also gave the largest total turnover rate. However, the difference between Pt and Rh, the least active metal, is within one order of magnitude. With respect to selectivity, aniline was barely formed on Ru or Ir, showing that these two metals have little activity for dehydrogenation to aniline. On the other hand, aniline formation was observed on Rh, Pd, and Pt, among which Pd showed the highest selectivity to aniline. This nature of catalyst metals agrees very much with the work by Ono and Ishida on phenol amination,[13] where aniline was formed in high selectivity on Pd, Pt, and Ph/Al_2O_3 while aniline was not detected on Ru/Al_2O_3. Another point to be noted is that the elimination of amino or hydroxyl group was observed on Rh and Pt, resulting in the formation of cyclohexane and benzene.

Taking high activity into consideration, all the following studies were done with Pt/SiO_2.

Effect of Reaction Conditions. The effect of reaction temperature on cyclohexanol amination was examined in the temperature range of 478—539 K and

is shown in Fig. 1. Both cyclohexylamine and aniline yield increased with temperature. But the selectivity shifts to aniline at high temperatures. Therefore, high temperature is desirable for aniline formation. In fact, Richardson et al.[10] obtained aniline in high selectivity at 573 K.

In Fig. 2 is shown the effect of contact time on the conversion and yield. The yield of each product increased almost proportionally with contact time within the range to 3.5 g h mol^{-1}. The selectivity change with contact time is plotted in Fig. 3, which shows that the selectivity to dicyclohexylamine increases and that to cyclohexylamine decreases. This suggests that the former originates by condensation reaction of two molecules of the latter. Similarly, *N*-cyclohexylaniline is thought to be formed by condensation of cyclohexylamine and aniline, although this conclution is not so clear as in the case of dicyclohexylamine.

When the yield of these dimers is divided and added to their component compounds (cyclohexylamine and aniline), the selectivity does not change much within the whole range of the experiment. This result indicates that cyclohexylamine and aniline are formed from cyclohexanol not in the consecutive process but in the parallel process.

Reaction Mechanism. In order to elucidate the reaction mechanism, several related reactions were performed. The results are summerized in Table 2. First, when cyclohexanol and hydrogen were passed over Pt/SiO_2 with inert N_2 instead of NH_3, cyclohexanone was formed as the only product, the cyclohexanol conversion being almost the same. Next, cyclohexanone was fed instead of cyclohexanol in the amination reaction. In this case, the conversion was much larger, but the product distribution was almost the same except for the ratio of monomers to dimers. Therefore, it is inferred that amination of cyclohexanone is a facile reaction, producing the same products in the same selectivity as the amination of cyclohexanol. In order to examine the formation pathway of cyclohexylamine or aniline, cyclohexylamine or aniline was passed at 493 K over Pt/SiO_2 in an atmosphere of ammonia and hydrogen. It was found that cyclohexylamine is not formed from aniline and the reverse reaction occurs to only a little extent. This means that conversion from cyclohexylamine to aniline is a difficult reaction under these

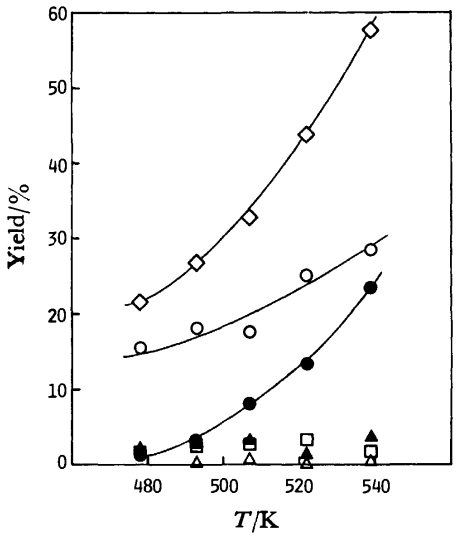

Fig. 1. Effect of reaction temperature on cyclohexanol amination on 0.50% Pt/SiO_2.
The data have been transformed to fit the reaction condition that 1 g of the catalyst is used.
◇: Total, ○: cyclohexylamine, ●: aniline, △: dicyclohexylamine, ▲: *N*-cyclohexylaniline, □: cyclohexane+benzene.

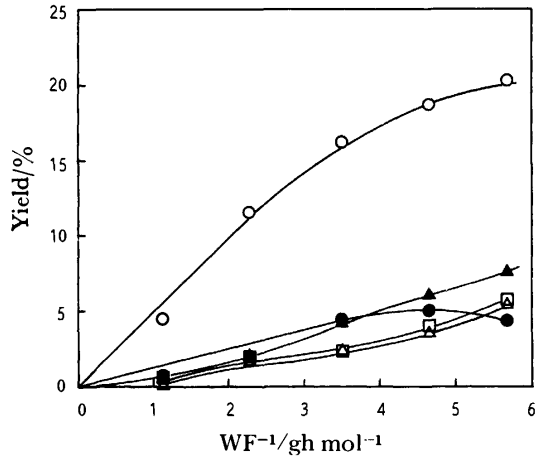

Fig. 2. Effect of contact time on the product yield in cyclohexanol amination at 493 K on 0.50% Pt/SiO_2.
○: Cyclohexylamine, ●: aniline, △: dicyclohexylamine, ▲: *N*-cyclohexylaniline, □: cyclohexane+benzene.

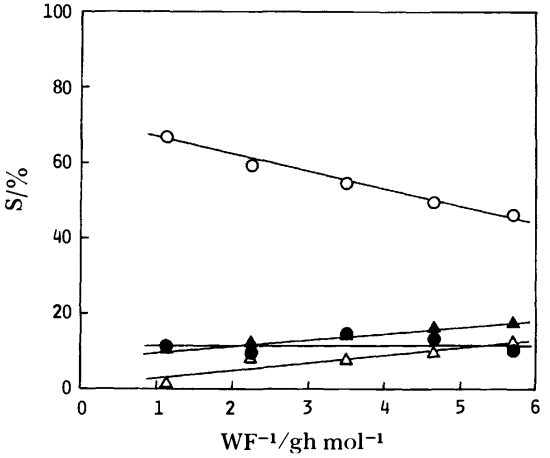

Fig. 3. Effect of contact time on the product selectivity in cyclohexanol amination at 493 K on 0.50% Pt SiO_2.
○: Cyclohexylamine, ●: aniline, △: dicyclohexylamine, ▲: *N*-cyclohexylaniline.

Table 2. Results of Related Reactions[a]

Reactant	Yield/%						
	Cyclohexanol	Cyclohexyl-amine	Aniline	Dicyclohexyl-amine	*N*-cyclohexyl-aniline	Cyclohexane +Benzene	Cyclohexanone
Cyclohexanol/NH_3/H_2	—	1.52	0.26	0.069	0.119	0.099	0
Cyclohexanol/N_2/H_2	—	0	0	0	0	0	1.51
Cyclohexanone/NH_3/H_2	1.30	13.63	1.58	21.85	4.42	0.45	0
Cyclohexylamine/NH_3/H_2	0	—	1.33	4.31	2.21	0.57	0
Aniline/NH_3/H_2	0	0	—	0	0.33	0.72	0

a) Catalyst: 0.99 wt% Pt/SiO_2 0.07 g. Reaction temperature: 493 K. Reactant gas flow rate: 49/98/98 mmol h^{-1}.

reaction conditions or vice versa. Therefore, these two compounds are considered to originate not in the consecutive process but in the parallel process. It is unlikely that cyclohexylamine and aniline are in equilibrium. Ono and Ishida[13] pointed out that cyclohexylamine and aniline are formed in equilibrium in the case of phenol amination at 523 K. The difference may be attributed to different catalysts and reaction conditions.

From these results, a reaction scheme represented by Fig. 4 can be given. The first step, which is rate-determining, is the dehydrogenation of cyclohexanol to cyclohexanone intermediate. Then, cyclohexylamine and aniline are formed simultaneously via cyclohexylideneamine by amination of cyclohexanone. The presence of cyclohexylideneamine intermediate has been proposed and proved in studies on amination reactions[13,14] or hydrogenation of aniline.[15]

Structure Sensitivity. Catalytic reactions on metal catalysts can be classified into two groups, one is structure-sensitive and the other structure-insensitive, depending on the manner how the catalytic activity is influenced by metal particle size or crystallographic plane.[16] To investigate structure sensitivity of this amination reaction, six Pt/SiO_2 catalysts with different Pt particle size were prepared by changing Pt loading from about 0.30 to 6.5 wt%. With decreasing Pt loading, Pt dispersion increased from 16 to 73% and Pt particle size decreased consequently from 7.2 to 1.6 nm. The reaction results are shown in Table 3. It was found that catalytic activity per surface metal atom and product selectivity do not change much with Pt particle size. Therefore, it can be concluded that cyclohexanol amination on Pt/SiO_2 is a structure-insensitive reaction. This conclusion is also supported by the result of Table 1 that the catalytic activity is not so sensitive to the nature of the catalyst metal.[17] Most of hydrogenation and dehydrogenation reactions have been found to be structure-insensitive. Therefore, this amination reaction can be expected to be structure-insensitive because the rate-determining step is the dehydrogenation of cyclohexanol to cyclohexanone. Thus, improving metal dispersion has no more effect than making metal surface area larger.

Strictly speaking, however, the product distribution seems to be affected by Pt particle size, because the selectivity to aniline decreased and the selectivity to

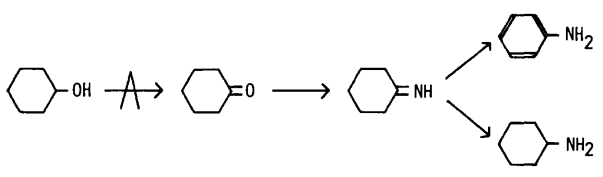

Fig. 4. Reaction scheme of cyclohexanol amination.

Table 3. Effect of Pt Particle Size[a]

Catalyst				Conversion %	Turnover rate 10^{-3} s^{-1} (Selectivity %)				
L[b] wt%	D[c] %	d[d] nm	Weight g		Total	Cyclohexyl-amine	Aniline	Dicyclohexyl-amine	*N*-cyclohexyl-aniline	Cyclohexane +Benzene
0.30	73	1.6	0.354	6.72	106.02	67.13(63.3)	12.66(11.9)	2.77(2.6)	14.27(13.5)	9.19(8.7)
0.50	64	1.8	0.248	7.28	114.87	77.23(67.2)	12.90(11.2)	1.89(1.6)	12.14(10.6)	10.72(9.3)
0.99	49	2.3	0.188	6.69	83.22	53.24(64.0)	9.37(11.3)	4.27(5.1)	6.09(7.3)	10.25(12.3)
2.9	22	5.2	0.132	4.50	58.49	41.24(70.5)	4.49(7.7)	3.18(5.4)	1.65(2.8)	7.93(13.6)
6.5	16	7.2	0.071	5.39	90.23	50.94(56.5)	6.49(7.2)	5.06(5.6)	2.27(2.5)	25.48(28.2)

a) Reaction temperature: 493 K. b) L is the Pt loading. c) D is the Pt dispersion. d) d is the Pt particle size.

cyclohexane plus benzene increased with Pt particle size, as can be seen from Table 3. Especilally on 6.5% Pt/SiO_2, considerable elimination of amino or hydroxyl group was observed, resulting in 28% selectivity to cyclohexane plus benzene. Hence, highly dispersed Pt/SiO_2 is favorable for obtaining aniline in higher selectivity.

Deactivation of Catalysts. Figure 5 shows a typical change of the product yield with time on stream. The yield of each product dropped with time especially at the beginning of the reaction. It should be noted, however, that the product selectivity remains unchanged. Considering that this reaction is structure-insensitive, it is suggested that the number of surface Pt atoms decreases as the catalyst deactivation proceeds. In fact, Table 4 indicates that the catalyst deactivation is closely related to the decrease of

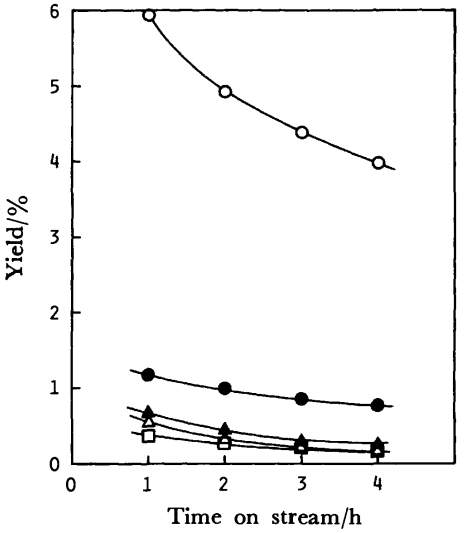

Fig. 5. Change in the product yield with time on stream in cyclohexanol amination at 493 K on 0.50% Pt/SiO_2. ○: Cyclohexylamine, ●: aniline, △: dicyclohexylamine, ▲: *N*-cyclohexylaniline, □: cyclohexane+benzene.

Table 4. Change in Percentage Pt Exposed by Reaction[a]

L[b]/%	D[c]/%	
	Fresh	Used
0.30	73	36
0.50	63	35
0.99	49	35
2.9	22	19
6.5	16	14

a) Catalyst amount: 1.8 g. Reactions conditions: 523 K, 5 h. b) L is the Pt loading. c) D is the percentage Pt exposed, which is equal to Pt dispersion for fresh catalysts.

percentage Pt exposed, and that the extent of decrease is larger as the Pt loading is smaller.

Deactivation may be caused by sintering or surface fouling by carbonaceous or polymeric materials. In the case of this reaction, surface fouling is more likely because the catalyst weight increased by 10% after performing amination reaction. This conclution agrees with the work by Richardson and Lu.[10] However, regeneration of the deactivated catalysts by calcination with air and/or hydrogen has been unsuccessful so far.

References

1) P. S. Sabatier and A. Mailhe, *Compt. Rend.*, **153**, 1204 (1912).
2) N. S. Kozlow and L. Akhmetschina, *Dokl. Akad. Nauk SSSR*, **85**, 91 (1952).
3) A. W. C. Taylor, Brit. Patent 679014 (1952).
4) A. W. C. Taylor, P. Davies, and P. W. Reynolds, U. S. Patent 2636902 (1953).
5) Y. Omote, K. Iwase, and J. Nakamura, *Kogyo Kagaku Zasshi*, **70**, 1508 (1967).
6) A. Guyot and M. Fournier, *Bull. Soc. Chim.*, **47**, 203 (1930).
7) R. S. Baker, U. S. Patent 3442950 (1960).
8) R. V. Carruba and R. L. Golden, U. S. Patent 3347921 (1967).
9) N. Goetz, L. Hupfer, W. Hoffmann, and M. Baumann, Eur. Pat. Appl. EP 50229 (1982); *Chem. Abstr.*, **97**, P127236q (1982).
10) J. T. Richardson and W.-C. Lu, *J. Catal.*, **42**, 275 (1976).
11) H. S. Hwang, Ph. D. Thesis, Stanford University, Stanford, U. S. A., 1975.
12) J. R. Anderson, "Structure of Metallic Catalysts," Academic Press, London (1975), p. 360.
13) Y. Ono and H. Ishida, *J. Catal.*, **72**, 121 (1981).
14) H. Hamada, T. Matsuzaki, and K. Wakabayashi, *Nippon Kagaku Kaishi*, **1979**, 248.
15) H. Greenfield, *J. Org. Chem.*, **29**, 3082 (1964).
16) M. Boudart, *Adv. Catal. Relat. Subj.*, **20**, 153 (1969).
17) M. Boudart and G. Djega-Mariadassou, "Kinetics of Heterogeneous Catalytic Reactions," Princeton University Press, Princeton, New Jersey (1984), p. 190.

 © 1987 The Chemical Society of Japan Bull. Chem. Soc. Jpn., 60, 61—68 (1987)

A High Resolution ^{23}Na NMR Study of Sodium Complexes with Ionophores in Solution. Stability of Complexes as Viewed from Displacements of ^{23}Na Chemical Shifts as Referred to Those in the Solid State

Hazime Saitô* and Ryoko Tabeta
Biophysics Division, National Cancer Center Research Institute,
Tsukiji 5-Chome, Chuo-ku, Tokyo 104
(Received June 26, 1986)

We have recorded ^{23}Na NMR spectra of sodium complexes with naturally occurring and synthetic ionophores in chloroform and methanol solution, to gain insight into conformational stability of these complexes as examined from the displacements of ^{23}Na chemical shifts with respect to those in the solid state. Interestingly, the ^{23}Na chemical shifts of sodium complexes with monensin and tetranactin obtained in chloroform solution are very close to those in the solid, as a result of adopting similar conformation between the solid and solution. For the rest of complexes, however, the ^{23}Na NMR signals are displaced downfield in solution as compared with those of the solid state. Such downfield shifts are well interpreted in terms of the presence of conformational fluctuation and/or sodium ions interacting with solvent or anions. Therefore, downfield displacement is more significant in methanol which can be good ligand molecules. The presence of fluctuation-induced quadrupole coupling constants is consistent with our view about ^{23}Na chemical shifts. These quadrupole interactions were reduced in methanol solution, owing to the presence of exchange with solvents.

It is well-recognized that ionic permeability of alkaline cations in biological or artificial membranes is strongly enhanced by the presence of naturally occurring or synthetic ionophores.[1-4] This phenomenon can be interpreted in terms of a mobile carrier model of ionophores in which most important step is complexation of metal ions to these ionophores at interface and interior of membrane lipids.[2] These ligand molecules should undergo marked conformational change to achieve stability and ion selectivity for particular metal ions. Nevertheless, it has not yet been fully explored whether or not conformations of these ionophores in the crystalline state are retained in the liquid phase or membrane-bound state because of lack in suitable experimental means. One of the most promising new approach to this end is to examine displacements of the conformation-dependent ^{13}C chemical shifts (up to 8 ppm) which are varied upon particular conformations, as manifested from our previous high-resolution solid-state ^{13}C NMR studies of a variety of crystalline free and complexed ionophores.[5-8]

Alternatively, we can utilize ^{23}Na chemical shifts of sodium complexes in solution as compared with those of the solid state. For this purpose, we have recently demonstrated that ^{23}Na chemical shifts of solid sodium salts and complexes are significantly displaced (up to 60 ppm) depending on a variety of anions or ligand molecules and the Na–O interatomic distances,[9,10] as determined by magic angle spinning (MAS) method. The advantage of recording ^{23}Na NMR spectra in the solid state is that NMR signals of the individual species of the ion–ion, ion-solvent, and ion-ligand interactions were observed separately in the solid state, free from any chemical exchange process as encountered in solution. For the latter, extensive conventional high-resolution ^{23}Na NMR studies have been performed to obtain the kinetic and thermodynamic data of complexation in solution[11-25] although separate observation of such species is difficult owing to the presence of fast chemical exchange. Accordingly, use of these solid-state ^{23}Na NMR data provides one unambiguous reference data to assess whether or not conformations achieved in the solid state are retained in solution or membrane-bound state. For this purpose, it seems to be essential to utilize solvent of lower polarity such as chloroform to reproduce hydrophobic environment as in interior of biomembranes, although previous ^{23}Na NMR study by Haynes et al.[12] was mainly conducted for sodium complexes in methanol solution owing to the encountered difficulty in recording substantially broadened spectra in chloroform.

In this paper, we aimed to compare ^{23}Na chemical shifts of sodium complexes with some naturally occurring (valinomycin, nonactin, tetranactin, monensin, and lasalocid) and synthetic (cryptands 22, 221, 222, and 18-crown-6) ionophores (see Fig. 1) in chloroform and methanol solution with those obtained in the solid state previously reported.[10] Surprisingly, we noted that the linewidths of ^{23}Na NMR signals in these systems are substantially increased (up to 2.2 kHz for the complex with valinomycin). In addition, the ^{23}Na chemical shifts of monensin and tetranactin in chloroform solution were very close to the data of solid state, indicating the similarity of conformations between the solid and solution. Nevertheless, solid-state conformations are not retained for the rest of complexes in chloroform and methanol solution, because of the presence of rapid conformational fluctuation and ligand ex-

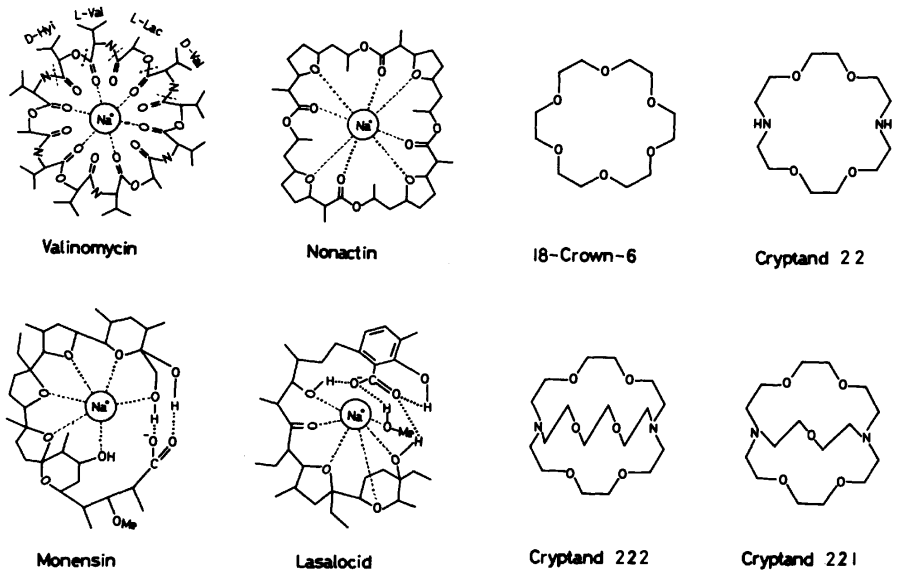

Fig. 1. Schematic representation of some sodium complexes with naturally occurring and synthetic ionophores.

change between the ionophores and solvent molecules.

Experimental

Sodium complexes of valinomycin (Sigma Chemical Company, MI, USA), nonactin (Boehringer-Mannheim GmbH, Germany), and tetranactin (Chugai Pharmaceutical Co. Ltd., Tokyo) (see Fig. 1) were prepared from ethyl acetate solution containing 10% excess NaSCN as described previously.[7] Complex formation was confirmed by the characteristic changes of ^{13}C NMR signals in the crystalline complexes as determined by the cross polarization-magic angle spinning (CP-MAS) NMR method.[7,8] Monensin (Na salt) and lasalocid (Na salt) were purchased from Sigma Chemical Company, MI, USA. These samples were recrystallized from diethyl ether-petroleum ether (1:1) containing small amount of acetone or methanol. Cryptands 22, 221, and 222 were purchased from Aldrich Chemical Company, WI, USA. 18-Crown-6 (18C6) was purchased from Aldrich Chemical Company, WI, USA. Sodium complexes with these cryptands and 18C6 were prepared by the method previously reported.[8]

High-resolution ^{23}Na NMR spectra were recorded on a Bruker CXP-300 spectrometer operating at 79.35 MHz. The crystalline complexes obtained by the procedure described above were dissolved (10 mg ml^{-1}) in deuterated chloroform (Merck Company, Germany) or methanol solution and transferred to 10 mm o.d. quartz NMR sample tubes (Shigemi Standard Joint Company, Tokyo), to avoid undesirable intense signal arising from standard Pyrex sample tubes. Spectral width and data points were usually taken as 10 kHz and 4 K, respectively. To record extremely broadened ^{23}Na NMR signal from the sodium complex with valinomycin, we utilized spectral width 25 kHz and data point 1 K. Free induction decays were accumulated usually 100—500 times. We further confirmed that the observed ^{23}Na signals did not arise from empty sample tube. ^{23}Na chemical shifts were referred to the resonance peak of 1 M† NaCl solution. Proton-decoupled ^{13}C NMR spectra were recorded on the same spectrometer operating at 75.46 MHz. ^{13}C spin-lattice relaxation times were measured for the same samples observed for ^{23}Na NMR spectra by the standard pulse-sequence of the inversion recovery.

Results

Figure 2 illustrates high-resolution ^{23}Na NMR spectra of some sodium complexes with naturally occurring ionophores in chloroform solution. Generally, the ^{23}Na NMR peaks of these sodium complexes were resonated at higher field region than the reference peak of 1 M NaCl solution. In particular, the ^{23}Na NMR peak of Na^+-tetranactin complex appears at the highermost peak-position (−27.8±0.3 ppm). Obviously, ^{23}Na NMR signals of complexes with lasalocid, monensin and valinomycin in chloroform solution are significantly broadened (up to 2200 Hz) but those of nonactin and tetranactin are not. By contrast, these signals were considerably narrowed in methanol solution and the extent of displacements of peaks was significantly reduced in methanol solution, as shown in Fig. 3. Note that relative peak position was also altered between chloroform and methanol solution. In a similar manner, Figs. 4 and 5 summarize ^{23}Na NMR spectra of some sodium complexes with synthetic ionophores in chloroform and methanol solution, respectively. In chloroform solution, a ^{23}Na NMR signal of very low intensity is clearly seen at the peak position of 1 M NaCl solution (Fig. 4). Undoubtedly, this peak arose from the ^{23}Na

† 1 M=1 mol dm^{-3}.

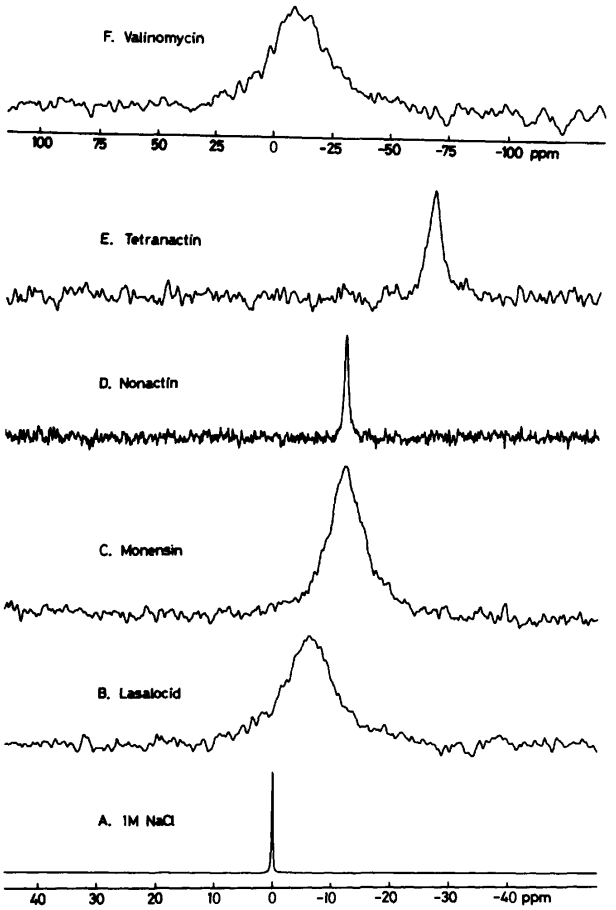

Fig. 2. 79.35 MHz ^{23}Na NMR spectra of some sodium complexes with naturally occurring ionophores in chloroform solution. Note that horizontal scale of F is expanded 2.5 times as that of A–E.

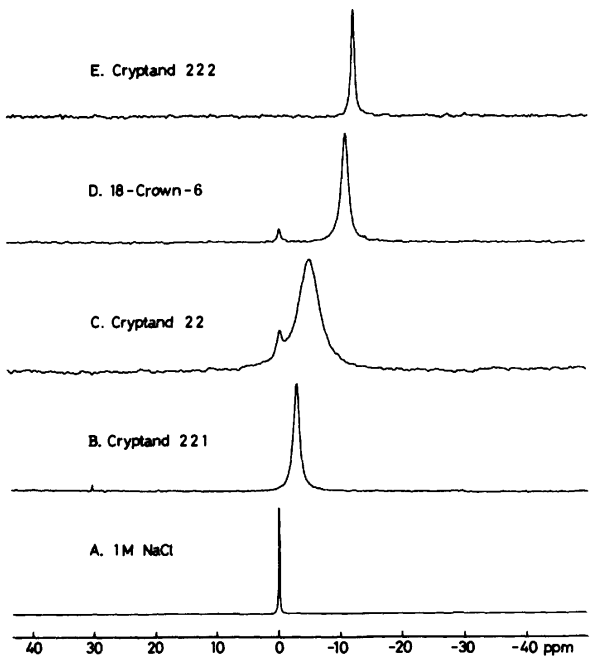

Fig. 4. 79.35 MHz ^{23}Na NMR spectra of some sodium complexes with synthetic ionophores in chloroform solution.

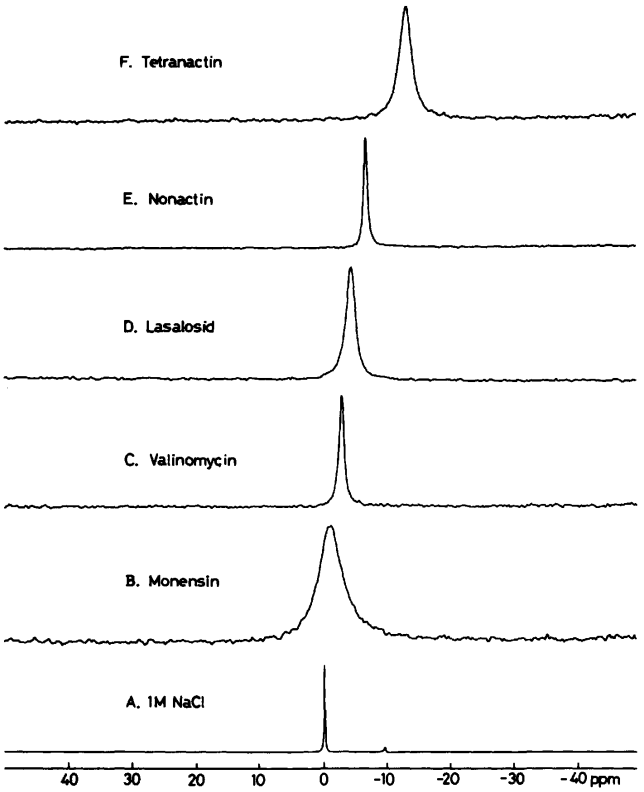

Fig. 3. 79.35 MHz ^{23}Na NMR spectra of some sodium complexes with naturally occurring ionophores in methanol solution.

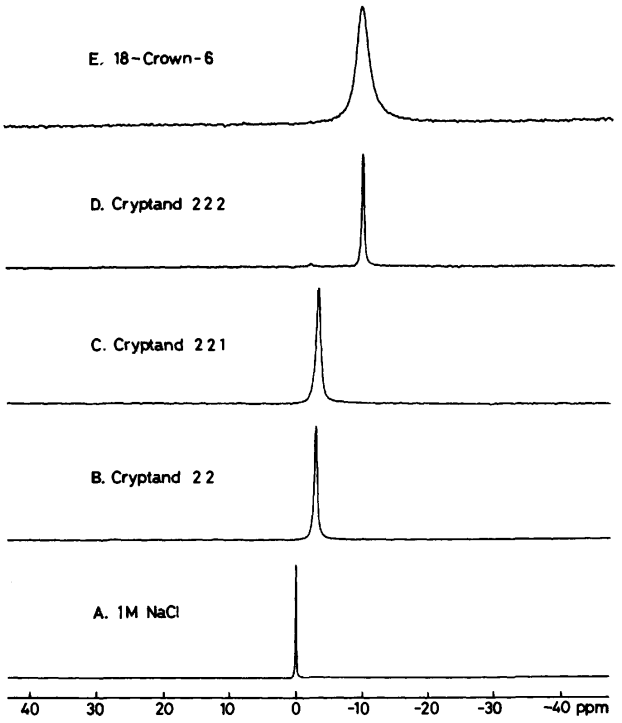

Fig. 5. 79.35 MHz ^{23}Na NMR spectra of some sodium complexes with synthetic ionophores in methanol solution.

Table 1. ^{23}Na Chemical Shifts of Some Sodium Complexes with Naturally Occurring and Synthetic Ionophores in the Solid and Solution (Referred to 1 M NaCl)

	Solid[a]		Solution			
	Chemical Shift ppm	Linewidth Hz	in $CDCl_3$		in CH_3OH	
			Chemical Shift ppm	Linewidth Hz	Chemical Shift ppm	Linewidth Hz
Valinomycin	−23.3±4.7	3000	−7.7±3.5	2200	−2.6±0.1	70
Lasalocid	−11.6±3.3	2100	−6.2±1.1	710	−4.0±0.2	130
Monensin	−14.2±3.4	2800	−12.4±0.8	520	−0.7±0.6	370
Nonactin	−18.2±1.0	680	−12.1±0.1	60	−6.3±0.1	50
Tetranactin	−24.0±1.2	740	−27.8±0.3	210	−12.7±0.3	170
22	−18.3±3.5	2200	−5.0±0.5	320	−3.0±0.1	40
222	−16.2±1.7	1040	−12.2±0.1	50	−10.3±0.1	28
221	−16.4±2.8	1700	−2.9±0.1	90	−3.6±0.1	60
18C6	−16.0±0.9	530	−10.9±0.1	98	−10.3±0.1	160

a) Data taken from Ref. 10.

Table 2. Effective Quadrupole Coupling Constants, Correlation Times, and ^{13}C Spin-Lattice Relaxation Times of Some Sodium Complexes with Naturally Occurring and Synthetic Ionophores

	e^2qQ/h (MHz)		τ_C s	^{13}C Spin-Lattice Relaxation Times (T_1's) (ms)[a]	
	$CDCl_3$	CH_3OH		CH	CH_2
Valinomycin	4.7	0.86	7.8×10^{-11}	605±72	
Lasalocid	2.2	0.94	1.2×10^{-10}	400±16	249±23
Monensin	2.0	1.7	1.0×10^{-10}	460±39	295±14
Nonactin	0.82	0.75	7.1×10^{-11}	668±63	356
Tetranactin	1.4	1.2	9.0×10^{-11}	527±13	216
22	3.3 (4.4)[b]	1.2 (1.6)[b]	2.3×10^{-11}		1025±67
222	1.4 (1.7)[b]	1.0 (1.3)[b]	2.1×10^{-11}		1145±53
221	2.1 (2.4)[b]	1.7 (1.9)[b]	1.7×10^{-11}		1370±83
18C6	1.9 (2.4)[b]	2.4 (3.1)[b]	2.2×10^{-11}		1094

a) Averaged value of several T_1 values from different peak positions. b) Calculated based on the T_1 value of 1.85 s (Ref. 18).

ion coordinated to either anion or water molecules present in trace amount in chloroform (slow chemical exchange). No such a peak was seen in methanol solution, because of the presence of rapid ligand exchange between the ionophores and solvents, if any. The relative peak positions in both the solvent systems were also altered. Table 1 summarizes these ^{23}Na chemical shifts and linewidths, together with those obtained in the solid state. We summarize ^{13}C spin-lattice relaxation times of these complexes measured in chloroform solultion in Table 2 (spectra not shown).

Discussion

^{23}Na Chemical Shifts. As demonstrated in our previous papers,[9,10] the ^{23}Na chemical shifts of sodium salts and complexes in the solid state are strongly influenced by a variety of anions and ligand moieties (C=O, OH, or ether), and Na-O distance. Interestingly, the Na-O distances of the sodium complexes with ionophores studied in this paper are usually longer than those of open-chain ligand molecules to be able to take optimal configuration.[26] As a result, it appears that the ^{23}Na NMR signals of these complexes are resonated at a higher field position by about 10—20 ppm, as compared with those complexes with open-chain ligand molecules.[10] As a clue for an explanation of this trend, it has been mentioned that the ^{23}Na chemical shifts are strongly influenced by the extent of electron transfer from the ligand molecule to a 3p orbital of the central metal cation, which in turn induces downfield displacement of peaks through contribution of paramagnetic shielding effect.[11a] Otherwise, it is impossible to account for the displacement of peaks as large as 60 ppm by means of the diamagnetic shielding term alone which is caused by 2s electrons of Na atom. In fact, we showed on the basis of an ab initio molecular orbital calculation that the extent of electron transfer

from ligand molecule to a 3p orbital could be increased when the Na–O distance is decreased until 2.5 Å: under these conditions, ^{23}Na NMR signal would be displaced downfield together with a decrease of the Na–O distance.[10]

By contrast, interpretation of the ^{23}Na chemical shifts in solution state is much complicated, because the observed ^{23}Na shift, δ_{obsd}, consists of time-averaged values of the following several contributions:

$$\delta_{obsd} = p_1\delta_{complex} + p_2\delta_{solvent} + p_3\delta_{ion}$$
$$p_1 + p_2 + p_3 = 1 \quad (1)$$

where $\delta_{complex}$, $\delta_{solvent}$, and δ_{ion} stand for the ^{23}Na chemical shifts of the sodium ions interacting with the ionophores, solvent molecules, and anions, respectively. To be used for reference data of $\delta_{complex}$, $\delta_{solvent}$, and δ_{ion} values, we have already recorded ^{23}Na NMR spectra of a variety of corresponding crystalline samples by high-resolution solid-state ^{23}Na NMR method, as pointed out previously.[9,10] It is cautioned, however, that these data obtained in the solid state are not necessary the same as those in solution, if molecular conformation achieved in the solid is not always retained in solution state. This will happen for a variety of complexes in which the Na–O distance of the complex is much larger than the sum of crystallographic radii of sodium (0.99 Å) and oxygen (1.40 Å) atoms as in the case of Na^+-valinomycin[10] and/or resultant conformational fixation of ligand molecule by metal-binding is not sufficient in solution. In such cases, it is conceivable that the Na–O bond distance would be instantaneously decreased to gain more effective ion-dipolar interaction as a result of thermal fluctuation of ligand moiety, leading to the downfield displacement of the ^{23}Na NMR peaks in view of the data as mentioned above. Then, the $\delta_{complex}$ value obtained in the solid could be modified to some extent. At the same time a plausible instantaneous decrease in the cation–anion distance during thermal fluctuation of ligand molecules would also cause downfield displacement of ^{23}Na peaks, although anions in crystalline sodium complexes are not in the vicinity of sodium ions and do not affect the ^{23}Na NMR peak position in the complexes.[10]

In chloroform solution, contribution from $\delta_{solvent}$ can be neglected because chloroform is not served as ligand molecules for the cation.. It is emphasized that peaks from the remaining two factors, $\delta_{complex}$ and δ_{ion}, are independently observed or at least in slow exchange in chloroform solution, as seen as two separate peaks in Fig. 4. Therefore, it is expected that the ^{23}Na chemical shifts of the complexes in chloroform solution should be the same as those observed in the solid, if there exists no conformational change between these two systems, as in the sodium complexes with monensin and tetranactin (Table 1). This finding is consistent with our previous data concerning with the similarity of the conformation-dependent ^{13}C chemical shifts of ligand molecules between the solid and solution.[7,27]

Nevertheless, it is obvious from Table 1 that the ^{23}Na NMR peaks are displaced downfield in chloroform solution for the rest of complexes (valinomycin, lasalocid, nonactin, 22, 221, 222, and 18C6). This observation strongly suggests that molecular conformation of these complexes could be effectively distorted by thermal fluctuation of ligand molecules in solution, because downfield displacements of peaks were noted in chloroform solution, consistent with our view as described above. In fact, such a downfield displacement of ^{23}Na NMR peaks in solution is most significant for the complex with valinomycin (15.6 ppm). As to Na^+-valinomycin complex, no detailed data of molecular conformation in the solid state are available from X-ray diffraction study. However, we previously demonstrated on the basis of the conformation-dependent ^{13}C chemical shifts[7] that conformation of Na^+-valinomycin complex in the solid state is not significantly different from that of K^+-valinomycin.[26] Nevertheless, the size of cavity with the Na–O distances[28] 2.69—2.83 Å, which is optimal for K^+ ion (1.33 Å), seems to be too large to accommodate smaller sodium ion (0.99 Å). As a result, acquired stabilization energy of the ion-dipolar interaction will be decreased for the sodium complex than that of the potassium complex. This is one of reasons why ionic selectivity of K^+ ion is larger than that of Na^+ ion by 1.7×10^4.[3] Accordingly, the above-mentioned conformation achieved in the solid state might be easily deformed to gain more favorable interaction energy by the metal-ligand interaction. Obviously, such a deformation of ligand molecule from the octahedral symmetry[28] would result in creation of a large electric field gradient around the sodium ion, thermal fluctuation of which is responsible for the extensive line broadening of the ^{23}Na NMR signal in solution.

On the contrary, it was previously shown by X-ray diffraction studies of K^+- and Na^+-complexed nonactin and tetranactin[29] that the cubic coordination by eight equidistant oxygen atoms obtained in the K^+ complexes (K^+–O: 2.8—2.9 Å) is deformed in the Na^+ complexes (Na–C=O: 2.40—2.45 Å. Na–O(ether): 2.74—2.83 Å).[30–32] In spite of such a close conformational similarity between the two types of sodium complexes, there appears a substantial difference in stability of such complexes in chloroform solultion, as manifested from the difference of ^{23}Na chemical shifts between the solid and solution: Na^+-tetranactin is stable, while Na^+-nonactin is not. This observation is again consistent with our previous high-resolution solid-state ^{13}C NMR study of Na^+-nonactin complex in which ^{13}C chemical shifts of the C=O carbons are substantially displaced upfield in chloroform solution

as compared with those of the solid, by reflecting instability of the complex.[7] In a similar manner to that of Na^+-valinomycin complex, the downfield displacement of ^{23}Na signal could be explained by the presence of conformational flexibility which would modify either the Na-O or Na-anion distances. Consistent with this view, nonactin molecule is more flexible than tetranactin in the sodium complexes, as manifested from the observed differences in the ^{13}C spin-lattice relaxation times (and resultant correlation times), as described later (see Table 2).

Lasalocid[33-35] and monensin[36,37] are charged carboxyl ionophores in which there is no symmetry around the sodium ion, because sodium ion is coordinated by ether, hydroxyl or carboxyl groups, as depicted schematically in Fig. 1. In addition to the monomeric form[35] of the sodium complex of lasalocid in which methanol is also complexed, dimeric form is also known to exist both in the solid[33,34] and nonpolar solvent[38,39] such as cyclohexane. The structure of the dimeric form consists of a sandwich type in which the cation resides in a cavity between the two ionophores.[33,34] Thus, a plausible conversion from the monomeric crystalline form to the dimeric form or thermal fluctuation of ligand molecules in chloroform solution could nicely account for the downfield displacement (by 5.0 ppm) of peaks by going from the solid to chloroform solution (see Table 1).

In a similar manner, ^{23}Na chemical shifts of sodium complexes with cryptands and 18C6 in chloroform are resonated downfield as compared with those of the solid state. Obviously, similar explanation to these downfield shifts applies straightforwardly to these samples by taking into account of flexibility of this class of compounds. In this connection, it is interesting to note that deviation of the ^{13}C chemical shifts in chloroform solution from those in the solid is most significant in Na^+-221 complex,[8] as compared with the sodium complexes with 22 and 222. In parallel with this observation, the downfield displacement of ^{23}Na NMR signal is most pronounced in the complex with 221.

In methanol solution, the ^{23}Na NMR signal of the above-mentioned complexes are substantially displaced downfield, due to the presence of ligand-exchange process with solvent molecules. Among them, significant displacements of ^{23}Na NMR signals in the complexes with monensin and tetranactin are noteworthy (11.7 and 15.1 ppm, respectively). Naturally, the original conformations of these complexes achieved both in the solid and chloroform solution are not any more retained in methanol solution. In this connection, it is interesting that the ^{23}Na chemical shifts of sodium complexes with cryptands and 18C6 are not strongly different between solutions of chloroform and methanol.

^{23}Na NMR Linewidths. Surprisingly, the linewidth of ^{23}Na NMR signal of Na^+-valinomycin complex in chloroform solution is in the same order of magnitude observed in the solid state, as summarized in Table 1. On the contrary, the linewidths of the other complexes are reduced to 1/3—1/20 of the solid state. As pointed out in the previous section, location of the sodium ion within the cavity of asymmetric electric field gradient creates strong field gradient eq. Thus, the interaction of this field gradient with the nuclear quadrupole moment eQ produces the efficient pathway of nuclear relaxation.

Under the condition of extreme narrowing ($w^2\tau_C^2 \ll 1$), the linewidth $W_{1/2}$ is written as,[40]

$$W_{1/2} = 1/\pi T_2 = 2\pi/5(e^2qQ/h)^2\tau_C \quad (2)$$

where w and τ_C are Larmor frequency and the correlation time which characterizes the fluctuation of the electric field gradient, respectively, e^2qQ/h is the quadrupole coupling constant. The correlation time τ_C can be independently determined by measurement of the ^{13}C spin-lattice relaxation time (T_1),[41]

$$1/T_1 = N\hbar^2\gamma_C^2\gamma_H^2 r^{-6}\tau_C \quad (3)$$

where N is number of proton(s) attached to carbon nuclei in question, γ_C and γ_H are gyromagnetic ratio of the carbon and proton, respectively, and r is the C–H distance.

By combination of Eqs. 2 and 3,[42] it is now possible to calculate the quadrupole coupling constant e^2qQ/h, which is a very important parameter to determine the linewidths of ^{23}Na NMR signals, from a knowledge of the correlation time τ_C, as deduced by the ^{13}C spin-lattice relaxation times. As listed in Table 2, the quadrupole coupling constants of some complexes in chloroform solution are in parallel with the degree of asymmetry in the electric environment of sodium atoms. It is now possible to estimate ^{23}Na NMR linewidths of these complexes under various situation, if correlation times of molecular tumbling are known. For instance, ^{23}Na NMR linewidths of these complexes incorporated in biological membranes are estimated as 0.5—50 kHz on the basis of Eq. 2 using the quadrupole coupling constant 2 MHz and correlation times 10^{-8}—10^{-10} s.[43] Accordingly, it appears that ^{23}Na NMR spectra of these complexes might be substantially broadened in biomembranes. To make this situation worse, presence of slower collective motion tends to further broaden linewidth ($T_2 \ll T_1$).[43] In fact, we were not successful in recording ^{23}Na NMR spectra of these ionophores incorporated into sonicated lipid bilayers of egg phosphatidylcholine (unpublished finding).

Strictly speaking, the correlation times τ_C in methanol solution might be different from those in

chloroform. However, we neglected such a difference to qualitatively estimate the quadrupole coupling constants. Further, it is also desirable to remove residual oxygen molecules, by freezing-and-thawing, to obtain reliable spin-lattice relaxation times longer than about 1000 ms. Instead, we used published T_1 value[18] of 18C6 under the conditions of degassing to evaluate the quadrupole coupling constants of some sodium complexes with cryptands and 18C6, as shown in the parentheses of Table 2. Interestingly, the estimated quadrupole coupling constants of sodium complexes with cryptands and 18C6 (in parentheses of Table 2) by this treatment became larger than those of the naturally occurring ionophores, reflecting inherent asymmetric nature of the complexes.

When ligand-exchange process occurs as in methanol solution, the ^{23}Na NMR linewidths are substantially decreased, as summarized in Table 1. Analogous to the expression of the ^{23}Na chemical shifts given in Eq. 1, the observed quadrupole coupling constant $(e^2qQ/h)_{obsd}$ is given by Eq. 4.

$$(e^2qQ/h)_{obsd} = p_1(e^2qQ/h)_{complex} + p_2(e^2qQ/h)_{solvent} + p_3(e^2qQ/h)_{ion}, \quad (4)$$

where subscripts, complex, solvent and ion, have the same meaning as those described already. If we can neglect fractions of sodium complexes of mixed ligands with ionophores and solvents, the second and third terms $(e^2qQ/h)_{solvent}$ and $(e^2qQ/h)_{ion}$ become nearly zero because of symmetric property. Therefore, the linewidths will be reduced in proportion to the fraction of the complexed species. In particular, such reduction of the linewidth is remarkable from 2200 Hz to 70 Hz in methanol for the complex with valinomycin. Thus, it is likely that sodium ion in this case is not mainly coordinated to valinomycin but to methanol. For the complexes with other ionophores, this trend is not drastic as in the case of the above-mentioned valinomycin but is still significant.

In conclusion, we have demonstrated that comparison of high-resolution ^{23}Na NMR spectra of sodium complexes in solution with those obtained in the solid is very useful to reveal conformational stability of these complexes in solution, as a complementary means to ^{13}C NMR spectroscopy utilizing the conformation-dependent ^{13}C chemical shifts.

We are grateful to Chugai Pharmaceutical Co. Ltd., Tokyo for generous gift of tetranactin.

References

1) Yu. A. Ovchinnikov, V. T. Ivanov, and A. M. Shkrob, "Membrane Active Complexones," B. B. A. Library, Vol. 12 Elsevier, New York (1974).

2) B. C. Pressman, *Ann. Rev. Biochem.*, **45**, 501 (1976).

3) F. de Jong and D. N. Reinhoudt, *Adv. Phys. Org. Chem.*, **17**, 1 (1981).

4) B. Dietrich, "Inclusion Compounds," ed by J. C. Atwood, J. E. Davies, and D. M. MacNicol, Academic Press, London (1984), Vol. 2, Chap. 10.

5) H. Saitô, R. Tabeta, A. Shoji, T. Ozaki, I. Ando, and T. Asakura, "Magnetic Resonance in Biology and Medicine," ed by G. Govil, C. L. Kheterapal, and A. Saran, Tata McGraw-Hill, New Delhi (1985), p. 195.

6) H. Saitô, *Magn. Reson. Chem.*, **24**, 835 (1986).

7) R. Tabeta and H. Saitô, *Biochemistry*, **24**, 7696 (1985).

8) R. Tabeta and H. Saitô, *Bull. Chem. Soc. Jpn.*, **58**, 3215 (1985).

9) R. Tabeta and H. Saitô, *Chem. Lett.*, **1984**, 293.

10) R. Tabeta, M. Aida, and H. Saitô, *Bull. Chem. Soc. Jpn.*, **59**, 1957 (1986).

11) For review: a) P. Laszlo, *Angew. Chem. Int. Ed. Engl.*, **17**, 254 (1978); b) M. M. Civan and M. Shporer, "Biological Magnetic Resonance," ed by L. J. Berliner and J. Reuben, Plenum Press, New York and London (1978), Chap. 1; c) B. Lindman and S. Forsen, "NMR and the Periodic Table," ed by R. K. Harris and B. E. Mann, Academic Press, London (1978), Chap. 6.

12) D. H. Haynes, B. C. Pressman, and A. Kowalsky, *Biochemistry*, **10**, 852 (1971).

13) M. Shporer, H. Zemel, and Z. Luz, *FEBS Lett.*, **40**, 357 (1974).

14) E. Shchori, J. Jagur-Grodzinski, Z. Luz, and M. Shporer, *J. Am. Chem. Soc.*, **93**, 7133 (1971).

15) E. Shchori, J. Jagur-Grodzinski, and M. Shporer, *J. Am. Chem. Soc.*, **95**, 3842 (1973).

16) M. Shamsipur and A. I. Popov, *J. Am. Chem. Soc.*, **101**, 4051 (1979).

17) B. O. Strasser, K. Hellenga, and A. I. Popov, *J. Am. Chem. Soc.*, **107**, 789 (1985).

18) B. Eliasson, K. M. Larsson, and J. Kowalewski, *J. Phys. Chem.*, **89**, 258 (1985).

19) J. M. Ceraso and J. L. Dye, *J. Am. Chem. Soc.*, **95**, 4432 (1973).

20) J. P. Kintzinger and J. M. Lehn, *J. Am. Chem. Soc.*, **96**, 3313 (1974).

21) J. M. Ceraso, P. B. Smith, J. S. Landers, and J. L. Dye, *J. Phys. Chem.*, **81**, 760 (1977).

22) J. D. Lin and A. I. Popov, *J. Am. Chem. Soc.*, **103**, 3773 (1981).

23) R. C. Phillips, S. Khazaeli, and J. L. Dye, *J. Phys. Chem.*, **89**, 606 (1985).

24) J. M. Ceraso and J. L. Dye, *J. Chem. Phys.*, **61**, 1585 (1974).

25) J. L. Dye, C. W. Andrews, and J. M. Ceraso, *J. Phys. Chem.*, **79**, 3076 (1975).

26) See Table 2 of Ref. 10 for compilation of the Na–O distances for a variety of sodium complexes with ionophores.

27) Unpublished finding for monensin by high-resolution solid-state ^{13}C NMR spectra.

28) K. Neupert-Laves and M. D. Dobler, *Helv. Chim. Acta*, **58**, 432 (1975).

29) Chemical structure of tetranactin is similar to that of nonactin, except for the presence of four ethyl groups in place of four methyl groups which are drawn inside the macrocyclic ring in Fig. 1.

30) M. Dobler, J. D. Dunitz, and B. T. Kilbourn, *Helv. Chim. Acta*, **52**, 2573 (1969).
31) M. Dobler and R. P. Phizackerley, *Helv. Chim. Acta*, **57**, 664 (1974).
32) T. Sakamaki, Y. Iitaka, and Y. Nawata, *Acta Crystallogr. Sect. B*, **32**, 768 (1976).
33) P. G. Schmidt, A. H. -J. Wang, and I. C. Paul, *J. Am. Chem. Soc.*, **96**, 6189 (1974).
34) G. D. Smith, W. L. Duax, and S. Forsen, *J. Am. Chem. Soc.*, **100**, 6725 (1978).
35) C. Shen and D. I. Patel, *Proc. Natl. Acad. Sci. U. S. A*, **73**, 4277 (1970).
36) M. Pinkerton and L. K. Steinrauf, *J. Mol. Biol.*, **49**, 533 (1970).
37) W. K. Lutz, F. K. Winkler, and J. Dunitz, *Helv. Chim. Acta*, **54**, 1103 (1971).
38) C. C. Chang and I. C. Paul, *Science*, **196**, 1441 (1977).
39) G. R. Painter, R. Pollack, and B. C. Pressman, *Biochemistry*, **21**, 5613 (1982).
40) A. Abragam, "Principle of Nuclear Magnetism," Claredon Press, Oxford (1961), Chap. 8.
41) A. Allerhand, D. Doddrell, and R. Komoroski, *J. Chem. Phys.*, **55**, 189 (1971).
42) H. Saitô, H. H. Mantsch, and I. C. P. Smith, *J. Am. Chem. Soc.*, **95**, 8453 (1973).
43) M. F. Brown, *J. Chem. Phys.*, **77**, 1576 (1982).

 © 1987 The Chemical Society of Japan Bull. Chem. Soc. Jpn., 60, 69—75 (1987)

Formulation of Enthalpy, Entropy, and Volume Changes Accompanying Association Reaction in Solution in Terms of Molecular Distribution Functions

Yosuke YOSHIMURA* and Masaru NAKAHARA*
Department of Chemistry, Faculty of Science, Kyoto University,
Oiwake-cho, Kitashirakawa, Sakyo-ku, Kyoto 606
(Received June 27, 1986)

The equilibrium constant of the chemical reaction in solution is formulated by means of the distribution function at the semiclassical level. The equivalence of the present expression and the traditional one that is based on the standard chemical affinity is proved. The changes of the thermodynamic quantities (enthalpy, entropy, and volume) at constasnt temperature and pressure are expressed on the basis of the present formulation. They are composed of the following three terms: (i) the internal change, (ii) the translational change, and (iii) the solvation change. Each term is evaluated for the dimerization of nitrogen dioxide. It is shown that the volume change is a good measure for the solvation change because it does not contain the internal change. Since the solvation change is explicitly expressed by means of the radial distribution function and its temperature or pressure derivative in an explicit manner, it is useful for discussing the solvent effect on the chemical reaction from the point of view of the liquid structure.

Our molecular understanding of chemical reactions is much less advanced in the liquid phase than in the gas phase because of the presence of many-body interactions characteristic of the liquid phase; most fundamental theories have been developed primarily for the gas-phase reaction which is free from complicated intermolecular interactions due to solvent. It is desired to improve the situation by applying statistical thermodynamics of liquids to reacting systems. We concentrate on the molecular interpretation of the widely used thermodynamic and activation parameters, such as enthalpy, entropy, and volume changes accompanying the chemical reaction in the condensed phase; these parameters are obtainable from the application of thermodynamics and transition state theory to the experimental study on the effect of temperature and pressure on the equilibrium and rate constants for the liquid-phase reaction.[1] We take advantage of the present knowledge of the liquid state at equilibrium in order to provide a theoretical framework or perspective for the molecular interpretation of the thermodynamic and activation parameters which have been used to characterize the mechanism of the reaction in solution.

It is still an open problem how the liquid structure of solvent influences the thermodynamic and activation parameters associated with chemical reactions in solution. When we consider this problem, it is of primary importance to clearly define what we mean by the solvent liquid structure. The radial distribution function is meaningful in this respect. In the previous papers,[2,3] we have successfully applied the distribution function theory of liquids to the problem of reaction and activation volumes to unveil the molecular aspects of the volume properties. This potential approach is extended here to apply to enthalpy and entropy changes to have an insight into the solvent effect on these macroscopic quantities from a molecular point of view; this kind of generalization is not yet completely fulfilled after such a new direction has been suggested by Chandler and co-workers[4-6] and followed by some others.[2,3,7] In the present work we intend to examine the macroscopic reaction parameters mentioned above beyond the primitive view that their changes are nothing more than a difference between the reactant and the product (or transition) states.

One of the merits of the distribution function theory is the capability of continuously treating a reaction process starting just from the reactant state as in the MO calculation of the potential energy supersurface. In the present approach, the transition and product states are represented by the configuration where the coordinates of the atoms involved in the reactants are specified. Thus we can regard the chemical reaction as a continuous variation of the distribution (configuration or arrangement) of constituent atoms or groups composing the reactant molecules; in the liquid-phase reaction, not only the reactants but also the third bodies like solvent molecules have to be included in the definition of the distribution. In the distribution function theory, we define a probability (density) of finding a configuration that varies with the extent (or coordinates) of a reaction, and its equilibrium and rate constans are given in terms of such probabilities. Since the distribution function theory is applicable to both the liquid and the gas phases, it enables us to disclose the key role of solvent molecules in differentiating the liquid-phase reaction from the gas-phase one.

Molecular Model for Association Reaction in Solution

Consider a reversible association reaction in solution at infinite dilution where two spherical molecules A and B form the adduct C in an excessive

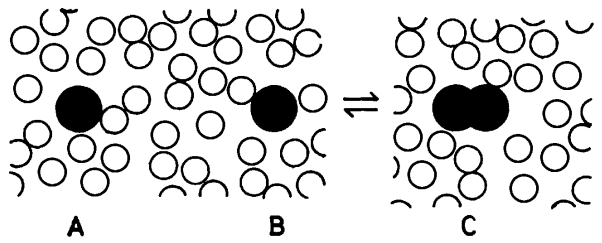

Fig. 1. Model of the bimolecular association reaction in solution illustrated in a two-dimensional way. The white circles denote the solvent molecules and the black the reactants.

amount of solvent as shown in Fig. 1. The potential energy Φ of the reaction system is assumed to be given by the pairwise additive intermolecular potentials u_{ij} as

$$\Phi = \sum u_{ij}, \tag{1}$$

where the pair potential u_{ij} is assumed to act only in the short range between the ith and jth species. The pair potential between the reactants A and B corresponds to the "potential energy supersurface" of the association reaction.

In the present paper, we neglect the quantum effect on the intramolecular behavior of the product molecule C because it is not easy to incorporate this effect into the distribution function formalism; the system is described here at the semiclassical level in the sense that the difference between the energy states is small enough compared with the thermal energy.

The behavior of the model system in the semiclassical limit can be predicted when we specify the form of the potential energy functions in the above scheme; here, however, we are concerned not with the numerical calculation but with the formalism. There remains another fundamental problem as to how to identify the product molecule C. There can be two ways to define C. One may define the product C as a molecular pair when the distance r between A and B lies between l and $l+\varepsilon$; here l and ε can be defined in an arbitrary manner independent of the environments, and l corresponds to the "bond length" when ε is in a sufficiently small range. The other may define C as a molecular pair which has the highest population at a value of r in the ensemble. We take the former definition for the sake of convenience.

Equilibrium Constant in Terms of Distribution Function

Expression for Equilibrium Constant. Since the total number N_C of the product C is the number of the molecular pair A-B which lies between l and $l+\varepsilon$ as described above, it is evaluated by using the radial distribution function $g_{AB}(r)$ as[2]

$$N_C = V\int n_A n_B g_{AB}(r)\cdot\chi(r)4\pi r^2 dr, \tag{2}$$

where V, n_A, n_B, and $\chi(r)$ denote the volume of the system, the number densities of A and B, and the characteristic function for identifying C, respectively. The explicit form of $\chi(r)$ is given here as

$$\chi(r) = \begin{cases} 1 & l \leqq r \leqq l+\varepsilon \\ 0 & r<l \text{ or } r>l+\varepsilon, \end{cases} \tag{3}$$

where ε is the distance in the range of which the molecular pair is recognized as the product C. When ε is small enough, Eq. 2 is written as

$$n_C = n_A n_B g_{AB}(l)\cdot\delta, \tag{4}$$

where n_C is the number density of C and δ is $4\pi l^2\varepsilon$. Since the concentrations of the reactants are at infinite dilution, n_C is negligibly small compared with n_A or n_B, and hence the equilibrium constant K is given as

$$K = n_C/n_A n_B = g_{AB}(l)\cdot\delta. \tag{5}$$

This simple expression is important because the molecular nature of solvent and solute molecules is taken into account in a natural manner.[8,9]

Equation 5 can be easily extended to the association between the same molecules, i.e., A=B, or the aggregation among a number of molecules. In the former case, Eq. 5 is rewritten as

$$K = n_C/n_A^2 = \frac{1}{2}g_{AA}(l)\cdot\delta, \tag{6}$$

where the factor 1/2 is necessary to avoid the double counting of the molecular pair in Eq. 2.

Radial Distribution Function in Terms of Cavity Distribution Function. Since the potential energy of the system is pairwise additive, the radial distribution function is expressed as the product of the Boltzmann factor for the "bond energy" $u_{AB}(l)$ at a fixed distance l and the cavity distribution function $y_{AB}(l)$ which is defined as[4]

$$g_{AB}(l) = \exp(-u_{AB}(l)/kT)\cdot y_{AB}(l), \tag{7}$$

where k and T are the Boltzmann constant and the temperature, respectively. The solute-solvent interactions are included in the cavity distribution function; the cavity distribution function is the radial distribution function between the hypothetical molecules which have no interactions between themselves and have interactions as usual with the solvent molecules. The cavity distribution function is introduced to represent the indirect interactions between A and B through the solvent molecules. The direct interaction $u_{AB}(l)$ between reactant molecules is separated unambiguously from the radial distribution function so that we may abstract the effect of the solvent-solvent interaction on the thermodynamic quantities of our interest.

Comparison of Distribution Function and Partition Function Expressions

Standard Chemical Affinity. The traditional scheme for treating the changes in the thermodynamic quantities is based on the standard chemical affinity A^0.[10] The standard chemical affinity is defined as

$$A^0 = -\sum \nu_i \mu_i^0, \tag{8}$$

where μ_i^0 is the standard chemical potential of species i; i runs for all the reactants ($\nu_i<0$) and the product ($\nu_i>0$); the symbol ^{0} denotes the standard state. The equilibrium constant K is related to the standard chemical affinity as follows:

$$A^0 = kT \ln K - \sum \nu_i kT \ln c^0, \tag{9}$$

where c^0 is the concentration of the standard state that is conventionally taken to be unity in most cases. The thermodynamic changes, such as enthalpy, entropy, and volume are derived by differentiating the standard chemical affinity. Furthermore, the standard chemical affinity is expressed by the partition functions Z_R^0 and Z_P^0 for the reactants and products, respectively, as

$$A^0 = kT \ln (Z_P^0/Z_R^0). \tag{10}$$

Thus we can diagnose the changes in the thermodynamic quantities by dividing into the contributions from each degree of freedom as shown below. However, the traditional treatment does not tell us the significance of the liquid structure on the chemical reaction. In this chapter, we try to find a relationship between the present and traditional schemes based on the distribution function and the partition function, respectively; remember that the liquid structure of solvent is taken into account in an explicit manner in the former approach.

Components of Standard Chemical Affinity. The standard chemical affinity of the model association reaction is composed of several factors, such as the translational, rotational, and vibrational degrees of freedom of the molecules involved in the reaction and the solute–solvent interactions. First, we briefly review the traditional formulation of the standard chemical affinity in terms of partition functions. The contributions of the solute–solvent interactions to the standard chemical potentials of A, B, and C in solution are considered to be expressed by the corresponding standard chemical potential for the process of their transfer from the ideal gas into the solvent. These are called the solvation free energies, and denoted as α_A, α_B, and α_C for A, B, and C, respectively. The internal degrees of freedom are assumed here to be unperturbed by this process. In consequence, we have the following expressions of the standard chemical potentials for species A, B, and C:

$$\mu_A^0 = kT \ln \left[\left(\frac{h^2}{2\pi m_A kT} \right)^{3/2} c^0 \right] + \alpha_A, \tag{11}$$

$$\mu_B^0 = kT \ln \left[\left(\frac{h^2}{2\pi m_B kT} \right)^{3/2} c^0 \right] + \alpha_B, \tag{12}$$

$$\mu_C^0 = -kT \ln Z_{int} + kT \ln \left[\left(\frac{h^2}{2\pi (m_A+m_B) kT} \right)^{3/2} c^0 \right] + \alpha_C, \tag{13}$$

where h, and m_A, and m_B are Planck's constant and the masses of A and B, respectively, and Z_{int} is the partition function for the internal degree of freedom. Using Eqs. 11—13 we have the standard chemical affinity in the form

$$A^0 = -\mu_C^0 + (\mu_A^0+\mu_B^0) = kT \ln Z_{int} + kT \ln (\lambda^3 c^0) - \Delta\alpha, \tag{14}$$

where

$$\lambda = (h^2/2\pi m_r kT)^{1/2}, \tag{15}$$

$$m_r = m_A m_B/(m_A+m_B), \tag{16}$$

$$\Delta\alpha = \alpha_C - (\alpha_A+\alpha_B). \tag{17}$$

Here we call the first term in Eq. 14 the internal contribution, the second the translational contribution, and the third the solvation contribution. Such a simple expression for the chemical affinity comes from the fact that the translational contribution is the same in the gas and liquid phases at the semiclassical level and the assumption that the internal structure of the molecule is unchanged by the solvation.

Comparison of Distribution Function and Partition Function Approaches. Although at first sight, Eqs. 5 and 14 seem to have no relation, the semiclassical expressions for the internal partition functions lead to a simple relation between them. The first term on the right-hand side of Eq. 14 comes from the following three factors; the rotational and vibrational degrees of freedom of the associated molecule C and the difference in the zero point of the energy between reactants A and B and product C. The last factor is equal to the bond energy $u_{AB}(l)$ that is negative in sign contrary to the convention. Hence it follows that

$$kT \ln Z_{int} = kT \ln Z^{rot} + kT \ln Z^{vib} - u_{AB}(l), \tag{18}$$

where Z^{rot} and Z^{vib} denote the partition functions of the rotational and vibrational motions of C, respectively.

The rotational partition function in the semiclassical approximation is written as

$$Z^{rot} = \frac{1}{s} \lambda^{-2} \cdot 4\pi l^2, \tag{19}$$

where s is the symmetry number of the associated molecule C, and the vibrational partition function as

$$Z^{vib} = \lambda^{-1} \varepsilon. \tag{20}$$

In the semiclassical approximation, the rotational

partition function is equivalent to the partition function of the two-dimensional translational motion for the particle of the mass m_r in an area $4\pi l^2$ (which is the surface area of the sphere of the radius l), and the vibrational partition function is equivalent to the partition function of the one dimensional translational motion of the particle in a length ε. Thus the internal partition function is written as

$$Z_{\text{int}} = \frac{1}{s}\lambda^{-3}4\pi l^2\varepsilon \cdot \exp\left(-u_{AB}(l)/kT\right). \tag{21}$$

When Eqs. 18—20 are used in Eq. 14 the standard chemical affinity is written as

$$A^0 = kT\ln\left(c^0 \cdot 4\pi l^2\varepsilon\right) - kT\ln s - u_{AB}(l) - \Delta\alpha. \tag{22}$$

This equation can be interpreted thermodynamically by considering a process by which the associated molecule C is formed. Suppose a gas mixture of the reactants A and B at the standard state the concentration of which is c^0. The first term on the right-hand side of Eq. 22 is the change due to the compression of reactant A (or B) from the free space to the concentration $1/(4\pi l^2\varepsilon)$ in the restricted space around B (or A); $4\pi l^2\varepsilon$ is the volume where one of the reactants can move in the neighborhood of the other. If A and B are the same, only either A or B is involved in the initial gas mixture at the standard state (the concentration c^0), so that the concentration of the resultant C is one half of c^0. Therefore, it is necessary to add $kT\ln 2$ to bring the product gas C into the standard state. This correction is made through the symmetry number s=2. Finally, the reversible work $\Delta\alpha$ accompanying the transfer of the product from the gas phase into the solvent is added as shown in Eq. 22.

According to Eq. 9, the equilibrium constant is expressed by the standard chemical affinity and the sum of the stoichiometric number -1 ($-\nu_A=-\nu_B=\nu_C=1$). Putting Eq. 22 into Eq. 9 we obtain

$$K = \frac{1}{s}\exp\left(-(u_{AB}(l)+\Delta\alpha)/kT\right)\cdot 4\pi l^2\varepsilon. \tag{23}$$

Comparison of Eqs. 5 and 23 leads to the following equation:

$$y_{AB}(l) = \exp\left(-\Delta\alpha/kT\right). \tag{24}$$

This equation is also derivable from the fact that $-kT\ln y_{AB}(l)$ is equal to the reversible work accompanying the approach of A and B at a large separation to the distance l[4]; this is called the potential of mean force by the solvent molecules and equivalent to the difference of the solvation free energy $\Delta\alpha$. In the classical scheme, the change $\Delta\alpha$ due to solvation is treated as the standard chemical affinity associated with the formation or the destruction of the solvation shell. This is contained naturally in the cavity distribution function treated here.

Free Volume Theory vs. Distribution Function Theory. Let us inspect the relation between the present framework based on the distribution function theory and the old one based on the free volume theory. It has been asserted by some authors[1b,11] that the difference in the equilibrium constant between the gas and the liquid phases arises from the restriction of the translational freedom in the liquid phase, and that the "free volume" is useful as a measure of the restriction. In this framework, the chemical potential change is simply written as

$$A^0 = A^0(\text{ideal}) + kT\ln\left(v^0 v_C^f/v_A^f v_B^f\right), \tag{25}$$

where A^0(ideal) is the standard chemical affinity without the solute–solvent interaction that is equal to the standard chemical affinity in the ideal gas, and v^0 and v_X^f are the volume per particle $1/c^0$ and the free volume per particle X, respectively. Although the free volume is often claimed to be ambiguous, its concept can be made clear by the present molecular approach as shown below.

According to Eq. 25, the reversible work α_X introduced into Eqs. 11—13 is expressed as

$$\alpha_X = -kT\ln\left(v_X^f/v^0\right). \tag{26}$$

Putting Eq. 26 into Eq. 24, we obtain the relation

$$y_{AB}(l) = v^0 v_C^f/v_A^f v_B^f \tag{27}$$

$$= p_C/p_A p_B, \tag{28}$$

where p_X is the ratio of v_X^f to v^0. Suppose dissolution of solute X into the solvent. The probability of the allowed occupation of an arbitrary place in the solvent is assumed to be equal to the ratio p_X of the free volume to the total volume. The cavity distribution function at a distance l is the ratio of the probability of finding the A–B pair at the distance l to that of finding the pair without correlation between A and B; the former and the latter probabilities are given by p_C and $p_A p_B$, respectively. Thus we can explain Eq. 25 in the probabilistic manner.

Components of Changes in Thermodynamic Quantities and Their Significance

The formulation in the previous section enables us to divide the changes of the thermodynamic quantities into the following three terms in an additive manner: (i) the change due to the direct interaction between the reactants which brings about the internal degree of freedom of the product (called the "internal change"), (ii) the change due to the translational motion (called the "translational change"), and (iii) the change due to the indirect interactions between the reactants through the solvent molecules (called the "solvation change"). The term "solvation" is used here in a broad sense, whereas it is often used for strong

solute-solvent interactions. In this section, we clarify the significance of each component of the enthalpy, entropy, and volume changes accompanying the association reaction proceeding under isobaric conditions. Numerical value for each component in an actual system is shown in the Appendix to see the relative importance.

Internal Contribution. The internal change in the chemical potential is represented by the first term in Eq. 14. Differentiation of the term leads to the following expressions:

$$\Delta\bar{H}^0(\text{int}) = u_{AB}(l) + \frac{3}{2}kT, \tag{29}$$

$$\Delta\bar{S}^0(\text{int}) = k\ln(\lambda^{-3}\cdot 4\pi l^2\varepsilon) + \frac{3}{2}k, \tag{30}$$

$$\Delta\bar{V}^0(\text{int}) = 0. \tag{31}$$

The internal changes are the same both in the ideal gas and in solution according to the present model. The first term in the enthalpy change is the pair potential change between the reactants. And the second term due to the energy of the internal degree of freedom of the associated molecule that is equal to $(3/2)kT$ as expected from the equipartition law of energy.[12]

Different aspects are shown by the internal enthalpy and entropy changes. While the enthalpy change depends on the strength of the bond, $u_{AB}(l)$, the entropy change depends on the "softness" of the bond, ε. Though the semiclassical term $(3/2)kT$ in the enthalpy change arises from the internal motion which is attributed to the "softness" of the A-B bond, the contribution of the term is usually small (3.7 kJ mol^{-1} at 25 °C) compared with the bond energy. Thus the standard chemical affinity is meaningfully split into the enthalpy and the entropy changes.

It is interesting that the internal contribution does not appear in the volume change. The present result discloses that whatever the internal change takes place the volume change is not observed without the solute-solvent interactions not the direct interaction betwee the solute and the vessel. Thus the "intrinsic volume change" has no real physical meaning, as referred to previously.[3]

Translational Contribution. The translational chemical potential change is represented by the second term in Eq. 14. Differentiation of this term leads to the following expressions:

$$\Delta\bar{H}^0(\text{trans}) = -\frac{3}{2}kT - \alpha_p kT^2, \tag{32}$$

$$\Delta\bar{S}^0(\text{trans}) = k\ln(\lambda^3 c^0) - \frac{3}{2}k - \alpha_p kT, \tag{33}$$

$$\Delta\bar{V}^0(\text{trans}) = -\kappa_T kT, \tag{34}$$

where α_p and k_T are the isobaric expansibility and the isothermal compressibility of the solvent, respectively. Since these translational changes are determined not only by the momentum of the molecule but also by the direct interaction between the molecule and the container's walls,[11] these equations contain the response function of the volume of the system with respect to the temperature (α_p) or the pressure (κ_T) as shown by the last term on the right hand-side of each equation.[13,14] These terms have been treated as the "correction term" in calculating the change of the thermodynamic quantity from the equilibrium constant expressed in molarity.[1a] The role of the last terms in Eqs. 32—34 was pointed out in a different manner in the "noninteracting solution"[11] where the solute molecule had only the translational degree of freedom in the container. We have previously elucidated the significance of the translational volume change on the basis of the virial theorem.[3,15]

Solvation Contribution. The solvation contribution to the standard chemical affinity is represented by the third term in Eq. 14. Differentiation of this term leads to the following expressions:

$$\Delta\bar{H}^0(\text{solv}) = kT^2\left(\frac{\partial\ln y_{AB}(l)}{\partial T}\right)_P, \tag{35}$$

$$\Delta\bar{S}^0(\text{solv}) = k\ln y_{AB}(l) + kT\left(\frac{\partial\ln y_{AB}(l)}{\partial T}\right)_P, \tag{36}$$

$$\Delta\bar{V}^0(\text{solv}) = -kT\left(\frac{\partial\ln y_{AB}(l)}{\partial P}\right)_T. \tag{37}$$

These formal expressions tell us that the solvation changes are determined by the liquid structure through the temperature or pressure derivative of the cavity distribution function. Comparison of Eqs. 29—37 reveals that the volume change is a more direct measure of the solvent effect than are the chemical affinity, and the entropy and enthalpy changes because the volume change is independent of the internal structure of the associated molecule C except for the bond length which is assumed to be unaffected by the environments.

The nature of the solvation change is more complicated than that of the internal of the translational change, which results from the fact that the cavity distribution function is determined by multibody interactions among the molecules. If the density of the solvent is small enough, the expansion of the cavity distribution function in powers of density can be truncated to the first several terms and served for a rigorous discussion of their explicit form of Eqs 35—37, an example is shown elsewhere[3] for the volume change in the dilute gas. But such a treatment breaks down in usual liquids where multibody interactions are dominant. Hence we should explore the liquid structure in a more sophisticated manner to establish a solid basis for the treatment of the solvation effects on the chemical reaction; e.g., such "extra-thermodynamic" relation-

ships as linear free energy relationship and the entropy-enthalpy compensation may be obtained along this line. The present-day liquid theory[16] will be useful for justifying the extra-thermodynamic rules empirically found. Our work along this line will appear in near future.

Appendix

Evaluation of the Internal, Traslational, and Solvation Contributions in an Actual System. Although the theoretical framework presented here is insufficient for understanding the molecular nature of the chemical reaction because of the complexity of the internal structure in the actual reaction system, at least, the translational and solvation contributions can be elucidated. The relative weights of the internal, translational, and solvation contributions vary from one thermodynamic quantity to another. Here, we show the significance of the three components in the changes of the thermodynamic quantities, enthalpy, entropy, and volume in an association reaction.

The dimerization of nitrogen dioxide in solution

$$2NO_2 \rightleftharpoons N_2O_4, \tag{38}$$

is a prototype association reaction studied experimentally[17-20] and theoretically[4,6] in both the gas and liquid phases. Although this reaction is complicated enough as referred to above, the translational and solvation contributions can be estimated by applying the experimental imformation in the present formulation.

We adopt the experimental data for the enthalpy and entropy changes in carbon tetrachloride which are obtained by measuring the solution susceptibility,[18] while there exists a discrepancy in the experimental data.[18,19] The isothermal compressibility and the isobaric expansibility are taken from Ref. 21.

The evaluated values for the three components at 25 °C and 1 atm (1 atm=1.013×10^5 Pa) are summarized in Table 1. The largest contribution to the entropy change comes from the translational change. If the internal freedom exists only in the associated molecule as in the present model, the internal entropy change is expected to be positive. However, since both nitrogen dioxide and dinitrogen tetroxide molecules have the internal freedom, the dimerization reaction may have the negative internal entropy change as shown in Table 1; the largest contribution to the internal entropy change comes from the rotational entropy change that is calculated here as -55 J K^{-1} mol^{-1}. The internal contribution plays the most important role in the enthalpy change. The volume change is dominated by the solvation change, and the translational volume change is rather small in solution, though the translational contribution to the volume change is dominant in the gas phase where the volume change amounts to -24 dm^3 mol^{-1}.

Table 1. Values of the Components of Changes of the Thermodynamic Quantities Accompanying the Dimerization of Nitrogen Dioxide in Carbon Tetrachloride at 25 °C and 1 atm[a,b]

	Internal	Translational	Solvation
$\Delta\bar{H}^0$ (kJ mol^{-1})	-50.9	-4.6	-5.6
$\Delta\bar{S}^0$ (J K^{-1} mol^{-1})	-28	-116	$+11$
$\Delta\bar{V}^0$ (cm^3 mol^{-1})	0	-3	-20

a) The standard state is taken to be 1 mol dm^{-3}. b) The internal changes of the enthalpy and entropy, which are assumed to be the same in the gas and the liquid phases, are calculated from the data of the gas-phase reaction[17] by subtracting the translational changes which are obtained from Eqs. 34 and 35. The experimental data of the volume change is obtained from Ref. 20.

The entropy change has been used in the characterization of the chemical reaction in solution with such a view that the entropy change (activation entropy) reflects the "softness" or "randomness" of the product (transition state). As shown here, however, the entropy change accompanying the association reaction contains a large amount of translational contribution which is independent of the molecular parameters except for the mass. Thus we must subtrac the translational contribution before discussing the mechanism of the association or addition reaction in terms of the entropy change.

The authors are grateful for the support of the present work by the Research Grant-in-Aid from the Ministry of Education, Science and Culture (No. 61134043).

References

1) a) L. P. Hammet, "Physical Organic Chemistry," McGraw-Hill, New York (1970); b) S. W. Benson, "The Foundations of Chemical Kinetics," McGraw-Hill, New York (1960); c) S. G. Entelis and R. P. Tiger, "Reaction Kinetics in the Liquid Phase," translated by R. Kondor, John Wiley, New York (1976).

2) Y. Yoshimura and M. Nakahara, *J. Chem. Phys.*, **81**, 4080 (1984).

3) Y. Yoshimura and M. Nakahara, *Ber. Bunsenges. Phys. Chem.*, **90**, 58 (1986).

4) D. Chandler and L. R. Pratt, *J. Chem. Phys.*, **65**, 2925 (1976).

5) L. R. Pratt, C. S. Hsu, and D. Chandler, *J. Chem. Phys.*, **68**, 4202 (1978).

6) D. Chandler, *Faraday Discuss. Chem. Soc.*, **66**, 184 (1978).

7) B. M. Ladanyi and J. T. Hynes, *J. Am. Chem. Soc.*, **108**, 585 (1986).

8) When we ignore the ion charge in the Fuoss equation for ion-pair formation,[9] the equilibrium constant is given by

$$K = \frac{4\pi}{3}a^3,$$

where a is the center-to-center distance between the two contact spheres. This equation has no real physical meaning, and should read better as

$$K = 4\pi a^2 \varepsilon,$$

which is equal to Eq. 5 when $g(a)$ is assumed to be unity.

9) R. M. Fuoss, *J. Am. Chem. Soc.*, **80**, 5059 (1958).

10) I. Prigogine and R. Defay, "Kagaku-Netsurikigaku (Chemical Thermodynamics)," translated by M. Seno, Misuzu, Tokyo (1977).
11) R. P. Bell and O. Gatty, *Phil. Mag.*, **9**, 75 (1935).
12) Since the Hamiltonian for the internal motion of C can be regarded to be independent of the coordinates, the energy partitioned is $(3/2)kT$. If the Hamiltonian depends on the coordinates, this is not the case; e.g., the harmonic oscillator shares an energy of $2kT$.
13) The translational volume change arises from the translational pressure change $(-kT/V)$ under the isochoric condition,[3] and the last terms of the translational enthalpy and entropy changes are attributed to the translational volume change. The enthalpy and entropy changes under isochoric condition are reduced to the following[14]:

$$(\Delta\bar{U}^0)_{T,V} = \Delta\bar{H}^0 - (\alpha_P/\kappa_T)T\Delta\bar{V}^0,$$
$$(\Delta\bar{S}^0)_{T,V} = \Delta\bar{S}^0 - (\alpha_P/\kappa_T)\Delta\bar{V}^0,$$

where $(\Delta\bar{U}^0)_{T,V}$ is the internal energy change under isochoric condition. When the translational volume change $k_T kT$ is used in the last terms of the above equations, they become equal to the corresponding term in Eqs. 32 and 33. Thus it is verified that the last terms in Eqs. 32 and 33 are attributed to the change of the direct interaction between the molecule and the container's walls.
14) S. B. Brummer and G. J. Hills, *Trans. Faraday Soc.*, **57**, 1816 (1961).
15) Y. Yoshimura, J. Osugi, and M. Nakahara, *Ber. Bunsenges. Phys. Chem.*, **89**, 25 (1985).
16) a) J. A. Barker and D. Henderson, *Rev. Mod. Phys.*, **48**, 587 (1976); b) H. C. Andersen, D. Chandler, and J. D. Weeks, *Adv. Chem. Phys.*, **34**, 105 (1976).
17) I. C. Hisatsune, *J. Phys. Chem.*, **65**, 2249 (1961).
18) T. F. Redmond and B. B. Wayland, *J. Phys. Chem.*, **72**, 1626 (1968).
19) P. Gray and P. Rathbone, *J. Chem. Soc.*, **1958**, 3550.
20) A. H. Ewald, *Discuss. Faraday Soc.*, **22**, 138 (1956).
21) J. S. Rowlinson and F. L. Swinton, "Liquids and Liquid Mixtures," 3rd Ed., Butterworth, London (1982).

 © 1987 The Chemical Society of Japan Bull. Chem. Soc. Jpn., 60, 77—81 (1987)

Laser Flash Photolysis of Azocumenes. Direct Observation of Stepwise Decomposition

Takashi SUMIYOSHI,* Mikiharu KAMACHI,† Yoko KUWAE,† and Wolfram SCHNABEL††
Department of Atomic Science and Nuclear Engineering, Faculty of Engineering, Hokkaido University, Sapporo 060
†Department of Macromolecular Chemistry, Faculty of Science, Osaka University, Toyonaka, Osaka 560
††Hahn-Meitner-Institut für Kernforschung Berlin, Bereich Strahlenchemie, Glienicker Straße 100, D-1000 Berlin 39, Germany
(Received July 5, 1986)

The mechanism of the decomposition of α,α′-azocumene and 2,2′-di-*p*-tolyl-2,2′-azopropane was studied by means of laser flash photolysis (λ=347 nm) and the optical absorption of 1-methyl-1-phenylethyl (α-cumyl) and α-cumyldiazenyl radicals was observed. The α-cumyl radicals were formed in two modes, a fast mode occurring during the flash and a slow mode after the flash. The ratio of the optical densities pertaining to the two modes depended on the absorbed dose rate. The higher the absorbed dose per flash, the more dominant was the fast mode. The transient band at λ=285 nm which decayed simultaneously with the grow- in of the α-cumyl radicals was assigned to α-cumyldiazenyl radicals. The experimental results strongly suggested the occurrence of the stepwise decomposition mechanism. The dose rate dependent kinetics of the slow formation process was explained in terms of the competition between the unimolecular decomposition and the dimerization of α-cumyldiazenyl radicals. The rate constants of the decomposition and the dimerization were estimated to be 1.1×10^5 s^{-1} and 5×10^9 M^{-1} s^{-1}, respectively.

Azo compounds are well-known as very effective initiators for the free radical polymerization of vinyl compounds.[1] Both thermal and photochemical decomposition reactions of azo alkanes were studied by several workers, and two mechanisms were discussed: simultaneous scission of the two C-N bonds (Eq. 1)[2] and stepwise cleavage of the C-N bonds involving the diazenyl radical as a transient (Eq. 2).[3]

$$R_1\text{-}N{=}N\text{-}R_2 \longrightarrow R_1\cdot + N_2 + \cdot R_2 \quad (1)$$

$$R_1\text{-}N{=}N\text{-}R_2 \longrightarrow R_1\text{-}N{=}N\cdot + \cdot R_2 \longrightarrow R_1\cdot + N_2 + \cdot R_2 \quad (2)$$

As far as *thermolysis* is concerned, Engel[4] arrived at the conclusion that "azoalkane thermolysis seems to proceed by a continuum of mechanisms between 1 and 2; the more unsymmetrical the azo compound the more unsymmetrically it cleaves." Actually, evidence for a concerted two bond cleavage according to reaction 1 was obtained for the thermolysis of symmetrical azo compounds: 1,1′-diphenylazoethane,[5] α,α′-azocumene,[6,7] and a cyclic azoalkane:[8]

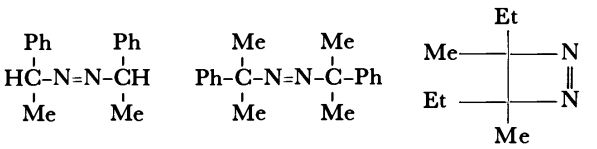

1,1′-diphenylazoethane | α,α′-azocumene | dl-3,4-diethyl-3,4-dimethyldiazetine

On the other hand, the occurrence of the heat-induced stepwise decomposition according to reaction 2 was evidenced in the case of *cis*-1,1′-azoadamantane, a symmetrical compound.[9] Dannenberg and Rocklin[10] carried out a theoretical study on the thermolysis of trans-azoethane, also a symmetrical compound, and arrived at the conclusion that the initial step is trans → cis isomerization which is followed by dissociation into diazenyl and ethyl radicals.

The mechanism of the *photolysis* of azo compounds was studied by relatively few researchers up to now. Porter et al.[11] postulated a stepwise mechanism based on their work with unsymmetrical compounds such as Ph-N=N-C(CH$_3$)$_2$Ph and Ph$_2$CH-N=N-CH$_2$Ph. Upon irradiation *trans*-1-(1,1-dimethylallylazo)alkanes of the type R-N=N-C(CH$_3$)$_2$CH=CH$_2$ with UV light (337 nm) evidence was obtained by Engel and Gerth[12] for the intermediacy of thermally labile cis-isomers. Diazenyl radicals were found to play "a more general role" in the decomposition of the cis isomers with R equal to phenyl, methyl, cyclohexyl, ethyl etc. In these cases the recombination of diazenyl and 1,1′-dimethylallyl radicals (occurring at the allylic site) was observed. However, with the symmetrical compound (R: H$_2$C=CHC(CH$_3$)$_2$) this turn-around reaction was not observed.

Rather recently, the photofragmentation of azomethane in the vapor phase was studied.[13] In this case, the fragmentation was complete within 2 ns and by coherent anti-Stokes Raman spectroscopy the nascent vibrational distribution appeared consistent with a theoretical prediction of stepwise bond scission.

The present paper describes results obtained upon the laser flash photolysis of α,α′-azocumenes in solution. These compounds were selected because, in spite of their UV band at 367 nm, they possess an absorption window between 270 and 340 nm. This enabled us to observe the absorption of transient species, i.e., 1-methyl-1-phenylethyl (α-cumyl, hereafter) and diazenyl radicals. As will be shown below

the photolysis of the α,α′-azocumenes occurred according to the stepwise mechanism.

Experimental

Materials. α,α′-Azocumene (AC) and 2,2′-di-*p*-tolyl-2,2′-azopropane (DMAC) were synthesized by a procedure described in the literature.[14] Cyclohexane of Uvasol(R) quality was obtained from E. Merck and was used without further purification.

Irradiations. Solutions of α,α′-azocumenes freed from oxygen by bubbling with purified argon were irradiated by 347 nm laser flashes of a ruby laser operated in conjunction with a frequency doubler. The flash duration was about 20 ns.

Actinometry was performed with benzene solutions of benzophenone (1.15×10^{-3} M†) containing naphthalene (1.03×10^{-1} M). The absorbed dose per flash was calculated from the concentration of naphthalene triplets formed by energy transfer from benzophenone with $\varepsilon_{T\text{-}T}=1.32\times10^{4}$ M^{-1} cm^{-1} at 425 nm[15] and $\phi(T)=1$. The maximum laser output was 4.5×10^{-4} Einstein per dm^3. The laser beam diameter was 0.6 cm at the sample position.

Results

Figure 1 shows transient absorption spectra with peaks at 272, 310, and 322 nm of a solution of AC in cyclohexane (4.7×10^{-3} M) photolyzed with an absorbed dose of 7.9×10^{-5} E l^{-1}.* These peaks were observed immediately at the end of the flash. The peaks at 272 and 322 nm grew-in further after the pulse. The three bands, which were also observed with DMAC in cyclohexane solution, are similar to those reported for benzyl,[16] *o*-, *m*-, *p*-methylbenzyl[17] and cumyl radicals.[18] They are, therefore, assigned to α-cumyl and 1-methyl-1-(*p*-tolyl)ethyl radicals, for AC and DMAC, respectively.

In addition to the absorption of α-cumyl radicals, a fast decaying transient absorption was observed in the region between 270 and 305 nm. The difference

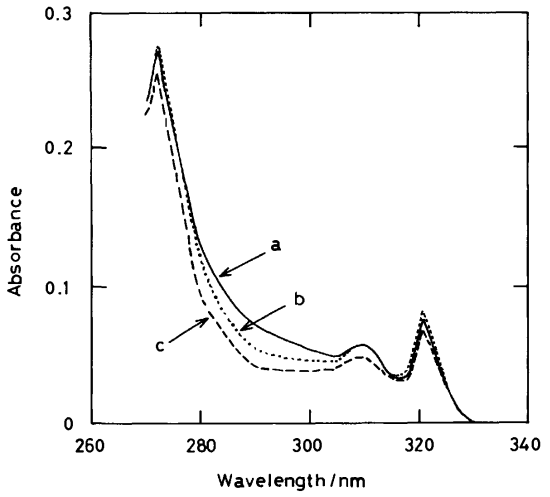

Fig. 1. Transient absorption spectra of 4.7×10^{-3} M α,α′-azocumene in cyclohexane recorded at the end of the flash (a), 8 μs (b), and 16 μs (c) later. $D_{abs}=7.9\times10^{-5}$ Einstein/l.

† 1 M=1 mol dm^{-3}, * l=dm^3.

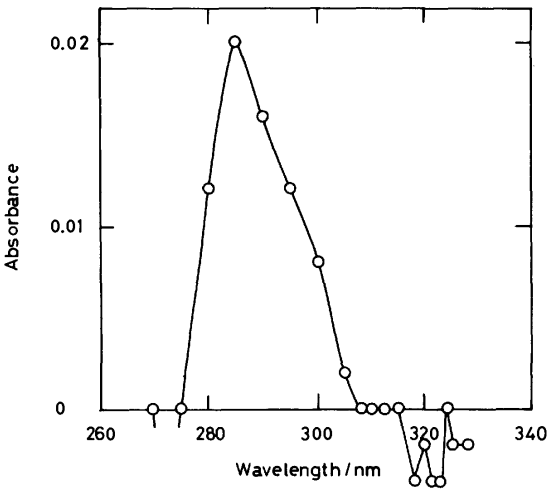

Fig. 2. Difference spectrum obtained by subtraction of spectrum (b) from spectrum (a) in Fig. 1.

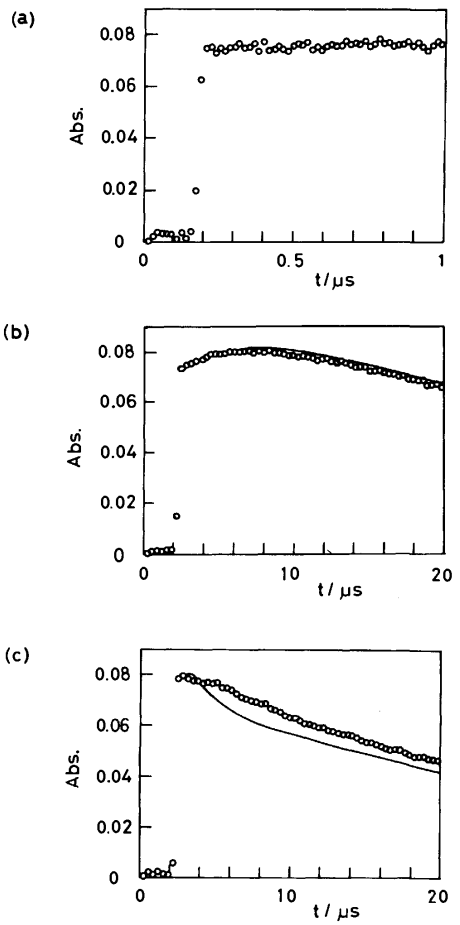

Fig. 3. Kinetic traces observed with 4.7×10^{-3} M α,α′-azocumene in cyclohexane (O), and simulated kinetic traces (—) at 322 (a) and (b), and 290 nm (c).

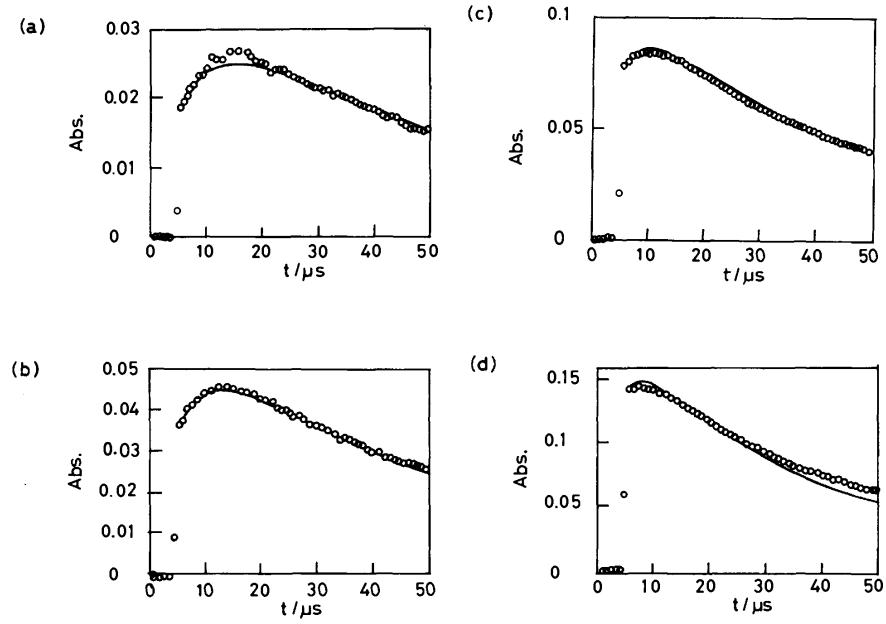

Fig. 4. Kinetic traces demonstrating changes in the 322 nm band observed with 4.7×10^{-3} M α,α'-azocumene in cyclohexane at absorbed doses of 2×10^{-5} (a), 3.7×10^{-5} (b), 8×10^{-5} (c), and 1.5×10^{-4} Einstein l^{-1} (d) (○).
Kinetic traces simulated with $\phi=0.36$ and $\varepsilon=4500\ M^{-1}\ cm^{-1}$ (—). Rate constants used are given in the text.

spectrum obtained by subtracting spectrum (b) from spectrum (a) in Fig. 1 is shown in Fig. 2. It has an absorption maximum at 285 nm.

Figure 3 shows kinetic traces recorded at 290 and 322 nm at an absorbed dose of 7.8×10^{-5} E l^{-1}. As can be seen from Fig. 3a, the absorption at 322 nm was formed to some extent during the flash. It increased further within about 5 μs and then decreased, as is shown in Fig. 3b. At 290 nm, on the other hand, the absorption formed during the flash decreased steadily after the flash.

Figure 4 shows kinetic traces obtained at 322 nm at various absorbed doses. It can be seen that with increasing absorbed dose the initial absorption increased while the extent of the grow-in absorption did not increase. Moreover, the grow-in rate depended significantly on the absorbed dose per flash. At $D_{absd}=2\times10^{-5}$ E l^{-1}, for example, the absorption increased until 10 μs but, at $D_{absd}=1.4\times10^{-4}$ E l^{-1}, only until 2 μs after the flash. The decay of the 322 nm band dose not fit first order or second order kinetics. However, the half lifetime slightly decreased with increasing absorbed dose, suggesting the occurrence of radical-radical reactions as will be dealt with in the next section. A similar kinetic behavior was observed with DMAC. In Fig. 5 the initial optical density (OD_0) and the maximum optical density (OD_{max}) at 322 nm were plotted against the absorbed dose per flash. Straight lines passing through the origin were obtained for OD_0 but not for OD_{max}. From the slope of the straight line (OD_0 vs. D_{absd}) the following $\phi\varepsilon$ values were

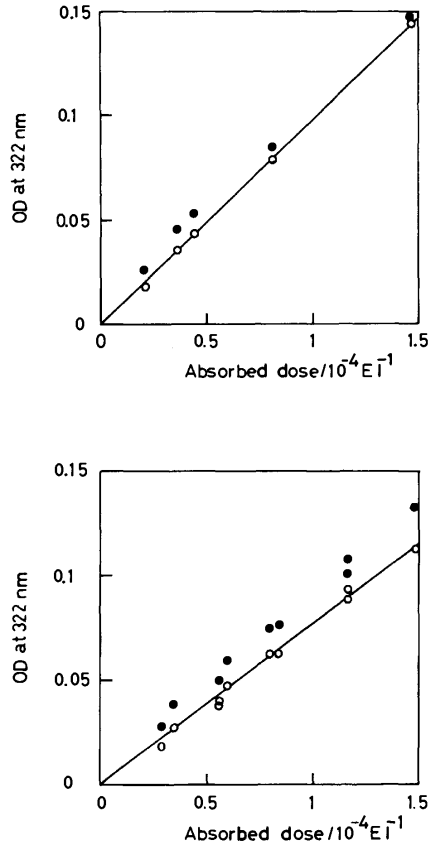

Fig. 5. Absorbed dose dependences of the initial (○) and the maximum (●) optical density observed at 322 nm.
(a) 4.7×10^{-3} M α,α'-azocumene in cyclohexane (b) 5.0×10^{-3} M 2,2'-di-*p*-tolyl-2,2'-azopropane in cyclohexane.

calculated for the α-cumyl radicals produced during the flash: 1630 and 1280 M^{-1} cm^{-1} for AC and DMAC, respectively.

Discussion

Engel and Steel have shown that the triplet-sensitized decomposition of AC (ϕ=0.31) occurs as efficient as the direct photolysis (0.36).[19] This fact suggests the intermediacy of the triplet AC in C-N bond scission.

For many azo compounds, it is well-known that the cis-isomers undergo remarkably facile thermal decomposition. *cis*-AC produced by UV irradiation of *trans*-AC in a poly(methyl methacrylate) matrix at −196 °C had a half lifetime of the order of 10 min at −100 °C,[20] while *trans*-AC has a lifetime of 20 min in toluene at 69 °C.[14] Thus, photoinduced trans-cis isomerization and the thermal instability of *cis*-AC suggest the intermediacy of *cis*-AC in decomposition. The present experimental results show that there exist two sources for α-cumyl radical production. On the basis of the fast mode of the α-cumyl radical formation that was completed during the laser pulse, it is assumed that both the triplet and the cis-isomer of α,α′-azocumene at room temperature have lifetimes much shorter than the laser pulse width of 20 ns.

The experimental results of the photolysis of α,α′-azocumenes in cyclohexane can be accounted for by the following equations:

$$\text{Ph-C(CH}_3)_2\text{-N=N-C(CH}_3)_2\text{-Ph} \longrightarrow \text{Ph-C(CH}_3)_2\text{-N=N}\cdot + \cdot\text{C(CH}_3)_2\text{-Ph} \quad (3)$$

$$\text{Ph-C(CH}_3)_2\text{-N=N}\cdot \longrightarrow \text{Ph-C(CH}_3)_2\cdot + \text{N}_2 \quad (4)$$

$$\text{Ph-C(CH}_3)_2\text{-N=N}\cdot + \text{Ph-C(CH}_3)_2\text{-N=N}\cdot \longrightarrow \text{Ph-C(CH}_3)_2\text{-N=N-N=N-C(CH}_3)_2\text{-Ph} \quad (5)$$

$$\text{Ph-C(CH}_3)_2\cdot \longrightarrow \text{product} \quad (6)$$

$$\text{Ph-C(CH}_3)_2\cdot + \text{Ph-C(CH}_3)_2\cdot \longrightarrow \text{product} \quad (7)$$

Figure 6 shows a plot of the ratio OD_{max}/OD_0 vs. the absorbed dose per flash which corresponds to the absorbed dose rate. It seems that both curves (obtained with AC and DMAC, respectively) are approaching the value of two on extrapolation of the absorbed dose rate to zero. At low absorbed dose rates the ratio of the concentrations of α-cumyl radicals formed by reaction 3, i.e., during the pulse, and reaction 4, i.e., after the pulse, is expected to be unity because the dimerization reaction 5 cannot compete with the unimolecular decomposition of diazenyl radicals according to reaction 4. This condition results in OD_{max}/OD_0=2. Reaction 6 stands for the reaction of α-cumyl radicals with intact α,α′-azocumene, the solvent and impurities.

To estimate the individual rate constants, a series of kinetic traces obtained within a wide range of absorbed doses (2×10^{-5}—1.5×10^{-4} E l^{-1}, see Fig. 4)

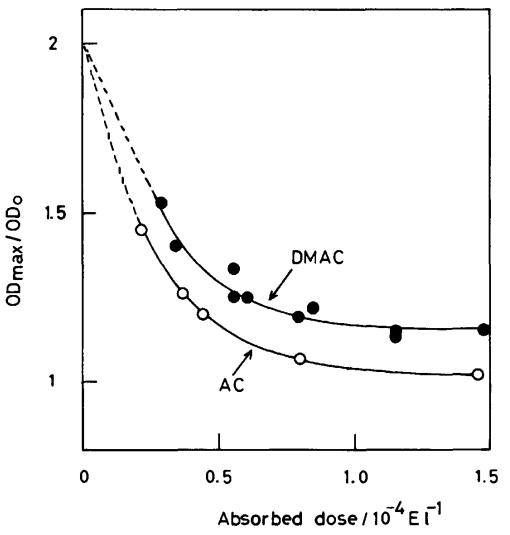

Fig. 6. Absorbed dose dependence of OD_{max}/OD_0 at 322 nm for α,α′-azocumene (○) and 2,2′-di-*p*-tolyl-2,2′-azopropane (●).

were simulated with the aid of a personal computer.

One can write equations for the rate of disappearance of the α-cumyldiazenyl radicals and the α-cumyl radicals:

$$-dA/dt = k_4A + 2k_5A^2 \quad (8)$$

$$-dB/dt = -k_4A + k_6B + 2k_7B^2 \quad (9)$$

where A and B represent the instantaneous concentrations of the α-cumyldiazenyl radicals and α-cumyl radicals respectively.

Equation 8 can be resolved to give[21]

$$\ln\{A_0(k_4+2k_5A)/A(k_4+2k_5A_0)\} = k_4t, \quad (10)$$

where A_0 is the initial concentration of the α-cumyldiazenyl radicals produced by reaction 3. Equation 10 may be rearranged to give

$$A = A_0k_4/\{(k_4+2k_5A_0)\exp(k_4t)-2k_5A_0\}. \quad (11)$$

By substituting this value for A into Eq. 9, we obtain

$$dB/dt = A_0k_4^2/\{(k_4+2k_5A_0)\exp(k_4t)-2k_5A_0\} - k_6B - 2k_7B^2. \quad (12)$$

This differential equation can be solved numerically by the Runge-Kutta method,[22] with the condition A_0=B_0 at t=0, where B_0 is the initial concentration of the α-cumyl radicals.

To estimate values of A_0 and B_0 one has to know the extinction coefficient of the α-cumyl radical at 322 nm. According to Nelsen and Bartlett[14] the quantum yield of the photodecomposition of α,α′-azocumene in benzene at 26.3 °C is 0.6. This rather high value very probably dose not only refer to scission of C-N bonds according to reactions 1 and 2 but also to other AC consuming reactions. For the

present case it appears more relevant to refer to the quantum yield of N_2 formation in order to estimate the quantum yield of α-cumyl radicals formed according to reactions 1 and 2. $\phi(N_2)=0.36$ has been determined by Engel and Steel[19] in the photolysis of AC in benzene. Dividing the slope of the straight line in Fig. 5a by 0.36 yields $\varepsilon(322\text{ nm})=4500\ M^{-1}\ cm^{-1}$ for AC. This extinction coefficient is quite similar to those obtained for *o*-, *m*-, *p*-methylbenzyl radicals which fall in the range 3000—6000.[17]

An iterative curve fitting procedure on the basis of Eq. 12 was applied to the experimental kinetic traces of Fig. 4. The solid lines in Fig. 4 are best fits obtained with the following rate constants: $k_4=1.1\times10^5\ s^{-1}$, $k_5=5\times10^9\ M^{-1}\ s^{-1}$, $k_6=1.65\times10^4\ s^{-1}$, and $k_7=1.8\times10^8\ M^{-1}\ s^{-1}$. With these rate constants the kinetic traces observed with DMAC in cyclohexane could also be reproduced. The unimolecular decay rate constant of the α-cumyldiazenyl radical k_4 can be compared with rate constants $(1.8—330)\times10^5\ s^{-1}$ obtained for substituted phenyldiazenyl radicals in water/*t*-butyl alcohol mixture.[23] The dimerization rate constant of the α-cumyldiazenyl radical is the same as that obtained for the phenyldiazenyl radical.[23]

The full line in Fig. 3 is the simulated kinetic trace representing the absorbances of both the α-cumyldiazenyl radical and the α-cumyl radical on the assumption that extinction coefficients at 290 nm are equal to 2000 and 2600 $M^{-1}\ cm^{-1}$, respectively. The difference between the experimental and the simulated curves might be explained on the basis of strongly absorbing products formed in the dimerization of α-cumyl radicals. According to Skinner et al.[24] the dimerization of α-cumyl radicals gives the following distribution of isomers: 1,2-diphenylethane:*o*-semibenzene:*p*-semibenzene=1:0.1:0.2.[24] The *p*-semibenzene is characterized by its strong UV absorption band peaked at 262 nm in cyclohexane and the extinction coefficient is estimated to be 25000—40000 $M^{-1}\ cm^{-1}$. From the spectrum of p-semibenzene the extinction coefficient at 290 nm can be estimated to be about 3500—6000 $M^{-1}\ cm^{-1}$.[24] Thus we can expect a contribution of about 10% of p-semibenzene to the transient absorption at 290 nm which compares well with the difference shown in Fig. 3c.

In conclusion, the present results clearly indicate the stepwise decomposition of α,α'-azocumenes on photolysis. This contrasts strongly the conclusion arrived at in the thermolysis studies,[6,7] where it is shown that on heating α,α'-azocumene is decomposed by a concerted process according to reaction 1. It can be conjectured that upon UV irradiation an electronically excited repulsive state is produced resulting in the occurrence of rapid fragmentation. This problem could probably be solved by a highly time-resolved flash photolysis technique.

The authors are grateful to Dr. G. Beck for maintaining the flash photolysis set-up and to Dr. J. Lilie for assisting in the computer evaluation of the data. M. K. and Y. K. wish to express their sincere appreciation to Professor Shun-ichi Nozakura, Osaka University, for his encouragement.

References

1) G. Odian, "Principle of Polymerization," 2nd ed, John-Wiley, New York (1981), p. 194.
2) C. Rüchardt, *Angew. Chem., Int. Ed. Engl.*, **9**, 830 (1970).
3) S. W. Benson and H. E. O'Neal, Nat. Stand. Ref. Data Ser., Nat. Bur. Stand., No. 21, 31 (1970).
4) P. S. Engel, *Chem. Rev.*, **80**, 99 (1980).
5) S. Seltzer, *J. Am. Chem. Soc.*, **83**, 2625 (1961); **85**, 14 (1963).
6) R. C. Neuman, Jr. and M. J. Amrich, Jr., *J. Org. Chem.*, **45**, 4629 (1980).
7) W. A. Pryor and K. Smith, *J. Am. Chem. Soc.*, **92**, 5403 (1970).
8) D. K. White and F. D. Greene, *J. Am. Chem. Soc.*, **100**, 6760 (1978).
9) R. C. Neuman, Jr. and G. A. Binegar, *J. Am. Chem. Soc.*, **105**, 134 (1983).
10) J. J. Dannenberg and D. Rocklin, *J. Org. Chem.*, **47**, 4529 (1982).
11) N. A. Porter, L. J. Marnett, C. H. Lochmüller, G. L. Closs, and M. Shobataki, *J. Am. Chem. Soc.*, **94**, 3664 (1972).
12) P. S. Engel and D. B. Gerth, *J. Am. Chem. Soc.*, **105**, 6849 (1983).
13) P. L. Holt, K. E. McCurdy, J. S. Adams, K. A. Burton, R. B. Weisman, and P. S. Engel, *J. Am. Chem. Soc.*, **107**, 2180 (1985).
14) S. F. Nelsen and P. D. Bartlett, *J. Am. Chem. Soc.*, **88**, 137 (1966).
15) R. Bensasson and E. J. Land, *Trans. Faraday Soc.*, **67**, 1904 (1971).
16) A. Habersbergerová, I. Janovský, and J. Teplý, *Radiat. Res. Rev.*, **1**, 109 (1968).
17) K. Sehested, H. Corfitzen, H. C. Christensen, and E. J. Hart, *J. Phys, Chem.*, **79**, 310 (1975).
18) K. Sehested and J. Holcman, *Nukleonika*, **24**, 942 (1979).
19) P. S. Engel and C. Steel, *Acc. Chem. Res.*, **6**, 275 (1973).
20) P. S. Engel and D. J. Bishop, *J. Am. Chem. Soc.*, **97**, 6754 (1975).
21) S. W. Benson, "The Foundations of Chemical Kinetics," McGraw-Hill, Book Company, Inc. (1960), p. 32.
22) H. Margenau and G. M. Murphy, "The Mathematics of Physics and Chemistry," 2nd ed., D. Van Nostrand Company, Inc., Princeton, New Jersey (1956), Chap, 13.
23) O. Brede, R. Mehnert, W. Naumann, and H. G. O. Becker, *Ber. Bunsenges. Phys. Chem.*, **84**, 666 (1980).
24) K. J. Skinner, H. S. Hochster, and J. M. McBride, *J. Am. Chem. Soc.*, **96**, 4301 (1974).

The Pulse-Photoconductivity of Poly(1-vinylpyrene)

Akira ITAYA* and Ken-ichi OKAMOTO
Department of Chemical Engineering, Faculty of Engineering, Yamaguchi University, Tokiwadai, Ube 755
(Received July 7, 1986)

The migration of electronic excitation energy, the steady-state photoconductivity, the hole-drift mobility and the carrier-photogeneration efficiency of holes in poly(1-vinylpyrene)(PVPy) films were investigated and compared with those in poly(*N*-vinylcarbazole)(PVCz) films. Although the concentration of the excimer-forming sites in PVPy films was about twenty times as large as that in PVCz films, the magnitude of the steady-state photoconductivity of PVPy was comparable to that of PVCz. The hole mobility in PVPy films was about one-half as large as that in PVCz films. The electric field and temperature dependence of the mobility fit Gill's empirical equation. The carrier-photogeneration efficiency, ϕ, of PVPy was larger than that of PVCz. The filed dependence of ϕ of PVPy for all the excitation bands was in good agreement with the Onsager theory of geminate recombination. The high photoconductivity of PVPy could be explained on the basis of these results.

A number of papers have appeared in the literature concerning carrier-photogeneration and charge transport in both aromatic vinyl polymers and molecularly-doped polymers from theoretical and practical standpoints.[1] It has been revealed that the concentration of excimer-forming sites is one of the important factors determining the magnitude of the photoconductivity; that is, the excimer-forming sites act as traps of both singlet excitation energy and hole carriers.[2,3]

Considerable data on the photoconductivity of poly(*N*-vinylcarbazole)(PVCz) have been accumulated because of an interest in highly photoconductive polymers.[4,5] *N*-Ethylcarbazole, which is a monomeric model compound of PVCz, shows no excimer fluorescence in either concentrated fluid solutions or the solid state[6] and is a typical compound which forms no excimer. On the other hand, 1-ethylpyrene shows an excimer fluorescence in concentrated fluid solutions and is a typical compound which forms an excimer. Poly(1-vinylpyrene) (PVPy) almost exclusively shows the excimer fluorescence in dilute solutions[7,8] and is, therefore, expected to have a high concentration of the excimer-forming sites in solid films.

In the present paper, the pulse photoconductivity of PVPy has been investigated in comparison with that of PVCz, poly(5-vinylbenzo[*b*]carbazole) (P5VBCz) and poly(7-vinylbenzo[*c*]carbazole) (P7VBCz).

Experimental

The PVPy was prepared by the polymerization of a 0.15 M†† toluene solution of purified 1-vinylpyrene in the presence of 2 mol% $BF_3 \cdot OEt_2$ under a nitrogen atmosphere at −35 °C for 1 h and was purified by reprecipitation from a tetrahydrofuran solution with methanol two times. The sample was stored in tubes within an argon atmosphere in the dark. Films were cast on NESA-coated conductive quartz plates from a chloroform solution containing 0.5% ethanol and were dried in vacuo. A semitransparent gold electrode with a typical area of 1 cm^2 was evaporated on a film to prepare a sandwich-type cell. Polymer-film thickness was determined from the weight and density (1.22 g cm^{-3}) of a film with a certain known area and/or by a capacitive method. The dielectric constant, ε, of the films was determined to be 3.28 from capacitance measurements at the frequency of 1 KHz at 298 K.

The fluorescence spectra and the steady-state photocurrent were measured with the apparatus described in a previous paper.[9,10]

The drift mobility and the carrier-photogeneration efficiency of holes were measured with the apparatus described in a previous paper by means of a conventional time-of-flight method in a vacuum of 2.6×10^{-3} Pa.[4,5] A 3 μs light pulse from an air-gap flash was irradiated onto a sample through appropriate narrow band-pass filters. The precautions described in a previous paper were taken in all the procedures in order to obtain reproducible results.[4]

Results and Discussion

Concentration of Excimer-Forming Sites. The fluorescence spectrum of PVPy films is composed of only one component and is assigned to the excimer fluorescence.[7,8] In PVPy films doped with dimethyl terephthalate (DMTP), where a long-range single-step energy transfer is impossible, the host fluorescence is significantly quenched (Fig. 1). The application of a random-hopping model of monomer-exciton migration to the quenching process of the host-sensitized energy transfer gives the concentration of trap sites (excimer-forming sites and non-fluorescent trap sites) for the singlet exciton migration.[2,11] The concentration of the trap sites in PVPy films was dependent on the excitation wavelength used in the quenching experiment and was 8.6×10^{-2} and 4.9×10^{-2} mol mol^{-1} basic unit for the 345 and 379 nm excitation,

* Present address: Department of Polymer Science and Engineering, Kyoto Institute of Technology, Matsugasaki, Kyoto 606.

†† 1 M=1 mol dm^{-3}.

respectively.

It has been reported that the process of photooxidation of PVCz films proceeds near the surface of films.[4,12] The absorption coefficient of 345 nm in the ^1L_a band (1.9×10^5 cm^{-1}) of PVPy films is about twenty times as large as that of 379 nm in the ^1L_b band (7.8×10^3 cm^{-1}) and 90% of the exciting light of 345 and 379 nm was absorbed within layers of less than 0.12 and 3.0 μm in depth, respectively. Therefore, the higher concentration of trap site obtained for the 345 nm excitation may be attributable to a high concentration of nonfluorescent photooxidation products. If the concentration of excimer-forming sites in PVPy films is taken to be 4.9×10^{-2} mol mol^{-1} basic unit, it is about twenty times as large as the value for PVCz films (2.7×10^{-3} mol mol^{-1} basic unit).[11]

Steady-State Photocurrent. Photocurrents with positive and negative electrode illumination of PVPy films (abbreviated to i_{ph}^+ and i_{ph}^-, respectively) showed a superlinearity on applied voltage in fields higher than ca. 70 and 130 kV cm^{-1}, respectively, although they were proportional to the applied voltage in the lower field. This field dependence of i_{ph}^+ is quite similar to that of PVCz.[13] Both i_{ph}^+ and i_{ph}^- of PVPy were always proportional to the light intensity (10^{11}—10^{13} photons cm^{-2} s^{-1}) in every wavelength region over the whole range of the applied voltage. The spectral dependence of the photocurrent (Fig. 2) was obtained by normalizing the observed photocurrent values to the values for a constant light intensity of 1×10^{13} photons cm^{-2} s^{-1}, according to the light-intensity dependence. This spectral dependence of i_{ph}^+ corresponds symbatically to the absorption spectrum, but that of i_{ph}^- does antibatically to the spectrum. This behavior of PVPy is also quite similar to that of PVCz in the field higher than 10^4 V cm^{-1}.[13] The magnitude of i_{ph}^+ is larger than that of i_{ph}^- in the UV wavelength region shorter than 385 nm (the absorption edge of the thick film), although they are nearly equal to each other in the wavelength region longer than 385 nm. The magnitude of both i_{ph}^- and i_{ph}^+ of PVPy was almost the same as that of PVCz.[13] Considering the difference in the concentration of excimer-forming sites between PVPy and PVCz, this result is noteworthy.

Hole-Drift Mobility. A transient photoresponse was detected for the positive electrode illumination and was attributed to hole transport. In the transient-response curve, a shoulder corresponding to a transit time (t_r) was observed above about 338 K. When no shoulder of the transient response curve was observed, the transit time (t_r*) was determined from the bilogarithmic plots, based on the theory of Scher and Montroll.[14] The hole-drift mobilities calculated from t_r and t_r* were abbreviated as μ_p and μ_p*, respectively.

Figure 3 shows the absorption spectrum of a PVPy thin film and the transmittance of the band-pass filters used. The hole-drift mobility was independent of the excitation bands of ^1L_a, ^1B_b, and ^1B_a. The results mentioned below concerning the hole mobility were obtained by the excitation of the ^1L_a absorption band.

Figure 4 shows the electric field dependence of the hole mobility of PVPy at 338 K. The results for PVCz, P5VBCz, and P7VBCz samples are also shown for the sake of a comparison. The straight lines in plots of log μ against the square root of the electric field show that the Poole-Frenkel type relation holds for these polymers. At 338 K and 9×10^4 V cm^{-1}, the hole mobility of PVPy was about one-half as large as that of PVCz and was larger than those of P5VBCz and P7VBCz. The monomeric model compounds of

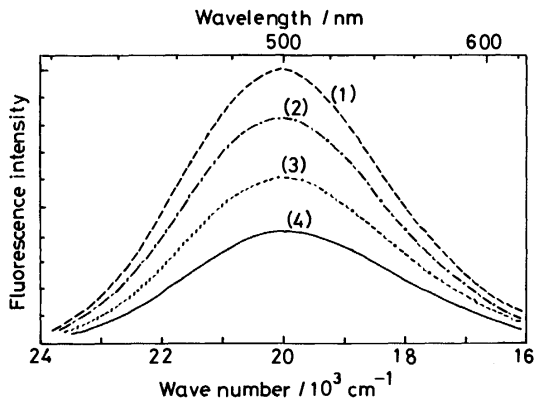

Fig. 1. Fluorescence spectra of PVPy films doped with DMTP at room temperature. DMTP concentration; (1): 0, (2): 1.20×10^{-2}, (3): 3.00×10^{-2}, (4): 7.50×10^{-2} (mol/VPy unit mol). Excitation wavelength; 379 nm.

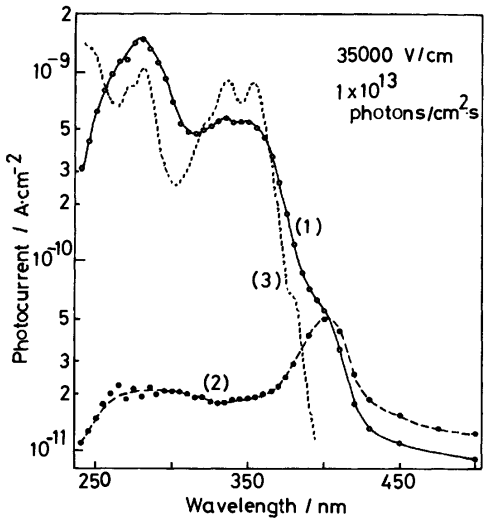

Fig. 2. Spectral dependence of steady-state photocurrent of PVPy in a high vacuum under 35000 V cm^{-1} at room temperature (1) i_{ph}^+ (2) i_{ph}^-. Absorption spectrum of PVPy films is shown by curve (3).

P5VBCz and P7VBCz also show no excimer fluorescence in concentrated solutions[15] and, therefore, these polymers are expected to have a low concentration of excimer-forming sites in films as well as PVCz. Therefore, the magnitude of the hole mobility is not simply related to the concentration of excimer-forming sites.

Figure 5 shows the temperature dependence of the hole mobility of PVPy and PVCz under various electric fields. The electric field dependence of the activation energies, ΔE_a, of PVPy, PVCz, P5VBCz, and P7VBCz is shown in Fig. 6. These figures indicate that the hole mobility of PVPy also follows Gill's empirical equation,[16] as is the case with carbazolyl- and benzocarbazolyl-pendant polymers:[5,16,17]

$$\mu_p = \mu_0 \exp\{-(\Delta E_0 - \beta\sqrt{E})/kT_{eff}\} \quad (1)$$

$$1/T_{eff} = 1/T - 1/T_0 \quad (2)$$

where k is the Boltzmann constant; E, the electric field; T, the film temperature, and μ_0, ΔE_0, T_0, and β; the characteristic parameters. The values of the parameters obtained are listed in Table 1. Remarkable differences in parameter values between PVPy and PVCz were found in μ_0 and T_0. The T_0 value of PVPy

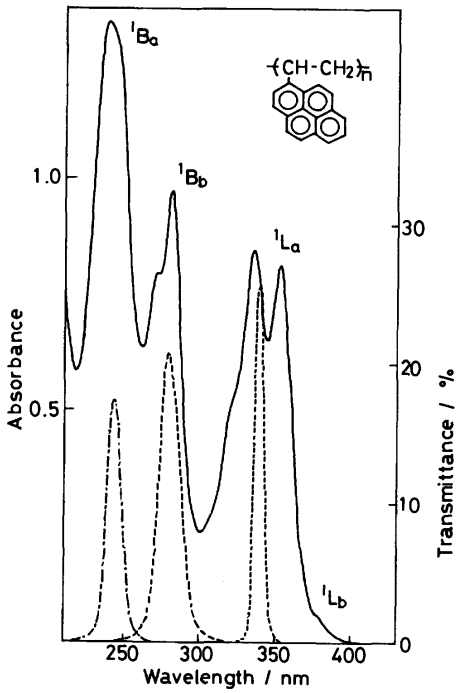

Fig. 3. Absorption spectrum of a PVPy film (1) and transmittance of band pass filters ((2)—(4)).

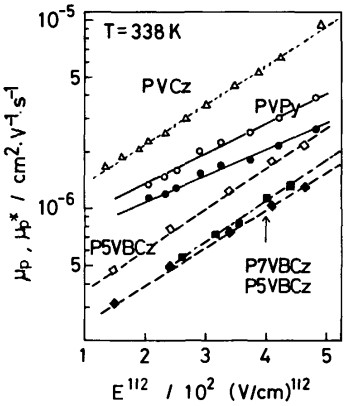

Fig. 4. Field dependence of the hole drift mobility at 338 K.

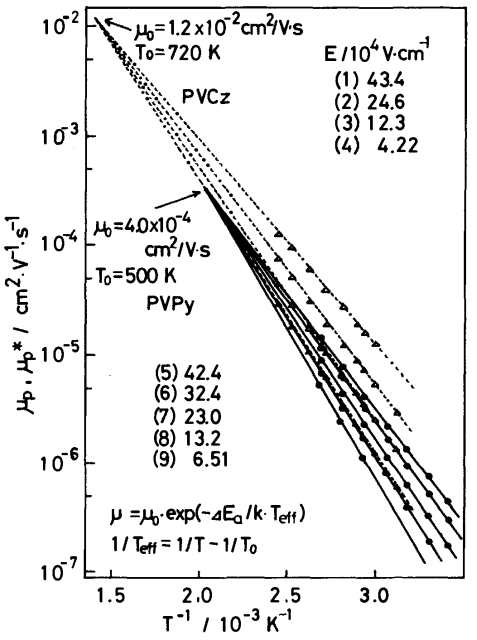

Fig. 5. Dependence of the hole drift mobility on temperature with electric field as a parameter.

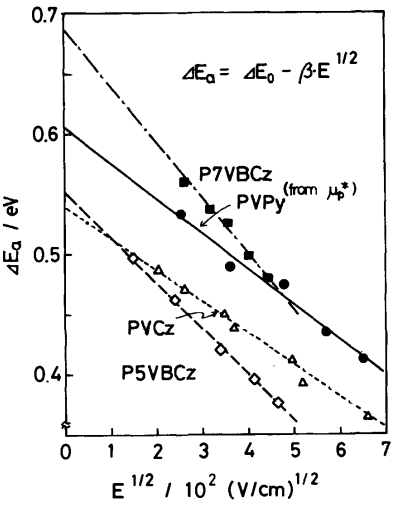

Fig. 6. Dependence of the activation energy $\Delta E_a (= \Delta E_0 - \beta\sqrt{E})$ on the electric field.

Table 1. Transport Parameters[a] and Glass Transition Temperature, T_g

Sample	μ_0 10^{-3} cm²/V·s	T_0 K	E_0 eV	β 10^{-4} eV/$\sqrt{V/cm}$	T_g K
PVPy	* 0.40	500	0.61	3.0	504
PVCz	* 8.5	730	0.53	2.6	501
P5VBCz	* 0.14	530	0.54	3.4	>544
P7VBCz	* 0.21	490	0.69	4.7	544
PVCz	15	725	0.54	2.6	501
P5VBCz	0.23	530	0.55	3.9	>544

a) *: Values were determined from μ_p*.

was much lower than that of PVCz and close to those of the benzocarbazolyl-pendant polymers. It has been suggested that T_0 is related to the freezing-in temperature of the micro motion of chromophores themselves acting as hopping sites; their micro motion destroys some structural traps preventing the hole transport and promotes the transport and that T_0 is the transition temperature from the glassy state to the supercooled liquid state in the hole-transport phenomena.[5,18] The pyrenyl chromophores connected to a skeletal chain at the 1-position have unsymmetric molecular structure, being different from carbazolyl chromophores connected to skeletal chain at the 9-position. Therefore, the packing between chromophores in PVPy may be loose as compared with chromophores in PVCz and the pyrenyl chromophores may tend to move to destroy the structual traps at lower temperatures.

The μ_0 value of PVPy was much smaller than that of PVCz by a factor of ca. 20 and close to those of the benzocarbazolyl-pendant polymers. It has been reported that the μ_0 value is related to a molecular interaction between chromophores[16] and is close to the value of the trap-free drift mobility.[19,20] Although a sample with a high value of T_0 tends to have a high value of μ_0, it is noted that the μ_0 value of PVCz is extremely high among the aromatic vinyl polymers investigated. Therefore, PVCz is considered to be a special case and the molecular interaction between carbazolyl chromophores in PVCz is considered to be very strong with regard to hole transport.

The value of the exponential term related to the temperature in Eq. 1 is larger for PVPy than for PVCz. However, the μ_0 value is much lower for PVPy than for PVCz. Consequently, the mobility of PVPy is one-half as large as that of PVCz. Although the concentration of excimer-forming sites in PVPy films is about twenty times as large as that in PVCz films, the difference in the mobility between PVPy and PVCz is small. This is considered to be attributed to the low T_0 value caused by the loose packing between chromophores in PVPy.

Carrier-Photogeneration Efficiency. In order to excite the ^1L_a, ^1B_b, and ^1B_a absorption bands, narrow band-pass filters of 340, 280, and 240 nm were used, respectively (Fig. 3). Figure 7 shows the field dependence of the carrier-photogeneration efficiency, ϕ, of PVPy for the various excitation bands, including that of PVCz for the sake of comparisons. The ϕ increases in the order of the ^1L_a, ^1B_b, and ^1B_a bands, as is the case of PVCz.

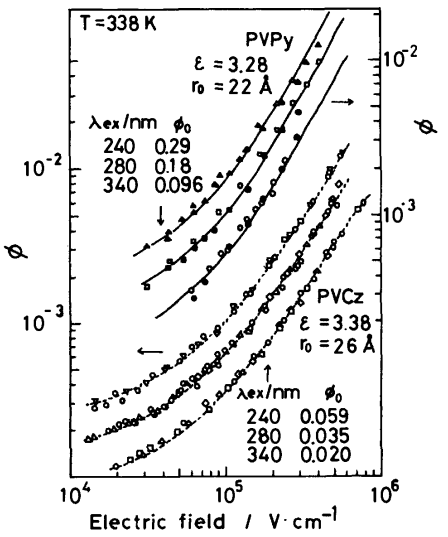

Fig. 7. Field dependence of the carrier-photogeneration efficiency in PVPy and PVCz films for various excitation bands. The solid lines were calculated from Eq. 3 with r_0 and ϕ_0 values presented in the figure.

The ϕ is given as the product of a primary yield, ϕ_0, of a bound electron-hole pair with an interionic separation of r_0 and the dissociation probability, P(E):[4]

$$\phi = \phi_0 \cdot P(E). \quad (3)$$

The P(E) is given by the Onsager theory[21] as the function of r_0. The solid lines in Fig. 7 were calculated from Eq. 3 with r_0 of 22 Å and with ϕ_0 of 0.096, 0.18, and 0.29 for the ^1L_a, ^1B_b, and ^1B_a bands, respectively. They are in good agreement with the experimental data. The carrier-photogeneration efficiency of PVCz fit also the Onsager theory with both ϕ_0 values increasing from 0.02 to 0.059 and a constant r_0 value of 26 Å.[4] Therefore, the carrier-photogeneration mechanism of PVPy is considered to be the same as that of PVCz.[4,11] That is, the extrinsic carrier-photogeneration via nonrelaxed exciplexes formed between singlet excitons and acceptor-like impurities or photooxidation products is also predominant in PVPy films for all the excitation bands.

The ϕ_0 values of PVPy are about five times as large as those of PVCz, although the concentration of excimer-forming sites of PVPy is higher than that of PVCz. This indicates that the concentration of acceptor-like impurities and/or photooxidation products is much higher for PVPy than for PVCz under these experimental conditions. Judging from that the

excimer-forming site is susceptible to photooxidation[12] and also that a PVPy film has a fairly low ionization potential (7.13 eV), concentration of photooxidation products in a PVPy film seems to be higher than that in a PVCz film. It has been reported for PVCz that the ϕ_0 value is higher for the excitation band having higher absorption coefficient,[4] because the concentration of photooxidation products becomes higher on going from the bulk to the surface. The similar concentration profile of the photooxidation products is also held in PVPy films, as indicated by the above-mentioned results of the singlet energy migration. The absorption coefficient of the ^1L_a band of PVPy (2.4×10^5 cm^{-1}) is larger than those of the ^1L_b and ^1L_a bands of PVCz (5×10^4 cm^{-1} and 1.5×10^5 cm^{-1}, respectively). Therefore, the large ϕ_0 value of PVPy is attributed to both the excitation of the film surface including photooxidation products in very high concentrations and the low ionization potential of a PVPy film.

In conclusion, the carrier-photogeneration efficiency of PVPy is twice as large as that of PVCz. On the other hand, the hole-drift mobility of PVPy is one-half as large as that of PVCz. Consequently, there is no significant difference in the steady-state photocurrent between PVPy and PVCz.

The cost of the present investigation was partly defrayed by the Grant-in-Aid from the Japanese Ministry of Education, Science, and Culture to AI(60550627). KO wishes to acknowledge the financial support of the Mita Kogyo Co. Ltd., for this work.

References

1) J. Mort and G. Pfister, "Electronic Properties of Polymers," ed by J. Mort and G. Pfister, Wiley-Interscience, New York (1982), Chap. 6.

2) W. Klöpffer, *J. Chem. Phys.*, **50**, 2337 (1969).

3) M. Yokoyama, K. Akiyama, N. Yamamori, H. Mikawa, and S. Kusabayashi, *Polymer J.*, **17**, 545 (1985).

4) K. Okamoto and A. Itaya, *Bull. Chem. Soc. Jpn.*, **57**, 1626 (1984) and references cited therein.

5) A. Itaya, K. Okamoto, and S. Kusabayashi, *Polymer J.*, **17**, 557 (1985) and references cited therein.

6) M. Yokoyama, T. Tamamura, M. Atsumi, M. Yoshimura, Y. Shirota, and H. Mikawa, *Macromolecules*, **8**, 101 (1975).

7) M. Yokoyama, T. Tamamura, T. Nakano, and H. Mikawa, *Chem. Lett.*, **1972**, 499.

8) J. R. McDonald, W. E. Echols, T. R. Price and R. B. Fox, *J. Chem. Phys.*, **57**, 1746 (1972).

9) A. Itaya, K. Okamoto, and S. Kusabayashi, *Bull. Chem. Soc. Jpn.*, **49**, 2082 (1976).

10) K. Okamoto, A. Itaya, and S. Kusabayashi, *Polymer J.*, **7**, 622 (1975).

11) A. Itaya, K. Okamoto, and S. Kusabayashi, *Bll. Chem. Soc. Jpn.*, **50**, 22 (1977).

12) A. Itaya, K. Okamoto, and S. Kusabayashi, *Bull. Chem. Soc. Jpn.*, **52**, 2218 (1979).

13) K. Okamoto, S. Kusabayashi, and H. Mikawa, *Bull. Chem. Soc. Jpn.*, **46**, 2324 (1973).

14) H. Scher and E. W. Montroll, *Phys. Rev. B*, **12**, 2455 (1975).

15) A. Itaya, K. Okamoto, and S. Kusabayashi, *Bull. Chem. Soc. Jpn.*, **51**, 79 (1978).

16) W. D. Gill, *J. Appl. Phys.*, **43**, 5033 (1972).

17) A. Itaya, K. Okamoto, and S. Kusabayashi, *Bull. Chem. Soc. Jpn.*, **58**, 2078 (1985).

18) M. Fujino, Y. Kanayama, H. Mikawa, S. Kusabayashi and M. Yokoyama, *Solid State Commun.*, **49**, 575 (1984).

19) B. Reimer and H. Bässler, Phys. *Status. Solidi A*, **51**, 445 (1979).

20) M. Fujino, H. Mikawa, and M. Yokoyama, *Photogr. Sci. Eng.*, **26**, 84 (1982).

21) L. Onsager, *J. Chem. Phys.*, **2**, 599 (1934); *Phys. Rev.* **54**, 554 (1938).

 © 1987 The Chemical Society of Japan Bull. Chem. Soc. Jpn., 60, 89—94 (1987)

Effects of Surfactants and Surface Treatment on Aqueous Dispersion of Silicon Carbide

Kenjiro MEGURO, Takahisa USHIDA, Tetsuya HIRAOKA, and Kunio ESUMI*
Department of Applied Chemistry and Institute of Colloid and Interface Science, Science University of Tokyo, Kagurazaka, Shinjuku-ku, Tokyo 162
(Received July 9, 1986)

The effects of the addition of surfactants and of the surface treatment upon the aqueous dispersion of silicon carbide were examined. In the case of β-SiC, the addition of nonionic surfactants having relatively longer lengths of hydrocarbon and oxyethylene chain to the β-SiC treated with a silane coupling agent enhanced the dispersion stability. On the other hand, the lack of a difference for the dispersion stability was observed between a silane coupling treated α-SiC and an untreated one by the addition of surfactants. These differences in the surface property of two kinds of SiC were confirmed by measuring the zeta potential and the heat of immersion in water.

In recent years particle-reinforced composites have become attractive for many fields because of their excellent properties. Particularly, interest in electrodeposited composite coatings has increased rapidly. The purposes for composite plating are improved abrasion resistance, friction resistance, corrosion resistance, functional plating and so on. The detailed properties and applications of such plating have been reported.[1-5] From many studies, it has been confirmed[6,7] that agitation and current density are two major factors that affect the rate of entrapment of electrodeposite composite plating.

Besides, it is important to disperse the component particles in the plating solution in order to obtain a homogeneous surface of composite plating. The dispersion of solid particles in an aqueous solution is often considerably influenced by the addition of a small amount of water-soluble substances. The dispersion effect by nonionic ethoxylated surfactants[8-10] is dependent on their chemical structure and on the kind of particles to be dispersed. Since nonionic ethoxylated surfactants have both hydrophilic and hydrophobic parts, it is expected that their adsorption behavior will be affected not only by their affinity to solids, but also by the affinity to the medium in the suspensions. It is also suggested that the adsorption of nonionic surfactants is strong when either the particle or medium is polar and the other is nonpolar.

In this study, interactions between treated silicon carbide with a silane coupling agent or an untreated one and nonionic surfactants in an aqueous solution of high concentration of electrolytes were investigated by measuring the zeta-potential, the particle size, the turbidity and the heat of immersion from the standpoint of basic electrodeposited composite plating.

Experimental

Materials. α-SiC was provided from Showa Denkou Co., Ltd., and β-SiC from Ibiden Co., Ltd.

The physical properties of silicon carbides are as follows: a density of 3.2 g cm^{-3} and a specific surface area of 9.5 m^2 g^{-1} for α-SiC and 3.2, 17.0 for β-SiC,

The nonionic surfactants were obtained from Nikko Chemical Co., Ltd.; their types and structural formula are

$C_{16}H_{33}$-O-$(CH_2CH_2O)_n$H (BC-*n*),
$C_{22}H_{45}$-O-$(CH_2CH_2O)_n$H (BB-*n*),
$C_{18}H_{35}$-O-$(CH_2CH_2O)_n$H (BO-*n*), and
$C_{18}H_{37}$-CO-O-$(CH_2CH_2O)_n$H (MYS-*n*),

where *n* indicates the mole number of oxyethylene units included in the surfactant.

Sodium dodecyl sulfate was provided from Wako Pure Chemical Industrial Ltd. and purified by recrystallization from ethanol.

Sodium chloride, calcium chloride and aluminum chloride were of commercial high pure grade reagents.

A nickel sulfamate aqueous solution was used as the plating solution. It was provided by the Electroplating Engineers of Japan Ltd.

The treatment of silicon carbide was carried out with a 5 w% solution of trimethylchlorosilane (TMCS), provided by Chisso Co., Ltd., in isopropyl alcohol by stirring for 2 h. After the treatment, the silicon carbide was washed five times with pure isopropyl alcohol. Then, the treated powder was dried for 2 h at 140 °C.

The water used in all experiments was purified by passing it through an ion-exchanged column followed by filtration in a Milli-Q Water Purification System.

Apparatus and Procedure. 0.5 g of silicon carbide was added to a nonionic surfactant solution (1 L) with a high electrolyte concentration and agitated with an ultrasonic bath for 10 min. Then, after shaking for 1 h at 25 °C, the absorbance of the suspension was recorded every 5 min during 1 h at 500 nm by means of a Hitachi 220-A-type double-beam spectrophotometer using 0.2-cm cells at 25 °C.

The stability of the suspension can be expressed as

$$[O.D]_t/[O.D]_5,$$

where $[O.D]_5$ is the absorbance after 5 min and $[O.D]_t$ is the absorbance after *t* minutes.

The heat of immersion in water for these samples was measured using a calorimeter (Tokyo Rikou Co., Ltd.) at 25 °C: after silicon carbide was placed into a glass ample tube and evacuated at 1×10^{-2} Torr for 1 h, the glass ample tube was sealed and set in a calorimeter with water, until it reached thermal equilibrium at 25 °C. Then, the glass

ample tube was broken and the silicon carbide was immersed in water. The liberated heat was recorded and calibrated by the normal procedure.

The zeta-potential of silicon carbide was measured by an electrophoresis apparatus Laser Zee TM Model 500 (PEN KEM, Inc.). The mean particle size was measured by a particle sizer (Malvern Co., Ltd.).

The pH of the silicon carbide suspension was measured using a pH meter 130 (Corning Co., Ltd.).

The surface of silicon carbide was measured by FTIR-ATR (Japan Spectroscopic Co. Ltd.).

Results and Discussion

1. Dispersion of Silicon Carbide in Aqueous Solution. Variations in the zeta-potential of α-SiC and β-SiC as a function of pH are given in Fig. 1. The silicon carbide particles had a positive charge at a low pH; their charges became negative with an increase in the pH. The isoelectric point of α-SiC was found to be in the vicinity of pH 2.3, and of β-SiC in the vicinity of pH 5. The pH of dispersion (0.5 g L^{-1}) of α-SiC and β-SiC in pure water was 5.6, at which the zeta potential of α-SiC was about -30 mV, and of β-SiC was about -7 mV, and their mean particle sizes were about 470 and 7300 nm, respectively.

Variations in the zeta-potential of silicon carbide with the concentration of each electrolyte solution are given in Fig. 2. The zeta-potential of silicon carbide in aqueous solution was altered from negative to zero by the addition of an electrolyte. By a further addition of the electrolyte, the charge of the particles became positive. In the case of aluminum chloride, upon a further addition, the charge of the particles again became zero.

On the other hand, the zeta-potential became high with the valency of cationic ions. Accordingly, the isoelectric point (i.e.p.) of silicon carbide was remarkably shifted to the low concentration with an increase in the valency of cationic ions.

It was found that both α-SiC and β-SiC had the highest positive charge by the addition of 1×10^{-4} M† $AlCl_3$. At this concentration, the absorbance of dispersion of α-SiC was initially 0.73, but greatly decreased to 0.01 after 24 h, while that of β-SiC gradually decreased from 1.45 to 0.85.

Variations in the zeta-potential of α-SiC and β-SiC

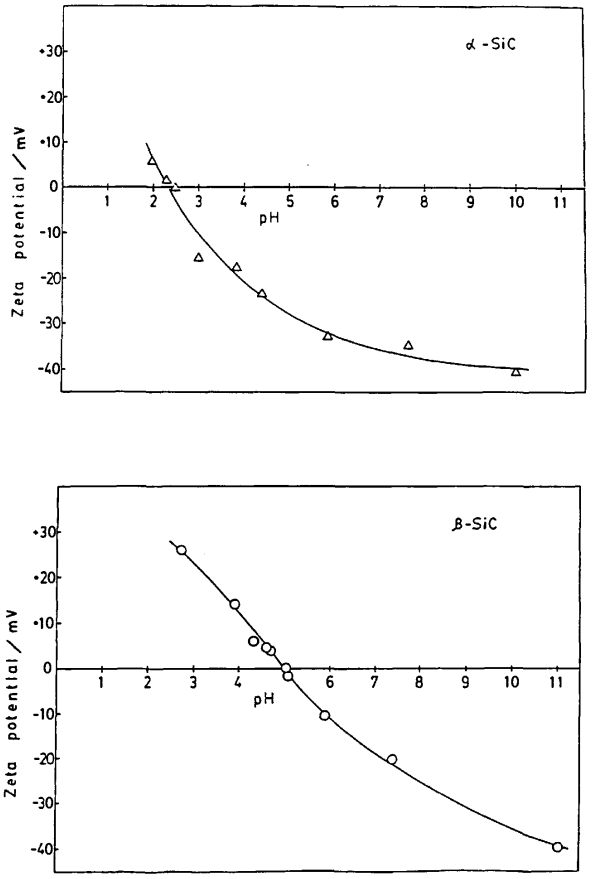

Fig. 1. Variation in zeta potential of silicon carbide as a function of pH.

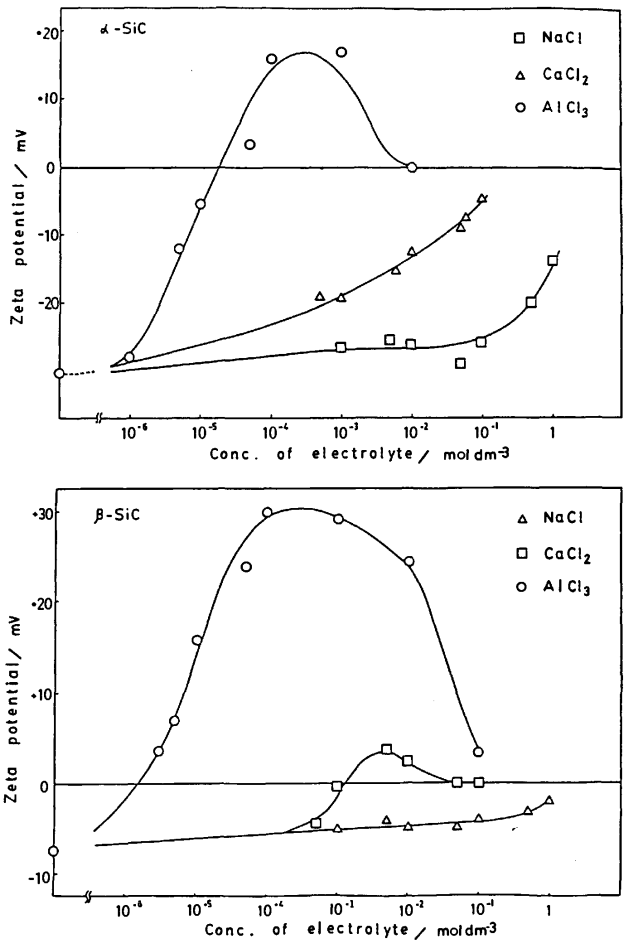

Fig. 2. Variation in zeta potential of silicon carbide with concentration of electrolyte.

† 1 M=1 mol dm^{-3}.

having a positive charge in a 1×10^{-4} M $AlCl_3$ aqueous solution with the concentration of an anionic surfactant (SDS) are given in Fig. 3. Particles of α-SiC and β-SiC had a positive charge during the initial state, and the mean particle sizes of α-SiC and β-SiC were about 800 and 300 nm, respectively. These positive charges of α-SiC and β-SiC decreased to zero upon the addition of a small amount of SDS whose concentrations were 2×10^{-4} and 5×10^{-4} M, respectively. Then, the SiC flocculated and the mean particle sizes of those flocculate were about 4000 and 5000 nm, respectively. Upon a further addition of SDS, α-SiC and β-SiC became negatively charged, and the flocs redispersed again. This resulted in a mean particle sizes of about 600 and 250 nm, respectively.

From these results, the processes of flocculation and redispersion of silicon carbide were observed by the addition of SDS. The stability of the dispersion of silicon carbide by the addition of 1×10^{-2} M SDS was altered as follows: The absorbance of the α-SiC suspension was initially 0.86 but decreased to 0.46 after 24 h, while that of β-SiC suspension gradually decreased from 1.44 to 1.00.

The absorbance at 500 nm for a suspension of α-SiC and β-SiC, which had flocculated by addition of SDS, changed with the concentration of added nonionic surfactant (BB-n). The results given in Fig. 4 show

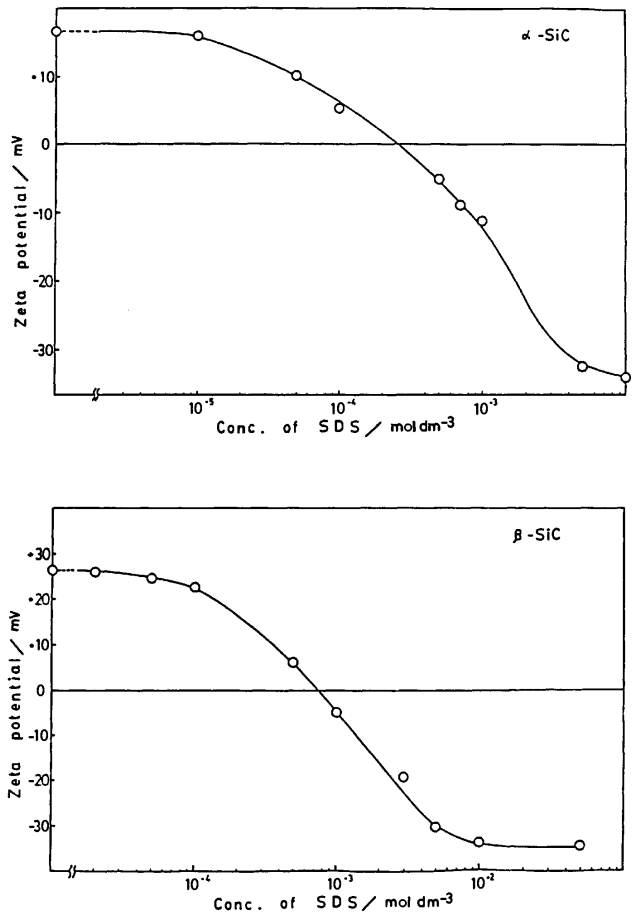

Fig. 3. Variation in zeta potential of silicon carbide in $AlCl_3$ solution(1×10^{-3} M) with a concentration of SDS.

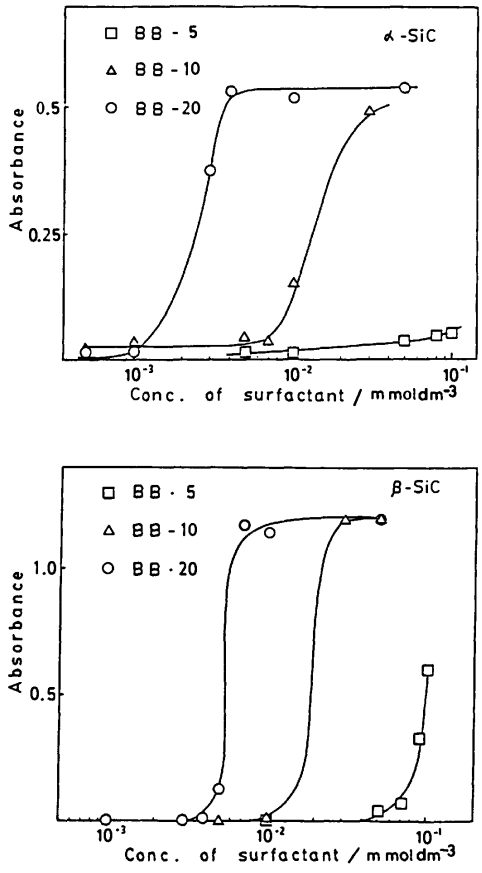

Fig. 4. Variation in absorbance for silicon carbide suspension, flocculated by addition of SDS, with addition of BB-5, BB-10, and BB-20.

Table 1. Dispersion Stability of Silicon Carbide

Sample	α-SiC		β-SiC	
	$[O.D]_0$	$[O.D]_{1d}{}^{a)}/[O.D]_0$	$[O.D]_0$	$[O.D]_{1d}{}^{a)}/[O.D]_0$
$AlCl_3$	0.73	0.01	1.45	0.59
$AlCl_3$+SDS	0.86	0.54	1.44	0.69
$AlCl_3$+SDS+BB-20	0.92	0.58	1.53	0.78

a) 1d indicates 1 day.

that the absorbance increases and becomes constant with the addition of BB-5, BB-10, and BB-20, indicating that a redispersion of α-SiC and β-SiC could be attained. A well redispersion was obtained by a smaller addition of a nonionic surfactant which had a longer oxyethylene chain, at which the mean particle sizes of α-SiC and β-SiC were about 800 and 310 nm, respectively. However, the addition of BB-5, scarcely gave a well redispersion.

The mechanisms of flocculation and redispersion can be explained in terms of a "two-fold adsorption layer," similar to that suggested earlier[11-14] That is, silicon carbide becomes positively charged in an aqueous aluminum chloride solution, providing a well dispersed state characterized by a minimum in the mean particle size and a maximum in the zeta-potential. By the addition of low concentrations of SDS, the particles are discharged and the size of flocculated particles increases. As the hydrocarbon chains of SDS are oriented outward, the particles become hydrophobic and flocculation takes place. On a further addition of SDS, the adsorption of this surfactant occurs by a chain interaction resulting in a two-fold layer with the ionized groups of the second layer oriented towards the solution. Accordingly, the particles become recharged and a redispersion is achieved due to the electric repulsion. A redispersion upon the addition of nonionic surfactants, on the other hand, is most likely due to a steric hindrance between the adsorbed nonionic surfactant molecules.

Table 1 shows the above results for the stability of dispersion. It is recognized that the positive charged particles flocculated by the addition of SDS are redispersed by the addition of a nonionic surfactant which has relatively longer lengths of the oxyethylene chain (BB-20); also, the stability of redispersion is remarkably enhanced.

2. Dispersion of Silicon Carbide in Aqueous Solution with High Concentration of Electrolyte. A well dispersion stability of silicon carbide treated with SDS and BB-20 was not obtained in a 0.1-M $AlCl_3$ aqueous solution since the zeta-potentials of α-SiC

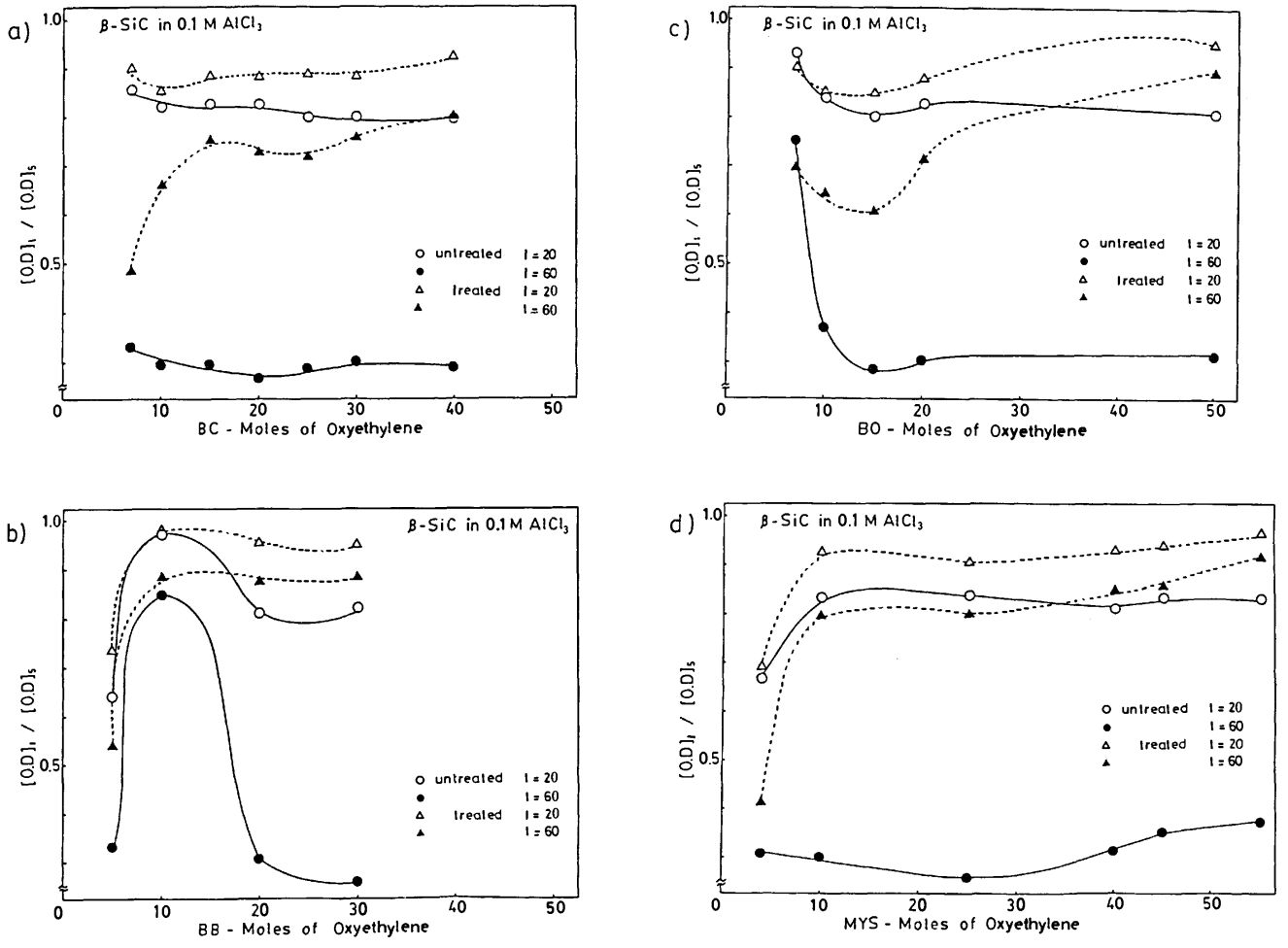

Fig. 5. Variation in $[0.D]_t/[0.D]_5$ of treated and untreated β-SiC with mole of oxyethylene included in nonionic surfactants in 0.1 M $AlCl_3$ aqueous solution.

and β-SiC are almost zero in a 0.1-M $AlCl_3$ aqueous solution or a 1-M $CaCl_2$ aqueous solution and the adsorption of SDS and BB-20 hardly occurred on the surface of silicon carbide. Therefore, a surface treatment of silicon carbide by a silane coupling agent was performed and the effect was examined. Variations in $[O.D]_t/[O.D]_5$ of TMCS-treated α-SiC and untreated α-SiC with the mole of oxyethylene included in each nonionic surfactants in a 0.1-M $AlCl_3$ aqueous solution were measured. Particularly, a well dispersion stability by the addition of BC-*n* or BB-*n* or MYS-*n* (n=10), and BO-*n* (n=7) was obtained. However, the effects of treatments with TMCS were not observed.

The results for TMCS-treated β-SiC and untreated β-SiC are given in Figs. 5 (a-d). In the case of β-SiC, the addition of nonionic surfactants, which had longer lengths of hydrocarbon and oxyethylene chains enhanced a dispersion stability of the treated sample significantly.

Similar results to that of α-SiC and β-SiC were also obtained in a 1.0-M $CaCl_2$ aqueous solution.

It was recognized through an FTIR-ATR measurement that silanol group exists on the surface of silicon carbide. Therefore, the reaction of trimethylchlorosilane with silanol would occur in the following manner[15-17]:

$$\text{-}\overset{|}{\underset{|}{\text{Si}}}\text{-OH} + (CH_3)_3SiCl \longrightarrow \text{-SiOSi}(CH_3)_3 + HCl.$$

Table 2 shows the immersional heat into water of untreated α-SiC, TMCS-treated α-SiC, untreated β-SiC and TMCS-treated β-SiC. In the case of β-SiC, by the reaction with TMCS, the heat was reduced, indicating that the surface of silicon carbide becomes appreciably hydrophobic under the treatment. As for α-SiC, the lack of difference in the heat between untreated α-SiC and TMCS-treated α-SiC implies that the surface of silicon carbide is not covered with TMCS.

As a general rule, interactions at water-solid surfaces are due to the van der Waals force, hydrogen bonding of water to hydroxyl groups and an electrostatic force (proportional to the surface charge). The hydrophilicity of a solid surface is mainly due to the latter two forces. Therefore, the dispersion stability of silicon carbide in water can be improved by the addition of an electrolyte, an anionic surfactant and a nonionic surfactant.

Table 2. Heat of Immersion of Silicon Carbide in Water ($J\,m^{-2}$) at 25 °C

	α-SiC	β-SiC
Untreated	0.20	0.17
TMCS-treated	0.19	0.11

However, in an aqueous solution with a high electrolyte concentraiton, silicon carbide hardly disperses, because the forces for adsorption of surfactants are very weak when particles are discharged due to a depression of electric double layer.

On the other hand, with an increase in the amount of the combined trimethylsilyl group, the silicon carbide particles start to float on the water surface without surfactants, and obviously reveal the surface hydrophobicity. Therefore, the mechanisms of dispersion of TMCS-treated β-SiC is explained as follows: the hydrocarbon chain of nonionic surfactants is oriented to the hydrophobic surface of TMCS-treated β-SiC. The force of adsorption is stronger between the surface and the hydrocarbon chain when the surface of β-SiC becomes hydrophobic. Accordingly, a well dispersed state is obtained when the length of the oxyethylene chain of a nonionic surfactant is relatively longer, even in an aqueous solution with a high electrolyte concentration.

For an application of electrodeposition, the SiC dispersion in a nickel sulfamate aqueous solution (plating bath) was studied. The results were similar to those for a in 1.0-M $CaCl_2$ aqueous solution or a 0.1-M $AlCl_3$ aqueous solution. Furthermore, the proportion of co-deposit TMCS-treated β-SiC on the plating surface to the concentration of TMCS-treated β-SiC in a plating bath by the addition of BC-40 or without BC-40 is given in Fig. 6. From this result, it is apparent that the amount of co-deposit after treatment with TMCS increases twice that without the treatment. Thus, the above result demonstrates that the dispersion of SiC is an important factor for an electrodeposite composite.

The authors are indebted to the Electroplating Engineers of Japan Ltd. for their help with the electroplating study.

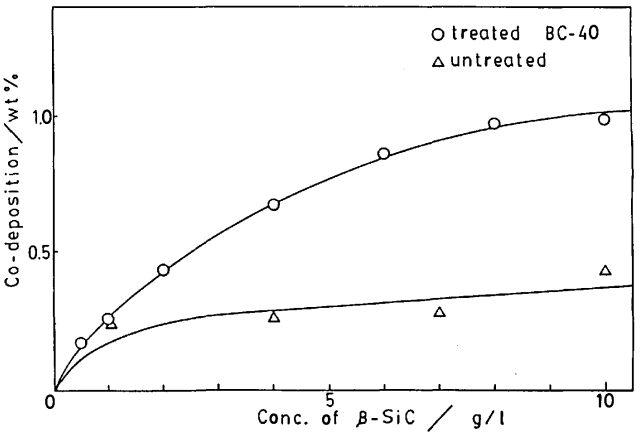

Fig. 6. Variation in amount of co-deposit of silicon carbide as a function of concentration of silicon carbide.

References

1) T. Hayashi, *Hyomen*, **11**, 220 (1973).
2) E. C. Kedward and B. Kiernan, *Metal Finishing J.*, **13**, 116 (1967).
3) E. C. Kedward, C. Addison, and A. A. B. Tennett, *Trans. IMF*, **54**, 8 (1976).
4) V. P. Greco and W. Baldauf, *Plating*, **55**, 250 (1968).
5) N. Guglielmi, *J. Electrochem. Soc*, **119**, 1009 (1972).
6) J. Foster and B. Cameron, *Trans. IMF*, **54**, 178 (1976).
7) A. M. J. Kariapper and J. Foster, *Trans. IMF*, **52**, 87 (1974).
8) H. Kuno and R. Abe, *Kolloid-Z.*, **177**, 40 (1961).
9) K. G. Mathai and R. H. Ottewill, *Trans. Faraday Soc.*, **62**, 750 (1966).
10) J. M. Corkill, J. F. Goodman, and J. R. Tate, *Trans. Faraday Soc.*, **62**, 979 (1966).
11) K. Meguro and T. Kondo, *Nippon Kagaku Zasshi*, **76**, 642 (1955).
12) K. Meguro, *Kogyo Kagaku Zasshi*, **58**, 905 (1955).
13) E. Matijevíc and R. H. Ottewill, *J. Colloid Sci.*, **13**, 42 (1958).
14) K. Meguro, S. Tomioka, N. Kawashima, and K. Esumi, *Progr. Colloid and Polymer Sci.*, **68**, 97 (1983).
15) M. R. Rosen, *J. Coatings Technology*, **50**, 70 (1978).
16) A. Krysztafkiewicy, L. Domka, and W. Wieczorek, *Colloid and Polymer Sci.*, **263**, 804 (1985).
17) K. Tsutsumi and H. Takahashi, *Colloid and Polymer Sci.*, **263**, 506 (1985).

 © 1987 The Chemical Society of Japan Bull. Chem. Soc. Jpn., 60, 95—97 (1987)

Surface Characterization of Silica Modified with Aminosilane Compounds

Seiichi KONDO,* Tatsuo ISHIKAWA, Naoki YAMAGAMI, Kiyotaka YOSHIOKA, and Yoshiko NAKAHARA†
School of Chemistry, Osaka University of Education, 4-88 Minamikawahori-cho, Tennoji-ku, Osaka 543
†Government Industrial Research Institute, Osaka, Midorigaoka, Ikeda 563
(Received July 14, 1986)

Adsorption behaviors, IR spectroscopy and surface electric properties were studied on the surfaces of well-defined mesoporous silica gels modified with triethoxy(3-aminopropyl)silane (TAS) and [3-(dimethylamino)propyl]diethoxymethylsilane (DDS). Surface free silanol groups react with ethoxyl groups of these compounds rigidly. Isoelectric points and points of zero charge of modified silicas shift from pH 3 of pure material to alkali, but DDS-modified silica gels dissolve themselves in aqueous phase because of their strong alkali environment.

Silica gels modified with a large variety of silane derivatives are used for the liquid/solid and gas/solid adsorption chromatography,[1] and there are substantial studies such as states of modifications and adsorption behaviors.[2,3] However, the surfaces of silica gels in these studies were usually not well-characterized in view of, for example, the species and population of surface silanol groups which are substituted with various modifying agents and thence the degree of surface coverage of functional groups per unit area. Therefore, there are still some ambiguities on the state of modified compounds on the surface. On this point of view, surface characterization of ethoxylated mesoporous silica gels was carried out in this laboratory with the result that one ethanol molecule reacts with one free silanol group which covers the surface with a population of 3/nm^2.[4]

The purpose of this report is to clarify details of surface modification with coupling agents which have plural number of reacting functional groups per molecule such as triethoxy(3-aminopropyl)silane (TAS) and [3-(dimethylamino)propyl]diethoxymethylsilane (DDS) by means of well-characterized mesoporous silica gels as a starting material.

Experimental

Materials. Thin transparent plates of mesoporous silica gels of about 0.1 to 0.05 mm thick were made as mentioned elsewhere.[4] Specific surface areas (A_s), pore volumes (V_p) and mean pore radii (r_p) of sample S1 were 718 m^2 g^{-1} 0.63 cm^3 g^{-1} and 1.8 nm respectively. Surfaces of these materials were modified with TAS and DDS by immersing the material in toluene solution of these coupling agents in various concentrations relative to total amount of free hydroxyl groups in these silica gels, and by warming at 323 K for 5 h. The products were washed with toluene and ethanol and dried in vacuo at room temperature.

Adsorption Properties. Specific surface areas, pore volumes and mean pore radii were obtained from nitrogen isotherms using B. E. T. and Cranston-Inkley equations.

IR Spectroscopy. Ft-nir spectrometer of Digilab FTS15E with a PbSe detector was used with 2 cm^{-1} resolution, in the range from room temperature to about 1000 K in vacuo.

Chemical Analysis. The amount of carbon and nitrogen atoms contained in modified samples was measured both by simultaneous TG-DTA and by CHN elements analyzer of Yanagimoto Co. Total number of OH groups, N_{OH}/nm^2, being obtained from ignition loss between 423 and 1373 K were 7.2 and 6.5 for S1 and S2 sillca gels respectively.

Surface Electric Charges. ζ Potentials were measured with ground powders suspended and pH-equilibrated in water by means of ζ meter of Penkem Co. model 501. Points of zero charges (pzc) were estimated from pH change caused by adding a known amount of hydrogen chloride or potassium hydroxide to the solution obtained by immersing 100 mg of powdered samples in the 0.1 mol l^{-1} solution of potassium chloride under nitrogen gas stream at 302.3 K.

Results and Discussion

The nitrogen adsorption isotherms of original and modified samples with TAS are typical to mesoporous materials as is shown in Fig. 1 in which N_n is the number of nitrogen atoms of TAS reacted with the surface per unit surface area and is equal to the

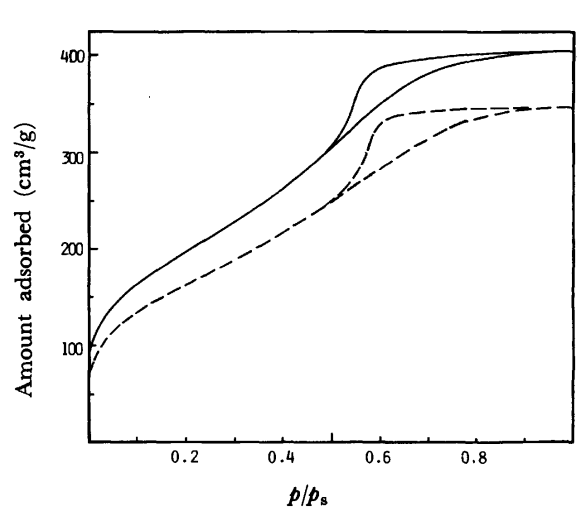

Fig. 1. The nitrogen adsorption isotherms of sample S1 (full line) and that modified with TAS to N_n= 0.49/nm^2 (broken line).

number of modified functional groups. Pore sizes are fairly uniform looking from pore size distribution curves in Fig. 2 with smaller maximum for larger amount of modification with TAS. Specific surface areas (A_s $m^2 g^{-1}$) and pore volumes (V_p $ml\ g^{-1}$) being computed from nitrogen gas adsorption isotherms of sample S2 decreased as the degree of modification with TAS and DDS was increased, whereas it was rather unusual to see that mean pore radii (r_p nm) did not decrease significantly as is seen in Table 1. The same tendency was observed with sample Sl.

The monolayer capacity of adsorbed water decreases by increasing degree of modification, such as from 4.7 water molecules/nm^2 to 1.5/nm^2 on sample modified with DDS to N_n=0.7. This shows that the sample became less hydrophilic by DDS modification, which was also true in case of TAS modification.

The reaction of these coupling agents on silica surface proceeds further to give the amount reacted much higher than monolayer of these substituted functional groups such as N_n=1.0. The ratio of nitrogen atoms to carbon atoms contained in silica gels after reaction was nearly equal to 0.7:3.0, as is seen in Fig. 3. This value is smaller than the ratio of these atoms in one molecule (1.0:3.0). This indicates that roughly one out of three ethoxy groups of a molecule did not react with surface silanol groups, the reason for which was explained by IR spectroscopy as is mentioned later. A_s, V_p, and r_p become smaller because of pore filling. However, the amount of these agents enough to cover the surface and form monolayer can not be precisely estimated from these results only.

Original mesoporous silica gels have mainly three types of silanol groups such as free silanol groups having a surface concentration of about 3/nm, inner OH groups and interparticle hydrogen-bonded silanol groups whose wave numbers are 3740, 3670 and about 3500 cm^{-1} respectively as was discussed elsewhere,[4] and as is partly seen in the ir spectra of unmodified sample Sl in Fig. 4. After modifying this sample with TAS and DDS, the absorbance of OH fundamental stretching band of free silanol groups decreases, and C-H and N-H bands in case of TAS increased. The absorbances of N-H band in case of TAS were proportional to the amount of nitrogen atoms contained in the sample, but free OH band disappears at nearly N_n=0.7 as is seen in Fig. 5. This was also true in case of DDS. This may be interpreted as that roughly two surface free silanol groups reacted with TAS or DDS, which agrees with the above mentioned result. The amino or dimethylamino groups of the substituted functional groups may be hydrogen-bonded to the

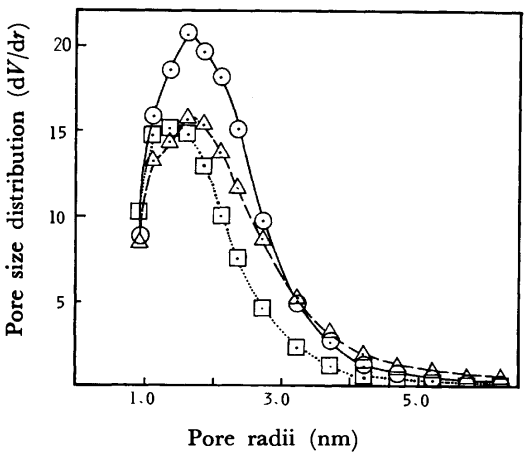

Fig. 2. Pore size distribution curves of sample Sl (circles), those modified with TAS to N_n=0.49 (triangles) and N_n=1.54 (squares).

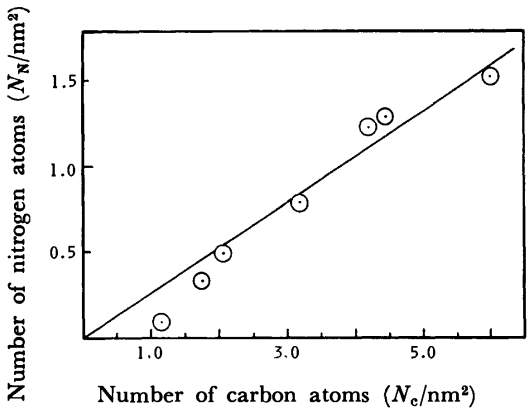

Fig. 3. The relation between number of nitrogen and carbon atoms contained in sample Sl modified with TAS.

Table 1. Nitrogen BET Specific Surface Areas (As) Pore Volumes (V_p) and Mean Pore Radii (r_p) of Sample S2 as the Function of Numbers of Modified Functional Groups Per Unit Surface Area

Number of substituted functional groups/N_n/nm^2		A_s m^2/g	B.E.T. parameter c	V_p/cm^3/g	r_p/nm
—	0	706	93	0.71	2.0
TAS	0.32	502	74	0.52	2.1
TAS	0.82	443	73	0.40	1.8
DDS	0.27	525	64	0.52	2.0
DDS	0.52	489	39	0.57	2.3
DDS	0.90	413	32	0.43	2.1

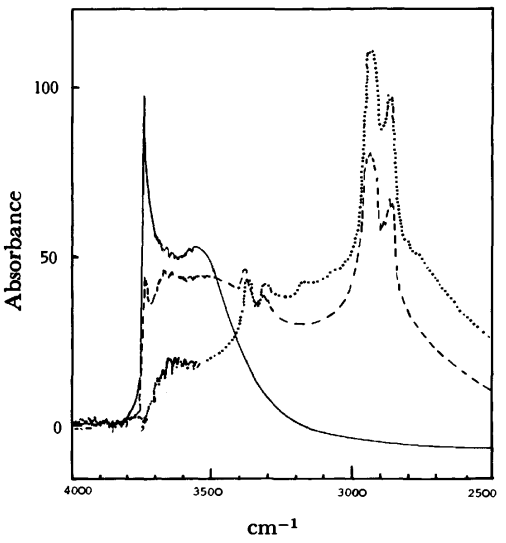

Fig. 4. IR spectra of sample S1 (full line), those modified with TAS to $N_n=0.49$ (broken line), and to $N_n=1.54$ (dotted line).

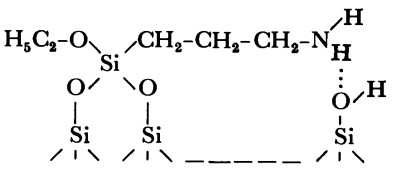

remaining one free silanol group as follows.

Thus, free silanol band disappeared and all three free silanol groups per nm² might have been used to form a monomolecular layer of functional groups. Modifying functional groups more than monolayer seem to react with each other forming some kind of polymers and lie over these modified surfaces to fill pores.

ζ Potentials and pzc were mearsured on these original and modified samples as the function of pH. The values of isoelectric points (iep) and pzc of the same sample agreed well to each other and were higher by increasing the amount of modification. Surface electric charges changed greatly by amine

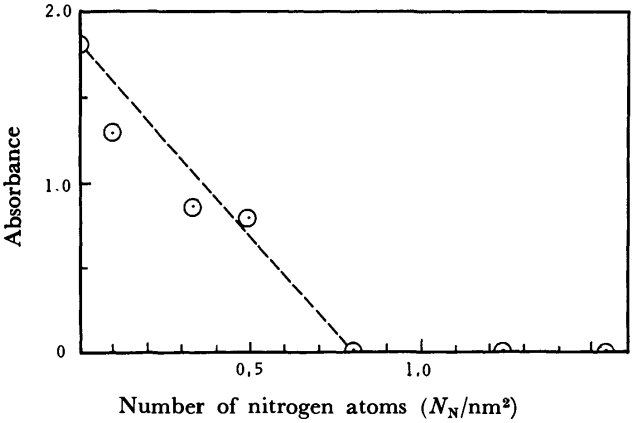

Fig. 5. The absorbance of O–H band as a function of number of nitrogen atoms contained in sample S1.

modification as one can expect. The iep and pzc of TAS modified samples were both about 8.0 and were stable for a prolonged period of time. On the other hand, initial values of iep and pzc of the DDS modified sample were equal to about 9.8 which is much higher than that of TAS, but went down to about 8.5 in 1 d. In this case, particles of this material dispersed in distilled water at room temperature are dissolved and disappeared after a few hours under microscope because of high pH produced by strong basicity of its surface. The free OH band emerged again after immersing this DDS-modified material in distilled water for several hours. These materials absorb alkyl halides irreversibly as is reported elsewhere.[5]

References

1) K. Unger, "Porous Sillica," Elsevier, Amsterdam (1979).

2) "Catalysis," ed by J. A. Anderson and M., Boudart, Springer-Verlag, Berlin (1983). Vol. 4, p. 155.

3) "Kagaku Sosetsu," No. 44, ed by S. Suzuki, Gakkai Publication Center, 1984, p. 34.

4) S. Kondo, *Hyomen*, **24**, 177 (1986).

5) T. Ishikawa, N. Yamagami, and S. Kondo, *Bull. Chem. Soc. Jpn.*, **59**, 3729 (1986).

 © 1987 The Chemical Society of Japan Bull. Chem. Soc. Jpn., 60, 99—103 (1987)

^{81}Br Nuclear Quadrupole Resonance of Cs_2ZnBr_4 and Crystal Stability of Compounds of A_2MX_4 Type

Hirokazu NAKAYAMA,† Nobuo NAKAMURA, and Hideaki CHIHARA*
Department of Chemistry, Faculty of Science, Osaka University,
Toyonaka, Osaka 560
(Received July 16, 1986)

The temperature dependences of ^{81}Br nuclear quadrupole resonance frequencies and quadrupolar relaxation times of Cs_2ZnBr_4 were measured. The librational motion of $[ZnBr_4]^{2-}$ about the Zn–Br axis parallel to the a axis in the crystal is more active than those about the other axes. The reason why this compound shows no phase transition can be accounted for by the molecular packing, especially the packing of $[ZnBr_4]^{2-}$ along the a axis. General examination of the relative size of cation/anion in the class of compounds of A_2MX_4 type led to a criterion which may be used to rationalize existence and absence of a phase transition.

A large number of A_2MX_4 type of compounds crystallize in the isomorphous structure with the space group *Pnma* and undergo analogous sequence of phase transitions. Among them much attention has recently been focused on Rb_2ZnBr_4 and Rb_2ZnCl_4 from experimental and theoretical points of view because they assume typical incommensurate structure in certain temperature regions. Cs_2HgBr_4[1] and Cs_2CdBr_4[2] also belong to this group and have interested us as they[3–6] show similar successive phase transitions from the normal room temperature phase to the phase of incommensurate structure and then to the commensurate phase on further cooling. We studied the microscopic structure of the incommensurate phases of these latter two materials by relating the nuclear quadrupole resonance results with a model calculation of the electric field gradients at the bromine sites.[7]

Cs_2ZnBr_4 also has the A_2MX_4 composition and crystallizes in the *Pnma* structure.[8] However no phase transition has been found in this compound so far.[3] These facts suggest that the structural stability of this type of compounds depends on a very intricate balance of interatomic forces and that the phase transition phenomena have to occur when such an intricate balance is destroyed. Hence it will be of great interest to uncover a factor or factors which govern the crystal stability and the cooperative phase change phenomena of such series of materials.

This paper is aimed first at deducing some information about the feature of the molecular motion in Cs_2ZnBr_4 from the temperature dependence of nuclear quadrupole resonance frequencies and spin-lattice relaxation times. The second purpose is to pin down the physical properties that determine the crystal structure and trigger the phase transition of these materials.

† Present address: Institute of Chemistry, College of General Education, Osaka University, Toyonaka, Osaka 560.

Experimental

Crystalline Cs_2ZnBr_4[8] was obtained by slow evaporation of aqueous solution of the stoichiometric amounts of CsBr and $ZnBr_2$ at room temperature. The sample was recrystallized twice from aqueous solution, ground and sealed in an ampule with helium gas for the NQR measurements.

The ^{81}Br NQR signal was observed with a home-built pulsed FT spectrometer based on a MATEC spectrometer. The matching unit was placed in the cryostat in order to make impedance matching easy. Details of the apparatus and its operation were reported elsewhere.[9]

The temperature dependence was determined by using a simple cryostat with liquid nitrogen as the refrigerant. The temperature, kept constant to within ±0.1 K during the NQR measurements, was measured with Chromel P-Constantan thermocouples.

Results and Discussion

Cs_2ZnBr_4. The temperature dependence of the nuclear quadrupole resonance frequencies is shown in Fig. 1. There are three resonance lines in the temperature range between 77 and 300 K in accordance with the X-ray structure data.[8] Our frequency data agree with those by Plesko et al.[3] within 100 kHz in the temperature range measured. We may assign the three resonance lines ν_1, ν_2, and ν_3 to the bromine 1, 2, and 3 in the structure data[8] respectively by reference to the NQR data of the isomorphous Cs_2CdBr_4.[6] One sees from this figure that the temperature coefficient of the resonance line at the site 1 is only $-2\,kHz\,K^{-1}$ in comparison with -6.5 kHz for the line at the site 2, indicating that the librational motion of the $[ZnBr_4]^{2-}$ tetrahedron is highly anisotropic. Since the direction of the bond between the bromine at the site 1 and the central metal almost coincides with the crystallographic a-axis, the above fact means that only the libration of the anion about the a-axis is highly excited. This interpretation is also supported by the relaxation time measurements. The temperature dependence of the ^{81}Br spin-lattice relaxation time, T_1, is shown in Fig. 2. The relaxation rate, T_1^{-1}, obeys the T^2 law[10] for all the

lines between 77 and 300 K, indicating that the relaxation of the bromine nuclei at all the sites is governed by the librational motion of the $[ZnBr_4]^{2-}$ tetrahedron. According to the theory of the quadrupolar relaxation[10] due to vibration,

$$T_1^{-1}(\nu_1) : T_1^{-1}(\nu_2) : T_1^{-1}(\nu_3) = \nu_1^2 : \nu_2^2 : \nu_3^2$$

holds if the molecular or the ionic motion is isotropic. Hence, the relaxation time of the ν_1 line would be the shortest if the isotropic anionic librations were excited. The experimental T_1 of the ν_1 is, however, more than twice as long as those of the other two lines, which supports again that the libration about the a-axis, which does not essentially affect the T_1 for ν_1, is sufficiently excited but those about the other axes have only small amplitudes.

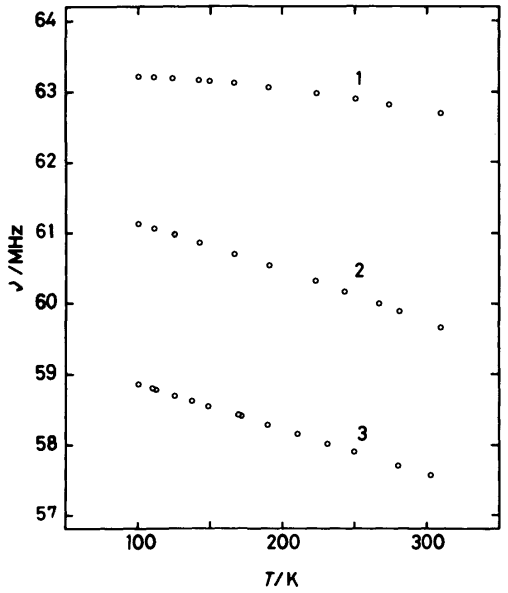

Fig. 1. Temperature dependence of ^{81}Br NQR frequencies in Cs_2ZnBr_4.

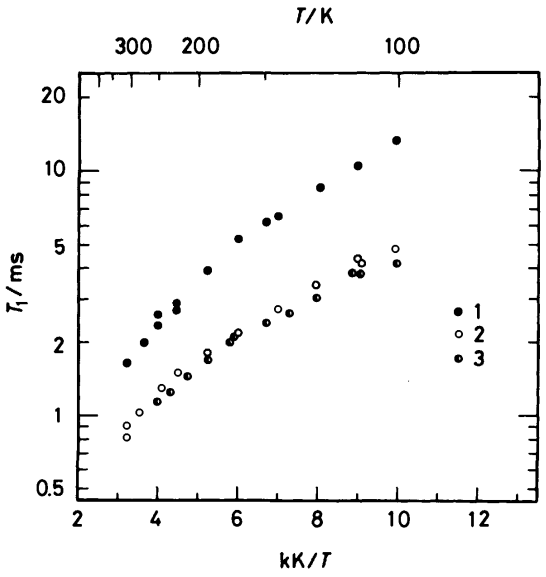

Fig. 2. Temperature dependence of ^{81}Br NQR spin-lattice relaxation times in Cs_2ZnBr_4.

In a previous paper[7] we showed that in Cs_2MBr_4 (M=Hg, Cd) the librational motion of the $[MBr_4]^{2-}$ (M=Cd, Hg) tetrahedron about the a-axis is highly excited in their normal phases and that such anisotropic libration is responsible for the phase transition to the incommensurate phase in which the rotational displacement of the anions about the a-axis generates the incommensurate wave along the a-axis.

Thus, we see that the compounds Cs_2MBr_4 (M=Hg, Cd) and Cs_2ZnBr_4 have a common feature; i.e., the librational mode is highly excited about the a-axis in the *Pnma* phase of each substance and it may be the cause of existence or non-existence of successive phase transitions in these isomorphous substances.

Phase Relation and Stability of A_2MX_4 Structure. The compounds Cs_2CdBr_4[3,5,6] and Cs_2HgBr_4[1,3-5] show successive phase transitions and become incommensurate in a certain temperature region. Their structures and phase transitions such as the transition temperature, the length and distance of the incommensurate wave vectors and the phase relation below T_c, etc., are very similar to each other. On the other hand, Cs_2ZnBr_4[3] shows no phase transition although its crystal structure[8] at room temperature is isomorphous to Cs_2HgBr_4[1] and Cs_2CdBr_4,[2] and these three compounds show common characteristic as mentioned in the preceding section. In an attempt to uncover a factor or factors which govern the phase relations and the stability of the *Pnma* structure, a comparison will be made of the structural characteristics of a variety of A_2MX_4 type compounds.

The space group of the highest temperature phase of each of A_2MX_4 type compounds (A=K, Na, Rb, Cs; B=Hg, Cd, Zn, Co, Mn, Cu; X=Cl, Br, I)[1,2,8,11-25] is listed in Table 1. From this table two interesting

Table 1. Space Group of A_2MX_4 Type of Compounds

Complex anion	Cation			
	Na	K	Rb	Cs
$HgCl_4$				*Pnma*[11]
$HgBr_4$				*Pnma*[1]
HgI_4				$P2_1$[12]
$CdCl_4$	*Pbam*[13]			$I4/mmm$[14]
$CdBr_4$				*Pnma*[2]
CdI_4				
$ZnCl_4$	*Pnma*[15]	*Pnma*[16]	*Pnma*[17]	*Pnma*[18]
$ZnBr_4$			*Pnma*[19]	*Pnma*[3]
ZnI_4			$P2_1/m$[20]	*Pnma*[21]
$CoCl_4$	*Pnma*[15]	*Pnma*[22]	*Pnma*[23]	*Pnma*[24]
$CoBr_4$		*Pnma*[25] $P2_1/m$[20]	*Pnma*[25]	*Pnma*[25]
CoI_4		$P2_1/m$[22]	$P2_1/m$[22]	*Pnma*[22]

properties can be extracted.

1) The compounds that have the common cation and the anion of almost the same size crystallize in the same space group irrespective of the chemical species of metallic element. A_2CoX_4 and A_2ZnX_4 have the same space group when A and X are common. Thus the space group of both Cs_2CoCl_4 and Cs_2ZnCl_4 is *Pnma* and the space group of Rb_2CoI_4 and Rb_2ZnI_4 is $P2_1/m$. Moreover, the lattice constants in A_2CoX_4 and A_2ZnX_4 are almost the same as shown in Table 2. The same relation can be seen between A_2HgBr_4 and A_2CdBr_4.

Table 2. Space Group and Lattice Parameters of A_2ZnX_4 and A_2CoX_4

Compound	Space group	Lattice constant		
		a/Å	*b*/Å	*c*/Å
Na_2ZnCl_4	*Pnma*[15]	8.053	6.402	13.695
Na_2CoCl_4	*Pnma*[15]	8.073	6.428	13.713
K_2ZnCl_4	*Pnma*[16]	8.926	7.256	12.402
K_2CoCl_4	*Pnma*[22]	8.933	7.240	12.421
Rb_2ZnCl_4	*Pmcn*[17]	7.282	12.726	9.257
Rb_2CoCl_4	*Pmcn*[23]	7.283	12.723	9.272
Cs_2ZnCl_4	*Pnma*[18]	9.758	7.400	12.970
Cs_2CoCl_4	*Pnma*[24]	9.737	7.392	12.972
Rb_2ZnBr_4	*Pmcn*[19]	7.656	13.343	9.708
Rb_2CoBr_4	*Pmcn*[25]	7.651	13.371	9.718
Cs_2ZnBr_4	*Pnma*[3]	10.196	7.770	13.517
Cs_2CoBr_4	*Pnma*[25]	10.181	7.723	13.492
Rb_2ZnI_4	$P2_1/m$[20]			
Rb_2CoI_4	$P2_1/m$[22]	10.383	8.144	7.657
Cs_2ZnI_4	*Pmcn*[21]	8.29	14.45	10.84
Cs_2CoI_4	*Pmcn*[22]	8.297	14.414	10.833

Table 3. Existence of Phase Transition or Transitions in A_2MX_4 Compounds

Complex anion	Cation			
	Na	K	Rb	Cs
$HgCl_4$				YES[26]
$HgBr_4$				YES[1,4,7]
HgI_4				
$CdCl_4$				
$CdBr_4$				YES[4,5]
CdI_4				
$ZnCl_4$	?	YES[28]	YES[28]	NO[29]
$ZnBr_4$			YES[28]	NO[4]
ZnI_4				YES[30]
$CoCl_4$	?	?	?	NO[31]
$CoBr_4$		?	?	?
CoI_4		?	?	?

2) The relative size of the cation and the complex anion governs the space group of the highest temperature phase. Those are the properties that

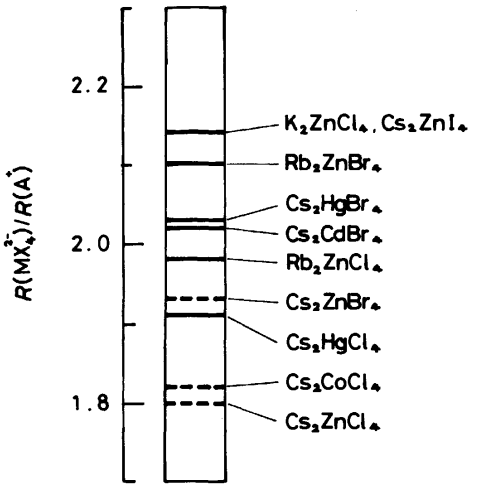

Fig. 3. Ratio of the effective radius of the complex anion $[MX_4]^{2-}$ to the radius of cation A^+ for various compounds.
——: Indicates a compound which has one or more phase transitions.
- - -: Indicates a compound which has no phase transition.

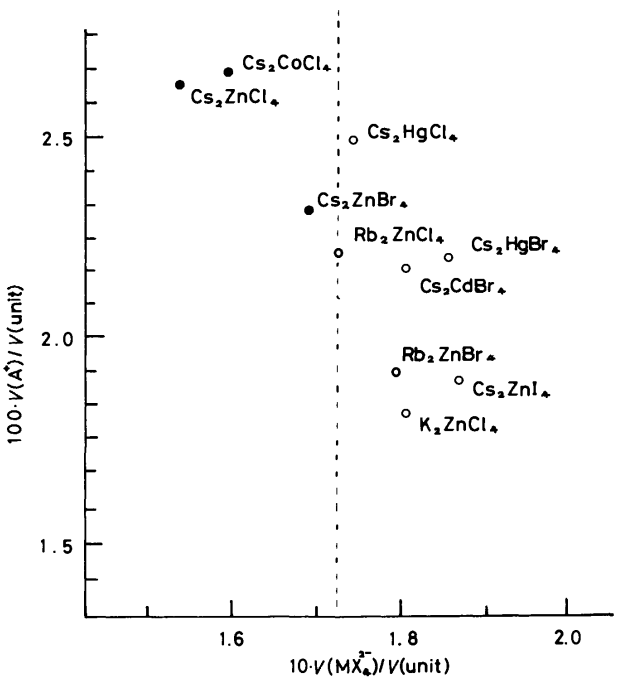

Fig. 4. The effective volume of the complex anion $[MX_4]^{2-}$ is plotted against the volume of the cation A^+ both reduced by the volume of the unit cell.
●: Indicates a compound which has phase transitions.
○: Indicates a compound which has no phase transition.

determine not only the crystal structure but also the phase relation. Table 3[1,3-6,26-31] suggests that the key factor for the highest temperature phase to undergo a phase transition into an incommensurate phase is the relative size of the cation and the complex anion. In order to show that it is the key factor in a more quantitative manner, the relative sizes of the cation and the anion were calculated for each of these compounds and the result is shown in Fig. 3. The ionic radii of the cations were taken from reference 32 as 1.52 Å for K^+, 1.66 Å for Rb^+ and 1.81 Å for Cs^+. The ionic radii of $[MX_4]^{2-}$ complex anions were obtained by adding interatomic distance of M–X and the atomic radius of the X atom. The ratios between the ionic radii, $R([MX_4]^{2-})/R(A^+)$, calculated from these data are arranged in Fig. 3, where the solid lines represent compounds which undergo a phase transition or transitions and the broken lines those without any transition. This graph shows that the compounds with the ratio value between 1.9 and 2.2 show a phase transition except for slight displacement of Cs_2ZnBr_4. If, on the other hand, the volume occupied by a cation is plotted against the volume occupied by a complex anion, both reduced by the unit cell volume (Fig. 4), the compounds for which $V([MX_4]^{2-})/V$(unit cell) is larger than 0.172 undergo at least one phase transition almost independent of the value of $V(A^+)/V$(unit cell). It thus seems that $V([MX_4]^{2-})/V$(unit cell)=0.172 is the critical value for A_2MX_4 type compounds; it serves as a gross criterion for distinguishing whether a compound with A_2MX_4 type structure undergoes any phase transition or not.

We saw in the preceding section that the anisotropic interaction plays an important role in the phase transition phenomena in the A_2MX_4 type of substances. In order to search for an anisotropic property

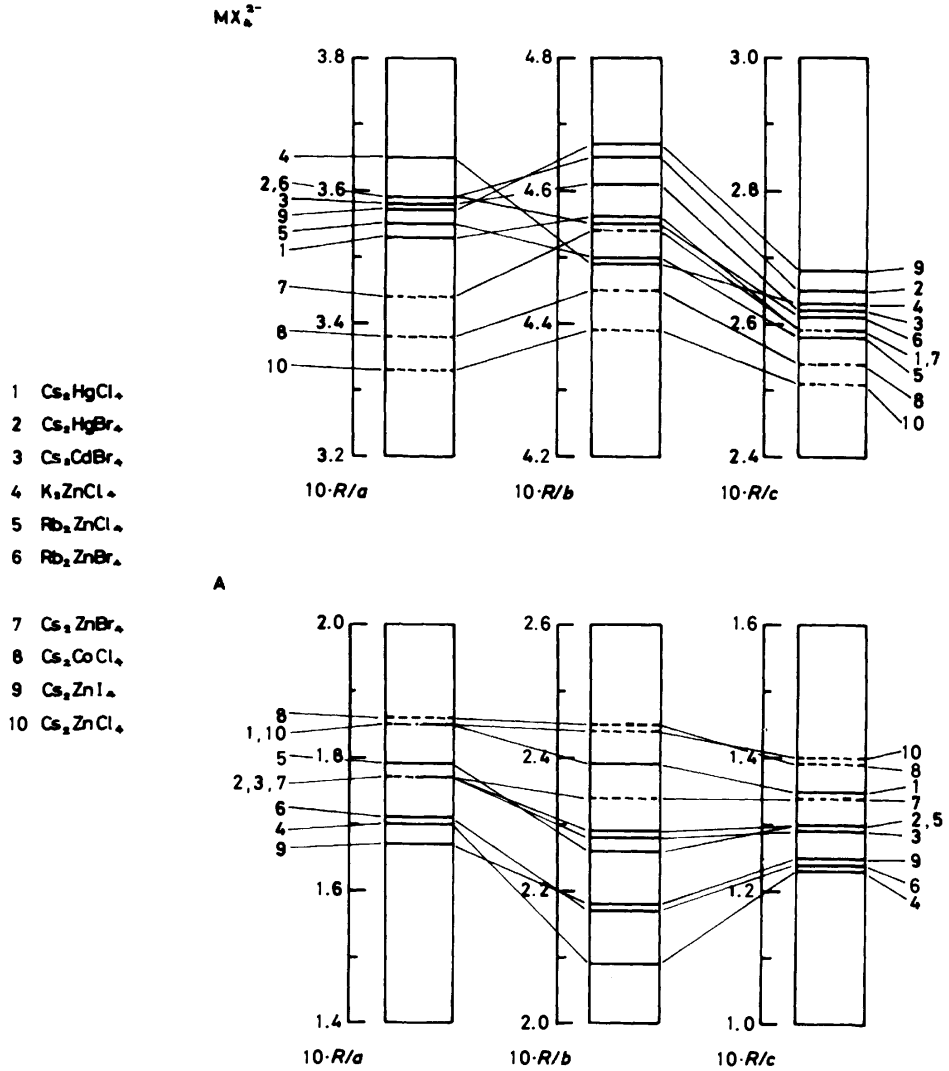

Fig. 5. Ratio of the radius of the complex anion $[MX_4]^{2-}$ and that of the cation A^+ to the individual lattice constants in various compounds are shown in the upper and the lower figures, respectively.
– – –: Indicates a compound which has no phase transition.

governing the crystal stability, we arranged the ionic radius $R(A^+)$ or $R([MX_4]^{2-})$ reduced by each of the lattice constants in the order of their magnitude as shown in Fig. 5. The compounds with and without any phase transition are highlighted by the solid and broken lines, respectively. These diagrams suggest that the compounds composed of a small cation and a large complex anion undergo a phase change. Especially, this tendency is distinct in regard to the quantity $R([MX_4]^{2-})/a$, i.e. the compounds with this ratio greater than 0.35 undergo some kind of phase transition. This finding is very important in that the compounds which possess an incommensurate phase show the incommensurate wave vector directed in the a-axis. Even the compounds that do not have an incommensurate phase show tripled unit cell in the a axis direction in the low temperature phase. We can therefore state that the ionic interaction along the a-axis mainly govern the stability of a particular crystal structure with regard to incommensurate modulation.

In this way we can interpret the fact that both Cs_2HgBr_4 and Cs_2CdBr_4 undergo successive phase transitions while the isomorphous Cs_2ZnBr_4 doesn't exhibit any phase transition: The anisotropic interaction along the crystallographic a-axis in Cs_2ZnBr_4 is small whereas in the former two compounds a strong cooperative interaction exists along the a-axis and may drive these materials to undergoing phase transitions on cooling.

We can now use our finding to predict the phase transition of the A_2MX_4 type of materials, i.e., a compound of A_2MX_4 type in which the value of $R([MX_4]^{2-})/a$ is slightly smaller than 0.35 is a candidate which undergoes a phase transition at high pressure because external pressure will increase this ratio up to 0.35 and then the original structure may become less stable.

References

1) G. K. Semin, I. M. Alymov, V. M. Burbelo, V. I. Pakhomov, and P. M. Fedorov, *Izv. Akad. Nauk. SSSR, Ser. Fiz.*, **42**, 2095 (1978).

2) D. Altermatt, H. Arend, A. Niggli, and W. Petter, *Mat. Res. Bull.*, **14**, 1391 (1979).

3) S. Plesko, R. Kind, and H. Arend, *Phys. Stat. Sol.*, (*a*), **61**, 87 (1980).

4) S. Plesko, V. Dvorák, R. Kind, and A. Treindl, *Ferroelectrics*, **36**, 331 (1981).

5) D. Altermatt, H. Arend, V. Gramlich, A. Niggli, and W. Petter, *Acta Crystallogr., Sect. B*, **40**, 347 (1984).

6) S. Plesko, R. Kind, and H. Arend, *Ferroelectrics*, **26**, 703 (1980).

7) H. Nakayama, N. Nakamura, and H. Chihara, to be published.

8) B. Morosin and E. C. Lingafelter, *Acta Crystallogr.*, **12**, 744 (1959).

9) H. Nakayama, Dissertation, Osaka University, 1985.

10) J. Van Kranendonk and M. Walker, *Phys. Rev. Lett.*, **18**, 701 (1967).

11) S. A. Linde, A. Ya Mikhailova, V. I. Pakhomov, V. V. Kirilenko, and V. G. Shul'ga, *Koord. Khim.*, **9**, 998 (1983).

12) V. I. Pakhomov and P. M. Fedorov, *Kristallografiya*, **17**, 942 (1972).

13) J. Goodyear, S. A. D. Ali, and G. A. Steigmann, *Acta Crystallogr., Sect. B*, **27**, 1672 (1971).

14) S. Stanley and G. Elizabeth, *Acta Crystallogr.*, **17**, 790 (1964)

15) C. J. J. van Loon and D. Visser, *Acta Crystallogr., Sect. B*, **33**, 188 (1977).

16) F. Milia, R. Kind, and J. Slak, *Phys. Rev.*, **B27**, 6662 (1983).

17) M. Wada, A. Sawada, and Y. Ishibashi, *J. Phys. Soc. Jpn.*, **47**, 1185 (1979).

18) J. A. McGinnety, *Inorg. Chem.*, **13**, 1057 (1974).

19) T. Ueda, S. Iida and H. Terauchi, *J. Phys. Soc. Jpn.*, **51**, 3953 (1982).

20) W. J. Asker, D. E. Scaife, and J. A. Watts, *Aust. J. Chem.*, **25**, 2301 (1972).

21) D. E. Scaife, *Aust. J. Chem.*, **24**, 1315 (1971).

22) H. J. Seifert and L. Stäudel, *Z. Anorg. Allg. Chem.*, **429**, 105 (1977).

23) M. Amit, A. Horowitz, and J. Makovsky, *Israel J. Chem.*, **10**, 715 (1972).

24) M. A. Porai-Koshits, *Kristallografia*, **1**, 291 (1956).

25) H. J. Seifert and I. Al-Khudair, *J. Inorg. Nucl. Chem.*, **37**, 1625 (1975).

26) V. V. Petrov, V. G. Pitsyuga, V. A. Gordeev, A. V. Bogdanova, M. A. Bagina, and A. Yu. Khalakhan, *Sov. Phys. Solid State*, **25**, 1995 (1983).

27) V. V. Danilov, V. V. Onopko, A. V. Bogdanova, and V. G. Shul'ga, *Sov. Phys. Solid State*, **23**, 1459 (1982).

28) Y. Yamada and N. Hamaya, *J. Phys. Soc. Jpn.*, **52**, 3466 (1983).

29) P. T. T. Wong, *J. Chem. Phys.*, **64**, 2186 (1976).

30) K. Gesi, *J. Phys. Soc. Jpn.*, **20**, 3535 (1981).

31) T. P. Melia and R. Merrifield, *J. Chem. Soc.*, (*A*), **1971**, 1258.

32) R. D. Shannon and C. T. Prewitt, *Acta Crystallogr., Sect. B*, **25**, 925 (1969).

 © 1987 The Chemical Society of Japan Bull. Chem. Soc. Jpn., 60, 105—109 (1987)

Multinuclear Solid-State NMR Study of Dehydration of Na-Y Type Zeolites

Shigenobu HAYASHI, Kikuko HAYAMIZU, and Osamu YAMAMOTO
National Chemical Laboratory for Industry, Tsukuba, Ibaraki 305
(Received July 22, 1986)

High-resolution solid-state NMR spectra of ^{23}Na, ^{27}Al, and ^{29}Si nuclei were measured for dehydrated Na-Y type zeolites as well as undehydrated and rehydrated samples using magic angle sample spinning technique. ^{1}H NMR spectra, X-ray diffraction patterns, and thermal properties were measured as well. ^{23}Na NMR results indicate that there are three types of Na sites with different symmetries in the faujasite framework; two types with high and slightly low symmetries are detected by NMR, while the third cannot because of its very low symmetry. Na ions in high-symmetry sites are moved into slightly-low and very-low-symmetry sites by the dehydration. On the other hand, the Na ions in the amorphous region are located in low and very-low-symmetry sites. ^{27}Al and ^{29}Si NMR lines are broadened by the dehydration, due to the distortion of AlO_4 tetrahedra and the interaction with ^{27}Al nuclei, respectively. The ^{29}Si spin-lattice relaxation time becomes longer by the dehydration, which indicates that water molecules play some role in the relaxation.

Zeolites are crystalline aluminosilicates with many pores inside it. SiO_4 and AlO_4 tetrahedra are connected by sharing their oxygen atoms, and positive ions and water are located in the cage constructed by the SiO_4 and AlO_4 tetrahedra. The structures and properties of zeolites are largely influenced by the water molecules.

High-resolution solid-state NMR has been extensively used to study the structure of zeolites in recent years.[1] ^{29}Si NMR can distinguish Si atoms in zeolites according as the number of Al atoms coordinating to the Si atoms through oxygen atoms.[2] ^{27}Al NMR can resolve four-coordinated and six-coordinated Al,[3] i.e., lattice and extra-lattice Al. A number of NMR spectra have been measured for various zeolites so far, and comparisons have been made between them. But even if the network structures are the same, it is possible that the spectra are different depending on the hydration state. Actually, spectral changes caused by thermal treatment have been reported for the ^{29}Si spectra of ZSM-5[4] and the ^{27}Al spectra of ZSM-5 and H-Y zeolites[5,6] No extensive studies, however, have been published up to now.

In the present work, ^{23}Na, ^{27}Al, and ^{29}Si NMR spectra have been measured for dehydrated Na-Y zeolites as well as undehydrated and rehydrated samples, using magic-angle sample-spinning (MAS) technique,[7]) to study the effect of the hydration state on the NMR spectra. ^{1}H NMR spectra, X-ray diffraction pattern, and thermal properties were measured as well. Changes of the microscopic structure shown by the NMR results are discussed in relation to the hydration state. Since the NMR spectra have been measured for several nuclei in the same samples, the relations between the spectra of different nuclei are also discussed.

Experimental

Materials. Na-Y zeolite, coded JRC-Z-Y4.8, was supplied by Sansho-Shokubai-Iinkai, Catalysis Society of Japan. Dehydration was carried out in air at elevated temperatures. Dehydrated samples are called DE400, DE600, and DE800, which were dehydrated at 400 °C for 4 h, at 600 °C for 5 h, and at 800 °C for 5 h, respectively. Rehydration was performed by contacting the dehydrated samples with an excess of liquid water at room temperature for 2.5 d, after which the sample was dried at 70 °C for 1 d. Rehydrated samples are called RExxx, whose xxx denotes the dehydration temperature.

Measurements. High-resolution solid-state NMR spectra were measured by a JEOL FX-200 pulsed spectrometer equipped with an accessary for MAS. The resonance frequencies were 52.80, 52.00, and 39.60 MHz for ^{23}Na, ^{27}Al, and ^{29}Si nuclei, respectively. An ordinary one-pulse cycle was used under a MAS condition with a spinning speed of about 3.5 kHz. ^{1}H NMR spectra were also measured by a Bruker CXP-100 pulsed spectrometer, operating at a resonance frequency of 90.03 MHz and using the ordinary one-pulse cycle. Shift values are referred to NaCl aqueous solution for the ^{23}Na spectra (The shift of solid NaCl was 6.7 ppm with respect to this standard.), to $AlCl_3$ aqueous solution for the ^{27}Al spectra, and to tetramethylsilane for the ^{29}Si and ^{1}H spectra. All the measurements were carried out at room temperature.

Powder X-ray diffraction patterns were measured by a Rigaku Geiger-flex diffractometer, and thermal analysis was performed by a Rigaku Thermoflex.

Results

^{23}Na NMR. Figure 1 shows ^{23}Na MAS NMR spectra of undehydrated and dehydrated samples. Since the maximum intensity of the central line ($m=1/2\rightarrow-1/2$) of half-integer spins is obtained at a flip angle of $\pi/(2I+1)$(I :spin number),[8] the flip angle of the excitation pulse was set at $\pi/4$ for ^{23}Na spin ($I=3/2$). The undehydrated sample has a symmetric peak at -12 ppm with a 1.2-kHz width. On the other hand, DE400 and DE600 have asymmetric line shapes, whose tops are located at the same position as the undehydrated sample. DE800 shows a markedly different line shape centered at -28 ppm with a

2.8-kHz width. The spectral intensities per unit sample weight are 20% for DE400 and DE600 and 40% for DE800 with respect to the undehydrated sample.

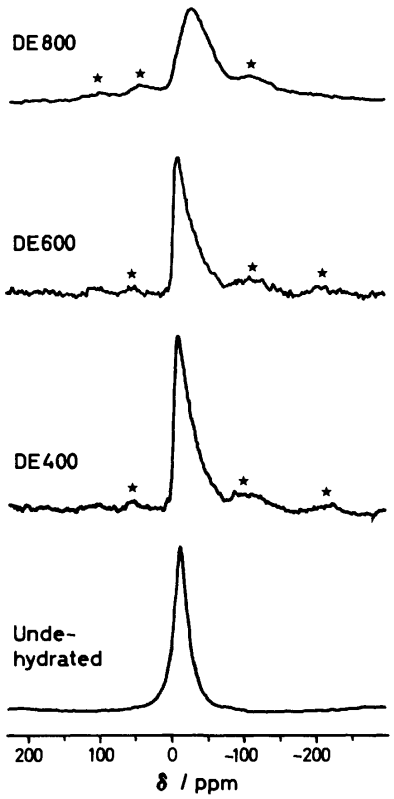

Fig. 1. ^{23}Na MAS NMR spectra of undehydrated and dehydrated Na–Y zeolites. The flip angle of the excitation pulse was $\pi/4$ and the recycle time was 1 s. The intensity is not normalized, and the mark ★ denotes spinning sideband.

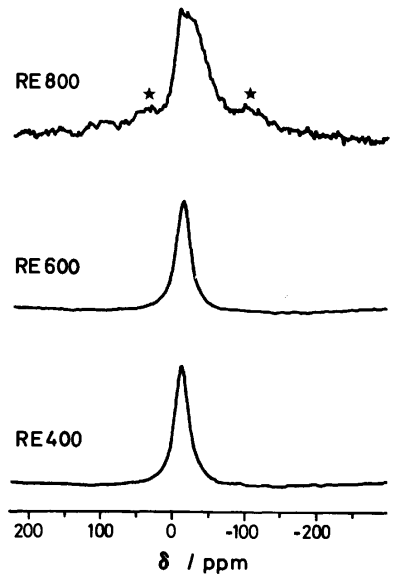

Fig. 2. ^{23}Na MAS NMR spectra of rehydrated Na–Y zeolites under the same measuring conditions as in Fig. 1.

Figure 2 shows the spectra of rehydrated samples. The spectra of RE400 and RE600 agree with that of the undehydrated sample, while the spectrum of RE800 is a superposition of the spectra of DE800 and the undehydrated sample.

Table 1. Summary of ^{23}Na and ^{27}Al MAS NMR

Sample	^{23}Na NMR[a]		^{27}Al NMR[b]	
	Peak	FWHM[c]	Peak	FWHM[c]
	ppm	kHz	ppm	kHz
Undehydrated	−12	1.2	53	1.0
DE400	−10	1.4	45	2.6
DE600	−11	1.4	42	2.7
DE800	−28	2.8	45	2.1
RE400	−13	1.2	51	1.3
RE600	−15	1.2	51	1.3
RE800	−11, −21	2.7	47	2.1

a) Resonance frequency of 52.80 MHz. b) Resonance frequency of 52.00 MHz. c) Full width at half-maximum.

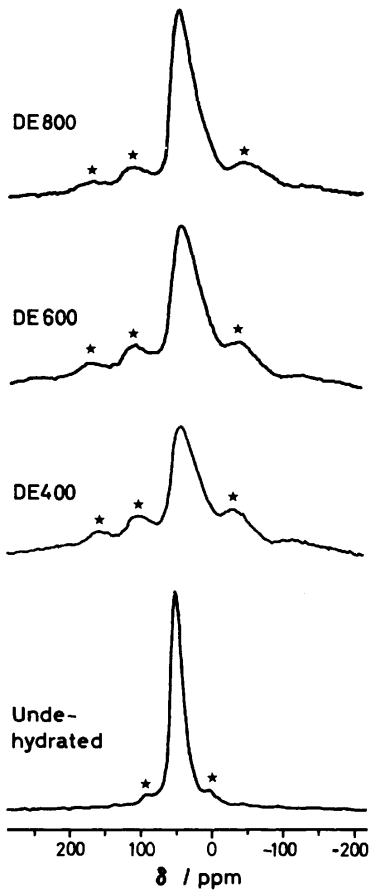

Fig. 3. ^{27}Al MAS NMR spectra of undehydrated and dehydrated Na–Y zeolites with the flip angle of $\pi/6$ and the recycle time of 1 s. The intensity is not normalized, and the mark ★ denotes spinning sideband.

The results are summarized in Table 1.

^{27}Al NMR. Figure 3 shows ^{27}Al MAS NMR spectra of the undehydrated and dehydrated samples. The undehydrated sample has a peak at 53 ppm with a 1.0-kHz width. DE400, DE600, and DE800 have a peak at about 45 ppm with a width of about 2.6 kHz, and their total intensities per unit sample weight decrease to the extent of 80—90% of that of the undehydrated sample. For the rehydrated samples, RE400 and RE600 have spectra similar to the undehydrated sample, while RE800 shows a spectrum similar to DE800. The results are usmmarized in Table 1.

^{29}Si NMR. Figure 4 shows ^{29}Si MAS NMR spectra of the undehydrated and dehydrated samples. The undehydrated sample has four peaks at −88.7, −93.7, −99.3, and −105.1 ppm, which are attributed to Si(3Al), Si(2Al), Si(1Al), and Si(OAl), respectively, in which Si(nAl) denotes the Si atom coordinated by n aluminum atoms and (4-n) silicon atoms through oxygen atoms. Assuming that Loewenstein's rule[9] is valid, the [Si]/[Al] ratio of the faujasite framework is estimated to be 2.75 using the equation in Ref. 10. The T_1 value is 6.3±0.7 s for all the four peaks. DE400 has four peaks also, but their widths are wider than those in the undehydrated sample, resulting in lower resolution. The two peaks assigned to Si(3Al) and Si(2Al) are shifted in the higher-field direction by about 1.5 ppm compared to those of the undehydrated sample, while other two peaks are not shifted. DE600 has the same line shape as DE400, and the line shape is independent of the recycle time, which indicates that the four peaks have the same T_1 value. The T_1 value is 13±3 s, longer than that of the undehydrated sample. DE800 has a negligible fine structure, and the total linewidth is broader than that of DE600.

Figure 5 shows the spectra of the rehydrated samples. RE400 and RE600 have the same spectra as the undehydrated sample. On the other hand, RE800 has a little fine structure, and the whole line shape is similar to the sum of the spectra of DE600 and DE800.

^{1}H NMR. ^{1}H results are summarized in Table 2. The undehydrated sample contains a large amount of water, whose proton shows a peak at 5.0 ppm with a 0.22-kHz width. The ^{1}H nuclei are in a motionally-narrowed state. On the other hand, the DE samples

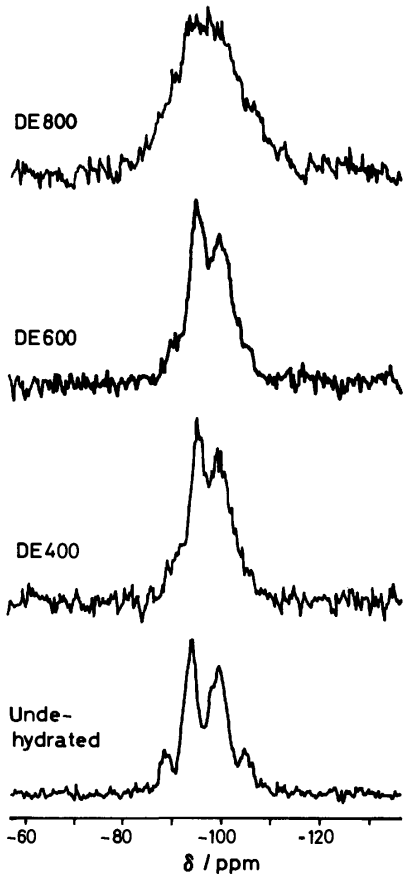

Fig. 4. ^{29}Si MAS NMR spectra of undehydrated and dehydrated Na-Y zeolites with the flip angle of about $\pi/2$ and the recycle time of 10 s. The intensity is not normalized.

Table 2. ^{1}H NMR Results

Sample	Peak / ppm	FWHM / kHz	C_H[a)]
Undehydrated	5.0	0.22	100
DE400	12	2.50	3.2
DE600	8.6	0.92	1.9
DE800	4.2	0.34	2.8

a) Relative hydrogen content with respect to the unit cell of the framework.

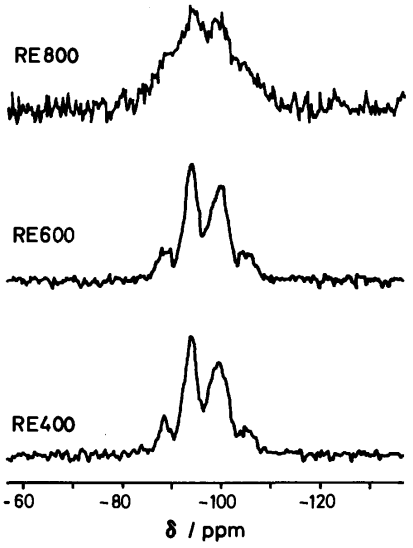

Fig. 5. ^{29}Si MAS NMR spectra of rehydrated Na-Y zeolites under the same measuring conditions as in Fig. 4.

lose most of their water. Though DE800 has a higher hydrogen content than DE600, it is probably caused by the absorption of water from atmospheric moisture after the dehydration process. The motionally-narrowed line which (0.34 kHz) of DE800 supports that the hydrogen is present in the form of mobile H_2O.

X-Ray Diffraction. The undehydrated sample shows a typical pattern of faujasite framework. Some peaks of the faujasite framework split into doublet in the pattern of DE400, indicating the lowering of the crystal symmetry. On the other hand, DE600 has the same pattern as the undehydrated sample, recovering the crystal symmetry. DE800 has a broad peak in addition to the pattern of the faujasite framework, which demonstrates that the framework structure is partially decomposed.

Thermal Analysis. Most of water molecules were desorbed in the temperature range between 35 and 350 °C, whose weight is 24.4% of the undehydrated sample. Weight decreased gradually up to 900°C, and finally 25.1% of the weight was lost.

Discussion

The DE samples lose most of their water, as demonstrated by ^{1}H NMR. X-Ray diffraction results indicate that DE400 and DE600 retain their network structure, while DE800 is a mixture of the faujasite network and an amorphous silica-alumina. Rehydration can reproduce the undehydrated state from DE400 and DE600, while it cannot from DE800, which is clearly demonstrated by ^{23}Na, ^{27}Al, and ^{29}Si NMR results.

^{23}Na NMR. Since ^{23}Na spin has quadrupole moment, the linewidth of the central line is broadened mainly by second-order quadrupole interaction,[11,12] reflecting coordination symmetry of the Na ion. The spectrum of the undehydrated sample shows a sharp line at −12 ppm without any spinning sidebands, which indicates that the Na ions are located in high-symmetry sites, coordinated by water molecules. On the other hand, the spectra of DE400 and DE600 have asymmetric line shapes and are accompanied by many spinning sidebands, suggesting that the Na ions are located in slightly-low-symmetry sites. The Na ions lose water molecules coordinating to themselves by the dehydration, as shown by the ^{1}H NMR results, and they approach to the framework atoms. Thus the coordination symmetry of the Na ions becomes slightly lower. The spectrum of DE800 shows a broad line centered at −28 ppm with many spinning sidebands, demonstrating that the Na ions are located in low-symmetry sites. It must be noted that a small shoulder is observed at about −10 ppm in the spectra of DE800, which can be ascribed to the Na ions in the faujasite framework left undecomposed.

By the rehydration, the Na ions in DE400 and DE600 recover their site symmetry, coordinated by water molecules. On the other hand, the spectrum of RE800 is composed of two lines centered at about −10 and −30 ppm. A part of Na ions in DE800 recover their symmetry, which are considered to be located not in the amorphous region but in the faujasite framework.

Consequently, three kinds of Na ions are observed with different site-symmetries. The difference in the signal position is originated from second-order quadrupole shift[12] and/or chemical shift.

The total signal intensities are largely reduced by the dehydration. Though the quadrupole interaction reduces the signal intensity,[13] the observed large reduction indicates the presence of undetectable nuclei, which are considered to be located at sites with very low symmetry. A simplified calculation suggests that 85 at% of Na ions are not observed in DE400 and DE600, while 70 at% in DE800.

A simple model is presented which can express the correlation between the Na sites and the NMR spectra. In the faujasite framework there are three kinds of occupied sites with different symmetries. The Na ions in the first site are coordinated by water molecules and have high symmetry, producing the narrow NMR line at −12 ppm without sidebands. The second site has slightly low symmetry, giving the asymmetric line at −10 ppm with many spinning sidebands, and the third site has very low symmetry, giving no detectable line. Only the first site is occupied in the hydrated state, while Na ions are distributed over the second and third sites in the dehydrated state. On the other hand, the amorphous region has low-symmetry sites and the third sites. The Na ions in this region cannot be hydrated to form symmetrical Na–H_2O clusters, probably because the ions are trapped on sites having an insufficient space for the cluster.

^{27}Al NMR. ^{27}Al spectra have only one peak which can be attributed to four-coordinated Al. DE400 and DE600 have larger linewidths than the undehydrated sample, which is considered to be broadened by second-order quadrupole effect. The AlO_4 tetrahedra is considered to be distorted by the approach of Na ions on dehydration. The approach of Na ions to the AlO_4 tetrahedra also gives rise to the lowering of Na site symmetry, as described above.

The broadening of the ^{27}Al resonance line on dehydration has been reported for H-ZSM-5 and H-Y, but in the case of Na-ZSM-5 the broadening is so large that the resonance line disappears.[5,6] On the contrary, a signal can be observed in the present case of Na-Y, but the intensity corresponding to 30–40 at% of Al atoms decreases. The decrease is partly explained by the increase in quadrupole interaction which reduces the intensity of the central line. Thus the value of 30—40 at% is only the upper limit of the

undetected Al atoms.

Rehydration can reproduce the ^{27}Al spectrum, since Na ions are removed from the neighborhood of the AlO_4 tetrahedra by coordination of water molecules. On the other hand, the spectrum of DE800 does not change by the rehydration, although DE800 indicates the same line shape and intensity as DE400 and DE600. The symmetry of the AlO_4 tetrahedra in DE800 is lowered by the decomposition of the network, not only by the neighboring Na ions.

^{29}Si NMR. The width of each Si(nAl) line is broadened by the dehydration, which is caused by dipolar interaction with ^{27}Al perturbed by its quadrupole interaction and/or chemical shift dispersion. Line broadening of a $I=1/2$ spin bonded to a $I \geqq 1$ spin has been reported for ^{13}C spectra of α-carbon atoms in amino acids.[14] The increase of electric field gradient on the Al nuclei makes the ^{29}Si resonance line broader in the present case. Chemical shift dispersion may be produced by lowering of the crystal symmetry. The results of X-ray diffraction and ^{29}Si NMR however indicate that the crystal symmetry does not influence the line width very much in this case, as explained below. Although DE400 has an X-ray diffraction pattern with lower crystal symmetry than the undehydrated sample and DE600, the ^{29}Si NMR spectra of DE400 and DE600 agree with each other. Furthermore, the ^{29}Si spectra of DE600 and the undehydrated sample are different in spite that they have the same X-ray diffraction pattern.

The peaks ascribed to Si(3Al) and Si(2Al) are shifted towards higher field by the dehydration. The shift is considered to be caused by the interaction with Al, since the shift is only observed for the Si atom coordinated by more than one Al atom.

In the case of ZSM-5 the ^{29}Si spectral structure is not directly correlated with the hydration state.[4] Heat treatment causes line narrowing instead of broadening, which is attributed to temoval of lattice defects such as Si-OH. This behavior is different from the present results of Na-Y. Since the Na-Y sample has a much higher Al content than ZSM-5, the ^{29}Si NMR spectrum of Na-Y is inevitably influenced by the Al nuclei.

By heating at 800 °C, the network structure is broken, and the amorphous part produces a broad ^{29}Si line without any fine structure. The structure cannot be reconstructed by the rehydration, so that the spectrum of the amorphous part does not change. Though RE800 shows a little fine structure, it is produced by a crystalline part left undecomposed.

The T_1 value of ^{29}Si nuclei is also changed by the dehydration, though the network structure retains. The mechanism of the ^{29}Si relaxation is not established now, but paramagnetic impurities have been reported to have some role in the relaxation.[15] From the present study, it can be concluded that water in the cage plays some role in the ^{29}Si relaxation. Water molecules are considered to be a transport medium of paramagnetic impurities.

In summary, ^{23}Na, ^{27}Al, and ^{29}Si MAS NMR spectra can reflect the hydration state of Y-type zeolites very well. Line shape, position, and width of the spectra and spin-lattice relaxation time are changed by dehydration and hydration treatments.

The authors acknowledge useful discussion to Dr. Shigemitsu Shin and Dr. Kunio Suzuki of this Laboratory. They also acknowledge the supply of the material to Catalysis Society of Japan, and the thermal analysis to Rigaku Denki Co. Ltd. Thanks are also expressed to the referee for his useful comments.

References

1) J. Klinowski, *Prog. NMR Spectrosc.*, **16**, 237 (1984).
2) E. Lippmaa, M. Mägi, A. Samoson, M. Tarmak, and G. Engelhardt, *J. Am. Chem. Soc.*, **103**, 4992 (1981).
3) D. Müller, G. Gessner, H.-J. Behrens, and G. Scheler, *Chem. Phys. Lett.*, **79**, 59 (1981).
4) G. Boxhoorn, A. G. T. G. Kortbeek, G. R. Hays, and N. C. M. Alma, *Zeolites*, **4**, 15 (1984).
5) A. P. M. Kentgens, K. F. M. G. J. Scholle, and W. S. Veeman, *J. Phys. Chem.*, **87**, 4357 (1983).
6) J. B. Nagy, Z. Gabelica, G. Debras, E. G. Derouane, J.-P. Gilson, and P. A. Jacobs, *Zeolites*, **4**, 133 (1984).
7) E. R. Andrew, *Prog. NMR Spectrosc.*, **8**, 1 (1972).
8) A. Abragam, "The principles of Nuclear Magnetism," Oxford University Press, London (1961), p. 36.
9) W. Loewenstein, *Am. Mineral.*, **39**, 92 (1954).
10) J. Klinowski, S. Ramdas, and J. M. Thomas, *J. Chem. Soc., Faraday Trans. 2*, **78**, 1025 (1982).
11) E. Kundla, A. Samoson, and E. Lippmaa, *Chem.Phys. Lett.*, **83**, 229 (1981).
12) H.-J. Behrens and B. Schnabel, *Physica*, **114B**, 185 (1982).
13) D. Fenzke, D. Freude, T. Frölich, and J. Haase, *Chem. Phys. Lett.*, **111**, 171 (1984).
14) C. J. Groombridge, R. K. Harris, K. J. Packer, B. J. Say, and S. F. Tanner, *J. Chem. Soc., Chem. Commun.*, **1980**, 174.
15) T. Watanabe, H. Shimizu, A. Masuda, and H. Saito, *Chem. Lett.*, **1983**, 1293.

The Phase Transition of 1,4-Dialkyl-1,4-diazoniabicyclo[2.2.2]octane Dibromides, C_n-DABCO-C_{n+1}-Br_2 ($10 \leqq n \leqq 17$)

Kengo IMAMURA, Takashi NOGAMI,* and Yasuhiko SHIROTA
Department of Applied Chemistry, Faculty of Engineering, Osaka University, Yamadaoka, Suita, Osaka 565
(Received July 26, 1986)

The phase transitions of 1,4-dialkyl-1,4-diazoniabicyclo[2.2.2]octane dibromide (bis(quaternary alkyl bromide salts) of DABCO) in which the difference in the carbon numbers of the two alkyl groups is one, were studied on the basis of measurements of differential scanning calorimetry, infrared absorption spectroscopy, and bromide-anion conductivities. The DSC measurements showed that an endothermic transition occurred at T_{c1} when the sample was heated from room temperature. An exothermic transition occurred at T_{c2}($T_{c2}<T_{c1}$) when the sample was cooled after it had been heated above T_{c1}. The transition temperatures (T_{c1} and T_{c2}), the transition enthalpies, and the transition entropies increased as the increase in the alkyl-chain lengths. T_{c1} was found to be governed by the even numbers of the alkyl group. The temperature dependence of the IR absorption spectra showed that the *trans*-zigzag conformation of the alkyl chain was destroyed by a conformational change above T_{c1}, and that the annealed sample existed as a metastable phase. The temperature dependence of the bromide-anion conductivities showed abrupt increases in the conductivities by three orders of magnitude at around the transition temperatures. The temperatures of the conductivity jump of the virgin samples were usually higher than those of the annealed samples. The differences in these two temperatures tended to become smaller as the increase in the alkyl-chain lengths. This fact can be explained as that the solid-state properties of the unsymmetric bis(quaternary salts) of DABCO tend to resemble those of the symmetric bis(quaternary salts) of DABCO as the increase in the alkyl-chain lengths.

A series of 1,4-dialkyl-1,4-diazoniabicyclo[2.2.2]octane dihalides (denoted as bis(quaternary salts) of DABCO) were found to exhibit phase transitions above room temperature by us.[1-4] The phase transition was studied by means of a DSC, IR absorption spectra, and a study of halide-anion conductivities. The phase transition of the symmetric bis(quaternary salts) was quite different from that of the unsymmetric bis(quaternary salts). In the case of the symmetric salts, almost a reversible transition was observed.[1,2] On the other hand, the unsymmetric salts were converted to the metastable phase when they were heated above the transition temperature, and then cooled.[3,4] The thermodynamic properties of the unsymmetric salts were explained by free energy-temperature relation. Some of the unsymmetric salts showed the conversion from the metastable phase to the stable phase during several days when they were kept at room temperature. The larger the difference in the carbon numbers of the two alkyl groups attached to DABCO nitrogens, the faster was the conversion rate from the metastable phase to the stable phase.[4] When the difference in the carbon numbers of the two alkyl groups was two, the conversion rates were too slow to be followed.[3] If we designate the bis(quaternary alkyl halide salt) of DABCO by the halide anion and by the numbers of the alkyl carbons (see Refs. 3 and 4),[5] the thermodynamic properties of the symmetric salts, C_n-DABCO-C_n-X_2 (X=Cl, Br, and I; $10 \leqq n \leqq 22$),[1,2] are quite different from those of the unsymmetric salts, C_n-DABCO-C_{n+2}-Br_2 ($10 \leqq n \leqq 16$)[3] and C_{10}-DABCO-C_n-Br_2 ($13 \leqq n \leqq 22$).[4] Thus, the phase transitions of a series of the unsymmetric salts, C_n-DABCO-C_{n+1}-Br_2, are interesting, because they seem to belong to the borderline of the different behaviors of the phase transitions. We studied the phase transitions of the bis(quaternary alkyl bromide salts) of DABCO, C_n-DABCO-C_{n+1}-Br_2 ($10 \leqq n \leqq 17$), by means of DSC, IR absorption spectra, and the measurements of the bromide-anion conductivities. The materials studied are shown in Fig. 1.

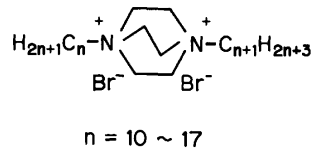

Fig. 1. Unsymmetric bis(quaternary alkyl bromide salts) of DABCO, C_n-DABCO-C_{n+1}-Br_2.

Experimental

Syntheses of Unsymmetric Bis(quaternary salts) of DABCO. The unsymmetric salt of DABCO was synthesized by two steps of the reactions, i.e., a synthesis of the mono(quaternary salt) by the reaction of DABCO with an equimolar amount of alkyl bromide, followed by a reaction of the resultant mono(quaternary salt) with another alkyl bromide. Detailed procedures were described previously.[3,4] All of the materials were recrystallized four or five times. The solvents of the recrystallization are acetonitrile for C_n-DABCO-C_{n+1}-Br_2 ($10 \leqq n \leqq 14$) and ethanol for C_n-DABCO-C_{n+1}-Br_2 ($15 \leqq n \leqq 17$) respectively.

Measurements. The DSC, the bromide-anion conductivities, and the IR absorption spectra were measured by the methods described previously.[2-4]

Results and Discussion

DSC Measurements. The DSC measurements were made while changing the temperature by 5 °C min^{-1}. When virgin samples[6] were heated from room temperature, endothermic signals ($\Delta H_{en,1}$) were obtained at T_{c1}. C_{11}-DABCO-C_{12}-Br_2 and C_n-DABCO-C_{n+1}-Br_2 (n=10, 13, and 15) showed three and two endothermic signals respectively. On the other hand, C_n-DABCO-C_{n+1}-Br_2 (n=12, 14, 16, and 17) showed only one endothermic signal. When the samples were cooled after they had once been heated above T_{c1}, all of them showed one exothermic signal ($\Delta H_{ex,1}$) at T_{c2} which was lower than T_{c1}; $T_{c1}>T_{c2}$. The succeeding heating-cooling cycles showed reproducible endothermic ($\Delta H_{en,2}$) and exothermic ($\Delta H_{ex,1}$) signals at around T_{c2}. The absolute values of $\Delta H_{ex,1}$ and $\Delta H_{en,2}$ were equal within the experimental error. Figure 2 shows the observed thermogram of C_{10}-DABCO-C_{11}-Br_2 as a typical example. The endothermic signals $\Delta H_{en,1}$ were usually broader[7] than $\Delta H_{en,2}$ for all of the materials studied. The observation of at least two transition temperatures (T_{c1} and T_{c2}) can be explained by the free energy-temperature relation as described before.[3,4] According to this, the sample exists as a metastable phase (C_M) when it is heated above T_{c1} and then cooled. Even if the sample was left at room temperature for weeks after it had been heated above T_{c1}, it showed endothermic ($\Delta H_{en,2}$) and exothermic ($\Delta H_{ex,1}$) signals at around T_{c2}. This fact shows that the potential barrier from the C_M phase to the stable phase (C_L) is too high for the C_M phase to go back to the C_L phase. Similar phenomena were also observed for C_n-DABCO-C_{n+2}-Br_2 ($10 \leqq n \leqq 16$).[3] This is consistent with the previous observation[3,4] that the conversion rate from C_M to C_L becomes slower as the decrease in the differences in the carbon numbers of the two alkyl chains attached to DABCO nitrogens. Part of Table 1 shows some materials, T_{c1}, T_{c2}, $\Delta H_{en,1}$,[8] ΔS_1 ($=\Delta H_{en,1}/T_{c1}$),[8] $\Delta H_{en,2}$, and ΔS_2 ($=\Delta H_{en,2}/T_{c2}$). Here ΔS_1 and ΔS_2 denote the transition entropies at T_{c1} and T_{c2} respectively. Since the virgin samples of C_n-DABCO-C_{n+1}-Br_2 (n=10, 11, 13, 15) showed more than one transitions, all of the transition temperatures and the corresponding transition enthalpies and transition entropies are shown for these materials in this table. The transition temperatures were obtained by the onsets of the endothermic signals. Figure 3 plots the transition temperatures (T_{c1} and T_{c2}) against the carbon numbers (n) of the alkyl groups of C_n-DABCO-C_{n+1}-Br_2. The transition temperatures of the symmetric salts, C_n-DABCO-C_n-Br_2 and C_{n+1}-DABCO-C_{n+1}-Br_2,[2] are also plotted for the sake of comparison. The following characteristics can be seen from Fig. 3. (1) The transition temperatures tend to increase as the increase in the alkyl-chain length. (2) The separation between T_{c1} and T_{c2} becomes smaller as the increase in the alkyl-chain length. (3)

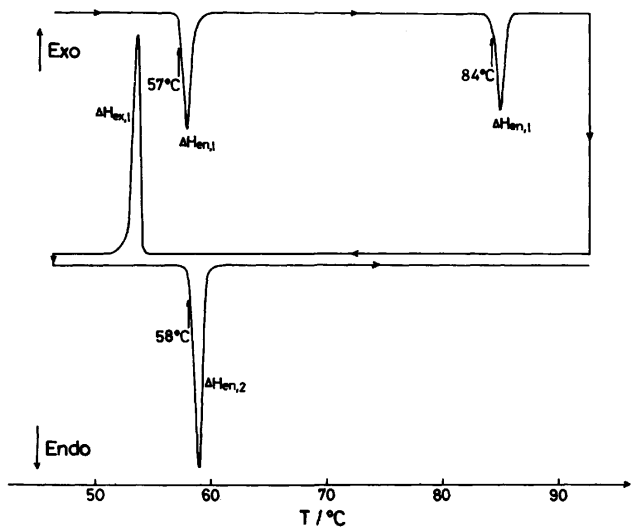

Fig. 2. DSC thermogram of C_{10}-DABCO-C_{11}-Br_2. Note that the sum of the two endothermic heats of transition ($\Delta H_{en,1}$) is close to the value of $\Delta H_{en,2}$.

Table 1. Materials, and the Transition Temperatures, Transition Enthalpies, Transition Entropies, and the Ratios of the Bromide-Anion Conductivities Before and After the Transitions

Materials	T_{c1} / °C	$\Delta H_{en,1}$ / kJ mol^{-1}	ΔS_1 / J/(mol deg)	σ_h/σ_1[a]	T_{c2} / °C	$\Delta H_{en,2}$ / kJ mol^{-1}	ΔS_2 / J/(mol deg)	σ_h/σ_1[b]
C_{10}-DABCO-C_{11}-Br_2	57, 84	27.1, 22.6	82, 63	820, 4[c]	58	48.9	148	1900
C_{11}-DABCO-C_{12}-Br_2	69, 77, 82	16.2, 22.7, 25.8	47, 65, 73	4500	65	51.7	153	2100
C_{12}-DABCO-C_{13}-Br_2	77	62.3	178	6000	72	59.7	173	5800
C_{13}-DABCO-C_{14}-Br_2	86, 87	69.3	193	1600	78	68.0	194	1500
C_{14}-DABCO-C_{15}-Br_2	88	76.9	213	1000	83	76.1	214	3200
C_{15}-DABCO-C_{16}-Br_2	89, 91	78.7	217	3300	87	78.4	218	3200
C_{16}-DABCO-C_{17}-Br_2	92	85.7	235	1700	90	87.3	240	1800
C_{17}-DABCO-C_{18}-Br_2	92	90.2	247	3100	92	96.1	263	1800

a) For the virgin samples. b) For the annealed samples. c) As shown in Fig. 6, two steps of the conductivity jumps were observed.

T_{c1}'s of C_n-DABCO-C_{n+1}-Br_2[9] are close to either the corresponding transition temperatures of C_n-DABCO-C_n-Br_2 or those of C_{n+1}-DABCO-C_{n+1}-Br_2. It is noteworthy that T_{c1}'s of C_n-DABCO-C_{n+1}-Br_2 (n= odd number) and those of C_n-DABCO-C_{n+1}-Br_2 (n=even number) are close to the transition temperatures of C_{n+1}-DABCO-C_{n+1}-Br_2 and C_n-DABCO-C_n-Br_2 respectively.[10]

The characteristic (1) above can be explained as follows. Since the phase transition is caused mainly by a conformational change in the alkyl groups,[2-4] a parallel relation between the transition temperature and the alkyl-chain length arises from an increase in the van der Waals force between molecules as the increase in the alkyl-chain length. The characteristic (2) can be explained as follows. The molecular shape of the unsymmetric bis(quaternary salt) of DABCO tends to resemble that of the symmetric salt as the increase in the alkyl-chain length. Thus, C_{17}-DABCO-C_{18}-Br_2 showed reversible transition (only one transition temperature) like the cases of the symmetric bis(quaternary alkyl halide salts) of DABCO.[1,2] Although the characteristic (3) is interesting, the reason is as yet not clear. Since the present materials possess both even and odd numbers of the alkyl carbons, the following expression (3)′ is simpler for the characteristic (3). (3)′ The transition temperature (T_{c1}) of C_n-DABCO-C_{n+1}-Br_2 is determined by the alkyl group of the even numbers of carbons, and it is close to that of the corresponding symmetric salt possessing the same (even) number of alkyl carbons.

Figure 4 plots the transition enthalpies ($\Delta H_{en,1}$ and $\Delta H_{en,2}$) against the carbon numbers (n) of the alkyl groups of C_n-DABCO-C_{n+1}-Br_2. This figure also shows similar plots of the transition enthalpies of the symmetric bis(quaternary salts),[2] C_n-DABCO-C_n-Br_2 and C_{n+1}-DABCO-C_{n+1}-Br_2, for the sake of comparison. The dotted circles of C_n-DABCO-C_{n+1}-Br_2 (n=10, 11) mean the sums of the transition enthalpies ($\Delta H_{en,1}$) of these materials. The following three characteristics can be seen from Fig. 4. (1) Both $\Delta H_{en,2}$ and $\Delta H_{en,1}$ tend to increase as the increase in the alkyl-chain length. (2) $\Delta H_{en,1}$'s are close to $\Delta H_{en,2}$'s for

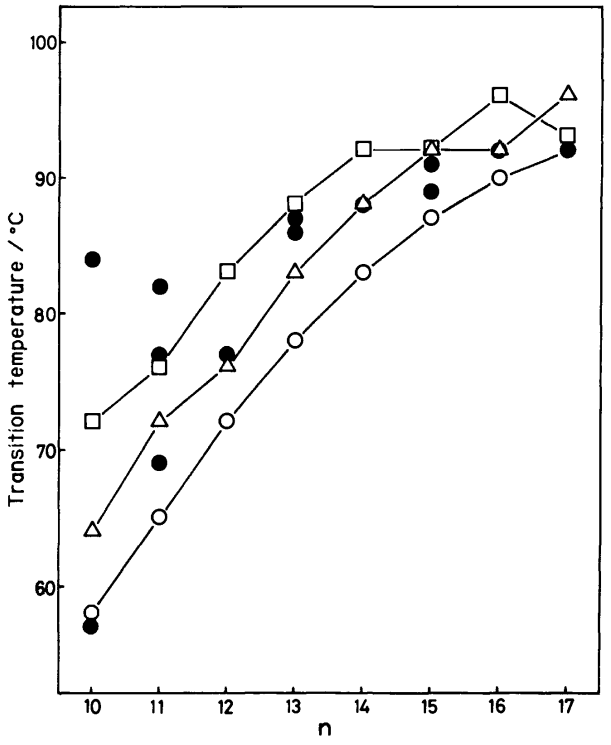

Fig. 3. The plot of the transition temperatures (T_{c1} and T_{c2}) against the carbon numbers (n) of alkyl group of C_n-DABCO-C_{n+1}-Br_2. The transition temperatures of the symmetric salts, C_n-DABCO-C_n-Br_2 and C_{n+1}-DABCO-C_{n+1}-Br_2, are also plotted for the sake of comparison.
●: T_{c1} of C_n-DABCO-C_{n+1}-Br_2, ○: T_{c2} of C_n-DABCO-C_{n+1}-Br_2. △: T_c of C_n-DABCO-C_n-Br_2, □: T_c of C_{n+1}-DABCO-C_{n+1}-Br_2.

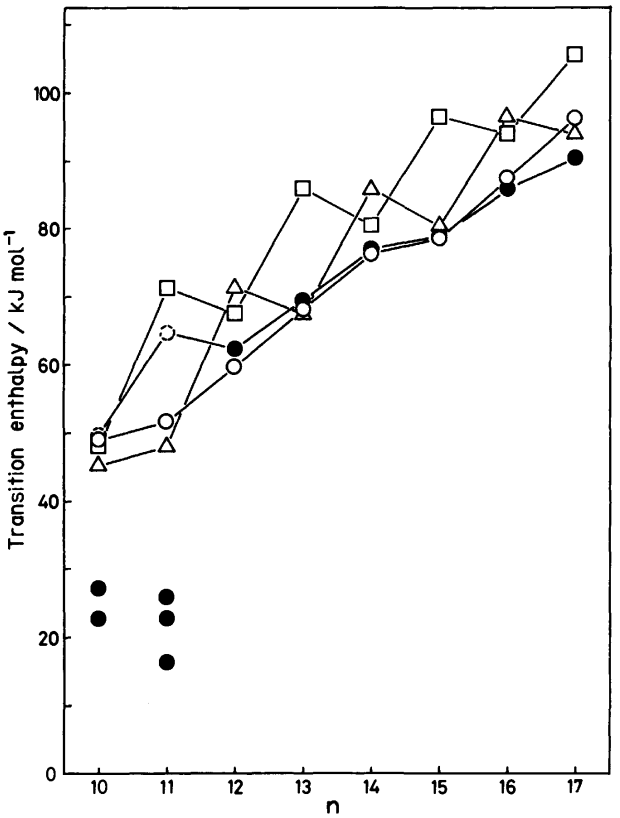

Fig. 4. The plot of the transition enthalpies ($\Delta H_{en,1}$ and $\Delta H_{en,2}$) against the carbon numbers (n) of alkyl group of C_n-DABCO-C_{n+1}-Br_2. The transition enthalpies of the symmetric salts, C_n-DABCO-C_n-Br_2 and C_{n+1}-DABCO-C_{n+1}-Br_2, are also plotted for the sake of comparison. Dotted circles mean the sum of the two transition enthaplies ($\Delta H_{en,1}$)for C_{10}-DABCO-C_{11}-Br_2 and that of the three transition enthalpies ($\Delta H_{en,1}$) for C_{11}-DABCO-C_{12}-Br_2.
●: $\Delta H_{en,1}$ of C_n-DABCO-C_{n+1}-Br_2, ○: $\Delta H_{en,2}$ of C_n-DABCO-C_{n+1}-Br_2. △: ΔH of C_n-DABCO-C_n-Br_2, □: ΔH of C_{n+1}-DABCO-C_{n+1}-Br_2.

C_n-DABCO-C_{n+1}-Br_2 ($12 \leqq n \leqq 17$). In the case of C_{10}-DABCO-C_{11}-Br_2, the sum of the two transition enthalpies ($\Delta H_{en,1}$) is close to $\Delta H_{en,2}$ (see also Fig. 2). (3) Comparison of $\Delta H_{en,2}$'s with the transition enthalpies of the symmetric salts gives the following rules: $\Delta H_{en,2}$'s of C_n-DABCO-C_{n+1}-Br_2 (n=odd number) are close to the transition enthalpies of the corresponding symmetric salts, C_n-DABCO-C_n-Br_2; if n is an even number, the following order holds except for C_{10}-DABCO-C_{11}-Br_2 (ΔH for C_n-DABCO-C_n-Br_2 > ΔH for C_{n+1}-DABCO-C_{n+1}-Br_2 > $\Delta H_{en,2}$ for C_n-DABCO-C_{n+1}-Br_2). Figure 5 plots the transition entropies (ΔS_1 and ΔS_2) against the carbon numbers (n) of the alkyl group of C_n-DABCO-C_{n+1}-Br_2. This figure also shows similar plots of the transition entropies of the symmetric bis(quaternary salts),[2,3] C_n-DABCO-C_n-Br_2 and C_{n+1}-DABCO-C_{n+1}-Br_2, for the sake of comparison. The dotted circles of C_n-DABCO-C_{n+1}-Br_2 (n=10, 11) mean the sum of the transition entropies (ΔS_1) of these materials. From Fig. 5, the characteristics (1)—(3) above of the transition enthalpies also hold in the cases of the transition entropies. From the Boltzmann relation, $\Delta S = R \ln W$, the numbers of sites (W) above the transition temperatures were estimated to be in the range of 300—5.7×10^{13} for the virgin and the annealed samples.[6,11] The large values of W suggest that the conformational change occurs at the every carbon site of the alkyl groups.

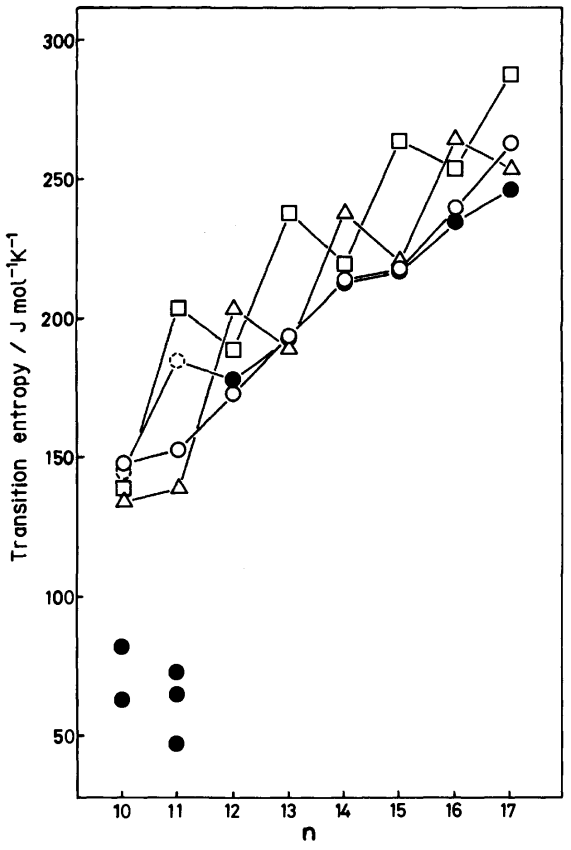

Fig. 5. The plot of the transition entropies (ΔS_1 and ΔS_2) against the carbon numbers (n) of alkyl group of C_n-DABCO-C_{n+1}-Br_2 ($\Delta S_1 = \Delta H_{en,1}/T_{c1}$, $\Delta S_2 = \Delta H_{en,2}/T_{c2}$). The transition entropies of the symmetric salts, C_n-DABCO-C_n-Br_2 and C_{n+1}-DABCO-C_{n+1}-Br_2, are also plotted for the sake of comparison. Dotted circles mean the sum of the two transition entropies for C_{10}-DABCO-C_{11}-Br_2 and that of the three transition entropies for C_{11}-DABCO-C_{12}-Br_2 respectively.
●: ΔS_1 of C_n-DABCO-C_{n+1}-Br_2, ○: ΔS_2 of C_n-DABCO-C_{n+1}-Br_2. △: ΔS of C_n-DABCO-C_n-Br_2, □: ΔS of C_{n+1}-DABCO-C_{n+1}-Br_2.

The characteristic (1) for the transition enthalpies is explained by the increase in the van der Waals force between molecules as the increase in the alkyl-chain length. The characteristic (1) for the transition entropies could be explained as follows. Since the phase transition is mainly caused by a conformational change in the alkyl group, the number of the sites after the transition increase as the increase in the alkyl-chain length. This gives rise to an increase in the transition entropies as an increase in the alkyl-chain length. The characteristic (2) for the transition enthalpies and entropies suggests that the structure of the C_M phase is not very different from that of the C_L phase. Since the difference in the numbers of the alkyl carbons is one in the present materials, their thermodynamic properties resemble those of the symmetric salts which have shown no clear indication of the presence of the metastable phase. The characteristic (2) is in common with the cases of the unsymmetric salts, C_n-DABCO-C_{n+2}-Br_2,[3] but is in sharp contrast to the cases of the unsymmetric salts, C_{10}-DABCO-C_n-Br_2.[4] In the latter cases, $\Delta H_{en,1}$ and ΔS_1 were larger than $\Delta H_{en,2}$ and ΔS_2 respectively. These facts show that the structural difference between C_L and C_M is small for C_n-DABCO-C_{n+1}-Br_2 and C_n-DABCO-C_{n+2}-Br_2, and that it tends to become larger with an increase in the alkyl-chain length. It is noteworthy that the sum of the two transition enthalpies ($\Delta H_{en,1}$) and that of the two transition entropies (ΔS_1) are close to $\Delta H_{en,2}$ and ΔS_2, respectively, in C_{10}-DABCO-C_{11}-Br_2. However, these relations do not hold in the case of C_{11}-DABCO-C_{12}-Br_2; the sums of the transition enthalpies and the transition entropies are larger than $\Delta H_{en,2}$ and ΔS_2 respectively. In order to clarify the thermodynamic properties described above, the determinations of the crystal structures of the present materials seem to be crucial.

Infrared Absorption Spectroscopy. The temperature dependence of the infrared absorption spectra of C_{13}-DABCO-C_{14}-Br_2 was measured as an example in order to obtain more information regarding the phase transition. It showed a similar change in the IR spectra as has been observed in the cases of the unsymmetric bis(quaternary alkyl bromide salts) of DABCO.[3,4] The virgin sample exhibited band

progressions originating from 720 cm^{-1}. This is the evidence for the *trans*-zigzag conformation of the alkyl groups. The band progressions suddenly disappeared at T_{c1} when the sample was heated from room temperature, and they appeared again at T_{c2} upon cooling the sample. This fact shows that the *trans*-zigzag conformation of the alkyl group is destroyed in the high temperature phase, and that the annealed sample[6] exists as a metastable phase. This is consistent with the DSC results. The detailed

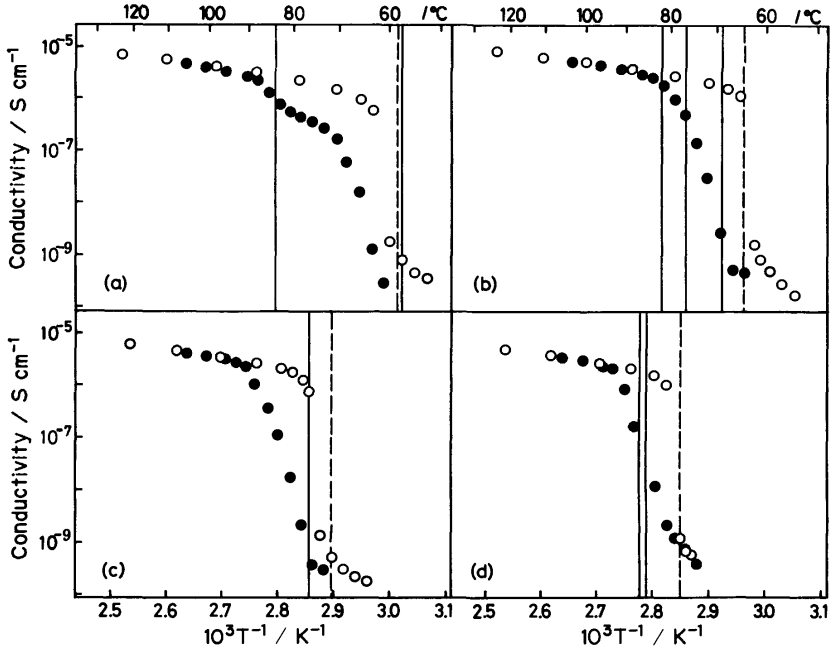

Fig. 6. Temperature dependence of the bromide-anion conductivities of C_n-DABCO-C_{n+1}-Br_2 ($10 \leqq n \leqq 13$) (●: virgin sample, ○: annealed sample). The vertical solid- and dotted-lines represent T_{c1} and T_{c2} respectively.
(a) $n=10$, (b) $n=11$, (c) $n=12$, (d) $n=13$.

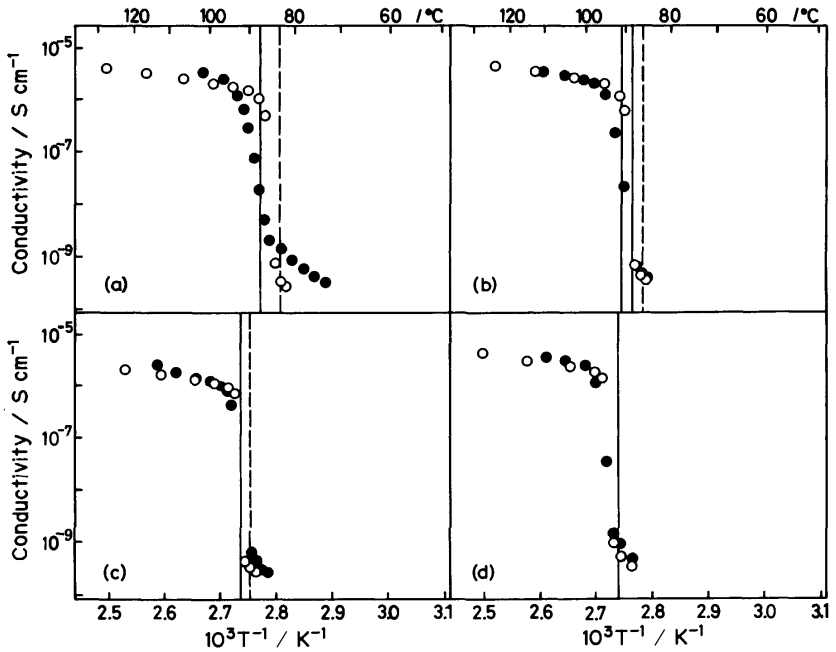

Fig. 7. Temperature dependence of the bromide-anion conductivities of C_n-DABCO-C_{n+1}-Br_2 ($14 \leqq n \leqq 17$) (●: virgin sample, ○: annealed sample). The vertical solid- and dotted-lines represent T_{c1} and T_{c2} respectively.
(a) $n=14$, (b) $n=15$, (c) $n=16$, (d) $n=17$.

discussion was given in the previous papers.[3,4]

Bromide-Anion Conductivities. All of the samples were confirmed to be bromide-anion conductors by the method described previously.[1] The bromide-anion conductivities were measured for the compressed pellet sample by an AC impedance method.[1-4] The conductivities of the virgin samples[6] were measured first by heating the sample slowly (0.5 °C min^{-1}) from room temperature across T_{c1}. The sample was then allowed to cool to room temperature, and the conductivities of the annealed sample[6] were measured by heating the sample again. Figures 6 and 7 show the temperature dependences of the bromide-anion conductivities of C_n-DABCO-C_{n+1}-Br_2 ($10 \leqq n \leqq 13$) and C_n-DABCO-C_{n+1}-Br_2 ($14 \leqq n \leqq 17$) respectively. Each figure shows both conductivities of the virgin and the annealed samples . The vertical solid- and dotted-lines represent T_{c1} and T_{c2} respectively. The conductivities less than 10^{-9} S cm^{-1} were below the limit of our measurements. All of the samples showed abrupt increases in the bromide-anion conductivities by three orders of magnitude at around the transition temperatures; the virgin and the annealed samples showed the conductivity jumps at around T_{c1} and T_{c2} respectively. Table 1 shows the ratios of the conductivities before (σ_l) and after (σ_h) the transition for the virgin and the annealed samples. They were found to be in the range of 1000 to 6000 for the virgin samples and in that of 1800 to 5800 for the annealed samples. The conductivity jump (σ_h/σ_l=6000) of C_{12}-DABCO-C_{13}-Br_2 is the largest of all of the materials studied hitherto.[2-4] To see closely Figs. 6 and 7, the following three characteristics are noteworthy. (1) The difference in the temperatures of the conductivity jumps between the virgin and the annealed samples tends to become smaller as the increase in the alkyl-chain lengths. (2) The conductivity jump becomes sharper as the increase in the alkyl-chain lengths. (3) Although the conductivities are quite different below the transition temperatures, they are almost similar above the transition temperatures with the activation energies of about 30 kJ mol^{-1}.

The characteristics (1) and (2) above are consistent with the results of the DSC measurements; the thermodynamic properties of the unsymmetric salts tend to resemble those of the symmetric salts as the increase in the alkyl-chain lengths. Since the symmetric salts showed only slight hysteresis of the conductivity jumps,[2] the characteristic (1) can be understood as a natural phenomenon. The characteristic (2) can also be deduced from the sharp conductivity jumps observed for the symmetric salts.[1,2] The characteristic (3) is a common phenomenon of all of the bis(quaternary alkyl halide salts) of DABCO, irrespective of the symmetric and unsymmetric salts, and it was discussed before.[2] From Figs. 6 and 7 and Table 1, it can not be said generally whether the virgin samples exhibit larger conductivity jumps than the annealed samples or not. The conductivity jump is caused by the formation of a large number of voids as a result of the conformational movement of the alkyl groups above the transition temperature.

Figures 6 and 7 also show the relations between the conductivity jumps and the transition temperatures (T_{c1} and T_{c2}). T_{c2}'s were located at the onsets of the conductivity jumps of the annealed samples except for C_{11}-DABCO-C_{12}-Br_2. T_{c1}'s were also located at the onsets of the conductivity jumps of the virgin samples for C_n-DABCO-C_{n+1}-Br_2(n=10, 11, 12, 17). However, T_{c1}'s were located at around the middle points of the conductivity jumps of the virgin samples for C_n-DABCO-C_{n+1}-Br_2(n=13, 14, 15, 16). The second T_{c1} of C_{10}-DABCO-C_{11}-Br_2 corresponds to the second conductivity jump. The second and the third T_{c1}'s of C_{11}-DABCO-C_{12}-Br_2 were located at around the end points of the conductivity jump. Although the complex behaviors of the relations between T_{c1}'s and the conductivity jumps are as yet not clear, they will reflect the difference in the formations of the voids as a result of the conformational change in the alkyl groups.

Summary. The phase transitions of bis(quaternary alkyl bromide salts) of DABCO, C_n-DABCO-C_{n+1}-Br_2 ($10 \leqq n \leqq 17$), were studied by means of the DSC, the infrared absorption spectroscopy, and the measurements of the bromide-anion conductivities. As described in the Introduction, these materials seem to belong to the borderline of the solid-state properties between the symmetric and unsymmetric bis(quaternary salts) which have been studied previously.[1-4] As expected, the present materials showed both properties of the symmetric and the unsymmetric salts as will be shown below. (1) C_n-DABCO-C_{n+1}-Br_2 showed at least two transition temperatures (T_{c1} and T_{c2}), and the annealed samples were found to be converted to the metastable phase by the DSC and the IR absorption spectra. These properties are similar to the cases of the unsymmetric salts.[3,4] (2) The separation between T_{c1} and T_{c2} tends to become smaller with an increase in the alkyl-chain length. C_{17}-DABCO-C_{18}-Br_2, which has the longest alkyl groups of the present materials, showed only one transition temperature; this is similar to the cases of the symmetric salts.[1,2] These facts show that the thermodynamic properties of C_n-DABCO-C_{n+1}-Br_2 tend to resemble those of the symmetric salts as the increase in the alkyl-chain length. (3) T_{c1}'s are close to the transition temperatures of the corresponding symmetric salts. It is especially interesting that T_{c1} is governed by the alkyl group possessing even number of carbons. (4) $\Delta H_{en,1}$'s and ΔS_1's are close to $\Delta H_{en,2}$ and ΔS_2 respectively. These facts suggest that the structure of

the metastable phase (C_M) is not very different from that of the low temperature phase (C_L). This is interesting in connection with the following observations; the symmetric salts did not show any presence of the C_M phase, but the unsymmetric salts showed C_M phase; when the difference in the carbon numbers of the two alkyl groups is larger than two, the structure of the C_M phase was assumed to be quite different from that of the C_L phase, unlike the cases of the present materials. Thus, C_n-DABCO-C_{n+1}-Br_2 can be said to possess intervening properties between the symmetric and unsymmetric salts. (5) The measurements of the bromide-anion conductivities revealed that conductivity jumps occurred at around T_{c1} and T_{c2} for the virgin and the annealed samples respectively. These phenomena are similar to the cases of the unsymmetric salts.[2,3] However, the differences in the two temperatures of the conductivity jumps tend to become smaller, and the conductivity jumps, themselves, tend to become sharper with an increase in the alkyl-chain lengths. These facts show that the temperature dependences of the bromide-anion conductivities tend to resemble those of the symmetric salts as the increase in the alkyl-chain lengths. The conductivity jump of C_{12}-DABCO-C_{13}-Br_2 was the largest of all of the materials studied hitherto.

We are grateful to Professor Shigekazu Kusabayashi and Dr. Shunsuke Takenaka, Faculty of Engineering, Osaka University, for the use of the DSC apparatus.

References

1) J. Shimizu, T. Nogami, and H. Mikawa, *Solid State Commun.*, **54**, 1009 (1985).

2) J. Shimizu, K. Imamura, T. Nogami, and H. Mikawa, *Bull. Chem. Soc. Jpn.*, **59**, 1443 (1986).

3) K. Imamura, J. Shimizu, and T. Nogami, *Bull. Chem. Soc. Jpn.*, **59**, 2699 (1986).

4) J. Shimizu, K. Imamura, T. Nogami, and H. Mikawa, *Bull. Chem. Soc. Jpn.*, **59**, 3367 (1986).

5) For example, 1-decyl-4-undecyl-1,4-diazoniabicyclo-[2.2.2]octane dibromide is abbreviated as C_{10}-DABCO-C_{11}-Br_2.

6) The virgin and the annealed samples mean the sample synthesized and the sample heated above T_{c1} at least once respectively.

7) The widths of all of the endothermic signals, $\Delta H_{en,2}$, were found to lie within 5 °C. However, those of the $\Delta H_{en,1}$ were broader than 5 °C, and are as follows: 5 °C and 5 °C, corresponding to two transitions for n=10; 11 °C, 8 °C, and 8 °C, corresponding to three transitions for n=11; 15 °C for n=12; 10 °C for n=13; 11 °C for n=14; 7 °C for n=15; 8 °C for n=16; 5 °C for n=17.

8) The two endothermic signals of C_n-DABCO-C_{n+1}-Br_2 (n=13, 15) were not separated well because of the proximity of the two transition temperatures. Thus, $\Delta H_{en,1}$'s were obtained by the total enthalpies of the two transitions, and ΔS_1 by dividing $\Delta H_{en,1}$ with the average transition temperatures (T_{c1}(average)=86.5°C for n=13, and T_{c1} (average)=90 °C for n=15).

9) The virgin samples of C_n-DABCO-C_{n+1}-Br_2 (n=11, 13, 15) possess more than one transition temperatures (T_{c1}). The second transition temperatures of these materials are close to the transition temperatures of the corresponding symmetric DABCO salts.

10) The characteristic (3) does not hold in the case of C_{10}-DABCO-C_{11}-Br_2. It showed large separation of the two transition temperatures (T_{c1}=57 °C, 84 °C).

11) The estimated numbers of sites (W) of C_n-DABCO-C_{n+1}-Br_2 above the transition temperatures are as follows. Virgin samples: 1.9×10^4 and 2000, corresponding to two transitions for n=10; 300, 2400, and 6200, corresponding to three transitions for n=11; 2×10^9 for n=12; 1.2×10^{10} for n=13; 1.3×10^{11} for n=14; 2.1×10^{11} for n=15; 1.8×10^{12} for n=16; 8.1×10^{12} for n=17. Annealed samples: 5.2×10^7 for n=10; 9.8×10^7 for n=11; 1.1×10^9 for n=12; 1.3×10^{10} for n=13; 1.5×10^{11} for n=14; 2.4×10^{11} for n=15; 3.7×10^{12} for n=16; 5.7×10^{13} for n=17.

 © 1987 The Chemical Society of Japan Bull. Chem. Soc. Jpn., 60, 119—123 (1987)

Stereochemistry of the (Iminodiacetato or *N*-Methyliminodiacetato)-(ethylenediamine-*N*-acetato)cobalt(III) Complexes

Tomoharu AMA,* Ryuichi NIIYAMA, Hiroshi KAWAGUCHI,* and Takaji YASUI*
Department of Chemistry, Faculty of Science, Kochi University,
Akebono-cho, Kochi 780
(Received May 24, 1986)

Four geometrical isomers of [Co(mida)(edma)] were prepared in the first time and their structures were determined on the basis of their visible and UV absorption spectral data. Three of the isomers were optically resolved by the use of a column containing QAE-Sephadex of the $Sb_2(d\text{-}tart)_2^{2-}$ form. Absolute configurations of the facially chelated isomers of [Co(mida)(edma)] were determined by measuring the ^1H NMR spectra of the optically resolved isomers with an asymmetric carbon-containing edma (obtained from the stereospecifically deuterated $(-)_{543}^{CD}$ C_2-*trans*(O)-$[Co(edma)_2]^{2+}$). Absolute configuations of the facially chelated isomers of [Co(ida)(edma)] were determined on the basis of their CD spectral data.

Either [Co(ida)(edma)] or [Co(mida)(edma)] (ida=iminodiacetato; edma=ethylenediamine-*N*-acetato; and mida=*N*-methyliminodiacetato) provides four geometrical isomers,[1] as shown in Fig. 1. In the present paper, chromatographic methods to separate and to resolve the isomers of [Co(ida)(edma)] and [Co(mida)-(edma)] which are uncharged complexes will be described.

The absolute configuration of the complex containing edma is closely related to the chirality of the asymmetric nitrogen arising from coordination of the ligand. The determination of the chirality of the asymmetric nitrogen make it possible to determine the absolute configuration of the edma chiral complex. On this basis, a ^1H NMR method to determine the absolute configurations of the isomers of $[Co(edma)_2]^+$ was reported in the previous paper.[2] In the present paper, we report on a modification of the method to determine the absolute configurations, which was applied to the isomers of [Co(mida)(edma)].

Experimental

Ligands. *N*-Methyliminodiacetic acid (H_2mida) and ethylenediamine-*N*-acetic acid (Hedma) were synthesized as described in the previous papers.[3-5]

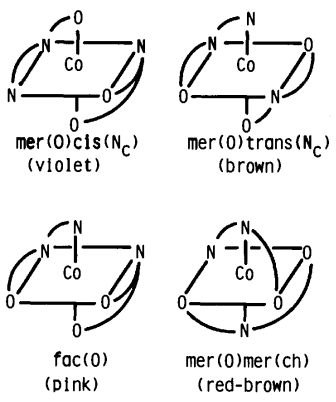

Fig. 1. The four geometrical isomers of [Co(ida)-(edma)] or [Co(mida)(edma)].

Preparation of the Complexes. Four Geometrical Isomers of the [Co(mida)(edma)] Complexes: A solution containing 2.4 g of $CoCl_2 \cdot 6H_2O$, 1.5 g of *N*-methyliminodiacetic acid (H_2mida) and 2.3 g of ethylenediamine-*N*-acetic acid dihydrochloride dihydrate (Hedma·2HCl·$2H_2O$) in 100 cm^3 of water was adjusted to pH 5 with a 2 mol dm^{-3} NaOH solution. The pH being kept constant at 5, 24 g of PbO_2 was stirred into the solution in small portions at 30 °C. After 1 h, the insoluble materials were removed by filtration. A solution containing neutral complexes was obtained by passing the filtrate through a QAE-Sephadex (SO_4^{2-} form) column and then an SP-Sephadex (K^+ form) column (eluent: water). This solution was evaporated to about 10 cm^3 and poured onto an SP-Sephadex (K^+ form) column. A band adsorbed on the column was separated into three parts by recyclic development with water: the first was an overlapped band (brown and red-brown); the second a violet band; and the third a pink band. Crude violet crystals were obtained by addition of methanol to the concentrated solution of the second eluant. Crude pink crystals were obtained by the same method as for the violet crystals. The solution obtained from the first part was acidified with a few drops of acetic acid and then concentrated under reduced pressure. Methanol was added to the concentrated solution. Brown crystals (unresolved) were deposited and were filtered off. The filtrate was evaporated almost to dryness to remove methanol and diluted with a small amount of water. The solution was repeatedly developed on a QAE-Sephadex column ($Sb_2(d\text{-}tart)_2^{2-}$ form; eluent: water), $(+)_{561}^{CD}$-brown (resolved; trace amount), red-brown (unresolved), and $(-)_{561}^{CD}$-brown band (resolved; trace amount) were separated (in the order of elution). The red-brown eluant (acidified with acetic acid) was concentrated under reduced pressure, and then acetone was added to the concentrated solution to obtain crude red-brown crystals. Each of the brown (unresolved), violet, and pink isomers was recrystallized from water by adding methanol and the red-brown isomer was next recrystallized from methanol by adding acetone. Yields of the isomers: the brown (unresolved), 420 mg; the violet, 650 mg; the red-brown, 10 mg; and the pink, 130 mg. Anal. Found for the brown isomer: C, 30.92; H, 5.64; N, 12.10%. Found for the red-brown isomer: C, 31.07; H, 5.46; N, 11.94%. Calcd for [Co(mida)(edma)]·$1.5H_2O$=$C_9H_{19}N_3O_{7.5}Co$: C, 31.05; H, 5.50; N, 12.07%. Found for the violet isomer: C, 31.74; H, 5.33; N, 12.31%. Calcd for [Co(mida)(edma)]·H_2O=$C_9H_{18}N_3O_7Co$: C, 31.87; H, 5.35;

N, 12.39%.

Four Geometrical Isomers of [Co(ida)(edma)]: These isomers were prepared according to the method reported in the previous paper.[1]

Optical Resolution. Isomers of [Co(ida)(edma)]: The racemic brown isomer of [Co(ida)(edma)] (ca. 50 mg) was dissolved in a small amount of warm water. The solution was poured onto a QAE-Sephadex column ($Sb_2(d\text{-}tart)_2^{2-}$ form, 3.7 cm×70 cm) and the adsorbed band developed with water. Developing was repeated on the same column using a micropump until the adsorbed band completely separated into two bands (recycle-times: 2). The earlier eluted isomer was $(+)_{565}^{CD}$ and the later eluted was $(-)_{565}^{CD}$. Each eluting solution from the two bands was concentrated to a small volume under reduced pressure at 35—40 °C. A crude complex was obtained by adding methanol to the concentrated solution: it was recrystallized from water by addition of methanol. The violet isomer of [Co(ida)(edma)] was resolved by the same method as that described above (recycle-times: 4). The earlier eluted isomer was $(+)_{563}^{CD}$ and the later eluted was $(-)_{563}^{CD}$. Though the pink isomer was chromatographed by the same method as that described for the brown isomer, the adsorbed band of the isomer was not separated into two bands upon 40 recycle-times. However, the faster eluted part showed (−) CD sign at 554 nm and the later one did (+). Fine needle crystals were obtained by adding methanol to each of the concentrated solutions. Found for $(+)_{565}^{CD}$ brown isomer: C 31.20; H, 4.55; N, 13.74%. Calcd for [Co(ida)(edma)]=$C_8H_{14}N_3O_6Co$: C, 31.28; H, 4.59; N, 13.68%. Found for $(+)_{563}^{CD}$ violet isomer: C, 29.41; H, 5.05; N, 12.89%. Calcd for [Co(ida)(edma)]·H_2O: C, 29.55; H, 4.96; N, 12.92%.

Isomers of [Co(mida)(edma)]: The brown and pink isomers of [Co(mida)(edma)] were resolved by the same method as that used for [Co(ida)(edma)]. The recycle times to attain complete separation of the enantiomers of the brown isomers were 5 and those of the pink isomer were 8. The earlier eluted bands of the brown and pink isomers showed (+) CD sign at 561 nm and at 565 nm, respectively. The resolution of the violet isomer was incomplete on the chromatograph using a QAE-Sephadex column ($Sb_2(d\text{-}tart)_2^{2-}$ form). However, it separated into enantiomers by 15 times recyclic development on a Sephadex G-10 column. Found for $(+)_{561}^{CD}$ brown isomer: C, 31.79; H, 5.51; N, 12.39%. Found for $(-)_{572}^{CD}$ violet isomer: C, 31.84; H, 5.35; N, 12.34%. Calcd for [Co(mida)(edma)]·H_2O=$C_9H_{18}N_3O_7Co$: C, 31.87; H, 5.35; N, 12.39%. Found for $(+)_{565}^{CD}$ pink isomer: C, 30.22; H, 5.70 N, 11.77%. Calcd for [Co(mida)(edma)]·$2H_2O$: C, 30.26; H, 5.64; N, 11.76%.

Determination of the Absolute Configuration of [Co(mida)(edma)]. A buffer solution (pH 10) was prepared by adding a suitable amount of 2 mol dm^{-3} DCl-D_2O to a solution containing 530 mg of Na_2CO_3 in 50 cm^3 of D_2O. About 1.0 g of $(-)_{543}^{CD}$ ($\Delta\Lambda\Delta(N_R,N_R)$) C_2-*trans*(O)-[Co(edma)$_2$]Cl·$2H_2O$[2] was dissolved into the buffer solution. The stereospecific deuteration reaction on the coordinating edma was allowed to proceed (40 °C, 25 min) and then stopped as described in the previous paper[1] (being adjusted the pH of the solution to 5 by addition of 1 mol dm^{-3} HCl). The complex solution was mixed with 10 g of zinc powder to reduce the central cobalt(III) and the mixture was stirred for 5 min. After the excess of zinc was filtered off, 0.64 g of $CoCl_2·6H_2O$ and 0.79 g of H_2mida were added to the filtrate and then the pH of the solution was adjusted to 5 with 2 mol dm^{-3} NaOH solution. After 15 g of PbO_2 was added to the solution, the mixture was stirred for 30 min at room temperature and the reactant solution was filtered. The filtrate was treated on a column chromatograph as described for separation of the racemic isomers of [Co(mida)(edma)]. Each facially chelated isomer so obtained was resolved into enantiomeric isomers by the chromatographic method described in the previous section. The ^1H NMR spectra of these isomers are illustrated in Fig. 5.

Spectral Measurements. The visible and UV absorption and CD spectra were recorded on a Hitachi 557 spectrophotometer and a JASCO J-22 spectropolarimeter in aqueous solutions, respectively. ^1H NMR spectra were recorded on a JEOL MH-100 spectrometer using DSS as an internal standard in D_2O or 0.1 mol dm^{-3} DCl-D_2O solutions.

Results and Discussion

Structural Assignments for the Isomers of [Co(mida)(edma)]. Each of the [Co(ida)(edma)] and [Co(mida)(edma)] complexes provides four geometrical isomers, as shown in Fig. 1. The structural assignments for the geometrical isomers of the former complex have been reported in the previous paper:[1] violet, *mer*(O)*cis*(N_c); brown, *mer*(O)*trans*(N_c); red-brown, *mer*(O)*mer*(ch); and pink, *fac*(O). The isomeric structures of the latter complex can be assigned by comparing their absorption spectra with those of the isomers of [Co(ida)(edma)]: violet, *mer*(O)*cis*(N_c); brown, *mer*(O)*trans*(N_c); red-brown, *mer*(O)*mer*(ch); and pink, *fac*(O) (Figs. 2 and 3). These assignments are also supported by the observation that the CD spectral behavior of an isomer of [Co(ida)-(edma)] is similar to that of the corresponding isomer of [Co(mida)(edma)] (vide infra).

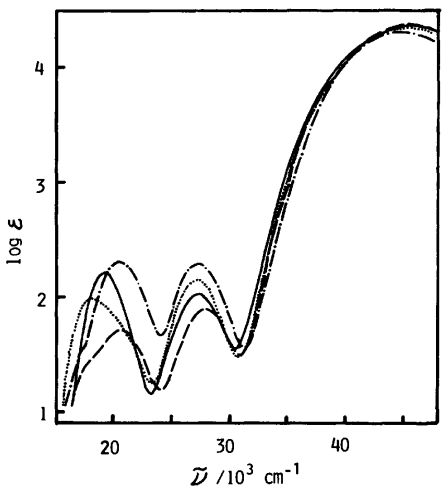

Fig. 2. Absorption spectra of [Co(ida)(edma)] in water: violet (·····), brown (– – –), pink (——), and red-brown (—·—).

^{1}H NMR Spectra. Table 1 shows the ^{1}H NMR data of the glycinate methylene protons of the edma complexes. The ^{1}H NMR spectra of the isomers which contain facially coordinating edma were measured in 0.1 mol dm^{-3} DCl-D_2O and in D_2O. The glycinate-ring (G-ring) signal for each isomer was observed as four peaks (an AB quartet) in D_2O, but it appeared as eight peaks in DCl because of the J_{H_a,H_b}, $J_{N\text{-}H,H_a}$, and $J_{N\text{-}H,H_b}$ couplings (Table 1). The $J_{N\text{-}H,H_b}$ and $J_{N\text{-}H,H_a}$ values are ca. 8 Hz's (for the peaks at lower field) and 1 Hz's (for those at higher field), respectively. On the basis of the Karplus equation,[6] the following assignments are possible: the dihedral angles of the proton resonating at higher field against the N-H proton (H-C-N-H) is about 90°, and the proton can be assigned to H_a (inside; Fig. 4 (A)). The angle of the proton (which is assigned to H_b (outside)) resonating at lower field is about 30°. Similar assignments for the G-ring methylene protons have been made for the isomers of $[Co(edma)_2]^{2+}$ [2] and for edda-Co(III) complexes.[7,8] When the N-H proton on the facially coordinating edma was deuterated, the signal of the G-ring methylene protons appeared as an AB quartet.

The G-ring methylene protons in the facially coordinating edma are known to be stereospecifically deuterated.[2,9-13] A new singlet appeared between the two higher-field peaks of the AB quartet, with intensity loss of the AB quartet. In other words, the deuteration rates are different between the two protons; the deuteration of the higher-field proton is much slower than that of the lower-field one. (The new singlet signal disappeared after a long period). Sudmeier and Occupati[9] found that the deuteration of the inside proton of the facial G-ring is slower than that of the outside proton for the edda-Co(III) complexes. The application of this to the present edma complexes leads to the conclusion that the two lower-field peaks of the AB quartet arise from the outside proton which is easily deuterated, while the two higher field peaks arise from the inside proton. These assignments are consistent with those made by the Karplus equation mentioned above.

Correlation between the Absolute Configuration Around the Cobalt Center and the Chirality of Asymmetric Nitrogen. When the edma ligand coor-

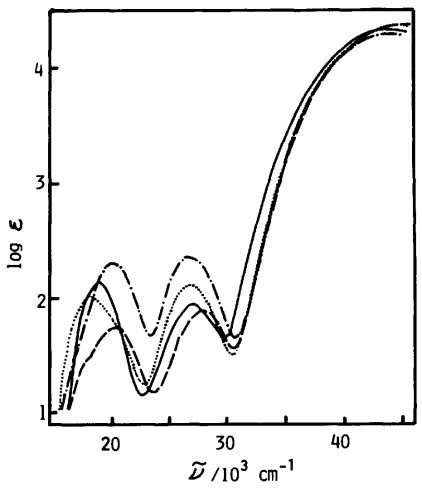

Fig. 3. Absorption spectra of [Co(mida)(edma)] in water: violet (·····), brown (– – –), pink (——), and red-brown (—·—).

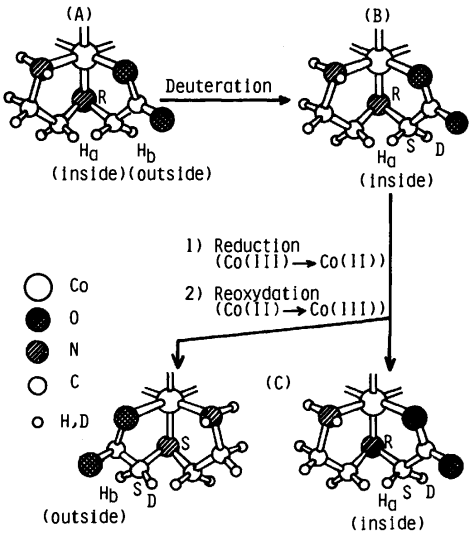

Fig. 4. Chemical environment of the facially coordinating edma. (A): undeuterated, (B): deuterated, and (C): reprepared by oxydizing the reduction product of (B) (See Experimental).

Table 1. ^{1}H NMR Data of the G-Ring Protons of edma in the [Co(mida)(edma)] Complexes

Geometrical Isomer	δ		J_{H_a,H_b} /Hz	$J_{N\text{-}H,H_a}$ /Hz	$J_{N\text{-}H,H_b}$ /Hz
	H_a	H_b			
mer(O)*cis*(N_c)	3.18	4.14	18	0	8
mer(O)*trans*(N_c)	3.40	4.22	18	0	8
fac(O)	3.15	4.00	18	2	9
mer(O)*mer*(ch)	3.84	3.84	—	7	9

Table 2. Possible Configurations and CD Signs of [Co(mida)(edma)] Complexes Containing Facially Coordinating edma

Geometrical Isomer	Possible Configuration		CD sign
	around cobalt(III)	asymmetric nitrogen	
mer(O)*cis*(N_c)	*ΛΔΛ*	N_S	$(+)^{CD}_{573}$
(violet)	*ΔΛΔ*	N_R	$(-)^{CD}_{573}$
mer(O)*trans*(N_c)	*ΔΛ*	N_S	$(+)^{CD}_{561}$
(brown)	*ΛΔ*	N_R	$(-)^{CD}_{561}$
fac(O)	*ΛΔΛ*	N_R	$(+)^{CD}_{565}$
(pink)	*ΔΛΔ*	N_S	$(-)^{CD}_{565}$

dinates to a cobalt(III) ion in the facial form, the secondary nitrogen (C-NH-C) becomes an asymmetric center (Fig. 4).[2] Where a geometrical structure of the edma complex is given, the absolute configuration around the cobalt(III) is restricted by the chirality of the asymmetric nitrogen. For example, in the *fac*(O) isomer of [Co(mida)(edma)], if the asymmetric nitrogen has R chirality (N_R), the absolute configuration around the cobalt(III) is *ΔΔΔ*. The correlation between the configurations around cobalt(III) and the chirality of asymmetric nitrogen is shown in Table 2.

Determination of Absolute Configurations by ^{1}H NMR. An outline of the method to determine the absolute configurations is illustrated in Fig. 4. The $(-)^{CD}_{543}$ C_2-*trans*(O)-$[Co(edma)_2]^{2+}$ isomer, the structure of which was determined in the previous work, has the configuration *ΔΔΔ*(N_R,N_R).[2] One of the G-ring $-CH_2-$ protons in this complex is stereospecifically deuterated in basic D_2O. When the outside proton (H_b in Fig. 4 (A)) was deuterated, the methylene carbon becomes an asymmetric center with the S chirality (C_S) (Fig. 4 (B)). Using this edma which contains C_S (edma(C_S)), the isomers of [Co(mida)(edma(C_S))] were prepared and resolved as described in the experimental section. In that experimental procedure, the C_S chirality was retained but the N_R chirality was not retained (yielded a 1:1 mixture of N_R and N_S). It is noteworthy that, when the nitrogen atom of the facially coordinating edma(C_S) takes N_R chirality, the undeuterated proton (-CHD-) occupies an inside position (Fig. 4 (C)). (When edma(C_S) takes N_S chirality, the -CHD- proton occupies an outside position.) In $(+)^{CD}_{561}$ *mer*(O)*trans*(N_c)-[Co(mida)(edma(C_S))], the NMR signal of G-ring -CHD- in edma(C_S)

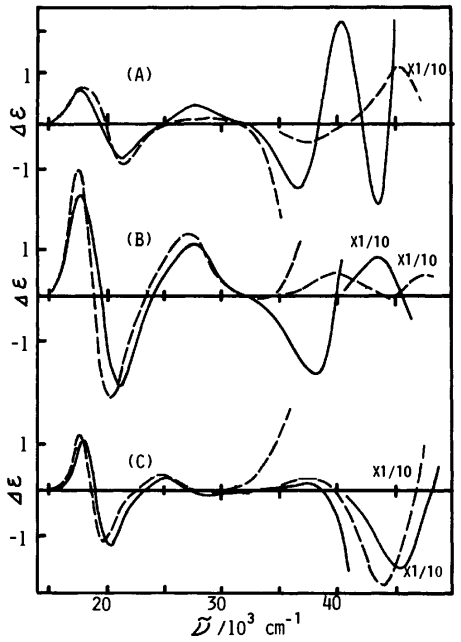

Fig. 6. CD spectra of the isomers of [Co(ida)(edma)] (——) and [Co(mida)(edma)] (– – –). (A) brown isomers of $(+)^{CD}_{565}$ [Co(ida)(edma)] and $(+)^{CD}_{561}$ [Co(mida)(edma)]; (B) violet isomers of $(+)^{CD}_{568}$ [Co(ida)(edma)] and $(+)^{CD}_{572}$ [Co(mida)(edma)]; and (C) pink isomers of $(+)^{CD}_{554}$ [Co(ida)(edma)] and $(+)^{CD}_{588}$ [Co(mida)(edma)].

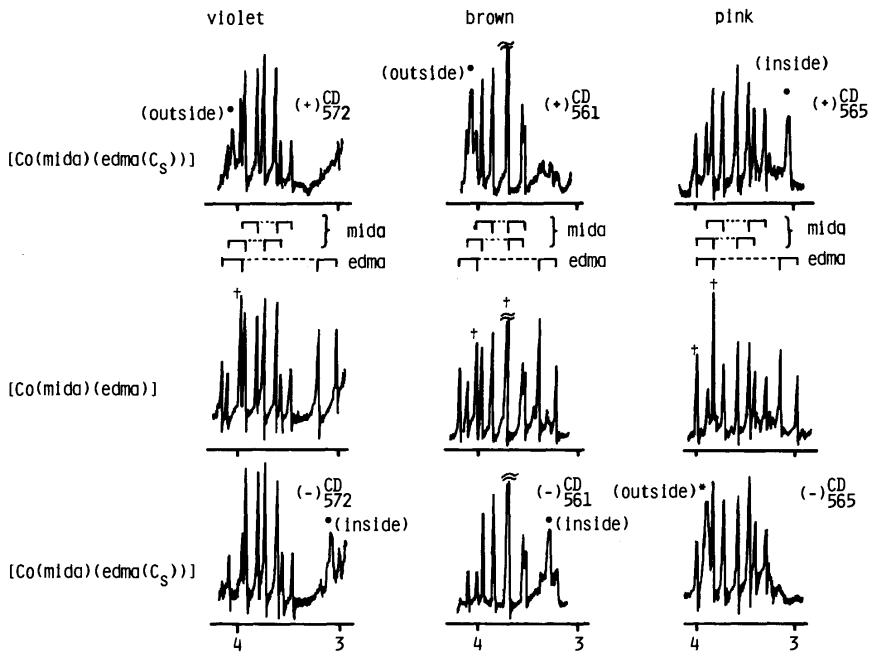

Fig. 5. ^{1}H NMR spectra of the optically active isomers of [Co(mida)(edma(C_S))] and those of the undeuterated isomers of [Co(mida)(edma)]. (Asterisked peaks: G-ring -CHD- of edma. Daggered peaks: Overlapped peaks.)

appeared at the chemical shift that corresponds to the outside proton (H_b; lower field) (Fig. 5). Accordingly, the chirality of the asymmetric nitrogen is N_S in $(+)^{CD}_{561}$ *mer*(O)*trans*(N_c)-[Co(mida)(edma(C_S))]. On the other hand, in $(-)^{CD}_{561}$ *mer*(O)*trans*(N_c)-[Co(mida)(edma(C_S))] the signal of -CHD- appeared at higher field (corresponding to the inside proton). This isomer should have N_R chirality. In a similar manner, the absolute configurations of three isomers of [Co(mida)-(edma)] were determined. These are summarized in Table 2 and Fig. 5.

CD Spectra of the Complexes. The CD spectra of the complexes examined are illustrated in Fig. 6. The facially chelated isomers of [Co(ida)(edma)] show similar CD patterns in the first and second band regions to those of the corresponding isomers (with the same colors) of [Co(mida)(edma)] except that the CD bands of the violet and pink isomers of [Co(mida)(edma)] shift slightly to the lower energy side than those of the corresponding isomers of [Co(ida)(edma)]. No shift was observed in the CD bands of the brown isomer of [Co(mida)(edma)]. Since the violet and pink isomers belong to *cis*(N_c) type isomers (violet, *mer*(O)*cis*(N_c); pink, *fac*(O) (Fig. 1)), steric compression between the methyl group of mida and the ethylene or methylene groups of edma is large in these isomers. The shift to the lower energy side results from this compression. Such compression is not expected in the brown isomer (*trans*(N_c) type) of [Co(mida)(edma)].

The first absorption bands of the *fac*(O)-[Co(N_3)-(O_3)] type complexes are sharp but those of *mer*(O)-[Co(N_3)(O_3)] are broad or not sharp with accompanying shoulder bands.[14,15] However, both isomers show two CD bands with opposite signs in the first absorption band region. This may be a general feature of the bis(terdentate)cobalt(III) type complex containing five membered chelate rings, even though the vicinal CD from the ligand may make the feature vague. The u-fac isomers of $[Co(ida)_2]^-$[16] and $[Co(dien)_2]^{3+}$[17] also show similar spectral patterns in the first absorption band region.

The $(+)^{CD}_{572}$ *ΔΔΔ* *mer*(O)*cis*(N_c)-[Co(mida)(edma)] gives two component CD bands with (+) and (−) signs at the lower and higher energy sides in the first absorption band region and the intensities (absolute values) are larger than those of $(+)^{CD}_{565}$ *fac*(O)-[Co(mida)(edma)]. The low CD intensities of the *fac*(O) isomer may result from one of the following two reasons: (1) although the *fac*(O) isomer has *ΔΔΔ* configuration the same as the *mer*(O)*cis*(N_c) isomer does, the N_R chirality of the coordinating edma in the *fac*(O) isomer is different from the N_S chirality in the *mer*(O)*cis*(N_c); (2) the split of the CD components in the first absorption band is smaller in the *fac*(O) isomer than in the *mer*(O)*cis*(N_c).

The CD intensities of $(+)^{CD}_{561}$ *mer*(O)*trans*(N_c) are the smallest among three resolved isomers of [Co(mida)-(edma)]. As this isomer has *Δ* and *Λ*-configurational ring pair, the CD contribution from the configurational effect is the smallest among three isomers and the vicinal CD from the N_S is dominant in this isomer.

References

1) T. Ama, H. Kawaguchi, and T. Yasui, *Bull. Chem. Soc. Jpn.*, **59**, 1471 (1986).
2) T. Ama, H. Kawaguchi, T. Yasui, K. Matsumoto, and S. Ooi, *Bull. Chem. Soc. Jpn.*, **58**, 2561 (1985).
3) M. Mori, M. Shibata, E. Kyuno, and F. Maruyama, *Bull. Chem. Soc. Jpn.*, **35**, 75 (1962).
4) G. J. Berchet, *Org. Synth.*, Coll Vol. 2, 397 (1956).
5) Y. Fujii, E. Kyuno, and R. Tsuchiya, *Bull. Chem. Soc. Jpn.*, **43**, 786 (1970).
6) M. Karplus, *J. Chem. Phys.*, **30**, 11 (1959).
7) J. I. Legg and D. W. Cooke, *Inorg. Chem.*, **4**, 1576 (1965).
8) L. N. Schoenberg, D. W. Cook, and C. F. Liu, *Inorg. Chem.*, **7**, 2386 (1968).
9) J. L. Sudmeier and G. Occupati, *Inorg. Chem.*, **7**, 2524 (1968).
10) P. F. Coleman, J. I. Legg, and J. Steele, *Inorg. Chem.*, **9**, 937 (1970).
11) C. W. Maricondi and C. Maricondi, *Inorg. Chem.*, **13**, 1110 (1974).
12) D. Radanovic and B. E. Douglas, *Inorg. Chem.*, **14**, 6 (1975).
13) D. H. Williams and D. H. Busch, *J. Am. Chem. Soc.*, **87**, 4644 (1965).
14) H. Yamatera, *Bull. Chem. Soc. Jpn.*, **31**, 95 (1958).
15) N. Matsuoka, J. Hidaka, and Y. Shimura, *Bull. Chem. Soc. Jpn.*, **40**, 1868 (1967).
16) T. Yasui, H. Kawaguchi, N. Koine, and T. Ama, *Bull. Chem. Soc. Jpn.*, **56**, 127 (1983).
17) M. Kojima, M. Iwagaki, Y. Yoshikawa, and J. Fujita, *Bull. Chem. Soc. Jpn.*, **52**, 3216 (1977).

 © 1987 The Chemical Society of Japan Bull. Chem. Soc. Jpn., 60, 125—129 (1987)

Crystal Structures of Bis(*r*-1,*c*-3,*c*-5-cyclohexanetriamine)cobalt(III) Iodide and Tricyano(*r*-1,*c*-3,*c*-5-cyclohexanetriamine)-cobalt(III) Monohydrate

Minoru Ishii,* Michiko Umehara, and Masayoshi Nakahara
Department of Chemistry, Faculty of Science, Rikkyo (St. Paul's) University,
Nishiikebukuro 3, Toshima-ku, Tokyo 171
(Received June 13, 1986)

The crystal structures of bis(*r*-1,*c*-3,*c*-5-cyclohexanetriamine)cobalt(III) iodide (**1**) and tricyano(*r*-1,*c*-3*c*-5-cyclohexanetriamine)cobalt(III) monohydrate (**2**) were determined by the X-ray diffraction technique. **1** is monoclinic with space group *A*2/*a*,[1] *a*=10.437(2), *b*=16.131(2), *c*=12.486(2) Å, and *β*=94.36(3)°, and **2** is orthorhombic with space group *Pbca*, *a*=12.599(1), *b*=16.818(2), and *c*=11.659(1) Å, the final *R* values for **1** and **2** were 0.048 and 0.045, respectively. In both the complexes, all six-membered chelate rings formed by the *r*-1,*c*-3,*c*-5-cyclohexanetriamine ligand and central cobalt atom assume chair conformations. The presence of the six-membered chelate rings does not introduce. much distortion on the octahedral geometry of the chromophores. These findings are in fair agreement with spectroscopic data on these complexes.

r-1,*c*-3,*c*-5-Cyclohexanetriamine (Fig. 1; abbreviated as chta) can act as a terdentate ligand and coordinate to the central metal in only one topological way (facial). Two kinds of complexes containing chta ligand, $[Co(chta)_2]^{3+}$ [2] and $[CoX_3(chta)]$[3] (X=CN^-, Cl^-, and CH_3COO^-), have been prepared. It is expected that a chta ligand coordinates to form a triplet six-membered ring, leading to existence of three six-membered chelate rings in $[CoX_3(chta)]$ (X=CN^-, Cl^-, and CH_3COO^-) and that of six in $[Co(chta)_2]^{3+}$. The d-d absorption bands of cobalt(III) complexes shift to the lower energy side as the number of chelate rings increases.[4] Rather large shifts were observed also for complexes of the type $[Co(triamine)_2]^{3+}$: for example, 19400 and 27200 cm^{-1} for $[Co(dpt)_2]^{3+}$ (dpt=bis(3-aminopropyl)amine)[5] and 21800 and 30000 cm^{-1} for *s*-*fac*-$[Co(dien)_2]^{3+}$ (dien=diethylenetriamine).[6] Although their band maxima are in lower energy sides than those of five-membered chelate polyamine complexes, they are located quite close to those of the corresponding ammine complexes: $[Co(chta)_2]Cl_3$, 20900 and 29200 cm^{-1},[2] $[Co(NH_3)_6]Cl_3$, 20960 and 29400 cm^{-1},[7] $[Co(CN)_3(chta)]$, 26300 and 33000 cm^{-1},[3] *fac*-$[Co(CN)_3(NH_3)_3]$, 26300 and 33000 cm^{-1}.[8] These facts suggest that the chta chelate assumes a undistorted structure in the complex. A study with scaled models has suggested that the chta ligand can build up a robust structure with the central atom. This work deals with the molecular structures of bis(*r*-1,*c*-3,*c*-5-cyclohexanetriamine)cobalt(III) iodide, $[Co(chta)_2]I_3$,[9] and tricyano(*r*-1,*c*-3,*c*-5-cyclohexanetriamine)cobalt(III) monohydrate, $[Co(CN)_3(chta)]\cdot H_2O$.

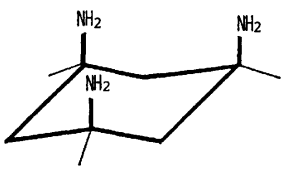

Fig. 1. *r*-1, *c*-3, *c*-5-Cyclohexanetriamine. (*cis*,*cis*-1,3,5-cyclohexanetriamine)

Experimental

Both the complexes were prepared according to the literatures.[2,3] The crystal of $[Co(chta)_2]I_3$ is of orange-red hexagonal prism and that of $[Co(CN)_3(chta)]\cdot H_2O$ is of yellow cube. Anal. for $[Co(chta)_2]I_3$. Found: C, 20.45; H, 4.32; N, 11.88; I, 54.54%. Calcd for $CoC_{12}H_{30}N_6I_3$: C, 20.65; H, 4.34; N, 12.04; I, 54.54%. Anal. for $[Co(CN)_3(chta)]\cdot H_2O$. Found: C, 37.44; H, 6.03; N, 28.95%. Calcd for $CoC_9H_{17}N_6O$: C, 38.04; H, 6.03; N, 29.57%. Specific gravities were determined by the floating method. Lattice constants were first approximately determined from Weissenberg photographs obtained with Cu *Kα* radiation and then refined. Crystal data of both the complexes are listed in Table 1. Intensities were collected on a Rigaku AFC-5 four-circle diffractometer (Josai University) with graphite-monochromated Mo *Kα* radiation (*λ*=0.7107 Å) up to 2*θ*=60°, the *θ*—2*θ* scan technique being employed. The usual corrections for Lorentz and polarization effects were made with both the crystals, and further corrections for absorption and

Table 1. Crystal Data

Compound	$[Co(chta)_2]I_3$	$[Co(CN)_3(chta)]\cdot H_2O$
Formula	$CoC_{12}N_{12}H_{60}I_3$	$CoC_9N_9H_{32}O$
Formula weight	698.11	284.25
Crystal system	Monoclinic	Orthorhombic
Space group	*A*2/*a*	*Pbca*
a/Å	10.437(2)	12.599(1)
b/Å	16.131(2)	16.818(2)
c/Å	12.486(2)	11.659(1)
β/°	94.36(3)	
V/Å^3	2096.05(5)	2470.2(5)
D_m/Mg m^{-3}	2.20	1.53
D_x/Mg m^{-3}	2.21	1.53
Z	4	8
μ(Mo *Kα*)/mm^{-1}	5.187	

extinction were made with $[Co(chta)_2]I_3$. Calculations were carried out on a Univac 1100 computer at the Rikkyo University Computer Center and partially on a HITAC 200 H computer at the Computer Center of the University of Tokyo.

Crystal Structure Determination. **a) $[Co(chta)_2]I_3$:** The observed systematic absence of $h\,k\,l$ for $k+l=2n+1$ and $h\,0\,l$ for $h=2n+1$ indicated that possible space groups would be $A2/a$ or Aa. Then, two refinements were carried out independently by assuming the two space groups.[10] In the case of Aa, some C–C and C–N bond lengths were abnormal and the coordinates and temperature factors had unusually high values, whereas no anomalies were found in the case of $A2/a$. Independent 2794 reflections with $|F_o|>3\sigma(|F_o|)$ were used for structure determination. The structure was solved by the heavy-atom method with a local version of UNICS.[11] The final refinement was carried out by using the full-matrix least squares program LINUS[12] with anisotropic temperature factors for non-hydrogen atoms and isotropic ones for hydrogen atoms. The final R and R_2 values were 0.048 and 0.055,[13] respectively. The positions of all hydrogen atoms were determined from the difference-Fourier map.

b) $[Co(CN)_3(chta)]\cdot H_2O$: From the observed systematic absence of $0\,k\,l$ for $k=2n+1$, $h\,0\,l$ for $l=2n+1$, and $h\,k\,0$ for $h=2n+1$, the space group was uniquely determined to be $Pbca$. Independent 2674 reflections with $|F_o|>3\sigma(|F_o|)$ were used. The structure was solved by the Patterson-Fourier method with UNICS.[11] The refinement was carried out by using the block-diagonal least squares program HBLS IV. With anisotropic temperature factors for non-hydrogen atoms and isotropic ones for hydrogen atoms, the final R and R_2 values were 0.045 and 0.049, respectively. Fourteen of fifteen hydrogen atoms, except those of the water molecule, were located from the difference-Fourier map. The position of the remaining hydrogen atom was determined theoretically.

The final atomic parameters and temperature factors of both the complexes are given in Tables 2 and 3.[14]

Table 2. Final Atomic Coordinates/10^{-4} with Estimated Standard Deviations in Parentheses, and Their Equivalent Isotropic Temperature Factors

Atom	x	y	z	B_{eq}/Å^2 a)
I (1)	2500	1169(<1)	0	3.5_3
I (2)	4142(<1)	6649(<1)	8855(<1)	3.1_8
Co	5000	7500	2500	1.8_2
N (1)	4387(6)	6489(3)	1716(5)	2.6_0
N (2)	5362(6)	6835(3)	3827(5)	2.5_5
N (3)	6777(5)	7283(3)	2089(5)	2.5_3
C (1)	5140(7)	5704(4)	1860(6)	2.7_9
C (2)	5219(7)	5428(4)	3013(7)	3.0_3
C (3)	6041(7)	6009(4)	3742(6)	2.9_3
C (4)	7351(7)	6133(5)	3334(7)	3.2_3
C (5)	7293(6)	6409(4)	2166(7)	3.0_6
C (6)	6469(7)	5834(5)	1442(7)	3.3_9

a) $B_{eq}=4/3(B_{11}a^2+B_{22}b^2+B_{33}c^2+B_{12}ab\cos\gamma+B_{13}ac\cos\beta+B_{23}bc\cos\alpha)$.

Table 3. Final Atomic Coordinates/10^{-4} with Estimated Standard Deviations in Parentheses, and Their Equivalent Isotropic Temperature Factors

Atom	x	y	z	B_{eq}/Å^2 a)
Co	2358(<1)	2275(<1)	609(<1)	1.4_1
N1A	1292(2)	1862(2)	1745(2)	2.1_5
N2A	1940(2)	1428(2)	−501(2)	2.1_5
N3A	3463(2)	1575(2)	1309(2)	1.7_4
C1C	3344(3)	2686(2)	−456(3)	1.9_9
C2C	1335(3)	2976(2)	−8(3)	2.1_3
C3C	2774(3)	3103(2)	1600(3)	1.9_4
N4C	3936(3)	2942(2)	−1108(3)	2.7_7
N5C	698(3)	3399(2)	−360(3)	3.2_0
N6C	3050(3)	3602(2)	2193(3)	2.7_2
C4A	1242(3)	982(2)	1935(3)	1.9_6
C5A	949(3)	561(2)	823(3)	2.3_4
C6A	1831(3)	599(2)	−66(3)	2.1_1
C7A	2889(3)	314(2)	404(3)	2.6_3
C8A	3182(3)	724(2)	1534(3)	2.6_1
C9A	2292(3)	672(2)	2397(3)	2.2_4
O	352(3)	3774(3)	2548(4)	7.3_8

a) $B_{eq}=4/3(B_{11}a^2+B_{22}b^2+B_{33}c^2+B_{12}ab\cos\gamma+B_{13}ac\cos\beta+B_{23}bc\cos\alpha)$.

Results and Discussion

Projections of the crystal structures of $[Co(chta)_2]I_3$ along the b axis and of $[Co(CN)_3(chta)]\cdot H_2O$ along the c axis are shown in Figs. 2 and 3. Perspective drawings of the complexes are shown in Figs. 4 and 5.

In both the complexes, the chta ligands are spanned on a face of an octahedron, that is, they coordinate in the facial positions, as expected.

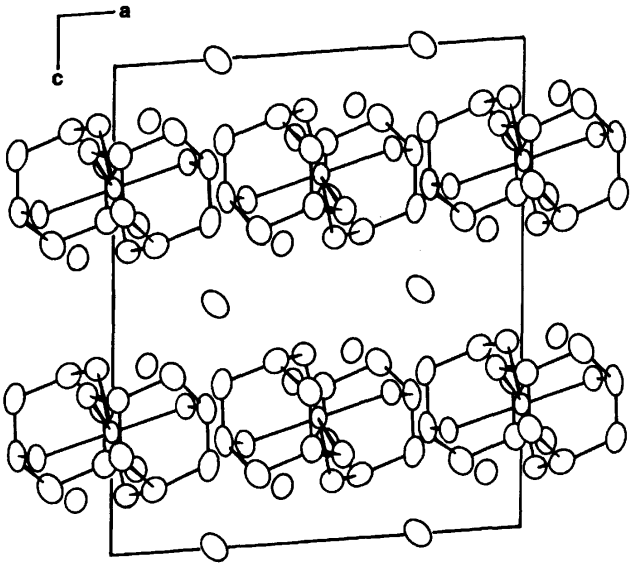

Fig. 2. Crystal structure of $[Co(chta)_2]I_3$ projected along the b-axis.

Bond distances and angles within the complex ion and molecule are listed in Tables 4 and 5, together with estimated standard deviations. Between both the complexes there are no remarkable differences with respect to the chta chelate. The Co-N(amine) bond distances which range from 1.948(6) to 2.010(3) Å are similar to those of some CoN_6 complexes with six-membered chelate rings.[15,16] These values are also in good agreement with the Co-N(NH_3) bond lengths of the corresponding ammine complexes (2.01 Å for *fac*-$[Co(CN)_3(NH_3)_3]$[8] and 1.979(1) Å for $[Co(NH_3)_6][Cr(CN)_6]$). The angles N(amine)-Co-N(amine) in the

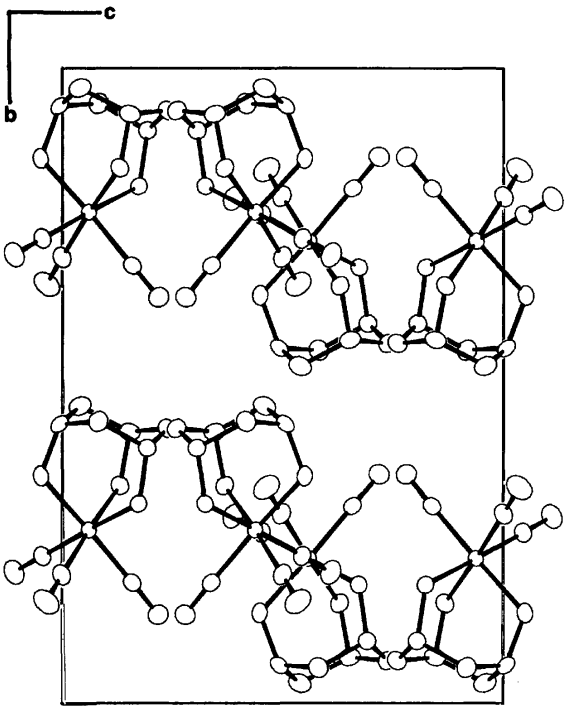

Fig. 3. Crystal structure of $[Co(CN)_3(chta)]$ projected along the *a*-axis.

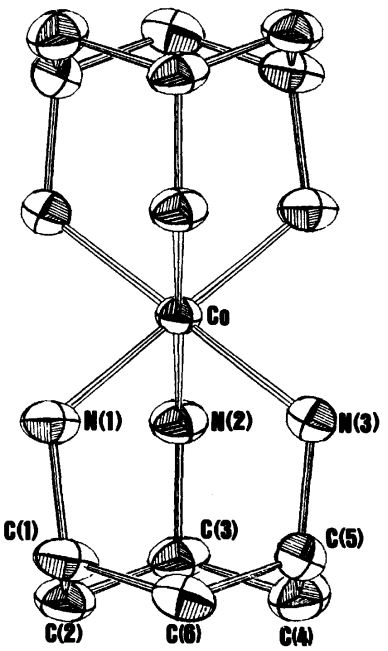

Fig. 4. Perspective drawing of the $[Co(chta)_2]^{3+}$.

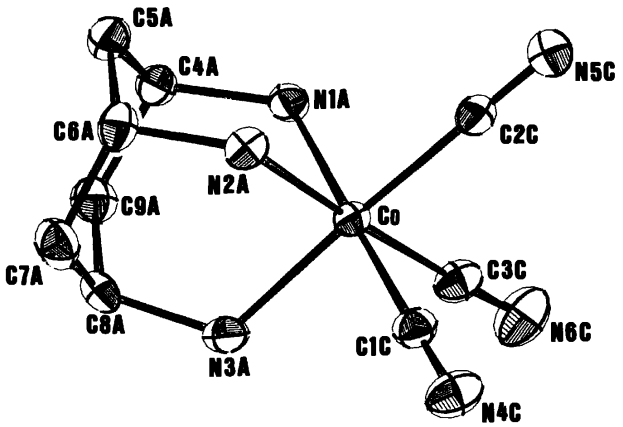

Fig. 5. Perspective drawing of the $[Co(CN)_3(chta)]$.

Table 4. Bond Distances and Angles within Cation $[Co(chta)_2]^{3+}$ with Estimated Standard Deviations in Parentheses

Bond distances *l*/Å		Bond angles ϕ/°			
Co-N(1)	1.984(6)	N(1)-Co-N(2)	90.1(3)	C(1)-C(2)-C(3)	112.2(7)
Co-N(2)	1.986(6)	N(1)-Co-N(3)	90.0(3)	C(2)-C(3)-C(4)	111.3(7)
Co-N(3)	1.992(7)	N(2)-Co-N(3)	89.9(3)	C(3)-C(4)-C(5)	113.0(7)
				C(4)-C(5)-C(6)	111.8(7)
N(1)-C(1)	1.494(10)	Co-N(1)-C(1)	119.3(5)	C(5)-C(6)-C(1)	111.6(7)
N(2)-C(3)	1.517(10)	Co-N(2)-C(3)	118.4(5)	C(6)-C(1)-C(2)	112.4(7)
N(3)-C(5)	1.510(10)	Co-N(3)-C(5)	118.9(5)		
C(1)-C(2)	1.502(11)	N(1)-C(1)-C(2)	110.9(6)		
C(2)-C(3)	1.524(11)	N(1)-C(1)-C(6)	108.9(6)		
C(3)-C(4)	1.508(12)	N(2)-C(3)-C(2)	109.7(6)		
C(4)-C(5)	1.522(12)	N(2)-C(3)-C(4)	110.4(6)		
C(5)-C(6)	1.516(12)	N(3)-C(5)-C(4)	108.8(7)		
C(6)-C(1)	1.534(12)	N(3)-C(5)-C(6)	110.4(7)		

Table 5. Bond Distances and Angles within Complex $[Co(CN)_3(chta)]$ with Estimated Standard Deviations in Parentheses

Bond distances l/Å			Bond angles ϕ/°		
Co-N1A	2.010(3)	N1A-Co-N2A	90.3(1)	C4A-C5A-C6A	112.5(3)
Co-N2A	1.996(3)	N2A-Co-N3A	91.7(1)	C5A-C6A-C7A	112.5(3)
Co-N3A	1.997(3)	N3A-Co-N1A	89.6(1)	C6A-C7A-C8A	112.3(3)
				C7A-C8A-C9A	111.7(3)
Co-C1C	1.888(3)	C1C-Co-C2C	88.3(1)	C8A-C9A-C4A	112.9(3)
Co-C2C	1.890(3)	C2C-Co-C3C	87.8(1)	C9A-C4A-C5A	110.7(3)
Co-C3C	1.884(3)	C3C-Co-C1C	87.1(1)		
N1A-C4A	1.498(4)	Co-N1A-C4A	117.8(2)		
N2A-C6A	1.490(4)	Co-N2A-C6A	118.1(2)		
N3A-C8A	1.498(5)	Co-N3A-C8A	118.0(2)		
C4A-C5A	1.523(5)	Co-C1C-N4C	179.3(3)		
C5A-C6A	1.522(5)	Co-C2C-N5C	178.3(3)		
C6A-C7A	1.519(5)	Co-C3C-N6C	178.3(3)		
C7A-C8A	1.532(5)				
C8A-C9A	1.509(5)	N1A-C4A-C5A	110.1(3)		
C9A-C4A	1.521(5)	N1A-C4A-C9A	110.8(3)		
		N2A-C6A-C5A	109.8(3)		
C1C-N4C	1.148(5)	N2A-C6A-C7A	109.7(3)		
C2C-N5C	1.148(5)	N3A-C8A-C7A	109.6(3)		
C3C-N6C	1.142(5)	N3A-C8A-C9A	110.4(3)		

chta chelate, close to 90°, are in agreement with those of analogous complexes.[15] Between both the complexes there is few difference in bond length and angle with respect to the triplet six-membered chelate rings, in contrast to the case of $[Co(diamine)_3]^{3+}$ complexes containing six-membered chelate rings.[15,16] The C-N(amine) and C-C bond distances are normal as such single bonds. The N(amine)-C-C angles are also normal as regular tetrahedral angles, but the Co-N(amine)-C ones are larger than those angles. Thus, these six-membered chelate rings are significantly flattened out. Absolute values of deviations from the plane Co-N-N(in chelate) are 0.91—0.96 Å (C(1)) and 0.56—0.62 Å (C(2)) for $[Co(chta)_2]^{3+}$ and 0.90—0.97 Å (C4A) and 0.53—0.67 Å (C5A) for $[Co(CN)_3(chta)]$. These six-membered rings assume more stable and less undistorted chair conformations than $[Co(tn)_3]^{3+}$[17] (Fig. 6). In complex $[Co(CN)_3(chta)]$, the Co-C-(cyano) and C-N(cyano) bond lengths agree with those of $[Co(CN)_3(NH_3)_3]$.[8] The C(cyano)-Co-C-(cyano) angles are smaller than 90°. The dihedral angle between the opposite N-N-N planes in $[Co(chta)_2]^{3+}$ is 0° as deduced necessarily from this symmetry, and that between the N-N-N and C-C-C planes in $[Co(CN)_3(chta)]$ is smaller than 1°. The octahedra of the CoN_6 and CoN_3C_3 chromophores are compressed or elongated along the quasi-threefold axes only slightly; the distance between the upper and lower triangles (2.292—2.297 Å) agrees with that estimated for a regular octahedron (2.294 Å).

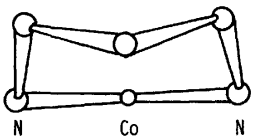

Fig. 6. Conformation of chta chelate ring.

These facts suggest that the distortion of the chromphores, although six-membered rings are formed by the chta ligands, is fairly alleviated by to the presence of the chta itself and that the octahedra retain approximately the O_h symmetry. The structures of the complex and ion, as determined in this work, are in good agreement with the speculations based on the absorption spectra.

References

1) Standard space group is $C2/c$ (No. 15).

2) R. A. D. Wentworth and J. J. Felton, *J. Am. Chem. Soc.*, **90**, 621 (1968).

3) M. Umehara, M. Ishii, T. Nomura, I. Muramatsu, and M. Nakahara, *Nippon Kagaku Kaishi*, **1980**, 657.

4) M. Kojima, H. Yamada, H. Ogino, and J. Fujita, *Bull. Chem. Soc. Jpn.*, **50**, 2325 (1977).

5) S. Yamada, M. Umehara, M. Ishii, and M. Nakahara, *Nippon Kagaku Kaishi*, **1983**, 1733.

6) Y. Yoshikawa and K. Yamasaki, *Bull. Chem. Soc. Jpn.*, **45**, 179 (1972).

7) J. Fujita and Y. Shimura, *Bull. Chem. Soc. Jpn.*, **36**, 1281 (1963).

8) Y. Yamamoto, *Nippon Kagaku Kaishi*, **1974**, 259.
9) M. Ishii, M. Umehara, T. Nomura, and M. Nakahara, *Chem. Lett.*, **1983**, 541.
10) The reliability indices were 0.060 for *A2/a* (the number of reflections 2794 and that of parameteres 110) and 0.063 for *Aa* (the number of reflections 2933 and that of parameters 200). The positions of the non-hydrogen atoms (I, Co, C, N) were determined by using anisotropic temperature factors.
11) T. Sakurai, UNICS, the Universal Crystallographic Computing System, Tokyo: The Crystallographic Society of Japan (1967).
12) P. Coppens and W. C. Hamilton, *Acta. Crystallogr., Sect. A*, **26**, 71 (1970).
13) $R=\Sigma||F_o|-|F_c||/\Sigma|F_o|$.
14) The complete F_o—F_c data are deposited as Document No. 8701 at the Office of the Editor of the Bull. Chem. Soc. Jpn.
15) S. Sato and Y. Saito, *Acta. Crystallogr., Sect. B*, **31**, 1378 (1975).
16) S. Sato and Y. Saito, *Acta. Crystallogr., Sect. B*, **34**, 420 (1978).
17) R. Nagao, F. Marumo, and Y. Saito, *Acta Crystallogr., Sect. B*, **29**, 2438 (1973).

 © 1987 The Chemical Society of Japan Bull. Chem. Soc. Jpn., 60, 131—139 (1987)

Magnetic Properties of Some Molybdenum(V) Dimeric Coordination Compounds with Terminal Oxo-Ligands and Di-μ-oxo-, Di-μ-sulfido- or μ-Oxo-μ-sulfido- Bridges

Hanako KOBAYASHI,* Takashi SHIBAHARA,† and Norikiyo URYŪ††
Faculty of Science and Technology, Keio University, Kohoku-ku, Yokohama 223
†Department of Chemistry, Okayama University of Science, Ridai-cho, Okayama 700
††Department of Applied Science, Faculty of Engineering, Kyushu University, Higashi-ku, Fukuoka 812
(Received June 18, 1986)

Magnetic susceptibilities and electron spin resonances of Mo(V) dimers, $Cs_2[Mo_2O_2S_2(ox)_2(H_2O)_2]\cdot 2H_2O$, $Ba[Mo_2O_4(ox)_2(H_2O)_2]\cdot 3H_2O$, $(pyH)_4[Mo_2O_2S_2(NCS)_6]$, $(pyH)_4[Mo_2O_4(NCS)_6]\cdot H_2O$ and $(pyH)_4[Mo_2O_3S(NCS)_6]$ were observed at temperatures from 2 K to room temperature. The paramagnetic part of the magnetic susceptibilities of these compounds was small and approached zero with decreasing temperature. Under an applied magnetic field strength of 40 kOe, the susceptibilities had temperature independent regions but the spin susceptibilities derived from the electron spin resonances, observed at a magnetic flux density of about 3000 G, showed temperature dependences like antiferromagnetic dimers. This discrepancy was explained by a quasi alternating linear chain antiferromagnetic model. The corrections of the diamagnetic susceptibilities are discussed.

Molybdenum coordination compounds with sulfur containing ligands are found in many enzyme systems. The magnetic properties of such molybdenum coordination compounds are of interest because the mechanism of enzyme activity is strongly correlated with their magnetism. Within a limited moiety of molybdenum coordination compounds, that is, a Mo(V) dimeric ion with double bridges of oxygen or sulfur, there are many residual problems. A salt $[C_5H_5MoO_2]_2$,[1] which has oxygen double bridges, is known to be diamagnetic from NMR observations. On the other hand, $Na_2[Mo_2O_4(edta)]\cdot 4H_2O$[2] and $Ba[MoO_2(ox)]_2\cdot 5H_2O$,[3] both are oxygen double bridged, are reported to be paramagnetic. A salt sulfur-bridged $Na_2[Mo_2O_2S_2(histidine)_2]\cdot H_2O$,[4] which seems to be similar to $Na_2[Mo_2O_4(edta)]\cdot 4H_2O$ from the view point of magnetism, is diamagnetic and $Ba[Mo_2O_4(C_2O_4)_2]\cdot 5H_2O$[5] is considered to be diamagnetic. The molecular and crystal structures of paramagnetic $(pyH)_4[Mo_2O_4(NCS)_6]\cdot H_2O$ were analyzed by Jezowska-Trzebiatowska et al.[6] together with several related coordination compounds. She reported the molar magnetic susceptibilities of $(pyH)_4[Mo_2O_4(NCS)_6]$ in the range $(74—281)\times 10^{-6}$ CGSemu at room temperature.[7] The magnetic susceptibility of $(pyH)_4[Mo_2O_4(NCS)_6]$ reported by Mitchell and Williams,[2] is paramagnetic with a value of 157×10^{-6} (CGSemu) at 120 K and 147×10^{-6} (CGSemu) at 293 K. We have synthesized its homologous series $[Mo_2O_3S(NCS)_6]$ and $[Mo_2O_2S_2(NCS)_6]$ salts[8] and observed their magnetic susceptibilities and electron paramagnetic resonances, together with those of $[Mo_2O_4(NCS)_6]$ salt.[6] The two dimeric salts $[Mo_2O_2S_2(ox)_2(H_2O)_2]$ and $[Mo_2O_4(ox)_2(H_2O)_2]$ also were prepared and measured to examine some common properties among 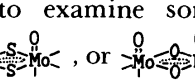 , or 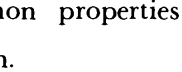 skelton.

Experimental

Preparation of Samples. Caesium di-μ-sulfido-bis[aquaoxalatooxomolybdate(V)] dihydrate ($Cs_2[Mo_2O_2S_2(ox)_2(H_2O)_2]\cdot 2H_2O$ (**1**)) and barium di-μ-oxo-bis[aquaoxalatooxomolybdate(V)] trihydrate ($Ba[Mo_2O_4(ox)_2(H_2O)_2]\cdot 3H_2O$ (**2**)) were prepared following Refs. 5, 9, and 10. Pyridinium di-μ-sulfido-bis[tris(isothiocyanato)oxomolybdate(V)] ($(pyH)_4[Mo_2O_2S_2(NCS)_6]$ (**3**)) and pyridinium di-μ-oxo-bis[tris(isothiocyanato)oxomolybdate(V)]monohydrate ($(pyH)_4[Mo_2O_4(NCS)_6]\cdot H_2O$ (**4**)) were prepared by the method reported in Refs. 6,7, and 11. Pyridinium μ-oxo-μ-sulfido-bis[tris(isothiocyanato)oxomolybdate(V)]($(pyH)_4[Mo_2O_3S(NCS)_6]$ (**5**)) was prepared following the method in Ref. 8. Chemical analysis results were: Found: N, 14.64; C, 32.51; H, 2.36%. Calcd for **3**: N, 14.64; C, 32.64; H, 2.53%. Found: N, 15.11; C, 33.26; H, 2.57%. Calcd for **4**: N, 14.86; C, 33.12; H, 2.78%. Found: N, 14.87; C, 33.29; H, 2.50%. Calcd for **5**: N, 14.89; C, 33.19; H, 2.57%.

Measurements of Magnetic Properties. Magnetic susceptibilities of samples **1**,**2**,**3**,**4**, and **5** were observed on powders in the temperature range from about 2 K to about 280 K by a magnetic balance (Oxford Instruments) of the Faraday method, which applies magnetic fields of a constant strength and a homogeneous gradient.[12,13] In order to prevent the powder sample from changing water content, it was put into a quartz cell together with minimum amount of liquid paraffin of special grade sufficient to cover the powder. The absolute values of the measured magnetic susceptibilities were small. Therefore, a constant magnetic field of 4×10^4 Oe and an inhomogeneous magnetic field with gradient of 390 Oe cm^{-1} were mainly used. The thermometer is fixed to the cryostat wall. The measurements of the $[Cr(NH_3)_6]Cl_3$ powder, which is paramagnetic in the temperature range from about 2 to 280 K, were made to correct the thermometer indications. For each measurement the sample cell site in the cryostat was checked, as were the pressures of the heat exchange gas and the time schedules of the temperature variation to get precise magnetic susceptibilities.

Electron spin resonances were observed on powder

samples and in CH_3CN solutions by a JEOL PE-3X with a microwave oscillator ES-SCXA. A thin-wall quartz cell was used. For CH_3CN solutions, signals were recorded with 1000 G/32 min scanning under 10 G modulation and input power of 0.8 mW. For powder samples measurements in the temperature range from about 2 K to 200—300 K were made using an Oxford Instruments' cryostat. Observations were made at 1000 G/40 min or 1000 G/16 min scanning rate under 1 or 10 G modulation with input power of 0.8 mW or 10^{-2} mW. The thermometer at the cryostat was calibrated by measurements of a Au(Co)-Cu thermocouple set at the sample position at a range of temperature variation made under the same conditions of changing rates and pressure of the atmosphere with the sample measurements. The magnetic flux densities were checked by diluted $Mn^{II}O$ hyperfine interaction signals and the H_1 effect measurements were also checked by the diluted $Mn^{II}O$ marker. The "H_1 effects" were observed in a range of input powers from 10^{-3} to 20 mW.

Units. The nonrationalized CGSemu are used in the present paper. The relations between the SI and the CGSemu systems on the units used in this paper are listed in Ref. 14.

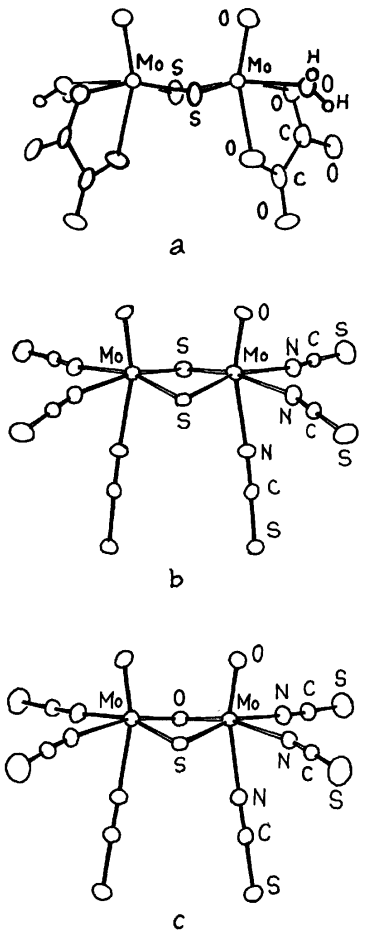

Fig. 1. Structures of complex ions from Ref. 8. (a): $[Mo_2O_2S_2(ox)_2(H_2O)_2]^{2-}$ ion, (b): $[Mo_2O_2S_2(NCS)_6]^{4-}$ ion, (c): $[Mo_2O_3S(NCS)_6]^{4-}$ ion.

Results and Discussion

Magnetic Susceptibility. The molybdenum complex ions of samples **1**,**3**, and **5** have the structures shown in Fig. 1. The structures of samples **2** and **4** are considered to be similar to **1** and **3**, respectively.

The measured magnetic susceptibilities of samples **3**, **4**, and **5** were corrected for diamagnetism following Pascal's law. As no absorption was observed in the wavenumber region of the spectra below 10^4 cm^{-1}, no correction for the temperature independent paramagnetism was made. The molar magnetic susceptibilities of samples **3**, **4**, and **5** at room temperature obtained in this way were 1.7×10^{-4}, -0.27×10^{-4}, and -4.4×10^{-4} cm^3, respectively. However, the electron paramagnetic resonances observed on all the three samples in the temperature range from about 2 to 280 K showed that they were paramagnetic, and the results of chemical analyses and molecular structure analyses by X-ray diffraction,[6,8] also established that the three were dimers of Mo (V), which may have $S=1/2$ spin on each Mo ion. The values of the molar magnetic susceptibilities reported above show that they need more corrections for diamagnetic susceptibilities, namely, at least the corrections of anisotropic diamagnetic susceptibilities due to the looped structures, that is, the pyridinium ion and the 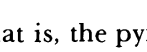 , 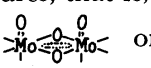 or 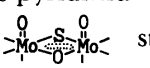 structures. Lonsdale[15] showed that the aromatic rings gave rise to anisotropic diamagnetic susceptibilities. An aromatic π-bonding structure with an effective radius r has an anisotropic diamagnetic susceptibility of $\chi_{ring}=(-Ne^2/4mC^2)\sum_p r^2$, where N is the Avogadro number, p is the number of p-electrons in the π-bonding loop and other symbols have their usual meanings. The unit of χ_{ring} is CGSemu except e and r which are CGSesu and Å respectively. The projections of the area of π-bonding looped structures on the planes perpendicular to the external manetic field directions of the samples were calculated in order to estimate the anisotropic diamagnetic susceptibilities. For the pyridinium ion, which is analogous to benzene, 6 electrons were taken as mobile electrons under the applied magnetic field. For the 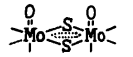 group, the following electronic

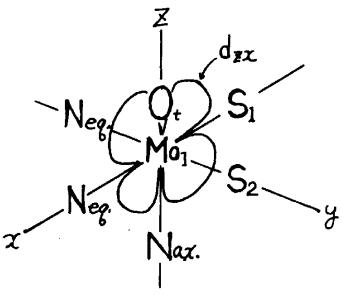

Fig. 2. Axes of atomic orbitals.

structure is assumed; a Mo^{5+} ion is basically six-coordinated with σ-bonding by two p-electrons from each bridged S^{2-} ion, two p-electrons from a terminal O^{2-} ion, two p-electrons from each equatorial N and two p-electrons from an axial N. If x, y, and z axes are taken as in Fig. 2, π-bondings are made up between d_{zx} of Mo_1 and p_z of S_1, and d_{yz} of Mo_1 and p_z of S_2, and, through the dimeric structure, a linked π-bonding is constructed. The π-bonding is a bound state like that in the aromatic benzene ring, but in this case the π-electrons might not be as mobile as those of the aromatic π-electrons. Thus, when the magnetic field is applied, four p_z-electrons of S-double bridges and two paramagnetic 4d electrons of two Mo^{5+} circulate along the π-bonding. The four p_z-electrons will contribute to the diamagnetism and two 4d electrons will effectively contribute to the paramagnetism; they have a spin of 1/2 respectively and would have super-exchange interactions of antiferromagnetic through the diamagnetic electrons as is predicted from the temperature dependence of the magnetic susceptibility derived from the ESR experiments as will be seen later. The electronic structure mentioned above is the simplest assumption for the Larmor rotation. The terminal O^{2-} would be coordinated to the Mo by four additional 2p-electrons, that is, between the Mo and the terminal O^{2-}, the bond order would therefore be higher than two. If so, the p orbitals might overlap with d_{zx} and d_{yz} of Mo. When the four $3p_z$-electrons which originally belonged to the bridged S^{2-} ions rotate in the external magnetic field, eight 2p-electrons from two terminal O^{2-} ions and four p-type electrons from the equatorial two N atoms, where sp hybridization is considered, would also be brought into the π-bonding rotation. This is because the $2p_z$ orbitals of the equatorial two N atoms are overlapped with d_{yz} and d_{zx} respectively. If this extended π-bonding is assumed, a total of 16 electrons will rotate along the linkage. If sp hybridizations are assumed in the bridged S^{2-}, four additional electrons, making a total of 20 might contribute to the anisotropic dia-

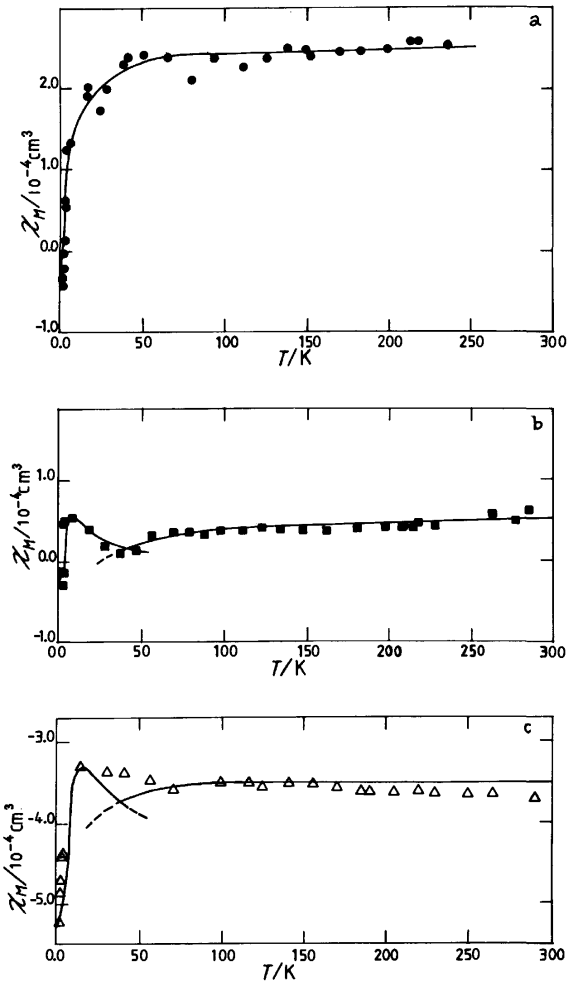

Fig. 3. Molar magnetic susceptibilities. (a): $(pyH)_4[Mo_2O_2S_2(NCS)_6]$ (**3**) (●: Experimental values. The diamangetic susceptibility -582×10^{-6} cm^3 is corrected. The thin curve is a fitted $C_3\exp(-5/T)$). (b): $(pyH)_4[Mo_2O_4(NCS)_6]\cdot H_2O$ (**4**) (■: Experimental values. The diamagnetic susceptibility -527×10^{-6} cm^3 is corrected. The thin curves are fitted $C_{41}T^{-1/2}\exp(-14/T^2)$ and $C_4\exp(-30/T)$). (c): $(pyH)_4[Mo_2O_3S(NCS)_6]$ (**5**) (△: Experimental values. The diamagnetic susceptibility -577×10^{-6} cm^3 is corrected. The thin curves are fitted $C_{51}T^{-1/2}\exp(-60/T^2)$ and $C_5\exp(-10/T)$).

Table 1. The Diamagnetic Susceptibilities[a] Used for the Correction of the Molar Magnetic Susceptibilities

	χ_{atomic}/(CGSemu)[b]	χ_{ring}/(CGSemu)[c] cation	χ_{ring}/(CGSemu)[d] anion
Sample (**1**)	−0.000268		−0.000004, −0.000014
Sample (**2**)	−0.000243		−0.000004, −0.000014
Sample (**3**)	−0.000502	−0.000072	−0.000008, −0.000034
Sample (**4**)	−0.000448	−0.000072	−0.000007, −0.000026
Sample (**5**)	−0.000498	−0.000072	−0.000007, −0.000030

a) The values are for one mol of the sample in CGSemu, then, their units are cm^3. b) The magnetic susceptibility for mol due to the atomic diamagnetism. c) The magnetic snsceptibility for mol due to four pyridinium ions. d) The magnetic susceptibility for mol due to a π-orbital containing two Mo(V)'s. The former value is the case of 4 mobile p-electrons and the latter value is of 16 mobile p-electrons.

magnetism. For the 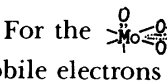 and 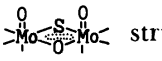 structures, the mobile electrons were similarly considered. The anisotropic diamagnetic molar susceptibilities are shown together with atomic diamagnetic susceptibilities in Table 1. The molar magnetic susceptibilities corrected for the diamagnetic susceptibilities are shown in Fig. 3.

The corrected value of sample **4** is in the same order value with that measured by Mitchell and Williams[2] for $(pyH)_4[Mo_2O_4(NCS)_6]$. Jezowska-Trzebiatowska et al.[7] measured more than five pyridinium salts of di-μ-oxo- and μ-oxo-μ-(sulfido, perchlorate, oxalato, or etc.)-bis[oxomolybdate(V)], the molar magnetic susceptibilities of which are in the same region with our data at room temperature. The temperature dependence of the molar magnetic susceptibilities of samples **3**, **4**, and **5** under the applied magnetic field of 40 kOe is roughly as follows. At very low temperature the molar magnetic suseptibilities increase exponentially with rising temperature from small values, reaching a maximum around 10—20 K, and retaining the same magnitude up to room temperature. This temperature dependence at very low temperatures shows that it can be expressed in the form of $\exp(E/kT)$, where E is an activation energy and E/k would be about 10—20 K (k: Boltzmann's const.= 1.380662×10^{-16} erg K^{-1}). The susceptibilities seem to decrease to zero at absolute zero K showing that the spins condense to a spin singlet state rather than to a long range ordered state. On the other hand from the temperature independent susceptibilities at higher temperatures we infer the existence of an ordered state. The isolated dimer spin system does not have any ordered state, and therefore an alternating linear chain system[16] or some other dimeric systems with

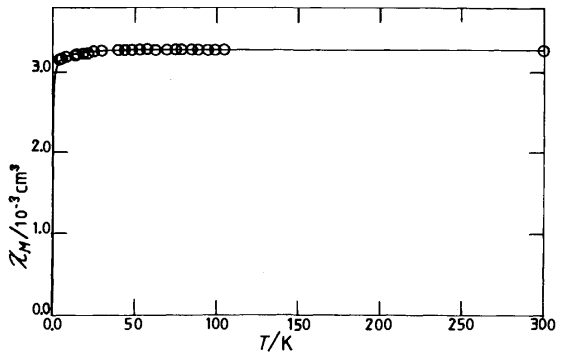

Fig. 4. The molar magnetic susceptibility of $Cs_2[Mo_2O_2S_2(ox)_2(H_2O)_2]\cdot 2H_2O$ (**1**). (○: Experimental values. The diamagnetic susceptibility -272×10^{-6} cm^3 is corrected. The thin curve is a fitted $C_1\exp(-0.2/T)$).

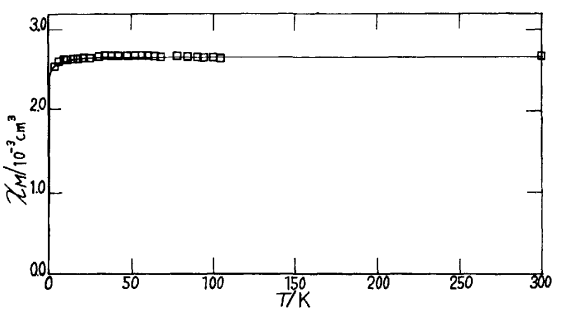

Fig. 5. The molar magnetic susceptibility of $Ba[Mo_2O_4(ox)_2(H_2O)_2]\cdot 3H_2O$ (**2**). (□: Experimental values. The diamagnetic susceptibility -247×10^{-6} cm^3 is corrected. The thin curve is a fitted $C_2\exp(-0.2/T)$).

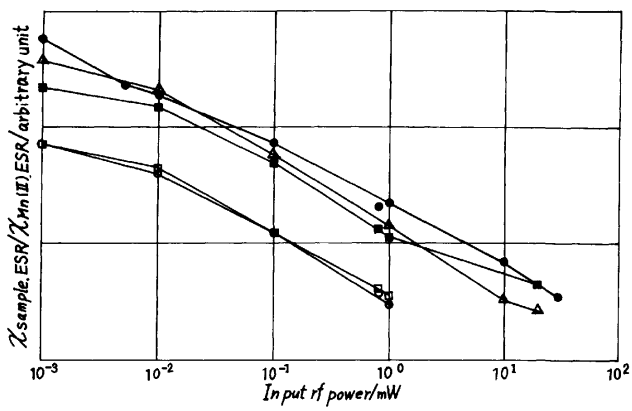

Fig. 6. The spin susceptibilities of the samples deduced from ESR's relative to that of diluted Mn^{2+} used as a reference versus input rf power. ○: $Cs_2[Mo_2O_2S_2(ox)_2(H_2O)_2]\cdot 2H_2O$ (**1**), □: $Ba[Mo_2O_4(ox)_2(H_2O)_2]\cdot 3H_2O$ (**2**), ●: $(pyH)_4[Mo_2O_2S_2(NCS)_6]$ (**3**), ■: $(pyH)_4[Mo_2O_4(NCS)_6]\cdot H_2O$ (**4**), △: $(pyH)_4[Mo_2O_3S(NCS)_6]$ (**5**).

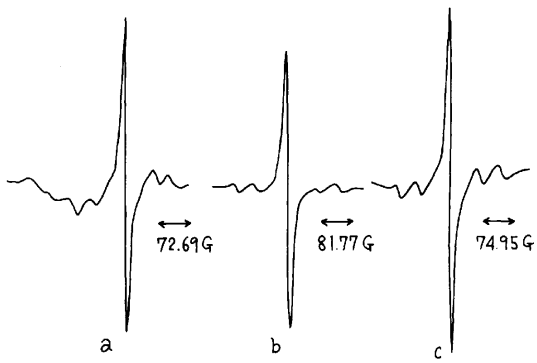

Fig. 7. ESR spectra. (a): $(pyH)_4[Mo_2O_2S_2(NCS)_6]$(**3**) in CH_3CN solution at room temperature (Experimental conditions: 9.455 GHz, 0.8 mW, 3400±500 G/64 min scanning, and 10 G moduration. Results are listed in Table 2), (b): $(pyH)_4[Mo_2O_4(NCS)_6]\cdot H_2O$ (**4**) in CH_3CN solution at room temperature (Experimental conditions: 9.456 GHz, 0.8 mW, 3400±500 G/32 min scanning, and 10 G moduration. Results are listed in Table 2), (c): $(pyH)_4[Mo_2O_3S(NCS)_6]$ (**5**) in CH_3CN solution (Experimental conditions: 9.456 GHz, 0.8 mW, 3400±500 G/64 min scanning and 10 G moduration. Results are listed in Table 2).

interactions among the dimers should be present. As shown in Figs. 4 and 5, samples **1** and **2** showed similar and clearer temperature dependence of the magnetic susceptibilities with those of sample **3**. The effective Bohr magneton numbers of the samples at 100 K were **1**:1.6, **2**:1.5, **3**:0.45, and **4**:0.21, respectively. Sample **5** was diamagnetic after the above diamagnetic corrections.

Electron Spin Resonance. The electron spin resonances were first observed to see if the samples are paramagnetic or not. All the samples showed paramagnetic resonances in the temperature region from 2 K to room temperature, in spite of the diamagnetic static susceptibility of sample **5**. As mentioned in the section of the experimental the electron paramagnetic resonances were observed under unusual conditions. In Fig. 6, the magnetic susceptibilities derived from the ESR signals at room temperature divided by the magnetic susceptibilities of the diluted Mn^{2+} compounds used as a reference of the ESR signals were plotted for the ESR input powers. All the samples showed decreasing intensities with increasing input powers, namely, a saturation effect called the "H_1 effect" was observed. Input power of 10^{-3} m W does not give the maximum signal intensity. This H_1 effect might be the reason why they reported that no ESR was observed in some Mo(V) dimeric coordination compounds.[6] The values of H_1 were not measured, but as at the same input power the diluted Mn^{2+} compound did not show any saturation. We believe that the input power of 0.8 mW was less than several G^2 as H_1^2. Which of T_1, T_2, or, both of T_1 and T_2 are responsible for the ESR signal saturations cannot be decided, but this effect is never found in the reports of ESR of Mo(V) monomer, then, the "H_1 effect" would arise from the dimeric structures of the samples. The distances between the Mo(V) ions in the dimers are about 2.5—2.8 Å, but the effective superexchange interactions between the paired Mo(V) ions might be small, making T_2 long, alternatively spins in the π-molecular orbitals might have a large relaxation time to the lattice of the bath.

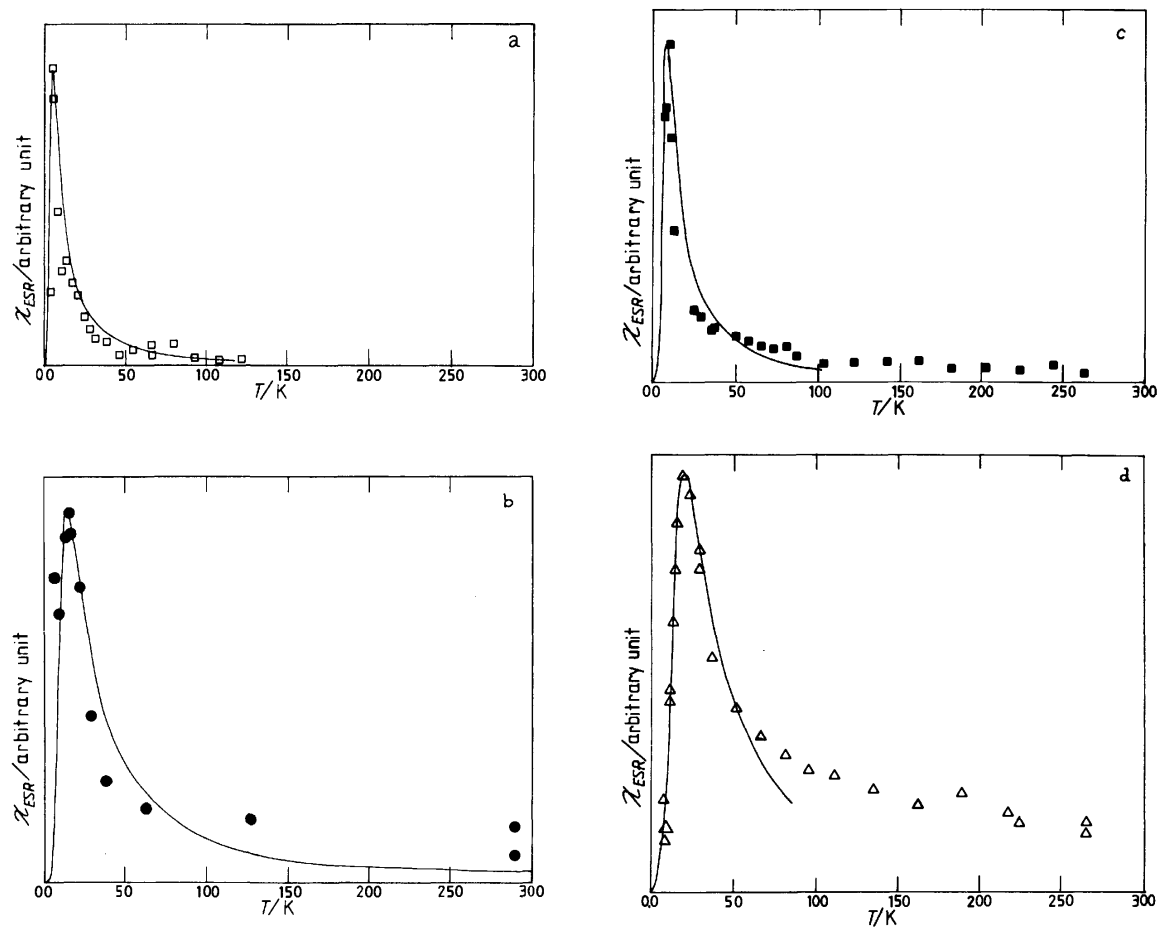

Fig. 8. Spin susceptibilities deduced from the ESR derivative curves versus temperatures. (a): Ba-$[Mo_2O_4(ox)_2(H_2O)_2]\cdot 3H_2O$ (**2**) (□: Experimental values and the thin curve is a fitted $B_2T^{-3/2}\exp(-20/T^2)$). (b): $(pyH)_4[Mo_2O_2S_2(NCS)_6]$ (**3**) (●: Experimental values and the thin curve is a fitted $B_3T^{-3/2}\exp(-160/T^2)$), (c): $(pyH)_4[Mo_2O_4(NCS)_6]\cdot H_2O$ (**4**) (■: Experimental values and the thin curve is a fitted $B_4T^{-3/2}\exp(-40/T^2)$), (d): $(pyH)_4[Mo_2O_3S(NCS)_6]$ (**5**) (△: Experimental values and the thin curve is a fitted $B_5T^{-3/2}\exp(-260/T^2)$).

In Fig. 7, ESR derivative curves of samples **3**, **4**, and **5** in CH_3CN solutions at room temperature are shown, of which averaged g-values, H_{msl}'s (separation of maximum slope) and the hyperfine interaction splittings observed at 0.8 mW input power are listed in Table 2. The hyperfine interaction splittings were observed also on powder samples as listed in Table 3 together with g-values and H_{msl}'s. The ESR signals of samples **3**, **4**, and **5** showed isotropic g-values. Samples **1** and **2** showed g-values of axial anisotropy. Relative intensities of g_1,g_2, and g_3 signals of sample **2** showed temperature dependences.

In Fig. 8, the spin susceptibilities obtained from the ESR signals by integration of the derivative curves of samples, **2**, **3**, **4**, and **5** respectively are shown in arbitrary units in the temperature region from 2 K to room temperature. The values at low temperatures seem to decrease to zero with decreasing temperatures. The spin susceptibilities have maxima at rather low temperatures; at higher temperatures they decrease with increasing temperature. This behavior is that of dimer spins or alternating linear spins[16] or ladder model spins,[16] though the peaks of the maxima are too steep to fit the theoretical dimer or alternating linear chain models. The different temperature dependences of a static magnetic susceptibility and a dynamic magnetic susceptibility are known as characteristic of the itinerant ferromagnetism in the theory on the weak ferromagnetic metals.[17] This is an attractive theory having various suggestive ideas. However in our samples, the itinerant interactions are limited within the π-molecular orbitals, therefore it

Table 2. ESR Results of CH_3CN Solutions and Powder Samples at Room Temperature

	CH_3CN solution			Powder		
	g_{av}-value	Hyperfine splitting/G	H_{msl}/G	g_{av}-value	Hyperfine splitting/G	H_{msl}/G
Sample (**1**)				1.995		4.53
Sample (**2**)				1.996		4.19
Sample (**3**)	1.933	48.95	13.6	1.933	50.24	14.4
Sample (**4**)	1.934	49.29	15.0	1.935	39.80	24.5
Sample (**5**)	1.931	49.06	13.6	1.935	36.76	18.7

Table 3. Crystal Structure Parameters

	Space group Z	Lattice constants /Å /degree	Mo-Mo distance in a dimer /Å	Effective area of π-orbital linked two Mo's /(Å)^2	Effective area of π-orbital of pyridinium ion /(Å)^2	Mo-Mo distance of the nearest in the nearest neighbour /Å
Sample (**1**)	$P2_1/c$ 4	$a=12.427$ $b=16.197$ $c=9.590$ $\beta=109.77$	2.52—2.54	1.99		4.07—6.63
Sample (**2**)	$P3_121$ 6	$a=10.630$ $b=10.630$ $c=11.65$ $\gamma=120$	2.54	1.99		5.64
Sample (**3**)	$P2_1/m$ 2	$a=15.669$ $b=13.106$ $c=9.173$ $\beta=96.77$	2.83	4.77	6.70	15.0
Sample (**4**)	$Pna2_1$ 4	$a=26.161$ $b=15.106$ $c=9.755$	2.58[a]	3.59	6.70	
Sample (**5**)	$P2_1/m$ 2	$a=15.898$ $b=13.207$ $c=9.085$ $\beta=94.04$	2.69	4.17	6.70	13.5

a) Ref. 6.

should not be considered in the present case.

Alternating Linear Chain Magnet Model. The arrangements of the molecules in the crystals of the five dimer samples were investigated.[5,8] Their space groups, lattice constants, numbers of Mo in a unit cell, distances between two Mo's of intra dimer and between a Mo and the nearest Mo in the nearest neighbour dimer, effective areas of the π-orbitals containing two Mo's and the π-orbital of pyridinium ion are listed in Table 3. In sample **1**,[8] the dimer complex ions make linear chains along the *c* axis, but it is not distinctly so, rather it should be said the dimer complex ions make two dimensional arrangements on the *bc* planes. Sample **2** has a spiral structure along the *c* axis where the molecular axes of the three dimer complex ions in a unit cell point in different directions consistent with the complx *g*-values observed in the ESR. Samples **3** and **5** have linear chains of the dimer complex ions along the *b* axis respectively. The details of sample **4** are not yet clear, but the five dimer samples are considered as magnetically alternating linear chains or dimers having low dimensional magnetic interactions among them.

The magnetic ordered state induced by the applied magnetic field was experimentally found on an alternating linear chain compound $Cu(NO_3)_2 \cdot 2.5H_2O$ by Amaya et al. and discussed by Tachiki et al., Bonner et al., and others.[16] In Fig. 9, a phase diagram of the alternating linear chain of Heisenberg spins proposed by Bonner is shown. She considers that the ordered SF(spin flop) phase has a temperature independent magnetic susceptibility and at lower applied magnetic fields than the SF phase region the spins behave as an alternating linear chain. She reported the results of the exact calculations of the magnetic and thermal properties of the alternating linear chain of a finite number of spins up to 10 and extended them to the infinite number of spins. On the other hand, she gave a rough temperature dependence of the magnetic susceptibility of the alternating linear chain under applied magnetic fields lower than the critical SF phase field as $\chi = T^{-1/2}\exp(-\Delta E_1/kT)$. This is a good approximation at low temperatures. As desctribed above, samples **1**, **2**, **3**, and **4** measured at 40 kOe of an applied magnetic field and sample **5** measured at 10 kOe of an applied field showed temperature independent magnetic susceptibilities at higher temperatures than some temperatures characteristic to each sample. If the molar magnetic susceptibilities at temperatures above the constant values under the applied magnetic fields are expressed as C_i, where the base line is set at the value of zero K, the molar magnetic susceptibilities of the samples **1**, **2**, **3**, **4**, and **5** under the magnetic fields are $C_1\exp(-0.2/T)$, $C_2\exp(-0.2/T)$, $C_3\exp(-5/T)$, $C_4\exp(-30/T)$, and $C_5\exp(-10/T)$, respectively, which are shown in Figs. 4,5, and 3 a,b, and c. It can be assumed that the samples take ordered states under high applied magnetic fields having the magnetic susceptibilities of the C_i's. If the spins are localized at atomic sites the magnetic susceptibilities will take the values of the ordered states as soon as the magnetic fields are applied at a low temperature. However the Mo(V) spins in the present samples are in the π-bonding linked orbitals. When the magnetic field is applied for the measurements at a low temperature, the mobile electrons and electron spins will begin the Larmor rotations. The rotations of the spins will attenuate with rising temperature to some velocities characteristic to each linked orbital and the spins will gradually take the ordered state values following the temperature dependences as shown in the graphs. The rotations of the nonmagnetic electrons will not have this temperature dependence. The electron spin resonances were observed at the magnetic flux densities of about 3000±15 G. The observed temperature dependences of the spin susceptibilities derived from the ESR signals show that 3000±15 G is lower than the critical fields of the SF ordered states, but the Larmor rotation will similarly affect the mobile electrons when the magnetic field is applied. At least the temperature dependence of the alternating linear chain magnetic susceptibilities of the five samples might have a term $\exp(-\Delta E'/T^2)$ instead of the Bonner's term $\exp(-\Delta E_1/T)$. The fitted magnetic susceptibilities to the experimental values of samples **2**, **3**, **4**, and **5** were $B_2T^{-3/2}\exp(-20/T^2)$, $B_3T^{-3/2}\exp(-160/T^2)$, $B_4T^{-3/2}\exp(-40/T^2)$, and $B_5T^{-3/2}\exp(-260/T^2)$, respectively, where B_i's are arbitrary constants. These fitted curves are drawn in Fig. 8 a, b, c, and d. The term T^{-1} multiplied to the Bonner's term $T^{-1/2}$ might come from the rf field. We cannot decide whether this temperature dependence comes from an isothermal effect or from some relaxation effect due to

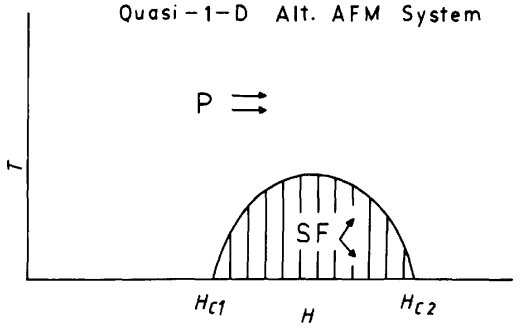

Fig. 9. A phase diagram of the quasi-1D alternating antiferromagnetic Heisenberg spins from Ref. 16. P $\rightleftarrows$ shows paramagnetic phase under applied magnatic field, SF$\rightleftarrows$ shows spin flopped phase of magnetic ordered phase induced by applied magnetic field; H_{c1} and H_{c2} are the critical magnetic fields at zero temperature.

the method of ESR measurements. The curves of the fitted magnetic susceptibilities agree with the experimental curves at low temperatures, but at temperatures higher than the susceptibility maximum, the fittings become poorer with rising temperature as the curves never approach the Curie-Weiss type temperature dependence. The static magnetic susceptibility of sample **4** shows a different behavior. Its Larmor rotation effect is $C_4\exp(-30/T)$ as mentioned above. Then before the spins reach the ordered state value the behavior as an alternating linear chain with the rotation effect appears with a fitted formula $C_{41}T^{-1/2}\exp(-14/T^2)$, as shown in Fig. 3. Sample **5** showed negative susceptibility after the above-mentioned atomic (Pascal) and molecular (π-orbital) orbital diamagnetism corrections have been applied. This sample was measured at an applied field of 40 kOe in the lower temperature region and at 10 kOe above 100 K. In the lower temperature region an alternating linear chain type susceptibility fitted to $C_{51}T^{-1/2}\exp(-60/T^2)$ is observed. For the superexchange interaction parameter J between two paramagnetic ions of spin 1/2 with double bridges each through one anion path are known to show a larger value than one hundred K, if it is expressed as $|J|/k$. For the present samples, if the exponential term of the spin susceptibilities derived from ESR signals indicates the band gap energy, then the superexchange interaction parameters of samples **2**, **3**, **4**, and **5** are $|-100|$, $|-32|$, $|-1.3|$, and $|-26|$K, respectively, where the rotation effects are removed. These values are small, though they are not inconsistent with the "H_1 effect".

The problem remains that sample **5** is diamagnetic after all the above-mentioned diamagnetic corrections have been applied. There may be some diamagnetism with large absolute values, not only in the sample **5** but in all the samples. The atomic daimagnetic susceptibility is $\chi=(-Ne^2/6mc^2)$ $(\sum_i r_i^2)$, which was deduced from Larmor's theorem by Langevin and Pauli, [18] that is, the Larmor's rotation in the atomic core is considered as the ideal one, where electrons rotate along an orbital on a plane energy level. This assumption is used in the case of benzene π-orbital by Lonsdale. The static magnetic susceptibility is $\chi=M/H$, where M is magnetization and H is magnetic field strength, when the magnetic induction B is defined as $B=\mu H=H+4\pi M$, $\chi=(\mu-1)/4\pi$. When the sample is a superconductor, B is zero, that is, permeability μ should be zero. We consider, here, for normal substances, therefore, $0<\mu$. On the other hand, we consider diamagnetism, therefore, χ should be negative, that is $\mu<1$. When the electrons obey the ideal Larmor's theorem, $\chi\fallingdotseq-10^{-6}\,\mathrm{cm}^3$, that is $1-\mu=+10^{-6}\times4\pi$, namely, B/H is very near to 1. In the present samples, when a magnetic field is applied, mobile electrons circulate along molecular orbitals which are 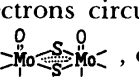 , or 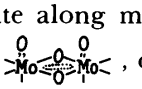 , or 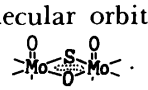 . In the above-mentioned corrections we have assumed ideal Larmor rotations, but, the results show us that the assumptions used were not suitable. B/H may be much smller than 1 and the samples may have diamagnetic susceptibilities with large absolute values. If so the symmetry of the molecular orbital of sample **5** is lower than those of samples **3** and **4**, and has diamagnetic susceptibility with the largest absolute value. This is consistent with the above considerations. Another possibility for the diamagnetism with a large absolute value, was proposed by Ginzburg[19] concerning the diamagnetism of CuCl and CdS. The diamagnetism would be due to the toroidal moment. He did not discuss coordination compounds, but if ring structures with mobile electrons take a toroidal coil arrangement in a crystal, the toroidal moment will appear. That possibility cannot be denied in samples **3**, **4**, and **5**.

The authors wish to express their sincere thanks to Professor Minoru Kinoshita and Dr, Tadashi Sugano, the University of Tokyo, for the valuable discussions all over this work. The authors wish to express their thanks to the Institute for Molecular Science, Okazaki, and the Institute for Solid State Physics, the University of Tokyo, for the measurements of the magnetic susceptibilities and Professor Tadamasa Shida, Kyoto University, for the observations of the electron spin resonances. One of the authors(H. K.) would like to thank Professor Ikuji Tsujikawa, Dr. Yoshitami Ajiro, and Dr. Kiminori Ushida, Kyoto University, for the valuable discussions and Dr. Keisaku Kimura and Mr. Shunji Bandow, Institute for Molecular Science, for their thoughtful advice and helps with the measurements.

References

1) M. Cousins and M. L. H. Green, *J. Chem. Soc.*, **1964**, 1567.
2) P. C. H. Mitchell and R. J. P. Williams, *J. Chem. Soc.*, **1962**, 4570.
3) C. M. French and J. H. Garside, *J. Chem. Soc.*, **1962**, 2006.
4) B. Spivak and Z. Dori, *J. Chem Soc., D*, **1970**, 1716.
5) F. A. Cotton and Sheila M. Morehouse, *Inorg. Chem.* **4**-10, 1377 (1965).
6) B. Jezowska-Trzebiatowska, T. Glowiak, M, F. Rudolf, M. Sabat, and J. Sabat, *Russ. J. Inorg. Chem.*, **22**, 1590 (1977).
7) B. Jezowska-Trzebiatowska, M. F. Rudolf, L. Natkaniec, and H. Sabat, *Inorg. Chem.*, **13**, 617 (1974).
8) T. Shibahara, H. Kuroya, K. Matsumoto, and S. Ooi, *Bull. Chem. Soc. Jpn.*, **56**, 2945 (1983), W. S. McDonald, *Acta Crystallogr., Sect. B*, **34**, 2850 (1978).
9) F. A. Armstrong, T. Shibahara, and A. G. Sykes, *Inorg. Chem.* **17**, 189 (1978).
10) R. G. James and W. Wardlaw, *J. Chem. Soc.*, **1927**, 2152.

11) N. H. Furman and C. O. Miller, *Inorg. Synth.* **3**, 160 (1950).
12) M. Takahashi, T. Sugano, and M. Kinoshita, *Bull. Chem. Soc. Jpn.*, **57**, 26 (1984).
13) K. Kimura and S. Bandow, *Kotai Butsuri*, **19**, 31 (1984).
14) List of units and conversions

	SI unit system	CGSemu non-rationalized system of unit
B: Magnetic flux density	$T=Wbm^{-2}$	G
H: Strength of magnetic field	Am^{-1}	Oe
M: Magnetization	Am^{-1}	
χ_M: Molar magnetic susceptibility	m^3	cm^3

3.336×10^{-10}/coulombs = 1/e.s.u. of elec. charge
$10^{-4}/T = 1/G$
$10^3\times4\pi/Am^{-1} = 1/Oe$
$(\chi_M$ in SI$)/m^3 = 4\pi\times10^{-6}(\chi_M$ in CGSemu$)/cm^3$

15) K. Lonsdale, *Proc. R. Soc. London, Ser. A.* **159**, 149 (1936).
16) J. C. Bonner, S. A. Friedberg, H. Kobayashi, D. L. Meier, and H. W. J. Blote, *Phys. Rev. B* **27**, 248 (1983).
17) T. Moriya and A. Kawabata, *J. Phys. Soc. Jpn*, **34** 639 (1973), *ibid*, **35**, 669 (1973); H. Hasegawa and T. Moriya, *J. Phys. Soc. Japan*, **36**, 1542 (1974); T. Moriya, *J. Magn. Magn. Mag.* **14**, 1 (1979); H. Capellmann, *Z. Physik, B* **34**, 29 (1979).
18) J. H. Van Vleck, "The Theory of Electric and Magnetic Susceptibilities," Oxford University Press (1932), p. 89.
19) L. V. Ginzburg, A. A. Gorbatsevich, Yu. V. Kopayev, and B. A. Volkov, *Solid State Commun.* **50**, 339 (1984).

 © 1987 The Chemical Society of Japan Bull. Chem. Soc. Jpn., 60, 141—148 (1987)

Stereochemical Properties of Copper(II) Complexes of (*S*)-3-Aminohexahydroazepine. Crystal and Molecular Structure of Bromobis[(*S*)-3-aminohexahydroazepine]copper(II) Perchlorate [CuBr(*S*-ahaz)$_2$]ClO$_4$

Masahiko SABURI,* Kazuo MIYAMURA, Masatoshi MORITA, Yasuo MIZOGUCHI, Sadao YOSHIKAWA, Sei TSUBOYAMA,*,† Tosio SAKURAI,† and Kaoru TSUBOYAMA†

Department of Synthetic Chemistry, Faculty of Engineering, The University of Tokyo, Hongo, Bunkyo-ku, Tokyo 113

†Institute of Physical and Chemical Research, Wako, Saitama 351-01

(Received July 11, 1986)

A series of copper(II) complexes of (*S*)-3-aminohexahydroazepine (abbreviated as *S*-ahaz) were prepared. The molecular structure of bromobis[(*S*)-3-aminohexahydroazepine]copper(II) perchlorate, [CuBr(*S*-ahaz)$_2$]-ClO$_4$, was determined using single-crystal X-ray diffraction method. The complex crystallizes is space group $P2_12_12_1$ with a=13.449(6), b=17.411(11), c=7.937(2) Å, and Z=4. The structure was solved by the direct method and refined by the least squares to R value of 0.068 for 1853 unique reflections. The Cu^{2+} ion has the square-pyramidal five-coordination geometry with four nitrogen atoms as basal donors and a bromide as an apical donor. The structures of other copper(II) complexes of *S*-ahaz were assigned on the basis of the above X-ray analysis result, together with electronic spectral and conductivity measurements. The complexes having the formula Cu(*S*-ahaz)$_2$X(ClO$_4$) (X$^-$=Cl$^-$, I$^-$, NCS$^-$, ONO$^-$) were assigned to have square-pyramidal five-coordinated structures. The *S*-ahaz complexes Cu(*S*-ahaz)$_2$X$_2$ (X$^-$=Cl$^-$, Br$^-$, NO$_3^-$) were also considered to have similar five-coordination geometries, while the complexes Cu(*S*-ahaz)$_2$X$_2$ (X$^-$=ClO$_4^-$, BF$_4^-$) to be four-coordinated in the crystalline state.

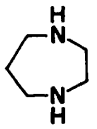

(1)

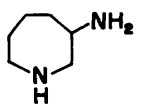

(2)

Musker and collaborators reported that 1,4-diazacycloheptane (**1**), abbreviated as dach, acts as a bidentate ligand for certain transition metal ions.[1,2] The structure of the copper(II) complex obtained from dach and Cu(NO$_3$)$_2$·6H$_2$O was determined by an X-ray crystallographic study,[3] which revealed that two Cu^{II} species, [Cu(NO$_3$)(dach)$_2$]$^+$ and [Cu(H$_2$O)(dach)$_2$]$^{2+}$, with square-pyramidal five-coordination geometries, were involved in the crystal. The molecular structure of [CuX(dach)$_2$]$^{n+}$ (X=NO$_3^-$ or H$_2$O), illustrated in Fig. 1 (I), indicated that the access of another monodentate ligand to the sixth coordination site is sterically blocked by the ligand methylene chains.

3-Aminohexahydroazepine (**2**), abbreviated hereafter as ahaz, is a unique chiral 1,2-diamine having C- and N-substituents which are fused into a seven-membered mono-azaheterocycle, while dach can be regarded as an *N*,*N*'-disubstituted 1,2-ethanediamine. If ahaz acts as a bidentate ligand for a metal ion, the ring carbon chain is required to orient nearly perpendicular to the five-membered chelate ring as in Fig. 1 (II). The ring carbon chain of ahaz should hang over the central metal ion in a similar manner as that of dach. Therefore, the coordination of a further ligand to the apical site should be significantly restricted for ahaz complexes due also to steric interactions with the ring methylenes.

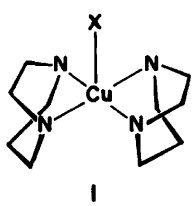

I

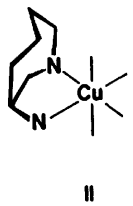

II

Fig. 1. The five-coordinated structure of [CuX(dach)$_2$]$^{n+}$ ion (I),[3] and a possible structure of ahaz coordinating to a metal ion, (II).

It seems interesting to compare the stereochemical and other properties of metal complexes of ahaz with those of dach. This paper describes the results on the preparation and stereochemical properties of copper(II) complexes of the optically active form of ahaz, i.e., (*S*)-3-aminohexahydroazepine (=S-ahaz), and, further, those of the X-ray structural analysis of a square-pyramidal copper(II) complex of *S*-ahaz, [CuBr(*S*-ahaz)$_2$]ClO$_4$.

Experimental

Measurements. Visible reflectance and absorption spectra were recorded with a Hitachi 340 spectrophotometer. Infrared spectra were obtained with a Jasco IRA-2 spectrophotometer. Electric conductivities were measured by a Toa Electronics CM-20A conductivity meter. Magnetic susceptibilities were measured at room temperature using a Shimadzu MB-100 magnetic balance (Faraday method). Optical rotations were measured with a Jasco DIP-360 polarimeter.

(*S*)-3-Aminohexahydroazepine (*S*-ahaz). To a suspension of lithium tetrahydridoaluminate (17.5 g) in dry tetrahydrofuran (THF, 400 cm^3) was added (*S*)-3-aminohexahydro-2-azepinone hydrochloride (25.0 g) in small

portions with stirring. The mixture was stirred and heated under reflux for 24 h, and then cooled to room temperature. To the mixture was added water (33 cm^3) drop by drop with stirring, and the resultant slurry was heated under reflux for 1 h. The cooled slurry was filtered off, and the solid mass was washed with THF. The solid was stirred with THF (150 cm^3) under reflux for 1 h, filtered, and washed as above. All the filtrates and washings were united, neutralized with dilute hydrochloric acid, and rotary-evaporated. The oily residue was dissolved in water (100 cm^3), and solid sodium hydroxide was added in small portions to make the mixture strong alkaline. The amine which separated from the aqueous layer was extracted with diethyl ether (total 250 cm^3), and the extracts were combined and dried over solid potassium hydroxide. The solvent was removed under reduced pressure, and the residual amine was distilled under reduced pressure. Bp, 92 °C/23 mmHg (3066 Pa). Yield; 9.5 g. α_{obsd} (neat, 589.3 nm, 1 cm cell)=−0.167°±0.002°.

In the same manner, (*S*)-3-aminohexahydro-2-azepinone prepared from L-lysine methyl ester dihydrochloride by the reported method,[4] was converted to *S*-ahaz. The product thus obtained was slightly racemized. α_{obsd} (neat, 589.3 nm, 1 cm cell)=−0.150°±0.002°.

(*RS*)-3-Aminohexahydroazepine (*RS*-ahaz). This was obtained by the same procedure for preparing *S*-ahaz, except the use of (*RS*)-3-aminohexahydro-2-azepinone hydrochloride in place of the *S*-enantiomer.

Preparation of Cu(*S*-ahaz)$_2$X$_2$ (X^-=ClO_4^-, NO_3^-, Cl^-, and Br^-). $CuX_2 \cdot nH_2O$ (5 mmol) dissolved in ethanol (5—10 cm^3) was added drop by drop to an ethanol solution (5 cm^3) of *S*-ahaz (11 mmol). Diethyl ether was added to complete the precipitation of copper(II) complex. The crystals formed were collected, washed with diethyl ether, and air-dried. The crude product was recrystallized from hot methanol.

Cu(*S*-ahaz)$_2$(BF_4)$_2$ was obtained similarly using 45% aqueous solution of Cu(BF_4)$_2$. Diethyl ether (100 cm^3) was added to an aqueous ethanol solution of the crude product to induce the precipitation of the complex. The analytical data of copper(II) complexes are given in Table 1.

Preparation of Cu(*S*-ahaz)$_2$X(ClO_4) (X^-=Cl^-, Br^-, I^-, NCS^-, and ONO^-). To a methanol solution of Cu(*S*-ahaz)$_2$(ClO_4)$_2$ (0.93 g; 2 mmol) was added a methanol solution of LiX(X^-=Cl^-, Br^-, or I^-) or NaX(X^-=NCS^- or NO_2^-) (3 mmol). The crystals which appeared were collected, and washed with methanol and diethyl ether. The product was recrystallized from methanol-water mixture (3:1 v/v). Table 1 lists the analytical data of the heteroanion[5] complexes obtained as above.

X-Ray Diffraction Analysis. A violet needle crystal, 0.20×0.38×0.57 mm, was used for the X-ray analysis. Diffraction data were collected on a Rigaku AFC-5 four-circle diffractometer with graphite-monochromatized Mo $K\alpha$ radiation (λ=0.71073 Å) at 296 K. Unit cell parameters were derived from a least squares fit of 16 2θ values in the range $20° < 2\theta < 30°$

Crystal Data. $C_{12}H_{28}BrClCuN_4O_4$, M=471.28, Orthorhombic, a=13.449(6), b=17.411(11), c=7.937(2) Å, U=1859(2) Å^3, space group $P2_12_12_1$, Z=4, D_m=1.66 (298 K), D_x=1.684 g cm^{-3}, $F(000)$=964, μ(Mo $K\alpha$)=3.47 mm^{-1}. Data were collected by ω and ω—2θ (2θ>30°) scan mode and at scan rate, 4.0° min^{-1}. The three standard reflections were monitored every 150 reflections and their intensities varied by<0.06. A total 1906 reflections obtained in the range of 2θ<55°, of which 1853 independent reflections with $|F_o| > 3\sigma(|F_o|)$ were used for the structure determination. The intensities data were corrected for Lorentz and polarization factors, but not for absorption.

Solution and Refinement. The structure was solved by the direct method, and was refined by using a block diagonal least-squares procedure based on $|F_o|$. Unit weight was used for all reflections. H-Atom coordinates were generated assuming the standard bond lengths and angles. All non-hydrogen atoms are anisotropic and H atoms are isotropic (321 parameters). The final indices R ($=(|F_o|-|F_c|)/|F_o|$) and R_w ($=[w(|F_o|-|F_c|)^2/w|F_o|^2]^{1/2}$) were 0.068 and 0.079 respectively. The largest shift to error value on the final cycle is 0.13. The maximum height in the final difference Fourier maps was 1.8 e Å^{-3} near the disordered perchlorate, O(3).

Atomic scattering factors are taken from International

Table 1. Elemental Analyses, Electric Conductivity, and Magnetic Susceptibility Data of Copper(II) Complexes

Complex	Elemental analyses[a]			Conductivity[b]	μ_{eff}
	C (%)	H (%)	N (%)	S 10^{-3} m^2 mol^{-1}	BM
Cu(*S*-ahaz)$_2$(ClO_4)$_2$	29.49(29.36)	5.55(5.75)	11.28(11.42)	151	1.76
Cu(*RS*-ahaz)$_2$(ClO_4)$_2$[c]	29.05(29.36)	5.60(5.75)	11.40(11.42)	161	1.78
Cu(*S*-ahaz)$_2$(BF_4)$_2$	30.38(30.96)	6.36(6.06)	11.74(12.04)	174	
Cu(*S*-ahaz)$_2$(NO_3)$_2$	34.76(34.65)	6.97(6.78)	19.96(20.21)	84	
Cu(*S*-ahaz)$_2$$Cl_2$	39.21(39.72)	7.85(7.78)	15.15(15.44)	71	1.73
Cu(*S*-ahaz)$_2$$Br_2$	31.16(31.90)	6.55(6.25)	12.25(12.41)	81	
Cu(*S*-ahaz)$_2$Cl(ClO_4)	33.38(33.77)	6.50(6.61)	12.90(13.13)	97	1.77
Cu(*S*-ahaz)$_2$Br(ClO_4)	30.61(30.58)	5.84(5.99)	12.24(11.89)	97	1.83
Cu(*S*-ahaz)$_2$I(ClO_4)	27.02(27.81)	5.67(5.44)	10.44(10.81)	102	1.81
Cu(*S*-ahaz)$_2$(NCS)(ClO_4)	34.02(34.74)	6.65(6.28)	15.17(15.59)	102	
Cu(*S*-ahaz)$_2$(ONO)(ClO_4)	32.35(32.95)	6.19(6.45)	16.06(16.02)	100	

a) The calculated values are in parentheses. b) Obtained for nitromethane solution (4×10^{-4} mol dm^{-3}) at 19 °C. c) The orange-red complex of racemic ahaz.

Tables for X-ray Crystallography.[6] The crystallographic calculations were performed on a FACOM M-380 computer of The Institute of Physical and Chemical Research using program MULTAN 78[7] and the UNICS III program system.[8] Their positional parameters for non-hydrogen atoms are listed in Table 2.[9]

Results

Isolation of Violet and Orange-Red Forms of $Cu(ahaz)_2(ClO_4)_2$. In our first examination, we prepared the ligand *S*-ahaz by lithium tetrahydridoaluminate reduction of (*S*)-3-aminohexahydro-2-azepinone (**3**), which was obtained via the cyclization of methyl L-lysinate[4] (Scheme 1). The copper(II)

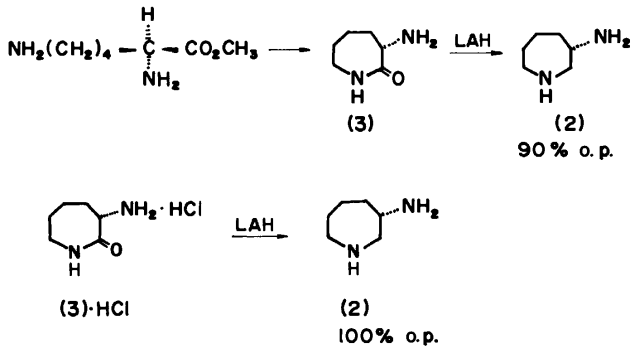

Scheme 1.

Table 2. Positional Parameters ($\times 10^4$) and Equivalent Isotropic Temperature Factors for Non-Hydrogen Atoms in $[CuBr(S\text{-ahaz})_2]ClO_4$

Atom	*x*	*y*	*z*	B_{eq}(Å^2)
Cu	1153(1)	4046(1)	4583(2)	2.8(0.0)
Br	2998(1)	4790(1)	4215(2)	4.1(0.0)
N(1)	548(9)	5028(7)	5535(19)	4.0(0.3)
C(2)	441(13)	5527(9)	4224(32)	5.6(0.6)
C(3)	−3(12)	5124(11)	2583(25)	4.9(0.5)
C(4)	−1098(13)	4915(13)	2732(27)	6.0(0.6)
C(5)	−1409(13)	4488(13)	4331(36)	7.1(0.7)
C(6)	−1294(14)	4930(15)	5866(32)	8.0(0.8)
C(7)	−313(14)	4986(13)	6648(27)	6.2(0.6)
N(8)	608(10)	4424(8)	2398(17)	4.0(0.4)
N(1)'	1818(10)	3076(8)	3716(19)	4.4(0.4)
C(2)'	2448(12)	2792(10)	4960(27)	5.0(0.5)
C(3)'	1898(15)	2806(10)	6706(24)	5.1(0.5)
C(4)'	1142(19)	2166(11)	7022(33)	7.0(0.7)
C(5)'	654(20)	1787(13)	5568(44)	9.2(1.0)
C(6)'	323(15)	2247(12)	4122(35)	7.0(0.7)
C(7)'	1123(16)	2490(11)	2958(25)	5.9(0.6)
N(8)'	1403(12)	3563(8)	6855(17)	4.7(0.4)
Cl	3709(4)	1961(3)	490(7)	6.2(0.1)
O(1)	4616(13)	1615(11)	467(28)	10.6(0.7)
O(2)	2919(13)	1495(11)	330(35)	12.6(0.9)
O(3)	3729(20)	2497(13)	−674(45)	17.0(1.3)
O(4)	3628(21)	2364(20)	1942(38)	19.2(1.4)

complex obtained from the above-mentioned ahaz (α_{obsd} (neat, 598.3 nm, 1 cm cell)=−0.150°±0.002°) and $Cu(ClO_4)_2\cdot 6H_2O$ consisted of two crystalline forms of different color, the dominant violet and the minor orange-red ones. Because the latter was less soluble than the former, they could be separated from each other by recrystallization from methanol.

In spite of the clear difference in their color, the elemental analysis results of these two forms agreed adequately with the expected values for the formula $C_{12}H_{28}Cl_2CuN_4O_8=Cu(C_6H_{14}N_2)_2(ClO_4)_2$. Electric conductivity measurements showed that they dissociated as bi-univalent electrolites in nitromethane. Further, magnetic susceptibility measurements suggested that both were mononuclear Cu^{II} species. The electric conductivity and magnetic susceptibility data of copper(II) complexes of ahaz are also summarized in Table 1.

A remarkable distinction between the two forms, which could be noticed finally with a surprise, was that the orange-red form was optically inactive, while the violet one optically active. Thus, the violet crystals evidently involve the optically active ahaz, the chiral carbon center of which should assume the *S*-configuration, because the starting material of the present ligand was L-lysine (Scheme 1). On the other hand, the orange-red form was thought to include the racemic ahaz. These results indicated that *S*-ahaz employed here was partially racemized.

To confirm the difference between copper(II) complexes caused by employing either the racemate or the optically-active *S*-enantiomer as the ligand, we synthesized both modifications of ahaz. The enantiomerically pure *S*-ahaz was prepared from the pure (*S*)-3-aminohexahydro-2-azepinone hydrochloride ((**3**)·HCl) (Scheme 1). The optically-pure *S*-ahaz showed an optical rotation α_{obsd} (neat, 589.3 nm, 1 cm cell)=−0.167°±0.002°, and gave rise to only the violet form. On the other hand, the orange-red form was the sole product for the reaction of *RS*-ahaz (*RS*-ahaz=racemic ahaz) with $Cu(ClO_4)_2$. These observations confirm that the violet form involves the pure *S*-antipode of ahaz.

Preparation of Copper(II) Complexes of *S*-ahaz. It was observed that the homo-anion[10] copper(II) complexes of *S*-ahaz, $Cu(S\text{-ahaz})_2X_2$, obtained by mixing $CuX_2\cdot nH_2O$ and twice the molar of *S*-ahaz were violet ($X^-=ClO_4^-$, BF_4^-, NO_3^-) or blue-violet ($X^-=Br^-$, Cl^-). As these complexes gave no single crystals suitable for X-ray structural analysis, their exact structures have not been clarified yet. The circular dichroism spectral feature of the S-ahaz complex has been reported.[11]

The hetero-anion[5] copper(II) complexes of *S*-ahaz having the formula $Cu(C_6H_{13}N_2)_2X(ClO_4)$ were obtained by either of the following two methods; (i) the addition of an excess amount of LiX ($X^-=Cl^-$, Br^-, I^-)

or NaX (X^-=NCS^-, NO_2^-) to a methanol solution of $Cu(S\text{-ahaz})_2(ClO_4)_2$ (Eq. 1), and (ii) the addition of $LiClO_4$ to a methanol solution of $Cu(S\text{-ahaz})_2X_2$ (X^-=Cl^-, Br^-) (Eq. 2).

$$Cu(S\text{-ahaz})_2(ClO_4)_2 + MX \rightarrow Cu(S\text{-ahaz})_2X(ClO_4) + MClO_4 \quad (1)$$

(M^+=Li^+ or Na^+; X^-=Cl^-, Br^-, I^-, NCS^-, ONO^-)

$$Cu(S\text{-ahaz})_2X_2 + LiClO_4 \rightarrow Cu(S\text{-ahaz})_2X(ClO_4) + LiX \quad (2)$$

(X^-=Cl^-, Br^-)

These hetero-anion complexes formed well-developed single crystals so that the molecular structure of the bromo complex, $Cu(S\text{-ahaz})_2Br(ClO_4)$, was determined using the single-crystal X-ray diffraction method.

The Molecular Structure of Bromobis[(*S*)-3-aminohexahydroazepine]copper(II) Ion. Figure 2 shows the perspective views of the complex cation, $[CuBr(S\text{-ahaz})_2]^+$. The selected bond parameters are listed in Table 3. The absolute configuration of the complex were assigned from the known absolute configuration of the ligand as an internal reference. The complex ion has a square-pyramidal structure with the bromide at the apex. Two *S*-ahaz ligands coordinate to Cu^{2+} ion in the trans fashion, and, expectedly, the seven-membered rings orient perpendicular to the CuN_4 basal plane. The seven-membered rings extend toward the same side of the basal plane, and disturb obviously the access of additional ligand to the sixth coordination site.

It is noticeable that the seven-membered ring of *S*-ahaz depicted on the left side of the structure in Fig.2 with the non-primed atoms N(1), C(2), ···N(8) has a different conformation from that of the right side *S*-ahaz with the primed atoms N(1)′, C(2)′, ···N(8)′. In spite that the seven-membered rings of both *S*-ahaz adopt the preferred twist-chair conformation,[12] the cyclic sequence of dihedral angles in the non-primed *S*-ahaz is different from that of the primed one as shown in Fig. 3. This is the reason for that the complex ion lacks the true C_2 symmetry. Both five-membered chelate rings take the λ conformation, though the chelate of the primed ligand is deformed to an envelope. The coordinating secondary asymmetric nitrogen center adopts the *R*-configuration.

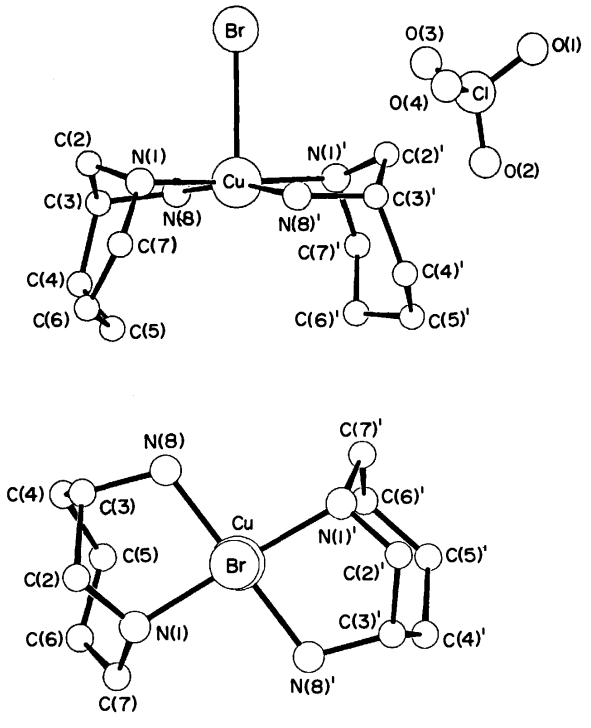

Fig. 2. Perspective views of $[CuBr(S\text{-ahaz})_2]^+$ ion.

Table 3. Bond Lengths (*l*/Å) and Angles (φ/°)

Cu-Br	2.813(2)		
N(8)-Cu	2.00(1)	N(8)'-Cu	2.02(1)
Cu-N(1)	2.04(1)	Cu-N(1)'	2.03(1)
N(1)-C(2)	1.36(3)	N(1)'-C(2)'	1.39(2)
C(2)-C(3)	1.60(3)	C(2)'-C(3)'	1.57(3)
C(3)-N(8)	1.48(2)	C(3)'-N(8)'	1.48(2)
C(3)-C(4)	1.52(2)	C(3)'-C(4)'	1.53(3)
C(4)-C(5)	1.53(3)	C(4)'-C(5)'	1.48(4)
C(5)-C(6)	1.45(4)	C(5)'-C(6)'	1.47(4)
C(6)-C(7)	1.46(3)	C(6)'-C(7)'	1.48(3)
C(7)-N(1)	1.46(2)	C(7)'-N(1)'	1.51(2)
Cl-O(1)	1.36(2)		
Cl-O(2)	1.34(2)		
Cl-O(3)	1.31(3)		
Cl-O(4)	1.35(3)		
N(8)-Cu-Br	94.7(4)	N(8)'-Cu-Br	98.0(5)
N(1)-Cu-Br	90.3(3)	N(1)'-Cu-Br	87.7(4)
N(8)-Cu-N(1)	84.2(6)	N(8)'-Cu-N(1)'	83.3(6)
Cu-N(1)-C(2)	107(1)	Cu-N(1)'-C(2)'	109(1)
Cu-N(1)-C(7)	120(1)	Cu-N(1)'-C(7)'	115(1)
N(1)-C(2)-C(3)	112(1)	N(1)'-C(2)'-C(3)'	110(1)
C(2)-C(3)-N(8)	104(1)	C(2)'-C(3)'-N(8)'	107(1)
C(4)-C(3)-N(8)	110(2)	C(4)'-C(3)'-N(8)'	110(2)
C(3)-N(8)-Cu	113(1)	C(3)'-N(8)'-Cu	112(1)
C(7)-N(1)-C(2)	114(1)	C(7)'-N(1)'-C(2)'	115(1)
N(1)-C(2)-C(3)	112(1)	N(1)'-C(2)'-C(3)'	110(1)
C(2)-C(3)-C(4)	114(2)	C(2)'-C(3)'-C(4)'	116(2)
C(3)-C(4)-C(5)	116(1)	C(3)'-C(4)'-C(5)'	119(2)
C(4)-C(5)-C(6)	114(2)	C(4)'-C(5)'-C(6)'	120(2)
C(5)-C(6)-C(7)	119(2)	C(5)'-C(6)'-C(7)'	115(2)
C(6)-C(7)-N(1)	118(2)	C(6)'-C(7)'-N(1)'	113(2)
O(1)-Cl-O(2)	116(1)		
O(1)-Cl-O(3)	107(2)		
O(1)-Cl-O(4)	108(2)		
O(2)-Cl-O(3)	112(2)		
O(2)-Cl-O(4)	109(2)		
O(3)-Cl-O(4)	103(2)		

The three possible N-O hydrogen-bond distances are 3.20 [N(8)—O(1^{i})], 3.07 [N(1)—O(4^{ii})], and 3.22 Å [N—O(1^{iii})]. The symmetry codes are (i) $x-1/2$, $-y+1/2$, $-z$, (ii) x, y, z, and (iii) $x-1/2$, $-y+1/2$, $-z+1$. There are no particularly short intermolecular distances.

Discussion

Square-Pyramidal Geometry of [CuBr(*S*-ahaz)$_2$]$^{2+}$ Ion. As has been described, one of the apical coordination site of Cu^{2+} ion in the title complex is effectively shielded from the coordination of a ligand by the seven-membered ring of *S*-ahaz. Similar five-coordination geometries of copper(II) complexes containing diamine ligands were established for [CuX(dach)$_2$]$^{n+}$ (X=NO_3^- or H_2O)[3] and [CuCl(1,3-dach)$_2$]$^+$ (1,3-dach=*cis*-1,3-cyclohexanediamine).[13] In the case of 1,3-dach complex, the methylene chains of the ligands shield one of the apical coordination sites in a closely similar manner to that of *S*-ahaz or dach.[13]

It was indicated for a number of copper(II) complexes with square-pyramidal coordination that the ratio of the apical Cu-X distance to the mean value of in-plane bond lengths (ca. 2.0 Å), i.e., (Cu-N/Cu-X), is 0.83 on an average, which is correlated to the geometry and/or electronic energy level.[14,15] The value of the present complex is 0.72, indicating that the Cu-Br distance is fairly longer than the average value for typical square-pyramidal configuration, and that the bromide ion binds to Cu^{2+} rather weakly. Concomitantly, the deviation of Cu^{2+} from the basal plane is very small (0.0097 Å).

Stereochemistries of Hetero-Anion Copper(II) Complexes of *S*-ahaz. Figure 4 shows the possible geometries of *S*-ahaz complex in which four amino nitrogen atoms occupy the basal coordination plane. The secondary (or primary) amino groups of the diamines are located in the cis relationship for (III) and in the trans fashion for (IV). The seven-membered rings are depicted in a twist-chair conformation, though certain other conformations will be plausible as well. The methylene chain of the ligand should strictly prevent the anion coordination at the apical site close to it, so that the cis isomer is necessary to take the four-coordination geometry (III), while the trans isomer may adopt either four- or five-coordination depending on the coordinating abilities of the anion present, since one of the apical sites in (IV) is not blocked by the ring methylenes. When the fifth coordination site of (IV) is occupied by a monodentate ligand, a square pyramidal five-coordination geometry (V) is effected. The X-ray diffraction study on [CuBr(*S*-ahaz)$_2$]ClO_4 clearly indicates the presence of such geometry as (V).

The hetero-anion complexes of *S*-ahaz other than [CuBr(*S*-ahaz)$_2$]ClO_4 were blue-violet, and their

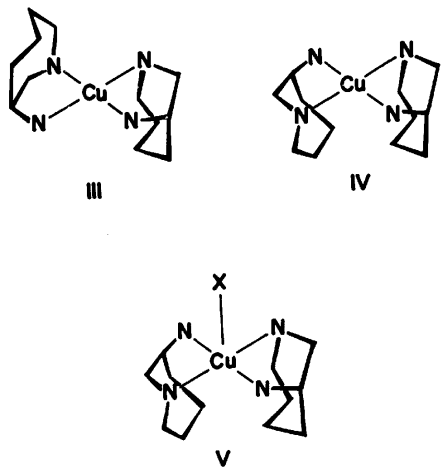

Fig. 4. Possible geometries of *S*-ahaz complexes. The four-coordinated cis form, (III); the four-coordinated trans form, (IV); the five-coordinated trans form (V). (X represents a coordinating anion).

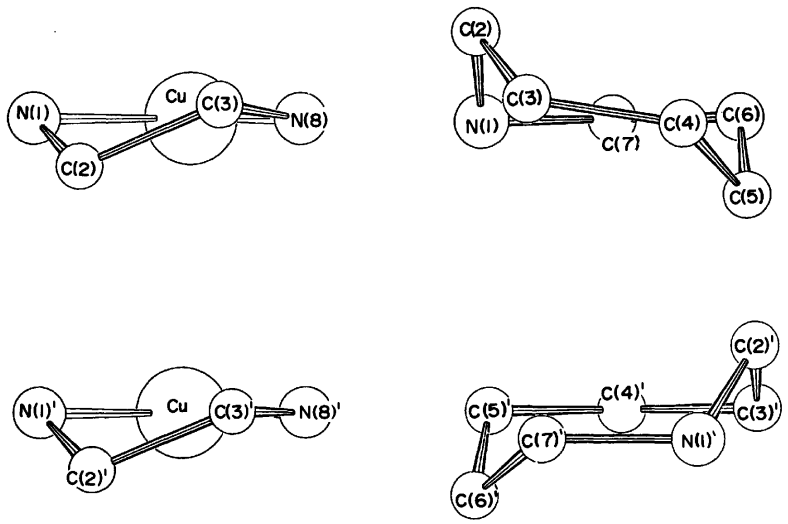

Fig. 3. Structures of five-membered chelate rings and seven-membered rings of *S*-ahaz.

reflectance spectra resembled one another as shown in Fig. 5 (see also Table 4). Further, all these complexes were found to dissociate uni-univalently in nitromethane (Table 1). This indicates that the halides or pseudohalides (NCS^-, ONO^-) with relatively high coordinating ability enter into the fifth coordination site to give rise to the complexes having the five-coordination structure (V) in a way similar to the $[CuBr(S\text{-ahaz})_2]^+$ ion. We concluded, therefore, that the hetero-anion complexes are thoroughly five-coordinated, and can be formulated as $[CuX(S\text{-ahaz})_2]ClO_4$ ($X^-=Cl^-$ etc.).

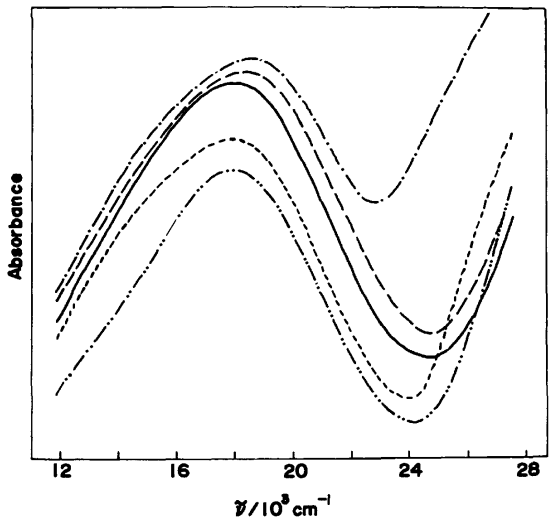

Fig. 5. Reflectance spectra of $[CuX(S\text{-ahaz})_2]ClO_4$: $X^-=Cl^-$ (——), $X^-=Br^-$ (— —), $X^-=I^-$ (—·—), $X^-=NCS^-$ (—··—), $X^-=ONO^-$ (----).

Table 4. Electronic Spectral Data of Copper(II) Complexes

Complex	Solvent[a]	$\bar{\nu}_{max}/cm^{-1}$	ε_{max}
$Cu(S\text{-ahaz})_2(ClO_4)_2$	R	18950	
	A	19420	97
	B	19050	84
$Cu(RS\text{-ahaz})_2(ClO_4)_2$	R	21100	
$Cu(S\text{-ahaz})_2(BF_4)_2$	R	19200	
	A	19530	103
	B	19050	84
$Cu(S\text{-ahaz})_2(NO_3)_2$	R	18950	
$Cu(S\text{-ahaz})_2Cl_2$	R	18590	
	A	17040	118
$Cu(S\text{-ahaz})_2Br_2$	R	18700	
	A	17210	117
$Cu(S\text{-ahaz})_2Cl(ClO_4)$	R	18200	
	A	17210	107
$Cu(S\text{-ahaz})_2Br(ClO_4)$	R	18300	
	A	17210	113
	B	18520	91
$Cu(S\text{-ahaz})_2I(ClO_4)$	R	18500	
	A	17860	108
$Cu(S\text{-ahaz})_2(NCS)(ClO_4)$	R	17850	
$Cu(S\text{-ahaz})_2(ONO)(ClO_4)$	R	17900	

a) R; reflectance spectra. A; obtained for nitromethane solution using 5 cm cells. B; obtained for methanol solution using 5 cm cells.

The infrared spectra of $[CuX(S\text{-ahaz})_2]ClO_4$ ($X^-=NCS^-$ and NO_2^-) were examined to clarify the coordination mode of these ambidentate anions. The complex with NCS^- showed bands at 2070 cm^{-1} for $\nu(CN)$ and at 856 cm^{-1} for $\nu(CS)$, and no band around 720—690 cm^{-1}. These are characteristic for the N-coordination of NCS^- ion.[16] The NO_2^- complex has bands at 1464 and 1452 cm^{-1} for $\nu(N=O)$ and at 1058 cm^{-1} for $\nu(N-O)$, indicative of the O-coordination of the NO_2^- group.[16]

Musker and Hussain described the preparation of hetero-anion complexes $[CuX(dach)_2]ClO_4$ ($X^-=Cl^-$, Br^-, NCS^-), and postulated their structures to be five-coordinated on the basis of electronic spectral and conductivity data.[1] The evidence of the square-pyramidal five-coordination geometry (Fig. 1 (I)) was provided by the X-ray analysis study on $[Cu(dach)_2(NO_3)]NO_3$,[3] which suggested that the other hetero-anion complexes of dach also took square pyramidal structures.

Stereochemistries of Homo-Anion Copper(II) Complexes of *S*-ahaz. The above-mentioned structure determination of $[CuBr(S\text{-ahaz})_2]ClO_4$ could imply the possible stereochemistries of the complex ions in $Cu(S\text{-ahaz})_2X_2$. Since the reflectance spectra of these complexes (Fig. 6 and Table 4) showed no significant change from those of the hetero-anion complexes, it seems likely that all the complexes adopt five-coordinated structures such as (V). However, these complexes were found to be classified into two groups on the basis of their conductivity behaviors.

The first group, which involves $Cu(S\text{-ahaz})_2X_2$ ($X^-=Cl^-$, Br^-, and NO_3^-), are uni-univalent electrolites in nitromethane, indicating that the complex ions have five-coordinated structures $[CuX(S\text{-ahaz})_2]^+$ in

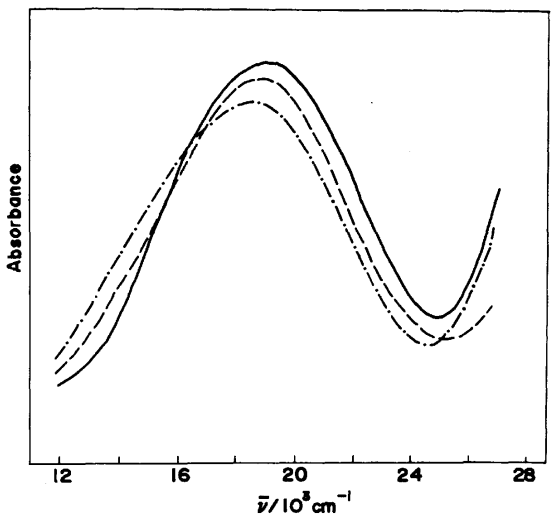

Fig. 6. Reflectance spectra of $Cu(S\text{-ahaz})_2X_2$: $X^-=ClO_4^-$ (——), $X^-=Cl^-$ (— —), $X^-=Br^-$ (—·—).

nitromethane solution. Because the rapid rearrangement and exchange of ligands are generally effected for labile copper(II) complexes in solution, it is difficult on the basis of conductivity and spectral data alone to determine unambiguously whether the crystalline state structures of these *S*-ahaz complexes are five-coordinated square-pyramidal as (V) or four-coordinated as (IV). Nevertheless we consider it to be more likely that these complexes adopt the structures (V) in a similar manner as $[CuBr(S\text{-ahaz})_2]ClO_4$ and can be formulated as $[CuX(S\text{-ahaz})_2]X$, because of that for most metal complexes such anions as halides tend to coordinate to the central metal ion in the crystalline state.

The second group, which involves the complexes with relatively weak coordinating anions as ClO_4^- and BF_4^-, were found to dissociate uni-bivalently in nitromethane. This indicates no coordination of the anion to Cu^{2+} in solution, and suggests that the interaction between the anions and Cu^{2+} for these complexes is negligible, or, if any, very weak even in the crystalline state. We supposed, therefore, that these two may adopt four-coordination structures, either (III) or (IV), and the complexes be formulated as $[Cu(S\text{-ahaz})_2]X_2$ ($X^-=ClO_4^-$, BF_4^-). We have not obtained any direct evidence of the above presumption yet, but a helpful information for considering the stereochemistry of above complexes is provided by the structural determination study of $[Cu(deen)_2](ClO_4)_2$ (deen=*N*,*N*-diethyl-1,2-ethanediamine).[17]

It is well-known that $[Cu(deen)_2]X_2$ exhibits reversible thermochromism between the red lower temperature form and the blue higher temperature form, when X^- is of low coordinating ability as ClO_4^- and BF_4^-.[17-22]. The structural change which may accompany with the color change had been studied from various aspects,[17,19-22] and conclusively demonstrated was that the most apparent stereochemical change in the course of the transformation from the red to blue form is the coformational inversion of one of the deen chelates.[17]

The red form has a strictly four-coordinated structure illustrated as (VI) in Fig. 7, in which the chelates assume the opposite conformation with each other.[17] On the other hand, the structure of the complex ion in the blue form can be depicted by (VII) in Fig. 7 or its antipode, where the chiralities of both chelate conformations are the same and the complex ion has a two-fold rotation axis perpendicular to the CuN_4 plane.[17] The coordination of perchlorate group to Cu^{2+} ion was indicated not to take place in the blue form, since the interatomic distance of Cu-O is not shorter than 4 Å.[17] This means that the color change mentioned above does not necessary mean the transformation from four to five coordination around Cu^{2+}. It is interesting to note that the stereochemical features of (VII), the presence of a two-fold rotation axis perpendicular to the CuN_4 plane and the identical chiralities of the conformation of both chelates, are same as those of (IV), one of the possible structures for $[Cu(S\text{-ahaz})_2]X_2$ ($X^-=ClO_4^-$, BF_4^-). We consider, therefore, that the S-ahaz complexes of perchlorate series ($X^-=ClO_4^-$, BF_4^-) has the four-coordination geometry (IV), and can be formulated as $[Cu(S\text{-ahaz})_2]X_2$.

The structure of the orange-red complex containing *RS*-ahaz is remained unsolved in the present paper. The structure determination of this and related complexes will be presented in a following paper.

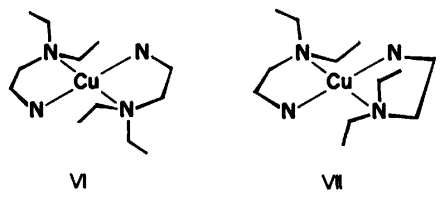

Fig. 7. Structures of $[Cu(deen)_2]^{2+}$ ion in the red form, (IV), and in the blue form, (VII).[16]

The authors wish to thank Dr. Yutaka Fukuda of Ochanomizu University for his help in obtaining the magnetic susceptibility data, and to Toray Co. for supplying the samples of (*S*)- and (*RS*)-3-amino-hexahydro-2-azepinone hydrochloride.

References

1) W. K. Musker and M. S. Hussain, *Inorg. Chem.*, **8**, 528 (1969).

2) W. K. Musker and E. D. Steffen, *Inorg. Chem.*, **13**, 1951 (1974).

3) M. S. Hussain and H. Hope, *Acta Crystallogr., Sect. B*, **25**, 1866 (1974).

4) D. W. Adamson, *J. Chem. Soc.*, **1943**, 39.

5) The term "hetero-anion" indicates that the complexes contain two kinds of the anions, one of which is perchlorate in this study. Thus, the hetero-anion complexes are shown in the form $Cu(diamine)_2X(ClO_4)$ ($X^-=Cl^-$, Br^- etc.).

6) International Tables for X-ray Crystallography, Vol. IV, Kynoch Press, Birmingham (1974).

7) P. Main, S. E. Hull, L. Lessinger, G. Germain, J.-P. Declercq, and M. M. Woolfson, MULTAN. A computer Program for the Automatic Solution of Crystal Structures from X-ray Diffraction Data. Univ. of York, England and Louvain, Belgium (1978).

8) T. Sakurai and K. Kobayashi, *Rikagaku Kenkyusho Hokoku*, **55**, 69 (1979).

9) Tables of the coordinates of hydrogen atoms, the anisotropic thermal parameters of the non-hydrogen atoms, selected torsional angles, and observed and calculated structure factors are kept as Document No. 8707 at the Chemical Society of Japan.

10) The term "homo-anion" indicates that the complexes contain only one kind of the anion, so that the complexes

are represented in the form $Cu(diamine)_2X_2$ (X^-=Cl^-, ClO_4^- etc.).

11) M. Morita and S. Yoshikawa, *J. Chem. Soc., Chem. Commun.* **1972**, 578; M. Morita and S. Yoshikawa, *Inorg. Nucl. Chem. Lett.*, **8**, 199 (1972).

12) J. Dale, *Top. Stereochem.*, **9**, 199 (1976), and references cited therein.

13) K. Kamisawa, K. Matsumoto, S. Ooi, R. Saito, and Y. Kidani, *Bull. Chem. Soc. Jpn.*, **54**, 1072 (1981).

14) B. J. Hathaway, *Struct. Bonding (Berlin)*, **14**, 49 (1973).

15) B. J. Hathaway and P. G. Hodgson, *J. Inorg. Nucl. Chem.*, **35**, 4071 (1973).

16) K. Nakamoto, "Infrared and Raman Spectra of Inorganic and Coordination Compounds," 3rd ed, Wiley, (1978), pp. 220, 270.

17) I. Grenthe, P. Paoletti, M. Sandstrom, and S. Glikberg, *Inorg. Chem.*, **18**, 2687 (1979).

18) P. Pfeiffer and H. Glaser, *J. Prakt. Chem.*, **151**, 134 (1938).

19) A. P. B. Lever and E. Mantovani, *Inorg. Chem.*, **10**, 817 (1971).

20) A. P. B. Lever, E. Mantovani, and J. C. Donini, *Inorg. Chem.*, **10**, 2424 (1971).

21) L. Fabbrizzi, M. Micheloni, and P. Paoletti, *Inorg. Chem.*, **13**, 3019 (1974).

22) J. R. Ferraro, L. J. Basile, L. R. Garcia-Ineguez, P. Paoletti, and L. Fabbrizzi, *Inorg. Chem.*, **15**, 2342 (1976).

 © 1987 The Chemical Society of Japan Bull. Chem. Soc. Jpn., 60, 149—157 (1987)

Comparative Studies of 2-, 3-, and 4-Pyridylpalladium(II) Complexes: Synthesis and Properties

Kiyoshi Isobe,* Yukio Nakamura, Toshio Miwa, and Shinichi Kawaguchi†
Department of Chemistry, Faculty of Science, Osaka City University,
Sumiyoshi-ku, Osaka 558
†School of Medicine(Premedical Bldg.), Kinki University,
Sayama-cho, Minamikawachi-gun, Osaka 589
(Received July 12, 1986)

Oxidative addition reactions of bromopyridines to tetrakis(triphenylphosphine)palladium(0) gave [{PdBr(2-pyridyl)(PPh_3)$_2$}] (**1b**), *trans*-[PdBr(3-pyridyl)(PPh_3)$_2$] (**2b**), and *trans*-[PdBr(4-pyridyl)(PPh_3)$_2$] (**3b**), which were converted on treatment with triethylphosphine to *trans*-[PdBr(2-, 3-, and 4-pyridyl)(PEt_3)$_2$] complexes (**1d**, **2d**, **3d**, respectively). Titration with perchloric acid in dioxane–water (1:1 by volume) indicated the basicity sequence of these complexes: 2-pyridyl≫4-pyridyl>3-pyridyl. The bromide ligand in **1b**—**3b** can readily be replaced by Cl^-, I^-, N_3^-, NCO^-, and NCS^-. In each corresponding series the relative thermal stability is in the sequence of 2-pyridyl>4-pyridyl>3-pyridyl. The pyridyl complexes containing triphenylphosphine react with carbon monoxide at ambient temperature and pressure to afford acyl complexes, which produce the corresponding esters by reactions with methanol. They also act as catalysts for cross coupling reactions of bromopyridines.

Oxidative addition of organic halides to palladium(0) complexes is one of the most convenient methods to prepare the σ bonded organopalladium(II) complexes.[1] In a previous paper we have reported on the 2-pyridylpalladium(II) complexes which were prepared by the reactions of 2-halopyridines with tetrakis(triphenylphosphine)palladium(0), $Pd(PPh_3)_4$.[2] Although the 2-pyridylnickel(II) complexes, [{NiX(C_5H_4N-C^2)(PPh_3)$_2$}] (X=halide and pseudohalide ligands), are quite stable, the corresponding 3-pyridyl complex [{NiCl(C_5H_4N-C^3)(PPh_3)}$_2$] is less stable and the 4-pyridyl complex has not been prepared.[3] On the contrary, stable 3- and 4-pyridyl palladium(II) complexes have been obtained. This paper reports on the comparative studies of these complexes. A preliminary account and X-ray molecular structures of these compounds have appeared.[4]

Experimental

Unless otherwise stated, air-sensitive materials were handled under a nitrogen atmosphere. Solvents used in these experiments were redistilled in nitrogen, and vessels and reagents were also purged with nitrogen. Dioxane was distilled over Linde molecular sieves 4A before use through a fractionating column.

Commercial reagents such as halopyridines, tertiary phosphines, Grignard reagents, and carbon monoxide were used without further purification. 4-Bromopyridine was freed from its hydrogen chloride adduct by action of triethylamine. The starting complex $Pd(PPh_3)_4$ was prepared by Coulson's method.[5] The dinuclear 2-pyridyl complexes [{PdX(C_5H_4N-C^2)(PPh_3)}$_2$], X=Cl (1a) and Br (1b) were prepared by the reactions of $Pd(PPh_3)_4$ with 2-chloro- and 2-bromopyridines as described already.[2]

Preparation of the *trans*-Bromo(3- and 4-pyridyl)bis(triphenylphosphine)palladium(II) Complexes, *trans*-[PdBr(C_5H_4N-C^3, and -C^4)(PPh_3)$_2$] (2b and 3b, respectively). 3-Bromo- or 4-bromopyridine (3.95 g, 25.0 mmol) was added to a solution of $Pd(PPh_3)_4$ (4.21 g, 3.63 mmol) in toluene (50 cm^3) and the mixture was allowed to react at 90 °C for 4 h. A white precipitate of 2b separated out in a 90% yield from the reaction mixture after standing for 5 h at room temperature. In the case of **3b**, the solution was concentrated to ca. 25 cm^3 and kept in a refrigerator for 24 h to deposit a white precipitate in a 73% yield.

Preparation of the *trans*-Halogeno- and *trans*-Pseudohalogeno(3- and 4-pyridyl)bis(triphenylphosphine)palladium(II) Complexes, *trans*-[PdX(C_5H_4N-C^3)(PPh_3)$_2$] with Cl (2a), I (2c), N_3 (2f), NCO (2g) and NCS (2h) as X and *trans*-[PdX(C_5H_4N-C^4)(PPh_3)$_2$] with Cl (3a), I (3c), N_3 (3f), NCO (3g), and NCS (3h) as X. Methanol (10 cm^3) was added to a solution of **2b** or **3b** (0.151 g, 0.190 mmol) in dichloromethane (30 cm^3). To this solution was added a methanol solution of ten times molar amount of sodium chloride (0.112 g), iodide (0.283 g), azide (0.121 g), cyanate (0.122 g), or thiocyanate (0.151 g). In the case of sodium chloride or cyanate, a mixture (15 cm^3) of methanol and water (2:1 by volume) was used because of their poor solubilities in methanol. After the reaction at 40 °C for 1 h (for 72 h in the case of NaCl), dichloromethane was distilled away under reduced pressure to deposit a white precipitate, which was recrystallized from dichloromethane–methanol. The yields were 85 (**2a**), 84 (**2b**), 65 (**2f**), 60 (**2g**), 81 (**2h**), 75 (**3a**), 93 (**3c**), 71 (**3f**), 68 (**3g**), and 78% (**3h**), respectively.

Preparation of the *trans*-Bromo(2-, 3-, and 4-pyridyl)bis(triethylphosphine)palladium(II) Complexes, *trans*-[PdBr(C_5H_4N-C^2, -C^3, and -C^4)(PEt_3)$_2$] (1d, 2d, and 3d, respectively). Triethylphosphine (0.340 g, 2.88 mmol) was added to a suspension of **1b** (0.611 g, 0.580 mmol), **2b** (0.915 g, 1.16 mmol), or **3b** (0.915 g, 1.16 mmol) in diethyl ether (30 cm^3) and the mixture was stirred at room temperature for 24, 5, and 5 h, respectively, to result in a clear colorless solution. After concentration to 5 cm^3, petroleum ether (20 cm^3) was added and the mixture was kept at −78, 0, and 0 °C, respectively, to precipitate white crystals in 30 (**1d**), 65 (**2d**), and 75% (**3d**) yields. Complexes **2d** and **3d** were recrystallized from diethyl ether–petroleum ether. Complex **1d** was dissolved in a mixture of water and methanol to be freed from triphenylphosphine and then recrystallized from petroleum ether. In order to prevent oxidation of triethylphosphine, preparation and purification of these

complexes were carried out under an argon atmosphere.

Preparation of *trans*-Bromo(2-, 3-, and 4-pyridylium)bis(triethylphosphine)palladium(II) 2,4-Dinitrophenolates, *trans*-[PdBr(C_5H_4NH-C^2, -C^3, and -C^4)(PEt_3)$_2$][2,4-$(NO_2)_2C_6H_3O$] (1e, 2e, and 3e, respectively). A dichloromethane solution (5 cm^3) of 2,4-dinitrophenol (0.0730 g, 0.395 mmol) was added to a solution of **1d**, **2d**, or **3d** (0.198 g, 0.395 mmol) in dichloromethane (5 cm^3) to convert the colorless solution to yellow instantaneously. Diethyl ether (10 cm^3) was added to the solution and the mixture was kept at 0 °C for 3 h to precipitate yellow crystals in 61, 64, and 63% yields, respectively, which were recrystallized from dichloromethane-diethyl ether.

Preparation of the *trans*-Bromo(3- and 4- pyridylcarbonyl)bis(triphenylphosphine)palladium(II) Complexes, *trans*-[PdBr(C_5H_4N-C^3-CO and -C^4-CO)(PPh_3)$_2$] (2i and 3i, respectively). Carbon monoxide was passed for 5 h through a solution of **2b** or **3b** (0.118 g, 0.150 mmol) in tetrahydrofuran at room temperature to convert the colorless solution to yellow. The solution was concentrated to 20 cm^3 by evaporation under reduced pressure. After addition of diethyl ether (60 cm^3), the mixture was left standing at room temperature for 24 h to obtain yellow crystals of **2i** and **3i** in 80 and 81% yields, respectively, which were recrystallized from dichloromethane–diethyl ether.

Reactions of the Acyl Complexes 2i and 3i with Methanol. Methanol (10 cm^3) was added to a solution of **2i** or **3i** (0.131 g, 0.160 mmol) in dichloromethane (20 cm^3) with changing color of the solution from yellow to red and finally to brown. After standing for 24 h, the solvent was distilled away to dryness under reduced pressure and the residue was extracted with diethyl ether. The solvent was vaporized again and the residue was dissolved in dichloromethane-d_2 and identified by the ^1H NMR assay to be methyl nicotinate and isonicotinate, respectively.

pH Titration of Complexes 1d, 2d, and 3d. To a solution of **1d** or **2d** (0.0879 g, 0.176 mmol) in dioxane (10 cm^3) was added an aqueous solution (10 cm^3) of sodium perchlorate which had been adjusted to μ=0.2, and the mixture containing the complex in 8.78×10^{-3} mol dm^{-3} was kept at 25.0±0.2 °C under a nitrogen atmosphere. Dioxane and an aqueous solution of perchloric acid (9.43×10^{-3} mol dm^{-3}) adjusted to μ=0.2 with sodium perchlorate were added from separate burettes to the sample solution.

Each time exactly the same volumes of titrants were added and the mixture was stirred for several minutes before recording the pH value. Standardization of the perchloric acid solution had been performed in advance with a standard solution of sodium carbonate dried at 200 °C using a mixture of Bromocresol Green and Methyl Red as an indicator. For comparison pyridine dissolved in a mixture of dioxane and water (1:1 by volume) was also titrated in a similar manner as above.

Unfortunately titration of **3d** in this way was not successful, since it is soluble in a mixture of dioxane and water (1:1 by volume) but not in the presence of sodium perchlorate to adjust the ionic strength. In order to compare relative basicities of **1d**, **2d**, and **3d**, titration as above was carried out in the absence of sodium perchlorate.

Measurements. Infrared spectra were taken in Nujol or hexachlorobutadiene mull on JASCO IR-E (4000—650 cm^{-1}), Hitachi EPI-L (700—200 cm^{-1}), and FIS-3 (400—30 cm^{-1}) spectrophotometers. ^1H NMR spectra were measured at 100 MHz in CD_2Cl_2 with Me_4Si as internal reference by means of a JEOL JNM MH-100 spectrometer. A JEOL JNM FX-100 instrument was used to record ^{13}C NMR spectra in $CDCl_3$ with Me_4Si as external reference at 25.0 MHz. Gas-chromatograms were obtained with a Yanagimoto G-180 instrument using nitrogen as a carrier gas through a Silicone DC-550 column, samples being injected at 200 °C. A Beckman Century SS-1 pH meter was used for titration together with glass and calomel electrodes. The Beckman buffer solution at pH 7.00 was used at 25 °C to calibrate the pH meter. The molecular weight was determined by vapor pressure osmometry in dichloromethane at 25 °C with an instrument manufactured by Knauer in Berlin, West Germany. The decomposition temperature was measured in a capilary tube under nitrogen.

Results and Discussion

Tetrakis(triphenylphosphine)nickel(0) reacts with 2- and 3-halopyridines promptly at room temperature to afford the 2- and 3-pyridylnickel(II) complexes.[3] Although the former is stable, the latter complex is not so stable as to allow full characterization and the 4-pyridyl complex has not yet been obtained. On the other hand, the reactions of $Pd(PPh_3)_4$ with 2-, 3-, and 4-bromopyridines did not proceed appreciably at room temperature, but occurred in toluene at 90 °C and completed after 4 h to form stable complexes. The 2-pyridylpalladium(II) complex is yellow and dinuclear as was reported previously,[2] while the 3- and 4-pyridyl complexes are white and mononuclear. The triphenylphosphine ligands in these complexes are readily replaced by triethylphosphine, an excess amount of which gives the mononuclear 2-pyridyl complex ultimately. Table 1 lists the complexes prepared in this study.

Halogeno Pyridyl Complexes. The analytical and molecular-weight data in Table 1 indicate that complexes **1d**, **2a—d**, and **3a—d** are all mononuclear. As is seen in Table 2, decomposition temperature of these complexes is high. In the cases of 2-pyridyl nickel(II)[3] and palladium(II)[2] complexes, the relative thermal stability of halogeno complexes was in the sequence of Cl>Br>I. The same sequence holds for the 4-pyridyl complexes **3a—c**, but in the case of 3-pyridyl complexes the bromo complex **2b** decomposes at appreciably higher temperature than the chloro complex **2a** does.

Among complexes containing the same halogeno ligand, the 4-pyridyl complexes are more stable than the corresponding 3-pyridyl complexes. The triethylphosphine complexes having distinct melting points show the decomposition temperature in the sequence of 2-pyridyl(**1d**)>4-pyridyl(**3d**)>3-pyridyl(**2d**).

Infrared spectra of these complexes show a single ν(Pd-P) band in the 410—430 cm^{-1} region in conformity with the presumed trans structure and the ν(Pd-Cl):ν(Pd-Br):ν(Pd-I) ratio is 1:0.75:0.59 for

2a—**c**, resembling to that for the 2-pyridyl complexes (1:0.75:0.55),[2a] although the corresponding ratio (1:0.62:0.50) for **3a**—**c** is a little smaller.

The methyl protons in **1d**, **2d**, and **3d** resonate at 1.0—1.1 ppm as a 1:4:6:4:1 quintet (J=ca. 9 Hz), indicating the trans arrangement of the triethylphosphine ligands.[6] As is listed in Table 3, the ring protons of the triphenylphosphine ligands in **2a** and **3a** exhibit two multiplets at about 7.4 and 7.6 ppm, the former being assigned to the meta and para protons, and the latter to the ortho protons.[7]

The NMR signals attributable to the pyridine-ring protons in **1d**, **2d**, and **3d** are shown in Fig. 1. The ring protons of 2-substituted pyridines such as methyl-, ethyl-, methoxy-, and chloropyridines show an ABB'X pattern, H^3 and H^5 resonating at the highest field with almost the same chemical shifts, and H^4 and H^6 at lower fields in this sequence.[8] In the case of complex **1d**, the $PdBr(PEt_3)_2$ moiety attached to C^2 effects the strongest influence on H^3, of which the signal shifts to lower field to overlap with that of H^4. Thus the signal at the highest field is assigned to H^5

Table 1. Analytical Data for the σ-Pyridyl Palladium(II) Complexes

Complex		Found (Calcd)			
		C (%)	H (%)	N (%)	Mol wt
$[PdBr(C_5H_4N\text{-}C^2)(PEt_3)_2]$	**1d**	40.50	6.75	2.81	497
		(40.78)	(6.84)	(2.80)	(501)
$[PdBr(C_5H_4NH\text{-}C^2)(PEt_3)_2]$-$[2,4\text{-}(NO_2)_2C_6H_3O]$	**1e**	40.61	5.53	6.02	
		(40.34)	(5.54)	(6.14)	
$[PdCl(C_5H_4N\text{-}C^3)(PPh_3)_2]$	**2a**	65.31	4.41	1.86	740
		(66.14)	(4.60)	(1.88)	(745)
$[PdBr(C_5H_4N\text{-}C^3)(PPh_3)_2]$	**2b**	61.51	4.28	1.76	781
		(62.42)	(4.34)	(1.78)	(789)
$[PdI(C_5H_4N\text{-}C^3)(PPh_3)_2]$	**2c**	58.70	4.08	1.70	821
		(58.91)	(4.10)	(1.68)	(836)
$[PdBr(C_5H_4N\text{-}C^3)(PEt_3)_2]$	**2d**	40.96	6.84	2.79	499
		(40.78)	(6.84)	(2.80)	(501)
$[PdBr(C_5H_4NH\text{-}C^3)(PEt_3)_2]$-$[2,4\text{-}(NO_2)_2C_6H_3O]$	**2e**	40.31	5.58	6.09	
		(40.34)	(5.59)	(6.14)	
$[PdCl(C_5H_4N\text{-}C^4)(PPh_3)_2]$	**3a**	65.65	4.82	1.76	730
		(66.14)	(4.60)	(1.88)	(745)
$[PdBr(C_5H_4N\text{-}C^4)(PPh_3)_2]$	**3b**	61.71	4.30	1.70	770
		(62.42)	(4.34)	(1.78)	(789)
$[PdI(C_5H_4N\text{-}C^4)(PPh_3)_2]$	**3c**	58.33	4.22	1.59	810
		(58.91)	(4.10)	(1.68)	(836)
$[PdBr(C_5H_4N\text{-}C^4)(PEt_3)_2]$	**3d**	41.15	6.84	2.77	490
		(40.78)	(6.84)	(2.80)	(501)
$[PdBr(C_5H_4NH\text{-}C^4)(PEt_3)_2]$-$[2,4\text{-}(NO_2)_2C_6H_3O]$	**3e**	40.45	5.61	6.05	
		(40.34)	(5.59)	(6.14)	
$[PdN_3(C_5H_4N\text{-}C^3)(PPh_3)_2]$	**2f**	65.22	4.53	7.15	740
		(65.57)	(4.56)	(7.46)	(751)
$[PdNCO(C_5H_4N\text{-}C^3)(PPh_3)_2]$	**2g**	66.97	4.59	3.71	744
		(67.16)	(4.56)	(3.73)	(751)
$[PdNCS(C_5H_4N\text{-}C^3)(PPh_3)_2]\frac{1}{2}H_2O$	**2h**	64.58	4.72	3.54	730
		(64.99)	(4.55)	(3.61)	(776)
$[PdN_3(C_5H_4N\text{-}C^4)(PPh_3)_2]$	**3f**	65.01	4.41	7.06	748
		(65.57)	(4.56)	(7.46)	(751)
$[PdNCO(C_5H_4N\text{-}C^4)(PPh_3)_2]$	**3g**	66.82	4.39	3.41	760
		(67.16)	(4.56)	(3.73)	(751)
$[PdNCS(C_5H_4N\text{-}C^4)(PPh_3)_2]$	**3h**	65.31	4.30	3.39	751
		(65.76)	(4.47)	(3.65)	(767)
$[PdBr(C_5H_4N\text{-}C^3\text{-}CO)(PPh_3)_2]$	**2i**	61.46	4.20	1.46	810
		(61.75)	(4.19)	(1.71)	(817)
$[PdBr(C_5H_4N\text{-}C^4\text{-}CO)(PPh_3)_2]$	**3i**	61.76	4.22	1.71	805
		(61.75)	(4.19)	(1.71)	(817)

and that at the lowest field to H^6. The ABMX pattern of the ring proton signals from **2d** is similar to that from methyl nicotinate,[8,9] and four signals are assigned as is seen in Fig. 1. The 4-pyridyl complex **3d** has the highest symmetry and exhibits only two doublets, of which the higher-field one is attributed to H^3 and H^5, and the lower-field one to H^2 and H^6. Assignment of signals from pyridine ring protons in **2a** and **3a** was made by reference to **2d** and **3d**, respectively.

Table 4 lists the ^{13}C NMR data from complexes **1d**, **2d**, and **3d**. The methyl and methylene carbons of triethylphosphine resonate at about 8 and 15 ppm, respectively, and the latter signal appears as a triplet with J(C-P)=ca. 13 Hz, indicating the trans arrangement of the two phosphine ligands.[10] Assignment of the pyridine-ring carbons was made based on both the completely and selectively ^1H-decoupled studies as well as measurements without ^1H-decoupling.

Figure 2 shows the ^{13}C NMR spectra of **1d**, **2d**, and **3d** under ^1H-decoupled (A_1, B_1, and C_1) and nondecoupled (A_2, B_2, and C_2) conditions. The ^1J(C-H) values given therein were determined by spectral measurements without proton irradiation. The triplet signal at 179.7 ppm lacks in ^1H-coupling and assigned to C^2 in **1d**. All of the other signals for pyridine-ring carbons exhibit ^1H-coupling (A_2). Irradiation at the resonance frequency of H^6 (8.3 ppm) reduced only the doublet at 149.1 ppm to a singlet, which is then assigned to C^6. In a similar way the 117.5 ppm signal was attributed to C^5. The remaining two signals at 133.3 and 132.5 ppm are so close to each other that the spin-decoupling method is not applicable. However the triplet at 133.3 ppm is assigned to C^3 because of its coupling to ^{31}P, since the carbon atoms adjacent (ortho) to the quaternary carbon bonded to the metal in **2d** and **3d** showed coupling to ^{31}P (Fig. 2 and Table 4).

In a similar manner the $^{13}C\{^1H\}$ spectra of **2d** (B_1) and **3d** (C_1) in Fig. 2 were assigned to each pyridine-ring carbon. It is worth noting that the value of ^1J(C-H) decreases with the distance of the carbon from the nitrogen atom in the sequence of $^1J(C^2\text{-}H)>{}^1J(C^3\text{-}H)>{}^1J(C^4\text{-}H)$ and $^1J(C^6\text{-}H)>{}^1J(C^5\text{-}H)>{}^1J(C^4\text{-}H)$. This is analogous to the situation observed for free pyridine.[11] All of the spectral data obtained for **1d**, **2d**, and **3d** are consistent with their trans structures which were confirmed by X-ray analysis.[4]

Compared with the ^{13}C shieldings for uncoordinated pyridine carbons (C^2, 149.7; C^3, 123.6; C^4, 135.5 ppm),[12] ring carbons in **1d**, **2d**, and **3d** show the following tendency. (i) The carbon atom bonded to palladium shows a very large down-field shift of ca. 30 ppm. (ii) The carbon atoms adjacent to the quaternary carbon also shift to lower field by 6–10 ppm, appearing as triplets due to coupling to ^{31}P as does the metal-bonded carbon. (iii) Carbons at the meta position of the quaternary carbon suffer the least effect on coordination, showing up-field shift less than 3 ppm. (iv) Carbons at the para position of the quaternary carbon also experience up-field shift by about 6 ppm.

Substituent effect similar to (i) has been reported for monosubstituded benzenes[13,14] and pyridines,[12,15] showing that the quaternary carbon is susceptible

Table 2. Decomposition Temperatures and Some FIR Data

Complex	Dec. temp[a] °C	ν(Pd-X) cm^{-1}	ν(Pd-P) cm^{-1}
1d	181 (79)		412 m
2a	165	297 s	420 w
2b	182	223 m	420 w
2c	147	175 m	418 w
2d	149 (121)		416 m
3a	215	305 s	430 m
3b	210	189 m	430 m
3c	170	154 w	425 m
3d	175 (128)		415 m

a) Figure in parenthesis is melting point.

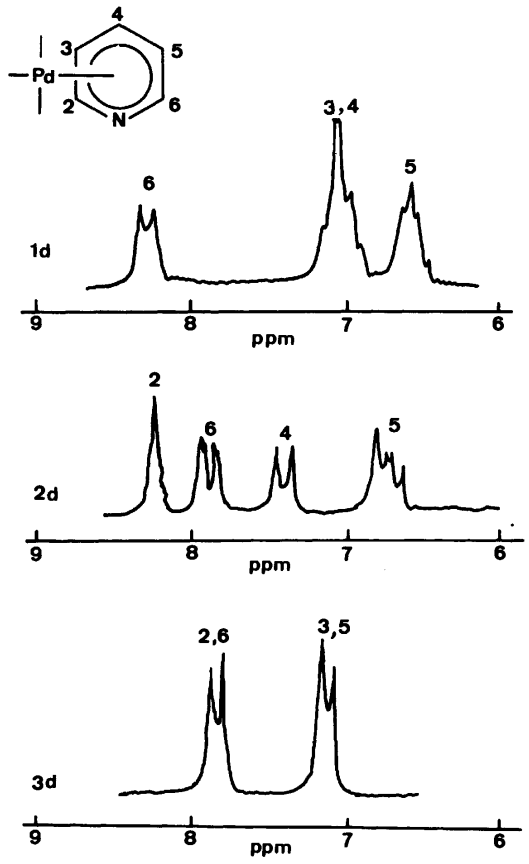

Fig. 1. ^1H NMR spectra at 100 M Mz in CD_2Cl_2 with Me_4Si as internal reference for pyridine ring protons in *trans*-[$PdBr(C_5H_4N$-C^2, C^3, and $C^4)(PEt_3)_2$] (**1d**, **2d**, and **3d**, respectively).

Table 3. ^1H Chemical Shifts in CD_2Cl_2 (ppm from internal Me_4Si)

Complex	Pyridine ring protons					Benzene ring protons					Other protons
	H^2	H^3	H^4	H^5	H^6	H^3	H^4	H^5	H^2	H^6	
1d		7.06 m	7.06 m	6.62 m	8.28 d						1.08 q (CH_3)[a]
											1.57 m (CH_2)
1e		7.75 d	7.68 m	7.26 m	8.52 d	8.80 d		7.94 dd		6.66 d	1.06 q (CH_3)[a]
											1.70 m (CH_2)
											14.76 br (NH)
2a	7.95 s		6.83 m	6.10 m	6.83 m	——	7.41 m	——	7.58 m	——	
2d	8.32 s		7.47 d	6.86 dd	7.95 dd						1.04 q (CH_3)[a]
											1.56 m (CH_2)
2e	8.40 br		7.96 br	7.28 br	8.16 br	8.83 d		8.04 br		6.88 d	1.04 q (CH_3)[a]
											1.60 m (CH_2)
											13.14 s (NH)
3a	b)	6.75 m		6.75 m	b)	——	7.44 m	——	6.63 m	——	
3d	7.96 d	7.22 d		7.22 d	7.96 d						1.07 q (CH_3)[a]
											1.61 m (CH_2)
3e	8.02 br	7.81 br		7.81 br	8.02 br	8.83 d		8.06 br		6.80 d	1.08 q (CH_3)[a]
											1.64 m (CH_2)
2f	7.93 s		6.85 m	6.16 m	6.85 m	——	——	7.45 m	——	——	
2g	7.92 s		6.83 m	6.15 m	6.83 m	——	——	7.44 m	——	——	
2h	7.91 s		6.81 m	6.17 m	6.81 m	——	——	7.49 m	——	——	
3f	b)	6.74 m		6.74 m	b)	——	——	7.45 m	——	——	
3g	b)	6.75 m		6.75 m	b)	——	——	7.47 m	——	——	
3h	b)	6.75 m		6.75 m	b)	——	——	7.49 m	——	——	
2i	8.96 s		6.89 m	6.89 m	8.38 m	——	7.77 m	——	7.41 m	——	
3i	8.23 d	b)		b)	8.23 d	——	7.77 m	——	7.44 m	——	
py[c]	8.60 m	7.25 m	7.64 m	7.25 m	8.60 m						

a) 1 : 4 : 6 : 4 : 1 quintet with J=ca. 9 Hz. b) Indiscernible due to overlapping with the phenyl protons. c) Uncoordinated pyridine in $CDCl_3$ (from Ref. 7). s: singlet, d: doublet, dd: a doublet of doublets, m: multiplet.

Table 4. ^{13}C Chemical Shifts (ppm from external Me_4Si) and Coupling Constants (Hz) in $CDCl_3$

Complex	Pyridine ring carbons					Phosphine ligand (PEt_3 or PPh_3)			
	C^2	C^3	C^4	C^5	C^6	CH_2 C^1	CH_3 C^2	C^3	C^4
1d	179.7	133.3	132.5	117.5	149.1	14.9	8.1		
		^1J(C-H)=163.2	^1J(C-H)=161.8	^1J(C-H)=163.2	^1J(C-H)=176.5	^1J(C-H)=129.4	^1J(C-H)=129.4		
	^2J(C-P)=6.0	^3J(C-P)=7.3				J(C-P)=13.0			
2b	164.6	152.8	135.7	130.1	151.4	138.2	142.4	134.9	137.2
	^3J(C-P)=3.4	^2J(C-P)=3.6	^3J(C-P)≈3			J(C-P)=23.0	J(C-P)=5.0	J(C-P)=4.4	
2d	155.3	150.8	144.0	123.9	143.7	15.0	8.1		
	^1J(C-H)=177.2		^1J(C-H)=160.3	^1J(C-H)=161.0	^1J(C-H)=179.4	^1J(C-H)=133.8	^1J(C-H)=128.0		
	^3J(C-P)=3.7	^2J(C-P)=6.1	^3J(C-P)=2.4			J(C-P)=13.4			
3b	155.2	140.8	186.5	140.8	155.2	137.9	142.2	134.8	137.2
		^3J(C-P)=3.9	^2J(C-P)≈5	^3J(C-P)=3.9		J(C-P)=23.5	J(C-P)=6.5	J(C-P)=5.0	
3d	146.8	133.8	170.8	133.8	146.8	14.8	8.0		
	^1J(C-H)=175.0	^1J(C-H)=160.3		^1J(C-H)=160.3	^1J(C-H)=175.0	^1J(C-H)=133.8	^1J(C-H)=128.0		
		^3J(C-P)=3.7	^2J(C-P)=5.9	^3J(C-P)=3.7		J(C-P)=13.5			
py[a]	149.7	123.6	135.5	123.6	149.7				
	^1J(C-H)=170.0	^1J(C-H)=163.0	^1J(C-H)=152.0	^1J(C-H)=163.0	^1J(C-H)=170.0				

a) Data for uncoordinated pyridine from Ref. 10 and 11.

to the inductive, resonance, and anisotropic effects of the substituent.[16] However, variation in shielding for the present complexes is the highest among values reported so far. Thus the ^{13}C shieldings of the benzene-ring carbons in *trans*-$[Pt(C_6H_5)L(AsMe_3)_2]PF_6$ with various neutral ligands as L show a quite similar pattern to (i)—(iv) above,[17] but the extent of downfield shift for the carbon bonded to platinum is not so large as the present case.

The deshielding effect on the adjacent carbons (ii) may be attributed to the anisotropic effect by the palladium moiety rather than σ, π-inductive and resonance effects.[16,17] The $PtX(PEt_3)_2$ group with a variety of negative ligands as X, when bound to fluorobenzene, was said to be an electron donor in both the inductive and resonance senses.[6] On the other hand a bonding model was proposed for *trans*-$[Pt(C_6H_5)L(AsMe_3)_2]PF_6$ in which σ rather than π interactions are dominant in the phenyl-platinum bond,[17] whereas evidence was presented supporting the presence of significant π interactions between platinum and an aryl ligand in a series of complexes of the type *trans*-$[PtX(C_6H_5)(PEt_3)_2]$.[16] The effects (iii) and (iv) in the present case may be due to inductive and/or resonance effects of palladium.

The pyridine ring carbons in **2b** and **3b** except C^4 in **2b** resonate at lower fields than corresponding carbons in **2d** and **3d** (Table 4). These results may be related to the lower electron-donating ability of palladium in **2b** and **3b** than that in **2d** and **3d**, respectively, caused by lower basicity and higher π-acceptability of triphenylphosphine compared with triethylphosphine. Ring carbons of the triphenylphosphine ligands in **2b** resonate in a usual region, appearing as triplets except the para carbon in conformity with the proposed trans configuration. The chemical shifts and the coupling constants for carbons in the triphenylphoshine ligands in **3b** are very close to those for **2b** (Table 4).

pH Titration of the *trans*-Bromo(2-, 3-, and 4-pyridyl)bis(triethylphosphine)palladium(II) Complexes. Complexes **1d** and **2d** as well as pyridine are readily soluble in dioxane-water (1:1 by volume) adjusted to μ=0.1 with sodium perchlorate, and were titrated with perchloric acid. Complex **3d**, on the other hand, is enough soluble in dioxane-water only in the absence of sodium perchlorate and titration was carried out under these conditions to compare the basicity of **3d** with that of **1d** and **2d**. Titration curves at μ=0.1 are shown in Fig. 3. In a mixture of dioxane and water the reading of a pH meter is usually 0.10 higher than the true value of $-\log[H^+]$ in the whole range.[18] The pK_a values of the conjugate acids of **1d**, **2d**, and py were calculated to be 8.04, 5.47 and 4.47, respectively, by using corrected values of $[H^+]$. Thus the basicity of **1d** is ca. 3700 times higher than that of uncoordinated pyridine, indicating substantial charge donation from the $PdBr(PEt_3)_2$ moiety to nitrogen.

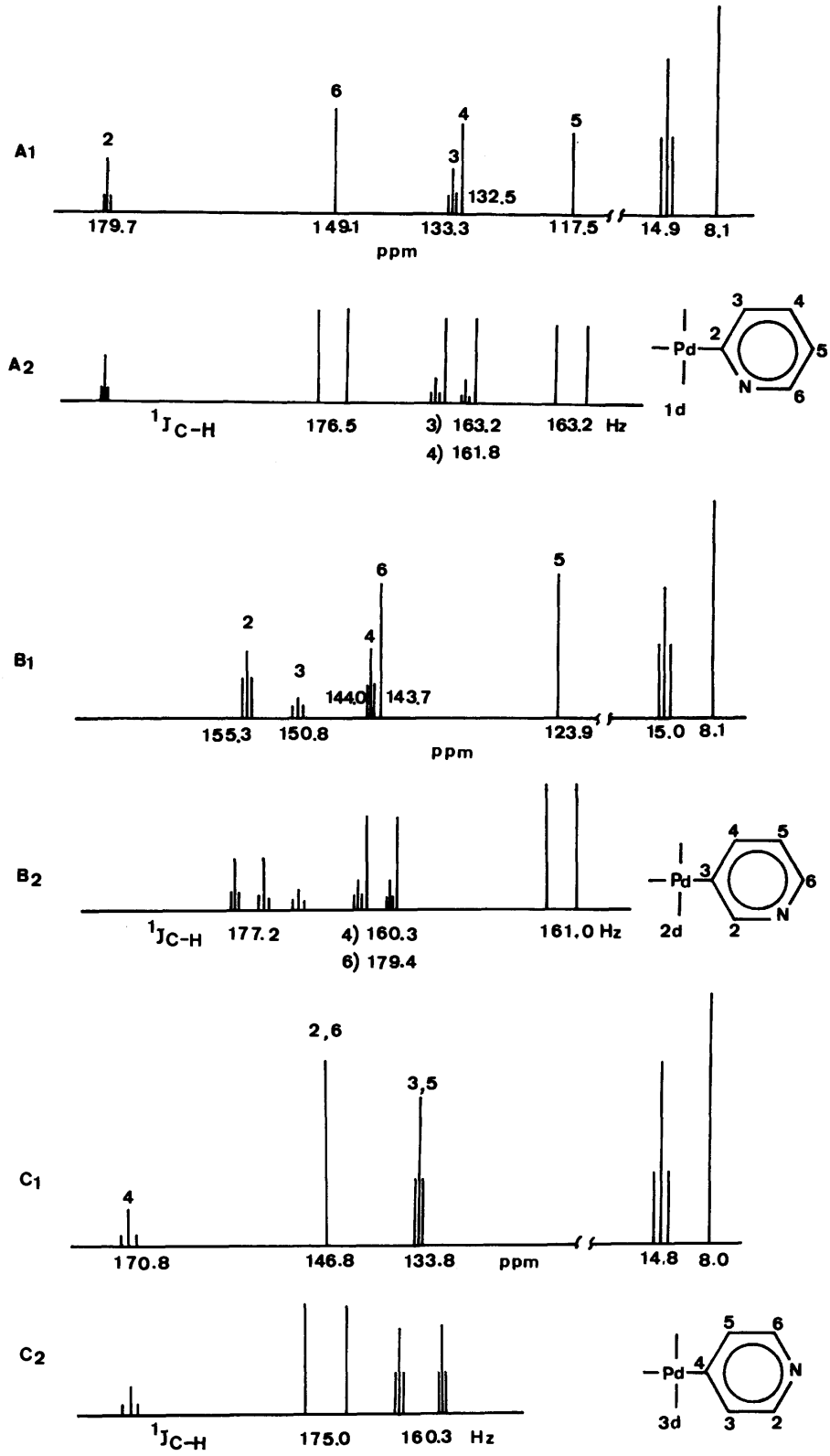

Fig. 2. ^{13}C NMR spectra at 25.0 MHz in $CDCl_3$ of *trans*-[PdBr(C_5H_4N-C^2, C^3, and C^4)(PEt_3)$_2$] (**1d**, **2d**, and **3d**, respectively) under ^1H-decoupled (A_1, B_1, and C_1) and nondecoupled (A_2, B_2, and C_2) conditions, the chemical shift being given in ppm from external Me_4Si and the ^1J(C–H) in Hz.

Titration in the absence of supporting electrolytes gave the pK_a values of 7.44, 5.01, and 5.38 to **1d**, **2d**, and **3d**. Thus the relative basicity is in the sequence of 2-pyridyl (**1d**)>4-pyridyl (**3d**)>3-pyridyl (**2d**).

The enhancement of basicity of pyridine by substitution with electron-donating groups such as CH_3 and NH_2 also depends upon the position attached on the ring and is in the sequence of 4>2>3.[19] The relative basicities of the present complexes do not follow this sequence and may not be rationalized only by simple inductive effect as applied to the methyl and amino substituents. The charge density donated by the $PdBr(PEt_3)_2$ substituent attached to C^2 seems not to be dissipated throughout the ring but to be accumulated at the adjacent nitrogen. The extraordinarily large ^3J(C-P) value of 7.3 at C^3 in **1d** as compared with ^3J(C-P) values for carbons adjacent to the quaternary carbons in **2d** and **3d** might be brought by a similar mechanism.

Johnson and Winterton[20] also found that the pK_a values of pyridinium salts with the $CH_2Co(CN)_5^{3-}$ substituent depend on the position of substitution, decreasing in the sequence of 2(10.6)>4(9.2)>3(8.3). In order to compare the bonding parameters and distribution of charge densities in **1d**, **2d**, and **3d**, X-ray analysis and MO calculations of these complexes have been carried out and the results were reported previously.[4]

Pyridylium Complexes. An equimolar amount of 2,4-dinitrophenol reacts with **1d**, **2d**, and **3d** to afford adducts **1e**, **2e**, and **3e**, respectively. Fig. 4 compares the IR bands related to the $\rangle C{=}\overset{+}{N}\langle_{H}$ group of these complexes and pyridinium 2,4-dinitrophenolate(A). The frequencies of vibration due to the iminium group in **1e** and **3e** are appreciably higher than those for **A** and **2e** which are comparable.

The NH^+ proton in these complexes resonates at substantially lower field than that of **A** does. When compared at a constant concentration of 0.409 mol dm^{-3}, the chemical shifts were 14.76, 13.14, 14.07, and 11.03 ppm for **1e**, **2e**, **3e**, and **A**, respectively, though they varied somewhat with concentration. (The OH proton of free 2,4-dinitrophenol resonates at 10.94 ppm.)

On adduct formation the pyridine-ring protons in the complexes show large down-field shifts (Table 3) and the phenol-ring protons do large up-field shifts compared with those in a free molecule (H^3, 9.06; H^5, 8.43; H^6, 7.34 ppm). The extent of variation is much larger than that for **A** in which the pyridine-ring protons resonate at 8.97 (H^2 and H^6), 7.36 (H^3 and H^5), and 7.78 (H^4) ppm, the phenol-ring protons appearing at 8.97 (H^3), 8.42 (H^5), and 7.31 (H^6) ppm. These IR and ^1H NMR evidences indicate that proton is more strongly interacting with nitrogen in these adducts than in **A** probably in the sequence of 2-pyridyl(**1e**)>4-pyridyl(**3e**)>3-pyridyl(**2e**)>**A**.

Pseudohalogeno Pyridyl Complexes. The pseudohalogeno 3- and 4-pyridyl complexes **2f—h** and **3f—h** were derived in high yields from **2b** and **3b**, respectivery, by ligand substitution with pseudohalides. Analytical and molecular-weight data in Table 1 as well as single ν(Pd-P) bands in the 420—435 cm^{-1} region (Table 5) indicate that these complexes have the trans mononuclear structure. Frequencies of the ν(CN) and ν(CS) vibrations observed for **2h** and **3h** indicate that each NCS ligand in these complexes is

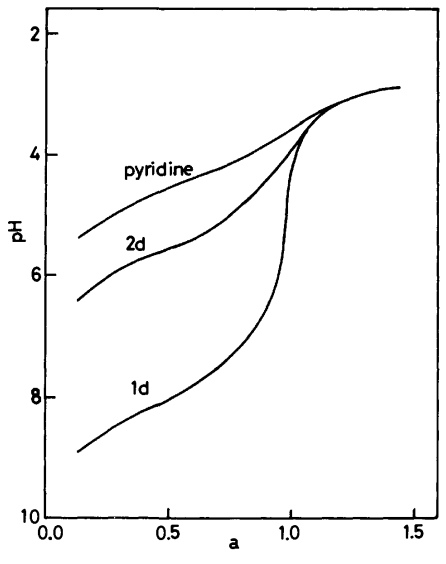

Fig. 3. pH Titration of *trans*-[PdBr(C_5H_4N-C^2 and C^3)$(PEt_3)_2$] (**1d** and **2d**, respectively) and pyridine with perchloric acid in dioxane-water (1 : 1 by volume) at 25.0 °C and μ=0.1 ($NaClO_4$) under nitrogen. The absissa gives the mole ratio of (acid added/complex): a.

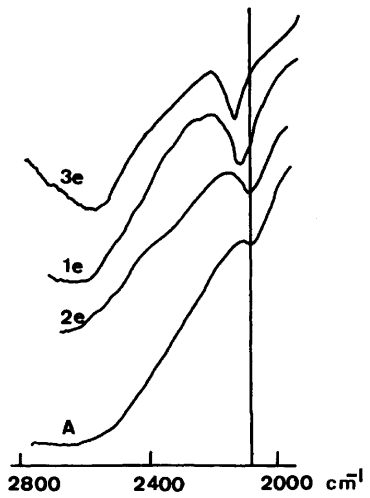

Fig. 4. IR spectra in the 2000—2800 cm^{-1} region of pyridinium 2,4-dinitrophenolate (**A**) and *trans*-[PdBr(C_5H_4NH-C^2, C^3, and C^4)$(PEt_3)_2$][2,4-$(NO_2)_2$-C_6H_3O (**1e**, **2e**, and **3e**, respectively) in Nujol.

Table 5. Characteristic IR in Nujol(cm^{-1}) for the Pseudohalogeno Complexes[a)]

Complex	ν(CN) or ν_a(NNN)	ν(CY) or ν_b(NNN)	δ(NCY) or δ(NNN)	ν(Pd-P)
2f	2048 vs	1330 m	595 w	433 m
2g	2215 vs	1328 m	605 m	430 m
2h	2082 vs	820 w	b)	430 m
3f	2040 vs	1330 m	594 w	430 m
3g	2210 vs, 2195 vs	1328 w	605 w	430 m
3h	2080 vs	818 m	b)	423 m

a) Y=O or S. b) Indiscernible.

N-bonded.[21] Preliminary X-ray analysis has confirmed the proposed molecular structure of **2h** unequivocally.[22]

Similarly the ν(CN), ν(CO), and δ(NCO) frequencies for the cyanate ligand in **2g** and **3g** (Table 5) are in the range assigned to N-bonding.[21] In accordance with the fact that each of the pseudohalides in **2f—h** and **3f—h** is bound to palladium through the same donor atom, the chemical shifts of pyridine-ring protons in **2f—h** and **3f—h** completely coincide with each other, respectively, in the range of experimental error (Table 3).

The *trans*-Bromo(3- and 4-pyridylcarbonyl)bis(triphenylphosphine)palladium(II) Complexes. Complexes **2b** and **3b** reacted with carbon monoxide in THF at room temperature to give the insertion products **2i** and **3i**. The analytical and molecular-weight data in Table 1 as well as the single ν(Pd-P) band at 427 and 430 cm^{-1} for **2i** and **3i**, respectively, suggest that they are mononuclear complexes of trans structure. The ν(CO) bands are observed at 1642(**2i**) and 1644(**3i**) cm^{-1}, respectively. Both of these complexes readily reacted with methanol in the absence of base to produce methyl nicotinate (CH_3, 3.98 s; H^2, 9.20d; H^4, 8.20 m; H^5, 7.35 m; H^6, 8.85 m ppm) and isonicotinate (CH_3, 4.00 s; H^2, H^6, 8.80 d; H^3, H^5, 7.90 d ppm) in 48 and 54% yields, respectively. As was reported in a previous paper,[2a] $[PdBr(C_5H_3(6\text{-}Cl)N\text{-}C^2)(PPh_3)_2]$ is also carbonylated. It may be interesting from the standpoint of organic synthesis that one carbon unit can easily be added to any carbon of pyridine. It should also be noted that the corresponding triethylphosphine complexes **1d**, **2d**, and **3d** are not carbonylated. The Pd-C bonds in these complexes seem again to be more stable and/or more inert than those in the corresponding triphenylphosphine complexes.

Cross Coupling Reactions. Catalysis of the 2-pyridyl palladium(II) complexes on the cross coupling reactions of 2-chloro- and 2,6-dichloropyridines with methylmagnesium bromide was reported in a previous paper.[2a] Now one-hundredth molar amount of **2b** and **3b** were found to promote the reactions of 3- and 4-bromopyridines with methylmagnesium bromide in refluxing THF to give 3- and 4-methylpyridines in 12 and 6% yields, respectively, although the reactions did not occur at room temperature. Further improvement in yields may be desirable to make these catalytic reactions useful in organic synthesis.

We wish to thank Mr. Junichi Gohda for elemental analyses.

References

1) e.g. R. F. Heck, *Acc. Chem. Res.*, **2**, 10 (1969); "Organotransition Metal Chemistry," Academic Press, New York (1974), p. 29.

2) a) K. Isobe, K. Nanjo, Y. Nakamura, and S. Kawaguchi, *Bull. Chem. Soc. Jpn.*, **59**, 2141 (1986); b) K. Nakatzu, K. Kinoshita, H. Kanda, K. Isobe, Y. Nakamura, and S. Kawaguchi, *Chem. Lett.*, **1980**, 913; c) K. Isobe and S. Kawaguchi, *Heterocycles*, **16**, 1603 (1981).

3) K. Isobe, Y. Nakamura, and S. Kawaguchi, *Bull. Chem. Soc. Jpn.*, **53**, 139 (1980).

4) K. Isobe, E. Kai, Y. Nakamura, K. Nishimoto, T. Miwa, S. Kawaguchi, K. Kinoshita, and K. Nakatsu, *J. Am. Chem. Soc.*, **102**, 2475 (1980).

5) D. R. Coulson, *Inorg. Synth.*, **13**, 121 (1972).

6) G. W. Parshall, *J. Am. Chem. Soc.*, **88**, 704 (1966).

7) R. Keat, *Chem. Ind. (London)*, **1968**, 1362.

8) T. J. Batterham, "NMR Spectra of Simple Heterocycles," Wiley, New York (1973).

9) C. J. Pouchert and J. R. Campbell, "The Aldrich Library of NMR Spectra," Aldrich Chemical Co., Milwaukee, Wis. (1974), Vol. 9, p. 48.

10) B. E. Mann, B. L. Shaw, and R. E. Stainbank, *J. Chem. Soc., Chem. Commun.*, **1972**, 151; P. Diehl, E. Fluck, and R. Kosfeld, "^{31}P and ^{13}C NMR of Transition Metal Phosphine Complexes," Springer-Verlag, New York (1979), p. 65.

11) G. E. Maciel, J. W. McIver, Jr., N. S. Ostlund, and J. A. Pople, *J. Am. Chem. Soc.*, **92**, 1 (1970).

12) H. L. Retcofsky and R. A. Friedel, *J. Phys. Chem.*, **72**, 2619 (1968).

13) G. E. Maciel and J. J. Natterstad, *J. Chem. Phys.*, **42**, 2427 (1965).

14) J. B. Stothers, "Carbon-13 NMR Spectroscopy," Academic Press New York (1972), pp. 90—100.

15) H. L. Retcofsky and R. A. Friedel, *J. Phys. Chem.*, **71**, 3592 (1967); **72**, 290 (1968).

16) D. R. Coulson, *J. Am. Chem. Soc.*, **98**, 3111 (1976).

17) H. C. Clark and J. E. H. Ward, *J. Am. Chem. Soc.*, **96**, 1741 (1974).

18) S. Takamoto, Q. Fernando, and H. Freiser, *Anal. Chem.*, **37**, 1249 (1965).

19) L. G. Sillén and A. E. Martell, "Stability Constants of Metal-Ion Complexes. Supplement No. 1," The chemical Society, London (1971); K. Kahmann, H. Sigel, and H. Erlenmeyer, *Helv. Chim. Acta*, **7**, 1754 (1964).

20) M. D. Johnson and N. Winterton, *J. Chem. Soc. (A)*, **1970**, 507.

21) R. A. Bailey, S. L. Kozak, T. W. Michelsen, and W. N. Mills, *Coord. Chem. Rev.*, **6**, 407 (1971); A. H. Norbury, *Advan. Inorg. Chem. Radiochem.*, **17**, 231 (1975).

22) K. Nakatsu and K. Kinoshita, private communication.

 © 1987 The Chemical Society of Japan Bull. Chem. Soc. Jpn., 60, 159—169 (1987)

The Crystal and Molecular Structure of the Hydrated Light Lanthanoid(III) Chloroacetates, $[\{M(ClCH_2CO_2)_3\}_3(H_2O)_5]_n$, (M=La, Pr, Nd, and Eu)

Takashi Imai, Mamoru Shimoi, and Akira Ouchi*
Department of Chemistry, College of Arts and Sciences, The University of Tokyo, Komaba, Meguro-ku, Tokyo 153
(Received May 19, 1986)

The crystal and molecular structures of the hydrated lanthanum(III), neodymium(III), and europium(III) chloroacetates indicated in the title were determined by the single-crystal X-ray diffraction method; these three salts as well as the praseodymium(III) salt are apparently isomorphous. By the same synthetic technique, gadolinium(III) or heavier lanthanoid(III) did not give the isomorphous salts. Their crystals are monoclinic with the space group of $P2_1/c$, and the cell constants of the neodymium(III) salt, for example, are, a=14.805(4), b=18.765(4), c=14.403(5) Å, β=95.13(3)°. There are crystallographically independent three kinds of nine-coordinated metal atoms: Nd(1), Nd(2), and Nd(3). Among them, Nd(1) and Nd(2) are best approximated as being in a tricapped trigonal prism geometry. The Nd(3) is best regarded as being in a monocapped square-antiprism geometry, although one more additional oxygen atom, O(35), approaches one side face. In the lanthanum(III) complex, O(35) is thought to be ligated to La(3), while in the europium(III) complex O(35) is perfectly removed from Eu(III), being accompanied by a change in the coordination geometry of the ligand. In the crystal, the metal atoms are bridged by carboxylato ligands, forming polymeric chains approximately along [−110] or [110] axis. There are no carboxylato bridges between respective chains, although there are some hydrogen-bondings linking them with each other.

The variety of the coordinating structures of metal carboxylates, where the metal atoms are linked by the ligands, is one of the interesting thèmes of structural chemistry.[1] Especially, the lanthanoid(III) carboxylates are found to form many kinds of the chain structures where the carboxylate ions act as the bridges between the metal atoms.[2-9] Although the lanthanoid formate can make a two-dimensional polymeric structure,[10] the carboxylates generally form a dimer or a linear polymeric chain.[4]

In the case of cerium(III) acetate, it is in a polymeric form, where the respective pairs of the metal atoms, being nine-coordinated in a tricapped trigonal prism geometry, are bridged by three acetato ligands.[7] On the other hand, the holmium(III) acetate is in a dimer form, in which the metal atom is nine-coordinated, being bridged by two carboxylate ions.[6]

The neodymium(III) (methylthio)acetate has the nine-coordinated neodymium(III) atoms in the tricapped trigonal prism geometry, being bridged by two to four carboxylato ligands into a linear polymeric chain.[2] On the other hand, in the case of ytterbium(III) (methylthio)acetate, which is also in a linear polymeric form, respective pairs of side-by-side metal atoms are linked only with one carboxylate ion.[9]

From these results, we deduced that the size of the central metal ion as well as the substituted groups on the carboxylato ligands are the reasons for forming such a variety of the linkages in the polymeric structure.

This time, we have obtained the chloroacetates of a series of the lanthanoid elements, which were expected to have some characteristic structures. Moreover, the type of complexes indicated in the title could be obtained only for lanthanum(III) to europium(III), while gadolinium(III) and heavier lanthanoids did not give isomorphous complexes. Therefore, some effect of the central metal-ionic size to its structure is also expected to be found even in the series of the isomorphous complexes, as in cases of the tetraacetatolanthanoidates(III),[4] and of lanthanoid(III) *m*-hydroxybenzoates.[3] For these reasons, the authors have tried to determine the structures of the series of the complexes by the single-crystal X-ray diffraction method.

Experimental

Synthesis of Neodymium(III) Chloroacetate, $[\{Nd(ClCH_2CO_2)_3\}_3(H_2O)_5]$, and Its Isomorphous Complexes. Freshly obtained neodymium(III) hydroxide, by mixing solutions of neodymium(III) chloride hexahydrate (0.72 g, 2.0 mmol) and excess sodium hydroxide, was mixed with chloroacetic acid (0.57 g, 6.0 mmol). After stirring several minutes, the obtained aqueous solution was filtered and the filtrate was left standing for several days in a silica gel desiccator; care was taken that the solution did not become dry. The deposited crystals were filtered off and washed with a small portion of water. They were then dried in open air overnight and kept in a sealed bottle, where they remained stable. Yield: 0.55 g, 60%. Some additional lot, about 0.2 g, was obtained from the residual mother liquor, which almost had the same purity.

By applying the same synthetic technique, lanthanum(III), praseodymium(III), and europium(III) salts, which are apparently isomorphous with each other, were obtained almost in the same yield. Anal. ($M_3C_{18}H_{28}O_{23}Cl_9$) M, C, H. (where M=La, Pr, Nd, or Eu).

When this synthetic method was applied to obtain gadolinium(III) or heavier lanthanoid(III) salts, triclinic-type crystals were obtained instead. Chemical analyses

showed that they also include 5/3 molecules of water per one metal atom and are isomorphous with each other.

Although our synthetic results regarding the title complexes are reproducible, the compositions as well as the crystallographic data (obtained by the X-ray powder diffraction method) of the lanthanoid(III) chloroacetates shown in a reference,[11] did not agree with our results. Probably, the crystallizing conditions and, consequently, the number of the included water molecules of the salts were different from each other.

Single-Crystal X-Ray Analysis. From the crystallographic data obtained by the single-crystal X-ray diffraction method, the lanthanum(III), praseodymium(III), neodymium(III), and europium(III) chloroacetates indicated in the title are apparently isomorphous, although (as shown later) there are some discrepancies in their detailed structures. They are monoclinic with the space group $P2_1/c$, $Z=4$ (for the title formula; twelve metal atoms are included in one unit cell). Their crystallographic data are shown in Table 1 and some other experimental conditions are tabulated in Table 2. The reflections shown in Table 2 were collected on a Rigaku AFC-6A automated four-circle X-ray diffractometer with graphite monochromated Mo $K\alpha$ radiation (scan speed was 4° min^{-1} (θ)), the ω—2θ scan technique being employed.

Structure Determination. The structure of the neodymium(III) complex was solved by the heavy-atom method. The positions of the metal and some ligated oxygen atoms were deduced from a three-dimensional Patterson map, while all the other non-hydrogen atoms were located by means of successive Fourier syntheses and refined by the block-diagonal least-squares method. In the last cycle of the refinement with anisotropic temperature factors for all atoms, all the parameter shifts were less than one-third of the corresponding standard deviations. The structures of the isomorphous complexes were solved by starting with the final parameters of the neodymium(III) complex and were refined in the same way. All of their parameters converged in the same grade.

All the calculations were carried out on a HITAC M-280H apparatus at the Computer Center of the University of Tokyo, using the local version of the UNICS program.[12] The atomic scattering factors were taken from Ref. 13.

Infrared Spectrum Measurements. Their infrared spectra were obtained by means of a JASCO 202-A grating infrared spectrophotometer, using Nujol or hexachloro-1,3-butadiene mull.

Results and Discussion

The final atomic parameters of the complex are listed in Table 3 (1—3), while selected bond lengths and bond angles as well as some interatomic distances (which are thought to be the hydrogen-bonding types) are tabulated in Table 4.[14] A perspective drawings of the neodymium(III) complex around the metal atoms (Nd(1), Nd(2), and Nd(3)) as well as the numbering scheme of the atoms are shown in Figs. 1—3, and the crystal packing diagram in Fig. 4, respectively.

Table 1. Crystallographic Data of the Complexes $[\{M(ClCH_2CO_2)_3\}_3(H_2O)_5]_n$ (M=La, Pr, Nd, and Eu)

M=	La	Pr	Nd	Eu
F.W.	449.40	451.40	454.73	462.45
$a(l/Å)$	14.918(4)	14.817(6)	14.805(4)	14.716(9)
$b(l/Å)$	18.972(5)	18.825(5)	18.765(4)	18.671(4)
$c(l/Å)$	14.514(6)	14.421(6)	14.403(5)	14.365(6)
$\beta(\phi/°)$	95.18(3)	95.11(3)	95.13(3)	95.36(4)
$U(v/Å^3)$	4091(3)	4002(3)	3986(2)	3930(3)
$D_m(d/Mg\ m^{-3})$	2.19(3)	2.23(3)	2.24(3)	2.34(3)
$D_x(d/Mg\ m^{-3})$	2.19	2.25	2.27	2.35
μ(Mo $K\alpha$) (n/mm^{-1})	3.18	4.28	4.57	5.45

Table 2. Some Experimental Conditions to Obtain the Reflection Intensities

Metal	La	Nd	Eu
Number of reflections measured	7500	7310	7205
Reflections used for the calculation[a]	5527	5874	5693
Measured range ($2\theta/°$)	3—50	3—50	3—50
R[b]	0.043	0.037	0.049
R_{welght}[b]	0.052	0.050	0.059
Size of the crystal (v/mm^3)	0.15×0.15×0.3	0.3×0.3×0.25	0.3×0.3×0.3
Scan width ($\theta/°$)	1.04+0.5 tan θ	1.12+0.5 tan θ	1.05+0.5 tan θ
S[c]	2.157	2.547	3.322

a) Reflections with $|F_o|>3\sigma(|F_o|)$ were used. b) $R=\Sigma||F_o|-|F_c||/\Sigma|F_o|$; $R_{welght}=[\Sigma w(|F_o|-|F_c|)^2/\Sigma wF_o^2]^{1/2}$, where $w=1/[\{\sigma(|F_o|)\}^2+(F_{welght}\times F_o)^2]$, $F_{welght}=0.015$. c) $S=[\Sigma w(|F_o|-|F_c|)^2/(N_o-N_p)]^{1/2}$, where N_o=number of reflections, N_p=number of parameters.

Table 3. Final Atomic Coordinates ($\times 10^4$) and Equivalent Isotropic Temperature Factors (B_{eq}/Å^2) of Non-Hydrogen Atoms, with Estimated Standard Deviations in Parentheses

3.1. Lanthanum Complex					3.2. Neodymium Complex				
Atom	x	y	z	B_{eq}/Å^2 a)	Atom	x	y	z	B_{eq}/Å^2 a)
La(1)	4254.9(3)	898.6(2)	481.5(3)	1.6$_4$	Nd(1)	4257.0(3)	898.4(2)	475.5(3)	1.5$_1$
La(2)	716.0(3)	4080.1(2)	297.0(3)	1.6$_6$	Nd(2)	711.7(3)	4089.3(2)	283.0(3)	1.5$_8$
La(3)	2384.3(3)	2568.6(2)	1915.7(3)	1.6$_5$	Nd(3)	2410.4(3)	2572.1(2)	1921.5(3)	1.7$_0$
O(11)	5036(4)	271(3)	1919(4)	2.8$_9$	O(11)	5046(4)	294(3)	1889(4)	2.5$_1$
O(12)	3562(4)	296(3)	1866(4)	3.0$_1$	O(12)	3577(4)	298(3)	1835(4)	2.7$_4$
O(13)	2619(4)	889(4)	79(5)	3.3$_0$	O(13)	2646(4)	914(3)	116(4)	2.9$_1$
O(14)	1924(4)	1829(3)	575(4)	2.7$_8$	O(14)	1927(4)	1868(3)	590(4)	2.5$_2$
O(15)	4204(4)	−386(3)	78(4)	2.2$_7$	O(15)	4214(4)	−368(3)	78(4)	2.2$_8$
O(16)	4161(4)	−1452(3)	−491(5)	3.2$_0$	O(16)	4193(4)	−1452(3)	−466(4)	2.7$_6$
O(21)	−110(4)	5048(3)	997(4)	2.6$_1$	O(21)	−137(4)	5023(3)	967(4)	2.6$_6$
O(22)	−1170(4)	5730(3)	1442(4)	2.9$_3$	O(22)	−1172(4)	5727(3)	1441(4)	2.8$_1$
O(23)	1355(5)	4209(4)	1968(5)	3.8$_1$	O(23)	1327(4)	4227(4)	1945(4)	3.7$_1$
O(24)	2686(4)	3812(3)	2511(4)	2.9$_8$	O(24)	2653(4)	3801(3)	2495(4)	2.7$_7$
O(25)	929(4)	6137(4)	5(5)	3.6$_1$	O(25)	896(4)	6137(3)	100(6)	4.5$_3$
O(26)	1688(4)	5142(3)	321(5)	2.7$_8$	O(26)	1680(3)	5128(3)	353(4)	2.7$_0$
O(31)	2206(4)	3496(3)	477(4)	2.2$_4$	O(31)	2172(3)	3505(3)	487(4)	2.1$_8$
O(32)	3570(4)	3152(3)	902(4)	2.7$_5$	O(32)	3537(3)	3144(3)	895(4)	2.3$_9$
O(33)	4009(4)	1819(3)	1656(4)	2.0$_3$	O(33)	4018(4)	1804(3)	1635(3)	2.0$_8$
O(34)	3946(4)	2561(3)	2807(4)	2.3$_8$	O(34)	3944(4)	2568(3)	2780(3)	2.3$_9$
O(35)	598(4)	2962(3)	1197(5)	3.3$_0$	O(35)	526(6)	3007(4)	1182(5)	5.3$_8$
O(36)	771(4)	2284(4)	2409(4)	3.3$_4$	O(36)	815(4)	2326(4)	2369(4)	4.1$_7$
C(11)	4290(7)	73(4)	2211(6)	2.6$_0$	C(11)	4315(6)	80(4)	2178(5)	2.5$_0$
C(12)	4395(9)	−477(6)	2977(8)	4.7$_3$	C(12)	4429(8)	−475(5)	2952(7)	4.4$_5$
C(13)	1934(6)	1256(5)	184(6)	2.2$_2$	C(13)	1950(5)	1289(4)	203(5)	2.0$_0$
C(14)	1085(6)	933(6)	−303(9)	4.5$_0$	C(14)	1090(6)	960(5)	−309(7)	3.8$_0$
C(15)	3799(6)	−964(4)	−88(6)	2.1$_4$	C(15)	3817(5)	−963(4)	−88(5)	1.8$_8$
C(16)	2880(7)	−1011(5)	262(8)	3.6$_1$	C(16)	2876(6)	−1015(5)	253(7)	3.4$_1$
C(21)	−670(6)	5214(5)	1570(6)	2.6$_0$	C(21)	−682(6)	5196(4)	1560(6)	2.5$_1$
C(22)	−683(10)	4696(9)	2374(10)	7.5$_7$	C(22)	−699(8)	4686(7)	2376(8)	6.1$_3$
C(23)	2092(6)	4276(5)	2411(6)	2.5$_0$	C(23)	2057(5)	4275(5)	2402(5)	2.4$_7$
C(24)	2357(7)	4967(5)	2909(8)	3.9$_0$	C(24)	2330(7)	4960(5)	2926(7)	3.8$_4$
C(25)	1615(6)	5794(5)	286(7)	2.5$_6$	C(25)	1598(5)	5782(4)	344(6)	2.8$_5$
C(26)	2421(7)	6265(5)	580(9)	4.0$_2$	C(26)	2402(6)	6266(5)	610(8)	4.1$_3$
C(31)	3043(5)	3530(4)	415(5)	1.7$_0$	C(31)	3015(5)	3537(4)	413(5)	1.7$_2$
C(32)	3338(6)	4052(5)	−274(7)	3.2$_5$	C(32)	3318(6)	4053(5)	−279(6)	3.1$_1$
C(33)	4386(6)	2171(4)	2322(6)	2.0$_9$	C(33)	4397(5)	2169(4)	2294(5)	1.8$_0$
C(34)	5386(6)	2096(6)	2463(7)	3.7$_5$	C(34)	5392(6)	2104(5)	2440(6)	3.6$_5$
C(35)	284(5)	2598(5)	1812(6)	2.2$_8$	C(35)	270(5)	2633(4)	1789(5)	2.3$_5$
C(36)	−728(6)	2537(7)	1740(7)	4.2$_3$	C(36)	−732(7)	2504(7)	1783(9)	5.6$_7$
Cl(11)	3343(4)	−776(3)	3285(3)	9.4$_8$	Cl(11)	3380(3)	−773(2)	3298(3)	8.0$_3$
Cl(12)	74(2)	1318(2)	24(3)	5.8$_6$	Cl(12)	78(2)	1328(2)	31(3)	5.4$_6$
Cl(13)	2333(2)	−1821(2)	−21(3)	5.1$_8$	Cl(13)	2336(2)	−1829(1)	−44(2)	4.9$_3$
Cl(21)	−1286(4)	4932(3)	3236(3)	10.6$_7$	Cl(21)	−1302(3)	4931(2)	3250(3)	8.9$_2$
Cl(22)	1490(3)	5595(2)	2867(3)	8.7$_8$	Cl(22)	1464(3)	5601(2)	2892(3)	8.5$_9$
Cl(23)	3383(2)	5777(2)	1018(3)	5.0$_7$	Cl(23)	3385(2)	5779(2)	1033(2)	4.9$_8$
Cl(31)	4496(2)	3986(2)	−427(2)	4.9$_0$	Cl(31)	4485(2)	3977(2)	−431(2)	4.8$_7$
Cl(32)	5867(2)	2601(2)	3417(2)	4.8$_3$	Cl(32)	5872(2)	2613(2)	3409(2)	4.6$_2$
Cl(33)	−1154(2)	2666(3)	2817(3)	8.3$_7$	Cl(33)	−1137(2)	2697(3)	2855(3)	8.0$_2$
O(W1)	4031(4)	2117(3)	−308(4)	2.8$_2$	O(W1)	4034(4)	2102(3)	−298(4)	2.5$_6$
O(W2)	607(5)	2959(3)	−743(4)	3.2$_8$	O(W2)	634(4)	2969(3)	−730(4)	3.2$_5$
O(W3)	2412(4)	1317(3)	2513(4)	2.6$_3$	O(W3)	2417(4)	1334(3)	2493(4)	2.4$_8$
O(W4)	2284(5)	2617(4)	3672(4)	3.7$_7$	O(W4)	2285(4)	2601(4)	3651(4)	3.4$_5$
O(W5)	4132(4)	854(3)	−1258(4)	2.8$_3$	O(W5)	4122(4)	850(3)	−1239(4)	2.7$_0$

Table 3. Continued.

3.3. Europium Complex

Atom	x	y	z	B_{eq}/Å^2 a)	Atom	x	y	z	B_{eq}/Å^2 a)
Eu(1)	4255.1(3)	903.4(2)	462.5(3)	1.4_3	C(21)	−725(7)	5174(6)	1552(7)	2.0_7
Eu(2)	677.9(3)	4095.2(3)	292.7(3)	1.4_8	C(22)	−742(10)	4676(8)	2364(9)	4.3_5
Eu(3)	2494.4(3)	2556.2(3)	1905.3(3)	1.4_6	C(23)	2054(7)	4248(5)	2394(7)	2.1_0
O(11)	5058(5)	307(4)	1856(5)	2.1_3	C(24)	2326(8)	4933(6)	2918(8)	2.8_5
O(12)	3573(5)	308(4)	1804(5)	2.6_1	C(25)	1550(7)	5769(6)	529(8)	2.2_6
O(13)	2665(5)	933(4)	121(6)	2.7_4	C(26)	2388(8)	6253(7)	739(11)	3.9_0
O(14)	1943(5)	1905(4)	541(5)	2.4_4	C(31)	2958(6)	3533(5)	403(7)	1.6_3
O(15)	4201(5)	−351(4)	85(5)	2.3_6	C(32)	3255(7)	4066(6)	−290(8)	2.5_9
O(16)	4222(5)	−1437(4)	−455(5)	2.6_9	C(33)	4440(7)	2173(5)	2281(7)	1.7_8
O(21)	−249(4)	4949(4)	927(5)	1.9_0	C(34)	5461(7)	2110(7)	2395(9)	3.6_4
O(22)	−1150(5)	5743(4)	1442(5)	2.6_1	C(35)	172(7)	2738(6)	1768(7)	2.2_7
O(23)	1299(5)	4188(4)	1935(5)	2.5_5	C(36)	−569(8)	2284(8)	2142(10)	4.5_2
O(24)	2663(5)	3765(4)	2483(5)	2.2_4	Cl(11)	3397(3)	−755(3)	3299(4)	7.1_3
O(25)	823(5)	6113(4)	454(6)	2.7_1	Cl(12)	76(2)	1295(2)	88(3)	5.4_3
O(26)	1664(5)	5111(4)	449(5)	2.3_1	Cl(13)	2345(2)	−1839(2)	−118(3)	5.1_6
O(31)	2117(4)	3493(4)	495(5)	1.9_0	Cl(21)	−1280(4)	4958(3)	3287(3)	8.3_6
O(32)	3519(4)	3141(4)	869(5)	2.1_9	Cl(22)	1418(3)	5554(2)	2934(3)	6.0_2
O(33)	4036(4)	1801(4)	1613(4)	1.8_7	Cl(23)	3408(2)	5773(2)	1046(3)	4.7_9
O(34)	3993(5)	2563(4)	2769(5)	2.3_0	Cl(31)	4420(2)	3989(2)	−459(3)	4.8_8
O(35)	−46(7)	3224(5)	1212(7)	4.6_4	Cl(32)	5932(2)	2615(2)	3391(3)	4.4_7
O(36)	958(6)	2552(5)	2032(8)	4.7_7	Cl(33)	−1165(4)	2765(3)	2892(5)	10.9_6
C(11)	4322(8)	92(5)	2156(7)	2.3_2	O(W1)	4020(5)	2097(4)	−307(5)	2.4_0
C(12)	4446(10)	−450(7)	2941(9)	3.8_4	O(W2)	622(5)	2903(4)	−555(6)	3.4_7
C(13)	1961(7)	1307(5)	180(7)	2.0_5	O(W3)	2406(5)	1338(4)	2442(5)	2.4_0
C(14)	1101(8)	964(7)	−300(10)	3.9_4	O(W4)	2270(6)	2559(5)	3590(5)	3.5_1
C(15)	3819(7)	−951(5)	−85(7)	1.8_7	O(W5)	4126(5)	853(4)	−1227(5)	2.5_8
C(16)	2884(8)	−1032(7)	215(10)	3.7_1					

a) The equivalent isotropic temperature factors were computed using the following expression: $B_{eq}=4/3(B_{11}a^2+B_{22}b^2+B_{33}c^2+B_{13}ac\cos\beta)$. The B_{ij}'s are defined by: $T=\exp[-(h^2B_{11}+k^2B_{22}+l^2B_{33}+2klB_{23}+2hlB_{13}+2hkB_{12})]$.

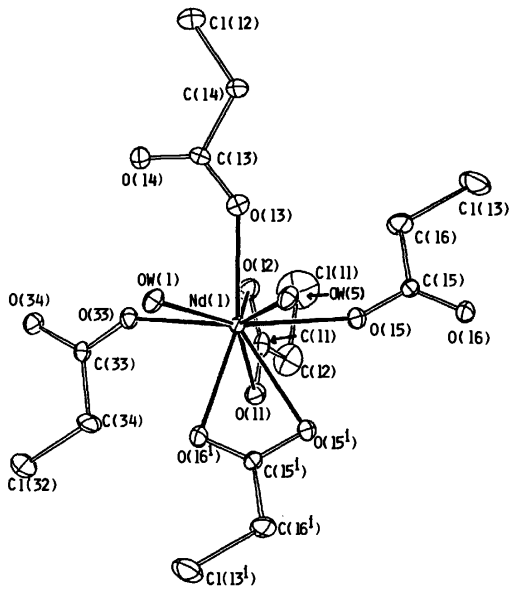

Fig. 1. A perspective drawing of the complex around Nd(1) atom with the numbering scheme of the atoms.

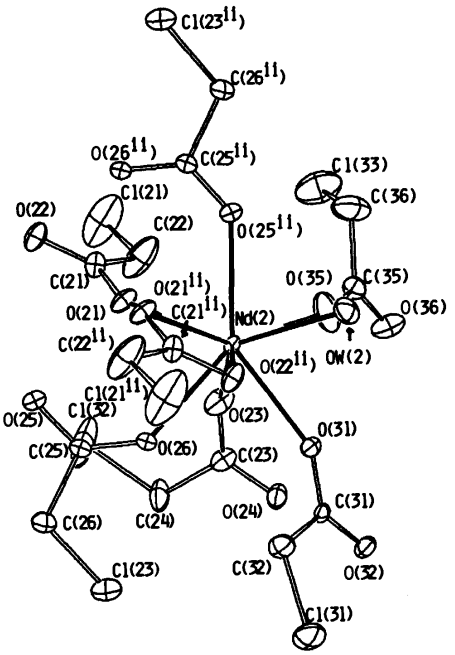

Fig. 2. A perspective drawing of the complex around Nd(2) atom with the numbering scheme of the atoms.

Schematic presentations to show the coordination geometries of the ligating atoms around the Nd(1), Nd(2), and Nd(3) atoms are shown in Figs. 5.1, 5.2, and 5.3. As shown in these figures, in the neodymium-(III) complex, Nd(1) and Nd(2) atoms are approximately in a tricapped trigonal prism geometry. The Nd(3) atom is regarded as being in a monocapped square-antiprism geometry,[15] however other than these nine oxygen atoms, another oxygen atom, O(35), also approaches the metal atom above one side face of the square-antiprism, Nd(3)···O(35)=3.009(8) Å, although the distance is much longer than the other Nd-O bond lengths of this complex.[15]

As shown in Table 5, the average of eighteen Nd-O bond lengths around the Nd(1) and Nd(2) atoms is 2.493 Å, while that of nine Nd-O bond lengths around the Nd(3) atom is 2.553 Å. The former is about the same as the sum of the radii of the tervalent Nd (Coordination number (CN)=9) and O (Valence (Val)=2−, CN=2) ions, 2.51 Å;[16] however the latter is too long. It is rather near to the sum of the Nd(CN=10) and O ions, 2.56 Å (see the footnote g of Table 5). Concerning their lengths, the Nd-O bonds around the Nd(3) atom are like those of ten-coordination. This fact is probably because the O(35) atom, which is not very far from the coordination area around the metal atom, giving some steric hindrance effect to the other coordinated ligands.

The respective Nd-O bond lengths around the Nd(1) or Nd(2), and Nd(3) atoms are distributed in the ranges shown in Table 5 by the ratios of the maximum and minimum values to the average lengths, respectively. In the high-coordination-number geometries, such a discrepancy regarding the respective M-O bond lengths around one metal atom is sometimes found.

The coordinating carboxylate ions found in the neodymium(III) complex are classified into three groups, depending on their forms (as previously shown in Ref. 4). The **A**-, **B**-, and **C**-type ions (as

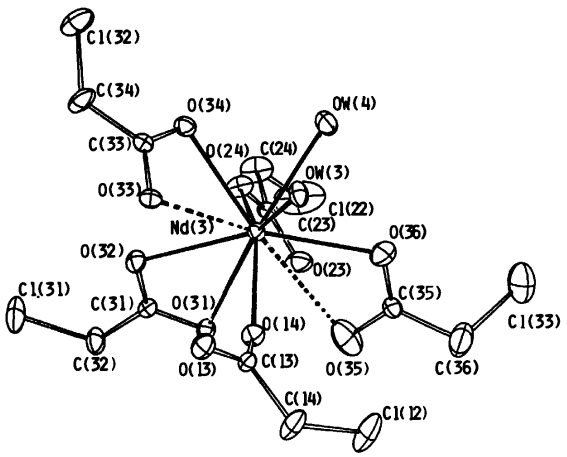

Fig. 3. A perspective drawing of the complex around Nd(3) atom with the numbering scheme of the atoms.

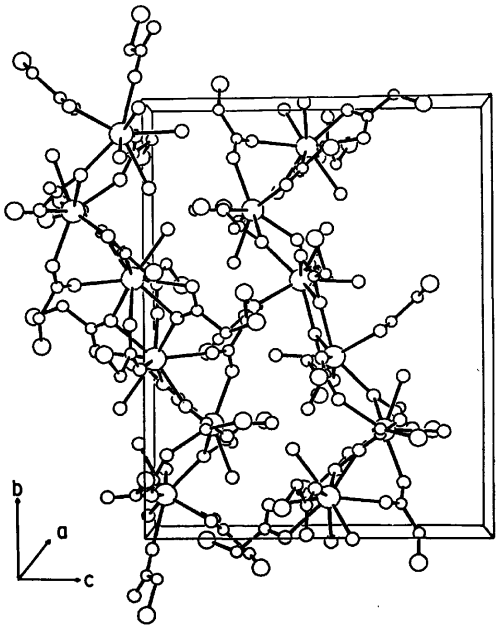

Fig. 4. Crystal packing diagram of the neodymium(III) complex.

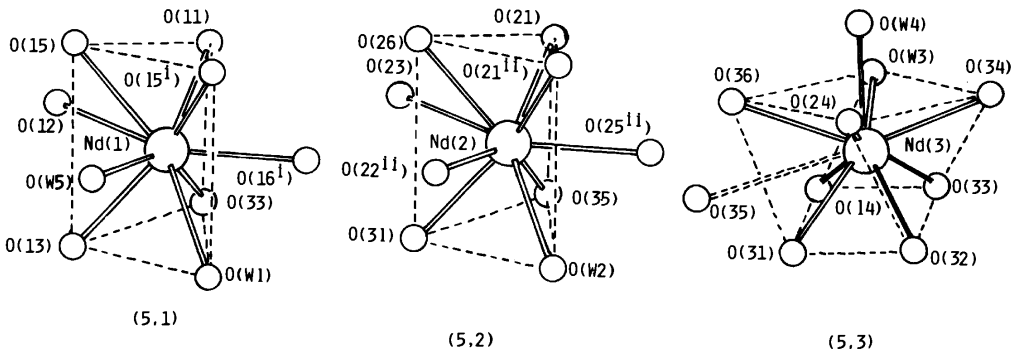

Fig. 5. Schematic presentation of the complex with the numbering scheme of the ligating atoms: 5.1, 5.2, and 5.3 show the coordination geometries around Nd(1), Nd(2), and Nd(3), respectively.

Table 4. Interatomic Distances and Bond Angles of the Complexes, with the Standard Deviations in Parentheses

M	La(l/Å)	Nd(l/Å)	Eu(l/Å)	M	La(ϕ/°)	Nd(ϕ/°)	Eu(ϕ/°)
M(1^{i})···M(1)	4.368(1)	4.315(1)	4.301(1)	O(33)-M(1)-O(16^{i})	84.4(2)	84.48(18)	84.3(2)
M(1)···M(3)	4.817(1)	4.764(1)	4.641(2)	O(16^{i})-M(1)-O(W1)	73.8(2)	73.27(18)	74.0(2)
M(3)···M(2)	4.345(1)	4.352(1)	4.429(2)	O(W1)-M(1)-O(33)	69.9(2)	69.93(18)	70.1(3)
M(2)···M(2^{ii})	4.142(1)	4.060(1)	3.974(1)	O(11)-M(1)-O(13)	123.7(2)	124.08(19)	124.6(3)
M(3)···M(2^{iii})	6.501(2)	6.455(2)	6.539(2)	O(13)-M(1)-O(W5)	77.0(2)	78.1(2)	78.9(3)
M(1)···M(3^{iv})	6.358(2)	6.278(2)	6.215(2)	O(W5)-M(i)-O(11)	141.5(2)	141.5(2)	140.9(3)
M(1)-O(11)	2.586(7)	2.524(6)	2.490(8)	O(12)-M(1)-O(15^{i})	118.9(2)	118.10(19)	117.7(3)
M(1)-O(12)	2.605(8)	2.544(7)	2.513(9)	O(15^{i})-M(1)-O(15)	65.53(18)	64.63(17)	64.5(2)
M(1)-O(13)	2.457(6)	2.395(5)	2.346(7)	O(15)-M(1)-O(12)	75.4(2)	75.26(19)	74.6(3)
M(1)-O(15)	2.505(6)	2.445(5)	2.404(7)	O(11)-M(1)-O(33)	81.6(2)	81.10(19)	81.0(3)
M(1^{i})-O(15)	2.688(6)	2.660(6)	2.679(8)	O(12)-M(1)-O(33)	71.7(2)	71.9(2)	72.0(3)
M(1^{i})-O(16)	2.584(6)	2.520(5)	2.454(7)	O(11)-M(1)-O(12)	50.0(2)	50.7(2)	51.7(3)
M(1)-O(33)	2.491(6)	2.430(6)	2.396(7)	O(21)-M(2)-O(21^{ii})	70.9(2)	70.2(2)	70.9(3)
M(1)-O(W1)	2.587(6)	2.527(6)	2.497(7)	O(21^{ii})-M(2)-O(26)	70.0(2)	70.17(19)	67.4(2)
M(1)-O(W5)	2.516(8)	2.461(7)	2.419(9)	O(26)-M(2)-O(21)	72.8(2)	74.12(19)	78.1(2)
M(2)-O(21)	2.479(6)	2.416(6)	2.337(7)	O(23)-M(2)-O(25^{ii})	117.6(2)	120.1(2)	133.4(3)
M(2)-O(23)	2.536(9)	2.498(8)	2.456(9)	O(25^{ii})-M(2)-O(22^{ii})	100.6(2)	97.9(2)	84.8(3)
M(2)-O(26)	2.480(6)	2.417(5)	2.386(7)	O(22^{ii})-M(2)-O(23)	141.1(3)	141.3(2)	141.6(3)
M(2^{ii})-O(21)	2.603(7)	2.543(6)	2.539(8)	O(35)-M(2)-O(W2)	66.9(2)	67.4(2)	71.0(3)
M(2^{ii})-O(22)	2.696(8)	2.656(7)	2.666(9)	O(W2)-M(2)-O(31)	72.8(2)	71.98(19)	68.5(3)
M(2^{ii})-O(25)	2.488(6)	2.432(6)	2.395(7)	O(31)-M(2)-O(35)	70.8(2)	72.5(2)	92.7(3)
M(2)-O(31)	2.477(5)	2.419(5)	2.391(6)	O(21)-M(2)-O(23)	72.2(2)	72.1(2)	75.9(3)
M(2)-O(35)	2.505(8)	2.437(8)	2.407(11)	O(21)-M(2)-O(35)	110.6(2)	107.5(2)	86.7(3)
M(2)-O(W2)	2.605(7)	2.556(7)	2.535(9)	O(14)-M(3)-O(W3)	74.3(2)	74.84(19)	75.9(3)
M(3)-O(14)	2.447(7)	2.385(6)	2.383(8)	O(14)-M(3)-O(31)	76.1(2)	74.65(19)	71.5(3)
M(3)-O(24)	2.539(6)	2.464(6)	2.410(7)	O(31)-M(3)-O(24)	70.3(2)	69.88(18)	70.0(2)
M(3)-O(31)	2.725(7)	2.707(6)	2.694(8)	O(32)-M(3)-O(34)	70.1(2)	71.07(18)	70.0(2)
M(3)-O(32)	2.644(7)	2.562(6)	2.470(8)	O(34)-M(3)-O(W4)	68.3(2)	69.7(2)	72.4(3)
M(3)-O(34)	2.561(6)	2.486(5)	2.427(7)	O(W4)-M(3)-O(36)	66.5(2)	66.5(2)	72.5(3)
M(3)-O(36)	2.628(7)	2.546(7)	2.285(9)	O(24)-M(3)-O(32)	72.1(2)	73.66(19)	75.2(3)
M(3)-O(W3)	2.526(6)	2.464(5)	2.409(7)	O(32)-M(3)-O(W3)	126.4(2)	127.18(18)	131.6(3)
M(3)-O(W4)	2.569(9)	2.515(8)	2.473(10)	O(W3)-M(3)-O(36)	72.6(2)	73.8(2)	83.6(3)
M(3)-O(33)	2.865(6)	2.845(5)	2.736(7)	O(36)-M(3)-O(24)	103.7(2)	101.3(2)	92.7(3)
M(3)-O(35)	2.872(7)	3.009(8)	3.978(10)	M(1)-O(11)-C(11)	93.5(6)	93.5(5)	93.4(6)
O(11)-C(11)	1.283(12)	1.260(11)	1.267(14)	M(1)-O(12)-C(11)	93.9(6)	93.4(5)	93.1(7)
O(12)-C(11)	1.229(12)	1.228(10)	1.237(13)	M(1)-O(13)-C(13)	140.1(6)	142.2(5)	144.1(7)
O(13)-C(13)	1.257(11)	1.263(9)	1.259(13)	M(3)-O(14)-M(13)	149.4(7)	147.1(6)	142.1(8)
O(14)-C(13)	1.227(11)	1.222(10)	1.231(13)	M(2)-O(23)-C(23)	138.7(7)	139.1(6)	138.6(8)
O(15)-C(15)	1.265(10)	1.273(9)	1.267(12)	M(3)-O(24)-C(23)	120.9(6)	123.3(5)	125.6(7)
O(16)-C(15)	1.245(12)	1.227(10)	1.231(13)	M(2^{ii})-O(25)-C(25)	137.5(6)	137.7(5)	134.8(7)
O(21)-C(21)	1.270(13)	1.269(12)	1.261(15)	M(2)-O(26)-C(25)	139.4(6)	138.1(5)	134.9(7)
O(22)-C(21)	1.235(11)	1.237(10)	1.236(13)	M(2)-O(21)-C(21)	146.3(6)	147.7(6)	152.7(7)
O(23)-C(23)	1.229(12)	1.217(10)	1.242(13)	M(2^{ii})-O(21)-C(21)	96.2(6)	96.7(5)	98.0(7)
O(24)-C(23)	1.248(11)	1.252(10)	1.268(12)	M(2^{ii})-O(21)-M(2)	109.1(3)	109.9(3)	109.1(3)
O(25)-C(25)	1.248(11)	1.257(10)	1.244(12)	M(2^{ii})-O(22)-C(21)	92.7(6)	92.1(5)	92.1(7)
O(26)-C(25)	1.243(11)	1.233(10)	1.246(13)	M(1)-O(15)-C(15)	153.1(5)	153.9(5)	155.4(7)
O(31)-C(31)	1.261(10)	1.263(9)	1.259(12)	M(1^{i})-O(15)-C(15)	92.0(5)	90.4(4)	88.7(6)
O(32)-C(31)	1.237(10)	1.235(9)	1.251(12)	M(1)-O(15)-M(1^{i})	114.5(2)	115.4(2)	115.5(3)
O(33)-C(33)	1.263(11)	1.262(10)	1.285(13)	M(1^{i})-O(16)-C(15)	97.5(5)	98.2(5)	100.4(6)
O(34)-C(33)	1.249(11)	1.258(10)	1.242(14)	M(2)-O(31)-C(31)	148.6(5)	147.9(5)	145.8(6)
O(35)-C(35)	1.252(13)	1.208(12)	1.231(15)	M(3)-O(31)-C(31)	93.4(5)	91.9(4)	89.0(6)
O(36)-C(35)	1.232(12)	1.248(11)	1.234(13)	M(2)-O(31)-M(3)	113.2(2)	116.1(2)	121.0(3)
O(W4)···O(W2^{iii})	2.926(10)	2.882(9)	2.948(13)	M(3)-O(32)-C(31)	98.0(5)	99.6(5)	99.8(6)
O(34)···O(W1^{iii})	2.795(10)	2.829(9)	2.832(12)	M(1)-O(33)-C(33)	144.2(6)	144.6(5)	144.2(7)
O(W4)···O(W1^{iii})	2.923(10)	2.934(8)	2.964(11)	M(3)-O(33)-C(33)	87.7(5)	86.4(4)	85.5(6)
O(36)···O(W2^{iii})	2.754(12)	2.830(11)	3.647(17)	M(3)-O(33)-M(1)	128.1(2)	129.0(2)	129.3(3)
O(W5)···O(24^{iv})	2.738(10)	2.788(8)	2.799(11)	M(3)-O(34)-C(33)	102.6(6)	103.5(5)	102.2(7)
				M(2)-O(35)-C(35)	152.5(6)	157.8(7)	138.8(9)
				M(3)-O(35)-C(35)	89.5(6)	85.8(6)	54.9(6)
				M(2)-O(35)-M(3)	107.6(2)	105.6(3)	84.0(3)
				M(3)-O(36)-C(35)	101.9(6)	107.8(6)	151.8(9)

Key to the symmetry operations: i, $1-x$, $-y$, $-z$; ii, $-x$, $1-y$, $-z$; iii, x, $0.5-y$, $0.5+z$; iv, x, $0.5-y$, $-0.5+z$.

follows) are schematically given in Fig. 6.

(**A**) Chelating ion: The ion **11**,[17] belongs to this group. Its COM and CO'M angles are 93.5(3) and 93.4(5)°, which are normal (in the range of 90—95°) for this group ions.[4]

(**B**) *Z,Z*-Type bridging bidentate ions: (*syn-syn* type bridge according to the classification by Chatteric.[18]) The ions **12**, **22**, and **23** belong to this group. In the standard form of this type ion, 2(M-O')/(M-O+M'-O') is about 1.6—1.7, the angles MO'C and M'OC, and COM and CO'M' are about 60 and 135—150°, respectively. The bond lengths and angles of these ions are found to be in the normal ranges, respectively, although C(23)-O(24)-Nd(3) is an exception (123.3(5)°).

(**C**) Tridentate-type bridging ions: (One oxygen atom of a carboxylato chelate around a metal atom is also bonded to another metal atom, consequently as a whole the ligand acts as a tridentate.) Ions **21**, **13**, **31**, **32**, and **33** are the members. In the typical form, the bond lengths (M-O, M-O', and M'-O') as well as the bond angles (MOC and MO'C, about 90—100°) are about the same, respectively, and the angle M'O'C is in the range 140—150°. Bonds O'-M' and C-O are at the opposite sides of the C-O' bond from each other. As previously shown,[4] many of the actually found ligands of this type are deformed from the ideal shape. When it deforms, the M-O' length as well as the COM angle increase, while the CO'M angle decreases. In this complex, the type of ligands deforms approximately in the given order. Their bond lengths and bond angles are compared with each other in Table 6, where the corresponding data regarding those of the lanthanum(III) and europium(III) complexes are also shown. As shown in the Table, for ion **21** of the neodymium(III) complex (which is almost in the standard form) the M-O' length is not much different from that of M-O and M'-O' and angles MOC and MO'C are within the normal range. On the other hand, in cases of the other deformed ligands, the bond lengths and bond angles deviate as mentioned above. The deformation in the form of the tridentate-type ligand is thought to tend toward the *Z,E*-type bidentate one (where M-O and C-O' bonds are at the same side of the C-O bond, while M'-O' and C-O bonds are at the opposite sides of the C-O' bond from each other, respectively). Angles COM and CO'M' are in the range 140—145° (CO'M is about 60°) and M-O' length is about 1.6- to 1.7-times the average of the M-O and M'-O' lengths in standard *Z,E*-type bidentate ion.[4] Therefore, even the most deviated ion, **33**, of the neodymium(III) complex is far from the normal *Z,E*-type bidentate.

The coordination type of the respective carboxylate ions, their bridging positions as well as the number of the intermetallic bridges are schematically shown in Fig. 7. As shown in this figure, the pairs of the

Table 5. The Comparison of the Metal-Oxygen Bondings of the Complexes

Metal	La	Nd	Eu
$M\text{-}O_{calc(CN=9)}$ [b]	2.57	2.51	2.47
$M\text{-}O_{calc(CN=10)}$ [b]	2.62	(2.56)[g]	(2.52)[g]
$M\text{-}O_{av(M(1),M(2))}$ [c]	2.54_9	2.49_3	2.46_2
$M\text{-}O_{av(M(3),9)}$ [d]	2.61_2	2.55_3	2.47_6
$M\text{-}O_{av(M(3),10)}$ [d]	2.63_8	2.59_8	2.62_7
$M\text{-}O_{min(M(1),M(2))}/M\text{-}O_{av(M(1),M(2))}$ [e]	0.96	0.97	0.95
$M\text{-}O_{max(M(1),M(2))}/M\text{-}O_{av(M(1),M(2))}$ [e]	1.06	1.07	1.09
$M\text{-}O_{min(M(3))}/M\text{-}O_{av(M(3),9)}$ [f]	0.94	0.93	0.92
$M(3)\text{-}O(35)/M\text{-}O_{av(M(3),10)}$ [f]	1.09	1.16	1.51
$M(3)\text{-}O(33)/M\text{-}O_{av(M(3),9)}$ [f]	1.09	1.11	1.11

b) The sum of the Shannon's ionic radii.[16] The valence of the central metal is 3+, and its coordination number *n* is shown by CN=*n*. c) Average of the 18 M-O bond lengths around M(1) and M(2) atoms. d) Average of written numbers of the M-O bond lengths around M(3) atom. (In the case of 9, M(3)-O(35) one is rejected.) e) The shortest (shown by min) or the longest (shown by max) M-O bond length around the M(1) and M(2) atoms is divided by the average of all the M-O bond lengths around the metal atoms. f) The written bond length is divided by the average M-O bond length around M(3) atom, where "av(M(3), 9)" means the average of nine M-O bond lengths excluding M(3)-O(35), while "av(M(3), 10)" that of all ten bond lengths around the metal atom. g) As Shannon did not give the ionic radii of neodymium(III) and europium(III) in ten-coordination, the values 0.05 Å longer than the corresponding nine-coordination radii are tentatively adopted.

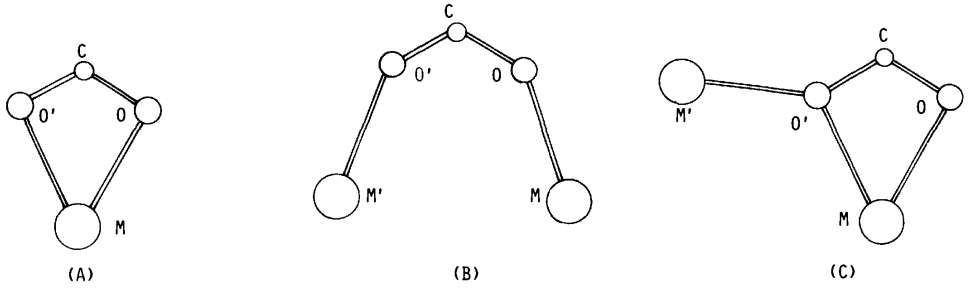

Fig. 6. Schematic presentation of the three types of ligands.

neodymium(III) atoms, Nd(1^{i}) and Nd(1), Nd(1) and Nd(3), Nd(3) and Nd(2), and Nd(2) and Nd(2^{ii}) (where the key to the symmetry operations: i, $1-x$, $-y$, $-z$; ii, $-x$, $1-y$, $-z$) are bridged by: two **C**-type ions; one **B**-and one **C**-type ion; one **B**-, one **C**- and one extremely deformed **C**-type ion; and two **B**- and two **C**-type ions, respectively. The respective inter-metal-atomic distances are: 4.315(1), 4.764(1), 4.352(1), and 4.060(1) Å. Therefore, judging from these data, the effect of a **C**-type bridge to shorten the intermetallic distance is greater than that of a **B**-type bridge.

Thus, the metal atoms in the complex are arranged in the order of ···Nd(1^{i})···Nd(1)···Nd(3)···Nd(2)···Nd(2^{ii})···, approximately along [−110] axis, although in a zig-zag way. The next chain on the *z*-axis direction, ···Nd(1^{iv})···Nd(1^{iii})···Nd(3^{iii})···Nd(2^{iii})···Nd(2^{v})···, (where the key to the symmetry operations: iii, x, $0.5-y$, $0.5+z$; iv $1-x$ $0.5+y$, $0.5-z$; v, $-x$, $-0.5+y$, $0.5-z$), is laid along [110] axis. Thus, the polymeric chains along both axes are aligned alternately. Between these side-by-side chains, no coordinated carboxylato bridges are found, though some hydrogen bondings are expected to exist (as shown by some interatomic distances in Table 4).

The structures of the lanthanum(III) and europium-(III) complexes resemble that of the neodymium(III) complex. However, there are some differences between them (mentioned below) regarding their detailed structures.

In the lanthanum(III) complex, an average of eighteen La-O bond lengths around the La(1) and La(2) atoms is 2.549 Å; this is slightly shorter than the

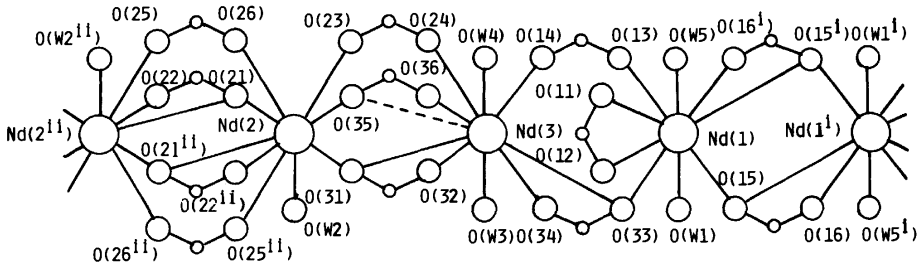

Fig. 7. Schematic presentation of the bridgings between the metal atoms. (Key to the symmetric operations: i, $1.0-x$, $-y$, $-z$; ii, $-x$, $1.0-y$, $-z$).

Table 6. Some Comparative Data about Interatomic Distances and Bond Angles of Tridentate-Type Ligands of the Complexes[h)]

Lanthanum(III) Complex

Ligand	21	11	31	32	33
(M-O+M'-O')/2	2.588	2.545	2.561	2.526	2.567
2(M'-O)/(M-O+M'-O')	1.02	1.06	1.06	1.13	1.12
MOC(ϕ/°)	92.7(6)	97.5(5)	98.0(5)	102.6(6)	101.9(6)
MO'C(ϕ/°)	96.2(6)	92.0(5)	93.4(5)	87.7(5)	89.5(6)
M'O'C(ϕ/°)	146.3(6)	153.1(5)	148.6(5)	144.2(6)	152.5(6)

Neodymium(III) Complex

Ligand	21	11	31	32	33
(M-O+M'-O')/2	2.536	2.483	2.491	2.458	2.492
2(M'-O)/(M-O+M'-O')	1.00	1.07	1.09	1.16	1.21
MOC(ϕ/°)	92.1(5)	98.2(5)	99.6(5)	103.5(5)	107.8(6)
MO'C(ϕ/°)	96.7(5)	90.4(4)	91.9(4)	86.4(4)	85.8(6)
M'O'C(ϕ/°)	147.7(6)	153.9(5)	147.9(5)	144.6(5)	157.8(7)

Europium(III) Complex

Ligand	21	11	31	32	33
(M-O+M'-O')/2	2.502	2.429	2.431	2.412	2.346
2(M'-O)/(M-O+M'-O')	1.01	1.10	1.11	1.13	1.70
MOC(ϕ/°)	92.1(7)	100.4(6)	99.8(6)	102.2	151.8(9)
MO'C(ϕ/°)	98.0(7)	88.7(6)	89.0(6)	85.5(6)	54 9(6)
M'O'C(ϕ/°)	152.7(7)	155.4(7)	145.8(6)	144.2(7)	138.8(9)

h) The nominations of the atoms shown in this Table are the same as those of Fig. 6(C).

sum of the tervalent La(CN=9) and O ionic radii, 2.57 Å.[16] The average of ten La–O bond lengths, including La(3)–O(35), around the La(3) atom is 2.638 Å; this is almost the same as the sum of the tervalent La(CN=10) and O ionic radii, 2.62 Å[16] (the average of nine La–O lengths, excluding La(3)–O(35), is 2.612 Å, which is not much different from the latter sum, too).

The corresponding La–O bonds, except La(3)–O(35), are all longer than the respective Nd–O bonds; the differences between them are in the range of 0.028—0.068 Å around the M(1) and M(2) atoms, and 0.017—0.082 Å around the M(3) atom. The relatively long La(3)–O(35) distance is, on the contrary, 0.137 Å shorter than that of the neodymium(III) complex. Even other than this bond, La(1^{i})–O(15), La(3)–O(31), and La(3)–O(33), which are relatively long, are also not very elongated when the central metal atom is changed from neodymium(III) to lanthanum(III). Consequently, the range between the shortest and the longest M–O bond lengths of the lanthanum(III) complex is widened in the neodymium(III) complex (Table 5).

Table 6 gives a comparison of the respective tridentate-type ions of the neodymium(III) complex with the corresponding ones of lanthanum(III) complex; the deviations from the ideal values of the relative M–O′ lengths, and of the MOC as well as MO′C angles are a little greater in the neodymium(III) complex.

As the ionic radius of the neodymium(III) is shorter than that of lanthanum(III), due to the lanthanoid contraction effect, the spherical area around the neodymium(III) atom to be occupied by the ligating atoms is smaller than that of the lanthanum(III) ion. Therefore, in the neodymium (III) complex, there are more steric interactions between the ligating atoms and between the ligand molecules. These steric hindrance effects work unequally on the respective ligands. Consequently, the respective M–O bond lengths do not decrease equally, and the M–O bond lengths of the neodymium(III) complex disperse over a wider range.

Of course, even in the lanthanum(III) complex, as the restrictions such as the bonding directions of the respective ligating atoms, and the definite distance between each pair of the oxygen atoms of the same ligand still remain, the discrepancy of the respective La–O bond lengths and the deformation of the coordination geometries around the respective metal atoms are also found.

Although the disproportional changes of several M–O bond lengths are found when the central metal atom of the lanthanum(III) complex is substituted by the neodymium(III) atom; no change of the bonding type of the ligands is found. This kind of the unequal bond-length change in a series of the isomorphous complexes was also reported in a series of guanidinium tetraacetatolanthanoidates(III).[4]

In the europium(III) complex, an average eighteen Eu–O bond lengths around the Eu(1) and Eu(2) atoms is 2.462 Å; this is about the same as the sum of the tervalent Eu(CN=9) and O ionic radii: 2.47 Å.[16] However, the differences between the respective Eu–O and the corresponding Nd–O bond lengths distribute over a wider range than those between the Nd–O and La–O lengths: 0.079—−0.019 Å (negative value means that the Eu–O is longer). The relatively long Nd–O bonds, such as Nd(1^{i})–O(15) and Nd(2^{ii})–O(25), are rather elongated in the europium(III) complex. On the other hand, some M–O bonds other than the elongated type of the same ligand are greatly shortened: M(1^{i})–O(16) and M(2)–O(21) are the examples.

The Eu(3) atom is regarded as being nine-coordinated. The average of the nine Eu–O bond lengths around it is 2.476 Å; this is about the same as the sum of the radii of tervalent Eu(CN=9) and O ions. No such discrepancy, as was found in the lanthanum(III) or the neodymium(III) complexes, was recognized. From this aspect, the Eu(3) atom is in pure nine-coordination geometry. Around the Eu(3) atom, except Eu(3)–O(35), all the Eu–O lengths are shorter than the corresponding Nd–O lengths of the neodymium(III) complex by 0.002 to 0.261 Å.

The general tendency of the change of the M–O bond lengths around the Eu(3) atom is about the same as that around the Eu(1) and Eu(2) atoms, although in more drastic way. The distance Eu(3)···O(35) is 0.969 Å longer than that of the neodymium(III) complex; consequently the O(35) atom of the europium(III) complex is perfectly out of the bonding distance. Moreover, it is thought to be even out of the sterically affecting region around the metal atom. On the other hand, the bond Eu(3)–O(36) is extremely short, 2.285(9) Å, although almost the same short Nd–O bond (2.312(10) Å) was already found in another polymeric-type carboxylato complex of neodymium(III).[2] Such disproportional changes of the M–O bond lengths of the same ligands are also found in ions **31**, and **32**. As shown in Table 4 (compared with the corresponding ions of the neodymium(III) complex), in the ion **31** the shorter bond is very shortened, while the longer one is shortened only a little, in the europium(III) complex. On the other hand, in the ion **32** the longer bond is more shortened.

According to the data shown in Table 6, four tridentate-type ions (except **33**) of the europium(III) complex are found to be in the forms approximately the same as the corresponding ones of the neodymium-(III) or lanthanum(III) complexes; the grade of their deviations from the respective values of the standard types are not much different from those of the former two complexes.

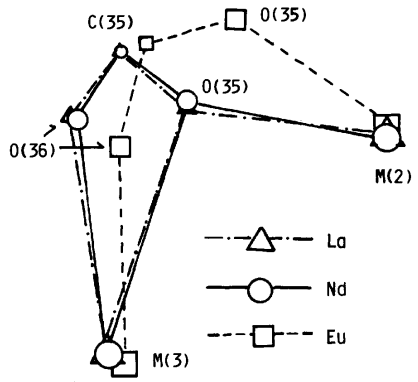

Fig. 8. The projection of **33** and the bonded metal atoms of the complexes to the (001) plane. The origin of the unit cell, the a-axis, and the scaling in length are taken commonly.

On the other hand (as shown in Fig. 8) in ion **33** of the europium(III) complex, bonds O(35)-Eu(2) and O(36)-C(35) are at the same side of bond C(35)-O(35) (*Z*-type), while the corresponding bonds of the neodymium(III) and lanthanum(III) complexes are at the opposite sides of the C(35)-O(35) bond from each other (*E*-type). As shown in Table 6, in the europium(III) complex, the bond length ratio 2(M-O')/(M-O+M'-O'), and the bond angles C(35)-O(36)-Eu(3) (COM) and C(35)-O(35)-Eu(2) (CO'M') are in the respective standard ranges of the *Z,Z*-type ion, while in those of the other two complexes the values are in the range of the tridentate-type ion, although they are a little deviated.

Thus, in the europium(III) complex, there are not only the unequal change of the respective M-O bond lengths, but also the change of the type of the coordinating ligand, depending on the change of the atomic number (i.e., the ionic size of the central metal atom). This is the first example of this kind of the discrepancy of the structure in the series of the apparently isomorphous lanthanoid complexes.

Such change of the M-O bond lengths in the complex of the smaller size metal causes some stress on the coordination geometry around the metal atom; also, the degree of the stress should affect the stability of the complex. As a result, in an europium(III) complex, the modification of the ligand form also took place, although its apparent crystal system did not change yet.

The infrared spectra of the series of the complexes were examined, and we found continuous changes in the intensities of the ν_{as}(COO) peaks as well as of the splitting of the ν_s(COO) band, depending on the increase of the metal atomic number.

The main peak of the ν_{as}(COO) band of lanthanum(III) and praseodymium(III) complexes appeared at about 1580 cm^{-1}, together with small shoulders at about 1565 and 1605 cm^{-1}, while in the neodymium(III) complex, both of the 1565 and 1580 cm^{-1} peaks were dominant (former one is stronger). On the other hand, in the europium(III) complex, only the 1565 cm^{-1} peak was dominant together with a new small peak at 1650 cm^{-1}; no shoulders could be recognized at 1580 and 1605 cm^{-1}.

The ν_s(COO) band of the lanthanum(III) and praseodymium(III) complexes appears at 1415 cm^{-1} as a broad peak, while in the neodymium(III) and europium(III) complexes, the peak splits clearly into three equal height ones at 1396, 1420, and 1440 cm^{-1}.

Although at present, it is impossible to assign these peaks exactly, at least we can deduce that there are some changes in the bonding modes (not only the continuous change of bond strengths) of the carboxylate ions. This depends on the increase in the atomic number of the central metal atom; this fact may correspond with the X-ray analysis results mentioned above.

The authors wish to thank Shin-Etsu Chemical Ind. Co. Ltd., for presenting us with the highly pure lanthanoid oxides.

References

1) R. C. Mehrotra and R. Bohra, "Metal Carboxylates," Academic Press, London, U. K. (1983), p. 757, and references cited in it.

2) S. Kondo, M. Shimoi, A. Ouchi, and T. Takeuchi, *Bull. Chem. Soc. Jpn.*, **55**, 2840 (1982).

3) Y. Koizumi, H. Sawase, Y. Suzuki, T. Takeuchi, M. Shimoi, and A. Ouchi, *Bull. Chem. Soc. Jpn.*, **57**, 1809 (1984).

4) H. Sawase, Y. Koizumi, Y. Suzuki, M. Shimoi, and A. Ouchi, *Bull. Chem. Soc. Jpn.*, **57**, 2730 (1984), and the references cited in it.

5) M. S. Khiyalov, I. R. Amiraslanov, Kh. S. Mamedov, and E. M. Movsmov, *Koord. Khim.*, **7**, 445 (1981).

6) J. W. Bats, R. Kalus, and H. Fuess, *Acta Crystallogr., Sect. B*, **35**, 1225 (1979).

7) G. G. Sadikov, G. A. Kukina, and M. A. Porai-Koshits, *Zh. Strukt. Khim.*, **8**, 551 (1967).

8) G. G. Sadikov, G. A. Kukina, and M. A. Porai-Koshits, *Zh. Strukt. Khim.*, **12**, 859 (1971).

9) A. Ouchi, M. Shimoi, and S. Kondo, *Bull. Chem Soc. Jpn.*, **58**, 1053 (1985).

10) A. S. Antsyshkina, M. A. Porai-Koshits, I. V. Ar-Khangel'ski, and L. A. Butman, *Koord. Khim.*, **2**, 565 (1976).

11) E. R. Birmingham, "Rare Earth Element Coordination Compounds, D5," of Gmelin's Handbook of Inorganic Chemistry, 8th ed (1984), p. 61.

12) "Universal Crystallographic Computation Program System (UNICS)," ed by T. Sakurai, Crystallograghic Society of Japan, Tokyo (1967).

13) "International Tables for X-Ray Crystallography," Kynoch Press, Birmingham (1974), Vol. IV, pp. 72, 150.

14) Some additional data regarding bond lengths and bond angles, the final thermal parameters, and the final F_o–F_c tables are deposited as Document 8709 at the office of the editor of Bull. Chem. Soc. Jpn.

15) Although in many papers each coordination geometry (where the coordination number is higher than 7) around the lanthanoid or such heavy metal atom is approximated to some type, generally it is only an approximation and it is deformed from the ideal shape. Some other geometry may also be applicable in place of the written one. In the title complex, for the geometry of Nd(1) and Nd(2) atoms, the tricapped trigonal-prism is thought to be the best approximation, although they are deformed. When the geometry is assumed as schematically shown in Fig. 5 as 5.1 and 5.2, the dihedral angles between the side rectangulars are within the range of 55.8 to 63.5°, while those between the planes of the both end triangles and of the side rectangulars are within the range of 77.4 to 99.2°. The dihedral angles between two end triangle planes are 21.2 and 17.0°. Around the Nd(3) atom, if the O(33) and O(35) atoms are rejected, the coordination geometry of the metal atom is regarded as a deformed dodecahedron, where the atoms [O(32), O(34), O(W4), and O(36)] and [O(24), O(31), O(14), and O(W3)] are on the apexes of the both trapezia, respectively. Moreover, if only the O(35) is rejected, a tricapped trigonal-prism geometry can be adopted, where both end triangles are [O(36), O(W3), and O(14)] and [O(24), O(32), and O(34)], while O(W4), O(33), and O(31) are capped above the respective faces.

However, as the O(35) atom only in the lanthanum(III) complex is not very far from the metal atom (compared with the other ligated oxygen atoms), it is preferable to adopt a common structure available to all three complexes which includes the O(35) atom. In the two above-mentioned geometries, we cannot give any reasonable position around the assumed polyhedron to the O(35) atom. On the other hand, if we assume the *cis*-bicapped square-antiprism geometry around the M(3) atom, we can consider it reasonable as a cap above one side face, although the geometry is deformed to some grade. Moreover, as the monocapped square-antiprism is a more common geometry, we can imagine an additional capping atom above a side face, O(35), is less strongly ligated.

16) R. D. Shannon, *Acta Crystallogr., Sect. A*, **32**, 751 (1976). The presented ionic radii are as follows (the valence of the metals is 3+, and of oxygen ion 2−; the coordination numbers of the metal ions (8, 9, or 10) are shown by the respective numbers (unit is in *l*/Å): r_{La}, 8=1.160, 9=1.216, 10=1.27 Å; r_{Nd}, 8=1.109, 9=1.163 Å; r_{Eu}, 8=1.066, 9=1.120 Å; r_O, 2=1.35 Å.

17) Hereafter, each carboxylate ion is numbered according to that of the chlorine atom in it; ions ***n*1**, ***n*2**, and ***n*3** (where ***n***=1, 2, and 3) include the carboxylato group atoms of C(n1), O(n1), O(n2); C(n3), O(n3), O(n4); and C(n5), O(n5), O(n6), respectively.

18) J. Chatteric and P. Thornton, "Advances in Inorganic Chemistry and Radiochemistry," Academic Press, New York (1977), Vol. 20, p. 291.

 © 1987 The Chemical Society of Japan Bull. Chem. Soc. Jpn., 60, 171—178 (1987)

The Crystal and Molecular Structure of Heavy Lanthanoid(III) Chloroacetates in the Hydrated Form, $[M_3(ClCH_2CO_2)_9(H_2O)_4]_n \cdot nH_2O$ (M=Gd, Dy, Er, and Yb)

Yoshihiko SUGITA and Akira OUCHI*
Department of Chemistry, College of Arts and Sciences, The University of Tokyo, Komaba, Meguro-ku, Tokyo 153
(Received July 21, 1986)

The crystal and molecular structures of the chloroacetato complexes of gadolinium(III), erbium(III), and ytterbium(III) indicated in the title were determined by the single-crystal X-ray diffraction method. In addition to these three complexes, the isomorphous dysprosium(III) salt was also obtained. Their chemical composition, $M_3L_9 \cdot 5H_2O$ (where M=Gd, Dy, Er, or Yb; HL=chloroacetic acid), is the same as that of the light lanthanoid(III) (La—Eu) chloroacetates, though the latter crystals are monoclinic. The cell constants of the ytterbium(III) salt, for example, are: triclinic, space group $P\bar{1}$, a=13.278(10), b=13.624(6), c=12.067(4) Å α=96.62(3), β=100.68(5), γ=67.40(4)°, Z=2 (including 6 metal atoms). There are three kinds of crystallographically independent metal atoms; Yb(1), Yb(2), and Yb(3): Yb(1) and Yb(2) are octa-coordinated (square-antiprism geometry) and Yb(3) is ennea-coordinated (monocapped square-antiprism geometry). Two oxygen atoms around the last type of the metal atom are the more separated in the higher atomic-number lanthanoid(III) complex, while the other M-O bond lengths decrease, depending on the increase of the metal atomic number. The metal atoms are bridged by carboxylate ions in a chair form along the [111] axis, though in a way different from that of the light lanthanoid(III) complexes.

The variety of the coordination geometries of the central metal atom as well as the carboxylate ions in the lanthanoid carboxylate complexes are one of the interesting thème of structural chemistry.[1] Among them, chloroacetates of light lanthanoid(III) (La through Eu) were found to have a complicated linear polymeric structure bridged by carboxylate ions.[2]

Using the same synthetic technique, the chloroacetates of heavy lanthanoid(III) (Gd through Yb) in the hydrated form were obtained. From a preliminary check of their single crystals by the X-ray diffraction method, they were found to be isomorphous with each other since their cell constants resemble each other. However, their crystal system is triclinic, not monoclinic like that of the light lanthanoid(III) salts, though the results of their chemical analyses show that the heavy and light lanthanoid(III) chloroacetates have the same chemical composition: $ML_3 \cdot 5/3\ H_2O$ (where M=Gd, Dy, Er, or Yb, as well as La, Pr, Nd, or Eu; HL=chloroacetic acid).[2]

It was recognized in many other cases that the crystals of the complexes of the heavy and light lanthanoids(III) are different from each other, even when the used synthetic technique is the same. For example, in the case of acetates, the cerium(III) salt is in a linear polymeric structure, while the holmium-(III) salt is in a dimer form.[3,4] In cases of the Lewis base (L') adducts of tris(O,O'-dialkyl dithiophosphato)lanthanoid(III) ($Ln(R_2dtp)_3$), light and heavy lanthanoids(III) gave $[Ln(R_2dtp)_3L'_2]$ and $[Ln(R_2dtp)_2L'_3][R_2dtp]$ type complexes, respectively. The border of both series of complexes exists between praseodymium and neodymium in the case of the triphenylphosphine oxide adducts,[5] and at gadolinium in the case of the benzamide adducts (both types of adducts were obtained for gadolinium).[6,7]

Therefore, it is interesting to examine the difference in the structures between the light and heavy lanthanoid(III) complexes of the same ligand; we have determined the crystal and molecular structures of the latter complexes by the X-ray diffraction technique using their single crystals.

Experimental

Synthesis of Ytterbium(III) Chloroacetate, $[Yb_3(ClCH_2CO_2)_9(H_2O)_4] \cdot H_2O$, and Its Isomorphous Complexes. The synthetic technique is about the same as that for the neodymium(III) salt.[2] Ytterbium(III) hydroxide was obtained by mixing aqueous solutions of ytterbium(III) chloride (obtained by dissolving ytterbium(III) oxide (Yb_2O_3, 0.39 g, 1.0 mmol) in excess of hydrochloric acid), and of excess sodium hydroxide. After the ytterbium hydroxide and chloroacetic acid (0.57 g, 6.0 mmol) were mixed and stirred for several minutes, the obtained solution was filtered and the filtrate was left standing in a silica gel desiccator for several days. About two-thirds of the water was removed and crystals were deposited. They were first separated and dried in the open air overnight and then kept in a sealed glass bottle. They were stable there at least for several months. Yield: 0.75 g, 78%.

Applying the same technique, gadolinium(III), dysprosium(III), and erbium(III) salts, which were isomorphous with each other, were obtained in about the same yield. Anal. ($M_3L_9 \cdot 5H_2O = M_3C_{18}H_{28}O_{23}Cl_9$), M, C, H (where M=Gd, Dy, Er, or Yb).

It was reported that the number of water molecules in the lanthanoid chloroacetates $ML_3 \cdot n'H_2O$ were: n'=4 for the Ho salt, 5 for the Er salt, and 3 for the Tm, Yb and Lu salts.[8] However, according to our synthetic method, only one type of crystal, $M_3L_9 \cdot 5H_2O$, could be obtained for the heavy lanthanoids(III).

Single-Crystal X-Ray Analysis. The crystals used for the analysis were obtained by the above-mentioned syntheses. From the crystallographic data obtained by the single-

crystal X-ray diffraction technique, the four above-mentioned chloroacetates were all found to be isomorphous with each other. They are triclinic with the space group of $P\bar{1}$, Z=2 (for the title formula with n=1; six metal atoms are included in a unit cell).

Their crystallographic data are given in Table 1 and some experimental conditions to obtain the intensity data are tabulated in Table 2. The reflections were collected on a Rigaku AFC-6A automated four-circle X-ray diffractometer with graphite monochromated Mo $K\alpha$ radiation (the scan speed was 4° min^{-1} (θ)), using the ω—2θ scan technique.

Structure Determination. The structure of the ytterbium(III) complex was solved by the heavy-atom method. The positions of the metal and some oxygen atoms were deduced from a three-dimensional Patterson map; the other non-hydrogen atoms were located successively by repeated Fourier syntheses. Their positional, isotropic and then anisotropic thermal parameters were refined by a block-diagonal least-squares method. At the last cycle of the refinement with anisotropic temperature factors for all non-hydrogen atoms, all the parameter shifts were less than one-third of the corresponding standard deviations. The structures of the isomorphous complexes were solved starting with the final parameters of the ytterbium(III) complex, and were refined in the same way. All the hydrogen atoms were fixed at the calculated positions assuming their C-H bond lengths to be 1.08 Å and their B_{iso}'s to be 8.0.

As shown in Table 3, the temperature factors of Cl(22), Cl(31), Cl(32), and Cl(33) atoms of all the complexes are large, and the apparent bond lengths of their C(36)-Cl(33) are a little too short. Attempts to determine the disorders of these atoms (i.e., to divide each atomic position into two with respective appropriate occupancy factors for them) were not successful; all the trials did not give any improvement to their temperature factors and to their R value. It is likely that these atoms are distributed in a wide region around the most probable position. Thus, these chlorine atoms as well as some carbon atoms of the ligands which take their positions far from the central metal atom are not well fixed; such position ambiguity regarding some ligand atoms was often encountered in structure determinations of some lanthanoid(III) complexes.[2,6,7,9-11]

All the calculations were carried out on a HITAC M-680H at the Computer Center of the University of Tokyo using a local version of the UNICS program.[12] The atomic scattering factors were taken from Ref. 13.

Infrared Spectrum Measurements. Their infrared spectra were obtained by means of a JASCO 202A grating infrared spectrophotometer using Nujol and hexachloro-1,3-butadiene mull.

Results and Discussion

The final atomic parameters and their equivalent thermal parameters of the complexes are listed in

Table 1. Crystallographic Data of the Complexes $[M_3(ClCH_2CO_2)_9(H_2O)_4]_n \cdot nH_2O$ (M=Gd, Dy, Er, and Yb)

M=	Gd	Dy	Er	Yb
F.W. (n=1)	1403.24	1419.00	1433.27	1450.61
a(l/Å)	13.428(6)	13.418(12)	13.333(5)	13.278(10)
b(l/Å)	13.736(6)	13.722(17)	13.671(4)	13.624(6)
c(l/Å)	12.185(5)	12.162(11)	12.111(3)	12.067(4)
α(ϕ/°)	96.55(4)	96.63(9)	96.65(2)	96.62(3)
β(ϕ/°)	100.65(4)	100.72(8)	100.67(3)	100.68(5)
γ(ϕ/°)	67.23(3)	67.13(7)	67.35(2)	67.40(4)
U(v/Å^3)	2034.3(16)	2025(4)	1999.6(11)	1978(2)
D_m(d/Mg m^{-3})	2.29(3)	2.31(3)	2.39(3)	2.41(3)
D_x(d/Mg m^{-3})	2.29	2.33	2.38	2.44
μ(Mo $K\alpha$)(n/mm^{-1})	5.65	6.36	7.16	8.09

Table 2. Some Experimental Conditions to Obtain the Reflection Intensities

Metal	Gd	Er	Yb
Number of reflections measured	7211	6957	7038
Reflections used for the calculation[a]	6104	5978	5952
Measured range (2θ/°)	3—50	3—50	3—50
R[b]	0.050	0.063	0.045
R_{welght}[b]	0.061	0.075	0.054
Size of the crystal (v/mm^3)	0.3×0.25×0.2	0.3×0.2×0.15	0.3×0.25×0.25
Scan width (θ/°)	1.04+0.5 tan θ	1.20+0.5 tan θ	1.15+0.5 tan θ
S[c]	1.696	2.115	1.592

a) Reflections with $|F_o| > 3\sigma(|F_o|)$ were used. b) $R=\sum||F_o|-|F_c||/\sum|F_o|$; $R_{welght}=[\sum(|F_o|-F_c|)^2/\sum wF_o^2]^{1/2}$, where $w=1/[\{\sum(|F_o|)\}^2+(F_{welght}\times F_o)^2]$, $F_{welght}=0.020$. c) $S=[\sum w(|F_o|-|F_c|)^2/(N_o-N_p)]^{1/2}$, where N_o= number of reflections, N_p=number of parameters.

Table 3. Final Atomic Coordinates ($\times 10^4$) and Equivalent Isotropic Temperature Factors (B_{eq}/Å^2) of Non-Hydrogen Atoms, with Estimated Standard Deviations in Parentheses

3.1 Gadolinium Complex					3.2 Erbium Complex				
Atom	x	y	z	B_{eq}/Å^2 a)	Atom	x	y	z	B_{eq}/Å^2 a)
Gd(1)	573.6(4)	712.9(4)	1406.1(4)	2.1$_7$	Er(1)	568.8(5)	703.8(5)	1401.4(5)	2.0$_8$
Gd(2)	3043.5(4)	1647.4(3)	3411.1(4)	2.0$_7$	Er(2)	3048.6(5)	1638.6(5)	3394.5(5)	2.0$_7$
Gd(3)	4855.8(4)	3719.5(3)	3871.4(4)	2.0$_7$	Er(3)	4859.5(5)	3715.7(5)	3843.0(5)	2.1$_9$
O(11)	2045(6)	−123(7)	286(7)	3.9$_2$	O(11)	2007(9)	−111(10)	294(9)	4.1$_3$
O(12)	2476(5)	663(5)	1834(6)	2.8$_0$	O(12)	2452(7)	675(7)	1866(8)	2.5$_2$
O(13)	1337(7)	−1047(6)	2105(6)	3.8$_2$	O(13)	1304(9)	−1017(8)	2102(9)	3.6$_0$
O(14)	318(6)	−965(5)	462(6)	2.6$_6$	O(14)	277(8)	−935(7)	456(8)	2.7$_1$
O(15)	113(7)	2488(6)	1306(7)	4.0$_1$	O(15)	149(9)	2425(8)	1285(9)	3.5$_7$
O(16)	1319(6)	2925(5)	2598(6)	3.1$_4$	O(16)	1336(8)	2893(8)	2607(9)	3.0$_8$
O(21)	3350(6)	2320(6)	1873(6)	3.4$_3$	O(21)	3351(9)	2302(8)	1876(8)	3.3$_4$
O(22)	3729(7)	3773(6)	2220(7)	4.2$_2$	O(22)	3750(10)	3759(8)	2206(9)	3.9$_3$
O(23)	722(9)	1101(7)	3256(7)	5.4$_2$	O(23)	654(11)	1087(9)	3211(9)	4.5$_9$
O(24)	1748(6)	1730(7)	4529(7)	4.4$_2$	O(24)	1778(9)	1670(9)	4445(9)	3.8$_7$
O(25)	4887(6)	626(6)	3204(7)	3.5$_0$	O(25)	4858(8)	685(8)	3216(9)	3.2$_8$
O(26)	5514(7)	1927(6)	3591(7)	3.9$_7$	O(26)	5548(9)	1961(7)	3580(9)	3.5$_3$
O(31)	3095(6)	3286(5)	4129(6)	2.8$_0$	O(31)	3108(8)	3250(7)	4096(8)	2.8$_9$
O(32)	3104(6)	4862(5)	4479(7)	3.3$_1$	O(32)	3144(9)	4814(8)	4431(9)	3.5$_6$
O(33)	4775(6)	5465(5)	3944(6)	3.1$_6$	O(33)	4782(8)	5423(7)	3925(9)	3.0$_9$
O(34)	5038(6)	6939(5)	4288(6)	3.0$_2$	O(34)	5052(8)	6879(8)	4353(8)	3.1$_0$
O(35)	5850(7)	3683(7)	2415(7)	4.4$_0$	O(35)	5830(10)	3673(10)	2399(10)	4.4$_3$
O(36)	7505(7)	2463(7)	2710(7)	4.4$_9$	O(36)	7516(10)	2467(10)	2721(10)	4.5$_4$
C(11)	2728(8)	145(8)	946(9)	2.8$_6$	C(11)	2702(11)	170(11)	976(11)	2.3$_5$
C(12)	3859(9)	−110(10)	714(11)	4.3$_7$	C(12)	3859(13)	−129(15)	735(15)	4.4$_2$
C(13)	888(9)	−1486(8)	1297(9)	2.9$_9$	C(13)	864(12)	−1460(11)	1299(12)	2.8$_5$
C(14)	995(11)	−2596(9)	1313(10)	4.3$_9$	C(14)	986(16)	−2584(12)	1302(15)	4.5$_7$
C(15)	523(8)	3125(7)	1856(9)	2.6$_2$	C(15)	553(12)	3100(11)	1828(12)	2.8$_2$
C(16)	−109(11)	4249(9)	1488(12)	4.4$_4$	C(16)	−76(15)	4215(12)	1446(16)	4.2$_5$
C(21)	3344(9)	3181(9)	1592(10)	3.3$_0$	C(21)	3363(12)	3147(12)	1593(13)	3.0$_5$
C(22)	2901(12)	3507(11)	419(10)	4.9$_9$	C(22)	2913(18)	3501(16)	384(15)	5.4$_4$
C(23)	955(9)	1489(9)	4209(9)	3.1$_9$	C(23)	940(12)	1477(11)	4176(12)	2.7$_9$
C(24)	138(14)	1637(17)	4977(15)	8.1$_6$	C(24)	141(17)	1655(20)	4975(18)	6.6$_2$
C(25)	5629(8)	986(7)	3307(8)	2.3$_9$	C(25)	5628(11)	1038(11)	3317(11)	2.5$_1$
C(26)	6768(9)	278(8)	3133(10)	3.3$_4$	C(26)	6755(13)	285(12)	3139(14)	3.4$_3$
C(31)	2671(8)	4218(8)	4490(8)	2.5$_3$	C(31)	2683(11)	4186(11)	4451(12)	2.8$_9$
C(32)	1629(11)	4496(11)	4958(12)	5.2$_6$	C(32)	1629(15)	4479(15)	4917(16)	5.1$_0$
C(33)	4909(8)	6223(7)	3627(8)	2.3$_3$	C(33)	4916(11)	6190(11)	3608(12)	2.5$_9$
C(34)	4903(13)	6246(11)	2415(10)	5.2$_5$	C(34)	4913(20)	6252(16)	2421(15)	5.9$_1$
C(35)	6750(11)	3117(9)	2150(11)	4.4$_9$	C(35)	6727(16)	3113(13)	2125(15)	4.4$_0$
C(36)	6919(19)	3231(15)	992(16)	9.5$_2$	C(36)	6939(27)	3181(21)	925(23)	9.3$_3$
Cl(11)	4246(3)	−1108(3)	−352(3)	4.8$_2$	Cl(11)	4235(4)	−1102(4)	−333(4)	4.7$_5$
Cl(12)	2037(4)	−3334(3)	2336(4)	6.5$_2$	Cl(12)	2026(5)	−3314(4)	2348(5)	6.3$_4$
Cl(13)	578(4)	5105(3)	1969(4)	7.1$_9$	Cl(13)	589(5)	5085(4)	1952(5)	6.7$_1$
Cl(21)	2093(4)	2854(4)	−357(3)	7.3$_6$	Cl(21)	2097(5)	2842(5)	−384(4)	7.3$_3$
Cl(22)	343(8)	2311(11)	6198(7)	22.2	Cl(22)	405(9)	2386(12)	6193(8)	17.7
Cl(23)	6837(3)	−951(2)	2454(3)	5.5$_5$	Cl(23)	6806(4)	−946(3)	2456(4)	5.3$_2$
Cl(31)	1413(5)	5522(5)	5955(5)	11.8	Cl(31)	1460(7)	5500(7)	5963(7)	12.0
Cl(32)	5316(9)	7182(6)	2048(4)	18.7	Cl(32)	5368(13)	7182(8)	2102(6)	19.6
Cl(33)	6546(9)	4320(5)	465(6)	17.1	Cl(33)	6556(13)	4322(7)	458(8)	17.8
O(W1)	−1172(6)	874(7)	1658(7)	4.1$_6$	O(W1)	−1153(9)	891(9)	1649(9)	4.0$_0$
O(W2)	3594(6)	−116(6)	4062(7)	3.8$_0$	O(W2)	3618(9)	−102(8)	4008(9)	3.6$_6$
O(W3)	2364(8)	8803(7)	4301(7)	4.9$_7$	O(W3)	2390(11)	8798(10)	4322(10)	4.9$_4$
O(W4)	6809(5)	3200(5)	4674(6)	2.7$_8$	O(W4)	6760(8)	3237(7)	4667(8)	2.6$_8$
O(W5)	4082(7)	1529(6)	5382(6)	3.5$_5$	O(W5)	4075(9)	1522(8)	5344(8)	3.3$_9$

Table 3. Continued.

3.3 Ytterbium Complex

Atom	x	y	z	B_{eq}/Å^2 a)	Atom	x	y	z	B_{eq}/Å^2 a)
Yb(1)	568.8(3)	702.3(3)	1398.7(4)	1.6_6	C(21)	3362(8)	3135(8)	1595(10)	2.4_3
Yb(2)	3047.3(3)	1636.5(3)	3385.3(4)	1.6_9	C(22)	2921(12)	3486(10)	405(11)	3.9_8
Yb(3)	4862.6(4)	3714.8(3)	3828.7(4)	1.8_5	C(23)	929(8)	1469(8)	4141(10)	2.5_8
O(11)	2010(6)	−108(7)	307(6)	3.1_6	C(24)	144(13)	1663(15)	4981(13)	5.8_3
O(12)	2438(5)	689(5)	1879(6)	2.2_5	C(25)	5629(8)	1043(7)	3315(8)	1.9_1
O(13)	1318(7)	−1020(5)	2096(7)	2.9_4	C(26)	6764(9)	277(8)	3138(10)	2.7_9
O(14)	271(6)	−930(5)	451(6)	2.3_7	C(31)	2669(8)	4170(8)	4433(9)	2.0_8
O(15)	143(7)	2421(6)	1282(7)	3.0_3	C(32)	1614(11)	4498(12)	4912(13)	4.9_9
O(16)	1341(6)	2877(5)	2599(7)	2.5_7	C(33)	4928(7)	6182(7)	3653(8)	1.6_7
O(21)	3333(7)	2295(6)	1866(6)	2.8_9	C(34)	4920(13)	6248(10)	2428(11)	4.4_4
O(22)	3740(7)	3739(6)	2215(7)	3.4_2	C(35)	6743(11)	3102(9)	2116(11)	3.7_2
O(23)	660(7)	1071(6)	3207(7)	3.4_0	C(36)	6948(20)	3201(15)	942(16)	8.6_1
O(24)	1793(6)	1660(7)	4440(6)	3.0_0	Cl(11)	4236(3)	−1111(3)	−328(3)	4.2_3
O(25)	4854(6)	706(6)	3211(7)	2.8_5	Cl(12)	2032(3)	−3310(3)	2349(4)	5.5_5
O(26)	5561(6)	1966(6)	3587(7)	2.9_2	Cl(13)	591(4)	5078(3)	1938(4)	5.8_0
O(31)	3105(6)	3217(5)	4090(6)	2.6_3	Cl(21)	2094(4)	2843(4)	−393(3)	6.5_8
O(32)	3148(6)	4795(5)	4420(6)	2.5_2	Cl(22)	415(6)	2419(8)	6189(5)	14.0
O(33)	4781(6)	5401(6)	3898(7)	2.9_9	Cl(23)	6801(3)	−942(2)	2459(3)	4.6_2
O(34)	5058(6)	6865(6)	4370(6)	2.5_3	Cl(31)	1476(5)	5482(5)	5965(5)	10.6
O(35)	5827(7)	3664(7)	2383(7)	3.9_4	Cl(32)	5403(9)	7186(6)	2127(5)	17.3
O(36)	7521(7)	2468(7)	2723(8)	4.0_7	Cl(33)	6575(9)	4326(5)	454(6)	16.0
C(11)	2703(8)	154(8)	964(9)	2.1_0	O(W1)	−1140(6)	874(7)	1651(7)	3.2_0
C(12)	3855(10)	−120(10)	751(11)	3.8_2	O(W2)	3630(6)	−112(6)	3988(7)	3.2_5
C(13)	870(9)	−1460(8)	1304(9)	2.4_6	O(W3)	2389(8)	8798(7)	4315(7)	4.0_6
C(14)	980(11)	−2578(8)	1315(11)	3.8_2	O(W4)	6746(6)	3265(5)	4662(6)	2.4_6
C(15)	565(8)	3070(7)	1844(9)	2.2_3	O(W5)	4075(7)	1514(6)	5342(6)	3.0_7
C(16)	−107(11)	4206(8)	1441(12)	3.5_8					

a) The equivalent isotropic temperature factors were computed using the following expression: $B_{eq}=4/3(B_{11}a^2+B_{22}b^2+B_{33}c^2+B_{12}ab\cos\gamma+B_{13}ac\cos\beta+B_{23}bc\cos\alpha)$. The B_{ij}'s are defined by: $T=\exp[-(h^2B_{11}+k^2B_{22}+l^2B_{33}+2hlB_{23}+2hlB_{13}+2hkB_{12})]$.

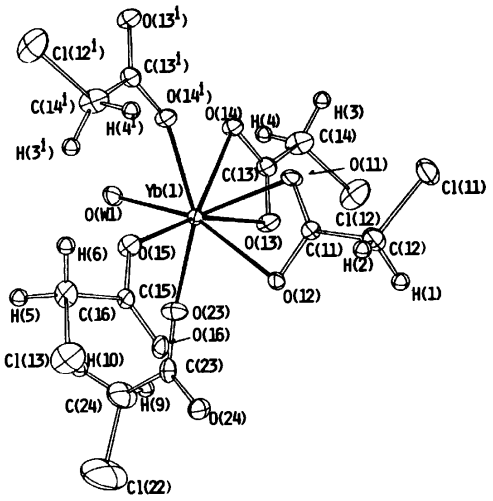

Fig. 1. A perspective drawing of the complex around Yb(1).[15]

Table 3 (3.1—3.3), while selected bond lengths and angles are given in Table 4.[14] Perspective drawings of the ytterbium(III) complex around the metal atoms (Yb(1), Yb(2), and Yb(3)) as well as the numbering scheme of the atoms are shown in Figs. 1—3 and the crystal packing diagram in Fig. 4, respectively.

Schematic presentations of the coordination geometries of the ligating atoms around the Yb(1), Yb(2), and Yb(3) atoms are shown in Fig. 5 (5.1—5.3), respectively.

The structures of these complexes are completely different from those of the light lanthanoid(III) complexes, as mentioned in the following paragraph.

In these complexes, one water oxygen atom is not coordinated to any metal atoms, though all of the water molecules are coordinated in the light lanthanoid(III) salts. The coordination numbers of the metal atoms of the title complexes are smaller than those of the light lanthanoid(III) ones; there are two octa- and one ennea-coordinated metal atoms in the former complexes, while two ennea- and one deca- (or ennea-) coordinated metal atoms in the latter complexes.

The Yb(1) and Yb(2) atoms are octa-coordinated (square-antiprism geometry) while the Yb(3) atom is ennea-coordinated (monocapped square-antiprism geo-

Table 4. Interatomic Distances and Bond Angles of the Complexes, with the Standard Deviations in Parentheses[15]

M	Gd(l/Å)	Er(l/Å)	Yb(l/Å)	M	Gd(ϕ/°)	Er(ϕ/°)	Yb(ϕ/°)
M(1^{I})···M(1)	4.009(2)	4.044(2)	4.023(2)	O(11)-M(1)-O(12)	52.0(3)	53.4(4)	53.7(3)
M(1)···M(2)	4.266(2)	4.240(2)	4.218(3)	O(12)-M(1)-O(15)	84.0(3)	82.9(4)	82.7(3)
M(2)···M(3)	4.339(2)	4.316(2)	4.305(2)	O(15)-M(1)-O(14^{I})	79.3(3)	79.3(4)	79.3(3)
M(3)···M(3^{II})	4.306(2)	4.321(2)	4.325(2)	O(11)-M(1)-O(14^{I})	75.7(3)	74.3(4)	74.6(3)
M(1)-O(11)	2.443(10)	2.383(14)	2.365(9)	O(13)-M(1)-O(14)	52.0(3)	53.0(4)	53.3(3)
M(1)-O(12)	2.487(8)	2.456(10)	2.436(8)	O(14)-M(1)-O(W1)	74.3(3)	74.3(4)	73.9(3)
M(1)-O(13)	2.419(8)	2.365(11)	2.356(8)	O(W1)-M(1)-O(23)	81.6(4)	79.4(5)	79.3(4)
M(1)-O(14)	2.572(8)	2.529(10)	2.516(8)	O(13)-M(1)-O(23)	79.7(4)	79.3(5)	78.9(3)
M(1)-O(15)	2.284(8)	2.215(11)	2.203(8)	O(12)-M(2)-O(16)	77.5(3)	77.0(4)	76.3(3)
M(1)-O(23)	2.246(11)	2.186(15)	2.174(11)	O(16)-M(2)-O(24)	73.7(3)	73.2(4)	73.5(3)
M(1)-O(W1)	2.342(9)	2.283(13)	2.264(9)	O(24)-M(2)-O(W2)	73.6(3)	73.7(5)	73.9(3)
M(1)-O(14^{I})	2.364(9)	2.320(12)	2.301(9)	O(12)-M(2)-O(W2)	75.3(3)	74.6(4)	74.5(3)
M(2)-O(12)	2.401(8)	2.343(11)	2.311(8)	O(21)-M(2)-O(25)	74.8(3)	74.5(4)	74.6(3)
M(2)-O(16)	2.413(7)	2.371(9)	2.349(7)	O(25)-M(2)-O(W5)	75.5(3)	74.6(4)	74.5(3)
M(2)-O(21)	2.346(11)	2.304(15)	2.282(11)	O(W5)-M(2)-O(31)	68.4(3)	68.6(4)	68.4(3)
M(2)-O(24)	2.362(12)	2.285(15)	2.265(11)	O(21)-M(2)-O(31)	77.4(3)	77.1(5)	77.9(3)
M(2)-O(25)	2.371(7)	2.296(10)	2.279(7)	O(22)-M(3)-O(26)	86.6(3)	87.5(4)	87.6(3)
M(2)-O(31)	2.341(7)	2.293(10)	2.246(8)	O(26)-M(3)-O(W4)	77.2(2)	76.6(3)	76.9(3)
M(2)-O(W2)	2.425(9)	2.366(12)	2.361(8)	O(W4)-M(3)-O(33)	87.3(2)	86.6(4)	86.2(3)
M(2)-O(W5)	2.533(9)	2.489(13)	2.488(10)	O(22)-M(3)-O(33)	97.7(3)	98.0(4)	98.6(3)
M(3)-O(22)	2.273(10)	2.235(13)	2.217(10)	O(31)-M(3)-O(32)	48.9(3)	49.1(4)	49.3(3)
M(3)-O(33)	2.350(8)	2.287(11)	2.250(8)	O(22)-M(3)-O(35)	72.7(4)	72.1(5)	72.9(4)
M(3)-O(26)	2.279(7)	2.221(9)	2.206(7)	O(26)-M(3)-O(35)	84.8(3)	83.9(5)	83.8(4)
M(3)-O(31)	2.730(9)	2.721(13)	2.748(10)	O(33)-M(3)-O(35)	77.2(3)	77.8(5)	77.9(4)
M(3)-O(32)	2.463(8)	2.388(11)	2.375(8)	O(W4)-M(3)-O(35)	71.7(3)	73.1(5)	73.5(4)
M(3)-O(33^{II})	2.802(9)	2.853(13)	2.897(10)	O(32)-M(3)-O(34^{II})	76.3(3)	75.3(4)	74.6(3)
M(3)-O(34^{II})	2.472(10)	2.385(14)	2.368(8)	O(33^{II})-M(3)-O(34^{II})	48.1(3)	47.3(4)	47.1(3)
M(3)-O(35)	2.396(12)	2.343(17)	2.329(12)	O(31)-M(3)-O(34^{II})	65.0(3)	65.0(4)	64.6(3)
M(3)-O(W4)	2.471(7)	2.405(10)	2.382(7)	C(35)-O(35)-M(3)	135.6(10)	136.1(15)	135.9(10)
C(11)-O(11)	1.243(15)	1.27(2)	1.232(15)	C(15)-O(15)-M(1)	131.7(7)	133.6(10)	131.7(7)
C(11)-O(12)	1.251(16)	1.24(2)	1.278(16)	C(15)-O(16)-M(2)	147.9(7)	147.3(9)	147.3(7)
C(13)-O(13)	1.275(16)	1.26(2)	1.248(16)	C(23)-O(23)-M(1)	162.0(11)	158.1(14)	157.4(10)
C(13)-O(14)	1.260(15)	1.27(2)	1.281(15)	C(23)-O(24)-M(2)	125.2(10)	130.7(13)	129.2(9)
C(15)-O(15)	1.273(15)	1.30(2)	1.287(15)	C(21)-O(21)-M(2)	138.7(9)	139.3(13)	138.8(9)
C(15)-O(16)	1.228(14)	1.236(19)	1.208(14)	C(21)-O(22)-M(3)	139.0(9)	137.8(12)	139.2(9)
C(21)-O(21)	1.265(17)	1.25(2)	1.243(16)	C(25)-O(25)-M(2)	124.7(7)	127.3(10)	128.7(7)
C(21)-O(22)	1.245(16)	1.25(2)	1.235(16)	C(25)-O(26)-M(3)	165.1(7)	162.1(9)	160.9(7)
C(23)-O(23)	1.259(18)	1.28(2)	1.245(17)	C(11)-O(11)-M(1)	95.0(8)	94.3(10)	95.8(8)
C(23)-O(24)	1.219(16)	1.22(2)	1.252(15)	C(11)-O(12)-M(1)	92.7(7)	91.7(10)	91.2(7)
C(25)-O(25)	1.256(15)	1.27(2)	1.261(15)	M(1)-O(12)-M(2)	121.6(3)	124.1(5)	125.4(3)
C(25)-O(26)	1.256(13)	1.233(18)	1.234(13)	C(13)-O(13)-M(1)	97.3(7)	97.5(10)	97.5(7)
C(31)-O(31)	1.248(12)	1.243(17)	1.257(12)	C(13)-O(14)-M(1^{I})	156.2(8)	155.7(11)	155.7(8)
C(31)-O(32)	1.234(15)	1.24(2)	1.246(15)	M(1)-O(14)-M(1^{I})	112.2(3)	113.0(4)	113.2(3)
C(33)-O(33)	1.236(15)	1.24(2)	1.229(15)	C(31)-O(31)-M(2)	153.4(7)	153.1(10)	153.2(8)
C(33)-O(34)	1.244(14)	1.27(2)	1.235(14)	C(31)-O(32)-M(3)	101.3(7)	103.6(10)	104.7(7)
C(35)-O(35)	1.237(16)	1.23(2)	1.240(16)	M(2)-O(31)-M(3)	117.5(3)	118.5(4)	118.8(3)
C(35)-O(36)	1.216(15)	1.25(2)	1.237(15)	C(31)-O(31)-M(3)	88.1(6)	87.2(9)	86.4(6)
O(36)···O(W4)	2.677(15)	2.68(2)	2.676(15)	C(33)-O(33)-M(3)	155.8(7)	155.8(11)	159.2(8)
O(34)···O(W5^{II})	2.746(13)	2.808(18)	2.820(13)	C(33)-O(33)-M(3^{II})	87.0(7)	86.4(10)	82.3(7)
O(W3)···O(W4^{II})	2.875(12)	2.892(17)	2.922(14)	C(33)-O(34)-M(3^{II})	102.7(7)	108.6(11)	108.1(8)
O(W1)···O(36^{III})	2.602(12)	2.595(17)	2.605(13)	M(3)-O(33)-M(3^{II})	113.1(4)	113.9(5)	113.7(4)
O(W3)···O(13^{IV})	2.765(15)	2.80(2)	2.778(15)				
O(W3)···O(W2^{IV})	2.682(16)	2.71(2)	2.708(16)				
O(W2)···O(W5^{V})	2.965(10)	2.951(14)	2.925(10)				

metry). Table 4 compares the gadolinium(III), erbium(III), and ytterbium(III) complexes with each other. It can be seen that the respective M–O bond lengths, except for M(3)–O(31), and M(3)–O(33^{ii}),[15] decrease in the order of the metal atomic number, due to a decrease in the metal atomic radius.

The observed lengths of the M–O bonds of these complexes are distributed relatively over a wide range; no clear difference between the lengths to the carboxylato oxygen and to the water oxygen atoms could be found. The average M–O bond lengths around M(1) and M(2) atoms are 2.397(2.246–2.572), 2.343(2.186—2.529), and 2.325(2.174—2.516) Å for the gadolinium, erbium, and ytterbium complexes, respectively. These are comparable to the respective sums of Shannon's ionic radii of the metals (Valence(Val)=3+, Coordination number(CN)=8) and oxygen (Val=2−, CN=2); the calculated M–O bond lengths, where M=Gd, Er, and Yb, are 2.40, 2.35, and 2.34 Å in the order.[16]

The average of the nine M–O bond lengths around the M(3) atom is 2.471(2.273—2.802), 2.426(2.221—2.853), and 2.419(2.206—2.897) Å, for the gadolinium, erbium, and ytterbium complexes, respectively. These

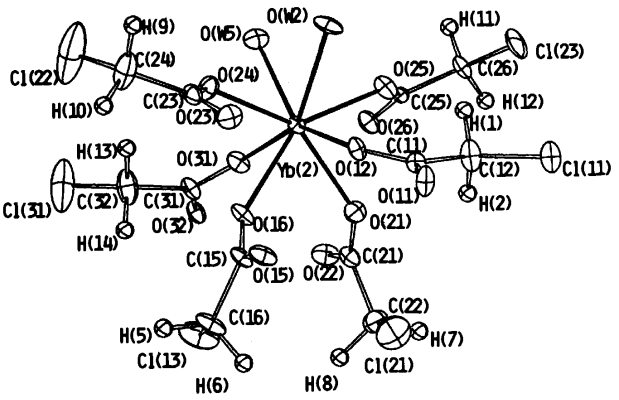

Fig. 2. A perspective drawing of the complex around Yb(2).[15]

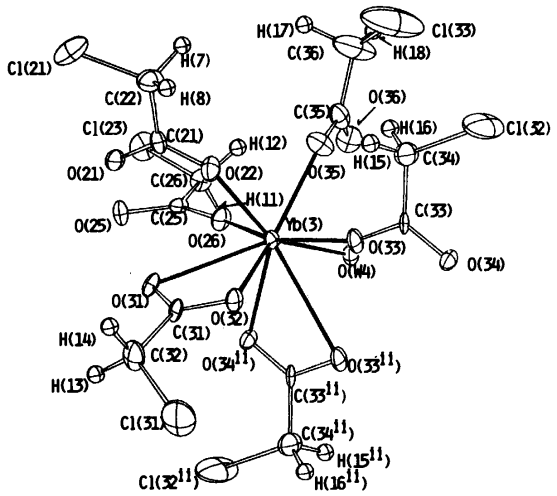

Fig. 3. A perspective drawing of the complex around Yb(3).[15]

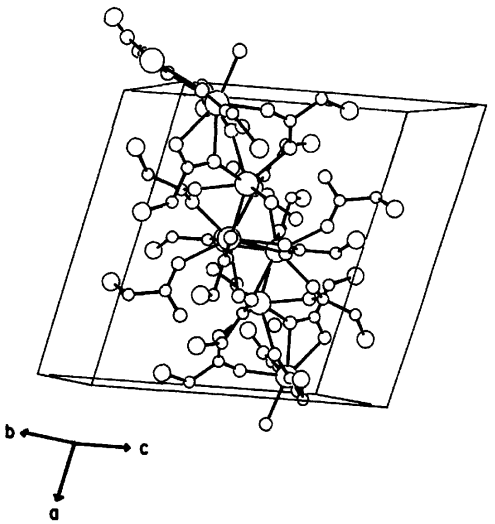

Fig. 4. Crystal packing diagram of the complex.

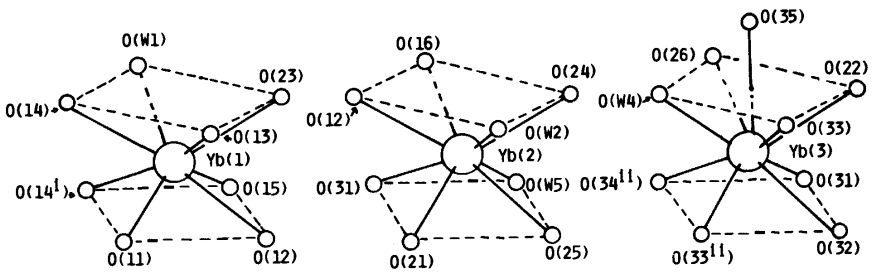

(5.1) (5.2) (5.3)

Fig. 5. Schematic presentation of the complex with the numbering scheme of the ligated oxygen atoms: 5.1, 5.2, and 5.3 show the coordination geometries around Yb(1), Yb(2), and Yb(3) atoms, respectively.[15]

are slightly longer than the respective sums of the ionic radii of metal(Val=3+, CN=9) and oxygen; the calculated M–O bond lengths, where M=Gd, Er, and Yb, are 2.46, 2.41, and 2.39 Å.[16] Except for the two long bonds, M(3)–O(31) and M(3)–O(33^{ii}), the average lengths of the other seven M–O bonds around the M(3) atom are 2.394, 2.337, and 2.318 Å, respectively, for the three complexes. These are much longer than the respective sums of the ionic radii of the metal (Val=3+, CN=7) and oxygen; 2.35, 2.295, and 2.275 Å for M=Gd, Er, and Yb. Consequently, around the M(3) atom, it is better to adopt the ennea-coordination geometry.

In the series of lanthanoid(III) elements, its ionic radius decreases depending on the increase of their atomic number due to the lanthanoid contraction effect. Therefore, the coordination area to be occupied by the ligating atoms around each metal atom decreases depending on the increase of the atomic number, too. In such case, the weakly ligating atoms, such as O(31) and O(33^{ii}), are kept further away than the other coordinating atoms, while the other M–O lengths decrease.[2]

All the carboxylate ions in the complex are coordinated to the metal atoms, and their coordination geometries are classified into three types (as follows). The chelating-type ions, found in the light lanthanoid(III) salts, were not found in the heavy lanthanoid(III) complexes, while the unidentate-type ions were not found in the former.

(**A**) Unidentate type: The ion **35**,[17] is type one. The O(35) atom is ligated to the M(3) atom, while the O(36) atom is not coordinated to any metal atom; but it is hydrogen-bonded with a water oxygen atom, O(W4), which is ligated to the M(3) atom. The bond lengths O(35)–C(35) and O(36)–C(35) are not very different from each other, and the C=O double bond of the carboxyl group is probably not very localized.

(**B**) *Z,Z*-Type bidentate bridging type: Ions **15**, **21**, **23**, and **25** are members.[17] Although the MOC angles of this type ion in the standard form should be in the range 140—150°, some of the determined angles of the title complexes are out of the range, and the differences between both the M–O bond lengths of the same ligands are relatively large: in the ytterbium(III) complex, for example, they are in the range 0.065—0.146 Å. Therefore, the deformation of this type ion is thought to be greater than those of the light lanthanoid(III) complexes.

(**C**) Tridentate type:[18] The ideal form of this type ion is that the carboxyl group COO′ makes a chelate ring with a metal atom M. At the same time, one oxygen atom, O′, approaches another metal atom, M′. Ions **11**, **13**, **31**, and **33**,[17] are members (where the more deformed one is written the later). In the most deformed ones, **31** and **33**,[17] the M–O′ bond lengths are much longer than M–O or M′–O′ bond lengths of the complex. However, as shown in Table 4, their MOC angles are in the range 101—109°, while the angles MO′C are in the range 82—89°. Therefore, their deformations are not the range-out ones of this type ion. The change of the coordination type, found in an europium(III) complex in the series of light lanthanoid(III) complexes,[2] could not be found.

Respective types and numbers of the bridges between the metal atoms are schematically shown in Fig. 6, and the intermetallic distances are shown in Table 4. As shown in the Figure, the pairs of metal atoms, M(1^{i})···M(1) and M(3)···M(3^{ii}) are bridged by two tridentate type ions, while M(1)···M(2) and M(2)···M(3) by one tridentate type and two *Z,Z*-type bidentate bridging type ions, respectively. No clear relation was found between the numbers as well as the types of the bridging ions and the intermetallic distances.

The metal atoms are lined in a linear polymeric chain of Yb(1^{i})···Yb(1)···Yb(2)···Yb(3)···Yb(3^{ii})···, which spans approximately along [111] axis. Thus, in the heavy lanthanoid(III) complexes, all the polymeric chains are parallel, though in the light lanthanoid-(III) salts, two kinds of the lines along [110] and [−110] are alternately placed. As shown in Table 4, there are some hydrogen bondings through a coordinated water oxygen and O(36) as well as

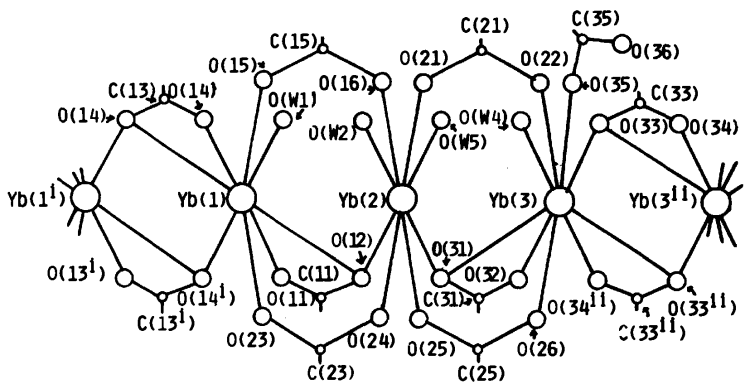

Fig. 6. Schematic presentation of the bridgings between the metal atoms.[15]

O(W3) atoms to the side-by-side chains; however, no carboxylato bridgings between them were found.

This kind of the complicated bridging is also found in various other lanthanoid(III) carboxylates.[2,19]

The general feature of the infrared spectra of the gadolinium, dysprosium, erbium, and ytterbium chloroacetates are about the same, although it is different from those of the light lanthanoid(III) chloroacetates.[2] As the ν_{as}(COO) band, two strong peaks appeared at 1570 and 1620 cm^{-1}, with smaller peaks at 1620—1630 and at 1650—1660 cm^{-1}. As the ν_s(COO) band, two strong peaks appeared at 1398 and 1440 cm^{-1}, with two shoulders at both sides of the main peaks. The maximum wavenumbers of these peaks of the four complexes are not very different from each other.

The authors wish to thank the Shin-Etsu Chemical Ind. Co., Ltd., for presenting us with the highly pure lanthanoid oxides.

References

1) R. C. Mehrotra and R. Bohra, "Metal Carboxylates," Acad. Press, London, U. K. (1983), p. 757, and the references cited in it.

2) T. Imai, M. Shimoi, and A. Ouchi, *Bull. Chem. Soc. Jpn.*, **60**, 159 (1987).

3) G. G. Sadikov, G. A. Kukina, and M. A. Porai-Koshits, *Zh. Strukt. Khim.*, **8**, 551 (1967).

4) W. Bats, R. Kalus, and H. Fuess, *Acta Crystallogr., Sect. B*, **35**, 1225 (1977).

5) A. A. Pinkerton and D. Schwarzenbach, *J. Chem. Soc., Dalton Trans.*, **1976**, 2466.

6) K. Nagai, R. Nakamura, M. Shimoi, and A. Ouchi, *Bull. Chem. Soc. Jpn.*, **57**, 2725 (1984).

7) R. Nakamura, K. Nagai, M. Shimoi, and A. Ouchi, *Bull. Chem. Soc. Jpn.*, **57**, 2919 (1984).

8) L. M. Vdovina and O. V. Dubinina, *Zh. Neorg. Khim.*, **28**, 76 (1983); E. R. Birnbaum, "Gmelin's Handbook of Inorganic Chemistry," 8th ed, System No. 39, Part D5 (1984), p. 65.

9) Y. Ohki, M. Nakamura, Y. Suzuki, K. Nagai, M. Shimoi, and A. Ouchi, *Bull. Chem. Soc. Jpn.*, **58**, 1593 (1985).

10) T. Imai, M. Shimoi, and A. Ouchi, *Bull. Chem. Soc. Jpn.*, **59**, 669 (1986).

11) T. Imai, M. Nakamura, K. Nagai, Y. Ohki, Y. Suzuki, M. Shimoi, and A. Ouchi, *Bull. Chem. Soc Jpn.*, **59**, 2115 (1986).

12) "Universal Crystallographic Computation Program System (UNICS)," ed by T. Sakurai, Crystallographic Society of Japan, Tokyo (1967).

13) "International Tables for X-Ray Crystallography," Kynoch Press, Birmingham (1974), Vol. IV, pp. 72, 150.

14) Some additional data of bond lengths, the final thermal parameters, and the final F_o—F_c tables are deposited as Document No. 8708 at the office of the Editor of Bull. Chem. Soc. Jpn.

15) Key to the symmetry operations: i, $-x$, $-y$, $-z$; ii $1-x$, $1-y$, $1-z$, iii, $-1+x$, y, z; iv, x, $1+y$, z; v, $1-x$, $-y$, $-z$.

16) R. D. Shannon, *Acta Crystallogr., Sect. A*, **32**, 751 (1976). (r_{Gd}(Val=3+), CN=7, 1.00, CN=8, 1.053, CN=9, 1.107; r_{Er}(Val=3+), CN=7, 0.945, CN=8, 1.004, CN=9, 1.062; r_{Yb}(Val=3+), CN=7, 0.925, CN=8, 0.985, CN=9, 1.042; r_O(Val=2−), CN=2, 1.35 Å.

17) Each carboxylate ion is numbered by that of the chlorine atom in it; the ions ***n*1**, ***n*2**, and ***n*3** (where n=1, 2, or 3) include the carboxylato group atoms of C(n1), O(n1), O(n2); C(n3), O(n3), O(n4); and C(n5), O(n5), O(n6), respectively.

18) H. Sawase, Y. Koizumi, Y. Suzuki, M. Shimoi, and A. Ouchi, *Bull. Chem. Soc. Jpn.*, **57**, 2730 (1984).

19) S. Kondo, M. Shimoi, A. Ouchi, and Takeuchi, *Bull. Chem. Soc. Jpn.*, **55**, 2840 (1982).

 © 1987 The Chemical Society of Japan Bull. Chem. Soc. Jpn., 60, 179—183 (1987)

The Syntheses and the X-Ray Crystal Structure of Tetramethylammonium Tetrakis- and Tris(thiocyanato)cadmates(II), $[(CH_3)_4N]_2[Cd(SCN)_4]$ and $[(CH_3)_4N][Cd(SCN)_3]$

Yasumitsu KUNIYASU,† Yasuo SUZUKI,† Masahiro TANIGUCHI,* and Akira OUCHI
Department of Chemistry, College of Arts and Sciences, The University of Tokyo, Komaba, Meguro-ku, Tokyo 153
†Department of Industrial Chemistry, Faculty of Engineering, Meiji University, Higashi-Mita, Tama-ku, Kawasaki, Kanagawa 214
(Received July 31, 1986)

The crystal and molecular structure of the two new thiocyanatocadmate(II) complexes indicated in the title were determined by the single-crystal X-ray-diffraction technique. $[(CH_3)_4N]_2[Cd(SCN)_4]$ (**1**) is triclinic, with a space group of $P\bar{1}$; a=7.300(2), b=13.019(4), c=5.8920(9) Å, α=96.32(2), β=93.080(18), γ=104.63(2)°, and Z=1, while $[(CH_3)_4N][Cd(SCN)_3]$ (**2**) is orthorhombic with a space group of $Pna2_1$; a=10.506(3), b=13.797(5), c=9.4506(18) Å, Z=4. In both complexes, the cadmium atom is in an octahedral geometry. In **1**, the metal atom is at the center of symmetry, and respective pairs of side-by-side metal atoms are bridged by two thiocyanate (SCN) ions, where one SCN ion is *S*-coordinated and the other is *N*-coordinated to the same-side metal atom. Also bonded with two nitrogen atoms of unidentate SCN ions, the metal atom is 4*N*2*S*-hexa-coordinated, and they line up along the c-axis in a polymeric form. In **2**, respective pairs of side-by-side metal atoms are bridged by three SCN ions, two of those SCN ions being *S*-coordinated, and one *N*-coordinated, to the same-side metal atom; each metal atom is 3*S*3*N*-hexa-coordinated, and the chain of the polymeric complex lines up along the a-axis. The tetramethylammonium ions bond with the polymeric complex only by the ionic bonding. The final R values obtained are **1**=0.039 and **2**=0.050.

It was already known that some thiocyanate complexes of cadmium(II) are in the polymeric form. For example, cadmium(II) thiocyanate itself is in a three-dimensional polymeric form, where each cadmium(II) atom is 4*S*2*N*-hexa-coordinated, being in an octachedral geometry.[1] It is also well-known that some Lewis base adducts of cadmium(II) thiocyanate are in the linear polymeric form, where respective pairs of the side-by-side cadmium(II) atoms are bridged by two thiocyanate (SCN) ions[2-5] or by the base molecules.[6] The cesium salt of tris(thiocyanato)cadmate(II) has a three-dimensional polymeric structure, where the two kinds of cadmium(II) atoms are 6*S*- and 6*N*-hexa-coordinated, while its rubidium salt has a two-dimensional polymeric structure, where the two kinds of cadmium(II) atoms are 4*N*2*S*- and 2*N*4*S*-hexa-coordinated.[7] On the other hand, in $K_2[Cd(SCN)_4]\cdot 2H_2O$, the tetrakis(thiocyanato)cadmate(II) ions are discrete; the cadmium atom is 2*N*4*S*-hexa-coordinated although the octahedron around the metal atom is deformed.[8]

From these results, the bridging structure of the thiocyanatocadmate(II) can be expected to depending on the kind of counter cation. As the rubidium and cesium salts have the respective types of polymeric structures, it can also be expected that, if a different kind of counter cation is introduced, some complex with another type of polymeric structure will be obtained. From this expectation, we started the syntheses of some tetraalkylammonium salts of the thiocyanatocadmate(II), and have thus obtained the title complexes; their crystal and molecular structures were determined by the single-crystal X-ray-diffraction technique.

Experimental

Syntheses of Tetramethylammonium Tetrakis(thiocyanato)cadmate(II) (1), and Tetramethylammonium Tris(thiocyanato)cadmate(II) (2). The cadmium(II) thiocyanate (**3**) and tetramethylammonium thiocyanate (**4**) were obtained by metathetical reactions between the respective chlorides and potassium thiocyanate in a methanol medium, as in cases of the other thiocyanates.[9]

To synthesize Complex **1**, the solutions of **3** and **4** in the mol ratio of 1:2 (**3**, 0.57 g, 2.5 mmol in 20 cm³ of acetone; **4**, 0.66 g, 5.0 mmol in 10 cm³ of acetone) were mixed and left standing overnight at the ambient temperature. Crystals of **1** were thus deposited. Yield, 0.68 g; 1.38 mmol, 58%.

To obtain Complex **2**, aqueous solutions of equimol amounts of **3** and **4** (0.57 g (2.5 mmol) and 0.33 g (2.5 mmol), respectively, in 10 cm³ of water) were mixed and left standing overnight in a silica gel desiccator. Crystals of **2** were thus deposited. Yield, 0.37 g; 1.03 mmol, 41%. An additional lot, which was almost of the same purity, was also obtained from the filtrate.

Intensity Data Collection. The crystallographic data of both complexes are listed in Table 1, while some of the experimental conditions used to obtain the intensity data are tabulated in Table 2. The reflections were collected on a Rigaku AFC-6A automated four-circle X-ray diffractometer, with graphite-monochromated Mo $K\alpha$ radiation (the scan speed was 4° min⁻¹ (θ), and the ω—2θ scan-technique was employed).

Structure Determination. Their structures were solved by the heavy-atom method. The positions of the metal and sulfur atoms were deduced from the three-dimensional Patterson map; the other non-hydrogen atoms were located by means of successive Fourier syntheses. Their positional, isotropic, and then anisotropic thermal parameters were refined by means of a block-diagonal least-squares method. Eight hydrogen atoms of **1** were found on the difference

Fourier map, while the other hydrogen atoms were situated at their respective positions assuming C-H=1.08 Å and B_{iso}=6.0. In the final cycle, all the hydrogen atoms were fixed. The positions of any hydrogen atoms of **2** were not determined exactly on the difference Fourier map, and so we gave up adding their parameters to the calculation.

All the calculations were carried out on a HITAC M 680H computer at the Computer Center of the University of Tokyo, using a local version of the UNICS program.[10] The atomic scattering factors were taken from Ref. 11.

Infrared Spectrum Measurements. The infrared spectra of the samples were obtained by means of a JASCO 202A grating infrared spectrophotometer, using Nujol and hexachloro-1,3-butadiene mulls.

Results and Discussion

The final atomic parameters of the non-hydrogen atoms of **1** and **2** are listed in Table 3 as 3.1 and 3.2, while the bond lengths and bond angles of **1** and **2** are tabulated in Table 4 and Table 5 respectively.[12] Perspective drawings of the skeleton of the polymeric chains of Complexes **1** and **2**, together with the numbering scheme of the atoms, are shown in Figs, 1 and 3 respectively. The crystal packing diagrams of **1** and **2** are shown in Figs. 2 and 4.

In **1**, the cadmium(II) atom is at the center of symmetry and is 4*N*2*S*-hexa-coordinated, being in a slightly deformed octahedral geometry. Two nitrogen atoms of unidentate SCN ions, two nitrogen atoms, and two sulfur atoms of the respective bridging SCN ions are coordinated. The Cd-N bond lengths of the unidentate SCN (Cd-N(2)=2.357(3) Å) is longer than that of the bridging SCN (Cd-N(1)=2.269(2) Å), but both of them are shorter than the sum of Shannon's ionic radii, 2.41 Å.[13] This is probably because the assumed valence of the nitrogen atom is not appropriate, for the charge on the SCN ion is much delocalized. The observed Cd-S bond length is 2.742(1) Å (Cd-S(1^i)), about the same as the sum of Shannon's ionic radii, 2.79 Å.[13] These values are not much different from the respective values of Lewis base adducts of the cadmium(II) thiocyanate, which have the same type of doubly bridged SCN ions in their polymeric structures.[2-5] The Cd-N(1)-C(1), Cd-N(2)-C(2), and Cd-S(1^i)-C(1^i) angles are 165.8(2), 158.0(2), and 98.65(8)° respectively, while the average

Table 1. Crystallographic Data of the Complexes

Chemical formulae	$[(CH_3)_4N]_2[Cd(SCN)_4]$	$[(CH_3)_4N][Cd(SCN)_3]$
F.W.	493.02	360.79
Crystal system	triclinic	orthorhombic
Space group	$P\bar{1}$	$Pna2_1$
$a(l/Å)$	7.300(2)	10.506(3)
$b(l/Å)$	13.019(4)	13.797(5)
$c(l/Å)$	5.8920(9)	9.4506(18)
$\alpha(\phi/°)$	96.32(2)	90.0
$\beta(\phi/°)$	93.080(18)	90.0
$\gamma(\phi/°)$	104.63(2)	90.0
$U(v/Å^3)$	536.5(3)	1370.0(7)
$D_m(d/Mg\ m^{-3})$	1.51(3)	1.73(3)
$D_x(d/Mg\ m^{-3})$	1.52	1.75
μ(Mo $K\alpha$) (n/mm^{-1})	1.39	2.00
Z	1	4

Table 2. Some Experimental Conditions Used to Obtain the Reflection Intensities

Chemical formulae	$[(CH_3)_4N]_2[Cd(SCN)_4]$	$[(CH_3)_4N][Cd(SCN)_3]$
Number of reflections Measured	5104	2850
Reflections used for the calculation[a]	4258	1551
Measured range $(2\theta/°)$	3—72	3—65
R[b]	0.039	0.050
R_{weight}[b]	0.042	0.058
Size of the crystal (v/mm^3)	0.30×0.20×0.25	0.30×0.25×0.27
Scan width $(\theta/°)$	1.02+0.5 tan θ	1.11+0.5 tan θ
S[c]	1.38	1.88

a) Reflections with $|F_o|>3\sigma(|F_o|)$ were used. b) $R=\Sigma||F_o|-|F_c||/\Sigma|F_o|$; $R_{weight}=[\Sigma(|F_o|-|F_c|)^2/\Sigma wF_o^2]^{1/2}$, where $w=1/[\{\Sigma(|F_o|)\}^2+(F_{weight}\times F_o)^2]$, $F_{weight}=0.015$. c) $S=[\Sigma w(|F_o|-|F_c|)^2/(N_o-N_p)]^{1/2}$, where N_o=number of reflections and N_p=number of parameters.

of the S-C-N angle of the SCN ions is 178.6°. Both of the Cd-N-C angles can be said to be almost in the normal range, because in other thiocyante complexes, the M-N-C (SCN) bond angles have been shown to be 160—180°.[14]

The respective pairs of the neighboring cadmium(II) atoms are bridged by two SCN ions; one of them is *S*-coordinated, and the other is *N*-coordinated, to the same-side metal atom, thus forming a polymeric linear chain structure along the [001] axis. Thus, it has been shown that the tetrakis(thiocyanato)cadmate ion in its tetramethylammonium salt takes a linear

Table 3. Final Non-Hydrogen Atomic Coordinates ($\times 10^4$) of $[(CH_3)_4N]_2[Cd(SCN)_4]$ (3.1) and $[(CH_3)_4N][Cd(SCN)_3]$ (3.2) Together with Their Equivalent Isotropic Temperature Factors (Estimated Standard Deviations are Shown in Parentheses)

3.1 $[(CH_3)_4N]_2[Cd(SCN)_4]$

Atom	x	y	z	B_{eq}/Å^2 d)
Cd	0.0	0.0	0.0	2.7_4
S (1)	3302(1)	361(1)	7852(1)	3.3_7
S (2)	2092(1)	4011(1)	453(2)	5.2_8
C (1)	2385(3)	220(2)	5208(3)	2.8_6
C (2)	1111(3)	2753(2)	522(4)	3.4_3
N (1)	1798(3)	116(2)	3327(3)	4.6_0
N (2)	404(4)	1867(2)	581(5)	5.1_3
N (3)	6503(3)	3072(2)	4438(3)	3.3_3
C (3)	4902(4)	3214(2)	5804(5)	5.0_1
C (4)	5742(4)	2275(2)	2384(5)	4.7_6
C (5)	7413(5)	4109(9)	3626(7)	6.1_7
C (6)	7865(6)	2698(4)	5839(7)	7.6_3

3.2 $[(CH_3)_4N][Cd(SCN)_3]$

Atom	x	y	z	B_{eq}/Å^2 d)
Cd	734.3(5)	2091.0(5)	0.0	3.5_8
S (1)	2248(2)	471(2)	−9(11)	4.9_1
S (2)	4370(3)	3848(2)	−1978(4)	4.5_9
S (3)	4445(3)	3655(3)	2255(4)	4.6_6
C (1)	3567(7)	1117(6)	68(27)	3.2_2
N (1)	4494(6)	1554(6)	−57(23)	4.2_4
C (2)	3050(10)	3215(8)	−1853(13)	3.8_2
N (2)	2049(8)	2870(7)	−1650(12)	4.4_5
C (3)	3019(10)	3213(8)	1799(13)	3.6_7
N (3)	2116(9)	2839(7)	1668(13)	4.6_9
N (4)	3524(8)	1066(5)	5014(25)	4.4_7
C (5)	2500(16)	1801(12)	4810(30)	8.4_5
C (6)	4567(18)	1398(20)	5885(30)	$13._6$
C (7)	3002(22)	262(14)	5873(30)	$13._3$
C (8)	3904(19)	678(15)	3677(20)	9.3_1

d) The equivalent isotropic temperature factors were computed using the following expression: $B_{eq}=4/3(B_{11}a^2+B_{22}b^2+B_{33}c^2+B_{12}ab\cos\gamma+B_{13}ac\cos\beta+B_{23}bc\cos\alpha)$ for (3.1), and $B_{eq}=4/3(B_{11}a^2+B_{22}b^2+B_{33}c^2)$ for (3.2). The B_{ij}'s are defined by: $T=\exp[-(h^2B_{11}+k^2B_{22}+l^2B_{33}+2klB_{23}+2hkB_{12}+2hlB_{13})]$.

Table 4. Bond Lengths and Bond Angles of $[(CH_3)_4N]_2[Cd(SCN)_4]$

Bond Length	(l/Å)	Bond Length	(l/Å)
Cd-N (1)	2.269(2)	Cd-N (2)	2.357(3)
Cd-S (1^i)	2.742(1)	S (1)-C (1)	1.634(2)
C (1)-N (1)	1.148(3)	S (2)-C (2)	1.619(2)
C (2)-N (2)	1.144(3)	N (3)-C (3)	1.492(4)
N (3)-C (4)	1.487(3)	N (3)-C (5)	1.488(4)
N (3)-C (6)	1.467(5)		
Bond Angle	**(ϕ/°)**	**Bond Angle**	**(ϕ/°)**
N(1)-Cd-N(2)	89.76(8)	N(2)-Cd-S(1^i)	91.79(6)
N(1)-Cd-(S^i)	92.40(6)	Cd-N(1)-C(1)	165.8(2)
Cd-N(2)-C(2)	158.0(2)	Cd-S(1^i)-C(1^i)	98.65(8)
N(1)-C(1)-S(1)	177.7(2)	N(2)-C(2)-S(2)	179.4(2)
C(3)-N(3)-C(4)	109.3(2)	C(3)-N(3)-C(5)	108.8(2)
C(3)-N(3)-C(6)	109.8(3)	C(4)-N(3)-C(5)	107.7(2)
C(4)-N(3)-C(6)	109.7(3)	C(5)-N(3)-C(6)	111.6(3)

Key to the symmetry operation: i, $-x$, $-y$, $1-z$.

Table 5. Bond Lengths and Bond Angles of $[(CH_3)_4N][Cd(SCN)_3]$

Bond Length	(l/Å)	Bond Length	(l/Å)
Cd-S (1)	2.743(3)	Cd-S (2^{ii})	2.689(4)
Cd-S (3^{ii})	2.727(4)	Cd-N (1^{ii})	2.280(7)
Cd-N (2)	2.344(11)	Cd-N (3)	2.378(12)
S (1)-C (1)	1.649(8)	C (1)-N (1)	1.151(11)
S (2)-C (2)	1.643(11)	C (2)-N (2)	1.170(14)
S (3)-C (3)	1.673(11)	C (3)-N (3)	1.087(14)
N (4)-C (5)	1.491(19)	N (4)-C (6)	1.44(3)
N (4)-C (7)	1.48(3)	N (4)-C (8)	1.43(3)
Cd···Cd^i	5.373(3)		
Bond Angle	**(ϕ/°)**	**Bond Angle**	**(ϕ/°)**
S(1)-Cd-S(2^{ii})	85.08(10)	S(1)-Cd-S(3^{ii})	89.02(10)
S(2^{ii})-Cd-S(3^{ii})	95.54(12)	S(1)-Cd-N(3)	90.1(3)
S(1)-Cd-N(2)	91.7(3)	S(2^{ii})-Cd-N(1^{ii})	94.3(2)
S(2^{ii})-Cd-N(2)	94.2(3)	S(3^{ii})-Cd-N(1^{ii})	92.5(2)
S(3^{ii})-Cd-N(3)	87.1(3)	N(1^{ii})-Cd-N(3)	90.5(3)
N(1^{ii})-Cd-N(2)	86.9(3)	N(3)-Cd-N(2)	83.2(4)
S(1)-Cd-N(1^{ii})	178.36(19)	S(2^{ii})-Cd-N(3)	174.5(3)
S(3^{ii})-Cd-N(2)	170.3(3)		
Cd^i-N(1)-C(1)	155.5(7)	Cd-N(2)-C(2)	145.6(10)
Cd-N(3)-C(3)	144.5(11)	Cd-S(1)-C(1)	92.7(3)
Cd^i-S(2)-C(2)	98.3(4)	Cd^i-S(3)-C(3)	96.1(4)
S(1)-C(1)-N(1)	171.5(11)	S(2)-C(2)-N(2)	170.6(11)
S(3)-C(3)-N(3)	169.5(11)	C(5)-N(4)-C(6)	114.0(14)
C(5)-N(4)-C(7)	108.2(14)	C(5)-N(4)-C(8)	110.0(18)
C(6)-N(4)-C(7)	101.9(19)	C(6)-N(4)-C(8)	114.3(15)
C(7)-N(4)-C(8)	107.9(14)		

Key to the symmetry operations: i, $0.5+x$, $0.5-y$, z; ii, $-0.5+x$, $0.5-y$, z.

polymeric chain structure, while its potassium salt has discrete anions, although the latter is in a dihydrate form.[8]

In **2**, the cadmium(II) atom is *3N3S*-hexacoordinated, being in a slightly deformed octahedral geometry, where three nitrogen atoms and, accordingly three sulfur atoms, also- are in the *fac*-configuration; around one metal atom, each sulfur atom is at the *trans*-position of a nitrogen atom. The average Cd-S and Cd-N bond lengths are 2.720 and 2.334 Å respectively. Therefore, the average values are not very different from the respective values of **1** or from the Lewis base adducts of cadmium(II) thiocyanate, although as is shown in Table 5, the respective Cd-N bond lengths as well as Cd-S bond lengths of **2** are a little different from each other. However, all of them are shorter than the respective sums of Shannon's ionic radii; 2.41 and 2.79 Å.[13] The average bond angles of Cd-N-C, Cd-S-C, and S-C-N are 148.5, 95.7, and 170.4° respectively. Although the angles of the latter two are not much different from the corresponding values of **1**, nor from those of the Lewis base adducts of cadmium(II) thiocyanate,[2-5] the Cd-N-C angles of **2**, especially Cd-N(2)-C(2) and Cd-N(3)-C(3), are much smaller than the normal value.[14] This structural deformation is probably caused by the mutual steric interaction of the

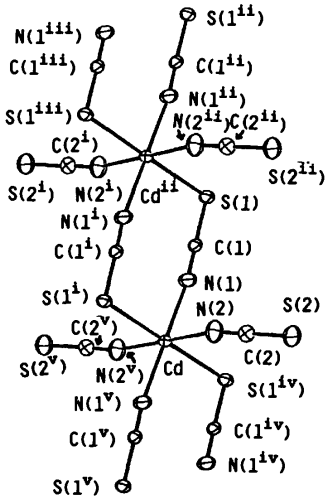

Fig. 1. A perspective drawing of the structure of $[(CH_3)_4N]_2[Cd(SCN)_4]$, with the numbering scheme of the atoms. Key to the symmetry operations: i, $-x$, $-y$, $1-z$; ii, x, y, $1+z$; iii, $-x$, $-y$, $2-z$; iv, x, y, $-1+z$; v, $-x$, $-y$, $-z$.

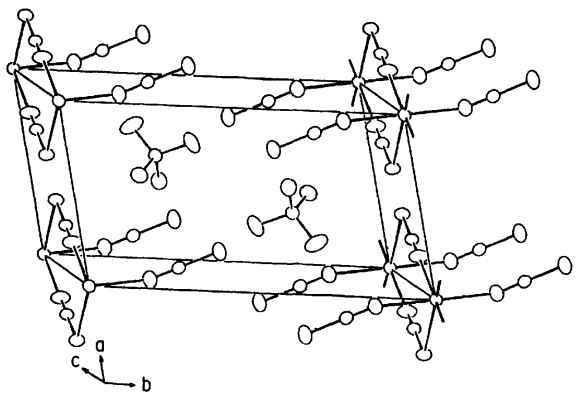

Fig. 2. Crystal packing diagram of $[(CH_3)_4]_2[Cd(SCN)_4]$.

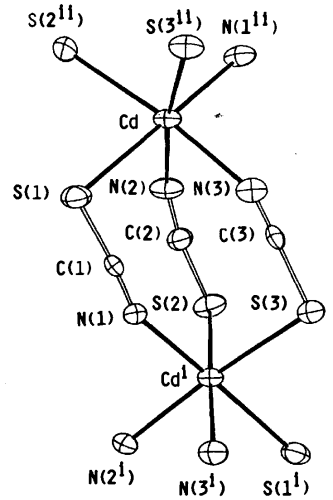

Fig. 3. A perspective drawing of the structure of $[(CH_3)_4N][Cd(SCN)_3]$, with the numbering scheme of the atoms. Key to the symmetry operations: i, $0.5+x$, $0.5-y$, z; ii, $-0.5+x$, $0.5-y$, z.

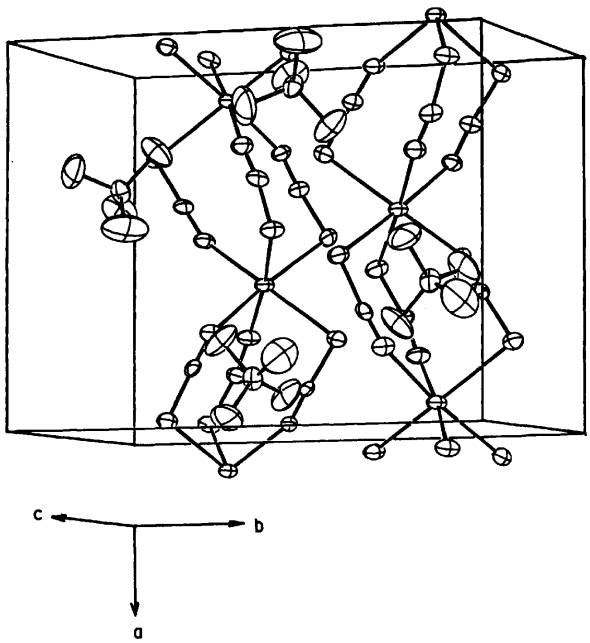

Fig. 4. Crystal packing diagram of $[(CH_3)_4N][Cd(SCN)_3]$.

respective SCN ions in a limited packing space of the crystal, thus forming such a type of triple chain.

The respective pairs of the neighboring cadmium(II) atoms are bridged by three SCN ions, where one of them is *N*-coordinated, and the other two are *S*-coordinated to a one-side metal atom. Thus, in **2**, the side-by-side metal atoms are triply bridged by three SCN ions, thus forming a polymeric linear chain structure along the [100] axis, although in a zig-zag way.

Although many kinds of bridging structures have been found in cadmium(II) thiocyanate complexes, no such triply bridged one has yet been found; this is a new type of polymeric chain of the thiocyanate ions.

The tetramethylammonium ions in **1** and **2** are not bridged, but are isolated from the complex chain; only mutual electrostatic interaction is expected.

In the infrared spectrum of **1**, the ν(CN) and δ(SCN) bands appear as doublets: the maximum wavenumbers are 2070, 2105(s), and 453, 464(m) cm^{-1} respectively, although the ν(CS) band at 768(w) cm^{-1} is found to be a singlet. On the. other hand, in the spectrum of **2**, the ν(CN), δ(SCN), and ν(CS) bands are all singlet; their maximum wave numbers are 2100(s), 460(m), and 758(w) cm^{-1} respectively. These facts may be due to the existence of two kinds of SCN ions in **1**, as has been shown by the structure analysis, while the bond strengths of the three SCN ions in **2** are not very different from each other. The absorption bands of the tetramethylammonium ion are found at 1480(s), 1378(s), and 941(s) cm^{-1}; they are about the same in the spectra of **1** and **2**.

References

1) M. Cannas, G. Carta, A. Cristini, and G. Marongiu, *J. Chem. Soc., Dalton Trans.*, **1976**, 300.

2) L. Cavalca, M. Nardelli, and G. Fava, *Acta Crystallogr.*, **13**, 125 (1960).

3) J. G. Haasnoot, G. C. M. de Keyzer, and G. C. Verschoor, *Acta Crystallogr., Sect. C*, **39**, 1207 (1983).

4) R. G. Goel, W. P. Henry, M. J. Olivier, and A. L. Beauchamp, *Inorg. Chem.*, **20**, 3924 (1981).

5) M. Taniguchi, M. Shimoi, and A. Ouchi, *Bull. Chem. Soc. Jpn.*, **59**, 2299 (1986).

6) L. R. Groeneveld, G. Vos, G. C. Verschoor, and J. Reedijk, *J. Chem. Soc., Chem. Commun.*, **1982**, 620.

7) G. Thiele and D. Messer, *Z. Anorg. Allgem. Chem.*, **464**, 255 (1980).

8) V. V. Sanadze and G. S. Zdanov, *Dokl. Akad. Nauk. SSSR*, **73**, 111 (1950); *Structure Report*, **16**, 303 (1952).

9) P. P. Singh and A. K. Gupta, *Inorg. Chem.*, **17**, 1 (1978).

10) "Universal Crystallographic Computation Program System (UNICS)," ed by T. Sakurai, Crystallographic Society of Japan, Tokyo (1967).

11) "International Tables for X-Ray Crystallography," Kynoch Press, Birmingham (1974), Vol. IV, pp. 72, 150.

12) The positions and isotropic temperature factors of the hydrogen atoms in **1**, the anisotropic thermal parameters of the non-hydrogen atoms of **1** and **2**, and the final F_o—F_c tables of both complexes are deposited as Document No. 8713 at the Office of the Editor of Bull. Chem. Soc. Jpn.

13) R. D. Shannon, *Acta Crystallogr., Sect. A*, **32**, 751 (1976). (r_{Cd}(Valence (Val)=2+, Coordination number (CN)=6), 0.95; r_S (Val=2−, CN=6), 1.84; r_N(Val=3−, CN=4), 1.46 Å).

14) A. F. Wells, "Structural Inorganic Chemistry," 5th ed, Clarendon, Oxford, U. K. (1984), p. 935.

 © 1987 The Chemical Society of Japan Bull. Chem. Soc. Jpn., 60, 185—191 (1987)

Reactions of 3-(2-Methyl-1,3-dioxolan-2-yl)tropolone Methyl Ethers with Hydrazines, Thiourea, Guanidine, and Amidines

Kimiaki IMAFUKU,* Yosuke KIKUCHI,† and Bing-Zhu YIN††
Department of Chemistry, Faculty of Science, Kumamoto University,
Kurokami, Kumamoto 860
(Received May 16, 1986)

3-(2-Methyl-1,3-dioxolan-2-yl)tropolone, prepared from 3-acetyltropolone, was methylated with diazomethane to afford 2-methoxy-3-(2-methyl-1,3-dioxolan-2-yl)tropone (**3a**) and 2-methoxy-7-(2-methyl-1,3-dioxolan-2-yl)tropone (**3b**). The methyl ether **3a** reacted with hydrazine to afford 2-hydrazono-3-(2-methyl-1,3-dioxolan-2-yl)-3,5-cycloheptadien-1-one and 3-methyl-1,8-dihydrocycloheptapyrazol-8-one. The reaction with methylhydrazine afforded 3-(2-methyl-1,3-dioxolan-2-yl)-2-methylhydrazono-3,5-cycloheptadien-1-one and 1,3- and 2,3-dimethyl-dihydrocycloheptapyrazol-8-ones. Another methyl ether **3b** reacted with hydrazine to afford 2-hydrazino-7-(2-methyl-1,3-dioxolan-2-yl)tropone, while the reaction with methylhydrazine gave 2-(2-methyl-1,3-dioxolan-2-yl)-7-(2-methylhydrazino)tropone, 2-(2-methyl-1,3-dioxolan-2-yl)-7-(1-methylhydrazino)tropone, and 1,3-dimethyl-8-methylhydrazono-1,8-dihydrocycloheptapyrazole. On the other hand, the methyl ether **3a** reacted with guanidine, acetamidine, and benzamidine to give 4-(2-methyl-1,3-dioxolan-2-yl)-2-amino-, 2-methyl-, and 2-phenylcycloheptimidazole, respectively. The reaction of the methyl ether **3b** also gave the same products. The reaction of **3b** with thiourea afforded 2-mercapto-4-(2-methyl-1,3-dioxolan-2-yl)cycloheptimidazole but **3a** resulted in the rearrangement to ethyl 2-(2-methyl-1,3-dioxolan-2-yl)benzoate.

We found that 3-acetyltropolone is useful as starting material for the synthesis of heterocycle-fused troponoid compounds, because it has β-diketone structure.[1] On the other hand, the acetyl group not only enhances the reactivity of the tropolone nucleus but also becomes the reaction center for nucleophilic reactions. For example, 3-acetyltropolone and its methyl ether reacted with hydrazines to give 1,8-dihydrocycloheptapyrazol-8-one derivatives.[2-4] We also reported reactions of 3-acetyltropolone methyl ethers, 2-acetyl-7-methoxytropone and 3-acetyl-2-methoxytropone, with guanidine and amidines.[5] In these reactions, we found that the former produced the usual cycloheptimidazole derivatives but the latter produced 9*H*-cyclohepta[*d*]pyrimidine derivatives.

In the present work, 3-acetyltropolone (**1**) reacted with ethylene glycol in the presence of *p*-toluenesulfonic acid to afford 3-(2-methyl-1,3-dioxolan-2-yl)tropolone (**2**), which was methylated with diazomethane to give two isomeric methyl ethers, 2-methoxy-3-(2-methyl-1,3-dioxolan-2-yl)tropone (**3a**) and 2-methoxy-7-(2-methyl-1,3-dioxolan-2-yl)tropone (**3b**). All of the other isomers, 2-methoxy-4-, -5-, and -6-(2-methyl-1,3-dioxolan-2-yl)tropones, have been reported.[6]

Furthermore, we describe reactions of 2-methoxy-3-(2-methyl-1,3-dioxolan-2-yl)tropone and 2-methoxy-7-(2-methyl-1,3-dioxolan-2-yl)tropone (**3a** and **3b**) with hydrazines, urea, thiourea, guanidine, and amidines.

Results and Discussion

Synthesis of 3-(2-Methyl-1,3-dioxolan-2-yl)tropolone (2) and Its Methyl Ethers (3a and 3b). 3-Acetyltropolone (**1**)[2] reacted with ethylene glycol in dry benzene in the presence of *p*-toluenesulfonic acid to give 3-(2-methyl-1,3-dioxolan-2-yl)tropolone (**2**) as colorless prisms. Ketalization was confirmed by spectral data, such as a disappearance of the acetyl carbonyl absorption in the IR spectrum and the appearance of an ethylenedioxy resonance as an A_2B_2 pattern in the ^1H NMR spectrum.

Methylation of **2** with diazomethane gave two isomeric methyl ethers as crystals which were determined to be 2-methoxy-3-(2-methyl-1,3-dioxolan-2-yl)tropone (**3a**) (mp 80—81 °C) and 2-methoxy-7-(2-methyl-1,3-dioxolan-2-yl)tropone (**3b**) (mp 121—122 °C) by their spectral data.

Reactions with Hydrazine. It is well known that reactive troponoids, such as 2-methoxy-, 2-tosyloxy-, and 2-chlorotropones, react with hydrazine to afford 2-hydrazinotropones.[7] Previously, it was reported that 2-methoxy-4-, -5-, and -6-(2-methyl-1,3-dioxolan-2-yl)tropones reacted with hydrazine to afford, respectively, 2-hydrazino-4-, -5-, and -6-(2-methyl-1,3-dioxolan-2-yl)tropones.[6]

A solution of 2-methoxy-3-(2-methyl-1,3-dioxolan-2-yl)tropone (**3a**) and hydrazine hydrate in methanol was refluxed for 1 h to afford 2-hydrazono-3-(2-methyl-1,3-dioxolan-2-yl)-3,5-cycloheptadien-1-one (**4**) and 3-methyl-1,8-dihydrocycloheptapyrazol-8-one (**5**)[2] in 19 and 36% yields, respectively. The former is a tautomer of 2-hydrazino-3-(2-methyl-1,3-dioxolan-2-yl)tropone. Its structure was determined by its spectral data. The ^1H NMR spectrum shows peaks at δ 1.84 (3H, s) for CH_3, 3.01 (2H, d, J=6 Hz) for 7-CH_2, 3.5—4.2 (4H, m) for OCH_2CH_2O, 5.71 (1H, dt, J=9.5 and

† Present address: Fujirebio Inc., Komiya-cho, Hachioji, Tokyo 192.

†† Permanent address: Department of Chemistry, Yanbian University, Yanji, Jilin-sheng, China.

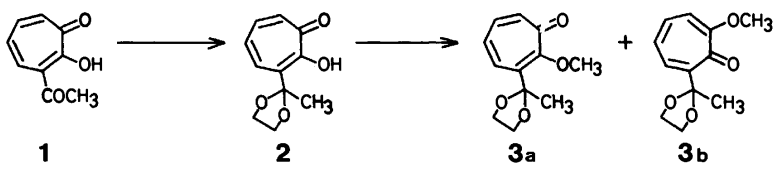

Scheme 1.

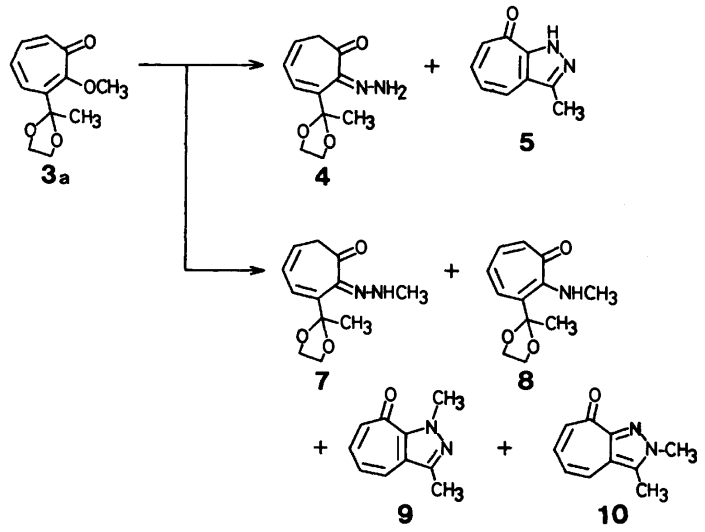

Scheme 2.

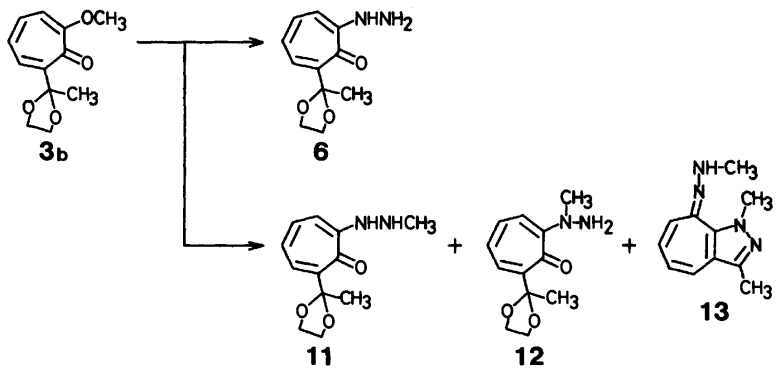

Scheme 3.

6 Hz) for H-6, 6.21 (1H, dd, J=9.5 and 5.5 Hz) for H-5, 6.67 (1H, d, J=5.5 Hz) for H-4, and 10.5 (2H, br) for NH_2. The UV spectrum is different from those of 2-hydrazino-4-, -5-, and -6-(2-methyl-1,3-dioxolan-2-yl)tropones.[6] It is thought that the tropone ring cannot maintain a planar hydrazino-substituted structure by steric hindrance of the vicinal bulky 2-methyl-1,3-dioxolan-2-yl group at the 3-position and, thus, tautomerized to a non-planar hydrazono-substituted structure.

The 2-methyl-1,3-dioxolan-2-yl group in compound **4** was hydrolyzed with 2 M (1 M=1 mol dm^{-3}) hydrochloric acid and did not give 3-acetyl-2-hydrazinotropone but, rather, its cyclized product **5** in 89% yield.

Another methyl ether **3b** in methanol was refluxed for 6 h with hydrazine hydrate to give 2-hydrazino-7-(2-methyl-1,3-dioxolan-2-yl)tropone (**6**) in 74% yield; it was determined by its elemental analysis and spectral data. The UV spectrum is similar to those of its isomers, 2-hydrazino-4-, -5-, and -6-(2-methyl-1,3-dioxolan-2-yl)tropones. Thus, all of the isomers have been obtained except for 2-hydrazino-3-(2-methyl-1,3-dioxolan-2-yl)tropone, which exsists in tautomeric form, 2-hydrazono-3-(2-methyl-1,3-dioxolan-2-yl)-3,5-cycloheptadien-1-one (**4**).

Reactions with Methylhydrazine. A solution of the methyl ether **3a** and methylhydrazine in methanol was refluxed for 8 h to afford 3-(2-methyl-1,3-dioxolan-2-yl)-2-methylhydrazono-3,5-cycloheptadien-1-

one (**7**), 2-methylamino-3-(2-methyl-1,3-dioxolan-2-yl)tropone (**8**), 1,3-dimethyl-1,8-dihydrocycloheptapyrazol-8-one (**9**)[3] and 2,3-dimethyl-2,8-dihydrocycloheptapyrazol-8-one (**10**)[3] in 7, 9, 3, and 13% yields, respectively. Product **7** was isolated as a tautomer of 3-(2-methyl-1,3-dioxolan-2-yl)-2-(2-methylhydrazino)tropone. Its structure was determined by its spectral data. The UV spectrum is similar to that of compound **4**. The ^{1}H NMR spectrum also shows a similar pattern. The methylene protons at the 7-position was observed at δ 2.91 as a doublet peak (J=7 Hz). Compound **7** was heated with 2 M hydrochloric acid on a water bath to afford the cyclized product **10** in 91% yield. Compound **8** was also confirmed spectroscopically. Methyl ether **3a** reacted with methylamine to give the same product **8** in 10% yield.

A mixture of methyl ether **3b** and methylhydrazine in methanol was refluxed for 24 h to afford 2-(2-methyl-1,3-dioxolan-2-yl)-7-(2-methylhydrazino)tropone (**11**), 2-(2-methyl-1,3-dioxolan-2-yl)-7-(1-methylhydrazino)tropone (**12**), and 1,3-dimethyl-8-methylhydrazono-1,8-dihydrocycloheptapyrazole (**13**)[3] in 31, 29, and 8% yields, respectively. Compound **11** was determined by its spectral data. The UV spectrum is similar to that of compound **6**. The structure of the compound **12** was also confirmed by its spectral data. The ^{1}H NMR spectrum shows peaks at δ 1.90 (3H, s) for C-CH_3, 3.32 (3H, s) for N-CH_3, 3.5—4.2 (4H, m) for OCH_2CH_2O, 4.2 (2H, br) for NH_2, 6.2—7.2 (3H, m) for H-4,5,6, and 7.43 (1H, dd, J=9 and 2 Hz) for H-3. Previously, we reported that similar-type compounds could be obtained by the reactions of 2-tosyloxy- and 2-chlorotropones with methylhydrazine.[8]

Reactions with Urea and Thiourea. It is well known that 2-methoxytropones react with guanidine and thiourea to afford cycloheptimidazole derivatives.[9,10] However, reactions with urea do not give cycloheptimidazole, except for the case of 4-(*p*-nitrostyryl)tropolone methyl ethers.[11] Reactions of both methyl ethers of 3-acetyltropolone with urea gave 2-acetylbenzoic acid as a rearrangement product.

A mixture of the methyl ether **3a** and urea in absolute ethanol was refluxed for 1 h in the presence of sodium ethoxide to afford the rearrangement product, ethyl 2-(2-methyl-1,3-dioxolan-2-yl)benzoate (**14**), in 83% yield. Its IR spectrum shows an ester carbonyl absorption at 1720 cm^{-1}. The ethyl group in the ester and the ethylenedioxy group were confirmed by the ^{1}H NMR spectrum.

The reaction of **3b** with urea in the presence of sodium ethoxide gave 3-(2-methyl-1,3-dioxolan-2-yl)tropolone (**2**) as a hydrolysis product and 2-ethoxy-7-(2-methyl-1,3-dioxolan-2-yl)tropone (**15**) as the alkoxy-exchanged product in 45 and 47% yields, respectively. For the latter, the introduction of an ethoxyl group into the 2-position was confirmed by the ^{1}H NMR spectrum. The UV spectrum is very similar to that of the methyl ether **3b**.

The methyl ether **3a** was heated in the presence of sodium ethoxide to give **14** in 82% yield. In a similar manner, **3b** gave **2** and **15** in 22 and 61% yields, respectively. The use of potassium hydroxide instead of sodium ethoxide gave also similar results. Namely, **3a** gave **14** in 72% yield, while **3b** gave **2** and **15** in 21 and 44% yields, respectively. Thus, these results show that urea does not participate in the reactions. This type of rearrangement with alkali or alkoxide is well known.[12,13]

A solution of **3a** and thiourea was refluxed for 2 h in the presence of sodium ethoxide gave a rearrangement product **14** in 80% yield. On the other hand, the

Table 1. Reactions of 3-(2-Methyl-1,3-dioxolan-2-yl)tropolone Methyl Ethers (**3a** and **3b**)

Substrate	Reagent	Base	Reaction time / h	Product/Yield/%			
3a	NH_2NH_2[a]	—	1	**4**(19)	**5**(36)		
3b	NH_2NH_2[a]	—	6	**6**(74)			
3a	CH_3NHNH_2	—	8	**7**(7)	**8**(9)	**9**(3)	**10**(13)
3b	CH_3NHNH_2	—	24	**11**(31)	**12**(29)	**13**(8)	
3a	$(H_2N)_2C=O$	NaOEt	1		**14**(83)		
3b	$(H_2N)_2C=O$	NaOEt	0.5		**15**(47)	**2**(45)	
3a	$(H_2N)_2C=S$	NaOEt	1		**14**(80)		
3b	$(H_2N)_2C=S$	NaOEt	2	**16**(81)			
3a	$(H_2N)_2C=NH$[b]	KOH	2	**17**(5)	**14**(64)		
3a	$(H_2N)_2C=NH$[c]	—	24	**17**(21)	**14**(37)		
3b	$(H_2N)_2C=NH$[b]	KOH	2	**17**(62)	**15**(21)		
3b	$(H_2N)_2C=NH$[c]	—	24	**17**(74)			
3a	$CH_3C(=NH)NH_2$[b]	NaOEt	2	**18**(4)	**14**(78)		
3b	$CH_3C(=NH)NH_2$[b]	NaOEt	3	**18**(30)	**15**(11)		
3a	$PhC(=NH)NH_2$[b]	NaOEt	2	**19**(14)	**14**(45)		
3b	$PhC(=NH)NH_2$[b]	NaOEt	8	**19**(69)	**15**(4)		

a) Hydrate. b) Hydrochloride. c) Carbonate.

reaction of **3b** afforded 2-mercapto-4-(2-methyl-1,3-dioxolan-2-yl)cycloheptimidazole (**16**) as reddish-orange prisms in 81% yield. Its UV spectrum [235 (log ε 4.26), 256 (4.53), 313 (3.88), and 450 nm (4.26)] is very similar to those of isomers, 5-(2-methyl-1,3-dioxolan-2-yl)- [227 (log ε 4.26), 253 (4.55), 310 (3.78), and 440 nm (4.23)] and 6-(2-methyl-1,3-dioxolan-2-yl)-2-mercaptocycloheptimidazole [230 (log ε 4.64), 305 (3.84), 440 nm (4.37)].[14]

Reactions with Guanidine. A mixture of the methyl ether **3a** and guanidine hydrochloride in absolute ethanol was refluxed for 2 h in the presence of potassium hydroxide to give 2-amino-4-(2-methyl-1,3-dioxolan-2-yl)cycloheptimidazole (**17**) as yellow prisms in 5% yield, in addition to the rearrangement product **14** in 64% yield. The UV spectrum of the former is very similar to those of isomeric 2-amino-5- and -6-(2-methyl-1,3-dioxolan-2-yl)cycloheptimidazoles.[14] The ^{1}H NMR spectrum shows peaks at δ 2.07 (3H, s) for CH_3, 3.7—4.3 (4H, m) for OCH_2CH_2O, 7.2—7.8 (2H, m) for H-6 and -7, 7.60 (2H, br) for NH_2, 7.97 (1H, dm, J=9 Hz) for H-5, and 8.30 (1H, dd, J=10 and 2.5 Hz) for H-8. On the other hand, the reaction of **3a** with guanidine carbonate improved the yield of **17** to 21%. The cycloheptimidazole **17** was hydrolyzed to afford 4-acetyl-2-aminocycloheptimidazole (**20**)[5] in 83% yield.

The reaction of **3b** with guanidine hydrochloride gave cycloheptimidazole **17** and the alkoxy-exchanged product **15** in 62 and 21% yields, respectively.

Reactions with Amidines. A mixture of methyl ether **3a** and acetamidine hydrochloride in absolute ethanol was refluxed for 2 h in the presence of sodium ethoxide to afford 2-methyl-4-(2-methyl-1,3-dioxolan-2-yl)cycloheptimidazole (**18**) as yellow prisms and the rearrangement product **14** in 4 and 78% yields, respectively. The ^{1}H NMR spectrum of the former shows two singlet peaks at δ 2.44 for the 2-CH_3 and 2.95 for the acetal CH_3 and three multiplet peaks at δ 3.7—4.4 for the OCH_2CH_2O, 7.75—8.15 for H-6 and -7, and 8.3—8.8 for H-5 and -8 protons. In the UV spectrum, four absorption bands were observed at 228 (log ε 4.42), 260 (4.62), 323 (4.01), and 399 nm (3.14). The reaction of the methyl ether **3b** with acetamidine afforded the same cycloheptimidazole **18** and the alkoxy-exchanged product **15** in 30 and 11% yields, respectively. The cycloheptimidazole **18** was decomposed by heating with dilute hydrochloric acid and

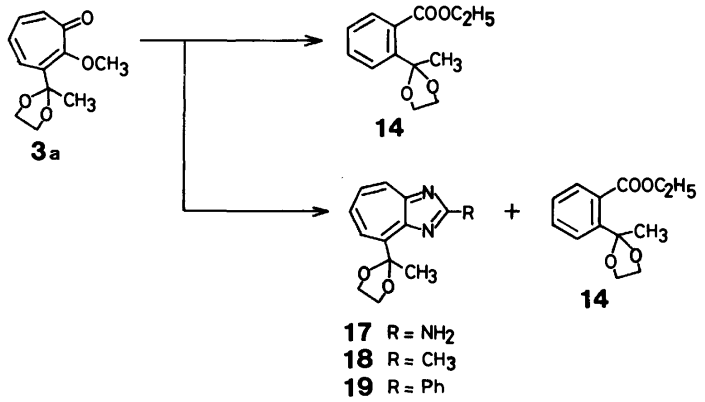

Scheme 4.

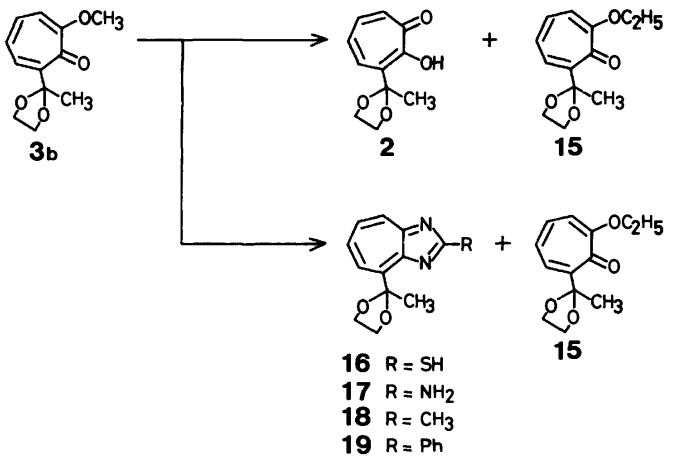

Scheme 5.

did not give the hydrolysis product, 4-acetyl-2-methylcycloheptimidazole.

With benzamidine, the reaction of **3a** gave 4-(2-methyl-1,3-dioxolan-2-yl)-2-phenylcycloheptimidazole (**19**) as yellow needles and the rearrangement product **14** in 14 and 45% yields, respectively. The UV spectrum of the former exhibits the absorption bands at 259 (log ε 4.53), 277 sh (4.46), 356 sh (4.39), 366 (4.40), and 415 nm sh (3.25). Compound **19** was hydrolyzed with dilute hydrochloric acid to afford 4-acetyl-2-phenylcycloheptimidazole (**21**)[5] in 65% yield.

Methyl ether **3b** also reacted with benzamidine to give the cycloheptimidazole **19** and the alkoxy-exchanged product **15** in 69 and 4% yields, respectively.

Experimental

Measurements. The melting points were determined with a Yanagimoto MP-S2 apparatus and are uncorrected. The IR spectra were taken on a JASCO A-102 spectrophotometer, and the UV spectra on a Hitachi EPS-3T spectrophotometer. The ^{1}H NMR spectra were recorded with a Hitachi-Perkin-Elmer R-24 spectrometer (60 MHz). The high-resolution mass spectra were obtained with a JEOL DX-300 apparatus.

3-(2-Methyl-1,3-dioxolan-2-yl)tropolone (2). A mixture of 3-acetyltropolone (**1**) (3.76 g, 20 mmol) and ethylene glycol (40 ml) in dry benzene (120 ml) was refluxed under stirring in the presence of *p*-toluenesulfonic acid (0.4 g). As water produced in the reaction was removed by azeotropic distillation with benzene, dry benzene (1000 ml) was gradually added into the reaction mixture. After refluxing for 10 h, the reaction mixture was diluted with water and extracted with benzene. The benzene extract was washed with water. The evaporation residue from the extract yielded 3-(2-methyl-1,3-dioxolan-2-yl)tropolone (**2**) (3.4 g, 71%) as colorless prisms (from benzene–hexane): Mp 86—87 °C; IR ($CHCl_3$) 1600 cm^{-1} (C=O); UV (CH_3OH) 247 (log ε 4.38), 253 sh (4.30), 310 sh (3.78), 324 (3.88), 362 (3.84), 376 (3.82), 404 nm sh (3.00); ^{1}H NMR ($CDCl_3$) δ=1.85 (3H, s, CH_3), 3.7—4.3 (4H, m, OCH_2CH_2O), 6.8—7.5 (3H, m), 8.00 (1H, dm, *J*=9 Hz, H-7), 9.50 (1H, br, OH). Found: C, 63.61; H, 5.84%. Calcd for $C_{11}H_{12}O_4$: C, 63.45; H, 5.81%.

Methylation of 3-(2-Methyl-1,3-dixolan-2-yl)tropolone (2). To a solution of **2** (5.2 g, 25 mmol) in chloroform (50 ml), an ethereal solution of diazomethane was added dropwise until the resulting mixture gave no colorlation with an iron(III) chloride solution. After removing the solvent, the residue was chromatographed on a Wakogel C-100 column (600 g) using ethyl acetate as an eluant. The evaporation residue from the former fractions was twice rechromatographed on four Wakogel B-10 plates (30×30 cm) with chloroform to give 2-methoxy-3-(2-methyl-1,3-dioxolan-2-yl)tropone (**3a**) (1.9 g, 34%) as pale yellow crystals (from benzene–hexane): Mp 80—81 °C; IR ($CHCl_3$) 1580 cm^{-1} (C=O); UV (CH_3OH) 239 (log ε 4.21), 330 nm (3.82); ^{1}H NMR ($CDCl_3$) δ=1.71 (3H, s, CH_3), 3.75—4.1 (4H, m, OCH_2CH_2O), 3.89 (3H, s, OCH_3), 6.6—7.3 (3H, m), 7.50 (1H, dm, *J*=10 Hz, H-7). Found: C, 64.75; H, 6.53%. Calcd for $C_{12}H_{14}O_4$: C, 64.85; H, 6.53%. The evaporation residue from the latter fractions gave 2-methoxy-7-(2-methyl-1,3-dioxolan-2-yl)tropone (**3b**) (2.9 g, 52%) as colorless prisms (from benzene–hexane): Mp 121—122 °C; IR ($CHCl_3$) 1600 cm^{-1} (C=O); UV (CH_3OH) 243 (log ε 4.18), 308 sh (3.70), 322 (3.74), 345 sh (3.69), 355 nm (3.68); ^{1}H NMR ($CDCl_3$) δ=1.88 (3H, s, CH_3), 3.8—4.1 (4H, m, OCH_2CH_2O), 3.88 (3H, s, OCH_3), 6.4—7.45 (3H, m), 7.75 (1H, d, *J*=10 Hz, H-3). Found: C, 65.05; H, 6.30%. Calcd for $C_{12}H_{14}O_4$: C, 64.85; H, 6.35%.

General Procedure for the Reactions of the Methyl Ethers (3a and 3b) with Hydrazines. A solution of the methyl ether **3a** or **3b** (444 mg, 2 mmol) and the reagent (4 mmol) in methanol (20 ml) was refluxed. After removing the solvent, the residue was triturated with water and extracted with chloroform. The products were separated by chromatography on Wakogel B-10 plates (30×30 cm) with ethyl acetate. These results are summarized in Table 1.

2-Hydrazono-3-(2-methyl-1,3-dioxolan-2-yl)-3,5-cycloheptadien-1-one (4): Yellow crystals (from benzene–hexane); mp 120 °C (decomp); IR ($CHCl_3$) 3440 (NH), 3370 (NH), 1600 cm^{-1} (C=O); UV (CH_3OH) 281 (log ε 3.65), 335 nm (3.72); ^{1}H NMR ($CDCl_3$) δ=1.84 (3H, s, CH_3), 3.01 (2H, d, *J*=6 Hz, 7-CH_2), 3.5—4.2 (4H, m, OCH_2CH_2O), 5.71 (1H, dt, *J*=9.5, 6 Hz, H-6), 6.21 (1H, dd, *J*=9.5, 5.5 Hz, H-5), 6.67 (1H, d, *J*=5.5 Hz, H-4), 10.5 (2H, br, NH_2). Found: *m/z* 222.0971. Calcd for $C_{11}H_{14}N_2O_3$: M, 222.1004.

3-Methyl-1,8-dihydrocycloheptapyrazol-8-one (5): Orange plates; mp 183—184 °C (lit,[2] 183—184 °C).

2-Hydrazino-7-(2-methyl-1,3-dioxolan-2-yl)tropone (6): Orange needles (from benzene–hexane); mp 161 °C (decomp); IR ($CHCl_3$) 3300 (NH), 3240 (NH), 1600 cm^{-1} (C=O); UV (CH_3OH) 232 (log ε 4.39), 343 (4.11), 410 nm (4.09); ^{1}H NMR ($CDCl_3$) δ=1.90 (3H, s, CH_3), 3.5—4.5 (4H, m, OCH_2CH_2O), 6.60 (1H, ddd, *J*=12, 9, 3 Hz, H-4), 7.0—7.4 (2H, m, H-5,6), 7.81 (1H, d, *J*=9 Hz, H-3), 8.8 (1H, br, NH). Found: C, 59.43; H, 6.52; N, 12.41%. Calcd for $C_{11}H_{14}N_2O_3$: C, 59.45; H, 6.35; N, 12.60%.

3-(2-Methyl-1,3-dioxolan-2-yl)-2-methylhydrazono-3,5-cycloheptadien-1-one (7): Yellow oil; IR ($CHCl_3$) 3450 (NH), 1640 cm^{-1} (C=O); UV (CH_3OH) 216 (log ε 4.23), 287 (3.86), 350 nm (4.02); ^{1}H NMR ($CDCl_3$) δ=1.82 (3H, s, *C*-CH_3), 2.91 (2H, d, *J*=7 Hz, 7-CH_2), 3.33 (3H, s, *N*-CH_3), 3.5—4.2 (4H, m, OCH_2CH_2O), 5.69 (1H, dt, *J*=9.5, 6 Hz, H-6), 6.18 (1H, dd, *J*=9.5, 5.5 Hz, H-5), 6.55 (1H, d, *J*=5.5 Hz, H-4), 12.95 (1H, br, NH). Found: *m/z* 236.1071. Calcd for $C_{12}H_{16}N_2O_3$: M, 236.1161.

2-Methylamino-3-(2-methyl-1,3-dioxolan-2-yl)tropone (8): Pale yellow needles (from benzene–hexane); mp 125—126 °C; IR ($CHCl_3$) 3300 (NH), 1600 cm^{-1} (C=O); UV (CH_3OH) 212 (log ε 3.88), 256 (4.37), 342 (4.04), 412 nm (3.96); ^{1}H NMR ($CDCl_3$) δ=1.06 (3H, s, *C*-CH_3), 2.97 (3H, d, *J*=6 Hz, *N*-CH_3), 3.5—4.2 (4H, m, OCH_2CH_2O), 6.3—7.6 (5H, m, H-4,5,6+NH). Found: *m/z* 221.1013. Calcd for $C_{12}H_{15}N_2O_3$: M, 221.1052.

1,3-Dimethyl-1,8-dihydrocycloheptapyrazol-8-one (9): Pale yellow needles; mp 100—101 °C (lit,[3] 96—98 °C).

2,3-Dimethyl-2,8-dihydrocycloheptapyrazol-8-one (10): Pale yellow needles; mp 178—180 °C (lit,[3] 178—179 °C).

2-(2-Methyl-1,3-dioxolan-2-yl)-7-(2-methylhydrazino)tropone (11): Yellow needles (from benzene–hexane); mp 151 °C (decomp); IR ($CHCl_3$) 3260 (NH), 1590 cm^{-1} (C=O); UV (CH_3OH) 247 (log ε 4.13), 344 (4.27), 412 nm (4.05); ^{1}H NMR ($CDCl_3$) δ=1.80 (3H, s, *C*-CH_3), 2.62 (3H, s,

N-CH_3), 3.5—4.2 (4H, m, OCH_2CH_2O), 4.09 (1H, br, NH), 6.55 (1H, ddd, J=12, 9, 3 Hz, H-4), 6.9—7.3 (2H, m, H-5,6), 7.71 (1H, d, J=9 Hz, H-3), 8.6 (1H, br, NH). Found: m/z 236.1063. Calcd for $C_{12}H_{16}N_2O_3$: M, 236.1161.

2-(2-Methyl-1,3-dioxolan-2-yl)-7-(1-methylhydrazino)tropone (12): Yellow plates (from benzene-hexane); mp 149 °C (decomp); IR ($CHCl_3$) 3500 (NH), 3300 (NH), 1600 cm^{-1} (C=O); UV (CH_3OH) 216 (log ε 4.13), 260 (4.17), 355 (4.08), 422 nm (3.86); ^1H NMR ($CDCl_3$) δ=1.90 (3H, s, *C*-CH_3), 3.22 (3H, s, *N*-CH_3), 3.5—4.2 (4H, m, OCH_2CH_2O), 4.2 (2H, br, NH_2), 6.2—7.2 (3H, m, H-4,5,6), 7.43 (1H, dd, J=9, 2 Hz, H-3). Found: m/z 236.1058. Calcd for $C_{12}H_{16}N_2O_3$: M, 236.1161.

1,3-Dimethyl-8-methylhydrazono-1,8-dihydrocycloheptapyrazole (13): Reddish orange needles; mp 113—114 °C (lit,[3] 112—113 °C).

Hydrolysis of the Hydrazone (4) with Hydrochloric Acid. The hydrazone **4** (111 mg, 0.5 mmol) in 2 M hydrochloric acid (5 ml) was heated for 1 h on a water bath. The mixture was diluted with water and extracted with chloroform. The extract was washed with water and dried over sodium sulfate. The evaporation of the solvent gave the cycloheptapyrazol-8-one **5** (71 mg, 89%).

Hydrolysis of the Hydrazone (6) with Hydrochloric Acid. The hydrazone **6** (118 mg, 0.5 mmol) in 2 M hydrochloric acid (5 ml) was heated for 1 h on a water bath. The mixture was worked up, as mentioned above, to give the cycloheptapyrazol-8-one **10** (80 mg, 92%).

Reaction of the Methyl Ether (3a) with Methylamine. A mixture of **3a** (122 mg, 0.5 mmol) and 40% methylamine solution (2 ml) in methanol (5 ml) was allowed to stand for 4 d at room temperature. After removing the solvent, the residue was dissolved in chloroform, washed with water, and dried over sodium sulfate. The evaporation residue from the chloroform solution was chromatographed on a Wakogel B-10 plate (30×30 cm) with ethyl acetate to afford the methylaminotropone **8** (12 mg, 10%).

General Procedure for the Reactions of the Methyl Ethers (3a and 3b) with Urea, Thiourea, Guanidine, and Amidines. A solution of the methyl ether **3a** or **3b** (222 mg, 1 mmol) in absolute ethanol (5 ml) was added a solution of the reagent (2 mmol) and the base (2 mmol) (indicated in Table 1) in absolute ethanol (5 ml). After removing the solvent, the residue was triturated with water, made slightly acidic with 10% acetic acid, and extracted with chloroform. The products were separated by chromatography on Wakogel B-10 plates (30×30 cm) with chloroform or ethyl acetate. These results are summarized in Table 1.

Ethyl 2-(2-Methyl-1,3-dioxolan-2-yl)benzoate (14): Colorless prisms (from cyclohexane); mp 49—50 °C; IR ($CHCl_3$) 1720 cm^{-1} (C=O); ^1H NMR ($CDCl_3$) δ=1.36 (3H, t, J=7 Hz, $CH_2C\underline{H}_3$), 1.78 (3H, s, CH_3), 3.4—4.2 (4H, m, OCH_2CH_2O), 4.30 (2H, q, J=7 Hz, $C\underline{H}_2CH_3$), 7.2—7.7 (4H, m). Found: C, 66.02; H, 6.83%. Calcd for $C_{13}H_{16}O_4$: C, 66.08; H, 6.65%.

2-Ethoxy-7-(2-methyl-1,3-dioxolan-2-yl)tropone (15): Colorless prisms (from benzene-hexane); mp 108—109 °C; IR ($CHCl_3$) 1620 cm^{-1} (C=O); UV (CH_3OH) 244 (log ε 4.23), 323 (3.92), 353 nm (3.86); ^1H NMR ($CDCl_3$) δ=1.50 (3H, t, J=7 Hz, $CH_2C\underline{H}_3$), 1.89 (3H, s, CH_3), 3.6—4.2 (4H, m, OCH_2CH_2O), 4.06 (2H, q, J=7 Hz, $C\underline{H}_2CH_3$), 6.5—7.25 (3H, m), 7.75 (1H, dd, J=7, 2 Hz, H-3). Found: C, 66.20; H, 6.89%. Calcd for $C_{13}H_{16}O_4$: C, 66.08; H, 6.83%.

2-Mercapto-4-(2-methyl-1,3-dioxolan-2-yl)cycloheptimidazole (16): Reddish orange prisms (from benzene-hexane); mp 228—229 °C; UV (CH_3OH) 235 (log ε 4.26), 256 (4.53), 274 sh (4.13), 313 (3.88), 450 nm (4.26); ^1H NMR ($CDCl_3$) δ=1.75 (3H, s, CH_3), 3.7—4.4 (4H, m, OCH_2CH_2O), 7.3—8.2 (4H, m), 10.85 (1H, br, SH). Found: C, 58.32; H, 4.88; N, 10.99%. Calcd for $C_{12}H_{12}N_2O_2S$: C, 58.06; H, 4.84; N, 11.29%.

2-Amino-4-(2-methyl-1,3-dioxolan-2-yl)cycloheptimidazole (17): Yellow prisms (from ethanol); mp 208—209 °C; UV (CH_3OH) 240 sh (log ε 4.29), 263 (4.52), 290 sh (4.01), 360 nm (4.24); ^1H NMR ($CDCl_3$) δ=2.07 (3H, s, CH_3), 3.7—4.3 (4H, m, OCH_2CH_2O), 7.2—7.8 (2H, m, H-6,7), 7.60 (2H, br, NH_2), 7.97 (1H, dm, J=9 Hz, H-5), 8.30 (1H, dd, J=10, 2.5 Hz, H-8). Found: C, 62.05; H, 5.93; N, 18.32%. Calcd for $C_{12}H_{13}N_3O_2$: C, 62.32; H, 5.67; N, 18.23%.

2-Methyl-4-(2-methyl-1,3-dioxolan-2-yl)cycloheptimidazole (18): Yellow prisms (from cyclohexane); mp 119—120 °C; UV (CH_3OH) 228 (log ε 4.42), 260 (4.62), 307 sh (3.93), 323 (4.01), 399 nm (3.14); ^1H NMR ($CDCl_3$) δ=2.14 (3H, s, CH_3), 2.95 (3H, s, 2-CH_3), 3.7—4.4 (4H, m, OCH_2CH_2O), 7.75—8.15 (2H, m, H-6,7), 8.3—8.8 (2H, m, H-5,8). Found: C, 67.78; H, 6.19; N, 12.10%. Calcd for $C_{13}H_{14}N_4O_2$: C, 67.81; H, 6.19; N, 12.17%.

4-(2-Methyl-1,3-dioxolan-2-yl)-2-phenylcycloheptimidazole (19): Yellow needles (from cyclohexane); mp 155—156 °C; UV (CH_3OH) 259 (log ε 4.53), 277 sh (4.46), 356 sh (4.39), 366 (4.40), 415 nm sh (3.25); ^1H NMR ($CDCl_3$) δ=2.28 (3H, s, CH_3), 3.6—4.2 (4H, m, OCH_2CH_2O), 7.2—7.6 (3H, m, H-3′,4′,5′), 7.65—8.0 (2H, m, H-6,7), 8.3—8.5 (1H, m, H-5), 8.55—8.9 (3H, m, H-2′,6′,8). Found: C, 74.05; H, 5.63; N, 9.52%. Calcd for $C_{18}H_{16}N_4O_2$: C, 73.95; H, 5.52; N, 9.58%.

Rearrangement of the Methyl Ether (3a) with Sodium Ethoxide or Potassium Hydroxide. (a) To a sodium ethoxide solution, prepared from sodium (28 mg, 1.2 mmol) and absolute ethanol (6 ml), was added **3a** (113 mg, 0.6 mmol). The mixture was refluxed for 30 min to give **14** (116 mg, 82%).

(b) A mixture of **3a** (266 mg, 1.2 mmol) and potassium hydroxide (67 mg, 1.2 mmol) in absolute ethanol (10 ml) was refluxed for 1 h to give **14** (204 mg, 72%).

Reaction of the Methyl Ether (3b) with Sodium Ethoxide or Potassium Hydroxide. (a) Methyl ether **3b** (222 mg, 1 mmol) in sodium ethoxide solution, prepared from sodium (46 mg, 2 mmol) and absolute ethanol (10 ml), was refluxed for 30 min to give **2** (45 mg, 22%) and **15** (145 mg, 62%).

(b) A mixture of **3b** (222 mg, 1 mmol) and potassium hydroxide (56 mg, 1 mmol) in absolute ethanol (10 ml) was refluxed for 1 h to give **2** (44 mg, 21%) and **15** (105 mg, 44%).

Hydrolysis of the Cycloheptimidazole (17). Compound **17** (231 mg, 1 mmol) in 2 M hydrochloric acid (20 ml) was heated on a water bath for 20 min. The mixture was diluted with water, neutralized with a saturated sodium hydrogencarbonate solution, and extracted with chloroform. The evaporation residue from the extract was chromatographed on a Wakogel B-10 plate (30×30 cm) with ethyl acetate to give 4-acetyl-2-aminocycloheptimidazole (**20**) (155 mg, 83%) as yellow needles (from ethanol): mp 218—219 °C (lit,[5] 213—214 °C).

Hydrolysis of the Cycloheptimidazole (19): Compound **19** (81 mg, 0.28 m mol) in 1 M hydrochloric acid (4 ml) was heated on a water bath for 20 min. The mixture was worked

up, as mentioned above, to give 4-acetyl-2-phenylcycloheptimidazole (**21**) (43 mg, 65%) as yellow needles (from cyclohexane): mp 148—149 °C (lit,[5] 142—143 °C).

We wish to thank Dr. Hiromichi Matsuura, Wakunaga Pharmaceutical Co., Ltd., for his kind measurements of the high-resolution mass spectra. The present work was partly supported by a Grant-in-Aid for Scientific Research (No. 60540336) from the Ministry of Education, Science and Culture.

References

1) K. Imafuku and Z.-T. Jin, *Yanbian Daxue Xuebao*, **1983**, 35.

2) A. Yamane, M. Nagayoshi, K. Imafuku, and H. Matsumura, *Bull. Chem. Soc. Jpn.*, **52**, 1972 (1979).

3) A. Yamane, K. Imafuku, and H. Matsumura, *Bull. Chem. Soc. Jpn.*, **53**, 1461 (1980).

4) K. Imafuku, A. Yamane, and H. Matsumura, *J. Heterocycl. Chem.*, **17**, 1293 (1980).

5) Z.-T. Jin, K. Imafuku, and H. Matsumura, *J. Chem. Soc., Perkin Trans., 1*, **1982**, 1037.

6) I. Murata, *Bull. Chem. Soc. Jpn.*, **34**, 577 (1961).

7) T. Nozoe, K. Takase, and H. Matsumura, "Dai Yuki Kagaku," ed by M. Kotake, Asakura Shoten, Tokyo (1960), Vol. 13, p. 343.

8) K. Imafuku, K. Kamachi, Y. Matsuda, and H. Matsumura, *Bull. Chem. Soc. Jpn.*, **52**, 2447 (1979).

9) T. Nozoe and K. Kikuchi, "Dai Yuki Kagaku," ed by M. Kotake, Asakura Shoten, Tokyo (1960), Vol. 13, p. 579.

10) F. Pietra, *Chem. Rev.*, **73**, 293 (1973).

11) H. Matsumura and S. Kitahara, presented at the 9th National Meeting of the Chemical Society of Japan, Kyoto, 1956.

12) T. Nozoe, "Non-benzenoid Aromatic Compounds," ed by D. Ginsburg, Interscience, New york (1959), p. 410.

13) T. Nozoe, K. Takase, and H. Matsumura, "Dai Yuki Kagaku," ed by M. Kotake, Asakura Shoten, Tokyo (1960), Vol. 13, p. 186.

14) I. Murata, *Bull. Chem. Soc. Jpn.*, **34**, 580 (1961).

 © 1987 The Chemical Society of Japan Bull. Chem. Soc. Jpn., 60, 193—200 (1987)

Thermal Condensation in Solid State of *N*-Hydroxyalkyl-2-imidazolidinone

Choichiro SHIMASAKI,* Ryosei KANAYAMA, Hiroaki YOSHIDA, and Makoto YUGAMIDANI
Faculty of Engineering, Toyama University, Gofuku, Toyama 930
(Received May 22, 1986)

N-(1-Hydroxyalkyl)-2-imidazolidinones (**1**) were prepared by a reaction of 2-imidazolidinone with form-, acet-, propion-, and butyraldehyde. In all of these reactions, **1** were unstable and moisture-sensitive substances. The pyrolysis reaction of **1** was found to be a thermal decomposition via a condensation reaction stage after a molten state. The condensation stage obeyed 1/2- and the first-order kinetics. The kinetic data regarding the condensation reaction were evaluated by analyses of the dependences of the area of isothermal DSC curves upon the reaction time. It may be concluded that the difference provided by the reaction order and the activation parameters were caused by the number of the hydrogen atoms on the β-carbon atom adjacent to the carbon attacked the hydroxyl group of side chain in **1**. In the decomposition by electron impact of **1** and dimer of **1**, the cleavage of the five-membered ring which corresponded to the molecular-ion peak for 2-imidazolidinone (*m/z* 86) was considered to take place after a successive cleavage of the side chain. On the basis of both kinetic studies and ESR or Mass spectral observations, the dimerization mechanism is fully discussed.

Thermosetting resins are characterized by irreversible chemical and physical changes that take place during a "cure." The resin is polymerized into a substance of a three-dimensional network which is no longer soluble or fusible. Whenever basic studies regarding this resin or its chemical structures and curing reactions are investigated, a determination of the experimental conditions involves many difficulties. Recently, Ishida et al.[1] have a convenient method using computer simulation for the initial polymerization mechanism of the trimer (at most). However, a study regarding the reaction products and the mechanism of the thermal condensation for *N*-(1-hydroxyalkyl)-2-imidazolidinone (**1**) in the solid state has not yet been carried out.

2-Imidazolidinone (**2**) has many advantages over any other substituted ureas. Furthermore, **2** has two active imino groups similar to the amino groups of urea. **2** can not produce compounds which have an intermolecular ether formation such as uron. If **1** are cured at a certain temperature, the curing process must be similar to those of the main-chain formation for the urea resin. The present authors investigated the curing reaction of **1** under no alkaline and acid catalyst conditions by IR, ^{1}H and ^{13}C NMR measurements, as well as mass spectrum, ESR, and DSC measurements. DSC is a useful tool for measuring the thermally induced conformation transition of macromolecules[2] as well as the polymerization process. An application of DSC to the study of polymerization provides available information for a kinetic data, such as a reaction parameter. The present authors have already reported that **2**, 2-imidazolidinethione, and their *N*,*N*′-bis(hydroxymethyl) derivatives are of great value as thermally stable agents.[3] The object of the present work is divided into two parts: (1) The characterization and experimental verification of reactions related to the proposed process. (2) The condensation of the material and reaction mechanism to estimate the overall reaction for the monomer by a thermochemical analysis.

Experimental

Materials. The **2** (paraformaldehyde, ethanol, and methanol) were of reagent grade and were used without further purification. The acet-, propion-, and butyraldehyde were distilled before use.

Preparation of Samples. A preparation of *N*-(1-hydroxymethyl)-2-imidazolidinone (**1a**) (**2** 43 g(0.5 mol) and paraformaldehyde 15 g(0.5 mol)) was suspended in 25 ml of ethanol under a nitrogen atmosphere. The ethanol solution was controlled at pH 12 with a 2M† -NaOH aq soln. as the catalyst. After an elevation of the temperature by the reaction heat, the ethanol solution was cooled below 10 °C with ice. White crude crystals were filtered with suction and washed with cooled acetone in order to remove any solvents and the 2M-NaOH aq soln. A white crystal of **1a** was obtained by recrystallization from chroloform.

A preparation of *N*-(1-hydroxyethyl)-2-imidazolidinone (**1b**), *N*-(1-hydroxypropyl)-2-imidazolidinone (**1c**), and *N*-(1-hydroxybutyl)-2-imidazolidinone (**1d**) (*N*-substituted hydroxyalkyl derivatives such as **1b**, **1c**, and **1d**) were all prepared according to the reported method for monomethylolurea.[4]

Measurements. DSC and TG: A sample was heated at the rate 5 °C min^{-1} in air using a Rigakudenki TG-DSC apparatus.

IR spectrophotometry: An IR spectrum of the sample was recorded on a Nipponbunko IR-810 using the KBr-disc method.

Mass spectrum: A mass spectrum of the sample was taken with an ionization potential of between 20 and 70 eV using a JEOL-JMS-D300.

^{1}H and ^{13}C NMR measurements: **1a** and **1c** were dissolved in a deuterated dimethyl sulfoxide solution, and **1b** and **1d** in a deuterated chloroform solution, respectively. The ^{1}H and ^{13}C NMR spectra of each solution was taken on a JNM-FX-90-FT-NMR instrument.

ESR measurement: The ESR spectrum of the sample was

† 1 M=1 mol dm^{-3}.

taken under 50 and 100 kHz fields (modulation using a JEOL FE 3X spectrometer). The sample tube that fed **1c** was sealed in a vacuum system (10^{-3} mmHg (1 mmHg=133.322 Pa)) using a Hickman vacuum apparatus.

Paper chromatography: A one-dimensional paper chromatographic separation was carried out on the species using a developing solvent of 1-butanol–ethanol–water (4:1:2). The color was developed using a color-producing reagent of sodium pentacyanonitrosylferrate(III) and potassium hexacyanoferrate(III).[5]

Results and Discussion

Syntheses of 1. The physical properties of **1** are summarized in Table 1. As Table 1 shows, the observed values in the elemental analysis are in accord with the calculated values. The R_f values of the samples by paper chromatography increases upon increasing of the length of the alkyl group in the side chain. Similarly, the melting point of the sample rises upon increasing the molecular weight of **1** (except for **1d**). In the IR spectra, these samples do not show any change in the characteristic absorption due to ν_{C-H} at 2950 cm^{-1} increases with an increase in the length of the side chain. The NMR data of these samples indicate that the structure of **1** is in accord with that proposed in Scheme 1. In the mass spectra of these samples, the parent peak can be detected in the spectrum of **1a** at *m/z* 116. In the spectra of other samples, however, the parent peak can not be detected. The peak of $(M-H_2O)^+$ can be detected at a high intensity similar to that of the mass spectra of tertiary alcohol. The analytical and spectroscopic data regarding the structure of **1** are consistent with that proposed in Scheme 1.

Thermal Analysis. Figure 1 shows a DSC–TG curve for **1c**, as determined by a heating rate of 5 °C min^{-1}. The DSC curve exhibited two endother-

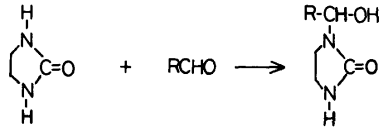

2-imidazolidinone aldehyde *N*-(1-hydroxyalkyl)-2-imidazolidinone

R: -H **1a**
$-CH_3$ **1b**
$-CH_2CH_3$ **1c**
$-(CH_2)_2CH_3$ **1d**

Scheme 1.

Table 1. Physical Properties of **1a**, **1b**, **1c**, and **1d**

		1a	**1b**	**1c**	**1d**
Elemental analysis/%	C	40.93 (41.37) [a]	45.77 (46.14)	50.06 (49.99)	53.17 (53.15)
	H	6.83 (6.94)	7.65 (7.75)	8.48 (8.39)	8.95 (8.92)
	N	24.42 (24.12)	21.52 (21.52)	19.48 (19.43)	17.65 (17.71)
Melting point (θ_m/°C)		54.5	62.5	84.5	81.0
IR spectra (cm^{-1})	ν_{NH}	3320	3340	3340	3340
	ν_{CH}	2950	2950	2950	2950
	$\nu_{C=O}$	1680	1690	1690	1690
	ν_{C-O}	1030	1100	1030	1030
R_f value [b]		0.52	0.72	0.77	0.80
Yield/%		71.3	55.1	81.7	60.5
^{1}H NMR position/ppm	In ring				
(Relative intensity:	$-(CH_2)_2-$	3.356 (4H: m)	3.458 (4H: m)	3.265 (4H: m)	3.508 (4H: m)
multiplicity) [c]	-NH	6.199 (1H: s)	5.665 (1H: s)	6.369 (1H: s)	5.780 (1H: s)
	In side chain				
	CH_3-	—	1.340 (3H: t)	0.796 (3H: t)	0.931 (3H: t)
	$(CH_3)CH_2-$	—	—	1.479 (2H: m)	1.478 (2H: m)
	$-CH_2-$	4.531 (2H: d)	—	—	1.478 (2H: m)
	-CH-	—	5.542 (1H: m)	4.964 (1H: m)	5.301 (1H: m)
	-OH	5.636 (1H: d)	4.773 (1H: d)	5.406 (1H: d)	4.812 (1H: d)
^{13}C NMR	In ring				
	$-(CH_2)_2-$	40.000 [d]	38.298, 39.030	40.000 [d]	38.274, 38.932
	-C=O	158.920	162.702	161.556	162.946
	In side chain				
	CH_3-	—	20.014	9.775	13.700
	$(CH_3)CH_2-$	—	—	27.011	18.576
	$-CH_2-$	66.675	—	—	35.738
	-CH-	—	72.452	76.109	75.622

a) Calculated values in parentheses. b) For paper chromatograpy. c) s: Singlet, d: doublet, t: Triplet, m: multiplet. d) Values were overlapped with the signal of DMSO-d_6.

mic peaks and an exothermic peak. The first endothermic peak is attributed to the melting point. The second endothermic peak is due to the formation of a dimer; this is confirmed by the IR, mass, and NMR spectra of samples obtained before and after the second endothermic peak (described later). The final DSC peak is found over a wide temperature range, in which the sample decomposed with the evolution of gases. The TG curve shows that the pyrolysis process for a sample takes place in two stages. In Fig. 1, the first plateau of the TG curve is probably due to a condensation of the sample to a dimer compound. The other plateau corresponds to a thermal degradation and a decomposition reaction. The kinetic consideration is carried out by this condensation. First, the present authors discuss the kinetic analysis using for an example McGhie method.[6] The DSC measurements are carried out by the method in which the sample was hermetically sealed in an aluminum pan and in a DSC cell using an isothermal mode. Condensation was studied in the temperature range of 90—150 °C. Figure 2 shows typical isothermal condensation curves for **1c**. After an induction period, during which condensation occurred at a slow rate, there was a rapid increase in the endothermic heat of the condensation region (apparently obeying 1/2- and first-order kinetics). By calling the representative total area under a given isothermal curve a, and the fractional area up to the time t, x, the 1/2- and the first-order kinetics plots of $2\times[a^{1/2}-(a-x)^{1/2}]$ and $\ln[a/(a-x)]$ vs. $t-t_0$ for each curve are linear. Figures 3 and 4 show these plots for the isothermal condensation of four samples at any temperature. The data was normalized with respect to time by plotting the time after the induction period t_0. Thus, each isothermal curve yielded two important quantities, t_0 and k. The 1/2- and the first- order rate constant was obtained from the slope of the curve in Figs. 3 and 4. The rate constant for the condensation of **1** is summarized in Table 2. Second, Arrhenius plots are shown in Fig. 5. The activation energy was obtained by the slope and the frequency factor was obtained by the intercept of these lines (Fig. 5). The results of these calculations are summarized in Table 3. The reaction order of **1a** is different from the other three samples. **1b** has an activation energy about half that of **1c** or **1d** and **1b** has an activation entropy about two-times that of **1c** or **1d**. **1c** has an activation energy and the activation entropy that are the same order as **1d**. It can be assumed that the difference provided by the reaction order and the

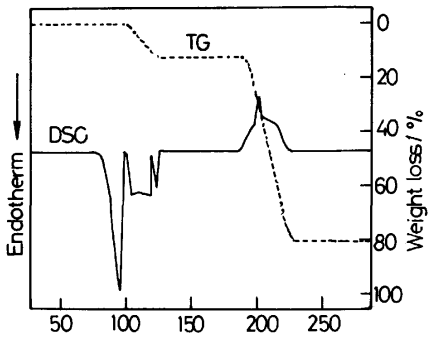

Fig. 1. DSC and TG curves of **1c**.

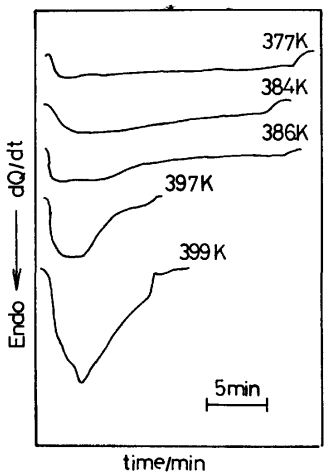

Fig. 2. Isothermal polycondensation DSC curves for **1c**.

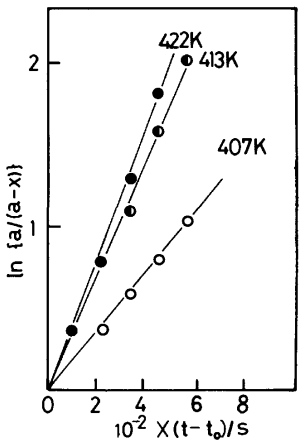

Fig. 3. First order kinetic plots of $\ln[a/(a-x)]$ vs. $t-t_0$ for the isothermal polycondensation of **1a**.

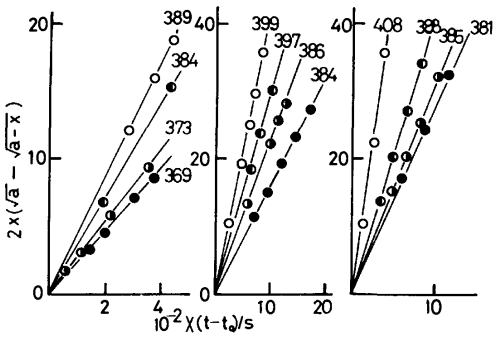

Fig. 4. 1/2 order kinetic plots of $2\times[a^{1/2}-(a-x)^{1/2}]$ vs. $t-t_0$ for the isothermal polycondensation of **1b**, **1c**, **1d**.

activation parameters is caused by the number of the hydrogen atom (β-hydrogen atom) on β-carbon atom adjacent to the carbon attached to the hydroxyl group of the side chain in **1**. These compounds may be grouped, therefore, into three general classes: (1) no β-hydrogen atom (**1a**); (2) three β-hydrogen atoms (**1b**) and (3) two β-hydrogen atoms (**1c**, **1d**).

Thermal Condensation of 1. The TG analysis shows that a dehydration of the samples can be expected for the thermal condensation of **1** since the weight loss of the first plateau at the temperature range of the condensation corresponds to that of about one mole of water. The IR spectra of the condensation products show that the absorption due to ν_{C-O} at 1030 cm^{-1} decreases in intensity (Fig. 6). The ^{13}C NMR spectra of **1c** and its condensation product is given as an example in Fig. 7. This figure shows that the signal at δ 161.556 due to the carbonyl group separates into two signals, and the signal due to the α-carbon atom attached to the hydroxyl group splits after condensation. These results show that the formation process of dimer seemed to be dehydrated as intermolecular combination (Scheme 2). The mass spectra of the condensation products also support this dimer formation. The mass spectra of the condensation products are summarized in Table 4. In this Table 4 **1a**-H, **1b**-H, **1c**-H, and **1d**-H are used for symboliz-

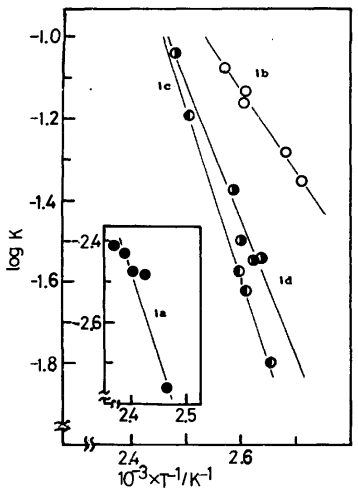

Fig. 5. Arrehnius plots of the first order rate constants for the polycondensation of **1a**, and 1/2 order for the polycondensation of **1b**, **1c**, and **1d**.

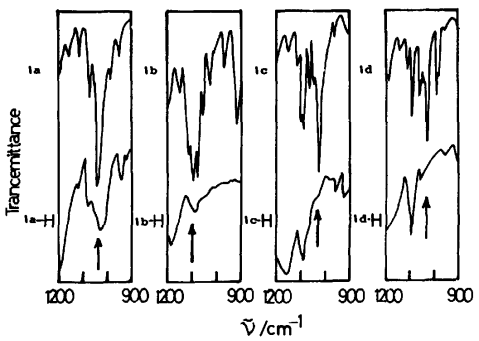

Fig. 6. Change of ν_{C-O} absorption on IR spectra of *N*-hydroxyalkyl derivatives.

Table 2. Reaction Rate for the Condensation of **1**

Compound	Temp/K	Reaction order	Rate constant[a]
	407		1.72×10^{-3}
	413		3.34×10^{-3}
1a	416	1.0	3.36×10^{-3}
	419		3.72×10^{-3}
	422		3.84×10^{-3}
	369		4.39×10^{-2}
	373		5.15×10^{-2}
1b	383	0.5	7.09×10^{-2}
	384		7.37×10^{-2}
	389		8.52×10^{-2}
	377		1.62×10^{-2}
	384		2.37×10^{-2}
1c	386	0.5	2.78×10^{-2}
	397		5.70×10^{-2}
	399		6.51×10^{-2}
	381		2.85×10^{-2}
	382		2.87×10^{-2}
1d	385	0.5	3.13×10^{-2}
	388		4.23×10^{-2}
	408		9.30×10^{-2}

a) Unit in 1.0(reaction order); s^{-1}. Unit in 0.5; $mol^{1/2}$ $l^{-1/2}$ s^{-1}.

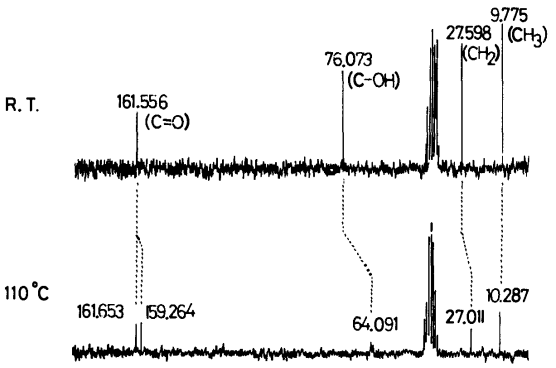

Fig. 7. ^{13}C NMR spectra of **1c** and **1c**-H.

Table 3. Kinetic Data for the Condensation of **1**

Compound	A[a]	ΔE_a / kJ mol^{-1}	ΔS^* / e.u.
1a	3.98×10^{7}	8.07	−26.40
1b	1.65×10^{4}	39.37	−41.65
1c	2.16×10^{9}	80.46	−18.24
1d	1.59×10^{8}	71.30	−23.43

a) Unit in **1a**: s^{-1}, Unit in **1b**, **1c**, and **1d**: $mol^{1/2}$ $l^{-1/2}$ s^{-1}.

ing the thermal condensation products of **1a**, **1b**, **1c**, and **1d**, respectively. There are no peaks due to trimer or oligomer in these mass spectra. The observed fragment ions in the mass spectra of the condensation products support the main fragmentation mechanism of the dimer by the typical representative **1c** (Fig. 8). The amount of aldehyde liberated during the thermal reaction of **1** was about 10% (in quantities of the sample fed with the flask). The elimination of the corresponding aldehyde due to the pyrolysis of **1** is a reverse reaction of *N*-hydroxyalkylation. Consequently, the pyrolysis of **1** leads to the production of **2** (10% of the amount of the samples fed with the flask). A

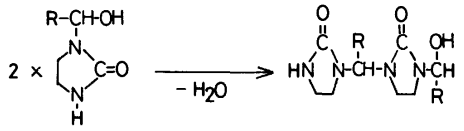

Scheme 2.

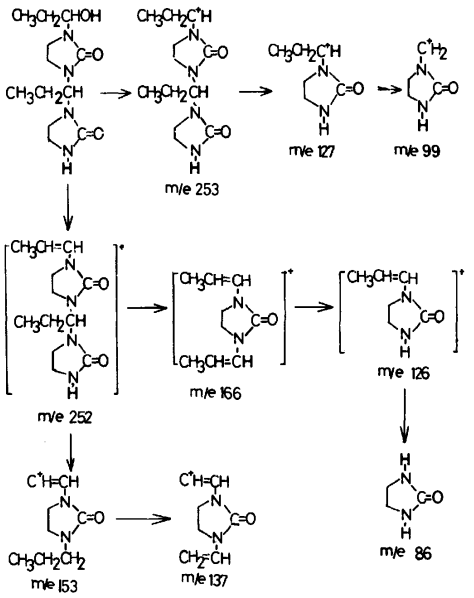

Fig. 8. Main fragmentation for **1c**–H.

Table 4. Mass Spectral Data for **1a**-H, **1b**-H, **1c**-H, and **1d**-H

m/z	Relative intensity[a]	Observed molecular weight	U.S.[c]	Probable ion composition
(I) **1a**-H				
86.0	43.60	86.0498 (86.0932)[b]	2.0	$C_3H_6N_2O$
99.0	100.00	99.0557 (99.1121)	2.5	$C_4H_7N_2O$
113.0	12.96	113.0650 (113.1389)	2.5	$C_5H_9N_2O$
183.0	15.60	183.0802 (183.1895)	4.5	$C_7H_{11}N_4O_2$
196.0	4.80	196.1038 (196.2084)	5.0	$C_8H_{12}N_4O_2$
(II) **1b**-H				
86.0	100.00	86.0496 (86.0932)	2.0	$C_3H_6N_2O$
112.0	21.83	112.0630 (112.1310)	3.0	$C_5H_8N_2O$
113.0	1.61	113.0633 (113.1381)	2.5	$C_5H_9N_2O$
138.0	4.89	138.0819 (138.1688)	4.0	$C_7H_{10}N_2O$
139.0	0.81	139.0844 (139.1716)	3.5	$C_7H_{11}N_2O$
(III) **1c**-H				
86.0	32.20	86.0295 (86.0932)	2.0	$C_3H_6N_2O$
99.0	6.55	99.0645 (99.1121)	2.5	$C_4H_7N_2O$
126.0	55.41	126.0771 (126.1578)	3.0	$C_6H_{10}N_2O$
127.0	100.00	127.0845 (127.1657)	2.5	$C_6H_{11}N_2O$
137.0	4.94	137.0797 (137.1609)	4.5	$C_7H_9N_2O$
153.0	1.36	153.1029 (153.2035)	3.5	$C_8H_{13}N_2O$
166.0	6.49	166.1119 (166.2224)	4.0	$C_9H_{14}N_2O$
252.0	1.99	252.1603 (252.3156)	5.0	$C_{12}H_{20}N_2O_2$
253.0	0.34	253.1727 (253.3235)	4.5	$C_{12}H_{21}N_2O_2$
(IV) **1d**-H				
86.0	67.87	86.0295 (86.0932)	2.0	$C_3H_6N_2O$
99 0	6.43	99.0569 (99.1121)	2.5	$C_4H_7N_2O$
125.0	100.00	125.0719 (125.1499)	3.5	$C_6H_9N_2O$
139.0	6.46	139.0829 (139.1716)	3.5	$C_7H_{11}N_2O$
153.0	2.73	153.1009 (153.2035)	3.5	$C_8H_{13}N_2O$
165.0	13.67	165.0997 (165.2145)	4.5	$C_9H_{13}N_2O$
179.0	14.62	179.1192 (179.2413)	4.5	$C_{10}H_{15}N_2O$
194.0	2.66	194.1424 (194.2760)	4.5	$C_{11}H_{17}N_2O$

a) Relative intensity referred to base peak of spectrum as 100. b) Calculated values. c) U.S.=Degree of unsaturation.

separation of the various mixtures into the liberated **2** could not be verified. Thus, the observed values through elemental analyses are not in full agreement with calculated ones.

Reaction Mechanism for Thermal Condensation in Solid State. Dimerization of **1a**: **1a** has a γ-lactam structure. Therefore, **1a** shows a "tautomeric change" as shown in Scheme 3. In the DSC measurement over the high-temperature range, it is expected that an activated complex is formed from two molecules of the lactim (enol isomer) of **1a** (Scheme 4). These equilibrium conditions for Scheme 4 lie far to the right, showing the reaction process during a smooth formation of the activation complex. At this equilibrium, therefore, the reaction for dimerization apparently obeys first-order kinetics. The expected process for the dimerization of **1a** is as follows.

The reaction mechanism for the dimerization of **1b**, **1c**, and **1d**: As described in the previous section, the dimerization of **1** shows first-order kinetics, whereas in **1b**, **1c**, and **1d**, the order of reaction is to the 1/2 order. It is expected that the dimerization of **1b**, **1c**, and **1d** proceeds by the same mechanism. The use of the results of ESR and mass spectra clarifies the difference in the order of the reaction. ESR measurements were carried out for **1c** at room temperature, 70, 100, 130, and 150 °C. **1c** was in a solid state at room temperature and at other temperatures melted. As Fig. 9 shows, the signal may be due to an intermediate material which participates in the thermal condensation, since this signal was observed alone at the temperature range of the thermal-condensation process. It shows that the intermediate material is considered to form at the pertinent temperature range (70—130 °C). Also, this signal deviates from 0 G to a low magnetic field, and shows a discernible shoulder at the low-magnetic-field side of the main signal. The above results do not indicate that **1c** thermally polymerizes to form the radical. Therefore, the present authors conclude that **1c** in this system forms the electron-transfer complex. After the ESR measurement of **1c** (at 100 °C), the sample tube fed with **1c** was cooled to room temperature. During the ESR measurement under these conditions, the same signal (observed at 100 °C) was reproduced in the ESR spectrum of this sample. This result seems to show that the thermal condensation stops and the resulting activity species remain unaltered. This behavior resembles ordinary very closely living polymerization regarding chemical properties. The possible structure of intermediates formed during the activated state in the course of the dimerization process for **1b**, **1c**, and **1d** is the activated complex (A) and the enol type (B) like lactim (Scheme 5).

The presence of (A) was confirmed by the ESR measurements, and (B) gave no direct evidence concering its existence in the solid state. In the melted state, however, the presence of (B) have likewise been formed in the case of cyanuric acid. By a comparison of structures (A) and (B), the hydroxyl group of (A) was easier to eliminate than that of (B). In the next step, the activated complex (C) (Scheme 5) was formed

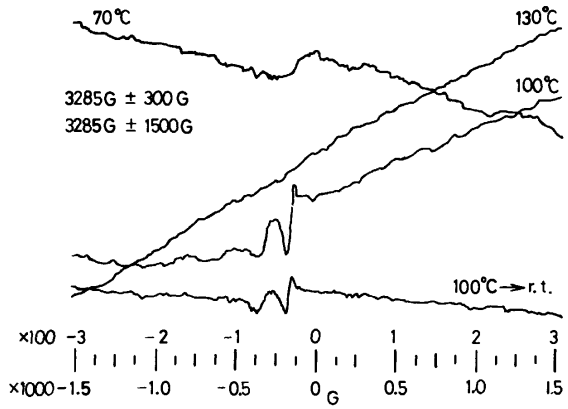

Fig. 9. ESR spectra of **1c**.

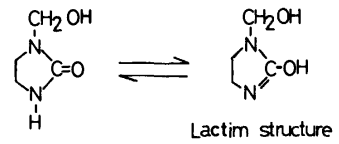

Scheme 3.

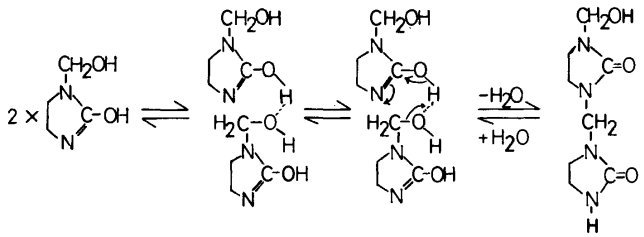

Scheme 4.

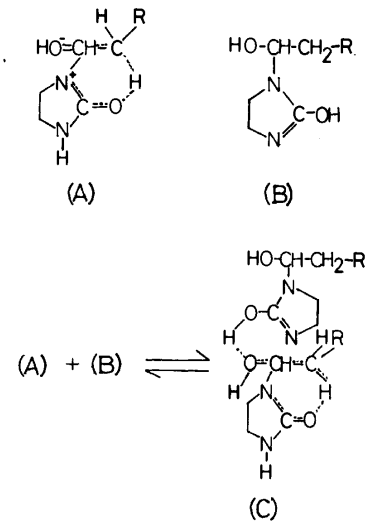

Scheme 5.

from (A) and (B). Now, on the assumption that the overall reaction of dimerization of **1** proceeds with the apparent first-order reaction (such as the dimerization of **1a**), the main conclusion to be drawn from these results is as follows. The concentration of **1**, (A), (B), and (C) are symbolized as [M], [A], [B], and [C], respectively. The equation for each process is as follows:

For the formation of (A)

$$M \rightleftharpoons A \qquad K_1[M] = [A]. \tag{1}$$

For the formation of (B)

$$M \rightleftharpoons B \qquad K_2[M] = [B]. \tag{2}$$

For the formation of (C)

$$A + B \rightleftharpoons C \qquad K_3[A][B] = [C], \tag{3}$$

where K_1, K_2, and K_3 are the equilibrium constants for each process. If the values of [A] and [B] in Eq. 3 are replaced by the corresponding expressions as Eqs. 1 and 2, it is found that

$$K_1 \cdot K_2 \cdot K_3[M]^2 = [C]. \tag{4}$$

According to the previous assumption, for an overall reaction,

$$\text{Reaction rate} = k_0[M], \tag{5}$$

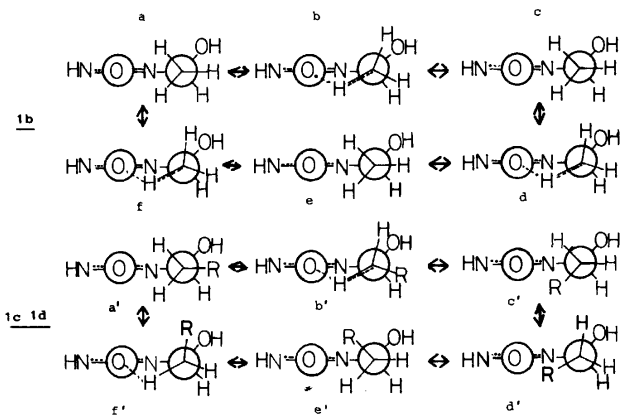

Fig. 10. Conformations of **1b**, **1c**, and **1d**.

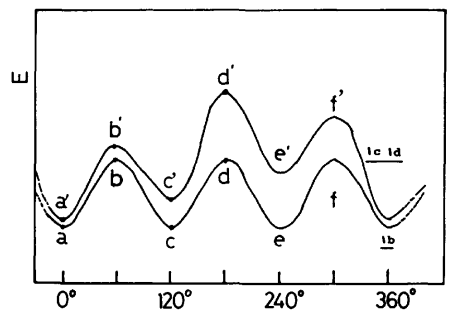

Fig. 11. Rotational energy profiles for **1b**, **1c**, and **1d**.

where k_0 is the rate constant for the overall reaction. When the value of [M] in Eq. 4 is substituted into Eq. 5,

$$\text{Reaction rate} = k_0\{1/(K_1 \cdot K_2 \cdot K_3)\}^{1/2}[C]^{1/2}. \tag{6}$$

When $k_0\{1/(K_1 \cdot K_2 \cdot K_3)\}^{1/2}$ is substituted for k, Eq. 6 becomes

$$\text{Reaction rate} = k[C]^{1/2}. \tag{7}$$

Equation 7 shows that the reaction for the dimerization of **1b**, **1c**, and **1d** proceeds by a 1/2-order reaction. This result agrees with those of the DSC measurements. It is expected for **1b**, **1c**, and **1d** that the DSC measurement was taken in order to obtain information regarding the formation of (C) to the dimer. From these results, it is clear that (A), (B), and (C) are formed during the induction period. The effect of the number of β-hydrogen atoms on the activation parameters must be discussed. **1c** and **1d** have methyl and ethyl groups on the β-carbon atom, respectively. The difference in the activation parameters between **1c** and **1d** for the dimerization is negligibly small. Therefore, the effect of these alkyl groups as the electron donor on the electron-transfer complex (A) is negligible. Figure 10 shows conformations of **1b**, and **1c** and **1d** which are concerned with a rotation about the bond between the α- and the β-carbon atoms attached to the hydroxyl group. Their interconversion processes are represented by the Newman projection formulae. The formation of the electron-transfer complex in the case of **1b** is formed at b, d, and f (Fig. 10). However, in the case of **1c** and **1d**, the formation of the electron-transfer complex is formed at b′ and f′. The formation of (A) at b, b′, d, f, and f′ should be unstable forms owing to their eclipsed geometries. This is the reason for the formation of (A), which is only at the pertinent temperature range (as shown in the ESR spectra). Figure 11 shows the rotational-energy profiles for **1b**, **1c**, and **1d**. According to these profiles, it is definite in the case of **1c** and **1d** that the rotational-energy of structures b′ and f′ is higher than that for b and f in **1b**. This is the reason for the difference in the activation parameters between **1b** and **1c** or **1d**.

We acknowledge the good advice of Prof. Eiichi Tsukurimichi and Dr. Toshiaki Yoshimura. We thank Mr. Yoshiharu Yoneyama for NMR measurements and Miss Misao Shinoda for the Mass spectra. We thank Prof. Shigeya Takeuchi for good advice regarding DSC measurement.

References

1) S. Ishida, *Netsukokaseijushi*, **1**, 40 (1980).
2) Y. Fujita and Y. Noda, *Bull. Chem. Soc. Jpn.*, **57**, 2177 (1984).

3) C. Shimasaki, A. Uchida, H. Oonishi, Y. Iwai, and M. Wakabayashi, *Nippon Kagaku Kaishi*, **1983**, 1761.
4) S. Takeuchi, "Yukikagobutsugoseiho," ed by Yukigosei Kagakukyokai, Gihodo, (1969), pp. 27, 61.
5) M. Takimoto and K. Koeda, *Kogyo Kagaku Zasshi*, **63**, 797 (1960).
6) A. R. McGhie, P. S. Kalyanaraman, and A. F. Garito, *J. Polym. Sci., Polym. Lett. Ed.*, **16**, 335 (1978).

 © 1987 The Chemical Society of Japan Bull. Chem. Soc. Jpn., 60, 201—204 (1987)

The Nucleophilic Reaction upon Electron-Deficient Pyridone Derivatives. VIII.[1] Novel Fragmentation of 3,5-Dinitro-2-pyridone by Primary Amine

Yasuo TOHDA,* Masahiro ARIGA, Toshihide KAWASHIMA, and Eizo MATSUMURA
Department of Chemistry, Osaka Kyoiku University,
Minamikawahoricho 4-88, Tennoji-ku, Osaka 543
(Received June 17, 1986)

Fragmentation of 3,5-dinitro-2-pyridone (**1**) by primary amine gave nitroacetamide (**2**) and nitromalonaldehyde diimine. In the case of *N*-methyl derivative (**1c**), the reaction was completely suppressed by the product **2** to give an anionic σ-adduct of **1c** with **2**. The mechanism of the reaction was discussed.

In previous papers, we reported a ring transformation of 3,5-dinitro-2-pyridone (**1**) with various ketones into *p*-nitrophenols[2] or *p*-nitroanilines.[3] Three types of the intermediates were isolated and characterized, i.e., an anionic σ-adduct,[4] a 2-azabicyclo[3.3.1]nonane derivative,[2,3] and an α-nitro-α-(2-nitro-2,4-hexadienyl)acetamide derivative.[3] (Scheme 1) The reaction of **1** is unusual in the reactions of heteroaromatic compounds, because most ring transformations of electron-deficient heterocyclic compounds with ketones or other nucleophiles proceed through open chain intermediates rather than through such bicyclic compounds.[5] It is analogous to the reaction of 1,3,5-trinitrobenzene with acetone and diethylamine to give *N,N*-diethyl-*p*-nitroaniline,[6] because an anionic σ-adduct[7] and a bicyclo[3.3.1]nonane derivative[8] were recognized as the intermediates.

In our study on electron-deficient pyridone derivatives, we found a novel fragmentation of 3,5-dinitro-2-pyridone (**1**) by primary amine. The mechanism of the reaction which appears to be closely related to those of the above reactions will be discussed.

Results and Discussion

The reaction of 3,5-dinitro-1-(4-nitrophenyl)-2-pyridone (**1a**) with excessive aliphatic or aromatic primary amine in pyridine at room temperature gave a nitroacetamide (**2a**) and nitromalonaldehyde diimine (**3**) (Eq. 1). The aliphatic amines reacted faster and gave better yields of **2** and **3** than the aromatic amines. The reaction of **1a** with cyclohexylamine was completed within 5 min. Similarly, 1-(2-pyridyl) derivative (**1b**) reacted with these amines according to Eq. 1. On the other hand, 1-methyl derivative (**1c**) reacted with excess of the aliphatic primary amines at 50 °C to give **3** and a Michael-type adduct (**4**) as indicated in Eq. 2. No aromatic primary amines reacted with **1c** at 50 °C due to their low basicity. The results are summarized in Table 1. The structure of **3** was confirmed by comparing **3b** with an authentic sample prepared by the reaction of sodium salt of nitromalonaldehyde with *p*-anisidine. The product **4** showed characteristics of anionic σ-adduct of **1c** by the UV and ^{1}H NMR spectra.[4] The addition site of nucleophilic carbon or nitrogen is C-6 of **1c**. Chemical shifts of H-6 of **4a** (cyclohexylammonium salt) or **4b** (*t*-butylammonium salt) were found at δ of 6.2. The values are about 1 ppm lower than those of anionic σ-adducts of **1c** with usual carbon nucleophiles. This is attributed to strong diamagnetic anisotropic effect of anionic part of α-(*N*-methyl-carbamoyl)-α-nitromethylene of **4**. Coupling between H-4 and H-6 was not observed. Treatment of **4a** with hydrochloric acid gave **1c**, *N*-methyl-α-nitroacetamide (**2c**), and cyclohexylammonium chloride in 85, 45, and 90% yields, respectively. An authentic sample of **4a** was obtained by mixing its components in pyridine at room temperature. From these facts, **4** were identified as dianionic salts as indicated in Eq. 2.

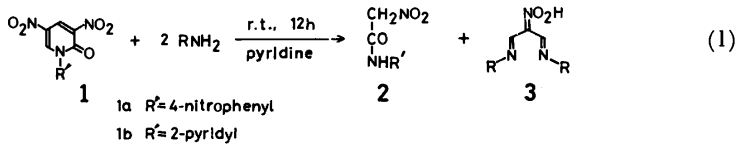

(1)

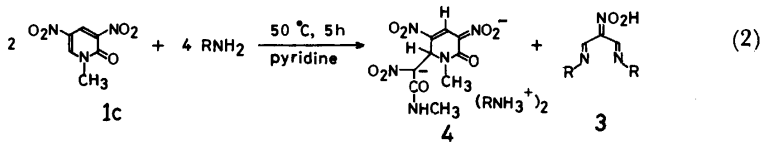

(2)

The different results between **1a**, **1b**, and **1c** can be interpreted by the hard-soft concept. **1c** is a softer electrophile than **1a** and **1b**, because **1c** is a weaker electrophile for hard amines but has stronger affinity for soft nucleophilic carbon of nitroacetamide (**2**) than **1a** and **1b**. In the case of **1c**, the reaction indicated by Eq. 1 is completely suppressed by the product **2c** which gives adduct **4** by addition to **1c**. The difference in reactivity between **1a** and **1c** explains the following facts. In the presence of excess acetone, the reaction of **1c** with cyclohexylamine at 70 °C gave *N*-cyclohexyl-*p*-nitroaniline quantitatively. The fragmentation in Eqs. 1 and 2 is thus completely suppressed by acetone nucleophile. On the other hand, in the case of the reaction of **1a** under similar conditions, competitive reactions between the fragmentation and the ring transformation occurred to give a mixture of **3a** and *N*-cyclohexyl-*p*-nitroaniline in 41 and 19% yields, respectively.

When the reaction of a mixture of **1c** and excess of cyclohexylamine (1:6 mol ratio) in pyridine-d_5 was monitored at 37 °C by ^{1}H NMR spectra, the first observable species was only an anionic σ-adduct (**5**) of **1c** with the amine; δ=3.18 (s, NCH_3), 5.68 (d, H-6, J=1.0 Hz), and 9.37 (d, H-4, J=1.0 Hz). The chemical shifts and coupling patterns were similar to those of the secondary amine adducts of **1c**.[4] As the peaks of **5** decreased slowly, the peaks of the products **3a** and **4a** increased. The change did not obey the first-order kinetics as expected from the mechanism. Neither other intermediate nor by-product was detected. Transformation of **5** to an intermediate is the rate-determining step. The pyridone **1c** also reacted with strong secondary amines such as pyrrolidine and diethylamine in pyridine-d_5 to give anionic σ-adducts immediately, but the further fragmentation did not occur under the similar conditions. On the other hand, the reactive pyridone **1a** was rapidly decom-

Table 1. Fragmentation of 3,5-Dinitro-2-pyridone (**1**) by Primary Amine

Substrate[a]	Amine	Reaction Temperature	Products	(Yields/%)[c]
1a	Cyclohexylamine	r.t.	**2a** (80)	**3a** (88)
1a	*p*-Anisidine	r.t.	**2a** (15)	**3b** (73)
1a	Aniline	r.t.	**2a** (0)	**3c** (59)
1b	Cyclohexylamine	r.t.	**2b'**[b] (75)	**3a** (86)
1b	*p*-Anisidine	r.t.	**2b** (56)	**3b** (82)
1b	Aniline	r.t.	**2b** (0)	**3c** (58)
1c	Cyclohexylamine	50 °C	**4a** (94)	**3a** (88)
1c	*t*-Butylamine	50 °C	**4b** (92)	**3d** (88)
1c	*p*-Anisidine	100 °C	—	**3c** (6)

a) Notations of the compounds are described in Eqs. 1 and 2. b) Isolated as a cyclohexylammonium salt. c) In the reaction of **1a** and **1b**, yields are based on Eq. 1. In the reaction of **1c**, yields are based on Eq. 2.

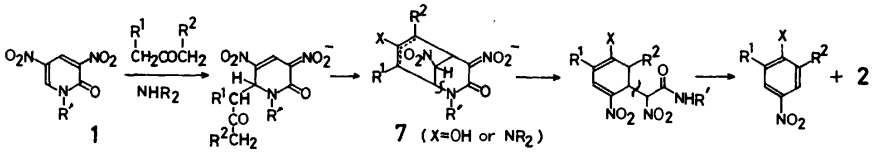

Scheme 1.

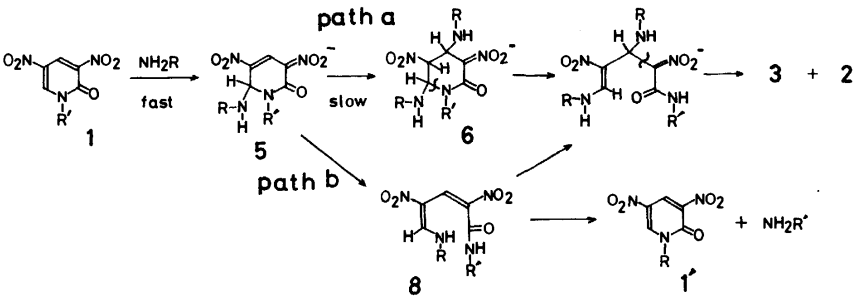

Scheme 2.

posed to unidentifiable products by pyrrolidine.

There are two possible courses of the reaction. The one involves a complex (**6**) formed by twofold addition of the primary amine. (Scheme 2, path a) The complex **6** corresponds to the bicyclic intermediate (**7**) in the ring transformation (Scheme 1).[2,3] Although diadduct formation such as **6** has been exemplified in the reaction of 1,3,5-trinitrobenzene and other electron-deficient aromatic systems,[9] this type of fragmentation has not been reported. Easy heterolysis of C_6–N_1 bond of **6** explains the fragmentation of **1**, whereas lack of such a bond in the diadduct of trinitrobenzene would result no fragmentation.

The alternative course which involves an open-chain intermediate (**8**) can be considered. (path b) The similar intermediate has been postulated in the reactions of 3,5-dinitro-4-pyridone with sodium salt of ethyl acetoacetate[10] or with primary amine.[11] In the latter reaction, recyclization of the open-chain intermediate gives another 4-pyridone, in which an original *N*-substituent is exchanged for the primary amine. Since such a substitution product (**1'**) was not found in the present reaction, path a is more probable than path b.

Thus the fragmentation is a characteristic reaction of 3,5-dinitro-2-pyridone (**1**) and unique reaction of electron-deficient aromatic compounds.

Experimental

The infrared spectra were measured in nujol by means of a Hitachi 260-10 spectrophotometer, ^{1}H NMR spectra by a Hitachi R-20 B spectrometer, and ultraviolet spectra by a Shimadzu UV-240 spectrophotometer.

3,5-Dinitro-(4-nitrophenyl)-2-pyridone (1a). Nitration of 1-(4-nitrophenyl)-2-pyridone with fuming nitric acid (d 1.42) at 130 °C for 7 h gave **1a** in 65% yield. Pale yellow needles (AcOH–H_2O 3:1); mp 221.5—222 °C. ^{1}H NMR (DMSO-d_6) δ=7.91 (d, 2H, J=9.1 Hz), 8.46 (d, 2H, J=9.1 Hz), 9.17 (d, 1H, J=3.1 Hz), 9.51 (d, 1H, J=3.1 Hz), IR: 1710 cm^{-1} (C=O), 1577, 1530, 1346, 1324 cm^{-1} (NO_2). Found: C, 43.10; H, 2.05; N, 18.27%. Calcd for $C_{11}H_6N_4O_7$: C, 43.15; H, 1.98; N, 18.30%.

Reaction of 1a with Cyclohexylamine. To a solution of 0.61 g of **1a** in 15 ml of pyridine 1.21 g of cyclohexylamine in 5 ml of pyridine was added at 0 °C. The mixture was allowed to stand at room temperature for 12 h. After removal of the solvent in vacuo, residual oil was extracted with hexane to give 0.49 g of the diimine **3a**; colorless needles (hexane); mp 86—87 °C. ^{1}H NMR ($CDCl_3$) δ=1.0—2.2 (m, 20H), 3.0—3.5 (m, 2H), 8.70 (s, 2H), 11.0 (broad, 1H). IR: 1650, 1600 cm^{-1} (C=N). Found: C, 64.74; H, 9.00; N, 14.99%. Calcd for $C_{15}H_{25}N_3O_2$: C, 64.48; H, 9.02; N, 15.04%. The residue was dissolved in water and slightly excess hydrochloric acid was added to the solution. Precipitates were recrystallized from ethanol to give 0.36 g of α-nitro-*N*-(4-nitrophenyl)acetamide (**2a**); pale yellow needles; decomp 177—179 °C. ^{1}H NMR (DMSO-d_6) δ=5.59 (s, 2H), 7.83 (d, 2H, J=9.2 Hz), 8.23 (d, 2H, J=9.2 Hz), 11.07 (broad s, 1H). IR: 3360 cm^{-1} (N–H), 1703 cm^{-1} (C=O). Found: C, 42.90; H, 3.17; N, 18.69%. Calcd for $C_8H_7N_3O_5$: C, 42.67; H, 3.13; N, 18.66%.

Reaction of 3,5-Dinitro-1-(2-pyridyl)-2-pyridone (1b) with *p*-Anisidine. To a solution of 0.52 g of **1b** in 15 ml of pyridine was added 0.74 g of *p*-anisidine in 5 ml of pyridine at 0 °C. The mixture was allowed to stand at room temperature for 12 h. Water was added to the mixture and resulted precipitates were recrystallized from ethanol to give 0.54 g of **3b**. Yellow needles; mp 133—135 °C. ^{1}H NMR ($CDCl_3$) δ=3.82 (s, 6H), 6.94 (d, 4H, J=9.1 Hz), 7.19 (d, 4H, J=9.1 Hz), 8.99 (s, 2H), 13.5 (broad, 1H). IR: 1642, 1563 cm^{-1} (C=N). Found: C, 62.50; H, 5.36; N, 12.74%. Calcd for $C_{17}H_{17}N_3O_4$: C, 62.37; H, 5.24; N, 12.84%. After the solvent was removed in vacuo, the residue was recrystallized from chloroform to give 0.21 g of **2a**.[2]

Similarly, nitromalonaldehyde dianil (**3c**) was obtained. Yellow needles; mp 93—95 °C. ^{1}H NMR ($CDCl_3$) δ=7.0—7.6 (m, 10H), 9.10 (s, 2H), 13.5 (broad, 1H). IR: 1650, 1567 cm^{-1} (C=N). Found: C, 67.54; H, 4.88; N, 15.47%. Calcd for $C_{15}H_{13}N_3O_2$: C, 67.40; H, 4.90; N, 15.72%.

Reaction of 1-Methyl-3,5-dinitro-2-pyridone (1c) with Cyclohexylamine. To a solution of 0.40 g of **1c** in 15 ml of pyridine 1.21 g of cyclohexylamine in 5 ml of pyridine was added. The mixture was heated at 50 °C for 3 h. After the solvent was removed in vacuo, residual oil was extracted with hexane. The extract was recrystallized from hexane to give 0.25 g of **3a**. The residue was dissolved in hot ethanol containig a few drops of cyclohexylamine. After cooling, 0.43 g of **4a** was obtained as orange powder; decomp 118—123 °C. ^{1}H NMR (DMSO-d_6) δ=0.9—2.2 (m, 20H), 2.71 (s, 3H), 2.71 (d, 3H, J=5.2 Hz), 2.4—3.2 (m, 2H), 6.20 (s, H-6), 5.8—7.0 (broad, 8H), 8.60 (s, H-4), 10.04 (broad q, 1H, J=5.2 Hz). IR: 3260, 2650, 2550 cm^{-1} (NH_3^+), 1626 cm^{-1} (C=O). UV (MeOH, 8.38×10^{-5} mol l^{-1}, ε depends on the concentration of **4a**): λ_{max} (ε) 489 nm (1.96×10^4), 302 nm (1.37×10^4). Found: C, 47.27; H, 7.30; N, 18.42%. Calcd for $C_{21}H_{39}N_7O_9$ (monohydrate): C, 47.27; H, 7.37; N, 18.38%.

Similarly **3d** and **4b** were obtained from reaction of **1c** with *t*-butylamine.

3d: Colorless needles (hexane); mp 142—143 °C. ^{1}H NMR ($CDCl_3$) δ=1.34 (s, 18H), 8.73 (s, 2H), 12.6 (broad, 1H). IR: 1640, 1592 cm^{-1} (C=N). Found: C, 58.02; H, 9.29; N, 18.43%. Calcd for $C_{11}H_{21}N_3O_2$: C, 58.12; H, 9.31; N, 18.49%.

4b: Orange powder (ethanol–*t*-butylamine); decomp 120—127 °C. ^{1}H NMR (DMSO-d_6) δ=1.24 (s, 18H), 2.70 (s, 3H), 2.71 (d, 3H, J=4.9 Hz), 6.28 (s, H-4), 6.7 (broad, 9H), 8.61 (s, H-6), 10.04 (broad q, 1H, J=4.9 Hz). IR: 2610, 2500 cm^{-1} (NH_3^+), 1627 cm^{-1} (C=O). UV (MeOH, 8.38×10^{-5} mol l^{-1}): λ_{max} (ε) 489 nm (1.71×10^4), 301 nm (1.61×10^4). Found: C, 41.83; H, 7.10; N, 20.22%. Calcd for $C_{17}H_{36}N_7O_{9,5}$ (1.5 hydrate): C, 41.63; H, 7.40; N, 19.99%.

Reaction of 1a with Cyclohexylamine in the Presence of Acetone. A solution of 0.31 g of **1a**, 0.61 g of cyclohexylamine, and 0.58 g of acetone in 20 ml of pyridine was heated at 70 °C for 3 h. The solvent was removed in vacuo and residue was treated by column-chromatograph with silica gel. Benzene elute gave 42 mg of *N*-cyclohexyl-*p*-nitroaniline; mp 99 °C; yellow needles (hexane). Chloroform elute gave 82 mg of 3-cyclohexylamino-2-nitro-2-propenal; mp 130—131 °C; pale yellow needles (hexane). Found: C, 54.58; H, 7.12; N, 14.35%. Calcd for $C_9H_{14}N_2O_3$: C, 54.53; H, 7.12; N, 14.13%. This compound was quantitatively obtained by treatment of **3a** with silica gel.

References

1) For the preceding paper: M. Ariga, Y. Tohda, and E. Matsumura, *Bull. Chem. Soc. Jpn.*, **58**, 393 (1985).

2) E. Matsumura, M. Ariga, and Y. Tohda, *Bull. Chem. Soc. Jpn.*, **52**, 2413 (1979).

3) E. Matsumura, Y. Tohda, and M. Ariga, *Bull. Chem. Soc. Jpn.*, **55**, 2174 (1982).

4) Y. Tohda, M. Ariga, T. Kawashima, and E. Matsumura, *Chem. Lett.*, **1983**, 715.

5) For example in pyridine system: A. N. Kost, S. P. Gromov, and R. S. Sagitullin, *Tetrahedron*, **37**, 3423 (1981).

6) T. Abe, *Bull. Chem. Soc. Jpn.*, **32**, 997 (1959).

7) R. Foster and C. A. Fyfe, *Tetrahedron*, **22**, 1831 (1966).

8) M. J. Strauss and H. Schran, *J. Am. Chem. Soc.*, **91**, 3974 (1969); H. Schran and M. J. Strauss, *J. Org. Chem.*, **36**, 856 (1971); L. M. Gnanadoss and D. Kalaivani, *ibid.*, **50**, 1174 (1985); *idem, ibid.*, **50**, 1178 (1985).

9) M. J. Strauss, *Chem. Rev.*, **70**, 688 (1970).

10) E. Matsumura, M. Ariga, and Y. Tohda, *Bull. Chem. Soc. Jpn.*, **53**, 2891 (1980).

11) E. Matsumura, M. Ariga, Y. Tohda, and T. Kawashima, *Tetrahedron Lett.*, **22**, 757 (1981); E. Matsumura, H. Kobayashi, T. Nishikawa, M. Ariga, Y. Tohda, and T. Kawashima, *Bull. Chem. Soc. Jpn.*, **57**, 1961 (1984).

 © 1987 The Chemical Society of Japan Bull. Chem. Soc. Jpn., 60, 205—213 (1987)

Synthesis of Shikalkin (±Shikonin) and Related Compounds[1)]

Akira TERADA,* Yasuhiro TANOUE, Akira HATADA, and Hiroshi SAKAMOTO
Department of Chemistry, Kyushu Institute of Technology, Sensui-cho, Tobata, Kitakyushu 804
(Received June 18, 1986)

The key intermediate, 2-formyl-1,4,5,8-tetramethoxynaphthalene, was prepared through 1,4,5,8-tetramethoxynaphthalene, which was obtained from 1,5-naphthalenediol via three steps or from naphthazarin via one step. A total synthesis of shikalkin and dihydroshikalkin have been accomplished with this aldehyde via a side-chain introductions with Grignard reactions and the following demethylations.

A root of *Lithospermum erythrorhizon* Sieb. et Zucc. found in Japan, China, and Korea is called Shikon and contains purple pigments (about 1 wt%) under the bark. Two kinds of Shikon are available in the market. One is called "Ko-shikon," which is the root of the above, and the other is "Nan-shikon," which is the root of *Macrotomia euchroma* Pauls. From ancient times the purple pigments have been used as dyes, which are well known as Kodaimurasaki. They can be represented by shikonin and its esters as Fig. 1.

These compounds have antiinflammatory,[4)] antibacterial,[5)] and antitumor actions,[6)] and are also used as raw materials for dyes[7)] and cosmetics.[8)]

Alkanna tinctoria in Europe contains alkannin,[9)] an enantiomer of shikonin. According to a proposal of R. Kuhn, Brockmann named the racemate shikalkin, an equimolar mixture of shikonin and alkannin. Japanese shikonin also contains 20% shikalkin.[10)]

Kuroda[11)] and Brockmann[9)] reported on shikonin's structure and a synthesis of its derivatives, but there was no report concerning the total synthesis of shikonin itself. First, Kuroda had proposed that all three hydroxyl groups in shikonin were bonded to the naphthazarin skeleton; finally, however, formula **1-a** was established by Brockmann.[9a)] Arakawa et al.[12)] showed that the absolute configuration of the α-hydroxyl group in shikonin is *R*.

Shikonin and alkannin are so labile that they must be delicately handled during their extraction.[9b, 11)] The fact that shikonin cyclizes easily by Lewis acid[13)] to cycloshikonin has posed difficulties in attempts toward its total synthesis. Until recently, cycloshikonin and cycloalkannin had been considered to possess structure **2**, but Sankawa et al.[14)] proved that the real structure was the ether **3** Fig. 2.

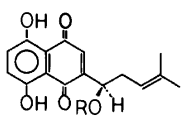

1a—f

(**a**) Shikonin R : H. (**b**) Acetylshikonin R : $COCH_3$. (**c**) 3-Methyl-2-butenoylshikonin R : $COCH{=}C(CH_3)_2$.[2)] (**d**) Isobutyrylshikonin R : $COCH(CH_3)_2$.[2)] (**e**) 3,4-Dimethyl-3-pentenoylshikonin R : $COCH_2C(CH_3){=}C(CH_3)_2$.[3)] (**f**) β-Hydroxyisovalerylshikonin R : $COCH_2C(OH)(CH_3)_2$.[3)]

Fig. 1.

In a recent communication we reported on the total synthesis of shikalkin[(±)shikonin].[15)] The present paper describes the total synthesis in detail in addition to related compounds of shikalkin, and a new synthetic method of 1,4,5,8-tetramethoxynaphthalene.

Results and Discussion

Methylation of 1,5-naphthalenediol with dimethyl sulfate provided 1,5-dimethoxynaphthalene (**4**).[16)] Bromination of **4** gave 4,8-dibromo-1,5-dimethoxynaphthalene (**5**).[17)] Zweig et al.[18)] reported that the compound **5** gave 1,4,5,8-tetramethoxynaphthalene (**6**) (19%) when treated with sodium methoxide and copper(I) oxide in DMF. By using copper(I) iodide[19)] instead of copper(I) oxide we were able to obtain **6** in a good yield (84%). The treatment of **6** with Vilsmeier reagent ($POCl_3$, DMF)[20)] gave 2-formyl-1,4,5,8-tetramethoxynaphthalene (**7**) in 99% yield.

Compound **6** was also synthesized from naphthazarin, which was easily prepared by a treatment of

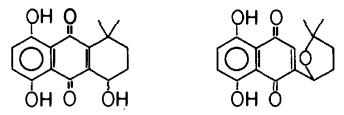

2 3

Fig. 2.

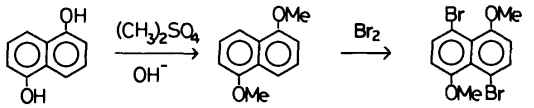

4 5

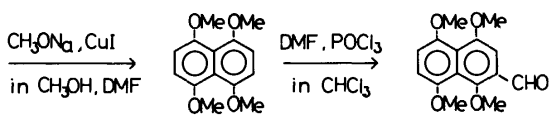

6 7

Fig. 3.

maleic anhydride with hydroquinone in a molten mixture of aluminum chloride and sodium chloride.[11b] According to Thomson's procedure, methylation of naphthazarin with methyl *p*-toluenesulfonate gave 5,8-dimethoxy-1,4-naphthoquinone (**8**) in 44% yield.[21] Reduction of the quinone **8** and methylation were simultaneously accomplished with sodium dithionite and dimethyl sulfate to give the tetramethyl ether **6** (48%). The ether **6** was also directly prepared in 44% yield from naphthazarin without the isolation of the quinone **8**.

First, the synthesis of dihydroshikalkin was tried. A treatment of the aldehyde **7** with isopentylmagnesium bromide gave 2-(1-hydroxy-4-methylpentyl)-1,4,5,8-tetramethoxynaphthalene (**9**) (95%). Methylation of **9** with methyl iodide gave 2-(1-methoxy-4-methylpentyl)-1,4,5,8-tetramethoxynaphthalene (**10**) (81%), which was transformed into a 1,4-naphthoquinone derivative **11** (42%)[22] by oxidation using cerium(IV) ammonium nitrate [$Ce(NH_4)_2(NO_3)_6$, CAN].[23]

Demethylation of **11** with aluminum chloride[24] gave 5,8-dihydroxy-2-(1-methoxy-4-methylpentyl)-1,4-naphthoquinone (**12**) in 49% yield. The ^1H NMR spectrum showed signals at δ 12.49 (1H), 12.59 (1H) due to phenolic hydroxyl groups whose protons form strong hydrogen bonds. The presence of a signal at δ 3.32 (3H) due to the methoxyl group suggested that no demethylation in the side chain had occurred. Therefore, a similar reaction was carried out without the protection of the hydroxyl group (shown in the scheme of Fig. 6).

Oxidation of **9** with CAN gave 2-(1-hydroxy-4-methylpentyl)-5,8-dimethoxy-1,4-naphthoquinone (**13**) (52%) as a major product. Further demethylation of the quinone **13** with aluminum chloride gave crude products, which were purified by silica-gel chromatography to afford two products.

The IR of the product eluted first barely showed a broad absorption at 3100—3700 cm^{-1}, which is similar to the spectrum of naphthazarin. The lack of a secondary alcoholic hydroxyl group was also proved by the IR spectrum which showed no C-O stretching band at 1060 cm^{-1}. The ^1H NMR spectrum showed signals at δ 12.47 (1H), 12.61 (1H) due to the phenolic hydroxyl groups; however, no signal was found at δ 3—6. Therefore, it was thought that there was no other hydroxyl group present. The mass spectrum (*m/z*, 274, M^+)[25] and the above spectral data revealed that the structure was **15**. Kyogoku et al.[26] had obtained this from the natural product. The formation mechanism of **15** will be investigated more and reported in the near future.

The product eluted next (in 48% yield) was similar to shikonin under an IR comparison. The presence of a secondary alcoholic hydroxyl group was confirmed by a broad absorption at 3050—3700 cm^{-1} and a C-O band at 1060 cm^{-1}. The ^1H NMR spectrum showed

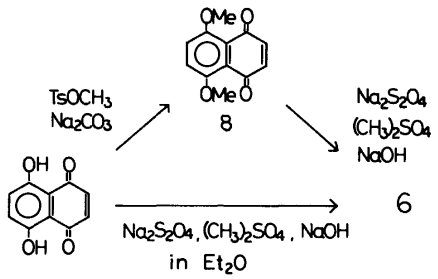

Fig. 4.

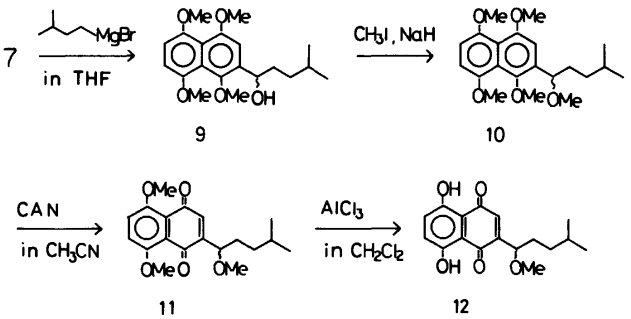

Fig. 5.

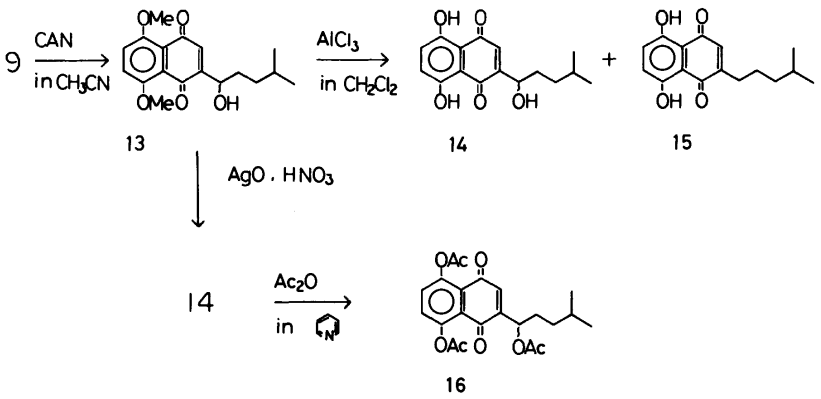

Fig. 6.

signals at δ 12.46 (1H), 12.58 (1H) due to hydrogen-bonded phenolic hydroxyl groups, and at δ 4.87 (1H) due to a proton of the methine attached to the secondary hydroxyl group. The mass spectrum of the product clearly exhibited a molecular ion peak at *m/z* 290. These data as well as an elemental analysis clearly indicated that this was the proposed dihydroshikalkin, 5,8-dihydroxy-2-(1-hydroxy-4-methylpentyl)-1,4-naphthoquinone (**14**). Sankawa et al.[6] had obtained this from the natural product.

Since demethylation using aluminum chloride is accompanied by various side reactions; Parker et al. used AgO–HNO_3[27] as a demethylation reagent. In an analogous way, demethylation of **13** with AgO–HNO_3 gave **14** in 28% yield. Treatment of **14** with acetic anhydride in pyridine afforded triacetate **16**.

The total synthesis of shikalkin is described below.

Treatment of methyl vinyl ketone with hydrogen bromide by the procedure of Gerlach et al.[28]; and acetalization with ethylene glycol in the presence of an acid catalyst gave 4-bromo-2-butanone ethylene acetal **17**. The treatment of the aldehyde **7** with the Grignard reagent of **17** afforded 2-[4,4-(ethylenedioxy)-1-hydroxypentyl]-1,4,5,8-tetramethoxynaphthalene (**18**) in 96% yield. Methylation of **18** with methyl iodide gave an ether, which was converted into 2-(1-methoxy-4-oxopentyl)-1,4,5,8-tetramethoxynaphthalene (**19**) by deacetalization in the presence of an acid. The ketone **19** was treated with methylmagnesium iodide to give 2-(1-methoxy-4-hydroxy-4-methylpentyl)-1,4,5,8-tetramethoxynaphthalene (**20**) in 86% yield. Dehydration of the alcohol **20** with thionyl chloride in pyridine at −18 °C gave 2-(1-methoxy-4-methyl-4-pentenyl)-1,4,5,8-tetramethoxynaphthalene (**22**) and 2-(1-methoxy-4-methyl-3-pentenyl)-1,4,5,8-tetramethoxynaphthalene (**21**). The ratio of these two isomers was about 3:5 as judged by gas chromatography.

A variety of reagents such as HBr, $AlCl_3$, $(CH_3)_3SiI$, BBr_3, etc.,[29,30] are available for the demethylation of methyl ethers; however, hard reaction conditions are usually required except for BBr_3 and $(CH_3)_3SiI$. Our preliminary attempt to treat 1,4,5,8-tetramethoxynaphthalene **6** with BBr_3 at −78 °C gave the naphthazarin (**23**) in 68% yield. Then, a demethylation of **21** with BBr_3 in CH_2Cl_2 at −70—−80 °C afforded the cyclic ether **3** in 5% yield instead of the desired shikalkin **24**. A cleavage of the ether **21** with $AlCl_3$ or $(CH_3)_3SiI$ was unsuccessful.

A synthesis of shikalkin was attempted while considering the following two points: 1) that the carbon–carbon double bond of the side chain should be introduced as late as possible, and 2) the selection of a protecting group for the secondary alcoholic hydroxyl group which could be easily removed under mild conditions.

Deacetalization of **18** with an acid afforded the ketone **25** and a treatment of **25** with methylmagnesium iodide gave 2-(1,4-dihydroxy-4-methylpentyl)-1,4,5,8-tetramethoxynaphthalene (**26**). Oxidation of **26** with CAN afforded 5,8-dimethoxy-2-(1,4-dihydroxy-4-methylpentyl)-1,4-naphthoquinone (**27**) as a major product, and further demethylation of **27** with AgO–HNO_3 yielded 5,8-dihydroxy-2-(1,4-dihydroxy-4-methylpentyl)-1,4-naphthoquinone (**28**). Acetylation of **28** with acetic anhydride in pyridine gave the

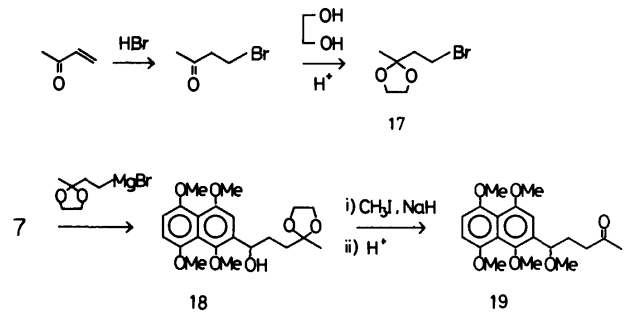

Fig. 7.

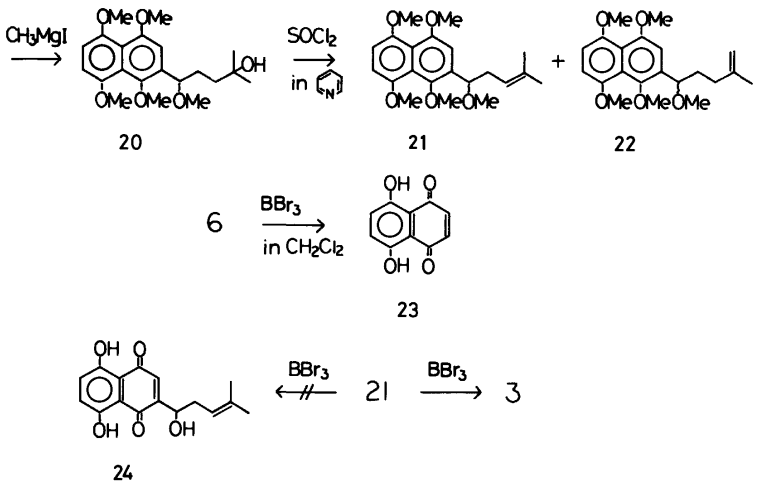

Fig. 8.

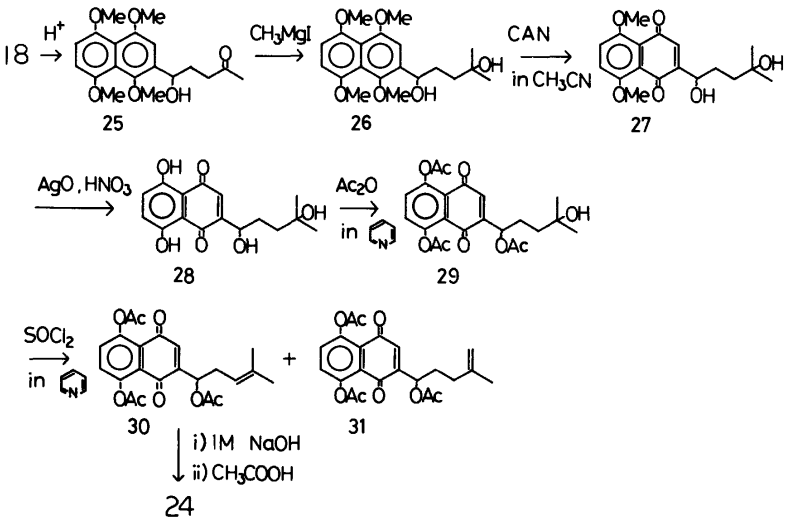

Fig. 9.

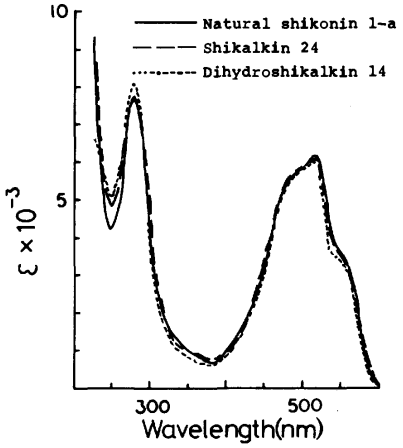

Fig. 10.

triacetate **29**. The secondary hydroxyl group of **28** was acetylated, but tertiary one was not because of a steric hindrance. The treatment of **29** with thionyl chloride in pyridine at −38 °C afforded a mixture of dehydrated compounds, **30** and **31**, in 46% yield. The ratio of these two isomers **30**:**31** was ca. 3:1 as judged by the ^{1}H NMR. Compound **30** was separated by chromatography on silica-gel and was then hydrolyzed by an alkali; and neutralization with acetic acid gave shikalkin **24** in 37% yield.

The ultraviolet spectra of natural shikonin extracted from shikon, synthetic shikalkin **24**, and dihydroshikalkin **14** are shown in Fig. 10. In the spectra of all compounds the benzenoid and quinonoid electron-transfer (E.T.) bands appear at 278 nm, and the benzenoid E.T. band at 515 nm.

Experimental

^{1}H NMR spectra were taken on a JEOL JNM-FX60 spectrometer using tetramethylsilane as an internal standard and the chemical shifts were reported in δ values. Mass spectral data were obtained with a JEOL DX-300. Infrared spectra were recorded on a Hitachi 260—30 infrared spectrometer and the UV spectra on a Shimadzu recording spectrometer UV-200S. Analytical GLC was performed on a Shimadzu GC-6A gas chromatography using Silicone SE-30. High-performance liquid chromatography (HPLC) was performed with a EYELA PLC-10 using TC-ODS 1171. Column chromatography was performed on silica gel (Wakogel C-200) and alumina (Sumitomo activated alumina, KCG-30). Melting points were determined with a Yanagimoto micromelting point apparatus and were uncorrected.

1,5-Dimethoxynaphthalene **4**, mp 181—182 °C (lit,[16] 183—184 °C) was prepared by the method of Benthey.[16]

4,8-Dibromo-1,5-dimethoxynaphthalene (5). Bromine (49.3 g, 0.32 mol) in carbon tetrachloride (50 ml) was added to a solution of 1,5-dimethoxynaphthalene (30.3 g, 0.16 mol) *in carbon tetrachloride (600 ml) at 70—71 °C. After stirring* at 70 °C for 30 min, the solution was concentrated and the residue was recrystallized from carbon tetrachloride to give 32.4 g (58%) of **5**, mp 187—189 °C (lit,[17] 187 °C). Found: C, 41.64; H, 2.93%. Calcd for $C_{12}H_{10}O_2Br_2$: C, 41.65; H, 2.91%.

1,4,5,8-Tetramethoxynaphthalene (6). A 6 from 5. A mixture of 4,8-dibromo-1,5-dimethoxynaphthalene (11 g, 32 mmol), sodium methoxide (5.7 g, 106 mmol), copper(I) iodide (20 g, 106 mmol), *N,N*-dimethylformamide (360 ml) and methanol (360 ml) was refluxed for 30 h. The cooled mixture was poured into ice water and the resulting precipitate was filtered, washed with water and dried. It was extracted with chloroform, and evaporation of the solvent gave a solid residue which was chromatographed on alumina. The fractions taken from the column were recrystallized from ligroin to give 6.66 g (84%) of **6** as white needles, mp 168.5—169 °C (lit.,[17] 167—168 °C). Found: C, 67.53; H, 6.58%. Calcd for $C_{14}H_{16}O_4$: C, 67.73; H, 6.50%.

B 6 from 8. 5,8-Dimethoxy-1,4-naphthoquinone (**8**) was prepared according to the method described in the literature.[20] To a solution of the quinone **8** (2.19 g, 10 mmol) in methanol (10 ml) was added 40% aqueous sodium hydroxide (5 ml). The solution was alternatively

treated with sodium dithionite (8.5 g, 49 mmol) in water (10 ml), and dimethyl sulfate (6 g, 49 mmol) under reflux for 8 h. After cooling, the reaction mixture was diluted with water and extracted with chloroform. The chloroform solution was washed with brine, dried, and evaporated. The residue was chromatographed on alumina and recrystallized from ligroin to give 1.20 g (48%) of **6**, mp 168—169 °C.

C. 6 from Naphthazarin. To a solution of naphthazarin (0.19 g, 1 mmol) in ether (40 ml) was added sodium dithionite (0.53 g, 3 mmol) in water (10 ml) with stirring. After 30 min, the solution was alternatively treated with sodium hydroxide (5 g) in water (10 ml) and dimethyl sulfate (7.5 g, 60 mmol) at room temperature for 3 h. To the solution was again added the above-mentioned amounts of aqueous sodium hydroxide, dimethyl sulfate and aqueous sodium dithionite; and the mixture was then stirred at room temperature for 12 h. The reaction mixture was acidified by the addition of hydrochloric acid and extracted with chloroform. After the usual work-up, column chromatography on alumina gave 0.11 g (44%) of **6**, mp 167—168 °C.

2-Formyl-1,4,5,8-tetramethoxynaphthalene (7). A solution of **6** (6.0 g, 25 mmol) in chloroform (50 ml) was added to a mixture of phosphoryl chloride (19.0 g, 125 mmol) and *N,N*-dimethylformamide (9.0 g, 125 mmol) and the mixture was refluxed for 6 h. It was then decomposed with ice water and extracted with chloroform. The chloroform solution was washed with brine and dried over anhydrous sodium sulfate. Evaporation of the solvent gave a residue which could be recrystallized from hexane-benzene to afford 6.72 g (99%) of **7** as yellow crystals, mp 124—125.5 °C. IR (KBr) 1673 (C=O), 2845, and 1067 cm^{-1} (OCH_3); MS *m/z* 276 (M^+) and 248 (M^+-CO); ^1H NMR ($CDCl_3$) δ=3.91, 3.92, 3.98, 3.99 (each s, 3H, OCH_3), 6.96, 7.00, 7.20 (3H, ArH), and 10.56 (s, 1H, CHO). Found: C, 65.44; H, 5.94%. Calcd for $C_{15}H_{16}O_5$: C, 65.21; H, 5.84%.

2-(1-Hydroxy-4-methylpentyl)-1,4,5,8-tetramethoxynaphthalene (9). The aldehyde **7** (2.0 g, 7.3 mmol) was added to the Grignard solution of isopentylmagnesium bromide (21.9 mmol) in tetrahydrofuran (40 ml) and the mixture was stirred at room temperature for 3 h, decomposed with aqueous ammonium chloride and extracted with chloroform. The chloroform solution was treated as usual and left a crude oil. This oil was purified by alumina chromatography to give 2.4 g (95%) of **9**. IR (neat) 3470 (OH) and 1065 cm^{-1} (OCH_3); MS *m/z* 348 (M^+) and 330 (M^+-H_2O); ^1H NMR ($CDCl_3$) δ=0.83, 0.92 (6H, $2CH_3$) 1.1—1.9 (5H, $2CH_2$, CH), 2.22 (1H, OH), 3.74 (s, 3H, OCH_3), 3.89 (s, 3H, OCH_3), 3.93 (s, 6H, $2OCH_3$), 5.20 (t, 1H, -C<u>H</u>(OH)-), 6.81 (s, 2H, ArH), and 6.97 (s, 1H, ArH).

2-(1-Methoxy-4-methylpentyl)-1,4,5,8-tetramethoxynaphthalene (10). A solution of the alcohol **9** (0.61 g, 1.76 mmol) in dry tetrahydrofuran (15 ml) was chilled to 0—5 °C, and sodium hydride (ca. 60% in oil, 0.35 g, 8.8 mmol) was added. Methyl iodide (1.25 g, 8.8 mmol) was added to this solution at 0—5 °C with strring. The mixture was allowed to stand overnight at room temperature, then poured into ice water, and extracted with chloroform. The chloroform solution was washed with brine and dried over anhydrous sodium sulfate. The solvent was removed by a rotary evaporator to give an oil. Chromatography on alumina with chloroform as an eluent gave a purified oil of **10** (0.51 g, 81%). IR (neat) 2840 and 1060 cm^{-1} (OCH_3); MS *m/z* 362 (M^+), 330, and 291; ^1H NMR ($CDCl_3$) δ=0.83, 0.91 (6H, $2CH_3$), 1.1—1.9 (m, 5H, $2CH_2$ and CH), 3.24 (s, 3H, -CH($OC\underline{H}_3$)-), 3.76, 3.90 (each s, 3H, OCH_3), 3.94 (s, 6H, $2OCH_3$), 4.78 (t, 1H, -C<u>H</u>(OCH_3)-), 6.83 (s, 2H, ArH), 6.92 (s, 1H, ArH). Found: C, 69.00; H, 8.22%. Calcd for $C_{21}H_{30}O_5$: C, 69.59; H, 8.34%.

2-(1-Methoxy-4-methylpentyl)-5,8-dimethoxy-1,4-naphthoquinone (11). A solution of the ester **10** (1.34 g, 3.7 mmol) in acetonitrile (30 ml) was cooled in an ice bath. To this solution was added a solution of cerium(IV) ammonium nitrate (6 g, 11.1 mmol) in water (10 ml). The mixture was stirred for 30 min, diluted with water, and extracted with chloroform. After working up as usual, the crude product was purified by silica-gel chromatography to yield 0.52 g (42%) of **11**, mp 97—99 °C. IR (KBr) 1655(C=O) and 1060 cm^{-1} (OCH_3); MS *m/z* 332 (M^+), 317, and 216; ^1H NMR($CDCl_3$) δ=0.82, 0.90 (6H, $2CH_3$), 1.1—2.0 (m, 5H, $2CH_2$ and CH), 3.29 (s, 3H, OCH_3), 3.97 (s, 6H, $2OCH_3$), 4.43 (t, 1H, -C<u>H</u>(OCH_3)-), 6.78 (s, 1H, quinonoid ring H), 7.32 (s, 2H, benzenoid ring H).

5,8-Dihydroxy-2-(1-methoxy-4-methylpentyl)-1,4-naphthoquinone (12). A solution of 1,4-naphthoquinone **11** (0.18 g, 0.54 mmol) in dichloromethane (8 ml) was cooled in an ice bath. Aluminum chloride (1 g, 5.4 mmol) was added to this solution and the mixture was stirred at room temperature for 1 h. The reaction mixture was decomposed by the addition of ice water and extracted with ether. The usual work-up and purification of the crude product by silica-gel chromatography gave 80 mg (49%) of **12** as a viscous oil. IR (KBr) 1610 (C=O), 1570, and 1100 cm^{-1}; MS *m/z* 304 (M^+), 277, 232, and 229; ^1H NMR ($CDCl_3$) δ=0.83, 0.92 (6H, $2CH_3$), 1.1—1.9 (m, 5H, $2CH_2$ and CH), 3.32 (s, 3H, OCH_3), 4.50 (t, 1H, -C<u>H</u>(OCH_3)-), 7.12 (s, 1H, quinonoid ring H), 7.17 (s, 2H, benzenoid ring H), 12.49 and 12.59 (each s, 1H, ArOH).

2-(1-Hydroxy-4-methylpentyl)-5,8-dimethoxy-1,4-naphthoquinone (13). A solution of the alcohol **9** (1.3 g, 3.7 mmol) in acetonitrile (15 ml) was cooled to 10—20 °C. To this solution was added dropwise a solution of cerium(IV) ammonium nitrate(5.1 g, 9.25 mmol) in water (15 ml) under stirring. The reaction mixture was stirred at room temperature for 30 min, diluted with water and extracted with chloroform. Usual work-up and chromatography on silica-gel gave two products as viscous oils. The first eluate gave 0.20 g (17%) of an isomer of **13**, 6-(1-hydroxy-4-methylpentyl)-5,8-dimethoxy-1,4-naphthoquinone. IR (KBr) 3500 (OH), 1650 (C=O), 1580, 1560, and 1050 cm^{-1}; ^1H NMR ($CDCl_3$) δ=0.84, 0.93 (6H, $2CH_3$), 1—2 (m, 5H, $2CH_2$ and CH), 2.60 (broad, 1H, OH), 3.82 (s, 3H, OCH_3), 3.96 (s, 3H, OCH_3), 5.16 (m, 1H, -C<u>H</u>(OH)-), 6.77 (2H, quinonoid ring 2H), and 7.51 (s, 1H, benzenoid ring H).

The second eluate gave 0.62 g (52%) of **13**. IR (KBr) 3500 (OH), 1650 (C=O), 1580, 1560, and 1050 cm^{-1}; ^1H NMR ($CDCl_3$) δ=0.84, 0.93 (6H, $2CH_3$), 1—2 (m, 5H, $2CH_2$ and CH), 2.60 (broad, 1H, OH), 3.96 (s, 6H, $2OCH_3$), 4.70 (m, 1H, -C<u>H</u>(OH)-), 6.77 (1H, quinonoid ring H), and 7.31 (s, 2H, benzenoid ring H).

5,8-Dihydroxy-2-(1-hydroxy-4-methylpentyl)-1,4-naphthoquinone (14) and 5,8-Dihydroxy-2-(4-methylpentyl)-1,4-naphthoquinone (15). A, Demethylation with $AlCl_3$. Aluminum chloride (41 mg, 3.1 mmol) was added to a solution of the quinone **13** (98 mg, 0.31 mmol) in dichloromethane (5 ml) cooled in an ice bath. The reaction

mixture was stirred at room temperature for 1 h, decomposed by the addition of water (50 ml) and 5% aqueous oxalic acid (100 ml), and extracted with chloroform. After the usual work-up, the crude product was purified by silica-gel chromatography to yield two crystalline products: 22 mg (26%) of **15** from the first eluate, mp 55—70 °C (lit,[26] 99 °C). IR (KBr) 1609 (C=O) and 1570 cm^{-1}; MS *m/z* 274 (M^+), 205, and 204. Calcd for $C_{16}H_{18}O_4$: *m/z* 274.1205, Found: 274.1210. ^1H NMR ($CDCl_3$) δ=0.85, 0.94 (6H, $2CH_3$), 1.1—1.9 (m, 5H, $2CH_2$ and CH), 2.60 (t, 2H, *J*=7 Hz, $ArCH_2$-), 6.85 (s, 1H, quinonoid ring H), 7.20 (s, 2H, benzenoid ring H), 12.47 and 12.62 (each s, 1H, ArOH).

The second eluate gave 43 mg (48%) of **14**, mp 78—81 °C (lit,[6] 100—107 °C). IR (KBr) 3600—3100 (broad, OH), 1610 (C=O), 1570, and 1065 cm^{-1} (OH); MS Found: *m/z* 290.1143. Calcd: 290.1154. ^1H NMR ($CDCl_3$) δ=0.85, 0.95 (6H, $2CH_3$), 1.1—2.0 (m, 5H, $2CH_2$ and CH), 2.24 (broad, 1H, -CH(O<u>H</u>)-), 4.87 (t, 1H, -C<u>H</u>(OH)-), 7.14 (s, 1H, quinonoid ring H), 7.19 (s, 2H, benzenoid ring H), 12.46 and 12.58 (each s, 1H, ArOH). Found: C, 65.95; H, 6.45%. Calcd for $C_{16}H_{18}O_5$: C, 66.20; H, 6.25%.

B Demethylation with AgO-HNO_3. To a solution of the quinone **13** (1.10 g, 3.5 mmol) and AgO (4.27 g, 35 mmol) in acetone (50 ml), was added dropwise 40% HNO_3 (45 ml) at 15—20 °C over 5 min. The mixture was stirred at room temperature for 5 min and extracted with dichloromethane (100 ml). The dichloromethane solution was washed with brine and dried over Na_2SO_4. The solvent was evaporated and the crude product was purified by silica-gel chromatography to afford 0.21 g (28%) of **14**, mp 79.5—81.5 °C.

5,8-Diacetoxy-(1-acetoxy-4-methylpentyl)-1,4-naphthoquinone (16). Acetic anhydride (1 ml) was added to a solution of dihydroshikalkin **14** (65 mg, 0.224 mmol) in pyridine (2.5 ml) at 0—5 °C, and stirred at 0—5 °C for 2 h. After concentration under reduced pressure at room temperature, the crude product was chromatographed on silica-gel to give 85 mg (91%) of **16**, mp 98—100 °C. IR (KBr) 1775 (ester C=O), 1745 (ester C=O), 1667 (quinone C=O), and 1188 cm^{-1}; MS *m/z* 374, 332, 272, 229, and 43 (CH_3CO^+), and no parent peak was observed. ^1H NMR ($CDCl_3$) δ=0.83, 0.92 (6H, $2CH_3$), 1.1—1.9 (m, 5H, $2CH_2$ and CH), 2.11 (s, 3H, -CH(OCOC<u>H</u>$_3$)-), 2.43 (s, 6H, ArOAc), 5.82 (t, 1H, -C<u>H</u>(OCOCH$_3$)-), 6.65 (s, 1H, quinonoid ring H), and 7.37 (s, 2H, benzenoid ring H).

4-Bromo-2-butanone Ethylene Acetal (17). Hydrogen bromide was bubbled into a freshly distilled methyl vinyl ketone (192 g, 2.74 mol) to saturate for 5 h at −80 °C; then the solution gradually solidified. To this solution was added ethylene glycol (340 g, 5.48 mol) and *p*-toluenesulfonic acid monohydrate (10 g, 0.052 mol) at −80 °C; the mixture was then stirred at −80—−40 °C for 3 h. Acetonitrile (250 ml) was added to the mixture and the solvent was evaporated at room temperature under reduced pressure; this procedure was repeated 3 times. The solution was combined with 1 M† KOH (1000 ml) and the product was extracted with hexane. After the usual work-up, the crude product was distilled under reduced pressure to yield 143 g (28%) of **17**, bp 55—56 °C/1.5 mmHg (lit,[28] 64—68 °C/9 mmHg). Found: C, 37.06; H, 5.78%. Calcd for $C_6H_{11}O_2Br$: C, 36.95; H, 5.68%.

2-[4,4-(Ethylenedioxy)-1-hydroxypentyl]-1,4,5,8-tetramethoxynaphthalene 18. The Grignard solution of the ethylene acetal **17** (26.3 mmol) in tetrahydrofuran (30 ml) was added to the aldehyde **7** (2.4 g, 8.76 mmol) and the reaction mixture was stirred at room temperature for 3 h. After a decomposition with aqueous ammonium chloride, extraction with chloroform, and usual procedures, the crude product was purified by chromatography on alumina with chloroform to give 3.28 g (96%) of **18** as an oil. IR (neat) 3480 (OH), 2850 (OCH_3), and 1060 cm^{-1} (OCH_3); MS *m/z* 392 (M^+), 374 (M^+-H_2O), and 330; ^1H NMR ($CDCl_3$) δ=1.34 (s, 3H, CH_3), 1.6—2.2 (m, 5H, $2CH_2$ and OH), 3.76 (s, 3H, OCH_3), 3.89 (s, 3H, OCH_3), 3.94 (s, 4H, $2CH_2$), 3.96 (s, 6H, $2OCH_3$), 5.20 (t, 1H, CH), 6.82 (s, 2H, ArH), and 7.01 (s, 1H, ArH).

2-(1-Methoxy-4-oxopentyl)-1,4,5,8-tetramethoxynaphthalene (19). A solution of the alcohol **18** (3.28 g, 8.4 mmol) in dry tetrahydrofuran (30 ml) was cooled to 0—5 °C, and sodium hydride (ca. 60% in oil, 1 g, 25.2 mmol) was added. Methyl iodide (5.94 g, 25.2 mmol) was added at 0—5 °C, and the mixture was allowed to stand at room temperature overnight; then it was poured into ice water and extracted with chloroform. The chloroform solution was washed with brine and dried over Na_2SO_4. After removing the solvent an oil was obtained. To the solution of this oily product in acetone (10 ml) was added *p*-toluenesulfonic acid monohydrate (100 mg). The solution was kept in a freezer for 3 h, diluted with ice water, and extracted with chloroform. After the usual work-up, the crude product was purified by silica-gel chromatography to yield **19** (1.73 g, 57%) as an oil. IR (neat) 2850 (OCH_3), 1710 (C=O), and 1060 cm^{-1} (OCH_3); MS *m/z* 362 (M^+), and 315; ^1H NMR ($CDCl_3$) δ=2.14 (s, 3H, $COCH_3$), 2.0—2.8 (m, 4H, $2CH_2$), 3.23 (s, 3H, -CH(OC<u>H</u>$_3$)-), 3.76 (s, 3H, OCH_3), 3.89 (s, 3H, OCH_3), 3.94 (s, 6H, $2OCH_3$), 4.78 (t, 1H, CH), 6.84 (s, 2H, ArH), 6.89 (s, 1H, ArH). Found: C, 65.66; H, 7.40%. Calcd for $C_{20}H_{26}O_6$: C, 66.28; H, 7.23%.

2-(4-Hydroxy-1-methoxy-4-methylpentyl)-1,4,5,8-tetramethoxynaphthalene (20). Methylmagnesium iodide (6.5 mmol) in ether (10 ml) was added to a solution of the ketone **19** (0.47 g, 1.3 mmol) in tetrahydrofuran (20 ml) at 0—5 °C and the mixture was stirred at room temperature for 3 h. After decomposition with aqueous ammonium chloride, extraction with chloroform, and usual procedure, a crude oil was chromatographed on alumina to afford 0.42 g (86%) of **20**. IR (neat) 3470 (OH), 2845, and 1075 cm^{-1}; MS *m/z* 378 (M^+), 360 (M^+-H_2O), and 291; ^1H NMR ($CDCl_3$) δ=1.20 (s, 6H, $2CH_3$), 1.4—2.0 (m, 4H, $2CH_2$), 2.21 (s, 1H, OH), 3.25 (s, 3H, -CH(OC<u>H</u>$_3$)-), 3.76 (s, 3H, OCH_3), 3.90 (s, 3H, OCH_3), 3.94 (s, 6H, $2OCH_3$), 4.81 (t, 1H, -C<u>H</u>(OCH_3)-), 6.83 (s, 2H, ArH), and 6.92 (s, 1H, ArH).

2-(1-Methoxy-4-methyl-3-pentenyl)-1,4,5,8-tetramethoxynaphthalene (21) and 2-(1-Methoxy-4-methyl-4-pentenyl)-1,4,5,8-tetramethoxynaphthalene (22). Alcohol **20** (191 mg, 0.51 mmol) in dry pyridine (1 ml) was treated with thionyl chloride (70 mg, 0.61 mmol) at 0—5 °C. This mixture was kept in a freezer for 17 h, diluted with ice water and extracted with chloroform. The chloroform solution was washed with dil hydrochloric acid, aqueous sodium hydrogencarbonate, brine, and dried over Na_2SO_4. The solvent removal provided a crude oil which was shown by GLC analysis to be a mixture of **21** and **22** (5:3). The chromatographic separation using alumina succeeded in giving two pure oils. The former eluate gave 62 mg of **22**. IR (neat) 1648 (C=CH_2),

† 1 M=1 mol dm^{-3}.

885 ($C=CH_2$), 1602, and 1073 cm^{-1}; MS *m/z* 306 (M^+); ^1H NMR ($CDCl_3$) δ=1.55 (s, 3H, $CH_2=C(C\underline{H}_3)$-), 1.8—2.2 (m, 4H, $2CH_2$), 3.25 (s, 3H, $CH(OC\underline{H}_3)$), 3.76 (s, 3H, OCH_3), 3.90 (s, 3H, OCH_3), 3.95 (s, 6H, $2OCH_3$), 4.73 (s, 2H, $C\underline{H}_2=C(CH_3)$-), 6.83 (s, 2H, ArH), and 6.94 (s, 1H, ArH).

The latter eluate afforded 104 mg of **21**. IR (neat) 1602, and 1073 cm^{-1}; MS *m/z* 360 (M^+), 328, and 291; ^1H NMR ($CDCl_3$) δ=1.55, 1.69 (6H, $2CH_3$), 2.50 (t, 2H, CH_2), 3.24 (s, 3H, -$CH(OC\underline{H}_3)$-), 3.75 (s, 3H, OCH_3), 3.90 (s, 3H, OCH_3), 3.95 (s, 6H, $2OCH_3$), 4.85 (t, 1H, *J*=6.6 Hz, -$C\underline{H}(OCH_3)$-), 5.26 (t, 1H, *J*=7.1 Hz, $(CH_3)_2C=C\underline{H}$-), 6.83 (s, 2H, ArH), and 6.95 (s, 1H, ArH). Found: C, 69.73; H, 7.85%. Calcd for $C_{21}H_{28}O_5$: C, 69.98; 7.83%.

5,8-Dihydroxy-1,4-naphthoquinone (Naphthazarin) (23). To a solution of 1,4,5,8-tetramethoxynaphthalene (**6**) (124 mg, 5 mmol) in dichloromethane (6 ml) was added dropwise BBr_3 (0.5 g, 20 mmol) in dichloromethane (6 ml) at −70 °C. After stirring at −70 °C for 2 h, the solution was allowed to warm to room temperature and to stand overnight. It was then poured into ice water and extracted with ether. After the usual work-up, sublimation of the crude product afforded 65 mg (68%) of pure **23**, mp 200—202 °C (lit,[31] 201—202 °C). IR (KBr) 1610 (C=O), 1565, and 1225 cm^{-1}; MS *m/z* 190 (M^+), 136, 134, and 108; ^1H NMR ($CDCl_3$) δ= 7.14 (s, 4H, ArH), and 12.39 (s, 2H, ArOH).

5,8-Dihydroxy-2-(5,5-dimethyl-2-tetrahydrofuranyl)-1,4-naphthoquinone (3). To the above obtained olefin **21** (119 mg, 0.33 mmol) dissolved in dichloromethane (2.5 ml) was added dropwise BBr_3 (248 mg, 0.99 mmol) in dichloromethane (2.5 ml) at −78 °C. After stirring at −78 °C for 2 h, the solution was allowed to warm to room temperature and to stand overnight. The solution was then poured into aqueous 1 M sodium hydroxide (30 ml) cooled in an ice bath, stirred for 1 h, and centrifuged to settle the precipitate. To the clean layer was added aqueous ammonium chloride (300 ml) and extracted with ether. After the usual work-up, column chromatography of the residue on silica gel afforded 5 mg (5%) of **3**, mp 79—80.5 °C (lit,[9a] 79—80 °C). IR (KBr) 1610 (C=O), 1570, and 1065 cm^{-1}; MS *m/z* 288 (M^+), and 219; ^1H NMR ($CDCl_3$) δ=1.36 (s, 6H, $2CH_3$), 1.80—1.85 and 2.39—2.81 (m, 4H, $2CH_2$), 5.14 (t, 1H, CH), 7.19 (s, 3H, ArH), and 12.51 (s, 2H, ArOH).

2-(1-Hydroxy-4-oxopentyl)-1,4,5,8-tetramethoxynaphthalene (25). A solution of the acetal **18** (7.53 g, 19.2 mmol) in acetone (30 ml) was cooled to 0—5 °C and *p*-toluenesulfonic acid monohydrate (250 mg) was added. The solution was kept in a refrigerator for 3 h with occasional shaking, diluted with ice water, and extracted with chloroform. After the usual work-up, the crude product was purified by chromatography of alumina to give 5.8 g (87%) of **25** as an oil. IR (neat) 3450 (OH), 1705 (C=O), 1600, and 1062 cm^{-1}; MS Found: *m/z* 348.1577. Calcd for $C_{19}H_{24}O_6$: *m/z* 348.1573. ^1H NMR ($CDCl_3$) δ=2.15 (s, 3H, $COCH_3$), 1.8—2.8 (m, 5H, $2CH_2$ and OH), 3.74 (s, 3H, OCH_3), 3.88 (s, 3H, OCH_3), 3.93 (s, 6H, $2OCH_3$), 5.21 (t, 1H, *J*=6.6 Hz, -$C\underline{H}(OH)$-), 6.81 (s, 2H, ArH), and 6.98 (s, 1H, ArH).

2-(1,4-Dihydroxy-4-methylpentyl)-1,4,5,8-tetramethoxynaphthalene (26). Methylmagnesium iodide (0.15 mol) in ether (30 ml) was added to a solution of ketone **25** (6.26 g, 0.018 mol) in tetrahydrofuran (120 ml) at 0—5 °C, and the mixture was stirred at room temperature for 3 h. After the usual procedures, the crude product was purified by alumina chromatography to afford 5.62 g (86%) of **26**. Recrystallization from ligroin-benzene (4:1) gave crystals, mp 114—115 °C. IR (KBr) 3400 (broad, OH), 1600, and 1070 cm^{-1}; MS Found: *m/z* 364.1900; Calcd: 364.1884. ^1H NMR ($CDCl_3$) δ=1.25 (s, 6H, $2CH_3$), 1.6—2.2 (m, 6H, $2CH_2$ and 2OH), 3.76, 3.89, 3.94, 3.95 (each s, 3H, OCH_3), 5.25 (t, 1H, -$C\underline{H}(OH)$-), 6.82 (s, 2H, ArH), and 7.01 (s, 1H, ArH). Found: C, 65.23; H, 7.73%. Calcd for $C_{20}H_{28}O_6$: C, 65.92; H, 7.74%.

2-(1,4-Dihydroxy-4-methylpentyl)-5,8-dimethoxy-1,4-naphthoquinone (27). A solution of cerium(IV) ammonium nitrate (7.57 g, 14 mmol) in water (25 ml) was added dropwise to a solution of the ether **26** (2.01 g, 6 mmol) in a mixed solvent of chloroform (5 ml) and acetonitrile (25 ml) at room temperature for 5 min. The mixture was stirred at room temperature for 10 min, diluted with ice water, and extracted with chloroform. After the usual work-up, the chromatography on alumina gave two products. The first eluate gave 0.28 g (15%) of an isomer of **27**, 6-(1,4-dihydroxy-4-methylpentyl)-5,8-dimethoxy-1,4-naphthoquinone, as a viscous oil. IR (KBr) 3430, 1650, 1588, and 1052 cm^{-1}; MS Found: *m/z* 334.1429. Calcd for $C_{18}H_{22}O_6$: 334.1417. ^1H NMR ($CDCl_3$) δ=1.24 (s, 6H, $2CH_3$), 1.5—2.1 (m, 4H, $2CH_2$), 2.2—2.6 (broad, 2H, OH), 3.81 (s, 3H, OCH_3), 3.99 (s, 3H, OCH_3), 5.15 (m, 1H, CH), 6.76 (s, 2H, quinonoid ring H), and 7.58 (s, 1H, benzenoid ring H).

The second eluate gave 1.29 g (70%) of **27**. Recrystallization from ligroin-benzene-chloroform mixture gave crystals, mp 127.5—130.5 °C. IR (KBr) 3430 (broad, OH), 1650 (C=O), 1588, and 1052 cm^{-1}; MS *m/z* 334 (M^+); ^1H NMR ($CDCl_3$) δ=1.24 (s, 6H, $2CH_3$), 1.5—2.1 (m, 4H, $2CH_2$), 2.2—2.6 (broad, 2H, 2OH), 3.94 (s, 6H, $2OCH_3$), 4.77 (m, 1H, CH), 6.84 (d, 1H, quinonoid ring H), and 7.29 (s, 2H, benzenoid ring H). Found: C, 64.06; H, 6.73%. Calcd for $C_{18}H_{22}O_6$: C, 64.66; H, 6.63%.

2-(1,4-Dihydroxy-4-methylpentyl)-5,8-dihydroxy-1,4-naphthoquinone (28). To a mixture of the 1,4-naphthoquinone **27** (503 mg, 1.51 mmol) and AgO (1.86 g, 15.1 mmol) in acetone (35 ml) was added 40% HNO_3 (28 ml) at 15—20 °C over 10 min. The reaction mixture was stirred at room temperature for 10 min and extracted with chloroform. The chloroform solution was washed with brine and dried over Na_2SO_4. The solvent was removed to give a crude product; this was purified by silica-gel chromatography to afford 124 mg (27%) of **28**, mp 151—152 °C. IR (KBr) 3300, 3200 (each broad, OH), 1610 (C=O), 1570, 1210, and 1080 cm^{-1}; MS Found: *m/z* 306.1079; Calcd: 306.1103. ^1H NMR ($CDCl_3$) δ=1.25 (s, 6H, $2CH_3$), 1.5—2.7 (m, 6H, $2CH_2$ and 2OH), 4.93 (t, 1H, -$C\underline{H}(OH)$-), 7.19 (s, 3H, ArH), 12.49 and 12.59 (each s, 1H, ArOH). Found: C, 62.43; H, 6.00%. Calcd for $C_{16}H_{18}O_6$: C, 62.74; H, 5.92%.

5,8-Diacetoxy-2-(1-acetoxy-4-hydroxy-4-methylpentyl)-1,4-naphthoquinone (29). Acetic anhydride (1 ml) was added to a solution of the tetraol **28** (69 mg, 0.225 mmol) in pyridine (2 ml) at 0—5 °C, and the mixture was stirred at 0—5 °C for 2 h. Excess of the reagent was removed under reduced pressure at room temperature, and the crude product was chromatographed on silica-gel to give 86 mg (88%) of the triacetate **29**. Recrystallization from ligroine-benzene gave crystals, mp 156.5—158.5 °C. IR (KBr) 3500 (broad, OH), 1770 (ester C=O), 1740 (ester C=O), 1660 (quinone C=O), and 1185 cm^{-1}; MS *m/z* 372, 371 (M^+−61),

288, 232, 219, and 43 (CH_3CO^+), and no parent peak was observed. ^1H NMR ($CDCl_3$) δ=1.20 (s, 6H, $2CH_3$), 1.4—2.4 (m, 5H, $2CH_2$ and OH), 2.12 (s, 3H, CH(OCOC$\underline{H}_3$)), 2.43 (s, 6H, ArOCOC$\underline{H}_3$), 5.87 (t, 1H, CH), 6.66 (s, 1H, ArH), and 7.37 (s, 2H, ArH). Found: C, 61.04; H, 5.57%. Calcd for $C_{22}H_{24}O_9$: C, 61.11; H, 5.59%.

5,8-Diacetoxy-2-(1-acetoxy-4-methyl-3-pentenyl)-1,4-naphthoquinone (30) and 5,8-Diacetoxy-2-(1-acetoxy-4-methyl-4-pentenyl)-1,4-naphthoquinone (31). The triacetate **29** (213 mg, 0.49 mmol) in dry pyridine (1.5 ml) was chilled to −38 °C, and thionyl chloride (70.4 mg, 0.59 mmol) was added. The mixture was stirred at −38 °C for 7 min and then poured into ice water. The reaction mixture was extracted with dichloromethane, and washed with brine, dried over Na_2SO_4, and concentrated. Column chromatography of the residue on silica-gel brought two viscous oils of **30** and **31** (3:1). The former eluate gave 23 mg (12%) of **31**. IR (KBr) 1770 (ester C=O), 1750 (ester C=O), 1665 (quinone C=O), and 888 cm^{-1} (C=C); ^1H NMR ($CDCl_3$) δ=1.56 (s, 3H, CH_2=C($C\underline{H}_3$)-), 1.9—2.5 (m, 4H, $2CH_2$), 2.09 (s, 3H, -CH(OCOC$\underline{H}_3$)-), 2.43 (s, 6H, ArOCOCH_3), 4.69 (s, 2H, $C\underline{H}_2$=C(CH_3)-), 5.87 (t, 1H, CH), 6.65 (s, 1H, ArH), and 7.37 (s, 2H, ArH).

The latter eluate afforded 70 mg (34%) of **30**. IR (KBr) 1770, 1750 (each ester C=O), and 1665 cm^{-1} (quinone C=O); ^1H NMR ($CDCl_3$) δ=1.56, 1.67 (6H, $2CH_3$), 1.9—2.5 (m, 4H, $2CH_2$), 2.09 (s, 3H, -CH(OCOC$\underline{H}_3$)-), 2.43 (s, 6H, ArOCOCH_3), 5.07 (t, 1H, $(CH_3)_2$C=C$\underline{H}$-), 5.87 (t, 1H, -C$\underline{H}$(OAc)-), 6.65 (s, 1H, ArH), and 7.37 (s, 2H, ArH).

5,8-Dihydroxy-(1-hydroxy-4-methyl-3-pentenyl)-1,4-naphthoquinone (24). The triacetate of the internal olefin **30** (63 mg, 0.15 mmol) was dissolved in aqueous 1 M sodium hydroxide (50 ml) and stirred during 3 h. The solution was filtered and the filtrate was acidified by addition of acetic acid until the solution turned red. The product was extracted with dichloromethane, washed with aqueous sodium hydrogencarbonate, brine, and dried over Na_2SO_4. The solvent was evaporated and the crude product was purified by silica-gel chromatography to afford 16 mg (37%) of **24**, mp 146—148 °C (lit,[9a] 148 °C). IR (KBr) 3400, 3100 (each broad, OH), 1613 (C=O), 1570, and 1075 cm^{-1}; MS Found: *m/z* 288.0999. Calcd: *m/z* 288.0997. ^1H NMR ($CDCl_3$) δ=1.66, 1.76 (6H, $2CH_3$), 2.1—2.9 (m, 3H, CH_2 and OH), 4.97 (t, 1H, -C$\underline{H}$(OH)-), 5.19 (t, 1H, (CH_3)C=C$\underline{H}$-), 7.20 (s, 3H, ArH), 12.49 and 12.59 (each s, 1H, ArOH). Found C, 66.34; H, 5.60%. Calcd for $C_{16}H_{16}O_5$: C, 66.66; H, 5.59%.

Isolation of Shikonin 1-a. Shikonin **1-a** was isolated from "Ko-shikon" according to the procedure described by Toribara,[9b] mp 146—147.5 °C (lit,[13] 147—149 °C). Found: C, 66.32; H, 5.66%. Calcd for $C_{16}H_{16}O_5$: C, 66.66; H, 5.59%.

We thank Mr. Takayuki Ōmori and Mr. Takeshi Hanamoto for their technical assistances, Mr. Yoshiharu Okada for the elemental analyses, Mrs. Miyako Kage for the NMR spectra, and Mrs. Keiko Yamaguchi for the MS spectra. We also thank Professor Alfred Hassner (Bar Ilan University, Israel) for reading this manuscript.

References

1) Paper II on Synthesis of Naphthoquinone Derivatives. For paper I, see Ref. 15.
2) I. Morimoto, T. Kishi, S. Ikegami, and Y. Hirata, *Tetrahedron Lett.*, **1965**, 4737.
3) I. Morimoto, and Y. Hirata, *Tetrahedron Lett.*, **1966**, 3677.
4) M. Hayashi, *Folia Pharmacol. Japon.*, **73**, 193 (1977).
5) K. Kyogoku, H. Terayama, Y. Tachi, T. Suzuki, and M. Komatsu, *Syoyakugaku Zasshi*, **27**, 31 (1973); Y. Tanaka and T. Odani, *Yakugaku Zasshi*, **92**, 525 (1972).
6) U. Sankawa, Y. Ebizuka, T. Miyazaki, Y. Isomura, H. Otsuka, S. Shibata, M. Inomata, and F. Fukuoka, *Chem. Pharm. Bull.*, **25**, 2392 (1977).
7) T. Yoshioka, "Tennen Senryo no Kenkyū," Mitsumura Suiko Shoin, Kyōto (1974), p. 157.
8) H. Futagoishi and T. Abe, *Cosmet. Perfumery*, **88**, 51 (1973).
9) a) H. Brockmann, *Justus Liebigs Ann. Chem.*, **521**, 1 (1935); b) T. Y. Toribara and A. L. Underwood, *Anal, Chem.*, **21**, 1352 (1949).
10) V. P. Papageorgiou, *Planta Med.*, **38**, 193 (1980).
11) a) C. Kuroda, *J. Chem. Soc. Tokyo*, **39**, 1051 (1918). b) C. Kuroda, and M. Wada, *Sci. Papers Inst. Phys. Chem. Research (Tokyo)*, **34**, 1740 (1938).
12) H. Arakawa and M. Nakazaki, *Chem. and Ind. (London)*, **1961**, 947.
13) S. Coffey, "Rodd's Chemistry of Carbon Compounds," Elsevier Sci. Publ., Amsterdam (1978), III G, p. 238.
14) U. Sankawa, H. Otsuka, Y. Kataoka, Y. Iitaka, A. Hoshi, and K. Kuretani, *Chem. Pharm. Bull.*, **29**, 116 (1981).
15) A. Terada, Y. Tanoue, A. Hatada, and H. Sakamoto, *J. Chem. Soc., Chem. Commun.*, **1983**, 987.
16) W. H. Benthey, R. Robinson, and C. Weizmann, *J. Chem. Soc.*, **1907**, 104.
17) A. H. Carter, E. Race, and F. M. Rowe, *J. Chem. Soc.*, **1942**, 236.
18) A. Zweig, A. H. Maurer, and B. G. Roberts, *J. Org. Chem.*, **32**, 1332 (1967).
19) R. G. R. Bacon and S. C. Rennison, *J. Chem. Soc. (C)*, **1969**, 312; A. Mckillop, B. D. Howorth, and R, J. Kobylecki, *Synth. Commun.*, **4**, 35 (1974).
20) I. M. Godfrey, M. V. Sargent, and J. A. Elix, *J. Chem. Soc., Perkin Trans. 1*, **1974**, 1353.
21) D. B. Bruce and R. H. Thomson, *J. Chem. Soc.*, **1955**, 1089.
22) The ^1H NMR spectrum of **11** showed signals at δ 6.78 (1H) due to quinonoid ring proton and 7.32 (2H) due to benzenoid ring proton. Because signals of quinonoid ring protons are usually observed at upper field than those of benzenoid ring protons.

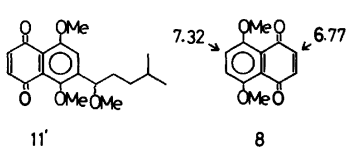

11 8

Fig. 11.

The structure 11′ was excluded because of these two protons being in the quinonoid ring. These are also supported with the NMR spectrum of dimethoxynaphthazarin **8**, whose spectrum showed signals at δ 6.77 due to the quinonoid ring protons and δ 7.32 the benzenoid ring protons.

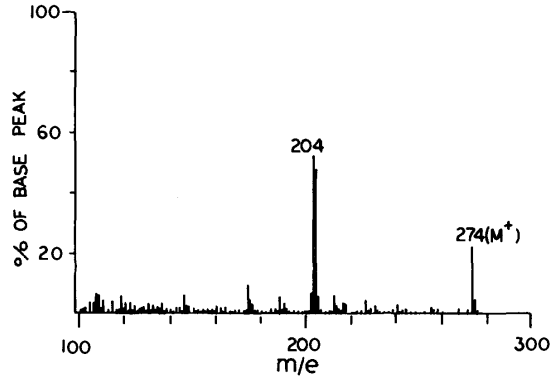

Fig. 12.

23) P. Jacob, III, P. S. Callery, A. T. Shulgin, and N. Castagoli, Jr., *J. Org. Chem.*, **41**, 3627 (1976). T.-t. Li, and R. H. Ellison, *J. Am. Chem. Soc.*, **100**, 6263 (1978); T. Kometani and E. Yoshii, *J. Chem. Soc., Perkin Trans, 1*, **1981**, 1191 and 1197.

24) C. M. Wong, D. Popien, R. Schwenk, and J. Te Raa, *Can. J. Chem.*, **49**, 2712 (1971).

25) The mass spectrum of **15** is shown in Fig. 12.

26) K. Kyogoku, H. Terayama, Y. Tachi, T. Suzuki, and M. Komatsu, *Syoyakugaku Zasshi*, **27**, 24 (1973).

27) K. A. Parker and J. Kallmerten, *J. Am. Chem. Soc.*, **102**, 5881 (1980); C. D. Snyder and H. Rapoport, *ibid.*, **94**, 227 (1972); C. D. Snyder, W. E. Bondinell, and H. Rapoport, *J. Org. Chem.*, **36**, 3951 (1971).

28) H. Gerlach and P. Künzler, *Helv. Chim. Acta*, **60**, 638 (1977).

29) M. V. Bhatt and S. U. Kulkarnin, *Synthesis*, **1983**, 253.

30) W. Schaefer and B. Frank, *Chem. Ber.*, **99**, 160 (1966).

31) The Chemical Society of Japan "Kagakubinran," 2nd ed., Maruzen, Tokyo (**1975**), p. 213.

 © 1987 The Chemical Society of Japan Bull. Chem. Soc. Jpn., 60, 215—222 (1987)

Highly Regioselective α-Addition of Alkynyl and Alkenyl Grignard Reagents to 1-Alkoxycarbonylpyridinium Salts and Its Application to Synthesis of 1-Azabicycloalkanes and (±)-Solenopsin A

Ryohei YAMAGUCHI,* Yutaka NAKAZONO, Toshitsugu MATSUKI, Ei-ichiro HATA, and Mituyosi KAWANISI
Department of Industrial Chemistry, Faculty of Engineering, Kyoto University, Yoshida, Kyoto 606
(Received June 20, 1986)

Nucleophilic addition of a variety of alkynyl and alkenyl Grignard reagents to 1-methoxycarbonylpyridinium chloride takes place at the α-position in a highly regioselective manner to give 2-substituted 1-methoxycarbonyl-1,2-dihydropyridines exclusively, while, with alkyl Grignard reagents, a lack of the regioselectivity is observed. These results may be explained by the HSAB principle. The high α-regioselectivity is preserved in the cases of 2-substituted pyridines as well, giving 2,6-disubstituted 1,2-dihydropyridines exclusively, which can be transformed stereoselectively into *cis*- and *trans*-2,6-dialkylated piperidines. These highly regioselective α-alkynylations of 1-methoxycarbonylpyridinium salts are exploited in synthesis of 1-azabicycloalkanes as well as (±)-solenopsin A.

Nucleophilic addition of organometallic reagents to 1-acylpyridinium salts has been utilized to prepare 2- and 4-substituted 1,2- and 1,4-dihydropyridines, which have proved to be valuable synthetic intermediates for nitrogen heterocycles.[1] The regioselectivity of these reactions has been of critical importance in synthetic and mechanistic points of view. There have been several organometallic reagents which favor the γ-attack on 1-acylpyridinium salts; organocopper reagents,[2] trialkylalkynylborates,[3] enol silyl ethers,[4] and titanium enolates[5] produce regioselectively the 4-substituted 1,4-dihydropyridines.

On the other hand, only a few organometallics, i.e. Grignard[6] and organocadmium reagents,[6c] have been reported to predominantly attack on the α-position. The regioselectivity of these reactions, however, is apparently biased, because 4- and/or 3-substituted pyridines have been used as the starting material in most of the cases.

Then, we have examined the reaction of 1-methoxycarbonylpyridinium chloride itself with a variety of Grignard reagents and found that the regioselectivity is highly dependent on the nature of Grignard reagent. Thus, with alkyl Grignard reagents, 4-alkyl-1,4- and 2-alkyl-1,2-dihydropyridines are produced in variable ratios, uncovering a lack of the regioselectivity.[7,8]

In this report we describe that alkynyl and alkenyl Grignard reagents add to the α-position of the pyridinium salt in a highly regioselective manner to afford 2-substituted 1,2-dihydropyridines exclusively and that this methodology provides an easy access to the synthesis of 1-azabicycloalkanes as well as 2,6-dialkylated piperidines.[9]

Results and Discussion

When we reexamined the reaction of 1-methoxycarbonylpyridinium chloride (**1**) with butylmagnesium

Table 1. Reactions of 1-Methoxycarbonylpyridinium Chloride (**1**) with Alkyl Grignard Reagents and Other Organometallic Reagents

Entry	R	M	Temp °C	Method[a]	Yield[b] %	Ratio(2/3)[c]
1	*n*-Bu	MgBr	0	A	41	78/22[d]
2	*n*-Bu	MgBr	−78	A	99	67/33
3	*n*-Bu	MgBr	−78	B	79	60/40
4	*n*-Bu	MgCl	−78	A	86	67/33
5	Me	MgI	0	A	54	92/8
6	Et	MgBr	−78	A	51	57/43
7	*i*-Pr	MgBr	−78	A	99	37/63
8	*n*-Bu	ZnCl[e]	0	A	99	19/81
9	*n*-Bu	Li	−78	B	f)	
10	*n*-Bu	Cu·BF_3	−78	B		0.5/99.5[g]

a) Method A: Methyl chloroformate was added to a mixture of pyridine and organometallic reagent in THF. Method B: **1** was preformed before adding organometallic reagent. b) Combined yield. c) Determined by GLC and/or ^{1}H NMR. d) A small amount of 5-butyl-5-nonanol was obtained. e) Prepared by adding $ZnCl_2$ to *n*-BuMgBr. f) Pentanoic anhydride was obtained. g) Taken from Ref. 2b.

bromide in THF at 0 °C according to the Fraenkel method,[6a] we found that 2-butyl-1-methoxycarbonyl-1,2-dihydropyridine (**2a**) and 4-butyl-1-methoxycarbonyl-1,4-dihydropyridine (**3a**) were produced in a ratio of 78:22, along with a small amount of 5-butyl-5-nonanol. The reaction conducted at −78 °C gave again a mixture of **2a** and **3a** in a ratio of 67:33. Since these results were inconsistent with that of Fraenkel et al., who reported the exclusive formation of **2a**, we decided to investigate the reaction of **1** with a couple of alkyl Grignard reagents as well as other organometallic reagents in more detail (Scheme 1, Table 1).

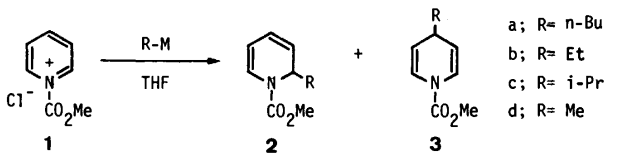

Scheme 1.

Table 1 evidently demonstrates that the regioselectivity is dependent on the character of metals. It has been suggested that the regioselectivity of the attack on the pyridinium cation by nucleophiles may be explained by the HSAB principle[10,11] (Fig. 1); with such relatively hard nucleophiles as hydroxide and amide ions the preferential α-attack (an arrow b) is observed, while with such soft ones as cyanide and enolate ions an attack on the γ-position (an arrow a) is predominant.[11] The above reactions with the organometallic reagents may be rationalized in the same context; the very soft organocopper reagents almost exclusively attack at the γ-position, as has been recently suggested by Akiba et al. (Entry 10).[2b,2c] The organozinc reagent, which is slightly harder than organocopper reagent, reveals a slightly less γ-selectivity (Entry 8). With harder alkyl Grignard reagents, both of α- and γ-attack occur in variable ratios (Entries 1—7). Furthermore, we have found that much harder organolithium reagent gives pentanoic anhydride exclusively (Entry 9), probably through the attack on the carbonyl moiety, the hardest position of the pyridinium salt (an arrow c in Fig. 1).

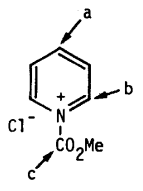

Fig. 1. Three possible positions attacked by nucleophiles.

While the above results led to the conclusion that alkyl Grignard reagents generally showed no appreciable α-regioselectivity, we were interested in that, among alkyl Grignard reagents, methyl Gignard reagent showed more than the 90% of the α-addition (Entry 5). We have thought that this is because the α-regioselectivity is enhanced by harder methyl group than other alkyl ones. Accordingly, in order to obtain 2-substituted 1,2-dihydropyridine selectively which may be a potential intermediate for alkaloid synthesis,[1] we have next examined the reaction of **1** with alkynyl as well as alkenyl Grignard reagents, considering that these organic moieties are supposed to be harder than alkyl ones (Scheme 2). The results are summarized in Table 2. As is shown in Table 2, the α-regioselectivity is far better than the expected; with a variety of alkynyl and alkenyl Grignard reagents the α-attack takes place exclusively to afford 2-alkynyl- and 2-alkenyl-1,2-dihydropyridines in good to excellent yields.[12,13]

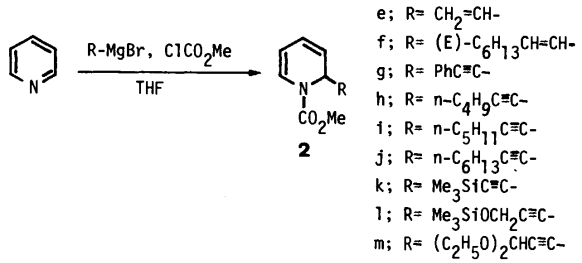

Scheme 2.

Tabe 2. Reactions of **1** with Alkynyl and Alkenyl Grignard Reagents[a]

Entry	R	Yield[b,c] %
1	CH_2=CH-	81
2	(*E*)-*n*-C_6H_{13}CH=CH-	71[d]
3	PhC≡C-	98
4	*n*-C_4H_9C≡C-	97
5	*n*-C_5H_{11}C≡C-	93
6	*n*-C_6H_{13}C≡C-	93
7	Me_3SiC≡C-	99
8	Me_3SiOCH$_2$C≡C-	98
9	$(EtO)_2$CHC≡C-	87

a) All reaction were carried out by Method A at 0° C, unless otherwise noted. b) Isolated yield. c) The α-regioselectivity was shown to be >98% by GLC and/or ^{1}H NMR analysis in all of the cases. d) The reaction was conducted at −40 °C.

To our further delight, it has been found that the above high α-regioselectivity is completely preserved in the reactions of 2-substituted pyridines (Scheme 3). The results are summarized in Table 3. Thus, reactions of 2-methyl- or 2-ethylpyridine with alkynyl Grignard reagents in the presence of methyl chloroformate proceeded in a highly regioselective manner to give exclusively 2,6-disubstituted 1-methoxycarbonyl-1,2-dihydropyridines, in spite of their steric congestion.[14]

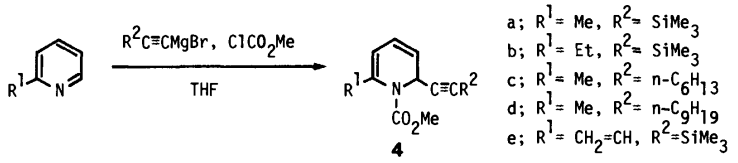

Scheme 3.

Table 3. Reactions of 2-Substituted 1-Methoxycarbonylpyridinium Chlorides with Alkynyl Grignard Reagents[a)]

Entry	R^1	R^2	Yield[b)] / %
1	Me	$SiMe_3$	79
2	Et	$SiMe_3$	66
3	Me	n-C_6H_{13}	73
4	Me	n-C_9H_{19}	79
5	CH_2=CH-	$SiMe_3$	26

a) All reactions carried out by Method A at 0 °C.
b) Isolated yield.

Synthesis of Indolizidine and Quinolizidine through Highly Regioselective α-Alkynylation of Pyridinium Salt. Indolizidine and quinolizidine skeletons are incorporated in a number of alkaloids and much effort has been made for constructing these systems.[15)] We describe here an application of the above reactions to synthesis of 1-azabicycloalkanes (Scheme 4).

Reactions of pyridine with alkynyl Grignard reagents possessing protected hydroxyl group **5** in the presence of methyl chloroformate gave exclusively 1-methoxycarbonyl-2-alkynyl-1,2-dihydropyridines (**6a** and **6b**), which were successively hydrogenated on Rh-Al_2O_3 and deprotected to afford 2-(3-hydroxypropyl)- and 2-(4-hydroxybutyl)piperidine derivatives (**7a** and **7b**), respectively, in good yields. Demethoxycarbonylation[16)] of **7**, followed by cyclization of the resulting amino alcohols (**8a** and **8b**) with PPh_3 and CBr_4,[17)] furnished indolizidine (**9a**) and quinolizidine (**9b**), respectively.

Synthesis of *cis*- and *trans*-2,6-Dialkylated Piperidines and (±)-Solenopsin A via 1-Methoxycarbonyl-2,6-disubstituted-1,2-dihydropyridines. 2,6-Dialkylated piperidines constitute the principal structure of a number of piperidine alkaloids.[18,19)] Accordingly, we next examined the stereoselective transformation of 2,6-disubstituted 1-methoxycarbonyl-1,2-dihydropyridine obtained above into *cis*- and *trans*-2,6-dialkylated piperidines and an application of this sequence to synthesis of (±)-solenopsin A, a piperidine alkaloid isolated from the venom of the fire ant.[20,21)]

At first we have found that careful hydrogenation of **4c** over 5% Pd-C can give a partially hydrogenated, crucial intermediate, 2,6-dialkylated 1,2,3,4-tetrahydropyridine (**10**) in 83% yield. Further hydrogenation of **10** over Pd-black, followed by demethoxycarbonylation with iodotrimethylsilane,[22)] afforded *cis*-2-methyl-6-octylpiperidine (**11**) exclusively (Scheme 5).

On the other hand, a cyclic imine (**12**) could be obtained, when **10** was demethoxycarbonylated with iodotrimethylsilane. According to the Yamamoto's elegant method for stereoselective reduction of this type of cyclic imine,[21a)] **12** was reduced by lithium tetrahydroaluminate in THF at −78 °C to afford *trans*-2-methyl-6-octylpiperidine (**13**), along with a small amount of the cis-isomer **11** (**13**:**11**=78:22).

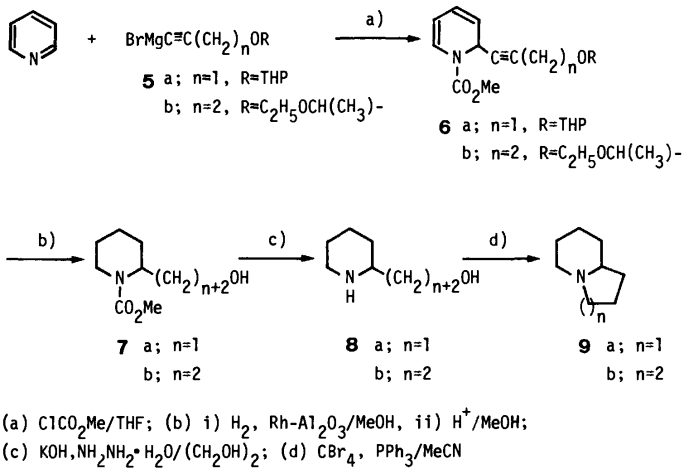

Scheme 4.

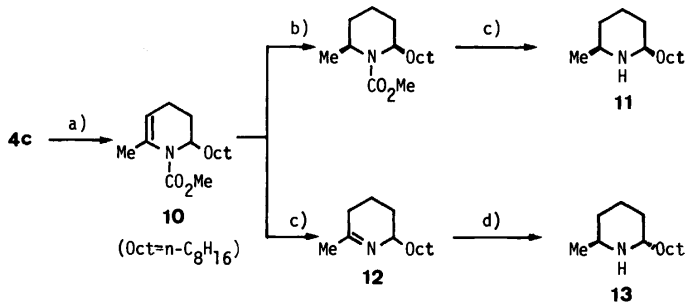

(a) H_2, Pd-C/MeOH; (b) H_2, Pd/MeOH; (c) $Me_3SiI/CHCl_3$; (d) $LiAlH_4$/THF, -78°C

Scheme 5.

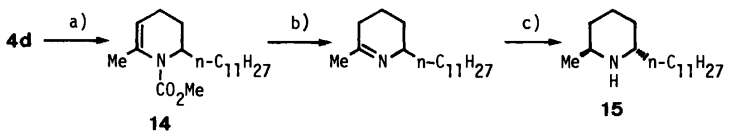

(a) H_2, Pd-C/MeOH; (b) $Me_3SiI/CHCl_3$; (c) $LiAlH_4$, Me_3Al/THF, -78°C

Scheme 6.

Thus, it has been shown that 2,6-disubstituted 1,2-dihydropyridine is a versatile precursor for *cis*- and *trans*-2,6-dialkylated piperidines.[23]

Consequently, the above sequence has been applied to the regio- and stereoselective synthesis of (±)-solenopsin A, *trans*-2-methyl-6-undecylpiperidine (Scheme 6). Careful hydrogenation of **4d** over 5% Pd-C in methanol gave 1,2,3,4-tetrahydropyridine derivative (**14**). Demethoxycarbonylation of **14** followed by reduction with lithium tetrahydroaluminate in the presence of trimethylaluminium[21a] afford (±)-solenopsin A (**15**) in 90% yield based on **14**, along with a small amount of its epimer. Thus, the present route provides one of the most practical and efficient method for the synthesis of (±)-solenopsin A (43% overall yield in 4 steps from 2-methylpyridine).[24]

Experimental

All the temperatures were uncorrected. The IR spectra were obtained on a Hitachi 215 or JASCO IR-810 spectrometer. The mass spectra were taken by using a Hitachi RMS-4 mass spectrometer. The ^1H and ^{13}C NMR spectra were obtained on Varian EM-390 and CFT-20 or JEOL FX-90Q spectrometers, Me_4Si being chosen as the internal standard. Analytical GLC were carried out on a Shimadzu GC-4C gas chromatography with 10% SE-30, 10% HVSG, or 10% PEG-20M on Chromsorb W columns. The microanalyses were performed by Kyoto University Elemental Analysis Center. All the reactions were carried out under Ar atmosphere, otherwise noted. THF was distilled from benzophenone ketyl before use.

General Procedure for the Reaction of 1-Methoxycarbonylpyridinium Chloride (1) with Alkyl Grignard Reagents. Method A. To a mixture of butylmagnesium bromide (5 mL, 2.0 M†, 10.0 mmol) and pyridine (0.396 g, 5.0 mmol) in THF (7.5 mL) was added methyl chloroformate (0.473 g, 5.0 mmol) at −78 °C. The reaction mixture was stirred for 5 h and quenched by adding water (0.75 mL) at that temp. The mixture was poured onto water and extracted with CH_2Cl_2. The organic layer was washed with brine and dried (Na_2SO_4). The solvent was evaporated and the residue was passed through a short silica-gel column eluting with CH_2Cl_2 to give a mixture of **2a**[3a] and **3a**[2a] (0.966 g, 99%). The ratio of **2a** to **3a** was 67:33 by GLC analysis.

Method B. To a solution of pyridine (0.396 g, 5.0 mmol) in THF (20 mL) were added methyl chloroformate (0.473 g, 5.0 mmol) at 0 °C. The mixture was stirred for 1 h and cooled to −78 °C. To this mixture was added butylmagnesium bromide (10.0 mmol in 15 mL of THF) and the reaction mixture was stirred for 5 h. The usual work-up gave a mixture of **2a** and **3a** (0.767 g, 79%). The ratio of **2a** to **3a** was 59:41 by GLC analysis.

The reactions of **1** with other alkyl Grignard reagents were conducted in a similar manner to the above. The yields and the ratios are described in Table 1.[2a]

Reaction of 1 with Butyllithium. To a mixture of **1**, prepared from pyridine (0.158 g, 2.0 mmol) and methyl chloroformate (0.189 g, 2.0 mmol), in THF (6 mL) was added *n*-BuLi (0.64 mL, 1.56 M, 1.0 mmol) in hexane at −78 °C. After 15 min, water (0.5 mL) was added to the mixture. The usual work-up gave valeric anhydride (0.091 g, 98%).

General Procedure for the Reaction of 1 with Alkenyl and Alkynyl Grignard Reagents. To a mixture of pyridine

† 1 M=1 mol dm^{-3}.

(0.211 g, 2.7 mmol) and alkenyl or alkynyl Grignard reagent (2.7—5.0 mmol) in THF (6—10 mL) was added a solution of methyl chloroformate (0.230 g, 2.4 mmol) in THF (2 mL) dropwise under ice-cooling. After 30 min, the mixture was poured onto 1 M aq NH_4Cl and extracted with CH_2Cl_2. The organic solution was washed with water and dried (Na_2SO_4). The solvent was evaporated and the residue was passed through a short silica-gel column eluting with CH_2Cl_2 to give **2**. The yield of each product is described in Table 2.

1-Methoxycarbonyl-2-vinyl-1,2-dihydropyridine (2e): MS *m/z* (%) 165 (M^+, 36), 138 (100); IR (neat): 1715 cm^{-1}; ^1H NMR ($CDCl_3$) δ=6.68 (br d, 1H, *J*=6 Hz), 4.66—6.02 (m, 7H), 3.74 (s, 3H); ^{13}C NMR ($CDCl_3$) δ=169.7 (s), 134.6 (d), 125.2 (d), 122.0 (d), 120.5 (d), 115.1 (t), 105.4 (d), 54.1 (d), 53.1 (q). Found: C, 65.45; H, 6.81%. Calcd for $C_9H_{11}NO_2$: C, 65.44; H, 6.71%.

1-Methoxycarbonyl-2-[(*E*)-1-octenyl]-1,2-dihydropyridine (2f): MS *m/z* (%) 249 (M^+, 11), 138 (100); IR (neat): 1720 cm^{-1}; ^1H NMR ($CDCl_3$) δ=6.65 (br d, 1H, *J*=6 Hz), 6.00—7.00 (m, 6H), 3.76 (s, 3H), 1.89—2.50 (br m, 2H), 1.08—1.70 (m, 8H), 0.88 (t, 3H, *J*=7 Hz); ^{13}C NMR ($CDCl_3$) δ=154.0 (s), 126.4 (d), 125.2 (d), 121.4 (d), 120.9 (d), 105.3 (d), 105.1 (d), 52.9 (q), 50.2 (d), 32.2 (t), 31.8 (t), 29.9 (t), 29.1 (t), 22.7 (t), 14.0 (q). Found: C, 72.38; H, 9.46%. Calcd for $C_{15}H_{23}NO_2$: C, 72.25; H, 9.30%.

1-Methoxycarbonyl-2-phenylethynyl-1,2-dihydropyridine (2g): MS *m/z* (%) 239 (M^+, 100); IR (neat): 2200, 1720 cm^{-1}; ^1H NMR ($CDCl_3$) δ=7.15—7.50 (m, 5H), 6.60—7.15 (br, 1H), 5.18—6.12 (m, 4H), 3.76 (s, 3H); ^{13}C NMR ($CDCl_3$) δ=153.9 (s), 131.9 (2d), 128.3 (d), 128.2 (2d), 125.1 (d), 122.8 (s), 122.3 (d), 118.7 (d), 105.5 (d), 86.7 (s), 83.2 (s), 53.4 (q), 44.3 (d). Found: C, 75.06; H, 5.73%. Calcd for $C_{15}H_{13}NO_2$: C, 75.30; H, 5.48%.

1-Methoxycarbonyl-2-(1-hexynyl)-1,2-dihydropyridine (2h): MS *m/z* (%) 219 (M^+, 79), 218 (74), 79 (100); IR (neat): 2000, 1710 cm^{-1}; ^1H NMR ($CDCl_3$) δ=6.66 (br d, 1H, *J*=6 Hz), 5.10—5.98 (m, 4H), 3.78 (s, 3H), 1.97—2.25 (m, 2H), 1.10—1.62 (m, 4H), 0.82 (t, 3H, *J*=7 Hz); ^{13}C NMR ($CDCl_3$) δ=153.9 (t), 125.0 (d), 121.7 (d), 119.7 (d), 105.3 (d), 83.9 (s), 77.9 (s), 53.3 (q), 44.0 (d), 30.8 (t), 21.9 (t), 18.5 (t), 13.5 (q). Found: C, 71.13; H, 7.98%. Calcd for $C_{13}H_{17}NO_2$: C, 71.21; H, 7.81%.

1-Methoxycarbonyl-2-(1-heptynyl)-1,2-dihydropyridine (2i): MS *m/z* (%) 263 (M^+, 83), 262 (100); IR (neat): 2200, 1710 cm^{-1}; ^1H NMR ($CDCl_3$) δ=6.67 (br d, 1H, *J*=6 Hz), 5.07—6.00 (m, 4H), 3.79 (s, 3H), 1.92—2.25 (m, 2H), 1.10—1.61 (m, 6H), 0.87 (t, 3H, *J*=7 Hz); ^{13}C NMR ($CDCl_3$) δ=154.0 (s), 125.0 (d), 121.6 (d), 119.7 (d), 105.3 (d), 84.0 (s), 77.8 (s), 53.3 (q), 44.0 (d), 31.1 (t), 28.3 (t), 22.2 (t), 18.8 (t), 13.9 (q). Found: C, 72.14; H, 8.29%. Calcd for $C_{14}H_{19}NO_2$: C, 72.07; H, 8.21%.

1-Methoxycarbonyl-2-(1-octynyl)-1,2-dihydropyridine (2j): MS *m/z* (%) 247 (M^+, 100); IR (neat): 2245, 1730 cm^{-1}; ^1H NMR ($CDCl_3$) δ=6.68 (br d, 1H, *J*=7 Hz), 5.15—6.00 (m, 4H), 3.78 (s, 3H), 1.98—2.27 (m, 2H), 1.10—1.60 (m, 8H), 0.88 (t, 3H, *J*=7 Hz); ^{13}C NMR ($CDCl_3$) δ=153.9 (s), 125.1 (d), 121.7 (d), 119.7 (d), 105.3 (d), 84.0 (s), 77.9 (s), 53.3 (q), 44.0 (d), 31.4 (t), 28.6 (t), 28.5 (t), 22.6 (t), 18.9 (t), 14.0 (q). Found: C, 72.58; H, 8.61%. Calcd for $C_{15}H_{21}NO_2$: C, 72.84; H, 8.66%.

1-Methoxycarbonyl-2-trimethylsilylethynyl-1,2-dihydropyridine (2k): MS *m/z* (%) 235 (M^+, 67), 234 (66), 73 (100); IR (neat): 2160, 1735 cm^{-1}; ^1H NMR ($CDCl_3$) δ=6.65 (br d, 1H, *J*=7 Hz), 5.17—6.00 (m, 4H), 3.77 (s, 3H), 0.15 (s, 9H); ^{13}C NMR ($CDCl_3$) δ=153.9 (s), 125.2 (d), 122.3 (d), 118.9 (d), 105.5 (d), 102.9 (s), 87.8 (s), 53.4 (q), 44.5 (d), 0.0 (q). Found: C, 61.19; H, 7.26%. Calcd for $C_{12}H_{17}NO_2Si$: C, 61.24; H, 7.28%.

1-Methoxycarbonyl-2-(3-trimethylsilyloxy-1-propynyl)-1,2-dihydropyridine (2l): MS *m/z* (%) 265 (M^+, 81), 73 (100); IR (neat): 1720 cm^{-1}; ^1H NMR ($CDCl_3$) δ=6.63 (br d, 1H, *J*=6 Hz), 5.03—5.95 (m, 4H), 4.16 (s, 2H), 3.69 (s, 3H), 0.06 (s, 9H); ^{13}C NMR ($CDCl_3$) δ=153.4 (s), 124,8 (d), 122.0 (d), 118.2 (d), 105.1 (d), 82.3 (s), 81.4 (s), 53.1 (q), 50.9 (t), 43.5 (d), −0.5 (q). Found: C, 58.65; H, 7.15.% Calcd for $C_{13}H_{19}NO_3Si$: C, 58.84; H, 7.22%.

1-Methoxycarbonyl-2-(3,3-diethoxy-1-propynyl)-1,2-dihydropyridine (2m): MS *m/z* (%) 265 (M^+, 35), 138 (100); IR (neat): 1730 cm^{-1}; ^1H NMR ($CDCl_3$) δ=6.68 (br d, 1H, *J*=7 Hz), 5.22—6.07 (m, 4H), 5.20 (s, 1H), 3.80 (s, 3H), 3.31—3.75 (m, 4H), 1.20 (t, 6H, *J*=7 Hz); ^{13}C NMR ($CDCl_3$) δ=157.5 (s), 125.0 (d), 122.7 (d), 118.1 (d), 105.5 (d), 91.3 (d), 82.6 (s), 78.5 (s), 60.8 (2t), 53.5 (q), 43.6 (d), 15.1 (2q). Found: C, 63.12; H, 7.36%. Calcd for $C_{14}H_{13}NO_4$: C, 63.38; H, 7.22%.

General Procedure for the Reactions of 2-Substituted 1-Methoxycarbonylpyridinium Salts with Alkynyl Grignard Reagents. To a mixture of 2-substituted pyridine (5.3 mmol) and alkynylmagnesium bromide, prepared from the corresponding alkyne (2.7 mmol) and ethylmagnesium bromide (2.7 mmol), in THF (17 mL) was slowly added a solution of methyl chloroformate (0.255 g, 2.7 mmol) in THF (6 mL) over 1.5 h under ice-cooling. The mixture was stirred for 1.5 h and poured onto 10% aq NH_4Cl. The usual work-up and the subsequent short-column chromatography on silica-gel eluting with CH_2Cl_2 gave **4**. The yield of each product is described in Table 3.

1-Methoxycarbonyl-6-methyl-2-trimethylsilylethynyl-1,2-dihydropyridine (4a): mp 63.2—64.0 °C; MS *m/z* (%) 249 (M^+, 86), 174 (100); IR (nujol): 2150, 1715, 830 cm^{-1}; ^1H NMR ($CDCl_3$) δ=5.29—5.96 (m, 4H), 3.64 (s, 3H), 2.07 (s, 3H), 0.07 (s, 9H); ^{13}C NMR ($CDCl_3$) δ=154.3 (s), 135.3 (s), 123.5 (d), 120.1 (d), 112.2 (d), 103.2 (s), 87.4 (s), 53.1 (q), 45.0 (d), 21.6 (q), 0.1 (q). Found: C, 62.63; H, 7.66%. Calcd for $C_{13}H_{19}NO_2Si$: C, 62.61; H, 7.68%.

1-Methoxycarbonyl-6-ethyl-2-trimethylsilylethynyl-1,2-dihydropyridine (4b): MS *m/z* (%) 263 (M^+, 69), 234 (100); IR (neat): 2175, 1720, 845 cm^{-1}; ^1H NMR ($CDCl_3$) δ=5.41—5.71 (m, 4H), 3.94 (s, 3H), 2.01—3.04 (m, 2H), 1.04 (t, 3H, *J*=7 Hz), 0.11 (s, 9H); ^{13}C NMR ($CDCl_3$) δ=154.3 (s), 140.8 (s), 123.6 (d), 120.8 (d), 111.6 (d), 102.8 (s), 87.5 (s), 53.1 (q), 45.1 (d), 27.5 (t), 12.5 (q), 0.0 (q). Found: C, 63.58; H, 8.06%. Calcd for $C_{14}H_{21}NO_2Si$: C, 63.84; H, 8.04%.

1-Methoxycarbonyl-6-methyl-2-(1-octynyl)-1,2-dihydropyridine (4c): MS *m/z* (%) 261 (M^+, 100); IR (neat): 2220, 1720 cm^{-1}; ^1H NMR ($CDCl_3$) δ=5.36—5.94 (m, 4H), 3.73 (s, 3H), 2.15 (s, 3H), 1.90—2.28 (m, 2H), 1.05—1.57 (m, 8H), 0.85 (t, 3H, *J*=7 Hz); ^{13}C NMR ($CDCl_3$) δ=154.4 (s), 135.1 (s), 122.7 (d), 120.7 (d), 111.8 (d), 83.4 (s), 77.5 (s), 52.9 (q), 44.5 (d), 31.4 (t), 28.7 (t), 28.4 (t), 22.6 (t), 21.5 (q), 18.9 (t), 14.0 (q). Found: C, 73.50; H, 9.11%. Calcd for $C_{16}H_{23}NO_2$: C, 73.53; H, 8.87%.

1-Methoxycarbonyl-6-methyl-2-(1-undecynyl)-1,2-dihydropyridine (4d): MS *m/z* (%) 303 (M^+, 100); IR (neat): 2220, 1715 cm^{-1}; ^1H NMR ($CDCl_3$) δ=5.37—5.97 (m, 4H), 3.75 (s,

3H), 2.17 (s, 3H), 2.00—2.40 (m, 2H), 1.07—1.70 (m, 14H), 0.87 (t, 3H, J=7 Hz); ^{13}C NMR ($CDCl_3$) δ=154.4 (s), 135.0 (s), 122.7 (d), 120.6 (d), 111.8 (d), 83.4 (s), 77.3 (s), 53.0 (q), 44.3 (d), 32.0 (t), 29.6 (t), 29.3 (t), 29.2 (t), 28.8 (t), 28.7 (t), 22.8 (t), 21.5 (q), 18.8 (t), 14.1 (q). Found: C, 75.18; H, 9.92%. Calcd for $C_{19}H_{29}NO_2$: C, 75.20; H, 9.63%.

1-Methoxycarbonyl-2-trimethylsilylethynyl-6-vinyl-1,2-dihydropyridine (4e): MS m/z (%) 261 (M^+, 77), 202 (100); IR (neat): 2170, 1710, 840 cm^{-1}; ^{1}H NMR ($CDCl_3$) δ=4.92—6.45 (m, 7H), 3.64 (s, 3H), 0.04 (s, 9H); ^{13}C NMR ($CDCl_3$) δ=154.8 (s), 136.3 (s), 134.1 (d), 128.5 (d), 123.6 (d), 114.3 (t), 113.7 (d), 102.2 (s), 88.5 (s), 53.1 (q), 45.1 (d), 0.0 (q). Found: C, 64.19; H, 7.35%. Calcd for $C_{14}H_{19}NO_2Si$: C, 64.33; H, 7.33%.

1-Methoxycarbonyl-2-(3-hydroxypropyl)piperidine (7a). To a mixture of pyridine (1.242 g, 12.6 mmol) and 3-(2-tetrahydropyranyloxy)propynylmagnesium bromide, prepared from tetrahydro-2-(2-propynyloxy)-2*H*-pyran (1.396 g, 9.97 mmol) and ethylmagnesium bromide (6.0 mL, 1.88 M, 11.3 mmol), in THF (20 mL) was added a solution of methyl chloroformate (1.000 g, 10.5 mmol) in THF (10 mL) slowly over 1.5 h under ice-cooling. The mixture was stirred for 2 h, poured onto 10% aq NH_4Cl, and extracted with CH_2Cl_2. The organic solution was washed with water and brine, and dried (Na_2SO_4). The solvent was evaporated to give almost pure **6a**: ^{1}H NMR ($CDCl_3$) δ=6.76 (br d, 1H, J=7 Hz), 5.20—6.21 (m, 4H), 4.80 (br s, 1H), 4.27 (s, 2H), 3.83 (s, 3H), 3.47—4.02 (m, 2H), 1.30—1.97 (m, 6H); ^{13}C NMR ($CDCl_3$) δ=153.7 (s), 124.8 (d), 122.0 (d), 118.2 (d), 105.1 (d), 96.6 (d), 83.2 (t), 78.6 (s), 61.8 (t), 54.2 (t), 53.4 (q), 43.6 (d), 30.3 (t), 25.5 (t), 19.1 (t). Without purification, **6a** was dissolved in dry MeOH (15 mL) and completely hydrogenated over 5% Rh-Al_2O_3 (0. 20 g) under 8 kg cm^{-2} pressure of H_2. After the catalyst was removed by filtration through Celite, the solvent was evaporated. The residue was dissolved in dry MeOH (10 mL) and to this solution was added Amberlyst H-15 (0.15 g). The mixture was stirred at 45 °C for 1 h and Amberlyst H-15 was removed by filtration. The solvent was evaporated and the residue was purified through bulb-to-bulb distillation to give **7a** (1.621 g, 81%): Bp 110—120 °C/80 Pa; MS m/z (%) 201 (M^+, 4), 142 (100); IR (neat): 3450, 1680 cm^{-1}; ^{1}H NMR ($CDCl_3$) δ=3.83—4.50 (m, 2H), 3.68 (s, 3H), 3.53—3.83 (m, 2H), 2.63—3.10 (m, 1H), 2.53 (s, 1H), 1.20—1.90 (m, 10H); ^{13}C NMR ($CDCl_3$) δ=156.3 (s), 61.8 (t), 52.4 (q), 50.8 (d), 39.1 (t), 29.5 (t), 28.7 (t), 26.1 (t), 25.7 (t), 19.0 (t).

1-Methoxycarbonyl-2-(4-hydroxybutyl)piperidine (7b). To a mixture of pyridine (1.27 g, 12.9 mmol) and 4-(1-ethoxyethoxy)-1-butynylmagnesium bromide, prepared from 4-(1-ethoxyethoxy)-1-butyne (1.43 g, 10.1 mmol) and ethylmagnesium bromide (7.8 mL, 1.42 M, 11.1 mmol), in THF (20 mL) was added a solution of methyl chloroformate (1.00 g, 10.5 mmol) in THF (10 mL) slowly over 1.5 h under ice-cooling. The mixture was stirred for 2 h and the usual work-up gave **6b**: ^{1}H NMR ($CDCl_3$) δ=6.80 (br d, 1H, J=7 Hz), 5.38—6.13 (m, 4H), 4.75 (q, 1H, J=6 Hz), 3.83 (s, 3H), 3.36—3.80 (m, 4H), 2.43 (t, 2H, J=6 Hz), 1.30 (d, 3H, J=6 Hz), 1.13 (t, 3H, J=6 Hz); ^{13}C NMR ($CDCl_3$) δ=153.6 (s), 124.7 (d), 121.7 (d), 119.2 (d), 105.3 (d), 99.5 (d), 80.6 (s), 78.6 (s), 63.1 (t), 60.8 (t), 53.3 (q), 43.6 (d), 20.5 (t), 19.7 (q), 15.3 (q). Without purification, **6b** was hydrogenated in a similar manner to the above. In this case, 1-ethoxyethyl group was removed during this hydrogenation. Purification through bulb-to-bulb distillation gave **7b** (1.61 g, 75%): Bp 110—130 °C/67 Pa; IR (neat): 3400, 1690 cm^{-1}; ^{1}H NMR ($CDCl_3$) δ=3.80—4.33 (m, 2H), 3.65 (s, 3H), 3.57 (t, 2H, J=6 Hz), 2.60—3.07 (m, 2H), 1.10—1.83 (m, 12H); ^{13}C NMR ($CDCl_3$) δ=156.4 (s), 62.4 (t), 52.4 (q), 50.7 (d), 39.1 (t), 32.6 (t), 29.4 (t), 28.4 (t), 25.7 (t), 22.5 (t), 19.0 (t).

2-(3-Hydroxypropyl)piperidine (8a). A mixture of **7a** (0.699 g, 3.5 mmol), KOH (5.11 g), and 100% $NH_2NH_2 \cdot H_2O$ (0.85 mL) in ethylene glycol (26 mL) was heated under reflux for 1.5 h. The reaction mixture was poured onto water and extracted with CH_2Cl_2. The organic solution was washed with 30% aq NaOH and dried (Na_2SO_4). The solvent was evaporated to give almost pure **8a** (0.473 g, 95%): MS m/z (%) 143 (M^+, 9), 142 (100); ^{1}H NMR ($CDCl_3$) δ=3.57 (s, 2H), 3.53 (t, 2H, J=6 Hz), 2.90—3.20 (m, 1H), 2.30—2.77 (m, 2H), 0.93—1.90 (m, 14H); ^{13}C NMR ($CDCl_3$) δ=62.6 (t), 56.9 (d), 46.6 (t), 35.9 (t), 32.2 (t), 30.4 (t), 26.6 (t), 24.8 (t).

2-(4-Hydroxybutyl)piperidine (8b). A mixture of **7b** (0.263 g, 1.2 mmol), KOH (1.80 g), and 100%$NH_2NH_2 \cdot H_2O$ (0.3 mL) in ethylene glycol (9 mL) was heated under reflux for 1.5 h. The similar work-up to the above gave almost pure **8b** (0.179 g, 93%): ^{1}H NMR ($CDCl_3$) δ=3.55 (t, 2H, 6 Hz), 2.84—3.20 (m, 1H), 2.80 (br s, 2H), 2.27—2.77 (m, 2H), 0.97—1.90 (m, 12 H); ^{13}C NMR ($CDCl_3$) δ=61.5 (t), 56.8 (d), 47.0 (t), 37.0 (t), 32.9 (t), 32.8 (t), 26.4 (t), 24.8 (t), 22.2 (t).

Indolizidine (9a). A solution of **8a** (0.258 g, 1.8 mmol), PPh_3 (0.890 g, 3.3 mmol), and CBr_4 (1.320 g, 4.0 mmol) in dry CH_3CN (18 mL) was stirred at room temp overnight. The mixture was poured onto 10% aq HCl and washed with AcOEt. The aqueous layer was basified by adding 2 M aq NaOH and K_2CO_3, and extracted with ether. The organic layer was dried (K_2CO_3) and the solvent was evaporated. The residue was purified through bulb-to-bulb distillation (80 °C/6000 Pa) to give **9a** (0.130 g, 58%): Picrate, mp 229—231.5 °C (lit,[25] 233—234 °C); ^{1}H NMR ($CDCl_3$) δ=2.90—3.23 (m, 2H), 1.03—2.63 (m, 13H); ^{13}C NMR ($CDCl_3$) δ=64.4 (d), 54.3 (t), 53.2 (t), 31.1 (t), 30.6 (t), 25.6 (t), 24.7 (t), 20.7 (t).

Quinolizidine (9b). A solution of **8b** (0.164 g, 1.04 mmol), PPh_3 (0.520 g, 2.00 mmol), and CBr_4 (0.770 g, 2.33 mmol) in dry CH_3CN (11 mL) was heated under reflux for 2 h. The similar work-up to the above and purification through bulb-to-bulb distillation (80 °C/2666 Pa) gave **9b**: Picrate, mp 195—198 °C (lit,[26] 198—199 °C); ^{1}H NMR ($CDCl_3$) δ=2.60—2.97 (m, 2H), 0.90—2.23 (m, 15H); ^{13}C NMR ($CDCl_3$) δ=63.0 (d), 56.7 (t), 33.6 (t), 26.0 (t), 24.7 (t).

1-Methoxycarbonyl-6-methyl-2-octyl-1,2,3,4-tetrahydropyridine (10). A mixture of **4c** (0.783 g, 3.0 mmol) and 5% Pd-C (0.157 g) in dry MeOH (30 mL) was stirred under atmospheric pressure of H_2. The reaction was carefully monitored by TLC. As soon as the starting material disappeared, the reaction was stopped. The catalyst was removed by filtration through Celite and the solvent was evaporated. The residue was passed through a short silica-gel column eluting with hexane-CH_2Cl_2 (4:1) to give **10** (0.667 g, 83%): MS, m/z (%) 267 (M^+, 34), 196 (100); IR (neat): 1710 cm^{-1} ^{1}H NMR ($CDCl_3$) δ=4.85 (br s, 1H), 4.35 (br s, 1H), 3.66 (s, 3H), 2.00 (s, 3H), 1.10—2.10 (m, 18H), 0.87 (t, 3H, J=6 Hz); ^{13}C NMR ($CDCl_3$) δ=154.4 (s), 132.9 (s), 111.7 (d), 52.7 (d), 52.3 (q), 32.0 (t), 31.7 (t), 29.9 (t), 29.7 (t), 29.4 (t), 26.5 (t), 26.0 (t), 22.7 (t), 22.7 (q), 19.6 (t), 14.1 (q). Found: C, 75.18; H, 9.92%. Calcd for $C_{16}H_{29}NO_2$: C, 75.20; H, 9.63%.

***cis*-2-Methyl-6-octylpiperidine (11).** A mixture of **10** (0.203 g, 0.76 mmol) and Pd-black (0.02 g) in dry MeOH (5 mL) was stirred under atmospheric pressure of H_2 for 20 h. The catalyst was removed by filtration through Celite and the solvent was evaporated. The residue (0.126 g) was dissolved in dry $CHCl_3$ (2.0 mL) and to this solution was added iodotrimethylsilane (0.10 mL, 0.6 mmol). The reaction mixture was stirred at 50—60 °C for 3 h and then, after addition of MeOH (0.06 mL), at room temp for 0.5 h. The mixture was condensed under reduced pressure, diluted with 0.1 M aq NaOH, and extracted with CH_2Cl_2. The organic layer was dried (Na_2SO_4) and the solvent was evaporated to give **11** (0.103 g, 64%), which was identical with the authentic **11** prepared by a different route (vide infra).

***trans*-2-Methyl-6-octylpiperidine (13).** To a mixture of **10** (0.134 g, 0.50 mmol) in dry $CHCl_3$ (2.0 mL) was added iodotrimethylsilane (0.10 mL, 0.60 mmol). The mixture was stirred at 50—60 °C for 1.5 h and then, after addition of MeOH (0.06 mL), at room temp for 0.5 h. The mixture was condensed under reduced pressure, diluted with 0.1 M aq NaOH, and extracted with CH_2Cl_2. The solvent was evaporated to give a imine (**12**) (0.103 g): IR (neat): 1655 cm^{-1}. To a suspension of $LiAlH_4$ (0.475 g, 12.5 mmol) in THF (8.0 mL) was added a solution of **12** (0.103 g) in THF (8.0 mL) at −78 °C. The mixture was stirred at −78 °C for 1 h, −45 °C for 1 h, −20 °C for 1 h, and 0 °C for 1 h. The usual work-up and column chromatography on alumina eluting with ether gave **13**, along with a small amount of **11** (0.081 g, 70%, **13**:**11**=78:22 by GLC analysis).

Preparation of 11 and 13 by MacConell's Method.[22] To a mixture of 2,6-dimethylpyridine (2.15 g, 20 mmol) in ether (20 mL) was added PhLi in ether (17 mL, 1.33 M, 22 mmol) and the mixture was heated at reflux for 15 min. To this solution was added heptyl bromide (3.59 g, 20 mmol) over 30 min and the mixture was heated at reflux for 1 h. Usual work-up and distillation gave 2-methyl-6-octylpyridine (2.78 g, 68%). To a solution of 2-methyl-6-octylpyridine (0.48 g, 2.3 mmol) in dry EtOH (100 mL) was added Na (5.00 g, 217 mmol) in portionwise under reflux for 5 h. Usual work-up gave a mixture of **11** and **13** (0.412 g, 85%, 69:31 by GLC analysis), each of which was separated by column chromatography on alumina eluting with pentane–ether (9:1 to 0:10). **11**: MS *m/z* (%) 211 (M^+, 1), 98 (100); IR (neat): 1320 cm^{-1}; ^1H NMR ($CDCl_3$) δ=2.30—2.80 (m, 2H), 1.14—1.86 (m, 21H), 1.03 (d, 3H, J=6 Hz), 0.87 Hz (t, 3H, J=6 Hz); ^{13}C NMR ($CDCl_3$) δ=57.4 (d), 52.7 (d), 37.7 (t), 34.8 (t), 32.6 (t), 32.0 (t), 29.7 (t), 26.1 (t), 25.1 (t), 23.2 (q), 22.7 (t), 14.1 (q). **13**: MS *m/z* (%) 211 (M^+, 1), 98 (100); IR (neat): 1320 cm^{-1}; ^1H NMR ($CDCl_3$) δ=2.70—3.14 (m, 2H), 1.15—1.80 (m, 21H), 1.04 (d, 3H, J=6 Hz), 0.86 (t, 3H, J=6 Hz); ^{13}C NMR ($CDCl_3$) δ=51.1 (d), 46.1 (d), 34.4 (t), 33.3 (t), 32.0 (t), 31.1 (t), 29.9 (t), 29.7 (t), 29.4 (t), 26.6 (t), 22.7 (t), 21.3 (q), 19.8 (t), 14.1 (q).

1-Methoxycarbonyl-6-methyl-2-undecyl-1,2,3,4-tetrahydropyridine (14). A mixture of **4d** (0.303 g; 1.0 mmol) and 5% Pd–C (0.060 g) in dry MeOH (10 mL) was stirred under atmospheric pressure of H_2. The reaction was followed by GLC. After **4d** disappeared, the catalyst was removed by filtration through Celite and the solvent was evaporated. The residue was chromatographed on silica gel. Elution by hexane–CH_2Cl_2 (4:1) gave **14** (0.185 g, 60%): MS *m/z* (%) 309 (M^+, 31), 196 (100); IR (neat): 1715 cm^{-1}; ^1H NMR ($CDCl_3$) δ=4.87 (br s, 1H), 4.35 (br s, 1H), 3.69 (s, 3H), 2.02 (s, 3H), 1.07—2.07 (m, 24H), 0.87 (t, 3H, J=6 Hz); ^{13}C NMR ($CDCl_3$) δ=155.3 (s), 132.6 (s), 111.7 (d), 52.5 (q), 52.4 (d), 32.0 (t), 29.7 (6t), 29.4 (t), 26.4 (t), 25.8 (t), 22.7 (t), 22.7 (q), 19.5 (t), 14.1 (q). Found: C, 73.74; H, 11.40%. Calcd for $C_{19}H_{35}NO_2$: C, 74.06; H, 11.81%.

(±)-Solenopsin A, *trans*-2-Methyl-6-undecylpiperidine (15). To a mixture of **14** (0.155 g, 0.50 mmol) in dry $CHCl_3$ (2.0 mL) was added iodotrimethylsilane (0.10 mL, 0.60 mmol). The mixture was stirred at 50—60 °C for 1 h and, after addition of MeOH (0.06 mL), at room temp for 10 min. The solvent was evaporated and diluted with CH_2Cl_2. The solution was washed with 0.1 M aq NaOH and dried (Na_2SO_4). The solvent was evaporated and the residue was dissolved in THF (8.0 mL). This solution was added to a suspension of $LiAlH_4$ (0.133 g, 3.5 mmol) in THF (8.0 mL) at −78 °C. To this mixture was added trimethylaluminium in hexane (3.5 mL, 1.0 M, 3.5 mmol) and the mixture was stirred at −78 °C and warmed gradually to room temp over 2 h. Usual work-up and column chromatography on alumina eluting with ether gave **15** (0.113 g, 90%), which was shown to contain the cis-isomer (10%) by GLC analysis.[27] **15**: IR (neat): 1370 cm^{-1} (weak); ^1H NMR ($CDCl_3$) δ=2.70—3.13 (m, 2H), 1.13—1.87 (m, 27H), 1.05 (d, 3H, J=6 Hz), 0.87 (t, 3H, J=6 Hz); ^{13}C NMR ($CDCl_3$) δ=50.9 (d), 45.9 (d), 34.1 (t), 33.0 (t), 31.9 (t), 30.7 (t), 29.8 (t), 29.7 (t, 5C), 29.4 (t, 2C), 26.5 (t), 22.7 (t), 21.2 (q), 19.6 (t), 14.1 (q).

References

1) For reviews on dihydropyridine chemistry: a) U. Eisner and J. Kuthan, *Chem. Rev.*, **72**, 1 (1972); b) D. M. Stout and A. I. Meyers, *ibid.*, **82**, 223 (1982).

2) a) E. Piers and M. Soucy, *Can. J. Chem.*, **52**, 3536 (1974); b) K. Akiba, Y. Iseki, and M. Wada, *Tetrahedron Lett.*, **23**, 429 (1982); c) *Bull. Chem. Soc. Jpn.*, **57**, 1994 (1984); d) D. L. Comins and A. H. Adbullah, *J. Org. Chem.*, **47**, 4315 (1982); e) D. L. Comins, *Tetrahedron Lett.*, **24**, 2807 (1983); f) D. L. Comins and N. B. Mantlo, *ibid.*, **24**, 3683 (1983); g) *Idem, J. Heterocycl. Chem.*, **20**, 1239 (1983); h) D. L. Comins, E. D. Strout, and J. J. Herrick, *Heterocycles*, **22**, 151 (1984); i) D. L. Comins, R. K. Smith, and E. D. Strout, *ibid.*, **22**, 339 (1984).

3) A. Peleter and K. J. Gould, *J. Chem. Soc., Chem. Commun.*, **1974**, 347.

4) K. Akiba, Y. Nishihara, and M. Wada, *Tetrahedron Lett.*, **24**, 5269 (1983) and **26**, 3267 (1985).

5) D. L. Comins and J. D. Brown, *Tetrahedron Lett.*, **25**, 3297 (1984).

6) a) G. Fraenkel, J. W. Cooper, and C. M. Fink, *Angew. Chem. Int. Ed. Engl.*, **9**, 523 (1970); b) R. E. Lyle and E. White V, *J. Org. Chem.*, **36**, 772 (1971); c) L. M. Thiessen, J. A. Lepoivre, and F. C. Alderweireldt, *Tetrahedron Lett.*, **1974**, 59; d) R. E. Lyle and D. L. Comins, *J. Org. Chem.*, **41**, 3250 (1976); e) R. E. Lyle, J. L. Marshall, and D. L. Comins, *Tetrahedron Lett.*, **1977**, 1015; f) D. L. Comins, A. H. Abdullah, N. B. Mantlo, *Tetrahedron Lett.*, **25**, 4867 (1984); g) D. L. Comins and N. B. Mantlo, *J. Org. Chem.*, **50**, 4410 (1985); h) D. L. Comins and J. D. Brown, *Tetrahedron Lett.*, **27**, 2219 (1986).

7) During this research, the similar observation to the

ours has been reported, see Refs. 2c and 2d.

8) A part of this research has appeared in a preliminary form: a) R. Yamaguchi, Y. Nakazono, and M. Kawanisi, *Tetrahedron Lett.*, **24**, 1801 (1983); b) Y. Nakazono, R. Yamaguchi, and M. Kawanisi, *Chem. Lett.*, **1984**, 1129.

9) For our studies on reactions of 1-acylpyridinium salts with organotin reagents, see a) R. Yamaguchi, M. Moriyasu, M. Yoshioka, and M. Kawanisi, *J. Org. Chem.*, **50**, 287 (1985); b) R. Yamaguchi, M. Moriyasu, and M. Kawanisi, *Tetrahedron Lett.*, **27**, 211 (1986).

10) R. G. Pearson, *J. Chem. Educ.*, **45**, 581 and 643 (1986).

11) a) R. H. Hudson, *Angew. Chem. Int. Ed. Engl.*, **12**, 36 (1973); b) I. Fleming, "Frontier Orbitals and Organic Chemical Reactions," John Wiley & Sons, N.Y. (1976), p. 66. c) T.-L. Ho, "Hard and Soft Acids and Bases Principles in Organic Chemistry," Academic Press, N.Y. (1977).

12) Recently, reactions of 1-acylpyridinium salts with alkynyl Grignard reagents have been reported without the discussion on the regioselectivity: M. Natume and M. Ogawa, *Heterocycles*, **20**, 601 (1983).

13) It has been reported that the reaction of pyridine with silver phenylacetylide in the presence of benzoyl chloride gave 1-benzoyl-2-phenylethynyl-1,2-dihydropyridine: T. Agawa and S. I. Miller, *J. Am. Chem. Soc.*, **83**, 449 (1960).

14) It should be noted that a bulky 1-substituent (e.g., triphenylmethyl or *t*-butyldimethylsilyl group) induces the preferential γ-addition.[2c,d,6e]

15) For the recent report on this matter: P. D. Edwards and A. I. Meyers, *Tetrahedron Lett.*, **25**, 939 (1984), and references cited therein.

16) T. Shono, Y. Matsumura, K. Uchida, K. Tsubata, and A. Makino, *J. Org. Chem.*, **49**, 300 (1984).

17) a) V. Stoilova, L. S. Trifonov, and A. S. Orahovats, *Synthesis*, **1979**, 105; b) P. G. Sammes and S. Smith, *J. Chem. Soc., Perkin Trans. 1*, **1984**, 2415.

18) J. D. Hunt and A. C. McKillop, "Rodd's Chemistry of Carbon Compounds," ed by S. Coffey, Elsevier, Amsterdam (1978), Vol IV, Part G, p. 115.

19) V. Baliak, R. Jeyaraman, and L. Chandorasekaran, *Chem. Rev.*, **83**, 379 (1983).

20) J. G. MacConell, M. S. Blum, and H. M. Fales, *Tetrahedron*, **27**, 1129 (1971).

21) For stereoselective synthesis of (±)-solenopsin A: a) Y. Matsumura, K. Maruoka, and H. Yamamoto, *Tetrahedron Lett.*, **23**, 1929 (1982); K. Maruoka, T. Miyazaki, M. Ando, Y. Matsumura, S. Sakane, K. Hattori, and H. Yamamoto, *J. Am. Chem. Soc.*, **105**, 2831 (1983); b) M. Bonin, J. R. Romero, D. S. Grierson, and H.-P. Husson, *Tetrahedron Lett.*, **23**, 3369 (1982), and references cited therein.

22) M. E. Jung and M. A. Lyster, *J. Chem. Soc., Chem. Commun.*, **1978**, 315.

23) It should be noted that reductions of 2,6-dialkylated pyridines give exclusively or predominantly *cis*-2,6-dialkylated piperidines.[19,20]

24) Another route which also starts from 2-methylpyridine provides (±)-solenopsin A in 28% overall yield in 7 steps.[21b]

25) R. Lukes and Z. Vesely, *Coll. Czech. Chem. Commun.*, **24**, 944 (1959).

26) V. Boekelheide and S. Rothchild, *J. Am. Chem. Soc.*, **71**, 879 (1949).

27) The stereoselectivity (90%) was slightly lower than the reported one (95%),[21a] probably because **14** was slightly contaminated by the perhydrogenated compound.

 © 1987 The Chemical Society of Japan Bull. Chem. Soc. Jpn., 60, 223—228 (1987)

Reactivities of Stable Rotamers. XVIII. Reactions of 9-[2-(1-Hydroxyethyl)-1-naphthyl]fluorene Rotamers with Sulfuric Acid and Thionyl Chloride[1)]

Michinori Ōki,* Jiro Tsukahara, Kazuhiro Moriyama, and Nobuo Nakamura
Department of Chemistry, Faculty of Science, The University of Tokyo,
Bunkyo-ku, Tokyo 113
(Received June 21, 1986)

Treatment of the title compound with 70% sulfuric acid in 1,2-dimethoxyethane caused cyclization for the *ap* isomer, whereas it did dehydration to produce a vinyl compound smoothly for the *sp*. The same treatment with 10% sulfuric acid in 1,2-dimethoxyethane afforded the corresponding vinyl compounds from both rotamers. Treatment of the alcohol with thionyl chloride afforded the corresponding chloride in the case of the *sp*-alcohol, while it gave the *sp*-vinyl compound in addition to the *ap*-chloride in the case of the *ap*-alcohol. The change in solvents in the reaction of the *ap* form caused the change in the ratio of the olefin vs. the chloride: The polar solvents enhance the rates of formation of the chloride. Introduction of three deuteriums to the methyl group of the *ap*-form of the title compound suppressed the formation of the olefin to some extent. The results are explained on the grounds of steric effects in the ion-pair formation from the chlorosulfites and the contribution of the C–H stretching in the transition state of the elimination.

In previous papers of this series, it was postulated that a reaction is slow in the ap conformer of 9-arylfluorenes, one of which examples is 9-(2-substituted 1-naphthyl)fluorene (**1**), if the reaction takes a space-demanding transition state[2,3)] and that a cation formed in the benzylic position of the aryl group shows intramolecular interactions with the π-electron system of the fluorene moiety.[4)] Since 9-[2-(1-hydroxyethyl)-1-naphthyl]fluorene (**2**) should form a cationic species if treated with an acid and derivation of the alcohol to the corresponding chloride with the use of thionyl chloride should proceed with a cyclic transition state,[5)] the rotamers of compound **2** might show interesting difference in their behaviors in these reactions. Thus we investigated these reactions of the alcohol **2**. This paper is to report the results of the investigation and to discuss the origin of the difference.

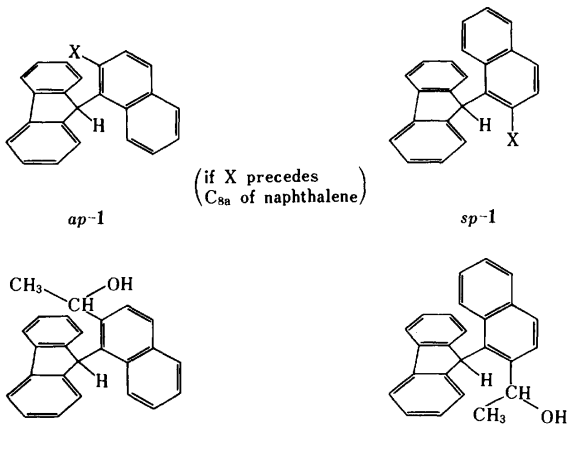

ap-1 *sp*-1

ap-2 *sp*-2

The barrier to rotation about the C_9(fluorene)-to-C_1(naphthalene) bond in the compound **2** has not been determined but may be assumed to be high enough to examine reactions without giving any complexity due to isomerization at room temperature for the following reasons. The barrier to rotation in 9-(2-methyl-1-naphthyl)fluorene (**1**: X=CH_3) is known to be ca. 29 kcal mol^{-1} (1 cal=4.18 J).[6,7)] Substitution of one of the hydrogens in the methyl group of 9-(2-methyl-1-naphthyl)fluorene does not significantly affect the barrier height (ca. 29 kcal mol^{-1}).[8)] In a series of 9-(2-substituted phenyl)fluorenes, the change in the substituent from methyl to ethyl and then to isopropyl causes a slight increase in the barrier height (16, 17, and 18 kcal mol^{-1}, respectively, for the *ap*→*sp* process).[6,9)] Similarly, 9-[2-(1-methoxycarbonylethyl)phenyl]fluorene exhibits ca. 18 kcal mol^{-1} barrier.[10)] Furthermore, the barrier to rotation in 9-[2-(α-hydroxybenzyl)-1-naphthyl]fluorene (*ap*→*sp*) is known to be ca. 30 kcal mol^{-1} at room temperature.[2b)] Thus the barrier to rotation about the C_9(fluorene)–C_1-(naphthalene) bond should be higher than 29 kcal mol^{-1}.

Reaction with Sulfuric Acid. Treatment of *ap*-**2** in 1,2-dimethoxyethane with sulfuric acid, of which concentration was high in the same solvent, afforded a product of which elemental analysis was consistent with a structure derived by dehydration of *ap*-**2**. From the ^{1}H NMR spectrum of the product and from our experience that has shown cyclization be possible for the *ap*-isomer if a cation is formed,[4)] we assigned a planar structure **3** for the product. By contrast, the *sp*-isomer afforded *ap*-9-(2-vinyl-1-naphthyl)fluorene (**4**) in good yields. If the concentration of sulfuric acid in 1,2-dimethoxyethane was low, both *ap*-**2** and *sp*-**2** afforded the respective rotamer of **4**, although the former is often contaminated by **3**.

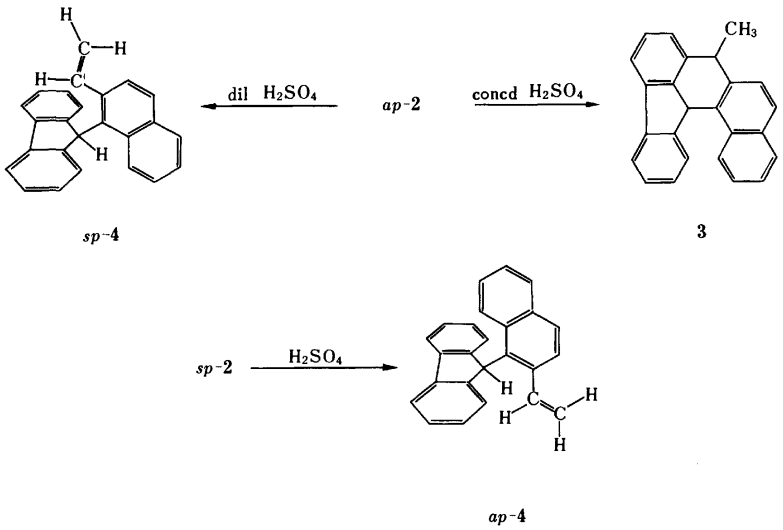

The reason for the fact that, whereas the *ap* form of **2** cyclized, *sp*-**2** failed to give any cyclized product, must be the geometry of the cation that is formed during the reaction. The cation from *sp*-**2** is in the plane of the fluorene ring. Since rotation about the C_9(fluorene)–C_1(naphthalene) bond must take place for the cation from *sp*-**2** for cyclization, of which barrier is high, deprotonation from the cation is a preferred process even in the concentrated sulfuric acid medium. In contrast, cyclization is favored in the cation from *ap*-**2** because the cationic center is very close to the π-system of the fluorene ring. It seems that, if the concentration of sulfuric acid is low, water or hydrogensulfate anion can remove a proton from the intervening cation from *ap*-**2** favorably.

If the π-participation in forming the benzylic cation from *ap*-**2** is really important, the dehydration of the *ap*-alcohol may be facilitated relative to the *sp*-alcohol, since formation of the cation is expected to be rate-determining. Competitive dehydration of *sp*-**2** and *ap*-**2** revealed that the relative rate, k_{sp}/k_{ap}, was 0.36, as determined by the formation of the olefins. Although this ratio might seem small, it must be taken as an indication that the π-participation is considerable, especially because the solvent molecules are good at stabilizing carbocations. For the cation from *ap*-**2**, solvation shell is formed by participation of the fluorene ring in addition to the solvent molecules, the latter being more favorable than the former.[4]

As to the stereostructure of **3**, there are two possibilities, *cis* and *trans*, with respect to the 8-H and 14c-H. For the stereochemical assignments of 9,10-dihydroanthracene derivatives, coupling constants in ^{1}H NMR are known to be useful.[11] Since the 14c-H should take the axial position because of the geometrical requirement, if the methyl group at the 8-position is equatorial, a large coupling constant between the protons in question is expected. Since they showed a small coupling constant, the ^{1}H NMR spectrum supports the stereochemistry in that the 8-H and the 14c-H are *trans* with each other.

Consideration of the reaction mechanism also supports the conclusion drawn from the ^{1}H NMR spectrum. The alcohol (**2**) will form a cationoid species when it is treated with sulfuric acid, since it is a benzylic alcohol.[12] Then there are two over-simplified reaction intermediates (**6** and **7**) possible, as

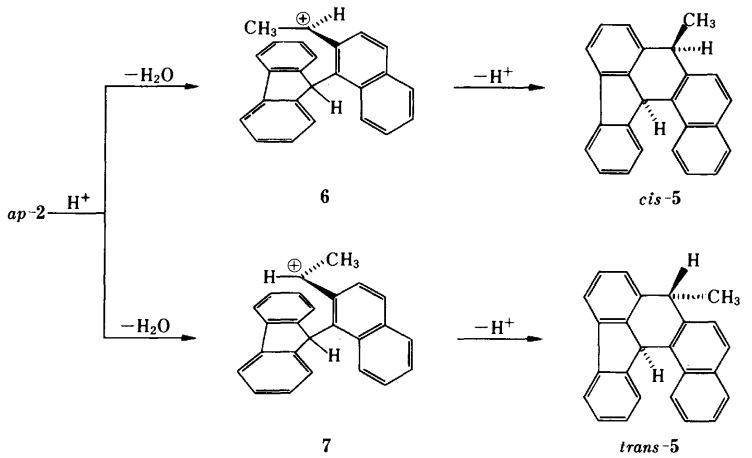

shown in the preceding page. Of the two, the one in which the methyl group is located over the fluorene ring **6** should be of high energy than the other **7** in which the hydrogen is over the fluorene ring. If cyclization takes place from **6**, the 8-H/14c-H stereochemistry is *cis*, whereas it is *trans* when cyclization takes place from **7**. Thus, *trans* stereochemistry should be favored in the product. In support of this, we observed formation of another isomer, of which ^{1}H NMR doublet signal appeared at δ 1.82 due to the methyl protons, in addition to the main product which showed the same peak at δ 1.53, in the reaction run by adding sulfuric acid to 1,2-dimethoxyethane solutions of *ap*-**2**, when temperature rose spontaneously.

Reactions with Thionyl Chloride. The reactions of the alcohol (**2**) with thionyl chloride was carried out generally as dichloromethane solutions at 0 °C. *sp*-**2** afforded the corresponding chloride (**8**) smoothly, whereas *ap*-**2** afforded *sp*-9-(2-vinyl-1-naphthyl)fluorene (**4**) in addition to the chloride (**8**). Since the reaction of 1-(2-naphthyl)ethanol under the same conditions gave the corresponding chloride only, as had been reported,[13] the anomaly is in *ap*-**2** rather than in *sp*-**2**. Formation of olefins in treatment of secondary alcohols with thionyl chloride has been reported in purely aliphatic series,[14] but not for the benzylic alcohols. We have examined whether hydrogen chloride reacted with *sp*-**4** to form *ap*-**8** and *ap*-**8** decomposed to produce *sp*-**4** under the conditions. The results were all negative. Thus the ratio *sp*-**4**/*ap*-**8** can be taken as intrinsic.

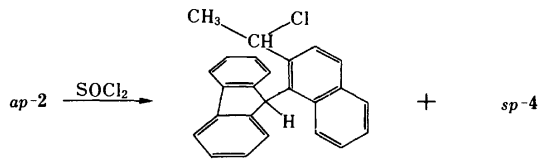

ap-**8**

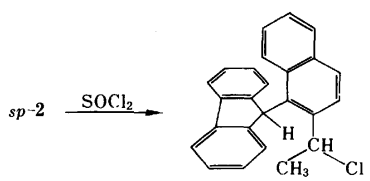

sp-**8**

The formation of a chloride from a chlorosulfite ester which is derived by the reaction of an alcohol with thionyl chloride is believed to proceed via an ion pair that is produced by a cyclic transition state.[5b] The rate-determining step in the olefin formation from secondary alcohols and thionyl chloride has been deduced to be the formation of the ion pair as well from the kinetic isotope effect.[15] However, it is necessary for the chloride anion to move in the deprotonation from the methyl group in the case of *ap*-**2**. Therefore, if the elimination to form *sp*-**4** and the substitution to form *ap*-**8** are competing, solvent effects due to the polarity are expected. Thus we carried out the reactions of **2** with thionyl chloride in various solvents. The results are shown in Table 1. The olefin **4** is never found in the product of the reaction of *sp*-**2**, as far as the present method of detection concerns, but the formation of the olefin from *ap*-**2** is dependent on the polarity of the solvent used: The more polar is the solvent, the more is the chloride produced.

Table 1. Dehydration versus Chlorination in the Reaction of **2** with Thionyl Chloride

Solvent	Dielectric constant of solvent	From *ap*-alcohol (*sp*-**4**/*ap*-**8**)	From *sp*-alcohol (*ap*-**4**/*sp*-**8**)
Hexane	1.88[b]	71/29	<5/>95
Dioxane	2.21[b]	67/33	<5/>95
Dichloromethane	8.93[b]	60/40	<5/>95
Thionyl chloride	9.25[c]	38/62	<5/>95
Nitromethane	35.9[b]	20/80	<5/>95

a) Reactions were carried out with ice-cooling except for the hexane solutions which were heated at 40 °C. b) From Ref. 16. c) From Ref. 17.

In order to get further insight into the reaction, we measured ^{1}H NMR spectra of mixtures of **2** and thionyl chloride in dichloromethane at 0 °C. Surprisingly, we found signals due to the starting material and the products, the olefin **4** and/or the chloride **8**, but not those due to chlorosulfites. Whereas the signals due to **2** decreased in their intensities and those due to the products increased in their intensities, we did not observe any signals ascribable to the chlorosulfite. This means either that the rate determining step in the reaction is not the step leading to the cyclic transition state or that the chlorosulfite is highly unstable, though its decomposition is rate-determining. It is not possible to conclude which is the case from the results of the present work. The rate determining step may vary also, as the polarity of the solvent changes.

We further carried out the reaction of *ap*-**2**-methyl-d_3 under the same conditions with the protium compound in dioxane to find that the ratio *sp*-**4**/*ap*-**8** changed from 2.0 in the protium compound to 1.0 in the deuterium compound. Although it was not possible to run the kinetic studies due to the fact that the chlorosulfites were unstable and thus the kinetic isotope effects were not determined, this change in the product ratio is interesting. The results would mean that the hydrogen-abstraction step is contributing to the overall reaction rates.

The implication of the results made it necessary to reexamine the reported kinetic isotope effect.[15] Close examination of the reported rates of decomposition of

1-methylbutyl-methyl,2,2-$d_{4.3}$ chlorosulfite reveals that the isotope effects are 1.4 and 3.3 in dioxane and isooctane, respectively. The secondary α-kinetic isotope effects are normally 10—15% per deuterium for the S_Ni type ionizations.[18] While the β-kinetic isotope effects are stereochemistry-dependent, they never exceeds 2.0.[19] The data obtained for the dioxane solutions are within the range for normal ionization reactions, but those for the isooctane solutions exceeds the range of the normal ionization, if the secondary isotope effects are assumed. This would mean that solvents change the mechanisms or the contributions to the transition states of the rate-determining step considerably, because the solvent polarity affects the transition state energy.

The isotope effects on the product ratio then could be used for the diagnosis of the reaction mechanisms, since the primary isotope effects are expected to be more than 3.0 for the normal cases.[20] From the data of the solvent effects on the product ratios, it was expected that the isotope effects on the product ratio *sp*-**4**/*ap*-**8** were to be the highest in hydrocarbons. Accordingly, examination of the product ratio *sp*-**4**/*ap*-**8** in hexane would be interesting. The reaction had to be carried out at 40 °C in hexane because of its slowness, while reactions were practically complete at 0 °C in other solvents. This operation will cause reduction in the *sp*-**4**/*ap*-**8** ratio relative to the data at 0 °C in other solvents.[21] Yet the ratio was 7:3 for the protium compound, a little higher value than that obtained with the dioxane solution at 0 °C (Table 1). Thus the solvent effect on the *sp*-**4**/*ap*-**8** ratio, favoring the formation of *sp*-**4** in less polar media, is still valid. The same treatment of *ap*-**2**-methyl-d_3 in hexane gave the *sp*-**4**/*ap*-**8** ratio of 1.5, which is still higher than that obtained with the dioxane solution of the deuterium compound.

From the above results, we can conclude that 1) the olefin formation from *ap*-**2** is favored in less polar media than in more polar media and 2) the deuterium isotope effects on the product ratio is more significant in less polar media than in the more polar. Any explanation of the mechanisms must accommodate these facts together with the results that have been published.

The formation of the olefin (*sp*-**4**) from *ap*-**2** may be explained by the steric effects. Molecular models of the cyclic transition state to form an ion pair from the *ap*-chlorosulfite suggest that the transition state of the reaction receives considerable steric hindrance from the fluorene ring. In nonpolar media, the ion pair must be tight, while it is loose in polar media. This will mean that the transition state for the ion-pair formation in polar media is attained earlier than that in nonpolar media. Since the $C_\alpha \cdots Cl$ distance in this assumed transition state in nonpolar media is shorter than that in polar media, the steric effect that is received by the former must be severer than the latter. By contrast, the elimination reaction which involves the contribution of the C–H stretching will receive far less steric effect of the fluorene ring because one of the C–H bonds in the methyl group is always far from the fluorene moiety. In addition to the above, there is a factor that must be taken into account. That is, the ionic reactions, that form the chloride in this case, are generally favored in polar solvents, whereas the olefin formation should be less affected by the polarity of the media, as judged from the participation of the C–H stretching to the olefin formation, which means that the nonionic cyclic transition state is contributing. Thus we conclude that due to the factors discussed above the chloride formation becomes relatively favored in polar media, while the olefin formation is favored in nonpolar media.

Experimental

9-[2-(1-Hydroxyethyl)-1-naphthyl]fluorene (2). A solution of 2.0 g (5.9 mmol) of a rotameric mixture (ca. 1:1) of 9-(2-formyl-1-naphthyl)fluorene[2] in 150 mL of ether was added to a Grignard solution, which was prepared from 0.37 g (15 mmol) of magnesium, 1.1 mL (18 mmol) of methyl iodide, and 15 mL of ether. The mixture was stirred for several minutes and decomposed with aqueous ammonium chloride. The ether layer was separated and the aqueous layer was extracted with ether. The combined ether layer was dried over magnesium sulfate and the solvent was evaporated to afford a mixture of the rotameric alcohols. The mixture was separated by silica-gel chromatography (hexane–ether eluent) to give 1.0 g each of *sp* and *ap* rotamers, which were identical with those previously reported.[2]

ap-9-[2-(2,2,2-Trideuterio-1-hydroxyethyl)-1-naphthyl]fluorene (*ap*-**2**-methyl-d_3) was similarly prepared from methyl-d_3 iodide and the *ap*-aldehyde (**1**: X=CHO) and purified by thin-layer chromatography (3:2 dichloromethane–hexane). MS (*m/z*): 339 (M^+, $C_{25}H_{17}D_3O$), 321 (base peak, $M-CD_3$), 320 (M−HDO). ^1H NMR ($CDCl_3$) δ=3.77 (1H, s), 6.10 (1H, s), 7.1—8.0 (13H, m), 8.4—8.6 (1H, m). The OH proton signal was not detected.

Reaction with Dilute Sulfuric Acid. A solution of 1.0 g of the *sp*-alcohol (**2**) in 50 mL of 1,2-dimethoxyethane was mixed with a mixture of 10 mL of concentrated sulfuric acid and 150 mL of 1,2-dimethoxyethane with ice-cooling. The mixture was stirred for 5 d at room temperature, poured into water, and extracted with ether. The ethereal extract was washed with aqueous sodium hydrogencarbonate and dried over magnesium sulfate. After evaporation of the solvent, the residue was chromatographed on silica gel (hexane eluent). The product was recrystallized from pentane to give pure *ap*-9-(2-vinyl-1-naphthyl)fluorene (**4**), mp 119.0—119.5 °C, in 90% yield. Found: C, 94.14; H, 5.41%. Calcd for $C_{25}H_{18}$: C, 94.30; H, 5.70%. ^1H NMR ($CDCl_3$) δ=5.4—5.9 (2H, m), 5.87 (1H, s), 6.3—8.0 (15H, m).

Similar treatment of the *ap*-alcohol (**2**) with sulfuric acid afforded *sp*-olefin (**4**), mp 134.5—135.5 °C, in 85% yield. Found: C, 94.58; H, 5.41%. Calcd for $C_{25}H_{18}$: C, 94.30; H, 5.70%. ^1H NMR ($CDCl_3$) δ=4.4—5.3 (2H, m), 5.4—5.8 (1H,

m), 6.11 (1H, s), 7.1—8.0 (13H, m), 8.4—8.7 (1H, m).

Reaction with Concentrated Sulfruic Acid. A solution of 1.0 g of *ap*-alcohol (**2**) in 10 mL of 1,2-dimethoxyethane was mixed with a mixture of 30 mL of 1,2-dimethoxyethane and 30 mL of concentrated sulfuric acid and stirred overnight at room temperature. The mixture was poured into water and extracted with ether. The ethereal extract was washed with aqueous sodium hydrogencarbonate and dried over magnesium sulfate. The solvent was evaporated and the residue was chromatographed on silca gel (hexane eluent) to afford *trans*-8-methyl-8,14c-dihydrodibenz[*a*,*l*]aceanthrylene (**5**), mp 173.0—174.0 °C, in 90% yield. Found: C, 94.27; H, 5.40%. Calcd for $C_{25}H_{18}$: C, 94.30; H, 5.70%. ^{1}H NMR ($CDCl_3$) δ=1.53 (3H, d, J=7 Hz), 4.11 (1H, dq, J=1 and 7 Hz), 5.14 (1H, d, J=1 Hz), 6.9—8.8 (13H, m).

Similar treatment of the *sp*-alcohol afforded the *ap*-olefin only which was identical with that described above.

Competitive Reaction of *ap*-2 and *sp*-2 with Sulfuric Acid. A solution of 20 mg each of *ap*-**2** and *sp*-**2** in 50 mL of 1,2-dimethoxyethane was mixed with a mixture of 10 mL of concentrated sulfuric acid and 50 mL of 1,2-dimethoxyethane with ice-cooling. The whole was stirred at room temperature for 3 h and treated similarly as above thereafter. The conversion was less than 10% under the conditions. The ratio of the rotameric olefins, *sp*-**4**/*ap*-**4**, was analyzed with the use of HPLC. The HPLC instrument was a Waters M-600 Chromatograph equipped with a UV detecter at 254 nm. At a flow rate of 3.1 mL min^{-1} of hexane on a Microporasil column, the retention times were, *ap*-**4** 6.1 min and *sp*-**4** 7.1 min. The formation ratio, *sp*-**4**/*ap*-**4**, was 0.36.

Since the reaction can be assumed to be first-order in each of the substrate and sulfuric acid is used in large excess and since the reaction was discontinued at early stages, the formation ratios were taken as the relative rates of the reaction.

9-[2-(1-Chloroethyl)-1-naphthyl]fluorene](8). A solution of 100 mg (0.30 mmol) of the *sp*-alcohol in 50 mL of nitromethane was mixed with 0.5 mL (4.3 mmol) of thionyl chloride which was freshly distilled from a mixture of thionyl chloride and triphenyl phosphite, with ice-cooling. The mixture was stirred at 40 °C for 10 min and the solvent was evaporated. The residue was chromatographed on silica-gel TLC to give ca. 80% *sp*-chloride, oil, which was rather unstable. High resolution MS gave very weak M^+ peak at m/z 354.1192, whereas the calcd value for $C_{25}H_{19}{}^{35}Cl$ is 354.1175. ^{1}H NMR ($CDCl_3$) δ=2.13 (3H, d, J=7 Hz), 5.86 (1H, s), 6.00 (1H, q, J=7 Hz), 6.3—8.0 (14H, m). No impurity was detected by ^{1}H NMR spectra.

Similar treatment of the *ap*-alcohol gave a mixture of *sp*-9-(2-vinyl-1-naphthyl)fluorene and *ap*-9-[2-(1-chloroethyl)-1-naphthyl]fluorene in 18 and 72% crude yields, respectively. The *ap*-chloride, oil, was again unstable but showed a very weak M^+ peak in high resolution MS at m/z 354.1166, whereas the calcd value for $C_{25}H_{19}{}^{35}Cl$ is 354.1175. No impurity peaks were detected in the ^{1}H NMR spectra of *ap*-**8**. ^{1}H NMR ($CDCl_3$) δ=1.02 (3H, d, J=7 Hz), 4.03 (1H, q, J=7 Hz), 6.10 (1H, s), 7.0–8.0 (13H, m), 8.4–8.6 (1H, m).

Solvent Dependence of the Thionyl Chloride Reaction with the Alcohol (2). Except for hexane solutions, the following is the typical procedure. The alcohol (*ap*-**2**) (30 mg) in appropriate solvent (50 mL) was mixed with 0.5 mL of thionyl chloride, which was purified as above, with ice-cooling, and the mixture was stirred for 5 min at that temperature and then at 40 °C for 10 min. The reaction mixture was treated similarly as above and the ratios (olefin/chloride) were determined by ^{1}H NMR spectra of the products in chloroform-*d* with the use of a Varian EM-390 spectrometer.

For hexane solutions, the reaction was carried out for 10 h at 40 °C with the same ratios of the reactants and the solvent and the mixture was treated similarly as above. Under the competitive conditions, 15% of the *ap*-alcohol remained unreacted, whereas 28% of the *sp*-alcohol was found unreacted after 10 h at 40 °C, when 50 mg each of the rotameric alcohols and 0.5 mL of thionyl chloride in 80 mL of hexane were used.[22]

Reaction of *ap*-2-Methyl-d_3 with Thionyl Chloride. The reaction was carried out in either dioxane or hexane as described in the Solvent Dependence section and the product ratios were determined by ^{1}H NMR spectra. The alcohol was less reactive than the protium compound, giving 35.5% unreacted alcohol after 10 h in hexane at 40 °C. The following ^{1}H NMR spectra were recorded. *ap*-**8**-methyl-d_3: 4.01 (1H, s), 6.10 (1H, s), 7.0—8.0 (13H, m), 8.4—8.6 (1H, m). *sp*-**4**-methylene-d_2: 5.54 (1H, s), 6.10 (1H, s), 7.0—8.0 (13H, m), 8.4—8.6 (1H, m).

This work was supported by a Grant in Aid for Scientific Research of the Ministry of Education, Science and Culture, to which our thanks are due.

References

1) For Part XVII, see M. Nakamura and M. Ōki, *Chem. Lett.*, **1986**, 1363.

2) a) M. Ōki and R. Saito, *Chem. Lett.*, **1981**, 649; b) R. Saito and M. Ōki, *Bull. Chem. Soc. Jpn.*, **55**, 3267 (1982).

3) S. Murata, S. Kanno, Y. Tanabe, M. Nakamura, and M. Ōki, *Bull. Chem. Soc. Jpn.*, **57**, 525 (1984).

4) S. Murata, S. Kanno, Y. Tanabe, M. Nakamura, and M. Ōki, *Angew. Chem., Int. Ed. Engl.*, **20**, 606 (1981); *Bull. Chem. Soc. Jpn.*, **55**, 1522 (1982).

5) a) W. A. Cowdrey, E. D. Hughes, C. K. Ingold, S. Masterman, and A. D. Scott, *J. Chem. Soc.*, **1937**, 1267; b) D. J. Cram, *J. Am. Chem. Soc.*, **75**, 332 (1953).

6) T. H. Siddall, III and W. E. Stewart, *J. Org. Chem.*, **34**, 233 (1969).

7) S. Murata, T. Mori, and M. Ōki, *Bull. Chem. Soc. Jpn.*, **57**, 1970 (1984).

8) R. Saito and M. Ōki, *Bull. Chem. Soc. Jpn.*, **55**, 2508 (1982).

9) M. Nakamura, N. Nakamura, and M. Ōki, *Bull. Chem. Soc. Jpn.*, **50**, 2986 (1977).

10) H. Iwamura and K. Yoshimura, *J. Am. Chem. Soc.*, **96**, 2652 (1974).

11) P. W. Rabideau, *Acc. Chem. Res.*, **11**, 141 (1978); A. W. Brinkma, M. Gordon, R. G. Harvey, P. W. Rabideau, J. B. Stothers, and A. L. Ternay, *J. Am. Chem. Soc.*, **92**, 5912 (1970).

12) C. K. Ingold, "Structure and Mechanism in Organic Chemistry," Cornell University Press, Ithaca (1953), p. 324.

13) P. A. Levene and L. A. Mikeska, *J. Biol. Chem.*, **75**, 587 (1927).

14) E. S. Lewis and C. E. Boozer, *J. Am. Chem. Soc.*, **74**,

308 (1952).
15) C. E. Boozer and E. S. Lewis, *J. Am. Chem. Soc.*, **76**, 794 (1954).
16) C. Reichardt, "Solvent Effects in Organic Chemistry," Verlag Chemie, Weinheim (1979), pp. 270—272.
17) "Gmelin Handbuch der Anorganischen Chemie," 8-Aufl. Schwefel Erg.-Bd. 1, 35 (1978).
18) E. A. Halevi, *Progr. Phys. Org. Chem.*, **1**, 109 (1963).
19) B. K. Carpenter, "Determination of Organic Reaction Mechanisms," John-Wiley, New York (1984), pp. 96—99.
20) V. Gold and D. P. N. Satchell, *Quart. Rev.*, **9**, 51 (1955); K. B. Wiberg, *Chem. Rev.*, **55**, 713 (1955); F. H. Westheimer, *ibid.*, **61**, 265 (1961); N. S. Isaacs, "Reactive Intermediates in Organic Chemistry," John-Wiley, New York (1974), pp. 38—43.
21) In one experiment in which thionyl chloride was added to a nitromethane solution of *ap*-**2** at room temperature followed by heating at 40 °C, no detectable amount of the olefin (*ap*-**4**) was formed. This lends support as well to the idea that the olefin formation is suppressed at a high temperature.
22) In hexane, it seems that the rate-determining step is the decomposition of the corresponding chlorosulfites, because addition of thionyl chloride to a hexane solution of *sp*-**2** caused a change in the chemical shift due to the methine proton in ^{1}H NMR spectra. However, the huge peaks due to the solvent prevented us performing any reliable, quantitative study.

 © 1987 The Chemical Society of Japan Bull. Chem. Soc. Jpn., 60, 229—240 (1987)

Concurrent Anodic Cyanation and Methoxylation of Methylated Furans. Oxidation Potential and Reactivity, and Stereochemical Control of Addition

Kunihisa Yoshida* and Takayuki Fueno
Department of Chemistry, Faculty of Engineering Science, Osaka University, Toyonaka, Osaka 560
(Received June 23, 1986)

The potentiostatic electrooxidation of a series of methyl-substituted furans was performed in MeOH that contains NaCN at a Pt anode in a divided cell. In all instances, the 1,4-additions of cyano and/or methoxyl group(s) across the furan ring were achieved. Replacement of an aromatic hydrogen by a cyano group occurred concurrently in some cases. The relative rates of cation radicals toward two different nucleophiles (CN^- ion and the solvent MeOH (or the MeO^- ion as a result of the equilibrium between CN^- ion and the solvent MeOH)) at the electrode surface were determined from the yields of products by using the rate expressions of competitive reactions. There is a linear correlation between the relative reactivity of the furans (on a log scale) and their oxidation potential. The ratio of stereoisomers formed in an electrooxidation of 2,5-dimethylfuran (2,5-DMF) changes with addition of adsorbable compound as well as substrate concentration and this is thought to be due to the influence of concentration (or coadsorbate) on substrate orientation in the adsorption layer.

Previously we reported the electrooxidation of 2.5-dimethylfuran (2,5-DMF) in MeOH that contains NaCN.[1-4] Stereoselective 1,4-addition of cyano and/or methoxyl group(s) to the furan ring occurred. The process consists of two successive competitive reactions; the first one is addition of two different nucleophiles, CN^- ion and the solvent MeOH (or the MeO^- ion as a result of the equilibrium between CN^- and MeOH), to the 2,5-DMF cation radical and the second one is to the benzenium-type ion formed by means of an ECE process. If this system is applied to a series of sequentially substituted furans, the mode and yields of products may well reflect the competitive reactions toward each cationic intermediate. It should provide information on the relative reactivity of a series of related cations toward two competing nucleophiles at the electrode.

In an attempt to determine the relative concentrations of those two nucleophiles at the electrode from oxidation products of 1,4-dimethoxybenzene (1,4-DMB) in the same solvent-electrolyte system using a competitive technique, Weinberg and co-workers assumed that the relative rates of 1,4-DMB cation radical and of substituted benzenium ions toward two nucleophiles would be both equal to those of relatively stable carbenium ions such as triarylmethyl cations, arenediazonium ions, and tropylium ions.[5] There is, however, no foundation for such a hypothesis. The idea that the relative (if not absolute) reactivity changes with the structure is rather natural.

The present paper describes the competitive anodic cyanation and methoxylation of a series of sequentially methyl-substituted furans. The relative reactivity of furans cation radicals toward two competing nucleophiles at the electrode has been estimated by studying the products. The relative reactivity changes widely with the substrate structure, and correlates with the oxidation potential at that. Addition to the furan ring, especially the second nucleophilic addition, is sterically controlled by the electrode. The influence of substrate concentration, aromatic additive, and electrode material on the ratio of stereoisomeric products has been investigated.[6]

Results

Cyclic Voltammetry (CV). Cyclic voltammograms were recorded for each compound using a solution of 0.4 M† NaCN in MeOH. The background current with this system began to increase at potentials more anodic than 1.60 V. The E_p values are collected in Table 2. 2,5-DMF gave a single anodic peak. The electrochemical data revealed that the height of the peak varied linearly with concentration, and there was no evidence of a reversible cathodic peak for any of the furans. The current function, $i_p/v^{1/2}$, where i_p is the peak current and v is the sweep rate, decreased, and E_p shifted more positive with increasing sweep rate. Similar voltammetric data were noted for other substituted furans (Table 1). All of the preceding data are consistent with a fast chemical reaction following the electron transfer.

Product Studies. The reactions were performed potentiostatically in a divided cell with a Pt anode at room temperature. The reference electrode was an SCE. The electroreaction medium was MeOH–0.4 M NaCN. The products were isolated by preparative GLC and were identified by the elemental and ^1H NMR, IR, and mass spectroscopic analyses.

The 1,4-addition of cyano and/or methoxyl group(s) across the diene system of a furan took place for all of the molecules investigated, and besides the replacement of an aromatic hydrogen by a cyano group at a free 2 (or 5) position occurred concurrently

† 1 M=1 mol dm^{-3}.

for furans lacking the substituent on either 2 or 5 (or both) position(s). Nuclear cyanation at the 3 position also occurred slightly for 2,5-DMF. In some cases, small amounts of side-chain-methoxylation products were produced. Some of cyanation products undergo base-catalyzed reaction[5,7] in the reaction medium, yielding methyl imidates. Small amounts of 1,4-dicarbonyl compounds and their monoacetals were occasionally obtained. Structural formulas of products are shown below and the results of preparative electroreaction are given in Table 2. The Table also contains the results of both the electrooxidation of 2,5-diethylfuran (2,5-DEF) in the same solvent-electrolyte system and the electroreaction of 2,5-DMF in EtOH that contains NaCN.

Table 1. Cyclic Voltammetric Data for the Electrooxidation of Methylated Furans in 0.4 NaCN-MeOH[a]

Compd	Sweep rate, mV/s	i_p, mA	$i_p/v^{1/2}$, mA $s^{1/2}/V^{1/2}$	E_p, V vs. SCE
2,5-DMF	10	1.3	13.0	1.28
	50	2.4	10.7	1.33
	100	3.1	9.8	1.35
	300	5.2	9.5	1.42
2,3,4-TMF	30	1.9	11.0	1.33
	100	2.9	9.2	1.37
	300	4.3	7.8	1.48
2,3,5-TMF	10	1.1	11.0	1.16
	100	2.8	8.9	1.25
	300	4.4	8.0	1.32
TetMF	10	1.0	10.0	1.06
	100	2.8	8.9	1.13
	300	4.2	7.7	1.24

a) Pt wire electrode, 0.322 cm^2. 2×10^{-2} M substrate.

Structure of Isomeric Pairs. The extensive and detailed studies on geometrical isomerism in 2,5-dihydro-2,5-dimethoxyfurans[8-11] make possible the structural assignments to isomeric pairs of the relevant 1,4-mixed addition products. The basis for the structural assignments resides in the fact that the chemical shift of a group in the 2 position of the furan ring is affected both by the other group at the 2 position and the magnetic influence exerted by the group at the 5 position that is cis to it. Thus, if a 2-methyl is cis to a 5-methoxyl (or a 5-cyano) it will resonate at lower field and raise the δ value than if it is

Table 2. Electrooxidation of Furans. Voltammetric Data and Products[a]

Compd	E_p, V[b]	Product	Isomer ratio (cis/trans)	CE[c] %	Compd	E_p, V[b]	Product	Isomer ratio (cis/trans)	CE[c] %
Unsubstituted	≈2.0	**1a**	1.7	27[d]	2,5-DMF[f]		**1y**[g]	3.4	53
		3a		0.5			**1z**	0.4	5
2-MF	1.61	**1b**	0.8	10			**2m**		Trace
		1c	1.6	32	3,4-DMF	1.61	**2h**		3
		2a		5			**2i**		1
3-MF	1.78	**2b**		0.5			**1m**		3
		1d	1.3	63			**1n**	1.5	60
		3b		0.5	2,3,4-TMF	1.37	**1o**	1.2	22
2,3-DMF	1.51	**1e**	2.0	27			**1p**		7
		1f	1.1	17			**1q**	1.2	13
		3c		2			**2j**		11
2,4-DMF	1.55	**1g**	1.3	10			**2k**		9
		1h		1	2,3,5-TMF	1.25	**1r**		5
		1i		2			**1s**	2.7	71
		1j	1.0	28			**1t**	2.5	7
		2c		21			**1u**	0.5	1.5
		2d		7	TetMF	1.13	**1v**	1.0	14
		3d		2			**1w**	3.2	75
2,5-DMF	1.35	**1k**	2.5	69			**1x**		Trace
		1l	0.5	3			**2l**		Trace
		2e		2	2,5-DEF	1.36	**1aa**[h]	3.0	58
		2f		e)			**1bb**	1.0	2
		2g		e)					

a) Oxidation in MeOH solvent, unless otherwise stated. The potential was set at the peak potential of the substrate. b) Peak potential from CV; Pt anode, MeOH, 0.4 M NaCN, SCE reference. Sweep rate is 0.1 V/s. Substrate concentration is 2×10^{-2} M. All voltammograms showed no cathodic peak corresponding to reversible reduction of a cation radical. c) Current efficiency. d) The remainder of the current is consumed by concurrent discharge of the solvent-electrolyte system. e) A small amount. f) Oxidation in EtOH. g) Equilibrium mixture at room temperature: cis/trans=1.5. h) Equilibrium mixture at room temperature: cis/trans=1.7.

cis to another 5-methyl (or 5-protio) group (Table 3). The same reasoning can be applied to the methoxyl peaks and permits the indicated structural assignments for the two isomers.

Stereochemical Experiments. Table 4 summarizes the isomer compositions of the products of electrooxidative cyanomethoxylation of 2,5-DMF conducted under various experimental conditions. The product mixture was analyzed in very early stages of the run to avoid the shift of the substrate concentration. Consequently, samples were withdrawn and analyzed after passage of 1 to 5% of the charge calculated for a two-electron transfer process, and the average of two or more runs was then taken to be the isomer ratio.

The reaction is sterically controlled by a Pt electrode. The ratio of the resultant stereoisomers depends on the concentration of the substrate, the highest value (3.1 : 1) being obtained in the most dilute solution. The ratio also changed with the type and concentration of aromatic additives. Among aromatic additives, 1,4-DMB and pyridine cause greater changes in the cis-to-trans ratio. On the contrary, addition of aromatic molecules such as bis(*p*-methoxyphenyl)-amine, triphenylamine, tris(*p*-bromophenyl)amine, and tri-*p*-tolylamine, of which oxidation potentials are lower than that of the substrate, prevented the reaction. These aromatic compounds are apparently inert under the present conditions even though they discharge practically. The current is consumed by the regeneration of the additive as a consequence of homogeneous electron transfer between the electrogenerated cation radical and CN^- ion.

In contrast to the Pt electrode, a vitreous C anode gives an isomer ratio approaching that of the equilibrium mixture.

Acid-Catalyed Reactions of 1,4-Mixed Addition Products. It was confirmed that neither of the isomers *cis*-**1k** and *trans*-**1k** undergoes interconversion under the reaction conditions. Both of them also remained intact on GLC. However, a trace of a strong acid converted either isomer into an equilibrium mixture of the two isomers. To obtain a value for the equilibrium isomer composition, cis-trans isomerization was carried out in MeOH in the presence of 1% CF_3COOH at 25.0 °C. The equilibrium was reached within 1 h. The equilibrium value for the ratio *cis*-**1k**:*trans*-**1k** was 1.5:1. Moreover, a temperature change had a negligible effect on the K value at 0 to 100 °C. The acid-catalyzed isomerization also occurs in other solvents such as $CHCl_3$ and CCl_4, but in EtOH it gives place to the alcohol exchange accompanying the isomerization equilibrium.

$$\mathbf{1k} \xrightarrow[\text{EtOH}]{H^+} \mathbf{1y} \qquad (1)$$

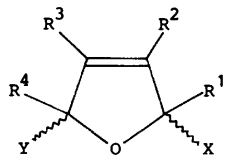

1a, $R^1=R^2=R^3=R^4=H$; X= Y=OMe
1b, $R^1=Me$; $R^2=R^3=R^4=H$; X=CN; Y=OMe
1c, $R^1=Me$; $R^2=R^3=R^4=H$; X=Y=OMe
1d, $R^1=R^3=R^4=H$; $R^2=Me$; X=Y=OMe
1e, $R^1=R^2=Me$; $R^3=R^4=H$; X=CN; Y=OMe
1f, $R^1=R^2=Me$; $R^3=R^4=H$; X=Y=OMe
1g, $R^1=R^3=Me$; $R^2=R^4=H$; X=CN; Y=OMe
1h, $R^1=R^3=Me$; $R^2=R^4=H$; X=C(OMe)=NH; Y=OMe
1i, $R^1=R^3=Me$; $R^2=R^4=H$; X=OMe; Y=CN
1j, $R^1=R^3=Me$; $R^2=R^4=H$; X=Y=OMe
1k, $R^1=R^4=Me$; $R^2=R^3=H$; X=CN; Y=OMe
1l, $R^1=R^4=Me$; $R^2=R^3=H$; X=Y=OMe
1m, $R^1=R^4=H$; $R^2=R^3=Me$; X=CN; Y=OMe
1n, $R^1=R^4=H$; $R^2=R^3=Me$; X=Y=OMe
1o, $R^1=R^2=R^3=Me$; $R^4=H$; X=CN; Y=OMe
1p, $R^1=R^2=R^3=Me$; $R^4=H$; X=OMe; Y=C(OMe)=NH
1q, $R^1=R^2=R^3=Me$; $R^4=H$; X=Y=OMe
1r, $R^1=R^2=R^4=Me$; $R^3=H$; X, Y=CN, C(OMe)=NH
1s, $R^1=R^2=R^4=Me$; $R^3=H$; X=CN; Y=OMe
1t, $R^1=R^2=R^4=Me$; $R^3=H$; X=OMe; Y=CN
1u, $R^1=R^2=R^4=Me$; $R^3=H$; X=Y=OMe
1v, $R^1=R^2=R^3=R^4=Me$; X= Y=CN
1w, $R^1=R^2=R^3=R^4=Me$; X= CN; Y=OMe
1x, $R^1=R^2=R^3=R^4=Me$; X= Y=OMe
1y, $R^1=R^4=Me$; $R^2=R^3=H$; X=CN; Y=OEt
1z, $R^1=R^4=Me$; $R^2=R^3=H$; X=Y=OEt
1aa, $R^1=R^4=Et$; $R^2=R^3=H$; X=CN; Y=OMe
1bb, $R^1=R^4=Et$; $R^2=R^3=H$; X=Y=OMe

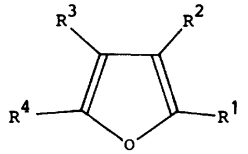

2a, $R^1=Me$; $R^2=R^3=H$; $R^4=C(OMe)=NH$
2b, $R^1=C(OMe)=NH$; $R^2=Me$; $R^3=R^4=H$
2c, $R^1=R^3=Me$; $R^2=H$; $R^4=CN$
2d, $R^1=R^3=Me$; $R^2=H$; $R^4=C(OMe)=NH$
2e, $R^1=R^4=Me$; $R^2=CN$; $R^3=H$
2f, $R^1=CH_2OMe$; $R^2=R^3=H$; $R^4=Me$
2g, $R^1=CH_2OMe$; $R^2=R^3=H$; $R^4=CH_2OMe$
2h, $R^1=CN$; $R^2=R^3=Me$; $R^4=H$
2i, $R^1=C(OMe)=NH$; $R^2=R^3=Me$; $R^4=H$
2j, $R^1=R^2=R^3=Me$; $R^4=CN$
2k, $R^1=R^2=R^3=Me$; $R^4=C(OMe)=NH$
2l, $R^1=CH_2OMe$; $R^2=R^3=R^4=Me$
2m, $R^1=CH_2OEt$; $R^2=R^3=H$; $R^4=Me$

$R^1CR^2_2CHR^3CHR^4COOMe$

3a, $R^1=R^3=R^4=H$; $R^2=OMe$
3b, $R^1=R^3=H$; $R^2=OMe$; $R^4=Me$
3c, $R^1=R^3=Me$; $R^2=1/2O$; $R^4=H$
3d, $R^1=R^4=Me$; $R^2=1/2O$; $R^3=H$

Table 3. Spectroscopic Data of Electrooxidation Products

Product	^{1}H NMR,[a] δ, ppm (J in Hz)	MS m/z (M^+)	IR ν, cm^{-1}
cis-**1a**	3.40 (6 H, s), 5.60 (2 H, s), 6.04 (2 H, s)		
trans-**1a**	3.40 (6 H, s), 5.88 (2 H, s), 6.04 (2 H, s)		
3a	1.76—2.04 (2 H, m), 2.20—2.48 (2 H, m), 3.32 (6 H, s), 3.67 (3 H, s), 4.38 (1 H, t, J=6.0)	161[b]	1740 (C=O), 2840 (H_3≡CO)
cis-**1b**	1.47 (3 H, s), 3.49 (3 H, s), 5.70 (1 H, dd, J=5.7, 1.1), 5.72 (1 H, m), 6.19 (1 H, dd, J=5.7, 1.1)		
trans-**1b**	1.67 (3 H, s), 3.43 (3 H, s), 5.78 (1 H, m), 5.99 (1 H, dd, J=5.7, 0.9), 6.06 (1 H, dd, J=5.7, 0.9)		
cis-**1c**	1.52 (3 H, s), 3.20 (3 H, s), 3.50 (3 H, s), 5.47 (1 H, m), 5.90 (1 H, dd, J=6.0, 0.9), 5.96 (1 H, dd, J=6.0, 0.9)		
trans-**1c**	1.57 (3 H, s), 3.12 (3 H, s), 3.42 (3 H, s), 5.75 (1 H, m), 5.90—5.98[c] 1.48 (3 H, s), 2.99 (3 H, s), 3.30 (3 H, s), 5.56 (1 H, m), 5.71 (1 H, dd, J=5.7, 1.0), 5.79 (1 H, dd, J=5.7, 1.0)[d]		
2a	2.34 (3 H, m), 3.89 (3 H, s), 6.02 (1 H, m), 6.2—6.9 (1 H, b), 6.63 (1 H, d, J=3.6)	139	3320 (NH), 1655 (C=N)
2b	2.24 (3 H, s), 3.90 (3 H, s), 6.0—6.5 (1 H, b), 6.26 (1 H, d, J=1.9), 7.33 (1 H, m)	139	3320 (NH), 1650 (C=N)
cis-**1d**	1.80 (3 H, m), 3.38 (3 H, s), 3.40 (3 H, s), 5.35 (1 H, m), 5.50 (1 H, m), 5.64 (1 H, m)		
trans-**1d**	1.78 (3 H, m), 3.34 (3 H, s), 3.38 (3 H, s), 5.60—5.68 (2 H, m), 5.70—5.80 (1 H, m)		
3b	1.18 (3 H, d, J=7.0), 1.65—2.20 (2 H, m), 2.36—2.72 (1 H, m), 3.32 (6 H, s), 3.67 (3 H, s), 4.38 (1 H, t, J=6.0)	175[b]	1740 (C=O), 2840 (H_3≡CO)
cis-**1e**	1.63 (3 H, s), 1.92 (3 H, s), 3.42 (3 H, s), 5.68 (2 H, m)		
trans-**1e**	1.70 (3 H, s), 1.92 (3 H, m), 3.39 (3 H, s), 5.60 (1 H, m), 5.71 (1 H, m)		
cis-**1f**	1.44 (3 H, s), 1.72 (3 H, m), 3.14 (3 H, s), 3.47 (3 H, s), 5.34 (1 H, m), 5.60 (1 H, m)		
trans-**1f**	1.51 (3 H, s), 1.72 (3 H, m), 3.05 (3 H, s), 3.40 (3 H, s), 5.62 (2 H, m)		
3c	1.15 (3 H, d, J=7.0), 2.21 (3 H, s), 2.3—2.8 (2 H, m), 2.8—3.2 (1 H, m), 3.65 (3 H, s)	144	1715 (C=O), 1730 (C=O)
cis-**1g**	1.62 (3 H, s), 1.80 (3 H, m), 3.40 (3 H, s), 5.54 (1 H, m), 5.70 (1 H, m)		
trans-**1g**	1.69 (3 H, s), 1.80 (3 H, m), 3.40 (3 H, s), 5.60 (1 H, m), 5.70 (1 H, m)		
cis(or *trans*)-**1h**	1.48 (3 H, s), 1.71 (3 H, s), 3.38 (3 H, s), 3.72 (3 H, s), 5.57 (1 H, m), 5.75 (1 H, s), 7.3—7.9 (1 H, b)		3320 (NH), 1655 (C=N)
cis(or *trans*)-**1i**	1.56 (3 H, s), 1.90 (3 H, m), 3.30 (3 H, s), 5.4—5.8[c]		
cis-**1j**	1.38 (3 H, s), 1.70 (3 H, s), 3.06 (3 H, s), 3.37 (3 H, s), 5.04 (1 H, m), 5.32 (1 H, m)[d]		
trans-**1j**	1.44 (3 H, s), 1.70 (3 H, s), 2.99 (3 H, s), 3.30 (3 H, s), 5.32 (2 H, m)[d]		
2c	2.16 (3 H, s), 2.30 (3 H, d, J=0.9), 5.98 (1 H, m)	121	2260 (C≡N)
2d	2.18 (3 H, s), 2.27 (3 H, d, J=0.9), 3.90 (3 H, s) 4.4—5.2 (1 H, b), 5.88 (1 H, m)	153	3320 (NH), 1645 (C=N)
3d	1.17 (3 H, d, J=6.3), 2.14 (3 H, s), 2.25—3.1 (3 H, m), 3.66 (3 H, s)	144	1720 (C=O), 1735 (C=O)
cis-**1k**	1.54 (3 H, s), 1.68 (3 H, s), 3.28 (3 H, s), 5.87 (1 H, d, J=5.7), 6.08 (1 H, d, J=5.7)		
trans-**1k**	1.60 (3 H, s), 1.74 (3 H, s), 3.16 (3 H, s), 5.93 (1 H, d, J=5.7), 6.03 (1 H, d, J=5.7)		
cis-**1l**	1.48 (6 H, s), 3.30 (6 H, s), 5.86 (2 H, s)		

Table 3. (Continued)

Product	^{1}H NMR,[a] δ, ppm (J in Hz)	MS m/z (M^+)	IR ν, cm^{-1}
trans-**1l**	1.58 (6 H, s), 3.20 (6 H, s), 5.88 (2 H, s)		
2e	2.25 (3 H, m), 2.42 (3 H, s), 6.02 (1 H, s)	121	2240 (C≡N)
2f	2.27 (3 H, m), 3.34 (3 H, s), 4.31 (2 H, s), 5.82—5.92 (1 H, m), 6.10—6.20 (1 H, m)		
2g	3.34 (3 H, s), 4.36 (2 H, s), 6.25 (1 H, s)		
2h	1.98 (3 H, d, J=1.0), 2.12 (3 H, s), 7.23 (1 H, m)	121	2245 (C≡N)
2i	1.93 (3 H, d, J=1.1), 2.15 (3 H, s), 3.89 (3 H, s), 7.16 (1 H, m), 7.3—7.9 (1 H, b)	153	3300 (NH), 1650 (C=N)
cis(or *trans*)-**1m**	1.70 (3 H, s), 1.82 (3 H, s), 3.38 (3 H, s), 5.05 (1 H, m), 5.56 (1 H, m)		
cis-**1n**	1.66 (6 H, s), 3.34 (6 H, s), 5.31 (2 H, s)		
trans-**1n**	1.66 (6 H, s), 3.34 (6 H, s), 5.59 (2 H, s)		
cis-**1o**	1.60 (3 H, s), 1.68 (3 H, m), 1.78 (3 H, m), 3.37 (3 H, s), 5.50 (1 H, m)		
trans-**1o**	1.66 (3 H, s), 1.68 (3 H, m), 1.78 (3 H, m), 3.37 (3 H, s), 5.53 (1 H, m)		
cis(or *trans*)-**1p**	1.44 (3 H, s), 1.60 (3 H, m), 1.74 (3 H, m), 3.19 (3 H, s), 3.79 (3 H, s), 4.68 (1 H, m), 7.5—7.9 (1 H, b)		1650 (C=N)
cis-**1q**	1.42 (3 H, s), 1.61 (3 H, m), 1.67 (3 H, m), 3.08 (3 H, s), 3.48 (3 H, s), 5.16 (1 H, m)		
trans-**1q**	1.48 (3 H, s), 1.61 (3 H, m), 1.67 (3 H, m), 3.00 (3 H, s), 3.36 (3 H, s), 5.46 (1 H, m)		
2j	1.88 (3 H, m), 2.08 (3 H, s), 2.23 (3 H, m)	135	2230 (C≡N)
2k	1.85 (3 H, m), 2.12 (3 H, s), 2.22 (3 H, m), 3.92 (3 H, s), 5.5—6.2 (1 H, b)	167	3330 (NH), 1650 (C=N)
cis(or *trans*)-**1r**	1.52 (3 H, s), 1.68 (3 H, s), 1.82 (3 H, d, J=1.4), 3.75 (3 H, s), 5.74 (1 H, m), 7.3—8.0 (1 H, b)		3320 (NH), 1655 (C=N)
cis-**1s**	1.48 (3 H, s), 1.63 (3 H, s), 1.90 (3 H, d, J=1.6), 3.25 (3 H, s), 5.48 (1 H, m)		
trans-**1s**	1.56 (3 H, s), 1.69 (3 H, s), 1.90 (3 H, d, J=1.6), 3.14 (3 H, s), 5.54 (1 H, m)		
cis-**1t**	1.46 (3 H, s), 1.62 (3 H, s), 1.74 (3 H, d, J=1.6), 3.22 (3 H, s), 5.69 (1 H, m)		
trans-**1t**	1.53 (3 H, s), 1.68 (3 H, s), 1.74 (3 H, d, J=1.6), 3.10 (3 H, s), 5.65 (1 H, m)		
cis-**1u**	1.44 (3 H, s), 1.47 (3 H, s), 1.75 (3 H, d, J=1.6), 3.26 (3 H, s), 3.32 (3 H, s), 5.54 (1 H, m)		
trans-**1u**	1.54 (3 H, s), 1.58 (3 H, s), 1.75 (3 H, d, J=1.6), 3.18 (3 H, s), 3.22 (3 H, s), 5.54 (1 H, m)		
cis-**1v**	1.64 (6 H, s), 1.79 (6 H, s)	176	2245 (C≡N)
trans-**1v**	1.68 (6 H, s), 1.79 (6 H, s)	176	
cis-**1w**	1.42 (3 H, s), 1.58 (3 H, s), 1.62 (3 H, s), 1.79 (3 H, s), 3.14 (3 H, s)		2245 (C≡N)
trans-**1w**	1.49 (3 H, s), 1.62 (3 H, s), 1.64 (3 H, s), 1.79 (3 H, s), 3.02 (3 H, s)	181	
cis-**1x**	1.39 (6 H, s), 1.62 (6 H, s), 3.23 (6 H, s)		
trans-**1x**	1.49 (6 H, s), 1.62 (6 H, s), 3.10 (6 H, s)		
2l	1.84 (3 H, s), 1.92 (3 H, s), 2.16 (3 H, s), 3.32 (3 H, s), 4.28 (2 H, s)		
cis-**1y**	1.21 (3 H, t, J=7.0), 1.61 (3 H, s), 1.66 (3 H, s), 3.24—3.76 (2 H, m), 5.89 (1 H, d, J=5.6), 6.03 (1 H, d, J=5.6)		
trans-**1y**	1.17 (3 H, t, J=7.0), 1.59 (3 H, s), 1.71 (3 H, s), 3.12—3.74 (2 H, m), 5.93 (1 H, d, J=5.6), 5.97 (1 H, d, J=5.6)		

Table 3. (Continued)

Product	^{1}H NMR,[a] δ, ppm (J in Hz)	MS m/z (M^+)	IR ν, cm^{-1}
cis-**1z**	1.17 (6 H, t, J=7.2), 1.48 (6 H, s), 3.16—3.84 (4 H, m), 5.86 (2 H, s)		
trans-**1z**	1.17 (6 H, t, J=7.0), 1.57 (6 H, s), 3.18—3.82 (4 H, m), 5.87 (2 H, s)		
2m	1.21 (3 H, t, J=7.0), 2.28 (3 H, m), 3.51 (2 H, q, J=7.0), 4.36 (2 H, s), 5.82—5.92 (1 H, m), 6.08—6.18 (1 H, m)		
cis-**1aa**	0.90 (3 H, t, J=7.6), 1.14 (3 H, t, J=7.4), 1.50—2.00 (4 H, m), 3.29 (3 H, s), 5.87 (1 H, d, J=6.0), 6.11 (1 H, d, J=6.0)		
trans-**1aa**	0.98 (3 H, t, J=7.6), 1.20 (3 H, t, J=7.2), 1.64—2.10 (4 H, m), 3.18 (3 H, s), 5.91 (1 H, d, J=6.0), 6.09 (1 H, d, J=6.0)		
cis-**1bb**	0.91 (6 H, t, J=7.6), 1.52—2.06 (4 H, m), 3.29 (6 H, s), 5.93 (2 H, s)		
trans-**1bb**	0.96 (6 H, t, J=7.6), 1.60—2.16 (4 H, m), 3.20 (6 H, s), 5.95 (2 H, s)		

a) 100 MHz, $CDCl_3$ solution unless otherwise noted. b) M−1 peak. c) Unresolved. d) CCl_4 solution.

Table 4. Isomer Ratio of the Products of Cyanomethoxylation of 2,5-DMF[a]

Concn of 2,5-DMF, M	Additive[b] (E_p, V[c])	E, V[d]	Isomer ratio (cis/trans[e])
0.02	None	1.30	3.1
0.10	None	1.30	3.0
0.20	None	1.30	2.9
0.20[f]	None	1.30	1.8
0.20	None	1.40	2.8
0.20	None	1.50	2.8
0.20	None	1.70	2.7
2.00	None	1.30	2.2
0.20	Benzene[g]	1.30	3.0
0.20	Anisole[g]	1.30	2.9
0.20	1,3,5-TMB[h] (1.44)	1.30	2.5
0.20	1,3,5-TMB	1.44	2.6
0.20	1,2-DMB (1.38)	1.30	2.2
0.20	1,2-DMB	1.38	2.1
0.20	1,3-DMB (1.50)	1.30	2.1
0.20	1,3-DMB	1.50	2.0
0.20	Pyridine[g]	1.30	1.8
0.20	1,4-DMB (1.24)	1.30	1.6

a) Pt anode unless otherwise stated. SCE reference. 0.4 M NaCN. b) [Additive]=0.20 M. c) Peak potential from CV. 0.02 M substrate. Scan rate is 0.1 V s^{-1}. Values are obtained on first scan. d) Potential for preparative electroreaction. e) Equilibrium value is 1.5. f) Vitreous C electrode. g) In these cases the oxidation wave was not observed due to the large background current from the concurrent electrolysis of the solvent-electrolyte system, i.e. >1.6. h) Trimethoxybenzene.

The adduct **1m**, which has a hydrogen on the 2 position geminate to a cyano group, differs in behavior. It smoothly loses MeOH to afford **2h** with a trace of CF_3COOH in $CHCl_3$.

$$\mathbf{1m} \xrightarrow{H^+/-MeOH} \mathbf{2h} \qquad (2)$$

Discussion

Mechanism. Both addition to and substitution on the furan ring are formally a 2-equiv change. Coulometry supports this experimentally. The voltammetric characteristics (Table 1) indicate that oxidation is initiated by electron transfer from the substrate molecule, followed by a fast chemical reaction. By analogy with anodic cyanation and methoxylation of other aromatic compounds,[3] the ECEC mechanism involving a cation-radical intermediate would be reasonable. The ionization potential of furan and the methylated derivatives is relatively low,[12-14] and the existence of their cation radicals has clearly been recognized in mass spectrometry[15] and studied by ESR.[16,17]

The cation radical mechanism is given in Scheme 1, illustrated for 2,3,4-trimethylfuran (2,3,4-TMF). The first step is the electron-transfer step which involves the direct discharge of the substrate. The cation radical **4** and the benzenium-type ions **5**—**8** react competitively with CN^- ion and the solvent MeOH (or the MeO^- ion as a result of the equilibrium between CN^- and MeOH). Part of **7** could undergo deprotonation to afford **2j**. We may denote rate constants as k_1, k_2,···, and k_{13}, and CEs as **1ox**, **1oy**, **1px**, **1py**, **1qx**, **1qy**, **2j**, **9x**, and **9y**. Thus **9x** and **9y**

represent the CE of product **9** formed in the first and third branches of Scheme 1, respectively. Treating the reactions in Scheme 1 as a system of competitive reactions[5,18] one can derive the following relationships.

$$\frac{k_1'}{k_2'}=\left(\frac{k_1}{k_2}\right)\left(\frac{CN^-}{MeOH}\right)=\frac{\mathbf{1ox}+\mathbf{9x}}{\mathbf{1px}+\mathbf{1qx}} \quad (3)$$

$$\frac{k_3'}{k_4'}=\left(\frac{k_3}{k_4}\right)\left(\frac{CN^-}{MeOH}\right)=\frac{\mathbf{1py}+\mathbf{2j}+\mathbf{9y}}{\mathbf{1oy}+\mathbf{1qy}} \quad (4)$$

$$\frac{k_5'}{k_6'}=\left(\frac{k_5}{k_6}\right)\left(\frac{CN^-}{MeOH}\right)=\frac{\mathbf{9x}}{\mathbf{1ox}} \quad (5)$$

$$\frac{k_7'}{k_8'}=\left(\frac{k_7}{k_8}\right)\left(\frac{CN^-}{MeOH}\right)=\frac{\mathbf{1px}}{\mathbf{1qx}} \quad (6)$$

$$\frac{k'_{10}}{k'_{11}}=\left(\frac{k_{10}}{k_{11}}\right)\left(\frac{CN^-}{MeOH}\right)=\frac{\mathbf{9y}}{\mathbf{1py}} \quad (7)$$

$$\frac{k'_{12}}{k'_{13}}=\left(\frac{k_{12}}{k_{13}}\right)\left(\frac{CN^-}{MeOH}\right)=\frac{\mathbf{1oy}}{\mathbf{1qy}} \quad (8)$$

where

$$\mathbf{9x}+\mathbf{9y}=\mathbf{9}=0.1 \quad (9)$$

$$\mathbf{1ox}+\mathbf{1oy}=\mathbf{1o}=22 \quad (10)$$

$$\mathbf{1px}+\mathbf{1py}=\mathbf{1p}=7 \quad (11)$$

$$\mathbf{1qx}+\mathbf{1qy}=\mathbf{1q}=13 \quad (12)$$

Here $k_1'=k_1(CN^-)$, $k_2'=k_2(MeOH)$,$\cdots$, $k_{13}'=k_{13}(MeOH)$.

We would like to evaluate the relative magnitudes of k_1 and k_2. In order to solve Eqs. 3—12, it is necessary to obtain information on the relative concentration of nucleophiles in the vicinity of the electrode. In the reactions containing a fast chemical step following the electron transfer, the concentration distribution of available, i.e., physisorbed, nucleo-

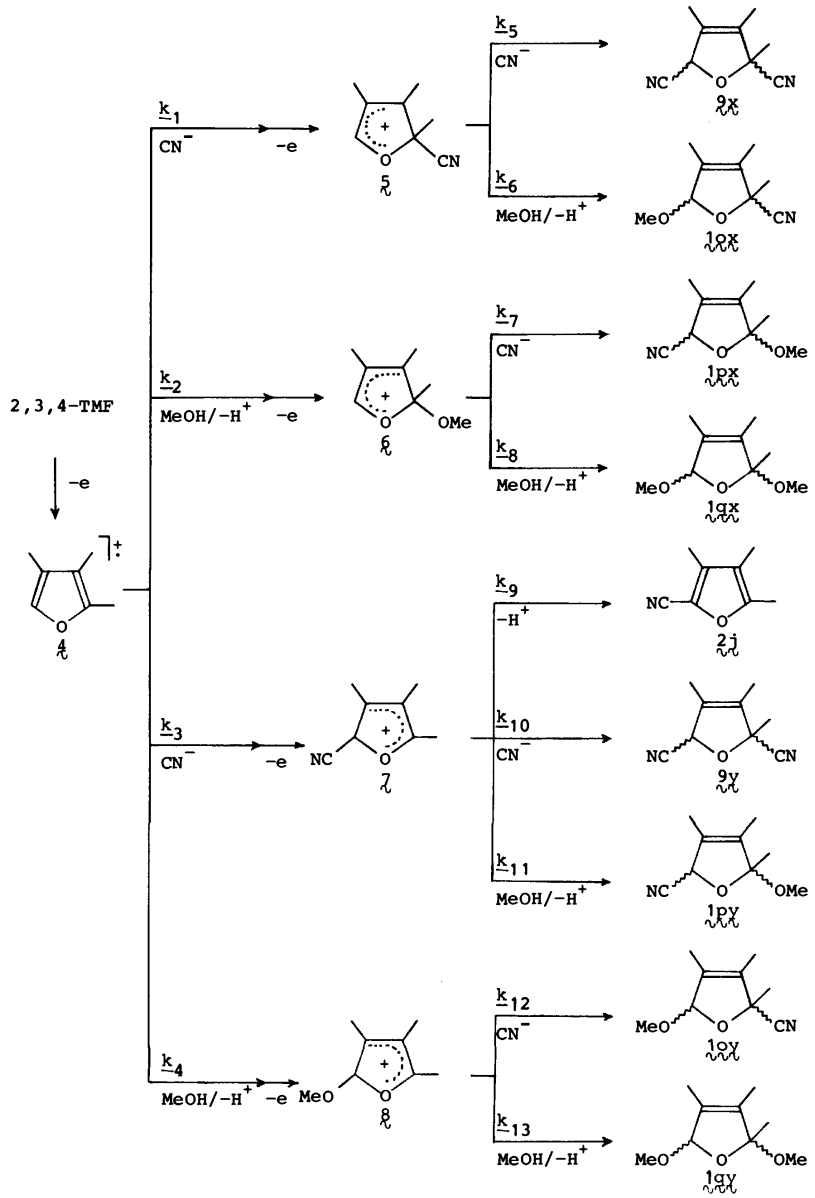

Scheme 1.

philes in the electrical double layer would be kept steadily constant by the competition[19] between mass transfer and chemical reaction. Prior to this, adsorption saturation of nucleophiles at the electrode surface may bear a part in duration of the spatially constant concentration. The observed independence of the product distribution obtained on competitive anodic cyanation and methoxylation of 2,5-DMF on the bulk concentration of CN^- ion or potential[2] supports this. Accordingly, the quantity (CN^-/MeOH) should actually be designated as (CN^-/MeOH)$_E$, i.e., referring to relative steady-state concentrations of these nucleophiles in the region of solution adjacent to the anode as compared to the bulk. Furthermore, it is assumed that $k_1/k_2=k_3/k_4$, $k_5\cong k_7$, $k_6\cong k_8$, $k_{10}\cong k_{12}$, and $k_{11}\cong k_{13}$. These assumptions would be reasonable since the electronically significant part of the structures of the corresponding cationic species are identical. The 2,5-dicyano adduct **9** was not detected and thus the lowest limit (0.1% CE) of product analysis in the present experiments was allotted to **9**. Substituting the assumed values for the relative quantities k_1/k_3, we can solve Eqs. 3—12.

Likewise, the relative rate constants of the cation radicals of other methylated furans toward two different nucleophiles have been evaluated. The results obtained are shown in Table 5, together with the observed anodic peak potential. As can be seen from Table 5, methyl substitution lowers the oxidation potential of the neutral substrate while it raises the relative reactivity k_1'/k_2' of its cation radical. A plot of log relative rate constant versus anodic peak potential gives a linear relationship (Fig. 1). The cation-radical intermediates derived from compounds having lower oxidation potentials would be less reactive and hence more discriminating than the cation radicals of substrates having higher oxidation potentials. Thus, the cation radical of 2,3,4,5-tetramethylfuran (TetMF) is highly selective for nucleophiles and preferentially combines with a powerful nucleophile, that is, the CN^- ion, whereas the cation radical of 3-methylfuran (3-MF) preferentially combines with an abundant nucleophile, namely, the solvent MeOH.

Table 5. Relative Reactivity of Methylated Furans Toward Two Different Nucleophiles

Compd	E_p, V	$(k_1/k_3)^{-1}$ a)	k_1'/k_2' b)
3-MF	1.78	0.2	0.01
3,4-DMF	1.61		0.1
2-MF	1.60	0.5—1.0	0.4b)
2,4-DMF	1.55	2.7—3.0	1.4b)
2,3-DMF	1.51	0	1.6
2,3,4-TMF	1.37	1.23	3.8
2,5-DMF	1.35		23
2,3,5-TMF	1.25	0.1—0.16	52
TetMF	1.13		742

a) Assumed values. b) Average values.

The mechanism presented in Scheme 2 can also account for the electrooxidation of 2-methylated furans. The cation radical **10** could undergo deprotonation to afford an analogue of a benzylic radical intermediate, which would subsequently undergo anodic oxidation (or homogeneous electron-transfer oxidation by the cation radical **10**) to give a cation **11**, followed by nucleophilic attack by CN^- ion (or MeOH) to give a 2,5-dihydro-5-methylenefuran **12**, which should be eventually transferred to **13**. Indeed, a compound of the type of **12** is probable as a reaction intermediate: e.g., 2,5-dihydro-5-methylene-2-furancarbonitrile and its homologues are the primary products of abnormal product formation in the reaction of 2-(chloromethyl)furans with aqueous cyanide solution.[20] The final step is the homogeneous chemical reaction. If the anodic reaction followed this reaction path, the observed cis-to-trans isomer ratio in the products would be consistent with the isomer composition for the homogeneous equilibrium. However, the anodic reaction of 2,5-DMF gives a high cis-to-trans reaction compared with the equilibrium value. Thus this pathway is not important in the

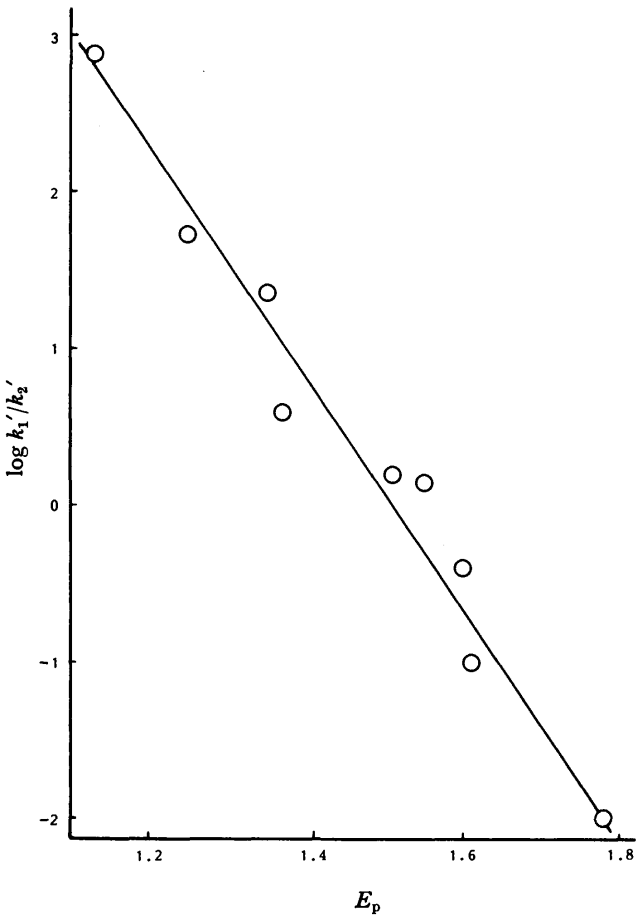

Fig. 1. Plot of log relative rate constant vs. E_p.

anodic reaction. Alternatively, the compound **12** could be aromatized in protic solvents for furans lacking the substituent on the 5 position (R_3=H). This mechanism was previously discussed in anodic nuclear substitution of 1,2-dimethylpyrrole and has been precluded on the basis of no incorporation of deuterium in the 2-methyl group upon the reaction in methanol-*d*.[21]

1,4-Dicarbonyl derivatives (**3**) would be formed in the acid-catalyzed ring fission[22,23] of 2-methoxyfurans obtained by either anodic nuclear methoxylation or 1,4-elimination[24,25] of MeOH element from the primary 2,5-dihydro-2,5-dimethoxyfurans.

Positional Reactivity. The values of k_1/k_3 given in Table 5 reveal the relative regioreactivity of the initial nucleophilic attack to the cation radicals of unsymmetrical methylfurans. The reaction occurs preferentially at the 2 (and 5) position. When a methyl group is attached at the 2 position, the initial nucleophilic attack occurs comparably at both 2 (ipso) and 5 (para) positions. The introduction of the methyl substituent in the 3 position activates dominantly the 2 (ortho) position.

Comparison with Electrooxidation of 1,4-DMB. Weinberg and co-workers investigated the electrooxidation of 1,4-DMB at a Pt electrode in MeOH that contains NaCN.[5] 1,4-DMB undergoes the additions of cyano and/or methoxyl group(s) across the aromatic nucleus in competition with methoxyl displacement. The CEs of *p*-methoxybenzonitrile **15** and of *p*-benzoquinone bis(dimethyl acetal) **18** are highly potential dependent, whereas the CE of 3-cyano-3,6,6-trimethoxy-1,4-cyclohexadiene **16** taken together with its base-catalyzed methanolysis product **17** is found to be independent of potential. A similar trend appears on changing the concentration of CN^- ion in the bulk solution. Curiously enough, there are discrepancies between their observations on 1,4-DMB and our previous results[2] on 2,5-DMF at the same material electrode. In the latter case, the product distribution was independent of anode potential or the bulk concentration of CN^- ion. Apparent potential dependency of the CEs of **15** and **18** in the former case may be ascribable to that, the 1,4-DMB cation radical is not adsorbed as strongly as is 2,5-DMF cation radical (or, the 1,4-DMB cation radical that reacts really with two competing nucleophiles may be formed by the homogeneous electron-transfer reaction between the primary product in the inner region and the parent uncharged molecule in the outer region), diffuses into the bulk solution which contains a greater relative concentration of MeO^- ion, and consequently produces a greater part of **18** with the decreasing in NaCN or with the lowering in anode potential.

An attempt by Weinberg and co-workers[5] to determine the relative concentrations of two nucleophiles at the electrode from electrooxidation products

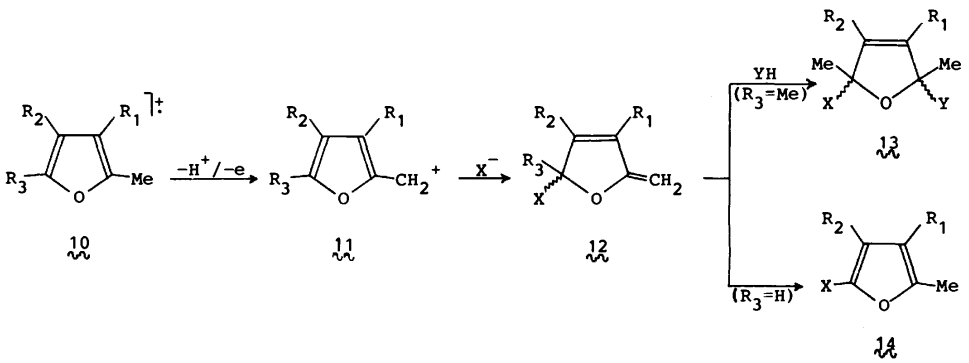

R_1, R_2, R_3 = H, Me

X, Y = CN, MeO

Scheme 2.

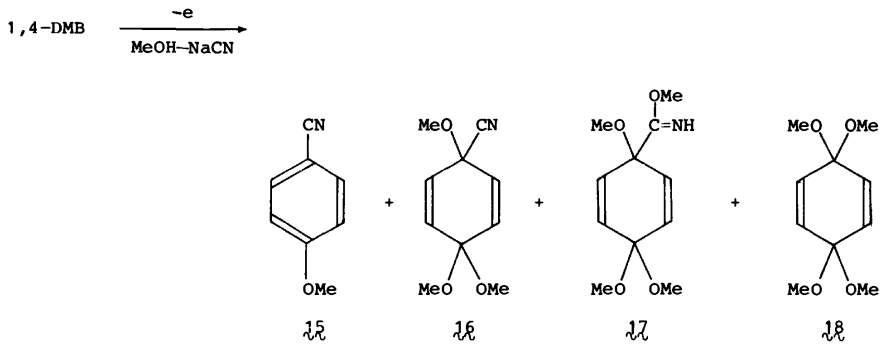

(13)

by using the rate expressions of competitive reactions met with failure. Their assumptions and results are not reasonable as mentioned previously.[26]

Stereochemical Control of Addition. The stereochemistry of electrochemical incremental reactions could be brought about by the orientation of the substrate molecule on the electrode surface during the reaction, especially in a *final* bond-formation step. The present anodic mixed 1,4-addition to 2,5-DMF is sterically controlled by the Pt electrode. The dependence observed of the ratio of the stereoisomeric products on the concentration of the substrate would be ascribable to the orientational transition which occurs as the substrate concentration is changed. The orientation of adsorbed aromatic molecules has been studied as a function of adsorbate molecular structure and its concentration.[27-29] At low concentrations, aromatic molecules generally adopt a flat orientation on the Pt surface in which the ring is more or less parallel to the electrode surface plane. Cis addition to the adsorbed furan ring would dominate. Transitions from flat to vertical (endwise or edgewise) orientations occur at higher concentrations. In the endwise orientation a C-H bond (or other substituent) of the ring is perpendicular to the surface, and in the edgewise orientation one edge is parallel and the ring is perpendicular to the surface. The ratio of isomeric products should reflect thermodynamic control.

The ratio of the stereoisomeric products also varies significantly with the addition of adsorbable compounds. Deviations from the ratio obtained in the blank experiment are explicable in terms of the changes in orientation. The changes in orientation of aromatic molecules under the influence of a surface-active anion, iodide, have recently been detected in aqueous solutions.[30] When a layer of molecules adsorbed in the planar orientation to the surface is exposed to a solution of a coadsorbate such as iodide, reorientation to an edgewise orientation occurs for most of the compounds. A similar phenomenon, that is, change of positional reactivity under aromatic additives, has been detected in other electrode reactions, for example, anodic nuclear acetoxylation of anisole.[31]

Infrared and Mass Spectral Intensity. 2-Furonitriles have a strong band in the region of the C≡N stretching vibration in IR spectra, whilst the intensity of the nitrile absorption band in nonaromatic 2,5-dihydro-2-furonitriles is very weak or undetectable. Marked declines in C≡N intensities are commonly observed when the oxygen-containing group is attached to the same carbon atom as the cyano group.[32]

The parent peaks are very weak or cannot be detected at all in the mass spectra of 2,5-dihydro-5-methoxy-2-furonitriles and of 2,5-dihydro-2,5-dimethoxyfurans. The absence of a parent peak in the mass spectrum of ethers is usually observed.[33]

Other Synthetic Method. The synthesis of a pertinent 2-cyano-5-methoxy compound by nonelectrochemical reaction of a 2,5-dimethoxy adduct (**1a**) and cyanotrimethylsilane has recently been reported.[34]

Experimental

Equipment. A JEOL FX-100 NMR spectrometer, a JASCO Model IR-E IR spectrophotometer, and a Hitachi Model RMS-4 mass spectrometer were used for structure determination.

CV was performed in a two-compartment cell in which the calomel reference electrode with an agar bridge was separated from the Pt anode and the cathode by a glass frit. The working electrode was a 1-cm Pt wire sealed in glass, and the auxiliary electrode was a Pt sheet. A Hokuto Denko HB-107A voltage scanner, HA-104 potentiostat, and Yokogawa Type 3083 XY recorder were used. All measurements were carried out at room temperature.

Controlled-potential electroreactions were performed by using a three-compartment cell (which separated the anode, cathode, and reference electrode solutions by glass frits). The anode compartment held 50 ml of anolyte, the cathode held 20 ml of catholyte, and the reference held 5 ml of an electrolyte solution. A Pt sheet (2×2 cm) anode was employed. A Pt wire was used as the cathode, and an SCE with an agar bridge as the reference. Anode potential was controlled by means of the potentiostat mentioned above.

Coulometry was carried out with a Hokuto Denko Model HF-108 A current integrator.

Materials. MeOH and NaCN were used without purification. Furan and 2-MF were obtained commercially and were purified by distillation.

3-MF was prepared by a three-step method starting with

Table 6. ^{1}H NMR Data of Alkylfurans[a]

Compd	Chemical shift δ, ppm
Furan	6.40 (2 H, m), 7.47 (2 H, m)
2-MF	2.29 (3 H, s), 6.00 (1 H, m), 6.28 (1 H, m), 7.30 (1 H, m)
3-MF	2.03 (3 H, m), 6.22 (1 H, m), 7.16 (1 H, m), 7.29 (1 H, m)
2,3-DMF	1.93 (3 H, m), 2.19 (3 H, m), 6.12 (1 H, m), 7.16 (1 H, m)
2,4-DMF	1.96 (3 H, s), 2.22 (3 H, s), 5.80 (1 H, m), 6.99 (1 H, m)
2,5-DMF	2.24 (3 H, m), 5.80 (1 H, m)
3,4-DMF	1.95 (3 H, m), 7.11 (1 H, m)
2,3,4-TMF	1.85 (3 H, m), 1.90 (3 H, m), 2.16 (3 H, s), 6.99 (1 H, m)
2,3,5-TMF	1.87 (3 H, m), 2.14 (3 H, s), 2.19 (3 H, s), 5.70 (1 H, s)
TetMF	1.84 (3 H, s), 2.16 (3 H, s)
2,5-DEF	1.21 (3 H, t), 2.60 (2 H, q), 5.83 (1 H, s)

a) 100 MHz, $CDCl_3$ solution.

2-methylallyl chloride and ethyl orthoformate.[35-37]

2,3-DMF was prepared by lithium aluminum hydride reduction of 3-chloromethyl-2-methylfuran,[38] which was obtained in 3 steps from chloroacetaldehyde and ethyl acetoacetate.[39]

2,4-DMF[40] was obtained by thermal decomposition of the δ-sultone[41] which was prepared by sulfonation of mesityl oxide.

2,5-DMF was prepared by dehydration of acetonylacetone according to the method of Gaertner and Tonkyn.[42]

3,4-DMF was synthesized by the hydrogenation of 3,4-bis(chloromethyl)furan[43] in the presence of Pd in barium sulfate.[44]

2,3,4-TMF was made from 3-hydroxymethyl-2,4-dimethylfuran, which was obtained by reduction of 2,4-dimethyl-3-furancarboxylic acid[45] with lithium aluminum hydride, using the procedure of Winberg, Fawcett, Mochel, and Theobald.[38]

2,3,5-TMF was prepared by a four-step procedure starting with ethyl acetoacetate and 3-chloro-2-butanone.[46]

TetMF was obtained by the dehydration of 3,4-dimethyl-2,5-hexanedione with acetic anhydride and zinc chloride.[42] 3,4-Dimethyl-2,5-hexanedione was prepared by the reaction of 2-butanone and di-*t*-butyl peroxide by a modification of the procedure of Moore.[47] Decomposition of the peroxide was accomplished by photodissociation instead of thermal decomposition. A solution of 2-butanone (250 ml) and di-*t*-butyl peroxide (25 g) was irradiated through a Pyrex filter by a 450-W high-pressure Hg vapor lamp at room temperature for 40 h. Colorless 3,4-dimethyl-2,5-hexanedione was collected at 94 °C/16 mmHg (1 mmHg=133.322 Pa), 8 g. No attempt was not made to optimize the yield.

2,5-DEF was prepared by the reaction of 2,5-bis(chloromethyl)furan[48] and methylmagnesium bromide.[49]

NMR data of furans were given in Table 6.

Authentic samples of *cis*- and *trans*-2,5-dihydro-2,5-dimethoxy-2,5-dimethylfuran were prepared by anodic methoxylation of 2,5-DMF.[11,50]

2,5-Bis(methoxymethyl)furan was prepared by the bromination of 2,5-DMF with *N*-bromosuccinimide, followed by treatment with NaOMe.[11]

2-Methoxymethyl-5-methylfuran was obtained according to the same method as above except that 1 equiv of *N*-bromosuccinimide was used.

2,5-Dimethyl-3-furancarbonitrile was prepared by reaction of 2,5-DMF and chlorosulfonyl isocyanate followed by treatment of the intermediate with *N*,*N*-dimethylformamide.[51]

General Electrooxidation Procedure. The anolyte (50 ml) was made up of the organic substrate (5 mmol) in a methanolic solution of NaCN (0.4 M). The catholyte was the same medium in the absence of the substrate. The anode and cathode compartments were kept under an atmosphere of nitrogen and the anolyte was stirred magnetically. The reaction was carried out at a controlled anode potential at room temperature. The potential was set at the peak potential of the substrate. During the run the current dropped with time and was discontinued when either 2 faradays/mol of furan added was passed or the current dropped to some low value near the original background level. To the product mixture were added internal standards for GLC analyses, the mixture was treated with water, and the organic material was extracted with ether. The ethereal solution was concentrated and analyzed by GLC using a PEG 6000 column at 65 °C. Each isomeric product was separated in pure form by preparative GLC. They were identified by the elemental and ^{1}H NMR, IR, and mass spectroscopic analyses (Table 3). The intensity of the C≡N stretching vibration in IR spectra varied with structure. Methyl imidates showed characteristic bands at the region of 3320 (NH) and 1650 cm^{-1} (C=N). *Caution*: a cyanide salt in MeOH must be handled in a fume hood, as it contains HCN as a result of the equilibrium between CN^- and the solvent MeOH.

Isomerization Equilibrium. Isomerization was carried out in MeOH (1 ml) containing either of the two isomers *cis*-**1k** and *trans*-**1k** (0.01 g) and 1% CF_3COOH as catalyst. The reaction mixture was kept at 25.0 °C by a thermostat. At specified intervals, samples were withdrawn and analyzed by GLC after neutralization with sodium carbonate.

References

1) K. Yoshida and T. Fueno, *Bull. Chem. Soc. Jpn.*, **42**, 2411 (1969).

2) K. Yoshida and T. Fueno, *J. Org. Chem.*, **36**, 1523 (1971).

3) K. Yoshida, "Electrooxidation in Organic Chemistry," Wiley-Interscience, New York (1984).

4) K. Yoshida, "The Chemistry of Functional Groups, Suppl. C," ed by S. Patai and Z. Rappoport, Wiley-Interscience, London (1983), p. 221.

5) N. L. Weinberg, D. H. Marr, and C. N. Wu, *J. Am. Chem. Soc.*, **97**, 1499 (1975).

6) Preliminary communication: K. Yoshida, *J. Chem. Soc., Chem. Commun.*, **1978**, 20.

7) F. C. Schaefer and G. A. Peters, *J. Org. Chem.*, **26**, 412 (1961).

8) D. Gagnaire and P. Vottero, *Bull. Soc. Chim. Fr.*, **12**, 2779 (1963).

9) T. Hiraoka, T. Iwashige, and I. Iwai, *Chem. Pharm. Bull.*, **13**, 285 (1965).

10) A. Aito, T. Matsuo, and C. Aso, *Bull. Chem. Soc. Jpn.*, **40**, 130 (1967).

11) S. D. Ross, M. Finkelstein, and J. J. Uebel, *J. Org. Chem.*, **34**, 1018 (1969).

12) P. Linda, G. Marino, and S. Pignataro, *J. Chem. Soc., B*, **1971**, 1585.

13) G. G. Aloisi, S. Santini, and G. Savelli, *J. Chem. Soc., Faraday Trans. 1*, **71**, 2045 (1975).

14) L. Klasinc, A. Sabljić, G. Kluge, J. Rieger, and M. Scholz, *J. Chem. Soc., Perkin Trans. 2*, **1982**, 539.

15) K. Heyns, R. Stute, and H. Scharmann, *Tetrahedron*, **22**, 2223 (1966).

16) M. Shiotani, Y. Nagata, M. Tasaki, J. Sohma, and T. Shida, *J. Phys. Chem.*, **87**, 1170 (1983).

17) D. N. Ramakrishna Rao and M. C. R. Symons, *J. Chem. Soc., Perkin Trans. 2*, **1983**, 135.

18) E. S. Gould, "Mechanism and Structure in Organic Chemistry," Henry Holt, New York (1959), p. 171.

19) H. Wendt, *Angew. Chem., Int. Ed. Engl.*, **21**, 256 (1982).

20) S. Divald, M. C. Chun, and M. M. Joullié, *J. Org. Chem.*, **41**, 2835 (1976).

21) K. Yoshida, *J. Am. Chem. Soc.*, **99**, 6111 (1977); **101**, 2116 (1979).
22) J. A. Hirsch and A. J. Szur, *J. Heterocycl. Chem.*, **9**, 523 (1972).
23) J. E. Garst and G. L. Schmir, *J. Org. Chem.*, **39**, 2920 (1974).
24) G. F. D'Alelio, C. J. Williams, Jr., and C. L. Wilson, *J. Org. Chem.*, **25**, 1028 (1960).
25) E. Sherman and A. P. Dunlop, *J. Org. Chem.*, **25**, 1309 (1960).
26) K. Yoshida, *J. Am. Chem. Soc.*, **98**, 254 (1976).
27) A. J. Fry, "Synthetic Organic Electrochemistry," Haper & Row, New York (1972), Chap. 4.
28) M. P. Soriaga and A. T. Hubbard, *J. Am. Chem. Soc.*, **104**, 2735 (1982).
29) M. P. Soriaga and A. T. Hubbard, *J. Am. Chem. Soc.*, **104**, 3937 (1982).
30) M. P. Soriaga and A. T. Hubbard, *J. Am. Chem. Soc.*, **104**, 2742 (1982).
31) W. J. M. Van Tilborg, J. J. Scheele, and L. Eberson, *Acta Chem. Scand., B*, **32**, 36 (1978).
32) L. J. Bellamy, "The Infra-red Spectra of Complex Molecules," 2nd ed, Wiley, New York (1958), pp. 263—266.
33) J. H. Beynon, "Mass Spectrometry and Its Application to Organic Chemistry," Elsevier, Amsterdam (1960), pp. 362—367.
34) K. Utimoto, Y. Wakabayashi, T. Horiie, M. Inoue, Y. Shishiyama, M. Obayashi, and H. Nozaki, *Tetrahedron*, **39**, 967 (1983).
35) J. W. Cornforth and M. Firth, *J. Chem. Soc.*, **1958**, 1098.
36) J. W. Cornforth, *J. Chem. Soc.*, **1958**, 1310.
37) J. P. Kutney, J. Cable, W. A. F. Gladstone, H. W. Hanssen, G. V. Nair, E. J. Torupka, and W. D. C. Warnock, *Can. J. Chem.*, **53**, 1796 (1975).
38) H. E. Winberg, F. S. Fawcett, W. E. Mochel, and C. W. Theobald, *J. Am. Chem. Soc.*, **82**, 1428 (1960).
39) K. C. Rice and J. R. Dyer, *J. Heterocycl. Chem.*, **12**, 1325 (1975).
40) Th. Morel and P. E. Verkade, *Recl. Trav. Chim. Pays-Bas*, **51**, 667 (1932).
41) R. H. Eastman and D. Gallup, *J. Am. Chem. Soc.*, **70**, 864 (1948).
42) R. Gaertner and R. G. Tonkyn, *J. Am. Chem. Soc.*, **73**, 5872 (1951).
43) K. Yu. Novitskii, Yu. K. Yur'ev, V. N. Zhingareva, and E. F. Egorova, *Dokl. Akad. Nauk SSSR*, **148**, 856 (1963).
44) K. Yu. Novitskii, G. T. Khachaturova, and Yu. K. Yur'ev, *Khim. Geterotsikl. Soedin.*, **5**, 406 (1969); *Chem. Heterocycl. Comp. (Engl. Transl.)*, **5**, 303 (1969); *Chem. Abstr.*, **71**, 124295k (1969).
45) T. Reichstein and H. Zschokke, *Helv. Chim. Acta*, **15**, 1105 (1932).
46) T. Reichstein, H. Zschokke, and W. Syz, *Helv. Chim. Acta*, **15**, 1112 (1932).
47) C. G. Moore, *J. Chem. Soc.*, **1951**, 236.
48) O. Moldenhauer, G. Trautmann, R. Pfluger, and H. Döser, *Justus Liebigs Ann. Chem.*, **580**, 176 (1953).
49) K. Yu. Novitskii, V. P. Volkov, L. P. Shaiderova, and Yu. K. Yur'ev, *Zh. Obshch. Khim.*, **31**, 136 (1961).
50) A. J. Baggaley and R. Brettle, *J. Chem. Soc., C*, **1968**, 969.
51) A. J. Floyd, R. G. Kinsman, Y. Roshan-Ali, and R. W. Brown, *Tetrahedron*, **39**, 3881 (1983).

 © 1987 The Chemical Society of Japan Bull. Chem. Soc. Jpn., 60, 241—247 (1987)

Methanol-Incorporated Photoaddition of *N*-Methyl-1,2-naphthalenedicarboximide with Alkenes and Dienes

Yasuo KUBO,* Mariko MIHARA, and Takeo ARAKI
Department of Chemistry, Faculty of Science, Shimane University, Matsue 690
(Received June 24, 1986)

Irradiation of acetonitrile-methanol solutions of *N*-methyl-1,2-naphthalenedicarboximide (**1b**) with 1,1-diphenylethylene gave a methanol-incorporated adduct at a carbonyl carbon atom in **1b** together with 2,2-diphenylethyl methyl ether as a typical electron-transfer photosensitized product. The photoreaction of **1b** with α-methylstyrene, styrene (**2c**), or 2-methyl-2-butene in the same solvent system gave a regio-isomeric pair of a mixture of two diastereomers of methanol-incorporated adducts at carbonyl carbon atoms. The irradiation of **1b** with 2,3-dimethyl-2-butene and ethyl vinyl ether (**2h**) in benzene–methanol afforded methanol-incorporated adducts, although no reaction was observed for irradiation in acetonitrile–methanol. The irradiation of **1b** with 2,5-dimethyl-2,4-hexadiene in acetonitrile–methanol also resulted in the formation of methanol-incorporated adducts. The values of the free-energy change associated with an electron-transfer (ΔG_{et}) from the alkenes to the singlet excited state of **1b** and fluorescence quenching rate constants support the photochemical single-electron-transfer mechanism for the addition. A preferential addition at the carbonyl carbon atom in **1b** as well as that at the more sterically hindered carbonyl carbon atom in the reaction of **1b** with **2c** and **2h** is explainable on the basis of the spin densities of the radical anion of **1b** derived by a photochemical single-electron-transfer.

Recently, photoreactions involving electron-transfer processes have received much attention with regard to both synthetic and mechanistic aspects in organic photochemistry.[1] During the course of studies on the photochemistry of imides, our and other groups have found a variety of alcohol (solvent)-incorporated intramolecular cyclization[2] and intermolecular addition products[3] in the photoreactions of phthalimide-alkene systems, possibly via a single-electron-transfer processes. However, imide compounds employed in the previous investigations have been confined to phthalimides, and only little information has been reported on the effect of the arene structures of arenedicarboximides. Mazzocchi and his co-workers reported that in the photoreaction of *N*-methyl-1,8-naphthalenedicarboximide (**1a**) and α-methylstyrene (**2b**) a methanol-incorporated addition occurred solely at a naphthalene ring carbon atoms.[4] We have recently reported that in the photolyses of *N*-(3-phenylallyl)arenedicarboximides methanol-incorporated intramolecular cyclization occurs at the carbonyl carbon atom.[5] Here, we report on the results of the intermolecular photoreaction of *N*-methyl-1,2-naphthalenedicarboximide (**1b**) with alkenes and dienes in solvents containing methanol. The results show that the methanol-incorporated addition generally occurs at the carbonyl carbon atoms, in contrast to the reaction of **1a**. The effect of the arene structure of the imides is discussed on the basis of spin densities in the imide radical anions derived by the photochemical single-electron-transfer.

We have already reported the photoreactions of **1b** and alkenes in benzene.[6] The predominant reaction in benzene was an insertion of the alkene into C(=O)–N bonds of **1b**, in contrast to the fact that the predominant photoreactions of **1a** and its 2,3-isomer were cyclobutane[6a,7] and oxetane formation,[6a] respectively.

Results and Discussion

Irradiation (>320 nm) of a mixture of **1b** and 1,1-diphenylethylene (**2a**) in N_2-purged acetonitrile–methanol (2/1 v/v) gave a methanol-incorporated adduct at the carbonyl carbon atom (**3a**), 2,2-diphenylethyl methyl ether (**5a**), and two naphthoazepinediones (**6a** and **7a**) (Eq. 1 and Table 1). The

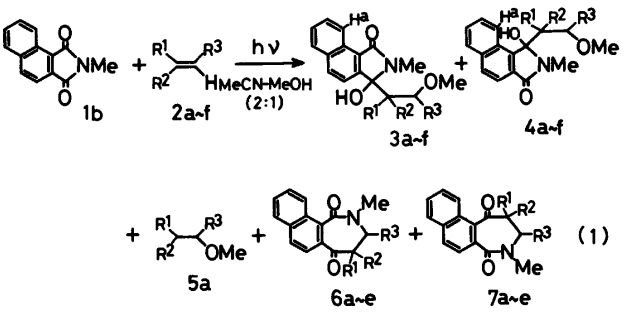

(1)

last two products (**6a** and **7a**) are the main products obtained in the photolysis of **1b** and **2a** in benzene and are formed by the insertion of **2a** into C(=O)–N bonds of **1b**.[6b] Other examples of the photoreactions of **1b** with alkenes (**2b—f**) are summarized in Table 1, which indicates that the methanol-incorporated addition to the carbonyl carbon atoms is characteristic of the reactions of **1b** with some ethylenes substituted by a phenyl group, **2b** and styrene (**2c**), and with an ethylene substituted by three alkyl groups, 2-methyl-2-butene (**2f**). No reaction was observed in the photolysis of **1b** with 1-hexene (**2d**), an ethylene substituted by one alkyl group. Only an insertion to give **6e** and **7e** was observed in the reaction with 2-

methylpropene (**2e**).[6c] The result shows that **1b** is less reactive toward a methanol-incorporated addition than *N*-methylphthalimide (**1c**) since irradiation of **1c** with **2e** gave the methanol-incorporated adduct together with the insertion product.[3d]

In the reaction with **2b**, **2c**, or **2f** a regioisomeric pair of a mixture of two diastereomers of the methanol-incorporated adduct (**3b,c,f** and **4b,c,f**) was obtained, although in the reaction with **2a** one of the regioisomers (**4a**) could not be isolated in a pure form because of the trace amount. The structures of the adducts are supported by a spectral resemblance to the benzo analogues obtained by the photoreactions of **1c**.[3d] The regiochemistry of the adducts shown in the structural formulas are deduced from the chemical shift of an aromatic proton H^a which was observed as ortho- and meta-coupled double doublets. The H^a protons in **3f** was observed in a lower field region (δ=9.18, 9.35) than those in **4f** (δ=8.62, 8.79) and the difference in chemical shift was 0.39—0.73 ppm. The molecular model examination indicates that the H^a proton in **3f** should be deshielded by the proximate lactam carbonyl group. This analysis is applicable to determination of the regiochemistry of the isomeric pairs of adducts having phenyl substituents (**3a—c** and **4b,c**), in which slight higher field shift of H^a protons compared with those in **3f** and **4f** is observed possibly due to the shielding effect of the phenyl substituent: H^a protons in **3a—c** and **4b,c** appear at δ=8.78—9.08 and at δ=8.36—8.52, respectively, and the difference in chemical shift is 0.26—0.72 ppm.

In the irradiation of **1b** (19 mM†) and 2,3-dimethyl-2-butene (**2g**, 480 mM), an ethylene substituted by four alkyl groups, in acetonitrile-methanol (2/1 v/v) no reaction was observed (at least with respect to conversion of **1b**). However, irradiation in benzene-methanol (19/1 v/v), a less-polar solvent, gave a methanol-incorporated adduct (**3g**, 32%) and **8** (14%) (Scheme 1). The keto amide structure of **8** was assigned on the basis of the spectral data: ^{1}H NMR

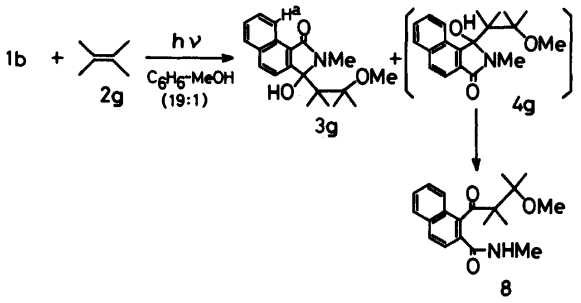

Scheme 1.

δ=2.90 (d, NH*Me*, coalesced to a singlet after D_2O exchange), 6.10 (br s, NH, disappeared after the D_2O exchange); IR 1678 (ketone), 1646 (amide) cm^{-1}. The regiochemistry shown in the structural formula was tentatively assigned on the basis of the assumption that **8** was derived by a ring-opening reaction which accompanied the hydrogen-migration of the initially formed **4g** (Scheme 1); it was not isolated in this system although both of the regioisomers were obtained in the other reaction systems (such as in the reaction with **2f**). Such a ring-opening reaction was reported to occur in the photoreaction of **1c** with **2g**.[3b]

A similar solvent effect to reactions with **2g** was observed in reactions with ethyl vinyl ether (**2h**). No reaction was observed during irradiation in acetonitrile-methanol (2:1 v/v), but irradiation of **1b** (19 mM) and **2h** (560 mM) in benzene-methanol (9/1 v/v) gave methanol-incorporated adducts (**3h**, 26% and **4h**, 34%) (Eq. 2). An addition at the more

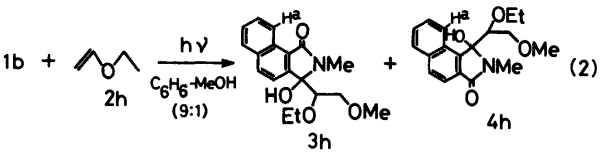

sterically hindered carbonyl carbon atom in **1b** predominated, as in the reaction with **2c**.

Table 1. Yields of Photoproducts from *N*-Methyl-1,2-naphthalenedicarboximide (**1b**) and Alkenes **2a—f** in Acetonitrile-Methanol (2/1 v/v)[a]

R^1	R^2	R^3	2	[2] mM	Yield[b]/% 3	4	5	6	7
Ph	Ph	H	**2a**	152	**3a** 70	**4a** 13	**5a** 105	**6a** 10	**7a** 5
Ph	Me	H	**2b**	340	**3b** 38	**4b** 26	—	—	—
Ph	H	H	**2c**	385	**3c** 27	**4c** 36	—	—	—
Bu	H	H	**2d**	476	**3d** 0	**4d** 0	—	**6d** 0	**7d** 0
Me	Me	H	**2e**	714	**3e** 0	**4e** 0	—	**6e** 56	**7e** 42
Me	Me	Me	**2f**	571	**3f** 31	**4f** 25	—	—	—

a) Reaction conditions: [**1b**] = 19 mM. b) Yields were based on consumed **1b**.

† 1 M=1 mol dm^{-3}.

As for the reaction with dienes, photoreaction with 1,3-butadiene and 2,3-dimethyl-1,3-butadiene, poorly alkyl substituted dienes, in acetonitrile–methanol (2/1 v/v) gave no methanol-incorporated adducts, but the irradiation of **1b** (19 mM) with 2,5-dimethyl-2,4-hexadiene (**9**, 360 mM) gave methanol-incorporated adducts (**10**, 43% and **11**, 27%) (Eq. 3). The trans-

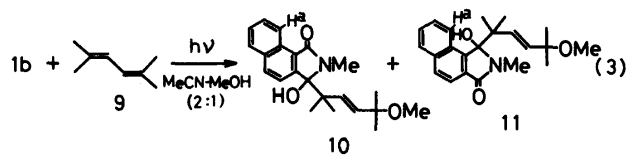

configurations of the aliphatic double bonds in **10** and **11** were assigned on the basis of the large coupling constants between the vinyl hydrogens (16.7 and 16.8 Hz, respectively). This reaction is the first example of an alcohol-incorporated addition of diene to arenedicarboximide.

A possible mechanism which can be used to interpret the general feature of the methanol-incorporated addition is shown in Scheme 2, in which alkenes are denoted as **12**. The initial step of the reaction is a single-electron-transfer from **12** to the singlet excited state of **1b**. The approximate values of the free-energy change associated with the electron-transfer (ΔG_{et}) can be estimated[8] by using

$$\Delta G_{et} = 96.49[E(D/D^+) - E(A^-/A)] - \Delta E_{0,0}. \quad (4)$$

In this equation $E(D/D^+)$ is the oxidation potential of the alkenes, $E(A^-/A)$ is the reduction potential of **1b**, and $\Delta E_{0,0}$ is the singlet excitation energy of **1b**. With these values, we can calculate the ΔG_{et} values for reactions with **2a,d—g** (Table 2). This table shows that the methanol-incorporated addition occurs only in the cases having negative ΔG_{et} values as expected from the electron-transfer mechanism.

An addition of alkenes (**2e—g**) to air-saturated acetonitrile solutions of **1b** (1×10^{-5} M) resulted in a reduction of the fluorescence of **1b** without varying the shape and the position of the emission. Stern-Volmer plots of the fluorescence quenching by **2e—g** gave straight lines against concentration of **2e—g**. Fluorescence quenching rate constants (k_q) in acetonitrile calculated from the Stern-Volmer slopes ($k_q\tau$) using the lifetime of the fluorescence of **1b**, together with k_q values in benzene, are shown in Table 3. The k_q values in acetonitrile are larger than those in benzene. The large k_q values obtained in quenching by **2f** and **2g** in acetonitrile and by **2g** in benzene may also support the electron-transfer mechanism.

Concerning the electron-transfer mechanism, the by-product **5a** in the reaction with **2a** could be one of the typical electron-transfer photosensitized products,

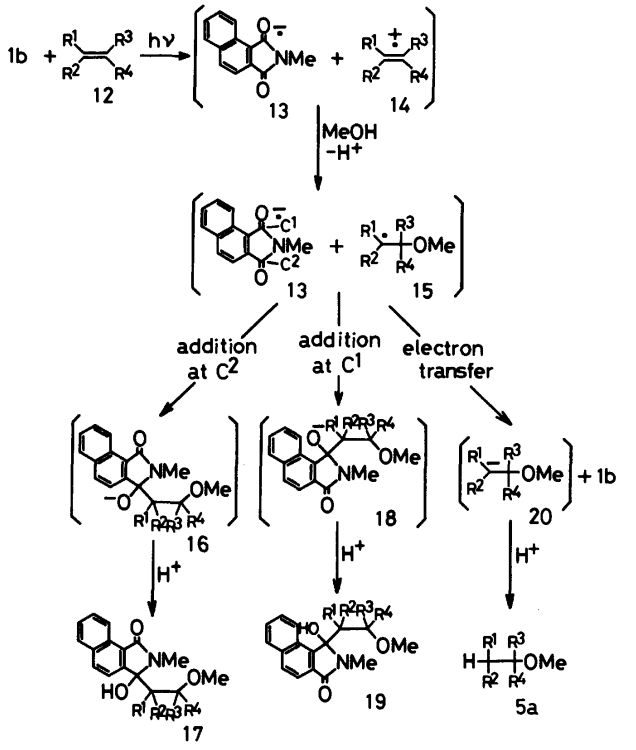

Scheme 2.

Table 2. Calculated Free Energy Changes (ΔG_{et}) Associated with Electron Transfer from Alkenes **2a, d—g** to the Singlet Excited State of *N*-Methyl-1,2-naphthalenedicarboximide (**1b**)

Alkenes	$E(D/D^+)$/V	ΔG_{et}[a]/kJ mol^{-1}
2a	1.48[b]	−56.4
2d	2.64[c]	+55.4
2e	2.39[c]	+31.3
2f	1.79[c]	−26.5
2g	1.63[c]	−42.0

a) Calculated by Eq. 4: $E(A^-/A) = -1.13$ V (in 0.5 M Et_4NClO_4/acetonitrile vs. Ag/0.01 M $AgClO_4$) from Ref. 7, $\Delta E_{0,0} = 308$ kJ mol^{-1} from Ref. 6b. b) Ref. 9. c) Ref. 3b.

Table 3. Fluorescence Quenching Rate Constants (k_q) for *N*-Methyl-1,2-naphthalenedicarboximide (**1b**) and Alkenes **2d, e—g** Systems[a]

Alkenes	$k_q\tau$[b] / dm^3 mol^{-1}	k_q[c] / dm^3 mol^{-1} s^{-1}	k_q[d] / dm^3 mol^{-1} s^{-1}
2d	0	0	0
2e	0.39	7.13×10^8	5.5×10^8
2f	48.7	8.90×10^8	6.1×10^7
2g	600	1.10×10^{10}	2.8×10^9

a) Conditions: [**1b**] $= 1\times10^{-5}$ mol dm^{-3}, at 25 °C, in air-saturated acetonitrile. b) Stern-Volmer slopes for the flnorescence quenching. c) Calculated from $k_q\tau$ using the lifetime ($\tau = 54.7$ ns) of the fluorescence of **1b**. d) In air-saturated benzene from Ref. 6b.

as reported by Arnold and his co-workers.[10] The electron-transfer photosensitized addition of methanol to **2a** giving **5a** and the methanol-incorporated addition of **2a** to **1b** giving **17** and **19** appear to be closely related processes via common intermediates (**13**+**15**). A combination reaction of the two components at the carbonyl carbon atoms (C^2 and C^1) of **1b** results in the formation of **17** and **19**, and the back electron-transfer from **13** to **15** results in the formation of **1b** and **5a** (Scheme 2).

A similar electron-transfer mechanism (Scheme 3) can be used to interpret the methanol-incorporated addition of **9** to **1b**. The addition of methanol to the radical cation **21** to give a radical **22** and a radical coupling at the tertiary carbon atom of **22** has already been reported.[11]

In the reaction with **2g** and **2h** peculiar solvent effects were observed. Thus, in a polar solvent system, acetonitrile–methanol (2/1 v/v), **1b** did not change upon irradiation, but in nonpolar solvent systems, benzene–methanol, an methanol-incorporated addition was observed. These results may be interpreted on the basis of an inclusion of different reaction intermediates. There is significant interest in the mechanism of reactions proceeded by a single-electron-transfer, particularly with respect to whether contact ion pairs and solvent separated ion pairs are involved.[1b,12] Solvent-separated ion pairs should be formed in a polar solvent if a sufficient electron-transfer could occur. Thus, in reactions with electron-donating alkenes such as **2g** and **2h** the solvent separated ion pair of **13** and **14** (Scheme 2) may be formed in a polar solvent and may reproduce **1b** by reaction pathways other than the methanol-incorporated addition, and the methanol-incorporated addition may arise only from the contact ion pair formed in nonpolar solvent.

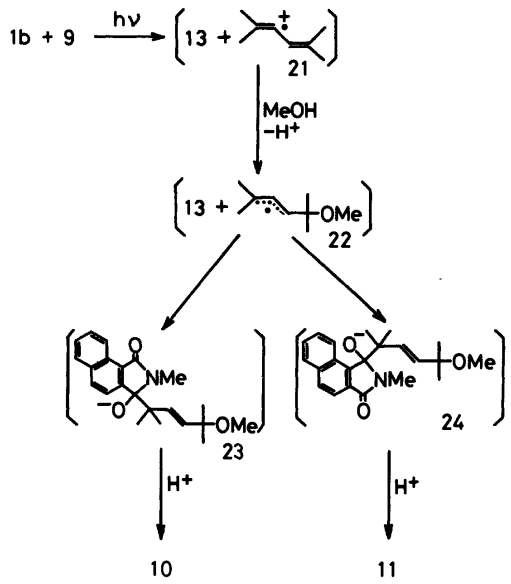

Scheme 3.

It should be emphasized here that the variation of the imide ring size caused a remarkable change in the reaction. Thus, a methanol-incorporated addition of **1b** as well as **1c**, possessing a five-membered imide ring, occurs exclusively at the carbonyl carbon atoms, while that of **1a**, possessing six-membered imide ring, occurs at the naphthalene ring carbon atom.[4] Whether the carbonyl carbon atom is attacked or the naphthalene ring carbon atom is attacked may depend on the reactivity of the respective carbon in the imide radical anion toward alkyl radicals such as **15** (Scheme 2). The relative spin density in the imide radical anion can be used as an index for the reactivity. The spin density of radical anions of 1,8-naphthalenedicarboximide (**25a**),[13] 1,2-naphthalenedicarboximide (**25b**),[5] and phthalimide (**25c**)[13] calculated by McLachlan method[14] as model compounds for radical anions of **1a**, **1b**, and **1c**, respectively, is shown in Fig. 1. That the spin density at the carbonyl carbon atom in **25a** is remarkably low compared with that at the naphthalene ring C^4 carbon atom in **25a** as well as that at the carbonyl carbon atom in **25b** and **25c** may support the preferential methanol-incorporated addition at the naphthalene ring carbon atom observed in the photoreaction of **1a**. The result that the spin density distribution in **25b** is similar to that in **25c** might account for the similar photoreaction pattern of **1b** and **1c**.

Another problem related to the spin density is which of the two types of carbonyl carbon atoms in **1b** is attacked during the methanol-incorporated addition. The spin density at the C^1 carbonyl carbon atom in a radical anion of **25b** is relatively high compared

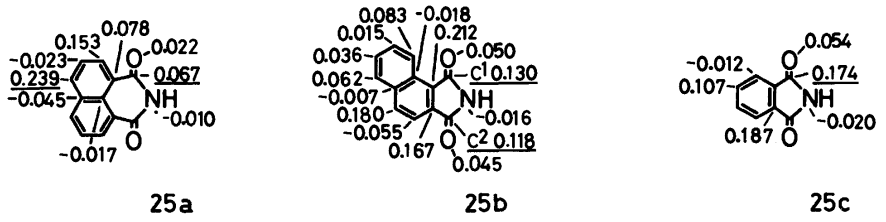

Fig. 1. Spin density of radical anions of 1,8-naphthalenedicarboximide (**25a**), 1,2-naphthalenedicarboximide (**25b**), and phthalimide (**25c**) calculated by McLachlan method.

with that at the C^2 carbon atom, although the difference in the spin density is not so large. Therefore, an addition at the C^1 carbon atom should be favorable to some extent. Since the C^1 carbonyl carbon atom is essentially more sterically hindered than the C^2 atom, the result that in the photolysis of **1b** with **2c** the yield of the products **4c** from the addition at the C^1 carbonyl carbon atom is larger than that of the products **3c** from the addition at C^2 atom may reflect the inherent preference of the addition at the C^1 atom because of the high spin density. A similar preference regarding an addition at the C^1 carbonyl carbon atom was observed in a reaction with **2h**, which was also an ethylene having only one substituent. In a series of reactions with **2c**, **2b**, and **2a**, the ratio of the products from the addition at the C^1 carbonyl carbon atom to those from the addition at the C^2 atom decreased in that order, probably due to a steric effect of the substituent of the alkenes on the addition.

Experimental

The mps were measured by a Yanagimoto micromelting-point apparatus and are uncorrected. ^{1}H NMR spectra were determined on a JEOL JNM-MH-100 (100 MHz) in $CDCl_3$ solution. IR spectra were obtained with a Hitachi 260-50 spectrophotometer. Mass spectra were measured on a JEOL JMS-DX-300 apparatus. Fluorescence spectra and the lifetimes were recorded by a Hitachi 850 spectrophotometer and a HORIBA NAES-1100 time-resolved spectrofluorometer, respectively. Microanalyses were performed on a Yanagimoto CHN corder MT-2.

Materials. *N*-Methylnaphthalene-1,2-dicarboximide (**1b**) was prepared and purified as described previously.[6b] Alkenes (**2a—h**) and dienes (**9**, 1,3-butadiene, and 2,3-dimethyl-1,3-butadiene) were commercially available and purified by distillation for liquid materials.

General Procedure for Irradiation and Product Isolation. Unless otherwise noted, UV irradiation of **1b** (19 mM) with alkenes (**2a—h**) and dienes (**9**, 1,3-butadiene, and 2,3-dimethyl-1,3-butadiene) in 25 ml of N_2 purged acetonitrile–methanol (2/1 v/v) was carried out with an Eikosha EHB-W-300 high-pressure Hg-lamp through aq $CuSO_4$ filter about 1 cm in thickness (>320 nm) at ambient temperature. The reaction was monitored by TLC (Merk, Kieselgel 60 F_{254}) analyses and ^{1}H NMR measurements. After an evaporation of the solvent, the residue was subjected to column chromatography (Wakogel C-200). Dichloromethane-ether was used as the eluant for the separation of the products. Yields were determined by measurement of the weight of the isolated products.

Irradiation of 1b and 1,1-Diphenylethylene (2a). 2,2-Diphenylethyl methyl ether (**5a**) was identical with a sample prepared by irradiation of **2a**, *p*-dicyanobenzene, and phenanthrene (sensitizer) in methanol.[15]

3-(1,1-Diphenyl-2-methoxyethyl)-3-hydroxy-2-methyl-2,3-dihydro-1*H*-benz[*e*]isoindol-1-one (**3a**): Mp 182—185 °C; ^{1}H NMR δ=2.93 (s, 3H, NMe), 3.23 (s, 3H, OMe), 4.31 and 4.62 (ABq, J=11 Hz, 2H, CH_2), 5.78 (s, 1H, OH), 6.8—7.9 (m, 15H, Arom H), 8.79 (dd, 1H, H^a); IR (KBr) 3250 (OH), 1665 (lactam), 1428, 1108, 712 cm^{-1}. Found: C, 79.65; H, 6.03; N, 3.41%; M^+-H_2O, 405. Calcd for $C_{28}H_{25}NO_3$: C, 79.41; H, 5.95; N, 3.31%; $M-H_2O$, 405.

Irradiation of 1b and α-Methylstyrene (2b). A mixture of diastereomers of 3-hydroxy-3-(2-methoxy-1-methyl-1-phenylethyl)-2-methyl-2,3-dihydro-1*H*-benz[*e*]isoindol-1-one (**3b**): Mp 166—172 °C; ^{1}H NMR of one diastereomer δ=1.20 (s, 3H, CMe), 2.88 (s, 3H, NMe), 3.33 (s, 3H, OMe), 3.74 and 3.93 (ABq, 2H, CH_2), 6.43 (s, 1H, OH), 7.1—8.0 (m, 10H, Arom H), 9.08 (dd, 1H, H^a); ^{1}H NMR of another diastereomer δ=1.37 (s, 3H, CMe), 2.60 (s, 3H, NMe), 3.37 (s, 3H, OMe), 3.80 (s, 2H, CH_2), 6.35 (s, 1H, OH), 7.1—8.0 (m, 10H, Arom H), 9.04 (dd, 1H, H^a); IR (KBr) 3300 (OH), 1662 (lactam), 1448, 1382, 1108, 702 cm^{-1}. Found: C, 76.63; H, 6.56; N, 3.96%; M^+-H_2O, 343. Calcd for $C_{23}H_{23}NO_3$: C, 76.43; H, 6.41; N, 3.88%; $M-H_2O$, 343.

A mixture of diastereomers of 1-hydroxy-1-(2-methoxy-1-methyl-1-phenylethyl)-2-methyl-1,2-dihydro-3*H*-benz[*e*]isoindol-3-one (**4b**): Mp 158—160 °C; ^{1}H NMR of one diastereomer δ=1.18 (s, 3H, CMe), 2.85 (s, 3H, NMe), 3.37 (s, 3H, OMe), 3.65 and 4.05 (ABq, 2H, CH_2), 5.85 (s, 1H, OH), 7.8—8.0 (m, 10H, Arom H), 8.39 (dd, 1H, H^a); ^{1}H NMR of another diastereomer δ=1.48 (s, 3H, CMe), 2.77 (s, 3H, NMe), 3.37 (s, 3H, OMe), 3.72 (s, 2H, CH_2), 5.82 (s, 1H, OH), 7.8—8.0 (m, 10H, Arom H), 8.36 (dd, 1H, H^a); IR (KBr) 3310 (OH), 1692 (lactam), 1461, 1386, 1106, 702 cm^{-1}. Found: C, 76.64; H, 6.52; N, 3.93%; M^+-H_2O, 343. Calcd for $C_{23}H_{23}NO_3$: C, 76.43; H, 6.41; N, 3.88%; $M-H_2O$, 343.

Irradiation of 1b and Styrene (2c). A mixture of diastereomers of 3-hydroxy-3-(2-methoxy-1-phenylethyl)-2-methyl-2,3-dihydro-1*H*-benz[*e*]isoindol-1-one (**3c**): Mp 153—161 °C; ^{1}H NMR of one diastereomer δ=2.85 (s, 3H, NMe), 3.42 (s, 3H, OMe), 3.4—4.0 (m, 2H), 4.1—4.3 (m, 1H), 5.21 (s, 1H, OH), 6.4—8.1 (m, 10H, Arom H), 8.83 (dd, 1H, H^a); ^{1}H NMR of another diastereomer δ=3.06 (s, 3H, NMe), 3.21 (s, 3H, OMe), 3.4—4.0 (m, 3H), 5.21 (s, 1H, OH), 6.4—8.1 (m, 10H, Arom H), 8.78 (dd, 1H, H^a); IR (KBr) 3320 (OH), 1680 (lactam), 1424, 1384, 1120, 760, 702 cm^{-1}. Found: C, 76.25; H, 6.18; N, 4.11%; M^+-H_2O, 329. Calcd for $C_{22}H_{21}NO_3$: C, 76.06; H, 6.09; N, 4.03%; $M-H_2O$, 329.

A mixture of diastereomers of 1-hydroxy-1-(2-methoxy-1-phenylethyl)-2-methyl-1,2-dihydro-3*H*-benz[*e*]isoindol-3-one (**4c**): Mp 146—152 °C; ^{1}H NMR of one diastereomer δ=3.26 (s, 3H, NMe), 3.50 (s, 3H, OMe), 3.5—4.4 (m, 3H), 6.15 (s, 1H, OH), 6.4—8.1 (m, 10H, Arom H), 8.52 (dd, 1H, H^a); ^{1}H NMR of another diastereomer δ=2.89 (s, 3H, NMe), 3.32 (s, 3H, OMe), 3.5—4.4 (m, 3H), 6.18 (s, 1H, OH), 6.4—8.1 (m, 10H, Arom H), 8.52 (dd, 1H, H^a); IR (KBr) 3300 (OH), 1680 (lactam), 1424, 1384, 1118, 760, 702 cm^{-1}. Found: C, 76.30; H, 6.27; N, 4.14%; M^+-H_2O, 329. Calcd for $C_{22}H_{21}NO_3$: C, 76.06; H, 6.09; N, 4.03%; $M-H_2O$, 329.

Irradiation of 1b and 2-Methyl-2-butene (2f). A mixture of diastereomers of 3-(1,1-dimethyl-2-methoxypropyl)-3-hydroxy-2-methyl-2,3-dihydro-1*H*-benz[*e*]isoindol-1-one (**3f**): Mp 148—151 °C; ^{1}H NMR of one diastereomer δ=0.52 (s, 3H, CMe), 1.18 (d, 3H, CH*Me*), 1.36 (s, 3H, CMe), 3.14 (s, 3H, NMe), 3.47 (s, 3H, OMe), 3.89 (q, 1H, C*H*Me), 6.28 (s, 1H, OH), 7.2—8.2 (m, 5H, Arom H), 9.35 (dd, 1H, H^a); ^{1}H NMR of another diastereomer δ=0.57 (s, 3H, CMe), 1.08 (d, 3H, CH*Me*), 1.25 (s, 3H, CMe), 3.09 (s, 3H, NMe), 3.30 (s, 3H, OMe), 3.75 (q, 1H, C*H*Me), 5.67 (s, 1H, OH), 7.4—8.18

(m, 5H, Arom H), 9.18 (dd, 1H, H^a); IR (KBr) 3280 (OH), 1694 (lactam), 1462, 1428, 1392, 1104 cm^{-1}. Found: C, 72.95; H, 7.54; N, 4.51%; M^+-H_2O, 295. Calcd for $C_{19}H_{23}NO_3$: C, 72.82; H, 7.40; N, 4.47%; $M-H_2O$, 295.

A mixture of diastereomers of 1-(1,1-dimethyl-2-methoxypropyl)-1-hydroxy-2-methyl-1,2-dihydro-3*H*-benz[*e*]-isoindol-3-one (**4f**): Mp 145—148 °C; ^1H NMR of one diastereomer δ=0.40 (s, 3H, CMe), 1.18 (d, 3H, CH*Me*), 1.27 (s, 3H, CMe), 3.22 (s, 3H, NMe), 3.52 (s, 3H, OMe), 3.95 (q, 1H, C*H*Me), 7.17 (s, 1H, OH), 7.5—8.1 (m, 5H, Arom H), 8.79 (dd, 1H, H^a); ^1H NMR of another diastereomer δ=0.49 (s, 3H, CMe), 0.99 (d, 3H, CH*Me*), 1.22 (s, 3H, CMe), 3.17 (s, 3H, NMe), 3.32 (s, 3H, OMe), 3.89 (q, 1H, C*H*Me), 6.71 (s, 1H, OH), 7.5—8.2 (m, 5H, Arom H), 8.62 (dd, 1H, H^a); IR (KBr) 3280 (OH), 1694 (lactam), 1376, 1122, 1102, 758 cm^{-1}. Found: C, 72.97; H, 7.54; N, 4.51%; M^+-H_2O, 295. Calcd for $C_{19}H_{23}NO_3$: C, 72.82; H, 7.40; N, 4.47%; $M-H_2O$, 295.

Irradiation of 1b and 2,3-Dimethyl-2-butene (2g). 3-Hydroxy-3-(2-methoxy-1,1,2-trimethylpropyl)-2-methyl-2,3-dihydro-1*H*-benz[*e*]isoindol-1-one (**3g**): Mp 158—161 °C; ^1H NMR δ=0.97 (s, 3H, CMe), 1.07 (s, 6H, CMe), 1.22 (s, 3H, CMe), 3.05 (s, 3H, NMe), 3.10 (s, 3H, OMe), 4.85 (s, 1H, OH), 7.6—8.0 (m, 5H, Arom H), 9.25 (dd, 1H, H^a); IR (KBr) 3280 (OH), 1666 (lactam), 1394, 1060, 800 cm^{-1}. Found: C, 73.54; H, 7.83; N, 4.33%; M^+-H_2O, 309. Calcd for $C_{20}H_{25}NO_3$: C, 73.36; H, 7.70; N, 4.28%; $M-H_2O$, 309.

N-Methyl-1-(3-methoxy-1-oxo-2,2,3-trimethylbutyl)-2-naphthalenecarboxamide (**8**): Mp 200—202 °C; ^1H NMR δ=1.12 (s, 3H, CMe), 1.19 (s, 3H, CMe), 1.26 (s, 3H, CMe), 1.38 (s, 3H, CMe), 2.90 (d, 3H, NH*Me*), 3.15 (s, 3H, OMe), 6.10 (br s, 1H, NH), 7.4—8.0 (m, 6H, Arom H); IR (KBr) 3380 (NH), 1678 (ketone), 1646 (amide), 1538, 1298, 1058, 762 cm^{-1}. Found:C, 73.51; H, 7.82; N, 4.31%; M^+, 327. Calcd for $C_{20}H_{25}NO_3$:C, 73.36; H, 7.70; N, 4.28%; M, 327.

Irradiation of 1b and Ethyl Vinyl Ether (2h). A mixture of diastereomers of 3-(1-ethoxy-2-methoxyethyl)-3-hydroxy-2-methyl-2,3-dihydro-1*H*-benz[*e*]isoindol-1-one (**3h**): Mp 155—158 °C; ^1H NMR of one diastereomer δ=1.29 (t, 3H, OCH_2Me), 2.99 (s, 3H, NMe), 3.11 (s, 3H, OMe), 2.9—3.5 (m, 2H), 3.6—4.2 (m, 3H), 5.53 (s, 1H, OH), 7.4—8.1 (m, 5H, Arom H), 9.07 (dd, 1H, H^a); ^1H NMR of another diastereomer δ=1.23 (t, 3H, OCH_2Me), 3.02 (s, 3H, NMe), 3.09 (s, 3H, OMe), 2.9—3.5 (m, 2H), 3.6—4.2 (m, 3H), 5.50 (s, 1H, OH), 7.4—8.1 (m, 5H, Arom H), 9.00 (dd, 1H, H^a); IR (KBr) 3320 (OH), 1665 (lactam), 1130, 1114, 702 cm^{-1}. Found: C, 68.62; H, 6.63; N, 4.54%; M^+-H_2O, 297. Calcd for $C_{18}H_{21}NO_4$: C, 68.55; H, 6.71; N, 4.44%; $M-H_2O$, 297.

One of the diastereomers of 1-(1-ethoxy-2-methoxyethyl)-1-hydroxy-2-methyl-1,2-dihydro-3*H*-benz[*e*]isoindol-3-one (**4h**): Mp 176—177 °C; ^1H NMR δ=1.41 (t, 3H, OCH_2Me), 2.96 (s, 3H, NMe), 3.11 (s, 3H, OMe), 2.7—3.4 (m, 2H), 3.6—4.2 (m, 2H), 4.45 (dd, 1H, CH), 4.82 (s, 1H, OH), 7.6—8.1 (m, 5H, Arom H), 8.35 (dd, 1H, H^a); IR (KBr) 3280 (OH), 1681 (lactam), 1428, 1392, 1115, 768 cm^{-1}. Found: C, 68.62; H, 6.88; N, 4.43%; M^+-H_2O, 297. Calcd for $C_{18}H_{21}NO_4$: C, 68.55; H, 6.71; N, 4.44%; $M-H_2O$, 297.

Another of the diastereomers of 1-(1-ethoxy-2-methoxyethyl)-1-hydroxy-2-methyl-1,2-dihydro-3*H*-benz[*e*]-isoindol-3-one (**4h**): Mp 136—139 °C; ^1H NMR δ=0.95 (t, 3H, OCH_2Me), 2.90 (s, 3H, NMe), 3.11 (s, 3H, OMe), 2.8—3.7 (m, 4H), 4.08 (dd, 1H, CH), 5.14 (s, 1H, OH), 7.3—8.0 (m, 5H, Arom H), 8.66 (dd, 1H, H^a); IR (KBr) 3280 (OH), 1682 (lactam), 1422, 1103, 1062, 702 cm^{-1}. Found: C, 68.72; H, 6.98; N, 4.51%; M^+-H_2O, 297. Calcd for $C_{18}H_{21}NO_4$: C, 68.55; H, 6.71; N, 4.44%; $M-H_2O$, 297.

Irradiation of 1b and 2,5-Dimethyl-2,4-hexadiene (9). 3-Hydroxy-3-(4-methoxy-1,1,4-trimethyl-2-pentenyl)-2-methyl-2,3-dihydro-1*H*-benz[*e*]isoindol-1-one (**10**): Mp 176—178 °C; ^1H NMR δ=0.98 (s, 3H, CMe), 1.15 (s, 3H, CMe), 1.21 (s, 3H, CMe), 1.24 (s, 3H, CMe), 2.77 (s, 3H, NMe), 3.06 (s, 3H, OMe), 3.52 (s, 1H, OH), 5.35 and 6.09 (ABq, J=16.8 Hz, 2H, CH=CH), 7.4—8.0 (m, 5H, Arom H), 9.11 (dd, 1H, H^a); IR (KBr) 3320 (OH), 1662 (lactam), 1424, 1380, 1068, 768 cm^{-1}. Found: C, 74.81; H, 7.83; N, 4.03%; M^+-H_2O, 335. Calcd for $C_{22}H_{27}NO_3$: C, 74.75; H, 7.70; N, 3.96%; $M-H_2O$, 335.

1-Hydroxy-1-(4-methoxy-1,1,4-trimethyl-2-pentenyl)-2-methyl-1,2-dihydro-3*H*-benz[*e*]isoindol-3-one (**11**): Mp 139—142 °C; ^1H NMR δ=0.88 (s, 3H, CMe), 1.09 (s, 6H, CMe), 1.14 (s, 3H, CMe), 2.79 (s, 3H, NMe), 2.97 (s, 3H, OMe), 4.46 (s, 1H, OH), 5.20 and 5.87 (ABq, J=16.7 Hz, 2H, CH=CH), 7.3—8.0 (m, 5H, Arom H), 8.58 (dd, 1H, H^a); IR (KBr) 3270 (OH), 1668 (lactam), 1422, 1384, 1070, 763 cm^{-1}. Found: C, 74.97; H, 7.84; N, 4.04%; M^+-H_2O, 335. Calcd for $C_{22}H_{27}NO_3$: C, 74.75; H, 7.70; N, 3.96%; $M-H_2O$, 335.

The present work was partially supported by a Grant-in-Aid for Scientific Research No. 60740276 from the Ministry of Education, Science and Culture.

References

1) a) P. S. Mariano, *Acc. Chem. Res.*, **16**, 130 (1983); b) S. L. Mattes and S. Farid, *Org. Photochem.*, **6**, 233 (1983); c) J. Y. Lan and G. B. Schuster, *J. Am. Chem. Soc.*, **107**, 6710 (1985); d) T. Hamada, A. Nishida, and O. Yonemitsu, *ibid.*, **108**, 140 (1986).

2) K. Maruyama, Y. Kubo, M. Machida, K. Oda, Y. Kanaoka, and K. Fukuyama, *J. Org. Chem.*, **43**, 2303 (1978); K. Maruyama and Y. Kubo, *J. Am. Chem. Soc.*, **100**, 7772 (1978); M. Machida, K. Oda, K. Maruyama, Y. Kubo, and Y. Kanaoka, *Heterocycles*, **14**, 779 (1980); K. Maruyama and Y. Kubo, *J. Org. Chem.*, **46**, 3612 (1981); K. Maruyama, T. Ogawa, Y. Kubo, and T. Araki, *J. Chem. Soc., Perkin Trans., 1*, **1985**, 2025.

3) a) K. Maruyama and Y. Kubo, *Chem. Lett.*, **1978**, 851; b) P. H. Mazzocchi, S. Minamikawa, and P. Wilson, *Tetrahedron Lett.*, **1978**, 4361; c) P. H. Mazzocchi and F. Khachik, *ibid.*, **22**, 4189 (1981); d) K. Maruyama and Y. Kubo, *J. Org. Chem.*, **50**, 1426 (1985); e) P. H. Mazzocchi, S. Minamikawa, and P. Wilson, *ibid.*, **50**, 2681 (1985).

4) P. H. Mazzocchi, C. Somich, and H. Ammon, *Tetrahedron Lett.*, **25**, 3551 (1984).

5) Y. Kubo, N. Asai, and T. Araki, *J. Org. Chem.*, **50**, 5484 (1985).

6) a) Y. Kubo, S. Tojo, M. Suto, R. Toda, T. Araki, *Chem. Lett.*, **1984**, 2075; b) Y. Kubo, R. Toda, K. Yamane, and T. Araki, *Bull. Chem. Soc. Jpn.*, **59**, 191 (1986).

7) Y. Kubo, M. Suto, S. Tojo, and T. Araki, *J. Chem. Soc., Perkin Trans., 1*, **1986**, 771.

8) D. Rehm and A. Weller, *Isr. J. Chem.*, **8**, 259 (1970).

9) D. R. Arnold and A. J. Maroulis, *J. Am. Chem. Soc.*, **98**, 5931 (1976).

10) R. A. Neunteufel and D. R. Arnold, *J. Am. Chem. Soc.*, **95**, 4080 (1973).

11) K. Mizuno, C. Pac, and H. Sakurai, *J. Am. Chem. Soc.*, **96**, 2993 (1974).
12) F. D. Lewis, B. E. Zebrowski, and P. E. Correa, *J. Am. Chem. Soc.*, **106**, 187 (1984); W. Hub, S. Schneider, F. Dorr, J. D. Oxman, and F. D. Lewis, *ibid.*, **106**, 708 (1984).
13) R. E. Sioda and W. S. Koski, *J. Am. Chem. Soc.*, **89**, 475 (1967).
14) A. D. McLachlan, *Mol. Phys.*, **1**, 233 (1958).
15) C. Pac, A. Nakasone, and H. Sakurai, *J. Am. Chem. Soc.*, **100**, 5806 (1977); T. Majima, C. Pac, A. Nakasone, and H. Sakurai, *ibid.*, **103**, 4499 (1981).

 © 1987 The Chemical Society of Japan Bull. Chem. Soc. Jpn., 60, 249—253 (1987)

Asymmetric Catalytic Hydrogenations of *N*-Pyruvoyl-(*S*)-proline Esters

Toratane MUNEGUMI, Manabu FUJITA, Tetsuya MARUYAMA, Shozo SHIONO, Michiaki TAKASAKI, and Kaoru HARADA*
Department of Chemistry, The University of Tsukuba, Sakura-Mura, Niihari-Gun, Ibaraki 305
(Received June 25, 1986)

Asymmetric catalytic hydrogenations of the entitled compounds were carried out over palladium on charcoal in various solvents to afford *N*-[(*S*)-lactoyl]-(*S*)-proline esters with a d.e.(=diastereoisomeric excess) of up to 59%. The stereochemistry of the catalytic hydrogenation was explained by the "chelation mechanism." And the effects of temperature and bulkiness of the ester groups on the asymmetric induction were also described.

Many studies on homogeneous asymmetric reactions have been reported[1,2] and the stereochemical models of those asymmetric inductions have been proposed. Prelog's model[3] and Cram's model[4] are typical examples. However, there are few general stereochemical models to explain the mechanism of the asymmetric induction in the heterogeneous hydrogenations. A hypothesis which explains the stereochemistry of the heterogeneous catalytic hydrogenations of α-keto acid derivatives was proposed.[5] We speculated a five-membered cyclic intermediate with the palladium catalyst as shown in Fig. 1. Many experimental results have supported the hypothesis which was named "chelation mechanism"[5,6] as a general model for asymmetric induction in the heterogeneous catalytic hydrogenations of α-keto acid derivatives.

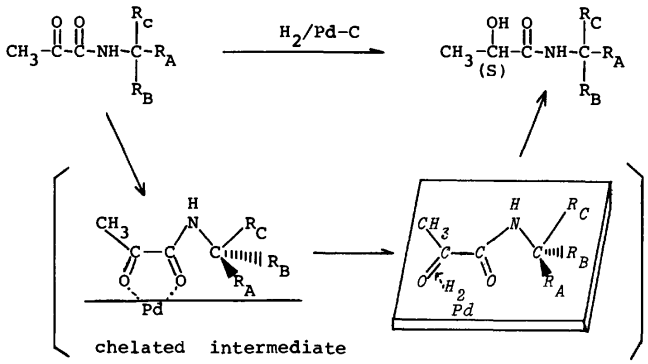

Fig. 1. Chelation mechanism in the catalytic hydrogenations of pyruvamides. R_A is bulkier than R_B.

In the previous papers,[6-8] the steric courses of asymmetric catalytic hydrogenations of several chiral pyruvamides over palladium on charcoal have been explained by the "chelation mechanism."[5,6] Of these asymmetric catalytic hydrogenations, the pyruvamides which contain amino acid esters as chiral sources gave low asymmetric yields[diastereoisomeric excess (d.e.)<24%].[8] Those low asymmetric yields seemed to be caused by the free rotation around the N–C bond between the amide nitrogen and chiral carbon (Fig. 1). Thus, there would be several possible "chelation intermediates" which took different conformations, and a mixture of these conformers was catalytically hydrogenated to afford lower d.e.

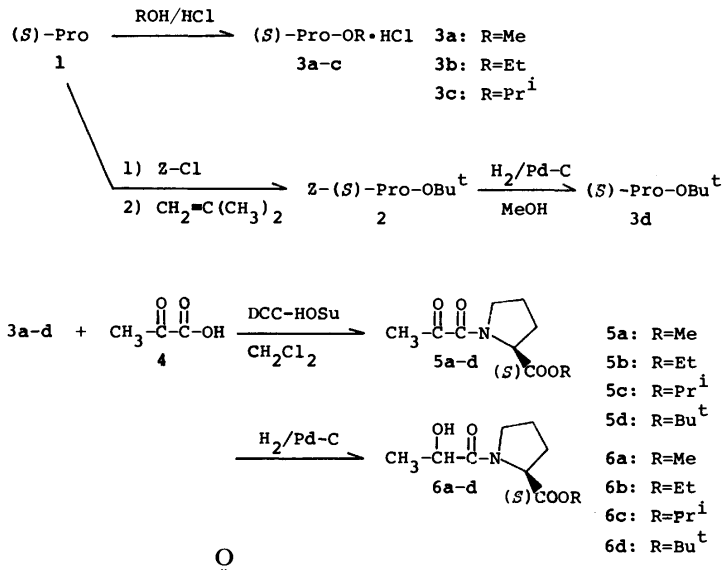

Scheme 1. Z: $C_6H_5CH_2O-\overset{O}{\overset{\|}{C}}-$, Bu^t: $(CH_3)_3C-$, DCC: dicyclohexylcarbodiimide, HOSu: *N*-hydroxysuccinimide.

In this paper, we wish to report the catalytic hydrogenations of pyruvamides having the N-C bond which does not rotate. We chose *N*-pyruvoyl-(*S*)-proline esters (methyl=Me, ethyl=Et, isopropyl=Pr^i, *t*-butyl=Bu^t) as the substrates for the asymmetric catalytic hydrogenations. The *N*-pyruvoyl-(*S*)-proline esters[9,10] were prepared by the manner as shown in Scheme 1. Substrates **5a—d** were hydrogenated in various solvents (methanol=MeOH, ethanol=EtOH, isopropyl alcohol=Pr^{i}OH, *t*-butyl alcohol=Bu^{t}OH, ethyl acetate=AcOEt, and tetrahydrofuran=THF) at 30 °C over palladium on charcoal. The hydrogenations in MeOH, EtOH, Pr^{i}OH were carried out at different temperatures (−30, −10, +10, +30, 50 °C). The diastereomeric mixtures of the hydrogenation products[*N*-lactoyl-(*S*)-proline esters] were separated to each diastereomer by a gas chromatography equipped with a chiral glass capillary column (Chirasil-Val).[11] Those diastereomers were identified by comparing the retention times with those of the authentic lactamides which were prepared separately from (*S*)-lactic acid[or (*R,S*)-lactic acid] and corresponding proline esters with dicyclohexylcarbodiimide as described in the literature.[12]

Results and Discussion

Substrates **5a—d** were hydrogenated over 5% palladium on charcoal to give diastereomeric mixtures of lactamides **6a—d** using various solvents at 30 °C as shown in Scheme 1. The results of the catalytic hydrogenations are shown in Table 1. All the catalytic hydrogenations of substrates **5a—d** gave *N*-[(*S*)-lactoyl]-(*S*)-proline esters[(*S,S*)-lactamides] in excess over *N*-[(*R*)-lactoyl]-(*S*)-proline esters[(*R,S*)-lactamides].

Table 1. Solvent Effect on the Catalytic Hydrogenations of Substrates **5a—d** at 30 °C

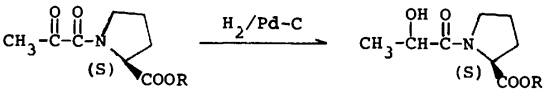

R	Confign.[a]	Solvent(ε)[b]	Chemical Yield/%	d.e.[c] %	Confign.[d]
Me	*S*	MeOH(33)	100	56	*S*
	S	EtOH(25)	99	50	*S*
	S	Pr^{i}OH(20)	80	49	*S*
	S	Bu^{t}OH(12)	49	51	*S*
	S	THF(8)	5	49	*S*
	S	AcOEt(6)	6	48	*S*
Et	*S*	MeOH	100	58	*S*
	S	EtOH	71	56	*S*
	S	Pr^{i}OH	75	50	*S*
	S	Bu^{t}OH	18	51	*S*
	S	THF	6	55	*S*
	S	AcOEt	11	52	*S*
Pr^i	*S*	MeOH	98	57	*S*
	S	EtOH	85	51	*S*
	S	Pr^{i}OH	92	49	*S*
	S	Bu^{t}OH	89	47	*S*
	S	THF	75	48	*S*
	S	AcOEt	76	45	*S*
Bu^t	*S*	MeOH	93	51	*S*
	S	EtOH	86	48	*S*
	S	Pr^{i}OH	68	42	*S*
	S	Bu^{t}OH	89	41	*S*
	S	THF	15	43	*S*
	S	AcOEt	16	39	*S*

a) Configuration of the chiral source. b) Dielectric constant of solvents. c) Diastereoisomeric excess= $[((S,S)-(R,S))/((S,S)+(R,S))]\times 100$ (%). d) Configuration of the newly formed chiral moiety.

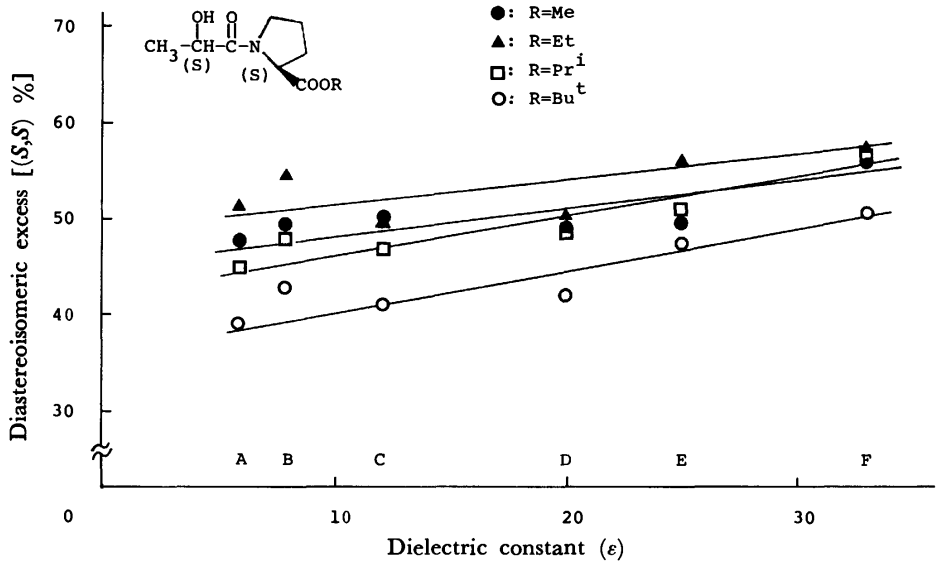

Fig. 2. Solvent effect on d.e. of hydrogenation products.
Solvent: A, AcOEt; B, THF; C, Bu^{t}OH; D, Pr^{i}OH; E, EtOH; F, MeOH.

The values of the d.e. of the asymmetric catalytic hydrogenations in Table 1 were plotted against the dielectric constants of the solvents used for the hydrogenations in Fig. 2. In most cases, the d.e. of the hydrogenation products were slightly higher in the solvents with higher dielectric constants than in the solvents with lower dielectric constants. The values of the d.e. were plotted against the bulkiness of R(Me<Et<Pr^i<Bu^t) as shown in Fig. 3. Substrate **5b** gave higher d.e. than **5a**. Substrate **5c** gave slightly lower d.e. than **5b**. Substrate **5d** gave the lowest d.e. In all solvents used, substrates **5a—d** gave (*S,S*)-lactamide in excess over (*R,S*)-lactamide with rather higher d.e. (up to 58%) than *N*-pyruvoyl-(*S*)-amino acid esters used in the previous study.[8] These results suggested that the fixation of the N-C bond gave stable conformers to make the d.e. of the resulting (*S,S*)-lactamide higher.

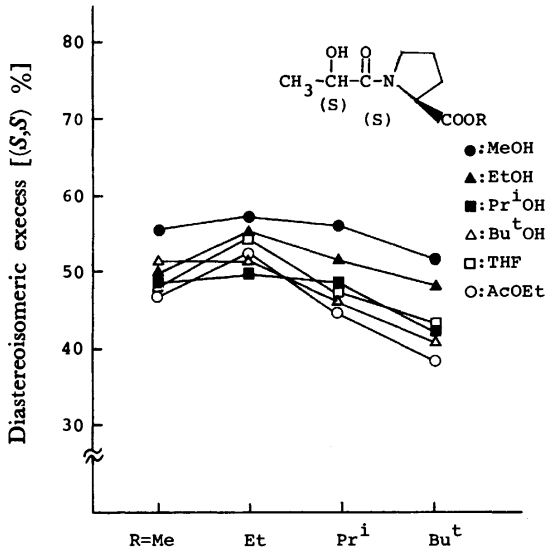

Fig. 3. Effect of bulkiness of substituent group on d.e.

There are two possible steric courses (A and B) through which substrates give (*S,S*)-lactamides in excess in the catalytic hydrogenations (Fig. 4). In the first step (A-1) of the steric course A, the two carbonyl groups take a s-trans conformation owing to their electrostatic repulsion, and the amide bond formed by pyruvic acid and proline ester moieties take a cis[13] conformation as shown in Fig. 4. The substrate molecule taking this conformation would be adsorbed on the palladium surface at the less bulky side of the molecule and be hydrogenated from the catalyst side to give (*S,S*)-lactamide. Thus, in the steric course A, the substrate molecule would be hydrogenated through one step adsorption on the palladium surface and then be hydrogenated. However, this steric course A seemed to contribute little to the asymmetric induction, because A-1 would be unstable due to the steric repulsion between $CH_3C{=}O$ and COOR group binding to the chiral center.

The steric course B which is the "chelation mechanism" could explain the stereochemistry of the catalytic hydrogenations as follows. In the first step (B-1), the substrate molecule would stand on the catalyst surface by the two carbonyl oxygens which take a s-cis conformation, and the amide bond would be trans[13] as shown in Fig. 4. This is the "chelated intermediate." In the second step(B-2), the intermediate would then be adsorbed at the less bulky side of the substrate on the catalyst. And the substrate molecule would be hydrogenated from the catalyst side to give (*S,S*)-lactamide in excess. Thus, in the steric course B, the "chelated intermediate" would be formed first between the substrate molecule and the palladium catalyst and then hydrogenated. Thus, the steric course B could explain the experimental results that (*S,S*)-lactamide was obtained in excess over (*R,S*)-lactamide with the fairly high d.e. (39—59%).

However, while the d.e. of the hydrogenation products would increase with the increase of the

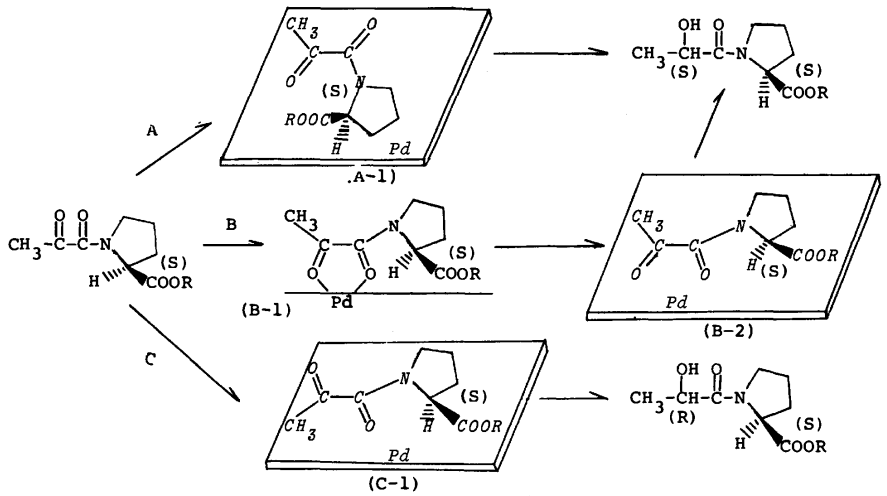

Fig. 4. Possible steric cuorses in the hydrogenations of substrates **5a—d**.

bulkiness of the ester moiety, acturely the d.e. decreased a little in the hydrogenations of substrates **5c,d** (R=Pr^i, Bu^t) as shown in Fig. 3. This could be due to the larger steric repulsion between the ester moiety of substrate **5c** or **5d** and the catalyst surface. Thus, the steric repulsion would inhibit the formation of the "chelated intermediate." And the molecular model of these substrate supported this possibility. Therefore, as the R group becomes larger, the proportion of the substrate molecule which takes other conformation as C-1 on the catalyst increased to give (*R,S*)-lactamide. And the d.e. of (*S,S*)-lactamide in the hydrogenation of substrates **5c,d** might slightly drcrease.

The hydrogenations of substrates **5a—d** were performed in MeOH, EtOH, and Pr^{i}OH at various temperatures. The results of these hydrogenations are shown in Table 2. Substrates **5a—c** gave similar d.e. at each temperature in each solvent. Substrate **5d** gave slightly higher d.e. at lower temperatures. The d.e. from **5d** reached to 59% (*S,S*) at −30 °C.

From the experimental results described above, we could conclude that the asymmetric induction of substrates **5a—d** would be explained by the chelation mechanism. And these experimental results might be useful to speculate the steric course of other heterogeneous asymmetric hydrogenation reactions.

Experimental

The melting points were uncorrected. Optical rotations were measured with a Jasco DIP-181 Digital polarimeter.

Table 2. Temperature Effect on the Catalytic Hydrogenations of Substrates **5a—d**

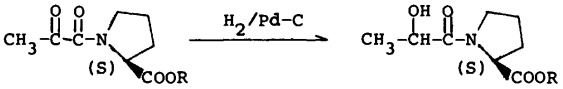

R	Confign.[a]	Solvent	Temperature °C	Chemical Yield/%	d.e.[b] %	Confign.[c]
Me	*S*	MeOH	−30	85	45	*S*
	S	MeOH	+10	100	56	*S*
	S	EtOH	−10	88	51	*S*
	S	EtOH	+30	99	50	*S*
	S	Pr^{i}OH	−30	50	49	*S*
	S	Pr^{i}OH	+10	87	50	*S*
	S	Pr^{i}OH	+30	80	49	*S*
Et	*S*	MeOH	−10	84	51	*S*
	S	MeOH	+30	100	58	*S*
	S	EtOH	−30	46	42	*S*
	S	EtOH	+10	70	55	*S*
	S	EtOH	+50	70	47	*S*
	S	Pr^{i}OH	−10	97	52	*S*
	S	Pr^{i}OH	+30	75	50	*S*
Pr^i	*S*	MeOH	−30	97	34	*S*
	S	MeOH	+10	100	47	*S*
	S	EtOH	−30	100	42	*S*
	S	EtOH	+10	100	44	*S*
	S	EtOH	+50	99	46	*S*
	S	Pr^{i}OH	−30	93	41	*S*
	S	Pr^{i}OH	+30	92	49	*S*
	S	Pr^{i}OH	+50	73	34	*S*
Bu^t	*S*	MeOH	−30	94	58	*S*
	S	MeOH	−10	100	53	*S*
	S	MeOH	+30	93	51	*S*
	S	EtOH	−30	94	59	*S*
	S	EtOH	+10	100	48	*S*
	S	EtOH	+50	60	45	*S*
	S	Pr^{i}OH	−30	71	50	*S*
	S	Pr^{i}OH	−10	78	45	*S*
	S	Pr^{i}OH	+30	68	42	*S*

a) Configuration of the chiral sources. b) Diastereoisomeric excess. c) Configuration of the newly formed chiral moiety.

The gas chromatographic analyses were carried out with a Hitachi 163 gas chromatograph, and the peaks on the chromatograms were integrated with a Shimazu C-R3A Chromatopac. NMR spectra were measured with a Hitachi R-24 High Resolution NMR spectrometer. IR spectra were measured with a Hitachi 260-50 infrared spectrometer. Palladium on charcoal(5%) was purchased from Nippon Engelhald.

Materials. *N*-Benzyloxycarbonyl-(*S*)-proline *t*-Butyl Ester (2):[14,15] The compound **2** was prepared from *N*-benzyloxycarbonyl-(*S*)-proline(Mp 73.5—74.5 °C $[\alpha]_D^{20}$ −38.0° (*c* 1.09, MeOH)) and isobutene in dichloromethane in the presence of H_2SO_4. Yield, 93%. Mp 40—41 °C. $[\alpha]_D^{24}$ −45.3° (*c* 1.00, AcOEt).

(*S*)-Proline Methyl, Ethyl, and Isopropyl Ester Hydrochloride (3a—c): These compounds **3a—c** were prepared by the esterification of **1** with HCl in the corresponding alcohols (MeOH, EtOH, and Pr^{i}OH).

(*S*)-Proline *t*-Butyl Ester (3d): *N*-Benzyloxycarbonyl-(*S*)-proline *t*-butyl ester **2** (2.08 g, 6.8 mmol) was hydrogenated in ethyl acetate in the presence of 5% palladium on charcoal. After the catalyst was removed off, the filtrate was evaporated in vacuo to give an oily product. This oil was redissolved in ethyl acetate and was used for preparation of **5d**.

***N*-Pyruvoyl-(*S*)-proline Methyl Ester (5a):**[9] (*S*)-Proline methyl ester hydrochloride (**3a**) (3.03 g, 20 mmol) was liberated with triethylamine (1.76 g, 20 mmol) and was coupled with pyruvic acid (**4**) by using dicyclohexyl-carbodiimide (4.54 g, 22 mmol) in ethyl acetate in the presence of *N*-hydroxysuccinimide (2.76 g, 24 mmol). The reaction was carried out for two hours at 0 °C and for 24 h at room temperature. After usual work-up, an oily crude product was obtained and was purified with silica-gel column chromatography (eluting solvent: benzene-ethyl acetate (12:1)) to give 1.29 g oil (32%). $[\alpha]_D^{15}$ −76.5° (*c* 1.25, EtOH). ^{1}H NMR (CCl_4) δ=1.50—2.50 (4H, br), 2.35 (3H, d), 3.64 (3H, s), 3.50 (2H, t), 4.75 (1H, br). IR: 1630, 1700, 1730 cm^{-1}. Found: C, 54.65; H, 6.83; N, 6.76%. Calcd for $C_9H_{13}NO_4$: C, 54.26; H, 6.57; N, 6.73%.

***N*-Pyruvoyl-(*S*)-proline Esters 5b—d.**[9] Substrates **5b—d** were prepared by the similar method to prepare **5a**. The physical data are shown as follows: **5b.** $[\alpha]_D^{17}$ −75.5° (*c* 1.22, EtOH). ^{1}H NMR (CCl_4) δ=1.25 (3H, t), 1.50—2.50 (4H, br), 2.30 (3H, d), 3.60 (2H, br), 4.05 (2H, br), 4.70 (1H, br). IR, 1630, 1710, 1730 cm^{-1}. Found: C, 56.02; H, 7.13; N, 6.47%. Calcd for $C_{10}H_{13}NO_4$: C, 56.32; H, 7.09; N, 6.56%. **5c.** $[\alpha]_D^{17}$ −65.5° (*c* 1.08, EtOH). ^{1}H NMR ($CDCl_3$) δ=1.15—1.30 (6H, dd), 1.80—2.25 (4H, br), 2.32—2.38 (3H, d), 3.40—3.90 (2H, br), 4.20—4.50 (1H, br). IR, 1620, 1700, 1710 cm^{-1}. Found: C, 57.88; H, 7.60; N, 6.22%. Calcd for $C_{12}H_{19}NO_4$: C, 58,13; H, 7.54; N, 6.16%. **5d.** $[\alpha]_D^{17}$ −71.4° (*c* 1.07, AcOEt). ^{1}H NMR ($CDCl_3$) δ=1.44 (9H, s), 2.07 (4H, br), 2.40 (3H, d), 3.50—3.83 (2H, br), 4.60—4.83 (1H, br). IR, 1640, 1720—1740 cm^{-1}. Found: C, 59.81; H, 8.11; N, 6.08%. Calcd for $C_{13}H_{21}NO_4$: C, 59.73; H, 7.93; N, 5.80%.

Catalytic Hydrogenations of Substrates 5a—d. Substrates **5a—d** (0.10 mmol) were dissolved in 5 ml solvents (MeOH, EtOH, Pr^{i}OH, Bu^{t}OH, THF, and AcOEt) in the presence of 20 mg of 5% palladium on charcoal and were hydrogenated at 30 °C. After 2—7 d hydrogenations, the catalyst was filtered off and the filtrate was evaporated in vacuo to give an oily product. Chemical yields and d.e. (=diastereoisomeric excess) of the hydrogenation products were determined by using gas liquid chromatography. Catalytic hydrogenations of **5a—d** at some different temperatures (−30, −10, +10, and +50 °C) were also carried out by the same manner.

***N*-Lactoyl-(*S*)-Proline Ester 6a—d.** Authentic *N*-lactoyl-(*S*)-proline esters were prepared from (*S*)-lactic acid[or (*R*,*S*)-lactic acid] and the corresponding (*S*)-proline esters as described in the literatuere.[12]

Gas Liquid Chromatographic Analyses. All the diastereomer mixture of the hydrogenation products were not derivatized and directly separated to each diastereomer by using a Hitachi gas chromatograph with a fused glass capillary column (Chirasil-Val[11] 25 m×0.25 mm I.D.) which was purchased from Alltech Associates, Inc. Applied Science Labs. Il 60015 U.S.A. Carrier gas was helium. The column temperature during the analyses was 170 °C (constant). Flame thermionic detector was used for these analyses.

References

1) J. D. Morrison, H. S. Mosher, "Asymmetric Organic Reactions," Prentice-Hall, Inc., New Jersey (1971).
2) D. Valentine, Jr. and J. W. Scot, *Synthesis*, **1978**, 329.
3) V. Prelog, *Helv. Chim. Acta*, **36**, 308 (1953).
4) D. J. Cram and F. A. Abd. Elhafez, *J. Am. Chem. Soc.*, **74**, 5828 (1950).
5) K. Harada and K. Matsumoto, *J. Org. Chem.*, **32**, 1794 (1967); K. Harada, Asymmetric Catalytic Hydrogenation, "Asymmetric Synthesis," ed by J. D. Morrison, Academic Press, New York (1985), Vol. 5, pp. 345—383.
6) K. Harada and T. Munegumi, *Bull. Chem. Soc. Jpn.*, **57**, 3203 (1984), cited therein.
7) K. Harada, T. Munegumi, and S. Nomoto, *Tetrahedron Lett.*, **22**, 111 (1981).
8) K. Harada and T. Munegumi, *Bull. Chem. Soc. Jpn.*, **56**, 2774 (1983).
9) B. W. Bycroft and G. R. Lee, *J. Chem. Soc., Chem. Commun.*, **1975**, 988.
10) K. Soai, K. Komiyama, H. Hasegawa, and A. Ookawa, *J. Chem. Soc., Chem. Commun.*, **1982**, 1282; K. Soai and H. Hasegawa, *J. Chem. Soc., Perkin Trans. 1*, **1985**, 769.
11) H. Frank, G. J. Nicholson, and E. Bayer, *J. Chromatogr.*, **146**, 197 (1978).
12) T. Munegumi and K. Harada, *J. Chromatogr.*, **291**, 354 (1984).
13) D. E. Dorman and F. A. Bovey, *J. Org. Chem.*, **38**, 2379 (1973).
14) W. Brenner and W. Huber, *Helv. Chim. Acta*, **36**, 1109 (1953).
15) R. W. Roeske, *J. Org. Chem.*, **28**, 1251 (1963).

 © 1987 The Chemical Society of Japan Bull. Chem. Soc. Jpn., 60, 255—259 (1987)

Synthesis of 1,4-Diaminocyclitol Antibiotics. I. Synthesis of 4′-Hydroxyfortimicin D

Kazuaki KANAI, Itsuki SAKAMOTO, Yasunobu MIYAMOTO, Seiichiro OGAWA,* and Tetsuo SUAMI†
Department of Applied Chemistry, Faculty of Science and Technology, Keio University, Hiyoshi, Yokohama 223
(Received June 25, 1986)

The 4′-hydroxy analog of fortimicin D has been synthesized by condensation of 4-*O*-acetyl-2,6-bis(2,4-dinitrophenylamino)-2,3,6-trideoxy-α-D-*ribo*-hexopyranosyl chloride with a partially protected aminocyclitol, 1,2:4,5-di-*N*,*O*-carbonylfortamine B, followed by deprotection.

Fortimicins are isolated from a fermentation broth of *Micromonospora olivoasterospora*,[1,2] and belong to members of 1,4-diaminocyclitol antibiotics. The structural features of the antibiotics are pseudo-disaccharides consisting of the aminocyclitol, fortamine, and the diamino sugar, 6-epipurpurosamine B. As a member of anitibiotic fortimicin-group, sporaricins,[3] istamycins,[4] sannamycins,[5] SF-2052,[6] and SF-1854[7] have been known. A number of chemical modifications has extensively been carried out, and the relationship between the structure and antimicrobial activity has gradually been made clear. However, most studies have been centered around the aminocyclitol moiety.[8] Therefore, in order to elucidate the role of the diamino sugar moiety in the antimicrobial activity, we have undertaken a modification of the amino sugar moiety.

We now describe a chemical synthesis of the 4′-hydroxy analog (**17**) of fortimicin D.[9] The synthesis involved preparation of the glycosyl chloride, 4-*O*-acetyl-2,6-bis(2,4-dinitrophenylamino)-2,3,6-trideoxy-α-*ribo*-hexopyranosyl chloride (**8**) and condensation of **8** with the partially protected aminocyclitol, 1,2:4,5-di-*N*,*O*-carbonylfortamine B (**9**).[10,11]

Results and Discussion

The glycosyl chloride **8** has been prepared by the following sequence. Methyl 2-acetamido-4,6-*O*-benzylidene-2,3-dideoxy-α-D-*ribo*-hexopyranoside (**3**)[12–15] was obtained in high yield (80%, 2 steps) from methyl 2-acetamido-4,6-*O*-benzylidene-2-deoxy-α-D-glucopyranoside (**1**)[6] by modified Barton's deoxygenation reaction.[17] Catalytic hydrogenation of methyl 2-acetamido-6-azido-2,3,6-trideoxy-α-D-*ribo*-hexopyranoside (**4**),[18] which was accessible from **3**, gave the 6-amino derivative **5** as an acetate form in 84% yield. Hydrolysis of **5** in refluxing 2 M†† hydrochloric acid solution gave the 2,6-diamino sugar **6**, which was converted into 1,4-di-*O*-acetyl-2,6-bis(2,4-dinitrophenylamino)-2,3,6-trideoxy-D-*ribo*-hexopyranose (**7**, 55%) by treatment with 2,4-dinitrofluorobenzene and triethylamine, followed by acetylation. The chloride **8** was obtained as yellow crystals (54%) by chlorination of **7** with 15% HCl–dioxane and acetyl chloride.

Condensation of **9** with **8** in dioxane in the presence of silver trifluoromethanesulfonate afforded 28% yield of the condensate **10** as an anomeric mixture, which was directly used for the following step. *O*-Deacetylation of **10** with 0.02 M sodium hydroxide gave two products (**11**, 5% based on **9**) and (**12**, 11%). The ^{1}H NMR spectrum of **11** revealed the presence of the anomeric proton of the α-D-glycoside as a doublet at δ 5.62 (J=4.5 Hz). The spectrum of **12** showed a doublet at δ 5.15 (J=7.5 Hz) attributable to the anomeric proton of the β-D-glycoside. Removal of the dinitrophenyl group of **11** with Amberlite IRA-400 (OH^-) resin, followed by hydrolysis in refluxing 1 M sodium hydroxide solution gave, in 76% yield, 4′-hydroxyfortimicin KE (**13**), which was characterized by conversion into the hepta-*N*,*O*-acetyl derivative (**14**). Selective *N*-benzyloxycarbonylation of **13** with *N*-(benzyloxycarbonyloxy)succinimide gave 1,2′,6′-tris[*N*-(benzyloxycarbonyl)]-4′-hydroxyfortimicin KE (**15**) in 50% yield. Tetrakis[*N*-(benzyloxycarbonyl)] derivative of 4′-hydroxyfortimicin D (**16**) was obtained in 67% yield by introduction of *N*-(benzyloxycarbonyl)-glycyl group into methyl amino group at C-4 of **15** with *N*-[*N*-(benzyloxycarbonyl)glycyloxy]succinimide and triethylamine. Hydrogenolysis of **16** in ethanol containing 0.1 M hydrochloric acid in the presence of

Table 1. Antimicrobial Activity of **17** and Fortimicin A[a]

Test Organisms	**17**	Fortimicin A
Streptococcus faecalis KY4280	>100	3.1
Pseudomonas aeruginosa KY4276	50	3.1
Staphylococcus aureus KY4279	6.3	<0.05
Escherichia coli KY4271	25	0.39
Bacillus subtilis KY4273	3.1	0.1
Shigella sonnei KY4281	50	0.78
Klebsiella pneumoniae KY4275	6.3	<0.05

a) Minimum inhibitory concentration in μg ml^{-1}.

† Present address: Department of Chemistry, Faculty of Science and Technology, Meisei University, Hodokubo, Hino, Tokyo 191.

†† 1 M=1 mol dm^{-3}.

10% palladium on charcoal gave 4′-hydroxyfortimicin D (**17**) as the hydrochloride.

The minimum inhibitory concentrations of **17** against seven organisms were compared with those of fortimicin A (Table 1). Antimicrobial activity of **17** was lower than that of fortimicin A.

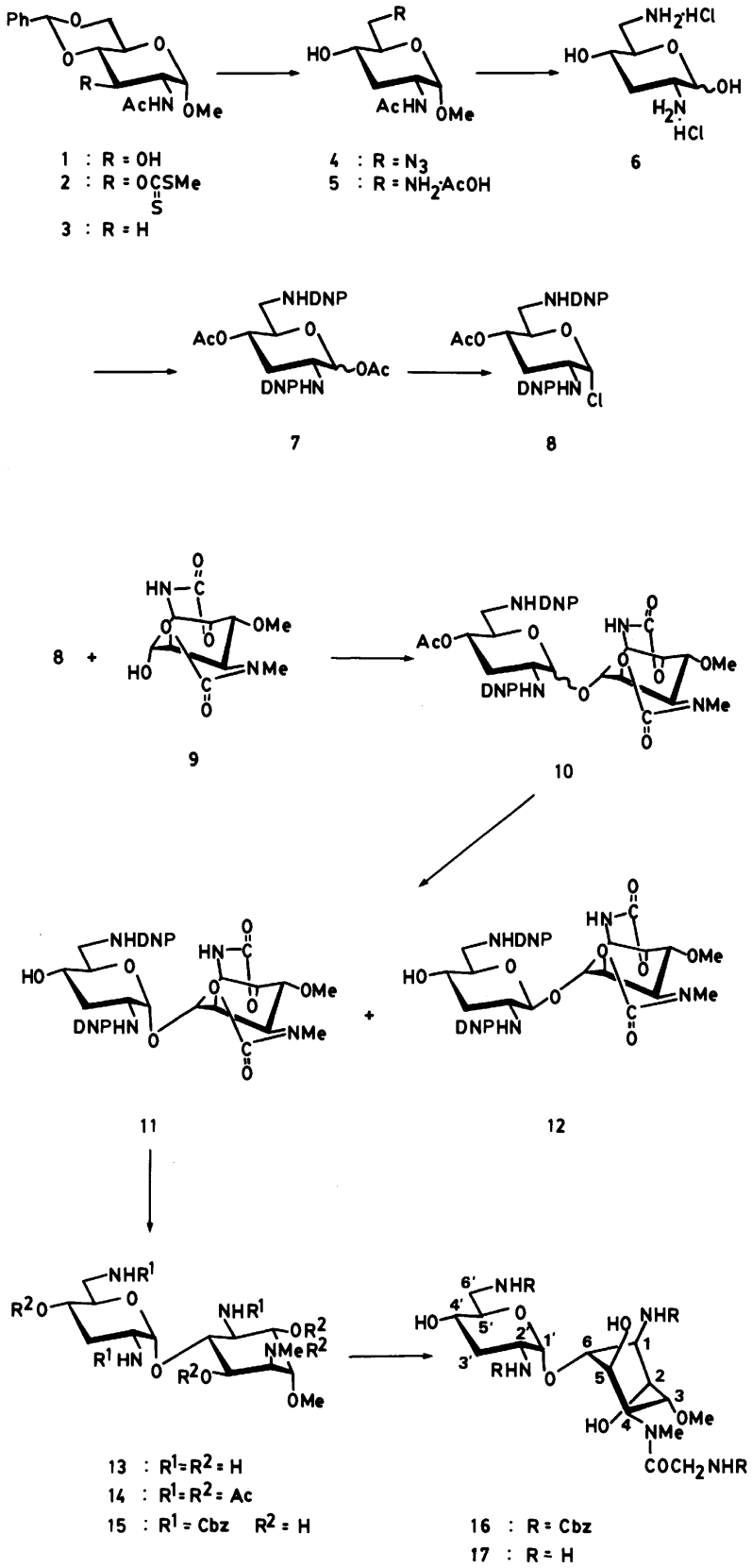

Experimental

General Procedures. Melting points were determined in capillary-tubes and are uncorrected. Optical rotations were measured on a JASCO DIP-4 polarimeter. IR and Mass spectra were recorded on Hitachi HPL-225 spectrophotometer and Hitachi M-80 and M-80A (SIMS) spectrometers, respectively. ^{1}H NMR spcetra with TMS or DSS as internal standard were recorded on Varian EM-390 (90 MHz). TLC and column chromatography were performed on Silica Gel 60F-254 (E. Merck) and Wakogel C-200, C-300 or Kieselgel 60, respectively. Concentration were carried out under reduced pressure below 40 °C.

Methyl 2-Acetamido-4,6-*O*-benzylidene-2-deoxy-3-*O*-[methylthio(thiocarbonyl)]-α-D-glucopyranoside (2). To a solution of methyl 2-acetamido-4,6-*O*-benzylidene-2-deoxy-α-D-glucopyranoside[16] (28.5 g) in *N*,*N*-dimethylformamide (400 ml), a suspension of 60% sodium hydride (5.40 g) in *N*,*N*-dimethylformamide (10 ml) and catalytic amount of imidazole were added. After stirring for 1 h at 50 °C, carbon disulfide (54 ml) was added to the mixture. After 15 min, methyl iodide (40 ml) was added and stirring was continued for 30 min. The mixture was then poured into ice water (500 ml) and extracted with chloroform (300 ml). The extracts were washed with 0.1 M hydrochloric acid, saturated aqueous $NaHCO_3$ and water, and dried. After evaporation of the solvent, the residue was crystallized from ethanol to afford **2** (29.1 g, 81%): Mp 182—183 °C; $[\alpha]_D^{14}$ −23.8° (*c* 0.93, chloroform); IR (KBr) 1665, 1520 (NHC=O), 1200 (C=S) cm^{-1}; ^{1}H NMR ($CDCl_3$) δ=1.92 (3H, s, NAc), 2.54 (3H, s, SMe), 3.41 (3H, s, OMe), 4.75 (1H, d, *J*=3.5 Hz, H-1), 5.53 (1H, s, C<u>H</u>C$_6$H$_5$), 5.90 (1H, d, *J*=9 Hz, NH), 6.31 (1H, t, *J*=9 Hz, H-3), 6.92—7.53 (5H, m, phenyl).

Found: C, 52.51; H, 5.56; N, 3.35; S, 15.26%. Calcd for $C_{18}H_{23}NO_6S_2$: C, 52.28; H, 5.61; N, 3.39; S, 15.51%.

Methyl 2-Acetamido-4,6-*O*-benzylidene-2,3-dideoxy-α-D-*ribo*-hexopyranoside (3). To a boiling solution of **2** (30 g) in toluene (750 ml), a solution of *n*-Bu_3SnH (38.8 ml) in toluene (62 ml) and catalytic amount of α, α′-azobisisobutyronitrile were added under nitrogen atmosphere. After 5 min, the mixture was cooled and concentrated to give a gelatinous residue, which was chromatographed on silica gel with chloroform–acetone (1:1). The fractions [R_f 0.38; toluene–acetone (3:1)] were concentrated to afford **3** (22.2 g, 99%) as an amorphous solid: Mp 248—249 °C; $[\alpha]_D^{16}$ +54.5° (*c* 1.27, chloroform), Lit.[14] mp 245 °C, $[\alpha]_D$ +55.5° (*c* 0.95).

Found: C, 62.38; H, 7.02; N, 4.55%. Calcd for $C_{16}H_{21}NO_5$: C, 62.52; H, 6.89; N, 4.56%.

Methyl 2-Acetamido-6-amino-2,3,6-trideoxy-α-D-*ribo*-hexopyranoside Acetate (5). A solution of methyl 2-acetamido-6-azido-2,3,6-trideoxy-α-D-*ribo*-hexopyranoside (**4**)[18] (2.62 g) in methanol (25 ml) containing acetic acid (0.1 ml) was hydrogenated with Raney nickel in the initial hydrogen pressure of 3.4 kg cm^{-2} for 17 h. The catalyst was filtered and the filtrate was concentrated to a residue, which was washed with ether to give **5** (2.52 g, 84%) as a white powder: Mp 150 °C; $[\alpha]_D^{22}$ +115° (*c* 0.65, methanol); ^{1}H NMR (CD_3OD) δ=1.97 (3H, s, NAc), 3.47 (3H, s, OMe), 4.64 (1H, d, *J*=3.3 Hz, H-1).

Found: C, 47.21; H, 7.75; N, 10.23%. Calcd for $C_9H_{18}N_2O_4 \cdot CH_3COOH$: C, 47.47; H, 7.97; N, 10.07%.

1,4-Di-*O*-acetyl-2,6-bis(2,4-dinitrophenylamino)-2,3,6-trideoxy-D-*ribo*-hexopyranose (7). A solution of **5** (9.52 g) in 2 M hydrochloric acid (200 ml) was refluxed for 4 h. The mixture was concentrated and the residue was dissolved in methanol (100 ml) and acetone (70 ml). 2,4-Dinitrofluorobenzene (17.9 g) and triethylamine (26.9 ml) were added to it under ice cooling and the mixture was stirred for 12 h at room temperature. The mixture was concentrated to half volume and partitioned between ethyl acetate (200 ml) and water (200 ml). The organic layer and the extracts (400 ml) were combined and dried. After concentration, the residue was chromatographed on silica gel with toluene–acetone (5:1) as an eluent to afford the *N*-(2,4-dinitrophenyl) derivative of **6** (14.7 g, 68%) as a yellow powder: Mp 138—139.5 °C; $[\alpha]_D^{19}$ +19.1° (*c* 1.1, acetone); IR (KBr) 1520, 1335 (NO_2) cm^{-1}. To a solution of the powder (14.6 g) in pyridine (150 ml), acetic anhydride (56 ml) was added under ice cooling and the mixture was stirred for 13 h at room temperature. The reaction solution was concentrated and the residue gave **7** (7.11 g) as a yellow powder upon addition of ethyl acetate. An additional crop of **7** (6.72 g, total yield 55%) was obtained by chromatography of the mother liquor on silica gel using toluene–acetone (8:1): Mp 190 °C (decomp); $[\alpha]_D^{25}$ +14.3° (*c* 0.34, chloroform); IR (KBr) 1745 (ester), 1525, 1340 (NO_2) cm^{-1}; ^{1}H NMR (pyridine-d_5) δ=2.12 and 2.26 (each 3H, s, OAc), 5.30 (1H, dt, *J*=5 Hz, 10 Hz, H-4), 6.63 (1/4H, d, *J*=8.5 Hz, H-1), 6.66 (3/4H, d, *J*=3.5 Hz, H-1).

Found: C, 45.55; H, 3.92; N, 14.46%. Calcd for $C_{22}H_{22}N_6O_{13}$: C, 45.68; H, 3.83; N, 14.53%.

4-*O*-Acetyl-2,6-bis(2,4-dinitrophenylamino)-2,3,6-trideoxy-α-D-*ribo*-hexopyranosyl Chloride (8). A solution of **7** (4.0 g) in 15% HCl–dioxane (175 ml) containing acetyl chloride (10 ml) was stirred at 50 °C for 4 h. The mixture was concentrated, and the residue was washed with ether and recrystallized from chloroform to afford **8** (2.10 g, 54%): Mp 127 °C (decomp); $[\alpha]_D^{17}$ +86.0° (*c* 1.66, acetone); ^{1}H NMR (acetone-d_6) δ=2.10 (3H, s, OAc), 4.80 (1H, ddt, *J*=4 Hz, 9 Hz, 12 Hz, H-2), 5.10 (1H, dt, *J*=4.5 Hz, 11.5 Hz, H-4), 6.54 (1H, d, *J*=4 Hz, H-1), 7.27 and 7.46 (each 1H, d, *J*=9 Hz, H-3 of DNP), 8.26 (2H, dd, *J*=3 Hz, 9 Hz, H-5 of DNP×2), 8.98 (2H, d, *J*=3 Hz, H-6 of DNP×2).

Found: C, 43.10; H, 3.60; N, 14.88; Cl, 6.45%. Calcd for $C_{20}H_{19}N_6O_{11}Cl$: C, 43.29; H, 3.45; N, 15.15; Cl, 6.39%.

4′-*O*-Acetyl-1,2:4,5-di-*N*,*O*-carbonyl-2′,6′-bis[*N*-(2,4-dinitrophenyl)]-fortimicin KE and -1′-epifortimicin KE (10). 1,2:4,5-Di-*N*,*O*-carbonylfortamine B (**9**)[10,11] (404 mg) was dissolved in freshly distilled dioxane (16 ml) at 100 °C. After the solution had been cooled to room temperature, **8** (1.95 g) and silver trifluoromethanesulfonate (990 mg) were added, and the mixture was stirred under argon atmosphere in the dark for 66 h. An insoluble material was filtered and washed with acetone. The filtrate was concentrated and the residual product was purified by a column chromatography using toluene–acetone (5:1). Fractions [R_f 0.33, toluene–acetone (5:2)] were concentrated to give the anomeric mixture of **10** (342 mg, 28%) and the aglycon **9** (200 mg) recovered.

1,2:4,5-Di-*N*,*O*-carbonyl-2′,6′-bis[*N*-(2,4-dinitrophenyl)]-4′-hydroxyfortimicin KE (11) and -1′-epi-4′-hydroxyfortimicin KE (12). To a solution of **10** (342 mg) in acetone (30 ml) and methanol (30 ml), 0.02 M sodium hydroxide (20 ml) was added and the mixture was stirred for 5 min. The mixture

was neutralized with Amberlite IR-120 (H^+) resin and concentrated. The residue was purified by chromatography with chloroform–acetonitrile (5:1). Fractions [R_f 0.46, chloroform–acetonitrile (3:1)] were concentrated to give **11** (58 mg, 5% based on **9**): Mp 163—167 °C; $[\alpha]_D^{23}$ +0.83° (*c* 0.84, acetone); IR (KBr) 1760 (cyclic carbamate), 1620, 1590 (aromatic), 1335 (NO_2) cm^{-1}; ^1H NMR (acetone-d_6) δ=2.86 (3H, s, NMe), 3.54 (3H, s, OMe), 5.62 (1H, d, *J*=4.5 Hz, H-1′).

Found: C, 45.49; H, 4.12; N, 14.98%. Calcd for $C_{28}H_{30}N_8O_{16}$: C, 45.78; H, 4.12; N, 15.25%.

The fractions (R_f 0.37) gave **12** (122 mg, 11% based on **9**): Mp 180—184 °C; $[\alpha]_D^{23}$ −32.2° (*c* 0.90, acetone); IR (KBr) 1760, 1620, 1590, 1335 cm^{-1}; ^1H NMR (acetone-d_6) δ=2.86 (3H, s, NMe), 3.48 (3H, s, OMe), 5.15 (1H, d, *J*=7.5 Hz, H-1′).

Found: C, 45.52; H, 4.17; N, 14.99%. Calcd for $C_{28}H_{30}N_8O_{16}$: C, 45.78; H, 4.12; N, 15.25%.

4′-Hydroxyfortimicin KE (13). A mixture of **11** (80 mg) in acetone (10 ml), methanol (10 ml) and water (5 ml), and Amberlite IRA-400 (OH^-) resin (2 ml) was stirred overnight. The resin was filtered and the filtrate was concentrated and the residue was partitioned between ethyl acetate (20 ml) and water (20 ml). The organic layer was washed with water (20 ml) and the aqueous layers were concentrated to give a syrup of *N*-de(2,4-dinitrophenyl)ated derivative of **11** (67 mg). To a refluxing solution of 1 M sodium hydroxide (10 ml), a solution of the syrup (67 mg) in water was added and the mixture was stirred for 1 h. The mixture was cooled to room temperature and neutralized with 1 M hydrochloric acid. After concentration, the residue was chromatographed on a column of Amberlite CG-50 (NH_4^+, 40 ml) resin with 0—0.16 M aq ammonia with gradient increase in concentration. Fractions [R_f 0.41, isopropyl alcohol–chloroform–concd aq ammonia (4:1:2)] were collected and concentrated to give 4′-hydroxyfortimicin KE **13** (29 mg, 76%): $[\alpha]_D^{17}$ +19.1° (*c* 0.43, water); ^1H NMR (D_2O) δ=2.72 (3H, s, NMe), 3.43 (3H, s, OMe).

1,4,2′,6′-Tetra-*N*-acetyl-2,5-di-*O*-acetyl-fortimicin KE (14). Compound **13** was acetylated in the usual way to give **14**: $[\alpha]_D^{17}$ +84.9° (*c* 0.85, methanol); IR (KBr) 1740 (ester), 1650 (NHC=O) cm^{-1}; ^1H NMR (CD_3OD) δ=1.89, 1.94, 1.96, 2.02, 2.05, 2.08 and 2.11 (each 3H, s, NAc×4 and OAc×3), 3.02, and 3.10 (3H in total, each s, NMe), 3.40 (3H, s, OMe).

Found: *m/z*, 645.2979. Calcd for $C_{28}H_{45}N_4O_{13}$: M+1, 645.2979.

1,2′,6′-Tris[*N*-(benzyloxycarbonyl)]-4′-hydroxyfortimicin KE (15). To a solution of **13** (29 mg) in water–methanol (1:2, 5 ml), *N*-(benzyloxycarbonyloxy)succinimide (64 mg) was added under ice cooling. After stirring for 3 h at 0 °C, the mixture was stirred for 20 h at room temperature. The mixture was concentrated, and the residue was extracted with chloroform (40 ml) and dried. After concentration, the residue was purified by preparative TLC with toluene–ethanol (4:1) to give **15** (31 mg, 50%): $[\alpha]_D^{21}$ +16.8° (*c* 0.30, methanol); ^1H NMR ($CDCl_3$) δ=2.30 (3H, s, NMe), 3.41 (3H, s, OMe), 5.06 (6H, s, benzyl×3), 5.28 (1H, d, *J*=3.8 Hz, H-1′), 7.31 (15H, s, phenyl×3).

Found: C, 59.89; H, 6.42; N, 7.21%. Calcd for $C_{38}H_{48}N_4O_{12}\cdot 2/3H_2O$: C, 59.68; H, 6.50; N, 7.33%.

1,2′,6′-Tris[*N*-(benzyloxycarbonyl)]-4-[*N*-[*N*-(benzyloxycarbonyl)glycyl]]-4′-hydroxyfortimicin KE (16). To a solution of **15** (18 mg) in dioxane (1.5 ml), *N*-[*N*-(benzyloxycarbonyl)-glycyloxy]succinimide (19 mg) and triethylamine (0.02 ml) were added and the mixture was stirred at 60 °C for 12 h. The mixture was cooled to room temperature and concentrated to give a residue which was extracted with chloroform (40 ml). The extract was dried and concentrated to the residue, which was purified by preparative TLC with toluene–ethanol (6:1) to give **16** (15 mg, 67%): $[\alpha]_D^{27}$ +53.0° (*c* 0.63, chloroform); ^1H NMR ($CDCl_3$) δ=2.82 (3H, s, NMe), 3.22 (3H, s, OMe), 5.07 (8H, s, benzyl×4), 7.32 (20H, s, phenyl×4).

Found: C, 60.86; H, 6.09; N, 7.16%. Calcd for $C_{48}H_{57}N_5O_{15}$: C, 61.07; H, 6.09; N, 7.42%.

4′-Hydroxyfortimicin D (17). To a solution of **16** (13.8 mg) in ethanol (3 ml), a mixture of 0.1 M hydrochloric acid (0.6 ml) and water (0.5 ml) was added. The mixture was hydrogenated in the presence of 10% palladium on charcoal (23 mg) at an initial hydrogen pressure of 3.4 kg cm^{-2} for 6 h. After removal of the catalyst, the filtrate was concentrated to afford a white solid of **17** (8.0 mg, quant.) as the hydrochloride: $[\alpha]_D^{22}$ +42.5° (*c* 0.4, water); ^1H NMR (D_2O) δ=3.13 (3H, s, NMe), 3.48 (3H, s, OMe), 4.10 (2H, bs, $COCH_2NH_2$), 5.48 (1H, d, *J*=4.8 Hz, H-1′). MS (SIMS) Found: *m/z*, 408. Calcd for $C_{16}H_{34}N_5O_7$: M+1, 408.

The authors wish to express their thanks to Drs. Kunikatsu Shirahata and Hiroshi Sano of Kyowa Hakko Co. for antibacterial assay. We also would like to thank Dr. Yoshimasa Fukuda of Meiji Seika Co. for measurement of mass spectrum, Mr. Saburo Nakada of the University for elemental analyses.

References

1) T. Nara, M. Yamamoto, I. Kawamoto, K. Takayama, R. Okachi, S. Takasawa, T. Sato, and S. Sato, *J. Antibiot.*, **30**, 533 (1977).

2) R. Okachi, S. Takasawa, T. Sato, S. Sato, M. Yamamoto, I. Kawamoto, and T. Nara, *J. Antibiot.*, **30**, 541 (1977).

3) T. Deushi, A. Iwasaki, K. Kamiya, T. Kunieda, T. Mizoguchi, M. Nakayama, H. Itoh, T. Mori, and T. Oda, *J. Antibiot.*, **32**, 174 (1979).

4) Y. Okami, K. Hotta, M. Yoshida, D. Ikeda, S. Kondo, and H. Umezawa, *J. Antibiot.*, **32**, 964 (1979).

5) I. Watanabe, T. Deushi, T. Yamaguchi, K. Kamiya, M. Nakayama, and T. Mori, *J. Antibiot.*, **32**, 1066 (1979).

6) S. Inouye, K. Ohba, T. Shomura, M. Kojima, T. Tsuruoka, J. Yoshida, M. Ito, S. Amano, S. Omoto, N. Ezaki, T. Ito, T. Niida, and K. Watanabe, *J. Antibiot.*, **32**, 1354 (1979).

7) S. Inouye, T. Shomura, K. Ohba, H. Watanabe, S. Omoto, T. Tsuruoka, M. Kojima, and T. Niida, *J. Antibiot.*, **33**, 510 (1980).

8) T. Suami, K. Tadano, and K. Matsuzawa, *J. Antibiot.*, **33**, 1289 (1980).

9) Fortimicin D is a minor component of Fortimicins; T. Iida, M. Sato, I. Matsubara, Y. Mori, and K. Shirahata, *J. Antibiot.*, **32**, 1274 (1979).

10) J. Tadanier, J. R. Martin, R. Hallas, R. Rasmussen, D. Grampovnik, W. Rosenbrook, Jr., W. Arnold, and E.

Schuber, *Carbohydr. Res.*, **98**, 11 (1981).
11) Y. Honda, and T. Suami, *Bull. Chem. Soc. Jpn.*, **55**, 1156 (1982).
12) A. Rosental, and P. Catsoulaus, *Can. J. Chem.*, **47**, 2748 (1969).
13) K. Kitahara, S. Takashi, H. Shibata, N. Kurihara, M. Nakajima, *Agric. Biol. Chem.*, **33**, 748 (1969).
14) C. L. Brewer, and R. D. Guthrie, *J. Chem. Soc., Parkin Trans. 1*, **1974**, 657.
15) T. F. Gallagher and D. Horton, *Carbohydr. Res.*, **116**, 227 (1983).
16) A. Neuberger, *J. Chem. Soc.*, **1941**, 50.
17) D. H. R. Barton and W. B. Motherwell, "Organic Synthesis Today and Tomorrow" ed by B. M. Trost and C. R. Hutchinson, Pergamon Press (1981), pp. 1—17.
18) M. M. Abuaan, J. S. Brimacombe, and L. C. N. Tucker, *Carbohydr. Res.*, **132**, 51 (1984).

 © 1987 The Chemical Society of Japan Bull. Chem. Soc. Jpn., 60, 261—266 (1987)

Synthesis on 1,4-Diaminocyclitol Antibiotics. II. Synthesis of 7′-Propylfortimicin A[1]

Kazuaki KANAI, Junji NISHIGAKI, Seiichiro OGAWA,* and Tetsuo SUAMI†
Department of Applied Chemistry, Faculty of Science and Technology, Keio University, Hiyoshi, Yokohama 223
(Received June 25, 1986)

7′-Propylfortimicin A has been synthesized by a condensation of newly prepared 1-*O*-acetyl-2,6-bis(2,4-dinitrophenylamino)-2,3,4,6,7,8,9,10-octadeoxy-L-*lyxo*-decopyranose with 2,5-di-*O*-benzoyl-1,4-bis-*N*-(methoxycarbonyl)fortamine B, followed by deprotection.

Since fortimicin A was discovered by Nara et al. in 1977,[2] its chemical modifications have extensively been studied.[3,4] In continuation of our study on modification of the diamino sugar moiety,[5] an extension of its sidechain would be of interest in connection with increase in its hydrophobic nature. We now describe the synthesis of 7′-propylfortimicin A (**17**).

Results and Discussion

1-*O*-Acetyl-2,6-bis(2,4-dinitrophenylamino)-2,3,4,6,7,8,9,10-octadeoxy-L-*lyxo*-decopyranose (**9**) has been prepared from the known methyl 2-acetamido-2,3,4-trideoxy-α-D-*erythro*-hexopyranoside (**1**)[6] as shown in Scheme.

Treatment of **1** with *p*-toluenesulfonyl chloride in pyridine gave the tosylate **2** in 76% yield. Displacement of the tosyloxy group with sodium iodide, followed by treatment with sodium nitrite in *N*,*N*-dimethylformamide and dimethyl sulfoxide, afforded the nitro derivative **4** in 48% yield. The nitro aldol reaction of **4** with butyraldehyde was effected in the presence of CsF in acetonitrile for 5 h at room temperature and the product was successively acetylated with acetic anhydride and BF_3 etherate to give **5** as a diastereoisomeric mixture. The reaction using KF instead of CsF resulted in a poor yield. Hydrogenation of **5** with sodium borohydride in dimethyl sulfoxide afforded a mixture of methyl 2-acetamido-2,3,4,6,7,8,9,10-octadeoxy-6-nitro-α-D-*ribo* and -β-L-*lyxo*-decopyranoside (**6**) in 41% yield based on **4**. Catalytic hydrogenation of **6** with Raney nickel in methanol, followed by *N*-acetylation with acetic anhydride, gave two products (**7**, 57% and **8**, 19%) after chromatography.

The stereochemistry at C-6 in **7** and **8** has been established by the values of specific rotations, and chemical shifts of C-7 in ^{13}C NMR spectra. The values of the specific rotations of **7** and **8**, together with those of methyl 2,6-di-*N*-acetyl-α-purpurosaminide B[7] and -6-*epi*-α-purpurosaminide B[6,8] are shown in Table 1.

† Present address: Department of Chemistry, Faculty of Science and Technology, Meisei University, Hodokubo, Hino, Tokyo 191.

From these data, we could assume that the values of specific rotations of the compounds with α-D-*ribo* configuration are more dextrorotatory than those of the corresponding β-L-*lyxo* isomers. In the ^{13}C NMR spectra on **7** and **8**, the signal of C-7 of **8** shifted upfield by 1.99 ppm compared to that of **7**. Chmielewski et al. observed this upfield shift for the related compounds, and assumed that it was due to the antiperiplanar arrangement of C-7/C-6/C-5/O-5.[9,10] In addition, the ^1H NMR spectrum of **8** revealed the H-5 signal (δ 3.60) with 6 Hz splitting, the dihedral angle around H-5 and H-6 being about 60°. The stereochemistry at C-6 of **7** and **8** has thus been confirmed as shown in Scheme.

Hydrolysis of **7** with 2 M†† hydrochloric acid, followed by successive *N*-(2,4-dinitrophenyl)ation and

Table 1. Specific Rotations of **7** and **8**

	7	**8**	a	b
$[\alpha]_D$	+43.4°	+147°	+62.5°	+185.7°

a: Methyl 2,6-di-*N*-acetyl-6-*epi*-α-purpurosaminide B.[7]
b: Methyl 2,6-di-*N*-acetyl-α-purpurosaminide B.[7]

Table 2. ^{13}C NMR Chemical Shifts[a] of **7** and **8**

	7	**8**
C-1	99.539	99.441
C-2	49.769	49.623
C-3	24.933	25.201
C-4	28.144	28.120
C-5	70.494	71.273
C-6	53.223	53.734
C-7	32.352	30.358
C-8	29.628	29.384
C-9	23.546	23.546
C-10	14.376	14.351
OMe	55.364	55.169
$\underline{C}OCH_3$	173.220	172.928
	172.782	172.758
$CO\underline{C}H_3$	22.525	22.598
	22.525	22.525

a) In parts per million downfield from TMS.

†† 1 M=1 mol dm^{-3}.

O-acetylation gave **9** in 26% yield. On the other hand, the aglycon, 2,5-di-*O*-benzoyl-1,4-bis[*N*-(methoxycarbonyl)]fortamine B (**12**), has been prepared from fortimicin B in the following way. Treatment of fortimicin B with methyl chloroformate in aqueous acetone gave 1,4,2′,6′-tetrakis[*N*-(methoxycarbonyl)]-fortimicin B (**10**) in 98% yield. Benzoylation of **10** with benzoyl chloride in pyridine afforded 65% yield of the 2,5-dibenzoate (**11**), which was hydrolyzed with acetic acid containing 2 M hydrochloric acid to give the aglycon **12** in 79% yield. Judging from the ^{1}H NMR data, **12** is assumed to adopt the skew-boat form as depicted in Scheme. However, the conformations of the fortamine moieties in pseudo-disaccharides could not be deduced by analogy with these results.

Condensation of **9** with **12** in 1,2-dichloroethane in the presence of trimethylsilyl trifluoromethanesulfonate under argon gave single compound **13** in 49% yield. The ^{1}H NMR spectrum of **13** exhibited the signal of H-1′ (δ 5.28) with a small coupling constant ($J_{1',2'}$=3 Hz), supporting that the anomeric proton is equatorial of the α-D-glycoside. Hydrolysis of **13** in refluxing aqueous dioxane with barium hydroxide, followed by removal of the dinitrophenyl group with Amberlite IRA-400 (OH^-) resin, afforded 7′-propylfortimicin B (**14**) in 68% yield. The tris[*N*-(benzyloxycarbonyl)] derivative **15** was prepared in 60% yield by treatment of **14** with *N*-(benzyloxycarbonyloxy)succinimide. Treatment of **15** with *N*-[*N*-(benzyloxycarbonyl)glycyloxy]succinimide and triethylamine gave 1,4,2′,6′-tetrakis[*N*-(benzyloxycarbonyl)] derivative **16** in 86% yield. Catalytic hydrogenation of **16** in the presence of 10% palladium on charcoal gave quantitatively the free base, which was characterized as crystalline 7′-propylfortimicin A disulfate (**17**).

Table 3. Antimicrobial Activity of **17** and Fortimicin A[a)]

Test Organisms	**17**	Fortimicin A
Streptococcus faecalis KY4280	12.5	12.5
Pseudomonas aeruginosa KY4276	50.0	12.5
Staphylococcus aureus KY4279	0.4	0.4
Escherichia coli KY4271	1.6	1.6
Bacillus subtillis KY4273	0.4	0.4
Shigella sonnei KY4281	3.1	6.3
Klebsiella pneumoniae KY4275	0.4	0.4

a) Minimum inhibitory concentration in $\mu g\,ml^{-1}$.

The minimum inhibitory concentration of **17** was compared with those of fortimicin A (Table 3). 7′-propylfortimicin A (**17**) exhibited almost similar activity to that of fortimicin A against many micro organisms except *Pseudomonas*.

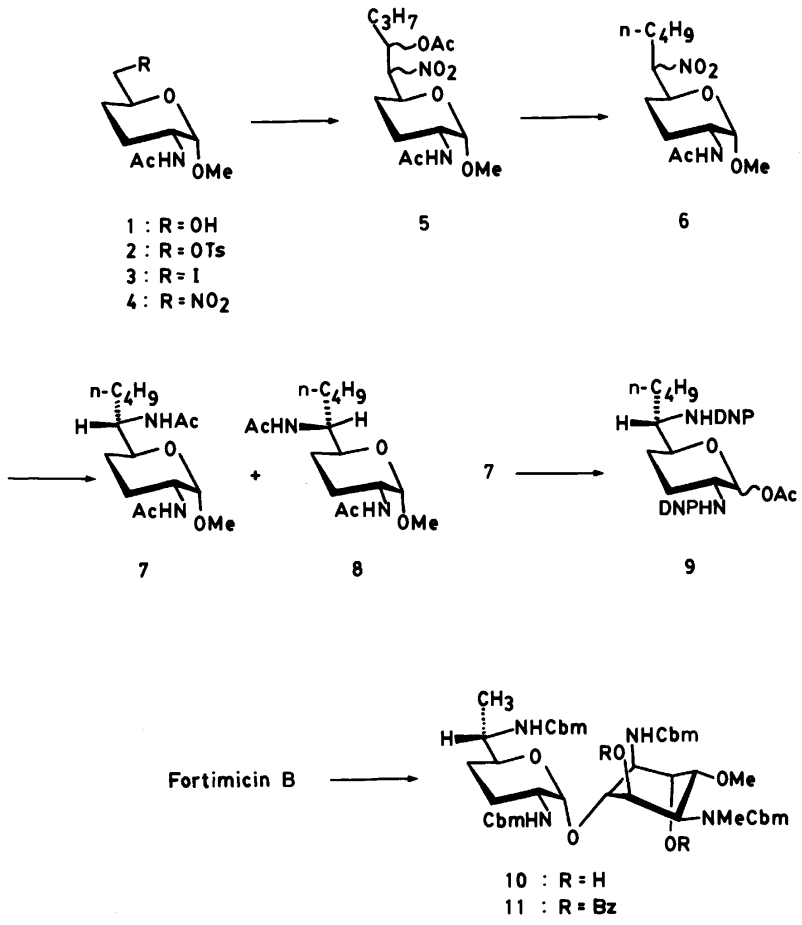

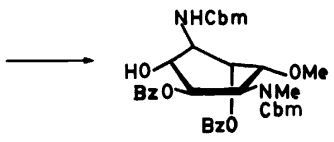

12

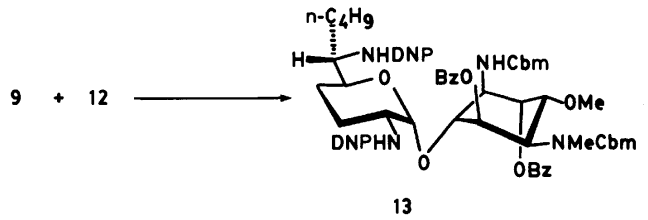

13

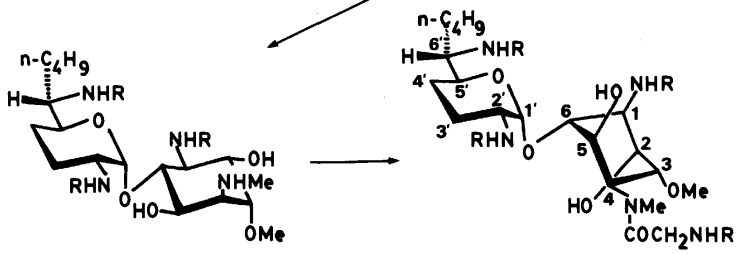

14 : R = H
15 : R = Cbz

16 : R = Cbz
17 : R = H

Experimental

General Procedures. Melting points were determined in capillary tubes and are uncorrected. Optical rotations were measured on a JASCO DIP-4 polarimeter. IR and Mass spectra were recorded on Hitachi HPL-225 spectrophotometer and Hitachi M-80 and M-80A (SIMS) spectrometers, respectively. ^{1}H NMR spectra with TMS or DSS as internal standard were recorded on Varian EM-390 (90 MHz) or JEOL FX-200 (200 MHz), and ^{13}C NMR spectra with TMS on JEOL FX-200 (50 MHz). TLC and column chromatography were performed on Silica Gel 60F-254 (E. Merck) and Kieselgel 60. Organic solutions were concentrated under reduced pressure below 40 °C.

Methyl 2-Acetamido-2,3,4-trideoxy-6-*O*-tosyl-α-D-*erythro*-hexopyranoside (2). To a solution of methyl 2-acetamido-2,3,4-trideoxy-α-D-*erythro*-hexopyranoside (**1**)[6] (1.03 g) in pyridine (20 ml), *p*-toluenesulfonyl chloride (2.50 g) was added under ice cooling and the mixture was poured into ice water (200 ml) and the solution was extracted with chloroform (200 ml). The extract was washed successively with 1 M hydrochloric acid (100 ml), saturated aqueous $NaHCO_3$ (100 ml) and water (100 ml), and dried. After concentration, the residue was chromatographed on silica gel with toluene–ethanol (10:1) to give **2** (1.38 g, 76%). Recrystallization from ethyl acetate–pentane afforded an analytical sample: Mp 98—99 °C; $[\alpha]_D^{20}$ +68.3° (*c* 1.29, chloroform); IR (KBr) 1355, 1170 (SO_2) cm^{-1}; ^{1}H NMR ($CDCl_3$) δ=1.39—2.05 (4H, m, H-3,4), 1.91 (3H, s, NAc), 2.43 (3H, s, Me of tosyl), 3.31 (3H, s, OMe), 4.50 (1H, d, *J*=3 Hz, H-1), 5.66 (1H, d, *J*=9 Hz, NH), 7.34 and 7.80 (each 2H, d, *J*=8.5 Hz, tosyl).

Found: C, 53.96; H, 6.44; N, 4.10; S, 8.71%. Calcd for $C_{16}H_{23}NO_6S$: C, 53.77; H, 6.49; N, 3.92; S, 8.97%.

Methyl 2-Acetamido-2,3,4,6-tetradeoxy-6-nitro-α-D-*erythro*-hexopyranoside (4). To a stirred solution of **2** (897 mg) in 2-butanone (30 ml), sodium iodide (1.50 g) was added and the mixture was refluxed for 2.5 h. The mixture was cooled to room temperature, and the solid was filtered. The filtrate was concentrated to dryness and was diluted with ethyl acetate (150 ml). The solution was washed successively with 30% aqueous sodium thiosulfate (100 ml) and water (100 ml), and dried. Evaporation of the solvent gave crude **3** (738 mg). To a solution of **3** (738 mg), without purification, in *N*,*N*-dimethylformamide (2 ml) and dimethyl sulfoxide (8 ml), sodium nitrite (938 mg) and phloroglucinol dihydrate (1.12 g) were added and the mixture was stirred for 6 d at room temperature. To the mixture, ice water (30 ml) was added and the mixture was extracted with chloroform (100 ml). The extract was washed with water (150 ml) and dried. After concentration, the residue was recrystallized from chloroform–petroleum ether to afford **4** (274 mg, 48% based on **2**): Mp 169 °C (decomp); $[\alpha]_D^{20}$ +138° (*c* 0.78, methanol); IR (KBr) 1545, 1365 (NO_2) cm^{-1}; ^{1}H NMR ($CDCl_3$) δ=1.89 (3H, s, NAc), 3.31 (3H, s, OMe), 4.51 (1H, d, *J*=3 Hz, H-1).

Found: C, 46.48; H, 6.78; N, 11.77%. Calcd for $C_9H_{16}N_2O_5$: C, 46.55; H, 6.94; N, 12.06%.

Methyl 2-Acetamido-2,3,4,6,7,8,9,10-octadeoxy-6-nitro-α-D-*ribo*- and β-L-*lyxo*-decopyranoside (6). To a solution of **4** (1.55 g) in acetonitrile (15 ml), butyraldehyde (1.20 ml) and CsF (1.01 g) were added and the mixture was stirred for 5 h at room temperature. The mixture was partitioned between ethyl acetate (20 ml) and water (20 ml). The aqueous layer

was extracted with ethyl acetate (40 ml) and the organic layer and the extract were combined, and dried. After evaporation of the solvent, a crude syrup of the condensation product (1.91 g) was obtained. To a solution of the condensate (1.91 g) in acetic anhydride (20 ml), BF_3 etherate (3 ml) was added under ice cooling. After stirring for 1 h at 0 °C, the mixture was poured into ice water (200 ml) and the solution was extracted with chloroform (300 ml). The extracts were washed successively with saturated aqueous $NaHCO_3$ (600 ml) and water (200 ml), and dried. After concentration, the residue was chromatographed on silica gel with ethyl acetate–2-butanone (10:1). Fractions [R_f 0.66, chloroform–methanol (10:1)] gave **5** (951 mg) as a syrup: IR ($CHCl_3$) 1740 (ester), 1665, 1560 (NHC=O), 1510, 1370 (NO_2) cm^{-1}; ^1H NMR ($CDCl_3$) δ=1.95 (3H, s, NAc), 2.11 (3H, s, OAc), 3.38 and 3.40 (3H in total, each s, OMe), 4.57 (1H, d, J=3 Hz, H-1), 5.26 (1H, m, H-7), 5.72 (1H, d, J=9 Hz, NH). The fractions [R_f 0.55, chloroform–methanol (10:1)] recovered **4** (359 mg).

To a solution of **5** (951 mg) in dimethyl sulfoxide (10 ml), a suspension of sodium borohydride (250 mg) in dimethyl sulfoxide (5 ml) was added. After stirring for 1 h at room temperature, the mixture was acidified with Amberlite IR-120 (H^+) resin and partitioned between dichloromethane (100 ml) and water (100 ml). The aqueous layer was extracted with dichloromethane (200 ml). The organic layer and the extracts were combined and washed with water (200 ml), and dried. After concentration, the residue was recrystallized from chloroform–petroleum ether to afford **6** (484 mg). Chromatography of the mother liquor on silica gel with ethyl acetate–2-butanone (10:1) gave an additional crop of **6** (310 mg, total yield 41% based on **4**): Mp 110 °C (decomp); $[\alpha]_D^{27}$ +124° (c 1.0, methanol); ^1H NMR ($CDCl_3$) δ=0.91 (3H, m, H-10), 1.17—2.19 (10H, m, H-3,4,7,8,9), 1.96 (3H, s, NAc), 3.33 and 3.38 (3H in total, each s, OMe), 4.54 (1H, d, J=3 Hz, H-1), 5.70 (1H, d, J=9 Hz, NH).

Found: C, 54.23; H, 8.17; N, 9.46%. Calcd for $C_{13}H_{24}N_2O_5$: C, 54.15; H, 8.39; N, 9.72%.

Methyl 2,6-Diacetamido-2,3,4,6,7,8,9,10-octadeoxy-β-L-*lyxo*-decopyranoside (7) and α-D-*ribo*-decopyranoside (8). A solution of **6** (730 mg) in methanol (10 ml) was hydrogenated in the presence of Raney nickel at an initial hydrogen pressure of 3.4 kg cm^{-2} for 18 h. After removal of the catalyst, the filtrate was concentrated. The residue was treated with acetic anhydride (4 ml) in methanol (10 ml) for 2 h. The mixture was concentrated and was chromatographed on silica gel with toluene–ethanol (10:1). Fractions [R_f 0.45, toluene–ethanol (3:1)] gave **7** (434 mg, 57%) as an amorphous solid: Mp 224—225.5 °C; $[\alpha]_D^{22}$ +43.4° (c 1.0, methanol); ^1H NMR (CD_3OD) δ=0.90 (3H, t, J=7 Hz, H-10), 1.32 (4H, m, H-8,9), 1.43—1.89 (6H, m, H-3,4,7), 1.92 and 1.98 (each 3H, s, NAc), 3.38 (3H, s, OMe), 3.74 (1H, dt, J=3.5 Hz, 10 Hz, H-5), 3.86 (1H, dt, J=3.5 Hz, 7 Hz, H-6), 3.88 (1H, ddd, J=3.5 Hz, 5.5 Hz, 12 Hz, H-2), 4.61 (1H, d, J=3.5 Hz, H-1).

Found: C, 59.89; H, 9.24; N, 9.08%; m/z, 300.2041. Calcd for $C_{15}H_{28}N_2O_4$: C, 59.98; H, 9.40; N, 9.33%; M^+, 300.2047.

The fractions [R_f 0.41, toluene–ethanol (3:1)] gave **8** (143 mg, 19%): Mp 252.5—254 °C; $[\alpha]_D^{22}$ +147° (c 0.86, methanol); ^1H NMR (CD_3OD) δ=0.90 (3H, t, J=7 Hz, H-10), 1.27—1.83 (10H, m, H-3,4,7,8,9), 1.92 and 1.94 (each 3H, s, NAc), 3.36 (3H, s, OMe), 3.60 (1H, ddd, J=2 Hz, 6 Hz, 11 Hz, H-5), 3.76 (1H, ddd, J=3 Hz, 6 Hz, 10 Hz, H-6), 3.88 (1H, ddd, J=3.5 Hz, 6.5 Hz, 10.5 Hz, H-2), 4.60 (1H, d, J=3.5 Hz, H-1).

Found: C, 59.70; H, 9.21; N, 8.94%; m/z, 301.2121. Calcd for $C_{15}H_{28}N_2O_4$: C, 59.98; H, 9.40; N, 9.33%; M+1, 301.2125.

1-*O*-Acetyl-2,6-bis(2,4-dinitrophenylamino)-2,3,4,6,7,8,9,10-octadeoxy-L-*lyxo*-decopyranose (9). A stirred solution of **7** (430 mg) in 2 M hydrochloric acid (10 ml) was refluxed for 23 h. The mixture was cooled to room temperature and concentrated, and dried in vacuum. To a solution of the residue in methanol (15 ml) containing 2,4-dinitrofluorobenzene (0.38 ml), triethylamine (0.8 ml) was added dropwise under ice cooling. After stirring for 1 h at 0 °C, the mixture was partitioned between ethyl acetate (50 ml) and water (30 ml). The aqueous layer was extracted with ethyl acetate (80 ml), and the organic layer and the extract were combined and dried. After concentration, the residue was treated with acetic anhydride (5 ml) in pyridine (10 ml) for 4 h at room temperature. The mixture was poured into ice water (100 ml) and the solution was extracted with dichloromethane (200 ml). The extract was successively washed with 1 M hydrochloric acid (200 ml) and water (200 ml), and dried. After concentration, the residue was chromatographed on silica gel with toluene–2-butanone (50:1—30:1) to afford **9** (218 mg, 26% based on **7**) as yellow syrup: $[\alpha]_D^{24}$ −42.4° (c 1.0, chloroform); ^1H NMR ($CDCl_3$) δ=1.99 and 2.25 (3H in total, each s, OAc), 5.65 (1/4H, d, J=9 Hz, H-1β), 6.35 (3/4H, d, J=3 Hz, H-1α), 6.91 and 7.31 (each 1H, d, J=11 Hz, H-3 of DNP), 8.24 and 8.33 (each 1H, dd, J=3 Hz, 11 Hz, H-5 of DNP), 8.48 and 8.86 (each 1H, d, J=10 Hz, NH-2,6), 9.10 and 9.15 (each 1H, d, J=3 Hz, H-6 of DNP).

Found: m/z, 576.1823. Calcd for $C_{24}H_{28}N_6O_{11}$: M^+, 576.1814.

1,4,2′,6′-Tetrakis[*N*-(methoxycarbonyl)]fortimicin B (10). To a solution of fortimicin B (5.80 g) in aqueous acetone (1:1, 200 ml), anhydrous sodium carbonate (5.29 g) and methyl chloroformate (7.85 ml) were added and the mixture was stirred for 20 min under ice cooling. The mixture was concentrated and the residue was partitioned between water (150 ml) and chloroform (150 ml). The aqueous layer was extracted with chloroform (250 ml), and the organic layer and the extract were combined and dried. After concentration, the residue was washed with petroleum ether to give **10** (9.50 g, 98%): Mp 85—92 °C; $[\alpha]_D^{19}$ +63.5° (c 1.21, chloroform); ^1H NMR ($CDCl_3$) δ=1.08 (3H, d, J=6 Hz, H-7′), 3.62, 3.65, 3.70, and 3.75 (each 3H, s, Cbm), 3.00 (3H, s, NMe), 3.42 (3H, s, OMe), 4.84 (1H, d, J=3 Hz, H-1′).

2,5-Di-*O*-benzoyl-1,4,2′,6′-tetrakis[*N*-(methoxycarbonyl)]-fortimicin B (11). To a solution of **10** (1.0 g) in pyridine (10 ml), benzoyl chloride (1.2 ml) was added and the mixture was stirred for 65 h at 60 °C. After cooling to room temperature, the mixture was poured into ice water (100 ml). The mixture was extracted with ethyl acetate (200 ml) and the extract was washed successively with 1 M hydrochloric acid (100 ml), saturated aqueous $NaHCO_3$ (100 ml), and water (100 ml), and dried. After concentration, the residue was chromatographed on silica gel with chloroform–methanol (40:1). Fractions [R_f 0.58, chloroform–methanol (20:1)] were concentrated and the residue was crystallized from ether–chloroform–petroleum ether to give **11** (890 mg, 65%): Mp 115—121 °C; $[\alpha]_D^{27}$ +13.4° (c 1.19, chloroform); ^1H NMR ($CDCl_3$) δ=1.09 (3H, d, J=6 Hz, H-7′), 2.92 (3H, s,

NMe), 3.49 (3H, s, OMe), 3.55, 3.64, 3.67, and 3.77 (each 3H, s, Cbm), 5.04 (1H, d, J=3 Hz, H-1′).

Found: C, 56.13; H, 6.04; N, 6.98%. Calcd for $C_{37}H_{48}N_4O_{15}$: C, 56.34; H, 6.13; N, 7.10%.

2,5-Di-*O*-benzoyl-1,4-bis[*N*-(methoxycarbonyl)]fortamine B (12). A solution of **11** (890 mg) in acetic acid (4 ml) containing 2 M hydrochloric acid (1 ml) was stirred for 4 h at 80 °C. After cooling to room temperature, the mixture was diluted with water (20 ml). The mixture was extracted with dichloromethane (100 ml) and the extract was washed successively with saturated aqueous $NaHCO_3$ (200 ml), brine (100 ml) and water (100 ml), and dried. After concentration, the residue was chromatographed on silica gel with chloroform–methanol (99:1). Fractions [R_f 0.32, chloroform–methanol (50:1)] gave **12** (476 mg, 79%). Recrystallization from ether–petroleum ether afforded an analytical sample: mp 104—113 °C; $[\alpha]_D^{22}$ +18.0° (c 0.65, chloroform); ^{1}H NMR ($CDCl_3$) δ=3.00 (3H, s, NMe), 3.29 (1H, bs, OH-6), 3.48 (3H, s, OMe), 3.60 and 3.64 (each 3H, s, Cbm), 4.04 (1H, dd, J=3 Hz, 8 Hz, H-3), 4.28 (2H, m, H-1,6), 4.97 (1H, dd, J=5 Hz, 8 Hz, H-4), 5.29 (1H, d, J=8 Hz, NH-1), 5.69 (1H, dd, J=5 Hz, 7 Hz, H-5), 5.78 (1H, dd, J=3 Hz, 7 Hz, H-2), 7.40—7.62 (6H, m, benzoyl), 7.98—8.10 (4H, m, benzoyl).

Found: C, 58.66; H, 5.69; N, 5.16%. Calcd for $C_{26}H_{30}N_2O_{10}$: C, 58.86; H, 5.70; N, 5.28%.

2,5-Di-*O*-benzoyl-2′,6′-bis[*N*-(2,4-dinitrophenyl)]-1,4-bis-[*N*-(methoxycarbonyl)]-7′-propylfortimicin B (13). To a mixture of **9** (218 mg), **12** (200 mg), and powdered molecular sieve 4A (200 mg) in 1,2-dichloroethane (5 ml) was added trimethylsilyl trifluoromethanesulfonate (0.07 ml) and the mixture was stirred for 2 h under argon. The mixture was diluted with dichloromethane (40 ml) and an insoluble material was filtered. The filtrate was washed with saturated aqueous $NaHCO_3$ (40 ml) and water (40 ml), and dried. After concentration, the residue was chromatographed on silica gel eluting with toluene–2-butanone (50:1—20:1) to give **13** (195 mg, 49%): Mp 127—132 °C; $[\alpha]_D^{27}$ + 0.8° (c 0.4, chloroform); ^{1}H NMR ($CDCl_3$) δ=2.82 (3H, s, NMe), 3.43 (3H, s, OMe), 3.52 and 3.64 (each 3H, s, Cbm), 3.70 (2H, m, H-2′,6′), 3.95 (1H, m, H-1), 4.09 (1H, dd, J=3 Hz, 10 Hz, H-3), 4.54 (1H, m, H-6), 4.88 (1H, m, H-4), 5.18 (1H, d, J=9 Hz, NH-1), 6.28 (1H, d, J=3 Hz, H-1′), 5.44 (1H, m, H-5), 5.77 (1H, m, H-2), 6.86 and 7.02 (each 1H, d, J=9 Hz, H-3 of DNP), 7.22—7.66 (6H, m, benzoyl), 7.88 and 8.16 (each 2H, d, J=8.5 Hz, bezoyl), 8.16 and 8.28 (each 1H, dd, J=3 Hz, 9 Hz, H-5 of DNP), 8.64 (2H, m, NH-2′,6′), 9.12 and 9.14 (each 1H, d, J=3 Hz, H-6 of DNP).

Found: C, 54.65; H, 5.20; N, 10.88%. Calcd for $C_{48}H_{54}N_8O_{19}$: C, 55.07; H, 5.20; N, 10.70%.

7′-Propylfortimicin B (14). A stirred solution of **13** (204 mg) in aqueous dioxane (1:2, 15 ml) containing barium hydroxide octahydrate (3.80 g) was refluxed for 14 h. The mixture was cooled to room temperature and the solid was filtered. Carbon dioxide was introduced to the filtrate and an insoluble material was filtered. After concentration, the residue was treated with Amberlite IRA-400 (OH^-) resin (13 ml) in a mixture of water (10 ml), methanol (15 ml) and acetone (15 ml). After stirring for 15 h, the resin was filtered, and the filtrate was neutralized with 1% H_2SO_4. After concentration of the solution, the residue was chromatographed on a column of Amberlite CG-50 (NH_4^+) resin (35 ml) with 0—0.20 M aq ammonia with gradient increase in concentration. Fractions [R_f 0.60, isopropyl alcohol–chloroform–concd aq ammonia (4:1:1)] gave **14** (51 mg, 68%): $[\alpha]_D^{27}$ +8.6° (c 1.54, water); IR (KBr) 3350, 2930, 1570, 1460, 1370, 1090 cm^{-1}; ^{1}H NMR (D_2O) δ=0.89 (3H, m, H-10′), 1.20—1.90 (10H, m, H-3′,4′,7′,8′,9′), 2.40 (3H, s, NMe), 2.82—2.96 (2H, m, H-2′,6′), 3.01 (1H, t, J=9.5 Hz, H-1), 3.11 (1H, dd, J=4 Hz, 4.5 Hz, H-4), 3.48 (3H, s, OMe), 3.53 (1H, t, J=9.5 Hz, H-6), 3.69 (1H, t, J=4 Hz, H-3), 3.72 (1H, dd, J=4 Hz, 9.5 Hz, H-2), 3.82 (1H, m, H-5′), 4.01 (1H, dd, J=4.5 Hz, 9.5 Hz, H-5), 5.16 (1H, d, J=3 Hz, H-1′).

Found: C, 52.80; H, 9.14; N, 13.29%; m/z, 391. Calcd for $C_{18}H_{38}N_4O_5 \cdot 1/2H_2CO_3$: C, 52.71; H, 9.32; N, 13.29%; M+1, 391.

1,2′,6′-Tris[*N*-(benzyloxycarbonyl)]-7′-propylfortimicin B (15). To a solution of **14** (49 mg) in aqueous methanol (1:2, 6 ml), *N*-(benzyloxycarbonyloxy)succinimide (97 mg) was added under ice cooling and the mixture was stirred for 3 h at 0 °C, and stirring was continued for 23 h at room temperature. After addition of 5% aqueous $NaHCO_3$ (10 ml) to the solution, the mixture was extracted with chloroform (30 ml) and the extract was dried. After concentration, the residue was chromatographed on silica gel with chloroform–methanol (30:1) to give **15** (59 mg, 60%): $[\alpha]_D^{27}$ +11.4° (c 1.66, chloroform); ^{1}H NMR ($CDCl_3$) δ=2.26 (3H, s, NMe), 3.39 (3H, s, OMe), 5.00 (6H, bs, benzyl×3), 7.27 (15H, s, phenyl×3).

1,2′,6′-Tris[*N*-(benzyloxycarbonyl)]-4-[*N*-[*N*-(benzyloxycarbonyl)glycyl]]-7′-propylfortimicin B (16). To a solution of **15** (57 mg) in dioxane (5 ml), *N*-[*N*-(benzyloxycarbonyl)-glycyloxy]succinimide (27 mg) and triethylamine (0.01 ml) were added and the mixture was stirred for 13 h at 60 °C. After cooling to room temperature, 5% aqueous $NaHCO_3$ (20 ml) was added to the mixture and the mixture was extracted with chloroform (30 ml). The extract was washed with water (30 ml), and dried. After concentration, the residue was chromatographed on silica gel with chloroform–methanol (50:1) to give **16** (62 mg, 86%): $[\alpha]_D^{25}$ +21.2° (c 1.16, chloroform); ^{1}H NMR ($CDCl_3$) δ=2.78 (3H, s, NMe), 3.27 (3H, s, OMe), 4.78 (1H, d, J=3 Hz, H-1′), 5.06 (8H, s, benzyl×4), 7.31 (20H, s, phenyl×4).

Found: C, 63.46; H, 6.65; N, 6.87%. Calcd for $C_{52}H_{66}N_5O_{14}$: C, 63.40; H, 6.75; N, 7.11%.

7′-Propylfortimicin A (17). A solution of **16** (53 mg) in methanol (5 ml) was hydrogenated in the presence of 10% palladium on charcoal (50 mg) at an initial hydrogen pressure of 3.4 kg cm^{-2} for 4 h. The catalyst was removed and the solution was concentrated. The residue was dissolved in water and passed through a column of Amberlite IRA-400 (OH^-) resin using water as an eluent. Fractions [R_f 0.39, isopropyl alcohol–chloroform–concd aq ammonia (4:1:1)] were collected and the solution was adjusted to pH 5 with 1% H_2SO_4. The mixture was concentrated to a residue, which was recrystallized from methanol–acetone to give **17** (25 mg, 70%) as the disulfate: $[\alpha]_D^{25.5}$ +63.5° (c 0.47, water); IR (KBr) 3430, 2920, 1485, 1110, 1030 cm^{-1}; ^{1}H NMR (D_2O) δ=0.92 (3H, t, J=7 Hz, H-10′), 1.41, 1.65, and 2.02 (10H in total, each m, H-3′,4′,7′,8′,9′), 3.16 (3H, s, NMe), 3.52 (3H, s, OMe), 4.88 (1H, dd, J=2 Hz, 12 Hz, H-4), 5.33 (1H, d, J=3.5 Hz, H-1′).

Found: C, 35.72; H, 7.04; N, 9.80%; m/z, 448. Calcd for $C_{20}H_{41}N_5O_6 \cdot 2H_2SO_4 \cdot 2H_2O$: C, 35.35; H, 7.27; N, 10.30%; M+1, 448.

The authors wish to express their thanks to Drs. Kunikatsu Shirahata and Hiroshi Sano of Kyowa Hakko Co. for performing antibacterial assay. We also would like to thank Dr. Yoshimasa Fukuda and Mr. Osamu Sakanaka of Meiji Seika Co. for measurement of mass, ^{13}C and ^{1}H NMR spectra, and Mr. Saburo Nakada and Mr. Akio Takahashi of the University for elemental analyses.

References

1) T. Suami, K. Kanai, J. Nishigaki, and S. Yokoi, 52rd National Meeting of the Chemical Society of Japan, Kyoto, April 1986, Abstr. No. 4N02.

2) T. Nara, M. Yamamoto, I. Kawamoto, K. Takayama, R. Okachi, S. Takasawa, T. Sato, and S. Sato, *J. Antibiot.*, **30**, 533 (1977).

3) S. Kondo and D. Ikeda, *Yuki Gosei Kagaku Kyokai Shi*, **40**, 902 (1982).

4) T. Suami, K. Tadano, and K. Matsuzawa, *J. Antibiot.*, **33**, 1289 (1980).

5) K. Kanai, I. Sakamoto, Y. Miyamoto, S. Ogawa, and T. Suami, *Bull. Chem. Soc. Jpn.*, **60**, 255 (1987).

6) T. Suami, Y. Honda, T. Kato, M. Masu, and K. Matsuzawa, *Bull. Chem. Soc. Jpn.*, **53**, 1372 (1980).

7) Y. Honda and T. Suami, *Bull. Chem. Soc. Jpn.*, **54**, 2825 (1981).

8) R. S. Eagan, R. S. Stanaszek, M. Cirovic, S. L. Mueller, J. Tadanier, J. R. Martin, P. Collum, A. W. Goldstein, R. L. D. Vault, A. D. Sinclair, E. E. Fager, and L. A. Mitscher, *J. Antibiot.*, **30**, 552 (1977).

9) M. Chmielewski, A. Konowal, and A. Zamojski, *Carbohydr. Res.*, **70**, 275 (1979).

10) E. L. Eliel, W. F. Bailey, L. D. Kopp, R. L. Willer, D. M. Grant, R. Bertrand, K. A. Christenses, D. K. Dalling, M. W. Duch, E. Wenkert, F. M. Schell, and D. W. Cochran, *J. Am. Chem. Soc.*, **97**, 322 (1975).

 © 1987 The Chemical Society of Japan Bull. Chem. Soc. Jpn., 60, 267—271 (1987)

A Simple and Convenient Method for the Synthesis of Iminomethylene Analogs of Peptides

Hidekazu Oyamada and Masaaki Ueki*
Department of Applied Chemistry, Science University of Tokyo,
1-3 Kagurazaka, Shinjuku-ku, Tokyo 162
(Received June 26, 1986)

The synthesis of pseudopeptides in which a part of the peptide bonds has been replaced by other isosteric bonds has been studied in order to obtain long-lasting peptide drugs and also to study the structure-activity relationships of peptides with biological activity. A simple and convenient method for the synthesis of pseudo[CH_2-NH]peptides was established by improving the conditions for the selective reduction of the peptide bond of *N*-protected dipeptide esters by borane. Among the ester residues investigated, the *t*-butyl ester gave the best result. During reactions no racemization occurred. [L-Pheψ[CH_2-NH]L-Leu$^{4-5}$]leucine-enkephalin was synthesized in good yield starting from *N*-benzyloxycarbonyl-L-phenylalanyl-L-leucine *t*-butyl ester.

Numbers of biologically active peptides which can be isolated or the sequences of which are determined by gene technical methods have been increasing. In the study of their physiological roles and their applications as drugs, native peptides have a substantial restriction due to their rapid degradation by peptidase. As a method for increasing the stability of peptides towards proteolytic enzymes, (and at the same time to determine the contribution of a specific amino acid residue to the biological activity,) syntheses of analogues with some residues replaced by unnatural amino acids such as *N*-methyl amino acids or D-amino acids have been tried with success.

As another approach to this problem, the syntheses of pseudopeptides in which a specific peptide bond is replaced by an appropriate isosteric bond stable to hydrolysis (such as CH=CH, CH_2-CO, CH_2-CH_2, CH_2-S, or CH_2-NH) have been studied. Among these isosteric bonds, the CH_2-NH bond has the characteristic that it maintains the amine function with a capacity as a hydrogen-bond donor. However, ψ[CH_2-NH]peptides have so far not been widely utilized since methods for the introduction of this bond to any desired position in a sequence of peptide have not been established. This study offers the first general method for the preparation of an *N*-protected ψ[CH_2-NH]dipeptide acid unit necessary for the synthesis of ψ[CH_2-NH]peptides.

The synthesis of ψ[CH_2-NH]peptides have been approached from two routes: 1) by direct CH_2-NH bond formation from a peptide aldehyde and a peptide ester, either through a Schiff-base formation followed by hydrogenation[1,2] or by a reductive alkylation[3] and 2) by the incorporation of a protected ψ[CH_2-NH]dipeptide acid unit by a usual peptide synthetic method.[4] The ψ[CH_2-NH]dipeptide acid units have been prepared from 2-(protected amino)ethyl tosylate[4] or halo acid[5] by a substitution reaction, or from protected dipeptide esters (either by the selective reduction of the peptide bond by borane followed by hydrolysis[6] or by reduction by sodium bis(2-methoxyethoxy)aluminium hydride followed by oxidation[4]). Most of these routes, however, can not be the general method owing to the complexity of the reactions. Only one exception, a reduction by borane, has a substantial possibility to be a general method. However, the procedure proposed by Roeske's group is not practically applicable because of the poor yield and difficulty of separation of the desired product from the by-products.[4] In this study we reinvestigated the conditions for a reduction of protected dipeptide esters by borane in order to establish a general method for the incorporation of the CH_2-NH bond in any desired position of the peptides.

A retention of asymmetry at chiral centers during the reduction and the necessity of protecting the generated secondary amine function during peptide bond elongation steps are also discussed.

Results and Discussion

Borane is known to reduce amide bonds selectively, but in the case of a protected dipeptide ester, a reduction of the ester moiety often accompanies this reaction. Roeske's group reported that a concurrent reduction of the ester bond was minimized by carrying out the reaction at −20 °C with 2 mol of BH_3 for 4—5 h. However, the fact that such selectivity is obtained only in a low conversion-stage restricted the practical application of their procedure. Then, we examined in detail the conditions for the reduction of protected dipeptide esters by borane and the effects of ester residues on the product yields.

Optimization of the conditions of the reduction of protected dipeptide esters by borane was tried by using *N*-benzyloxycarbonyl(Z)-L-phenylalanyl-L-Phenylalanine 2-methoxyethyl ester (**1a**) as a model compound.

$$X\text{-}AA^1\text{-}AA^2\text{-}CO_2Y \xrightarrow{BH_3\text{-}THF}$$
(**1a—g**)

$$X\text{-}AA^1\psi[CH_2\text{-}NH]AA^2\text{-}CO_2Y + X\text{-}AA^1\text{-}AA^2\text{-}CH_2OH$$
(**2a—g**) (**3a,b,e—g**)

$$+ X\text{-}AA^1\psi[CH_2\text{-}NH]AA^2\text{-}CH_2OH$$
(**4a,b,e—g**)

a: X=Z, AA^1=L-Phe, AA^2=L-Phe, Y=$CH_2CH_2OCH_3$
b: X=Z, AA^1=L-Phe, AA^2=L-Leu, Y=$CH_2CH_2OCH_3$
c: X=Z, AA^1=L-Phe, AA^2=L-Leu, Y=CH_3
d: X=Z, AA^1=L-Phe, AA^2=L-Leu, Y=$C(CH_3)_3$
e: X=Z, AA^1=L-Phe, AA^2=D-Leu, Y=$C(CH_3)_3$
f: X=Z, AA^1=Gly, AA^2=L-Phe, Y=$C(CH_3)_3$
g: X=Boc, AA^1=L-Phe, AA^2=L-Leu, Y=CH_3

Borane-tetrahydrofuran (THF) was added to a solution of **1a** in THF at −20 °C and then the temperature was increased to the point to be studied. After having been stirred at that temperature for an appropriate period, the remaining borane was quenched by the addition of methanol and the mixture was further treated with 1 M† HCl for 15 min to destroy boron-nitrogen bonds in products. Then, products were separated and isolated by preparative thin-layer chromatography (TLC) on silica gel. The results are summarized in Table 1 together with the results of a reduction of various kinds of protected dipeptide esters.

When the reaction temperature was raised between −5 and 0 °C, the yield of the corresponding pseudopeptide ester **2a** increased, while some part of it was further reduced to the pseudopeptide alcohol **4a** (Entries 3—5). In this case, the product of the selective reduction of the ester moiety, peptide alcohol **3a**, was not obtained. When the temperature was further raised to 30 °C, no further improvement in the conversion ratio of the starting material and yield of the desired product was obtained (Entry 6). Thus, the highest yield of the protected pseudodipeptide ester was obtained when a reduction of the protected dipeptide ester was carried out by use of 10 mol of BH_3 at 0 °C for 10 h (Entry 5).

In Entries 7—9 the effects of ester residues on the yield of the products were shown. The structure of the ester moiety has an important role in determining the ratio of the products. As expected, *t*-butyl ester (Entry 9) gave the highest yield of the desired pseudopeptide ester. However, a low yield was encountered in the case of Z-Gly-L-Phe-OBu^t, reflecting the lower reactivity of BH_3 toward α-unsubstituted amides[7] (Entry 11). On the other hand, these conditions are also applicable to *N*-*t*-butoxycarbonyl-dipeptide ester (Entry 12).

Racemization during the reduction was checked for two pseudopeptides, Z-L-Pheψ[CH_2-NH]L-Leu-OBu^t (**2d**) and Z-L-Pheψ[CH-NH]D-Leu-OBu^t (**2e**). Compounds **2d** and **2e** were deprotected by HBr in acetic acid and the free pseudodipeptides obtained were analyzed by reverse-phase HPLC.[8] Both compounds were eluted separately, and L-Pheψ[CH_2-NH]D-Leu was not detected in a sample of synthesized L-Pheψ[CH_2-NH]L-Leu. Since D-Pheψ[CH_2-NH]L-Leu, a mirror image of the L-Pheψ[CH_2-NH]D-Leu, should be eluted at the same position as L-Pheψ[CH_2-NH]D-Leu it can be concluded that racemization does not occur during the reduction at both chiral centers of the dipeptides.

In planning the synthesis of ψ[CH_2-NH]peptides by utilizing the ψ[CH_2-NH]dipeptide unit thus obtained, the necessity of protecting the secondary amine function should be considered. Most of the syntheses used so far protecting groups,[4] but syntheses without protection have also been reported.[1,2] In order to clarify this point and at the same time to determine the effect of a displacement of the peptide bond by an isosteric bond on the biological activity, we synthesized a pseudopeptide analogue of Leu-

Table 1. Reduction of *N*-Protected Dipeptide Esters **1a—g** by Borane

Entry	Compound	Reaction Conditions			Yield/%[a]			Recovery/%[a]
		Temp/°C	BH_3/**1** (mol mol^{-1})	Time/h	**2**	**3**	**4**	**1**
1	**1a**	−10	10	5	24	0	0	66
2	**1a**	−5	5	2	47	0	0	43
3	**1a**	−5	5	10	61	0	0	28
4	**1a**	0	5	10	60	0	7	21
5	**1a**	0	10	10	69	0	13	11
6	**1a**	30	5	1	41	0	12	10
7	**1b**	0	10	10	58	5	9	ND
8	**1c**	0	10	10	64	7	10	ND
9	**1d**	0	10	10	75	ND	5	ND
10	**1e**	0	10	10	49	ND	ND	ND
11	**1f**	0	10	10	16	ND	ND	ND
12	**1g**	0	10	10	47	ND	ND	ND

a) Isolated yield. ND: not determined.

† 1 M=1 mol dm^{-3}.

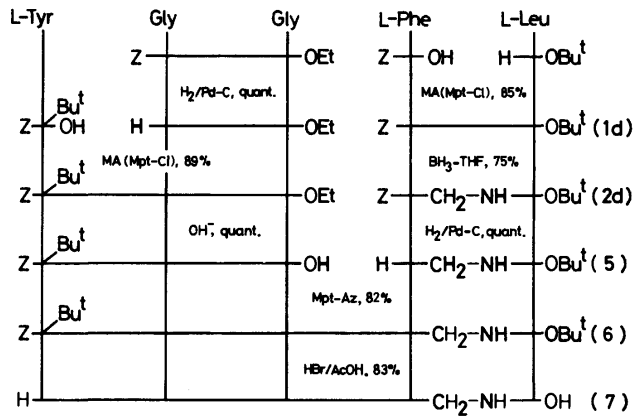

Scheme 1. Synthesis of [L-Pheψ[CH_2–NH]L-Leu$^{4-5}$]-leucine-enkephalin.

enkephalin, in which a peptide bond between Phe^4 and Leu^5 residues was replaced by the CH_2–NH bond. The synthetic route is shown in Scheme 1.

The benzyloxycarbonyl group of **2d** was removed by catalytic hydrogenolysis to give H-L-Pheψ[CH_2–NH]L-Leu-OBu^t (**5**) in quantitative yield as dihydrochloride. The coupling of **5** with a protected *N*-terminal tripeptide acid unit was carried out with the use of dimethylphosphinothioic azide as a coupling reagent[9,10] to afford the desired protected pseudopentapeptide ester, Z-L-Tyr(Bu^t)-Gly-Gly-L-Pheψ-[CH_2–NH]L-Leu-OBu^t (**6**), in 82% yield. In this reaction no significant amount of side products could be detected, showing that the protection of the secondary amine function was not necessary. The removal of all the protecting groups by HBr in acetic acid, followed by purification by preparative TLC and gel chromatography on Sephadex LH-20 gave chromatographically homogeneous [L-Pheψ[CH_2–NH]L-Leu$^{4-5}$]leucine-enkephalin (**7**) in 83% yield.

Measurements of the pharmacological activity of **7** in in vitro isolated tissue preparations are now being studied. Results will be reported elsewhere.

Experimental

All the melting points were uncorrected. TLC was performed on silica-gel plates (Merck 60 GF_{254}) in the following solvent systems(v/v): chloroform-methanol (9:1, R_f^1), chloroform-methanol (49:1, R_f^2), ether-petroleum ether (1:1, R_f^3), ethyl acetate (R_f^4), chloroform-methanol-water (65:25:4, R_f^5), chloroform-methanol-acetic acid (85:25:20, R_f^6), chloroform-methanol-acetic acid (95:5:3, R_f^7), 1-butanol-acetic acid-water (4:1:1, R_f^8). Diborane solution in THF was prepared from $NaBH_4$ and boron trifluoride etherate and standardized before use. For most of the experiments the concentration was approximately 2 M in BH_3. All the stepwise syntheses of protected di- and tripeptides were mediated with the mixed anhydride method with the use of dimethylphosphinothioic chloride (Mpt-Cl) as the coupling reagent.[11]

H-L-Phe-$OCH_2CH_2OCH_3$·HCl (8) and H-L-Leu-$OCH_2CH_2OCH_3$·HCl (9): These compounds were prepared from the corresponding amino acids and 2-methoxyethanol by the usual method using thionyl chloride. **8**: Mp 173.0—175.6 °C; $[\alpha]_D^{22}$ +15.7° (*c* 2.0, abs. EtOH); **9**: Mp 124.8—125.2 °C; $[\alpha]_D^{22}$ +12.5° (*c* 2.0, abs. EtOH).

Z-L-Phe-L-Phe-$OCH_2CH_2OCH_3$ (1a): The Mpt-Cl (2.57 g, 20 mmol) was added at rt to a stirred mixture of Z-L-Phe-OH (5.99 g, 20 mmol) and triethylamine (2.79 ml, 20 mmol) in chloroform (20 ml). After 30 min, to this solution, **8** (5.20 g, 20 mmol) in chloroform (20 ml) and triethylamine (5.58 ml, 40 mmol) were added at 0 °C and the solution was stirred at rt for 11 h. All the volatile materials were removed in vacuo. The residue was taken in ethyl acetate and the solution washed in the usual manner and dried. After evaporation of the solvent, the crude material was recrystallized from ethyl acetate-petroleum ether. Yield 8.57 g (85%); mp 119.5—120.0 °C; $[\alpha]_D^{27}$ +24.8° (*c* 1.0, $CHCl_3$); R_f^2=0.60, R_f^3=0.10; ^{1}H NMR ($CDCl_3$) δ=2.9—3.2 (m, 4H), 3.3—3.7 (m, 5H), 4.1—4.9 (m, 4H), 5.0 (s, 2H), 5.3—5.6 (d, 1H), 6.3—6.7 (d, 1H), 6.9—7.4 (aromatic protons, 15H).

Found: C, 68.71; H, 6.36; N, 5.40%. Calcd for $C_{29}H_{32}O_6N_2$: C, 69.03; H, 6.39; N, 5.55%.

Z-L-Phe-L-Leu-$OCH_2CH_2OCH_3$ (1b): This compound was obtained using **9** in the same way as described above. Crude products were recrystallized from ether-petroleum ether. Yield 62%; mp 77.0—77.8 °C; $[\alpha]_D^{27}$ −4.7° (*c* 1.0, $CHCl_3$); R_f^2=0.55, R_f^3=0.13; ^{1}H NMR($CDCl_3$) δ=0.8—1.0 (d, 6H), 1.4—1.9 (m, 3H), 3.0—3.2 (d, 2H), 3.35 (s, 3H), 3.5—3.7 (t, 2H), 4.1—4.8 (m, 4H), 5.07 (s, 2H), 5.2—5.5 (broad, 1H), 6.1—6.6 (broad, 1H), 7.1—7.4 (aromatic protons, 10H).

Found: C, 66.22; H, 7.24; N, 5.96%. Calcd for $C_{26}H_{34}O_6N_2$: C, 66.36; H, 7.28; N, 5.95%.

General Procedure for the Reduction of *N*-Protected Dipeptide Esters by BH_3-THF (Table 1): Borane-THF solution (2.5—5.0 mmol) was slowly added to the stirred solution of **1** (0.5 mmol) in THF at −20 °C. The reaction mixture was stirred at an appropriate temperature for an appropriate period (see Table 1). The reaction was quenched by the addition of methanol (5 ml) and then 1 M HCl (5 ml). After stirring for 15 min, the pH of the mixture was adjusted to 7—8 by a 5% aq $NaHCO_3$ solution. After removing THF in vacuo the desired product was extracted with chloroform or ethyl acetate. The combined extracts were washed, dried and evaporated under a reduced pressure, and the residue was purified by preparative silica-gel TLC.

Reduction of Z-L-Phe-L-Phe-$OCH_2CH_2OCH_3$ (1a): The reaction was carried out according to the general procedure. The purification by TLC was performed twice using different solvent systems; ether-petroleum ether (2:1 v/v) and then chloroform-methanol (20:1 v/v). **2a** was obtained as pale-yellow crystals; mp 63.0—63.2 °C; $[\alpha]_D^{26}$ +15.2° (*c* 2.6, $CHCl_3$); R_f^2=0.57, R_f^3=0.17; ^{1}H NMR ($CDCl_3$) δ=1.77 (broad, 1H), 2.15—3.1 (m, 6H), 3.1—4.4 (m, 9H), 4.9—5.3 (m, 3H), 6.8—7.4 (aromatic protons, 15H).

Found: C, 70.88; H, 6.97; N, 5.69%. Calcd for $C_{29}H_{34}O_5N_2$: C, 71.00; H, 6.99; N, 5.71%.

4a was obtained as colorless crystals. An analytical sample was recrystallized from ethyl acetate-petroleum ether; mp 111.0—111.7 °C; $[\alpha]_D^{26}$ +16.0° (*c* 0.6, $CHCl_3$); R_f^1=

0.49, R_f^5=0.38; ^{1}H NMR ($CDCl_3$) δ=2.25 (broad, 2H), 2.5—2.9 (m, 7H), 3.1—4.2 (m, 3H), 4.9—5.3 (m, 3H), 6.9—7.4 (aromatic protons, 15H).

Found: C, 74.32; H, 7.21; N, 6.57%. Calcd for $C_{26}H_{30}O_3N_2$: C, 74.61; H, 7.23; N, 6.69%.

Reduction of Z-L-Phe-L-Leu-OCH$_2$CH$_2$OCH$_3$ (1b): The reaction of **1b** (235 mg, 0.5 mmol) was carried out according to the general procedure. Purification by TLC was performed twice using different solvent systems; ether–petroleum ether (2:1 v/v) and then chloroform–methanol (10:1 v/v) to give **2b** as pale-yellow crystals; mp 54.0—55.0 °C; $[\alpha]_D^{19}$ −16.2° (*c* 1.0, $CHCl_3$); R_f^2=0.56, R_f^3=0.25; ^{1}H NMR ($CDCl_3$) δ=0.8—1.1 (d, 6H), 1.3—1.9 (m, 4H), 2.3—3.0 (m, 4H), 3.1—4.3 (m, 9H), 5.0—5.3 (m, 3H), 7.1—7.4 (aromatic protons, 10H).

Found: C, 67.94; H, 7.88; N, 5.92%. Calcd for $C_{26}H_{36}O_5N_2$: C, 68.39; H, 7.95; N, 6.14%.

3b (10.4 mg, 5.2%) was identical with the authentic sample prepared by the reduction of Z-L-Phe-L-Phe-OMe by $NaBH_4$; mp 119.0—121.3 °C; R_f^1=0.69, R_f^4=0.74.

4b (18.7 mg, 9.7%) was obtained as colorless crystals; mp 100.7—102.0 °C; R_f^1=0.44; R_f^4=0.13; ^{1}H NMR ($CDCl_3$) δ=0.7—1.0 (m, 6H), 1.0—1.9 (m, 3H), 2.1—4.4 (m, 10H), 5.0—5.3 (m, 3H), 7.1—7.6 (aromatic protons, 10H).

Reduction of Z-L-Phe-L-Leu-OMe (1c): According to the general procedure, **1c** (213 mg, 0.5 mmol) was reduced. **2c** was obtained as colorless crystals; 133 mg (64%); mp 66.0—68.0 °C; $[\alpha]_D^{19}$ −16.7° (*c* 1.0, $CHCl_3$); R_f^2=0.68; R_f^3=0.44; ^{1}H NMR ($CDCl_3$) δ=0.8—1.1 (d, 6H), 1.2—2.0 (m, 4H), 2.2—3.4 (m, 5H), 3.6—4.2 (m, 4H), 5.0—5.2 (m, 3H), 7.0—7.4 (aromatic protons, 10H).

Found: C, 69.72; H, 7.74; N, 6.48%. Calcd for $C_{24}H_{32}O_4N_2$: C, 69.88; H, 7.82; N, 6.79%.

Reduction of Z-L-Phe-L-Leu-OBu^t (1d): According to the general procedure, **1d** (217 mg, 0.5 mmol) was reduced. **2d** was obtained as colorless oil (158 mg, 75%); $[\alpha]_D^{19}$ −13.4° (*c* 1.1, $CHCl_3$); R_f^2=0.70; R_f^3=0.48.

Found: C, 70.47; H, 8.33; N, 5.76%. Calcd for $C_{27}H_{38}O_4N_2 \cdot 1/3H_2O$: C, 70.40; H, 8.46; N, 6.08%.

The acetic acid salt of **2d** was obtained as colorless crystals: Mp 76.8—78.6 °C; $[\alpha]_D^{27}$ −7.5° (*c* 1.0, $CHCl_3$).

Found: C, 67.47; H, 8.20; N, 5.47%. Calcd for $C_{29}H_{42}O_6N_2$: C, 67.68; H, 8.23; N, 5.44%.

Reduction of Z-L-Phe-D-Leu-OBu^t (1e): According to the general procedure, **1e** (141 mg, 0.30 mmol) was reduced. TLC purification in the solvent system of ether–petroleum ether (2:3 v/v) gave **2e** as a pale-yellow oil; 67.3 mg (49%); $[\alpha]_D^{25}$ +5.3° (*c* 3.8, $CHCl_3$); R_f^2=0.69; R_f^3=0.46. ^{1}H NMR ($CDCl_3$) δ=0.8—1.1 (d, 6H), 1.2—1.9 (m, 13H), 2.3—3.2 (m, 5H), 3.6—4.1 (broad, 1H), 5.0—5.3 (m, 3H), 7.1—7.4 (aromatic protons, 10H).

Found: C, 71.29; H, 8.37; N, 6.29%. Calcd for $C_{27}H_{38}O_4N_2$: C, 71.33; H, 8.43; N, 6.16%.

Reduction of Z-Gly-L-Phe-OBu^t (1f): According to the general procedure, **1f** (170 mg, 0.41 mmol) was reduced. TLC purification using ether as a solvent gave colorless oil of **2f**; 27.2 mg (17%); $[\alpha]_D^{27}$ +6.9° (*c* 3.0, methanol); R_f^1=0.80; R_f^5=0.56. ^{1}H NMR ($CDCl_3$) δ=1.35 (s, 9H), 1.65 (s, 1H), 2.6—3.6 (m, 7H), 5.0—5.3 (m, 3H), 7.1—7.4 (aromatic protons, 10H).

Found: C, 69.07; H, 7.56; N, 7.13%. Calcd for $C_{23}H_{30}O_4N_2$: C, 69.32; H, 7.59; N, 7.03%.

Reduction of Boc-L-Phe-L-Leu-OMe (1g): According to the general procedure, **1g** (157 mg, 0.40 mmol) was reduced. TLC purification using ether then chloroform–methanol (20:1 v/v) gave **2g** as colorless crystals; 71.7 mg (47%); mp 83.0—85.0 °C; $[\alpha]_D^{26}$ −2.3° (*c* 2, $CHCl_3$); R_f^2=0.63, R_f^3=0.48; ^{1}H NMR ($CDCl_3$) δ=0.6—1.1 (m, 6H), 1.4—2.0 (m, 13H), 2.2—3.5 (m, 5H), 3.5—4.3 (m, 4H), 4.4—4.9 (broad, 1H), 7.2 (aromatic protons, 5H).

Found: C, 66.58; H, 9.00; N, 7.57%. Calcd for $C_{21}H_{34}O_4N_2$: C, 66.63; H, 9.05; N, 7.40%.

Preparation of Z-L-Tyr(Bu^t)-Gly-Gly-L-Pheψ[CH$_2$-NH]L-Leu-OBu^t (6): Compound **2d** (145 mg, 0.32 mmol) was hydrogenolyzed in the presence of 10% Pd-C (50 mg) in methanol (4 ml) containing conc HCl (0.1 ml) to give 125.6 mg (quantitative) of H-L-Pheψ[CH$_2$-NH]L-Leu-OBu^t·2HCl, which was dissolved together with Z-L-Tyr(Bu^t)-Gly-Gly-OH (155 mg, 0.32 mmol) in *N*,*N*-dimethylformamide (DMF) (1.0 ml) and triethylamine (134 μl, 0.958 mmol). To this solution (cooled at 0 °C) dimethylphosphinothioic azide (47.6 mg, 0.352 mmol) in DMF (0.3 ml) was added and the mixture was stirred at this temperature for 24 h. The solution was diluted with ethyl acetate and washed with water, a 5% aq $NaHCO_3$ solution, water and saturated NaCl solution, dried over anhydrous sodium sulfate and evaporated. The oily residue was purified by silica-gel column chromatography to give **6** as amorphous solid; 207.8 mg (82%); $[\alpha]_D^{27}$ −13.4° (*c* 1.0, methanol); R_f^4=0.44, R_f^7=0.51. ^{1}H NMR ($CDCl_3$) δ=0.7—1.8 (m, 27H), 2.1—3.2 (m, 8H), 3.3—5.1 (m, 8H), 6.3—8.0 (m, 18H).

Found: C, 66.79; H, 7.76; N, 9.10%. Calcd for $C_{44}H_{61}O_8N_5$: C, 67.07; H, 7.80; N, 8.89%.

Preparation of H-L-Tyr-Gly-Gly-L-Pheψ[CH$_2$-NH]L-Leu-OH (7): 25% HBr in acetic acid (0.4 ml) was added to a solution of **6** (54.7 mg, 0.069 mmol) in acetic acid (0.2 ml) containing anisole (0.1 ml) and the solution stirred at room temperature for 2 h. After evaporation, the residue was washed with ether by trituration. The crude product was purified by silica-gel TLC by a solvent system of chloroform–methanol–29% aqueous ammonia (65:25:4) followed by gel chromatography on Sephadex LH-20 (eluted with methanol) to give chromatographically homogeneous monohydrobromide dihydrate of **7** as amorphous solid; 38.0 mg (83%); $[\alpha]_D^{27}$ +23.0° (*c* 1.9, methanol); R_f^5=0.25, R_f^8=0.54.

Found: C, 51.01; H, 6.42; N, 10.41%. Calcd for $C_{28}H_{42}O_7N_5Br$: C, 51.06; H, 6.73; N, 10.63%.

The present work was partially supported by a Grant from the Fujisawa Foundation.

References

1) J. Martinez, J.-P. Bali, M. Rodriguez, B. Castro, R. Magous, J. Laur, and M.-F. Lignon, *J. Med. Chem.*, **28**, 1874 (1985).

2) M. Rodriguez, J.-P. Bali, R. Magous, B. Castro, J. Martinez, *Int. J. Pept. Prot. Res.*, **27**, 2293 (1986).

3) M. J. Parry, A. B. Russell, and M. Szelke, "Chemistry and Biochemistry of Peptides," ed by J. Meienhofer, Ann Arbor Science Publishers, Ann Arbor (1972), p. 541.

4) M. Szelke, D. Hudson, R. Sharpe, I. MacIntyre, G. Fink, and A. M. C. Pickering, "Molecular Endocrinology,"

ed by I. MacIntyre and M. Szelke, Elsevier/North-Holland Biomedical Press, Amsterdam (1977), p. 57.

5) E. Atherton, H. O. Law, S. Moor, D. F. Elliott, and R. Wade, *J. Chem. Soc., (C)*, **1971**, 3393.

6) R. W. Roeske, F. L. Weitl, K. U. Prasad, and R. M. Thompson, *J. Org. Chem.*, **41**, 1260 (1976).

7) H. C. Brown, and P. Heim, *J. Org. Chem.*, **38**, 912 (1973).

8) HPLC analysis was performed on a Shimadzu LC3A liquid chromatograph; column: Nucleosil 5C18 (4×150 mm); temp. 40 °C; flow rate: 2.0 ml min^{-1}; eluent: 0.1 M H_3PO_4–K_2HPO_4 (pH 4.5)/CH_3CN (85/15); detection: 210 nm; retention time, H-L-Pheψ[CH_2–NH]L-Leu-OH: 5.80 min, H-L-Pheψ[CH_2–NH]D-Leu-OH: 3.65 min.

9) M. Ueki, K. Okazaki, Y. Sano, and S. Ikeda, "Peptide 1984," ed by U. Ragnarsson, Almqvist & Wiksell International, Stockholm (1984), p. 125.

10) M. Ueki, K. Okazaki, and S. Ikeda, "Peptide Chemistry 1984," ed by N. Izumiya, Protein Research Foundation, Osaka (1985), p. 67.

11) M. Ueki and T. Inazu, *Chem. Lett.*, **1982**, 45.

 © 1987 The Chemical Society of Japan Bull. Chem. Soc. Jpn., 60, 273—276 (1987)

ESR Studies of the Reaction of the Calcium Atom with Substituted Benzene Vapors[1)]

Kunio MOCHIDA* and Yasuhisa MIZUNO
Department of Chemistry, Faculty of Sciences, Gakushuin University,
1-5-1 Mejiro, Tokyo 171
(Received June 30, 1986)

The reaction of the calcium atom with substituted benzene vapors was examined by means of ESR. The anion radicals of substituted benzenes as intermediates were directly observed.

The study of metal-vapor reactions has been of considerable interest in organometallic chemistry and organic synthesis during the last few decades.[2)] With these methods, it is proving feasible to synthesize organometallic compounds which would be difficult, if not impossible, to prepare by other methods, and to study their reactive intermediates. The unstable intermediates (molecules and molecular fragments) produced by metal-vapor reactions are generally stabilized at cryogenetic temperatures in a solid matrix.

The unstable intermediates in metal-vapor reactions are mainly being examined by means of matrix infrared and Raman spectroscopy.[2)] Matrix electron spin resonance (ESR) is also potentially useful in these studies. However, there have been few reports on a convenient apparatus for high-boiling metal matrix ESR.[3)]

We previously reported the activation of the C–H bonds[4)] and C–X bonds[5)] of substituted benzenes by a calcium atom, followed by the formation of the corresponding arylcalcium hydrides and arylcalcium halides respectively. In these studies, the anion radicals of substituted benzenes were proposed to be reactive intermediates.

In this paper, we will describe the preparation of a convenient apparatus for high-boiling metal matrix ESR and also ESR studies of the reactions of the calcium atom with substituted benzene vapors using this apparatus.

Results and Discussion

In studying the activation of C–H bonds[4)] and C–X bonds[5)] of substituted benzene vapors with the calcium atom, the color of the intial products at 77 K turned green or blue, probably because of the anion radicals of substituted benzenes, depending on the aromatic compounds.

Apparatus. In order to observe directly the anion radicals of substituted benzenes produced by the reactions of the calcium atom with substituted benzene vapors, the apparatus for metal-atom matrix ESR illustrated in Fig. 1 was made. The cryostat assembly attaches directly to the assembly for metal vaporization and is pumped out as part of the complete vacuum system. Metal is vaporized using a filament of tungsten. During the vaporization of the metal, an organic substrate is introduced as vapor through an organic-substrate inlet tube. The co-condensation product of the metal atom and the organic substrate vapor condenses on a stainless-steel drum filled with liquid nitrogen. The co-condensation product of the metal-organic substrate at 77 K is transferred to the ESR tube using a scratching bar.

Miles and his co-workers have recently reported on matrix ESR in a rotating cryostat.[3)] The rotating cryostat has been used to deposit the metal atom onto the frozen layer of an organic substrate at 77 K. Our apparatus for the metal atom matrix ESR can similarly and coincidently be used to deposit the co-condensation products formed by the reactions of the metal atom with the organic-substrate vapor.

ESR Studies of Co-Condensation Products of the Calcium Atom and Substituted Benzene Vapors. The co-condensation products of the calcium atom with benzene, alkylbenzenes, and phenyltrimethylsilane respectively were examined by means of ESR. The ESR data of the products of the calcium atom and benzene (No. 1), alkylbenzenes (Nos. 2—5), and phenyltrimethylsilane (No. 6) are summarized in Table 1. Figure 2 shows the ESR spectrum of the product formed by the reaction of the calcium atom with benzene vapor. Although the spectrum is poorly

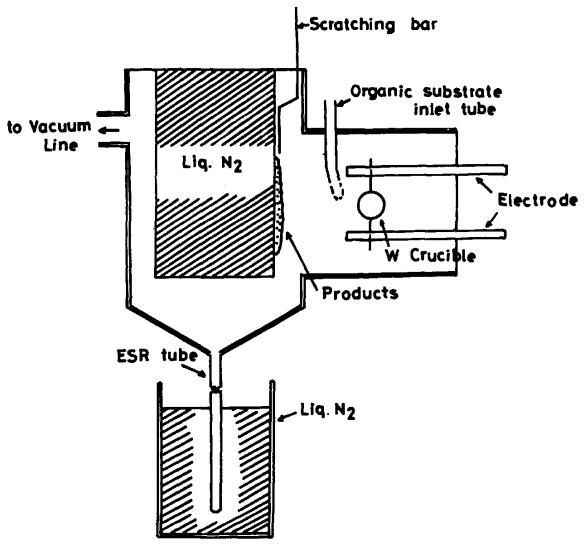

Fig. 1. The apparatus for metal atom matrix ESR.

resolved, it consists of a septet, and the line width is ca. 0.39 mT. The outermost lines of the septet are lost in the noise. The ESR spectrum of the calcium atom-benzene vapor product can safely be assigned to the benzene anion radical by comparison with that of a reference sample.[6,7] The experimental spectrum was reproduced by computer simulation, with the hyperfine splitting constants (hfsc) listed in Table 1. The signal gradually disappeared as the temperature was warmed at 0 °C. Figure 3 shows the ESR spectrum of the product by the reaction of the calcium atom with ethylbenzene vapor. The ESR spectrum is also poorly resolved, and the line width is ca. 0.56 mT. The ESR spectrum of the calcium atom-ethylbenzene vapor product can easily be assigned to the ethylbenzene anion radical by comparison with the ESR data of a reference of sample[6,7] and by computer simulation. The ESR spectra of the products formed by the reactions of the calcium atom with toluene, isopropylbenzene, *t*-butylbenzene, and phenyltrimethylsilane vapors were found to be broad singlets. Such broad singlets may result from the high concentrations of

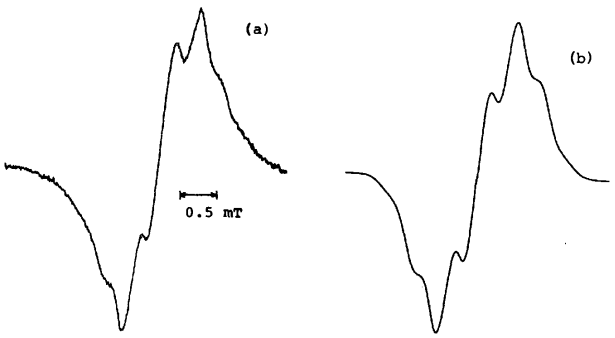

Fig. 2. (a) The observed ESR spectrum of calcium atom-benzene vapor product at −60 °C. (b) Computer simulated spectrum using Lorentzian line shape and a line width of 0.39 mT.

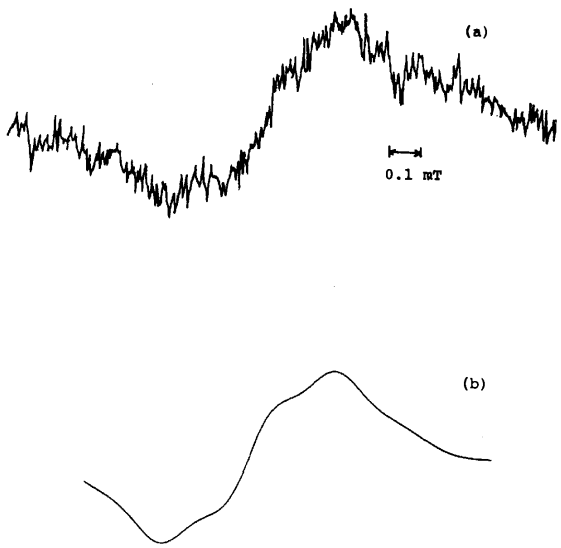

Fig. 3. (a) The observed ESR spectrum of calcium atom-ethylbenzene vapor product at −120 °C. (b) Computer simulated spectrum using Lorentzian line shape and a line width of 0.56 mT.

Table 1. ESR Data for Products of the Calcium Atom with Substituted Benzene Vapors

NO.	Compound	T/K	Hfs/mT (ring proton)	g[a]	Reference
1		213	0.35 0.404	2.0027 2.0028	This work [6, 7]
2	-Me	153	b) 0.554 (*o*-H), 0.569 (*m*-H) 0.013 (*p*-H)	2.0025 2.0028	This work [6, 7]
3	-Et	153	0.5[c] 0.540 (*o*-H), 0.615 (*m*-H) 0.018 (*p*-H)	2.0031 2.0029	This work [6, 7]
4	-Pr^i	153	b) 0.557 (*o*-H), 0.573 (*m*-H) 0.035 (*p*-H)	2.0030 2.0029	This work [6, 7]
5	-Bu^t	193	b) 0.531 (*o,m*-H), 0.172 (*p*-H)	2.0032	This work [6]
6	-SiMe$_3$	153	b) 0.266 (*o*-H), 0.106 (*m*-H) 0.813 (*p*-H)	2.0034	This work [8]
7	-F	173	b)	2.0035	This work
8	-Cl	173	b)	2.0034	This work

a) The g factors were determined by reference to that of Fremy's salt (g=2.0055). b) Not resolved. c) Hfs due to the para proton was not resolved.

the reaction intermediates or from the matrix conditions. Although no hyperfine structures due to the ring protons were resolved, these signals can safely be assigned to the anion radicals of the corresponding aromatic compounds on the basis of the ESR results for benzene and ethylbenzene vapors-calcium atom described above and on the basis of the reported g factors of these anion radicals. As a typical example, Fig. 4 shows the ESR spectrum of the product formed by the reaction of the calcium atom with toluene vapor.

The co-condensation products of the calcium atom with fluorobenzene and chlorobenzene vapors respectively were also examined. The ESR spectra of the products formed by the reactions of the calcium atom with fluorobenzene and chlorobenzene vapors respectively were found to be broader singlets than those of alkylbenzene vapors. The signal for the calcium atom-fluorobenzene vapor product was stable at −60 °C. On the other hand, the signal for the calcium atom-chlorobenzene vapor product was unstable and disappeared even at −60 °C. With bromobenzene, attempts to observe the anion radical failed. Although there have been studies of halogenated aromatic compound anion radicals by means of ESR, there has been no report on g factors of fluorobenzene and chlorobenzene anion radicals.[9] No hfs constants of calcium atom-fluorobenzene vapor product or of calcium atom-chlorobenzene vapor product were obtained in this study. Therefore, we could not determine whether the signals obtained by the reactions of the calcium atom with halobenzenes were those of the corresponding anion radicals or not.

These ESR results suggest that the anion radicals of substituted benzenes are produced in the reactions of the calcium atom with substituted benzene vapors.

In this experiment, we made a convenient apparatus for high-boiling metal atom matrix ESR and observed directly by means of ESR anion radicals of substituted benzenes as reaction intermediates in the reactions of the calcium atom with substituted benzene vapors. This apparatus will give further information on reaction intermediates in metal-vapor reactions.

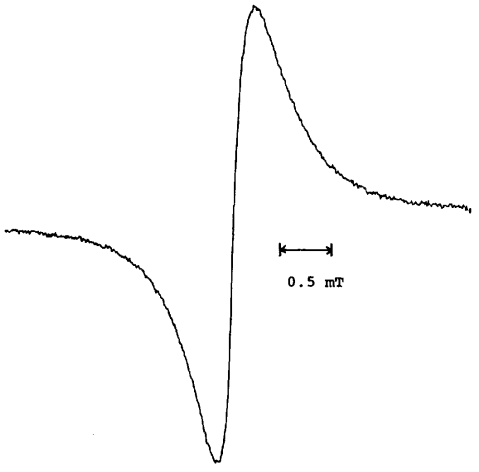

Fig. 4. The observed ESR spectrum of calcium atom-toluene vapor product at −120 °C.

Experimental

ESR Measurements. All the ESR spectra were obtained using a Varian E-9 ESR spectrometer. The field sweep of the spectrometer was calibrated with an aqueous solution of Fremy's salt (a_N=1.307 mT). The g factors were determined by reference to that of Fremy's salt (g=2.0055) using a dual cavity.

Materials. Substituted benzenes were dried and distilled prior to use.

Experimental Procedure. As a typical experiment, the reaction of the calcium atom with benzene vapor is described. Calcium metal (0.15 g, 3.7 mmol) was vaporized at a temperature of ca. 900 °C using a filament of tungsten in vacuo (ca. 5×10^{-3} Torr, 1 Torr=133.322 Pa) at a rate of ca. 20 mg min^{-1}. During the vaporization of the calcium metal, benzene (4 cm^3, 45 mmol) was introduced as vapor. The benzene vapor-calcium atom product condensed on a stainless-steel drum filled with liquid nitrogen. The product of calcium atom-benzene vapor at 77 K was transferred to the ESR tube using a scratching bar.

We wish to thank Messrs. Masayoshi Hamano, Hiroshi Miyagi, and Yuji Shimokawa of the machine shop of Gakushuin University for making the apparatus for the metal-atom matrix ESR studies. We also wish to thank Professor Tadashi Suehiro of Gakushuin University for providing the Varian E-9 ESR spectrometer. Partial financial support of this research by a Grant-in-Aid from the Ministry of Education, Science, and Culture of Japan is greatly acknowledged.

References

1) Preliminary results of this study were reported in *Chem. Lett.*, **1986**, 1125.

2) For example; J. R. Blackborow, and D. Young, "Metal Vapor Synthesis in Organometallic Chemistry," Springer-Verlag, New York (1979); K. J. Klabunde, "Reactive Intermediates," ed by R. A. Abramovitch, Plenum Press, New York (1980); K. J. Klabunde, "Chemistry of Free Atoms and Particles," Academic Press, New York (1980).

3) For example; P. H. Kasai, E. Hedaya, and E. B. Whipple, *J. Am. Chem. Soc.*, **91**, 4364 (1969); B. Miles, *Angew, Chem.*, **80**, 519 (1968); J. E. Bennett, B. Miles, and A. Tomas, *Proc. R. Soc. London, Ser. A*, **293**, 246 (1966); J. E. Bennett, B. Miles, A. Tomas, and B. Ward, *Adv. Phys. Org. Chem.*, **8**, 1 (1970); A. J. Buck, B. Miles, and J. A. Howard, *J. Am. Chem. Soc.*, **105**, 3381 (1983); J. A. Howard, R. Sutcliffe, H. Dahmane, and B. Miles, *Organometallics*, **4**, 697 (1985).

4) K. Mochida, H. Takeuchi, Y. Hiraga, and H. Ogawa, *Chem. Lett.*, **1984**, 1989.

5) K. Mochida and H. Ogawa, *J. Organomet. Chem.*, **243**, 131 (1983).

6) M. T. Jones, T. G. Kuechler, and S. Metz, *J. Mag.*

Resonance, **10**, 149 (1973).
7) M. T. Jones, S. Metz, and T. C. Kuechler, *Mol. Phys.*, **33**, 717 (1977).
8) J. A. Bedford, J. R. Bolton, A. Carrington, and R. H. Prince, *Trans. Faraday Soc.*, **59**, 53 (1963).
9) For example; A. Namiki, *J. Chem. Phys.*, **62**, 990 (1975); M. B. Yim and D. E. Wood, *J. Am. Chem. Soc.*, **98**, 2053 (1976).

 © 1987 The Chemical Society of Japan Bull. Chem. Soc. Jpn., 60, 277—282 (1987)

Photochemical C-P Bond Cleavage of Nitrobenzylphosphonate Ions

Yoshiki Okamoto,* Narimasa Iwamoto, Susumu Toki, and Setsuo Takamuku
The Institute of Scientific and Industrial Research, Osaka University,
Mihogaoka 8-1, Ibaraki, Osaka 567
(Received June 30, 1986)

Upon UV-irradiation, the C-P bond of *p*-nitrobenzylphosphonate ions cleaved with a quantum yield of about 0.7 in an aqueous alcohol solution to give 1,2-bis(4-nitrophenyl)ethane, *p*-nitrotoluene, orthophosphate, and alkyl dihydrogenphosphate. Whereas in an aqueous solution 1,2-bis(4-nitrophenyl)ethane was produced as a main product, in an alcohol solution only *p*-nitrotoluene was produced. This photolysis may proceed via intramolecular electron transfer from PO_3^{2-} group to nitro aromatic moiety to form an excited state, which undergoes C-P bond cleavage to give *p*-nitrobenzyl anion and monomeric metaphosphate anion as intermediates. The C-P bond cleavage of *p*-nitrobenzylphosphonate ion occurred more readily than those of *o*- and *m*-nitrobenzylphosphonate ions.

The chemical and thermal stability of C-P bond in free alkylphosphonic acid is well-known and chemical reactions involving C-P bond cleavage are not common.[1] The thermal decomposition of 2-haloalkylphosphonic acid is one of a few examples.[2] The C-P bond of this acid is easily cleaved into the fragments of 1-alkene, halide, and orthophosphate in a basic aqueous solution. The photochemical C-P bond cleavage of free phosphonic acid has not been reported before our previous letter.[3] Upon UV-irradiation of a basic 80% ethanol solution of *p*-nitrobenzylphosphonic acid (**1**), the formations of *p*-nitrotoluene (**2**), and salts of ethyl dihydrogenphosphate (**3**) and orthophosphoric acid (**4**) were observed.[3] We have suggested that this process involves an unimolecular C-P bond cleavage to give *p*-nitrobenzyl anion (**5**) and monomeric metaphosphate anion (**6**) as intermediates (Scheme 1). When anhydrous alcohol solutions of **1** containing 2 molar equivalents of 1,8-diazabicyclo[5.4.0]undec-7-ene (DBU) were irradiated, alkyl dihydrogenphosphates were obtained in almost quantitative yields.[4]

In the present paper, we will report the more detail investigation of photolysis of nitrobenzylphosphonic acids.

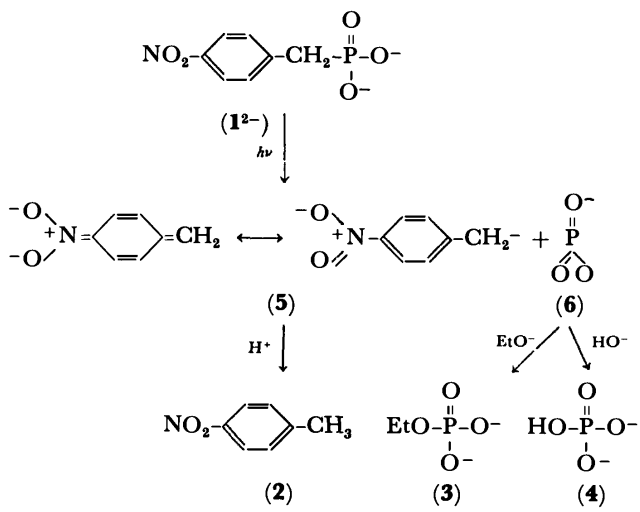

Scheme 1.

Results and Discussion

Photolysis of *p*-Nitrobenzylphosphonate Ion. In an aqueous solution, the absorption maximum of **1** is 290 nm at pH 5 and shifts to longer wavelength (305 nm) with increasing pH (Fig. 1). This shift may be due to an intramolecular charge transfer.[5] In an ethanol solution (containing 2 molar equivalents of DBU), this band shifts to shorter wavelength (298 nm). Upon exposure to ultraviolet light, an aqueous solution of dianion of **1** (50 mmol dm^{-3}) rapidly formed a precipitate, which was identified as 1,2-bis(4-nitrophenyl)ethane (**7**). Small amount of **2** was also detected. The quantum yield of C-P bond cleavage based on the yields of **7** and **2** was 0.86. The photolysis products and their quantum yields varied with the solvent (see below). By ^{31}P NMR observation, the quantitative yield of **4** (δ=2.6, H_2O, pH 12) was also observed after 1 h irradiation (Eq. 1).

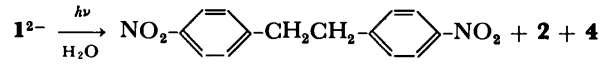

(7) (1)

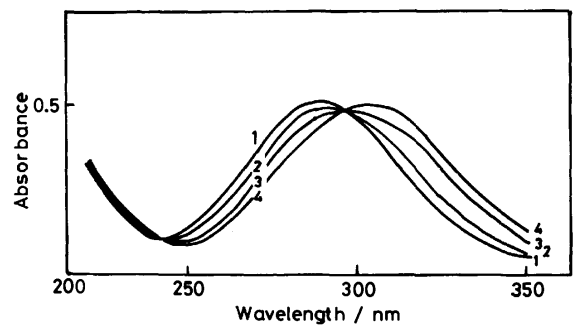

Fig. 1. Absorption spectra of **1** in an aqueous solution (5.0×10^{-2} mmol dm^{-3}) under different pH.
1: at pH ≈5.0, 2: at pH 6.8, 3: at pH 7.2, 4: at pH 8.0≈.

The photolysis of **1** was dependent on pH of the solution (80% EtOH) as shown in Fig. 2. The C–P bond cleavage did not occur below pH 5. It began above pH 5, which corresponds to the concentration of hydronium ion required for second ionization of **1** (pK_a^1 3.9, pK_a^2 9.3 in 80% EtOH). The yields of photolysis products **2** were constant above pH 9 (ϕ=0.76). Ethyl *p*-nitrobenzylphosphonate ion (**8**) did not undergo the C–P bond cleavage even at pH 10 (Eq. 2).

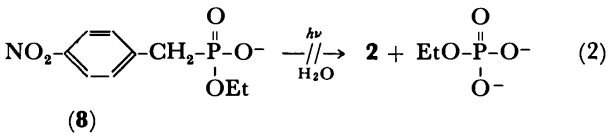

(8) (2)

Our results indicate that the undissociated or monodissociated **1** undergoes no C–P bond cleavage. The complete dissociation of the acid **1** is required for the photo-cleavage of C–P bond. Hammett σ_p constant of phosphono group ($-P(O)(OH)_2$) is 0.29, but that of complete dissociated phosphono group ($-PO_3^{2-}$) is −0.16.[6] Its electron-donor character increases by the complete dissociation. *p*-Nitrotoluene (**2**) could be produced by the reaction of **5** with H^+. This process is supported by a labelling experiment: The photolysis of $\mathbf{1}^{2-}$ in ethanol-*d*/deuterium oxide (v/v=3/2) gave *p*-nitrotoluene-*α*-*d* as a main product (81%). No phosphonic acid ($HPO(OH)_2$), resulted by homolytic C–P bond cleavage, could be detected by ^{31}P NMR observation of both the irradiated aqueous and ethanolic solutions of **1**. This photolysis was essentially the same in the presence or absence of oxygen: The yield of **4** was not be affected under bubbling of oxygen, although the yield of **2** was slightly reduced owing to a formation of *p*-nitrobenzaldehyde. Consequently, we conclude that the photolysis dose not proceed via radical mechanism, but via heterolytic C–P bond cleavage: The photoexcited **1** dianion may undergo heterolytic C–P bond cleavage to give **5** and **6**. The constancy of quantum yield of C–P bond cleavage with differences in the concentration of **1** also provides an evidence in favor of a direct C–P bond cleavage.

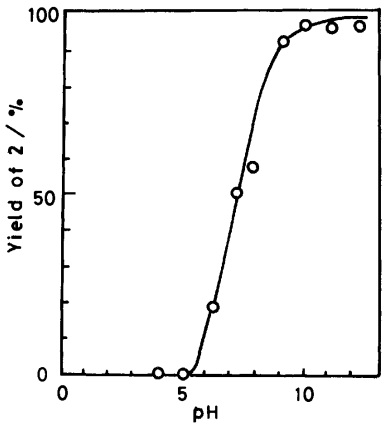

Fig. 2. Effect of pH on photolysis of **1** in 80% EtOH (50 mmol dm^{-3}, 1 h, in N_2).

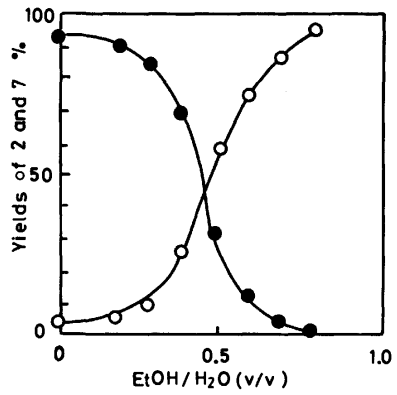

Fig. 3. Change of the product ratio **7/2** by the ratio of EtOH/H_2O (**1**, 50 mmol dm^{-3}, pH 10, 1 h, in N_2). —●—: **7**, —○—: **2**.

The product ratio of **7/2** decreased with an increase of the ratio of ethanol/water as shown in Fig. 3. In an anhydrous ethanol solution of **1** (containing 2 equivalents of DBU) only **2** was given (ϕ=0.50). The mechanism for the formation of **7** is not clear, and it is being investigated in more detail in our laboratory. The formation of product **7** via **5** by action of strong base on **2** in aqueous solution was reported by other investigator.[7]

Transient Intermediates. Although it is conceivable as an alternative path that **5** is formed by rapid electron transfer from phosphoranyl radical to benzyl radical after homolytic C–P bond cleavage, we can exclude this possibility by the results obtained with laser flash photolysis. The presence of two transient species was revealed by flash photolysis of an aqueous solution of $\mathbf{1}^{-2}$ with 15 ns flash of 308 nm light (Fig. 4). One is a transient species having absorption maximum at 360 nm, which is in agreement with that of **5** reported by Miller and Pobiner from the reaction of **2** with potassium *t*-butoxide in *t*-butyl alcohol.[8] The absorbance of the transient species was constant above pH 9, but below this was dependent upon the pH and at pH 5 could not be observed. The decrease of its absorbance may be comparable with the decrease of concentration of dianion of **1**. The difference of yields of the transient species in the presence or absence of oxygen was within experimental error. These results are consistent with the results from product analysis. The rate of formation of this absorption band followed first-order kinetics and the rate constant was 1.2×10^7 s^{-1} in aqueous solution (5.0×10^{-5} mol dm^{-3}, pH 12). The formation rate constant was not affected by the change of pH. In ethanol solution, the absorption maximum was identical with that in an aqueous solution, but the

formation rate constant reduced to $0.5\times10^7\ s^{-1}$. The lifetime of this transient species was very long and the decay behavior could not be followed by the ns-flash photolysis technique.

The other short-lived transient having absorption maximum at about 300 nm was also observed, although it could not be analyzed accurately, because the absorption maximum overlapped with that of **1** dianion (305 nm) (Fig. 4). This absorption band decayed together with an weak and broad absorption band at 500—800 nm. The decay rate of the latter band followed first-order kinetics and its rate constant was about $5.8\times10^6\ s^{-1}$. The decay of this transient absorption band may be correlated with the formation of 360-nm band, although there was a small difference in their rate constants. Thus, this short-lived transient intermediate may be a precursor of the 360-nm band and assigned as a diradical dianion **9** resulted by intramolecular electron transfer from PO_3^{2-} to nitro aromatic moiety (Scheme 2). Nagakura, et al. reported that radical anion of **2** has the absorption maxima at 302, 607, and 875 nm in THF.[10]

In an aqueous solution, the decay of 360-nm absorption band after short time exposure (2 s) of ultraviolet light with a high pressure mercury lamp could be observed with moderately high speed scanning using a UV spectrometer (Fig. 5). The lifetime was about 60 s, which is similar to that reported by Margerum (53 s) under the similar reaction conditions.[9] The rate constant for its absorption decay followed second-order kinetics.

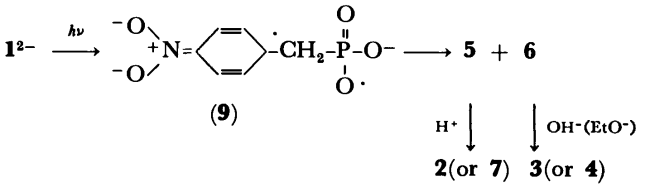

Scheme 2.

Photolysis of Other Nitrobenzylphosphonate Ions. Dianions of *o*- (**10**) and *m*-nitrobenzylphosphonic acids (**11**) also exhibited a clearly promoted reactivity on illumination, but their photochemical reactivities were more less than that of *p*-derivative (Table 1). Our results do not follow the photochemical patterns observed by Havinga et al., in the solvolysis of *m*- and *p*-nitrophenyl phosphates,[11] or by Zimmerman and Somasekhara, in the solvolysis of *m*- and *p*-nitrophenyl trityl ethers:[12] Readier C-P bond cleavage of **1** do not fit the mechanisms of Zimmerman on photolysis of nitrophenyl phosphates (**12**) in which the excited state of a *m*-nitro structure is considered to be favorable and that of a *p*-nitro unfavorable, for heterolytic cleavage.[13] Other different photochemical behavior of **12** is that the bond cleavage occurs with a definite efficiency between pH 5 and 12.[11]

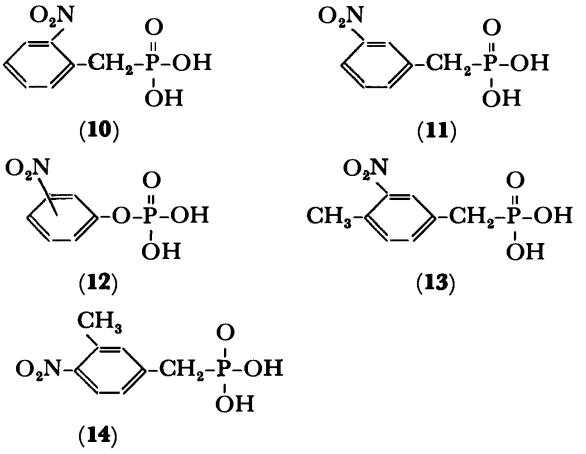

Whereas absorption maximum of *p*-derivatives of **12** in a basic aqueous solution is 310 nm, this band did not shift by increasing pH from 5 to 12. This fact indicates that there is no or little intramolecular charge transfer between PO_3^{-2} and nitro aromatic moiety in **12**. The electronic structure of photoexcited

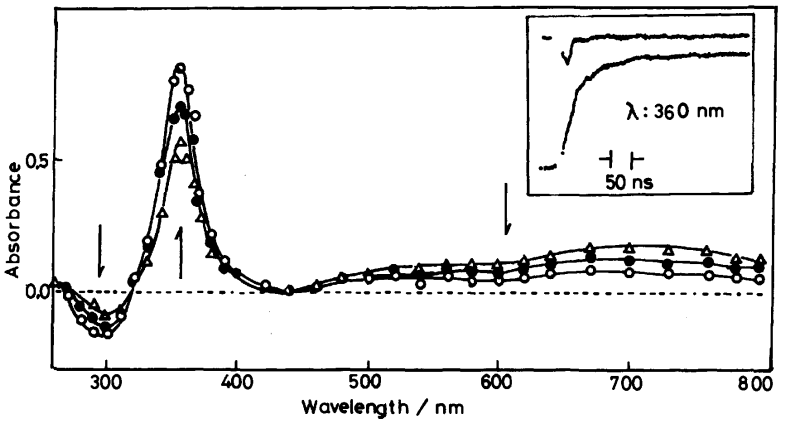

Fig. 4. Flash photolysis spectra from **1** in an aqueous solution (5.0×10^{-2} mmol dm^{-3}, pH 12, in Ar).
—△—: After 50 ns, —●—: after 100 ns, —○—: after 300 ns.
The insert figure shows a profile of the formation of transient absorption at 360 nm.

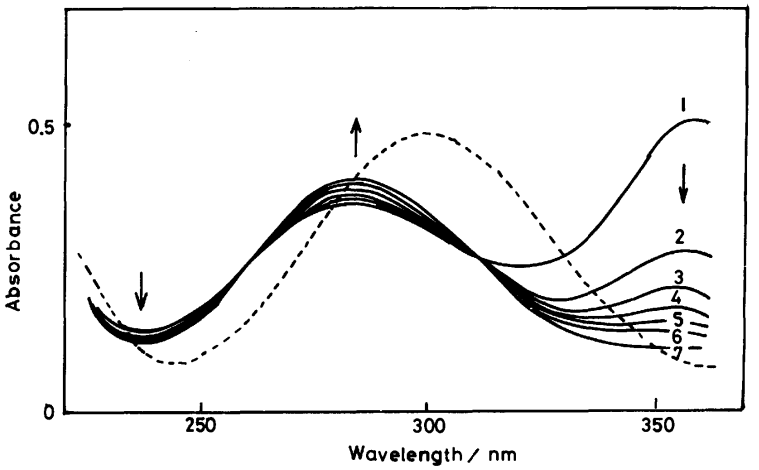

Fig. 5. Change of absorption spectra of **1** in an aqueous solution (5.0×10^{-2} mmol dm^{-3}, pH 12, in N_2) after 2 s irradiation with a high pressure mercury lamp (350 W).
·····: Unirradiated, 1: after 20 s, 2: after 50 s, 3: after 80 s, 4: after 120 s, 5: after 150 s, 6: after 300 s, 7: after 500 s.

Table 1. Quantum Yields of C-P Bond Cleavage of the Dianions of **11**, **10**, **1**, and *o*-, *m*-, and *p*-Nitrophenyl Phosphate (**12**)

Compound	Quantum yield
o-Nitrobenzylphosphonate dianion (**11**$^{-2}$)	0.024[a]
m-Nitrobenzylphosphonate dianion (**10**$^{-2}$)	0.039[a]
p-Nitrobenzylphosphonate dianion (**1**$^{-2}$)	0.76[a]
o-Nitrophenyl phosphate dianion	0.003[b]
m-Nitrophenyl phosphate dianion	0.05[b]
p-Nitrophenyl phosphate dianion	0.002[b]

a) Concentration 50 mmol dm^{-3}, 50% EtOH/H_2O, pH 12. b) The aqueous solutions of **12** (0.2 mmol dm^{-3}, 10 mmol dm^{-3} NaOH) were irradiated with monochromatic light of 313 nm.[11]

1 dianion may be entirely different from that of **12** anion. It is well-known that intermolecular electron transfer from an electron donor to *p*-nitrobenzyl chloride give *p*-nitrobenzyl chloride radical anion, which undergoes homolytic bond cleavage to afford *p*-nitrobenzyl radical and chloride anion.[14] In these reaction, numerious instances of light effects have been found, and some of them very large.[15] The fact that the dianion of **10** underwent C-P bond cleavage at a rate one-tenth that of **1** is readily understood in view of Geske's report that *o*-nitrotoluene is significantly more difficult to be reduced than **2**.[16] This is reasonably assumed to be due to steric hindrance to coplanarity in the ortho isomer, which lowers the reducibility of the system by tending electronically to isolate the nitro group from the ring.

Under identical photolysis conditions, dianions of (3-methyl-4-nitrophenylmethyl)phosphonic acid (**13**) and (4-methyl-2-nitrophenylmethyl)phosphonic acid (**14**) hardly underwent C-P bond cleavage.

These behaviors of photochemical C-P bond cleavage of **1** are similar to those of photochemical decarboxylation of nitrophenylacetate ions.[9]

Experimental

All mp and bp were uncorrected. Following spectrometers were used for spectral measurements: UV: Hitachi 323; Excimer laser Lambda Physik EMG 501; ^{1}H and ^{31}P NMR: Bruker WM 360.

Materials. Ethanol and other solvents were dried and distilled by the usual methods.

***p*-Nitrobenzylphosphonic Acid (1):** The acid **1** was prepared by the procedure reported previously.[3] Mp 230—232 °C. UV_{max} (H_2O, pH 12) 305 nm (ε 10,500). ^{1}H NMR (D_2O, DSS, pH 12) δ=2.98 (2H, d, J_{PH}=20 Hz), 7.1—8.1 (m, 4H). ^{31}P NMR (H_2O, 80% H_3PO_4, pH 12) δ=15.2 (t, J_{PH}=20 Hz).

***o*-Nitrobenzylphosphonic Acid (10):** After an equimolar mixture of *o*-nitrobenzyl bromide and triethyl phosphite was refluxed for 1 h, the mixture was distilled to give diethyl *o*-nitrobenzylphosphonate. Bp 160—165 °C/0.1 mmHg.† It was hydrolyzed by refluxing with hydrobromic acid for 12 h. The hydrolyzed acid **10** was recrystallized from water. Mp 190—191 °C, UV_{max} (H_2O, pH 12) 270 nm (ε 6,600). ^{1}H NMR (D_2O, DSS, pH 12) δ=3.65 (2H, d, J_{PH}=22.0), 7.1—8.0 (4H, m). Found: C, 38.56; H, 3.69; N, 6.58; P, 14.12%. Calcd for $C_7H_8NO_5P$: C, 38.72; H, 3.71; N, 6.45; P 14.27%.

***m*-Nitrobenzylphosphonic Acid (11):** The acid **11** was prepared by the same method as described above. Diethyl *m*-nitrobenzylphosphonate, bp 186—187 °C/0.5 mmHg, **11**, mp 186—187 °C. UV_{max} (H_2O, pH 12) 280 nm (ε 7,300). ^{1}H NMR (D_2O, pH 12) δ=2.84 (2H, d, J_{PH}=18.0 Hz), 7.1—8.0 (4H, m). Found: C, 38.81; H, 3.68; N, 6.38; P, 12.41%. Calcd for $C_7H_8NO_5P$: C, 38.72; H, 3.71; N, 6.45; P, 12.63%.

Ethyl *p*-Nitrobenzylphosphonate (8): The phosphonate **8** was prepared by nitration of ethyl benzylphosphonate with fuming nitric acid at 0 °C. Ethyl benzylphosphonate (mp 63—64 °C) was prepared by partial hydrolysis of diethyl

† 1 mmHg=133.3 Pa.

benzylphosphonate with 1 mol dm^{-3} NaOH 50% ethanol solution. **8**, mp 156—157 °C. UV_{max} (H_2O, pH 12) 290 nm (ε 10,600). ^1H NMR (D_2O, DSS, pH 12) δ=1.17 (t, 3H, J_{HH}=7.0 Hz), 3.10 (d, 2H, J_{PH}=20 Hz), 3.80 (quint, 2H, J_{HH}=7.0 Hz), 7.3—8.2 (m, 4H). Found: C, 44.25; H, 5.06; N, 5.69; P, 14.54%. Calcd for $C_9H_{12}NO_5P$: C, 44.09; H, 4.93; N, 5.71; P, 14.40%.

(3-Methyl-4-nitrophenylmethyl)phosphonic Acid (13): *m*-Methylbenzylphosphonic acid was nitrated with a nitric acid-sulfuric acid mixture (v/v=1:3) at 0 °C. Mp 219—220 °C. UV_{max} (H_2O, pH 12) 268 nm (ε 5,100). ^1H NMR (D_2O, DSS, pH 12) δ=2.58 (s, 3H), 3.35 (d, 2H, J_{PH}=20 Hz) 7.3—8.4 (m, 4 H). Found: C, 41.48; H, 4.27; N, 6.21; P, 13.37%. Calcd for $C_8H_{10}NO_5P$: C, 41.57; H, 4.36; N, 6.06; P, 13.40%.

(4-Methyl-3-nitrophenylmethyl)phosphonic Acid (14): *p*-Methylbenzylphosphonic acid was nitrated as described above. Mp 209—210 °C, UV_{max} (H_2O, pH 12) 274 nm (ε 3,800). ^1H NMR (D_2O, DSS, pH 12) δ=2.37 (s, 3H), 2.92 (d, 2H, J_{PH}=19 Hz), 7.0—8.0 (m, 3H). Found: C, 41.39; H, 4.18; N, 6.21; P, 13.49%. Calcd for $C_8H_{10}NO_5P$: C, 41.57; H, 4.36; N, 6.06; P, 13.40%.

Product Identification. The insoluble product was separated from the photolyzed aqueous solution of **1** by extraction with chloroform. The chloroform extract was evaporated, and the residue was recrystallized from acetone-ethanol to give **7**, pale yellow-needle (mp 181—183 °C) and it was identified by GLC with an authentic sample.

From a photolyzed ethanol solution of **1**, **2** was isolated. The ethanol was evaporated, and the residue was recrystallized from water-ethanol to give **2** (mp 51—52 °C), and identified by GLC with an authentic sample.

Typical Procedure of Photolysis. Five ml of a 50% ethanol solution of **1** (50 mmol dm^{-3}) was adjusted at pH 12 with a 10% aqueous solution of sodium hydroxide. Nitrogen was bubbled through the solution before irradiation. The solution was irradiated in a Pyrex tube (ϕ=10 mm) with a high-pressure mercury lamp (350 W) for 1 h under cooling with running water. The progress of the photolysis was directly monitored by a GLC analysis using biphenyl as an internal standard [Silicone OV-17 (2%) on Chromosorb W AW DMCS] of **2** or **7**. When the photolysis in a aqueous solution was carried out, chloroform (5 ml) was added and the mixture was shaken sufficiently. Analyses were performed on the chloroform extracts.

Photolysis of 1 in the Presence of Oxygen. The 80% ethanol solution of **1** (50 mmol dm^{-3}, pH 12) was irradiated in the same manner described above. Oxygen was bubbled into the solution during the irradiation. After irradiation, the solution was directly analyzed by GLC. *p*-Nitrobenzaldehyde, other than **2**, has been detected by comparison with an authentic sample (5.2%). As another oxidation product, a trace amount of *p*-nitrobenzyl alcohol was also detected.

Photolysis of 1 in Ethanol-*d*/Deuterium Oxide. One ml of ethanol-*d*/deuterium oxide solution (v/v=3/2) of **1** (50 mmol dm^{-3}) containing two equivalents of sodium deuteroxide was irradiated in the same manner as described above. The product was extracted with chloroform-*d*, and the extract was subjected to ^1H NMR analysis. *p*-Nitrotoluene-α-*d* [^1H NMR ($DCCl_3$, TMS) δ=2.46 (t, 2H, J_{DH}=2.2 Hz), 7.3—8.1 (m, 4H)] content in the product was 81%. When the ethanol-*d*/deuterium oxide solutions of **1** and **2** were allowed to stand for 24 h without UV-irradiation, isotopic hydrogen exchange on the methylene and the methyl groups of them could not be observed.

Measurement of the Quantum Yield. The quantum yields were determined on the basis of generated nitrotoluene and/or **7**, and chemical actinometry using 2-hexanone. The sample solutions (50 mmol dm^{-3}) were irradiated in a merry-go-round apparatus employing 313-nm monochromatic light according to the procedures previously described.[4]

Flash Photolysis. Flash photolyses were carried out by using a XeCl excimer laser Lambda Physik EMG 501 supplying 15 ns pulses of 308 nm light (energy 100 mJ/pulse). The solutions of **1** (5×10^{-2} mmol dm^{-3}, pH 12) were prepared freshly before irradiation and were deoxygenated by bubbling with argon gas. Irradiated solutions were replaced by a fresh solution for each pulse. The transmissions of samples were monitored using an optical system consisting of Xe-pulse lamp (Osram OPG 450), a monochromater (Nikon G-250), and a photomutiplier tube (Hamamatsu Photonics R928).

The authors are grateful to Mrs. Fusako Fukuda and Mr. Yoshio Takai of Material Analysis Center in the Institute of Scientific and Industrial Research, Osaka University, for the elemental analysis and the measurement of ^1H and ^{31}P NMR spectra.

The present work was partially supported by a Grant-in-Aid for Scientific Research No. 61223019 from the Ministry of Education, Science and Culture.

References

1) K. Sasse, "Organische Phosphorverbindungen Teil 1," in "Methoden der Organischen Chemie Band XXII/1," ed by E. Müller, Georg Thieme, Verlag. Stuttgart (1963), p. 85; L. D. Freedman and G. O. Doak, Chem. Rev., **57**, 489 (1957); T. Hori, M. Horiguchi, and A. Hayashi, "Biochemistry of Natural C-P Compounds," Japanese Association for Research on the Biochemistry of C-P Compounds, Otsu (1984), p. 14.

2) J. A. Maynard and J. M. Swan, *Aust. J. Chem.*, **16**, 596 (1963).

3) Y. Okamoto, N. Iwamoto, and S. Takamuku, *Chem. Lett.*, **1984**, 2091.

4) N. Iwamoto, Y. Okamoto, and S. Takamuku, *Bull. Chem. Soc. Jpn.*, **59**, 1505 (1986).

5) R. M. Issa, A. M. G. Nassar, A. M. Hindawey, F. M. Issa, and G. B. El-Hefnawey, *Spectrochim. Acta, Part A*, **31**, 199 (1975).

6) H. H. Jaffé, L. D. Freedman, and G. O. Doak, *J. Am. Chem. Soc.*, **75**, 2209 (1953).

7) G. A. Russell and E. G. Janzen, *J. Am. Chem. Soc.*, **89**, 300 (1967).

8) J. M. Miller and H. Pobiner, *Anal. Chem.*, **36**, 238 (1964).

9) J. D. Margerum and C. T. Petrusis, *J. Am. Chem. Soc.*, **91**, 2467 (1969); J. D. Margerum, *J. Am. Chem. Soc.*, **87**, 3772 (1965).

10) A. Ishitani, K. Kuwata, H. Tsubomura, and S.

Nagakura, *Bull. Chem. Soc. Jpn.*, **36**, 1357 (1963).
11) E. Havinga, R. O. de Jongh, and W. Dorst, *Recl. Trav. Chim. Pays-Bas*, **75**, 378 (1956); R. O. de Jongh and E. Havinga, *Recl. Trav. Chim. Pays-Bas*, **87**, 1318, 1327 (1968); E. Havinga and R. O. de Jongh, *Bull. Soc. Chim. Belg.*, **71**, 803 (1962).
12) H. E. Zimmerman and S. Somasekhara, *J. Am. Chem. Soc.*, **85**, 922 (1963).
13) H. E. Zimmerman and V. R. Sandel, *J. Am. Chem. Soc.*, **85**, 915 (1963).
14) R. C. Kerber, G. W. Urry, and N. Kornblum, *J. Am. Chem. Soc.*, **87**, 4520 (1965).
15) N. Kornblum, *Angew. Chem., Int. Ed. Engl.*, **14**, 734 (1975).
16) D. H. Geske, J. L. Ragle, M. A. Bambenek, and A. L. Balch, *J. Am. Chem. Soc.*, **86**, 987 (1964).

 © 1987 The Chemical Society of Japan Bull. Chem. Soc. Jpn., 60, 283—287 (1987)

A Novel Method for Determining the Chelation Ability of the Cysteine-Containing Peptides with 3,4-Toluenedithiol. Application to [2Fe-2S]-Ferredoxin Model Systems

Norikazu Ueyama, Satoru Ueno, and Akira Nakamura*
Department of Macromolecular Science, Faculty of Science, Osaka University, Toyonaka, Osaka 560
(Received July 2, 1986)

The chelating ability of a bidentate ligand, Cys-X-Y-Cys (X, Y=amino acid residue), in 2Fe-2S peptide model complexes was examined by a ligand-exchange method using 3,4-toluenedithiol (tdt-H_2) or *o*-xylene-α,α'-dithiol. The addition of tdt-H_2 to an *N,N*-dimethylformamide solution of $[Fe_2S_2(Z\text{-cys-Ala-Ala-cys-OMe})_2]^{2-}$ results in the cleavage pf Fe-S* (S*=inorganic sulfur) bond and in the formation of hydrogen sulfide and mononuclear Fe(III) peptide thiolate complex, $[Fe(Z\text{-cys-Ala-Ala-cys-OMe})(tdt)]^{1-}$. In the case of $[Fe_2S_2(Z\text{-Ala-cys-OMe})_4]^{2-}$, $[Fe_2S_2(tdt)^2]^{2-}$ was obtained by the substitution of Z-Ala-Cys-OMe with the chelating reagent. On the other hand, *o*-xylene-α,α'-dithiol expels both Z-Cys-Ala-Ala-Cys-OMe and Z-Ala-Cys-OMe ligands from these complexes.

An inherent lability of teterahedrally coordinated Fe(II) or Fe(III) species in solution is manifest in the observed ease in the core extrusion from iron–sulfur proteins or in the thiolate ligand exchange of their synthetic model complexes, e.g. $[Fe_2S_2(SR)_4]^{2-}$.[1] Bridging μ-sulfido ligands are also labile in these iron complexes and interconversion among [4Fe-4S], [3Fe-4S], and [2Fe-2S] clusters has been recently found in many iron–sulfur proteins.[2] Similar changes in cluster structures are studied for some model complexes.[3] Thus, we have reported a smooth conversion of $[Fe_2S_2(peptide)_4]^{2-}$ to $[Fe_4S_4(peptide)_4]^{2-}$ upon one-electron reduction.[4] All these reactions depend on the lability of the Fe-S bonds which is important for their functions in biological systems.

The high lability of monodentate thiolate ligands in Fe(II) complexes or the instability in Fe(III) complexes has been found to decrease by effective chelation.[5] Thus, remarkable thermal stability of oxidized rubredoxin (Fe(III) state) is ascribed to the multiple chelation of the protein. In the related model complex, $[Fe(Z\text{-cys-Pro-Leu-cys-OMe})_2]^{1-,2-}$ (Z=benzyloxycarbonyl), we have found a remarkable stabilizing effect due to chelation.[6,7] In native [2Fe-2S]-ferredoxins, the oxidized state is also stable by chelation where an invariant peptide sequence, Cys-A-B-C-D-Cys-X-Y-Cys chelates in tridentate fashion.[8] Here, the Cys-X-Y-Cys part is bridging the two Fe(III) ions and Cys-A-B-C-D-Cys part is chelating.

In the previous paper we reported the chelation of a tetrapeptide Cys-X-Y-Cys to $[Fe_2S_2]^{2+}$ ion.[9] However, we could not determine whether the Cys-X-Y-Cys bridges between the two Fe(III) ions of $[Fe_2S_2]^{2+}$ or chelates to one Fe(III) ion of $[Fe_2S_2]^{2+}$.

In this paper, we describe a novel method for determination of the mode of chelation of Cys-X-Y-Cys to $[Fe_2S_2]^{2+}$ core utilizing the ligand-exchange reaction with 3,4-toluenedithiol. This reagent has been employed for attempt to extrude some inorganic clusters from iron-sulfur proteins.[10]

Experimental

All manipulations involving solvent purifications, air-sensitive iron thiolate, and peptide complexes were carried out under argon atmosphere.

Materials. 3,4-Toluenedithiol (tdt-H_2) was obtained from Nakarai Chemical Co. and used without purification. Tetrahydrofuran (THF) was purified by distillation after sufficient refluxing over sodium metal. *N,N*-Dimethylformamide (DMF) was purified by distillation under reduced pressure before use. *o*-Xylene-α,α'-dithiol (*o*-xyl-$(SH)_2$) was prepared by the literature method.[11] $[NEt_4]_2[Fe_2S_2(S\text{-}t\text{-}Bu)_4]$ (**1**), $[NEt_4]_2[Fe_2S_2(Z\text{-Ala-cys-OMe})_4]$ (**2**),[12] and $[NEt_4]_2[Fe_2S_2(Z\text{-cys-Ala-Ala-cys-OMe})_2]$ (**3**) were synthesized by the method reported in the previous paper.[9] $[NEt_4]_2[Fe_2S_2(S_2\text{-}o\text{-xyl})_2]$ (**4**) was prepared according to the reported procedure.[13]

$[NEt_4]_2[Fe_2S_2(tdt)_2]$ (tdt=3,4-toluenedithiolate). To a solution of $[NEt_4]_2[Fe_2S_2(S\text{-}t\text{-Bu})_4]$ (200 mg, 2.5×10^{-4} mol) in acetonitrile (20 cm^3) was added 3,4-toluenedithiol (36 mg, 2.3×10^{-4} mol) with stirring at room temperature. The solution was concentrated under reduced pressure and the residue was washed with fresh THF. The powder obtained was recrystallized with acetonitrile and ether and gave black microcrystals. Found: C, 46.73; H, 7.39; N, 3.33. Calcd for $C_{30}H_{62}N_2S_6Fe_2$: C, 48.38; H, 7.04; N, 3.76. Absorption maxima (DMF); 550 nm (ε 4000), 496 nm (ε 5260), 475 nm (sh, ε 4800), 383 nm (ε 9100), and 320 nm (ε 9700). ^1H NMR spectrum; *o*-CH_3, δ=4.5; Ph-H, δ=10.2 and 10.5 (Me_2SO-d_6).

Detection of H_2S. Argon gas was bubbled into a DMF solution (2 cm^3) of $[NEt_4]_2[Fe_2S_2(Z\text{-cys-Ala-Ala-cys-OMe})_2]$ (30.3 mg, 2.1×10^{-5} mol) and the gas was vented through an 8 mM silver nitrate aqueous solution. After addition of tdt-H_2 (6.4 mg, 4×10^{-5} mol) into the DMF solution, the silver nitrate solution gave a black precipitate upon bubbling argon gas at room temperature. The black precipitate was collected with filtration. Yield 7 mg of silver sulfide (68%).

Methods. The visible spectrum (a) was obtained with a DMF solution of [2Fe-2S] complex (3×10^{-7} mol) in a

specially designed quartz 1 mm-cell equipped with stop-cocks for the measurements of visible and circular dichroism (CD) spectra. The ligand-exchange reaction (b) was carried out by the addition of a DMF solution of tdt-H_2 (3×10^{-7} mol) at room temperature. The difference visible spectra of the above systems were obtained by subtracting (a) from (b) to give a spectrum corresponding to the spectrum of a DMF solution of the authentic $[NEt_4]_2[Fe_2S_2(tdt)_2]$. The addition of *o*-xyl-$(SH)_2$ to [2Fe–2S] complexes was also carried out by the above method.

Physical Measurements. The visible spectra of the [2Fe–2S] complexes were obtained on a Jasco UVIDEC-5A spectrophotometer. CD spectra were recorded using a Jasco J-40 spectropolarimeter. The calibration of the spectropolarimeter was carried out with *epi*-androsterone in dioxane.[14] The values of ε and $\Delta\varepsilon$ were given in the unit of $M^{-1}cm^{-1}$.

Results and Discussion

Ligand-Exchange Reaction. A ligand-exchange method using 3,4-toluenedithiol (tdt-H_2) or *o*-xylene-α,α'-dithiol (*o*-xyl-$(SH)_2$) was employed to determine a chelation ability of Z–Cys–X–Y–Cys–OMe to $[Fe_2S_2]^{2+}$ core in DMF at room temperature. The proposed ligand-exchange reactions for the 2Fe–2S complexes with the dithiols are shown in the following scheme.

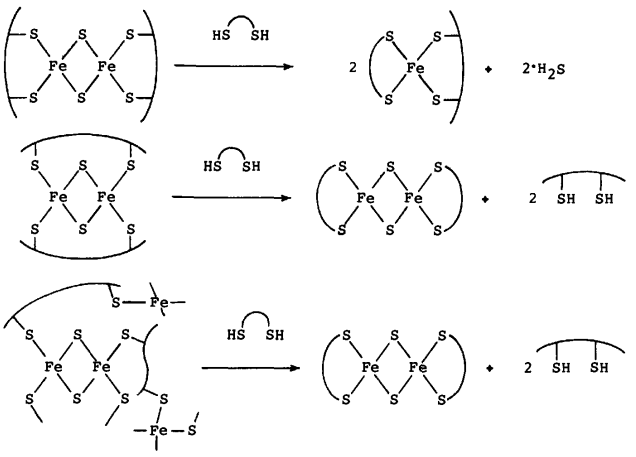

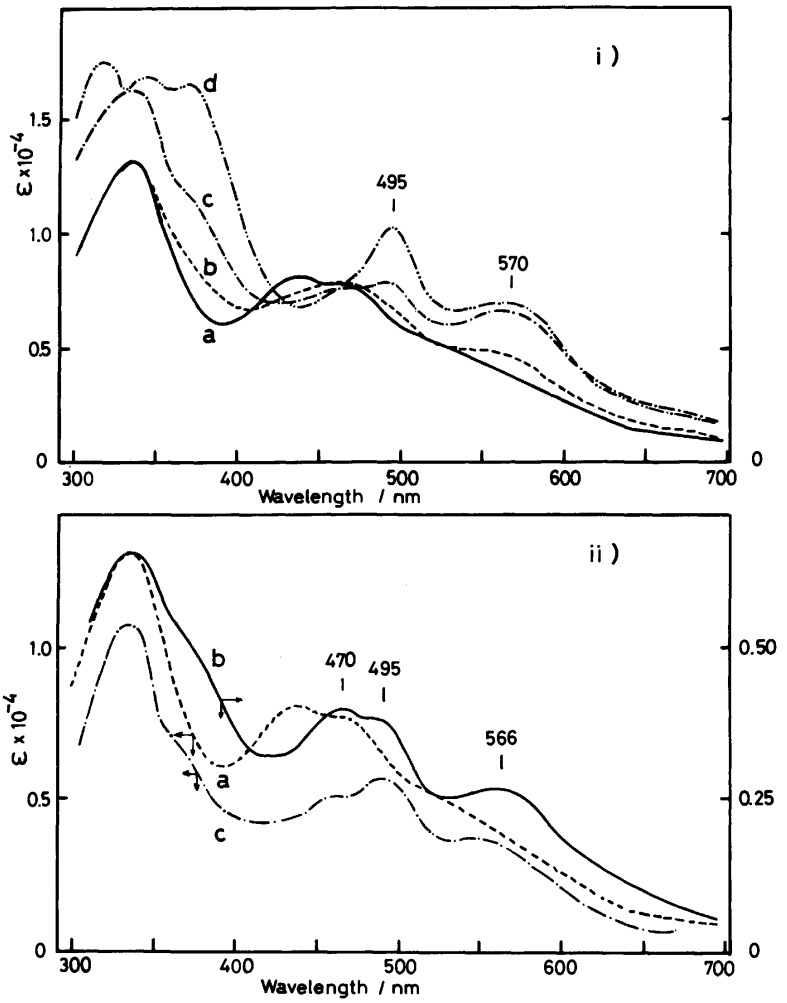

Fig. 1. Visible spectra of i) (a) a DMF solution of $[NEt_4]_2[Fe_2S_2(S\text{-}t\text{-}Bu)_4]$ at room temperature, (b) solution-(a)+tdt-H_2(1 equiv), (c) solution-(a)+tdt-H_2(2 equiv,) and (d) the solution-(a)+tdt-H_2(4 equiv) and ii) (a) a DMF solution of $[NEt_4]_2[Fe_2S_2(S\text{-}t\text{-}Bu)_4]$, (b) the difference visible spectrum of the reaction mixture of $[NEt_4]_2[Fe_2S_2(S\text{-}t\text{-}Bu)_4]$ and tdt-H_2 (1 : 1), and (c) the visible spectrum of a DMF solution of $[NEt_4]_2[Fe_2S_2(tdt)_2]$ at room temperature.

Monodentate ligand, *t*-Bu-S$^-$, in $[Fe_2S_2(S\text{-}t\text{-}Bu)_4]^{2-}$ can be easily expelled by Cys-containing peptides such as Z-Ala-Cys-OMe and Z-Cys-Ala-Ala-Cys-OMe. This ligand-exchange reaction in the following equation was utilized for the synthesis of [2Fe-2S] Cys-containing peptide complexes[9] as well as the synthesis of [4Fe-4S] peptide complexes.[15-17] The authentic $[NEt_4]_2[Fe_2S_2(tdt)_2]$ was synthesized by the same method.

$$[Fe_2S_2(S\text{-}t\text{-}Bu)_4]^{2-} \xrightarrow{RS^-} [Fe_2S_2(SR)_4]^{2-} + t\text{-BuSH} \quad (1)$$

(SR^- = $tdt^{2-}/2$, Cys-containing peptides$^-$)

Examination of Chelation of Peptide Ligands on $[Fe_2S_2]^{2+}$ Core by Ligand-Exchange Reaction with 3,4-Toluenedithiol. The dithiol readily exchanges with the monodentate ligand of [2Fe–2S] complexes as shown in $[NEt_4]_2[Fe_2S_2(S\text{-}t\text{-}Bu)_4]$ (**1**) and $[NEt_4]_2[Fe_2S_2$-(Z-Ala-cys-OMe)$_4$] (**2**).

Figure 1-i or 2 shows the visible spectra of **1** or **2** in DMF and the spectral change by the addition of various molar equivs of tdt-H_2. The addition of less than 2 equiv of tdt-H_2 to $[NEt_4]_2[Fe_2S_2(S\text{-}t\text{-}Bu)_4]$ resulted in formation of a new species giving an isosbestic point at 465 nm. The visible spectrum of the new species obtained by the addition of 1 equiv of tdt-H_2 is shown in Fig. 1-b. One of the figures shows a difference spectrum between **1** and the reaction mixture. The new species exhibits absorption maxima at 566, 495, 470, 375 (sh), and 336 nm for **1** or 566, 493, 470, 373 (sh), and 335 nm for **2** in DMF. The absorption maximum at 566 nm is assignable to a characteristic ligand-metal charge-transfer (LMCT) band for $[Fe_2S_2(SR)_4]^{2-}$ complex. The species having these absorption maxima (550, 496, 470, 370, 320 nm) was thus identified as the authentic $[Fe_2S_2(tdt)_2]^{2-}$ complex. The formation of $[Fe_2S_2(tdt)_2]^{2-}$ was observed by ^1H NMR spectrum of a reaction mixture of $[Fe_2S_2(Z\text{-cys-Ala-OMe})_4]^{2-}$ with tdt-H_2 in Me_2SO-d_6. Two broad peaks at δ 10.8 and 10.2 were found and assignable to the phenyl protons of tdt ligand, since the authentic tdt complex exhibited two Ph-H signals at δ 10.2 and 10.5 in Me_2SO-d_6. The methyl proton peaks of the ligand were overlapped with *t*-Bu peaks at δ 4.7.

The addition of tdt-H_2 to $[Fe_2S_2(Z\text{-Ala-cys-OMe})_4]^{2-}$ results in formation of $[Fe_2S_2(tdt)_2]^{2-}$ with a smooth substitution reaction of Z-Ala-Cys-OMe with the tdt ligand. In this case, the $[Fe_2S_2]^{2+}$ core remains until the addition of over 5 equiv of tdt-H_2.

The addition of over 3—4 equivs of tdt-H_2 to **1** resulted in formation of another new species having absorption maxima at 495 nm (ε 14500), 375 nm (ε 27400), and 313 nm (ε 19500). The addition of tdt-H_2 to a DMF solution of $[Fe_2S_2(S_2\text{-}o\text{-xyl})_2]^{2-}$ (**3**) (Fig. 3) or $[Fe_2S_2(Z\text{-cys-Ala-Ala-cys-OMe})_2]^{2-}$ (**4**) (Fig. 4) at

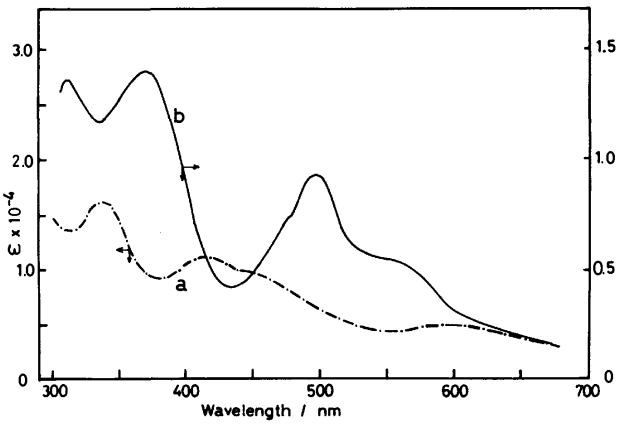

Fig. 3. Visible spectra of a) $[NEt_4]_2[Fe_2S_2(S_2\text{-}o\text{-xyl})_2]$ and b) the difference visible spectrum of the species forming from the ligand-exchange reaction (solution-(a) + tdt-H_2 (1 : 1)) in DMF at room temperature.

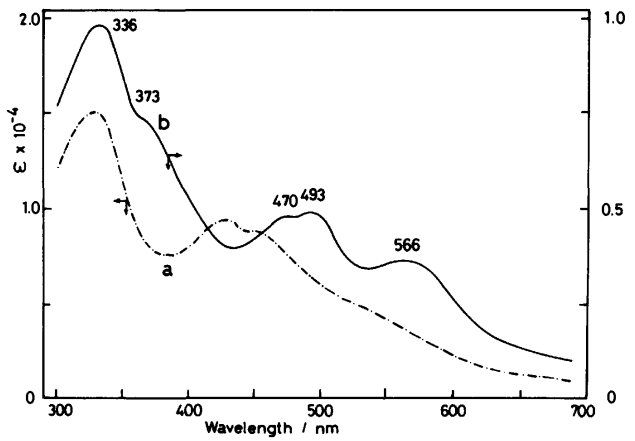

Fig. 2. Visible spectra of a) $[NEt_4]_2[Fe_2S_2(Z\text{-Ala-cys-OMe})_4]$ and b) the difference visible spectrum of the species obtained from the ligand-exchange reaction (solution-(a) + tdt-H_2 (1 : 1)) in DMF at room temperature.

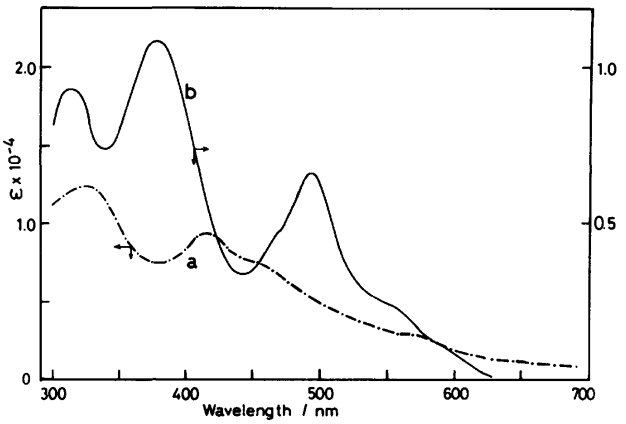

Fig. 4. Visible spectra of a) $[NEt_4]_2[Fe_2S_2(Z\text{-cys-Ala-Ala-cys-OMe})_2]$ and b) the difference visible spectrum of the species forming from the ligand-exchange reaction (solution-(a) + tdt-H_2 (1 : 1)) in DMF at room temperature.

(1 : 1) molar ratio gave another species which exhibits absorption maxima at 492 nm (ε 9700), 370 nm (sh, ε 13000), and 339 nm (ε 16000). The difference spectrum of the species is shown in Fig 4-b. The chelation of two tdt ligands is expected for Fe(III), but the absorption maxima of $[Fe(tdt)_2]^{1-}$ in DMF were reported to be observed at 645 nm (ε 100), 503 nm (ε 10000), and 386 nm (ε 17000).[18] The bis(peptide)Fe(III) complex, $[Fe(Z\text{-cya-Ala-Ala-cys-OMe})_2]^{1-}$ has been found to have absorption maxima at 495 nm (ε 3400) and 353 nm (ε 5500).[5] Therefore, these two bis-chelated species are not present at (1 : 1) ratio. Then, the new species suggests the formation of [Fe(tdt)-(Z-cys-Ala-Ala-cys-OMe)]$^{1-}$. This ligand-exchange reaction gave hydrogen sulfide which was detected as silver sulfide in 68% yield. The addition of tdt-H_2 to a DMF soultion of **4** results in preferential cleavage of Fe-S* at (1 : 1) molar ratio.

Addition of *o*-Xylene-α,α′-dithiol (*o*-xyl-(SH)$_2$) to a Solution of 2Fe-2S Peptide Complex. *o*-Xyl-(SH)$_2$ is also one of effective chelating reagents for Fe(III) ion. The succesive addition of 1—5 equiv of *o*-xyl-(SH)$_2$ to a DMF solution of $[Fe_2S_2(Z\text{-Ala-cys-OMe})_4]^{2-}$ and $[Fe_2S_2(Z\text{-cys-Ala-Ala-cys-OMe})_2]^{2-}$ showed a visible maximum at 588 nm with high-molar absorption coefficient which is assignable to a LMCT absorption maximum (ε 4800) of $[Fe_2S_2(S_2\text{-}o\text{-xyl})_2]^{2-}$ (Fig. 5). The addition of *o*-xyl-(SH)$_2$ to a solution of the peptide complexes results in formation of the same 2Fe-2S complex after the ligand substitution reaction. This titration was monitored by the CD spectral method and resulted in observation of 20% of the Δε value at 580 nm (Fig. 6). Clear isosbestic points in the CD spectra were observed at 350, 395, and 437 nm. The results indicate a monotonous substitution of Z-Cys-Ala-Ala-Cys-OMe with *o*-xyl-(SH)$_2$ giving mixed ligand [2Fe-2S] complexes as shown in the following scheme. The *K* value ($K_1 \cdot K_2$) obtained by the CD

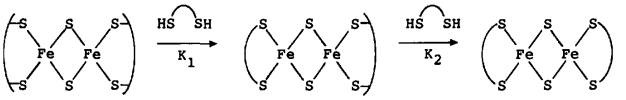

method is 0.4 (K_1=0.2, K_2=2.0) in DMF. On the contrary, the successive addition of *o*-xyl-(SH)$_2$ to $[Fe_2S_2(Z\text{-Ala-cys-OMe})_4]^{2-}$ results in gradual appearance of an absorption maximum at 592 nm. *K* value for the ligand-exchange reaction of $[Fe_2S_2(Z\text{-Ala-cys-OMe})_4]^{2-}$ is 0.0007 mol^2 in DMF (by the CD

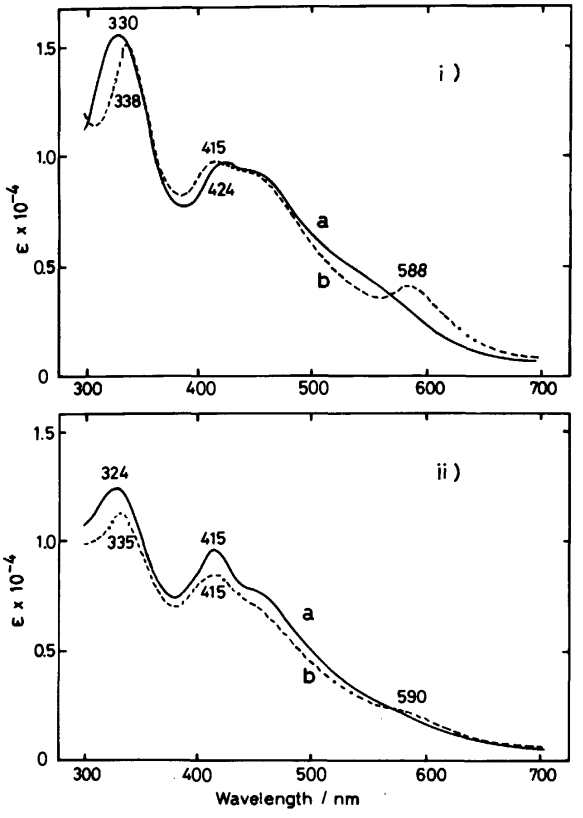

Fig. 5. Visible spectral change of the ligand-exchange reaction of i) (a) $[NEt_4]_2[Fe_2S_2(Z\text{-Ala-cys-OMe})_4]$ and (b) solution-(a) + *o*-xyl-(SH)$_2$ (1 : 2) and ii) (a) $[NEt_4]_2[Z\text{-cys-Ala-Ala-cys-OMe})_2]$ and (b) solution-(a) + *o*-xyl-(SH)$_2$ (1 : 2) in DMF at room temperature.

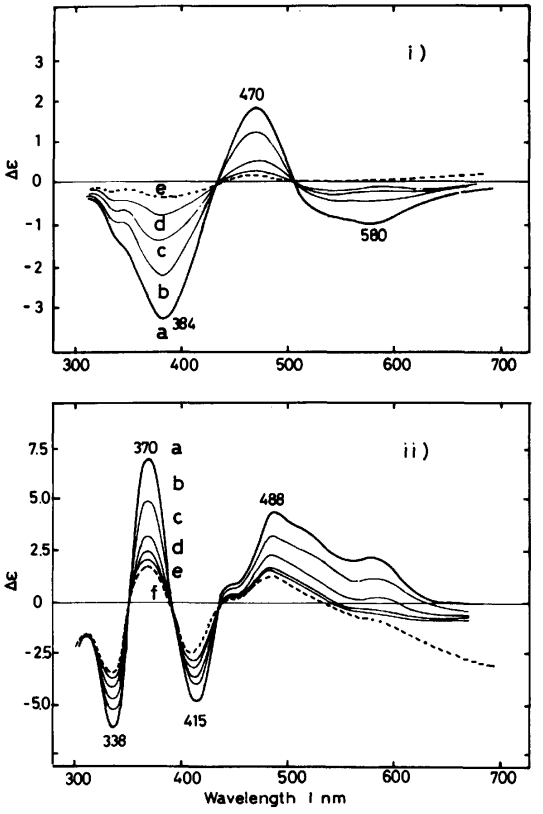

Fig. 6. CD spectral change of the ligand-exchange reaction of i) (a) $[NEt_4]_2[Fe_2S_2(Z\text{-Ala-cys-OMe})_4]$, (b) solution-(a) + *o*-xyl-(SH)$_2$ (1 : 1), (c) (1 : 2), (d) (1 : 3), and (e) (1 : 4) and ii) (a) $[NEt_4]_2[Z\text{-cys-Ala-Ala-cys-OMe})_2]$, (b) solution-(a) + *o*-xyl-(SH)$_2$ (1 : 1), (c) (1 : 2), (d) (1 : 3), (e) (1 : 4), and (f) (1 : 5) in DMF at room temperature.

method).

Chelating Ability of Z-Cys-Ala-Ala-Cys-OMe. The displacement reaction by tdt-H_2 with Cys-containing 2Fe–2S complexes in DMF was found to be different from that by *o*-xyl-$(SH)_2$. The addition of *o*-xyl-$(SH)_2$ to **1** and **2** results in formation of $[Fe_2S_2(S_2\text{-}o\text{-xyl})_2]^{2-}$ with a characteristic absorption maximum at 592 nm, which corresponds to the reported maximum at 590 nm (ε 4800) in DMF.[13] The difference between the K values (0.0007 for **2** and 0.4 mol^2 for **3**) is ascribed to the chelation effect of Z–Cys–Ala–Ala–Cys–OMe in **4**. The presence of the clear isosbestic point of the CD spectra with addtion of *o*-xyl-$(SH)_2$ to **3** indicates absence of a bridged Z–Cys–Ala–Ala–Cys–OMe ligand since the bridging ligand must be substituted first with tdt ligand. The successful employment of *o*-xyl-$(SH)_2$ for the core extrusion of [2Fe–2S]adrenal ferredoxin has already been reported.[1,10]

The addition of tdt-H_2 to a DMF solution of **2** and **3** results in the cleavage of Fe–S* bond in the $Fe_2S_2^{2+}$ core, giving $[Fe(tdt)(S_2\text{-}o\text{-xyl})]^{1-}$ or $[Fe(tdt)(Z\text{–cys–Ala–Ala–cys–OMe})]^{1-}$ with the following reaction scheme.

$$[Fe_2S_2(S_2\text{-}R)_2]^{2-} \xrightarrow{\text{tdt-}H_2} [Fe(tdt)(S_2\text{-}R)]^{1-} + H_2S \xrightarrow{\text{tdt-}H_2} 2[Fe(tdt)_2]^{1-} + (HS)_2\text{-}R \quad (2)$$

$(S_2\text{-}R^{2-} = S_2\text{-}o\text{-xyl}^{2-}$, Z-Cys-Ala-Ala-Cys-$OMe^{2-})$

Previously, we reported that $[Fe(Z\text{–cys–Ala–Ala–cys–OMe})_2]^{1-}$ exhibits CD extrema at 560 nm ($\Delta\varepsilon$ +1.3) and 500 nm ($\Delta\varepsilon$ −1.6) in DMF. The (1:1) species, $[Fe(tdt)(Z\text{–cys–Ala–Ala–cys–OMe})]^{1-}$, exhibits an absorption maximum at 494 nm (ε 12000) and CD extrema at 550 nm ($\Delta\varepsilon$ −0.6), 495 nm ($\Delta\varepsilon$ −1.0), and 335 nm ($\Delta\varepsilon$ −13.0). Formation of hydrogen sulfide was confirmed by precipitation of silver sulfide from silver nitrate. The satisfactory yield (68%) of silver sulfide indicates that the addition of tdt-H_2 to **3** preferentially cleavages the Fe–S* bonds according to the Eq 2. Averil et al. have reported the core extrusion of [2Fe–2S] adrenodoxin with tdt-H_2.[10] They speculated the formation of $[Fe(tdt)_2]^{2-}$ with addition of 19 equivs of tdt-H_2 to adrenodoxin. The reduction of $[Fe(tdt)_2]^{1-}$ should be involved in this case because the mononuclear bis(1,2-dithiolene)Fe(III) complex has a relatively positive redox potential and is easily reduced by the dithiol giving (2−) species ($[Fe^{II}(tdt)_2]^{2-}$). Our results suggest that, upon the core extrusion from iron-sulfur proteins, some of dithiols destroy a native cluster itself.

Thus we found that the addition of one equiv of tdt-H_2 to $[Fe_2S_2(SR)_4]^{2-}$ complex results in the formation of either $[Fe(tdt)(SR)_2]^{1-}$ or $[Fe_2S_2(tdt)_2]^{2-}$. The former complex is formed by cleavage of Fe–S* and the later product is obtained by the substitution of SR with tdt ligand. Thus, although we have examined only a few cases of the ligand exchange reactions for Cys-containing peptide complexes, the chelation of the peptide thiolate ligand to $[Fe_2S_2]^{2+}$ core was conveniently determined by using tdt-H_2.

In conclusion, the chelation of Z–Cys–Ala–Ala–Cys–OMe to each Fe(III) ion in the [2Fe–2S] complex is confirmed. The bridging coordination of this sequence in native [2Fe–2S]ferredoxins is thus enforced by the peptide sequence of the other parts.

References

1) a) J. Cambray, R. W. Lane, A. G. Wedd, R. W. Johnson, and R. H. Holm, *Inorg. Chem.*, **16**, 2565 (1977); b) W. O. Gillum, L. E. Mortenson, J.-S. Chen, and R. H. Holm, *J. Am. Chem. Soc.*, **99**, 584 (1977).

2) H. Beinert and A. J. Thomson, *Arch. Biochem. Biophys.*, **222**, 333 (1983).

3) a) K. S. Hagen, J. G. Reynolds, and R. H. Holm, *J. Am. Chem. Soc.*, **103**, 4054 (1981); b) K. S. Hagen, A. D. Watson, and R. H. Holm, *J. Am. Chem. Soc.*, **105**, 3905 (1983).

4) N. Ueyama, S. Ueno, M. Nakata, and A. Nakamura, *Bull. Chem. Soc. Jpn.*, **57**, 984 (1984).

5) N. Ueyama, M. Nakata, and A. Nakamura, *Bull. Chem. Soc. Jpn.*, **54**, 1727 (1981).

6) M. Nakata, N. Ueyama, T. Terakawa, and A. Nakamura, *Bull. Chem. Soc. Jpn.*, **56**, 3647 (1983).

7) N. Ueyama, M. Nakata, M. Fuji, T. Terakawa, and A. Nakamura, *Inorg. Chem.*, **24**, 2190 (1985).

8) T. Tsukihara, K. Fukuyama, H. Tahara, Y. Katsube, Y. Matsuura, N. Tanaka, M. Kakudo, K. Wada, and H. Matsubara, *J. Biochem.*, **84**, 1645 (1978).

9) S. Ueno, N. Ueyama, A. Nakamura, and T. Tsukihara, *Inorg. Chem.*, **25**, 1000 (1986).

10) B. A. Averill, J. R. Bale, and W. H. Orme-Johnson, *J. Am. Chem. Soc.*, **100**, 3034 (1978).

11) C. K. Mann, *Electroanal. Chem.*, **1969**, 3.

12) Small letter cys refers to the Cys residue involved in coordination.

13) J. J. Mayerle, S. E. Denmark, B. V. DePamphilis, J. A. Ibers, and R. H. Holm, *J. Am. Chem. Soc.*, **97**, 1032 (1975).

14) K. Tuzimura, T. Konno, H. Meguro, M. Hatano, T. Murakami, K. Kashiwabara, K. Saito, Y. Kondo, and T. Suzuki, *Anal. Biochem.*, **81**, 167 (1977).

15) L. Que, Jr., J. R. Anglin, M. A. Bobrik, A. Davison, and A. Holm, *J. Am. Chem. Soc.*, **96**, 6042 (1974).

16) N. Ueyama, T. Terakawa, M. Nakata, and A. Nakamura, *J. Am. Chem. Soc.*, **105**, 7098 (1983).

17) N. Ueyama, A. Kajiwara, T. Terakawa, and A. Nakamura, *Inorg. Chem.*, **24**, 4700(1985).

18) J. A. McCleverty, N. M. Atherton, N. G. Connelly, and C. J. Winscom, *J. Chem. Soc. (A)*, **1969**, 2242.

 © 1987 The Chemical Society of Japan Bull. Chem. Soc. Jpn., 60, 289—293 (1987)

Hydroxylation of Acetoxy-*p*-menthenes in the Cultured Cells of *Nicotiana tabacum*. Epoxidation of the Carbon-Carbon Double Bond

Toshifumi HIRATA, Shunsuke IZUMI, Teiji EKIDA, and Takayuki SUGA*
Department of Chemistry, Faculty of Science, Hiroshima University,
Higashisenda-machi, Naka-ku, Hiroshima 730
(Received July 7, 1986)

The process of the formation of glycols in the biotransformation of 1-acetoxy-*p*-menth-4(8)-ene and 8-acetoxy-*p*-menth-1-ene in the cultured cells of *Nicotiana tabacum* was examined. The formation of the glycols was found to result from epoxidation of the C–C double bond, followed by hydrolysis of the resulting epoxides.

Recent studies on the biotransformation of acetoxy-*p*-menthenes in the cultured cells of *Nicotiana tabacum* showed that the cells have the ability to hydroxylate regio- and stereoselectively the C–C double bond and its allylic position to yield the corresponding glycols and allyl alcohols.[1-3] Also the hydroxylation of 8-acetoxy-*p*-menth-1-ene was enantioselective;[3,4] the C–C double bond of the 4*S* enantiomer was hydroxylated in preference to the 4*R* one, whereas the hydroxylation at the allylic position was in favor of the 4*R* isomer. Such a difference in enantioselectivity in two types of the hydroxylation remarked us that the mechanism may differ from one another. We have investigated the process of hydroxylation of the C–C double bond in the cultured cells of *N. tabacum*.

Results and Discussion

Formation of Epoxides in the Biotransformation of Acetoxy-*p*-menthenes. In order to find intermediates in the hydroxylation of the C–C double bond, each of 1-acetoxy-*p*-menth-4(8)-ene (**1**) and (±)-8-acetoxy-*p*-menth-1-ene (**2**) was incubated for 2 d with a suspension of cultured cells of *N. tabacum* similarly to the manner described in our previous paper,[1] and careful TLC and GLC analyses indicated that the products were composed of unidentified products (**3**—**6**), in addition to the previously described hydroxylated products, such as *t*-1-acetoxy-*p*-menthane-*r*-4,8-diol (**7**) and 8-acetoxy-*c*-4-*p*-menthane-*r*-1,*t*-2-diol (**8**).[1,3] The unidentified products **3**—**6** were proved to be the corresponding epoxides of the acetoxy-*p*-menthenes by comparison of TLC, GLC, and GLC-MS with those of synthetic specimens described in the next section. Incubation of **1** gave *r*-1-acetoxy-*t*-4,8-epoxy-*p*-menthane (**3**) and *r*-1-acetoxy-*c*-4,8-epoxy-*p*-menthane (**4**) in 3.8 and 1.0% yields, respectively. On the other hand, incubation of **2** gave 8-acetoxy-*r*-1,*c*-2-epoxy-*c*-4-*p*-menthane (**5**) and 8-acetoxy-*r*-1,*c*-2-epoxy-*t*-4-*p*-menthane (**6**) in 2.0 and 0.1% yields, respectively.

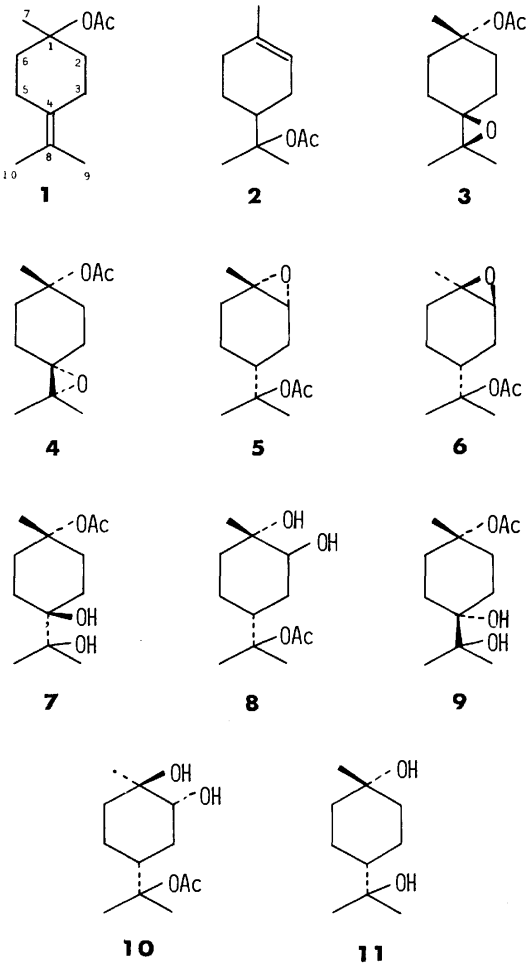

The time-courses in the biotransformation of the acetoxy-*p*-menthenes **1** and **2** in a suspension of the cultured cells were followed. In the case of **1**, the formation of the epoxides **3** and **4** was observed at an earlier period of incubation, but their content gradually decreased with the lapse of time after incubation for 4 d, as shown in Fig. 1a. Similar phenomenon was also observed in the case of 8-acetoxy-*p*-menth-1-ene (**2**) (Fig. 1b). Such a decrease in the amount of the epoxides is probably due to further transformation to other products such as glycols, which had been the main products in the

biotransformation of the acetoxy-*p*-menthenes.[1,3]

To elucidate the conversion of the epoxides to the glycols, each of the epoxides **3**—**6** was incubated under the same conditions as described above. The remarkable formation of the corresponding glycols was observed as shown in Fig. 2. The epoxides **3** and **6** were transformed to a single product, *t*-1-acetoxy-*p*-menthane-*r*-4,8-diol (**7**) and 8-acetoxy-*c*-4-*p*-menthane-*r*-1,*t*-2-diol (**8**), respectively, whereas the epoxides **4** and **5** gave a mixture of glycols, the glycol (**7**) and *c*-1-acetoxy-*p*-menthane-*r*-4,8-diol (**9**) in a ratio of 1:6 from **4** and the glycol **8** and 8-acetoxy-*t*-4-*p*-menthane-*r*-1,*t*-2-diol (**10**) in a ratio of 4:1 from **5**. Exclusive formation of the glycol **8** in the conversion of the epoxide **6** indicates occurrence of the cleavage of the epoxy ring at only C-1 and not at C-2. Such an exclusive conversion is probably due to the difference in the stability of intermediate cations in the transition state, as indicated by the MO calculation[5] that the total energy of the cation having a positive charge at C-1 is lower by 26 kcal† mol^{-1} than that of the cation at C-2. The transformation of the epoxides to the glycols was also found when the epoxides were treated with Murashige and Skoog's solution[6] used as culture medium. These findings clearly indicate that the epoxides are chemically converted to the corresponding glycols with this solution. The rate of the transformation of the epoxide **6** to the glycol **8** was very fast, as shown in Fig. 2d; this may be responsible for a little accumulation of the epoxide **6** in the biotransformation of **2**.

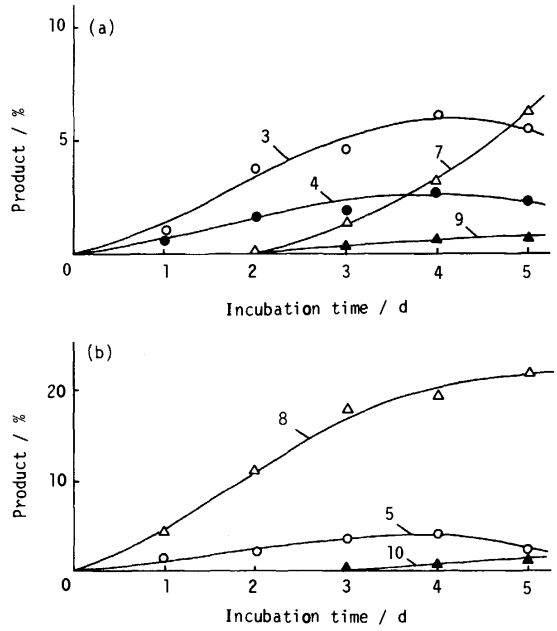

Fig. 1. Formation of the epoxides **3**—**5** and the glycols **7**—**10** in the biotransformation of (a) 1-acetoxy-*p*-meth-4(8)-ene (**1**) and (b) 8-acetoxy-*p*-menth-1-ene (**2**) in the cultured cells of *N. tabacum*.

The transformation of the acetoxy-*p*-menthenes to glycols in the cultured cells of *N. tabacum* was thus found to involve epoxidation of the double bond by a biological process, followed by hydrolysis of the resulting epoxides by a chemical one.

Structure Elucidation of the Synthetic Epoxides. For identification of the stereochemical structures of the epoxides produced in the biotransformation of the

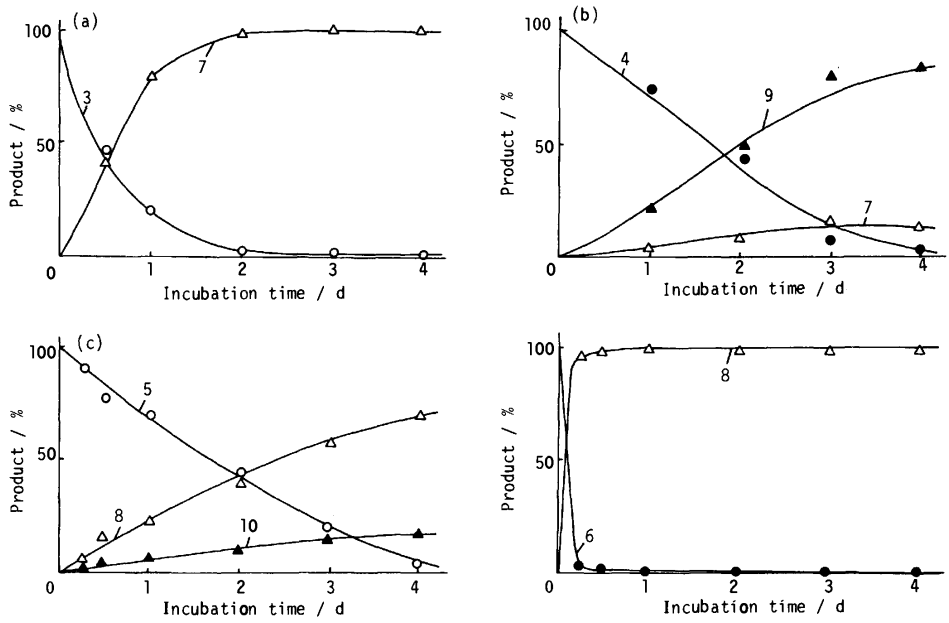

Fig. 2. The time-courses in the biotransformation of (a) *r*-1-acetoxy-*t*-4,8-epoxy-*p*-menthane (**3**), (b) *r*-1-acetoxy-*c*-4,8-epoxy-*p*-menthane (**4**), (c) 8-acetoxy-*r*-1,*c*-2-epoxy-*c*-4-*p*-menthane (**5**) and 8-acetoxy-*r*-1,*c*-2-epoxy-*t*-4-*p*-menthane (**6**) in the cultured cells of *N. tabacum*.

† 1 cal=4.184 J.

acetoxy-*p*-menthenes in the cultured cells, epoxides were prepared from **1** and **2** by epoxidation with *m*-chloroperbenzoic acid to determine their relative spatial arrangements between the epoxy ring and the 1-acetoxyl and 1-acetoxy-1-methylethyl groups, as described below. Epoxidation of **1** gave a 3:7 mixture of epoxides A and B which were identical with the products **4** and **3** in the biotransformation of **1**, respectively, in all respects of their spectra and chromatographic behavior. The fragmentation pattern in the mass spectrum of the epoxide A was quite similar to that of the epoxide B; this implies the epoxide A to be a geometrical isomer of the epoxide B. The epoxides A and B exhibited the ^{1}H NMR signals at δ 1.36 and 1.33, respectively, due to a tertiary *gem*-dimethyl group, instead of the signal (δ 1.67) due to the methyl groups attached to the 4(8)-double bond of **1**. Accordingly, the epoxides A and B were suggested to be 4,8-epoxides of **1**. However, these spectral data did not give any reliable informations for determining the relative orientation between the epoxy ring and the 1-acetoxyl group in the epoxides. The structure of the epoxide A was finally determined by X-ray crystallography. An ORTEP drawing[7] of the epoxide A is given in Fig. 3; the epoxy ring was found to be cis to the acetoxyl group. The epoxide A was thus established to be *r*-1-acetoxy-*c*-4,8-epoxy-*p*-menthane (**4**). Therefore, the epoxide B should be *r*-1-acetoxy-*t*-4,8-epoxy-*p*-menthane (**3**).

Epoxidation of **2** gave a 9:11 mixture of epoxides C and D which were identical with the epoxides **5** and **6** in the biotransformation of **2**, respectively. The relative orientation between the epoxy ring and the 1-acetoxy-1-methylethyl group in these epoxides was evidenced by ^{1}H NMR spectral analysis as described below. On the basis of Karplus's equation[8] and the ^{1}H NMR data reported for limonene 1,2-oxide,[9] ^{1}H–^{1}H coupling patterns for the C-2 proton of both the epoxides were predicted to be a doublet (J=4—7 Hz) for a *cis*-epoxide and a broad singlet or a triplet (J=0—2 Hz) for a *trans*-epoxide. The observed signals were a doublet (J=4.6 Hz) at δ 2.81 for the epoxide C and a broad singlet at δ 2.87 for the epoxide D; this observation suggests the relative orientation between the epoxy ring and the 1-acetoxy-1-methylethyl group in the epoxide C to be cis and that of the epoxide D to be trans. The suggested structure for the epoxide C was supported by the formation of *c*-4-*p*-menthane-*r*-1,8-diol (**11**)[10] on reduction with lithium aluminum hydride. The epoxides C and D were thus established to be 8-acetoxy-*r*-1,*c*-2-epoxy-*c*-4-*p*-menthane (**5**) and 8-acetoxy-*r*-1,*c*-2-epoxy-*t*-4-*p*-menthane (**6**), respectively. All the epoxides prepared above were used as authentic samples for the purpose of identification.

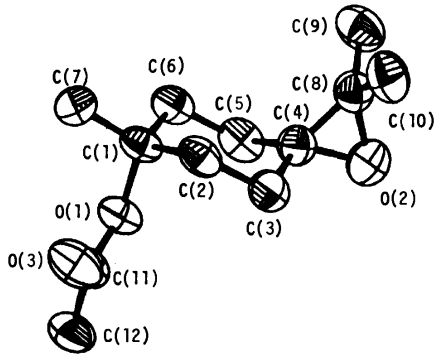

Fig. 3. ORTEP drawing of the epoxide A.

Experimental

Analytical TLC and preparative TLC were carried out on 0.25 mm and 0.75 mm thick silica-gel plates (Merck silica gel 60, GF_{254}), respectively. GLC analyses were performed on a Shimadzu GC-6A gas chromatograph equipped with an FID and a glass column (3 mm×2 m) packed with 15% DEGS and 2% OV-17 on Chromosorb W (AW-DMCS; 80—100 mesh) by programming the column temperature at 100—200 °C with a rate of 3 °C min^{-1} for DEGS and at 90—250 °C with a rate of 2 °C min^{-1} for OV-17. GLC-MS were recorded on a Shimadzu QP-1000 mass spectrometer which was equipped with an EI ion source operating at 70 eV and installed with a gas chromatograph equipped with an OV-17 column operating at 80—200 °C with a rate of 3 °C min^{-1}.

Substrate. 1-Acetoxy-*p*-menth-4(8)-ene (**1**) [IR ν_{max} (film) 1740 cm^{-1} (ester C=O); ^{1}H NMR ($CDCl_3$) δ=1.49 (3H, s, 7-Me), 1.67 (6H, bs, 9- and 10-Me), and 1.98 (3H, s, OAc); *m/z* (rel intensity) 136 (M$^+$—AcOH, 80%), 121 (100), and 93 (65)] was prepared from limonene (Ogawa Perfumery Co. Ltd.), according to the procedure described in our previous paper.[1]

(±)-8-Acetoxy-*p*-menth-1-ene (**2**) [IR ν_{max} (film) 1730 cm^{-1} (ester C=O); ^{1}H NMR ($CDCl_3$) δ=1.43 (6H, s, 9- and 10-Me), 1.64 (3H, bs, 7-Me), 1.96 (3H, s, OAc), and 5.32 (1H, bs, >C=CH-); *m/z* (rel intensity) 136 (M$^+$—AcOH, 85%), 121 (100), and 93 (63)] was prepared from (±)-*p*-menth-1-en-8-ol (*α*-terpineol) (Takasago Perfumery Co. Ltd.) by acetylation, followed by chromatography on a silica-gel column with hexane-ethyl acetate (97:3, v/v). Both the substrates used were >99.5% pure on GLC.

Incubation of Acetoxy-*p*-menthenes 1 and 2 in a Suspension of the Cultured Cells. A suspension of the cultured cells of *N. tabacum* "Bright Yellow" were prepared as described in our previous paper;[1] the cells were cultured in each 300-ml conical flask containing 100 ml of Murashige and Skoog's solution.[6] To the flask containing a suspension of the cultured cells, 10 mg of the substrate, such as 1-acetoxy-*p*-menth-4(8)-ene (**1**) and (±)-8-acetoxy-*p*-menth-1-ene (**2**), were administered; the total amount of the substrate used was 100 mg. The mixture was incubated at 25 °C for 2 d on a rotary shaker (70 rpm) in the dark. The cultured mixture was worked up in a manner similar to that described in our previous paper.[1] An incubation product obtained was subjected to the repeated TLC with hexane-ethyl acetate (7:3 and 1:1, v/v). Constituents of the product were identified by comparing their TLC, GLC, and GLC-MS with those of authentic specimens.

Time-Courses in the Biotransformation of Acetoxy-*p*-menthenes 1 and 2 and Epoxides 3—6. Each of the substrates was administered to a suspension of the precultured cells in each flask, as described above. A part of the incubation mixture (10 ml) was pipetted out and extracted with ether at a regular time interval. Each ether extract was dissolved in ethyl acetate and then subjected to GLC. The products were identified by comparison (co-GLC and GLC-MS) with authentic samples.[1,3] Yields of the products were determined on the basis of the peak areas on GLC and are expressed as the relative percent for the total amount of a whole reaction product extracted. The time-courses in the biotransformation are given in Figs. 1 and 2.

Treatment of Acetoxy-*p*-menthenes 1 and 2 and Epoxides 3—6 with Murashige and Skoog's Solution. Each of the substrates (10 mg) were shaken with 100 ml of Murashige and Skoog's solution (pH 5.8) at 25 °C for 4 d in the dark. A reaction mixture was extracted with ether to give an oily substance, which was subjected to TLC, GLC, and GLC-MS. The oily substance was composed of only the unchanged acetoxy-*p*-menthene in both the cases of the acetoxy-*p*-menthenes **1** and **2**.

The epoxides **3—6** were completely converted to the corresponding glycols. These glycols were identified by comparison of their TLC, GLC, and GLC-MS with those of authentic samples.[1,3] Each of the oily substances (9 and 10 mg) obtained in the reactions of **3** and **6** with Murashige and Skoog's solution was composed of only *t*-1-acetoxy-*p*-menthane-*r*-4,8-diol (**7**) and 8-acetoxy-*c*-4-*p*-menthane-*r*-1,*t*-2-diol (**8**), respectively, by GLC and GLC-MS analyses. In the case of the epoxide **4**, the oily substance (10 mg) was composed of the glycol **7** and *c*-1-acetoxy-*p*-menthane-*r*-4,8-diol (**9**) in a ratio of 1:6 on the basis of the peak areas on GLC. On the other hand, the oily substance (9 mg) from the epoxide **5** was composed of the glycol **8** and 8-acetoxy-*t*-4-*p*-menthane-*r*-1,*t*-2-diol (**10**) in a ratio of 4:1. The time-courses of the conversion of the epoxides **3—6** to the corresponding glycols in Murashige and Skoog's solution were quite similar to those in the case of the transformation of the epoxides in a suspension of the cultured cells (Fig. 2).

Table 1. Final Atomic Coordinates and Thermal Parameters of the Epoxide **4** with Standard Deviations in Parentheses

Atom	$10^4 x$	$10^4 y$	$10^4 z$	B_{eq}[a)]/Å^2
C(1)	6117 (7)	4790 (9)	1682 (4)	4.2
C(2)	6791 (7)	4292 (9)	2700 (4)	4.5
C(3)	8269 (7)	4490 (9)	2998 (5)	4.5
C(4)	8594 (7)	6330 (9)	2806 (5)	4.3
C(5)	8041 (7)	6765 (9)	1775 (5)	5.1
C(6)	6565 (7)	6601 (8)	1480 (5)	4.5
C(7)	4636 (7)	4690 (10)	1414 (5)	5.3
C(8)	8895 (7)	7690 (10)	3532 (5)	4.7
C(9)	8697 (8)	9598 (10)	3268 (6)	6.3
C(10)	8909 (8)	7307 (11)	4524 (5)	6.2
C(11)	6386 (7)	1990 (9)	971 (5)	4.8
C(12)	6924 (9)	1199 (10)	271 (5)	6.2
O(1)	6586 (5)	3690 (5)	1045 (3)	4.6
O(2)	9933 (5)	6843 (7)	3261 (4)	5.9
O(3)	5819 (5)	1188 (7)	1419 (4)	7.0

a) $B_{eq}=(B_{11}+B_{22}+B_{33})/3$.

Preparation of Authentic Samples. i) *r*-1-Acetoxy-*t*-4,8-epoxy-*p*-menthane (**3**) and *r*-1-acetoxy-*c*-4,8-epoxy-*p*-menthane (**4**). Following the procedure described in the reference,[11] 1-acetoxy-*p*-menth-4(8)-ene (**1**) (66 mg) dissolved in dichloromethane (4 ml) was epoxidized with *m*-chloroperbenzoic acid (75 mg) at 0 °C for 4 h. The reaction mixture, after working-up as usual, was subjected to preparative TLC with hexane-ethyl acetate (9:1, v/v) to afford the epoxide **3** [35 mg; IR ν_{max} (film) 1730 cm^{-1} (ester C=O); ^{1}H NMR ($CDCl_3$) δ=1.33 (6H, s, 9- and 10-Me), 1.54 (3H, s, 7-Me), and 2.02 (3H, s, OAc); *m/z* (rel intensity) 152 (M^+—AcOH, 6), 110 (45), and 79 (100)] and the epoxide **4** [15 mg; mp 86.5—87.0 °C, IR ν_{max} (film) 1735 cm^{-1} (ester C=O); ^{1}H NMR ($CDCl_3$) δ=1.36 (6H, s, 9- and 10-Me), 1.54 (3H, s, 7-Me), and 2.04 (3H, s, OAc); *m/z* (rel. intensity) 152 (M^+—AcOH, 2), 110 (44), and 79 (100)].

ii) 8-Acetoxy-*r*-1,*c*-2-epoxy-*c*-4-*p*-menthane (**5**) and 8-acetoxy-*r*-1,*c*-2-epoxy-*t*-4-*p*-menthane (**6**). Epoxidation of 8-acetoxy-*p*-menth-1-ene (**2**) (1.02 g) with *m*-chloroperbenzoic acid (1.2 g) in dichloromethane (25 ml) at 5 °C for 4 h, followed by working-up in the same manner as above, gave the epoxide **5** [269 mg; IR ν_{max} (film) 1729 (ester C=O); ^{1}H NMR ($CDCl_3$) δ=1.23 (3H, s, 9-Me), 1.29 (3H, s, 9-Me), 1.31 (3H, s, 10-Me), 1.88 (3H, s, OAc), and 2.81 (1H, d, *J*=4.6 Hz, 2-H); *m/z* (rel intensity) 152 (M^+—AcOH, 8), 137 (7), 126 (21), and 43 (100)] and the epoxide **6** [335 mg; IR ν_{max} (film) 1725 cm^{-1}; ^{1}H NMR ($CDCl_3$) δ=1.26 (3H, s, 7-Me), 1.38 (6H, s, 9- and 10-Me), 1.88 (3H, s, OAc), and 2.87 (1H, bs, 2-H); *m/z* (rel intensity) 152 (M^+—AcOH, 5), 137 (7), 126 (25), and 43 (100)].

Reduction of the Epoxide 5. The epoxide **5** (10 mg) dissolved in ether (2 ml) was refluxed with a suspension of $LiAlH_4$ (10 mg) in ether (2 ml) for 30 min. The reaction mixture, after working-up as usual, gave a crude product (6 mg). This crude product, after PTLC with hexane-ethyl acetate (7:3, v/v), gave *c*-4-*p*-menthane-*r*-1,8-diol (**11**):[10] 6 mg; mp and mmp 105—106 °C (lit,[12] mp 104—105 °C); IR ν_{max} (film) 3450 cm^{-1} (OH); ^{1}H NMR ($CDCl_3$) δ=1.18 (6H, s, 9- and 10-Me) and 1.21 (3H, s, 7-Me); *m/z* (rel intensity) 136 (M^+-2H_2O, 1), 96 (23), and 81 (100).

X-Ray Crystallographic Analysis of the Epoxide 4. The X-ray crystallographic analysis was performed on a Syntex R3 diffractometer using graphite-monochromated Mo $K\alpha$ radiation. The crystal analyzed was 0.62 mm×0.35 mm×0.87 mm in size. Crystal data: $C_{12}H_{20}O_3$, monoclinic, a=10.891 (5), b=7.747 (7), c=15.112 (8) Å, β=108.47 (4)°, U=1209.4 Å^3, Z=4, D_c=1.17 g cm^{-3}, D_m=1.20 g cm^{-3}, μ(Mo $K\alpha$)=0.9 cm^{-1}, space group $P2_1/c$. A total of 1316 reflections were collected by ω-scan ($2\theta_{max}$=50.0) and used in the structure determination. The phases of 204 reflections with $|E|>1.30$ were determined by MULTAN.[13] An E map for the best solution yielded positions for all non-hydrogen atoms. Anisotropic refinement for carbon and oxygen atoms and isotropic refinement for hydrogen atom by full-matrix least-squares calculation reduced the R index finally to 0.042. Final atomic coordinates are shown in Table 1. The lists of anisotropic thermal parameters and final structure factors have been deposited as Document No. 8718 at the Office of the Editor of the Chemical Society of Japan.

We acknowledge the assistance of Mr. Hidetoshi Sugimoto in the incubation of 1-acetoxy-4,8-epoxy-*p*-menthanes with the cultured cells and Messrs. Kiyotaka Munesada, Akira Nishikawa, and Satoru Murakami in the preparation of the authentic samples of 1-acetoxy-4,8-epoxy-*p*-menthanes. We thank Takasago Perfumery Co., Ltd. for a gift of the sample of α-terpineol and Ogawa Perfumery Co., Ltd., for a gift of the sample of limonene. The present work was supported in part by Grant-in-Aids for Developmental Scientific Research No. 57840030 (1982) and No. 59840013 (1984) from the Ministry of Education, Science and Culture.

References

1) Y. S. Lee, T. Hirata, and T. Suga, *J. Chem. Soc., Perkin Trans. 1*, **1983**, 2475.

2) T. Suga, Y. S. Lee, and T. Hirata, *Bull. Chem. Soc. Jpn.*, **56**, 784 (1983).

3) Y. S. Lee, *J. Sci. Hiroshima Univ., Ser. A*, **47**, 21 (1983).

4) T. Suga, T. Hirata, and Y. S. Lee, *Chem. Lett.*, **1982**, 1595.

5) J. A. Pople, D. L. Beveridge, "Approximate Molecular Orbital Theory," McGraw-Hill Inc., New York (1960).

6) T. Murashige and F. Skoog, *Physiol. Plant.*, **15**, 473 (1962).

7) C. K. Johnson, *ORTEP*. Oak Ridge National Laboratory Report ORNL-3794 (1965).

8) M. Karplus, *J. Am. Chem. Soc.*, **85**, 2870 (1963).

9) R. Wylde and J.-M. Teulon, *Bull. Soc. Chim. Fr.*, **1970**, 758.

10) T. Suga, T. Hirata, and T. Aoki, *Bull. Chem. Soc. Jpn.*, **55**, 914 (1982).

11) R. M. Bowman, A. Chambers, and W. R. Jackson, *J. Chem. Soc. (C)*, **1966**, 1296.

12) B. Singaram, P. M. Abraham, G. M. Saraswathi, and J. Verghese, *Indian J. Chem.*, **14B**, 934 (1976).

13) G. Germain, P. Main, and M. M. Woolfson, *Acta Crystallogr., Sect. A*, **27**, 368 (1971).

 © 1987 The Chemical Society of Japan Bull. Chem. Soc. Jpn., 60, 295—299 (1987)

Radical Switch Reaction. A Novel Reaction between Two Free Radicals in a Solvent Cage

Michio KOBAYASHI,* Michiko GOTOH, and Masato YOSHIDA
Department of Chemistry, Faculty of Science, Tokyo Metropolitan University, Fukazawa, Setagaya-ku, Tokyo 158
(Received July 10, 1986)

Studies on the thermal decomposition of *t*-butyl phenylazo sulfone suggested the occurrence of a radical switch reaction, a novel type of reaction between two radicals. A primary geminate radical pair, *t*-butanesulfonyl and phenyl radical pair, exchange sulfur dioxide to form a new radical pair consisting of *t*-butyl and benzenesulfonyl radicals. The generation of benzenesulfonyl radical was confirmed by its ESR spectrum and the isolation of products containing a benzenesulfonyl group.

The thermal decomposition of arylazo aryl sulfones (Ar-N=N-SO_2Ar') can be considered to be initiated by the homolytic cleavage of the S-N bond to give a diazenyl radical and a sulfonyl radical; the diazenyl radical further decomposes to an aryl radical and nitrogen.[1-5] In continuing studies on the decomposition mechanism of azo sulfones, we are interested in the decomposition of *t*-butyl phenylazo sulfone (Ph-N=N-SO_2-*t*-Bu **1**). Since the 1,1-dimethylethanesulfonyl radical, which is expected to be generated by homolytic cleavage of the S-N bond of **1**, is known to decompose readily to a *t*-butyl radical and sulfur dioxide,[6] the mechanism and products of the decomposition of **1** may be different from that of arylazo aryl sulfones. During the study of the decomposition mechanism of **1** by product analysis, chemically induced dynamic nuclear polarization (CIDNP) and ESR, we have observed the occurrence of a new type of reaction between two geminate radicals in a solvent cage. The results will be described in this paper.

Results and Discussion

The rate constant of the decomposition of the azo sulfone **1** was determined in benzene in the presence of 3 mol of pyridine per mol of **1**; pyridine was added in order to suppress the autocatalyzed decomposition of **1** by acidic products.[2] The reaction was monitored by UV absorption at 296 nm. The rate was found to be first order in **1**. The observed first order rate constants were 48.3 (65.2 °C), 23.3 (60.2 °C), 8.84 (55.2 °C), and 6.05×10^{-5} s^{-1} (50.8 °C). Activation parameters estimated from these value are ΔH^*=133.7 kJ mol^{-1} and ΔS^*=126.7 J K^{-1} mol^{-1}.

The products of decomposition of **1** under these conditions are summarized below.

Detection of biphenyl among the products suggested the generation of a phenyl free radical. This was further confirmed by the examination of the orientation in the phenylation of the aromatic ring in the thermal decomposition of **1** in nitrobenzene: The isomer ratio of the nitrobiphenyl produced was *o*-72.2%; *m*- 5.2%; *p*- 22.6%. The total yield of nitrobiphenyls amounted to 28%. The isomer distribution (*o,p*-orientation) is the characteristic of homolytic

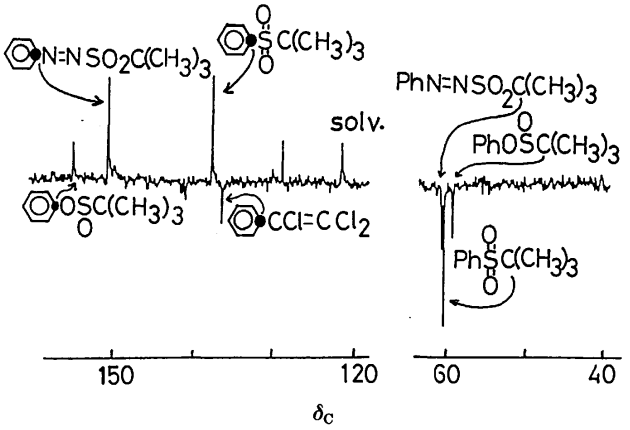

Fig. 1. The CIDNP spectra obtained in the thermal decomposition of azo sulfone **1** in tetrachloroethylene.

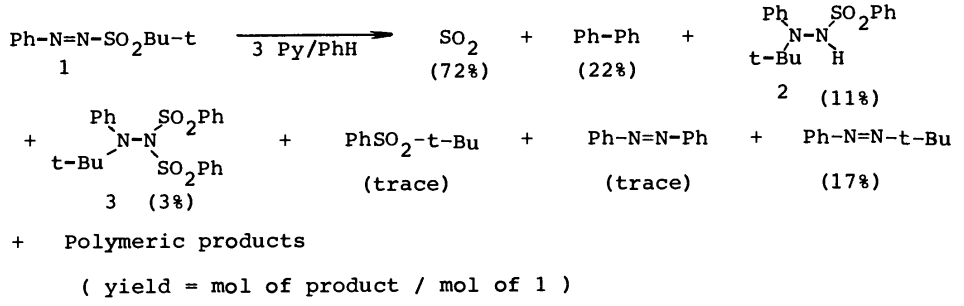

Scheme 1.

substitution by the phenyl radical.[7] The production of sulfur dioxide indicates the generation of the 1,1-dimethylethanesulfonyl radical followed by rapid decomposition to sulfur dioxide and a *t*-butyl radical.

We further examined the decomposition of azo sulfone **1** using the ^{13}C-CIDNP technique. When **1** was decomposed in tetrachloroethylene in a ^{13}C-NMR probe, several ^{13}C-CIDNP signals were observed as shown in Fig. 1. The enhanced absorption of C_1 and the emission signal of C_α of azo sulfone **1** itself indicates that the first step of the decomposition of **1** to give phenyldiazenyl-sulfonyl radical pair is reversible as shown in Eq. 1.

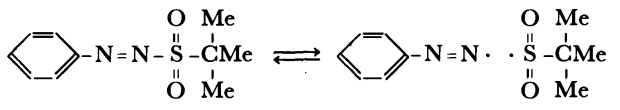

(1)

The mode of the CIDNP signals attributable to *t*-butyl phenyl sulfone and phenyl 1,1-dimethylethanesulfinate was also characteristic of the cage recombination products.[8] This suggests that in the second step, the primary geminate radical pair consisting of the phenyldiazenyl and 1,1-dimethylethanesulfonyl radicals decomposes to form a secondary radical pair consisting of phenyl and 1,1-dimethylethanesulfonyl radicals.

A considerable degree of a spin selection must occur in this radical pair before recombination or diffusion out of the solvent cage. Since the sulfonyl radical is ambident, recombination of these radicals in the solvent cage may give both sulfone and sulfinic ester. Although phenyl 1,1-dimethylethanesulfinate is unstable and could not be isolated as such among the final products of the decomposition of **1**, the ^{13}C-CIDNP spectrum shown in Fig. 1 cleary indicates that sulfinic ester is produced as the cage product during the thermal decomposition of **1**. In the previous paper,[1] we reported that the arenesulfonyl radical was ambident and acted either as a S- or O-centered radical.[5] Now the 1,1-dimethylethanesulfonyl radical is also shown to behave as a S- and O-centered radical.

Although considerable amounts of *t*-butylbenzene and benzene were detected among the decomposition products, they did not exhibit the CIDNP signals. The formation of *t*-butylbenzene and benzene indicates that the 1,1-dimethylethanesulfonyl radical decomposes to a *t*-butyl radical and sulfur dioxide in the third step to give the *t*-butyl and phenyl radical pair in the solvent cage. This radical pair may give *t*-butylbenzene as a recombination product, and benzene and isobutene as disproportionation products. Failure to observe CIDNP signals due to *t*-butylbenzene or benzene may be explained by the small difference between the *g* values of the phenyl and *t*-butyl radicals. Results of CIDNP studies of the decomposition of **1** in tetrachloroethylene are summarized in Scheme 2.

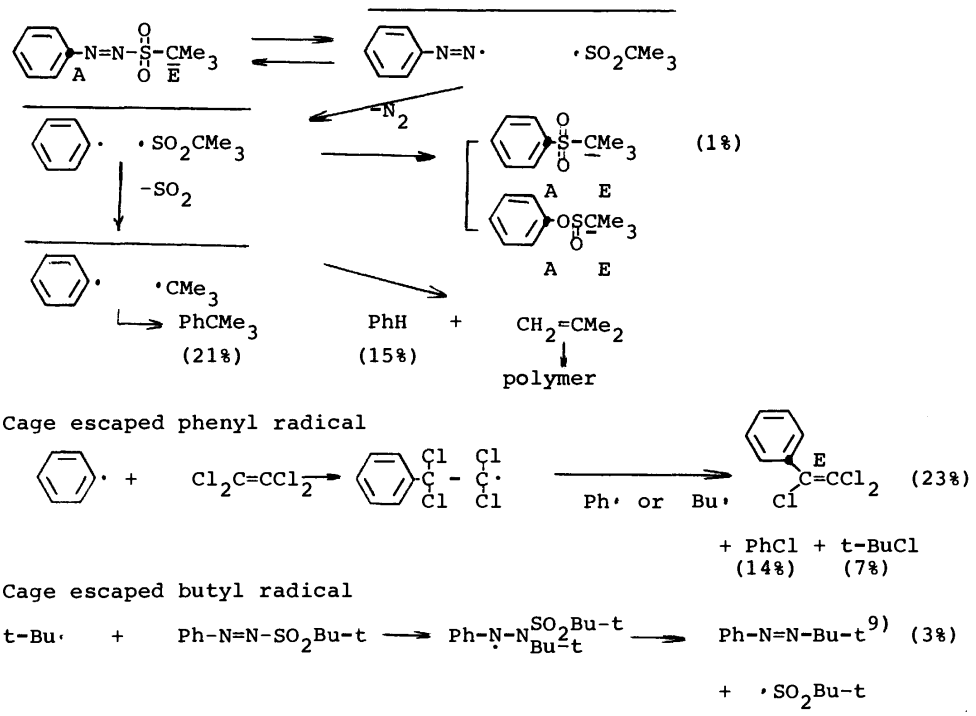

Compound **3** was also isolated in a yield of 1%.
· or — shows the polarized carbons. A: enhanced absorption, E: emission signal.

Scheme 2.

The above-mentioned results obtained by product analysis and CIDNP technique are those expected from the usual homolytic decomposition of an azo sulfone. A remarkable result was the isolation of some unexpected products, phenylsulfonylhydrazine **2** and **3**, in considerable yields. The products were characterized by ^{1}H, ^{13}C-NMR, IR, and MS spectra. In order further to confirm the structure of **2**, it was reduced by zinc dust in aq. NaOH. The production of *N*-(*t*-butyl)phenylamine and benzenesulfinic acid is consistent with the structure suggested by the spectral data.

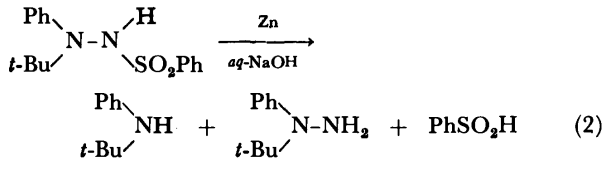

(2)

Formation of these phenylsulfonylhydrazine indicates the generation of benzenesulfonyl radical ($PhSO_2\cdot$) during the decomposition of **1**. Once sulfur dioxide splits off from 1,1-dimethylethanesulfonyl radical and diffuses out of the cage, the likelyhood of an encounter with a phenyl radical must be very small. As a phenyl radical is very reactive, a cage escaped phenyl radical should react with solvent benzene to give biphenyl before an encounter with sulfur dioxide. Thus, the only chance for the generation of a benzenesulfonyl radical is the recombination of the geminate phenyl radical and sulfur dioxide within the solvent cage.

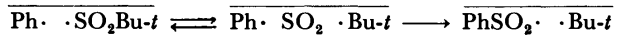

(3)

This exchange of sulfur dioxide between phenyl and 1,1-dimethylethanesulfonyl radicals to give benzenesulfonyl and *t*-butyl radical pair is a new type of reaction between two free radicals, which has no precedent. The driving force of this radical switch reaction must be the higher thermal stability of benzenesulfonyl radical than the 1,1-dimethylethanesulfonyl radical. The reaction of an aryl radical and sulfur dioxide to give a sulfonyl radical is well known, so the recombination of a phenyl radical and sulfur dioxide within the cage is plausible. Formation of **2** and **3** may be explained as shown in Scheme 3. The addition of a free radical to an N=N double bond to form a relatively stable hydrazyl radical (>N–N–Ar) must be thermally an easy process, although it has received little attention.[5,10,11] The addition of a benzenesulfonyl radical to the N=N bond of azo sulfone **1** will give the hydrazyl radical **4**, which may decompose to afford phenylazo phenyl sulfone and a *t*-butyl radical. The *t*-butyl radical then further attacks the azo sulfone to give the radical **5**. The radical **5** substituted by both electron-donor and -acceptor groups is expected to be rather stable (captodative substituent effect).[12,13] The hydrazyl radical **5** may give hydrazine **2** and **3** in benzene; in tetrachloroethylene it will give **3**. The hydrogen source for the formation of **2** should be a cyclohexadienyl radical formed by the addition of a phenyl radical to the solvent benzene.

Phenyl, butyl, and benzenesulfonyl radicals escape from the solvent cage. These radicals could be trapped by spin trapping reagents such as nitrosodurene, 2-nitroso-2-methylpropane, or *N*-(*t*-butyl)-α-phenylnitrone to give nitroxide radicals which may be detected by ESR. As shown in Scheme 4, the formation of the benzenesulfonyl radical along with *t*-butyl and phenyl radicals was verified by spin trapping.

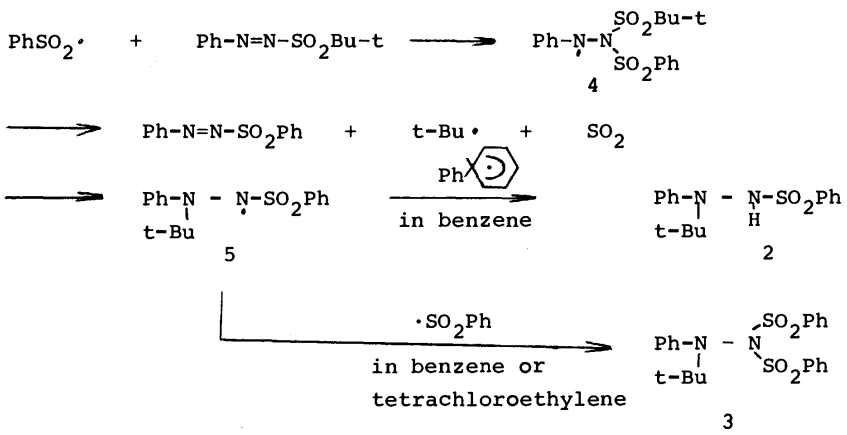

Scheme 3.

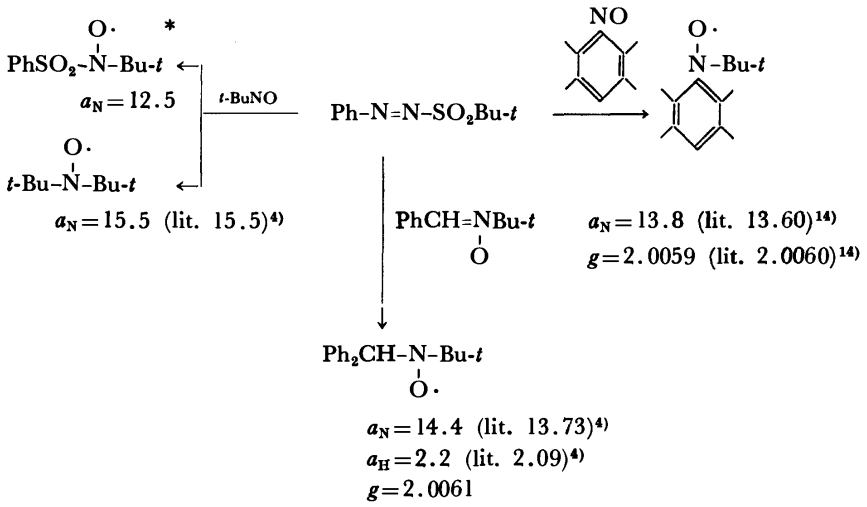

* The signal was assigned by the comparison with that obtained from benzenesulfonyl iodide and 2-nitroso-2-methylpropane under photo-irradiation.

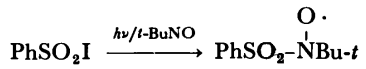

Scheme 4.

Experimental

Materials. Azo sulfone **1** was prepared from benzenediazonium tetrafluoroborate and sodium 1,1-dimethylethanesulfinate in water and recrystallized from hexane-benzene. Mp 65—66 °C (decomp), ^{1}H-NMR ($CDCl_3$) δ_H=1.63 (9H, s), 7.32—7.90 (5H, m), Found: C, 52.98; H, 6.31; N, 12.43%. Calcd for $C_{10}H_{14}N_2SO_2$: C, 53.08; H, 6.24; N, 12.43%. *t*-Butyl phenyl sulfone was prepared by the oxidation with hydrogen peroxide of *t*-butyl phenyl sulfide which was synthesized from isobutene and thiophenol. ^{13}C-NMR (Cl_2C=CCl_2) δ_C=23.0, 58.2, 127.6, 129.9, 132.0, 135.9.

Product Analysis of Thermal Decomposition of 1 in Benzene. After the decomposition was completed, the reaction mixture was washed with water. The organic layer was dried over magnesium sulfate and evaporated to give the oily residue, which was subjected to column chromatography. Sulfur dioxide was determined by the iodometric titration with a standard sodium thiosulfate solution.

Product Analysis of Thermal Decomposition of 1 in Tetrachoroethylene. The yields of the products shown in Scheme 2 were determined by gas chromatography except the sulfone, yield of which was an isolated yield by column chromatography.

CIDNP Spectra. A solution of **1** (1 mmol) and pyridine (3 mmol) in 10 cm^3 tetrachloroethylene was inserted in an NMR probe which had been heated at 100 °C, and ^{13}C NMR was measured: pulse flipping angle 45°; data points 8192; accumulation 30, pulse interval 2 s. A JEOL Fx-60 FT NMR spectrometer was used. The CIDNP signals were assigned by comparison with the chemical shifts of the authentic samples. The chemical shifts of the sulfinate were estimated from the related compounds. The sign of the net polarization as calculated according to Kaptein's rule agreed with the observed one.[8]

Spectral Data of 2 and 3. **2**: Mp 140 °C (decomp) ^{1}H-NMR ($CDCl_3$) δ=1.10 (s, 9H), 6.80—7.70 (m, 15H), ^{13}C-NMR ($CDCl_3$) δ=27.4, 59.8, 115.8, 116.3, 126.2, 128.3, 128.8, 132.7, IR 3240 (NH), 1323, 1160 cm^{-1} (SO_2), MS *m/z* 305, 304 (M^+), 163 (base), 107, 77, 57. Found: C, 63.06; H, 6.68; N, 9.19%. Calcd for $C_{16}H_{20}SO_2N_2$: C, 63.13; H, 6.62; N, 9.20%. **3**: Mp 120 °C (decomp) ^{1}H-NMR ($CDCl_3$) δ=1.38 (s, 9H), 6.9—8.0 (m, 16H), ^{13}C-NMR ($CDCl_3$) δ=29.7, 62.3, 125.0, 127.6, 127.8, 128.5, 129.4, 133.7, 139.9, 143.3, IR 1360, 1340, 1179, 1162 cm^{-1} (SO_2), MS *m/z* 444 (M^+), 303, 247, 163, 125, 105 (base), 77, 57. Found: C, 59.65; H, 5.41; N, 6.56%. Calcd. for $C_{22}H_{24}S_2O_4N_2$: C, 59.44; H, 5.44; N, 6.30%.

References

1) M. Kojima, H. Minato, and M. Kobayashi, *Bull. Chem. Soc. Jpn.*, **45**, 2032 (1972).

2) M. Kobayashi, H. Minato, M. Kojima, and N. Kamigata, *Bull. Chem. Soc. Jpn.*, **44**, 2501 (1971).

3) M. Kobayashi, S. Fujii, and H. Minato, *Bull. Chem. Soc. Jpn.*, **45**, 2039 (1972).

4) M. Kobayashi, E. Akiyama, H. Minato, and N. Kito, *Bull. Chem. Soc. Jpn.*, **47**, 1504 (1974).

5) M. Yoshida, N. Furuta, and M. Kobayashi, *Bull. Chem. Soc. Jpn.*, **54**, 2356 (1981).

6) R. T. van Aller, R. B. Scott, Jr., and E. L. Brockenbank, *J. Org. Chem.*, **31**, 2357 (1966).

7) M. J. Perkins, "Free Radicals," J. K. Kochi ed., Chap. 16, John Wiley & Sons, New York (1973).

8) R. Kaptein and J. Osterhoff, *Chem. Phys. Lett.*, **4**, 195, 214 (1969).

9) There is another plausible mechanism for the formation of Ph-N=N-Bu-*t*.

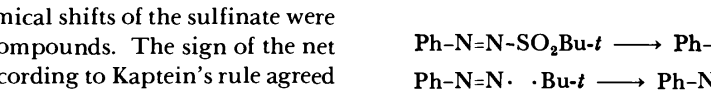

This cage recombination mechanism was rejected since in the decomposition of **1** in the presence of DPPH (2,2-

diphenyl-1-picryl hydrazyl: 1.5 mol per mol of **1**) as a radical scavenger, formation of Ph-N=N-Bu-*t* was completely suppressed.

10) J. L. Kice and R. S. Gabrielsen, *J. Org. Chem.*, **35**, 1004 (1970).

11) W. A. Pryor and H. Guard, *J. Am. Chem. Soc.*, **86**, 1150 (1964).

12) H. G. Viehe, R. Merenyi, L. Stella, and Z. Janousek, *Angew. Chem. Int. Ed. Engl.*, **18**, 917 (1979). H. G. Viehe, Z. Janousek, R. Merenyi, and L. Stella, *Acc. Chem. Res.*, **18**, 148 (1985).

13) D. Kost, M. Raban, and K. Aviram, *J. Chem. Soc., Chem. Commun.*, **1986**, 346.

14) S. Terabe, K. Kuruma, and R. Konaka, *J. Chem. Soc., Perkin Trans. 2*, **1973**, 1252.

 © 1987 The Chemical Society of Japan Bull. Chem. Soc. Jpn., 60, 301—310 (1987)

α,β-Epoxy Sulfoxides as Useful Intermediates in Organic Synthesis. IX.[1] A Novel Synthesis of Alkyl Vinyl Ketones and Divinyl Ketones from Carbonyl Compounds and 1-Chloro-3-phenylthiopropyl Phenyl Sulfoxide as a Three-Carbon Homologating Agent

Tsuyoshi SATOH, Takumi KUMAGAWA, Atsushi SUGIMOTO, and Koji YAMAKAWA*
Faculty of Pharmaceutical Sciences, Science University of Tokyo,
Ichigaya-funagawara-machi, Shinjuku-ku, Tokyo 162
(Received July 16, 1986)

The α,β-epoxy sulfoxides easily derived from carbonyl compounds and 1-chloro-3-phenylthiopropyl phenyl sulfoxide were treated with sodium benzeneselenolate to give β-phenylthio carbonyl compounds in excellent yields. The phenylthio group was oxidized to the sulfinyl group and was then treated with a base to afford alkyl vinyl ketones in quite good yields. This reaction presents a novel method for the preparation of alkyl vinyl ketones from carbonyl compounds by three-carbon homologation. The treatment of α,β-epoxy sulfoxides mentioned above with benzenethiolate gave α,β′-bis(phenylthio) ketones. The elimination of the both thio groups afforded divinyl ketones.

α,β-Unsaturated carbonyl compounds have received much attention for long time regarding synthetic organic reactions. They are quite useful as the dienophiles in the Diels-Alder reactions[2] and as the acceptors of Michael-type reactions.[3] Among the α,β-unsaturated carbonyl compounds, alkyl vinyl ketones and divinyl ketones are most important in the chemistry of carbon-carbon bond formation. Many methods have already been reported for the synthesis of vinyl ketones. The most widely used one is a two-carbon homologation method; one is the reaction of a vinylmetalic reagent, such as vinyllithium with carboxylic acids,[4] or with aldehydes followed by oxidation;[5] the other is a palladium-catalyzed acylation of alkenylzinc,[6] alkenyltin,[7] or alkenylcopper.[8] Another method for the synthesis of vinyl ketones is three-carbon homologation; one is the alkylation of alkyl halides or the addition of carbonyl

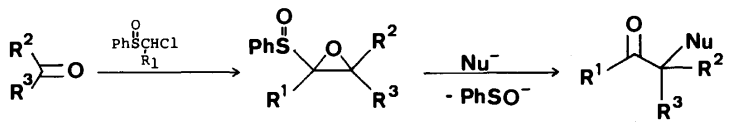

Scheme 1.

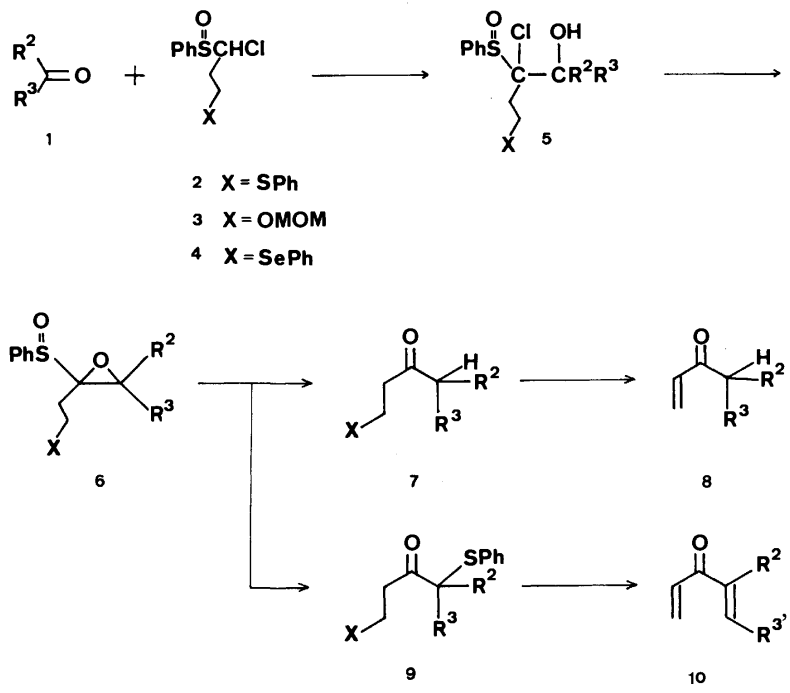

Scheme 2.

compounds with vinyl ketone anion equivalents (acyl anion equivalent)[9] and the other is a coupling of the α,β-unsaturated carboxylic acid chloride with transition-metal reagents[10] or with alkyltin[11] or alkyl iodides[12] by promotion of palladium. On the other hand, an excellent method for the synthesis of divinyl ketones was recently reported by Stille.[13]

Recently, we reported[14] a new method for the homologation of carbonyl compounds through α,β-epoxy sulfoxides upon a treatment with nucleophiles (Scheme 1). In these reactions if R_1 is to be a vinyl group or its equivalent this sequence must lead to a novel synthetic method for the preparation of alkyl vinyl ketones from carbonyl compounds by three-carbon homologation. In this paper we report a novel and versatile method for a synthesis of alkyl vinyl ketones **8** and divinyl ketones **10** from carbonyl compounds (**1**) and 1-chloro-3-phenylthiopropyl phenyl sulfoxide (**2**) as a three-carbon homologating agent through α,β-epoxy sulfoxides **6**.[15] The whole sequence is shown in Scheme 2.

Results and Discussion

A Synthesis of Alkyl Vinyl Ketones from Carbonyl Compounds Through α,β-Epoxy Sulfoxides by the Use of 1-Chloro-3-phenylthiopropyl Phenyl Sulfoxide as Three-Carbon Homologating Agent. As the three-carbon homologating agents, we selected three kinds of 3-substituted 1-chloropropyl phenyl sulfoxides **2**—**4**. 1-Chloro-3-phenylthiopropyl phenyl sulfoxide (**2**) was synthesized from 3-bromo-1-propanol via **11** in very good overall yields as shown in Scheme 3. Addition of **2** with benzaldehyde followed by treatment with a slight excess potassium *t*-butoxide in *t*-butyl alcohol gave the desired **12** in 92% yield. A treatment of **12** with excess sodium benzeneselenolate[14a] afforded β-phenylthio ketone **13** in 78% yield without any problem. Next, the sulfur group of **13** was oxidized with one equivalent of *m*-chloroperbenzoic acid (*m*-CPBA) to give the desired sulfoxide. In this reaction, we observed some vinyl ketone **14** during the work-up stage (alkali washing of the etheral extract of the product). On the basis of this observation we established the conditions of the derivation of β-phenylthio ketone to the vinyl ketone as follows. β-Phenylthio ketone (0.2 mmol) was treated with 1.1 equivalent of *m*-CPBA in CH_2Cl_2 (2 ml) at −60 °C for 20 min. Ether (4 ml) and 10% sodium hydroxide (4 ml) was added to the reaction mixture and the whole (two phases) was vigorously stirred at room temperature. In this one-pot oxidation β-elimination sequence the β-phenylthio ketone **13** gave the desired vinyl ketone **14** in 80% overall yield. A thermal elimination of the sulfinyl group[16] was also possible; however, we found that an alkaline treatment was much more convenient owing to higher yields and a one-pot operation.

The results of the preparation of alkyl vinyl ketones from α,β-epoxy sulfoxides are summarized in Table 1. As shown in the Table, various kinds of aldehydes and ketones were converted to alkyl vinyl ketones through the α,β-epoxy sulfoxides in good overall yields. The reaction time for the elimination of the phenylsulfinyl group was dependent on the substrate varied from 15 min to 2 d. It is noteworthy that this kind of reductive three-carbon homologation has been

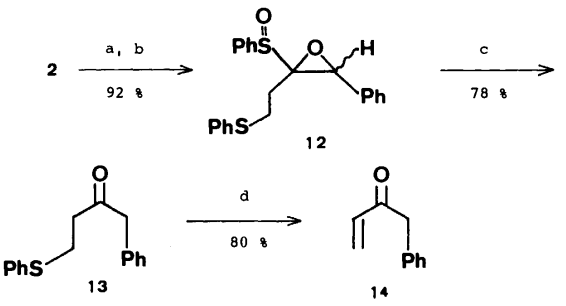

Scheme 4.

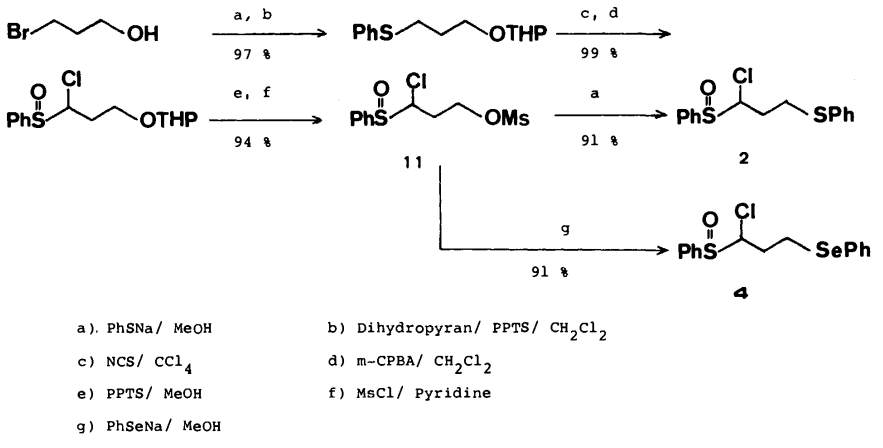

Scheme 3.

reported by Murai et al.[17] by using allylsilane chemistry; however, their procedure was reported to be useful only when unhindered aldehydes, not ketones, were used. In contrast with their results, the present method is quite useful for various kinds of aldehydes and ketones.

At the same time, we studied this vinyl ketone synthesis by using the three carbon homologating agents having a methoxymethoxy group or a phenylseleno group as the leaving group. 1-Chloro-3-(methoxymethoxy)propyl phenyl sulfoxide (**3**) was synthesized from 3-bromo-1-propanol in good overall yield (Scheme 5). The addition of **3** with benzaldehyde followed by a treatment with excess aqueous potassium hydroxide gave the α,β-epoxy sulfoxide **15** in quantitative yield; this was treated with sodium benzeneselenolate and afforded the desired ketone **16** having a leaving group at β-position.

Several acidic or basic conditions for the elimination of the methoxymethoxy group of **16** were tried; however, only disappointing results were obtained. For instance, a treatment of **16** with *p*-toluenesulfonic acid in benzene at 40 °C for 2.5 h or with 10% aqueous potassium hydroxide in benzene at room temperature for 3 h gave **14** in 33 and 24% yields, respectively.

Next, 1-chloro-3-(phenylseleno)propyl phenyl sulfoxide (**4**) was synthesized from **11** (Scheme 3). The addition of **4** with 4,4-(ethylenedioxy)cyclohexanone

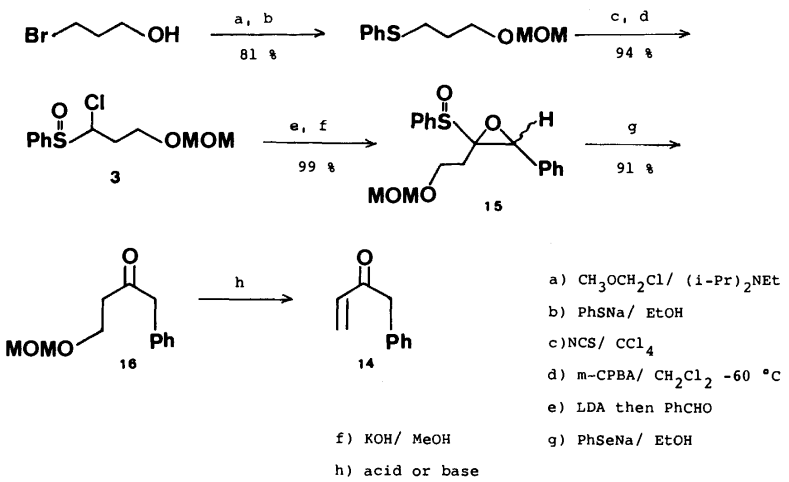

Scheme 5.

Table 1. Preparation of Alkyl Vinyl Ketones from α,β-Epoxy Sulfoxides through β-Phenylthio Ketones

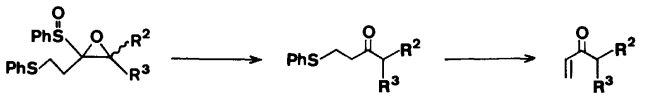

α,β-Epoxy Sulfoxide R_2	R_3	β-Phenylthio Ketone Yield/%		Time[a]	Alkyl Vinyl Ketone		Yield[b] %
H	Ph	(**12**) 78	(**13**)	1.5 h	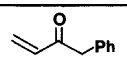	(**14**)	80
H	Cl-C$_6$H$_4$-	(**22**) 86	(**28**)	1.5 h	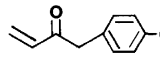	(**34**)	74
H	$CH_3(CH_2)_8$	(**23**) 85	(**29**)	2 d	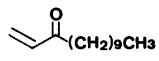	(**35**)	95
H	C$_6$H$_5$-	(**24**) 89	(**30**)	1 d	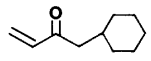	(**36**)	94
$-(CH_2)_5-$		(**25**) 94	(**31**)	3 h	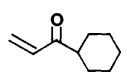	(**37**)	74
$-(CH_2)_2-C(O_2C_2H_4)-(CH_2)_2-$		(**26**) 96	(**32**)	15 min	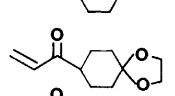	(**20**)	85
$-(CH_2)_6-$		(**27**) 96	(**33**)	1 d	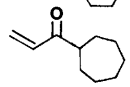	(**38**)	85

a) Reaction time for the alkaline treatment. b) Isolated purified yield.

was carried out in the usual way but in this case, after the addition of **4** with ketone, an elevation of the reaction temperature from −78 °C to room temperature gave the desired **17** in 74% yield.

We came across a problem in next step. A treatment of **17** with excess sodium benzeneselenolate in refluxing ethanol for 1 h gave an unseparable mixture of the desired seleno ketone **18** and an undesired thio ketone **19**. This was confirmed from the fact that the oxidation of the mixture with hydrogen peroxide[18] gave the vinyl ketone **20** and the sulfone **21** in a ratio of about 2 to 5.

A Synthesis of Divinyl Ketones from Carbonyl Compounds with Three-Carbon Homologation. As already reported, a treatment of α,β-epoxy sulfoxides with a thiolate gave α-sulfenylated ketones in good yields.[14b] In the case of the α,β-epoxy sulfoxides **23**—**27** this reaction should afford α,β′-bis(phenylthio) ketones; these compounds must give divinyl ketones by the elimination of both phenylthio groups. First of all, a treatment of the α,β-epoxy sulfoxide **23** with sodium benzenethiolate, prepared from thiophenol and sodium hydride in ethanol, gave a rather complex mixture in which some amount of the desired bis(phenylthio) ketone **39** was observed. This complexity of this reaction was thought to be due to the strong basicity of the conditions. Based on this consideration, sodium benzenethiolate was prepared from diphenyl disulfide by the reduction with sodium borohydride in refluxing ethanol for 30 min. Treatment of **23** with thus obtained sodium benzenethiolate in this solution at 0 °C for 1 h gave the desired

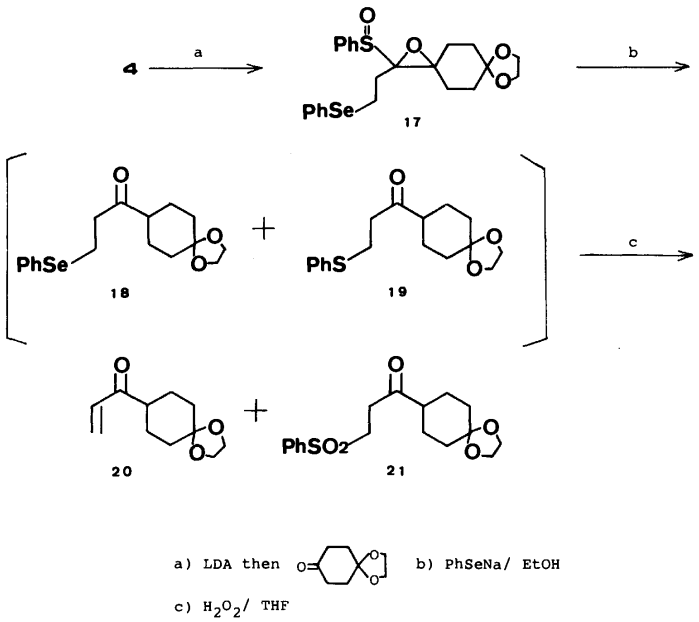

Scheme 6.

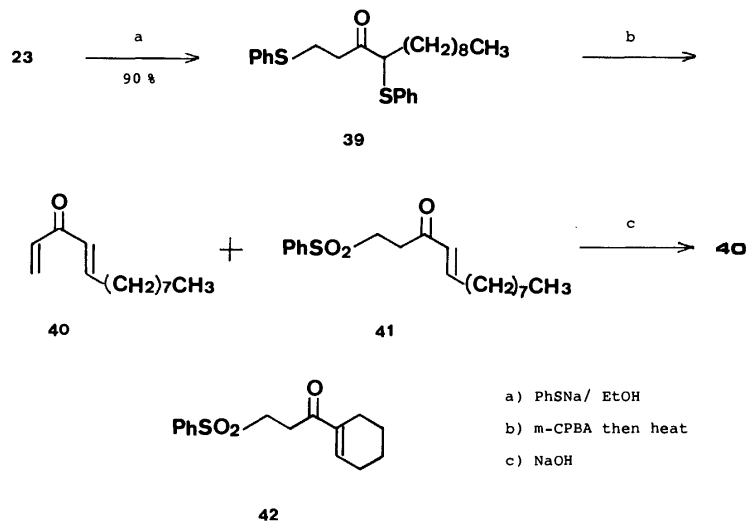

Scheme 7.

bis(phenylthio) ketone **39** as a sole product in 90% yield. This method for the sulfenylation was used throughout this study. Similar kinds of differences of the two conditions as mentioned above were reported by Liotta et al.[19] in the selenolate case.

A successive oxidation followed by pyrolytic elimination was our initial plan for the conversion of **39** to the desired divinyl ketone **40**. Bis(phenylthio) ketone **39** was oxidized with two equivalents of *m*-CPBA at −40 °C. The product, bis(phenylsulfinylated) ketone, was roughly purified by silica-gel column chromatography and heated in refluxing toluene for 15 min. In this reaction the desired **40** (66%) and the unexpected sulfone **41** (26%) were obtained. Finally, this mixture was treated with a base (as described for the synthesis of alkyl vinyl ketones) to give pure divinyl detone **40** in 79% yield. The oxidant for the formation of this sulfone was not determined certainly, but was thought to be the eliminated sulfinate. In the case of the bis(phenylthio) ketone derived from the α,β-epoxy sulfoxide **25**, the yield of the sulfone **42** came up to 50%. The results of the preparation of various kinds of divinyl ketones from α,β-epoxy sulfoxides through bis(phenylthio) ketones is shown in Table 2.

In conclusion, a novel and versatile procedure for the synthesis of vinyl and divinyl ketones from carbonyl compounds with three-carbon homologation was realized. As these unsaturated ketones are quite useful as the building blocks of compounds having a complex carbon framework, especially divinyl ketones are good precursors for cyclopentenone derivatives by Nazarov type cyclization;[20] the procedure presented in this paper contributes to the synthesis of complex natural products as well.

Experimental

All melting points are uncorrected. Infrared (IR) spectra were measured directly on a NaCl plate or in KBr disks with a Hitachi 215 spectrometer. ^{1}H Nuclear magnetic resonance (NMR) spectra were measured in a $CDCl_3$ solution with a JEOL FX-100 spectrometer using Me_4Si as an internal standard. Ultraviolet (UV) spectra were measured with a Hitachi 200 spectrometer. Electron-impact mass spectra (MS) were obtained on a Hitachi M-80 double-focusing spectrometer at 70 eV by direct insertion. Silica-gel BW-127 ZH (Fuji-Devison) containing 2% fluoresence reagent 254 and quartz column were used for column chromatography and the products having UV absorption were detected by UV irradiation.

1-Chloro-3-(methylsulfonyloxy)propyl Phenyl Sulfoxide (11). To a solution of sodium benzenethiolate (21 mmol) in MeOH (30 ml) was added 3-bromo-1-propanol (1.8 g; 20 mmol); the mixture was stirred under N_2 at room temperature for 45 min. Excess NH_4Cl was added and the MeOH was evaporated; then, the residue was extracted with ether. The product was distilled (bp 130 °C/2 mmHg (1 mmHg=133.322 Pa)) to give 3.36 g (99%) of 3-phenylthio-1-propanol as a colorless oil. IR (neat): 3350 (OH) cm^{-1}; ^{1}H NMR δ=1.89 (2H, quintet, J=7 Hz), 3.06 (2H, t, J=7 Hz), 3.78 (2H, t, J=7 Hz), 7.0—7.5 (5H, m). 3-Phenylthio-1-propanol (3.36 g; 20 mmol) was treated with dihydropyran (2.7 ml; 30 mmol) and pyridinium *p*-toluenesulfonate (PPTS) (250 mg; 1 mmol) in CH_2Cl_2 (20 ml) at room temperature for 1 h. After the workup according to Miyashita's procedure[21] the product was distilled (bp 150 °C/2 mmHg) to afford 4.9 g (97%) of 1-phenylthio-3-(tetrahydro-2-pyranyloxy)propane as a colorless oil. ^{1}H NMR δ=3.07 (2H, t, J=7 Hz), 4.58 (1H, bs). This sulfide (5.05 g; 20 mmol) was added to a suspension of NCS (21 mmol) in 40 ml of CCl_4 and the reaction mixture was stirred at room temperature for 2 h. The precipitate was filtered off and the filtrate was evaporated. The residue was dissolved in 60 ml of CH_2Cl_2 and cooled to −50 °C and *m*-CPBA (21 mmol) was added to the solution and stirred for

Table 2. Preparation of Divinyl Ketones from α,β-Epoxy Sulfoxides through Bis(phenylthio)ketones

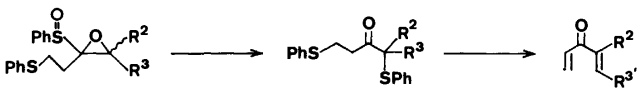

α,β-Epoxy Sulfoxide	Bis(phenylthio) Ketone Yield/%	Conditions of the Elimination			Divinyl Ketone		Yield[c] %
		Temp[a]	Time[a]	Time[b]			
23	90	110 °C	15 min	1 d	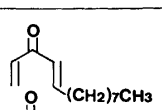	(**40**)	79
25	94	110 °C	1 h	17 h	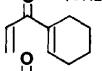	(**43**)	65
26	97	110 °C	1.5 h	2 h	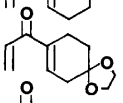	(**44**)	76
27	94	r.t.	2 h	1 d	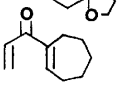	(**45**)	77

a) The conditions of the thermal elimination of the phenylsulfinyl group at α-position of the ketone. Refluxing in toluene. b) The time for the alkaline treatment at room temperature. c) Isolated purified yield.

1 h. The reaction mixture was diluted with 60 ml of CH_2Cl_2 and the whole was washed, successively, with 10% NaOH and sat. NH_4Cl. The usual work-up gave a crude product, which was purified by silica-gel column chromatography to afford 5.99 g (99%) of 1-chloro-3-(tetrahydro-2-pyranyloxy)-propyl phenyl sulfoxide (diastereomeric mixture) as a colorless oil. IR (neat): 1050, 1035 (SO) cm^{-1}. This product (769 mg; 2.54 mmol) was dissolved in 20 ml of MeOH and 64 mg of PPTS was added. The mixture was stirred at 50 °C for 2 h. After the usual work-up[21] 557 mg (99%) of the alcohol was obtained as a colorless oil. IR (neat): 3400 (OH), 1050 (SO) cm^{-1}. To a solution of the alcohol (3.17 g; 14.5 mmol) in 13 ml of pyridine was added methanesulfonyl chloride (2.3 ml; 29 mmol) at 0 °C and the solution was stirred for 1 h. The reaction mixture was diluted with benzene and washed, successively, with 10% HCl, sat. $NaHCO_3$, and sat. NH_4Cl. The product was purified by silica-gel column chromatography to give the desired **11** (4.06 g; 94%) as a colorless oil. IR (neat): 1360, 1180 (SO_2), 1050 (SO) cm^{-1}; ^1H NMR δ=2.0—2.9 (2H, m), 3.03, 3.07 (each s, OSO_2CH_3); MS *m/z* (%): 171 ([M−PhSO]$^+$, 21), 79 (42), 77 (57), 75 (100).

1-Chloro-3-phenylthiopropyl Phenyl Sulfoxide (2). To a solution of sodium benzenethiolate (14.4 mmol) in 21 ml of MeOH was added a solution of **11** (4.06 g; 13.7 mmol) in MeOH (5 ml). The reaction mixture was stirred at room temperature for 3 h. Excess NH_4Cl was added to the mixture and the MeOH was evaporated. The product was purified by the usual way to give 3.64 g (86%) of **2** as a colorless oil (diastereomeric mixture) and 0.24 g (6%) of recovered **11**. IR (neat): 1060 (SO) cm^{-1}; ^1H NMR δ=1.8—2.7 (2H, m), 2.8—3.4 (2H, m), 4.07 (dd, *J*=9, 4 Hz), 4.83 (dd, *J*=10, 4 Hz), 7.1—7.8 (10H, m); MS *m/z* (%): 310 (M$^+$, 8), 185 ([M−PhSO]$^+$, 28), 149 (32), 123 (100); Found: *m/z* 310.0237. Calcd for $C_{15}H_{15}ClOS_2$: M, 310.0251.

1,2-Epoxy-1-phenyl-2-phenylsulfinyl-4-phenylthiobutane (12). To a solution of LDA (2.1 mmol) in 9 ml of THF at −60 °C was added a solution of **2** (2 mmol) in 1 ml of THF dropwise with stirring. The stirring was continued for 15 min; then, 0.22 ml (2.1 mmol) of benzaldehyde was added. After 5 min the reaction was quenched by sat. aq NH_4Cl and the whole was extracted with benzene. The usual workup gave chlorohydrin-L[14a] and chlorohydrin-P[14a] in 43 and 54% yields, respectively. Chlorohydrin-L: Colorless oil; IR (neat): 3330 (OH), 1050 (SO) cm^{-1}; ^1H NMR δ=2.2—3.5 (4H, m), 5.00 (1H, s), 7.1—8.0 (15H, m); MS *m/z* (%): 290 ([M−PhSOH]$^+$, 35), 180 (27), 145 (46), 117 (77), 77 (100). Chlorohydrin-P: Colorless prisms; mp 112—114 °C (benzene-hexane); IR (KBr): 3350 (OH), 1040 (SO) cm^{-1}; ^1H NMR δ=1.6—3.1 (4H, m), 5.17 (1H, d, *J*=3 Hz), 7.0—7.8 (15H, m); MS *m/z* (%): 290 ([M−PhSOH]$^+$, 61), 180 (56), 145 (73), 117 (100); Found: C, 63.55; H, 5.04; Cl, 8.42; S, 15.53%. Calcd for $C_{22}H_{21}ClO_2S_2$: C, 63.37; H, 5.08; Cl, 8.50; S, 15.38%. To a solution of the chlorohydrin-L (1.10 g; 2.36 mmol) in 2 ml of benzene and 12 ml of *t*-BuOH was added a suspension of *t*-BuOK (234 mg; 3.03 mmol) in 2 ml of *t*-BuOH at room temperature with stirring. The reaction was quenched after 5 min by adding NH_4Cl and the solvent was evaporated. The residue was dissolved with benzene. After the usual workup, the product was purified by silica gel column chromatography to give 1.03 g (99%) of **12-L** as a colorless oil. IR (neat): 1055 (SO) cm^{-1}; ^1H NMR δ=1.5—2.1 (2H, m), 2.3—3.1 (2H, m), 4.82 (1H, s), 6.9—7.8 15H, m); MS *m/z* (%): 256 (33), 255 ([M−PhSO]$^+$, 18), 199 (38), 123 ([M-$C_{15}H_{13}O_2S$]$^+$, 100). **12-P**: Yield 92%; IR (neat): 1050 (SO) cm^{-1}; ^1H NMR δ=1.7—3.2 (4H, m), 4.53 (1H, s), 7.0—7.8 (15H, m); MS *m/z* (%): 199 (3), 125 (8), 109 ([M−$C_{16}H_{15}O_2S$]$^+$, 7), 78 (100).

1-Phenyl-4-phenylthio-2-butanone (13). To a suspension of diphenyl diselenide (1.46 g; 4.65 mmol) in 9 ml of EtOH was added $NaBH_4$ (353 mg; 9.3 mmol) by portions with stirring at room temperature. After vigorous hydrogen gas evolution ceased, the solution was cooled in an ice bath and a solution of **12** (0.93 mmol) in 0.5 ml of EtOH was added. The reaction mixture was stirred at 0 °C under N_2 for 20 min then the reaction was quenched by sat. aq NH_4Cl and then the EtOH was evaporated. The residue was extracted with benzene. After the usual workup, the product was purified by silica-gel column chromatography to give **13** in 78% yield as a colorless oil. IR (neat): 1720 (CO) cm^{-1}; ^1H NMR δ=2.7—2.9 (2H, m), 3.0—3.2 (2H, m), 3.70 (2H, s), 7.1—7.4 (10H, m); MS *m/z* (%): 256 (M$^+$, 65), 165 ([M−$PhCH_2$]$^+$, 23), 137 ([M−C_8H_7O]$^+$, 62), 123 ([M−C_9H_9O]$^+$, 100); Found: *m/z* 256.0914. Calcd for $C_{16}H_{16}OS$: M, 256.0920.

Oxidation of 13 with *m*-CPBA Followed by Treatment with Alkali. To a solution of **13** (48 mg; 0.91 mmol) in 2 ml of CH_2Cl_2 was added 44 mg (0.21 mmol) of *m*-CPBA at −60 °C with stirring. The stirring was continued for 20 min and then ether (4 ml) and 10% NaOH (4 ml) were added to the reaction mixture. This was vigorously stirred at room temperature for 1.5 h. The reaction mixture was neutralized by NH_4Cl and the whole was extracted with CH_2Cl_2, washed and dried. After the usual workup, the product was purified by silica-gel column chromatography to afford 22 mg (80%) of 1-phenyl-3-buten-2-one (**14**) as a colorless oil. IR (neat): 1690, 1670 (CO), 1615 (C=C) cm^{-1}; ^1H NMR δ=3.91 (2H, s), 5.85 (1H, dd, *J*=8, 3.5 Hz), 6.36 (1H, dd, *J*=18, 3.5 Hz), 6.45 (1H, dd, *J*=18, 8 Hz), 7.1—7.5 (5H, m); UV λ_{max}^{EtOH} 210, 256 nm; MS *m/z* (%): 146 (M$^+$, 21), 118 ([M−CO]$^+$, 13), 91 ([M−C_3H_3O]$^+$, 64), 55 (100); Found: *m/z* 146.0734. Calcd for $C_{10}H_{10}O$: M, 146.0731.

1-Chloro-3-(methoxymethoxy)propyl Phenyl Sulfoxide (3). Chloromethyl methyl ether (3.8 ml; 50 mmol) was added to a solution of 3-bromo-1-propanol (1.4 g; 10 mmol), *N,N*-diisopropylethylamine (5 ml; 29 mmol) in THF (0.5 ml) at 0 °C and the mixture was stirred at 0 °C for 30 min. The reaction mixture was poured into a mixture of ice and diluted HCl and the whole was extracted with ether. The ether extract was washed with sat. aq $NaHCO_3$, dried over Na_2SO_4 and the ether was evaporated. The residue was distilled (bp 100 °C/2 mmHg) to give 1.63 g (88%) of 1-bromo-3-(methoxy)methoxypropane as a colorless oil. ^1H NMR δ=2.10 (2H, quintet, *J*=6 Hz), 3.30 (3H, s), 3.45, 3.60 (each 2H, t, *J*=6 Hz), 4.55 (2H, s). This bromide (1 g; 5.5 mmol) was added to a solution of sodium benzenethiolate (6 mmol) in 6 ml of dry EtOH and the mixture was stirred at room temperature for 1.5 h under an N_2 atmosphere. The reaction mixture was neutralized by NH_4Cl and the EtOH was evaporated. The residue was dissolved with benzene and washed, successively, with 5% NaOH and sat. NH_4Cl. The product was distilled (bp 130 °C/2 mmHg) to give 1.07 g (92%) of 1-(methoxy)methoxy-3-phenylthiopropane as a colorless oil. ^1H NMR δ=1.95

(2H, quintet, J=6 Hz), 3.00 (2H, t, J=6 Hz), 3.31 (3H, s), 3.60 (2H, t, J=6 Hz), 4.55 (2H, s), 7.0—7.5 (5H, m). This product (1.07 g; 5 mmol) was chlorinated then oxidized according to the procedure described for the synthesis of **11** to afford 1.25 g (94%) of **3** as a colorless oil (diastereomeric mixture). IR (neat): 1050 (SO) cm^{-1}; ^1H NMR δ=3.28, 3.30 (each s, CH_3), 3.72 (m), 4.53, 4.55 (each s, $-OCH_2O-$).

1,2-Epoxy-4-(methoxymethoxy)-1-phenyl-2-phenylsulfinylbutane (15). Addition of **3** with benzaldehyde according to the procedure described for the synthesis of **12** gave two chlorohydrins. Chlorohydrin-L: Yield 40%, colorless prisms (benzene-hexane) mp 116—118 °C; IR (KBr): 3220 (OH), 1035, 1025 (SO) cm^{-1}; ^1H NMR δ=3.35 (3H, s), 4.60 (2H, s), 5.00 (1H, s), 7.25 (5H, s), 7.4—8.0 (5H, m). Chlorohydrin-P: Yield 60%, colorless prisms (AcOEt-hexane) mp 85 °C (decomp); IR (KBr): 3310 (OH), 1065, 1035, 1015 (SO) cm^{-1}; ^1H NMR δ=3.29 (3H, s), 4.47 (2H, s), 5.20 (1H, s), 7.2—7.8 (10H, m). **15-L**: Yield 99%, colorless oil, IR (neat): 1050 (SO) cm^{-1}; ^1H NMR δ=1.24—2.05 (2H, m), 3.29 (3H, s), 3.45 (2H, m), 4.49 (2H, s), 4.91 (1H, s), 7.10—7.94 (10H, m); MS m/z (%): 271 ([M−$C_2H_5O_2$]$^+$, 0.1), 207 ([M−PhSO]$^+$, 0.4), 125 (5), 91 (9), 45 (100). **15-P**: Yield 98%, colorless oil, IR (neat): 1050 (SO) cm^{-1}; ^1H NMR δ= 1.58—1.90 (1H, m), 2.47—2.78 (1H, m), 3.34 (3H, s), 3.56 (2H, t, J=6 Hz), 4.56 (2H, s), 4.61 (1H, s), 7.24—7.75 (10H, m); MS m/z (%): 271 ([M−$C_2H_5O_2$]$^+$, 0.1), 207 ([M−PhSO]$^+$, 0.4), 125 (3), 45 (100).

4-(Methoxymethoxy)-1-phenyl-2-butanone (16). The α,β-epoxy sulfoxide **15** was treated with sodium benzeneselenolate as described above to give **16** in 91% yield as a colorless oil. IR (neat): 1720, 1715 (CO) cm^{-1}; ^1H NMR δ=2.71 (2H, t, J=6 Hz), 3.33 (3H, s), 3.72 (2H, s), 3.76 (2H, t, J=6 Hz), 4.56 (2H, s), 7.0—7.4 (5H, m); MS m/z (%): 208 (M$^+$, 0.3), 177 ([M-CH_3O]$^+$, 2), 117 ([M−$PhCH_2$]$^+$, 16), 91 (51), 45 (100); Found: m/z 208.1092. Calcd for $C_{12}H_{16}O_3$: M, 208.1098.

Treatment of 16 with Acid or Base. Acidic conditions: A solution of **16** (35 mg) and p-TsOH·$2H_2O$ (3.2 mg) in 1.7 ml of benzene was stirred at 40 °C under N_2 for 2.5 h. The mixture was passed through a short pad of Na_2CO_3 and the product was purified by silica-gel column chromatography to give 8 mg (33%) of **14** as a colorless oil. Basic conditions: A mixture of **16** (42 mg) in 2 ml of benzene and 1.5 ml of 10% KOH was vigorously stirred at room temperature for 3 h to give 7 mg (24%) of **14** and several by-products.

1-Chloro-3-phenylselenopropyl Phenyl Sulfoxide (4). To a suspension of diphenyl diselenide (815 mg; 2.61 mmol) in 15 ml of MeOH was added $NaBH_4$ (200 mg; 5.23 mmol) by portions with stirring. After vigorous hydrogen gas evolution ceased, a solution of **11** (1.41 g; 4.75 mmol) in 2 ml of MeOH was added and the reaction mixture was stirred at room temperature for 2 h. Excess NH_4Cl was added and the MeOH was evaporated. After the usual work-up, the product was purified by silica-gel column chromatography to give 1.54 g (91%) of **4** as a colorless oil (diastereomeric mixture). IR (neat): 1055 (SO) cm^{-1}; ^1H NMR δ=2.0—2.7 (2H, m), 2.8—3.4 (2H, m), 4.69, 4.82 (each dd, J=9, 4 Hz), 7.1—7.8 (5H, m); MS m/z (%): 358 (M$^+$, 13), 233 ([M−PhSO]$^+$, 30), 201 ([M−PhSe]$^+$, 25), 171 (54), 101 (95), 77 (100).

2″-Phenylsulfinyl-2″-(2-phenylseleno)ethyldispiro[1,3-dioxolane-2,1′-cyclohexane-4′,1″-oxirane] (17). To a LDA (3.5 mmol) solution in THF (30 ml) at −78 °C was added a solution of **4** (118 g; 3.3 mmol) in 2 ml of THF dropwise with stirring. The stirring was continued for 30 min then a solution of 4,4-(ethylenedioxy)cyclohexanone (0.77 g; 5 mmol) in THF was added. After 5 min the cooling bath was removed and the mixture was stirred at room temperature for 1 h. Sat. aq NH_4Cl was added to the reaction mixture and the whole was extracted with benzene. After the usual work-up, the product was purified by silica-gel column chromatography to give 1.17 g (74%) of **17** as a colorless oil. In this reaction 0.28 g (24%) of **4** was recovered. IR (neat): 1145, 1100, 1090 (COC), 1050 (SO) cm^{-1}; ^1H NMR δ=1.1—2.9 (12H, m), 4.00 (4H, s), 7.1—7.7 (10H, m); MS m/z (%): 352 ([M−PhSO]$^+$, 27), 297 (25), 157 (34), 99 (100).

8-(1-Oxo-2-propenyl)-1,4-dioxaspiro[4.5]decane (20) and 8-(1-Oxo-3-phenylsulfonylpropyl)-1,4-dioxaspiro[4.5]decane (21). To a solution of sodium benzeneselenolate (5 mmol) in 9 ml of EtOH was added a solution of **17** (238 mg; 0.5 mmol) in 1 ml of EtOH and the mixture was refluxed for 1 h under N_2. Excess NH_4Cl was added and the EtOH was evaporated. The residue was extracted with benzene. After the usual work-up, te products were purified by silica-gel column chromatography to give 146 mg of unseparable mixture of **18** and **19**. IR (neat): 1715 (CO) cm^{-1}; MS m/z (%): 354 (M$^+$; $C_{17}H_{22}O_3Se$; 3), 306 (M$^+$; $C_{17}H_{22}O_3S$; 26), 99 (100). To a solution of the mixture (53 mg) in 1.5 ml of THF was added 35% H_2O_2 (0.5 ml) and the mixture was stirred at room temperature for 30 min. The whole was extracted with ether and washed, dried over Na_2SO_4. The products were separated by silica-gel column chromatography to afford 9 mg of **20** and 39 mg of **21**. **20**: Colorless oil; IR (neat): 1705, 1685 (CO), 1625 (C=C) cm^{-1}; UV λ_{max}^{EtOH} 214 nm; ^1H NMR δ=1.4—2.0 (8H, m), 2.5—2.8 (1H, m), 3.97 (4H, s), 5.77 (1H, dd, J=9, 3 Hz), 6.32 (1H, dd, J=18, 3 Hz), 6.50 (1H, dd, J=18, 9 Hz); MS m/z (%): 196 (M$^+$, 0.5), 168 ([M−C_2H_4]$^+$, 4), 141 ([M−C_3H_3O]$^+$, 4) 99 (100). **21**: Colorless prisms (benzene-hexane); mp 102—104.5 °C; IR (KBr): 1715 (CO), 1310 (SO_2) cm^{-1}; ^1H NMR δ=1.4—2.0 (8H, m), 2.2—2.6 (1H, m), 2.9—3.1 (2H, m), 3.3—3.5 (2H, m), 3.96 (4H, s), 7.4—8.0 (5H, m); MS m/z (%): 338 (M$^+$, trace), 197 ([M−$PhSO_2$]$^+$, 18), 141 ([M−$C_9H_9O_3S$]$^+$, 11), 99 (100); Found: C, 60.54; H, 6.53; S, 9.41%. Calcd for $C_{17}H_{22}O_5S$: C, 60.34; H, 6.55; S, 9.47%.

α,β-Epoxy Sulfoxides 22—27. All α,β-epoxy sulfoxides **22—27** were synthesized from **2** and carbonyl compounds as described for **12**.

1,2-Epoxy-1-(4-chlorophenyl)-2-phenylsulfinyl-4-phenylthiobutane (22). Chlorohydrin-L: Colorless oil; yield 42%; IR (neat): 3330 (OH), 1050 (SO) cm^{-1}; ^1H NMR δ=2.0—3.5 (4H, m), 4.91 (1H, s), 7.0—8.9 (14H, m), Chlorohydrin-P: Colorless powder: yield 42%; IR (KBr): 3490 (OH), 1050 (SO) cm^{-1}; ^1H NMR δ=1.6—3.1 (4H, m), 5.18 (1H, s), 7.0—7.7 (14H, m), **22-L**: Colorless oil; yield 86%; IR (neat): 1090, 1050 (SO) cm^{-1}; ^1H NMR δ=1.3—3.1 (4H, m), 4.72 (1H, s), 6.9—7.7 (14H, m); MS m/z (%): 414 (M$^+$, trace), 398 ([M−O]$^+$, 1.6), 341 (0.7), 289 (47), 233 (75), 125 (100). **22-P**: Colorless oil; yield 89%; IR (neat): 1090, 1050 (SO) cm^{-1}; ^1H NMR δ=1.6—3.1 (4H, m), 4.45 (1H, s), 7.0—7.7 (14H, m); MS m/z (%): 288 ([M−C_6H_6SO]$^+$, 12), 233 (100).

3,4-Epoxy-3-phenylsulfinyl-1-phenylthiotridecane (23). Chlorohydrin: Diastereomeric mixture; colorless oil; IR (neat): 3350 (OH), 1045 (SO) cm^{-1}; ^1H NMR δ=0.88, 0.90 (each t, J=7 Hz), 7.2—7.9 (10H, m); MS m/z (%): 340

([M−PhSOH]$^+$, 23), 230 (23), 284 (23), 110 (100). Less polar **23**: Colorless oil; yield 36%; IR (neat): 1055 (SO) cm^{-1}; ^{1}H NMR δ=0.90 (3H, bt, J=6 Hz), 1.0—3.1 (20H, m), 3.32 (1H, t, J=7 Hz), 7.1—7.8 (10H, m); MS m/z (%): 304 ([M−PhSOH]$^+$, 5), 249 (34), 218 (25), 186 (31), 125 (100). More polar **23**: Colorless oil; yield 45%; IR (neat): 1045 (SO) cm^{-1}; ^{1}H NMR δ=0.90 (3H, bt, J=6 Hz), 1.0—3.1 (20H, m), 3.67 (1H, m), 7.1—7.7 (10H, m); MS m/z (%): 305 ([M−PhSO]$^+$, 52), 249 (69), 123 (100).

1-Cyclohexyl-1,2-epoxy-2-phenylsulfinyl-4-phenylthiobutane (24). Chlorohydrin: Diastereomeric mixture; colorless oil; yield 95%; IR (neat): 3370 (OH), 1055 (SO) cm^{-1}; MS m/z (%): 296 ([M−PhSOH]$^+$, 15), 126 (53), 110 (100). Less polar **24**: Colorless oil; yield 38%; IR (neat): 1050 (SO) cm^{-1}; ^{1}H NMR δ=1.0—3.0 (15H, m), 3.04 (1H, d, J=8 Hz), 7.1—7.8 (10H, m); MS m/z (%): 386 (M$^+$, 0.2), 261 (23), 205 (31), 123 (100). More polar **24**: Colorless oil; yield 32%; IR (neat): 1055 (SO) cm^{-1}; ^{1}H NMR δ=0.8—3.4 (15H, m), 3.44 (1H, d, J=8 Hz), 7.1—8.0 (10H, m); MS m/z (%): 386 (M$^+$, trace), 261 (11), 185 (19), 123 (100).

2′-Phenylsulfinyl-2′-(2-phenylthioethyl)spiro[cyclohexane-1,1′-oxirane] (25). Chlorohydrin: Colorless plate; mp 100—102 °C (benzene-hexane); yield 77%; IR (KBr): 3210 (OH), 1030 (SO) cm^{-1}; ^{1}H NMR δ=0.8—3.2 (14H, m), 7.1—7.8 (10H, m); MS m/z (%): 282 ([M−PhSOH]$^+$, 28), 126 (31), 110 (100); Found: C, 61.65; H, 6.09; Cl, 8.60; S, 15.59%. Calcd for $C_{21}H_{25}ClO_2S_2$: C, 61.67; H, 6.16; Cl, 8.67; S, 15.68%. Epoxy sulfoxide **25**: Colorless prisms; mp 86—87 °C (benzene-hexane); yield 93%; IR (KBr): 1050 (SO) cm^{-1}; ^{1}H NMR δ=1.3—2.9 (14H, m), 7.1—7.7 (10H, m); MS m/z (%): 372 (M$^+$, trace), 247 ([M−PhSO]$^+$, 43), 123 (100); Found: C, 67.87; H, 6.46; S, 17.30% m/z 372.1191. Calcd for $C_{21}H_{24}O_2S_2$: C, 67.70; H, 6.49; S, 17.21% M, 372.1216.

2″-Phenylsulfinyl-2″-(2-phenylthioethyl)dispiro[1,3-dioxrane-2,1′-cyclohexane-4′,1″-oxirane] (26). Chlorohydrin: Colorless oil; yield 94%; IR (neat): 3400 (OH), 1040 (SO) cm^{-1}; ^{1}H NMR δ=1.4—3.2 (12H, m), 3.98 (4H, s), 7.1—7.8 (10H, m); MS m/z (%): 340 ([M−PhSOH]$^+$, 26), 203 (22), 99 (100). Epoxy sulfoxide **26**: Colorless oil; yield 99%; IR (neat): 1100 (COC), 1050 (SO) cm^{-1}; ^{1}H NMR δ=1.2—3.0 (12H, m), 4.02 (4H, s), 7.1—7.7 (10H, m); MS m/z (%): 414 ([M−O]$^+$, 0.2), 305 ([M−PhS]$^+$, 54), 249 (73), 99 (100).

2′-Phenylsulfinyl-2′-(2-phenylthio)ethylspiro[cycloheptane-1,1′-oxirane] (27). Chlorohydrin: Colorless oil; yield 97%; IR (neat): 3410 (OH), 1050 (SO) cm^{-1}; ^{1}H NMR δ=1.2—3.1 (16H, m), 7.1—7.8 (10H, m); MS m/z (%): 296 ([M−PhSOH]$^+$, 19), 278 (4), 234 (17), 186 (34), 149 (19), 125 (100). Epoxy sulfoxide **27**: Colorless oil; yield 68%; IR (neat): 1090, 1050 (SO) cm^{-1}; ^{1}H NMR δ=1.3—3.0 (16H, m), 7.0—7.7 (10H, m); MS m/z (%): 261 ([M−PhSO]$^+$, 17), 205 (100).

1-(4-Chlorophenyl)-4-phenylthio-2-butanone (28). Colorless crystals (EtOH-hexane); mp 52—55 °C; IR (KBr): 1720 (CO) cm^{-1}; ^{1}H NMR δ=1.64—1.85 (2H, m), 3.00—3.20 (2H, m), 3.62 (2H, s), 6.95—7.32 (9H, m); MS m/z (%): 290 (M$^+$, 38), 165 (25), 137 (64), 123 (100); Found: m/z 290.0526. Calcd for $C_{16}H_{15}OClS$: M, 290.0530.

1-Phenylthio-3-tridecanone (29). Colorless oil; IR (neat): 1715 (CO) cm^{-1}; ^{1}H NMR δ=0.89 (3H, bt, J=7 Hz), 1.1—1.7 (16H, m), 2.40 (2H, t, J=8 Hz), 2.75 (2H, m), 3.18 (2H, m), 7.2—7.4 (5H, m); MS m/z (%): 306 (M$^+$, 58), 165 (22), 137 (65), 123 (100).

1-Cyclohexyl-4-phenylthio-2-butanone (30). Colorless oil; IR (neat): 1720 (CO) cm^{-1}; ^{1}H NMR δ=0.5—2.1 (11H, m), 2.18 (2H, d, J=7 Hz), 2.72 (2H, m), 3.16 (2H, m), 7.1—7.4 (5H, m); MS m/z (%): 262 (M$^+$, 57), 137 (41), 125 (72), 109 (35), 97 (60), 55 (100).

1-Cyclohexyl-3-phenylthio-1-propanone (31). Colorless oil; IR (neat): 1715 (CO) cm^{-1}; ^{1}H NMR δ=0.8—2.0 (10H, m), 2.1—2.3 (1H, m), 2.6—2.9 (2H, m), 3.0—3.3 (2H, m), 7.1—7.6 (5H, m); MS m/z (%): 248 (M$^+$, 77), 191 (14), 165 (17), 137 (49), 123 (51), 109 (42), 83 (100); Found: m/z 248.1221. Calcd for $C_{15}H_{20}OS$: M, 248.1233.

8-(1-Oxo-3-phenylthiopropyl)-1,4-dioxaspiro[4.5]decane (32). Colorless oil; IR (neat): 1715 (CO) cm^{-1}; ^{1}H NMR δ=1.3—2.0 (8H, m), 2.1—2.5 (1H, m), 2.7—2.9 (2H, m), 3.0—3.3 (2H, m), 3.96 (4H, s), 7.1—7.4 (5H, m); MS m/z (%): 306 (M$^+$, 30), 192 (12), 169 (6), 137 (7), 123 (14), 99 (100); Found m/z 306.1291. Calcd for $C_{17}H_{22}O_3S$: M, 306.1288.

1-Cycloheptyl-3-phenylthio-1-propanone (33). Colorless oil; IR (neat): 1710 (CO) cm^{-1}; ^{1}H NMR δ=1.2—2.0 (12H, m), 2.3—2.6 (1H, m), 2.6—2.9 (2H, m), 3.0—3.2 (2H, m), 7.0—7.6 (5H, m); MS m/z (%): 262 (M$^+$, 95), 180 (6), 165 (23), 137 (58), 123 (70), 97 (87), 55 (100); Found: m/z 262.1372. Calcd for $C_{16}H_{22}OS$: M, 262.1389.

1-(4-Chlorophenyl)-3-buten-2-one (34). Colorless oil; IR (neat): 1690 (CO), 1620 (C=C) cm^{-1}; ^{1}H NMR δ=3.83 (2H, s), 5.85 (1H, dd, J=8, 3.5 Hz), 6.28 (1H, dd, J=17.5, 3.5 Hz), 6.37 (1H, dd, J=17.5, 8 Hz), UV λ_{max}^{EtOH} 218.5 nm; MS m/z (%): 180 (M$^+$, 24), 125 ([M−C_3H_3O]$^+$, 43), 55 ([M−C_7H_6Cl]$^+$, 100); Found: m/z 180.0333. Calcd for $C_{10}H_9OCl$: M, 180.0341.

1-Tridecen-3-one (35). Colorless oil; IR (neat): 1705, 1690 (CO), 1620 (C=C) cm^{-1}; ^{1}H NMR δ=0.89 (3H, t, J=7 Hz), 1.0—1.8 (16H, m), 2.61 (2H, t, J=7 Hz), 5.83 (1H, dd, J=9, 3 Hz), 6.26 (1H, dd, J=17.5, 3 Hz), 6.40 (1H, dd, J=17.5, 9 Hz); UV λ_{max}^{EtOH} 212 nm, MS m/z (%): 196 (M$^+$, 2), 167 ([M−C_2H_5]$^+$, 11), 139 ([M−C_4H_9]$^+$, 12), 70 ([M−C_9H_{18}]$^+$, 100); Found: m/z 196.1820. Calcd for $C_{13}H_{24}O$: M, 196.1825.

1-Cyclohexyl-3-buten-2-one (36). Colorless oil; IR (neat): 1700, 1685 (CO), 1620 (C=C) cm^{-1}; ^{1}H NMR δ=0.6—2.1 (11H, m), 2.47 (2H, d, J=7 Hz), 5.83 (1H, dd, J=9, 3 Hz), 6.23 (1H, dd, J=17.5, 3 Hz), 6.40 (1H, dd, J=17.5, 9 Hz); UV λ_{max}^{EtOH} 213 nm; MS m/z (%): 152 (M$^+$, 17), 134 ([M$^+$−H_2O]$^+$, 4), 109 ([M−C_3H_3O]$^+$, 18), 70 (100); Found: m/z 152.1182. Calcd for $C_{10}H_{16}O$: M, 152.1200.

1-Cyclohexyl-2-propen-1-one (37). Colorless oil; IR (neat): 1700, 1680 (CO), 1620 (C=C) cm^{-1}; ^{1}H NMR δ=1.0—2.0 (10H, m), 2.4—2.8 (1H, m), 5.77 (1H, dd, J=9, 3 Hz), 6.36 (1H, dd, J=18, 3 Hz), 6.45 (1H, dd, J=18, 9 Hz); UV λ_{max}^{EtOH} 212 nm.

1-Cycolheptyl-2-propen-1-one (38). Colorless oil; IR (neat): 1700, 1680 (CO), 1615 (C=C) cm^{-1}; ^{1}H NMR δ=1.1—2.1 (12H, m), 2.6—2.9 (1H, m), 5.71 (1H, dd, J=9, 3 Hz), 6.22 (1H, dd, J=18, 3 Hz), 6.38 (1H, dd, J=18, 9 Hz); UV λ_{max}^{EtOH} 212.5 nm; MS m/z (%): 152 (M$^+$, 7), 123 (10), 97 ([M−C_3H_3O]$^+$, 26), 55 ([M−C_7H_{13}]$^+$, 100).

General Procedure for the Preparation of Divinyl Ketones from α,β-Epoxy Sulfoxides Through Bis(phenylthio) Ketones. A synthesis of (*E*)-1,4-tridecadien-3-one (**40**) is described. A solution of diphenyl disulfide (660 mg; 3 mmol) and $NaBH_4$ (230 mg; 6 mmol) in 11 ml of dry EtOH was refluxed under N_2 for 30 min. This solution was cooled in an ice bath and a solution of **23** (260 mg; 0.6 mmol) in 1 ml of EtOH was added. The whole mixture was stirred at 0 °C for 1 h. The reaction was quenched by adding NH_4Cl

and the EtOH was evaporated. The residue was extracted with benzene and the organic layer was washed with sat. aq NH_4Cl and dried over Na_2SO_4. The product was purified by slilca-gel column chromatography to afford 226 mg (90%) of **39** as a colorless oil. IR (neat): 1710 (CO) cm^{-1}; ^1H NMR δ=0.88 (3H, bt, J=7 Hz), 1.0—2.0 (16H, m), 2.8—3.3 (4H, m), 3.62 (1H, t, J=7 Hz), 7.1—7.4 (10H, m); MS m/z (%): 414 (M^+, 6), 304 ([M−PhSH]$^+$, 10), 249 ([M−C_9H_9OS]$^+$, 100). To a solution of **39** (66 mg; 0.16 mmol) in 3 ml of CH_2Cl_2 at −40 °C was added *m*-CPBA (0.35 mmol) and the mixture was stirred for 5 min. The whole mixture was treated with short silica-gel column chromatography to remove the excess *m*-CPBA and *m*-chlorobenzoic acid. The crude product was heated in refluxing toluene (6 ml) for 15 min. The reaction mixture was cooled to room temperature and ether (6 ml) and 10% NaOH (3 ml) were added. The whole mixture (two phases) was vigorously stirred at room temperature for 1 d. The product was extracted with benzene and after the usual workup and silica-gel column chromatography, 24.5 mg (79%) of **40** was obtained as a colorless oil. IR (neat): 1670 (CO), 1640, 1620 (C=C) cm^{-1}; ^1H NMR δ=0.89 (3H, bt, J=7 Hz), 1.0—1.8 (12H, m), 2.1—2.4 (2H, m), 5.83 (1H, dd, J=10, 2 Hz), 6.32 (1H, dd, J=17.5, 2 Hz), 6.37 (1H, dt, J=16, 1.5 Hz), 6.70 (1H, dd, J=17.5, 10 Hz), 6.99 (1H, dt, J=16, 6.5 Hz); MS m/z (%): 194 (M^+, 2), 167 ([M−C_2H_4]$^+$, 9), 124 (16), 109 (32), 83 (63), 55 ([M−$C_{10}H_{19}$]$^+$, 100); Found: m/z 194.1641. Calcd for $C_{13}H_{22}O$: M, 194.1668.

(*E*)-1-Phenylsulfonyl-4-tridecen-3-one (41). Colorless oil; IR (neat): 1680 (CO), 1635 (C=C), 1310, 1155 (SO_2) cm^{-1}; ^1H NMR δ=0.89 (3H, bt, J=6.5 Hz), 1.0—1.7 (12H, m), 2.0—2.4 (2H, m), 2.96—3.20 (2H, m), 3.36—3.56 (2H, m), 6.09 (1H, dt, J=16, 1.5 Hz), 6.82 (1H, dt, J=16, 7 Hz), 7.4—8.1 (5H, m).

1-(1-Cyclohexenyl)-3-phenylsulfonyl-1-propanone (42). Colorless oil; IR (neat): 1665 (CO), 1305, 1150 (SO_2) cm^{-1}; ^1H NMR δ=1.40—1.80 (4H, m), 1.90—2.40 (4H, m), 2.96—3.25 (2H, m), 3.26—3.55 (2H, m), 6.90 (1H, m), 7.35—8.05 (5H, m); MS m/z (%): 278 (M^+, 14), 136 ([M−$PhSO_2H$]$^+$, 100), 109 (94).

1-(1-Cyclohexenyl)-2-propen-1-one (43). α,β′-Bis(phenylthio) ketone: Colorless oil; IR (neat): 1695 (CO) cm^{-1}; ^1H NMR δ=1.0—2.0 (10H, m), 3.12 (4H, m), 7.0—7.4 (10H, m); MS m/z (%): 356 (M^+, 6), 248 (6), 191 ([M−C_9H_9OS]$^+$, 86), 110 ([M−$C_{15}H_{18}OS$]$^+$, 100). **43**: Colorless oil; IR (neat): 1660 (CO), 1635, 1610 (C=C) cm^{-1}; ^1H NMR δ=1.64 (4H, m), 2.25 (4H, m), 5.65 (1H, dd, J=10.5, 2 Hz), 6.20 (1H, dd, J=17, 2 Hz), 6.90 (1H, m), 6.91 (1H, dd, J=17, 10.5 Hz); UV λ_{max}^{EtOH} 248.5 nm; MS m/z (%): 136 (M^+, 67), 108 ([M−C_2H_2]$^+$, 53), 81 ([M−C_3H_3O]$^+$, 100).

8-(1-Oxo-2-propenyl)-1,4-dioxaspiro[4.5]dec-7-ene (44). α,β′-Bis(phenylthio) ketone: Colorless oil; IR (neat): 1690 (CO), 1090 (COC) cm^{-1}; ^1H NMR δ=1.2—2.2 (8H, m), 2.9—3.4 (4H, m), 3.96 (4H, bs), 7.1—7.5 (10H, m); MS m/z (%): 414 (M^+, 13), 249 ([M−C_9H_9OS]$^+$, 100). **44**: Colorless oil; IR (neat): 1665 (CO), 1645, 1610 (C=C) cm^{-1}; ^1H NMR δ=1.82 (2H, bt, J=6 Hz), 2.4—2.7 (4H, m), 4.04 (4H, s), 5.73 (1H, dd, J=10.5, 2 Hz), 6.26 (1H, dd, J=17, 2 Hz), 6.83 (1H, m), 6.96 (1H, dd, J=17, 10.5 Hz); UV λ_{max}^{EtOH} 248.5 nm; MS m/z (%): 194 (M^+, 16), 86 ([M−C_7H_8O]$^+$, 100), Found: m/z 194.0940. Calcd for $C_{11}H_{14}O_3$: M, 194.0941.

1-(1-Cycloheptenyl)-2-propen-1-one (45). α,β′-Bis(phenylthio) ketone: Colorless oil; IR (neat): 1700 (CO) cm^{-1}; ^1H NMR δ=1.2—2.2 (12H, m), 3.0—3.4 (4H, m), 7.1—7.5 (10H, m); MS m/z (%): 370 (M^+, 5), 262 (44), 205 ([M−C_9H_9OS]$^+$, 100). To a solution of this bis(phenylthio) ketone (66 mg; 0.18 mmol) in 4 ml of CH_2Cl_2 at −70 °C was added *m*-CPBA (0.38 mmol) and stirred for 5 min. The cooling bath was removed and the mixture was stirred at room temperature for 2 h. To the reaction mixture was added ether (5 ml) and 10% NaOH (4 ml) and the whole (two phases) was vigorously stirred under N_2 for 1 d. The usual work-up and purification by silica-gel column chromatography gave **45** (20.6 mg; 77%) as a colorless oil. IR (neat): 1660 (CO), 1635, 1610 (C=C) cm^{-1}; ^1H NMR δ=1.3—2.0 (6H, m), 2.2—2.7 (4H, m), 5.72 (1H, dd, J=10, 2 Hz), 6.23 (1H, dd, J=17, 2 Hz), 6.95 (1H, dd, J=17, 10 Hz), 7.10 (1H, t, J=6 Hz); UV λ_{max}^{EtOH} 255 nm; MS m/z (%): 150 (M^+, 60), 135 (27), 95 (100); Found: m/z 150.1030. Calcd for $C_{10}H_{14}O$: M, 150.1043.

The authors are grateful to Dr. Sei-ichi. Saito, Tanabe Seiyaku Co. for the elemental analysis and Miss Noriko Sawabe, Mrs. Noriko Yamatani, and Miss Mutsumi Ohne of this laboratory for the NMR and mass spectral measurements.

References

1) Part VIII: T. Satoh, Y. Kaneko, and Koji Yamakawa, *Bull. Chem. Soc. Jpn.*, **59**, 2463 (1986).

2) M. C. Koletzel, *Org. React.*, **4**, 1 (1948); H. L. Holmes, *ibid.*, **4**, 60 (1948); L. W. Butz and A. W. Rytina, *ibid.*, **5**, 136 (1949); J. Sauer, *Angew. Chem., Int. Ed. Engl.*, **5**, 211 (1966), **6**, 16 (1967); G. Desimoni and G. Tacconi, *Chem. Rev.*, **75**, 651 (1975); G. Brieger and J. N. Bennett, *ibid.*, **80**, 63 (1980); M. Petrzilka, *Synthesis*, **1981**, 753; A. G. Fallis, *Can. J. Chem.*, **62**, 183 (1984); E. Ciganek, *Org. React.*, **32**, 1 (1984).

3) E. D. Bergmann, D. Ginsburg, and R. Pappo, *Org. React.*, **10**, 179 (1959); G. Posner, *ibid.*, **19**, 1 (1972); W. Carruthers, *Chem. Ind.*, **1973**, 931; M. E. Jung, *Tetrahedron*, **32**, 3 (1976); O. W. Lever, Jr., *ibid.*, **32**, 1943 (1976); R. E. Gawley, *Synthesis*, **1976**, 777.

4) J. C. Floyd, *Tetrahedron Lett.*, **1974**, 2877.

5) B. M. Trost and R. A. Kunz, *J. Am. Chem. Soc.*, **97**, 7152 (1975).

6) E. Negishi, V. Bagheri, S. Chatterjee, F.-T. Luo, J. A. Miller, and T. Stoll, *Tetrahedron Lett.*, **24**, 5181 (1983).

7) J. W. Labadie and J. K. Stille, *Tetrahedron Lett.*, **24**, 4283 (1983); *J. Am. Chem. Soc.*, **105**, 6129 (1983); J. W. Labadie, D. Tueting, and J. K. Stille, *J. Org. Chem.*, **48**, 4634 (1983).

8) N. Jabri, A. Alexakis, and J. F. Normant, *Tetrahedron Lett.*, **24**, 5081 (1983).

9) G. Stork and L. Maldonado, *J. Am. Chem. Soc.*, **93**, 5286 (1971); R. M. Jacobson, G. P. Lahm, and W. Clader, *J. Org. Chem.*, **45**, 395 (1980); P. Tuchinda, V. Prapansiri, W. Naengchomnong, and V. Reutrakul, *Chem. Lett.*, **1984**, 1427.

10) L. S. Hegedus, S. M. Lo, and D. E. Bloss, *J. Am. Chem. Soc.*, **95**, 3040 (1973); C. U. Pittman, Jr., and R. M. Hanes, *J. Org. Chem.*, **42**, 1194 (1977).

11) D. Milstein and J. K. Stille, *J. Am. Chem. Soc.*, **100**, 3636 (1978).

12) Y. Tamaru, H. Ochiai, F. Sanda, and Z. Yoshida,

Tetrahedron Lett., **26**, 5529 (1985).
13) W. F. Goure, M. E. Wright, P. D. Davis, S. S. Labadie, and J. K. Stille, *J. Am. Chem. Soc.*, **106**, 6417 (1984); G. T. Crisp, W. J. Scott, and J. K. Stille, *ibid.*, **106**, 7500 (1984).
14) a) T. Satoh, Y. Kaneko, T. Izawa, K. Sakata, and K. Yamakawa, *Bull. Chem. Soc. Jpn.*, **58**, 1983 (1985); b) T. Satoh, T. Kumagawa, and K. Yamakawa, *ibid.*, **58**, 2849 (1985); c) T. Satoh, Y. Kaneko, K. Sakata, and K. Yamakawa, *ibid.*, **59**, 457 (1986); d) T. Satoh, S. Motohashi, and K. Yamakawa, *ibid.*, **59**, 946 (1986).
15) A part of this study was reported as a communication: T. Satoh, T. Kumagawa, and K. Yamakawa, *Tetrahedron Lett.*, **27**, 2471 (1986).
16) B. M. Trost and T. N. Salzmann, *J. Am. Chem. Soc.*, **95**, 6840 (1973).
17) A. Murai, A. Abiko, N. Shimada, and T. Masamune, *Tetrahedron Lett.*, **25**, 4951 (1984).
18) D. L. J. Clive, *Tetrahedron*, **34**, 1049 (1978).
19) D. Liotta, U. Sunay, H. Santiesterban, and W. Markiwicz, *J. Org. Chem.*, **46**, 2605 (1981).
20) C. Santelli-Rouvier and M. Santelli, *Synthesis*, **1983**, 429.
21) M. Miyashita, A. Yoshikoshi, and P. A. Grieco, *J. Org. Chem.*, **42**, 3772 (1977).

 © 1987 The Chemical Society of Japan Bull. Chem. Soc. Jpn., 60, 311—324 (1987)

Hydrophobic Vitamin B_{12}. V. Electrochemical Carbon-Skeleton Rearrangement as Catalyzed by Hydrophobic Vitamin B_{12}: Reaction Mechanisms and Migratory Aptitude of Functional Groups†

Yukito MURAKAMI,* Yoshio HISAEDA, Toshiaki OZAKI, Takako TASHIRO, Teruhisa OHNO, Yutaro TANI, and Yoshihisa MATSUDA

Department of Organic Synthesis, Faculty of Engineering, Kyushu University, Hakozaki, Higashi-ku, Fukuoka 812

(Received July 19, 1986)

The carbon-skeleton rearrangements as catalyzed by heptamethyl cobyrinate perchlorate, [Cob(II)7C1ester]-ClO_4, were investigated under electrochemical conditions. The controlled-potential electrolysis of 2,2-bis(ethoxycarbonyl)-1-bromopropane, which is considered to be a model substrate for methylmalonyl-CoA mutase, was catalyzed by [Cob(II)7C1ester]ClO_4 in *N,N*-dimethylformamide to give the rearrangement product, 1,2-bis(ethoxycarbonyl)propane, as a major one at −1.5 V vs. SCE in the presence of acetic acid and at potentials more cathodic than −1.8 V vs. SCE without acetic acid in the dark. The electrochemical carbon-skeleton rearrangement was postulated to proceed via formation of anionic intermediates. The electrolyses of 1-bromo-2-cyano-2-ethoxycarbonylpropane, 2-acetyl-1-bromo-2-ethoxycarbonylpropane, and 1-bromo-2-[(ethylthio)carbonyl]propane with [Cob(II)7C1ester]ClO_4 also afforded the corresponding carbon-skeleton rearrangement products. The results indicated that substrates with two electron-withdrawing groups placed on the β-carbon atom with combinations of one carboxylic ester and one of carboxylic ester, acetyl, and cyano moieties readily gave the corresponding rearrangement products which were derived from individual migration of the substituent groups. Substrates with only one of the electron-withdrawing groups, carboxylic ester, acetyl, and cyano, did not give any rearrangement product, but a substrate with one thioester group afforded the corresponding rearrangement product. The migratory aptitude of electron-withdrawing groups was found to decrease in the order: COSR>COR>COOR>CN. Both electronic character and steric bulkiness of the migrating groups are apparently reflected on this tendency, even though relative contributions of these effects are much dependent on the nature of β-substituents.

We have previously prepared the cobalt complex of 1,19-dimethyl-A,D-didehydrocorrin (Hbdhc), having additional double bonds at peripheral positions and an additional angular methyl group as compared with the parent corrinoid, and investigated its structural properties in connection with vitamin B_{12} chemistry.[1,2] The bdhc complex is quite analogous to the corrinoid as far as electronic properties are concerned on the basis of its spectroscopic, electrochemical, and axial coordination behavior. On the other hand, the angular methyl groups in the complex exert an unusually large steric effect in the bimolecular reactions of Co^{I}(bdhc) with alkyl donors which result in the formation of an alkyl–cobalt bond. Even though the bdhc complex is considered to be a good B_{12} model, it does not catalyze the 1,2-migration reaction observed with vitamin B_{12}. This is indeed originated from the steric repulsion effect provided by the angular methyl group which prevents an alkyl fragment initially formed through the Co–C cleavage from staying close to the nuclear cobalt. In order to improve this stereochemical situation, it became necessary to develop another good vitamin B_{12} model.

Various cobalt complexes have been synthesized as model complexes,[3] but all of those complexes cannot be qualified as favorable model complexes in the light of the following aspects. (i) Redox behavior of the central cobalt, which is mainly controlled by basicity of an equatorial ligand, must be similar to that for the naturally occurring vitamin B_{12}. (ii) Electronic properties must be equivalent to those of the natural B_{12}, which are provided by the corrin ring with eight double bonds and the direct bond between A and D rings. (iii) The steric effects, which are caused by the methyl moiety and the hydrogen atom at C(1) and C(19) positions in the corrin ring, respectively, and by four propanamides and three acetamides placed at the α- and β-peripheral sites, respectively, must be retained by model complexes.

In order to simulate various functions of vitamin B_{12} as exerted in the hydrophobic active sites of enzymes concerned, we have been dealing with hydrophobic vitamin B_{12} derivatives which have ester groups in place of the peripheral amide moieties of the naturally occurring vitamin B_{12}.[4-12] These modified cobalt complexes satisfy all the above requirements and are readily soluble in a wide range of organic solvents.

Most of the vitamin B_{12} model reactions so far carried out are concerned merely with cleavage of the Co–C bond of the corresponding alkylated complexes[13] and cannot be regarded as catalytic ones.[14] Because the alkylated complexes in these reactions were prepared from cobalt complexes and alkyl halides in the presence of chemical reductants such as $NaBH_4$, it was difficult to establish the catalytic cycle and to eliminate an undesirable effect caused by reductants on the reaction. In order to overcome these

† Contribution No. 840 from this Department.

difficulties and set up clean reaction systems, we have adopted electrochemical means for reduction.[11] Recently, electrochemical reactions catalyzed by vitamin B_{12} derivatives or model complexes have been carried out rather extensively,[15-20] but catalytic isomerization reactions accompanied with the carbon-skeleton rearrangement, which are considered to be typical coenzyme B_{12}-dependent enzymatic reactions, have not been successfully performed yet.

In the present work, we have carried out the rearrangement reactions by electrochemical means for the first time as catalyzed by heptamethyl cobyrinate perchlorate, [Cob(II)7C$_1$ester]ClO_4, and reaction mechanisms involved in the electrolyses were clarified by means of various spectroscopic methods. Furthermore, we studied the migratory aptitude of functional groups in the carbon-skeleton rearrangement by employing several substrates having electron-withdrawing groups such as carboxylic ester, thioester, acetyl, and cyano moieties.

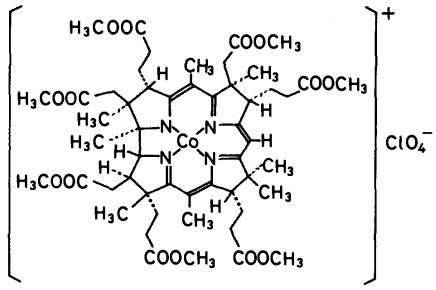

[Cob(III)7C$_1$ester]ClO_4

Results and Discussion

We have previously pointed out that [Cob(II)7C$_1$ester]ClO_4 is readily reduced to the univalent cobalt species of highly nucleophilic character by electrochemical means in nonaqueous media,[5] and catalytic reaction cycles shown in Scheme 1 were established. An alkylated complex, generated by the reaction between a univalent cobalt complex and an alkyl halide (RX), is generally decomposed by photolysis[10] or electrolysis to afford reduction and/or rearrangement products. First, we adopted 2,2-bis(ethoxycarbonyl)-1-bromopropane (**1**) which is considered to be a model substrate for methylmalonyl-CoA mutase. This bromide was originally used by Rétey et al. as a model substrate,[21] but Tada et al. reported that the photochemical decomposition of the corresponding alkylated cobaloxime complex gave only the reduction product, 2,2-bis(ethoxycarbonyl)-propane, and the rearrangement product, 1,2-bis-(ethoxycarbonyl)propane, was not detected.[22] Furthermore, the ethoxycarbonyl group of this substrate does not migrate during the reaction with tributyltin hydride which acts to generate the corresponding free radical in the course of the reaction without a cobalt complex.[23]

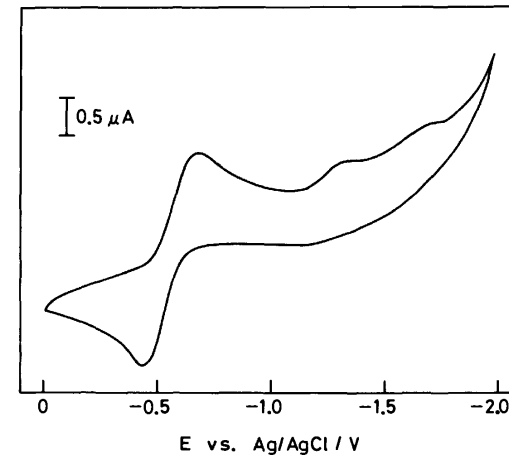

Fig. 1. Cyclic voltammogram of [Cob(II)7C$_1$ester]ClO_4 (7.2×10^{-4} mol dm^{-3}) in DMF containing 2,2-bis(ethoxycarbonyl)-1-bromopropane (0.10 mol dm^{-3}) and TBAF (0.10 mol dm^{-3}) at 20±2 °C in the dark; sweep rate, 100 mV s^{-1}.

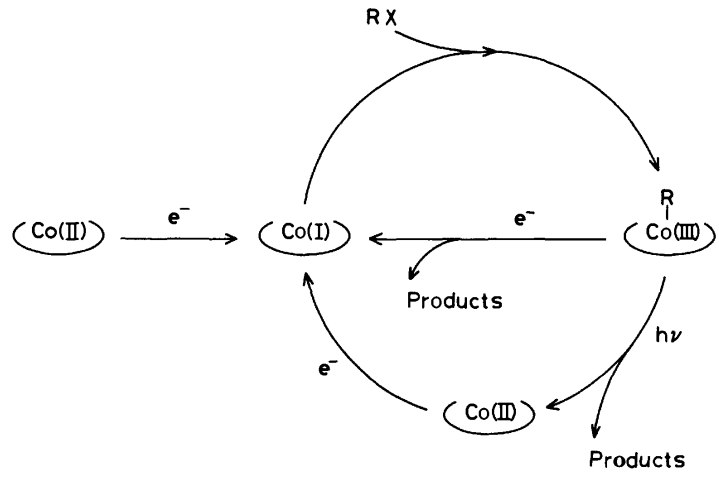

Scheme 1.

Redox Behavior. The redox behavior of [Cob(II)-7C$_1$ester]ClO_4 in *N*,*N*-dimethylformamide (DMF) containing 2,2-bis(ethoxycarbonyl)-1-bromopropane in a large excess and tetrabutylammonium tetrafluoroborate (TBAF) as a supporting electrolyte was examined by means of cyclic voltammetry as shown in Fig. 1.[12] The redox potential for the Co(II)/Co(I) couple on [Cob(II)7C$_1$ester]ClO_4 in DMF was observed at −0.56 V vs. Ag/AgCl in the presence of the alkyl bromide, while the corresponding potential in DMF was observed at −0.58 V vs. Ag/AgCl (−0.61 V vs. SCE) without the alkyl bromide.[5] An irreversible reduction peak was observed at ca. −1.3 V vs. Ag/AgCl and assigned to the formation of the one-electron reduction intermediate of the alkylated complex, which was generated by the reaction between the Co^I species and the alkyl halide. This value is in agreement with the one for heptamethyl methylaquacobyrinate perchlorate, [$(CH_3)(H_2O)$Cob(III)7C$_1$-ester]ClO_4, in DMF; −1.29 V vs. Ag/AgCl (−1.32 V vs. SCE). Its cathodic peak current was small in comparison with that for Co(II)/Co(I) due to the slow rate of reaction between the Co^I species and the substrate. In addition, the second irreversible reduction peak was observed at ca. −1.8 V vs. Ag/AgCl. This peak was assigned to the formation of the two-electron reduction intermediate of the alkylated complex as confirmed by coulometry and controlled-potential electrolysis described below. The first reduction peak for substrate **1** was observed at −2.7 V vs. Ag/AgCl by cyclic voltammetry in DMF without the hydrophobic vitamin B_{12}, so that the peaks observed in the range of −2.0—0 V vs. Ag/AgCl are not originated from the substrate itself. Consequently, the electrochemical behavior shown in Fig. 1 is consistent with the reduction processes shown in Scheme 5, indicating generation of mutually different intermediates by the electrolysis at −1.0, −1.5, and −2.0 V vs. SCE.[24]

Catalytic Reaction. The electrolysis of 2,2-bis(ethoxycarbonyl)-1-bromopropane was carried out upon addition of [Cob(II)7C$_1$ester]ClO_4 under various conditions. The following findings were obtained on the basis of the product analyses given in Table 1 (refer to Eq. 1). (i) At −1.0 V vs. SCE: products were

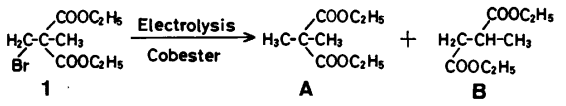

(1)

obtained only when the reaction mixture was irradiated with the visible light, and the major product was the reduced one (**A** in Eq. 1). (ii) At −1.5 V vs. SCE in the dark: the rearrangement product (**B** in Eq. 1) was the major one when an efficient proton source such as acetic acid or propionic acid was added,[25] while the reduction product (**A**) was largely obtained when 2-propanol was added or without any additive. (iii) At −1.5 V vs. SCE under irradiation with the visible light: the major product was the reduced one even in the presence of acetic acid. (iv) At potentials more cathodic than −1.8 V vs. SCE in the dark: the rearrangement product (**B**) was largely obtained even in the absence of acetic acid. The catalysis was very efficient at −2.0 V vs. SCE, so that the rearrangement product was obtained in yields

Table 1. Product Analyses for Controlled-Potential Electrolysis of 2,2-Bis(ethoxycarbonyl)-1-bromopropane as Catalyzed by Hydrophobic Vitamin B_{12}[a]

Entry	Electrolysis conditions					Yield/%[e]	
	Potential V vs. SCE	Irradiation[b]	Additive[c]	Charge[d] F mol^{-1}	Period h	**A**	**B**
1	−1.0	Irradiation	CH_3COOH	0.2	9	9—12	Trace
2	−1.5	Irradiation	CH_3COOH	3.0	12	36—41	3—10
3	−1.5	In the dark	CH_3COOH	3.0	6	16—18	40—46
4	−1.5	In the dark	C_2H_5COOH	3.0	9	15—17	25—28
5	−1.5	In the dark	$(CH_3)_2CHOH$	1.0	23	32—37	Trace
6	−1.5	In the dark	None	1.0	23	25—36	ca. 1
7	−1.8	In the dark	CH_3COOH	2.0	6	12—13	32—36
8	−1.8	In the dark	None	2.0	23	24—28	23—31
9	−2.0	In the dark	None	2.0	2	11—18	76—84

a) Electrolysis was carried out in a two-compartment cell equipped with Pt electrodes at 20±2 °C under argon atmosphere. Starting solutions composed of: [Cob(II)7C$_1$ester]ClO_4, 30 mg (2.6×10^{-5} mol): 2,2-bis(ethoxycarbonyl)-1-bromopropane, 1.0 g (3.8×10^{-3} mol); 30 mL of DMF containing 0.50 mol dm^{-3} TBAF. b) Irradiated with a 300-W tungsten lamp from a distance of 50 cm. c) CH_3COOH, 0.50 g (8.3×10^{-3} mol); C_2H_5COOH, 0.61 g (8.3×10^{-3} mol); $(CH_3)_2CHOH$, 0.50 g (8.3×10^{-3} mol). d) Electrical charge passed per mol of the substrate. e) Based on an initial amount of the substrate; the rest was the unreacted substrate (a small amount of $(CH_3CO_2)CH_2C(CH_3)(CO_2C_2H_5)_2$ was obtained when CH_3COOH was added); analyzed by GLC. Recovery of the catalyst: 80—90% at −1.0 V; 60—70% at −1.5 V; ca. 50% at −1.8 and −2.0 V vs. SCE.

equivalent to 100—110 times as much as a molar quantity of the hydrophobic vitamin B_{12} after 2 h of the reaction.

Reaction Mechanisms. The reaction mechanisms for controlled-potential electrolyses were investigated by means of electronic spectroscopy, product analyses, and coulometry as well as by the spin-trapping ESR technique.

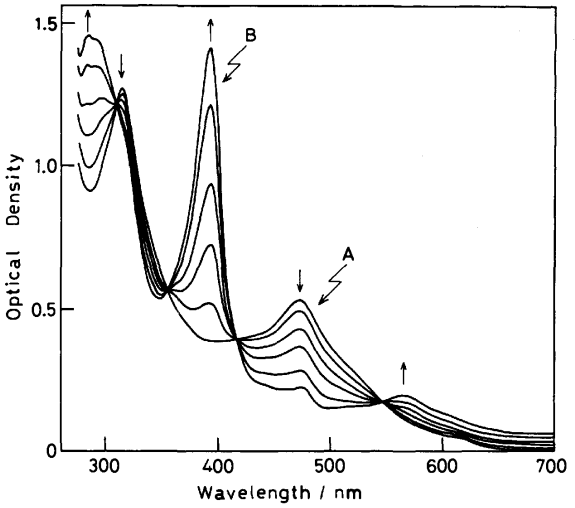

Fig. 2. Spectral change during electrochemical reduction of [Cob(II)7C$_1$ester]ClO_4 (5.2×10^{-5} mol dm^{-3}) in DMF containing 0.20 mol dm^{-3} TBAF at -1.0 V vs. SCE and 20.5 ± 0.1 °C: A, [Cob(II)7C$_1$ester]ClO_4; B, Cob(I)7C$_1$ester. Trends of spectral change with time are shown by arrows.

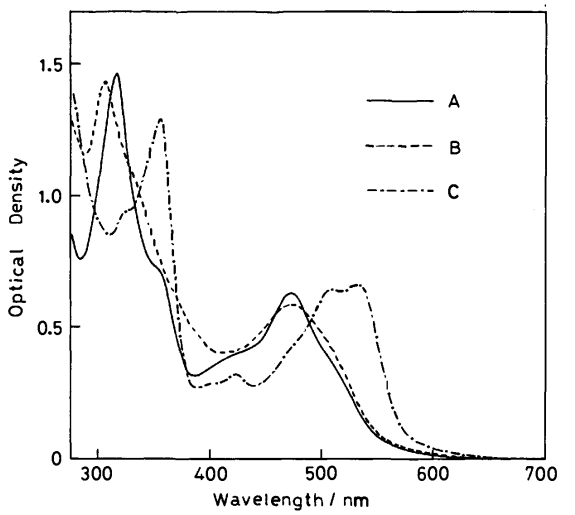

Fig. 3. Electronic spectra observed for a DMF solution containing [Cob(II)7C$_1$ester]ClO_4 (5.2×10^{-5} mol dm^{-3}), 2,2-bis(ethoxycarbonyl)-1-bromopropane (1.5×10^{-2} mol dm^{-3}), TBAF (0.20 mol dm^{-3}), and acetic acid (1.2×10^{-2} mol dm^{-3}) at 20.5 ± 0.1 °C under the following conditions: A, before electrolysis under argon atmosphere; B, electrolysis at -1.0 V vs. SCE under argon atmosphere; C, sample B being irradiated with a 150-W tungsten lamp from a distance of 20 cm for 1 min under aerobic conditions.

(a) Electrolysis at -1.0 V vs. SCE. The controlled-potential electrolysis was followed by electronic spectroscopy. [Cob(II)7C$_1$ester]ClO_4 was reduced to Cob(I)7C$_1$ester, having an absorption maximum at 394 nm as shown in Fig. 2, when the electrolysis was carried out at -1.0 V vs. SCE in the absence of an alkyl halide. When the electrolysis with 2,2-bis(ethoxycarbonyl)-1-bromopropane was carried out at -1.0 V vs. SCE in the dark, [Cob(II)7C$_1$ester]ClO_4 was transformed into the corresponding alkylated complex with absorption maxima at 305 and 474 nm (curve B in Fig. 3). Upon irradiation of this complex with the visible light for a short period of time under aerobic conditions, the electronic spectrum indicated cleavage of the Co-C bond[10] (curve C in Fig. 3). These spectral changes apparently reflect the fact that the alkylated complex is formed at -1.0 V vs. SCE and subsequently decomposed under irradiation conditions.

The reaction was also examined by the spin-trapping technique with α-phenyl-*N*-(*t*-butyl)nitrone (PBN).[26] An ESR spectrum for the PBN spin adduct formed in the course of electrolysis at -1.0 V vs. SCE is shown in Fig. 4. An ESR signal was not observed in the dark (A in Fig. 4), but clear signals for the PBN spin adduct (A_N=14.9 G, A_H=2.7 G; 10^4G=1 T) were detected upon irradiation with the visible light under anaerobic conditions (B in Fig. 4). The identical signals were observed in the absence of acetic acid. The result indicates that the radical species is generated as the intermediate under irradiation conditions.

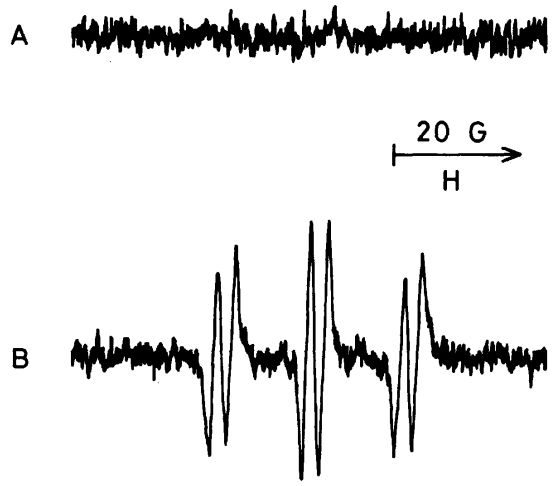

Fig. 4. ESR spectra observed during electrolysis (at -1.0 V vs. SCE) of a DMF solution containing [Cob(II)7C$_1$ester]ClO_4 (2.4×10^{-3} mol dm^{-3}), 2,2-bis-(ethoxycarbonyl)-1-bromopropane(0.29 mol dm^{-3}),PBN (0.12 mol dm^{-3}), acetic acid (0.56 mol dm^{-3}), and TBAF (0.10 mol dm^{-3}) at room temperature: A, in the dark; B, irradiated with a 300-W tungsten lamp from a distance of 60 cm.

In the light of the spectral measurements and the product analyses for the electrolysis at −1.0 V vs. SCE, a reaction cycle takes place as shown in Scheme 2. The Co^{II} complex is first converted into the Co^{I} species by the electrochemical reduction. The alkylated complex is formed in the second place by the reaction of the super-nucleophilic Co^{I} species with 2,2-bis(ethoxycarbonyl)-1-bromopropane. The complex is then decomposed by the visible light to give the Co^{II} species and the alkyl radical. The radical species abstracts a hydrogen atom to afford the reduction product (**A**), and the Co^{II} complex repeatedly acts as a mediator.

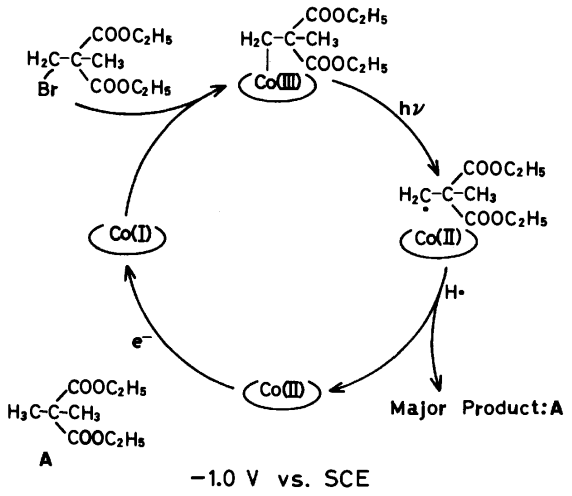

Scheme 2.

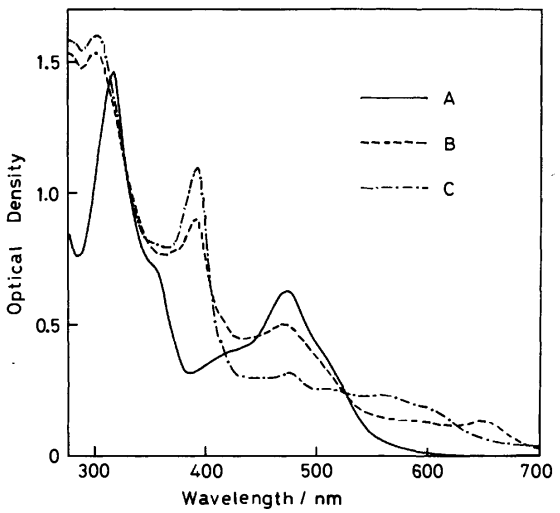

Fig. 5. Electronic spectra observed steadily during electrolysis of a DMF solution containing [Cob(II)7C_1-ester]ClO_4 (5.2×10^{-5} mol dm^{-3}), 2,2-bis(ethoxycarbonyl)-1-bromopropane (1.5×10^{-2} mol dm^{-3}), TBAF (0.20 mol dm^{-3}), and acetic acid (1.2×10^{-2} mol dm^{-3}) at 20.5±0.1 °C: A, before electrolysis; B, at −1.5 V vs. SCE; C, at −1.5 V vs. SCE without acetic acid.

(b) Electrolysis at −1.5 V vs. SCE. When the electrolysis was carried out at −1.5 V vs. SCE, absorption maxima were observed at 280, 302, 391, and 474 nm (curve B in Fig. 5). The spectrum indicates the formation of the alkylated complex and Cob(I)7C_1-ester. A similar spectral change was observed even in the absence of acetic acid (curve C in Fig. 5), but the absorbance intensity originated from Cob(I)7C_1ester was greater than that observed in the presence of acetic acid. These spectral features indicate that the alkylated complex is electrochemically decomposed at −1.5 V vs. SCE.

The electrolysis reaction without irradiation was also examined by the spin-trapping technique. ESR spectra for the PBN spin adducts formed in the course of electrolysis in the dark are shown in Fig. 6. ESR signals attributable to the PBN spin adducts were clearly observed (A in Fig. 6), while the signal intensities became much weaker upon addition of acetic acid (B in Fig. 6). Spin Hamiltonian parameters for the spin adducts are as follows: A_N=14.9 G, A_H=2.7 G; A_N=14.3 G, A_H=6.3 G. Only a single radical species with the former set of parameters was detected at the initial stage of the electrolysis. These values are identical with those observed for the electrolysis at −1.0 V vs. SCE under irradiation conditions. The latter set of parameters was assigned to another species formed in some secondary reactions. The result confirms that the radical species is generated as the electrolysis intermediate at −1.5 V vs. SCE without acetic acid while an efficient proton source such as acetic acid inhibits the formation of the radical species to a large extent.

A relationship between electrical quantity and

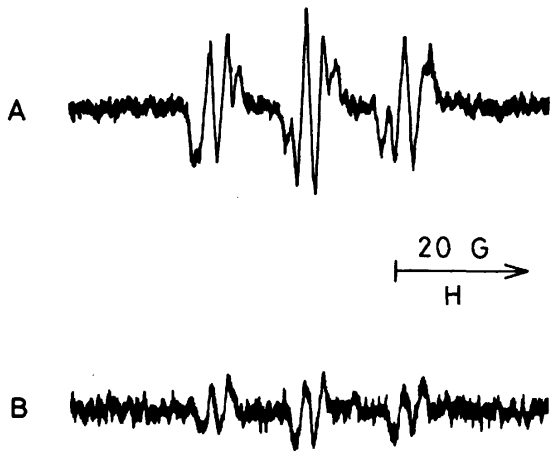

Fig. 6. ESR spectra observed during electrolysis (at −1.5 V vs. SCE) of a DMF solution containing [Cob(II)7C_1ester]ClO_4 (1.7×10^{-3} mol dm^{-3}), 2,2-bis(ethoxycarbonyl)-1-bromopropane (0.25 mol dm^{-3}), PBN (0.10 mol dm^{-3}), and TBAF (0.10 mol dm^{-3}) at room temperature in the dark: A, without acetic acid; B, in the presence of acetic acid (0.56 mol dm^{-3}).

product yield at the initial stage of electrolysis in the dark without acetic acid at −1.5 V vs. SCE is shown in Fig. 7. The reciprocal value (n) of the slope gives a number of electrons needed for the reaction; n=1.2 indicates one-electron reduction.

In order to identify the role of acetic acid, the electrolysis was carried out in the presence of the deuterated acetic acid (CH_3COOD) at −1.5 V vs. SCE in the dark. The product analysis by means of ^{1}H-NMR and mass spectral measurements clarified that the rearrangement product containing one deuterium, $(H_5C_2O_2C)CH_2CD(CH_3)(CO_2C_2H_5)$, was primarily obtained (refer to Eq. 2).[27] Its isotopic purity was

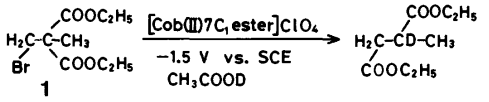

(2)

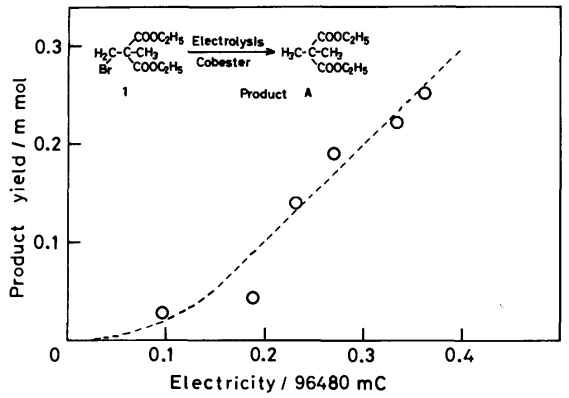

Fig. 7. Relationship between quantity of electricity and yield of the reduction product, 2,2-bis(ethoxycarbonyl)-propane, for electrolysis at −1.5 V vs. SCE and 20± 2 °C in the dark. Initial solution: [Cob(II)7C$_1$ester]-ClO_4, 30 mg (2.6×10^{-5} mol); 2,2-bis(ethoxycarbonyl)-1-bromopropane, 1.0 g (3.8×10^{-3} mol); 30 mL of DMF containing 0.50 mol dm^{-3} TBAF.

estimated to be 55—60%D. Even when CD_3COOD was used, the isotopic purity remained the same. Reasons for the formation of the product without deuterium may be given as follows: (i) proton-exchange between the deuterated acetic acid and a trace amount of water involved in DMF takes place;[28,29] (ii) proton donation from formic acid formed by decomposition of DMF occurs;[28] (iii) a proton is abstracted from the quaternary ammonium salt, the supporting electrolyte (Hofmann elimination).[30] The electrochemical carbon-skeleton rearrangement is postulated here to proceed via formation of an anionic intermediate, and the proton from acetic acid attacks on the β-carbon of the substrate bound to the hydrophobic vitamin B_{12}.

In the light of the above results, the electrolysis at −1.5 V vs. SCE proceeds via reaction cycles shown in Scheme 3. The mechanism for alkylation of the hydrophobic vitamin B_{12} is identical with that at −1.0 V vs. SCE (vide supra). The alkylated complex is then reduced to the one-electron reduction intermediate at −1.5 V vs. SCE in the dark. The electronic structure for the intermediate seems to be represented by two canonical forms I_A and I_B (Scheme 3). The proton attack on the β-carbon of the substrate induces the carbon-skeleton rearrangement, followed by the cobalt-carbon bond cleavage. On the other hand, the one-electron reduction intermediate is spontaneously decomposed to afford the Co^{I} chelate and the alkyl radical in the absence of an efficient proton source. The reduction product (**A**) is mainly produced from the alkyl radical by rapid abstraction of the hydrogen atom.

(c) Electrolysis at −2.0 V vs. SCE. When the electrolysis was carried out at −1.8 V vs. SCE, the absorbance originated from Cob(I)7C$_1$ester was more intense than that observed during the electrolysis at −1.5 V vs. SCE (Fig. 8). The alkylated complex was

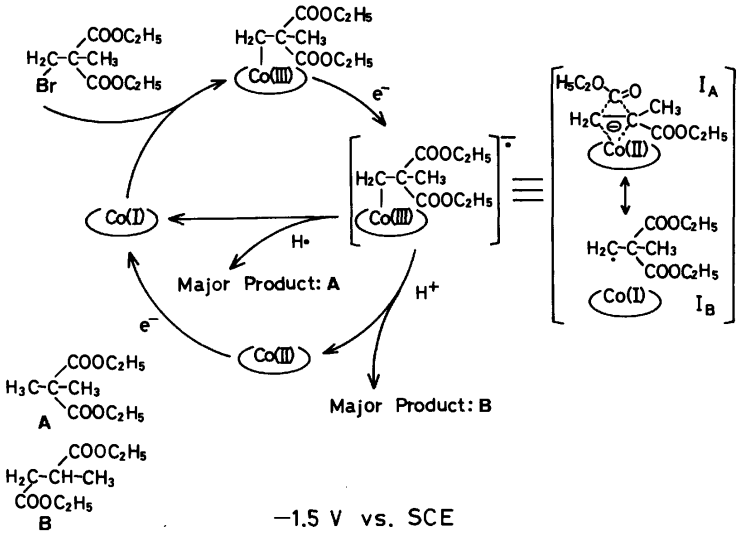

Scheme 3.

decomposed to the Co^{I} complex at potentials more cathodic than −1.8 V vs. SCE in the dark, since the Co^{I} species was steadily observed by electronic spectroscopy during the electrolysis. The spin-trapping technique was not applicable to the electrolysis at −2.0 V vs. SCE, because spin adducts were formed to a limited extent by electrolysis of the substrate itself even in the case without the hydrophobic vitamin B_{12}.

A relationship between electrical quantity and product yield for the electrolysis at −2.0 V vs. SCE in the dark is shown in Fig. 9; the n value of 2.3 indicates the electrolysis takes place via two-electron reduction (line C). Thus, the reaction at −2.0 V vs. SCE must proceed through a cycle shown in Scheme 4. The alkylated complex, which is generated in a manner as observed at −1.0 V vs. SCE, is converted into the two-electron reduction intermediate in the dark. This intermediate is decomposed to the Co^{I} chelate and the anionic species, and rearrangement product is obtained from the latter.

(d) Overall feature of electrolysis mechanisms. The formation conditions for the reduction and rearrangement products in the electrolysis of 2,2-bis(ethoxycarbonyl)-1-bromopropane as catalyzed by the hydrophobic vitamin B_{12} are summarized in Scheme 5. The rearrangement product is obtained primarily from the anionic intermediates, I_A and I_C, while the simple reduction product is mainly

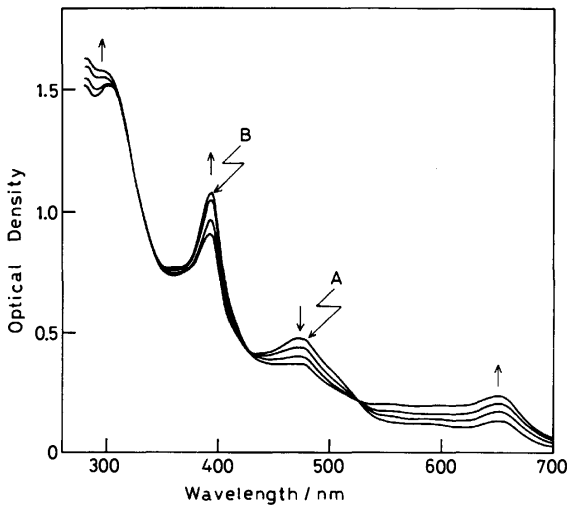

Fig. 8. Electronic spectra observed during electrolysis of a DMF solution containing [Cob(II)$7C_1$ester]ClO_4 (5.2×10^{-5} mol dm^{-3}), 2,2-bis(ethoxycarbonyl)-1-bromopropane (1.5×10^{-2} mol dm^{-3}), TBAF (0.20 mol dm^{-3}), and acetic acid (1.2×10^{-2} mol dm^{-3}) at 20.5 ±0.1 °C: A, steady state at −1.5 V vs. SCE; B, steady state at −1.8 V vs. SCE (electrolysis potential was reset at −1.8 V vs. SCE after state A was attained; trends of spectral change are shown by arrows).

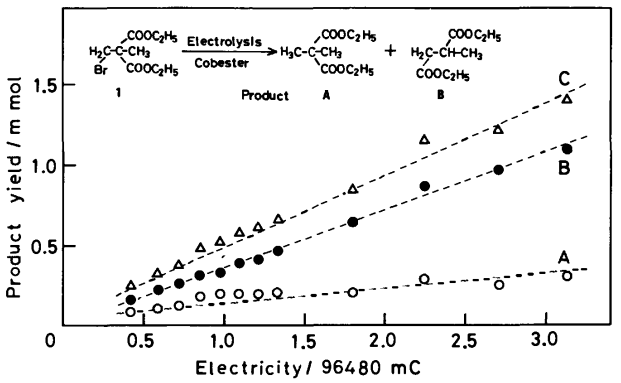

Fig. 9. Relationships between quantity of electricity and product yield for electrolysis at −2.0 V vs. SCE and 20±2 °C in the dark: A, yield of the reduction product, 2,2-bis(ethoxycarbonyl)propane; B, yield of the rearrangement product, 1,2-bis(ethoxycarbonyl)-propane; C, total yield. Initial solution: [Cob(II)-$7C_1$ester]ClO_4, 30 mg (2.6×10^{-5} mol); 2,2-bis(ethoxycarbonyl)-1-bromopropane, 1.0 g (3.8×10^{-3} mol); 30 mL of DMF containing 0.50 mol dm^{-3} TBAF.

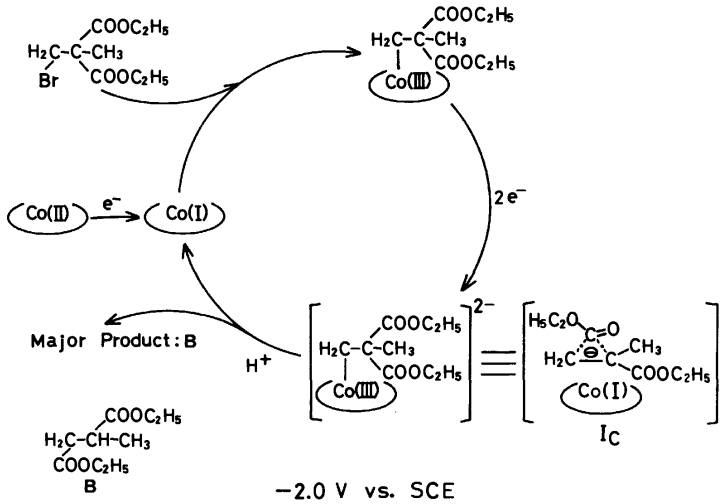

Scheme 4.

produced from the radical species. In particular, the two-electron reduction intermediate (Ic) is more effective in affording the rearrangement product. Since the identical radical species, which is produced by the reaction of the present substrate with tributyltin hydride[23] or by the photolysis of the present substrate bound to cobaloxime,[22] does not give the rearrangement product, the anionic reaction intermediates are the primary source for the rearrangement product. The present study demonstrates the first example of the rearrangement as catalyzed by a vitamin B_{12} model under electrochemical conditions.

Electrolyses of Various Substrates. In order to make further characterization of the catalytic proficiency of the hydrophobic vitamin B_{12} and clarify the migratory aptitude of functional groups in the electrochemical rearrangement reaction, other substrates were also used here. These substrates and the corresponding products are shown in Eqs. 3—8. All the substrates showed their first reduction peaks at -2.7 ± 0.1 V vs. Ag/AgCl as confirmed by cyclic voltammetry.

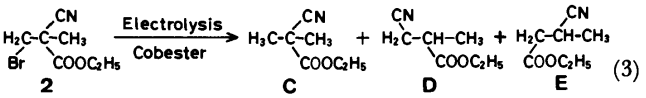

(3)

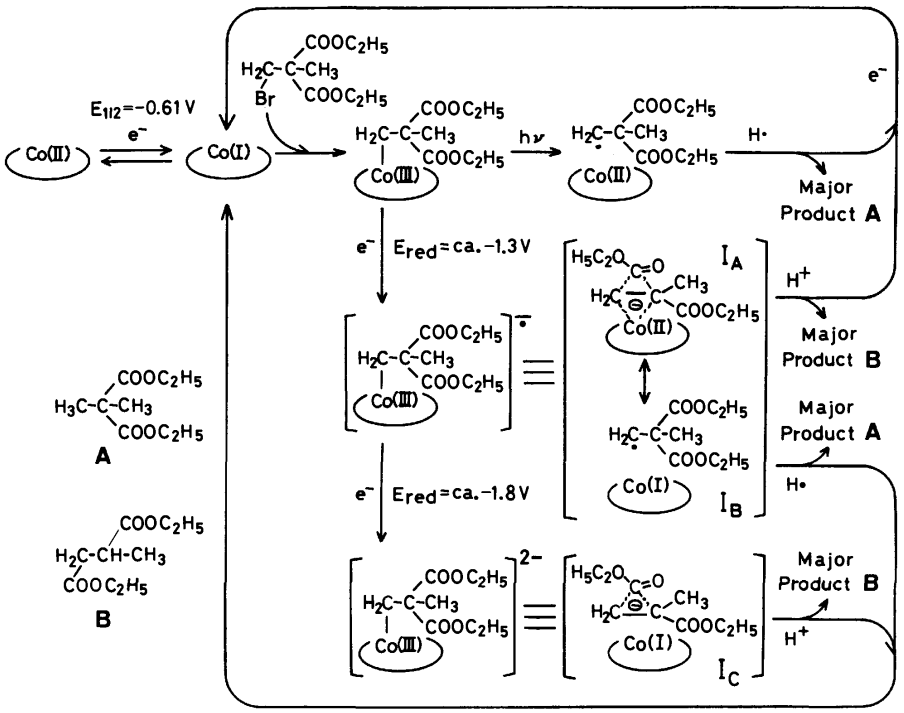

Scheme 5.

Table 2. Product Analyses for Controlled-Potential Electrolysis of 1-Bromo-2-cyano-2-ethoxycarbonylpropane as Catalyzed by Hydrophobic Vitamin B_{12}[a]

Entry	Electrolysis conditions					Yield/%[e]		
	Potential V vs. SCE	Irradiation[b]	Additive[c]	Charge[d] F mol^{-1}	Period h	C	D	E
1	−1.0	Irradiation	None	0.3	8	5	Trace	Trace
2	−1.5	In the dark	None	1.0	21	32—34	Trace	ca. 1
3	−1.5	In the dark	CH_3COOH	3.0	6	31—32	2—3	56—63
4	−2.0	In the dark	None	2.0	8	28—32	2—3	60—64

a) Electrolysis was carried out in a two-compartment cell equipped with Pt electrodes at 20 ± 2 °C under argon atmosphere. Starting solutions composed of: [Cob(II)7C$_1$ester]ClO_4, 30 mg (2.6×10^{-5} mol); 1-bromo-2-cyano-2-ethoxycarbonylpropane, 1.0 g (4.5×10^{-3} mol); 30 mL of DMF containing 0.50 mol dm^{-3} TBAF. b) Irradiated with a 300-W tungsten lamp from a distance of 50 cm. c) CH_3COOH, 0.50 g (8.3×10^{-3} mol). d) Electrical charge passed per mol of the substrate. e) Based on an initial amount of the substrate; the rest was the unreacted substrate (a small amount of $(CH_3CO_2)CH_2C(CH_3)(CO_2C_2H_5)(CN)$ was obtained when CH_3COOH was added); analyzed by GLC. Recovery of the catalyst: 80—90% at −1.0 V; 60—70% at −1.5 V; ca. 50% at −2.0 V vs. SCE.

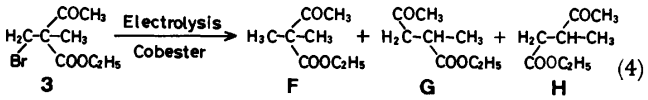

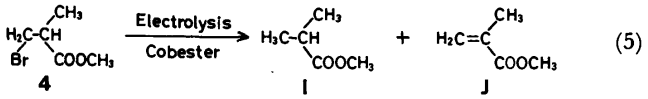

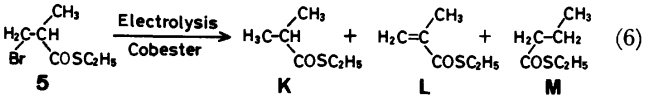

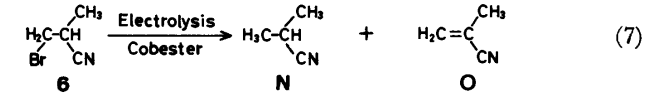

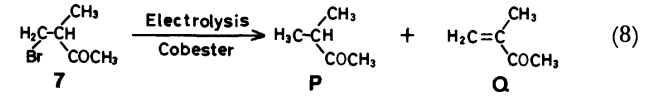

(a) Substrates with two electron-withdrawing groups. The product analyses for the electrolyses of 1-bromo-2-cyano-2-ethoxycarbonylpropane (**2**) and 2-acetyl-1-bromo-2-ethoxycarbonylpropane (**3**) are respectively shown in Tables 2 and 3. The following findings are based on the product analyses for the reaction with substrate **2** (Table 2; refer to Eq. 3). (i) At −1.0 V vs. SCE: products were obtained only when the reaction mixture was irradiated with the visible light, and the major product was the reduced one, 2-cyano-2-ethoxycarbonylpropane (**C**). (ii) At −1.5 V vs. SCE in the dark: the ester-migrated product, 2-cyano-1-ethoxycarbonylpropane (**E**), was the major one when acetic acid was added, while the reduction product (**C**) was largely obtained without any proton source. (iii) At −2.0 V vs. SCE in the dark: the rearrangement product (**E**) was the major one even in the absence of a proton source. (iv) The ester-migrated product (**E**) was produced more readily than the cyano-migrated one, 1-cyano-2-ethoxycarbonylpropane (**D**), under all the conditions; **E**:**D**=96:4.

The following results provide the basis for clarification of the reaction mechanisms concerned. (i) As for cyclic voltammetry performed in DMF on the alkylated complex[31] derived from the hydrophobic vitamin B_{12} and **2**, the first reduction wave was observed at −1.25 V vs. Ag/AgCl and the second one at −1.80 V vs. Ag/AgCl. (ii) On the basis of the relation between electrical quantity and product yield, one-electron reduction (n=1.1) and two-electron reduction (n=2.0) took place at −1.5 and −2.0 V vs. SCE, respectively. (iii) When CH_3COOD was used as a proton source at −1.5 V vs. SCE in the dark, the rearrangement product containing one deuterium, $(H_5C_2O_2C)CH_2CD(CH_3)(CN)$, was obtained as the major product. Its isotopic purity was estimated to be 50—60%D. These results are comparable to those obtained for the reaction with **1**. It may be concluded that the electrolyses of **2** catalyzed by the hydrophobic vitamin B_{12} proceed via formation of intermediates identical in electronic nature with those given in Scheme 5. It became apparent that the ester group has a higher tendency to migrate than the cyano group. This is in contrast with a previous result reported by Rétey et al.,[32] showing that the cyano-migrated product was obtained as a major one by photolysis of the alkylated complex derived from cobalamin and **2**. They concluded that the cyano group has a somewhat higher tendency to migrate than the ethoxycarbonyl group. Since their experimental conditions allow to generate primarily the radical species, the migratory aptitude of cyano and ester groups seems to become reversed under the present conditions which allow to give the anionic intermediates.

The electrolysis of substrate **3** gave the following

Table 3. Product Analyses for Controlled-Potential Electrolysis of 2-Acetyl-1-bromo-2-ethoxycarbonylpropane as Catalyzed by Hydrophobic Vitamin B_{12}[a]

Entry	Electrolysis conditions					Yield/%[e]		
	Potential V vs. SCE	Irradiation[b]	Additive[c]	Charge[d] F mol^{-1}	Period h	**F**	**G**	**H**
1	−1.0	Irradiation	None	1.0	20	2—3	7—10	Trace
2	−1.5	In the dark	None	1.0	20	10—13	53—60	ca. 1
3	−1.5	In the dark	CH_3COOH	3.0	10	15—20	73—83	ca. 1
4	−2.0	In the dark	None	2.0	12	2—5	90—93	3—4

a) Electrolysis was carried out in a two-compartment cell equipped with Pt electrodes at 20±2 °C under argon atmosphere. Starting solutions composed of: [Cob(II)7C_1ester]ClO_4, 30 mg (2.6×10^{-5} mol); 2-acetyl-1-bromo-2-ethoxycarbonylpropane, 1.0 g (4.2×10^{-3} mol); 30 mL of DMF containing 0.50 mol dm^{-3} TBAF. b) Irradiated with a 300-W tungsten lamp from a distance of 50 cm. c) CH_3COOH, 0.50 g (8.3×10^{-3} mol). d) Electrical charge passed per mol of the substrate. e) Based on an initial amount of the substrate; the rest was the unreacted substrate (a small amount of $(CH_3CO_2)CH_2C(CH_3)(COCH_3)(CO_2C_2H_5)$ was obtained when CH_3COOH was added); analyzed by GLC. The catalyst was recovered to the same extents as given in Table 2.

results on the basis of product analyses (Table 3; refer to Eq. 4). (i) The major product was the acetyl-migrated one, 1-acetyl-2-ethoxycarbonylpropane (**G**) under all the electrolysis conditions such as at −1.0 V vs. SCE under irradiation with the visible light, at −1.5 V vs. SCE in the dark with or without acetic acid, and at −2.0 V vs. SCE in the dark. (ii) A proportion of the rearrangement products was the highest under the electrolysis conditions at −2.0 V vs. SCE. (iii) The acetyl-migrated product (**G**) was much more favorably obtained than the ester-migrated one, 2-acetyl-1-ethoxycarbonylpropane (**H**), under all the conditions. These results are different from those for the electrolysis of **1** and indicate that the acetyl group can also migrate via a radical mechanism. This concept is in agreement with previous results which demonstrate that the acetyl group very readily undergoes the 1,2-migration via formation of radical intermediates.[22,33]

The following results may give some insight into the reaction mechanism. (i) The second reduction wave for the alkylated complex was scarcely detected by cyclic voltammetry carried out on [Cob(II)7C$_1$-ester]ClO$_4$ in DMF containing **3** in a large excess. The corresponding alkylated complex was quite labile and could not be isolated by ordinary procedures.[9,34] (ii) Numbers (n) of electrons consumed during the electrolysis was 1.3 and 1.6 at −1.5 and −2.0 V vs. SCE, respectively. (iii) When CH$_3$COOD was used as a proton source at −1.5 V vs. SCE in the dark, the rearrangement product containing one deuterium on the β-carbon was obtained as the major product.[35]

It is not apparent from the above results if the electrolysis at −2.0 V vs. SCE proceeds along with two-electron reduction or not so. The reaction mechanism for the electrolysis of **3** catalyzed by the hydrophobic vitamin B$_{12}$ may be different from that given in Scheme 5, but the detail is not clear at present. The acetyl group may also migrate via a radical mechanism, but the acetyl-migrated rearrangement reaction proceeds much favorably as the electrolysis potential becomes more cathodic.

(b) Substrates with only one electron-withdrawing group. The electrolyses of 1-bromo-2-methoxycarbonylpropane (**4**), 1-bromo-2-[(ethylthio)carbonyl]propane (**5**), 1-bromo-2-cyanopropane (**6**), and 1-bromo-2-acetylpropane (**7**), each with only one electron-withdrawing group, were carried out in the same manner. The β-elimination products were obtained primarily; 2-methoxycarbonylpropene (**J**), 2-cyanopropene (**O**), and 2-acetylpropene (**Q**) from substrates **4**, **6**, and **7**, respectively (refer to Eqs. 5, 7, and 8). Only the electrolysis of substrate **5**, having one thioester group on the β-carbon, afforded the corresponding rearrangement product, 1-[(ethylthio)carbonyl]propane (**M**) as shown in Table 4 (refer to Eq. 6). (i) At −1.5 V vs. SCE in the dark: the reduction product, 2-[(ethylthio)carbonyl]propane (**K**) was the major one without any additive, while the rearrangement one (**M**) was obtained when acetic acid was added. (ii) At −2.0 V vs. SCE in the drak: the rearrangement product (**M**) was dominantly obtained even in the absence of acetic acid. (iii) The β-elimination product, 2-[(ethylthio)carbonyl]-1-propene (**L**), was also largely obtained under the conditions that allow the formation of **M**. Thus, the rearrangement reaction during the electrolysis of **5** must proceed via reaction mechanisms similar to those given in Scheme 5.

(c) Migratory aptitude. The following aspects became apparent for the electrolyses of substrates **1**—**7**. (i) Substrates with two electron-withdrawing groups on the β-carbon atom tend to give the corresponding rearrangement products which are derived from individual migration of the groups (refer to Eqs. 1, 3, and 4). (ii) Substrates with only one of the electron-withdrawing groups do not give the rearrangement products (refer to Eqs. 5, 7, and 8), except for the substrate with one thioester group (refer to Eq. 6). The sulfur atom with d-orbitals seems to stabilize the anionic intermediates which subsequently afford the rearrangement product. (iii) The rearrangement reaction readily proceeds under the electrolysis

Table 4. Product Analyses for Controlled-Potential Electrolysis of 1-Bromo-2-[(ethylthio)carbonyl]-propane as Catalyzed by Hydrophobic Vitamin B$_{12}$[a]

Entry	Electrolysis conditions				Yield/%[d]		
	Potential / V vs. SCE	Additive[b]	Charge[c] / F mol^{-1}	Period / h	**K**	**L**	**M**
1	−1.5	None	1.0	5	37—41	ca. 1	ca. 1
2	−1.5	CH$_3$COOH	1.0	3	8—16	7—13	15—21
3	−2.0	None	2.0	3	18—22	22—28	33—41

a) Electrolysis was carried out in a two-compartment cell equipped with Pt electrodes at 20±2 °C under argon atmosphere in the dark. Starting solutions composed of: [Cob(II)7C$_1$ester]ClO$_4$, 6 mg (4.4×10^{-6} mol); 1-bromo-2-[(ethylthio)carbonyl]propane, 200 mg (9.0×10^{-4} mol); 7 mL of DMF containing 0.50 mol dm^{-3} TBAF. b) CH$_3$COOH, 0.10 g (1.7×10^{-3} mol). c) Electrical charge passed per mol of the substrate. d) Based on an initial amount of the substrate; the rest was the unreacted substrate; analyzed by GLC. The catalyst was recovered to the same extents as given in Table 2.

conditions which allow the formation of anionic intermediates.

In the light of the above results, the migratory aptitude of electron-withdrawing groups decreases in the following sequence: COSR>COR>COOR>CN. Both electronic character and steric bulkiness of the migrating groups must be responsible for this tendency. For the formation of the *quasi*-cyclopropane ring in the intermediate stage shown in Scheme 5, attack of the α-carbanion on the β-substituent group is progressively enhanced as the substituent becomes more electron-withdrawing (refer to Eq. 9).

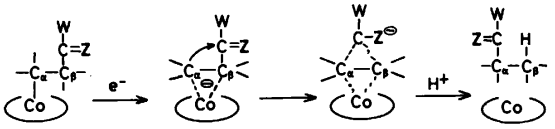

(9)

Stabilization of the anionic intermediates may be achieved through delocalization of negative charge within the *quasi*-cyclopropane ring, and its extent controls the migratory aptitude. On the other hand, a more bulky substituent on the β-carbon atom must be placed at the *anti*-position to the cobalt atom when the alkylated complex is formed (refer to Eq. 10) so

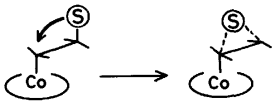

(10)

that such a bulky group readily migrates via formation of the *quasi*-cyclopropane ring. Relative contributions of both electronic and steric effects are much dependent on the nature of β-substituents.

Conclusion. The present study demonstrates for the first time the carbon-skeleton rearrangements catalyzed by a vitamin B_{12} model under electrochemical conditions. The carbon-skeleton rearrangement was postulated to proceed via formation of the anionic intermediates. In the light of the reactions with various substrates, the migratory aptitude of functional groups was clarified. However, it is not relevant to apply these mechanisms directly to the corresponding vitamin B_{12}-dependent enzymatic reactions, since the reduction potential as high as -2.0 V vs. SCE would not be expected in vivo. The rearrangement reaction is generally considered to proceed via radical mechanisms in vivo, but the nature of such radical species must be different from those in homogeneous solution. The reactivity of radical species may be subjected to change by the microenvironmental properties provided by apoenzymes at the reaction sites. In this regard, we have studied the catalytic behavior of the hydrophobic vitamin B_{12} in apoenzyme models such as hydrophobic cyclophanes and bilayer membranes.[34,36]

In the light of the present study, it became apparent that the rearrangement reactions of model substrates readily proceed under stronger reduction conditions. Hydrophobic vitamin B_{12}'s are expected to be widely utilized as specific catalysts for fine organic syntheses via the 1,2-migration process of various functional groups.

Experimental

General Analyses and Measurements. Elemental analyses were performed at the Microanalysis Center of Kyushu University. IR spectra were taken on a JASCO IR-810 infrared spectrophotometer, while electronic absorption spectra were recorded on a Hitachi 340 spectrophotometer. ESR spectra were obtained on a JEOL JES-ME3 X-band spectrometer equipped with a 100 kHz field modulation unit; a standard MgO/Mn^{II} sample calibrated with a NMR magnetometer was employed for calibration of the magnetic field. ^{1}H-NMR spectra were taken on a Hitachi R-24B or a JEOL JNM-FX100 spectrometer, and mass spectroscopic analyses were performed on a JEOL JMS-01SG-2 spectrometer.[37] Cyclic voltammograms were obtained on a Yanaco P-8 polarograph or an apparatus composed of a Hokuto Denko HA-501 potentiostat/galvanostat and a Hokuto Denko HB-104 function generator. An applied potential between the working and reference electrodes in the electrolysis was maintained constant with a Hokuto Denko HA-305 potentiostat/galvanostat and the electrical quantity was recorded on a Hokuto Denko HF-201 coulomb/ampere-hour meter. GLC analyses were carried out on a Shimadzu GC-4C or a Shimadzu GC-9A apparatus equipped with a Shimadzu C-R3A-FFC chromatopac.

Cyclic Voltammetry. An elecrtochemical cell similar to that reported in literature[38] was used and equipped with platinum wire of 0.5-mm diameter as working and auxiliary electrodes. A saturated calomel electrode (SCE) or an Ag/AgCl electrode was served as a reference which was separated from a bulk electrolyte solution by a salt bridge prepared with benzylidene-D-sorbitol[39] and a DMF solution of tetrabutylammonium tetrafluoroborate (TBAF; supporting electrolyte) (5.0×10^{-2} mol dm^{-3}). DMF solutions containing the cobalt complex, TBAF, and the inside of the cell were maintained under argon atmosphere throughout each measurement. All measurements were carried out at 20 ± 2 °C, and the scan rate was varied in a range from 10 through 200 mV s^{-1}. Half-wave potentials ($E_{1/2}$) and anodic and cathodic currents were evaluated according to the method described previously.[40]

Catalytic Reactions. The electrolyses of various substrates were carried out upon addition of [Cob(II)7C$_1$ester]-ClO_4 in a cylindrical three-electrode cell which was divided into two internal compartments with a single sheet of microporous polypropylene membrane and equipped with platinum mesh as working and auxiliary electrodes (Fig. 10). A DMF solution of [Cob(II)7C$_1$ester]ClO_4, a substrate, an additive, and TBAF was subjected to electrolysis at an appropriate controlled-potential under argon atmosphere. Then, the reaction mixture was distilled in vacuo and analyzed for products by means of GLC. Identification of the reaction products was performed by coinjection of the distilled sample and the corresponding authentic samples into columns of Silicone DC-550, Silicone SE-30, and Dioctyl phthalate. A capillary column of Polyethylene

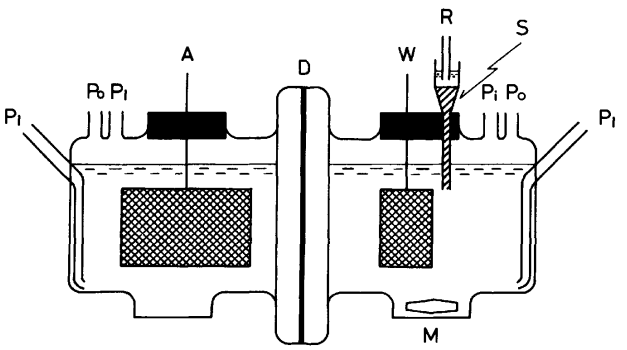

Fig. 10. Three-electrode cell for controlled-potential electrolysis: A, auxiliary electrode (Pt mesh); D, diaphram(Duragard: microporous polypropylene membrane); M, magnetic stirrer; P_i, inert gas inlet; P_o, inert gas outlet; R, reference electrode (SCE); S, salt bridge (prepared with benzylidene-D-sorbitol and a nonaqueous solution of TBAF); W, working electrode (Pt mesh).

Glycol-20M was used for identification of isomers having similar structures such as **D** and **E** or **G** and **H**. Each product separated by preparative GLC on Silicone DC-550 was identified by means of ^{1}H-NMR and mass spectroscopy.

Spectroscopic Measurements. Controlled-potential electrolyses under various conditions were carried out in a three-electrode cell modified for electronic and ESR spectral measurements, as described previously.[40] An applied potential between the working and reference electrodes was maintained constant with a conventional potentiostat and monitored with a Takeda Riken TR-6656 digital multimeter.

Materials. Heptamethyl dicyanocobyrinate, $(CN)_2$Cob(III)7C$_1$ester, was derived from cyanocobalamin after the method of Werthemann et al.[41] Preparation of [Cob(II)7C$_1$ester]ClO_4 from $(CN)_2$Cob(III)7C$_1$ester has been described previously.[4] Tetrabutylammonium tetrafluoroborate (TBAF) was prepared after the reported procedure.[42] α-Phenyl-*N*-(*t*-butyl)nitrone (PBN) as a spin-trapping agent, CH_3COOD (98 atom %D) (both from Aldrich Chemical Co., U.S.A.), and CD_3COOD (99.6 atom %D) of Commissariat á l'Enerqie Atomique, France were used as supplied. *N,N*-Dimethylformamide (DMF) was dried and purified just before use according to the standard procedure.[28] The substrates were prepared by the following procedures.

2,2-Bis(ethoxycarbonyl)-1-bromopropane (1). A solution of diethyl methylmalonate (11.2 g, 0.064 mol) in dry benzene (40 mL) and subsequently a solution of dibromomethane (16.0 g, 0.092 mol) in dry DMF (40 mL) were added dropwise to a suspension of sodium hydride (1.54 g, 0.064 mol) in dry benzene (20 mL) with vigorous stirring at room temperature under nitrogen atmosphere. After the reaction mixture being stirred for 2 h at room temperature, a saturated aqueous ammonium chloride (100 mL) was added to it. The resulting product was extracted with diethyl ether (100 mL×2), and the extract was washed with distilled water and dried over sodium sulfate. The product was recovered by distillation under reduced pressure (75—76 °C/5.3 Pa), and its purity was confirmed by GLC: Yield 12.0 g (70%); IR (neat) 1735 cm^{-1} (ester C=O); ^{1}H-NMR ($CDCl_3$, TMS) δ=1.30 (6H, t, $CH_2C\underline{H}_3$), 1.50 (3H, s, CH_3), 3.80 (2H, s, CH_2Br), and 4.20 (4H, q, $C\underline{H}_2CH_3$).

Found: C, 40.60; H, 5.68%. Calcd for $C_9H_{15}BrO_4$: C, 40.47; H, 5.66%.

1-Bromo-2-cyano-2-ethoxycarbonylpropane (2). This compound was derived from 1-cyano-1-ethoxycarbonylethane[43] (16.2 g, 0.128 mol) in a manner similar to that described above. The product was recovered by distillation under reduced pressure (80—90 °C/40—66 Pa) and further purified by preparative GLC on Silicone DC-550: Yield 16.2 g (68%); IR (neat) 2240 (C≡N) and 1740 cm^{-1} (ester C=O); ^{1}H-NMR ($CDCl_3$, TMS) δ=1.16 (3H, t, $CH_2C\underline{H}_3$), 1.54 (3H, s, CH_3), 3.46 (2H, m, CH_2Br), and 4.12 (2H, q, $C\underline{H}_2CH_3$).

Found: C, 38.42; H, 4.54; N, 6.52%. Calcd for $C_7H_{10}BrNO_2$: C, 38.20; H, 4.58; N, 6.36%.

2-Acetyl-1-bromo-2-ethoxycarbonylpropane (3). This substrate was prepared from ethyl 2-methylacetoacetate[44] (20 g, 0.14 mol) in a manner similar to that described above. The product was recovered by distillation under reduced pressure (70—72 °C/102 Pa) and purified further by preparative GLC on Silicone DC-550: Yield 12 g (36%); IR (neat) 1740 (ester C=O) and 1720 cm^{-1} (ketone C=O); ^{1}H-NMR ($CDCl_3$, TMS) δ=1.18 (3H, t, $CH_2C\underline{H}_3$), 1.41 (3H, s, CH_3), 2.10 (3H, s, $COCH_3$), 3.61 (2H, s, CH_2Br), and 4.13 (2H, q, $C\underline{H}_2CH_3$).

Found: C, 40.41; H, 5.36%. Calcd for $C_8H_{13}BrO_3$: C, 40.53; H, 5.53%.

1-Bromo-2-methoxycarbonylpropane (4). 3-Bromo-2-methylpropionic acid (51.3 g, 0.31 mol), which was obtained by the reaction of methacrylic acid with hydrogen bromide in acetic acid,[45] was esterified with methanol (100 mL) containing sulfuric acid (1 mL). The product was extracted with diethyl ether and recovered from the extract by distillation under reduced pressure (72.5—73.0 °C/2530 Pa): Yield 50.0 g (90%); IR (neat) 1750 cm^{-1} (ester C=O); ^{1}H-NMR ($CDCl_3$, TMS) δ=1.28 (3H, d, CH_3), 2.84 (1H, m, CH), 3.47 (2H, m, CH_2Br), and 3.66 (3H, s, CO_2CH_3).

Found: C, 33.27; H, 4.98%. Calcd for $C_5H_9BrO_2$: C, 33.17; H, 5.01%.

1-Bromo-2-[(ethylthio)carbonyl]propane (5). This was prepared according to a reported procedure.[1]

1-Bromo-2-cyanopropane (6). This compound was prepared by the reaction of 2-cyanopropene (15.0 g, 0.22 mol) with 30%(w/w) hydrogen bromide in acetic acid (100 mL) in a usual manner,[45] bp 35—40 °C/107 Pa: Yield 17.0 g (51%); IR (neat) 2240 cm^{-1} (C≡N); ^{1}H-NMR ($CDCl_3$, TMS) δ=1.44 (3H, d, CH_3), 3.10 (1H, m, CH), and 3.45 (2H, d, CH_2Br).

Found: C, 32.46; H, 4.11; N, 9.38%. Calcd for C_4H_6BrN: C, 32.46; H, 4.09; N, 9.46%.

1-Bromo-2-acetylpropane (7). This substrate was prepared by the reaction of 2-acetylpropene (5.0 g, 0.059 mol) with hydrogen bromide in methanol,[45] bp 60 °C/2670 Pa: Yield 1.0 g (10%); IR (neat) 1705 cm^{-1} (ketone C=O); ^{1}H-NMR ($CDCl_3$, TMS) δ=1.18 (3H, d, CH_3), 2.20 (3H, s, $COCH_3$) 2.29 (1H, m, CH), and 3.51 (2H, m, CH_2Br). This compound was so labile that its elemental analysis was not possible.

Authentic Samples. 2,2-Bis(ethoxycarbonyl)propane (**A**), 2-methoxycarbonylpropane (**I**), 2-methoxycarbonylpropene (**J**), 2-cyanopropane (**N**), 2-cyanopropene (**O**), 2-acetylpropane (**P**), and 2-acetylpropene (**Q**) were purchased from Nakarai Chemicals and purified by distillation before use; confirmed to be sufficiently pure by ^{1}H-NMR and GLC.

2-Cyano-1-ethoxycarbonylpropane (**E**),[46] 2-acetyl-2-ethoxycarbonylpropane (**F**),[44] 1-acetyl-2-ethoxycarbonylpropane (**G**),[47,48] 2-acetyl-1-ethoxycarbonylpropane (**H**),[47] 2-[(ethylthio)carbonyl]propane (**K**),[1] 2-[(ethylthio)carbonyl]-1-propene (**L**),[1] and 1-[(ethylthio)carbonyl]propane (**M**),[1] were prepared according to the methods described in literatures and confirmed to be sufficiently pure by ^{1}H-NMR and GLC.

1,2-Bis(ethoxycarbonyl)propane (B). This compound was derived from the corresponding carboxylic acid (10 g, 0.08 mol) by refluxing it in ethanol containing sulfuric acid, bp 74—75 °C/670 Pa: Yield 7.8 g (54%); IR (neat) 1735 cm^{-1} (ester C=O); ^{1}H-NMR ($CDCl_3$, TMS) δ=1.25 (6H, t, $CH_2C\underline{H}_3$), 1.30 (3H, d, CH_3), 2.60 (2H, m, CH_2), 2.90 (1H, m, CH), and 4.20 (4H, q, $C\underline{H}_2CH_3$).

2-Cyano-2-ethoxycarbonylpropane (C). This was obtained by the reaction of 1-cyano-1-ethoxycarbonylethane (5.0 g, 0.039 mol) with methyl iodide in a manner similar to that adopted for the preparation of **1**, bp 95 °C/4000 Pa: Yield 3.0 g (54%); IR (neat) 2240 (C≡N) and 1740 cm^{-1} (ester C=O); ^{1}H-NMR ($CDCl_3$, TMS) δ=1.30 (3H, t, $CH_2C\underline{H}_3$), 1.58 (6H, s, CH_3), and 4.18 (2H, q, $C\underline{H}_2CH_3$).

2-Cyano-1-ethoxycarbonylpropane (D). This compound was prepared by the reaction of 1-bromo-2-ethoxycarbonylpropane (5.0 g, 0.026 mol) with potassium cyanide (2.5 g, 0.038 mol) in a manner similar to that reported previously,[43] bp 85 °C/4000 Pa: Yield 0.30 g (10%); IR (neat) 2240 (C≡N) and 1735 cm^{-1} (ester C=O); ^{1}H-NMR ($CDCl_3$, TMS) δ=1.28 (3H, t, $CH_2C\underline{H}_3$), 1.32 (3H, d, CH_3), 2.62 (2H, br s, CH_2), 2.70 (1H, m, CH), and 4.12 (2H, q, $C\underline{H}_2CH_3$).

We wish to thank Mr. Hideki Horiuchi, glassworker of our department, for his skill in preparing specific three-electrode cells used for catalytic reactions, electronic and ESR spectroscopy, and cyclic voltammetry.

References

1) Y. Murakami, Y. Aoyama, and K. Tokunaga, *J. Am. Chem. Soc.*, **102**, 6736 (1980).

2) Y. Murakami, "Vitamin B_{12} Models with Macrocyclic Ligands," in "Biomimetic Chemistry," ed by D. Dolphin, C. McKenna, Y. Murakami, and I. Tabushi, Advances in Chemistry Series 191, American Chemical Society, Washington, D. C. (1980), pp. 179—199.

3) See for example: J. Halpern, "Chemistry and Significance of Vitamin B_{12} Model Systems," in "B_{12}," ed by D. Dolphin, John Wiley, New York (1982), Vol. 1, pp. 501—542.

4) Y. Murakami, Y. Hisaeda, and A. Kajihara, *Bull. Chem. Soc. Jpn.*, **56**, 3642 (1983).

5) Y. Murakami, Y. Hisaeda, A. Kajihara, and T. Ohno, *Bull. Chem. Soc. Jpn.*, **57**, 405 (1984).

6) Y. Murakami, Y. Hisaeda, and T. Ohno, *Bull. Chem. Soc. Jpn.*, **57**, 2091 (1984).

7) Y. Murakami, Y. Hisaeda, and T. Ozaki, *Chem. Lett.*, **1985**, 473.

8) Y. Murakami, Y. Hisaeda, T. Ohno, and T. Ozaki, *Chem. Lett.*, **1985**, 477.

9) Y. Murakami and Y. Hisaeda, *Bull. Chem. Soc. Jpn.*, **58**, 2652 (1985).

10) Y. Murakami, Y. Hisaeda, T. Ozaki, and T. Ohno, *Chem. Lett.*, **1985**, 1711.

11) Y. Murakami, Y. Hisaeda, T. Tashiro, and Y. Matsuda, *Chem. Lett.*, **1985**, 1813.

12) Y. Murakami, Y. Hisaeda, T. Tashiro, and Y. Matsuda, *Chem. Lett.*, **1986**, 555.

13) Recent model reactions are as follows, while the previous studies were already cited in Ref. 1. Models for methylmalonyl-CoA→succinyl-CoA conversion: A. I. Scott, J. Kang, D. Dalton, S. K. Chung, *J. Am. Chem. Soc.*, **100**, 3603 (1978); H. Flohr, W. Pannhorst, and J. Rétey, *Helv. Chim. Acta*, **61**, 1565 (1978); A. I. Scott, J. B. Hansen, and S. K. Chung, *J. Chem. Soc., Chem. Commun.*, **1980**, 388; M. Fountoulakis and J. Rétey, *Chem. Ber.*, **113**, 650 (1980); J. H. Grate, J. W. Grate, and G. N. Schrauzer, *J. Am. Chem. Soc.*, **104**, 1588 (1982); S. Wollowitz and J. Halpern, *ibid.*, **106**, 8319 (1984); P. Dowd and M. Shapiro, *Tetrahedron*, **40**, 3063 (1984); P. Dowd and B. K. Trivedi, *J. Org. Chem.*, **50**, 206 (1985); M. Tada, K. Inoue, K. Sugawara, M. Hiratsuka, and M. Okabe, *Chem. Lett.*, **1985**, 1821; M. Tada, K. Inoue, and M. Okabe, *ibid.*, **1986**, 703. Models for methylitaconate→α-methyleneglutarate conversion: J. W. Grate and G. N. Schrauzer, *Z. Naturforsch.*, **39b**, 821 (1984); P. Dowd and M. Shapiro, *Tetrahedron*, **40**, 3069 (1984); P. Dowd, B. K. Trivedi, M. Shapiro, and L. K. Marwaha, *J. Chem. Soc., Perkin Trans. 2*, **1985**, 413. Other rearrangements: B. T. Golding, C. S. Sell, and P. J. Sellers, *J. Chem. Soc., Perkin Trans. 2*, **1980**, 961; P. Muller and J. Rétey, *J. Chem. Soc., Chem. Commun.*, **1983**, 1342; R. G. Finke, D. A. Schiraldi, and B. J. Meyer, *Coord. Chem. Rev.*, **54**, 1 (1984).

14) A. I. Scott, J. Kang, P. Dowd, and B. K. Trivedi, *Bioorg. Chem.*, **9**, 227 (1980).

15) L. Walder, G. Rytz, K. Meier, and R. Schefford, *Helv. Chim. Acta*, **61**, 3013 (1978).

16) R. Schefford and E. Amble, *Angew. Chem., Int. Ed. Engl.*, **19**, 629 (1980).

17) R. Schefford, M. Dike, T. Herold, and L. Walder, *J. Am. Chem. Soc.*, **102**, 3642 (1980).

18) R. Schefford and R. Orlinski, *J. Am. Chem. Soc.*, **105**, 7200 (1983).

19) R. Schefford, G. Rytz, L. Walder, R. Orlinski, and Z. Chilmonczyk, *Pure Appl. Chem.*, **55**, 1791 (1983).

20) A. Ruhe, L. Walder, and R. Schefford, *Helv. Chim. Acta*, **68**, 1301 (1985).

21) G. Bildingmaier, H. Flohr, U. M. Kempe, T. Krebs, and J. Rétey, *Angew. Chem., Int. Ed. Engl.*, **14**, 822 (1975).

22) M. Tada, S. Akinaga, and M. Okabe, *Bull. Chem. Soc. Jpn.*, **55**, 3939 (1982).

23) U. Aeberhard, R. Keese, E. Stamm, U. C. Vögeli, W. Lau, and J. K. Kochi, *Helv. Chim. Acta*, **66**, 2740 (1983).

24) Both SCE and Ag/AgCl were used as reference electrodes; potentials vs. SCE are more cathodic by 30 mV relative to those vs. Ag/AgCl.

25) A small amount of $(CH_3CO_2)CH_2C(CH_3)(CO_2C_2H_5)_2$ was detected when acetic acid was used.

26) K. A. Bard, J. C. Gilbert, and R. D. Goodin, *J. Am. Chem. Soc.*, **96**, 620 (1974); E. E. Bancroft, H. N. Blount, and E. G. Janzen, *ibid.*, **101**, 3692 (1979).

27) It was confirmed that the proton exchange did not take place between 1,2-bis(ethoxycarbonyl)propane and the deuterated acetic acid in DMF at −1.5 V vs. SCE.

28) J. A. Riddick and W. B. Bunger, "Organic Solvents,"

Wiley-Interscience, New York (1970), pp. 836—840.
29) A. J. Fry and R. G. Reed, *J. Am. Chem. Soc.*, **94**, 8475 (1972).
30) A. J. Fry and R. G. Reed, *J. Am. Chem. Soc.*, **93**, 553 (1971).
31) [((CN)(CH_3)($CO_2C_2H_5$)CCH_2)(H_2O)Cob(III)7C_1-ester]ClO_4 was prepared by the reaction of [Cob(II)7C_1-ester]ClO_4 with substrate **2** in the presence of $NaBH_4$ and purified by column chromatography. Found: C 54.97; H, 6.59; N, 5.27%. Calcd for $C_{59}H_{85}ClCoN_5O_{21}$: C, 54.73; H, 6.62; N, 5.41%.
32) J. Rétey, "Vitamin B_{12}," ed by B. Zagalak and W. Friedrich, Walter de Gruyter, Berlin (1979), pp. 439—460.
33) C. L. Karl, E. J. Mass, and W. Reusch, *J. Org. Chem.*, **37**, 2834 (1972); M. Okabe, T. Osawa, and M. Tada, *Tetrahedron Lett.*, **22**, 1899 (1981); M. Tada, K. Miura, M. Okabe, S. Seki, and H. Mizukami, *Chem. Lett.*, **1981**, 33.
34) Y. Murakami, Y. Hisaeda, T. Ohno, and Y. Matsuda, *Chem. Lett.*, **1986**, 731.
35) Deuterium was further introduced partly into the acetyl moiety of the rearrangement product as confirmed by ^{1}H-NMR and mass spectroscopy. The reason is not clear at present.
36) Y. Murakami, Y. Hisaeda, J. Kikuchi, T. Ohno, M. Suzuki, and Y. Matsuda, *Chem. Lett.*, **1986**, 727.
37) Mass spectra were measured by courtesy of Prof. M. Tashiro of Kyushu University.
38) R. P. V. Duyne and C. N. Reilley, *Anal. Chem.*, **44**, 142 (1972).
39) F. Endo, *Yakugaku Zasshi*, **79**, 595 (1959).
40) Y. Matsuda, S. Yamada, and Y. Murakami, *Inorg. Chem.*, **20**, 2239 (1981).
41) L. Werthemann, R. Keese, and A. Eschenmoser, unpublished results; see L. Werthemann, Dissertation, ETH Zürich (Nr. 4097), Juris Druck und Verlag, Zürich (1968).
42) H. O. House, E. Feng, and N. P. Peet, *J. Org. Chem.*, **36**, 2371 (1971).
43) W. A. Bone and W. H. Perkin, Jr., *J. Chem. Soc.*, **1895**, 416.
44) K. Folkers and H. Adkins, *J. Am. Chem. Soc.*, **53**, 1416 (1931).
45) R. Mozingo and L. A. Patterson, *Org. Synth.*, Coll. Vol. 3, 576 (1955).
46) J. Bredt and J. Kallen, *Justus Liebigs Ann. Chem.*, **293**, 338 (1897).
47) C. Bischoff, *Justus Liebigs Ann. Chem.*, **205**, 313 (1880).
48) B. R. Baker, R. E. Schaub, and J. H. Williams, *J. Org. Chem.*, **27**, 116 (1952).

Synthesis of Hexahydroindenones through a Diels-Alder Cycloaddition and Nazarov Cyclization Sequence of Triene Alcohols

Eiji WADA, Isamu FUJIWARA, Shuji KANEMASA, and Otohiko TSUGE*
Research Institute of Industrial Science, and Department of Molecular Science and Technology, Interdisciplinary Graduate School of Engineering Sciences, Kyushu University, Kasugakoen, Kasuga 816
(Received June 26, 1986)

The Diels-Alder cycloaddition of 4-methylene-1,5-hexadien-3-ols with olefinic dienophiles such as dimethyl maleate, fumarate, and *N*-methylmaleimide produces 1-(1-cyclohexenyl)-2-propen-1-ols. These diene alcohols are oxidized with activated manganese(IV) oxide to give dienones, which are then treated with acid catalysts to undergo ready electrocyclization leading to hexahydroindenones with functional groups. Stereoselectivity at the electrocyclization step is found to depend upon the stereostructures of cyclohexene skeleton of the dienones as well as the reaction conditions.

2-Lithio-1,3-butadiene serves as a reagent which introduces a 1-methylene-2-propenyl unit into carbonyls by a regioselective nucleophilic addition.[1] In the preceding paper, we have already demonstrated that 1-aryl-2-methylene-3-buten-1-ols thus prepared undergo a sequence of Diels-Alder cycloaddition with electron-deficient olefins and acid-catalyzed cyclization leading to tetrahydrofluorene skeletons.[2] This sequence belongs to a new [6.5] annelation method to a benzene ring, while [6.6] annelation processes to acyclic and cyclic ketones have been established through stepwise sequence of two Diels-Alder reactions on 1-methylene-2-propenyl carbinols.[3]

The present article presents a new version of [6.5] annelation method by a sequence of two ring-forming reactions: The Diels-Alder cycloaddition of 4-methylene-1,5-hexadien-3-ols with olefins, oxidation of the diene alcohols as cycloadducts into dienones, and subsequent Nazarov cyclization. Although Nazarov reaction has been long utilized as a key reaction for natural product synthesis,[4] there are only limited examples known for the cyclization of dienones which are carrying several carbonyl functionalities.[5]

Results and Discussion

4-Methylene-1,5-hexadien-3-ols (**1**) as starting materials in the present work can be readily prepared from the regioselective reactions of 2-lithio-1,3-butadiene with 2-alkenals (Scheme 1).[1] Although some of the triene alcohols **1** were contaminated by a small amount of their isomers, 1,5,6-heptatrien-3-ols (**2**), these mixtures were able to be used for the following Diels–Alder cycloadditions without serious trouble. After the cycloaddition was over, the allene alcohols **2** were recovered unchanged and easily separated from the cycloadducts by column chromatography over silica gel.

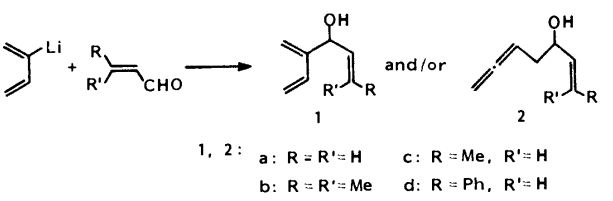

Scheme 1.

The triene alcohols **1a—d** were employed in the Diels-Alder reactions with dienophiles such as dimethyl maleate (**3**), dimethyl fumarate (**4**), and *N*-methylmaleimide (**5**). The reactions took place smoothly under reflux in benzene to give excellent yields of cycloadducts **6—8** as mixtures of two diastereomers (Scheme 2 and Table 1).

The oxidation of 1,4-pentadien-3-ols into pentadienones is not a well-studied transformation[6] and this oxidation should be done with care because pentadienones as products are, in general, labile compounds. We used activated manganese(IV) oxide for this purpose since its versatility in the oxidation of allyl alcohol has been well-achieved.[7] Thus, the diene

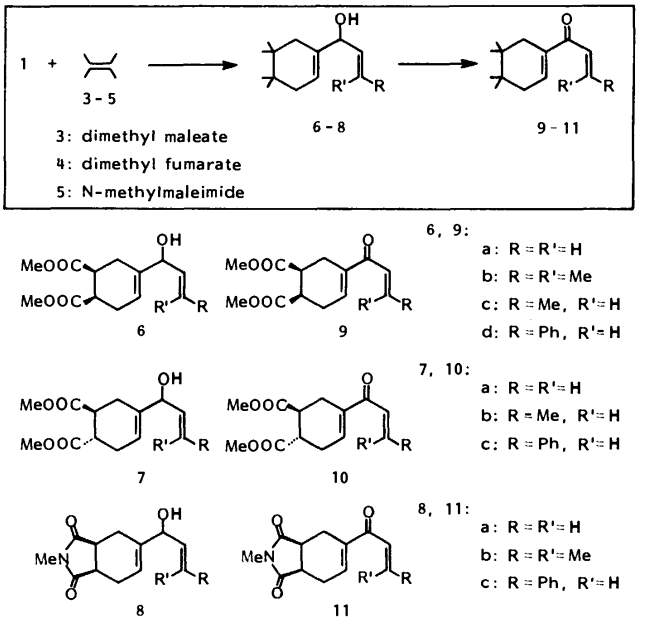

Scheme 2.

alcohols **6**—**8** were successfully oxidized with activated manganese(IV) oxide in dichloromethane at room temperature to give satisfactory yields of dienones **9**—**11** as unstable compounds (Scheme 2 and Table 2).

Although details will be discussed later, electrocyclization of the dienones **9**—**11** afforded two types of enones (tetrasubstituted endo olefins **12**, **14**, and trisubstituted exo olefins **13**, **15**) as cyclized products depending upon the reaction conditions as well as the structure of starting dienones **9**—**11** (Scheme 3). In all cases, no trace of the other cyclopentenones, double-bond isomers of **12** and **14**, was even detected. This is consistent with the reported examples for the electrocyclizations of dienones including cyclohexene moiety as an olefin part.[5,8,9]

Table 1. Diels-Alder Cycloaddition of Triene Alcohols **1**[a]

Triene alcohol	Dienophile (equiv)	Time h	Cycloadduct	Yield[b] %
1a[c]	3 (2.3)	48	**6a**	88
1b	3 (2.2)	48	**6b**	86
1c	3 (1.8)	48	**6c**	94
1d[d]	3 (3.4)	48	**6d**	83
1a[c]	4 (2.9)	48	**7a**	88
1c	4 (2.0)	48	**7b**	90
1d[e]	4 (1.6)	24	**7c**	87
1a	5 (1.0)	15	**8a**	83
1b	5 (1.1)	16	**8b**	90
1d[f]	5 (1.0)	12	**8c**	99

a) All reactions were carried out under reflux in dry benzene under nitrogen. b) Isolated yields. c—f) Contaminated by the corresponding allene alcohols: c) **1a**:**2a**=10:1; d) **1d**:**2d**=19:1; e) **1d**:**2d**=10:1; f) **1d**:**2d**=7:9.

Table 2. Oxidation of Diene Alcohols **6**—**8** with Manganese(IV) Oxide[a]

Diene alcohol	MnO_2/DA[b]	Temp °C	Time h	Product	Yield[c] %
6a	23	rt	2.5	**9a**	80
6b	27	rt	17	**9b**	72
6c	22	rt	5	**9c**	79
6d	30	rt	0.5	**9d**	56
7a	25	0	1	**10a**	84
7b	22	rt	5	**10b**	79
7c	28	rt	2.5	**10c**	78
8a	5	rt	20	**11a**	46[d]
8b	24	rt	2	**11b**	52
8c	18	rt	20	**11c**	53

a) All reactions were carried out in dichloromethane. b) Molar ratio (DA: diene alcohols **6**—**8**). c) Isolated yield. d) The starting material **8a** was recovered in 16% yield.

A wide variety of acid catalysts including both Brønsted and Lewis acids have served in the electrocyclization of dienones and their equivalents.[5] We hoped to avoid the use of aqueous acids since the dienones **9**—**11** are all bearing some substituents sensitive to hydrolysis and since aqueous acids sometimes cause abnormal cyclization.[10] In addition, a cyclization procedure under mild conditions was desired, under which stereoselective cyclization would be achieved and acid-catalyzed epimerization of the cyclized products would be suppressed.

First we tested the electrocyclization of the dienone **9a** in the presence of *p*-toluenesulfonic acid (*p*-TsOH). This reaction gave 55% of expected product **12a** when heated under reflux in benzene for 4.5 h, but the reaction temperature and time are both unacceptable. So, some Lewis acid catalysts were examined in dichloromethane (Table 3); gallium(III) chloride was found much more effective than some other Lewis acids such as titanium(IV) chloride, aluminum(III) chloride, tin(IV) chloride, boron trifluoride, and trimethylsilyl trifluoromethanesulfonate. For example, the cyclization was completed within 30 min below 0 °C to give 73% of **12a** when two equimolar amounts of gallium(III) chloride were employed.

Other maleate cycloadducts **9b**—**d** underwent smooth cyclization in the presence of gallium(III) chloride to give tetrasubstituted olefins **12b**—**d** and/or trisubstituted olefins **13b**—**d**, both with high stereoselectivities (Scheme 4 and Table 4). In each case, the crude reaction mixture was found to be consisting of two major products by TLC and ^1H NMR spectrum, one of which was identical with **12**. When this

Table 3. Electrocyclization of Dienone **9a** in the Presence of Various Lewis Acid Leading to **12a**[a]

Lewis acid (equiv)	Temperature °C	Time h	Yield % of **12a**[b]
$TiCl_4$ (1.0)	rt	1	22
$AlCl_3$ (2.0)	rt	2	25
$BF_3 \cdot OEt_2$ (2.0)	rt	7 d	26
Me_3SiOTf (1.0)	rt	5	47
$SnCl_4$ (0.5)	−8 to rt	20	39
$SnCl_4$ (0.5)	rt	4	52
$GaCl_3$ (1.0)	rt	0.5	63
$GaCl_3$ (2.0)	−20 to 0	0.5	73

a) All reactions were carried out in dry dichloromethane under nitrogen. b) Isolated yield.

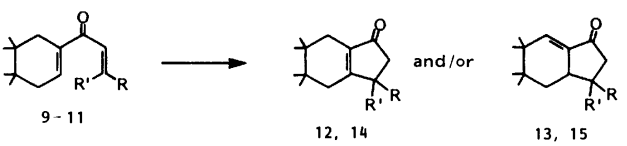

Scheme 3.

mixture was subjected to column chromatography over silica gel, the other product **A** completely isomerized into **13** which was also obtained from the electrocyclization of fumarate cycloadducts **10** as will be mentioned below. It is thus clear that the unstable primary products **A** and **13** are carrying cis and trans two adjacent ester groups, respectively.

Fumarate cycloadducts **10a—c** were similarly treated with gallium(III) chloride under the conditions listed in Table 4 to give tetrasubstituted olefins **14** together with aforementioned trisubstituted olefins **13c** and **13d**.

Structures of **12**, **13**, and **14** were determined mainly on the basis of spectral data except that the stereochemistry at the 3-positions of **12** and **13** could not be assigned only on their spectroscopic basis. Therefore, mechanistic consideration was taken into account. In the preceding paper,[2] we found that

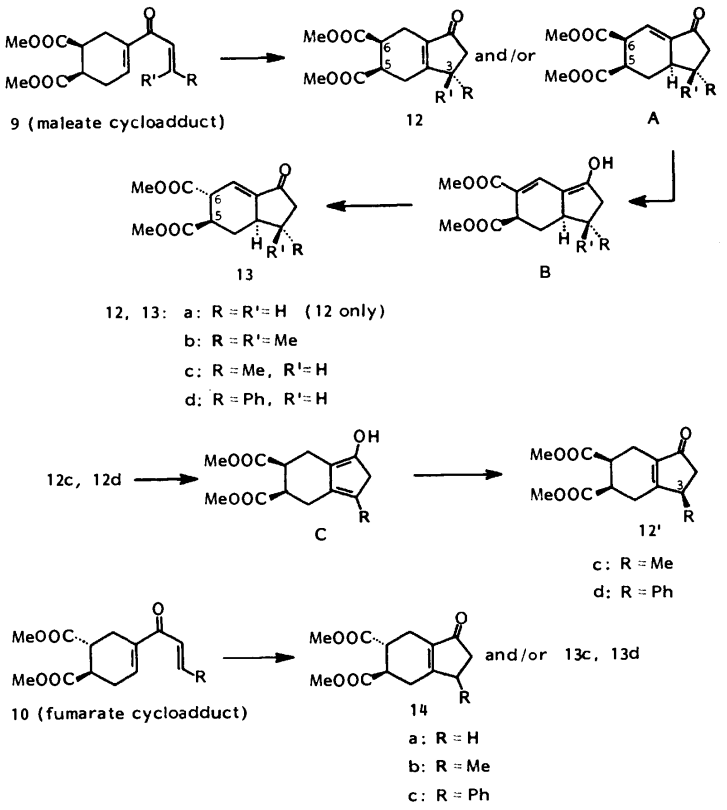

Scheme 4.

Table 4. Acid-Catalyzed Electrocyclization of Dienones **9—11**

Dienone	Acid (equiv)	Solvent[a]	Temperature °C	Time h	Product (yield)[b] %
9a	$GaCl_3$ (1.0)	DCM	−20 to 0	0.5	**12a** (73)
	p-TsOH (0.5)	BZ	reflux	4.5	**12a** (55)
9b	$GaCl_3$ (1.0)	DCM	rt	5 d	**12b** (68), **13b** (29)
	p-TsOH (1.0)	T	reflux	24	**12b** (57)
9c	$GaCl_3$ (1.0)	DCM	rt	24	**12c** (40), **13c** (49)
	p-TsOH (0.5)	BZ	reflux	6.5	**12c**+**12c'** (1:1, 59)
9d	$GaCl_3$ (1.0)	DCM	rt	5	**12d** (81), **13d** (5)
	p-TsOH (0.5)	T	reflux	12	**12d**+**12d'** (1:1, 63), **13d** (33)
10a	$GaCl_3$ (1.0)	DCM	rt	3	**14a** (90)
10b	$GaCl_3$ (1.0)	DCM	rt	3	**14b** (62),[c] **13c** (26)
10c	$GaCl_3$ (2.0)	DCM	rt	18	**14c** (80), **13d** (4)
11a	$GaCl_3$ (1.0)	DCM	rt	6	**15a** (17)
11b	$GaCl_3$ (2.0)	DCM	rt	6 d	**15b**+**15b'** (1:1, 90)
11c	$GaCl_3$ (1.0)	DCM	rt	2 d	**15c**+**15c'** (1:2, 46)

a) DCM: dichloromethane; BZ: benzene; T: toluene. b) Isolated yield. The isomer ratios were determined by ^1H NMR. c) A 1:1 mixture of stereoisomers.

dimethyl 4-(α-hydroxybenzyl)-4-cyclohexene-1,2-dicarboxylates underwent highly stereoselective electrocyclization leading to dimethyl 3,4a-*cis*-1*H*-2,3,4,4a-tetrahydrofluorene-2,3-dicarboxylate. The high stereoselectivity observed above in the Nazarov cyclization of maleate cycloadducts **9** presumably resulted in the same manner (Fig. 1): Pentadienyl cation **D** as an intermediate cyclizes through one of two possible conrotatory rotations to form allyl anion **E** which is sterically less hindered than the isomeric anion derived by the other rotation. Deprotonation of **E** at the 3a- or 7-position leads to **12** or **A**, respectively. Thus, the substituent R in **9** becomes cis to 5-H.

Small couplings of J_{5-6} (3.6 Hz) indicates the validity of 5,6-cis geometry of tetrasubstituted olefins **12** derived from **9**. On the other hand, trans configuration of epimerized products **13** is confirmed by relatively large couplings of J_{5-6} (10.0 Hz). One of

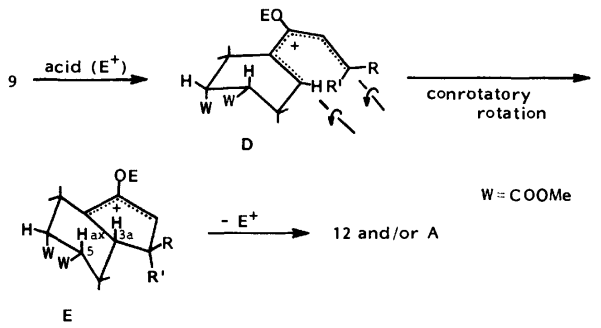

Fig. 1. Stereoselective cyclization of maleate cycloadducts **9** through conrotatory rotation of pentadienyl cation **D**.

4-methylene hydrogens of **13b** couples with two adjacent methine hydrogens (3a-H and 5-H) with 12.0 Hz of diaxial couplings, indicating 3a,5-cis structure (Fig. 2). The stereostructures of tetrasubstituted olefins **14b** and **14c** derived from fumarate cycloadducts **10b** and **10c** could not be assigned by spectral data.

The aforementioned ready epimerization at the 6-position of a trisubstituted olefin **A** probably took place through an acid-catalyzed dienolization (via **B**, Scheme 4). Contrary to the highly stereoselective electrocyclization of **9** in the presence of gallium(III) chloride, similar cyclizations with *p*-TsOH occurred in a nonstereoselective fashion. For example, a mixture of two stereoisomers **12c+12c′** (1:1) or **12d+12d′** (1:1) was obtained when the cyclization of **9c** or **9d** was carried out under reflux in benzene or toluene with *p*-TsOH, respectively (Table 4). As **12d** was found to isomerize into **12d′** in the presence of *p*-TsOH under comparable conditions, it is easily understood that **12d** undergoes a similar acid-catalyzed epimerization via dienol **C** (Scheme 4).

Even in the presence of gallium(III) chloride, maleimide cycloadducts **11** experienced nonstereoselective cyclization giving trisubstituted olefins **15** and/or **15′** (Scheme 5 and Table 4). This selectivity looks the same to that previously observed on the related cyclization.[2] No formation of tetrasubstituted olefins may be due to the serious steric hindrance anticipated to exist in the folded conformation of cyclohexene ring. The structures of **15** and **15′** were confirmed mainly on the basis of ^{1}H NMR data which were already shown in Fig. 2. The axial hydrogen (8-H_{ax}) of **15c** couples with both 7a-H and 8a-H with

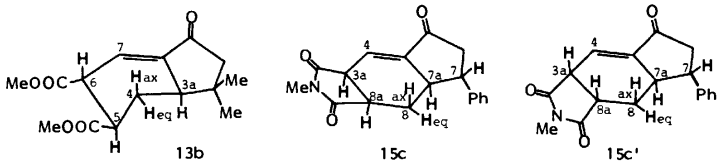

13b	15c	15c'
*J*4ax-3a=12.0	*J*8ax-7a=10.0	*J*8ax-7a=10.5
*J*4ax-5=12.0	*J*8ax-8a=12.5	*J*8ax-8a=6.0
*J*4ax-4eq=12.0	*J*8ax-8eq=11.0	*J*8ax-8eq=12.5
*J*4eq-3a=5.0	*J*8eq-8a=6.0	*J*8eq-8a=2.0
*J*4eq-5=3.0	*J*8a-3a=8.5	*J*8a-3a=8.0

*J*5-6=10.0

Fig. 2. Stereostructures and coupling constants (Hz) of **13b**, **15c**, and **15c′**.

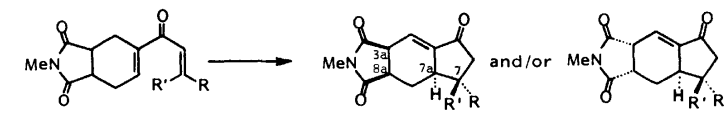

15, 15′: a: R=R′=H (15 only)
b: R=R′=Me
c: R=Ph, R′=H

Scheme 5.

large coupling (10.0 and 12.5 Hz), whereas 8-H_{ax} of **15c'** shows a small coupling constant toward 8a-H (6.0 Hz).

Experimental

General. Melting points were determined on a Yanagimoto melting point apparatus and are uncorrected. IR spectra were taken with a JASCO IRA-1 or a JASCO A-702 spectrometer. ^{1}H NMR spectra were recorded on a Hitachi R-40 (90 Hz), a JEOL FX-100 instrument (100 MHz), or Bruker AM 360 (360 MHz), and ^{13}C NMR on a JEOL FX-100 spectrometer at 25.05 MHz. Chemical shifts are expressed in parts per million downfield from tetramethylsilane as an internal standard. Mass spectra were measured with a JEOL-01SG-2 spectrometer at 70 eV of ionization energy. GC-Mass spectra as well as high resolution mass spectra (HRMS) were also obtained on the same instrument. Elemental analyses were performed on a Hitachi 026 CHN analyzer. Thin-layer chromatography (TLC) was accomplished on 0.2 mm precoated plates of silica gel 60 F-254 (Merck) or of aluminum oxide 60 F-254 type-E (Merck); visualization was with ultraviolet light (254 and 365 nm), iodine, molybdophosphoric acid (5% in ethanol), or *p*-anisaldehyde (5% in ethanol containing 5% of sulfuric acid). For preparative column chromatography, Wakogel C-200, C-300 (Wako), and Silicagel 60 (Merck) were employed. Flash chromatography was carried out on an EYELA EF-10 apparatus using a column (20×180 mm) packed with Silicagel 60 (Merck, size: 0.04—0.063 mm). Preparative high-performance liquid chromatography (HPLC) was performed on a Kusano KHLC-201 apparatus with a UV-detector Uvilog-III using a column (22×300 mm) packed with silica gel (Wakogel LC-50H). Gas liquid chromatography (GLC) was accomplished on a Yanaco G-2800 gas chromatograph (Yanagimoto) with a flame ionization detector using a glass column (SE-30, 3×2000 mm) or a glass capillary column (Silicone GE, SE-30, 0.25×5000 mm). Micro vacuum distillation was carried out on a Sibata GTO-250R Kugelrohr distilling apparatus. Solvents were evaporated with a Tokyo Rikakikai rotary evaporator type-V at about 50 °C unless otherwise stated.

Materials and Solvents. 4-Methylene-1,5-hexadien-3-ol (**1a**), 6-methyl-3-methylene-1,5-heptadien-4-ol (**1b**), *trans*-3-methylene-1,5-heptadien-4-ol (**1c**), and *trans*-4-methylene-1-phenyl-1,5-hexadien-3-ol (**1d**) were prepared from 2-lithio-1,3-butadiene and the corresponding aldehydes according to the reported method.[1] Although some of these triene alcohols **1** were often contaminated by the corresponding allene alcohols **2**, the mixtures were used for the following Diels-Alder reactions without purification. Gallium(III) chloride was prepared from metal gallium and dry hydrogen chloride and purified by distillation.

General Procedure for the Diels-Alder Reactions of Triene Alcohols 1 with Olefinic Dienophiles 3—5 Leading to Cycloadducts 6—8. Triene alcohols **1a—d** were heated under reflux in dry benzene with a slightly excess amount of dimethyl maleate (**3**), dimethyl fumarate (**4**), or *N*-methylmaleimide (**5**) under the reaction conditions listed in Table 1. The benzene was evaporated in vacuo and the residue was chromatographed over silica gel with hexane-ethyl acetate (4:1 to 1:3 v/v) or hexane-diethyl ether (1:1 v/v) to give cycloadducts **6—8** which were all mixtures of two diastereomers. The results are summarized in Table 1.

6a: Colorless liquid; IR (neat) 3400 and 1750 cm^{-1}; ^{1}H NMR ($CDCl_3$) δ=2.2—3.2 (7H, m, CH_2, CH, and OH), 3.66 (6H, s, COOMe), 4.48 (1H, br d, J=5.5 Hz, CHOH), 5.10 (1H, dt, J=10.0, 1.5, and 1.5 Hz, =CH_2 (cis)), 5.25 (1H, dt, J=17.5, 1.5, and 1.5 Hz, =CH_2 (trans)), 5.70 (1H, br s, 2-H), and 5.82 (1H, ddd, J=17.5, 10.0, and 5.5 Hz, CH=); ^{13}C NMR ($CDCl_3$) δ=24.83, 25.01, 25.48, 25.60 (each t, 3- and 6-C), 39.75, 39.86, 39.98 (each d, 4- and 5-C), 51.84 (q, COOMe), 76.09, 76.27 (each d, -CHOH-), 115.25 (t, =CH_2), 120.71, 120.88 (each d), 137.09, 137.20 (each s, 1-C), 138.61, 138.79 (each d), and 173.55 (s, COOMe); MS *m/z* (rel intensity, %) 236 (M^+−18, 9), 176 (52), 117 (100), and 79 (20).

Found: C, 61.45; H, 7.13%. Calcd for $C_{13}H_{18}O_5$: C, 61.40; H, 7.13%.

6b: Unstable colorless liquid; IR (neat) 3500 and 1725 cm^{-1}; ^{1}H NMR ($CDCl_3$) δ=2.1—3.2 (7H, m, CH_2, CH, and OH), 2.69, 2.73 (each 3H, d, J=1.0 Hz, =CMe_2), 3.65, 3.68 (6H, each s, COOMe), 4.70 (1H, d, J=9.0 Hz, CHOH), 5.18 (1H, br d, J=9.0 Hz, CH=), and 5.66 (1H, br s, 2-H); ^{13}C NMR ($CDCl_3$) δ=18.30, 18.53 (each q, =CMe_2), 25.12, 25.35, 25.71, 25.88 (each t, 3- and 6-C), 40.09, 40.12 (each d, 4- and 5-C), 51.95 (q, COOMe), 71.89, 72.01 (each d, CHOH), 119.19, 119.60 (each t, =CH_2), 125.89, 126.24 (each d), 133.65, 135.19, 135.83, 138.48 (each s), 173.77, and 173.95 (each s, COOMe); MS *m/z* (rel intensity, %) 282 (M^+, 2), 264 (19), 204 (26), 145 (100), 91 (30), 83 (27), 79 (29), and 77 (23).

6c: Colorless liquid; IR (neat) 3500 and 1725 cm^{-1}; ^{1}H NMR ($CDCl_3$) δ=1.70 (3H, d, J=6.0 Hz, =CHMe), 2.3—2.6 (5H, m, CH_2 and OH), 2.9—3.2 (2H, m, CH), 3.65 (6H, s, COOMe), 4.40 (1H, br d, J=5.5 Hz, CHOH), and 5.3—5.8 (3H, m, CH=); ^{13}C NMR ($CDCl_3$) δ=17.69 (q, =CHMe), 25.14, 25.48, 25.63 (each t, 3- and 6-C), 39.81, 40.06 (each d, 4- and 5-C), 51.80 (q, COOMe), 75.92 (d, CHOH), 119.83, 120.11, 127.28, 131.77, 131.96 (each d), 137.81 (s, 1-C), and 173.57 (s, COOMe); MS *m/z* (rel intensity, %) 268 (M^+, 1), 250 (22), 191 (20), 190 (44), 131 (100), and 69 (20).

Found: C, 62.71; H, 7.46%. Calcd for $C_{14}H_{20}O_5$: C, 62.67; H, 7.51%.

6d: Pale yellow liquid; IR (neat) 3400 and 1725 cm^{-1}; ^{1}H NMR ($CDCl_3$) δ=2.1—3.2 (7H, m, CH_2, CH, and OH), 3.56, 3.60 (each 3H, s, COOMe), 4.02 (1H, br d, J=6.0 Hz, CHOH), 5.72 (1H, br s, 2-H), 6.14 (1H, dd, J=16.0 and 6.0 Hz, CH=), 6.54 (1H, dd, J=16.0 and 3.0 Hz, =CHPh), and 7.0—7.2 (5H, m, Ph); ^{13}C NMR ($CDCl_3$) δ=25.05, 25.58 (each t, 3- and 6-C), 39.72, 39.91 (each d, 4- and 5-C), 51.80 (q, COOMe), 75.87 (d, CHOH), 120.66, 126.41, 127.48, 128.45, 130.26, 130.50 (each d), 136.64, 137.32, 137.42 (each s), 173.48, and 173.57 (each s, COOMe); MS *m/z* (rel intensity, %) 330 (M^+, 8), 312 (26), 270 (35), 211 (19), 194 (25), 193 (100), 178 (21), 131 (21), 115 (65), 105 (22), 103 (26), 91 (58), 79 (25), and 77 (34).

Found: C, 68.88; H, 6.77%. Calcd for $C_{19}H_{22}O_5$: C, 69.07; H, 6.71%.

7a: Colorless liquid; IR (neat) 3450 and 1725 cm^{-1}; ^{1}H NMR ($CDCl_3$) δ=2.0—2.5 (5H, m, CH_2 and OH), 2.7—3.0 (2H, m, CH), 3.66 (6H, s, COOMe), 4.50 (1H, br d, J=5.5 Hz, CHOH), 5.15 (1H, dt, J=10.0, 1.5, and 1.5 Hz, =CH_2 (cis)), 5.26 (1H, dt, J=17.5, 1.5, and 1.5 Hz, =CH_2 (trans)), 5.74 (1H, br s, 2-H), and 5.83 (1H, ddd, J=17.5, 10.0,

and 5.5 Hz, CH=); ^{13}C NMR ($CDCl_3$) δ=26.76, 27.00, 27.63, 27.78 (each t, 3- and 6-C), 41.27, 41.42 (each d, 4- and 5-C), 51.90 (q, COOMe), 75.82 (d, CHOH), 115.54, 115.64 (each t, =CH_2), 120.27, 120.75 (each d), 136.98, 137.27 (each s, 1-C), 138.44, 138.64 (each d), and 175.09 (s, COOMe); MS *m/z* (rel intensity, %) 236 (M^+−18, 3), 204 (32), 177 (20), 176 (84), 117 (100), 91 (21), 79 (33), and 77 (19).

Found: C, 61.11; H, 7.08%. Calcd for $C_{13}H_{18}O_5$: C, 61.40; H, 7.13%.

7b: Colorless liquid; IR (neat) 3500 and 1725 cm^{-1}; ^{1}H NMR ($CDCl_3$) δ=1.70 (3H, d, *J*=6.0 Hz, =CHMe), 1.9—2.7 (5H, m, CH_2 and OH), 2.7—2.9 (2H, m, CH), 3.66 (6H, s, COOMe), 4.40 (1H, d, *J*=5.5 Hz, CHOH), 5.3—5.9 (2H, m, CH=CHMe), and 5.70 (1H, br s, 2-H); ^{13}C NMR ($CDCl_3$) δ=17.71 (q, =CHMe), 27.12, 27.53, 27.88 (each t, 3- and 6-C), 41.47 (d, 4- and 5-C), 52.00 (q, COOMe), 75.88 (d, CHOH), 119.60, 120.13, 127.89, 131.89, 132.01 (each d), 137.89, 138.18 (each s, 1-C), and 175.60 (s, COOMe); MS *m/z* (rel intensity, %) 268 (M^+, 1), 218 (11), 190 (32), 131 (77), 91 (28), 79 (33), and 77 (30).

Found: C, 62.49; H, 7.49%. Calcd for $C_{14}H_{20}O_5$: C, 62.67; H, 7.51%.

7c: Colorless liquid; IR (neat) 3450 and 1730 cm^{-1}; ^{1}H NMR ($CDCl_3$) δ=1.8—3.0 (7H, m, CH_2 CH, and OH), 3.64, 3.66 (each 3H, s, COOMe), 4.66 (1H, br d, *J*=6.0 Hz, CHOH), 5.76 (1H, br s, 2-H), 6.14 (1H, dd, *J*=16.0 and 6.0 Hz, CH=), 6.58 (1H, d, *J*=16.0 Hz, =CHPh), and 7.0—7.4 (5H, m, Ph); ^{13}C NMR ($CDCl_3$) δ=27.00, 27.30, 27.77, 27.88 (each t, 3- and 6-C), 41.36 (d, 4- and 5-C), 52.06 (q, COOMe), 75.89 (d, CHOH), 120.54, 121.07, 128.01, 128.83, 130.01, 130.13, 131.24 (each d), 136.72, 137.48, 137.78 (each s), and 175.48 (s, COOMe); MS *m/z* (rel intensity, %) 330 (M^+, 32), 312 (19), 280 (25), 270 (79), 253 (25), 252 (53), 211 (43), 193 (100), 179 (20), 165 (25), 131 (36), 115 (48), 105 (33), 103 (33), 91 (66), 79 (39), and 77 (22).

Found: C, 68.91; H, 6.63%. Calcd for $C_{19}H_{22}O_5$: C, 69.07; H, 6.71%.

8a: Colorless liquid; IR (neat) 3500 and 1680 cm^{-1}; ^{1}H NMR ($CDCl_3$) δ=2.0—2.8 (5H, m, CH_2 and OH), 2.88, 2.90 (each 3H, s, NMe), 3.0—3.2 (2H, m, CH), 4.47 (1H, br d, *J*=5.5 Hz, CHOH), 5.0—5.3 (2H, m, =CH_2), and 5.5—5.9 (2H, m, CH= and 6-H); ^{13}C NMR ($CDCl_3$) δ=23.54 (t, 4- and 7-C), 24.61 (q, NMe), 39.03, 39.28 (each d, 3a- and 7a-C), 74.70, 75.38 (each d, CHOH), 115.24, 115.39 (each t, =CH_2), 121.19, 121.39, 137.76, 137.95 (each d), 140.54, 140.68 (each s), 179.66, and 179.91 (each s, CON); MS *m/z* (rel intensity, %) 221 (M^+, 100), 203 (24), 193 (34), 192 (21), 166 (38), 126 (35), 118 (77), 117 (63), 113 (46), 112 (68), 109 (22), 107 (43), 92 (29), 91 (43), 81 (60), 80 (38), 79 (78), 78 (29), and 77 (65).

Found: C, 65.82; H, 6.81; N, 6.40%. Calcd for $C_{12}H_{15}NO_3$: C, 65.14; H, 6.83; N, 6.33%.

8b: Unstable colorless liquid; IR (neat) 3500, 1770, and 1680 cm^{-1}; ^{1}H NMR ($CDCl_3$) δ=1.64, 1.70 (each 3H, s, =CMe_2), 2.0—3.0 (5H, m, CH_2 and OH), 2.86, 2.88 (each 3H, s, NMe), 3.0—3.2 (2H, m, CH), 4.67 (1H, br d, *J*=8.5 Hz, CHOH), 5.03 (1H, m, CH=), and 5.76 (1H, br s, 6-H); ^{13}C NMR ($CDCl_3$) δ=17.93 (q, =CMe_2), 23.49, 23.78, 24.26 (each t, 4- and 7-C), 24.51, 25.53 (each q, NMe), 39.23, 39.42 (each d, 3a- and 7a-C), 70.41, 71.00 (each d, CHOH), 119.63, 119.92, 124.99, 125.14 (each d), 134.93, 135.22, 141.76, 141.85 (each s), 179.52, 179.86 (each s, CON); MS *m/z* (rel intensity, %) 249 (M^+, 10), 131 (11), and 43 (100).

8c: Pale yellow needles (diethyl ether-hexane); mp 100—102 °C; IR (KBr) 3200, 1680, and 1620 cm^{-1}; ^{1}H NMR ($CDCl_3$) δ=2.0—2.8 (5H, m, CH_2 and OH), 2.78 (3H, s, NMe), 3.0—3.2 (2H, m, CH), 4.64 (1H, br d, *J*=7.0 Hz, CHOH), 5.88 (1H, m, 6-H), 6.06 (1H, dd, *J*=16.0 and 7.0 Hz, CH=), 6.52 (1H, d, *J*=16.0 Hz, =CHPh), and 7.1—7.4 (5H, m, Ph); ^{13}C NMR ($CDCl_3$) δ=23.77, 23.94 (each t, 4- and 7-C), 24.77 (q, NMe), 39.36, 39.53 (each d, 3a- and 7a-C), 74.41, 75.71 (each d, CHOH), 121.71, 126.60, 127.83, 128.65, 129.77, 130.77, 131.19, (each d), 136.66, 141.42 (each s), 180.18, and 180.36 (each s, CON); MS *m/z* (rel intensity, %) 297 (M^+, 95), 279 (33), 194 (23), 193 (34), 192 (55), 186 (29), 165 (23), 116 (23), 115 (59), 113 (24), 112 (35), 105 (46), 104 (25), 103 (46), 91 (75), 80 (41), 79 (100), 78 (33), and 77 (84).

Found: C, 72.85; H, 6.33; N, 4.70%. Calcd for $C_{18}H_{19}NO_3$: C, 72.70; H, 6.44; N, 4.71%.

General Procedure for Oxidation of Diene Alcohols 6—8 with Activated Mangnese(IV) Oxide Leading to Dienones 9—11. Diene alcohols **6—8** and activated manganese(IV) oxide were stirred in dry dichloromethane (10—20 ml per 1 mmol of the alcohols) at room temperature under the reaction conditions listed in Table 2. The oxide was filtered off through Celite 545 and the filtrate was evaporated in vacuo. The residue was chromatographed over silica gel with hexane-ethyl acetate (1 : 1 to 2 : 1 v/v) to give **9—11**. The results are summarized in Table 2.

9a: Colorless liquid; IR (neat) 1730 and 1650 cm^{-1}; ^{1}H NMR ($CDCl_3$) δ=2.4—3.3 (6H, m, CH_2 and CH), 3.67, 3.69 (each 3H, s, COOMe), 5.72 (1H, dd, *J*=10.5 and 2.0 Hz, =CH_2 (cis)), 6.24 (1H, dd, *J*=17.1 and 2.0 Hz, =CH_2 (trans)), 6.89 (1H, m, 2-H), and 6.94 (1H, dd, *J*=17.1 and 10.5 Hz, CH=); ^{13}C NMR ($CDCl_3$) δ=24.42, 26.54 (each t, 3- and 6-C), 39.16, 39.45 (each d, 4- and 5-C), 52.02 (q, COOMe), 128.34 (t, =CH_2), 131.10 (d, COCH=), 137.32 (s, 1-C), 138.20 (d, 2-C), 172.92, 173.01 (each s, COOMe), and 190.16 (s, CO); MS *m/z* (rel intensity, %) 252 (M^+, 19), 221 (24), 220 (17), 192 (35), 133 (100), 105 (16), and 77 (29).

Found: C, 61.59; H, 6.19%. Calcd for $C_{13}H_{16}O_5$: C, 61.89; H, 6.39%.

9b: Colorless needles (diethyl ether-hexane); mp 94—97 °C; IR (KBr) 1725, 1650, and 1600 cm^{-1}; ^{1}H NMR ($CDCl_3$) δ=1.92, 2.08 (each 3H, d, *J*=1.3 Hz, =CMe_2), 2.5—3.2 (6H, m, CH_2 and CH), 3.64, 3.66 (each 3H, s, COOMe), 6.38 (1H, m, *J*=1.3 Hz, COCH=), and 6.78 (1H, m, 2-H); ^{13}C NMR ($CDCl_3$) δ=20.85 (q, =CMe_2), 24.46, 26.37 (each t, 3- and 6-C), 27.68 (q, =CMe_2), 39.31, 39.65 (each d, 4- and 5-C), 52.05 (q, COOMe), 120.65 (d, COCH=), 136.08 (d, 2-C), 138.76 (s, 1-C), 154.20 (s, =CMe_2) 173.38, 173.48 (each s, COOMe), and 192.04 (s, CO); MS *m/z* (rel intensity, %) 280 (M^+, 69), 249 (32), 220 (24), 161 (100), 160 (25), 83 (66), and 55 (36).

Found: C, 64.54; H, 7.29%. Calcd for $C_{15}H_{20}O_5$: C, 64.27; H, 7.19%.

9c: Colorless needles (diethyl ether-hexane); mp 80—83 °C; IR (KBr) 1725, 1660, and 1610 cm^{-1}; ^{1}H NMR ($CDCl_3$) δ=1.90 (3H, d, *J*=6.0 Hz, =CHMe), 2.3—3.2 (6H, m, CH_2 and CH), 3.66, 3.68 (each 3H, s, COOMe), and 6.5—7.2 (3H, m, CH=CHMe and 2-H); ^{13}C NMR ($CDCl_3$) δ=18.32 (q, =CHMe), 24.51, 26.46 (each t, 3- and 6-C), 39.18, 39.52 (each d, 4- and 5-C), 51.85 (q, COOMe), 126.16 (d, COCH=), 136.93 (d, 2-C), 137.42 (s, 1-C), 142.42 (d, =CHMe), 172.94, 173.09 (each s, COOMe), and 189.90 (s, CO); MS *m/z* (rel intensity, %) 266 (M^+, 52), 235 (28), 206 (27), 148 (100), 84 (18), and 69

(51).

Found: C, 63.19; H, 6.77%. Calcd for $C_{14}H_{18}O_5$: C, 63.15; H, 6.81%.

9d: Colorless needles (diethyl ether-hexane); mp 111—112 °C; IR (KBr) 1725, 1640, and 1595 cm^{-1}; ^1H NMR ($CDCl_3$) δ=2.2—3.3 (6H, m, CH_2 and CH), 3.65, 3.67 (each 3H, s, COOMe), 6.96 (1H, br s, 2-H), 7.24, 7.63 (each 1H, d, J=15.7 Hz, CH=CHPh), and 7.3—7.6 (5H, m, Ph); ^{13}C NMR ($CDCl_3$) δ=24.60, 26.48 (each t, 3- and 6-C), 39.10, 39.45 (each d, 4- and 5-C), 51.96 (q, COOMe), 120.77, 128.11, 128.75, 130.10 (each d), 134.86 (s), 137.03 (d, 2-C), 137.91 (s, 1-C), 142.96 (d, PhCH=), 172.85, 173.01 (each s, COOMe), and 189.52 (s, CO); MS m/z (rel intensity, %) 328 (M^+, 29), 268 (18), 210 (19), 209 (100), 131 (71), 105 (21), 103 (66), and 77 (75).

Found: C, 69.27; H, 5.98%. Calcd for $C_{19}H_{20}O_5$: C, 69.50; H, 6.14%.

10a: Colorless liquid; IR (neat) 1725 and 1650 cm^{-1}; ^1H NMR ($CDCl_3$) δ=2.2—3.0 (6H, m, CH_2 and CH), 3.70 (6H, s, COOMe), 5.74 (1H, dd, J=10.5 and 2.0 Hz, $=CH_2$ (cis)), 6.26 (1H, dd, J=17.0 and 2.0 Hz, $=CH_2$ (trans)), 6.90 (1H, br s, 2-H), and 6.92 (1H, dd, J=17.0 and 10.5 Hz, COCH=); ^{13}C NMR ($CDCl_3$) δ=25.83, 28.41 (each t, 3- and 6-C), 40.28, 40.80 (each d, 4- and 5-C), 52.08 (q, COOMe), 128.63 (t, $=CH_2$), 130.86 (d, 2-C), 137.50 (s and d, 1-C and COCH=), 174.37 (s, COOMe), and 189.81 (s, CO); MS m/z (rel intensity, %) 253 (M^++1, 2), 221 (23), 220 (54), 192 (83), 133 (100), and 55 (52).

Found: C, 62.12; H, 6.42%. Calcd for $C_{13}H_{16}O_5$: C, 61.96; H, 6.54%.

10b: Colorless prisms (diethyl ether-hexane); mp 67—69 °C; IR (KBr) 1725 and 1650 cm^{-1}; ^1H NMR ($CDCl_3$) δ=1.90 (3H, dd, J=6.5 and 1.0 Hz, =CHMe), 2.1—3.0 (6H, m, CH_2 and CH), 3.68 (6H, s, COOMe), 6.60 (1H, dd, J=15.0 and 1.0 Hz, COCH=), 6.7—6.9 (1H, m, 2-H), and 6.88 (1H, dq, J=15.0 and 6.5 Hz, =CHMe); ^{13}C NMR ($CDCl_3$) δ=18.41 (q, =CHMe), 26.12, 28.47 (each t, 3- and 6-C), 40.47, 41.00 (each d, 4- and 5-C), 52.12 (q, COOMe), 126.18 (d, COCH=), 136.54 (d, 2-C), 137.83 (s, 1-C), 143.42 (d, MeCH=), 174.84 (s, COOMe), and 189.90 (s, CO); MS m/z (rel intensity, %) 267 (M^++1, 2), 206 (13), 147 (52), 105 (16), 91 (17), 79 (27), 78 (22), 77 (47), and 69 (100).

Found: C, 63.14; H, 6.80%. Calcd for $C_{14}H_{18}O_5$: C, 63.15; H, 6.81%.

10c: Colorless prisms (dichloromethane-hexane); mp 130—131 °C; IR (KBr) 1725 and 1640 cm^{-1}; ^1H NMR ($CDCl_3$) δ=2.1—3.1 (6H, m, CH_2 and CH), 3.70 (6H, s, COOMe), 6.92 (1H, br s, 2-H), 7.2—7.6 (5H, m, Ph), 7.22, and 7.63 (each 1H, d, J=15.7 Hz, CH=CHPh); ^{13}C NMR ($CDCl_3$) δ=26.18, 28.47 (each t, 3- and 6-C), 40.47, 41.00 (each d, 4- and 5-C), 52.12 (q, COOMe), 120.89, 128.42, 129.07, 130.48 (each d), 135.12 (s), 136.60 (d, 2-C), 138.36 (s, 1-C), 143.54 (d, PhCH=), 174.71 (s, COOMe), and 189.54 (s, CO); MS m/z (rel intensity, %) 328 (M^+, 25), 297 (25), 296 (48), 268 (53), 209 (100), 131 (62), 105 (19), 103 (52), and 77 (38).

Found: C, 69.72; H, 6.07%. Calcd for $C_{19}H_{20}O_5$: C, 69.50; H, 6.14%.

11a: Unstable colorless liquid; IR (neat) 1690 and 1650 cm^{-1}; ^1H NMR ($CDCl_3$) δ=2.2—3.3 (6H, m, CH_2 and CH), 2.90 (3H, s, NMe), 6.74 (1H, dd, J=10.5 and 2.0 Hz, $=CH_2$ (cis)), 7.22 (1H, dd, J=17.0 and 2.0 Hz, $=CH_2$ (trans)), 7.88 (1H, dd, J=17.0 and 10.5 Hz, COCH=), and 7.90 (1H, m, 6-H); ^{13}C NMR ($CDCl_3$) δ=21.55, 24.60 (each t, 4- and 7-C), 24.76 (q, NMe), 38.16, 38.63 (each d, 3a- and 7a-C), 128.81 (t, $=CH_2$), 130.34 (d, COCH=), 138.67 (d, 6-C), 139.90 (s, 5-C), 178.59, 179.00 (each s, CON), and 188.16 (s, CO); MS m/z (rel intensity, %) 219 (M^+, 37), 134 (16), 133 (21), 108 (24), 105 (30), 80 (20), 79 (81), 78 (29), and 77 (68).

Found: C, 66.01; H, 5.79; N, 6.12%. Calcd for $C_{12}H_{13}NO_3$: C, 65.74; H, 5.98; N, 6.39%.

11b: Colorless prisms (diethyl ether-hexane); mp 111—113 °C; IR (KBr) 1680 cm^{-1}; ^1H NMR ($CDCl_3$) δ=1.92, 2.08 (each 3H, d, J=1.0 Hz, $=CMe_2$), 2.1—3.3 (6H, m, CH_2 and CH), 2.92 (3H, s, NMe), 6.37 (1H, m, J=1.0 Hz, COCH=), and 6.88 (1H, m, 6-H); ^{13}C NMR ($CDCl_3$) δ=20.72 (q, $=CMe_2$), 21.60, 24.54 (each t, 4- and 7-C), 24.83 (q, NMe), 27.59 (q, $=CMe_2$), 38.34, 38.87 (each d, 3a- and 7a-C), 119.42 (d, COCH=), 135.97 (d, 6-C), 141.43 (s, 5-C), 155.11 (s, $=CMe_2$), 178.77, 179.24 (each s, COOMe), and 189.28 (s, CO); MS m/z (rel intensity, %) 247 (M^+, 22), 148 (24), 135 (20), 126 (25), 122 (42), 121 (21), 105 (22), 91 (25), 83 (97), 79 (57), 78 (50), and 77 (100).

Found: C, 67.91; H, 6.95; N, 5.81%. Calcd for $C_{14}H_{17}NO_3$: C, 68.00; H, 6.93; N, 5.66%.

11c: Colorless needles (diethyl ether-hexane); mp 161—162 °C; IR (KBr) 1680 cm^{-1}; ^1H NMR ($CDCl_3$) δ=2.2—2.9 (4H, m, CH_2), 2.92 (3H, s, NMe), 3.0—3.3 (2H, m, CH), 7.06 (1H, m, 6-H), 7.18, 7.62 (each 1H, d, J=16.0 Hz, CH=CHPh), and 7.2—7.6 (5H, m, Ph); ^{13}C NMR ($CDCl_3$) δ=22.08, 24.83 (each t, 4- and 7-C), 25.01 (q, NMe), 38.46, 38.92 (each d, 3a- and 7a-C), 120.18 128.16, 128.81, 130.28 (each d), 134.68 (s), 137.50 (d, 6-C), 140.96 (s, 5-C), 143.72 (d, PhCH=), 178.77, 179.18 (each s, COOMe), and 187.81 (s, CO); MS m/z (rel intensity, %) 295 (M^+, 100), 294 (40), 209 (11), 184 (20), 183 (19), 131 (73), 103 (52), and 77 (53).

Found: C, 73.15; H, 5.90; N, 4.92%. Calcd for $C_{18}H_{17}NO_3$: C, 73.20; H, 5.80; N, 4.74%.

General Procedure for Acid-Catalyzed Electrocyclic Reaction of Dienones 9—11 Leading to 12—15. Use of *p*-toluenesulfonic acid as a catalyst: To a solution of *p*-toluenesulfonic acid in dry benzene or toluene (15—20 ml per 1 mmol of substrate) was added a dienone. The mixture was heated under reflux for the reaction time listed in Table 4. After cooled to room temperature, the resulting mixture was poured into ice water and extracted with diethyl ether. The ether extract was dried over anhydrous magnesium sulfate and evaporated in vacuo. The residue was chromatographed over silica gel with hexane-ethyl acetate (4:1 to 1:2 v/v). Use of gallium(III) chloride: A dienone in dichloromethane was slowly added at −20 °C to a solution of freshly prepared gallium(III) chloride in dry dichloromethane (20—30 ml per 1 mmol of substrate). After the reaction was completed (checked on TLC), the mixture was poured into ice water. The same separation procedure as above gave the cyclized products **12—15**. All the results are listed in Table 4.

12a: Colorless liquid; IR (neat) 1730, 1690, and 1650 cm^{-1}; ^1H NMR ($CDCl_3$) δ=2.4—2.5 (2H, m), 2.5—2.6 (2H, m), 2.6—2.7 (3H, m) 2.94 (1H, dd, J=19.8 and 7.2 Hz, one of 4-H), 3.10 (1H, ddd, J=7.2, 6.3, and 3.6 Hz, 5-H), 3.21 (1H, dt, J=5.8, 5.8, and 3.6 Hz, 6-H), 3.65, and 3.68 (each 3H, s, COOMe); ^{13}C NMR ($CDCl_3$) δ=21.31, 28.77, 29.41 (each t, 3-, 4-, and 7-C), 34.52 (t, 2-C), 39.34, 39.98 (each d, 5- and 6-C), 51.84 (q, COOMe), 136.27 (s, 7a-C), 170.61 (s, 3a-C), 172.61,

172.72 (each s, COOMe1/2 and 207.37 (s, 1-C); MS *m/z* (rel intensity, %) 252 (M^+, 38), 221 (23), 193 (39), 192 (23), 133 (100), 105 (43), and 91 (36).

Found: C, 61.96; H, 6.54%. Calcd for $C_{13}H_{16}O_5$: C, 61.89; H, 6.39%.

12b: Colorless liquid; IR (neat) 1725, 1680, and 1650 cm^{-1}; ^1H NMR ($CDCl_3$) δ=1.17, 1.20 (each 3H, s, 3-Me), 2.30 (2H, br s, 2-H), 2.43 (1H, ddt, J=18.2, 6.0, 2.0, and 2.0 Hz, one of 4-H), 2.57 (1H, br dd, J=19.7 and 6.5 Hz, one of 7-H), 2.63 (1H, ddd, J=18.2, 6.0, and 2.0 Hz, the other of 4-H), 2.86 (1H, ddd, J=19.7, 6.5, and 2.0 Hz, the other of 7-H), 3.10 (1H, dt, J=6.5, 6.5, and 3.6 Hz, 6-H), 3.15 (1H, dt, J=6.0, 6.0, and 3.6 Hz, 5-H), 3.66, and 3.68 (each 3H, s, COOMe); ^{13}C NMR ($CDCl_3$) δ=21.31, 23.84 (each t, 4- and 7-C), 26.60 (q, 3-Me), 39.45, 40.39 (each d, 5- and 6-C), 40.57 (s, 3-C), 51.37 (t, 2-C), 51.96, 52.08 (each q, COOMe), 134.33 (s, 7a-C), 172.72, 172.84 (each s, COOMe), 177.54 (s, 3a-C), and 205.96 (s, 1-C); MS *m/z* (rel intensity, %) 280 (M^+, 30), 240 (21), 221 (40), 209 (22), 161 (58), 121 (100), 119 (30), 105 (19), and 42 (71).

Found: C, 64.13; H, 7.28%. Calcd for $C_{15}H_{20}O_5$: C, 64.27; H, 7.19%.

12c: Colorless liquid; IR (neat) 1730, 1700, and 1650 cm^{-1}; ^1H NMR ($CDCl_3$) δ=1.15 (3H, d, J=7.1 Hz, 3-Me), 1.99 (1H, dd, J=18.5 and 2.9 Hz, one of 2-H), 2.43 (1H, ddd, J=18.0, 6.0, and 2.2 Hz, one of 4-H), 2.50 (1H, ddd, J=19.0, 6.8, and 2.0 Hz, one of 7-H), 2.64 (1H, dd J=18.0 and 6.0 Hz, the other of 4-H), 2.65 (1H, dd, J=18.5 and 6.8 Hz, the other of 2-H), 2.76 (1H, m, 3-H), 2.78 (1H, dd, J=19.0, and 6.8 Hz, the other of 7-H), 3.15 (1H, dt, J=6.0, 6.0, and 3.6 Hz, 5-H), 3.20 (1H, dt, J=6.8, 6.8, and 3.6 Hz, 6-H), 3.63, and 3.66 (each 3H, s, COOMe); ^{13}C NMR ($CDCl_3$) δ=18.67 (q, 3-Me), 21.49, 26.71 (each t, 4- and 7-C), 35.93 (d, 3-C), 39.51, 40.27 (each d, 5- and 6-C), 43.65 (t, 2-C), 51.96, 52.08 (each q, COOMe), 135.74 (s, 7a-C), 172.77, 174.42, 174.66 (each s, COOMe and 3a-C), and 206.60 (s, 1-C); MS *m/z* (rel intensity, %) 266 (M^+, 8), 207 (21), 206 (21), 148 (100), 119 (20), 105 (66), 91 (42), and 77 (31).

Found: C, 62.92; H, 6.94%. Calcd for $C_{14}H_{18}O_5$: C, 63.15; H, 6.82%.

12c' could not be separated from the mixture with **12c**. Its formation was confirmed by the appearance of additional peaks in ^{13}C NMR ($CDCl_3$) δ=21.31 (t) and 135.86 (s, 7a-C).

12d: Colorless liquid; IR (neat) 1730, 1700, 1650, and 1600 cm^{-1}; ^1H NMR ($CDCl_3$) δ=2.35 (1H, dd, J=19.0 and 5.9 Hz, one of 4-H), 2.42 (1H, dd, J=19.0 and 2.2 Hz, one of 2-H), 2.58 (1H, ddd, J=17.8, 6.5, and 2.1 Hz, one of 7-H), 2.70 (1H, dd, J=19.0 and 5.9 Hz, the other of 4-H), 2.77 (1H, ddd, J=17.8, 6.5, and 2.1 Hz, the other of 7-H), 2.95 (1H, dd, J=19.0 and 6.9 Hz, the other of 2-H), 3.01 (1H, dt, J=6.5, 6.5, and 3.6 Hz, 6-H), 3.19 (1H, dt, J=5.9, 5.9, and 3.6 Hz, 5-H), 3.68, 3.69 (each 3H, s, COOMe), 3.85 (1H, dd, J=6.9 and 2.2 Hz, 3-H), and 7.1—7.4 (5H, m, Ph); ^{13}C NMR ($CDCl_3$) δ=21.55, 26.95 (each t, 4- and 7-C), 39.45, 40.28 (each d, 5- and 6-C), 45.03 (t, 2-C), 47.50 (d, 3-C), 52.08 (q, COOMe), 127.17, 129.05 (each d), 136.91, 141.14 (each s), 172.43, 172.67, 172.84 (each s, COOMe and 3a-C), and 206.66 (s, 1-C).

Found: C, 69.53; H, 6.35%. Calcd for $C_{19}H_{20}O_5$: C, 69.50; H, 6.14%.

12d': Colorless prisms (diethyl ether-hexane); mp 86—87 °C; IR (KBr) 1730, 1700, 1650, and 1600 cm^{-1}; ^1H NMR ($CDCl_3$) δ=2.36 (1H, dd, J=18.9 and 2.2 Hz, one of 2-H), 2.45 (1H, dd, J=19.7 and 6.2 Hz, one of 4-H), 2.56 (1H, ddd, J=18.0, 5.9, and 2.0 Hz, one of 7-H), 2.60 (1H, dd, J=19.7 and 6.8 Hz, the other of 4-H), 2.84 (1H, ddt, J=18.0, 5.9, 2.0, and 2.0 Hz, the other of 7-H), 2.95 (1H, dd, J=18.9 and 6.9 Hz, the other of 2-H), 3.11 (1H, ddd, J=6.8, 6.2, and 3.6 Hz, 5-H), 3.20 (1H, dt, J=5.9, 5.9, and 3.6 Hz, 6-H), 3.63, 3.68 (each 3H, s, COOMe), 3.87 (1H, dd, J=6.9 and 2.2 Hz, 3-H), and 7.0—7.3 (5H, m, Ph); ^{13}C NMR ($CDCl_3$) δ=21.64, 27.24 (each t, 4- and 7-C), 39.57, 40.37 (each d, 5- and 6-C), 45.37 (t, 2-C), 47.52 (d, 3-C), 51.95 (q, COOMe), 127.23, 128.89 (each d), 137.62, 141.02 (each s), 171.87, 172.51, 172.75 (each s, COOMe and 3a-C), and 207.00 (s, 1-C); MS *m/z* (rel intensity, %) 328 (M^+, 86), 297 (22), 269 (49), 268 (30), 209 (100), 167 (49), 165 (28), 103 (22), 77 (22), and 59 (95).

Found: C, 69.49; H, 6.13%. Calcd for $C_{19}H_{20}O_5$: C, 69.50; H, 6.16%.

13b: Colorless prisms (diethyl ether-hexane); mp 99—101 °C; IR (KBr) 1725 and 1650 cm^{-1}; ^1H NMR ($CDCl_3$) δ=0.80, 1.23 (each 3H, s, 3-Me), 1.40 (1H, q, J=12.0 Hz, one of 4-H), 2.20 (2H, br s, 2-H), 2.24 (1H, ddd, J=12.0, 5.0, and 3.0 Hz, the other of 4-H), 2.50 (1H, ddd, J=12.0, 5.0, and 3.0 Hz, 3a-H), 3.05 (1H, ddd, J=12.0, 10.0, and 3.0 Hz, 5-H), 3.70, 3.72 (each 3H, s, COOMe), 3.80 (1H, m, 6-H), and 6.70 (1H, t, J=3.0 Hz, 7-H); ^{13}C NMR ($CDCl_3$) δ=22.60, 26.89 (each q, 3-Me), 26.07 (t, 4-C), 36.87 (s, 3-C), 41.80, 44.91, 47.97 (each d, 3a-, 5-, and 6-C), 52.19, 52.49 (each q, COOMe), 54.60 (t, 2-C), 127.40 (d, 7-C), 141.08 (s, 7a-C), 171.60, 174.49 (each s, COOMe), and 203.84 (1-C); MS *m/z* (rel intensity, %) 280 (M^+, 15), 249 (25), 248 (63), 221 (30), 220 (39), 192 (27), 165 (37), 164 (100), 161 (43), 136 (44), 119 (20), 106 (20), 105 (91), 91 (34), 78 (38), and 77 (50).

Found: C, 64.46; H, 7.29%. Calcd for $C_{15}H_{20}O_5$: C, 64.27; H, 7.19%.

13c: Unstable colorless liquid; IR (neat) 1730 and 1660 cm^{-1}; ^1H NMR ($CDCl_3$) δ=1.22 (3H, d, J=6.0 Hz, 3-Me), 1.30 (1H, q, J=12.0 Hz, one of 4-H), 1.5—2.6 (6H, m), 3.06 (1H, ddd, J=12.0, 10.0, and 3.0 Hz, 5-H), 3.72, 3.74 (each 3H, s, COOMe), 3.76 (1H, m, 6-H), and 6.64 (1H, t, J=3.0 Hz, 7-H); ^{13}C NMR ($CDCl_3$) δ=18.03 (q, 3-Me), 30.53 (t, 4-C), 36.58 (d, 3-C), 41.74, 44.85, 45.21 (each d, 3a-, 5-, and 6-C), 46.21 (t, 2-C), 52.25, 52.54 (each q, COOMe), 126.40 (d, 7-C), 142.31 (s, 7a-C), 171.60, 174.37 (each s, COOMe), and 204.19 (s, 1-C); MS *m/z* (rel intensity, %) 266 (M^+, 3), 206 (13), 148 (27), 105 (59), 91 (35), 79 (19), 78 (38), 77 (47), and 59 (100).

HRMS Found: *m/z* 266.1153. Calcd for $C_{14}H_{18}O_5$: M, 266.1153.

13d: Colorless liquid; IR (neat) 1730, 1665, and 1615 cm^{-1}; ^1H NMR ($CDCl_3$) δ=1.36 (1H, q, J=12.0 Hz, one of 4-H), 2.32 (1H, dt, J=12.0, 3.5, and 3.5 Hz, the other of 4-H), 2.4—2.9 (4H, m), 3.02 (1H, ddd, J=12.0, 10.0, and 3.0 Hz, 5-H), 3.68, 3.74 (each 3H, s, COOMe), 3.78 (1H, m, 6-H), 6.76 (1H, t, J=3.0 Hz, 7-H), and 7.1—7.5 (5H, m, Ph); ^{13}C NMR ($CDCl_3$) δ=30.59 (t, 4-C), 41.63, 44.97, 45.32 (each d, 3a-, 5-, and 6-C), 46.26 (t, 2-C), 47.56 (d, 3-C), 52.13, 52.55 (each q, COOMe), 126.99, 127.17, 128.82 (each d), 140.32, 141.67 (each s), 171.37, 174.13 (each s, COOMe), and 202.84 (s, 1-C).

Found: C, 69.42; H, 6.07%. Calcd for $C_{19}H_{20}O_5$: C, 69.50; H, 6.14%.

14a: Colorless needles (diethyl ether-hexane); mp 106—108 °C; IR (KBr) 1725 and 1700 cm^{-1}; ^1H NMR ($CDCl_3$) δ=2.28 (1H, ddt, J=19.0, 5.3, 2.2, and 2.2 Hz, one of 4-H),

2.4—2.6 (6H, m), 2.72 (1H, dd, J=19.0 and 5.9 Hz, one of 7-H), 2.95 (1H, dt, J=9.2, 9.2, and 5.3 Hz, 5-H), 3.05 (1H, dt, J=9.2, 9.2, and 5.9 Hz, 6-H), 3.68, and 3.70 (each 3H, s, COOMe); ^{13}C NMR ($CDCl_3$) δ=22.49, 29.41, 30.24 (each t, 3-, 4-, and 7-C), 34.70 (t, 2-C), 40.63, 41.04 (each d, 5- and 6-C), 52.19 (q, COOMe), 136.56 (s, 7a-C), 169.90 (s, 3a-C), 174.02, 174.13 (each s, COOMe), and 207.06 (s, 1-C); MS m/z (rel intensity, %) 252 (M^+, 5), 220 (28), 193 (26), 192 (42), 133 (100), 105 (45), 91 (43), and 57 (20).

Found: C, 62.12; H, 6.42%. Calcd for $C_{13}H_{16}O_5$: C, 61.96; H, 6.54%.

14b (Mixture of 1:1 stereoisomers): Colorless liquid; IR (neat) 1730, 1700, and 1650 cm^{-1}; ^{1}H NMR ($CDCl_3$) δ=1.17 (3H, d, J=7.0 Hz, 3-Me), 2.7—3.2 (9H, m), 3.87, and 3.90 (each 3H, s, COOMe); ^{13}C NMR ($CDCl_3$) δ=18.53, 18.71 (each q, 3-Me), 22.41, 22.65, 27.65, 28.35 (each t, 4- and 7-C), 35.65, 36.13 (each d, 3-C), 40.65, 40.77, 41.24 (each d, 5- and 6-C), 43.83 (t, 2-C), 52.18 (q, COOMe), 136.01 (s, 7a-C), 174.00, 174.37, 174.48 (each s, COOMe and 3a-C), and 206.53 (s, 1-C); MS m/z (rel intensity, %) 266 (M^+, 3), 207 (17), 206 (42), 147 (100), 119 (21), 105 (64), 91 (38), 79 (19), 77 (29), and 59 (22).

HRMS Found: m/z 266.1164. Calcd for $C_{14}H_{18}O_5$: M, 266.1153.

14c: Colorless liquid; IR (neat) 1730 and 1700 cm^{-1}; ^{1}H NMR ($CDCl_3$) δ=2.2—2.5 (3H, m), 2.66 (1H, br s), 2.8—3.1 (4H, m), 3.62, 3.69 (each 3H, s, COOMe), 3.87 (1H, br d, J=5.5 Hz, 3-H), and 7.0—7.5 (5H, m, Ph); ^{13}C NMR ($CDCl_3$) δ=22.71, 28.59 (each t, 4- and 7-C), 40.53, 41.06 (each d, 5- and 6-C), 45.18 (t, 2-C), 47.71 (d, 3-C), 52.18 (q, COOMe), 129.24 (d), 137.36, 140.89 (each s), 171.78, 174.19, 174.42 (each s, COOMe and 3a-C), and 206.48 (s, 1-C); MS m/z (rel intensity, %) 328 (M^+, 5), 268 (22), 209 (54), 167 (36), 166 (19), 165 (37), 131 (21), 115 (21), 105 (25), 104 (29), 103 (34), 91 (20), 78 (29), 77 (43), and 59 (100).

Found: C, 68.75; H, 6.15%. Calcd for $C_{19}H_{20}O_5$: C, 69.50; H, 6.14%.

15a: Colorless needles (diethyl ether-hexane); mp 170—173 °C; IR (KBr) 1710 and 1670 cm^{-1}; ^{1}H NMR ($CDCl_3$) δ=1.1—1.5 (2H, m), 2.2—2.5 (4H, m), 2.78 (1H, ddd, J=13.0, 5.0, and 2.0 Hz, one of 8-H), 2.96 (3H, s, NMe), 3.22 (1H, ddd, J=8.0, 5.5, and 2.0 Hz, 8a-H), 3.72 (1H, ddd, J=8.0, 5.2, and 2.8 Hz, 3a-H), and 6.70 (1H, dd, J=5.2 and 2.8 Hz, 4-H); ^{13}C NMR ($CDCl_3$) δ=25.07 (q, NMe), 27.77, 29.65 (each t, 7- and 8-C), 34.34 (d, 8a-C), 37.75 (t, 6-C), 39.86 (d, 3a-C), 42.15 (d, 7a-C), 124.82 (d, 4-C), 142.90 (s, 4a-C), 175.01, 178.24 (each s, 1- and 3-C), and 204.66 (s, 5-C); MS m/z (rel intensity, %); 219 (M^+, 15), 134 (29), 105 (35), 92 (100), 91 (59), 78 (83), 77 (47), and 51 (31).

Found: C, 65.85; H, 6.04%. Calcd for $C_{12}H_{13}NO_3$: C, 65.74; H, 5.98%.

15b+15b′: The crude reaction mixture was consisting of **15b**, **15b′**, and a small amount of **11b**. Pure **15b′** was isolated from the other two by column chromatography.

15b′: Colorless prisms (diethyl ether-hexane); mp 181—182 °C; IR (KBr) 1720, 1680, and 1650 cm^{-1}; ^{1}H NMR ($CDCl_3$) δ=0.82, 1.24 (each 3H, s, 7-Me), 1.50 (1H, ddd, J=12.8, 11.5, and 5.5 Hz, one of 8-H), 2.22 (1H, dddd, J=11.5, 5.0, 3.5, and 3.0 Hz, 7a-H), 2.18 (2H, br s, 6-H), 2.56 (1H, ddd, J=12.8, 5.0, and 2.5 Hz, the other of 8-H), 2.95 (3H, s, NMe), 3.26 (1H, ddd, J=8.0, 5.5, and 2.5 Hz, 8a-H), 3.70 (1H, ddd, J=8.0, 5.0, and 3.0 Hz, 3a-H), and 6.70 (1H, dd, J=5.0 and 3.5 Hz, 4-H); ^{13}C NMR ($CDCl_3$) δ=20.47 (t, 8-C) 22.59, 24.94, 26.77 (each q, NMe and 7-Me), 37.00 (s, 7-C), 39.53, 41.94, 43.77 (each d, 3a-, 7a-, and 8a-C), 54.18 (t, 6-C), 125.48 (d, 4-C), 142.60 (s, 4a-C), 175.31, 178.37 (each s, 1- and 3-C), and 203.78 (s, 5-C); MS m/z (rel intensity, %) 247 (M^+, 28), 191 (26), 163 (41), 106 (30), 105 (43), 79 (18), 78 (100), and 77 (34).

Found: C 67.92; H, 6.93; N, 5.60%. Calcd for $C_{14}H_{17}NO_3$: C, 68.00; H, 6.93; N, 5.66%.

The formation of **15b** was deduced only on the basis of ^{1}H NMR ($CDCl_3$) of the mixture with **11b**: δ=0.76, 1.24 (each 3H, s, 7-Me), 2.95 (3H, s, NMe), and 6.83 (1H, m, 4-H).

15c+15c′: Only **15c′** was separated in pure form through column chromatography of the mixture containing **15c** and **15c′**. However, **15c** was still contaminated by a small amount of **15c′**. **15c′**: Colorless prisms (dichloromethane-hexane); mp 246—248 °C; IR (KBr) 1770, 1690, and 1650 cm^{-1}; ^{1}H NMR ($CDCl_3$) δ=1.36 (1H, ddd, J=12.5, 10.5, and 6.0 Hz, one of 8-H), 2.3—2.9 (6H, m), 2.94 (3H, s, NMe), 3.19 (1H, ddd, J=8.0, 6.0, and 2.0 Hz, 8a-H), 3.74 (1H, ddd, J=8.0, 5.0, and 2.5 Hz, 3a-H), 6.78 (1H, dd, J=5.0 and 2.5 Hz, 4-H), and 7.28 (5H, m, Ph); MS m/z (rel intensity, %) 295 (M^+, 17), 184 (24), 163 (46), 106 (20), 105 (35), 104 (20), 77 (100), and 76 (26).

Found: C, 73.31; H, 5.91; N, 4.94%. Calcd for $C_{18}H_{17}NO_3$: C, 73.20; H, 5.80; N, 4.74%.

15c: IR (KBr) 1770, 1690, and 1650 cm^{-1}; ^{1}H NMR ($CDCl_3$) δ=1.04 (1H, ddd, J=12.5, 11.0, and 10.0 Hz, one of 8-H), 2.4—3.0 (4H, m), 2.98 (3H, s, NMe), 3.00 (1H, ddd, J=12.5, 8.5, and 6.0 Hz, 8a-H), 3.50 (1H, dt, J=8.5, 3.0, and 3.0 Hz, 3a-H), 7.00 (1H, t, J=3.0 Hz, 4-H), and 7.1—7.5 (5H, m, Ph).

^{13}C NMR of mixture of **15c** and **15c′** in $CDCl_3$: δ=24.77, 24.95 (each q, NMe), 25.77, 29.94 (each t, 8-C), 38.98, 39.57, 41.10, 41.92 (each d, 3a- and 8a-C), 44.56 (d, 7a—C), 47.32, 47.79 (each t, 6-C), 124.88, 125.23, 126.75, 126.87, 127.11, 128.69 (each d), 140.08, 140.26, 142.72, 143.37 (each s), 174.78, 177.60, 177.78 (each s, 1- and 3-C), 202.02, and 202.43 (each s, 5-C).

References

1) E. Wada, S. Kanemasa, I. Fujiwara, and O. Tsuge, *Bull. Chem. Soc. Jpn.*, **58**, 1942 (1985).

2) E. Wada, S. Kanemasa, and O. Tsuge, *Bull. Chem. Soc. Jpn.*, **59**, 2451 (1986).

3) O. Tsuge, E. Wada, S. Kanemasa, and H. Sakoh, *Chem. Lett.*, **1984**, 469 and 709.

4) K. E. Stevens and L. A. Paquette, *Tetrahedron Lett.*, **22**, 4393 (1981); H. Schostarez and L. A. Paquette, *Tetrahedron*, **37**, 4431 (1981); T. Hiyama, M. Shinoda, H. Saimoto, and H. Nozaki, *Bull. Chem. Soc. Jpn.*, **54**, 2747 (1981).

5) As a review on Nazarov cyclization: C. Santelli-Rouvier and M. Santelli, *Synthesis*, **1983**, 429.

6) E. A. Braude and J. A. Coles, *J. Chem. Soc.*, **1952**, 1430 and **1950**, 2014.

7) As a review: A. J. Fatiadi, *Synthesis*, **1976**, 65 and 133.

8) I. N. Nazarov and L. N. Pinkina, *Zh. Obshch. Khim.*, **18**, 675 and 681 (1948) (*Chem. Abst.*, **43**, 116 and 117 (1949)); R. M. Jacobson and G. P. Lahm, *J. Org. Chem.*, **44**, 462 (1979); R. M. Jacobson, G. P. Lahm, and J. W. Clader, *ibid.*, **45**, 395 (1980); T. Hiyama, M. Shinoda, and H. Nozaki, *J. Am. Chem. Soc.*, **101**, 1599 (1979); F. Cooke, R. Moerck, J.

Schwindeman, and P. Magnus, *J. Org. Chem.*, **45**, 1046 (1980); L. A. Paquette, W. E. Fristad, D. S. Dime, and T. R. Bailey, *ibid.*, **45**, 3017 (1980); J. P. Marino and R. J. Linderman, *ibid.*, **46**, 3696 (1981).

9) Silicon-directed Nazarov cyclization is an exception: S. E. Denmark and T. K. Jones, *J. Am. Chem. Soc.*, **104**, 2642 (1982); T. K. Jones and S. E. Denmark, *Helv. Chim. Acta*, **66**, 2377 and 2397 (1983).

10) S. Hirano, S. Takagi, T. Hiyama, and H. Nozaki, *Bull. Chem. Soc. Jpn.*, **53**, 169 (1980).

 © 1987 The Chemical Society of Japan Bull. Chem. Soc. Jpn., 60, 335—342 (1987)

Synthesis of Arylthio-Substituted 3,8-Diphenyl-1,2-diazacycloocta-2,4,6,8-tetraenes and Their Thermolysis

Seiichi YOGI,* Kozo HOKAMA, and Otohiko TSUGE†,*
Department of Chemistry, Faculty of Science, Ryukyu University,
Nakagami-gun, Okinawa 903-01
†Research Institute of Industrial Science, Kyushu University,
Kasugakoen, Kasuga 816
(Received June 28, 1986)

Nucleophilic substitution of 4,7-dichloro-3,8-diphenyl-1,2-diazocine with arenethiols gave stable 4-arylthio-7-chloro- and/or 4,7-bis(arylthio)-1,2-diazocines. Unsymmetrical 4,7-bis(arylthio)- and 4-acetoxy-7-phenylthio-1,2-diazocines were also prepared from 4-chloro-7-phenylthio-1,2-diazocine. Thermolysis of all the diazocines afforded only arylthio-substituted pyridines with extrusion of benzonitrile.

1,2-Diazacycloocta-2,4,6,8-tetraenes (1,2-diazocines) free of benzo groups were not known until Trost et al.[1] succeeded in an elegant synthesis of the parent 1,2-diazocine (**1**), which decomposed slowly in solution at room temperature and rapidly neat. However, experiments that might have yielded substituted monocyclic 1,2-diazocines, in which compound **2** had been pyrolyzed, failed to give stable eight-membered rings, for although these probably formed, under the conditions of their preparation they seemingly valence tautomerized and extruded nitrogen, giving substituted benzene instead.[2]

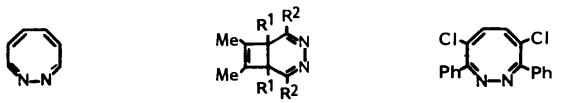

1 2 3

We have recently reported[3] a convenient method for the synthesis of 4,7-dichloro-3,8-diphenyl-1,2-diazocine (**3**), which is the first example of stable substituted monocyclic 1,2-diazocine, via a chlorination-dehydrochlorination sequence starting from readily available 3,8-diphenyl-1,2-diazacycloocta-2,8-diene,[4] and the conversion of **3** into stable mono(acyloxy)- and bis(acyloxy)-1,2-diazocines by nucleophilic substitutions of chlorine atoms on **3** with carboxylate anions. In addition, it has been found that in contrast to the parent 1,2-diazocine (**1**), which thermally decomposed to benzene and pyridine with comparable rates,[1] these stable 1,2-diazocines had been pyrolyzed to give only pyridines with the extrusion of benzonitrile: This provided a new route for the synthesis of chloro- and acyloxy-substituted pyridines which are difficult to prepare by other methods.

Nucleophilic substitutions of chlorine atoms on the 1,2-diazocine (**3**) with a carboxylate anion (Y=OCOR) can be understood by the processes as illustrated in Scheme 1. The 1,2-diazocine (**3**) is thermally isomerized into its valence isomer (**A**), which gives a mono(acyloxy)-1,2-diazocine (**D**) through the process **B**→**C**, and then the 1,2-diazocine (**D**) is similarly converted into a bis(acyloxy)-1,2-diazocine (**H**) via the processes **E**→**F**→**G**.[3]

Thus, it is indicated that a route to new 4,7-disubstituted 1,2-diazocines is opened by the reaction of 4,7-dichloro-1,2-diazocine (**3**) with various nucleophiles. In this paper we describe the synthesis of arylthio-substituted 1,2-diazocines, and their thermolysis leading to pyridines.

Results and Discussion

Synthesis of Arylthio-Substituted 1,2-Diazocines. Although the reaction of 4,7-dichloro-1,2-diazocine (**3**) with sodium benzenethiolate in benzene under reflux gave the expected 4-chloro-7-phenylthio- (**4a**) and 4,7-

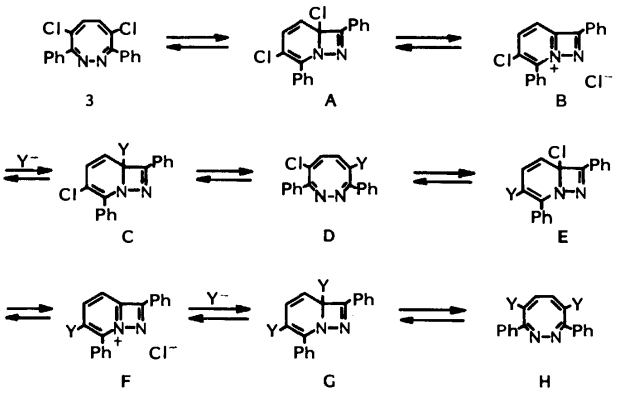

Scheme 1.

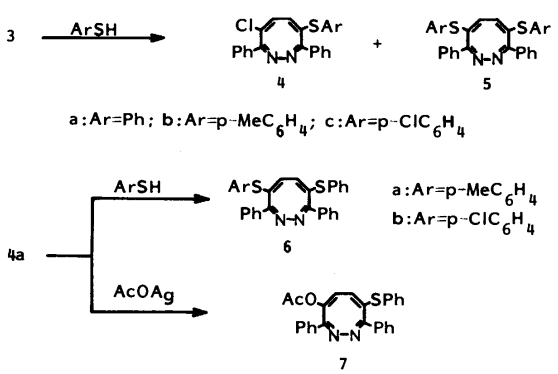

Scheme 2.

bis(phenylthio)-1,2-diazocine (**5a**), the reaction using benzenethiol in place of the thiolate brought about more satisfactory results. When heated with four equivalents of benzenethiol under similar conditions, **3** was converted into a mixture of **4a** and **5a** in good yield, whose relative yields depended upon the reaction time. Similarly, the 1,2-diazocine (**3**) reacted with *p*-methyl- and *p*-chlorobenzenethiol to give the corresponding mono(arylthio)- (**4b** and **4c**) and bis-(arylthio)-1,2-diazocines (**5b** and **5c**), respectively.[5] The results are given in Table 1.

In the reaction of mono(phenylthio)-1,2-diazocine (**4a**) with *p*-substituted benzenethiols under similar conditions, the corresponding unsymmetrical bis-(arylthio)-1,2-diazocines (**6a** and **6b**) were obtained in good yields, respectively. A longer reaction time was required for the preparation of **6a** than for **6b** (Table 1). Also, the 1,2-diazocine (**4a**) reacted with silver acetate in refluxing benzene to give 4-acetoxy-7-phenylthio-1,2-diazocine (**7**) (Scheme 2). Structural elucidation of all the 1,2-diazocines (**4**—**7**) was accomplished on the basis of spectral data.

Thermolysis of Arylthio-Substituted 1,2-Diazocines. It is evident that the mono(arylthio)- (**4**) and bis(arylthio)-1,2-diazocines (**5**) are thermally isomerized into their valence isomers, diazabicyclooctatrienes like **E** and **G** (Y=ArS), respectively (Scheme 1). Thus, in analogy with acyloxy-substituted 1,2-diazocines,[3] thermolysis of the 1,2-diazocines (**4** and **5**) can be expected to afford mono(arylthio)- and bis(arylthio)-substituted pyridines with the extrusion of benzonitrile, respectively.

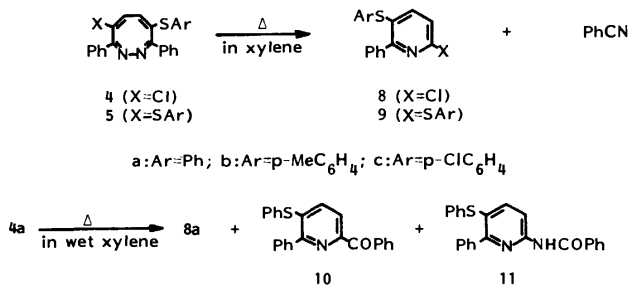

Scheme 3.

In fact, the 1,2-diazocines (**4** and **5**) decomposed in dry xylene under reflux to give the corresponding 3-arylthio-6-chloro-2-phenylpyridine (**8**) and 3,6-bis-(arylthio)-2-phenylpyridines (**9**) in good yields respectively, together with benzonitrile (Table 2). On the other hand, when heated in wet xylene under reflux for 6 h, the 1,2-diazocine (**4a**) afforded the pyridine (**8a**), 6-benzoyl-2-phenyl-3-phenylthiopyridine (**10**), and 6-benzoylamino-2-phenyl-3-phenylthiopyridine (**11**) in 12, 63, and 7% yields, respectively (Scheme 3): This is closely similar to the formation of 3,6-dichloro-2-phenyl-, 6-benzoyl-3-chloro-2-phenyl-, and 6-benzoyl-amino-3-chloro-2-phenylpyridine in the thermolysis of 4,7-dichloro-1,2-diazocine (**3**) in wet toluene.[3]

The structures of pyridines (**8**—**11**) were confirmed on the basis of spectral data as well as on the chemical conversions.

The mono(phenylthio)pyridine (**8a**) was allowed to react with sodium methoxide in methanol under reflux to give 6-methoxy-2-phenyl-3-phenylthiopyridine (**12**), which on heating with hydrobromic acid was converted into a mixture of 6-phenyl-2-pyridone (**13**)[6] and diphenyl disulfide. The pyridone (**13**) was

Table 2. Thermolysis of Arylthio-Substituted 1,2-Diazocines[a]

1,2-Diazocine	Reaction time/h	Products/%	
		Pyridine	PhCN
4a	5	**8a** 75	93
4b	6	**8b** 73	63
4c	6	**8c** 86	72
5a	6	**9a** 85	93
5b	6	**9b** 92	78
5c	6	**9c** 79	84

a) The thermolysis was carried out in dry xylene under reflux.

Table 1. Reactions of Chloro-Substituted 1,2-Diazocines with Nucleophiles[a]

Starting Diazocine (SD)	Nucleophile (Nu)	SD/Nu mol/mol	Reaction time/h	Products yield/%	Unreacted SD/%
3	PhSNa	1/3	5	**4a** 38 **5a** 17	15
3	PhSH	1/4	6	**4a** 65 **5a** 32	3
3	PhSH	1/4	18	**4a** 2 **5a** 70	2
3	*p*-MeC_6H_4SH	1/4	4	**4b** 59 **5b** 12	28
3	*p*-MeC_6H_4SH	1/4	18	**5b** 98	0
3	*p*-ClC_6H_4SH	1/3	7	**4c** 43 **5c** 34	—[b]
4a	*p*-MeC_6H_4SH	1/1.5	7	**6a** 35	41
4a	*p*-MeC_6H_4SH	1/3	24	**6a** 78	—[b]
4a	*p*-ClC_6H_4SH	1/1.5	7	**6b** 75	8
4a	MeCOOAg	1/4.8	20	**7** 61	20

a) The reactions were carried out in benzene under reflux. b) The unreacted diazocine was not isolated.

identical with an authentic sample prepared from hydrolysis of 2-acetoxy-6-phenylpyridine.[7]

Oxidations of the mono(arylthio)- (**8**) and bis(arylthio)pyridines (**9**) with potassium permanganate in acetic acid or 35% hydrogen peroxide gave the corresponding mono(arylsulfonyl) (**14**) and bis(arylsulfonyl)pyridines (**15**) in good yields, respectively. On treatment with sodium methoxide in methanol under reflux, both the pyridines (**14** and **15**) were converted into the same 3-arylsulfonyl-6-methoxy-2-phenylpyridines (**16**). When heated with hydrobromic acid, 6-methoxy-2-phenyl-3-phenylsulfonylpyridine (**16a**) was converted into 6-phenyl-5-phenylsulfonyl-2-pyridone (**17**) (Scheme 4).

On the other hand, the reaction of the benzoylpyridine (**10**) with hydroxylamine afforded a mixture of stereoisomeric oximes (**18**), which on the Beckmann rearrangement using polyphosphoric acid gave 2-phenyl-6-phenylcarbamoyl-3-phenylthiopyridine (**19**) in good yield. Hydrolysis of the pyridine (**19**) gave 6-phenyl-5-phenylthio-2-pyridinecarboxylic acid (**20**), which on heating at 230—250 °C was converted into 2-phenyl-3-phenylthiopyridine (**21**). The pyridine (**21**) was also obtained by the reduction of the pyridine (**8a**) with zinc dust in acetic acid.

Hydrolysis of the (benzoylamino)pyridine (**11**) with an ethanolic alkali solution gave 6-amino-2-phenyl-3-phenylthiopyridine (**22**), which was then converted, by diazotization, into 6-phenyl-5-phenylthio-2-pyridone (**23**). Oxidation of the pyridone (**23**) gave the phenylsulfonylpyridone (**17**).

Next, thermolysis of unsymmetrical bis(arylthio)-1,2-diazocines (**6**) was investigated. In dry xylene under reflux for 5 h, the 4-(*p*-methylphenylthio)-7-phenylthio-1,2-diazocine (**6a**) gave benzonitrile and oil, which consisted of a 1:1 mixture of 6-(*p*-methylphenylthio)-2-phenyl-3-phenylthio- (**24a**) and 3-(*p*-methylphenylthio)-2-phenyl-6-phenylthiopyridine (**25a**), in 78 and 68% yields, respectively. Although it was very difficult to isolate pure **24a** and **25a** from the mixture, the formation of **24a** and **25a** was confirmed by the conversion, via the corresponding bis(arylsulfonyl)pyridines (**26a** and **27a**),

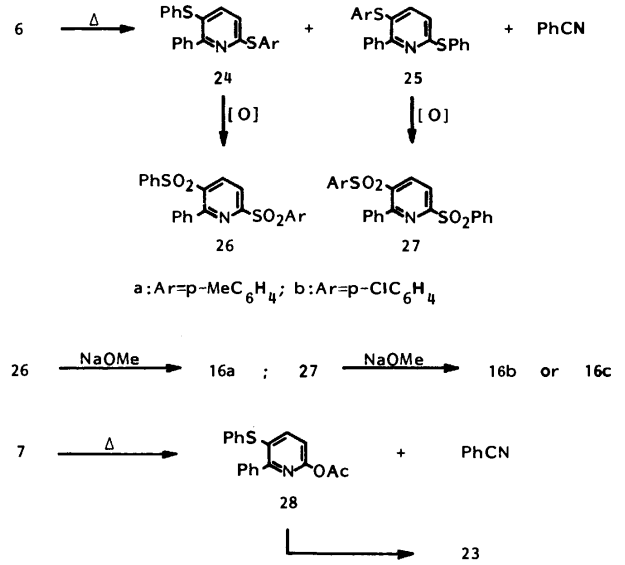

Scheme 5.

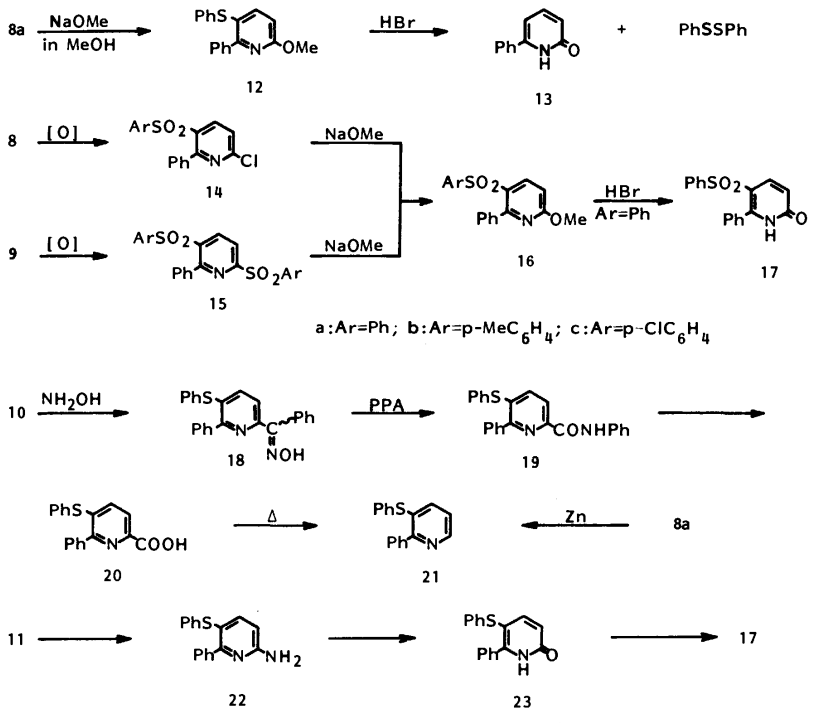

Scheme 4.

into the methoxypyridines (**17a** and **17b**), respectively.

Similarly, thermolysis of the 4-(*p*-chlorophenylthio)-7-phenylthio-1,2-diazocine (**6b**) afforded benzonitrile and a mixture of 6-(*p*-chlorophenylthio)-2-phenyl-3-phenylthio- (**24b**) and 3-(*p*-chlorophenylthio)-2-phenyl-6-phenylthiopyridine (**25b**) in 76 and 84% yields, respectively. The pyridines (**24b** and **25b**) were again converted into the methoxypyridines (**17a** and **17c**) via the corresponding bis(arylsulfonyl)pyridines (**26b** and **27b**), respectively (Scheme 5).

Thermolysis of the 4-acetoxy-7-phenylthio-1,2-diazocine (**7**) was performed under similar conditions: Benzonitrile and 6-acetoxy-2-phenyl-3-phenylthiopyridine (**28**) were obtained in 69 and 87% yields, respectively. The acetoxypyridine (**28**) was readily converted into the pyridone (**23**) on an ethanolic alkali hydrolysis.

Experimental

IR spectra were obtained on a JASCO A-302 spectrometer. ^{1}H NMR spectra were recorded on a Hitachi R-24 or a JEOL FX-100 instrument, and ^{13}C NMR spectra were measured on a JEOL FX-100 spectrometer at 25.05 MHz. Chemical shifts are expressed in parts per million downfield from tetramethylsilane. Mass spectra were taken with a Hitachi RMU-6L spectrometer at 70 eV ionization energy. Elemental analyses were performed on a Yanaco MT 2 CHN corder instrument.

Reaction of Dichloro-1,2-diazocine (3) with Sodium Benzenethiolate. A solution of benzenethiol (1.10 g, 10 mmol) in methanol (10 ml) was added to a solution of sodium methoxide in methanol, which was prepared from metallic sodium (0.3 g) and methanol (10 ml), and then the resultant mixture was concentrated in vacuo to leave sodium benzenethiolate as white powder. A solution of 1.08 g (3.3 mmol) of the dichloro-1,2-diazocine (**3**) in benzene (50 ml) was refluxed with the thiolate for 5 h. The reaction mixture was washed with water, and the benzene layer was concentrated in vacuo, and the residue was chromatographed on silica gel using benzene–hexane (3:7) as an eluent to give 0.17 g (15%) of unreacted **3**, 0.42 g (38%) of the mono(phenylthio)-1,2-diazocine (**4a**) and 0.23 g (17%) of the bis(phenylthio)-1,2-diazocine (**5a**).

4a: Mp 143—144 °C (decomp); colorless needles; ^{1}H NMR ($CDCl_3$) δ=6.17, 6.49 (each 1H, d, =CH, J=4.8 Hz), 7.10—7.50 (13H, m), 7.51—7.80 (2H, m); MS m/z 402, 400 (M^+). Found: C, 71.98; H, 4.26; N, 7.11%. Calcd for $C_{24}H_{17}N_2SCl$: C, 71.90; H, 4.27; N, 6.99%.

5a: Mp 156—157 °C; colorless needles; ^{1}H NMR ($CDCl_3$) δ=6.27 (2H, s, =CH), 7.00—7.50 (16H, m), 7.51—7.70 (4H, m); ^{13}C NMR ($CDCl_3$) δ=153.47 (s), 137.56 (s), 134.80 (s), 132.80 (s), 131.80, 129.99, 129.16, 128.34, 128.22 (each d); MS m/z 474 (M^+). Found: C, 75.80; H, 4.62; N, 6.08%. Calcd for $C_{30}H_{22}N_2S_2$: C, 75.92; H, 4.67; N, 5.90%.

Reaction of 3 with Arenethiols. i) With Benzenethiol. After a solution of **3** (0.65 g, 2 mmol) and benzenethiol (0.88 g, 8 mmol) in benzene (50 ml) was refluxed for 6 h, the reaction mixture was washed with a 10% aqueous sodium hydroxide solution, and then water. The benzene layer was concentrated in vacuo, and the residue was chromatographed (silica gel, benzene) to give 20 mg (3%) of unreacted **3**, 0.52 g (65%) of **4a** and 0.30 g (32%) of **5a**. The result of the reaction for 18 h is shown in Table 1.

ii) With *p*-Methylbenzenethiol. A solution of **3** (0.65 g, 2 mmol) in benzene (30 ml) refluxed with *p*-methylbenzenethiol (1.0 g, 8 mmol) for 4 h. Similar work-up of the reaction mixture gave 0.18 g (28%) of unreacted **3**, 0.49 g (59%) of the mono(*p*-methylphenylthio)-1,2-diazocine (**4b**), and 0.12 g (12%) of the bis(*p*-methylphenylthio)-1,2-diazocine (**5b**). The result of the reaction for 18 h is given in Table 1.

4b: Mp 131—132 °C; colorless prisms; ^{1}H NMR ($CDCl_3$) δ=2.28 (3H, s), 6.10, 6.50 (each 1H, d, =CH, J=4.2 Hz), 6.80—7.80 (14H, m); MS m/z, 416, 414 (M^+). Found: C, 72.48; H, 4.46; N, 6.70%. Calcd for $C_{25}H_{19}N_2SCl$: C, 72.36; H, 4.62; N, 6.75%.

5b: Mp 172—173 °C; colorless needles; ^{1}H NMR ($CDCl_3$) δ=2.26 (6H, s), 6.20 (2H, s, =CH), 6.80—7.80 (18H, m); MS m/z 502 (M^+). Found: C, 76.58; H, 5.26; N, 5.34%. Calcd for $C_{32}H_{26}N_2S_2$: C, 76.45; H, 5.21; N, 5.57%.

iii) With *p*-Chlorobenzenethiol. A solution of **3** (1.2 g, 3.68 mmol) in benzene (30 ml) was refluxed with *p*-chlorobenzenethiol (1.59 g, 11 mmol) for 7 h. Similar work-up gave 0.68 g (43%) of the mono(*p*-chlorophenylthio)-1,2-diazocine (**4c**) and 0.67 g (34%) of the bis(*p*-chlorophenylthio)-1,2-diazocine (**5c**).

4c: Mp 99—101 °C; colorless needles; ^{1}H NMR ($CDCl_3$) δ=6.18, 6.42 (each 1H, d, =CH, J=4.2 Hz), 7.03 (4H, s), 7.16—7.86 (10H, m); MS m/z 438, 436, 434 (M^+). Found: C, 66.39; H, 3.78; N, 6.56%. Calcd for $C_{24}H_{16}N_2SCl_2$: C, 66.21; H, 3.70; N, 6.43%.

5c: Mp 196—197 °C (decomp); yellow needles; ^{1}H NMR ($CDCl_3$) δ=6.32 (2H, s, =CH), 7.15 (8H, s), 7.20—7.70 (10H, m); MS m/z 546, 544, 542 (M^+). Found: C, 66.57; H, 3.46; N, 4.92%. Calcd for $C_{30}H_{20}N_2S_2Cl_2$: C, 66.29; H, 3.71; N, 5.15%.

4-(*p*-Methylphenylthio)-7-phenylthio-1,2-diazocine (6a). A solution of 1.0 g (2.5 mmol) of the mono(phenylthio)-1,2-diazocine (**4a**) in benzene (50 ml) was refluxed with *p*-methylbenzenethiol (1.0 g, 8.1 mmol) for 24 h. Similar work-up gave 0.95 g (78%) of the diazocine (**6a**): Mp 132—133 °C; colorless needles; ^{1}H NMR ($CDCl_3$) δ=2.22 (3H, s), 6.15, 6.24 (each 1H, d, =CH, J=4.2 Hz), 6.75—7.90 (19H, m); MS m/z 488 (M^+). Found: C, 76.02; H, 4.90; N, 5.82%. Calcd for $C_{31}H_{24}N_2S_2$: C, 76.20; H, 4.95; N, 5.73%.

The result of the reaction for 7 h is given in Table 1.

4-(*p*-Chlorophenylthio)-7-phenylthio-1,2-diazocine (6b). A solution of 0.64 g (1.6 mmol) of the diazocine (**4a**) in benzene (30 ml) was refluxed with *p*-chlorobenzenethiol (0.35 g, 2.4 mmol) for 7 h. Similar work-up afforded 50 mg (8%) of unreacted **4a** and 0.61 g (75%) of the diazocine (**6b**): Mp 129—130 °C; yellow needles; ^{1}H NMR ($CDCl_3$) δ=6.30, 6.37 (each 1H, d, =CH, J=4.2 Hz), 7.03—7.73 (19H, m); MS m/z 510, 508 (M^+). Found: C, 70.68; H, 3.94; N, 5.61%. Calcd for $C_{30}H_{21}N_2S_2Cl$: C, 70.78; H, 4.16; N, 5.50%.

4-Acetoxy-7-phenylthio-1,2-diazocine (7). A solution of 1.0 g (2.5 mmol) of the diazocine (**4a**) in benzene (50 ml) was refluxed with silver acetate (2.0 g, 12 mmol) for 20 h. The reaction mixture was filtered, and the precipitate was washed with benzene (50ml). The combined benzene solution was concentrated in vacuo, and the residue was chromatographed (silica gel, benzene) to give 0.2 g (20%) of

unreacted **4a** and 0.65 g (61%) of the diazocine (**7**): Mp 161—163 °C (decomp); colorless needles; ^{1}H NMR ($CDCl_3$) δ=1.95 (3H, s), 6.25 (2H, s, =CH), 7.20—7.90 (15H, m); MS *m/z* 425 (M^+). Found: C, 73.31; H, 4.51; N, 6.74%. Calcd for $C_{26}H_{20}N_2O_2S$: C, 73.56; H, 4.75; N, 6.60%.

Thermolysis of 4-Chloro-7-phenylthio-1,2-diazocine (4a). i) In Dry Xylene. A solution of **4a** (1.60 g, 4 mmol) in dry xylene (20 ml) was refluxed for 5 h. The reaction mixture was concentrated in vacuo, and the residue was chromatographed (silica gel, benzene) to give 0.38 g (93%) of benzonitrile and 0.89 g (75%) of 6-chloro-2-phenyl-3-phenylthiopyridine (**8a**).

8a: Oil; ^{1}H NMR ($CDCl_3$) δ=7.06, 7.53 (each 1H, d, PyH, *J*=8.0 Hz), 7.20—7.90 (10H, m); MS *m/z* 299, 297 (M^+). Found: C, 68.85; H, 4.05; N, 4.91%. Calcd for $C_{17}H_{12}NSCl$: C, 68.56; H, 4.06; N, 4.70%.

Thermolysis of 4-chloro-7-(*p*-methylphenylthio)- (**4b**) and 4-chloro-7-(*p*-chlorophenylthio)-1,2-diazocine (**4c**) under similar conditions afforded 6-chloro-3-(*p*-methylphenylthio)-2-phenyl- (**8b**) and 6-chloro-3-(*p*-chlorophenylthio)-2-phenylpyridine (**8c**) together with benzonitrile, respectively. The results are shown in Table 2.

8b: Oil; ^{1}H NMR ($CDCl_3$) δ=2.31 (3H, s), 6.98 (1H, d, PyH, *J*=8.4 Hz), 7.02—7.82 (10H, m, ArH and PyH); MS *m/z* 311 (M^+). Found: C, 69.54; H, 4.34; N, 4.65%. Calcd for $C_{18}H_{14}NSCl$: C, 69.33; H, 4.53; N, 4.49%.

8c: Oil; ^{1}H NMR ($CDCl_3$) δ=7.08 (1H, d, PyH, *J*=8.4 Hz), 7.10—7.80 (10H, m, ArH and PyH); MS *m/z* 335, 333, 331 (M^+). Found: C, 61.20; H, 3.61; N, 4.08%. Calcd for $C_{17}H_{11}NSCl_2$: C, 61.45; H, 3.34; N, 4.22%.

ii) In Wet Xylene. A solution of **4a** (1.60 g, 4 mmol) in xylene (20 ml) containing 3 drops of water was refluxed for 6 h. Similar work-up and chromatography (silica gel, benzene) of the pyrolysate gave 0.14 g (12%) of the pyridine (**8a**), 0.92 g (63%) of 6-benzoyl-2-phenyl-3-phenylthiopyridine (**10**) and 0.11 g (7%) of 6-benzoylamino-2-phenyl-3-phenylthiopyridine (**11**).

10: Mp 120—121 °C; colorless prisms; IR (KBr) 1646 cm^{-1}; ^{1}H NMR ($CDCl_3$) δ=7.21 (5H, s), 7.65, 8.23 (each 1H, d, PyH, *J*=8.2 Hz), 7.30—7.65 (8H, m), 7.80—8.02 (2H, m); MS *m/z* 367 (M^+). Found: C, 78.32; H, 4.59; N, 3.50%. Calcd for $C_{24}H_{17}NOS$: C, 78.44; H, 4.66; N, 3.81%.

11: Mp 120—121 °C; yellow prisms; IR (KBr) 3300, 3200, 1655 cm^{-1}; ^{1}H NMR ($CDCl_3$) δ=7.04—8.04 (16H, m, ArH and PyH), 8.29 (1H, d, PyH, *J*=8.4 Hz), 8.74 (1H, broad, NH); MS *m/z* 382 (M^+). Found: C, 75.14; H, 4.91; N, 7.10%. Calcd for $C_{24}H_{18}N_2OS$: C, 75.36; H, 4.74; N, 7.33%.

Thermolysis of 4,7-Bis(phenylthio)-1,2-diazocine (5a). A solution of 0.95 g (2 mmol) of the diazocine (**5a**) in dry xylene (20 ml) was refluxed for 6 h. Similar work-up and chromatography (silica gel, benzene) of the pyrolysate gave 0.19 g (93%) of benzonitrile and 0.63 g (85%) of 3,6-bis(phenylthio)-2-phenylpyridine (**9a**).

9a: Mp 77—78 °C; colorless prisms; ^{1}H NMR ($CDCl_3$) δ=6.61 (1H, d, PyH, *J*=7.2 Hz), 7.10—7.80 (16H, m, ArH and PyH); MS *m/z* 371 (M^+). Found: C, 74.40; H, 4.31; N, 3.79%. Calcd for $C_{23}H_{17}NS_2$: C, 74.35; H, 4.61; N, 3.77%.

Similar thermolysis of 4,7-bis(*p*-methylphenylthio)- (**5b**) and 4,7-bis(*p*-chlorophenylthio)-1,2-diazocine (**5c**) afforded 3,6-bis(*p*-methylphenylthio)-2-phenyl- (**9b**) and 3,6-bis(*p*-chlorophenylthio)-2-phenylpyridine (**9c**), together with benzonitrile, respectively. The results are given in Table 2.

9b: Mp 102—103 °C; colorless prisms; ^{1}H NMR ($CDCl_3$) δ=2.29, 2.45 (each 3H, s), 6.57 (1H, d, PyH, *J*=8.4 Hz), 7.02—8.03 (14H, m, ArH and PyH); MS *m/z* 399 (M^+). Found: C, 74.97; H, 5.51; N, 3.53%. Calcd for $C_{25}H_{21}NS_2$: C, 75.14; H, 5.30; N, 3.51%.

9c: Oil; ^{1}H NMR ($CDCl_3$) δ=6.67 (1H, d, PyH, *J*=8.4 Hz), 7.10—7.70 (14H, m, ArH and PyH); MS *m/z* 443, 441, 439 (M^+). Found: C, 62.81; H, 3.17; N, 3.20%. Calcd for $C_{23}H_{15}NS_2Cl_2$: C, 62.72; H, 3.43; N, 3.18%.

6-Methoxy-2-phenyl-3-phenylthiopyridine (12). In a solution of sodium methoxide in methanol, which was prepared from metallic sodium (1.0 g) in methanol (30 ml), 0.5 g (1.7 mmol) of the pyridine (**8a**) was heated under reflux for 5 h. The reaction mixture was poured into water (100 ml), and the mixture was extracted with benzene (50 ml×2). The extract was concentrated in vacuo, and the residue was chromatographed (silica gel, benzene) to give 0.41 g (82%) of the methoxypyridine (**12**): Mp 68—69 °C; colorless prisms; ^{1}H NMR ($CDCl_3$) δ=3.85 (3H, s), 6.54, 7.48 (each 1H, d, PyH, *J*=8.4 Hz), 7.13—7.38 (3H, m), 7.02 (5H, s), 7.53—7.73 (2H, m); MS *m/z* 293 (M^+). Found: C, 73.58; H, 5.02; N, 4.60%. Calcd for $C_{18}H_{15}NOS$: C, 73.69; H, 5.15; N, 4.77%.

Conversion of the Methoxypyridine (12) into 6-Phenyl-2-pyridone (13). A suspension of 0.15 g (0.5 mmol) of the pyridine (**12**) in 48% hydrobromic acid (1 ml) was heated under reflux for 4 h. To the reaction mixture was added water (10 ml), and the mixture was extracted with benzene. The benzene extract was concentrated in vacuo, and the residue was chromatographed (silica gel, benzene) to give 30 mg (27%) of diphenyl disulfide which was identical with an authentic sample. An aqueous acidic layer was alkalized with an aqueous sodium carbonate solution to precipitate 40 mg (46%) of the pyridine (**13**), mp 196—197 °C (lit,[6] mp 197 °C), which was identical with an authentic sample prepared from hydrolysis of 2-acetoxy-6-phenylpyridine.[7]

6-Chloro-2-phenyl-3-phenylsulfonylpyridine (14a). To a stirred solution of 0.3 g (1 mmol) of the phenylthiopyridine (**8a**) in acetic acid (30 ml), added slowly a 6.6% aqueous potassium permanganate solution at room temperature; when about 5 ml of the permanganate solution was added, reddish violet color of the reaction mixture did not disappear. A 10% aqueous sodium hydrogensulfite solution (10 ml) was added to the colored solution, and then the resultant clear solution was poured into water (50 ml) to give a precipitate. Filtration and recrystallization of the precipitate from petroleum ether to give 0.27 g (82%) of the phenylsulfonylpyridine (**14a**): Mp 131—133 °C; colorless needles; IR (KBr) 1320 cm^{-1}; ^{1}H NMR ($CDCl_3$) δ=7.05—7.45 (10H, m), 7.47, 8.65 (each 1H, d, PyH, *J*=8.4 Hz); ^{13}C NMR ($CDCl_3$) δ=159.75, 154.40, 139.67, 139.32, 136.44, 133.81, 129.57, 129.22, 128.52, 127.87, 127.64, 123.17; MS *m/z* 331, 329 (M^+). Found: C, 61.75; H, 3.97; N, 4.43%. Cacld for $C_{17}H_{12}NO_2SCl$: C, 61.91; H, 3.67; N, 4.25%.

Similar oxidations of *p*-methylphenylthio- (**8b**) and *p*-chlorophenylthiopyridine (**8c**) gave the corresponding arylsulfonylpyridines **14b** and **14c** in 61 and 76% yields, respectively.

14b: Mp 143—145 °C; colorless needles; IR (KBr) 1320 cm^{-1}; ^{1}H NMR ($CDCl_3$) δ=2.33 (3H, s), 6.95—7.45 (9H, m), 7.51, 8.62 (each 1H, d, PyH, *J*=8.4 Hz); MS *m/z* 345, 343 (M^+). Found: C, 62.66; H, 3.91; N, 3.78%. Calcd for

$C_{18}H_{14}NO_2SCl$: C, 62.88; H, 4.10; N, 4.07%.

14c: Mp 149—150 °C; colorless needles; IR (KBr) 1320 cm^{-1}; ^1H NMR ($CDCl_3$) δ=7.13—7.43 (9H, m), 7.55, 8.65 (each 1H, d, PyH, J=8.4 Hz); MS m/z 367, 365, 363 (M^+). Found: C, 56.27; H, 2.99; N, 3.61%. Calcd for $C_{17}H_{11}NO_2SCl_2$: C, 56.06; H, 3.04; N, 3.85%.

3,6-Bis(phenylsulfonyl)-2-phenylpyridine (15a). i) A solution of 0.50 g (1.4 mmol) of the bis(phenylthio)pyridine (**9a**) in acetic acid (30 ml) was refluxed with 35% hydrogen peroxide (5 ml) for 3 h. After it had been cooled to room temperature, water (100 ml) was added to it. The mixture was extracted with benzene (50 ml×2), and the extract was concentrated in vacuo to leave a residue which was recrystallized from petroleum ether to give 0.48 g (81%) of the pyridine (**15a**): Mp 187—189 °C; yellow needles; IR (KBr) 1320 cm^{-1}: ^1H NMR ($CDCl_3$) δ=7.20—7.72 (13H, m), 7.96—8.01 (2H, m), 8.32, 8.88 (each 1H, d, PyH, J=8.4 Hz); ^{13}C NMR ($CDCl_3$) δ=160.98, 159.75, 140.20, 139.55, 138.56, 136.33, 134.22, 133.51, 129.87, 129.39, 129.10, 128.63, 128.05, 127.52, 120.30; MS m/z 371 ($M^+ - SO_2$). Found: C, 63.51; H, 4.17; N, 3.28%. Cacld for $C_{23}H_{17}NO_4S_2$: C, 63.43; H, 3.93; N, 3.22%.

ii) A 6.6% aqueous potassium permanganate solution was slowly added, at room temperature, to a stirred solution of 0.37 g (1 mmol) of the pyridine (**9a**) in acetic acid (30 ml); when about 9 ml of the permanganate solution was added, reddish violet color of the reaction mixture did not disappear. After a 10% aqueous sodium hydrogensulfite solution (20 ml) was added to the reaction mixture, the resultant clear solution was poured into water (50 ml) to give a precipitate. Filtration and recrystallization of the precipitate from petroleum ether to give 0.28 g (64%) of the pyridine (**15a**).

Similar oxidations of the bis(*p*-methylphenylthio)- (**9b**) and bis(*p*-chlorophenylthio)pyridine (**9c**) with potassium permanganate in acetic acid gave the corresponding bis(arylsulfonyl)pyridines **15b** and **15c** in 69 and 76% yields, respectively.

15b: Mp 231—232 °C; colorless needles; IR (KBr) 1330 cm^{-1}; ^1H NMR ($CDCl_3$) δ=2.31, 2.39 (each 3H, s), 6.91—7.46 (11H, m), 7.71—8.01 (2H, m), 8.26, 8.86 (each 1H, d, PyH, J=8.4 Hz); MS m/z 399 ($M^+ - SO_2$). Found: C, 64.66; H, 4.70; N, 3.28%. Calcd for $C_{25}H_{21}NO_4S_2$: C, 64.77; H, 4.57; N, 3.02%.

15c: Mp 227—228 °C; colorless needles; IR (KBr) 1330 cm^{-1}; ^1H NMR ($CDCl_3$) δ=7.02—7.62 (11H, m), 7.82—8.02 (2H, m), 8.30, 8.88 (each 1H, d, PyH, J=8.4 Hz); MS m/z 443, 441, 439 ($M^+ - SO_2$). Found: C, 54.72; H, 2.79; N, 2.70%. Calcd for $C_{23}H_{15}NO_4S_2Cl_2$: C, 54.77; H, 3.00; N, 2.78%.

6-Methoxy-2-phenyl-3-phenylsulfonylpyridine (16a). i) In a solution of sodium methoxide in methanol, which was prepared from metallic sodium (1.0 g) in methanol (30 ml), 0.66 g (2 mmol) of the pyridine (**14a**) was refluxed for 5 h. The mixture was poured into water (100 ml), and extracted with benzene (50 ml×2). The benzene extract was concentrated in vacuo, and the residue was chromatographed (silica gel, benzene) to give 0.52 g (80%) of the pyridine (**16a**): Mp 84—85 °C; yellow prisms; IR (KBr) 1320 cm^{-1}; ^1H NMR ($CDCl_3$) δ=3.90 (3H, s), 6.84, 8.52 (each 1H, d, PyH, J=8.4 Hz), 7.10—7.50 (10H, m); MS m/z 325 (M^+). Found: C, 66.51; H, 4.89; N, 4.33%. Calcd for $C_{18}H_{15}NO_3S$: C, 66.44; H, 4.65; N, 4.31%.

ii) In a solution of sodium methoxide in methanol, which was prepared from metallic sodium (0.5 g) in methanol (30 ml), 0.40 g (0.9 mmol) of the pyridine (**15a**) was refluxed for 5 h. Similar work-up and chromatography (silica gel, benzene) of the residue gave 0.22 g (75%) of the pyridine (**16a**).

The bis(*p*-methylphenylsulfonyl)- (**15b**) and bis(*p*-chlorophenylsulfonyl)pyridine (**15c**) reacted with sodium methoxide in methanol under similar conditions to give the corresponding methoxypyridines **16b** and **16c** in 67 and 70% yields, respectively.

16b: Mp 107—108 °C; colorless prisms; IR (KBr) 1320 cm^{-1}; ^1H NMR ($CDCl_3$) δ=2.32 (3H, s), 3.92 (3H, s, OCH_3), 6.83, 8.50 (each 1H, d, PyH, J=8.4 Hz), 6.95—7.35 (9H, m); MS m/z 339 (M^+). Found: C, 67.41; H, 4.99; N, 4.34. Calcd for $C_{19}H_{17}NO_3S$: C, 67.23; H, 5.05; N, 4.13%.

16c: Mp 143—144 °C; colorless prisms; IR (KBr) 1320 cm^{-1}; ^1H NMR ($CDCl_3$) δ=3.90 (3H, s), 6.79, 8.46 (each 1H, d, PyH, J=8.4 Hz), 7.02—7.30 (9H, m); MS m/z 361, 359 (M^+). Found: C, 59.87; H, 3.79; N, 3.74%. Calcd for $C_{18}H_{14}NO_3SCl$: C, 60.08; H, 3.92; N, 3.89%.

6-Phenyl-5-phenylsulfonyl-2-pyridone (17). A suspension of 0.16 g (0.5 mmol) of the methoxypyridine (**16a**) in 48% hydrobromic acid (4 ml) was refluxed for 4 h; during which time it turned into a clear solution. When it had been cooled to room temperature, crystals separated out. The crystals were filtered and washed well with a 10% aqueous sodium carbonate solution, and recrystallized from ethyl acetate to give 60 mg (40%) of the pyridone (**17**): Mp 267—268 °C; colorless needles; IR (KBr) 2700—3100, 1660, 1650, 1300 cm^{-1}; ^1H NMR ($CDCl_3$) δ=6.41, 8.15 (each 1H, d, PyH, J=11.0 Hz), 7.10—7.50 (10H, m); MS m/z 311 (M^+). Found: C, 65.31; H, 4.00; N, 4.63%. Calcd for $C_{17}H_{13}NO_3S$: C, 65.58; H, 4.21; N, 4.50%.

Conversion of 6-Benzoyl-2-phenyl-3-phenylthiopyridine (10) into 2-Phenyl-6-phenylcarbamoyl-3-phenylthiopyridine (19). A solution of 0.49 g of the benzoylpyridine (**10**) in ethanol (30 ml) was refluxed with an aqueous hydroxylamine solution, which was prepared by the treatment of hydroxylamine hydrochloride (1.5 g) with a 7% aqueous sodium hydroxide solution (10 ml), for 2 h. The reaction mixture was poured into water (100 ml), and the resultant mixture was acidified with hydrochloric acid, and then extracted with chloroform (50 ml×2). The chloroform extract was concentrated in vacuo, and the residue was chromatographed (silica gel, chloroform) to give 0.27 g (54%) of a mixture of isomeric oximes (**18**). Without further purification, a mixture of oximes (**18**) was used for the Beckmann rearrangement: 0.3 g (0.8 mmol) of the oximes (**18**) was heated with polyphosphoric acid (3 ml) at 90—100 °C for 2 h. The mixture was poured into water (50 ml), and extracted with chloroform (30 ml×2). The extract was concentrated in vacuo, and the residue was chromatographed (silica gel, benzene) to give 0.24 g (88%) of the phenylcarbamoylpyridine (**19**).

19: Mp 145—146 °C; yellow prisms; IR (KBr) 3250, 1735 cm^{-1}; ^1H NMR ($CDCl_3$) δ=7.33, 7.90 (each 1H, d, PyH, J=8.4 Hz), 7.41—7.70 (15H, m), 8.93 (1H, broad, NH); MS m/z 382 (M^+). Found: C, 75.49; H, 4.65; N, 7.12%. Calcd for $C_{24}H_{18}N_2OS$: C, 75.36; H, 4.74; N, 7.33%.

2-Phenyl-3-phenylthiopyridine (21). i) From the Phenylcarbamoylpyridine (19). A suspension of 0.3 g (0.8 mmol)

of the pyridine (**19**) in an ethanolic potassium hydroxide solution, which was prepared from potassium hydroxide (0.5 g) in ethanol (20 ml), was refluxed for 3 h. The mixture was poured into water (20 ml) and extracted with benzene (20 ml×2). The aqueous layer was acidified with hydrochloric acid, and extracted with chloroform (30 ml×2). The chloroform extract was concentrated in vacuo to give 0.15 g (61%) of 6-phenyl-5-phenylthio-2-pyridinecarboxylic acid (**20**). After 0.2 g of the carboxylic acid (**20**) was heated at 230—250 °C for 15 min, the product was purified by chromatography (silica gel, benzene) to give 60 mg (35%) of the pyridine (**21**).

20: Mp 141—142 °C; colorless prisms; IR (KBr) 2800—3050, 1700 cm^{-1}; MS *m/z* 307 (M^+). Found: C, 70.51; H, 4.33; N, 4.44%. Calcd for $C_{18}H_{13}NO_2S$: C, 70.33; H, 4.26; N, 4.56%.

21: Oil; ^1H NMR ($CDCl_3$) δ=7.01 (1H, dd, PyH(β), J=4.8, 8.0 Hz), 7.39 (1H, dd, PyH(γ), J=1.2, 8.0 Hz), 7.20—7.55 (8H, m), 7.55—7.80 (2H, m), 8.45 (1H, dd, PyH(α), J=1.2, 4.8 Hz); MS *m/z* 263 (M^+). Found: C, 77.80; H, 4.68; N, 5.26%. Calcd for $C_{17}H_{13}NS$: C, 77.53; H, 4.98; N, 5.32%.

ii) From 6-Chloro-2-phenyl-3-phenylthiopyridine (8a). A solution of 0.23 g (0.8 mmol) of the chloropyridine (**8a**) in acetic acid (20 ml) was refluxed with zinc dust (1.5 g) for 8 h. The hot reaction mixture was filtered and the precipitate was washed with benzene (30 ml). The filtrate was poured into water (100 ml), and the resultant mixture was extracted with benzene (50 ml). The benzene extract was concentrated in vacuo and the residue was chromatographed (silica gel, benzene) to give 0.1 g (49%) of the pyridine (**21**).

6-Amino-2-phenyl-3-phenylthiopyridine (22). In a 10% ethanolic potassium hydroxide solution (20 ml) was heated 0.1 g of the (benzoylamino)pyridine (**11**) under reflux for 4 h. After the reaction mixture was concentrated in vacuo, the residue was triturated with water (10 ml), and then extracted with chloroform (30 ml). The extract was concentrated in vacuo, and the residue was chromatographed (silica gel, chloroform) to give 30 mg (41%) of the aminopyridine (**22**): Mp 177—178 °C; yellow needles; IR (KBr) 3460, 3300, 2950, 1635 cm^{-1}; ^1H NMR ($CDCl_3$) δ=4.66 (2H, broad, NH_2). 6.41, 7.52 (each 1H, d, PyH, J=8.4 Hz), 6.96—7.56 (10H, m); MS *m/z* 278 (M^+). Found: C, 73.20; H, 4.79; N, 9.80%. Cacld for $C_{17}H_{14}N_2S$: C, 73.35; H, 5.07; N, 10.06%.

6-Phenyl-5-phenylthio-2-pyridone (23). After diazotization of 0.1 g of the aminopyridine (**22**) with sodium nitrite (50 mg) in aqueous sulfuric acid (conc sulfuric acid (1 ml) and water (10 ml)) was carried out at 0—5 °C, the reaction mixture was heated at 50—60 °C for 1 h. Water (10 ml) was added to the mixture and the mixture was extracted with chloroform (20 ml×2). The extract was concentrated in vacuo, and the residue was chromatographed (silica gel, chloroform) to give 30 mg (30%) of the pyridone (**23**): Mp 206—208 °C; colorless needles; IR (KBr) 2700—3100, 1640 cm^{-1}; ^1H NMR ($CDCl_3$) δ=6.43 (1H, d, PyH, J=9.0 Hz), 7.00—7.60 (11H, m, ArH and PyH); MS *m/z* 279 (M^+). Found: C, 73.29; H, 4.41; N, 5.26%. Calcd for $C_{17}H_{13}NOS$: C, 73.10; H, 4.69; N, 5.01%.

Oxidation of the Pyridone (23). A solution of 0.1 g of the pyridone (**23**) in acetic acid (20 ml) was heated with 35% hydrogen peroxide (2 ml) under reflux for 3 h. The reaction mixture was concentrated in vacuo, and the residue was chromatographed (silica gel, chloroform–ethyl acetate (7:3)) to give 50 mg (45%) of the phenylsulfonylpyridone (**17**).

Thermolysis of the 4-(*p*-Methylphenylthio)-7-phenylthio-1,2-diazocine (6a). A solution of 0.73 g (1.5 mmol) of the 1,2-diazocine (**6a**) in dry xylene (20 ml) was refluxed for 5 h. The mixture was concentrated in vacuo, and the residue was chromatographed (silica gel, benzene) to give 0.12 g (78%) of benzonitrile and 0.39 g (63%) of a mixture of 6-(*p*-methylphenylthio)-2-phenyl-3-phenylthio- (**24a**) and 3-(*p*-methylphenylthio)-2-phenyl-6-phenylthiopyridine (**25a**) whose ratio was found to be 1:1 on the basis of ^1H NMR spectrum (δ=2.28, 2.34 (each s, CH_3)). It was very difficult to isolate pure **24a** and **25a** from the mixture.

Oxidation of the Mixture of 24a and 25a. A 6.6% aqueous potassium permanganate solution was slowly added, at room temperature, to a stirred solution of 0.17 g (0.4 mmol) of the mixture of **24a** and **25a** in acetic acid (30 ml); when about 6 ml of the permanganate solution was added, reddish violet color of the reaction mixture did not disappear. After a 10% aqueous sodium hydrogensulfite solution (12 ml) was added to the reaction mixture, the resultant clear solution was poured into water (50 ml) to give 0.14 g (71%) of a 1:1 mixture of 6-(*p*-methylphenylsulfonyl)-2-phenyl-3-phenylsulfonyl- (**26a**) and 3-(*p*-methylphenylsulfonyl)-2-phenyl-6-phenylsulfonylpyridine (**27a**): Mp 171—176 °C; ^1H NMR ($CDCl_3$) δ=2.29, 2.37 (each s, CH_3, relative intensity 1:1). Again it was very difficult to isolate pure **26a** and **27a** from the mixture.

Conversion of the Mixture of 26a and 27a into the Methoxypyridines 16a and 16b. In a solution of sodium methoxide in methanol, which was prepared from metallic sodium (0.5 g) in methanol (30 ml), 0.14 g (0.3 mmol) of the mixture of **26a** and **27a** was heated under reflux for 5 h. The reaction mixture was poured into water (50 ml), and the mixture was extracted with benzene (50 ml×2). The extract was concentrated in vacuo, and the residue was chromatographed (silica gel, benzene) to give 30 mg (30%) of 6-methoxy-2-phenyl-3-phenylsulfonylpyridine (**16a**) and 40 mg (36%) of 6-methoxy-3-(*p*-methylphenylsulfonyl)-2-phenylpyridine (**16b**), respectively.

Thermolysis of 4-(*p*-Chlorophenylthio)-7-phenylthio-1,2-diazocine (6b). A solution of 0.69 g (1.4 mmol) of the 1,2-diazocine (**6b**) in dry xylene (20 ml) was refluxed for 5 h. Similar work-up and chromatography (silica gel, benzene) of the residue gave 0.13 g (76%) of benzonitrile and 0.46 g (84%) of a mixture of 6-(*p*-chlorophenylthio)-2-phenyl-3-phenylthio- (**24b**) and 3-(*p*-chlorophenylthio)-2-phenyl-6-phenylthiopyridine (**25b**). Since it was very difficult to isolate pure **24b** and **25b**, the mixture was subjected to oxidation. A similar oxidation of 0.27 g of the mixture of **24b** and **25b** with potassium permanganate in acetic acid gave 0.14 g (45%) of 6-(*p*-chlorophenylsulfonyl)-2-phenyl-3-phenylsulfonylpyridine (**26b**) and 70 mg (23%) of 3-(*p*-chlorophenylsulfonyl)-2-phenyl-6-phenylsulfonylpyridine (**27b**), respectively.

26b: Mp 183—185 °C; colorless needles; IR (KBr) 1325 cm^{-1}; ^1H NMR ($CDCl_3$) δ=7.00—7.60 (6H, m), 7.80—8.10 (2H, m), 8.29, 8.86 (each 1H, d, PyH, J=8.4 Hz); MS *m/z* 407, 405 (M^+-SO_2). Found: C, 58.82; H, 3.58; N, 3.10%. Calcd for $C_{23}H_{16}NO_4S_2Cl$: C, 58.78; H, 3.43; N, 2.98%.

The sulfonylpyridines **26b** and **27b** reacted with sodium methoxide in methanol to give the methoxypyridines **16a** and **16c**, respectively.

Thermolysis of the 4-Acetoxy-7-phenylthio-1,2-diazocine

(**7**). A solution of 1.0 g (2.4 mmol) of the 1,2-diazocine (**7**) in dry xylene (20 ml) was refluxed for 5 h. Similar work-up and chromatography (silica gel, benzene) of the residue gave 0.17 g (69%) of benzonitrile and 0.66 g (87%) of 6-acetoxy-2-phenyl-3-phenylthiopyridine (**28**).

28: Oil; IR (neat) 1760 cm^{-1}; ^1H NMR ($CDCl_3$) δ=2.30 (3H, s), 6.87, 7.45 (each 1H, d, PyH, J=7.8 Hz), 7.20—7.70 (10H, m); MS m/z 321 (M^+). Found: C, 71.23; H, 4.66; N, 4.23%. Calcd for $C_{19}H_{15}NO_2S$: C, 71.00; H, 4.70; N, 4.36%.

Hydrolysis of the Acetoxypyridine (28) to the Pyridone (23). A solution of 0.5 g (1.6 mmol) of the pyridine (**28**) in an ethanolic alkali solution (sodium hydrogencarbonate (1.0 g) in ethanol (50 ml)) was refluxed for 4 h. After the mixture was concentrated in vacuo, the residue was triturated with water (30 ml), and extracted with chloroform (30 ml×2). The extract was concentrated in vacuo, and the residue was chromatographed (silica gel, chloroform) to give 0.27 g (62%) of the pyridone (**23**).

References

1) B. M. Trost and R. M. Cory, *J. Am. Chem. Soc.*, **93**, 5573 (1971); B. M. Trost, P. H. Schudder, R. M. Cory, N. J. Turro, V. Ramamurthy, and T. J. Katz, *J. Org. Chem.*, **44**, 1264 (1979).

2) G. Maier, V. Heep, M. Wießler, and Straßer, *Chem. Ber.*, **102**, 1928 (1969).

3) S. Yogi, K. Hokama, and O. Tsuge, *Chem. Lett.*, **1982**, 1579; S. Yogi, K. Hokama, K. Ueno, and O. Tsuge, *Bull. Chem. Soc. Jpn.*, **59**, 1087 (1986).

4) C. G. Overberger and I. Tashlick, *J. Am. Chem. Soc.*, **81**, 217 (1959).

5) The reaction of the diazocine (**3**) with alkanethiols gave also the corresponding mono(alkylthio)- and bis-(alkylthio)-1,2-diazocines: The results will be reported elsewhere.

6) A. Dornow and E. Neuse, *Chem. Ber.*, **84**, 296 (1951).

7) Bruce E. Witzel, Conrad P. Dorn, and Tsung-Ying Shen, Ger. Offen., 1810822 (*Chem. Abstr.*, **71**, 124270y (1969)).

 © 1987 The Chemical Society of Japan Bull. Chem. Soc. Jpn., 60, 343—347 (1987)

Preparation of Arylsulfonyl-Substituted 3,8-Diphenyl-1,2-diazacycloocta-2,4,6,8-tetraenes and Their Thermolysis

Seiichi Yogi,* Kozo Hokama, and Otohiko Tsuge†,*
Department of Chemistry, Faculty of Science, Ryukyu University,
Nakagami-gun, Okinawa 903-01
†Research Institute of Industrial Science, Kyushu University,
Kasugakoen, Kasuga 816
(Received July 24, 1986)

Nucleophilic substitution of 4,7-dichloro-3,8-diphenyl-1,2-diazocine with benzenesulfinate gave stable 7-chloro-4-phenylsulfonyl- and 4,7-bis(phenylsulfonyl)-1,2-diazocine. The 4-mono(arylsulfonyl)- and 4,7-bis-(arylsulfonyl)-1,2-diazocines were obtained by oxidation of the corresponding mono(arylthio)- and bis(arylthio)-1,2-diazocines, respectively. 4-Phenylsulfonyl-7-phenylthio-1,2-diazocine was also prepared. Thermolysis of all the diazocines gave only pyridine derivatives, and the feature of the thermolysis was also described.

Although Trost et al.[1] succeeded in an elegant synthesis of 1,2-diazacycloocta-2,4,6,8-tetraene, the parent 1,2-diazocine, substituted monocyclic 1,2-diazocines were not known until we reported the synthesis of stable 4,7-disubstituted 3,8-diphenyl-1,2-diazocines: 4,7-Dichloro-3,8-diphenyl-1,2-diazocine (**1**),[2] which can be readily obtained through a chlorination–dehydrochlorination sequence starting from 3,8-diphenyl-1,2-diazacycloocta-2,8-diene,[3] reacted with nucleophiles such as carboxylate anions[2] and arenethiols[4] to give the corresponding 4-substituted and 4,7-disubstituted 1,2-diazocines. In addition, it has been found that in contrast to the parent 1,2-diazocine, which decomposed slowly in solution at room temperature and rapidly neat to benzene and pyridine with comparable rates,[1] thermolysis of these stable 1,2-diazocines in refluxing toluene or xylene gave only pyridines with the extrusion of benzonitrile. This provided a new route for the synthesis of 3,6-disubstituted 2-phenylpyridines.

In order to obtain further information on thermal behavior of stable 1,2-diazocines, we have investigated the preparation of 1,2-diazocines bearing electron-withdrawing arenesulfonyl groups in place of electron-donating groups such as acyloxy[2] and arylthio groups,[4] and their thermolysis.

Results and Discussion

Preparation of Arylsulfonyl-Substituted 1,2-Diazocines. As expected, the dichloro-1,2-diazocine (**1**) reacted with two equivalents of silver benzenesulfinate in benzene under reflux for 6 h to give 7-chloro-3,8-diphenyl-4-phenylsulfonyl- (**2a**) and 4,7-bis(phenylsulfonyl)-3,8-diphenyl-1,2-diazocine (**3a**) in 83 and 3% yields, respectively. It has been found, however, that oxidations of the 4-arylthio-7-chloro- (**4a—c**)[4] and 4,7-bis(arylthio)-1,2-diazocines (**5a—e**)[4] with potassium permanganate or hydrogen peroxide in acetic acid afforded the corresponding mono(arylsulfonyl)-, **2a—c**, and bis(arylsulfonyl)-1,2-diazocines, **3a—e**, in fairly good yields, respectively (Scheme 1).

On the other hand, 3,8-diphenyl-4-phenylsulfonyl-7-phenylthio-1,2-diazocine (**6**) was obtained from the reaction of the mono(phenylsulfonyl)-1,2-diazocine (**2a**) with benzenethiol or the reaction of the mono(phenylthio)-1,2-diazocine (**4a**) with lead benzenesulfinate in benzene under reflux, respectively.

Structural elucidation of all the 1,2-diazocines, **2**, **3**, and **6**, was accomplished on the basis of spectral data.

Thermolysis of Arylsulfonyl-Substituted 1,2-Diazocines. We have first investigated the thermolysis of the mono(arylsulfonyl)-1,2-diazocines (**2**). When a solution of the phenylsulfonyl-1,2-diazocine (**2a**) in dry xylene was heated under reflux for 5 h, three pyridines, 3-chloro-2-phenyl-6-phenylsulfonyl- (**7a**), 6-benzoyl-2-phenyl-3-phenylsulfonyl- (**8a**), and 6-benzoyl-3-chloro-2-phenylpyridine (**9**) were isolated together with benzonitrile in small amounts.

Thermolysis of the (*p*-tolylsulfonyl)- (**2b**) and (*p*-chlorophenylsulfonyl)-1,2-diazocine (**2c**) under simi-

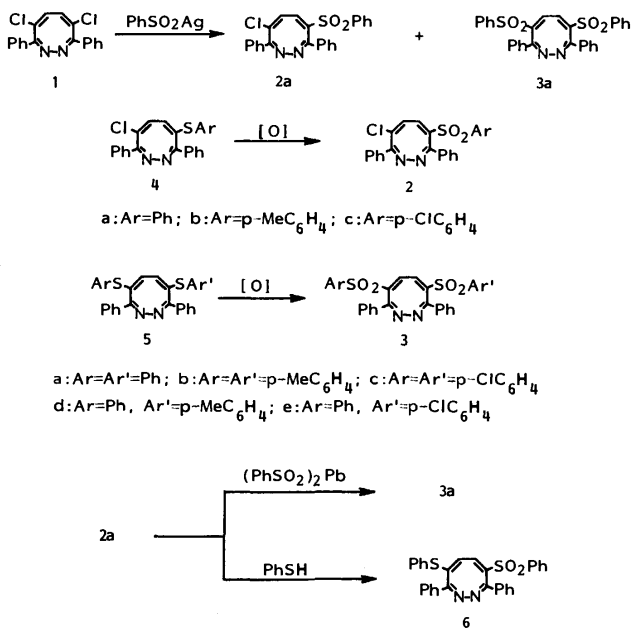

Scheme 1.

lar conditions gave the corresponding 6-arylsulfonyl-3-chloro-2-phenyl- (**7b** and **7c**), 3-arylsulfonyl-6-benzoyl-2-phenylpyridines (**8b** and **8c**) and the pyridine **9**, accompanied by trace amounts of benzonitrile, respectively (Scheme 2).

The structures of the pyridines, **7** and **8**, were confirmed on the basis of spectral data. In addition, the reaction of the pyridines, **7a—c**, with sodium methoxide in methanol afforded the same product, 3-chloro-6-methoxy-2-phenylpyridine (**10**), which was identical with an authentic sample prepared from 3,6-dichloro-2-phenylpyridine (**11**).[2] The pyridine **8a** was also obtained by the oxidation of 6-benzoyl-2-phenyl-3-phenylthiopyridine (**12**).[4] The pyridine **9** was identical with the product obtained from the thermolysis of the dichloro-1,2-diazocine (**1**) in wet toluene under reflux.[2]

As reported previously,[2,4] 4,7-disubstituted 3,8-diphenyl-1,2-diazocines are thermally isomerized into their valence isomers, diazabicyclooctatrienes. In the case of unsymmetrically 4,7-disubstituted 1,2-diazocines **A**, two valence isomers, **B-1** and **B-2**, are possible. 4-Acyloxy-7-chloro-[2] and 4-arylthio-7-chloro-1,2-diazocines[4] are exclusivly isomerized into their valence isomers **B-1** (X=OCOR and SAr), which decomposed into the corresponding 6-chloropyridines **C-1** (X=OCOR and SAr) with the extrusion of benzonitrile, respectively (Scheme 3).

As illustrated in Scheme 2, however, the mode of decomposition of the arylsulfonyl-substituted 1,2-diazocines (**2**) is somewhat different from those of the acyloxy- and arylthio-substituted 1,2-diazocines. The 1,2-diazocines **2** seem to be preferentially isomerized into **B-2** (X=SO_2Ar) rather than **B-1** (X=SO_2Ar). It is evident that the pyridines, **7** and **9**, are derived from the **B-2**: The extrusion of benzonitrile from the **B-2** gives the pyridines **7**, and the pyridine **9** corresponds to the hydrolytic compounds **F-2** (X=SO_2Ar) of the imidoylpyridines **E-2** (X=SO_2Ar) arising from ring opening of the azonia intermediates **D-2** (X=SO_2Ar).[5]

In analogy with the formation of **9**, the pyridines **8** form via the processes, **B-1**→**D-1**→**E-1**→**F-1** (each X=SO_2Ar) (Scheme 3). Taking into account the formation of the pyridines, **8** and **9**, it should be emphasized that the arenesulfonyl group suppresses the extrusion of benzonitrile from the valence isomers, **B-1** and **B-2**, respectively.

Next, the thermolysis of the bis(arylsulfonyl)-1,2-diazocines (**3**) was carried out under similar conditions. The symmetrical bis(arylsulfonyl)-1,2-diazocines (**3a—c**) gave the corresponding 3-arylsulfonyl-6-benzoyl-2-phenylpyridines (**8a—c**) as the main products, together with small amounts of the corresponding 3,6-bis(arylsulfonyl)-2-phenylpyridines (**13a—c**),[4] respectively (Scheme 4). In the thermolysis of the unsymmetrical bis(arylsulfonyl)-1,2-diazocine (**3d** or **3e**), two 3-arylsulfonyl-6-benzoyl-2-phenylpyridines (**8a** and **8b**) or (**8a** and **8c**) were obtained together with trace amounts of a mixture of the corresponding 6-arylsulfonyl-2-phenyl-3-phenylsulfonyl- (**14**) and 3-arylsulfonyl-2-phenyl-6-phenylsulfonylpyridine (**15**), respectively.

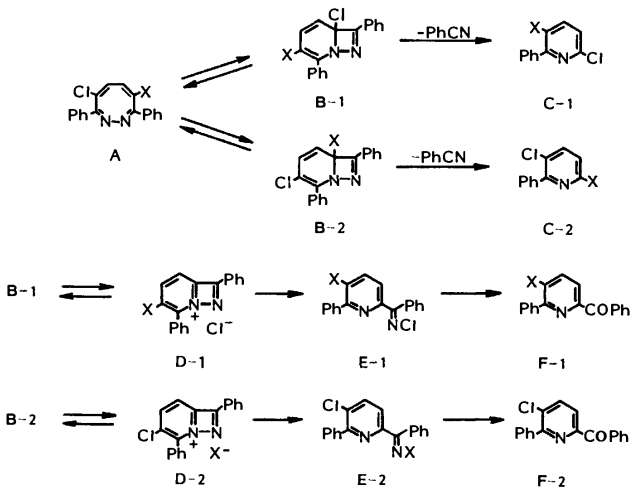

Scheme 3.

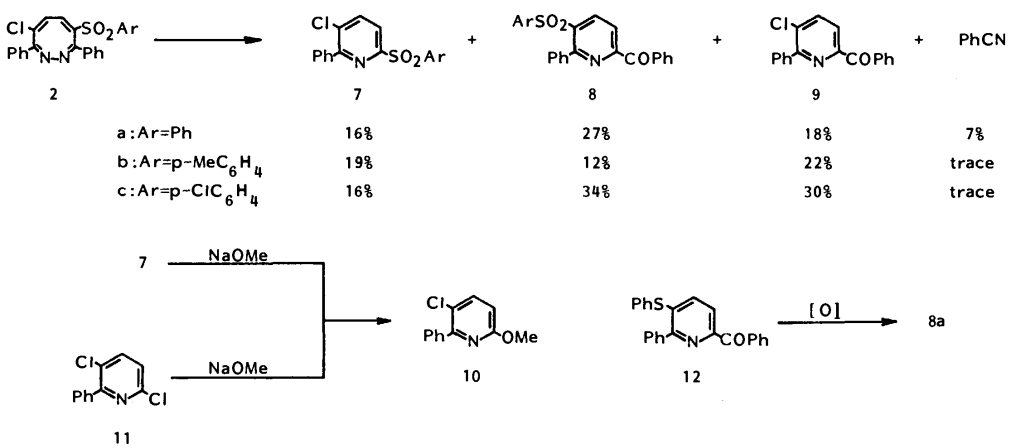

Scheme 2.

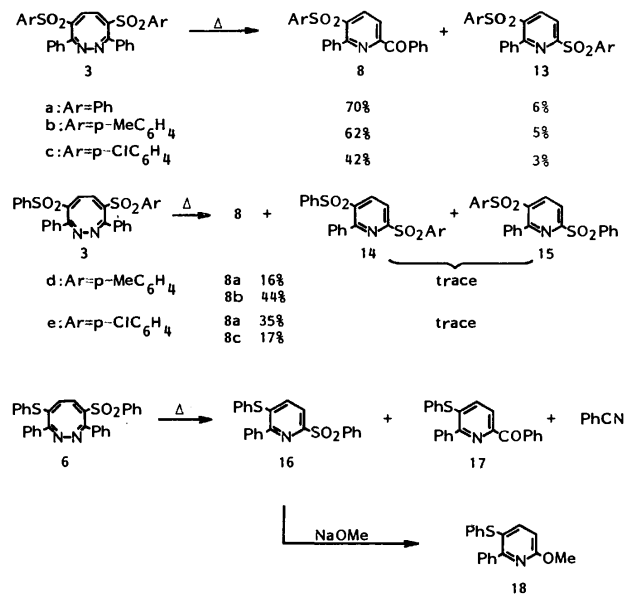

Scheme 4.

When the 4-phenylsulfonyl-7-phenylthio-1,2-diazocine (**6**) was pyrolyzed under similar conditions, 2-phenyl-6-phenylsulfonyl-3-phenylthio- (**16**) and 6-benzoyl-2-phenyl-3-phenylthiopyridine (**17**)[4] were obtained together with benzonitrile. The pyridine **16** was converted into 6-methoxy-2-phenyl-3-phenylthiopyridine (**18**)[4] (Scheme 4).

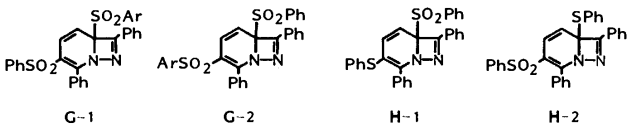

On the basis of the results shown in Scheme 4, it is clear that the unsymmetrical bis(arylsulfonyl)-1,2-diazocines (**3d** and **3e**) decomposed via two possible valence isomers, **G-1** and **G-2**. However, the decomposition of **3d** occurs somewhat more preferentially via **G-2** than **G-1**, and the reverse in **3e**. On the other hand, the 1,2-diazocine **6** exclusively decomposes via **H-1**, but not **H-2**.

Experimental

IR spectra were obtained on a JASCO A-302 spectrometer. ^{1}H NMR spectra were recorded on a Hitachi R-24 or a JEOL FX-100 instrument, and ^{13}C NMR spectra were measured on a JEOL FX-100 spectrometer at 25.05 MHz. Chemical shifts are expressed in parts per million downfield from tetramethylsilane. Mass spectra were taken with a Hitachi RMU-6L spectrometer at 70 eV ionization energy. Elementary analyses were performed on a Yanaco MT 2 CHN corder instrument.

Reaction of the Dichloro-1,2-diazocine (1) with Silver Benzenesulfinate. A solution of the diazocine **1**[2] (1.3 g, 4mmol) in benzene (50 ml) was refluxed with silver benzenesulfinate (2.0 g, 8 mmol) for 6 h. The reaction mixture was filtered, and the precipitate was washed with benzene (50 ml). The combined benzene solution was concentrated in vacuo, and the residue was chromatographed on silica gel to give 1.42 g (83%) of the mono(phenylsulfonyl)-1,2-diazocine (**2a**) (from benzene elution) and 60 mg (3%) of the bis(phenylsulfonyl)-1,2-diazocine (**3a**).

2a: Mp 180—181 °C (decomp); colorless needles; IR (KBr) *1320 cm^{-1}*; ^{1}H NMR (CDCl$_3$) *δ=6.60 (1H, d, =CH, J=4.2 Hz)*, 7.20—7.80 (16H, m, =CH and ArH); ^{13}C NMR (CDCl$_3$) δ=149.29, 148.36, 142.61, 141.61, 139.90, 133.86, 132.21 (each s), 131.22, 130.63, 130.16, 128.58, 128.39, 128.11, 127.69; MS *m/z* 434, 432 (M$^+$). Found: C, 66.58; H, 3.87; N, 6.38%. Calcd for $C_{24}H_{17}N_2O_2SCl$: C, 66.58; H, 3.96; N, 6.47%.

3a: Mp 227—229 °C (decomp); colorless needles; IR (KBr) 1320 cm^{-1}; ^{1}H NMR (CDCl$_3$) δ=7.75 (2H, s, =CH), 7.40—7.70 (20H, m); MS *m/z* 538 (M$^+$). Found: C, 66.83; H, 4.05; N, 5.42%. Calcd for $C_{30}H_{22}N_2O_4S_2$: C, 66.89; H, 4.12; N, 5.20%.

Oxidation of the 4-Arylthio-7-chloro-1,2-diazocines (4). Typical run is illustrated for the phenylthiodiazocine **4a**.

i) With Hydrogen Peroxide: A solution of 0.8 g (2 mmol) of **4a**[4] in acetic acid (30 ml) was refluxed with 35% hydrogen peroxide (10 ml) for 1.5 h. The reaction mixture was poured into water (50 ml) to precipitate solid, which on recrystallization from benzene gave 0.52 g (60%) of the mono(phenylsulfonyl)-1,2-diazocine (**2a**).

ii) With Potassium Permanganate. A 6.6% aqueous potassium permanganate solution was slowly added, at room temperature, to a stirred solution of 0.8 g (2 mmol) of **4a** in acetic acid (40 ml); when about 8 ml of the permanganate solution was added, reddish violet color of the reaction mixture did not disappear. After a 10% aqueous sodium hydrogensulfite solution (18 ml) was added to the reaction mixture, the resultant clear solution was poured into water (50 ml) to give 0.5 g (58%) of **2a**.

Similar oxidations of the 4-chloro-7-(*p*-methylphenylthio)- (**4b**)[4] and 4-chloro-7-(*p*-chlorophenylthio)-1,2-diazocine (**4c**)[4] with potassium permanganate in acetic acid gave the corresponding mono(arylsulfonyl)-1,2-diazocines **2b** and **2c** in 50 and 58% yields, respectively.

2b: Mp 186—188 °C (decomp); colorless needles; IR (KBr) 1320 cm^{-1}; ^{1}H NMR (CDCl$_3$) δ=2.32 (3H, s), 6.67 (1H, d, =CH, *J*=4.2 Hz), 6.98—7.80 (15H, m, =CH and ArH); MS *m/z* 449, 446 (M$^+$). Found: C, 67.29; H, 4.01; N, 6.16%. Calcd for $C_{25}H_{19}N_2O_2SCl$: C, 67.18; H, 4.29; N, 6.27%.

2c: Mp 177—179 °C (decomp); colorless needles; IR (KBr) 1330 cm^{-1}; ^{1}H NMR (CDCl$_3$) δ=6.64 (1H, d, =CH, *J*=4.2 Hz), 7.01—7.71 (15H, m, =CH and ArH); MS *m/z* 470, 468, 466 (M$^+$). Found: C, 61.80; H, 3.61; N, 5.76%. Calcd for $C_{24}H_{16}N_2O_2SCl_2$: C, 61.67; H, 3.45; N, 5.99%.

Oxidation of the 4,7-Bis(arylthio)-1,2-diazocines (5). Typical run is illustrated for the bis(phenylthio)diazocine **5a**.

i) With Hydrogen Peroxide. A solution of 0.95 g (2 mmol) of **5a**[4] in acetic acid (30 ml) was refluxed with 35% hydrogen peroxide (10 ml) for 1.5 h. The reaction mixture was poured into water (50 ml) to precipitate solid, which on recrystallization from petroleum ether gave 0.68 g (63%) of the bis(phenylsulfonyl)-1,2-diazocine (**3a**).

ii) With Potassium Permanganate. To a stirred solution of **5a** (0.5 g, 1 mmol) in acetic acid (40 ml), a 6.6%

aqueous potassium permanganate solution was slowly added at room temperature; when about 9 ml of the permanganate solution was added, reddish violet color of the reaction mixture did not disappear. After a 10% aqueous sodium hydrogensulfite solution (20 ml) was added to the reaction mixture, the resultant clear solution was poured into water (50 ml) to give 0.41 g (76%) of **3a**.

Similar oxidations of the bis(*p*-methylphenylthio)- (**5b**)[4] and bis(*p*-chlorophenylthio)-1,2-diazocine (**5c**)[4] with potas sium permanganate in acetic acid gave the bis(*p*-tolylsulfonyl)- (**3b**) and bis(*p*-chlorophenylsulfonyl)-1,2-diazocine (**3c**) in 62 and 53% yields, respectively.

3b: Mp 245—247 °C (decomp); colorless needles; IR (KBr) 1320 cm^{-1}; MS *m/z* 566 (M^+). Found: C, 68.15; H, 4.50; N, 4.91%. Calcd for $C_{32}H_{26}N_2O_4S_2$: C, 67.82; H, 4.62; N, 4.94%.

3c: Mp 173—174 °C (decomp); colorless needles; IR (KBr) 1330 cm^{-1}; ^1H NMR ($CDCl_3$) δ=7.64 (2H, s, =CH), 7.02—7.57 (18H, m); MS *m/z* 610, 608, 606 (M^+). Found: C, 59.53; H, 3.11; N, 4.86%. Calcd for $C_{30}H_{20}N_2O_4S_2Cl_2$: C, 59.31; H, 3.32; N, 4.61%.

4-Phenylsulfonyl-7-phenylthio-1,2-diazocine (6). i) A solution of 0.58 g (1.3 mmol) of the mono(phenylsulfonyl)-1,2-diazocine (**2a**) in benzene (30 ml) was refluxed with 0.33 g (3 mmol) of benzenethiol for 4 h. After the reaction mixture was washed with a 10% aqueous sodium hydroxide solution and then water, the benzene solution was concentrated in vacuo to leave the residue. Chromatography (silica gel, benzene) of the residue gave 0.45 g (78%) of unreacted **2a** and 0.14 g(21%) of the 1,2-diazocine **6**.

ii) A solution of 0.8 g (2 mmol) of the phenylthiodiazocine **4a** in benzene (50 ml) was heated with 1.0 g (2 mmol) of lead benzenesulfinate under reflux for 18 h. The reaction mixture was filtered, and the precipitate was washed with benzene (30 ml). The combined benzene solution was concentrated in vacuo, and chromatography (silica gel, benzene) of the residue afforded 0.17 g (21%) of unreacted **4a** and 0.52 g (51%) of **6**.

6: Mp 203—204 °C (decomp); colorless needles; IR (KBr) 1320 cm^{-1}; ^1H NMR ($CDCl_3$) δ=6.20 (1H, d, =CH, *J*=4.2 Hz), 7.01—7.81 (21H, m, -CH and ArH); MS *m/z* 506 (M^+). Found: C, 69.97; H, 4.09; N, 5.75%. Calcd for $C_{30}H_{22}N_2O_2S_2$: C, 71.12; H, 4.38; N, 5.53%.

Thermolysis of the 7-Chloro-4-phenylsulfonyl-1,2-diazocine (2a). A solution of 1.0 g (2.3 mmol) of **2a** in dry xylene (20 ml) was refluxed for 5h. The reaction mixture was concentrated in vacuo, and the residue was chromatographed (silica gel, benzene) to give 20 mg (7%) of benzonitrile, 0.12 g (16%) of 3-chloro-2-phenyl-6-phenylsulfonylpyridine (**7a**), 0.25 g (27%) of 6-benzoyl-2-phenyl-3-phenylsulfonylpyridine (**8a**), and 0.12 g (18%) of 6-benzoyl-3-chloro-2-phenylpyridine (**9**), mp 119—120 °C (lit.[2] mp 119—120 °C).

7a: Mp 132—133 °C; yellow prisms; IR (KBr) 1320 cm^{-1}; ^1H NMR ($CDCl_3$) δ=7.97, 8.05 (each 1H, d, PyH, *J*=8.4 Hz), 7.32—7.82 (8H, m), 7.97—8.22 (2H, m); ^{13}C NMR ($CDCl_3$) δ=156.98, 156.46, 139.50, 138.61, 136.33, 133.86, 133.63, 129.57, 129.58, 129.05, 127.99, 121.06; MS *m/z* 267, 265 (M^+-SO_2). Found: C, 61.82; H, 3.56; N, 4.07%. Calcd for $C_{17}H_{12}NO_2SCl$: C, 61.91; H, 3.67; N, 4.25%.

8a: Mp 159—160 °C; yellow needles; IR (KBr) 1665, 1320 cm^{-1}; ^1H NMR ($CDCl_3$) δ=8.11, 8.86 (each 1H, d, PyH, *J*=8.2 Hz), 7.10—7.60 (13H, m), 7.97—8.12 (2H, m); ^{13}C NMR ($CDCl_3$) δ=191.87, 157.81, 157.40, 139.14, 138.88, 138.20, 137.15, 135.09, 133.39, 133.16, 130.98, 129.63, 128.87, 128.52, 128.16, 127.87, 127.45, 122.70; MS *m/z* 399 (M^+). Found: C, 71.95; H, 4.51; N, 3.65%. Calcd for $C_{24}H_{17}NO_3S$: C, 72.16; H, 4.29; N, 3.51%.

Thermolysis of the 4-Chloro-7-(*p*-tolylsulfonyl)-1,2-diazocine (2b). A solution of 0.7 g (1.6 mmol) of **2b** in dry xylene (20 ml) was refluxed for 5h. Similar work-up and chromatography (silica gel, benzene) of the pyrolysate gave trace amounts of benzonitrile, 0.1 g (19%) of 3-chloro-2-phenyl-6-(*p*-tolylsulfonyl)pyridine (**7b**), 80 mg (12%) of 6-benzoyl-2-phenyl-3-(*p*-tolylsulfonyl)pyridine (**8b**), and 0.1 g (22%) of the pyridine **9**.

7b: 142—143 °C; colorless needles; IR (KBr) 1320 cm^{-1}; ^1H NMR ($CDCl_3$) δ=2.40 (3H, s), 7.33—7.83 (8H, m, PyH and ArH) 7.83—8.13 (3H, m, PyH and ArH); MS *m/z* 281, 279 (M^+-SO_2). Found: C, 63.01; H, 4.26; N, 4.33%. Calcd for $C_{18}H_{14}NO_2SCl$: C, 62.88; H, 4.10; N, 4.07%.

8b: Mp 163—164 °C; colorless prisms; IR (KBr) 1655, 1320 cm^{-1}; ^1H NMR ($CDCl_3$) δ=2.33 (3H, s), 8.06, 8.81 (each 1H, d, PyH, *J*=8.4 Hz), 6.76—7.56 (12H, m), 7.86—8.16 (2H, m): MS *m/z* 413 (M^+). Found: C, 72.37; H, 4.50; N, 3.43%. Calcd for $C_{25}H_{19}NO_3S$: C, 72.62; H, 4.63; N, 3.39%.

Thermolysis of the 4-Chloro-7-(*p*-chlorophenylsulfonyl)-1,2diazocine (2c). A solution of 0.8 g (1.7 mmol) of **2c** in dry xylene (20 ml) was refluxed for 5 h. Similar work-up and chromatography (silica gel, benzene) of the pyrolysate gave trace amounts of benzonitrile, 0.1 g (16%) of 3-chloro-6-(*p*-chlorophenylsulfonyl)-2-phenylpyridine (**7c**), 0.25 g (34%) of 6-benzoyl-3-(*p*-chlorophenylsulfonyl)-2-phenylpyridine (**8c**), and 0.15 g (30%) of the pyridine **9**.

7c: Mp 132—133 °C; colorless needles; IR (KBr) 1320 cm^{-1}; ^1H NMR ($CDCl_3$) δ=7.29—7.69 (8H, m, PyH and ArH), 7.94—8.19 (3H, m, PyH and ArH); MS *m/z* 303, 301, 299 (M^+-SO_2). Found: C, 56.06; H, 3.04; N, 3.85%. Calcd for $C_{17}H_{11}NO_2SCl_2$: C, 55.77; H, 3.21; N, 3.69%.

8c: Mp 147—148 °C; colorless needles; IR (KBr) 1660, 1330 cm^{-1}; ^1H NMR ($CDCl_3$) δ=8.13, 8.85 (each 1H, d, PyH, *J*=8.4 Hz), 7.09—7.59 (12H, m), 7.78—8.19 (2H, m); MS *m/z* 435, 433 (M^+). Found: C, 66.21; H, 3.60; N, 3.49%. Calcd for $C_{24}H_{18}NO_3SCl$: C, 66.43; H, 3.72; N, 3.23%.

Conversion of the 3-Chloro-2-phenyl-6-phenylsulfonylpyridine (7a) to 3-Chloro-6-methoxy-2-phenylpyridine (10). The pyridine **7a** (0.2 g, 0.6 mmol) was heated in a solution of sodium methoxide in methanol, which was prepared from metallic sodium (0.5 g) in methanol (20 ml), under reflux for 5 h. The reaction mixture was poured into water (50 ml), and the mixture was extracted with benzene (50 ml×2). The benzene extract was concentrated in vacuo, and chromatography (silica gel, benzene) of the residue gave 0.1 g (76%) of the pyridine **10**.

10: Oil; ^1H NMR ($CDCl_3$) δ=3.89 (3H, s), 6.59, 7.52 (each 1H, d, PyH, *J*=8.4 Hz), 7.27—7.52 (3H, m), 7.67—7.87 (2H, m); MS *m/z* 221, 219 (M^+). Found: C, 65.37; H, 4.62; N, 6.51%. Calcd for $C_{12}H_{10}NOCl$: C, 65.61; H, 4.59; N, 6.38%.

Similar treatments of 3-chloro-2-phenyl-6-(*p*-tolylsulfonyl)- (**7b**) and 3-chloro-6-(*p*-chlorophenylsulfonyl)-2-phenylpyridine (**7c**) with sodium methoxide in methanol afforded the pyridine **10** in 67 and 50% yields, respectively. The pyridine **10** was identical with the product from the reaction of 3,6-dichloro-2-phenylpyridine (**11**)[2] with sodium

methoxide in methanol under similar conditions.

Thermolysis of the Symmetrical Bis(arylsulfonyl)-1,2-diazocines. Typical run is illustrated for the bis(phenylsulfonyl)-1,2-diazocine (**3a**). A solution of **3a** (1.0 g, 1.9 mmol) in dry xylene (20 ml) was refluxed for 5 h. The reaction mixture was concentrated in vacuo, and the residue was chromatographed on silica gel to give 0.52 g (70%) of the pyridine **8a** (from benzene elution) and 50 mg (6%) of 3,6-bis(phenylsulfonyl)-2-phenylpyridine (**13a**), mp 187—189 °C (lit,[4] mp 187—189 °C) (from chloroform elution).

Thermolysis of the bis(*p*-tolylsulfonyl)- (**3b**) or bis(*p*-chlorophenylsulfonyl)-1,2-diazocine (**3c**) in dry xylene under similar conditions gave the pyridine **8b** and 3,6-bis(*p*-tolylsulfonyl)-2-phenylpyridine (**13b**), mp 231—232 °C (lit,[4] mp 231—232 °C), or the pyridine **8c** and 3,6-bis(*p*-chlorophenylsulfonyl)-2-phenylpyridine (**13c**), mp 227—228 °C (lit,[4] mp 227—228 °C), respectively. The results are shown in Scheme 4.

Thermolysis of the Unsymmetrical Bis(arylsulfonyl)-1,2-diazocines. A solution of 0.7 g (1.3 mmol) of the 4-phenylsulfonyl-7-(*p*-tolylsulfonyl)-1,2-diazocine (**3d**) in dry xylene (20 ml) was refluxed for 5 h. The reaction mixture was concentrated in vacuo, and the pyrolysate was chromatographed on silica gel to give 80 mg (16%) of **8a** and 0.23 g (44%) of **8b** (each from benzene elution), together with 10 mg of a mixture of 2-phenyl-3-phenylsulfonyl-6-(*p*-tolylsulfonyl)- (**14**) and 2-phenyl-6-phenylsulfonyl-3-(*p*-tolylsulfonyl)pyridine (**15**) (each Ar=*p*-MeC_6H_4) (from chloroform elution) whose ratio was not determined.

In the thermolysis of the 7-(*p*-chlorophenylsulfonyl)-4-phenylsulfonyl-1,2-diazocine (**3e**) under similar thermolytic conditions, two benzoylpyridines, **8a** and **8c**, were obtained accompanied by small amounts of a mixture of two the corresponding 3,6-bis(arylsulfonyl)-2-phenylpyridines, **14** and **15** (Ar=*p*-ClC_6H_4). whose ratio was not determined (See Scheme 4).

Thermolysis of the 4-Phenylsulfonyl-7-phenylthio-1,2-diazocine (6). A solution of **6** (0.6 g, 1.2 mmol) in dry xylene (20 ml) was refluxed for 5 h. Similar work-up and chromatography (silica gel, benzene) of the pyrolysate gave 60 mg (49%) of benzonitrile, 0.3 g (63%) of 2-phenyl-6-phenylsulfonyl-3-phenylthiopyridine (**16**), and 0.1 g (23%) of 6-benzoyl-2-phenyl-3-phenylthiopyridine (**17**), mp 120—121 °C (lit,[4] mp 120—121 °C). The pyridine **16** was converted into 6-methoxy-2-phenyl-3-phenylthiopyridine (**18**), mp 68—69 °C (lit,[4] mp 68—69 °C).

16: Mp 143—145 °C; colorless prisms; ^1H NMR ($CDCl_3$) δ=7.1—8.3 (m, PyH and ArH); MS *m/z* 399 (M^+-SO_2). Found: C, 68.17; H, 4.15; N, 3.67%. Calcd for $C_{23}H_{17}NO_2S_2$: C, 68.46; H, 4.25; N, 3.47%.

References

1) B. M. Trost and R. M. Cory, *J. Am. Chem. Soc.*, **93**, 5573 (1971); B. M. Trost, P. H. Schudder, R. M. Cory, N. J. Turro, V. Ramamurthy, and T. J. Katz, *J. Org. Chem.*, **44**, 1264 (1979).

2) S. Yogi, K. Hokama, K. Ueno, and O. Tsuge, *Bull. Chem. Soc. Jpn.*, **59**, 1087 (1986).

3) C. G. Overberger and I. Tashlick, *J. Am. Chem. Soc.*, **81**, 217 (1959).

4) S. Yogi, K. Hokama, and O. Tsuge, *Bull. Chem. Soc. Jpn.*, **57**, 335 (1987).

5) The intervention of azonia intermediates like D and imidoylpyridines like **E** in the thermal reaction of 4,7-disubstituted 1,2-diazocines can be strongly supported by the isolation of 3-acetoxy-6-(*N*-chlorobenzimidoyl)-2-phenyl pyridine (Ref. 2).

 © 1987 The Chemical Society of Japan Bull. Chem. Soc. Jpn., 60, 349—354 (1987)

Synthesis of Dichlorocyclobuta[*b*]benzofuran-2a-carboxylic Derivatives and 3-(Trichloroethenyl)coumarin through Cross Photocycloadduct of Coumarin and Tetrachloroethylene[1)]

Shinji NONOYAMA, Noriyuki YONEZAWA, Kazuhiko SAIGO,
Masaki HASEGAWA,* and Yoichi IITAKA†
Department of Synthetic Chemistry, Faculty of Engineering, The University of Tokyo,
Hongo, Bunkyo-ku, Tokyo 113
†Faculty of Pharmaceutical Science, The University of Tokyo, Hongo, Bunkyo-ku, Tokyo 113
(Received July 25, 1986)

Photoirradiation of coumarin and tetrachloroethylene with a high-pressure mercury lamp through Pyrex filter in the presence of benzene and benzophenone gave cross cycloadduct (**3**) in a moderate yield. By treatment with bases or nucleophiles at room temperature, **3** underwent ring-contraction reaction through lactone-opening, cyclobutene formation, and intramolecular S_N2' displacement to yield dichlorocyclobuta[*b*]-benzofurancarboxylic derivatives exclusively. By use of a non-nucleophilic base, 3-(trichloroethenyl)coumarin was alternatively obtained through [2+2] cycloreversion of cyclobutene intermediate in a good yield.

[2+2] Photocycloadducts of olefins occasionally have particular reactivities based on their strain arisen from the highly restricted geometry. For example, we have reported the highly enhanced reactivities of coumarin dimers and their lactone-opened derivatives,[2)] and their application to polymer synthesis and polymer reaction.[3)] Our continuing studies on [2+2] photocycloadducts led us to investigate the reaction of the compounds having dissymmetrical structures. Recently, we carried out cross photocycloaddition reaction of coumarin (**1**) and tetrachloroethylene (**2**) with an expectation that cyclobutane-fused pyrone compounds would undergo easily lactone-opening reaction to lead some attractive reactions such as ring-expansion and rearrangement.[4)] The reaction of the obtained cross photocycloadduct, 1,1,2,2-tetrachloro-1α,2α,2aα,8bα-tetrahydro-3*H*-cyclobuta[*c*][1]benzopyran-3-one (**3**), with nucleophiles or bases resulted in the ring-contraction or cycloreversion to give two types of compounds. One is dichlorocyclobuta[*b*]benzofuran-2a-carboxylic derivatives (**6**), which would be yielded via lactone-opening, cyclobutene formation, and intramolecular S_N2' displacement. The other is 3-(trichloroethenyl)coumarin (**9**) obtained by cycloreversion of the cyclobutene intermediate.

In this paper, we wish to report these reactions in detail with the X-ray structural analysis of the new type of compound having 4,5,6-fused ring system.

Results and Discussion

The cross photocycloaddition between coumarin (**1**) and tetrachloroethylene (**2**) was undertaken by irradiation with the light of a high-pressure mercury lamp. When the irradiation was carried out in the absence of benzene, the photoreaction did not proceed at all. Moreover, when benzophenone was not present, the formation of homodimers of coumarin, anti head-to-head, anti head-to-tail, and syn head-to-head coumarin dimers, overcame the production of cross cycloadduct (**3**). Accordingly, for the synthesis of **3** in a high yield, presence of both benzene and benzophenone was proved to be essential. Under the optimum conditions, 52% conversion to **3** and 39% isolated yield were achieved (Scheme 1).

Treatment of **3** with methanol at room temperature gave simply lactone-opened derivative **4a** as a sole product (Run 1), which would be obtained in analogy with the lactone-opening reaction of coumarin dimers.[2a)] When the reaction was undertaken at reflux temperature, cyclobutene compound **5a** and 3-(trichloroethenyl)coumarin (**9**) were formed (Runs 2 and 3). Though easy relactonization of cyclobutanecarboxylate **4a** to lactone **3** on heating or under acidic conditions such as contact with silica gel disturbed the isolation, the formation of **4a** was ascertained by ^{1}H and ^{13}C NMR spectra of the reaction mixture, which showed two doublets of cyclobutane ring protons [δ=4.49 and 4.89 (J=10 Hz), in $CDCl_3$] and four peaks of cyclobutane ring carbons [δ=51.9 (d), 59.0 (d), 89.2 (s), and 93.0 (s), in $CDCl_3$], together with other peaks appearing in the reasonable regions for **4a**. Isolation of cyclobutenecarboxylate **5a** was also unsuccessful, because of the spontaneous transformation to trichloroethenylcoumarin (**9**). The formation of **5a** was also confirmed by the ^{1}H NMR spectrum of the reaction mixture, which showed singlet for methoxyl protons (3H) at δ=3.81, singlet for cyclobutene ring proton (1H) at δ=5.07, and multiplet for aromatic protons

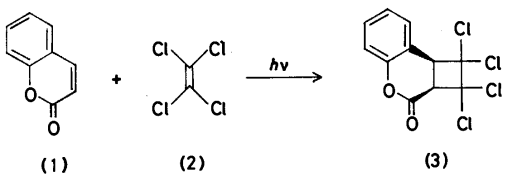

Scheme 1.

(4H) at δ=6.75—6.95.

However, when butylamine or an alkali was used, two types of compounds (**5** and **6**) were obtained in the ratio depending on the basicity and/or the amount of the nucleophile used. Simply lactone-opened derivatives **4b**, **4c** were not detected. This result indicates that in the reaction of **3** with butylamine or an alkali, lactone-opening reaction initially took place to produce cyclobutanecarboxylic derivatives **4**, followed by immediate dehydrochlorination reaction yielding cyclobutenes **5**, and finally intramolecular S_N2' displacement occurred by the attack of the phenolate anion on the sp^2 carbon of the cyclobutene ring.

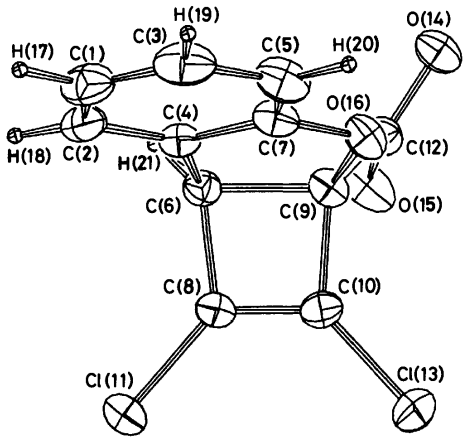

Fig. 1. Perspective view of cyclobutabenzofurancarboxylic acid (**6c**) drawn by ORTEP[12] program. Atoms (except hydrogen) are shown by ellipsoids of 30% probability.

The intramolecular S_N2' displacement for ring closure was more influenced by the basicity of the nucleophile than the cyclobutene formation (Runs 5—11). The reaction mentioned above resulted finally in an almost quantitative contraction of the cyclobutenefused benzofuran systems (Runs 7, 9, and 11).

Reactions of **3** with nucleophiles or bases are summarized in Table 1.

The structures of these compounds were determined by ^1H and ^{13}C NMR spectra, IR spectra, and elemental analyses. The structure of cyclobutabenzofurancarboxylic acid (**6c**) was confirmed by X-ray analysis. The perspective view is shown in Fig. 1, and the atomic coordinates, the bond lengths, and the bond angles are shown in Tables 2—4.

As methanol has not enough basicity, in the reaction with **3** at room temperature methanol did not act other than a weak nucleophile and there existed an equilibrium between lactone-opened and -closed compounds. Then a mixture of lactone **3** and ester **4a** was obtained. But when the reaction mixture was heated at methanol reflux temperature, thermal dehydrochlorination of cyclobutanecarboxylate **4a** would occur to give cyclobutenecarboxylate **5a**. At such high temperature, by further [2+2] cycloreversion the plausible intermediate, methyl *cis*-3-(2-hydroxyphenyl)-2-(trichloroethenyl)-2-propenoate (**7a**), would be gradually formed from **5a**. Then, **7a** should smoothly undergo thermal or acid-catalyzed relactonization to give trichloroethenylcoumarin (**9**) without formation of cyclobutabenzofuran **6a**, because methanol cannot produce phenolate anion from

Table 1. Reaction of Cross Cycloadduct **3**

Run	Base	Equiv	Solvent	Time h	Temp[b]	Conversion[a] (Isolated Yield) %				Recovery[a] %
						4	**5**	**6**	**9**	**3**
1	MeOH	1250	MeOH–Acetone (5:1)	240	r.t.	52	0	0	0	48
2	MeOH	1000	MeOH–Acetone (2:3)	60	reflux	40	3	0	11	46
3	MeOH	12000	MeOH	60	reflux	21	12	0	19	48
4	$BuNH_2$	1	Acetone	1	r.t.	0	48	0	0	52
5	$BuNH_2$	2	Acetone	1	r.t.	0	100(67)	0	0	0
6	$BuNH_2$	4	Dioxane	1	r.t.	0	40	60	0	0
7	$BuNH_2$	10	Acetone	1.5	r.t.	0	0	100(96)	0	0
8	$NaHCO_3$	10	H_2O–Acetone (1:1)	42	r.t.	0	90(31)	10	0	0
9	Na_2CO_3	30	H_2O–MeOH (3:2)	97	r.t.	0	0	100	0	0
10	NaOH	1	H_2O–Acetone (1:10)	4	r.t.	0	28	12	0	60
11	NaOH	10	H_2O–MeOH (5:1)	1	r.t.	0	0	100(90)	0	0
12	Et_3N	45	Benzene	0.25	r.t.	0	0	0	100(82)	0

a) Conversion and recovery were determined on the basis of the ^1H NMR spectra of the crude products. b) r.t. means room temperature.

phenolic hydroxyl group.

The exclusive formation of **9** was performed by treatment of **3** with triethylamine. As triethylamine has not nucleophilicity, the six-membered lactone-ring should be maintained all over the reaction steps. Then, by dehydrochlorination plausible 6,6,4-fused ring intermediate **8**, which is considered to be very unstable because of its highly restricted structure, would be formed, and immediate cycloreversion to **9** should exclusively proceed in a similar manner to the dehydrochlorination and cyclocleavage reactions of the photoadduct of cyclohexanone and dichloroethylene.[5]

On the contrary, the reaction path from cyclobutenecarboxylate **5a** to **9** via cyclobutene **8** seems unsuitable, since heating *N*-butylcyclobutenecarboxamide (**5b**) in benzene afforded **9** exclusively. The spontaneous lactonization of *cis*-cinnamamide derivative **7b** is reasonable, but the formation of very unstable 6,6,4-fused ring compound (**8**) together with cleavage of amide linkage looks very disadvantageous, and under such drastic conditions [2+2] cycloreversion of cyclobutene **5b** to diene **7** must proceed far rapidly.

The overall feature of these reactions is summarized in Scheme 2.

By the reactions mentioned above, cyclobutenecarboxylic derivatives fused benzofuran ring (**6**) were readily obtained through three sequential stepwise

Table 2. Atomic Coordinates and Equivalent Isotropic Temperature Factors for Cyclobutabenzofurancarboxylic Acid (**6c**) with Standard Deviations in Parentheses

No	Atom	x 10^4	y 10^4	z 10^4	B_{eq} Å^2
1	C(1)	973(3)	1782(10)	3501(6)	4.95(0.10)
2	C(2)	810(3)	2007(9)	5020(6)	3.86(0.08)
3	C(3)	1222(3)	−26(11)	2978(6)	5.33(0.10)
4	C(4)	906(2)	368(8)	5963(5)	3.09(0.07)
5	C(5)	1318(3)	−1700(10)	3910(6)	4.61(0.09)
6	C(6)	827(2)	179(7)	7646(5)	2.94(0.06)
7	C(7)	1146(2)	−1433(8)	5422(5)	3.44(0.07)
8	C(8)	1481(2)	634(7)	8612(5)	2.89(0.06)
9	C(9)	1070(2)	−2069(7)	7907(5)	2.91(0.06)
10	C(10)	1694(2)	−1241(8)	8788(5)	3.05(0.06)
11	Cl(11)	1838(1)	2853(2)	9230(2)	4.46(0.02)
12	C(12)	573(2)	−3403(7)	8786(5)	3.12(0.07)
13	Cl(13)	2403(1)	−2312(2)	9703(2)	4.64(0.02)
14	O(14)	278(2)	−4860(5)	8151(4)	3.89(0.05)
15	O(15)	500(2)	−2888(6)	10149(4)	5.16(0.07)
16	O(16)	1205(2)	−2948(5)	6479(4)	3.57(0.05)
No	Atom	x 10^3	y 10^3	z 10^3	B_{eq} Å^2
17	H(17)	90(3)	293(10)	278(7)	7(2)
18	H(18)	63(3)	327(9)	536(6)	6(1)
19	H(19)	132(4)	−20(11)	189(8)	9(2)
20	H(20)	149(3)	−294(10)	348(7)	7(2)
21	H(21)	30(3)	71(11)	791(7)	8(2)

Table 3. Bond Lengths of Cyclobutabenzofurancarboxylic Acid (**6c**) with Standard Deviations in Parentheses

C(1)-C(2)	1.396(7) Å
C(1)-C(3)	1.383(10)
C(2)-C(4)	1.384(7)
C(3)-C(5)	1.396(9)
C(4)-C(6)	1.504(6)
C(4)-C(7)	1.379(7)
C(5)-C(7)	1.397(7)
C(6)-C(8)	1.500(6)
C(6)-C(9)	1.586(7)
C(7)-O(16)	1.378(6)
C(8)-C(10)	1.323(7)
C(8)-Cl(11)	1.709(5)
C(9)-C(10)	1.488(6)
C(9)-C(12)	1.527(7)
C(9)-O(16)	1.424(5)
C(10)-Cl(13)	1.690(5)
C(12)-O(14)	1.243(6)
C(12)-O(15)	1.264(6)

Table 4. Bond Angles of Cyclobutabenzofurancarboxylic Acid (**6c**) with Standard Deviations in Paretheses

C(2)-C(1)-C(3)	120.4(5)°
C(4)-C(2)-C(1)	117.6(5)
C(5)-C(3)-C(1)	122.8(6)
C(6)-C(4)-C(2)	130.1(4)
C(6)-C(4)-C(7)	108.4(4)
C(2)-C(4)-C(7)	121.3(4)
C(7)-C(5)-C(3)	115.5(5)
C(8)-C(6)-C(4)	115.6(4)
C(8)-C(6)-C(9)	83.4(3)
C(4)-C(6)-C(9)	100.6(3)
O(16)-C(7)-C(4)	115.2(4)
O(16)-C(7)-C(5)	122.5(4)
C(4)-C(7)-C(5)	122.3(5)
C(10)-C(8)-C(6)	96.4(4)
C(10)-C(8)-Cl(11)	132.3(4)
C(6)-C(8)-Cl(11)	131.3(3)
C(10)-C(9)-C(6)	86.5(3)
C(10)-C(9)-C(12)	116.0(4)
C(10)-C(9)-O(16)	116.8(4)
C(6)-C(9)-C(12)	116.7(4)
C(6)-C(9)-O(16)	108.9(3)
C(12)-C(9)-O(16)	110.1(4)
Cl(13)-C(10)-C(8)	133.3(4)
Cl(13)-C(10)-C(9)	133.0(4)
C(8)-C(10)-C(9)	93.7(4)
O(14)-C(12)-C(9)	120.0(4)
O(14)-C(12)-O(15)	125.4(4)
C(9)-C(12)-O(15)	114.6(4)
C(7)-O(16)-C(9)	106.5(3)

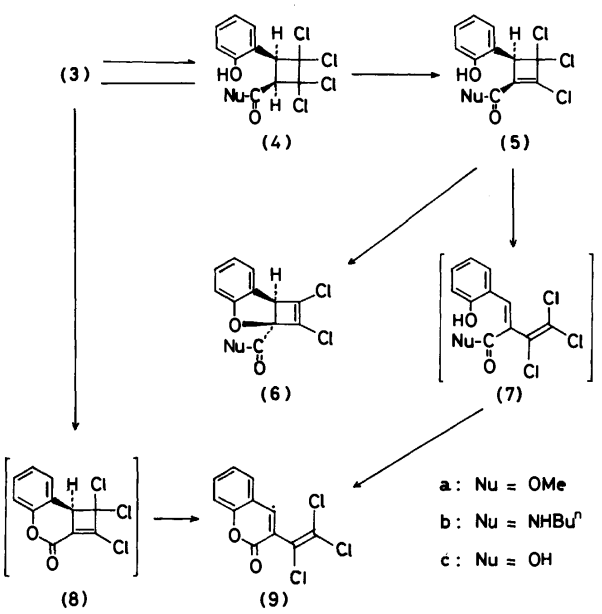

Scheme 2.

reactions, and trichloroethenyl lactone (**9**) was easily prepared by dehydrochlorination and cycloreversion. In addition, both of these reactions proceeded under very mild conditions with high yields. The syntheses of cyclobutene-fused benzofuran systems were reported by Tinnemans and Neckers[6] along with a large number of reports about the 4,5,6-fused ring systems of nitrogen and sulfur analogues.[7] According to their method the cyclobutene-fused benzofurans were synthesized by the cross photocycloaddition between benzofurans and an alkyne, but initial photoadducts easily underwent photoisomerization, resulting in the formation of complicated mixtures of the rearranged isomers. By contrast, cyclobutabenzofurans **6b**, **6c** were formed exclusively from cyclobuta[1]benzopyran-3-one **3**, which was readily prepared as a pure material in an adequate yield. In addition, compared to the related nucleophilic and/or thermal ring transformation reactions of pyrone derivatives to give furans,[8] the ring contraction of **3** proceeded under mild conditions even when butylamine was used as a nucleophile at room temperature. For the occurrence of this ring contraction, the ring-opening reaction must occur before dehydrochlorination, and the S_N2' displacement must proceed much faster than the [2+2] cycloreversion. If either reaction is slow, a considerable amount of trichloroethenylcoumarin (**9**) would be formed. Thus, this result clearly shows the highly enhanced ring-opening tendency of the lactone ring of cross cycloadduct **3**. This high reactivity is considered to be attributed to the strain of the lactone rings which is brought about by cyclobutanation. Although under such weakly basic conditions, the equilibrium between the phenolic hydroxyl group and the phenolate anion does not favor the phenolate anion; the neighboring group effect. should permit the nucleophilic attack of the phenolate anion to proceed so rapid that it competes effectively with the thermal cycloreversion.

Experimental

All melting points were measured on a MELTEMP micro melting point apparatus and are uncorrected. IR and NMR spectra were recorded on a JASCO IR-810 spectrophotometer and JEOL GX-400 nuclear magnetic spectrometric instrument, respectively. Photoirradiation was undertaken with an Eiko-sha EHB-WI(F)-500 high-pressure mercury lamp (500 W).

All the reagents and solvents were purified by the methods described in the literature.[9] Anti head-to-head, anti head-to-tail, and syn head-to-head coumarin dimers were prepared according to the methods described in the literature,[10] and used as authentic samples for the identification and the quantification of the photoproducts by ^{1}H NMR spectroscopy.

Unless specified otherwise, the following experimental conditions were used. The reactions were carried out under an argon atmosphere. The extracts were washed with saturated aqueous sodium chloride before drying. The solution was dried overnight and the desiccant was removed by filtration. The solvents were taken off on a flash evaporator at the temperature below 10 °C. The conversions were determined by ^{1}H NMR spectrum of the reaction mixture in $CDCl_3$. Separations of the products by column chromatography were carried out using silica gel (Wako-gel C-200, 100—200 mesh). The chemical shifts in ^{1}H and ^{13}C NMR spectra were referred to tetramethylsilane (TMS) signals.

Synthesis of 1,1,2,2-Tetrachloro-1α,2α,2aα,8bβ-tetrahydro-3*H*-cyclobuta[*c*][1]benzopyran-3-one (3): 14.54 g (0.10 mol) of coumarin (**1**) and 3.14 g (0.017 mol) of benzophenone were dissolved in a mixture of tetrachloroethylene (**2**) (633.6 g, 3.82 mol) and benzene (36.0 g). The solution was irradiated with the 500 W high-pressure mercury lamp through Pyrex filter for 28.5 h. On the basis of ^{1}H NMR spectrum of the reaction mixture, 42% of **1** was found to convert to **3**, accompanying 13% of anti head-to-head coumarin dimer and a trace amount (less than 0.5%) of syn head-to-head coumarin dimer. No other product could be detected. After concentration of the reaction mixture under reduced pressure, silica-gel column chromatographic separation using benzene as an eluant gave 9.52 g (30.5%) of **3**: Mp 144—145 °C; IR (KBr) 1770 (C=O), 930 (cyclobutane), 820, 805, 775, 745, 700 cm^{-1}; ^{1}H NMR (400 MHz $CDCl_3$) δ=4.22 (1H, d, J=10 Hz, cyclobutane ring proton), 4.59 (1H, d, J=10 Hz, cyclobutane ring proton), 7.07—7.43 (4H, m, aromatic protons); ^{13}C NMR (100 MHz $CDCl_3$) δ=50.7 (d), 50.8 (d), 89.8 (s), 93.9 (s), 114.3 (s), 117.5 (d), 125.2 (d), 129.5 (d), 131.0 (d), 151.6 (s), 158.9 (s); Found: C, 42.23; H, 2.06; Cl, 45.04%. Calcd for $C_{11}H_6Cl_4O_2$: C, 42.35; H, 1.93; Cl, 45.46%.

When 7.27 g (50 mmol) of coumarin (**1**) was irradiated for 141 h under same conditions described above, 39% (5.97 g) of **3** was obtained (conversion was 52%).

Reaction of Cross Adduct (3) with Methanol at Room Temperature: A solution of **3** (156 mg, 0.5 mmol) in methanol (100 ml) was stirred for 240 h at room temperature,

followed by evaporation of excess methanol. The ^{1}H NMR spectrum of the residue thus obtained in $CDCl_3$ showed a singlet of methoxyl protons (δ=3.83, 3H), two doublets of cyclobutane ring protons (δ=4.49 and 4.89, each 1H, J=10 Hz), and a multiplet for aromatic ring protons (δ=6.70—7.30, 4H) together with the peaks of **3**. In its ^{13}C NMR spectrum in $CDCl_3$, four carbons of cyclobutane ring [δ=51.9 (d), 59.0 (d), 89.2 (s), and 93.0 (s)], a methoxyl carbon [δ=51.8 (q)], aromatic carbons [δ=115.1 (d), 119.9 (s), 120.2 (d), 128.7 (d), 128.8 (d), and 153.5 (s)], and a carbonyl carbon [166.6 (s)] were observed. These NMR data were consistent with the structure of methyl 2,2,3,3-tetrachloro-*c*-4-(2-hydroxyphenyl)-*r*-1-cyclobutanecarboxylate (**4a**). Based on the integration intensities in the ^{1}H NMR spectrum, content of ester **4a** was calculated to be 52% and that of **3** to be 48%. But isolation of **4a** was unsuccessful since relactonization took place easily on silica-gel column or on standing at room temperature.

Reaction of Cross Cycloadduct (3) with Methanol at Reflux Temperature: **3** (156 mg, 0.5 mmol) was dissolved in methanol (70 ml) at room temperature, and the solution was stirred for 60 h at reflux temperature. The solution was concentrated under reduced pressure to yield a solid. On the basis of the ^{1}H NMR spectrum of the solid thus obtained, it was confirmed that 21% of **3** converted to cyclobutanecarboxylate **4a**, 12% to cyclobutenecarboxylate **5a**, and 19% to trichloroethenylcoumarin (**9**). Chromatography on silica gel using benzene as an eluant afforded **5a** (20 mg, 14%), along with a mixture of starting material (**3**) and **9**. Data for cyclobutene **5a**; ^{1}H NMR ($CDCl_3$) δ=3.81 (3H, s, OMe), 5.07 (1H, s, cyclobutene ring proton), and 6.75—6.95 (4H, m, aromatic protons). On silica-gel column, **4a** was considered to be decomposed to **5a** or lactone **3**, and resulted cyclobutenecarboxylate **5a** was also very unstable and spontaneously decomposed to **9** on standing at room temperature. So elemental analysis and measurement of mp were unsuccessful.

***N*-Butyl-2,3,3-trichloro-4-(2-hydroxyphenyl)-1-cyclobutenecarboxamide (5b):** Butylamine (73 mg, 1.0 mmol) was added to a stirred acetone solution (10 ml) of **3** (156 mg, 0.5 mmol) at room temperature. After stirring for 1 h, the solution was poured into 1 M† HCl (20 ml), and extracted with benzene (50 ml×3). The extracts were combined, dried ($MgSO_4$), and concentrated to leave viscous liquid, which was washed with chloroform (10 ml×3) to give cyclobutenecarboxamide **5b** (116 mg, 67%): glass; IR (KBr) 1655 (amide I), 1530 (amide II), 760, 595 cm^{-1}; ^{1}H NMR ($CDCl_3$) δ=0.95 [3H, t, J=7.5 Hz, $(CH_2)_3CH_3$], 1.20—1.80 (4H, m, $CH_2CH_2CH_2CH_3$), 3.29—3.50 [2H, m, $NCH_2(CH_2)_2CH_3$], 5.15 (s, 1H, cyclobutene ring proton), 6.14 (1H, br s, NH), 6.60—7.25 (4H, m, aromatic protons), 7.96 (1H, br s, ArOH); ^{13}C NMR ($CDCl_3$) δ=13.7 (q), 20.0 (t), 31.3 (t), 39.5 (t), 59.3 (d), 84.5 (s), 115.3 (d), 119.6 (d), 120.5 (s), 128.3 (d), 129.8 (d), 134.3 (s), 134.8 (s), 155.2 (s), 160.0 (s); Elemental analysis was unsuccessful since cyclobutene **5b** was transformed to trichloroethenylcoumarin (**9**) on a silica-gel column.

2,3,3-Trichloro-4-(2-hydroxyphenyl)-1-cyclobutenecarboxylic Acid (5c): To a stirred solution of **3** (156 mg, 0.5 mmol) in acetone (10 ml), 10 ml of sodium hydrogencarbonate (1 M) was added at room temperature. After stirring at room temperature for 42 h, the reaction mixture was poured into 15 ml of 1 M HCl and extracted with benzene (50 ml×3). The extracts were combined, dried ($MgSO_4$), and concentrated to yield a white powder, which was washed with chloroform (10 ml×3) to give cyclobutenecarboxylic acid (**5c**) (46 mg, 31%): mp 132°C (decomp.); IR (KBr) 1705 (C=O), 885, 740, 600 cm^{-1}; ^{1}H NMR [$(CD_3)_2SO$] δ=4.97 (1H, s, cyclobutene ring proton), 6.67—6.90 (3H, m, aromatic protons), 7.15—7.20 (1H, m, aromatic proton), 9.89 (1H, s, NH), 13.8 (1H, br s, CO_2H); ^{13}C NMR [$(CD_3)_2CO$] δ=60.8 (d), 85.9 (s), 115.9 (d), 120.2 (d), 122.1 (s), 129.6 (d), 130.5 (d), 133.8 (s), 140.3 (s), 156.9 (s), and 161.2 (s); Elemental analysis was unsuccessful because cyclobutenecarboxylic acid (**5c**) was transformed to **9** on a silica-gel column.

***N*-Butyl-1,2-Dichloro-2aα,7bα-dihydrocyclobuta[*b*]benzofuran-2a-carboxamide (6b):** Butylamine (365 mg, 5.0 mmol) was added to a stirred acetone solution (10 ml) of **3** (156 mg, 0.5 mmol) at room temperature. After stirring for 1.5 h, the solution was poured into 1 M HCl (7.5 ml), and extracted with benzene (50 ml×3). The extracts were combined, dried ($MgSO_4$), and concentrated to give a white solid. The crude product was recrystallized from hexane to give cyclobutabenzofurancarboxamide (**6b**) as needles (150 mg, 96%): Mp 94—95°C; IR (KBr) 1665 (amide I), 1555 (amide II), 875, 740, 635 cm^{-1}; ^{1}H NMR ($CDCl_3$) δ=0.94 (3H, t, J=7.5 Hz, $(CH_2)_3CH_3$), 1.31—1.41 (2H, m, $CH_2CH_2CH_2CH_3$), 1.50—1.60 (2H, m, $CH_2CH_2CH_2CH_3$), 3.26—3.36 (1H, m, $CH_2CH_2CH_2CH_3$), 3.38—3.48 (1H, m, $CH_2CH_2CH_2CH_3$), 4.62 (1H, s, cyclobutene ring proton), 6.68 (1H, br s, NH), 6.96—7.06 (2H, m, aromatic protons), 7.26—7.34 (2H, m, aromatic protons); ^{13}C NMR ($CDCl_3$) δ=13.7 (q), 20.0 (t), 31.5 (t), 39.4 (t), 58.9 (d), 91.4 (s), 112.3 (d), 122.4 (d), 124.4 (s), 124.6 (s), 125.2 (d), 129.8 (d), 136.7 (s), 161.1 (s), 165.1 (s); Found: C, 57.43; H, 4.74; N, 4.53; Cl, 22.71%. Calcd for $C_{15}H_{15}Cl_2NO_2$: C, 57.71; H, 4.84; N, 4.49; Cl, 22.71%.

1,2-Dichloro-2aα,7aα-dihydrocyclobuta[*b*]benzofuran-2a-carboxylic Acid (6c): To a stirred methanol solution (50 ml) of **3** (189 mg, 0.61 mmol) aqueous sodium hydroxide (1 M, 6.1 ml) was added at room temperature. After stirring for 1 h at room temperature, the solution was poured into 1 M HCl (20 ml), and extracted with benzene (50 ml×3). The extracts were combined, dried ($MgSO_4$), and concentrated under reduced pressure, and the residue was recrystallized from benzene-hexane to afford white blocks of cyclobutabenzofurancarboxylic acid (**6c**) (140 mg, 90%): Mp 144°C (decomp); IR (KBr) 1730, 1700 (C=O and cyclobutene), 750 cm^{-1}; ^{1}H NMR ($CDCl_3$) δ=4.66 (1H, s, cyclobutene ring proton), 6.98—7.04 (2H, m, aromatic protons), 7.24—7.30 (2H, m, aromatic protons), 9.46 (1H, s, CO_2H); ^{13}C NMR ($CDCl_3$) δ=60.27 (d), 89.8 (s), 113.3 (d), 123.0 (d), 124.7 (s), 125.0 (s), 125.8 (d), 130.9 (d), 138.3 (s), 162.1 (s), 172.5 (s); Found: C, 51.53; H, 2.50; Cl, 26.99%. Calcd for $C_{11}H_6O_3Cl_2$: C, 51.39; H, 2.35; Cl, 27.58%.

3-(Trichloroethenyl)coumarin (9): Triethylamine (730 mg, 7.2 mmol) was added to a stirred benzene solution (20 ml) of **3** (50 mg, 0.16 mmol) at room temperature. After stirring at room temperature for 15 min, reaction mixture was poured into 1 M HCl (40 ml) and extracted with benzene (50 ml×3). The extracts were combined, dried ($MgSO_4$), and concentrated under reduced pressure to leave a white solid (39.4 mg), which was purified on a silica-gel column using

† 1 M=1 mol dm^{-3}.

benzene as an eluant to give pure **9** as white powder (36.2 mg, 82%). Recrystallization from hexane gave needles: Mp 129—130 °C; IR (KBr) 1725, 1700 (pyrone ring), 890, 815, 770 cm^{-1}; ^1H NMR ($CDCl_3$) δ=7.32—7.40 (2H, m, aromatic protons), 7.54—7.65 (2H, m, aromatic protons), 7.87 (1H, s, olefinic proton); ^{13}C NMR ($CDCl_3$) δ=117.6 (d), 118.9 (s), 124.2 (s), 124.6 (s), 124.7 (s), 125.6 (d), 129.3 (d), 133.9 (d), 145.4 (d), 154.8 (s), 158.0 (s); Found: C, 47.78; H, 1.98; Cl, 38.64%. Calcd for $C_{11}H_5Cl_3O_2$: C, 47.95; H, 1.83; Cl, 38.60%.

Crystallographic Measurement of Cyclobutabenzofurancarboxylic Acid (6c): Crystal Data. $C_{11}H_6Cl_2O_3$, M=257.1. Monoclinic, a=18.814(10), b=6.688(5), c=8.825(5) Å, β=92.38(5)°, V=1109 Å^3, space group $P2_1/n$, Z=4, D_x=1.538 g cm^{-3}, μ for Cu $K\alpha$=52.9 cm^{-1}.

The crystal of approximate dimensions 0.25×0.20×0.35 mm was mounted on a Philips PW1100 diffractometer and the integrated intensities were measured by a 2θ—θ scan method using graphite monochromated Cu $K\alpha$ radiation. 2042 Independent reflections were measured as above the 2σ(I) level out of 2542 theoretically possible ones in the 2θ range 6° through 156°. The intensities were corrected for Lorentz and polarization factors but not for absorption.

The crystal structure was determined by the direct method[11] and refined by the block-diagonal-matrix least-squares calculations. The R value was reduced to 0.067 for 2042 observed structure factors including 5 hydrogen atoms which were located on a difference electron-density map and assessed isotropic temperature factors. The carboxyl group may be protonated at O(15) since C(12)-O(15) is longer than C(12)-O(14) and C(9)-C(12)-O(15) is quite smaller than C(9)-C(12)-O(14), but this hydrogen atom was not found in the difference map.

The complete F_o—F_c data are deposited as Document No. 8715 at the Office of the Editor of Bull. Chem. Soc. Jpn.

References

1) Preliminary communication, N. Yonezawa, S. Nonoyama, K. Saigo, and M. Hasegawa, *J. Org. Chem.*, **50**, 3026 (1985).

2) a) N. Yonezawa and M. Hasegawa, *Bull. Chem. Soc. Jpn.*, **56**, 367 (1983); b) N. Yonezawa, T. Yoshida, and M. Hasegawa, *J. Chem. Soc., Perkin Trans. 1*, **1983**, 1083; c) N. Yonezawa, Y. Ikebe, T. Yoshida, T. Hirai, K. Saigo, and M. Hasegawa, *Bull. Chem. Soc. Jpn.*, **57**, 1608 (1983); d) N. Yonezawa, T. Yamashita, T. Kanoe, K. Saigo, and M. Hasegawa, *Ind. Eng. Chem., Prod. Res. Dev.*, **24**, 593 (1985).

3) a) M. Hasegawa, K. Saigo, H. Katsuki, N. Yonezawa, and T. Kanoe, *J. Polym. Sci., Polym. Chem. Ed.*, **21**, 2345 (1983); b) N. Yonezawa, T. Kanoe, K. Saigo, Y. Chen, K. Tachibana, and M. Hasegawa, *J. Polym. Sci., Polym. Lett. Ed.*, **23**, 617 (1985); c) K. Saigo, Y. Chen, N. Yonezawa, K. Tachibana, T. Kanoe, and M. Hasegawa, *Chem. Lett.*, **1985**, 1891.

4) a) J. W. Hanifin and E. Cohen, *J. Org. Chem.*, **33**, 2811 (1968); b) J. W. Hanifin and E. Cohen, *J. Org. Chem.*, **36**, 910 (1971); c) D. J. Haywood, R. G. Hunt, C. J. Potter, and S. T. Reid, *J. Chem. Soc., Perkin Trans. 1*, **1977**, 2458; d) T. Shimo, K. Somekawa, S. Kuwakino, O. Tsuge, and S. Kanemasa, *Chem. Lett.*, **1984**, 1503.

5) T. S. Cartrell, W. S. Haller, and J. C. Williams, *J. Org. Chem.*, **34**, 509 (1969).

6) A. H. A. Tinnemans and D. C. Neckers, *J. Org. Chem.*, **42**, 2374 (1977).

7) D. C. Neckers and A. H. A. Tinnemans, "Synthetic Organic Photochemistry," ed by W. M. Horspool, Plenum Press, New York (1984), p. 285.

8) N. A. Orlow and W. W. Tistschenko, *Chem. Ber.*, **63**, 2948 (1930); R. Fittig and G. Ebert, *Justus Liebigs Ann. Chem.*, **216**, 161 (1882); V. A. Zagorevskii and N. V. Dudykina, *Zh. Obshch. Khim.*, **32**, 2383 (1962); [*Chem. Abstr.*, **58**, 5617e (1963)]; F. C. Cheng and S. F. Tan, *J. Chem. Soc. (C)*, **1968**, 543. D. A. Brent, J. D. Hribar, and D. C. DeJongh, *J. Org. Chem.*, **35**, 135 (1970).

9) D. D. Perrin, W. L. F. Armarego, and D. R. Perrin, "Purification of Laboratory Chemicals," 2nd ed., Pergamon Press, Oxford (1980).

10) C. H. Krauch, S. Farid, and G. O. Schenck, *Chem. Ber.*, **99**, 625 (1966).

11) G. Germain, P. Main, and M. M. Woolfson, *Acta Crystallogr., Sect. A*, **27**, 368 (1971).

12) C. K. Johnson, ORTEP, Report ORNL-3794, Oak Ridge National Laboratory, Oak Ridge, Tennessee, U.S.A., 1965.

 © 1987 The Chemical Society of Japan Bull. Chem. Soc. Jpn., 60, 355—363 (1987)

Syntheses of 23-C-Substituted Derivatives of Mycaminosyl Tylonolide and 4′-Deoxymycaminosyl Tylonolide[1)]

Shuichi SAKAMOTO, Norio KAJIKAWA, Tsutomu TSUCHIYA,* and Sumio UMEZAWA
Institute of Bioorganic Chemistry, 1614 Ida, Nakahara-ku, Kawasaki 211
(Received July 26, 1986)

23-C-Substituted derivatives of mycaminosyl tylonolide (MT) and 4′-deoxymycaminosyl tylonolide (DT) have been prepared by the reaction of protected 23-aldehyde derivatives, 2′,4′-di-*O*-acetyl-3-*O*-*t*-butyldimethylsilyl-23-deoxy-23-oxomycaminosyl tylonolide diethyl acetal (**5**) and 2′-*O*-acetyl-3-*O*-*t*-butyldimethylsilyl-23,4′-dideoxy-23-oxomycaminosyl tylonolide diethyl acetal (**26**), with several Grignard reagents and methyllithium. The final products were (23*S*)- and (23*R*)-23-C-methyl (**13a, 13b**), -ethyl (**14a, 14b**), -butyl (**15a, 15b**), -phenyl (**16b, 16a**), -allyl (**17a, 17b**), -vinyl (**18a, 18b**), -ethynyl (**19b, 19a**) derivatives of MT, and (23*S*)- and (23*R*)-23-C-methyl (**28a, 28b**), -vinyl (**29a, 29b**), and -ethynyl (**30b, 30a**) derivatives of DT. Their configurations at 23-position were determined by the NOE difference spectroscopy on **13a** and **13b**.

As previously reported,[2)] 23-dialkylamino-23-deoxymycaminosyl tylonolides and their 4′-deoxy analogs had considerable antibacterial activities against both Gram-positive and -negative bacteria. Since, generally, macrolide antibiotics are active only against Gram-positive bacteria, the species of the substituents at C-23 of mycaminosyl tylonolides seem important in terms of antibacterial spectrum. This prompted us to modify the substituents at C-23 with new ones. This paper describes[1)] the syntheses of 23-C-alkyl and 23-C-aryl derivatives of mycaminosyl tylonolide (MT) and 4′-deoxymycaminosyl tylonolide[3)] (DT) by way of the C-23- aldehyde intermediates.

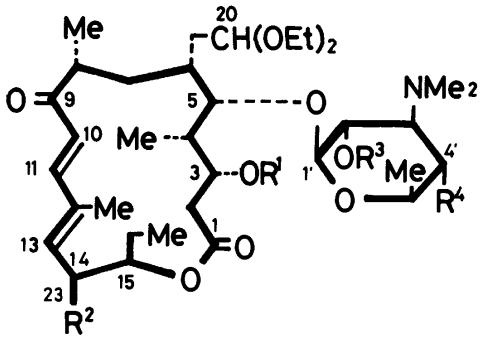

	R^1	R^2	R^3	R^4
1	H	CH_2OH	Ac	OAc
2	$SiMe_2tBu$	CH_2OSiMe_2tBu	Ac	OAc
3	H	CH_2OSiMe_2tBu	Ac	OAc
4	$SiMe_2tBu$	CH_2OH	Ac	OAc
5	$SiMe_2tBu$	CHO	Ac	OAc
8	$SiMe_2tBu$	CH_2OH	H	OH
9	$SiMe_2tBu$	CHO	H	OH
11a	$SiMe_2tBu$	(*S*)CH(OH)Me	Ac	OAc
11b	$SiMe_2tBu$	(*R*)CH(OH)Me	Ac	OAc
12a	$SiMe_2tBu$	(*S*)CH(OH)Me	H	OH
12b	$SiMe_2tBu$	(*R*)CH(OH)Me	H	OH
20	$SiMe_2tBu$	CH_2OSiMe_2tBu	H	OH
21	$SiMe_2tBu$	CH_2OSiMe_2tBu	H	$OSO_2CH_2C_6H_5$
22	$SiMe_2tBu$	CH_2OSiMe_2tBu	H	I
23	$SiMe_2tBu$	CH_2OSiMe_2tBu	H	H
24	$SiMe_2tBu$	CH_2OSiMe_2tBu	Ac	H
25	$SiMe_2tBu$	CH_2OH	Ac	H
26	$SiMe_2tBu$	CHO	Ac	H
27a	$SiMe_2tBu$	(*S*)CH(OH)Me	Ac	H
27b	$SiMe_2tBu$	(*R*)CH(OH)Me	Ac	H

2′,4′-Di-*O*-acetylmycaminosyl tylonolide diethyl acetal[3)] (**1**) was treated with *t*-butylchlorodimethylsilane in the presence of imidazole in *N*,*N*-dimethylformamide (DMF), whereupon the 3,23-di-*O*-silyl derivative (**2**) was obtained almost quantitatively with slight amount of 23-*O*-silyl derivative **3**. Selective removal of the 23-*O*-silyl group of **2** was carried out by treatment with tetrabutylammonium fluoride in oxolane. The *O*-silyl protection proved to be superior to *O*-tetrahydrofuranylation, -tetrahydropyranylation, or -methoxymethylation, because the 3,23-di(acetal) derivatives prepared were difficult to remove selectively their 23-*O*-protecting groups. Oxidation of the resulting 23-hydroxy compound **4** was examined with several reagents; pyridinium chlorochromate (PCC) oxidized the dimethylamino group in addition to the 23-hydroxyl group, dimethyl sulfoxide (DMSO)–acetic anhydride gave a large amount of 23-*O*-(methylthiomethyl) by-product, DMSO-$(COCl)_2$ in the presence of triethylamine (Swern oxidation) gave a large amount of open-macrolactone compound **6**, and only DMSO–dicyclohexylcarbodiimide (DCC) in

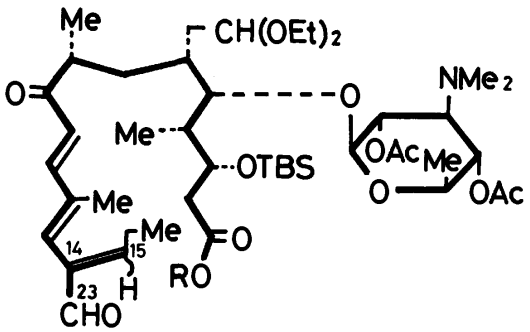

6 R: H
7a, b R: Me

TBS: *t*-butyldimethylsilyl

the presence of pyridinium trifluoroacetate gave the desired product **5** in high yield with slight **6**. The isolated **5** was unstable and readily converted to **6** by β-elimination in the presence of base such as triethylamine or its own basicity caused by 3′-dimethylamino group. The ^{1}H-NMR spectrum of **6** showed, by the decoupling method, that **6** had a new double bond between C-14 and C-15, and was a mixture of two geometrical isomers (the ratio being changed between 2:3—2:1 depending upon the slight change in experimental conditions; but the cause was not pursued). Methylation of **6** with diazomethane gave the corresponding esters **7a** and **7b** proving the presence of a carboxylic acid in **6**.

We next tried to prepare the unprotected 23-oxo derivative (**10**) of MT from **5**. De-*O*-acetylation of **5** in an usual manner[3] (in methanol, 50 °C, 24 h), however, gave the desired de-*O*-acetyl derivative (**9**) in only low yield, possibly by the presence of the unstable 23-aldehyde group. We therefore converted **4** to the 3-*O*-silyl-2′,4′-diol (**8**) which was oxidized by the DMSO–DCC method as described above to afford the 23-oxo derivative (**9**) in a moderate yield (50%). Removal of the acetal and 3-*O*-silyl protecting groups with 5% hydrofluoric acid in acetonitrile gave the 23-oxo compound **10** in a low yield. Efforts to improve the yield were unsuccessful. The presence of two aldehyde groups in **10** was proved by the ^{1}H-NMR spectrum, the signal of the new 23-CHO proton being appeared at δ 9.69.

Methylation of **5** with methylmagnesium bromide in oxolane gave the two 23-C-methyl derivatives (*S* and *R*) in low yields with several by-products including the reduction product **4**; formation of this kind of reduction product **4** sometimes occurs in the reaction with the Grignard reagent. The low yields of the methyl products **11a**, **11b** may be resulted from the partial reaction of the carbonyl group at C-9 of **5** with the Grignard reagent as well as opening of the macrolactone ring during the reaction. In the ^{1}H-NMR spectra, the major product **11a** showed new methyl signals (doublet) at δ 1.12, and the minor (**11b**), at δ 1.22. Since **4** was produced from **5** with limited amount of sodium cyanotrihydroborate, the same R-configuration[4,5] at C-14 of **11a,b** with that of MT was concluded. This was supported by the ^{1}H-NMR spectra of **11a** and **11b**, in that both $J_{13,14}$ and $J_{14,15}$ showed, respectively, almost identical values with those of MT.[5] When **5** was methylated with methyllithium in ether, **11a** was obtained in a better yield. Methanolysis of **11a** and **11b** gave the deacetyl derivatives (**12a** and **12b**), which were led, by deblocking with hydrochloric acid in acetonitrile, to the final 23-C-methyl products **13a**, **13b**.

In the ^{1}H-NMR spectra of **13a** and **13b**, the signals of Me-24 appeared at δ 1.15 and 1.24 (each doublet), respectively, and the methyl configurations were determined by the NOE difference spectroscopy[6] (Fig. 1). Irradiation at δ 1.15 (Me-24) of **13a** caused pronounced positive signal enhancements of H-13, -14, and -23 (the signals of H-5′ were also slightly enhanced possibly by the simultaneous irradiation of Me-6′), whereas irradiation at δ 1.24 (Me-24; Me-21 and Me-6′ were also irradiated simultaneously inevitably) of **13b** caused similar enhancements of H-13, -15, and -23, as well as those of H-10 and 5′. The sharp difference between **13a** and **13b** was that **13a** gave enhancement of H-14, and **13b**, H-15. To satisfy the above result on **13a**, the Me-24 should come stereochemically to the position to bisect the projection angle formed by the C(13)–C(14) and C(14)–H(14) sides (Fig. 1). On the other hand, the small value of $J_{14,23}$(=2 Hz) indicates that H-23 should take gauche (not antiperiplanar) position with respect

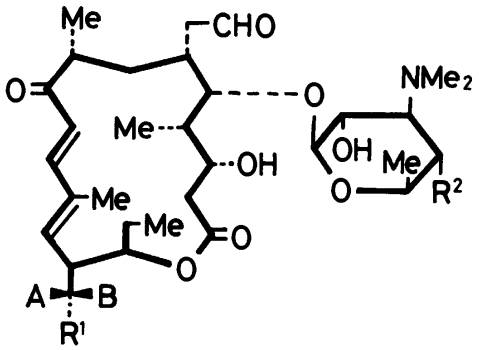

	ac*	A	B	R^1	R^2
MT		H	H	OH	OH
DT		H	H	OH	H
10		=O		H	OH
13a	*S*	OH	H	Me	OH
13b	*R*	H	OH	Me	OH
14a	*S*	OH	H	Et	OH
14b	*R*	H	OH	Et	OH
15a	*S*	OH	H	Bu	OH
15b	*R*	H	OH	Bu	OH
16a	*R*	OH	H	C_6H_5	OH
16b	*S*	H	OH	C_6H_5	OH
17a	*S*	OH	H	$CH_2CH{=}CH_2$	OH
17b	*R*	H	OH	$CH_2CH{=}CH_2$	OH
18a	*S*	OH	H	$CH{=}CH_2$	OH
18b	*R*	H	OH	$CH{=}CH_2$	OH
19a	*R*	OH	H	C≡CH	OH
19b	*S*	H	OH	C≡CH	OH
28a	*S*	OH	H	Me	H
28b	*R*	H	OH	Me	H
29a	*S*	OH	H	$CH{=}CH_2$	H
29b	*R*	H	OH	$CH{=}CH_2$	H
30a	*R*	OH	H	C≡CH	H
30b	*S*	H	OH	C≡CH	H

* Absolute configuration at C-23 by Cahn-Ingold-Prelog specifications.

to H-14 (the projection angle of H(14)-C(14)-C(23)-H(23) should be 68° according to a literature[7]). This conclusion was also supported by another NOE experiment: irradiation of H-23 of **13a** caused positive signal enhancement only of H-14 (12.6%). These results indicate that the absolute configuration at C-23 of **13a** is *S*. In the case of **13b**, the Me-24 was concluded to take the position to bisect the projection angle formed by the C(13)-C(14) and C(14)-C(15) sides. Again from the $J_{14,23}$ value (=6 HZ), the gauche relationship between H-14 and H-23 is concluded (the projection angle of H(14)-C(14)-C(23)-H(23) should be 50°[7]). This conclusion was also supported by another NOE experiment: irradiation of H-23 of **13b** caused positive signal enhancements of H-14 (5%) and H-15 (8%). The absolute configuration at C-23 of **13b** is, therefore, determined to be *R*. Another aspect worthy to mention was that, in **13b**, NOE was observed (not clear in **13a**) between Me-21 and H-10, suggesting close spatial relationship between them.

Other 23-C-substituted derivatives of MT were prepared by treatment of **5** with several other Grignard reagents, that is, ethyl-, butyl-, phenyl-, allyl-, vinyl-, and ethynylmagnesium bromides. In all cases two

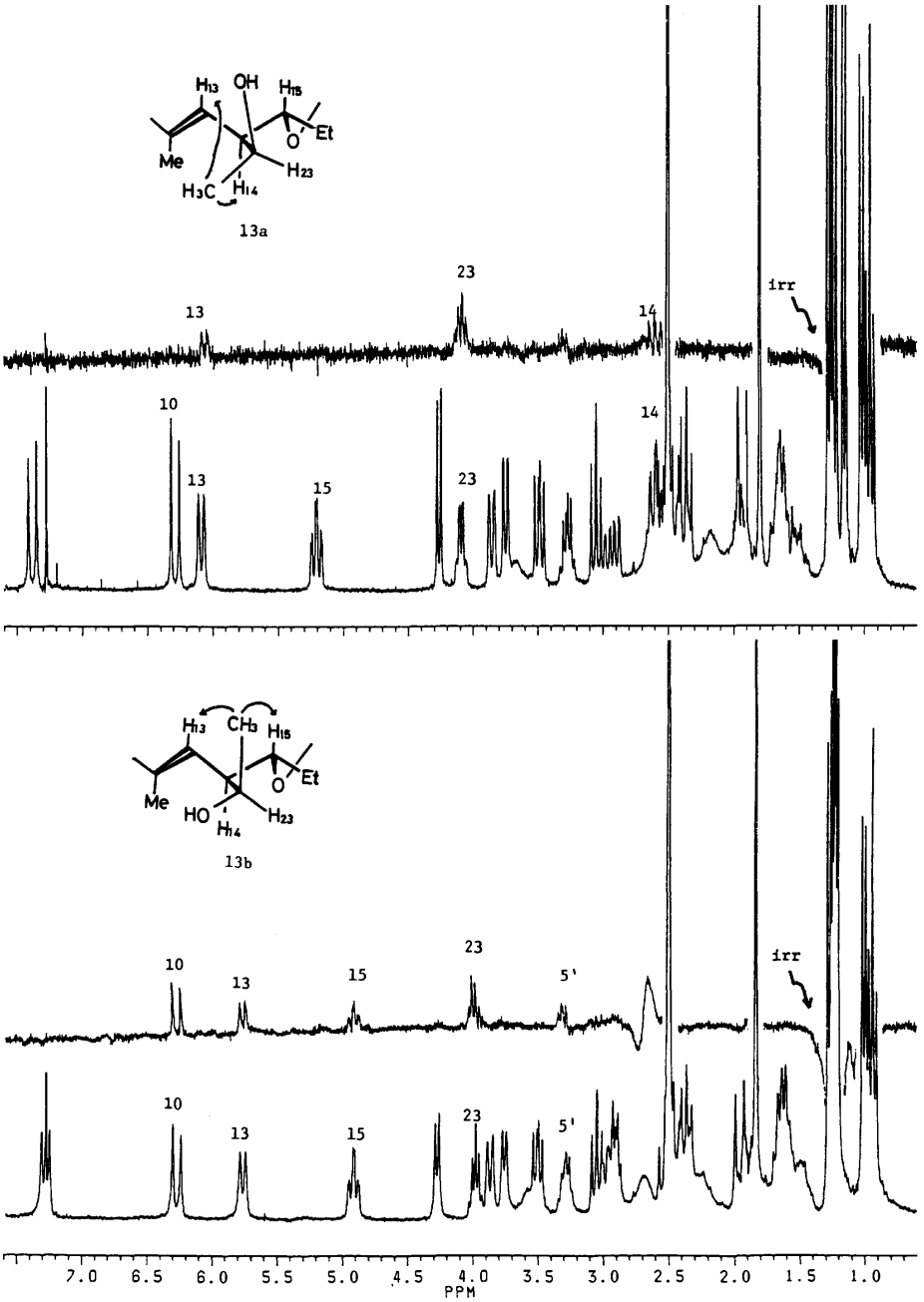

Fig. 1.

products, namely, (*S*)- and (*R*)-23-C-ethyl (**14a**, **14b**), (*S*)- and (*R*)-23-C-butyl (**15a**, **15b**), (*R*)- and (*S*)-23-C-phenyl (**16a**, **16b**), (*S*)- and (*R*)-23-C-allyl (**17a**, **17b**), (*S*)- and (*R*)-23-C-vinyl (**18a**, **18b**), and (*R*)- and (*S*)-23-C-ethynyl derivatives (**19a**, **19b**) of mycaminosyl tylonolide (MT) were produced with by-products accompanied. These products were purified by column chromatography, but with difficulty owing to their close mobilities between products and by-products. The faster-moving products (compounds attached "**a**" to the numbers) had, in all cases, small $J_{14,23}$ values (2—3 Hz) in their ^{1}H-NMR spectra, being the same with the value of **13a**, and the slower-moving (compounds attached "**b**" to the numbers), larger $J_{14,23}$ values (5.5—6.8 Hz), being the same with the value of **13b**. These data are shown in Table 1 with some chemical shifts. The absolute configurations at C-23 of the faster- and slower-moving products were, therefore, specified L and D, respectively, independent of the RS specifications by Cahn-Ingold-Prelog. The fact that L-isomers were always predominating except for the ethynyl derivatives (**19a**,**b**) will be reasonable from the Felkins model[8] describing the approach of the Grignard reagent to a carbonyl carbon (Fig. 2).

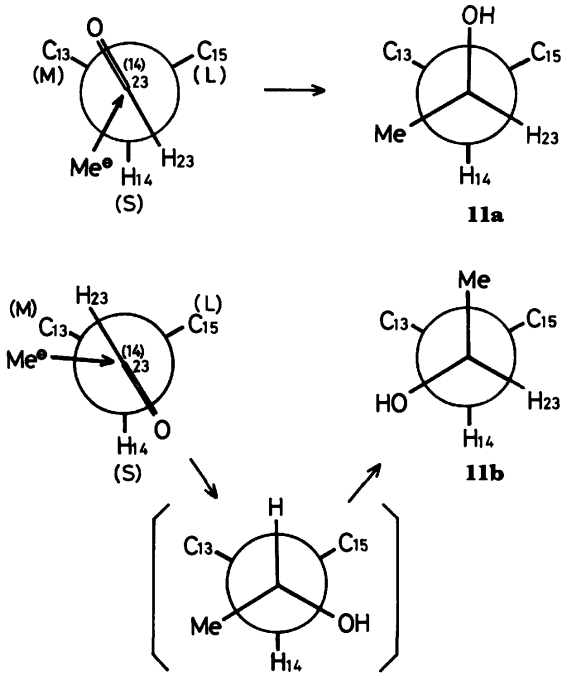

Fig. 2.

The 4′-deoxy analogs (DT-series) of the above MT-series having 23-C-methyl (**28a**,**b**), -vinyl (**29a**,**b**), and -ethynyl (**30a**,**b**) groups were next prepared. In order to remove the C-4′ hydroxyl group before 23-C-alkylation, **2** was solvolyzed with hot methanol, and the 2′,4′-diol (**20**) was treated with phenylmethanesulfonyl chloride. The 4′-*O*-benzylsulfonyl derivative (**21**) was then treated with sodium iodide in 2-butanone, and the 4′-iodo derivative (**22**) was reduced

Table 1. Proton Chemical Shift Data[a] of the Products Prepared [the structure at C-23 is -CHR(OH)]

Compound	R[b]	H-10	H-11	H-13	H-14	H-15	Me-17	Me-18	Me-21	Me-22	H-23	3′-NMe$_2$	$J_{14,23}$[c]
MT	H	6.27	7.30	5.88	2.88	4.98	0.95	1.01	1.22	1.83	3.73	2.55	5.5
13a	Me	6.28	7.38	6.08	2.60	5.20	0.95	1.02	1.22	1.80	4.09	2.50	2
13b	Me	6.27	7.27	5.76	2.91	4.91	0.94	1.01	1.22	1.84	3.98	2.51	6
14a	Et	6.28	7.36	6.07	2.68	5.24	0.95	1.02	1.22	1.81	3.75	2.51	2
14b	Et	6.25	7.24	5.72	2.90	4.96	0.94	1.01	1.22	1.84	3.69	2.51	6.3
15a	Bu	6.27	7.34	6.05	2.66	5.23	0.96	1.01	1.21	1.80	3.82	2.50	2
15b	Bu	6.25	7.25	5.72	2.88	4.97	0.94	1.00	1.21	1.83	3.73	2.51	6.3
16a	Ph	6.14	7.29	6.15	2.88	5.32	1.01	1.00	1.17	1.46	5.03	2.50	2.5
16b	Ph	6.14	7.08	5.55	3.15	4.97	0.95	0.99	1.18	1.72	4.84	2.49	6.8
17a	all	6.30	7.39	6.11	2.69	5.25	0.95	1.02	1.22	1.79	3.90	2.50	2
17b	all	6.26	7.26	5.70	2.86	4.98	0.93	1.00	1.22	1.83	3.8	2.50	6.8
18a	vin	6.27	7.35	6.05	2.75	5.22	0.97	1.01	1.22	1.78	4.37	2.51	2.5
18b	vin	6.26	7.27	5.76	3.03	4.92	0.95	1.01	1.22	1.84	4.31	2 50	5.5
19a	eth	6.32	7.39	6.10	2.91	5.22	0.96	1.02	1.22	1.84	4.62	2.51	2.5
19b	eth	6.30	7.42	6.11	3.11	5.08	0.96	1.02	1.22	1.84	4.56	2.50	5
28a	Me	6.32	7.42	6.12	2.58	5.20	0.95	1.09	1.21	1.79	4.11	2.28	2
28b	Me	6.33	7.31	5.80	2.94	4.89	0.94	1.08	1.20	1.83	3.99	2.27	6.3
29a	vin	6.30	7.39	6.08	2.73	5.22	0.96	1.09	1.21	1.70	4.39	2.27	2.5
29b	vin	6.30	7.32	5.78	3.0	4.89	0.95	1.08	1.21	1.82	4.32	2.27	5.8
30a	eth	6.34	7.41	6.12	2.90	5.23	0.95	1.09	1.21	1.83	4.63	2.27	3.0
30b	eth	6.34	7.42	6.10	3.10	5.07	0.96	1.10	1.27	1.84	4.55	2.27	5.5
Multipl.		d	d	d	ddd	dt	t	d	d	s or d		s	

a) Measured at room temperature; 50 °C for compounds MT, **15a** and **15b**. b) Abbreviations: all=allyl, vin=vinyl, and eth=ethynyl. c) Multiplicities of H-23 were dq (for 23-L products) and quintet (23-D products).

with tributylstannane to give the 4′-deoxy derivative (**23**). The above reaction sequence is fundamentally the same with the procedure previously reported.[3] Acetylation of **23** gave the 2′-*O*-acetyl-4′-deoxy derivative (**24**). The all-protected derivative was then subjected to the procedure described in the MT-series, that is, 23-de-*O*-silylation (to give **25**), oxidation (to give the 23-oxo derivative, **26**), alkylation with methylmagnesium bromide or the other Grignard reagents (to give **27a**, **27b**, and other 23-C-alkyl derivatives), and deblocking to give the final products (**28a,b**, **29a,b**, and **30a,b**). Elemental analyses of the products are shown in Table 2 with some other data.

Antibacterial spectra[1] of these products showed diverse activity results, but D-series products always had stronger activities than those of the corresponding L-isomers. Compound **10** showed markedly decreased antibacterial activity.

Experimental

General. Grignard reagents (MeMgBr, EtMgBr, *n*-BuMgBr, PhMgBr, AllylMgBr) were purchased from Tokyo Kasei Kogyo Co., Ltd., and methyllithium (1.5 M solution in diethyl ether 1 M=1 mol dm^{-3}), from Aldrich Chem. Co. Thin-layer chromatography (TLC) was carried out on kieselgel 60 F-254 silica gel (E. Merck) with detection by spraying with sulfuric acid, followed by slight heating. Column chromatography was performed on Wakogel C-200 or Kieselgel 60, 230—400 mesh (E. Merck). Optical rotations were measured with a Perkin-Elmer 241 polarimeter. ^{1}H-NMR spectra were recorded at 250 MHz at room temperature, unless otherwise stated, in the FT mode with a Bruker WM 250 spectrometer, or at 90 MHz with a Varian EM-390 spectrometer.

2′,4′-Di-*O*-acetyl-3,23-bis(*O*-*t*-butyldimethylsilyl)mycaminosyl Tylonolide Diethyl Acetal (2). To a mixture of **1**[3] (22.5 g) and imidazole (12.1 g) in dry *N*,*N*-dimethylformamide (23 ml) was added *t*-butylchlorodimethylsilane (22.4 g) and the solution was heated at 75 °C overnight. Evaporation with several additions of xylene gave a residue, that was extracted with benzene (2 L). The solution was washed with saturated aqueous sodium hydrogencarbonate, saturated aqueous sodium sulfate, dried (Na_2SO_4), and evaporated to give a solid (29 g). The solid showed, on TLC with toluene–ethyl acetate (2:1), spots at R_f 0.7 (**2**), 0.65 (trace, **3**), and 0 (cf **1**: R_f=0.15). An analytical sample of **2** was prepared by silica-gel column chromatography with toluene–ethyl acetate (3:1), $[\alpha]_D^{22}$ −11° (*c* 1, $CHCl_3$); ^{1}H-NMR ($CDCl_3$) δ=−0.04, 0.03, 0.04, and 0.17 (each 3H s, $SiMe_2$×2), 0.87 (18H s, Si-*t*Bu×2), 1.78 (3H s with slight splittings, Me-22), 2.06 and 2.07 (each 3H s Ac×2), 2.34 (6H s, NMe_2), 3.67 (2H, H-23a,b), 3.98 (1H sl. br d, $J_{2b,3}$[7] ≈6.5 Hz, H-3), 4.35 (1H br d, *J*≈7.5 Hz, H-1′), 4.75 (1H t, J=10 Hz, H-4′), 4.89 (1H dd, *J*=7.5 and 10 Hz, H-2′), 5.78 (1H d, $J_{13,14}$=10.5 Hz, H-13), 6.25 (1H d, $J_{10,11}$=15 Hz, H-10), 7.18 (1H d, H-11).

Found: C, 62.47; H, 9.32; N, 1.56%. Calcd for $C_{51}H_{93}NO_{13}Si_2$: C, 62.26; H, 9.46; N, 1.42%.

3: $[\alpha]_D^{22}$ −12° (*c* 1, $CHCl_3$); ^{1}H-NMR ($CDCl_3$) δ=0.05 and 0.06 (each 3H s, $SiMe_2$), 0.89 (9H s, Si-*t*-Bu), 1.79 (3H s with slight splittings, Me-22), 2.06 and 2.07 (each 3H s,

Table 2.

Compound	Yield[a]	$[\alpha]_D^{22}$ (*c* 1, $CHCl_3$)	Formula	C (%)		H (%)		N (%)	
				Found	Calcd	Found	Calcd	Found	Calcd
13a	26	−10°	$C_{32}H_{53}NO_{10}$	62.50	62.85	8.54	8.67	2.21	2.29
13b	7.8	+16°	$C_{32}H_{53}NO_{10}$	62.54	62.85	8.66	8.67	2.25	2.29
14a	21	−6°	$C_{33}H_{55}NO_{10}\cdot H_2O$	61.89	61.58	8.61	8.86	1.94	2.17
14b	4	+9°	$C_{33}H_{55}NO_{10}$	63.31	63.36	8.84	8.80	2.28	2.24
15a	8	+7°	$C_{35}H_{59}NO_{10}$	64.34	64.32	9.03	9.04	2.32	2.14
15b	2.3	+30°	$C_{35}H_{59}NO_{10}$	64.07	64.32	9.01	9.04	2.16	2.14
16a	21	+81°	$C_{37}H_{55}NO_{10}$	66.01	65.97	8.36	8.17	1.95	2.08
16b	9.2	+30°	$C_{37}H_{55}NO_{10}\cdot 2/3H_2O$	64.73	64.82	8.24	8.13	2.09	2.04
17a	7	+40°	$C_{34}H_{55}NO_{10}$	63.89	64.05	8.60	8.63	2.23	2.20
17b	3.8	−10°	$C_{34}H_{55}NO_{10}\cdot H_2O$	62.55	62.29	8.41	8.70	2.07	2.14
18a	29	−3°	$C_{33}H_{53}NO_{10}\cdot H_2O$	61.69	61.78	8.23	8.58	2.27	2.18
18b	7	0°	$C_{33}H_{53}NO_{10}$	63.32	63.56	8.56	8.51	2.05	2.25
19a	13	+65°	$C_{33}H_{51}NO_{10}$	63.61	63.77	8.47	8.21	2.02	2.25
19b	14	−39°	$C_{33}H_{51}NO_{10}\cdot H_2O$	61.42	61.97	7.96	8.29	2.21	2.19
28a	20	−16°	$C_{32}H_{53}NO_9$	64.25	64.54	8.80	8.91	2.41	2.35
28b	7	+12°	$C_{32}H_{53}NO_9\cdot 1/2H_2O$	63.81	63.58	8.87	8.94	2.44	2.32
29a	18	0°	$C_{33}H_{53}NO_9$	64.97	65.24	8.76	8.73	2.50	2.31
29b	8	0°	$C_{33}H_{53}NO_9$	65.46	65.24	8.81	8.73	2.27	2.31
30a	6.2	+7°	$C_{33}H_{51}NO_9$	65.71	65.45	8.54	8.43	2.29	2.31
30b	6.3	−36°	$C_{33}H_{51}NO_9$	65.10	65.45	8.30	8.43	2.23	2.31

a) Based on **4** or **25** and after purification; the 23-L and 23-D products were, respectively, purified in the same manner; in **13b** and **14b**, however, the yields were estimated from the mixture of the product and MT owing to difficulty of separation.

AcX2), 2.34 (6H s, NMe_2), ≈3.68 (H-23a,b), 3.78 (1H dd, $J_{3,OH}$≈4.5, $J_{2b,3}$=10 Hz, H-3), 4.40 (1H d, J=7.5 Hz, H-1'), 4.77 (1H t, H-4'), 4.91 (1H dd, H-2'), 5.87 (1H d, H-13), 6.31 (1H d, H-10), 7.25 (1H d, H-11); Irradiation at δ 2.46 (dd, H-2b)[7] collapsed the double doublets of H-3 to a doublet.

Found: C, 62.22; H, 8.99; N, 1.42%. Calcd for $C_{45}H_{79}NO_{13}Si$: C, 62.14; H, 9.09; N, 1.61%.

2',4'-Di-*O*-acetyl-3-*O*-*t*-butyldimethylsilylmycaminosyl Tylonolide Diethyl Acetal (4). To an ice-cold solution of crude **2** (29 g) in oxolane (290 ml) was added a M solution (29.5 ml) of tetrabutylammonium fluoride (1 moler equivalent for **2**) in oxolane (the solution contained <5% of water, Aldrich Chem. Co., Wisconsin, U.S.A.), and the solution was kept at room temperature for 1 h. On cheking by TLC with toluene–ethyl acetate (1:1), the solution showed a major spot at R_f 0.45. Evaporation gave a residue, that was extracted with benzene (1 L). The organic solution was washed with saturated aqueous sodium hydrogencarbonate, saturated aqueous sodium sulfate, dried (Na_2SO_4), and evaporated. The residue was chromatographed on a silica-gel column with toluene–ethyl acetate (3:2) to give a solid of **4**, 19.7 g (72% from **1**); $[\alpha]_D^{22}$ −10° (*c* 1, $CHCl_3$); ^{1}H-NMR ($CDCl_3$) δ=−0.04 and 0.175 (each 3H s, $SiMe_2$), 0.87 (9H s, Si-*t*-Bu), 1.82 (3H, Me-22), 2.06 and 2.07 (each 3H s, AcX2), 2.34 (6H s, NMe_2), 3.98 (1H d, $J_{2b,3}$=7 Hz, H-3), 4.35 (1H br d, H-1'), 4.74 (1H t, H-4'), 4.89 (1H dd, H-2'), 5.74 (1H d, H-13), 6.28 (1H d, H-10), 7.18 (1H d, H-11).

Found: C, 62.35; H, 8.98; N, 1.53%. Calcd for $C_{45}H_{79}NO_{13}Si$: C, 62.14; H, 9.09; N, 1.61%.

2',4'-Di-*O*-acetyl-3-*O*-*t*-butyldimethylsilyl-23-deoxy-23-oxomycaminosyl Tylonolide Diethyl Acetal (5). A mixture of **4** (2.24 g), pyridinium trifluoroacetate (747 mg) and dicyclohexylcarbodiimide (2.13 g) in benzene–dimethyl sulfoxide (1:1, 45 ml) was stirred at room temperature overnight. Oxalic acid dihydrate (1.95 g) in 1,4-dioxane (22.5 ml) was added and the mixture was stirred for 30 min. The resulting precipitates were filtered off with aid of benzene, and the organic solution was concentrated. The residue was extracted with benzene and the solution was thoroughly washed with saturated aqueous sodium hydrogencarbonate (to remove dimethyl sulfoxide), saturated aqueous sodium sulfate, dried (Na_2SO_4), and evaporated. The residue showed, on TLC with toluene–ethyl acetate (1:1), two spots at R_f 0.55 (**5**) and R_f 0.3 (minor, **6**). Column chromatography of the residue with toluene–ethyl acetate (2:1→1:1) gave solids of **5**, 1.93 g (86%) and **6**, 0.32 g (14%).

5: $[\alpha]_D^{22}$ −40° (*c* 1, $CHCl_3$); ^{1}H-NMR ($CDCl_3$) δ=−0.04 and 0.17 (each 3H s, $SiMe_2$), 0.88 (9H s, Si-*t*-Bu), 1.85 (3H, Me-22), 2.07 and 2.08 (each 3H s, AcX2), 2.36 (6H s, NMe_2), 3.57 (1H dt, H-14), 3.99 (1H d, H-3), 4.37 (1H d, H-1'), 4.75 (1H t, H-4'), 4.89 (1H dd, H-2'), 5.25 (1H dt, H-15), 5.77 (1H d, H-13), 6.33 (1H d, H-10), 7.18 (1H d, H-11), 9.67 (1H d, H-23); $J_{2b,3}$=7,5, $J_{10,11}$=16, $J_{13,14}$=10, $J_{14,15}$=9, $J_{14,23}$=3.8, $J_{15,16a}$=9.5, $J_{15,16b}$=2.5, $J_{1',2'}$=7.5 Hz. Irradiation of H-14 collapsed the double triplets of H-15 to a broadened doublet, and the doublets of H-13 and H-23 to a singlet, respectively. Irradiation of H-23 collapsed the double triplets of H-14 to a triplet.

Found: C, 62.24; H, 8.77; N, 1.49%. Calcd for $C_{45}H_{77}NO_{13}Si$: C, 62.28; H, 8.88; N, 1.61%.

6: $[\alpha]_D^{25}$ −32° (*c* 1, $CHCl_3$); ^{1}H-NMR ($CDCl_3$; the ratio of the components of **6** changed (A/B=2/1—2/3) depending on the experimental conditions, on which no study was carried out): δ=0.06 (for A/2) and 0.09 (A/2 +B) (6H in total, each s, $SiMe_2$), 0.90 (9H d, Si-*t*-Bu), 1.25(B) and 1.69(A) (3H in total, each s with small splittings, Me-22), 2.06 (6H s, AcX2), 2.34 (6H s, NMe_2), ≈2.3 (H-16), ≈2.5 (H-2), 3.96 (1H m, H-3), 4.38 (1H d, H-1'), 4.59 (1H m, H-20), 4.74 (1H t, H-4'), 4.90 (1H dd, H-2'), 6.26(B) and 6.28(A) (1H in total, each d, H-10), 6.36 (1H sl. br s, H-13), 6.69(A) and 6.72(B) (1H in total, each t, H-15), 7.11(B) and 7.33(A) (1H in total, each d, H-11), 9.44(A) and 9.46(B) (1H in total, each s, H-23); $J_{10,11}$=15.5, $J_{13,16}$≦1, $J_{15,16a}$=$J_{15,16a}$=7.5 Hz. Irradiation of H-16 collapsed the triplet of H-15 to a singlet and sharpened the broad singlet of H-13. Irradiation of H-13 sharpened the signals of both H-16 and H-23.

Esterification of 6 (obtained by a run) with Diazomethane (to give 7a and 7b). To a solution of **6** (65.4 mg) in chloroform (0.65 ml) was added 0.3 M diazomethane in ether (1.8 ml) and the solution was kept at room temperature for 1 h. The solution showed, on TLC with toluene–ethyl acetate (2:1), two spots at R_f 0.35 and R_f 0.25. Evaporation gave a residue, that was subjected to column chromatography with hexane–ethyl acetate (4:1→2:1) to give solids of **7a** (R_f=0.35), 25.4 mg (38%) and **7b** (R_f=0.25), 19.5 mg (29%).

7a: ^{1}H-NMR ($CDCl_3$) δ=0.04 and 0.08 (each 3H s, $SiMe_2$), 0.89 (9H s, Si-*t*-Bu), 2.04 and 2.06 (each 3H s, AcX 2), 2.25 (2H quintet, H-16), 2.34 (6H s, NMe_2), a set of eight signals typical for the AB part of an ABX system centered at 2.50 (2H, J=6.75 and 15 Hz, H-2a,b), 3.67 (3H s, CO_2Me), 4.03 (1H m, H-3), 4.40 (1H d, J=7.5 Hz, H-1'), 4.55 (1H m, H-20), 4.72 (1H t, H-4'), 4.89 (1H dd, H-2'), 6.25 (1H sl. br s, H-13), 6.35 (1H d, H-10), 6.67 (1H sl, br t, H-15), 7.11 (1H d, H-11), 9.46 (1H s, H-23); $J_{10,11}$=15.5, $J_{15,16a}$=$J_{15,16b}$=7.5 Hz.

7b: ^{1}H-NMR ($CDCl_3$) δ=0.04 and 0.08 (each 3H s, $SiMe_2$), 0.89 (9H s, Si-*t*-Bu), 2.05 (6H s, AcX2), 2.27 (2H quintet, H-16), 2.34 (6H s, NMe_2), 2.52 (2H, H-2a,b), 3.69 (3H s, CO_2Me), 4.05 (1H, br, H-3), 4.41 (1H d, H-1'), 4.58 (1H t, H-20), 4.72 (1H t, H-4'), 4.89 (1H dd, H-2'), 6.27 1H d, H-10), 6.35 (1H sl. br s, H-13), 6.63 (1H t, $J_{15,16a}$=$J_{15,16b}$=7.5 Hz, H-15), 7.32 (1H d, H-11), 9.46 (1H s, H-23).

In the 250 MHz ^{1}H shift-correlated 2D NMR spectrum, Me-17 could be correlated to H-16, and the latter, to H-15.

3-*O*-*t*-Butyldimethylsilylmycaminosyl Tylonolide Diethyl Acetal (8). A solution of **4** (100 mg) in methanol (2 ml) was heated at 50 °C for 24 h. Evaporation was followed by extraction of the residue with chloroform. The organic solution was washed with saturated aqueosu sodium hydrogencarbonate, saturated aqueous sodium sulfate, dried (Na_2SO_4), and evaporated to give a solid of **8**, 89 mg (98%); $[\alpha]_D^{22}$ −2° (*c* 1, $CHCl_3$); ^{1}H-NMR ($CDCl_3$) δ=−0.04 and 0.18 (each 3H s, $SiMe_2$), 0.85 (9H s, Si-*t*-Bu), 0.93 (3H t, Me-17), 0.99 (3H d, Me-18), 1,83 (3H, Me-22), 2.50 (6H s, NMe_2), 3.03 (1H t, H-4'), 3,53 (1H dd, H-2'), 4.02 (1H sl. br d, H-3), 4.27 (1H sl. br d, H-1'), 4.73 (1H br dd, H-20), 4.90 (1H dt, H-15), 5.77 (1H d, H-13), 6.27 (1H d, H-10), 7.21 (1H d, H-11); $J_{2b,3}$=6, $J_{4,18}$=7, $J_{10,11}$=16, $J_{13,14}$=10, $J_{14,15}$=$J_{15,16a}$=9, $J_{15,16b}$=2.5, $J_{1',2'}$=6.5, $J_{2'3'}$=$J_{3'4'}$=$J_{4'5'}$=10Hz.

Found: C, 62.77; H, 9.41; N, 1.71%. Calcd for $C_{41}H_{75}NO_{11}Si$: C, 62.68; H, 9.55; N, 1.78%.

3'-*O*-*t*-Butyldimethylsilyl-23-deoxy-23-oxomycaminosyl

Tylonolide Diethyl Acetal (9). From 5. A solution of **5** (22.2 mg) in methanol (0.1 ml) was heated at 50 °C for 24 h. TLC (chloroform–methanol–28% aqueous ammonia= 10:1:0.1) of the reaction mixture showed two spots at R_f 0.3 (**9**) and R_f 0.01 (major). Evaporation was followed by extraction of the residue with chloroform. The solution was washed with saturated aqueous sodium sulfate, dried (Na_2SO_4), and evaporated. The residue was chromatographed on a silica-gel column with chloroform–methanol–28% aqueous ammonia (20:1:0.1) to give a solid of **9**, 6.9 mg (34%).

From 8. A mixture of **8** (300 mg), pyridinium trifluoroacetate (74 mg) and dicyclohexylcarbodiimide (315 mg) in benzene–dimethyl sulfoxide (1:1, 6 ml) was stirred at room temperature overnight. The solution showed, on TLC with chloroform–methanol–28% aqueous ammonia (10:1:0.1), a spot at R_f 0.3 (major, **9**) with several minors. The solution was then treated as usual to give, after chromatography (chloroform–methanol–28% aqueous ammonia=10:1:0.1), a solid of **9**, 150 mg (50%); $[\alpha]_D^{23}$ −40° (*c* 1, $CHCl_3$); ^{1}H-NMR ($CDCl_3$) δ=−0.04 and 0.16 (each 3H s, $SiMe_2$), 0.89 (9H s, Si-*t*-Bu), 1.85 (3H d, $J\approx1$ Hz, Me-22), 2.56 (6H s, NMe_2), 4.02 (1H d, H-3), 4.35 (1H d, H-1′), 5.25 (1H dt, H-15), 5.78 (1H d, H-13), 6.32 (1H d, H-10), 7.19 (1H d, H-11), 9.66 (1H d, H-23); $J_{14,15}\approx9$, $J_{14,23}$=3.8 Hz.

Found: C, 62.53; H, 9.13; N, 1.90%. Calcd for $C_{41}H_{73}NO_{11}Si$: C, 62.83; H, 9.32; N, 1.42%.

23-Deoxy-23-oxomycaminosyl Tylonolide (10). To a solution of **9** (20 mg) in acetonitrile (0.1 ml) in a silicone vessel was added 10% aqueous hydrofluoric acid (0.1 ml) and the solution was kept at 27 °C overnight. The solution showed, on TLC with chloroform–methanol–28% aqueous ammonia (5:1:0.1), spots at R_f 0.38 (**10**) and R_f 0. Afrer addition of saturated aqueous sodium hydrogencarbonate (0.5 ml), the reaction mixture was extracted with chloroform. The organic solutioon was washed with saturated aqueous sodium sulfate, dried (Na_2SO_4), and evaporated. The residue was chromatographed over silica gel with chloroform–methanol (7:1) to give an unstable solid of **10**, 3.9 mg (26%); $[\alpha]_D^{22}$ −60° (*c* 1, $CHCl_3$); ^{1}H-NMR ($CDCl_3$) δ=0.96 (3H t, Me-17), 1.02 (3H d, Me-18), 1.22 (3H d, Me-21), 1.27 (3H d, Me-6′), 1.87 (3H d, $J\approx1$ Hz, Me-22), 1.96 (1H d, H-2a), 2.40 (1H t, H-3′), 2.52 (6H s, NMe_2), 2.56 (1H dd, H-2b), 2.96 (1H ddd, H-19b), 3.07 (1H t, H-4′), 3.27 (1H m, H-5′), 3.49 (1H dd, H-2′), 3.65 (1H dt, H-14), 3.74 (1H dd, H-5), 3.87 (1H d, H-3), 4.27 (1H d, H-1′), 5.30 (1H dt, H-15), 5.83 (1H d, H-13), 6.36 (1H d, H-10), 7.31 (1H d, H-11), 9.69 (1H d, H-23), 9.71 (1H s, H-20); $J_{13,14}$= $J_{14,15}$=10, $J_{14,23}$=3.8 Hz; other *J* values were almost the same with those of the related compounds reported.[7] Irradiation of H-14 collapsed the double triplets of H-15 to double doublets, and the doublets of H-13 and H-23 to a singlet, respectively.

Found: C, 61.47; H, 8.41; N, 2.44%. Calcd for $C_{31}H_{49}NO_{10}\cdot1/2\ H_2O$: C, 61.59; H, 8.28; N, 2.32%.

(23*S*)- and (23*R*)-2′4′-Di-*O*-acetyl-3-*O*-*t*-butyldimethylsilyl-23-C-methylmycaminosyl Tylonolide Diethyl Acetal (11a, 11b). Procedure A. To a cold (−78 °C) solution of **5** (570 mg) in oxolane (7 ml) was added methylmagnesium bromide (1 ml of M solution in oxolane) and the mixture was stirred at the temperature for 1.5 h, then kept at room temperature for 1 h. The reaction mixture was poured into an ice-cold half-saturated aqueous ammonium chloride (30 ml) and extracted with chloroform. The organic solution combined was washed with saturated aqueous sodium sulfate, dried (Na_2SO_4), and evaporated to give a residue. Silica-gel column chromatography of the residue with toluene–ethyl acetate (2:1) gave, from the earlier fractions, a solid of **11a**, 236 mg (36%), and from the later, a mixture of **11b** and **4**, 114 mg, the both compounds had the same mobility on chromatogram.

11a: $[\alpha]_D^{21}$ −10° (*c* 1, $CHCl_3$); ^{1}H-NMR ($CDCl_3$) δ=−0.04 and 0.18 (each 3H s, $SiMe_2$), 0.87 (9H s, Si-*t*Bu), 1.12 (3H d, Me-24), 1.78 (3H short-spaced d, Me-22), 2.06 and 2.08 (each 3H s, Ac×2), 2.35 (6H s, NMe_2), 2.45 (1H dd, $J_{2,3}$=7, $J_{2a,b}$=19 Hz, H-2b), 2.49 (1H dt, H-14), 2.73 (1H t, H-3′), 3.98 (1H br d, H-3), 4.10 (H-23), 4.36 (1H br d, H-1′), 4.68 (1H, br, H-20), 4.75 (1H t, H-4′), 4.89 (1H dd, H-2′), 5.13 (1H dt, H-15), 5.96 (1H d, H-13), 6.27 (1H d, H-10), 7.23 (1H d, H-11); $J_{13,14}$=10, $J_{14,15}$=9, $J_{14,23}$=2.5, $J_{23,Me\text{-}24}$=7 Hz. Irradiation of H-23 collapsed the doublet of Me-24 and the double triplets of H-14 to a singlet and a triplet, respectively.

Found: C, 62.59; H, 9.17; N, 1.67%. Calcd for $C_{46}H_{80}NO_{13}Si$: C, 62.59; H, 9.07; N, 1.59%.

11b: $[\alpha]_D^{21}$ +11° (*c* 1, $CHCl_3$); ^{1}H-NMR ($CDCl_3$) δ=−0.04 and 0.18 (each 3H s, $SiMe_2$), 0.87 (9H s, Si-*t*Bu), 1.22 (3H d, Me-24), 1.83 (3H short-spaced d, Me-22), 2.06 and 2.07 (each 3H s, Ac×2), 2.34 (6H s, NMe_2), 2.47 (1H dd, H-2b), 2.73 (1H t, H-3′), 2.88 (1H dt, H-14), 3.98 (1H br d, H-3), 3.98 (1H br d, H-23), 4.35 (1H d, H-1′), 4.68 (1H, br, H-20), 4.75 (1H t, H-4′), 4.85 (1H, H-15), 4.89 (1H dd, H-2′), 5.73 (1H d, H-13), 6.27 (1H d, H-10), 7.18 (1H d, H-11); $J_{13,14}$=$J_{14,15}$=10, $J_{14,23}$=6, $J_{23,Me\text{-}24}$=6.5 Hz. Irradiation at δ=3.98 collapsed the doublet of Me-24 and double triplets of H-14 to a singlet and a triplet, respectively.

Procedure B. To a cold (−78 °C) solution of **5** (310 mg) in dry diethyl ether (3.1 ml) was added methyllithium (0.25 ml of 1.5 M solution in diethyl ether) and the mixture was stirred in the cold for 1.5 h, then the resulting yellow suspension was kept at room temperature for 1 h. Work-up as described for Procedure A gave a crude mixture. Silica-gel column chromatography of the mixture with toluene–ethyl acetate (2:1→1:1) gave solids of **11a**, 140 mg (44%) and **11b**, 36 mg (≈11%, slightly contaminated with **4**).

(23*S*)-23-C-Methylmycaminosyl Tylonolide (13a). A solution of **11a** (236 mg) in methanol (2.4 ml) was heated at 50 °C overnight. Evaporation gave a solid of **12a**. To a solution of the solid in acetonitrile (1.2 ml) was added M aqueous hydrochloric acid (1.2 ml) and the solution was kept at 37 °C overnight. On TLC with chloroform–methanol–28% aqueous ammonia (9:1:0.1), the solution showed a spot (R_f=0.23). Addition of saturated aqueous sodium hydrogencarbonate (10 ml) was followed by extraction of the mixture with chloroform. The organic solution isolated was washed with saturated aqueous sodium sulfate, dried (Na_2SO_4), and evaporated to give a solid (178 mg). Silica-gel column chromatography with chloroform–methanol–28% aqueous ammonia (20:1:0.1→10:1:0.1) gave a solid of **13a**, 121 mg (74%).

13a: ^{1}H-NMR ($CDCl_3$) δ=1.15 (3H d, Me-24), 1.27 (3H d, Me-6′), 2.36 (1H t, J=10 Hz, H-3′), 2.93 (1H ddd, J=1.5, 10, and 17.5 Hz, H-19b), 3.05 (1H t, J=10 Hz, H-4′), 3.27 (1H m, H-5′), 3.49 (1H dd, H-2′), 3.75 (1H d, H-5), 3.86 (1H sl. br d, H-3), 4.26 (1H d, J=7.5 Hz, H-1′), 9.69 (1H

s, H-20); $J_{13,14}$=10.8, $J_{14,15}=J_{15,16a}$=9.5, $J_{15,16b}$=3, $J_{23,Me\cdot24}$= 7.5 Hz. Irradiation of H-14 collapsed the signals of H-13, H-15, and H-23 to a singlet, a broad doublet, and a quartet, respectively. Irradiation of H-23 collapsed the doublet of Me-24 to a singlet.

(23*R*)-23-C-Methylmycaminosyl Tylonolide (13b). A solution of crude **11b** (114 mg obtained by Procedure A) was treated as described for **13a** and the products were twice chromatographed (to remove MT accompanied) as described, to give solids of **13b**, 39 mg (7.8% from **4**) and mycaminosyl tylonolide (19 mg).

13b: ^{1}H-NMR ($CDCl_3$) δ=1.24 (3H d, Me-24), 1.27 (3H d, Me-6'), 2.37 (1H t, H-3'), 3.05 (1H t, H-4'), 3.28 (1H m, H-5'), 3.50 (1H dd, H-2'), 3.76 (1H d, H-5), 3.87 (1H d, H-3), 4.28 (1H d, H-1'), 9.70 (1H s, H-20); $J_{13,14}$=10.5, $J_{14,15}=J_{15,16a}$=9.0, $J_{15,16b}$=3, $J_{23,Me\cdot24}\approx$6 Hz. Irradiation of H-23 collapsed the signals of H-14 and Me-24 to a triplet and a singlet, respectively.

General Procedure for the Syntheses of 14a,b—19a,b. A mixture of **4** (900 mg), pyridinium trifluoroacetate (300 mg) and dicyclohexylcarbodiimide (850 mg) in benzene–dimethyl sulfoxide (1:1 18 ml) was stirred at room temperature for **6 h** and the mixture was treated as described for **5** to give, without chromatography, a crude product (900 mg). To a cold (−78 °C) solution of the product in dry oxolane (9 ml) was added ethylmagnesium bromide (0.8 ml of 3 M solution in ether; for the preparation of **14a,b**), butylmagnesium bromide (1.2 ml of 2 M solution in oxolane, for **15a,b**), phenylmagnesium bromide (1.2 ml of 2 M solution in oxolane, for **16a,b**), allylmagnesium bromide (2.4 ml of M solution in ether, for **17a,b**), vinylmagnesium bromide [prepared from magnesium turnings (960 mg) and vinyl bromide (3.5 ml) in oxolane (20 ml) and used 2 ml of this solution; for **18a,b**] or ethynylmagnesium bromide [prepared by dropwise addition of EtMgBr (5 ml of 3 M solution in ether) to acetylene saturated in oxolane (10 ml) at 0—5 °C and used 4 ml of this red solution; for **19a,b**], and the mixture was kept at −78 °C for 1 h (at 0—5 °C for **19**), then kept at room temperature for 1 h. Work-up as described for **11a,b** gave, after column chromatography with toluene–ethyl acetate (2:1), a mixture of reaction products. Each product mixture was then methanolized and hydrolyzed as described for **13a** to give, after column chromatography with chloroform–methanol–28% aqueous ammonia (20:1:0.1→10:1:0.1), a final set of products as the solids of **14a,b—19a,b** (see Table 2).

3,23-Bis(*O*-*t*-butyldimethylsilyl)-4'-deoxymycaminosyl Tylonolide Diethyl Acetal (23). A solution of **2** (14.4 g) in methanol (144 ml) was heated at 50 °C overnight. Evaporation gave a residue, that was extracted with chloroform. The organic solution was washed with saturated aqueous sodium hydrogencarbonate, saturated aqueous sodium sulfate, dried (Na_2SO_4), and evaporated to give a solid of **20** (12.7 g, 96%). To a cold (−40 °C) solution of the solid (12.7 g) in pyridine (127 ml) was added phenylmethanesulfonyl chloride (2.7 g initially, and 1.38 g after 1 hour) and the solution was kept at −40 °C for 5.5 h in total. After addition of water (0.5 ml), the solution was concentrated to give a residue, that was extracted with chloroform. The organic solution was washed with saturated aqueous sodium hydrogencarbonate, saturated aqueous sodium sulfate, dried (Na_2SO_4), and evaporated. The residue showed, on TLC with toluene–ethyl acetate (2:1), a spot at R_f 0.65 (major, **21**) with trace spots of R_f 0.8 and R_f 0. A mixture of the residue and sodium iodide (4.2 g) in 2-butanone (127 ml) was heated at 80 °C for 1 h. TLC (toluene–ethyl acetate 2:1) of the solution showed a spot (**22**) of the same R_f value with that of **21**. Filtration followed by evaporation gave a solid, that was extracted with benzene. The organic solution was washed with 0.1 M aqueous sodium thiosulfate, saturated aqueous sodium sulfate, dried (Na_2SO_4), and evaporated to give a solid. To a solution of the solid in benzene (127 ml) was added tributylstannane (12.3 g) and the solution was refluxed for 9 h. TLC (cyclohexane–acetone 7:4) of the solution showed a major spot at R_f 0.25 (**23**). Evaporation gave a syrup, that was twice chromatographed over silica gel with chloroform–methanol (20:1) to give solids of **23**, 10.3 g (82%) and **20**, 0.31 g. **23**: $[\alpha]_D^{20}$ −7° (*c* 1, $CHCl_3$).

^{1}H-NMR ($CDCl_3$) δ=−0.05, 0.02, 0.03, and 0.18 (each 3H s, $SiMe_2$×2), 1.78 (3H d, Me-22), 2.28 (6H s, NMe_2), 4.00 (1H d, H-3), 4.24 (1H d, H-1'), 4.75 (1H m, H-20), 4.93 (1H dt, H-15), 5.79 (1H d, H-13), 6.26 (1H d, H-10), 7.20 (1H d, H-11).

Found: C, 63.68; H, 9.81; N, 1.79%. Calcd for $C_{47}H_{88}NO_{10}Si_2$: C, 63.95, H, 9.98; N, 1.59%.

2'-*O*-Acetyl-3,23-bis(*O*-*t*-butyldimethylsilyl)-4'-deoxymycaminosyl Tylonolide Diethyl Acetal (24). A mixture of **23** (8.56 g) and acetic anhydride (1.17 ml) in acetonitrile (86 ml) was kept at room temperature for 6 h. Evaporation with several additions of toluene gave a residue, that was extracted with chloroform. The organic solution was washed with saturated aqueous sodium hydrogencarbonate, saturated aqueous sodium sulfate, dried (Na_2SO_4), and evaporated to give a residue. Silica-gel column chromatography with toluene–ethyl acetate (1:1→1:2) gave a solid of **24**, 7.42 g. (82%); $[\alpha]_D^{22}$ +1° (*c* 1, $CHCl_3$).

^{1}H-NMR ($CDCl_3$) δ=−0.05, 0.03, 0.05, and 0.18 (each 3H s, SiM_2×2), 1.78 (3H d, Me-22), 2.08 (3H s, Ac), 2.27 (6H s, NMe_2), 4.28 (1H d, H-1'), ≈4.7 (2H, H-2', 20), 4.93 (1H dt, H-15), 5.78 (1H d, H-13), 6.25 (1H d, H-10), 7.19 (1H d, H-11).

Found: C, 63.49; H, 9.68; N, 1.48%. Calcd for $C_{49}H_{90}NO_{11}Si_2$: C, 63.63; H, 9.74; N, 1.52%.

2'-*O*-Acetyl-3-*O*-*t*-butyldimethylsilyl-4'-deoxymycaminosyl Tylonolide Diethyl Acetal (25). To an ice-cold solution of **24** (7.3 g) in oxolane (73 ml) was added a M solution of tetrabutylammonium fluoride in oxolane (8.7 ml) and the mixture was kept at room temperature for 2 h. Work-up as described for **24** gave a crude product, having, on TLC (chloroform–acetone 1:1), a single spot (R_f 0.5). It was purified by column chromatography with chloroform–acetone (6:5) to give a solid of **25**, 6 g (93%); $[\alpha]_D^{20}$ +4° (*c* 1, $CHCl_3$).

^{1}H-NMR ($CDCl_3$) δ=−0.05 and 0.18 (each 3H s, $SiMe_2$), 1.82 (3H s, Me-22), 2.08 (3H s, Ac), 2.27 (6H s, NMe_2), 4.29 (1H d, H-1'), ≈4.75 (2H, H-2', 20), 4.89 (1H dt, H-15), 5.75 (1H d, H-13), 6.30 (1H d, H-10), 7.18 (1H d, H-11).

Found: C, 62.80; H, 9.21; N, 1.80%. Calcd for $C_{43}H_{77}NO_{11}Si\cdot1/2\ H_2O$: C, 62.93; H, 9.51; N, 1.71%.

(23*S*)- and (23*R*)-2'-*O*-Acetyl-3-*O*-*t*-butyldimethylsilyl-4'-deoxy-23-C-methylmycaminosyl Tylonolide Diethyl Acetal (27a, 27b). To a solution of **25** (900 mg) in benzene–dimethyl sulfoxide (1:1, 18 ml) were added pyridinium tri-

fluoroacetate (230 mg) and dicyclohexylcarbodiimide (914 mg) and the mixture was stirred at room temperature for 4 h. After addition of oxalic acid dihydrate (372 mg) in 1,4-dioxane (9 ml), the mixture was stirred for 1 h. Filtration followed by concentration of the solution gave a syrup. A benzene solution of the syrup was washed with saturated aqueous sodium hydrogencarbonate, saturated aqueous sodium sulfate, dried (Na_2SO_4), and evaporated to give a solid, 900 mg; TLC: R_f 0.5 with toluene–acetone (3:2). The ^{1}H-NMR spectrum (90 MHz, in $CDCl_3$) of this solid showed a doublet ($J_{14,23}$=3 Hz) at δ 9.75 (CHO at C-23).

To a cold (−78 °C) solution of the solid (900 mg) in dry oxolane (9 ml) was added methylmagnesium bromide in oxolane (1.6 ml of M solution) and the solution was kept at −78 °C for 1 h. The reaction mixture was poured into an ice-cold half-saturated aqueous ammonium chloride (30 ml) and extracted with chloroform. The organic solution was washed with saturated aqueous sodium sulfate, dried (Na_2SO_4), and evaporated to give a solid, that showed several spots including R_f 0.47 (major, **27a**) and 0.41 (minor, **27b** and **25**) on TLC with toluene–acetone (3:2). Column chromatography with toluene–acetone (4:1→1:1) gave solids of crude **27a**, 384 mg (≈42%) and **27b**, 131 mg (contaminated with **25**).

27a: ^{1}H-NMR ($CDCl_3$) δ=−0.04 and 0.18 (each 3H s, $SiMe_2$), 1.12 (3H d, $J_{23,Me\text{-}24}$=7.5 Hz, Me-24), 1.78 (3H d, Me-22), 2.09 (3H s, Ac), 2.26 (6H s, NMe_2), 2.47 (1H m, H-14), 4.09 (1H dq, $J_{14,23}$=2.5 Hz, H-23), 5.14 (1H dt, H-15).

27b: ^{1}H-NMR ($CDCl_3$; the signals for **25** were not recorded) δ=1.20 (3H d, $J_{23,Me\text{-}24}$=6 Hz, Me-24), 2.09 (3H s, Ac), 2.89 (1H m, H-14), 4.30 (1H d, H-1′).

(23*S*)- and (23*R*)-4′-Deoxy-23-C-methylmycaminosyl Tylonolide (28a, 28b). A solution of **27a** (384 mg) in methanol (7 ml) was heated at 50 °C overnight. Evaporation gave a residue of the deacetylated product. To a solution of the residue in acetonitrile (1.5 ml) was added M aqueous hydrochloric acid (1.5 ml) and the solution was kept at 37 °C overnight. After addition of saturated aqueous sodium hydrogencarbonate (10 ml), the mixture was extracted with chloroform. The organic solution was washed with saturated aqueous sodium sulfate, dried (Na_2SO_4), and evaporated. Column chromatography of the residue with chloroform–methanol–28% aqueous ammonia (15:1:0.1) gave a solid of **28a**, 130 mg (50% from **27a**). Compound **27b** (131 mg) was likewise treated as described above to give, after column chromatography, solids of **28b**, 47 mg (7% from **25**) and DT, 20 mg.

General Procedure for the Syntheses of 29a,b and 30a,b. A mixture of **25** (900 mg), dicyclohexylcarbodiimide (914 mg), and pyridinium trifluoroacetate (230 mg) in benzene–dimethyl sulfoxide (1;1, 18 ml) was stirred at room temperature overnight. Work-up as described for **27a,b** gave the final products.

We are grateful to Mrs. Yukiko Otsuka and Miss Yoshiko Koyama of our Institute for measurements of the NMR spectra, to Mr. Saburo Nakada of Keio University for elemental analysis, and to Mrs. Machiko Yamazoe for preparation of the manuscript.

References

1) Preliminary communication: T. Tsuchiya, S. Sakamoto, N. Kajikawa, S. Umezawa, M. Hamada, and H. Umezawa, *J. Antibiot.*, **39**, 1021 (1986).

2) A. Tanaka, T. Tsuchiya, Y. Okada, S. Umezawa, M. Hamada, and H. Umezawa, *J. Antibiot.*, **35**, 113 (1982).

3) A. Tanaka, T. Tsuchiya, S. Umezawa, and H. Umezawa, *J. Antibiot.*, **34**, 1374 (1981).

4) S. Omura, H. Matsubara, A. Nakagawa, A. Furusaki, and T. Matsumoto, *J. Antibiot.*, **33**, 915 (1980).

5) S. Sakamoto, T. Tsuchiya, T. Miyake, A. Tanaka, and S. Umezawa, *Bull. Chem. Soc. Jpn.*, **57**, 3536 (1984).

6) For example see: L. D. Hall and J. K. M. Sanders, *J. Chem. Soc., Chem. Commun.*, **1980**, 368.

7) A. Tanaka, A. Watanabe, R. Kobayashi, T. Tsuchiya, S. Umezawa, M. Hamada, and H. Umezawa, *J. Antibiot.*, **34**, 1137 (1981).

8) M. Chérest, H. Felkin, and N. Prudent, *Tetrahedron Lett.*, **1968**, 2199; M. Chérest and H. Felkin, *ibid*, **1968**, 2205; N. T. Anh, Topics in Current Chemistry, **88**, 145, Springer-Verlag (1980).

 © 1987 The Chemical Society of Japan Bull. Chem. Soc. Jpn., 60, 365—368 (1987)

Syntheses of Bis(vinylenedithio)tetrathiafulvalene and Bis(methylvinylenedithio)tetrathiafulvalene

Tadashi NAKAMURA, Shin-ichi IWASAKA, Hideyuki NAKANO, Kazuhiko INOUE, Takashi NOGAMI,* and Hiroshi MIKAWA†

Department of Applied Chemistry, Faculty of Engineering, Osaka University, Yamadaoka, Suita, Osaka 565

(Received July 28, 1986)

Bis(vinylenedithio)tetrathiafulvalene (BVDT-TTF) and bis(methylvinylenedithio)tetrathiafulvalene (BMVDT-TTF) were synthesized as attractive donor molecules for highly conductive organic salts. These molecules have analogous structures to BEDT-TTF, but are expected to possess more planar structures. They have higher oxidation potentials than BEDT-TTF. The synthetic method of BVDT-TTF by using a phase-transfer catalyst was also studied.

Bis(ethylenedithio)tetrathiafulvalene (BEDT-TTF) is known to give superconductive organic salts.[1,2] BEDT-TTF salts possess a two-dimensional electrical-conductivity character due to the presence of eight sulfur atoms in the donor molecule. Since BEDT-TTF has two ethylene units at both sides of the molecule, it is nonplanar.[3] One of the important factors for donor and acceptor molecules which give highly conductive salts is their planar structures. A replacement of the ethylene units of BEDT-TTF with carbon–carbon double bonds would give an attractive donor molecule since it has an analogous structure to BEDT-TTF and is expected to possess a more planar structure. The IBM group has reported the syntheses of bis(vinylenedithio)tetrathiafulvalene (BVDT-TTF) and bis(dimethylvinylenedithio)tetrathiafulvalene (BDMVDT-TTF) without a detailed description of the synthetic procedures.[4] They synthesized these donor molecules, starting from a reaction of 1,3,4,6-tetrathiapentalene-2,5-dione with a phase-transfer catalyst and Na_2CO_3. We also synthesized BDMVDT-TTF[5] by a different route. We have now synthesized BVDT-TTF and bis(methylvinylenedithio)tetrathiafulvalene (BMVDT-TTF) by different routes from those of the IBM group. The IBM method is assumed to be broadly applicable to the syntheses of the related donor molecules, and deserves to be studied in detail. We synthesized 4,5-(vinylenedithio)-1,3-dithiol-2-one, which is a precursor to BVDT-TTF, by the method reported by the IBM group. Since no detailed synthetic procedure has been disclosed for this method, and some researchers claim that this method is difficult,[6] it will be worth describing the synthetic procedures. We found that our method is superior to the IBM method.

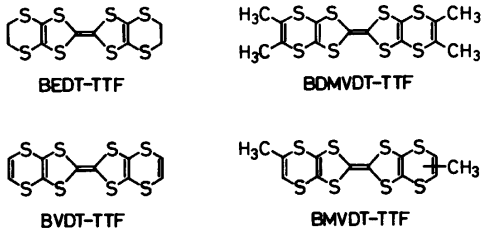

Results and Discussion

Synthesis of BVDT-TTF. BVDT-TTF was synthesized by four reaction steps (Scheme 1). The synthesis of the starting material, $(Et_4N)_2[Zn(dmit)_2]$ (**1**),[7] was made by the reported method.[8] The synthesis of 4,5-(ethoxyethylenedithio)-1,3-dithiole-2-thione (**2**) was made by a reaction of **1** with 1,2-dichloroethyl ethyl ether in refluxing acetone. A dilution method is crucial for the synthesis of **2**, since its yield was poor without the dilution method. An elimination reaction of ethanol from **2** was made by refluxing a benzene solution of **2** and anhydrous *p*-toluenesulfonic acid to give 4,5-(vinylenedithio)-1,3-dithiole-2-thione (**3**). Since the coupling reaction of **3** with triethyl phosphite gave BVDT-TTF in low yield, **3** was converted to 4,5-(vinylenedithio)-1,3-dithiol-2-

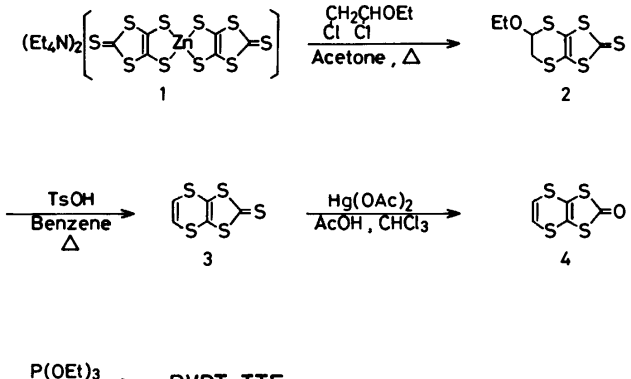

Scheme 1.

† Present address: Department of Environment and Safety Engineering, Faculty of Engineering, Fukui Institute of Technology, Gakuencho, Fukui 910.

one (**4**) by treating with mercury(II) acetate. The coupling reaction of **4** was made by heating it in neat triethyl phosphite, and BVDT-TTF was obtained as red needles. The cyclic voltammetry of BVDT-TTF in THF (0.1 M n-Bu_4NClO_4, Pt electrode, 20 mV s^{-1}) exhibited one wave: $E_{1/2}$=0.83 V vs SCE. This value was higher than those of the BEDT-TTF observed in THF ($E_{1/2}(1)$=0.69 V, $E_{1/2}(2)$=0.82 V vs SCE).

Synthesis of BMVDT-TTF. BMVDT-TTF was also synthesized by a four step reaction (Scheme 2). Reaction of **1** with propargyl bromide in refluxing acetone gave 4,5-(2-methylene-1,2-ethanediyldithio)-1,3-dithiole-2-thione (**5**). The dilution method is also crucial for this reaction. Without this method, two successive substitution reactions occurred to give 4,5-bis(propargylthio)-1,3-dithiole-2-thione (**8**) as the main product (judging from the mass and IR spectra). Product **5** was isomerized to 4,5-(methylvinylenedithio)-1,3-dithiole-2-thione (**6**) by treating **5** with p-toluenesulfonic acid monohydrate in toluene. Since the coupling reaction of **6** with neat triethyl phosphite gave BMVDT-TTF in low yield (16%), **6** was converted to 4,5-(methylvinylenedithio)-1,3-dithiol-2-one (**7**) by treating with mercury(II) acetate. The coupling reaction of **7** with neat triethyl phosphite gave BMVDT-TTF as light-yellow needles. The cyclic voltammetry of BMVDT-TTF in THF also gave one redox wave ($E_{1/2}$=0.80 V vs. SCE). This value was also higher than those of BEDT-TTF.

Synthesis of BVDT-TTF by Using Phase-Transfer Catalyst. Since the IBM group has disclosed no detailed synthetic procedure for the syntheses of BVDT-TTF and the related donor molecules,[4] we studied the synthetic conditions of BVDT-TTF by their method. The reaction route is shown in Scheme 3. The synthesis of 1,3,4,6-tetrathiapentalene-2,5-dione (**9**) was made by the reported method.[9] A benzene/water solution containing **9**, Aliquat 336,[10] and sodium carbonate was stirred at 40—45 °C to give 2-oxo-1,3-dithiole-4,5-dithiolate (**10**) in benzene phase. Then, the aqueous phase was eliminated by a syringe. Without the elimination of the aqueous phase, another carbonyl group also reacted to give tetrathiolate. The reaction of **10** with 1,2-dichloroethyl ethyl ether gave 4,5-(ethoxyethylenedithio)-1,3-dithiol-2-one (**11**). The elimination of ethanol from **11** was made by treating with p-toluenesulfonic acid in chlorobenzene to give **4**, which is a precursor to BVDT-TTF.

We have studied two different synthetic routes of BVDT-TTF (Schemes 1 and 3). Comparing these methods, the method shown in Scheme 1 is better than that in Scheme 3 from the following reasons. (1) The starting material, $(Et_4N)_2[Zn(dmit)_2]$,[7] in Scheme 1 can be obtained on a large scale (about 150 g) in one day. Therefore, the succeeding synthesis can be made on a large scale. On the other hand, a large-scale synthesis of **9** is not only difficult, but its synthesis requires several days. Although **9** can be commercially obtained, it is expensive. Furthermore, **9** sensitizes and produces skin rashes on some individuals. (2) All of the reaction products in Scheme 1 can be easily purified by recrystallization or chromatography. On the other hand, the product in Scheme 3 must be purified by column chromatography, followed by recrystallization, mainly due to the contamination of Aliquat 336. Thus, a much longer time is required for the purification. The loss of the product during these procedures is also a serious problem.

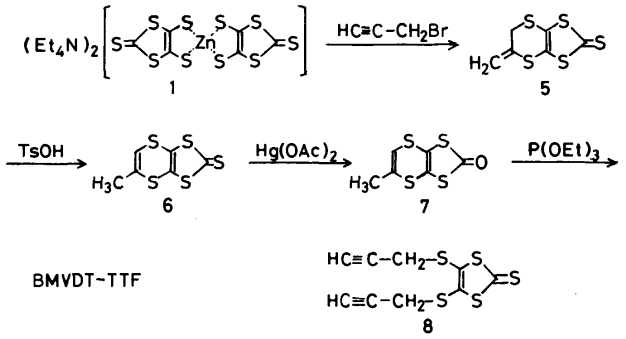

Scheme 2.

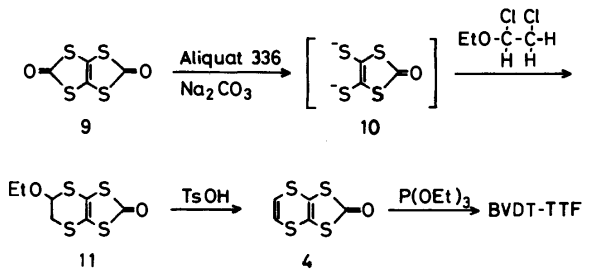

Scheme 3.

Experimental

The reaction was made under a nitrogen atmosphere, except for the syntheses of **4** and **7**. In the following reactions, second crops of **2**, **3**, **4**, BVDT-TTF, **5**, **6**, **7**, and BMVDT-TTF could be obtained by concentrating the mother solutions of the recrystallizations.

4,5-(Ethoxyethylenedithio)-1,3-dithiole-2-thione (2). A two-liter flask containing 1.7 l of acetone was equipped with two dropping funnels. The funnels contained an acetone solution (200 ml) of **1** (25 g) and an acetone solution (100 ml) of 1,2-dichloroethyl ethyl ether (10 g), respectively. After refluxing the acetone in the flask, the acetone solutions of **1** and 1,2-dichloroethyl ethyl ether were simultaneously dropped into the flask with vigorous stirring for a 3-h period; the solution was then refluxed for another 21 h. After cooling to room temperature, an orange precipitate was filtered off, and the acetone in the filtrate was evaporated. The residue was extracted with benzene, washed with water, dried over Na_2SO_4, recrystallized from acetonitrile, and then from the mixed solvent of hexane and

chloroform (2:1) to give yellowish-brown needles of **2** (9.3 g, 50% yield based on **1**). Mp 108 °C. Found: C, 2.89; H, 31.19; S, 59.78%. Calcd for $C_7H_8OS_5$: C, 3.00; H, 31.32; S, 59.72%. MS *m/z* 268 (M^+).

4,5-(Vinylenedithio)-1,3-dithiole-2-thione (3). The azeotropic distillation of 100 ml of benzene from the benzene solution (105 ml) of *p*-toluenesulfonic acid monohydrate ($TsOH \cdot H_2O$, 7.086 g) eliminated water in the solution. Benzene (895 ml) was added to the solution, and 100 ml of benzene was distilled again. After the benzene solution of TsOH was refluxed, a benzene solution (200 ml) of **2** (5 g) was added from a dropping funnel. The solution was refluxed for 24 h with vigorous stirring. The reddish-yellow solution gradually became dark brown. After cooling to room temperature, the solution was washed with water, then with aqueous $NaHCO_3$, finally with water, and dried over Na_2SO_4. After evaporating the benzene, the residue was chromatographed on silica gel by using benzene as an eluent. The second red fraction contained **3**. It was chromatographed again on silica gel by using hexane and chloroform (2:1) to give pure **3** as yellow powders (890 mg, 23.7%). Mp 143—144 °C. Found: C, 27.09; H, 0.85; S, 71.91%. Calcd for $C_5H_2S_5$: C, 27.01; H, 0.85; S, 71.91%. MS *m/z* 222 (M^+). ^{1}H-NMR (CS_2) δ=6.63 (s).

4,5-(Vinylenedithio)-1,3-dithiol-2-one (4). To the chloroform solution (30 ml) of **3** (300 mg) was added 30 ml of acetic acid and 1.075 g of mercury(II) acetate; the solution was stirred for 20 min at room temperature. A white precipitate was filtered off, and the filtrate was washed with water, then with aqueous $NaHCO_3$, finally with water, and dried over Na_2SO_4. After evaporating the solvent, the residue was chromatographed on silica gel by using hexane and chloroform (1:1) as an eluent. The second orange fraction gave **4** as pale yellow powders (158 mg, 57%). Mp 99 °C. Found: C, 29.02; H, 0.91; S, 61.94%. Calcd for $C_5H_2OS_4$: C, 29.11; H, 0.91; S, 62.15%. MS *m/z* 206 (M^+). ^{1}H-NMR (CS_2) δ=6.59 (s).

Bis(vinylenedithio)tetrathiafulvalene (BVDT-TTF). Two hundred mg of **4** was added to 5 ml of triethyl phosphite (freshly distilled), and the solution was stirred for 2 h at 100—105 °C. After cooling to room temperature, the precipitate was collected, washed with methyl alcohol, and dried to give BVDT-TTF (132 mg, 72%). It was recrystallized from chloroform to give red needles of BVDT-TTF. Mp 227 °C (decomp). Found: C, 31.85; H, 1.02; S, 67.13%. Calcd for $C_{10}H_4S_8$: C, 31.56; H, 1.06; S, 67.38%. MS *m/z* 380 (M^+). ^{1}H-NMR (CS_2) δ=6.5 (s). λ_{max}^{THF} (log ε): 316 nm (3.83), 340 nm (3.84).

4,5-(2-Methylene-1,2-ethanediyldithio)-1,3-dithiole-2-thione (5). To the refluxing acetone (480 ml) was added (dropwise) an acetone solution (60 ml) of **1** (7.19 g) and acetone solution (30 ml) of propargyl bromide (2.38 g) simultaneously for a 8-h period. The solution was refluxed for another 18 h. The residue was filtered off, acetone was evaporated, and the oil was extracted with benzene. It was washed with water, dried over Na_2SO_4, and chromatographed on silica gel by using hexane and chloroform (4:1) as an eluent. The first yellow fraction contained **5** and **8**. It was chromatographed again on silica gel by using hexane and chloroform (6:1) as an eluent, and the first fraction gave **5** (802 mg, 17%). It was recrystallized from acetonitrile to give orange needles. Mp 114—116 °C. Found: C, 30.50; H, 1.61; S, 67.62%. Calcd for $C_6H_4S_5$: C, 30.49; H, 1.71; S, 67.81%. MS *m/z* 236 (M^+). ^{1}H-NMR (CS_2) δ=3.71 (2H, s), 5.29 (1H, s), 5.39 (1H, s).

4,5-(Methylvinylenedithio)-1,3-dithiole-2-thione (6). A toluene solution (50 ml) of **5** (250 mg) and *p*-toluenesulfonic acid monohydrate ($TsOH \cdot H_2O$, 0.4 g) was refluxed for 1 h, and TsOH was filtered off. The filtrate was washed with water and dried over Na_2SO_4. After evaporating the solvent, **6** was extracted with acetonitrile. It was recrystallized from acetonitrile to give **6** as orange needles (150 mg, 61%). Mp 103 °C. Found: C, 30.50; H, 1.61; S, 67.62%. Calcd for $C_6H_4S_5$: C, 30.49; H, 1.71; S, 67.81%. MS *m/z* 236 (M^+). ^{1}H-NMR (CS_2) δ=2.20 (3H, s), 6.18 (1H, s).

4,5-(Methylvinylenedithio)-1,3-dithiol-2-one (7). Mercury(II) acetate (0.34 g) and **6** (0.1 g) was added to the mixed solvent of chloroform (10 ml) and acetic acid (10 ml), and the solution was stirred for 15 min at room temperature. A white precipitate was filtered off and the filtrate was washed with water, then with aqueous $NaHCO_3$, finally with water, and dried over Na_2SO_4. It was chromatographed on silica gel by using the mixed solvent of hexane and chloroform (1:1). The first pale yellow fraction gave **7** (75 mg, 80%). Recrystallization from methanol gave analytically pure **7**. Mp 80.5—81 °C. Found: C, 32.64; H, 1.85; S, 58.17%. Calcd for $C_6H_4OS_4$: C, 32.71; H, 1.83; S, 58.20%. MS *m/z* 220 (M^+). ^{1}H-NMR (CS_2) δ=2.20 (3H, s), 6.12 (1H, s).

Bis(methylvinylenedithio)tetrathiafulvalene (BMVDT-TTF). To triethyl phosphite (8 ml, freshly distilled) was added 0.2 g of **7**, and the mixture was stirred for 2 h at 110 °C. The yellow product was collected (157 mg, 92%), washed with methyl alcohol, and recrystallized from chloroform to give BMVDT-TTF as yellow needles. Mp: gradually decomposes at around 204 °C. Found: C, 35.12; H, 2.11; S, 61.74%. Calcd for $C_{10}H_8S_8$: C, 35.27; H, 1.97; S, 62.76%. MS *m/z* 408 (M^+). ^{1}H-NMR (CS_2) δ=2.12 (3H, s), 6.03 (1H, s). λ_{max}^{THF} (log ε): 316 nm (3.69), 342 nm (3.69).

4,5-(Ethoxyethylenedithio)-1,3-dithiol-2-one (11). A four-necked flask containing **9** (624 mg, 3 mmol), Na_2CO_3 (636 mg, 6 mmol), benzene (40 ml), and water (40 ml) was equipped with two dropping funnels, which contained a benzene solution (40 ml) of Aliquat 336 (2.5 g) and benzene solution (40 ml) of 1,2-dichloroethyl ethyl ether (429 mg, 3 mmol), respectively. The solution in the reaction vessel was heated to 40—45 °C, and a benzene solution of Aliquat 336 was dropped for a 40-min period with vigorous stirring, then stirred for another 20 min. After cooling to room temperature, the aqueous phase was eliminated by a syringe. The dithiolate (**10**) was produced as a reddish benzene solution. The benzene solution of 1,2-dichloroethyl ethyl ether was then added dropwise to the above solution for a 30-min period with stirring at room temperature, and the solution was stirred for another 90 min at 40—45 °C. Filtration of the solution, followed by the evaporation of the solvent, gave dark red oil. It was extracted with benzene, washed with water, and dried over Na_2SO_4. After evaporating the benzene, the residue was chromatographed on silica gel by using a mixed solvent of hexane and chloroform (4:1) as an eluent. The second yellow fraction contained almost pure **11** as a reddish-yellow oil (454 mg, 60%). MS *m/z* 252 (M^+). It was difficult to purify **11** completely by repeated chromatographies due to the contamination of Aliquat 336. Thus, the crude product was

used directly in the next step of the reaction.

4,5-(Vinylenedithio)-1,3-dithiol-2-one (4) from 11. To *p*-toluenesulfonic acid monohydrate (5.538 g) was added the mixed solvent of benzene (80 ml) and chlorobenzene (80 ml). An azeotropic distillation of benzene eliminated any water in the solution. A chlorobenzene solution (10 ml) of **11** (1.157 g) was added to the above solution and was then refluxed for 4 h. After cooling to room temperature, the solution was washed with water and dried over Na_2SO_4. After evaporating chlorobenzene, the residue was chromatographed on silica gel by using a mixed solvent of hexane and chloroform (1 : 1) as an eluent. The first yellow fraction gave **4** (234 mg, 25%), which was recrystallized from acetonitrile to give light yellow needles. Mp 99.5—100.5 °C. Found: C, 29.19; H, 0.92; S, 61.26%. Calcd for $C_5H_2S_4O$: C, 29.11; H, 0.98; S, 62.15%. MS *m/z* 206 (M^+). ^{1}H-NMR (CS_2) δ=6.60.

The present work was partially supported by a Grant-in-Aid for Special Research Project on New Superconductive Materials (No. 59221012) from the Ministry of Education, Science and Culture.

References

1) J. M. Williams, M. A. Beno, H. H. Wang, P. C. W. Leung, T. J. Emge, U. Geiser, and K. D. Carlson, *Acc. Chem. Res.*, **18**, 261 (1985).

2) J. M. Williams, *Prog. Inorg. Chem.*, **33**, 183 (1985).

3) H. Kobayashi, A. Kobayashi, Y. Sasaki, G. Saito, and H. Inokuchi, *Bull. Chem. Soc. Jpn.*, **59**, 301 (1986).

4) R. R. Schumaker, V. Y. Lee, and E. M. Engler, *J. Phys.*, **44**, C3-1139 (1983).

5) K. Inoue, Y. Tasaka, O. Yamazaki, T. Nogami, and H. Mikawa, *Chem. Lett.*, **1986**, 781.

6) Private communication from Professor Patrick Cassoux, Laboratoire de Chimie de Coordination du CNRS, 31400 Toulouse, France.

7) H_2(dmit)=4,5-dimercapto-1,3-dithiole-2-thione.

8) G. Steimecke, H. J. Sieler, R. Kirmse, and E. Hoyer, *Phosphorus and Sulfur*, **7**, 49 (1979).

9) R. R. Schumaker, V. Y. Lee, and E. M. Engler, *J. Org. Chem.*, **49**, 564 (1984).

10) Aliquat 336 is a mixture of quaternary alkylammonium chlorides. Trioctylmethylammonium chloride is the main compound.

 © 1987 The Chemical Society of Japan Bull. Chem. Soc. Jpn., 60, 369—373 (1987)

Battle River Coal Liquefaction and Its Co-Processing with Tar-Sand Bitumen

Ryoichi Yoshida,* Makoto Miyazawa,† and Yosuke Maekawa
Government Industrial Development Laboratory, Hokkaido, 2-Jo 17-Chome, Tsukisamu-Higashi, Toyohira-ku, Sapporo 004
†Nippon Kokan K. K., 1-1 Minamiwatarida-cho, Kawasaki-ku, Kawasaki 210
(Received February 24, 1986)

Battle River coal from Canada shows an excellent applicability to liquefaction. At 450 °C, anthracene oil and Cold Lake tar-sand bitumen show the solvent effect as a vehicle oil in the initial stage of liquefaction. A definite advantage is gained by tar-sand bitumen co-processing, where hydrogen consumption is comparatively lower than that of anthracene oil derived from coal to produce a similar yield of oil.

As part of a study program of coals from the Pan-Pacific Basin area at the Government Industrial Development Laboratory, Hokkaido, their basic properties[1] and their reaction characteristics in liquefaction[2,3] have been studied. In a previous paper,[2] the behavior during liquefaction of Wandoan coal, Australian subbituminous coal, was investigated. As to Battle River coal, Canadian subbituminous coal, the liquefaction test by a 0.1 T/D continuous plant was carried out.[3,4] However, the detailed behavior during liquefaction is not sufficiently understood.

In the present paper, the reactivity in the liquefaction of Battle River coal from Canada was studied without vehicle oil and with tar-sand bitumen from Cold Lake, Canada, and anthracene oil derived from coal as vehicle oil in a batch autoclave in order to obtain fundamental data on the liquefaction and co-processing characteristics.

Experimental

The analytical data of Battle River coal, anthracene oil, and tar-sand bitumen are shown in Table 1. The experimental procedure and reaction conditions of coal liquefaction in a shaking-type, 500 ml autoclave are given in detail elsewhere.[2,5] In the experiments of coal liquefaction, 10 g of Battle River coal, 1 g of a dry red-mud catalyst, 0.1 g of sulfur as a promoter, and 15 g of vehicle oil were charged in an authoclave. The initial pressure of hydrogen was adjusted to reach a reaction pressure of 220—230 kg cm^{-2}. The reaction temperature was 400 °C or 450 °C. Liquid and solid products were extracted with hexane and toluene successively, and they were separated into 3 fractions: a hexane-soluble fraction (oil), a hexane-insoluble/toluene-soluble fraction (asphaltene), and a toluene insoluble fraction (unreacted coal). The coal conversion was calculated on the basis of the unreacted coal.

Results and Discussion

Battle River coal (Fig. 1) and tar-sand bitumen (Fig. 2), were hydrogenated, respectively, with red-mud and sulfur without vehicle oil. In the liquefaction of the Battle River coal (Fig. 1), the conversion and the asphaltene yield at 400 °C tend to increase with an increase in the reaction time. The conversion reaches the equilibrium value at 450 °C, where the asphaltene yield decreases, and the gas yield, oil yield, and hydrogen consumption increase, with the increase in the reaction time. These results show that the secondary hydrogenolysis of the products occurs at 450 °C. Such a reaction trend is similar to that of Wandoan coal reported in a previous paper.[2] However, the conversion of Battle River coal is 96 wt% daf at 450 °C and at 60—120 min, higher by about 3 wt% daf than that of Wandoan coal under the same reaction conditions.

The results of the hydrogenolysis of tar-sand bitumen itself as a blank run are shown in Fig. 2. As has been reported in a previous paper,[2] the whole quantity of original anthracene oil is soluble in hexane, i.e., oil; hence, the whole quantity of the products after hydrogenolysis is also soluble in hexane. However, original tar-sand bitumen contains 15 wt% of the hexane insoluble/toluene soluble fraction, i.e., asphaltene. After hydrogenolysis, 3.3—

Table 1. Analysis of Sample Coal and Vehicle Oils

Coal and vehicle	Ultimate analysis/wt%					Atomic ratio		
	C	H	N	O	S	H/C	N/C	O/C
Battle River coal	70.0[a)]	4.7[a)]	1.7[a)]	23.1[a)]	0.6[a)]	0.80	0.021	0.247
Anthracene oil	90.0	6.2	1.1	2.4	0.3	0.83	0.011	0.020
Cold Lake tar-sand bitumen	83.7	11.4	0.3	0.6	4.0	1.64	0.003	0.005

a) d.a.f. coal basis. b) Proximate analysis of Battle River coal/wt%, Moisture: 11.9, Ash: 10.1, Volatile Matter: 34.1, Fixed Carbon: 43.3.

5.4 wt% of asphaltene remains in the products at 400 °C, while 0.6—2.1 wt% of asphaltene remains in the products at 450 °C. The hydrogen consumption is ca. 0.5 wt%[2] and is almost constant during the hydrogenolysis of anthracene oil, but when tar-sand bitumen is hydrogenated, the hydrogen consumption tends to increase with the increase in the reaction time; especially at 450 °C, it increases from 1 to 3 wt%. Regarding the gaseous products, the formation of hydrogen sulfide from tar-sand bitumen is remarkable and at 400 °C exceeds that of hydrocarbon gases, such as methane, ethane, and propane. No carbon monoxide or carbon dioxide formation was observed.

Figure 3 shows the results of the liquefaction of Battle River coal with anthracene oil and with tar-sand bitumen co-processing. The product yields are calculated as the difference between blank runs and those charged with coal. In this experiment, the effect of vehicle oil on the reactivity of the liquefaction of Battle River coal was examined. The conversion in the initial stage at 400 °C is about 30 wt% daf without vehicle oil (Fig. 1) and with tar-sand bitumen (Fig. 3), while it is about 80 wt% daf with anthracene oil (Fig. 3).

At 450 °C, the conversion, the asphaltene yield, and the oil yield in the initial stage up to the reaction time of 60 min show differences depending on the nature of the vehicle oil (tar-sand bitumen or anthracene oil) and on the presence or the absence of the vehicle oil. The effect of vehicle oil on the initial stage of liquefaction is clearly observed. Anthracene oil and tar-sand bitumen are different in the degree of the effect of vehicle oil in the initial stage; tar-sand bitumen contains more resins, asphaltene, and the heavy fraction boiling off above 400 °C, which should make it more viscous than anthracene oil, as is shown in Table 2. The fluidity of the reactants must be less in the initial stage when vehicle oil is tar-sand bitumen. Therefore, the reactivity of the reactants must be less.[6] However, as the reaction time and reaction temperature increase, the tar-sand bitumen decomposes (Fig. 2) and/or its viscosity must drop substantially. Therefore, as vehicle oil tar-sand bitumen shows an effect comparable to that of

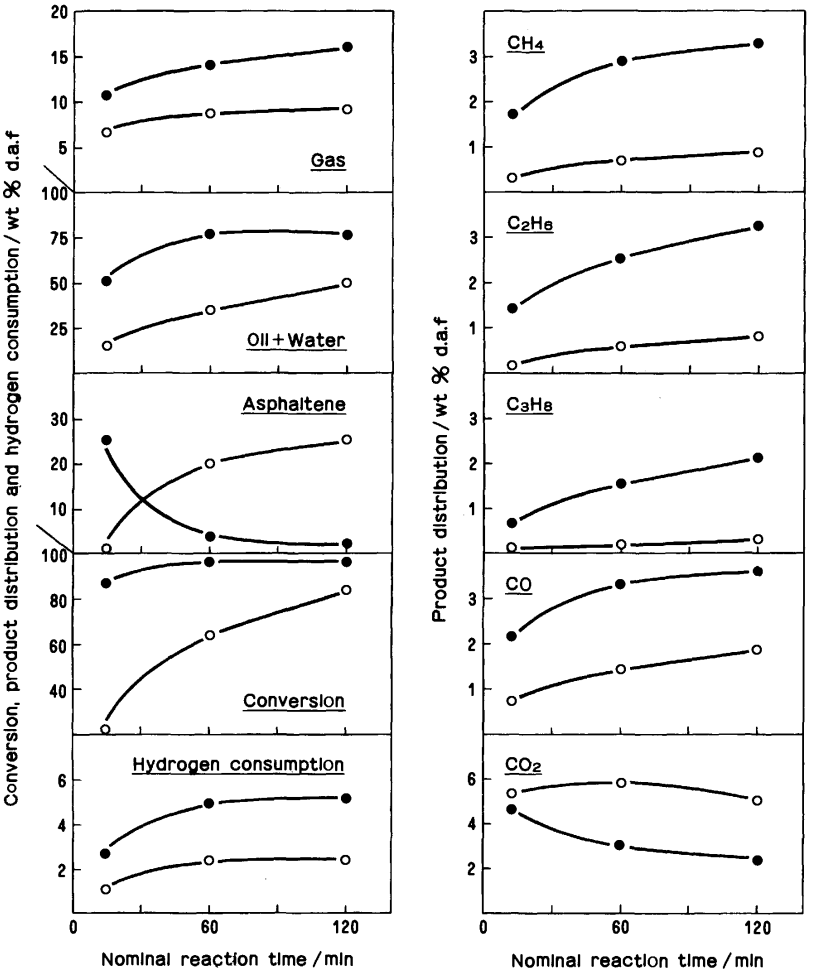

Fig. 1. Conversion, product distribution and hydrogen consumption vs. nominal reaction time on Battle River coal hydrogenolysis with red-mud/sulfur catalyst. ○: 400 °C, ●: 450 °C.

anthracene oil at 450 °C, as has been reported by Moschopedis.[7] Hydrogen consumption and gas formation are the highest with anthracene oil, and they increase with an increase in the reaction time; subsequently, the oil yield tends to decrease. When tar-sand bitumen is used, the hydrogen consumption is lower and is considered to be the effect of hydrogen sulfide.[8-10] Hydrogen sulfide starts to decompose to hydrogen and sulfur above 400 °C, and it is easily decomposed to hydrogen and sulfur in the presence of iron sulfide.[8] The hydrogen formed immediately after the decomposition of hydrogen sulfide can be more active than normal hydrogen, and the hydrocracking ability and the hydrogen-donor ability may play some role in the coal conversion.[8-10] The lower formation of gaseous products is remarkable.

In Table 3, the analytical data of the hexane-soluble fraction are shown. The hexane-soluble fraction in Table 3 is a mixture of the hexane-soluble fraction from Battle River coal and vehicle oil. In the presence of tar-sand bitumen, the hydrogen contents in the hexane-soluble fraction produced are higher than the

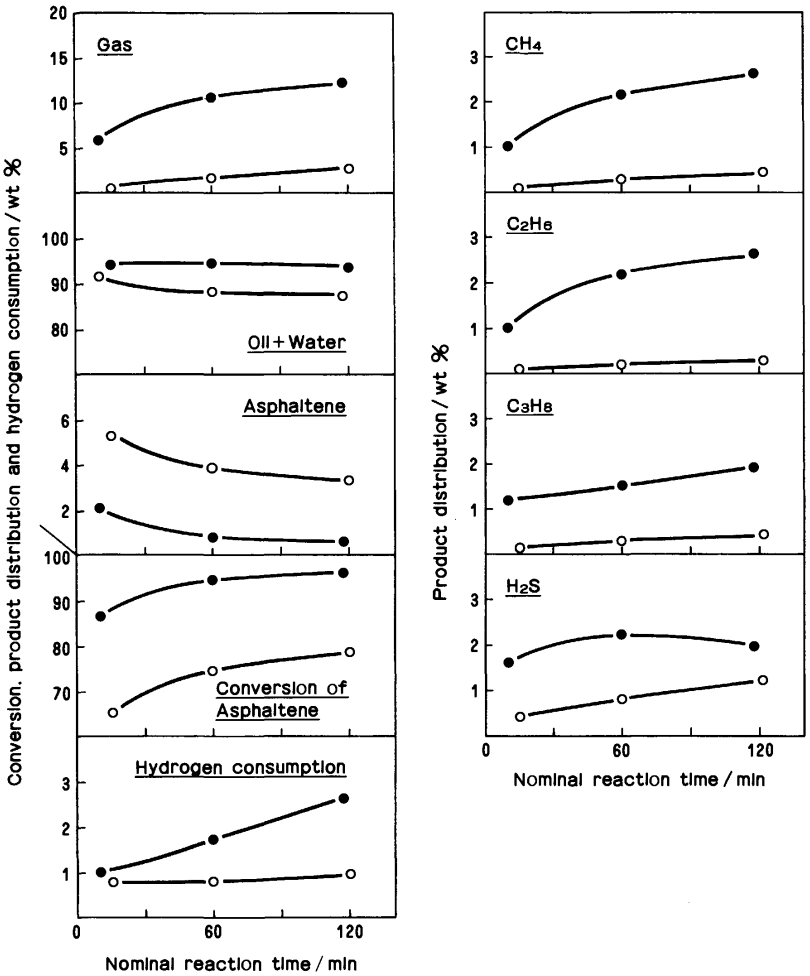

Fig. 2. Conversion, product distribution and hydrogen consumption vs. nominal reaction time on Cold Lake tar sand bitumen hydrogenolysis with redmud/sulfur catalyst. ○: 400 °C, ●: 450 °C.

Table 2. Analytical Data of Vehicle Oils

Vehicle oil	Type analysis/wt%				Boiling-range distribution/wt%			
	Saturated hydrocarbons	Aromatics	Resin	Asphaltene	Naphtha Fr. (IBP—200 °C)	Middle Fr. (200—325 °C)	Heavy Fr. (325—400 °C)	Residue (400 °C—FBP)
Anthracene oil	0.0	90.3	9.7	0.0	1.6	37.6	39.6	21.2
Tar-sand bitumen	18.3	56.2	10.5	15.0	1.6	46.0	24.3	28.2

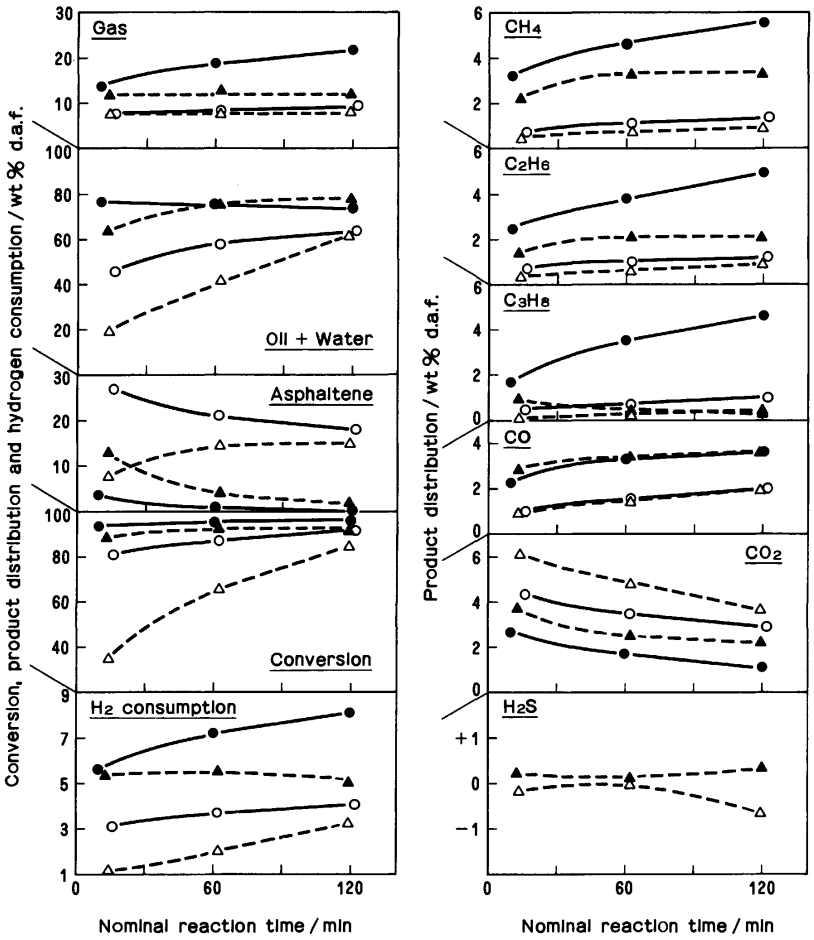

Fig. 3. Conversion, product distribution and hydrogen consumption vs. nominal reaction time on Battle River coal hydrogenolysis with red-mud/sulfur catalyst and anthracene oil and Cold Lake tar sand bitumen.
With anthracene oil, ○: 400° C, ●: 450 °C.
With Cold Lake tar sand bitumen, △: 400 °C, ▲: 450 °C.

Table 3. Analytical Data of Oil Produced from Battle River Coal

Reaction temp/°C	Reaction time/min	Ultimate analysis/wt%, d.a.f.					Atomic ratio			
		C	H	N	O	S	H/C	N/C	O/C	S/C
					Anthracene oil					
400	16	89.4	6.9	1.2	2.3	0.23	0.93	0.012	0.019	0.001
400	62	89.0	7.2	1.2	2.4	0.18	0.97	0.012	0.020	0.001
400	122	88.5	7.4	1.2	2.4	0.53	1.00	0.012	0.020	0.002
450	10	89.3	7.1	1.3	2.1	0.13	0.95	0.012	0.018	0.001
450	60	89.2	7.4	1.2	2.1	0.12	1.00	0.012	0.018	0.001
450	120	89.3	7.4	1.1	2.0	0.16	0.99	0.011	0.017	0.001
					Tar-sand bitumen					
400	14	83.7	11.1	0.63	1.1	3.4	1.59	0.006	0.010	0.015
400	62	84.3	11.0	0.81	1.4	2.5	1.57	0.008	0.012	0.011
400	119	84.8	10.9	0.76	1.4	2.2	1.54	0.008	0.012	0.010
450	13	85.4	10.3	1.0	1.5	1.7	1.45	0.010	0.013	0.007
450	62	86.2	9.8	1.0	1.5	1.5	1.36	0.010	0.013	0.007
450	119	86.2	9.7	1.1	1.6	1.5	1.35	0.011	0.014	0.007

hydrogen contents in the hexane-soluble fraction produced when anthracene oil was used. The H/C atomic ratio in the hexane-soluble fraction produced from co-processing with tar-sand bitumen is 1.4 to 1.6, higher by 1.4 to 1.7 times than the H/C atomic ratio in the hexane-soluble fraction produced when anthracene oil was used. Tar-sand bitumen seems to be associated with the lowering of the nitrogen content and the oxygen content in the hexane-soluble fraction. However, the sulfur in tar-sand bitumen was probably transferred to the hexane-soluble fraction.

Conclusion

In summary, Battle River coal shows an excellent reactivity to liquefaction, for the maximum conversion attainable is ca. 90 wt% daf at 400 °C and ca. 96 wt% daf at 450 °C. In the presence of anthracene oil as the vehicle oil, Battle River coal shows a liquefaction behavior similar to that of Wandoan coal. At 400 °C, anthracene oil is excellent as a vehicle oil to facilitate the liquefaction reaction during the heating period up to 400 °C. The conversion at 400 °C and 16 min reaches about 80 wt% daf. When tar-sand bitumen is used as the vehicle oil at 400 °C, the conversion shows a change, depending on the reaction time, similar to the conversion change in the case of no vehicle oil. Tar-sand bitumen shows the effect of vehicle oil on the increase in the oil yield. At 450 °C, anthracene oil and tar-sand bitumen show the effect of vehicle oil in the initial stage up to 60 min, and they facilitate the increase in the conversion and the oil yield and the decrease in the asphaltene yield. When tar-sand bitumen is used, it may be surmised that the conversion of tar-sand bitumen itself proceeds and that, at the same time, the conversion of coal-derived asphaltene to the oil fraction is also facilitated at 450 °C.

References

1) R. Yoshida, M. Miyazawa, H. Narita, and Y. Maekawa, *J. Fuel Soc. Jpn.*, **63**, 871 (1984).

2) M. Miyazawa, R. Yoshida, T. Yoshida, S. Yokoyama, Y. Nakata, and Y. Maekawa, *J. Fuel Soc. Jpn.*, **64**, 107 (1985).

3) Y. Hasegawa, S. Ueda, R. Yoshida, S. Yokoyama, T. Okutani, Y. Nakata, T. Yoshida, H. Narita, Y. Maekawa, N. Sakai, M. Miyazawa, and S. Ibaragi, Proceedings of the 20th Conference on Coal Science (1983), p. 140.

4) M. Suzuki, S. Oshima, K. Shimada, M. Yumura, T. Takematsu, Y. Kuriki, H. Yoshitome, M. Oba, Y. Sugimoto, and S. Yamadaya, Proceedings of the 20th Conference on Coal Science (1983), p. 143.

5) R. Yoshida, M. Miyazawa, and Y. Maekawa, *Chem. Lett.*, **1984**, 1113.

6) Y. Maekawa, K. Shimokawa, T. Ishii, and G. Takeya, *Kogyo Kagaku Zasshi*, **73**, 2347 (1970).

7) S. E. Moschopedis, *Liquid Fuels Technol.*, **2**, 177 (1984).

8) T. Okutani, S. Yokoyama, R. Yoshida, and T. Ishii, *Ind. Eng. Chem., Prod. Res. Dev.*, **18**, 367 (1979).

9) E. A. Sondreal, W. G. Wilson, and V. I. Stenberg, *Fuel*, **61**, 925 (1982).

10) R. M. Baldwin and S. Vinciguerra, *Fuel*, **62**, 498 (1983).

 © 1987 The Chemical Society of Japan Bull. Chem. Soc. Jpn., 60, 375—380 (1987)

Structure, Properties, and Na^+ Transport Membrane of Polyelectrolyte Complexes Consisting of Glycol Chitosan and Poly(vinyl sulfate)

Yasuo KIKUCHI* and Naoji KUBOTA
Department of Environmental Chemistry and Engineering, Faculty of Engineering, Oita University, Dannoharu, Oita 870-11
(Received April 28, 1986)

Glycol chitosan (GC) was allowed to react with poly(vinyl sulfate) (PVSK) to form many different water-insoluble polyelectrolyte complexes (PECs) in aqueous solution at various hydrogen ion concentrations. According to elemental analyses, IR spectroscopy, and solubilities of PECs, molecular structures of each PEC depend on $[H^+]$. This result is attributable to change with $[H^+]$ in the degree of dissociation and conformation of GC and PVSK. PEC membranes were made by casting solutions of all kinds of PECs, and transport phenomena through a membrane of the PEC prepared in a solution of 4 v/v% HCl were investigated under various conditions. The transport ratio of Na^+ and the electric potential difference between the left and right sides of the membrane were measured, with a result that the higher value the membrane potential difference was long allowed to maintain, the higher the transport ratio became. According to this result, the driving force of transport is dependent on the membrane potential, Donnan potential and diffusion potential, between both sides of the membrane. The Cl^- exclusion (Donnan exclusion), however, is small due to the small cation-exchange capacity, so that the membrane potential difference is caused to decrease rather rapidly by Cl^- permeation.

Polyelectrolyte complexes (PECs) are expected to find many-sided applications[1-3] because of the diversity of their structures and properties. For example, PECs may be prepared in the form of cationic or anionic as well as neutral polymer complex because of the applicability of a variety of components, mixing ratios, and solvent pHs, and may be cast into membranes with various ion-exchange capacities (0—2 mequiv g^{-1} dry membrane).[4] Consequently, when PEC membranes with high permeability[5] are used, it is possible to control the active transport of alkali metal and halide ions, of which a great number of studies have recently been made.[6-11] Investigation on PEC membrane is, however, confined almost to synthetic polymers, and there have been only a few papers on PEC membranes of naturally occurring polysaccharides. We have already reported that PEC membranes of glycol chitosan–poly(vinyl sulfate),[12] methyl glycol chitosan–(carboxymethyl)dextran–poly(vinyl sulfate),[13] and [2-(diethylamino)ethyl]dextran hydrochloride–(carboxymethyl)dextran–poly(vinyl sulfate)[14] systems are capable of active and selective transport of alkali metal ions.

This paper deals with chemical reactions of glycol chitosan (GC) with poly(vinyl sulfate) (PVSK) and general characteristics of resulting PECs. In addition, a description will be made on active transport of Na^+ through a membrane of PEC prepared in 4v/v% HCl solution, with particular reference to the relationship between transport ratio and membrane potential.

Experimental

Glycol chitosan (GC) (nitrogen content, 6.09%; intrinsic viscosity, 1.68 dl g^{-1} in 1 mol dm^{-3} NaCl solution at 25 °C) as a polycation and poly(vinyl sulfate) (PVSK) (sulfur content, 18.67%; intrinsic viscosity, 0.66 dl g^{-1} in 1 mol dm^{-3} NaCl solution at 25 °C) as a polyanion were used to prepare PECs. Sodium poly(*p*-styrenesulfonate) (NaSS) and poly(*p*-styrenesulfonic acid) (HSS) with molecular weights 1.0×10^4 and 5.0×10^5 were adopted in the active transport experiment. Reactions were run in 7, 4, and 1% HCl, at pHs 2.0, 4.5, 6.5, 11.0, and 13.0, and in 5% NaOH, considering that the degree of dissociation of polyelectrolytes and their conformation are influenced by hydrogen ion concentration. GC solution (2 g dm^{-3}) was added dropwise to PVSK solution (2 g dm^{-3}) and vice versa, for the adjustment to the same $[H^+]$, at a rate of 50 cm^3/30 min with stirring at ca. 22 °C. Water-insoluble PECs were thus obtained. After 30 min, the precipitate was separated by centrifugation. Then, it was washed with methanol, and dried in vacuo at room temperature until there occurred no further decrease in weight. Estimation of the nitrogen in PEC was carried out by the Kjeldahl method, and quantitative analysis of sulfur was performed at the Institute of Physical and Chemical Research. IR spectra of PEC in a KBr pellet were taken with a Hitachi 285 spectrophotometer. The miscibility of GC, PVSK, or PEC with the ternary solvent system, NaBr/acetone/water, was examined as previously described.[15]

PEC membrane was obtained from a PEC prepared in 4% HCl solution by casting. The method of casting into membrane and the experimental conditions were described in a previous paper.[12] A diaphragm type cell, made of poly(methyl methacrylate) and consisting of two chambers, was used in the active transport experiment for Na^+. After well washing with water, the PEC membrane was fixed tightly with silicone rubber between both chambers of the cell having an effective area of 4.0 cm^2. In the right-side chamber of the cell was placed 25 cm^3 of 0.1 mol dm^{-3} NaOH solution, and simultaneously 25 cm^3 of HCl (or HSS) solution of one of various concentrations containing 0.1 mol dm^{-3} NaCl (or 0.1 mol dm^{-3} NaSS unit) in the left-side chamber. The cell was then put in a thermostat controlled at 30 °C. At proper intervals, 0.1 cm^3 samples

from both the side chambers of the cell were withdrawn and analyzed for the concentration of Na^+ with an atomic absorption spectrophotometer (Shimadzu AA-640). At the same time, the concentration of Cl^- was determined by volumetric titration with $Hg(NO_3)_2$, and the concentration of SS^- from the absorbance at 260 nm (Hitachi 100-10 spectrophotometer). The electric potential difference between the left and right sides of the membrane was obtained by measurement with a Horiba F-7 potentiometer and Ag-AgCl electrodes. The ion-exchange capacity of the membrane was determined as follows.[16] The PEC membrane was first immersed in 1 mol dm^{-3} HCl solution. After washing with water, this membrane was in turn immersed in 30 cm^3 of 1 mol dm^{-3} NaCl solution three times every two hours. After washing with water again, washings and immersing solvents were titrated with 0.05 mol dm^{-3} NaOH solution. The ion-exchange capacity was evaluated by dividing the measured value by the dry membrane weight.

Results and Discussion

Polyelectrolyte Complex. Figure 1 shows the dependence, upon hydrogen ion concentration, of the molar ratio of the reacting groups in PVSK and GC in a reaction mixture solution at the start and end of coagulation of PEC. The molar ratio, S(PVSK)/N(GC), increased with increasing $[H^+]$ and no coagulation was observed in solutions of lower $[H^+]$ than pH 6.5, i.e., larger amounts of PVSK solution were necessary to coagulate GC solution containing PEC as the hydrogen ion concentration was increased. The reason for above is that the degree of dissociation of GC decreases with decreasing $[H^+]$ and reaches zero eventually, whereas that of PVSK remains unchanged. In the pH 6.5 solution, the following strange phenomenon was observed. A coagulation occurred when PVSK solution was added to GC solution, while none when GC solution was added to PVSK solution. A probable reason for this phenomenon is that the concentration of PEC and the ionic strength in the reaction mixture for which PVSK solution was added to GC solution, were initially higher than those in the reaction mixture for which GC solution was added to PVSK solution.[3] Further investigation on this point should be made. Experimental conditions, yields of products, and results of elemental analyses for each PEC prepared after coagulation are given in Table 1. As seen in Table 1, the sulfur and nitrogen contents in the PECs which reflect the molar ratio of PVSK to GC are roughly equal, except for the PEC prepared in pH 6.5 solution. As a result, it appears that the reactions proceeded in the same manner when PEC was prepared after coagulation in the solutions of

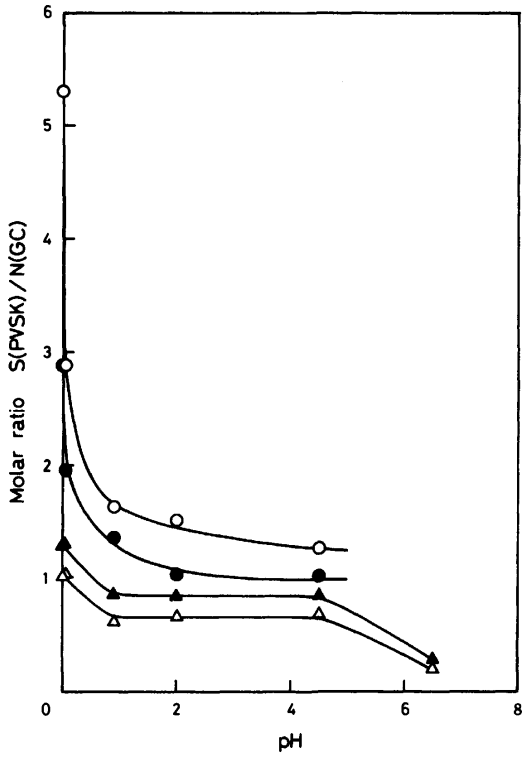

Fig. 1. Starting and end points of coagulation.
○△: Starting point of coagulation, ●▲: end point of coagulation, ○●: GC solution was added dropwise to PVSK solution, △▲: PVSK solution was added dropwise to GC solution.

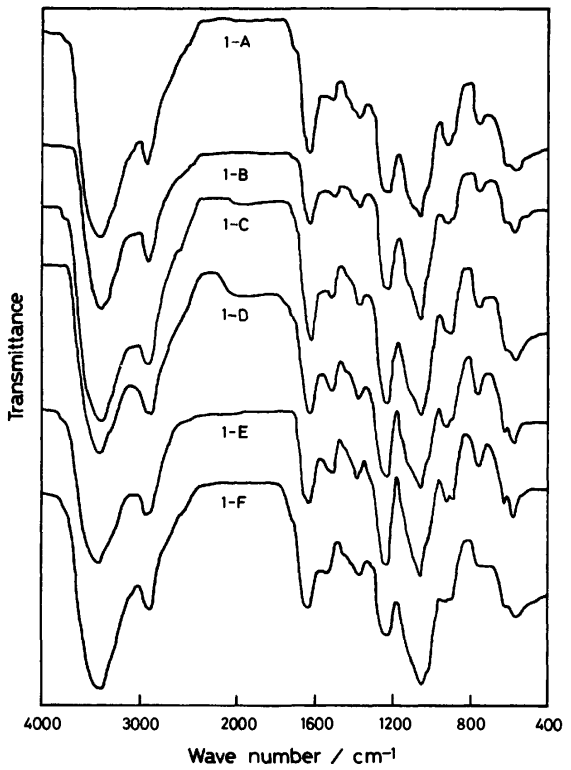

Fig. 2. IR spectra of the PEC. Sample codes correspond to those in Table 1.

$[H^+]$>pH 6.5. Thus, the hydrogen ion concentration in this system plays an important role in determining the ratio of PVSK/GC in the PEC.

Since the IR spectra of the PECs prepared in the cases where PVSK solution was added to GC solution are identical with those in the cases where GC solution was added to PVSK solution, only the former are shown in Fig. 2. The IR spectra of the PECs are almost the same as that of a mixture of PVSK and GC, differing from one another only in details. The absorption band at 1540 cm^{-1} assigned to $-NH_3^+$ in GC is present in all PECs, whereas that assigned to $-NH_2$ which should appear at 1590 cm^{-1} is absent. The absorption bands at 1230 and 800—600 cm^{-1}, which are also present in each PEC, are assigned to $-OSO_3^-$ in PVSK. The intensity of these absorptions is nearly equal in all PECs except the one prepared in pH 6.5 solution, whose absorbances at 1230 and 800—600 cm^{-1} are weak. These results imply that the PECs were produced in the same way, and this viewpoint coincides with the result of elemental analyses in Table 1. Furthermore, the absorption bands around 3500 cm^{-1} assigned to -OH groups are found in every PEC, and this proves that inter- and intramolecular hydrogen bonds between -OH groups are formed. These IR spectra have revealed that the PECs prepared in 7% HCl—pH 4.5 solutions consist of a greater fraction of PVSK, whereas the PVSK contents in the PECs prepared in pH 6.5 solution are low.

PECs are insoluble in general organic solvents, e.g., *N,N*-dimethylformamide, *N,N*-dimethylacetamide, and dimethyl sulfoxide, but soluble in ternary solvent mixtures, e.g., NaBr/acetone/H_2O and $CaCl_2$/1,4-dioxane/H_2O, and also in 36% HCl solution without heating. Phase diagrams were obtained for all kinds of PECs in the system of NaBr/acetone/H_2O and are shown in Fig. 3. There is a small region in the solvent composition field where PEC remains in the solution to form a homogeneous, viscous sirup. The miscibility limit of each PEC is approximately constant except for the PEC prepared in the solution of pH 6.5.

These experimental results support the concept that the PECs prepared in 7% HCl—pH 4.5 solutions have common constituents and similar compositions, but that the PEC prepared in pH 6.5 solution is different from them. This concept is in turn reduced to the dependence that the degree of dissociation of GC and PVSK changes with $[H^+]$.

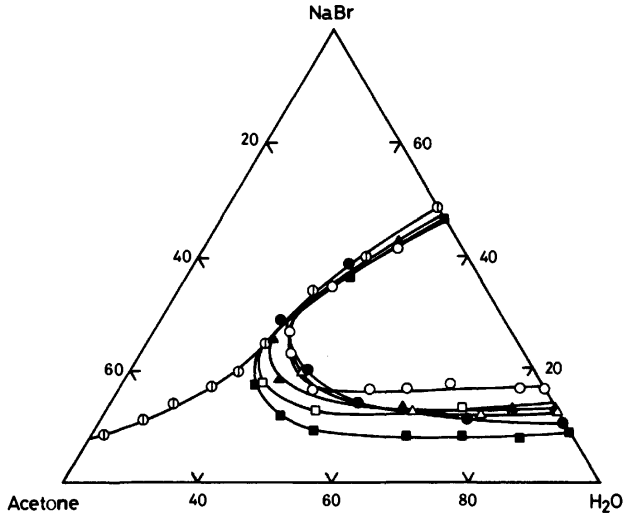

Fig. 3. Phase diagrams of the PEC in the ternary solvent system at 30 °C. ⓘ: NaBr/acetone/H_2O, ○: 1-A, ●: 1-B, △: 1-C, ▲: 1-D, □: 1-E, ■: 1-F.

Table 1. Experimental Conditions, Yields, and Elemental analyses of PECs

Sample code[a)]	Conditions		Yield/g	Sulfur content/%	Nitrogen content/%	Molar ratio of S(PVSK)/N(GC) in PEC
	Hydrogen ion concentration	Molar ratio of S(PVSK)/N(GC) in mixture				
1-A	7 v/v% HCl	2.00	0.304	7.03	2.67	1.15
1-B	4 v/v% HCl	1.60	0.314	7.40	2.59	1.25
1-C	1 v/v% HCl	1.10	0.282	7.73	2.29	1.48
1-D	pH 2.0	1.00	0.281	7.61	2.18	1.53
1-E	pH 4.5	0.90	0.293	7.41	2.10	1.54
1-F	pH 6.5	0.50	0.079	4.64	5.19	0.39
2-A	7 v/v% HCl	2.00	0.221	7.04	2.15	1.43
2-B	4 v/v% HCl	1.60	0.246	6.51	2.02	1.41
2-C	1 v/v% HCl	1.10	0.322	7.01	2.07	1.48
2-D	pH 2.0	1.00	0.409	7.85	2.43	1.41
2-E	pH 4.5	0.90	0.438	8.13	2.60	1.37

a) Series 1: PVSK solution was added dropwise to GC solution (100 cm^3). Series 2: GC solution was added dropwise to PVSK solution (100 cm^3).

Polyelectrolyte Complex Membrane. The membrane obtained by casting the PEC prepared in 4% HCl solution was adopted for the study on the transport of alkali metal ion Na^+, because this membrane was most stable in acidic and alkaline solutions. The concentrations of Na^+ in the left- and right-side chambers of the cell were set the same initially. The left-side chamber contained HCl as well, while the right-side chamber NaOH. Figure 4 shows concentration changes for Na^+, Cl^-, and H^+ with time in both the side chambers containing 0.1 mol dm^{-3} HCl. Despite the fact that both the sides of the membrane were originally equal in the concentration of Na^+, an increase of Na^+ in the left side was observed and the change in the right side was quite reverse. This suggests that the active transport of Na^+ took place from the right side, alkaline solution, to the left side, acidic solution, through the membrane. The concentration of Na^+ in the left side increased up to a maximum, and then decreased with the passage of time. This back transport of concentrated Na^+ is due to decrease in the hydrogen ion concentration difference between both sides of the membrane and to the permeation of Cl^-. The ratios of the transported ions are calculated by

$$\text{Transport ratio } (\%) = \frac{[Na^+]_{max} - [Na^+]_0}{[Na^+]_0} \times 100, \quad (1)$$

where $[Na^+]_{max}$ is the mole number of Na^+ in the left-side chamber at the maximum, and $[Na^+]_0$ is the mean of the initial mole numbers of Na^+ in both the side chambers. The dependence of the transport ratio of Na^+ on the concentration of H^+ in the left-side chamber is shown in Fig. 5. The transport ratio corresponds to the $[H^+]$, and it is high at $[H^+]$ above pH 1.0, whereas low at $[H^+]$ below pH 2.0. Hence, it is thought that the driving force for the transport of Na^+ will be the hydrogen ion concentration difference between both the side chambers which causes an electric potential gradient. Accordingly, the membrane potential difference needs to be measured. Figure 6 indicates that the membrane potential difference gets greater as the concentration of HCl in the left side is increased, and this tendency is consistent with the result in Fig. 5. The membrane potential difference, however, decreases with time. This decrease in the potential difference is not only due to the transport of Na^+ from the right to left side

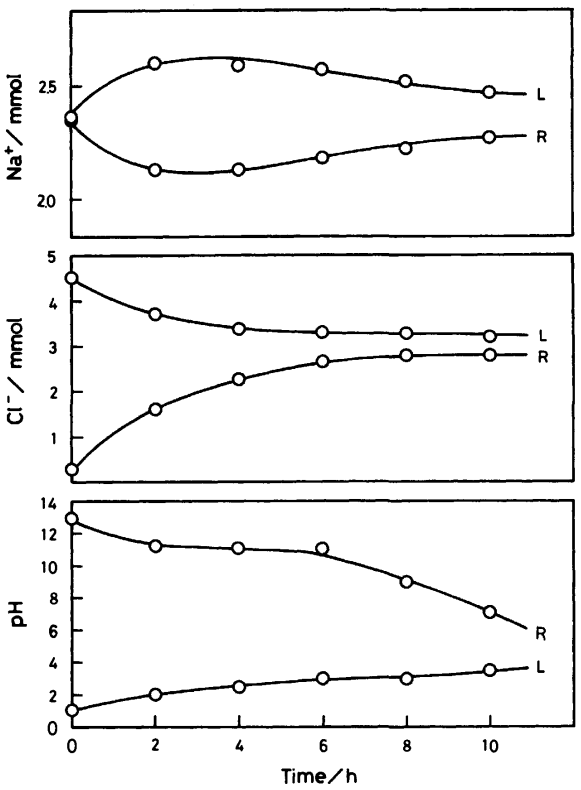

Fig. 4. Changes in the concentration of Na^+, Cl^-, and H^+ at the active transport

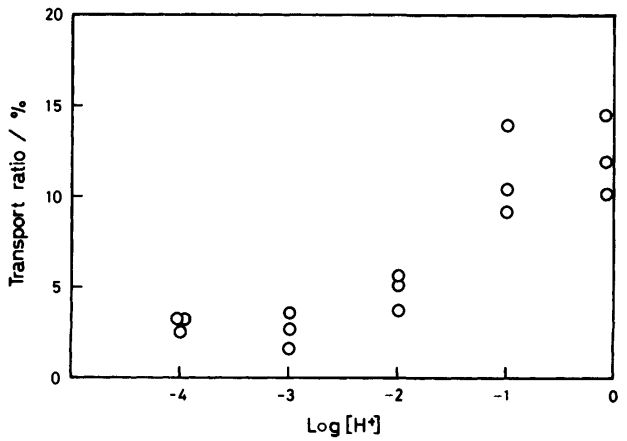

Fig. 5. Effect of the hydrogen ion concentration on the transport ratio of Na^+ in the case HCl was used.

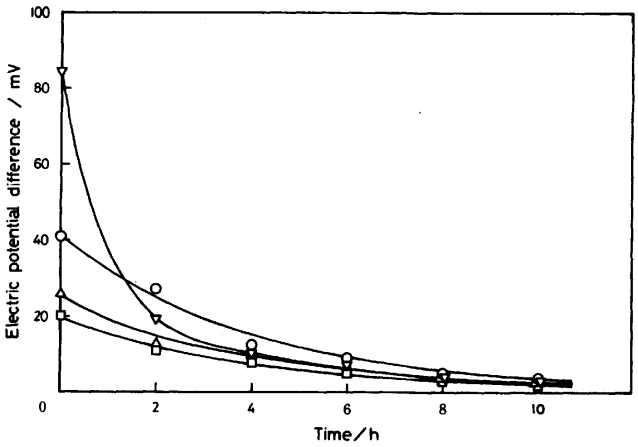

Fig. 6. Changes of the electric potential difference with time. ▽: 1 mol dm^{-3} HCl, ○: 0.1 mol dm^{-3} HCl, △: 0.01 mol dm^{-3} HCl, □: 0.001 and 0.0001 mol dm^{-3} HCl.

but also due to the permeation of Cl^- from the left to right side. As shown in Fig. 4, this Cl^- permeation is large, so that an investigation on the transport in cases where all negative charges are kept fixed in the left side of the membrane, was attempted, results obtained being analyzed in the light of the above conclusion.

The results in the case where HSS and NaSS were adopted instead of HCl and NaCl, respectively, are shown in Figs. 7 and 8. The transport ratios were evaluated by Eq. 1 by taking into consideration the transfer of water based on the Donnan osmosis. The concentration of Na^+ in the left-side chamber increased and that in the right-side one decreased with the passage of time in a similar manner as in the case of HCl. On the other hand, the concentration of SS^- was unchanged, in contrast with Cl^- in the case of HCl. Moreover, the transport ratios of Na^+ were much larger than those in the case of HCl, as shown in Fig. 8. This is compatible with the assumption that the membrane potential difference would be maintained for a long time because SS^- is kept fixed well in the left side of the membrane. This assumption is supported by the result in Fig. 9. The membrane potential difference was maintained for more than 24 h.

Therefore, on the basis of the results described above we speculate that the transport of Na^+ will be effected in the following manner. The PEC membrane is considered to be a sort of charged membrane for which the functional groups of $-OSO_3^-$ in PVSK are responsible. The permeation phenomena in the case where a charged membrane is used or a certain ion is fixed in one side of the membrane, is explained in terms of the Donnan membrane equilibrium. It is difficult to analyze such a system as in this study comprising many kinds of ions. However, on the assumption that the membrane potential is the concentration membrane potential raised by HCl or HSS, the membrane potential $\Delta\phi$ can be regarded as the sum of the Donnan potentials $\Delta\phi_{Don,L}$ and $\Delta\phi_{Don,R}$ at the two solution-membrane interfaces and the diffusion potential $\Delta\phi_{Dif}$ in the membrane.[17] Tentative membrane potential and transfer of Na^+ deduced

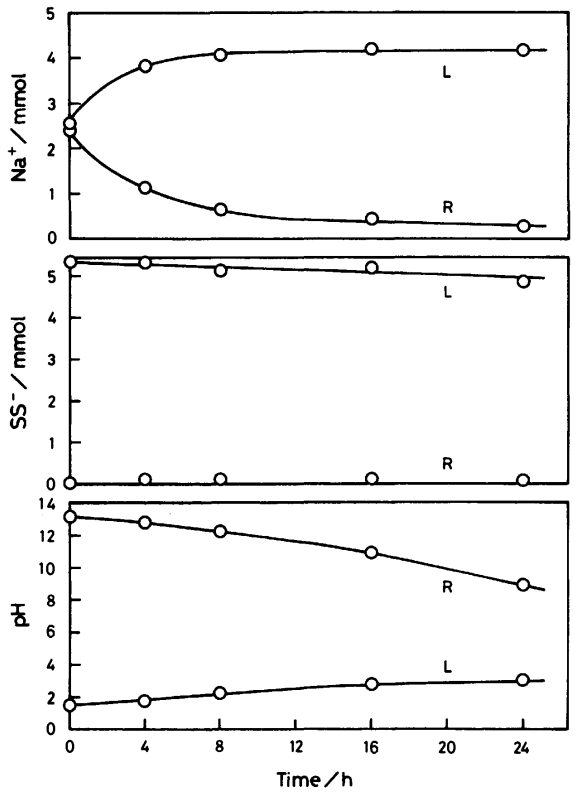

Fig. 7. Changes in the concentration of Na^+, SS^-, and H^+ at the active transport.

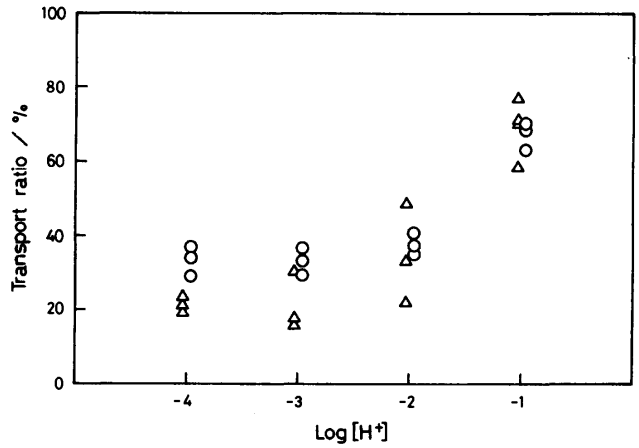

Fig. 8. Effect of the hydrogen ion concentration on the transport ratio of Na^+ in the case HSS was used. ○: $M_w = 1.0 \times 10^4$, △: $M_w = 5.0 \times 10^5$.

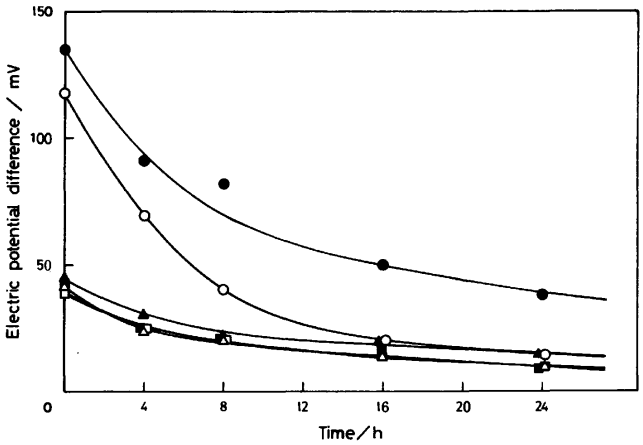

Fig. 9. Changes of the electric potential difference with time. ○: 0.1 mol dm^{-3} HSS($M_w = 1.0 \times 10^4$), △: 0.01 mol dm^{-3} HSS($M_w = 1.0 \times 10^4$), □: 0.001 and 0.0001 mol dm^{-3} HSS($M_w = 1.0 \times 10^4$), ●: 0.1 mol dm^{-3} HSS($M_w = 5.0 \times 10^5$), ▲: 0.01 mol dm^{-3} HSS($M_w = 5.0 \times 10^5$), ■: 0.001 and 0.0001 mol dm^{-3} HSS($M_w = 5.0 \times 10^5$).

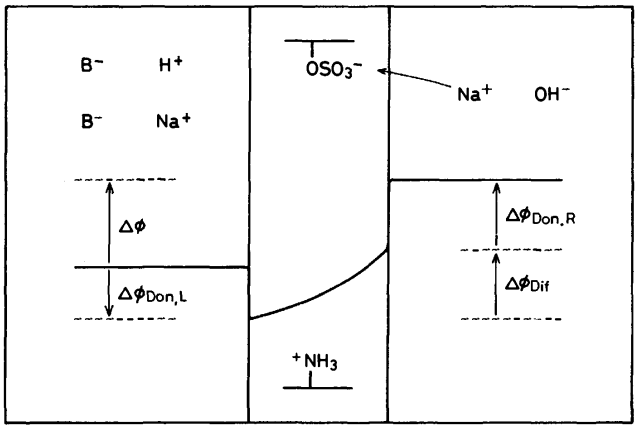

Fig. 10. Schematic representation of the membrane potential.

from the conclusions described above are illustrated in Fig. 10. In this system, the membrane surface potential is low because PEC membrane is anionic, and the potential in the membrane increases in the direction toward the right because of the large mobility of H^+. Thus, as a result, the right side is higher than the left side in electric potential. Na^+ was transported from the right to left side, i.e., from the alkaline to acidic side, through the membrane in accord with the gradient of electric potential. It seems that $-OSO_3^-$ groups in the membrane serve as carriers for Na^+.[8] However, the Donnan exclusion for Cl^- is small due to the small cation-exchange capacity (0.14 mequiv g^{-1} dry membrane) and there are $-N^+$ groups in the membrane capable of attracting Cl^-, so that the membrane potential difference is not maintained constant so long by Cl^- permeation. Then, the transport ratio of Na^+ seems low in the case of HCl. In the case of HSS, on the contrary, $\Delta\phi_{Don,L}$ and $\Delta\phi_{Dif}$ are larger than those in the case of HCl for the fixed SS^-, although $\Delta\phi_{Don,R}$ is equal; moreover, the maintenance time of constant membrane potential difference is long. Therefore, the transport of Na^+ in accord with the membrane potential gradient is appreciable.

References

1) Y. Mori and H. Tanzawa, *Kobunshi*, **22**, 616 (1973).
2) A. Nakajima, *Kagaku To Kogyo*, **27**, 750 (1974).
3) E. Tsuchida and K. Abe, *Adv. Polym. Sci.*, **45**, 18 (1982).
4) L. L. Markley, H. J. Bixler, and R. A. Cross, *J. Biomed. Mater.*, **2**, 145 (1968).
5) H. J. Bixler and A. S. Michaels, *Encycl. Polymer Sci. Tech.*, **10**, 765 (1969).
6) T. Shimidzu, M. Yoshikawa, M. Hasegawa, and K. Kawakatsu, *Macromolecules*, **14**, 170 (1981).
7) T. Shimidzu and M. Yoshikawa, *Nippon Kagaku Kaishi*, **1983**, 958.
8) T. Uragami, R. Nakamura, and M. Sugihara, *Polymer*, **24**, 559 (1983).
9) T. Uragami, F. Yoshida, and M. Sugihara, *J. Appl. Polym. Sci.*, **28**, 1361 (1983).
10) N. Ogata, K. Sanui, and H. Fujimura, *J. Appl. Polym. Sci.*, **25**, 1914 (1980).
11) M. Yoshikawa, H. Ogata, and K. Sanui, *Polym. J.*, **15**, 609 (1983).
12) Y. Kikuchi and N. Kubota, *Bull. Chem. Soc. Jpn.*, **58**, 2121 (1985).
13) Y. Kikuchi and N. Kubota, *Nippon Kagaku Kaishi*, **1985**, 1592.
14) Y. Kikuchi and N. Kubota, *Nippon Kagaku Kaishi*, **1985**, 111; *J. Appl. Polym. Sci.*, **30**, 2565 (1985).
15) Y. Kikuchi, K. Hori, and Y. Onishi, *Nippon Kagaku Kaishi*, **1980**, 1157.
16) M. Senoo and Y. Tanaka, "Makugaku Jikkenho," ed by M. Nakagaki, Kitami Shobo, Tokyo (1984), p. 194.
17) T. Hanai, "Maku To Ion," Kagaku Dojin, Kyoto (1978), p. 232.

 © 1987 The Chemical Society of Japan Bull. Chem. Soc. Jpn., 60, 381—383 (1987)

Neutralization Dialysis for Deionization

Manabu IGAWA,* Kiyoyuki ECHIZENYA, Takashi HAYASHITA, and Manabu SENO†
Department of Applied Chemistry, Faculty of Engineering, Kanagawa University,
Rokkakubashi, Kanagawa-ku Yokohama 221
†Institute of Industrial Science, The University of Tokyo,
Roppongi, Minato-ku, Tokyo 106
(Received June 30, 1986)

In neutralization dialysis, cations are exchanged with protons across a cation-exchange membrane, while anions are exchanged with hydroxide ions across an anion-exchange membrane, and the effective deionization and the neutralization occur simultaneously on the base of Donnan equilibrium. The ion-exchange membranes are much more permeable to the electrolytes than the nonelectrolytes and their mutual separation is possible by this method.

Donnan dialysis is an ion-exchange membrane process based on Donnan equilibrium[1] and it has been used for salt enrichment.[2-5] Recently, we proposed a novel deionization method based on the principle of Donnan dialysis by the simultaneous use of a cation-exchange membrane and an anion-exchange membrane.[6] When a salt solution is separated from an acid solution with a cation-exchange membrane and from a base solution with an anion-exchange membrane, the cations in the salt solution are exchanged with protons, while the anions are exchanged with hydroxide ions, and deionization and neutralization occur simultaneously. This process can be called "neutralization dialysis," because salts are transported rapidly across the membrane by the great concentration gradients of protons and hydroxide ions caused by neutralization in the deionization compartment. Neutralization dialysis is a simple, continuous, and very effective process and its principle must also play an important role in biomembranes. Active transports coupled with proton antiport have been reported as the model of biomembranes,[7] but the ion transport will be enhanced much when it is coupled with neutralization reaction. This method will be quite profitable for desalination because of requiring a low energy and low cost and it may be able to substitute this deionization process for the ion-exchange process on ion-exchange resin. The ion-exchange membranes are much more permeable to electrolytes than nonelectrolytes and their complete mutual separation will be also reported in this report.

Experimental

The neutralization-dialysis cell, which is similar to the macromosaic cell,[8] and the schematic ion transport are shown in Fig. 1. Each compartment is 0.5 mm thick with a 2×10 cm^2 area. The solutions in deionization compartment D, in acid compartment A, and in base compartment B were cycled from respective reservoirs with tube pumps at a rate of 40 cm min^{-1}. The ion-exchange membranes in the cell were Selemion AMV and CMV(Asahi Glass Co., Ltd.). In the dialysis experiment, 3 cm^3 samples were collected from the solution of compartment D at a regular interval and the cation concentration, the specific resistance, and pH were measured with an atomic absorption spectrophotometer, a conductance cell, and a pH meter, respectively. The separation of electrolytes from nonelectrolytes was investigated with a mixed aqueous solution of potassium chloride and methyl alcohol. The concentration of methyl alcohol was measured with a total organic carbon analyzer.

Results and Discussion

A deionization experiment was carried out with the neutralization-dialysis cell and Fig. 2 shows the changes with time of the cation concentration, pH, and the specific resistance of the solution in compartment D. The ion concentration decreased and the specific resistance increased rapidly with time, and a deionized water with a specific resistance of 1 MΩ cm were obtained after 1.5 h.

In this process, Donnan equilibrium is set up across a membrane after an ample time and the ratios of the

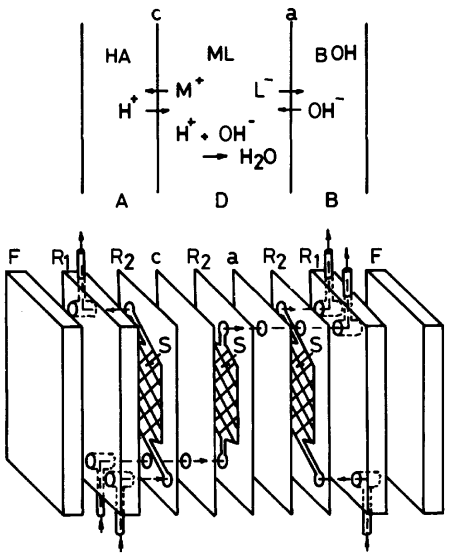

Fig. 1. Neutralization-dialysis cell and the schematic ion transport. a: Anion-exchange membrane, c: cation-exchange membrane. R_1 and R_2: silicone rubber sheet, S: spacer, F: acrylic resin frame.

ion concentrations in each compartment become

$$C_A^M/C_A^H = C_D^M/C_D^H, \quad (1)$$

$$C_B^L/C_B^{OH} = C_D^L/C_D^{OH}, \quad (2)$$

From the standpoint of thermodynamics, activities should be used for describing Donnan equilibrium but activity coefficients are assumed to be unity and concentrations are used in these equations for simplifying the discussion. In the equations, C is concentration, M, L, H, and OH are a monovalent cation, a monovalent anion, proton, and hydroxide ion, respectively, and A, B, and D are symbols of the compartments. When the volume of the acid solution is equal to that of the base solution and $C_A^H=C_B^{OH}$, $C_A^M=C_B^L$ and $C_D^M=C_D^L$. The material balance for the metal ion is

$$C_A^M V_A + C_D^M V_D = C_{0,D}^M V_D + C_{0,A}^M V_A, \quad (3)$$

where the amount of the ion in the cation-exchange membrane is ignored, and V and C_0 show the volume and the initial metal ion concentration of the solutions, respectively. From Eqs. 1 and 3, the final concentration of the metal ion in the deionization compartment is

$$C_D^M = (C_{0,D}^M V_D + C_{0,A}^M V_A)/(C_A^H V_A/C_D^H + V_D). \quad (4)$$

Since protons and hydroxide ions combine to be water and their concentrations become 10^{-7} mol dm^{-3} ideally in compartment D, the equilibrated concentration in compartment D is calculated to be 3.8×10^{-10} mol dm^{-3} according to this equation in the case of Fig. 2. The pH decreased appreciably in the initial stage of the dialysis as shown in Fig. 2, because the transport rate of protons in the cation-exchange membrane differs from that of hydroxide ions in the anion-exchange membrane. Sulfuric acid and calcium hydroxide were used for acid and base in this experiment to decrease the leakage of co-ions across the membrane because polyvalent co-ions repel ion-exchange membranes strongly, but it can not be ignored in highly deionized solution.

In neutralization dialysis, the diffusion flux of metal ion across the membrane, J_M can be derived as the function of the ion concentration in the bulk solution. The ion flux is proportional to the concentration difference in the membrane as generally recognized[9] and it is

$$J_M = P(\bar{C}_D^M - \bar{C}_A^M), \quad (5)$$

where P, C_D^M, and C_A^M are the permeation constant, the concentration in the membrane adjacent to the deionization compartment, and that adjacent to the acid compartment, respectively.[4] The ion-exchange equilibriums apply at the interfaces of the membranes and the equilibrium constant, K is

$$K = (\bar{C}_A^M/C_A^M)/(\bar{C}_A^H/C_A^H) = (\bar{C}_D^M/C_D^M)/(\bar{C}_D^H/C_D^H), \quad (6)$$

where K is assumed to be constant on either side of the membrane. When the concentration of the exchangeable cation in the cation-exchange membrane is shown as C_{ex}, the relationship between each ion concentration in the membrane is

$$\bar{C}_A^M + \bar{C}_A^H = \bar{C}_D^M + \bar{C}_D^H = C_{ex}. \quad (7)$$

From Eqs. 5—7, J_M is expressed as the function of the ion concentration in the bulk solution by

$$J_M = C_{ex}P[1/(1+C_D^H/KC_D^M) - 1/(1+C_A^H/KC_A^M)]. \quad (8)$$

According to this equation, it is predicted that J_M increases with increasing the ratio of C_A^H to C_A^M and becomes zero when Donnan equilibrium is attained across the membrane as shown in Eq. 1. J_M also increases with the decrease of C_D^H but the optimum value of C_D^H is 10^{-7} mol dm^{-3} because the anion flux can be also described in the same form as Eq. 8 and it should be equal to J_M for the most efficient

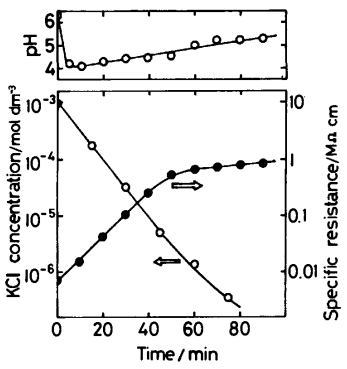

Fig. 2. Deionization by neutralization dialysis. Compartment A, 0.01 mol dm^{-3} H_2SO_4 (1 dm^3). Compartment B, 0.01 mol dm^{-3} $Ca(OH)_2$ (1 dm^3). Compartment D, 0.001 mol dm^{-3} KCl (75 cm^3).

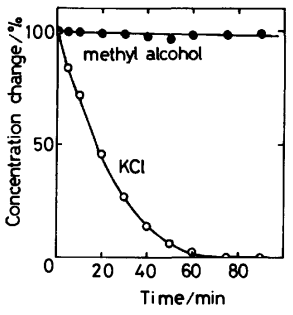

Fig. 3. Separation of potassium chloride from methyl alcohol. Compartment D, 0.1 mol dm^{-3} methyl alcohol+0.01 mol dm^{-3} KCl aqueous solution (100 cm^3). The other experimental conditions are the same as those of Fig. 2.

deionization.

The deionization capability was also confirmed when KCl was initially added to both acid and base solutions to be 0.1 mol dm^{-3} in the case of Fig. 2. The permeation rate decreased and the time taken to reach 10% of the initial concentration of the deionization compartment becomes about 5 times longer, but KCl was transported against its concentration difference as expected by above equations.

A dialytic separation of potassium chloride from methyl alcohol was also tried in this system and the result is shown in Fig. 3. The concentration change of methyl alcohol could be ignored (within 2%), while potassium chloride was effectively removed and its concentration became 0.2% of the initial concentration after 1.5 h. Since permeabilities of nonelectrolytes decreases rapidly with the increase of the molecular weight,[8] the loss of nonelectrolytes during the dialysis is much smaller in almost all the case than that showm in Fig. 3. A dialytic deionization of a mixed solution of electrolytes and nonelectrolytes is achieved effectively in this process.

References

1) F. G. Donnan, *Chem. Rev.*, **1**, 73 (1924).
2) R. M. Wallace, *Ind. Eng. Chem., Process Des. Dev.*, **6**, 423 (1967).
3) J. A. Cox and J. E. DiNunzio, *Anal. Chem.*, **49**, 1272 (1977).
4) M. A. Lake and S. S. Melsheimer, *AIChE J.*, **24**, 130 (1978).
5) J. A. Cox, K. Slonawska, D. Gatchell, and A. G. Hiebert, *Anal. Chem.*, **56**, 650 (1984).
6) M. Igawa, K. Echizenya, T. Hayashita, and M. Senō, *Chem. Lett.*, **1986**, 237.
7) E. M. Choy, D. F. Evans, and E. L. Cussler, *J. Am. Chem. Soc.*, **96**, 7085 (1974).
8) M. Igawa, T. Tachibana, I. Ueki, M. Tanaka, and M. Senō, *Ind. Eng. Chem., Fundam.*, **24**, 485 (1985).
9) O. Kedem and A. Katchalsky, *Biochim. Biophys. Acta*, **27**, 229 (1958).

 © 1987 The Chemical Society of Japan Bull. Chem. Soc. Jpn., 60, 385—390 (1987)

Polymer-Protected Metal Complex for Gas Separation. III. Water-Resistivity of Polystyrene Resin-Supported Aluminium Copper(I) Chloride as Solid Carbon Monoxide Adsorbent[1)]

Hidefumi HIRAI,* Susumu HARA, and Makoto KOMIYAMA
Department of Industrial Chemistry, Faculty of Engineering, The University of Tokyo, Hongo, Bunkyo-ku, Tokyo 113
(Received July 14, 1986)

Solid adsorbents of carbon monoxide are prepared from aluminium chloride, copper(I) chloride, and a macroreticular type polystyrene resin by use of various solvents, and their resistivities against water vapor are investigated. The adsorbing capacities of the adsorbents prepared by use of carbon disulfide and dichloromethane remain virtually unchanged even after repeated (3—5 times) contacts of the adsorbents with nitrogen gas containing 10 mol% water with respect to the charged copper(I) chloride (water contents: 5600 and 4600 ppm). The adsorbents obtained with the use of benzene and toluene as preparation solvents, however, exhibit small but gradual decreases in the adsorbing capacities on the repeated contacts with nitrogen gas containing water. Scanning electron microscopy and energy dispersive X-ray microanalysis on the water-resistant adsorbents, prepared with the use of carbon disulfide and dichloromethane, show that the active species for the adsorption, aluminium copper(I) chloride, uniformly distributes in the beads of the polystyrene resin without formation of aggregates. Almost all of aluminium copper(I) chloride is located in the apolar microporosities of the polystyrene resin here, and is effectively protected from water vapor.

Carbon monoxide (CO), which is one of the most important raw materials in chemical industry,[2)] is usually obtained as gas mixtures with hydrogen, nitrogen, oxygen, methane, carbon dioxide, and water vapor.[3)] Thus, CO must be separated from the gas mixtures prior to effective utilization.

In previous papers,[4,5)] the authors reported that toluene solutions of polystyrene-protected aluminium copper(I) chloride ($AlCuCl_4$) reversibly absorbed CO under mild conditions. These absorbents were stable against water vapor, and thus were applicable to separation of CO from gas mixtures containing considerable amounts of water vapor. In the absence of the polystyrene, however, $AlCuCl_4$ in toluene was rapidly deactivated by water vapor due to irreversible reaction of $AlCuCl_4$ with water.[6)]

Furthermore, the authors succeeded in the preparation of the macroreticular type cross-linked polystyrene resin-supported $AlCuCl_4$ as solid adsorbents for CO.[1,7,8)] With the use of them, separations of CO from gas mixtures were successfully achieved both by pressure-swing method and by thermal-swing method.

This paper reports on the resistivities against water vapor for the macroreticular type polystyrene resin-supported $AlCuCl_4$. Effects of preparation solvents on the water-resistivities of the adsorbents are described. Furthermore, the results of scanning electron microscopy and energy dispersive X-ray microanalysis on the surface and the cross-section of the adsorbents are shown. The mechanism of water-resistivities is discussed in terms of the microstructures of the adsorbents.

Experimental

Materials. A macroreticular type cross-linked polystyrene resin (8:2 styrene–divinylbenzene copolymer; 20—50 mesh; 296—740 μm in diameter; average pore diameter 9 nm; surface area 300 $m^2 g^{-1}$)[9)] was obtained from Bio-Rad Laboratories (Bio-Beads SM-2). The resin was successively washed with the following solvents under the specified conditions: aqueous hydrochloric acid solution, 4 mol dm^{-3}, 55 °C, 2 h; aqueous sodium hydroxide solution, 2 mol dm^{-3}, 55 °C, 2 h; distilled water, 55 °C, 2 h; methanol, room temperature, 1 h; dichloromethane, room temperature, 1 h.

Aluminium chloride was purified by sublimation. Copper(I) chloride was reprecipitated from a concentrated aqueous hydrochloric acid solution by the addition of distilled water, followed by washing successively with ethanol and diethyl ether, and then dried overnight in vacuo at 100 °C.

Carbon disulfide and dichloromethane were dried over diphosphorus pentaoxide and were distilled. Toluene and benzene were distilled after being dried over metallic sodium.

Carbon monoxide and nitrogen, which had purities of 99.95 and 99.999%, respectively, were passed through columns of molecular sieve 3A immediately before use.

Preparation of CO Adsorbents. The solid CO adsorbents were prepared by refluxing aluminium chloride, copper(I) chloride, and the macroreticular type polystyrene resin in various solvents under dry nitrogen.[8)] Charged molar ratios of aluminium chloride and styryl residue in the resin, respectively, to copper(I) chloride were 1.0 and 1.2. After 6 h, the solvents were removed from the mixtures by evaporation at 4 mmHg (1 mmHg=133.3 Pa) for 4—6 h. Evaporation temperature was gradually elevated from room temperature to 80 °C, as the evaporation proceeded.

Adsorption and Desorption of CO. The adsorption of CO by the adsorbent, continuously stirred by use of a magnetic stirrer, was carried out at 25 °C, 1 atm, and was

followed by measuring the uptake of CO with the use of a gas burette.[8]

The desorption of adsorbed CO was achieved by subjecting the adsorbent to a reduced pressure (7 mmHg) at 25 °C for 10 min.

Contacts of CO Adsorbents with Water Vapor. The contacts of the adsorbents with water vapor were effected by circulating 10 dm^3 of nitrogen gas, which contained 10 mol% water to the charged CuCl, over the adsorbents at 25 °C for 10 min by use of a gas-circulating pump. The contents of water were in the range of 4600—6100 ppm. During the contacts, the adsorbents were stirred using a magnetic stirrer. The nitrogen containing water vapor was prepared by the introduction of distilled water into 10 dm^3 of evacuated vessel using a microsyringe, followed by the addition of dry nitrogen in an amount required to make the total pressure atmospheric.

Effects of contacts of the adsorbents with dry nitrogen, in place of nitrogen containing water vapor, were investigated in similar ways in order to evaluate precisely the effects of water vapor on the capacities of the adsorbents.

Scanning Electron Microscopy and Energy Dispersive X-Ray Microanalysis on CO Adsorbents. Scanning electron microscopy and the energy dispersive X-ray microanalysis were simultaneously carried out by use of a system composed of a Hitachi model S-550 scanning electron microscope and a KEVEX model 7000-75 energy dispersive X-ray spectrometer.[10] Data analysis was made on a DEC type PDP 11/34 mini computer.

The specimens for the analysis of the cross-sections of the beads of the adsorbents were prepared by embedding the beads in an epoxy resin. The resultant composites were scraped with sand paper so that the cross-sections of the beads could be analyzed. Alternatively, the beads of the adsorbents were divided into two parts by using a stainless steel blade, and were used for the analysis.

Results

Effect of Water Vapor on Adsorbing Ability of Macroreticular Type Polystyrene Resin-Supported Aluminium Copper(I) Chloride Prepared Using Carbon Disulfide As Solvent. Open circles in Fig. 1 show the adsorption of CO at 25 °C, 1 atm by the adsorbent prepared from 3.03 g (22.7 mmol) of aluminium chloride ($AlCl_3$), 2.25 g (22.7 mmol) of copper(I) chloride (CuCl), and 2.84 g (26.1 mequiv. of styryl residue) of the macroreticular type cross-linked polystyrene resin (divinylbenzene content 20%) by use of 20 cm^3 of carbon disulfide as solvent. The adsorption is rapid and the equilibrium molar ratio of the adsorbed CO to the charged CuCl is 1.07. The amount of adsorbed CO per 1 g of the adsorbent is 67 cm^3 (standard temperature and pressure).

After the first adsorption, the adsorbent is contacted with 10 dm^3 of dry nitrogen at 25 °C for 10 min, and then is subjected to a reduced pressure (7 mmHg) at 25 °C for 10 min. In the second adsorption, the adsorbent promptly adsorbs CO and the equilibrium molar ratio of adsorbed CO to the charged CuCl is 0.54, as shown by the solid circles in Fig. 1.

The open triangles in Fig. 1 depict the third adsorption of CO. Before the adsorption, the adsorbent is contacted with nitrogen containing 10 mol% water to the charged CuCl (water content: 5600 ppm) for 10 min, and is kept at 7 mmHg, 25 °C for 10 min. The equilibrium molar ratio of the adsorbed CO to the charged CuCl is 0.54, which is identical with the value in the second adsorption. In the fourth, the fifth, the sixth, and the seventh adsorptions, the time courses of CO adsorptions are virtually the same as those for the second and the third adsorptions. Prior to each of these adsorptions, the adsorbent is contacted with nitrogen containing 10 mol% water (water content: 5600 ppm).

Water Resistivities of CO Adsorbents Prepared by Use of Various Solvents. Figure 2 depicts the plots of the CO adsorbing capacities of the adsorbents as functions of numbers of repeated adsorptions of CO. Prior to each of the third and the later adsorptions, the adsorbents are contacted with nitrogen containing 10 mol% water with respect to the charged CuCl, as indicated by the arrows. Before the second adsorptions the adsorbents are contacted with dry nitrogen.

In the first adsorptions, all the adsorbents, prepared by use of carbon disulfide, dichloromethane, toluene, and benzene, adsorb CO approximately equimolar to the charged CuCl.

The adsorbing capacity of the adsorbent prepared by use of carbon disulfide remains constant at 0.54 in the second to the seventh adsorption (see the open circles). Thus, no measurable decrease in the capacity

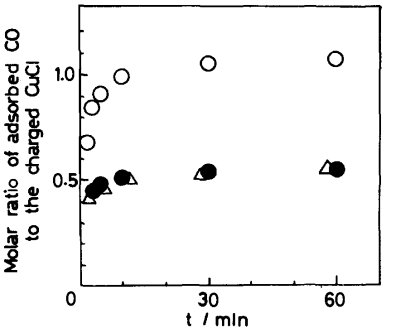

Fig. 1. Adsorption of CO at 25 °C, 1 atm by the adsorbent prepared from the macroreticular type (divinylbenzene content 20%) polystyrene resin, $AlCl_3$, and CuCl by use of carbon disulfide as solvent: the first adsorption (○), the second adsorption (●), and the third adsorption (△); the desorptions of CO were carried out by subjecting the adsorbent to a reduced pressure (7 mmHg) at 25 °C for 10 min; prior to the third adsorption, the adsorbent was contacted with 10 dm^3 of nitrogen containing 10 mol% water to the charged CuCl (water content 5600 ppm) at 25 °C for 10 min; the adsorbent was prepared from 3.03 g (22.7 mmol) of $AlCl_3$, 2.25 g (22.7 mmol) of CuCl, and 2.84 g (26.1 mequiv. in styryl residue) of the polystyrene resin with the use of 20 cm^3 of carbon disulfide.

is perceived even after five times of the contacts of the adsorbent with nitrogen containing water vapor. The capacity of the adsorbent prepared using dichloromethane is also unchanged after three times of the contacts with nitrogen containing water vapor (the closed circles). In contrast, the CO adsorbing capacities of the adsorbents prepared by use of toluene and benzene as solvents gradually decrease on the contacts with water vapor, as depicted by the open triangles and the closed triangles, respectively.

The differences between the adsorbing capacities in the first adsorptions and those in the second adsorptions are ascribed to the amounts of CO adsorbed in equilibria under the desorption conditions employed (7 mmHg at 25 °C for 10 min), as described in the previous paper.[8] When the CO adsorption-desorption cycles are repeated without the contacts of the adsorbents with water vapor, the adsorbing capacities of all the four adsorbents in the third and the later adsorptions are identical with the values in the corresponding second adsorptions.[8]

Scanning Electron Microscopy (SEM) on Surface of CO Adsorbents. Figure 3 depicts the SEM photographs of the surface of the adsorbents. The surface of the adsorbent prepared using carbon disulfide as solvent is smooth and deposition of metal salts is hardly detected, as exhibited by the photograph (a). On the surface of the adsorbent prepared with the use of toluene as solvent, however, depositions of considerable amount of metal salts are clearly observed (the photograph (b)).

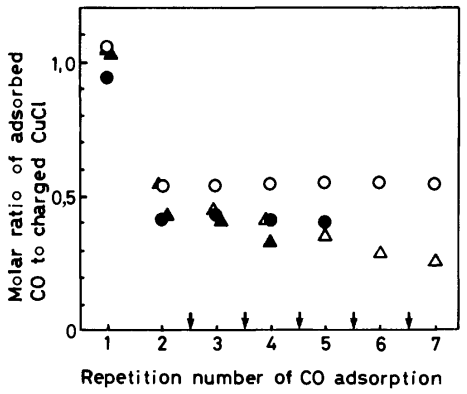

Fig. 2. Effects of water vapor on the CO adsorbing capacities at 25 °C, 1 atm for the adsorbents prepared from the macroreticular type polystyrene resin, $AlCl_3$, and CuCl by use of carbon disulfide (○), dichloromethane (●), toluene (△), and benzene (▲) as solvents: the arrows refer to the contacts of the adsorbents with nitrogen containing 10 mol% water to the charged CuCl at 25 °C for 10 min; the desorptions of CO were carried out by subjecting the adsorbents to a reduced pressure (7 mmHg) at 25 °C for 10 min.

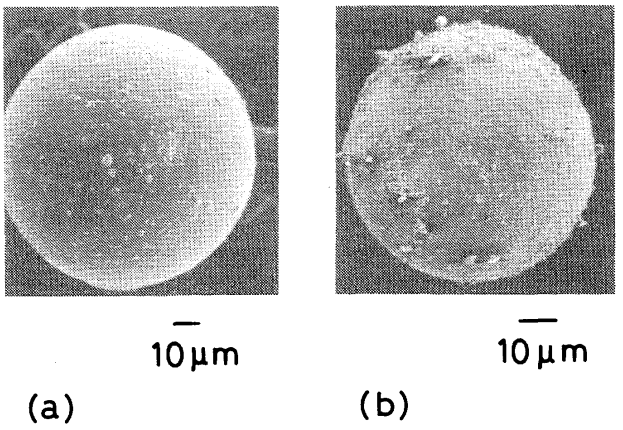

Fig. 3. SEM photographs of the surface of the CO adsorbents prepared from the macroreticular type polystyrene resin, $AlCl_3$, and CuCl by use of (a) carbon disulfide and (b) toluene as solvents.

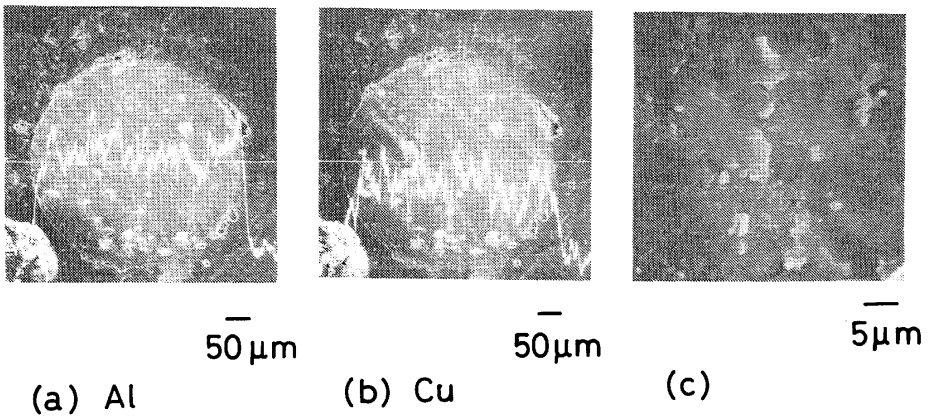

Fig. 4. SEM photographs as well as distributions of Al and Cu atoms for the cross-section of the CO adsorbent prepared from the macroreticular type polystyrene resin, $AlCl_3$, and CuCl by use of carbon disulfide as solvent: the waved lines show the distributions of (a) Al atoms and (b) Cu atoms along the corresponding white straight lines.

Scanning Electron Microscopy (SEM) and Energy Dispersive X-Ray Microanalysis on Cross-Sections of Beads of CO Adsorbents. Figures 4—6 depict SEM photographs of the cross-sections of the beads of the adsorbents. The waved lines refer to the distributions of Al and Cu atoms along the corresponding white straight lines on the cross-sections of the beads.

For the adsorbent prepared by use of carbon disulfide, both Al atoms and Cu atoms uniformly distribute in the cross-section of the bead, as shown by the waved lines in the photographs (a) and (b) in Fig. 4. Even at a larger magnitude of magnification (the photograph (c) in Fig. 4), no depositions of metal salts are detected.

In the adsorbent obtained with the use of toluene, Al atoms exist largely on or near the surface of the bead, as depicted in the photograph (a) in Fig. 5. The Cu atoms, however, are abundantly present in the inner portion of the bead with small population near the surface of the bead (the photograph (b) in Fig. 5). Thus, the distributions of Al and Cu atoms are different from each other. In addition, many granules are perceived mostly in the inner portion of the bead.

Figure 6 shows SEM photographs of the inner portion of the bead prepared with the use of toluene. Here, the middle parts of the cross-section of the bead in Fig. 5 (a) and (b) are analyzed at larger magnitudes of magnification. A number of crystalline deposits are observed in the photographs (a) and (b), while highly grown columnar crystals are seen in the photograph (c).

As depicted by the waved line in Fig. 6 (b), the distribution of the Cu atoms exhibits maxima at the positions where the crystalline deposits are present on the white straight line. In contrast, the distribution of the Al atoms shows minima at the positions of the deposits (Fig. 6 (a)). Thus, most of the Al atoms are located in the portions where no deposits exist. The X-ray microanalysis on one of the deposits, which involves signals from the region of diameter around 1—2 μm, has showed that the atomic ratio of Cu, Cl, and Al is 37.5:57.6:4.9.

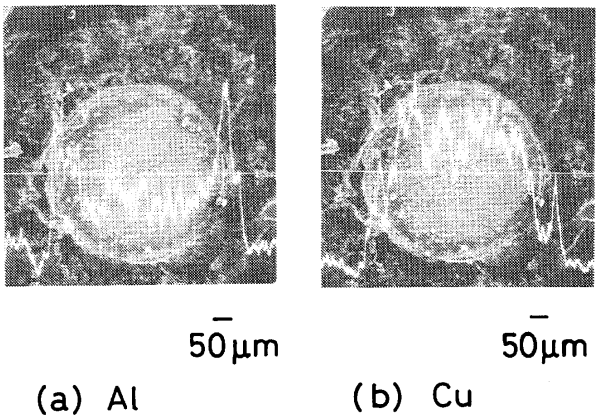

Fig. 5. SEM photographs as well as distributions of Al and Cu atoms for the cross section of the CO adsorbent prepared from the macroreticular type polystyrene resin, $AlCl_3$, and CuCl by use of toluene as solvent: The waved lines show the distributions of (a) Al atoms and (b) Cu atoms along the corresponding white straight lines.

Discussion

Water-Resistivity of Macroreticular Type Polystyrene Resin-Supported $AlCuCl_4$ As CO Adsorbent. The macroreticular type polystyrene resin-supported

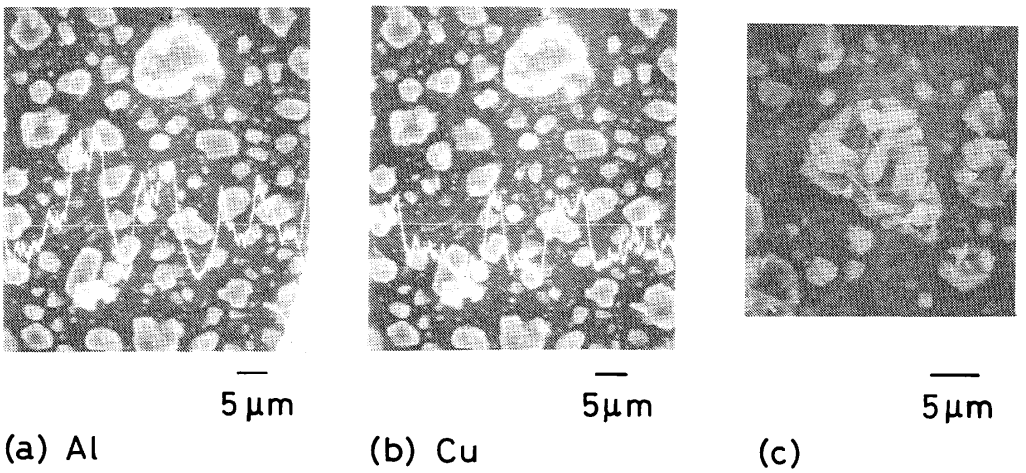

Fig. 6. SEM photographs as well as distributions of Al and Cu atoms for the inner portions of the bead of the CO adsorbent prepared from the macroreticular type polystyrene resin, $AlCl_3$, and CuCl by use of toluene as solvent: The middle parts of the cross-section of the bead in Fig. 5 (a) and (b), where many fine deposits of metal salts are observed, are analyzed at larger magnitudes of magnification; the waved lines refer to the distributions of (a) Al and (b) Cu atoms along the corresponding white straight lines.

$AlCuCl_4$ is stable against water vapor, as shown in Fig. 2, when carbon disulfide and dichloromethane are used as preparation solvents. No measurable decreases in the adsorbing capacities are observed after five and three repeated contacts of the adsorbents (total periods of contacts 50 and 30 min) with nitrogen containing 5600 and 4600 ppm of water, respectively. The water-resistivities of these adsorbents are quite important from the viewpoints of practical applications, since almost all of the CO sources in industry contain considerable amounts of water vapor.

These results are highly in contrast with the fact that the CO absorbing abilities of toluene solutions of $AlCuCl_4$ rapidly and significantly decrease on the contacts with water vapor.[4-6] Thus, CO separation processes using these liquid absorbents require pretreatments of feed gas to reduce the amount of water vapor to 1 ppm or smaller.[6] The water-resistivities of the present solid CO adsorbents are definitely attributable to protection of $AlCuCl_4$ by the polystyrene resin. As shown previously,[4,5] linear polystyrene exhibits effective protection of $AlCuCl_4$ from water vapor in toluene, resulting in water-resistant liquid CO absorbents.

In contrast to the water-resistivities of the adsorbents prepared by use of carbon disulfide and dichloromethane, the capacities of the adsorbents prepared by using toluene and benzene gradually decrease on the repeated contacts with water vapor (Fig. 2). The CO adsorbing and desorbing abilities of solid of $AlCuCl_4$ without the polystyrene resin are small.[8]

Microstructures of CO Adsorbents Prepared by Use of Various Solvents. In the polystyrene-supported $AlCuCl_4$ prepared by use of carbon disulfide as solvent, $AlCuCl_4$ uniformly disperses without formation of aggregates in the beads of the polystyrene resins (Fig. 4).

With the use of toluene as preparation solvent, however, the distribution of Cu atoms and that of Al atoms in the adsorbents are different from each other, and many deposits are formed in the beads (Fig. 5). The deposits are assignable to solid of CuCl on the basis of the atomic ratio (37.5:57.6:4.9) of Cu, Cl, and Al atoms. Both the deviation of the ratio (1.54) of Cl to Cu from the theoretical value (1.0) for CuCl and the presence of small amount of Al atoms are associated with the fact that the ratio has been determined by the analysis on a region of diameter around 1—2 μm. Thus the analysis involves signals from the parts other than the deposit, which are abundant in $AlCl_3$ (see Fig. 6 (a)), in addition to the signals from the deposit. Subtraction of three times (14.7) of the observed value (4.9) for Al atom from that (57.6) for Cl atom results in an estimated value (42.9) for Cl atom which exists in fact in the deposit. This subtraction is based on the assumption that all the Al atoms are present in the forms of $AlCl_3$. The ratio of the estimated value (42.9) for Cl atom to the observed value (37.5) for Cu atom is 1.14, which is close to the theoretical value (1.0) for CuCl.

The significant dependence of the distributions of the metal salts in the CO adsorbents on the preparation solvents is attributable to differences in the solubilities of the salts in the solvents. All the four solvents used, carbon disulfide, dichloromethane, benzene, and toluene, are good solvents for polystyrene.

When CuCl, $AlCl_3$, and the polystyrene resin are refluxed in carbon disulfide or dichloromethane, $AlCuCl_4$, formed in situ in the reaction mixtures, promptly penetrates into the polystyrene beads due to formation of molecular complexes between the double salt and the aromatic rings of the polystyrene resin. The amounts of $AlCuCl_4$ in the liquid phase after refluxing are virtually none.[8] Both carbon disulfide and dichloromethane are poor solvents for $AlCuCl_4$, $AlCl_3$, and CuCl. In the resin, $AlCuCl_4$ is located in the microporosities, and interacts with multiple aromatic rings there. Location of the $AlCuCl_4$ on the surface of the macroporosities of the resin in the adsorbents is energetically less favorable, since the number of the aromatic rings which can interact with one molecule of the double salt is smaller. On the subsequent evaporation of the liquid phase, homogeneous and molecular dispersion of $AlCuCl_4$ in the microporosities of the beads is achieved.

These arguments are supported by the finding[11] of strong charge-transfer bands having absorption maxima around 460 nm for the toluene solutions of $AlCuCl_4$ containing linear polystyrene. In the absence of the polystyrene, such charge-transfer bands were not detected at all.

On refluxing CuCl, $AlCl_3$, and the polystyrene resin in toluene or benzene, however, the $AlCuCl_4$ is present both in the polystyrene beads and in the liquid phase, since $AlCuCl_4$ effectively dissolves in benzene and toluene due to molecular complex formations with the aromatic solvents.[12,13] On the evaporation, most of the $AlCuCl_4$ in the liquid phase precipitates either on the surface of the macroporosities or on the surface of the beads.

The formation of deposits of CuCl in the beads of the adsorbents prepared with these aromatic solvents (Figs. 5 and 6) is probably associated with decomposition of some portion of $AlCuCl_4$ in the liquid phase to $AlCl_3$ and CuCl on the evaporation. Here, the CuCl aggregates each other to crystalline solids, and the $AlCl_3$ forms molecular complexes[14] with the aromatic rings around the macroporosities. As the evaporation proceeds still more, a part of the $AlCl_3$ dissolves in the solvents which are subsequently drawn out of the innermore parts of the beads. These $AlCl_3$ molecules gradually move towards the outside of the beads

together with the solvents, and at the final stage of the evaporation they precipitate either on the surface of the polystyrene beads or in the vicinity of their surface. The CuCl, which shows virtually no solubility in the solvents, retains the crystalline forms. These arguments are consistent with the large population of Al atoms on and near the surface of the beads (Fig. 5 (a)) and with the large population of Cu atoms in the inner portion of the beads (Fig. 5 (b)).

Mechanism of Water-Resistivities of CO Adsorbents. For the adsorbents prepared by use of carbon disulfide and dichloromethane as solvents, most of the $AlCuCl_4$ is located in the microporosities of the polystyrene resin. Inside of the microporosities, composed of aromatic rings and methylene residues, is highly apolar and the concentration of water vapor there is quite small even when the adsorbents are present under the atmosphere containing considerable amounts of water vapor. In addition, the aromatic rings interacting with the $AlCuCl_4$ in the microporosities prevent the access of water vapor to the double salt by steric hindrance. These effects, both of which suppress the irreversible reaction between the $AlCuCl_4$ and water, function cooperatively, giving rise to the water-resistivities of the adsorbents.

Rather small water-resistivities of the adsorbents prepared with the use of toluene and benzene are ascribed to location of some of $AlCuCl_4$ on the surface of the beads of the polystyrene resin and on the surface of macroporosities. These $AlCuCl_4$ molecules without sufficient protection by the aromatic rings of the polystyrene are rapidly deactivated with water vapor due to irreversible reaction.[5,6]

The above arguments are supported by the fact that the catalytic activity of $AlCl_3$ incorporated in a gel type polystyrene resin remains intact even after the resin-$AlCl_3$ composites are washed with water.[15] Porosity of gel type polystyrene resin exists only in swollen states in good solvents.[16]

The proposed mechanism for the water-resistivities of the present adsorbents is consistent with that for the water-resistivities of the toluene solutions of the linear polystyrene-protected $AlCuCl_4$ as liquid CO absorbents.[5] There, $AlCuCl_4$ is effectively protected by the adjacent aromatic rings of linear polystyrenes from water vapor.

In conclusion, water-resistant solid adsorbents for carbon monoxide, the macroreticular type polystyrene resin-supported aluminium copper(I) chloride, are prepared from copper(I) chloride, aluminium chloride, and the resin. The use of solvents such as carbon disulfide and dichloromethane, which are good solvents for the resin and poor solvents for the double salt, is essential for the adsorbents to be sufficiently stable against water vapor.

The authors wish to express their thanks to Mr. Shigeru Ohtsuka and Mr. Mitsuhiro Adachi at the University of Tokyo for the assistance in the scanning electron microscopy and the energy dispersive X-ray microanalysis.

References

1) A preliminary communication: H. Hirai, S. Hara, and M. Komiyama, *Chem. Lett.*, **1982**, 1685.
2) "New Syntheses with Carbon Monoxide," ed by J. Falbe, Springer-Verlag, Berlin (1980).
3) A. L. Kohl and F. C. Riesenfeld, "Gas Purification," 3rd ed, Gulf Publishing Co., Houston (1979).
4) H. Hirai, M. Komiyama, and S. Hara, *Makromol. Chem., Rapid Commun.*, **2**, 495 (1981).
5) H. Hirai, S. Hara, and M. Komiyama, *Bull. Chem. Soc. Jpn.*, **59**, 109 (1986).
6) D. J. Haase and D. G. Walker, *Chem. Eng. Prog.*, **70**, 74 (1974).
7) H. Hirai, M. Komiyama, and S. Hara, *Makromol. Chem., Rapid Commun.*, **3**, 95 (1982).
8) H. Hirai, S. Hara, and M. Komiyama, *Bull. Chem. Soc. Jpn.*, **59**, 1051 (1986).
9) "Materials, Equipment and Systems for Chromatography Electrophoresis Immunochemistry and HPLC," Catalog G, Bio-Rad Laboratories Ltd., (1981), p. 28.
10) S. Ohtsuka, K. Okaya, and T. Inoue, *Funtai Kogaku Kaishi*, **17**(12), 709 (1980).
11) H. Hirai, K. Kanaka, and M. Komiyama, *Polym. Prep. Jpn.*, **34(3)**, 484 (1985).
12) R. W. Turner and E. L. Amma, *J. Am. Chem. Soc.*, **88**, 1877 (1966).
13) H. Hirai, M. Nakamura, and M. Komiyama, *Bull. Chem. Soc. Jpn.*, **56**, 2519 (1983).
14) S. J. Costanzo and N. B. Jurinski, *Tetrahedron*, **23**, 2571 (1967).
15) D. C. Neckers, D. A. Kooistra, and G. W. Green, *J. Am. Chem. Soc.*, **94**, 9284 (1972).
16) W. L. Sederel and G. J. Dejang, *J. Appl. Polym. Sci.*, **17**, 2815 (1973).

A Kinetic Study of Pressure Effect upon an Outer Sphere Electron-Transfer Reaction Involving Free Radicals

Masahiro EBIHARA, Yoichi SASAKI,† Shozo TERO-KUBOTA, and Kazuo SAITO*
Coordination Chemistry Laboratories, Institute for Molecular Science, Myodaiji, Okazaki 444
(Received July 14, 1986)

Synopsis. Volume of activation for the redox reaction between $[(en)_2Co^{III}(\mu\text{-}NH_2,O_2^{(-)})Co^{III}(en)_2]^{4+}$ (en, ethylenediamine) and 2,2,6,6-tatramethyl-1-piperidinyloxyl radical is zero. The result endorses our previous discussion that the changes in solvation and in intrinsic volume of reactants are respectively responsible for determining the precursor and transition state.

Usefulness of pressure effect for elucidating the reaction mechanism of electron-transfer reactions has been widely understood,[1-3] but experimental data are available only for limited variety of redox pairs.[4] When the charge sign of the oxidant and reductant is different from each other, the equilibrium constant for the precursor formation K_{os} and the electron-transfer rate constant k_e are kinetically analyzed.[5-8] Hence the molar volume change accompanied by the precursor formation ΔV°_{os} and the activation volume of the electron-transfer stage $\Delta V^{\neq}_e$ are individually known, particularly when the charge numbers are high.[4,9-11] We have discussed that the ΔV°_{os} is mostly governed by the environmental effect, i.e. the observed positive values are due to the release of hydrated water molecules in the second hydration sphere on the formation of precursor ion pair.[10] Such a consideration may be endorsed by use of a reductant without charge. We have chosen 2,2,6,6-tetramethyl-1-pyperidinyloxyl (TMPNO) which is soluble in water and stable in air as reductant and binuclear cobalt(III) complex doubly bridged by hyperoxide and amide as oxidant. This paramagnetic complex has its localized unpaired electron at the hyperoxide moiety and the two Co^{III} atoms have low spin configuration, which is retained in the reduced form, diamagnetic μ-peroxo-μ-amido bridged species. Hence the change in overall structure before and after the redox reaction is expected to be very small. The stoichiometry of the reaction is as follows.

$$[(en)_2Co^{III}(\mu\text{-}NH_2, O_2^{(-)})Co^{III}(en)_2]^{4+} + \text{TMPNO radical} \longrightarrow [(en)_2Co^{III}(\mu\text{-}NH_2, O_2^{(2-)})Co^{III}(en)_2]^{3+} + \text{TMPNO cation}$$

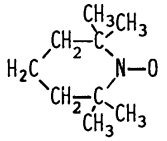

2,2,6,6-tetramethyl-1-pyperidinyloxyl (TMPNO)

Table 1. Kinetic Data for the Redox Reaction between $[(en)_2Co^{III}(\mu\text{-}NH_2, O_2^{(-)})Co^{III}(en)_2]^{4+}$ and 2,2,6,6-Tetramethyl-1-piperidinyloxyl Radical in Aqueous Solution

t/°C	I/M	Buffer	pH	$k_{obsd}/10^4$ M^{-1} s^{-1}
4.8	0.10	Acetate	3.92	1.30±0.03
15.0	0.10	Perchlorate	2.85	2.57±0.13
15.0	0.10	Perchlorate	3.95	2.75±0.06
15.0	0.10	Acetate	3.92	2.71±0.11
15.0	0.10	Acetate	5.00	2.68±0.16
15.0	0.50	Acetate	3.95	4.56±0.09
24.8	0.10	Acetate	3.92	5.17±0.24
$\Delta H^{\neq}$/kJ mol^{-1}		45.0±0.3		
$\Delta S^{\neq}$/J mol^{-1} K^{-1}		−3.7±1.2		
$\Delta V^{\neq}_{obsd}$/cm^3 mol^{-1}		0.2±0.5	(I=0.1 M)	
(cf. Fig. 1)		−1.4±1.3	(I=0.5 M)	

Experimental

The oxidant was synthesized by the known method[12] in pure chloride form. Commercial TMPNO was sublimed in vacuo. pH Titration gave no sign of protonation at pH 2 to 11. The standard redox potentials for TMPNO· to $TMPNO^+ + e^-$ are +0.478 and +0.475 V vs. SCE at ionic strengths 0.1 and 0.5 M (NaCl), respectively. The pH was adjusted with acetate buffer (acetate concentration 0.01 M) or perchloric acid to 2.85 to 5.00. The ionic strength was adjusted to 0.1 and 0.5 M with sodium perchlorate (M=mol dm^{-3}).

The kinetics were followed at 4.8 to 24.8 °C under the following conditions: [oxidant]=(0.73 to 7.3)×10^{-5} M, [reductant]=(2.0 to 10.0)×10^{-4} M. A Union Giken Stopped-flow spectrophotometer was used for the kinetic measurement. The pressure effect was measured (up to 200 MPa) by a High Pressure Stopped-flow Apparatus FIT 3 exploited in Department of Chemistry, Nagoya University.[13] The pressure was measured with a strain-type gauge calibrated with a standard Heize gauge. The pressure remained constant within less than 1 MPa.

Results

When the kinetics were followed by this method at 306 nm (absorption peak of the oxidant) in the presence of a large excess of the reductant, the pseudo first order plots with respect to the oxidant concentration were linear for more than three half period of the reaction. The first order rate constant is independent of the initial concentration of the oxidant and proportional to that of reductant.

$$\text{Rate} = k_{obsd}[\mu\text{-}NH_2, O_2^{(-)}][\text{TMPNO}]$$

Table I shows that the rate constant is independent of

† Present address: Department of Chemistry, Faculty of Science, Tohoku University, Sendai 980.

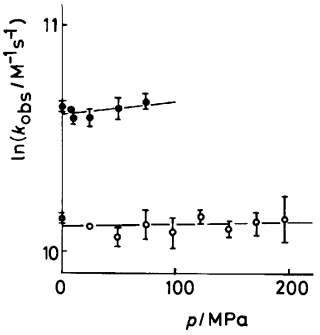

Fig. 1. Dependence of the observed second order rate constant upon the pressure.
○ at I=0.1 M, ● at I=0.5 M 15.0 °C
Bars indicate the range of 70% certainity.

the pH and the buffering agent. It increases significantly with increase in ionic strength. The activation parameters included in the Table clearly indicate that the volume of activation is zero (Fig. 1) and so is the activation entropy. Ligand substitution of the oxidant complex is very slow under the given conditions.

Discussion

It is generally understood that the influence of ionic strength upon reaction rates is feasible in the precursor formation stage rather than in the electron-transfer stage.[7] The observed increase in k_{obsd} with ionic strength can be interpreted that the interaction between the oxidant in less strongly hydrated form and the reductant results in effective precursor. Since the reductant is a chargeless radical, this fact implies that the precursor formation will not bring about significant change in the solvation state of the precursor formation, to make the ΔV°_{os} almost zero. Since $\Delta V^{*}_{obsd}=\Delta V^{\circ}_{os}+\Delta V^{*}_{e}$, the volume of activation at the electron-transfer stage is also very likely near to zero.

Consideration on the basis of crystallographic data of $[(en)_2Co^{III}(\mu\text{-}NH_2,O_2^{(-)})Co^{III}(en)_2]^{4+}$,[14] $[(en)_2Co^{III}(\mu\text{-}NH_2,\ O_2^{(2-)})Co^{III}(en)_2]^{3+}$,[15] TMPNO,[16] and its oxidized cation[17] indicates that the change in molar volume of these species is not significant. The Co–Co distances of the hyperoxide- and peroxide bridged species are 3.25 and 3.27 Å, and the configuration of ethylenediamine ligand around Co^{III} as well as the Co–N distance is very similar to each other. The Co–O–O–Co moiety has planar (O–O 1.36 Å) and gauche (1.48 Å) structure, respectively, but the transition from O_2^- to O_2^{2-} will proceed without siginificant change in structure of that part. TMPNO and its oxidized cation have almost equal bond distances to each other including N–O (1.296 and 1.19 Å, respectively). The angles of N–O bond to the C–N–C plane of piperidine are 19.4 and 0°, respectively, but they are within the four methyl groups on 2- and 6- position and the small angle change will not cause big change in molar volumes of the two species. Thus the change in intrinsic molar volume of the oxidant and reductant on electron transfer will be very small. This fact indicates that the change in solvation state around the precursor will not be appreciable since the ΔV^{*}_{e} is near to zero. This consideration is supported by the very small absolute value of activation entropy.

When an electron is transferred from the chargeless TMPNO to the +4 oxidant in the precursor, a change in dipole moment may be expected, which could increase the hydration around the precursor, because +4 vs. 0 pair could give stronger hydration than +3 vs. +1 pair does. If this effect gave significant contribution to increase ΔV^{*}_{e} value, there should be some other contribution to compensate the increase in volume of the system. Careful examination of the molar volumes of participating species as well as the hydration around them did not suggest any possibility of decrease in volume of the system. Hence we conclude that in the present system both ΔV°_{os} and ΔV^{*}_{e} will be near to zero. The present result seems to support our previous conclusion that the contributions of change in solvation sphere and in the intrinsic volume of the reactants are respectively responsible for determining the precursor and the transition state of redox systems involving charged oxidant and reductant.

This work was supported by the Grant-in-Aid of the special research project No. 60129031 from Ministry of Education, Science and Culture to K.S, to which the authors' thanks are due.

References

1) D. R. Stranks, *Pure Appl. Chem.*, **38**, 303 (1974).
2) D. A. Palmer, H. Kelm, *Coord. Chem. Rev.*, **36**, 89 (1981).
3) T. W. Swaddle, ACS Symp. Ser., No. 198, 39 (1982).
4) Latest example, I. Krack, and R. van Eldik, *Inorg. Chem.*, **25**, 1743 (1986), and the references therein.
5) A. Neves, W. Herrmann, and K. Wieghardt, *Inorg. Chem.*, **23**, 3435 (1985).
6) E. Kremer, G. Cha, M. Morkevicius, M. Seaman, and A. Haim, *Inorg. Chem.*, **23**, 3028 (1984).
7) Y. Sasaki, *Bull. Chem. Soc. Jpn.*, **50**, 1939 (1977).
8) S. Kondo, Y. Sasaki, and K. Saito, *Inorg. Chem.*, **20**, 429 (1981).
9) Y. Sasaki, F. B. Ueno, and K. Saito, *J. Chem. Soc., Chem. Commun.*, **1981**, 1135.
10) M. Kanesato, M. Ebihara, Y. Sasaki, and K. Saito, *J. Am. Chem. Soc.*, **105**, 5711 (1983).
11) R. van Eldik and H. Kelm, *Inorg. Chim. Acta*, **73**, 91 (1983).
12) M. B. Stevenson and A. G. Sykes, *J. Chem. Soc., Dalton Trans.*, **1969**, 2293.
13) S. Funahashi, K. Ishihara, and M. Tanaka, *Inorg. Chem.*, **22**, 2564 (1983); *Rev. Sci. Instr.*, **53**, 1231 (1982).
14) U. Thewalt and R. E. Marsh, *J. Am. Chem. Soc.*, **89**, 6364 (1967).
15) U.Thewalt, *Z. Anorg. Allg. Chem.*, **393**, 1 (1972).
16) P. A. Capiomont and J. Lajzerowicz-Bonneteau, *Acta Crystallogr., Sect. B.*, **26**, 1198 (1970).
17) L. O. Atovmyan, V. A. Golubev, N. I. Gdovina, and G. A. Klitskaya, *Zh. Struk. Khim.*, **16**, 92 (1975).

Molecular Structure of $(+)^{CD}_{550}\cdot(+)^{CD}_{370}$-(2-Aminoethanesulfenato)bis(1,3-propanediamine)-cobalt(III) Perchlorate

Ken-ichi OKAMOTO,* Takumi KONNO, Hisahiko EINAGA,[1] and Jinsai HIDAKA
Department of Chemistry, University of Tsukuba, Sakura, Ibaraki 305
(Received July 15, 1986)

Synopsis. The molecular structure of the title complex, $(+)^{CD}_{550}\cdot(+)^{CD}_{370}$-[Co(aese)(tn)$_2$](ClO$_4$)$_2$, has been determined by the X-ray analysis. This isomer having the Λ configuration takes S configuration for the sulfur donor atom and one of the two 1,3-propanediamine chelate rings takes a chair form and the other an asymmetric skew-boat one.

In the previous papers,[2,3] we reported the preparation and the spectro- and stereochemical properties of the [Co(aese)(diamine)$_2$]$^{2+}$-type complexes, where the aese denotes 2-aminoethanesulfenate and the diamine is 1,2-ethanediamine (en) and 1,3-propanediamine (tn). In *Λ*-[Co(aese)(en)$_2$]$^{2+}$ generated by the oxidation reaction of *Λ*-[Co(2-aminoethanethiolato)(en)$_2$]$^{2+}$ with hydrogen peroxide, the formation ratio of the two isomers, *Λ*-(*R*) and *Λ*-(*S*),[4] is about 3:1.[2] While, the formation ratio of the two isomers for *Λ*-[Co(aese)-(tn)$_2$]$^{2+}$ obtained from a similar oxidation reaction is *Λ*-(*R*):*Λ*-(*S*)≈5:6.[3] In order to elucidate the difference in these formatiom ratios between the en and tn complexes, we determined in this work the molecular structure of $(+)^{CD}_{550}\cdot(+)^{CD}_{370}$-[Co(aese)(tn)$_2$](ClO$_4$)$_2$ by the X-ray diffraction method. The structure of the present tn complex is discussed in comparison with that of the corresponding [Co(aese)(en)$_2$]$^{2+}$ complex.[5]

Experimental

X-Ray Data Collection. $(+)^{CD}_{550}\cdot(+)^{CD}_{370}$-[Co(aese)(tn)$_2$]-(ClO$_4$)$_2$ was prepared by the method of the literature.[3] The resultant precipitate of the $(+)^{CD}_{550}\cdot(+)^{CD}_{370}$ isomer was collected by filtration. When the filtrate was kept in a refrigerator for 2 h, fairly large needle crystals, which showed the identical absorption and CD spectra with the $(+)^{CD}_{550}\cdot(+)^{CD}_{370}$ isomer, were obtained. The unit cell parameters and intensity data for the single crystal (ca. 0.18×0.24×1.00 mm^3) were measured on a Rigaku-denki four-circle diffractometer (AFC-5) with graphite-monochromatized Mo *Kα* radiation. The systematic absence led to either the space groups $P6_1$ or $P6_5$, which could not be determined by using the anomalous scattering factors for the Mo *Kα* radiation. Taking the absolute configuration based on the CD spectral behavior into consideration,[3] the space group is tentatively determined to be $P6_5$. The crystal data are as follows; $C_8H_{26}N_5O_9SCl_2Co$, a=9.367(1), c=37.878 (15) Å, V=2878.5(13) Å^3, hexagonal, $P6_5$, D_m=1.73 g cm^{-3}, D_x=1.724 g cm^{-3}, Z=6, and μ(Mo *Kα*)=13.6 cm^{-1}.

The intensity data were collected by a ω—2θ scan technique up to 2θ=60° with a scan rate of 3° min^{-1}. During the cource of the data collection, three reflections were monitored every 40 reflections. The intensity data were converted to F_o data in the usual manner. Absorption corrections were not applied. A total of 1020 indepedent reflections with $F_o > 3\sigma(|F_o|)$ were considered as 'observed' and used for the structure analysis.

Determination of Crystal Structure. The position of the cobalt atom was obtained from a three-dimensional Patterson function. Difference Fourier maps, based on the cobalt position, revealed all the non-hydrogen atoms. The structure was refined by a full-matrix least-squares refinement of the positional and anisotropic thermal parameters of all the non-hydrogen atoms (program RFINE by L. W. Finger was used[6]). The neutral atomic scattering factors for the non-hydrogen atoms were taken from the literature.[7] The final R and R_w values are 0.089 and 0.079, respectively. The final positional parameters and equivalent isotropic temperature factors for the non-hydrogen atoms are listed in Table 1. Tables of structure factors, anisotropic temperature factors, and bond lengths and angles are kept at the Chemical Society of Japan (Document No. 8714).

Table 1. Positional and Thermal Parameters

Atom	x	y	z	B_{eq}/Å^2 [a]
Co	0.3504(4)	0.1852(3)	0.1500	2.36
S	0.1968(8)	0.1124(8)	0.1978(2)	3.77
N1	0.139(3)	0.068(3)	0.1213(6)	4.99
N2	0.342(3)	0.396(3)	0.1461(8)	5.25
N3	0.554(3)	0.299(2)	0.1777(7)	4.12
N4	0.367(3)	−0.018(2)	0.1537(6)	4.22
N5	0.482(3)	0.259(3)	0.1031(8)	5.32
C1	0.010(4)	−0.045(3)	0.1769(10)	5.54
C2	−0.006(3)	0.026(4)	0.1438(8)	5.34
C3	0.383(5)	0.506(4)	0.1738(10)	6.88
C4	0.573(4)	0.570(4)	0.1824(12)	7.64
C5	0.579(4)	0.425(4)	0.2036(12)	6.69
C6	0.480(4)	−0.042(4)	0.1314(8)	6.26
C7	0.489(7)	−0.001(5)	0.0950(12)	9.78
C8	0.564(6)	0.171(5)	0.0875(18)	15.34
O3	0.252(2)	0.025(3)	0.2243(6)	5.31
CL1	0.0040(9)	0.5450(9)	0.1351(2)	4.93
CL2	0.6550(9)	0.6907(8)	0.0671(3)	5.29
O11	0.057(6)	0.584(6)	0.1689(14)	17.15[b]
O12	0.089(4)	0.689(4)	0.1141(9)	8.92[b]
O13	−0.160(4)	0.504(5)	0.1351(12)	13.94[b]
O14	0.017(4)	0.414(4)	0.1218(9)	9.64[b]
O21	0.542(4)	0.646(4)	0.0947(9)	10.65[b]
O22	0.839(6)	0.793(5)	0.0752(14)	15.87[b]
O23	0.612(4)	0.779(4)	0.0373(11)	12.17[b]
O24	0.635(4)	0.543(4)	0.0500(10)	10.49[b]

a) B_{eq} is the equivalent isotropic temperature factors defined by Hamilton.[15] b) Isotropic temperature factor.

Results and Discussion

The perspective drawing of $(+)^{CD}_{550}\cdot(+)^{CD}_{370}$-[Co(aese)-(tn)$_2$]$^{2+}$ is shown in Fig. 1. The coordination geometry

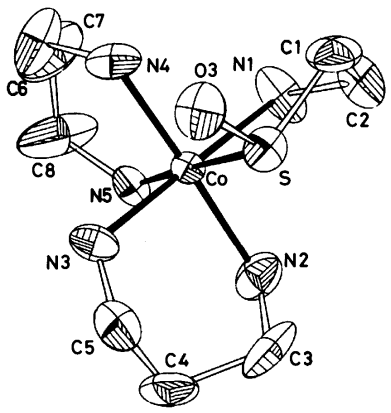

Fig. 1. A perspective drawing of $(+)_{550}^{CD}\cdot(+)_{370}^{CD}$-[Co(aese)$(tn)_2]^{2+}$ with the numbering scheme of the atoms.

around the cobalt atom is approximately octahedral. The 2-aminoethanesulfenate coordinates to the cobalt atom with the nitrogen and sulfur atoms. The asymmetric sulfur donor atom in $(+)_{550}^{CD}\cdot(+)_{370}^{CD}$-[Co(aese)$(tn)_2]^{2+}$ takes the (*S*) configuration for the Λ configuration which was suggested from the CD spectral behavior.[3] The five-membered chelate ring of the coordinated aese ligand, S-C1-C2-N1, takes the reasonable gauche form with a δ conformation (Fig. 1).[8] The six-membered 1,3-propanediamine chelate ring N2-C3-C4-C5-N3, takes the chair conformation, as in the case of the tn ligand in $[Co(tn)_3]^{3+}$,[9] $[Co(X)_2(tn)_2]^{n+}$ ($(X)_2$=$(NCS)_2$[10,11] and 2,4-pentanedionato (acac)[12]), and $[Co(en)_2(tn)]^{3+}$.[13] The other tn chelate ring, N4-C6-C7-C8-N5, however, has the asymmetric skew-boat form (Fig. 1). This irregular conformation seems to be caused by the intramolecular hydrogen bond between the sulfenato oxygen atom, O3, and the nitrogen atom, N4, of the amino group, because the distance between the oxygen atom and nitrogen one is 2.986 Å.

The coordination angles in the tn chelate rings, N2-Co-N3 and N4-Co-N5, are 90.6° and 93.4°, respectively, which are slightly smaller than those found in $(-)_{589}$-$[Co(tn)_3]^{3+}$ (mean 94.5°)[9] and $(-)_{589}$-$[Co(acac)(tn)_2]^{2+}$ (mean 96°).[12] The average bond lengths of Co-N2, Co-N3, and Co-N4, where the nitrogen atoms are cis position to the sulfur donor atom, is 1.991 Å, and this value is in consistent with that of Co-N in other (1,3-propanediamine)cobalt(III) complexes.[9-13] On the other hand, the trans Co-N5 bond length (2.074 Å) is longer than the average cis Co-N one. A similar trans effect has been observed in the bis(1,2-ethanediamine)cobalt(III) complexes with a coordinated sulfenato sulfur atom; $[Co(aese)(en)_2]^{2+}$[5] and [Co(L-cysteinesulfenato-*N*,*S*)$(en)_2]^{2+}$.[14] The bond lengths and angles associated with the aese ligand are similar to those of the corresponding bis(1,2-ethanediamine) complex,[5] although the Co-S bond length (2.199 Å) is somewhat shorter and Co-N1 one (2.033 Å) somewhat longer than those in $[Co(aese)(en)_2]^{2+}$ (Co-S=2.253 Å and Co-N=1.987 Å).

In *Λ*-(*S*)-$[Co(aese)(tn)_2]^{2+}$ (Fig. 1), the tn chelate ring, of which amine proton may participate in an intramolecular hydrogen bond with the oxygen atom of the aese ligand, takes the asymmetric skew-boat form, although the other tn chelate ring takes a chair form, as in the case of the tn chelate rings in $[Co(tn)_3]^{3+}$,[9] $[Co(X)_2(tn)_2]^{n+}$ ($(X)_2$=$(NCS)_2$[10,11] and acac[12]), and $[Co(en)_2(tn)]^{3+}$.[13] The Λ-(*R*) tn isomer can also be expected to take a similar intramolecular hydrogen bond to the Λ-(*S*) isomer because of the flexibility of the tn chelate ring. This stereochemical similarity of the Λ-(*R*) and Λ-(*S*) tn isomers is probably related to the fact that the two isomers are formed in roughly equal amounts. In crystal of *Λ*-(*R*)-$[Co(aese)(en)_2]^{2+}$,[5] both of the aese and en chelate rings, which take a lel conformation (δ conformation), form a similar intramolecular hydrogen bond to the Λ-(*S*) tn isomer. While, molecular model constructions reveal that the Λ-(*S*) en isomer can not be expected to have such interaction as the Λ-(*R*) en isomer because of the rigidity of the five-membered chelate rings. The stereochemical difference between the two Λ-$[Co(aese)(en)_2]^{2+}$ isomers suggests that the Λ-(*R*) isomer is more abundantly formed by the intramolecular hydrogen bond than the Λ-(*S*) isomer. In other words, the difference in the formation ratio between the isomers, (*R*) and (*S*), of *Λ*-$[Co(aese)(en)_2]^{2+}$ and those of *Λ*-$[Co(aese)(tn)_2]^{2+}$ is considered to be associated with that in the flexibility of the tn or en chelate ring and simultaneously with that in the formation of the intramolecular hydrogen bond.

References

1) Present address: Institute of Materials Science, University of Tsukuba, Sakura, Ibaraki 305.
2) T. Konno, K. Okamoto, and J. Hidaka, *Bull. Chem. Soc. Jpn.*, **57**, 3104 (1984).
3) T. Konno K. Okamoto, H. Einaga, and J. Hidaka, *Bull. Chem. Soc. Jpn.*, **58**, 1119 (1985).
4) Λ and Δ denote the absolute configuration due to the skew pair of the chelate rings, and (*R*) and (*S*) denote the absolute configuration of the sulfur donor atom in the aese.
5) I. K. Adzamli, K. Libson, J. D. Lydon, R. C. Elder, and E. Deutsch, *Inorg. Chem.*, **18**, 303 (1979).
6) L. W. Finger, RFINE-2, Geophysical Lab. Carnegie Institution, Washington D. C. 1972.
7) "International Tables for X-Ray Crystallography," The Kynoch Press Birmingham (1974), Vol. IV.
8) C. J. Hawkins, "Absolute Configuration of Metal Complexes," John Wiley & Sons, Inc., New York (1971).
9) T. Nomura, F. Marumo, and Y. Saito, *Bull. Chem. Soc. Jpn.*, **42** 1016 (1969).
10) K. Matsumoto, M. Yonezawa, H. Kuroya, H. Kawaguchi, and S. Kawaguchi, *Bull. Chem. Soc. Jpn.*, **43**, 1269 (1970).
11) K. Matsumoto, S. Ooi, H. Kawaguchi, M. Nakano and S. Kawaguchi, *Bull. Chem. Soc. Jpn.*, **55**, 1840 (1982).
12) K. Matsumoto, H. Kawaguchi, H. Kuroya, and S. Kawaguchi, *Bull. Chem. Soc. Jpn.*, **46**, 2424 (1973).
13) H. V. F. S. Jensen, *Acta Chem. Scand.*, **26**, 3421 (1972).
14) W. G. Jackson, A. M. Sargeson, and P. O. Whimp, *J. Chem. Soc., Chem. Commun.*, **1976**, 934.
15) W. C. Hamilton, *Acta Crystallogr.*, **12**, 609 (1959).

Catalytic Behavior of Optically Active Amino Alcohol-Borane Complex in the Enantioselective Reduction of Acetophenone Oxime *O*-Alkyl Ethers

Shinichi Itsuno,* Yoshiki Sakurai, Koichi Ito, Akira Hirao,† and Seiichi Nakahama†

School of Materials Science, Toyohashi University of Technology, Tempaku-cho, Toyohashi 440
†Department of Polymer Science, Tokyo Institute of Technology, Ohokayama, Meguro-ku, Tokyo 152

(Received July 7, 1986)

Synopsis. In the presence of the optically active amino alcohol-borane complex, an oxime ether was reduced with various hydride reducing agents to give a chiral primary amine of high optical purity. Catalytic use of the chiral complex was also investigated.

We have reported previously that a tetrahydrofuran (THF) solution of a chiral reducing agent prepared from an optically active amino alcohol and borane reduced ketones and ketone oxime *O*-alkyl ethers quantitatively with high enantioselectivity to give optically active secondary alcohols[1] and primary amines,[2] respectively. In most studies for asymmetric reduction, a stoichiometric amount of chiral metal hydrides has been required. For the practical purpose, catalytic use of the expensive chiral auxiliary has been intensely desired as well as high enantioselectivity of the reaction.[4] In this context, we studied the catalytic behaviour of the chiral amino alcohol-borane complex in the reduction of oxime ethers.

The optically active amino alcohol such as **1** reacted with an excess borane in THF to generate hydrogen. After evaporation of unreacted free borane and THF under reduced pressure at room temperature, chiral complex was obtained as a white powder. Although this chiral complex has a B-H bond which was easily detected by infra-red spectroscopy (2500 cm^{-1}) and hydrogen evolution by acid hydrolysis, a THF solution of this white powder could not reduce any oxime ether within one day at room temperature. However, interesingly, when THF-borane (1:1) was added to the mixture of a THF solution of the chiral complex and acetophenone *O*-methyl oxime, optically pure (*S*)-1-phenylethylamine was obtained quantitatively in 20 h at room temperature, after hydrolysis (Table 1, Run 1). In the presence of the above chiral complex prepared from **1** and borane, the oxime ether was reduced asymmetrically also with metal hydrides such as lithium alminum hydride ($LiAlH_4$) and aluminum hydride (AlH_3) in place of borane. The reduction with sodium borohydride did not proceed due to its low reactivity. Results are summarized in Table 1.

On the basis of these results, catalytic use of the chiral complex was investigated. For example, in the presence of 1 equiv of the chiral complex, 1 equiv of acetophenone *O*-benzyl oxime was reduced asymmetrically in a THF solution containing excess of free borane (4 equiv) to give (*S*)-1-phenylethylamine of 95% ee (see Experimental). Under the same conditions, 4 equiv of the oxime ether could also be reduced to give the chiral amine in 90% ee. These results show that the reduction is catalyzed by the chiral complex. The chiral complex would interact with the oxime ether to accelerate the borane reduction and induce asymmetry. Indeed, borane alone reduced the oxime ether slowly in THF at ambient temperatute. Even 10 equiv of the oxime ether was reduced quantitatively with 10 equiv of borane in the presence of only 1 equiv of the chiral complex to give the chiral amine (52%ee). This somewhat low enantioselectivity indicates that the reduction of the oxime ethers with free borane proceeded competitively when a small amount of the chiral complex was employed. To use the chiral complex more effectively, the following procedure was attempted. After asymmetric reduction of 5 mmol of acetophenone *O*-methyl oxime with borane in the presence of the chiral complex prepared from 5 mmol of the chiral amino alcohol, another 5 mmol of the oxime ether and borane was introduced again without work-up procedure. Overall, 10 mmol of the oxime ether may interact with the chiral complex successively. Isolated 9 mmol of the amine exhibited 85% of the optical purity. This result demonstrates that the chiral complex induces the asymmetric reduction also for the borane reduction of the second added substrate. The successive asymmetric reduction of the oxime ether was repeated five times. Total amount of the amine isolated was 43 mmol by use of only 5 mmol of the complex, optical purity of the amine being 67% ee. A gradual decrease of enantioselectivity would be caused by the accumulation of chiral amino borane after asymmetric reduction of the oxime ether.

Table 1. Enantioselective Reduction of Acetophenone *O*-Methyloxime in the Presence of Chiral Complex Prepared from **1** and Borane

Run	Reducing agent	I-Phenylethylamine			
		Yield/% (Isolated)	$[\alpha]_D^{22}$	%ee[a]	Config.[a]
1	BH_3	90	−40.3	100	S
2	$NaBH_4$	0	—	—	—
3	$LiAlH_4$	85	−30.6	76	S
4	AlH_3	79	−17.7	44	S

a) Values for maximum rotation and configuration taken from Ref. 7).

Although the exact structure of the chiral complex was not clear, this complex possessed interesting characteristics in the asymmetric reduction of oxime ethers; (1) The reduction with borane was accelerated by the presence of the complex. (2) The complex itself could not reduce oxime ether. (3) The high level of asymmetry was induced by the complex. (4) By the use of small amount of the complex, more than stoichiometric amount of the oxime ether was reduced asymmetrically. Consequently, we supposed tentatively that this chiral complex prepared from optcally active amino alcohol and borane may be a chiral catalyst, not a reagent, for asymmetric reduction of oxime ethers. The realization of higher efficiency of the chiral catalyst is now under investigation.

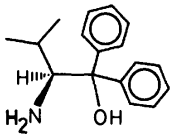

1

Experimental

All reactions were carried out under a nitrogen atmosphere. GLPC analyses were carried out on a Yanaco G180 gas chromatograph with a 3 m×3 mm column packed with PEG20 M on Diasolid L. Optical rotations were measured on a JASCO DIP-140 digital polarimeter using a 1 cm or 10 cm thermostated microcell. ^{1}H NMR spectra were taken in $CDCl_3$ (internal Me_4Si) on a JEOL JNM-PMX 60 or a JEOL JNM-GX 270 spectrometer. Melting points were determined on a Yanagimoto micromelting point apparatus.

Materials. Tetrahydrofuran (THF) was dried over sodium wire and distilled over $LiAlH_4$ and stored under nitrogen. AlH_3 was prepared by adding the theoretical quantity of 100% sulfuric acid to the standardized THF solution of $LiAlH_4$.[5] Borane was prepared by the reaction of $NaBH_4$ with diethyl ether–trifluoroborane (1:1) according to the procedure of Brown.[6] (*S*)-(−)-2-amino-3-methyl-1,1,-diphenyl-1-butanol (**1**) and acetophenone oxime *O*-alkyl ethers were prepared by previously described procedures.[2]

Enantioselective Reduction of Acetophenone *O*-Methyloxime with $LiAlH_4$ in the Presence of 1-Borane Complex. A solution of borane (20 mmol) in THF (10 ml) was added to a solution of **1** (10 mmol) at 0 °C during ca. 20 min. The resulting solution was stirred at 0 °C for 8 h. The excess of free borane and solvent were evaporated off in vac. at room temperature to give a white solid (the chiral complex). The chiral complex was dissolved in dry THF (20 ml) and acetophenone *O*-methyl oxime (10 mmol) in THF (5 ml) was then added dropwise at 0 °C. After addition was complete a THF solution of $LiAlH_4$ (10 mmol) was added at 0 °C. The reaction mixture was warmed to room temperature, stirred for 24 h, and then decomposed by the dropwise addition of Na_2SO_4 saturated water and 2M HCl(1 M=1 mol dm^{-3}). After hydrolysis, evaporation of THF deposited the **1**-HCl as a white solid, which was collected on a glass filter and washed with water. The aqueous acid extract was shaken with ether, cooled, made basic with aqueous ammonia, and extracted with ether. The ether layer was dried ($MgSO_4$) and evaporated to give a colorless oil which upon distillation (bulb-to-bulb) furnished 1-phenylethylamine: 85% yield. This was characterized by IR and ^{1}H NMR spectroscopy and shown to be homogeneous by GLPC analysis. The optical rotation was $[\alpha]_D^{22}$ −30.6° (neat)(lit,[7] $[\alpha]_D^{22}$ −40.3° (neat)). The optical yield, 76%, was calculated by the observed optical rotation and the kwown maximum rotation of 1-phenylethylamine.

Enantioselective Reduction of Acetophenone *O*-Benzyloxime with Borane in the Presence of 1-Borane Complex. A THF solution of the chiral complex was prepared from **1** (10 mmol) and borane (20 mmol) according to the above procedure. To the solution, a solution of acetophenone *O*-benzyl oxime (10 mmol) in THF (5 ml) was added and then borane (40 mmol) was added dropwise at 0 °C. The reaction mixture was warmed to room temperature and stirred for 24 h. After hydrolysis with 2M HCl, **1**-HCl was filtered off and benzyl alcohol was extracted. The aqueous layer was basified with aqueous ammonia and extracted with ether. The ether layer was dried ($MgSO_4$) and evaporated to give a colorless oil which upon distillation (bulb-to-bulb) furnished (*S*)-1-phenylethylamine: 80% yield, $[\alpha]_D^{22}$ −38.3°, 95% ee.

References

1) a) S. Itsuno, K. Ito, A. Hirao, and S. Nakahama, *J. Chem. Soc., Perkin Trans., 1*, **1984** 2887; b) S. Itsuno, K. Ito, A. Hirao, and S. Nakahama, *J. Org. Chem.* **49**, 555 (1984).

2) S. Itsuno, M. Nakano, K. Miyazaki, H. Masuda, K. Ito, A. Hirao, and S. Nakahama, *J. Chem. Soc., Perkin Trans., 1*, **1985**, 2039.

3) "Asymmetric Synthesis," ed by J. D. Morrison, Academic Press Inc., London (1983), Vol. 2.

4) a) "Asymmetric Synthesis," J. D. Morrison, Academic Press Inc., New York (1985), Vol. 5; b) I. Ojima, *Yuki Gosei Kagaku Kyokai Shi*, **44**, 499 (1986).

5) S. Krishnamurthy and H. C. Brown, *J. Org. Chem.* **45**, 849 (1980).

6) "Organic Syntheses via Boranes," ed by H. C. Brown Wiley, New York (1975).

7) W. Theilaker and H. G. Winkler, *Chem. Ber.* **87**, 691 (1954).

Regioselective Addition of Organic Chlorides to Epoxides in the Presence of Quaternary Ammonium Chloride

Xue-Ping GU, Isao IKEDA, and Mitsuo OKAHARA*
Department of Applied Chemistry, Faculty of Engineering, Osaka University, Yamadaoka 2-1, Suita, Osaka 565
(Received July 9, 1986)

Synopsis. By a reaction of epoxides with organic chlorides in the presence of dodecyltrimethylammonium chloride as a catalyst, a series of 2-substituted 1-(chloromethyl)ethyl ethers were synthesized regioselectively in high yields under mild conditions.

Epoxides are useful materials in organic synthetic chemistry and industry based on its active epoxy ring, and many kinds of reactions with various reagents have been widely utilized. However, the reaction of epoxides with organic halides had not attracted much attention until the reaction with chloroacetate was reported, where the effect of a catalyst on this reaction was studied.[1] In the course of the investigation regarding the reactivity of epichlorohydrin under phase-transfer catalytic conditions,[2] we found that dodecyltrimethylammonium chloride is a very effective catalyst for the preparation of a wide variety of 2-substituted 1-(chloromethyl)ethyl ethers by the reactions of epoxides with various organic chlorides under mild conditions.

There are several reports concerning the application of 2-substituted 1-(chloromethyl)ethyl ethers. For example, 2-chloro-1-(chloromethyl)ethyl ethers can afford the corresponding azetidines by reactions with primary amines,[3] and are also used to modify the properties of rubber or cellulose.[4-7] At present, we found that 2-chloro-1-(chloromethyl)ethyl methoxymethyl ether (**3a**) is a very effective acetonylation reagent to convert a series of hydroxyl compounds to the corresponding acetonyl ethers.[8]

The reaction may proceed via the intermediate of 2-substituted 1-(chloromethyl)ethoxide as shown in Scheme 1, where Q^+ represents quaternary ammonium ion.

Several novel 2-substituted 1-(chloromethyl)ethyl ethers were synthesized in good yields using dodecyltrimethylammonium chloride as a catalyst. The synthetic conditions and results are shown in Table 1. Products are characterized by spectral and elemental analyses. In the mass spectra, all products gave the characteristic fragment peak based on the elimination of chloromethyl group, and no fragment peak based on dehydrochlorination appeared, showing that this addition reaction of organic chlorides to epoxide in the presence of dodecyltrimethylammonium chloride is regioselective, regardless of substitution group in the substrate epoxide within this experiment.

In the case of methallyl chloride with epichlorohydrin, no reaction proceeded at 85 °C. In the reaction of chloroacetone with epichlorohydrin, 2-chloro-1-(chloromethyl)ethanol was isolated in 57% yield as the main product rather than the anticipated 2-chloro-1-

Table 1. Synthesis of 2-Substituted 1-(Chloromethyl)ethyl Ethers

Product		Reaction conditions: Temperature °C	Reaction conditions: Time h	Yield[a] %
2,4-$Cl_2C_6H_3$-OCH_2OCH_3	**3a**	30	20	93
2-Cl-4-$C_{11}H_{23}C_6H_3$-OCH_2OCH_3	**3b**	30	6	98
2-Cl-4-$C_{10}H_{21}OC_6H_3$-OCH_2OCH_3	**3c**	30	6	78
2-Cl-4-(4-tolyl-S)C_6H_3-OCH_2OCH_3	**3d**	30	6	90
2,4-$Cl_2C_6H_3$-O-$Si(CH_3)_3$	**3e**	10	3	91
2,4-$Cl_2C_6H_3$-$OCH_2OC_2H_5$	**3f**	30	20	75
2,4-$Cl_2C_6H_3$-$OC(O)$-C_6H_5	**3g**	80	3	90
2,4-$Cl_2C_6H_3$-$OCH_2C(O)OCH_3$	**3h**	80	20	58
2,4-$Cl_2C_6H_3$-OCH_2-C_6H_5	**3i**	100	20	30

a) Isolated yield. The catalyst used is commercial dodecyltrimethylammonium chloride without further purification.

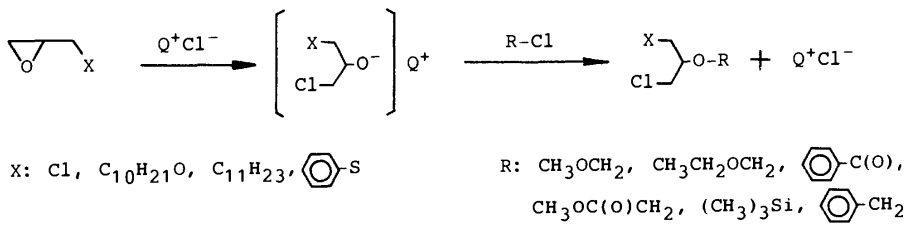

Scheme 1.

(chloromethyl)ethyl acetonyl ether, possibly due to the too acidic methyl or methylene group of chloroacetone.

Experimental

General Procedure for Preparation of 2-Substituted 1-(Chloromethyl)ethyl Ethers. 2-Chloro-1-(chloromethyl)ethyl Methoxymethyl Ether (3a): The mixture of chloromethyl methyl ether 24.6 g (0.30 mol), epichlorohydrin 31.4 g (0.36 mol) and dodecyltrimethylammonium chloride 3.9 g (0.015 mol) is stirred with a magnetic stirrer at 30 °C for 20 h. Then, by fractional distillation at reduced pressure, **3a** was obtained as a colorless liquid; yield: 48.3 g (93%); bp 94—95 °C/30 Torr (1 Torr=133.322 Pa). A GLC of the reaction product showed only one peak, except for excess epichlorohydrin. Another run of the same reaction was carried out at 50 °C for 3 h, yielding 74% of **3a**. Without the catalyst, the yield of **3a** was only 18%, even after a prolonged reaction time (48 h) at 30 °C. ^{1}H NMR ($CDCl_3$) δ=3.42 (s, 3H), 3.70—3.76 (d, 4H), 3.88—4.10 (m, 1H), 4.75 (s, 2H); MS, *m/z* (rel intensity) 173 (M^++1), 171 (M^+−1), 123 (12), 75 (12), 45 (100); IR (neat) 2970, 1460, 1170, 1060, 923, 770 cm^{-1}. Found: C, 34.66; H, 5.98; Cl, 41.14%. Calcd for $C_5H_{10}Cl_2O_2$: C, 34.71; H, 5.83; Cl, 40.97%.

1-(Chloromethyl)tridecyl Methoxymethyl Ether (3b): Synthesized by the reaction of 1,2-epoxytetradecane (0.1 mol) and chloromethyl methyl ether (0.11 mol); bp 100 °C/0.05 Torr (Kugelrohr distillation). ^{1}H NMR ($CDCl_3$) δ=0.80—1.00 (t, 3H), 1.10—1.80 (m, 22H), 3.40 (s, 3H), 3.46—3.65 (d, 2H), 3.65—3.80 (m, 1H), 4.74 (s, 2H); MS, *m/z* (rel intensity) 243 (5), 45 (100); IR (neat) 2950, 1050 cm^{-1}. Found: C, 65.57; H, 11.52; Cl, 11.98%. Calcd for $C_{16}H_{33}ClO_2$: C, 65.61; H, 11.36, Cl, 12.10%.

1-Chloromethyl-2-(decyloxy)ethyl Methoxymethyl Ether (3c): Synthesized by the reaction of decyl glycidyl ether (0.1 mol) and chloromethyl methyl ether (0.11 mol); bp 115 °C/0.04 Torr. ^{1}H NMR ($CDCl_3$) δ=0.76—1.10 (t, 3H), 1.06—1.80 (m, 16H), 3.40 (s, 3H), 3.42—3.80 (m, 6H), 3.80—4.00 (m, 1H), 4.74 (s, 2H); MS, *m/z* (rel intensity) 294 (12), 57 (52), 45 (100); IR (neat) 2950, 1110, 1040 cm^{-1}. Found: C, 60.93; H, 10.87; Cl, 11.82%. Calcd for $C_{15}H_{31}ClO_3$: C, 61.10; H, 10.60; Cl, 12.02%.

1-Chloromethyl-2-(phenylthio)ethyl Methoxymethyl Ether (3d): Synthesized by the reaction of phenyl glycidyl sulfide (0.1 mol) and chloromethyl methyl ether (0.11 mol); bp 90 °C/0.01 Torr. ^{1}H NMR ($CDCl_3$) δ=3.10—3.30 (d, 2H), 3.40 (s, 3H), 3.60—3.80 (d, 2H), 3.80—4.00 (m, 1H), 4.78 (s, 2H); MS, *m/z* (rel intensity) 246 (M^+), 123 (61), 45 (100); IR (neat) 2950, 1590, 1460, 1440, 1160, 1110, 1040 cm^{-1}. Found: C, 53.52; H, 6.08%. Calcd for $C_{11}H_{15}ClO_2S$: C, 53.54; H, 6.13%.

2-Chloro-1-(chloromethyl)ethyl Trimethylsilyl Ether (3e): Synthesized by the reaction of epichlorohydrin (0.11 mol) and chlorotrimethylsilane (0.1 mol); bp 81 °C/20 Torr. ^{1}H NMR ($CDCl_3$) δ=0.10 (s, 9H), 3.40—3.60 (q, 4H), 3.80—4.00 (m, 1H); MS, *m/z* (rel intensity) 185 (24), 151 (47), 93 (100) 73 (62); IR (neat) 2950, 1250, 1100, 840 cm^{-1}. Found: C, 35.62; H, 7.03; Cl, 35.17%. Calcd for $C_6H_{14}Cl_2OSi$: C, 35.82; H, 7.01; Cl, 35.24%.

2-Chloro-1-(chloromethyl)ethyl Ethoxymethyl Ether (3f): Synthesized by the reaction of epichlorohydrin (0.11 mol) and chloromethyl ethyl ether (0.1 mol); bp 85 °C/20 Torr. ^{1}H NMR ($CDCl_3$) δ=1.14—1.26 (t, 3H), 3.56—3.90 (m, 6H), 3.90—4.12 (m, 1H), 4.80 (s, 2H); MS, *m/z* (rel intensity) 187 (M^++1), 185 (M^+−1), 137 (14), 75 (14), 59 (100), 31 (32); IR (neat) 3000, 2900, 1450, 1140, 1060, 770 cm^{-1}. Found: C, 38.24; H, 6.47; Cl, 37.70%. Calcd for $C_6H_{12}Cl_2O_2$: C, 38.52; H, 6.47; Cl, 37.90%.

2-Chloro-1-(chloromethyl)ethyl Benzoate (3g): Synthesized by the reaction of epichlorohydrin (0.11 mol) and benzoyl chloride (0.1 mol); bp 89 °C/0.02 Torr. ^{1}H NMR ($CDCl_3$) δ=3.84—3.92 (d, 4H), 5.32—5.52 (m, 1H), 7.24—7.68 (m, 3H), 8.00—8.16 (m, 2H); MS, *m/z* (rel intensity) 234 (M^+), 232 (M^+), 123 (34), 122 (49), 105 (100); IR (neat) 1730, 1295, 1122, 730 cm^{-1}. Found: C, 51.48; H, 4.40; Cl, 30.20%. Calcd for $C_{10}H_{10}Cl_2O_2$: C, 51.53; H, 4.30; Cl, 30.40%.

2-Chloro-1-(chloromethyl)ethyl Methoxycarbonylmethyl Ether (3h): Synthesized by the reaction of epichlorohydrin (0.11 mol) and chloroacetic acid methyl ester (0.1 mol); bp 78 °C/0.02 Torr. ^{1}H NMR ($CDCl_3$) δ=3.72—4.00 (m, 8H), 4.30 (s, 2H); MS, *m/z* (rel intensity) 201 (M^++1), 199 (M^+−1), 151 (46), 93 (100), 75 (45); IR (neat) 2975, 1760, 1440, 1230 cm^{-1}. Anal. Calcd for $C_6H_{10}Cl_2O_3$: C, 35.84; H, 5.01; Cl, 35.26%. Found: C, 36.06; H, 5.07; Cl, 35.07%.

Benzyl 2-Chloro-1-(chloromethyl)ethyl Ether (3i): Synthesized by the reaction of epichlorohydrin (0.12 mol) and benzyl chloride (0.1 mol); bp 80 °C/0.05 Torr. ^{1}H NMR ($CDCl_3$) δ=3.60—4.00 (m, 5H), 4.68 (s, 2H), 7.16 (s, 5H); MS, *m/z* (rel intensity) 220 (M^+), 218 (M^+), 91 (100); IR (neat) 2800, 1460, 1120, 1090, 760, 720 cm^{-1}. Found: C, 54.43; H, 5.70; Cl, 32.17%. Calcd for $C_{10}H_{12}Cl_2O$: C, 54.81; H, 5.52; Cl, 32.35%.

References

1) T. Takeda, S. Yasuhara, and S. Watanabe, *Bull. Chem. Soc. Jpn.*, **53**, 2566 (1980); *Kagaku To Kogyo (Osaka)*, **55**, 25 (1981).

2) X.-P. Gu, I. Ikeda, and M. Okahara, *Synthesis*, **1985**, 649.

3) A. D. Jr. Cale, H. Jenkins, *Ger. Offen.*, 1932219 (1970); *Chem. Abstr.*, **72**, 100478s (1970).

4) M. S. Brouwer, A. Hulkenberg, J. G. J. Kok, R. Van Moorselaar, W. R. M. Overbeek, and P. G. J. Wesselman, *Recl. Trav. Chim. Pays-Bas*, **98**, 316 (1979).

5) N. B. Sattur, I. Hussain, G. R. Phalgumani, P. Bajaj, M. L. Malhotra, and V. B. Chipalkatti, *J. Text. Ass.*, **33**, 227 (1972).

6) G. R. Phalgumani, A. P. Singh, and R. Kumar, *Colourage*, **22**, 23 (1975).

7) C. Mircea, D. Larica, H. Cornel, F. Steliana, C. Constantin, P. Ion, M. Elisabeta, F. Rodica, and S. Paul, *Rom.*, 56965 (1974); *Chem. Abstr.* **83**, 165515y (1975).

8) X.-P. Gu, I. Ikeda, M. Okahara, *J. Org. Chem.*, **52**, xxx (1987).

Mechanism of Photochemical Reaction from Benzyl Chloride to Toluene in Solution

Takeshi TAKEMURA* and Masahisa FUJITA
Research Institute of Applied Electricity, Hokkaido University, Sapporo 060
(Received June 25, 1986)

Synopsis. The photochemical reaction from benzyl chloride to toluene has been investigated in rigid glasses and fluid solutions. The experimental results indicate that toluene formation from benzyl chloride in 2-methylpentane proceeds via hot benzyl radicals or higher triplet states that are isoenegitic to the vibrationless level of the S_1 state of BzCl and proceeds negligibly from stable benzyl radicals.

Benzyl chloride (BzCl) is photochemically very active and its photochemistry has been widely studied.[1-4] Although it is known that upon irradiation with UV light, BzCl in alkane solvents yields a variety of photochemical products, several problems for the reaction mechanism remain unsettled, especially concerning intermediates in the excited state leading to photoproducts. This note is concerned with the mechanism of the photochemical reaction from BzCl to toluene, which was believed to proceed via benzyl radicals (Bz radicals) as a reaction intermediate.[1-4]

On the other hand, it is difficult to observe any emission of the fluorescence and phosphorescence of BzCl in the usual organic solvents at any temperature.[1,5-7] This suggests that the lifetime of the S_1 state of BzCl in solution is very short (less than 10^{-12} s; cf. Results and Discussion) and that the T_1 state is poorly populated because the intersystem crossing rate from the S_1 state to an excited triplet state is unlikely to be as fast as 10^{12} s^{-1}. Accordingly, the photochemistry of BzCl in solution is considered to proceed exclusively from the S_1 state and/or from the higher triplet states. This consideration corresponds to the results by Cristol and Bindel, who indicated that the photoreaction of BzCl in *t*-butyl alcohol occurs via a short-lived upper state, S_1, or a higher triplet state.[2]

In this study, we attempt to elucidate the photochemical processes concerning the formation of toluene from BzCl as a prototype of the homolytic photochemical reaction and to reveal the energy-relaxation processes in the excited states of BzCl as a series of studies on those of halogenated benzenes.[7-11]

Experimental

Benzyl chloride (Wako Chemical Co.) was purified by repeated vaccum distillations. 2-Methylpentane (Tokyo Kasei Co.) was purified after the method described in a previous paper.[8] Absorption and emission spectra were measured, respectively, with a Hitachi 228 spectrophotometer and a high-sensitivity fluorescence and phosphorescence spectrophotometer by means of the photon-counting technique using a Hamamatsu R585 photomultiplier. Unless otherwise stated, the photochemical experiments were made at 77 K using 1-cm square quartz cell and irradiation was carried out at 265 nm with a bandwidth of 10 nm by the use of light from a 150-W xenon arc passed through a monochromator.

Upon irradiation of BzCl in 2-methylpentane (2-MP) at 77 K, the contents of Bz radicals and toluene produced are quantitatively obtained by monitoring the fluorescence of Bz radicals and the phosphorescence of toluene. In measurements of the fluorescence of Bz radicals and of the phosphorescence of toluene, the excitations were carried out at an absorption band of 318 nm for Bz radicals and at a band of 254 nm for toluene (with a bandwidth of 2 nm). The concentrations of BzCl in 2-MP examined were in the range 10^{-4}—10^{-5} M.

Results and Discussion

Upon irradiation with a UV light shorter than 270 nm, BzCl in 2-MP at 77 K reacts to form Bz radicals and toluene. Bz radicals show a structured fluorescence spectrum commencing at 465 nm and has a very strong absorption band at 318 nm. Therefore, the formation of Bz radicals can be quantitatively observed by monitoring the fluorescence spectrum excited at 318 nm. Toluene produced can also be detected by monitoring the phosphorescence of toluene by means of time-resolved spectroscopy.[8,9] The fluorescence from toluene can not be used as a quantitative measure of toluene because of the very low concentration of toluene produced and because of interference from the Raman scattering light due to solvents. It should be noted here that the fluorescence of BzCl could not be detected within our experimental accuracies (the quantum yield is less than 10^{-5}).

Also, no phosphorescence from BzCl could be observed. Fresh BzCl in 2-MP at 77 K did not show any emission with a lifetime longer than 10^{-3} s (the quantum yield is less than 10^{-5}). Although no fresh BzCl showed a structured emission spectrum starting at 390 nm with a lifetime of 3—5 ms, which is similar to the phosphorescence spectrum reported in Ref. 5, it was found from the excitation spectrum of the

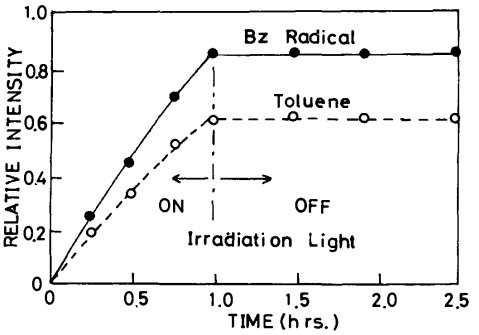

Fig. 1. Plots of the fluorescence intensities of Bz radicals (-●—●-) and the phosphorescence intensities of toluene (-○- -○-) as a function of the time with and without irradiation light of 265 nm of BzCl in 2-MP at 77 K.

emission that the emission is due to an impurity: maybe benzaldehyde. The emission with a lifetime of 2 s (produced by irradiation) can be attributed to toluene on the basis of the phosphorescence and its excitation spectra.

In Fig. 1 the fluorescence intensities of Bz radicals and the phosphorescence intensities of toluene are plotted as a function of the time with and without irradiation of BzCl in 2-MP at 77 K with a light of 265 nm. The concentrations of Bz radicals and toluene increase with the irradiation time and show no change for at least 3 h after irradiation. This is consistent with the observation that stable Bz radicals ("stable" means Bz radicals are in the vibrationless level in the ground state) in rigid glass solutions at 77 K react negligibly with solvents.[1)]

Figure 2 shows the formation rates of Bz radicals and toluene against the intensities of the irradiation light, indicating that each of the rates is linear to the light intensities under experimental conditions; that is, the photoreaction from BzCl to toluene as well as to Bz radicals is a one-photon process.

Now we are in a position to consider the mechanism regarding the photoreaction from BzCl to toluene. On the basis of the experimental results described above, we can give three mechanisms as candidates of a plausible path for the toluene formation from BzCl: (1) a reaction of toluene←stable Bz radical involves an appropriate orientation between the Bz radical and solvent molecules concerned and is accompanied by considerable amounts of the activation energy; (2) stable Bz radicals react with alkyl radicals produced by the reaction between the solvent and the chlorine atom (comes photochemically from BzCl) to form toluene with a negligible amount of the activation energy; and (3) toluene arises from a hot Bz radical or a higher triplet state isoenergitic to the vibrationless level of the S_1 state of BzCl and arises negligibly from stable Bz radicals. Mechanisms (1) and (2) involve the concentrations of stable Bz radicals, while (3) does not.

In order to decide which mechanism is acceptable, it is desirable to examine the oxygen effect on the photochemical reaction in question in a fluid solution. The lifetime of Bz radicals is found to be considerably long in a degassed alkane solvent and decreases with an increase in the concentration of oxygen.[1)] Accordingly, if the photochemical reaction in the fluid solution was influenced by aeration, mechanism (3) would be excluded from a possible mechanism. On the contrary, if the aeration effect on the reaction in the fluid solution is negligible, the contributions from (1) and (2) are less for the photochemistry in interest, and (3) is favorable.

BzCl in 2-MP at room temperature was irradiated for 3 h under deaerated and aerated conditions; then, the phosphorescence of toluene produced was quantitatively observed at 77 K. For both samples, deaerated and aerated solutions, the contents of the toluene produced by irradiation were almost equal to each other within our experimental accuracies. That is, the effect of oxygen on the reaction could not be clearly observed. The experimental results also showed that the toluene formation under fluid conditions was not in an order of magnitude appreciably different from those in rigid glass at 77 K. These facts indicate that the reaction of interest had no appreciable amounts of activation energy and involved no relatively long-lived species as intermediates (such as stable Bz radicals and the T_1 state of BzCl). In addition, the fact that the rate of the toluene formation is linear against the intensity of the irradiation light (as described before), excludes mechanism (2) from a possible path for the photoreaction.

Thus, the experimental results described above lead us to the conclusion that the photochemical reaction from BzCl to toluene proceeds via a very short-lived Bz radical (hot Bz radical) as the reaction intermediate and does not via stable Bz radicals and the T_1 state of BzCl. That is, hot Bz radicals produced from the S_1 state or the isoenergitic higher triplet state transform into toluene during the very short lifetime. These reaction processes seem to correspond to the mechanism of the heterolytic photoreaction of BzCl in *t*-butyl alcohol which is considered to occur via the short-lived S_1 state or a higher triplet state.[2)]

Figure 3 schematically shows the photochemical mechanism proposed. For BzCl in 2-MP, the lifetime of the S_1 state can be estimated to be shorter than one picosecond from the fluorescence quantum yield ($\leqslant 10^{-5}$) and radiative lifetime ($\approx 10^{-7}$ s estimated from the oscillator strength of S_0—S_1 absorption). This indicates that the S_1 state deactivates dominantly

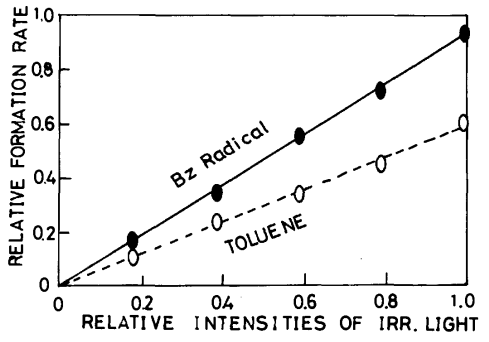

Fig. 2. Plots of the formation rates of Bz radicals (-●—●-) and of toluene (-O- -O-) against the intensities of the irradiation light.

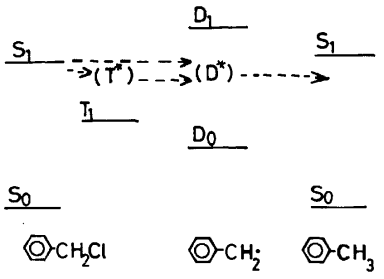

Fig. 3. Possible mechanism for photochemical reaction from BzCl to toluene in alkane solvent. The reaction proceeds along arrows in competition with vibrational relaxations.

to the radical formation directly or to higher triplet states. Although we could not decide whether the hot Bz radicals were formed directly from the S_1 state or via a higher triplet state, hot Bz radicals are actually regarded as being produced almost directly from the S_1 state.[12]

Finally, we shall show the results of a photochemical reaction for benzyl bromide (BzBr). BzBr also shows no fluorescence and phosphorescence under any condition and gives almost no Bz radicals. However, toluene is considerably produced from BzBr in 2-MP at 77 K upon irradiation with UV light. This seems to give some evidence that the photochemical process of toluene formation proceeds along the mechanism shown in Fig. 3.

References

1) G. Porter and E. Strachan, *Trans. Faraday Soc.*, **54**, 1595 (1958).
2) S. J. Cristol and T. H. Bindel, *J. Am. Chem. Soc.*, **103**, 7287 (1981).
3) S. J. Cristol and B. E. Greenwald, *Tetrahedron Lett.*, **1976**, 2105.
4) T. Ichimura and Y. Mori, *J. Chem. Phys.*, **57**, 1677 (1972).
5) T. Ichimura, T. Hikida, and Y. Mori, *J. Phys. Chem.*, **79**, 291 (1975).
6) T. Ichimura, and Y. Mori, *J. Chem. Phys.*, **82**, 4723 (1985).
7) T. Takemura, M. Fujita, S. Nagaoka, and H. Baba, Abstracts, Annual Symposium on Molecular Structure, Nagoya, Japan (Oct. **1984**), p. 68.
8) T. Takemura, Y. Yamada, and H. Baba, *Chem. Phys.*, **68**, 171 (1982).
9) T. Takemura, Y. Yamada, M. Sugawara, and H. Baba, *J. Phys. Chem.*, **90**, 2324 (1986).
10) S. Nagaoka, T. Takemura, and H. Baba, *Bull. Chem. Soc. Jpn.*, **58**, 2082 (1985).
11) S. Nagaoka, T. Takemura, H. Baba, N. Koga, and K. Morokuma, *J. Phys. Chem.*, **90**, 759 (1986).
12) T. Ichimura, Y. Mori, M. Sumitani, and K. Yoshihara, *J. Chem. Phys.*, **80**, 962 (1984).

Crystal Structure of the Mixed-Stacked Salt of Bis(ethylenedithio)-tetrathiafulvalene (BEDT-TTF) and Tetracyanoquinodimethane (TCNQ)

Takehiko Mori* and Hiroo Inokuchi
Institute for Molecular Science, Okazaki 444
(Received July 17, 1986)

Synopsis. The crystal structure of the monoclinic form of (BEDT-TTF)(TCNQ) is determined by X-ray analysis. The donor (BEDT-TTF) and the acceptor (TCNQ) molecules are planar and form alternating stacks.

Recently the discoveries of superconductivity have aroused much interest in BEDT-TTF complexes. Although the organic superconductors based on BEDT-TTF have been found among the salts with inorganic anions such as ReO_4^-, I_3^-, IBr_2^-, and AuI_2^-,[1] the conventional type of charge-transfer complex (BEDT-TTF)(TCNQ) was already prepared as early as 1978 when BEDT-TTF was first synthesized,[2] and this complex has been reported to be highly conductive by the measurements on compressed samples.[2,3] On the way to characterize this complex by means of the X-ray analysis and the measurements of physical properties by using single crystals, we found two different types of crystals: The monoclinic form and the triclinic form. The triclinic form of (BEDT-TTF)(TCNQ) is composed of segregated stacks, where TCNQ molecules are stacked face to face, while BEDT-TTF molecules are arranged side by side along the TCNQ stacks. This complex shows comparatively high conductivity and undergoes a characteristic metal-insulator transition around room temperature.[4] In the present paper we report the crystal structure of the other form, the monoclinic form of (BEDT-TTF)(TCNQ).

Experimental

Single crystals for structure analysis were obtained by the direct reaction of the donor and the acceptor in various organic solvent.[4] The donor and the acceptor were dissolved together in a hot organic solvent such as 1,1,1- and 1,1,2-trichloroethane, 1,2-dichloroethane, and THF, and the solution was allowed to evaporate at room temperature. By keeping for several weeks, black crystals of the complex in the form of elongated plates were grown. The triclinic form was obtained together with the monoclinic form from the same solution, and it was difficult to control reaction conditions so as to obtain only one form. Since these two forms were quite similar in shape, they were only distinguished by X-ray investigations.

Crystal Data. $C_{22}H_{12}N_4S_8$, F.W. 588.89, monoclinic, space group $P2_1/n$, a=23.897(4), b=7.327(2), c=7.053(2) Å, β=98.37(2), U=1221.8(5) Å^3, Z=2, D_x=1.601 gcm^{-1}, and μ(Mo $K\alpha$)=7.23 cm^{-1}. Intensity data were measured by the θ—2θ scan technique on a Rigaku AFC-5R automated four-circle diffractometer with graphite-monochromatized Mo $K\alpha$ radiation ($2\theta<60°$) and corrected for usual Lorentz and polarization effects, but not for the absorption. The structure was solved by the direct method and refined by the block-diagonal least-squares procedure to an R value of 0.052, by using 2294 independent reflections ($|F_o|>3\sigma(|F_o|)$). Anisotropic thermal parameters were adopted for all non-hydrogen atoms, and the hydrogen atoms were refined isotropically.

Results and Discussion

The atomic coordinates are listed in Table 1.[5] The crystal sturcture is shown in Fig. 1. The donors and the acceptors are stacked alternately along the b axis (the crystal long axis). Each molecule is present on an inversion center. The donor and the acceptor molecules are planar (see Fig. 1). As shown in Table 2, the planarity of BEDT-TTF is as good as those observed in the BEDT-TTF salts with various inorganic anions; the deviation of each atom from the optimal plane is within 0.04 Å except the terminal ethylene groups. This contrasts with the nonplanar structure of the neutral molecule.[6]

It is noteworthy that BEDT-TTF and TCNQ form either segregated (the triclinic form) or mixed (the monoclinic form) stacks with the same 1:1 composition. This is largely related to the similar molecular size. The rectangle of the outer sulfur atoms of BEDT-TTF, 9.6×3.7=36 Å^2 has almost the same size as that of TCNQ, 8.5×4.1=35 Å^2. In this context, the terminal ethylene group of BEDT-TTF plays an exceptional role, because there is no overlap between this part and TCNQ (Fig. 1) due to the steric repulsion of this out-of-plane aliphatic moiety.

Table 1. Atomic Parameters (×10^4) of the Monoclinic (BEDT-TTF)(TCNQ)

Atom	x	y	z	B_{eq}
S (1)	4503(1)	383(1)	2357(1)	3.4
S (2)	4241(1)	983(1)	−1821(1)	3.1
S (3)	3384(1)	1545(2)	3196(1)	4.3
S (4)	3091(1)	2329(1)	−1795(1)	3.7
C (1)	4737(1)	284(4)	116(4)	2.8
C (2)	3825(1)	1222(5)	1452(5)	2.9
C (3)	3710(1)	1518(4)	−424(4)	2.7
C (4)	2873(2)	3064(6)	1929(6)	4.6
C (5)	2619(1)	2391(6)	−11(6)	4.7
C (6)	427(1)	500(5)	3919(4)	3.0
C (7)	−63(1)	−158(5)	3003(4)	3.0
C (8)	516(1)	698(4)	5968(4)	2.6
C (9)	1019(1)	1362(4)	6915(4)	2.7
C (10)	1479(1)	1938(4)	5951(4)	2.8
C (11)	1126(1)	1495(5)	8964(5)	3.3
N (1)	1852(1)	2407(4)	5242(4)	3.8
N (2)	1219(1)	1579(5)	10587(4)	5.0

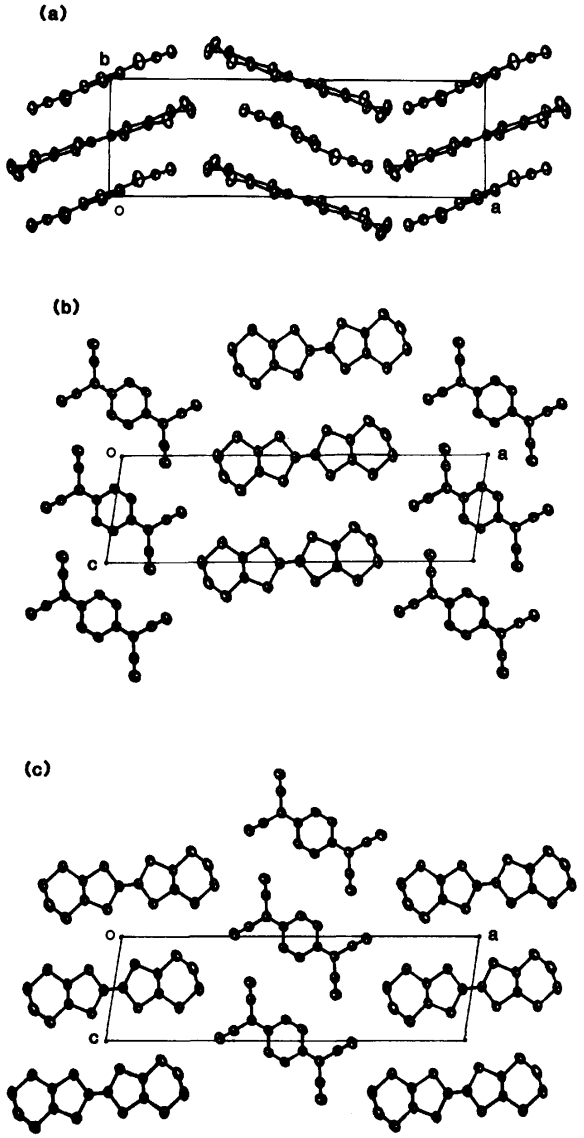

Fig. 1. Crystal structure of the monoclinic (BEDT-TTF)(TCNQ).
(a) Projection on the ab plane. (b) Projection along the b axis, the molecules on the $y=0$ inversion centers and (c) on the $y=0.5$ inversion centers.

Table 2. Least Squares Planes and Deviations (Å); X, Y, Z are Coordinates (Å) Referred to the Orthogonal Axes a, b, and c*

(a) TTF skeleton of BEDT-TTF					
$0.3267X+0.9372Y+0.1219Z=3.4333$					
S (1)	0.004	C (2)	0.004	S (4)	−0.015
S (2)	0.011	C (3)	−0.013	C (4)	−0.542
C (1)	0.004	S (3)	0.037	C (5)	0.219
(b) TCNQ					
$0.3684X-0.9276Y+0.0624Z=0.0284$					
C (6)	−0.030	C (9)	0.018	N (1)	0.004
C (7)	−0.041	C (10)	0.009	N (2)	−0.032
C (8)	0.015	C (11)	0.002		

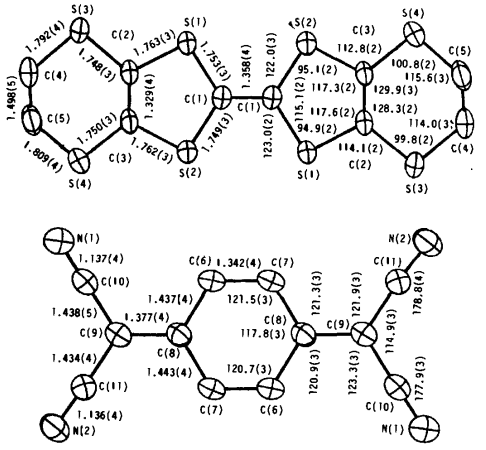

Fig. 2. Molecular geometry of BEDT-TTF and TCNQ.

Table 3. A Comparison of the Averaged Bond Lengths (mmm Molecular Symmetry) of BEDT-TTF and TCNQ with Those of the Neutral Species, BEDT-TTF$^{+1/2}$ in α-(BEDT-TTF)$_2$PF$_6$, and TCNQ$^{-1/2}$ in (Ph$_4$P)(TCNQ)$_2$ and (TMPD)(TCNQ)$_2$[6-8]

	BEDT-TTF^0	Present Complex	BEDT-TTF$^{+1/2}$
C (1)-C (1)	1.319	1.358	1.365
C (1)-S (1)	1.757	1.751	1.740
C (2)-S (1)	1.754	1.763	1.750
C (2)-C (3)	1.332	1.329	1.345
	TCNQ^0	Present Complex	TCNQ$^{-1/2}$
C (6)-C (7)	1.346	1.342	1.353
C (6)-C (8)	1.448	1.440	1.434
C (8)-C (9)	1.374	1.377	1.396
C (9)-C (10)	1.441	1.434	1.428
C (10)-N (1)	1.14	1.14	1.17

The molecular geometry is depicted in Fig. 2. In order to estimate the degree of charge transfer, η, the molecular geometries of the constituents are analyzed in comparison with the molecular geometries in which the degrees of charge transfer are evident from their composition (Table 3). As for BEDT-TTF, the central C=C bond length and the C(1)-S(1) bond length are between those of $\eta=0$ and $\eta=1/2$ species. On the other hand, since the population of the LUMO of TCNQ is largest on C(8) and C(9),[9] the bond lengths associated with these atoms are sensitive to η; these bond lengths are also between $\eta=0$ and $\eta=1/2$. As a whole, we can conclude the degree of charge transfer to be between $\eta=0$ and $\eta=1/2$, probably about $\eta=0.2$—0.3.

The electrical resistivity measured by the usual four-probe method is in the order of 10^6 Ωcm. Saito et al. have briefly mentioned two forms of (BEDT-TTF)(TCNQ); one affords a broad infrared spectrum and the other affords a sharp spectrum.[3] The broad

spectrum is considered to be that of the triclinic form, and is associated with its high conductivity. On the other hand, the sharp spectrum is that of the present low-conductive monoclinic form.

References

1) S. S. P. Parkin, E. M. Engler, R. R. Schumaker, R. Lagier, V. Y. Lee, J. C. Scott, and R. L. Greene, *Phys. Rev. Lett.*, **50**, 270 (1983); E. B. Yagubskii, J. F. Shchegolev, V. N. Laukhin, P. A. Kononovich, M. V. Kartsovnic, A. V. Zvarykina, and L. I. Buravov, *Pis'ma Zh. Eksp. Teor. Fiz.*, **39**, 12 (1984); J. M. Williams, H. H. Wang, M. A. Beno, T. J. Emge, L. M. Sowa, P. T. Copps, F. Behroozi, L. N. Hall, K. D. Carlson, and G. W. Crabtree, *Inorg. Chem.*, **23**, 3839 (1984); H. H. Wang, M. A. Beno, U. Geiser, M. A. Firestone, K. S. Webb, L. Nunez, G. W. Crabtree, K. D. Carlson, J. M. Williams, L. J. Azevedo, J. F. Kwak, and J. E. Schirber, *Inorg. Chem.*, **24**, 2465 (1985); H. Kobayashi, R. Kato, A. Kobayashi, Y. Nishio, K. Kajita, and W. Sasaki, *Chem. Lett.*, **1986**, 789, 833.

2) M. Mizuno, A. F. Garito, and M. P. Cava, *Chem. Commun.*, **1978**, 18.

3) G. Saito, H. Hayashi, T. Enoki, and H. Inokuchi, *Mol. Cryst. Liq. Cryst.*, **120**, 341 (1985).

4) T. Mori and H. Inokuchi, *Solid State Commun.*, **59**, 355 (1986).

5) The parameters of the hydrogen atoms, the anisotropic thermal parameters, and the list of the structure factors are deposited at the office of the Chemical Society of Japan (Document No. 8705).

6) H. Kobayashi, A. Kobayashi, Y. Sasaki, G. Saito, and H. Inokuchi, *Bull. Chem. Soc. Jpn.*, **59**, 301 (1986).

7) H. Kobayashi, R. Kato, T. Mori, A. Kobayashi, Y. Sasaki, G. Saito, T. Enoki, and H. Inokuchi, *Mol. Cryst. Liq. Cryst.*, **107**, 33 (1984).

8) R. E. Long, R. A. Sparks, and K. N. Trueblood, *Acta Crystallogr.*, **18**, 932 (1965); A. W. Hanson, *Acta Crystallogr., Sect. B*, **24**, 768 (1968); P. Goldstein, K. Seff, and K. N. Trueblood, *Acta Crystallogr., Sect. B*, **24**, 778 (1968).

9) J. P. Lowe, *J. Am. Chem. Soc.*, **102**, 1262 (1980).

Viscosity Behavior of Poly(2-vinylpyridine) of a Low Molecular Weight

Masafumi YOSHIDA,* Kikuo ITOH, Noriyuki SAKAMOTO, and Shizuo ARICHI
Department of Chemistry, Faculty of General Education, Kumamoto University, Kurokami 40-1, Kumamoto 860
(Received May 28, 1986)

Synopsis. For the data of the limiting viscosity number of poly(2-vinylpyridine) of a low molecular weight M_w=2.26—0.21×10⁴ in benzene and methanol, the value of the thickness parameter, b, and the energy difference, E, between the gauche and trans state were discussed in terms of the theory of Rossi and Perico. It is possible to use this theory for the viscosity data in the molecular weight range of 0.35—1.30×10⁴. The values of E and b were thus estimated; E depended on the nature of the solvent for this polymer, while b was constant (0.3 nm). The temperature dependence of the calculated limiting viscosity number, $d\ln[\eta]/dT$, in benzene and dioxane was discussed, together with the measured values.

In the relation of the limiting viscosity number and the molecular weight for the range of low molecular weights, the equation $[\eta]=KM^{0.5}$ holds. Here, the constant, K, is independent of the nature of a solvent.[1] For poly(2-vinylpyridine), the present authors previously reported that the constant, K, is equal to the value of Flory's K_θ, which is itself related to the unperturbed mean-square radius gyration of the chain molecule.[2] Consequently, it was deduced that it was possible to evaluate the characteristic ratio from the measurement of the limiting viscosity number for a low molecular weight.

On the other hand, according to the precepts of statistical mechanics, the properties of chain molecules should be evaluated by averaging all the conformations generated by varying all angles and all bond lengths to the extent permitted by the chain structure. The subsequent calculation for a long chain, is indeed formidable, but they can be greatly abbreviated though the adoption of a rotation angle.[3] Furthermore, Rossi and Perico reported the theoretical treatment of a short-chain polymer.[4] They showed that the limiting viscosity number of a short-chain polymer could be evaluated from a model of the independent hindered rotation by introducing b, a thickness parameter.

In this paper, the energy difference, E, between the gauche and trans states and thickness parameter, b, will be discussed on the basis of the limiting viscosity number for the low-molecular-weight range of poly(2-vinylpyridine) in benzene and methanol, using the theory of Rossi and Perico.[4] These values in several solvents will then be evaluated, and the temperature dependence of the calculated limiting viscosity number will be discussed.

Experimental

Poly(2-vinylpyridine) was polymerized, with butyllithium as the initiator, in tetrahydrofuran at −27 °C for the BL-sample, while A-1-V was polymerized with $\alpha\alpha'$-azobisisobutyronitrile in benzene at 25 °C. The polymer samples were obtained by the method of fractional precipitation. Benzene and petroleum ether were used as solvent and precipitant. The limiting viscosity number was measured with a Ubbelohode-type viscometer.

The weight average molecular weight of the polymer fraction was determined with a Fica-50 automatic light scattering photometer in methanol at 25 °C for scattered angles of 30—150°. The measurement of the specific refractive-index increment was carried out by the use of a Shimadzu-DR-3-type differential refractometer.

Results and Discussion

The relation of the limiting viscosity number and the molecular weight for short chain polymers was represented by the theory of Rossi and Perico.[4] The relation was as follows:

$$[\eta] = \phi 6^{3/2}(R_s^3/M)$$
$$R_s = \langle s^2\rangle_0^{1/2} + b$$

Table 1. Results from the Calculation and the Viscosity Measurements

Sample	$M_w \times 10^{-3}$	N_c[a]	$\langle s^2\rangle_{0,\,calcd}^{1/2}$[b] nm	Benzene $[\eta]_{calcd}$	Benzene $[\eta]_{meas}$	$\langle s^2\rangle_{0,\,calcd}^{1/2}$[c] nm	Methanol $[\eta]_{calcd}$	Methanol $[\eta]_{meas}$
BL-6-2	22.9	435	3.61	0.110	0.111	4.04	0.151	0.170
BL-6-3	13.1	249	2.70	0.0869	0.089	3.01	0.117	0.117
BL-6-4	9.46	179	1.98	0.0748	0.075	2.51	0.0989	0.099
BL-6-5	7.49	141	1.98	0.0671	0.065	2.19	0.0874	0.086
BL-6-6	5.46	103	1.66	0.0582	0.057	1.83	0.0747	0.074
BL-6-7	4.95	93	1.57	0.0557	0.055	1.72	0.0702	0.073
BL-6-8	3.55	67	1.29	0.0478	0.043	1.41	0.0594	0.057
BL-6-9	2.10	39	0.92	0.0336	0.039	0.99	0.0397	0.043

a) Bond number of the polymer chain. b) and c) A root mean-square radius gyration for E=1.0 and 1.15 kcal mol^{-1} respectively. (1 cal=4.184 J).

where ϕ was a hydrodynamic parameter and was constant (2.87×10^{21}) for the number of monomeric units $N_c>20$; M was the molecular weight. $<s^2>_0$ was a mean-square radius gyration and was calculated for the chain with an independent bond rotational potential according to the rotational-isomer method[5]; b was the thickness of the polymer chain.

The limiting viscosity number for a low molecular weight was calculated by choosing the appropriate values of E and b yielding the best-fitting point. In Table 1 the calculated results are shown, together with the measured values, which have been reported before in benzene and methanol at 25 °C.[2] The calculated values were in very good agreement with all the measured values except with the data of BL-6-2 in methanol and with those of BL-6-9 in both solvents. The value of E is 1.0 kcal mol^{-1} in benzene and 1.15 kcal mol^{-1} in methanol. As to the disagreement with the value of E in benzene and methanol, it is possible to explain it as follows. The specific interaction between poly(2-vinylpyridine) and a solvent was investigated; alcohol is solvated to the pyridine nitrogen of this polymer through hydrogen bonding. However, there has been no report of the specific interaction in benzene for this polymer. On the other hand, the value of b is the same, 0.3 nm, in both solvents (the size of the pyridine ring: 0.3 nm). This value is reasonable. Furthermore, the relation of the calculated limiting viscosity number and the molecular weight is represented by the Mark-Houwink-Sakurada empirical equation: $[\eta]_\theta=K_\theta M^{0.5}$ That is, E is affected by the nature of a solvent, but b is independent of this polymer.

As to the discrepancy between the calculated and measured viscosity data of BL-6-2 in methanol and BL-6-9 in both solvents, it may be explained that, for the former, the theory of Rossi and Perico can not be accepted because of the presence of the excluded volume;[2] as for the latter, it is difficult to determine the accurate limiting viscosity number for very a low viscosity.

From the above conclusion that b is independent of the nature of a solvent, it is possible to evaluate E from one point of the limiting viscosity number over the suitable-molecular weight range: 3500—13000 for this polymer. Consequently, the value of E is calculated from the data of BL-6-7 in ethyl methyl ketone and dioxane and from those of A-1-V ($M_w=7.87\times10^3$) in ethanol and chloroform.[7] The value of E in ethyl methyl ketone and dioxane, which are very poor solvent for this polymer, are 0.95 and 1.05 kcal mol^{-1} respectively. On the other hand, in ethanol, E is 1.15 kcal mol^{-1} and in chloroform, 1.25 kcal mol^{-1}.

The Temperature Dependence of the Limiting Viscosity Number. The temperature coefficient of the limiting viscosity number for poly(2-vinylpyridine) was previously reported from the temperature dependence on the limiting viscosity number.[2] Therefore, the limiting viscosity number could be calculated from the above equation at several temperatures. Table 2 shows the results of the calculated limiting viscosity numbers together with the measured limiting viscosity numbers (BL-6-7) in benzene, dioxane and ethyl methyl ketone at several temperatures. It is found that the calculated values agreed with the respective measured values. The values of the temperature coefficient of the limiting viscosity numbers, as calculated by means of the method of least squares, are -5.1×10^{-3} in dioxane, -4.9×10^{-3} in benzene, and -4.6×10^{-3} in ethyl metyl ketone. On the other hand, the measured values are -4.5×10^{-3} in dioxane, -3.9×10^{-3} in benzene, and -3.7×10^{-3} in ethyl methyl ketone. From the agreement with the calculated and measured limiting viscosity number and/or these temperature coefficients, it is considered that the theory of Rossi and Perico is acceptable and that the E and b values for the low-molecular-weight poly(2-vinylpyridine) are reasonable.

Flory's K_θ value of the polymer was indirectly determined in a non-θ-solvent using an extrapolation method based on the two-parameter theory for a dilute solution. Flory's K_θ or K value of a low molecular weight for a non-polar polymer is independent of the nature of a solvent at the same temperature; E and b are constant. The solvent effect on Flory's K_θ value of a polar polymer has also been investigated.[7]

The results of the investigation of poly(4-vinylpyridine) by Hirai and Yanagida indicate that the hydrogen bonding and solvation for the side chain of a polymer must result in an increase in the values of E and b.[8] The values of E and b are 1.1—1.3 kcal mol^{-1} and 0.45—0.67 nm respectively for poly(4-vinylpyridine). The values of E and b for that polymer are a little larger than those for the present observation, and b is variable.

Table 2. Results from the Calculation and the Viscosity Measurements at Several Temperature

Temperature °C	Dioxane		Benzene		Ethyl methyl ketone	
	$[\eta]^{a)}_{calcd}$	$[\eta]_{meas}$	$[\eta]^{b)}_{calcd}$	$[\eta]_{meas}$	$[\eta]^{c)}_{calcd}$	$[\eta]_{meas}$
20	0.0618	0.0627	0.0570	0.0575	0.0526	0.0532
25	0.0601	0.0611	0.0555	0.0568	0.0512	0.0529
30	0.0584	0.0588	0.0540	0.0560	0.0500	0.0518
35.1	0.0569	0.0580	0.0526	0.0556	0.0487	0.0507
45	0.0541	0.0564	0.0502	0.0538	0.0466	0.0498
60	0.0504	0.0520	0.0469	0.0489	0.0437	0.0459

a) $E=1.05$ kcal mol^{-1}. b) $E=1.0$ kcal mol^{-1}. c) $E=0.95$ kcal mol^{-1}.

Now, the steric factor, σ, which is defined as the ratio between the actual steric hindrance, assuming a free rotation, is obtained from Flory's K_θ value. The effect of the substituent volume of the polymer chain on the value of is quite small-for example, polypropylene; 1.76, and polyisobutylene 1.80.[9] That is, the effect of the increase in the substituent volume, which results in the hydrobonding or solvation of this polymer, may not have an effect on σ or on Flory's K_θ value. This is perhaps to be explained by the fact that, in a polymer chain, a huge group of atoms corresponding to the remaining part of the chain is always attached to the carbon atom being considered; therefore, the substituent volume may have only a minor effect on the hindering potential for rotation about the C-C bond. In other words, it is suitable that b is constant and that the nature of the solvent affects the rotation of the chain.

In conclusion, the results of the above calculation suggest that the value of E and b can be evaluated from the limiting viscosity number of the low molecular weight for poly(2-vinylpyridine) in the range of 3500—13000 according to the theory of Rossi and Perico,[4] and that E is affected by the nature of a solvent, while b is constant.

References

1) U. Bianchi and A. Paterson, *J. Polymer Sci., Part A-2*, **6**, 1759 (1968).
2) M. Yoshida, S. Yamaguchi, N. Sakamoto, and S. Arichi, *Bull. Chem. Soc. Jpn.*, **58**, 1023 (1985).
3) P. J. Flory, "Statistical Mechanics of Chain Molecules," Interscience, New York (1969).
4) C. Rossi and A. Perico, *J. Chem. Phys.*, **53**, 1223 (1970).
5) H. Benoit and P. M. Doty, *J. Phys. Chem.*, **57**, 958 (1953).
6) S. Arichi, M. Matsuura, Y. Yamamoto, and H. Murata *Bull. Chem. Soc. Jpn.*, **39**, 434 (1966).
7) A. Dondos and H. Benoit, *Macromolecules*, **4**, 279 (1971).
8) Y. Hirai and T. Yanagida, *Bull. Chem. Soc. Jpn.*, **51**, 2421 (1978).
9) M. Kurata and W. H. Stockmayer, *Fortschr. Hochpolym. Forsch.*, **3**, 196 (1963).

The Structure of μ-Aquabis(μ-trichloroacetato)bis[aquabis(trichloroacetato)-erbium(III)] Hydrate, $[\{Er(CCl_3CO_2)_2(H_2O)\}_2(CCl_3CO_2)_2(H_2O)]_n \cdot nH_2O$

Takashi IMAI and Akira OUCHI*
Department of Chemistry, College of Arts and Sciences, The University of Tokyo, Komaba, Meguro-ku, Tokyo 153
(Received June 21, 1986)

Synopsis. The structure of the title complex has been determined by the single-crystal X-ray diffraction method. A crystal of $Er_2C_{12}H_8O_{16}Cl_{18}$, F. W. 1380.86 is triclinic, with the space group of $P\bar{1}$, a=12.787(8), b=15.209(7), c=11.685(7) Å, α=102.24(5), β=114.43(5), γ=70.59(4)°, Z=2 (for the dimer formula), D_x=2.36, D_m=2.34(3) Mg m^{-3}, and μ(Mo $K\alpha$)=5.74 mm^{-1}. All the carboxylate ions act as bidentate bridges, and each pair of the side-by-side metal atoms is bridged by four carboxylate ions, or by two carboxylate ions and one water-oxygen atom, alternately, forming a polymeric chain approximately parallel to the [011] axis. The chains are arrayed in layers parallel to the (100) plane, and the respective layers are separated by the trichloromethyl groups.

We have reported previously about the lanthanoid(III) 2-naphthalenesulfonate enneahydrate, where the crystal is composed of alternate layers of hydrophilic metal cores and hydrophobic naphthalene rings.[1] However, such a layer structure was not always found, even when the ligand has a large hydrocarbon group in it; for example, in neodymium(III) 1-hydroxy-2-naphthoate–water–ethanol (1/2/2), the ligand-metal cores are surrounded by naphthalene rings.[2]

As the layer structure is very interesting, we have been trying to find another example. Along this line, the title complex was chosen, because the trichloromethyl groups in the ligands were also expected to act as a hydrophobic part.

Moreover, as many lanthanoid(III) carboxylates have a complicated polymeric form in their crystals,[3,4] it is interesting to compare the structure of the title complex with them. Therefore, its crystal and molecular structure has been determined by the X-ray-diffraction method using a single crystal.

Experimental

Preparation of μ-Aquabis(μ-trichloroacetato)bis[aquabis(trichloroacetato)erbium(III)] Hydrate. Wet erbium(III) hydroxide, freshly prepared from an hydrochloric acid solution of erbium(III) oxide (0.38 g, containing 2.0 mmol of Er(III)) and an excess of sodium hydroxide, was treated with trichloroacetic acid (0.98 g, 6.0 mmol). The aqueous solution thus obtained (about 8 cm^3) was left standing in a desiccator over silica gel for several days at the ambient temperature; about two-thirds of the water was then removed, and crystals were deposited. They were filtered and washed with a little water. Yield: 0.62 g, 45%. Although the crystals were stable in a sealed bottle for several months, they easily lost a part of the water in the open air.

The dysprosium(III) complex, which is thought to be isomorphous, is also obtained by the same technique. (a=12.818(15), b=15.247(16), c=11.648(12) Å, α=102.01(9), β=114.62(9), γ=70.99(9)°, U=1950(4) Å^3).

Anal. ($M_2C_{12}H_8O_{16}Cl_{18}$) M=Er or Dy, C, H.

Single-crystal X-Ray Analysis. A crystal with dimensions of 0.25×0.25×0.15 mm^3 was used for the measurement after its edges have been ground off. The reflections within the range of $3°<2\theta<50°$ were collected on a Rigaku AFC-6A four-circle automated X-ray diffractometer with Mo $K\alpha$ radiation, employing the ω—2θ scan technique. Of the 6957 independent reflections, 4642 reflections with $|F_o|>3\sigma(|F_o|)$ were used for the refinement. The intensities were corrected for the Lorentz and polarization factors, but no correction was made for the absorption and extinction. All the calculations were carried out on a HITAC M-280H computer at the Computer Center of the University of Tokyo, using the local version of UNICS.[5] The scattering factors were taken from Ref. 6.

Structure Determination. The structure was solved by the heavy-atom method, and all the non-hydrogen atoms were found. However, as the temperature factors of the five chlorine atoms were found to be large, at the final step of the refinement their positions were fixed assuming their B_{iso} value to be 15.0. The final R value thus obtained, by applying the anisotropic temperature factors for the other atoms, was 0.084.[7] Although the thermal parameters of some chlorine atoms of this complex are found to be abnormally large, the same kind of positional ambiguities of some atoms are also found in the structural determination of some lanthanoid(III) complexes,[8–11] with regard to some carbon atoms of the hydrocarbon groups, or even some sulfur atoms which are apart from the central metal core and are in the hydrophobic moiety in the crystal.

Results and Discussion

Some selected bond lengths and bond angles are tabulated in Table 1.[12] The respective perspective drawings of the complex around Er(1) and Er(2) atoms are shown in Figs. 1 and 2; a schematic presentation to show the coordination geometries around the metal atoms as well as the bridging modes, in Fig. 3, and the crystal packing diagram, in Fig. 4.

All the metal atoms are octa-coordinated and are in the square-antiprism geometry. The Er–O bond lengths of the carboxylato oxygen atoms are 2.28 Å on the average (maximum, Er(1)–O(16^i)=2.387(13) and minimum, Er(2)–O(21)=2.227(17) Å),[13] while the Er–O(water) bond lengths are longer than they (2.45 Å on the average, except the Er(2)–O(W2)). The Er(2)–O(W2) is the longest one (3.10(2) Å), and this bond is thought to be very weak.

All the carboxylato ligands act as Z,Z-type bidentate bridges.[3] Their COM angles of the carboxyl groups are about 140—147°, except for some abnormal ones in **15** and **25**.[14]

One oxygen atom, O(W4) is not ligated with any

Table 1. Selected Bond Lengths and Bond Angles of the Complex[13]

Bond length	l/Å	Bond length	l/Å	Bond length	l/Å
Er(1)-O(12)	2.28(2)	Er(1)-O(13)	2.268(16)	Er(1)-O(15)	2.26(2)
Er(1)-O(22)	2.288(15)	Er(1)-O(W1)	2.43(3)	Er(1)-O(W2)	2.537(17)
Er(1)-O(16^{I})	2.387(13)	Er(1)-O(11^{I})	2.277(17)	Er(2)-O(14)	2.244(14)
Er(2)-O(21)	2.227(17)	Er(2)-O(23)	2.29(3)	Er(2)-O(25)	2.233(18)
Er(2)-O(W2)	3.10(2)	Er(2)-O(W3)	2.36(3)	Er(2)-O(24^{II})	2.304(17)
Er(2)-O(26^{II})	2.300(19)	O(11)-C(11)	1.23(3)	O(12)-C(11)	1.26(4)
O(13)-C(13)	1.24(3)	O(14)-C(13)	1.23(3)	O(15)-C(15)	1.22(3)
O(16)-C(15)	1.23(3)	O(21)-C(21)	1.24(3)	O(22)-C(21)	1.25(3)
O(23)-C(23)	1.26(4)	O(24)-C(23)	1.23(3)	O(25)-C(25)	1.22(3)
O(26)-C(25)	1.24(3)				
Bond angle	ϕ/°	**Bond angle**	ϕ/°	**Bond angle**	ϕ/°
O(12)-Er(1)-O(16^{I})	74.6(6)	O(16^{I})-Er(1)-O(11^{I})	75.4(5)	O(W2)-Er(1)-O(13)	73.5(5)
O(13)-Er(1)-O(W1)	71.5(7)	O(12)-Er(1)-O(15)	77.5(8)	O(15)-Er(1)-O(11^{I})	74.6(7)
O(W2)-Er(1)-O(22)	71.8(5)	O(22)-Er(1)-O(W1)	69.7(7)	O(14)-Er(2)-O(W3)	74.6(8)
O(W3)-Er(2)-O(21)	73.9(8)	O(21)-Er-(2)-O(W2)	65.7(6)	O(W2)-Er(2)-O(14)	67.3(5)
O(23)-Er(2)-O(25)	76.7(8)	O(25)-Er(2)-O(26^{II})	122.3(7)	O(24^{II})-Er(2)-O(23)	125.5(8)
O(26^{II})-Er(2)-O(24^{II})	78.7(6)				

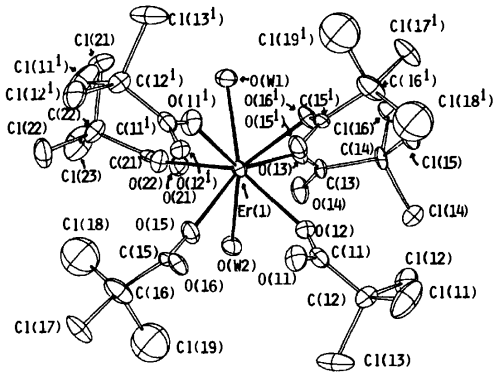

Fig. 1. A perspective drawing of the complex around Er(1) atom, with the numbering scheme of the atoms.[13]

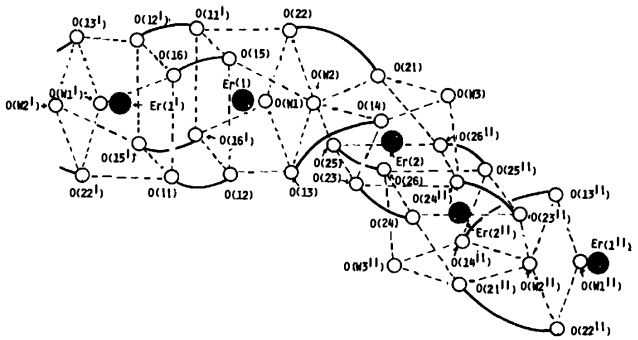

Fig. 3. Schematic presentation to show the coordination geometries around the metal atoms, as well as the bridgings between them.[13]

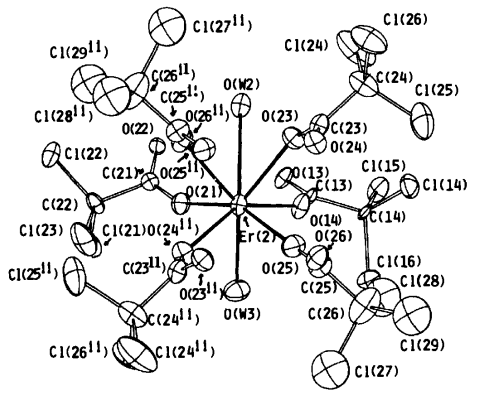

Fig. 2. A perspective drawing of the complex around Er(2) atom, with the numbering scheme of the atoms.[13]

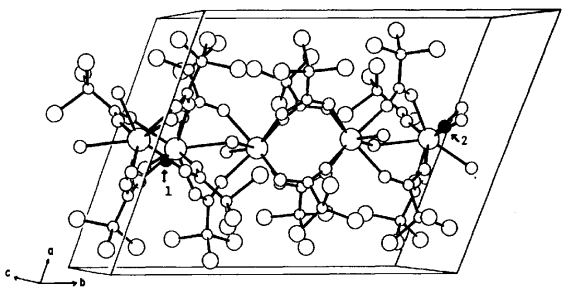

Fig. 4. Crystal packing diagram of the complex. ● atoms are: 1, O(W4); 2, O($W4^{II}$).[13]

metal atom, but it is hydrogen-bonded with O(W1), O(W3), and O(W1^{iii}) atoms.[13]

As is shown in Fig. 3, Er(1^{i})···Er(1), and Er(2)···Er(2^{ii}) are bridged by four carboxylate ions, while Er(1)···Er(2) is bridged by two carboxylate ions and one water oxygen atom O(W2), although Er(2)–O(W2) is a little too long. The dihedral angles of the respective pairs of the square planes above and below the Er(1) and Er(2) atom are 2.8 and 4.8° respectively, while that of the two squares joined by O(W2) is 62.3°. The intermetallic distances of Er(1^{i})···Er(1), Er(1)···Er(2), and Er(2)···Er(2^{ii}) are 4.430(4), 4.823(3), and 4.267(3) Å respectively, and they are aligned approximately along the [011] axis.

As is shown in Fig. 4, the polymeric chains are arrayed in a layer parallel to the (100) plane, and the chlorine atoms of the ligands take positions in the parallel layes on both sides of it. Thus, the layer structure of this complex resemble that of lanthanoid(III) 2-naphthalenesulfonate;[1] the hydrophobic-trichloromethyl group layers act as those of the naphthalene-ring layers of the latter complex.

The authors are greatly obliged to the Shin-Etsu Chemical Ind. Co., Ltd., for presenting them with highly pure lanthanoid oxides.

References

1) Y. Ohki, Y. Suzuki, M. Nakamura, M. Shimoi, and A. Ouchi, *Bull. Chem. Soc. Jpn.*, **58**, 2968 (1985).

2) Y. Ohki, Y. Suzuki, T. Takeuchi, M. Shimoi, and A. Ouchi, *Bull. Chem. Soc. Jpn.*, **59**, 1015 (1986).

3) H. Sawase, Y. Koizumi, Y. Suzuki, M. Shimoi, and A. Ouchi, *Bull. Chem. Soc. Jpn.*, **57**, 2730 (1984), and the references cited there in.

4) M. C. Favas, D. L. Kepert, B. W. Skelton, and A. H. White, *J. Chem. Soc., Dalton Trans.*, **1980**, 454.

5) "Universal Crystallographic Computation Program System (UNICS)," ed by T. Sakurai, Crystallographic Society of Japan, Tokyo (1967).

6) "International Tables for X-Ray Crystallography," Kynoch Press, Birmingham (1974), Vol. IV, pp. 72, 150.

7) $R=\sum||F_o|-|F_c||/\sum|F_o|$.

8) K. Nagai, R. Nakamura, M. Shimoi, and A. Ouchi, *Bull. Chem. Soc. Jpn.*, **57**, 2725 (1984).

9) R. Nakamura, M. Shimoi, and A. Ouchi, *Bull. Chem. Soc. Jpn.*, **57**, 2919 (1984).

10) Y. Ohki, M. Nakamura, Y. Suzuki, K. Nagai, M. Shimoi, and A. Ouchi, *Bull. Chem. Soc. Jpn.*, **58**, 1593 (1985).

11) T. Imai, M. Nakamura, N. Nagai, Y. Ohki, Y. Suzuki, M. Shimoi, and A. Ouchi, *Bull. Chem. Soc. Jpn.*, **59**, 2115 (1986).

12) The final positional and anisotropic thermal parameters, the F_o—F_c table, and some additional bond-length and bond-angle data are deposited as Document No. 8702 at the Office of the Editor of the Bull. Chem. Soc. Jpn.

13) Key to the symmetry operation: i, $1-x$, $-y$, $-z$; ii, $1-x$, $1-y$, $1-z$; iii, $1-x$, $-y$, $1-z$.

14) In this paper, the numbering of the respective carboxylate ions is shown by the number of the carboxyl-carbon atoms of the respective ions. Therefore, the ***n*1**, ***n*3**, and ***n*5** ions (where $n=1$, 2, or 3) include O(n1) and O(n2); O(n3) and O(n4); and O(n5) and O(n6) atoms, respectively.

Synthesis and Electrocatalytic Properties of Rare Earth Platinum or Palladium Bronzes

Ken-ichi MACHIDA,* Michio ENYO, Gin-ya ADACHI,† and Jiro SHIOKAWA †
Research Institute for Catalysis, Hokkaido University, Sapporo 060
†Department of Applied Chemistry, Faculty of Engineering, Osaka University, Yamadaoka, Suita, Osaka 565
(Received June 26, 1986)

Synopsis. Dysprosium platinum and palladium bronzes, DyM_3X_4 (M=Pt or Pd; X=O, S, Se, or Te) were synthesized, except for $DyPt_3S_4$, by a solid state technique. They were found to have a high electric conductivity with ρ=0.3—2.6×10^{-5} Ω cm and among them, the oxide bronzes crystallized in $Na_xPt_3O_4$ type structure. The platinum oxide bronzes in particular showed a high activity for the methanol electrooxidation as compared with ordinary platinum electrodes.

Metal bronzes can be candidates for electrode materials,[1] since they often show a good electric conductivity and some of them possess a high corrosion resistivity in acid or alkali solutions. Shannon et al.[2] have tested a series of $M'_xPt_3O_4$ (M'=Li, Na, Mg, Ca, Zn, Cd, Co, and Ni), and found them promising as brine electrolyzer anodes or H_2-O_2 fuel cell electrocatalysts. Recently, rare earth palladium sulfide analogues of the platinum oxide bronzes, $LnPd_3S_4$(Ln=rare earth elements), have been reported by Keszler and Ibers.[3]

Methanol electrooxidation characteristics of platinum electrodes in acid solution are known to be considerably influenced by a trace amount of foreigen elements.[4] Among them, rare earth elements, typically dysprosium, have been reported to possess a significant degree of activity enhancement effect on the reaction.[4c] In this note, dysprosium platinum or palladium bronzes are prepared and the electric and electrocatalytic properties were studied.

Experimental

Preparation Method. The rare earth platinum (or palladium) bronzes were prepared by a solid state technique: Appropriate amounts of Dy_2O_3 and PtO_2 (or PdO) for oxygen bronzes or elemental Dy, Pt (or Pd), and X' (X'=S, Se, or Te) for other chalcogenide analogues were mixed. The former was heated at 773 K under oxygen stream for 40 h and the latter in an evacuated silica tube at 1073 K for 60 h. A structural analysis of the samples prepared was performed by X-ray diffraction (XRD) using monochrmatized Mo $K\alpha$ radiation (λ=0.70926 Å) and the atomic ratio was checked by X-ray fluorescent spectroscopy.

Electrical and Electrochemical Measurements. The electric resistivity of the sintered samples were measured using a four probe method in air at room temperature. The methanol electrooxidation experiments were carried out according to the method described elsewhere.[5]

X-Ray Photoelectron Spectroscopy Measurements. The XPS signals were obtained with an ESCA VG-III apparatus using Al $K\alpha$ radiation.

Results and Discussion

Preparation of Bronzes. The samples obtained were found to give powder XRD patterns different from those of the raw materials, except for the case of the Dy-Pt-S mixture. The XRD data have indicated that the oxides are crystallized in a $Na_xPt_3O_4$ type structure (cubic, $Pm3n$).[6] Preparation of the rare earth platinum or palladium oxide bronzes is the first case reported in so far as we know. The XRD data are listed in Table 1 and the phase relations are summarized in Table 2, together with those of the other chalcogenide systems Dy-M-X'. Since the oxide samples have been mixed with the remaining Dy_2O_3 and Pt (or Pd and PdO) or the reaction has not been stoichiometrically achieved, they are expected to be of the form $Dy_xM_3O_4$ with $x\leqq1$ and not DyM_3O_4. The lattice constants of the platinum and palladium oxide bronzes were determined by a least-square treatment to be a=5.665(3) and 5.651(2) Å, respectively. The

Table 1. X-Ray Diffraction Data for $Dy_xM_3O_4$ (M=Pt, Pd)

hkl	$Dy_xPt_3O_4$			$Dy_xPd_3O_4$		
	d_o/Å	d_c/Å	I/I_0	d_o/Å	d_c/Å	I/I_0
110	3.997	4.000	17	3.978	3.996	33
200	2.851	2.833	13	2.810	2.826	17
210	2.538	2.534	100	2.527	2.527	100
211	2.319	2.313	22	2.311	2.307	22
220	2.009	2.003	13	2.000	1.998	16
310	1.792	1.791	13	1.789	1.787	11
222	1.637	1.635	17	1.632	1.631	28
320	1.571	1.571	35	1.568	1.567	28
321	1.513	1.514	17	1.511	1.510	17
400	1.414	1.416	9	1.411	1.413	17

Table 2. Lattice Constant and Specific Resistivity of the Product Phases Prepared from Dy : M : X = 1 : 3 : 4 Mixtures

X	Lattice constant/Å		$\rho/10^{-5}$ Ω cm	
	Pt	Pd	Pt	Pd
O	a=5.665(3) Å[a] (Dy_2O_3, Pt)	a=5.651(2) Å[a] (Dy_2O_3, PdO, Pd)	1.9	2.6
S	(PtS)[b]	a=6.646(2) Å[a]	110	1.4
Se	Unknown	Unknown	1.0	0.8
Te	Unknown	Unknown	0.3	0.3

a) These are isostructural with $Na_xPt_3O_4$.[6] Starting materials in parentheses remained as impurities. b) The phase is assigned according to the XRD powder file.[7]

observed fact that the lattice constant of the platinum oxide bronze is about 0.2% larger than that of palladium appears to be reasonable from the difference between their ionic radii.

The crystal structure of $Dy_xM_3O_4$ is shown in Fig. 1. Each Dy atom is located in the hole of M_3O_4 framework and is surrounded by 8 O atoms. The M_3O_4 framework consists of M–O bonds of which each M or O atom is linked to 4 O and 3 M atoms with 1.998—2.003 Å. Particularly, the M and O atoms form a coplanar square or a triangle configuration with O atoms and M, respectively, which allow the chemical bonds between M and O atoms via interactions of their dsp^2 and sp^2 hybrid orbitals, etc. These covalently bonded atom groups must be closely related to their electrical properties as described later.

For the sulfide systems, the Dy-Pt-S specimen gives only those XRD patterns which are derived from PtS. Thus, no bronze was likely to be formed under the experimental conditions employed. Exceptionally, however, the palladium sulfide bronze, $DyPd_3S_4$ was formed in a single phase, which did not contain starting materials as impurities. The crystal data [cubic, a=6.646(2) Å] corresponded with that of the lanthanum analogue [cubic, a=6.7394(1) Å][3] which is isostructural with $Na_xPt_3O_4$ as well as the above oxide bronzes.

On the other hand, the selenide and telluride specimens showed new XRD patterns (Table 3) which were not assigned as that of the $Na_xPt_3O_4$ type bronze nor of other selenides or tellurides of Dy, Pt, and Pd; their structures were not determined. However, since they showed a high electric conductivity characteristic of bronzes as described later and the atomic ratio determined by the X-ray fluorescent spectra agreed with that in the starting mixtures, the new XRD patterns might be derived from the DyM_3X_4 type bronzes.

Electric Conductivity. The specific resistivity data of the specimens are summarized in Table 2. They were found to be good electric conductors (ρ=0.3—2.6×10^{-5} Ω cm), except for the specimen in the Dy–Pt–S system (ρ=1.1×10^{-3} Ω cm). The results seem to be in harmony with their phase formations: The high conductivity is realized with the formation of bronzes whilie the Dy–Pt–S mixture [of which the major phase is PtS (semiconductor)] has low conductivity. Along this line, the formation of bronzes in the selenide and telluride systems may be suggested from their high conductivity, although their structure has not been identified by the XRD method.

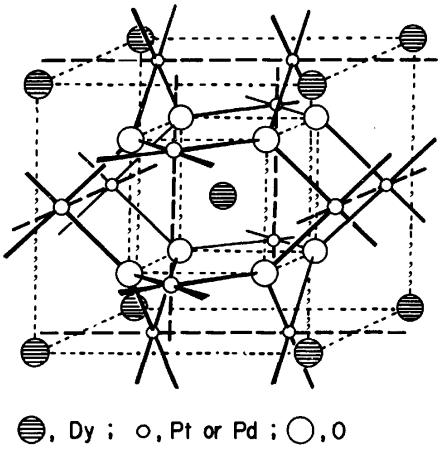

Fig. 1. Crystal structure of $Dy_xM_3O_4$ (M=Pt or Pd) based on the $Na_xPt_3O_4$ structure.[6]

X-Ray Photoelectron Spectroscopy. Typical XPS spectra of $Dy_xPt_3Se_4$ are shown in Fig. 2. The spectrum derived from Se 3 d electrons consisted of two bands at 52.8 and 57.1 eV, which might be assigned to those of Se^{2-} and Se^{4+} ions, respectively. The Pt 4f electrons gave two sets of XPS signals at 70.9—74.2 and 73.6—77.0 eV, which might be attributed to neutral Pt atoms and Pt^{2+} ions, respectively. Since H_2SeO_3 and Pt have never been detected on the XRD pattern of $DyPt_3Se_4$, such ionic species are likely to be formed only near the surface by hydrolysis with moisture in air. For the dysprosium, a broad band at about 153.0 eV was observed which might be originated from the 4d electrons of Dy^{3+} ions. Similar valence relations among the elements were also observed on the other bronzes. Thus, the DyM_3X_4

Table 3. X-Ray Diffraction Data[a] for $DyPt_3X_4$ (X=Se, Te)

$DyPt_3Se_4$		$DyPt_3Te_4$	
d_0/Å	I/I_0	d_0/Å	I/I_0
7.53	5	11.95	12
5.47	68	5.94	100
5.10	100	5.26	51
3.81	4	3.96	6
3.42	6	2.959	5
3.28	10	2.907	21
3.24	8	2.856	42
2.996	14	2.594	5
2.935	15	2.396	9
2.780	21	2.140	12
2.730	60	2.094	16
2.673	13	2.042	13
2.646	13	1.998	7
2.552	8	1.745	5
2.471	13	1.658	5
2.384	6	1.576	13
2.344	15	1.560	7
2.093	6		
1.995	32		
1.924	5		
1.874	29		
1.815	46		
1.755	10		
1.699	5		

a) Similar XRD patterns were obtained for the $DyPd_3X_4$ bronze counterparts, respectively.

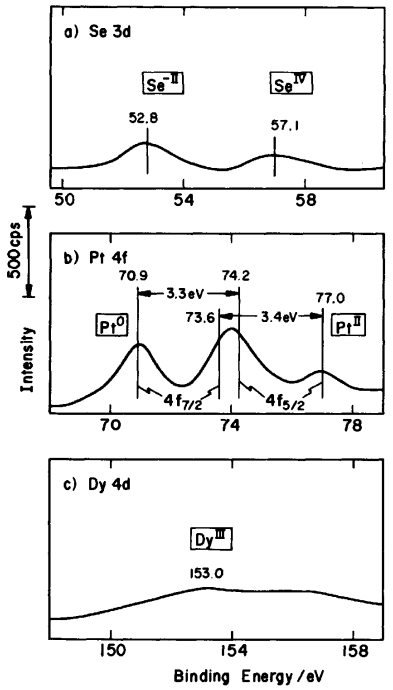

Fig. 2. X-Ray photoelectron spectra of Se 3d, Pt 4f, and Dy 4d electrons of $DyPt_3Se_4$.

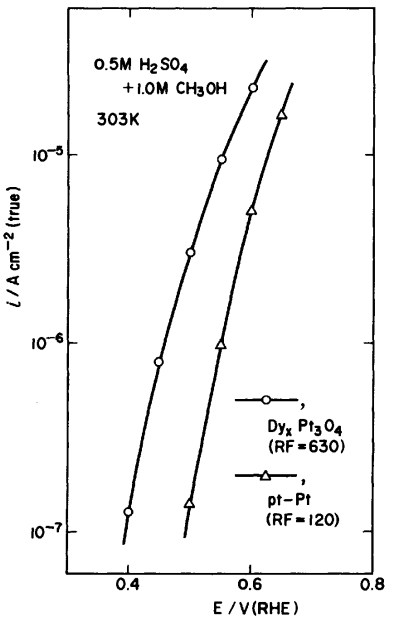

Fig. 3. Anodic polarization behaviours of the $Dy_xPt_3O_4$ and pt–Pt electrodes in methanol electrooxidation. *RF*: roughness factor.
0.5 M H_2SO_4+1.0 M CH_3OH, 303 K.

bronzes generally consist of the elements of Dy^{III}, M^{II}, and X^{-II}. Accordingly, these bronzes can generally be formulated as $[DyM_3X_4+e^-]$ and the resulting electrons are presumably sent to the conduction bands formed by the covalently bonded M_3O_4 framework. This model of supplying electrons can perhaps describe their metallic conductivity.

Methanol Electrooxidation Characteristics. The oxide bronzes, particularly $Dy_xPt_3O_4$, were found to have a high level of catalytic activity for the methanol electrooxidation. The other chalcogenide analogues were, however, unstable in acid solutions. The Tafel relation observed on a $Dy_xPt_3O_4$ electrode with the roughness factor (R_F; the value was determined by amounts of the under-potential hydrogen adsorption) of 630 is shown in Fig. 3, together with that of a platinized Pt (pt-Pt) electrode (R_F=120); the large R_F value of the bronze may be caused by the dissolution of one of the starting material, viz. Dy_2O_3, existed as an impurity in the bronze. The electrode showed the rest potential around 0.35 V (RHE) which was more negative, and hence suggested a better catalytic activity, than that of Pt itself at which it was usually 0.40—0.45 V. Indeed, the specific activity per true unit surface area of $Dy_xPt_3O_4$ was observed to be about one order of magnitude higher than that of ordinary Pt electrode.

References

1) D. B. Sepa, A, Damjanovic, and J. O' M. Bockris, *Electrochim. Acta*, **12**, 746 (1967); A. Damjanovic, D. B. Sepa, and J. O' M. Bockris, *J. Res. Inst. Catal., Hokkaido Univ.*, **16**, 1 (1968); B. Broyde, *J. Catal.*, **10** 13 (1968).

2) R. D. Shannon, T. E. Gier, P. F. Carcia, P. E. Bierstedt, R. B. Flippen, and A. J. Vega, *Inorg. Chem.*, **21**, 3372 (1982).

3) D. A. Keszler and J. A. Ibers, *Inorg. Chem.*, **22**, 3366 (1983).

4) a) J. O' M. Bockris and H. Wroblowa, *J. Electroanal. Chem.*, **7**, 428 (1964); b) K. J. Cathro, *J. Electrochem. Soc.*, **116**, 1608 (1969); c) M. M. P. Janssen and J. Moolhuysen, *Electrochim. Acta*, **21**, 869 (1976).

5) K. Machida, M, Enyo, I. Toyoshima, Y. Toda, and T. Masumoto, *Surf. Coatings Technol.*, **27**, 359 (1986).

6) a) J. Waser and E. D. McClanahan, Jr., *J. Chem. Phys.*, **19**, 413 (1951); b) J. Waser and E. D. McClanahan, Jr., *ibid.*, **20**, 199 (1952); c) A. F. Wells, "Structural Inorganic Chemistry," Clarendon, Oxford (1975), p. 456.

7) The file of X-ray powder diffraction standards by the American Society for Testing and Materials. Inorganic compounds: 18-972.

Kinetic Studies on Dehydrogenation Reaction of 5,6-Dihydro-2,4(1*H*,3*H*)-pyrimidinediones in Aqueous Solution Induced by Argon Arc Plasma or Hydrogen-Oxygen Flame

Hiroshi NARAOKA, Michiaki TAKASAKI, Shinya NOMOTO, and Kaoru HARADA*
Department of Chemistry, University of Tsukuba, Sakura, Niihari, Ibaraki 305
(Received June 13, 1986)

Synopsis. 5,6-Dihydro-2,4(1*H*,3*H*)-pyrimidinediones underwent dehydrogenation at the 5- and 6-position producing 2,4(1*H*,3*H*)-pyrimidinediones in aqueous solution induced by argon arc plasma or flames. From consideration based on the kinetic study of this reaction, it was found that abstraction of a hydrogen atom took place preferentially at the 6-position of the dihydropyrimidinediones.

Although various types of plasma chemistry have been reported,[1] most of these are chemical reactions in the gaseous phase or onto the solid phase. Few organic reactions in aqueous solution using plasma have been performed except for contact glow discharge electrolysis.[2] We recently reported a few aqueous-phase reactions induced by argon arc plasma or flames.[3-5] When argon arc plasma or flames of various gases mixed with oxygen were kept in contact with aqueous solution containing organic compounds, a very powerful and clean oxidation reaction took place without adding any oxidizing agent. For example, aliphatic amines were oxidized to amino acids,[3] and direct hydroxylation of aromatic rings proceeded in aqueous solution of phenyl-containing amino acids.[4] The active oxidizing species could be hydroxyl radicals which exist in flames, or which are produced by dissociation of water by high energy argon arc plasma.

In the present study, it was found that 5,6-dihydro-2,4(1*H*,3*H*)-pyrimidinediones underwent dehydrogenation at the 5- and 6-position producing 2,4(1*H*,3*H*)-pyrimidinediones in aqueous solution induced by argon arc plasma or flames. This paper reports the kinetics of the dehydrogenation and the reaction mechanism.

Results and Discussion

The substrates used here were 5,6-dihydro-5-methyl-2,4(1*H*,3*H*)-pyrimidinedione (**1a**), 5.6-dihydro-2,4(1*H*, 3*H*)-pyrimidinedione (**1b**) and 5,6-dihydro-6-methyl-2,4(1*H*,3*H*)-pyrimidinedione (**1c**) (Scheme 1). The time courses of the yield of product (**2c**) and the decay curves of the substrate (**1c**) are shown in Figs. 1 and 2, which were obtained by using argon arc plasma and hydrogen-oxygen flame, respectively. The yields of pyrimidinediones increased with the reaction time and then decreased because of the decomposition of the products. Table 1 shows the maximum yield and its reaction time for each substrate. The order of the maximum yields of the products are as follows: **2c>2b>2a**, in both energy sources.

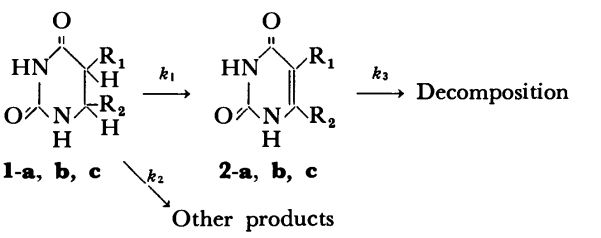

1a, 2a: $R_1=CH_3$, $R_2=H$ **1b, 2b**: $R_1=H$, $R_2=H$ **1c, 2c**: $R_1=H$, $R_2=CH_3$

Scheme 1.

Table 1. Maximum Yields and Thier Reaction Times for Each Substrate and the Energy Source

	1a-2a	**1b-2b**	**1c-2c**
Ar arc plasma	1.0% (40 min)	2.3% (60 min)	6.8% (40 min)
H_2-O_2 flame	2.4% (60 min)	4.0% (100 min)	6.4% (60 min)

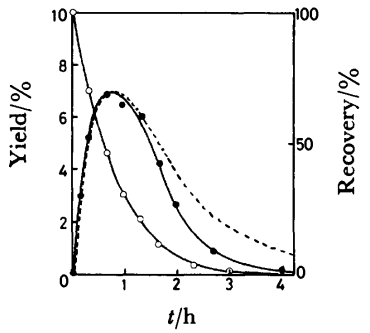

Fig. 1. The time course of the yield of **2c** through dehydrogenation reaction of **1c** by argon arc plasma; (○—○) **1c**, (●—●) **2c**.

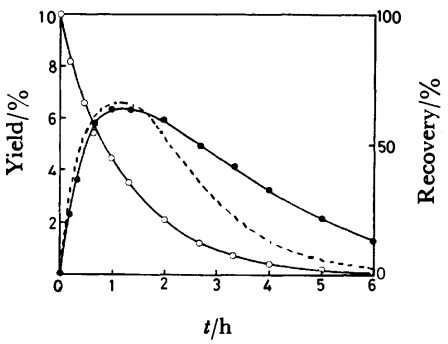

Fig. 2. The time course of the yield of **2c** through dehydrogenation reaction of **1c** by hydrogen-oxygen flame; (○—○) **1c**, (●—●) **2c**.

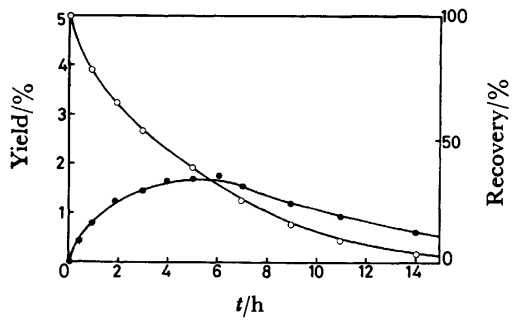

Fig. 3. The time course of the yield of **2b** through dehydrogenation reaction of **1b** by acetylene–oxygen flame; (O—O) **1b**, (●—●) **2b**.

This dehydrogenation reaction could proceed by the action of hydroxyl radicals, which were produced through dissociation of water molecule by high energy argon arc plasma, or transferred into the aqueous reaction mixture from the flames.[3–5] The dehydrogenation reaction was also effected by an acetylene(C_2H_2)–oxygen flame instead of a hydrogen–oxygen flame (Fig. 3). The rate of the dehydrogenation reaction with this flame was lower than that with a hydrogen–oxygen flame. This could be due to the lower hydroxyl radical abundunce in the acetylene–oxygen flame.

This reaction proceeded as a first-order reaction with respect to the decay of the substrate. This result was attributed to the large number of active species provided. Accordingly, it was also confirmed that the decay of the product proceeded as a first-order reaction from individual experiments. The reaction pathway could be explained as shown in Scheme 1, where k_1+k_2 and k_3 are the rate constants for the decay of the substrate and the product, respectively. The rate expression for the reaction is given by

$$\frac{d[P]}{dt} = k_1[DHP_0]e^{-(k_1+k_2)t} - k_3[P], \quad (1)$$

where [P] represents the concentration of the product, and [DHP_0] stands for the concentration of the substrate at t=0. Eq. 1 gives

$$[P] = -\frac{k_1}{k_1+k_2}[DHP_0](e^{-(k_1+k_2)t}-1) - k_3\int_0^t [P]dt. \quad (2)$$

The value of k_1+k_2, k_3, and k_1 are shown in Table 2. The theoretical curves are represented in Fig. 1 and Fig. 2 by dotted line, using Eq. 3 which is obtained from Eq. 1.

$$[P] = \frac{k_1}{k_3-k_1-k_2}[DHP_0](e^{-(k_1+k_2)t}-e^{-k_3t}). \quad (3)$$

The value of $k_1/(k_1+k_2)$, which represents the ratio of the dehydrogenation reaction, are shown in Table 2. It is apparent that the ratio of $k_1/(k_1+k_2)$ on **1c** was higher than that of others. These results show that the dehydrogenation reaction of **1c** took place easier than the others.

It has been known that the radical abstraction of a hydrogen atom is observed at the site with higher electron density.[6] For the substrates used, the electron density is lower at the 5-position than at the 6-position owing to the electron-withdrawing effect of a carbonyl group at the 4-position. In addition, in the case of **1c**, the electron density at the 6-position should be highest owing to the inductive effect of the methyl group.

Based on the considerations mentioned above, the experimental results suggest that the preferential redical abstraction took place at the 6-position. Therefore, **1c** had the highest value of $k_1/(k_1+k_2)$.

The chemical reactions in aqueous solution induced by flames or argon arc plasma are a new type of chemistry. The reaction is also interesting from the chemical evolutionary point of view. The reaction could be regarded as a model for the solar plasma-induced reaction in the primitive hydrosphere, when the primitive Earth had no magnetic field and low atmospheric pressure.

Table 2. Rate Constants of Dehydrogenation Reaction for Each Substrate and Energy Source

Substrates	Rate constants (min^{-1})			$k_1/(k_1+k_2)$
	k_1+k_2[a]	k_3[b]	k_1[c]	
1a–2a*	2.02×10^{-2}	2.14×10^{-2}	6.38×10^{-4}	0.032
1b–2b*	2.11×10^{-2}	2.04×10^{-2}	1.07×10^{-3}	0.028
1c–2c*	1.97×10^{-2}	2.06×10^{-2}	3.73×10^{-3}	0.19
1a–2a**	1.33×10^{-2}	3.03×10^{-2}	1.21×10^{-3}	0.096
1b–2b**	1.25×10^{-2}	2.94×10^{-2}	1.63×10^{-3}	0.16
1c–2c**	1.27×10^{-2}	2.76×10^{-2}	3.59×10^{-3}	0.28

* Ar arc plasma. ** H_2–O_2 flame.

a) The values k_1+k_2 were obtained from the data up to 80 min after the begining of the reaction for both argon arc plasma and hydrogen-oxygen flame. b) The values k_3 were obtained from the data up to 80 min or 40 min after the begining of the reaction for argon arc plasma or hydrogen-oxygen flame, respectively. c) Using Eq. 2, the values of k_1 were estimated by averaging the values of each 20 min after 20 min up to 80 min or 180 min of the reaction, carried out by argon arc plasma or hydrogen-oxygen flame, respectively. The term $\int_0^t [P]dt$ was estimated by the area of the figure in comparison with that of a standard.

Experimental

Materials. Compound **1b** was prepared by the method of Dakin.[7] Other substrates were commercial products. Their purities were checked by high performance liquid chromatography (HPLC).

Apparatus and Procedures. The apparatus used is shown in Fig. 4. The plasma torch used for the plasma induced reaction was a non-transferred type plasma torch (Nippon Welling Co., Wellpen NP-7). The conditions to produce plasma jet were: argon, 1.5 dm^3 min^{-1}; electric current, 40 A; electric voltage, 15 V. The plasma torch was immersed into the solution of the substrate 1 cm below the surface and the plasma jet was directly applied into the solution. The flame used in the dehydrogenation reaction was a hydrogen–oxygen flame, and the flow rates of gas

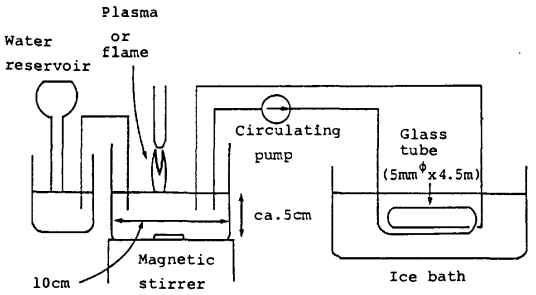

Fig. 4. Apparatus for the plasma- or flame-induced reaction.

($dm^3\ min^{-1}$) were 1.5 (hydrogen) and 0.8 (oxygen). A flame from a burner nozzle was blown onto the solution 3 cm above the surface. The temperature of the solution was kept at 40—50 °C throughout the reaction by circulating the solution through a glass tube immersed in an ice bath. The concentration of the substrates were 2.5×10^{-2} mol dm^{-3} and the volumes of the reaction mixture were 0.3 and 0.5 dm^3 for the flame and plasma, respectively. At appropriate time intervals, 0.5 ml aliquots of the solution were withdrawn and analyzed with HPLC. The column used for HPLC was Finepak C_{18} (JASCO 4.6 mm i.d.×25 cm; eluent: H_2O–CH_3OH) and UV detector (230 nm) was used. Quantitative analyses were carried out by comparison with authentic samples.

References

1) J. D. Hollahan and T. Bell, "Techniques and Application of Plasma Chemistry," Wiley-Interscience, New York (1974).

2) K. Harada, "Molecular Evolution and Protobiology," ed by K. Matsuno, K. Dose, K. Harada, and D. L. Rohlfing, Plenum Press, New York (1984), p. 83.

3) S. Nomoto, M. Takasaki, N. Sakata, and K. Harada, *Tetrahedron Lett.*, **24**, 3357 (1983).

4) M. Takasaki and K. Harada, *Tetrahedron Lett.*, **25**, 885 (1984).

5) M. Takasaki and K. Harada, *Tetrahedron*, **41**, 4463 (1985).

6) G. A. Russel, "Free Radicals," ed by J. K. Kochi, John Wiley and Sons, New York (1973), Vol 1, p. 275.

7) H. D. Dakin, *Am. Chem. J.*, **44**, 48 (1910).

Preparation and Structures of Acetylene Adducts of 4,6-*O*-Isopropylidene- and 4-*O*-Acetyl-6-*O*-triphenylmethyl-1,5-anhydro-2-deoxy-D-*erythro*-hex-1-en-3-uloses[1)]

Takanao MATSUI,* Takashi MOROOKA, and Mitsuru NAKAYAMA†
Faculty of Engineering, Miyazaki University, Kumano, Miyazaki 889-21
†Department of Agricultural Chemistry, College of Agriculture, University of Osaka Prefecture, Sakai, Osaka 591
(Received June 23, 1986)

Synopsis. Cyclobutene adducts were formed stereoselectively in good yields by the irradiation of acetone solutions of 4,6-*O*-isopropylidene- and 4-*O*-acetyl-6-*O*-triphenylmethyl-1,5-anhydro-2-deoxy-D-*erythro*-hex-1-en-3-uloses, derived from D-glucal triacetate, in the presence of acetylene. The stereochemistry at the ring junction was achieved by a single-crystal X-ray analysis and a chemical correlation with the derived compounds.

Carbohydrate enones can be used to produce chiral compounds with four- and six-membered rings by the photochemical addition and Diels–Alder reaction of olefins, although in certain cases there are problems of regio- and stereochemical-selectivity in cycloadduct formation. In recent reports,[2)] Fraser-Reid et al. have demonstrated that annulated pyranosids obtained from carbohydrate α-enones can be converted into a variety of natural products and analogues. We have been concerned with the use of an enone system in pyranone compounds in order to prepare thermal and photochemical cycloadducts, e.g., the Diels–Alder adducts[3)] of methyl 2-oxo-2*H*-pyran-5-carboxylate with isoprene and the acetylene adducts[1)] of 7-methoxychromone, which are rearranged to cyclic skeletons and transformed into aromatic compounds.[1,4)] In the present investigation, conversions of carbohydrates into the chiral pyranone compounds and the use of their enone systems in cycloaddition reactions have been studied. This paper describes how photochemical reactions of 4,6-*O*-isopropylidene- and 4-*O*-acetyl-6-*O*-triphenylmethyl-1,5-anhydro-2-deoxy-D-*erythro*-hex-1-en-3-uloses (**1** and **2**), derived from readily available D-glucal triacetate,[5)] with acetylene gave stereoselectively the optically active cyclobutene adducts (**3** and **4**); the stereochemistry of the products was revealed by a single-crystal X-ray analysis and a chemical correlation.

Irradiation of **1** in an acetone solution saturated with a stream of acetylene by means of a 500-W high-pressure mercury lamp afforded [2+2]-cycloadduct (**3**) as a single compound in 81% yield. The single-crystal X-ray analysis confirmed the syn relationship of the cyclobutene ring to the proton at the C-5 position,[6)]

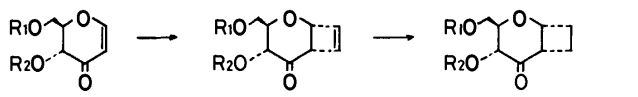

1 $R_1+R_2=C(CH_3)_2$ 3 $R_1+R_2=C(CH_3)_2$ 5 $R_1=H$, $R_2=Ac$
2 $R_1=CPh_3$, $R_2=Ac$ 4 $R_1=CPh_3$, $R_2=Ac$ 6 $R_1=CPh_3$, $R_2=Ac$
7 $R_1=R_2=H$
8 $R_1+R_2=C(CH_3)_2$

Scheme 1.

indicating that acetylene approaches from the least hindered side of the molecule. Under similar conditions, enone **2** underwent a photochemical cycloaddition with acetylene to give the same type adduct (**4**) in 75% yield. The structural proof of **4** was based on a chemical correlation with **3**. That is, treatment of **4** with H_2 over Pd-C followed by deacetylation of the resulting cyclobutane acetate (**5**) afforded cyclobutane diol (**7**), which was identical in all respects with the product obtained from **3** (Scheme 1). Thus, the stereoselectivity of these cycloadditions seems to derive from the steric influence of the isopropylidene and triphenylmethyl substituents that blocks approach of acetylene from the β-face of the enone molecules.

As an application, we have examined the photochemical behavior of **3** and **4** having a bicyclic β,γ-unsaturated ketone system.[8)] When both **3** and **4** were irradiated in acetone and acetonitrile, the photoreduction products **8** and **6** were obtained in detectable amounts (27 and 20% yields), which were identical with the samples prepared by isopropylidenation of **7** and isolated from catalytic hydrogenation of **4**, respectively.

Experimental

Melting points are uncorrected. IR spectra were measured in $CHCl_3$ with a Hitachi 260-50 spectrophotometer. ^1H and ^{13}C NMR spectral data were obtained in $CDCl_3$ on a JEOL JNM-PMX 60 spectrometer and a JEOL JNM-FX 60 Fourier transform spectrometer, respectively. Chemical shifts are

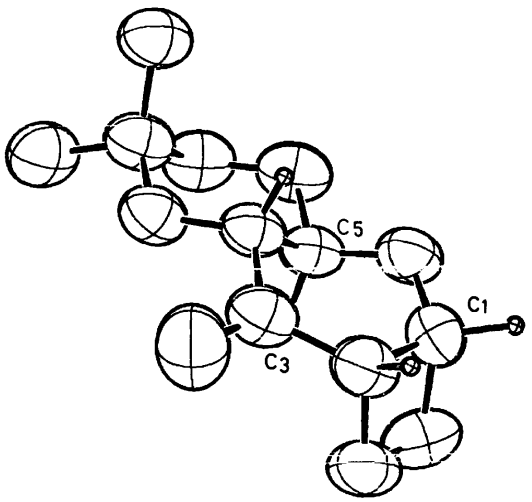

Fig. 1. ORTEP drawing of the molecular structure of **3**.[7)]

reported in δ values (ppm) downfield from an internal TMS reference. The mass spectra were measured with a JEOL JMS-D 300S spectrometer. Optical rotations were taken on a JASCO DIP-SL polarimeter. X-Ray diffraction data were obtained on an Enraf-Nonius CAD-4 automated four-circle diffractometer with a SDP program package. All irradiations were carried out with a 500-W high-pressure mercury lamp (Eikosha EHB-WI-500).

Photoaddition of Acetylene to 4,6-*O*-Isopropylidene- and 4-*O*-Acetyl-6-*O*-triphenylmethyl-1,5-anhydro-2-deoxy-D-*erythro*-hex-1-en-3-uloses (1 and 2). (a) To 1. A solution of **1** (120 mg) in dry acetone (250 ml) was irradiated through a Pyrex filter at room temperature for 30 min under a continuous introduction of acetylene. The removal of the solvent under reduced pressure and chromatography of the residue on silica gel using hexane-ethyl acetate (4:1) as eluent gave **3** (112 mg, 81% yield); mp 117—118.5 °C (hexane-ethyl acetate); $[\alpha]_D^{24}$ +103° (*c* 0.54 in EtOH); IR: 1725, 1390, 1380, and 1125 cm^{-1}; ^1H NMR δ=1.51 (6H, s, -C(CH$_3$)$_2$), 3.7—4.4 (5H, m), 5.14 (1H, d, *J*=2 Hz, -OCHCH=), and 6.2—6.4 (2H, m, -CH=CH-); ^{13}C NMR δ=18.6, 28.6, 55.9, 62.4, 63.2, 75.4, 77.6, 100.2, 137.0, 140.0, and 200.1; MS: *m/z* 210 (M^+); Found: C, 62.85; H, 6.92%. Calcd for $C_{11}H_{14}O_4$: C, 62.84; H, 6.71%.

(b) To 2. A solution of **2** (200 mg) in dry acetone (600 ml) was irradiated through a Pyrex filter at room temperature for 30 min under a continuous introduction of acetylene. After removing the solvent, the residue was subjected to column chromatography on silica gel using hexane-ethyl acetate (9:1) as eluent to afford **4** (158 mg, 75% yield); mp 157—158 °C (hexane-acetone); $[\alpha]_D^{24}$ +187° (*c* 0.53 in EtOH); IR: 1745, 1720, and 1600 cm^{-1}; ^1H NMR δ=1.78 (3H, s, OAc), 2.97 and 3.36 (each 1H, dd, *J*=3 and 10 Hz, -CH$_2$OCPh$_3$), 3.66 (1H, d, *J*=4 Hz, -COCH-), 4.10 (1H, dt, *J*=3 and 10 Hz, Ph$_3$COCH$_2$CH-), 5.05 (1H, d, *J*=4 Hz, -OCHCH=), 5.23 (1H, d, *J*=10 Hz, -CHOAc), 6.08 (2H, s, -CH=CH-), and 7.0—7.5 (15H, m, 3×Ph); ^{13}C NMR δ=20.3, 55.9, 62.1, 69.5, 74.9, 127.0, 127.1, 127.9, 128.8, 129.7, 137.0, 140.9, 143.6, 169.1, and 200.3; MS: *m/z* 454 (M^+); Found: C, 76.57; H, 5.91%. Calcd for $C_{29}H_{26}O_5$: C, 76.63; H, 5.77%.

Conversion of 3 and 4 to 7. (a) From 3. A mixture of **3** (100 mg) and 5% Pd-C (25 mg) in ethanol (15 ml) was stirred under a hydrogen atmosphere at room temperature for 90 min until it absorbed ca. 18 ml of H_2. The catalyst was removed by filtration and the solvent was evaporated to give an oil (100 mg); this was chromatographed on silica gel using benzene-ethyl acetate (1:1) as eluent to afford **7** (colorless oil, 80 mg). IR: 3600, 3500, and 1715 cm^{-1}; ^1H NMR δ=1.6—2.6 (4H, m, -CH$_2$CH$_2$-), 2.84 (2H, bs, 2×OH), 3.0—3.6 (1H, m, -COCH-), 3.72 (1H, dd, *J*=3 and 10 Hz, -OCHCH$_2$OH), 3.91 (2H, d, *J*=3 Hz, -CH$_2$OH), 4.37 (1H, d, *J*=10 Hz, -CHOH), and 4.90 (1H, dd, *J*=8 and 15 Hz, -OCH-); MS: *m/z* 173 ([M+1]$^+$).

Isopropylidene Derivative (8) of 7. *p*-Toluenesulfonic acid (43 mg) was added to a mixed solution of **7** (110 mg), 2,2-dimethoxypropane (10 ml) and dry *N*,*N*-dimethylformamide (0.5 ml), and then the mixture was stirred at room temperature for 50 min. A usual work-up and purification by silica-gel column chromatography (hexane-ethyl acetate, 9:1) gave **8** in 32% yield; mp 138—139 °C (hexane-ethyl acetate); IR: 1730, 1390, and 1380 cm^{-1}; ^1H NMR δ=1.54 (6H, s, -C(CH$_3$)$_2$), 1.7—2.7 (4H, m, -CH$_2$CH$_2$-), 3.0—3.5 (1H, m, -COCH-), 3.8—4.5 (2H, m, -OCHCHO-), 3.93 (2H, d, *J*=3 Hz, -OCH$_2$-), and 4.84 (1H, dd, *J*=8 and 15 Hz, -OCH-); MS: *m/z* 212 (M^+); Found: C, 62.24; H, 7.75%. Calcd for $C_{11}H_{16}O_4$: C, 62.25; H, 7.60%.

(b) From 4. A mixture of **4** (200 mg) and 5% Pd-C (120 mg) in ethyl acetate (20 ml) was stirred with H_2 at room temperature for 17 min. After ca. 20 ml of H_2 had been consumed, a similar work-up to that described above gave 210 mg of oily product, which was chromatographed on silica gel using hexane-ethyl acetate (98:2, 95:5, and 50:50) as developing agent to afford triphenylmethanol (75 mg), **6** (65 mg), and **5** (60 mg) in the order of elution. **5**: Colorless oil; IR: 3580, 3500, 1740, and 1720 cm^{-1}; ^1H NMR δ=1.5—2.7 (4H, m, -CH$_2$CH$_2$-), 2.21 (3H, s, OAc), 3.0—3.4 (2H, m, -COCH- and OH), 3.80 (2H, d, *J*=2 Hz, -CH$_2$OH), 4.07 (1H, dt, *J*=2 and 10 Hz, -CHCH$_2$OH), 4.87 (1H, dd, *J*=7 and 15 Hz, -OCH-), and 5.23 (1H, d, *J*=10 Hz, -CHOAc). **6**: Mp 130—131 °C (ethanol); IR: 1740, 1730, 1600, 1490, and 1450 cm^{-1}; ^1H NMR δ=1.90 (3H, s, OAc), 1.5—3.3 (5H, m, -CH$_2$CH$_2$- and -COCH-), 3.11 and 3.42 (each 1H, dd, *J*=3 and 10 Hz, -CH$_2$OCPh$_3$), 4.01 (1H, dt, *J*=3 and 10 Hz, Ph$_3$COCH$_2$CH-), 4.81 (1H, dd, *J*=8 and 14 Hz, -OCH-), and 5.34 (1H, d, *J*=10 Hz, -CHOAc). Alkaline hydrolysis of **5** (25 mg of **5**, 5 ml of methanol, 55 mg of Na_2CO_3, and stirring at room temperature for 25 h) gave **7** which was identical with the above material.

Irradiation of 3. A solution of **3** (203 mg) in anhydrous acetone (500 ml) was irradiated through a Pyrex filter at room temperature for 60 min. After removing the solvent, the residue was chromatographed on silica gel using hexane-ethyl acetate (7:3) as an eluent to afford **8** (55 mg, 27% yield); this was identical in all respects with the sample prepared by isopropylidenation of **7**.

Irradiation of 4. Irradiation of a solution of **4** (200 mg) in anhydrous acetonitrile (600 ml) through a Pyrex filter at room temperature for 30 min, followed by a silica-gel column chromatographic work-up of the residual oil using hexane-ethyl acetate (95:5) as an eluent afforded **6** (40 mg, 20% yield); this was identical with the compound previously obtained from the catalytic hydrogenation of **4**.

We wish to thank the Research Center for Material Analysis in Miyazaki University for the NMR and MS measurements and the X-ray crystallographic analyses.

References

1) This work is Part 3 of "Cycloadditions in Pyrones," Part 2: T. Matsui and M. Nakayama, *Bull. Chem. Soc. Jpn.*, **56**, 3531 (1983).

2) B. J. Fitzsimmons and B. Fraser-Reid, *Tetrahedron*, **40**, 1279 (1984) and references therein.

3) T. Matsui, T. Inoue, M. Nakayama, and J. D. White, *Bull. Chem. Soc. Jpn.*, **56**, 647 (1983); M. Nakayama, J. Kuramoto, T. Matsui, and J. D. White, *Bull. Chem. Soc. Jpn.*, **58**, 3051 (1985).

4) T. Imagawa, T. Nakagawa, M. Kawanisi, and K. Sisido, *Bull. Chem. Soc. Jpn.*, **52**, 1506 (1979).

5) C. D. Hurd and H. Jenkins, *Carbohydr. Res.*, **2**, 240 (1966); W. Roth and W. Pigman, "Methods in Carbohydr. Chem.," ed by R. L. Whistler, M. L. Wolfrom, and J. N. BeMiller, Academic Press, New York (1963), Vol. 2, pp. 405—408.

6) The final Fo and Fc data are deposited at the Office of the Editor of the Bulletin of the Chemical Society of Japan (Document No. 8716).

7) C. K. Johnson, ORTEP. Oak Ridge National Laboratory Report ORNL-3794 (1965).

8) For photorearrangement examples of β,γ-unsaturated carbonyl systems, an oxa-di-π-methane rearrangement of an acyclic β,γ-unsaturated ketone (W. G. Dauben, M. S. Kellogg, J. I. Seeman, and W. A. Spitzer, *J. Am. Chem. Soc.*, **92**, 1786 (1970)) and a construction of the bicyclobutane compound from 5-methoxy-2a,8a-dihydro-8*H*-benzo[*b*]cyclobuta[*e*]pyran-8-one (see Ref. 1).

Kinetic Studies on the Oxidation of Thiols by Coenzyme PQQ

Shinobu ITOH, Nobuyuki KATO, Minae MURE, and Yoshiki OHSHIRO*
Department of Applied Chemistry, Faculty of Engineering, Osaka University,
Yamadaoka 2-1, Suita, Osaka 565
(Received July 14, 1986)

Synopsis. Kinetic studies on the oxidation of thiols by coenzyme PQQ are carried out under anaerobic conditions. A bell shaped pH-rate profile having a maximum rate at around pK_a of the thiol is observed. The rate-determining step changes between acidic and basic sides of the profile indicating the existence of at least one intermediate in the course of the reaction.

Mercapto groups are important in biological systems due to the widespread occurrence of this functional group in many proteins and in natural compounds such as glutathione, cysteine, coenzyme A, and lipoic acid. In particular, reversible oxidation-reduction to the disulfide stage is an essential process in such systems, and thus mechanistic details on the oxidation of thiols by flavins have been demonstrated.[1,2] On the other hand, we have found that coenzyme PQQ (4,5-dihydro-4,5-dioxo-1*H*-pyrrolo[2,3-*f*]-quinoline-2,7,9-tricarboxylic acid) is an efficient catalyst in air oxidation of thiols.[3] In this paper, we wish to report the kinetic studies on the reaction between PQQ and thiols.[4]

Results and Discussion

Treatment of PQQ (3.4×10^{-2} mmol) and 10-fold excess of benzenethiol in 20% CH_3CN neutral aqueous solution under anaerobic conditions gave $PQQH_2$ (4,5-dihydroxy-1*H*-pyrrolo[2,3-*f*]quinoline-2,7,9-tricarboxylic acid, 84%) and diphenyl disulfide (99% based on PQQ) as shown in Eq. 1. This reaction was followed spectrophotometrically under pseudo-first-order conditions ([PQQ] ≪ [PhSH], Fig. 1). PQQ was reduced rapidly to $PQQH_2$ with isosbestic points at 274, 336, and 399 nm at pH* 4.65 (see Experimental), and the reaction followed pseudo-first-order rate law up to 90% conversion (Fig. 2). When the concentration of the thiol was kept constant and the pH* was varied using 0.05 M acetate, phosphate, and carbonate (containing 20% CH_3CN, μ=0.2 with KCl), it was found that a plot of log k_{obsd} vs. pH* exhibited a "bell-shaped curve" (Fig. 3). Interestingly, the reaction was found to be first-order in benzenethiol concentration at the acidic side of the bell-shaped curve (pH* 6.3), while it was second-order in benzenethiol concentration at the basic conditions (pH* 9.9) as shown in Fig. 4. This result shows an evidence for a change in rate-determining step between the acidic and the basic conditions. This implies the existence of at least one intermediate, and all one-step mechanisms such as a net hydride transfer may be ruled out.

From these results, we assume the following reaction path (Eq. 2).

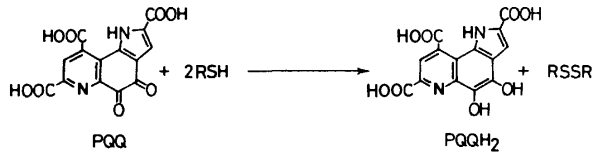

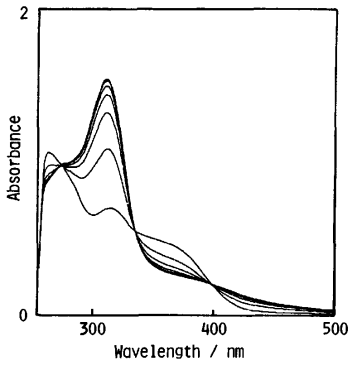

Fig. 1. Sepctral change along the progress of the oxidation of PhSH (4.0×10^{-3} M) by PQQ (4.0×10^{-5} M) in 0.05 M acetate buffer (pH* 4.65, μ=0.2 with KCl, 20% CH_3CN) at 30 °C under anaerobic conditions.

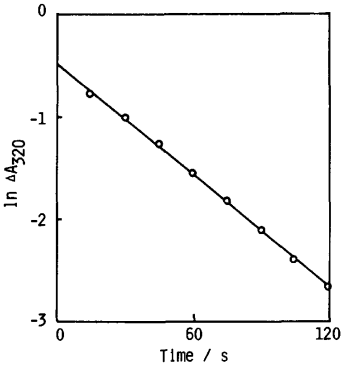

Fig. 2. Pseudo-first-order plot for the oxidation of PhSH by PQQ at pH* 4.65.

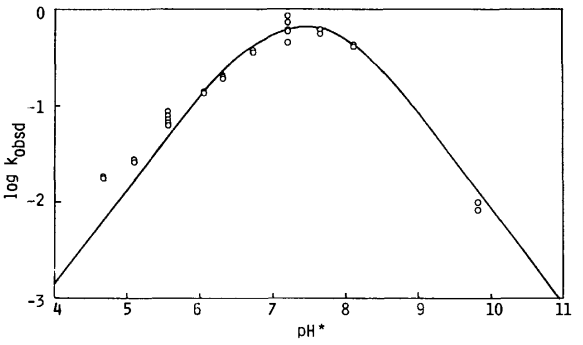

Fig. 3. The pH-rate profile for the oxidation of PhSH by PQQ.

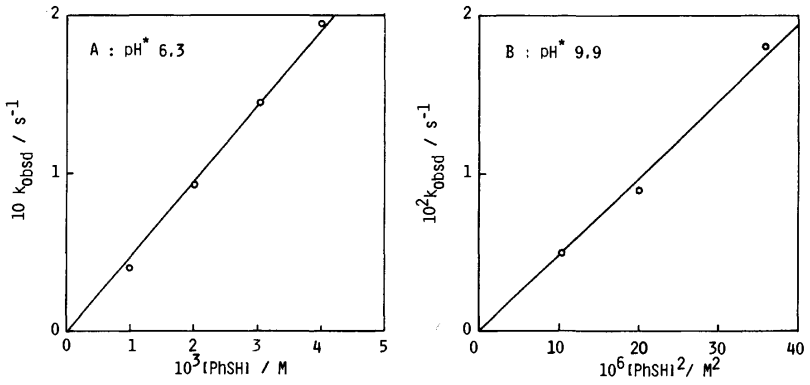

Fig. 4. Dependence of k_{obsd} on benzenethiol concentration at pH* 6.3 (A) and 9.9 (B).

$$PQQ \underset{k_{-1}}{\overset{k_1[RS^-]}{\rightleftharpoons}} I^- \underset{k_{-H}}{\overset{k_H[H^+]}{\rightleftharpoons}} IH \xrightarrow{k_2[RS^-]} PQQH^- + RSSR \quad (2)$$

(I: intermediate)

If it is assumed that protonation of I^- occurs rapidly relative to the establishment of the PQQ-I^- equilibrium ($k_H[H^+] \gg k_{-1}$), the rate law can be given as

$$k_{obsd} = \frac{k_1 k_2 K_a^2 a_H [RSH]_T^2}{k_{-1} K_H (K_a + a_H)^2 + k_2 K_a a_H (K_a + a_H)[RSH]_T} \quad (3)$$

where K_a is the apparent dissociation constant of benzenethiol and K_H is k_{-H}/k_H. Curve-fitting of Eq. 3 (solid line in Fig. 3) by using pK_a value (6.9) determined by spectrophotometric titration under the kinetic conditions provides the following values; k_1=325 $M^{-1}s^{-1}$, $k_2/k_{-1}K_H$=1.6×10^{10} M^{-2}. Using these values, kinetic behaviors mentioned above can be explained with this equation. Namely, under acidic conditions ($K_a \ll a_H$), Eq. 3 can be simplified to Eq. 4 in which k_{obsd} is proportional to $[RSH]_T$ and a_H^{-1}, respectively. On the other hand, under basic conditions ($K_a \gg a_H$), Eq. 5 is an approximated form where k_{obsd} is proportional to $[RSH]_T^2$ and a_H, respectively. Aliphatic thiols such as 2-mercaptoethanol, cysteine, and 1,4-butanedithiol were also oxidized rapidly at around their pK_as as shown in Table.

$$k_{obsd} = k_1 a_H^{-1} K_a [RSH]_T \quad (4)$$

$$k_{obsd} = k_1 k_2 k_{-1}^{-1} K_H^{-1} a_H [RSH]_T^2 \quad (5)$$

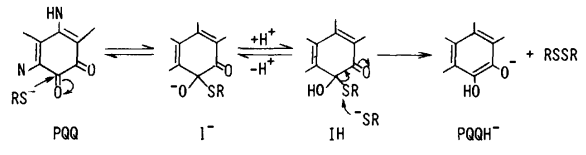

Scheme

From buffer dilution studies (0.1—0.5 M at pH* 6.3 and 9.9), it could be concluded that the oxidation of benzenethiol by PQQ is not subject to buffer catalysis. One of the possible mechanism is that involving C-5 attack of the thiolate ion followed by breakdown to reduced PQQ and the corresponding disulfide as shown in Scheme. In this mechanism, the first thiolate ion attack to the quinone is the rate-determining step under the acidic conditions, while the breakdown step is rate-determining under the basic conditions. It is well-known that C-5 quinone carbonyl of PQQ is easily attacked by nucleophiles.[5] Jencks and his co-worker have demonstrated that the addition of a thiolate ion to carbonyl group shows no general acid catalysis.[6] So there may be no general acid catalysis in the first thiolate ion attack to the quinone carbonyl. Further, the acid-base dissociation constant of the quinol group of $PQQH_2$ is determined to be 7.08×10^{-10} M (pK_a 9.15) by spectrophotometric titration. Thus, the breakdown step would not also be subject to general acid catalysis.

Table 1. Pseudo-First-Order Rate Constants for the Oxidation of Thiols by Coenzyme PQQ[a]

Thiol	pK_a	pH*	k_{obsd}/s^{-1} [b]
PhSH	6.9	7.2	6.5×10^{-1}
$HOCH_2CH_2SH$	9.7	9.8	8.1×10^{-2}
$HS(CH_2)_4SH$[c]	10.3	9.1	3.3×10^{-1}
$HOOCCH(NH_2)CH_2SH$	8.5	8.1	3.4×10^{-2}

a) [PQQ]=4.0×10^{-5} M, [thiol]=4.0×10^{-3} M, 0.05 M buffer solution (μ=0.2 with KCl, containing 20% CH_3CN) at 30 °C under anaerobic conditions. b) Average values of 3—5 kinetic runs. c) In 40% CH_3CN buffer solution.

Alternatively, free radical mechanism (one-electron transfer; I^-=PQQ^-) may be applicable since stepwise one electron oxidation of thiols is well documented.[7] In that case, however, the reactions at all pH region investigated should be first-order in benzenethiol concentration, since the PQQ semiquinone radical is well-known to be unstable to disproportionate rapidly to PQQ and $PQQH_2$ under these aqueous conditions.[8] If the PQQ semiquinone radical should be comparably stable, kinetics indicative of autocatalytic process would be observed. From these considerations, the ionic mechanism (Scheme) is preferable for the present oxidation.

Experimental

Kinetics. Kinetic measurements for the oxidation of thiols by PQQ were carried out under anaerobic pseudo-first-order conditions. An anaerobic 20% acetonitrile aqueous solution (1.5 ml) containing a thiol (8.0×10^{-3} M) was mixed with 1.5 ml of a 20% acetonitrile buffer solution (0.05 M acetate, phosphate, and carbonate, μ=0.2 with KCl) containing PQQ (8.0×10^{-5} M) under anaerobic conditions in a Thunberg cuvette. The reaction was followed by monitoring the appearance of $PQQH_2$ at 320 nm at 30 °C (Shimadzu UV-240 spectrophotometer equipped with a temperature controlled cell holder, Shimadzu TCC-240). The pH* is a corrected pH value by adding 0.11 to measured pH value in an aqueous buffer solution containing 20% CH_3CN.[9]

The present work was partially supported by a Grant-in-Aid for Co-operative Research (No. 60304027) from the Ministry of Education, Science, and Culture to which our thanks are due.

References

1) I. Yokoe and T. C. Bruice, *J. Am. Chem. Soc.*, **97**, 450 (1975).

2) E. L. Loechler and T. C. Hollocher, *J. Am. Chem. Soc.*, **102**, 7312, 7322, 7328 (1980).

3) S. Itoh, N. Kato, Y. Ohshiro, and T. Agawa, *Chem. Lett.* **1985**, 135.

4) Reoxidation of reduced PQQ by molecular oxygen has already been investigated; S. Itoh, Y. Ohshiro, and T. Agawa, *Bull. Chem. Soc., Jpn*, **59**, 1911 (1986).

5) R. H. Dekker, J. A. Duine, J. Frank, P. E. J. Verwiel, and J. Westerling, *Eur. J. Biochem.*, **125**, 69 (1982).

6) G. E. Liehard and W. P. Jencks, *J. Am. Chem. Soc.*, **88**, 3982 (1966).

7) Patai, S. "The Chemistry of the Thiol Group," Wiley; New York (1974).

8) Mixing of PQQ and $PQQH_2$ under appropriate anaerobic conditions did not give the semiquinone radical. Only under strongly alkaline conditions (pH 13), the semiquinone radical can be detected by UV-visible absorption spectroscopy: J. A. Duine, J. Frank, and P. E. J. Verwiel, *Eur. J. Biochem.*, **118**, 395 (1981).

9) G. Douheret, *Bull. Soc. Chim., Fr*, **1968**, 3122.

Influences of Lewis Acids on the Photochemical Cyclodimerization of Cyclopentenone

Takuji OGAWA,* Yoshiyuki MASUI, Shoshi OJIMA, and Hitomi SUZUKI*
Department of Chemistry, Faculty of Science, Ehime University, Bunkyo-cho, Matsuyama 790
(Received February 5, 1986)

Synopsis. In the presence of tin(IV) chloride, photochemical dimerization of cyclopentenone gave a cis-transoid-cis head-to-head dimer as predominant product. Other Lewis acids such as zinc(II) bromide, boron trifluoride etherate, tin(II) chloride, and silver(I) trifluoromethylsulfonate, however, showed little influence. Tris-(2,2,6,6-tetramethyl-3,5-heptanedionato)lanthanum(III) and tris(2,2,6,6-tetramethyl-3,5-heptanedionato)europium(III) affected regiochemistry of the reaction in a way to favor a head-to-tail dimer.

Photochemical (2+2) cycloaddition of cyclopentenones to form tricyclic ring systems has been widely used for the synthesis of natural products.[1] Since these tricyclic compounds are of difficult access via ordinary ionic reactions, photochemical route appears to be more attractive for their preparation. However, photochemical (2+2) cycloaddition is generally known to be difficult to control its regio- and/or stereochemistry and many possible isomers are formed together. In order to improve the selectivity, micellar effect[2] and salt effect[3] have been studied, but no satisfactory results have been obtained as yet. We thought that the coordinative ability of Lewis acids or lanthanoid complexes to carbonyl oxygen may be exploited to control the mode of photochemical cyclodimerization of cyclopentenon in solution.

Results and Discussion

Dry dichloromethane solutions containing 0.6 mol dm^{-3} cyclopentenone (**1**) and various amounts of tin(IV) chloride(**2**) were irradiated using a merry-go-round apparatus with a high-pressure mercury lamp under a nitrogen atmosphere. Product analyses were performed by gas chromatographic comparison with authentic samples[4] and typical results are tabulated in Table 1.

Table 1. Effect of $SnCl_4$ on the Photochemical Dimerization of Cyclopentenone

$SnCl_4$ mole ratio[a]	Time h	Conversion %	Yields/%[b] HH	HT	Ratio HH/HT
0.00	5.5	55	15	41	27/73
0.00	2.5	27	19	43	30/70
0.00	0.1	1	20	45	30/70
0.13	5.5	35	13	18	43/58
0.25	5.5	38	14	16	47/53
0.53	5.5	16	24	3	89/11
0.63	5.5	20	9	1	90/10

a) Mole ratio of $SnCl_4$/cyclopentenone. b) Yields are based on cyclopentenone consumed.

As a tendency, the yields of a cis-transoid-cis head-to-tail dimer (HT) decreased while those of a cis-transoid-cis head-to-head dimer (HH) increased as the

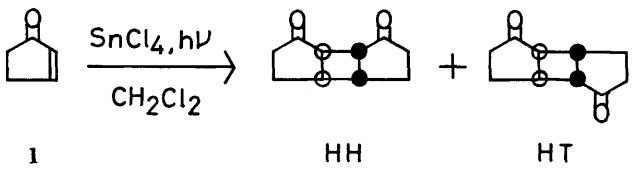

Scheme

Table 2. Relative Rate of Degradation of HH and HT Dimers in the Presence of **2**[a]

2 mole ratio[b]	Time h	Filter	HH %	HT[c] %	HH/HT ratio
0.0	0.0	None	33	67	33/67
0.0	5.0	None	0	34	0/100
0.5	5.0	None	7	38	16/84
0.0	5.5	$CuSO_4$[d]	10	56	15/85
0.5	5.5	$CuSO_4$[d]	20	59	25/75

a) About 0.1 mol dm^{-3} of HH and HT dimer solution in dichloromethane was irradiated and amounts of the dimers were determined by gas chromatography using xanthone as the internal standard. b) Mole ratio of $SnCl_4$/dimers. c) Amounts of HH and HT dimers remained. d) $CuSO_4$; 1 cm thickness of saturated $CuSO_4$ aqueous solution filter.

Table 3. Effect of Lewis Acids on the Photochemical Dimerization of Cyclopentenone

Lewis acid mole ratio[a]	Conversion %	Ratio HH/HT
$ZnBr_2$(0.13)	30	34/66
$ZnBr_2$(0.25)	30	35/65
$ZnBr_2$(0.50)	10	31/69
$BF_3 \cdot OEt_2$(0.30)	40	23/77
$BF_3 \cdot OEt_2$(0.55)	50	38/62
$SnCl_2$(0.50)	30	31/69
AgOTf(0.25)	34	37/63
AgOTf(0.50)	13	53/46
La(thd)$_3$(0.05)	25	20/80
Eu(thd)$_3$(0.05)	23	20/80

a) Mole ratio of the Lewis acid/cyclopentenone.
Tf=trifluoromethanesulfonate
thd=2,2,6,6-tetramethyl-3,5-heptanedionato

mole ratio (**2**/**1**) changed from zero to 0.53, the HH/HT ratios finally rising up to ca. 9.

Effect of **2** on the photodegradation of the dimers was also studied. No matter whether **2** was present or not, HH dimer was degraded faster than HT dimer (Table 2). Thus, the observed improvement of the selectivity cannot simply be attributed to the preferential degradation of HT dimer by **2**.

Total yields (HH+HT) were not so high and decreased as the conversion increased. It was because that the dimers underwent further photochemical reactions by absorbing light competitively with cyclopentenone.

With an expectation to increase yields by suppression of decomposition of the dimers, cyclopentenone solution was irradiated through $CuSO_4$ filter. HH dimer had the absorption maximum at 300 nm ($\varepsilon \fallingdotseq 60$) and $CuSO_4$ filter cut off lights shorter than 310 nm. As shown in Table 2, $CuSO_4$ filter suppressed the decomposition, although small amounts of dimers decomposed because of a small overlap of absorption edge of the dimers around 310—320 nm and light through $CuSO_4$ filter. However, the yields of dimers did not increase by using $CuSO_4$ filter, because absorption of cyclopentenone shifted to the shorter wavelength by coordination with **2** (Fig. 1) and cyclopentenone coordinate with **2** was not absorb light through $CuSO_4$ filter efficiently.

Effects of other Lewis acids such as zinc(II) bromide, boron trifluoride etherate, tin(II) chloride, and silver(I) trifluoromethanesulfonate were also examined in THF solutions. However, no significant influence of these Lewis acids was observed (Table 3). Acidity of these Lewis acids may be too weak to form such a rigid complex with **1** as to effect the regiochemistry.

When a low concentration of tris(2,2,6,6-tetramethyl-3,5-heptanedionato)lanthanum(III) ($La(thd)_3$; **3**) or tris(2,2,6,6-tetramethyl-3,5-heptanedionato)europium(III) ($Eu(thd)_3$; **4**) was added to the solution of **1** (mole ratio **3**/**1** or **4**/**1**=0.05), the ratio of regioisomers (HH/HT) decreased a little (Table 3). Addition of the increasing amount of **3** or **4** to the solution resulted in the formation of a complex of **1** with **3** or **4** which did not liberate **1** or its dimers at all under the conditions employed.

The results mentioned above are quite different from those observed in the cases of aromatic enones (cinnamate[5a] and coumarin[5b]). In the case of coumarin the quantum yield was highest when 0.125 equiv of boron trifluoride was present, and the predominant dimer was head-to-head in the absence of the Lewis acid, and head-to-tail in the presence of boron trifluoride. It is believed that the excited complex of coumarin with boron trifluoride reacts with another molecule of coumarin at the ground state, leading to the observed dependence of quantum yields on concentration.[5]

Contrarily, in the case of cyclopentenone small amounts of **2** (**2**/**1**=0.1—0.2) were not effective, and the addition of about 0.5 mol of **2** to 1 mol of **1** was necessary to achieve high HH/HT ratio (Table 1). Furthermore, the regiochemistry changed from head-to-tail to head-to-head by the addition of **2**. These results can be explained by an assumption that two molecules of cyclopentenone coordinate on one tin(IV) chloride from one side through the carbonyl oxygen atom and the photochemical dimerization occurs within the complex thus formed. Formation of 1:2 complex of **2** with **1** was supported by UV absorptivity change of **1** in the presence of various mole ratio of **2** (Fig. 2). The 1:2 complex formation is in consistent with the favored head-to-head regiochemistry in the presence of **2**, because the most favored conformation of two molecules of **1** in the complex would give the head-to-head dimer.

If the photochemical reaction occurs between the Lewis acid complex of **1** and non-coordinated **1**, the effect should be observed even at low Lewis acid/cyclopentenone ratio as was the case with coumarin. Coordinated cyclopentenone would be unable to react with ground state cyclopentenone by two reasons; small absorptivity of coordinated cyclopentenone as is shown in Fig. 1 and steric crowding around the tin(IV) atom.

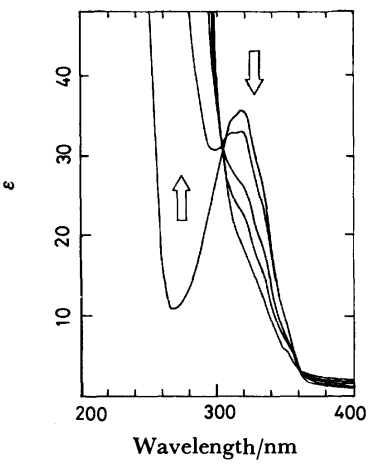

Fig. 1. UV absorption spectra of cyclopentenone in the presence of tin(IV) chloride.[a]
a) Arrows indicate the direction of spectral changes observed when 0.0 to ca. 0.5 mol ratio of $SnCl_4$ was added to a CH_2Cl_2 solution of cyclopentenone.

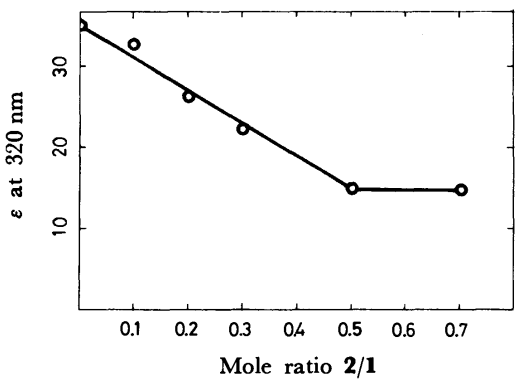

Fig. 2. Absorptivity change of **1** at 320 nm by adding various mole ratio of **2**.

Experimental

Materials. Cyclopentenone was prepared according to the reported method.[6] Tin(II) chloride, zinc(II) bromide, boron trifluoride etherate and silver(I) trifluoromethanesulfonate were commercial products and used as such. Lanthanoid complexes were prepared according to the literature method.[7] Dichloromethane was dried over P_2O_5, distilled under nitrogen, and stored with molecular sieves 3A.

Irradiation of Solutions. About 6 mmol of **1** and the Lewis acid were dissolved in 10 dm^{-3} of dry dichloromethane and were irradiatd under a nitrogen atmosphere in Pyrex tubes, using a 300-W high-pressure mercury arc lamp. In instances where equal irradiation of several samples was required, a merry-go-round apparatus was used.

Products Analyses. Dimer ratios and relative yields were analyzed by gas chromatography, using a 20% PEG-6000 (1 m) or 25% DEGS (1 m) column, and xanthone was used as an internal standard. Column temperature was 170 °C. Retention times of samples were as follows. In the case of PEG-6000: **1**, 11 min; HT, 27 min; HH, 38 min. In the case of DEGS: **1**, 3 min; HT, 6 min; HH, 9 min.

References

1) J. Kossanyi, *Pure Appl. Chem.*, **51**, 181 (1979).
2) K-H. Lee and P. de Mayo, *J. Chem. Soc., Chem. Commun.*, **1979**, 493.
3) R. Hoffman, P. Wells, and H. Morrison, *J. Org. Chem.*, **36**, 102 (1971).
4) P. E. Eaton, *J. Am. Chem. Soc.*, **84**, 2344 (1962).
5) a)F. D. Lewis and J. D. Oxman, *J. Am. Chem. Soc.*, **106**, 466 (1984); b)F. D. Lewis, D. K. Howard, and J. D. Oxman, *ibid.*, **105**, 3344 (1983).
6) M. Rosenblum, *J. Am. Chem. Soc.*, **79**, 3179 (1957).
7) K. J. Eisentraut and R. E. Sievers, "Inorganic Synthesis," (1968), Vol.11, p.94.

Syntheses of Steroidal *trans*-Iodo Acetates

C. Akira HORIUCHI* and J. Yasuo SATOH
Department of Chemistry, Rikkyo (St. Paul's) University, Nishi-Ikebukuro, Toshima-ku, Tokyo 171
(Received June 27, 1986)

Synopsis. The reaction of the following steroidal olefins with iodine–copper(II) acetate in acetic acid afforded the corresponding steroidal *trans*-iodo acetates: 5α-cholest-1-, -2-, and -3-ene; and 5β-cholest-1-, -2-, and -3-ene.

trans-1-Iodo-2-acetates are important as intermediates of Prévost reaction. There have been known many procedures for syntheses of *trans*-1-iodo-2-acetates, namely, *trans*-addition to olefins using iodine–silver(I) acetate,[1] *N*-iodosuccinimide–acetic acid,[2] iodine–mercury(II) acetate,[3] and iodine–thallium acetate.[4] Recently, Georgoulis and Valery[5] reported a convenient procedure for the preparation of vicinal alkoxy-iodoalkanes from alkene by means of copper(II) acetate and iodine. In part of the paper, they mentioned that the reaction of cyclohexene with iodine–copper(II) acetate in acetic acid yielded *trans*-iodo(acetoxy)cyclohexane.

We have been investigating a novel iodination method using iodine–copper(II) acetate; and as early steps in this research project, we have already reported the α-iodination of ketones;[6] the regioselective iodination of estradiol, estriol, and estrone;[7a,7b] a convenient procedure for iodination of electron-rich aromatic compounds;[8] and α-iodination of carboxylic acid.[9]

Now in the present paper, we would like to report that the reaction of the following steroidal olefins readily yielded the corresponding steroidal *trans*-iodo acetates: 5α-cholest-1- (**1**), -2- (**2**), and -3-ene (**3**); and 5β-cholest-1- (**4**), -2- (**5**), and -3-ene (**6**).

The reaction of 5α-cholest-1-ene (**1**) with iodine–copper(II) acetate in acetic acid at 60 °C for 10 h yielded the *trans*-iodo acetate (**7**), mp 113—114 °C. The NMR spectrum of **7** showed two multiplets due to the C_1- and C_2-proton at δ 4.46 (W/2=6.0 Hz) and 5.45 ppm (W/2=6.0 Hz), respectively. From this spectrum, however, it would not be determined the structure of **7**; and so the following procedure was carried out: The iodo acetate (**7**) was reduced with lithium aluminium hydride to give the 2β-hydroxyl derivative (**18**). By treating the iodo acetate (**7**) with potassium hydroxide, the 1β, 2β-epoxide (**13**) was obtained. From these results an acetoxyl group and an iodine atom of the iodo acetate were shown to be *trans*; this led to a 1α-iodo-2β-acetoxy-5α-cholestane structure for this iodo acetate. Similarly, 5α-cholest-2-ene (**2**) gave the 3α-iodo-2β-acetoxy derivative (**8**) (85%).[10] In the case of 5α-cholest-3-ene (**3**), a needle crystalline material (**9**), mp 83—85 °C was obtained. This product was presumed to be 3α-iodo-4β-acetoxy-5α-chlolestane on the basis of the NMR spectral data. The iodo acetate (**9**) was then converted to the 3β,4β-epoxide (**14**). The reaction of **9** with lithium aluminium hydride gave the 4β-ol derivative (**19**). Similarly, the reaction of 5β-cholest-1- (**4**) and -2-ene (**5**) gave 1β-iodo-2α-acetoxy- (**10**) and 3β-iodo-2α-acetoxy derivatives (**11**), respectively. These structures were determined from the NMR spectra and the chemical methods described above. The reaction of 5β-cholest-3-ene (**6**) gave *trans*-iodo acetate (**12**); mp 125—126 °C. The NMR spectrum showed a triplet (J=10.5 Hz) and a multiplet (W/2=15 Hz) at δ 4.50 and δ 5.02, respectively. By treating **12** with potassium hydroxide according to the method above, 3α, 4α-epoxide (**17**) was obtained. From this fact, *trans*-iodo acetate (**12**) was confirmed to be 4β-iodo-3α-acetoxy-5β-cholestane.

Moreover, the reaction is applicable to the synthesis of hindered *cis*-diols. The *trans*-iodo acetate (**8**) was converted with *m*-chloroperbenzoic acid to give 2β-acetoxy-5α-cholestan-3β-ol (**22**) (90%). Then the hydrolysis of **22** afforded the 2β,3β-diol (**23**) in good yield.

Thus, on the basis of all of the foregoing results, it can be concluded that the reagent used in this work [iodine–copper(II) acetate in acetic acid] is applicable to the steroidal olefins. In the reactions of 5α- and 5β-steroidal olefins with this reagent, the products in the case of the 5α-steroidal olefins were the α-iodo-β-acetoxy derivatives, in which the iodine attacked from the α-face; while the products in the case of the 5β-olefins were the β-iodo-α-acetoxy derivatives, in which the iodine attacked from the β-face. These results are also in agreement with the facts that the

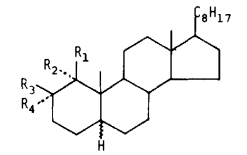

7: 5α-H, R_1=R_4=H, R_2=I, R_3=OAc
10: 5β-H, R_1=I, R_2=R_3=H, R_4=OAc

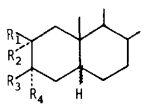

8: 5α-H, R_1=OAc, R_2=R_3=H, R_4=I
11: 5β-H, R_1=R_4=H, R_2=OAc, R_3=I

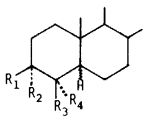

9: 5α-H, R_1=R_4=H, R_2=I, R_3=OAc
12: 5β-H, R_1=R_4=H, R_2=OAc, R_3=I

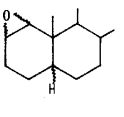

13: 5α-H, 1β,2β-O-
15: 5β-H, 1α,2α-O-

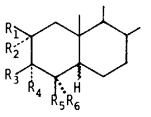

18: 5α-H, R_1=OH, R_2=R_3=R_4=R_5=R_6=H
19: 5α-H, R_1=R_2=R_3=R_4=R_6=H, R_5=OH
20: 5β-H, R_1=R_3=R_4=R_5=R_6=H, R_2=OH
21: 5β-H, R_1=R_2=R_3=R_5=R_6=H, R_4=OH
22: 5α-H, R_1=OAc, R_3=OH, R_2=R_4=R_5=R_6=H
23: 5α-H, R_1=R_3=OH, R_2=R_4=R_5=R_6=H

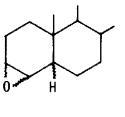

14: 5α-H, 3β,4β-O-
17: 5β-H, 3α,4α-O-

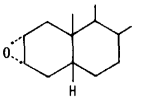

16

Table 1. Yields and Physical Data of *trans*-Iodo Acetates (**7**—**12**)

Materials	Products	Isolated yields/%	Mp θ_m/°C	IR (KBr, cm^{-1})	NMR (CCl_4, δ, ppm)	Elemental analysis/%	
1	**7**	80	113—114	1741 1240	2.05 (3H, s) 4.46 (1H, m, W/2=6.0 Hz) 5.45 (1H, m, W/2=6.0 Hz)	Found (Calcd for $C_{29}H_{49}O_2I$)	
						C	H
						63.03	9.05
						(62.58)	(8.87)
2	**8**	85	96—98 (lit, 96—97[10])	1744 1233	2.03 (3H, s) 4.54 (1H, m, W/2=7.0 Hz) 5.18 (1H, m, W/2=8.0 Hz)	62.60	8.92
3	**9**	76	83—85	1741 1231	2.03 (3H, s) 4.54 (1H, m, W/2=7.5 Hz) 5.18 (1H, m, W/2=7.5 Hz)	62.71	8.93
4	**10**	85	75—76	1740 1235	2.07 (3H, s) 4.99 (1H, m, W/2=6.0 Hz) 5.45 (1H, m, W/2=6.0 Hz)	62.39	8.89
5	**11**	79	87—88	1740 1233	2.06 (3H, s) 4.55 (1H, m, W/2=9.0 Hz) 5.10 (1H, m, W/2=9.0 Hz)	62.59	8.90
6	**12**	83	125—126	1741 1231	2.11 (3H, s) 4.50 (1H, t, J=10.5 Hz) 5.02 (1H, m, W/2=15.0 Hz)	62.42	8.84

α-face of 5α-steroidal olefins is less hindered than the β-face, and that the β-face of 5β-steroidal olefins is less hindered than the α-face.

Experimental

All the melting points are uncorrected. The IR and NMR spectra were measured using a Hitachi model 215 grating infrared spectrometer and a nuclear magnetic resonance spectrometer, Hitachi-Perkin Elmer R-20A, in carbon tetrachloride and deuteriochloroform, with TMS as the internal standard.

General Procedure. A mixture of steroidal olefin (1.349×10^{-3} mol), copper(II) acetate monohydrate (1.349×10^{-3} mol), iodine (1.349×10^{-3} mol), and acetic acid (50 ml) was stirred at 55—60 °C. After 10—30 h, the reaction mixture turned to brown; and then it was filtered to remove copper(I) iodide produced. The filtrate was taken up in ether, and the ether extracts were washed with sodium hydrogencarbonate solution and with water, and then dried and evaporated. Crystallization of the residue from ethanol gave *trans*-iodo acetate.

Confirmation of Configuration of 1α-Iodo-2β-acetoxy-5α-cholestane (7). The *trans*-iodo acetate (**7**) (180 mg) in dry ether (18 ml) was treated with lithium aluminium hydride (13 mg). After the usual work-up, the resulting oil, on crystallization from ethanol, gave 5α-cholestan-2β-ol (**18**) (140 mg), mp 161—163 °C (154—155 °C[16]).

The *trans*-iodo acetate (**7**) (20 mg) in ethanol was treated with potassium hydroxide. After the usual work-up, the resulting oil, on crystallization from ethanol, yielded 1β,2β-epoxy-5α-cholestane (**13**) (9 mg), mp 93—94 °C (94—95 °C[16]).

Confirmation of Configuration of 3α-Iodo-4β-acetoxy-5α-cholestane (9). By practically the same method as that in the case of **7** above, **9** (40 mg) was converted to 5α-cholestan-4β-ol (**19**) (17 mg), mp 131—133 °C (132—135 °C[17]) and 3β,4β-epoxy-5α-cholestane (**14**) (16 mg), mp 96—98 °C (98—99 °C[18]) respectively.

Confirmation of Configuration of 1β-Iodo-2α-acetoxy-5β-cholestane (10). The *trans*-iodo acetate (**10**) (70 mg) in dry ether was treated with lithium aluminium hydride. After the usual work-up, the resulting oil, on crystallization from ethanol, gave 5β-cholestan-2α-ol (**20**) (41 mg), mp 105—106 °C (106—107 °C[19]).

The *trans*-iodo acetate (**10**) (70 mg) in ethanol (10 ml) was treated with potassium hydroxide (76 mg). After the usual work-up, the resulting oil, on crystallization from ethanol, gave 1α,2α-epoxy-5β-cholestane (**15**) (45 mg); IR (KBr): 847 cm^{-1}, ^1H NMR (CCl_4) δ=2.63 (1H, d, J=3.6 Hz) and 3.05 (1H, m, W/2=6.75 Hz).

Found: C, 83.43; H, 11.89%. Calcd for $C_{27}H_{46}O$; C, 83.87 H, 11.99%.

Confirmation of Configuration of 3β-Iodo-2α-acetoxy-5β-cholestane (11). The *trans*-iodo acetate (**11**) (30 mg) in dry ether was treated with lithium aluminium hydride. After the usual work-up, the resulting oil, on crystallization from ethanol gave 5β-cholestan-2α-ol (**20**) (17 mg), mp 105—106 °C (106—107 °C[19]). The *trans*-iodo acetate (**11**) (70 mg) in ethanol was treated with potassium hydroxide. After the usual work-up, crystallization of the residue from ethanol gave 2α,3α-epoxy-5β-cholestane (**16**) (38 mg), mp 74—76 °C; IR (KBr): 810 and 800 cm^{-1}, ^1H NMR (CCl_4) δ=2.75—3.10 (2H, m).

Found: C, 83.50; H, 11.90%. Calcd for $C_{27}H_{46}O$; C, 83.87 H, 11.99%.

Confirmation of Configuration of 4β-Iodo-3α-acetoxy-5β-cholestane (12). By practically the same method as that in the case of **11** above, **12** (40 mg) was converted to 5β-cholestan-3α-ol (**21**) (14 mg), mp 113—115 °C (107—108 °C[20]) and 3α,4α-epoxy-5β-cholestane (**17**) (18 mg), mp 53—55 °C (55—56 °C[21]), respectively.

The Reaction of 2β-Acetoxy-3β-iodo-5α-cholestane (8) with *m*-Chloroperbenzoic Acid. A mixture of **8** (200 mg) in

methylene dichloride (20 ml) and *m*-chloroperbenzoic acid (137 mg) was stirred at room temperature for 4 h. After the usual work-up, the resulting oil, on crystallization from ethanol, 2β-acetoxy-5α-cholestan-3β-ol (**22**) (144 mg), mp 136—137 °C (136—138 °C[22]).

Hydrolysis of 2β-Acetoxy-5α-cholestan-3β-ol (22). A mixture of **22** (100 mg) in methanol (10 ml) and potassium hydroxide (10 mg) in water (0.5 ml) was refluxed for 0.5 h. After evaporation of the reaction mixture, the residue was dissolved in ether. The ethereal solution was washed with water, dried, and evaporated. Crystallization of the residue from methanol gave plates of **23** (90 mg), mp 174—177 °C (175—176 °C[22]).

We are indebted to Toyo Jozo Co., Ltd. for the elemental analyses.

References

1) L. Birckenbach, J. Goubeau, and E. Berninger, *Ber.*, **65**, 1339 (1932).
2) M. Adinolfi, M. Parrilli, G. Barone, G. Laonigro, and L. Mangoni, *Tetrahedron Lett.*, **1976**, 3661.
3) C. Georgoulis and J. M. Valery, *Bull. Soc. Chim. Fr.*, **1975**, 1431.
4) R. C. Cambie, R. C. Hayward, J. L. Roberts, and P. S. Rutledge, *J. Chem. Soc., Perkin Trans. 1*, **1974**, 1858.
5) C. Georgoulis and J. M. Valery, *Synthesis*, **1978**, 402.
6) C. A. Horiuchi and J. Y. Satoh, *Synthesis*, **1981**, 312.
7) C. A. Horiuchi and J. Y. Satoh, *J. Chem. Soc., Chem. Commun.*, **1982**, 671; C. A. Horiuchi, A. Haga, and J. Y. Satoh, *Bull. Chem. Soc. Jpn.*, **59**, 2459 (1986).
8) C. A. Horiuchi and J. Y. Satoh, *Bull. Chem. Soc. Jpn.*, **57**, 2691 (1984).
9) C. A. Horiuchi and J. Y. Satoh, *Chem. Lett.*, **1984**, 150.
10) D. G. Hey, G. D. Meakins, and M. W. Pemberton, *J. Chem. Soc.*, **1966**, 1331.
11) T. Nakano, M. Hasegawa, and C. Djerassi, *Chem. Pharm. Bull.*, **11**, 465 (1963).
12) J. Mckenna, J. K. Norymberski, and R. D. Stubbs, *J. Chem. Soc.*, **1959**, 2502.
13) K. Abe and J. Y. Satoh, *Bull. Chem. Soc. Jpn.*, **51**, 941 (1978).
14) B. R. Davis and P. D. Woodgate, *J. Chem. Soc.*, **1966**, 2006.
15) S. E. Bruce and R. E. Gall, *J. Chem. Soc.*, **1972**, 2319.
16) A. Kasal, *Collect. Czech. Chem. Commun.*, **41**, 140 (1976).
17) D. N. Jones, J. R. Lewis, C. W. Shoppee, and G. H. R. R. Summers, *J. Chem. Soc.*, **1955**, 2876.
18) A. Furst and R. Scotoni Jr., *Helv. Chim. Acta.*, **36**, 1332 (1953); D. H. R. Barton, *J. Chem. Soc.*, **1953**, 1027.
19) M. Tomoeda and T. Koga, *Tetrahedron Lett.*, **1965**, 3231.
20) D. N. Kirk and V. Petrow, *J. Chem. Soc.*, **1959**, 1691.
21) V. Sanda and J. Fajkos, *Collect. Czech. Chem. Commun.*, **32**, 3726 (1967).
22) E. Glotter and A. Schwartz, *J. Chem. Soc., Perkin Trans. 1*, **1976**, 1660.

Photoreactions of *N*-Methyl-1,2-naphthalenedicarboximide with Dienes. Formation of Naphthazepinediones and Their Secondary Reactions

Yasuo KUBO,* Rie TODA, and Takeo ARAKI
Department of Chemistry, Faculty of Science, Shimane University, Matsue, Shimane 690
(Received June 24, 1986)

Synopsis. In the photolysis of a benzene solution of *N*-methyl-1,2-naphthalenedicarboximide (**5**) in the presence of dienes, i.e., 2,3-dimethyl-1,3-butadiene and 1,3-butadiene, insertion of one of the double bond in the dienes into a C(=O)-N bond of **5** was observed to give naphthazepinediones. These products were found to convert further into cyclobutanes and α,β-unsaturated ketones via photochemical intramolecular cycloaddition and via hydrogen migration, respectively.

In recent years, the photochemistry of imides has been the subject of intensive investigations.[1] A characteristic photoreaction of arenedicarboximides in the presence of alkenes is the insertion of the alkene into a C(=O)-N bond of the imide moiety.[2] Concerning the reactions with dienes, Mazzocchi and his co-workers have reported that the photoreaction of *N*-methylphthalimide (**1**) with, for example, 1,3-butadiene (**2a**) gives **4a** and **4b** by insertion of one of the double bonds in **2a** into a C(=O)-N bond of **1** (**1**+**2a**→**3**) and successive photochemical hydrogen-migration (**3**→**4a**+**4b**) (Eq. 1).[2a,f]

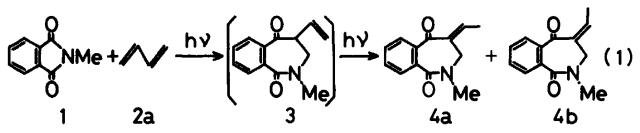

1 2a 3 4a 4b (1)

systematic investigation of the photochemistry of arenedicarboximides with alkenes, we have established that the arene structure played a crucial role in determining the reaction pathways.[3] This paper describes the photoreactions of *N*-methyl-1,2-naphthalenedicarboximide (**5**) with dienes in benzene. The predominant reaction of **5** with dienes is found to be insertion of one of the double bonds in the dienes into a C(=O)-N bond of **5** (naphthazepinedione formation). New types of secondary reactions are observed at the same time.

Results and Discussion

Irradiation of a benzene solution of **5** (10 mM, 1 M=1 mol dm^{-3}) and 2,3-dimethyl-1,3-butadiene (**2b**) (100 mM) by a light of >320 nm (aq $CuSO_4$ filter) for a short time gave naphthazepinedione (**6**, 27%) and two regio-isomeric cyclobutanes (**8**, 17% and **9**, 38%) (Scheme 1). Prolonged irradiation of the same system gave only **8** (42%) and **9** (40%), and irradiation of **6** alone in benzene afforded **8** quantitatively. These results clearly show that **8** is a secondary photoproduct of **6**. Although **7** could not be isolated, product **9** seems to be formed similarly from the corresponding

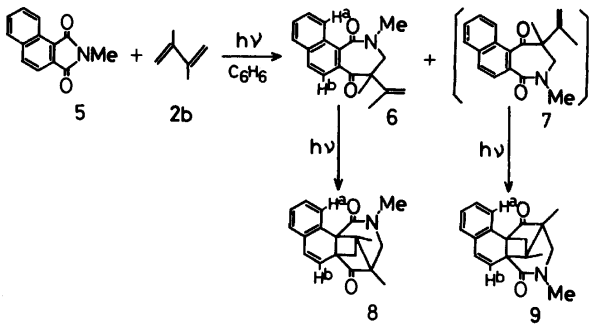

5 2b 6 7 8 9

Scheme 1.

precursor **7** which is more reactive than **6** under the photochemical conditions used.

The structure of **6** was supported by the spectral resemblance to the analogous naphthazepinediones obtained by the photoreactions of **5** with alkenes.[3b] The regiochemistry was deduced mainly from the chemical shift of H^b, which generally appeared at a lower field region than that of H^a in such a regio-isomer.[3b] The structures of **8** and **9** were assigned on the basis of IR and ^{1}H NMR spectra. The IR spectra of **8** and **9** show characteristic five-membered carbonyl absorption bands at 1758 and 1762 cm^{-1}, respectively. The H^a signal of **8** shifted considerably to a lower field (δ=7.95) than that of **9**, probably due to the deshielding effect of the lactam carbonyl group. Molecular model examination shows that the five-membered carbonyl groups in **8** and **9** are fixed in configurations where no anisotropic effects of the carbonyl groups exerts on H^a and H^b.

After irradiation of a benzene solution of **5** (10 mM) and **2a** (100 mM) for a short time, chromatography of the resultant mixtures on silica-gel column gave a mixture of **12a** and **12b** (45%, isomer-ratio=2.9:1) and a mixture of **13a** and **13b** (40%, isomer-ratio=2.6:1), respectively (Scheme 2). These products were only weakly observed in the ^{1}H NMR spectrum of the original mixture before chromatography. Judged from the ^{1}H NMR spectra of the original mixtures, the main products seem to be **10** and **11** (not isolated) because of their spectral resemblance to the naphthazepinediones obtained by the reactions of **5** with alkenes.[3b] These results may indicate that the initially formed **10** and **11** were converted by silica-gel treatment to a mixture of **12a** and **12b**, and a mixture of **13a** and **13b**, respectively.

On the other hand, prolonged irradiation of **5** and **2a** gave a mixture of **12a** and **12b** (38%, isomer-

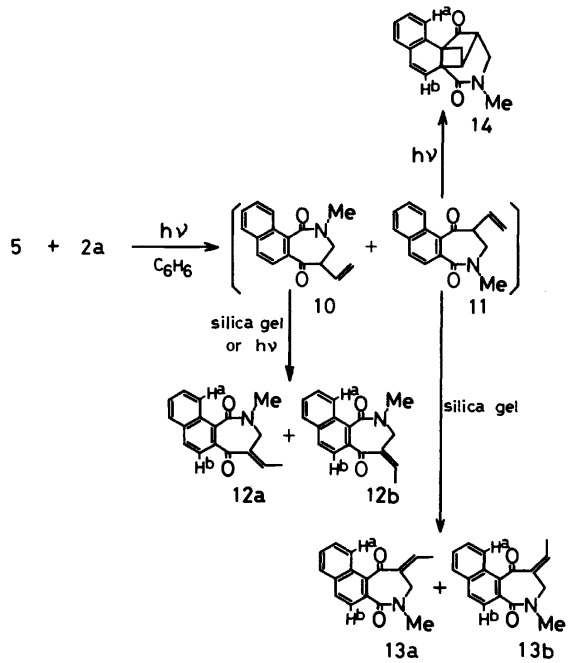

Scheme 2.

ratio=2.0:1), and **14** (33%) together with a trace amount of a mixture of **13a** and **13b**. In this case, the ^{1}H NMR spectrum of the irradiation mixture was a simple combination of those of the isolated products, indicating that the unchanged products were isolated by chromatography.

The structures of **12a,b** and **13a,b** were supported by the spectral resemblance to the benzo analogues.[2a,f] The regiochemistry was deduced from the chemical shifts of H^a and H^b as in the case of the regiochemistry-determination of the naphthazepinediones obtained by the reactions of **5** with alkenes.[3b] The structure of **14** was supported by the spectral resemblance to **9**.

The photoreaction of **5** and 2,5-dimethyl-2,4-hexadiene (**2c**) was slow and only gave a mixture of unidentified minor products.

The results obtained here indicate that the insertion of one of the double bonds in dienes into a C(=O)–N bond of **5** is a predominant reaction in the photoreaction of **5** with dienes. The predominance of the insertion is a characteristic nature of the excited state of **5**, since no significant predominance was observed in the reactions of *N*-methyl-1,8- and -2,3-naphthalenedicarboximides with dienes.[3c] In the present system a new type of secondary photoreaction is found, i.e., intramolecular cycloaddition, which was not observed in the reaction of the benzo analogue. The hydrogen-migration (**10**→**12a,b**) is found to occur by the action of silica gel as well as by already known photochemical process. The photochemical pathways from **10** and **11** were strongly structure-dependent, i.e., β-naphthyl ketone (**10**) or α-naphthyl ketone (**11**) structure determines whether hydrogen-migration (**10**→**12a,b**) or cycloaddition (**11**→**14**) is favored.

Experimental

The mps were measured by a Yanagimoto micromelting point apparatus, and are uncorrected. ^{1}H NMR spectra were determined on a JEOL JNM-MH-100 (100 MHz) in $CDCl_3$ solution. IR spectra were obtained with a Hitachi 260-50 spectrophotometer. Mass spectra were measured on a JEOL JMS-DX-300 apparatus. Microanalyses were performed on a Yanagimoto CHN corder MT-2.

Materials. *N*-Methyl-1,2-naphthalenedicarboximide (**5**) was prepared and purified as previously described.[3b] Dienes (**2a—c**) were commercially available and **2b,c** were purified by distillation.

General Procedure for Irradiation and Product Isolation. UV irradiation of 25 cm^3 of N_2 purged benzene solutions containing 10 mM of **5** and 100 mM of dienes (**2a—c**) was carried out with an Eikosha EHB-W-300 high-pressure Hg-lamp through aq $CuSO_4$ filter about 1 cm in thickness (>320 nm) at ambient temperature. The reaction was monitored by ^{1}H NMR measurements. After evaporation of the solvent, the residue was subjected to column chromatography (Wakogel C-200). Dichloromethane-ether was used as the eluant for the separation of the products.

Irradiation of 5 and 2,3-Dimethyl-1,3-butadiene (2b). 4-Isopropenyl-2,4-dimethyl-3,4-dihydro-1*H*-naphth[1,2-*c*]-azepine-1,5(2*H*)-dione (**6**): Mp 145—148 °C; ^{1}H NMR δ=1.55 (s, 3H, CMe), 1.87 (s, 3H, =CMe), 3.28 (s, 3H, NMe), 3.27 and 4.38 (ABq, *J*=14 Hz, 2H, CH_2), 4.84 and 5.08 (br s, 2H, $=CH_2$), 7.4—7.7 (m, 2H, Arom H), 7.7—8.1 (m, 3H, Arom H), 8.12 (d, 1H, H^b); IR (KBr) 1698 (ketone), 1643 (lactam), 1482, 1406, 1384, 1080 cm^{-1}. Found: C, 77.93; H, 6.74; N, 4.82%; M$^+$, 293. Calcd for $C_{19}H_{19}NO_2$: C, 77.79; H, 6.53; N, 4.77%; M, 293.

12,14,15-Trimethyl-12-azapentacyclo[12.2.1.$0^{1,10}$.$0^{4,9}$.$0^{10,15}$]-heptadecane-2,4,6,8-tetraene-11,17-dione (**8**): Mp 242—245 °C; ^{1}H NMR δ=1.21 (s, 6H, CMe), 1.77 and 3.08 (ABq, *J*=8 Hz, 2H, cyclobutane CH_2), 2.82 (s, 3H, NMe), 3.32 (s, 2H, NCH_2), 5.95 and 6.93 (ABq, *J*=10 Hz, 2H, $CH=CH^b$), 7.1—7.4 (m, 3H, Arom H), 7.95 (dd, 1H, H^a); IR (KBr) 1758 (ketone), 1648 (lactam), 1496, 1332, 796 cm^{-1}. Found: C, 77.92; H, 6.67; N, 4.86%; M$^+$, 293. Calcd for $C_{19}H_{19}NO_2$: C, 77.79; H, 6.53; N, 4.77%; M, 293.

12,14,15-Trimethyl-12-azapentacyclo[12.2.1.$0^{1,10}$.$0^{2,7}$.$0^{10,15}$]-heptadecane-2,4,6,8-tetraene-11,17-dione (**9**): Mp 235—238 °C; ^{1}H NMR δ=1.20 (s, 3H, CMe), 1.38 (s, 3H, CMe), 1.72 and 2.66 (ABq, *J*=8 Hz, 2H, cyclobutane CH_2), 2.87 (s, 3H, NMe), 3.32 and 3.51 (ABq, *J*=12 Hz, 2H, NCH_2), 6.19 and 6.68 (ABq, *J*=10 Hz, 2H, $CH=CH^b$), 7.2—7.6 (m, 4H, Arom H); IR (KBr) 1762 (ketone), 1658 (lactam), 1386, 1338, 1239, 801 cm^{-1}. Found: C, 78.04; H, 6.79; N, 4.63%; M$^+$, 293. Calcd for $C_{19}H_{19}NO_2$: C, 77.79; H, 6.53; N, 4.77%; M, 293.

Irradiation of 5 and 1,3-Butadiene (2a). A mixture of (*E*)- and (*Z*)-4-ethylidene-2-methyl-3,4-dihydro-1*H*-naphth[1,2-*c*]azepine-1,5(2*H*)-dione (**12a+12b**, the isomer ratio=3:4): Mp 132—136 °C; ^{1}H NMR of **12a**, δ=2.05 (d, *J*=7 Hz, 3H, =CMe), 3.23 (s, 3H, NMe), 4.27 (br s, 2H, NCH_2), 7.19 (q, 1H, =CH), 7.4—8.1 (m, 6H, Arom H); ^{1}H NMR of **12b**, δ=2.39 (d, *J*=7 Hz, 3H, =CMe), 3.29 (s, 3H, NMe), 4.13 (br s, 2H, NCH_2), 6.23 (q, 1H, =CH), 7.4—8.1 (m, 6H, Arom H); IR (KBr) 1675 (ketone), 1641 (lactam), 1475, 1395, 1245, 773 cm^{-1}. Found: C, 77.16; H, 5.83; N, 5.31%; M$^+$, 265. Calcd for $C_{17}H_{15}NO_2$: C, 76.96; H, 5.70; N, 5.28%; M, 265.

A mixture of (*E*)- and (*Z*)-2-ethylidene-4-methyl-3,4-dihydro-1*H*-naphth[2,1-*c*]-azepine-1,5(2*H*)-dione (**13a+13b**, the isomer ratio=1:3): Mp 152—158 °C; ^{1}H NMR of **13a**, δ=2.04 (d, *J*=7 Hz, 3H, =CMe), 3.27 (s, 3H, NMe), 4.08 and 4.43 (ABq, *J*=16 Hz, 2H, NCH_2), 7.32 (q, 1H, =CH), 7.5—7.8 (m, 2H, Arom H), 7.77 (d, *J*=8 Hz, 1H, Arom H), 7.9—8.0

(m, 1H, Arom H), 8.05 (d, 1H, J=8 Hz, 1H, H^b), 8.51 (dd, 1H, H^a); ^{1}H NMR of **13b**, δ=2.34 (d, J=7 Hz, 3H, =CMe), 3.27 (s, 3H, NMe), 3.44 and 4.58 (br ABq, 2H, NCH_2), 6.36 (q, 1H, =CH), 7.5—7.8 (m, 3H, Arom H), 7.9—8.0 (m, 1H, Arom H), 8.05 (d, 1H, J=8 Hz, 1H, H^b), 8.51 (dd, 1H, H^a); IR (KBr) 1672 (ketone), 1643 (lactam), 1476, 1386, 1248, 786 cm^{-1}. Found: C, 77.23; H, 5.95; N, 5.36%; M^+, 265. Calcd for $C_{17}H_{15}NO_2$: C, 76.96; H, 5.70; N, 5.28; M, 265.

12-Methyl-12-azapentacyclo[12.2.1.$0^{1,10}$.$0^{2,7}$.$0^{10,15}$]heptadecane-2,4,6,8-tetraene-11,17-dione (**14**): Mp 243—246 °C; ^{1}H NMR δ=1.61 (d, J=7 Hz, 1H, 1H of cyclobutane CH_2), 2.81 (s, 3H, NMe), 2.91 (dd, J=4, 7 Hz, 1H, 1H of cyclobutane CH_2), 2.9—3.1 (m, 1H, COCH), 3.2—3.3 (m, 1H, cyclobutane CH), 3.5—3.8 (m, 2H, NCH_2), 6.00 and 6.52 (ABq, J=10 Hz, 2H, $CH{=}CH^b$), 7.0—7.4 (m, 4H, Arom H); IR (KBr) 1768 (ketone), 1640 (lactam), 1342, 1244, 800 cm^{-1}. Found: C, 76.88; H, 5.95; N, 5.01%; M^+, 265. Calcd for $C_{17}H_{15}NO_2$: C, 76.96; H, 5.70; N, 5.28%; M, 265.

References

1) For reviews see: P. H. Mazzocchi, "Organic Photochemistry," ed by A. Padwa, Marcel Dekker, New York (1981), Vol. 5, p. 421; Y. Kanaoka, *Acc. Chem. Res.*, **11**, 407 (1978).

2) a) P. H. Mazzocchi, M. Bowen, and N. Narian, *J. Am. Chem. Soc.*, **99**, 7063 (1977); b) P. H. Mazzocchi, S. Minamikawa, and M. Bowen, *J. Org. Chem.*, **43**, 3079 (1978); c) K. Maruyama and Y. Kubo, *Chem. Lett.*, **1978**, 769; d) Y. Kanaoka, K. Yoshida, and Y. Hatanaka, *J. Org. Chem.*, **44**, 664 (1979); e) P. H. Mazzocchi, S. Minamikawa, and P. Wilson, *ibid.*, **44**, 1186 (1979); f) P. H. Mazzocchi, S. Minamikawa, P. Wilson, M. Bowen, and N. Narian, *ibid.*, **46**, 4846 (1981); g) P. H. Mazzocchi, F. Khachik, P. Wilson, and R. Highet, *J. Am. Chem. Soc.*, **103**, 6498 (1981); h) P. H. Mazzocchi, P. Wilson, F. Khachik, L. Klingler, and S. Minamikawa, *ibid.*, **48**, 2981 (1983); i) K. Maruyama, T. Ogawa, Y. Kubo, and T. Araki, *J. Chem. Soc., Perkin Trans., 1*, **1985**, 2025; j) K. Maruyama and Y. Kubo, *J. Org. Chem.*, **51**, 1426 (1985).

3) a) Y. Kubo, S. Tojo, M. Suto, R. Toda, and T. Araki, *Chem. Lett.*, **1984**, 2075; b) Y. Kubo, R. Toda, K. Yamane, and T. Araki, *Bull. Chem. Soc. Jpn.*, **59**, 191 (1986); c) Y. Kubo, M. Suto, S. Tojo, and T. Araki, *J. Chem. Soc., Perkin Trans., 1*, **1986**, 771.

Molecular Structure of the exo-Diels-Alder-Adduct of 5-Methoxy-2-methyl-4-(*p*-nitrophenyl)oxazole with *N*-Methylmaleimide

Toshikazu IBATA,* Jiro TOYODA, Hatsue TAMURA, and Kazuhide OGAWA
Institute of Chemistry, College of General Education, Osaka University,
Toyonaka, Osaka 560
(Received June 24, 1986)

Synopsis. The molecular structure of the exo-Diels-Alder adduct of 5-methoxy-2-methyl-4-(*p*-nitrophenyl)oxazole with *N*-methylmaleimide was determined by X-ray analysis. The crystals are triclinic, space group $P\bar{1}$, with a=9.160(2), b=11.182(2), c=8.816(1) Å, α=92.39(1), β=116.47(1), γ=100.60(1)°, Z=2, D_x=1.455 Mg m^{-3}, D_m=1.458 Mg m^{-3}, μ(Cu $K\alpha$)=9.76 cm^{-1}. The configuration of the exo-adduct is consistent with that predicted on the basis of the NMR data.

The Diels–Alder reaction is one of the most useful reactions in organic synthesis, and widely studied for the preparation of six-membered compounds.[1] Oxazoles have a conjugate azadiene system and are available for the diene component of the Diels–Alder reaction to prepare nitrogen-containing bicyclic compounds.[2,3] In these cycloadditions, the determination of the stereochemistry of the adducts is indispensable from the synthetic and mechanistic view points. However, because of the extreme unstability of the Diels–Alder adducts of oxazoles, no structural determination has been studied yet. The authors have reported that the reaction of 5-methoxy-2-methyl-4-(*p*-nitrophenyl)oxazole (**1**) and *N*-methylmaleimide (**2**) gave two adducts, **3** and **4**, in 32 and 58% yields, respectively.[3] The structures of **3** and **4** were

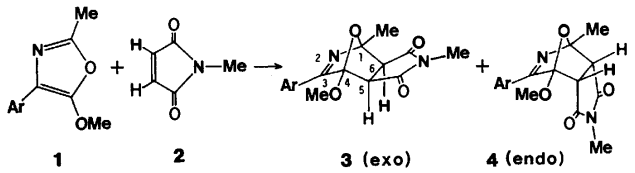

1 **2** **3 (exo)** **4 (endo)**

Ar=p-$NO_2C_6H_4$

determined tentatively to exo- and endo-adducts on the basis of NMR spectra. The high-field shift of N–CH_3 signal of the adduct (**4**) at δ 2.55, in comparison with that of **3** at δ 3.04, was attributed to the shielding effect of *p*-nitrophenyl group located near the N–CH_3. In this manner **4** was assumed to have endo-structure and **3** to have exo-structure.[3] In order to confirm the above assumption we performed X-ray analysis of the adduct. Of these two adducts endo-adduct (**4**) was found difficult to obtain good crystals for X-ray analysis because of its unstability owing to the retro-Diels–Alder reaction.

Experimental

The Diels–Alder reaction of **1** and *N*-methylmaleimide was carried out by the method previously described.[3] Colorless crystals of the exo-adduct (**3**) were obtained by the several recrystallizations from a mixed solvent of benzene and hexane after the separation of the reaction products by silica-gel column chromatography.

The cell dimensions and diffraction intensities were measured on a Rigaku four-circle diffractometer with Ni-filtered Cu $K\alpha$ radiation. Among 2338 independent reflections with 2θ values up to 120°, 2294 with $|F_o|>0$ were used for the structure determination. No correction was made for absorption.

The structure was solved by the MULTAN 80 program.[4] The positions of the hydrogen atoms were obtained from the difference Fourier synthesis. The structural parameters were obtained by the block-diagonal least-squares method. Anisotropic thermal parameters were applied to the non-hydrogen atoms and isotropic parameters, to the hydrogen atoms. The final R values was 0.046. The function minimized was $\sum w(|F_o|-|F_c|)^2$ with the following weighting scheme: $w=(\sigma^2(F_o)+0.0072|F_o|+0.0009|F_o|^2)^{-1}$.

All the atomic scattering factors were taken from the "International Tables for X-Ray Crystallography".[5] The computations were carried out on an ACOS-850 computer at the Crystallographic Research Center, Institute for Protein Research Laboratory, Osaka University, using "The

Table 1. Atomic Positional (×10^4) and Thermal Parameters for exo-Adduct (**3**)

Atom	x	y	z	B_{eq}/Å^2
O1	766(1)	3878(1)	1337(2)	3.3
O2	−139(2)	1766(1)	365(2)	3.9
O3	3962(2)	6123(1)	325(2)	5.1
O4	880(2)	2330(2)	−2425(2)	5.7
O5	4924(2)	−954(2)	8595(2)	6.1
O6	3582(3)	−2242(2)	6325(2)	7.9
N1	2962(2)	3846(1)	3967(2)	3.5
N2	2205(2)	4346(2)	−1370(2)	4.0
N3	4018(2)	−1209(2)	7061(2)	4.5
C1	2417(2)	4563(2)	2510(2)	3.2
C2	3456(2)	4289(2)	1573(2)	3.2
C3	3277(2)	5060(2)	168(2)	3.7
C4	1734(2)	3121(2)	−1224(2)	4.0
C5	2518(2)	2977(2)	657(2)	3.4
C6	1201(2)	2709(2)	1331(2)	3.3
C7	2250(2)	2733(2)	3277(2)	3.3
C8	2456(3)	5871(2)	2981(3)	4.0
C9	1707(3)	4825(3)	−2995(3)	5.4
C10	−1409(3)	1570(2)	929(3)	5.2
C11	2609(2)	1681(2)	4223(2)	3.3
C12	3478(2)	1902(2)	6008(2)	3.7
C13	3925(3)	957(2)	6945(2)	3.8
C14	3489(2)	−212(2)	6066(2)	3.6
C15	2604(3)	−474(2)	4309(3)	4.2
C16	2157(3)	488(2)	3383(2)	4.0

Universal Crystallographic Computing System-Osaka".[6] Table 1 lists the final atomic coordinates with equivalent isotropic temperature factors.[7]

Results and Discussion

Molecular Structure. The perspective view of the adduct (**3**) determined by the X-ray analysis is depicted in Fig. 1. The molecule has the exo-structure as has

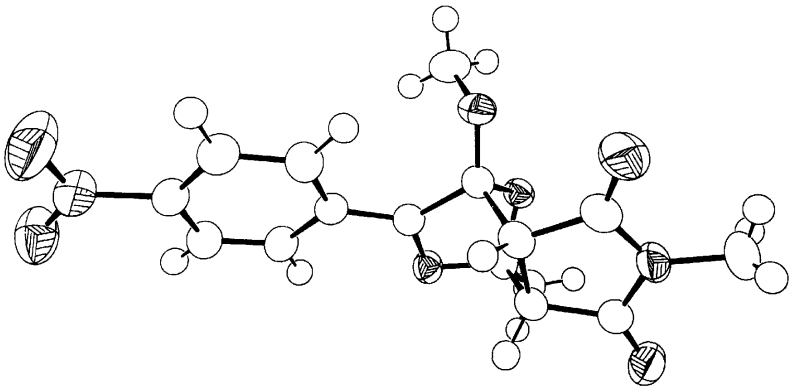

Fig. 1. Perspective view of the exo-adduct (**3**).

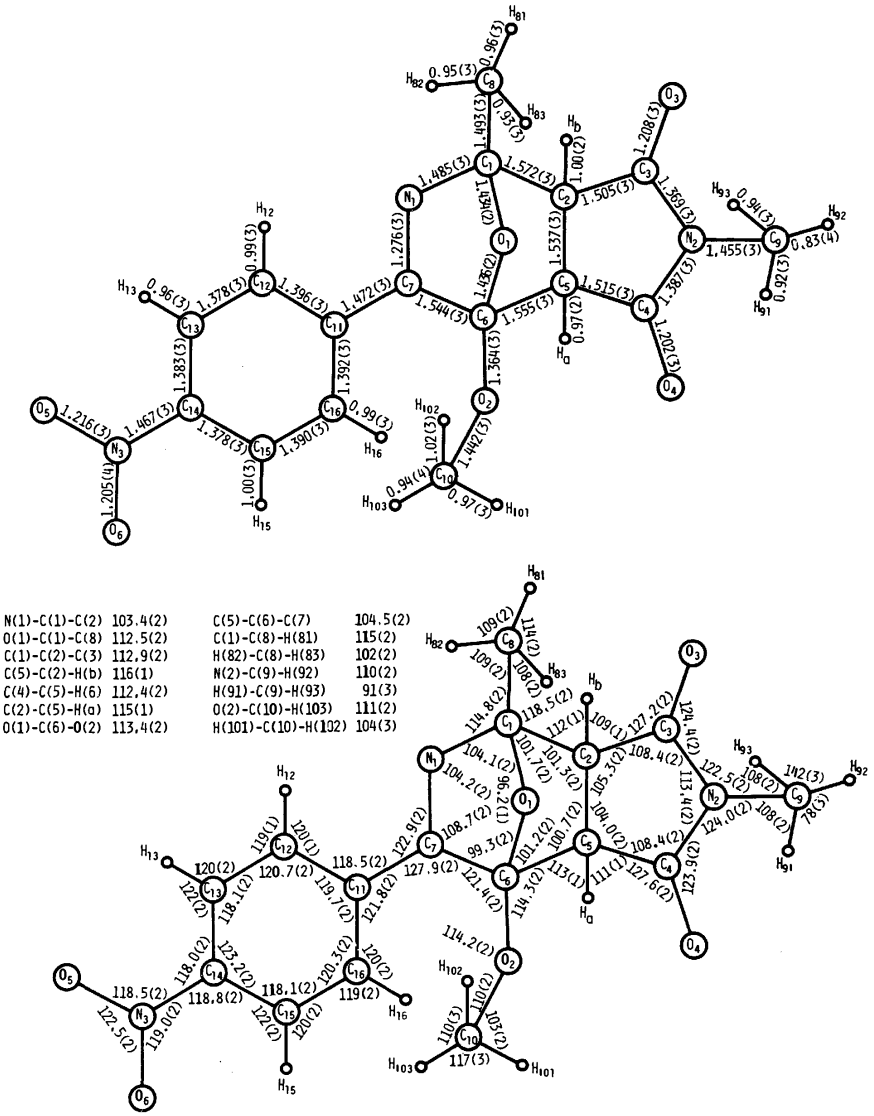

Fig. 2. Bond lengths (l/Å) and angles (ϕ/°).

been deduced on the basis of the NMR data. Bond distances and angles are given in Fig. 2.

The bond lengths and bond angles of *N*-methyltetrahydrofuran-3,4-dicarboximide ring system of the adduct (**3**) agree fairly well with those of the corresponding parts of the exo-(**5**) and endo-adduct (**6**) between *N*-methylmaleimide and 1-methoxy-2-benzopyrylium-4-olate[8] except for the following points. The bond lengthes, O(1)–C(1) and O(1)–C(6) of **3** are equal within the limits of experimental errors, while the differences between the corresponding bonds in the exo- and endo-adducts (**5** and **6**) are regarded as significant. The observation that the C(1)–O(1)–C(6) bond angle (96.2°) of **3** is smaller than those of **5** (104.1°) and **6** (105.0°) may be ascribed to the difference of the ring system which consists of a five-membered ring in **3** in contrast to a six-membered rings in **5** and **6**.

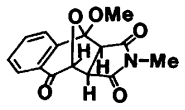

5

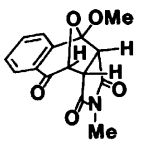

6

There is no appreciable interaction between the hydrogen atoms of the methoxyl group and the bridged oxygen atom, while the corresponding intramolecular distances in the exo-2:1-adduct between 1-methoxy-2-benzopyrylium-4-olate and acenaphthylene are shorter than the van der Waals distance.[10] The intramolecular distance (2.49 Å) between imide-carbonyl oxygen O(4) and one of the *N*-methyl hydrogen H(91) is shorter than the van der Waals distance. The torsion angle C(13)–C(14)–N(3)–O(5) is 6°, which is comparable to some of the corresponding torsion angles of the nitrobenzene derivatives.[11]

Coupling Constant and Ring-Current Effect. The coupling constant between the vicinal protons of the exo-adduct (**3**) $J_{5,6}$=6.3 Hz is consistent with the calculated value (8.19 Hz) according to the Karplus's Equation.[9] The distance (4.40 Å) between imide-methyl group and bridged oxygen in **3** is far enough to cause the anisotropic deshielding effect of bridged oxygen on chemical shift of *N*-methyl group. In fact, chemical shift of *N*-methyl of **3**, δ 3.04, is quite similar to the value of *N*-methylsuccinimide (δ 2.98). Therefore, the value of chemical shift (δ 2.55) of the endo-adduct (**4**) may be attributed to the anisotropic shielding effect of a *p*-nitrophenyl group located near the *N*-methyl group; that is distance between the *N*-methyl carbon and the center of phenyl group is approximated to 4.5 Å by the CPK model inspection of **4**.

References

1) J. Sauer, *Angew. Chem. Internat. Edit.*, **5**, 211 (1966); J. Sauer, *ibid*, **6**, 16 (1967); D. L. Boger, *Tetrahedron*, **39**, 2869 (1983).

2) T. Naito, K. Ueno, M. Sano, Y. Omura, I. Itoh, and F. Ishikawa, *Tetrahedron Lett.*, **1968**, 5767.

3) T. Ibata, S. Nakano, H. Nakawa, J. Toyoda, and Y. Isogami, *Bull. Chem. Soc. Jpn.*, **59**, 433 (1986).

4) P. Main, S. J. Fiske, S. E. Hull, L. Lessinger, G. Germain, J-P. Declercq, and M. M. Woolfson, "MULTAN 80. A System of Computer Programs for the Automatic Solution of Crystal Structures from X-Ray Diffraction Data," Univ. of York, England and Louvain, Belgium (1980).

5) "International Tables for X-Ray Crystallography," Kynoch Press, Birmingham (1974), Vol IV, p. 71.

6) T. Ashida, "HBLS V, p. 53 and DAPH, p. 61, The Universal Crystallographic Computing System-Osaka", The Computation Center, Osaka University (1979).

7) The F_o and F_c tables, anisotropic temperature factors, and hydrogen positional and isotropic thermal parameters are kept as Document No. 8650 at the Chemical Society of Japan.

8) H. Tamura, T. Ibata, and K. Ogawa, *Bull. Chem. Soc. Jpn.*, **57**, 926 (1984).

9) M. Karplus, *J. Chem. Phys.*, **30**, 15 (1959).

10) J. Toyoda, T. Ibata, H. Tamura, K. Ogawa, T. Nishino, and M. Takebayashi, *Bull. Chem. Soc. Jpn.*, **58**, 2212 (1985).

11) T. C. W. Mark and J. Trotter, *Acta Crystallogr.*, **18**, 68 (1965); P. Coppens, G. M. J. Schmidt, *Acta Crystallogr.*, **18**, 654 (1965); A. T. McPhail, G. A. Sim, *J. Chem. Soc.*, **1965**, 227; E. G. Boonstra, *Acta Crystallogr.*, **16**, 816 (1963).

Convenient Synthesis of Alkanediyl Bis(alkyl trithiocarbonate)s from Alkanedithiols with Alkyl Halides and Carbon Disulfide in the Presence of Phase-Transfer Catalyst

Akira SUGAWARA,* Ken HASEGAWA, Ken-ichi SUZUKI, Yukio TAKAHASHI, and Ryu SATO*,†

Department of Industrial Chemistry, Tsuruoka Technical College, Tsuruoka, Yamagata 997
†Department of Resource Chemistry, Faculty of Engineering, Iwate University, Morioka 020

(Received July 4, 1986)

Synopsis. Alkanediyl bis(alkyl trithiocarbonate)s were conveniently synthesized by treating alkanedithiols with alkyl halides and carbon disulfide in the presence of a phase-transfer catalyst.

It is known that trithiocarbonates, R-S-C(=S)-S-R, exhibit insecticidal and fungicidal activities.[1] Therefore, many chemists have investigated the synthesis of trithiocarbonates, for example, by reactions of (i)sodium trithiocarbonate with alkyl halides,[2] (ii) thiophosgene with benzenethiols,[3] (iii)arylchlorodithioformates with alkanethiols,[4] (iv)lithium alkyltrithiocarbonates derived from lithio 2-alkylthio-1,3-dithiolanes with alkyl halides,[5] and (v)alkanethiols and haloalkanenitriles with carbon disulfide in the presence of tetrabutylammonium sulfate.[6] Recently, we also reported the one-pot synthesis of alkyl aryl trithiocarbonates by treating thiols with alkyl halides and carbon disulfide in the presence of a phase-transfer catalyst.[7] However, bis(trithiocarbonate)s, R-S-C(=S)-S-$(CH_2)_n$-S-C(=S)-S-R, which may have synthetic potential due to the presence of two trithiocarbonate groups are yet difficult to obtain. To our knowledge, there have been only two reports on the preparation of two 1,2-ethanediyl bis(alkyltrithiocarbonate)s from 2,2′-[1,2-ethanediylbis(thio)]bis[1,3-dithiolane].[8] Here, we wish to report a convenient preparation of (*S*,*S*′-)alkanediyl bis(alkyl trithiocarbonate)s (**2**) from α,ω-alkanedithiols (**1**) with alkyl halides and carbon disulfide in the presence of a phase-transfer catalyst (PTC) (Eq. 1).

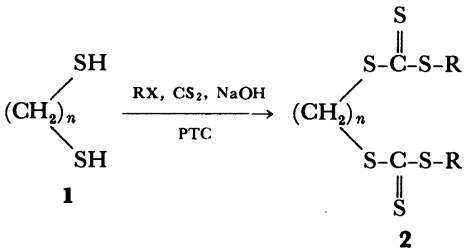

1 **2** (1)

Since a marked difference was not observed in the use of other catalysts, we employed trioctylmethylammonium chloride as a phase-transfer catalyst. Various (*S*,*S*′-)alkanediyl bis(alkyl trithiocarbonate)s (**2aa**–**2de**) were synthesized from α,ω-alkanedithiols (**1**), for example, 1,2-ethane-, 1,3-propane- and 1,6-hexanedithiols, in good yields as shown in Table 1. The absence of PTC resulted in a poor yield of (*S*,*S*′-)alkanediyl bis(alkyl trithiocarbonate)s (**2**). All reactions proceeded smoothly at an ambient temperature.

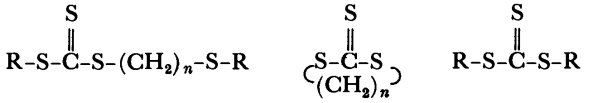

3 **4** **5**

The use of alkyl iodides rather than bromides gave better results (Runs 5—6). Bulky alkyl iodides such as isopropyl iodide did not yield the desired (*S*,*S*′-)alkanediyl bis(alkyl trithiocarbonate)(**2**) (Run 10). It is noted that 1,6-hexanedithiol gave **2** selectively. Bis(trithiocarbonate)s **2ab**–**2ac** and **2ba**–**2de** obtained by this method were new compounds.

This novel method for the preparation of (*S*,*S*′-) alkanediyl bis(alkyl trithiocarbonate)s is convenient, and has synthetic utility.

Experimental

All Melting points were uncorrected. ^{1}H NMR spectra were measured with a HITACHI R-20B, using tetramethylsilane as internal standard. IR spectra were obtained on a JASCO-G spectrophotometer. Elemental analysis were determined with YANAGIMOTO MT-3.

General Procedure. To a solution of α,ω-alkanedithiol (**1**) (3.5 mmol) and sodium hydroxide (10.5 mmol) in water (5 ml), carbon disulfide (10.5 mmol) and trioctylmethylammonium chloride (0.07 mmol) was added and then stirred at 10—30 °C for 2 h. Alkyl halide (10.5 mmol) in benzene (5 ml) was added to the solution and further stirring was continued at the temperature for 3 h. After completion of the reaction benzene layer was washed with water and then dried on sodium sulfate. Yellow oil obtained by evaporation of benzene was chromatographed on silica gel using chloroform as eluent, to give the desired (*S*,*S*′-)alkanediyl bis(alkyl trithiocarbonate)s (**2**) together with by-products (**3**, **4**, and **5**). The structure of the products were characterized by ^{1}H NMR, IR, MS, and elemental analysis.

1,2-Ethanediyl Bis(methyl trithiocarbonate) 2aa: Mp 53.3 °C;[8] IR (KBr) 2900, 1380, 1040, and 810 cm^{-1}; ^{1}H NMR ($CDCl_3$) δ=2.75 (s, 6H, CH_3) and 3.67 (s, 4H, CH_2); Found: C, 26.38; H, 3.55%. Calcd for $C_6H_{10}S_6$: C, 26.25; H, 3.67%.

1,2-Ethanediyl Bis(ethyl trithiocarbonate) 2ab: Mp 35.0 °C; IR (KBr) 2900, 1383, 1058 and 805 cm^{-1}; ^{1}H NMR ($CDCl_3$) δ=1.38 (t, 6H, 7.2 Hz, CH_3), 3.35 (q, 4H, 7.2 Hz, CH_2) and 3.64 (s, 4H, CH_2); Found: C, 31.78; H, 4.62%. Calcd for $C_8H_{14}S_6$: C, 31.76; H, 4.66%.

1,2-Ethanediyl Bis(propyl trithiocarbonate) 2ac: Mp 32.0 °C; IR (KBr) 2900, 1390, 1039, and 800 cm^{-1}; ^{1}H NMR ($CDCl_3$) δ=0.97 (t, 6H, 6.8 Hz, CH_3), 1.68 (m, 4H, 6.8, 7.2 Hz, CH_2), 3.25 (t, 4H, 7.2 Hz, CH_2) and 3.51 (s, 4H, CH_2); Found: C, 36.68; H, 5.30%. Calcd for $C_{10}H_{18}S_6$: C, 36.33; H, 5.49%.

1,2-Ethanediyl Bis(methoxycarbonylmethyl trithiocarbonate) 2ad: Mp 65.0 °C[8]; IR (KBr) 2900, 1730, 1160, and 1055 cm^{-1}; ^{1}H NMR ($CDCl_3$) δ=3.70 (s, 4H, CH_2), 3.77 (s,

Table 1. Reaction of Alkanedithiols with Alkyl Halides and Carbon Disulfide in the Presence of PTC[a)]

Run	Alkanedithiol	Alkyl halide	React.		Yield of product/%[b)]			
			Temp/°C	Time/h	**2**	**3**	**4**	**5**
1	Ethane	CH_3I	10	3	82 (**2aa**)	10 (**3aa**)	8	Trace
2			r.t.	3	73 (**2aa**)	24 (**3aa**)	Trace	Trace
3			40	3	50 (**2aa**)	44 (**3aa**)	6	5
4[c)]			10	3	4 (**2aa**)	54 (**3aa**)	20	22
5		C_2H_5I	10	3	86 (**2ab**)	11 (**3ab**)	Trace	Trace
6		C_2H_5Br	10	3	35 (**2ab**)	36 (**3ab**)	29	27
7		n-C_3H_7I	20	5	45 (**2ac**)	8 (**3ac**)	45	20
8		n-C_3H_7Br	20	5	7 (**2ac**)	19 (**3ac**)	16	Trace
9		n-C_3H_7Cl	20	5	0	0	20	0
10		i-C_3H_7I	30	20	0	0	67	16
11		CH_3OCOCH_2Br	10	5	90 (**2ad**)	Trace	4	0
12	Propane	CH_3I	20	5	81 (**2ba**)	11 (**3ba**)	8	Trace
13		C_2H_5I	20	5	83 (**2bb**)	9 (**3bb**)	8	8
14		n-C_3H_7I	20	5	76 (**2bc**)	6 (**3bc**)	12	11
15		CH_3OCOCH_2Br	20	5	92 (**2bd**)	Trace	4	0
16		$C_6H_5CH_2Br$	20	5	83 (**2be**)	16 (**3be**)	Trace	Trace
17	Butane	CH_3I	20	5	86 (**2ca**)	12 (**3ca**)	Trace	Trace
18		C_2H_5I	20	5	87 (**2cb**)	12 (**3cb**)	Trace	Trace
19		n-C_3H_7I	20	5	78 (**2cc**)	10 (**3cc**)	Trace	Trace
20		CH_3OCOCH_2Br	20	5	90 (**2cd**)	8 (**3cd**)	Trace	0
21		$C_6H_5CH_2Br$	20	5	84 (**2ce**)	14 (**3ce**)	Trace	Trace
22	Hexane	CH_3I	20	3	100 (**2da**)	0	0	0
23		C_2H_5I	20	3	100 (**2db**)	0	0	0
24		n-C_3H_7I	20	8	96 (**2dc**)	0	0	0
25		CH_3OCOCH_2Br	20	3	91 (**2dd**)	Trace	6	0
26		$C_6H_5CH_2Br$	20	5	100 (**2de**)	0	0	0

a) Trioctylmethylammonium chloride was used as a PTC. b) Isolated yield. c) Reaction in the absence of PTC.

6H, CH_3) and 4.20 (s, 4H, CH_2); Found: C, 30.51; H, 3.88%. Calcd for $C_{10}H_{14}O_4S_6$: C, 30.75; H, 3.61%.

1,3-Propanediyl Bis(methyl trithiocarbonate) 2ba: Oil; IR (neat) 2890, 1405, 1070, and 812 cm^{-1}; ^1H NMR ($CDCl_3$) δ=2.08 (quint, 2H, 7.0 Hz, CH_2), 2.72 (s, 6H, CH_3) and 3.45 (t, 4H, 7.0 Hz, CH_2); Found: C, 29.12; H, 4.09%. Calcd for $C_7H_{12}S_6$: C, 29.14; H, 4.19%.

1,3-Propanediyl Bis(ethyl trithiocarbonate) 2bb: Oil; IR (neat) 2910, 1446, 1252, 1075, and 815 cm^{-1}; ^1H NMR ($CDCl_3$) δ=1.34 (t, 6H, 7.2 Hz, CH_3), 2.07 (quint, 2H, 6.8 Hz, CH_2), 3.34 (t, 4H, 7.2 Hz, CH_2) and 3.43 (t, 4H, 6.8 Hz, CH_2); Found: C, 34.21; H, 4.95%. Calcd for $C_9H_{16}S_6$: C, 34.14; H, 5.09%.

1,3-Propanediyl Bis(propyl trithiocarbonate) 2bc: Oil; IR (neat) 2900, 1398, 1063, 1045, and 813 cm^{-1}; ^1H NMR ($CDCl_3$) δ=1.03 (t, 6H, 6.8 Hz, CH_3), 1.68 (m, 4H, 6.8 Hz, 7.0 Hz, CH_2), 2.06 (quint, 2H, 7.0 Hz, CH_2), 3.32 (t, 4H, 7.0 Hz, CH_2) and 3.43 (t, 4H, 7.0 Hz, CH_2); Found: C, 38.29; H, 5.87%. Calcd for $C_{11}H_{20}S_6$: C, 38.33; H, 5.85%.

1,3-Propanediyl Bis(methoxycarbonylmethyl trithiocarbonate) 2bd: Mp 65.0 °C; IR (KBr) 2850, 1725, 1162, 1060, and 805 cm^{-1}; ^1H NMR ($CDCl_3$) δ=2.13 (m, 2H, 7.0 Hz, CH_2), 3.49 (t, 4H, 7.0 Hz, CH_2), 3.76 (s, 6H, CH_3) and 4.19 (s, 4H, CH_2); Found: C, 32.92; H, 3.91%. Calcd for $C_{11}H_{16}O_4S_6$: C, 32.65; H, 3.99%.

1,3-Propanediyl Bis(benzyl trithiocarbonate) 2be: Mp 58.0 °C; IR (KBr) 3040, 2900, 1450, 1073, 1060, 830, and 697 cm^{-1}; ^1H NMR ($CDCl_3$) δ=2.07 (quint, 2H, 7.0 Hz, CH_2), 3.43 (t, 4H, 7.0 Hz, CH_2), 4.59 (s, 4H, CH_2) and 7.25 (s, 10H, arom); Found: C, 51.58; H, 4.47%. Calcd for $C_{19}H_{20}S_6$: C, 51.78; H, 4.57%.

1,4-Butanediyl Bis(methyl trithiocarbonate) 2ca: Mp 54.9 °C; IR (KBr) 2900, 1407, 1065, and 820 cm^{-1}; ^1H NMR ($CDCl_3$) δ=1.78 (t, 4H, 6.0 Hz, CH_2), 2.69 (s, 6H, CH_3) and 3.36 (t, 4H, 6.0 Hz, CH_2); Found: C, 31.81; H, 4.44%. Calcd for $C_8H_{14}S_6$: C, 31.76; H, 4.66%.

1,4-Butanediyl Bis(ethyl trithiocarbonate) 2cb: Mp 34.0 °C; IR (KBr) 2920, 1448, 1073, 1022, and 815 cm^{-1}; ^1H NMR ($CDCl_3$) δ=1.33 (t, 6H, 7.2 Hz, CH_3), 1.78 (m, 4H, CH_2), 3.15—3.52 (m, 4H, CH_2) and 3.33 (q, 4H, 7.2 Hz, CH_2); Found: C, 36.64; H, 5.49%. Calcd for $C_{10}H_{18}S_6$: C, 36.33; H, 5.49%.

1,4-Butanediyl Bis(propyl trithiocarbonate) 2cc: Mp 27.4 °C; IR (KBr) 2930, 1448, 1075, 1022, and 810 cm^{-1}; ^1H NMR ($CDCl_3$) δ=0.92 (t, 6H, 7.0 Hz, CH_3), 1.63 (sextet, 4H, 7.0 Hz, CH_2), 1.72 (t, 4H, 7.0 Hz, CH_2), 3.28 (t, 4H, 7.0 Hz, CH_2) and 3.31 (t, 4H, 7.0 Hz, CH_2); Found: C, 40.19; H, 5.94%. Calcd for $C_{12}H_{22}S_6$: C, 40.18; H, 6.18%.

1,4-Butanediyl Bis(methoxycarbonylmethyl trithiocarbonate) 2cd: Mp 66.2 °C; IR (KBr) 2860, 1746, 1165, and 1070 cm^{-1}; ^1H NMR ($CDCl_3$) δ=1.80 (m, 4H, CH_2), 3.40 (m, 4H, CH_2), 3.74 (s, 6H, CH_3) and 4.15 (s, 4H, CH_2); Found: C, 34.65; H, 4.14%. Calcd for $C_{12}H_{18}O_4S_6$: C, 34.43; H, 4.33%.

1,4-Butanediyl Bis(benzyl trithiocarbonate) 2ce: Mp 95.5 °C; IR (KBr) 3010, 2900, 1452, 1052, 810, and 700 cm^{-1}; ^1H NMR ($CDCl_3$) δ=1.79 (m, 4H, CH_2), 3.39 (t, 4H, 6.5 Hz, CH_2), 4.60 (s, 4H, CH_2) and 7.38 (s, 10H, arom); Found: C, 52.53; H, 4.85%. Calcd for $C_{20}H_{22}S_6$: C, 52.58; H, 4.88%.

1,6-Hexanediyl Bis(methyl trithiocarbonate) 2da: Mp 72.0 °C; IR (KBr) 2900, 1409, 1262, 1064, and 808 cm^{-1};

^{1}H NMR ($CDCl_3$) δ=1.54 (m, 8H, CH_2), 2.77 (s, 6H, CH_3) and 3.39 (t, 4H, 8.0 Hz, CH_2); Found: C, 36.12; H, 5.32%. Calcd for $C_{10}H_{18}S_6$: C, 36.33; H, 5.49%.

1,6-Hexanediyl Bis(ethyl trithiocarbonate) 2db: Mp 42.0 °C; IR (KBr) 2910, 1410, 1250, 1089, and 838 cm^{-1}; ^{1}H NMR ($CDCl_3$) δ=1.32 (t, 6H, 7.2 Hz, CH_3), 1.44 (m, 8H, CH_2), 3.37 (q, 4H, 7.2 Hz, CH_2) and 3.35 (m, 4H, CH_2); Found: C, 40.39; H, 6.11%. Calcd for $C_{12}H_{22}S_6$: C, 40.19; H, 6.18%.

1,6-Hexanediyl Bis(propyl trithiocarbonate) 2dc: Mp 46.0 °C; IR (KBr) 2900, 1416, 1228, 1060, and 815 cm^{-1}; ^{1}H NMR ($CDCl_3$) δ=1.02 (t, 6H, 7.0 Hz, CH_3), 1.53 (m, 8H, CH_2), 1.69 (sextet, 4H, 7.0 Hz, CH_2) and 3.35 (t, 8H, 7.0 Hz, CH_2); Found: C, 43.12; H, 6.65%. Calcd for $C_{14}H_{26}S_6$: C, 43.48; H, 6.78%.

1,6-Hexanediyl Bis(methoxycarbonylmethyl trithiocarbonate) 2dd: Mp 63.0 °C; IR (KBr) 2780, 1747, 1165, and 1076 cm^{-1}; ^{1}H NMR ($CDCl_3$) δ=1.50 (m, 8H, CH_2), 3.37 (t, 4H, CH_2), 3.74 (s, 6H, CH_3) and 4.17 (s, 4H, CH_2); Found: C, 37.40; H, 4.85%. Calcd for $C_{14}H_{22}O_4S_6$: C, 37.64; H, 4.96%.

1,6-Hexanediyl Bis(benzyl trithiocarbonate) 2de: Mp 86.0 °C; IR (KBr) 3010, 2920, 1454, 1060, 822, 798, and 701 cm^{-1}; ^{1}H NMR ($CDCl_3$) δ=1.50 (bs, 8H, CH_2), 3.35 (t, 4H, 7.0 Hz, CH_2), 4.60 (s, 4H, CH_2) and 7.28 (s, 10H, arom); Found: C, 54.62; H, 5.49%. Calcd for $C_{22}H_{26}S_6$: C, 54.73; H, 5.43%.

Methyl 2-(Methylthio)ethyl Trithiocarbonate 3aa: Oil; IR (neat) 2900, 1410, 1055, 1040, and 810 cm^{-1}: ^{1}H NMR ($CDCl_3$) δ=2.17 (s, 3H, CH_3), 2.74 (s, 3H, CH_3), 2.70 (t, 2H, 7.8 Hz, CH_2) and 3.59 (t, 2H, 7.8 Hz, CH_2); Found: C, 30.04; H, 4.83%. Calcd for $C_5H_{10}S_4$: C, 30.28; H, 5.08%.

Ethyl 2-(Ethylthio)ethyl Trithiocarbonate 3ab: Oil; IR (neat) 2900, 1450, 1252, 1070, and 810 cm^{-1}; ^{1}H NMR ($CDCl_3$) δ=1.28 (t, 3H, 7.2 Hz, CH_3), 1.37 (t, 3H, 7.2 Hz, CH_3), 2.63 (q, 2H, 7.2 Hz, CH_2), 2.78 (t, 2H, 4.8 Hz, CH_2), 3.36 (q, 2H, 7.2 Hz, CH_2) and 3.56 (t, 2H, 4.8 Hz, CH_2); Found: C, 36.84; H, 6.12%. Calcd for $C_7H_{14}S_4$: C, 37.13; H, 6.23%.

Propyl 2-(Propylthio)ethyl Trithiocarbonate 3ac: Oil; IR (neat) 2900, 1054, 1039, and 808 cm^{-1}; ^{1}H NMR ($CDCl_3$) δ=0.99 (t, 3H, 6.8 Hz, CH_3), 1.01 (t, 3H, 6.8 Hz, CH_3), 1.62 (m, 2H, 6.8, 7.2 Hz, CH_2), 1.72 (m, 2H, 6.8, 7.2 Hz, CH_2), 2.54 (t, 2H, 7.2 Hz, CH_2), 2,80 (m, 2H, CH_2), 3.31 (t, 2H, 7.2 Hz, CH_2) and 3.50 (m, 2H, CH_2); Found: C, 42.21; H, 6.84%. Calcd for $C_9H_{18}S_4$: C, 42.48; H, 7.13%.

Methyl 3-(Methylthio)propyl Trithiocarbonate 3ba: Oil; IR (neat) 2880, 1417, 1070, and 812 cm^{-1}; ^{1}H NMR ($CDCl_3$) δ=2.03 (s, 3H, CH_3), 2.53 (quint, 2H, 7.0 Hz, CH_2), 2.72 (s, 3H, CH_3) and 3.46 (t, 4H, 7.0 Hz, CH_2); Found: C, 33.77; H, 5.53%. Calcd for $C_6H_{12}S_4$: C, 33.93; H, 5.70%.

Ethyl 3-(Ethylthio)propyl Trithiocarbonate 3bb: Oil; IR (neat) 2900, 1445, 1250, 1075, 1025, and 815 cm^{-1}; ^{1}H NMR ($CDCl_3$) δ=1.22 (t, 3H, 7.0 Hz, CH_3), 1.34 (t, 3H, 7.0 Hz, CH_3), 1.92 (quint, 2H, 7.5 Hz, CH_2), 2.41 (t, 2H, 7.5 Hz, CH_2), 2.49 (q, 2H, 7.0 Hz, CH_2), 3.34 (q, 2H, 7.0 Hz, CH_2) and 3.44 (t, 2H, 7.5 Hz, CH_2); Found: C, 39.77; H, 6.56%. Calcd for $C_8H_{16}S_4$: C, 39.96; H, 6.71%.

Propyl 3-(Propylthio)propyl Trithiocarbonate 3bc: Oil; IR (neat) 2900, 1440, 1060, 1040, and 810 cm^{-1}; ^{1}H NMR ($CDCl_3$) δ=1.03 (t, 6H, 6.8 Hz, CH_3), 1.50—2.90 (m, 8H, 6.8, 7.0 Hz, CH_2), 3.32 (t, 4H, 7.0 Hz, CH_2) and 3.43 (t, 4H, 7.0 Hz, CH_2); Found: C, 44.61; H, 7.59%. Calcd for $C_{10}H_{20}S_4$: C, 44.73; H, 7.51%.

Benzyl 3-(Benzylthio)propyl Trithiocarbonate 3be: Oil; IR (neat) 3020, 2880, 1498, 1060, 798, and 694 cm^{-1}; ^{1}H NMR ($CDCl_3$) δ=2.00 (quint, 2H, 7.0 Hz, CH_2), 3.04 (t, 2H, 7.0 Hz, CH_2), 3.42 (t, 2H, 7.0 Hz, CH_2), 4.16 (s, 2H, CH_2), 4.54 (s, 2H, CH_2) and 7.18—7.21 (m, 10H, arom); Found: C, 59.33; H, 5.43%. Calcd for $C_{18}H_{20}S_4$: C, 59.30; H, 5.53%.

Methyl 4-(Methylthio)butyl Trithiocarbonate 3ca: Oil; IR (neat) 2920, 1420, 1065, and 810 cm^{-1}; ^{1}H NMR ($CDCl_3$) δ=1.67—1.84 (m, 4H, CH_2), 1.96 (s, 3H, CH_3), 2.40 (t, 2H, 7.0 Hz, CH_2), 2.66 (s, 3H, CH_3) and 3.32 (t, 2H, 7.0 Hz, CH_2); Found: C, 37.38; H, 6.18%. Calcd for $C_7H_{14}S_4$: C, 37.13; H, 6.23%.

Ethyl 4-(Ethylthio)butyl Trithiocarbonate 3cb: Oil; IR (neat) 2950, 1450, 1075, 1022, and 810 cm^{-1}; ^{1}H NMR ($CDCl_3$) δ=1.16 (t, 3H, 7.0 Hz, CH_3), 1.29 (t, 3H, 7.0 Hz, CH_3), 1.70 (m, 4H, CH_2), 2.41 (q, 2H, 7.0 Hz, CH_2), 2.42 (t, 2H, 7.0 Hz, CH_2), 3.29 (q, 2H, 7.0 Hz, CH_2) and 3.30 (t, 2H, 7.0 Hz, CH_2); Found: C, 42.28; H, 6.96%. Calcd for $C_9H_{18}S_4$: C, 42.48; H, 7.13%.

Propyl 4-(Propylthio)butyl Trithiocarbonate 3cc: Oil; IR (neat) 2920, 1455, 1060, 1038, and 800 cm^{-1}; ^{1}H NMR ($CDCl_3$) δ=1.02 (t, 3H, CH_3), 1.28 (t, 3H, CH_3), 1.83 (m, 8H, CH_2), 2.80 (m, 2H, CH_2) and 3.39 (m, 6H, CH_2); MS (13.5 eV) *m/z* 283 (M^+), 239, 164, 120, and 43.

Methoxycarbonylmethyl 4-(Methoxycarbonylmethylthio)-butyl Trithiocarbonate 3cd: Mp 43.0 °C; IR (KBr) 2840, 1740, 1430, 1060, and 800 cm^{-1}; ^{1}H NMR ($CDCl_3$) δ=1.84 (m, 4H, CH_2), 3.44 (m, 4H, CH_2), 3.74 (s, 3H, CH_3), 3.76 (s, 3H, CH_3), 4.20 (s, 2H, CH_2) and 4.31 (s, 2H, CH_2); MS (10 eV) *m/z* 343 (M^+), 254, 193, 160, 91, and 74.

Benzyl 4-(Benzylthio)butyl Trithiocarbonate 3ce: Oil; IR (neat) 3020, 2900, 1450, 1060, and 810 cm^{-1}; ^{1}H NMR ($CDCl_3$) δ=1.63 (m, 4H, CH_2), 2.30 (m, 2H, CH_2), 3.26 (m, 2H, CH_2), 3.58 (s, 2H, CH_2), 4.52 (s, 2H, CH_2) and 7.17 (s, 10H, arom); Found: C, 60.57; H, 5.89%. Calcd for $C_{19}H_{22}S_4$: C, 60.27; H, 5.86%.

References

1) J. T. Bashour, U. S. Patent, 2676129 (1954) [*Chem. Abstr.*, **48**, 8472i (1954)]; *ibid*, 2731487 (1956) [*Chem. Abstr.*, **50**, 15583h (1956)]; H. J. Renner, G. Schneider, and J. Weissflog, Ger. (East), 15431 (1958) [*Chem. Abstr.*, **54**, 2650f (1960)].

2) F. Runge, Z. El-Hewehi, H. J. Renner, and E. Taeger, *J. Prakt. Chem.*, **11**, 284 (1960).

3) F. Runge and Z. El-Hewehi, *J. Prakt. Chem.*, **10**, 268 (1959); M. Zbirovsky and V. Ettel, *Chem. Listy*, **51**, 2094 (1957) [*Chem. Abstr.*, **52**, 6318g (1958)].

4) H. C. Godt, Jr. and A. E. Wann, *J. Org. Chem.*, **26**, 4047 (1961).

5) S. Tanimoto, T. Oida, H. Ikehira, and M. Okano, *Bull. Chem. Soc. Jpn.*, **55**, 1977 (1982).

6) P. J. Wepplo and D. P. Wright, Jr., Ger. Often., 2937334 (1980) [*Chem. Abstr.*, **93**, 149828d (1980)].

7) A. Sugawara, M. Shirahata, S. Sato, and R. Sato, *Bull. Chem. Soc. Jpn.*, **57**, 3353 (1984).

8) S. Tanimoto, T. Oida, K. Ikehira, and T. Sugimoto, *Tetrahedron Lett.*, **22**, 655 (1981); S. Tanimoto, T. Oida, T. Kokubo, and M. Okano, *Bull. Chem. Soc. Jpn.*, **55**, 339 (1982).

Effect of $Ru_3(CO)_{12}$ and Triisopropylphosphine on the Catalytic Activity of CO Hydrogenation by $Co_2(CO)_8$

Kazuhisa MURATA,* Akio MATSUDA, Takashi MASUDA, Masaru ISHINO,† and Mitsuhisa TAMURA†
National Chemical Laboratory for Industry, Yatabe, Tsukuba, Ibaraki 305
†Takatsuki Research Laboratory, Sumitomo Chemical Co. Ltd., Tsukahara, Takatsuki, Osaka 569
(Received June 24, 1986)

Synopsis. A catalyst system, containing $Co_2(CO)_8$ coupled with $Ru_3(CO)_{12}$ and triisopropylphosphine($(i\text{-Pr})_3P$), was found to be effective for the ethylene glycol formation by homogeneous hydrogenation of CO: The most active catalyst, the activity of glycol formation of which was ca. 3 times higher than that of $Co_2(CO)_8$ alone, was obtained at phosphorus:Co:Ru ratio of 2:1:1.

Many efforts have been made to prepare ethylene glycol directly from syngas ($CO+H_2$) using homogeneous catalyst of Group 8 metals.[1] Rhodium,[1b,c] ruthenium,[1a,b,c] and cobalt[1b,c] metals are particularly favorable. Recently, it has been reported that the use of mixed metals, Rh and Ru, as catalyst precursors results in an improved catalytic activity.[2]

We have reported a direct synthesis of the glycol from syngas, where $Co_2(CO)_8$ in toluene solvent is employed under the standard conditions of 1800 atm (180 MPa) and 230 °C.[3] Also, we have found that, in the cobalt-catalyzed glycol production from formaldehyde and syngas, the addition of $Ru_3(CO)_{12}$ is effective for enhancing the glycol productivity.[4] The addition of phosphines has proved to be effective in the case of Rh-amide catalyst.[5] These findings prompt us to try Co-Ru or Co-Ru-P mixed catalysts for the hydrogenation of CO to give ethylene glycol under high pressure and high temperature. Now we describe here some of our results.

Results and Discussion

Some typical examples are shown in Fig. 1, where total amount of metals is held constant at 0.4 (Co+Ru) mmol. In our system involving cobalt coupled with ruthenium and triisopropylphosphine-($(i\text{-Pr})_3P$), ethylene glycol (EG), methanol (MeOH), and methyl formate (MF) are mainly produced with a small amount of ethanol (EtOH) (See Table 1). The results are summarized as follows:

i) A small but clear synergism was observed in the absence of $(i\text{-Pr})_3P$(●).

ii) The addition of $(i\text{-Pr})_3P$ resulted in enhancing the CO hydrogenation activity of Co–Ru system (○): The most active catalyst, the cativity of glycol formation of which was ca. 3 times higher than that of $Co_2(CO)_8$ alone, was obtained at phosphorus:Co:Ru ratio of 2:1:1. Further addition of the phosphine reduced the glycol formation. The effectiveness of other phosphines was in the order: $(i\text{-Pr})_3P(1.59)$>$(n\text{-Bu})_3P(1.14)$>$Cy_3P(0.93)$(Cy:cyclohexyl)>none(0.55)>

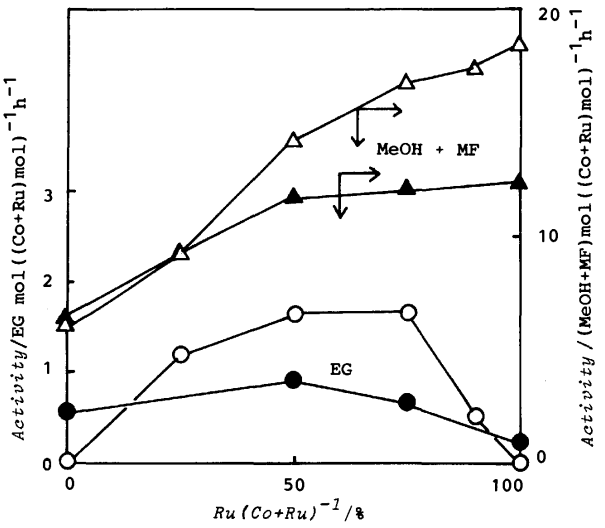

Fig. 1. CO hydrogenation activity vs. ruthenium mole fraction. Co+Ru=0.4 mmol, $(i\text{-Pr})_3P$ 0.4 mmol, dioxane 20 ml, 270 °C, 5 h, 1000 atm, $H_2/CO=1$.
○△ with $(i\text{-Pr})_3P$, ●▲ without $(i\text{-Pr})_3P$.

Table 1. Effect of H_2/CO Ratio under 2000 atm[a]

H_2/CO Ratio	T/°C	Product/mmol				N_{EG}[b]	Sel.$_{EG}$[c]	N_{C_1}[d]
		MeOH	MF	EtOH	EG	mol/g-atom. h	%	mol/g-atom. h
1	270	3.95	4.4	0.01	3.03	22.8	42	62.8
2	270	8.78	4.46	0.09	4.23	31.8	39	99.5
3	270	11.2	3.49	0.01	2.49	18.7	25	111
1	250	0.79	1.53	0.01	1.27	9.5	52	17.4
3	250	3.18	2.05	0.01	1.96	14.7	43	39.3

a) Conditions: $Co_2(CO)_8$ 0.0335 mmol, $Ru_3(CO)_{12}$ 0.0223 mmol, $(i\text{-Pr})_3P$ 0.133 mmol, toluene 7 ml, 2000 atm, 1 h. b) Turnover frequency relative to the total amounts of Co and Ru. c) Sel.$_{EG}$=2EG×100/(MeOH+MF+2(EG+EtOH)). d) MeOH+MF.

$(PhO)_3P(0.25)>Ph_3P(0.07)>Cy_2P(CH_2)_2PCy_2(0.012)$(Cy: cyclohexyl)(numerical values refer to turnover frequency of the glycol (N_{EG})). It was found for the first time that the addition of ruthenium-phosphine was effective for the cobalt-catalyzed CO hydrogenation.[6]

iii) After the reaction, the data of which is shown in Fig. 1, each catalyst solution, which is pale red-brown color, is truly homogeneous. Isotope-labelling studies using dioxane-d_8 conclusively demonstrated that the glycol was primary product and not solvent-derived by hydrogenation of dioxane.

iv) Replacement of $Ru_3(CO)_{12}$ by other metal carbonyls such as $Re_2(CO)_{10}$, $Mo(CO)_6$, $Fe(CO)_5$, and $Cr(CO)_6$ resulted in negative effects on the activity, whereas $Rh_4(CO)_{12}$ promoted the reaction, but the extent was less than $Ru_3(CO)_{12}$. Catalytic behaviors of Co-Ru-P system were examined, in comparison with $Co_2(CO)_8$ alone. For Co-Ru-P (1:1:2) system, the pressure dependence of the glycol formation was greater than fourth-order, while that for C_1-(MeOH+MF) formation process was in the vicinity of first- to second-order, as shown in Fig. 2 (○,△). Analogous dependences were observed in the cobalt catalyst (Fig. 2, ●, ▲). The glycol formation increased with either increases in partial pressure of H_2 or CO; the C_1 formation increased with the increase in P_{H2} and decreased with the increase in P_{CO}. Similar trends were obtained for $Co_2(CO)_8$. The activity of Co-Ru-P system was affected by the initial H_2/CO ratio (Table 1): The maximum activity was achieved at the ratio of 2 at 270 °C. The activation energy for the glycol formation was 105 kJ mol^{-1} and that for C_1 products was 142 kJ mol^{-1}, in the case of Co-Ru-P in toluene solvent under 2000 atm.[7] For $Co_2(CO)_8$ alone in the same solvent, the energies for glycol and C_1 have been found to be 100 and 138 kJ mol^{-1}, respectively.[3]

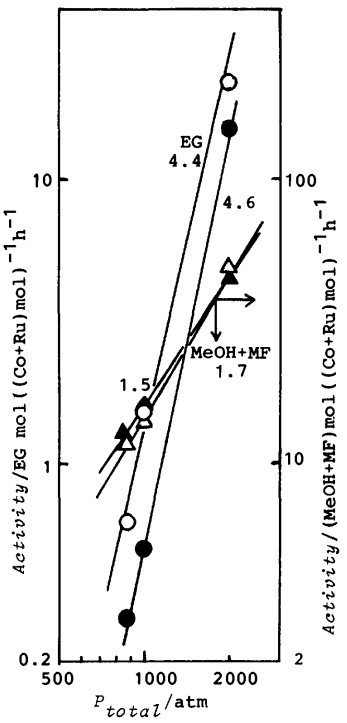

Fig. 2. Effect of total pressure.
toluene 7 ml, 270 °C, 5 h, $H_2/CO=1$.
○△ $Co_2(CO)_8$ 0.1 mmol, $Ru_3(CO)_{12}$ 0.0667 mmol, $(i\text{-Pr})_3P$ 0.4 mmol, ●▲ $Co_2(CO)_8$ 0.2 mmol.

The IR spectroscopic measurements were undertaken under the conditions of 20 atm at room temperature.[8] The hexane solution of Co-Ru-P system exhibited IR absorptions characteristic of $Co_2(CO)_8$(2075 m, 2045 m, 2025 s, 1857 m cm^{-1})[9], $Ru(CO)_5$(2040 s, 2002 s cm^{-1}),[10] and $Ru(CO)_4[(i\text{-Pr})_3P]$ (1982 m, 1940 vs cm^{-1}).[11,12] Mixed cobalt-ruthenium carbonyl cluster species[13] were not detected. For comparison, the Ru-P system, the spectra of which showed $Ru(CO)_5$ and $Ru(CO)_4[(i\text{-Pr})_3P]$[14], possessed high productivity of C_1 compounds but not glycol (Fig. 1) and, on the other hand, the Co-Ru system, exhibiting $Co_2(CO)_8$ and $Ru(CO)_5$ carbonyl bands,[14] was favorable in the glycol formation but a little inferior to the Co-Ru-P system (Fig. 1). There findings demonstrate that the presence of $Co_2(CO)_8$ species seems to be essential for the glycol formation and that the presences of both $Ru(CO)_5$ and $Ru(CO)_4[(i\text{-Pr})_3P]$ contribute to the enhancement of total catalytic activity.

Experimental

Materials. Phosphines, solvents, and $Ru_3(CO)_{12}$ were obtained commercially and used with no further purification. $Co_2(CO)_8$ was prepared according to an usual procedure.

Reaction Procedure. A catalyst solution containing $Co_2(CO)_8$, $Ru_3(CO)_{12}$, and phosphine in solvent was placed in a Hastelloy C(100 ml)- or Inconnel(20 ml)-autoclave, which was subsequently charged with syngas ($H_2/CO=1$). After the reaction, the reaction vessel was cooled to room temperature and the solution was analyzed by GLC. IR spectra were measured with a JEOL A-302 type spectrometer.

This work is a part of "C_1 Chemistry Project," a National Research and Development Program of Agency of Industrial Science and Technology, Ministry of International Trade and Industry (M. I. T. I.), Japan.

References

1) a) B. D. Dombek. *J. Am. Chem. Soc.*, **103**, 6508 (1981); b) W. Keim, M. Berger, and J. Schlupp, *J. Catal.*, **61**, 359 (1980); c) D. R. Fahey, *J. Am. Chem. Soc.*, **103**, 136 (1981); d) J. F. Knifton, *ibid.*, **102**, 6855 (1980); f) W. Keim, M. Anstock, M. Roper, and J. Schlupp, *C_1 Mol. Chem.*, **1**, 21 (1984); g) A. Deluzarche, R. Fonseca, G. Jenner, and A. Kiennemann, *Erdoel Kohle, Erdgas, Petrochem, Brennst.-Chem.*, **32**, 313 (1979).

2) a) J. F. Kniftor, *J. Chem. Soc., Chem. Commun.*, **1983**, 729; b) R. Whyman, *ibid.*, **1983**, 1439; c) B. D. Dombek, *Organometallics*, **4**, 1707 (1985).

3) T. Masuda, K, Murata, T. Kobayashi, and A, Matsuda, *Nippon Kagaku Kaishi*, **1986**, 171.

4) K. Murata, A. Matsuda, and T. Masuda, 51st National Meeting of the Chemical Society of Japan, Kanazawa, October 1985, Abstr., No. 4 M01.

5) M. Tamura, M. Ishino, T. Deguchi, and S.

Nakamura, The third Symposium of C_1 Catalysis (at Tokyo, Japan), 1986, No. 9; E. Watanabe, Y. Hara, K. Wada, and T. Onoda, *Chem. Lett.*, **1986**, 285.

6) B. D. Dombek, *Adv. Catal.*, **32**, 325 (1983).

7) For Ru-I system in 18-crown-6 solvent, observed activation energies of 37.7 and 75.4 kJ mol^{-1} have been seen for the glycol and methanol productions. B. D. Dombek, *J. Organomet. Chem.*, **250**, 467 (1983).

8) A standard catalyst solution which is subjected to the IR analysis was prepared as follows; a hexane solution (20 ml) containing $Co_2(CO)_8$(0.2 mg-atom), $Ru_3(CO)_{12}$(0.2 mg-atom), and (i-Pr)$_3$P(0.4 mmol) was treated under the conditions of 1000 atm of syngas and 270 °C for 5 h. After the autoclave was cooled to room temp. and depressurized up to 20 atm, an aliquot sample was withdrawn from the vessel to a high pressure IR cell.

9) R. Whyman, *J. Organomet. Chem.*, **81**, 97 (1974).

10) J. S. Bradley, *J. Am. Chem. Soc.*, **101**, 7419 (1979).

11) F. Piacenti, M, Bianchi, E, Benedetti, and G, Braca, *Inorg. Chem.*, **7**, 1815 (1968).

12) UV spectra of the solution at atmospheric pressure were also consistent with the presence of $Co_2(CO)_8$(350 nm) and the absence of cluster $Ru_3(CO)_{12}$(390 nm). We also observed a weak IR band of $Co_2(CO)_7$[(i-Pr)$_3$P](1994 cm^{-1}).[10] But little glycol is generated in $Co_2(CO)_8$/(i-Pr)$_3$P system under the conditions (Fig. 1).

13) W. L. Gladfelter, G. L. Geoffroy, and J. C. Calabrese, *Inorg. Chem*, **19**, 2569 (1980). Also, the UV spectra under 80 atm at ambient temp. exhibited no cluster absorptions.

14) In the Ru/(i-Pr)$_3$P system, $Ru_3(CO)_{12}$ species was not present and, on the contrary, the cluster was present in Co-Ru system (UV spectra).

Interaction between Copper(I) Chloride and Active Carbon in Active Carbon-Supported Copper(I) Chloride as Solid Carbon Monoxide Adsorbent

Hidefumi HIRAI,* Keiichiro WADA, and Makoto KOMIYAMA
Department of Industrial Chemistry, Faculty of Engineering, The University of Tokyo
7-3-1, Hongo, Tokyo 113
(Received July 14, 1986)

Synopsis. Magnetic susceptibility (-4.7×10^{-9} m^3 kg^{-1}) of the carbon monoxide adsorbent prepared from 10.0 g of active carbon and 1.4 g of copper(I) chloride is in paramagnetic side with respect to the value (-10.1×10^{-9} m^3 kg^{-1}) estimated from the susceptibilities of the components. Almost all the copper atoms are in their monovalent states, as shown by X-ray photoelectron spectroscopy. These results have indicated specific interaction between active carbon and copper(I) chloride in the adsorbent.

Separation of carbon monoxide from gas mixtures is an important process in industry, since carbon monoxide is usually obtained as mixtures with nitrogen, hydrogen, methane, and carbon dioxide.[1]

In previous papers,[2,3] the authors showed that the active carbon-supported copper(I) chloride rapidly and reversibly adsorbed carbon monoxide under mild conditions. The adsorbing capacities of the adsorbents were much larger than the sum of the capacities of the active carbon and copper(I) chloride, indicating some interaction between them in the adsorbents.

This paper reports the results of magnetic susceptibility measurements and X-ray photoelectron spectroscopy on the active carbon-supported copper(I) chloride, which shed light on the interaction between active carbon and copper(I) chloride in the adsorbents.

Experimental

Active carbon was purchased from Kureha Chemical Industries Co. (BAC G-70R, Lot No. 810117; beads of average diameter ca 0.7 mm) and was subjected to a reduced pressure (6 mmHg) at 200 °C for 5 h immediately before use. The active carbon-supported copper(I) chloride was prepared by stirring 10.0 g of the active carbon in 15 cm^3 of aqueous hydrochloric acid solution (3 mol dm^{-3}) containing various amounts of copper(I) chloride at room temperature for 1 h, followed by the removal of the liquid phase at 6 mmHg, 100 °C.[2,3] The amount of copper(I) chloride supported onto the active carbon was determined by atomic absorption spectroscopy.

Magnetic susceptibilities were measured at room temperature by use of a CAHN Instrument Co. Model RG Automatic Electrobalance, which took advantage of the Gouy's method.[4] The permanent magnetic field, the magnetic field gradient, and the balance sensitivity were 5 kG (1 G=10^{-4} T), 4.841×10^6 G^2 cm^{-1}, and 0.1 μg, respectively. Specimens (100—500 mg) were charged into Pyrex glass vessels of diameter 8 mm and depth 10 mm under nitrogen. The susceptibilities of the specimens were determined by subtraction of the susceptibilities for the vessels without the specimens from the values for the vessels with them.

X-Ray photoelectron spectra were measured on a Shimadzu Electron Spectrometer ESCA 750 with Mg X-ray anode. Chemical shifts were determined by use of the $4f_{7/2}$ band of metallic gold at 84.0 eV as reference.

Results and Discussion

Figure 1 depicts the X-ray photoelectron spectra for the Cu_{2p} region of the active carbon-supported copper(I) chloride as carbon monoxide adsorbents, copper(I) chloride, and copper(II) chloride. The adsorbents exhibit spectra (a and b) having two bands at 933 and 953 eV, which are virtually identical with that (c) of copper(I) chloride. The spectra of the adsorbents, however, are significantly different from that (d) of copper(II) chloride, which shows four bands at 937, 944, 957, and 964 eV. Thus, almost all the copper atoms in the adsorbents are present in the monovalent states.

Table 1 lists the mass magnetic susceptibility of the adsorbent (Active Carbon/CuCl) composed of 10.0 g of the active carbon (Active Carbon) and 1.4 g of copper(I) chloride (CuCl) together with the values of the components. All of the adsorbent, the active carbon, and copper(I) chloride are diamagnetic, as shown by the negative values of the susceptibilities. The absolute value (4.7×10^{-9} m^3 kg^{-1}) of the susceptibility of the adsorbent is considerably smaller than that (10.1×10^{-9} m^3 kg^{-1}) estimated from the susceptibilities (-11.0×10^{-9} and -3.9×10^{-9} m^3 kg^{-1}, respec-

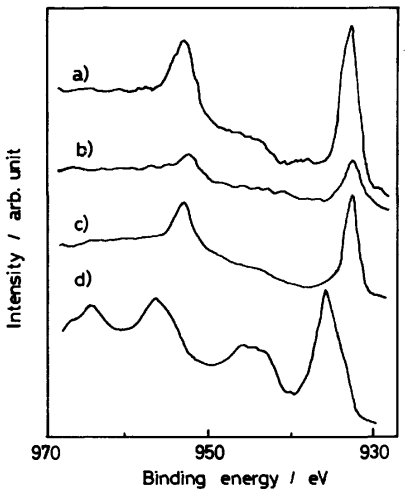

Fig. 1. X-Ray photoelectron spectra in the Cu_{2p} region for (a) the adsorbent prepared from 2.5 g of copper(I) chloride and 10.0 g of the active carbon, (b) the adsorbent prepared from 1.5 g of copper(I) chloride and 10.0 g of the active carbon, (c) solid of copper(I) chloride, and (d) solid of copper(II) chloride.

Table 1. Mass Magnetic Susceptibility of the Carbon Monoxide Adsorbent Prepared from 10.0 g of the Active Carbon and 1.4 g of Copper(I) Chloride as well as the Values for the Components

Specimen	Magnetic susceptibility[a] 10^{-9} m^3 kg^{-1}
Active carbon/CuCl	−4.7
Active carbon	−11.0
CuCl	−3.9

a) Negative signs refer to diamagnetic properties.

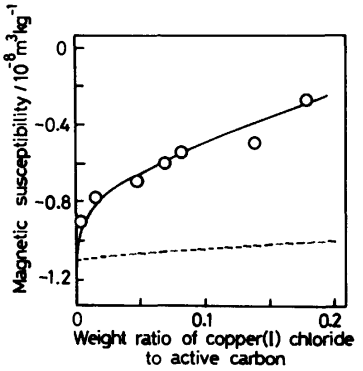

Fig. 2. Plot of mass magnetic susceptibility of the carbon monoxide adsorbent prepared from the active carbon and copper(I) chloride against the weight ratio of copper(I) chloride to the active carbon: the negative signs in the susceptibilities refer to diamagnetic properties; the broken line is a theoretical line evaluated from the susceptibilities of the components under the assumption that the additivity rule is valid.

tively) of the active carbon and copper(I) chloride under the assumption that the additivity rule is applicable here. In the rule proposed by Wiedemann,[5] the susceptibility is expressed by linear combination of the values of the components with the use of weight fractions as coefficients. This indicates that some paramagnetic species are formed by the interaction between the active carbon and copper(I) chloride.

The open circles in Fig. 2 depict the plot of the mass magnetic susceptibility for the adsorbent composed of the active carbon and copper(I) chloride as a function of the weight ratio of copper(I) chloride to the active carbon. The broken line refers to theoretical values evaluated by use of the additivity rule. All the experimental points are located in considerably paramagnetic sides with respect to the theoretical line. The magnitude of the deviation of the experimental point from the theoretical line significantly increases with increase in the weight ratio of copper(I) chloride to the active carbon.

These results show that some electronic interaction is operative between the active carbon and copper(I) chloride in the adsorbent. The interaction is probably associated with formation of pi-type complex between them. Electron donation from the active carbon to the copper(I) chloride as well as back donation from the copper atoms to the active carbon results in unpaired electrons both on the copper atoms and in the condensed aromatic rings of the active carbon, giving rise to the increase in the paramagnetic characters of the adsorbents.

These arguments are supported by the formation of pi-complexes between copper(I) ion and various olefins.[6] In the present adsorbents almost all the copper(I) chloride are present in their monomeric or dimeric forms.[3]

Virtually the same X-ray photoelectron spectra (a and b in Fig. 1) of the adsorbents with that (c) of copper(I) chloride is ascribed to rather small dependence of the chemical shifts of copper(I) ions on their chemical circumstances. The chemical shifts of Cu_{2p} bands for the complexes between copper(I) chloride and various ligands are identical with each other within 1.6 eV.[7]

The interaction between copper(I) chloride and active carbon in the adsorbents has been also examined by electron spin resonance spectroscopy. Detection of signals from the paramagnetic species in the adsorbents, however, has not been successful yet, probably due to both effective shielding of them from magnetic field by the active carbon and background signals from the active carbon.

High dispersion of copper(I) chloride on the surface of the active carbon in the active carbon-supported copper(I) chloride, which is essential for the large adsorbing ability of the adsorbents,[3] is attributable to the specific interaction between the active carbon and the copper(I) chloride. Without the interaction, copper(I) chloride is promptly bound each other through chlorine bridges, forming aggregates with minimal adsorbing capacities. In addition, decreases of the electron densities in the d-orbitals of the copper(I) ions, due to back donation from them to the active carbon, suppress back donation from the copper atoms to carbon monoxide. This weakens coordination bonds between the carbon monoxide and the copper(I) ions in the adsorbents, resulting in the effective desorption of the adsorbed carbon monoxide under mild conditions.

In conclusion, the magnetic susceptibility measurements as well as X-ray photoelectron spectroscopy have showed specific interaction between active carbon and copper(I) chloride in the active carbon-supported copper(I) chloride as solid carbon monoxide adsorbents. Effective and reversible adsorptions of carbon monoxide by the adsorbents are ascribed to the interaction.

The authors would like to thank Prof. Shunichi Kobayashi at the University of Tokyo for his help in the measurements of magnetic susceptibilities.

References

1) L. Kohl and F. C. Riesenfeld, "Gas Purification," 3rd ed, Gulf Publishing Co., Houston (1979).

2) H. Hirai, K. Wada, and M. Komiyama, *Chem. Lett.*, **1983**, 361.

3) H. Hirai, K. Wada, and M. Komiyama, *Bull. Chem. Soc. Jpn.*, **59**, 2217 (1986).
4) L. F. Bates, "Modern Magnetism," 3rd ed, Cambridge University Press, London (1951), p. 115.
5) Ref. 4, p. 14.
6) F. A. Cotton and G. Wilkinson, "Advanced Inorganic Chemistry," 4th ed, John Wiley & Sons, New York (1980) pp. 809—810.
7) D. C. Frost, A. Ishitani, and C. A. McDowell, *Mol. Phys.*, **24**, 861 (1972).

Adsorption of Cu^{2+} or Hg^{2+} Ion on Resins Prepared by Crosslinking Metal-Complexed Chitosans

Kazuya OHGA* Yoshiaki KURAUCHI, and Hiroshi YANASE
Department of Environmental Chemistry and Engineering, Faculty of Engineering, Oita University, Dannoharu, Oita 870-11
(Received June 21, 1986)

Synopsis. Crosslinking metal-complexed chitosans (metal ions=Cu(II), Cd(II), Zn(II), Ni(II), and Fe(III)) with (chloromethyl)oxirane yields resins having higher abilities to adsorb Cu^{2+} than a resin obtained from chitosan in the absence of metal ion. Resins from Cd(II)-chitosan complex can act as effective adsorbents for Hg^{2+}; their Langmuir's adsorption parameters depend on the quantity of (chloromethyl)oxirane used.

Chitosan has been used as an effective coagulating

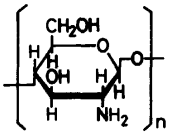

Chitosan

agent in activated sludge plants and for recovering proteins from food processing factories. This inexpensive polysaccharide can also act as an adsorbent for transition metal ions through chelation,[1-7] in which the amino group of the 2-amino-2-deoxy-D-glucose (glucosamine) unit plays an important role. The amino group is also responsible for dissolution of chitosan in acidic media.[2,3,5,7] This is one serious disadvantage from the practical viewpoint; thus, we attempted to crosslink chitosan with (chloromethyl)oxirane.[8] However, the crosslinking resulted in significant lowering of adsorptive activity, as will be described later. In the present paper, we describe that this problem can be largely overcome by crosslinking metal-complexed chitosan. Central metal ions of complexes are most likely to protect the amino group effective for the adsorption against the attack of the crosslinking agent and, at the same time, to preserve adsorption domains.

Experimental

Chitosan (Tokyo Kasei) was purified through gelation of its aqueous acetic acid solution with KOH, lyophilized, and sufficiently dried in vacuo (<0.13 Pa) for 2 d. The other reagents were of reagent or higher grade and used without further purification. All solutions were prepared with distilled, deionized water.

Preparation of Crosslinked Chitosan. Chitosan (5 g) was crosslinked with (chloromethyl)oxirane (2.9 g, equimolar to the glucosamine unit on the assumption that the chitosan is deacetylated completely[9]) accoding to the procedure reported by Noguchi et al.[10] The resin (NM-R) obtained was dried in vacuo (<0.13 Pa) to a constant weight 6.5 g.

Crosslinking of Metal-Complexed Chitosans. A 0.2 mol dm^{-3} NaOH solution was added dropwise to a 0.3 mol dm^{-3} acetic acid solution (40 cm^3) containing chitosan (500 mg) and a metal chloride ($CuCl_2$, $CdCl_2$, $ZnCl_2$, $NiCl_2$, or $FeCl_3$, equimolar to the glucosamine unit) with vigorous stirring to get a gelatinous metal-complexed chitosan.[5] The addition of the NaOH solution was stopped just before the solution pH got abruptly increased. The gel isolated after centrifugation was crosslinked with (chloromethyl)oxirane (2.9 g, ten times the molar quantity of the glucosamine unit) by the above method. The resin obtained was washed with 1.2 mol dm^{-3} HCl and 0.3 mol dm^{-3} acetic acid repeatedly to remove the metal ion and uncrosslinked chitosan, except for the Fe(III) complex which required conc. HCl to get rid of Fe^{3+} ion completely. The metal-free resin was washed subsequently with 0.2 mol dm^{-3} NaOH and with deionized water to neutral pH, and then dried similarly to the chitosan resin prepared in the absence of metal ion. The yields of the resins from the Cu(II)-, Cd(II)-, Ni(II)-, Zn(II)-, or Fe(III)-complex (abbreviated as Cu-R, Cd-R, Ni-R, Zn-R, or Fe-R, respectively) were 479, 477, 489, 487, and 250 mg, respectively. Likewise, crosslinking of the Cd(II) complex at (chloromethyl)oxirane/glucosamine unit molar ratios of 0.5, 1.0, 4.0, and 6.0 gave resins Cd-$R_{0.5}$, Cd-R_1, Cd-R_4, and Cd-R_6 in yields of 368, 394, 432, and 456 mg, respectively.

Equilibrium Adsorption Test. The resin was ground and sieved to 100—200 mesh size. After having been dried to constant weight, the sieved resin (10 mg) was placed in glass test tubes (16.5×165 mm), to which were added 0.05 mol dm^{-3} acetic acid/sodium acetate buffer solution (pH 5.0, 5 cm^3) containing a metal chloride (0.500—5.00 mmol dm^{-3} for Cu^{2+} or 1.00—8.00 mmol dm^{-3} for Hg^{2+}). The mixture was shaken at a shaking rate of ca. 110 strokes/min at 30.0±0.1 °C for 24 h. The equilibrated mixture was centrifuged, and then the supernatant solution was analyzed for the metal ion by atomic absorption spectrophotometry (Shimadzu AA-640-12). Hg^{2+} ion was determined by the cold vapor technique (Shimadzu mercury vaporizer unit MVU-1A). The quantity of metal ion adsorbed by the resin was obtained by subtracting the concentration in the supernatant solution from the initial concentration. A commercially available chelate resin, Chelex 100 (100—200 mesh; water content 68.8%), was also used for comparison.

Results and Discussion

Adsorption of Cu^{2+}. The ability of NM-R (the chitosan resin obtained in the absence of metal ion) to adsorb Cu^{2+} was first examined but no appreciable adsorption was observed. The resins prepared by crosslinking the metal-complexed chitosans adsorbed Cu^{2+} effectively. As Fig. 1 shows, the experimental isotherms obey the Langmuir equation, $C_{eq}/X=1/X_m b+C_{eq}/X_m$, where C_{eq} and X represent the equilibrium concentration of Cu^{2+} and the quantity of Cu^{2+} adsorbed, respectively. Adsorption parameters, binding constants b, and the quantities, X_m, of adsorbed Cu^{2+} ion with which the resins are saturated, are evaluated from the intercepts and slopes. The numerical data are summarized in Table 1, together

Table 1. Parameters for Cu^{2+} Adsorption

Adsorption parameters	Resins[a]					
	Cu-R	Cd-R	Zn-R	Ni-R	Fe-R	Chelex 100
X_m/mmol g^{-1}	1.4	1.2	0.92	0.78	0.67	2.3
b/$mmol^{-1}$ dm^3	1.1	1.1	1.0	0.51	0.73	1.9

a) Chitosan resins were prepared by crosslinking at a (chloromethyl)oxirane/glucosamine unit molar ratio of 10.

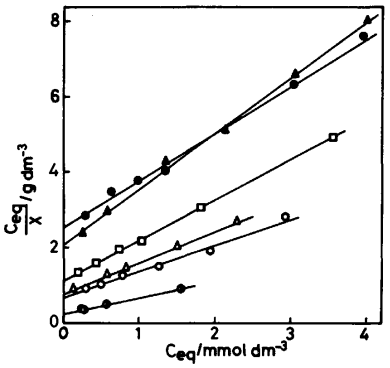

Fig. 1. Adsorption isotherms of Cu^{2+} on Cu-R(○), Cd-R(△), Zn-R(□), Ni-R(●), Fe-R(▲), and Chelex 100(◑) at 30.0 °C.

Table 2. Parameters for Hg^{2+} Adsorption

Adsorption parameters	Resins					
	Cd-R	Cu-R	Fe-R	Ni-R	NM-R[a]	Chelex 100
X_m/mmol g^{-1}	1.6	1.5	1.3	1.1	0.85	1.5
b/$mmol^{-1}$ dm^3	2.6	0.98	0.51	0.56	1.6	2.4

a) Prepared by crosslinking with (chloromethyl)oxirane of equimolar quantity to the glucosamine unit. For the other chitosan resins, see the footnote in Table 1.

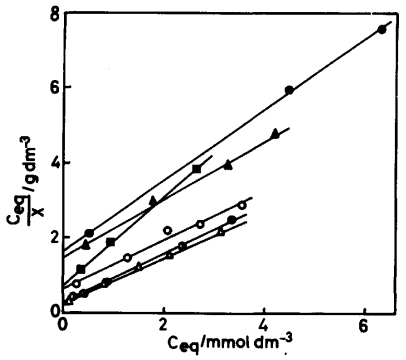

Fig. 2. Adsorption isotherms of Hg^{2+} on Cu-R(○), Cd-R(△), Ni-R(●), Fe-R(▲), NM-R(■), and Chelex 100(◑) at 30.0 °C. C_{eq} and X represent the equilibrium concentration of Hg^{2+} and the quantity of Hg^{2+} adsorbed, respectively.

with those for the commercial resin, Chelex 100. The quantities of Cu^{2+} uptake on the chitosan resins steeply decrease below pH 3, probably due to the protonation of the amino gourp of the glucosamine unit prevailing over its coordination to Cu^{2+}. The adsorption behavior was thus investigated at pH 5.0 where the precipitate of copper(II) hydroxide is not formed.

It is important to note here that lowering of the adsorption ability of parent chitosan by crosslinking was so small when the Cu(II)–chitosan complex (for resin (Cu-R), which of the chitosan resins has the largest adsorption parameters) was used; the uptake of Cu^{2+} from 5 cm^3 of an unbuffered solution ($[Cu^{2+}]=1.17$ mmol dm^{-3}) onto Cu-R or chitosan powder (10 mg) were 52 and 62%, respectively, at adsorption equilibrium. Thus, the central metal ions of the chitosan complexes serve to retain the adsorption ability of chitosan. This suggests that the metal ions can successfully leave domains available for the adsorption upon the removal of the ions from the resins. It is probable that the coordination of the amino groups to the metal ions leads to crosslinking between the hydroxyl groups so that the amino groups survive in the adsorption domains. Moreover, the fact that Cu-R has the largest adsorption parameters of the chitosan resins used, supports the idea that the Cu^{2+} ion in the complex serves, to some extent, as a template ion.[11] The parameters for Cd-R, comparable to those for Cu-R, can be explained in terms of the large ionic radius of Cd^{2+}.

Table 1 also demonstrates that the abilities of the chitosan resins to adsorb Cu^{2+} are lower than that of Chelex 100. However, it should be emphasized that, for the adsorption of Hg^{2+}, Cd-R was found to possess a high ability comparable to that of Chelex 100 known as an excellent chelating resin for Hg^{2+},[6] as will be mentioned in the following subsection.

Adsorption of Hg^{2+}. The isotherms for Hg^{2+} adsorption are also of Langmuir's type as shown in Fig. 2. The parameters obtained are summarized in Table 2.

Of the metal ions used for complexing with chitosan, Cd^{2+} has the largest ionic radius, so that Cd-R could be expected to have the greatest advantage for the adsorption of Hg^{2+} having a large ionic radius. This anticipation has been embodied by the large adsorption parameters of Cd-R, especially by its quite large binding constant comparable to that of Chelex 100.

NM-R has a moderate ability to adsorb Hg^{2+}. This adsorption behavior, different from the case of the Cu^{2+} adsorption, seems due to the coordination to Hg^{2+} of the hydroxyl groups and the ethereal oxygen atoms originating from the parent chitosan and (chloromethyl)oxirane. Thus, in the case of the resins from the metal–chitosan complexes also it is necessary to take into account the participation of these oxygen atoms.

Figure 3 and Table 3 are for the resins prepared by crosslinking the Cd(II)–chitosan complex with reduced quantities of (chloromethyl)oxirane. As Fig. 3

Table 3. Parameters for the Adsorption of Hg^{2+} on Resins Prepared by Crosslinking the Cd(II)-Chitosan Complex with Different Quantities of (Chloromethyl)oxirane

Adsorption parameters	Resins[a]			
	Cd-R_6	Cd-R_4	Cd-R_1	Cd-$R_{0.5}$
X_m/mmol g^{-1}	1.8	1.9	2.5	2.6
b/mmol^{-1} dm^3	1.8	1.7	1.5	1.2

a) The numbers appearing after Cd-R denote the molar ratio of the (chloromethyl)oxirane used for crosslinking to the glucosamine unit.

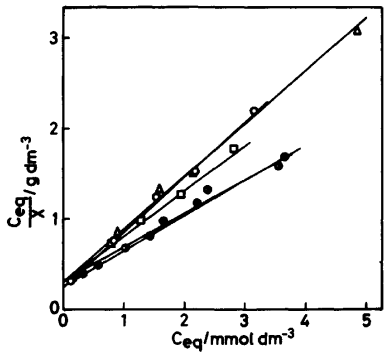

Fig. 3. Adsorption isotherms of Hg^{2+} on Cd-R_6(△), Cd-R_4(□), Cd-R_1(●), and Cd-$R_{0.5}$(◑) at 30.0 °C. For comparison, the isotherm for Cd-R(○) was plotted again. For C_{eq} and X, see the footnote in Fig. 2.

shows, Cd-R_4, Cd-R_1, and Cd-$R_{0.5}$ adsorb Hg^{2+} in larger quantities than Cd-R_6 and Cd-R do. Table 3 indicates that the X_m value progressively increases with decrease in the amount of (chloromethyl)oxirane used. The b value, on the contrary, tends to decrease. Thus, the above improvement of the adsorption ability by use of reduced quantities of oxirane, for which the resulting reduced degree of crosslinking is most probably responsible, is due to the increment in the X_m value prevailing over the decrement in the b value. The X_m value of Cd-R_1 is three times as large as that of NM-R (Table 2), which was crosslinked with the same molar quantity of (chloromethyl)oxirane as Cd-R_1. This again verifies the effectiveness of the central ion, Cd^{2+}, for leaving the domains available for the adsorption of Hg^{2+}.

Separation of Cu^{2+}, Hg^{2+}, and Cd^{2+} Ions. A great difference in the b value was observed between the adsorptions of Cu^{2+} and Hg^{2+} on the Cd-R resin (Tables 1 and 2). Moreover, Cd^{2+} was not adsorbed appreciably on Cd-R or Cd-R_6 under the same conditions as those for the Cu^{2+} or Hg^{2+} adsorption. These findings suggest that a selective separation of Cu^{2+}, Hg^{2+}, and Cd^{2+} ions is feasible by using an appropriate resin obtainable from the Cd(II)-complexed chitosan. Figure 4 illustrates that this separation may be achieved with 95—100% recovery by using a small column (8.0 cm×0.4 cm i.d.) containing 40 mg of Cd-R_6. The following solutions were successively used as eluents: 0.05 mol dm^{-3} acetate buffer, 1.00 mmol dm^{-3} HNO_3, and 0.5 mol dm^{-3} HNO_3. In addition, almost the same chromatograms were obtained when the metal ions were loaded into the column again after complete washing with deionized water, which indicates an effective durability in repeated use.

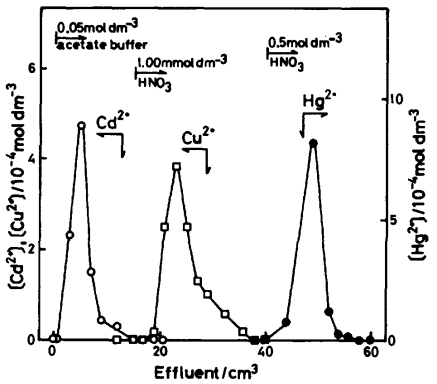

Fig. 4. Separation of Cd^{2+}, Cu^{2+}, and Hg^{2+} ions with a Cd-R_6 column (8.0 cm × 0.4 cm i.d., 40 mg of Cd-R_6). The quantities of the metal ions loaded were 2 μmol for Cd^{2+}, 3 μmol for Cu^{2+}, and 4 μmol for Hg^{2+}. The flow rate was 2 cm^3/h.

References

1) K. Kurita, Y. Koyama, and A. Taniguchi, *J. Appl. Polym. Sci.*, **31**, 1169 (1986).
2) Y. Kobayashi and T. Nakayama, *Mizu Shori Gijutsu*, **26**, 303 (1985).
3) M. S. Masri, V. G. Randall, and A. G. Pittman, *Am. Chem. Soc., Polym. Prepr.*, **19**, 483 (1978).
4) R. A. A. Muzzarelli and L. Sipos, *Talanta*, **18**, 853 (1971).
5) R. A. A. Muzzarelli, *Anal. Chim. Acta*, **54**, 133 (1971).
6) R. A. A. Muzzarelli, G. Raith, and O. Tubertini, *J. Chromatogr.*, **47**, 414 (1970).
7) R. A. A. Muzzarelli and O. Tubertini, *Talanta*, **16**, 1571 (1969).
8) Crosslinking with pentanedial has also been reported to give insoluble chitosan resins.[1,3]
9) The molar ratios mentioned hereinafter are also based on this assumption.
10) J. Noguchi, S. Tokura, M. Inomata, and C. Asano, *Kogyo Kagaku Zasshi*, **68**, 904 (1965).
11) a) The selective adsorption of a template ion has also been observed with chelating resins prepared by crosslinking metal-poly(4-vinylpyridine) complexes;[11b] b) H. Nishide and E. Tsuchida, *Macromol. Chem.*, **177**, 2295 (1976).

 © 1987 The Chemical Society of Japan Bull. Chem. Soc. Jpn., 60, 447—451 (1987)

Acridine Derivatives. I. Molecular Structure of the Novel Acridinyl-Substituted Uracil, 5-(9-Acridinyl)-6-amino-1,3-dimethyluracil

Michio Kimura
Niigata College of Pharmacy, 5829 Kamishin'ei-cho, Niigata 950-21
(Received April 25, 1986)

The reaction of enamine between 9-chloroacridines and 6-aminouracil derivatives give novel acridine substituted uracils, the structures of which have been determined by means of an X-ray analysis of 5-(acridin-9-yl)-6-amino-1,3-dimethyluracil hydrochloride dihydrate, $C_{19}H_{16}N_4O_2 \cdot HCl \cdot 2H_2O$. The crystal is triclinic with a space group $P\bar{1}$; also, $a=8.763(3)$, $b=16.130(9)$, $c=7.620(2)$ Å, $\alpha=117.51(4)$, $\beta=83.81(3)$, $\gamma=94.21(4)°$, $Z=2$, $V=949.3$ Å^3, $D_c=1.16$ g cm^{-3}, and $\mu=5.30$ cm^{-1} for Cu $K\alpha$. The structure was solved by a direct method and refined by a block-diagonal least-squares procedure: $R=0.074$ for 2810 reflections with $|F_o|>3\sigma(|F_o|)$. The crystal is composed of the title compound, chloride anion, and two molecules of water held together by hydrogen bonds (described in Table 4).

DNA has a reversible-binding ability for accepting planar molecules which can be inserted between the base pairs of a double helix.[1-4] Most intercalators are mutagens or compounds that have some significant biological and physicochemical properties.[5-9] It is thus of considerable interest to find new type intercalators and to understand the detailed manner of their binding modes within the confines of a double-helical structure. The recent synthesis and study of the 9-anilinoacridines (**5**) (Scheme 1)[10-19] which have antibacterial, antimalarial, mutagenic and carcinogenic properties by intercalating to DNA have encouraged us to investigate a synthesis of novel acridine derivatives and their molecular geometries. During this work the author observed the reaction of enamine between 9-chloroacridines (**2**) and 6-aminouracil derivative (**6**); this gives novel acridinyl-substituted uracils (**7**) instead of 6-(9-acridinylamino)uracils (**8**) corresponding to 9-anilinoacridines (**5**). In order to establish the structure of **7**, the title compound ($R_1=R_2=H$) was chosen for X-ray diffraction studies. The preparation of the novel acridinyl-substituted uracils, (**7**) shown in Scheme 1, followed general procedures: Jourdan-Ullmann condensation of an appropriate 2-chlorobenzoic acid and an aromatic amine formed an *N*-arylanthranilic acid (**1**). The acridine ring formation was carried out in many cases with $POCl_3$ in order to provide 9-chloroacridines (**2**)[20] directly; these were then coupled with the appropriate 6-aminouracil derivatives. When ring formation with $POCl_3$ was not desirable, this reaction was effected with either H_2SO_4, polyphosphoric acid (PPA), or polyphosphate ester (PPE) to give the 9(10*H*)-acridinones (**3**). These were then converted to the desired 9-chloroacridines (**2**) with $SOCl_2$/DMF.[21]

This paper is concerned about the molecular structure of 5-(9-acridinyl)-6-amino-1,3-dimethyluracil (**7**, $R_1=R_2=H$) obtained by means of an X-ray diffraction of its hydrochloride dihydrate.

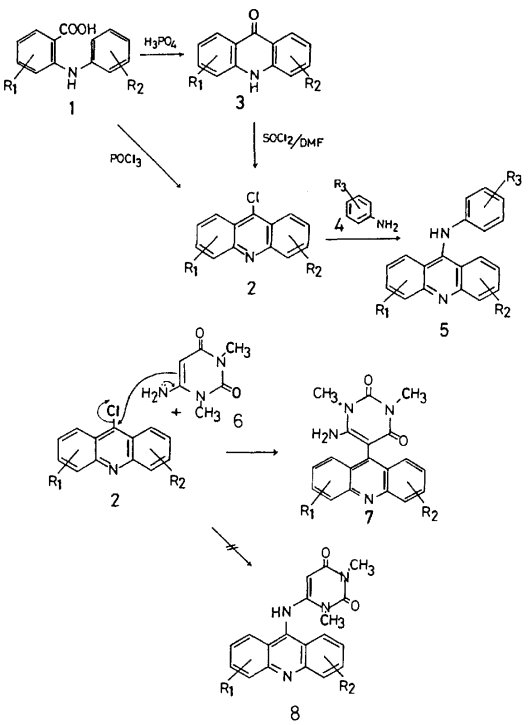

Scheme 1. Substituents R_1, R_2 and R_3 are alkyl, alkoxy, amino, nitro and methylsulfonylamino etc.[15]

Experimental

Preparation of 5-(9-Acridinyl)-6-amino-1,3-dimethyluracil. A mixture of 9-chloroacridine (1.0 g, 0.0047 moles) and 6-amino-1,3-dimethyluracil (0.73 g, 0.0047 moles) in 50 cm^3 of ethanol was stirred at room temperature for 20 h. At the end of this period the resulting red solid was filtered off and recrystallized from MeOH-H_2O (5 : 1 v/v) to give yellow crystals (1.33 g, 85%). Mp > 300 °C; TLC ($CHCl_3$ as an eluent) R_f=0.09; IR (KBr): 3500, 3170, 1690, 1640, 1580, 1500 cm^{-1}; ^{1}H NMR (DMSO) δ=3.24 (s, 3H), 3.46 (s, 3H), 6.65 (s, NH_2), 7.67—8.67 (m, 8H of acridine); MS *m/z* (rel intensity): 332 (M^+, 31), 174 (31), 141 (31), 97 (41), 81 (81), 70 (98), 57 (100).

Suitable crystals for X-ray investigation were obtained by a slow evaporation of an EtOH-H_2O solution added a drop of concd HCl at room temperature.

Collection and Reduction of Data. The crystal used for the X-ray study had approximate dimensions of 0.20×0.25×0.20 mm. The unit cell parameters at room temperature

were refined by least-squares using the Bragg angles (Cu $K\alpha$, λ=1.54178 Å) of 24 reflections ($30°<2\theta<40°$). The crystal data are given in Table 1. Intensity data were collected at room temperature on a Rigaku AFC diffractometer utilizing nickel-filtered Cu $K\alpha$ radiation. The θ—2θ scan mode was employed. The scan rate was 5° min^{-1} in θ, and the scan range in θ was varied by 1.2+0.15° tanθ. Background were counted for 7 s at both ends of the scan with an offset of 50% of the scan range from the calculated position of the $K\alpha$ peak. A total of 3479 unique reflections of the type $\pm h$, $\pm k$, l were measured in the range $2\theta<125°$. The intensities of three standard reflections measured after every 57 reflections dropped by an average of a few percent over the period of data collection; however, no correction was applied for this fluctuation. Lorentz and polarization corrections were applied but no absorption correction was applied (μ=5.30 cm^{-1} for Cu $K\alpha$). Standard deviations in the intensities, $\sigma(|F_o|)$, were derived directly from counting statistics.

Solution and Refinement of the Structure. The structure was solved by direct methods using *MULTAN* 78[22] to calculate phases for the 300 $|E|$ values with $|E|>1.50$. The E map computed from the phase set with the largest combined figure of merit (2.62) revealed all non-hydrogen atoms except for two oxygen atoms of water and one chlorine atom. The subsequent difference Fourier map readily gave the remaining atoms. Atomic parameters were refined by the block-diagonal least-squares procedure. The function minimized was $\sum w(|F_o|-|F_c|)^2$, where w was taken as $1/\sigma^2(F_o)$. All of the hydrogen atoms could be readily located from a difference Fourier map. During further refinement, anisotropic and isotropic thermal parameters were included for the non-hydrogen and hydrogen atoms, respectively. The refinement converged to a conventional $R=\sum||F_o|-|F_c||/\sum|F_o|$ of 0.057 and a weighted $R_w=\sum w(|F_o|-|F_c|)^2/\sum w|F_o|^2)^{1/2}$ of 0.079 with a GOF of 1.49 (Quality of fit=$[\sum w(|F_o|-|F_c|)^2/(N_{obsd}-N_{para})]^{1/2}$). The refinement was completed when the largest shift in any parameters among the non-hydrogen atoms was 0.05σ; the largest shift for hydrogen atoms was 0.08σ. The largest peak in the final difference map, 0.2 $eÅ^{-3}$, was located near the chlorine atom. Atomic scattering factors were taken from those of "International Tables for X-Ray Crystallography."[23] Mathematical and computational details are noted elsewhere.[24] Calculations were carried ouy by using the *UNICS*[25] program system on an ACOS 850 computer at the Crystallographic Research Center, Institute for Protein Research, Osaka University, and an ACOS 900 computer at Computation Center of Niigata University. The final positional parameters* of non-hydrogen and hydrogen atoms with equivalent isotropic and isotropic temperature factors are given in Table 2.

Table 1. Physical and Crystallographic Data

Formula unit	$C_{19}H_{16}N_4O_2 \cdot HCl \cdot 2H_2O$
M	332.34
Crystal system	triclinic
Space group	$P\bar{1}$
a/Å	8.763(3)
b/Å	16.130(9)
c/Å	7.620(2)
α/°	117.51 4)
β/°	83.81(3)
γ/°	94.21(4)
V/Å^3	949.3
Z	2
D_x/g cm^{-3}	1.163
Radiation	Cu $K\alpha$
λ/Å	1.54178
No. of reflections	
measured	3479
Observed [$\|F_o\|>3\sigma(\|F_o\|)$]	2810
R	0.057

Discussion

The estimated structure of the title compound has shown the novel acridine derivative substituted by uracil, which is obtained by the interesting reaction of the enamine of 9-chloroacridine and biological important uracil. The molecular structure and the atom labeling are illustrated by an ORTEP drawing in Fig. 1.[31] The bond lengths and angles are given in Table 3,

* Tables of anisotropic thermal parameters, coordinates of hydrogen atoms, least-squares planes, and the observed and calculated structure factors are kept as Document No. 8717 at the Chemical Society of Japan.

Table 2. Final Atomic Positional and Thermal Parameters with Estimated Standard Deviations in Parentheses

Atoms	x	y	z	B_{eq} (or B)/Å	Atoms	x	y	z	B_{eq} (or B)/Å
C 1	1.2119(6)	0.1252(4)	0.5562(7)	3.15	C15	1.0078(5)	0.2829(3)	0.7257(7)	2.48
C 2	1.3054(6)	0.0498(4)	0.4780(8)	3.96	C16	0.9224(6)	0.3037(3)	0.9084(7)	2.94
C 3	1.2634(6)	−0.0346(4)	0.3124(8)	3.97	N17	0.9782(5)	0.3795(3)	1.0765(6)	3.19
C 4	1.1300(6)	−0.0433(4)	0.2290(7)	3.32	C18	1.1032(6)	0.4345(4)	1.0705(7)	3.43
C 5	0.6604(6)	0.0823(4)	0.2048(8)	4.05	N19	1.1737(5)	0.4162(3)	0.8855(6)	2.92
C 6	0.5638(6)	0.1553(5)	0.2691(9)	5.20	C20	1.1298(5)	0.3404(3)	0.7136(7)	2.63
C 7	0.5990(6)	0.2437(5)	0.4248(9)	4.95	O21	0.8061(4)	0.2602(3)	0.9292(5)	3.86
C 8	0.7300(6)	0.2585(4)	0.5189(8)	3.77	C22	0.9098(8)	0.3947(5)	1.2744(8)	5.26
C 9	0.9706(5)	0.1953(3)	0.5484(7)	2.50	O23	1.1505(5)	0.4984(3)	1.2211(6)	4.89
N10	0.8978(5)	0.0262(3)	0.2295(6)	2.84	C24	1.3138(7)	0.4717(4)	0.8806(9)	4.40
C11	1.0730(5)	0.1201(3)	0.4721(7)	2.44	N25	1.2087(5)	0.3261(3)	0.5433(6)	3.26
C12	1.0330(5)	0.0345(3)	0.3088(7)	2.70	O26	0.5221(7)	−0.3020(4)	0.0006(9)	9.30
C13	0.8341(5)	0.1845(3)	0.4576(7)	2.69	O27	0.6107(6)	−0.4369(4)	−0.3881(7)	7.30
C14	0.7979(5)	0.0969(4)	0.2959(7)	2.95	CL	0.8014(2)	−0.1731(1)	−0.0748(2)	4.04

$B_{eq}=\frac{1}{3}(U_{11}+U_{22}+U_{33})$ (where $U_{11}=\frac{B_{11}}{8\pi^2 a^{*2}}$, etc.).

Table 3. Bond Distances and Angles with Estimated Standard Deviations in Parentheses

(a) Bond distances for non-hydrogen atoms (l/Å)

C 1-C 2 1.371(7)	C 1-C11 1.416(6)	C 2-C 3 1.422(8)	C15-C 9-C13 121.3(4)	C15-C 9-C11 119.2(4)
C 3-C 4 1.358(7)	C 4-C12 1.417(7)	C 5-C 6 1.367(8)	C13-C 9-C11 119.5(4)	C14-N10-C12 123.3(4)
C 5-C14 1.406(7)	C 6-C 7 1.410(9)	C 7-C 8 1.368(7)	C12-C11-C 9 119.1(4)	C 9-C11-C 1 118.0(4)
C 8-C13 1.424(7)	C 9-C11 1.418(6)	C 9-C13 1.406(6)	C 9-C11-C 1 122.9(4)	C11-C12-N10 119.5(4)
C 9-C15 1.481(7)	N10-C12 1.358(6)	N10-C14 1.357(6)	C11-C12-C 4 121.3(4)	N10-C12-C 4 119.2(4)
C11-C12 1.419(7)	C13-C14 1.424(7)	C15-C16 1.411(7)	C14-C13-C 9 119.4(4)	C14-C13-C 8 117.9(4)
C15-C20 1.388(6)	C16-N17 1.406(6)	C16-O21 1.233(6)	C 9-C13-C 8 122.7(4)	C13-C14-N10 119.2(4)
N17-C18 1.370(6)	N17-C22 1.476(7)	C18-N19 1.383(7)	C13-C14-C 5 121.2(4)	N10-C14-C 5 119.6(4)
O18-O23 1.224(6)	N19-C20 1.385(6)	N19-C24 1.474(7)	C20-C15-C16 121.0(4)	C20-C15-C 9 120.2(4)
C20-N25 1.330(6)			C16-C15-C 9 118.7(4)	O21-C16-N17 119.1(4)
			O21-C16-C15 125.0(5)	N17-C16-C15 115.9(4)
			C22-N17-C18 117.1(6)	C22-N17-C16 118.3(4)
(b) Bond angles (ϕ/°)			C18-N17-C16 124.2(4)	O23-C18-N19 120.7(5)
C11-C 1-C 2 120.4(5)	C 3-C 2-C 1 120.3(5)		O23-C18-N17 122.1(5)	N19-C18-N17 117.2(4)
C 4-C 3-C 2 121.4(5)	C12-C 4-C 3 118.6(5)		C24-N19-C20 120.4(4)	C24-N19-C18 116.9(4)
C14-C 5-C 6 118.7(5)	C 7-C 6-C 5 121.3(5)		C20-N19-C18 122.0(4)	N25-C20-N19 117.7(4)
C 8-C 7-C 6 120.8(5)	C13-C 8-C 7 120.0(5)		N25-C20-C15 123.0(4)	N19-C20-C15 119.3(4)

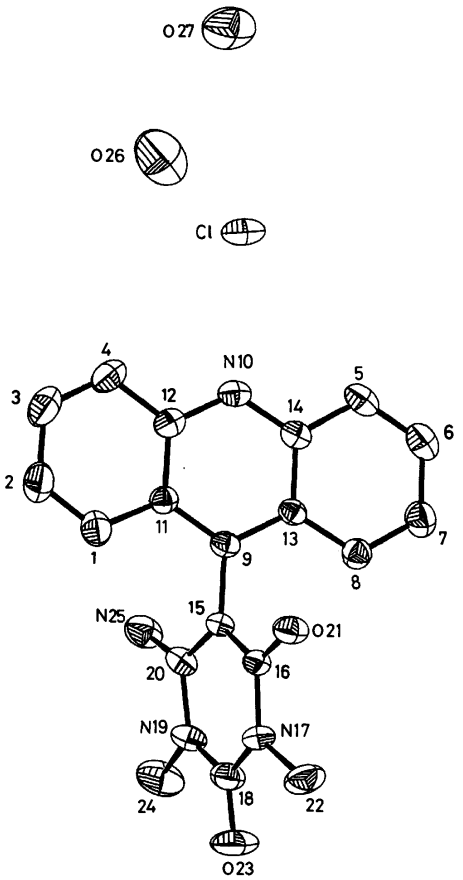

Fig. 1. An ORTEP[31] drawing of the title compound···Non-hydrogen atoms are drawn as thermal ellipsoids with 50% probability level.

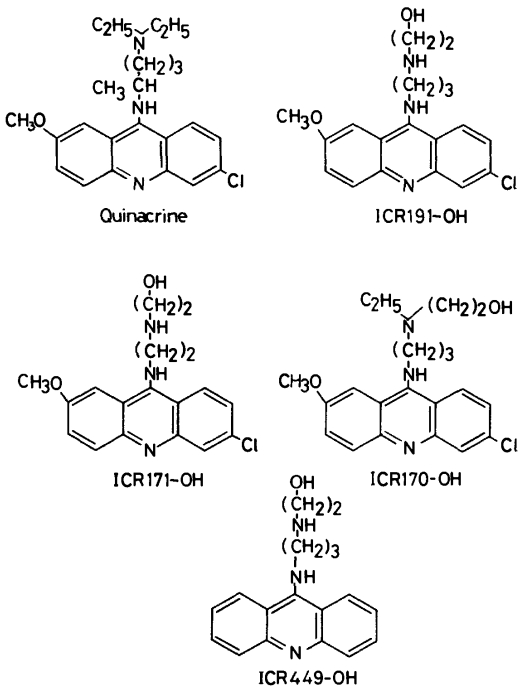

Fig. 2. Formulae of quinacrine and ICR series compounds.

together with estimated standard deviations. The average C-C distances of two benzene rings of acridine nucleus are 1.401 and 1.400 Å, respectively, while that of the C-N distances of the acridine nucleus is 1.358 Å. On the other hand, the uracil ring has average values of 1.386 Å in the C-N bond and 1.229 Å in the C=O bond. These values are normal, and the bond distances of the two benzene rings of acridine nucleus are exactly equivalent within experimental error. As shown in Fig. 1, the molecule consists of two planar portions. The derivatives from the least-squares planes through portions of the molecule are calculated and, the dihedral angle between the least-squares planes defined by the acridine ring and the uracil ring is 108.0°. The calculated dihedral angle is 2.5° between the best planes through the outer rings of the acridine ring system; these are compared with values of 8° for quinacrine,[26] 4.9° for ICR-191-OH,[27] 7.5° for ICR-171-OH,[28] 10.7°for ICR-170-OH,[29] and 12.5° for ICR-449-OH.[30] The formulate of the above ICR compounds are shown in Fig. 2. In these series of acridines, it seems that the more potent biological activities, such as antitumor and mutagenic activity,

Table 4. Hydrogen-Bond Distances (l/Å) and Angles (ϕ/°)

D-H···A	D-H	D···A	H···A	D-H···A
N10-HN10···Cl[a)]	0.94(8)	3.093(4)	2.20(8)	157.7(6.6)
N25-H1N25···Cl[a)]	0.84(6)	3.278(4)	2.47(6)	159.6(5.3)
N25-H2N25···O27[b)]	0.83(6)	2.870(7)	2.09(6)	157.2(6.3)
O26-H1O26···Cl	0.93(9)	3.271(6)	2.38(9)	159.9(7.6)
O26-H2O26···O21[c)]	1.11(7)	2.939(6)	1.83(7)	171.3(6.6)
O27-H2O27···O26	0.89(9)	2.813(9)	1.93(9)	167.4(7.7)
O27-H1O27···O23[d)]	1.03(7)	3.005(6)	2.00(7)	163.1(6.0)

Symmetry code: a) $1-x, -y, -z$; b) $1+x, y, z$; c) $x, y, z-1$; d) $x-1, y, z-1$

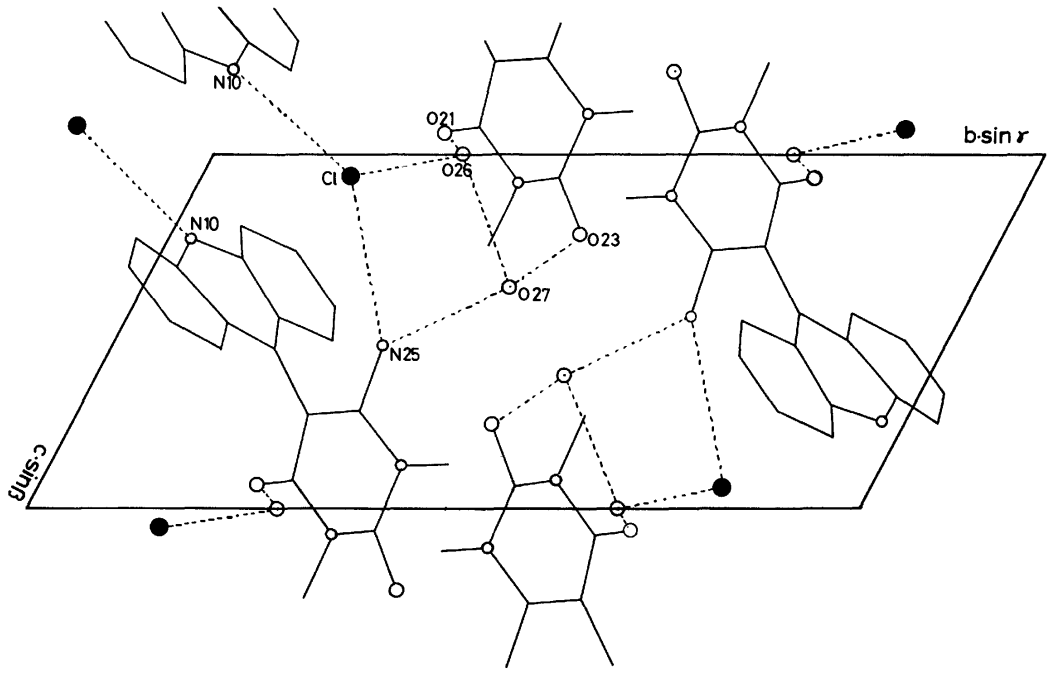

Fig. 3. Projection of the crystal structure along the a axis.

are caused by the flatter ring systems and better stacking ring systems as intercalators to DNA.

Hydrogen-bond distances and bond angles are given in Table 4. The molecules in the unit cell are connected by three-dimentional networks of hydrogen-bonds, composed of seven hydrogen atoms originating from atoms N25, O26, O27 and protonated N10, and corresponding hydrogen bonding acceptors (Fig. 3). That is, there are the hydrogen-bonds of 2.813 (9) Å between the water oxygen atom O27 and another water oxygen O26, and 2.939 (8) Å between the water oxygen atom O26 and the oxygen atom O21 of the uracil ring. Water oxygen atom O27 is also connected by oxygen O23 of the uracil ring and nitrogen atom N25 of the adjacent molecule by the hydrogen-bonds, 3.005 (8) and 2.870 (7) Å, respectively. On the other hand, the chloride anion has a hydrogen bonding interaction (3.093 (4) Å) with the protonated nitrogen atom N10 on which is also met a hydrogen atom (N10 ··· H=0.94 (8) Å).

In a similar synthetic method, the novel acridinyl-substituted uracils related to the title compound were also prepared. For those compounds, all the analytical and spectroscopic data are in accordance with the given structures (Scheme 1). The interesting physicochemical and biological properties of these compounds are expected, such as antitumor activity and their binding characteristics to DNA and to synthetic polynucleotide. The application of this reaction to other 6-aminouracil derivatives and nucleotide bases makes us such that we can find potent biologically active compounds as intercalators. Studies concerning the above topics are now in progress and results will be published in due course.

The author is grateful to Professor Masao Kakudo, Himeji Institute of Technology, and Professor Yukiteru Katsube and the staff of Crystallographic Research Center, Institute for Protein Research, Osaka University, for the use of diffractometer and ACOS 850 computer.

References

1) J. W. Drake, "The Molecular Basis of Mutation," Holdenday Inc., San Francisco (1970), p. 134.

2) S. Georghiou, *Photochem. Photobiol.*, **26**, 59 (1977).

3) D. J. Patel, *Biopolymers*, **16**, 2739 (1977).
4) F. S. Parker and J. L. Irvin, *J. Biol. Chem.*, **199**, 889 (1952).
5) M. J. Waring, *Eur. J. Cancer*, **12**, 995 (1976).
6) L. S. Lerman, *Proc. Natl. Acad. Sci. U.S.A.*, **49**, 94 (1963).
7) M. J. Waring, *Chem. Ind.*, **1975**, 105.
8) A. H. J. Wang, G. J. Quigley, and A. Rich, *Nucleic Acids Research*, **6**, 3879 (1979).
9) W. D. Wilson and R. H. James "Intercalation Chemistry," ed by M. S. Whittingham and A. J. Jacobson, Academic Press, New York (1982).
10) G. J. Atwell, B. F. Cain, and W. A. Denny, *J. Med. Chem.*, **20**, 520 (1977).
11) W. A. Denny, G. J. Atwell, and B. F. Cain, *J. Med. Chem.*, **20**, 1242 (1977).
12) W. A. Denny, G. J. Atwell, and B. F. Cain, *J. Med. Chem.*, **21**, 5 (1978).
13) W. A. Denny, G. J. Atwell, and B. F. Cain, *J. Med. Chem.*, **22**, 1453 (1979).
14) B. C. Baguley, W. A. Denny, G. J. Atwell, and B. F. Cain, *J. Med. Chem.*, **24**, 520 (1981).
15) W. A. Denny, B. F. Cain, G. J. Atwell, C. Hansch, A. Panthananickal, and A. Leo, *J. Med. Chem.*, **25**, 276 (1982).
16) W. A. Denny, G. J. Atwell, and B. C. Baguley, *J. Med. Chem.*, **26**, 1619 (1983).
17) G . J. Atwell, G. W. Rewcastle, W. A. Denny, B. F. Cain, and B. C. Baguley, *J. Med. Chem.*, **27**, 367 (1984).
18) G. W. Rewcastle, G. J. Atwell, B. C. Baguley, and W. A. Denny, *J. Med. Chem.*, **27**, 1053 (1984).
19) G. J. Atwell, B. F. Cain, B. C. Baguley, G. J. Finaly, and W. A. Denny, *J. Med. Chem.*, **27**, 1481 (1984).
20) A. Albert, "The Acridines," 2nd ed, Edward Arnold, London (1966), p. 403.
21) B. F. Cain, R. N. Seelye, and G. J. Atwell, *J. Med. Chem.*, **17**, 922 (1974).
22) P. Main, L. Lesseiger, M. M. Woolfson, G. Germain, and J. P. Declercq, *MULTAN* 78. A System of Computor Programs for the Automatic Solution of Crystal Structure from X-Ray Diffraction Data. Univs. of York, England and Louvain, Belgium (1978).
23) "International Tables for X-Ray Crystallography," Kynoch Press, Birmingham, Vol. IV (1974), p. 71, p. 102.
24) M. Kimura, *Bull. Chem. Soc. Jpn.*, **59**, 121 (1986).
25) T. Ashida and N. Yasuoka, *UNICS*-Osaka, Computation Center, Osaka University, 1979, and *UNICS* Niigata version at Niigata College of Pharmacy.
26) C. Courseille, B. Busetta, and M. Hospita , *Acta Crystallogr., Sect. B*, **29**, 2349 (1973).
27) H. L. Carrell, *Acta Crystallogr., Sect. B*, **28**, 1754 (1972).
28) J. P. Glusker, J. A. Minkin, and W. Orehowsky, Jr., *Acta Crystallogr., Sect. B*, **28**, 1 (1972).
29) H. M. Berman and J. P. Glusker, *Acta Crystallogr., Sect. B*, **28**, 590 (1972).
30) J. P. Glusker, B. Gallen, and H. L. Carrell, *Acta Crystallogr., Sect. B*, **29**, 2000 (1973).
31) C. K. Johnson, *ORTEP* II, Report ORNL-5138, Oak Ridge National Laboratory, Tennessee (1976).

 © 1987 The Chemical Society of Japan Bull. Chem. Soc. Jpn., 60, 453—456 (1987)

Liquid-Phase Hydration of Acrylonitrile to Acrylamide over the Manganese Dioxide Catalyst

Kazuo SUGIYAMA,* Hiroshi MIURA, Yasushi NAKANO, Hidehiro SUZUKI, and Tsuneo MATSUDA
Department of Applied Chemistry, Faculty of Engineering, Saitama University, Shimo-okubo, Urawa 338
(Received June 9, 1986)

The liquid-phase hydration of acrylonitrile to acrylamide was examined over a manganese dioxide catalyst at 65 °C. When the catalysts were treated at 110—500 °C, both the acidity and the reaction activity of the catalysts decreased at temperatures above 110 °C. The reduction of the solid acidity of heat-treated samples decreased the catalytic activity of the catalysts. It was confirmed that the solid acidity of manganese dioxide was derived from acidic hydroxyl groups on the catalyst surface through their dispersion in water. A good relationship between the number of surface hydroxyl groups and the catalytic activity of the manganese dioxide was observed; its hydration ability was depressed by the addition of an aqueous base as a NaOH solution. These results show that the acidic surface hydroxyl group of a manganese dioxide catalyst is the active site of acrylonitrile hydration. The kinetic behavior of both acrylonitrile and water was examined and the reaction rate showed both first and zero orders with respect to the acrylonitrile and water concentration, respectively. The hydration mechanism of acrylonitrile on the manganese dioxide catalyst is discussed.

In our previous papers,[1,2] it was reported that the heterogeneous hydration of acrylonitrile (AN) proceeded on various metal oxide catalysts in the liquid-phase. The hydration selectivity to the reaction products (acrylamide (AA), ethylene cyanohydrin and bis-(2-cyanoethyl) ether) was governed by the solid acid-base properties in the liquid phase. The acidic metal oxide catalysts selectively hydrated the C≡N triple bond of an AN molecule and only AA formed, while the basic metal oxide catalysts hydrated the C=C double bond rather than C≡N. AA is an especially useful material among those three products owing to such industrial uses as paper-strengthening agents, flocculants and crude-oil recovery agents. For AA production, manganese dioxide (MnO_2) was the most effective catalyst among the metal oxides since it exhibits a selectivity to AA.

The high catalytic ability of MnO_2 is well-known. A few examples include the oxidation of CO,[3,4] hydrocarbons[5,6] and the decomposition of H_2O_2.[7,8] Furthermore, since MnO_2 prepared by an electrolytic oxidation method has been used as a depolarizer of drycells, the surface properties of MnO_2 also have been studied by many investigators.[9-12] Regarding the catalytic abilities of MnO_2 on the liquid-phase hydration of AN to AA, they have been scarcely clarified. This study, therefore, aims to clarify the properties at the active sites of a MnO_2 catalyst as well as the hydration mechanism.

Experimental

Catalyst Preparation. A MnO_2 catalyst produced from the electrolytic oxidation of manganeous sulfate was supplied by Toyo Soda Manuf. Co. It was preheated at 110—500 °C for 1 h in air and then used for the hydration. MnO_2 catalysts having a differential surface coverage of Zn^{2+} ions were also prepared by an ion exchange of Zn^{2+} and the hydroxyl group on the MnO_2 samples preheated at 110 °C. The surface area was determined by the BET method. The crystal structure was identified by using the X-ray diffraction method.

Activity Measurement. The liquid-phase hydration of AN was carried out in a batch reactor system. Ordinary experimental conditions were as follows: reaction temperature of 65 °C, 6-h reaction time, 2.5-g catalyst, purified AN 8.5 and 100 ml of H_2O. A detailed description of the procedure was described in a previous paper.[2] The inhibition effects of the additives were examined by the addition of HNO_3, NaOH, AA, or acrylic acid in the reaction system suspended with a MnO_2 sample. After the reaction temperature reached 65 °C, AA was added.

Surface Hydroxyl Group. The amount of hydroxyl groups on the MnO_2 surface was determined in accordance with the manner described by Kozawa;[9,13,14] this method can be described as follows: a preheated MnO_2 sample (1.0 g) was placed into an Erlenmeyer flask with glass stopper, into which 25 ml of the zinc solution was poured. The zinc solution was prepared as follows: two moles of NH_4Cl and 0.1 mol of ZnO were dissolved in one liter of water and then adjusted to a pH of 7.0 by the addition of aqueous ammonia. The resulting suspension was shaken with the use of a vibrator for 12 h; it was then allowed to stand for 1 h. A portion of the supernatant solution was titrated by the EDTA method. The difference between the amount of Zn^{2+} adsorbed in this procedure and that consumed by the original solution corresponds to the number of Zn^{2+} ions. Another portion of the supernatant solution was titrated with a standard solution of HCl (0.01 mol dm^{-3}) using Methyl Orange as an indicator for determining the amount of released H^+. The difference between the amount of HCl consumed in this titration and that consumed by the original solution corresponds to the number of hydrogen ions released by the ion-exchange reaction.

Amount of AN Adsorbed. A preheated MnO_2 sample (2.5 g) was placed into an Erlenmeyer flask with a glass stopper; then, 100 ml of 2.5 wt% AN aqueous solution was poured into the flask. After stirring for 6 h, the sample was allowed to stand for 40 h at room temperature and was then kept at 40 °C for 4 h. The amount of adsorbed AN was determined from the difference of the concentration of AN before and after adsorption. The concentration of AN was measured by gas chromatography.

Acidic Properties. The surface acidity of MnO_2 samples was determined by an indicator titration method using

Table 1. Properties of the Manganese Dioxide Catalysts after Heat Treatment at Various Temperatures

Sample No.	Calcination temp(°C)	Surface area ($m^2 g^{-1}$)	Nitrile conv (%)[a]	Acid amount at pK_a=+4.8 (mmol g^{-1})	Equi-acid-base point/pH	X-ray diffraction analysis
1	110	33.2	13.3	0.078	3.6	γ-MnO_2 (amorphous)
2	200	28.5	10.9	0.051	4.1	γ-MnO_2
3	300	16.3	7.3	0.019	4.4	γ-MnO_2
4	400	13.3	5.4	0.029	5.2	γ-MnO_2
5	500	12.9	1.7	0.015	5.9	γ-MnO_2 (+ trace Mn_2O_3)

a) Reaction conditions: Reaction temperature; 65°C: Reaction time; 6h: Acrylonitrile 8.5ml, pure water 100ml: Catalyst weight; 2.5±0.1g.

Table 2. Amount of Adsorbed Zn^{2+} and Released H^+ Ion by the Ion-Exchange Reaction on the Manganese Dioxide Samples

Sample No.	Calcination temp(°C)	Amount of adsorbed Zn^{2+} (mmol g^{-1})	Amount of released H^+ (mmol g^{-1})	H^+/Zn^{2+} ratio	Amount of Surface OH groups (mmol g^{-1})[a]
1	110	0.26	0.54	2.1	0.52
2	200	0.23	0.44	1.9	0.46
3	300	0.19	0.40	2.1	0.38
4	400	0.07	0.14	2.0	0.14
5	500	0.05	0.11	2.2	0.10

a) Double molar quantity of the adsorbed Zn^{2+} was defined as the amount of surface OH groups on the MnO_2 samples on the basis of Kozawa's results.[9]

Methyl Red (pK_a=+4.8) as the indicator. The equi-acid-base point of MnO_2 samples, representing the solid acid-base properties of a metal oxide dispersed in water, was determined by a pH-shift method.[15] A detailed description of the procedure for both acidic property measurements was given in previous papers.[2,17]

Results and Discussion

Acidic Properties and Catalytic Activity. In one previous paper,[16] we reported that a large number of moderate-strength acid sites was present on the MnO_2 surface. The relationship between the acidic properties and the catalytic abilities of MnO_2 on the liquid-phase hydration of AN was investigated. As shown in Table 1, the catalytic activity (conversion of AN after a 6-h reaction) of MnO_2 catalysts decreased upon increasing the calcination temperature. A heat treatment of the catalysts simultaneously led to a reduction of both the specific surface area and the solid acidities, indicated by acid amounts at pK_a=4.8 and values of their equi-acid-base point. However, transformations of the crystal structure by heat treatments could not be observed, although the crystal growth was observed. The stability of the structure was also supported from the fact that neither the endothermic nor the exothermic peak was observed by a DTA analysis until 500°C. Therefore, it was concluded that the reduction of the catalytic activity by the heat-treatment was caused by a decrease in the acidic property of the catalysis accompanying a specific surface-area loss.

Surface Hydroxyl Groups. On the MnO_2 surface cation-exchangeable hydroxyl groups are present.[9,10] It was confirmed in a previous study[17] that the surface hydroxyl group had remained on the sample, even under a heat-treatment at 500°C. The number of surface hydroxyl groups on the MnO_2 dispersed in water was determined by the cation-exchange method. The obtained results are shown in Table 2. The number of adsorbed Zn^{2+} and released H^+ ions decreased upon increasing the heat-treatment temperature. The amount of released H^+ was twice that of adsorbed Zn^{2+}. This simple integral ratio indicates that a single Zn^{2+} ion exchanges with two H^+ ions of the surface hydroxyl groups as follows:

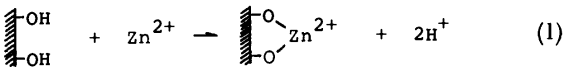

(1)

Therefore, a double molar quantity of the adsorbed Zn^{2+} was defined as the amount of surface hydroxyl groups on the MnO_2 samples.

The relation between the catalytic activity and the amount of surface hydroxyl groups of MnO_2 treated at 110—500°C was examined. The catalytic activity was directly proportional to the amount of surface hydroxyl groups (Fig. 1); the relationship between them can be described by

$$\text{ANconv.} = a[\text{-OH}]_s, \quad (2)$$

where a and $[\text{-OH}]_s$ are the constant of proportionality and the number of surface hydroxyl groups, respectively. The value of the correlation coefficient of a was determined to be 0.997. This result suggests that the acidic hydroxyl groups on the surface are the active sites for AN hydration.

The poisoning effects were examined. As shown in Fig. 2, the conversion of AN on the MnO_2 catalysts

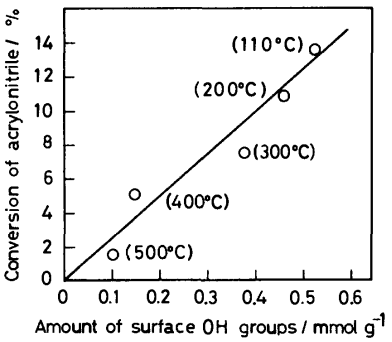

Fig. 1. Relationship between the conversion of acrylonitrile and amount of surface hydroxyl groups of the MnO_2 catalysts heat-treated at various temperature. The values in parentheses is that of calcination temperature. Reaction conditions are the same as those in Table 1.

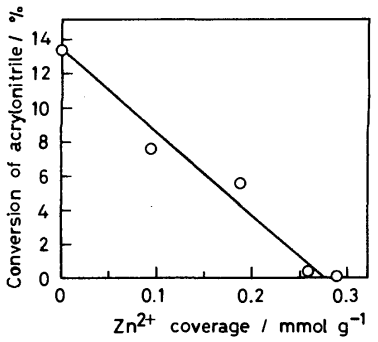

Fig. 2. Relationship between the conversion of acrylonitrile and surface covarage of Zn^{2+} ion on the MnO_2 catalysts treated at 110°C.

Table 3. Poisoning Effect of the Additives to MnO_2 Catalyst on the Hydration of Acrylonitrile[a)]

Additive	Nitrile conv(%)	Amide sel(%)
Blank	13.3	100
HNO_3 0.2 mmol	13.0	100
0.4 mmol	13.8	100
0.6 mmol	13.5	100
NaOH 0.2 mmol	12.2	100
0.4 mmol	10.1	90.6
0.6 mmol	7.1	73.1

a) Reaction conditions are the same as those in Table 1.

coated with various amounts of Zn^{2+} linearly decreased upon increasing the surface coverage of adsorbed Zn^{2+}. When acid or alkali was added to an AN solution the catalytic activity changed as shown in Table 3. The addition of HNO_3 had little effect on the catalytic activity and selectivity to AA; in the case of the addition of NaOH the catalytic abilities of MnO_2 decreased.

Consequently, we could conclude that the active site of a MnO_2 catalyst on the liquid-phase hydration of AN to AA is the acidic surface hydroxyl group.

Hydration Mechanism. The number of AN molecules adsorbed on the preheated MnO_2 samples was shown in Fig. 3. A good relationship between the number of adsorbed AN molecules and surface hydroxyl groups was observed with a slope of unity. Therefore, we concluded that an AN molecule adsorbs on a surface hydroxyl group.

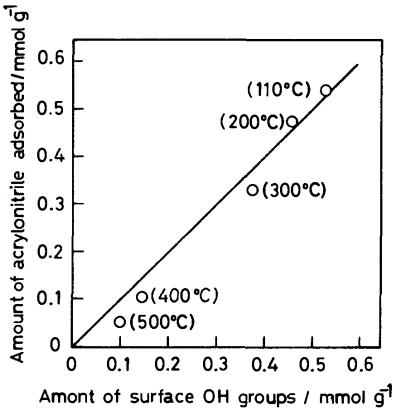

Fig. 3. Relationship between the amount of both adsorbed acrylonitrile and surface hydroxyl group of the MnO_2 catalysts treated at various temperature. Adsorption temperature: 40°C

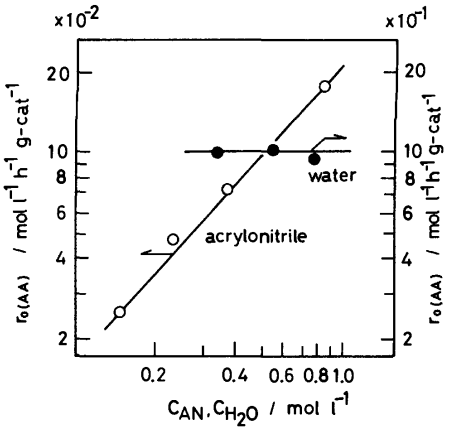

Fig. 4. Dependence on the concentration of acrylonitrile or water.
Reaction temperature: 65°C

The dependence of AN and the water concentration on the hydration rate of AN was examined and the results are given in Fig. 4. From this figure, the dependence on the concentration of each reactant was first order to the AN concentration and zero order to water. Consequently, the rate equation can be given as

$$r = k[\mathrm{AN}]^{1.0}[\mathrm{H_2O}]^{0}, \quad (3)$$

where k, [AN] and [H_2O] show a rate constant, concentration of AN and water, respectively. The rate equation shows that excess water is adsorbed on the catalyst surface and that its concentration on the surface is constant during hydration. The reaction between the adsorbed AN and adsorbed water is rate-determining. In addition, since the conversion of AN is proportional to the number of hydroxyl groups on the cata-

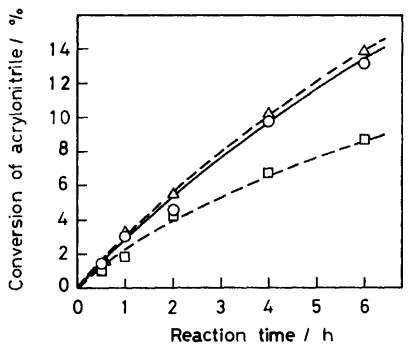

Fig. 5. Effect of additives.
(□): Acrylamide, (△): acrylic acid, (○): no addition
Reaction temperature: 65°C.

lyst surface, the equation can be rewritten as

$$r'=k'[\mathrm{AN}]^{1.0}[\mathrm{H_2O}]^{0}[\mathrm{-OH}]_{s}^{1.0}. \quad (4)$$

The catalytic abilities of MnO_2 were retarded by the addition of AA (Fig. 5). Thus, these results suggest that an accumulation of AA takes place on the MnO_2 surface during hydration in a batch reactor, retarding the reaction.

On the basis of the results described above, the hydration mechanism of AN to AA on the MnO_2 catalyst was postulated (Fig. 6). An acidic hydroxyl group exists on a Mn^{4+} ion of the MnO_2 surface and is surrounded by a large number of water molecules (see Fig. 6 (I)). An AN molecule first adsorbs on an acidic hydroxyl group (Fig. 6 (II)); then, a covalent coordination through N (2s) lone-pair electrons of a C≡N bond by the electrostatic force of attraction will take place on the surface hydroxyl group of MnO_2. Then, a hydroxide anion supplied from the surrounding water attacks the carbonium ion of the C≡N bond, whereas the residual proton adsorbs on Mn-$O^{\ominus}$ to regenerate hydroxyl group (III→IV). An amide group is formed by a 2,4-shift reaction of the precusor in the tautomerism system; then AA desorbs from the site (V). In this manner the liquid-phase hydration of AN to AA on the acidic hydroxyl group of MnO_2 will catalytically proceed as a Langmuir-Hinshelwood-type reaction mechanism.

Conclusion

The results of the liquid-phase hydration of AN to AA on a MnO_2 catalyst can be summarized as follows:

(1) The catalytic activity is proportional to the amount of the acidic surface hydroxyl group.

(2) An AN molecule adsorbs on a surface hydroxyl group.

(3) The reaction order is first-order with respect to AN and zero-order with respect to the water concentration, respectively.

(4) AA inhibits AN hydration.

It is concluded that active site of a MnO_2 catalyst is the acidic surface hydroxyl group and that hydration

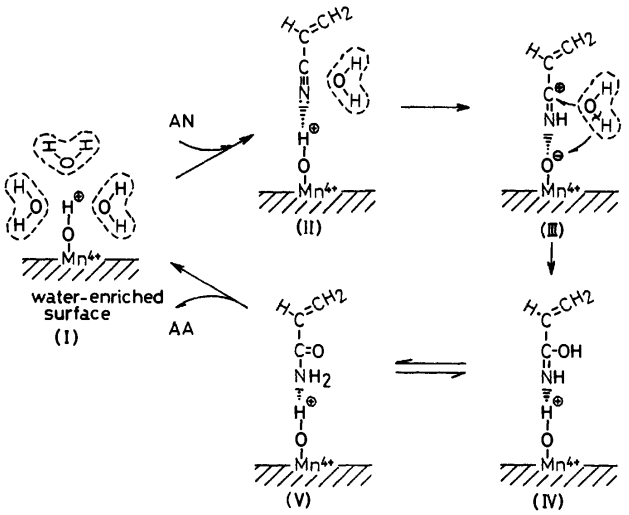

Fig. 6. Hydration scheme of acrylonitrile to acrylamide.

proceeds through a Langmuir-Hinshelwood-type mechanism between adsorbed AN and adsorbed water.

The authors greatly thanks the Toyo Soda Manuf. Co., Ltd. for supplying the MnO_2 sample.

References

1) H. Miura, K. Sugiyama, S. Kawakami, T. Aoyama, and T. Matsuda, *Chem. Lett.*, **1982**, 183.
2) K. Sugiyama, H. Miura, Y. Nakano, H. Sekiwa, and T. Matsuda, *Bull. Chem. Soc. Jpn.*, **59**, 2983 (1986).
3) G. Boreskov, "Advances in Catalysis," Academic Press (1965), Vol. 15, p. 285.
4) M. Kobayashi, H. Matsumoto, and H. Kobayashi, *J. Catal.*, **21**, 48 (1971).
5) J. M. Basset and W. F. Graydon, *J. Catal.*, **20**, 383 (1971).
6) H. J. Neuburg, M. J. Phillips, and W. F. Graydon, *J. Catal.*, **38**, 33 (1975).
7) J. Mooi and P. W. Selwood, *J. Am. Chem. Soc.*, **74**, 1750 (1952).
8) R. I. Razouk, G. M. Habashy, and N. Ph. Kelada, *J. Catal.*, **25**, 183 (1973).
9) A. Kozawa, *J. Electrochem. Soc.*, **106**, 552 (1959).
10) A. K. Covington, T. Cressey, B. G. Lever, and H. R. Thirsk, *Trans. Faraday Soc.*, **58**, 1975 (1962).
11) M. Yuyama, M. Anayama, S. Sakai, and K. Takahashi, *Denki Kagaku*, **34**, 962 (1966).
12) J. J. Laragne and J. Brenet, *Bull. Soc. Chim. Fr.*, **9**, 3499 (1968).
13) A.Kozawa, "Batteries, Vol. 1, Manganese Dioxide," ed by K. V. Kordesch, Marcel Dekker Inc. (1974), p. 385.
14) A. Kozawa, *Denki Kagaku*, **43**, 618 (1975).
15) I. Tari, K. Fujii, and T. Hirai, *Denki Kagaku*, **49**, 517 (1981).
16) K. Sugiyama, Y. Nakano, H. Miura, and T. Matsuda, *Bull. Chem. Soc. Jpn.*, **58**, 1825 (1985).
17) K. Sugiyama, Y. Nakano, S. Sano, H. Miura, T. Mitamura, and T. Matsuda, *Denki Kagaku*, **51**, 179 (1983).

 © 1987 The Chemical Society of Japan Bull. Chem. Soc. Jpn., 60, 457—462 (1987)

The Solvation Effect on the Reactions in Solution. I. The Solvation Model for the Interpretation of Entropy Changes in the Complex Formation of Dichlorodimethylstannane with Pyridine

Hideaki FUJIWARA,* Hiroyuki ARAKAWA, Saburo MURATA, Ikuzi OHTAKU, Motoko ISHII, and Yoshio SASAKI
Faculty of Pharmaceutical Sciences, Osaka University, 1-6 Yamada-Oka, Suita, Osaka 565
(Received July 9, 1986)

A complex-formation reaction has been studied for the Me_2SnCl_2 plus pyridine system in dimethyl phthalate (DMP) and dioctyl phthalate (DOP) by means of titration calorimetry. The resulting entropy changes in the reactions of A+B=AB and AB+B=AB_2, with A=Me_2SnCl_2 and B=pyridine, were compared with those calculated for the gas-phase reactions. The values in solution amounted only to 1/3—1/4 of the gas-phase values. Correction for the entropy of solution of each component failed to explain the observed values in the absence of a strong solvation. The solvation model is presented to allow for such a discrepancy, assuming a strong solvation for Me_2SnCl_2 as well as for the 1 : 1 pyridine complex by definite numbers of solvents. To test the applicability of the model, calculations were made based on molecular statistical thermodynamics. The results obtained were reasonable, indicating that a free molecule, Me_2SnCl_2, is solvated by 1.3 molecules of the solvent of DMP, which are released about half by half on the formation of the 1 : 1 and 1 : 2 complexes with pyridine.

Entropy changes upon reactions are generally expressed as the sum of the standard entropies of the products minus those of the starting materials. The standard entropy is equal to the (absolute) entropy of the compound in its standard state at an arbitrary temperature. Based on this concept, entropies of reactions have been calculated from the entropies of relevant compounds, which are either measured as thermodynamic third-law entropies in a calorimetric experiment or estimated statistically from the molecular theory for thermodynamic functions. The calculated entropies usually coincide well with those observed for gas-phase reactions, proving the thermodynamic third law. However, reactions in a solution are almost always accompanied by changes in solvation which affect the entropy change to a great extent. Therefore, solvation is essential for a full understanding of the entropy changes in a solution. In other words, entropy changes can be expected to offer important information regarding the solvation phenomena.

Hitherto, the thermodynamic aspects of reactions in solution have attracted attention mostly in terms of the enthalpy. The well-known Hammett substituent constants have been derived assuming a major contribution from the enthalpy term to the free energy change as a result of a negligible entropy term or a proportional enthalpy-entropy relationship. Some other empirical treatments, such as Drago's *E* and *C* parameters[1] and Gutmann's donor number,[2] have been developed for the enthalpy term in relation to acid-base reactions. Also, a classification of Pearson's hard and soft acids and bases (HSAB)[3] has been discussed quantum chemically[4] in relation to the enthalpy term, although the idea first came from a classification of the free energy changes. In contrast to this, the entropy term has long been overlooked in the discussion of the thermodynamic profiles. Hitherto, ion-pair formation has been discussed with regard to the entropy term, and the entropy of hydration has been obtained for different ion pairs.[5]

The present authors have previously reported that entropy changes upon the complex formation of some chloromethylstannanes with Lewis bases, as measured in halogenated hydrocarbon solvents, amount to only 1/3 of those estimated in the gas phase.[6,7] These results have been interpreted to indicate the release of a definite number of solvent molecules from the solvation sphere upon the complex formation. To take the solvation effect into consideration more exactly, in the present study the entropy term is discussed on the basis of thermochemical cycle. The solvents used are substituted phthalates, for which the entropies of solution can be measured by means of the gas-liquid chromatography.

Experimental

The Me_2SnCl_2 (Tokyo Kasei Co.) was purified by sublimation under a reduced pressure. The pyridine was dried over CaH_2 and distilled in a dry box. The dimethyl phthalate (DMP) and dioctyl phthalate (DOP) were distilled under reduced pressure in a dry box. Alkylbenzenes from commercial sources were used for the gas-liquid chromatography without further purification. The calorimetric titration experiments were performed on a Tronac 550 isothermal/isoperibol calorimeter under an isothermal mode. The details of this experiment were the same as those in Ref. 7. The gas-chromatographic retention data were collected on a Yanagimoto T-1880 gas chromatograph with a TCD detector. The column temperature was measured with a copper-constantan thermocouple. DMP and DOP were coated on 60/80 mesh Chromosorb W AW-DMCS (25 wt%). The temperature ranges measured were from 50 to 70 °C for DMP and from 85 to 135 °C for DOP. The retention data were extrapolated to the vanishing amount of the injection for each solute at each temperature.

Results

Our analysis of the calorimetric titration data is summarized in Table 1 for the complex formation of

Table 1. Analysis of Calorimetric Titration Data for the Me_2SnCl_2+Pyridine System in Dimethyl and Dioctyl Phthalates (DMP and DOP) at 25 °C

Solvent	K_1[a]	K_2[a]	$-\Delta H_1$[b]	$-\Delta H_2$[b]	$-\Delta S_1$[c]	$-\Delta S_2$[c]
DMP	26.7±0.7	4.0±0.2	30.8±0.3	30.7±2.5	76.1±0.9	91.4±8.2
DOP	22.4±0.8	3.8±0.2	32.5±2.1	34.9±0.3	83.3±7.1	106.0±2.1

a) $dm^3 mol^{-1}$. b) $kJ mol^{-1}$. c) $J K^{-1} mol^{-1}$.

Me_2SnCl_2 with pyridine in DMP and DOP. The successive formation of 1 : 1 and 1 : 2 complexes (Eqs. 1 and 2) has already been concluded from the analysis of the NMR[8] and of the calorimetric[9] titration data.

$$A+B=AB \qquad K_1,\ \Delta H_1,\ \Delta S_1 \tag{1}$$

$$AB+B=AB_2 \qquad K_2,\ \Delta H_2,\ \Delta S_2 \tag{2}$$

Table 1 shows that DMP and DOP resemble each other as solvents. Besides these two, the phthalates $C_6H_4(COOR)_2$ with R=C_2H_5, C_4H_9, C_7H_{15}, and C_9H_{19} were also tested, but the results showed no clear dependence on the carbon number in R.

The entropy of solution, which is necessary for the comparison of the entropies of reactions in solution and those in the gas phase, was derived from the retention data in gas-liquid chromatography. The basic equation used is as follows;[10]

$$\ln(V_g^0)+\ln(T\rho/273.15)=-\Delta H^s/RT+\Delta S^s/R, \tag{3}$$

where V_g^0 is the specific retention volume, T is the column temperature, ρ is the density of the liquid phase, and ΔH^S and ΔS^S are the enthalpy and entropy of solution, respectively. From the data of benzene, toluene, and ethyl-, propyl-, and isopropylbenzenes, the following relations were obtained between ΔS^S and the thermodynamic third-law entropy, $S^0_{298}(g)$:

$$\Delta S^s=-0.093\,S^0_{298}(g)-9.0 \qquad r=0.998 \text{ in DOP}, \tag{4}$$
$$(0.002)\quad(8.5)$$

$$\Delta S^s=-0.097\,S^0_{298}(g)+7.4 \qquad r=0.985 \text{ in DMP}. \tag{5}$$
$$(0.007)\quad(2.6)$$

Here, the values of $S^0_{289}(g)$ have been taken from Ref. 11. In Eqs. 4 and 5, r is the correlation coefficient and the standard errors are listed in parentheses.

Discussion

In the discussion of entropy changes upon complex-formation reactions in solution, rigorous calculation is very difficult because solvation contributes a great deal to the entropy of each component and because some physical properties, e.g., the fundamental vibrations at low frequencies and the physical properties of the complex especially, are frequently lacking. However, any discussion of the entropy changes in solution can be expected to disclose solvation phenomena in the reaction process. In this section, first, the entropy of reaction is estimated without assuming any specific solvation for each component; it will be compared with the experimental values.

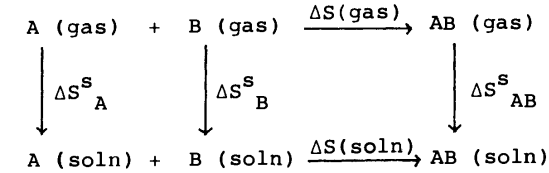

Fig. 1. A complex formation reaction of A+B=AB in gas phase and in solution. ΔS^s is the entropy of solution of each component.

i) Estimation of the Entropy Changes Assuming No Specific Solvation. For a simple reaction of A+B=AB, a thermochemical cycle will be given such as the one shown in Fig. 1. Generally, Eq. 6 holds for the gas-phase reaction, and a thermochemical consideration leads to Eq. 7:

$$\Delta S^0(gas)=S^0_{AB}(gas)-S^0_A(gas)-S^0_B(gas), \tag{6}$$

$$\Delta S^0(soln)=\Delta S^0(gas)+(\Delta S^s_{AB}-\Delta S^s_A-\Delta S^s_B). \tag{7}$$

In Eq. 6, $S^0_{AB}(gas)$, $S^0_A(gas)$, and $S^0_B(gas)$ are the standard entropies of AB, A, and B respectively in the gas phase at a standard state. Recently, Wertz proposed a simple relation between the entropy of solution, ΔS^S, and the thermodynamic third-law entropy, $S^0_{298}(g)$; he based this relation on a discussion of relatively simple molecules which interact only weakly with the solvent,[12] i.e.:

$$\Delta S^s=a\,S^0_{298}(g)+b. \tag{8}$$

The coefficents, a and b, in this equation were later reported to change slightly depending on the type of compound.[13] Here, it is clear that the entropy of solution of each component is actually non-vanishing, even if it does not interact strongly with the solvent. In the present case, Eq. 7 is converted to Eq. 9 (see Appendix 1).

$$\Delta S^0_{calcd}(soln)=(1+a)\,\Delta S^0(gas)-b-aR\ln 24.5 \tag{9}$$

where $\Delta S^0_{calcd}(soln)$ means $\Delta S^0(soln)$ as calculated from $S^0(gas)$ and Wertz's equation, $S^0(gas)$ being obtained from an experiment in the gas phase or from the molecular statistical method described above. Equation 9 is applicable to both steps of Eqs. 1 and 2 in the present study, but the coefficients a and b remain undetermined because of the unavailable third-law entropies in the gaseous and liquid states of DMP and DOP. To determine these coefficients, the entropies of solution were measured by means of gas-liquid chro-

matography for some hydrocarbons which interact only weakly with the phthalates (Eqs. 4 and 5). In this way, Eq. 9 proved to be Eqs. 10 and 11 in DOP and DMP, respectively for the reactions of both Eqs. 1 and 2:

$$\Delta S_{calcd}(soln) = 0.907\,\Delta S^0(gas) + 11.5 \quad \text{in DOP,} \quad (10)$$

$$\Delta S_{calcd}(soln) = 0.903\,\Delta S^0(gas) - 4.8 \quad \text{in DMP.} \quad (11)$$

Here, ΔS^0(gas) means S^0_{AB}(gas)-S^0_A(gas)-S^0_B(gas) and ΔS^0_{AB2}(gas)-S^0_{AB}(gas)-S^0_B(gas). In the present study, ΔS^0(gas) is obtained by means of the molecular statistical calculation (Appendix 2). As a first approximation, the vibrational part of the entropies was omitted in the calculation of ΔS^0(gas), for the contributions from the products and the starting materials were almost the same. Although detailed structural parameters are not required for the discussion below because of the minor dependence of the calculated entropies on the structural changes, references are cited for Me_2SnCl_2,[14] pyridine,[15] and $Me_2SnCl_2 \cdot (pyridine)_2$.[16] As for the 1:1 complex, two configurations were assumed, where either pyridine or the Cl group is located at an equatorial position besides the two methyl groups.[17] However, the resulting entropies were virtually unchanged. The comparison of the calculated values with the experimental value shown in Table 2 shows that the correction from the entropy of solution of each component is small and does not explain the difference between the entropies observed in solution and those calculated for the gas-phase reaction. Therefore, a model assuming no specific solvation fails to explain the results in the present study. Where, then, does this difference come from? If it were possible to measure ΔS^S for the AB complex similarly to those of A and B, ΔS^0(soln) could be estimated according to Eq. 7. However, this is impossible because of the labile character of the complex. For reference, the entropies of solution were measured for several methylstannanes (Table 3). These entropies decreased with an increase in the acidity of the stannanes: Me_4Sn exhibits no discernible tendency toward acid, whereas the acidity increases from Me_3SnCl to Me_2SnCl_2. Hence, this decrease is attributed to the increased solvation for the stannanes with increased acidity. In the following, a solvation model is presented which allows for the effect of strong solvation on the entropy of solution and helps to interpret the experimental entropies of reactions in solution measured above.

Table 2. Entropies of the Reactions in Solution and in the Gas Phase

	Solvent	Calculated[a]	Observed[a]
$(\Delta S^0_{soln})_1$	DOP	−209.5	−83.3
	DMP	−222.1	−76.1
	Gas phase	−270.3	—
$(\Delta S^0_{soln})_2$	DOP	−227.3	−106.0
	DMP	−239.8	−91.4
	Gas phase	−286.8	—

a) In units of $J\,K^{-1}\,mol^{-1}$.

ii) Solvation Model for the Interpretation of Entropy Changes in Solution. In Fig. 2 a solvation model is depicted for the reactions of A+B=AB and AB+B=AB_2, where A and AB are strongly solvated by m and n molecules of the solvent respectively, whereas AB_2, in which the tin atom possesses a coordination number of six, and B are not solvated, or are only weakly solvated, so that their entropies of solution are expressed by the Wertz-type equation. From a consideration of the

Table 3. Entropies of Solution ΔS^s for Several Methylstannanes as Determined by Means of Gas-Liquid Chromatography[a]

Mobile phase	Me_2SnCl_2	Me_3SnCl	Me_4Sn
DOP	−73.8±4.7	−58.1±5.6	−34.9±0.3
DMP	−98.6±0.7	−69.9±9.2	−37.6±1.5

a) In units of $J\,K^{-1}\,mol^{-1}$.

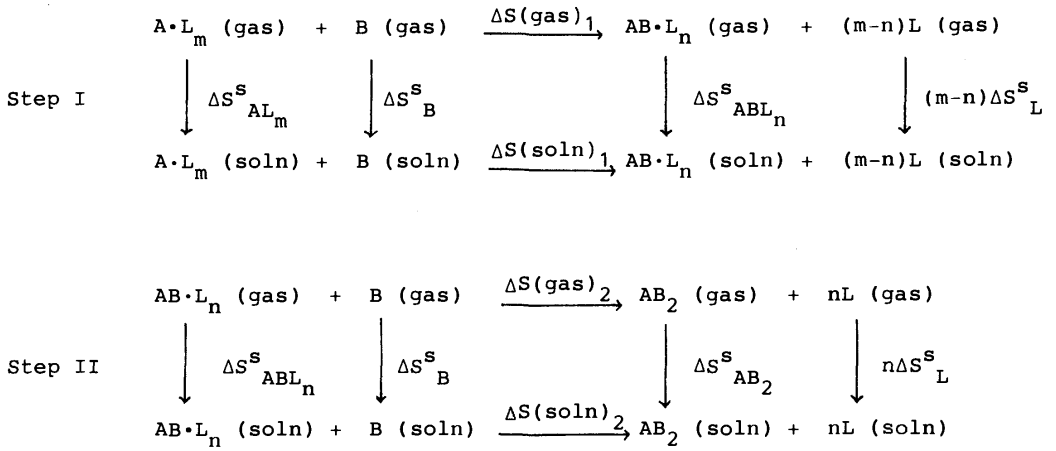

Fig. 2. The solvation model for the reactions of A+B=AB and AB+B=AB_2. A and AB are solvated strongly by m and n molecules of the solvent L, respectively.

thermochemical cycles in Fig. 2, the following equations are derived:

$$\Delta S^0(\text{soln})_1 = \Delta S^0(\text{gas})_1 + \Delta S^s_{ABL_n} + (m-n)\Delta S^s_L - (\Delta S^s_{AL_m} + \Delta S^s_B), \quad (12)$$

$$\Delta S^0(\text{soln})_2 = \Delta S^0(\text{gas})_2 + \Delta S^s_{AB_2} + n\Delta S^s_L - (\Delta S^s_{ABL_n} + \Delta S^s_B). \quad (13)$$

The substitution of Eq. A2 into Eqs. 12 and 13 leads to:

$$\Delta S^0(\text{soln})_1 = (1+a)\Delta S^0(\text{gas})_1 + (m-n-1)(b+aR\ln 24.5), \quad (14)$$

$$\Delta S^0(\text{soln})_2 = (1+a)\Delta S^0(\text{gas})_2 + (n-1)(b+aR\ln 24.5). \quad (15)$$

Here,

$$\Delta S^0(\text{gas})_1 = S^0_{ABL_n}(\text{gas}) + (m-n)S^0_L(\text{gas}) - S^0_{AL_m}(\text{gas}) - S^0_B(\text{gas}), \quad (16)$$

$$\Delta S^0(\text{gas})_2 = S^0_{AB_2}(\text{gas}) + nS^0_L(\text{gas}) - S^0_{ABL_n}(\text{gas}) - S^0_B(\text{gas}), \quad (17)$$

holds; also, the following equations hold when an additivity rule is assumed for the entropy of the strongly solvated species:

$$S^0_{AL_m}(\text{gas}) = S^0_A(\text{gas}) + m\{S^0_{AL}(\text{gas}) - S^0_A(\text{gas})\}, \quad (18)$$

$$S^0_{ABL_n}(\text{gas}) = S^0_{AB}(\text{gas}) + n\{S^0_{ABL}(\text{gas}) - S^0_{AB}(\text{gas})\}. \quad (19)$$

By substituting Eqs. 18 and 19 into 16 and 17, we obtain:

$$\Delta S^0(\text{gas})_1 = \Delta S^0_{AB}(\text{gas}) + n\Delta S^0_{ABL}(\text{gas}) - m\Delta S^0_{AL}(\text{gas}), \quad (20)$$

$$\Delta S^0(\text{gas})_2 = \Delta S^0_{AB_2}(\text{gas}) - n\Delta S^0_{ABL}(\text{gas}), \quad (21)$$

where, $\Delta S^0_{AB}(\text{gas}) = S^0_{AB}(\text{gas}) - S^0_A(\text{gas}) - S^0_B(\text{gas})$, $\Delta S^0_{ABL}(\text{gas}) = S^0_{ABL}(\text{gas}) - S^0_{AB}(\text{gas}) - S^0_L(\text{gas})$, $\Delta S^0_{AL}(\text{gas}) = S^0_{AL}(\text{gas}) - S^0_A(\text{gas}) - S^0_L(\text{gas})$, and $\Delta S^0_{AB_2}(\text{gas}) = S^0_{AB_2}(\text{gas}) - S^0_{AB}(\text{gas}) - S^0_B(\text{gas})$. Then, Eqs. 14 and 15 turn out to be:

$$\Delta S^0(\text{soln})_1 = (1+a)\Delta S^0_{AB}(\text{gas}) + n\Delta S^0_{ABL}(\text{gas}) - m\Delta S^0_{AL}(\text{gas}) + (m-n-1)(b+aR\ln 24.5), \quad (22)$$

$$\Delta S^0(\text{soln})_2 = (1+a)\Delta S^0_{AB_2}(\text{gas}) - n\Delta S^0_{ABL}(\text{gas}) + (n-1)(b+aR\ln 24.5). \quad (23)$$

The rearrangement of Eqs. 22 and 23 gives these expressions for m and n:

$$m = \frac{\Delta S^0(\text{soln})_1 - (1+a)\{\Delta S^0_{AB}(\text{gas}) + n\Delta S^0_{ABL}(\text{gas})\} + (n+1)(b+aR\ln 24.5)}{-(1+a)\Delta S^0_{AL}(\text{gas}) + (b+aR\ln 24.5)}, \quad (24)$$

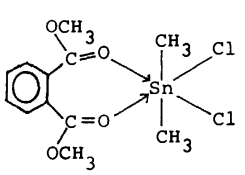

[Me_2SnCl_2·DMP]

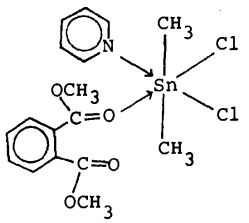

[Me_2SnCl_2·Py·DMP]

Fig. 3. Structures assumed as the strongly solvated species.

$$n = \frac{\Delta S^0(\text{soln})_2 - (1+a)\Delta S^0_{AB_2}(\text{gas}) + (b+aR\ln 24.5)}{-(1+a)\Delta S^0_{ABL}(\text{gas}) + (b+aR\ln 24.5)}, \quad (25)$$

Therefore, n can be determined from Eq. 25, the value of which will enable m to be determined from Eq. 24. In making these calculations, $\Delta S^0(\text{soln})_1$ and $\Delta S^0(\text{soln})_2$ can be replaced by experimental values, but definite structures need be assigned to AL and ABL in order to calculate the entropy of these strongly solvated species. The structures shown in Fig. 3 were assumed for the case of L=DMP. The molecular structures of pyridine[15] and DMP were taken to be the same in both free and complexed states, and also the structural data of the Me_2SnCl_2·(*N*,*N*-dimethylformamide)$_2$[18] complex was used for the Sn····O=C distance and angle in Me_2SnCl_2·DMP. The structure of DMP was determined on the basis of the standard bond lengths[19] and angles for sp^2 and sp^3 hybridization. Calculations were also performed under somewhat different structures for the complexes (e.g., a cis configuration with regard to the two Cl groups in Me_2SnCl_2·(pyridine)$_2$ or Me_2SnCl_2·pyridine·DMP), but the resulting entropies showed no discernible changes. In this way, m=1.34 and n=0.70 were obtained. This means that, when judged from the point of view of the entropy change, a free molecule of Me_2SnCl_2 is solvated by ca. 1.3 molecules of DMP, half of which are released when the 1 : 1 and 1 : 2 complexes are each formed with pyridine. As for the molecular structures of these strongly solvated species, the structures shown in Fig. 3 can be imagined. However, in the case of the solvated Me_2SnCl_2·pyridine complex, the solvent (DMP) molecule needs be either in a rapid exchange between the solvated state and a released state or in a rather weak solvation to make the averaged solvation number equal to 0.7. This number is probable since the tin atom is already coordinated by a strong base of pyridine before solvation occurs with a relatively weak base of DMP. Also, Me_2SnCl_2·DMP is solvated by an extra 0.3 molecule of DMP, on the average. This situation may be explained by a partial contribution from a solvated structure where two DMP molecules are involved.

iii) An Effect of the Entropy of Vibration in the Solvation Model. New vibrational degrees of freedom contribute to the entropy of reaction when new

chemical bonds are formed between the two participant molecules, leading to a complex. This number is six when one bond is formed to make a new complex, but such a vibrational term has been reported to be nontrivial from a comparison of the calculated sum of the translational and rotational entropies with the experimental total entropy for several gas-phase reactions.[20] When a linear relationship is assumed between the vibrational term, $\Delta S^0_{vib}(gas)$, and log μ according to Ref. 20, μ being the reduced mass of the complex, Eq. 26 is obtained from the data in the reference, excluding the complexes with a cyclic structure:

$$\Delta S^0_{vib}(gas) = 35.4 \log \mu - 20.4. \quad (24)$$

When this equation was used to estimate the vibrational terms in $\Delta S^0(gas)_1$, $\Delta S^0(gas)_2$, $\Delta S^0_{AL}(gas)$, and $\Delta S^0_{ABL}(gas)$, the latter values decreased by ca. 16% in absolute value and m=1.25 and n=0.65 resulted. That is, the conclusion given in this section does not change considerably even if the vibrational term is included in the calculation.

Appendix 1

Correction of Eq. 8 for the difference in standard states.

In Eq. 8, ΔS^s corresponds to the entropy changes of a gas at unit atm, and a and b are constants, which are determined from the entropies and other physical properties of the solvent. In the present study, the equilibrium constant is given in units of mol dm^{-3}: hence, ΔS^0(soln) and ΔS^0(gas) are given on that basis also, the standard state corresponding to a unit mol dm^{-3}. As this contrast, the third-law entropy, $S^0_{298}(g)$, is expressed relative to a standard state of 25 °C and 1 atm. Therefore, the gas-phase entropy, S^0(gas), in Eq. 6, which corresponds to a unit mol dm^{-3} at 25 °C, is connected with the $S^0_{298}(g)$ by the following equation under an ideal gas assumption:

$$S^0(gas) = S^0_{298}(g) - R \ln 24.5. \quad (A1)$$

Hence, Eq. 8 is converted to Eq. A2 for the present purposes:

$$\Delta S^s = a S^0(gas) + b + aR \ln 24.5, \quad (A2)$$

since ΔS^s itself does not change on this conversion of the standard state. The substitution of Eqs. 6 and A2 into Eq. 7 leads to Eq. 9.

Appendix 2

Calculation of entropies according to molecular statistical thermodynamics.

The entropy of a molecule is composed of several parts (translational, rotational, vibrational, and internal-rotational ones); i.e., $S = S_{tr} + S_{rot} + S_{vib} + S_{ir}$. Each part relates to the physical properties of the molecule:[21]

$$S_{tr} = R(1.5 \ln M + 2.5 \ln T - \ln P - 1.1650), \quad (A3)$$

$$S_{rot} = R(0.5 \ln I_A I_B I_C + 1.5 \ln T - \ln \sigma - 2.7106), \quad (A4)$$

$$S_{rot} = R(\ln I + \ln T - \ln \sigma - 2.1886) \text{ for linear molecules}, \quad (A5)$$

$$S_{vib} = R \sum_i [(\theta_i/T)\exp(-\theta_i/T)/\{1-\exp(-\theta_i/T)\} - \ln\{1-\exp(-\theta_i/T)\}], \quad \theta_i = h\nu_i/k, \quad (A6)$$

$$S_{ir} = S_{fir} - (S_f - S), \quad (A7)$$

where R is the gas constant, M is the molecular weight, T is the absolute temperature, h is Planck's constant, k is the Boltzmann constant, ν_1 is the wavenumber, and P is the pressure in atm, equal to 1/24.5 atm for an ideal gas of unit mol dm^{-3} at 25 °C. $I_A I_B I_C$ in Eq. A4 is the product of the principal moments of inertia and is calculated simply by using the moments of inertia with regard to any Cartesian axes x, y, or z, which go through the center of gravity:

$$I_A I_B I_C = \begin{vmatrix} I_{xx} & -I_{xy} & -I_{xz} \\ -I_{xy} & I_{yy} & -I_{yz} \\ -I_{xz} & -I_{yz} & I_{zz} \end{vmatrix} \quad (A8)$$

where $I_{xx} = \sum m_i(y_i^2 + z_i^2)$ and $I_{xy} = \sum m_i x_i y_i$.

σ is the symmetry number, which is equal to the number of rotational operations by which the molecule remains the same as before when all the atoms are numbered. Thus, the accurate calculation of entropies is feasible according to the above formalism. Some computer programs have also published,[22] in which several refinements such as "vibrational anharmonicity" are included.

References

1) R. S. Drago, *J. Chem. Educ.*, **51**, 300 (1974).
2) V. Gutmann, "Coordination Chemistry in Non-Aqueous Solutions," Springer-Verlag, Berlin (1968).
3) T-L. Ho, "Hard and Soft Acids and Bases," Academic Press, New York (1977).
4) G. Klopman, *J. Am. Chem. Soc.*, **90**, 223 (1968).
5) G. H. Nanchollas, *Quart. Rev.*, **14**, 402 (1960) and the references cited therein.
6) H. Fujiwara, F. Sakai, Y. Mikawa, and Y. Sasaki, *Bull. Chem. Soc. Jpn.*, **58**, 1741 (1985).
7) H. Fujiwara, F. Sakai, A. Kawamura, N. Shimizu, and Y. Sasaki, *Bull. Chem. Soc. Jpn.*, **58**, 2331 (1985).
8) H. Fujiwara, F. Sakai, and Y. Sasaki, *J. Phys. Chem.*, **83**, 2400 (1979).
9) F. Sakai, Ph. D. Thesis, Osaka University (1983).
10) E. F. Meyer, *J. Chem. Educ.*, **50**, 191 (1973).
11) D. R. Stull, E. F. Westrum, and G. C. Sinke, "The Chemical Thermodynamics of Organic Compounds," Wiley, New York (1969).
12) D. H. Wertz, *J. Am. Chem. Soc.*, **102**, 5316 (1980).
13) M. H. Abraham, *J. Am. Chem. Soc.*, **103**, 6742 (1981).
14) H. Fujii and M. Kimura, *Bull. Chem. Soc. Jpn.*, **44**, 2643 (1971).
15) B. Bak, L. H-Nygard, and J. R-Anderson, *J. Mol. Spectrosc.*, **2**, 36 (1958).
16) L. A. Aslanov, V. M. Ionov, V. M. Attiya, A. B. Permin, and V. S. Petrosyan, *Zh. Strukt. Khim.*, **19**, 185 (1978).
17) V. S. Petrosyan, N. S. Yashina, and O. A. Reutov, *Adv. Organomet. Chem.*, **14**, 63 (1976).
18) L. A. Aslanov, V. M. Ionov, V. M. Attiya, A. B. Permin, and V. S. Petrosyan, *Zh. Strukt. Khim.*, **19**, 109 (1978).
19) "Tables of Interatomic Distances and Configuration

in Molecules and Ions," Special Publication No. 11, A. D. Mitchell et al., General Eds., London, Chemical Society (1958).
20) A. Shepp and S. H. Bauer, *J. Am. Chem. Soc.*, **76**, 265 (1954).
21) G. Herzberg, "Molecular Spectra and Molecular Structure. II. Infrared and Raman Spectra of Polyatomic Molecules," Van Nostrand, New York (1945).
22) a) R. S. McDowell, QCPE Program No. 269, "Thermo," Indiana University; b) Y. Yoneda, "EROICA," Tokyo University Computation Center News, **14**, 119 (1982).

 © 1987 The Chemical Society of Japan Bull. Chem. Soc. Jpn., 60, 463—466 (1987)

Cationic Motions and Phase Transitions in $[(CH_3)_4N]GaBr_4$ Crystals as Studied by ^1H NMR and Differential Thermal Analysis Techniques

Setsuko SATO and Daiyu NAKAMURA*
Department of Chemistry, Faculty of Science, Nagoya University, Chikusa-ku, Nagoya 464
(Received August 6, 1986)

Two phase transitions were located for solid $[(CH_3)_4N]GaBr_4$ at 404 and 138 K. The temperature dependences of ^1H NMR spin-lattice relaxation times were determined mainly at 20 MHz. A shallow ^1H T_1 minimum appearing at ca. 400 K and a deep one below ca. 250 K were observed. The latter minimum could be explained by the occurrence of the overall reorientation of the cation as a whole with an activation energy of 14.5 kJ mol^{-1}. The shallow ^1H T_1 minimum may come from temperature dependent quadrupolar relaxation of bromine nuclei through the dipolar relaxation of the second kind.

Dynamical behavior of tetramethylammonium, $(tetMA)^+$, cations in various crystalline salts has been extensively studied mainly using ^1H NMR techniques,[1–13] because of several motional modes of the cation expected to be activated with increasing temperature. The motions of the cation which contribute to ^1H spin-lattice relaxation time, T_1, around room temperature were shown in various solids to be random reorientation of the CH_3 groups about each C–N bond axis by 120°, i.e., the CH_3 C_3 reorientation, and the overall reorientation of the cations about the center of gravity.

In some crystals such as (tetMA)X (X=Cl, Br, I),[3] the above two kinds of motional modes are activated successively at well-separated temperatures. However, it is shown from our NMR studies on $(tetMA)_2MX_6$[10,11] and $(tetMA)_2CdX_4$[12] type complexes and some clathrate hydrates of (tetMA)OH[13] that the above reorientational processes of the cation do not necessarily take place step by step distinctly with changing temperature. The present investigation of the motion of $(tetMA)^+$ cations in $(tetMA)GaBr_4$ crystals has been undertaken to find an example of crystals in which the cation performs a different type of motions from those already clarified.

Experimental

At first, we carried out synthetic experiments to obtain $(tetMA)_2Ga_2Br_6$ according to the method described in literature[14] except adding bromine. The synthetic procedure was as follows. Granular gallium was dissolved in hydrobromic acid involving bromine in a temperature range of 70—80 °C. When (tetMA)Br was added to the resulting solution, a white precipitate was obtained from the hot solution. When the solution was cooled to room temperature, the precipitate completely dissolved. The precipitate obtained at higher temperatures was $(tetMA)GaBr_4$ in contrast to the product reported in the literature.[14] The existence of $[GaX_4]^-$ (X= Cl, Br) had been reported elsewhere.[15,16] Purification was made by successive recrystallizations from a warm hydrobromic acid solution and finally from a CH_3NO_2 solution. Anal. Calcd for $[(CH_3)_4N]GaBr_4$: C, 10.4; H, 2.6%. Found: C, 10.4; H, 2.6%. The sample prepared was further identified by taking far IR spectra. The $\tilde{\nu}_3$ band of $[GaBr_4]^-$ was observed at 273 cm^{-1} with a shoulder at 280 cm^{-1} as already reported for the same complex.[16]

^1H T_1 was measured at various temperatures by use of pulsed NMR spectrometers already reported[10,17] at the Larmor frequencies of 20 and 10.5 (partly) MHz. The conventional inversion method to observe free induction decay signals was employed to determine T_1 values. Differential thermal analysis (DTA) experiments were carried out with a homemade apparatus already described.[18] Temperatures in the above two kinds of experiments were determined employing a copper vs. constantan thermocouple and could be estimated to be accurate within ±1 K. The 2nd moments of ^1H NMR absorptions were determined by means of a JEOL-MW-40S spectrometer at several temperatures measured with an accuracy of ±3 K.

Results and Discussion

Since many kinds of crystals involving $(tetMA)^+$ cations are known to exhibit structural phase transition in their solid phase,[3–7,9–13] we carried out the experiments of DTA. When the sample at room temperature was cooled to 80 K, no heat anomaly could be detected as shown in Fig. 1. However, a broad and small endothermic anomaly was recorded at ca. 138 K with increasing temperature fairly rapidly (≈3.4 K min^{-1}). When the sample was heated from room temperature, an endothermic anomaly showing marked thermal hysteresis appeared at 404 K. Accordingly, it can be concluded that $(tetMA)GaBr_4$ crystals undergo a first order phase transition at 404 K and an unusual small phase transition at ca. 138 K.

The temperature dependences of ^1H T_1 observed at 20 MHz in a temperature range of 96—440 K and at 10.5 MHz between 246 and 435 K are shown in Fig. 2.

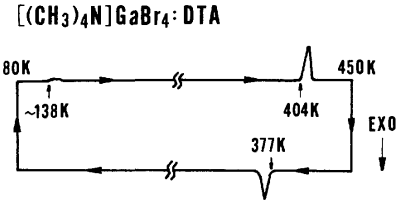

Fig. 1. Differential thermal analysis curves recorded for $[(CH_3)_4N]GaBr_4$.

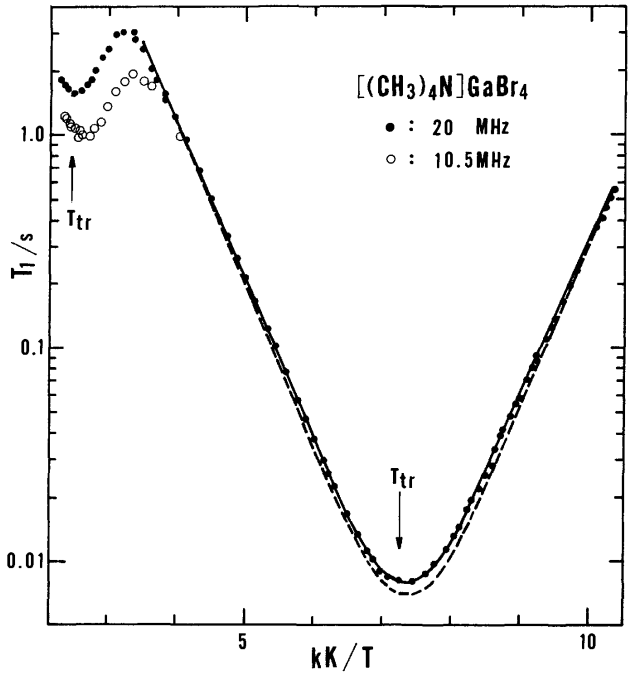

Fig. 2. Temperature dependence of ^1H T_1 observed for $[(CH_3)_4N]GaBr_4$ at 20 (●) and 10.5 (○) MHz. Solid and broken lines indicate the calculated curves using the BPP theory and the Takeda et al. method, respectively. T_{tr} indicates the phase transition temperatures determined from differential thermal analysis.

Below ca. 250 K, ^1H T_1 values determined formed a deep V-shaped curve, the minimum value of which was 8 ms obtained at ca. 135 K. On the other hand, ^1H T_1 values observed above ca. 250 K deviated from the V-shaped curve with increasing temperature and yielded a maximum around 310 K, above which temperature a very shallow T_1 minimum was obtained at ca. 400 K when observation was made at the Larmor frequency of 20 MHz. In this paper we mainly discuss about the T_1 curve having the deep minimum.

To assign the deep T_1 minimum to the motional mode of the cation, we determined the ^1H NMR 2nd moment, M_2, at several temperatures. The results are as follows: 24 G^2 at 77 K, 0.4 G^2 at 135, 167, and 215 K, 0.3_6 G^2 at 298 K, and 0.3_4 G^2 at 425 K. The rigid lattice M_2 value of an isolated $(tetMA)^+$ cation was calculated in a previous report[10] as 26.72 G^2 by use of the geometrical data reported by Andrew and Canepa.[1] For the present complex, the M_2 value observed at 77 K is very near to and only slightly smaller than the rigid lattice value. This suggests that the motions of the cation in $(tetMA)GaBr_4$ crystals are almost frozen at 77 K. On the other hand, very sharp ^1H NMR absorption lines were recorded above 135 K, indicating that the cations perform isotropic reorientation in the crystal. Accordingly, the deep T_1 minimum can be attributed to the isotropic reorientation, i.e., the C_2 and C_3 reorientations of the whole cation with or without the CH_3 C_3 reorientation of the four CH_3 groups.

According to the BPP theory,[19] T_1 due to magnetic dipolar relaxation mechanism can be written as

$$T_1^{-1} = C\left(\frac{\tau}{1+\omega^2\tau^2} + \frac{4\tau}{1+4\omega^2\tau^2}\right). \quad (1)$$

Here, ω, C, and τ represent the angular Larmor frequency employed, the motional constant, and the correlation time for the motion, respectively. By assuming the Arrhenius relation for the correlation time, one has

$$\tau = \tau_0 \exp(E_a/RT), \quad (2)$$

where τ_0 is the correlation time at the limit of infinite temperature and E_a is the activation energy for the motion.

^1H T_1 values observed below ca. 250 K were fitted to Eqs. 1 and 2 using E_a and the T_1 minimum values determined experimentally. The values of E_a and the T_1 minimum were 14.5 kJ mol^{-1} and 8 ms, respectively. The calculated BPP curve agrees very well with the observed data, suggesting that the motion of the cation can be described by a single motional mode, possibly the isotropic overall reorientation of the cation as a whole. However, we cannot say whether or not the CH_3 C_3 reorientation is involved in the cationic motional process giving rise to the deep T_1 minimum. The present type of motional process activated for $(tetMA)^+$ cations is a unique example in various crystalline salts containing the cation ever studied.

To confirm the adequacy of the above interpretation of the deep T_1 minimum obtained, we calculated quantitatively the T_1 curve based on the more general method developed by Takeda et al.,[20] which has been successfully employed for the analysis of the T_1 data obtained for some $(tetMA)^+$ salts of cadmium(II) complexes[12] and also clathrate hydrates of (tetMA)OH.[13]

In this calculation, each ^1H-^1H vector involved in the CH_3 C_3 reorientation, the cationic reorientation about its C_3 axes, and that about its C_2 axes was assumed to jump at the rates of ω_{CH_3}, ω_3, and ω_2, respectively, which gave transition matrices for intramethyl and intermethyl ^1H-^1H vectors. The transition matrices constructed at a given temperature were diagonalized numerically, where ω_{CH_3}, ω_3, and ω_2 were given as reciprocals of τ values expressed by Eq. 2 with E_a and τ_0 taken as adjustable parameters. For ω_3 and ω_2, the same E_a but the different τ_0 values were assumed. To obtain good agreement between the observed values and the calculated curve, the E_a value of $14._8$ kJ mol^{-1} was employed, which is slightly different from the foregoing value obtained from the BPP analysis. The bond lengths of C-H and C-N were assumed to be 1.09 and 1.50 Å, respectively, according to Albert et al.,[3] while the all bond angles of the cation to be tetrahedral. The present geometry is thought to be more suitable to check the adequacy of the above discussion than that of Andrew and Canepa[1] because the present com-

plex will form loosely packed crystals in contrast to those of (tetMA)X (X=Cl, Br, I) studied by Albert et al.[3] The calculated curve with the values of E_a=14.8 kJ mol^{-1} and τ_0=1.3×10^{-13} s for the all reorientations of the CH_3 C_3 and the whole cationic C_2 and C_3 is shown in Fig. 2. The calculated curve explains still fairly well the observed values although the T_1 minimum calculated is slightly smaller than the observed one.

In the above calculation, we assumed that the CH_3 C_3 and the overall cationic reorientations are activated simultaneously with the same E_a value. However, it is possible to assume alternatively that the overall reorientation of the cations occurs from lower temperatures with E_a similar to the above value whereas the CH_3 C_3 reorientation is activated at higher temperatures with a larger E_a value. In other words, we regarded the cation itself as in a rigid state with no CH_3 C_3 reorientation in the present temperature region. Even in this case, the same calculated T_1 curve could be obtained by taking very large E_a for the CH_3 C_3 process such as 50 kJ mol^{-1}.

When the cation keeping the four CH_3 groups in rigid performs overall reorientation rapidly, ^{1}H-^{1}H dipole interactions in the cation are completely averaged out. This means that any M_2 reduction does not occur even if the CH_3 C_3 reorientation is activated at a temperature higher than the T_1 minimum temperature at ca. 135 K. Therefore, we can say for this complex that the CH_3 C_3 reorientation occurs rapidly enough at the T_1 minimum temperature with the same E_a of 14.8 kJ mol^{-1} as that of the overall reorientation or at a higher temperature than ca. 135 K, and we cannot determine which is the true situation for this complex.

The present E_a value for the overall reorientation of the cation is very small indicating that the cation experiences a weak crystal field. Previously, we observed the small-angle reorientation of each CH_3 group of the cation in a lower temperature region of some hexahalometallates(IV) forming high symmetric crystals.[10,11] In these crystals, the cation also undergoes weak crystal field. For the present complex, however, we did not detect the small-angle reorientation of the CH_3 groups.

Since no structural data of the (tetMA)$GaBr_4$ crystal were available, we took X-ray powder patterns at room temperature by means of a Model VD-1A X-ray diffractometer from Shimadzu Seisakusho Co. However, the patterns shown in Fig. 3 could not be explained in terms of a cubic or a tetragonal crystal system indicating that (tetMA)$GaBr_4$ forms a crystal structure of lower symmetry. From the appearance of a shoulder for the IR $\bar{\nu}_3$ band of $[GaBr_4]^-$ in solid (tetMA)$GaBr_4$,[16] it can be said that the complex anion is located on a site having lower symmetry than cubic. Accordingly, it is highly probable that the cation is also located on a lower symmetry site. This may be the reason why the small-angle reorientation was not observed in the present complex.

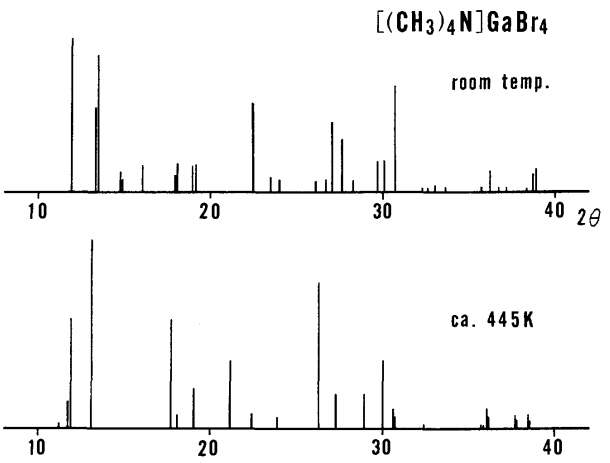

Fig. 3. X-Ray powder patterns taken at room temperature and at ca. 445 K for $[(CH_3)_4N]GaBr_4$.

In the higher temperature region above room temperature, (tetMA)$GaBr_4$ yielded a first order phase transition at 404 K. To know something about the crystal structure of the high temperature phase, we took X-ray powder patterns at ca. 445 K and obtained simpler patterns than those recorded at room temperature as shown in Fig. 3. The strong diffraction lines can be approximately interpreted in terms of a cubic structure with a lattice constant of ca. 15 Å. Since those strong lines have very weak side lines unexplainable by the cubic system, however, the crystal structure might belong to a less symmetric system, possibly a monoclinic one which is very close to the cubic system. It is very interesting that the phase transition did not give any detectable influence on the temperature dependence of ^{1}H T_1. This suggests that the motional state of the cation is not directly altered above and below the phase transition.

To obtain information for the characterization of the shallow T_1 minimum, we observed ^{1}H T_1 by a different Larmor frequency of 10.5 MHz as shown in Fig. 2. ^{1}H T_1 observed at both frequencies showed a clear frequency dependence in a temperature region of the shallow T_1 minimum. However, the ratios of T_1 values determined at the two frequencies measured at a given temperature were not ω^2 but nearly ω. This indicates that the relaxation mechanism yielding the shallow minimum cannot be attributed to the simple BPP type. Also the 2nd moment at 425 K was almost the same as that at room temperature, this is, no drastic decrease of the 2nd moment was found. The facts indicate that this T_1 minimum cannot be explained through a simple dipolar relaxation mechanism such as the self-diffusion of the cations. In a previous paper,[12] a ^{1}H T_1 decrease with increasing temperature observed at higher temperatures for (tetMA)$_2CdBr_4$ and (tetMA)$_2CdI_4$ was attributed to the ^{1}H relaxation through magnetic interactions between ^{1}H and halogen nuclei, where the quadrupolar relaxation of bro-

mine and iodine nuclei, respectively, is very fast because of a fluctuating electric field gradient possibly by the molecular or anionic reorientation. This relaxation mechanism named as dipolar relaxation of the second kind[21] may be the main origin for the present shallow T_1 minimum. The appearance of the T_1 minimum suggests that $[GaBr_4]^-$ reorients more rapidly than $[CdBr_4]^{2-}$ in almost the same high temperature region.

References

1) E. R. Andrew and P. C. Canepa, *J. Magn. Reson.*, **7**, 429 (1972).
2) M. Mahajan and B. D. Nageswara Rao, *J. Phys. C*, **7**, 995 (1974).
3) S. Albert, H. S. Gutowsky, and J. A. Ripmeester, *J. Chem. Phys.*, **56**, 3672 (1972).
4) A. A. V. Gibson and R. E. Raab, *J. Chem. Phys.*, **57**, 4688 (1972).
5) H. Rager and A. Weiss, *Z. Phys. Chem.*, **NF93**, 299 (1974).
6) T. Tsuneyoshi, N. Nakamura, and H. Chihara, *J. Magn. Reson.*, **27**, 191 (1977).
7) H. Rager and A. Weiss, *Ber. Bunsenges. Phys. Chem.*, **80**, 138 (1976).
8) H. Rager and A. Weiss, *Ber. Bunsenges. Phys. Chem.*, **82**, 535 (1978).
9) T. Tsang and D. B. Utton, *J. Chem. Phys.*, **64**, 3780 (1976).
10) L. S. Prabhumirashi, R. Ikeda, and D. Nakamura, *Ber. Bunsenges. Phys. Chem.*, **85**, 1142 (1981).
11) S. Sato, R. Ikeda, and D. Nakamura, *Ber. Bunsenges. Phys. Chem.*, **86**, 936 (1982).
12) S. Sato, R. Ikeda, and D. Nakamura, *Bull. Chem. Soc. Jpn.*, **59**, 1981 (1986).
13) S. Sato, R. Ikeda, and D. Nakamura, *J. Chem. Soc., Faraday Trans. 2*, **82**, 2053 (1986).
14) C. A. Evans and M. J. Taylor, *Chem. Commun.*, **1969**, 1201.
15) D. F. C. Morris, B. D. Andrews, and E. L. Short, *J. Inorg. Nuclear Chem.*, **28**, 2436 (1966).
16) M. J. Taylor, *J. Chem. Soc. A*, **1968**, 1780.
17) S. Gima, Y. Furukawa, R. Ikeda, and D. Nakamura, *J. Mol. Struct.*, **111**, 189 (1983).
18) Y. Kume, R. Ikeda, and D. Nakamura, *J. Magn. Reson.*, **33**, 331 (1979).
19) N. Bloembergen, E. M. Purcell, and R. V. Pound, *Phys. Rev.*, **73**, 679 (1948).
20) S. Takeda, G. Soda, and H. Chihara, *Mol. Phys.*, **47**, 501 (1982).
21) M. O. Norris, J. H. Strange, J. G. Powles, M. Rhodes, K. Marsden, and K. Krynicki, *J. Phys. C*, **1**, 422 (1968).

 © 1987 The Chemical Society of Japan Bull. Chem. Soc. Jpn., 60, 467—474 (1987)

^{1}H NMR Studies on the Motion of Cations in the Three Solid Phases of Methylammonium Perchlorate Including Cationic Self-Diffusion in Its Highest-Temperature Solid Phase

Hiroyuki Ishida, Ryuichi Ikeda, and Daiyu Nakamura*
Department of Chemistry, Faculty of Science, Nagoya University, Chikusa-ku, Nagoya 464
(Received August 25, 1986)

The temperature dependences of the second moment of ^{1}H NMR absorptions, the ^{1}H spin-lattice relaxation time, T_1, and the ^{1}H spin-spin relaxation time, T_2, of $CH_3NH_3ClO_4$ ($CH_3ND_3ClO_4$) were observed in the three solid phases existing over a wide range of temperature. In the phase I stable above 451 K, the onset of the isotropic reorientation as well as the self-diffusion of the cations with the activation energy of 36 kJ mol^{-1} was observed. In the phase II stable between 451 and 321 K, no remarkable change in the motional state of the cation was observed, but the dynamical orientational disorder of perchlorate anions was expected to occur. In the phase III stable below 321 K, the correlated reorientation defined as the C_3 reorientation of the cation having the rigid structure, was observed at lower temperatures for two nonequivalent cations in the crystal with small activation energies of 4.4 and 2.0 kJ mol^{-1}. The uncorrelated reorientation in which both CH_3 and NH_3^+ groups perform C_3 reorientation independently could be observed at a higher temperature with the activation energy of 6.4 kJ mol^{-1}. Nonexponential behavior appearing in the observation of T_1 below 40 K could be explained by the presence of a contribution to ^{1}H T_1 from the rotational tunneling of the cation.

Recently, we have found the presence of highly movable methylammonium $(MA)^+$ cations performing overall reorientation as well as self-diffusion in the highest-temperature solid phase of various simple $(MA)^+$ salts, such as (MA)I,[1,2] $(MA)NO_3$,[3,4] $(MA)ClO_4$,[3] and $(MA)_2SO_4$.[5] Furthermore, we also revealed the presence of such an unusual phase for $(CH_3)_3NHNO_3$[6] and $[C(NH_2)_3]ClO_4$[7] crystals. Very recently, Jurga and Spiess confirmed the existence of the unusual phase in $(MA)ClO_4$ crystals,[8] and also they found the appearance of a similar phase in $(CH_3)_2NH_2ClO_4$[9] and $(CH_3)_3NHClO_4$[10] crystals.

From our studies carried out up to date, it can be said that these highest-temperature solid phases of the above salts bear a strong resemblance to the plastic phase,[11] which is well-known to exist in molecular solids. Similarities are as follows. Both of the present and the plastic phases contain considerably freely moving constituents, i.e., molecule-like cations and such molecules, respectively. Additionally, an unusually large entropy change which is in some cases larger than that of melting, has been observed at the phase transition to the above phases with increasing temperature.[2,4,8,12]

Stammler et al.[13] carried out the experiments of differential thermal analysis (DTA) and powder X-ray diffraction and found three solid phases for $(MA)ClO_4$ above room temperature. The room-temperature phase (the phase III) obtainable below 321 K has a monoclinic unit lattice belonging to the space group $P2_1/n$.[14] With increasing temperature, this phase transforms at 321 K into the phase II, the crystal structure of which belongs to a tetragonal system.[14] The crystal of the highest-temperature phase (the phase I) existing above 451 K has a CsCl-type cubic structure.[14] The existence of the unusual solid phase in this salt was already reported as a letter.[3]

To obtain detailed information about dynamical properties of the cations in the above three phases, the present investigation of the temperature dependences of ^{1}H spin-lattice relaxation times (T_1) above 11 K, ^{1}H spin-spin relaxation times (T_2), and ^{1}H NMR second moments (M_2) has been undertaken for $(MA)ClO_4$ and $(CH_3ND_3)ClO_4$ [hereafter abbreviated as (MA-*d*)ClO_4]. Jurga and Spiess[8] reported ^{1}H NMR results obtained above 80 K for both salts. However, their data partly disagree with ours. Therefore, we again carried out sample preparations and ^{1}H T_1 measurements very carefully and confirmed our data presented here to be reasonable.

Experimental

$(MA)ClO_4$ was synthesized by neutralizing an aqueous solution of methylamine with perchloric acid by cooling the reaction vessel with an ice-bath. The resultant solution was placed in a desiccator, and crystals were separated after slowly evaporating water. The crystals obtained were purified by performing recrystallizations twice from isopropyl alcohol. A partially deuterated analog, (MA-*d*)ClO_4, was prepared from purified $(MA)ClO_4$ by successive crystallizations made three times from heavy water. These salts are so hygroscopic that the purified samples were dried over phosphorus pentaoxide in a vacuum desiccator for several weeks. After that, the samples, which had been put in glass ampoules for the measurements of NMR and DTA, were again dried by pumping out inner gas of the ampoules for ca. 8 h at ca. 90 °C before sealing them with a small amount of helium exchange gas.

DTA curves were recorded by using a homemade apparatus already described.[15] ^{1}H T_1, ^{1}H T_2, and M_2 of ^{1}H NMR absorptions were determined by use of apparatus already reported.[16,17] The T_1 measurements below 77 K were performed by employing a cryostat newly constructed by us. The cryostat could be used for the frequency variable pulsed spectrometer[17] for the measurements of NMR relaxation times between 4.2 and ca. 100 K. The sample temperature could be roughly controlled by adjusting the pressure of helium gas put in open space between the sample probe and

a glass cylinder which was immersed in liquid helium. To obtain a given and constant temperature, electric power supplied into a heater wound on the probe was controlled by means of an Oxford model DTC2 temperature controller. When measurements were carried out with this cryostat, sample temperatures were determined by use of a gold (0.07% iron) vs. chromel thermocouple with an accuracy of ±0.2 K. For the other T_1 and T_2 measurements as well as DTA experiments, sample temperatures were measured with a copper vs. constantan thermocouple with an estimated error of ±1 K.

Results

To confirm the phase transition temperatures (T_{tr}) reported,[13] DTA curves were recorded for $(MA)ClO_4$ and $(MA\text{-}d)ClO_4$ in the temperature range of 80—460 K. When $(MA)ClO_4$ was heated, two endothermic anomalies appeared at 321 and 451 K. These temperatures agree well with the T_{tr} values determined by Stammler et al.[13] from their DTA measurements and also by Jurga and Spiess from their DSC experiments.[8] However, the higher T_{tr} of 452 K observed for $(MA\text{-}d)ClO_4$ by us was higher by as much 15 K as that reported by Jurga and Spiess,[8] although the lower T_{tr} of 321 K obtained by us for the deuterated analog agreed well with their T_{tr} of 319.7 K reported.

The M_2 values of $(MA)ClO_4$ observed at 77 K and at various temperatures between 260 and 460 K are shown in Fig. 1, where an M_2 value of $(MA\text{-}d)ClO_4$ determined at 77 K is also included. At 77 K, $(MA)ClO_4$ and $(MA\text{-}d)ClO_4$ gave M_2 of $8._0$ and $7._0$ G^2, respectively. At 260 K, $(MA)ClO_4$ still yielded a large M_2 of $7._5$ G^2. With further increasing temperature from 260 to 450 K, a gradual M_2 decrease to ca. 6 G^2 was observed. However, no discontinuous decrease in M_2 was detected at T_{tr} from the phase III to the phase II [hereafter, such T_{tr} as this will be abbreviated as T_{tr}(III→

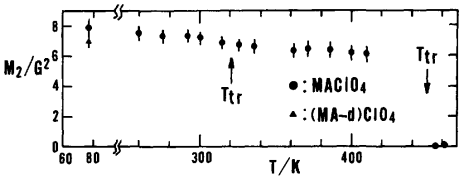

Fig. 1. ^1H NMR second moments (M_2) observed for $CH_3NH_3ClO_4$ at various temperatures. M_2 observed at 77 K for $CH_3ND_3ClO_4$ is also included. Vertical lines written on observed values are error bars estimated. T_{tr} with arrows indicates phase transition temperature.

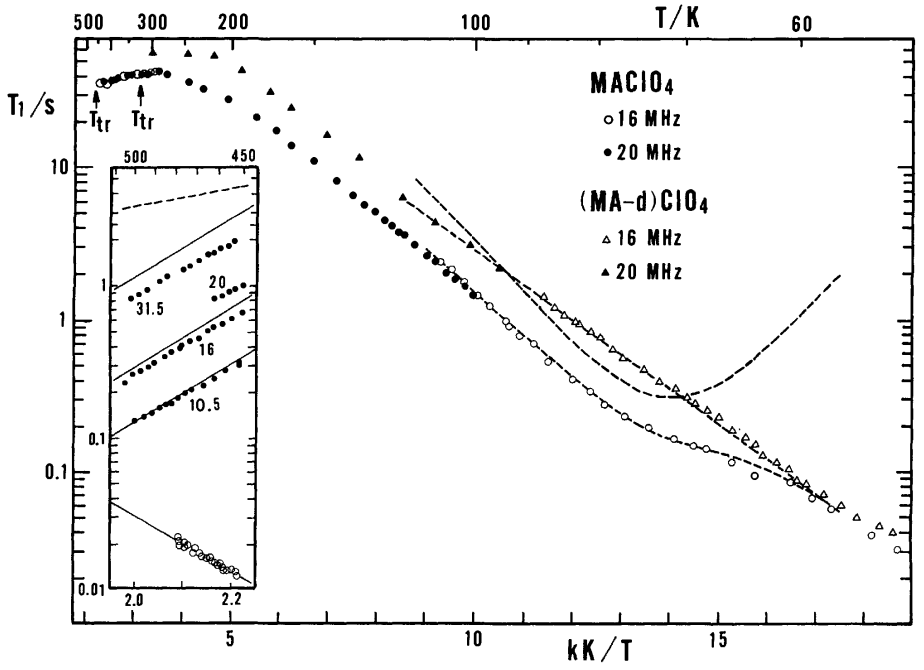

Fig. 2. Temperature dependences of ^1H T_1 observed for $CH_3NH_3ClO_4$ and $CH_3ND_3ClO_4$ at 16 and 20 MHz. A log T_1 vs. T^{-1} curve written by a broken line, which has a shallow minimum, indicates the BPP curve for the uncorrelated reorientation of the $CH_3NH_3^+$ cation, whereas a straight broken line is a hot-side fraction of the BPP curve corresponding to the correlated reorientation of the cation. The sum of the two curves is written by a broken line in agreement with the data of $CH_3NH_3ClO_4$. Temperature dependences of ^1H T_1 (●) observed at 10.5, 16, 20, and 31.5 MHz and ^1H T_2 (○) determined at 31.5 MHz for $CH_3NH_3ClO_4$ in its highest- temperature phase are shown as an inserted figure. Straight lines having negative temperature gradients denote T_{1d} derived at each Larmor frequency except 20 MHz, while the broken line indicates T_{1i}. The straight line having a positive temperature coefficient is the best-fitted line to the T_2 data observed.

II)], although Jurga and Spiess reported a clear M_2 decrease of 2.6 G^2 around 300 K.[8] At the higher T_{tr} of 451 K, M_2 decreased discontinuously to an extremely small value less than 0.05 G^2.

Temperature dependences of ^1H T_1 determined for $(MA)ClO_4$ and $(MA\text{-}d)ClO_4$ in relatively high-temperature regions are shown in Fig. 2. ^1H T_1 values of $(MA)ClO_4$ determined in the temperature ranges of 53—107 and 296—505 K at the Larmor frequency of 16 MHz and of 100—462 K at 20 MHz are depicted. For $(MA\text{-}d)ClO_4$, ^1H T_1 measurements at 16 MHz were made between 53 and 87 K, while those at 20 MHz were carried out between 95 and 300 K.

The $\log T_1$ vs. T^{-1} plots of both salts determined at 16 MHz increased with increasing temperature, and the plots extrapolated to higher temperatures agree well with those of the corresponding salts observed at 20 MHz as can be seen in Fig. 2. The $\log T_1$ value of $(MA\text{-}d)ClO_4$ increased almost linearly with decreasing T^{-1} in the present temperature range, whereas $(MA)ClO_4$ yielded a shallow T_1 minimum around 75 K. Almost the same temperature-dependence curve of ^1H T_1 observed at 20 MHz was obtained for both salts between ca. 100 and ca. 200 K.

$(MA)ClO_4$ yielded a broad T_1 maximum around 300 K, above which temperature almost the same ^1H T_1 values were observed at a given temperature for the measurements made at both Larmor frequencies of 16 and 20 MHz and the observed ^1H T_1 decreased gradually with increasing temperature up to T_{tr}. No discontinuity in the ^1H T_1 curve was observed at T_{tr} of 321 K. However, ^1H T_1 changed discontinuously at T_{tr} of 451 K, where ^1H T_2 also increased discontinuously by about three orders of magnitude.

The temperature variations of ^1H T_1 values determined for $(MA)ClO_4$ in its phase I are inserted in Fig. 2 as an enlarged figure on the T^{-1} scale. In this phase, ^1H T_1 was observed at 10.5 and 31.5 MHz in addition to the above frequencies in the temperature range of T_{tr}—ca. 500 K. With increasing temperature in the phase I, each ^1H T_1 measured at four different Larmor frequencies decreased monotonously, whereas ^1H T_2 determined at 31.5 MHz between T_{tr} and ca. 480 K increased linearly with decreasing T^{-1}. The temperature gradient of the $\log T_1$ vs. T^{-1} plots observed in this phase became gentler when the Larmor frequency employed increased.

The temperature dependences of ^1H T_1 observed for $(MA)ClO_4$ and $(MA\text{-}d)ClO_4$ in the temperature ranges of 11—110 and 18—90 K are shown in Figs. 3 and 4, respectively. Above ca. 40 K, each ^1H T_1 value of $(MA)ClO_4$ observed at 16 and 30.5 MHz yielded a deep T_1 minimum of 17 ms at 46 K and of 34 ms at 50 K, respectively. Similarly, $(MA\text{-}d)ClO_4$ gave a T_1 minimum of 31 ms at 49 K and of 53 ms at 51 K for the measurements made at 16 and 30.5 MHz, respectively.

Below ca. 40 K, nonexponential behavior was observed for the ^1H spin-lattice relaxation of both salts. If one assumes the presence of two independent relaxation processes having different relaxation times, $T_{1\ell}$ and T_{1s} ($T_{1\ell} > T_{1s}$), the ^1H magnetization $M_z(t)$ observed after each 90° pulse, where t is the time inter-

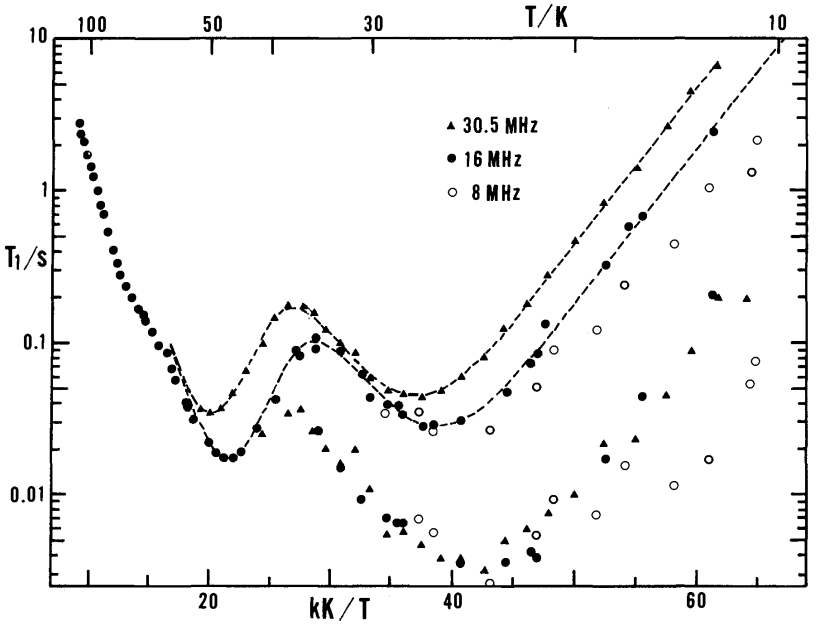

Fig. 3. Temperature dependences of ^1H T_1 observed for $CH_3NH_3ClO_4$ at 8, 16, and 30.5 MHz. Below ca. 40 K, long($T_{1\ell}$) and short (T_{1s}) components of T_1 for each Larmor frequency were obtained from nonexponential free induction decay curves observed. The sum of two independent BPP type T_1 curves corresponding to two kinds of crystallographically nonequivalent cations is written with broken lines for each frequency.

val between 180 and 90° pulses, can be given by

$$M_0 - M_z(t) = A_s \exp(-t/T_{1s}) + A_\ell \exp(-t/T_{1\ell}). \quad (1)$$

Here, M_0 denotes the M_z value under the thermal equilibrium of the spin system, i.e., $M_0 = M_z(\infty) = -M_z(0)$. To evaluate T_{1s} and $T_{1\ell}$, the $M_z(t)$ values observed at various intervals were fitted to Eq. 1 by use of the least-squares method under the condition of $A_s + A_\ell = 2M_0$. As an example, $M_z(t)$ values observed for $(MA)ClO_4$ at 19 K with the best-fitted M_z (t) recovery curve are shown in Fig. 5.

For $(MA\text{-}d)ClO_4$, it became difficult to obtain two T_1 values accurately around 40 K, because T_{1s} and $T_{1\ell}$ values come close to each other with increasing temperature. Accordingly, averaged T_1 values, T_{1av}, were evaluated from

$$T_{1av} = (t_{half})/\ln 2, \quad (2)$$

where (t_{half}) denotes the time interval t when a half-recovery value of the ^1H magnetization is reached. T_{1av} values derived from this method agree with the $T_{1\ell}$ values roughly estimated by using Eq. 1. Since these T_{1av} values were very near to the $T_{1\ell}$ curve extrapolated from the low-temperature side, T_{1av} was assumed to have the same origin of ^1H relaxation as $T_{1\ell}$ and plotted in Fig. 4.

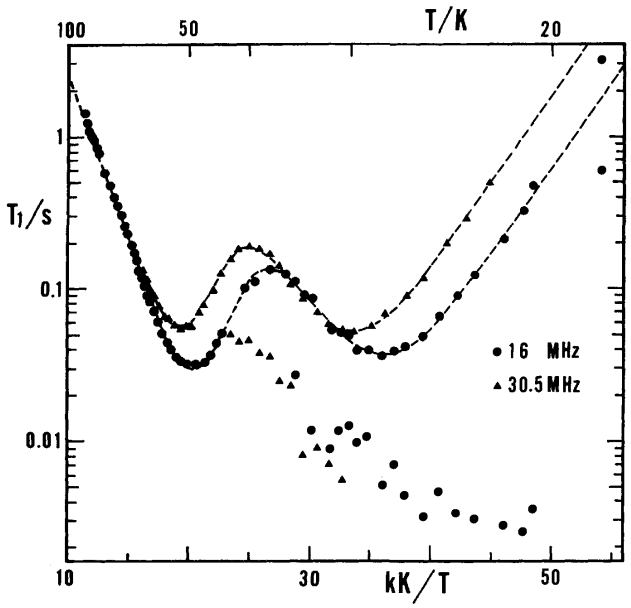

Fig. 4. Temperature dependences of ^1H T_1 observed for $CH_3ND_3ClO_4$ at 16 and 30.5 MHz. Below ca. 40 K, ^1H T_1 observed at each frequency showed nonexponential behavior and, $T_{1\ell}$ and T_{1s} could be determined as in the case of $CH_3NH_3ClO_4$ shown in Fig. 3. The sum of two different BPP curves arising from the two nonequivalent cations is indicated by broken lines calculated at each Larmor frequency. Around the high-temperature minima appeared, ^1H T_1 observed at both frequencies showed somewhat nonexponential behavior. However, it was difficult to obtain short T_1 component values accurately. Therefore, these values are omitted from the figure.

The T_1 curves of both salts thus obtained were connected smoothly to the respective T_1 curve observed in a higher-temperature region than 40 K. Each $T_{1\ell}$ curve of $(MA)ClO_4$ obtained from the measurements at 16 and 30.5 MHz exhibited a minimum of 28 ms at 26 K and 44 ms at 27 K, respectively. Similarly, $(MA\text{-}d)ClO_4$ yielded a $T_{1\ell}$ minimum of 36 ms at 28 K and 52 ms at 30 K for the measurements at 16 and 30.5 MHz, respectively. On the other hand, T_{1s} values measured at these two frequencies at a given temperature were approximately equal to each other in the temperature range where the nonexponential recovery curves could be observed for each analog. A minimum of 3.2 ms for the T_{1s} curve of $(MA)ClO_4$ could be located at 23 K, whereas no clear minimum could be found for $(MA\text{-}d)ClO_4$ down to 20 K.

Discussion

Second Moments of ^1H NMR Absorptions. According to the theoretical calculation of M_2 by use of Van Vleck's method,[18] $(MA)^+$ cations which rotate about the respective C-N bond axes give rise to ^1H M_2 of 8.9 G^2.[19,20] The fact that M_2 of 8.0 G^2 was observed for $(MA)ClO_4$ at 77 K indicates that the cations perform this motion with higher frequencies than 10^5 Hz even at 77 K.

A drastic decrease in M_2 to a value less than 0.05 G^2 at T_{tr} of 451 K clearly indicates the onset of the diffusional jumps as well as the isotropic rotation of the cations in the phase I. This is because M_2 observed in

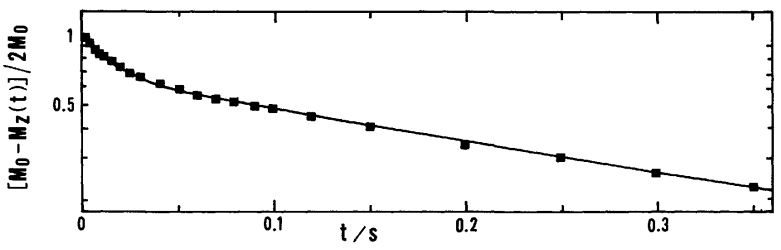

Fig. 5. ^1H magnetization recovery values, $[M_0 - M_z(t)]/2M_0$, observed for $CH_3NH_3ClO_4$ at 19 K by changing the interval time, t, between 180° and 90° pulses. M_0 denotes the thermal equilibrium value of the magnetization value. The solid line is the best fitted curve obtained by the least-squares method.

this phase is much smaller than the theoretical value of 0.8 G^2 calculated for the isotropically rotating cations in crystals using the crystal structure[13] of the phase I. A similar M_2 reduction has been already observed in some $(MA)^+$ salts.[1-6] For (MA)I[2] and $(MA)NO_3$[4] crystals, ^1H NMR and also electrical conductivity data obtained could be explained in terms of the above motional state of the cations.

Room-Temperature Phase (Phase III). (MA-*d*)ClO_4 yielded two deep minima of T_1 (including $T_{1\ell}$) below 100 K. These T_1 minima are attributable to magnetic dipolar relaxation because their frequency dependence is well explained by the BPP theory.[21] Since M_2 of 7.0 G^2 observed for this salt at 77 K is close to the theoretical value of 6.1 G^2 calculated for the cation reorienting about its C_3 axis,[19] these T_1 minima can be assigned to this motion. $(MA)ClO_4$ also showed two T_1 (including $T_{1\ell}$) minima at about the same temperatures as those of (MA-*d*)ClO_4. These results indicate the existence of two kinds of crystallographically nonequivalent $(MA)^+$ ions in the phase III crystal, in agreement with the results of X-ray diffraction analysis carried out by Zanazzi.[14] The fact that each of the T_1 and $T_{1\ell}$ minimum temperatures is approximately the same for both salts implies that the CH_3 and NH_3^+ groups in a cation have the correlation time of the C_3 reorientations very close to each other.

From the reason described below, this C_3 reorientation is attributable to the "correlated reorientation" of the cation, which has already been defined as the C_3 reorientation of the cation as a whole with keeping its rigid structure.[22] This motional mode is expected to exist for the cation in crystals where the C_3 rotation of the whole cation has a lower hindering barrier than the intracationic or internal C_3 rotation. The correlated reorientation of the $(MA)^+$ cation has been found in $(MA)_2MX_6$ (M=Sn, Te, Pt; X=Cl or Br) complexes, from the study of ^1H T_1 at lower temperatures.[22,23]

When the correlated reorientation of the cation takes place at a lower temperature, the "uncorrelated reorientation," which has been also defined before as the independent reorientation of the CH_3 and NH_3^+ groups in the identical cation,[22] is expected to occur with increasing temperature. In fact, a shallow T_1 minimum assignable to the uncorrelated reorientation was observed for the foregoing $(MA)_2MX_6$-type complexes.[22,23]

As shown in Fig. 2, $(MA)ClO_4$ gave a shallow T_1 minimum at ca. 75 K, whereas no such minimum was observed for (MA-*d*)ClO_4 in the same temperature range. The appearance of the shallow T_1 minimum is responsible for the averaging of magnetic-dipole interactions between protons belonging to the different groups in a cation, which reorient independently. Accordingly, the shallow minimum observed for $(MA)ClO_4$ can be assigned to the uncorrelated reorientation of the cation.

The ^1H T_1 curve around this minimum can be expressed as[24]

$$T_1^{-1}=(2/3)\gamma^2[\Delta M_{2c}g(\tau_c)+\Delta M_{2u}g(\tau_u)], \quad (3)$$

where

$$g(\tau)=\frac{\tau}{1+\omega^2\tau^2}+\frac{4\tau}{1+4\omega^2\tau^2}. \quad (4)$$

Here, γ, ω, and τ are the gyromagnetic ratio of a proton, the angular Larmor frequency, and the correlation time of a motion involved in the averaging of ^1H-^1H dipolar interactions, respectively. ΔM_{2c} is an M_2 reduction through the onset of the correlated reorientation of the cation from the rigid lattice M_2 value. ΔM_{2u} denotes the difference between the M_2 values for the cations performing the correlated reorientations and those having independently reorienting CH_3 and NH_3^+ groups. τ_c and τ_u indicate the correlation time for the correlated reorientation of the cation and for the uncorrelated reorientation which is the relative intracationic reorientation of the two groups, respectively. Each of these correlation times can be related to the activation energy, E_a, for the corresponding motion using the Arrhenius relationship given by

$$\tau=\tau_0\exp(E_a/RT), \quad (5)$$

where τ_0 is the correlation time at the limit of infinite temperature.

A fitting calculation of the ^1H T_1 values of $(MA)ClO_4$ observed between 57 and 110 K was carried out using the program SALS[25] at the Computation Center of Nagoya University. The best-fitted T_1 curve and the values of the unknown parameters determined from the calculation are given in Fig. 2 and Table 1, respectively. M_{2u} of 0.5 G^2 obtained agrees well with that of 0.4 G^2 calculated from the theoretical T_1 minimum for the same motion in the $(MA)_2MX_6$-type

Table 1. Activation Energy, E_a, the Correlation Time, τ_0, at the Limit of Infinite Temperature, and the Motional Mode of Methylammonium Ions in the Phases I and III of Methylammonium Perchlorates

Compound	Phase	E_a/kJ mol^{-1}	$\tau_0\times10^{13}$/s	Motional Mode (data obtained from)
$CH_3NH_3ClO_4$	III	2.0±0.2	5±3	Correlated C_3 reorient. ($T_{1\ell}$)
	III	4.4±0.1	0.8±0.1	Correlated C_3 reorient. (T_1)
	III	6.4±0.3	1.3±0.6	Uncorrelated C_3 reorient.(T_1)
	I	37±3	—	Self-diffusion (T_1)
	I	35±3	—	Self-diffusion (T_2)
$CH_3ND_3ClO_4$	III	2.2±0.2	5±3	Correlated C_3 reorient. ($T_{1\ell}$)
	III	4.4±0.1	1.3±0.1	Correlated C_3 reorient. (T_1)

complexes.[22] This means that two kinds of nonequivalent $(MA)^+$ cations existing in the crystal yielded their T_1 minima attributable to the uncorrelated reorientation at approximately the same temperature. This is expected from the foregoing discussion made on this reorientation which is hindered mostly by the intracationic potential barrier. E_a of 6.4 kJ mol^{-1} evaluated for this cationic motion in the present salt is lower than that of ca. 8 kJ mol^{-1} already reported for the same motion in $(MA)_2MX_6$-type complexes.[22] The present small E_a can be explained if the T_1 curve observed is broadened due to the presence of two different T_1 curves overlapping each other, which arise from the two nonequivalent cations, each of which gives the T_1 minimum at a little different temperature.

Next, we try to explain the ^1H T_1 and ^1H T_1 minima observed for both salts below 50 K by the BPP theory.[21] This theory predicts that the ratios of the T_1 minima observed at two different Larmor frequencies should be equal to the ratio of these frequencies. The ratios observed for the high-temperature T_1 minima, T_{1min}(30.5 MHz)/T_{1min}(16 MHz) were 1.9 and 1.8 for $(MA)ClO_4$ and (MA-*d*)ClO_4, respectively, in good agreement with the theoretical value of 1.91. On the other hand, the low-temperature T_1 minima yielded the ratios of 1.6 and 1.4 in the same order as above, which were much smaller than the theoretical value. Moreover, the squared ratios of T_1 observed at 30.5 MHz to that of 16 MHz at the same temperature on the low-temperature side of the minima were 2.5 and 2.6 for $(MA)ClO_4$ and (MA-*d*)ClO_4, respectively. These values were also much smaller than the theoretical value of 3.6 $[(30.5/16)^2]$ predicted from the BPP theory.[21]

These facts and the foregoing nonexponential T_1 behavior observed below 40 K cannot be explained by the usual mechanism, i.e., the averaging of magnetic dipolar interactions due to the cationic motions, and suggest the existence of some contribution to ^1H T_1 from the rotational tunneling of the cation in $(MA)ClO_4$ crystals.[26-28] Another fact that T_{1s} of $(MA)ClO_4$ has a minimum at 23 K, suggests that the tunneling frequency is of the order of 10^7 Hz around this temperature.[28]

Here, we roughly evaluate E_a values for the correlated reorientation of the $(MA)^+$ cation. Assuming that the T_1 and $T_{1\ell}$ curves observed at 16 MHz can be expressed by the superposition of two independent BPP curves, we have

$$T_1^{-1} = (1/2)[Cg(\tau_c) + C'g(\tau_c')], \quad (6)$$

where C and C' are the motional constants of the correlated reorientation of the two kinds of cations with the correlation times τ_c and τ_c', respectively. Equations 5 and 6 were fitted to the observed values by the least-squares method. The unknown parameters determined and the best-fitted T_1 curves are shown in Table 1 and Figs. [4, 5], respectively. The activation energies for the correlated reorientation of the cation in both salts were much smaller than the corresponding value of the uncorrelated reorientation. This supports our expectation that the whole-cation reorientation is less hindered than the intracationic reorientation of the CH_3 and NH_3^+ groups.

Intermediate Phase (Phase II). When the temperature was raised above 300 K, ^1H T_1 decreased monotonously in the phases III and II without showing any detectable anomaly at T_{tr}(III→II). Since no frequency dependence of ^1H T_1 was observed in this temperature range, this T_1 decrease cannot be attributed to magnetic dipolar relaxation. From the preceding discussion, it is apparent that the cations in $(MA)ClO_4$ crystals are considerably free. This suggests that the cations perform a rapid rotation around the C-N bond axis. Such a rapid axial rotation of the cations may give rise to spin-rotation relaxation which is known to yield frequency-independent T_1 decrease with increasing temperature even in solids.[29,30]

Jurga and Spiess have reported a clear M_2 decrease around T_{tr}(III→II) and assigned it to the onset of the precession of the cations about an axis inclined at an angle of 18° to each C-N bond axis.[8] However, neither T_1 minimum nor frequency-dependent T_1 corresponding to this M_2 decrease could be detected in the present study and also in their T_1 measurements.

If the above motional model of the cation proposed by Jurga and Spiess is considered, ^1H T_1 arising from this motion can be calculated by substituting the parameters (E_a, τ_0, and ΔM_2) of this motion given in their paper[8] into Eq. 5 and the following BPP equation[21]

$$T_1^{-1} = (\tfrac{2}{3})\gamma^2 \Delta M_2 g(\tau). \quad (7)$$

Therefore, the T_1 values roughly evaluated at the Larmor frequency of 20 MHz were ca. 16 and 1.2 s at 350 and 440 K, respectively. These results indicate that ^1H T_1 in the phase II should decrease more rapidly than the observed values with increasing temperature. Furthermore, these T_1 values should show frequency dependency due to magnetic dipolar relaxation caused by the precessional motion in contrast to the present experimental fact.

In our M_2 measurements, no marked change in M_2 was found around room temperature although a gradual decrease in M_2 with increasing temperature was found over a wide range of temperature. This M_2 decrease can be interpreted in terms of a gradual increase of the amplitude of lattice vibrations.[31,32] The activation of lattice vibrations usually gives no remarkable effect on T_1 which is consistent with our T_1 data observed in the phase II.

Jurge and Spiess[8] reported a large entropy change ΔS_{tr} (20.9 J K^{-1} mol^{-1}) of transition at T_{tr}(III→II) of 321 K for $(MA)ClO_4$, indicating that the ions forming the crystal obtain motional freedom considerably at T_{tr}(III→II). This ΔS_{tr} is larger than that (16.9 J K^{-1}

mol^{-1}) obtained at T_{tr}(II→I). However, the fact that no marked discontinuity in either ^1H T_1 or M_2 was observed at T_{tr}(III→II) indicates that the cationic motion is little affected through this transition. Accordingly, the large ΔS_{tr} observed at T_{tr}(III→II) suggests that a sudden increase in the motional freedom of ClO_4^- anions takes place at 321 K. That is, the onset of anionic rotation around each chlorine atom is expected to occur in the phase II. This expectation is consistent with the ^1H spin-lattice dipolar relaxation time, T_{1D}, data reported by Jurga and Spiess.[8] They observed a discontinuous decrease in T_{1D} at T_{tr}(III→II), and also a monotonous decrease of T_{1D} in the phase II with increasing temperature. These facts observed by them can be explained in terms of the averaging of the dipolar interactions between ^1H and ^{17}O nuclei caused by the anionic rotation.[33]

The ΔS_{tr} value of 16.9 $J K^{-1} mol^{-1}$ at T_{tr}(II→I)[8] can be compared with those of (MA)I[2] and $(MA)NO_3$[4] at the highest-temperature solid-solid phase transition. These salts perform the same kind of phase transitions as $(MA)ClO_4$ at high temperatures and transform into highly disordered crystals with a CsCl-type cubic structure. ΔS_{tr} of 15 $J K^{-1} mol^{-1}$ observed for (MA)I at T_{tr} to the ε phase[2] is comparable to that of $(MA)ClO_4$, whereas $(MA)NO_3$ gives a larger ΔS_{tr} of 28 $J K^{-1} mol^{-1}$ at the corresponding T_{tr}.[4] This ΔS_{tr} of the nitrate can be assigned to an increase in the motional freedom of both cations and anions at the phase transition. We have previously shown for the iodide, however, that only the cationic motion is responsible for the transition entropy observed.[2] Accordingly, the phase transition at 451 K occurring in $(MA)ClO_4$ crystals can be characterized mainly by the change in the motional state of the cation. This is consistent with our previous expectation that the dynamical orientational disorder of the anions will take place at the low-temperature T_{tr}.

High-Temperature Phase (Phase I). The discontinuous decrease of M_2 to a value less than 0.05 G^2 and the sudden increase of T_2 to 14 ms as well, occurring at T_{tr}(II→I), indicate the onset of the isotropic reorientation and the self-diffusion of the cations in the phase I. The log T_1 vs. T^{-1} plots of the phase I, as determined at four different Larmor frequencies shown in Fig. 2, increase almost linearly with increasing T^{-1} and the gradients against T^{-1} become gentler with increasing frequency. The T_1 behavior similar to this was also reported for the cubic phase of $(MA)NO_3$[4] and (MA)I.[2] According to the analysis of the T_1 data of these salts, the present T_1 values could also be expressed by the superposition of the two components, T_{1d} and T_{1i}, as written by

$$T_1^{-1} = T_{1d}^{-1} + T_{1i}^{-1}. \quad (8)$$

Here, T_{1d} and T_{1i} denote ^1H T_1 proportional to ω^2 and independent of ω, respectively. As the most probable origin of T_{1i}, the spin-rotation interaction due to the isotropic rotation of the cation can be considered. On the other hand, T_{1d} is assignable to the self-diffusion of the cations in agreement with the vanishingly small M_2 determined in this phase.

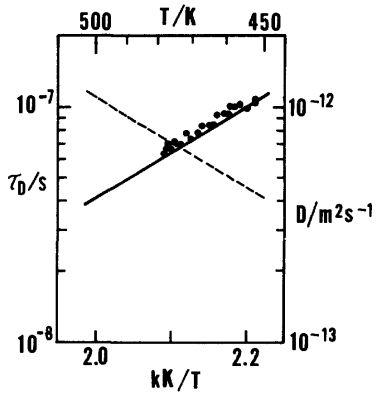

Fig. 6. The correlation times of the self-diffusion estimated from the ^1H T_2 values are shown by dots. The solid line indicates the calculated one from the T_{1d} values derived. The broken line indicates the temperature variations of the diffusion constant, D, calculated from T_{1d} values.

If the monovacancy mechanism proposed by Torrey[34] and Sholl[35] is applicable for the self-diffusion of the cations in the present crystal, we have[4]

$$T_{1d}^{-1} = (36/5)\gamma^4\hbar^2 a_0^{-6}\omega^{-2}\tau_D^{-1}(S_0 - S_1/Z). \quad (9)$$

Here, a_0, τ_D, and Z are the lattice constant of the phase I, the correlation time of the self-diffusion, and the number of the nearest neighbors in the simple cubic sublattice formed by the cations, respectively. The numerical values of S_0 and S_1 are given in Sholl's paper.[35] When we derived Eq. 9, we used the condition of $\omega\tau_D \gg 1$. By introducing ^1H T_1 values observed to Eq. 9 and using Z=6, we could estimate τ_D at various temperatures.

The diffusion constant D of the cations in the crystal can be expressed as[36]

$$D = <r^2>/6\tau_D, \quad (10)$$

where $<r^2>$ is the mean-square jump distance of the cations, which is taken as a_0^2 in the monovacancy mechanism. The values of τ_D and D calculated using the above equations are shown in Fig. 6.

τ_D can be also calculated independently from the ^1H T_2 data determined using the relation written by[4]

$$T_2^{-1} = (27/20)\gamma^4\hbar^2 a_0^{-6}\tau_D g(0). \quad (11)$$

Substituting $g(0)$=17.98[35] into Eq. 11, we obtained τ_D as shown by dots in Fig. 6. The τ_D values derived from the T_2 values agree well with the line calculated from T_{1d}.

For $(MA)^+$ cations in the highest-temperature solid phase of $(MA)ClO_4$, the D value of the order of 10^{-13} $m^2 s^{-1}$ was obtained. The same order of D for the diffusion of the same cation was also obtained in the highest-temperature solid phase of $(MA)NO_3$.[4] It is

known that many plastic crystals which are formed by neutral molecules have analogous D values of ca. 10^{-13} $m^2 s^{-1}$ observed near their melting temperatures (T_m) although they are distributed over a wide range of temperature.[36] τ_D values obtained in the phase I are very similar to those of $(MA)NO_3$ and also of the plastic crystals. By extrapolation to higher temperatures, τ_D of $(MA)ClO_4$ at T_m can be obtained from the log τ_D vs. T^{-1} curve as ca. 3×10^{-8} s. This is close to the value of 9.8×10^{-8} s evaluated for $(MA)NO_3$[4] and also to those τ_C values of the plastic crystals forming a bcc lattice, which are ca. 1×10^{-7} s on the average.[36] These facts suggest that the highest-temperature solid phase of the ionic crystals of $(MA)ClO_4$ and $(MA)NO_3$ has solid state properties similar in many respects to those of the plastic crystals.

The activation energies for the self-diffusion of the cations calculated from the T_{1d} and T_2 data employing Eq. 5 are given in Table 1. The E_a values obtained from both relaxation values agree well with each other within experimental errors. These E_a values of $(MA)ClO_4$ are very close to that (35 kJ mol^{-1}) of (MA)I for the same motion,[2] whereas they are much higher than 28 kJ mol^{-1} obtained for $(MA)NO_3$.[4] Since these phases of the three salts containing diffusive $(MA)^+$ cations have the isomorphous CsCl-type cubic structure, the E_a values obtained can be compared by considering the differences in the shape and the size of the anions. The bulky and nearly spherical ClO_4^- anions and also bulky I^- anions seem to provide higher barriers for the translational jumps of the cations than the planar NO_3^- anions.[37]

The authors express their thanks to Mr. Yoshisato Funahashi and Mr. Gunzo Takamatsu of our machine shop for the construction of the NMR cryostat usable down to liquid helium temperature.

References

1) H. Ishida, R. Ikeda, and D. Nakamura, *Phys. Status Solidi A*, **70**, K151 (1982).
2) H. Ishida, R. Ikeda, and D. Nakamura, *Bull. Chem. Soc. Jpn.*, **59**, 915 (1986).
3) H. Ishida, R. Ikeda, and D. Nakamura, *Chem. Lett.*, **1982**, 1943.
4) H. Ishida, R. Ikeda, and D. Nakamura, *J. Chem. Soc., Faraday Trans. 2*, **81**, 963 (1985).
5) H. Ishida, N. Matsuhashi, R. Ikeda, and D. Nakamura, *Chem. Lett.*, **1985**, 1859.
6) H. Ishida, R. Ikeda, and D. Nakamura, *Ber. Bunsenges. Phys. Chem.*, **90**, 598 (1986).
7) S. Gima, Y. Furukawa, and D. Nakamura, *Ber. Bunsenges. Phys. Chem.*, **88**, 939 (1984).
8) S. Jurga and H. W. Spiess, *Z. Naturforsch., A*, **40**, 602 (1985).
9) S. Jurga and H. W. Spiess, *Ber. Bunsenges. Phys. Chem.*, **89**, 763 (1985).
10) S. Jurga, *Phys. Status Solidi A*, **81**, 77 (1984).
11) N. Boden, "The Plastically Crystalline State," ed. J. N. Sherwood, Wiley, New York (1979).
12) J. Timmermans, *J. Phys. Chem. Solid*, **18**, 1 (1961).
13) M. Stammler, R. Bruenner, W. Schmidt, and D. Orcutt, *Advan. X-ray Anal.*, **9**, 170 (1966).
14) P. F. Zanazzi, *Acta Crystallogr., Sect B*, **24**, 499 (1968).
15) Y. Kume, R. Ikeda, and D. Nakamura, *J. Magn. Reson.*, **33**, 331 (1979).
16) L. S. Prabhumirashi, R. Ikeda, and D. Nakamura, *Ber. Bunsenges. Phys. Chem.*, **85**, 1142 (1981).
17) S. Gima, Y. Furukawa, R. Ikeda, and D. Nakamura, *J. Mol. Struct.*, **111**, 189 (1983).
18) J. H. Van Vleck, *Phys. Rev.*, **74**, 1168 (1948).
19) H. Ishida, R. Ikeda, and D. Nakamura, *J. Phys. Chem.*, **86**, 1003 (1982).
20) H. Ishida, R. Ikeda, and D. Nakamura, *Bull. Chem. Soc. Jpn.*, **55**, 3116 (1982).
21) A. Abragam, "The Principles of Nuclear Magnetism," Oxford University Press, London (1961).
22) R. Ikeda, Y. Kume, D. Nakamura, Y. Furukawa, and H. Kiriyama, *J. Magn. Reson.*, **24**, 9 (1976).
23) Y. Furukawa, H. Kiriyama, and R. Ikeda, *Bull. Chem. Soc. Jpn.*, **54**, 103 (1981).
24) G. Soda and H. Chihara, *J. Phys. Soc. Jpn.*, **36**, 954 (1974).
25) T. Nakagawa and Y. Koyanagi, Program Library in Computation Center of Nagoya University, Code Number 466.
26) J. Haupt, *Z. Naturforsch., A*, **26**, 1578 (1971).
27) S. Clough, *J. Phys. C*, **9**, 1553 (1976).
28) R. A. Wind, S. Emid, D. J. Ligthelm, J. F. J. M. Pourquie, and J. Smidt, *Bull. Magn. Reson.*, **6**, 71 (1984).
29) R. Ikeda and C. A. McDowell, *Chem. Phys. Lett.*, **14**, 389 (1972).
30) K. Shimomura, M. Yoshida, A. Sanjoh, and H. Negita, *Phys. Lett. A*, **81**, 189 (1981).
31) B. Pedersen, *J. Chem. Phys.*, **41**, 122 (1964).
32) U. Shmueli, M. Polak, and M. Sheinblatt, *J. Chem. Phys.*, **59**, 4535 (1973).
33) K. Morimoto and K. Shimomura, *J. Phys. Soc. Jpn.*, **54**, 3244 (1985).
34) H. C. Torrey, *Phys. Rev.*, **92**, 962 (1953).
35) C. A. Sholl, *J. Phys. C*, **7**, 3378 (1974); **8**, 1737 (1975).
36) J. M. Chezeau and J. H. Strange, *Phys. Reports*, **53**, 1 (1979).
37) T. C. Waddington, *Adv. Inorg. Chem. Radiochem.*, **1**, 180 (1959).

 © 1987 The Chemical Society of Japan Bull. Chem. Soc. Jpn., 60, 475—481 (1987)

Molecular Dynamics Simulation of Liquid Water

Kazuo TOKIWANO† and Kiyoshi ARAKAWA*
Research Institute of Applied Electricity, Hokkaido University, Sapporo 060
†Faculty of Engineering, Hokkaido University, Sapporo 060
(Received August 7, 1986)

A molecular dynamics simulation has been performed for a fluid system containing 1000 water molecules confined to a cubical box at mass density 1 g cm^{-3}, where the ST2 type intermolecular potential has been used. Newtonian equations of motion of molecules were solved according to the method of constraints proposed by Ryckaert et al. Atomic radial distribution functions and corresponding partial structure functions at 24 and 93 °C were given and compared with theoretical calculations for the pentamer-monomer mixture model and neutron diffraction data. The agreement among the three was found to be satisfactory on the whole. In order to investigate how profoundly the periodic boundary condition influences upon the calculated values, the difference between the hydrogen-bonding behavior of molecules near the boundary and that of those in the central part of the box was examined into details. The population of hydrogen bonds near the boundary was found to be about 10% lower than that in the central part including about 210 molecules. In addition to these static properties the self-diffusion process was investigated.

The study of the properties of computer model has played a very important role in the development of the theories of liquid. It has been the case in the theories of molecular fluids. With respect to liquid water, such models have provided valuable information[1,2] necessary for constructing theoretical models of the liquid.[3,4] Since the first comprehensive works by Rahman and Stillinger,[1] simulation calculations of liquid water have been performed for various potential models such as ST2, MCY etc.,[5-14] though no decisive results have been obtained until present.

The equilibrium structure of a molecular fluid is described in terms of partial structure functions, $a_{ss'}(Q)$, which is related to atom pair (s,s') correlations. Recently, we have calculated three partial structure functions, $a_{OO}(Q)$, $a_{OH}(Q)$, and $a_{HH}(Q)$,[15] according to a theoretical calculation procedure[15-17] proposed for obtaining structure factors of a fluid composed of molecular clusters of various sizes. A substantial agreement was found between the calculated and experimental values.

In order to push forward the study of the liquid structure of water further, we have attempted, here, a computer simulation study for the fluid system containing 1000 water molecules. It is straightforward to calculate the partial structure functions $a_{ss'}(Q)$ and others using computer simulation techniques. In this paper we present first the results of partial structure functions obtained from the molecular dynamics simulation. The results are compared with neutron diffraction data[17,18] and our preceding theoretical calculations for the pentamer-monomer mixture model.[15,17] Further discussions on the simulation calculation are given.

Molecular Dynamics Simulations

As a model of liquid water we used the ST2 molecules of Stillinger and Rahman.[2] Molecular dynamics simulations were performed for a system of N=1000 water molecules confined to a cubical box, being subjected to periodic boundary conditions. The mass density was fixed at 1 g cm^{-3}, so that the cube edge length was 31.03 A. In evaluating potentials and forces the interaction between two molecules was neglected when the oxygen-oxygen distance was larger than a cut-off distance r_c. The cut-off was placed at r_c=8.46 A.

Newtonian equations of motion were solved by the method of constraints described by Ryckaert et al.[19] This method was devised originally to deal with the problem of large molecules having internal degrees of freedom, and it has a general applicability. The method of constraints is based on the cartesian equations of motion of individual atoms, being simple to implement. The time increment Δt for numerical integration of the equations of motion was taken to be

$$\Delta t = 1.0 \times 10^{-16}\ \mathrm{s}.$$

To take the molecular dynamics statistical average, we utilized a period of 10000 Δt. Molecular dynamics runs were generated at two distinct temperatures, 24 and 93 °C; they correspond to fixed total energies of $-110\ \varepsilon$ and $-91\ \varepsilon$ respectively, where ε is 0.07575 kcal mol^{-1} (1 cal=4.184 J). The total energy was monitored every 10 steps of Δt, and if it had drifted by $\pm 0.04\ \varepsilon$ (on the average every 500 steps) all velocities were rescaled to recover the initial energy value.

Results and Discussion

Radial Distribution Functions. Figures 1 and 2 show the atomic radial distribution functions $g_{OO}(r)$, $g_{OH}(r)$, and $g_{HH}(r)$ obtained from the molecular dynamics runs for the ST2 model for 24 and 93 °C, respectively.

Partial Structure Functions. The partial structure functions $a_{ss'}(Q)$ are related to the atomic radial distribution functions $g_{ss'}(r)$ by the expression

$$a_{ss'}(Q) = 4\pi\rho\int_0^\infty [g_{ss'}(r) - 1] r^2 j_0(Qr)\mathrm{d}r, \qquad (1)$$

where $j_0(x)=\sin x/x$, s and s' label nucleus species, and $Q=|\vec{Q}|$ ($\vec{Q}$: the scattering vector).

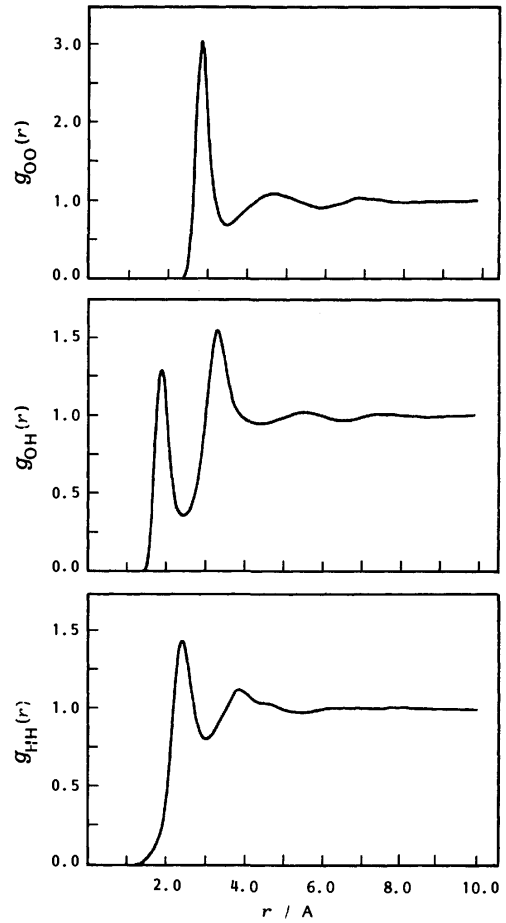

Fig. 1. Radial distribution functions at 24°C.

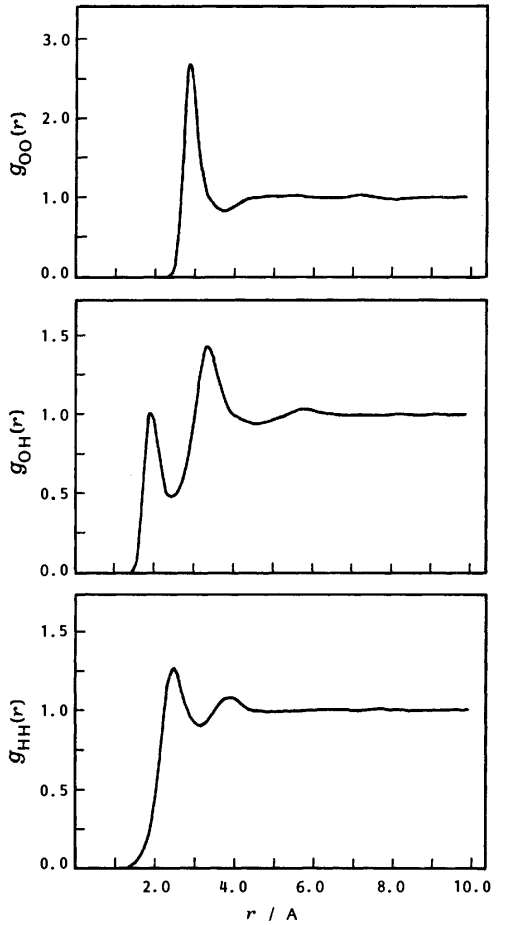

Fig. 2. Radial distribution functions at 93°C.

Now, we can calculate the partial structure functions $a_{ss'}(Q)$ for the ST2 model by using the molecular dynamics results of $g_{ss'}(r)$ given in Figs. 1 and 2. The calculated $a_{OO}(Q)$, $a_{OH}(Q)$, and $a_{HH}(Q)$ functions for 24°C are shown in Figs. 3—5, respectively, and are compared with the corresponding neutron diffraction data of Thiessen and Narten[18] as well as with the preceding theoretical calculations for the pentamer-monomer mixture model.[15] The agreement among those three is satisfactory on the whole.

We calculated the total coherent neutron structure factor $S_m(Q)$ by using the three partial structure functions $a_{ss'}(Q)$ given in Figs. 3—5. The structure factor $S_m(Q)$ is defined as a sum of partial structure factors $S_{ss'}(Q)$[15]

$$S_m(Q)=(b_O+2b_H)^{-2}[b_O^2S_{OO}(Q)+4b_Ob_HS_{OH}(Q)+4b_H^2S_{HH}(Q)], \quad (2)$$

where b_s is the coherent scattering length of nucleus s, and

$$S_{OO}(Q)=1+a_{OO}(Q),$$
$$S_{OH}(Q)=a_{OH}(Q)+Y_{OH}(Q),$$
$$S_{HH}(Q)=(1/2)+a_{HH}(Q)+(1/2)Y_{HH}(Q).$$

The $Y_{ss'}(Q)$ is generally approximated by

$$Y_{ss'}(Q)=j_0(Qr_{ss'})\exp(-\gamma_{ss'}Q^2),$$

where $r_{ss'}$ is the distance between the s and s' nuclei, and $(2\gamma_{ss'})^{1/2}$ the rms variation to the distance $r_{ss'}$. Figure 6 shows the calculated $S_m(Q)$ curve, together with the corresponding observed data[17] and the previous result for the pentamer-monomer mixture model.[17] As seen in Fig. 6, the present values are in good agreement with the observed data as well as with the ones for the pentamer-monomer mixture model.

Here, the $a_{OH}(Q)$ and $a_{HH}(Q)$ curves, shown in Figs. 4 and 5 respectively, are of particularly interest. First, taking account of experimental difficulties in determining partial structure functions, it can be said that the present $a_{OH}(Q)$ and $a_{HH}(Q)$ curves essentially reproduce the corresponding observed data, and also that the agreement between the $a_{OH}(Q)$ and $a_{HH}(Q)$ curves for the ST2 model and the pentamer-monomer mixture model is remarkably good on the whole. These results seem to show the effectiveness of the pentamer-monomer mixture model for describing the equilibrium structure of liquid water. The ST2 model has a strong tendency for water molecules to form tetrahedrally-coordinated structures. The dominance of a tetrahedral configuration as the local environment around a molecule on the average is essential for liquid water.

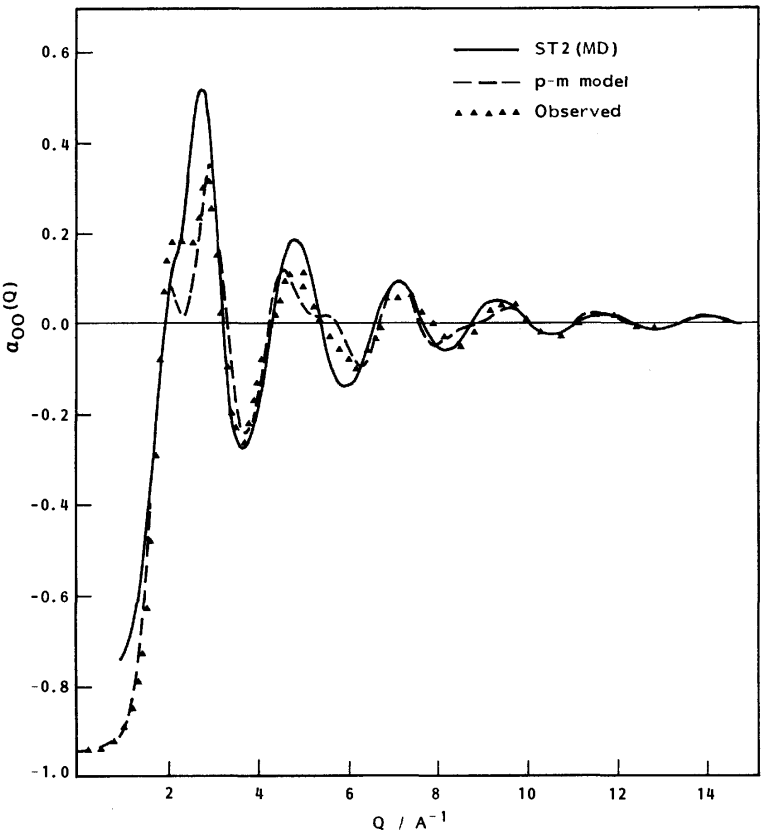

Fig. 3. O-O structure function $a_{OO}(Q)$ at 24°C in comparison with the observed data[18] and the calculated ones for pentamer-monomer mixture model (p-m model).[15]

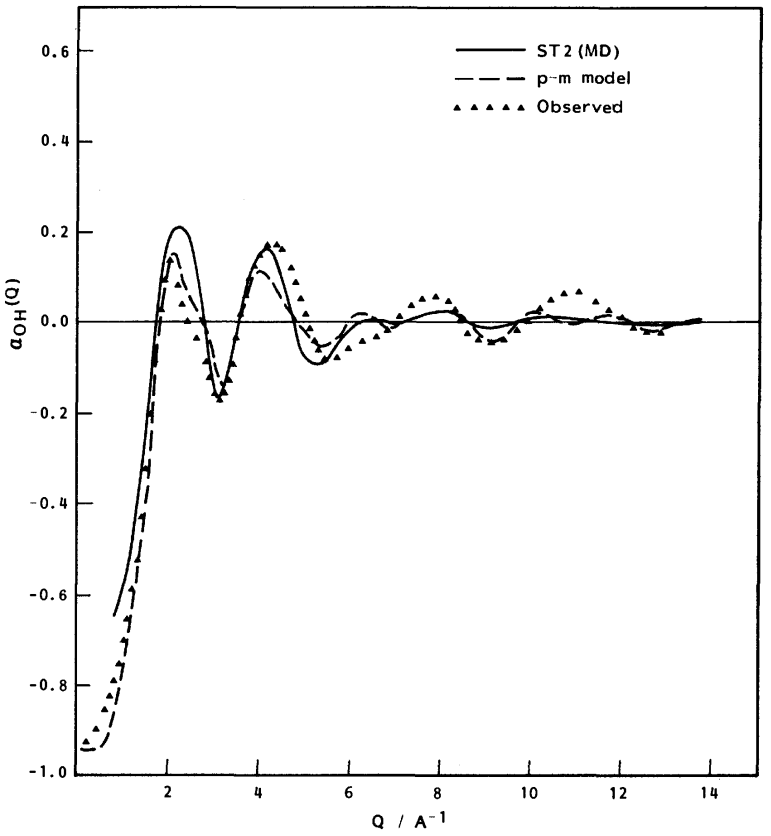

Fig. 4. O-H structure function $a_{OH}(Q)$ at 24°C in comparison with the observed data[18] and the calculated ones for pentamer-monomer mixture model.[15]

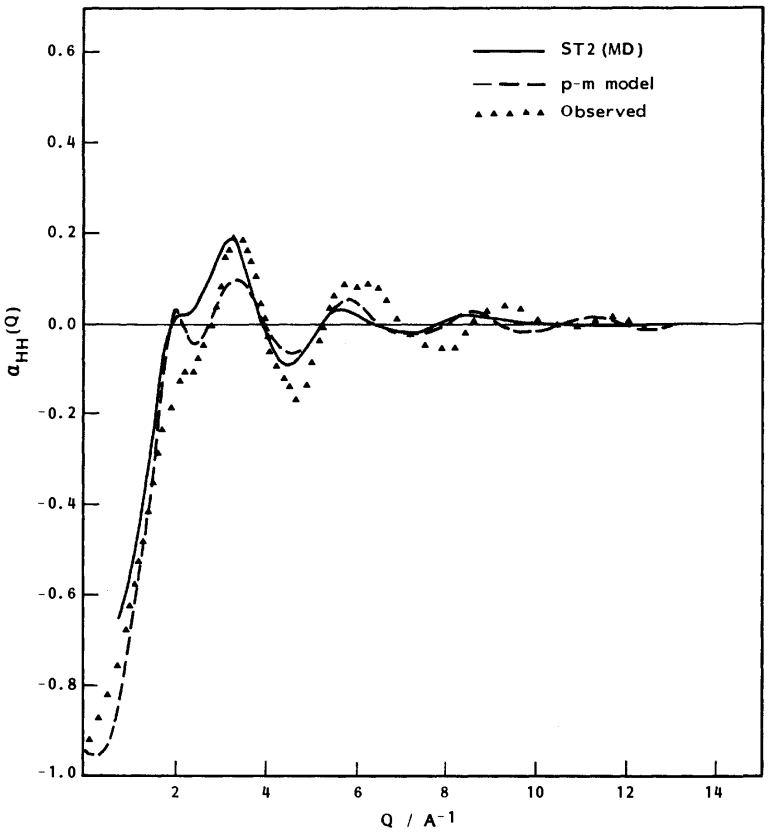

Fig. 5. H-H structure function $a_{HH}(Q)$ at 24°C in comparison with the observed data[18] and the calculated ones for pentamer-monomer mixture model.[15]

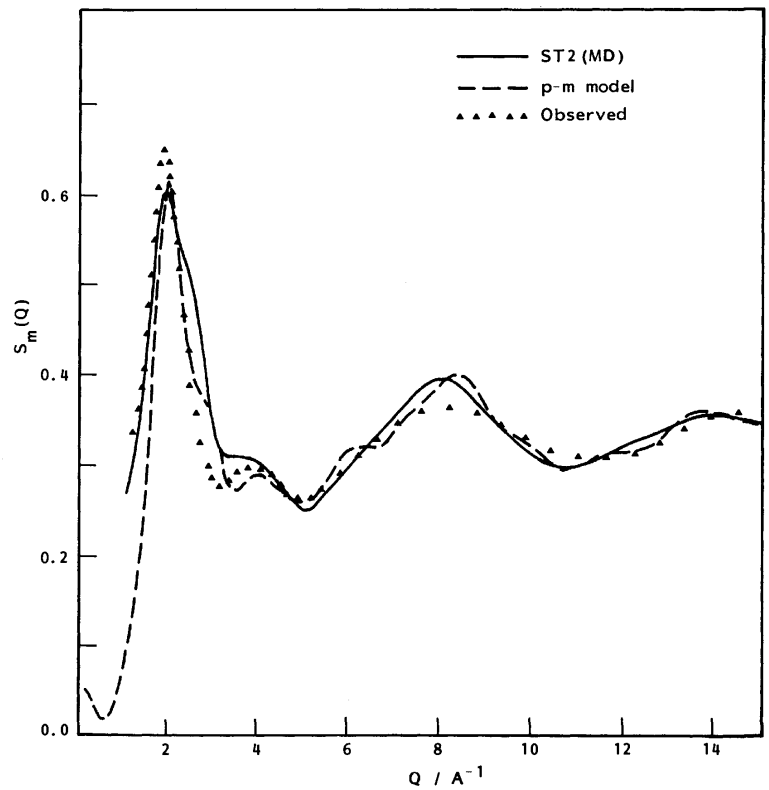

Fig. 6. Coherent neutron structure factor $S_m(Q)$ at 24°C in comparison with the observed data[17] and the calculated ones for pentamer-monomer mixture model.[17]

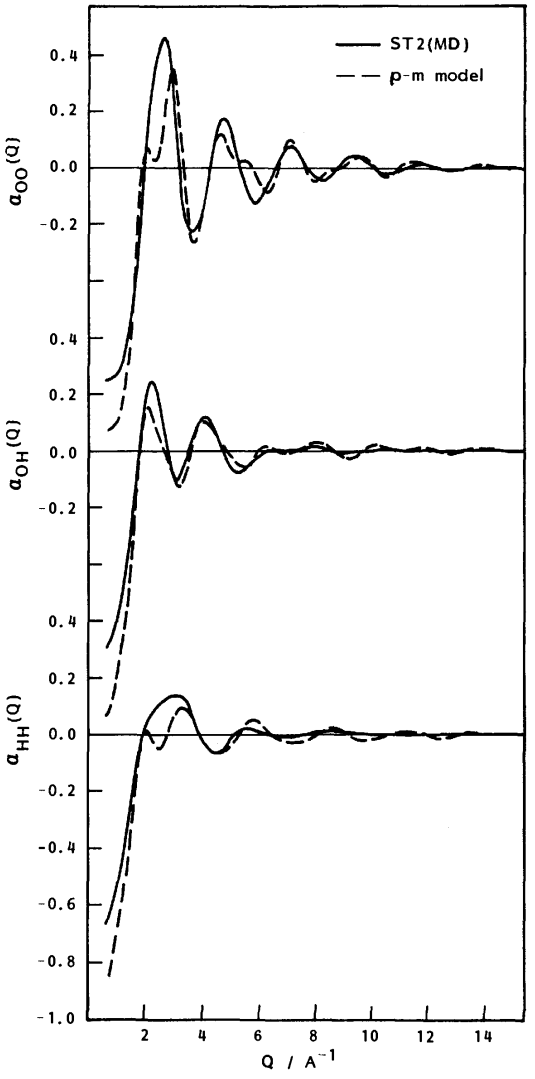

Fig. 7. Partial structure functions at 93°C in comparison with the corresponding ones calculated for pentamer-monomer mixture model.[17]

This feature should always be taken into consideration in constructing a theoretical model of water. In the pentamer-monomer mixture model, liquid water is regarded as an equilibrium mixture of the tetrahedral hydrogen-bonded pentamers and the non-hydrogen-bonded monomers.[3,17] The present results show that the pentamer-monomer mixture model can describe the overall structural properties of liquid water.

Seeing further details, some discrepancies are found for the $a_{OO}(Q)$ curves shown in Fig. 3; a double peak appears in the observed curve around Q=2.5 A^{-1}, but for the ST2 curve at 24 °C the double peak is quite less impressive and the right peak is too high. The similar situation was seen in the simulated X-ray scattering intensity curves due to Rahman and Stillinger for the BNS potential system at 34.3 °C.[1] An improvement is considered to be achieved by allowing the simulations to incorporate the nonrigidity of water molecules.[5,14]

In Fig. 7 the molecular dynamics $a_{ss'}(Q)$ curves for the ST2 system at 93 °C are given in comparison with the calculated curves for the pentamer-monomer mixture model. In Fig. 8 the $S_m(Q)$ curve for the ST2 system at 93 °C is shown, together with neutron diffraction data.[17]

Effects of the Periodic Boundary Conditions on Distributions of Hydrogen Bonds. In a molecular dynamics simulation of liquid systems, a periodic boundary condition is required in order to minimize surface effects, and the influences of artificial correlations imposed by the condition have been believed to be satisfactorily small for substantially large cells. For hydrogen-bonded fluids like water, however, there is a possibility that the periodicity condition affects the aspect of "hydrogen bonding" between molecules. In the following we examine the effects of the periodic boundary condition on distributions of hydrogen bonds.

In measuring the degree of hydrogen bonding, we follow a guideline due to Rahman and Stillinger.[1] If the interaction energy for a given pair of molecules lies below an assigned negative cut-off energy V_{HB}, the pair is hydrogen bonded and if their interaction equals or exceeds V_{HB}, they are not hydrogen bonded.

In order to see the degree of hydrogen bonding near the surface of the box, we classify molecules into two groups, and calculate separately the distributions of hydrogen bonds for each group;

$$\text{group I: } 0.2L < x_j, y_j, z_j < 0.8L$$

$$\text{group II: } x_j, y_j, z_j < 0.2L \text{ and } x_j, y_j, z_j > 0.8L$$

where L is the edge length of the cubic box and x_j, y_j, and z_j are the center of mass cartesian coordinates of molecule j.

In Fig. 9 we show the distributions of hydrogen bonds thus obtained for five different values of V_{HB}. These were determined by averaging over a period of 1000 Δt. From the comparison between the histograms for group I (about 210 molecules in the central part of the box) and those of group II (about 790 molecules near the surface), it is seen that the mean of the distribution for group II clearly shifts to lower numbers of hydrogen bonds. The population of hydrogen bonds which are destroyed near the surface is estimated roughly to be 10%. The cause of lowering of the degree of hydrogen bonding in group II is supposed as in the following. The periodic boundary condition clearly constrains the freedom of the molecules in motion near the surface of the box on the whole. This constraint subjected to the condition, probably that with respect to the rotationary degree of freedom of molecules, is considered resultantly to shift the degree of hydrogen bonding in group II to a lower magnitude than that in group I. Thus, it can be said that in the present simulation the molecules in group I (about 210 molecules) as the inner part resemble more exactly to the real water. In order to avoid such effects due to the

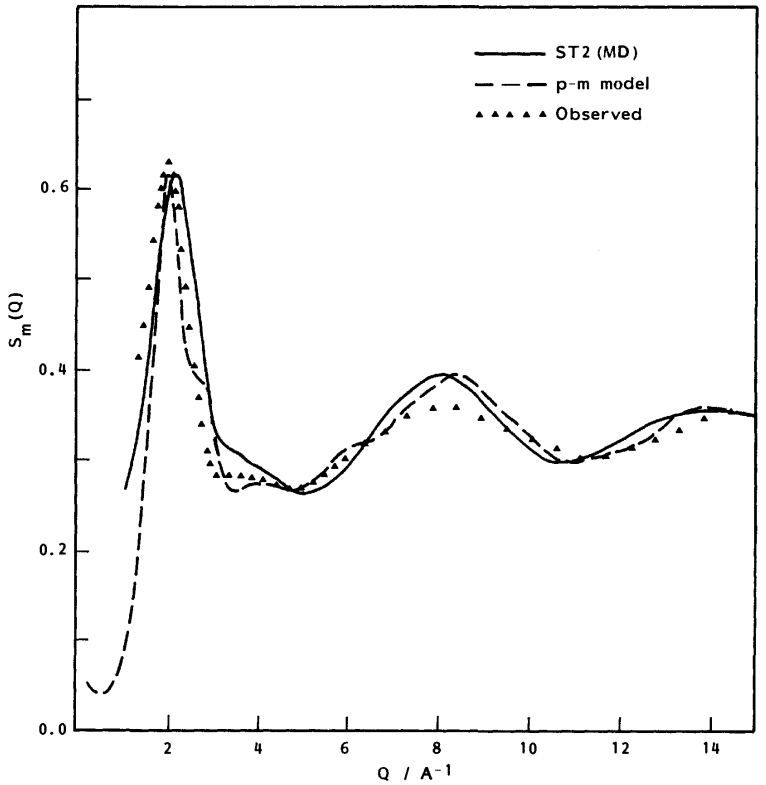

Fig. 8. Coherent neutron structure factor $S_m(Q)$ at 93°C in comparison with the observed data[17] and the calculated ones for pentamer-monomer mixture model.[17]

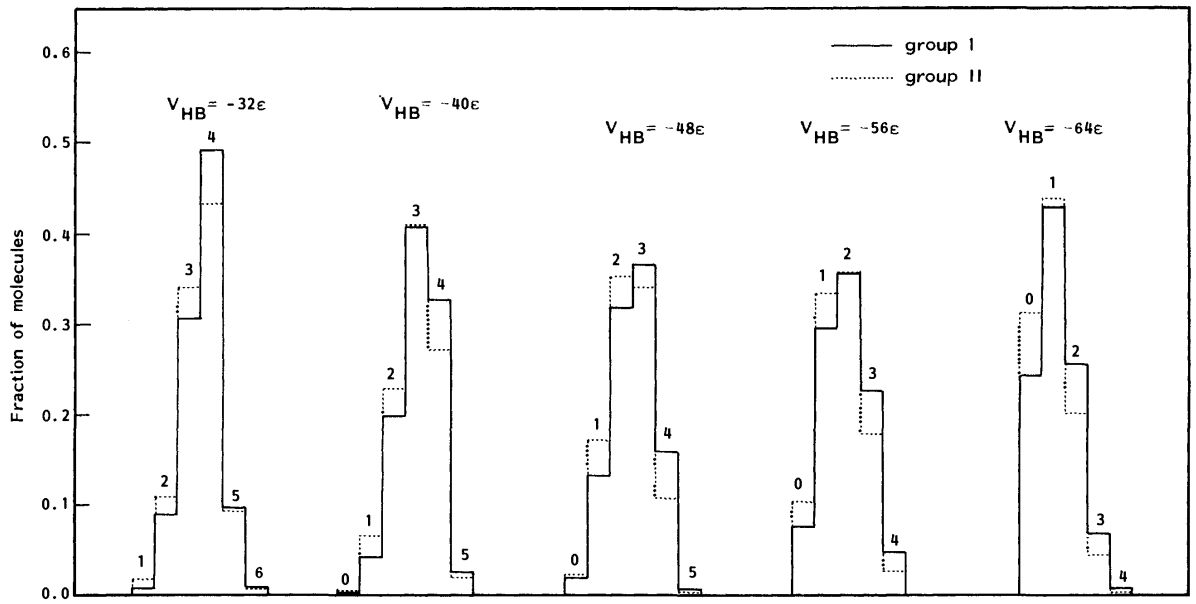

Fig. 9. Effects of periodic boundary conditions on distributions of hydrogen bonds. The results were obtained for 24°C.

periodic boundary conditions in a simulation of liquid water, the total number of molecules is desired to be as large as in the present simulation.

Self-Diffusion Process. The normalized velocity autocorrelation function for the molecular center of mass motion is given by

$$\psi(t) = <\frac{1}{N}\sum_j^N \vec{v}_j(0)\vec{v}_j(t)>/<\frac{1}{N}\sum_j^N \vec{v}_j(0)^2>, \quad (3)$$

where $\vec{v}_j$ is the center of mass velocity for molecule j. Figure 10 gives the normalized velocity autocorrelation function $\psi(t)$ at 24°C, including the simulation

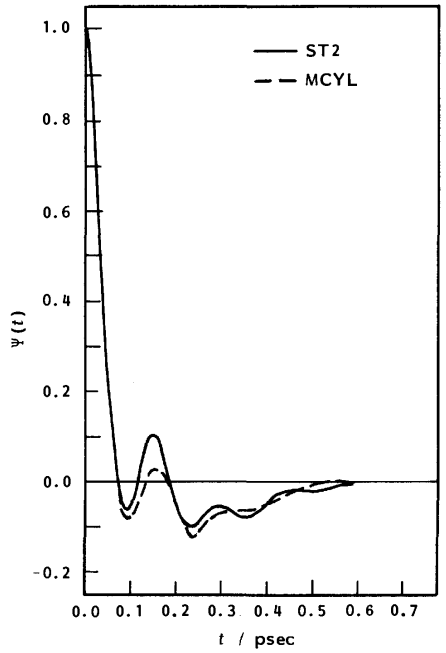

Fig.10. Velocity autocorrelation function for the molecular center of mass motion at 24°C in comparison with the ones for MCYL model given by Lie and Clementi.[14]

calculation of Lie and Clementi for the MCYL model at 27 °C.[14] The present result is consistent with the results of Stillinger and Rahman's simulations[2] expected at the corresponding temperature. Then, we find that the curves for the ST2 and MCYL models substantially resemble each other on the whole, although a more pronounced oscillatory behavior after the first negative region appears in the ST2 curve.

The self-diffusion coefficient D can be calculated by means of a Green-Kubo relation. Using the $\psi(t)$ curve given in Fig. 10, we obtain 2.8×10^{-5} cm^2s^{-1} for the ST2 model at 24 °C. This value is consistent with the results of Stillinger and Rahman extrapolated at the corresponding temperature.

References

1) A. Rahman and F. H. Stillinger, *J. Chem. Phys.*, **55**, 3336 (1971).
2) F. H. Stillinger and A. Rahman, *J. Chem. Phys.*, **60**, 1545 (1974).
3) K. Arakawa, K. Tokiwano, and K. Kojima, *Bull. Chem. Soc. Jpn.*, **50**, 65 (1977).
4) B. R. Lentz, A. T. Hagler, and H. A. Scheraga, *J. Phys. Chem.*, **78**, 1531 (1974).
5) A. Rahman, F. H. Stillinger, and H. L. Lemberg, *J. Chem. Phys.*, **63**, 5223 (1975); F. H. Stillinger and A. Rahman, *J. Chem. Phys.*, **68**, 666 (1978).
6) M. Rao, C. S. Pangali, and B. J. Berne, *Mol. Phys.*, **37**, 1773 (1979).
7) R. O. Watts, *Mol. Phys.*, **28**, 1069 (1974).
8) G. C. Lie, E. Clementi, and M. Yoshimine, *J. Chem. Phys.*, **64**, 2314 (1976).
9) J. C. Owicki and H. A. Scheraga, *J. Am. Chem. Soc.*, **99**, 7403 (1977).
10) J. R. McDonald and M. L. Klein, *J. Chem. Phys.*, **68**, 4875 (1978); R. W. Impey, M. L. Klein, and J. R. McDonald, *J. Chem. Phys.*, **74**, 647 (1981).
11) D. C. Rapaport and H. A. Scheraga, *Chem. Phys. Lett.*, **78**, 491 (1981).
12) G. Jancso, P. Bopp, and K. Heinzinger, *Chem. Phys.*, **85**, 377 (1984).
13) W. L. Jorgensen, J. Chandrasekhar, J. Madura, R. W. Impey, and M. L. Klein, *J. Chem. Phys.*, **79**, 926 (1983).
14) G. C. Lie and E. Clementi, *Phys. Rev. A*, **33**, 2679 (1986).
15) N. Ohtomo, K. Tokiwano, and K. Arakawa, *Bull. Chem. Soc. Jpn.*, **57**, 329 (1984).
16) N. Ohtomo, K. Tokiwano, and K. Arakawa, *Bull. Chem. Soc. Jpn.*, **54**, 1802 (1981).
17) N. Ohtomo, K. Tokiwano, and K. Arakawa, *Bull. Chem. Soc. Jpn.*, **55**, 2788 (1982).
18) W. E. Thiessen and A. H. Narten, *J. Chem. Phys.*, **77**, 2656 (1982).
19) J. P. Ryckaert, G. Ciccotti, and H. J. C. Berendsen, *J. Comput. Phys.*, **23**, 327 (1977); G. Ciccotti, M. Ferrario, and J. P. Ryckaert, *Mol. Phys.*, **47**, 1253 (1982).

 © 1987 The Chemical Society of Japan Bull. Chem. Soc. Jpn., 60, 483—487 (1987)

An ENDOR Study of Diphenyl Nitroxide and Its Methyl Derivatives, The Effect of the Methyl Substitution

Jun YAMAUCHI,* Keiichi OKADA, and Yasuo DEGUCHI
College of Liberal Arts and Sciences, Kyoto University, Kyoto 606
(Received August 9, 1986)

The ENDOR spectra of diphenyl nitroxide (DPNO) and its monomethyl derivatives were observed in ethylbenzene at −70 °C. The agreement between the ESR and ENDOR data is generally good. The MO calculations, however, indicate a few disagreements in the case of the *m*- and *o*-methyl DPNO derivatives. The methyl substitution at the meta-position destroys the equivalency of all protons at the meta-positions, which are divided into two sets of equivalent proton groups of the same number. The ortho-substitution weakens the coplanarity of the two benzene rings and increases the number of the equivalent proton groups, which are fully resolved in the ENDOR spectrum. The steric hindrance is taken into account in the MO calculation, which can predict these slightly different coupling groups-again except for those in the meta-positions. A satisfactorily simulated spectrum of the *o*-methyl DPNO is obtained on the basis of the ENDOR data.

Previously two of the present authors (J.Y. and Y.D.) have investigated the hyperfine structures of several neutral radicals by means of the electron spin resonance (ESR).[1] In this work, diphenyl nitroxide (DPNO) and its methyl derivatives have been discussed in detail from the point of view of steric effect. The hyperfine coupling constants of the nitrogen and protons have been greatly affected in the case of the ortho-substituted compounds. The steric hindrance has weakened the coplanarity of the two benzene rings and caused a redistribution of the spin density such that the number of the equivalent proton group is increased, giving rise to complex ESR spectra. This must be one of the reasons why the ESR spectra of the ortho-methylated compounds could not be analyzed completely, whereas unambiguous analyses and assignment have been done for the other derivatives.

Electron nuclear double resonance (ENDOR) is the most useful for establishing the detailed proton hyperfine coupling constants in complicated ESR spectra.[2] Thus, the application of the ENDOR to the methylated DPNO derivatives was attempted in order to confirm the steric effect of the ortho-substituted compounds. As far as we know, there has been no such ENDOR work, not even on the parent compound DPNO. Thus, in this paper a proton ENDOR study is reported on DPNO and its monomethyl derivatives, with an emphasis placed on the *o*-methyl DPNO; the effect of the methyl substitution is also discussed.

Nitroxide radicals have previously been investigated extensively by means of ENDOR. For example, there are several works on the neutral nitroxide radicals containing aliphatic and/or aromatic substituent;[3-7] also the ^{14}N-ENDOR of the nitroxides is another interesting subject.[8-12] ESR investigations of DPNO have been made in a solid[13] and in solution.[1] DPNO shows two isotropic hyperfine coupling constants A_1=1.91 and A_2=0.82 G (1 G=10^{-4} T) in ethylbenzene.[14] These are assigned to the six equivalent protons at the ortho- and para-positions, and to the four equivalent protons at the meta-positions, respectively.[1] The para- or meta-substitution of a methyl group has little influence on the spin density distribution. Thus, the ESR spectra are easily explained by considering the increased proton number on the substituted position. Ortho-substituted DPNO, on the other hand, shows a drastic redistribution of the spin density because of strong bond-twisting.[1] Recently a short communication about a general triple resonance experiment on DPNO has been published.[14] The general triple resonance made possible the determination of the relative signs of the hyperfine coupling constants of the protons; that is, the two coupling constants, A_1 and A_2, of DPNO have opposite signs, in agreement with the earlier result.[13]

Experimental

DPNO and its derivatives are fairly unstable; thus, one should use a radical compound synthesized freshly in order to prepare a sample of its solution. Synthetic methods were described in the previous paper.[1] Solution samples for ENDOR measurements were prepared by the standard technique, using ethylbenzene as the solvent. The ESR and ENDOR spectra were recorded at −2 and −70 °C respectively for the best resolution.

The ENDOR spectrometer consists basically of a commercial JEOL FE-3X ESR spectrometer, with a JEOL ES EDX2 ENDOR accessory equipped with a TE_{011} cavity. Moreover, a broad-band ENDOR accessory equipped with a TM_{110} was built. This is similar to the one reported previously.[15] A simple block diagram is shown in Fig. 1. The TM_{110} cavity contains a silver solenoid of 20 turns (30 mm length, 7 mm o.d., made of silver wire 1 mm in diameter) directly mounted on a thin quartz tube; it is supplied with microwave power through a coupling iris which connects the cavity with the wave guide. With this device, it is easier to adjust the coupling between the cavity and the transmission line of microwave power than with the coaxial-line method. A frequency generator (Hewlett-Packard HP8601A) generates the radio-frequency, which passes through a broad-band power amplifier (ENI A300) and the solenoid. Finally, its power is dissipated in a 50 Ω oil-cooled resistor (TRIO RF DUMMY LOAD RD 300). A linear amp simultaneously sweeps the 6.5 KHz FM frequency of the oscillator and drives the *X*-axis of the *X*-*Y* recorder. The phase-sensitively detected changes of the absorbed microwave power generate the signal voltage,

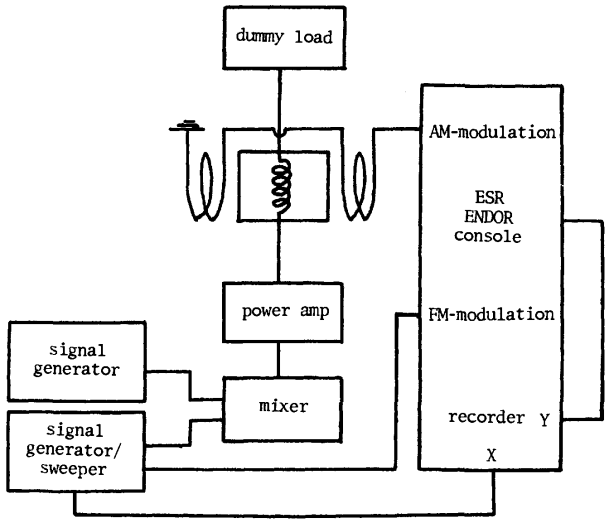

Fig. 1. A block diagram for ENDOR and triple experiments using a TM_{110} mode cavity.

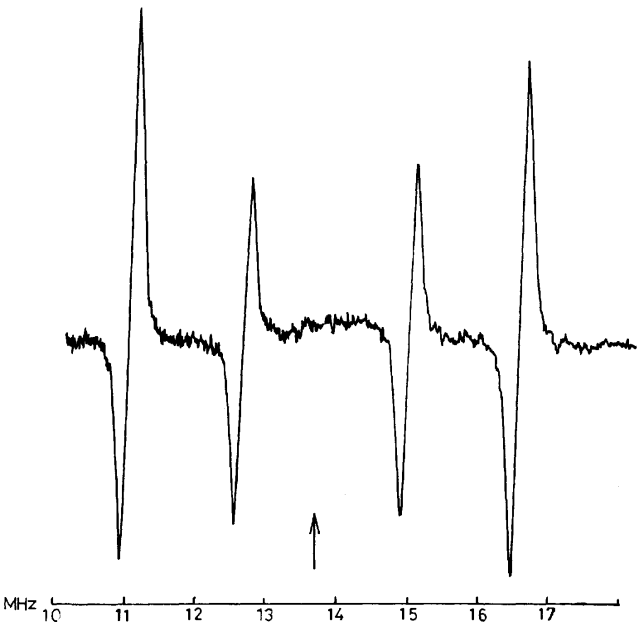

Fig. 2. ENDOR spectrum of DPNO in ethylbenzene at −70°C. The arrow indicates the frequency of free proton.

driving the Y-axis of the recorder. The ENDOR signals are observed in the systems of both TE_{011} and TM_{110} cavities. In the spectra themselves, there are no essential differences. However, the TM_{110} cavity system surely has certain advantages, as has been pointed out elsewhere[11,14-16] The ENDOR spectra shown in this paper were all recorded by means of the TM_{110} cavity.

Results

The ENDOR spectrum of DPNO is shown in Fig. 2, from which one can recognize that the protons on both benzene rings are to be classified into two different sets, such as one group of para- or ortho-protons and

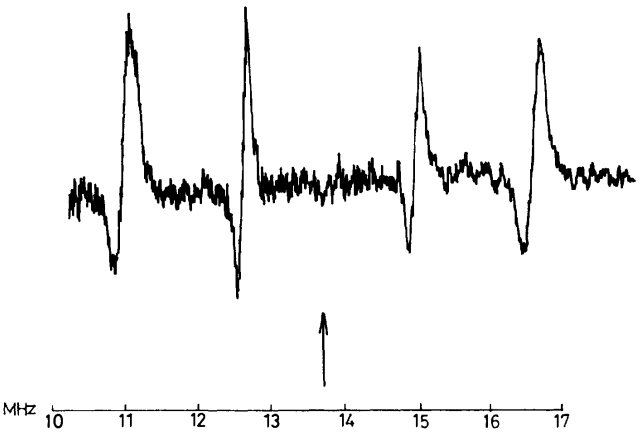

Fig. 3. ENDOR spectrum of *p*-methyl DPNO in ethylbenzene at −70°C. The arrow indicates the frequency of free proton.

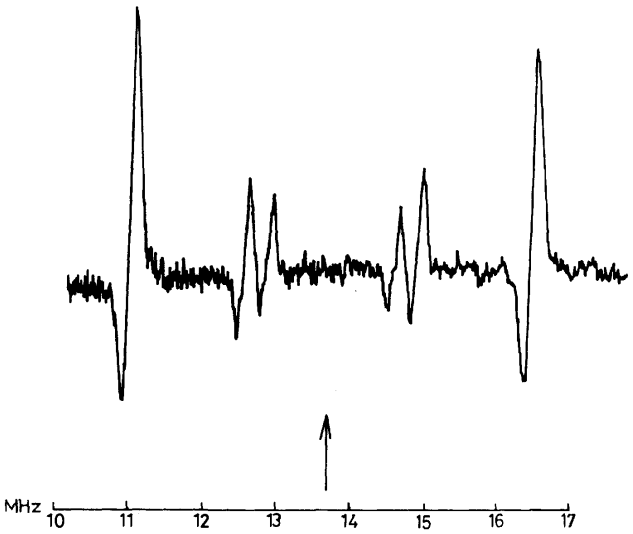

Fig. 4. ENDOR spectrum of *m*-methyl DPNO in ethylbenzene at −70°C. The arrow indicates the frequency of free proton.

another group of meta-protons. Features similar to those in DPNO appear in the cases of *p*-methyl and *m*-methyl DPNO (Figs. 3 and 4). The ortho-methylated derivative of DPNO, however, shows a fairly different appearance in its ENDOR spectrum, as is shown in Fig. 5; firstly, the overall width of the spectrum is about 8 MHz, about 2 MHz larger than that of DPNO. Secondly, the weak ENDOR absorption lines due to several sets of equivalent protons can be observed. The proton hyperfine coupling constants determined from the ENDOR spectra are summarized in Table 1, in which the data obtained from the ESR spectra are also listed for comparison. Two of the present authors (J.Y. and Y.D.) could not analyze the ESR spectrum of the *o*-methyl DPNO, but at this time the ESR spectral analysis could be made on the basis of the ENDOR results and the spectrum could be simulated using the hyperfine coupling constants listed in the table.

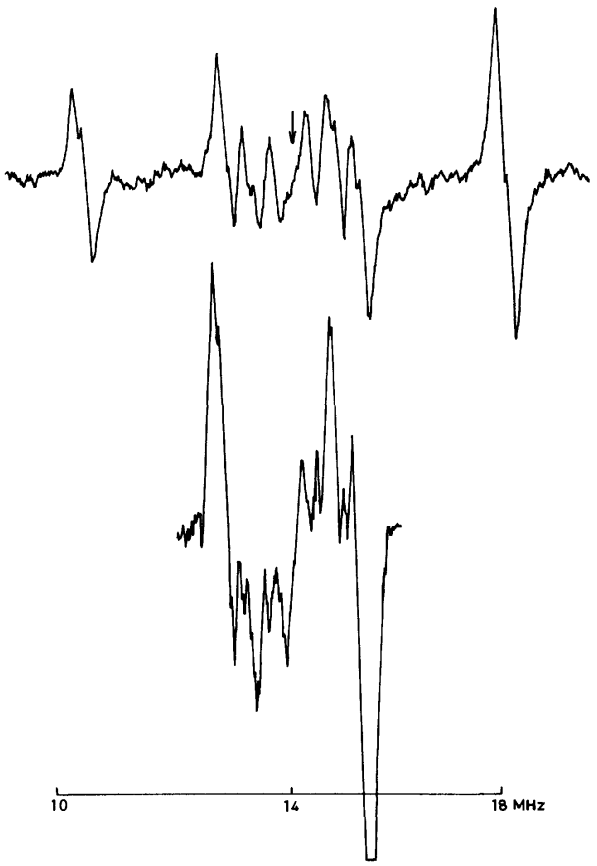

Fig. 5. ENDOR spectrum of *o*-methyl DPNO in ethylbenzene at −70°C. The arrow indicates the frequency of free proton. The central part of higher sensitivity and resolution is also shown.

Discussion

The agreement between the ESR and the ENDOR data is excellent, except in the case of *o*-methyl DPNO. For further comparison, the usual MO calculations were performed. The same MO parameters as in the previous paper were employed for the simple Hückel and McLachlan methods. Thus, the theoretically calculated hyperfine coupling constant in each position is also shown in Table 1, where the McConnel relation between the spin density and the hyperfine coupling constant is applied with a proportionality constant of $|Q|=27.3$ G. The calculations also support the assignment which has been made mainly on the basis of the ESR simulation. Here a comment about *m*-methyl DPNO is appropriate. In this radical, both ESR and ENDOR assure two kinds of equivalent proton sets in the meta-positions. The inner pair of absorption lines in DPNO and its *p*-methyl derivative splits into two lines *m*-methyl DPNO, giving 814 and 577 mG splittings. These are also ascertained by the ESR simulation; 810 and 580 mG. However, the equivalent proton numbers of both hyperfine coupling constants are found to be the same, so that there is no way to assign the larger hyperfine coupling to the methyl or the other meta-protons. Deuteron substitution (for example, trideuteriomethyl substitution at the meta-position) would be necessary to solve this problem. On the other hand, the MO calculation predicts only a minor difference, less than 30 mG, between

Table 1. ESR, ENDOR, and MO Calculation Results for DPNO and Its Derivatives

Compound		A_{H1}/G	A_{H2}/G	A_{H3}/G	A_{H4}/G	A_N/G
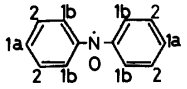	ESR	1.910	0.820			9.500
	ENDOR	1.914	0.817			—
	cal[a]	a 1.966	0.938			9.500[c]
		b 2.153				
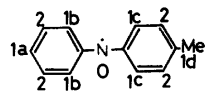	ESR	1.890	0.830			9.750
	ENDOR	1.980	0.834			—
	cal[a]	a 1.980	0.932			9.525[c]
		b 2.167				
		c 2.148				
		d 1.896				
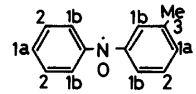	ESR	1.920	0.810	0.580		9.580
	ENDOR	1.923	0.814	0.577		—
	cal[a]	a 1.966	0.938	0.910		9.503[c]
		b 2.156				
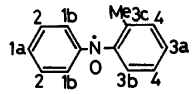	ESR	2.680	0.830	0.560	0.280	9.941
		2.610		0.500		
	ENDOR	2.731	0.881	0.600	0.249	—
	cal[b]	a 2.405	1.226	a 0.552	0.305	10.440[c]
		b 2.691		b 0.647		
				c 0.608		

a) A twisted angle of 45° is assumed. b) A twisted angle of 60° is assumed. c) A proportionality constant of $|Q|=27.3$ G is assumed so that the DPNO value is reprodued.

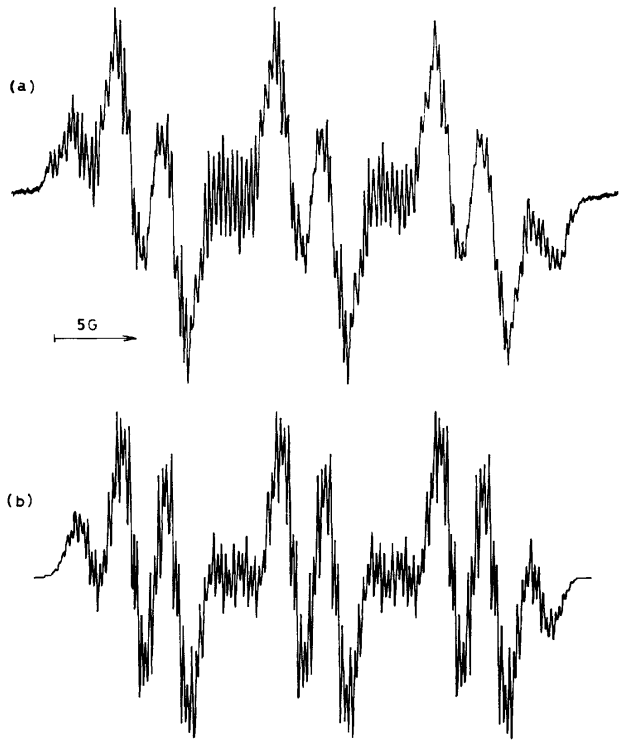

Fig. 6. ESR(a) and simulated(b) spectra of *o*-methyl DPNO.

these positions. We have no reasonable explanation about this discrepancy at present. In Table 1, therefore, the larger hyperfine coupling constant is assigned temporarily to the *m*-methyl protons, following the MO calculation.

The fact that the overall width of the ENDOR spectrum of *o*-methyl DPNO is larger than that of DPNO implies that the steric hindrance effect of the methyl group substituted at the ortho-position of the benzene ring is dominant in this case; that is, there is a greater population of electron on the N-O bond and the benzene ring of no-methyl substitution than on the twisted tolyl ring. In the earlier ESR, only the biggest proton coupling (2.70 G) was recognized except for the nitrogen one, which gave a quartet appearance in the spectrum (Fig. 6). A similar value, although the absorption line is slightly split, is also observed this time in the ENDOR spectrum (Fig. 5), from which three additional sets of equivalent protons are revealed in the smaller splitting groups. In a more highly sensitive spectrum, it seems that the smaller two groups split into two splittings further, as is shown in Fig. 5. All these slightly different values obtained experimentally can be predicted by the theoretical MO calculations, assuming the sterically hindered rotation of one phenyl ring containing the substituted methyl group away from the remaining π-electron framework, which includes the N-O nitroxide group. This assumption has been discussed in detail in the previous paper,[1] where a twisted angle of 55—60° was anticipated for a proton-methyl proton repulsion case. In Table 1 the results of the MO calculation (a twisted angle of 60° is assumed) are compared with the experimental results; the fit is excellent except for the second biggest proton coupling, which is assigned to the meta-positions of the unsubstituted benzene ring. Considering the tendency of the other protons, it is rather difficult to understand this value. The steric hindrance makes the unpaired electron highly populated on the ortho- and para-positions of the unsubstituted benzene ring. Nevertheless, the meta-proton hyperfine coupling constant increased less than 10%, whereas a 40% increase is observed in the para- and ortho-positions. On the other hand, the MO calculations show that all positions of the unsubstituted benzene ring are equally influenced to localize the unpaired electron ca. 40% more and that the calculated hyperfine coupling constants, except for this meta-position, are in good agreement with the experimental values. This quantitative singularity at the meta-position, together with the discrepancy discussed in the *m*-methyl DPNO, may be relevant to a special characteristic of the meta-positions of the benzene rings, that is, a negative spin density. A more sophisticated MO treatment and/or steric hindrance mechanism is necessary. This will be commented on in the Discussion section later. At any rate, the comparatively good agreement surely supports the validity of the steric hindrance mechanism developed in the earlier paper.[1]

The ESR simulation was carried out on the basis of the ENDOR results. DPNO and its *p*-methyl derivative are straightforward, and the *m*-methyl DPNO is almost the same. Even a stick-diagram construction can yield reliable values. It is found that the coupling constants of the *m*-methyl DPNO, 810 and 560 mG, which are assigned to the meta-positions, should be taken into account so as to produce quartet splittings. This means that three protons in each group should contribute as an equivalent proton group. Then the well-simulated spectrum can be reproduced. The assignment, however, is still ambiguous, although it is narrowly evidenced by the MO calculation. For the *o*-methyl DPNO, there are many sets of equivalent protons so that the assignment seems to be really intuitive for the smaller coupling groups. According to the MO calculation, however, the magnitude of the hyperfine coupling constants agrees well with the experimental values; thus, one can assign each hyperfine coupling so as to satisfy the order of its magnitude. Furthermore, if one takes into account several experimental facts, for instance, the facts that the ortho- and para-proton hyperfine coupling constants are almost equal and are bigger than the meta-protons, or that the unpaired electron is highly localized on the unsubstituted benzene ring, the analysis can be nearly perfect. By changing the coupling constants little by little from the ENDOR values we finally come to the simu-

lated spectrum shown in Fig. 5. Of course, a minor modification would still be necessary to complete it. Generally speaking, however, the ESR data of the sterically hindered *o*-methyl DPNO in Table 1 are considered to be reasonable.

The general triple resonance of DPNO was described in an earlier communication,[14] where it was clarified that the two hyperfine coupling groups of the meta- and para- or ortho-positions have opposite signs. Usually one may assume a positive spin density on the carbon atoms at the para- and ortho-positions and, therefore, a negative spin density at the meta-positions, as has been evidenced by several MO calculations. This means that the spin density on the carbon atoms at the meta-positions is rather small but, on the contrary, is easily influenced by many factors, for example, MO parameters, substituents, steric rotations, and solvents. Therefore, the discrepancy and the singularity observed in the meta-positions in this experiment may be attributed to these properties. To solve the problem, more precise work, such as deuteron substitution, a study of the solvent effect, and triple experiments for the methylated DPNO, will be necessary.

In conclusion, the ENDOR study supports the previous ESR work. In the para- and meta-methylated DPNO, only a few modifications of DPNO are necessary; that is, the methyl substitution in such positions results in little change in the spin density distribution. The ortho-methylated DPNO is twisted at one N–C bond, which is attached to the substituted benzene ring. The data calculated on the assumption that the twisted angle is 60° are reasonable and consistent with the spin density distribution and the steric hindrance consideration discussed previously.[1] We observed a minor but clear discrepancy and singularity in the meta-positions of the meta- or ortho-substituted DPNO.

References

1) J. Yamauchi, H. Nishiguchi, K. Mukai, Y. Deguchi, and H. Takaki, *Bull. Chem. Soc. Jpn.*, **40**, 2512 (1967).
2) L. Kevan and L. D. Kispert, "Electron Spin Double Resonance Spectroscopy," John Wiley and Sons, New York (1976).
3) R. D. Allendoerfer and J. H. Engelmann, *Mol. Phys.*, **20**, 569 (1971).
4) K. Ishizu, H. Nagai, K. Mukai, M. Kohno, and T. Yamamoto, *Chem. Lett.*, **1973**, 1261.
5) K. Ishizu, T. Yamamoto, M. Kohno, A. Nakajima, and Y. Deguchi, *Tetrahedron Lett.*, **1974**, 1537.
6) Y. Kotake and K. Kuwata, *Chem. Lett.*, **1984**, 83.
7) J. Yamauchi and Y. Deguchi, *Chem. Lett.*, **1985**, 111.
8) D. S. Leniart, J. C. Vendrine, and J. S. Hyde, *Chem. Phys. Lett.*, **6**, 637 (1970).
9) K. P. Dinse, K. Mobius, M. Plato, and R. Biehl, *Chem. Phys. Lett,*. **14**, 196 (1972).
10) N. M. Atherton and M. Brustolon, *Mol. Phys.*, **32**, 23 (1976).
11) J. Yamauchi and Y. Deguchi, *Chem. Lett.*, **1983**, 257.
12) E. G. Janzen and U. M. Dehler, *Chem. Lett.*, **1984**, 1233.
13) Y. Deguchi, *Bull. Chem. Soc. Jpn.*, **34**, 910 (1961).
14) Y. Deguchi, K. Okada, J. Yamauchi, and K. Fujii, *Chem. Lett.*, **1983**, 1611.
15) K. Mobius and R. Biehl,"Multiple Electron Resonance Spectroscopy," ed by M. M. Dorio and J. H. Freed, Plenum Press, New York (1979), Chap. 14.
16) J. Lopez, K. Okada, J. Yamauchi, and Y. Deguchi, *Bull. Chem. Soc. Jpn.*, **57**, 673 (1984).

 © 1987 The Chemical Society of Japan Bull. Chem. Soc. Jpn., 60, 489—492 (1987)

Oxygen-17 NMR Study of the Uranyl Ion. IV.[1] ^{17}O Nuclear Magnetic Relaxation and Chemical Shifts of Uranyl Oxygen Atoms and Coordinated Water

Woo-Sik Jung, Hiroshi Tomiyasu, and Hiroshi Fukutomi*
Research Laboratory for Nuclear Reactors, Tokyo Institute of Technology,
O-okayama, Meguro-ku, Tokyo 152
(Received August 13, 1986)

^{17}O nuclear magnetic relaxation times and chemical shifts of uranyl oxygen atoms (hereafter uranyl oxygens) and solvent water have been measured with changing concentration of the uranyl ion in aqueous solution. The ^{17}O resonance of the water molecule in the first-coordination sphere is determined to be at 90.1±1.2 ppm relative to free water at 25 °C. The effective correlation time for the ^{17}O quadrupolar relaxation of the coordinated water, which corresponds to the reorientation time for the hydrated uranyl ion, is about 8.7 times that of free water. The ^{17}O spin-lattice relaxation times (T_1) of uranyl oxygens have been measured at 25 °C. From the ^{17}O T_1 values the ^{17}O nuclear quadrupole coupling constant of uranyl oxygens has been estimated to be 0.44 MHz. This small value implies the high symmetry of electron distribution around uranyl oxygens.

Although ^1H resonances of the water molecule in the first-coordination sphere of a uranyl ion (UO_2^{2+}) have been observed,[2-5] it is impossible to observe directly the ^{17}O resonance of the coordinated water even at low temperature. The ^{17}O nuclear magnetic relaxation of acidified water is dominated by a quadrupolar relaxation process,[6] which is brought about by interaction of the nuclear electric quadrupole moment with fluctuations of the electric field gradient (EFG) at the oxygen nucleus. The equality of T_1 and T_2 (spin-spin relaxation time) holds for acidic solutions of pure water. In the limit of extreme narrowing, the ^{17}O longitudinal relaxation rate follows Eq. 1,[7]

$$\frac{1}{T_1} = \frac{12\pi^2}{125}\left(1+\frac{\xi^2}{3}\right)\left(\frac{e^2qQ}{h}\right)^2\tau_c, \quad (1)$$

where ξ is an asymmetry parameter of the electric field gradient, e^2qQ/h the quadrupole coupling constant (QCC) in Hz, h the Planck constant, and τ_c the effective correlation time for molecular reorientation. Approximate estimate of τ_c for isotropic tumbling may be made by application of the modified Stokes-Einstein-Debye formula,

$$\tau_c = 4\pi r^3 f\eta/3k_BT, \quad (2)$$

where f is the Gierer-Wirtz microviscosity correction factor,[8] r the molecular radius, η the viscosity, k_B the Boltzmann constant, and T the absolute temperature.

The τ_c value is expected to increase for water coordinated to diamagnetic ions in aqueous solution, thus causing the broadening of the ^{17}O resonance. If the exchange reaction of water between free and coordinated water in the ions is very fast, a single ^{17}O resonance of water is observed, which corresponds to the average of resonances in these environments.

In order to elucidate the behavior of the coordinated water in the uranyl ion, we have measured linewidths and chemical shifts of ^{17}O resonances of solvent water with changing concentration of the uranyl ion in aqueous solution. ^{17}O relaxation times of uranyl oxygens have been also measured and an ^{17}O QCC value of uranyl oxygens has been estimated.

Experimental

Uranyl nitrate hexahydrate $UO_2(NO_3)_2\cdot 6H_2O$ was purified by the extraction into diethyl ether from ammonium nitrate solution and recrystallized twice from aqueous solution. Preparation of uranyl perchlorate pentahydrate $UO_2(ClO_4)_2\cdot 5H_2O$ and ^{17}O-enriched uranyl oxygens has been described elsewhere.[9] The concentrations of uranyl ions were calculated on the assumption that the hydration number of the uranyl ion is 5.[4] The ^{17}O NMR spectra were obtained with a JEOL JNM-FX 100 FT-NMR spectrometer operating at 13.46 MHz. The measurements were performed with a 5-mm o.d. NMR sample tube, which was immersed in a 10-mm o.d. concentric NMR tube containing $(CD_3)_2CO$ (Merck). The samples were not degassed since the presence of oxygen makes no effect on the ^{17}O linewidth.[10]

Full linewidths ($\Delta\nu$) at half height were determined by a least-squares Lorentzian lineshape-fitting procedure. The positive chemical shift is downfield relative to the reference signal. Samples for measurements of ^{17}O linewidths and spin-lattice relaxation times of uranyl oxygens were prepared by the same method as described in the previous paper.[9] The ^{17}O T_1 measurements, which were carried out at 54.10 MHz on a JEOL JNM-GX 400 FT-NMR spectrometer, were made by using the inversion recovery pulse sequence.

Results and Discussion

^{17}O Chemical Shifts of Coordinated Water. ^{17}O chemical shifts of uranyl oxygens relative to solvent water tend to decrease with increasing concentration of the uranyl ion in nitrate solution, as shown in Fig. 1. If one adopts $(CD_3)_2CO$ as a reference for ^{17}O chemical shifts, it is possible to know how the concentration of the uranyl ion affects the respective ^{17}O chemical shifts of uranyl oxygens and solvent water. An example of the results is illustrated in Fig. 2. The ^{17}O chemical shifts of uranyl oxygens increase linearly with increasing concentration of the uranyl ion, where $d\delta(^{17}O)/d[UO_2^{2+}]=1.7$ ppm m^{-1} at 25 °C. This value is larger than that for the uranyl perchlorate complex,[1] and

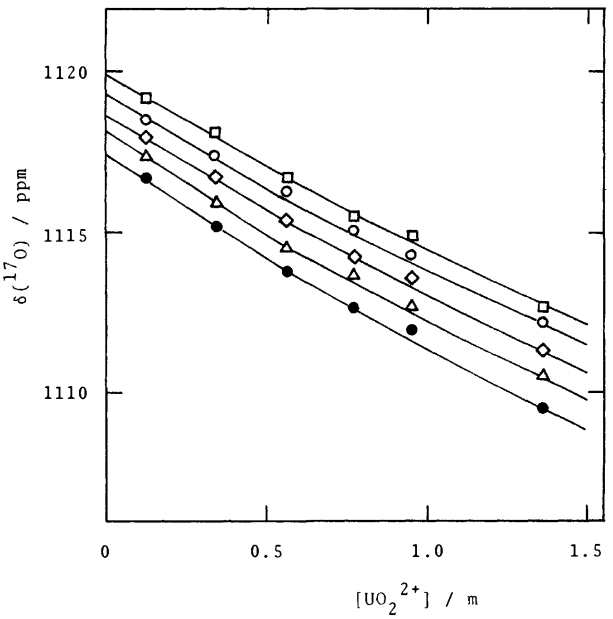

Fig. 1. Dependence of ^{17}O chemical shift of uranyl oxygens (relative to solvent water) on $[UO_2^{2+}]$ in nitrate solution at 20 (●), 25 (△), 30 (◇), 35 (○), and 40 (□)°C; 1 m=1 mol kg^{-1}.

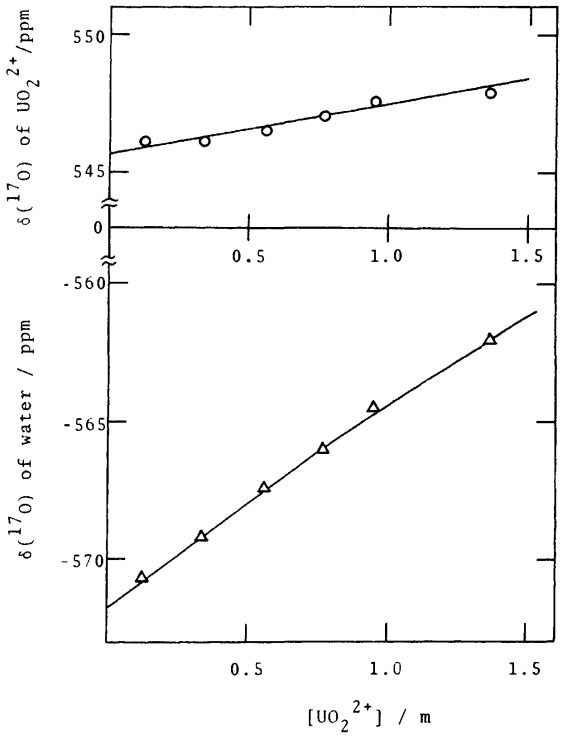

Fig. 2. Effects of $[UO_2^{2+}]$ on ^{17}O chemical shift (relative to acetone-d_6) of uranyl oxygens (○) and solvent water (△) in nitrate solution at 25°C.

this result is attributed to the formation of $UO_2NO_3^+$, the ^{17}O chemical shift of which is larger than that of UO_2^{2+} ion by 4.9 ppm at 25 °C.[1]

On the other hand, the ^{17}O resonances of solvent water shift downfield and the plot of $\delta(^{17}O)$ vs. $[UO_2^{2+}]$ deviates slightly from a linear relationship with increasing $[UO_2^{2+}]$ as shown in Fig. 2. This arises from the fact that since the exchange of water between free and coordinated water in the uranyl ion is very fast,[2,11] the observed ^{17}O resonance is the average of the resonances in these environments. The observed ^{17}O chemical shift is given by

$$\delta(^{17}O)_{obsd} = P_f\delta_f(^{17}O) + P_c\delta_c(^{17}O), \quad (3)$$

where P_f (or $\delta_f(^{17}O)$) and P_c (or $\delta_c(^{17}O)$) are mole fractions (or chemical shifts) of free and coordinated water, respectively. Assuming that the effect of NO_3^- ions on ^{17}O chemical shifts of water is negligible,[12] we calculated $\delta_f(^{17}O)$ and $\delta_c(^{17}O)$ by a nonlinear least-squares method. The results obtained are listed in Table 1. The ^{17}O chemical shifts of free water relative to $(CD_3)_2CO$ are in good agreement with the literature value.[13]

Figure 3 shows that the difference in ^{17}O chemical shift between free and coordinated water decreases with increasing temperature. Since $d\delta(^{17}O)/dT$ for

Table 1. ^{17}O Chemical Shifts[a] and Linewidths of Free and Coordinated Water in the Uranyl Ions at Various Temperature

Temp	$\delta_f(^{17}O)$	$\delta_c(^{17}O)$	$\Delta\nu_f$	$\Delta\nu_c$
°C	ppm	ppm	Hz	Hz
20	−570.6±0.1	−479.6±1.4	53.5±0.5	477±9
25	−571.8±0.1	−481.7±1.1	45.8±0.9	413±16
30	−571.7±0.1	−487.0±1.1	39.7±0.5	339±9
35	−572.4±0.1	−488.9±0.9	34.6±0.1	290±3
40	−573.0±0.1	−491.8±1.6	29.5±0.4	253±7

a) Relative to $(CD_3)_2CO$.

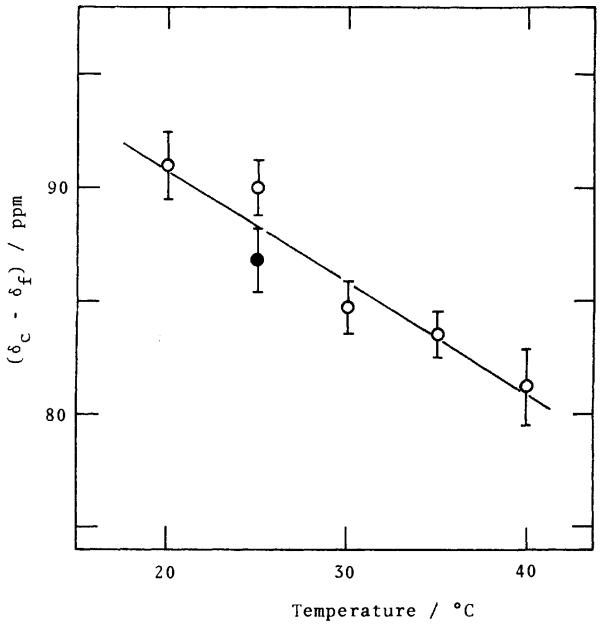

Fig. 3. Temperature dependence of the difference in ^{17}O chemical shift between free and coordinated water in nitrate (○) and perchlorate (●) solutions.

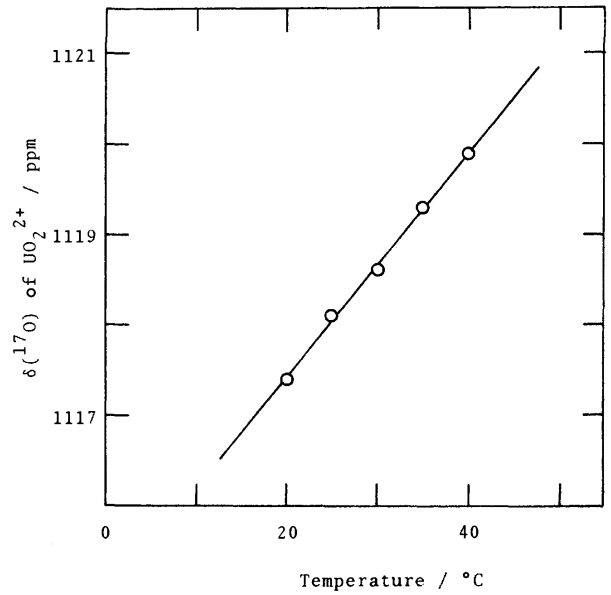

Fig. 4. Temperature dependence of ^{17}O chemical shift of uranyl oxygens (relative to pure water) at infinite dilution of the uranyl ion.

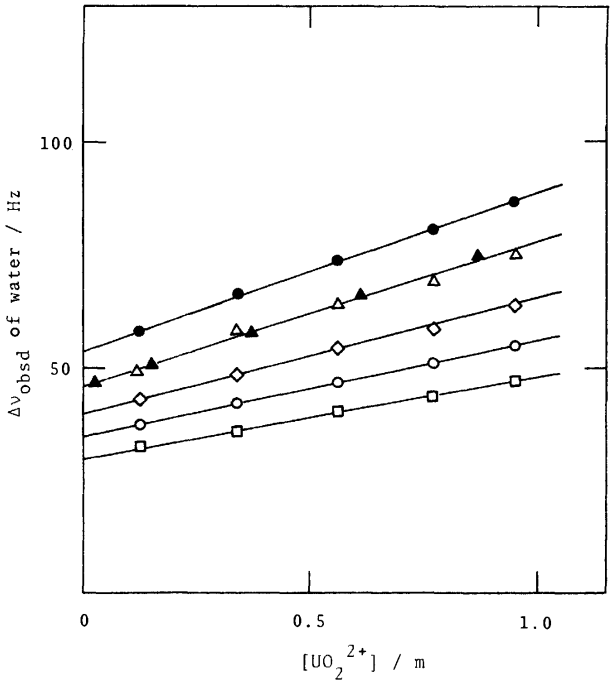

Fig. 5. Dependence of ^{17}O linewidth of solvent water on $[UO_2^{2+}]$ in nitrate solution at 20 (●), 25 (△), 30 (◇), 35 (○), and 40 (□)°C; 25°C (▲), in perchlorate solution.

pure water is −0.03 ppm °C^{-1},[12] then $d\delta(^{17}O)/dT$ for the coordinated water was calculated to be 0.52 ppm °C^{-1} from the slope in Fig. 3. The ^{17}O chemical shift of uranyl oxygens relative to free water at infinite dilution of the uranyl ion is given by (1114.9±0.1)+(0.12±0.01)×Temp (°C) as shown in Fig. 4. The second term agrees with the difference in $d\delta(^{17}O)/dT$ between uranyl oxygens (+0.087 ppm °C^{-1})[1] and pure water.

^{17}O Relaxation Times of Coordinated Water. The dependence of ^{17}O linewidth ($\Delta\nu_{obsd}$) of solvent water on $[UO_2^{2+}]$ is shown in Fig. 5. Assuming that the viscosity of the solution studied is equal to that of pure water and the rate of water exchange is slow relative to the rate of molecular reorientation,[14] $\Delta\nu_{obsd}$ is given by

$$\Delta\nu_{obsd} = P_f \Delta\nu_f + P_c \Delta\nu_c, \quad (4)$$

where $\Delta\nu_f$ and $\Delta\nu_c$ are linewidths of free and coordinated water, respectively. The values of $\Delta\nu_f$ and $\Delta\nu_c$ calculated by a nonlinear least-squares method are listed in Table 1. From the results that the values of $\Delta\nu_f$ and $\Delta\nu_c$ for the nitrate complex agree with those for the perchlorate complex within experimental errors (Fig. 5), the effect of formation of the $UO_2NO_3^+$ complex[1] on $\Delta\nu_c$ and $\Delta\nu_f$ is considered to be negligible in the concentration range studied.

Table 1 shows that the $\Delta\nu_f$ values are consistent with linewidths of pure water in the literature[15] within experimental errors and that the average ratio of $\Delta\nu_c$ to $\Delta\nu_f$, $(\Delta\nu_c/\Delta\nu_f)_{av}$, is about 8.7. Since an external charge has only a negligible effect on the ^{17}O electric field gradient of water,[16,17] the ^{17}O QCC and the asymmetry parameter of the coordinated water can be assumed to be the same as those of pure water (QCC=6.68 MHz; ξ=0.93).[16] The $(\Delta\nu_c/\Delta\nu_f)_{av}$ value should be, therefore, equal to the ratio of the tumbling time (τ_c) between coordinated and free water. The τ_c value for the coordinated water can be estimated from Eq. 2 on the assumption that the radius (3.82 Å) of the hydrated uranyl ion is taken to be the sum of the van der Waals radius (1.40 Å) of oxygen and the distance (2.42 Å)[4] between the uranium atom and the water of hydration. The estimated value of τ_c (1.9×10^{-11} s) at 25 °C for the coordinated water is longer than that (2.5×10^{-12} s) for pure water by a factor of 7.6, which is close to $(\Delta\nu_c/\Delta\nu_f)_{av}$. This supports the idea that the effective correlation time for the ^{17}O quadrupolar relaxation of the coordinated water in the uranyl ion corresponds to the reorientation time for the hydrated uranyl ion. It is worth noting that for 2+ diamagnetic ions such as Ca^{2+}, Mg^{2+}, and Cd^{2+}, τ_c for the water molecule in the first-coordination sphere corresponds to intramolecular rotation around the metal-oxygen axis.[18]

The quadrupolar relaxation rate is usually well represented by an Arrhenius-type function

$$1/T_2 = A \exp(E_Q/RT), \quad (5)$$

where E_Q is an activation energy for the reorientation. Plots of $\ln\Delta\nu_c$ or $\Delta\nu_f$ vs. $1/T$ were linear in the temperature range studied. The activation energies for free and coordinated water were determined to be 22.4±0.1 and 24.8±0.8 kJ mol^{-1}, respectively.

^{17}O Relaxation Times of Uranyl Oxygens. We measured ^{17}O T_1 relaxation times of uranyl oxygens (enriched by using $H_2{}^{17}O$ (42.1 atom%)) in aqueous

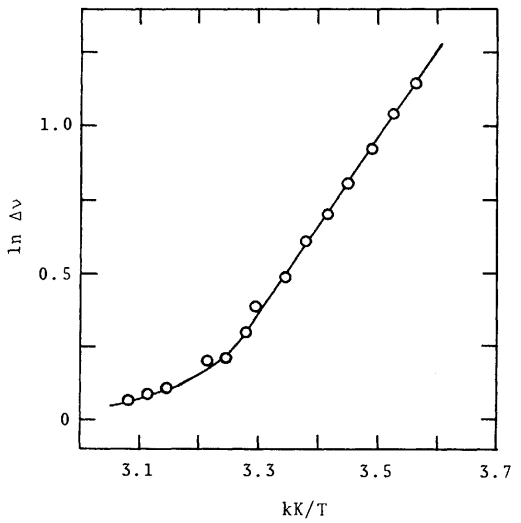

Fig. 6. A semilogarithmic plot of ^{17}O linewidths of uranyl oxygens against the reciprocal temperature. $[UO_2^{2+}]$=0.5 m and $[H^+]$=0.1 m in nitrate solution.

perchlorate solution ($H_2O:D_2O$=1:1 by weight), where $[UO_2^{2+}]$=0.098 m and $[H^+]$=0.23 m. The T_1 values were determined to be 0.245±0.001, 0.227±0.001, and 0.244±0.001 s at 25 °C for $[^{16}O=U=^{17}O]^{2+}$, $[^{17}O=U=^{17}O]^{2+}$, and $[^{18}O=U=^{17}O]^{2+}$, respectively. In view of the fact that three T_1 values become equal with increasing temperature,[19] the slightly smaller T_1 value for $[^{17}O=U=^{17}O]^{2+}$ may be attributed to overlapping of three ^{17}O resonances. When the values of 1.0 cp and 3.82 Å are taken as the viscosity of the solution studied and the molecular radius, respectively, the τ_c value for the hydrated uranyl ion was calculated to be 2.2×10^{-11} s from Eq. 2. The ^{17}O QCC of uranyl oxygens can be obtained from Eq. 1 by using values of T_1 (0.245 s) and τ_c and taking the asymmetry parameter ξ to be zero. The value obtained is 0.44 MHz, which appears to be the smallest of previously measured ^{17}O QCC values. For tetrahedral molecules such as MoO_4^-, RuO_4, and OsO_4, ^{17}O QCC's have been reported to be 0.72,[20] 1.12,[21] and 0.967 MHz,[21] respectively. The significantly small ^{17}O QCC of uranyl oxygens implies the high symmetry of the electron distribution around uranyl oxygen atoms.

We also measured ^{17}O linewidths of a $[^{16}O=U=^{17}O]^{2+}$ isotopomer in aqueous nitrate solution ($H_2O:D_2O$=1:2 by weight), where $[UO_2^{2+}]$=0.5 m and $[H^+]$=0.1 m. Figure 6 shows that an Arrhenius plot of the ^{17}O linewidth against temperature indicates a marked change in the activation energy around 40 °C. This result resembles the results of dynamic behavior of water, e.g. rotational[22] or translational processes,[23] where activation energies for both types of processes decrease with temperature. The activation energy obtained from Fig. 6 is 24.2±0.3 kJ mol^{-1} in the low-temperature range (7—35 °C). The activation energy value is very close to that for ^{17}O quadrupolar relaxation rate of the water molecule in the first-coordination sphere of the uranyl ion, indicating that there is a similarity in ^{17}O quadrupolar relaxation mechanisms between the uranyl oxygens and the coordinated water.

The authors wish to express their thanks to Dr. Kazumi Hata of JEOL, Ltd. for T_1 measurements on a JEOL JNM-GX 400 FT-NMR spectrometer.

References

1) Part III: W.-S. Jung, H. Tomiyasu, and H. Fukutomi, *Bull. Chem. Soc. Jpn.*, **59**, 3761 (1986).
2) Y. Ikeda, S. Soya, H. Fukutomi, and H. Tomiyasu, *J. Inorg. Nucl. Chem.*, **41**, 1333 (1979).
3) A. Fratiello, V. Kubo, R. E. Lee, and R. E. Schuster, *J. Phys. Chem.*, **74**, 3726 (1970).
4) M. Åberg, D. Ferri, J. Glaser, and I. Grenthe, *Inorg. Chem.*, **22**, 3986 (1983).
5) V. A. Sherbakov and L. L. Shcherbakov, *Radiokhimiya*, **18**, 207 (1976).
6) S. Meiboom, *J. Chem. Phys.*, **34**, 375 (1961); S. W. Rabideau and H. G. Hecht, *J. Chem. Phys.*, **47**, 544 (1967).
7) A. Abragam, "The Principle of Nuclear Magnetism," Oxford University Press, Oxford (1961), Chap. VIII.
8) A. Gierer and K. Wirtz, *Z. Naturforsch., A.* **8a**, 532 (1953).
9) W.-S. Jung, Y. Ikeda, H. Tomiyasu, and H. Fukutomi, *Bull. Chem. Soc. Jpn.*, **57**, 2317 (1984).
10) R. E. Connick and E. D. Stover, *J. Phys. Chem.*, **65**, 2075 (1961).
11) V. Frei and H. Wendt, *Ber. Bunsenges. Phys. Chem.*, **74**, 593 (1970).
12) Z. Luz and G. Yagil, *J. Phys. Chem.*, **70**, 554 (1966).
13) H. A. Christ, P. Diehl, HR. Schneider, and H. Dahn, *Helv. Chim. Acta*, **44**, 865 (1961).
14) J. E. Anderson and P. A. Fryer, *J. Chem. Phys.*, **50**, 3784 (1969).
15) J. C. Hindman, A. Svirmickas, and M. Wood, *J. Phys. Chem.*, **74**, 1266 (1970).
16) B. Halle and H. Wennerstrom, *J. Chem. Phys.*, **75**, 1928 (1981).
17) D. Fiat and R. E. Connick, *J. Am. Chem. Soc.*, **90**, 608 (1968).
18) R. E. Connick and K. Wüthrich, *J. Chem. Phys.*, **51**, 4506 (1969).
19) Unpublished data.
20) R. R. Vold and R. L. Vold, *J. Chem. Phys.*, **61**, 4360 (1974).
21) C. Brevard and P. Granger, *J. Chem. Phys.*, **75**, 4175 (1981).
22) K. Krynicki, *Physica (Utrecht)*, **32**, 167 (1966).
23) D. Eisenberg and W. Kauzmann, "The Structure and Properties of Water," Oxford University Press, London (1969), Chap. 4.

 © 1987 The Chemical Society of Japan Bull. Chem. Soc. Jpn., 60, 493—496 (1987)

Conductance of Potassium Iodide in Supercooled Water

Masaru NAKAHARA* and Masanobu ZENKE[1)]
Department of Chemistry, Faculty of Science, Kyoto University, Oiwake-cho, Kitashirakawa, Sakyo-ku, Kyoto 606
(Received August 22, 1986)

The conductance of potassium iodide was measured in water as a function of concentration (between 2×10^{-3} and 10^{-2} mol dm^{-3}) and temperature (between −6 and 0 °C). The effect of temperature on the mobility of such halide ions as I^- and Cl^- ions was discussed by taking the ionic residual friction coefficient $\Delta\zeta$, which was defined as the overall friction coefficient subtracted by the Stokes one for slip, instead of the conventional Walden product. We compared the experimental results with the predictions due to the Hubbard-Onsager dielectric friction theory. Of the monovalent ions so far studied, the iodide ion shows the largest negative value of $\Delta\zeta$ with the largest positive temperature coefficient; their signs are opposite to those theoretically predicted. These findings were explained in terms of the special ionic transport mechanism called the passing-through-cavities.

The conductivity measurement in electrolyte solution has made a great contribution to our understanding of the dynamic and static properties of electrolyte solution because of its high sensitivity and the availability of the single-ion property. We can probe the ion-ion and ion-solvent interactions through the concentration dependence of molar conductance and its limiting value, respectively; the latter quantity is involved in a theoretical equation of conductance to be determined experimentally. As reviewed elsewhere,[2,3)] however, our attention is now focused on the dynamics of the ion-solvent interaction as a result of the stimulation due to the recent advances in the theory of ion mobility.[4-7)]

The modern dielectric friction theory of ionic motion in solution developed by Hubbard and Onsager (HO)[4,5)] has been tested systematically against experiments on ion mobility (translational motion) under a variety of conditions in the previous papers.[8-16)] In the extensive test,[9-16)] the residual friction coefficient ($\Delta\zeta$), which is defined as the overall ionic friction coefficient subtracted by the Stokes one for slip,[9,17)] has been used successfully instead of the conventional Walden product, and led to the elucidation of the reliability and limitations of the HO theory; although the HO theory can describe the charge effect for small ions with a large surface charge density, it is unsuccessful in explaining the negative values of $\Delta\zeta$ for such medium-sized ions as the larger alkali metal and the halide ions in hydrogen-bonded solvents.

The validity of the HO theory indicates that the classical Stokes-Einstein-Walden framework for interpreting ion mobility has to be replaced by the modern HO framework as soon as possible. On the other hand, the disclosed limitations of the HO theory suggests the necessity of a new theory where the molecular nature and the liquid structure of solvent are taken into account in some manner. To explain the essential limitations of the continuum theory for ion transport, such a jump mechanism as the passing-through-cavities (PTC) has been proposed.[9-12,16)] The idea on the PTC mechanism has been hinted in the first study on conductances of the alkali metal ions in supercooled water.[9)] This important work is extended here to such halide ions as I^- and Cl^- to have more insights into the PTC mechanism.

Theoretical

We use the HO continuum model as a reference system to elucidate the effect of the solvent structure on the mechanism of ion transport process. For this purpose, first of all, we show in brief the significance of the HO theory and the procedure for its application.

Although the Stokes-Einstein-Walden (SEW) framework based on the Navier-Stokes (NS) hydrodynamic equation of motion is in general use in the interpretation of ion mobility, in principle, the NS hydrodynamic equation is inapplicable to ionic systems of our interest. HO have overcome the fundamental limitations of ordinary hydrodynamics by developing the dielectric friction theory and inventing the epoch-making electrohydrodynamic equation for migrating ions as follows:

$$\eta\nabla^2\boldsymbol{v} = \nabla p - \frac{1}{2}[\boldsymbol{E}_0\times(\nabla\times\boldsymbol{P}^*) + \boldsymbol{E}_0(\nabla\cdot\boldsymbol{P}^*)], \quad (1)$$

where η is the solvent viscosity, v the velocity field in the fluid, p the pressure, $\boldsymbol{E}_0$ the electrical field at $v=0$, and $\boldsymbol{P}^*$ the polarization deficiency. In this equation $\boldsymbol{P}^*$ expresses the departure of the orientational polarization of the Debye type from that at $v=0$ due to slow dielectric relaxation of the flowing solvent. Thus HO extended the NS hydrodynamic equation to ionic systems in a self-consistent manner by adapting the Debye dielectric relaxation theory to the flow system involving a charged sphere.

The second term on the right side of Eq. 1 represents the contribution of dielectric friction which is coupled to viscous friction. The full coupling of the two kinds of frictions renders the HO theory superior to ordinary hydrodynamics and the early dielectric friction theory[18,19)] in the treatment of ion dynamics in solution, as clearly shown elsewhere.[15,16,20,21)]

The essential difference between the modern (HO) and classical (NS) continuum models mentioned above is understandable from Eq. 1. When the charge on an ion is neglected ($\boldsymbol{E}_0=0$), Eq. 1 reduces to the

linearized form of the NS equation given by

$$\eta\nabla^2 v = \nabla p. \quad (2)$$

This equation leads to the following well-known Stokes law of the friction coefficient for a sphere with the radius R:

$$\zeta_S = 4\pi\eta R, \quad (3)$$

where ζ_S is the Stokes friction coefficient for the slip boundary condition. As mentioned elsewhere,[14] the slip boundary condition seems preferable to the stick on the molecular level, and R is usually taken to be the crystallographic radius of the ion.[22] Thus only the size effect of the solute can be handled by the NS hydrodynamic equation, whereas the charge effect as well as the size effect is treated by the HO electrohydrodynamic equation in a self-consistent manner.

The ionic friction coefficient ζ is related to the limiting conductance λ° as:

$$\zeta = |e| F/\lambda^\circ, \quad (4)$$

where F is the Faraday constant and e is the ionic charge. By using Eqs. 3 and 4 we can define the residual friction coefficient[9,17] as

$$\Delta\zeta = \zeta - \zeta_S. \quad (5)$$

Since the purely hydrodynamic friction is taken as a reference in Eq. 5, $\Delta\zeta$ reflects mainly the dielectric friction and all the other factors neglected in the primitive hydrodynamic model for ζ_S. As elucidated previously,[17] the residual friction coefficient is much more useful and meaningful than the so far widely used Walden product.

The numerical solutions to the linearized form of Eq. 1 are given in terms of the dimensionless quantity of the form

$$x = \zeta/\eta R_{HO}, \quad (6)$$

where R_{HO} denotes the Hubbard-Onsager radius, and x depends only on R and R_{HO}. A kind of solvent parameter R_{HO} is defined as

$$R_{HO} = \left[\frac{e^2}{16\pi\eta\varepsilon_0^2}(\varepsilon_0 - \varepsilon_\infty)\tau\right]^{1/4}, \quad (7)$$

where τ, ε_0 and ε_∞ are the dielectric relaxation time, the static, and high-frequency dielectric constants, respectively.

The HO theoretical value of the residual friction coefficient is expressed in the polynomial form[14,15]

$$\Delta\zeta = \eta(xR_{HO} - yR) = \eta R_{HO}\sum_{j=1}^{4} a_j (R_{HO}/R)^j, \quad (8)$$

where $y=4\pi$ for the slip boundary condition considered here and the universal coefficients are given as follows:

$$a_1 = -2.7866,$$
$$a_2 = 8.6216,$$
$$a_3 = -3.3425,$$

and

$$a_4 = 0.39550,$$

for $R/R_{HO} > 0.3$, which is satisfied by the I^- ion in water. When the physical properties of solvent involved in the HO radius expressed by Eq. 7 are all available, the HO value of the residual ionic friction coefficient $\Delta\zeta$ can be calculated for the ion characterized by the radius R and the charge e according to Eq. 8 under any conditions.

Table 1. Molar Conductances Λ ($S^{-1}cm^2mol^{-1}$) of KI in Supercooled Water at Various Concentrations C ($mol\,dm^{-3}$)

t/°C	$C^{a)}\times10^3$				
	2.167_6	4.066_1	5.953_0	7.924_2	9.863_6
0	81.09	80.52	80.14	79.85	79.64
−2	76.40	75.88	75.53	75.29	75.09
−4	71.80	71.31	71.00	70.77	70.57
−6	67.29	66.91	66.59	66.41	66.18

a) Concentrations at 0°C.

Table 2. Limiting Molar Conductances ($S^{-1}cm^2mol^{-1}$) of KI, K^+, and I^- in Water and Parameters in Eq. 9 as a Function of Temperature

t/°C	Λ°	$\lambda^\circ(K^+)^{a)}$	$\lambda^\circ(I^-)$	S	E	J
0	83.06	40.63	42.43	48.10	21.26	180
−2	78.22	38.25	39.97	44.97	20.05	176
−4	73.50	35.94	37.56	41.95	18.86	164
−6	68.91	33.67	35.24	39.03	17.72	156

a) From Ref. 9.

Experimental

Potassium iodide of high quality was supplied by Merck. The concentrations of the dilute solutions at 5 °C were determined by weight, and their variation with temperature was corrected by using the density of water. The conductivity of water was in the range of 5×10^{-7}—$8\times10^{-7}\,s^{-1}\,cm^{-1}$ at 0 °C. Molar conductances of KI measured in this way were reproducible within ±0.1%. The physical properties of water, such as density, dielectric properties, and viscosity, used in the present work are provided elsewhere.[9,23] Details of the experimental apparatus and procedure are described in the previous paper.[23]

Results

Table 1 shows the molar conductance (Λ) of KI in water measured as a function of concentration C ($mol\,dm^{-3}$) and temperature t (°C). The limiting molar conductances Λ°($S^{-1}\,cm^2\,mol^{-1}$) summarized in Table 2 are obtained by analyzing the conductance data in Table 1 with the aid of the Fuoss-Onsager equation of conductance for unassociated electrolyte[24,25]

$$\Lambda = \Lambda^\circ - SC^{-1/2} + EC\log C + JC, \quad (9)$$

where the parameters S, E, and J have the usual meaning and depend on the temperature and the solvent properties. Our value of Λ° (KI) at 0 °C agrees with that in the literature.[26]

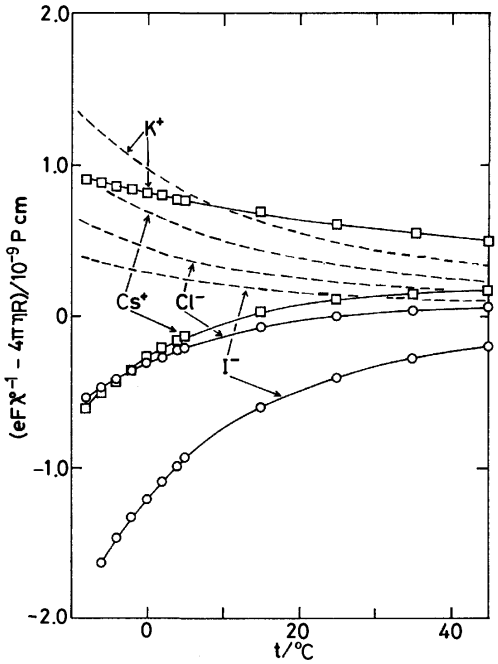

Fig. 1. Plots of the theoretical and experimental residual friction coefficients for several ions in water against temperature. The broken and full lines indicate the theoretical and experimental results, respectively. The square and circle symbols are used for the cations and anions, respectively.

As pointed out elsewhere,[9,11,23,27] the Fuoss-Onsager equation based on the sphere-in-continuum model describes well the concentration dependence of conductance in supercooled water. The validity of the continuum model for this case indicates that the relaxation and electrophoretic effects on ion mobility due to the ion-ion interactions in dilute solution can be presented in terms of the water radial distribution function that is effectively unity at a large ion-ion separation as in the continuum model. As discussed below, however, this is not the case for the ion-solvent interactions acting in the short range.

The limiting molar conductance of the iodide ion $\lambda°(I^{-1})$ listed in the fourth column of Table 2 is derived at each temperature by using the value of $\lambda°(K^+)$ previously determined;[9] the Kohlrausch law of independent migration of ions is applied. By using Eqs. 4 and 5 we have transformed the limiting ionic conductances of the iodide ion and some others[9] into the residual friction coefficients and plotted them against temperature in Fig. 1 for comparison with the HO theoretical prediction. The residual friction coefficients above 0 °C in Fig. 1 are computed from the conductance data in the literature.[26,28]

Discussion

Figure 1 shows how the HO dielectric friction theory of ion mobility predicts the temperature and ion-size dependencies of the residual friction coefficients for the medium-sized ions; the theory predicts that the positive ionic residual friction coefficient decreases with an increase in temperature and ion size. Although the K^+ ion ($R=1.33$ Å) has a negative temperature coefficient of $\Delta\zeta$ just as predicted, the I^- ($R=2.16$ Å) and Cl^- ($R=1.81$ Å) ions as well as the Cs^+ ion ($R=1.69$ Å) exhibit a positive temperature coefficient and a large negative value of $\Delta\zeta$ contrary to the theoretical prediction. Of the monovalent ions so far investigated, the iodide ion has the largest negative residual friction coefficient. However, the observed values of $\Delta\zeta$ are in the sequence $K^+ > Cs^+ > Cl^- > I^-$ in agreement with the HO prediction.

The unpredictable sign of the temperature coefficients of $\Delta\zeta$ for the medium-sized ions is originally related to their large negative values which become more negative as water is supercooled. The negative sign of $\Delta\zeta$ expressed by Eq. 5 indicates that the friction coefficients for these ions are even smaller than the lower limit (Eq. 3) set by the continuum model where the bulk properties of the solvent are used. The essential limitation of the continuum model for solvent is not ascribed to the charge effect of the ion but to the size effect because a similar limitation of the Stokes-Einstein law is found for diffusion of neutral molecules.[3,16,29,30] Thus it turns out that although the HO continuum theory is successful for small ions with a large surface charge density, it exhibits essential limitations for the medium-sized ions because of the neglect of many complicated factors in the vicinity of the ion. To explain the anomalous mobility, such a concept as the passing-through-cavities (PTC) mechanism has been introduced in the previous work.[9,10,12,16]

Figure 1 suggests that the stabilization or development of the hydrogen-bonded network in water favors the PTC mechanism. This is quite reasonable because the PTC process requires the framework formed by the hydrogen-bonded water molecules. The PTC process is assisted by such a cooperative fluctuating motion of the framework that it can reduce the potential barrier or friction for ion migration.[12] The role of the PTC mechanism increases when the extent of hydrogen bonds in water is promoted by any other factors than temperature; the PTC mechanism has so far been confirmed by changing the water structure through temperature,[9,11,12] pressure,[10-13] solvent isotope,[13] and organic cosolvent.[14,15] In this respect, this mechanism is analogous to that seen in the solid electrolyte.[31] Thus the PTC mechanism remains as a memory in the short-range order characteristic of the liquid state even after the long-range order is completely lost by melting. The corresponding limitations of the continuum model are shown also in the study of rotational motion of ions.[20]

Such an ion transport process as the PTC mechanism is expected to be important in highly viscous liquids, liquid crystals, and membranes in view of the features described above. This will be examined in our

experimental investigation in progress. Furthermore, a molecular theory of ionic or molecular diffusion in liquids is desired to be developed beyond hydrodynamics. The Wolynes molecular theory[6,7] cannot explain the negative value of $\Delta\zeta$ because it relies upon the hydrodynamic relation Eq. 3 in the expression of the friction coefficient due to the hard force-hard force correlation.

The authors are grateful for the financial support of this work by the Research Grant-in-Aid from the Ministry of Education, Science and Culture (No. 61134043).

References

1) Present address: Department of VLSI, NEC, Sagamihara City, Kanagawa Prefecture 239, Japan.
2) P. G. Wolynes, *Ann. Rev. Phys. Chem.*, **31**, 345 (1980).
3) M. Nakahara, *Kagaku (Chemistry)*, **38**, 489 (1983).
4) J. B. Hubbard and L. Onsager, *J. Chem. Phys.*, **67**, 4850 (1977).
5) J. B. Hubbard, *J. Chem. Phys.*, **68**, 1649 (1978).
6) P. G. Wolynes, *J. Chem. Phys.*, **68**, 473 (1978).
7) P. Colonomos and P. G. Wolynes, *J. Chem. Phys.*, **71**, 2644 (1979).
8) D. F. Evans, T. Tominaga, J. B. Hubbard, and P. J. Wolynes, *J. Phys. Chem.*, **83**, 2669 (1979).
9) N. Takisawa, J. Osugi, and M. Nakahara, *J. Phys. Chem.*, **85**, 3582 (1981).
10) M. Nakahara, T. Török, N. Takisawa, and J. Osugi, *J. Chem. Phys.*, **76**, 5145 (1982).
11) N. Takisawa, J. Osugi, and M. Nakahara, *J. Chem. Phys.*, **77**, 4717 (1982).
12) a) N. Takisawa, J. Osugi, and M. Nakahara, *J. Chem. Phys.* **78**, 2591 (1983); b) M. Nakahara, N. Takisawa, and J. Osugi, "High Pressure in Science and Technology," ed by C. Homan, R. K. MacCrown, and E. Whalley, North-Holland, New York (1984), Part II, p. 169.
13) M. Nakahara, M. Zenke, M. Ueno, and K. Shimizu, *J. Chem. Phys.*, **83**, 280 (1985).
14) K. Ibuki and M. Nakahara, *J. Chem. Phys.*, **84**, 2776 (1986).
15) K. Ibuki and M. Nakahara, *J. Chem. Phys.*, **84**, 6979 (1986).
16) K. Ibuki and M. Nakahara, *J. Phys. Chem.*, in press.
17) M. Nakahara and K. Ibuki, *J. Phys. Chem.*, **90**, 3026 (1986).
18) R. Zwanzig, *J. Chem. Phys.*, **38**, 1603 (1963).
19) R. Zwanzig, *J. Chem. Phys.*, **52**, 3625 (1970).
20) M. Nakahara and K. Ibuki, *J. Chem. Phys.*, **85**, 4654 (1986).
21) K. Ibuki and M. Nakahara, *J. Phys. Chem.*, **90**, 6362 (1986).
22) L. Pauling, "The Nature of the Chemical Bond," Cornell University, New York (1960).
23) M. Nakahara, N. Takisawa, and J. Osugi, *J. Phys. Chem.*, **85**, 112 (1981).
24) R. M. Fuoss and F. Accasoina, "Electrolytic Conductance," Interscience, New York (1959).
25) P. C. Carman, *J. Phys. Chem.*, **74**, 1653 (1970).
26) R. De Lisi, M. Goffredi, and V. T. Liveri, *J. Solution Chem.*, **10**, 351 (1981).
27) M. Nakahara, *J. Phys. Chem.*, **88**, 2138 (1984).
28) R. A. Robinson and R. H. Stokes, "Electrolyte Solutions," Butterworths, London (1968), Appendices.
29) a) D. F. Evans, T. Tominaga, and C. Chan, *J. Solution Chem.*, **8**, 461 (1979); b) D. F. Evans, T. Tominaga, and H. T. Davis, *J. Chem. Phys.*, **74**, 1298 (1981).
30) a) G. L. Pollack, *Phys. Rev. A*, **23**, 2660 (1981); b) G. L. Pollack and J. J. Enyeart, *Phys. Rev. A*, **31**, 980 (1985).
31) a) A. Ueda and Y. Kaneko, *Butsuri*, **40**, 866 (1985); b) M. Hokazono, A. Ueda, and Y. Hiwatari, *Solid State Ionics*, **13**, 151 (1984).

 © 1987 The Chemical Society of Japan Bull. Chem. Soc. Jpn., 60, 497—502 (1987)

The Structure of the Cyclodextrin Complex. XIX. Crystal Structures of Hexakis(2,3,6-tri-*O*-methyl)-α-cyclodextrin Complexes with (*S*)- and (*R*)-Mandelic Acid. Chiral Recognition through the Induced-Fit Conformational Change of the Macrocyclic Ring

Kazuaki HARATA,* Kaneto UEKAMA,† Masaki OTAGIRI,† and Fumitoshi HIRAYAMA†
Research Institute for Polymers and Textiles, 1-1-4 Yatabe-Higashi, Tsukuba, Ibaraki 305
†Faculty of Pharmaceutical Sciences, Kumamoto University, 5-1 Oe-honmachi, Kumamoto 862
(Received August 23, 1986)

Hexakis(2,3,6-tri-*O*-methyl)-α-cyclodextrin (methyl-α-CDx) forms crystalline inclusion complexes with (*S*)-mandelic acid (*S*-MA) and (*R*)-mandelic acid (*R*-MA). Both crystals are monoclinic, and the space group is $P2_1$ with cell dimensions: $a=13.123(2)$, $b=23.187(4)$, $c=13.113(2)$ Å, $\beta=107.19(1)°$ for the *S*-MA complex, $a=11.624(2)$, $b=23.739(4)$, $c=13.786(2)$ Å, $\beta=106.56(1)°$ for the *R*-MA complex. The structures were solved by inspection of a Patterson map and the R-map method, and refined by the block-diagonal least-squares method to the *R*-values of 0.087 for the *S*-MA complex and 0.055 for the *R*-MA complex. In the *S*-MA complex, the methyl-α-CDx molecule, which has a *pseudo* two-fold symmetry, loosely includes the phenyl group of *S*-MA. The hydroxyl and carboxyl groups of *S*-MA protrude from the O(2), O(3) side of the methyl-α-CDx cavity and form hydrogen bonds with water molecules located outside the host cavity. The methyl-α-CDx molecule in the *R*-MA complex tightly binds the *R*-MA molecule which is deeply inserted into the host cavity. The hydroxyl group of *R*-MA is hydrogen-bonded to an O(2) oxygen atom of host methyl-α-CDx. The comparison of the two structures suggests that the complex formation induces the conformational change of the host molecule to accommodate *S*-MA or *R*-MA more suitably within the cavity.

Cyclodextrins form diastereoisomers by including optically active guests. Many attempts have been made to resolve racemic compounds by the co-precipitation with cyclodextrins.[1] Except for some cases, however, cyclodextrins are not good reagents for this purpose. Since the intramolecular cavity of cyclodextrins is round and rather symmetrical, cyclodextrins does not seem to be sensitive to the chirality of included guests, as demonstrated in our earlier reports.[2,3] α-Cyclodextrin equally includes *R* -and *S*-isomers of 1-phenylethanol although the hydroxyl group attached to the assymmetric carbon atom is disordered.[2] In the crystal of the β-cyclodextrin complex with racemic Flurbiprofen, a pair of *S*- and *R*-isomers are packed within the cavity formed by two β-cyclodextrin molecules.[3]

Recently, it has been found that the permethylation markedly changes the macrocyclic conformation of cyclodextrins.[4] Permethylated cyclodextrins also form inclusion complexes with a variety of guests, but the geometry of the host-guest interaction differs from that of the parent cyclodextrin complexes because of the different size and shape of the macrocyclic cavity. Previously, we have briefly reported that permethylated cyclodextrins recognize the chirality of mandelic acid[5] and Flurbiprofen[6,7] in the crystalline state. This paper deals with the crystal structures of hexakis(2,3,6-tri-*O*-methyl)-α-cyclodextrin (methyl-α-CDx) complexes with (*S*)-mandelic acid (*S*-MA) and (*R*)-mandelic acid (*R*-MA), and will discuss the chiral recognition through the induced-fit conformational change of methyl-α-CDx.

Experimental

Materials and Measurements. Methyl-α-CDx complexes with *S*- and *R*-MA were crystallized at 50 °C by standing aqueous solutions containing methyl-α-CDx and each isomer with ca. 1 : 1 molar ratio. Lattice parameters and diffraction intensities were measured at room temperature on a Nicolet P3/F diffractometer with graphite-monochromated Cu $K\alpha$ radiation. Lattice parameters were refined by using 25 reflections with 2θ values in the range 40—45°. By using θ—2θ scan mode, 4837 (*S*-MA complex) and 4925 (*R*-MA complex) independent reflections with $|F_o| \geqq 3\sigma(F)$ were obtained up to 118° in 2θ. No corrections were made for absorption or extinction effects.

Crystal Data: (1) *S*-MA complex, $C_{54}H_{96}O_{30}\cdot C_8H_8O_3\cdot 3H_2O$, F.W.=1431.5, monoclinic, space group $P2_1$, $Z=2$, $a=13.123(2)$, $b=23.187(4)$, $c=13.113(2)$ Å, $\beta=107.19(1)°$, $V=3812(1)$ Å^3, $D_X=1.247$ g cm^{-3}, (2) *R*-MA complex, $C_{54}H_{96}O_{30}\cdot C_8H_8O_3\cdot 2H_2O$, F.W.=1413.5, monoclinic, space group $P2_1$, $Z=2$, $a=11.624(2)$, $b=23.739(4)$, $c=13.786(2)$ Å, $\beta=106.56(1)°$, $V=3646(1)$ Å^3, $D_X=1.289$ g cm^{-3}.

Determination and Refinement of the Structure. The orientation of the molecular axis of methyl-α-CDx was easily deduced from a Patterson map in both structures. The rotation around the molecular axis and the position of the molecule in the unit cell were determined from an R-map, which was calculated by using a model structure of methyl-α-CDx having a six-fold molecular symmetry. The orientation and position of each residue were corrected by the rigid-body least-squares method. After the refinement of atomic parameters of methyl-α-CDx, the guest and water molecules were found on Fourier and difference-Fourier maps. The block-diagonal least-squares refinement of the structure, including 42 hydrogen atoms (*S*-MA complex) and 96 hydrogen atoms (*R*-MA complex), achieved the *R*-value of 0.087 for the *S*-MA complex and 0.055 for the *R*-MA complex. The quantity minimized was $\sum w(|F_o|-|F_c|)^2$, with $w=1.0$ for all the reflections. Final atomic parameters and B_{eq} values are given in Table 1. Tables of observed and calculated structure factors, anisotropic temperature factors of non-hydrogen atoms, atomic parameters of hydrogen atoms, bond dis-

Table 1. Final Atomic Coordinates ($\times 10^4$) and B_{eq} Values[a)]

I. Methyl-α-CDx–*S*-MA complex

	x	y	z	B_{eq}/Å^2		x	y	z	B_{eq}/Å^2
C(1,G1)	5459(12)	3240(6)	5644(10)	7.30	C(8,G4)	237(15)	2868(7)	-3028(12)	9.47
C(2,G1)	6553(11)	2924(6)	5841(11)	7.82	C(9,G4)	-870(23)	2856(13)	3023(19)	17.35
C(3,G1)	6389(10)	2378(5)	5162(10)	6.24	O(2,G4)	-543(9)	1705(4)	-2322(8)	9.40
C(4,G1)	5492(10)	1996(5)	5332(9)	5.69	O(3,G4)	-434(8)	2932(4)	-2348(7)	7.90
C(5,G1)	4515(10)	2345(6)	5260(9)	5.97	O(4,G4)	503(5)	3400(3)	-254(6)	4.76
C(6,G1)	3704(13)	2018(7)	5713(13)	8.10	O(5,G4)	-910(6)	2112(4)	226(8)	6.91
C(7,G1)	7686(13)	3768(7)	6199(17)	11.58	O(6,G4)	-353(10)	2662(5)	2277(9)	10.37
C(8,G1)	7989(12)	2110(7)	4708(16)	9.93	C(1,G5)	2211(9)	209(5)	1593(9)	5.14
C(9,G1)	1933(20)	2096(13)	5814(22)	17.09	C(2,G5)	1967(9)	186(5)	369(9)	5.39
O(2,G1)	7320(7)	3273(4)	5542(9)	8.79	C(3,G5)	1618(9)	789(5)	-111(9)	5.16
O(3,G1)	7352(7)	2046(4)	5441(8)	7.80	C(4,G5)	668(9)	979(5)	274(9)	5.23
O(4,G1)	5260(6)	1583(3)	4502(6)	4.80	C(5,G5)	962(9)	966(5)	1499(9)	5.27
O(5,G1)	4771(8)	2860(4)	5931(7)	7.11	C(6,G5)	53(12)	1115(7)	1960(12)	8.02
O(6,G1)	2706(9)	2326(5)	5356(10)	10.39	C(7,G5)	2801(16)	-480(9)	-541(18)	12.57
C(1,G2)	3393(9)	4753(5)	2789(9)	5.41	C(8,G5)	1859(15)	1116(8)	-1742(12)	9.65
C(2,G2)	4619(9)	4797(5)	3015(9)	5.53	C(9,G5)	-1785(15)	935(10)	1779(21)	14.40
C(3,G2)	5087(8)	4191(5)	3377(9)	4.90	O(2,G5)	2908(6)	8(4)	110(7)	7.06
C(4,G2)	4727(9)	3994(5)	4327(9)	4.99	O(3,G5)	1304(7)	739(4)	-1227(6)	6.60
C(5,G2)	3495(9)	4011(5)	4036(9)	5.33	O(4,G5)	444(6)	1569(3)	-120(6)	5.32
C(6,G2)	3057(11)	3865(7)	4961(12)	7.54	O(5,G5)	1273(6)	385(3)	1847(6)	5.12
C(7,G2)	5535(19)	5450(9)	2211(16)	13.06	O(6,G5)	-885(8)	796(5)	1414(9)	8.82
C(8,G2)	6747(13)	3876(9)	3125(16)	10.42	C(1,G6)	5430(9)	993(5)	4783(9)	5.31
C(9,G2)	3189(19)	4029(10)	6777(14)	13.38	C(2,G6)	5761(8)	667(5)	3937(9)	5.40
O(2,G2)	4877(7)	4972(4)	2076(7)	6.63	C(3,G6)	4899(8)	709(5)	2864(8)	4.91
O(3,G2)	6231(6)	4242(4)	3683(7)	6.92	C(4,G6)	3859(9)	475(5)	3001(9)	5.12
O(4,G2)	5120(6)	3418(3)	4555(6)	5.34	C(5,G6)	3581(9)	736(5)	3947(9)	5.24
O(5,G2)	3162(6)	4591(3)	3729(6)	5.11	C(6,G6)	2697(10)	390(7)	4248(9)	6.76
O(6,G2)	3588(9)	4179(5)	5888(8)	8.77	C(7,G6)	7649(10)	586(8)	4405(14)	9.22
C(1,G3)	228(9)	3983(5)	-404(9)	5.27	C(8,G6)	5232(12)	741(8)	1160(12)	8.28
C(2,G3)	1062(9)	4301(5)	-775(8)	5.37	C(9,G6)	1500(16)	424(11)	5235(15)	12.64
C(3,G3)	2137(9)	4266(5)	105(8)	5.08	O(2,G6)	6738(6)	884(4)	3804(7)	6.83
C(4,G3)	2004(9)	4514(5)	1128(9)	5.29	O(3,G6)	5201(7)	391(4)	2083(7)	6.46
C(5,G3)	1042(8)	4247(5)	1422(8)	5.02	O(4,G6)	3056(6)	602(3)	2020(6)	4.89
C(6,G3)	749(9)	4581(6)	2283(10)	6.45	O(5,G6)	4484(6)	742(3)	4890(5)	5.12
C(7,G3)	626(14)	4387(7)	-2674(10)	8.87	O(6,G6)	2274(8)	751(5)	4874(8)	9.10
C(8,G3)	3833(11)	4231(8)	-247(12)	8.43	O(W1)	1948(20)	2463(22)	3102(23)	20.76
C(9,G3)	-211(15)	4548(10)	3503(15)	11.56	O(W2)	-3107(19)	738(10)	-725(19)	22.50
O(2,G3)	1193(7)	4089(4)	-1747(6)	6.64	O(W3)	5701(18)	4195(11)	8094(18)	22.48
O(3,G3)	2918(7)	4589(4)	-199(7)	6.91	C(1,SM)	4891(18)	2491(11)	100(22)	14.76
O(4,G3)	2990(5)	4375(3)	1941(6)	4.85	C(2,SM)	5412(24)	2483(12)	1201(18)	17.17
O(5,G3)	111(5)	4239(4)	506(6)	5.29	C(3,SM)	4775(19)	2441(11)	1805(16)	14.37
O(6,G3)	127(8)	4232(5)	2748(8)	9.09	C(4,SM)	3572(22)	2506(12)	1458(23)	16.54
C(1,G4)	-643(9)	1733(6)	-476(11)	6.47	C(5,SM)	3191(15)	2504(12)	277(23)	16.88
C(2,G4)	-791(11)	2050(6)	-1555(12)	8.05	C(6,SM)	3844(18)	2537(13)	-402(21)	16.42
C(3,G4)	-149(10)	2595(6)	-1408(9)	6.01	C(7,SM)	5547(20)	2280(18)	-750(36)	33.09
C(4,G4)	-332(9)	2972(5)	-507(10)	5.69	C(8,SM)	5807(20)	2834(17)	-1046(40)	30.64
C(5,G4)	-260(10)	2624(6)	499(10)	5.98	O(1,SM)	5082(16)	3080(11)	-1464(15)	20.61
C(6,G4)	-698(12)	2955(6)	1301(12)	7.54	O(2,SM)	6659(17)	3033(10)	-895(22)	22.90
C(7,G4)	-1207(18)	1204(7)	-2694(14)	12.28	O(3,SM)	6379(15)	1961(10)	-278(22)	23.61

II. Methyl-α-CDx–*R*-MA complex

	x	y	z	B_{eq}/Å^2		x	y	z	B_{eq}/Å^2
C(1,G1)	1084(5)	4726(3)	3433(5)	3.96	C(8,G4)	4031(8)	-790(6)	2147(9)	10.15
C(2,G1)	1976(5)	4853(3)	4473(5)	4.05	C(9,G4)	-2729(7)	1135(4)	-1105(6)	6.07
C(3,G1)	2292(5)	4343(3)	5141(5)	3.81	O(2,G4)	2455(5)	-216(2)	2333(4)	5.59
C(4,G1)	1219(5)	3971(3)	5134(5)	3.76	O(3,G4)	2777(5)	470(2)	698(4)	5.88
C(5,G1)	318(5)	3915(3)	4091(5)	3.74	O(4,G4)	1504(4)	1522(2)	582(3)	3.86
C(6,G1)	-882(6)	3700(3)	4199(5)	4.52	O(5,G4)	-405(4)	506(2)	1409(4)	4.39
C(7,G1)	3034(8)	5663(4)	4149(7)	7.10	O(6,G4)	-1543(4)	970(2)	-500(4)	5.14
C(8,G1)	4009(8)	4642(4)	6491(6)	7.72	C(1,G5)	768(6)	1073(3)	5768(5)	4.16
C(9,G1)	-1495(8)	3042(4)	2850(7)	7.43	C(2,G5)	1530(6)	554(3)	5771(5)	4.31
O(2,G1)	3081(4)	5078(2)	4375(4)	5.01	C(3,G5)	1781(6)	490(3)	4767(5)	4.22
O(3,G1)	2792(4)	4504(2)	6183(3)	5.21	C(4,G5)	638(6)	510(3)	3886(5)	4.14
O(4,G1)	1659(4)	3424(2)	5477(3)	3.86	C(5,G5)	-157(6)	1011(3)	3991(5)	4.43
O(5,G1)	68(3)	4468(2)	3626(3)	3.75	C(6,G5)	-1422(6)	967(4)	3262(6)	5.72
O(6,G1)	-1717(4)	3575(2)	3231(4)	4.91	C(7,G5)	2627(9)	507(6)	7521(6)	9.42
C(1,G2)	1255(6)	3934(3)	-87(5)	4.36	C(8,G5)	3574(8)	-26(5)	4749(7)	7.89
C(2,G2)	2169(6)	4380(3)	339(5)	4.34	C(9,G5)	-3191(9)	1467(7)	2696(10)	12.31
C(3,G2)	2453(5)	4404(3)	1475(5)	3.99	O(2,G5)	2661(4)	591(2)	6528(3)	4.84
C(4,G2)	1280(5)	4503(3)	1781(4)	3.69	O(3,G5)	2302(5)	-60(2)	4728(4)	5.61
C(5,G2)	255(6)	4120(3)	1194(5)	3.97	O(4,G5)	1026(4)	576(2)	2987(3)	4.14
C(6,G2)	-957(6)	4334(3)	1223(5)	4.83	O(5,G5)	-314(4)	1013(2)	4982(3)	4.25
C(7,G2)	3459(13)	4657(7)	-616(12)	14.70	O(6,G5)	-1975(5)	1502(3)	3261(5)	8.28
C(8,G2)	4380(7)	4705(5)	2471(7)	7.76	C(1,G6)	1580(6)	3264(3)	6455(5)	4.37
C(9,G2)	-3015(7)	4138(5)	725(8)	8.02	C(2,G6)	2628(6)	2895(3)	6973(5)	4.27
O(2,G2)	3255(4)	4269(2)	69(4)	5.58	C(3,G6)	2596(6)	2312(3)	6461(5)	4.21
O(3,G2)	3220(4)	4864(2)	1861(4)	4.80	C(4,G6)	1384(5)	2038(3)	6280(5)	3.87
O(4,G2)	1601(3)	4387(2)	2843(3)	3.57	C(5,G6)	392(6)	2454(3)	5774(5)	4.08
O(5,G2)	175(4)	4094(2)	133(3)	4.03	C(6,G6)	-900(6)	2242(3)	5621(6)	4.97
O(6,G2)	-1845(4)	3947(3)	732(4)	6.20	C(7,G6)	4374(11)	3324(7)	7968(7)	12.95
C(1,G3)	1554(6)	1699(3)	-380(5)	4.66	C(8,G6)	4379(7)	1751(4)	6730(7)	7.45
C(2,G3)	2711(6)	2018(3)	-307(5)	4.98	C(9,G6)	-2186(8)	2136(4)	6659(8)	8.04
C(3,G3)	2746(6)	2578(3)	257(5)	4.40	O(2,G6)	3729(4)	3166(2)	7011(4)	5.22
C(4,G3)	1607(6)	2922(3)	-254(5)	4.34	O(3,G6)	3483(4)	1968(2)	7123(3)	4.98
C(5,G3)	501(6)	2566(3)	-308(6)	5.02	O(4,G6)	1390(4)	1568(2)	5647(3)	3.84
C(6,G3)	-644(7)	2854(3)	-920(7)	6.88	O(5,G6)	499(4)	2963(2)	6368(3)	4.16

Table 1. (Continued)

	x	y	z	B_{eq}/Å^2		x	y	z	B_{eq}/Å^2
C(7,G3)	4621(10)	1621(6)	-271(9)	11.02	O(6,G6)	-1018(4)	2069(2)	6593(4)	5.75
C(8,G3)	4571(8)	3020(5)	1173(8)	8.63	O(W1)	-457(5)	1024(3)	7824(4)	6.52
C(9,G3)	-2709(9)	2817(5)	-978(13)	13.74	O(W2)	731(13)	-1004(6)	3284(13)	22.51
O(2,G3)	3708(4)	1682(2)	229(4)	5.90	C(1,RM)	4153(7)	2892(4)	4121(6)	5.57
O(3,G3)	3786(4)	2883(2)	201(4)	5.89	C(2,RM)	4552(9)	2345(4)	4222(7)	7.78
O(4,G3)	1661(4)	3405(2)	378(3)	4.14	C(3,RM)	3813(11)	1901(5)	3754(9)	9.90
O(5,G3)	567(4)	2051(2)	-858(3)	4.87	C(4,RM)	2666(10)	2022(5)	3159(9)	10.13
O(6,G3)	-1636(5)	2533(3)	-802(6)	8.70	C(5,RM)	2259(9)	2570(6)	3016(8)	10.22
C(1,G4)	524(6)	225(3)	2137(5)	4.51	C(6,RM)	2985(8)	3001(5)	3496(7)	7.76
C(2,G4)	1498(6)	75(3)	1651(5)	4.57	C(7,RM)	4927(7)	3359(4)	4693(7)	6.47
C(3,G4)	1996(6)	606(3)	1306(5)	4.20	C(8,RM)	6147(7)	3396(4)	4428(7)	6.40
C(4,G4)	996(6)	972(3)	637(5)	4.13	O(1,RM)	6047(5)	3561(3)	3524(4)	7.25
C(5,G4)	-50(5)	1048(3)	1105(5)	3.84	O(2,RM)	7089(5)	3322(3)	5102(6)	9.21
C(6,G4)	-1156(6)	1295(3)	393(5)	4.71	O(3,RM)	5215(5)	3297(3)	5743(5)	8.59
C(7,G4)	2503(14)	-790(4)	2147(13)	17.07					

a) $B_{eq}=8\pi^2(u_1^2+u_2^2+u_3^2)/3$, where u_i is the root-mean-square deviation in the i-th principal axis of the thermal ellipsoid.

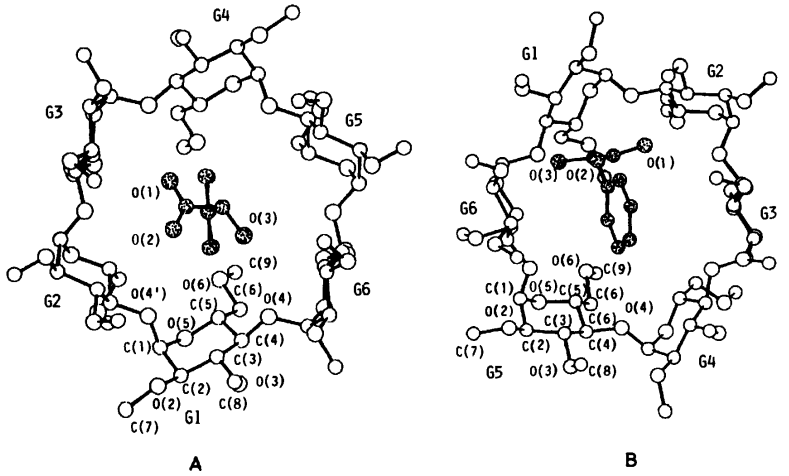

Fig. 1. The numbering scheme of the methyl-α-CDx complexes with *S*-MA (A) and *R*-MA (B). The guest molecules are shaded.

tances, angles, and conformation angles are kept at The Chemical Society of Japan (Document No. 8719). The computation was carried out on a FACOM M-380 computer at the Center of the Research Information Processing System (RIPS), Agency of Industrial Science and Technology, Tsukuba.

Description of the Structure

Conformation of Methyl-α-CDx. The numbering scheme of both complexes is shown in Fig. 1. The average bond distances and angles of 2,3,6-tri-*O*-methylglucose residues are shown in Fig. 2. Table 2 gives geometrical data describing the macrocyclic conformation of methyl-α-CDx.

Methyl-α-CDx in the *S*-MA Complex: The methyl-α-CDx molecule has a *pseudo* two-fold symmetry. The conformational difference among six 2,3,6-tri-*O*-methylglucose residues is observed in the orientation of C(6)–O(6) bonds. Two O(6)–C(6) bonds (G2 and G5 residues) are in a gauche-gauche conformation, while the others show a gauche-trans conformation. All O(6)–C(9) bonds are trans to the corresponding C(5)–C(6) bond. The O(2)–C(7) bonds point away from the center of the methyl-α-CDx ring. On the other hand, the O(3)–C(8) bonds are oriented to the opposite direction, turning to the inside of the methyl-α-CDx ring. The six glycosidic oxygen atoms form a nearly regular hexagon with the radius of 4.23—4.38 Å and the O(4)···O(4′) distance of 4.24—4.36 Å (Table 2). The O(2)···O(3′) distances are longer than those found in α-cyclodextrin complexes[2] because of the steric hindrance involving C(8)H_3 methyl groups.[4] The C(8) atoms are located at a position equidistant from O(2) and O(2′) atoms with the distance of 3.12—3.52 and 3.31—3.41 Å, respectively. The G3 and G6 residues are nearly perpendicular to the plane through the six O(4) atoms. The sharp inclination of the G1 and G4 residues (the tilt-angles of 35.9 and 34.6°, respectively) is supported by the included W1 water molecule which forms the O(6, G1)···W1···O(6, G4) hydrogen-bond bridge.

Methyl-α-CDx in the *R*-MA Complex: The methyl-α-CDx ring is less symmetrical than that of the *S*-MA complex. The C(6)–O(6) bonds show also two types of orientations. The gauche-gauche conformation is found in the G4 and G6 residues, and the C(6)–O(6) bonds in the other residues are in the gauche-trans conformation. Except for the O(6, G1)–C(9, G1) bond,

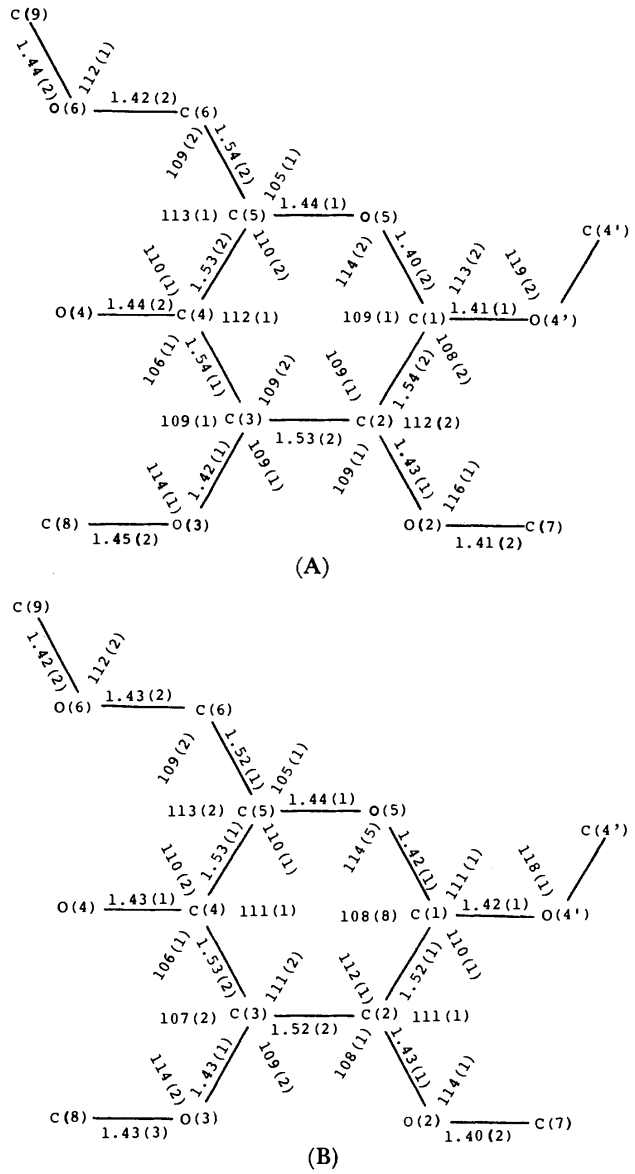

Fig. 2. Average bond distances and angles for the 2,3,6-tri-*O*-methylglucose residue in the methyl-α-CDx complexes with *S*-MA (A) and *R*-MA (B). Standard deviations given in parentheses were estimated according to $\sigma=[\sum_{i=1}^{6}(x_i-\bar{x})^2/5]^{1/2}$, where x_i is the bond distance or angle in the i-th residue and $\bar{x}$ is the average value.

all the O(6)–C(9) bonds are trans to the corresponding C(5)–C(6) bond. The O(6, G1)–C(9, G1) bond turns to the inside of the methyl-α-CDx ring, and the C(9,G1)H_3 methyl group caps the O(6) side of the cavity. The O(2)–C(7) and O(3)–C(8) bonds show the same conformations as those in the *S*-MA complex. The macrocyclic ring is rather elliptically distorted compared with the methyl-α-CDx ring in the *S*-MA complex. The diagonal O(4, G2)···O(4, G5) distance of 9.08 Å is 1 Å longer than the O(4, G1)···O(4, G4) distance (8.08 Å). The G3 and G6 residues, which face to each other, are nearly perpendicular to the plane through six O(4) atoms. The other residues incline

Table 2. Geometrical Data Describing the Macrocyclic Conformation of Methyl-α-CDx

I. Distance (l/Å) from the center of gravity of six O(4) atoms to each O(4) atom

	S-MA Complex	*R*-MA Complex
O(4, G1)	4.26	4.05
O(4, G2)	4.23	4.54
O(4, G3)	4.37	4.27
O(4, G4)	4.26	4.03
O(4, G5)	4.23	4.55
O(4, G6)	4.38	4.29
Average	4.29	4.29

II. O(4)···O(4′) distance (l/Å) between adjacent residues

	S-MA Complex	*R*-MA Complex
O(4, G1)···O(4, G2)	4.25	4.27
O(4, G1)···O(4, G6)	4.31	4.43
O(4, G2)···O(4, G3)	4.34	4.14
O(4, G3)···O(4, G4)	4.30	4.49
O(4, G4)···O(4, G5)	4.24	4.17
O(4, G5)···O(4, G6)	4.36	4.28
Average	4.30	4.30

III. O(2)···O(3′) distance (l/Å) between adjacent residues

	S-MA Complex	*R*-MA Complex
O(2, G1)···O(3, G2)	3.43	3.55
O(2, G2)···O(3, G3)	3.43	3.34
O(2, G3)···O(3, G4)	3.37	3.20
O(2, G4)···O(3, G5)	3.30	3.38
O(2, G5)···O(3, G6)	3.46	3.44
O(2, G6)···O(3, G1)	3.39	3.44
Average	3.40	3.39

IV. Deviation (d/Å) of O(4) atoms from their least-squares plane

	S-MA Complex	*R*-MA Complex
O(4, G1)	0.031	0.093
O(4, G2)	0.238	−0.153
O(4, G3)	−0.271	0.033
O(4, G4)	0.034	0.150
O(4, G5)	0.235	−0.204
O(4, G6)	−0.266	0.081
R.M.S. Deviation	0.207	0.132

V. Tilt-angle[a] (ϕ/°) of each 2,3,6-tri-*O*-methylglucose residue

	S-MA Complex	*R*-MA Complex
G1	35.9	29.3
G2	19.8	23.0
G3	7.9	1.9
G4	34.6	23.2
G5	18.7	26.6
G6	7.5	2.9
Average	20.7	17.8

a) The tilt-angle is defined as an angle made by the plane through six O(4) atoms and a plane through C(1), C(4), O(4), and O(4′) of each residue.

with their O(6) side turning to the inside of the methyl-α-CDx ring. In spite of the elliptical distortion of the methyl-α-CDx ring, the O(2)···O(3′) distances do not much differ from those of the *S*-MA complex. The

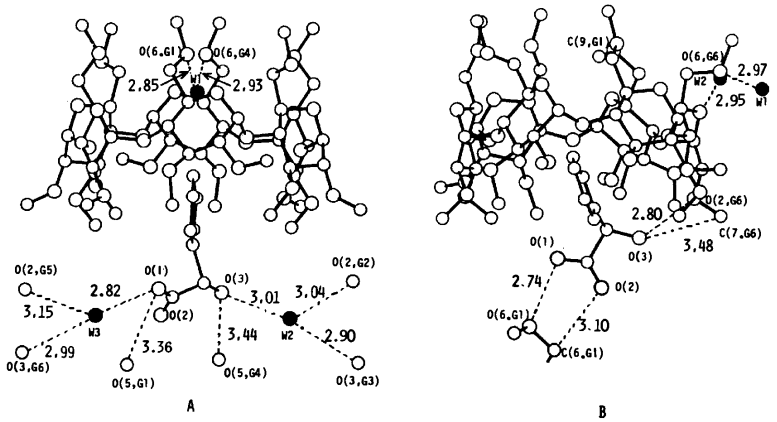

Fig. 3. The inclusion feature of the methyl-α-CDx complexes with *S*-MA (A) and *R*-MA (B). Water molecules are shown by full circles. Intermolecular contacts (Å) involving the guest and water molecules are shown by dashed lines.

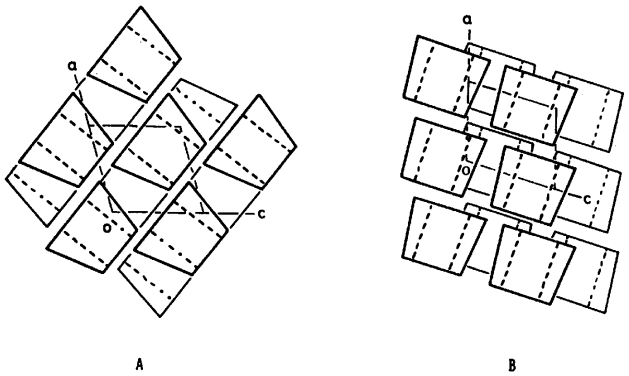

Fig. 4. Schematic drawings of the packing feature of methyl-α-CDx molecules in the crystals of the *S*-MA complex (A) and *R*-MA complex (B).

average O(2)···C(8) and O(2′)···C(8) distances (3.30 and 3.38 Å, respectively) indicate that the $C(8)H_3$ methyl group is located at an equidistant position from the two O(2) oxygen atoms.

Host-Guest Interaction. The inclusion feature of the complexes are shown in Fig. 3. In both complexes, the phenyl group is inserted into the methyl-α-CDx ring from the O(2), O(3) side, but the mode of the host-guest interaction differs between these complexes.

***S*-MA Complex:** The phenyl group is included within the host cavity parallel to the *pseudo* two-fold axis of methyl-α-CDx. The *S*-MA molecule is weakly bound at the O(2), O(3) side of the cavity, as indicated by the relatively large temperature factors of *S*-MA (Table 1), since the phenyl group is only partially inserted into the host cavity. The W1 water molecule is also included at the O(6) side of the cavity to fill the vacant space. The hydroxyl and carboxyl groups protrude outside the cavity, and form hydrogen bonds with the W2 and W3 water molecules, respectively. These water molecules are also hydrogen-bonded to oxygen atoms of adjacent methyl-α-CDx molecules.

***R*-MA Complex:** The host molecules are stacked along the a axis to form a channel-type structure, as shown in Fig. 4. The guest *R*-MA molecule is included within the methyl-α-CDx column. The phenyl group is more deeply inserted into the host cavity, and sandwiched between the G3 and G6 residues (Figs. 1 and 3). The phenyl plane makes an angle of 70.5° with the plane through six O(4) atoms. The hydroxyl group of *R*-MA is hydrogen-bonded to the O(2, G6) atom. The carboxyl group is located outside the host cavity, and forms hydrogen bond with the O(6, G1) oxygen atom of the adjacent methyl-α-CDx molecule.

Crystal Structure. The crystal structure of both complexes are shown in Figs. 5 and 6. In the *S*-MA complex, methyl-α-CDx molecules are arranged to form a layer parallel to the [10$\bar{1}$] plane (Fig. 4). Two adjacent layers are shifted by about half a molecule, forming a blick-work pattern. The O(6) side of the cavity is open to the intermolecular space of the next layer, where the W2 and W3 water molecules are located.

Methyl-α-CDx molecules in the *R*-MA complex are arranged along the a axis in a head-to-tail mode to form an endless column. The methyl-α-CDx ring is not perpendicular to the column axis, but the plane through six O(4) atoms makes an angle of 72.5° with the column axis. The guest *R*-MA molecule is arranged in the methyl-α-CDx column. Two water molecules are located outside the methyl-α-CDx column. W1 forms hydrogen bonds with O(6, G4) and O(6, G6), while W2 is hydrogen-bonded to O(5, G6).

Discussion

As shown in Figs. 1 and 3, the macrocyclic conformation of methyl-α-CDx differs depending on the included isomer. When methyl-α-CDx includes *S*-MA, the macrocyclic ring becomes symmetrical and has the *pseudo* two-fold symmetry. The symmetrical

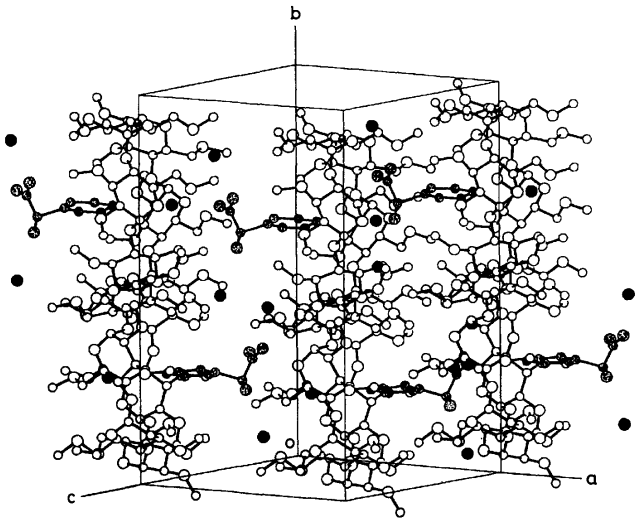

Fig. 5. The crystal structure of the methyl-α-CDx–*S*-MA complex.

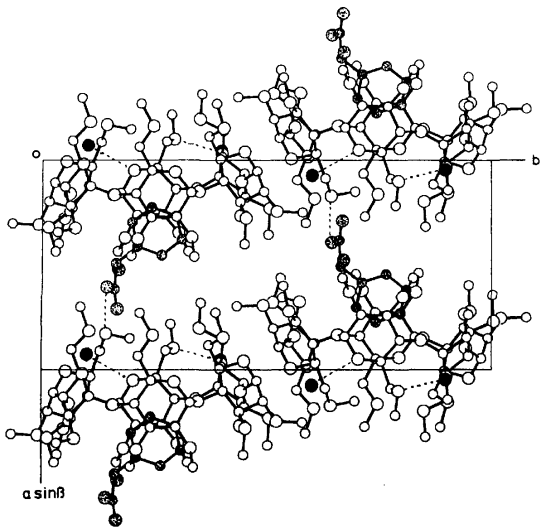

Fig. 6. The crystal structure of the methyl-α-CDx–*R*-MA complex viewed along the c axis.

cavity is favorable to accommodate the phenyl group which is located on the *pseudo* two-fold axis of methyl-α-CDx. The macrocyclic ring of the *R*-MA complex is less symmetrical and somewhat elliptically distorted. The elliptical change of the host cavity, which may be induced by the host-guest interaction, is suitable for the deep penetration of *R*-MA. The formation of the host-guest hydrogen bond between the hydroxyl group of *R*-MA and the O(2, G6) atom of methyl-α-CDx requires the inclination of *R*-MA towards the G1, G6 side of the methyl-α-CDx ring as well as the deep penetration. As the result, a long axis of the benzene ring becomes parallel to the O(4, G2)··· O(4, G5) diagonal, as shown in Fig. 1. The macrocyclic ring should become elliptical to include the phenyl group in such orientation. The methyl-α-CDx molecule seems to recognize the chirality of mandelic acid by the formation of the host-guest hydrogen bond. The hydrogen-bond formation with *S*-MA may be prevented by the steric hindrance involving methyl groups. When *R*-MA is replaced by *S*-MA, the hydroxyl group of *S*-MA should approach to the O(2) or O(3) atom of the G2 residue to form a hydrogen bond. But, such approach is blocked by the methyl group attached to the O(3, G2) atom. The hydrogen-bond formation of *S*-MA with water molecules does not require the deep penetration of *S*-MA into the host cavity.

The comparison of these structures with the α-cyclodextrin-1-phenylethanol complex[2] suggests the important role of methyl groups in the chiral recognition. Both isomers of 1-phenylethanol are equally included within the α-cyclodextrin cavity in the crystal except for the orientation of the hydroxyl group attached to the asymmetric carbon atom. The hydroxyl group of *R*- and *S*-isomers are hydrogen-bonded to the O(2)H and O(3)H hydroxyl groups of α-cyclodextrin, respectively. Such hydrogen bonding may be prevented by the methyl group attached to the O(3) oxygen atom when 1-phenylethanol is included in methyl-α-CDx. The induced-fit conformational change requires the flexibility of the macrocyclic ring. The macrocyclic ring of parent cyclodextrins is considerably rigid because of the intramolecular O(2)··· O(3′) hydrogen bond. The permethylation blocks the intramolecular hydrogen bond and makes the macrocyclic ring more flexible. The chiral recognition by permethylated cyclodextrins has been also observed in the permethylated β-cyclodextrin complexes with Flurbiprofen.[6]

References

1) W. L. Hinze, *Separation and Purification Methods*, **10**, 159 (1981).

2) K. Harata, *Bull. Chem. Soc. Jpn.*, **55**, 1367 (1982).

3) K. Uekama, F. Hirayama, T. Imai, M. Otagiri, and K. Harata, *Chem. Pharm. Bull.*, **31**, 3363 (1983).

4) K. Harata, K. Uekama, M. Otagiri, and F. Hirayama, *J. Inclusion Phenom.*, **1**, 279 (1984).

5) K. Harata, K. Uekama, M. Otagiri, and F. Hirayama, *Chem. Lett.*, **1983**, 1807.

6) K. Harata, F. Hirayama, T. Imai, K. Uekama, and M. Otagiri, *Chem. Lett.*, **1984**, 1549.

7) K. Harata, K. Uekama, M. Otagiri, and F. Hirayama, *J. Inclusion Phenom.*, **2**, 583 (1985).

 © 1987 The Chemical Society of Japan Bull. Chem. Soc. Jpn., 60, 503—507 (1987)

The Vaporization of the Various Trace Components from Aluminoborosilicate Glass

Noriko ITOH* and Tetsurō NAKAMURA
Research Laboratory of Engineering Material, Tokyo Institute of Technology,
4259 Nagatsuta, Midori-ku, Yokohama 227
(Received February 6, 1986)

The simultaneous vaporization of dopants in aluminoborosilicate glass was investigated by means of mass spectrometry using a Knudsen cell. The detected chemical species were Na, K, Ni, Zn, Rb, Ag, Te, TeO_2, and Cs in the temperature range of 650—800 °C. Their vapor pressures were 10^{-6}—10^{-4} Pa. The activation energy of vaporization was discussed in relation to the electrostatic force between the vaporizing specie and oxygen. However, lithium, alkali-earth metal elements, alomst all the transition metal elements (such as Fe, Cr, and Ru), and rare-earth metal elements were not detected in the vapor phase, though they were contained in the glass matrix.

The glass is often heated to several hundred degrees in the process of producing and using the enamel, the glass lining, or the glass matrix containing radioactive wastes. It is an important problem how many and what constituents vaporize from the glass. Numerous investigations have been reported.[1-9] They have, however, been concerned with the gross volatility[1-5] and volatility of a specified element.[2,6-9]

In this work, Knudsen's effusion cell and a mass spectrometer were used in order to determine simultaneously about thirty kinds of chemical species vaporizing from the aluminoborosilicate glasses. The volatilities of the detected elements were estimated by mean of a scale of activation energy.

Experimental

Glass Matrices. The glass matrices were SiO_2-Al_2O_3-B_2O_3-Na_2O glasses doped with a single modifier oxide (S-series) and doped with 26—35 kinds of modifier oxides (P-series). The S-series glasses were used in order to estimate the thermodynamic parameters of the vaporization of a certain modifier ion. The experimental data concerning S1 will be excluded hereinafter because neither Sr nor SrO was detected in the vapor from the S1 glass, where the SrO was the modifier oxide. The chemical compositions are shown in Table 1. The S2, S3, and S4 glass matrices were prepared in the weight ratio of $SiO_2 : B_2O_3 : Al_2O_3 : Na_2O : M_xO_y = 1 : 0.312 : 0.0797 : 0.220 : 0.0848$.

The P-series glasses were used to observe the simultaneous vaporization of the various modifier ions from the same matrix. The P5 and P7 glasses were prepared so that their frit compositions are the same as those of the S-series glasses, i.e., the weight ratio was $SiO_2 : B_2O_3 : Al_2O_3 = 1 : 0.326 : 0.0814$, but the weight ratios of the modifier oxides were different. The frit compositions of the P6 and P8 glasses were different from those of the S-series glasses. However, most of the modifier oxides of the P6 glass have a chemical composition analogous to that of the P5 glass. On the other hand the P8 glass is analogous to the P7 glass in the composition of most of the modifier oxides. The chemical compositions are listed in Table 2 in the order of (1) the components of the frit glass, (2) the components doped in the frit glass and detected in the

*Present address: Tokyo Metropolitan Institute of Technology, 6-6 Asahigaoka, Hino, Tokyo 191.

Table 1. Composition of S2-S4 Glass Matrices (wt.%)

	S2	S3	S4
SiO_2	59.0	59.0	59.0
B_2O_3	18.3	18.3	18.3
Na_2O	13.0	13.0	13.0
Al_2O_3	4.7	4.7	4.7
Cs_2O	5.0	—	—
La_2O_3	—	5.0	—
TeO_2	—	—	5.0
Sum	100	100	100

Table 2. Composition of Aluminoborosilicate Glass (wt.%)

		P5	P6	P7	P8
I	SiO_2	43.22	47.2	43.47	48.49
	B_2O_3	14.07	13.5	14.15	18.58
	Na_2O	8.42	9.34	10.00	11.30
	Al_2O_3	3.52	2.41	3.54	2.00
II	K_2O	2.01	0.96	—	—
	NiO	0.49	0.49	0.23	—
	ZnO	2.01	0.96	3.03	—
	Rb_2O	0.15	0.15	0.11	0.12
	Ag_2O	—	—	0.02	0.02
	TeO_2	0.26	0.26	0.19	0.18
	Cs_2O	1.02	1.02	0.75	0.84
III	Fe_2O_3	7.41	7.41	2.04	2.96
	Li_2O	3.02	1.93	3.54	1.87
	CaO	2.01	0.96	3.03	1.86
	BaO	0.68	1.64	3.52	0.57
	ZrO_2	2.00	2.00	1.46	2.52
	MoO_3	1.99	1.99	1.45	1.57
	RuO_2	1.02	1.02	0.74	0.86
	CeO_2	1.14	1.14	3.34	1.90
	Nd_2O_3	2.50	2.50	1.38	1.48
	Cr_2O_3	La_2O_3	Content of each oxide is 0.01—1.0 wt.%.		
	MnO_2	Pr_6O_{11}			
	SrO	Sm_2O_3			
	P_2O_5	Rh_2O_3			
	Y_2O_3	PdO			
	CdO			0.02	0.02
	SnO_2	—	—	⎫	⎫
	SeO_2			0.05	0.05
	Eu_2O_3				
	Sb_2O_3	—	—	—	0.005

vapor phase, and (3) the components doped in the frit glass but not detected in the vapor phase.

Mass Spectrometry. The instrument used was a JEOL-1A-type mass spectrometer equipped with the Knudsen cell. The conditions of measurement were as follows:

a) Realizable limit of vapor pressure: 10^{-6}—10^{-4} Pa,
b) Deviation of ion current I: ±20%,
c) Mass resolution at m=44: 2200,
d) Ionizing electron: 27.0 kV×100 μA,
e) Potential for accelerating the ions to the electric-magnetic field: 8 kV,
f) Temperature measurement: 400—840 °C by the use of a W5Re/W26Re thermocouple.

A glass sample of about 0.5 g was set in the Knudsen cell and heated step by step, such as: room temperature $\xrightarrow{1.5h}$ 400 °C(1h) $\xrightarrow{40m}$ 500 °C(1h) $\xrightarrow{40m}$ 600 °C(1h) $\xrightarrow{20m}$ 650 °C(1h) $\xrightarrow{20m}$ 700 °C(1h) $\xrightarrow{20m}$ 750 °C(1h) $\xrightarrow{20m}$ 800 °C(1h), or as: room temperature $\xrightarrow{40m}$ arbitrary temperature(1.5h). The steady ion currents were confirmed even after 150m at 700 °C. The weight loss of the glass between before and after heating was 1.5 mg.

Results and Discussion

The Shape of Mass Peak and Correction of the Peak Height. A mass spectrum is constituted of the background (BG) peaks and the sample peaks. Since the BG peaks appear at the positions of almost all the mass numbers, the mass spectrum of BG was used as the mass marker. As the BG molecules are composed of carbon, hydrogen and oxygen, the sample peak appears at a lower mass position than the BG peak when the mass number is the same. The typical shape of a mass peak is illustrated in Fig. 1. It can be seen that the peak height of ^{39}K started to grow at 650 °C and then continued to grow exponentially as the temperature was raised.

The heights of the BG peaks are quite different because of the change in the instrumental constant. Thus, the BG peak heights at every temperatures were normalized at constant values, and the observed heights of the sample peaks were corrected using the normalizing factor.

Establishment of the Steady Flow. The ion currents became constant after 10 min when the temperature of the sample reached the arbitrary value. This means that a steady flow from the Knudsen chamber to the ionizing chamber was established. The difference in pressure between inside and outside the Knudsen cell is calculated by means of Eq. 1, itself derived from the molecular corrision theory and the Maxwellian distribution of velocities[10,11]

$$P - P_{out} = G(2\pi RT/M)^{1/2}/(Ut), \quad (1)$$

where P: Pressure inside the Knudsen cell,
P_{out}: Pressure outside the Knudsen cell, i.e., in the ionizing chamber,
G: Effusion loss through the orifice of area U in an experimental time t,
T: Temperature in the Knudsen cell,
M: Molar weight of the effusion species.

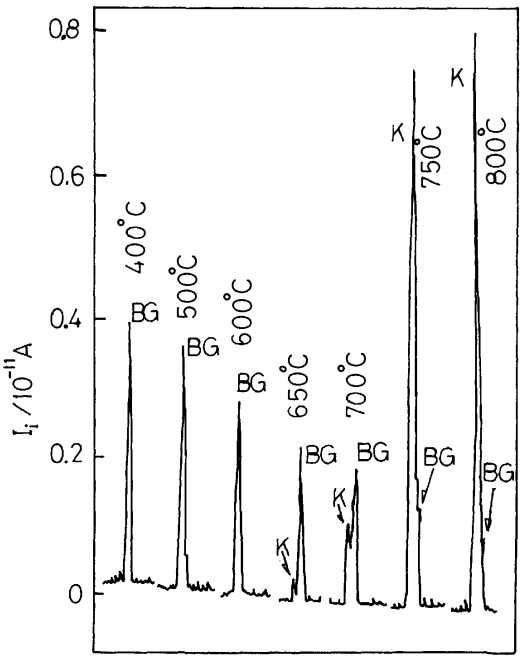

Fig. 1. Change of the mass peak pattern at m=39 for P6 glass matrix. BG: Back Ground, K: Potassium.

In view of the facts that the mean molar weight of various effusing species M is 100 g/mole and that t=4h because the effusion rate G/t increases steeply beyond 700 °C, and using the experimental values of G=1.5 mg, T=1000 K, U=0.25² π mm² and P_{out}=2×10⁻⁵ Pa, P=0.38 Pa was obtained. P=0.38 Pa corresponds to 3.1×10⁻⁹ mol from the ideal gas law, and it is comparable with the effusing rate per second G/t=1.0×10⁻⁹ mol s⁻¹. Thus a rapid but steady effusion and a similar vaporization were recognized.

Vaporizing Species and the Volatilities. The assignment of the chemical species was based on the agreement of the ion-beam current ratio with the natural abundance of isotopes. No parent-daughter relation was found between Na, NaO, Na_2O, and Na_2, or between Cs, CsO, and Cs_2O, by recording the ionization efficiency curves in the range of the ionizing voltage from 4 to 33 kV. Thus, it is presumed that the chemical formulae of the assigned ions are identical with those of the evaporating species.

The species vaporizing from every glass were Na, K, Rb, and Cs, but Li was not vaporized from any glass. Nickel and Zinc were vaporized from the P5 and P7 glasses, but not from the P6 glass. Tellurium was vaporized as Te from the P5, P6 and S4, while it was vaporized as Te and TeO_2 from the P7 and P8 glasses. The other modifier ions were not detected in the vapor phase of any glass. None of the network-former ions (Al, B, or their oxides) were detected in the vapor phase below 840 °C. The vaporizing species and the ion-beam currents observed are summarized in Table 3.

The ratios of the ion-beam current IT vs. the molar fractions of the positive ion in the glass matrix X are

Table 3. Observed Ion-Beam Currents ($\times 10^{-11}$ A) at Various Temperatures

	T/K	^{23}Na	^{39}K	^{58}Ni	^{64}Zn	^{85}Rb	^{107}Ag	^{130}Te	^{133}Cs	^{130}Te^{16}O$_2$
P5	933	0.4	1.0	2.4	0	.0	—	0	0.99	0
	962	1.3	3.2	8.7	0	0	—	0	1.7	0
	990	2.25	5.8	8.3	0.5	0.20	—	0.25	3.2	0
	1020	2.5	6.4	9.0	0.51	0.30	—	0.47	2.8	0
	1050	2.6	5.2	10.9	1.38	0.43	—	0.71	4.8	0
	1083	7.1	11.6	15.8	2.24	0.49	—	1.09	6.2	0
P6	989	3.77	1.88	0	0	0	—	0	1.54	0
	1022	3.66	2.42	0	0	0.535	—	0	2.53	0
	1050	5.83	4.36	0	0	0.893	—	0	12.6	0
	1077	12.6	7.69	0	0	0.654	—	0.128	8.21	0
	1110	19.3	13.6	0	0	1.61	—	0.313	15.7	0
P7	928	1.14	—	6.26	0	0.306	0.163	0	1.51	0
	960	1.11	—	14.6	0	Missed	0	0	4.6	0.043
	986	4.87	—	36.6	0	0.444	0.444	0	5.93	0.212
	1025	10.2	—	39.9	0.286	1.21	0.73	0.508	17.6	0.478
	1077	25.9	—	143	0.894	2.50	1.20	1.10	30.2	1.46
P8	930	0.881	—	—	—	0	0	0	0.610	0
	971	3.84	—	—	—	0	0	0.060	4.31	0
	1011	5.76	—	—	—	0.244	0.550	0.227	7.70	0
	1039	10.1	—	—	—	1.12	1.03	0.458	9.39	0
	1086	46.2	—	—	—	1.92	2.40	0.782	19.0	1.01
S2	933	0	—	—	—	—	—	—	0.06	—
	970	0	—	—	—	—	—	—	0.13	—
	1005	0.09	—	—	—	—	—	—	1.2	—
	1043	0.45	—	—	—	—	—	—	5.9	—
	1073	1.2	—	—	—	—	—	—	10.0	—
S3	930	0								
	979	0.016								
	1025	0.090								
	1057	0.34								
	1105	2.6								
S4	1001	0.061	—	—	—	—	—	0	—	—
	1030	0.341	—	—	—	—	—	0.120	—	—
	1060	0.807	—	—	—	—	—	0.532	—	—
	1095	2.95	—	—	—	—	—	1.11	—	—
	1110	4.8	—	—	—	—	—	1.88	—	—

Table 4. The Ratios of (Ion Current IT)/(Molar Fraction in the Glass X) at 800 °C (μA·K/mol%)

	S2	S3	S4	P5	P6	P7	P8
Li	—	—	—	0	0	0	0
Na	0.64	0.04	0.08	0.43	0.78	1.66	1.67
K	—	—	—	2.91	7.46	—	—
Rb	—	—	—	9.30	17.2	53.0	41.2
Cs	0.78	—	—	17.2	21.8	133	68.8
Ag	—	—	—	—	—	259	400
Ni	—	—	—	2.0	0	9.14	—
Zn	—	—	—	0.016	0	0.005	—
Te	—	—	0.004	0.13	0.047	0.18	0.14

shown in Table 4. The IT/X varies by several orders in magnitude with the different ions in the same glass. This means that the vaporization is incongruent. Supposing that the IT/X is a scale of the volatility, and that the species are confined to monovalent ions, silver is the most volatile; subsequently volatility order of Cs>Rb>K>Na follows silver. The exptremely high value of IT/X for silver is attributably to the rapid diffusion. The volatility of alkali metal ions is correlated with the ionic radius.

Thermodynamic Considerations. The total vapor pressure in the Knudsen cell was previously estimated as P=0.38 Pa. The partial pressure of the i-th ion P_i is proportional to the ion current I_i.[11]

$$P_i = I_i Tk/(\sigma_i S_i), \quad (2)$$

where k: Istrumental coefficient,
σ_i: Ionization cross-section,
S_i: Sensitivity coefficient of the secondary-electron multiplier.

In practice, the I_i and T are observed by means of mass spectrometry, but the estimation of the σ_i and S_i is impossible. Accordingly, the values of P_i are not

Table 5. Arrhenius Plots of the Ion-Current IT(AK); $\log(IT)=-a/T+b$

	S2		S3		S4	
	a	*b*	*a*	*b*	*a*	*b*
Na	17808	9.716	19416	9.973	19116	9.972
Te	—	—	—	—	16356	7.064
Cs	18440	9.318	—	—	—	—

	P5		P6		P7		P8	
	a	*b*	*a*	*b*	*a*	*b*	*a*	*b*
Na	7389	−0.3437	12840	5.056	10520	3.238	10740	3.486
K	6296	−1.082	10620	2.769	—	—	—	—
Ni	4766	−2.345	—	—	9098	2.616	—	—
Zn	8675	0.3754	—	—	10969	2.168	—	—
Rb	5304	−3.327	5627	−2.758	6867	−1.239	6551	−1.643
Ag	—	—	—	—	6344	−1.964	9772	1.420
Te	7705	−0.796	14505	5.148	7540	−0.9272	7145	−1.494
Cs	5579	−1.997	9774	2.027	9184	2.116	9463	2.134
TeO_2	—	—	—	—	11840	3.211	—	—

Table 6. Activation Energy ΔH_i^* (kJ mol^{-1}) and Network-Formers' Content (mol%)

	P5	P6	P7	P8	S2	S3	S4
Na	141.5	246	201.4	205.6	341.0	371.8	366.0
K	120.6	203	—	—	—	—	—
Ni	91.3	>300	174.2	—	—	—	—
Zn	166.1	>300	210.0	—	—	—	—
Rb	101.6	107.7	131.5	125.4	—	—	—
Ag	—	—	121.5	187.1	—	—	—
Te	147.5	278	144.4	136.8	—	—	313.2
Cs	106.8	187.2	175.8	181.2	353.2	—	—
$\sum_i X(i)$ (i=Si, B, Al)	60.53	63.99	60.87	67.90	77.86	78.04	78.02

determined by the use of Eq. 2.

Suppose that an *i*-th component in the glass matrix has an activation energy of vaporization, ΔH_i^*. The ΔH_i^* is, as well known, a coefficient of the Arrhenius plot of the vapor pressure:

$$\frac{d \ln P_i}{d(1/T)} = \frac{-\Delta H_i^*}{R} \tag{3}$$

By substituting Eq. 2 in Eq. 3, we obtain:

$$\frac{d \ln(I_i T)}{d(1/T)} = \frac{-\Delta H_i^*}{R} \tag{4}$$

The plots of $\ln(I_iT)$ vs. $1/T$ showed linear lines. The coefficients of lines *a* and *b* were calculated by means of the least-squares method, they are summarized in Table 5. The ΔH_i^* values were evaluated from the *a* value and Eq. 4. They were listed in Table 6. Tables 4 and 6 indicate that the volatility of Na, Te, or Cs in the S2, S3, and S4 (S-series) glasses is obviously smaller than in the P5, P6, P7, and P8 (P-series) glasses. This is attributable to the fact that the network-former ions in the S-series glass are richer than in the P-series glass: i.e., the sum of the molar fractions of Si, B, and Al in the S-series glass was about 78 mol%, while that in the P-series glass was 61—68 mol%.

From another point of view, the activation energies of monovalent modifier ions in the same glass decrease and then increase as the ionic radius increases. If the activation energy were exactly the energy needed for release from the electrostatic force between M^+ and O^{2-}, the activation energy would decrease monotonously as the ionic radius increased. Thus, another energy which increases with the increase in the ionic radius must be included in the activation energy. The high registivity of Cs against movement has been reported after the measurement of the self-diffusion coefficient. For instance, the values in $M_2O \cdot SiO_2$ glass at 500 °C are 5.8×10^{-10} cm^2 s^{-1} for M=Cs, while 2.3×10^{-8} cm^2 s^{-1} for M=Na.[13,14] It was assumed that the additional energy is elastic energy and is proportional to the cube of the ionic radius;

$$\Delta H_i^* = \Delta H_{i,\text{coul}}^* + \Delta H_{i,\text{elas}}^*, \tag{5}$$

$$\Delta H_{i,\text{coul}}^* = N\frac{2e^2\alpha}{r_o + r_i} = \frac{A}{r_o + r_i}, \tag{6}$$

$$\Delta H_{i,\text{elas}}^* = Dr_i^3. \tag{7}$$

As the Madelung constant is used to calculate the lattice energy, $\Delta H_{i,\text{coul}}^*$ is a product of $2e^2/(r_o+r_i)$ by a constant α. Thus, a simple expression, $A/(r_o+r_i)$, was obtained. It was previously noted that the observed

Table 7. Calculated and Observed Activation Energy ΔH_i^* (kJ mol^{-1})

i	r_i+r_o[a]	P5 $A=321.0$, $D=-0.244$				P6 $A=555.1$, $D=-6.89$				P7 $A=378.7$, $D=6.153$				P8 $A=455.6$, $D=1.13$			
		Calcd			Obsd	Calcd			Obsd	Calcd			Obsd	Calcd			Obsd
	nm	coul	elas	sum		coul	elas	sum		coul	elas	sum		coul	elas	sum	
Na^+	0.224	143	0	143	142	248	−4	244	246	169	4	173	201	203	1	204	206
Ag^+	0.255	—	—	—	—	—	—	—	—	148	9	157	122	179	2	181	187
K^+	0.278	115	−1	114	121	200	−18	182	203	—	—	—	—	—	—	—	—
Rb^+	0.292	110	−1	109	102	190	−24	166	108	130	22	152	132	156	4	160	125
Cs^+	0.303	106	−1	105	107	183	−30	153	187	125	27	152	176	150	5	155	181

a) Shannon's effective ionic radius of 6-coordinated ion; $r_o=0.140$ nm.[15]

ΔH_i^* showed different values depending on the mol% of the network-former ion: Si, B, and Al. The total mol% of the modifier cations and the middle ions in the P-series glasses were 32—39 mol%. This quantity is sufficient to determine the values of $\Delta H_{i,coul}^*$. It follows that a more precise chemical composition may also be effective. The A and D constants were calculated for the respective glass by the least-squares method, using the data of ΔH_i^* and Shannon's effective ionic radius.[15] The contributions of the electrostatic energy and the elastic energy to the total activation energy was summarized in Table 7. Almost all the $\Delta H_{i,calc'd}$ values are in agreement with the $\Delta H_{i,obs'd}$ values, but (1) the $\Delta H_{i,calc'd}$ values for every glass showed a monotonously decreasing curve with increase in r_o+r_i, and (2) the negative sign of D for the P5 and P6 glasses is unreasonable physically. The other functions, such as $A/(r_o+r_i)+B\exp[-(r_o+r_i)C]+Dr_i^3$ and $A/(r_o+r_i)+Dr_i^2$, gave quite unreasonable values of A, B, or C. The calculation based on the simple assumption suggested that the electrostatic energy is the major portion, while the elastic energy is a minor portion, of the activation energy.

Conclusion

When an aluminoborosilicate glass matrix is heated up to near the softening point, Na, K, Ni, Zn, Rb, Ag, Te, TeO_2, and Cs are detected in the vapor phase. The activation energy of vaporization was calculated from the Arrhenius plot of the observed ion currents.

References

1) D. Walmsley, B. A. Sammons, and J. R. Crover, AERE-R5777 (1969).
2) W. J. Gray, BNWL-2111 (1976).
3) L. A. Chick, G. F. Piepel, G. B. Mellinger, R. P. May, W. J. Gray, and C. Q. Buckwalter, PNL-3188 (1981).
4) N. Kassis and G. H. Frishat, *Commun. Am. Ceram. Soc.*, **1981**, C-28.
5) S. Murai, J. T. Wenzel, and D. M. Sanders, *Phys. Chem. Glasses*, **21**, 150 (1980).
6) A. S. Nikiforov, V. V. Kulichenko, N. V. Krylova, N. D. Musatov, and A. S. Polyakov, "Scientific Basis for Nuclear Waste Management," ed by G. J. Macarthy, Plenum Press, New York (1979), Vol. 1, pp. 117—121.
7) A. E. Albrethsen and L. C. Schwendiman, BNWL-338 (1967).
8) M. M. Schultz, V. L. Stolyarova, and G. A. Semenov, *J. Non-Crystal. Solids*, **38—39**, 581 (1980).
9) J. T. Wenzel and D. Sanders, *Phys. Chem. Glasses*, **23**, 47 (1982).
10) A. Harashima, "Thermodynamics and Staticdynamics," Baifūkan, Tokyo (1982), p. 190.
11) P. Goldfinger, "Mass Spectrometry," ed by R. I. Reed, Academic Press, London/New York (1965), pp. 268—272.
12) O. Kubaschewski, E. LL. Evans, and C. B. Alock, "Metallurgical Thermochemistry," Pergamon Press, Oxford/New York/Toronto/ Sydney (1967), pp. 409—420.
13) R. Terai, T. Kitaoka, and C. Ueno, *J. Ceram. Soc. Jpn*, **77**, 88 (1969).
14) R. Terai, *J. Ceram. Soc. Jpn*, **77**, 318 (1969).
15) R. D. Shannon and C. T. Prewitt, *Acta Crystallogr., Sect. B*, **25**, 925 (1969).

 © 1987 The Chemical Society of Japan Bull. Chem. Soc. Jpn., 60, 509—515 (1987)

The Polarographic Reduction of Acids in Pyridine. The Cause of the Differences in Half-Wave Potentials with Various Supporting Electrolytes

Masashi Hojo,* Yoshihiro Akita, Kazukiyo Nishikawa, and Yoshihiko Imai
Department of Chemistry, Faculty of Science, Kochi University, Kochi 780
(Received April 22, 1986)

The polarographic reductions of acetic, benzoic, *p*-toluenesulfonic, and perchloric acids have been examined in pyridine solutions with tetrabutylammonium, tetraethylammonium, sodium, and lithium perchlorate as the supporting electrolytes. The difference in the half-wave potentials of the acids was explained in terms of the difference in the degree of interaction between the pyridinium ion and the conjugate bases (e.g., CH_3COO^-) made of the acids. The alkali-metal ions interact with the acetate or benzoate ion to form $RCOO^-(M^+)_2$ (M=Li and Na). The formation constants of $RCOO^-(M^+)_2$ were evaluated by means of the positive shift in the half-wave potential of the pyridinium ion in the presence of a large excess of the alkali metal ions. Substituted acetic and benzoic acids and phenols were also examined so as to ascertain the effect of the substituent groups.

Hickey et al.[1] reported very interesting behavior in the polarographic reduction of some acids in pyridine: the pyridinium ion produced in 0.1 M† $LiClO_4$ is reduced at a more positive potential than that of the wave produced in 0.1 M Et_4NClO_4. The half-wave potential ($E_{1/2}$) of the pyridinium wave in Et_4NClO_4 depends on the acids from which the pyridinium ion is produced, whereas that in $LiClO_4$ is essentially independent of the acids (leveling effect). In spite of their great efforts to clarify the cause of the difference in $E_{1/2}$ between Et_4NClO_4 and $LiClO_4$, they were not able to reach the conclusion, probably because they not only lacked knowledge about the key chemical species but had also failed in preparing the compound ($C_6H_5COONEt_4$) essential for the study in a pure form. Tsuji and Elving[2] explained the leveling effect qualitatively in terms of the ion-association and ion-exchange reactions.

We have developed a polarographic method[3,4] to obtain a complex formation constant using the anodic (mercury dissolution) wave induced from a base. By the method, we have confirmed some new species, including the $RCOO^-(M^+)_2$ (M=Li and Na)-type species for the acetate and benzoate ions in acetonitrile.[4]

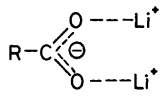

The formation of the $[CH_3COOLi_2]^+$ species in acetonitrile was first proposed by Itabashi in 1972.[5]

In the present investigation, the polarographic behavior of acetic, benzoic, *p*-toluenesulfonic, and perchloric acids in pyridine is examined using several supporting electrolytes. The leveling effect of the acids caused by Li^+ and Na^+ will be accounted for by the formation of the $RCOO^-(M^+)_2$ species. Methyl- and chloro-substituted acetic acids, and chloro-substituted benzoic acids and phenols will also be examined.

The reduction of the hydrogen ion at the dropping mercury electrode is usually accompanied by a high overvoltage in aqueous solutions. Mairanovskii,[6] however, assumed that some protonated bases (e.g., protonated pyridine) might be reduced reversibly, and he confirmed a normal reversible process for the catalytic hydrogen wave caused by pyridine in a 0.1 M borate buffer containing tetraethylammonium phenylmethanesulfonate.

† 1 M=1 mol dm^{-3}.

Experimental

Pyridine from Wako Pure Chemicals (GR grade) was dried with molecular sieves 4A.[7,8] The method of preparing pure tetraethylammonium benzoate was described in a previous paper.[4] The supporting electrolytes were prepared and dried by the methods described elsewhere.[9] Benzoic and *p*-toluenesulfonic acids were dried as has been described previously.[10] Commercial acetic acid (Wako, GR grade) and perchloric acid (Wako, GR grade, 60%) were used as received. The other acids and phenols, commercially obtained GR or EP grade, were used without further purification.

All the polarograms were recorded with a Yanagimoto polarograph, Model P-1000 and a Watanabe X-Y recorder, Model WX-4401-L0, with the potential sweep rate of 5 mV s^{-1}, at (25±0.2)°C. Two dropping mercury electrodes were used: the open-circuit characteristics of the electrodes at h=50 cm were m=2.02 mg s^{-1} and τ= ca. 4 s (capillary A), and m=1.79 mg s^{-1} and τ=4.0 s (capillary B), in 0.1 M Et_4NClO_4-pyridine. The drop time was regulated at 1.0 s for all the polarographic measurements. The reference electrode was a silver-silver perchlorate electrode, Ag/0.1 M $AgClO_4$-pyridine. Pure nitrogen was used for the deoxygenation of polarographic solutions.

Results and Discussion

Acetic, Benzoic, *p*-Toluenesulfonic, and Perchloric Acids. Benzoic acid gave a single cathodic wave at ca. −1.57 V in pyridine containing 0.1 M Et_4NClO_4 as the supporting electrolyte, as is shown in Fig. 1. The wave height was linear to the concentration of benzoic acid over the range of 0.1—1 mM. The wave was found to be diffusion-controlled, as is indicated by the relation of $i_l \propto \sqrt{h}$. With 0.1 M n-Bu_4NClO_4, a similar wave was observed at almost the same potential. With 0.1 M

Table 1. The d.c. Polarographic Data of Perchloric, *p*-Toluenesulfonic, Benzoic, and Acetic Acids in Pyridine with Various Supporting Electrolytes

Supporting electrolyte[a]	$E_{1/2}$[b]/V (Prewave)	i_l/μA	$E_{1/2}$/V	i_l/μA (Main wave)	Slope[c]/mV
$[HClO_4]=1.0$ mM					
n-Bu_4N^+	−1.0	0.15	−1.20	2.6	59
Et_4N^+	−1.07	0.2	−1.235	2.8	63
Na^+	−0.97	0.25	−1.215	2.75	56
Li^+	−1.01	0.2	−1.23	2.85	58
[*p*-TOs]=1.0 mM					
n-Bu_4N^+	−1.07	0.2	−1.21	2.3	74
Et_4N^+	−1.05	0.15	−1.245	2.1	58
Na^+	−0.98	0.2	−1.23	2.0	54
Li^+	−1.04	0.3	−1.24	2.35	47
$[C_6H_5COOH]=1.0$ mM					
n-Bu_4N^+	—		−1.585	2.5	80
Et_4N^+	—		−1.57	2.6	73
Na^+	−1.06	0.3	−1.30	2.5	75
Li^+	−1.03	0.3	−1.24	2.5	53
$[CH_3COOH]=0.96$ mM					
n-Bu_4N^+	—		−1.75	2.85	110
Et_4N^+	—		−1.69	2.95	100
Na^+	−1.125	0.25	−1.37	2.6	79
Li^+	−1.08	0.3	−1.285	2.4	63

a) 0.1 M perchlorate salts. b) vs. Ag/0.1 M $AgClO_4$–pyridine. c) $-E$ vs. $\log[i/(i_d-i)]$. Capillary A was used for measuring the data in Table 1.

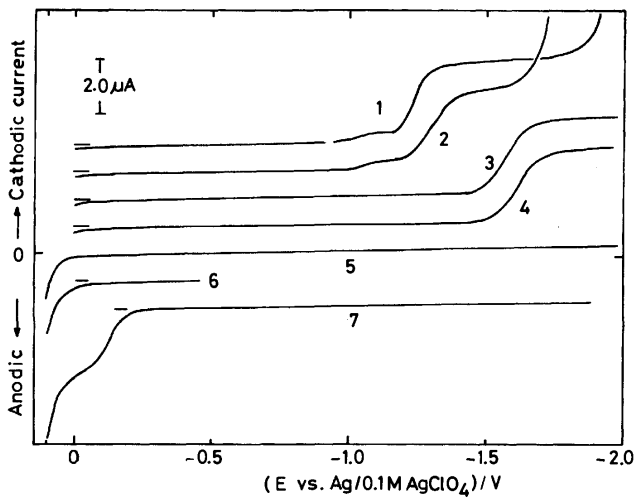

Fig. 1. D.c. polarograms of benzoic acid and the benzoate ion in pyridine containing various supporting electrolytes at 25°C.
[Benzoic acid]=1.0 mM for 1—4.
1: 0.1 M $LiClO_4$, 2: 0.1 M $NaClO_4$, 3: 0.1 M Et_4NClO_4, 4: 0.1 M Bu_4NClO_4, 5: the base current with 0.1 M Et_4NClO_4, 6: $[C_6H_5COOEt_4N]=0.99$ mM, 0.1 M $LiClO_4$ or $NaClO_4$, 7: $[C_6H_5COOEt_4N]=0.99$ mM, 0.1 M Et_4ClO_4.

$LiClO_4$ and $NaClO_4$, however, the wave was shifted to more positive potentials and the wave was accompanied by a prewave (Table 1). Similar behavior has been reported by Hickey et al.:[1] they attributed the main wave to the reduction of the pyridinium ion formed from benzoic acid and pyridine. Acetic acid gave a less reversible cathodic wave at a more negative potential than benzoic acid. The half-wave potential of the wave depended on the supporting electrolyte cation. On the other hand, the main waves for perchloric or *p*-toluenesulfonic acid (*p*-TOs) were observed at more positive potentials (−1.20—−1.245 V), being almost indifferent to the kind of supporting electrolyte cations.

The half-wave potentials of the main wave for the acids in the presence of the tetraalkylammonium ions are in this order: $HClO_4 \simeq p$-TOs>benzoic acid>acetic acid. The negative shift for the weaker acids may be accounted for by the interaction between the pyridinium ion and the conjugate-base anion ($PyH^+ \wedge\!\wedge\, RCOO^-$). Therefore, the effect of the benzoate ion on the $E_{1/2}$ for benzoic acid was examined. A ten-fold concentration increase (from 10 to 100 mM) of tetraethylammonium benzoate shifted the $E_{1/2}$ for benzoic acid (1 mM) ca. 120 mV negatively and decreased the wave height linearly down to half of the initial height at 100 mM of the salt. This shows a strong interaction between the pyridinium cation and the benzoate anion. The potential shift of ca. 120 mV with a 10-fold increase in the benzoate concentration suggested that the compound formed by the pyridinium ion and a large excess of the benzoate ion might be a 1:2 complex (pyridinium dibenzoate; cf. $[Li^+(C_6H_5COO^-)_2]$ in Ref. 4). At any rate, the benzoate and acetate ions seemed to be bound to the pyridinium ion so tightly because neither pyridinium benzoate nor acetate gave any anodic wave, although tetraethylammonium benzoate gave a well-defined anodic wave at −0.12 V with 0.1 M Et_4NClO_4 (Fig. 1).

The half-wave potentials of the reduction waves for

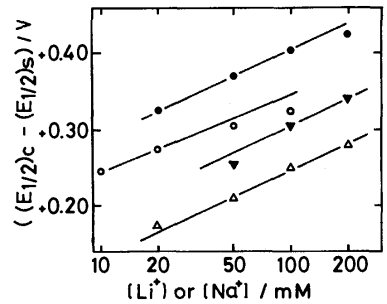

Fig. 2. Shifts of the half-wave potentials of the cathodic waves of acetic and benzoic acids (1 mM) with the addition of alkali metal ions. (●): Acetic acid, Li^+, (○): benzoic acid, Li^+, (▼): acetic acid, Na^+, (△): benzoic acid, Na^+. The total ionic strength is kept to be 0.1 M with Et_4NClO_4, except for 200 mM solutions of Li^+ and Na^+. See the text for $(E_{1/2})_c$ and $(E_{1/2})_s$.

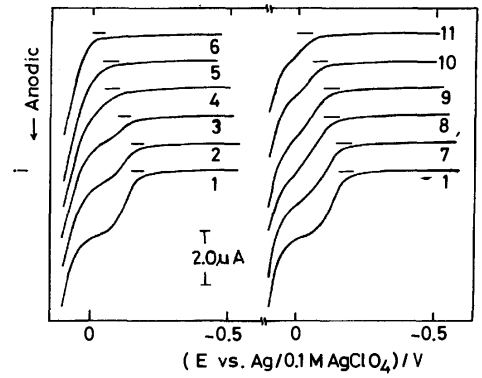

Fig. 3. Changes in the anodic wave from the benzoate ion in 0.1 M Et_4NClO_4-pyridine with the addition of $LiClO_4$ and $NaClO_4$.
$[C_6H_5COOEt_4N]$=0.99 mM.
1: Li^+ and Na^+ free, 2: 0.4, 3: 0.6, 4: 0.8, 5: 1.0, 6: 2.0 mM of Li^+, 7: 0.4, 8: 0.8, 9: 1.0, 10: 1.4, 11: 2.0 mM of Na^+.

acetic and benzoic acids were shifted positively by the supporting electrolyte cation in this order: $Li^+ > Na^+ > Et_4N^+ \simeq n\text{-}Bu_4N^+$. The positive shift by alkali metal cations suggested that the interaction between the pyridinium ion and the acetate or benzoate ion would be weakened by the interaction between the acetate or benzoate ion and the alkali-metal cations. Figure 2 shows the shifts in the $E_{1/2}$ for acetic and benzoic acids with the concentration changes in Li^+ and Na^+. The $E_{1/2}$ shifted ca. 120 mV positively upon a 10-fold increase in the concentration of the alkali-metal ions, except in the case of benzoic acid with Li^+ (ca. 100 mV). The waves became reversible and diffusion-controlled at higher concentrations of Li^+ or Na^+ ($\geqslant$ 20 mM) in most cases. However, for acetic acid, more than 50 mM of Na^+ was needed to obtain the reversible and diffusion-controlled wave.

The following equation was used to analyze the above data:

$$(E_{1/2})_c = (E_{1/2})_s + \frac{0.059}{n}\log K + \frac{0.059}{n} p \log [M^+], \quad (1)$$

where n is the number of electrons and p is the number of M^+ bound to a carboxylate ion. The term of $(E_{1/2})_c$ means the $E_{1/2}$ of an acid in the presence of an alkali-metal ion. As the standard ($(E_{1/2})_s$), the $E_{1/2}$ of the acid in the absence of alkali-metal ions (with 0.1 M Et_4NClO_4) was taken. K stands for the overall formation constant. The other conditions for Eq. 1 are similar to those given in Refs. 3, 4, or 11. In Eq. 1, we get p=2, since the pyridinium ion is reduced by one electron (n=1)[2,12,13] and the slope of $\Delta E_{1/2}/\Delta\log[M^+]$ is ca. 120 mV, as has been mentioned above.

Thus, the reaction for acetic acid is as follows:

$$PyH^+ \wedge\wedge\wedge\wedge CH_3COO^- + 2\,M^+ \overset{K}{\rightleftharpoons} PyH^+ \cdots\cdots CH_3COO^-(M^+)_2. \quad (2)$$

The formation constants of the ion pair (or complex) between the acetate ion and the lithium and sodium ions were found to be log (K/M^2)=ca. 8.8 and ca. 7.1 respectively. We ignored the irreversibility of the wave for acetic acid in the absence of an alkali-metal ion. For the benzoate ion, the values were log (K/M^2)= ca. 7.8 and ca. 6.2 with Li^+ and Na^+ respectively. In acetonitrile,[4] the formation constants of $CH_3COO^-(Li^+)_2$ and $C_6H_5COO^-(Li^+)_2$ in the reactions between $RCOONEt_4$ and Li^+ were obtained as log (K/M^2)=11.0 and ca. 9.0 respectively. The values of the formation constants are only approximate, however, because of some irreversibility in the waves and an incomplete dissociation of $M^+ClO_4^-$ in pyridine solutions.

In this study, the cathodic wave of the pyridinium ion was used as the indicator. The pyridinium ion is not bound to the alkali-metal ion directly, but through the acetate (or benzoate) ion.

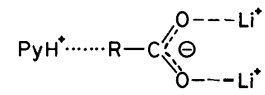

The relatively positive and constant values of the $E_{1/2}$ of $HClO_4$ and p-TOs with various supporting electrolytes indicate that the perchlorate and p-toluenesulfonate ions should interact only weakly with the pyridinium ion ($PyH^+ \cdots\cdots ClO_4^-$). If the interaction between the pyridinium ion and the conjugate base anion (from acetic or benzic acid) were completely removed by any interaction, the reduction potential of the weak acid would approach the positive value of $HClO_4$ or p-TOs.

Figure 3 shows the change in the anodic (mercury dissolution) wave from the benzoate ion (1 mM) in pyridine-0.1 M Et_4NClO_4 upon the addition of Li^+ and Na^+. The wave height of the anodic wave from the benzoate ion decreased linearly with the increase in the concentration of Li^+, and the wave disappeared completely at 1 mM of Li^+. Upon the addition of Na^+, a positive shift of the anodic wave was observed because

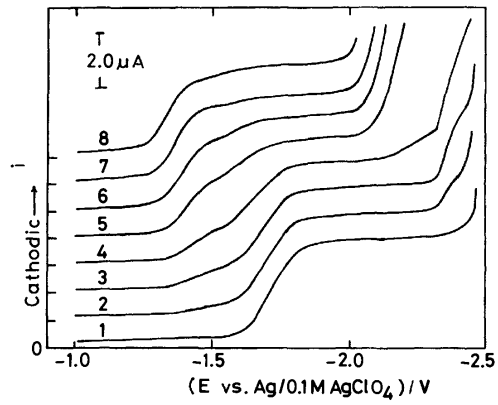

Fig. 4. Changes in the polarographic wave of 1 mM acetic acid (10 ml) with the addition of 0.1 M $LiClO_4$. The supporting electrolyte is 0.1 M Et_4NClO_4. 1: Li^+ free, 2: 40, 3: 100, 4: 200, 5: 500 μl, 6: 1, 7: 2, 8: 5 ml of 0.1 M $LiClO_4$ added. The total volume changes are not corrected.

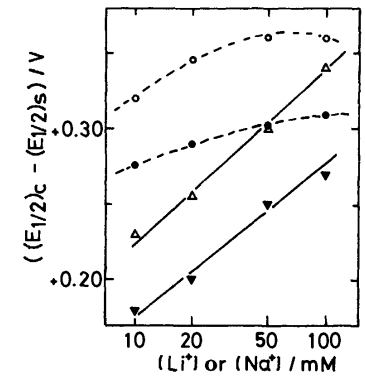

Fig. 5. Shifts in the half-wave potentials of cathodic waves of chloro-substituted benzoic acids (1 mM) with the addition of alkali metal ions.
(○): *p*-Chlorobenzoic, Li^+, (△): *p*-chlorobenzoic, Na^+, (●): 2,4-dichlorobenzoic, Li^+, (▼): 2,4-dichlorobenzoic acid, Na^+. The total ionic strength is kept to be 0.1 M with Et_4NClO_4. See Fig. 2 for $(E_{1/2})_c$ and $(E_{1/2})_s$.

the wave was not completely depressed, even at 2 mM of Na^+. In acetonitrile,[4] although the anodic wave from the benzoate ion disappeared at the equivalence point as a result of the formation of the white precipitate of lithium or sodium benzoate, the anodic wave was recovered again at a much more positive potential by the addition of a large excess of Li^+ or Na^+ (the formation of $C_6H_5COO^-(M^+)_2$). Unfortunately, the reappearance of the anodic wave was not observed, even at 0.1 M Li^+ or Na^+, in the pyridine solution, for the potential of the anodic wave was too close to the positive potential limit in the absence of any complex-forming agent (ca. +0.05 V). Thus, the formation of $C_6H_5COO^-(M^+)_2$ was not directly proved by the anodic wave from the benzoate ion in pyridine, unlike as in acetonitrile.

Figure 4 shows the change in the polarographic wave of acetic acid upon the addition of $LiClO_4$. Upon the addition of a small amount of $LiClO_4$, a small cathodic wave appeared at a more positive potential than that of the initial wave in 0.1 M Et_4NClO_4 as the supporting electrolyte. The wave height of the more positive wave increased with the increase in the concentration of $LiClO_4$. At last, the wave merged into the initial wave at high concentrations of $LiClO_4$. These experimental results suggest the successive formation of $RCOO^-Li^+$ and $RCOO^-(Li^+)_2$ from PyH^+ ∧∧∧ $RCOO^-$ and $LiClO_4$.

Hickey et al. described that specific differences in the effects of supporting-electrolyte cations appeared to be due to electrocapillary phenomena and perhaps also to the extent of the solvation of the ions.[1] However, the present study as well as the work by Tsuji and Elving[2] shows that the interaction between the pyridinium ion and the conjugate base from a weak acid plays an important role in the reduction potential of the acid in pyridine solutions.

In conclusion, the leveling effect of the carboxylic acids with Li^+ or Na^+ can be explained quantitatively by the formation of $RCOO^-(M^+)_2$-type species, instead of in terms of simple ion-exchange reactions, i.e., $PyH^+A^-+M^+ClO_4^- \rightleftarrows PyH^+ClO_4^-+M^+A^-$ (A^-=the conjugate base of an acid) proposed by Tsuji and Elving,[2] in pyridine solutions.

Methyl- or Chloro-Substituted Acetic and Benzoic Acids and Phenols. The polarographic data for propionic and pivalic ($(CH_3)_3CCOOH$) acids and for chloro-substituted acetic and benzoic acids in pyridine solutions are listed in Table 2. The polarographic behavior of these compounds was very similar to that of acetic and benzoic acids, except that trichloroacetic acid gave a very large wave (6 μA, cf. 3 μA for 1 mM acetic acid) with Et_4N^+ or n-Bu_4N^+ as the supporting-electrolyte cation. The large wave-height for trichloroacetic acid can be explained by the immediate reduction of a chlorine atom in the substituent group, besides the reduction of the pyridinium ion. Only the reduction of the pyridinium ion with one electron (n= 1) occurred for the other acids.

With Et_4N^+ or n-Bu_4N^+ as the supporting-electrolyte cation, the half-wave potential of an acid depends on its acid strength. The linear relation between $E_{1/2}$ and pK_a^{aq} (dissociation constant in water) for acids in pyridine has been reported by Tsuji and Elving.[13] With Li^+ or Na^+ as the supporting-electrolyte cation, however, the half-wave potentials of chloro-substituted acetic and benzoic acids were rather constant in value (−1.2—−1.4 V).

The effects of the concentrations of alkali-metal ions on the half-wave potentials of substituted acetic and benzoic acids were also examined. Figure 5 shows the effects of Li^+ and Na^+ on the reduction of *p*-chlorobenzoic and 2,4-dichlorobenzoic acids. The half-wave potential of *p*-chlorobenzoic and 2,4-dichlorobenzoic acids were shifted ca. 120 mV posi-

Table 2. The d.c. Polarographic Data of Other Acids and Phenols in Pyridine with Various Supporting Electrolytes

Supporting electrolyte[a]	$E_{1/2}$[b]/V (Prewave)	i_l/μA (Prewave)	$E_{1/2}$/V	i_l/μA (Main wave)	Slope[c]/mV
[CH_3CH_2COOH]=1.05 mM					
n-Bu_4N^+			−1.79	3.0	95
Et_4N^+			−1.72	3.1	95
Na^+	−1.42	0.15	−1.42	2.9	79
Li^+	−1.31	0.2	−1.31	2.8	58
[$(CH_3)_3CCOOH$]=0.99 mM					
n-Bu_4N^+			−1.81	2.9	89
Et_4N^+			−1.74	2.65	82
Na^+	−1.185	0.2	−1.44	2.35	74
Li^+	−1.11	0.25	−1.32	2.45	65
[$ClCH_2COOH$]=1.0 mM					
n-Bu_4N^+			−1.41	2.6	100
Et_4N^+			−1.47	2.65	92
Na^+	−0.965	0.25	−1.205	2.55	66
Li^+	−1.02	0.3	−1.23	2.5	53
[$Cl_2CHCOOH$]=1.0 mM					
n-Bu_4N^+			−1.235	2.5	89
Et_4N^+			−1.30	2.9	82
Na^+	−0.92	0.2	−1.13	2.25	63
Li^+	−1.03	0.2	−1.26	2.4	53
[Cl_3CCOOH]=0.99 mM					
n-Bu_4N^+			−1.95	5.9	173
Et_4N^+			−1.72	5.8	205
Na^+	−1.05	0.45	−1.24[d]	1.6	—
Li^+	−1.07	0.5	−1.25	1.9	58
[p-Chlorobenzoic acid]=1.0 mM					
n-Bu_4N^+			−1.57	2.55	105
Et_4N^+			−1.48	2.65	82
Na^+	−1.04	0.2	−1.31	2.3	68
Li^+	−1.00	0.2	−1.23	2.35	59
[2,4-Dichlorobenzoic acid]=1.0 mM					
n-Bu_4N^+			−1.48	2.35	92
Et_4N^+			−1.48	2.7	87
Na^+	−1.03	0.2	−1.29	2.65	53
Li^+	−1.04	0.25	−1.27	2.6	47
[C_6H_5OH]=1.0 mM					
n-Bu_4N^+			−2.065	1.95	142
Et_4N^+			−1.985	2.25	142
Na^+			—[e]		
Li^+			−1.79	3.1	77
[p-Chlorophenol]=0.93 mM					
n-Bu_4N^+			−1.98	2.1	152
Et_4N^+			−1.91	2.25	126
Na^+			—[e]		
Li^+			−1.72	2.4	100
[2,4-Dichlorophenol]=1.0 mM					
n-Bu_4N^+			−1.81	2.55	116
Et_4N^+			−1.735	2.6	108
Na^+			−1.555	1.8	84
Li^+			−1.45	2.1	84

a) 0.1 M perchlorate salts. b) vs. Ag/0.1 M $AgClO_4$-pyridine. c) $-E$ vs. $\log[i/(i_d-i)]$. d) A polarographic maximum was accompanied. e) No wave was observed up to the reduction of the Na^+ ion. Capillary B was used for measuring the data in Table 2.

tively by a 10-fold increase in the concentration of $NaClO_4$ ($\Delta E_{1/2}/\Delta\log[Na^+] \simeq 120$ mV). The analyses of the data by means of Eq. 1 gave formation constants of $\log(K/M^2)$=ca. 6.1 and ca. 4.9 for $ClC_6H_4COO^-(Na^+)_2$ and $Cl_2C_6H_3COO^-(Na^+)_2$, respectively. The effect of Li^+ on the waves of both acids is larger than that of Na^+, judging from the potential at each concentration of the aklali-metal ions. However, the

Table 3. The Values of the $\Delta E_{1/2}/\Delta\log[M^+]$ Slope and the Estimated Values of the Formation Constants of $RCOO^-(M^+)_2$

Acid	Li^+		Na^+	
	Slope/mV	Log K[a)]	Slope/mV	Log K[a)]
CH_3COOH	115	8.8	132	7.1
CH_3CH_2COOH	95	9.0	110	7.2
$(CH_3)_3CCOOH$	80	—	—[b)]	
$ClCH_2COOH$	25		80	—
$Cl_2CHCOOH$	0		20, 60[c)]	
Cl_3CCOOH	—[d)]		—[d)]	
C_6H_5COOH	100	7.8	120	6.2
p-Chlorobenzoic	≈50[e)]		117	6.1
2,4-Dichlorobenzoic	≈40[e)]		97	4.9

a) The formation constant, $K(M^{-2})$, in $RCOO^- + 2M^+ \rightleftarrows RCOO^-(M^+)_2$. b) The wave height was decreased by the addition of Na^+. c) The curve was separated into two parts, as is shown in Fig. 6. d) Another reaction seems to occur; see the text. e) The slope became smaller at higher concentrations of M^+.

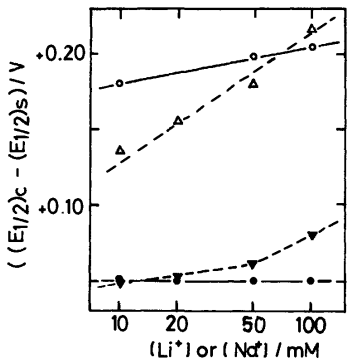

Fig. 6. Shifts in the half-wave potentials of cathodic waves of chloro-substituted acetic acids (1 mM) with the addition of alkali metal ions.
(○): Chloroacetic, Li^+, (△): chloroacetic, Na^+, (●): dichloroacetic, Li^+, (▼): dichloroacetic acid. Na^+. The total ionic strength is kept to be 0.1 M with Et_4NClO_4. See Fig. 2 for $(E_{1/2})_c$ and $(E_{1/2})_s$.

values of $\Delta E_{1/2}/\Delta\log[Li^+]$ are much smaller (40 or 50 mV) than 120 mV. Therefore, the species formed by the reaction between Li^+ and the conjugate base ($RCOO^-$) seems to be, at most, $RCOO^-Li^+$.

The slope of $\Delta E_{1/2}/\Delta\log[M^+]$ (M=Li and Na) were also small in value for chloro-substituted acetic acids, as Table 3 shows. Figure 6 illustrates the effect of Li^+ and Na^+ on the half-wave potentials of chloroacetic and dichloroacetic acids. In the case of dichloroacetic acid, the effect of Li^+ seems to be smaller than that of Na^+, judging from the potential at each concentration of M^+ and from the slope of $\Delta E_{1/2}/\Delta\log[M^+]$. Apparently, the interaction of Na^+ with the dichloroacetate ion is stronger than that of Li^+. This phenomenon may be explained by the difference in the degree of solvation between Li^+ and Na^+, and also by the weakness of the interaction of the dichloroacetate ion with the alkali-metal ions. A lithium ion will be solvated by pyridine more strongly than a sodium ion. We have found interaction between Li^+ and a monoamine as well as acyclic[14] and cyclic[15] polyamines in acetonitrile. The complexing of the lithium ion with pyridine was confirmed in acetonitrile.[16] It seems that the solvation of Li^+ by pyridine is so strong that the dichloroacetate ion cannot interact with Li^+ interact with Li^+ any more, for the basicity of the (dichloro)acetate ion is weakened by the substituted chlorine atoms.

Even the half-wave potentials of phenols were affected by the supporting-electrolyte cations (see Table 2). The interaction between a lithium ion and the anion from substituted phenol has been suggested on the basis of the UV and visible absorption spectra.[13]

We wish to express our thanks to Dr. Keiichi Tsuji of the Institute of Physical and Chemical Research for his helpful discussion. We would also like to thank Professor Kosuke Izutsu of Shinshu University for kind looking over the manuscript and for his valuable suggestions.

References

1) J. E. Hickey, M. S. Spritzer, and P. J. Elving, *Anal. Chim. Acta*, **35**, 277 (1966).
2) K. Tsuji and P. J. Elving, *Anal. Chem.*, **41**, 1571 (1969).
3) M. Hojo and Y. Imai, *Bunseki Kagaku*, **32**, E77 (1983).
4) M. Hojo and Y. Imai, *Bull. Chem. Soc. Jpn.*, **56**, 1963 (1983).
5) E. Itabashi, *J. Electroanal. Chem. Interfacial Electrochem.*, **36**, 179 (1972).
6) S. G. Mairanovskii, *Zh. Fiz. Khim.*, **33**, 691 (1959); J. Heyrovsky and J. Kuta, "Principles of Polarography," Academic Press, New York (1966), p. 416.
7) A. Cisak and P. J. Elving, *J. Electrochem. Soc.*, **110**, 160 (1963).
8) M. Asthana and L. M. Mukherjee, "Recommended Methods for Purification of Solvents and Tests for Impurities," ed by J. F. Coetzee, Pergamon Press, Oxford (1982), p. 44.
9) T. Fujinaga, S. Okazaki, and M. Hojo, *Bull. Inst. Chem. Res., Kyoto Univ.*, **56**, 139 (1978).
10) M. Hojo and Y. Imai, *Anal. Chem.*, **57**, 509 (1985).

11) M. E. Peover and J. D. Davies, *J. Electroanal. Chem.*, **6**, 46 (1963).
12) M. S. Spritzer, J. M. Costa, and P. J. Elving, *Anal. Chem.*, **37**, 211 (1965).
13) K. Tsuji and P. J. Elving, *Anal. Chem.*, **41**, 286 (1969).
14) M. Hojo and Y. Imai, *J. Electroanal. Chem. Interfacial Electrochem.*, **209**, 297 (1986).
15) M. Hojo and Y. Imai, *Anal. Sci.*, **1**, 185 (1985).
16) T. Nakamura, *Bull. Chem. Soc. Jpn.*, **48**, 1447 (1975).

 © 1987 The Chemical Society of Japan Bull. Chem. Soc. Jpn., 60, 517—523 (1987)

The Solubility of Benzene-Hydrocarbon Binary Mixtures in Water

Isao SANEMASA,* Yoshiko MIYAZAKI, Seiji ARAKAWA, Masaya KUMAMARU, and Toshio DEGUCHI
Department of Chemistry, Faculty of Science, Kumamoto University, Kurokami 2-39-1, Kumamoto 860
(Received July 21, 1986)

The solubility in water at 25.0 °C of benzene-hydrocarbon binary mixtures has been studied for different ratios between benzene and toluene, ethylbenzene, (*o*-, *m*-, *p*-)xylene, propylbenzene, chlorobenzene, and cyclohexane. Aqueous solutions saturated with mixed solutes were prepared by making use of the solute vapor. The solubility of individual constituent in the binary mixture was found to change linearly with mole fraction over a whole range of the composition. This is not the case for the benzene-cyclohexane system: the solubility of each component deviates positively from the linear change of solubility with composition. The solubility of each component of benzene-1-octanol mixture in water was also measured by adding the mixture of various compositions directly to water. The positive deviation for the solubility of each component was observed. The relationship between the 1-octanol/water partition coefficient of a solute and the aqueous solubility of pure liquid solute which forms a nonideal solution in 1-octanol was discussed.

We have previously reported a method of preparing aqueous solutions saturated with a solute such as benzene and alkylbenzenes.[1] The solute vapor in equilibrium with liquid solute is introduced into water and circulated in a closed system. The experimental characteristic of this method is that the equilibrium of the solute at different desired concentrations can be attained rapidly by adjusting the temperature of solute phase separated from aqueous phase, while the temperature of the aqueous phase is kept constant. We have demonstrated by this technique that the equilibrium solubility of sparingly soluble solutes in water changes linerly with the solute vapor pressure, in other words, the solubility obeys Henry's law.[1-3]

We will report further application of the method. Instead of changing the temperature of single liquid solute, mixed binary solutes of various compositions are used. The vapor pressure of the constituent solute varies with mole fraction in the mixed solute phase. The equilibrium solubility of each constituent is measured as a function of the mole fraction. We assume that Henry's law is applied to individual solute, because the concentration of solute in aqueous phase is usually very low. When Raoult's ideal solution law is held to mixed solute, the equilibrium solubility of the constituent solute in water is expected to be proportional to the mole fraction of solute mixture.

The solubility of a large variety of hydrocarbons has been extensively studied to accumulate data. There are, however, only a few reports concerning the aqueous solubility of mixed solutes in different composition. It is important to know what is the critical factor in determining the aqueous solubility of the constituent solute, because mixture of organic compounds rather than a solute is what we encounter in the natural aqueous environment, e.g., spilled oil on water surface.

The study of aqueous solubility of binary organic solutes is also important in considering partition of an organic solute in aqueous and organic phases. Partition coefficients of a number of chemicals in organic solvent and water, especially in 1-octanol/water system, have been extensively studied. The partition coefficient of the molecule is a measure of its relative solubility in two solvents; the coefficient has been determined under the condition that the solute concentration is extreamely low. When the solute forms a nonideal solution with organic solvent, we need to know how aqueous solubility of the solute changes with its concentration in the organic layer and what is the dominant factor in the aqueous solubility. Is there any solubilization effect of 1-octanol dissolved in water? The effect is probable only when there is an appreciable octanol-solute interaction in aqueous solution.[4] The benzene-1-octanol binary mixture was studied from interest in these problems.

Experimental

Materials. Deionized re-distilled water was used throughout this work. Benzene (99.5%), toluene (99%), ethylbenzene (98%), (*o*-, *m*-, and *p*-)xylene (each 98%), propylbenzene (97%), chlorobenzene (99%), cyclohexane (98%), and 1-octanol (95%) of analytical reagent grade with the minimum purity in the parentheses were used as solutes without further purification. When 1-octanol was used to prepare calibration curves for determining its concentrations in aqueous and benzene-1-octanol phases after equilibrium, 1-octanol was purified by distillation under reduced pressure.

Apparatus and Procedures. The apparatus used for preparing aqueous solutions saturated with solute vapor was essentially the same as that previously reported.[1]

The apparatus is composed of two main parts: A separatory funnel (300 cm^3) with a surrounding jacket and a pear-shaped flask (50 cm^3) which is immersed in a thermostated bath. We will call the former "solubility flask," and the latter "solute reservoir." These were connected to each other with Teflon or glass tubes. Water of 100 cm^3 and a binary liquid hydrocarbon mixture of 10 cm^3 were placed in the solubility flask and in the solute reservoir, respectively. The temperature of thermostated bath was kept at 25.0±0.1 °C, and that of solubility flask was also held at the same temperature by circulating water from the bath through surrounding jacket. The assembled apparatus was placed in a chamber, whose temperature was kept a little higher than 25 °C to avoid condensation of the solute vapor inside the apparatus. The solute vapor generated by bubbling air

through the solute reservoir via a sintered glass ball was introduced into the solubility flask by a Viton diaphragm airpump and was circulated at 1.5 dm^3 min^{-1}.

After the solubility equilibrium was attained (it takes 10 min), each 30 cm^3 portion of the aqueous solution was transferred successively by a stopcock attached to the bottom of solubility flask into three cylindrical separatory funnels of 50 cm^3 capacity, to which each 5 cm^3 volume of an extractant had been placed in advance. The organic extracts were analyzed by a Hitachi 164 gas chromatograph (column packing, PEG-1000; detector, hydrogen flame ionization). Cyclohexane or benzene was used as extractant; the latter was used only in the case of analyzing cyclohexane in benzene-cyclohexane system. A suitable volume of internal standard had been previously added to the extractant; *p*-xylene was used in benzene-toluene and benzene-cyclohexane systems, toluene in other systems.

The composition of mixed solute in the solute reservoir was analyzed in the following way. After the solubility equilibrium had been attained, a 5 cm^3 portion was pipetted off from the solute reservoir, diluted to 25 cm^3 with the same solvent used in extracting the solute from aqueous phase, and analyzed by gas chromatography. In this case, the solvent itself serves as an internal standard.

In the case of benzene-1-octanol system, an aqueous solution saturated with 1-octanol was not obtaied by the solute vapor circulation technique mentioned above. Then, each 60 cm^3 of mixed solute of various compositions was added to water (200 cm^3) in a 360 cm^3 glass bottle with a stopper and equilibrated by stirring overnight with a Teflon-enclosed magnet in a thermostated bath at 25.0±0.1 °C. The bottle was designed to make it easy to take out the aqueous solution through a stopcock attached to bottle side near the bottom. The solutes in 20 cm^3 portions of the aqueous solution were extracted with cyclohexane containing an internal standard and analyzed by gas chromatography. As the internal standard, toluene was used to analyze benzene and 1-hexanol to analyze 1-octanol. The solute phase after equilibrium was also analyzed by gas chromatography to determine the composition. A 5 cm^3 portion of the solute phase was taken out of the bottle and diluted to 25 cm^3 with cyclohexane which serves as internal standard.

Results

The Time Required for Attaining the Solubility Equilibrium. Aqueous solution to be saturated with solute vapor reached equilibrium with each solute of the binary mixture after 10 min at a circulation rate of vapor of 1.5 dm^3 min^{-1} (Fig. 1). In the case of benzene-1-octanol system, it was also confirmed that overnight stirring of the aqueous phase with the mixed solute solution is sufficient to attain equilibrium with each solute.

The Composition of Binary Solute Mixture and Solubility of Component Solutes in Water. The solubility of component solutes of binary mixture in water at 25.0 °C is given in Tables 1 to 3 and shown in Figs. 2 to 5 as a function of mole fraction of the component.

A single component solubility in water at 25.0 °C determined by circulating the solute vapor was 2.07×10^{-2} (benzene), 5.65×10^{-3} (toluene), 1.37×10^{-3} (ethylbenzene), 1.68×10^{-3} (*o*-xylene), 1.33×10^{-3} (*m*-xylene), 1.51×10^{-3} (*p*-xylene), 4.15×10^{-4} (propylbenzene), 3.78×10^{-3} (chlorobenzene), and 6.27×10^{-4} mol dm^{-3} (cyclohexane) and that determined by adding liquid solute directly to water was 2.22×10^{-2} (benzene) and 4.11×10^{-3} mol dm^{-3} (1-octanol). These values are in reasonable agreement with our previous estimations and with literature values.[1,5,6]

Discussion

The Technique to Prepare Aqueous Solutions Saturated with Solutes. Two techniques were used to prepare aqueous solutions saturated with solute: the circulation of solute vapor and the direct addition of liquid solute into water. The solubility of benzene determined by the latter technique was about 10% higher than that obtained by the former one. It is difficult at present to explain this discrepancy, but we suppose that the direct contact of liquid solute with water is liable to overestimated solubility due to formation of solute micro-emulsion dispersed in aqueous solution. The former technique being applied to the benzene-1-octanol system, the aqueous phase was saturated with benzene after circulation for 15 min, while the 1-octanol-saturated solution was not obtained even after 5 h at the same circulation rate. We first thought that the vapor circulation technique is inadequate for this system, because water dissolved in 1-octanol during circulation may prevent vaporization of 1-octanol (the solubility of water in 1-octanol is considerably high). Then, we tried to saturate water with 1-octanol vapor as follows; nitrogen gas was made to flow through the reservoir containing 1-octanol purified by distillation via a sintered glass ball or a glass capillary and introduced into the solubility flask. This technique, which we call the open method, gave aqueous solutions saturated with various solutes in the previous work.[1] In the case of 1-octanol, however, the

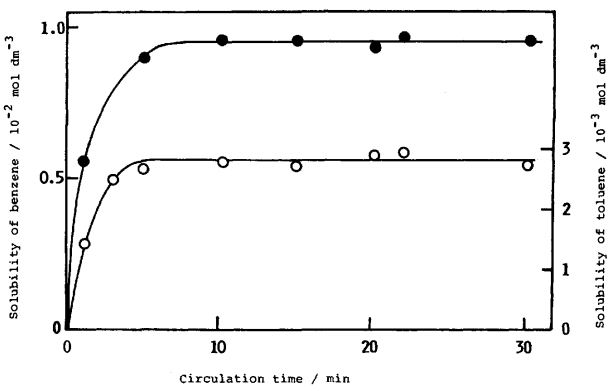

Fig. 1. The effect of the mixed solute vapor circulation time on the constituent solute solubility in water. The aqueous solubilities of benzene (●) and toluene (○) at 25°C. Mole fraction of benzene in the binary mixture is set at 0.48.

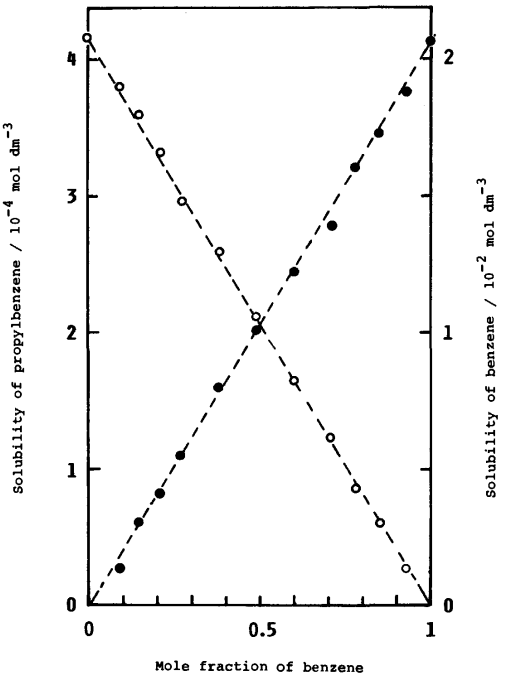

Fig. 2. Benzene-propylbenzene binary system. Aqueous solubilities of benzene (●) and propylbenzene (○) at 25°C as a function of the solute composition in the binary mixture.

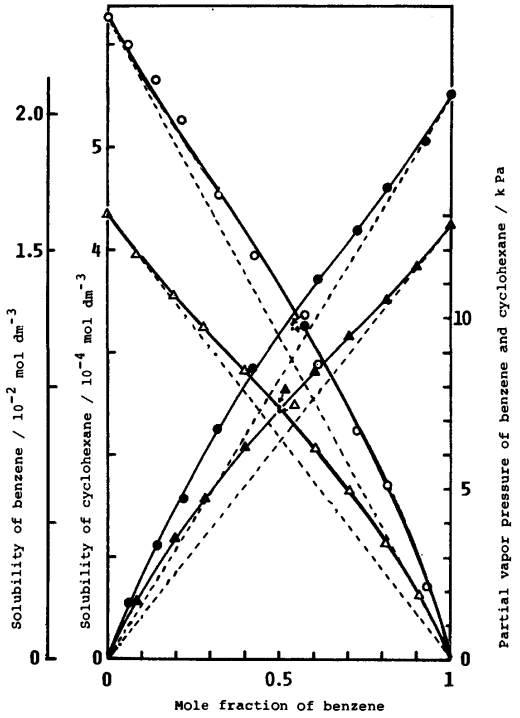

Fig. 4. Benzene-cyclohexane binary system. Aqueous solubilities of benzene (●) and cyclohexane (○) at 25°C and partial vapor pressures of benzene (▲) and cyclohexane (△) at 25°C as a function of the solute composition in the binary mixture (the vapor pressure data taken from Ref. 12).

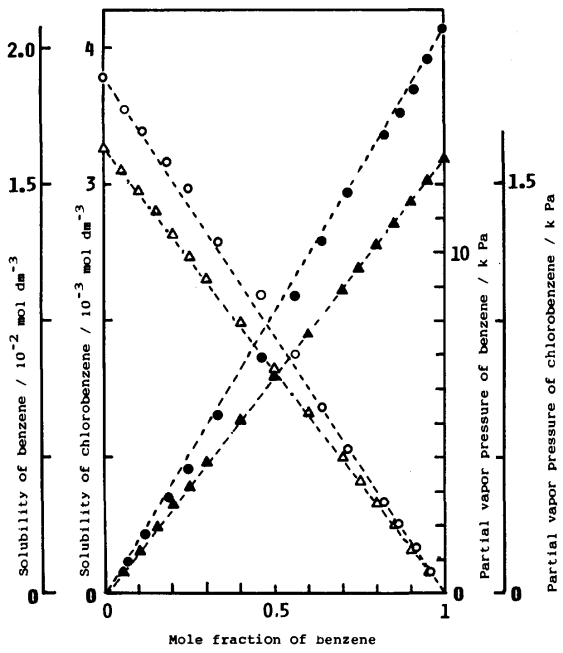

Fig. 3. Benzene-chlorobenzene binary system. Aqueous solubilities of benzene (●) and chlorobenzene (○) at 25°C and partial vapor pressures of benzene (▲) and chlorobenzene(△) at 25°C as a function of the solute composition in the binary mixture (the vapor pressure data taken from Ref. 10).

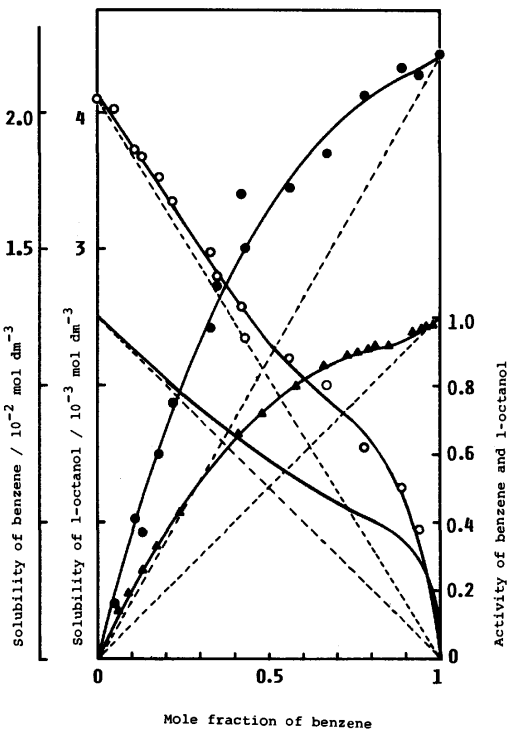

Fig. 5. Benzene-1-octanol binary system. Aqueous solubilities of benzene (●) and 1-octanol (○) at 25°C and activities of benzene(▲) and 1-octanol (△) at 20°C as a function of the solute composition in the binary mixture (the activity data taken from Ref. 14).

Table 1. Benzene-Toluene, -Ethylbenzene, -*o*-Xylene, -*m*-Xylene, -*p*-Xylene, -Propylbenzene, and -Chlorobenzene Binary Mixed Solute Solutions, the Aqueous Solubilities of Benzene and the Hydrocarbons at 25°C as a Function of the Solute Composition in the Binary Mixtures

Mole fraction		Solubility/ 10^{-3} mol dm^{-3}		Mole fraction		Solubility/ 10^{-3} mol dm^{-3}	
C_6H_6	The other component	C_6H_6	The other component	C_6H_6	The other component	C_6H_6	The other component
				0.565	0.435	10.9	1.76
	Benzene-Toluene			0.640	0.360	12.9	1.40
0	1.000	0	5.65	0.717	0.283	14.7	1.07
0.040	0.960	0.750	5.20	0.826	0.174	16.8	0.679
0.170	0.830	3.50	4.60	0.867	0.133	17.4	0.507
0.290	0.710	6.50	3.66	0.915	0.085	18.5	0.344
0.440	0.560	8.40	3.29	0.957	0.043	19.6	0.170
0.497	0.503	9.50	2.74	1.000	0	20.7	0
0.618	0.382	13.1	2.16				
0.673	0.327	13.4	1.83		Benzene-ethylbenzene		
0.702	0.298	14.2	1.67	0	1.000	0	1.37
0.833	0.167	17.4	0.959	0.147	0.853	2.86	1.18
0.916	0.084	18.1	0.459	0.268	0.732	5.02	1.03
1.000	0.000	20.7	0	0.384	0.616	7.42	0.857
				0.486	0.514	9.26	0.715
	Benzene-*o*-xylene			0.570	0.430	11.4	0.571
0	1.000	0	1.68	0.660	0.340	13.2	0.458
0.076	0.924	1.52	1.57	0.742	0.258	15.4	0.329
0.135	0.865	3.03	1.42	0.800	0.200	16.7	0.244
0.243	0.757	5.56	1.24	0.888	0.112	18.4	0.122
0.392	0.608	8.12	1.03	1.000	0	20.7	0
0.473	0.527	10.3	0.869				
0.576	0.424	12.2	0.721		Benzene-*m*-xylene		
0.695	0.305	14.4	0.537	0	1.000	0	1.33
0.768	0.232	16.4	0.391	0.072	0.928	1.56	1.21
0.831	0.169	17.9	0.264	0.139	0.861	3.05	1.18
0.923	0.077	19.8	0.129	0.208	0.792	4.15	1.03
1.000	0	20.7	0	0.268	0.732	5.23	0.974
				0.322	0.678	6.60	0.878
	Benzene-*p*-xylene			0.385	0.615	7.84	0.839
0	1.000	0	1.51	0.494	0.506	10.1	0.681
0.079	0.921	1.45	1.38	0.594	0.406	12.1	0.548
0.151	0.849	2.87	1.28	0.687	0.313	13.7	0.423
0.265	0735	5.44	1.11	0.773	0.227	16.4	0.337
0.400	0.600	7.92	0.914	0.854	0.146	17.9	0.201
0.495	0.505	9.97	0.775	0.929	0.071	19.4	0.104
0.580	0.420	12.1	0.629	1.000	0	20.7	0
0.690	0.310	14.1	0.498				
0.773	0.227	15.6	0.344		Benzene-propylbenzene		
0.853	0.147	17.5	0.236	0	1.000	0	0.415
0.914	0.086	19.0	0.113	0.086	0.914	1.37	0.379
0.958	0.042	20.3	0.0630	0.146	0.854	3.00	0.360
1.000	0	20.7	0	0.204	0.796	4.08	0.332
				0.266	0.734	5.47	0.297
	Benzene-chlorobenzene			0.375	0.625	7.97	0.259
0	1.000	0	3.78	0.489	0.511	10.1	0.211
0.068	0.932	1.16	3.55	0.598	0.402	12.2	0.164
0.114	0.886	2.20	3.39	0.706	0.294	13.9	0.123
0.185	0.815	3.51	3.16	0.776	0.224	16.1	0.0866
0.247	0.753	4.57	2.97	0.842	0.158	17.3	0.0600
0.334	0.666	6.57	2.58	0.925	0.075	18.8	0.0270
0.463	0.537	8.71	2.19	1.000	0	20.7	0

aqueous solution obtained in this manner was far from saturation even after 6 h at the aeration rate ranging from 0.02 to 1.5 dm^3 min^{-1}. Thus, the possibility that water in 1-octanol may prevent 1-octanol from vaporizing can be excluded. Different cause should be sought.

Concerning with the vapor circulation technique, it should be mentioned that, as was pointed out in the previous paper,[2] the liquid solute in the reservoir will gradually be in equilibrium with water during the

Table 2. Benzene-Cyclohexane Binary Mixed Solute Solution, the Aqueous Solubility and Henry's law Coefficient at 25 °C

Mole fraction		Solubility/ 10^{-3} mol dm^{-3}		Vapor pressure[a]/ kPa		K_H[b]/ 10^4 kPa	
C_6H_6	C_6H_{12}	C_6H_6	C_6H_{12}	C_6H_6	C_6H_{12}	C_6H_6	C_6H_{12}
0	1.000	0	0.627	0	13.01	—	115
0.067	0.933	2.10	0.601	1.348	12.18	3.57	113
0.149	0.851	4.26	0.567	2.768	11.21	3.61	110
0.222	0.778	5.92	0.528	3.873	10.33	3.62	109
0.325	0.675	8.40	0.455	5.253	9.27	3.48	113
0.424	0.576	10.7	0.393	6.438	8.136	3.33	115
0.541	0.459	12.0	0.323	7.727	6.946	3.58	119
0.612	0.388	14.0	0.288	8.468	6.129	3.36	118
0.725	0.275	15.8	0.222	9.636	4.809	3.38	120
0.814	0.186	17.3	0.171	10.57	3.451	3.39	112
0.924	0.076	19.0	0.073	11.79	1.475	3.45	112
1.000	0	20.7	0	12.71	0	3.41	—

a) The vapor pressure at desired mole fraction was estimated based on the data presented in Ref. 12. b) Henry's law coefficient: K_H=(vapor pressure in Pa)/(solubility in mole fraction).

Table 3. Benzene-1-Octanol Binary Mixed Solute Solution, the Aqueous Solubility at 25 °C, the Activity at 20 °C, and the Ratio

Mole fraction		Solubility/ 10^{-3} mol dm^{-3}		Activity[a]		Ratio[b] 10^3	Ratio[b] 10^4
C_6H_6	1-Octanol	C_6H_6	1-Octanol	C_6H_6	1-Octanol	C_6H_6	1-Octanol
0	1.000	0	4.11	—	1.00	—	1.35
0.048	0.952	2.06	4.02	0.112	0.954	3.02	1.32
0.106	0.894	5.07	3.73	0.207	0.905	2.27	1.35
0.178	0.822	7.53	3.52	0.332	0.838	2.44	1.32
0.219	0.781	9.33	3.36	0.394	0.799	2.35	1.32
0.329	0.671	12.1	2.98	0.548	0.706	2.51	1.32
0.352	0.648	13.6	2.79	0.580	0.686	2.37	1.37
0.435	0.565	15.0	2.35	0.676	0.624	2.50	1.48
0.559	0.441	17.2	2.19	0.780	0.540	2.52	1.37
0.666	0.334	18.6	2.01	0.853	0.477	2.55	1.32
0.780	0.220	20.7	1.55	0.913	0.413	2.45	1.48
0.894	0.106	21.6	1.26	0.954	0.329	2.45	1.45
0.942	0.058	21.3	0.953	0.965	0.278	2.52	1.62
1.000	0	22.2	0	1.00	—	2.50	—

a) The activity at 20 °C was evaluated at desired mole fraction from the activity vs. mole fraction curve illustrated in Ref. 14. b) The ratio of the activity at 20 °C to the aqueous solubility at 25 °C in mole fraction.

vapor circulation, and hence, the solute phase is no longer "pure" binary system. Yet we can neglect the contribution of water to the partial vapor pressure of constituent solute in the binary mixture, because the solubility of water in liquid hydrocarbons used in this study is as low as 3×10^{-3} in mole fraction.[7]

The Aqueous Solubility of Two Solutes Which Form Ideal or Near-Ideal Binary Mixtures. The solubility of the constituent solutes in the seven binary mixtures, benzene-toluene, -ethylbenzene, -(*o*-, *m*-, *p*-) xylene, -propylbenzene, and -chlorobenzene, changed almost linearly with its mole fraction over a whole range of the composition. Assuming that Henry's law holds for the dissolution of each component in water, the linear relationship between the aqueous solubility and the solute mole fraction indicates that the solute forms an ideal or nearly ideal solution with benzene.[8] In such a system, the solubility of the solute at any composition can be easily estimated by multiplying unit solubility by mole fraction of the component. It should be emphasized, however, that the mixed solute solution cannot be taken at once as being ideal, because an experimental error of 5% or so is inevitable in the solubility determinations. For instance, chlorobenzene does not form ideal solution with benzene.[9,10] Data in the literature[10] on the relationship between vapor pressure and mole fraction at 25 °C are plotted for each component in Fig. 3. The maximum deviations of vapor pressure from Raoult's law, 1.65% for chlorobenzene and 0.65% for benzene, both positive, occur at 0.5 mole fraction. The same positive deviations cannot be expected from the present study unless the accuracy of solubility measurements is improved.

The Aqueous Solubility of Two Solutes Which Form Non-Ideal Binary Mixtures. In the cases of benzene–cyclohexane and -1-octanol, the plots of the aqueous solubility of a component vs. the composition of binary solute mixture exhibit noticeable deviations from linear relationship. This arises from nonideality of these mixed solute solutions. It is well-known that benzene forms nonideal solution with cyclohexane.[11,12] We can evaluate the activity coefficients for cyclohexane, γ_a, and for benzene, γ_b, at respective mole fraction, X_a and X_b, by the equation,[13] $RT \ln \gamma_{a(b)} = X_{b(a)}^2[A_0 - A_1(1-4X_{a(b)}) + A_2(1-8X_{a(b)}+12X_{a(b)}^2)]$; the constants, A_0, A_1, and A_2 for each component are determined from the data presented in Ref. 12 to be 1318.8, −42.95, and 38.31 (cyclohexane) and 1312.9, −44.19, and 54.77 (benzene), respectively. The partial vapor pressure of the component, P_i, is expressed as $P_i = X_i\gamma_i P_i^\circ$, where X_i, γ_i, and P_i° is the mole fraction of component in the liquid solute mixture, the activity coefficient, and the pure solute vapor pressure, respectively. Figure 4 shows the partial vapor pressure as a function of the mole fraction. The solubility curve appears to be similar in shape to the corresponding vapor pressure curve. For a quantitative consideration, the ratio of the partial pressure to the equilibrium solubility in water for each component at the same mole fraction in binary mixture was determined (the ratio refers to Henry's law coefficient). We can see from Table 2 that the ratio is almost constant over a whole range of the mixed solute composition. This indicates that Henry's law is valid to the aqueous solubility of the constituent.

With respect to the benzene–1-octanol binary system, the activity of each component at 20 °C is available,[14] and literature data are plotted in Fig. 5. The activity and solubility curves for the corresponding component appear to resemble each other: both the activity and the solubility of 1-octanol change almost linearly in higher mole fraction region of 1-octanol and decrease steeply in its lower mole fraction region, while those of benzene exhibit large positive deviations from the postulated ideal linear lines in higher mole fraction region of benzene. However, as can be seen from Table 3 where ratios of the activity at 20 °C to the solubility at 25 °C are given, large discrepancies are noticeable for benzene and 1-octanol in each lower mole fraction region. These discrepancies may be attributable partly to inaccuracy of solubility measurements. It is doubtful, however, whether the activity determined in the absence of water is applicable to the present case. The water content in 1-octanol amounts to 0.25 mole fraction.[6] Yet the activity of each solute seems to dominate the aqueous solubility of benzene–1-octanol binary mixture.

The 1-Octanol/Water Partition and Aqueous Solubility of the Solute Which Forms Non-Ideal Solution with 1-Octanol. Chiou et al. have suggested a "solubilization" effect of 1-octanol;[15] the solubility of a solute in water which has been saturated with 1-octanol is larger than that in 1-octanol-free water. Miller et al., on the other hand, have demonstrated using polynuclear aromatic hydrocarbons and polychlorinated biphenyls that the presence of dissolved 1-octanol in water has little effect on the solubility of the substances in water.[4] Considerably low solubility in 1-octanol-saturated water is apparent in their data, though the authors did not mention it. This is presumably caused by the state of organic substances. The 1-octanol present saturated in water is transferred in part to the organic substances in the solid state. Then, the organic substance is no longer pure one-component system, that is, the mole fraction becomes lower than unity. This may be responsible for low solubility of the organic substances in 1-octanol-saturated water.

Our present results support Miller et al. The positive deviation of solubility of benzene in water from the ideal solubility line observed for the benzene–1-octanol system is not due to the solubilization effect by 1-octanol, but is caused by the formation of a nonideal solution from benzene and 1-octanol.

The 1-octanol/water partition coefficient, $K_{o/w}$, is commonly defined as

$$k_{o/w} = C_o/C_w, \tag{1}$$

where C_o and C_w denote the molar concentration of solute in 1-octanol saturated with water and that in water saturated with 1-octanol, respectively. Considering mutual solubility of 1-octanol and water, an equation which correlates the partition coefficient with the solubility of pure liquid solute in water, S, was proposed by Chiou et al.[15] as follows:

$$\log K_{o/w} = -\log S - \log \bar{V}^{o*} - \log \gamma_o^* + \log(\gamma_w^*/\gamma_w), \tag{2}$$

where $\bar{V}^{o*}$ is the partial molar volume of 1-octanol saturated with water, γ_o^* is the activity coefficient of the solute in 1-octanol saturated with water, and γ_w^* and γ_w refer to the activity coefficient of the solute in water saturated with 1-octanol and that in pure water, respectively. This equation is derived based on the assumption that the solute concentrations both in aqueous and 1-octanol phases are sufficiently low.

For various liquid solutes, especially for homologous series, the log $K_{o/w}$ vs. −log S plots have been found to be linear with inclinatios close to unity.[16] There have been published, however, some experimental data which clearly display the slopes significantly lower than unity.[4,15,16] Chiou et al. assumed that the solubilization effect of 1-octanol in water is one of the reasons of significantly lower inclination than the ideal value of −1.[15] We will propose the viewpoint that the liquid solute forms a nonideal mixed solution with 1-octanol. Let us consider the case of benzene–1-octanol. The $K_{o/w}$ of benzene, which is the reverse of tangent of aqueous solubility vs. solute concentration

in 1-octanol curve at infinitely diluted with 1-octanol, is not constant, but depends on the composition of octanol phase. In practice, $K_{o/w}$ is to be measured at a definite solute composition, and $K_{o/w}$ value thus determined is always larger than that expected under infinitely diluted condition. This causes the inclination of log $K_{o/w}$ vs. $-\log S$ plot to be smaller than unity. The circumstances are reversed when the solubility of the solute in water deviates negatively from the ideal solubility. The solute composition in 1-octanol should, therefore, be as low as possible, especially in such a case that the solute-1-octanol mixed solution is far from being ideal.

The Solvent Extraction and Aqueous Solubility of the Solute to be Extracted. When the solvent extraction is considered in general under the conditions that mutual solubility of extractant and water is low and further that the solute concentration in extractant and in water is sufficiently low, Eq. 2 can be written in the form;

$$\log K_{org/w} = -\log S - \log V^{org} - \log \gamma_{org}, \quad (3)$$

where $K_{org/w}$ is the partition coefficient of the solute between organic extractant and aqueous phase, V^{org} is the molar volume of pure extractant, and γ_{org} refers to the activity coefficient of the solute in pure extractant. Combining Eq. 1 with Eq. 3, we can derive $\%E$, the extraction percentage of the solute from an aqueous phase of v_w dm^3 to an organic phase of v_{org} dm^3,

$$\%E = 100/(1 + S\, V^{org} \gamma_{org} v_w v_{org}^{-1}). \quad (4)$$

This equation is useful in predicting the degree of extraction of the solute at a definite volume ratio of aqueous phase to organic phase with known values of solubility in water of pure solute to be extracted, the molar volume of pure extractant, and the solute activity coefficient in extractant. It should be emphasized that the $\%E$ depends on whether the extractant-solute system deviates positively or negatively from Raoult's law.

References

1) I. Sanemasa, M. Araki, T. Deguchi, and H. Nagai, *Bull. Chem. Soc. Jpn.*, **55**, 1054 (1982).

2) I. Sanemasa, S. Arakawa, M. Araki, and T. Deguchi, *Bull. Chem. Soc. Jpn.*, **57**, 1539 (1984).

3) I. Sanemasa, *Bull. Chem. Soc. Jpn.*, **48**, 1795 (1975); I. Sanemasa, T. Kobayashi, C. Y. Piao, and T. Deguchi, *ibid.*, **57**, 1352 (1984); I. Sanemasa, S. Arakawa, C. Y. Piao, and T. Deguchi, *ibid.*, **58**, 3033 (1985).

4) M. M. Miller, S. P. Wasik, G. L. Huang, W. Y. Shiu. and D. Mackay, *Environ. Sci. Technol.*, **19**, 522 (1985).

5) L. J. Andrews and R. M. Keefer, *J. Am. Chem. Soc.*, **71**, 3644 (1949); L. J. Andrews and R. M. Keefer, *J. Am. Chem. Soc.*, **72**, 3113 (1950); K. Kinoshita, H. Ishikawa, and K. Shinoda, *Bull. Chem. Soc. Jpn.*, **31**, 1081 (1958); D. Mackay, A. Bobra, W. Y. Shiu, and S. H. Yalkowsky, *Chemosphere*, **9**, 701 (1980); S. P. Wasik, M. M. Miller, Y. B. Tewari, W. E. May, W. J. Sonnefeld, H. DeVoe, and W. H. Zoller, *Residue Reviews*, **85**, 30 (1983); A. L. Horvath, "IUPAC Solubility Data Series, Vol. 20," ed by A. L. Horvath and F. W. Getzen, Pergamon, Oxford (1985), pp. 153—182 (chlorobenzene).

6) G. T. Hefter, "IUPAC Solubility Data Series, Vol. 15," ed by A. F. M. Barton, Pergamon, Oxford (1984), pp. 364—367 (1-octanol).

7) J. Polak and B. C.-Y. Lu, *Can. J. Chem.*, **51**, 4018 (1973).

8) J. Gmehling, U. Onken, and W. Arlt, "Vapor-liquid Equilibrium Data Collection, Aromatic Hydrocarbons. Chemistry Data Series Vol. I, Part 7," DECHEMA (Deutsche Gesellschaft für Chemisches Apparatewesen), Frankfurt (1980). It can be seen from the literature data cited in this data book that the benzene-toluene and -*m*-xylene make ideal systems, while the benzene-ethylbenzene, -*p*-xylene, and -propylbenzene make near ideal systems.

9) R. K. Nigam and N. N. Maini, *Indian J. Chem.*, **10**, 197 (1972); M. Diazpena, A. Compostizo, A. Crespo Colin, and I. Escudero, *J. Chem. Thermodyn.*, **13**, 869 (1981).

10) J. R. Khurma, O. Muthu, S. Munjal, and B. D. Smith. *J. Chem. Eng. Data.* **28**, 100 (1983); H. C. Van Ness and B. D. Smith, *Int. Data Ser., Selec. Data Mixtures. Ser., A*, **1983**, 181.

11) G. Scatchard, S. E. Wood, and J. M. Mochel, *J. Phys. Chem.*, **43**. 119 (1939); E. R. Brewster and M. L. McGlashan, *J. Chem. Soc., Faraday Trans. 1*, **69**, 2046 (1973); G. Arich. I. Kikic, and P. Alessi, *Chem. Eng. Sci.*, **30**, 187 (1975); W. J. Green and H. S. Frank, *J. Solution Chem.*, **8**, 187 (1979), A. Tasić, B. Djordjević, D. Grozdanić, N. Afgan, and D. Malić, *Chem. Eng. Sci.*, **33**, 189 (1978); R. A. Mentzer. R. A. Greenkorn, and K. C. Chao, *J. Chem. Thermodyn.*, **14**, 817 (1982).

12) T. Nitta, T. Akimoto, A. Matsui, and T. Katayama, *J. Chem. Eng. Jpn.*, **16**, 352 (1983).

13) "Shin Jikken Kagaku Kôza, Vol. 2," ed by The Chemical Society of Japan, Maruzen, Tokyo (1977), p. 403.

14) R. F. Platford, *J. Solution Chem.*, **5**, 645 (1976).

15) C. T. Chiou, D. W. Schmedding, and M. Manes, *Environ. Sci. Technol.*, **16**, 4 (1982).

16) S. C. Valvani, S. H. Yalkowsky, and T. J. Roseman. *J. Pharm. Sci.*, **70**. 502 (1981); Y. B. Tewari, M. M. Miller, S. P. Wasik, and D. E. Martire, *J. Chem. Eng. Data*, **27**, 451 (1982).

17) M. M. Miller, S. Ghodbane, S. P. Wasik, Y. B. Tewari, and D. E. Martire, *J. Chem. Eng. Data*, **29**, 184 (1984).

 © 1987 The Chemical Society of Japan Bull. Chem. Soc. Jpn., 60, 525—530 (1987)

Synthesis, Characterization, and Optical Resolution of Electrically Neutral Octahedral Cobalt(III) Complexes Containing the Tetradentate Ligand

Hiroshi NAKAZAWA, Hisaka OHTSURU, and Hayami YONEDA*
Department of Chemistry, Faculty of Science, Hiroshima University, Hiroshima 730
(Received July 28, 1986)

Three geometrical isomers of [Co(edda)(aa)] where edda=*N',N*-ethylenediaminediacetato, aa=glycinato (gly), β-alaninato (β-ala), have been synthesized and characterized. They have been completely resolved into the enantiomers, except *unsym-cis-fac*-[Co(edda)(β-ala)], by the bis(μ-*d*-tartrato)diantimonate(III) anion, $[Sb_2(d\text{-tart})_2]^{2-}$, form of QAE-Sephadex resin with water as the eluent, and their absolute configurations have been determined based upon the circular dichroism spectra. It has been revealed that the Δ enantiomer is favored more by $[Sb_2(d\text{-tart})_2]^{2-}$ than the Λ enantiomer irrespective of the kind of the geometrical isomers. Consideration on the mechanism of the optical resolution has been presented.

The optical resolution of electrically neutral transition metal complexes is difficult, compared with that of cationic or anionic metal complexes, because they do not form diastereomers with an optically active resolving agent. Chromatographic technique is very effective to achieve the optical resolution of such neutral complexes.[1] Some neutral complexes have been reported to be partially resolved into the enantiomers; *cis*-[Co(dimethylglyoximato)$_2$(NH_3)Cl] by using a quartz powder column,[2] *mer*- and *fac*-[Co(gly)$_3$], and *s-cis-mer*-[Co(edda)(gly)] by using a potato starch column,[3] where gly and edda stand for glycinato and *N,N'*-ethylenediaminediacetato, respectively. The first complete resolution of neutral complexes was reported in 1976 by Yoneda for *fac*-[Co(β-ala)$_3$] (β-ala=β-alaninato) on the Na^+ form of CM-Sephadex cation exchanger with an ethanol-water solution of sodium *d*-tartrate, Na_2(d-tart), as the eluent.[4] Thereafter, the complete resolution of a series of enantiomeric pairs of *fac*-[Co(D/L-ser)$_{3-n}$(β-ala)$_n$] (n=0 to 3, ser=serinato) was achieved on Na^+ form of TSK-211 cation exchanger with sodium bis(μ-*d*-tartrato)diantimonate(III), Na_2-$[Sb_2(d\text{-tart})_2]$, aqueous solution as the eluent.[5] An anion-exchange column has also been indicated to be useful to resolve neutral complexes into enantiomers. Two series of enantiomeric pairs of *fac*-[Co(gly)$_{3-n}$(β-ala)$_n$] and *fac*-[Co(D/L-α-ala)$_{3-n}$(β-ala)$_n$] were completely resolved on the $[Sb_2(d\text{-tart})_2]^{2-}$ form of TSK-220 anion exchanger with water as the eluent.[6] Complete resolution of the meridional isomer of tris(amino acidato)-cobalt(III) complexes has also been achieved. After success of optical resolution of *mer*-[Co(β-ala)$_3$],[7] enantiomeric pairs of *mer*-[Co(gly)$_3$] and *mer*-[Co(D/L-α-ala)$_3$] were resolved on the $[Sb_2(d\text{-tart})_2]^{2-}$ form of QAE-Sephadex resin with water as the eluent.[8]

Neutral complexes, other than tris(amino acidato)-complexes, have also been tried to be resolved. Tris-(acetylacetonato)transition-metal complexes, [M-(acac)$_3$] (M=Cr, Co, Rh, Ru) were partially resolved by the use of a *d*-lactose column[9] or a quartz column[10] and [M(acac)$_3$] (M=Cr, Co, Ru) and [M(gly)$_{3-n}$(acac)$_n$] (n=3 to 1) were also partially resoluved on a Δ-[Ni(phen)$_3$]-montmorillonite column (phen=1,10-phenanthroline).[11] Recently, [Co(acac)$_3$] and [Cr-(acac)$_3$] were completely resoluved by HPLC on a (+)-poly(triphenylmethyl methacrylate) column.[12]

Neutral complexes completely resolved so far into enantiomers are limited only to tris-chelates. We report here the complete resolution of neutral complexes containing a tetradentate ligand by column chromatography. As such complexes, we chose [Co(edda)(gly)] and [Co(edda)(β-ala)]. For both complexes, there are three geometrical isomers shown in Scheme 1.

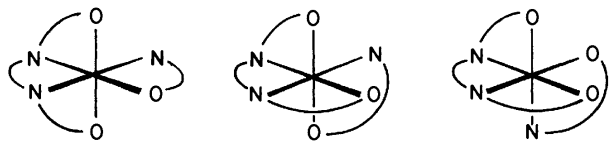

Scheme 1.

Experimental

General Remarks. *N,N'*-Ethylenediaminediacetic acid (H_2edda), glycine (Hgly), β-alanine (H-β-ala) were commercially available and were used without further purification. Na[Co(edda)(CO_3)]·1.5H_2O,[13] Co^{II}(edda),[14] and *s-cis-mer*-[Co(edda)(gly)][15] were prepared according to the literature methods. Absorption (AB) and circular dichroism (CD) spectra were recorded on a Shimadzu UV 200 and a JASCO J-40CS, respectively.

Synthesis and Separation of the Isomers of *u-cis-mer* and *u-cis-fac*-[Co(edda)(gly)]. To a solution of 4.00 g (0.012 mol) of Na[Co(edda)(CO_3)]·1.5H_2O in 30 cm^3 of water was added 0.90 g (0.012 mol) of glycine. The solution was heated to 50 °C, and 7.5 cm^3 of HCl aqueous solution containing 1.0 cm^3 of concentrated HCl was added dropwise. The heating was continued for 5 h. Then, the solution was filtered. The filtrate was placed on an anion-exchange column (Dowex 1-X8, Cl^- form) and eluted with water to remove any residual starting material or anionic products. The eluate was evaporated under an air stream to 10 cm^3 and again filtered to remove the s-cis-mer isomer. The filtrate was placed on a cation-exchange column (SP-Sephadex C-25, Na^+ form) and

washed through with water. The color materials separated into two bands, a blue-violet band and a slower moving red-violet band. The u-cis-mer isomer (1.2 g, 32%) and u-cis-fac isomer (1.0 g, 24%) were obtained from the first and the second eluted bands as crystals by concentration, respectively.

Found: C, 29.55; H, 5.09; N, 13.34%. Calcd for *u-cis-mer*-$[CoC_8H_{14}N_3O_6]\cdot 0.5H_2O$: C, 30.39; H, 4.78; N, 13.29%.

Found: C, 27.82; H, 5.07; N, 12.39%. Calcd for *u-cis-fac*-$[CoC_8H_{14}N_3O_6]\cdot 2H_2O$: C, 27.99; H, 5.29; N, 12.24%.

Synthesis of *s-cis-mer*-[Co(edda)(β-ala)]. The complex was prepared in the manner similar to that of the glycine analog. To 500 cm^3 of an aqueous solution containing 4.66 g (0.020 mol) of Co^{II}(edda) were added 2.00 g of activated charcoal and 1.78 g (0.020 mol) of β-alanine. A stream of air was passed through the suspended solution for ca. 8 h. Then, the solution was heated at 60 °C for 30 min. The charcoal was removed by filtration and washed with hot water several times. The filtrate and washings were combined, which were heated on a stream bath almost to dryness. Purple crystals were deposited as a crude product (2.3 g, 35%). The purple product (1.1 g, 17%) for elemantal analysis was obtained by recrystallization from hot water.

Found: C, 32.26; H, 5.16; N, 12.79%. Calcd for $[CoC_9H_{16}N_3O_6]\cdot 0.5H_2O$: C, 32.74; H, 5.19; N, 12.73%.

Synthesis and Separation of the Isomers of *u-cis-mer* and *u-cis-fac*-[Co(edda)(β-ala)]. The synthesis and separation were identical with that of the glycine analog except it was carried out using 1.13 g (0.013 mol) of β-alanine. Yield of the u-cis-mer isomer was 1.2 g (18%), and that of the u-cis-fac isomer was 1.0 g (15%).

Found: C, 32.56; H, 5.37; N, 12.57%. Calcd for *u-cis-mer*-$[CoC_9H_{16}N_3O_6]\cdot 0.5H_2O$: C, 32.74; H, 5.19; N, 12.73%.

Found: C, 32.20; H, 4.75; N, 12.48%. Calcd for *u-cis-fac*-$[CoC_9H_{16}N_3O_6]\cdot 0.5H_2O$: C, 32.74; H, 5.19; N, 12.73%.

Optical Resolution by Ion-Exchange Chromatography. A column of 1.0 cm inner diameter was filled with 82.5 cm length of QAE-Sephadex A-25 (anion exchanger) which had been treated with 0.1 mol aqueous solution of $K_2[Sb_2(d\text{-tart})_2]$. About 20 mg of each sample prepared in this paper was dissolved in ca. 2 cm^3 of water and the solution was loaded on the column. The elution was done with water at a flow rate 7.8×10^{-2} $cm^3\,min^{-1}$. The void volume was measured to be 30.9 cm^3 by using $[Fe(phen)_3]Cl_2$ (phen=1,10-phenanthroline) as a marker. An automatic fraction collector was connected to the end of the column to divide the eluate into fractions of 4 cm^3. The AB spectrum of each fraction was measured. Thus, the retention volumes were determined. Two fractions in which the concentration of the separated enantiomers was highest were passed through QAE-Sephadex A-25 (Cl^- form) with water as the eluent to remove $[Sb_2(d\text{-tart})_2]^{2-}$. The eluates obtained were subjected to AB and CD measurments.

Results and Discussion

Preparation and Assignment of Geometrical Isomers. *s-cis-mer*-[Co(edda)(gly)] complex was prepared from Co^{II}(edda), obtained from $CoCO_3$ and Ba(edda), and glycine according to the literature method.[15] The geometrical isomers of [Co(edda)(diamine)]$^+$ and [Co(edda)(L)] (L=gly, L-ala) prepared from Co^{II}(edda) were assigned exclusively to trans and s-cis-mer, respectively according to the absorption spectra and ^1H NMR spectra.[14,15] Therefore, [Co(edda)(β-ala)] prepared from Co^{II}(edda) and β-alanine can be thought to have s-cis-mer configuration. The similar absorption spectrum to that of *s-cis-mer*-[Co(edda)(gly)] also supports the s-cis-mer configuration. The purity was checked by elemental analysis and column chromatography.

The reaction of $Na[Co(edda)(CO_3)]$, prepared from $Na_3[Co(CO_3)_3]$ and H_2edda, with glycine produced the mixture of u-cis-mer and u-cis-fac isomers of [Co(edda)(gly)]. Although s-cis-mer isomer was also formed in this reaction as a minor product, it could be readily removed by filtration because of its low solubility in water. The two u-cis isomers were separated by pass-

Table 1. Absorption and Circular Dichroism Data of [Co(edda)(aa)]

Complex	Absorption Max./nm (ε)	Circular Dichroism Max./nm ($\Delta\varepsilon$)[a]
s-cis-mer-[Co(edda)(gly)]	542 (116) 470 sh 372 (133)	542 (−5.35) 465 (+2.17)
u-cis-mer-[Co(edda)(gly)]	525 (94) 370 (128)	543 (−2.48) 465 (+0.97)
u-cis-fac-[Co(edda)(gly)]	520 (223) 374 (167)	523 (−1.12)
s-cis-mer-[Co(edda)(β-ala)]	560 sh 505 (113) 374 (122)	550 (−3.67) 477 (+2.31)
u-cis-mer-[Co(edda)(β-ala)]	590 sh 505 (83) 373 (90)	553 (−1.58) 477 (+1.09)
u-cis-fac-[Co(edda)(β-ala)]	523 (252) 374 (147)	560 (−)[b] 500 (+)

a) For Δ-enantiomer. b) Partially resolved.

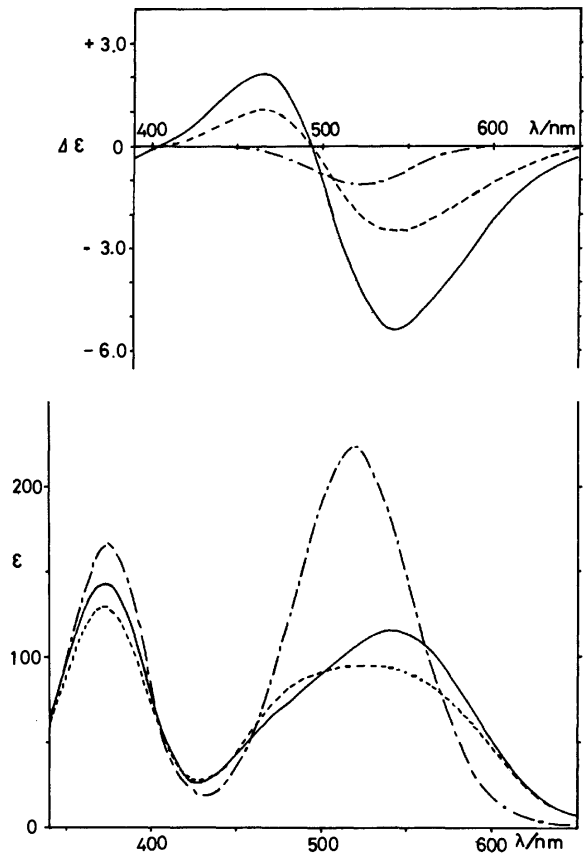

Fig. 1. Absorption spectra (below) and circular dichroism spectra (above) of *Δ*-[Co(edda)(gly)]; s-cis-mer (——), u-cis-mer (----), u-cis-fac (-·-·-).

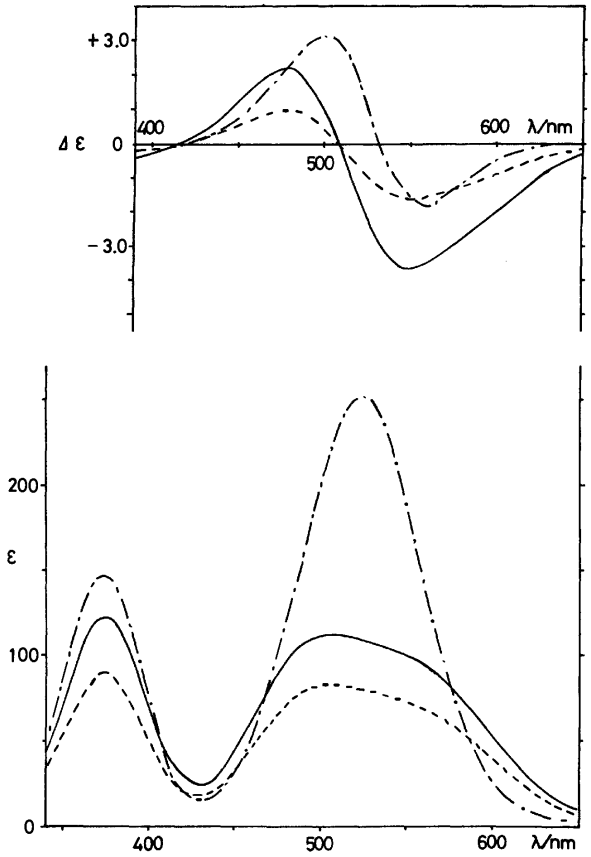

Fig. 2. Absorption spectra (below) and circular dichroism spectra (above) of *Δ*-[Co(edda)(β-ala)]; s-cis-mer (——), u-cis-mer (----), u-cis-fac(-·-·-). The scale is arbitrary for the u-cis-fac isomer due to the partial resolution.

ing through the SP-Sephadex C-25 column. The first eluted isomer was assigned to u-cis-mer and the second one to u-cis-fac, according to the reason mentioned below. The u-cis-mer and u-cis-fac isomers of [Co(edda)(β-ala)] were obtained in the manner identical with that of [Co(edda)(gly)].

The absorption (AB) and circular dichroism (CD) data of the neutral complexes prepared in this paper are given in Table 1. Figures 1 and 2 show the AB and CD spectra. The ligand field symmetry of the u-cis-fac isomer is higher than that of the u-cis-mer isomer. The decrease in symmetry from facial to meridional is expected to cause a splitting or at least a broadening of the lowest energy absorption band in the visible spectra. In [Co(edda)(gly)], broadening is obviously observed in the low-energy absorption band for the first eluted isomer. In [Co(edda)(β-ala)], a marginal shoulder is found for the first eluted isomers. In contrast, the second eluted isomers of [Co(edda)(gly)] and [Co(edda)-(β-ala)] exhibit a relatively sharp absorption band. Therefore, the first and the second eluted isomers for both [Co(edda)(gly)] and [Co(edda)(β-ala)] can be assigned to the u-cis-mer and u-cis-fac isomers, respectively. The similar assignment based upon the absorption spectra was done with respect to *u-cis-fac* and *u-cis-mer*-[Co(edda)(L-ala)] isomers.[13]

The assignment is consistent with the chromatographic behavior. Although both isomers are electrically neutral, the facial isomer has a greater dipole moment than the meridional isomer. Thus, the former is considered to interact more effectively with the functional group of SP-Sephadex C-25 cation exchanger than the later. Therefore, the facial isomer is expected to be eluted later than the meridional one. Such tendency has been actually observed (vide infra, see Table 2).

Circular Dichroism Spectra and Absolute Configurations. The partial optical resolution of *s-cis-mer*-[Co(edda)(gly)] has been attained and its absolute configuration has been established.[15] The CD spectrum of the *Λ* configuration consists of a dominant positive band at lower energy and a minor negative band at higher energy in the first d-d transition region. The sign of the dominant peak in the first d-d transition region of the CD spectrum can generally be related to the net chirality of the complex.[16,17] A *Δ* configuration of chelate rings is expected to produce a negative dominant peak in the d-d transition region while a *Λ* configuration would produce a positive dominant peak.[16] This argument has been applied to [Co(edda)(diamine)]$^{+}$[13] and *s-cis-mer*-[Co(edda)(aa)] (aa=gly, L-ala).[15] The CD spectra shown in Figs. 1 and 2 are

Table 2. Adjusted Retention Volumes and Separation Factors

Complex	Adjusted Retention Volume/cm³ First	Second	Separation Factor
s-cis-mer-[Co(edda)(gly)]	55.6 (*Λ*)[a]	63.6 (*Λ*)	1.14
u-cis-mer-[Co(edda)(gly)]	56.1 (*Λ*)	64.6 (*Λ*)	1.15
u-cis-fac-[Co(edda)(gly)]	197.1 (*Λ*)	221.1 (*Λ*)	1.12
s-cis-mer-[Co(edda)(*β*-ala)]	47.9 (*Λ*)	53.1 (*Λ*)	1.13
u-cis-mer-[Co(edda)(*β*-ala)]	45.1 (*Λ*)	53.1 (*Λ*)	1.17
u-cis-fac-[Co(edda)(*β*-ala)]	151.6[b]		—

a) Absolute configuration. b) Partial separation.

quite resemble to those of $[Co(edda)(diamine)]^+$ and *s-cis-mer*-[Co(edda)(aa)] (aa=gly, L-ala), although a minor positive band at higher energy is not observed in the case of *u-cis-fac*-[Co(edda)(gly)]. Therefore, the criterion to assign the absolute configuration from the sign of the CD spectra in the first d-d transition region should also be applicable to the u-cis-mer and u-cis-fac isomers of [Co(edda)(gly)] and [Co(edda)(*β*-ala)].

The CD spectra in Figs. 1 and 2 are for the second eluted enantiomers in the chromatographic separation. Since these CD spectra except that for *u-cis-fac*-[Co(edda)(*β*-ala)] comprise a dominant negative peak at lower energy and a minor positive peak at higher energy, the absolute configuration can be assigned to *Λ*. In the case of *u-cis-fac*-[Co(edda)(*β*-ala)], although the positive peak at higher energy is slightly greater than the negative peak at lower energy in intensity in its CD spectrum, it is highly likely that the absolute configuration is *Λ* from the quite similar CD pattern to those for the other complexes shown in Figs. 1 and 2.

Optical Resolution by Chromatography. The optical resolution was carried out by passing the neutral complexes through the $[Sb_2(d\text{-tart})_2]^{2-}$ form of QAE-Sephadex resin with water as the eluent. We chose $[Sb_2(d\text{-tart})_2]^{2-}$ as a resolving agent because $[Sb_2(d\text{-tart})_2]^{2-}$ is known to a very effective chiral selector not only for cationic transition metal complexes[1,18] but also for neutral complexes.[5-8] Water was used as the eluent in the present experiment. To obtain a good results, attention should be paid to the flow rate when neutral complexes are subjected to column chromatography in order to be resolved into enantiomers; the small flow rate seems to cause the better resolution. In the present experiment about 12 to 47 h, depending on complexes, were spent for each run. Two bands were clearly separated for every complex except for *u-cis-fac*-[Co(edda)(*β*-ala)]. The examination of the CD spectra of the eluates proved that the first eluted enantiomers have the *Λ* configurations (vide supra). In the case of *u-cis-fac*-[Co(edda)(*β*-ala)], though only one peak was obtained in the elution curve, the front and the rear fractions exhibited the enantiomeric CD spectra, indicating that the partial resolution was attained. The enantiomer in the front fraction had the *Λ* configuration. In the present chromatographic run, the chiral selector, $[Sb_2(d\text{-tart})_2]^{2-}$, was held in the stationary phase. Thus the second eluted enantiomer can be considered to have the greater affinity to $[Sb_2(d\text{-tart})_2]^{2-}$ than the first eluted enantiomer. For all neutral complexes examined in this paper, the *Λ* isomer is favored more by $[Sb_2(d\text{-tart})_2]^{2-}$ than the *Λ* isomer.

Before obtaining the adjusted retention volumes, the void volume of the column should be determined. Selection of a marker for determining the void volume is sometime difficult.[19] At first, we chose Blue Dextran 2000 as a marker since it is generally used for cation-exchange resin. However, it proved to be unsuitable because the band of Blue Dextran 2000 broadened considerably. Since QAE-Sephadex anion exchanger prevents to select anionic compounds as a marker, a cationic complex, $[Co(en)_3]Cl_3$, was used. This trial was, however, unsuccessful because it caused precipitation. The use of $[Cu(en)_2]Cl_2$ caused the greater retention volume than those of the neutral complexes. Finally, $[Fe(phen)_3]Cl_2$ proved to be a good marker to determine the retention volume of the QAE-Sephadex column. Since Sephadex contains many hydrophilic functional groups, $[Fe(phen)_3]^{2+}$ having hydrophobic ligands is presumed to have no significant interaction with the stationary phase. The resulting void volume, 30.9 cm³, may be a reasonable value, because the same void volume was obtained for SP-Sephadex-C25 cation-exchange column with the same diameter and length by using Blue Dextran as a marker, where QAE-Sephadex and SP-Sephadex resin used here have the same particle size.

The adjusted retention volumes and separation factors are listed in Table 2. For both the glycine and the *β*-alanine complexes, the retention volumes of the facial isomers are three to four times as large as those of the meridional isomers. This can be attributed to the greater dipole moment of the fac isomers. Between s-cis-mer and u-cis-mer isomers, there is no significant difference in the retention volumes. Comparison with the glycine and the *β*-alanine complexes in the same geometrical isomers reveals that the value for the glycine complex is greater than that for the *β*-alanine complex without exception. This tendency may be general because of the observation of the trend among tris(amino acidato)cobalt(III) complexes.[6,8] The

Table 3. Lists of Neutral Complexes Completely Resolved with $[Sb_2(d\text{-tart})_2]^{2-}$ Anion

Complex	Favorable enantiomer with $[Sb_2(d\text{-tart})_2]^{2-}$	Separation Factor	Reference[c]
fac-[Co(D/L-ser)$_3$]	Λ-D[a]	1.702	5
	Δ-D	1.510	5
fac-[Co(D/L-ser)$_2$(β-ala)]	Λ-D	1.349	5
	Δ-D	1.193	5
fac-[Co(D/L-ser)(β-ala)$_2$]	Λ-D	1.189	5
	Λ-L	1.060	5
fac-[Co(β-ala)$_3$]	Λ	1.060	5
fac-[Co(β-ala)$_3$]	Λ	1.152[b]	6
fac-[Co(β-ala)$_2$(gly)]	Λ	1.566[b]	6
fac-[Co(β-ala)(gly)$_2$]	Λ	1.456[b]	6
fac-[Co(gly)$_3$]	Λ	1.474[b]	6
fac-[Co(β-ala)$_2$(α-ala)]	Λ-D	1.293[b]	6
	Λ-L	1.323[b]	6
fac-[Co(β-ala)(α-ala)$_2$]	Λ-D	1.423[b]	6
fac-[Co(α-ala)$_3$]	Λ-D	1.993[b]	6
mer-[Co(gly)$_3$]	Δ	1.138	8
mer-[Co(β-ala)$_3$]	Δ	1.175	7, 8
mer-[Co(D/L-α-ala)$_3$]	Δ-L	1.512	8
	Δ-D	1.089	8
s-cis-mer-[Co(edda)(gly)]	Δ	1.14	This work
u-cis-mer-[Co(edda)(gly)]	Δ	1.15	This work
u-cis-fac-[Co(edda)(gly)]	Δ	1.12	This work
s-cis-mer-[Co(edda)(β-ala)]	Δ	1.13	This work
u-cis-mer-[Co(edda)(β-ala)]	Δ	1.17	This work

a) Λ and D stand for the configuration around Co(III) metal and of the amino acid ligand, respectively. This chromatographic separation was carried out for the enantiomeric pair of Λ-D and Δ-L. b) The values were calculated based upon the original data though these data are not shown in the literature. c) Brief chromatographic conditions: on Na^+ form of TSK-211 cation exchanger with $Na_2[Sb_2(d\text{-tart})_2]$ aqueous solution for Ref. 5; on $[Sb_2(d\text{-tart})_2]^{2-}$ form of TSK-220 anion exchanger with water for Ref 6; on $[Sb_2(d\text{-tart})_2]^{2-}$ form of QAE-Sephadex anion exchanger with water for Refs. 7, 8, and this work.

comparison among the separation factors in Table 2 reveals that there is no obvious defference (from 1.12 to 1.17).

Mechanistic Consideration of Optical Resolution. Table 3 summarizes the neutral complexes completely resolved so far with $[Sb_2(d\text{-tart})_2]^{2-}$, together with the absolute configuration of the favorable enantiomer with the chiral anion, and the separation factors. As can be seen, with respect to the facial tris(amino acidato)-cobalt(III) complexes, the Λ enantiomers are favored unless two or more functional groups (hydroxyl groups) exist in the chelate rings, while the Δ enantiomers are favored in the case of the meridional complexes. This trend is kept for *mer*-[Co(edda)(aa)] complexes. However, it is not held for *fac*-[Co(edda)(aa)].

We have proposed the L-J model as a stereoselective ion-association model between a metal complex cation and $[Sb_2(d\text{-tart})_2]^{2-}$ anion.[1,20] The L-shaped channel was defined in the previous papers as the L-shaped opening between chelate rings, and the J-shaped channel as the mirror images of the L-shaped chennel. The optically active $[Sb_2(d\text{-tart})_2]^{2-}$ anion can associate intimately with that enantiomer of a metal complex cation that has the L-shaped channel, but cannot associate closely with the enantiomer that has only the J-shaped channel. In the case of *fac*-[Co(aa)$_3$], the Λ enantiomer has L-shaped channels in a position where $[Sb_2(d\text{-tart})_2]^{2-}$ anion is able to access electrostatically. Recently, the stereoselective ion-association model which is modefied and refined the L-J model has been proposed.[21] The model also suggests that the $[Sb_2(d\text{-tart})_2]^{2-}$ anion produces a favorable pair with the Λ enantiomer of the tris-chelate than with the Δ enantiomer. Thus, it is clear that the Λ enantiomer is favored by $[Sb_2(d\text{-tart})_2]^{2-}$ in homo and hetero facial tris(amino acidato)cobalt(III) neutral complexes. The chromatographic behaviour of *u-cis-fac*-[Co(edda)(aa)] that the Δ enantiomer makes an intimate pair with $[Sb_2(d\text{-tart})_2]^{2-}$ seems to be peculiar. However, the complex has neither L-shaped nor J-shaped channel. Although why the Δ enantiomer is favored more with the chiral anion and how the anion discriminates the enantiomers are not clear at present, we think this result is providing some clues about the chiral discrimination.

In meridional isomers, the Δ enantiomer is favored more by $[Sb_2(d\text{-tart})_2]^{2-}$ exclusively. Let us consider the reason. *mer*-[Co(aa)$_3$] is electrically neutral as a whole, but there is charge localization. It can be thought that the oxgen donor atom possesses a slightly negative charge and nitrogen donor atom does a slightly positive charge. From the pure electrostatic point of view, the most probable direction of the access

toward *mer*-[Co(aa)$_3$] for the [Sb$_2$(*d*-tart)$_2$]$^{2-}$ is considered to be the one indicated by arrow 0 in Scheme 2(A). However, the anion coming along this direction can not recognize the chirality of the complex because it touches the complex at only NH_2 group shown as N_E in Scheme 2(A). Next electrostatically favored access for the [Sb$_2$(*d*-tart)$_2$]$^{2-}$ is either one of the directions indicated by arrow 1 and 2. Although the two approaches are slightly different, they allow the anion to touch the complex at two NH_2 groups, N_E-N_S for arrow 1 and N_E-N_N for arrow 2. Then the anion can discriminate the absolute configuration of the complex. We consider that either one or both these two association modes 1 and 2, seem to play an important role in chiral discrimination.

u-cis-mer-[Co(edda)(aa)], Scheme 2(B), corresponds to the complex that N_E and N_S of the *mer*-[Co(aa)$_3$] are connected by a CH_2CH_2 bridge. The bridging of CH_2CH_2 group between N_E and N_N of complex (A) produces *s-cis-mer*-[Co(edda)(aa)], complex (C). The ethylene bridge between N_E and N_S precludes the access of [Sb$_2$(*d*-tart)$_2$]$^{2-}$ from the direction of arrow 1, and that between N_E and N_N prevents the access of the chiral selector from the direction of arrow 2. The two isomers, *u-cis-mer* and *s-cis-mer*-[Co(edda)(aa)], are presumed to accept the oncoming anion only through either one of the two association modes 1 and 2.

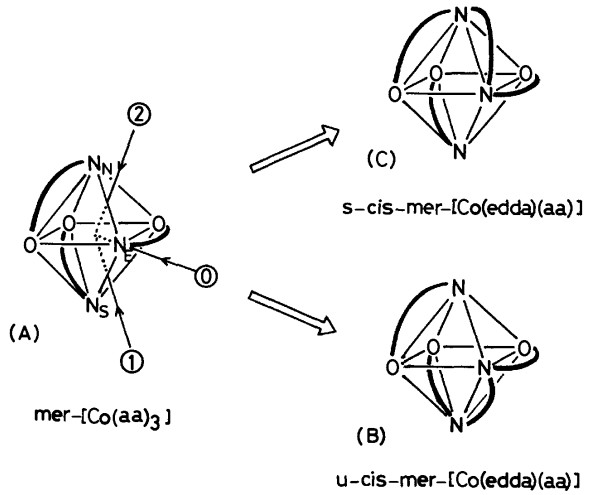

Scheme 2.

The retention volumes and the separation factors of the two isomers for both the glycine and β-alanine complexes exhibit no significant difference. Moreover, these separation factors are almost equal to those of *mer*-[Co(gly)$_3$] and *mer*-[Co(β-ala)$_3$]. Therefore, we can conclude that the two association models 1 and 2 are equally effecive on the chiral discrimination in *mer*-[Co(aa)$_3$] with using [Sb$_2$(*d*-tart)$_2$]$^{2-}$ as a resolving agent and only one mode is enough for complete resolution.

References

1) a) H. Yoneda, *J. Chromatogr.*, **313**, 59 (1985); b) H. Yoneda, *J. Liq. Chromatogr.*, **2**, 1157 (1979).
2) R. Tsuchida, M. Kobayashi, and A. Nakamura, *Bull. Chem. Soc. Jpn.*, **11**, 38 (1936).
3) a) H. Krebs and R. Rasche, *Z. Anorg. Allg. Chem.*, **276**, 236 (1954); b) B. E. Douglas and S. Yamada, *Inorg. Chem.*, **4**, 1561 (1965); c) J. I. Legg, D. W. Cooke, and B. E. Douglas, *Inorg. Chem.*, **6**, 700 (1967).
4) H. Yoneda and T. Yoshizawa, *Chem. Lett.*, **1976**, 707.
5) S. Yamazaki, T. Yukimoto, and H. Yoneda, *J. Chromatogr.*, **175**, 317 (1979).
6) T. Yukimoto and H. Yoneda, *J. Chromatogr.*, **22**, 477 (1981).
7) S. Yamazaki and H. Yoneda, *Inorg. Nucl. Chem. Lett.*, **15**, 195 (1979).
8) H. Yoneda, T. Yukimoto, Y. Kushi, and H. Nakazawa, *J. Liq. Chromatogr.*, **9**, 573 (1986).
9) a) T. Moeller and E. Gulyas, *J. Inorg. Nucl. Chem.*, **5**, 245 (1958); b) J. P. Collman, R. P. Blair, R. L. Marshall, and L. Slade, *Inorg. Chem.*, **2**, 576 (1963); c) R. C. Fay, A. Y. Girgis, and U. Klabunde, *J. Am. Chem. Soc.*, **92**, 7056 (1970).
10) T. S. Piper, *J. Am. Chem. Soc.*, **83**, 3908 (1961).
11) a) A. Yamagishi, *J. Chem. Soc., Chem. Commun.*, **1981**, 1168; b) A. Yamagishi, R. Ohnishi, and M. Soma, *Chem. Lett.*, **1982**, 85; c) A. Yamagishi, *Inorg. Chem.*, **21**, 3393 (1982); d) A. Yamagishi and R. Ohnishi, *Inorg. Chem.*, **21**, 4233 (1982).
12) Y. Okamoto, S. Honda, E. Yashima, and H. Yuki, *Chem. Lett.*, **1983**, 1221.
13) L. Halloran and J. I. Legg, *Inorg. Chem.*, **13**, 2193 (1974).
14) J. I. Legg and D. W. Cooke, *Inorg. Chem.*, **4**, 1576 (1965).
15) J. I. Legg, D. W. Cooke, and B. E. Douglas, *Inorg. Chem.*, **6**, 700 (1967).
16) A. J. McCaffery, S. F. Mason, and B. J. Norman, *J. Chem. Soc.*, **1965**, 5094.
17) J. I. Legg and B. E. Douglas, *J. Am. Chem. Soc.*, **88**, 2697 (1966).
18) Y. Yoshikawa and K. Yamasaki, *Coord. Chem. Rev.*, **28**, 205 (1979).
19) S. Yamazaki and H. Yoneda, *J. Chromatogr.*, **169**, 400 (1979).
20) a) H. Nakazawa and H. Yoneda, *J. Chromatogr.*, **160**, 89 (1978); b) H. Nakazawa, U. Sakaguchi, and H. Yoneda, *J. Chromatogr.*, **213**, 323 (1981).
21) a) K. Miyoshi, S. Izumoto, and H. Yoneda, *Bull. Chem. Soc. Jpn.*, **59**, 3475 (1986); b) K. Miyoshi, S. Izumoto, K. Nakai, and H. Yoneda, submitted for publication.

 © 1987 The Chemical Society of Japan Bull. Chem. Soc. Jpn., 60, 531—538 (1987)

Calorimetric and Spectrophotometric Studies of Chloro Complexes of Nickel(II) and Zinc(II) Ions in *N,N*-Dimethylformamide

Shin-ichi Ishiguro,* Kazuhiko Ozutsumi, and Hitoshi Ohtaki†
Coordination Chemistry Laboratories, Institute for Molecular Science, Myodaiji, Okazaki 444
†Department of Electronic Chemistry, Tokyo Institute of Technology at Nagatsuta, Nagatsuta, Midori-ku, Yokohama 227
(Received August 4, 1986)

Complexation of Ni(II) and Zn(II) with Cl^- ions has been studied by calorimetry and spectrophotometry in *N,N*-dimethylformamide (DMF) containing 0.4 mol dm^{-3} $(C_2H_5)_4NClO_4$ as a constant ionic medium at 25 °C. Calorimetric titration curves obtained in each system were well-explained in terms of formation of $[MCl_n]^{(2-n)+}$ (n=1—4 and M^{2+}=Ni^{2+} or Zn^{2+}), and their formation constants, enthalpies and entropies were determined. Formation of the nickel(II) chloro complexes in DMF was also supported by spectrophotometry. In the nickel(II) chloride system, the stepwise enthalpy ΔH_3° and entropy ΔS_3° values are remarkably large and positive as compared with the ΔH_n° and ΔS_n° (n=1, 2, and 4) values. Individual electronic spectra of nickel(II) ion, $[NiCl]^+$ and $[NiCl_2]$ are significantly different in both intensities and peak positions from those of $[NiCl_3]^-$ and $[NiCl_4]^{2-}$ over the range 300—850 nm. These thermodynamic and spectrophotometric results were explained in terms of formation of the octahedral $[NiCl]^+$ complex as well as $[Ni(dmf)_6]^{2+}$ and of formation of the tetrahedral $[NiCl_3]^-$ and $[NiCl_4]^{2-}$ complexes in DMF. On the other hand, in the zinc(II) chloride system, the ΔS_n° (n=1 and 2) values are large and positive, but the ΔS_n° (n=3 and 4) values are significantly small. The corresponding ΔH_n° (n=1 and 2) values are positive but the ΔH_n° (n=3 and 4) values are significantly negative. It is thus postulated that the $[ZnCl_n]^{(2-n)+}$ (n=2 and 3) complexes have the tetrahedral coordination structure as well as the $[ZnCl_4]^{2-}$ complex in DMF.

In previous papers, we reported complexation between copper(II) and chloride ions in *N,N*-dimethylformamide (DMF),[1] acetonitrile[2] and dimethyl sulfoxide (DMSO),[3] and in acetonitrile-DMF mixtures[4] by calorimetry and spectrophotometry. The complexation between copper(II) and chloride ions is markedly enhanced in these aprotic solvents as compared with that in water, which may mainly be ascribed to weaker solvent-solvent interactions in the former solvents than in the latter, as already noted by Ahrland.[5] The coordination structure around copper(II) ion changes in the course of the complexation of the metal ion with chloride ions, and the distorted octahedral $[Cu(dmf)_6]^{2+}$ and $[CuCl(dmf)_5]^+$ complexes and the distorted tetrahedral $[CuCl_3(dmf)]^-$ and $[CuCl_4]^{2-}$ complexes are formed in DMF according to an X-ray diffraction study.[6]

It has been established from measurements of electronic spectra of the tetrahalogenonickelate(II) complexes that they have the tetrahedral structure both in crystal and in solution.[7-9] The tetrahedral $[NiCl_4]^{2-}$ ion is slightly distorted in $(R_4N)_2NiCl_4$ (R=CH_3 or C_2H_5) but almost regular in the triphenylmethylarsonium compound.[10,11] The tetrahedral $[ZnCl_4]^{2-}$ entity has also been found in M_2ZnCl_4 (M^+=K^+, Rb^+ and Cs^+) crystals,[12-16] in $ZnCl_2$-KCl melts[17] and in a highly concentrated zinc(II) chloride aqueous solution.[18] Complexation between nickel(II) and halide ions has so far been studied by spectrophotometry in some aprotic solvents.[19,22] However, no quantitative result of their formation constants and enthalpies has been obtained in aprotic solvents. On the other hand, complexation of zinc(II) with halide ions has been well studied by potentiometry and calorimetry in DMSO,[23,24] although no reliable result has been reported in other aprotic solvents.[25]

Although the donicity of DMF and DMSO is not significantly different,[26] we pointed out in a previous paper[3] that the complexation of copper(II) with chloride ions is markedly weaker in DMSO than in DMF due to stronger solvent-solvent interactions in the bulk of the former. In this respect, DMF can be a better solvent than DMSO for studying weak complexation of metal ions such as nickel(II) and zinc(II) with chloride ions.

In this work, we therefore investigated complexation of Ni(II) and Zn(II) with chloride ions in DMF by calorimetry and spectrophotometry using similar procedures to those employed in previous works,[1-4] and thermodynamic quantities of formation of the metal chloro complexes were determined. Electronic spectra of individual nickel(II) chloro complexes in DMF were also estimated. On the basis of the thermodynamic and spectrophotometric results, changes in the coordination structure around nickel(II) and zinc(II) ions in the course of the complexation in DMF are discussed.

Experimental

Reagent. *Nickel(II) perchlorate DMF solvate* was obtained by dissolving nickel(II) perchlorate hexahydrate crystals in DMF and then by repeatedly recrystallizing from DMF in order to remove water, and was finally isolated by recrystallizing them from a 50% v/v DMF-acetone mixture. *Zinc(II) perchlorate DMF solvate* was prepared from zinc(II) perchlorate hexahydrate crystals by the similar procedure to that used for preparing nickel(II) perchlorate DMF solvate and was finally obtained by recrystallizing them from acetone. Each of nickel(II) and zinc(II) perchlorate DMF solvates thus prepared was dried at about 40 °C in a vacuum oven for several days and kept in a desiccator over P_2O_5. The value of x within $[M(ClO_4)_2 \cdot (dmf)_x]$ (M^{2+}=Ni^{2+} or Zn^{2+}) was found to be 6, as already noted by Schneider,[27] which

was confirmed by gravimetry using dimethylglyoxime and by titration with EDTA for nickel(II) and zinc(II) perchlorate DMF solvates, respectively.

Tetraethylammonium perchlorate and *tetraethylammonium chloride* of reagent grade were once recrystallized from water and dried at 100 °C.

N,N-Dimethylformamide was dried for several weeks over molecular sieves 4A 1/16 and then distilled at 40 °C under a reduced pressure (260 Pa) and stored over the molecular sieves in a dark bottle with a P_2O_5 drying-tube.

Measurements. Calorimetric and spectrophotometric measurements were carried out in a room thermostated at (25.0±0.2) °C. All test solutions prepared contained 0.4 mol dm^{-3} $(C_2H_5)_4NClO_4$ as a constant ionic medium.

Calorimetric measurements were performed in a thermostated water-bath controlled at (25.000±0.007) °C. 100 cm^3 of a metal perchlorate DMF solution was placed in a Dewar vessel which was filled with dry nitrogen gas and prevented from moisture with a P_2O_5 drying-tube, and then it was titrated with 0.4 mol dm^{-3} $(C_2H_5)_4NCl$ DMF solution. The concentration of metal ions in the initial test solution was varied over the range 5—15 and 5—20 mmol dm^{-3} for nickel(II) and zinc(II) ions, respectively. Heats of complexation observed at each titration point were ranged 1—5 J with a certainty ±0.05 J and were corrected for heats of dilution of the titrant which were determined in advance by separate experiments by titrating a 0.4 mol dm^{-3} $(C_2H_5)_4NClO_4$ DMF solution with the 0.4 mol dm^{-3} $(C_2H_5)_4NCl$ titrant solution. All of the measurements were carried out by using a fully automatic on-line system for calorimetry developed in our laboratory.[28] Details of the data treatment have been described elsewhere.[2,3]

Electronic spectra were measured with a HITACHI 340 spectrophotometer (HITACHI) equipped with a PC-9801F2 computer (NEC) which recorded data every 2 nm over the wavelength range 300—850 nm. A flow cell with a light-path length of 0.5 cm was connected with a titration vessel through Teflon and glass tubes. 20 cm^3 of a metal perchlorate solution was placed in a vessel under a dry nitrogen atmosphere and then titrated with the 0.4 mol dm^{-3} $(C_2H_5)_4NCl$ titrant solution.

Results and Discussion

Nickel(II) Chloro Complexes. Calorimetric titration curves obtained in the nickel(II) chloride system with varying concentrations of the metal ion are depicted in Fig. 1. In the figure, enthalpies $\Delta H^\circ = -q/(\delta v C_{X,tit})$ were plotted against C_X/C_M, where q, δv, C_X and C_M stand for the heat evolved, the volume of an aliquot of the titrant added and the concentrations of chloride and nickel(II) ions in solution, respectively, at each titration point, and $C_{X,tit}$ denotes the concentration of chloride ion in the titrant solution.

Complexation between nickel(II) and chloride ions in DMF is rather weak because, as seen in Fig. 1, the titration curves were strongly dependent on the concentration of nickel(II) ion in the solutions and appreciable endothermicities were still observed at $C_X/C_M>10$. The enthalpy ΔH° in each titration curve first decreased with increasing C_X/C_M and then increased after passing through a minimum. Each titration curve showed a maximum value around $C_X/C_M=3—7$ and then decreased to approach $\Delta H^\circ=0$.

The calorimetric data were analyzed by assuming the formation of plausible sets of nickel(II) chloro complexes and by simultaneously optimizing their formation constants and enthalpies by the least-squares method, the results being summarized in

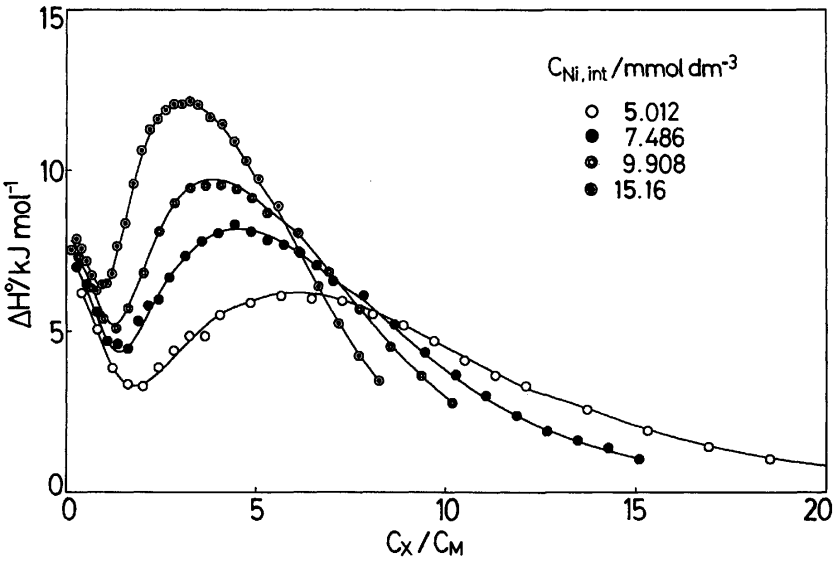

Fig. 1. Calorimetric titration curves of nickel(II) chloride DMF solutions containing 0.4 mol dm^{-3} $(C_2H_5)_4NClO_4$ at 25°C. Concentrations of nickel(II) ions, $C_{Ni,int}$/mmol dm^{-3}, in initial test solutions are given in the figure. The solid lines show the theoretical curves calculated by using the constants of the set (1—4) by calorimetry in Table 1.

Table 1. The Least-Squares Refinement of Overall Formation Constants, $\log(\beta_n/\mathrm{mol}^{-n}\,\mathrm{dm}^{3n})$, and Enthalpies, $\Delta H^\circ_{\beta n}/\mathrm{kJ\,mol}^{-1}$, of $[NiCl_n]^{(2-n)+}$ in *N*,*N*-Dimethylformamide Containing 0.4 mol dm^{-3} $(C_2H_5)_4NClO_4$ at 25 °C

	Calorimetry		Spectrophotometry	
	(1—4)	(1, 3, 4)	(1—4)	(1, 3, 4)
$\log\beta_1$	2.85(0.05)	2.72(0.03)	2.89(0.01)	2.97(0.01)
$\log\beta_2$	3.76(0.13)	—	3.75(0.05)	—
$\log\beta_3$	5.53(0.06)	5.56(0.04)	5.80(0.02)	5.93(0.01)
$\log\beta_4$	7.40(0.06)	7.19(0.03)	7.46(0.02)	7.54(0.01)
$\Delta H^\circ_{\beta 1}$	8.6(0.2)	9.4(0.1)	—	—
$\Delta H^\circ_{\beta 2}$	27.7(5)	—	—	—
$\Delta H^\circ_{\beta 3}$	90.6(9)	73.2(2.5)	—	—
$\Delta H^\circ_{\beta 4}$	77.2(0.8)	79.4(0.7)	—	—
U[a]	0.145	0.186	0.0165	0.0208
R[b]	0.0129	0.0146	0.0123	0.0138
N[c]	107	107	2100	2100

Values in parentheses refer to standard deviations. a) Error-square sum. b) The Hamilton *R*-factor. c) The number of data points.

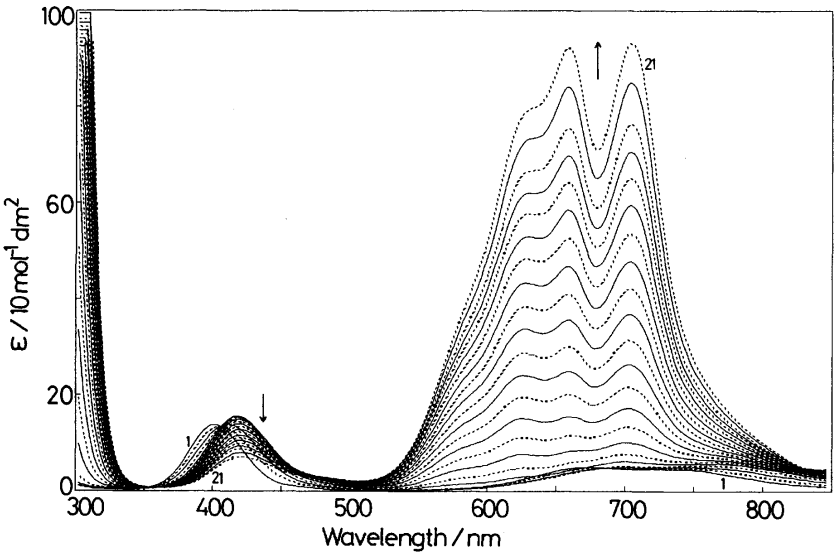

Fig. 2. Electronic spectra of nickel(II) chloride DMF solutions in the range 300—850 nm. Intensities are normalized with a unit concentration of the metal ion in solution. The spectra changed along the direction of the arrows with increasing C_X/C_M, the C_X/C_M value being varied from 0 of the solution No. 1 to 3.78 of the solution No. 21.

Table 1.

Among various sets examined, the set (1—4) assuming the formation of $[NiCl_n]^{(2-n)+}$ (n=1—4) and the set (1,3,4) eliminating $[NiCl_2]$ from the set (1—4) gave relatively small Hamilton *R*-factors (calculated by $\{\sum(q_{i,obsd}-q_{i,calcd})^2/\sum(q_{i,obsd})^2\}^{1/2}$), 0.0129 and 0.0146, respectively. Other sets such as (1, 2), (1, 3), (1, 4), (1, 2, 3), and (1, 2, 4) gave much larger values of the Hamilton *R*-factor. As seen in Fig. 1 by the solid lines, theoretical titration curves calculated by using the constants of the set (1—4) in Table 1 well reproduced the experimental points over the whole range of C_X/C_M examined. However, the set (1, 3, 4) could also reproduce the experimental points rather satisfactorily because the Hamilton *R*-factor of the set (1, 3, 4) was close to that of the set (1—4), and therefore, the $\Delta H^\circ_{\beta 2}$ and $\Delta H^\circ_{\beta 3}$ values evaluated from the calculation by using the set (1—4) contained relatively large uncertainties.

Electronic spectra of nickel(II) chloride DMF solutions measured with varying concentrations of the ligand ion are depicted in Fig. 2. Each spectrum should be represented as the sum of electronic spectra of individual nickel(II) chloro complexes by taking into account the distribution of species in solution. Therefore, absorbance data obtained at selected 30 wavelengths in the range 300—850 nm were analyzed by assuming the formation of plausible sets of nickel(II) chloro complexes and their formation constants and molar extincition coefficients of each complex at relevant wavelengths were optimized by the least-squares method. Among various sets of complexes

examined, again the sets (1—4) and (1, 3, 4), as seen in Table 1, gave relatively small Hamilton R-factors, 0.0123 and 0.0138, respectively. The same analysis was performed by using absorbance data at differently chosen 30 wavelengths in the range 300—850 nm in order to check the reproducibility of the formation constants thus evaluated, and the formation constants of each complex obtained by using the second set of data gave practically the same values as those evaluated by using the first set of absorbance data.

Since the formation constant log β_2 of the $[NiCl_2]$ complex, as well as the log β_n (n=1, 3, and 4) values of the other three nickel(II) chloro complexes obtained by calorimetry and spectrophotometry is in very good agreement with each other, as seen in Table 1, we concluded that the formation of the $[NiCl_2]$ complex should be taken into account together with the other three complexes in DMF. Consequently, we finally propose the formation of $[NiCl_n]^{(2-n)+}$ (n=1—4) in DMF. Distribution of the nickel(II) chloro complexes in DMF is depicted in Fig. 3, which was calculated by using the formation constants of the set (1—4) by calorimetry in Table 1.

Zinc(II) Chloro Complexes. Calorimetric titration curves for the zinc(II) chloride system obtained by using similar procedure to that employed in the previous section are depicted in Fig. 4. In contrast to the nickel(II) chloride system, the titration curves showed only a slight dependence on the concentration of zinc(II) ion in solution. In addition, the $\Delta H°$ values approached zero at C_X/C_M>4, indicating that the zinc(II) chloro complexes are more stable than the nickel(II) chloro complexes in DMF.

The calorimetric data were analyzed by assuming the formation of plausible sets of mononuclear $[ZnCl_n]^{(2-n)+}$($n\leq4$) complexes, and their formation constants and enthalpies were simultaneously refined. Among them, the sets (1—4) and (2—4) gave relatively small Hamilton R-factors, 0.0359 and 0.0500, respectively. The results of overall formation constants and enthalpies thus optimized for both sets are summarized

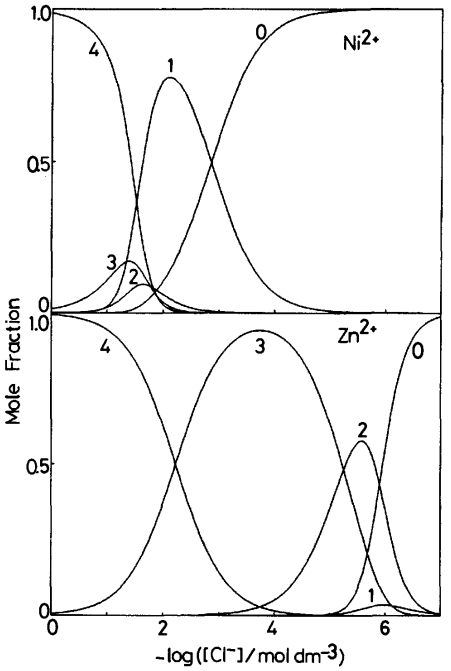

Fig. 3. Distribution of species of the chloro complexes of nickel(II) and zinc(II) ions in 0.4 mol dm^{-3} $(C_2H_5)_4NClO_4$ DMF solution. The numbers represent n within $[MCl_n]^{(2-n)+}$ (M^{2+}=Ni^{2+} and Zn^{2+}).

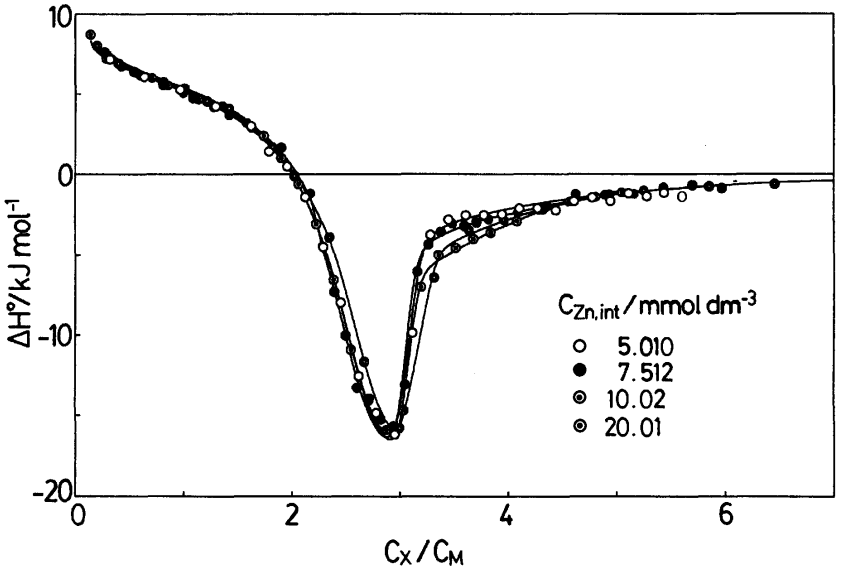

Fig. 4. Calorimetric titration curves of zinc(II) chloride DMF solutions containing 0.4 mol dm^{-3} $(C_2H_5)_4NClO_4$ at 25°C. Concentrations of zinc(II) ions, $C_{Zn,int}$/mmol dm^{-3}, in initial test solutions are given in the figure. The solid lines show the theoretical curves calculated by using the constants of the set (1—4) in Table 2.

Table 2. The Least-Squares Refinement of Overall Formation Constants, $\log(\beta_n/\text{mol}^{-n}\,\text{dm}^{3n})$, and Enthalpies, $\Delta H^\circ_{\beta n}$/kJ mol^{-1}, of $[NiCl_n]^{(2-n)+}$ in *N*,*N*-Dimethylforamide Containing 0.4 mol dm^{-3} $(C_2H_5)_4NClO_4$ at 25 °C

	(1—4)	(2—4)
$\log\beta_1$	4.81(0.14)	—
$\log\beta_2$	11.80(0.16)	11.66(0.20)
$\log\beta_3$	17.06(0.24)	16.56(0.29)
$\log\beta_4$	19.28(0.26)	18.77(0.32)
$\Delta H^\circ_{\beta1}$	14.7(2.9)	—
$\Delta H^\circ_{\beta2}$	16.1(0.1)	16.4(0.2)
$\Delta H^\circ_{\beta3}$	−1.5(0.1)	−1.6(0.1)
$\Delta H^\circ_{\beta4}$	−9.4(0.2)	−9.4(0.2)
U[a]	0.287	0.558
R[b]	0.0359	0.0500
N[c]	118	118

Values in parentheses refer to standard deviations. a) Error-square sum. b) The Hamilton *R*-factor. c) The number of data points.

Table 3. Thermodynamic Quantities, $\log(K_n/\text{mol}^{-1}\,\text{dm}^3)$, ΔG°_n/kJ mol^{-1}, ΔH°_n/kJ mol^{-1}, and ΔS°_n/J K^{-1} mol^{-1}, for the Stepwise Formation of $[NiCl_n]^{(2-n)+}$ and $[ZnCl_n]^{(2-n)+}$ in *N*,*N*-Dimethylformamide (DMF) and Dimethyl Sulfoxide (DMSO) at 25 °C

	Nickel(II)	Zinc(II)	
	DMF	DMF	DMSO[a]
$\log K_1$	2.85	4.81	1.94
$\log K_2$	0.91	6.99	3.90
$\log K_3$	1.77	5.26	2.25
$\log K_4$	1.87	2.22	—
ΔG°_1	−16.3	−27.5	−11.1
ΔG°_2	−5.2	−39.9	−22.3
ΔG°_3	−10.1	−30.0	−12.0
ΔG°_4	−10.7	−12.7	—
ΔH°_1	8.6	14.7	22.3
ΔH°_2	19.1	1.4	0.8
ΔH°_3	62.9	−17.6	−10.2
ΔH°_4	−13.4	−7.9	—
ΔS°_1	84	142	112
ΔS°_2	82	139	77
ΔS°_3	245	42	9
ΔS°_4	−9	16	—
$\Delta G^\circ_{\beta4}$[b]	−42.2	−110.0	—
$\Delta H^\circ_{\beta4}$[b]	77.2	−9.4	—
$\Delta S^\circ_{\beta4}$[b]	401	338	—

a) Ref. 24. b) Values of the overall formation of $[MCl_4]^{2-}$ (M^{2+}=Ni^{2+} and Zn^{2+}).

in Table 2. Considering the appreciably smaller Hamilton *R*-factor of the set (1—4) than that of the set (2—4), we finally propose the formation of $[ZnCl_n]^{(2-n)+}$ (n=1—4) in DMF. Distribution of species of the zinc(II) chloro complexes in DMF calculated by using the formation constants of the set (1—4) in Table 2 is also depicted in Fig. 3. As seen in Fig. 3, the formation of $[ZnCl]^+$ is so weak that the $\Delta H^\circ_{\beta1}$ value evaluated involves a rather large uncertainty.

Stepwise Thermodynamic Quantities. Stepwise formation constants, $\log(K_n/\text{mol}^{-1}\,\text{dm}^3)$, Gibbs energies, ΔG°_n/kJ mol^{-1}, enthalpies, ΔH°_n/kJ mol^{-1}, and entropies, ΔS°_n/J K^{-1} mol^{-1}, were then calculated, the results being summarized in Table 3.

Nickel(II) ion may be primarily coordinated with six DMF molecules in DMF as has been observed within the $Ni(ClO_4)_2\cdot(dmf)_6$ solvate crystal,[27] because the absorption spectrum of nickel(II) perchlorate DMF solutions showed practically the same spectral profile as the reflectance spectrum of the solvate crystal. Zinc(II) ion is suggested to be coordinated with six solvent molecules in zinc(II) perchlorate DMSO solutions and in the $Zn(ClO_4)_2\cdot(dmso)_6$ crystal.[29,30] Similarly, zinc(II) ion may be coordinated with six DMF molecules in zinc(II) perchlorate DMF solution as well as in the $Zn(ClO_4)_2\cdot(dmf)_6$ crystal.[27] Chloride ions stepwise coordinate to Ni(II) or Zn(II) ion to yield the tetrahedral $[MCl_4]^{2-}$ (M^{2+}=Ni^{2+} or Zn^{2+}) complex in the solutions[7,8] and thus all solvent molecules coordinating to the metal ions are liberated at the formation of the $[MCl_4]^{2-}$ complex. The structural change around Ni(II) and Zn(II) ions from octahedral to tetrahedral must thus take place at a certain step of complexation between the metal and chloride ions.

DMF molecules coordinating to metal ions lose their freedom of motion to a great extent. On the contrary, as the result of complexation between a metal and ligand ions, DMF molecules coordinating to the ions are liberated, the process being accompanied by an increase in the degree of freedom of the DMF molecules, i.e., the entropy change associated with the liberation of solvent molecules must be large and positive.

As seen in Table 3, the ΔH°_3 and ΔS°_3 values of stepwise formation of $[NiCl_3]^-$ are extremely large and positive as compared with the corresponding values of the $[NiCl_n]^{(2-n)+}$ (n=1, 2, and 4). Thus, DMF molecules coordinating to nickel(II) ion must be extensively liberated and the coordination number around the metal ion may be decreased at the formation of $[NiCl_3]^-$. Individual electronic spectra of $[NiCl_3]^-$ and $[NiCl_4]^{2-}$ in DMF show strong absorption bands over the range 550—750 nm which are not observed in the spectra of $[NiCl_n]^{(2-n)+}$ (n=0—2) as will be discussed in a later section. Thus, we propose the tetrahedral structure for the $[NiCl_3]^-$ complex as well as the tetrahedral $[NiCl_4]^{2-}$ complex. The trichloronickelate(II) complex may thus involve one DMF molecule within the coordination shell of the metal ion as represented by $[NiCl_3(dmf)]^-$. The metal-solvent bond within the complex may be weak because the subsequent stepwise formation of $[NiCl_4]^{2-}$ shows even negative enthalpy and entropy changes.

On the other hand, in the zinc(II) chloride system, an extensive liberation of solvent molecules may take place at the formation of the $[ZnCl]^+$ complex because

both ΔS_1° and ΔH_1° values shown in Table 3 are large and positive, and thus the coordination number around zinc(II) ion might be decreased within the $[ZnCl]^+$ complex. However, it is hard to conclude the coordination structure of $[ZnCl]^+$ (four-, five- or six-coordination) because the ΔS_n° (n=1 and 2) values involve rather large uncertainties due to the weak formation of the $[ZnCl]^+$ complex in DMF. The formation of $[ZnCl(dmso)_3]^+$ in DMSO[23,24] and of $[ZnCl(CH_3OH)_5]^+$ in methanol[31] has been suggested.

In contrast to large and positive ΔS_n° (n=1 and 2) values of formation of the $[ZnCl]^+$ and $[ZnCl_2]$ complexes, the ΔS_n° (n=3 and 4) values of $[ZnCl_3]^-$ and $[ZnCl_4]^{2-}$ are significantly small. The corresponding ΔH_n° (n=1 and 2) values are positive but the ΔH_n° (n=3 and 4) values are negative. The result indicates that the liberation of DMF molecules takes place to a great extent at each consecutive step of the formation of $[ZnCl]^+$ and $[ZnCl_2]$ but only to a small extent at the formation of $[ZnCl_3]^-$ and $[ZnCl_4]^{2-}$. It is thus expected that the $[ZnCl_2]$ and $[ZnCl_3]^-$ complexes may have a smaller coordination number than the $[Zn(dmf)_6]^{2+}$ and $[ZnCl]^+$ complexes in DMF. We therefore propose that the di- and trichloro complexes of Zn(II) have the tetrahedral four-coordinate structure in DMF, as represented by $[ZnCl_2(dmf)_2]$ and $[ZnCl_3(dmf)]^-$, respectively, which are similar to the tetrahedral $[ZnCl_4]^{2-}$ complex.

The metal-solvent interaction may be very weak within the $[ZnCl_n]^{(2-n)+}$ (n=2 and 3) complexes as indicated by negative ΔH_n° (n=3 and 4) values in spite of weaker metal-chloride bonds within higher complexes. The negative ΔH_n° value has also been observed at the stepwise formation of $[CuCl_4]^{2-}$,[1-4] as well as $[NiCl_4]^{2-}$ as discussed in a preceding section. The weakening of metal-solvent interactions may lead to an elongation of metal-solvent bonds within a metal complex. Structural evidence of elongation of a metal-solvent bond with an increase in the number of a ligand atom in the coordination shell which has a larger electron donicity than the solvent molecules has been obtained for the copper(II) chloro complexes in DMF[6] and the copper(II) and nickel(II) glycinato complexes in water[32-34] by means of X-ray diffraction.

Comparison between Formation of $[ZnCl_n]^{(2-n)+}$ in DMF and in DMSO. Complexation of zinc(II) with chloride ions has been studied in DMSO by Ahrland et al.,[23,24] and the formation of $[ZnCl_n]^{(2-n)+}$ (n=1—3) was indicated. According to their formation constants, the formation of $[ZnCl]^+$ is suppressed in DMSO as well as in DMF. It is noted that, as seen in Table 3, the formation constants of the zinc(II) chloro complexes in DMSO are markedly smaller than those in DMF, the result being mainly ascribed to smaller entropy changes in the former solvent than in the latter. When solvent molecules are liberated from the coordination sphere of an ion to enter the bulk solvent in the course of complexation, it is expected that the entropy of formation of a complex is positive. However, the positive entropy at the liberation of solvent molecules may be compensated for the structure formation of the solvent molecules in the bulk, if the solvent has rather strong solvent-solvent interactions. Since the donicity of DMF and DMSO is not largely different, the entropy increase at the liberation of solvent molecules from zinc(II) ion may be to a similar extent in both solvents. However, as described in a preceding paper,[3] DMSO has a long-range solvent-solvent interactions in the bulk than DMF has. Therefore, when solvent molecules subsequently enter the bulk phase, their degrees of freedom decrease more extensively in DMSO than in DMF, and thus, a less net entropy change of formation of a zinc(II) chloro complex results.

Electronic Spectra of Individual $[NiCl_n]^{(2-n)+}$ Complexes. Electronic spectra of individual nickel(II) chloro complexes were extracted from measured electronic spectra at varying concentrations of chloride ion in nickel(II) chloride DMF solutions over the wavelength range 300—850 nm, and the result is depicted in Fig. 5.

The nickel(II) DMF solvate complex shows an absorption peak at about 400 nm and very broad and very weak bands at 500—800 nm. The monochloronickel(II) complex shows a spectrum similar to that of the solvate complex, but the absorption peak at ca. 400 nm slightly shifted to a longer wavelength by ca. 20 nm than that of the solvate complex. The electronic spectra of these species are significantly different from the spectrum of $[NiCl_4]^{2-}$ which has the tetrahedral structure. Therefore, the $[NiCl]^+$ complex may have the octahedral type structure as well as $[Ni(dmf)_6]^{2+}$. The distorted octahedral structure of $[NiCl]^+$ in water has been suggested by X-ray diffraction.[35]

Although the spectrum of the dichloronickel(II) complex obtained is rather uncertain due to the weak formation of the complex in DMF, weak absorption bands ranging 400—600 nm are attributed to the complex, the spectrum being even slightly different from the spectra of $[Ni(dmf)_6]^{2+}$ or $[NiCl]^+$. It may be difficult to conclude the structure of the $[NiCl_2]$ complex from the spectral profile obtained here, but the different shape of the spectrum of the $[NiCl_2]$ complex suggests a different structure (a largely distorted six-coordinate or even a five-coordinate structure) of the complex from that of $[Ni(dmf)_6]^{2+}$ or $[NiCl(dmf)_5]^+$.

In the spectra of the tri- and tetrachloronickelate(II) complexes, absorption peaks appearing at 400—500 nm in the spectra of $[Ni(dmf)_6]^{2+}$, $[NiCl]^+$, and $[NiCl_2]$ almost disappear, while intense absorption peaks appear in the range 500—800 nm. The electronic spectrum of $[NiCl_4]^{2-}$ obtained has been ascribed to the absorption bands arising from the complex with the tetrahedral structure.[7-9] On the other hand, the electronic spectrum of trichloronickelate(II) complex has not been discussed in detail because overlapped spectra

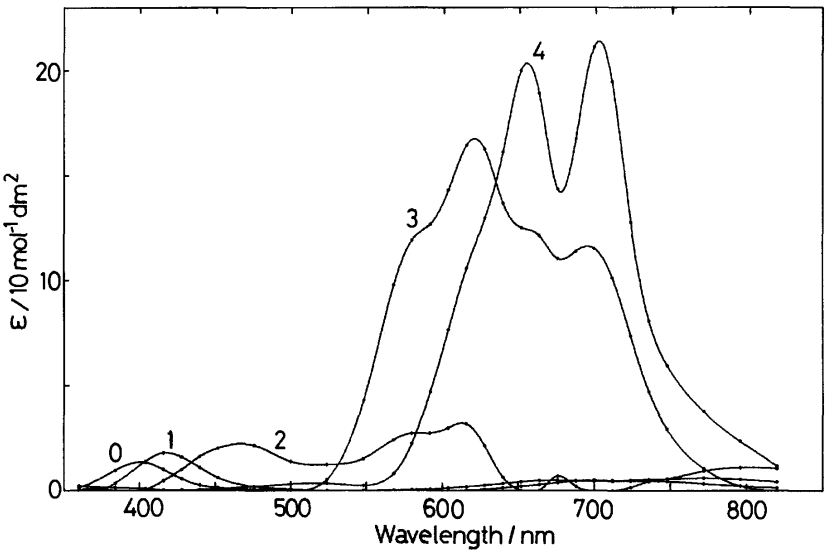

Fig. 5. Electronic spectra of individual nickel(II) chloro complexes in the range 350–850 nm obtained in 0.4 mol dm^{-2} $(C_2H_5)_4NClO_4$ DMF solution. The numbers represent n within $[NiCl_n]^{(2-n)+}$.

of $[NiCl_3]^-$ and $[NiCl_4]^{2-}$ are usually obtained in solution and it is difficult to extract the sole spectrum of $[NiCl_3]^-$. The electronic spectrum of $[NiCl_3]^-$ extracted in this work shows two peaks (ca. 620 and 695 nm) and two shoulders (ca. 575 and 660 nm). The similar intensities and peak positions of the bands of $[NiCl_3]^-$ to those of $[NiCl_4]^{2-}$ indicate that these complexes have the same type of coordination structure, i.e., the tetrahedral type structure, around the metal ion.

The similar spectrum to that of $[NiCl_3]^-$ in DMF has been observed for a nickel(II) chloride acetonitrile solution with the C_X/C_M ratio of 4,[21] the $[NiCl_3]^-$ complex probably being present as the main species in the acetonitrile solution. Similar electronic spectra of $[NiCl_3]^-$ observed in DMF and in acetonitrile in spite of a stronger donicity of DMF than that of acetonitrile suggest that the metal-solvent bonds within the $[NiCl_3(dmf)]^-$ and $[NiCl_3(acetonitrile)]^-$ complexes are so weak that the electronic spectra of the complex may not be appreciably influenced by the difference of the solvent molecules. Similar electronic spectra have also been obtained for the $[CuCl_3]^-$ complex in DMF and in acetonitrile.[1,2]

The present work has been financially supported by the Grant-in-Aid for Special Project Research No. 60540389 from the Ministry of Education, Science and Culture.

References

1) S. Ishiguro, B. G. Jeliazkova, and H. Ohtaki, *Bull. Chem. Soc. Jpn.*, **58**, 1143 (1985).
2) S. Ishiguro, B. G. Jeliazkova, and H. Ohtaki, *Bull. Chem. Soc. Jpn.*, **58**, 1749 (1985).
3) S. Ishiguro, H. Suzuki, B. G. Jeliazkova, and H. Ohtaki, *Bull. Chem. Soc. Jpn.*, **59**, 2407 (1986).
4) S. Ishiguro, B. G. Jeliazkova, and H. Ohtaki, *Bull. Chem. Soc. Jpn.*, **59**, 1073 (1986).
5) S. Ahrland, *Pure Appl. Chem.*, **54**, 1451 (1982); **51**, 2019 (1979); "The Chemistry of Nonaqueous Solvents (J. J. Lagowski, ed.)," Academic Press, New York (1978), Vol. **VA** p. 1.
6) K. Ozutsumi, S. Ishiguro, and H. Ohtaki, to be published.
7) N. S. Gill and R. S. Nyholm, *J. Chem. Soc.*, **1959**, 3997.
8) D. M. L. Goodgame, M. Goodgame, and F. A. Cotton, *J. Am. Chem. Soc.*, **83**, 4161 (1961).
9) D. M. Gruen and R. L. McBeth, *J. Phys. Chem.*, **63**, 393 (1959).
10) J. R. Weisner, R. C. Srivastava, C. H. L. Kennerd, M. Di Vaira, and E. C. Lingafelter, *Acta Crystallogr.*, **23**, 565 (1967).
11) D. M. L. Goodgame, M. Goodgame, and F. A. Cotton, *J. Am. Chem. Soc.*, **83**, 344 (1961).
12) B. Brehler, *Z. Krist.*, **109**, 68 (1957); **114**, 66 (1960).
13) V. Dvorak and R. Kind, *Phys. Status Solidi A*, **107**, K109 (1981).
14) N.E. Massa, *J. Phys., Colloq.*, 593 (1981).
15) M. Quilichini, J. P. Mathieu, and M. Le Postollec, *J. Phys. (Les Ulis, Fr.)*, **43**, 787 (1981).
16) R. Blinc, I. P. Aleksandrova, and A. S. Chaves, *J. Phys. C*, **15**, 547 (1982).
17) M. Itoh, K. Sakai, and T. Nakamura, *Inorg. Chem.*, **21**, 3552 (1982).
18) S. Hayashi, The Master Thesis (Tokyo Institute of Technology 1986).
19) F. C. Frederic and K. E. Johnson, *J. Inorg. Nucl. Chem.*, **43**, 1483 (1981).
20) F. A. Cotton and R. Francis, *J. Am. Chem. Soc.*, **82**, 2986 (1960).
21) M. Baaz, V. Gutmann, G. Hampel, and J. R. Masaguer, *Mh. Chem.*, **93**, 1416 (1962).
22) H. Hubacck, B. Stancic, and V. Gutmann, *Mh. Chem.*, **94**, 1119 (1963).

23) S. Ahrland and N-O. Björk, *Acta Chem. Scand., Ser. A*, **30**, 265 (1976).
24) S. Ahrland, N-O. Björk, and R. Portanova, *Acta Chem. Scand., Ser. A*, **30**, 270 (1976).
25) M.N. Hughes, *Coor. Chem. Rev.*, **37**, 297 (1981).
26) V. Gutmann, "The Donor-Acceptor Approach to Molecular Interactions," Prenum, New York (1978).
27) W. Schneider, *Helv. Chim. Acta*, **46**, 1842 (1963).
28) S. Ishiguro, K. Yamamoto, and H. Ohtaki, *Anal. Sci.*, **1**, 263 (1985).
29) M. Sandström, I. Persson, and S. Ahrland, *Acta Chem. Scand., Ser. A*, 607 (1978).
30) I. Persson, *Acta Chem. Scand., Ser. A*, **36**, 7 (1982).
31) H. Doe and T. Kitagawa, *Inorg. Chem.*, **21**, 2272 (1982).
32) K. Ozutsumi and H. Ohtaki, *Bull. Chem. Soc. Jpn.*, **56**, 3635 (1983).
33) K. Ozutsumi, T. Yamaguchi, H. Ohtaki, K. Tohji, and Y. Udagawa, *Bull. Chem. Soc. Jpn.*, **58**, 2786 (1985).
34) K. Ozutsumi and H. Ohtaki, *Bull. Chem. Soc. Jpn.*, **57**, 2605 (1984).
35) M. Magini, *J. Chem. Phys.*, **74**, 2523 (1981).

 © 1987 The Chemical Society of Japan Bull. Chem. Soc. Jpn., 60, 539—543 (1987)

Nocovalent Interactions in Metal Complexes. 14.[1] Proton NMR Spectroscopic Investigation on Stereoselectivity in Cobalt(III) Complexes of Various 3-Substituted 1-Phenyl-1,3-propanediones

Michio NAKAMURA, Hisashi ŌKAWA,* Tasuku ITO,[†,#1] Masako KATO,[†,#2] and Sigeo KIDA[#3]
Department of Chemistry, Faculty of Science, Kyushu University 33, Hakozaki, Higashiku, Fukuoka 812
[†]Department of Applied Molecular Science, Institute for Molecular Science,
Okazaki National Research Institute, Okazaki 444
(Received August 6, 1986)

1 : 3-Cobalt(III) complexes of 3-substituted 1-phenyl-1,3-propanediones (C_6H_5-CO-CH_2-CO-R) have been synthesized, and their stereoselectivities were studied with 400 MHz proton NMR spectroscopy. When the substituent (R) was ethyl, propyl, isopropyl, butyl, or isobutyl, the complexes were obtained in a mixture of fac and mer isomers with the fac/mer ratio of 1/3, demonstrating statistical distribution. When the substituent was *t*-butoxymethyl or cyclohexyloxymethyl the fac isomer was predominantly formed. The stereoselectivity in the geometrical isomer formation of the complexes was ascribed to the interligand CH/π-interaction occuring between the R group and the phenyl ring. The stereoselectivities of the complexes [Co(*l*-moba-X)$_3$] (*l*-moba-X^-=4-(*l*-menthyloxy)-1-(*p*-X-phenyl)-1,3-butanedionate ion; X=H, Br, CH_3) were also examined by means of ^{1}H NMR spectroscopy and compared with the CD spectral result previously reported.

Previously we reported the stereoselective formation of the fac-Δ isomer of tris{4-(*l*-menthyloxy)-1-phenyl-1,3-butanedionato}M(III) complexes, [M(*l*-moba)$_3$] (M=Co, Cr, Mn) (Fig. 1(a); X=H).[2] This stereoselectivity was presumed to be due to the intramolecular, interligand CH/π-interaction[3] operating between the phenyl group and the *l*-menthyl group (Fig. 2). This presumption is supported by the facts that (1) the stereoselectivity in tris{4-(*l*-menthyloxy)-1-(2-naphthyl)-1,3-butanedionato}M(III) [M(*l*-mona)$_3$] (Fig. 1(b)) is higher than that of [Co(*l*-moba)$_3$] because of the larger π-system of the naphthyl group compared with the phenyl group[4] and (2) the stereoselectivity of [M(*l*-moba-Br)$_3$], [M(*l*-moba)$_3$], and [M(*l*-moba-Me)$_3$] (see Fig. 1(a)) is enhanced in this order because the π-electron density of the ring increases in the order 4-BrC_6H_4<C_6H_5<4-$CH_3C_6H_4$.[5]

So far we have inspected the stereoselectivities of the complexes based on circular dichroism induced at d-d transition bands. In this study we aimed to obtain direct evidences for the stereoselectivities of cobalt(III) complexes by means of high-resolution (400 MHz) proton NMR spectroscopy. We have synthesized 1 : 3-cobalt(III) complexes of various 3-substituted 1-phenyl-1,3-propanediones (Fig. 1(c)). The stereoselectivity in the formation of geometrical isomers (fac and mer) of the complexes was examined by ^{1}H NMR spectroscopy and discussed in terms of intramolecular, interligand interaction. Further, the stereoselectivities of [Co(*l*-moba-X)$_3$] (X=H, Br, Me) were examined by means of ^{1}H NMR spectroscopy, and compared with the CD spectral result previously reported.[4]

3-Substituted 1-phenyl-1,3-propanediones used in

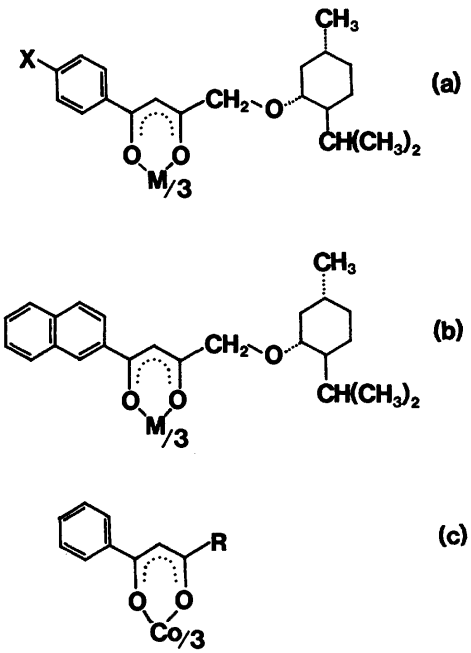

Fig. 1. Chemical structures of (a) [M(*l*-moba-X)$_3$] (X=H, Br, CH_3), (b) [M(*l*-mona)$_3$], and (c) [Co(L-R)$_3$].

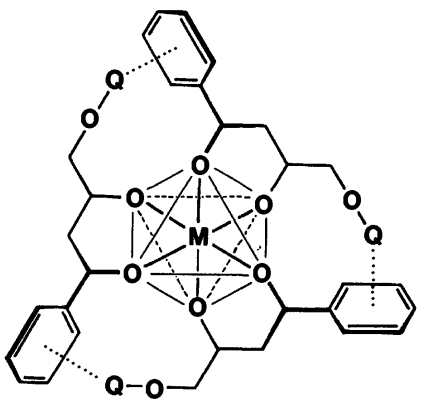

Fig. 2. Schematical representation of interligand CH/π-interaction in [M(*l*-moba)$_3$] (Q=*l*-menthyl).

[#1] Present address: Department of Chemistry, Faculty of Science, Tohoku University, Aoba, Aramaki, Sendai 980.
[#2] Present address: Department of Chemistry, Faculty of Science, Kyoto University, Sakyo-ku, Kyoto 606.
[#3] Present address: Coordination Chemistry Laboratories, Institute for Molecular Science, Okazaki National Research Institute, Okazaki 444.

Table 1. Abbreviations of 3-Substituted 1-Phenyl-1,3-diones[a)]

R	X	Ligand
$-\overset{\alpha}{C}H_2\overset{\beta}{C}H_3$	H	H(L-Et)
$-\overset{\alpha}{C}H_2\overset{\beta}{C}H_2\overset{\gamma}{C}H_3$	H	H(L-*n*Pr)
$-\overset{\alpha}{C}H(\overset{\beta}{C}H_3)_2$	H	H(L-*i*Pr)
$-\overset{\alpha}{C}H_2\overset{\beta}{C}H_2\overset{\gamma}{C}H_2\overset{\delta}{C}H_3$	H	H(L-*n*Bu)
$-\overset{\alpha}{C}H_2\overset{\beta}{C}H(\overset{\gamma}{C}H_3)_2$	H	H(L-*i*Bu)
$-\overset{\alpha}{C}H_2-C_6H_5$	H	H(L-Bz)
$-\overset{\alpha}{C}H_2O\overset{\delta}{C}(CH_3)_3$	H	H(L-BuO)
$-\overset{\alpha}{C}H_2O-C_6H_4$ (1–6)	H	H(L-CyO)
$-\overset{\alpha}{C}H_2O-C_6H_3(CH(CH_3)_2)$ (1–6)	H	H(*l*-moba)
$-\overset{\alpha}{C}H_2O-C_6H_3(CH(CH_3)_2)$ (1–6)	Br	H(*l*-moba-Br)
$-\overset{\alpha}{C}H_2O-C_6H_3(CH(CH_3)_2)$ (1–6)	CH_3	H(*l*-moba-Me)

a) See Fig. 1.

this study are given in Table 1, together with their abbreviations.

Experimental

Materials. Methyl ethyl ketone, methyl *n*-propyl ketone, methyl *i*-propyl ketone, methyl *n*-butyl ketone, methyl *i*-butyl ketone, acetophenone, *p*-bromoacetophenone, and *p*-methylacetophenone were purchased from Nakarai Chemical Co. *l*-Menthyloxyacetic acid was purchased from Tokyo Kasei Chemical Co. *t*-Butoxyacetic acid and cyclohexyloxyacetic acid were synthesized by the reaction of chloroacetic acid with *t*-butyl alcohol and cyclohexanol, respectively.[6)] Ethyl benzoate, ethyl *t*-butoxyacetate, and ethyl cyclohexyloxyacetate were synthesized by the esterification of the corresponding carboxylic acids.

Preparation. 3-Substituted 1-phenyl-1,3-propanediones (generally represented by H(L-R)) were synthesized by the Claisen condensation reaction[7)] between corresponding ester and ketone in the presence of sodium hydride as the base. The synthetic methods for H(*l*-moba-X) (X=H, Br, Me) have been described in the preceding papers.[2,5)]

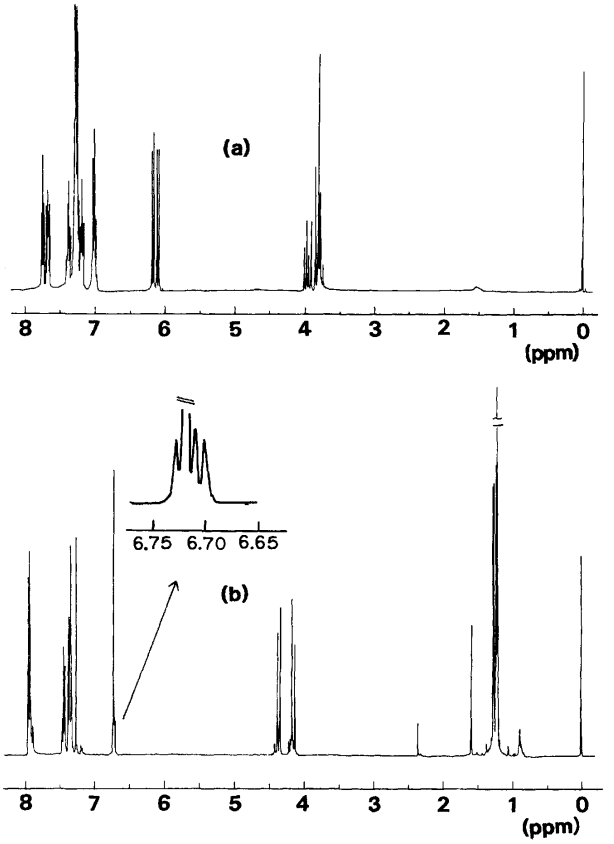

Fig. 3. Proton NMR spectra of (a) [Co(L-Bz)$_3$] and (b) [Co(L-BuO)$_3$].

Cobalt(III) complexes were obtained by the reaction of $Na_3[Co(CO_3)_3]\cdot 3H_2O$ and H(L-R)), in a way similar to that for tris(benzoylacetonato)cobalt(III).[8)] All the [Co(L-R)$_3$] complexes were obtained as green oily substances. They were purified by eluting through an alumina column (10 mm×100 mm) and identified by ^{1}H NMR spectra.

Measurements. ^{1}H NMR spectra were measured on a JEOL Fourier Transform NMR Spectrometer JNM GX-400 in $CDCl_3$. Tetramethylsilane was used as an internal standard.

Results and Discussion

For 1 : 3-cobalt(III) complexes of unsymmetrical 1,3-diketones, there are two geometrical isomers, fac and mer. The statistical ratio for the fac/mer isomers is 1/3. In the fac isomer three ligands are equivalent, whereas in the mer isomer no ligands are equivalent to each other.[9)] Therefore, in ^{1}H NMR spectra of tris(1,3-diketonato)cobalt(III) complexes, the methine proton in the chelate ring, for example, should be observed as four singlets with the same intensity (one from fac isomer and three from mer isomer) if there is no stereoselectivity in the formation of the complexes. When the interligand CH/π-interaction operates in the molecule to produce predominantly the fac isomer,

Table 2. ^{1}H NMR Spectral Data for 3-Substituted 1-Phenyl-1,3-propanediones and Their Cobalt(III) Complexes[a)]

	Ligand δ/ppm	Complex δ/ppm
H(L-Et)	met: 6.16(s) α: 2.45(qa) β: 1.20(t)	met: 6.19 6.22 6.23 6.24[b)] α: 2.52—2.65(m) β: 1.09—1.19(m)
H(L-*n*Pr)	met: 6.16(s) α: 2.39(t) β: 1.71(qa) γ: 0.99(t)	met: 6.18 6.20 6.21 6.22[b)] α: 2.43—2.65(m) β: 1.56—1.71(m) γ: 0.79—0.96(m)
H(L-*i*Pr)	met: 6.19(s) α: 2.61(mc) β: 1.22(d)	met: 6.21 6.23 6.27 6.30[b)] α: 2.81—2.86(m) β: 1.10—1.15(m)
H(L-*n*Bu)	met: 6.17(s) α: 2.15(t) β: 1.65(mc) γ: 1.40(mc) δ: 0.94(t)	met: 6.19 6.20 6.21 6.22[b)] α: 2.35—2.68(m) β: 1.56—1.64(m) γ: 1.18—1.39(m) δ: 0.68—0.92(m)
H(L-*i*Bu)	met: 6.15(s) α: 2.28(d) β: 2.17(mc) γ: 0.99(d)	met: 6.15 6.16 6.17 6.19[b)] α: 2.26—2.58(m) β: 2.10—2.14(m) γ: 0.76—0.97(m)
H(L-Bz)	met: 6.12(s) α: 3.73(s)	met: 6.08 6.11 6.16 6.19 α: 3.73—4.01(m)
H(L-BuO)	met: 6.60(s) α: 4.08(s) δ: 1.28(s)	met: 6.72 (6.70 6.71 6.73)[c)] α: 4.12 4.16 4.33 4.37[d)] δ: 1.21 (1.23 1.25 1.27)[c)]
H(L-CyO)	met: 6.57(s) α: 4.17(s)	met: 6.78 (6.77 6.79 6.80)[c)] α: 4.22 4.25 4.42 4.46[d)]
H(*l*-moba)	met: 6.56(s) α: 4.16(qa)[d)] 2-iPr: 0.95(d), 0.82(d) 5-Me: 0.93(d)	met: 6.69 6.70 6.73 α: 4.14—4.51(m) CH_3: 0.73—0.91(m)
H(*l*-moba-Br)		met: 6.63 6.64 6.65 6.67 α: 4.06—4.47(m) CH_3: 0.72—0.93(m)
H(*l*-moba-Me)		met: 6.66 α: 4.13—4.54(m) CH_3: 0.72—0.95(m)

a) See Fig. 1 and Table 1. Abbreviations: met=methine proton, s=singlet, d=doublet, t=triplet, qa=quartet, qi=quintet, mc=multiplet center, CH_3=three methyl groups of the *l*=menthyl group. b) Four peaks with nearly the same intensity. c) Weak peaks in parentheses. d) AB quartet.

only one singlet of the methine signal (or one intense and three weak singlets) should be observed. Thus, the stereoselectivity in tris(1,3-diketonato)cobalt(III) complexes can be inspected by the number of the methine proton signals and their relative intensities.

Each ^{1}H NMR spectrum of the free ligands H(L-R) shows a singlet peak in the 6.1—6.7 ppm which can be assigned to the methine proton on the chelate ring. The integrated intensity of this signal corresponds to one proton, clearly indicating that the diketones assume the enol form. The assignment of main ^{1}H NMR signals of the ligands are given in Table 2.

As shown in Fig. 3(a), the spectrum of [Co(L-Bz)$_3$] shows four singlets with the equal intensity in the 6.08—6.18 ppm region, attributable to the methine protons. Evidently the fac/mer ratio is the statistical one, indicating no stereoselectivity in this case. A similar ^{1}H NMR spectral feature (four methine signals)

was observed for [Co(L-Et)$_3$], [Co(L-*n*Pr)$_3$], [Co(L-*i*Pr)$_3$], [Co(L-*n*Bu)$_3$], and [Co(L-*i*Bu)$_3$] (Table 2). On the other hand, the NMR spectrum of [Co(L-BuO)$_3$] showed a strong peak at 6.72 ppm attributable to the methine proton of the fac isomer, together with three very weak peaks at 6.70, 6.71, and 6.73 ppm attributable to the methine proton of the mer isomer (Fig. 3(b)). The methine proton intensity of the fac isomer is about 10 times that of each peak for the mer isomer, indicating the fac/mer ratio of ca. 10/3 for this complex. The fac/mer ratio was also estimated by the proton signal intensities of *t*-butyl groups; the 1.21 ppm signal attributable to the fac isomer is about 10 times as strong as the signals at 1.23, 1.25, and 1.27 ppm attributable to the mer isomer. [Co(L-CyO)$_3$] also showed a similar spectral pattern in the methine signal region, demonstrating the predominant formation of the fac isomer (Table 2). The fac/mer ratio for this complex was estimated at ca. 3 from the methine peak intensities. The stereoselectivities found for [Co(L-BuO)$_3$] and [Co(L-CyO)$_3$] may be attributed to the intramolecular, interligand CH/π-interaction as supposed for [M(*l*-moba-X)$_3$][2,5] and [M(*l*-mona)$_3$][4] (see Fig. 2).

The Dreiding model considerations suggest that the substistuent R with a carbon chain longer than two-carbon chain (C_2) may come into contact with the neighbouring phenyl ring in [Co(L-R)$_3$] but such a contact is not feasible in the complex with the substituent of C_2 chain. No stereoselectivity in [Co(L-Et)$_3$] and [Co(L-*i*Pr)$_3$], therefore, is easily understandable. However, [Co(L-*n*Pr)$_3$], [Co(L-*n*Bu)$_3$], [Co(L-*i*Bu)$_3$], and [Co(L-Bz)$_3$] also showed no stereoselectivity in spite of their substituent longer than C_2 chain. In the case of [Co(L-Bz)$_3$], the phenyl and the benzyl rings cannot stack with each other from the steric requirement of the molecule, and this may be a reason for no stereoselectivity of this complex. In contrast to the above complexes, [Co(L-BuO)$_3$] and [Co(L-CyO)$_3$] showed a high stereoselectivity.

It is not straightforward to explain the marked difference in stereoselectivities between the two classes, ([Co(L-*n*Pr)$_3$], [Co(L-*n*Bu)$_3$], and [Co(L-*i*Bu)$_3$]) and ([Co(L-BuO)$_3$] and [Co(L-CyO)$_3$]). At the moment we only point out two geometrical features which might relate to the different stereoselectivity between the two classes; (1) the latter class contains the ether group at the β-position of the substituent whereas the β-group for the former class is the methylene group, and (2) the latter class contains an inflexible hydrophobic group (*t*-butyl or cyclohexyl) in the R substituent whereas former class contains a rather flexible group in the substituent.

Proton NMR technique was applied to the analysis of the stereoselectivities of [Co(*l*-moba-Br)$_3$], [Co(*l*-moba)$_3$], and [Co(*l*-moba-Me)$_3$]. The spectra in the methine proton region are given in Fig. 4. In the spectra of [Co(*l*-moba-Br)$_3$] and [Co(*l*-moba)$_3$], four

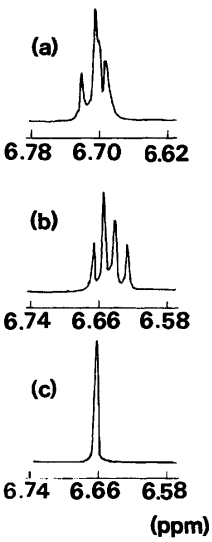

Fig. 4. NMR spectra (methine proton region) of (a) [Co(*l*-moba)$_3$], (b) [Co(*l*-moba-Br)$_3$], and (c) [Co(*l*-moba-Me)$_3$].

signals were observed. The result clearly indicates that each complex obtained is not of a pure isomer but a mixture of isomers. Since our CD spectral investigations have shown the predominant formation of the fac-isomer for these complexes,[5] the highest methine signal (6.65 ppm of [Co(*l*-moba-Br)$_3$] and 6.71 ppm of [Co(*l*-moba)$_3$]) may be assigned to this isomer. In the spectrum of [Co(*l*-moba-Me)$_3$], on the other hand, only one methine signal was observed at 6.66 ppm, clearly demonstrating that the fac-Δ isomer was selectively formed in this case. It is revealed from the present NMR spectral study that the stereoselectivity of [Co(*l*-moba-Br)$_3$], [Co(*l*-moba)$_3$], and [Co(*l*-moba-Me)$_3$] increases in this order, in accordance with the CD spectral result previously reported.[4]

It should be noted that the circular dichroism of [Co(*l*-moba-Me)$_3$], which is proved to be optically pure in this study, is 2.5 times as intense as that of optically pure [Co(acac)$_3$].[10,11] Judging from the fact that optical activity arising from the vicinal effect is at least two orders of magnitude smaller than that from the configurational effect,[12] it is suggested that the interligand CH/π-interaction enhances the distortion about the three-fold axis of the [Co(*l*-moba-Me)$_3$] molecule and thence increases the optical activity at the metal.

This work was supported by the Joint Studies Program (1984—1985) of the Institute for Molecular Science.

References

1) Part 13: H. Ōkawa, M. Nakamura, Y. Shuin, and S. Kida, *Bull. Chem. Soc. Jpn.*, **59**, 3657 (1986).

2) H. Ōkawa, K. Ueda, and S. Kida, *Inorg. Chem.*, **21**, 1594 (1982).

3) M. Nishio, *Kagaku No Ryoiki*, **31**, 998 (1977). The

weak interaction between an aromatic ring and proton of an alkyl or alicyclic group is designated as CH/π-interaction.

4) M. Nakamura, H. Ōkawa, and S. Kida, *Inorg. Chim. Acta*, **96**, 111 (1984).

5) M. Nakamura, H. Ōkawa, and S. Kida, *Bull. Chem. Soc. Jpn.*, **58**, 3377 (1985).

6) M. T. Leffler and A. E. Calkins, *Org. Synth.*, Col. Vol. III, p. 545.

7) F. W. Swamer and C. R. Hauser, *J. Am. Chem. Soc.*, **72**, 1352 (1950).

8) H. F. Bauer and W. C. Dinkard, *J. Am. Chem. Soc.*, **82**, 5031 (1960).

9) A. Y. Girgis and R. C. Fay, *J. Am. Chem. Soc.*, **92**, 7061 (1970).

10) R. B. Von Dreele and R. C. Fay, *J. Am. Chem. Soc.*, **93**, 4936 (1971).

11) R. R. Judkins and D. J. Royer, *Inorg. Chem.*, **13**, 945 (1974).

12) T. Yasui, J. Fujita, and Y. Shimura, *Bull. Chem. Soc. Jpn.*, **42**, 2081 (1969).

 © 1987 The Chemical Society of Japan Bull. Chem. Soc. Jpn., 60, 545—549 (1987)

The Solvent Extraction of Alkali and Alkaline Earth Metal Ions with Nonionic and Ionic Surfactants Having Poly(oxyethylene) Chain

Yukio SAKAI,*,† Masahiro SHINMURA,† Hajime OTSUKA,†† and Makoto TAKAGI††
†Faculty of Education, Miyazaki University, Funatsuka, Miyazaki 880
††Department of Organic Synthesis, Faculty of Engineering, Kyushu University, Hakozaki, Higashi-ku, Fukuoka 812
(Received August 11, 1986)

Extraction behavior of alkali and alkaline earth metal cations was investigated with a new extractant derived from polyethylene glycol mono[4-(1,1,3,3-tetramethylbutyl)phenyl]ether (Triton X-100; average number of oxyethylene group, 10) by introducing a phenolic(2-hydroxy-5-nitrobenzyl) group at the hydroxyl terminal of the polyethylene glycol chain. Alkali metal cations were extracted into 1,2-dichloroethane by forming 1 : 1 complex with the extractant. The overall extraction constant sequence was $K^+(10^{-9.15})>Rb^+(10^{-9.26})>Cs^+(10^{-9.28})>Na^+(10^{-10.08})>Li^+(10^{-10.36})$. The selectivity for K^+, Na^+, and Li^+ was discussed by comparing the extraction behavior with a mixture of nonionic surfactant or dicyclohexano-18-crown-6 and a proton-dissociable lipophilic dye. For alkaline earth metal cations, the extractability decreased in the order $Ba^{2+}>Sr^{2+}>Ca^{2+}\gg Mg^{2+}$. The metal extractability strongly depended on the nature of the anion in the aqueous phase.

In a previous paper,[1] we have reported the extraction behavior of alkaline earth metal cations with nonionic surfactants having a poly(oxyethylene) chain in the presence of lipophilic anions. Alkaline earth metal cations form cationic complexes with a poly(oxyethylene) chain, and the complexes are easily extractable into 1,2-dichloroethane together with lipophilic anions. The lipophilicity of the surfactant complexes seems to arise from the formation of a lipophilic shell around the cation. The extraction efficiency is strongly dependent on the lipophilicity of the counter anion.

Similar to alkaline earth metal cations, alkali metal cations also form cationic complexes with a poly(oxyethylene) chain.[2-4] Yanagida et al.[5] reported that potassium ions were extracted with poly(oxyethylene) compounds together with an anion in the aqueous phase and the extractability depended on the nature of the counter anion. The interaction between the poly(oxyethylene) chain and cations has been applied not only to the photometric determination of the nonionic surfactant using the potassium ion and such a colored lipophilic anion as picrate,[6,7] but also to the sensors based on ionic-selective electrodes.[8,9]

From the standpoint of metal separation, the introduction of an anionic group into a poly(oxyethylene) chain can be expected to give a new series of extractants similar to those reported for crown ethers.[10] Yamazaki et al.[11] synthesized some poly(oxyethylene) derivatives with a hydroxyl group and a carboxyl group at each end of the poly(oxyethylene) chain and studied a carrier mediated transport of alkali metal ions.

In the present study, an integration of a nonionic surfactant (Triton X-100) and a proton-dissociable dye is attempted in the hope to obtain a new extraction-photometric reagent for alkali and alkaline earth metal cations. The basic features of the metal extraction with the extractant have been investigated.

Experimental

Reagent. The extractant (TP) which contains both Triton X-100 and phenolic structures was synthesized from Triton X-100, ethylene glycol, and 2-hydroxy-5-nitrobenzyl bromide (known as Koshland-I reagent, Dojin Labs. Inc.) as described below.

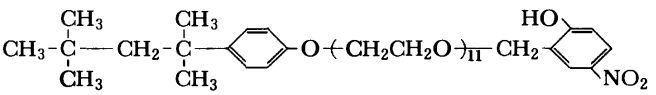

(TP)

Nonionic surfactants, Triton X-100 and polyethylene glycol mono(*p*-nonylphenyl)ethers (5PEGP, 10PEGP; 5 and 10 indicate the number of oxyethylene groups) were purchased from Tokyo Chemical Industry Co., Ltd. and used without further purification. Dicyclohexano-18-crown-6 (DCH18C6) was purchased from Nakarai Chemicals Co., Ltd. 2,5-Dinitro-4-(1,1,3,3-tetramethylbutyl)phenol (DNP) was synthesized by the method described in the preceding paper.[1] 1,2-Dichloroethane and metal salts were purchased from Wako Pure Chemical Industries, Ltd.. These reagents used were of best available grade.

2-(2-Hydroxy-5-nitrobenzyloxy)ethanol. 2-Hydroxy-5-nitrobenzyl bromide (3g, 13 mmol) was dissolved in 60 ml of ethylene glycol and stirred for 5 h at 60 °C. After the unreacted ethylene glycol was removed under reduced pressure, the resulting precipitates were recrystallized from a water–methanol mixture to give white crystals. The product was identified by means of IR and NMR spectrometry. Yield 2.53 g (93%), mp=132—133 °C. ^{1}H NMR ($CDCl_3$), 7.8—8.2 (2H, m, aromatic H), 6.9 (1H, s, aromatic H), 4.4 (2H, s, $ArCH_2$–), 3.6 (4H, s, OCH_2CH_2).

Synthesis of TP. Triton X-100 tosylate (6.5 g, 10 mmol), which was synthesized from tosyl chloride and Triton X-100 in a usual manner, was added to a suspension of sodium hydride (60% in oil; 1 g, 25 mmol) in DMF (13 ml) under nitrogen. To this solution, the DMF solution (13 ml) of 2-(2-hydroxy-5-nitrobenzyloxy)ethanol (2.1 g, 10 mmol) was slowly added at 0 °C and stirred for 24 h at room temperature. The temperature was then raised to 50—58 °C and after 2 h stirring, the mixture was concentrated under reduced pressure. The residue was taken up into chloroform and washed with water. The chloroform solution was con-

centrated and the residue was purified by column chromatography on silica gel (Wakogel C-200) with chloroform. Yield 57%. Yellow viscous oil. Found: C, 61.17; H, 8.95; N, 1.13%. Calcd for $C_{43}H_{71}O_{15}N$: C, 61.33; H, 8.50; N, 1.66%. ^1H NMR ($CDCl_3$), 8.0—8.2 (2H, m, aromatic H), 6.8—7.4 (5H, m, aromatic H), 4.8 (2H, s, $ArCH_2$-), 4.1—4.4 (2H, m, $ArOCH_2$-), 3.7—3.9 (44H, m, OCH_2CH_2), 1.85 (2H, s, $-CH_2-$), 1.5 (6H, s, $-C(CH_3)_2-$), 0.9 (9H, s, $-C(CH_3)_3$).

Determination of Acid Dissociation Constant of TP. The acid dissociation constant of TP in 20% dioxane was determined photometrically. An aliquot (20 ml) of dioxane solution of TP (4.0×10^{-4} mol dm^{-3}) was transferred to a 100 ml standard flask and an aliquot (7—10 ml) of aqueous alkali metal hydroxide or tetraethylammonium hydroxide solution (1.0 mol dm^{-3}) was added. After the mixture was diluted to 100 ml with water, the whole solution was transferred to a beaker and titrated with 1.0 mol dm^{-3} hydrochloric acid. The pH and the optical absorbance at 412 nm which corresponded to the absorption maximum of deprotonated TP were measured at 25 °C. The ionic strength was in the range 0.07—0.1.

Extraction Study. A pH-buffered aqueous solution (6 ml) of alkali or alkaline earth metal salt (0.1 mol dm^{-3}) was equilibrated with 1,2-dichloroethane solution (6 ml) of TP (10^{-4} mol dm^{-3}) or of mixture of PEGP and DNP by shaking mechanically for 20 min at 20 °C using a 50-ml centrifuge tube. After centrifuging for phase separation, the absorbances of both organic and aqueous phases at 300—450 nm and the pH of the aqueous phase were measured. When necessary, the concentration of metal ion in organic phase was determined by flame photometry (Nippon Jarrell Ash Co. Ltd., model AA-855) after back extraction with dilute hydrochloric acid.

Results and Discussion

The solubility of TP in 20% dioxane was so small that there appeared faintly milky turbidity even at 8×10^{-5} mol dm^{-3} TP concentration. The solubility increased with increasing pH of the solution. The increase is due to the proton dissociation of TP. On the other hand, TP was readily soluble in ordinary water-immiscible organic solvents. The distribution ratio of TP between water and 1,2-dichloroethane was more than 200. The deprotonated TP anion in 20% dioxane showed an absorption maximum at 412 nm, where a molar absorptivity was 14000 dm^3 mol^{-1} cm^{-1}. The acid dissociation constant was photometrically determined to be $10^{-6.90\pm0.05}$. The effect of a variety of alkali metal cations, including lithium, sodium and potassium, on the constant was investigated. However, the values obtained were similar to each other, suggesting that there were not appreciable interactions between TP (or TP anion) and alkali metal cations in this medium.

Alkali metal cations were extracted with TP into 1,2-dichloroethane. The extractability decreased in the order $K^+>Rb^+>Cs^+>Na^+>Li^+$. In preliminary experiments, it was found that the extraction was dependent only little on the concentration as well as the nature of the anion in the aqueous phase. Hence, the extraction equilibrium can be represented by the following equation:

$$M^+ + (HL)_o = (ML)_o + H^+,$$

where M^+ and HL represent alkali metal cation and TP, respectively, and the subscript "o" refers to the species in the organic phase. The extraction constant K_{ex} is defined by

$$K_{ex} = \frac{[ML]_o[H^+]}{[HL]_o[M^+]}. \quad (1)$$

In the present study, since a large excess of alkali metal cations is used as compared with the amount of the extractant, the concentration of M^+ in the aqueous phase remains constant before and after the extraction. In addition, the ratio of the concentration of complexed TP (TP anion) to that of free TP in the organic phase can be readily obtained from spectrophotometrical data. Under these conditions, it is possible to establish the stoichiometry of metal extraction by looking at the dependence of the ratio $[ML]_o/[HL]_o$ on pH, which also allows the evaluation of the extraction constant defined by Eq. 1.

The spectral parameters of alkali metal cation-TP complexes used for the calculation of extraction constants are summarized in Table 1. The molar absorptivities were calculated from the absorbance of organic phase and the concentration of extracted metal ion, which was obtained by flame photometry. All of these values, except for lithium, are similar to each other. The plots of logarithmic value of the ratio ($\log [ML]_o/[HL]_o$) against pH (which was assumed to be equal to $-\log [H^+]$) are shown in Fig. 1. Linear relationships with a slope of about 1 were obtained, indicating the validity of the proposed extraction equilibrium.

The validity of the proposed extraction reaction was also justified from the experiment on the effect of TP concentration on the metal distribution ratio (D=total concentration of metal in organic phase/total concentration of metal in aqueous phase). The results obtained are shown in Fig. 2. The plots of log D against $\log [TP]_o$ under constant pH conditions show a linear relationship with a slope of about 1.0, which indicates that TP extracts alkali metal ions by forming 1 : 1 complexes as assumed before.

Based on these results, the extraction constants were calculated and summarized in Table 1. It is noticeable that the extraction constants for potassium, rubidium and cesium are almost the same at about $10^{-9.2}$, while those of sodium and lithium are lower by one order at $10^{-10.08}$ and $10^{-10.36}$, respectively.

A similar selectivity for alkali metal cations was observed for the ion-pair extraction with noncyclic linear poly(oxyethylene) ligands and lipophilic anionic dye. Table 2 indicates the extraction constants for potassium and sodium with a combined use of such neutral ligands (5PEGP, 10PEGP, and DCH18C6) and

Table 1. Spectral Characteristics of Alkali Metal Complexes of TP and Extraction Constants (1,2-dichloroethane, 20°C)

Salts	Max. Wavelength	Molar absorptivity	$-\log K_{ex}$ [a]
	nm	$dm^3 mol^{-1} cm^{-1}$	
LiCl	406	14300	10.36
NaCl	413	16200	10.08
KCl	418	16400	9.15
RbCl	418	16400	9.26
CsCl	418	16400	9.28

a) K_{ex} according to Eq. 1.

Table 2. Extraction of Potassium and Sodium with Neutral Ligand and DNP. Extraction Constants ($\log K_{ex}$;[a] 1,2-dichloroethane, 20°C)

Salts	5PEGP	10PEGP	DCH18C6	DCH18C6[b]	DCH18C6[c]
NaCl	4.06	4.64	4.34	3.97	4.20
KCl	4.67	5.55	6.33	6.00	6.36

a) K_{ex} in $mol^{-2} dm^6$ according to Eq. 2. b) With picrate in chloroform at 25°C (Ref. 12). c) With picrate in dichloromethane at 20°C (Ref. 13).

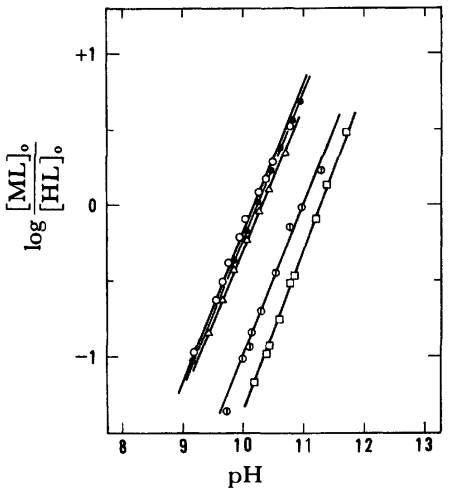

Fig. 1. Plots of $\log[ML]_o/[HL]_o$ against pH.
Concentration before equilibration:
Organic phase, $[HL]_o=1.09\times10^{-4}$ mol dm^{-3}.
Aqueous phase, $[MCl]=0.100$ mol dm^{-3}. ○: KCl, ●: RbCl, △: CsCl, Φ: NaCl, □: LiCl.

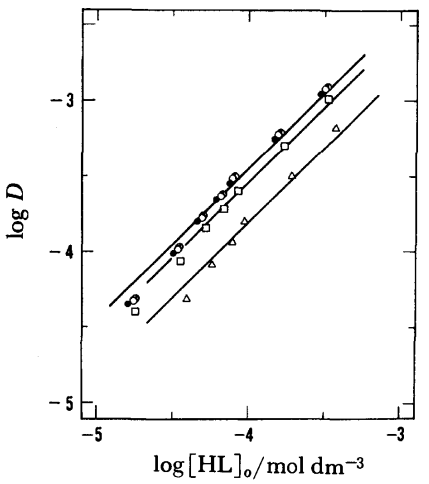

Fig. 2. Plots of distribution ratio ($\log D$) against $\log[HL]_o$ at constant pH.
Concentration before equilibration:
organic phase, $[HL]_o=2.18\times10^{-5}-4.36\times10^{-4}$ mol dm^{-3}. Aqueous phase, $[MCl]=0.100$ mol dm^{-3}. KCl(pH=9.79), ●: RbCl(9.88), △: CsCl(9.44), Φ: NaCl(10.73), □: LiCl(10.91).

DNP. The extraction constants are given by the following equation;

$$M^+ + (E)_o + A^- = (MEA)_o$$

$$K_{ex} = \frac{[MEA]_o}{[M^+][E]_o[A^-]}, \quad (2)$$

where $(E)_o$ and A^- represent the neutral ligand in organic phase and DNP anion in aqueous phase, respectively.

From Table 2, the extraction constant of potassium with DCH18C6 is about hundred times larger than that for sodium. This difference in the constants does not seem to depend much on the nature of anion and solvent used.[12,13]

As to PEGP system, Table 2 shows that the difference in extraction constant between potassium and sodium increases with increasing number of oxyethylene unit of nonionic surfactants. The constant with 10PEGP for potassium ($10^{5.55}$), for which the length of poly(oxyethylene) chain is close to that of TP, is by about one order of magnitude larger than that for sodium ($10^{4.64}$). The difference (0.91 in log unit) is consistent with that (0.93) of TP. Thus, it may be concluded from the comparison that an extractant having noncyclic-poly(oxyethylene) chain has inherently higher extraction preference toward potassium over sodium and that the selectivity constant (the ratio of extraction constant) between of potassium and

sodium with 10PEGP and TP is one tenth of that with DCH18C6.

If the acid dissociation constant and distribution ratio of the extractant remain the same on change in extractant structure, a selectivity of metal extraction can generally be related to both the stability constant of the complex formation in aqueous phase and the distribution ratio of the resultant complex between aqueous and organic phases.

Ono et al.[3,4] investigated the complexation between alkali metal cations and open-chain poly(oxyethylene) conductometrically in methanol and found that the stability constants for sodium ($10^{1.43}$) are by one order of magnitude smaller than that for potassium ($10^{2.72}$). The difference in the stability constants is close to those of the extraction constants in the present study, which suggests that the difference in sodium- and potassium-extractability is related to the complex-stability characteristics inherent to poly(oxyethylene) type ligands. This in turn suggests that the difference in distribution ratio among the alkali metal complexes of PEGP and TP is rather small. This seems reasonable, since a poly(oxyethylene) chain adopts a helical conformation[14,15] in its complex with alkali metals and such a solvation shell-type around the cation is thought to show similar lipophilicity.

It is generally accepted that small-size cations such as sodium and lithium are strongly hydrated in water, which makes it difficult to form stable complexes with PEGP. It is also reported that lithium ion does not bind with poly(oxyethylene) chain in methanol because of its strong solvation.[3,4] However, lithium was considerably extracted with TP in the present study. The extractability can be interpreted by a strong ionic interaction between lithium and *p*-nitrophenolate anion of TP. The extraction of potassium, sodium, and lithium with DNP was studied in strongly alkaline media (alkali metal hydroxide solution) to give the metal extraction constant in the absence of a neutral ligand; the constants (K'_{ex}= $[MA]_o/[M^+][A^-]$) obtained were $10^{-0.62}$, $10^{-0.94}$ and $10^{1.01}$, respectively. The extractability decreases in the following order; $Li^+ \gg K^+ > Na^+$. Takagi et al.[12] reported that the crown ether compounds having an anionic side chain interact favorably with sodium and lithium ions through ionic interaction, resulting in a net decrease in the alkali metal extraction selectivity based on the "size effect" of crown ethers. The same trend obviously holds for the extraction with the present noncyclic poly(oxyethylene) extractant having a proton dissociable site within the molecule.

Unlike the extraction of alkali metal cations, the extraction of alkaline earth metals by TP is considerably affected by the nature of inorganic anions present in the aqueous phase (Fig. 3). As shown in Fig. 3, the extactability of barium decreases with anions in the order, $ClO_4^- > SCN^- > Cl^-$. The sequence of the anions is compatible with the hydrophobicity of these anions.

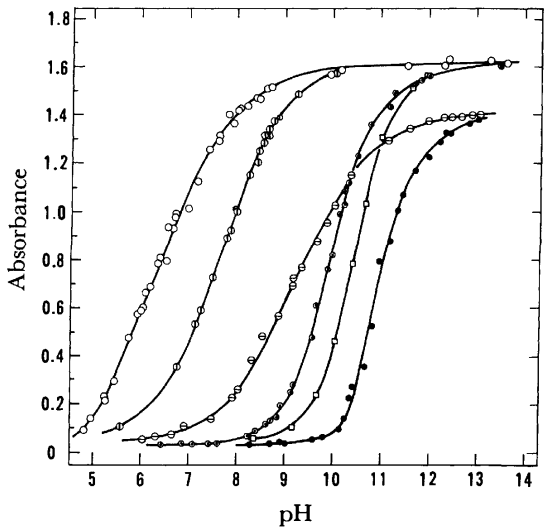

Fig. 3. Influence of pH on the extraction of alkaline earth metal ions with TP.
Concentration before equilibration:
organic phase, $[HL]_o = 1.00 \times 10^{-4}$ mol dm^{-3}
aqueous phase, $[MX_2] = 0.10$ mol dm^{-3}
○: $Ba(ClO_4)_2$ (absorbance measured at 403 nm), ◑: $Ba(SCN)_2$ (405 nm), ◉: $BaCl_2$ (410 nm), □: $SrCl_2$ (407 nm), ⊖: $Ca(ClO_4)_2$ (388 nm), ●: $CaCl_2$ (400 nm).

A similar effect was observed in the extraction of barium with a mixture of PEGP and DNP.[1] In the previous study, it was described that barium was extracted by forming a complex having a composition of Ba^{2+} : PEGP : DNP^- : inorganic anion = 1 : 1 : 1 : 1. In the present system, it is also possible that the TP anion extracts barium together with an inorganic anion in order to neutralize the charge on barium ion. However, there is a difference between the two systems (Ba^{2+}-PEGP-DNP^--X^- and Ba^{2+}-TP^--X^-) with regard to the effect of the inorganic anion on the distribution ratio of barium ion, i.e., the dependence of the extraction on the nature of the inorganic anion is much larger in the TP system than in the PEGP-DNP system. As shown in Fig. 3, the extractions of barium perchlorate and chloride with TP take place at pH 5.0 and 8.5, respectively, while corresponding pHs with PEGP and DNP were 6.0 and 7.0 (the ratio of extraction constants for barium perchlorate and barium chloride was about ten for the PEGP-DNP system[1]). This appears to arise from the dissociation of barium complex to the inorganic anion and the cationic barium complex in the organic phase, which is favorable for improving the extractability. This presumption is partly supported from the result of electric conductivity measurement on a barium-loaded organic phase. The apparent conductivity of organic phase increases in the order, $ClO_4^- > SCN^- > Cl^-$. This suggests that the dissociation constant of the barium complexes in the organic phase increases in the same order for these anions.

As to the selectivity of TP among alkaline earth metal cations, the following sequence was observed as

shown in Fig. 3: $Ba^{2+} > Sr^{2+} > Ca^{2+} \gg Mg^{2+}$. The extraction of magnesium ion is negligibly small and hence is not shown in Fig. 3. A detailed study on the extraction equilibrium and related constants is in progress.

In conclusion, the introduction of a proton-dissociable group into a poly(oxyethylene)-type surfactant molecule gave an efficient extractant for alkali and alkaline earth metal ions. The metal ions could be extracted into and back-extracted from organic solvents simply by changing the pH of the contacting aqueous solution, while the extractant stayed essentially in organic solution. This makes the extractant useful both in ordinary solvent extraction and in carrier-mediated liquid membrane separation processes. Unlike crown ether-based reagents, poly(oxyethylene)-based extractants are easy to prepare at low costs, and could be a candidate for a large scale separation of certain alkali metals in the future. On the other hand, poly(oxyethylene)-based extractants obviously can not be expected to offer a variety of metal extraction selectivity as has been proved possible with crown ether-based reagents. However, it is becoming increasingly clear that the extraction of alkali and alkaline earth metal ions depends remarkably on the nature of the incorporated anionic group (which is to make a direct interaction with the extracted metal ion), basicity and the extent of anionic charge delocalization within the proton-dissociating functional group.[16] In this sense, it would deserve further study to look at the effect of the nature of the anionic group on the extraction selectivity of metal ions.

References

1) Y. Sakai, H. Nakamura, M. Takagi, and K. Ueno, *Bull. Chem. Soc. Jpn.*, **59**, 381 (1986).
2) A. M. Y. Jaber, G. J. Moody, and J. D. R. Thomas, *J. Inorg. Nucl. Chem.*, **39**, 1689 (1977).
3) K. Ono, H. Konami, and K. Murakami, *J. Phys. Chem.*, **83**, 2665 (1979).
4) H. Awano, K. Ono, and K. Murakami, *Bull. Chem. Soc. Jpn.*, **55**, 2530 (1982).
5) S. Yanagida, K. Tanaka, and M. Okahara, *Bull. Chem. Soc. Jpn.*, **50**, 1386 (1977).
6) L. Favretto and F. Tunis, *Analyst*, **101**, 198 (1976).
7) L. Favretto, B. Stancher, and F. Tunis, *Analyst*, **104**, 241 (1979), **105**, 1254 (1980).
8) R. J. Levins, *Anal. Chem.*, **43**, 1045 (1971).
9) D. L. Jones, G. J. Moody, and J. D. R. Thomass, *Analyst*, **106**, 439 (1981).
10) M. Takagi and K. Ueno, "Crown Compounds as Alkali and Alkaline Earth Metal Ion Selective Chromogenic Reagents" in "Host Guest Complex Chemistry III" in "Topics in Current Chemistry," ed by F. L. Boschke, Springer-Verlag, Berlin (1984), Vol. 121, pp. 39—66.
11) N. Yamazaki, S. Nakahama, A. Hirano, and S. Negi, *Tetrahedron Lett.*, **1978**, 2429.
12) H. Otsuka, H. Nakamura, M. Takagi, and K. Ueno, *Anal. Chim. Acta.*, **147**, 227 (1983).
13) M. Jawaid and F. Ingman, *Talanta*, **25**, 91 (1978).
14) D. L. Hughes, C. L. Mortimer, D. G. Parsons, M. R. Truter, and J. N. Wingfield, *Inorg. Chim. Acta*, **21**, L23 (1977).
15) B. L. Papke, M. A. Ratner, and D. F. Shriver, *J. Phys. Chem. Solids*, **42**, 493 (1981).
16) Y. Katayama, R. Fukuda, and M. Takagi, *Anal. Chim. Acta*, in press.

 © 1987 The Chemical Society of Japan Bull. Chem. Soc. Jpn., 60, 551—556 (1987)

The Synthesis and Crystal and Molecular Structures of [Pentaaquabis(1-hydroxy-2-naphthoato)neodymium(III)] (1-Hydroxy-2-naphthoate) Dihydrate, $[Nd\{C_{10}H_6(OH)CO_2\}_2(H_2O)_5][C_{10}H_6(OH)CO_2]\cdot 2H_2O$

Yoshiyuki Ohki,† Yasuo Suzuki,† Mamoru Shimoi, and Akira Ouchi*
Department of Chemistry, College of Arts and Sciences, The University of Tokyo, Komaba, Meguro-ku, Tokyo 153
†Department of Industrial Chemistry, Faculty of Engineering, Meiji University, Higashi-Mita, Tama-ku, Kawasaki, Kanagawa 214
(Received August 14, 1986)

The title complex was synthesized, and its crystal and molecular structures were determined by the single-crystal X-ray-diffraction method. It is triclinic, with the space group of $P\bar{1}$; the cell constants are a=20.621 (4), b=22.288 (5), c=7.724 (1) Å, α=93.30 (2), β=96.78 (2), γ=107.43 (2)°, Z=4, and the final R value is 0.048. Although there are two kinds of crystallographically independent complexes, their structures are almost the same, with only a slight difference in the orientations of the naphthalene rings of the ligands. Both of the central metal atoms are ennea-coordinated and are in the tricapped trigonal-prism geometry: two carboxylato ligands make four-membered chelate rings, and they are also ligated five water oxygen atoms. No carboxylate ions bridge the metal atoms, but the oxygen atoms of the ligands, isolated carboxylate ions, and the crystalline water molecules are linked through hydrogen bondings along the bc-plane. The metal atoms lie on a plane parallel to (100), and the planes are separated by the layers of the naphthalene rings of the naphthoate ions.

The structures of many lanthanoid carboxylates have already been reported, and it has been found that almost all of them are in dimeric or polymeric forms, bridged by carboxylato ligands in various modes.[1-8] The present authors were interested especially in the structure of the lanthanoid carboxylates, whose ligands have some bulky substituents, such as phenyl or naphthyl rings. In crystals of such a type of complex, the large hydrophobic parts and the hydrophilic central metal-core parts are apt to take separate positions. For example, the lanthanoid(III) 2-naphthalenesulfonates, although they are not carboxylates, have been found to have an accumulated layer structure where the naphthalene-ring part and the metal-core part form hydrophobic and hydrophilic layers alternately.[9] We have previously obtained neodymium(III) 1-hydroxy-2-naphthoate from an ethanol-water mixed solution, where the ethanol and the water molecules are both coordinated to the same metal atom, and where the metal cores are surrounded by the naphthyl groups of the carboxylato ligands.[10]

When a 2-propanol-water solvent was used instead of ethanol-water, we could obtain alcohol-free neodymium(III) 1-hydroxy-2-naphthoate. This compound is stable in air, unlike the ethanol-coordinated complex, which effloresced quite rapidly.[10] To clarify this difference, we have determined its crystal structure using the single-crystal X-ray-diffraction method.

Experimental

Synthesis of [Pentaaquabis(1-hydroxy-2-naphthoato)-neodymium(III)] (1-Hydroxy-2-naphthoate) Dihydrate. An aqueous solution of neodymium(III) chloride hexahydrate (0.38 g, 1.0_5 mmol) was mixed with an excess of a solution of sodium hydroxide. The hydroxide thus precipitated was washed with water and then dissolved into 20 cm^3 of a warm 2-propanol-water mixture (2:1=v/v) together with 1-hydroxy-2-naphthoic acid (0.59 g, 3.1 mmol); some residue subsequently filtered off. The filtrate was left standing for several days; the crystalline salt was thus precipitated. Yield: 0.36 g, 0.43 mmol, 41%. Found: Nd, 17.30; C, 47.21; H, 4.13%. Calcd for $NdC_{33}H_{35}O_{16}$: Nd, 17.34; C, 47.65; H, 4.24%.

Single-Crystal X-Ray Analysis. A crystal 0.5×0.32×0.10 mm^3 in size was used as the sample without any shaping. The crystallographic data: $NdC_{33}H_{35}O_{16}$, F.W.=831.87, triclinic, space group $P\bar{1}$, a=20.621 (4), b=22.288 (5), c=7.724 (1) Å, α=93.30 (2), β=96.78 (2), γ=107.43 (2)°, U=3347.2 (12) $Å^3$, Z=4, D_m=1.63 (3), D_x=1.65 $Mg\,m^{-3}$, μ(Mo$K\alpha$)=1.65 mm^{-1}. The reflections were collected on a Rigaku AFC-6A automated four-circle X-ray diffractometer with graphite-monochromated Mo$K\alpha$ radiation (0.7107 Å), in the range of $3°<2\theta<55°$, the ω scan technique being employed (scan speed: 4° min^{-1} (θ)); scan width: 1.27+0.5 tan θ (θ/°)). Of the 15417 independent reflections observed, 7579 reflections with $|F_o|>3\sigma(|F_o|)$ were used for the refinement. The intensities were corrected for the Lorentz and polarization factors, as well as for the absorption.

Structure Determination. The structure was solved by the heavy-atom method. Because all the k-odd reflections were very weak, it was assumed that the crystal is formed by the alternate pile of almost identical structures along the b-axis. At first, the average positions of the metal atoms and some coordinated oxygen atoms were deduced from a Patterson map. The other non-hydrogen atoms were located by means of successive Fourier syntheses. The atomic parameters were refined successively by the block-diagonal least-squares method.

At this stage, the structure of the complex was almost converged, but the naphthalene rings parallel to (010) plane were quite deformed, and the difference Fourier synthesis showed the presence of another orientation of the ring. Therefore, the structure was refined with two independent structures, using all the reflections. At the end of the refinement, all the naphthalene rings were found to be in the normal form. The final R value was 0.048.[11]

All the calculations were carried out on a HITAC M-280H apparatus at the Computer Center of the University of Tokyo, using the local version of the UNICS program.[12] The atomic scattering factors were taken from Ref. 13.

Table 1. Final Atomic Coordinates ($\times 10^4$) of the Complex, together with the Equivalent Isotropic Temperature Factors, with their Estimated Standard Deviations in Parentheses

Atom	x	y	z	B_{eq}/Å$^{2a)}$	Atom	x	y	z	B_{eq}/Å$^{2a)}$
Nd(1)	4539.9(2)	3669.1(2)	2701.5(6)	2.2$_1$	Nd(2)	4570.1(2)	8663.3(2)	2695.8(6)	2.4$_2$
O(1)	3426(3)	3398(3)	3808(8)	3.8$_4$	O(7)	3352(3)	8388(3)	3542(9)	4.1$_1$
O(2)	3364(3)	3518(3)	1015(8)	4.1$_2$	O(8)	3446(4)	8393(4)	762(9)	4.7$_3$
O(3)	5678(3)	3471(3)	3163(9)	3.9$_9$	O(9)	5710(3)	8484(3)	3318(9)	3.6$_2$
O(4)	5758(3)	4472(3)	3601(8)	3.3$_4$	O(10)	5767(3)	9476(3)	3630(9)	3.7$_2$
O(5)	3999(4)	393(3)	1097(9)	4.4$_9$	O(11)	4012(3)	5429(3)	977(8)	3.3$_4$
O(6)	4282(3)	1432(3)	1850(8)	3.8$_3$	O(12)	4293(3)	6438(3)	1823(8)	3.3$_9$
O(W1)	4367(3)	4702(3)	3468(8)	3.5$_4$	O(W8)	4357(4)	9675(3)	3549(8)	4.0$_6$
O(W2)	4614(4)	2968(3)	4(8)	3.8$_6$	O(W9)	4683(4)	7973(3)	125(8)	3.9$_1$
O(W3)	4744(3)	4313(3)	219(8)	3.3$_9$	O(W10)	4759(4)	9307(3)	259(8)	3.9$_5$
O(W4)	4188(4)	2563(3)	3243(9)	4.7$_7$	O(W11)	4230(4)	7545(3)	3367(9)	4.5$_0$
O(W5)	4705(3)	3759(3)	5916(8)	3.5$_5$	O(W12)	4675(3)	8715(3)	5886(8)	3.7$_6$
O(W6)	6232(5)	707(5)	2403(10)	7.2$_3$	O(W13)	6201(4)	5645(3)	2485(9)	4.5$_4$
O(W7)	6488(10)	2004(9)	2379(25)	19.7	O(W14)	6492(4)	7048(3)	2181(9)	4.7$_3$
O(C1)	2419(3)	3299(3)	5504(8)	3.9$_1$	O(C31)	2229(4)	8414(4)	4510(11)	6.4$_7$
O(C11)	6668(4)	3075(3)	4227(10)	4.6$_2$	O(C41)	6683(3)	8109(3)	4406(8)	3.5$_2$
O(C21)	2822(4)	−213(3)	−436(11)	5.6$_8$	O(C51)	2829(3)	4830(3)	−623(10)	4.6$_6$
C(C1)	3083(4)	3428(4)	2392(12)	3.1$_4$	C(C4)	3095(5)	8369(5)	1969(14)	4.5$_6$
C(C2)	6030(4)	4018(5)	3766(12)	3.7$_6$	C(C5)	6051(4)	9065(4)	3844(11)	2.4$_9$
C(C3)	3867(4)	906(5)	1078(12)	3.5$_3$	C(C6)	3858(4)	5937(4)	1084(10)	2.5$_8$
C(1)	2077(4)	3342(4)	3975(11)	2.7$_3$	C(31)	1970(6)	8324(5)	2824(17)	5.5$_4$
C(2)	2354(4)	3404(4)	2408(11)	2.7$_5$	C(32)	2351(5)	8280(5)	1507(14)	4.2$_2$
C(3)	1942(5)	3446(5)	817(13)	4.2$_0$	C(33)	2049(6)	8161(6)	−323(16)	5.5$_1$
C(4)	1260(5)	3421(6)	826(15)	5.0$_1$	C(34)	1363(7)	8080(7)	−737(20)	7.2$_1$
C(5)	959(5)	3350(5)	2401(14)	4.1$_2$	C(35)	972(7)	8170(6)	531(22)	7.6$_0$
C(6)	263(5)	3331(6)	2449(16)	5.2$_5$	C(36)	236(8)	8110(8)	136(27)	10.7
C(7)	−34(7)	3209(7)	3966(18)	6.4$_9$	C(37)	−99(8)	8221(8)	1464(27)	10.9
C(8)	380(6)	3171(6)	5514(16)	5.6$_9$	C(38)	162(7)	8299(7)	3254(24)	9.1$_5$
C(9)	1059(5)	3197(6)	5508(14)	4.5$_7$	C(39)	881(7)	8369(7)	3792(24)	8.7$_3$
C(10)	1356(4)	3295(4)	3981(12)	3.3$_6$	C(40)	1237(6)	8276(5)	2385(20)	6.2$_1$
C(11)	7017(5)	3668(5)	4877(12)	3.6$_5$	C(41)	7037(4)	8735(4)	5016(11)	2.8$_1$
C(12)	6724(4)	4151(4)	4688(11)	2.6$_0$	C(42)	6774(4)	9219(4)	4755(11)	3.0$_6$
C(13)	7104(5)	4775(5)	5419(13)	4.2$_8$	C(43)	7144(4)	9837(4)	5438(13)	3.4$_8$
C(14)	7769(5)	4899(5)	6301(13)	3.7$_0$	C(44)	7790(5)	9982(6)	6370(16)	5.0$_5$
C(15)	8059(5)	4398(5)	6511(12)	4.0$_0$	C(45)	8091(5)	9481(5)	6579(14)	3.8$_6$
C(16)	8737(5)	4526(5)	7439(14)	4.4$_2$	C(46)	8776(6)	9632(7)	7550(15)	6.1$_1$
C(17)	8993(6)	4017(7)	7592(17)	6.4$_4$	C(47)	9050(6)	9144(6)	7789(15)	5.6$_6$
C(18)	8634(6)	3413(7)	6853(17)	5.9$_9$	C(48)	8679(6)	8501(7)	7110(16)	6.3$_1$
C(19)	7975(6)	3287(7)	5947(16)	6.5$_6$	C(49)	8015(5)	8342(5)	6178(14)	4.4$_9$
C(20)	7681(5)	3787(5)	5747(12)	3.5$_9$	C(50)	7729(4)	8848(5)	5951(12)	3.5$_9$
C(21)	2690(5)	340(5)	−536(13)	4.0$_4$	C(51)	2713(4)	5393(4)	−594(11)	2.8$_5$
C(22)	3167(5)	879(5)	195(12)	3.4$_5$	C(52)	3209(4)	5959(4)	191(11)	2.3$_8$
C(23)	3023(5)	1482(4)	6(12)	3.2$_7$	C(53)	3051(5)	6528(5)	204(14)	4.6$_5$
C(24)	2391(6)	1463(5)	−856(14)	4.6$_5$	C(54)	2423(5)	6561(5)	−566(15)	4.5$_5$
C(25)	1894(5)	893(6)	−1571(12)	4.3$_4$	C(55)	1925(5)	5988(5)	−1338(13)	4.1$_3$
C(26)	1215(6)	869(7)	−2434(15)	5.6$_7$	C(56)	1264(5)	6014(6)	−2128(15)	5.6$_2$
C(27)	764(6)	287(7)	−3055(17)	6.9$_5$	C(57)	764(6)	5456(6)	−2869(16)	5.4$_0$
C(28)	910(7)	−257(8)	−2878(20)	7.8$_7$	C(58)	906(5)	4875(6)	−2946(15)	5.1$_9$
C(29)	1547(6)	−289(7)	−2099(20)	7.3$_7$	C(59)	1550(5)	4844(5)	−2180(13)	3.8$_4$
C(30)	2036(5)	326(6)	−1433(14)	4.7$_3$	C(60)	2061(4)	5402(4)	−1378(11)	3.0$_2$

a) The equivalent isotropic temperature factors were computed using the following expression:
$B_{eq}=4/3(B_{11}a^2+B_{22}b^2+B_{33}c^2+B_{12}ab\cos\gamma+B_{13}ac\cos\beta+B_{23}bc\cos\alpha)$. The b_{ij}'s are defined by:
$T=\exp[-(h^2B_{11}+k^2B_{22}+l^2B_{33}+2klB_{23}+2hlB_{13}+2hkB_{12})]$.

Results and Discussion

The final atomic parameters and their equivalent isotropic temperature factors are listed in Table 1, while some bond lengths and bond angles, as well as some interatomic distances which are thought to be the hydrogen-bonding ones, are tabulated in Table 2. The projection of the two unit cells along the c-axis, along with the notation of the naphthalene rings, and the perspective drawings of the complex around the metal atoms, Nd(1) and Nd(2), are shown in Figs. 1, 2, and 3, respectively.[14]

Both the metal complexes have almost the same structure: the central metal atoms are ennea-coordinated and are in the tricapped trigonal-prism geometry, where four oxygen atoms of two chelating

Table 2. Selected Bond Lengths and Bond Angles with Their Standard Deviations in Parentheses[16)]

Bond length	(l/Å)	Bond length	(l/Å)
Nd(1)-O(1)	2.462(7)	Nd(2)-O(7)	2.574(7)
Nd(1)-O(2)	2.532(7)	Nd(2)-O(8)	2.491(7)
Nd(1)-O(3)	2.504(7)	Nd(2)-O(9)	2.497(7)
Nd(1)-O(4)	2.597(5)	Nd(2)-O(10)	2.578(5)
Nd(1)-O(W1)	2.483(7)	Nd(2)-O(W8)	2.490(8)
Nd(1)-O(W2)	2.579(7)	Nd(2)-O(W9)	2.518(7)
Nd(1)-O(W3)	2.461(7)	Nd(2)-O(W10)	2.429(7)
Nd(1)-O(W4)	2.429(7)	Nd(2)-O(W11)	2.483(6)
Nd(1)-O(W5)	2.454(6)	Nd(2)-O(W12)	2.441(6)
C(C1)-O(1)	1.247(12)	C(C4)-O(7)	1.260(13)
C(C1)-O(2)	1.268(12)	C(C4)-O(8)	1.241(14)
C(C2)-O(3)	1.246(11)	C(C5)-O(9)	1.290(9)
C(C2)-O(4)	1.301(14)	C(C5)-O(10)	1.234(12)
C(C3)-O(5)	1.252(14)	C(C6)-O(11)	1.266(12)
C(C3)-O(6)	1.288(10)	C(C6)-O(12)	1.258(9)
O(4)···O(W13)	2.726(10)	O(6)···O(W4)	2.753(11)
O(W1)···O(11)	2.756(10)	O(W6)···O(W7)	2.78(2)
O(W7)···O(C11)	2.61(2)	O(12)···O(W11)	2.722(10)
O(W13)···O(W14)	3.031(10)	O(W14)···O(C41)	2.742(10)
O(4)···O(W1^{i})	2.919(10)	O(6)···O(W12^{i})	2.719(10)
O(W4)···O(C41^{i})	2.870(10)	O(W5)···O(12^{i})	2.701(9)
O(W5)···O(W13^{i})	2.936(11)	O(W5)···O(W14^{i})	3.161(10)
O(W6)···O(W12^{i})	2.956(14)	O(W7)···O(W12^{i})	2.97(2)
O(C1)···O(W14^{i})	3.014(11)	O(C11)···O(W11^{i})	2.891(11)
O(2)···O(W14^{iv})	2.795(11)	O(5)···O(W10^{iv})	2.792(11)
O(6)···O(W9^{iv})	2.819(10)	O(W2)···O(12^{iv})	2.829(9)
O(W2)···O(W9^{iv})	2.888(11)	O(W2)···O(W14^{iv})	2.662(10)
O(W3)···O(W3^{iv})	2.980(12)	O(W3)···O(11^{iv})	2.739(9)
O(W3)···O(W13^{iv})	2.709(10)	O(W6)···O(W10^{iv})	2.713(11)
O(W7)···O(8^{iv})	2.57(2)	O(W7)···O(W9^{iv})	2.93(2)
O(W13)···O(C51^{iv})	2.993(12)	O(10)···O(W6^{v})	2.878(12)
O(W8)···O(5^{v})	2.725(11)	O(10)···O(W8^{vi})	2.888(10)
O(W10)···O(W10^{vii})	3.015(13)	O(W6)···O(C21^{viii})	3.020(15)
Bond angle	**(ϕ/°)**	**Bond angle**	**(ϕ/°)**
O(2)-Nd(1)-O(W1)	78.5(2)	O(8)-Nd(2)-O(W8)	85.6(2)
O(2)-Nd(1)-O(W3)	74.5(2)	O(8)-Nd(2)-O(W10)	73.4(2)
O(W1)-Nd(1)-O(W3)	71.1(2)	O(W8)-Nd(2)-O(W10)	72.6(2)
O(W4)-Nd(1)-O(W5)	79.0(2)	O(W11)-Nd(2)-O(W12)	75.0(2)
O(W4)-Nd(1)-O(3)	79.1(2)	O(W11)-Nd(2)-O(9)	78.5(2)
O(W5)-Nd(1)-O(3)	82.0(2)	O(W12)-Nd(2)-O(9)	81.0(2)
O(1)-Nd(1)-O(W2)	116.3(2)	O(7)-Nd(2)-O(W9)	114.4(2)
O(1)-Nd(1)-O(4)	137.3(2)	O(7)-Nd(2)-O(10)	139.5(2)
O(4)-Nd(1)-O(W2)	106.3(2)	O(10)-Nd(2)-O(W9)	106.1(2)
O(2)-Nd(1)-O(W4)	89.9(2)	O(8)-Nd(2)-O(W11)	87.1(2)
O(W1)-Nd(1)-O(W5)	77.3(2)	O(W8)-Nd(2)-O(W12)	76.3(2)
O(W3)-Nd(1)-O(3)	97.9(2)	O(W10)-Nd(2)-O(9)	100.5(2)
O(1)-Nd(1)-O(2)	51.8(2)	O(7)-Nd(2)-O(8)	50.9(2)
O(1)-Nd(1)-O(W1)	75.2(2)	O(7)-Nd(2)-O(W8)	72.4(2)
O(1)-Nd(1)-O(W5)	69.3(2)	O(7)-Nd(2)-O(W12)	72.2(2)
O(1)-Nd(1)-O(W4)	70.4(2)	O(7)-Nd(2)-O(W11)	72.3(2)
O(W2)-Nd(1)-O(2)	81.0(2)	O(W9)-Nd(2)-O(8)	75.0(2)
O(W2)-Nd(1)-O(W3)	70.8(2)	O(W9)-Nd(2)-O(W10)	72.5(2)
O(W2)-Nd(1)-O(3)	72.2(2)	O(W9)-Nd(2)-O(9)	72.9(2)
O(W2)-Nd(1)-O(W4)	69.4(2)	O(W9)-Nd(2)-O(W11)	70.6(2)
O(4)-Nd(1)-O(W1)	73.9(2)	O(10)-Nd(2)-O(W8)	74.4(2)
O(4)-Nd(1)-O(W3)	75.0(2)	O(10)-Nd(2)-O(W10)	75.4(2)
O(4)-Nd(1)-O(3)	50.8(2)	O(10)-Nd(2)-O(9)	50.7(2)
O(4)-Nd(1)-O(W5)	75.7(2)	O(10)-Nd(2)-O(W12)	77.9(2)
C(C1)-O(1)-Nd(1)	95.7(6)	C(C4)-O(7)-Nd(2)	91.3(6)
C(C1)-O(2)-Nd(1)	91.8(6)	C(C4)-O(8)-Nd(2)	95.7(7)
O(1)-C(C1)-O(2)	120.4(9)	O(7)-C(C4)-O(8)	121.3(10)
C(C2)-O(3)-Nd(1)	97.3(6)	C(C5)-O(9)-Nd(2)	95.8(5)
C(C2)-O(4)-Nd(1)	91.6(6)	C(C5)-O(10)-Nd(2)	93.4(5)
O(3)-C(C2)-O(4)	118.5(8)	O(9)-C(C5)-O(10)	119.1(7)
O(5)-C(C3)-O(6)	123.2(9)	O(11)-C(C6)-O(12)	120.2(8)

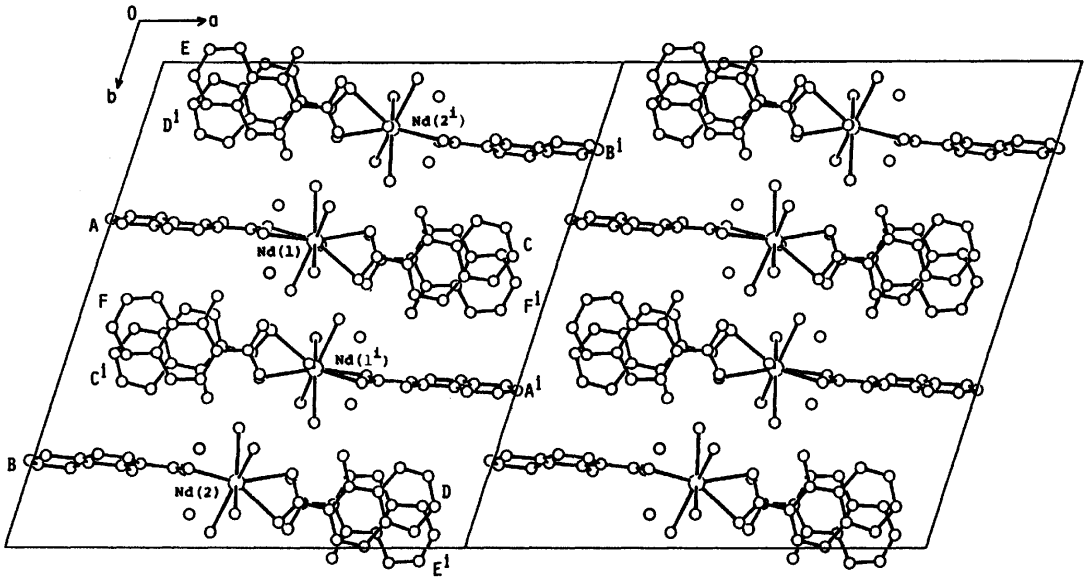

Fig. 1. Projection along the c-axis of the two unit cells with the notations of the naphthalene rings.[16]

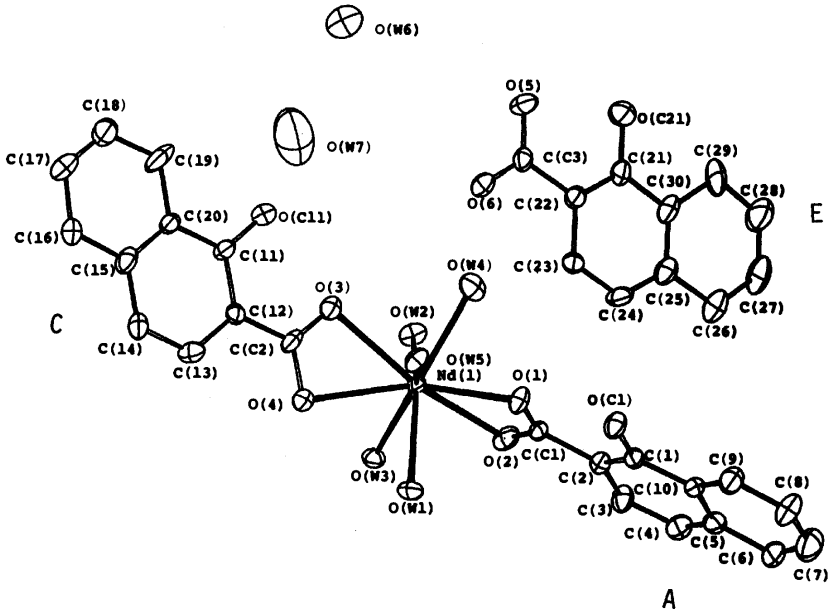

Fig. 2. Perspective drawing of the complex around Nd(1) atom and a non-coordinated naphthoate ion (**E**) with the numbering scheme.

ligands (forming four-membered rings) and five water oxygen atoms are coordinated. The main distinction between the geometries around the two metal atoms lies in the orientations of the A and B naphthoato ligands. As is shown by the schematic presentation in Fig. 4, around Nd(1) and Nd(2) both chelating ligands span the apexes of the trigonal prism and the cap positions respectively; such chelating positions are usual with this type of complex, because the distance between an apex and its nearest cap point is shorter than the edge between two apexes of the prism.[10]

No bridging by the carboxylate ions is found between metal atoms, and this type of the isolated complex is rather rare among lanthanoid carboxylates. The Nd-O bond lengths of the two carboxyl oxygen atoms of the same chelating ligand are not equal. The average lengths of the long and short bonds are 2.57 (2) and 2.49 (2) Å, respectively. However, there is no tendency for either the longer Nd-O bond to join the shorter C-O bond, or the reverse; that is, all the C-O bond lengths are not much different from the delocalized carboxyl C-O bond length. The Nd-O bond lengths in this compound are rather affected by the respective coordinating positions; generally, the Nd-O bonds at the cap positions are longer than those at the apexes of the trigonal prism. The average Nd-O bond

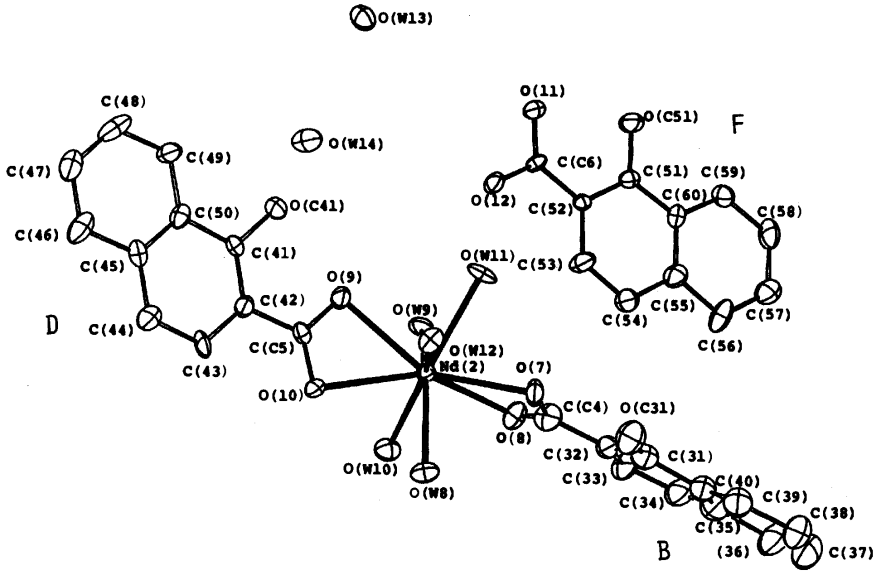

Fig. 3. Perspective drawing of the complex around Nd(2) atom and a non-coordinated naphthoate ion (**F**) with the numbering scheme.

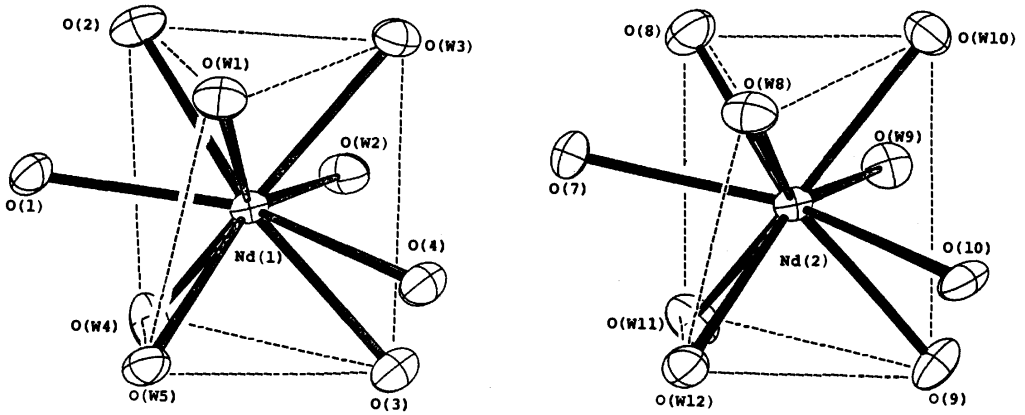

Fig. 4. Schematic presentation to show the coordination geometries around Nd(1) and Nd(2) atoms.

lengths of the water ligands are 2.48 (4) Å, which is a little shorter than that of the carboxylate oxygen atoms, 2.53 (5) Å.

The sum of the Shannon's ionic radii is 2.51 Å for the Nd-O bond (r_{Nd}(Valence(Val)=3+, Coordination Number (CN)=9)=1.163, and r_O(Val=2−, CN=2)=1.35 Å),[15] and both types of Nd-O bond lengths of this complex are not much different.

The other carboxylate anions (**E** and **F**) are not coordinated to the metal atom, and there are two more water molecules per metal atom which are not coordinated. Judging from the interatomic distances, it seems that there are some hydrogen bondings between the carboxyl and hydroxyl-group-oxygen atoms of the carboxylate ions, as well as between the coordinated and non-coordinated water oxygen atoms; many such bondings form a kind of network. Such interatomic distances are shown in Table 2.

As is shown in Fig. 1, the central metal atoms are arrayed almost entirely on (200). Both of the naphthalene rings of the chelate ligands extend to the direction approximately perpendicular to this plane. The naphthalene-ring planes of the ligands on both sides

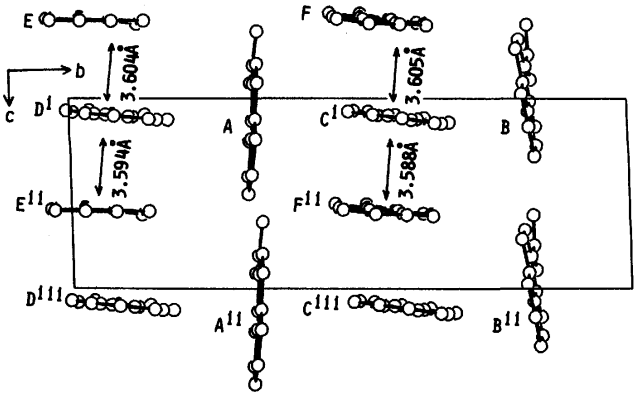

Fig. 5. Packing projection of the naphthalene rings on the plane perpendicular to the $\mathbf{D}^{i}$ ring plane, which is also approximately perpendicular to all the other naphthalene rings.[16]

of one metal atom, **A** and **C**, or **B** and **D**, are approximately orthogonal to each other, while those of the non-coordinated naphthoate ions are almost parallel to one of them, **F** and $\mathbf{C}^{i}$, or **E** and $\mathbf{D}^{i}$, with their hydroxyl groups directed in opposite directions. Thus, as is shown in Fig. 5, the series of naphthalene-ring planes, **E**, $\mathbf{D}^{i}$, $\mathbf{E}^{ii}$, ··· and **F**, $\mathbf{C}^{i}$, $\mathbf{F}^{ii}$, ··· are almost paralle:[16] the maximum dihedral angle between them is 4.7°. They are accumulated approximately in the c-direction. Their inter-planar distances are slightly longer than the thickness of an aromatic ring: $\mathbf{C}^{i}$-**F**, 3.605; $\mathbf{C}^{i}$-$\mathbf{F}^{ii}$, 3.588; **E**-$\mathbf{D}^{i}$, 3.604; and $\mathbf{D}^{i}$-$\mathbf{E}^{ii}$, 3.594 Å.[16] The overlappings of the naphthalene rings of **E**-$\mathbf{D}^{i}$, $\mathbf{D}^{i}$-$\mathbf{E}^{ii}$, **F**-$\mathbf{C}^{i}$, and $\mathbf{C}^{i}$-$\mathbf{F}^{ii}$ are 43, 50, 44, and 51% respectively.[b]

It is of interest to compare this structure with that of lanthanoid(III) 2-naphthalenesulfonate.[9] The latter is also two-dimensional network formed of hydrogen bonds between the coordinated and non-coordinated water molecules and sulfonato group, and the naphthalene rings are intercalated between the hydrophilic layers to form hydrophobic sheets. Naphthalene rings dangling from both sides of the hydrophilic sheets interlock with each other to form only one layer of naphthalene rings, and they are packed very closely, as is shown by the distances between the naphthalene rings, which are almost the thickness of the aromatic rings. In the case of the title complex, the naphthalene rings protruding from the hydrophilic layers do not interlock with each other, but form two sheets of naphthalene layers back to back. These differences may be due to the difference in the bulkiness of the sulfonato group and the carboxylato groups, and also to the participation of hydroxyl groups in the hydrogen bondings of the title complex.

The authors wish to thank the Shin-Etsu Chemical Ind. Co., Ltd., for presenting to them the highly pure lanthanoid oxides.

[b] When a naphthalene ring is projected on another naphthalene ring which is approximately parallel, the percentage of the overlapping area to the ring area is adopted.

References

1) H. Sawase, Y. Koizumi, Y. Suzuki, M. Shimoi, and A. Ouchi, *Bull. Chem. Soc. Jpn.*, **57**, 2730 (1984), and the references cited there in.

2) Y. Koizumi, H. Sawase, Y. Suzuki, T. Takeuchi, M. Shimoi, and A. Ouchi, *Bull. Chem. Soc. Jpn.*, **57**, 1809 (1984).

3) Y. Koizumi, H. Sawase, Y. Suzuki, M. Shimoi, and A. Ouchi, *Bull. Chem. Soc. Jpn.*, **57**, 1677 (1984).

4) S. Kondo, M. Shimoi, A. Ouchi, and T. Takeuchi, *Bull. Chem. Soc. Jpn.*, **55**, 2840 (1982).

5) J. W. Bats, R. Kalus, and H. Fuess, *Acta Crystallogr., Sect. B*, **35**, 1225 (1979).

6) M. S. Khiyalov, I. R. Amiraslanov, Kh. S. Mamedov, and E. M. Movsumov, *Zh. Strukt. Khim.*, **22**, 113 (1981).

7) L. A. Aslanov, I. D. Kiekbaev, I. K. Abdul'minev, and M. A. Porai-Koshits, *Kristallografiya*, **19**, 170 (1974).

8) R. C. Mehrotra and R. Bohra, "Metal Carboxylates," Acad. Press, New York, N. Y. (1983), p. 757.

9) Y. Ohki, Y. Suzuki, M. Nakamura, M. Shimoi, and A. Ouchi, *Bull. Chem. Soc. Jpn.*, **58**, 2968 (1985).

10) Y. Ohki, Y. Suzuki, T. Takeuchi, M. Shimoi, and A. Ouchi, *Bull. Chem. Soc. Jpn.*, **59**, 1015 (1986).

11) $R=\sum||F_o|-|F_c||/\sum|F_o|$.

12) "The Universal Crystallographic Computation Program System (UNICS)," ed by T. Sakurai, Crystallographic Society of Jpn., Tokyo (1967).

13) "International Tables for X-Ray Crystallography," Kynoch Press, Birmingham, U. K. (1974), Vol. IV, pp. 92, 150.

14) Some supplemental bond-length and bond-angle data, the final F_o-F_c table, and the anisotropic thermal parameters are deposited as Document No. 8720 at the Office of the Editors of the Bull. Chem. Soc. Jpn.

15) R. D. Shannon, *Acta Crystallogr., Sect. A*, **32**, 751 (1976).

16) Key to the symmetry operations: i, $1-x$, $1-y$, $1-z$; ii, x, y, $1+z$; iii, $1-x$, $1-y$, $2-z$; iv, $1-x$, $1-y$, $-z$; v, x, $1+y$, z; vi, $1-x$, $2-y$, $1-z$; vii, $1-x$, $2-y$, $-z$; viii, $1-x$, $-y$, $-z$.

 © 1987 The Chemical Society of Japan Bull. Chem. Soc. Jpn., 60, 557—562 (1987)

ESR Studies of a New $3d_{z^2}$-Type Copper(II)-Crown Ether Complex with Pentagonal Bipyramidal Geometry

Yong Li, Kunihiko Tajima, Kazuhiko Ishizu,* and Nagao Azuma†
Department of Chemistry, Faculty of Science, Ehime University, Matsuyama 790
†Faculty of General Education, Ehime University, Matsuyama 790
(Received August 15, 1986)

In the presence of the optimum amount of water, the copper(II) ion and 15-crown-5 (15C5) derivatives gave the dihydrated complex in boron trifluoride–diethyl ether (BF_3-ether). Based on optical and ESR spectrometric titrations, we found that the crown ether captures the copper(II) ion in the equivalent metal/ligand molar ratio. The d-d band absorptions of the complexes were detected in the near-infrared region. The complexes revealed the characteristic ESR g-anisotropies ($g_z<g_x$, g_y) which are typical of the copper(II) complexes with a $3d_{z^2}$ ground-state doublet. The superhyperfine splittings due to the ^{17}O isotope was successfully detected, and the fact of the axial ligation of the water molecule was demonstrated. The ESR parameters were determined by means of the computer simulation of the line shape, while the copper-ligand bonding parameters were estimated from the ESR parameters by means of Bleaney's calculation.

The crown ether showed a pronounced ability to bind various cations and anions, with marked conformational changes in the polyether-ring moiety upon the metal chelations. Their hydrophobic exterior allows them to solubilize ionic substances in non-aqueous solvents.[1] These novel properties of crown ethers have resulted in their use as ligands in the molecular design of a metal complex with an unusual metal coordination and a distinctive electronic structure.

For example, the first successful preparation of a Cu(II) complex with a $3d_{z^2}$ ground state has been reported for the systems composed of $CuCl_2$ and crown ethers containing five oxygen atoms. In this case, the ESR measurement clearly demonstrated that the unpaired electron occupies the $3d_{z^2}$ metal orbital, as judged from the typical g-anisotropies, $g_z<g_x$, g_y.[2] The positive detection of a superhyperfine splitting ascribed to the axially ligated two chlorine atoms ($I=3/2$) suggested that the coordination geometry of the complex is a pentagonal bipyramid.[3,4] The subsequent X-ray analysis of the Benzo-15-crown-5(B15C5)-$CuCl_2$ complex visualized the detailed molecular structure, in which the complex takes the pentagonal bipyramidal geometry with the five ethereal oxygen atoms in the equatorial positions and with the two chlorine atoms at the apical positions.[5]

One of the distinct characteristics of the bonding scheme of the complex is the shorter Cu-Cl distances (2.254 and 2.242 Å) seen in the axial bond length, in comparison with the equatorial bond length (2.240—2.337 Å) between the metal and the ethereal oxygen atoms. In contrast to the case of the 5-*O*-membered crown ether, the Cu(II) complexes of 4-*O*- and 6-*O*-membered crown ethers reveal the ESR anisotropies assigned to those of the $3d_{x^2-y^2}$ or $3d_{xy}$-type ground state. In this case, the copper atom binds with the two chlorine atoms at the equatorial positions, thus forming a distorted octahedral geometry, in which the apical Cu-O distances (2.343 and 2.403 Å) are much longer than the equatorial bond length (Cu-Cl=2.214 Å, Cu-O=2.218 and 2.113 Å).[6]

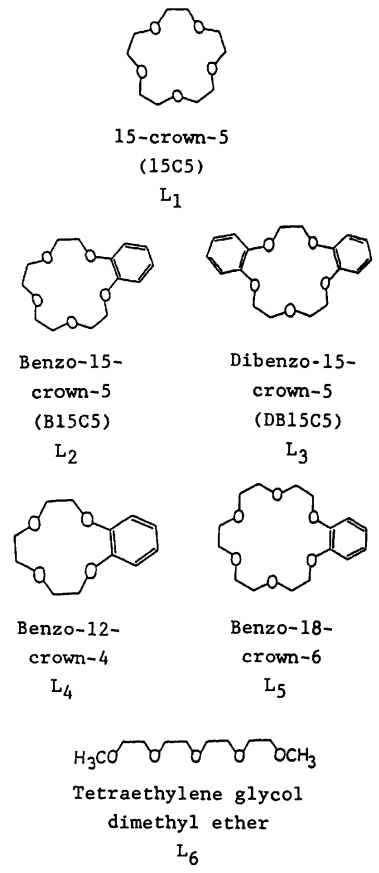

Fig. 1. Chemical structures of polyethers.

In order to elucidate in more detail the coordination chemistry with regard to the Cu(II) complex of 5-*O*-membered crown ether, we continued our efforts to obtain a similar Cu(II) complex generated in a BF_3-ether solution containing a small amount of water. Based on the spectrophotometric titration, we confirmed that the complex is a monomeric copper(II) complex, in which the Cu(II) ion is incorporated into the crown ether in the equivalent metal/ligand molar ratio. In the present paper, we wish to report the

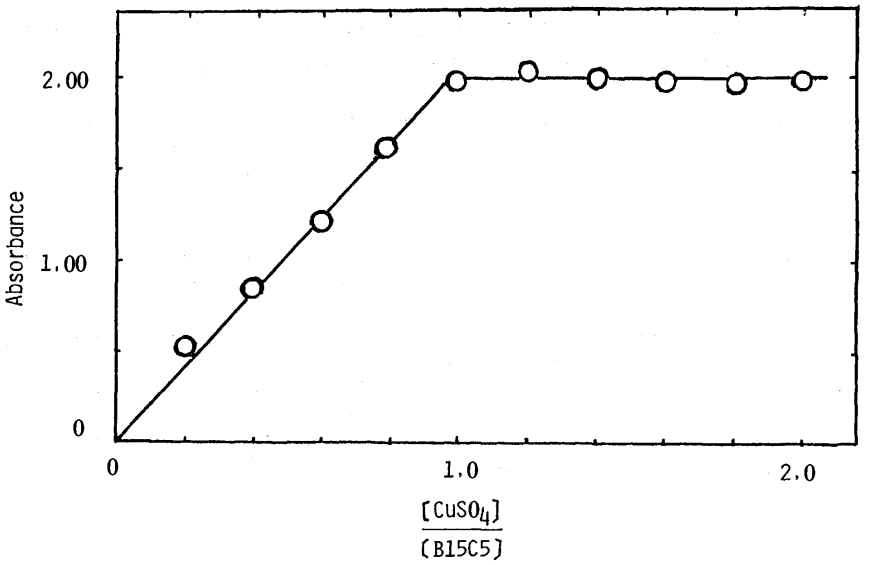

Fig. 2. Plot of the absorbance vs. the molar ratio of Cu(II) ion added to B15C5 solution.

spectroscopic properties of a new Cu(II)-5-*O*-membered crown ether complex in which two water molecules coordinate to the axial positions. The *g*-anisotropies measured, $g_z<g_x$, g_y, were indeed typical of Cu(II) complexes with the $3d_{z^2}$ ground state. The positive evidence for the axial ligation of the water molecule was successfully demonstrated by observing the ^{17}O-superhyperfine splitting, which is overlapped with each copper nuclear hyperfine splitting occurring at the g_z-component. By the aid of the MO scheme, the copper-ligand bonding nature was discussed in terms of the ^{17}O spin density.

Under the same reaction conditions, the complex formation was investigated between the Cu(II) ion and a crown ether with an even oxygen number, such as Benzo-12-crown-4(**L**$_4$) and Benzo-18-crown-6(**L**$_5$); the same experiment was also carried out for the 5-*O*-membered polyether with an open-chain structure(**L**$_6$, Fig. 1). In these cases, however, no experimental evidence to support the existence of a $3d_{z^2}$-type complex was obtained anywhere. It was thus confirmed that only 5-*O*-membered crown ethers gave the $3d_{z^2}$-type copper(II) complex in solution.

Experimental

The crown ethers used in this experiment were synthesized and purified according to Pedersen's procedure.[7] The tetraethylene glycol dimethyl ether and copper(II) salts were purchased at Wako Chemicals, Ltd., and they were used without further purification. A commercial grade of 47% BF_3-ether was used after dehydration and distillation.[8]

The electronic spectra were recorded with a JASCO UVIDEC-1 spectrometer and a JASCO UVIDEC-590 NIR spectrometer at room temperature. The ESR measurements were carried out at 77 K by using a JEOL-FE-2XG X-band spectrometer operating with a 100-KHz magnetic-field modulation. The *g*-values were determined by taking Li-TCNQ (g=2.0025) as a standard. The magnetic fields were calibrated based on the hyperfine splitting of Mn(II) in MgO (8.69 mT). All the measurements were performed at the Advanced Instrumental Center for Chemical Analysis, Ehime University.

Results and Discussion

Electronic Spectra. A 1.04×10^{-2} mol dm^{-3} solution (2.5 ml) of B15C5 dissolved in BF_3-ether was titrated with a 0.13 M $CuSO_4$ aqueous solution. By a step-by-step addition (0.04 ml) of the $CuSO_4$ solution, the growth in the absorption intensity was observed in the visible region of the electronic spectrum. An excellent linear increase in the visible absorption (λ_{max}=430 nm, ε=202 mol^{-1} dm^3 cm^{-1}) can be seen with an increase in the amount of $CuSO_4$ added, until the molar ratio of $CuSO_4$ to B15C5, [$CuSO_4$]/[B15C5], reaches unity (Fig. 2). When the total molar concentration of $CuSO_4$ exceeds that of B15C5, a sharp turning occurred on the linear plot, and no important changes in the absorption intensities were detected with a further increase in the [$CuSO_4$]/[B15C5] ratio. Based on the titration behavior between the B15C5 and the $CuSO_4$ solution, the Cu(II) complex formed in the present system is identified as a mononuclear copper(II) complex composed of the Cu(II) ion and the crown ether in an equivalent molar ratio. A similar titration behavior is obtained for the Dibenzo-15-crown-5(DB15C5)-Cu(II) complex by monitoring the characteristic absorption at λ_{max}=448 nm (ε=258 mol^{-1} dm^3 cm^{-1}).

The visible absorption bands thus characterized for DB15C5- and B15C5-Cu(II) complexes are probably to be attributed to the charge transfer between the benzene molecular orbital and the copper 3d atomic orbital, because no important absorption band can be detected for the 15C5-Cu(II) complex in the visible

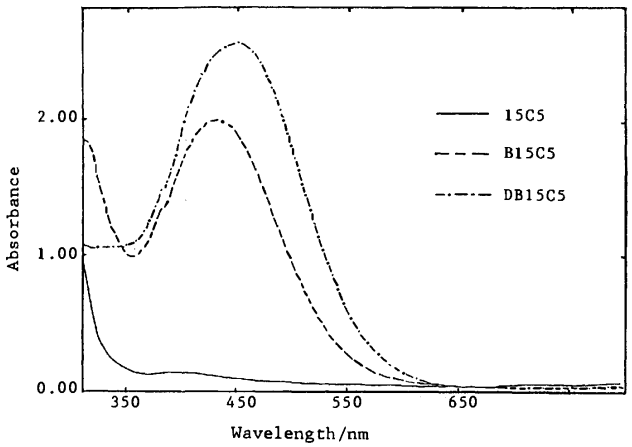

Fig. 3. Visible absorption spectra observed at room temperature for Cu(II)-complexes of L_1, L_2, and L_3.

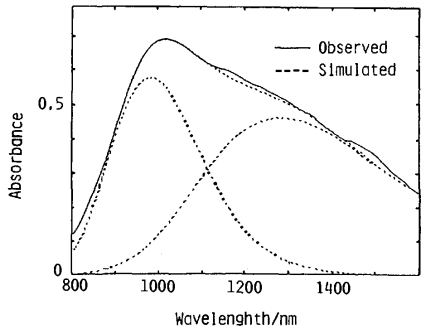

Fig. 4. Near infrared electronic absorption spectra observed at room temperature.

region of the electronic-absorption spectrum (Fig. 3). On the other hand, at the near-infrared band, broad, weak bands were found in the range from 850 to 1600 nm for all the Cu(II) complexes. The computer simulations show that the observed bands are resolved into two characteristic absorptions, occurring at 980 and 1300 nm, respectively (Fig. 4). The molar-extinction coefficients of the bands determined are of the order of 10; we thus assigned these bands to the copper d-d transition absorptions. Based on the ESR parameters (Table 2), the d-d transition energies, ΔE_{zx} and ΔE_{yz}, can be theoretically estimated as follows:

$$\Delta g_x = \frac{6\lambda'}{\Delta E_{zx}}, \quad \Delta g_y = \frac{6\lambda'}{\Delta E_{yz}}, \quad \lambda' = \alpha^2\lambda_0 \qquad (1)$$

where λ_0 (-828 cm^{-1}) is the spin-orbital interaction parameter of a copper(II)-free ion. The calculated wavelengths of the corresponding d-d absorptions (800 and 1000 nm) thus support the fact that the observed optical spectrum of each complex occurs at the near-infrared region, as is shown in Table 1.

ESR Spectra. In the same manner, the Cu(II) complexes were prepared by mixing the crown ethers (L_1, L_2, L_3) with $CuSO_4$ in BF_3-ether in the equivalent molar ratio. The ESR spectra were recorded at 77 K, as

Table 1. Absorption Spectral Data of the Crown Ether-Cu(II) Complexes

Ligand	λ_{max} [a]	ε [a]	λ_{max}	ε	λ_{max}	ε
L_1	—	—	980	8.8	1325	8.7
L_2	430	202	980	6.8	1285	6.3
L_3	448	258	995	9.4	1330	6.8

a) λ_{max} in nm and ε in mol^{-1}dm^{3}cm^{-1}.

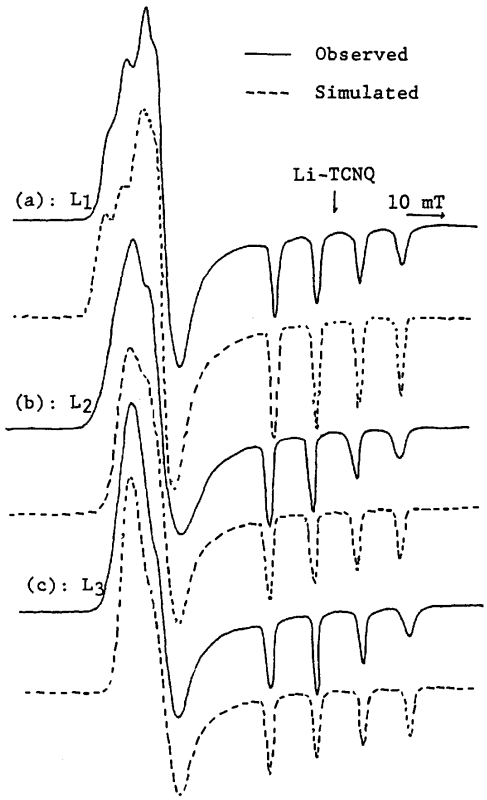

Fig. 5. ESR spectra observed at 77 K and simulated for the crown ether-copper(II) complexes in BF_3-ether. The simulations were carried out by taking the line width as follows: (a): σ_x=1.9 mT, σ_y=3.1 mT, σ_z=0.7 mT; (b): σ_x=2.8 mT, σ_y=2.7 mT, σ_z=0.7 mT; and (c): σ_x=2.2 mT, σ_y=2.8 mT, σ_z= 0.7 mT.

is shown in Fig. 5. The observed spectra together exhibit the rhombic g-anisotropies as are featured in the Cu(II) complexes with the $3d_{z^2}$ ground-state doublet. The computer simulation of the line shape (broken line) showed an excellent agreement with those of the observed spectra based on the ESR parameters summarized in Table 2. Based on the ESR intensity measured at 77 K, the complex formation between 15C5 and the Cu(II) ion was also investigated. A linear growth of the apparent ESR intensity was confirmed within the range in which the total concentration of Cu(II) ions added is less than the equivalent molar concentration of the crown ether (Fig. 6). When an excess amount of the Cu(II) ion is present in the reaction mixture, the ESR of another Cu(II) complex, which reveals the g-anisotropies typical of the $3d_{x^2-y^2}$ or

Table 2. ESR Parameters of the Crown Ether-Cu(II) Complexes

Ligand		g_x	g_y	g_z	A_x[a)]	A_y	A_z	A_z°
L_1	Obsd.	2.400	2.334	1.993	56.0	10.0	107.3	24.3
	Calcd.	—	—	—	40.5	14.8	—	—
L_2	Obsd.	2.387	2.310	1.992	15.0	5.0	112.0	23.5
	Calcd.	—	—	—	42.1	16.0	—	—
L_3	Obsd.	2.387	2.313	1.989	10.0	1.0	117.6	22.9
	Calcd.	—	—	—	47.1	22.4	—	—

a) A in 10^{-4} cm^{-1}.

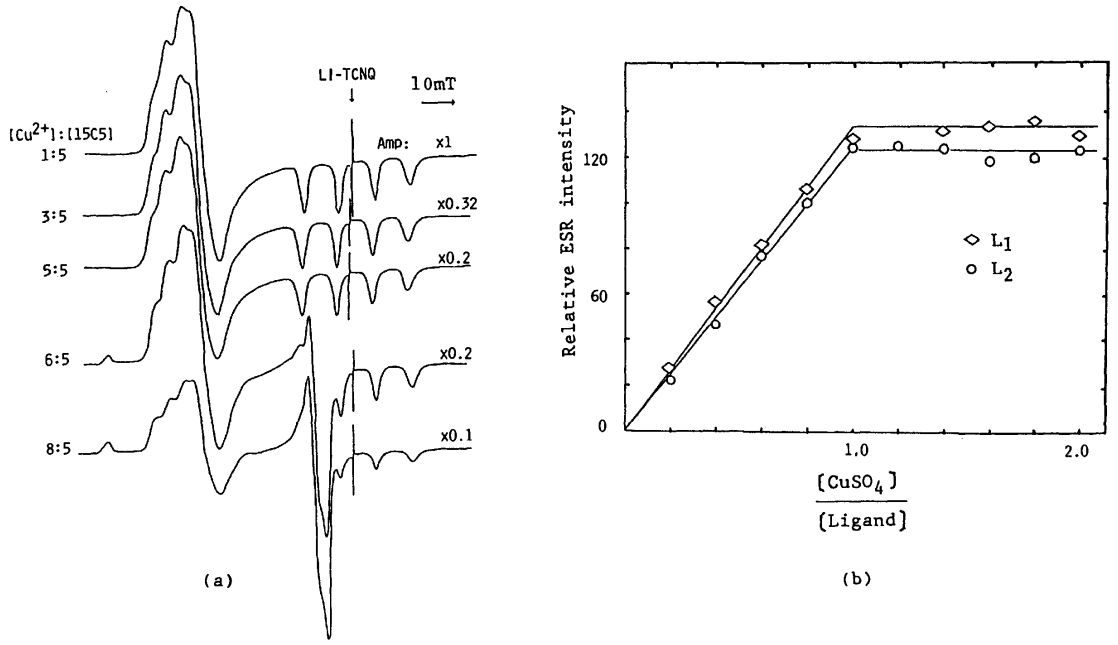

Fig. 6. ESR titration behavior observed for 15C5-Cu(II) systems. (a) ESR spectra observed at 77 K for 15C5-Cu(II) complex generated in the different copper(II) ion/ligand ratio. (b) Relation between the observed ESR intensities of 15C5-Cu(II) complex and the metal/ligand ratio during a titration.

$3d_{xy}$-type ground state, began to overlap with the ESR hyperfine structure of the 15C5-Cu(II) complex, as may be seen in Fig. 6(a). Further, we confirmed that the ESR hyperfine structure ascribed to the $3d_{z^2}$ ground state and that their intensities were not affected by the addition of another ether, 4-*O*-, 6-*O*-membered crown ether (L_4 and L_5) or 5-*O*-membered open-chain ether (L_6), in a large excess. The ESR spectra of the L_4, L_5, and L_6-Cu(II) complexes revealed the *g*-anisotropies, $g_z > g_x$, g_y, appreciate to the $3d_{x^2-y^2}$ or $3d_{xy}$ ground state. One can now conclude that the complexation between the polyether and the Cu(II) ion to give the $3d_{z^2}$ ground-state doublet is strictly limited to the case of the 5-*O*-membered crown ether.

In order to confirm the fact that the water molecules are coordinated to the Cu(II) ion at the apical positions, the L_1, L_2, and L_3-Cu(II) complexes have been obtained by using a $CuSO_4$ aqueous solution containing $H_2{}^{17}O$ (^{17}O atom%=10). The second derivative ESR spectra of the g_z-component measured are shown in Fig. 7, where the ligand superhyperfine splitting due to the ^{17}O isotope (I=5/2) may clearly be seen; the positive evidence of the water ligation is thus successfully demonstrated. Because of the lower concentration of the ^{17}O isotope contained in the H_2O used here, the possibility of the observation of superhyperfine interactions ascribed to the two ^{17}O atoms can be safely disregarded. The superhyperfine coupling constants, A_z°, are listed in Table 2.

With reference to the X-ray analysis of the molecular structure of the L_2-$CuCl_2$ complex,[5] one can now assume that the present complex has two water molecules axially coordinated above and below the pentagonal crown ring.

Calculation of Bonding Parameters. The appropriate molecular orbital occupied by an unpaired electron, which involves the metal $3d_{z^2}$ orbital and also the ligand orbital, can be expressed as follows, provided that the complexes take the pentagonal bipyramidal geometry, D_{5h}:

$$\psi_{z^2} = \alpha d_{3z^2} - \frac{\alpha'}{2\sqrt{10}}(\sqrt{10}\,Z_1 + \sqrt{10}\,Z_2 - 2\,Z_3 - 2\,Z_4 - 2\,Z_5 - 2\,Z_6 - 2\,Z_7) \quad (2)$$

Table 3. Bonding Parameters of the Crown Ether-Cu(II) Complexes

Ligand	Dihydrated				Dichlorinated			
	α^2	$P^{a)}$	κ	β^2	α^2	P	κ	β^2
L_1	0.763	275	0.1003	0.0806	0.914	329	0.1561	0.0875
L_2	0.771	277	0.0904	0.0859	0.914	329	0.1235	0.0995
L_3	0.777	280	0.0700	0.0950	0.916	330	0.0995	0.1085

a) P in 10^{-4} cm^{-1}.

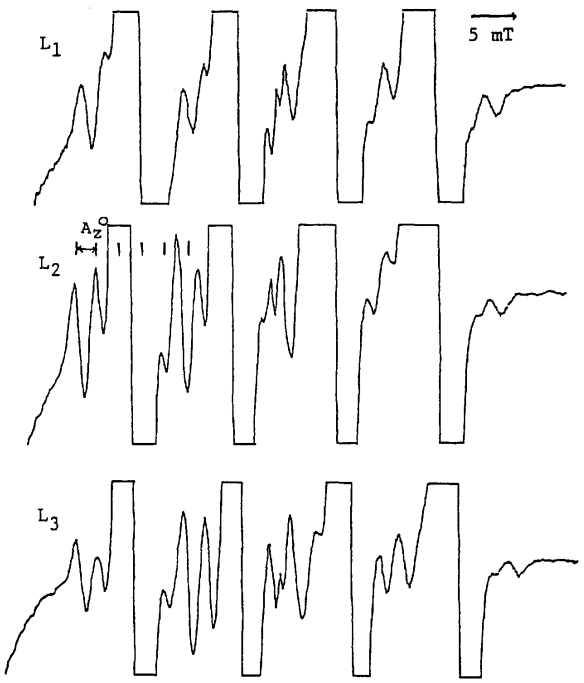

Fig. 7. Enlarged second derivative ESR spectra observed at 77 K for the g_z-components. The six-line superhyperfine structure is attributed to the ^{17}O atom of $H_2{}^{17}O$ which is axially coordinated to the Cu(II) complex.

where Z_1 and Z_2 denote the atomic orbitals in the axial ligands, where Z_3—Z_7 are those in the equatorial ligands, and where the atomic orbitals of the oxygen atoms axially coordinated are described in terms of the sp^3 hybridization, expressed as:

$$Z_i = np \pm \sqrt{1-n^2}\, s \quad (n^2 = 3/4) \tag{3}$$

The spin density on the apical ligand ^{17}O, ρ_0, was thus calculated by means of the following equation:

$$A_z^{\circ} = \rho_o(1-n^2)(A_f + 2A_p) \tag{4}$$

where A_f (-1544×10^{-4} cm^{-1}) and A_p (-48×10^{-4} cm^{-1}) are the isotropic and anisotropic hyperfine constants respectively for the unit spin density on a ^{17}O atom.[9] The total ligand spin densities thus obtained are 0.223—0.237 for the complexes, The magnitude of the spin density on the $3d_{z^2}$ copper atomic orbital, α^2, was estimated by neglecting the overlap integral between the copper and ligand orbitals. Based on the α^2 value thus determined, the Fermi contact term, κ, was calculated from the A_z value using Bleaney's equation,[10] expressed as:

$$A_x = P_0(-\kappa\alpha^2 + \Delta g_x + \frac{1}{14}\Delta g_y - \frac{2}{7}\alpha^2) \tag{5}$$

$$A_y = P_0(-\kappa\alpha^2 + \Delta g_y + \frac{1}{14}\Delta g_x - \frac{2}{7}\alpha^2) \tag{6}$$

$$A_z = P_0(-\kappa\alpha^2 + \Delta g_z - \frac{1}{14}(\Delta g_x + \Delta g_y) + \frac{4}{7}\alpha^2) \tag{7}$$

$$(\Delta g_x = g_x - g_e,\ \Delta g_y = g_y - g_e,\ \Delta g_z = g_z - g_e)$$

where P_0 (360×10^{-4} cm^{-1}) is the dipolar-term of a Cu(II)-free ion. The calculated bonding parameters of the Cu(II) complexes are summarized in Table 3. The magnitude of the calculated A_x and A_y values show an excellent accordance with the experimental tendency, $A_x > A_y$, which was determined by a computer simulation of the observed line shapes, (cf. Table 2). The anomalously small κ values estimated here may be attributed to the mixing of the 4s orbital into the $3d_{z^2}$ atomic orbital, in the correct symmetry, A_{1g}. The isotropic-interaction term measures the sum of the spin polarization attributable to the $3d_{z^2}$ and 4s electrons, written as:

$$-P_0\kappa = A_{3d}\alpha^2 + A_{4s}\beta^2 \tag{8}$$

where A_{3d}=-142×10^{-4} cm^{-1} and A_{4s}=896×10^{-4} cm^{-1}.[11]

In Table 3, the bonding parameters of the dihydrated crown ether-Cu(II) complexes are compared with those of the dichlorinated crown ether-Cu(II) complexes previously reported.[3] It was again confirmed that the contribution of about 8—9.5% from 4s reduces the κ values to a large extent. In both cases, one may see a common tendency for the Δg_z values, a measure of the admixture of $3d_{x^2-y^2}$ into the ground state, to approach that of the pure $3d_{z^2}$ ground state, Δg_z=-0.021,[10] with an increase in the number of fused benzene rings. A concomitant increase in the A_z value can be noted with the increase in the Δg_z and β^2 values. These findings imply that the planar-fused benzene restricts a conformational change in the crown ring upon the optimum metal coordination at the equatorial positions.

For the spin densities on the copper $3d_{z^2}$ orbital, however, one may note a large discrepancy between the values of the dichlorinated crown ether-Cu(II) complexes and those of the dihydrated crown ether-Cu(II) complexes. The considerable reduction in α^2 values noted for the dihydrated Cu(II) complexes means that

the covalent bonding nature between the copper and the axial ligand is more dominant in the present complexes than in the dichlorinated-Cu(II) complexes.

Finally, we would like to consider the reason why the formation of the Cu(II) complex with the $3d_{z^2}$ ground state is limited to cyclic 5-*O*-membered crown ether, not including either the cyclic 4-*O*-, 6-*O*-membered crown ethers or the open-chain 5-*O*-membered polyether. One of the ways to solve the puzzle is by a comparison of the metal-ion radii, which would give the best fit in the cavity of the 15C5. Of interest is the fact that the molecular structure of the dichlorinated B15C5-Cu(II) complex is very much like that of the B15C5-$Mg(NCS)_2$ complex, taking a pentagonal bipyramidal structure.[5,12] The effective radius reported for the Cu(II) ion (0.87 Å) is, indeed, close to that of the Mg(II) ion (0.86 Å).[13] On the other hand, the unpaired copper $3d_{z^2}$ orbital, A_{1g}, would be effectively stabilized in the pentagonal bipyramidal ligand field (D_{5h}), which has the proper symmetry with a metal atomic orbital in terms of the Jahn-Teller distortion.

It has been believed that a strict annihilation of all aerial moisture from the reaction mixture is necessary for the preparation of the crown ether-Cu(II) complex revealing the $3d_{z^2}$ ground state in solution.[3,4] In the present paper, however, the existence of a new dihydrated crown ether-Cu(II) complex with the $3d_{z^2}$ ground state has successfully been demonstrated. Thereafter, we could confirm that the ground-state electronic configuration of the crown ether-Cu(II) complex is greatly dependent on the number of ethereal oxygen donors of the crown ether, and that the $3d_{z^2}$ ground state is exactly limited to the case of the Cu(II) complex of 5-*O*-membered crown ether. In order to put our proposal on a more rigorous experimental base, ESR studies of the Cu(II) complexes with 3-*O*- and 7-*O*-membered crown ethers are now under way.

References

1) J. J. Christensen, D. J. Eatough, and R. M. Izatt, *Chem. Rev.*, **74**, 351 (1974).
2) K. Ishizu, T. Haruta, K. Nakai, K. Miyoshi, and Y. Sugiura, *Chem. Lett.*, **1978**, 579.
3) K. Ishizu, T. Haruta, Y. Kohno, K. Mukai, and Y. Sugiura, *Bull. Chem. Soc. Jpn.*, **53**, 3513 (1980).
4) J. Jezierska and J. B. Raynor, *J. Chem. Soc., Dalton, Trans.*, **1981**, 56.
5) T. Sakurai, K. Kobayashi, S. Tsuboyama, Y. Kohno, N. Azuma, and K. Ishizu, *Acta Crystallogr., Sect. C*, **39**, 206 (1983).
6) F. P. Van Remoorte, F. P. Bore, and E. C. Steiner, *Acta Crystallogr.*, **31**, 1420 (1975).
7) C. J. Pedersen, *J. Am. Chem. Soc.*, **89**, 7017 (1967).
8) G. Zweifel and H. C. Brown, *Org. Reactions*, **13**, 28 (1963).
9) J. E. Wertz and J. R. Bolton, "Electron Spin Resonance," McGraw-Hill, N. Y. (1972), "Table C. Nuclear spins, abundances, moments and hyperfine coupling for some common magnetic nuclei."
10) B. Bleaney, K. D. Bower, and M. H. L. Pryce, *Proc. R. Soc. London*, **228**, 147 (1955).
11) A. F. Garito and B. B. Wayland, *J. Am. Chem. Soc.*, **91**, 866 (1969).
12) J. D. Owen, *J. Chem. Soc., Dalton Trans.*, **1978**, 1418.
13) R. D. Shannon, C. T. Prewitt, *Acta Crystallogr.*, **25**, 925 (1969).

 © 1987 The Chemical Society of Japan Bull. Chem. Soc. Jpn., 60, 563—570 (1987)

Redox Reactions of *cis*-Dialkylcobalt(III) Complexes with Benzyl and Allyl Bromides, Induced by Thermal Cleavage of the Cobalt-Carbon Bond

Kunio Ishikawa, Shunichi Fukuzumi, and Toshio Tanaka*
Department of Applied Chemistry, Faculty of Engineering, Osaka Univeristy, Suita, Osaka 565
(Received August 25, 1986)

The thermal cleavage of the cobalt-carbon bond of *cis*-dialkylcobalt(III) complexes, *cis*-$[R_2Co(bpy)_2]^+$(R=Me, Et, and $PhCH_2$; bpy=2,2′-bipyridine), was enhanced by the presence of benzyl and allyl bromide, inducing the C-C bond formation to yield mainly 1,2-diphenylethane and 1,5-hexadiene, respectively. In the *cis*-$[(PhCH_2)_2Co(bpy)_2]^+$-allyl bromide system, a comparable amount of the cross-coupling product (4-phenyl-1-butene) was obtained together with the homo-coupling products (1,2-diphenylethane and 1,5-hexadiene). The enhancement of the thermal cleavage of the cobalt-carbon bond of *cis*-$[R_2Co(bpy)_2]^+$ by the reactions with benzyl and allyl bromides is caused by the high reactivity of the carbanion ligand of $[RCo(bpy)_2]^+$ produced by the homolytic cleavage of the cobalt-carbon bond of *cis*-$[R_2Co(bpy)_2]^+$, which undergoes the exchange, coupling, and cross-coupling reactions with benzyl and allyl groups of the bromides. Based on the kinetics and the activation parameters, the cobalt-carbon bond dissociation enthalpy of *cis*-$[(PhCH_2)_2Co(bpy)_2]^+$ has been estimated to be 92 kJ mol^{-1}.

The mechanisms of thermal decomposition of organotransition-metals[1,2] as well as the bond dissociation energies of the metal-carbon bonds[3] have been subjects of much interest, since the application of transition-metal reagents to organic, organometallic, and biochemical synthesis, stoichiometric or catalytic, requires the cleavage of metal-carbon bonds. Significant attention has been devoted to mono-organocobalt complexes, which relate to the naturally occurring coenzyme, vitamin B_{12}.[4-8] Although cobalt-carbon bonds of many mono- and di-organocobalt(III) complexes are thermally stable at moderate temperatures, the cleavage of cobalt-carbon bonds is known to be enhanced significantly by redox reactions with organic and inorganic oxidants.[9-13] The cleavage of cobalt-carbon bonds of di-organocobalt(III) complexes, which has been much less studied than mono-organocobalt(III) complexes, is of particular interest, since the cleavage of the cobalt-carbon bond may produce coordinately unsaturated mono-organocobalt(II) complexes which may be much more reactive than di-organocobalt complexes.[14,15]

We have previously reported that the photocleavage of cobalt-carbon bonds of *cis*-dialkylcobalt(III) complexes, *cis*-$[R_2Co(bpy)_2]^+$ (R=Me, Et, and $PhCH_2$; bpy=2,2′-bipyridine), induces C-C bond formation via the redox reactions with benzyl and allyl bromides to yield 1,2-diphenylethane and 1,5-hexadiene, respectively, as the main products.[16] In this study, we report that the thermal cleavage of the cobalt-carbon bond of *cis*-$[R_2Co(bpy)_2]^+$ also induces the C-C bond formation in redox reactions with benzyl and allyl bromides. The present study provides a nice opportunity to compare the thermal and photochemical redox reactions of *cis*-dialkylcobalt(III) complexes with organic halides, revealing both the common and the different aspects in mechanisms between the thermal and photochemical redox reactions.

Experimental

Materials. *cis*-Dialkylcobalt(III) complexes, *cis*-$[R_2Co(bpy)_2]^+$ (R=Me, Et, and $PhCH_2$), were prepared by the reaction of $CoCl_2 \cdot 6H_2O$ with an excess of $NaBH_4$ in the presence of the corresponding alkyl halides and the ligand bpy.[16,17] They were isolated as the perchlorate salts and recrystallized from methanol/water. The purity of the complexes was checked by the elemental analysis; *cis*-$[Me_2Co(bpy)_2]ClO_4$: Found: C, 52.7; H, 4.6; N, 11.1. Calcd for $C_{22}H_{22}N_4O_4CoCl$: C, 52.8; H, 4.4; N, 11.2. *cis*-$[Et_2Co(bpy)_2]ClO_4$ H_2O: Found: C, 52.1; H, 5.1; N, 10.0. Calcd for $C_{24}H_{28}N_4O_5CoCl$: C, 52.7; H, 5.2; N, 10.2. *cis*-$[(PhCH_2)_2Co(bpy)_2]ClO_4$: Found: C, 62.0; H, 4.6; N, 8.5. Calcd for $C_{34}H_{30}N_4O_4CoCl$: C, 63.0; H, 4.7; N, 8.7. Both $[Co(bpy)_3](ClO_4)_2$ and $[Co(bpy)_3]ClO_4$ were prepared by following the literature method.[18] Benzyl or allyl bromide obtained from Wako Pure Chemicals was washed with a 5% aqueous $NaHCO_3$ solution and water successively. After the solution was dried with $MgSO_4$, it was fractionally distilled in the dark under reduced pressure before use. Reagent grade acetonitrile was purified by the standard procedure,[19] followed by redistillation from calcium hydride. Acetonitrile-d_3 was stirred with freshly activated Molecular Sieve 4A (Wako Pure Chemicals) and then transferred in vacuum. Other reagents used for the product analyses were obtained commercially.

Analytical Procedure. Thermal decomposition of *cis*-$[R_2Co(bpy)_2]^+$ was carried out in a Pyrex tube (8 mm I.D.) which contained an MeCN solution (0.5 cm^3) of *cis*-$[R_2Co(bpy)_2]^+$ (1.0×10^{-2} mol dm^{-3}). The solution in the tube was thoroughly degassed by the repeated freeze-pump-thaw cycles before sealing. The top of sealed tube was covered with a reflux condenser and the bottom containing the solution was immersed in an oil bath which was thermostated at 353 K. After the reaction for 52 h, an atmospheric pressure of nitrogen was introduced to the tube, and the gaseous products were analysed by glc using a Unibeads 1S column (1 m).

The redox reactions of *cis*-$[R_2Co(bpy)_2]^+$ with benzyl and allyl bromides were monitored using a Japan Electron Optics JNM-PS-100 ^1H NMR spectrometer (100 MHz). Typically, *cis*-$[R_2Co(bpy)_2]^+$ (0.05 mmol) and benzyl bromide

Table 1. Product Distributions of Thermal and Photochemical Decomposition of *cis*-$[R_2Co(bpy)_2]^+$ under Degassed Conditions in Acetonitrile

cis-$[R_2Co(bpy)_2]^+$	Reaction	Time	Conversion	Product distribution
		h	%	%
R=Me[a]	Δ[c]	52	22	CH_4(66), C_2H_6(34)
	$h\nu$[d]	15	91	CH_4(91), C_2H_6(9)
R=Et[a]	Δ[c]	52	79	C_2H_6(67), C_2H_4(24), C_4H_{10}(9)
	$h\nu$[d]	15	76	C_2H_6(73), C_2H_4(27), C_4H_{10}(trace)
R=$PhCH_2$[b]	Δ[c]	5	57	$PhCH_3$(94), PhC_2H_4Ph(6),
	$h\nu$[d]	50	43	$PhCH_3$(47), PhC_2H_4Ph(51)

a) 1.0×10^{-2} mol dm^{-3}. b) 4.5×10^{-2} mol dm^{-3}. c) Thermolysis at 353 K. d) Photolysis was carried out under irradiation with visible light from a Xenon lamp through a Toshiba glass filter (O-36) which transmits light of $\lambda>360$ nm at 298 K (Ref. 16).

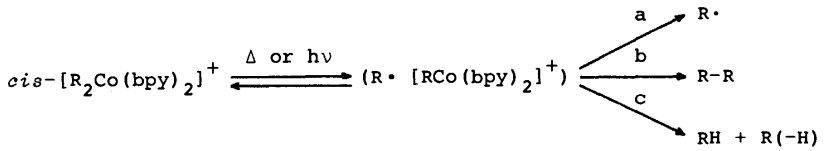

Scheme 1.

(0.05 mmol) was added to an NMR tube which contained 0.5 cm^3 CD_3CN. After the solution was degassed, the sealed NMR tube with a reflux condenser was immersed in an oil bath at 353 K. The NMR spectra were measured periodically at 298 K and the products were identified by comparing the spectra with those of authentic samples. The conversion of *cis*-$[R_2Co(bpy)_2]^+$ to $[Co(bpy)_3]^{2+}$ was confirmed by the appearance of the down field signals of the 2,2′-bipyridine ligand.[18] The organic products were analysed by glc using an OV-17 column (2 m).

Kinetic Measurements. Kinetic data were obtained by using a Union SM-401 spectrophotometer equipped with thermostated cell holders. Reaction rates were determined by the disappearance of the absorption band due to *cis*-$[R_2Co(bpy)_2]^+$ in MeCN (λ_{max}=472, 495, and 502 nm for R=Me, Et, and $PhCH_2$, respectively) under a degassed condition using a Schlenk tube equipped with a side arm fused to a square cuvette (1 or 10 mm I.D.). All the data followed pseudo-first-order kinetics, from which rate constants were determined by least-squares curve fitting using an NEC 9801F microcomputer.

Results and Discussion

Thermal Decomposition of *cis*-$[R_2Co(bpy)_2]^+$. *cis*-Dialkylcobalt(III) complexes are stable in MeCN at 298 K. When the temperature was raised to 353 K, *cis*-$[R_2Co(bpy)_2]^+$ decomposed slowly to undergo the dealkylation reaction. The product distributions are shown in Table 1, together with the data of the corresponding photodecomposition[16] for comparison. The product distributions between thermal and photodecomposition of *cis*-$[R_2Co(bpy)_2]^+$ are similar to each other, except for the ratio of the coupling products of the alkyl groups. For example, both the thermolysis and photolysis of *cis*-$[Me_2Co(bpy)_2]^+$ give methane and ethane, but the mol ratio of ethane to methane in the thermolysis at 353 K (34/66) is significantly larger than that in the photolysis at 298 K (9/91). In the case of *cis*-$[Et_2Co(bpy)_2]^+$ as well, an appreciable amount of the coupling product (butane) is obtained only in the thermolysis (Table 1). On the other hands, thermolysis of *cis*-$[(PhCH_2)_2Co(bpy)_2]^+$ gives a smaller amount of the coupling product (1,2-diphenylethane) than the photolysis (Table 1).

Such product distributions between the thermolysis and photolysis may be explained by Scheme 1, where both the thermolysis and photolysis of *cis*-$[R_2Co(bpy)_2]^+$ results in the homolytic cleavage of the cobalt-carbon bond to produce a geminate radical pair (R· $[RCo(bpy)_2]^+$) which undergoes (a) free radical reactions out of the cage to yield RH and R-R, (b) a coupling reaction in the cage to yield R-R, or (c) a β-hydrogen transfer in the cage to give RH and R(-H) with a 1 : 1 ratio when the alkyl group contains a β hydrogen. Such a homolytic cleavage of the Co-C bond in the photolysis of *cis*-$[R_2Co(bpy)_2]^+$ has been confirmed by the detection of alkyl radicals in the ESR measurements at 77 K.[16] In the case of R=Me or Et, the alkyl radical formed in the geminate radical pair may be reactive enough to undergo the coupling reaction in the cage at a high temperature (e.g., 353 K) to yield more coupling product R-R than the case of photolysis at 298 K. On the other hand, the activation barrier of hydrogen abstraction by benzyl radical from a solvent is known to be higher than that of bimolecular coupling reaction of benzyl radicals.[20] Thus, in the case of *cis*-$[(PhCH_2)_2Co(bpy)_2]^+$, the former becomes a major process in the thermolysis at 353 K to yield mainly toluene (Table 1). Although the stepwise homolytic processes (Scheme 1) appear to account for the product distribution in both the thermal and photochemical decomposition of *cis*-$[R_2Co(bpy)_2]^+$ in the absence and presence of benzyl or allyl bromide as discussed later in more detail, the present conclusion that the coupling R-R and olefin R(-H) products arise

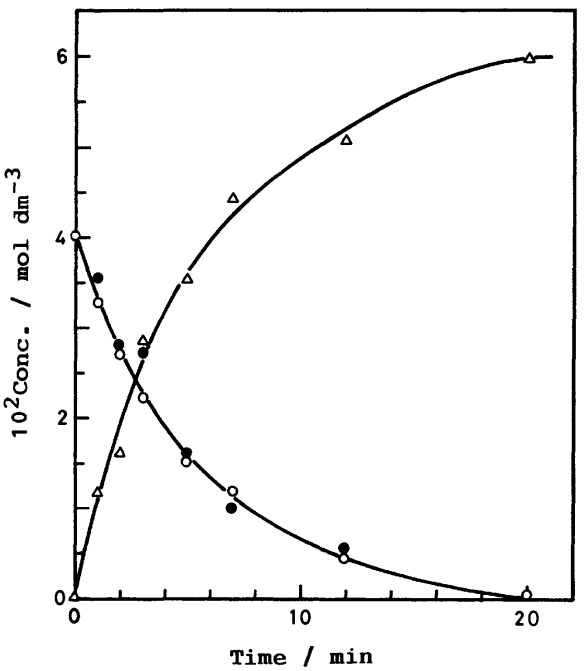

Fig. 1. Time course of the thermal reaction of *cis*-$[(PhCH_2)_2Co(bpy)_2]^+$ (4.0×10^{-2} mol dm^{-3}) with benzyl bromide (4.0×10^{-2} mol dm^{-3}) under a degassed condition in CD_3CN at 353 K; *cis*-$[(PhCH_2)_2Co(bpy)_2]^+$ (○), $PhCH_2Br$ (●), and PhC_2H_4Ph (△).

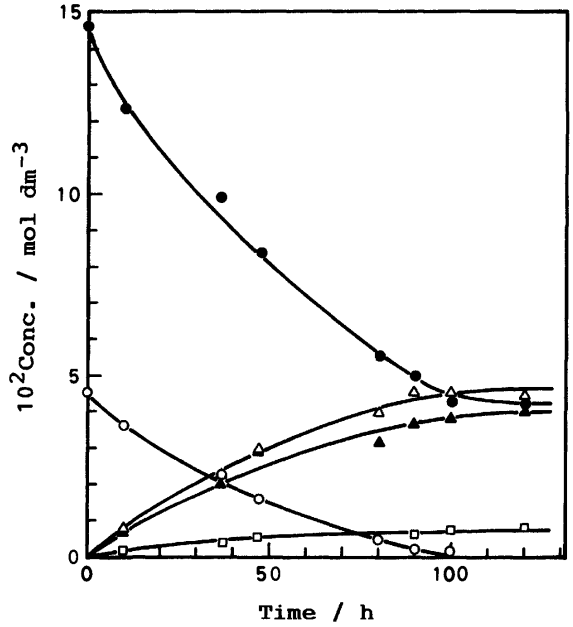

Fig. 2. Time course of the thermal reaction of *cis*-$[Me_2Co(bpy)_2]^+$ (4.5×10^{-2} mol dm^{-3}) with benzyl bromide (1.46×10^{-1} mol dm^{-3}) under a degassed condition in CD_3CN at 353 K; *cis*-$[Me_2Co(bpy)_2]^+$ (○), $PhCH_2Br$ (●), MeBr (△), PhC_2H_4Ph (△), and C_2H_6 (□).

via the homolytic cleavage of the cobalt-carbon bond must be accepted with reservation, since the concerted processes for the reductive coupling and β-elimination pathways are difficult to distinguish from the stepwise, homolytic processes.[21-24]

Redox Reactions of *cis*-$[R_2Co(bpy)_2]^+$ with Benzyl and Allyl Bromides. When the thermal decomposition of *cis*-$[(PhCH_2)_2Co(bpy)_2]^+$ is carried out in the presence of benzyl bromide at 353 K, the rate is enhanced significantly as shown in Fig. 1, where the reaction is completed in 20 min. In addition, the product distribution is changed drastically from toluene as a main product in the absence of benzyl bromide to 1,2-diphenylethane in the presence of benzyl bromide (Fig. 1). The approximate stoichiometry of the reaction is given by Eq. 1,

$$cis\text{-}[(PhCH_2)_2Co(bpy)_2]^+ + PhCH_2Br \xrightarrow{\Delta} \frac{3}{2}PhC_2H_4Ph + [Co(bpy)_2Br]^+ \quad (1)$$

which is the same as the corresponding photochemical reaction.[16]

Thermolysis rate of *cis*-$[Me_2Co(bpy)_2]^+$ is also enhanced by the presence of benzyl bromide, although the rate is much slower than that of *cis*-$[(PhCH_2)_2Co(bpy)_2]^+$, as shown in Fig. 2. The presence of benzyl bromide suppresses completely the formation of methane observed in the absence of benzyl bromide (Table 1), instead methyl bromide is formed as well as 1,2-diphenylethane as a main product, while the ethane formation is not suppressed completely (Fig. 2). The apparent stoichiometry of the reaction between *cis*-$[Me_2Co(bpy)_2]^+$ and benzyl bromide is 1 : 2.3. Such a stoichiometry in Fig. 2 may be explained by considering the occurrence of two different reactions; one is the same as the corresponding photochemical reaction (Eq. 2),[16]

$$cis\text{-}[Me_2Co(bpy)_2]^+ + 3PhCH_2Br \longrightarrow \frac{3}{2}PhC_2H_4Ph + 2MeBr + [Co(bpy)_2Br]^+, \quad (2)$$

where *cis*-$[Me_2Co(bpy)_2]^+$ reacts with three equivalent amounts of benzyl bromide to yield 1,2-diphenylethane and methyl bromide, and the other is the reaction with a 1 : 1 stoichiometry to yield ethane (Eq. 3),

$$cis\text{-}[Me_2Co(bpy)_2]^+ + PhCH_2Br \longrightarrow \frac{1}{2}PhC_2H_4Ph + [Co(bpy)_2Br]^+ + C_2H_6, \quad (3)$$

where benzyl bromide may be reduced by $[Co(bpy)_2]^+$ following the coupling reaction in the cage (Scheme 1-b). The occurrence of two different reactions (Eqs. 2 and 3) can also account for the product distribution in the thermolysis of *cis*-$[Et_2Co(bpy)_2]^+$ in the presence of benzyl bromide (Fig. 3), where one mol of *cis*-$[Et_2Co(bpy)_2]^+$ reacts with 1.4 mol of benzyl bromide to yield 1,2-diphenylethane, ethyl bromide, and butane with small amounts of toluene and ethylene.

Similar results are obtained in the thermolysis of *cis*-$[R_2Co(bpy)_2]^+$ in the presence of allyl bromide. Table 2 summarizes the product distribution includ-

Table 2. Product Yields in the Thermal Reactions of *cis*-$[R_2Co(bpy)_2]^+$ with Benzyl and Allyl Bromides under Degassed Conditions in Acetonitrile at 353 K

cis-$[R_2Co(bpy)_2]^+$[a]	R'Br[a]	Time / h	Product / %[b]
R=Me (4.5×10^{-2})	R'=$PhCH_2$ (1.46×10^{-1})	103	PhC_2H_4Ph(49), $PhCH_3$(1.0), C_2H_6(33), MeBr(98)
R=Et (9.6×10^{-2})	R'=$PhCH_2$ (9.6×10^{-2})	54	PhC_2H_4Ph(48), $PhCH_3$(2.1), C_4H_{10}(38), C_2H_4(10), EtBr(23)
R=Me (7.1×10^{-2})	R'=C_3H_5 (7.1×10^{-2})	100	C_6H_{10}(48), C_3H_6(3.3), C_4H_8(2.2), C_2H_6(32), MeBr(98)
R=Et (9.5×10^{-2})	R'=C_3H_5 (9.5×10^{-2})	30	C_6H_{10}(49), C_3H_6(1.8), C_5H_{10}(2.2), C_4H_{10}(37), C_2H_4(10), EtBr(22)
R=$PhCH_2$ (4.0×10^{-2})	R'=$PhCH_2$ (4.0×10^{-2})	0.5	PhC_2H_4Ph(147), $PhCH_3$(5.4)
R=$PhCH_2$ (4.0×10^{-2})	R'=C_3H_5 (4.0×10^{-2})	0.5	PhC_2H_4Ph(86), C_6H_{10}(35), PhC_4H_7(17), $PhCH_3$(12), C_3H_6(4.3)

a) The concentrations of the reactants in parentheses. b) Based on the cobalt complex.

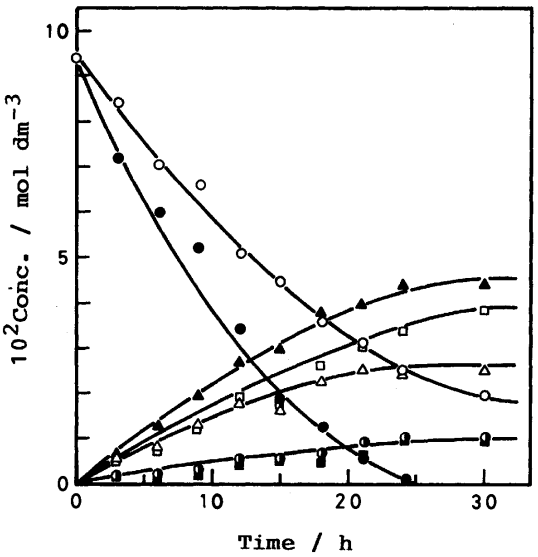

Fig. 3. Time course of the thermal reaction of *cis*-$[Et_2Co(bpy)_2]^+$ (9.4×10^{-2} mol dm^{-3}) with benzyl bromide (9.4×10^{-2} mol dm^{-3}) under a degassed condition in CD_3CN at 353 K; *cis*-$[Et_2Co(bpy)_2]^+$ (○), $PhCH_2Br$ (●), EtBr (△), PhC_2H_4Ph (▲), C_4H_{10} (□), C_2H_4 (■), and $PhCH_3$ (◑).

ing the minor products. In the reactions of *cis*-$[Me_2Co(bpy)_2]^+$ and *cis*-$[Et_2Co(bpy)_2]^+$ with benzyl and allyl bromides, the coupling products of the organic groups of the bromides (1,2-diphenylethane and 1,5-hexadiene, respectively) are obtained, and small amounts of cross-coupling products between the alkyl group of *cis*-$[R_2Co(bpy)_2]^+$ and the organic group of the bromides (e.g., ethylbenzene in the *cis*-$[Me_2Co(bpy)_2]^+$–benzyl bromide system) are formed as well as the products derived from hydrogen abstraction by benzyl and allyl radicals from a solvent (i.e., toluene and propene, respectively). The stoichiometry of these reactions is between 1 and 3 on the degree of the contribution of two different reactions (Eqs. 2 and 3). In the case of the reactions of *cis*-$[(PhCH_2)_2Co(bpy)_2]^+$ with benzyl bromide, however, the stoichiometry is 1 : 1 (Eq. 1) to yield mainly the homo-coupling product (1,2-diphenylethane) together with a small amount of toluene. When benzyl bromide is replaced by allyl bromide in the reaction with *cis*-$[(PhCH_2)_2Co(bpy)_2]^+$, the cross-coupling product between benzyl and allyl group, i.e., 4-phenyl-1-butene is formed together with the homo-coupling products (1,2-diphenylethane and 1,5-hexadiene) as shown in Table 2. Thus, the thermolysis of all the *cis*-dialkylcobalt(III) complexes in the presence of benzyl or allyl bromide results in the C–C bond formation to yield the homo- or cross-coupling products of benzyl and allyl groups as the main products together with small amounts of products derived from hydrogen abstraction by benzyl or allyl radical from a solvent.

Kinetics and Mechanism. The rate of thermal decomposition of *cis*-$[(PhCH_2)_2Co(bpy)_2]^+$ at 353 K is the fastest among *cis*-$[R_2Co(bpy)_2]^+$, and decreases in the order R=$PhCH_2$>Et>Me. The detailed kinetic study has been limited to the thermolysis of *cis*-$[(PhCH_2)_2Co(bpy)_2]^+$, since only *cis*-$[(PhCH_2)_2Co(bpy)_2]^+$ decomposed at measurable rates at relatively low temperatures (e.g., 323 K). The decomposition rates in both the absence and presence of benzyl bromide obeyed the pseudo-first-order kinetics, and the observed rate constant was increased significantly by the presence of benzyl bromide. Such enhancement of the rate by the presence of benzyl bromide may be explained by Scheme 2, where the cleavage of the cobalt–carbon bond (k_1 in Scheme 2) occurs to give a geminate radical pair ($PhCH_2\cdot[PhCH_2Co(bpy)_2]^+$). In the absence of benzyl bromide, the overall decomposition rate may be much lowered owing to the facile recombination of benzyl radical with $[PhCH_2Co(bpy)_2]^+$ in the cage (k_{-1}).[24] The recombination between free benzyl radical and $[PhCH_2Co(bpy)_2]^+$, which are escaped from the cage, may be neglected compared with the recombination of the geminate radical pair in Scheme 2, since the former unimolecular process may be much faster than the latter bimolecular process. Applying the steady-state approximation

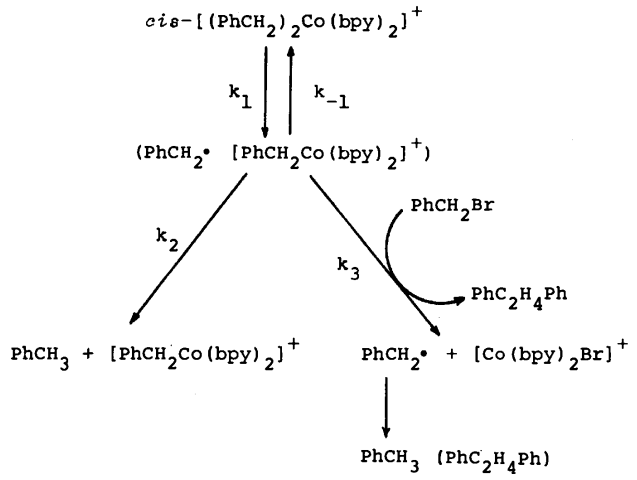

Scheme 2.

to the intermediate ($PhCH_2 \cdot [PhCH_2Co(bpy)_2]^+$) in Scheme 2, the observed rate constant k_0 in the absence of benzyl bromide is expressed by Eq. 4,

$$k_0 = k_1k_2/(k_{-1}+k_2), \quad (4)$$

where k_2 is the rate constant for hydrogen abstraction by benzyl radical from a solvent to yield toluene. Since the recombination process (k_{-1}) may be highly exothermic, k_{-1} may be much larger than k_2; $k_{-1} \gg k_2$, when Eq. 4 is reduced to Eq. 5.

$$k_0 = k_1k_2/k_{-1} \quad (5)$$

The benzyl group of $[PhCH_2Co(bpy)_2]^+$ produced by the homolytic cleavage of the cobalt-carbon bond of *cis*-$[(PhCH_2)_2Co(bpy)_2]^+$ is regarded as the benzyl anion ligand on the basis of the ESR spectrum of $[PhCH_2Co(bpy)_2]^+$ observed in the photolysis of *cis*-$[(PhCH_2)_2Co(bpy)_2]^+$ at 77 K.[15,16] Thus, in the presence of benzyl bromide, the benzyl anion ligand of $[PhCH_2Co(bpy)_2]^+$ may undergo the facile coupling reaction with benzyl bromide (k_3) to yield 1,2-diphenylethane as the case of the photoredox reaction of *cis*-$[(PhCH_2)_2Co(bpy)_2]^+$ with benzyl bromide.[16] Then, the observed rate constant k_{obsd} in the presence of benzyl bromide may be given by Eq. 6. Under the

$$k_{obsd} = \frac{k_1(k_2 + k_3[PhCH_2Br])}{k_{-1} + k_2 + k_3[PhCH_2Br]} \quad (6)$$

condition that $k_{-1} \gg k_2$, from Eqs. 5 and 6 is derived Eq. 7.

$$\frac{1}{k_{obsd} - k_0} = \frac{1}{k_1} + \frac{k_{-1}}{k_1k_3[PhCH_2Br]} \quad (7)$$

The validity of Eq. 7 is confirmed by the linear plots between $(k_{obsd}-k_0)^{-1}$ and $[PhCH_2Br]^{-1}$ at various temperatures as shown in Fig. 4. The rate constant k_1 and k_3k_1/k_{-1} at 323 are obtained as $7.7\times10^{-4}\,s^{-1}$ and $1.1\times10^{-2}\,dm^3\,mol^{-1}\,s^{-1}$, respectively. The rate constant k_{-1} for the cage recombination of an alkyl radical and cob(II)alamin has been reported to be $1.39\times10^9\,s^{-1}$.[5b] By using this value, the rate constant k_3 for the redox

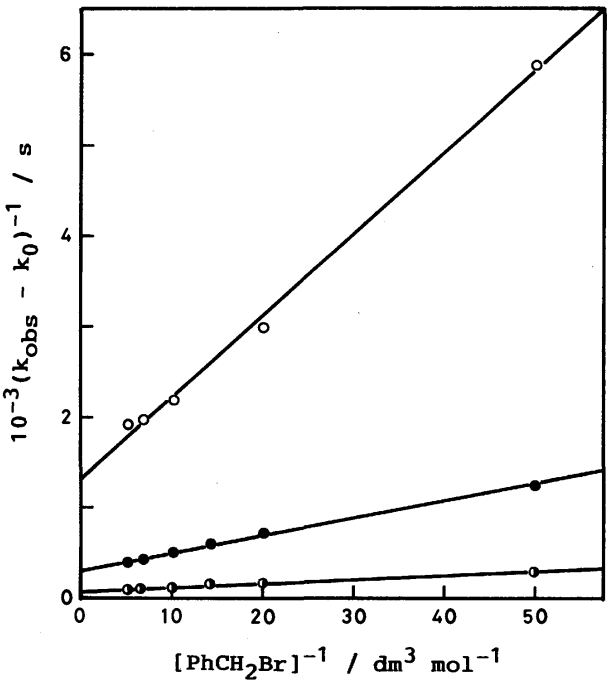

Fig. 4. Plots of $(k_{obsd}-k_0)^{-1}$ vs. $[PhCH_2Br]^{-1}$ for the thermal reaction of *cis*-$[(PhCH_2)_2Co(bpy)_2]^+$ (1.1×10^{-2} mol dm^{-3}) with benzyl bromide in MeCN at 323 (○), 338 (●), and 353 K (◑); see Eq. 7 in text.

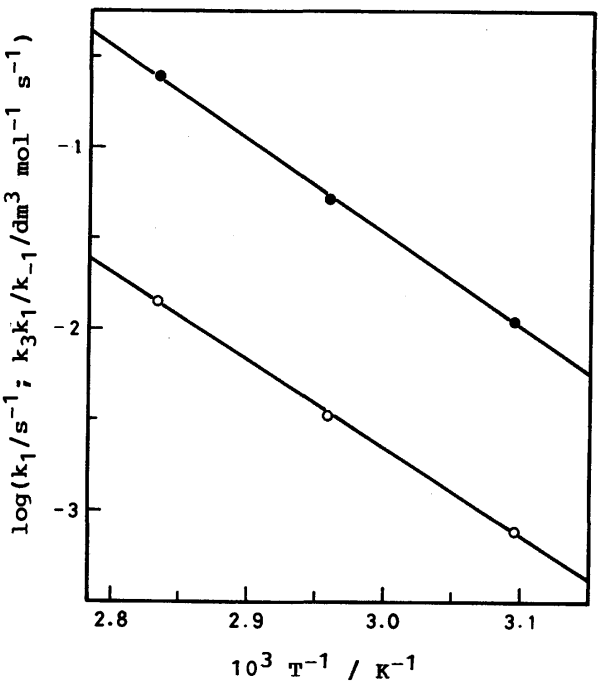

Fig. 5. Arrhenius plots of k_1 (○) and k_3k_1/k_{-1} (●) for the thermal reaction of *cis*-$[(PhCH_2)_2Co(bpy)_2]^+$ with benzyl bromide in MeCN.

reaction of $[PhCH_2Co(bpy)_2]^+$ with benzyl bromide is estimated as $2.0\times10^{10}\,dm^3\,mol^{-1}\,s^{-1}$, which is identical with the diffusion rate constant in MeCN.[25] Arrhenius plots of both k_1 and k_3k_1/k_{-1} give good straight lines with similar slopes to each other (Fig. 5), from which

the values of $\Delta H_1^{\neq}$ and $\Delta H_3^{\neq}+\Delta H_1$ are obtained as 92±4 and 96±4 kJ mol^{-1}, respectively.

Thus, the cobalt-carbon bond dissociation enthalpy ΔH_1 is estimated as 92±4 kJ mol^{-1} by assuming that $\Delta H_1^{\neq} \cong 0$, which is a reasonable approximation for the highly exothermic radical recombination process.[5,6,24] The ΔH_1 value obtained here is similar to those of many organocobalt(III) complexes reported in the literatures.[3a,5,6] The $\Delta H_3^{\neq}$ value may also be estimated as 4±4 kJ mol^{-1} from the values of ΔH_1 and $\Delta H_3^{\neq}+\Delta H_1$. Such a small $\Delta H_3^{\neq}$ value is compatible with the rate constant k_3 being diffusion controlled as described above. The facile reaction of $[PhCH_2Co(bpy)_2]^+$ with benzyl bromide may be responsible for the efficient C-C bond formation from *cis*-$[R_2Co(bpy)_2]^+$ and benzyl bromide, induced by the thermal cleavage of the cobalt-carbon bond. A cobalt-containing product $[Co(bpy)_2Br]^+$, which may be the initial product by the reaction of $[PhCH_2Co(bpy)_2]^+$ with benzyl bromide as confirmed by the ESR spectrum in the photolysis of the *cis*-$[R_2Co(bpy)_2]^+$-benzyl bromide system at 77 K,[16] is converted to $[Co(bpy)_3]^{2+}$ being the most stable form among the mono-, bis-, and tris(2,2′-bipyridine)-cobalt(II) complexes (see Experimental).[26] On the other hand, benzyl radicals produced by the homolytic cleavage of the cobalt-carbon bond of *cis*-$[R_2Co(bpy)_2]^+$ give 1,2-diphenylethane and a small amount of toluene (Table 2).[27] According to Scheme 2, the stoichiometry of the thermal reaction of *cis*-$[R_2Co(bpy)_2]^+$ with benzyl bromide is 1 : 1, agreeing with the observation in Fig. 1 (Eq. 2).

When the alkyl groups of the reactants (*cis*-$[R_2Co(bpy)_2]^+$ and R′Br) are different, the reaction scheme becomes more complicated as shown in Scheme 3, where the thermolysis of *cis*-$[R_2Co(bpy)_2]^+$ (R=Me and Et) also leads to the homolytic cleavage of the cobalt-carbon bond to produce the geminate radical pair ($R\cdot[RCo(bpy)_2]^+$). In the presence of R′Br (R′=$PhCH_2$ and C_3H_5), the alkyl radical (Me· and Et·) may be converted to the more stable radical ($PhCH_2\cdot$ and $C_3H_5\cdot$) by the reaction with R′Br as confirmed by the ESR spectrum in the photolysis of the *cis*-$[R_2Co(bpy)_2]^+$-R′Br system at 77 K.[16] The benzyl and allyl radicals give the homo-coupling products (1,2-diphenylethane and 1,5-hexadiene, respectively) with small amounts of by-products derived from the hydrogen abstraction from a solvent (toluene and propene, respectively) as shown in Table 2. The carbanion ligand in $[RCo(bpy)_2]^+$ may react readily with R′Br to produce the more stable carbanion ligand, and $[R'Co(bpy)_2]^+$ thus formed by the exchange reaction may undergo the homo-coupling reaction with R′Br to yield R′-R′ and $[Co(bpy)_2Br]^+$, while $[RCo(bpy)_2]^+$ may proceed also to the cross-coupling reaction with R′Br, which is shown by the broken line in Scheme 3, yielding R-R′ as a minor product in Table 2 (ethylbenzene, propylbenzene, 1-butene, and 1-pentene for the *cis*-$[Me_2Co(bpy)_2]^+$-$PhCH_2Br$, *cis*-$[Et_2Co(bpy)_2]^+$-$PhCH_2Br$, *cis*-$[Me_2Co(bpy)_2]^+$-C_3H_5Br, and *cis*-$[Et_2Co(bpy)_2]^+$-C_3H_5Br systems, respectively). In this case, the stoichiometry of the reaction of *cis*-$[R_2Co(bpy)_2]^+$ with R′Br is 1 : 3 (Eq. 2), in contrast with the case in Scheme 2.

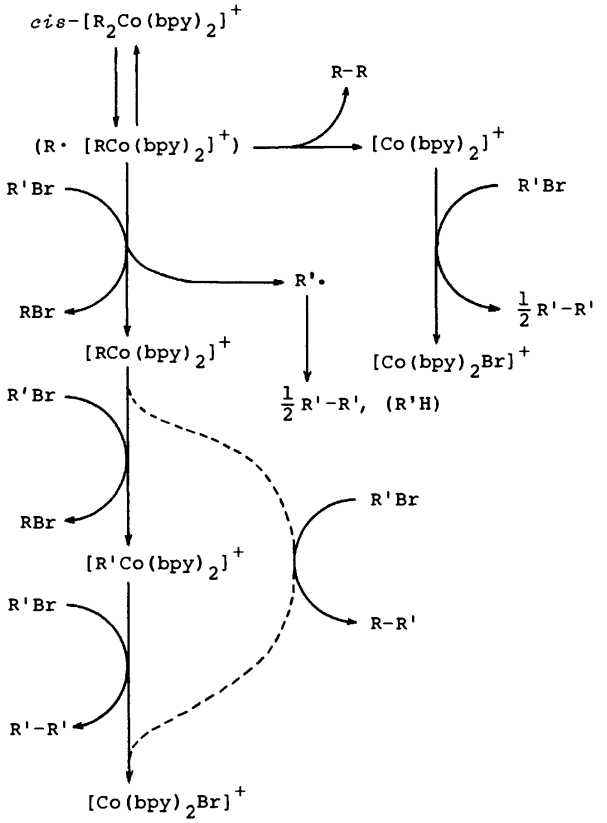

Scheme 3.

On the other hand, a coupling reaction in the geminate radical pair produced by the homolytic cleavage of the cobalt-carbon bond of *cis*-$[R_2Co(bpy)_2]^+$ may occur in the case of R=Me and Et to yield R-R and $[Co(bpy)_2]^+$ (Scheme 1-b).[28] A β-hydrogen transfer in the geminate radical pair may also occur in the case of R=Et which has a β-hydrogen to yield ethane and ethylene as well as $[Co(bpy)_2]^+$ (Scheme 1-c). In the presence of R′Br, such processes are suppressed by the facile reaction of $[RCo(bpy)_2]^+$ in the geminate radical pair with R′Br, but the reductive coupling process is not suppressed completely to yield R-R as well as $[Co(bpy)_2]^+$ which may readily reduce R′Br to give R′-R′ (Scheme 3). Although the reaction mechanism for the reduction of R′Br by $[Co(bpy)_2]^+$ is less clear than that for the reduction of R′Br by $[RCo(bpy)_2]^+$, a likely pathway may be proposed as shown by Eqs. 8—10, since the facile reduction of

$$[Co(bpy)_2]^+ + R'Br \longrightarrow [Co(bpy)_2Br]^+ + R', \quad (8)$$

$$R'\cdot + [Co(bpy)_2Br]^+ \longrightarrow [R'Co(bpy)_2Br]^+, \quad (9)$$

$$R'\cdot + [R'Co(bpy)_2Br]^+ \longrightarrow R'-R' + [Co(bpy)_2Br]^+, \quad (10)$$

alkyl halides by Co(I) complexes is known to occur to yield alkyl radicals and Co(II) complexes Eq. 8,[29] and

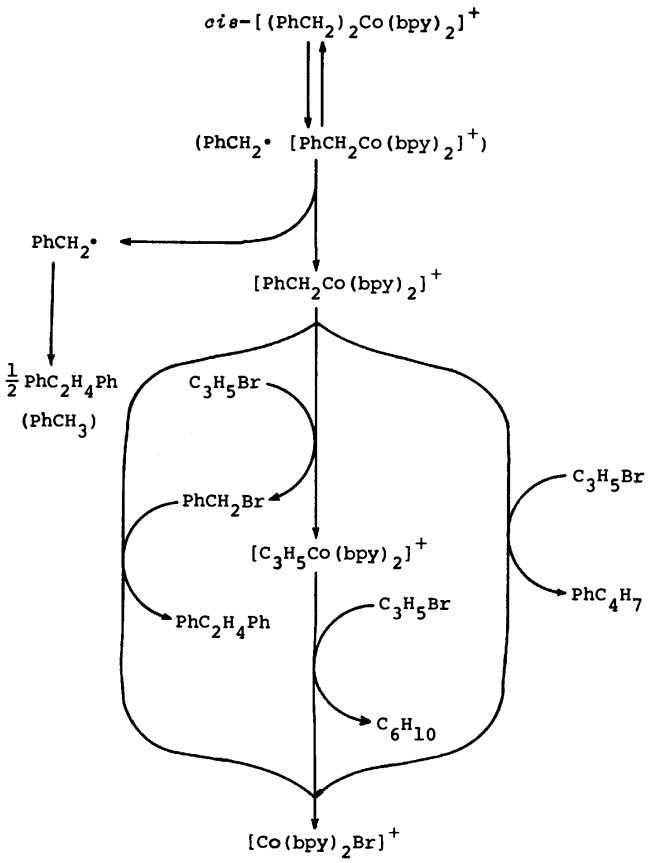

Scheme 4.

the coupling reaction of alkyl radicals may be enhanced in the presence of $[Co(bpy)_2Br]^+$ by the fast recombination with alkyl radicals (Eq. 9),[5,6,24] followed by the bimolecular homolytic displacement reactions (Eq. 10).[23,30] In this case, the stoichiometry is 1 : 1 (Eq. 3). Thus, these two different processes (Eqs. 2 and 3) in Scheme 3 can account for the observed stoichiometry as well as the product distribution in the reaction with R'Br (Figs. 2, 3, and Table 2).

Although the thermal reaction of *cis*-$[(PhCH_2)_2Co(bpy)_2]^+$ with allyl bromide (Scheme 4) is the most complicated case, the reaction scheme is identical with that for the corresponding photochemical reaction reported in the previous paper,[16] except that the thermal cleavage of the cobalt-carbon bond occurs instead of the photocleavage. The monobenzylcobalt(II) complex $[PhCH_2Co(bpy)_2]^+$ produced by the thermal cleavage of the cobalt-carbon bond of *cis*-$[(PhCH_2)_2Co(bpy)_2]^+$ can undergo the exchange, homo- coupling, and cross-coupling reactions with comparable rates, because of similar stabilities between benzyl and allyl anions, yielding 1,2-diphenylethane and 1,5-hexadiene as the homo-coupling products as well as 4-phenyl-1-butene as the cross-coupling product (Table 2). The benzyl radicals which are also produced by the thermal cleavage of the cobalt-carbon bond give 1,2-diphenylethane and toluene by the bimolecular coupling reaction and the hydrogen abstraction from a solvent, respectively (Table 2).[27,31]

In conclusion, the present study has demonstrated that monoalkylcobalt(II) complexes produced by the thermal cleavage of the cobalt-carbon bond of *cis*-dialkylcobalt(III) complexes are highly reactive in the reduction of benzyl and allyl bromides, undergoing the C-C bond formation to yield the homo- and cross-coupling products depending on the stability of the carbanion ligand. In addition to this process which is essentially the same as employed in the corresponding photoredox reaction, the reductive elimination process, where the pair of cobalt-carbon bonds of *cis*-$[R_2Co(bpy)_2]^+$ is cleaved thermally, is also involved in the reduction of benzyl and allyl bromides.

References

1) a) J. K. Kochi, "Organometallic Mechanisms and Catalysis," Academic Press, New York (1979); b) G. W. Parshall, "Homogeneous Catalysis," John Wiley and Sons, New York (1980); c) J. Halpern, *Inorg. Chim. Acta*, **50**, 11 (1981).

2) a) P. J. Davidson, M. F. Lappert, and R. Pearce, *Chem. Rev.*, **76**, 219 (1976); b) R. R. Schrock and G. W. Parshall, *ibid.*, **76**, 243 (1976); c) M. C. Baird, *J. Organomet. Chem.*, **64**, 289 (1974); d) P. S. Braterman and R. J. Cross, *Chem. Soc. Rev.*, **2**, 271 (1973); e) J. R. Norton, *Acc. Chem. Res.*, **12**, 139 (1979).

3) a) J. Halpern, *Acc. Chem. Res.*, **15**, 238 (1982); b) G. W. Kirker, A. Bakac, and J. H. Espenson, *J. Am. Chem. Soc.*, **104**, 1249 (1982); c) A. Bakac and J. H. Espenson, *ibid.*, **106**, 5197 (1984); d) J. H. Espenson, *Prog. Inorg. Chem.*, **30**, 189 (1983).

4) a) "B_{12}," ed by D. Dolphin, Wiley-Interscience, New York (1982); b) "Vitamin B_{12}, Proceedings of the 3rd European Symposium on Vitamin B_{12} and Intrinsic Factor," ed by B. Zagalak and W. Friedrick, Walter de Gruyter, New York (1979); c) J. Halpern, *Pure Appl. Chem.*, **55**, 1059 (1983); d) R. H. Abeles and D. Dolphin, *Acc. Chem. Res.*, **9**, 114 (1976); e) B. Babior, *ibid.*, **8**, 376 (1975).

5) a) T. T. Tsou, M. Loots, and J. Halpern, *J. Am. Chem. Soc.*, **104**, 623 (1982); b) J. Halpern, S.-H. Kim, and T. W. Leung, *ibid.*, **106**, 8317 (1984); **107**, 2199 (1985); c) F. T. T. Ng and G. L. Rempel, *ibid.*, **104**, 621 (1981); d) J. Halpern, F. T. T. Ng, and G. L. Rempel, *ibid.*, **101**, 7124 (1979).

6) a) H. B. Gjerde and J. H. Espenson, *Organometallics*, **1**, 435 (1982); b) R. G. Finke, B. L. Smith, B. J. Mayer, and A. A. Molinero, *Inorg. Chem.*, **22**, 3677 (1983); c) R. G. Finke and B. P. Hay, *ibid.*, **23**, 3041 (1984).

7) a) S. M. Chemaly and J. M. Pratt, *J, Chem. Soc., Dalton Trans.*, **1980**, 2274; b) J. H. Grate, J. W. Grate, and G. N. Schrauzer, *J. Am. Chem. Soc.*, **104**, 1588 (1982); c) G. N. Schrauzer and J. H. Grate, *ibid.*, **103**, 541 (1981); d) J. H. Grate and G. N. Schrauzer, *ibid.*, **101**, 4601 (1979); e) K. N. V. Duong, A. Ahond, C. Merienne, and A. Gaudemer, *J. Organomet. Chem.*, **55**, 375 (1973).

8) a) G. N. Schrauzer and R. J. Windgassen, *J. Am. Chem. Soc.*, **88**, 3738 (1966); b) G. Costa and G. Mestroni, *Tetrahedron Lett.*, **1967**, 4005; c) V. E. Magnuson and J. H. Weber, *J. Organomet. Chem.*, **92**, 233 (1975); d) M. W. Witman and J. H. Weber, *Inorg. Nucl. Chem. Lett.*, **11**, 591 (1975); e) T. Ikariya and A. Yamamoto, *J. Organomet. Chem.*, **120**, 257 (1976).

9) a) J. M. Wood, *Science*, **183**, 1049 (1974); b) U. Schmidt and F. Huber, *Nature*, **259**, 157 (1976); c) P. T. S. Wong, Y. K. Chau, and P. L. Luxon, *ibid.*, **253**, 263 (1975); d) Y. K. Chau, P. T. S. Wong, B. A. Silverberg, P. L. Luxon, and G. A. Bengert, *Science*, **192**, 1130 (1976).

10) a) J. Halpern, M. S. Chan, J. Hanson, T. S. Roche, and J. A. Topich, *J. Am. Chem. Soc.*, **97**, 1606 (1975); b) P. Abley, E. R. Dockal, and J. Halpern, *ibid.*, **95**, 3166 (1973); c) H. L. Fritz, J. H. Espenson, D. A. Williams, and G. A. Molander, *ibid.*, **96**, 2378 (1974); d) J. H. Espenson, W. R. Bushey, and M. E. Chmielewski, *Inorg. Chem.*, **14**, 1302 (1975); e) J. H. Espenson and T. D. Sellers, Jr., *J. Am. Chem. Soc.*, **96**, 94 (1974); f) R. J. Blau and J. H. Espenson, *ibid.*, **107**, 3530 (1985).

11) a) Y.-T. Fanchiang, *Organometallics*, **4**, 1515 (1985); b) Y.-T. Fanchiang, *J. Chem. Soc., Dalton Trans.*, **1985**, 1375; c) Y.-T. Fanchiang, *Inorg. Chem.*, **23**, 3428, 3983 (1984); **21**, 2344 (1982); d) Y.-T. Fanchiang, J. J. Pignatello, and J. M. Wood, *Organometallics*, **2**, 1748, 1752 (1983).

12) a) W. H. Tamblyn, R. J. Klingler, W. S. Hwang, and J. K. Kochi, *J. Am. Chem. Soc.*, **103**, 3161 (1981); b) M. W. Witman and J. H. Weber, *Inorg. Chim. Acta*, **23**, 263 (1977); c) J. H. Dimmit and J. H. Weber, *ibid.*, **16**, 2512 (1977); **15**, 2375 (1976); e) J. H. Espenson, H. L. Fritz, R. A. Heckman, and C. Nicolini, *ibid.*, **15**, 906 (1976).

13) a) S. Fukuzumi, K. Ishikawa, and T. Tanaka, *J. Chem. Soc., Dalton Trans.*, **1985**, 899; *Chem, Lett.*, **1984**, 417; b) S. Fukuzumi, K. Ishikawa, and T. Tanaka, *Nippon Kagaku Kaishi*, **1985**, 62; c) S. Fukuzumi, K. Ishikawa, and T. Tanaka, *Chem. Lett.*, **1986**, 1.

14) a) G. Costa, A. Puxeddu, and E. Reisenhofer, *J. Chem. Soc., Chem. Commun.*,**1971**, 993; b) M. D. Le Hoang, Y. Robin, J. Devynck, C. Bied-Charreton, and A. Gaudemer, *J. Organomet. Chem.*, **222**, 311 (1981).

15) a) M. Hoshino, S. Konishi, Y. Terai, M. Imamura, *Inorg. Chem.*, **21**, 89 (1982); b) D. N. R. Rao and M. C. R. Symons, *J. Organomet. Chem.*, **244**, C43 (1983); *J. Chem. Soc., Faraday Trans. 1*, **80**, 423 (1984).

16) S. Fukuzumi, K. Ishikawa, and T. Tanaka, *Chem. Lett.*, **1985**, 1355; *Organometallics*, in press.

17) G. Mestroni, A. Camus, and E. Mestroni, *J. Organomet. Chem.*, **24**, 775 (1970).

18) R. J. Fitzgerald, B. B. Huchinson, and K. Nakamoto, *Inorg. Chem.*, **9**, 2618 (1970).

19) D. D. Perrin, W. L. F. Armarego, and D. R. Perrin, "Purification of Laboratory Chemicals," Pergamon Press, New York (1966).

20) a) M. J. Gibian and R. C. Corley, *Chem. Rev.*, **73**, 441 (1973); b) R. D. Burkhart, *J. Phys. Chem.*, **73**, 2703 (1969).

21) For discussion of mechanisms of reductive elimination whether being concerted or stepwise, see: Refs. 1a, 2a, and 2b.

22) For a β-elimination pathway through a rate-determining homolysis, see: Refs. 3a, 5a, and 23.

23) M. D. Johnson, *Acc. Chem.. Res.*, **16**, 343 (1983).

24) a) T. S. Roche and J. F. Endicott, *J. Am. Chem. Soc.*, **94**, 8622 (1972); *Inorg. Chem.*, **13**, 1575 (1974); b) J. F. Endicott and G. J. Ferraudi, *J. Am. Chem. Soc.*, **99**, 243 (1977); c) J. F. Endicott and T. L. Netzel, *ibid.*, **101**, 4000 (1979); d) C. Y. Mok and J. F. Endicott, *ibid.*, **100**, 123 (1978); e) H. Elroi and D. Meyerstein, *ibid.*, **100**, 5540 (1978).

25) a) L. Eberson, *Adv. Phys. Org. Chem.*, **18**, 79 (1982); b) D. Rehm and A. Weller, *Isr. J. Chem.*, **8**, 259 (1970).

26) R. M. Smith and A. E. Martell, "Critical Stability Constants," Plenum Press, New York (1975), Vol. 2, p. 235.

27) The coupling reaction of benzyl radicals to yield 1,2-diphenylethane may be enhanced by the presence of $[Co(bpy)_2Br]^+$ (see Eqs. 9 and 10), which can account for the smaller yield of toluene in the presence of benzyl bromide (Table 2) than that in its absence (Table 1).

28) A cobalt-containing product was identified as $[Co(bpy)_3]^+$ by comparing the nmr spectrum in the course of the thermolysis of *cis*-$[Et_2Co(bpy)_2]^+$ in CD_3CN at 353 K with that of the authentic sample prepared by the reduction of $[Co(bpy)_3]^{2+}$ with $NaBH_4$ (see Ref. 18). The bis complex $[Co(bpy)_2]^+$ formed initially may be converted to the tris complex being the most stable form (Ref. 26).

29) a) A. M. Tait, M. Z. Hoffman, and E. Hayon, *J. Am. Chem. Soc.*, **98**, 86 (1976); b) S. Baral and P. Neta, *J. Phys. Chem.*, **87**, 1502 (1983).

30) a) R. C. McHatton, J. H. Espenson, and A. Bakac, *J. Am. Chem. Soc.*, **104**, 3531 (1982); b) A. E. Crease and M. D. Johnson, *ibid.*, **100**, 8013 (1978); c) B. D. Gupta, T. Funabiki, and M. D. Johnson, *ibid.*, **98**, 6697 (1976); d) P. Bougeard, B. D. Gupta, and M. D. Johnson, *J. Organomet. Chem.*, **206**, 211 (1981); e) A. E. Crease, B. D. Gupta, M. D. Johnson, and S. Moorhouse, *J. Chem. Soc., Dalton Trans.*, **1978**, 1821; f) A. Bury, S. T. Corker, and M. D. Johnson, *J. Chem. Soc., Perkin Trans. 1*, **1982**, 645.

31) Some benzyl radicals may be converted to allyl radicals by the reaction with allyl bromide as the case in Scheme 3, yielding 1,5-hexadiene and a small amount of propene (Table 2).

 © 1987 The Chemical Society of Japan Bull. Chem. Soc. Jpn., 60, 571—574 (1987)

Atmospheric Concentrations of Halocarbons in Japan in 1979—1986

Yoshihiro MAKIDE,* Akihito YOKOHATA, Yuji KUBO, and Takeshi TOMINAGA
Department of Chemistry, Faculty of Science, The University of Tokyo, Hongo, Bunkyo-ku, Tokyo 113
(Received September 5, 1986)

The average atmospheric concentrations of halocarbons in the mid-latitude Northern Hemisphere have been measured accurately for 7 years from 1979 to 1986. Atmospheric samples were collected in summer and winter in Hokkaido (40—45°N), and the halocarbons at 10—400 pptv (pptv=10^{-12} v/v) concentrations were determined with 0.5% precision. The concentrations of halocarbons with long lifetimes have been increasing steadily (CCl_2F_2: 18 pptv/year, CCl_3F: 8—9 pptv/year, CH_3CCl_3: 4 pptv/year, CCl_4: 2 pptv/year); those of short-lived halocarbons ($CHCl=CCl_2$ and $CCl_2=CCl_2$) are low (<25 pptv) and show only seasonal variations.

A great concern has been shown for the change in the Earth's environment caused by increasing atmospheric concentrations of trace gases released by human activities. Among them, two groups of compounds should be watched most carefully: CO_2 which causes "greenhouse effect" as released in huge amounts,[1] and halocarbons (halogenated hydrocarbons) with extremely long atmospheric lifetimes, which cause depletion of the stratospheric ozone.[2]

Since the possibility of stratospheric ozone depletion by chlorofluoromethanes (CCl_2F_2 and CCl_3F) was pointed out in 1974,[3] extensive efforts have been made to assess the effect in the future.[2,4] The depletion of ozone in the middle and upper stratosphere has been detected recently.[4]

Halocarbon concentrations in the atmosphere were measured since 1978 at ALE (Atmospheric Lifetime Experiment) stations in Ireland (52°N, 10°W); Oregon, USA (1980—, 45°N, 124°W); the Barbados (13°N, 59°W); American Samoa (14°S, 171°W); and Tasmania (41°S, 145°E), and the data observed up to 1981 have been published.[5] However, such measurements had calibration problems,[6] and no systematic measurement of the atmospheric concentrations has been attempted in Asia. Furthermore, reliable statistics of the world production and emission of halocarbons is hardly available.[7] Since the comparison of models and measurements has shown some disagreements,[4] accurate monitoring of the atmospheric halocarbon concentrations has become more and more important.

In view of such a situation, we started measuring the average atmospheric concentrations of halocarbons in 1979 by analyzing atmospheric samples collected in Hokkaido in summer and winter. The preparation of primary standards was improved, and calibration was repeated carefully. In this paper we wish to report definite atmospheric halocarbon concentrations based on carefully established calibration standards and the trends in their concentrations over the 7 years from 1979 to 1986.

Experimental

Analytical System and Calibration. We have developed an extremely clean, all-metal analytical system for accurate measurement of ultratrace amounts of CCl_2F_2, CCl_3F, CH_3CCl_3, CCl_4, $CHCl=CCl_2$, and $CCl_2=CCl_2$ at 10—400 pptv (pptv: parts per trillion by volume, 10^{-12} v/v) concentration level in the atmosphere.[8,9] A new technique of preparing primary calibration standards was developed for relatively unstable compounds, such as CH_3CCl_3 and CCl_4.[10]

A portion of the atmospheric sample or the standard sample was introduced into an evacuated sample loop (50 ml) up to a pressure of about 1/3 atm and then transferred into a gas chromatograph. A Silicone OV-101 column was used as the preconcentration/separation column with the temperature programmed from −40 to 70 °C. Each halocarbon thus separated was determined by means of an electron capture detector. Methane was mixed into the extremely pure nitrogen carrier gas flow as a make-up gas just before the detector in order to improve the S/N ratio.

The primary calibration standard for each compound was carefully prepared by three-step static dilution with highly purified zero air to a concentration close to the atmospheric concentration. Zero air saturated with water vapor at room temperature was introduced into the flask before the final dilution step so that the water-vapor pressure in the primary standards eventually became about 1 kPa. Several ambient air samples stored in large sample containers were calibrated for all components against each primary standard; they were then used as the secondary standards in routine analysis.

Atmospheric Sampling. All samples were collected by grab-sampling in highly evacuated, extremely clean, all-stainless steel canisters (of two-liter volume and equipped with a stainless-steel bellows valve). In the field, sample air was introduced into the canister up to the ambient pressure by simply opening the valve; no pump or compressor, which would inevitably cause contamination, was employed.

Sampling locations in Japan were extensively surveyed in 1979: in the main and southern parts of Japan, it was found difficult to avoid the influence of regionally polluted air from Japan or Korea.[8] Thus we have collected well-mixed air free from local pollution (called averaged-concentration air, or background air) on a remote coast or point of land mainly in Hokkaido (but occasionally on the west coast of the Tohoku area) every summer (late July to early August) and winter (late January to early February) since 1979. Typical sampling locations are Wakkasakanai in Moor Sarobetsugenya (45°N, 142°E), Nosappu-misaki Point (43°N, 146°E), Setana in Oshima Peninsula (42°N, 140°E), and Nyudozaki Point (40°N, 140°E). Samples were collected against the wind blowing from the ocean.

While the weather conditions are relatively stable in winter (i.e., a high atmospheric pressure overlying Siberia and a low atmospheric pressure overlying the North-west Pacific

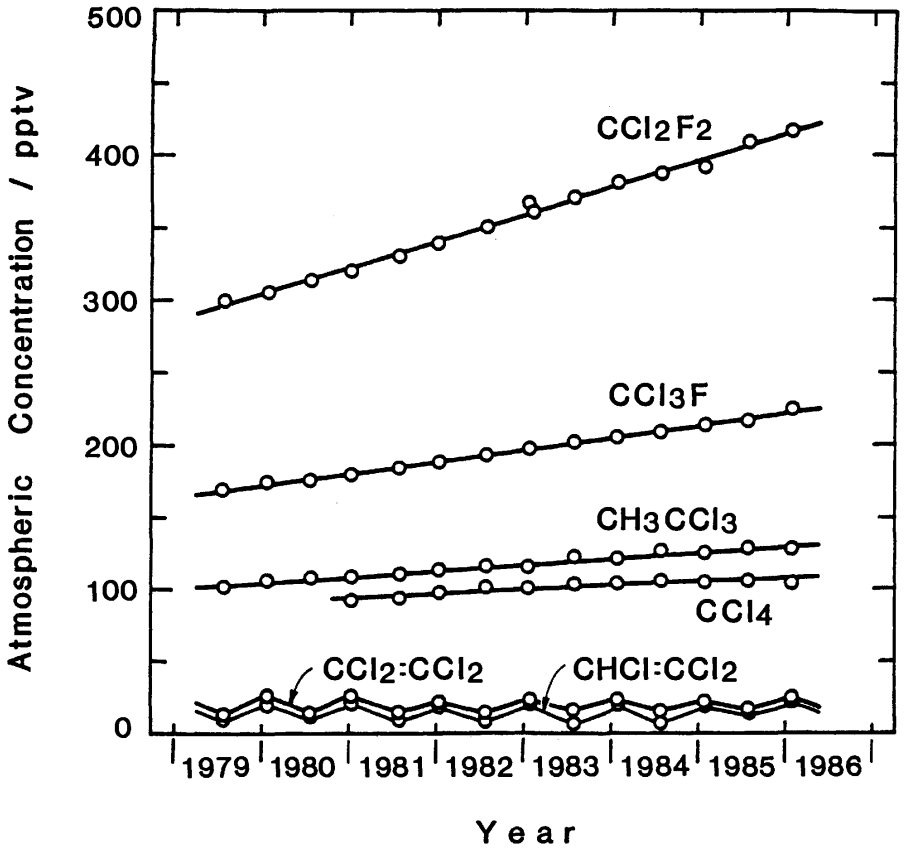

Fig. 1. Atmospheric concentrations of halocarbons in the mid-latitude Northern Hemisphere observed in Hokkaido (40—45°N) in 1979—1986. (pptv=10^{-12} v/v in dry air).

Ocean, causing strong west wind), they are changeable in summer according to the strength of the high atmospheric pressure over the Pacific Ocean. Thus, higher- or lower-latitude air was sometimes collected depending on the distribution of atmospheric pressure. All the collected samples were analyzed in our laboratory at the University of Tokyo within a few weeks of sampling.

Results and Discussion

Analysis. The primary standards for CCl_2F_2, CCl_3F, CH_3CCl_3, and CCl_4 were carefully prepared in different ways and repeatedly, and the concentration of each compound in a secondary standard was determined one by one. The calibration values for these compounds were determined definitely.

The precision of the measurement was within 0.5% at 100 pptv concentration level. The constancy of the calibration was often checked by using the same vacuum-line system and by analyzing several stored ambient air samples which contained enough water vapor to keep most components unchanged.

Trend of Halocarbon Concentrations Observed in Hokkaido. The atmospheric concentrations of CCl_2F_2, CCl_3F, CH_3CCl_3, CCl_4, $CHCl=CCl_2$, and $CCl_2=CCl_2$ observed in Hokkaido since 1979 are shown in Fig. 1.

The concentrations of CCl_2F_2, CCl_3F, and CH_3CCl_3 have been increasing almost linearly during the present period except for small fluctuations depending on the year, possibly due to the meteorological conditions and the limited number of samples. It is not clear whether or not such 2—3-year trends really reflect the variation in emission in the corresponding period.

The observed concentrations of CCl_2F_2 and CCl_3F at the end of January, 1986, were 417 and 225 pptv respectively. Our data of CCl_2F_2 and CCl_3F concentrations in 1980 agree reasonably well (within a possible range of accuracy: 4—5%) with those of the ALE measurements.[5] The increments of the CCl_2F_2 and CCl_3F concentrations we observed in the 6.5-year period were about 117 pptv (i.e., 18 pptv/year) and 56 pptv (i.e., 8.6 pptv/year) respectively; these values correspond to annual increase rates of 6.0 and 5.1% of the 1979 concentrations, or to those of 4.4 and 3.8% of the 1986 concentrations.

While the Chemical Manufacturers Association (CMA) gave estimates of world production and emission for CCl_2F_2 and CCl_3F up to 1982, it then discontinued the world estimates because of the alleged difficulty in estimating the production in the USSR and in Eastern European countries. The CMA data on CCl_2F_2 reported in 1981 were, however, revised upward in the

following year,[7] corresponding to the comments that the observed atmospheric concentrations were much higher than those expected from the 1981 CMA emission values.[11] The CMA attributed the revised amount mainly to unknown USSR emission.

In the 1980's, the world production of CCl_2F_2 and CCl_3F appears to have been roughly constant, or to be gradually increasing.[12] Even if the current emission level is maintained constant in the future (a very conservative assumption), the atmospheric concentrations of CCl_2F_2 and CCl_3F will keep increasing up to above 3000 and 1000 pptv respectively. If the emission of these halocarbons increases, as has been reported recently, the concentrations will become extremely high in the future[13] and a catastrophic change in the ozone layer can be anticipated.[14] The greenhouse effect is also predicted as a result of the strong IR absorption of halocarbons not overlapping with CO_2 absorption bands.[15]

The atmospheric concentration of CH_3CCl_3 has been increasing by about 4 pptv/year, reaching about 130 pptv in 1986. While the production and atmospheric release of CH_3CCl_3 (about 500 kilotons/year) exceed those of CCl_2F_2 and CCl_3F, the increment in its atmospheric concentration is smaller because CH_3CCl_3 is decomposed, mainly by the reaction with OH in the troposphere, and so has only a 6—7 year lifetime.[16]

The atmospheric concentration of CCl_4 increases rather slowly (about 2 pptv/year) because of its large accumulation in the atmosphere as a result of prolonged use since the 1920's, a smaller amount of release (about 100 kilotons/year) in recent years, and its lifetime of about 30 years.[10]

While our data on CCl_2F_2 and CCl_3F concentrations for the 1979—1981 period are similar to the ALE data, the CH_3CCl_3 and CCl_4 values were both about 30% lower than the ALE's.[5] Such large discrepancies in the observed CH_3CCl_3 and CCl_4 concentrations may be attributed to the calibration difficulties in their data, as we have previously pointed out.[6,10] Our new calibration method has solved the problem by adding water vapor in the preparation of standards for CH_3CCl_3 and CCl_4: otherwise, these compounds are readily adsorbed on the vessel's inner wall in extremely pure, dry gases in primary standards, thus mistakenly leading to apparently low concentrations in the standards and, consequently, high atmospheric concentrations, as might be the case with the ALE measurements.

While the $CHCl{=}CCl_2$ and $CCl_2{=}CCl_2$ concentrations in Tokyo often exceed 1000 pptv, those observed in Hokkaido were below 25 pptv, according to their short lifetimes (of a few weeks to a few months) in the troposphere; also, they showed seasonal variation (i.e., they were high in winter and low in summer). This seasonal variation in concentrations may reflect the seasonal difference in the photochemical activity (i.e., the higher OH radical concentration and faster reaction rate in summer) or a difference in the longitudinal transport of air masses from Europe to Hokkaido in the mid-latitude Northern Hemisphere (i.e., faster in winter than in summer). Such an obvious seasonal variation in $CHCl{=}CCl_2$ and $CCl_2{=}CCl_2$ concentrations has not been reported before. By analyzing the seasonal variation coupled with meteorological data, useful information regarding the photochemical activity and/or the global circulation of air masses can be obtained.

In addition to the halocarbons mentioned above, we have also observed other halocarbons, such as $CClF_2CClF_2$, CCl_2FCClF_2, and $CHCl_3$, in the same analytical run,[8,9] although their concentrations have not been determined quantitatively (because of the low concentration, contamination, or instability). CCl_2FCClF_2 has recently been increasingly used for cleaning fine electronic parts, etc. The stainless steel bellows valves of our sample canisters (Nupro SS-4H) had also been washed with this solvent (a standard procedure for meeting NASA specifications). Since we noticed that the CCl_2FCClF_2 concentration increased gradually and slightly in stored samples, even in carefully prepared sample canisters, we discontinued the quantitative determination of the CCl_2FCClF_2 concentration. However, its concentration in freshly collected samples has also been increasing because of its long atmospheric lifetime exceeding several decades.

The contamination of underground water with $CHCl{=}CCl_2$ and $CCl_2{=}CCl_2$ released by the semiconductor industry or dry cleaning has recently been observed in the USA and Japan, and more stable chlorofluorocarbons (e.g., CCl_2FCClF_2) have been proposed as substitutes for such unstable chlorocarbons. Although CCl_2FCClF_2 might be less toxic for human bodies if uptaken, it will instead contribute to the depletion of stratospheric ozone, as does CCl_2F_2. Accordingly, the use of halocarbons with extremely long lifetimes should be strictly checked for the protection of the Earth's atmosphere.

References

1) "Changing Climate," National Academy of Sciences, Washington, D. C., 1983.

2) "The Stratosphere 1981, Theory and Measurements," World Meteorological Organization, (WMO Global Ozone Research and Monitoring Project Report No. 11), Geneva, (1982).

3) M. J. Molina and F. S. Rowland, *Nature*, **249**, 810 (1974).

4) "Present State of Knowledge of the Upper Atmosphere: An Assessment Report," National Aeronautics and Space Administration, (NASA Reference Publication 1162), Washington, D.C., 1986.

5) R. G. Prinn, P. G. Simmonds, R. A. Rasmussen, R. D. Rosen, F. N. Alyea, C. A. Cardelino, A. J. Crawford, D. M. Cunnold, P. J. Fraser, and J. E. Lovelock, *J. Geophys. Res.*, **88**, 8353 (1983).

6) R. A. Rasmussen and J. E. Lovelock, *J. Geophys. Res.*, **88**, 8369 (1983).
7) "World Production and Release of Chlorofluorocarbons 11 and 12 through 1980," Chemical Manufacturers Association (1981); CMA (1982); CMA (1983).
8) Y. Makide, Y. Kanai, and T. Tominaga, *Nippon Kagaku Kaishi*, **1981**, 133.
9) Y. Makide, A. Yokohata, and T. Tominaga, *J. Trace Microprobe Techniques*, **1**, 265 (1983).
10) A. Yokohata, Y. Makide, and T. Tominaga, *Bull. Chem. Soc. Jpn.*, **58**, 1308 (1985).
11) F. S. Rowland, S. C. Tyler, D. C. Montague, and Y. Makide, *Geophys. Res. Lett.*, **9**, 481 (1982).
12) *Chem. Eng. News*, **64**, (April 28), 29 (1986).
13) R. E. Dickinson and R. J. Cicerone, *Nature*, **319**, 109 (1986).
14) M. J. Prather, M. B. McErloy, and S. C. Wofsy, *Nature*, **312**, 227 (1984).
15) V. Ramanathan, R. J. Cicerone, H. B. Singh, and J. T. Kiehl, *J. Geophys. Res.*, **90**, 5547 (1985).
16) Y. Makide and F. S. Rowland, *Proc. Natl. Acad. Sci. U.S.A.*, **78**, 5933 (1981).

 © 1987 The Chemical Society of Japan Bull. Chem. Soc. Jpn., 60, 575—581 (1987)

Synthesis, Characterization, and Isomerization of *trans*- and *cis*-$[CoCl_2(1,2\text{- or }1,3\text{-diphosphine})_2]^+$ and Related Complexes

Tomoji Ohishi, Kazuo Kashiwabara, and Junnosuke Fujita*
Department of Chemistry, Faculty of Science, Nagoya University, Chikusa-ku, Nagoya 464
(Received August 25, 1986)

A number of new diphosphine complexes of cobalt(III), *trans*- and *cis*-$[CoCl_2$(dmpe, dmpp, dbpe, or dpee$)_2]^+$, *trans*- and *cis*-$[CoBr_2(dmpe)_2]^+$, *trans*- and *cis*-$[CoCl(H_2O)(dmpe)_2]^{2+}$, *trans*-$[Co(I_2$ or BrI$)(dmpe)_2]^+$, and $[Co(CO_3)$(dmpp or dbpe)$]^+$ have been prepared and characterized, where dmpe, dmpp, dbpe, and dpee denote 1,2-bis(dimethylphosphino)ethane, 1,3-bis(dimethylphosphino)propane, 1,2-bis(dibutylphosphino)-ethane, and *cis*-1,2-bis(diphenylphosphino)ethylene, respectively. The trans isomers of the dihalogeno complexes are stable to aquation, while the cis isomers release one of the halide ions in water fairly rapidly to yield *cis*-$[CoX(H_2O)$(diphosphine$)_2]^+$ which isomerizes to the trans isomer on exposure of ultraviolet light. The *cis*-$[CoCl_2$(diphosphine$)_2]^+$ complexes in methanol or ethanol solution isomerize to the trans isomer, and the rates were followed spectrophotometrically in the temperature range of 39.0—65.0 °C. The rates have a first-order dependence on the complex concentration. Both the ΔH^* and ΔS^* values for the isomerization increase in the order diphosphine=dmpe<dmpp<dbpe<dpee. This order coincides with the increasing order in cone angle of phosphine ligands, and suggests that the difference in rates among the complexes comes from a steric factor. Absorption spectra of all the complexes have been recorded and the results compared with those of the corresponding ethylenediamine complexes.

Since the first synthesis of cobalt(III)-diphosphine complexes, *trans*-$[CoX_2\{(C_2H_5)_2PCH_2CH_2P(C_2H_5)_2\}_2]^+$ (X=Cl^-, Br^-, and I^-) by Wymore and Bailar,[1] several complexes of this type have been prepared with $(CH_3)_2PCH_2CH_2P(CH_3)_2$,[2,3] $(CH_3)_2PCH_2CH_2CH_2P(CH_3)_2$,[4] *o*-$C_6H_4[P(CH_3)_2]_2$,[5] *o*-$C_6H_4[P(C_6H_5)_2]_2$,[6] and *cis*-$(C_6H_5)_2PCHCHP(C_6H_5)_2$.[7] To our knowledge, however, no cis isomer of those complexes is known. This paper reports the first examples of *cis*-$[CoX_2$(diphosphine$)_2]^+$, where X is Cl^- or Br^-, and diphosphine is $(CH_3)_2PCH_2CH_2P(CH_3)_2$=dmpe, $(CH_3)_2PCH_2CH_2CH_2P(CH_3)_2$=dmpp, $(C_4H_9)_2PCH_2CH_2P(C_4H_9)_2$=dbpe, or *cis*-$(C_6H_5)_2PCHCHP(C_6H_5)_2$=dpee. A pair of trans and cis isomers of $[CoX_2$(diphosphine$)_2]^+$ will be useful for studying physical and chemical properties of a cobalt(III)-phosphine complex which consists of a hard Lewis acid and a soft Lewis base. In this paper we report synthesis, absorption spectra and cis to trans isomerization of the new complexes, and compare the results with those of the corresponding ethylenediamine (en) complexes.

Experimental

Phosphine ligands were handled under an atmosphere of nitrogen until they formed cobalt(III) complexes. All solvents used for preparing ligands and complexes were deoxygenated by bubbling nitrogen for 20 min immediately before use. Absorption and ^1H NMR spectra were recorded on a Hitachi 323 spectrophotometer and a Jeol-PMX 60 spectrometer, respectively.

Phosphine Ligands. The dpee ligand was obtained from Strem Chemicals, Inc. and used as received. The dmpe[8] and dmpp[4] ligands were prepared according to literature methods, and dbpe was prepared by the following method. To $(C_4H_9)_2PH$[9] (11.4 g, 78 mmol) in dry THF (400 cm^3) was added dropwise LiC_4H_9 (15% hexane solution, 39.94 g) with stirring. After 1 h 1,2-dichloroethane (3.86 g, 39 mmol) was added to the resulting orange solution. Stirring was continued for 3 h to give a colorless solution. The solvent was removed under reduced pressure, and the oily residue was shaken with a mixture of chloroform (100 cm^3) and water (100 cm^3) to extract LiCl into water. The chloroform layer was separated, dried over Na_2SO_4 (3 g), and evaporated under reduced pressure to yield a light yellow oil of dbpe, which was used for preparing complexes without further purification.

Preparation of Complexes.† *trans*-$[CoCl_2(dmpe)_2]ClO_4$. The complex was prepared by the published method.[2]

***trans*-$[CoBr_2(dmpe)_2]ClO_4$.** An ethanol solution (5 cm^3) of dmpe (2.06 g, 14 mmol) was added to an ethanol solution (250 cm^3) of $CoBr_2\cdot 6H_2O$ (2.02 g, 6.2 mmol) with stirring. After 1 h concd HBr (1 cm^3) was added, and air was bubbled through the solution for 10 h. The resulting green solution was concentrated to 100 cm^3 under reduced pressure. On addition of $NaClO_4$ (1 g) in ethanol (5 cm^3) the concentrate gave green crystals, which were filtered and recrystallized from hot methanol. Yield: 2.1 g (55%). Found: C, 23.45; H, 4.99%. Calcd for $C_{12}H_{32}Br_2ClCoO_4P_4$: C, 23.30; H, 5.21%. The complex is soluble in methanol, ethanol, and acetonitrile.

***trans*-$[CoI_2(dmpe)_2]ClO_4\cdot 0.5CH_3OH$.** This complex was prepared by a method similar to that for *trans*-$[CoBr_2(dmpe)_2]^+$. A methanol solution (100 cm^3) containing dmpe (240 mg, 1.6 mmol) and $CoI_2\cdot 6H_2O$ (337 mg, 0.8 mmol) was stirred for 20 min and then was mixed with concd HI (1 cm^3) and $NaClO_4$ (150 mg). Air was bubbled through the solution for 6 h. The resulting dark brown solution was concentrated to 50 cm^3 under reduced pressure. The concentrate was cooled at −5 °C for 10 h to give brownish-violet crystals, which were filtered, washed with a mixture (20 cm^3) of methanol and diethyl ether (2:1), and air-dried. Yield: 200 mg (33%). Found: C, 21.02; H, 4.59%. Calcd for $C_{12.5}H_{34}ClCoI_2O_{4.5}P_4$: C, 20.61; H, 4.84%. The complex is soluble in DMF and DMSO.

***cis*-$[CoCl_2(dmpe)_2]ClO_4$.** Crystals of $[Co(CO_3)(dmpe)_2]ClO_4\cdot 1.5NaClO_4\cdot H_2O$[10] (736 mg, 1.15 mmol) were soaked in ice-cold concd HCl (20 cm^3) at 0 °C. After 1 h the result-

†All of the perchlorate salts of cobalt(III)-phosphine complexes described below are potentially explosive, and should be handled carefully.

ing red solution was mixed with an ice-cold aqueous solution (3 cm^3) of $NaClO_4$ (300 mg) and was cooled at −5 °C for 10 h. Red crystals deposited were filtered and recrystallized from acetonitrile (20 cm^3) by adding diethyl ether (50 cm^3). Yield: 340 mg (52%). Found: C, 27.23; H, 6.45%. Calcd for $C_{12}H_{32}C_{13}CoO_4P_4$: C, 27.21; H, 6.09%. The complex is soluble in methanol and acetonitrile.

***cis*-[CoBr$_2$(dmpe)$_2$]ClO$_4$·0.5CH$_3$CN·H$_2$O.** The complex was prepared by the same method as for *cis*-$[CoCl_2(dmpe)_2]^+$ using concd HBr instead of concd HCl. Yield: 38%. Found: C, 21.71; H, 5.32, N, 1.21%. Calcd for $C_{13}H_{35.5}N_{0.5}Br_2ClCoO_5P_4$: C, 21.76; H, 5.45; N, 1.07%. The complex is soluble in methanol and acetonitrile.

***trans*-[CoCl$_2$(dmpp)$_2$]ClO$_4$·0.5H$_2$O.** The complex was prepared by the method of Cloyd and Meek.[4]

[Co(CO$_3$)(dmpp)$_2$]ClO$_4$·H$_2$O. To a solution of *trans*-$[CoCl_2(dmpp)_2]ClO_4 \cdot 0.5H_2O$ (200 mg, 0.35 mmol) in a mixture (100 cm^3) of acetonitrile and water (4:1) were added K_2CO_3 (97.6 mg, 0.7 mmol) in water (3 cm^3) and active charcoal (100 mg). The mixture was stirred for 30 min and filtered. The filtrate was evaporated to dryness under reduced pressure, and the complex was extracted with methanol (20 cm^3). On addition of diethyl ether (50 cm^3) the extract gave a yellow precipitate, which was filtered, washed with a mixture (50 cm^3) of methanol and diethyl ether (1:5), and air-dried. Yield: 150 mg (78%). Found: C, 31.74; H, 6.78%. Calcd for $C_{15}H_{38}ClCoO_8P_4$: C, 31.94; H, 6.17%. The complex is soluble in methanol and ethanol.

***cis*-[CoCl$_2$(dmpp)$_2$]ClO$_4$·0.5H$_2$O.** The complex was prepared from $[Co(CO_3)(dmpp)_2]ClO_4 \cdot H_2O$ and concd HCl by a method similar to that for *cis*-$[CoCl_2(dmpe)_2]^+$. Yield: 48%. Found: C, 29.54; H, 6.19%. Calcd for $C_{14}H_{37}Cl_3CoO_{4.5}P_4$: C, 29.67; H, 6.58%. The complex is soluble in methanol and acetonitrile.

***trans*-[CoCl$_2$(dbpe)$_2$]PF$_6$·H$_2$O.** An ethanol solution (100 cm^3) containing $CoCl_2 \cdot 6H_2O$ (193 mg, 0.81 mmol) and dbpe (684 mg, 1.62 mmol) was stirred for 40 min, and then concd HCl (1 cm^3) was added. Air was bubbled through the solution for 10 h. The resulting dark green solution was evaporated to dryness under reduced pressure, and the residue was dissolved in methanol (50 cm^3). The methanol solution was shaken with hexane (100 cm^3) to extract free dbpe into hexane. This procedure was repeated several times, and the methanol layer was separated and concentrated to 20 cm^3 under reduced pressure. To the concentrate were added water (10 cm^3) and NH_4PF_6 (500 mg) dissolved in a mixture (3 cm^3) of water and methanol (1:1). The mixture was stored in a refrigerator for 10 h to yield green crystals, which were filtered, washed with a mixture (30 cm^3) of water and ethanol (4:1), and air-dried. Yield: 110 mg (15%). Found: C, 46.46; H, 9.47%. Calcd for $C_{36}H_{82}Cl_2CoF_6OP_5$: C, 46.50; H, 8.89%. The complex is soluble in methanol, ethanol, chloroform, and diethyl ether.

[Co(CO$_3$)(dbpe)$_2$]PF$_6$·1.5H$_2$O. To *trans*-$[CoCl_2(dbpe)_2]PF_6 \cdot H_2O$ (200 mg, 0.22 mmol) in a mixture (100 cm^3) of methanol and water (4:1) were added K_2CO_3 (100 mg, 0.72 mmol) in water (5 cm^3) and active charcoal (ca. 100 mg). The mixture was stirred for 4 h and filtered. The filtrate was evaporated to dryness under reduced pressure, and the complex was extracted with ethanol (20 cm^3). The extract was concentrated to 10 cm^3 and mixed with a solution of NH_4PF_6 (500 mg) in a mixture (3 cm^3) of water and ethanol (4:1). The mixture was stored in a refrigerator for 10 h to yield orange crystals, which were filtered, washed with a mixture (30 cm^3) of water and ethanol (4:1), and air-dried. Yield: 80 mg (41%). Found: C, 47.89; H, 9.04%. Calcd for $C_{37}H_{83}CoF_6O_{4.5}P_5$: C, 47.89; H, 9.02%. The complex is soluble in methanol and ethanol.

***cis*-[CoCl$_2$(dbpe)$_2$]PF$_6$·H$_2$O.** Ice-cold concd HCl (1 cm^3) was added to an ethanol solution (2 cm^3) of $[Co(CO_3)(dbpe)_2]PF_6 \cdot 1.5H_2O$ (70 mg, 0.075 mmol) at 0 °C, the color of the solution changing slowly from yellow to red. To the red solution was added NH_4PF_6 (200 mg) in water (0.5 cm^3), and the mixture was stored in a refrigerator for 10 h to give red-violet crystals, which were filtered, washed with a mixture (10 cm^3) of ethanol and water (1:5), and air-dried. Yield: 20 mg (29%). Found: C, 46.83; H, 9.56%. Calcd for $C_{36}H_{82}Cl_2CoF_6OP_5$: C, 46.50; H, 8.89%. The complex is soluble in methanol and ethanol.

***trans*-[CoCl$_2$(dpee)$_2$]ClO$_4$.** The complex was prepared according to the literature method.[7]

***cis*-[CoCl$_2$(dpee)$_2$]BF$_4$.** Ice-cold concd HCl (1 cm^3) was added dropwise to an ethanol solution (6 cm^3) of $[Co(O_2)(dpee)_2]BF_4$[7] (100 mg, 0.103 mmol) at 0 °C. After a while the resulting red-violet solution was mixed with $NaBF_4$ (200 mg) in water (1 cm^3), and was allowed to stand at 5 °C for 10 h to yield red-violet crystals, which were filtered and dissolved in a minimum amount of ethanol–dichloromethane (5:1). The solution was applied on a column (ϕ 2.5×20 cm) of Toyopearl TSK-GEL, and the adsorbed products were eluted with ethanol. An yellow-green (major product) and a red-violet (minor product) band appeared. The eluate of the red-violet band was collected and evaporated to dryness under reduced pressure below 30 °C. The residue was dissolved in ethanol (5 cm^3), and diethyl ether (5 cm^3) was added. The solution was allowed to stand at 5 °C for 10 h to give violet crystals, which were filtered, washed with a mixture (20 cm^3) of diethyl ether and ethanol (5:1), and air-dried. Yield: 20 mg (19%). Found: C, 62.68; H, 4.62%. Calcd for $C_{52}H_{44}BCl_2CoF_4P_4$: C, 61.87; 4.39%. The complex is soluble in ethanol and dichloromethane.

***trans*-[CoBrI(dmpe)$_2$]ClO$_4$.** To a methanol solution (50 cm^3) of *trans*-$[CoBr_2(dmpe)_2]ClO_4$ (200 mg, 0.32 mmol) was added dropwise a methanol solution (3 cm^3) of NaI (50 mg, 0.33 mmol) with stirring. The solution was stirred for 3 h at 45 °C, and then concentrated under reduced pressure to 5 cm^3. On cooling at 0 °C brown crystals were precipitated, filtered, washed with a mixture (30 cm^3) of methanol and diethyl ether (1:1), and air-dried. Yield: 150 mg (70%). Found: C, 21.71; H, 4.87%. Calcd for $C_{12}H_{32}BrClCoIO_4P_4$: C, 21.66; H, 4.84%. The complex is soluble in methanol and ethanol.

***cis*-[CoCl(H$_2$O)(dmpe)$_2$](PF$_6$)$_2$·CH$_3$CN.** To an acetonitrile solution (3 cm^3) of *cis*-$[CoCl_2(dmpe)_2]ClO_4$ (100 mg, 0.19 mmol) was added water (40 cm^3). The solution was stirred at room temperature for 15 min, the color of the solution changing from red to yellow. On addition of NH_4PF_6 (500 mg) in water (3 cm^3) a yellow precipitate was obtained. It was filtered, washed with water (50 cm^3), and air-dried. Yield: 110 mg (85%). Found: C, 23.07; H, 5.01; N, 1.88%. Calcd for $C_{14}H_{37}NClCoF_{12}OP_6$: C, 22.61; H, 4.84; N, 2.04%. The complex is soluble in acetonitrile. The perchlorate of the complex can be obtained by use of $NaClO_4$ instead of NH_4PF_6, but tends to explode by mechanical shock.

***trans*-[CoCl(H$_2$O)(dmpe)$_2$](PF$_6$)$_2$·CH$_3$CN.** An acetonitrile solution (50 cm^3) of *cis*-$[CoCl(H_2O)(dmpe)_2](PF_6)_2 \cdot CH_3CN$ (50 mg, 0.067 mmol) was allowed to stand at room tempera-

ture. The color of the solution changed very slowly from yellow to red-orange in the dark, but the change was remarkably accelerated by sunlight. With slow evaporation of acetonitrile red-orange crystals were precipitated, filtered, and air-dried. Yield: 45 mg (90%). Found: C, 23.18; H, 4.92; N, 2.02%. Calcd for $C_{14}H_{37}NClCoF_{12}OP_6$: C, 22.61; H, 4.84; N, 2.04%. The complex is soluble in acetonitrile.

Kinetic Measurements. Isomerization reactions of *cis*-$[CoCl_2(L)_2]^+$ (L=dmpe, dmpp, dbpe, and dpee) and *cis*-$[CoBr_2(dmpe)_2]^+$ to the trans isomers in methanol or ethanol solution were monitored spectrophotometrically with a Jasco UNIDEC 610 spectrophotometer equipped with a thermostated cell compartment. The solvents of spectroscopic grade methanol and ethanol were dried over Molecular Sieves, and the complex concentrations were ca. 4×10^{-4}—1×10^{-3} mol dm^{-3}. The temperature of the solutions was in the range of 39.0—65.0 °C and kept constant within ±0.3 °C by use of a temperature-controlled circulating bath, Yamato-Komatsu CET-24W. Suitable wavelengths for following the isomerization reactions were in the range of 485—556 nm where the complexes show the first absorption band. In each kinetic run, the plot of $\ln(D_t-D_\infty)$ vs. time gave a straight line until at least five half-lives, where D_t and D_∞ denote the absorbance at time t and at infinite time, respectively. The slope gave the first-order rate constant of isomerization k, and Eyring treatment of $\log(k/T)$ vs. T^{-1} yielded the activation parameter. All the experiments should be carried out in the dark, because the isomerization reactions were accelerated by sunlight.

Results and Discussion

Preparation and Characterization of the Complexes. All the *trans*-$[CoX_2(diphosphine)_2]^+$ (X=Cl^-, Br^-, or I^-) complexes in this study can be easily prepared by oxidation of the cobalt(II)-diphosphine species in methanol or ethanol with air in moderate yields, although the yield of the dbpe complex was rather poor because of its high solubility. For *cis*-$[CoX_2(diphosphine)_2]^+$ (X=Cl^- or Br^-), the dmpe, dmpp, and dbpe complexes were prepared by treating the corresponding carbonato complexes with concd HX, while *cis*-$[CoCl_2(dpee)_2]^+$ was obtained by the reaction of $[Co(O_2)(dpee)_2]^+$ with concd HCl, the reaction with $[Co(CO_3)(dpee)_2]^+$ giving only the trans isomer. The former three complexes can also be prepared from the corresponding peroxo complexes.[10] The reactions with concd HX should be carried out at a low temperature, since the trans isomer is formed in larger amounts with an increasing reaction temperature. The $[Co(O_2)(dpee)_2]^+$ complex afforded a mixture of the cis and trans isomers by the reaction even at a low temperature. The formation of the trans isomer will be attributable to the following properties of the dpee complex; the $[Co(O_2)(dpee)_2]^+$ complex has less reactivity toward HX compared with other diphosphine-peroxo complexes,[10] and *cis*-$[CoCl_2(dpee)_2]^+$ isomerizes to the trans isomer much faster than other *cis*-$[CoCl_2(diphosphine)_2]^+$ do (vide infra). The reaction of $[CoCO_3(dmpe)_2]^+$ with concd HI yielded only the *trans*-diiodo complex. The cis isomer in which two large I^- ions are in the cis positions will be sterically unstable.

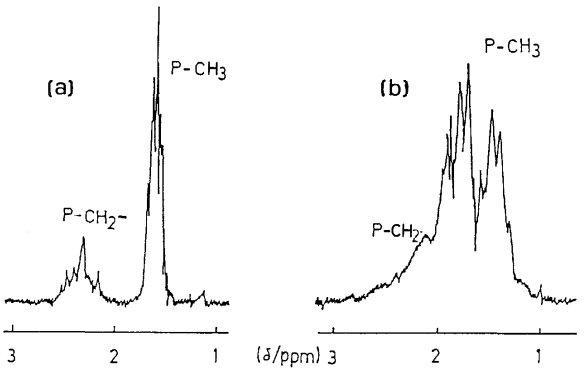

Fig. 1. ^1H NMR spectra of (a) *trans*-$[CoCl_2(dmpe)_2]^+$ and (b) *cis*-$[CoCl_2(dmpe)_2]^+$ (in CD_3CN, TMS reference).

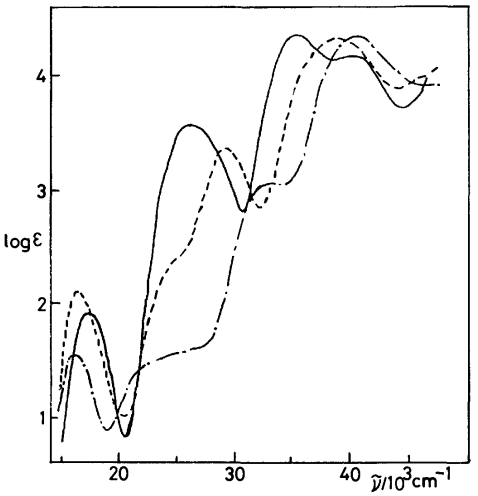

Fig. 2. Absorption spectra of *trans*-$[CoCl_2(dmpe)_2]^+$ (——), *trans*-$[CoCl_2(edmp)_2]^+$ (----), and *trans*-$[CoCl_2(en)_2]^+$ (-·-·-).

All the *cis*-$[CoX_2(diphosphine)_2]^+$ complexes in nonaqueous solvents are fairly stable in the dark, but easily isomerize to the trans isomer on exposure of ultraviolet light. The *cis*-$[CoCl_2(dmpe)_2]^+$ complex in acetonitrile afforded *cis*-$[CoCl(H_2O)(dmpe)_2]^+$ by the addition of water. The aqua complex in acetonitrile was stable in the dark, but isomerized to the trans aqua complex on exposure of ultraviolet light. Both cis and trans aqua complexes were isolated as the hexafluorophosphate. Detailed studies on these photochemical reactions are in progress.

Geometrical structures of the complexes were assigned from the ^1H NMR spectra, and from comparisons of the absorption spectra with those of other phosphine and ethylenediamine complexes. In the ^1H NMR spectrum, for example, *trans*-$[CoCl_2(dmpe)_2]^+$ shows a multiplet methyl signal at δ ca. 1.6, while the cis isomer gives many signals in the region of δ 1.5—2.0 (Fig. 1). The spectral pattern of the cis isomer is quite similar to those of $[CoCO_3(dmpe)_2]^+$ and

$[CoC_2O_4(dmpe)_2]^+$,[11] which have necessarily a cis geometry.

Figure 2 compares the absorption spectra of *trans*-$[CoCl_2(L)_2]^+$ (L= dmpe, edmp, and en), where edmp denotes $NH_2CH_2CH_2P(CH_3)_2$. For *trans*(Cl, Cl), *cis*(P, P)-$[CoCl_2(edmp)_2]^+$, we have assigned the peak at 16600 cm^{-1} to the Ia component of the first absorption band, the shoulder at ca. 23800 cm^{-1} to the second absorption band overlapped the Ib component of the first absorption band, the bands at 29500 and 39700 cm^{-1} to the Co-Cl charge-transfer band, and the shoulder at ca. 36500 cm^{-1} to the Co-P charge-transfer band, by comparing the spectrum with that of the en complex.[12] The spectrum of *trans*-$[CoCl_2(dmpe)_2]^+$ may be assigned in a similar manner; the band at 17300 cm^{-1} can be assigned to the Ia component of the first absorption band, the broad band at 26100 cm^{-1} to that involving three components, the second absorption band, the Ib component of the first absorption band, and the Co-Cl charge-transfer band, the band at 35400 cm^{-1} to the Co-P charge-transfer band, and the band at 40500 cm^{-1} to the Co-Cl charge-transfer band. In Fig. 3 the spectra of *trans*-$[CoX_2(dmpe)_2]^+$ (X=Br^- and I^-) are compared with that of *trans*-$[CoCl_2(dmpe)_2]^+$. The spectrum of the dibromo complex is similar to that of the dichloro complex, but that of the diiodo complex differs from those of other halogeno complexes. For *trans*-$[CoX_2(en)_2]^+$, the spectra of the dichloro and dibromo complexes are similar, but that of the diiodo complex also differs from others.[13] Other phosphine complexes, *trans*-$[CoCl_2(L)_2]^+$ (L=dmpp and dbpe), give spectra similar to that of the dmpe complex (Fig. 4(a)). The Ia band shifts to higher energy in the order L=dpee<dbpe<dmpp<dmpe (Table 1). This order coincides with the decreasing order in cone angle of

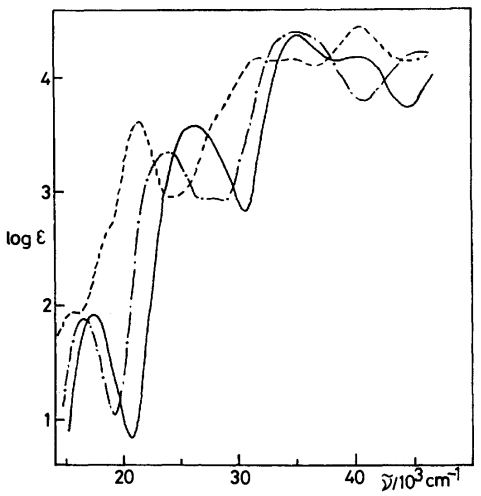

Fig. 3. Absorption spectra of *trans*-$[CoCl_2(dmpe)_2]^+$ in CH_3OH (——), *trans*-$[CoBr_2(dmpe)_2]^+$ in CH_3OH (-·-·-), and *trans*-$[CoI_2(dmpe)_2]^+$ in CH_3CN (----).

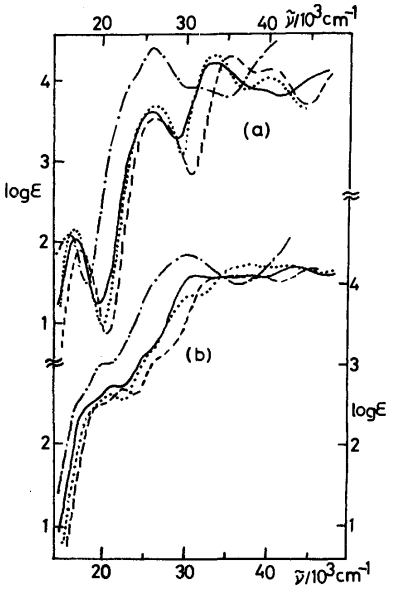

Fig. 4. Absorption spectra of (a) *trans*-$[CoCl_2(dmpe)_2]^+$ (----), *trans*-$[CoCl_2(dmpp)_2]^+$ (·····), *trans*-$[CoCl_2(dbpe)_2]^+$ (——), and *trans*-$[CoCl_2(dpee)_2]^+$ (-·-·-), and (b) *cis*-$[CoCl_2(dmpe)_2]^+$ (----), *cis*-$[CoCl_2(dmpp)_2]^+$ (·····), *cis*-$[CoCl_2(dbpe)_2]^+$ (——), and *cis*-$[CoCl_2(dpee)_2]^+$ (-·-·-). Solvent: CH_3OH except for the dpee complexes (CH_2Cl_2).

Table 1. Absorption Spectral Data[a]

Complex	$\tilde{\nu}/10^3\,cm^{-1}(\log\varepsilon)$			
trans-$[CoCl_2(dmpe)_2]^+$	17.30(1.92)	26.10(3.70)	35.40(4.35)	40.50(4.16)
cis-$[CoCl_2(dmpe)_2]^+$	19.7 (2.5)[b]	22.30(2.69)	26.60(3.06)	
trans-$[CoCl_2(dmpp)_2]^+$	16.66(2.19)	26.50(3.50)	33.50(4.34)	40.30(4.06)
cis-$[CoCl_2(dmpp)_2]^+$	19.5 (2.5)[b]	21.01(2.62)	25.0 (3.1)[b]	
trans-$[CoCl_2(dbpe)_2]^+$	16.61(2.05)	26.00(3.64)	33.20(4.26)	39.20(3.88)
cis-$[CoCl_2(dbpe)_2]^+$	18.2 (2.5)[b]	21.14(2.74)	24.80(3.08)	
trans-$[CoCl_2(dpee)_2]^+$	15.87(2.11)	22.7 (3.9)[b]	25.80(4.40)	31.00(3.94)
cis-$[CoCl_2(dpee)_2]^+$	17.0 (2.5)[b]	20.00(3.00)	26.0 (4.0)[b]	
trans-$[CoBr_2(dmpe)_2]^+$	16.39(1.89)	24.00(3.35)	35.09(4.39)	45.0(4.2)
trans-$[CoBrI(dmpe)_2]^+$	16.13(1.90)	22.47(3.38)	33.80(4.27)	
trans-$[CoI_2(dmpe)_2]^+$	15.38(1.94)	18.2 (2.6)[b]	22.30(3.60)	27.2(3.5)[b]
	31.70(4.15)	34.50(4.14)	40.40(4.43)	

a) Solvent: CH_3OH except for *trans*- and *cis*-$[CoCl_2(dpee)_2]^+$ (CH_2Cl_2) and *trans*-$[CoI_2(dmpe)_2]^+$ (CH_3CN).
b) Shoulder.

phosphine ligands.[14]

Figure 4(b) shows absorption spectra of *cis*-$[CoCl_2(L)_2]^+$ (L=dmpe, dmpp, dbpe, and dpee). The spectra in the region of 15000—25000 cm^{-1} are similar among the four complexes and have three bands or shoulders. These absorptions can be assigned to the first and second bands from a comparison with the spectrum of *cis*-$[CoCl_2(en)_2]^+$. This complex shows the first absorption band at 18600 cm^{-1} with a shoulder at ca. 17000 cm^{-1} and the second absorption band at 25500 cm^{-1}.[15] In a previous paper,[16] we reported that the first absorption band of the $[Co(N)_n(P)_{6-n}]^{3+}$-type complexes shifts to higher energy by replacing N with P, while the energy of the second absorption band remains almost unchanged. Thus the bands and shoulders in the region of 17000—22000 cm^{-1} of *cis*-$[CoCl_2(diphosphine)_2]^+$ are assigned to the first absorption band split into two components,[17] and the shoulders in the region of 25000—26000 cm^{-1} to the second absorption band. The higher energy first absorption band shifts to higher energy in the order diphosphine=dpee<dbpe<dmpp<dmpe. This order is the same as that observed for the corresponding trans isomer. The spectral patterns in the ligand field absorption band region of these *trans*- and *cis*-$[CoCl_2(diphosphine)_2]^+$ complexes are very similar to those of *trans*- and *cis*-$[CoCl_2(diarsine)_2]^+$, respectively, to which similar band assignments have been made.[18,19]

The chloride ions in *trans*-$[CoCl_2(diphosphine)_2]^+$ are quite inert to aquation compared with those in *trans*-$[CoCl_2(en)_2]^+$. For example, *trans*-$[CoCl_2(dmpe)_2]^+$ is stable in neutral water at room temperature for at least several days, while *trans*-$[CoCl_2(en)_2]^+$ liberates one chloride ion to aquate with the half-life time of 361 min (25 °C, pH 1).[20] The *trans*-$[CoCl_2\{NH_2CH_2CH_2P(CH_3)_2\}_2]^+$ complex is also stable to aquation.[12] The reactivity of *trans*-$[CoCl_2(diphosphine)_2]^+$ to the substitution reaction of CO_3^{2-} for the two chloride ions depends on the kind of phosphines. The reaction of the dmpe complex with K_2CO_3 occurs instantly at room temperature to yield $[CoCO_3(dmpe)_2]^+$, whereas those of the dmpp and dbpe complexes proceed at a higher temperature or the addition of active charcoal. Miskowski et al.[7] used Ag_2CO_3 to prepare $[CoCO_3(dpee)_2]^+$, from *trans*-$[CoCl_2(dpee)_2]^+$, the breaking of the Co–Cl bond being assisted by Ag^+. The *trans*-dichloro complexes containing bulky phosphine ligands seem to have less reactivity to substitution reactions for the chloride ions.

In contrast to *trans*-$[CoCl_2(diphosphine)_2]^+$, the corresponding cis isomers liberate rapidly one chloride ion in aqueous solution to yield *cis*-$[CoCl(H_2O)(diphosphine)_2]^{2+}$. The reaction of *cis*-$[CoCl_2(dmpe)_2]^+$ is complete within 15 min in neutral water at 25 °C, which is much faster than that of *cis*-$[CoCl_2(en)_2]^+$ ($t_{1/2}$=ca. 46 min, 25 °C, pH 1).[20] The lability of Cl^- in *cis*-$[CoCl_2(dmpe)_2]^+$ may be brought about by the strong trans effect of the phosphine ligand.[21] However, the subsequent reaction to liberate the second chloride ion is so slow that *cis*-$[CoCl(H_2O)(dmpe)_2]^{2+}$ can be isolated. A similar aquation reaction has been reported for *cis*-$[RuCl_2\{(C_2H_5)_2PCH_2CH_2P(C_2H_5)_2\}_2]$.[22]

The *trans*-$[CoI_2(dmpe)_2]^+$ complex, which was prepared from $[CoCO_3(dmpe)_2]^+$ and concd HI, can also be obtained by metathesis of *trans*-$[CoX_2(dmpe)_2]ClO_4$ (X=Cl^-, Br^-) and NaI. The mixed halogeno complexes, *trans*-$[CoXI(dmpe)_2]^+$ (X=Cl^-, Br^-), were isolated by similar reactions, although the pure chloroiodo complex was not obtained. Reverse reactions yielding the chloro and bromo complexes from the diiodo complex do not take place. These results indicate that the cobalt(III) ion in the dmpe complex has stronger affinity to I^- than to Cl^- and Br^-. The cobalt(III) ion which belongs to a hard acid may be softened by coordination of phosphine ligands, and may have stronger affinity to a more soft base I^- than Cl^- and Br^- as predicted by the principle of "Hard and Soft Acids and Bases."[23]

Isomerization Reactions. All the *cis*-$[CoX_2(diphosphine)_2]^+$ complexes prepared in this study isomerize in methanol or ethanol to the trans isomer. Figure 5 shows the change in absorption spectrum at intervals during the isomerization of *cis*-$[CoCl_2(dpee)_2]^+$ in methanol at 50 °C. Three isosbestic points were found at 363, 488, and 634 nm and the final spectrum was identical with that of a freshly prepared solution of *trans*-$[CoCl_2(dpee)_2]^+$. These results indicate that the cis isomer isomerizes to the trans isomer, and no reverse reaction occurs. The cis isomers of other phosphine complexes gave similar results. The rates of the isomerization were followed by measuring the change in absorbance at a given wavelength, and from

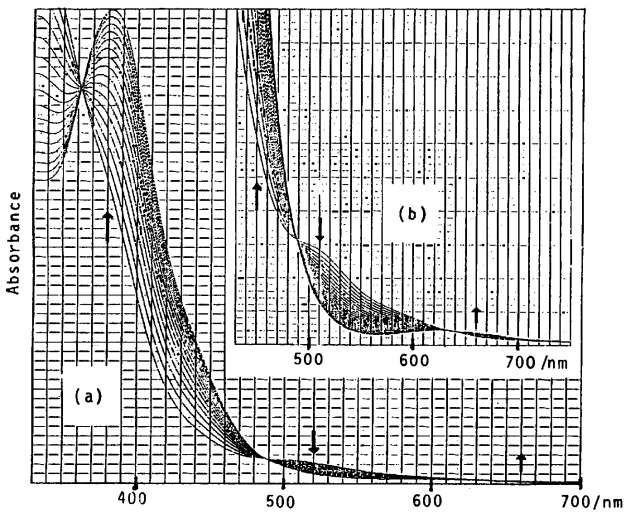

Fig. 5. Change in absorption spectrum of *cis*-$[CoCl_2(dpee)_2]BF_4$ in methanol at 50°C (recorded intervals: 30 min). Trends of spectral changes with time are shown by arrows.. In (b), the scale of absorbance is expanded.

the data the first-order rate constants were obtained (Experimental, Fig. 6, and Table 2). For *cis*-$[CoCl_2(dbpe)_2]^+$, the isomerization was also studied at 39 °C in the presence of 200 times as many moles of LiCl, but the rate was the same within the experimental error.

The mechanism for isomerization of the present complexes is not clear at present. However, the fact that the rate of isomerization of *cis*-$[CoCl_2(dbpe)_2]^+$ is not affected by the addition of LiCl suggests that the complex isomerizes by an intramolecular mechanism. Peloso and Tobe[24] proposed an intramolecular mechanism for the isomerization of *cis*-$[CoCl_2(diars)_2]^+$ (diars=*o*-phenylenebis(dimethylarsine)). This complex isomerizes to the trans isomer in methanol with a similar rate (1.67×10^{-6} s^{-1}, 55 °C) to that of *cis*-$[CoCl_2(dmpe)_2]^+$, and the rate increases only a little by the addition of LiCl. The *cis*-$[CoCl_2\{(CH_3)_2AsCH_2CH_2CH_2As(CH_3)_2\}_2]^+$ complex gives similar results in the isomerization to the trans isomer.[19] The *cis*-$[CoX_2(L)_2]^+$-type complexes (L=diphosphine and diarsine) in methanol seem to isomerize to the trans isomer intramolecularly by a similar mechanism. The *cis*-$[CoCl_2(en)_2]^+$ complex in methanol isomerizes to the trans isomer faster ($t_{1/2}$=3.6 h, 35 °C) than do the diphosphine and diarsine complexes, and the rate is dependent upon the LiCl concentration, for which a unimolecular mechanism involving a five-coordinate intermediate was proposed.[25]

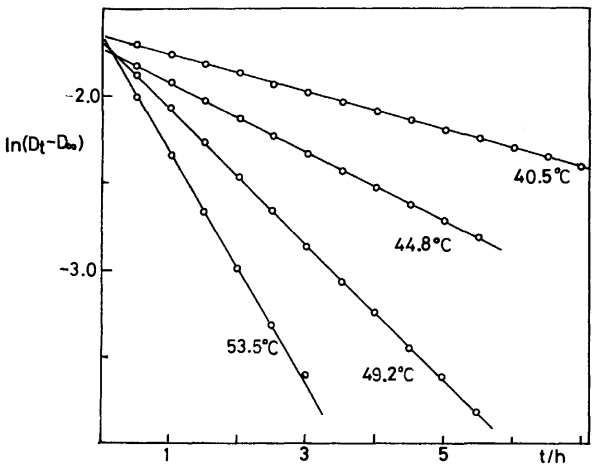

Fig. 6. Plots of $\ln(D_t-D_\infty)$ against time at 40.5, 44.8, 49.2, and 53.5°C for *cis*-$[CoCl_2(dpee)_2]BF_4$.

Table 2. Rate Constants for Isomerization of the Complexes

Complex	*t* / °C	*k* / $s^{-1}\times10^{-5}$
cis-$[CoCl_2(dpee)_2]BF_4$	40.5	2.91±0.01
	44.8	5.38±0.02
	49.2	10.72±0.02
	53.5	18.03±0.02
cis-$[CoCl_2(dbpe)_2]PF_6$	39.0	1.10±0.02
	43.3	2.06±0.03
	49.3	4.65±0.03
	52.3	7.29±0.05
cis-$[CoCl_2(dmpp)_2]BF_4$	46.4	3.27±0.02
	49.1	4.60±0.02
	51.7	6.48±0.02
	54.0	8.47±0.03
cis-$[CoCl_2(dmpe)_2]ClO_4$	55.0	0.13±0.02
	60.0	0.25±0.02
	62.3	0.28±0.04
	65.0	0.40±0.03
cis-$[CoBr_2(dmpe)_2]ClO_4$	50.0	1.15±0.03

Solvent: CH_3OH except for *cis*-$[CoCl_2(dmpe)_2]ClO_4$ (C_2H_5OH).

Table 3 lists the activation parameters for the isomerization. The ΔH^* values increase in the order, the dmpe < dmpp < dbpe < dpee complexes. However, the ΔG^* (25 °C) values are similar because of the positive ΔS^* values increasing in the same order as for the ΔH^* values. The orders in the ΔH^* and ΔS^* values coincide with the increasing order in cone angle of phosphine ligands, and suggest that the difference in rates among the complexes comes from a steric factor. If the isomerization is assumed to proceed intramolecularly , the increasing ΔH^* values with increasing bulkiness of a phosphine ligand may be conceivable, since the complex with a bulky phosphine ligand would require larger energy to reach a transition state by twisting the octahedral structure of the complex. For the change in ΔS^*, however, no appropriate explanation can be given at present, although there are fairly large differences among the complexes. More data are needed to discuss in detail.

The rate constant 1.15×10^{-5} s^{-1} at 50 °C of *cis*-$[CoBr_2(dmpe)_2]^+$ is larger by a factor of about 10 than that of *cis*-$[CoCl_2(dmpe)_2]^+$ at the same temperature. As stated previously, $[CoI_2(dmpe)_2]^+$ formed only the trans isomer by the reaction of $[CoCO_3(dmpe)_2]^+$ with HI. The cis isomer may isomerize very rapidly to the trans isomer during the reaction. The stability of *cis*-$[CoX_2(dmpe)_2]^+$ depends largely on the kind of halide ions and becomes low rapidly on going from a small Cl^- to a large I^- ion.

Table 3. Thermodynamic Parameters for Isomerization of the Complexes

Complex	ΔH^* / kJ mol^{-1}	ΔS^* / J mol^{-1} K^{-1}	$\Delta G^*_{25\,°C}$ / kJ mol^{-1}
cis-$[CoCl_2(dpee)_2]BF_4$	118.2±1.8	45.0±5.6	104.8±3.5
cis-$[CoCl_2(dbpe)_2]PF_6$	116.5±0.8	33.4±2.4	106.6±1.5
cis-$[CoCl_2(dmpp)_2]BF_4$	106.4±0.9	2.1±2.9	105.8±1.7
cis-$[CoCl_2(dmpe)_2]ClO_4$	95.6±3.4	−66.3±10	115.4±6.4

The authors wish to thank the Ministry of Education for Scientific Research Grant-in-Aid No. 60470046.

References

1) C. E. Wymore and J. C. Bailar, Jr., *J. Inorg. Nucl. Chem.*, **14**, 42 (1960).
2) T. Ohishi, K. Kashiwabara, and J. Fujita, *Chem. Lett.*, **1981**, 1371.
3) H. C. Jewiss, W. Levason, and M. Webster, *Inorg. Chem.*, **25**, 1997 (1986).
4) J. C. Cloyd, Jr. and D. W. Meek, *Inorg. Chim. Acta*, **6**, 480 (1972).
5) L. F. Warren and M. A. Bennett, *Inorg. Chem.*, **15**, 3126 (1976).
6) A. L. Hale, H. C. Jewiss, and W. Levason, *Inorg. Chim. Acta*, **97**, 85 (1985).
7) V. M. Miskowski, J. L. Robbins, G. S. Hammond, and H. B. Gray, *J. Am. Chem. Soc.*, **98**, 2477 (1976).
8) *Inorg. Synth.*, Vol. XV, p.188.
9) K. Issleib and A. Tzschach, *Chem. Ber.*, **92**, 704 (1959).
10) T. Ohishi, K. Kashiwabara, J. Fujita, S. Ohba, T. Ishii, and Y. Saito, *Bull. Chem. Soc. Jpn.*, **59**, 385 (1986).
11) T. Ohishi, K. Kashiwabara, and J. Fujita, *Bull. Chem. Soc. Jpn.*, **60**, 583 (1987).
12) I. Kinoshita, Y. Yokota, K. Matsumoto, S. Ooi, K. Kashiwabara, and J. Fujita, *Bull. Chem. Soc. Jpn.*, **56**, 1067 (1983).
13) M. Nakahara and M. Mitsuya, *Bull. Chem. Soc. Jpn.*, **45**, 2209 (1972).
14) C. A. Tolman, *Chem. Rev.*, **77**, 313 (1977).
15) Y. Shimura and R. Tsuchida, *Bull. Chem. Soc. Jpn.*, **29**, 311 (1956).
16) T. Ohishi, K. Kashiwabara, and J. Fujita, *Bull. Chem. Soc. Jpn.*, **56**, 3441(1983).
17) H. Yamatera, *Bull. Chem. Soc. Jpn.*, **31**, 95 (1958).
18) T. M. Dunn, R. S. Nyholm, and S. Yamada, *J. Chem. Soc.*, **1962**, 1564.
19) K. Iwata, M. Kojima, and J. Fujita, *Bull. Chem. Soc. Jpn.*, **58**, 3003 (1985).
20) R. G. Pearson, C. R. Boston, and F. Basolo, *J. Am. Chem. Soc.*, **75**, 3089 (1953), *J. Phys. Chem.*, **59**, 304 (1955).
21) F. Basolo and R. G. Pearson, "Mechanism of Inorganic Reactions," 2nd ed., John Wiley and Sons, New York (1967).
22) J. Chatt and R. G. Hayter, *J. Chem. Soc.*, **1961**, 896.
23) R. G. Pearson, *J. Chem. Educ.*, **45**, 581, 643 (1968).
24) A. Peloso and M. L. Tobe, *J. Chem. Soc.*, **1964**, 5063.
25) B. Bosnich, C. K. Ingold, and M. L. Tobe, *J. Chem. Soc.*, **1965**, 4074.

 © 1987 The Chemical Society of Japan Bull. Chem. Soc. Jpn., 60, 583—588 (1987)

Preparation and Properties of Cobalt(III)-1,2-Bis(dimethylphosphino)-ethane (dmpe) Complexes of the $[Co(L)(dmpe)_2]^{n+}$ Type

Tomoji Ohishi, Kazuo Kashiwabara, and Junnosuke Fujita*
Department of Chemistry, Faculty of Science, Nagoya University, Chikusa-ku, Nagoya 464
(Received September 8, 1986)

Seven new cobalt(III)-phosphine complexes of the type $[Co(L)(dmpe)_2]^{n+}$ were prepared from *trans*-[Co(Cl or Br)$_2$(dmpe)$_2$]$^+$, where dmpe denotes $(CH_3)_2PCH_2CH_2P(CH_3)_2$, and L is $C_2O_4^{2-}$, $NH_2CH_2COO^-$(gly), $NH_2CH(CH_3)COO^-$(ala), $(C_2H_5)_2NCS_2^-$(dtc), $(NCS^-)_2$, $(NCO^-)_2$, or $(CN^-)_2$. Reactions of *cis*-$[CoCl_2(dmpe)_2]^+$ with X^- (X^-=CN^-, NCS^-, and NCO^-) yielded only *trans*-$[CoX_2(dmpe)_2]^+$. Qualitative stabilities of the complexes containing a bidentate ligand in aqueous solution were found to decrease in the order L= $CH(CH_3CO)_2^-$(acac), $C_2O_4^{2-}$, dtc>CO_3^{2-}≫gly, ala>$NH_2CH_2CH_2NH_2$(en); the complexes containing O or S donor atoms are thermally more stable than those containing an amino donor group. The d-d absorption bands of the complexes were assigned by comparing the spectra with those of related Co(III)-phosphine and -en complexes. The IR and visible absorption spectra of the NCS^- and NCO^- complexes indicate an N coordination mode of these ambidentate ligands.

In a previous paper,[1] we have prepared all complexes of the series $[Co(acac)_x(en)_y(dmpe)_z]^{(3-x)+}$ and found that $[Co(acac)_{3-n}(dmpe)_n]^{n+}$ (n=1, 2) were more stable than $[Co(en)_{3-n}(dmpe)_n]^{3+}$ (n=1, 2), where acac, en and dmpe denote an acetylacetonate ion, ethylenediamine and 1,2-bis(dimethylphosphino)ethane, respectively. The en complexes in water are reduced to Co(II) on heating over 60 °C, and $[Co(en)(dmpe)_2]^{3+}$ in water containing excess chloride ions affords *trans*-$[CoCl_2(dmpe)_2]^+$ by heating, whereas the acac complexes remain unchanged under the same conditions. The acac ligand seems to stabilize the cobalt(III)-dmpe system.

To examine properties of cobalt(III)-phosphine complexes in more detail, we attempted to prepare cobalt(III)-dmpe complexes containing a variety of ligands. This paper reports the preparation and some properties of the $[Co(L)(dmpe)_2]^{n+}$-type complexes, where L denotes a bidentate ligand such as CO_3^{2-}, $C_2O_4^{2-}$, $NH_2CH_2COO^-$(gly), (*S*)-$NH_2CH(CH_3)COO^-$(*S*-ala) or $(C_2H_5)_2NCS_2^-$(dtc), and two unidentate ions such as NCS^-, NCO^-, CN^-, or H_2O.

Experimental

The dmpe ligand[2] was handled under an atmosphere of nitrogen until it formed cobalt(III) complexes. All solvents used for the preparation of dmpe and the complexes were deoxygenated by bubbling nitrogen for 20 min immediately before use. ^{1}H NMR, absorption, circular dichroism and IR spectra were recorded on a Jeol JNM-PMX 60 spectrometer, a Hitachi 323 spectrophotometer, a Jasco J-40CS spectropolarimeter, and a Jasco A-3 infrared spectrometer, respectively.

Preparation of the Complexes.† $[Co(CO_3)(dmpe)_2]ClO_4 \cdot 1.5NaClO_4 \cdot H_2O$[3] and *trans*-$[Co(H_2O)_2(dmpe)_2](ClO_4)_3 \cdot 2H_2O$[3] were prepared from *trans*-$[CoBr_2(dmpe)_2]ClO_4$[4] and the carbonato complex, respectively by reported methods.

$[Co(C_2O_4)(dmpe)_2]PF_6 \cdot 0.5NaPF_6$. An aqueous solution (5 cm^3) of $(NH_4)_2C_2O_4$ (5.36 mg, 0.38 mmol) was added to a solution of *trans*-$[CoCl_2(dmpe)_2]ClO_4$[5] (100 mg, 0.19 mmol) in a mixture of water and methanol (1 : 1, 50 cm^3), and the mixture was stirred for 10 h at room temperature. The resulting yellow solution was diluted with water (1 dm^3) and applied on a column (ϕ 3 cm×120 cm) of SP-Sephadex C-25. The adsorbed products were eluted with 0.1 mol dm^{-3} NaCl, giving a minor green and a major yellow band. The yellow eluate was collected and evaporated to dryness under reduced pressure. A yellow complex was extracted from the residue with methanol, and the extract was mixed with an aqueous solution (5 cm^3) of $NaPF_6$ (300 mg). The mixture was concentrated in a desiccator over P_4O_{10}, yielding yellow crystals, which were filtered, washed with a mixture (30 cm^3) of methanol and diethyl ether (1 : 1), and air-dried. Yield: 80 mg (72%). Found: C, 24.89; H, 5.30%. Calcd for $C_{14}H_{32}O_4F_9P_{5.5}Na_{0.5}Co$: C, 24.86; H, 4.76%. The complex is soluble in water, methanol and ethanol.

$[Co(dtc)(dmpe)_2](ClO_4)_2$. A methanol solution (30 cm^3) containing *trans*-$[CoBr_2(dmpe)_2]ClO_4$[4] (100 mg, 0.16 mmol) and sodium diethyldithiocarbamate (36.4 mg, 0.16 mmol) was stirred for 10 h at room temperature. The yellow crystals which precipitated were filtered, washed with a mixture (20 cm^3) of methanol and diethyl ether (1 : 1) and air-dried. Yield: 52 mg (72%). Found: C, 29.10; H, 6.00; N, 1.97%. Calcd for $C_{17}H_{42}NO_8P_4S_2Cl_2Co$: C, 28.91; H, 5.99; N, 1.98%. The complex is soluble in methanol, ethanol and acetonitrile.

$[Co(gly)(dmpe)_2](ClO_4)_2 \cdot 0.5NaClO_4 \cdot H_2O$. To *trans*-$[CoCl_2(dmpe)_2]ClO_4$[5] (100 mg, 0.19 mmol) in a mixture (50 cm^3) of water and methanol (1 : 1) were added an aqueous solution (5 cm^3) of sodium glycinate (37 mg, 0.38 mmol) and a small amount of active charcoal. The mixture was stirred for 10 h at room temperature, and then filtered to remove active charcoal. The filtrate was diluted with water (1 dm^3) and applied on a column (ϕ 3 cm×120 cm) of SP-Sephadex C-25. By elution with 0.2 mol dm^{-3} NaCl, a small red (probably $[Co(gly)_2(dmpe)]^+$) and then a yellow band appeared. The eluate of the yellow band was collected and evaporated to dryness under reduced pressure. The residue was treated with methanol (100 cm^3) to extract the complex. To the extract was added an aqueous solution (2 cm^3) of $NaClO_4$ (300 mg), and the mixture was concentrated in a vacuum desiccator over P_4O_{10}, yielding yellow crystals. The crystals were filtered, washed with cold methanol (10 cm^3) and air-dried. Yield: 67 mg (18%). Found: C, 26.10; H, 5.70; N, 2.24%. Calcd for $C_{14}H_{38}NO_{13}P_4Cl_{2.5}Na_{0.5}Co$: C, 26.21; H, 5.97; N, 2.18%. The complex is soluble in water and

†All of the perchlorate salts of cobalt(III)-phosphine complexes described below are potentially explosive, and should be handled carefully.

methanol.

[Co(*S*-ala)(dmpe)$_2$](ClO$_4$)$_2$·0.5NaClO$_4$. The complex was prepared by a method similar to that for the glycinato complex, using sodium (*S*)-alaninate. The separation of two diastereomers was not achieved by SP-Sephadex column chromatography. Yield: 10%. Found: C, 23.71; H, 4.97; N, 1.95%. Calcd for $C_{15}H_{38}NO_{12}P_4Cl_{2.5}Na_{0.5}Co$: C, 23.45; H, 4.95; N, 1.82%. The solubility of the complex is similar to that of the glycinato complex.

***trans*-[Co(CN)$_2$(dmpe)$_2$]ClO$_4$.** To a solution of *trans*-[CoBr$_2$(dmpe)$_2$]ClO$_4$ (480 mg, 0.776 mmol) in a mixture (15 cm^3) of acetonitrile and water (2 : 1) was added an aqueous solution (3 cm^3) of NaCN (100 mg, 2.04 mmol), and the mixture was stirred at room temperature. After 1 h the solution was concentrated to 5 cm^3 under reduced pressure and cooled at 0 °C. The white crystals which precipitated were filtered, washed with a small amount of cold methanol and air-dried. Yield: 205 mg (52%). Found: C, 32.93; H, 6.32; N, 5.49%. Calcd for $C_{14}H_{32}N_2O_4P_4ClCo$: C, 32.68; H, 6.29; N, 5.44%. The complex is soluble in water and methanol.

***trans*-[Co(NCS)$_2$(dmpe)$_2$]ClO$_4$·2NaClO$_4$.** A solution (50 cm^3) containing *trans*-[CoCl$_2$(dmpe)$_2$]ClO$_4$ (100 mg, 0.19 mmol) and KNCS (36.7 mg, 0.38 mmol) in a mixture of methanol and water (1 : 1) was stirred at 50 °C for 1 h, and then at room temperature for 10 h. The resulting orange solution was evaporated to dryness under reduced pressure, and the residue was dissolved in acetonitrile (10 cm^3). The solution was chromatographed by a column (ϕ 3 cm×40 cm) of Sephadex LH-20. By elution with a mixture of hexane and acetonitrile (1 : 1), a green (the starting dichloro complex) and an orange band appeared. The orange eluate was collected, evaporated to dryness under reduced pressure, and the residue was dissolved again in acetonitrile (5 cm^3). The solution was mixed with an acetonitrile solution (2 cm^3) of NaClO$_4$ (200 mg) and concentrated in a vaccum desiccator over P_4O_{10}. The orange crystals which were formed were filtered, washed with cold methanol (10 cm^3) and air-dried. Yield: 33 mg (21%). Found: C, 20.40; H, 4.06; N, 3.45%. Calcd for $C_{14}H_{32}N_2O_{12}P_4S_2Cl_3Na_2Co$: C, 20.51; H, 3.93; N, 3.41%. The complex is soluble in acetonitrile.

***trans*-[Co(NCO)$_2$(dmpe)$_2$]ClO$_4$·H$_2$O.** A solution containing *trans*-[CoBr$_2$(dmpe)$_2$]ClO$_4$ (300 mg, 0.49 mmol) and KNCO (119 mg, 1.47 mmol) in a mixture (100 cm^3) of methanol and water (2 : 1) was stirred for 3 h at room temperature. The resulting orange solution was diluted with water (1 dm^3) and applied on a column (ϕ 3 cm×120 cm) of SP-Sephadex C-25. By elution with 0.1 mol dm^{-3} NaCl, a green (the starting dibromo complex) and a yellow eluate were obtained. The yellow eluate was concentrated to dryness under reduced pressure, and the residue was dissolved in methanol (30 cm^3). The methanol solution was diluted with water (1 dm^3) and applied on a small column (ϕ 3cm×20 cm) of SP-Sephadex C-25. The adsorbed complex was eluted with 1 mol dm^{-3} NaClO$_4$, and the eluate was concentrated in a desiccator over P_4O_{10} to give yellow-orange crystals. The crystals were filtered, washed with a mixture (20 cm^3) of methanol and diethyl ether (1 : 1), and air-dried. Yield: 200 mg (72%). Found: C, 30.04; H, 5.80; N, 5.35%. Calcd for $C_{14}H_{34}N_2O_7P_4ClCo$: C, 29.99; H, 6.11; N, 5.00%. The complex is soluble in methanol and acetonitrile.

Optical Resolution of [Co(CO$_3$)(dmpe)$_2$]+. One g of [Co(CO$_3$)(dmpe)$_2$]ClO$_4$·1.5NaClO$_4$·H$_2$O in water (1 cm^3) was charged on the top of a column (ϕ 3 cm×30 cm) of SP-Sephadex C-25, and the complex was eluted with an aqueous solution of 0.1 mol dm^{-3} disodium (−)-di-*O*-benzoyltartrate. No resolution of the complex was achieved by this method. The yellow eluate was collected and concentrated to ca. 20 cm^3 under reduced pressure. Excess disodium (−)-di-*O*-benzoyltartrate was removed by chromatography with a column (ϕ 2.5 cm×30 cm) of Toyopearl TSK-GEL and an eluent water. The eluate was evaporated to dryness under reduced pressure, and the residue was dissolved in ethanol (20 cm^3). On addition of diethyl ether (20 cm^3) the solution gave a yellow precipitate. It was recrystallized three times from a mixture of ethanol and diethyl ether (1 : 4). Yield: 36 mg. The product was dissolved in water and the solution was applied on a column (ϕ 1.5 cm×10 cm) of SP-Sephadex C-25. The column was washed with water, and then the complex was eluted with 0.1 mol dm^{-3} NaClO$_4$. The eluate was concentrated to a small volume under reduced pressure, and the concentrate was used for CD measurements. The complex concentration was determined by reference to the ε values of the racemate.

Results and Discussion

The ease of preparation of [Co(L)(dmpe)$_2$]$^{n+}$ from *trans*-[Co(Cl or Br)$_2$(dmpe)$_2$]$^+$ and a bidentate ligand L differs appreciably by the kind of L. Reactions of *trans*-[Co(Cl or Br)$_2$(dmpe)$_2$]$^+$ with acac, CO_3^{2-}, $C_2O_4^{2-}$ or dtc proceeded smoothly at room temperature and the complexes were obtained in 70—90% yields, while those with gly or *S*-ala did not take place even at 50 °C and resulted in decomposition of the *trans*-dihalogeno complex to cobalt(II) species at a higher temperature. The gly and *S*-ala complexes were obtained in a poor yield, 18 and 10%, respectively by the reactions in the presence of active charcoal. The *trans*-[Co(Cl or Br)$_2$(dmpe)$_2$]$^+$ complex did not react with more bulky (*S*)-proline under similar conditions. The [Co(en)(dmpe)$_2$]$^{3+}$ complex is also obtained in a poor yield (18%) by a similar reaction with en.[1] The poor yield of [Co(L)(dmpe)$_2$]$^{n+}$ in which L has an amino donor group may be attributable to instability of the complex shown later.

The *trans*-[Co(Cl or Br)$_2$(dmpe)$_2$]$^+$ complex afforded only *trans*-[CoX$_2$(dmpe)$_2$]$^+$ by reactions with MX (M=Na$^+$ or K$^+$, X=CN$^-$, NCO$^-$ or NCS$^-$) at room temperature. Attempts to prepare the corresponding cis isomers were unsuccessful. The reaction of *cis*-[CoCl$_2$(dmpe)$_2$]$^+$ [4] with CN$^-$ took place easily at 0 °C, but only the trans isomer was formed, no fraction indicative of the cis isomer being obtained in column chromatography. The reactions with NCO$^-$ and NCS$^-$ proceeded hardly at 0 °C, and yielded the trans isomer at a higher temperature. Since cis-[CoX$_2$(dmpe)$_2$]$^+$ (X=Cl, Br) can be prepared from [Co(CO$_3$)(dmpe)$_2$]$^+$ by treating with HX at 0 °C,[4] no formation of cis-isomers of these pseudo-halogeno complexes would be due to kinetic reasons. When [Co(CO$_3$)(dmpe)$_2$]$^+$ is treated with HClO$_4$, instead of HX, *trans*-[Co(H$_2$O)$_2$(dmpe)$_2$]$^{3+}$ is formed.[3] For the dinitro complex, neither cis nor trans isomer was formed by the

Table 1. Absorption Spectral Data of $[Co(L)(dmpe)_2]^{n+}$

Complex	$\tilde{\nu}_1/10^3\,cm^{-1}$ (log ε)	$\tilde{\nu}_2/10^3\,cm^{-1}$ (log ε)	$\tilde{\nu}_2-\tilde{\nu}_1$	Solvent
$[Co(dtc)(dmpe)_2]^{2+}$	22.5(2.85)	25.1(3.02)	2600	CH_3CN
$[Co(CO_3)(dmpe)_2]^{+}$	23.5(2.96)	27.1(2.98)	3600	CH_3OH
$[Co(C_2O_4)(dmpe)_2]^{+}$	23.9(2.90)	27.4(2.93)	3500	CH_3OH
[Co(*S*-ala)$(dmpe)_2]^{2+}$	24.1(2.93)	28.4(3.00)	4300	H_2O
$[Co(gly)(dmpe)_2]^{2+}$	24.3(2.92)	28.4(3.01)	4100	H_2O
$[Co(en)(dmpe)_2]^{3+}$	24.8(2.86)	29.4(2.84)	4600	H_2O

reaction of *trans*-$[Co(Cl\text{ or }Br)_2(dmpe)_2]^{+}$ with $NaNO_2$. The result will be attributable to steric interactions between the NO_2^- and dmpe ligands as suggested by Miskowski et al.[6] for the corresponding *cis*-1,2-bis(diphenylphosphino)ethylene complex. The $[CoX_2(diars)_2]^{n+}$ (diars=*o*-phenylenebis(dimethylarsine)) complexes have somewhat different properties in chemical reactions. Although *cis*-$[CoCl_2(diars)_2]^{+}$ yields *trans*- $[Co(NCS)_2(diars)_2]^{+}$ by the reaction with KNCS,[7] the reaction of $[Co(CO_3)(diars)_2]^{+}$ with $HClO_4$ affords *cis*-$[Co(H_2O)_2(diars)_2]^{3+}$, from which various *cis*-$[CoX_2(diars)_2]^{n+}$ ($X=Cl^-$, NO_2^-, NO_3^-, CH_3CN) can be derived.[8]

Geometrical structures of $[CoX_2(dmpe)_2]^{n+}$can be easily assigned by comparing the ^1H NMR spectra with those of *cis*- and *trans*-$[CoX_2(dmpe)_2]^{+}$ ($X=Cl^-$, Br^-).[3]

The $C_2O_4^{2-}$ and dtc complexes appear to have stability similar to that of the acac complexes.[1] The complexes in water in the absence or presence of excess NaCl remain unchanged by heating (60—70 °C). The CO_3^{2-} complex is also stable in hot water, but gives a small amount of *trans*-$[CoCl_2(dmpe)_2]^{+}$ in the presence of excess NaCl by prolonged heating. On the other hand, the gly and *S*-ala complexes decompose to cobalt(II) species or yield *trans*-$[CoCl_2(dmpe)_2]^{+}$ under the same conditions. However, these complexes seem to be more stable than $[Co(en)(dmpe)_2]^{3+}$.[1] Thus it can be concluded qualitatively that $[Co(L)(dmpe)_2]^{n+}$ (L=a bidentate ligand) decreases the stability in the order acac, $C_2O_4^{2-}$, dtc > CO_3^{2-} ≫ gly, *S*-ala > en; the complexes containing an amino group are less stable than those with O or S donor atoms.

The NCS^- and NCO^- ligands are an ambidentate ligand to be able to coordinate to a metal ion through N or S, and N or O, respectively. In the IR spectrum *trans*-$[Co(NCS)_2(dmpe)_2]^{+}$ shows the C-S stretching band at 839 cm^{-1}, indicating the N-bonding of NCS^-.[9] Related complexes *cis*(NCS,NCS),*trans*(P,P)- and *trans* (NCS,NCS), *cis* (P,P)-$[Co(NCS)_2\{NH_2CH_2CH_2P(C_6H_5)_2\}_2]^{+}$[10] and *trans*-$[Co(NCS)_2\{cis\text{-}(C_6H_5)_2PCHCHP(C_6H_5)_2\}_2]^{+}$[6] have also been reported to have the N-bonding of NCS^-. For the coordination mode of NCS^-, Norbury et al.[11,12] pointed out that the NCS^- ligand in a hard metal complex containing π-acceptor ligands tends to coordinate through the S atom. A cobalt(III)-phosphine complex should be the case, but no S-bonding of NCS^- has been reported except for the so-called cobaloxime complexes.[13] The preference of N-bonding may come from a steric factor. The Co-NCS moiety is usually nearly linear (∠CoNC=170—180°), whereas the Co-SCN moiety is bent (∠CoSC=≈105°).[10,11] The atomic (ionic) radius of N should be much smaller than that of S. Thus the S-bonding of NCS^- will require greater space and will be unfavorable in a complex containing bulky ligands such as tertiary phosphines. The coordination mode of NCO^- in *trans*-$[Co(NCO)_2(dmpe)_2]^{+}$ could not be assigned from the IR spectrum, but will be the N-bonding, since the complex shows the absorption spectrum very similar to that of *trans*-$[Co(NCS)_2(dmpe)_2]^{+}$ in the first d-d band region (vide post).

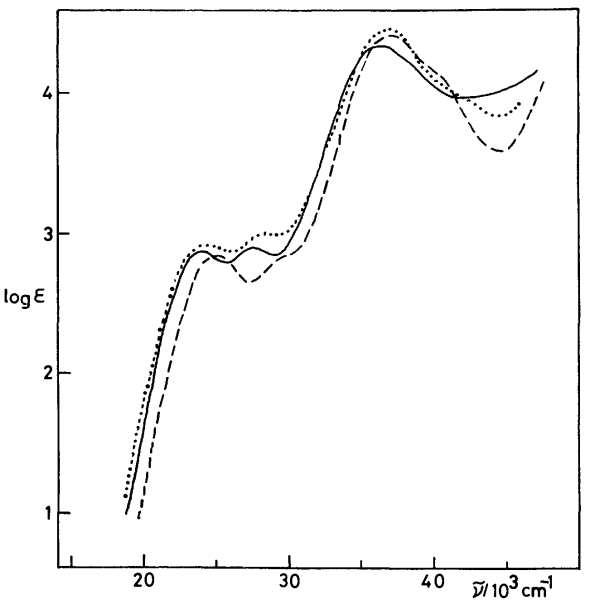

Fig. 1. Absorption spectra of $[Co(C_2O_4)(dmpe)_2]^{+}$ in methanol (——), $[Co(gly)(dmpe)_2]^{2+}$ in water (·····), and $[Co(en)(dmpe)_2]^{3+}$ in water (----).

Absorption spectra of $[Co(L)(dmpe)_2]^{n+}$ ($L=C_2O_4^{2-}$, gly, en) are shown in Fig. 1 and the data in Table 1. In a previous paper,[1] we assigned the band at 24750 cm^{-1} and the shoulder at 29400 cm^{-1} of the en complex to the first and the second d-d bands, respectively. The $C_2O_4^{2-}$ and gly complexes give two d-d bands similar to those of the en complex. The spectrum of the CO_3^{2-} complex is quite similar to that of the $C_2O_4^{2-}$ complex. These d-d bands shift to the low energy side with an increase in number of the O donor atom according to

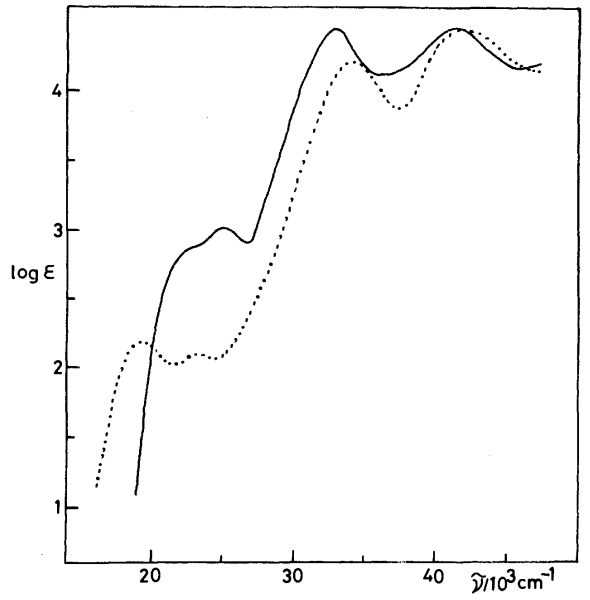

Fig. 2. Absorption spectra of $[Co(dtc)(dmpe)_2]^{2+}$ in acetonitrile (——) and $[Co(dtc)(en)_2]^{2+}$ in water (·····).

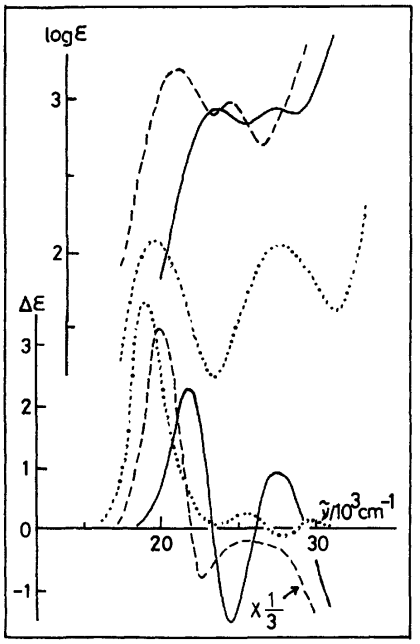

Fig. 3. Absorption and CD spectra of $(+)_{589}$-$[Co(CO_3)(dmpe)_2]^+$ in methanol (——), $(+)_{589}$-$[Co(CO_3)(diars)_2]^+$ in methanol (----),[16] and $(+)_{589}$-$[Co(CO_3)(en)_2]^+$ in water (·····).

the spectrochemical series.[14] However, the extent of shift is larger for the second d-d band than that for the first d-d band. As a result, the energy separation between the first and the second d-d bands becomes small with an increase in number of the O donor atom (Table 1). For $[Co(L)(en)_2]^{n+}$, the values of the energy separation are much larger than those of the dmpe complexes and are nearly the same among the L=en (8100 cm^{-1}), gly (8400 cm^{-1}), and $C_2O_4^{2-}$ (8100 cm^{-1}) complexes.[14]

The absorption spectrum of $[Co(dtc)(dmpe)_2]^{2+}$ is compared with that of $[Co(dtc)(en)_2]^{2+}$ [15] in Fig. 2. The bands at 19600 cm^{-1} ($\log\varepsilon$=2.21) and 23300 cm^{-1} ($\log\varepsilon$=2.11) of the en complex have been assigned to the first and the second d-d bands, respectively on the basis of the magnetic circular dichroism study.[15] The energy separation between these two bands (3700 cm^{-1}) is much smaller than that of $[Co(en)_3]^{3+}$ (8100 cm^{-1}), indicating largely reduced interelectronic repulsions between the ligand field levels. It is known that many dtc complexes show large reduction of the interelectronic repulsion.[15] Thus the shoulder at 22500 cm^{-1} and the band at 25100 cm^{-1} of $[Co(dtc)(dmpe)_2]^{2+}$ can be assigned to the first and the second d-d bands, respectively, although the energy separation between them is extremely small (2600 cm^{-1}) as a cobalt(III) complex.

Absorption and circular dichroism (CD) spectra of $(+)_{589}$-$[Co(CO_3)(dmpe)_2]^+$ are compared with those of the corresponding diars[16] and en[17] complexes in Fig. 3. The decreasing order in energy of the first d-d band is dmpe (23500 cm^{-1})>diars (21000 cm^{-1})> en (19600 cm^{-1}), while that of the second d-d band en (27900 cm^{-1})>dmpe (27100 cm^{-1})>diars (25000 cm^{-1}). From the data the ligand field splitting parameter (Δ) was estimated by assuming C=4B; 24400 cm^{-1} for dmpe, 22000 cm^{-1} for diars, and 21680 cm^{-1} for en complexes. The Δ values of the en and diars complexes are similar. However, en is a primary diamine and its ligand field strength is known to be much stronger than that of a tertiary diamine *N,N,N',N'*-tetramethylethylenediamine corresponding to dmpe and diars.[18] Thus it can be concluded that the spectrochemical series for group 5B elements is P>As>N. The same conclusion has been obtained by spectral studies of *trans*-$[CoCl_2(L)_2]^+$ (L=en, dmpe, 1,2-bis(dimethylarsino)ethane).[19]

The CD strength of $(+)_{589}$-$[Co(CO_3)(dmpe)_2]^+$ in Fig. 3 appears to be weak as compared with those of the en and diars complexes. It is not clear whether the weak strength is attributable to incomplete resolution. The $(+)_{589}$-$[Co(CO_3)(dmpe)_2]^+$ isomer exhibits a positive (21800 cm^{-1}, $\Delta\varepsilon$=+2.29) and a negative (24400 cm^{-1}, $\Delta\varepsilon$=−1.55) CD peaks in the first d-d band region. The absolute configurations of $(+)_{589}$-$[Co(CO_3)(en)_2]^+$ [17] and $(+)_{589}$-$[Co(CO_3)(diars)_2]^+$ [16] have been reported to be Λ. From a comparison of three CD spectra in Fig. 3, the $(+)_{589}$-isomer of the dmpe complex can also be assigned to the Λ configuration. The dmpe complex shows a relatively strong negative CD band in the first d-d band region. Similar strong negative bands have been observed for cobalt(III)-phosphine complexes such as Λ-$[Co(en)_n(dmpe)_{3-n}]^{3+}$ (n=1, 2)[1] or Λ-$[Co(en)_n(edmp)_{3-n}]^{3+}$ (n=0, 1; edmp=$NH_2CH_2CH_2P(CH_3)_2$).[20]

Figure 4 shows absorption spectra of *trans*-$[CoX_2(dmpe)_2]^{n+}$(X=H_2O, CN^-, NCO^-, NCS^-) and Table 2 lists the data. For *trans*-$[Co(H_2O)_2(dmpe)_2]^{3+}$, the

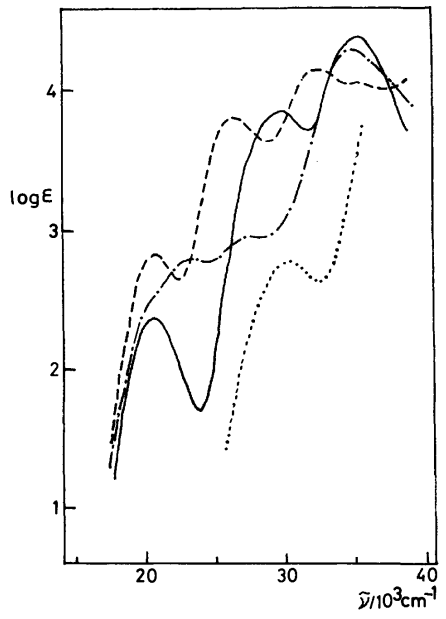

Fig. 4. Absorption spectra of *trans*-$[Co(NCS)_2(dmpe)_2]^+$ in acetonitrile (----), *trans*-$[Co(NCO)_2(dmpe)_2]^+$ in acetonitrile (——), *trans*-$[Co(OH_2)_2(dmpe)_2]^{3+}$ in 0.5 mol dm^{-3} $HClO_4$ (-·-·-), and *trans*-$[Co(CN)_2(dmpe)_2]^+$ in methanol (·····).

Table 2. Absorption Spectral Data of *trans*-$[CoX_2(dmpe)_2]^{n+}$

Complex	$\tilde{\nu}/10^3$ cm^{-1} (logε)	Solvent
trans-$[CoCl_2(dmpe)_2]^+$	17.3(1.92)	CH_3OH
	26.2(3.58)	
	35.1(4.36)	
	40.4(4.16)	
trans-$[Co(OH_2)(dmpe)_2]^{3+}$	20(2.4)[a]	b)
	23.3(2.80)	
	27.3(2.96)	
	34.7(4.30)	
trans-$[Co(NCS)_2(dmpe)_2]^+$	20.6(2.82)	CH_3CN
	26.3(3.81)	
	32.1(4.16)	
	35(4.2)[a]	
	41.5(4.51)	
trans-$[Co(NCO)_2(dmpe)_2]^+$	20.5(2.37)	CH_3CN
	29.6(3.86)	
	34.9(4.39)	
	42(3.8)[a]	
trans-$[Co(CN)_2(dmpe)_2]^+$	30.5(2.77)	CH_3OH
	40.5(4.63)	

a) Shoulder. b) 0.5 mol dm^{-3} $HClO_4$.

shoulder around 20000 cm^{-1} and the band at 23300 cm^{-1} can be assigned to two components of the splitting first d-d band, and the band at 27300 cm^{-1} to the second d-d band, since *trans*-$[Co(H_2O)_2(en)_2]^{3+}$ shows similar d-d bands with three peaks at 18200, 22500, and 29000 cm^{-1}.[21] The *trans*-$[Co(CN)_2(dmpe)_2]^+$ complex shows a single d-d band assignable to the first d-d band. The band is rather broad and appears to involve another band. However, it remains unknown whether the band consists of two components of the splitting first d-d band or of the first and second d-d bands with a very small energy difference. The *trans*-$[Co(CN)_2(en)_2]^+$ complex shows a clear splitting in the first d-d band, giving a shoulder around 21000 cm^{-1} and a band at 24400 cm^{-1}.[22] Neither *trans*-$[Co(NCO)_2(dmpe)_2]^+$ nor *trans*-$[Co(NCS)_2(dmpe)_2]^+$ shows splittings on the first d-d band. The *trans*-$[Co(NCS)_2(en)_2]^+$ complex does not exhibit splitting either, giving a single first d-d band at 19700 cm^{-1}.[23] The NCO^- complex gives the first d-d band at nearly the same position as that of the NCS^- complex, and can be assigned to the N-bonding isomer for NCO^-, since the NCS^- ligand in the latter complex has been indicated to coordinate through the N atom by the IR spectrum (vide ante). The energies of the first d-d bands of the NCO^- and NCS^- complexes are rather lower than that of the aqua complex, although the rankings of NCO^-, NCS^- and H_2O are similar in the spectrochemical series.[14] The phosphine[6] and arsine[24] complexes of cobalt(III) containing NCS^- bonded through the N atom have been reported to give the first d-d band at a lower wavenumber than that expected from the ranking of NCS^- in the spectrochemical series.

The authors wish to thank the Ministry of Education for Scientific Research Grant-in-Aid No. 60470046.

Reference

1) T. Ohishi, K. Kashiwabara, and J. Fujita, *Bull. Chem. Soc. Jpn.*, **56**, 3441 (1983).
2) *Inorg. Synth.*, **15**, 188 (1974).
3) T. Ohishi, K. Kashiwabara, J. Fujita, S. Ohba, T. Ishii, and Y. Saito, *Bull. Chem. Soc. Jpn.*, **59**, 385 (1986).
4) T. Ohishi, K. Kashiwabara, and J. Fujita, *Bull. Chem. Soc. Jpn.*, **60**, 575 (1987).
5) T. Ohishi, K. Kashiwabara, and J. Fujita, *Chem. Lett.*, **1981**, 1371.
6) V. M. Miskowski, J. L. Robbins, G. S. Hammond, and H. B. Gray, *J. Am. Chem. Soc.*, **98**, 2477 (1976).
7) A. Peloso and M. L. Tobe, *J. Chem. Soc.*, **1964**, 5063.
8) B. Bosnich, W. G. Jackson, and J. W. McLaren, *Inorg. Chem.*, **13**, 1133 (1974).
9) A. H. Norbury, *Adv. Inorg. Chem. Radiochem.*, **17**, 231 (1975).
10) M. Atoh, K. Kashiwabara, H. Ito, T. Ito, and J. Fujita, *Bull. Chem. Soc. Jpn.*, **57**, 3139 (1984).
11) A. H. Norbury, *J. Chem. Soc.(A)*, **1971**, 1089.
12) A. H. Norbury, P. E. Show, and A. I. P. Sinha, *J. Chem. Soc., Dalton Trans*, **1975**, 742.
13) K. A. Kargol, K. D. Lavin, R. W. Crecely, and J. L. Burmeister, *Inorg. Chem.*, **19**, 1515 (1980).
14) Y. Shimura and R. Tsuchida, *Bull. Chem. Soc. Jpn.*, **29**, 311 (1956).
15) M. Kita et al., *Inorg. Chem.*, submitted for publication, private communication.
16) W. G. Jackson and B. Bosnich, *Inorg. Chem.*, **22**, 2842 (1983).
17) A. J. McCaffery, S. F. Mason, and B. J. Norman, *J. Chem. Soc.*, **1965**, 5094.

18) Y. Ouyang, M. Kojima, and J. Fujita, *Bull. Chem. Soc. Jpn.*, **57**, 3574 (1984).
19) K. Iwata, M. Kojima, and J. Fujita, *Bull. Chem. Soc. Jpn.*, **58**, 3003 (1985).
20) I. Kinoshita, K. Kashiwabara, J. Fujita, K. Matsumoto, and S. Ooi, *Bull. Chem. Soc. Jpn.*, **54**, 2683 (1981).
21) R. A. D. Wentworth and T. S. Piper, *Inorg. Chem.*, **4**, 709, 1524 (1965).
22) K. Konya, H. Nishikawa, and M. Shibata, *Inorg. Chem.*, **7**, 1165 (1968).
23) K. Yamazaki, J. Hidaka, and Y. Shimura, *Bull. Chem. Soc. Jpn.*, **50**, 2624 (1977).
24) S. Yamada, *Coord. Chem. Rev.*, **2**, 83 (1967).

 © 1987 The Chemical Society of Japan Bull. Chem. Soc. Jpn., 60, 589—594 (1987)

Isomerization and Racemization of the Tris(2,2′-bipyridine *N,N′*-dioxide)chromium(III) Complex

Hideaki KANNO* and Junnosuke FUJITA†

Department of Chemistry, Faculty of Science, Shizuoka University, Oya, Shizuoka 422

†Department of Chemistry, Faculty of Science, Nagoya University, Chikusa-ku, Nagoya 464

(Received September 25, 1986)

Both racemic and optically active $[Cr(bpdo)_3](ClO_4)_3 \cdot 1.5H_2O$ (bpdo=2,2′-bipyridine *N,N′*-dioxide) were found to crystallize in the $lel_2 \cdot ob(\Delta(\lambda\lambda\delta), \Lambda(\delta\delta\lambda))$ isomer. The complexes isomerized spontaneously to the $lel_3(\Delta(\lambda\lambda\lambda), \Lambda(\delta\delta\delta))$ isomer upon dissolution in water with a rapid absorption spectral change, and then racemized ($\Delta \rightleftarrows \Lambda$) slowly. The rate constant for isomerization was 5.33×10^{-3} s^{-1} at 303.2 K, and that for racemization 1.93×10^{-4} s^{-1} at the same temperature. An intramolecular conformational inversion of the bpdo chelate ring ($\delta \rightleftarrows \lambda$) and an intramolecular twist mechanism were proposed for the isomerization and the racemization of the complex, respectively. Neither isomerization nor racemization was observed for $[Cr(en)(bpdo)_2]^{3+}$ in aqueous solution.

2,2′-Bipyridine *N,N′*-dioxide (bpdo) forms a skew seven-membered chelate ring upon coordination to a metal ion.[1,2] The skew chelate ring of bpdo was confirmed by X-ray analysis of $[La(bpdo)_4](ClO_4)_3$.[3] Since the skew conformation can exist in a pair of enantiomers, δ and λ as shown in Fig. 1, a tris-bpdo complex has four possible racemic pairs of diastereomers. By analogy with the stereoisomerism in $[M(en)_3]^{n+}$ (en= ethylenediamine),[4] these diastereomers can be designated as lel_3 ($\Delta(\lambda\lambda\lambda)$, $\Lambda(\delta\delta\delta)$), $lel_2 \cdot ob(\Delta(\lambda\lambda\delta), \Lambda(\delta\delta\lambda))$, $lel \cdot ob_2(\Delta(\lambda\delta\delta), \Lambda(\delta\lambda\lambda))$, and $ob_3(\Delta(\delta\delta\delta), \Lambda(\lambda\lambda\lambda))$. Bertini et al. reported that the dominant isomer of $[M(bpdo)_3](PF_6)_2$ ($M=Co^{2+}$, Ni^{2+}) in acetonitrile will be either the lel_3 or ob_3 one from ^1H NMR studies.[5] They also suggested that a rapid chelate ring interconversion ($\delta \rightleftarrows \lambda$) seems unlikely because of the anticipated high barrier to chelated bpdo interconversion.[5]

In previous papers, we reported that $[Cr(bpdo)_3]^{3+}$ [6] and $[Cr(mbdo)_3]^{3+}$ [7] (mbdo=3,3′-dimethyl-2,2′-bipyridine *N,N′*-dioxide) give one and three racemic pairs of diastereomers, respectively, and that the former complex racemizes spontaneously in aqueous solution. These results indicate that the bpdo chelate ring is flexible and changes its conformation ($\delta \rightleftarrows \lambda$) very easily. On the other hand, the mbdo chelate ring can not change its conformation because of the steric hindrance due to the methyl groups.[7] Recently, we also found that both racemic and $(-)_{589}$-$[Cr(acac)(bpdo)_2](ClO_4)_2 \cdot H_2O$ (acac=acetylacetonate(1−)) crystallize in the lel_2 ($\Delta(\lambda\lambda)$, $\Lambda(\delta\delta)$) isomer, but isomerize spontaneously to the $lel \cdot ob(\Delta(\lambda\delta), \Lambda(\delta\lambda))$ isomer and racemize in aqueous solution.[8] From kinetic studies, the isomerization of $[Cr(acac)(bpdo)_2]^{2+}$ was suggested to occur by intramolecular conformational inversion ($\delta \rightleftarrows \lambda$) of the bpdo chelate ring.[8] This result indicates that in some metal complexes, a favorable bpdo chelate ring conformation in a crystal is different from that in solution. Such a conformational change due to environment is known for $[Cr(en)_3]^{3+}$,[9] but the kinetics of conformational inversion of the en chelate ring can not be studied because of the very rapid interconversion in solution. This paper reports spontaneous isomerization of the tris-bpdo chromium(III) complex in aqueous solution sudied by absorption and circular dichroism (CD) spectroscopy. This paper also reports the results of reinvestigation on racemization of this complex.[6]

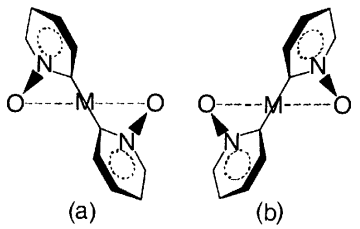

Fig. 1. The conformation of bpdo, (a) δ- and (b) λ-skew form.

Experimental

Materials. The bpdo ligand was prepared according to the literature.[10] The complexes, $[Cr(bpdo)_3](ClO_4)_3 \cdot 1.5H_2O$ and $[Cr(en)(bpdo)_2](ClO_4)_3 \cdot 1.5H_2O$ were prepared and resolved by the method reported previously.[6]

Kinetic Runs. Both racemic and optically active $[Cr(bpdo)_3](ClO_4)_3 \cdot 1.5H_2O$ in aqueous solution show a rapid absorption spectral change. The change in absorbance at 620 nm was continuously recorded on a Shimadzu MPS-50L spectrophotometer in the temperature range of 15.0 to 35.0 °C using a 1 cm quartz cell with a cell jacket to maintain the temperature constant within ±0.1 °C. The pH and ionic strength (I=0.1) of solutions were adjusted with an aqueous solution of NaCl-HCl. Because of insufficient solubility of $[Cr(bpdo)_3](ClO_4)_3 \cdot 1.5H_2O$ in water for the measurement (ca. 1.5 mmol dm^{-3} at 20 °C), the complex was converted into the chloride by the following method. A mixture of a Dowex 1-x8 anion exchanger in the chloride form (1 g) and an aqueous solution of NaCl (0.1 mol dm^{-3}, 20 cm^3) was kept at a constant temperature in a water bath. To the mixture, the finely ground complex (ca. 0.13 g) was added. After being stirred for 1 min, the Dowex anion exchanger was filtered off using a glass filter immersed in the same water bath. The complex concentrations were in the range of 5.0 to 7.6 mmol dm^{-3}. The rate of spectral change obeyed the first order kinetic law and the observed rate constant (k_{obsd}) is expressed as follows:

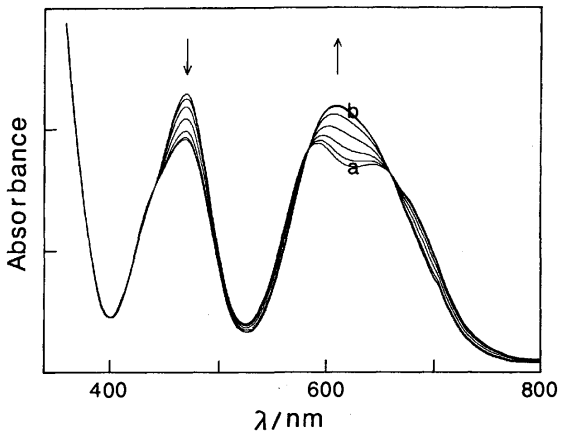

Fig. 2. Absorption spectral change in the visible region of $[Cr(bpdo)_3](ClO_4)_3 \cdot 1.5H_2O$ in aqueous solution at 15.0°C. Trends of the spectral change with time are shown by arrows. Reaction time (min): 2.5(a), 4, 8, 16, 32, 64, ∞(b).

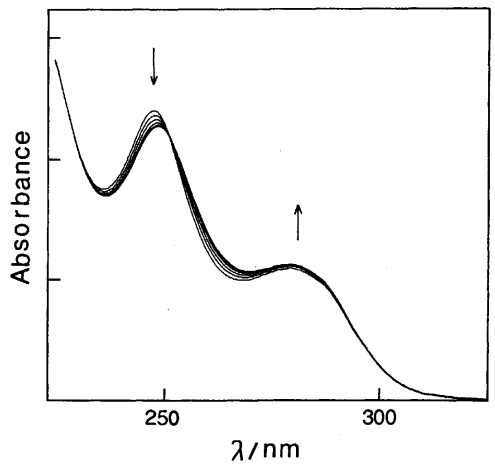

Fig. 3. Absorption spectral change in the ultraviolet region of $[Cr(bpdo)_3](ClO_4)_3 \cdot 1.5H_2O$ in aqueous solution at 18.0°C. Reaction time (min): 2, 4, 8, 16, 32, ∞.

$$k_{obsd} = -\ln[(A_t - A_\infty)/(A_0 - A_\infty)]/t,$$

where A's are absorbances at the time denoted by suffixes. For a comparison, the measurements were also carried out for the perchlorate of the complex without exchanging it into the chloride. The rate observed for the perchlorate agreed with that for the chloride within the experimental error.

A decrease in optical activity at 589 nm of $(-)_{589}$-$[Cr(bpdo)_3](ClO_4)_3 \cdot 1.5H_2O$ in aqueous solution was observed by similar procedures as described above using a Union PM-101 digital polarimeter and a 5 cm quartz cell. The perchlorate of the complex was used for the measurements. The temperatures and the complex concentrations were in the range of 25.0 to 45.0 °C and 1.0 to 1.5 mmol dm^{-3}, respectively. The complex lost the optical activity in two steps with different rates, the first rapid and the subsequent slow steps (vide post). In the latter step, the rate of decrease obeyed the first order kinetic law and the observed rate constant (k_{obsd}) is also expressed by the above equation, where A's are degrees of optical rotation.

For $[Cr(en)(bpdo)_2](ClO_4)_3$, the same experiments were carried out as those for $[Cr(bpdo)_3]^{3+}$ in the dark so as to avoid photoinduced reactions.[6] Neither absorption spectral change nor loss of optical activity was observed in acidic solution. However, the complex in neutral aqueous solution showed a slight decrease in absorbance (< 1% at 530 nm) after 2 h. The resulting solution contained a very small amount of a hydrolyzed product as detected by column chromatography.

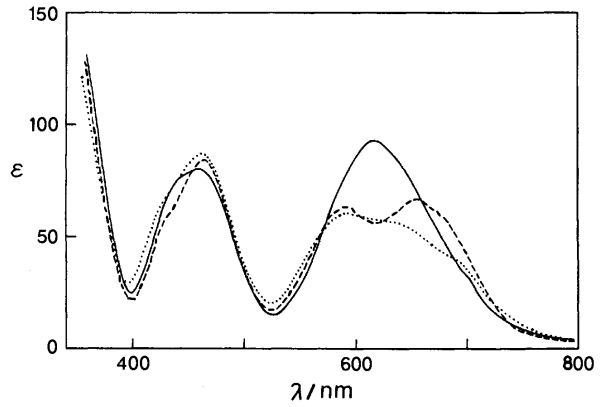

Fig. 4. Absorption spectra of three diastereomers of $[Cr(rac\text{-}mbdo)_3]^{3+}$ in the visible region in aqueous solution; *lel*$_3$ (——), *lel*$_2$·*ob* (----), and *lel*·*ob*$_2$ (·····).[7]

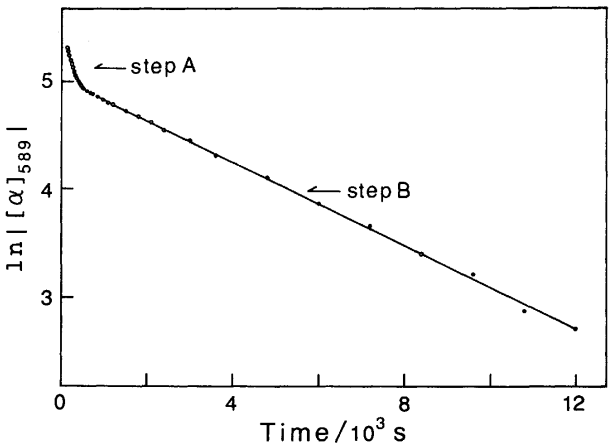

Fig. 5. Decrease in optical rotation (at 589 nm) of $(-)_{589}$-$[Cr(bpdo)_3](ClO_4)_3 \cdot 1.5H_2O$ with time in aqueous solution at 30.0°C. [Complex]=1.17×10^{-3} mol dm^{-3}; I=0.1.

Other Measurements. Absorption and circular dichroism spectra were recorded on a Shimadzu MPS-50L spectrophotometer and a Jasco J-500 spectropolarimeter, respectively. Optical rotations were measured with a Union PM-101 digital polarimeter.

Results and Discussion

Properties of the Complexes. Quagliano et al. first prepared bpdo complexes with a variety of metal ions including chromium(III).[2] As we reported previously,[6] $[Cr(bpdo)_3]^{3+}$ gives only one racemic pair of diastereomers of four possible ones. No indication for the formation of the other isomers was found by SP-Sephadex column chromatography. The optical resolution of the complex[6] was achieved by a chemical

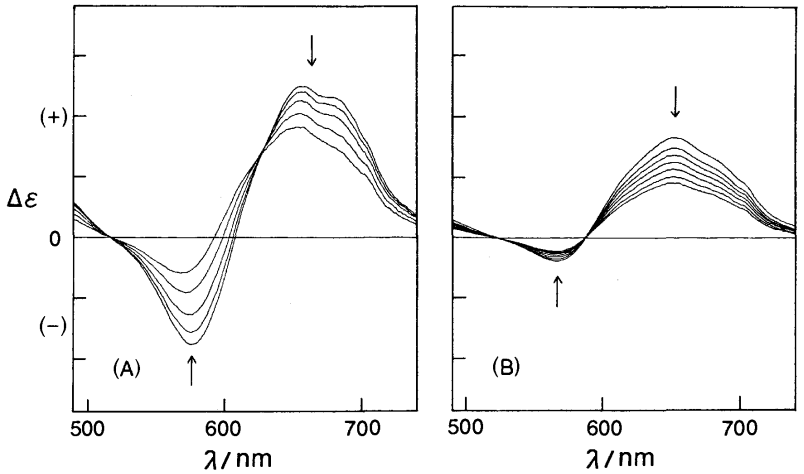

Fig. 6. CD spectral change in the region of the first absorption band of $(-)_{589}$-$[Cr(bpdo)_3](ClO_4)_3 \cdot 1.5H_2O$ in aqueous solution at 15.0°C. Trends of the spectral change with time are shown by arrows. Reaction time (min): (A): 2.5, 4, 7, 13, 25; (B): 50, 80, 110, 140, 170, 200, 230.

method using $(+)_{589}$-[Co(L-cysteinesulfinato(2−)-$S,N)_3]^{3-}$.[11] The optically active complex loses gradually its activity in aqueous solution at room temperature.

Both racemic and optically active $[Cr(bpdo)_3](ClO_4)_3 \cdot 1.5H_2O$ in aqueous solution show a rapid absorption spectral change with isosbestic points at 660, 584, 442, and 251 nm as shown in Figs. 2 and 3. The complexes are not hydrolyzed during the spectral change, no hydrolyzed product such as $[Cr(bpdo)_2(H_2O)_2]^{3+}$ [12] being detected on column chromatograms. These results suggest that the spectral change is caused by isomerization between two isomers of four possible ones of the complex. As Fig. 2 shows, the splitting first absorption band ($^4T_{2g} \leftarrow {}^4A_{2g}$) around 610 nm becomes a single peak with passage of time. All of the possible isomers of the complex have a $[CrO_6]$ chromophore in which the coordinated oxygen atoms are the same kind. However, actual symmetries of the lel_3 and ob_3 isomers will be D_3, and those of the $lel_2 \cdot ob$ and $lel \cdot ob_2$ isomers will lower to C_2. In the fields of D_3 and C_2 symmetries, the first absorption band of an octahedral parentage ($^4T_{2g}$) will split into two ($^4A_1$, ^4E) and three (2^4A, ^4B) components, respectively.[13] Figure 4 shows the absorption spectra of the isomers of $[Cr(rac\text{-mbdo})_3]^{3+}$.[7] The complex gives three racemic pairs of diastereomers, the lel_3, $lel_2 \cdot ob$, and $lel \cdot ob_2$ isomers. The ob_3 isomer will not be formed because of its extremely crowded structure.[6,7] By comparing the spectra in Figs. 2 and 4, it is seen that spectra a and b of the bpdo complex quite resemble those of the $lel_2 \cdot ob$ and lel_3 isomers of the mbdo complex, respectively. Thus the isomers corresponding to spectra a and b in Fig. 2 can be assigned to have the $lel_2 \cdot ob$ and lel_3 structures, respectively, and it is concluded that the spectral change in the bpdo complex is caused by isomerization of the complex, $lel_2 \cdot ob \rightleftarrows lel_3$. In the ultraviolet region, the spectra of the

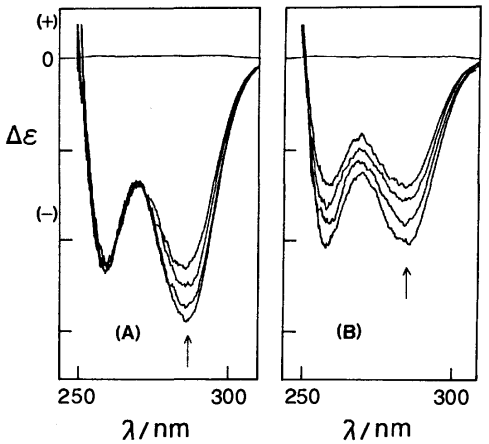

Fig. 7. CD spectral change in the ultraviolet region of $(-)_{589}$-$[Cr(bpdo)_3](ClO_4)_3 \cdot 1.5H_2O$ in aqueous solution at 18.0°C. Reaction time (min): (A): 2, 5, 11, 23; (B): 50, 80, 110, 140.

three isomers of the mbdo complex are similar.[7] The spectral change in the bpdo complex is also very small as shown in Fig. 3. Molecular models indicate that the $lel_2 \cdot ob$ isomer of the bpdo complex isomerizes to the lel_3 one without difficulty and vice versa, since the bpdo chelate ring is flexible and changes its comformation, $\delta \rightleftarrows \lambda$, very easily.[6-8]

As shown in Fig. 5, an aqueous solution of $(-)_{589}$-$[Cr(bpdo)_3](ClO_4)_3 \cdot 1.5H_2O$ loses the optical activity in two steps with different rates, the first rapid (step A) and the subsequent slow (step B) steps. In the former step, the decrease in activity accompanies the absorption spectral change stated above, while no spectral change was observed in the latter step. These results suggest that step A involves the isomerization reaction between the diastereomers, $lel_2 \cdot ob \rightleftarrows lel_3$, and step B the racemization reaction between the enantiomers, $\Delta \rightleftarrows \Lambda$, of the complex. Figures 6 and 7 show the CD

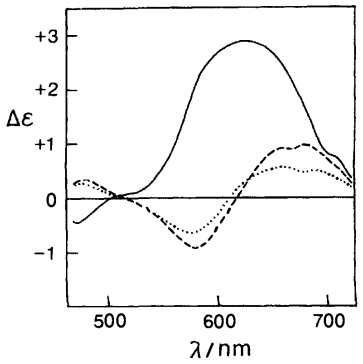

Fig. 8. CD spectra of three diastereomers of $(-)_{589}$-[Cr(rac-mbdo)$_3$]$^{3+}$ in the region of the first absorption band in aqueous solution; *lel*$_3$($\Lambda(\lambda\lambda\lambda)$) (——), *lel*$_2$·*ob*($\Lambda(\lambda\lambda\delta)$) (----), and *lel*·*ob*$_2$($\Lambda(\delta\lambda\lambda)$) (·····).[7]

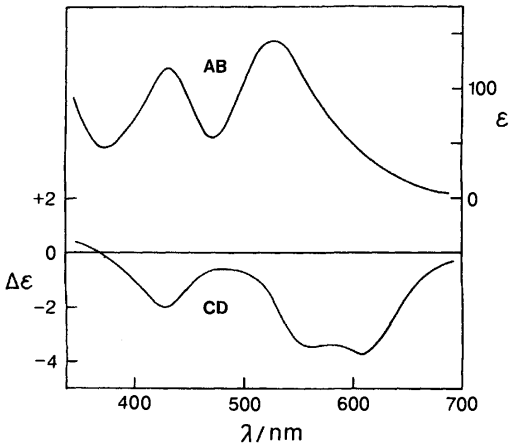

Fig. 9. Absorption and CD spectra in the visible region of $(+)_{589}$-[Cr(en)(bpdo)$_2$](ClO$_4$)$_3$·H$_2$O in 10^{-2} mol dm^{-3} hydrochloric acid.

spectral change of the $(-)_{589}$-isomer in the region of the first absorption band and in the ultraviolet region, respectively. In both regions, the spectrum varies in two steps. In the first rapid step (Figs. 6 (A) and 7 (A)), the spectrum shows a change in both magnitude and pattern and accompanies the absorption spectral change, while in the subsequent slow step (Figs. 6 (B) and 7 (B)), it only shows a decrease in magnitude and neither change in CD pattern nor in absorption spectrum was observed. In the region of the first absorption band, the complex exhibits two CD components of similar strength with opposite signs at the beginning of the reaction, but the negative component diminishes more rapidly than the positive component does. Figure 8 shows the CD spectra of the three isomers of $(-)_{589}$-[Cr(*rac*-mbdo)$_3$]$^{3+}$, *lel*$_3$($\Lambda(\lambda\lambda\lambda)$), *lel*$_2$·*ob*($\Lambda(\lambda\lambda\delta)$), and *lel*·*ob*$_2$($\Lambda(\delta\lambda\lambda)$), in the region of the first absorption band.[7] Both isomers of the *lel*$_2$·*ob* and *lel*·*ob*$_2$ show two CD components of similar strength with opposite signs, while the *lel*$_3$ one exhibits only one positive CD component. The CD spectra of these isomers suggest that the CD spectral change of the bpdo complex in the first rapid step is caused by isomerization of the complex, *lel*$_2$·*ob*($\Lambda(\lambda\lambda\delta)$)$\rightleftarrows$*lel*$_3$($\Lambda(\lambda\lambda\lambda)$). Although it is not clear from the CD spectra whether the initial isomer of the bpdo complex is *lel*$_2$·*ob* or *lel*·*ob*$_2$, it is assigned to the *lel*$_2$·*ob* isomer from the previous absorption spectral and kinetic studies (vide post). Thus it is concluded that $(-)_{589}$-[Cr(bpdo)$_3$](ClO$_4$)$_3$·1.5H$_2$O crystallizes in the $\Lambda(\lambda\lambda\delta)$(*lel*$_2$·*ob*) structure and rapidly isomerizes in aqueous solution to the $\Lambda(\lambda\lambda\lambda)$(*lel*$_3$) structure and then slowly racemizes, $\Lambda \rightleftarrows \Lambda$.

The [Cr(en)(bpdo)$_2$]$^{3+}$ complex[6] gives only one pair of diastereomers which was resolved by a chemical method using $(-)_{589}$-[As(1,2-benzenediolate(2−))$_3$]$^-$,[14] although the complex can have three possible racemic pairs of diastereomers, *lel*$_2$, *lel*·*ob*, and *ob*$_2$. Both racemic and $(+)_{589}$-[Cr(en)(bpdo)$_2$](ClO$_4$)$_3$ show no absorption and CD spectral changes in acidic solution (pH ca. 2) at room temperature, but they are slowly hydrolyzed in neutral aqueous solution (see Experimental). The slow loss of optical activity of the complex described in our previous paper[6] is attributable to the hydrolysis of the complex. Figure 9 shows the absorption and CD spectra of $(+)_{589}$-[Cr(en)(bpdo)$_2$]$^{3+}$ in the visible region recorded in this work. In the region of the first absorption band, the complex exhibits two positive CD components. In our previous work, the CD component on the low energy side could not be observed because it lies outside the region measurable by our instrument.[6] The corrected CD spectral data of the $(+)_{589}$-isomer in the visible region are as follows in $\tilde{\nu}$/cm^{-1} ($\Delta\varepsilon$/mol^{-1} dm^3 cm^{-1}); 16500 (−3.72), 17860 (−3.49), and 23360 (−1.99). The absolute configuration of the complex including chirality of bpdo could not be assigned from the CD spectrum, because its pattern is quite different from those of analogous complexes.[6] However, examination with molecular models indicates that in the *lel*·*ob* structure of the complex, the amino or methylene protons of the puckered en chelate ring comes very close to the pyridine ring of the *ob*-form bpdo ligand, whereas there is no such proximity among the ligands in the *lel*$_2$ structure. The *ob*$_2$ isomer will not be formed because of its extremely crowded structure. Thus [Cr(en)(bpdo)$_2$](ClO$_4$)$_3$ will be stabilized in the *lel*$_2$ structure and shows no isomerization in solution. The complex does not racemize either under the same conditions as for [Cr(bpdo)$_3$]$^{3+}$ and [Cr(acac)(bpdo)$_2$]$^{2+}$ described below. Although the reason for this remains unknown at the moment, racemization of the bpdo complex seems to take place with conformational inversion of the bpdo chelate ring, i.e. the isomerization of the complex. The stereoselective formation of *lel*$_2$-[Cr(en)(bpdo)$_2$]$^{3+}$ is in contrast to that of [Cr(acac)(bpdo)$_2$](ClO$_4$)$_2$ which was found to crystallize in the *lel*$_2$ isomer but isomerize to the *lel*·*ob* one and racemize in aqueous solution.[8] Molecular models indicate that

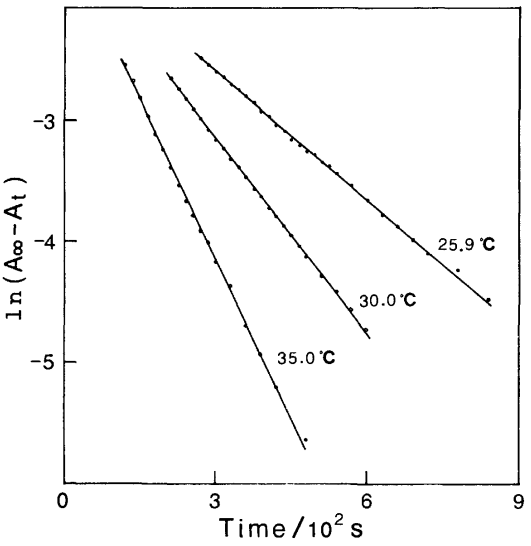

Fig. 10. Plots of $\ln(A_\infty - A_t)$ vs. time for change of absorbance (at 620 nm) of $[Cr(bpdo)_3]^{3+}$ in aqueous solution. [complex]=6.45×10^{-3} mol dm^{-3}; I=0.1.

there is no extreme proximity between the acac and bpdo ligands in these isomers. The difference in reactivity between the en and acac bis-bpdo complexes will be also attributable to such steric conditions. Recently, we found that the conformations of bpdo in mixed-ligand chromium(III) complexes are greatly influenced by other ligands in the complex.[6,8,15] For example, $[Cr(acac)_2(bpdo)]^+$ gives only a $lel(\Delta(\lambda), \Lambda(\delta))$ isomer,[8] whereas $[Cr(bpy)_2(bpdo)]^{3+}$ (bpy=2,2′-bipyridine) only an $ob(\Delta(\delta), \Lambda(\lambda))$ isomer.[15] Thus the bpdo chelate ligand changes its conformation very easily depending upon steric conditions in a complex.

Kinetics of Isomerization and Racemization of $[Cr(bpdo)_3]^{3+}$. The rate of isomerization of $[Cr(bpdo)_3]^{3+}$ in aqueous solution, $lel_2 \cdot ob \rightleftarrows lel_3$, was followed by monitoring the change in absorbance at 620 nm with time under the conditions described in Experimental part. As Fig. 10 shows, the rate of the spectral change obeyed the first order kinetic law for at least four half-lives, and the observed rate constant (k_{obsd}) was obtained from the slope of log ($A_\infty - A_t$) vs. time, where A's are absorbances at the time denoted by suffixes. The rate for the optically active complex agreed with that for the racemate within the experimental error. The values of k_{obsd} are listed in Table 1. Arrhenius treatment of log(k_{obsd}) vs. T^{-1} yielded an activation energy of (82.1±1.3) kJ mol^{-1} and Eyring treatment of log(k_{obsd}/T) vs. T^{-1} gave an activation enthalpy of (79.6±1.3) kJ mol^{-1} and an activation entropy of (−26.1± 4.3) J K^{-1} mol^{-1}. The rate was independent of concentrations of H^+ and the free ligand (bpdo). Hence it is suggested that the isomerization proceeds by an intramolecular mechanism. In a previous paper,[8] we have reported that $\Delta(\lambda\lambda)(lel_2)$-$[Cr(acac)(bpdo)_2]^{2+}$ isomerized to the $\Delta(\lambda\delta)(lel \cdot ob)$ isomer at a rate 3.31×10^{-3} s^{-1} (22.0 °C), and that the activation energy, enthalpy, and entropy values were 77.3 kJ mol^{-1}, 74.9 kJ mol^{-1}, and −38.5 J K^{-1} mol^{-1}, respectively. The rate and kinetic parameters of $[Cr(bpdo)_3]^{3+}$ are similar to those of $[Cr(acac)(bpdo)_2]^{2+}$ ($\lambda\lambda \rightleftarrows \lambda\delta$). Thus the isomerization reactions of these two complexes would proceed by the same mechanism, and the isomerization of $[Cr(bpdo)_3]^{3+}$ will not involve the reaction, $lel \cdot ob_2(\Delta(\lambda\delta\delta)) \rightleftarrows lel_3(\Delta(\lambda\lambda\lambda))$, in which simultaneous inversion of two bpdo chelate rings $\delta\delta \rightleftarrows \lambda\lambda$ takes place.

Table 1. Rate Constants for the Isomerization of $[Cr(bpdo)_3]^{3+}$ in Aqueous Solutions (I=0.1[a])

t/°C	$k_{obsd}\times10^3$/s^{-1}	t/°C	$k_{obsd}\times10^3$/s^{-1}
15.0	0.962±0.004[b]	30.0	5.33±0.03
18.5	1.43±0.01	30.0[c]	5.37±0.05
22.0	2.16±0.01	30.0[d]	5.30±0.04
22.0[c]	2.15±0.01	30.0[e]	5.34±0.06
22.0[d]	2.13±0.02	30.0[f]	5.36±0.06
22.0[e]	2.15±0.01	30.0[g]	5.36±0.05
22.0[f]	2.13±0.03	35.0	8.66±0.09
25.9	3.51±0.03		

a) Ionic strength adjusted with NaCl. b) Errors are standard deviations estimated by least squares. c) In 0.1 mol dm^{-3} HCl. d) In 0.05 mol dm^{-3} dpdo. e) For $(-)_{589}$-isomer. f) For the perchlorate of the complex (see Experimental). g) For $(+)_{589}$-isomer.

Table 2. Rate Constants for the Racemization of $(-)_{589}$-$[Cr(bpdo)_3]^{3+}$ in Aqueous Solutions (I=0.1[a])

t/°C	$k_{obsd}\times10^4$/s^{-1}	t/°C	$k_{obsd}\times10^4$/s^{-1}
25.0	1.13±0.02[b]	35.0	3.20±0.02
29.8[c]	1.90±0.01	39.8[d]	5.23±0.04
30.0	1.93±0.02	40.0	5.25±0.03
30.0[d]	1.93±0.03	40.0[c]	5.21±0.03
30.0[e]	1.91±0.02	45.0	8.38±0.06
30.0[f]	1.93±0.03	45.0[d]	8.41±0.05

a) Ionic strength adjusted with NaCl. b) Errors are standard deviations estimated by least squares. c) In 0.05 mol dm^{-3} dpdo. d) In 0.1 mol dm^{-3} HCl. e) For $(+)_{589}$-isomer. f) For the chloride of the complex prepared with a Dowex anion exchanger (see Experimental).

Our previous study on racemization of $[Cr(bpdo)_3]^{3+}$ in aqueous solution[6] was reinvestigated in this paper. The rate of loss of activity of $(-)_{589}$-$[Cr(bpdo)_3]^{3+}$ was followed by monitoring the change in optical rotation at 589 nm with time under the conditions described in Experimental part. As Fig. 5 shows, the rate in step B obeyed the first order kinetic law at least three half-lives, and the rate constant (k_{obsd}) was obtained from the slope of log$|\alpha_t|$ vs. time, where α is degrees of optical rotation. The values of k_{obsd} are given in Table 2. The rate of racemization was independent of concentrations of H^+ and the free ligand (bpdo). Hence the racemization ($\Delta \rightleftarrows \Lambda$) will also proceed by an intramolecular mechanism. The estimated values of activation energy, enthalpy, and entropy are (79.0±0.3)

kJ mol^{-1}, (76.5±0.3) kJ mol^{-1}, and (−64.0±1.0) J K^{-1} mol^{-1}, respectively, which agree with those estimated in our previous work.[6] From a comparison of these kinetic parameters with those of other complexes such as $[Cr(phen)_3]^{3+}$,[16] the racemization of $[Cr(bpdo)_3]^{3+}$ is suggested to proceed via an intramolecular twist mechanism. The small negative activation entropy value for the racemization of $[Cr(bpdo)_3]^{3+}$ seems to be consistent with such a mechanism.[17] In our previous work,[8] the rate of racemization of $(-)_{589}$-$[Cr(acac)(bpdo)_2]^{2+}$ in aqueous solution was found to be 1.51×10^{-4} s^{-1} at 25.0 °C with the activation energy, enthalpy, and entropy of 84.8 kJ mol^{-1}, 82.4 kJ mol^{-1}, and −41.7 J K^{-1} mol^{-1}, respectively. The rate and kinetic parameters of $[Cr(bpdo)_3]^{3+}$ are very similar to those of $[Cr(acac)(bpdo)_2]^{2+}$, and the racemization reactions of these two complexes would proceed by the same mechanism. For the intramolecular racemization of a tris(chelate)-type complex, several different twist mechanisms have been proposed.[18] However, it is difficult to determine which mechanism is the most probable for the present complexes.

This work was supported by a Grant-in-Aid for Scientific Research No. 60740330 from the Ministry of Education, Science and Culture.

References

1) R. G. Garvey, J. N. Nelson, and R. O. Ragsdale, *Coord. Chem. Rev.*, **3**, 375 (1968); N. M. Karayannis, L. L. Pytlewski, and C. M. Mikulski, *ibid.*, **11**, 93 (1973); N. M. Karayannis, A. N. Speca, D. E. Chasan, and L. L. Pytlewski, *ibid.*, **20**, 37 (1976).

2) P. G. Simpson, A. Vinciguerra, and J. V. Quagliano, *Inorg. Chem.*, **2**, 282 (1963); A. Vinciguerra, P. G. Simpson, Y. Kakiuti, and J. V. Quagliano, *ibid.*, **2**, 286 (1963).

3) A. R. Al-Karaghouli, R. O. Day, and J. S. Wood, *Inorg. Chem.*, **17**, 3702 (1978).

4) E. J. Corey and J. C. Bailar, Jr., *J. Am. Chem. Soc.*, **81**, 2620 (1959).

5) I. Bertini, D. Gatteschi, and L. J. Wilson, *Inorg. Chim. Acta*, **4**, 629 (1970).

6) H. Kanno, K. Kashiwabara, and J. Fujita, *Bull. Chem. Soc. Jpn.*, **52**, 761 (1979).

7) H. Kanno, K. Kashiwabara, and J. Fujita, *Bull. Chem. Soc. Jpn.*, **52**, 1408 (1979).

8) H. Kanno, T. Shimotori, S. Utsuno, and J. Fujita, *Chem. Lett.*, **1983**, 939; H. Kanno, S. Utsuno, and J. Fujita, *Bull. Chem. Soc. Jpn.*, **57**, 3443 (1984).

9) K. N. Raymond, P. W. R. Corfield, and J. A. Ibers, *Inorg. Chem.*, **7**, 842, 1362 (1968); K. N. Raymond and J. A. Ibers, *ibid.*, **7**, 2333 (1968).

10) I. Murase, *Nippon Kagaku Zasshi*, **77**, 682 (1956).

11) L. S. Dollimore and R. D. Gillard, *J. Chem. Soc., Dalton Trans.*, **1973**, 933.

12) H. Kanno, unpublished work; absorption spectral data of $[Cr(bpdo)_2(H_2O)_2]^{3+}$ prepared by aquation of $[CrCl_2(bpdo)_2]Cl\cdot 3H_2O$ in 0.01 mol dm^{-3} hydrochloric acid λ/nm (ε/mol^{-1} dm^3 cm^{-1}); 606 (48.7), 441 (70.0), 280 (19500), 250 (35300), and 218 (60400). The preparation of the dichloro complex will be described elsewhere.

13) F. A. Cotton, "Chemical Applications of Group Theory," 2nd ed, Wiley-Interscience, New York (1971).

14) R. F. Weinland and J. Heinzler, *Chem. Ber.*, **52**, 1316 (1919); G. E. Ryschkewitsch and J. M. Garrett, *J. Am. Chem. Soc.*, **90**, 7234 (1968).

15) H. Kanno, K. Kashiwabara, and J. Fujita, *Bull. Chem. Soc. Jpn.*, **53**, 2881 (1980); H. Kanno, S. Utsuno, and J. Fujita, *ibid.*, **59**, 1293 (1986).

16) N. A. P. Kane-Maguire and S. A. Edwards, *J. Inorg. Nucl. Chem.*, **38**, 1037 (1976); G. A. Lawrance and D. R. Stranks, *Inorg. Chem.*, **16**, 929 (1977).

17) S. S. Eaton, J. R. Hutchison, R. H. Holm, and E. L. Muetterties, *J. Am. Chem. Soc.*, **94**, 6411 (1972); M. C. Palazzotto, D. J. Duffy, B. L. Edgar, L. Que, Jr., and L. H. Pignolet, *ibid.*, **95**, 4537 (1973).

18) See for example: F. Basolo and R. G. Pearson, "Mechanisms of Inorganic Reactions," 2nd ed, Wiley-Interscience, New York (1967); J. J. Fortman and R. E. Sievers, *Coord. Chem. Rev.*, **6**, 331 (1971); N. Serpone and D. G. Bickley, *Prog. Inorg. Chem.*, **17**, 391 (1972).

 © 1987 The Chemical Society of Japan Bull. Chem. Soc. Jpn., 60, 595—601 (1987)

Preparation and Stereochemistry of Cobalt(III) Complexes with Ethylenediamine-*N*-acetate and 3-Azapentane-1,5-diamine or 3-Methyl-3-azapentane-1,5-diamine

Takaji YASUI,* Toshie SHIKIJI, Norio KOINE,† Tomoharu AMA, and Hiroshi KAWAGUCHI
Department of Chemistry, Faculty of Science, Kochi University, Akebono-cho, Kochi 780
†Department of Industrial Chemistry, Faculty of Engineering, Ehime University, Bunkyo-cho, Matsuyama 790
(Received September 9, 1986)

Four geometrical isomers possible in each of $[Co(edma)(dien)]^{2+}$ and $[Co(edma)(mdien)]^{2+}$, where edma, dien, and mdien denote ethylenediamine-*N*-acetate, 3-azapentane-1,5-diamine, and 3-methyl-3-azapentane-1,5-diamine respectively, and facial isomer of $[Co(edma)(NH_3)_3]^{2+}$ were prepared and resolved into optically active isomers by a column-chromatographic method. The structural assignments of these geometrical isomers were carried out on the basis of the absorption, ^1H NMR, and ^{13}C NMR spectral data. The absolute configurations of the optically active isomers containing facially coordinated edma were determined by ^1H NMR measurements of the glycinate-ring methylene (-CHD-) of edma stereospecifically deuterated in a weak basic D_2O. The relationship between the absolute configurations and the CD spectral behaviors of these isomers is also discussed.

The octahedral complexes of cobalt(III) with terdentate ligands, such as iminodiacetate (ida), *N*-methyliminodiacetate (mida), 3-azapentane-1,5-diamine (dien), 3-methyl-3-azapentane-1,5-diamine (mdien), and ethylenediamine-*N*-acetate (edma), provide varieties of geometrical and optical isomers. Therefore, the complexes with these ligands are useful for the investigations of spectroscopic properties, stereochemistry, and reactivity (isomerization and racemization reactions). Keene and coworkers first isolated three geometrical isomers (u-fac, s-fac, and mer) possible for $[Co(dien)_2]^{3+}$.[1] Thereafter, a complete series of geometrical isomers have been reported for the complexes of $[Co(ida)_2]^-$,[2] $[Co(mida)_2]^-$,[2] $[Co(ida)(mida)]^-$,[3] $[Co(ida)(dien)]^+$,[4] $[Co(mida)(dien)]^+$,[5] $[Co(ida)(mdien)]^+$,[5] $[Co(mida)(mdien)]^+$,[5] $[Co(dien)(mdien)]^{3+}$[6,7] (three isomers), $[Co(edma)_2]^+$ (six isomers),[8-10] [Co(ida)(edma)],[9,10] and [Co(mida)(edma)][11] (four isomers). However, there is no report for the mixed-ligand complexes of $[Co(edma)(dien)]^{2+}$ and $[Co(edma)(mdien)]^{2+}$. Both the complexes provide four geometrical isomers with chiral structure, as shown in Fig. 1.

In the present paper, the preparation and optical resolution of $[Co(edma)(dien)]^{2+}$, $[Co(edma)(mdien)]^{2+}$ and $[Co(edma)(NH_3)_3]^{2+}$ will be described, and the stereochemistry will be discussed on the basis of their absorption, ^1H NMR, ^{13}C NMR, and CD spectral data.

Experimental

Preparation and Optical Resolution of the Complexes. Preparation of Four Geometrical Isomers of [Co(edma)(mdien)]$^{2+}$: An aqueous solution containing 2.27 g (0.01 mol) of ethylenediamine-*N*-acetic acid dihydrochloride dihydrate[12] (Hedma·2HCl·$2H_2O$) and 2.26 g (0.01 mol) of 3-methyl-3-azapentane-1,5-diamine trihydrochloride[13] (mdien·3HCl) in 60 cm^3 of water was passed through an anion-exchange resin (Dowex 1×8, ClO_4^- form) column to convert the chloride ions to the perchlorate ions, and then the solution was evaporated to a volume of 20 cm^3. Similarly, an aqueous solution containing 2.23 g (0.01 mol) of $CoCl_2·6H_2O$ in 30 cm^3 of water was passed through an anion-exchange resin column of ClO_4^- form. These two solutions were mixed and the solution was adjusted to pH 6.5—6.9 with 1 mol dm^{-3} NaOH solution. Lead dioxide (8.0 g) was stirred into the solution in small portions at 40 °C over a 1 h period, the pH of the solution being kept at 6.5—6.9. After insoluble materials had then been removed by filtration, the filtrate (red-purple) was charged on an SP-Sephadex C-25 column (ϕ 4.7 cm×90 cm, NH_4^+ form). The adsorbed band was developed with 0.2 mol dm^{-3} $(NH_4)_2SO_4$ solution. The band was separated into several bands by recyclic developement: red-orange (a mixture of four isomers of $[Co(edma)_2]^+$), red (a mixture of two isomers of $[Co(edma)_2]^+$), orange (desired isomer, el 1), red-orange (el 2), orange (el 3), violet (unidentified complex), orange (el 4), and orange ($[Co(mdien)_2]^{3+}$) bands (formation ratio of el 1, el 2, el 3, and el 4 was 39 : 48 : 2 : 11). The eluate from each band of el 1—el 4 was evaporated under reduced pressure, and methanol was added to the concentrated solution. Ammonium sulfate deposited was removed by filtration and the filtrate was again evaporated. A crude complex was obtained from the concentrated solution by addition of methanol. The isomers of el 1, el 3, and el 4 were isolated in a crystal by recrystallizing the crude complexes from water-methanol

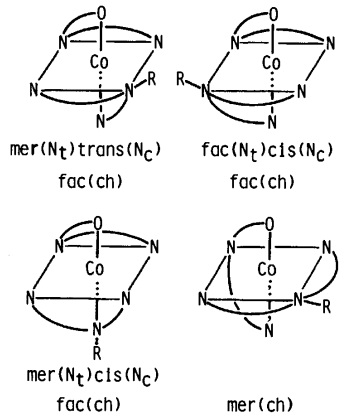

Fig. 1. Four geometrical isomers of $[Co(edma)(dien)]^{2+}$ (R=H) or $[Co(edma)(mdien)]^{2+}$ (R=CH_3). N_t and N_c denote terminal and central nitrogens, respectively, and fac(ch) and mer(ch) represent the isomers with facially and meridionally chelated ligands, respectively.

solvent. The isomer of el 2 was obtained as a crystal of bromide salt by converting the sulfate salt to the bromide salt using a short QAE-Sephadex (Br^- form) column. Found for el 1: C, 25.51; H, 6.45; N, 16.42%. Calcd for $[Co(edma)(mdien)]SO_4 \cdot 2H_2O = C_9H_{28}N_5O_8SCo$: C, 25.41; H, 6.64; N, 16.47%. Found for el 2: C, 23.60; H, 5.42; N, 14.97%. Calcd for $[Co(edma)(mdien)]Br_2 \cdot 0.5H_2O = C_9H_{25}N_5O_{2.5}Br_2Co$: C, 23.39; H, 5.45; N, 15.16%. Found for el 3: C, 24.96; H, 6.50; N, 16.15%. Calcd for $[Co(edma)(mdien)]SO_4 \cdot 2.5H_2O = C_9H_{29}N_5O_{8.5}SCo$: C, 24.89; H, 6.73; N, 16.12%. Found for el 4: C, 26.19; H, 6.76; N, 16.53%. Calcd for $[Co(edma)(mdien)]SO_4 \cdot 1.5H_2O = C_9H_{27}N_5O_{7.5}SCo$: C, 25.96; H, 6.54; N, 16.82%.

Resolution of $[Co(edma)(mdien)]^{2+}$: The racemates of el 1—el 4 were resolved into optically active isomers by a column-chromatographic method.

A solution containing ca. 1 g of each racemate of el 1—el 4 in a small amount of water was poured onto an SP-Sephadex column (ϕ 4.7 cm×50 cm, Na^+ form), and the adsorbed band was developed with a 0.2 mol dm^{-3} $Na_2Sb_2(d\text{-tart})_2$ solution. On each chromatographic run of el 1, el 3, and el 4, the adsorbed band separated completely into two bands by repeating recyclic developement 5—6 times, and each band was eluted out from the column. Whereas on the run of el 2, the band separation was incomplete. The front and rear fractions of the broadening band, which showed enantiomeric CD curves with (+) and (−) signs at 528 nm respectively, were eluted out. Each eluate was evaporated, and a saturated KCl solution was added to the concentrated solution to make deposit $K_2Sb_2(d\text{-tart})_2$ salt, which was removed by filtration. The filtrate was again evaporated, and methanol was added to the concentrated solution to eliminate KCl. The methanolic solution was evaporated, and the concentrated solution was charged on a short QAE-Sephadex (Br^- form) column to convert Cl^- ion to Br^- ion. The solution eluted with water was evaporated and methanol was added to the concentrated solution. A crude complex obtained was recrystallized from water by addition of methanol. Found for the early eluted $(-)^{CD}_{509}$ isomer of el 1: C, 23.22; H, 5.63; N, 14.95%. Found for the $(-)^{CD}_{528}$ isomer (from rear fraction) of el 2: C, 23.18; H, 5.65; N, 14.64%. Found for the early eluted $(-)^{CD}_{540}$ isomer of el 4: C, 22.92; H, 5.59; N, 15.03%. Calcd for $[Co(edma)(mdien)]Br_2 \cdot H_2O = C_9H_{26}N_5O_3Br_2Co$: C, 22.95; H, 5.56; N, 14.85%. Found for the early eluted $(+)^{CD}_{514}$ isomer of el 3: C, 23.65; H, 6.01; N, 14.30%. Calcd for $[Co(edma)(mdien)]Br_2 \cdot H_2O \cdot 0.5CH_3OH = C_{9.5}H_{28}N_5O_{3.5}Br_2Co$: C, 23.42; H, 5.79; N, 14.38%.

Preparation and Resolution of $[Co(edma)(dien)]^{2+}$: The crude isomers (el 1—el 4) of $[Co(edma)(dien)]SO_4$ were obtained by the same method as that used for the isomers of $[Co(edma)(mdien)]SO_4$. Formation ratio of el 1, el 2, el 3, and el 4 was 18 : 55 : 12 : 15. The sulfate salts were converted to the chloride salts using a QAE-Sephadex A-25 (Cl^- form) column. The crude complexes obtained were recrystallized from water by addition of methanol. The isomers of el 1 and el 3 were obtained in orange crystals and the isomers of el 2 and el 4 in red-orange crystals. Found for el 1: C, 27.03; H, 6.36; N, 19.34%. Calcd for $[Co(edma)(dien)]Cl_2 \cdot 0.5H_2O = C_8H_{23}N_5O_{2.5}Cl_2Co$: C, 26.75; H, 6.46; N, 19.50%. Found for el 2: C, 25.70; H, 6.67; N, 18.69%. Found for el 4: C, 25.44; H, 6.58; N, 18.54%. Calcd for $[Co(edma)(dien)]Cl_2 \cdot 1.5H_2O = C_8H_{25}N_5O_{3.5}Cl_2Co$: C, 25.48; H, 6.68; N, 18.57%. Found for el 3: C, 24.96; H, 6.78; N, 17.85%. Calcd for $[Co(edma)(dien)]Cl_2 \cdot 2H_2O = C_8H_{26}N_5O_4Cl_2Co$: C, 24.88; H, 6.79; N, 18.14%.

The optical resolutions of these isomers were carried out by the same method as that used for the four isomers of $[Co(edma)(mdien)]^{2+}$. Found for the late eluted $(+)^{CD}_{504}$ isomer of el 1: C, 25.70; H, 6.55; N, 18.27%. Calcd for $[Co(edma)(dien)]Cl_2 \cdot 1.5H_2O = C_8H_{25}N_5O_{3.5}Cl_2Co$: C, 25.48; H, 6.68; N, 18.57%. Found for the late eluted $(-)^{CD}_{514}$ isomer of el 2: C, 20.87; H, 5.33; N, 15.13%. Calcd for $[Co(edma)(dien)]Br_2 \cdot H_2O = C_8H_{24}N_5O_3Br_2Co$: C, 21.02; H, 5.29; N, 15.32%. Found for the early eluted $(-)^{CD}_{500}$ isomer of el 3: C, 22.61; H, 5.66; N, 15.08%. Calcd for $[Co(edma)(dien)]Br_2 \cdot CH_3OH = C_9H_{26}N_5O_3Br_2Co$: C, 22.95; H, 5.56; N, 14.86%. Found for the late eluted $(-)^{CD}_{527}$ isomer of el 4: C, 27.07; H, 6.41; N, 19.58%. Calcd for $[Co(edma)(dien)]Cl_2 \cdot 0.5H_2O = C_8H_{23}N_5O_{2.5}Cl_2Co$: C, 26.75; H, 6.46; N, 19.50%.

Preparation and Resolution of *fac*-$[Co(edma)(NH_3)_3]^{2+}$: Although the geometrical structure of this complex has been reported in the preceding paper,[14] the preparative method was not described. A solution containing 4.0 g of Hedma · 2HCl · $2H_2O$ in 40 cm^3 of water was poured onto a column containing anion-exchange resin (Dowex 1×8, NO_3^- form) and eluted out with water, in order to exchange Cl^- ion to NO_3^- ion. The eluate was evaporated to ca. 3 cm^3 and then added to a solution containing 6.0 g of $[Co(NH_3)_5(H_2O)](NO_3)_3$ in 250 cm^3 of 25% aqueous NH_3. The mixed solution was heated at 80 °C for 3 h and then cooled to room temperature. The resultant solution was evaporated to ca. 20 cm^3 to charge again on an SP-Sephadex column (ϕ 4.7 cm×50 cm, Na^+ form). The adsorbed band was developed with 0.5 mol dm^{-3} $NaNO_3$ solution. The second band of red-orange color was eluted out, and then the eluate was concentrated. Methanol was added to the concentrated eluate to make deposit $NaNO_3$ salt, which was removed by filtration. Red-orange complex was obtained from the filtrate by evaporation and by addition of methanol. This complex was used for the resolution without further purification.

The racemate obtained above was dissolved into 50 cm^3 of water to charge on an SP-Sephadex column (ϕ4.7 cm×50 cm, K^+ form). The adsorbed band was completely separated into two bands by developing it with a 0.1 mol dm^{-3} $K_2Sb_2(d\text{-tart})_2$ solution. Each band was eluted out with a 0.2 mol dm^{-3} KCl solution. The first and second eluates which exhibited (+) and (−) CD signs at 512 nm, respectively, were evaporated to ca. 5 cm^3 and 100 cm^3 of methanol was added to the concentrated solutions. Potassium chloride deposited was removed by filtration. Ethanol was added to the filtrates to obtain crude complexes, which were recrystallized from water by addition of ethanol. Found for the $(-)^{CD}_{512}$ isomer: C, 15.40; H, 6.35; N, 22.34%. Calcd for $[Co(edma)(NH_3)_3]Cl_2 \cdot H_2O = C_4H_{20}N_5O_3Cl_2Co$: C, 15.20; H, 6.38; N, 22.16%.

Determination of Absolute Configurations of the Complexes by ^1H NMR Technique. Determination of the absolute configurations of the optically active *fac*-$[Co(edma)(dien)]^{2+}$ and *fac*-$[Co(edma)(NH_3)_3]^{2+}$ complexes was carried out by the method modified that used for the $[Co(edma)_2]^+$ complex in our previous study.[8]

About 0.2 g of $(+)^{CD}_{504}$ el 1 $[Co(edma)(dien)]Cl_2 \cdot 1.5H_2O$ was dissolved into a buffer solution (pH 10), and the solution was allowed to stand at 40 °C for ca. 1 h to deuterate one of the two methylene protons on the edma glycinate ring (G-ring) (Fig. 2). The deuteration reaction was stopped by acidifing the solution (pH 5—6) with 1 mol dm^{-3} HCl, and zinc powder (2 g) was added to the solution. After stirring the mixture for 5 min at ca. 25 °C, unreacted zinc was removed

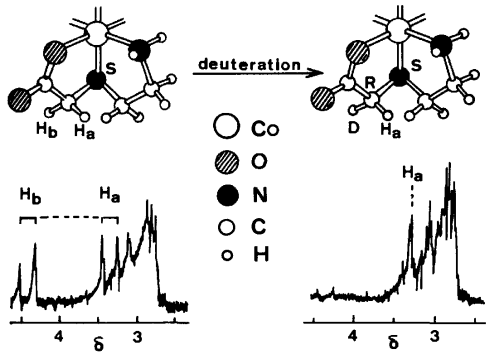

Fig. 2. Stereospecific deuteration on the G-ring $-CH_2-$ of coordinated edma in $(+)^{CD}_{504}$ el 1 of $[Co(edma)(dien)]^{2+}$

by filtration. To the filtrate, 52 mg of $CuSO_4 \cdot 5H_2O$ (to make produce a blue copper(II) complex of dien) and 95 mg of Hedma·2HCl·$2H_2O$ were added, and the solution was adjusted to pH 7.0—7.5 with 1 mol dm^{-3} NaOH. Lead dioxide (1.5 g) was added to the solution and the mixture was stirred for 15 min at ca. 25 °C. The reactant solution was filtered, and the filtrate was poured onto an SP-Sephadex column (ϕ 3 cm×35 cm, Na^+ form). The adsorbed band was separated into red, orange-red, and blue bands by elution with a 0.2 mol dm^{-3} NaCl solution. The red band including C_2- and C_1-*trans(O)*-$[Co(edma)_2]^+$ isomers was transfered to another SP-Sephadex column and developed with a 0.1 mol dm^{-3} Na_2Sb_2(d-tart)$_2$ solution. The band separated into three bands of $(-)^{CD}_{543}$ C_2-, C_1-, and $(+)^{CD}_{543}$ C_2-*trans(O)*-$[Co(edma)_2]^+$. Each band was eluted out and crystals of $(-)^{CD}_{543}$ and $(+)^{CD}_{543}$ isomers were obtained by the same procedure as that described in our previous paper,[9] and their ^{1}H NMR were measured.

Deuterations of the $(+)^{CD}_{514}$ el 2 and $(-)^{CD}_{527}$ el 4 isomers of $[Co(edma)(dien)]^{2+}$ and the $(-)^{CD}_{512}$ isomer of *fac*-$[Co(edma)(NH_3)_3]^{2+}$ were also carried out by the same method as that described for $(+)^{CD}_{504}$ el 1, except that $CuSO_4 \cdot 5H_2O$ was not used for the last isomer. The ^{1}H NMR spectra of the C_2-*trans(O)*-$[Co(edma)_2]^+$ (E-1) enantiomers obtained from the deuterated isomers are shown in Fig. 3.

Spectral Measurements. The absorption and CD spectra were measured by a Hitachi 557-type spectrometer and a JASCO J-22 spectropolarimeter, respectively. The ^{1}H NMR spectra were recorded on a JEOL MH-100 NMR spectrometer using DSS as an internal standard. The ^{13}C NMR spectra at 25 MHz were recorded on a JEOL JNM-FX 100 spectrometer. The peak positions were measured relative to internal dioxane (δ=67.40). The signals of the G-ring $-CH_2-$ carbons in coordinated edma were assigned by a ^{1}H selective decoupling method.

Results and Discussion

Assignments of Geometrical Isomers. As Fig. 1 shows, each of the mixed-ligand complexes, $[Co(edma)(mdien)]^{2+}$ and $[Co(edma)(dien)]^{2+}$, provides three facially chelated [fac(ch)] isomers of mer(N_t)-trans(N_c), fac(N_t)cis(N_c), and mer(N_t)cis(N_c) and one meridionally chelated [mer(ch)] isomer. All these isomers are chiral complexes which can be resolved into

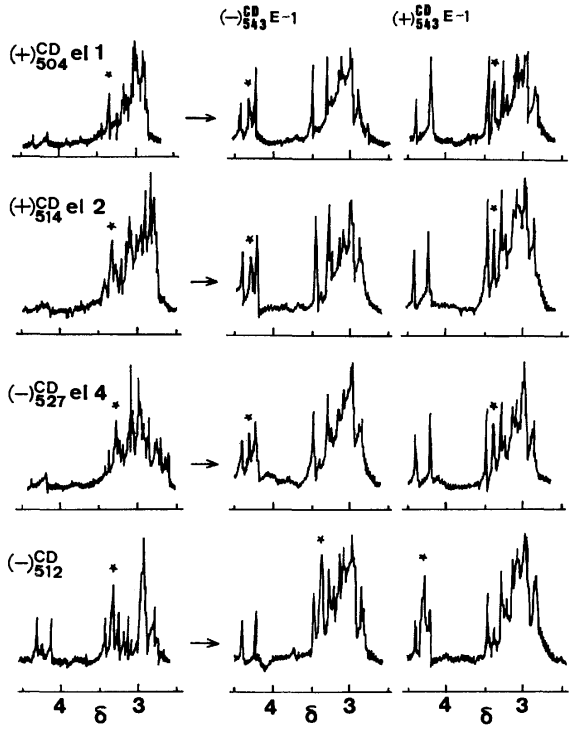

Fig. 3. ^{1}H NMR spectra of $(-)^{CD}_{543}$ $[\Delta\Delta\Delta(N_R,N_R)]$ and $(+)^{CD}_{543}$ $[\Lambda\Delta\Lambda(N_S,N_S)]$ C_2-*trans(O)*-$[Co(edma)_2]^+$ (E-1) obtained from the stereospecifically deuterated $(+)^{CD}_{504}$ el 1, $(+)^{CD}_{514}$ el 2, and $(-)^{CD}_{527}$ el 4 $[Co(edma)(dien)]^{2+}$ and $(-)^{CD}_{512}$ *fac*-$[Co(edma)(NH_3)_3]^{2+}$. (Aristerisked peaks: G-ring -CHD-.)

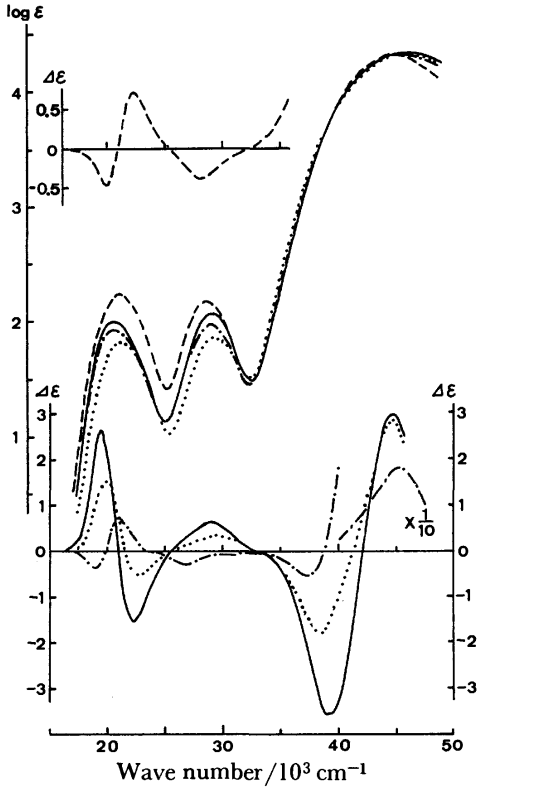

Fig. 4. Absorption and CD curves of $[Co(edma)(dien)]^{2+}$: ····· $(+)^{CD}_{504}$ el 1, —— $(+)^{CD}_{514}$ el 2, ---- $(-)^{CD}_{500}$ el 3 (in 0.1 mol dm^{-3} HCl solution), and -·-·- $(-)^{CD}_{527}$ el 4.

Table 1. Absorption Spectral Data of the edma Complexes

Isomer	Structure	First band[a)]	Second band[a)]	CT band[a)]
$[Co(edma)(dien)]^{2+}$				
el 1	*mer*(N_t)*trans*(N_c)	21.05 (1.822)	28.99 (1.865)	45.66 (4.309)
el 2	*fac*(N_t)*cis*(N_c)	20.66 (1.990)	28.99 (2.056)	46.08 (4.325)
el 3	*mer*(ch)	21.05 (2.223)	28.65 (2.163)	44.64 (4.296)
el 4	*mer*(N_t)*cis*(N_c)	20.62 (1.922)	28.99 (1.946)	45.87 (4.305)
$[Co(edma)(mdien)]^{2+}$				
el 1	*mer*(N_t)*trans*(N_c)	20.81 (1.890)	29.07 (1.878)	44.84 (4.294)
el 2	*fac*(N_t)*cis*(N_c)	20.28 (2.092)	28.41 (2.078)	45.05 (4.310)
el 3	*mer*(ch)	20.45 (2.191)	28.25 (2.217)	43.29 (4.262)
el 4	*mer*(N_t)*cis*(N_c)	19.92 (1.892)	28.49 (1.926)	43.67 (4.266)
$[Co(edma)(NH_3)_3]^{2+}$				
	fac	20.41 (1.840)	28.82 (1.925)	47.90 (4.280)

a) Wave numbers and logε values (in parenthesis) are given in $10^3\,cm^{-1}$ and $mol^{-1}\,dm^3\,cm^{-1}$, respectively.

optically active isomers. The four geometrical isomers have the same chromophore of the [Co N_5O] type, but they show spectral behaviors slightly different from each other, especially in the d-d absorption region (Fig. 4 and Table 1). The structures of these isomers can be assigned on the basis of the absorption, ^1H and ^{13}C NMR spectral data.

It is known that the molar absorption coefficient of the first absorption band is larger in a mer(ch) isomer than in a fac(ch) isomer of the terdentate ligand complexes, such as $[Co(ida)_2]^-$,[2] $[Co(edma)_2]^+$,[8] and $[Co(dien)_2]^{3+}$.[1,15] In the present complexes the band intensities of el 3 are more enhanced than those of the other isomers, suggesting that the structure of the former isomer may be assigned to mer(ch) and those of the latter isomers to fac(ch). These assignments are consistent with those done on the basis of the ^1H and ^{13}C NMR data (vide infra).

The ^1H NMR spectra of the four isomers of $[Co(edma)(mdien)]^{2+}$ are illustrated in Fig. 5 and their chemical shifts are given in Table 2, together with those of $[Co(edma)(dien)]^{2+}$. The G-ring methylene protons of el 3 resonate as a singlet-like peak at 3.73 ppm, while those of el 1, el 2, and el 4 do as four peaks of a AB quartet. Such a difference in signal pattern has also been observed between the mer(ch) and fac(ch) isomers of $[Co(edma)_2]^+$.[9] A comparison in signal pattern between the $[Co(edma)(mdien)]^{2+}$ complex and the $[Co(edma)_2]^+$ complex leads to assign el 3 to mer(ch) and el 1, el 2, and el 4 to fac(ch). Similarly, the mer(ch) and fac(ch) structures for the four isomers of $[Co(edma)(dien)]^{2+}$ are assigned from the ^1H NMR data of the G-ring methylene protons.

The el 1, el 2, and el 4 isomers of $[Co(edma)(mdien)]^{2+}$ show the methyl proton signals in the range of 2.5—2.8 ppm (Fig. 5). Previously, in the study of the (*S*)-alaninato cobalt(III) complex Berends and Brushmiller suggested that the methyl signal shifts to the lower-field side when the methyl group lies at the position deshielded by an anisotropic effect arising from the C-O bond.[16] The molecular model examinations of the three fac(ch) isomers of $[Co(edma)(mdien)]^{2+}$ show that the methyl group attaching to the central nitrogen of mdien lies at the deshielded position only in the mer(N_t)trans(N_c) structure. The methyl signal of el 1 (δ= 2.81) locates at a lower magnetic field than those of el 2 (2.63) and el 4 (2.54), which leads to assign the structure of el 1 to mer(N_t)trans(N_c).

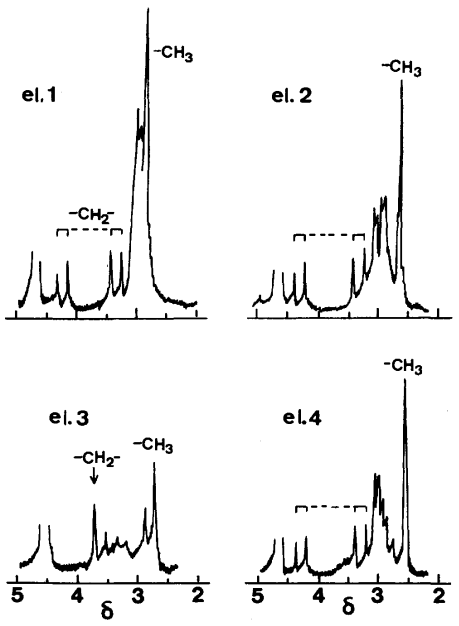

Fig. 5. ^1H NMR spectra of four geometrical isomers in $[Co(edma)(mdien)]^{2+}$.

The structural assignment of el 4 can be made on the basis of the ^{13}C NMR data. In our previous work[10] for the $[Co(edma)_2]^+$ and [Co(ida)(edma)] complexes, their geometrical structures were determined from the ^{13}C chemical shifts; the carbon neighboring to the central nitrogen (N_c) of a terdentate ligand resonates at a lower magnetic field when the trans position to N_c was occupied with oxygen atom than when the position was occupied with nitrogen atom. Figure 6(b) shows the ^{13}C NMR shift patterns of the four isomers of $[Co(edma)(mdien)]^{2+}$, and their shift data are summa-

Table 2. ^{1}H and ^{13}C NMR Data[a] of [Co(edma)(dien)]$^{2+}$ and [Co(edma)(mdien)]$^{2+}$

Isomer	Proton			J_{AB}	Carbon[b]				
	G-ring	$-CH_AH_B-$	$-CH_3$	Hz	a	*b, c	f, h	i	d, e, g
[Co(edma)(dien)]$^{2+}$									
el 1	4.63	2.89		18.5	184.93	57.21	53.94		44.20(d)
						*56.77	53.51		41.37
el 2	4.81	2.82		18.5	184.64	*57.11	54.63		45.08
						56.87	53.87		43.56
									41.32
el 3	3.92	3.64		16.5	183.56	*54.72	50.63		48.29
						53.07	50.39		47.46
									46.68
el 4	4.32	2.86		19.0	185.22	57.65	56.62		43.27
						*55.85	55.07		42.20
									41.42
[Co(edma)(mdien)]$^{2+}$									
el 1	4.23	3.33	2.81	18.0	184.44	57.31	63.93	51.26	42.59
						*57.16	62.96		42.44
									41.27
el 2	4.31	3.31	2.63	19.0	185.51	56.82	64.47	50.53	44.10
						*55.99	62.38		42.25
									40.98
el 3	3.73(s)		2.71	—	183.62	*54.43	61.50	45.80	46.20
						53.75	61.35		45.42
									45.27
el 4	4.26	3.28	2.54	19.0	184.88	*57.16	66.27	51.61	43.03
						57.06	66.08		41.71
									40.84

a) δ Values from DSS (^{1}H) and TMS (^{13}C). b) Labeling of carbons is given in Fig. 6. The marked (*) signal were determined by the selective decoupling method. (s): Singlet-like peak. (d): Doublet peak.

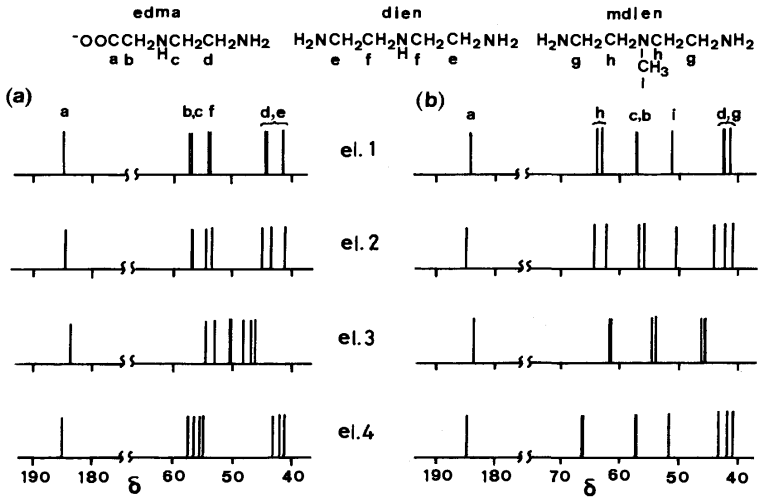

Fig. 6. ^{13}C NMR signal patterns of four geometrical isomers in (a) [Co(edma)(dien)]$^{2+}$ and in (b) [Co(edma)(mdien)]$^{2+}$.

rized in Table 2. Among three fac(ch) isomers, el 4 exhibited resonance peaks of h carbons at the lowest field: δ values for el 4, 66.08 and 66.27; for el 1, 62.96 and 63.93; for el 2, 62.38 and 64.47. Accordingly, the structure of el 4 is assigned to mer(N_t)cis(N_c), in which the trans position to N_c is occupied with oxygen atom.

The geometrical structure of el 2 was assigned on the basis of shift behavior of methyl carbon resonance. In our previous ^{13}C NMR study of [Co(ida)(mida)]$^{-}$, the higher-field shift of methyl carbon resonance observed for the u-fac isomer was ascribed to a steric interaction between the methyl group of the mida ligand and the G-ring methylene of the ida ligand.[3] Steric interaction is also expected to occur between the methyl group of mdien and the G-ring methylene of edma in [Co(edma)(mdien)]$^{2+}$ with fac(N_t)cis(N_c) structure. As given in Table 2, the methyl carbon of el 2 (δ=50.53) resonates at a higher-field relative to those of el 1

Table 3. CD Spectral Data and Absolute Configurations of the edma Complexes

Isomer	Absolute configuration[a]	First band region[b]	Second band region	CT band region[b]
$[Co(edma)(dien)]^{2+}$				
el 1 $(+)^{CD}_{504}$	$\Lambda(GE)\Delta(EE)(N_S)$	19.84 (+1.532)	29.41 (+0.345)	38.31 (−1.82)
		22.57 (−0.518)		45.05 (+2.84)
el 2 $(+)^{CD}_{514}$	$\Lambda(EE)\Delta(GE)\Lambda(GE)(N_S)$	19.46 (+2.611)	29.24 (+0.620)	39.06 (−3.594)
		22.27 (−1.547)		44.84 (+3.00)
el 3 $(-)^{CD}_{500}$[c]		20.00 (−0.437)	28.25 (−0.353)	
		22.22 (+0.705)		
el 4 $(-)^{CD}_{527}$	$\Delta(GE)\Lambda(EE)\Delta(EE)(N_S)$	18.98 (−0.373)	27.10 (−0.268)	37.45 (−0.508)
		21.05 (+0.697)		45.25 (+18.00)
$[Co(edma)(mdien)]^{2+}$				
el 1 $(+)^{CD}_{509}$	$\Lambda(GE)\Delta(EE)(N_S)$	19.65 (+2.011)	29.85 (+0.135)	38.17 (−3.22)
		22.37 (−0.490)		45.66 (+9.87)
el 2 $(+)^{CD}_{528}$	$\Lambda(EE)\Delta(GE)\Lambda(GE)(N_S)$	18.94 (+2.752)	28.57 (+0.735)	41.67 (−1.39)
		21.41 (−1.328)		45.05 (+5.46)
et 3 $(-)^{CD}_{514}$[c]		19.57 (−0.490)	28.41 (−0.165)	37.04 (+1.79)
		21.74 (+0.730)		
el 4 $(-)^{CD}_{540}$	$\Delta(GE)\Lambda(EE)\Delta(EE)(N_S)$	18.52 (−0.560)	26.32 (−0.392)	37.88 (−2.23)
		20.41 (+0.181)	30.21 (−0.042)	43.48 (+11.65)
		22.42 (−0.310)		
$[Co(edma)(NH_3)_3]^{2+}$				
fac $(+)^{CD}_{512}$	(N_S)	19.53 (+1.641)	29.41 (+0.306)	38.17 (−0.439)
		22.52 (−0.811)		

a) G and E denote glycinate-ring and ethylenediamine-ring, respectively. b) Wave numbers and $\Delta\varepsilon$ values (in parenthesis) are given in $10^{-3}cm^{-1}$ and $mol^{-1}dm^3cm^{-1}$, respectively. c) Measured in 0.1 mol dm^{-3} HCl solution.

(51.26) and el 4 (51.61) with the same facially chelated form. From this result we can assign the structure of el 2 to fac(N_t)cis(N_c).

The geometrical structures of el 1, el 2, and el 4 of $[Co(edma)(dien)]^{2+}$ were assigned by comparing their absorption and CD spectra in the d-d absorption region with those of el 1, el 2, and el 4 of $[Co(edma)(mdien)]^{2+}$.

Absolute Configurations of the fac(ch) Isomers. When unsymmetrical edma was facially coordinated to a cobalt(III) ion as a terdentate ligand, the secondary nitrogen becomes an asymmetric center. In the case that a geometrical structure is given for the edma complex, the configurational chirality around the cobalt(III) is restricted by the chirality (N_R or N_S) of the asymmetric nitrogen (vice versa).

In the previous works,[9,11] it has been shown that one of the G-ring -CH_2- protons of facially chelated edma is stereospecifically deuterated in basic D_2O. For example, when the secondary nitrogen of chelated edma takes N_S chirality, the outside proton (H_b in Fig. 2) is deuterated before the inside proton (H_a) is deuterated, and the methylene carbon becomes an asymmetric center (-CHD-) with C_R chirality. In this case NMR signal of the undeuterated G-ring methylene-proton is observed as a single peak in a higher magnetic field.

Stereospecific deuteration method was also applied to the fac(ch) isomers of $[Co(edma)(dien)]^{2+}$ and $[Co(edma)(NH_3)_3]^{2+}$ (detailed deuteration procedures are described in the Experimental section). Figure 3 shows the ^1H NMR spectra of $(-)^{CD}_{543}$ E-1 and $(+)^{CD}_{543}$ E-1 (of which the absolute configurations are $\Delta\Lambda\Delta(N_R, N_R)$ and $\Lambda\Delta\Lambda(N_S, N_S)$,[9] respectively) obtained from the deuterated $(+)^{CD}_{504}$ el 1, $(+)^{CD}_{514}$ el 2, and $(-)^{CD}_{527}$ el 4 isomers of $[Co(edma)(dien)]^{2+}$ and the deuterated $(-)^{CD}_{517}$ isomer of *fac*-$[Co(edma)(NH_3)_3]^{2+}$

When the deuterated $(+)^{CD}_{504}$ el 1 isomer was used as a starting material, a single peak (marked with *) due to G-ring -CHD- was observed at δ ca. 4.3 (lower-field side) for $(-)^{CD}_{543}$ E-1 and at δ ca. 3.35 (higher-field side) for $(+)^{CD}_{543}$ E-1. As described above (Fig. 2), the single peak at lower-field is assigned to outside proton (H_b) and the single peak at higher-field to inside proton (H_a). This indicates that the chirality of the deuterated methylene carbon is C_R. As the starting isomer containing C_R exhibited a single peak in the higher-field side, the absolute configuration should be assigned to $\Lambda(GE)\Delta(EE)(N_S)$ (where G and E denote glycinate ring and ethylenediamine ring, respectively). Similar considerations for the ^1H NMR spectral data of the $(+)^{CD}_{512}$ el 2 and $(-)^{CD}_{527}$ el 4 isomers lead to conclude that their absolute configurations are $\Lambda(EE)\Delta(GE)\Lambda(GE)(N_S)$ and $\Delta(GE)\Lambda(EE)\Delta(EE)(N_S)$, respectively, as given in Table 3.

When the deuterated $(-)^{CD}_{512}$ isomer of *fac*-$[Co(edma)(NH_3)_3]^{2+}$ was used as a starting material, a single peak appeared in the higher-field side for $(-)^{CD}_{543}$ E-1 and in the lower-field side for $(+)^{CD}_{543}$ E-1 (Fig. 3). Such signal patterns suggest that the chiralities of asymmetric nitrogens and carbons in $(-)^{CD}_{543}$ and $(+)^{CD}_{543}$ E-1 are N_RC_S and N_SC_S, respectively. Accordingly, the absolute con-

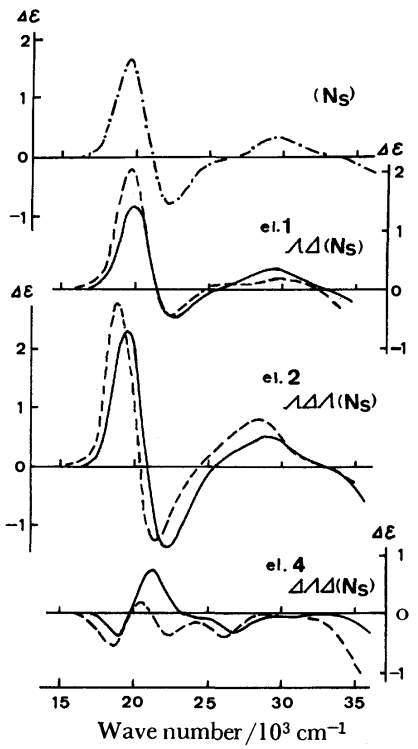

Fig. 7. The absolute configurations and CD spectra of the fac(ch) isomers in [Co(edma)-$(NH_3)_3]^{2+}$ (-·-·-), [Co(edma)(dien)]$^{2+}$ (——), and [Co(edma)(mdien)]$^{2+}$ (----).

figuration of the starting $(-)^{CD}_{512}$ isomer, which exhibited a single peak in the higher-field side, is assigned to N_R.

Absolute configurations for the optically active fac(ch) isomers of [Co(edma)(mdien)]$^{2+}$ were determined by comparing their CD spectral behaviors in the d-d absorption region with those of the corresponding fac(ch) isomers of [Co(edma)(dien)]$^{2+}$ (Table 3).

CD Spectra. The CD spectra and numerical data of the present edma complexes are shown in Figs. 4 and 7 and Table 3. The optical activities of the fac(ch) isomers of [Co(edma)(dien)]$^{2+}$ and [Co(edma)(mdien)]$^{2+}$ arise dominantly from two effects of configurational chirality due to skew pairs of the chelate rings and chirality due to the secondary nitrogen of coordinated edma. In the [Co(edma)(dien)]$^{2+}$ complex, the CD curve of $(+)^{CD}_{504}$ el 1 with Λ(GE)Δ(EE)(N_S) configuration is quite similar in pattern and intensity to that of $(+)^{CD}_{512}$ *fac*-[Co(edma)$(NH_3)_3]^{2+}$ with only N_S chirality (Fig. 7). This similarity suggests that the CD contributions from the configurational chiralities of Λ(GE) and Δ(EE) cancellate to each other. Similar considerations are also made on el 2 and el 4; the higher intense CD of $(+)^{CD}_{514}$ el 2 with ΛΔΛ(N_S) [net Λ(N_S)] is ascribed to the additive contribution from the Λ and N_S chiralities, while the lower intense CD of $(-)^{CD}_{527}$ el 4 with ΔΛΔ(N_S) [net Δ(N_S)] is ascribed to the differential contribution from the Δ and N_S chiralities.

The CD spectra of the mer(ch) isomers (el 3) of the dien and mdien complexes were measured in an acidic solution because their rapid racemization occurred in water.

The optical activity of the mer(ch) isomers arises from two effects due to chiral disposition of the nonplanar ligands and N chirality of coordinated edma. The relatively intense CD observed for two el 3, compared with the mer isomers of [Co$(dien)_2]^{3+}$,[17] [Co(mida)(dien)]$^{+}$,[18] and [Co(dien)(mdien)]$^{3+}$,[6] is ascribed to the summed effect of such two chiralities.

References

1) F. R. Keene, G. H. Searle, Y. Yoshikawa, A. Imai, and K. Yamasaki, *J. Chem. Soc., D*, **1970**, 784.
2) T. Yasui, H. Kawaguchi, N. Koine, and T. Ama, *Bull. Chem. Soc. Jpn.*, **56**, 127 (1983).
3) H. Kawaguchi, T. Ama, and T. Yasui, *Bull. Chem. Soc. Jpn.*, **57**, 2422 (1984).
4) J. I. Legg and D. W. Cooke, *Inorg. Chem.*, **5**, 594 (1966); K. Gailey, K. Igi, and B. E. Douglas, *J. Coord. Chem.*, **5**, 171 (1976).
5) Presented at the Symposium by the Chemical Society of Japan, Kochi, 1984, Abstract, p. 91.
6) M. Kojima, M. Iwagaki, Y. Yoshikawa, and J. Fujita, *Bull. Chem. Soc. Jpn.*, **50**, 3216 (1977).
7) G. H. Searle, F. R. Keene, and S. F. Lincoln, *Inorg. Chem.*, **17**, 2362 (1978); G. H. Searle, S. F. Lincoln, S. G. Teague, and D. G. Rowe, *Aust. J. Chem.*, **32**, 519 (1979).
8) T. Yasui, H. Kawaguchi, and T. Ama, *Chem. Lett.*, **1983**, 1277.
9) T. Ama, H. Kawaguchi, T. Yasui, K. Matsumoto, and S. Ooi, *Bull. Chem. Soc. Jpn.*, **58**, 2561 (1985).
10) T. Ama, H. Kawaguchi, and T. Yasui, *Bull. Chem. Soc. Jpn.*, **59**, 1471 (1986).
11) T. Ama, R. Niiyama, H. Kawaguchi, and T. Yasui, *Bull. Chem. Soc. Jpn.*, **60**, 119 (1987).
12) Y. Fujii, E. Kyuno, and R. Tsuchiya, *Bull. Chem. Soc. Jpn.*, **43**, 786 (1970).
13) K. Nakajima, T. Shin-uchi, and M. Tauchi, *Nippon Kagaku Zasshi*, **89**, 408 (1968).
14) T. Ama, H. Kawaguchi, and T. Yasui, *Bull. Chem. Soc. Jpn.*, **59**, 3597 (1981).
15) Y. Yoshikawa and K. Yamasaki, *Bull. Chem. Soc. Jpn.*, **45**, 179 (1972).
16) E. A. Berends and J. G. Brushmiller, *Inorg. Nucl. Chem. Lett.*, **6**, 847 (1970).
17) F. R. Keene and G. H. Searle, *J. Chem. Soc., D.* **1970**, 893.
18) N. Koine, T. Tanigaki, J. Hidaka, and Y. Shimura, *Chem. Lett.*, **1980**, 871.

 © 1987 The Chemical Society of Japan Bull. Chem. Soc. Jpn., 60, 603—607 (1987)

Pressure and Temperature Effects on Octahedral-Tetrahedral Equilibria in 3-Methylpyridine Solutions of Some Cobalt(II) Halides

Kazuo KOJIMA
Department of Chemistry, Faculty of Science and Engineering, Ritsumeikan University, Kita-ku, Kyoto 603
(Received September 11, 1986)

The visible absorption spectra of CoX_2 (X=Cl, Br) in 3-methylpyridine (3-Me-py) solutions have been measured in the pressure range of 1 bar—3 kbar at room temperature, and in the temperature range of ≈5—≈76 °C at 1 bar. The equilibrium, $[CoX_2(3\text{-Me-py})_2]$ (tetrahedral) + 2(3-Me-py) ⇄ $[CoX_2(3\text{-Me-py})_4]$ (octahedral), is found to be followed over this pressure range. Higher pressures favor the octahedral species with the volume changes −18—−19 $cm^3\,mol^{-1}$ at 1 bar. On the other hand, the above equilibrium holds fairly well at temperatures up to about 40 °C. Higher temperatures favor the tetrahedral species, the heats of reaction, being 56.7 $kJ\,mol^{-1}$ (5.0—44.8 °C) and 58.6 $kJ\,mol^{-1}$ (4.8—34.2 °C) for the chloro and bromo complexes, respectively. An intense and broad band appears around 400 nm at elevated temperatures especially for the bromo complex solution. This band may be assigned to a charge-transfer band occurring in a contact ion pair of solvent molecule 3-Me-py with X^- arising from the dissociation of the tetrahedral species $[CoX_2(3\text{-Me-py})_2]$.

King et al.[1,2] and Sawada et al.[3,4] have studied in detail the configurational equilibria between the octahedral $[CoX_2(R\text{-py})_4]$ and tetrahedral $[CoX_2(R\text{-py})_2]$ complexes in nonaqueous solvents such as nitromethane and 1,2-dichloroethane, where X=Cl, Br, or I and R-py=pyridine or methylpyridines. However, the pressure and temperature effects on the equilibria have not been discussed.

In the previous papers,[5,6] the effects of pressure and temperature on the octahedral-tetrahedral equilibria in pyridine solutions of Co(II) halides have been reported. From the variations in the visible absorption spectra with pressure and temperature, the values of ΔV and ΔH, the volume and the heat of the following reaction, were obtained

$$\underset{\text{(tetrahedral)}}{[CoX_2(py)_2]} + 2py \rightleftharpoons \underset{\text{(octahedral)}}{[CoX_2(py)_4]},$$

where X=Cl, Br, or I. Higher pressures favored the octahedral species but higher temperatures did the tetrahedral species. The ΔV values were −41, −29, and −6 $cm^3\,mol^{-1}$ at 1 bar and the ΔH values were 57.3, 60.7, and 65.3 $kJ\,mol^{-1}$ for X=Cl, Br, and I, respectively.

As a part of a series of the study, the present paper describes the spectrochemical investigations of the pressure and temperature dependence of the following equilibrium

$$\underset{\text{(tetrahedral)}}{[CoX_2(3\text{-Me-py})_2]} + 2(3\text{-Me-py}) \overset{K}{\rightleftharpoons} \underset{\text{(octahedral)}}{[CoX_2(3\text{-Me-py})_4]}, \quad (1)$$

where X=Cl or Br, and K is the equilibrium constant. Moreover, the above reaction may be accompanied by another reaction and the possibility will be also discussed.

Experimental

$CoCl_2$ and $CoBr_2 \cdot 6H_2O$ were used after drying and 3-Me-py was used after drying and distillation. Sample solutions of CoX_2 in 3-Me-py were prepared just before spectroscopic measurements.

High-pressure spectra were recorded on a Hitachi 340 spectrophotometer equipped with a clamp-type optical cell[7] and high-temperature spectra on a Shimadzu MPS-2000 instrument equipped with a pair of thermostated quartz cells.

The experimental details have been described in the previous paper.[5]

Results and Discussion

Spectra at Atmospheric Pressure and Room Temperature. The changes in the absorption spectra of CoX_2 solutions in 3-Me-py with pressure and temperature are shown in Figs. 1—4. The spectra are composed of the two main bands due to d-d transitions. The one is the O-band due to the $^4T_{1g}(F) \rightarrow {}^4T_{1g}(P)$ electronic transition of the octahedral complex $[CoX_2(3\text{-Me-py})_4]$ and the other the T-band due to the $^4A_2(F) \rightarrow {}^4T_1(P)$ transition of the tetrahedral complex $[CoX_2(3\text{-Me-py})_2]$.

At atmospheric pressure and room temperature, the O-band comprises the two peaks (503, 530 nm) and the shoulder (≈560 nm) for the chloro complex, and the two peaks (526, 543 nm) and shoulders (≈490, ≈570 nm) for the bromo complex. All of the peaks for both halo complexes lie in longer wavelength by 3—6 nm than those of the complexes $[CoX_2(py)_4]$ (X=Cl, Br) in pyridine solutions.[5]

Under atmospheric pressure and room temperature, the T-band comprises the three peaks (578, 613, and 640 nm) and the shoulder (≈665 nm) for the chloro complex, and the two peaks (597, 648 nm) and shoulders (≈626, ≈675 nm) for the bromo complex. All of these peaks for both halo complexes shift to longer wavelength by 3—7 nm in comparison with those of the $[CoX_2(py)_2]$ complexes in pyridine solutions.[5] This finding is in contrast to the results of Sawada et al.[3,4] They have found that the positions of the peaks for the tetrahedral complexes $[CoX_2(R\text{-py})_2]$ remain almost unchanged in 1,2-dichloroethane or in 1,2-dibromoethane regardless of pyridine and 3-Me-py. This

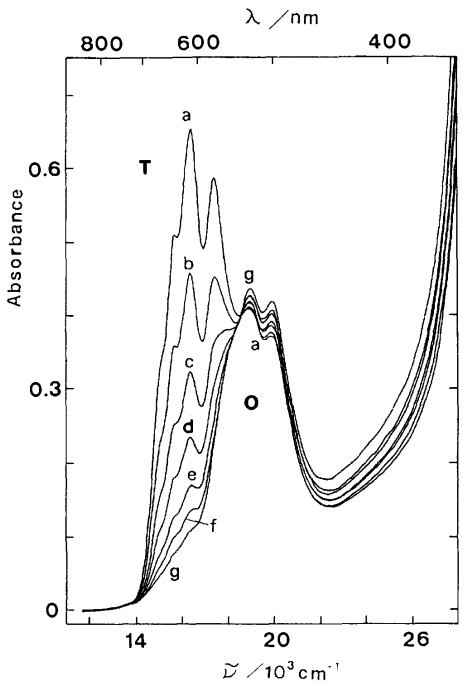

Fig. 1. Absorption spectra of $CoCl_2$ in 3-Me-py at high pressures (17.0°C), uncorrected for compression of solution. Concn: 1.38×10^{-2} mol dm^{-3}, optical path length: 1.6 cm.
a: 1 bar, b: 0.5 kbar, c: 1.0 kbar, d: 1.5 kbar, e: 2.0 kbar, f: 2.5 kbar, g: 3.0 kbar.

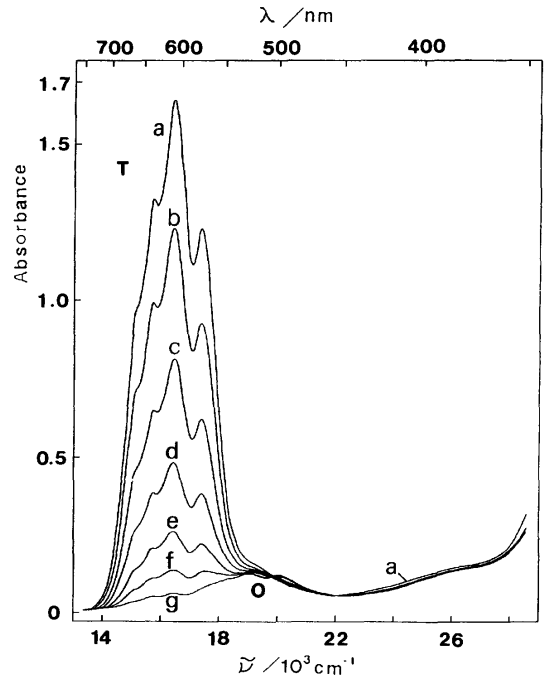

Fig. 3. Absorption spectra of $CoCl_2$ in 3-Me-py at various temperatures (1 bar), uncorrected for thermal expansion of solution. Concn: 7.01×10^{-3} mol dm^{-3}, optical path length: 0.98 cm.
a: 65.3°C, b: 55.2°C, c: 44.8°C, d: 35.0°C, e: 25.1°C, f: 16.1°C, g: 5.0°C.

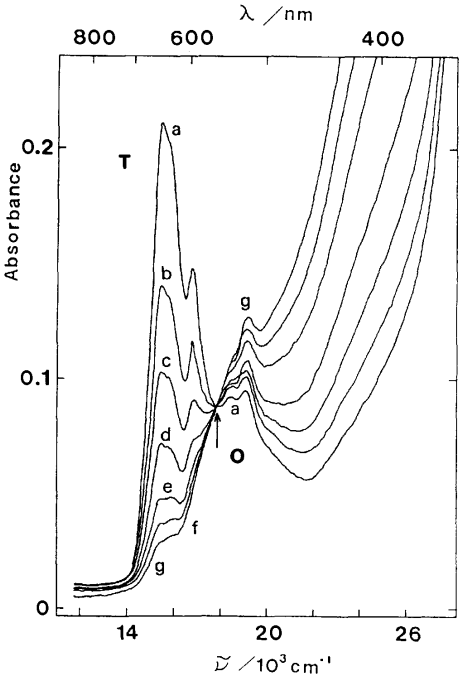

Fig. 2. Absorption spectra of $CoBr_2$ in 3-Me-py at high pressures (18.5°C), uncorrected for compression of solution. The curves d—g are drawn after shifting them along the ordinate so as to cross at a point indicated by an arrow. Concn: 2.98×10^{-3} mol dm^{-3}, optical path length: 1.6 cm.
a: 1 bar, b: 0.5 kbar, c: 1.0 kbar, d: 1.5 kbar, e: 2.0 kbar, f: 2.5 kbar, g: 3.0 kbar.

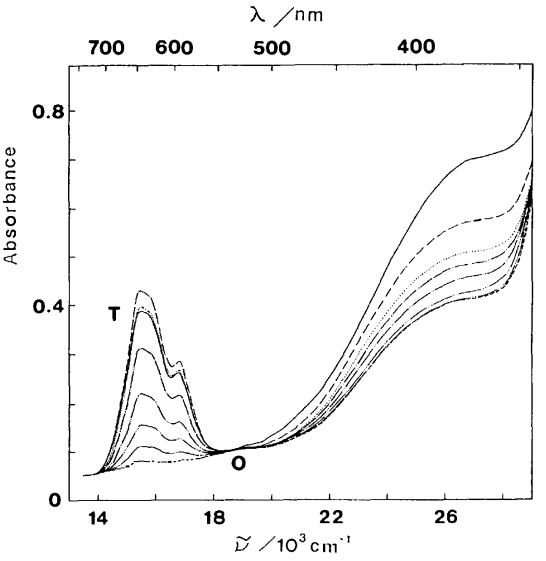

Fig. 4. Absorption spectra of $CoBr_2$ in 3-Me-py at various temperatures (1 bar), uncorrected for thermal expansion of solution. Concn: 2.33×10^{-3} mol dm^{-3}, optical path length: 0.98 cm.
——: 76.6°C, ------: 64.8°C, ·····: 54.4°C, —·—: 44.8°C, —··—: 34.2°C, —···—: 24.4°C, —·····—: 15.9°C, --------: 4.8°C.

contrast may be assumed to be caused by the solute-solvent interaction.

For both halo complexes, the intensity ratio of the T-band to the O-band is larger for the CoX_2-3-Me-py system in the present study than for the CoX_2-pyridine system[5] at atmospheric pressure and room temperature. This result suggests that the equilibrium constant of Eq. 1, K, is smaller in the 3-Me-py solutions than in the pyridine ones, being in agreement with the other results.[1-4]

Pressure Effect. Figures 1 and 2 show the pressure dependence of the spectra. The intensities of the T-bands decrease with increasing pressure. Because of an enhancement of the intensities in the shorter wavelength region than about 460 nm with increasing pressure, the changes in the O-bands are more obscure in this system than in the pyridine system.[5] However, for the chloro complex the O-band intensity is found to increase slightly with pressure. This is likely for the bromo complex, judging from a comparison with the result of the $CoBr_2$-pyridine system.[5] From the facts presented above, it can be concluded that the equilibrium of Eq. 1 shifts toward the octahedral species $[CoX_2(3\text{-Me-py})_4]$ with increasing pressure.[8]

Regarding $[CoX_2(3\text{-Me-py})_4]$ as the product, the volume change, ΔV, is estimated. As shown in Ref. 5, ΔV is calculated by

$$\Delta V = -RT\frac{d}{dP}\ln(I_o/I_t), \qquad (2)$$

where R is the gas constant, and I_o and I_t are the integrated intensities of the O-band and T-band, respectively.

Figure 5 shows the plots of $\ln(I_o/I_t)$ vs. pressure. These plots are fitted to the following equations by the least-squares method:

$$\ln(I_o/I_t) = -0.0960 + 0.765P + 0.125P^2,$$

for the chloro complex, and

$$\ln(I_o/I_t) = -0.463 + 0.772P, \text{ for the bromo complex.} \qquad (3)$$

From Eqs. 2 and 3, the values of ΔV are estimated for the chloro complex as −18, −21, −24, −27, −29, −32, −34 $cm^3\,mol^{-1}$ in the order of pressure from 1 bar to 3.0 kbar at intervals of 0.5 kbar, and for the bromo complex as −19 $cm^3\,mol^{-1}$ over the range of 1 bar −1.5 kbar. No reliable datum is obtained for the bromo complex at high pressures above 1.5 kbar.

ΔV equals $V_{oct}-(V_{tet}+2V_{sol})$, where V_{oct}, V_{tet}, and V_{sol} are the intrinsic volumes of the octahedral species, the tetrahedral species, and the solvent molecule, respectively. Moreover, the ΔV values are always negative in the CoX_2-3-Me-py and CoX_2-pyridine systems. Therefore, the larger the value of $V_{oct}-V_{tet}$ or the smaller that of $V_{tet}+2V_{sol}$ becomes, the smaller $|\Delta V|$ is obtained. $|\Delta V|$, at 1 bar, is 18 $cm^3\,mol^{-1}$ for the chloro complex and is 19 $cm^3\,mol^{-1}$ for the bromo complex in the CoX_2-3-Me-py system. On the other hand, in the

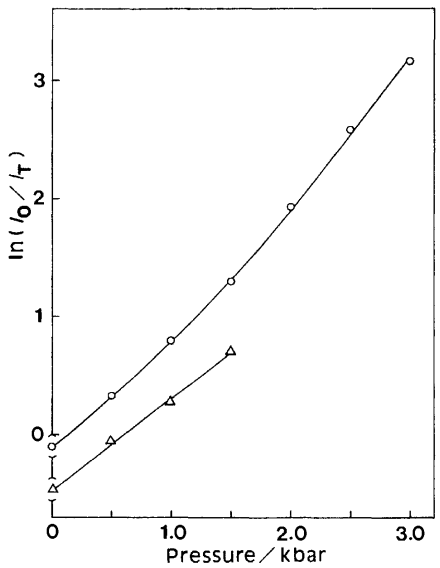

Fig. 5. Logarithm of the integrated-intensity ratio of the O-band to the T-band (I_o/I_t) vs. pressure.
O: $CoCl_2$, Δ: $CoBr_2$, ——: calculated fitting lines.

CoX_2-pyridine system, the $|\Delta V|$ values were 41 and 29 $cm^3\,mol^{-1}$ for the chloro and bromo complexes, respectively, as reported previously.[5] The values of $|\Delta V|$ for both halo complexes are found to be smaller in the CoX_2-3-Me-py system than in the CoX_2-pyridine system. This fact may imply that replacement of ligand pyridine molecules by ligand 3-Me-py ones makes the value of $V_{oct}-V_{tet}$ larger or makes the value of $V_{tet}+2V_{sol}$ smaller. For the 3-Me-py system, there is little difference in $|\Delta V|$ between the two halo complexes in contrast with the CoX_2-pyridine system. This fact may suggest that the contribution of X to V_{oct} and V_{tet} becomes relatively small in the CoX_2-3-Me-py system regardless of Cl and Br.

When the values of V_{oct} and V_{tet} are obtained, the quantitative interpretation upon ΔV can be formulated.

Temperature Effect. The variations in the spectra with temperature are shown in Figs. 3 and 4. The intensities of the T-bands increase steeply with increasing temperature. Although the changes in the O-bands with temperature are obscured due to the intense T-bands, the equilibrium of Eq. 1 probably shifts toward the tetrahedral species $[CoX_2(3\text{-Me-py})_2]$ with increasing temperature contrary to the pressure effect described above. This tendency is very similar to the CoX_2-pyridine system.[5]

However, a marked difference between the two systems should be pointed out here, that is, absorption bands at about 400 nm are observed only in the CoX_2-3-Me-py system. These bands show the following features: (i) They can be observed even at low temperatures. Those peak positions are not clear, but can be estimated at about 390 nm in the chloro complex solution and at about 400 nm in the bromo com-

plex solution. Another peak seems to lie around 430 nm in the latter. Anyway, there is little difference in the peak positions between these two halo complex systems. (ii) For the bromo complex system, the intensity of the 400-nm band increases markedly with increasing temperature simultaneously with suppression of the enhancement of the T-band intensity. The intensity of the T-band becomes smaller at 76.6 °C than at 64.8 °C. Even if the bromo complex solution heated to 76.6 °C is cooled to room temperature, the 400-nm band intensity remains almost unchanged, but the T-band intensity is reduced to a value slightly smaller than that at room temperature before heat of the solution (not shown); the variation in the intensity of the 400-nm band as a function of temperature is irreversible, but that of the T-band is almost reversible. For the chloro complex system, the similar trend for the spectral changes with temperature is observed but not significantly. These facts suggest that the 400-nm band occurs more easily for the bromo complex system than for the chloro complex one and that this band is the more strengthened, the T-band is the more suppressed. (iii) In relation to the 400-nm band, a weak and broad absorption is observed in the region of ≈350—≈440 nm in each of the spectrum of the 3-Me-py solution of KBr, $N(CH_3)_4Br$, $ZnBr_2$, or $NiBr_2$.[9]

By the way, Cabral et al.[2] have concluded that for the tetrahedral complex $[CoBr_2(3\text{-Me-py})_2]$ in nitromethane in the presence of an excess of 3-Me-py, the reaction of exchanging Br^- by 3-Me-py occurs at room temperature. Therefore, from the results of this investigation in addition to the conclusion of Cabral et al.,[2] besides the main reaction of Eq. 1, the following dissociation reaction of the tetrahedral complex occurs in the 3-Me-py solutions and shifts toward a new octahedral species with increasing temperature

$$\underset{\text{(tetrahedral)}}{[CoX_2(3\text{-Me-py})_2]} + (4-x)(3\text{-Me-py}) \longrightarrow \underset{\text{(octahedral)}}{[CoX_x(3\text{-Me-py})_{6-x}]^{(2-x)+}} + (2-x)X^-, \quad (4)$$

where x=0 or 1. The reaction of Eq. 4 is greatly dependent on the temperature for the bromo complex system, but is little for the chloro complex system.

Although any spectral evidence for the presence of the octahedral $[CoX_x(3\text{-Me-py})_{6-x}]^{(2-x)+}$ complex can not be obtained, a free X^- ion in 3-Me-py solutions is probably related to the appearance of the 400-nm band. That is, from the facts (i)—(iii) described above, the 400-nm band may be assigned to a charge-transfer band occurring in a contact ion pair of X^- with a solvent molecule of 3-Me-py.

To our knowledge, there have been some reports on the charge-transfer spectra of ion pairs between halide ions and another ions or molecules the absorption maxima of which lie in relatively long wavelength such as 400 nm. Briegleb et al.[10] have reported that in the interaction of halides e.g. LiI or LiBr (electron donor is I^- or Br^-) with trinitrobenzene in different kinds of solvents, the absorption maximum lies in 385—476 nm for the iodo complex and in 294—370 nm for the bromo complex. Dwivedi and Rao[11] have found that for the $(C_7H_{15})_4N^+X^-$-trinitrobenzene systems in CCl_4, $CHCl_3$, or CH_2Cl_2, the charge-transfer bands appear at 323 nm for X=Cl, at 371—383 nm for X=Br, and at 450—475 nm for X=I. In comparison with these authors' results, the assignment of the 400-nm band in the present study may be reasonable.

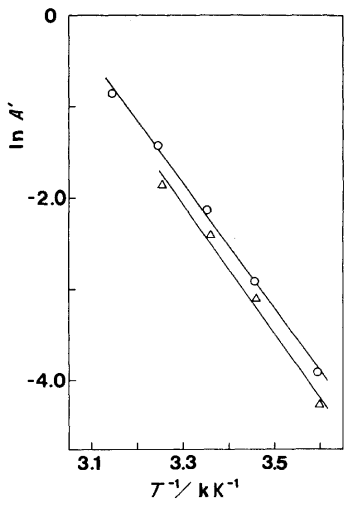

Fig. 6. Logarithm of the corrected absorbance A' vs. reciprocal of absolute temperature.
○: $CoCl_2$, △: $CoBr_2$, ——: calculated fitting lines.

The heat of reaction, ΔH, is estimated in the lower-temperature range (the tetrahedral $[CoX_2(3\text{-Me-py})_2]$ species is regarded as the product). As described in Ref. 5, the change in the equilibrium constant with temperature can be followed by the absorbance change of the 665-nm shoulder for the chloro complex and the 648-nm peak for the bromo complex. In Fig. 6, the logarithm of the corrected absorbance A' is plotted against the reciprocal of absolute temperature. As the thermal expansion coefficient of 3-Me-py has never been estimated, the corresponding value of pyridine ($0.001\ K^{-1}$)[12] is used as the approximate value for 3-Me-py over the temperature range in order to obtain the corrected absorbance A'.

As shown in Fig. 6, the plots are fitted to straight lines, indicating that ΔH is constant for each of the halo complex reaction of Eq. 1 over the lower-temperature range. From the slopes of the lines, ΔH is estimated for the chloro complex as 56.7 kJ mol^{-1} over the range of 5.0—44.8 °C and for the bromo complex as 58.6 kJ mol^{-1} between 4.8 and 34.2 °C.

The value of 56.7 kJ mol^{-1} for the chloro complex is compatible with 56.1 kJ mol^{-1} of Cabral et al.[2] Like the CoX_2-pyridine system,[5] ΔH is also larger for the bromo complex (58.6 kJ mol^{-1}) than for the chloro complex (56.7 kJ mol^{-1}) in this CoX_2-3-Me-py system.

This tendency is consistent with the proposal of King et al.[1] that ΔH is a measure of Co(II)-pyridine base dative π-bonding which increases with decrease in the electronegativity of X. For the chloro complexes, ΔH is larger for the pyridine system (57.3 kJ mol^{-1}) than for the 3-Me-py one (56.7 kJ mol^{-1}). The similar relation can be found between the two bromo complexes (60.7 and 58.6 kJ mol^{-1}). This tendency may be accounted for by the result of Cabral et al.[2] that ligand pyridine is a better π-accepter compared with ligand 3-Me-py.

The author would like to express his sincere thanks to Professor Jiro Matsuda of Ritsumeikan University for valuable discussions, critical reading of the manuscript, and continuous encouragements. The author also wishes to thank Professor Ikuji Tsujikawa of Kyoto University for his encouragements. Thanks are due to Mr. Masao Yoshikawa for his support in the experiment. This work was partially supported by a Grant-in-Aid for Scientific Research No. 59470038 from the Ministry of Education, Science and Culture.

References

1) H. C. A. King, E. Körös, and S. M. Nelson, *J. Chem. Soc., A*, **1963**, 5449.

2) J. de O. Cabral, H. C. A. King, S. M. Nelson, T. M. Shepherd, and E. Körös, *J. Chem. Soc., A*, **1966**, 1348.

3) K. Sawada and T. Suzuki, *J. Inorg. Nucl. Chem.*, **43**, 2301 (1981).

4) K. Sawada, K. Miura, and T. Suzuki, *Bull. Chem. Soc. Jpn.*, **55**, 780 (1982).

5) K. Kojima, M. Saida, M. Donoue, and J. Matsuda, *Bull. Chem. Soc. Jpn.*, **56**, 684 (1983).

6) K. Kojima, T. Miyashita, and J. Matsuda, *Bull. Chem. Soc. Jpn.*, **57**, 879 (1984).

7) K. Suzuki and M. Tsuchiya, *Bull. Chem. Soc. Jpn.*, **48**, 1701 (1975).

8) As will be described below in the temperature effect, an appearance of a 400-nm band is probably related to the existence of another kind of reaction besides the equilibrium of Eq. 1. However, it is observed that the 400-nm band scarcely changes with pressure and is also not the cause of the enhancement of the intensity below about 460 nm described above. Therefore, it is thought to be reasonable that only the equilibrium of Eq. 1 is influenced by pressure.

9) The experiment has been done as follows: The four kinds of bromide were dried under reduced pressure at about 105 °C to constant weight. After dried with anhydrous $CaSO_4$, 3-Me-py was distilled. Each salt was sealed with 3-Me-py into a glass tube, and then kept for a month at about 70 °C in a drying box. The spectra were recorded at room temperature. If the experiment for the salts of chloride is done, similar results with the bromide will be expected.

10) G. Briegleb, W. Liptay, and R. Fick, *Z. Electrochem.*, **66**, 851 (1962).

11) P. C. Dwivedi and C. N. R. Rao, *Spectrochim. Acta, A*, **26**, 1535 (1970).

12) R. F. Brunel and K. Van Bibber, "International Critical Tables," 1st ed, ed by E. W. Washburn et al., McGraw-Hill Book Company, New York (1928), Vol. III, p. 28.

 © 1987 The Chemical Society of Japan Bull. Chem. Soc. Jpn., 60, 609—612 (1987)

A Formylcarbonium Ion Synthon. Synthesis of 3-Thio-Substituted 2-Amino Acids and Thio-Substituted Enamines from 2-Acyloxyacrylonitriles[1)]

Akira Oku,* Naofumi Hori-ie, and Toshiro Harada
Department of Chemistry, Kyoto Institute of Technology, Matsugasaki, Sakyo-ku, Kyoto 606
(Received May 26, 1986)

The utilization of 2-acyloxy-3-phenylthiopropionitriles (**2**) which were prepared by the Michael addition of thiophenol to 2-acyloxyacrylonitriles (CH_2=C(CN)OCOR), as a formylcarbonium ion synthon, was demonstrated by the transformation of **2** into *S*-phenylcysteine and 2-phenylthio enamines.

2-Acyloxyacrylonitriles (**1**) are useful equivalents of ketenes utilizable as dienophiles,[2)] carbene acceptors and 1,3-dipolarophiles.[3)] Structures of **1** also tell us that they can be used as Michael acceptors to give **2**-substituted acetaldehyde cyanohydrins **5** which are equivalents of the corresponding **2**-substituted aldehydes **4**. In this regard, we have investigated the addition of thiols to **1** and verified that **1** can play a role of formylcarbonium ion synthon **3** (Eq. 1) as being demonstrated in the conversion of the adduct to 3-thio-2-amino acids, such as *S*-phenylcysteine, and also to 2-phenylthio enamines.

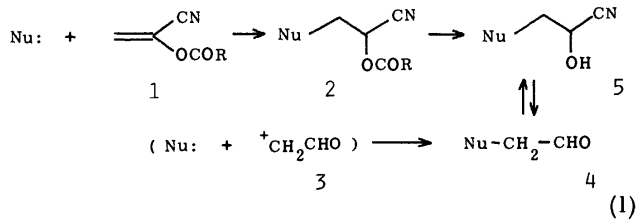

(1)

Results and Discussion

The polar addition of thiophenol to 2-benzoyloxyacrylonitrile (**1a**) in methanol at 0 °C in the presence of benzyltrimethylammonium hydroxide (Triton B, 40% in MeOH) gave 2-benzoyloxy-3-phenylthiopropionitrile.[4)] Results are summarized in Table 1 (see Eq. 2). Displacement at the carbonyl group also took place concomitantly besides the desired Michael addition. This side reaction, however, can be minimized by changing the acyloxy group: among three esters examined (benzoate **1a**, pivalate **1b**, and acetate **1c**), benzoate **1a** apparently favors the Michael addition more than the other esters.[5)] In addition, the phenyl group of **1a** may also suppress the displacement and eventually adduct **2a** predominates.[6)] The difference between **1b** and **1c** may be due to the steric effect of the *t*-butyl group that retards the displacement at the carbonyl group.

Free radical addition of thiophenol to **1c** under high-dilution conditions also yielded adduct **2c** in a better yield (55%) when pentane was the solvent. In cyclohexane, side reactions were suppressed and the isolation of **2c** was easier.

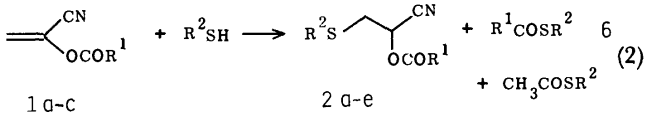

(2)

a, R^1 = Ph; b, R^1 = *t*-Bu; c, R^1 = CH_3
R^2 = Ph (a, b, c), R^2 = Et (d, e)

Adducts **2** were transformed effectively by the reaction with amines into 2-amino-3-phenylthiopropionitriles (**7**) (see Table 2 and Eq. 3) which are common intermediates for the synthesis of both title compounds. Pyrrolidine reacted with **2** exothermically and a diluent (ether) was required to control the reaction. Diethylamine reacted slowly at an ambient

Table 1. Reaction of 2-Acyloxyacrylonitrile (**1**) with Thiols

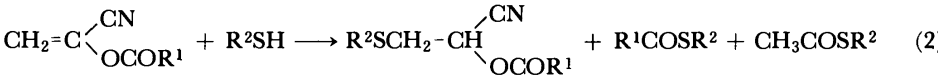

(2)

Acrylonitrile		RSH	Method[a)]	Solvent	Temp	Time	Product yield/%
	R^1	R^2			°C	h	
1a	Ph	Ph	A	EtOH	20	5	**2a** 62
1a	Ph	Ph	B	EtOH	20	4	**2a** 65
1b	*t*-Bu	Ph	A	EtOH	0	7.5	**2b** 42
1b	*t*-Bu	Ph	A	MeOH	0	2.2	**2b** 41
1c	Me	Ph	A	MeOH	0	2.5	**2c** 14
1c	Me	Ph	C	Pentane	0	20	**2c** 55
1a	Ph	Et	A	MeOH	0	2.5	**2d** 25
1b	*t*-Bu	Et	A	EtOH	0	4.0	**2e** 10

a) Method A: Triton-B was used as a base. Method B: K_2CO_3 was used. Method C: Irradiation by a medium pressure Hg lamp.

Table 2. Reaction of 2-Acyloxy-3-phenylthiopropionitrile (**2**) with Amines

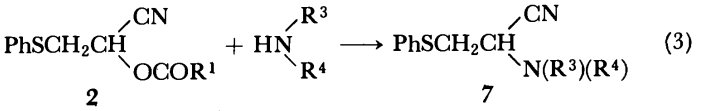

(3)

Entry	R^1	R^3	R^4	Solvent	Temp °C	Time h	Product yield/%[a]	Bp(θ_b/°C)/Torr
1	Me	$-(CH_2)_4-$		Et_2O	20	2	**7f** 88	117—125/0.04
2	Ph	$-(CH_2)_4-$		Et_2O	20	2	**7f** 71	
3	Me	Et	Et	MeOH	70	0.5	**7g** 96	115/0.02
4	*t*-Bu	Et	Et	MeOH	70	0.5	**7g** 81	
5	Me	Et	H	MeOH	70	0.5	**7h**[b]	Decomposed
6	Me	H	H	MeOH	20	2	**7i**[b]	Decomposed

a) Isolated yields. b) Not isolated but almost quantitative as determined by ^1H NMR analysis of the reaction mixture.

temperature without solvent but effectively in boiling methanol. Both ethylamine and ammonia reacted effectively with any compound of **2** but products were thermally too labile to be isolated by distillation. Eventually, reaction mixtures were subjected directly to the following hydrolysis. When the product mixture containing **7f** was chromatographed through a silica-gel column, 2-(phenylthio)acetaldehyde cyanohydrin (**8**, ca. 10%) was isolated, which readily reacted with diethylamine independently in methanol to give **7g** (92%). This finding is indicative of the intermediacy of **8** in the main reaction channel that leads **2** to **7**.

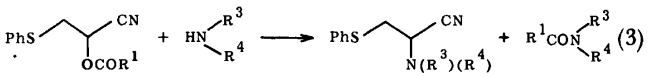

(3)

2 a-c 7 f-i

f, R^3-R^4 = $-(CH_2)_4-$; **g**, $R^3 = R^4$ = Et;
h, R^3 = Et, R^4 = H; **i**, $R^3 = R^4$ = H

The acid-catalyzed hydrolysis of **7i**[7] in aqueous HBr or H_2SO_4 gave *S*-phenylcysteine (**9**), the overall yield from **2** was 60—63% (Eq. 4). This procedure for the synthesis of **9** seems better than the reported not only in yield but also in simplicity.[8] The hydrolysis of 2-(1-pyrrolidinyl)nitrile (**7f**), however, did not give the expected amino acid, but a hydrolytic deamination took place to give 2-hydroxy-3-(phenylthio)propionic acid (**10**).[9] This is because the pyrrolidinyl group has a higher basicity than the $-NH_2$ group and hence it is protonated more easily and substituted by water.

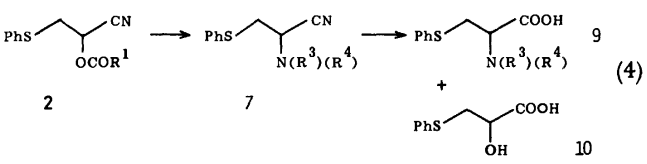

(4)

2 7 9 10

In addition to the synthesis of 3-substituted 2-amino acids such as **9**, amino nitriles **7** exhibited an interesting behavior which can be synthetically utilizable to the preparation of thio-substituted enamines. We found that, in general, propionitriles **7** are thermally labile and unable to be isolated or purified by distillation.[10] We thought this deserves to be explored and the pyrolysis of **7** was independently investigated.[11]

When a benzene solution of **7f** was heated at 240 °C, 1-phenylthio-2-(1-pyrrolidinyl)ethene (**11f**) was obtained as a mixture of cis and trans isomers in 83% yield (conversion 71%) (Eq. 5). Analogously **7g** gave the diethylamino enamine **11g**. The same pyrolytic behaviors of both **7f** and **7g** were also observed in their VPC analysis when the injection temperatures were above 200 °C. It is noteworthy that the cyano group is the most preferable leaving group to the other potentially removable ones (phenylthio and amino group).

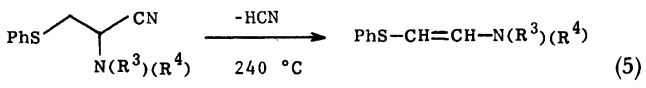

(5)

7 f, g 11 f, g

To summarize, 2-acyloxy-substituted acrylonitriles (**1**) have been proved to be a viable formylcarbonium ion synthon and they seem to provide us with easy access to several 2-substituted aldehyde derivatives.

Experimental

General Procedures. Boiling points are uncorrected. ^1H NMR spectra (chemical shifts are given in δ units in $CDCl_3$ solution) were recorded on Varian T-60A and IR spectra on JASCO IRA-1 spectrometers. Elemental Analyses were performed by Microanalysis Center of Kyoto University. Mass spectra including exact mass analyses were measured on a Hitachi M-80A mass spectrometer, and VPC anal ysis on Shimadzu GC-4CIT gas chromatograph (glass column; 10% Apiezon L on Chromosorb unless otherwise noted).

2-Acyloxyacrylonitriles (1). 2-Benzoyloxy- (**1a**), 2-pivaloyloxy- (**1b**), and 2-acetoxyacrylonitrile (**1c**) were synthesized from the corresponding acyl chlorides and acetyl cyanide according to our previous study.[12] Spectroscopic data of **1b** (for **1a**, **1c**, and **1d**, see Ref. 12) are as follows. ^1H NMR 1.27 (s, 9H), 5.65 (d×2, 2H, J=2.0 Hz). IR (liq film) 2960 (m), 1760 (s), 1630 (m), 1095 (s) cm^{-1}. $P^+(m/z)$ 153 (M^+).

Preparation of 3-Thio-substituted 2-Acyloxypropio-

Table 3. Spectroscopic Data of Products **2** and **7**

	^{1}H NMR[a,b]						IR cm^{-1}	P$^+$
	CH_2	CH	R^1	R^2	R^3	R^4	(liq film)	(m/z)
2a	3.47(d) J=6.6	5.64(t)	7—8(m)		—	—	1730, 1260, 1100	283(M^+)
2b	3.26(d) J=7	5.32(t)	1.15(s)	7.4(m)	—	—	1740, 1280, 1100	263(M^+)
2c	3.35(d) J=7	5.40(t)	2.03(s)	7.4(m)			1750, 1375, 1210, 1030	221(M^+)
2d	3.06(d) J=6.6	5.67(t)	7.5—8.2 (m)	1.30(t), 2.73(q) J=7	—	—	1740, 1270, 1100 720	174(M^+—EtS(61))
2e	2.93(d) J=6.6	5.36(t)	1.23(s)	1.26(t) 2.65(q) J=7	—	—		
7f	3.18 (ABX) J=13.0, 8.6, 6.8	3.85 (ABX) J=8.6, 6.8	—	—	1.8(m) 2.6(m)		2950, 2800, 1480, 1440, 740, 685	232(M^+) 205(M^+—HCN(27))
7g	3.20 (ABX) J=13.0, 9.2, 7.0	3.75 (ABX) J=9.2, 7.0	—	—	1.03(t) 2.5(q) J=7.0		2960, 2800, 1480, 1440, 740, 680	234(M^+) 207(M^+—HCN(27))
7h	3.20(m)	3.60(br m)	—	—	1.10(t) 2.8(m) J=7.8	1.5(m)	2980, 1485, 1445, 1030, 745, 695	
7i	3.17(br d) J=6.6	3.78(br t)	—	—	2.0(br s)			

a) Chemical shifts are in δ units and J values in Hz. b) Chemical shifts of Ph groups of **7** are abbreviated.

nitriles (2). Method A: To a mixture of acrylonitrile **1** (4 mmol) and thiol (R=Ph or Et, 5 to 6 mmol) in a solvent (MeOH, EtOH, *t*-BuOH, or Et_2O) was added a 40% MeOH solution of benzyltrimethylammonium hydroxide (Triton B, 40—80 μL) or K_2CO_3 (4 mmol). After stirring for a period at a desired temperature, the reaction mixture was extracted by a mixture of Et_2O and water, and the ethereal solution was dried ($MgSO_4$). Product **2** was separated after a silica-gel column chromatography.

Method B: Sodium metal (0.5 g, 20 mmol) was slowly added to a solution of PhSH (9.0 g, 90 mmol) and the mixture was warmed at 40 °C until sodium dissolved. The solution was cooled at −7 °C, **1c** (2.24 g, 20 mmol) was added, and the mixture was stirred for 1.5 h. The workup procedure was analogous to that of Method A.

Method C: In a photolysis apparatus equipped with a Pyrex filter and a medium pressure mercury lamp, a diluted pentane solution (200 mL) of PhSH (7.0 g) was charged and to which, under irradiation, a mixture of **1c** (3.9 g, 35 mmol) and PhSH (7.0 g) was added slowly over 2 h. After 20 h, **1c** disappeared. Adduct **2c** was isolated by a vacuum distillation. Bp 115—125 °C/1.5 mmHg (1 mmHg=133.3 Pa). Yield 55%.

Results are summarized in Table **1** and the spectroscopic data for **2** in Table 3. Exact mass of **2a**: Found, 283.0670. Calcd for $C_{16}H_{13}NO_2S$, 283.0667. **2b**: Found, 263.0978. Calcd for $C_{14}H_{17}NO_2S$, 263.0981. **2c**: Found, 221.0512. Calcd for $C_{11}H_{11}NO_2S$, 221.0511. Anal. of **2d**: Found: C, 61.53; H, 5.62; N, 5.93%. Calcd for $C_{12}H_{13}O_2NS$: C, 61.25; H, 5.57; N, 5.95%.

2-Amino-3-phenylthiopropionitriles (7). 2-Acyloxy-3-phenylthiopropionitrile (2, 1 mmol) in a solvent (Et_2O or MeOH) was mixed with an excess amount of amine (pyrrolidine, Et_2NH, 30% MeOH solution of $EtNH_2$, or NH_3 in MeOH; 3 to 20 equivalents), and the total mixture was stirred at an ambient temperature or 70 °C. 2-Amino-substituted 3-phenylthiopropionitriles (**7**) were obtained by distillation except the reactions with $EtNH_2$ and NH_3. In the latter cases products were thermally too labile to be distilled and, therefore, used directly in subsequent reactions. Results are listed in Table 2 and the spectroscopic data for **7** in Table 3.

Exact Mass of 7f: Found, 232.1038. Calcd for $C_{13}H_{16}N_2S$, 232.1036. Exact mass of the fragment peak corresponding to **11f**: Found, 205.0904. Calcd for $C_{12}H_{15}NS$, 205.0927. **7g**: Found, 234.1186. Calcd for $C_{13}H_{18}N_2S$, 234.1192. Exact mass of the fragment peak corresponding to **11g**: Found, 207.1065. Calcd for $C_{12}H_{17}NS$, 207.1083.

Acid-Hydrolysis of 2-Amino-3-phenylthiopropionitrile (7i). Nitrile **7i** (1.1 mmol) prepared quantitatively from **2c** and aqueous ammonia by the above procedure, but not isolated, was mixed with 0.2 mL of concd H_2SO_4 and 2 mL of water. The mixture was warmed at 120 °C for 24 h, cooled down to 20 °C, 2 mL of water was added, and neutralized by 28% aqueous ammonia to pH 8, After a small amount of charcoal was added, the solution was filtered, slightly acidified by diluted H_2SO_4 to pH 5, and cooled in dark to separate

S-phenylcysteine **9** in 63—70% yields. ^{1}H NMR 3.70 (br d, 2H, J=6.0 Hz), 4.50 (br q or t, 1H), 7.5 (m, 3H), 7.4 (m, 5H), 11.5 (s). IR (KBr) 2800 (broad), 1600 (s), 1500 (m), 1400 (s), 1360 (s), 720 (m) cm^{-1}.

Acid-Hydrolysis of 2-(1-Pyrrolidinyl)-3-phenylthiopropionitrile (7f). A mixture of **7f** (0.22 g, 0.95 mmol), water (0.5 mL), and 0.5 mL of 47% HBr was heated for 24 h under refluxing conditions. After the removal of water in vacuo, the residue was washed with a mixture of water and Et_2O, and the ethereal solution was analyzed to find that it consisted of only one product. The solution was esterified in MeOH by the Fischer method to give methyl 2-hydroxy-3-(phenylthio)-propionate **12** (30%). ^{1}H NMR 3.35 (s, 1H), 3.60 (s, 3H), 3.65 (br d, 2H, J=5.0 Hz), 4.37 (t, 1 H, J=5.0 Hz), 7.5 (m, 5H). IR (liq film) 3500 (broad, m), 1750 (s), 1595 (m), 1230 (broad, m), 1100 (s), 750 (m), 700 (m) cm^{-1}.

Pyrolysis of 2-(1-Pyrrolidinyl)-3-phenylthiopropionitrile (7f): Preparation of 1-Phenylthio-2-(1-pyrrolidinyl)ethene (11). A vertically fixed Pyrex column (30 cm length×10 mm i.d.) packed with glass beads was heated at 240 °C under a N_2 stream at 50 mmHg. A benzene solution (2 mL) of **7f** (0.4 mmol) was slowly injected from the top of the column and a product mixture was collected at −70 °C. 1-Phenylthio-2-(1-pyrrolidinyl)ethene (**11f**) was formed in 82% (conversion 71%). ^{1}H NMR 1.8 (m, 4H), 2.6 (m, 4H), 4.38 (d, 1H, J=12.8 Hz), 6.83 (d, 1H, J=12.8 Hz), 7.3 (m, 5H). For the exact mass of **11f**, see Experimental section corresponding to the preparation of **7f**. The same pyrolysis procedure on **7g** gave the thio enamine **11g** in 22% yield (conversion 49%). Mass spectrum of **11g**, m/z (relative intensity): 207 (M^+, 68), 174 (26), 116 (55), 91 (49), 56 (100). Exact mass: Found, 207.1070. Calcd for $C_{12}H_{17}NS$, 207.1083.

References

1) Ketene Equivalents, No. 11. For No. 10 see Ref. 3b.

2) a) D. A. Evans, W. L. Scott, and J. K. Truesdale, *Tetrahedron Lett.*, **1972**, 121; b) A. Oku, H. Hasegawa, J. Nishimura, and T. Harada, *J. Org. Chem.*, **46**, 4152 (1981); c) A. Oku, Y. Nozaki, J. Nishimura, and T. Harada, *J. Org. Chem.*, **48**, 4374 (1983).

3) a) A. Oku, T. Yokoyama, and T. Harada, *J. Org. Chem.*, **48**, 5333 (1983); b) A. Oku, T. Yokoyama, and T. Harada, *Tetrahedron Lett.*, **24**, 4699 (1983).

4) Thiol esters **6** (benzoate, pivalate) and thiol acetate were also formed as byproducts.

5) Not only the acidity constants of the acids corresponding to the respective ester but also the NMR chemical shift of the CH_2=proton of **1** may tell the relative reactivity toward Michael addition. Thus, the observed decreasing order in δ values of CH_2 (**1a** 5.87>**1c** 5.74>**1b** 5.67) may correspond to the reactivity order in the Michael addition. So does the IR(C=O) frequency the carbonyl reactivity toward thiolate ion, and the order in frequencies (**1c** 1765>**1b** 1760>**1a** 1740 cm^{-1}) may correspond to the reactivity in the displacement at the carbonyl.

6) Alcoholic solvents (MeOH, EtOH, *t*-BuOH) are more suitable for the reaction than ethers. When potassium carbonate was used instead of Triton B in the reaction of **1a**, the yield of **2a** slightly increased from 62 to 65% while **6a** decreased from 29 to 13%.

7) The reaction mixture of **2b** and NH_3 was directly hydrolyzed without isolating the intermediate **7i** (R^3=R^4=H)

8) L. Goodman, R. M. Moss, and B. R. Baker, *J. Org. Chem.*, **23**, 1251 (1958).

9) Product **10** was isolated as the Me ester after the treatment with MeOH.

10) Nitrile **7i** was also thermally labile under a VPC condition (injection 250 °C column 220 °C).

11) It was reported that 2-amino-2,3-diphenylpropionitrile was thermally unstable and underwent a dehydrocyanation to give the corresponding enamine. C. H. Hauser, A. M. Taylor, and T. G. Ledford, *J. Am. Chem. Soc.*, **82**, 1786 (1960).

12) A. Oku and S. Arita, *Bull. Chem. Soc. Jpn.*, **52**, 3337 (1979).

 © 1987 The Chemical Society of Japan Bull. Chem. Soc. Jpn., 60, 613—616 (1987)

Carbon-13 NMR and IR Spectroscopic Studies on Some 7-Oxabicyclo[2.2.1]heptanes and -heptenes. n-π Interaction and Hydrogen Bonding

Yasuhisa SENDA,*,† Akihiko OHNO, Jun-ichi ISHIYAMA, Shin IMAIZUMI, and Shin-ichi KAMIYAMA††,†††

Department of Engineering Science, Faculty of Engineering, Tohoku University, Aoba, Aramaki, Sendai 980

††Government Industrial Research Institute, Tohoku, Nigatake, Sendai 983

(Received June 5, 1986)

The ^{13}CNMR spectra of diastereomeric pairs of the title compounds together with some tetrahydrofurans were examined and the chemical shifts were compared with those for the corresponding bicyclo[2.2.1]heptanes and -heptenes. The intramolecular interaction between the n-orbital of an oxygen atom and the π-orbital of an olefinic bond was found in 2-methylene-7-oxabicyclo[2.2.1]heptane. Intramolecular hydrogen bonding between the 7-oxygen and the hydroxyl group occurs in *exo*-7-oxabicyclo[2.2.1]heptane-2-methanol.

The ^{13}CNMR spectra of substituted 7-oxabicyclo[2.2.1]heptanes (**1**—**6**) and -heptenes (**7** and **8**) and some tetrahydrofurans (**9** and **10**) were examined. The chemical shifts were compared with those for analogous carbocyclic compounds. Some intramolecular interactions were expected between the oxygen atom introduced at the 7-position of a bicyclo[2.2.1]heptane skeleton and the functional group in the molecule. The hydrogen bonding in 7-oxabicyclo[2.2.1]heptane-2-methanol (**4**) and the n-π interaction in 2-methylene-7-oxabicyclo[2.2.1]heptane (**6**) were also studied.

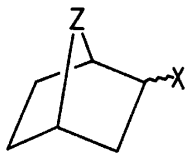

	X	Z
1:	H	O
2:	CH_3	O
3:	$COOCH_3$	O
4:	CH_2OH	O
5:	CH_2OCOCH_3	O
6:	$=CH_2$	O
11:	$=CH_2$	CH_2
13:	CH_3	CH_2

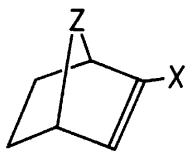

7:	H	O
8:	CH_3	O

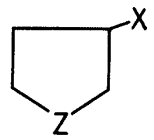

9:	$=CH_2$	O
10:	CH_2OH	O
12:	$=CH_2$	CH_2
14:	CH_3	O
15:	CH_3	CH_2

Results and Discussion

The new compounds employed in this study were **6** and 2-methyl-7-oxabicyclo[2.2.1]hept-2-ene (**8**). The former was prepared by the thermal decomposition of 7-oxabicyclo[2.2.1]heptane-2-methanol acetate (**5**) over Pyrex chips at 450 °C and the latter was obtained by a Diels-Alder reaction of 3-methylfuran with ethylene.

Table 1 summarized the ^{13}C chemical shifts of **1**—**10**. The introduction of an oxygen atom to the 7-position of a bicyclo[2.2.1]heptane skeleton caused a downfield shift of 38 ppm for the carbon α to the oxygen atom,[1] but no appreciable shift was observed on the carbon β to the oxygen atom. The γ carbons, which are the carbons of the substituents attached to the 7-oxabicyclo[2.2.1]heptane skeleton, showed small upfield shifts compared to those for the corresponding bicyclo[2.2.1]heptanes.[1] Considerable shielding differences were observed in two diastereomeric 7-oxabicyclo[2.2.1]heptane derivatives. The signals for C2, C6, and the carbon of the substituent attached to the ring skeleton of endo-isomers always appeared at higher fields than those for exo-isomers. The resonances for C2, C6, and the methyl group of *endo*-2-methyl-7-oxabicyclo[2.2.1]heptane (*endo*-**2**) were shielded by 4.0, 6.1 and 5.3 ppm, respectively, compared to those for *exo*-**2**. The signals for other ring carbons of endo-isomers did not always appear at higher fields than those for exo-isomers. No significant shielding difference between the two diastereoisomers was found for carbons which were not directly bonded to the bicyclic skeleton. The shielding difference of the methyls between stereoisomeric methoxycarbonyl groups was 0.2 ppm and that for the acetoxyl groups was only 0.1 ppm. The resonances for the methyl carbons of diastereomers **2** appeared at δ 21.3 (exo) and 16.0 (endo). These values are comparable with those of the equatorial and axial methyls on a cyclohexane ring in a chair conformation.[2]

In the 7-oxabicyclo[2.2.1]hept-2-ene series (**7** and **8**), the introduction of a methyl group into an sp^2 carbon causes an upfield shift of the other sp^2 carbon compared to the parent compound. The methyl carbon signal for the sp^2 carbon also appeared at a higher field than that for the sp^3 carbon of compound **2**, as experienced on bicyclo[2.2.1]hept-2-enes.[1]

†Present address: Department of Chemistry, Yamagata University, Koshirakawa, Yamagata 990.

†††Present address: Department of Applied Chemistry, Yamagata University, Jonan, Yonezawa 992.

Table 1. ^{13}C Chemical Shifts of 7-Oxabicyclo[2.2.1]heptanes, -heptenes and Related Compounds[a)]

Compound		Chemical shift (δ) Ring						Substituent		
		C1	C2	C3	C4	C5	C6	C8	C9	C10
7-oxabicyclo[2.2.1]heptane										
Parent (**1**)		76.1	30.3	30.3	76.1	30.3	30.3			
2-Methyl- (**2**)	exo	81.9	40.0	37.8	76.6	29.7	29.7	21.3		
	endo	80.2	36.0	39.1	77.5	31.1	23.6	16.0		
-2-carboxylic acid methyl ester (**3**)	exo	78.8	51.8	48.0	76.3	34.5	29.5	173.8	29.7	
	endo	77.7	51.7	47.9	77.5	33.3	26.4	172.8	29.9	
-2-methanol (**4**)	exo	77.9	45.8	34.0	76.3	30.0	29.5	65.0		
	endo	78.3	44.2	34.3	77.0	30.6	24.2	63.6		
-2-methanol acetate (**5**)	exo	75.5	42.5	34.1	76.0	29.9	29.3	66.5	170.7	20.9
	endo	77.9	40.6	34.4	76.8	30.5	24.3	65.4	170.5	20.8
2-Methylene- (**6**)		80.6	150.9	39.1	77.2	29.5	30.6	102.5		
7-Oxabicyclo[2.2.1]hept-2-ene										
Parent (**7**)		77.7	134.6	134.6	77.7	23.4	23.4			
2-Methyl- (**8**)		82.1	142.6	128.2	78.8	26.0	23.3	12.3		
3-Methylenetetrahydrofuran (**9**)			71.0	148.1	32.9	68.6		105.5		
Tetrahydrofuran-3-methanol (**10**)			70.6	41.5	28.7	67.8		64.0		

a) The carbon numbering is as follows:

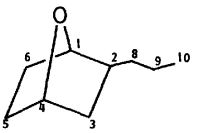

Table 2. Differences in β- and γ-Carbon Resonances between Unsaturated Compounds and between the Corresponding Saturated Ones (ppm)

Unsaturated compound	β	γ	Saturated compound	β	γ
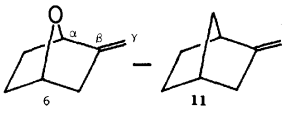 6 – 11	−4.7	+0.7	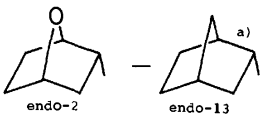 endo-2 – endo-13	+1.5	−1.5
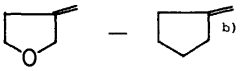 9 – 12	−0.5	+0.6	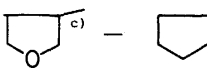 14 – 15	−1.5	−3.0

The chemical shifts were taken from[a)] Ref. 1. b) S. H. Grover and J. B. Stothers, *Can. J. Chem.*, **53**, 589 (1975). c) E. L. Eliel, V. S. Rao and K. M. Pietrusiewicz, *Org. Magn. Reson.*, **12**, 461 (1979). d) M. Christl, H. J. Reich and J. D. Roberts, *J. Am. Chem. Soc.*, **93**, 3463 (1971).

The ^{13}C chemical shifts for sp^2 carbons of **6** and 3-methylenetetrahydrofuran (**9**) were compared with those for the corresponding hydrocarbons (Table 2). The shielding differences, thus obtained, were compared with those for saturated compounds. The $\Delta\delta$ value for the carbon β to the oxygen atom between *endo*-**2** or 3-methyltetrahydrofuran (**14**) and the corresponding hydrocarbons (**13** or **15**) are +1.5 or −1.5, respectively, and that for the carbon γ to the oxygen atom being −1.5 or −3.0 ppm, respectively. On the other hand, the $\Delta\delta$ value between **6** or **9** and the corresponding hydrocarbon (**11** or **12**) are −4.7 and −0.5 for the β-carbon, and +0.7 and 0.6 ppm for the γ-carbon, respectively. The β carbon resonances for the unsaturated system which contains an oxygen atom were located at a higher field than those for the corresponding hydrocarbons. The γ carbon resonances, on the contrary, moved downfield compared to those for the corresponding hydrocarbons.

Molecular orbital interactions have been found between a nonbonding orbital of an oxygen and the π-orbital of the olefinic bond in a series of cyclic allylic ethers and alcohols in which the oxygen is placed at the anticlinal position with respect to the double bond.[3)] The Newman projection formula, viewed from C1 along the C1-C2 bond of **6** indicates that the dihedral angle between the O7-C1 bond and the C2-C8 (*exo*-methylene carbon) double bond is approximately 150°. This suggests the presence of the previously mentioned intramolecular orbital interac-

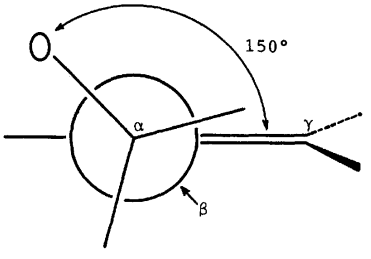

tion in this compound. The through-space interaction between the π-type n-orbital in the oxygen atom and the vacant p-π^*-orbital results in a decrease in the electron density at the oxygen atom. The enhanced effective electronegativity of the oxygen atom, therefore, induces a homoconjugative through-bond interaction between the C–O σ-orbital and the p-π-orbital.

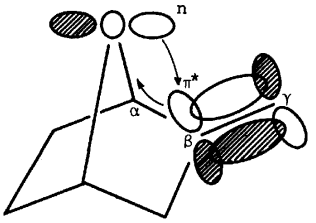

The electron delocalization of the π-orbital by such through-space and through-bond interaction results in an upfield shift of the β carbon resonances and a downfield shift of γ carbon resonances. The shielding differences observed in a series of **9** infer the presence of an analogous orbital interaction.

The stereochemistry of the hydrogenation of 2-substituted 5-methylene-1,3-dioxanes over Group-VIII transition metals made a sharp contrast with that of 4-substituted 1-methylenecyclohexanes.[3b] A high cis selectivity was observed with the former, while the latter exhibited a wide variety of diastereomeric product distributions. The stereochemistry of the reaction was interpreted in terms of the n–π orbital interaction. The hydrogenation of **6** and 2-methylenebicyclo[2.2.1]-heptane (**11**) was performed over Group-VIII noble-metal catalysts in order to examine the stereochemistry of the reaction. In this case, the steric factor was always predominant, giving more than 58% endo-isomer (Table 3). The introduction of an oxygen atom into the 7-position of the bicyclo[2.2.1]heptane skeleton resulted in an increase in the attack of the hydrogen from the endo side, which is the opposite side of the oxygen atom. This also supports the presence of the n–π orbital interaction in **6**.[3b]

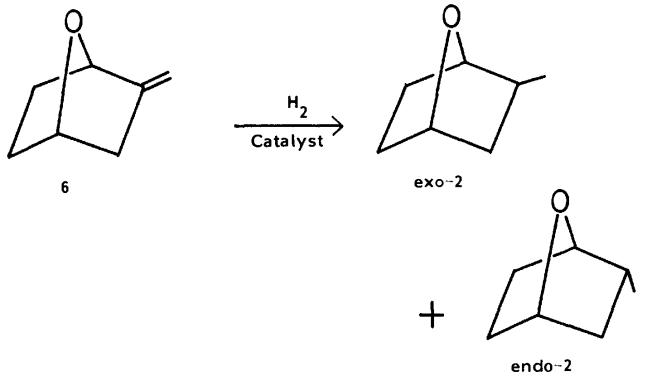

No evidence of intramolecular hydrogen bonding has been found in either *endo*- or *exo*-**4** by proton NMR spectroscopy.[4] In this work, the ν_{OH} vibration was carefully examined in these two diastereomers together with tetrahydrofuran-2-methanol (**10**) which corresponds to the partial structure of **4**. The spectra

Table 3. Stereochemistry on the Hydrogenation of **6** and **11**

Catalyst	Starting olefin **6** Product (*endo*/%)	Starting olefin **11** Product (*endo*/%)
Ru-black	71	74
Rh-black	69	73
Pd-black	82	90
Os-black	70	79
Ir-black	62	77
Pt-black	58	84

Table 4. The OH Stretching Absorption of Some Hydroxylic Compounds (cm^{-1})

Compound	ν_{OH}	ε	$\Delta\nu_{1/2}$[a]	$\Delta\nu$[b]
10	3639	86	22	
	3610	sh[c]	—	29
exo-**4**	3654	55	24	
	3533	17	84	121
endo-**4**	3653	91	22	

a) Half-band width. b) Separation of free and bonded hydroxyl bands. c) Shoulder.

were obtained under such conditions as suppress intermolecular hydrogen bonding (in carbon tetrachloride at 4×10^{-3} M). Table 4 shows the infrared absorption frequencies in a hydroxyl stretching region. Alcohol **10** showed absorption for a free hydroxyl group at 3639 cm^{-1} and a bonded hydroxyl group at 3610 cm^{-1} as a shoulder of the main absorption. The absorption of *endo*-**4** at 3653 cm^{-1} could be associated with a free hydroxyl group, while the absorptions of *exo*-**4** appeared at 3654 and 3533 cm^{-1} corresponded to a free and a bonded hydroxyl group, respectively. Since the apparent areas of the absorption of both bonded and free hydroxyl bands of *exo*-**4**

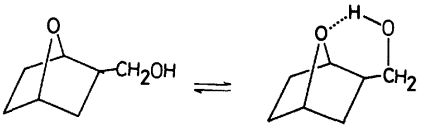

are roughly equal, the hydrogen bonded conformers and the alternative seem to be of equal population. Such an equilibrium between the bonded and free hydroxyl species in the system may make it difficult to determine the hydrogen bonding in an NMR time scale. Essentially, free pseudo-rotation occurs between the half-chair (C_2) and the envelope (C_s) conformation of the tetrahydrofuran skeleton of **10**, with the former form slightly preferred.[5] In some conformations intramolecular hydrogen-bond formation is possible, but the bonded conformation is insufficiently stabilized by the formation of the hydrogen bond. Consequently, only a very weak absorption of a bonded hydroxyl appears. As expected, no hydrogen bond is formed in *endo*-**4** in which the C1–O7 and C2–CH_2OH bonds are in opposite direction. The tetrahydrofuran ring in **4** has a fixed C_s form with the oxygen atom out of the five-membered ring plane.[5] The structural

analysis of tetrahydrofuran and 7-oxabicyclo[2.2.1]-heptane homologs by X-ray diffraction,[6] electron diffraction[7] and microwave analysis[8] suggests that the degree of puckering of the tetrahydrofuran moiety of 7-oxabicyclo[2.2.1]heptane skeleton is a little greater than that of tetrahydrofuran itself. Consequently, the distance between O7 and the hydroxyl oxygen becomes smaller than that for **10**. This also supports the formation of stronger hydrogen bonding in the bicyclic system. Using either the equation derived by Kuhn[9] or the modified equation by Brutcher and Bauer[10] relating the $\Delta\nu$ to the hydrogen bonded distance, the distance between O7 and hydroxyl hydrogen in *exo*-**4** was estimated to be 1.28 or 1.74 Å, respectively. Since Ouellette et al. reported that the minimum O7-hydroxyl oxygen distance is 2.6 Å from the examination of the model,[4] the distance between the hydroxyl hydrogen and O7 was estimated to be 1.64 Å by assuming that the distance between the hydrogen and the oxygen of a hydroxyl group is 0.96 Å. This is in fair agreement with the results obtained in the present work. If it is possible to apply the enthalpy vs. shift difference of the ν_{OH} band relationship ($-\Delta H$ (kcal mol^{-1})$=0.016\ \Delta\nu_{OH}+0.63$)[11] to this system, $-\Delta H$ between the free and bonded species is then 10.7 kJ mol^{-1}. In this connection, $-\Delta H$ of the hydrogen bonding between benzyl alcohol and dioxane is 8.8 kJ mol^{-1}.[12]

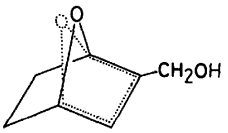

Experimental

Materials. Diels-Alder reaction of furan and methyl acrylate by refluxing for 5 weeks followed by hydrogenation over Pd-C gave 7-oxabicyclo[2.2.1]heptane-2-carboxylic acid methyl ester (**3**) in a yield of 19%.[13] The two diastereomers of **3** were separated by fractional distillation. Ester **3** was reduced with LAH in ether to give **4**, (72%)[13] which was treated with acetic anhydride in pyridine to give **5** (70%).[13] The tosylate of **4** was reduced with LAH to give **2** (60%).[13] 1,4-Cyclohexanediol was heated over Al_2O_3 to give 7-oxabicyclo[2.2.1]heptane (**1**) (45%).[14] Diels-Alder reaction of furan with ethylene at 155 °C for 6 h gave 7-oxabicyclo[2.2.1]-hept-2-ene (**7**) (5%).[15] A Wittig reaction of tetrahydrofuran-3-one and of bicyclo[2.2.1]heptan-2-one with methyltriphenylphosphonium bromide gave **9** (65%)[16] and **11** (65%),[17] respectively. Tetrahydrofuran-3-carboxylate was reduced with LAH to give **10** (65%).[18]

2-Methylene-7-oxabicyclo[2.2.1]heptane (6). The acetate (18 g, 0.106 mol) was passed through a heated (440—450 °C) Pyrex tube (50 cm×10 mm) packed with Pyrex chips. The crude mixture was digested with pentane which was washed with a saturated $NaHCO_3$ solution and a saturated NaCl solution and then dried over $CaCl_2$. Distillation yielded **6** (3.2 g, 0.029 mol, 27%), bp 37 °C/40 mmHg. Found: C, 76.56; H, 9.58%. Calcd for $C_7H_{10}O$: C, 76.33; H, 9.15%. ^{1}H NMR (100 MHz, $CDCl_3$) δ=1.49—2.16 (6H), 4.73 (3H, m), 4.89 (1H, brs).

2-Methyl-7-oxabicyclo[2.2.1]hept-2-ene (8). After the mixture of 3-methylfuran (20 g, 0.244 mol) and ethylene (40 kg cm^{-2}) was stirred in a 200-ml autoclave at 150 °C for 24 h, the crude product was extracted with pentane. Distillation gave **8** (2 g, 0.018 mol, 7%), bp 115—120 °C. Found: C, 76.53; H, 9.53%. Calcd for $C_7H_{10}O$: C, 76.33; H, 9.15%. ^{1}H NMR (100 MHz, $CDCl_3$) δ=1.17 (2H, m), 1.27 (2H, m), 1.80 (3H, d, J=1.4 Hz), 4.69 (1H, brd, J=3.7 Hz), 4.87 (1H, brs), and 5.75 (1H, brs).

Catalytic Hydrogenation. The substrate (0.5 mmol) and the catalyst (5 mg) in ethanol (3 ml) were stirred with hydrogen at atmospheric pressure and room temperature. After the reaction was completed the catalyst was removed by the centrifugal method and the mixture was analyzed by GLC.

Spectra. ^{1}H NMR spectra were obtained with a Jeol FX-100 spectrometer and ^{13}C NMR spectra were obtained with a Jeol MH-100 and FX-100 spectrometers in an FT-mode using TMS as an internal standard. $CDCl_3$ was used as a solvent. IR spectra were measured with a Hitachi model 260-10 spectrometer using a 30-mm optical-length quartz cell. CCl_4 was used as a solvent.

We are grateful to Professor Kaoru Hanaya and Mr. Takashi Muramatsu, Miyagi University of Education, for measurements of IR spectra at high dilution.

References

1) E. Lippmaa, T. Pehk, J. Paasivirta, N. Belikova, and P. Plate, *Org. Magn. Reson.*, **2**, 581 (1970).
2) Y. Senda and S. Imaizumi, *Tetrahedron*, **31**, 2905 (1975).
3) a) Y. Senda, J-I. Ishiyama, and S. Imaizumi, *Tetrahedron Lett.*, **1978**, 1085; b) J-I. Ishiyama, Y. Senda, and S. Imaizumi, *J. Chem. Soc., Perkin Trans. 2*, **1982**, 71.
4) R. J. Ouellette, K. Liptak, and G. E. Booth, *J. Org. Chem.*, **32**, 2394 (1967).
5) B. Fuchs, *Top. Stereochem.*, **10**, 1 (1978).
6) D. Gravel, R. Deziel, F. Brisse, and L. Hechler, *Can. J. Chem.*, **59**, 2997 (1981).
7) H. J. Geise, W. J. Adams, and L. S. Bartell, *Tetrahedron*, **25**, 3045 (1969).
8) G. G. Engerholm and A. C. Luntz, *J. Chem. Phys.*, **50**, 2446 (1969).
9) L. P. Kuhn, *J. Am. Chem. Soc.*, **74**, 2492 (1952).
10) F. V. Brutcher, Jr. and W. Bauer, Jr., *J. Am. Chem. Soc.*, **84**, 2236 (1962).
11) M. D. Joesten and R. S. Drago, *J. Am. Chem. Soc.*, **84**, 3817 (1962).
12) G. C. Pimentel and A. L. McClellan, "The Hydrogen Bond," Freeman and Company, San Francisco (1960), p. 234.
13) M. P. Kunstmann, D. S. Tarbell, and D. I. Davies, *J. Am. Chem. Soc.*, **84**, 4119 (1962).
14) E. A. Fehnel, S. Goodyear, and J. Berkowitz, *J. Am. Chem. Soc.*, **73**, 4979 (1951).
15) W. Nudenberg and L. W. Butz, *J. Am. Chem. Soc.*, **66**, 307 (1944).
16) Y. Infarnet, A. Accary, and J. Huet, *Bull. Soc. Chim. Fr.*, **1980**, *Partie II*, 261.
17) H. C. Brown and J. H. Kawakami, *J. Am. Chem. Soc.*, **92**, 1990 (1970).
18) H. Katsura, *Nippon Kagaku Zasshi*, **82**, 91 (1961).

 © 1987 The Chemical Society of Japan Bull. Chem. Soc. Jpn., 60, 617—620 (1987)

Ethylene Glycol from Synthesis Gas by Homogeneous Ruthenium and Ruthenium-Rhodium Catalysts

Yoshihisa KISO* and Kenji SAEKI
Research Center, Mitsui Petrochemical Industries, Ltd., Waki-cho, Kuga-gun, Yamaguchi 740
(Received June 6, 1986)

In the formation of ethylene glycol from synthesis gas, amines (especially imidazole and its derivatives) enhanced the catalytic activity of a ruthenium carbonyl mixed with alkali metal halides. A rhodium carbonyl complex further promoted the activity and selectivity of a ruthenium-alkali metal halide-imidazole catalyst.

The direct formation of ethylene glycol from synthesis gas has been expected to be one of the most attractive new methods for ethylene glycol production on a commercial scale.[1,2] A number of homogeneous catalysts have been reported, such as rhodium, ruthenium, cobalt and iridium complexes.[3-10] Although some promoters, such as halides (alkali metal salt.[6] iminium salt[10] etc.) or carboxylic acids,[6,7] for ruthenium catalyst were reported, research concerning other types of promoters has scarcely been reported. In the course of our research regarding the formation of methanol and ethylene glycol from synthesis gas by ruthenium-alkali metal halide catalysts, we found that organic amines (especially imidazole compounds) promoted the activity of a ruthenium catalyst for ethylene glycol formation.[11] We also found that a rhodium carbonyl complex further enhanced the activity and selectivity of a ruthenium-halide-imidazole catalyst for ethylene glycol formation. In this paper, we report on the direct formation of ethylene glycol from synthesis gas by these ruthenium and ruthenium-rhodium bimetallic catalysts.

Results and Discussion

Ruthenium Catalyst Promoted by Halide and Amine. Dombek[6] reported that methanol and ethylene glycol are formed from synthesis gas when using a ruthenium-alkali metal halide catalyst. We examined the effect of organic amines on this ruthenium-halide catalyst (Eq. 1.).

$$CO + H_2 \xrightarrow{\text{Ru-halide-amine}} CH_3OH + HOCH_2CH_2OH \quad (1)$$

Table 1 summarizes the results for the synthesis of ethylene glycol and methanol in the presence of $[Ru_3(CO)_{12}]$, halide and amine. It was shown that *N*-methylmorpholine, pyridine, 2-pyridinol, benzimidazole, imidazole, and its methyl derivatives promoted the activity of a $[Ru_3(CO)_{12}]$-CsI catalyst for ethylene glycol formation. Of these amines, imidaozle derivatives and 2-pyridinol were especially effective. Furthermore, imidazole promoted the formation of ethylene glycol using a $[Ru_3(CO)_{12}]$ catalyst combined with several types of halide compounds (CsBr, CsCl, KI, Me_4NI, Ph_4NI). On the contrary, 2,2′-bipyridyl, pyrazole and triazole supressed the formation of ethylene glycol.

The activities for ethylene glycol and methanol formation were influenced by the molar ratio of amine to ruthenium. The molar ratio suitable for ethylene glycol formation increased in the following order; *N*-methylmorpholine<imidazole<pyridine≪2-pyridinol. This sequence shows that the more basic the amine, the lower the suitable molar ratio (pK_a at 25 °C: *N*-methylmorpholine 7.38, imidazole 6.95, pyridine 5.21, 2-pyridinol 1.25).[12] This result suggests that the amine acts as a base for the ruthenium catalyst. On the other hand, methanol formation increased with an increasing molar ratio of imidazole to ruthenium; however in the case of other amines, the activities did not greatly depend on the molar ratio of amine to ruthenium. We examined the IR spectra of a recovered reaction mixture started from $[Ru_3(CO)_{12}]$-CsI-imidazole catalyst system under a synthesis-gas atmosphere at room temperature. The spectra were similar to those started from a $[Ru_3(CO)_{12}]$-CsI catalyst system which result in the formation of $[HRu_3(CO)_{11}]^-$(ν(CO) 2020s, 1985s, 1950m cm^{-1}),[6] although the catalytic activities were different from each other. This result suggests that active species of both catalyst systems are similar; also, the ruthenium cluster anion is thought to play an important role in active species, as shown by Dombek in ruthenium-iodide catalyst system.[6] Probably, the amine is converted to an ammonium ion which acts as a cation against the ruthenium anion in the active species **1** (Eq. 2). A similar effect of amine as a cation has been proposed by Kaplan in ethylene glycol formation with a rhodium-amine catalyst:[6]

$$[HRu_x] + R_3N \rightleftharpoons \underset{\mathbf{1}}{[R_3NH]^+[Ru_x]^-}. \quad (2)$$

In ethylene glycol formation from synthesis gas, formaldehyde and glycolaldehyde are thought to be important intermediates; the formation of hydroxymethyl complex **3** from a formaldehyde complex **2** is an important step.[13] It is thought that amine promotes the formation of **3** by a proton transfer from the ammonium ion to **2** (Scheme 1). Without the aid of the ammonium ion, the formation of the methoxy complex **4** from **2** may be favored; this will produce methanol, not ethylene glycol.

Effect of Imidazole on Rhodium and Cobalt Catalysts. Rhodium carbonyls and cobalt carbonyls have

Table 1. Effect of Amine on $[Ru_3(CO)_{12}]$-Halide Catalyst for Synthesis Gas Reaction[a)]

Halide	Amine	Amine concd[c)]	mol (Ru mol·h)$^{-1}$		Selectivity[b)]/%
			CH_3OH	$HOCH_2CH_2OH$	
CsI	None		1.34	0.13	9.1
CsI	*N*-Methylmorpholine	(1)	1.45	0.19	11.7
CsI	*N*-Methylmorpholine	(5)	1.61	0.17	9.5
CsI	*N*-Methylmorpholine	(50)	1.14	0.09	7.4
CsI	Pyridine	(5)	1.53	0.20	11.7
CsI	Pyridine	(20)	1.28	0.24	15.6
CsI	Pyridine	(50)	1.01	0.28	21.9
CsI	2-Pyridinol	(5)	1.43	0.21	12.8
CsI	2-Pyridinol	(50)	1.64	0.45	21.5
CsI	2,2′-Bipyridyl	(1)	0.22	0.01	3.7
CsI	Imidazole	(1)	1.98	0.36	15.2
CsI	Imidazole	(5)	2.17	0.64	22.9
CsI	Imidazole	(15)	2.32	0.62	20.9
CsI	Imidazole	(50)	5.82	0.44	7.0
CsI	1-Methylimidazole	(5)	1.61	0.43	21.3
CsI	2-Methylimidazole	(5)	2.74	0.30	9.9
CsI	4-Methylimidazole	(5)	2.24	0.46	17.0
CsI	Benzimidazole	(5)	2.19	0.37	14.6
CsI	Pyrazole	(5)	2.50	0.04	1.6
CsI	1,2,4-Triazole	(5)	0.48	0.02	3.3
CsBr	None		1.08	0.11	9.3
CsBr	Imidazole	(5)	2.21	0.48	17.9
CsCl	None		0.97	0.08	7.6
CsCl	Imidazole	(5)	1.90	0.27	12.6
KI	None		1.11	0.08	7.0
KI	Imidazole	(5)	2.00	0.48	18..9
Me_4NI	None		3.52	0.11	3.0
Me_4NI	Imidazole	(5)	1.69	0.27	13.8
Ph_4PI	None		2.01	0.17	7.7
Ph_4PI	Imidazole	(5)	2.10	0.47	18.4

a) Charge: $[Ru_3(CO)_{12}]$ 0.10 mmol, halide 1.80 mmol, sulfolane 7.5 cm^3; run conditions: CO/H_2 (1:1) 300 kg cm^{-2}, 200 °C, 4 h. b) $100\times(HOCH_2H_2OH)\,mol/(CH_3OH+HOCH_2CH_2OH)\,mol$. c) Molar ratio of amine against Ru atom.

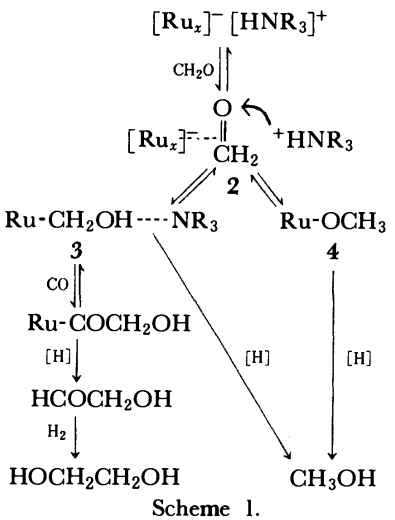

Scheme 1.

been known to be active catalysts for ethylene glycol formation from synthesis gas.[6)] Although the effect of amines on cobalt catalysts has scarcely been examined, amines such as alkylamines and pyridine derivatives have been reported to promote the activity of rhodium catalysts.[6)] In our research of ruthenium catalysts, imidazole derivatives were found to be effective promoters. Since the effect of imidazole derivatives on other metal catalysts has not been reported, we examined the effect of imidazole on a rhodium catalyst ($[Rh(CO)_2$(acac)] (acac=acetylacetonato) in sulfolane solvent) and a cobalt catalyst ($[Co_2(CO)_8]$ in toluene solvent), respectively (Table 2). These results showed that imidazole promoted the activity of a rhodium catalyst, though the level of activity was very low. On the contrary, a cobalt catalyst became deactivated upon adding imidazole.

Ruthenium-Rhodium Bimetallic Catalysts.[14)] As shown for ruthenium catalysts, the activity for ethylene glycol formation was promoted by amines. However, the selectivity to ethylene glycol was still low for the formation of a large amount of methanol. In order to increase the selectivity of the ruthenium catalyst, we examined the effect of a small amount of $[Rh(CO)_2$(acac)] on a ruthenium-CsI catalyst system, since several rhodium catalysts have been known to show a high selectivity to ethylene glycol. Table 3 summarizes the results of ruthenium-rhodium-CsI-imidazole catalyst. Although, rhodium itself did not show catalytic activity under the condition given in Table 3, it promoted the activity and selectivity of a ruthenium

Table 2. Effect of Imidazole on Rhodium or Cobalt Catalyst

Metal catalyst	Imidazole[c]	mol (metal mol·h)$^{-1}$	
		CH_3OH	$HOCH_2CH_2OH$
$[Rh(CO)_2(acac)]$[a]	0	0.11	<0.01
$[Rh(CO)_2(acac)]$[a]	5	0.25	0.08
$[Co_2(CO)_8]$[b]	0	0.62	0.02
$[Co_2(CO)_8]$	5	≈0	≈0

a) Charge: $[Rh(CO)_{12}(acac)]$ 0.3 mmol, sulfolane 7.5 cm^3; run conditions: CO/H_2 (1:1) 300 kg cm^{-2}, 240°C, 4 h. b) Charge: $[Co_2(CO)_8]$ 1.0 mmol, toluene 10 cm^3; run conditions: CO/H_2 (1:1) 500—600 kg cm^{-2}, 240°C, 4 h. c) Molar ratio of imidazole against Rh or Co atom.

Table 3. Synthesis Gas Reaction by Ruthenium-Rhodium Bimetallic Catalyst[a]

Ru	Rh	CsI	Imidazole	mmol h^{-1}	
mmol	mmol	mmol	mmol	CH_3OH	$HOCH_2CH_2OH$
0.3	0	1.8	1.5	1.005	0.230
0	0.1	1.8	1.5	0	0
0.3	0.1	1.8	1.5	0.618	0.465
0.3	0	1.8	0	0.678	0.085
0.3	0.1	1.8	0	0.372	0.212

a) Charge: $[Ru_3(CO)_{12}]$ $[Rh(CO)_2(acac)]$, CsI, Imidazole and *N*-methyl-2-pyrrolidone 7.5 cm^3; run conditions: CO/H_2 (1:1) 300 kg cm^{-2}, 200°C, 2 h.

Table 4. Synthesis Gas Reaction in the Presence of $[Ru_3(CO)_{12}]$-$Rh(CO)_2(acac)]$ Catalyst Promoted by CsI and Imidazole[a]

mol% of metal		mmol h^{-1}[b]	
Ru	Rh	CH_3OH	$HOCH_2CH_2OH$
100	0	6.51	0.97
86	14	4.07	2.18
75	25	2.65	2.16
50	50	1.84	1.86
0	100	0.05	0.11

a) Charge: Ru+Rh 0.4 mmol, CsI 2.4 mmol, Imidazole 2.0 mmol, *N*-methyl-2-pyrrolidone 10 cm^3; run conditions: CO/H_2 (1:1) 500 kg cm^{-2}, 200°C, 2 h. b) In addition to methanol and ethylene glycol, small amounts of other products were formed. For example in the case of catalyst Ru/Rh=75/25, methylformate 0.01 mmol h^{-1}, ethanol 0.08 mmol h^{-1} and 1,2-propanediol 0.22 mmol h^{-1} were formed.

catalyst for ethylene glycol formation. Furthermore, promotion by imidazole was also observed in ruthenium-rhodium-CsI catalysis.

In order to analyze the functions of ruthenium and rhodium metal centers, we examined the activity of ruthenium-rhodium bimetallic catalysts with various molar ratios of ruthenium/rhodium. Table 4 summarizes the results from synthesis gas reactions in the presence of $[Ru_3(CO)_{12}]$, $[Rh(CO)_2(acac)]$, CsI and imidazole. In these reactions, the total number of ruthenium and rhodium atoms were kept constant. Ethylene glycol and methanol were the main products, and small amounts of other products (methylformate, ethanol and 1,2-propanediol) were formed. The rate of ethylene glycol formation was maximum at a molar ratio of ruthenium to rhodium around 6:1—3:1.

As mentioned in the prior section, ethylene glycol and methanol are thought to be formed through the common intermediate, formaldehyde (Scheme 2).[15] Since little or no formaldehyde (or its derivatives) was detected by GC analyses, steps **b** and **c** may be faster than step **a**; therefore, the total rate of ethylene glycol and methanol formation may depend upon the rate of step **a**. This total rate (mol h^{-1}) was found to increase with increasing concentration of ruthenium (Fig. 1). This result suggests that step **a** is catalyzed mainly by ruthenium in ruthenium-rhodium bimetallic catalyst. The molar ratio of ethylene glycol to methanol, which depends upon the relative rate of step **b**/step **c**, increased upon increasing the concentration of rhodium (Fig. 1). Rhodium may promote the formation of ethylene glycol from formaldehyde. Thus, ruthenium and rhodium play important independent roles in bimetallic catalyst.

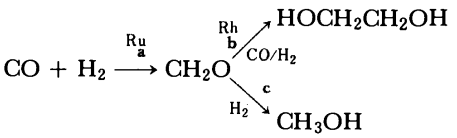

Scheme 2.

We analyzed the catalysts with IR spectra under a synthesis-gas atomsphere at room temperature. Rhodium anion species, $[Rh(CO)_4]^-$ (ν(CO) 1895s cm^{-1})[16] and minor $[Rh(CO)_2I_2]^-$ (ν(CO) 2010, 1975 cm^{-1})[17] were observed in the reaction mixture starting from rhodium-CsI-imidazole catalyst. An IR analysis of the reaction mixture starting from ruthenium-rhodium-CsI-imidazole catalyst showed the existance of $[HRu_3$-

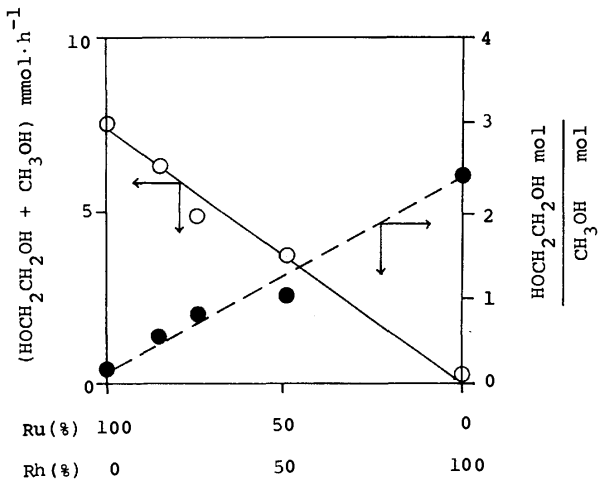

Fig. 1. Effect of molar ratio of ruthenium/rhodium on activities and selectivities of catalysts. ——○——, ($HOCH_2CH_2OH+CH_3OH$) mmol h^{-1}; ——●——, molar ratio of $HOCH_2CH_2OH$ against CH_3OH. Conditions; see Table 4.

$(CO)_{11}]^-$, $[Rh(CO)_4]^-$, and $[Rh(CO)_2I_2]^-$. No other species (such as mixed metal clusters) were observed. These results support Scheme 2 in which ruthenium and rhodium act independently.

Experimental

Catalytic expreiments were carried out in a 60-ml autoclave made of Hastelloy C-276. The reactor was charged with metal carbonyl ($[Ru_3(CO)_{12}]$, $[Rh(CO)_2(acac)]$, $[Co_2(CO)_8]$), an additive (halide, amine) and a solvent and was pressurized with CO/H_2 (1 : 1) gas and heated under stirring with a magnetic stirrer (300—600 kg cm^{-2}, 200—240 °C, 2—4 h). An analysis of the products was performed by gas chromatography (column; 10% PEG20M TPA/Chromosorb 102). Infrared spectra were recorded with a Shimadzu IR-420 spectrometer under a synthesis-gas atomsphere at room temperature.

This work was one part of the "C_1 Chemistry Project," a National Research and Development Program of Agency of Industrial Science and Technology, Ministry of International Trade and Industry (M. I. T. I.), Japan. We wish to thank Mr. Tetsuo Hayashi, Mr. Hideto Matsuoka, and Mr. Hiroyoshi Tarumoto for experimental assistance, and are grateful to Mr. Masahide Tanaka and the members of Ethylene Glycol Group of the Project for valuable discussions.

References

1) J. Koller, *Chemtech.*, **14**, 504 (1984).
2) J. Fable and C. D. Frohning, *J. Mol. Chem.*, **17**, 117 (1982).
3) R. L. Pruett and W. E. Walker (to Union Carbide Corp.), U. S. Patent, 3833634 (1974).
4) A. Deluzarche, A. Fonseca, G. Jenner, and A. Kiennemann, *Erdöl Kohle, Erdgas, Petrochem.*, **32**, 313 (1979).
5) W. Keim, M. Berger, and J. Schlupp, *J. Catal.*, **61**, 359 (1980).
6) B. D. Dombek, *J. Am. Chem. Soc.*, **102**, 6855 (1980); **103**, 6508 (1981); *J. Organomet. Chem.*, **250**, 467 (1983); *Adv. Catal.*, **32**, 325 (1983).
7) J. F. Knifton, *J. Am. Chem. Soc.*, **103**, 3959 (1981); *J. Chem. Soc., Chem. Commun.*, **1981**, 188; *J. Catal.*, **76**, 101 (1982).
8) D. R. Fahey, *Prepr. Div. Pet. Chem. A. C. S.*, **25**, 570 (1980).
9) W. Keim, M. Anstoch, M. Roper, and J. Schlupp, *C1 Mol. Chem.*, **1**, 21 (1984).
10) Y. Kiso, M. Tanaka, H. Nakamura, T. Yamasaki, and K. Saeki, *J. Organomet. Chem.*, **312**, 357 (1986).
11) Y. Kiso and K. Saeki, *J. Organomet. Chem.*, **303**, C17 (1986).
12) D. D. Perrin, Dissociation Constants of Organic Bases in Aqueous Solution, Butterworths, London, 1965.
13) D. R. Fahey, *J. Am. Chem. Soc.*, **103**, 136 (1981); L. C. Costa, *Catal. Rew. -Sci. Eng.*, **25**, 325 (1983).
14) Similar ruthenium-rhodium bimetallic catalysts were reported by Knifton and Dombek. We independently discovered the ruthenium-rhodium bimetallic catalyst. Y. Kiso, H. Nakamura, and K. Saeki, Japan. Patent, 128644 (1982); Y. Kiso and K. Saeki, Japan. Patent, 194827 (1983); K. Saeki, Y. Kiso, and M. Tanaka, The First Symposium on C_1 Catalysis, Tokyo, Japan, 1984 Abstr., No. 41; J. Knifton, *J. Chem. Soc., Chem. Commun.*, **1983**, 729; B. D. Dombek, *Organometallics*, **4**, 1707 (1985).
15) Recently, Nakamura et al. showed that ethylene glycol and methanol were formed through formaldehyde in Ru-halide and Ru-Rh-halide catalysts. S. Nakamura, T. Deguchi, T. Takano, M. Ishino, The Second Symposium on C_1 catalysis, Tokyo, Japan, 1985, Abstr., No. 108.
16) P. Chini and S. Martinengo, *Inorganica Chimica Acta*, **3**, 21 (1969).
17) L. M. Vallarino, *Inorg. Chem.*, **4**, 161 (1965).

 © 1987 The Chemical Society of Japan Bull. Chem. Soc. Jpn., 60, 621—626 (1987)

Photoadducts of 4,6-Dimethyl- and 4-Methoxy-6-methyl-2-pyrones with Chloroethylenes and Their Dehydrochlorination

Tetsuro SHIMO, Kenichi SOMEKAWA,* Yusuke WAKIKAWA, Hisako UEMURA, Otohiko TSUGE,† Kiyohisa IMADA,†† and Kimiko TANABE††
Department of Applied Chemistry, Faculty of Engineering, Kagoshima University, Korimoto, Kagoshima 890
†Research Institute of Industrial Science, Kyushu University, Kasugakoen, Kasuga 816
††Department of Industrial Chemistry, Faculty of Engineering, Miyazaki University, Kumano, Miyazaki 889-21
(Received June 20, 1986)

Sensitized photoreactions of 2-pyrones with chloroethylenes gave two kinds of [2+2]cycloadducts, 2-oxabicyclo[4.2.0]oct-4-en-3-ones (**4**, **8**) and across the C_3–C_4 double bond in 2-pyrone, benzene derivatives, and/or cyclobutanecarboxylic acids: Their relative yields greatly depended upon the nature of the reactants. The dehydrochlorination of the cycloadducts **4** and **8** across the C_5–C_6 double bonds in the pyrones with triethylamine in ethanol gave 5-ethenyl-2-pyrones, whose structures were previously incorrectly assigned as oxocinones, via a symmetry-allowed ring opening of 2-oxabicyclo[4.2.0]octa-4,6-dien-3-ones. Some 5-ethenyl-2-pyrones possessing a chlorinated ethenyl group finally affords 5-ethynyl-2-pyrones by an anti-elimination of hydrogen chloride. The X-ray crystallographic analyses of 5-ethenyl- and 5-ethynyl-2-pyrones are also described.

Although much attention has been denoted to the thermal cycloaddition reactions of 2-pyrones,[1] the investigation of their photochemical ones has not been extended beyond our reports[2,3] except dimerization.[4] The sensitized photochemical reaction of 4,6-dimethyl-2-pyrone (**1**) with such electron-deficient olefins as acrylonitrile and methyl acrylate gave two stereoisomeric [2+2]cycloadducts, as major products, across the C_5–C_6 double bond in **1**,[2] while methyl 2-pyrone-5-carboxylate afforded two stereoisomeric [4+2]cycloadducts in the reaction with acrylonitrile under similar conditions.[3]

Hanifin and Cohen[5] have first reported the formation of an eight-membered oxygen heterocycle, oxacyclooctatrienone (oxocinone) ring system, by the pyrolysis of a 3-chlorocoumarin photodimer with the elimination of hydrogen chloride. It was demonstrated, however, that the pyrolysis of photochemical [2+2]-cycloadducts between 2,6-dimethyl-4-pyrone with acetylenes gave no expected monocyclic oxocinones, but instead the adducts underwent a symmetry-allowed bicyclic Claisen rearrangement followed by aromatization to substituted phenols.[6] Thus, it has not been known monocyclic oxocinone ring system up to date. If [2+2]cycloadducts are again formed in the photochemical reaction of such 2-pyrones bearing an electron-donating group as **1** with halogen-substituted olefins, the halogenated cycloadducts would be expected to give monocyclic oxocinones by dehydrohalogenation with a concurrent ring expansion.

The purpose of this work was to prepare halogenated [2+2]cycloadducts to 2-pyrones in hope that they would serve as useful intermediates in the preparation of monocyclic oxocinones. This paper describes the sensitized photochemical reaction of 4,6-dimethyl- (**1**) and 4-methoxy-6-methyl-2-pyrone (**2**) with chlorinated olefins, and the dehydrochlorination of [2+2]cycloadducts. The previously proposed structures for dehydrochlorinated products[7] are also revised.

Results and Discussion

Photochemical Reactions. A solution of 4,6-dimethyl-2-pyrone (**1**) and 1,1-dichloroethylene (**3a**), trichloroethylene (**3b**), or 2-chloroacrylonitrile (**3c**), in the presence of benzophenone as a sensitizer, in acetonitrile was irradiated, through a Pyrex vessel, with a 400W high-pressure mercury lamp under nitrogen. As expected, [2+2]cycloadducts **4** were obtained in all reactions together with other products, **5**, **6** and/or **7**: Their relative yields greatly depended upon the nature of olefins (Table 1).

The products, **4a—c**, formed in all cases were assigned as regioselective [2+2]cycloadducts, 2-oxabicyclo-[4.2.0]oct-4-en-3-ones, across the C_5–C_6 double bond in **1**, and two isomers, **4c**-1 (major) and **4c**-2 (minor), which were formed in the reaction with **3c**, were deduced to be *endo*- and *exo*-7-cyano derivatives, respectively, on the basis of spectral data. Since two isomers, **4c**-1 and **4c**-2, as well as **4a** and **4b** did not change on treatment with basic alumina, which was used to infer the stereochemistry of ring junctions in photochemical [2+2]cycloadducts,[2,8] all the adducts **4** could be assigned as *cis*-fused. And, it seemed reasonable to assume that the configurations between hydrogens at 6- and 8-positions in all **4** are *cis*, because of showing a large value (2.0 Hz) of long range coupling.[9]

On the basis of comparison of spectral data of similar corresponding compounds,[2] the other products, **5**, **6**, and **7**, were easily assigned as the corresponding 3-oxabicyclo[4.2.0]oct-4-en-2-one, 2-acetonyl-2-methyl-1-cyclobutane carboxylic acids, and *m*-xylene derivatives, respectively (Scheme 1).

The photochemical reaction of 4-methoxy-6-methyl-2-pyrone (**2**) with **3a** under similar conditions gave the corresponding [2+2]cycloadduct **8a**, together with a cyclobutanecarboxylic acid **9a** as the major product. In the reaction with **3b**, **2** gave three products, [2+2]cycloadduct **8b**, cyclobutanecarboxylic acid **9b**, and 2,3-dichloro-5-methoxytoluene (**10b**). The results

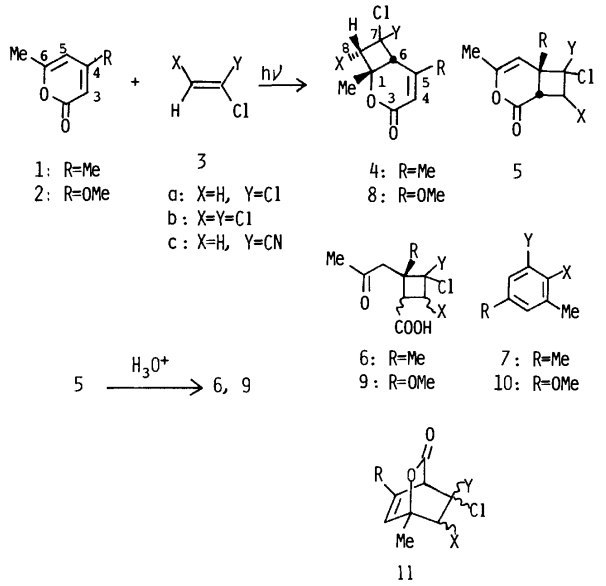

Scheme 1.

Table 1. Photochemical Reaction of 2-Pyrones with Chlorinated Ethylenes[a)]

2-Pyrone	Ethylene	Products (yield/%)
1	**3a**	**4a** (17), **5a** (34)
1	**3b**	**4b** (10), **6b** (5), **7b** (4)
1	**3c**	**4c** (23),[b)] **7c** (13)
2	**3a**	**8a** (16), **9a** (56)
2	**3b**	**8b** (23), **9b** (8), **10b** (17)

a) A solution of 2-pyrone and ethylene was irradiated in the presence of benzophenone. b) Two stereoisomers, **4c**-1 and **4c**-2, were isolated in 17 and 6% yields.

are also given in Table 1.

The [2+2]cycloadducts, **8a** and **8b**, were again assigned as regio- and stereoselective adducts, like **4a** and **4b**, across the C_5–C_6 double bond in **2**, respectively.

The cyclobutanecarboxylic acids, **6** and **9**, correspond to hydrolyzed products of [2+2]cycloadducts **5** across the C_3–C_4 double bonds in **1** and **2**, respectively. In fact, the cycloadduct **5a** (R=Me, X=H, Y=Cl) was quantitatively hydrolyzed to **6a** at room temperature. On the other hand, it is evident that toluene derivatives, **7** and **10** are formed from [4+2]cycloadducts like **11** with the decarboxylation followed by dehydrochlorination (Scheme 1).

Dehydrochlorination of the 2-Oxabicyclo[4.2.0]oct-4-en-3-ones. Dehydrochlorination of the [2+2]cycloadducts, **4** and **8**, with triethylamine in ethanol under reflux afforded three types of dehydrochlorinated products depending upon the nature of substituents on the adducts as well as the reaction conditions.

The reaction of dichloro-substituted adduct **4a** with triethylamine for 30 h afforded a product **14a** with the elimination of two moles of hydrogen chloride, while trichloro- **4b** and monochloro-substituted adduct **4c** (a mixture of two isomers) gave high yields of monodehydrochlorinated products, **13b** and **13c**, under similar conditions for 15 h. Similar treatment of the dichloro-substituted adduct **8a** with triethylamine afforded a mono- **16a** and di-dehydrochlorinated product **17a** depending upon the reaction conditions (Table 2).

Table 2. Dehydrochlorination of [2+2]Cycloadducts

[2+2]Cycloadduct	Conditions[a)] Time/h	Product Yield/%
4a	Et_3N 30	**14a** 41
4b	Et_3N 15	**13b** 97
4c[b)]	Et_3N 15	**13c** 89
8a	Et_3N 2	**16a** 95
8a	Et_3N 38	**17a** 89
8b	Et_3N 1.5	**12b** 82
12b[c)]	100 °C 2	**16b** 80

a) The reactions with Et_3N were carried out in EtOH under reflux. b) A mixture of **4c**-1 and **4c**-2 was used. c) Heated in DMSO.

The spectral data indicated that the products, **13b**, **13c**, **16a**, have similar structures each other. Although we have previously proposed the 2*H*-oxocin-2-one structures (**15**) for the compounds, **13b** and **13c**,[7)] they should be now revised to 5-ethenyl-2-pyrones on the basis of further inspection of spectral data. In addition, **13b** was finally confirmed to be 5-(*trans*-1,2-dichloroethenyl)-4,6-dimethyl-2-pyrone by the X-ray crystallographic analysis.

The di-dehydrochlorinated products, **14a** and **17a**, could be assigned as the corresponding 5-ethynyl-2-pyrones, respectively, on the basis of spectral data, and finally of X-ray crystallographic analysis of **14a**.

The X-ray crystallographic data of **13b** and **14a** will be shown in the next section.

On the other hand, the reaction of trichloro-substituted adduct **8b** with triethylamine for 1.5 h afforded another type of mono-dehydrochlorinated product **12b**, which was easily converted into an isomeric 5-ethenyl-2-pyrone (**16b**) on heating at 100 °C for 2 h (Table 2).

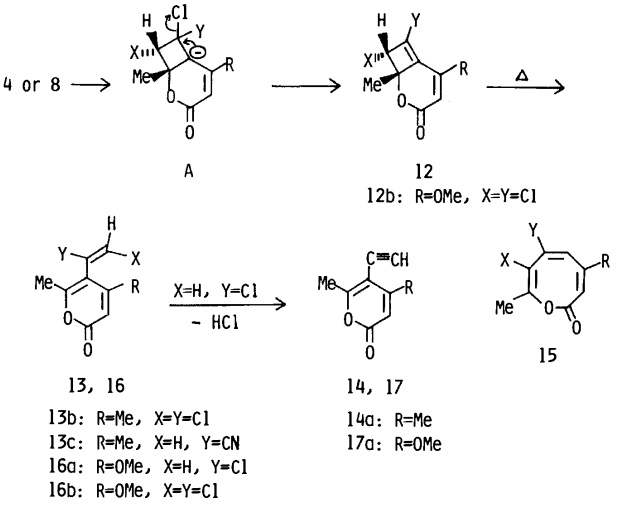

Scheme 2.

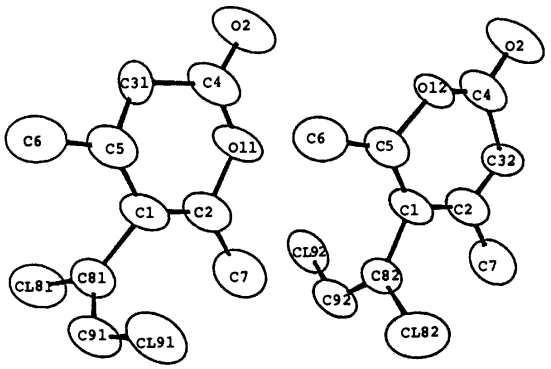

Fig. 1. Two possible molecules, **13b**, at a crystallographically equivalent site.

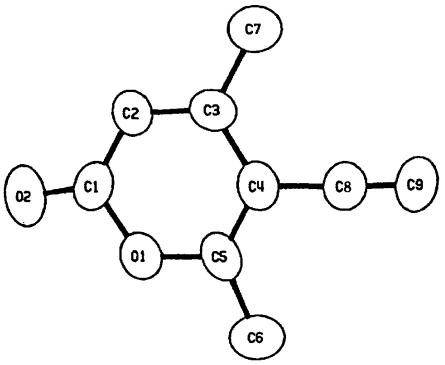

Fig. 2. Molecular structure of **14a**.

On the basis of spectral data the compound **12b** was deduced to be 7,8-dichloro-5-methoxy-1-methyl-2-oxabicyclo[4.2.0]octa-4,6-dien-3-one. Both its IR and ^{1}H NMR spectra are very similar to those of the starting [2+2]cycloadduct **8b**, except for an additional double bond absorption (1580 cm^{-1}) in the IR and a lack of a methine proton at 6-position in the ^{1}H NMR spectra. In the ^{13}C NMR spectrum, **12b** has two additional sp^2 carbons (δ 135.3 and 131.3) assigned to 6-and 7-C, accompanying lacks of sp^3 carbons (δ 53.5 and 85.3) in **8b**.

These dehydrochlorinations are summarized as follows; dichloro-**4a** → **14a**, trichloro-**4b** → **13b**, monochloro-**4c** → **13c**, dichloro-**8a** → **16a** → **17a**, trichloro-**8b** → **12b** → **16b**. The formation of **12b** from **8b** was effective in ethanol solvent, but not in benzene.

On the basis of the above results, the transformation sequence, **4** or **8** → **12** → **13** or **16** → **14** or **17**, can be illustrated as shown in Scheme 2. The elimination of a proton from **4** or **8** with triethylamine occurs at the 6-position but not at the 8-position, and generates an anionic intermediate A which is stabilized by the conjugated enone and by solvation in ethanol. Subsequent elimination of a chloride ion from A gives **12**, which then undergoes a symmetry-allowed ring opening to afford **13** or **16**. Finally, the chlorinated ethenyl-2-pyrones (**13**, **16**) (X=H, Y=Cl) give **14** and **17** by an anti-elimination of hydrogen chloride.

Table 3. Selected Bond Lengths (l/Å) and Angles (ϕ/°) in **13b** (Standard Deviations are in Parentheses)

O2-C4	1.21(7)	C2-O11-C4	129(6)
O11-C2	1.44(4)	C2-C1-C5	121(5)
O11-C4	1.23(6)	O11-C2-C1	113(3)
C1-C2	1.36(9)	O11-C4-C31	116(4)
C1-C5	1.38(9)	C1-C5-C31	129(3)
C1-C81	1.54(2)	C4-C31-C5	113(5)
C5-C31	1.24(6)	CL81-C81-C91	116(2)
C81-C91	1.30(2)	CL91-C91-C81	120(2)
C91-CL91	1.72(3)		
C4-C31	1.64(5)		

Table 4. Selected Bond Lengths (l/Å) and Angles (ϕ/°) in **14a** (Standard Deviations are in Parentheses)

O1-C1	1.395(7)	C1-O1-C5	122.4(5)
C1-O2	1.219(7)	O1-C1-C2	116.7(5)
C1-C2	1.403(9)	O2-C1-C2	128.2(7)
C2-C3	1.355(8)	C1-C2-C3	122.3(6)
C3-C7	1.498(9)	C2-C3-C4	118.3(6)
C3-C4	1.434(9)	C2-C3-C7	121.0(6)
C4-C5	1.347(9)	C3-C4-C5	120.5(6)
C4-C8	1.447(9)	C3-C4-C8	119.7(6)
C5-O1	1.370(7)	O1-C5-C4	119.7(6)
C5-C6	1.477(9)	C4-C5-C6	127.6(6)
C8-C9	1.185(8)	C4-C8-C9	178.5(8)

Table 5. Selected Tortional Angles (ϕ/°) in **13b**

C2-C1-C5-C31	1.9
C1-C81-C91-CL91	4.1
C2-C1-C81-C91	94.4
C2-C1-C5-C6	−179.0
C5-C1-C2-C7	−178.6
CL81-C81-C91-CL91	−178.7

X-Ray Crystal Structures of 5-Ethenyl- (13b) and 5-Ethynyl-2-pyrone (14a). The molecular structures of **13b** and **14a** are illustrated in Figs. 1 and 2, respectively. Bond lengths and angles for **13b** and **14a** are also listed in Tables 3 and 4, respectively.

The compound **13b** has some interesting and unusual features in its molecular geometry. The length of the bond C_1-C_{81} (1.54 Å) is fairly longer than that for a normal conjugated single bond (ca. 1.47 Å), while the double bond C_{81}-C_{91} is fairly short (1.30 Å) (Table 3). As shown in Fig. 1, the sp^2 face of the dichloroethenyl group (C_{81}-C_{91}-CL_{91}) is distorted against the 2-pyrone face (torsional angle of C_2-C_1-C_{81}-C_{91}=94.4°) (Table 5). The characteristic geometry can be easily explained on the basis of the steric repulsion between the 5-(1,2-dichloroethenyl) group and 4,6-dimethyl groups.

Experimental

General and Materials. All melting points were uncorrected. UV spectra were recorded on a Hitachi EPS-3 spectrometer and IR spectra were determined with JASCO A-3 spectrometer. ^{1}H and ^{13}C NMR spectra were measured for $CDCl_3$ solutions on a JEOL JNM-MH-100 (100 MHz) and JEOL FX-100 (25 MHz) spectrometers using TMS as the internal reference. Mass spectra were measured with a JEOL

JMS-0lSG spectrometer. The X-ray diffraction data were obtained on an Enraf-Nonius CAD-4 automated four-circle diffractometer with a SDP program package. All the photoaddition and synthetic application reactions were monitored by the use of GC, which was performed at 170 °C (column temp) on a Yanagimoto G80 instrument using a column of Silicone SE-30 (10%)/Chromosorb W (AW). Wakogel C200 was used for preparative column chromatography.

4,6-Dimethyl-2-pyrone (**1**)[10] and 4-methoxy-6-methyl-2-pyrone (**2**)[11] were prepared according to methods previously descrived in the literature.

Photoreaction of 1 with 3a. A solution of **1** (3.0 g, 24 mmol), **3a** (23 ml, 240 mmol), and benzophenone (0.5 g, 2.7 mmol) as a sensitizer in 200 ml of acetonitrile under nitrogen atmosphere was irradiated with a Riko immersion-type 400W high-pressure mercury lamp through a Pyrex vessel at 0—5 °C for 2.5 h. The solvent was removed by the use of a rotary evaporator. The residue was chromatographed on a silica-gel column with benzene-acetone (40 : 1) gave 1.81 g (34%) of **5a** (R=Me, X=H, Y=Cl), and with (20 : 1) gave 0.90 g (17%) of **4a**. Adding one drop of water to 11 mg of **5a** and left 10d at room temperature to give 12 mg (100%) of **6a**. Compound **5a** was detected by GC analysis at 1.8 min when **4a** was at 2.6 min.

4a: Colorless oil; IR (neat) 1720 cm^{-1}; ^1H NMR ($CDCl_3$) δ=1.62 (3H, s, Me), 2.06 (3H, br. s, Me), 3.24 (1H, dd, J_{gem}=16.0, $J_{8,6}$=2.0 Hz, 8-*exo*-H), 3.40 (1H, d, J_{gem}=16.0 Hz, 8-*endo*-H), 3.62 (1H, br. s, 6-H), 6.14 (1H, br. s, 4-H); MS *m/z* (220 M^+, 0.3%), 105 (base peak).

Found: C, 49.34; H, 4.56%. Calcd for $C_9H_{10}O_2Cl_2$: C, 48.90; H, 4.56%.

5a: Colorless plates from hexane; mp 78—79 °C; IR (KBr) 1765 cm^{-1}; ^1H NMR ($CDCl_3$) δ=1.43, 2.04 (each 3H, s, Me), 3.22 (3H, m, 1-H, 8-CH_2), 5.12 (1H, br. s, 5-H); MS *m/z* 220 (M^+, 2%), 82 (base peak).

Found: C, 48.80; H, 4.56%. Calcd for $C_9H_{10}O_2Cl_2$: C, 48.89; H, 4.53%.

6a: Colorless solid from acetone; mp 115—116 °C; IR (KBr) 1720, 1700 cm^{-1}; ^1H NMR ($CDCl_3$) δ=1.58, 2.15 (each 3H, s, Me), 2.82, 3.10 (each 1H, d, J_{gem}=18.5 Hz, 5-CH_2), 3.08—3.3 (2H, m, 1-, 4-H), 10.20 (1H, br. s, COOH); MS *m/z* 238 (M^+, 0.3%), 82 (base peack).

Found: C, 45.39; H, 5.08%. Calcd for $C_9H_{12}O_3Cl_2$: C, 45.21; H, 5.06%.

Photoreaction of 1 with 3b. A solution of **1** (5.0 g, 40 mmol), **3b** (28 ml, 310 mmol), and benzophenone (1.6 g, 9 mmol) in 200 ml of acetonitrile was irradiated for 28 h. The solvent was then removed to give 1.0 g (10%) of **4b**. The residue was chromatographed with benzene to afford 0.11 g (4%) of 4,5-dichloro-*m*-xylene (**7b**). The continued elution with benzene-acetone (5 : 1) gave 0.51 g (5%) of **6b**.

4b: Colorless needles from benzene; mp 192—193 °C; IR (KBr) 1722 cm^{-1}; ^1H NMR ($CDCl_3$) δ=1.55 (3H, s, Me), 2.03 (3H, d, Me), 3.48 (1H, d, $J_{6,8}$=2.0 Hz, 6-H), 4.76 (1H, d, $J_{8,6}$=2.0 Hz, 8-H), 6.00 (1H, br. s, 4-H); MS *m/z* 219 (M-Cl, 6%), 124 (base peak).

Found: C, 42.27; H, 3.52%. Calcd for $C_9H_9O_2Cl_3$: C, 42.30; H, 3.57%.

6b: Colorless needles from benzene-acetone (5 : 1); mp 132—135 °C; IR (KBr) 1738, 1698 cm^{-1}; ^1H NMR ($CDCl_3$) δ=1.60, 2.16 (each 3H, s, Me), 2.82, 3.14 (each 1H, d, J_{gem}=19.0 Hz, CH_2), 3.02 (1H, d, $J_{1,4}$=10.0 Hz, 1-H), 4.90 (1H, d, $J_{4,1}$=10.0 Hz, 4-H), 10.0 (1H, br. s, COOH); MS *m/z* 272 (M^+, 0.1%), 148 (base peak).

Found: C, 39.76; H, 4.13%. Calcd for $C_9H_{11}O_3Cl_3$: C, 39.53; H, 4.03%.

Photoreaction of 1 with 3c. A solution of **1** (3.0 g, 24 mmol), **3c** (9.5 ml, 120 mmol), and benzophenone (0.5 g, 2.7 mmol) in 200 ml of acetonitrile was irradiated for 1.5 h and the solvent was then removed. The chromatography of the residue with benzene gave 0.41 g (13%) of 3,5-dimethylbenzonitrile (**7c**). The continued elution with benzene-acetone (10 : 1) afforded 1.16 g of a mixture between **4c**-1 (17%) and **4c**-2 (6%), from which both of them were isolated by repeated chromatography.

4c-1: Colorless plates from diethyl ether; mp 100—102 °C; IR (KBr) 2250, 1720 cm^{-1}; ^1H NMR ($CDCl_3$) δ=1.64 (3H, s, Me), 2.10 (3H, br. s, Me), 2.92 (1H, dd, J_{gem}=14.0, $J_{8,6}$=2.0 Hz, 8-*exo*-H), 3.36 (1H, d, J_{gem}=14.0 Hz, 8-*endo*-H), 3.36 (1H, br.s, 6-H), 6.12 (1H, br.s, 4-H); MS *m/z* 212 (M^++1, 11%), 96 (base peak).

Found: C, 56.76; H, 4.88; N, 6.65%. Calcd for $C_{10}H_{10}NO_2Cl$: C, 56.75; H, 4.76; N, 6.62%.

4c-2: Colorless plates from diethyl ether; mp 110—113 °C; IR (KBr) 2250, 1720 cm^{-1}; ^1H NMR ($CDCl_3$) δ=1.64 (3H, s, Me), 2.05 (3H, br. s, Me), 3.10 (1H, d, J_{gem}=14.0 Hz, 8-*endo*-H), 3.30 (1H, dd, J_{gem}=14.0, $J_{8,6}$=2.0 Hz, 8-*exo*-H), 3.68 (1H, br. s, 6-H), 6.35 (1H, br. s, 4-H); MS *m/z* 212 (M^++1, 3%), 96 (base peak).

Found: C, 56.69; H, 4.78; N, 6.48%. Calcd for $C_{10}H_{10}NO_2Cl$: C, 56.75; H, 4.76; N, 6.62%.

Photoreaction of 2 with 3a. A solution of **2** (7.0 g, 50 mmol), **3a** (48 ml, 500 mmol), benzophenone (1.0 g, 5.4 mmol), and acetonitrile (500 ml) was irradiated at 0—5 °C for 4 h, the same work-up as mentioned above to give 7.2 g (56%) of **9a** from concentration and 1.7 g (16%) of **8a** from column chromatography with benzene-acetone (10 : 1). The precursor of **9a** was detected by GC analysis at 3.0 min when **8a** was at 5.5 min.

8a: Colorless leaflets from acetone-hexane (1 : 3); mp 98—99 °C; IR (KBr) 1700 cm^{-1}; ^1H NMR ($CDCl_3$) δ=1.66 (3H, s, Me), 3.20 (1H, dd, J_{gem}=15.0, $J_{8,6}$=2.0 Hz, 8-*exo*-H), 3.36 (1H, d, J_{gem}=15.0 Hz, 8-*endo*-H), 3.68 (1H, d, $J_{6,8}$=2.0 Hz, 6-H), 3.80 (3H, s, OMe), 5.36 (1H, s, 4-H); MS *m/z* 236 (M^+, 2%), 112 (base peak).

Found: C, 45.63; H, 4.22%. Calcd for $C_9H_{10}O_3Cl_2$: C, 45.60; H, 4.25%.

9a: Colorless prisms from acetone; mp 121—122 °C; IR (KBr) 1730, 1705 cm^{-1}; ^1H NMR ($CDCl_3$) δ=2.18 (3H, s, Me), 2.76 (2H, d, $J_{4,1}$=8.5 Hz, 4-CH_2), 3.19 (2H, s, 5-CH_2), 3.40 (3H, s, OMe), 3.44 (1H, t, $J_{1,4}$=8.5 Hz, 1-H), 10.5 (1H, br. s, COOH); MS *m/z* 237 (M−H_2O+1, 0.2%), 98 (base peak).

Found: C, 42.39; H, 4.76%. Calcd for $C_9H_{12}O_4Cl_2$: C, 42.54; H, 4.74%.

Photoreaction of 2 with 3b. A solution of **2** (5.1 g, 36 mmol), **3b** (38 ml, 430 mmol), benzophenone (2.0 g, 11 mmol), and acetonitrile (450 ml) was irradiated for 10 h and then removed the solvent to afford 2.3 g (23%) of **8b**. The column chromatography of the filtrate with benzene gave 1.2 g (17%) of 2,3-dichloro-5-methoxytoluene (**10b**) and with benzene-acetone (1 : 1) gave 0.9 g (8%) of **9b**. The precursor of **9b** was detected by GC analysis at 2.1 min when **8b** was at 11.0 min.

8b: Colorless plates from diethyl ether-hexane (2 : 1); mp 210—212 °C; IR (KBr) 1715 cm^{-1}; ^1H NMR ($CDCl_3$) δ=1.60

(3H, s, Me), 3.26 (1H, d, $J_{6,8}$=2.0 Hz, 6-H), 3.81 (3H, s, OMe), 4.77 (1H, d, $J_{8,6}$=2.0 Hz, 8-*exo*-H), 5.35 (1H, s, 4-H); MS *m/z* 270 (M^+, 0.2%), 112 (base peak).

Found: C, 39.87; H, 3.33%. Calcd for $C_9H_9O_3Cl_3$: C, 39.81; H, 3.34%.

9b: Colorless plates from chloroform-hexane (1 : 1); mp 156—157 °C; IR (KBr) 1720, 1710 cm^{-1}; ^1H NMR ($CDCl_3$) δ=2.24 (3H, s, Me), 3.12, 3.40 (each 1H, d, J_{gem}=19.0 Hz, CH_2), 3.42 (1H, d, $J_{4,1}$=10.0 Hz, 4-H), 3.43 (3H, s, OMe), 4.61 (1H, d, $J_{1,4}$=10.0 Hz, 1-H), 8.14 (1H, br.s, COOH); MS *m/z* 273 ($M-H_2O+1$, 0.1%), 98 (base peak).

Found: C, 37.33; H, 3.83%. Calcd for $C_9H_{11}O_4Cl_3$: C, 37.50; H, 3.80%.

Dehydrochlorination of 4a. A mixture of **4a** (0.28 g, 1.3 mmol), triethylamine (0.6 ml, 4.4 mmol), and ethanol (5 ml) was refluxed for 30 h. After concentration the residue was extracted with benzene to give 0.08 g (41%) of **14a**.

14a: Colorless prisms from chloroform; mp 139—140 °C; UV (MeOH) 309 (ε 3000), 245 nm (5000); IR (KBr) 3260, 2250, 1744 cm^{-1}; ^1H NMR ($CDCl_3$) δ=2.24, 2.44 (each 3H, s, Me), 3.40 (1H, s, 8-H), 6.04 (1H, s, 3-H); ^{13}C NMR ($CDCl_3$) δ=19.2, 20.9 (each q, Me), 75.9 (s, 7-C), 85.3 (d, 8-C), 102.6 (s, 5-C), 110.7 (d, 3-C), 156.3 (s, 4-C), 160.6 (s, 2-C), 166.8 (s, 6-C); MS *m/z* 148 (M^+, 87%), 120 (base peak).

Found: C, 73.04; H, 5.58%. Calcd for $C_9H_8O_2$: C, 72.99; H, 5.44%.

Dehydrochlorination of 4b. A mixture of **4b** (0.26 g, 1.0 mmol), triethylamine (0.2 ml, 1.5 mmol), and ethanol (5 ml) was refluxed for 15 h. After concentration the residue was extracted with diethyl ether to give 0.21 g (97%) of **13b**.

13b: Colorless prisms from hexane; mp 130—132 °C; UV (MeOH) 296 (ε 5930), 237 nm (6040); IR (KBr) 1720 cm^{-1}; ^1H NMR ($CDCl_3$) δ=2.13 (3H, d, Me), 2.25 (3H, s, Me), 6.05 (1H, br. s, 3-H), 6.60 (1H, s, 8-H); ^{13}C NMR ($CDCl_3$) δ=17.9, 19.3 (each q, Me), 111.5 (d, 3-C), 113.5 (s, 5-C), 120.8 (d, 8-C), 127.3 (s, 7-C), 154.5 (s, 4-C), 161.1, 161.2 (each s, 2-, 6-C); MS *m/z* 218 (M^+, 29%), 43 (base peak).

Found: C, 49.46; H, 3.67%. Calcd for $C_9H_8O_2Cl_2$: C, 49.32; H, 3.65%.

Dehydrochlorination of 4c. A mixture of **4c**-1 and **4c**-2 (4 : 1 mix. 0.32 g, 1.5 mmol), triethylamine (0.4 ml, 3.0 mmol), and ethanol (5 ml) was refluxed for 15 h. After concentration the residue was column chromatographed using benzene to afford 0.23 g (89%) of **13c**.

13c: White crystal; mp 63—64 °C; UV (MeOH) 296 (ε 7200), 214 nm (7700); IR (KBr) 2250, 1740, 1720 cm^{-1}; ^1H NMR ($CDCl_3$) δ=2.20, 2.30 (each 3H, s, Me), 5.96, 6.42 (each 1H, $=CH_2$), 6.06 (1H, br. s, 3-H), ^{13}C NMR ($CDCl_3$) δ=18.4, 20.3 (each q, Me), 111.8 (d, 3-C), 113.1, 116.1 (each s, 5-, 7-C), 116.8 (s, CN), 138.3 (t, 8-C), 154.4 (s, 4-, 6-C), 160.7 (s, 2-C); MS *m/z* 175 (M^+, 44%), 147 (base peak).

Found: C, 68.42; H, 5.19; N, 8.00%. Calcd for $C_{10}H_9NO_2$: C, 68.56; H, 5.17; N, 8.00%.

Dehydrochlorination of 8a. The refluxing of a mixture of **8a** (0.5 g, 2.1 mmol) and triethylamine (0.9 ml, 6.3 mmol) in 10 ml of ethanol for 2 h, followed by extraction with diethyl ether to give 0.4 g (95%) of **16a**. On the other hand, a mixture of **8a** (0.28 g, 1.2 mmol), triethylamine (0.8 ml, 6.0 mmol), and ethanol (5 ml) was refluxed for 38 h, and the same work-up as mentioned above afforded 0.17 g (89%) of **17a**.

16a: Colorless prisms from chloroform; mp 110—112 °C; UV (MeOH) 283 (ε 6500), 228 nm (8000); IR (KBr) 1720 cm^{-1}; ^1H NMR ($CDCl_3$) δ=2.28 (3H, s, Me), 3.84 (3H, s, OMe), 5.40, 5.74 (each 1H, d, J_{gem}=1.5 Hz, $=CH_2$), 5.46 (1H, s, 3-H); ^{13}C NMR ($CDCl_3$) δ=17.9, 56.4 (each q, Me), 87.5 (d, 3-C), 112.7 (s, 5-C), 121.1 (t, 8-C), 130.7 (s, 7-C), 161.2 (s, 2-C), 163.1 (s, 6-C), 168.7 (s, 4-C); MS *m/z* 200 (M^+, 84%), 165 (base peak).

Found: C, 53.94; H, 4.54%. Calcd for $C_9H_9O_3Cl$: C, 53.88; H, 4.52%.

17a: Colorless needles from chloroform-diethyl ether (1 : 1); mp 140—141 °C; UV (MeOH) 290 (ε 4300), 240 nm (7900); IR (KBr) 3300, 1745, 1723 cm^{-1}; ^1H NMR ($CDCl_3$) δ=2.42 (3H, s, Me), 3.37 (1H, s, 8-H), 3.87 (3H, s, OMe), 5.44 (1H, s, 3-H); ^{13}C NMR ($CDCl_3$) δ=19.2, 56.6 (each q, Me), 73.5 (s, 7-C), 85.3 (d, 8-C), 87.2 (d, 3-C), 97.7 (s, 5-C), 162.3 (s, 2-C), 167.9 (s, 6-C), 169.3 (s, 4-C); MS *m/z* 164 (M^+, base peak).

Found: C, 65.79; H, 4.93%. Calcd for $C_9H_8O_3$: C, 65.85; H, 4.91%.

Dehydrochlorination of 8b. The refluxing of a mixture of **8b** (0.82 g, 3.0 mmol) and triethylamine (1.6 ml, 12 mmol) in 30 ml of ethanol for 1.5 h and washing the residue with water to give the water-insoluble product **12b** (0.58 g, 82%). A solution of **12b** (15 mg, 0.06 mmol) in 0.3 ml of DMSO-d_6 was heated in the NMR sample tube at 100 °C for 2 h to give 11 mg (80%) of **16b**.

12b: Colorless prisms from chloroform; mp 124—126 °C; UV (MeOH) 281 nm (ε 2100); IR (KBr) 1720, 1670, 1580 cm^{-1}; ^1H NMR ($CDCl_3$) δ=1.61 (3H, s, Me), 3.81 (3H, s, OMe), 4.80 (1H, s, 8-H), 5.28 (1H, s, 4-H); ^{13}C NMR ($CDCl_3$) δ=21.7, 56.6 (each q, Me), 67.3 (d, 8-C), 78.3 (s, 1-C), 96.1 (d, 4-C), 131.3, 135.3 (each s, 6-, 7-C), 159.2 (s, 3-C), 164.6 (s, 5-C); MS *m/z* 234 (M^+, 2%), 199 (base peak).

Found: C, 46.07; H, 3.42%. Calcd for $C_9H_8O_3Cl_2$: C, 45.99; H, 3.43%.

16b: Colorless prisms from diethyl ether-hexane (2 : 1); mp 124—127 °C; UV (MeOH) 284 (ε 3020), 228 nm (6200); IR (KBr) 1710 cm^{-1}; ^1H NMR ($CDCl_3$) δ=2.24 (3H, s, Me), 3.84 (3H, s, OMe), 5.48 (1H, s, 3-H), 6.57 (1H, s, 8-H); ^{13}C NMR ($CDCl_3$) δ=18.6, 56.5 (each q, Me), 87.7 (d, 3-C), 107.5 (s, 5-C), 120.1 (d, 8-C), 126.4 (s, 7-C), 160.5 (s, 2-C), 163.7 (s, 6-C), 169.5 (s, 4-C); MS *m/z* 234 (M^+, 16%), 199 (base peak).

Found: C, 46.08; H, 3.42%. Calcd for $C_9H_8O_3Cl_2$: C, 45.99; H, 3.43%.

X-Ray Analyses of Compounds 13b and 14a. Compounds **13b** and **14a** were recrystallized from diethyl ether-hexane (1 : 1) and diethyl ether solutions as colorless prisms, respectively. Crystal size: **13b** 0.56×0.35×0.42 mm^3, **14a** 0.56×0.35×0.21 mm^3. All data sets were measured by the ω—2θ scan method on a CAD4 diffractometer with graphite monochromated Mo $K\alpha$ radiation (λ=0.71073 Å). SDP Program package[12] with the tables of atomic scattering factors[13] was used.

13b: Triclinic, space group $P\bar{1}$, a=7.405(4) Å, b=7.408 (4) Å, c=10.133(3) Å, α=71.44(7)°, β=71.44(7)°, γ=81.36(7)°, V=498.8(4) $Å^3$, d (calcd)=1.458 g cm^{-3} for z=2, μ (Mo $K\alpha$)= 11.90 cm^{-1}; 2911 unique reflections, solution by direct method (MULTAN 82),[14] and refined by least-squares method with full matrix, R=0.050, R_w=0.050, unit weights, for 172 variables and 1308 reflections with $I \geq 3.0 \times \sigma$ (I). All non-H atoms anisotropic with H atoms isotropic.

14a: Monoclinic, space group $P2_1/n$, a=9.854(12) Å, b=11.444(1) Å, c=20.439(2) Å, β=85.14(5)°, V=2297(3) $Å^3$, d (calcd)=1.285 g cm^{-3} for Z=4 (12 molecules), μ (Mo $K\alpha$)=0.846

cm^{-1}; 4158 unique reflections, solution by direct method (MULTAN 82),[14] and refined by least-squares method with full matrix, R=0.106, R_w=0.106, unit weights, for 298 variables and 2076 reflections with $I \geq 3.0 \times \sigma(I)$. All non-H atoms anisotropic with H atoms isotropic. The unsymmetric unit consists of three identical molecules of **14a**. Crystal data, positional and thermal parameters, bond distances and angles as well as ORTEP drawings[15] and structure factors for compounds **13b** and **14a** are kept in the office of the Chemical Society of Japan (Document No. 8721).

The authors appreciate to the Research Center for Material Analysis in Miyazaki University for the X-ray crystallographic analysis.

References

1) N. P. Shusherina, *Russ. Chem. Rev.*, **43**, 851 (1974).
2) T. Shimo, K. Somekawa, and S. Kumamoto, *Nippon Kagaku Kaishi*, **1983**, 394.
3) T. Shimo, K. Somekawa, M. Sato, and S. Kumamoto, *Nippon Kagaku Kaishi*, **1984**, 1927.
4) R. D. Rieke and R. A. Copenhafer, *Tetrahedron Lett.*, **1971**, 879.
5) J. W. Hanifin and E. Cohen, *J. Org. Chem.*, **33**, 2811 (1968).
6) J. W. Hanifin and E. Cohen, *J. Org. Chem.*, **36**, 910 (1971).
7) T. Shimo, K. Somekawa, J. Kuwakino, H. Uemura, S. Kumamoto, O. Tsuge, and S. Kanemasa, *Chem. Lett.*, **1984**, 1503.
8) P. J. Nelson, D. Ostrem, J. D. Lassila, and O. L. Chapman, *J. Org. Chem.*, **34**, 811 (1969).
9) I. Fleming and D. H. Williams, *Tetrahedron*, **23**, 2747 (1967).
10) N. R. Smith and R. H. Wiley, *Org. Synth.*, Coll. Vol. IV, 337 (1963).
11) J. D. Bu'Lock and H. G. Smith, *J. Org. Chem.*, **1960**, 502.
12) B. A. Frenz and Enraf-Nonius, SDP, Structure Determination Package (1982).
13) D. T. Cromer and J. T. Waber, "International Tables for Crystallography," Kynoch Press, Birmingham (1974), Vol. IV.
14 P. Main, *MULTAN* 11/82 (1982).
15) C. K. Johnson, "ORTEP, a Fortran Thermal-Ellipsoid Plot Program for Crystal Structure Illustrations," 3rd ed., Oak Ridge National Lab., ORNL-5138 (1976).

Methylation of Alcohols and Phenols Adsorbed on Silica Gel with Diazomethane

Haruo OGAWA, Toshikazu HAGIWARA, Teiji CHIHARA,† Shousuke TERATANI,* and Kazuo TAYA
Department of Chemistry, Tokyo Gakugei University, Koganei, Tokyo 184
†The Institute of Physical and Chemical Research, Wako, Saitama 351-01
(Received June 23, 1986)

Alcohols and phenols adsorbed on silica gel react with diazomethane and quantitatively afford the corresponding methyl ethers. Alumina and titanium dioxide are also effective adsorbents for the reaction.

Carboxylic acids are easily *O*-methylated with diazomethane to give the corresponding esters. Alcohols, however, do not react with diazomethane because of their weak acidity. The methylation of alcohols with diazomethane requires a Lewis acid catalyst such as boron trifluoride,[1] tetrafluoroboric acid,[2] zinc chloride[3] and aluminum chloride[4] in solution. Mineral acids are not suitable for the catalyst because they react with the reagent. Recently, silica gel suspended in ether was found to be effective for the methylation of unstable alcohols with diazomethane.[5] However, these types of catalysts are not always effective for a complete methylation of alcohols.

The use of solid adsorbents as a reaction medium is becoming increasingly widespread in organic syntheses[6] involving oxidation,[7] alkylation,[8] and condensation.[9] We have successfully utilized solid adsorbents in the acetylation of alcohols and phenols by ketene,[10] and a selective monomethyl esterification of dicarboxylic acids by diazomethane[11] or by dimethyl sulfate.[12] The advantages of solid adsorbents are simpler work-ups, milder reaction conditions and higher selectivities.

Recent spectroscopic studies[13] have proved that alcohols are chemisorbed on alumina or silica as alkoxides or a species in which O–H bonds are strongly polarized. These facts persuaded us to use these oxides as a reaction medium as well as the catalyst for the methylation of alcohols with diazomethane. We report here that gaseous diazomethane easily reacts with alcohols and phenols adsorbed on oxides to quantitatively give the corresponding methyl ethers.

Results and Discussion

Methylation of 1-Decanol. 1-Decanol, which had been adsorbed on silica gel, was treated with gaseous diazomethane. The reaction profile of the methylation of 1-decanol is shown in Fig. 1. 1-Decanol was methylated in proportion to the amounts of diazomethane introduced, and 1-methoxydecane was quantitatively obtained when about 20 molar equivalents of diazomethane were used.

In the absence of silica gel, 1-decanol in ether was hardly methylated even by the addition of 200 molar equivalents of diazomethane. Clearly, silica gel is essential for this reaction.

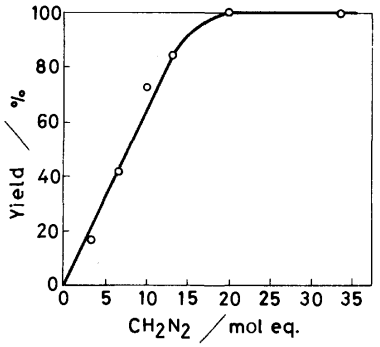

Fig. 1. Reaction profile of methylation of 1-decanol on silica gel.

Table 1. Methylation of Alcohols and Phenols on Silica Gel[a]

Substrate	CH_2N_2/mol equiv	Yield/%[b]
1-Decanol	34	99
1-Decanol[c]	159	83
1-Decanol[d]	200	< 1
Geraniol	34	96
Benzyl alcohol	34	99
1-Methyl-1-hexanol	68	99
Cyclohexanol	68	99
2-Methyl-2-hexanol	68	99
2-Methyl-2-butanol	68	99
Phenol	34	99
2-*t*-Butylphenol	34	93
2,6-Diisopropylphenol	34	79
2,6-di-t-Butylphenol	68	< 1
1-Naphthol	34	98
2-Naphthol	34	93

a) To a 1.0 g of silica gel 0.32 mmol of alcohol or phenol was added. b) Determined by GLC and/or HPLC. c) Silica gel suspended in ether. d) In an ether solution in the absence of silica gel.

Methylation of Alcohols and Phenols. Various kinds of alcohols and phenols were tested; the results are summarized in Table 1. As well as primary and secondary alcohols and phenol, tertiary alcohols and hindered phenols were quantitatively methylated. Geraniol, which holds two olefinic double bonds, was also methylated in a high yield with the bonds intact. However, 2,6-di-*t*-butylphenol was not methylated, even with 300 molar equivalents of diazomethane. On the basis of molecular models, 2,6-di-*t*-butylphenol could not be adsorbed on the silica gel surface with the hydroxyl group on account of a steric hindrance

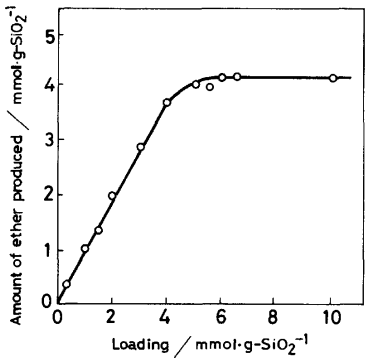

Fig. 2. Formation of 1-methoxydecane from the different amount of 1-decanol adsorbed on silica gel. The reaction was carried out with 34 molar equivalents of diazomethane.

involving the two *t*-butyl groups. These results suggest that the methylation requires the adsorption of hydroxyl group on the oxide.

While using silica gel suspended in ether, 1-decanol could not be quantitatively methylated and the product, 1-methoxydecane, was obtained in an 83% yield with a large excess of diazomethane (159 molar equivalents). Ohno et al.[5] reported that the maximum values of conversion for some alcohols such as geraniol, benzyl alcohol, and 2-methyl-2-butanol were no more than 25—54%. These less reactive alcohols could be exhaustively methylated by using our method.

Effect of Surface Coverage on Methylation. Adsorbed samples of 1-decanol with various amounts of loading were prepared and treated with diazomethane. As shown in Fig. 2, the amount of produced 1-methoxydecane was proportional to the amount of loading. Beyond the value of 4.0 mmol g^{-1}-SiO_2, however, the amount of 1-methoxydecane did not increase even upon the addition of large excess amounts of diazomethane.

The limiting value of loading (4.0 mmol g^{-1}-SiO_2) appears to be the saturation amount of 1-decanol on the silica gel surface. The surface area of the silica gel used was found to be 371 $m^2 g^{-1}$ by a BET measurement. Thus, one molecule of 1-decanol occupies 0.15 nm^2 on the silica gel surface. The critical cross section for aliphatic alcohols determined from their monomolecular layers spread over a flat surface of water is 0.216 nm^2.[14] The agreement between these two cross-sectional values implies that 1-decanol molecules are adsorbed as a monomolecular layer on silica gel. The methylation seems to occur on the silica gel surface by a reaction of diazomethane with the 1-decanol adsorbed as the monomolecular layer.

Effective Adsorbents. Various kinds of solid adsorbents were tested in the methylation of 1-decanol. A small amount of diazomethane was introduced into the reaction vessel in order to estimate the effectiveness of each adsorbent. Table 2 shows that the yields of 1-methoxydecane decreased in the following order:

Table 2. Effect of Adsorbent[a]

Adsorbent[b]	Yield/%[c]	Relative value
SiO_2	41.4	1
Al_2O_3	11.5	0.28
TiO_2	6.5	0.16
Zeolite(Na-Y type)	2.1	0.05
SiO_2–Al_2O_3[d]	2.0	0.05
Celite 545	1.3	0.03
ZnO	0.4	0.01
MgO	0.0	0.00
Non	0.0[e]	0.00

a) To a 1.0 g of adsorbent 0.32 mmol of 1-decanol was added. b) Dried at 110°C for one hour in a stream of N_2 before adsorption of 1-decanol. c) Yield of 1-methoxydecane, when 6.8 molar equivalents of diazomethane was introduced at room temperature. d) 28.6% Al_2O_3. e) In an ethyl ether solution in the absence of any additives.

$$SiO_2 > Al_2O_3 > TiO_2.$$

A sufficient amount of diazomethane resulted in a complete conversion on Al_2O_3 and/or TiO_2. On zeolite, silica-alumina, Celite 545, and zinc oxide the methylation occurred slightly. Magnesium oxide did not cause a reaction.

IR and inelastic electron tunneling spectroscopy clearly showed that surface-bound alkoxides or strongly polarized O–H bonds were formed when alcohols were introduced to silica or alumina.[13] The chemisorption of alcohol on the oxides undoubtedly facilitates a dissociation of protons from the hydroxyl group. It has been reported that methylation of alcohols is initiated by the portonation of diazomethane with the aid of a Lewis acid.[4] Probably, the protonation of diazomethane occurs on the oxides by accepting protons released from the adsorbed alcohol and the protonated diazomethane attacks the resulting alkoxide to form the methyl ether.

Experimental

Materials. A modified method was adopted for the preparation of diazomethane from *N*-methyl-*N*-nitroso-*p*-toluenesulfonamide.[15] Diazomethane is toxic and potentially explosive. All the operations were performed in a well ventilated hood and behind a safety screen. The following preparation of diazomethane is illustrative. In a 25 ml distillation flask, 2 g of potassium hydroxide, 3.2 ml of water and 11 ml of diethylene glycol dimethyl ether were placed. A stream of dry nitrogen (10 ml min^{-1}) was passed through the flask and led to a drying tube containing potassium hydroxide pellets. The flask was kept at 30°C and 6.88 g (31 mmol) of *N*-methyl-*N*-nitroso-*p*-toluenesulfonamide was added by small portions over 20 min. Nitrogen was passed for an additional 30 min in order to carry the diazomethane thoroughly into the reaction vessel for methylation. The total amount of dry diazomethane was measured to be 22 mmol (70% yield) by a GLC analysis instead of titration.[16] The amount of diazomethane was controlled by the amount of *N*-methyl-*N*-nitroso-*p*-toluenesulfonamide used.

Silica gel (Wako Chemicals; 200 mesh, for column chro-

matographic use), alumina (the reference catalyst of the Catalysis Society of Japan (JRC-ALO-5; 60—200 mesh) and titanium dioxide (JRC-TIO-1; powder), zeolite (JRC-Z-Y4.8; powder, Na-Y type), silica-alumina (JRC-SAH-1; powder, 38% alumina), Celite 545 (Johns-Manville), zinc oxide (Kokusan Chemicals), and Magnesium oxide (Kamishima Chemicals) were used. These solids were dried at 110 °C for a day and stored in a desiccator.

Other materials were commercial products and were used without further purification.

Reaction Procedure. Typically, 51 mg (0.32 mmol) of 1-decanol was added into a reaction vessel of a glass column (15-mm i.d.) containing 1.0 g of silica-gel powders. The reaction vessel was allowed to stand for a day, although lumps of silica gel usually disappeared within an hour. Then, a calculated amount of diazomethane was introduced into the reaction vessel in a stream of nitrogen at room temperature. After passage of the diazomethane through the vessel, the adsorbate was immediately eluted with ethyl acetate. The eluate was condensed and the product was analyzed by GLC and/or HPLC. 1-Methoxydecane was obtained in a 99% yield and no reaction other than methylation was observed.

The amount of diazomethane necessary for a complete methylation of 1-decanol could be reduced by the following method. The 3 molar equivalents of diazomethane were introduced into a reaction vessel maintained at −78 °C. The color of the silica gel near the entrance end of the reaction vessel changed to yellow. The vessel, sealed with septum, was allowed to stand for 12 h at room temperature to ensure a complete conversion.

References

1) M. Neeman and Y. Hashimoto, *J. Am. Chem. Soc.*, **84**, 2972 (1962).

2) M. Neeman, M. C. Caserio, J. D. Roberts, and W. S. Johnson, *Tetrahedron*, **6**, 36 (1959).

3) H. Meerwein and G. Hintz, *Liebigs Ann. Chem.*, **484**, 1 (1930).

4) E. Müller, R. Heischkeil, and M. Bauer, *Liebigs Ann. Chem.*, **677**, 55 (1964).

5) K. Ohno, H. Nishiyama, and H. Nagase, *Tetrahedron Lett.*, **1979**, 4405.

6) A. Mckillop and D. W. Young, *Synthesis*, **1979**, 401; G. H. Posner, *Angew. Chem. Int. Ed. Ergl.*, **17**, 487 (1978).

7) Z. Cohen, E. Keinan, Y. Mazur, and T. H. Varkony, *J. Org. Chem.*, **40**, 2141 (1975); E. Keinan and Y. Mazur, *ibid.*, **42**, 844 (1977), and references cited therein.

8) G. Bram and T. Fillebeen-Khan, *J. Chem. Soc., Chem. Commun.*, **1979**, 522.

9) E. Keinan and Y. Mazur, *J. Am. Chem. Soc.*, **99**, 3861 (1977); J. Muzard, *Synthesis*, **1982**, 60.

10) T. Chihara, S. Teratani, and H. Ogawa, *J. Chem. Soc., Chem. Commun.*, **1981**, 1120; T. Chihara, Y. Takagi, S. Teratani, and H. Ogawa, *Chem. Lett.*, **1982**, 1451.

11) H. Ogawa, T. Chihara, and K. Taya, *J. Am. Chem. Soc.*, **107**, 1365 (1985).

12) H. Ogawa, Y. Ichimura, T. Chihara, S. Teratani, and K. Taya, *Bull. Chem. Soc. Jpn.*, **59**, 2481 (1986).

13) S. D. Williams and K. W. Hipps, *J. Catalysis*, **78**, 96 (1982); H. Jeziorowski, H. Knözinger, W. Meye, and H. D. Müller, *J. Chem. Soc., Faraday Trans. 1*, **69**, 1744 (1973).

14) N. K. Adam, "Physics and Chemistry of Surface," 3rd. Oxford Univ. Press, London (1941), p. 50.

15) Th. J. de Boer, H. J. Backer, "Organic Syntheses," Wiley, New York, 1963, Coll. Vol. IV, p. 250.

16) F. Arndt, "Organic Syntheses," Wiley, New York, 1943, Coll. Vol. II, p. 165.

 © 1987 The Chemical Society of Japan Bull. Chem. Soc. Jpn., 60, 631—636 (1987)

Functionalization of 2-Deoxy-2,3-dehydro-*N*-acetylneuraminic Acid Methyl Ester[1)]

Kaoru Okamoto,† Tadao Kondo,††,* and Toshio Goto*
Laboratory of Organic Chemistry, Faculty of Agriculture, Nagoya University, Chikusa-ku, Nagoya 464
††Chemical Instrument Center, Nagoya University, Chikusa-ku, Nagoya 464
(Received July 3, 1986)

The acetyl protected 2-deoxy-2,3-dehydroneuraminic acid methyl ester was functionalized by modifying its 2,3-double bond to convert it into new glycosyl donors such as 2,3-dibromo-, 2,3-epoxy-, and 2-halo-3-hydroxyneuraminic acid derivatives.

In the glycosylation of *N*-acetylneuraminic acid (NeuAc), most reactions have so far been carried out by use of 2-chloro derivative of the pentaacetylated neuraminic acid methyl ester **1** first prepared by Kuhn et al.[2)] The largest problem in these reactions is that the main product is the 2-deoxy-2,3-dehydro-NeuAc derivative **2**[3)] generated by the competitive elimination of hydrogen chloride when the reactivity of the glycosyl acceptor is low. As it was difficult to prevent the elimination of hydrogen chloride in the 2-chloro derivative **1**, we have tried to utilize **2** having the 2,3-double bond to prepare new and useful glycosyl donors. The paucity of reports on reactivity of the 2,3-dehydro compound **2** prompted us to investigate it. We report here some functionalizations of **2**, which was easily prepared in 81% yield by treatment of **1** with DBU in benzene and by crystallization from hexane-ethyl acetate.

Reactivity of the 2,3-Double Bond of 2. First we carried out bromination of **2** by treatment with bromine in dichloromethane or by electrochemical oxidation of sodium bromide[4)] in acetonitrile-water (Pt-Pt electrodes) to give the 2β,3α-dibromide **3a**[5)] as white crystals in 93 or 98% yield, respectively (Table 1, Entries 1, 2). In ^{1}H NMR sepctrum the $J_{3eq,4}$ coupling constant of **3a** is 3.4 Hz, indicating that the configuration of the bromo groups is trans diaxial. The dibromide **3a** is a useful glycosyl donor for the glycosylation since the 3-axial position is blocked by the bromo group to prevent the elimination reaction.[5)]

Treatment of **2** with *N*-bromosuccinimide (NBS) in acetonitrile-water at 20 °C gave in 98% yield two bromohydrins which were separated by silica-gel column chromatography (Entry 3). The more mobile isomer was adduct **4b** having a trans diequatorial bromine (59% yield), and the slower was trans diaxial adduct **3b** (39% yield), which showed 11.0 and 3.7 Hz of $J_{3,4}$ coupling constant, respectively, in ^{1}H NMR spectra. Interestingly in this bromohydration, the product ratio was variable according to the reaction temperature. Thus, at a low temperature (−20 °C) the diequatorial adduct **4b** was obtained predominantly (dimethyl sulfoxide was used as the solvent since the reaction was very slow when acetonitrile was used), whereas at a high temperature (60—80 °C) the thermodynamically more stable diaxial isomer **3b** was formed in preference to **4b** (Entries 4, 5, 6). The use of *N*-iodosuccinimide (NIS) instead of NBS gave similar results but no adduct was obtained with *N*-chlorosuccinimide (NCS) (Entries 7, 8, 9).

Bromoacetoxylation of **2** was effective with NBS-sodium acetate-acetic acid system to give **3d** (41% yield) and **4d** (41% yield) (Entry 10). Without sodium acetate this reaction required a longer reaction time. Similar result was obtained in iodoacetoxylation of **2** except the ratio of yields of **3e** (80%) and **4e** (11%) (Entry 11). Chloroacetoxylation of **2** did not proceed similarly to the above chlorohydrin reaction (Entry 12). Treatment of **2** with NBS or 2,4,4,6-tetrabromo-2,5-cyclohexadien-1-one (TBCD) in methanol gave in quantitative yield a mixture of methyl 3-bromo glycosides **3f** and **4f** (Entries 13, 14), which was separated and the both glycosides were debrominated with tributylstannane to give methyl β-glycoside **5**[6)] (**3**: X=H, Y=OMe) and α-glycoside **6**[6)] (**4**: X=H, Y=OMe) in 96% yield. Iodomethoxylation was failed owing to decomposition of NIS with methanol (Entry 15). Attempts of haloglycosylation of **2** with NXS (X=Br, I)-sugar derivative combinations[7)] were unsuccessful.

Conversion of 3b and 3c to Glycosyl Donors 7 and 8a—c. Since direct epoxidation of **2** with various peroxides was unsuccessful, we have examined conversion of **3b** and **3c** to the epoxide **7**. Treatment of the

†Present address: Institute of Bio-Active Science (IBAS), Nippon Zoki Pharmaceutical Co., Ltd., Kinashi, Yashiro-cho, Kato-gun, Hyogo 673-14.

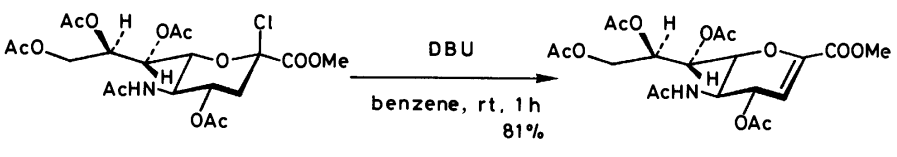

1 2

Scheme 1.

Table 1. Reaction of **2** with X^+-Y^-

Entry	Reaction System	Reaction		Product (Yield/%[a])			
		Temp/°C	Time/h	X	Y	**3** series	**4** series
1	Bromine CH_2Cl_2	0	0.2	Br	Br	**3a** (93)	—
2	NaBr, —e MeCN-H_2O	20	2.0	Br	Br	**3a** (98)	—
3	NBS MeCN-H_2O	20	6.0	Br	OH	**3b** (39)	**4b** (59)
4	NBS DMSO-H_2O	−20	0.5	Br	OH	**3b** (8)	**4b** (84)
5	NBS MeCN-H_2O	60	1.0	Br	OH	**3b** (71)	**4b** (26)
6	NBS MeCN-H_2O	80	0.2	Br	OH	**3b** (73)	**4b** (23)
7	NIS MeCN-H_2O	20	8.0	I	OH	**3c** (56)	**4c** (38)
8	NIS MeCN-H_2O	60	0.5	I	OH	**3c** (72)	**4c** (24)
9	NCS MeCN-H_2O	60	12.0	Cl	OH	—	—[b]
10	NBS AcONa-AcOH	20	1.5	Br	OAc	**3d** (41)	**4d** (41)
11	NIS AcONa-AcOH	20	1.0	I	OAc	**3e** (80)	**4e** (11)
12	NCS AcONa-AcOH	20	6.0	Cl	OAc	—	—[b]
13	NBS MeOH	20	1.0	Br	OMe	**3f** (37)	**4f** (55)
14	TBCD[c] CH_2Cl_2-MeOH	20	0.2	Br	OMe	**3f** (45)	**4f** (48)
15	NIS MeOH	20	2.0	I	OMe	—	—[b]

a) Isolated yield. b) **2** was recovered. c) 2,4,4,6-Tetrabromo-2,5-cyclohexadien-1-one.

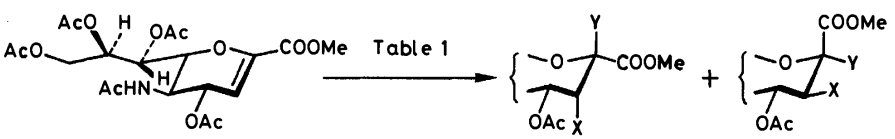

2 **3** series **4** series

a: X = Br, Y = Br
b: X = Br, Y = OH
c: X = I, Y = OH
d: X = Br, Y = OAc
e: X = I, Y = OAc
f: X = Br, Y = OMe

Scheme 2.

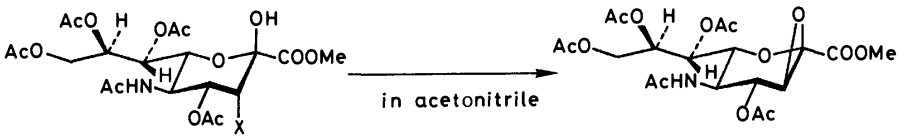

3b X=Br ($(>)_2$NEt, 4 h, 83%) 7
DBU, 10 min, 92%
3c X=I ($(>)_2$NEt, 2 h, 76%)

Scheme 3.

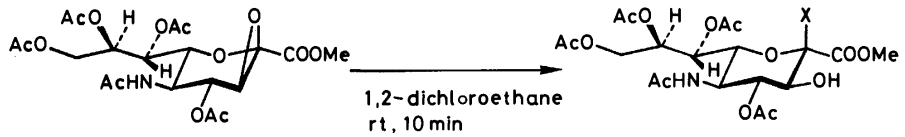

7 $BF_3 \cdot OEt_2$ 8a X=F (97%)
$TiCl_4$ 8b X=Cl (95%)
$TiBr_4$ 8c X=Br (98%)

Scheme 4.

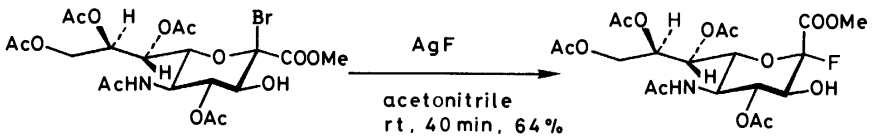

8c 8d

Scheme 5.

bromohydrin **3b** with *N*,*N*-diisopropylethylamine in anhydrous acetonitrile for 4 h gave the β-epoxide **7** as white crystals in 83% yield (Scheme 3). As some decomposition products were detected during the period of the reaction, **3b** was treated with DBU for 10 min to afford **7** in 92% yield. Similarly, the iodohydrin **3c** was converted with *N*,*N*-diisopropylethylamine to the epoxide **7** in 76% yield. In ^{1}H NMR spectrum of the epoxide **7**, the $J_{3,4}$ coupling constant was 0 Hz, and in mass (FAB) spectrum of **7**, molecular ion *m*/*z* 490 (M+1) was observed. On the other hand the diequatorial bromohydrins **4b** and **4c** were unreactive to the above epoxidation conditions.

We found that the epoxide **7** was very sensitive to the Lewis acids such as boron trifluoride–ether complex, titanium(IV) chloride, and titanium(IV) bromide. When the epoxide **7** was treated with boron trifluoride–ether complex in 1,2-dichloroethane, a single product was obtained. The vicinal coupling constant between H-3ax and fluoro group of the product was 22.6 Hz in ^{1}H NMR spectrum and the molecular ion *m*/*z* 510 was observed in mass (FAB) spectrum. From these data structure of the product was deduced as the fluorohydrin **8a** shown in Scheme 4. The treatment of **7** with titanium(IV) chloride or titanium(IV) bromide in 1,2-dichloroethane gave the 2-chloro compound **8b** or 2-bromo compound **8c** quantitatively. As the question still remained in the configuration of the anomeric position of **8b** and **8c**, the bromo derivative **8c** was treated with silver fluoride in acetonitrile to give the fluoride **8d** in concomitance with the epoxide **7**. The $J_{3ax,F}$ coupling constant of **8d** was 15.0 Hz and this value agreed with α configuration[8] of the fluorine atom, different from the β isomer **8a**.

The epoxide **7**, fluoride **8a**, chloride **8b**, and bromide **8c** are well-suited to be the glycosyl donors for the glycosylation reaction, since these derivatives are no longer the deoxysugar at **3** position and the competitive elimination reaction is suppressed.[9]

Experimental

General. Melting points were taken on a Mitamura Riken flat-bulb thermometer with a heating metal block and uncorrected. Elemental analyses were done on a Perkin-Elmer 240C elemental analyzer. Nuclear magnetic resonance spectra (NMR) were obtained with a JEOL GX-500 instrument in the FT mode. Chemical shifts were expressed in parts per million from internal tetramethylsilane (δ). Coupling constants are in hertz(Hz) and splitting pattern abbreviations are: s, singlet; d, doublet; dd, doublet of doublets; ddd, doublet of double doublets; br, broad. Mass spectra (MS) were obtained on a JEOL DX-300 spectrometer. Infrared spectra (IR) were recorded on a JASCO A-3 spectrophotometer. Optical rotations $[\alpha]_D$ were recorded on a JASCO DIP-181 digital polarimeter.

Table 2. ^{1}H NMR Data of **2**—**8d** in Chloroform-*d*

Compound	Chemical shifts, δ (multiplicity)													
	H-3eq (d)	H-3ax (d)	H-4 (dd)	H-5 (ddd)	H-6 (dd)	H-7 (dd)	H-8 (ddd)	H-9 (dd)	H-9′ (dd)	Me ester (s)	NH (d)	OH-2 (br.s)	OH-3 (d)	O-Ac, N-Ac (s)	Aglycon (s)
2[a]	6.00		5.52	4.38	4.41	5.51	5.37	4.20	4.60	3.81	5.55			1.94, 2.06, 2.07, 2.08, 2.13	
3a	5.05		5.77	4.51	4.46	5.42	5.25	4.15	4.45	3.91	5.54			1.96, 2.06, 2.09, 2.11, 2.16	
3b	4.62		5.44	4.42	4.38	5.35	5.29	4.15	4.89	3.82	6.03	5.92		1.93, 2.04, 2.08, 2.09, 2.19	
3c	4.71		4.80	4.32	4.42	5.33	5.28	4.15	4.96	3.82	6.13	5.92		1.93, 2.04, 2.07, 2.09, 2.20	
3d	4.65		5.65	4.09	4.32	5.33	5.13	4.22	4.58	3.83	5.63			1.94, 2.04, 2.04, 2.11, 2.19, 2.20	
3e	4.75		5.02	4.01	4.33	5.32	5.13	4.23	4.58	3.83	5.70			1.95, 2.03, 2.04, 2.11, 2.19, 2.21	
3f	4.61		5.47	4.37	4.09	5.36	5.29	4.19	4.87	3.84	5.43			1.91, 2.04, 2.08, 2.08, 2.18	3.30
4b		4.36	5.32	4.32	4.30	5.33	5.20	3.99	4.38	3.94	5.93	5.06		1.89, 2.03, 2.08, 2.09, 2.14	
4c		4.40	5.34	4.31	4.33	5.33	5.19	4.00	4.37	3.93	6.13	5.21		1.89, 2.02, 2.09, 2.10, 2.14	
4d		4.10	5.29	4.33	5.25	5.39	5.11	4.04	4.37	3.79	6.00			1.90, 2.04, 2.09, 2.10, 2.12, 2.15	
4e		4.19	5.27	4.29	5.22	5.38	5.11	4.04	4.37	3.80	6.01			1.89, 2.04, 2.08, 2.11, 2.12, 2.14	
4f		3.98	5.49	4.27	4.65	5.26	5.35	4.05	4.24	3.85	5.44			1.91, 2.03, 2.07, 2.08, 2.14	3.54
5	2.44[b]	1.89[b]	5.26	4.13	3.93	5.41	5.22	4.13	4.80	3.82	5.42			1.88, 2.02, 2.03, 2.08, 2.15	3.27
6	2.57[b]	1.94[b]	4.86	4.07	4.13	5.33	5.43	4.11	4.32	3.82	5.14			1.89, 2.03, 2.04, 2.14, 2.15	3.32
7		3.61	5.21	4.27	4.08	5.42	5.28	4.17	4.55	3.85	5.69			1.91, 2.05, 2.08, 2.12, 2.13	
8a		4.18[c]	5.22	4.31	4.34	5.38	5.20	4.04	4.36	3.89	6.19		3.82	1.88, 2.05, 2.08, 2.09, 2.14	
8b		4.18[b]	5.22	4.32	4.38	5.44	5.16	4.03	4.40	3.91	5.66		3.39	1.90, 2.06, 2.10, 2.10, 2.13	
8c		3.83[b]	5.24	4.37	4.34	5.46	5.16	4.04	4.42	3.92	5.83		3.65	1.90, 2.07, 2.10, 2.12, 2.13	
8d		3.99[c]	5.38	4.33	4.46	5.29	5.31	4.09	4.34	3.86	6.17		4.20	1.90, 2.03, 2.05, 2.11, 2.14	

Compound	First-order coupling constants, Hz											
	$J_{3eq,3ax}$	$J_{3eq,4}$	$J_{3ax,4}$	$J_{4,5}$	$J_{5,6}$	$J_{5,NH}$	$J_{6,7}$	$J_{7,8}$	$J_{8,9}$	$J_{8,9'}$	$J_{9,9'}$	$J_{OH,3ax}$	$J_{3ax,F}$
2		3.4		7.0	8.9	8.8	3.5	4.3	7.0	3.2	−12.5		
3a		3.4		10.0	10.7	9.9	1.8	7.0	5.5	2.8	−12.5		
3b		3.7		10.1	10.2	8.9	1.5	3.6	8.2	2.2	−12.5		
3c		4.0		10.1	10.4	9.5	1.8	2.0	8.6	2.3	−12.2		
3d		3.8		9.4	10.7	8.5	1.8	5.6	6.4	2.1	−12.5		
3e		4.0		10.4	10.7	8.6	1.8	5.5	6.4	2.4	−12.5		
3f		3.7		10.4	10.7	10.1	1.8	4.3	7.5	2.4	−12.5		
4b			11.0	10.7	10.0	9.5	1.8	6.9	7.0	2.4	−12.5		
4c			11.0	9.5	10.0	9.5	2.1	7.0	7.0	2.6	−12.5		
4d			10.1	10.4	11.0	10.4	2.5	6.1	6.1	2.4	−12.5		
4e			11.3	10.1	11.0	10.4	2.4	6.1	6.1	2.4	−12.5		
4f			10.7	10.4	10.8	10.4	2.1	8.5	6.1	2.2	−12.5		
5	−12.8	5.0	12.5	10.6	10.5	9.3	2.3	2.1	7.6	2.4	−12.5		
6	−12.8	4.6	12.5	10.1	10.2	9.8	2.1	8.5	5.5	2.7	−12.5		
7			0	7.6	8.5	10.1	3.7	4.9	7.0	2.8	−12.5		
8a			9.5	9.3	9.7	8.8	1.8	6.7	6.4	2.5	−12.5	7.9	−22.6
8b			9.5	9.5	9.7	10.1	2.2	7.3	5.8	2.7	−12.5	4.6	
8c			9.2	9.5	9.0	9.5	1.8	7.0	5.8	2.4	−12.5	3.4	
8d			8.9	9.8	10.7	10.1	1.0	7.5	5.8	2.0	−12.2	6.1	−15.0

a) Measured at 40 °C. b) Multiplicity: dd. c) Multiplicity: ddd.

Analytical thin-layer chromatography (TLC) was conducted on precoated TLC glass sheets (silica gel 60F-254, layer thickness 0.25 mm) manufactured by E. Merck. Detection was effected with 2% concentrated sulfuric acid in ethanol.

^{1}H NMR data were summarized in Table 2 and MS, elemental analyses, mp, R_f, $[\alpha]_D$, and IR data in Table 3.

Methyl 5-Acetamido-4,7,8,9-tetra-*O*-acetyl-2,3,5-trideoxy-D-*glycero*-D-*galacto*-non-2-enopyranosonate (2). Compound **1** (7.7 g, 15.1 mmol), freshly prepared by Kuhn's method,[2] was dissolved in dry benzene (70 ml). After addition of DBU (2.7 ml, 18.1 mmol), the mixture was stirred for 1 h at room temperature under argon atmosphere, washed with water and brine, dried over anhydrous Na_2SO_4, and evaporated in vacuo to give a crude material, which was chromatographed on a silica-gel column (benzene-acetone, 3:2) to give a syrup. This syrup was crystallized from hexane-ethyl acetate to give **2** (5.8 g, 81%) as white needles.

Methyl 5-Acetamido-4,7,8,9-tetra-*O*-acetyl-2,3-dibromo-2,3,5-trideoxy-β-D-*erythro*-L-*manno*-2-nonulopyranosonate (3a). Method A. To a solution of **2** (280 mg, 0.59 mmol) in dichloromethane (5 ml) was added bromine (0.04 ml, 0.78 mmol) at 0 °C under argon atmosphere. After stirring for 10 min, the mixture was evaporated in vacuo to give a syrup, which was crystallized from hexane-ethyl acetate to give **3a** (350 mg, 93%) as white needles.

Method B. A mixture of **2** (50 mg, 0.11 mmol) and sodium bromide (250 mg, 2.4 mmol) in acetonitrile (8 ml)-water (2 ml) was electrolyzed with platinum electrodes (1×2 cm^2) 5 mm apart under a constant current density of 5 mA cm^{-2} for 2 h. The mixture was evaporated to dryness and the residue was partitioned between ethyl acetate and water. The organic layer was washed with brine, dried over anhydrous Na_2SO_4, and evaporated in vacuo to give a crude material, which was treated in a similar manner as above.

Reaction of 2 with NXS (X=Br, I) in Acetonitrile (or Dimethyl Sulfoxide)-Water. To a solution of **2** (200 mg, 0.42 mmol) in acetonitrile (or dimethyl sulfoxide) (2 ml)-water (0.8 ml) was added NXS (0.48 mmol) at the temperature shown in Table 1. The mixture was stirred for 0.2—8 h

Table 3. MS, Elemental Analyses, Mp, R_f, $[\alpha]_D$, and IR Data of **2**—**8d**

Compound	Formula	MS[a] (M+H)		Anal. C(%)	H(%)	N(%)	Mp[b] θ_m/°C	R_f[c]	$[\alpha]_D^{21}$[d] (c)	ν_{max}^{KBr} NH, OH	ester	amide I	amide II
2	$C_{20}H_{27}NO_{12}$	474	Calcd	50.74	5.75	2.96	126—127	0.46	+79.9°(1.3)	3270	1738	1645	1565
			Found	50.84	5.46	2.76							
3a	$C_{20}H_{27}NO_{12}Br_2$	634	Calcd	37.93	4.30	2.21	156—157	0.52	−57.7°(1.1)	3400	1753	1649	1560
			Found	37.84	4.23	2.06							
3b	$C_{20}H_{28}NO_{13}Br$	570, 572	Calcd	42.12	4.95	2.45	118—120	0.36	+38.7°(1.1)	3380	1742	1640	1522
			Found	42.36	4.81	2.68							
3c	$C_{20}H_{28}NO_{13}I$	618	Calcd	38.91	4.57	2.27	168—170	0.37	+66.5°(1.1)	3310	1745	1658	1555
			Found	39.02	4.45	2.24							
3d	$C_{22}H_{30}NO_{14}Br$	612, 614	Calcd	43.15	4.94	2.29	—[e]	0.44	+2.9°(1.6)	3380	1743	1660	1540
			Found	43.22	4.69	2.17							
3e	$C_{22}H_{30}NO_{14}I$	660	Calcd	40.07	4.59	2.12	81—83	0.44	+12.1°(1.4)	3380	1740	1662	1538
			Found	40.07	4.46	1.99							
3f	$C_{21}H_{30}NO_{13}Br$	584, 586	Calcd	43.16	5.18	2.40	186—187	0.49	+35.7°(1.5)	3420	1748	1662	1565
			Found	43.07	5.03	2.25							
4b	$C_{20}H_{28}NO_{13}Br$	570, 572	Calcd	42.12	4.95	2.45	—[e]	0.48	−41.6°(1.5)	3370	1746	1660	1540
			Found	42.29	4.92	2.94							
4c	$C_{20}H_{28}NO_{13}I$	618	Calcd	38.91	4.57	2.27	—[e]	0.48	−56.4°(1.3)	3370	1745	1660	1540
			Found	39.21	4.47	2.02							
4d	$C_{22}H_{30}NO_{14}Br$	612, 614	Calcd	43.15	4.94	2.29	95—96	0.55	−38.5°(1.3)	3380	1745	1660	1540
			Found	43.26	4.81	2.34							
4e	$C_{22}H_{30}NO_{14}I$	660	Calcd	40.07	4.59	2.12	86—88	0.56	−51.9°(0.9)	3430	1745	1660	1538
			Found	40.34	4.56	2.00							
4f	$C_{21}H_{30}NO_{13}Br$	584, 586	Calcd	43.16	5.18	2.40	158—159	0.54	−69.6°(2.0)	3420	1748	1655	1540
			Found	43.51	5.28	2.34							
5	$C_{21}H_{31}NO_{13}$	506	Calcd	49.90	6.18	2.77	—[e]	0.43	−14.7°(1.5)	3400	1741	1660	1540
			Found	50.14	6.38	2.76							
6	$C_{21}H_{31}NO_{13}$	506	Calcd	49.90	6.18	2.77	87—89	0.43	−23.7°(1.1)	3420	1742	1660	1540
			Found	49.92	6.11	2.68							
7	$C_{20}H_{27}NO_{13}$	490	Calcd	49.08	5.56	2.86	177—178	0.46	−10.0°(1.3)	3420	1740	1650	1572
			Found	48.97	5.55	2.89							
8a	$C_{20}H_{28}NO_{13}F$	510	Calcd	47.15	5.54	2.75	—[e]	0.26	−37.3°(0.7)	3400	1745	1660	1540
			Found	47.48	5.43	2.86							
8b	$C_{20}H_{28}NO_{13}Cl$	526, 528	Calcd	45.68	5.37	2.66	—[e]	0.30	−66.0°(0.9)	3420	1742	1658	1540
			Found	45.79	5.09	2.51							
8c	$C_{20}H_{28}NO_{13}Br$	570, 572	Calcd	42.12	4.95	2.46	—[e]	0.35	−91.1°(0.6)	3420	1742	1660	1540
			Found	42.01	4.88	2.22							
8d	$C_{20}H_{28}NO_{13}F$	510	Calcd	47.15	5.54	2.75	—[e]	0.28	−26.9°(0.8)	3410	1742	1660	1540
			Found	47.15	5.79	2.64							

a) Fast atom bombardment method. b) Recrystallized from hexane–ethyl acetate. c) Solvent system is benzene–acetone (3:2). d) Measured in chloroform. e) Viscous syrup.

and dried up, and the residue was chromatographed on a silica-gel column (benzene–acetone, gradient elution from 3:1 to 3:2). The fast migrating zone was a 2,3-diequatorial isomer, methyl 5-acetamido-4,7,8,9-tetra-*O*-acetyl-3-bromo-3,5-dideoxy-α-D-*erythro*-L-*gluco*-2-nonulopyranosonate (**4b**) or methyl 5-acetamido-4,7,8,9-tetra-*O*-acetyl-3,5-dideoxy-3-iodo-α-D-*erythro*-L-*gluco*-2-nonulopyranosonate (**4c**), as a syrup and the slower migrating zone was a 2,3-diaxial isomer, methyl 5-acetamido-4,7,8,9-tetra-*O*-acetyl-3-bromo-3,5-dideoxy-β-D-*erythro*-L-*manno*-2-nonulopyranosonate (**3b**) or methyl 5-acetamido-4,7,8,9-tetra-*O*-acetyl-3,5-dideoxy-3-iodo-β-D-*erythro*-L-*manno*-2-nonulopyranosonate (**3c**), which was recrystallized from hexane–ethyl acetate.

Reaction of 2 with NXS (X=Br, I) in Sodium Acetate–Acetic Acid. A solution of **2** (200 mg, 0.42 mmol), NXS (0.48 mmol), and sodium acetate (200 mg) in glacial acetic acid (2 ml) was stirred for 1—1.5 h at 20 °C under argon atmosphere. After evaporation, the residue was partitioned between ethyl acetate and water. The organic layer was washed with 5% $NaHCO_3$, water, and brine, dried over anhydrous Na_2SO_4, and evaporated in vacuo to give a crude material, which was chromatographed on a silica-gel column (benzene–acetone, gradient elution from 3:1 to 2:1). The fast migrating zone was a 2,3-diequatorial isomer, methyl 5-acetamido-2,4,7,8,9-penta-*O*-acetyl-3-bromo-3,5-dideoxy-α-D-*erythro*-L-*gluco*-2-nonulopyranosonate (**4d**) or methyl 5-acetamido-2,4,7,8,9-penta-*O*-acetyl-3,5-dideoxy-3-iodo-α-D-*erythro*-L-*gluco*-2-nonulopyranosonate (**4e**), as a syrup and the slower migrating zone was a 2,3-diaxial isomer, methyl 5-acetamido-2,4,7,8,9-penta-*O*-acetyl-3-bromo-3,5-dideoxy-β-D-*erythro*-L-*manno*-2-nonulopyranosonate (**3d**) or methyl 5-acetamido-2,4,7,8,9-penta-*O*-acetyl-3,5-dideoxy-3-iodo-β-D-*erythro*-L-*manno*-2-nonulopyranosonate (**3e**), which was recrystallized from hexane–ethyl acetate.

Reaction of 2 with NBS or 2,4,4,6-Tetrabromo-2,5-cyclohexadien-1-one (TBCD) in Methanol. To a stirred solution of **2** (100 mg, 0.21 mmol) in absolute methanol (1.5 ml) was added NBS or TBCD (0.23 mmol) at 20 °C under argon atmosphere. The mixture was stirred for 0.2—2.0 h and evaporated in vacuo to give a residue. The residue was dissolved in ethyl acetate and the solution was washed with water and brine, dried over anhydrous Na_2SO_4, and evaporated in vacuo to give a syrup, which was chromatographed on a silica-gel column (benzene–acetone, 2:1). The fast migrating zone was a 2,3-diequatorial isomer, methyl (methyl 5-acetamido-4,7,8,9-tetra-*O*-acetyl-3-bromo-3,5-di-

deoxy-α-D-*erythro*-L-*gluco*-2-nonulopyranosid)onate (**4f**) and the slower migrating zone was a 2,3-diaxial isomer, methyl (methyl 5-acetamido-4,7,8,9-tetra-*O*-acetyl-3-bromo-3,5-dideoxy-β-D-*erythro*-L-*manno*-2-nonulopyranosid)onate (**3f**), which was recrystallized from hexane–ethyl acetate.

Methyl (Methyl 5-Acetamido-4,7,8,9-tetra-*O*-acetyl-3,5-dideoxy-β-D-*glycero*-D-*galacto*-2-nonulopyranosid)onate (5). To a solution of **3f** (30 mg, 0.05 mmol) in anhydrous tetrahydrofuran (0.6 ml) was added tributylstannane (0.034 ml, 0.13 mmol). The mixture was heated for 2 h at 60 °C with stirring under argon atmosphere and evaporated in vacuo to give a syrup, which was chromatographed on a silica-gel column (benzene–acetone, 3 : 2) to give **5** (25 mg, 96%) as a syrup.

Methyl (Methyl 5-Acetamido-4,7,8,9-tetra-*O*-acetyl-3,5-dideoxy-α-*glycero*-D-*galacto*-2-nonulopyranosid)onate (6). To a solution of **4f** (48 mg, 0.08 mmol) in anhydrous tetrahydrofuran (1 ml) was added tributylstannane (0.05 ml, 0.19 mmol). The mixture was worked up in a similar manner as **3f** and recrystallized from hexane–ethyl acetate to give **6** (40 mg, 96%) as a white amorphous powder.

Epoxidation of 3b. To a stirred solution of **3b** (500 mg, 0.88 mmol) in anhydrous acetonitrile (4 ml) was added *N,N*-diisopropylethylamine (0.22 ml, 1.26 mmol) or DBU (0.16 ml, 1.07 mmol). The mixture was stirred for 4 h or 10 min, respectively, at room temperature and evaporated in vacuo to give a crude material, which was chromatographed on a silica-gel column (benzene–acetone, 3 : 2) and crystallized from hexane–ethyl acetate to give methyl 5-acetamido-4,7,8,9-tetra-*O*-acetyl-2,3-anhydro-5-deoxy-β-D-*erythro*-L-*gluco*-2-nonulopyranosonate (**7**) (83 or 92%) as white needles.

Epoxidation of 3c. To a solution of **3c** (50 mg, 0.08 mmol) in anhydrous acetonitrile (0.6 ml) was added *N,N*-diisopropylethylamine (0.02 ml, 0.11 mmol). The mixture was stirred for 2 h at room temperature and worked up in a similar manner as **3b** to give **7** (30 mg, 76%) as white needles.

Reaction of 7 with Halogenating Agents ($BF_3 \cdot OEt_2$, $TiCl_4$, and $TiBr_4$). To a solution of **7** (200 mg, 0.41 mmol) in 1,2-dichloroethane (3 ml) was added boron trifluoride–ether complex, titanium(IV) chloride, or titanium(IV) bromide (0.45 mmol). The mixture was stirred for 10 min at room temperature and evaporated in vacuo to give a residue, which was dissolved in ethyl acetate. The organic layer was washed with saturated Na_2SO_4 solution (when boron trifluoride–ether complex was used, this operation was not required), 5% $NaHCO_3$, and brine, dried over anhydrous Na_2SO_4, and evaporated in vacuo to give a crude syrup, which was purified by chromatography on a silica-gel column (benzene–acetone, 1 : 1) to give methyl 5-acetamido-4,7,8,9-tetra-*O*-acetyl-2-fluoro-, chloro-, or bromo-2,5-dideoxy-β-D-*erythro*-L-*gluco*-2-nonulopyranosonate (**8a**), (**8b**), and (**8c**), respectively, in yields as shown in Scheme 4.

Fluorination of 8c with Silver Fluoride. A mixture of **8c** (150 mg, 0.26 mmol) and silver fluoride (130 mg, 1.0 mmol) in anhydrous acetonitrile was stirred for 40 min at room temperature in the dark. The mixture was filtered through a Celite 545 bed and the solid was washed with ethyl acetate. The combined filtrates and washings were evaporated to give a residue. The residue was dissolved in ethyl acetate, washed with 5% sodium thiosulfate and brine, dried over anhydrous Na_2SO_4, and evaporated in vacuo to give a crude material, which was chromatographed on a silica-gel column (benzene–acetone, gradient elution from 3 : 2 to 1 : 1). The fast migrating zone was the epoxide **7** (36 mg, 28%), which was obtained as white needle crystals, and the slow migrating zone was the α-fluoride, methyl 5-acetamido-4,7,8,9-tetra-*O*-acetyl-2,5-dideoxy-2-fluoro-α-D-*erythro*-L-*gluco*-2-nonulopyranosonate (**8d**) (86 mg, 64%) which was obtained as a syrup.

References

1) Synthetic Studies on Gangliosides 2.
2) R. Kuhn, P. Lutz, and D. L. MacDonald, *Chem. Ber.*, **99**, 611 (1966).
3) P. Meindl and H. Tuppy, *Monatsh. Chem.*, **100**, 1295 (1969).
4) S. Torii, K. Uneyama, H. Tanaka, T. Yamanaka, T. Yasuda, M. Ono, and Y. Kohmoto, *J. Org. Chem.*, **46**, 3312 (1981).
5) K. Okamoto, T. Kondo, and T. Goto, *Chem. Lett.*, **1986**, 1449.
6) M. M. Ponpipom, R. L. Bugianesi, and T. Y. Shen, *Can. J. Chem.*, **58**, 214 (1980); D. J. M. Van Der Vleugel, W. A. R. Van Heeswijk, and J. F. G. Vliegenthart, *Carbohydr. Res.*, **102**, 121 (1982).
7) I. Lundt, J. Thiem, and A. Prahst, *J. Org. Chem.*, **49**, 3063 (1984).
8) M. N. Sharma and R. Eby, *Carbohydr. Res.*, **127**, 201 (1984).
9) Glycosylation of these new glycosyl donors will be reported elsewhere.

 © 1987 The Chemical Society of Japan Bull. Chem. Soc. Jpn., 60, 637—643 (1987)

Glycosylation of 4,7,8,9-Tetra-*O*-acetyl-2-deoxy-2β,3β-epoxy-*N*-acetylneuraminic Acid Methyl Ester[1)]

Kaoru Okamoto,† Tadao Kondo,††,* and Toshio Goto*
Laboratory of Organic Chemistry, Faculty of Agriculture, Nagoya University, Chikusa-ku, Nagoya 464
††Chemical Instrument Center, Nagoya University, Chikusa-ku, Nagoya 464
(Received July 3, 1986)

Reaction of the 2β,3β-epoxyneuraminic acid derivative prepared from 2,3-dehydroneuraminic acid derivative with primary or secondary alcohol gave the corresponding glycoside(s) or ortho ester.

In the course of our glycosylation study on *N*-acetylneuraminic acid we have prepared some new glycosyl donors such as 2,3-dibromo-, 2,3-epoxy-, and 2-halo-3-hydroxy-*N*-acetylneuraminic acid derivatives from tetra-*O*-acetyl-2-deoxy-2,3-dehydro-*N*-acetylneuraminic acid methyl ester (**1**).[2)] We have already reported that the 2,3-dibromo compound is well-suited for the stereoselective β-glycosylation since the bromo group prevents the elimination reaction.[3)] We report here glycosylation of the 2,3-epoxy ccmpound **2**[2)] whose epoxy ring is β-oriented (Scheme 1). If the glycosylation reaction occurs in S_N2 type, **2** is suited to give α-glycosides.

Treatment of **2** with methanol in the presence of *d*-camphor-10-sulfonic acid or Amberlyst 15 catalyst (catalytic amount) gave only methyl α-glycoside **3** in nearly quantitative yield. To determine the anomeric configuration the glycoside **3** was treated with phenyl chlorocarbonothioate[4)] in the presence of 4-dimethylaminopyridine (DMAP) to give **5**, which was reduced with tributylstannane to the known α-glycoside **6**[5)] quantitatively. Antimony pentachloride (1.0 equiv) in methanol was also effective catalyst for this glycosylation. By use of 2 equivalents of methanol in the presence of antimony pentachloride or trimethylsilyl triflate (TMSOTf) catalyst, however, an inseparable mixture of α- and β-glycosides was obtained.

Treatment of **2** with methyl 2,3,4-tri-*O*-benzyl-α-D-glucoside (**8**)[6)] in the presence of boron trifluoride–ether complex or titanium(IV) chloride gave methyl 5-acetamido-4,7,8,9-tetra-*O*-acetyl-2,5-dideoxy-2-fluoro-β-D-*erythro*-L-*gluco*-2-nonulopyranosonate (**12**)[2)] or methyl 5-acetamido-4,7,8,9-tetra-*O*-acetyl-2-chloro-2,5-dideoxy-β-D-*erythro*-L-*gluco*-2-nonulopyranosonate (**7**)[2)] without any glycosides. The hydroxy-β-glycoside **9** was

†Present address: Institute of Bio-Active Science (IBAS), Nippon Zoki Pharmaceutical Co., Ltd., Kinashi, Yashiro-cho, Kato-gun, Hyogo 673-14.

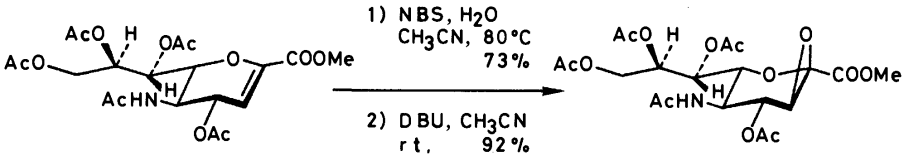

1 2

Scheme 1.

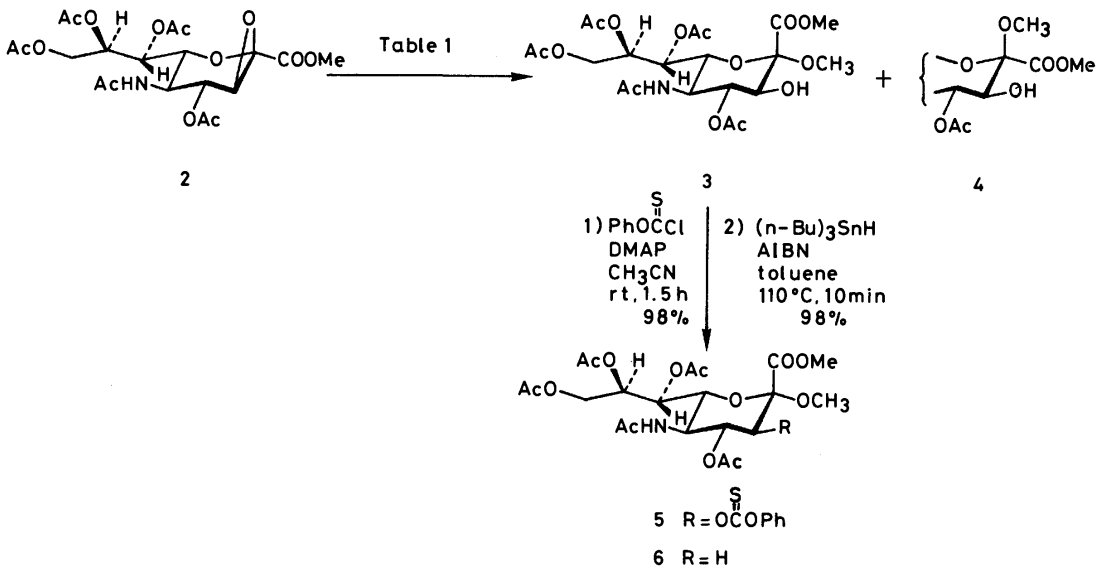

2 3 4

Scheme 2.

Table 1. Reaction of the Epoxide **2** and Methanol

Catalyst(equiv)	MeOH (equiv)	Solvent	Reaction		Yield/% of Product	
			Temp	Time	**3**	**4**
CSA (cat.)		Methanol	rt	15 min	99[a]	
Amberlyst 15 (cat.)		Methanol	rt	15 min	98[a]	
$SbCl_5$ (1.0)		Methanol	rt	15 min	89[a]	
$SbCl_5$ (1.0)	2.0	$ClCH_2CH_2Cl$	0°C	15 min	41[b]	20[b,c]
TMSOTf (1.0)	2.0	$ClCH_2CH_2Cl$	0°C	15 min	62[b]	29[b]

a) Isolated yield. b) Determined by ^1H NMR. c) Methyl 5-acetamido-4,7,8,9-tetra-*O*-acetyl-2-chloro-2,5-dideoxy-β-D-*erythro*-L-*gluco*-2-nonulopyranosonate (**7**) was also obtained in 37% yield.

Table 2. Reaction of the Epoxide **2** and Glucose Derivative **8**[a]

Catalyst(equiv)	Solvent	Reaction		Yield/%[b] of **9**
		Temp	Time/h	
CSA (cat.)	$ClCH_2CH_2Cl$	rt	0.5	no reaction
$BF_3 \cdot OEt_2$ (1.0)	THF	rt	0.2	c)
$TiCl_4$ (1.0)	$ClCH_2CH_2Cl$	rt	0.2	d)
$SbCl_5$ (1.0)	$ClCH_2CH_2Cl$	rt	0.2	49
TMSOTf[e] (1.0)	$ClCH_2CH_2Cl$	0°C	0.2	56

a) Two equivalents of **8** were used. b) Isolated yield. c) Methyl 5-acetamido-4,7,8,9-tetra-*O*-acetyl-2,5-dideoxy-2-fluoro-β-D-*erythro*-L-*gluco*-2-nonulopyranosonate (**12**) was obtained in 80% yield. d) Methyl 5-acetamido-4,7,8,9-tetra-*O*-acetyl-2-chloro-2,5-dideoxy-β-D-*erythro*-L-*gluco*-2-nonulopyranosonate (**7**) was obtained in 80% yield. e) Na_2HPO_4 was used as a buffer.

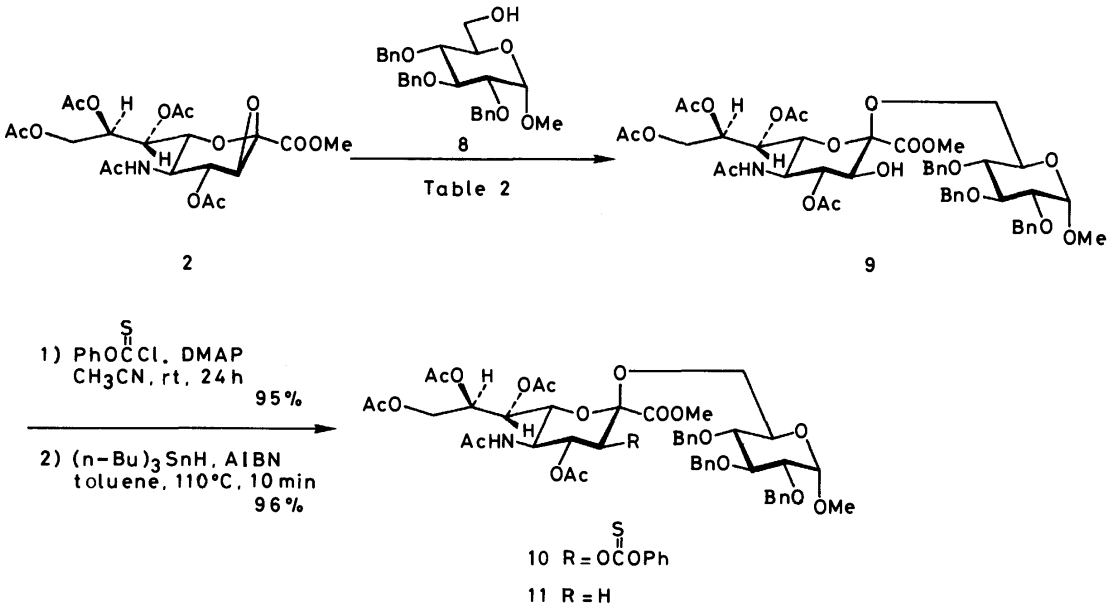

Scheme 3.

obtained in a moderate yield by the use of either antimony pentachloride or trimethylsilyl triflate. In the ^1H NMR spectrum of **9**, the coupling constant $J_{7,8}$ was 1.5 Hz and the $\Delta\delta$|H-9′-H-9| value was 0.94 ppm. In cases of the carbonothioate **10** and the glycoside **11**, the $J_{7,8}$ values were 1.5 and 2.2 Hz and the $\Delta\delta$|H-9′-H-9| values were 0.94 and 0.94 ppm, respectively. As **11** was determined to be a β-glycoside by comparing its physical data with those of the authentic sample,[3] it is safe to deduce the anomeric configuration of **9** from the $J_{7,8}$ and $\Delta\delta$|H-9′-H-9| values in ^1H NMR spectrum.[7,8] Similarly, reaction of **2** with methyl 2,4,6-tri-*O*-benzyl-β-D-galactopyranoside (**13**)[9] afforded in 64% yield only β-glycoside **14**, whose $J_{7,8}$ was 1.8 Hz and $\Delta\delta$|H-9′-H-9| value was 1.02 ppm. To make sure that the anomeric position was β configuration, the hydroxy-glycoside **14** was carbonothioated and reduced in the same manner as above to give the protected 3-*O*-(2β-neuraminyl)galactoside **16**, which was identical with the authentic sample.[3] Although the reaction of **2** with the acceptor **13** in the presence of mercury(II) chloride catalyst gave no glycosides, treatment of **2**

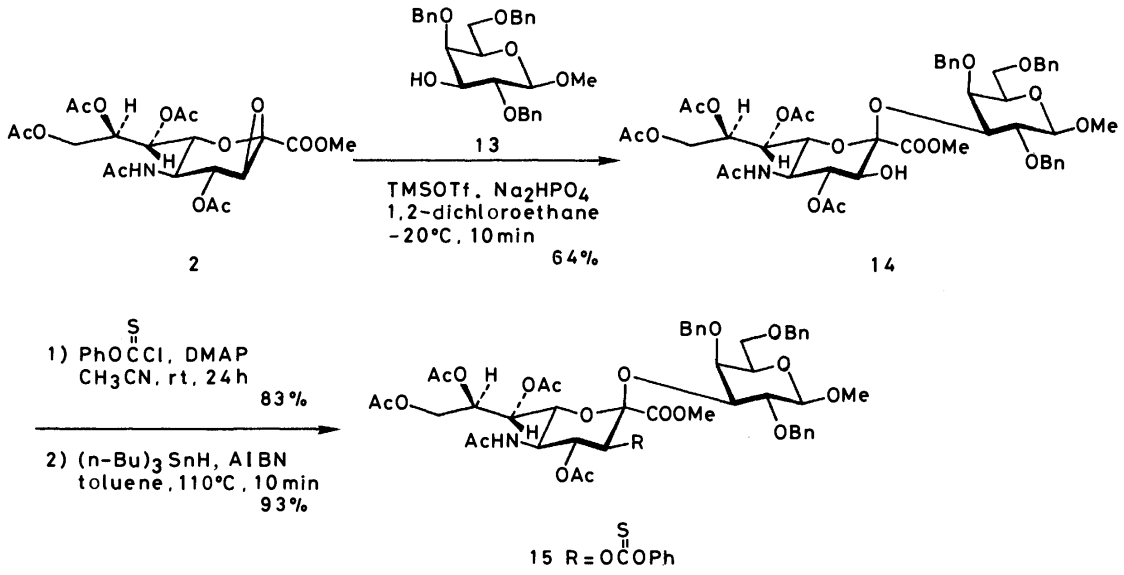

Scheme 4.

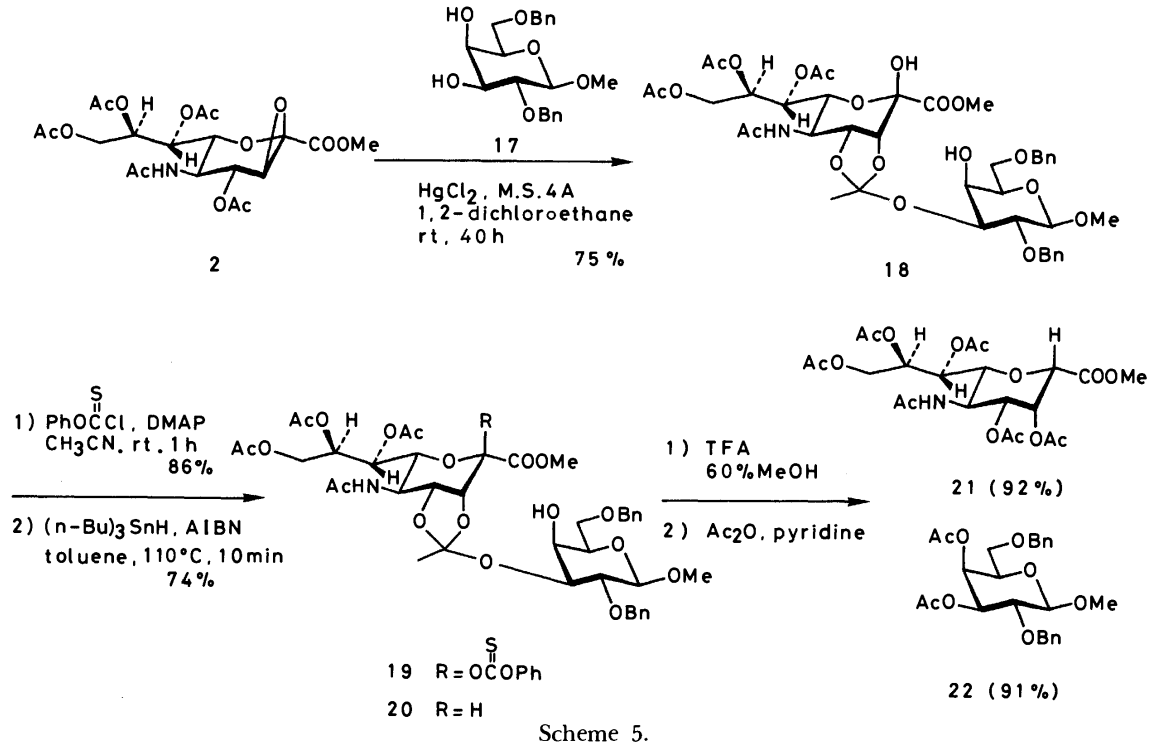

Scheme 5.

with a less sterically hindered acceptor **17** afforded an unstable product **18** in 75% yield. In its ^1H NMR spectrum, the coupling constant $J_{7,8}$ was 4.2 Hz and the $\Delta\delta|$H-9′-H-9$|$ value was 0.89 ppm, which were fit for neither α- nor β-glycoside. The product **18** was treated with phenyl chlorocarbonothioate to determine the structure. In spite of the presence of a carbonothioate group in **19** as evident from its ^1H NMR spectrum, the signal corresponding to H-3 of **19** was not shifted toward lower field. The carbonothioated **19** was reduced with tributylstannane to give **20**, which exhibited $J_{2ax,3eq}$ coupling constant as 2.4 Hz. From these data a series of compounds obtained by the reaction of **2** with **17** was revealed to be the ortho esters as illustrated in Scheme 5. Treatment of **20** with dilute trifluoroacetic acid in aqueous methanol gave almost instantaneously two degradation products, which were treated with acetic anhydride in pyridine to afford the acetylated compounds **21** and **22**. These compounds were characterized by IR, ^1H NMR, and mass spectra.

In summary, the epoxide **2** gave α-glycosides by the use of highly reactive acceptors such as methanol, and

β-glycosides by sugar derivatives such as a 6-unprotected glucoside and a 3-unprotected galactoside in the presence of antimony pentachloride or trimethylsilyl triflate. On the other hand, the ortho ester was yielded in the presence of mercury(II) chloride catalyst. The anomeric configuration of neuraminic acid derivatives was able to be determined from the $J_{7,8}$ coupling constant and the $\Delta\delta|$H-9′-H-9$|$ value in ^{1}H NMR spectrum. For example, 2β-glycosides showed ca. 2 Hz in $J_{7,8}$ and ca. 1 ppm of $\Delta\delta|$H-9′-H-9$|$ value, whereas 2α-glycosides showed more than 7 Hz in $J_{7,8}$ coupling constant and less than 0.5 ppm of $\Delta\delta|$H-9′-H-9$|$ value. These values in glycosides remain unaltered even if 3 position of NeuAc unit is substituted by any group.

Experimental

General. Melting points were taken on a Mitamura Riken flat-bulb thermometer with a heating metal block and uncorrected. Elemental analyses were done on a Perkin-Elmer 240C elemental analyzer. Nuclear magnetic resonance spectra (NMR) were obtained with a JEOL GX-500 instrument in the FT mode. Chemical shifts were expressed in parts per million from internal tetramethylsilane (δ). Coupling constants are in hertz(Hz) and splitting pattern abbreviations are: s, singlet; d, doublet; dd, doublet of doublets; ddd, doublet of double doublets; m, mutiplet; br, broad. Mass spectra (MS) were obtained on a JEOL DX-300 spectrometer. Infrared spectra (IR) were recorded on a JASCO A-3 spectrophotometer. Optical rotations $[\alpha]_D$ were recorded on a JASCO DIP-181 digital polarimeter.

Analytical thin-layer chromatography (TLC) was conducted on precoated TLC glass sheets (silica gel 60F·254, layer thickness 0.25 mm) manufactured by E. Merck. Detection was effected with 2% concentrated sulfuric acid in ethanol.

^{1}H NMR data were summarized in Tables 3, 4, and 5, and MS, elemental analyses, mp, R_f, $[\alpha]_D$, and IR data in Table 6.

Reaction of the Epoxide 2 and Methanol. Procedure A

Table 3. ^{1}H NMR Data of NeuAc Unit at 500 MHz in Chloroform-*d*

Compound	Chemical shifts, δ (multiplicity)																
	H-2ax (d)	H-3eq (d)	H-3ax (d)	H-4 (dd)	H-5 (ddd)	H-6 (dd)	H-7 (dd)	H-8 (ddd)	H-9 (dd)	H-9′ (dd)	Me ester (s)	NH (d)	OH-2 (br.s)	OH-3 (d)	O-Ac, N-Ac (s)	Phenyl (m)	Aglycon (s)
3			3.82[a]	5.15	4.22	4.54	5.28	5.37	4.08	4.32	3.84	5.63		3.02	1.89, 2.03, 2.08 2.09, 2.14		3.46
5			5.87	5.50	4.42	4.63	5.31	5.36	4.10	4.32	3.82	5.52			1.92, 2.04, 2.06 2.09, 2.16	7.04—7.44	3.51
6		2.57	1.94	4.86	4.07	4.13	5.33	5.43	4.11	4.32	3.82	5.14			1.89, 2.03, 2.04 2.14, 2.15		3.32
9			3.85[a]	5.05	4.21	4.30	5.35	5.24	4.04	4.98	3.80	5.39		2.53	1.87, 1.97, 2.04 2.06, 2.14		
10			5.87	5.43	4.41	4.44	5.41	5.28	4.08	5.02	3.68	5.63			1.88, 1.98, 2.05 2.06, 2.17	6.85—7.50	
11		2.47	1.88	5.16	4.11	4.27	5.38	5.27	4.13	5.07	3.72	5.49			1.86, 1.97, 2.01 2.05, 2.13		
14			3.90[a]	5.00	4.08	4.02	5.17	5.09	3.96	4.98	3.54	4.52		3.68	1.72, 1.93, 2.01 2.02, 2.08		
15			5.82	5.32	4.25	3.94	5.15	5.18	3.95	5.22	3.51	3.95			1.65, 1.99, 2.00 2.03, 2.09	6.90—7.65	
16		2.70	1.80	4.98	3.99	3.91	5.15	5.15	4.00	4.99	3.54	3.86			1.64, 1.98, 2.00 2.03, 2.06		
18		4.60		4.47	3.87	4.23	5.32	5.25	4.04	4.93	3.68	5.84	5.48		1.69, 1.93, 2.03 2.07, 2.13		
19		4.72		4.44	4.18	4.15	5.38	5.14	4.20	4.65	3.71	6.64			1.72, 1.92, 1.93 2.06, 2.13	7.10—7.50	
20	4.28	4.74[a]		4.53	3.39	3.79	5.24	5.30	4.18	4.61	3.66	5.69			1.65, 1.95, 2.03 2.06, 2.12		
21	4.37	5.71[a]		5.22	4.25	3.88	5.39	5.30	4.20	4.73	3.75	5.87			1.90, 1.99, 2.05 2.07, 2.13, 2.17		

Compound	First-order coupling constants, Hz												
	$J_{2ax,3ex}$	$J_{3eq,3ax}$	$J_{3eq,4}$	$J_{3ax,4}$	$J_{4,5}$	$J_{5,6}$	$J_{5,NH}$	$J_{6,7}$	$J_{7,8}$	$J_{8,9}$	$J_{8,9'}$	$J_{9,9'}$	$J_{OH,3ax}$
3				9.8	10.1	11.0	10.1	2.1	7.9	6.1	2.6	−12.5	6.1
5				8.6	10.4	11.0	9.8	2.1	8.0	6.3	2.5	−12.5	
6		−12.8	4.6	12.5	10.1	10.2	9.8	2.1	8.5	5.5	2.7	−12.5	
9				9.5	10.4	10.7	10.1	2.1	1.5	9.2	2.3	−12.5	7.3
10				9.8	9.8	10.1	9.5	2.0	1.5	9.2	2.1	−12.5	
11		−12.9	5.1	10.8	11.2	10.4	10.4	2.3	2.2	9.3	2.2	−12.5	
14				9.5	9.8	10.0	10.1	2.0	1.8	9.2	2.4	−12.5	7.0
15				9.8	10.4	10.5	10.5	2.1	2.1	8.9	2.2	−12.5	
16		−13.4	4.6	11.6	11.2	10.7	10.4	1.8	b)	8.5	2.1	−12.5	
18			5.2		8.2	10.7	9.8	2.1	4.2	7.9	2.1	−12.5	
19			5.5		7.6	10.0	9.2	2.7	2.7	7.6	2.1	−12.5	
20	2.4		5.8		7.6	11.3	8.2	1.8	5.5	6.7	2.4	−12.5	
21	1.2		3.5		10.7	9.4	9.8	2.1	4.9	7.3	2.4	−12.5	

a) Multiplicity: dd. b) Not assigned owing to the complexity of the spectrum.

Table 4. ^{1}H NMR Data of Glc or Gal Unit at 500 MHz in Chloroform-*d*

Compound	Chemical shifts, δ (multiplicity)									First-order coupling constants, Hz							
	H-1 (d)	H-2 (dd)	H-3 (dd)	H-4 (dd)	H-5 (ddd)	H-6 (dd)	H-6′ (dd)	OMe (s)	OH-4 (d)	$J_{1,2}$	$J_{2,3}$	$J_{3,4}$	$J_{4,5}$	$J_{5,6}$	$J_{5,6'}$	$J_{6,6'}$	$J_{OH,4}$
9	4.90	3.64	3.99	3.72	3.79	3.88	4.09	3.36		3.7	9.5	9.2	8.9	2.0	2.3	−10.9	
10	4.93	3.67	3.99	3.84	3.82	3.87	4.19	3.36		3.7	9.5	8.9	9.0	1.0	2.0	−10.3	
11	4.89	3.61	3.97	3.70	3.74	3.80	3.81	3.35		3.7	9.5	9.2	10.1	2.5	2.0	−10.8	
14	4.35	3.87	4.39	4.10	3.82	3.69	3.73	3.49		7.0	9.2	3.1	1.0	6.7	6.3	−10.0	
15	4.38	3.84	4.42	4.08[a]	3.88	3.77	3.79	3.47		7.3	9.8	3.1	0	7.2	7.1	−10.2	
16	4.34	3.75	4.09	3.94[a]	3.77	3.68	3.71	3.46		7.3	9.8	2.8	0	6.1	6.1	−9.8	
18	4.28	3.51	3.67	4.01	3.57	3.72	3.78	3.55	2.98	7.6	9.5	3.7	0	6.1	4.6	−10.1	1.5
19	4.29	3.53	3.70	3.90[b]	3.58	3.75	3.81	3.56	2.68	7.9	9.8	3.4	0.5	5.4	5.8	−10.1	2.5
20	4.27	3.50	3.69	3.95	3.56	3.72	3.79	3.55	2.64	7.9	9.5	3.4	0	5.8	5.5	−9.8	2.5
22	4.38	3.58	4.98	5.42	3.83	3.49	3.57	3.59		7.6	10.1	3.7	1.0	6.7	6.3	−9.8	

a) Multiplicity: d. b) Multiplicity: ddd.

Table 5. ^{1}H NMR Data of Other Groups at 500 MHz in Chloroform-*d*

Compound	Chemical shifts, δ (multiplicity)					First-order coupling constants, Hz
	PhC<u>H</u>$_2$ (AB quartet)			Ph (m)	O-Ac (s)	J_{gem}
9	4.74 and 4.89,	4.76 and 4.82,	4.85 and 4.97	7.23—7.45		−11.0, −11.9, −11.0
10	4.78 and 4.85,	4.88 and 4.96,	4.92 and 5.00	6.85—7.50		−11.9, −11.0, −11.0
11	4.70 and 4.87,	4.75 and 4.82,	4.84 and 4.97	7.20—7.50		−10.8, −12.0, −11.0
14	4.54 and 4.56,	4.74 and 4.87,	4.88 and 4.90	7.20—7.50		−11.9, −11.3, −13.7
15	4.60,[a]	4.82 and 5.02,	4.95 and 5.03	6.90—7.65		−11.9, −13.7
16	4.56,[a]	4.68 and 4.88,	4.79 and 4.80	7.20—7.50		−11.0, −12.5
18	4.57 and 4.61,	4.63 and 4.81,		7.25—7.50		−11.9, −11.0
19	4.58 and 4.60,	4.62 and 4.85,		7.10—7.50		−10.0, −10.7
20	4.57 and 4.61,	4.61 and 4.85,		7.23—7.45		−12.2, −11.0
22	4.44 and 4.55,	4.61 and 4.85,			1.94, 2.01	−11.9, −11.9

a) Multiplicity: s.

Table 6. MS, Elemental Analyses, Mp, R_f, $[\alpha]_D$, and IR Data of **3**—**22**

Compound	Formula	MS[a] (M+H)	Anal.	C(%)	H(%)	N(%)	Mp θ_m/°C	R_f	$[\alpha]_D$ (c)[b] (Temp)	ν_{max}^{KBr} NH, OH	ester	amide I	amide II
3	$C_{21}H_{31}NO_{14}$	522	Calcd	48.37	5.99	2.69	—[c]	0.27[d]	−34.3°(1.1)	3430	1743	1660	1540
			Found	48.35	5.89	2.75			(15°C)				
5	$C_{28}H_{35}NO_{15}S$	658	Calcd	51.14	5.36	2.13	—[c]	0.56[d]	−18.4°(1.2)	3430	1748	1660	1540
			Found	50.85	5.43	2.32			(15°C)				
6	$C_{21}H_{31}NO_{13}$	506	Calcd	49.90	6.18	2.77	87—89[e]	0.43[d]	−23.7°(1.1)	3420	1742	1660	1540
			Found	50.11	6.01	2.92			(21°C)				
9	$C_{48}H_{59}NO_{19}$	955	Calcd	60.43	6.23	1.47	—[c]	0.46[d]	+11.5°(1.3)	3430	1743	1665	1540
			Found	60.71	6.45	1.39			(21°C)				
10	$C_{55}H_{63}NO_{20}S$		Calcd	60.60	5.82	1.29	—[c]	0.60[f]	−5.6°(2.6)	3400	1748	1665	1540
			Found	60.23	5.78	1.44			(20°C)				
11	$C_{48}H_{59}NO_{18}$	938	Calcd	61.46	6.34	1.49	—[c]	0.52[f]	+23.3°(1.0)	3400	1748	1665	1540
			Found	61.59	6.34	1.31			(29°C)				
14	$C_{48}H_{59}NO_{19}$	955	Calcd	60.43	6.23	1.47	—[c]	0.48[f]	−15.7°(1.0)	3380	1743	1670	1540
			Found	60.56	6.57	1.59			(11°C)				
15	$C_{55}H_{63}NO_{20}S$		Calcd	60.60	5.82	1.29	—[c]	0.64[f]	+9.1°(0.7)	3420	1752	1660	1540
			Found	60.91	5.75	1.46			(12°C)				
16	$C_{48}H_{59}NO_{18}$	938	Calcd	61.46	6.34	1.49	—[c]	0.58[f]	+5.3°(1.0)	3400	1743	1660	1540
			Found	61.23	6.27	1.08			(29°C)				
18	$C_{48}H_{53}NO_{19}$		Calcd	57.00	6.18	1.62	—[c]	0.40[d]	+31.8°(1.2)	3400	1745	1660	1540
			Found	56.72	6.08	1.87			(11°C)				
19	$C_{48}H_{57}NO_{20}S$		Calcd	57.65	5.75	1.40	—[c]	0.54[f]	−9.5°(1.0)	3400	1748	1660	1530
			Found	57.83	5.41	1.42			(12°C)				
20	$C_{41}H_{53}NO_{18}$		Calcd	58.08	6.30	1.65	—[c]	0.40[f]	+12.3°(0.9)	3420	1742	1660	1530
			Found	57.82	6.07	1.36			(11°C)				
21	$C_{22}H_{31}NO_{14}$	534	Calcd	49.53	5.86	2.63	—[c]	0.26[f]	+49.8°(1.6)	3370	1748	1660	1540
			Found	49.50	5.79	2.38			(12°C)				
22	$C_{25}H_{30}O_8$	459	Calcd	65.49	6.60		—[c]	0.54[g]	+6.5°(2.0)		1740		
			Found	65.44	6.73				(12°C)				

a) Fast atom bombardment method. b) Measured in chloroform. c) Viscous syrup. d) Solvent system is benzene-acetone (3:2). e) Recrystallized from hexane-ethyl acetate. f) Solvent system is benzene-acetone (2:1). g) Solvent system is benzene-ethyl acetate (6:1).

(*d*-camphor-10-sulfonic acid or $SbCl_5$ catalyst in the presence of large excess methanol). To a solution of **2** (100 mg, 0.20 mmol) in absolute methanol (2.5 ml) was added *d*-camphor-10-sulfonic acid (cat. amount) or antimony pentachloride (26 μl, 0.20 mmol) at room temperature under argon atmosphere. After stirring for 15 min, the mixture was evaporated to dryness, and the residue was dissolved in ethyl acetate. The solution was washed with 5% $NaHCO_3$ and brine, dried over anhydrous Na_2SO_4. The solvent was removed in vacuo to give a syrupy residue, which was chromatographed on a silica-gel column (benzene-acetone, 1:1) to give methyl glycoside of methyl 5-acetamido-4,7,8,9-tetra-*O*-acetyl-5-deoxy-α-D-*erythro*-L-*gluco*-2-nonulopyranosonate (**3**) as a syrup.

Procedure B (Amberlyst 15 catalyst in the presence of large excess methanol). A mixture of **2** (100 mg, 0.20 mmol) and Amberlyst 15 (cat. amount) in absolute methanol (2.5 ml) was stirred for 15 min under argon atmosphere. It was filtered and the resin was washed well with methanol. The combined filtrate and washings were evaporated to a syrup, which was purified in the same manner as procedure A.

Procedure C ($SbCl_5$ catalyst in the presence of 2 equiv of methanol). To a solution of **2** (100 mg, 0.20 mmol) in 1,2-dichloroethane (2.0 ml) containing 0.2 M (1M=1 mol dm^{-3}) methanol (2.0 ml) was added antimony pentachloride (26 μl, 0.20 mmol) at 0 °C under argon atmosphere. The mixture was stirred for 15 min, diluted with chloroform, washed with 5% $NaHCO_3$ and brine, dried over anhydrous Na_2SO_4, and evaporated to dryness. The residue was purified in the same manner as procedure A. The fast migrating zone was methyl 5-acetamido-4,7,8,9-tetra-*O*-acetyl-2-chloro-2,5-dideoxy-β-D-*erythro*-L-*gluco*-2-nonulopyranosonate (**7**)[2] (40 mg, 37%) and the slow migrating zone was an inseparable mixture of **3** (41%) and **4** (20%).

Procedure D (TMSOTf catalyst in the presence of 2 equiv of methanol). To a solution of **2** (100 mg, 0.20 mmol) in 1,2-dichloroethane (2.0 ml) containing 0.2 M methanol was added trimethylsilyl triflate (40 μl, 0.20 mmol) at 0 °C under argon atmosphere. The mixture was worked up in the same manner as above to give **3** (62%) and **4** (29%).

Methyl (Methyl 5-Acetamido-4,7,8,9-tetra-*O*-acetyl-5-deoxy-3-*O*-[phenoxy(thiocarbonyl)]-α-D-*erythro*-L-*gluco*-2-nonulopyranosid)onate (5). A solution of **3** (50 mg, 0.096 mmol), 4-dimethylaminopyridine (50 mg, 0.41 mmol), and phenyl chlorocarbonothioate (27 μl, 0.20 mmol) in anhydrous acetonitrile (1.0 ml) was stirred for 1.5 h at room temperature under argon atmosphere. The mixture was evaporated to dryness and the residue, which was partitioned between ethyl acetate and water. The organic layer was separated, washed with water and brine, dried over anhydrous Na_2SO_4, and evaporated in vacuo to give a crude material, which was chromatographed on a silica-gel column (benzene-acetone, 5:2) to give **5** (64 mg, 98%) as a colorless syrup.

Methyl (Methyl 5-Acetamido-4,7,8,9-tetra-*O*-acetyl-3,5-dideoxy-α-D-*glycero*-D-*galacto*-2-nonulopyranosid)onate (6). To a solution of **5** (20 mg, 0.030 mmol) in toluene (1.0 ml) were added tributylstannane (20 μl, 0.074 mmol) and AIBN (cat. amount) under argon atmosphere. The mixture was heated at 110 °C for 10 min, evaporated to dryness and the residue was chromatographed on a silica-gel column (benzene-acetone, 2:1) to give crystals. Recrystallization from hexane-ethyl acetate gave **6** (15 mg, 98%) as white needles.

Reaction of the Epoxide 2 and 8. Procedure A ($BF_3 \cdot OEt_2$ catalyst). To a stirred solution of **2** (20 mg, 0.041 mmol) and **8**[6] (40 mg, 0.086 mmol) in tetrahydrofuran (0.6 ml) was added boron trifluoride-ether complex (5.2 μl, 0.041 mmol) at room temperature under argon atmosphere. After stirring for 0.2 h, the solvent was removed and the residue was dissolved in ethyl acetate. The solution was washed with 5% $NaHCO_3$ and brine, dried over anhydrous Na_2SO_4, and evaporated in vacuo to give a crude syrup, which was chromatographed on a silica-gel column (benzene-acetone, 1:1). Unreacted **8** (35 mg) was recovered and then methyl 5-acetamido-4,7,8,9-tetra-*O*-acetyl-2,5-dideoxy-2-fluoro-β-D-*erythro*-L-*gluco*-2-nonulopyranosonate (**12**)[2] (16.7 mg, 80%) was obtained.

Procedure B ($TiCl_4$ catalyst). To a solution of **2** (20 mg, 0.041 mmol) and **8** (40 mg, 0.086 mmol) in 1,2-dichloroethane (0.6 ml) was added titanium(IV) chloride (4.5 μl, 0.041 mmol) at room temperature under argon atmosphere. The mixture was stirred for 0.2 h, diluted with ethyl acetate, washed with saturated Na_2SO_4 and brine, dried over anhydrous Na_2SO_4, and evaporated in vacuo to give a residue, which was treated in the same manner as procedure A to give **8** (30 mg) and **7** (17.3 mg, 80%).

Procedure C ($SbCl_5$ catalyst). To a solution of **2** (20 mg, 0.041 mmol) and **8** (40 mg, 0.086 mmol) in 1,2-di chloroethane (0.6 ml) was added antimony pentachloride (5.2 μl, 0.041 mmol) at room temperature under argon atmosphere. The mixture was stirred for 0.2 h, diluted with ethyl acetate, washed with 5% $NaHCO_3$ and brine, dried over anhydrous Na_2SO_4, and evaporated in vacuo to give a crude material, which was chromatographed on a silica-gel column (benzene-acetone, 2:1) to give methyl 2,3,4-tri-*O*-benzyl-6-*O*-[methyl(5-acetamido-4,7,8,9-tetra-*O*-acetyl-5-deox -β-D-*erythro*-L-*gluco*-2-nonulopyranosyl)onate]-α-D-glucopyranoside (**9**) (19 mg, 49%) as a syrup.

Procedure D (TMSOTf catalyst). To a mixture of **2** (20 mg, 0.041 mmol), **8** (40 mg, 0.086 mmol), anhydrous disodium hydrogenphosphate (20 mg), and 1,2-dichloroethane (0.6 ml) was added trimethylsilyl triflate (8 μl, 0.041 mmol) at 0 °C under argon atmosphere. It was stirred for 0.2 h at the same temperature and worked up in the same manner as above to give **9** (22 mg, 56%).

Methyl 2,3,4-Tri-*O*-benzyl-6-*O*-[methyl(5-acetamido-4,7,8,9-tetra-*O*-acetyl-5-deoxy-3-*O*-[phenoxy(thiocarbonyl)]-β-D-*erythro*-L-*gluco*-2-nonulopyranosyl)onate]-α-D-glucopyranoside (10). A solution of **9** (22 mg, 0.023 mmol), 4-dimethylaminopyridine (6 mg, 0.049 mmol), and phenyl chlorocarbonothioate (7 μl, 0.051 mmol) in anhydrous acetonitrile (0.3 ml) was stirred for 24 h at room temperature under argon. The mixture was evaporated to dryness, and the residue was dissolved in ethyl acetate, washed with water and brine, dried over anhydrous Na_2SO_4, and evaporated in vacuo to give a crude material. This was chromatographed on a silica-gel column (benzene-acetone, 5:2), triturated with hexane-ethyl acetate, and washed with hexane to give **10** (24 mg, 95%).

Methyl 2,3,4-Tri-*O*-benzyl-6-*O*-[methyl(5-acetamido-4,7,8,9-tetra-*O*-acetyl-3,5-dideoxy-β-D-*glycero*-D-*galacto*-2-nonulopyranosyl)onate]-α-D-glucopyranoside (11). To a solution of **10** (20 mg, 0.018 mmol) in toluene (1 ml) were added tributylstannane (10 μl, 0.037 mmol) and AIBN (cat. amout) under argon atmosphere. The mixture was heated at 100 °C for 15 min and the solvent was removed in vacuo to give a crude material, which was chromatographed on a silica-gel

column (benzene–acetone, 2 : 1) to give **11** (16.5 mg, 96%) as a syrup.

Methyl 2,4,6-Tri-*O*-benzyl-3-*O*-[methyl(5-acetamido-4,7,8,9-tetra-*O*-acetyl-5-deoxy-β-D-*erythro*-L-*gluco*-2-nonulopyranosyl)-onate]-β-D-galactopyranoside (14). To a mixture of **2** (20 mg, 0.041 mmol), **13**[10] (40 mg, 0.086 mmol), anhydrous disodium hydrogenphosphate (20 mg), and 1,2-dichloroethane (0.3 ml) was added trimethylsilyl triflate (8 μl, 0.041 mmol) at −20 °C under argon atmosphere. It was stirred for 10 min, diluted with ethyl acetate, washed with 5% $NaHCO_3$ and brine, dried over anhydrous Na_2SO_4, and evaporated to dryness. The residue was chromatographed on a silica-gel column (benzene–acetone, 2 : 1) to give **14** (25 mg, 64%) as a syrup.

Methyl 2,4,6-Tri-*O*-benzyl-3-*O*-[methyl(5-acetamido-4,7,8,9-tetra-*O*-acetyl-5-deoxy-3-*O*-[phenoxy(thiocarbonyl)]-β-D-*erythro*-L-*gluco*-2-nonulopyranosyl)onate]-β-D-galactopyranoside (15). A solution of **14** (18 mg, 0.019 mmol), 4-dimethylaminopyridine (6 mg, 0.049 mmol), and phenyl chlorocarbonothioate (5 μl, 0.036 mmol) in anhydrous acetonitrile (0.3 ml) was stirred for 24 h at room temperature under argon atmosphere. After evaporation, the residue was partitioned between ethyl acetate and water. The organic layer was separated, washed with water and brine, dried over anhydrous Na_2SO_4, and evaporated in vacuo to give a crude material, which was chromatographed on a silica-gel column (benzene–acetone, 4 : 1) to give **15** as a syrup.

Methyl 2,4,6-Tri-*O*-benzyl-3-*O*-[methyl(5-acetamido-4,7,8,9-tetra-*O*-acetyl-3,5-dideoxy-β-D-*glycero*-D-*galacto*-2-nonulopyranosyl)onate]-β-D-galactopyranoside (16). To a solution of **15** (15 mg, 0.014 mmol) in toluene (1 ml) were added tributylstannane (7 μl, 0.026 mmol) and AIBN (cat. amount) under argon atmosphere. The mixture was heated at 110 °C for 10 min and evaporated to dryness. The residue was chromatographed on a silica-gel column (benzene–acetone, 4 : 1) to give a syrup. This was triturated with hexane–ethyl acetate and washed with hexane to give **16** (12 mg, 93%).

Reaction of the Epoxide 2 with 17. A mixture of **2** (100 mg, 0.20 mmol), **17**[10] (160 mg, 0.43 mmol), mercury(II) chloride (60 mg, 0.22 mmol), powdered molecular sieves 4A (200 mg), and 1,2-dichloroethane (3 ml) was stirred for 40 h. The reaction mixture was filtered and the solid was washed with chloroform. The combined filtrate and washings were washed with water and brine, dried over anhydrous Na_2SO_4, and evaporated in vacuo to give a residue, which was chromatographed on a silica-gel column (benzene–acetone, 3 : 2) to give the ortho ester **18** (132 mg, 75%).

To a solution of **18** (100 mg, 0.12 mmol) and 4-dimethylaminopyridine (60 mg, 0.49 mmol) in anhydrous acetonitrile (1.5 ml) was added phenyl chlorocarbonothioate (18 μl, 0.13 mmol) under argon atmosphere. The mixture was stirred for 1 h at room temperature, evaporated to dryness, and the residue was partitioned between ethyl acetate and water. The ethyl acetate layer was separated, washed with water and brine, dried over anhydrous Na_2SO_4, and evaporated in vacuo to give a syrup, which was chromatographed on a silica-gel column (benzene–acetone, 3 : 2) to give **19** (100 mg, 86%).

To a mixture of **19** (80 mg, 0.08 mmol), anhydrous sodium acetate (40 mg), and toluene (3 ml) was added tributylstannane (43 μl, 0.16 mmol) under argon atmosphere. The mixture was heated at 110 °C for 10 min, diluted with ethyl acetate, washed with water and brine, dried over anhydrous Na_2SO_4, and evaporated to dryness. The residue was chromatographed on a silica-gel cloumn (benzene–acetone, 3 : 2), triturated with hexane–ethyl acetate, and washed with hexane to give **20** (50 mg, 74%).

To a solution of **20** (100 mg, 0.12 mmol) in 60% aq methanol (3 ml) was added trifluoroacetic acid (1 drop) at room temperature. After stirring for 10 min, the mixture was evaporated to dryness and the residue was treated with acetic anhydride (0.4 ml) and pyridine (0.8 ml) for 10 h at room temperature under argon atmosphere. The resulting mixture was evaporated to a syrup, which was chromatographed on a silica-gel column (benzene–ethyl acetate, 6 : 1, followed by benzene–acetone, 1 : 1) to give methyl 3,4-di-*O*-acetyl-2,6-di-*O*-benzyl-β-D-galactopyranoside (**22**) (50 mg, 92%) and methyl 5-acetamido-3,4,7,8,9-penta-*O*-acetyl-2,5-dideoxy-D-*erythro*-L-*manno*-2-nonulopyranosonate (**21**) (51 mg, 91%) as a syrup.

References

1) Synthetic Studies on Gangliosides 3.
2) K. Okamoto, T. Kondo, and T. Goto, *Bull. Chem. Soc. Jpn.*, preceding paper in this issue.
3) K. Okamoto, T. Kondo, and T. Goto, *Chem. Lett.*, **1986**, 1449.
4) M. J. Robins and J. S. Wilson, *J. Am. Chem. Soc.*, **103**, 932 (1981).
5) M. M. Ponpipom, R. L. Bugianesi, and T. Y. Shen, *Can. J. Chem.*, **58**, 214 (1980).
6) P. Kovac, J. Alfödi, and B. Kosik, *Chem. Zveski.*, **28**, 820 (1974).
7) In the case of the α-glycoside, the coupling constant $J_{7,8}$ was 8.9 Hz and the $\Delta\delta$|H-9′-H-9| value was 0.24 ppm.[8]
8) H. Ogura, K. Furuhata, T. Osawa, S. Toyoshima, and M. Ito, Ger. Offen. DE3219209 (1982).
9) H. M. Flowers, *Carbohydr. Res.*, **39**, 245 (1975).

 © 1987 The Chemical Society of Japan Bull. Chem. Soc. Jpn., 60, 645—648 (1987)

A Synthesis of Optically Active 4-Diethoxyphosphinyl-3-(1-hydroxyethyl)-2-azetidinone: A Potential Precursor to (1-Aminoalkyl)-phosphonic Acid Derivatives

Masao SHIOZAKI* and Hidekazu MASUKO
Chemical Research Laboratories, Sankyo Co., Ltd. Hiromachi 1-2-58, Shinagawa-ku, Tokyo 140
(Received July 10, 1986)

Optically active 4-diethoxyphosphinyl-3-(1-hydroxyethyl)-2-azetidinone (**8**) was synthesized from (2*R*,3*R*)-*N*-diethoxyphosphinylmethyl-2,3-epoxybutyramide derivatives, and compound **8** was alternatively synthesized from (3*R*,4*R*)-4-acetoxy-3-[(*R*)-1-(*t*-butyldimethylsilyloxy)ethyl]-2-azetidinone via 3-[1-(*t*-butyldimethylsilyloxy)-ethyl] derivative.

4-Dialkoxyphosphinyl-2-azetidinone derivatives obtained by a treatment of the corresponding 4-acetoxy-2-azetidinone derivatives with trialkyl phosphites have already been reported by Campbell[1] as the starting material of alanyl dipeptide-containing organophosphorus moiety via β-phosphono-β-alanine derivatives. Such organophosphorus-containing molecules as the (1-aminoalkyl)phosphonic acid dipeptide (for example: alaphosphine–an inhibitor of alanine racemase) are becoming increasingly important for pharmaceutical use.

In this paper we wish to describe a new synthetic procedure for optically active 4-diethoxyphosphinyl-3-(1-hydroxyethyl)-2-azetidinone (**8**), as a potential precursor to one of the (1-aminoalkyl)phosphonic acid derivatives, by a ring closure of 2-bromo-3-hydroxybutyramides via the corresponding 2,3-epoxybutyramides which possess an activated methylene adjoining the amide nitrogen. This type of intramolecular concerted ring-closure reaction accompanied by an epoxide cleavage reaction to form a β-lactam derivative has already been reported.[2] On the other hand, (3*R*,4*R*)-4-acetoxy-3-[(*R*)-1-(*t*-butyldimethylsilyloxy)-ethyl]-2-azetidinone (**9**) is one of the key intermediates to carbapenem antibiotics,[3] and **9** may become a commercially available material. Therefore, we attempted to utilize compound **9** for the synthesis of **8**. As a result, it was revealed that **9** is a promising intermediate for the synthesis of **8**. Thus, we also wish to report here this alternative procedure.

The starting phosphorus-containing butyramides were synthesized as follows: A treatment of 4-methoxybenzylamine or *p*-anisidine with paraformaldehyde according to the procedure reported by Ratcliffe et al.[4] gave hexahydro-1,3,5-triazines, **1a** (95% yield; mp 113—115 °C) or **1b** (72% yield; mp 128—130 °C). A reaction of the hexahydro-1,3,5-triazines (**1a** and **1b**) with diethyl phosphite at 100 °C for 4—6 h gave secondery amines (**2a** and **2b**: 65 and 61% yields, respectively). An amide-formation reaction of the amines (**2a** and **2b**) with 1 equivalent of (2*S*,3*R*)-2-bromo-3-hydroxybutyric acid[5] in tetrahydrofuran

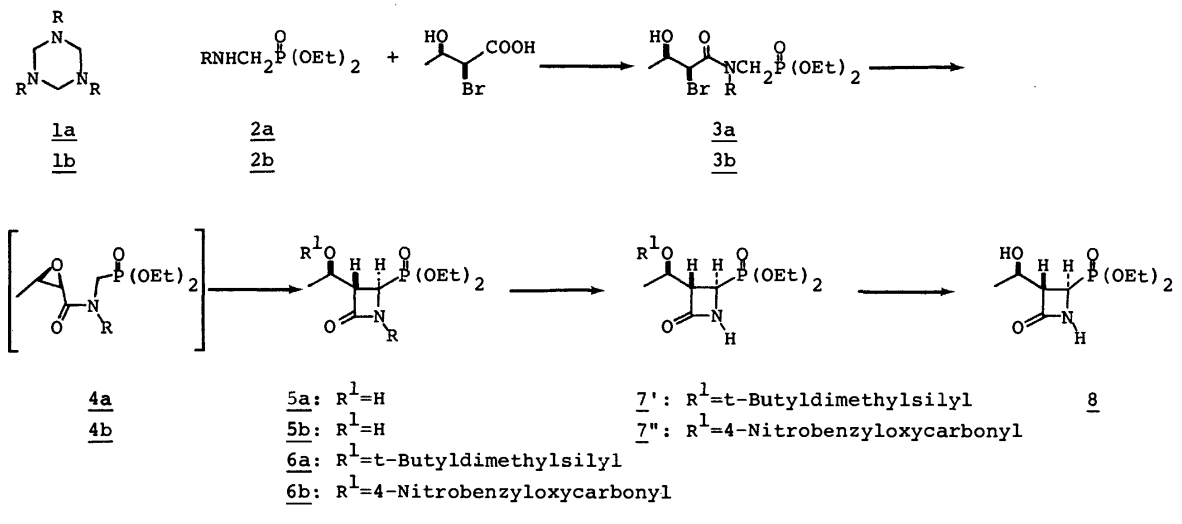

Scheme 1.

(THF) in the presence of 1 equivalent of dicyclohexylcarbodiimide (DCC) gave **3a** (77% yield) and **3b** (21% yield).

Next, these phosphorus-containing butyramides were cyclized to β-lactams in a stereospecific manner. A treatment of **3a** and **3b** with 1 equivalent of lithium hexamethyldisilazanide in tetrahydrofuran at ice-cooling temperature for 5 min, and then another 1 equivalent of $LiN(SiMe_3)_2$ at 24 °C gave chiral 4-diethoxyphosphinyl-3-(1-hydroxyethyl)-2-azetidinone derivatives (**5a** (37% yield) and **5b** (61% yield) via *cis*-epoxides, **4a** and **4b**); *cis*-β-lactams were not isolated. The protection of the hydroxyl group of **5b** with 4-nitrobenzyl chloroformate by use of 4-dimethylaminopyridine (DMAP) as a base in CH_2Cl_2 gave **6b** (79% yield) as a foam. The deprotection of the methoxyphenyl group of **6b** with 3 equivalents of cerium(IV) ammonium nitrite (CAN) in acetone-H_2O (3 : 2) gave **7″** (81% yield) as a crystalline solid; mp 74—76 °C. The hydrogenolysis of **7″** with 5% Pd-C/H_2 at room temperature gave **8** (92% yield); mp 70—71 °C; $[\alpha]_D^{24}$ −4.9° (*c* 0.59, $CHCl_3$). Similarly, protection of the hydroxyl group of **5a** with *t*-butyldimethylsilyl chloride by use of 4-dimethylaminopyridine (DMAP) as a base in *N*,*N*-dimethylformamide (DMF) gave **6a** (67%). Deprotection of the methoxybenzyl group of **6a** with $K_2S_2O_8$-K_2HPO_4 in MeCN-H_2O (1 : 1) at 70—75 °C under argon for 30 min gave *N*-unsubstituted β-lactam **7′** (57% yield) as a gum. This 3,4-trans compound (**7′**) was also alternatively synthesized in good yield without detecting the 3,4-cis isomer[1b] by a treatment of (3*R*,4*R*)-4-acetoxy-3-[(*R*)-1-(*t*-butyldimethylsilyloxy)-ethyl]-2-azetidinone (**9**) with triethyl phosphite according to Campbell's method,[1] and **7′**, obtained from both routes was identical in all respects. Compound **7′** was converted to **8** in 72% yield by a treatment with a tetrabutylammonium fluoride solution in tetrahydrofuran.

These compounds **5a**, **b**, **6a**, **b**, **7′**, **7″**, and **8** should be potential precursors to new 1-aminoalkylphosphonic acid analogues.

Experimental

Melting points were determined on a Yanagimoto micro-melting point apparatus and were uncorrected. Optical rotations were obtained by the use of a Perkin-Elmer 241 polarimeter. ^1H NMR spectra were recorded at 60 MHz with a Varian T-60 spectrometer using tetramethylsilane as an internal standard (δ value). The IR absorption spectra were determined on a Jasco IR A-2 spectrophotometer. Mass spectra were obtained on a JMS-01SG mass spectrometer. Preparative TLC was performed on silica-gel plates (Merck 60 PF_{245}), and column chromatography was carried out on columns packed with Merck silica-gel 60 using slightly increased pressure (1.5 atm) for elution. Elemental analyses were performed by the Analytical Center of the Analytical and Metabolic Research Laboratories, Sankyo Co., Ltd.

1,3,5-Tris(4-methoxybenzyl)hexahydro-1,3,5-triazine (1a). To a solution of 4-methoxybenzylamine (13.72 g, 0.10 mol) in dry ethanol (10 ml) was added formaldehyde (37 wt% solution in water, 7.5 ml) at room temperature with stirring. After 15 min, the reaction mixture was dissolved in EtOAc (100 ml). The solution was washed with water and brine, dried over $MgSO_4$, and concentrated in vacuo to give a triazine (14.22 g, 95% yield) as a crystalline solid; mp 113—115 °C. ^1H NMR ($CDCl_3$) δ=3.35 (6H, s), 3.55 (6H, s), 3.75 (9H, s), 6.65—7.25 (12H, m). MS *m/z* 447 (M^+). Found: C, 72.48; H, 7.38; N, 9.39%. Calcd for $C_{27}H_{33}O_3N_3$: C, 72.00; H, 7.40; N, 9.15%.

1,3,5-Tris(4-methoxyphenyl)hexahydro-1,3,5-triazine (1b). Treatment of *p*-anisidine and formaldehyde as described above gave **1b** in 72% yield as a crystalline solid; mp 128—130 °C. ^1H NMR ($CDCl_3$) δ=3.73 (3H, s), 4.65 (2H, s), 6.65—7.15 (4H, m). MS *m/z* 405 (M^+). Found: C, 70.63; H, 6.65; N, 10.22%. Calcd for $C_{24}H_{27}N_3O_3$: C, 71.09; H, 6.71; N, 10.36%.

***N*-(Diethoxyphosphinylmethyl)-4-methoxybenzylamine (2a).** A solution of the triazine **1a** (6.27 g, 14 mmol) in diethyl phosphite (5.4 ml, 42 mmol) was stirred for 6 h at 100 °C. After cooling, the reaction mixture was diluted with EtOAc (100 ml), which was washed with sat. $NaHCO_3$ aq and brine, dried over $MgSO_4$, and concentrated in vacuo to give an oily residue. Chromatography of the remaining residue on a silica-gel column (elution with cyclohexane-EtOAc (1 : 4)) gave an amine (7.30 g, 60.1%) as a viscous oil. ^1H NMR ($CDCl_3$) δ=1.25 (6H, t, *J*=6 Hz), 1.65 (1H, bs), 2.85 (2H, d, *J*=13 Hz), 3.65 (3H, s), 3.8—4.3 (6H, m), 6.6—7.25 (4H, m).

***N*-(Diethoxyphosphinylmethyl)-4-methoxyaniline (2b).** The same treatment of **1b** as described above in the formation of **2a** from **1a** gave **2b** in 61% yield as an oil. ^1H NMR ($CDCl_3$) δ=1.16 (6H, t, *J*=6 Hz), 3.30 (2H, d, *J*=6 Hz), 3.67 (3H, s), 3.8—4.3 (4H, m), 6.68 (4H, s). IR ν_{max}(film) cm^{-1}; 3300, 1520, 1260. MS *m/z* 273 (M^+).

(2*S*,3*R*)-*N*-(Diethoxyphosphinylmethyl)-*N*-(4-methoxybenzyl)-2-bromo-3-hydroxybutyramide (3a). To a solution of the amine **2a** (6.88 g, 24 mmol) and (2*S*,3*R*)-2-bromo-3-hydroxybutyric acid (4.39 g, 24 mmol) in THF (50 ml) was added DCC (4.66 g, 24 mmol) with stirring at room temperature. After 10 min, the reaction mixture was filtered to remove the precipitated DCC-H_2O. The filtrate was concentrated in vacuo to give an oily mixture, which was chromatographed on a silica-gel column. Elution with EtOAc gave an amide **3a** (8.32 g, 77% yield). ^1H NMR ($CDCl_3$) δ=1.1—1.4 (9H, m), 3.80 (3H, s), 3.85—4.45 (8H, m), 4.5—4.8 (2H, m), 6.85—7.20 (4H, m). MS *m/z* 451 (M^+).

(2*S*,3*R*)-*N*-(Diethoxyphosphinylmethyl)-*N*-(4-methoxyphenyl)-2-bromo-3-hydroxybutyramide (3b). The same treatment of **2b** as described above in the formation of **3a** from **2a** gave **3b** in 21% yield as a crystalline solid; mp 76—79 °C (from diisopropyl ether). ^1H NMR ($CDCl_3$) δ=1.22 (3H, t, *J*=8 Hz), 1.28 (6H, t, *J*=8 Hz), 3.78 (3H, s), 3.88—4.28 (8H, m), 6.74—7.30 (4H, m). MS *m/z* 437 (M^+). Found: C, 44.00; H, 5.78; N, 3.14; Br, 18.43; P, 7.70%. Calcd for $C_{16}H_{25}NO_6BrP$: C, 43.81; H, 5.70; N, 3.19; Br, 18.23; P, 7.16%.

(3*S*,4*R*)-4-Diethoxyphosphinyl-3-[(*R*)-1-hydroxyethyl]-1-(4-methoxybenzyl)-2-azetidinone (5a). To a solution of the amide **3a** (2.26 g, 5 mmol) in THF (10 ml) was added dropwise a solution of lithium hexamethyldisilazanide (15 mmol), which was prepared from hexamethyldisilazane (2.42 g) in THF (10 ml) and butyllithium (1.6 M in hexane, 9.38 ml), under nitrogen with stirring at 0—5 °C. After 30 min, the reaction mixture was diluted with EtOAc (100 ml), which was washed with 5% HCl, sat. $NaHCO_3$ and brine,

dried over Na_2SO_4, and concentrated in vacuo to give an oily mixture. Chromatography of the mixture on preparative silica-gel plates (developed with EtOAc) gave a β-lactam **5a** (0.68 g, 36.6% yield). IR ν_{max}(film) 1750 cm^{-1}; ^1H NMR ($CDCl_3$) δ=1.15—1.45 (9H, m), 2.95 (1H, bs), 3.20—3.55 (1H, m), 3.6—4.4 (7H, m), 4.75 (1H, d, J=15 Hz), 6.65—7.35 (4H, m). MS m/z 371 (M^+).

(3*S*,4*R*)-4-Diethoxyphosphinyl-3-[(*R*)-1-hydroxyethyl]-1-(4-methoxyphenyl)-2-azetidinone (5b). Treatment of **3b** with lithium hexamethyldisilazanide as described above in the formation of **5a** from **3a** gave **5b** in 61% yield as an oil. IR ν_{max}(film) cm^{-1}; 3400, 1760, 1260, 1520. ^1H NMR ($CDCl_3$) δ=1.20 (3H, d, J=6 Hz), 1.22 (6H, t, J=6 Hz), 2.15 (1H, bs), 3.70 (3H, s), 3.28—4.45 (7H, m), 6.68—7.48 (4H, m). MS m/z 357 (M^+).

(3*S*,4*R*)-3-[(*R*)-1-(*t*-Butyldimethylsilyloxy)ethyl]-4-diethoxyphosphinyl-1-(4-methoxybenzyl)-2-azetidinone (6a). To a solution of **5a** (520 mg, 1.4 mmol) and *t*-butyldimethylsilyl chloride (320 mg, 2.1 mmol) in DMF (2 ml) was added DMAP (260 mg, 2.1 mmol) at room temperature with stirring. After 15 h, the reaction mixture was diluted with EtOAc (100 ml), which was washed with 5% HCl aq, sat. $NaHCO_3$ and brine, dried over Na_2SO_4, and filtered. The filtrate was concentrated in vacuo to give an oily product which was chromatographed on a silica-gel column. Elution with cyclohexane-EtOAc (1 : 1) gave a silyl ether (**6a**, 451 mg, 67.2% yield). ^1H NMR ($CDCl_3$) δ=0.05 (6H, s), 0.75 (9H, s), 1.05—1.40 (6H, dt, J=8, 2 Hz; 3H, d, J=6 Hz), 3.27 (1H, dt, J=8, 3 Hz), 3.73 (3H, s), 3.73—4.30 (7H, m), 4.57 (1H, d, J=14 Hz), 6.65—7.30 (4H, m). IR ν_{max}(film) 1760, 1260 cm^{-1}. MS m/z 485 (M^+).

(3*S*,4*R*)-4-Diethoxyphosphinyl-1-(4-methoxyphenyl)-3-[(*R*)-1-(4-nitrobenzyloxycarbonyloxy)ethyl]-2-azetidinone (6b). To a solution of **5b** (140 mg, 0.4 mmol), 4-nitobenzyloxycarbonyl chloride (260 mg, 1.2 mmol) in dichloromethane (4 ml) was added DMAP (150 mg, 1.2 mmol) with stirring at room temperature. After 2 h, the reaction mixture was diluted with EtOAc, which was washed with dil. HCl, water, sat. $NaHCO_3$ and brine, dried over $MgSO_4$, and concentrated in vacuo to give a residual oil. Preparative TLC of the residue on silica-gel plates gave **6b** (210 mg, 97% yield) as an oil. IR ν_{max}(film) cm^{-1}; 1760, 1610, 1520, 1260. ^1H NMR ($CDCl_3$) δ=1.24 (6H, dt, J=6, 2 Hz), 1.49 (3H, d, J=4 Hz), 3.48—3.68 (1H, m), 3.79 (3H, s), 3.84—4.38 (6H, m), 5.20 (2H, s), 6.78—8.25 (8H, m). MS m/z 536 (M^+).

(3*S*,4*R*)-3-[(*R*)-1-(*t*-Butyldimethylsilyloxy)ethyl]-4-diethoxyphosphinyl-2-azetidinone (7′). (a) To a solution of **6a** (140 mg, 0.3 mmol) in MeCN-H_2O (1 : 1, 20 ml) was added K_2HPO_4 (490 mg, 2.8 mmol) and $K_2S_2O_8$ (900 mg, 3.3 mmol) under argon. The mixture was heated at 73 °C for 30 min with stirring. After concentration in vacuo, the residue was diluted with water (50 ml), and extracted with EtOAc (100 ml×2). The combined organic layer was washed with sat. $NaHCO_3$ and brine, dried over Na_2SO_4, filtered and concentrated in vacuo to give an oily residue. Chromatography on a preparative TLC plate (developed with cyclohexane-EtOAc (1 : 2) gave *N*-unsubstituted product **7′** (60 mg, 57% yield) as a gum. ^1H NMR ($CDCl_3$) δ=0.05 (6H, s), 0.85 (9H, s), 1.15 (3H, d, J=6 Hz), 1.35 (6H, t, J=8 Hz), 3.35 (1H, dt, J=8, 3 Hz), 3.7—4.5 (7H, m), 6.30 (1H, bs). MS m/z 366 (M^+).

(b) A mixture of (3*R*,4*R*)-4-acetoxy-3-[(*R*)-1-(*t*-butyldimethylsilyloxy)ethyl]-2-azetidinone (**9**, 1.2 g) and triethyl phosphite (4 ml) was heated to 100 °C for 1 h. The reaction mixture was concentrated in vacuo with a pump, and chromatographed on a silica-gel column. Elution with EtOAc-cyclohexane (1 : 1) gave **7′** in 92% yield, which was identical with that obtained in (a).

(3*S*,4*R*)-4-Diethoxyphosphinyl-3-[(*R*)-1-(4-nitrobenzyloxycarbonyloxy)ethyl]-2-azetidinone (7″). To a solution of **6b** (110 mg, 0.2 mmol) in acetone (1.5 ml) and water (1 ml) was added CAN (330 mg, 0.6 mmol) at 0 °C with magnetic stirring. After 30 min at 0 °C, the reaction mixture was diluted with EtOAc, which was washed with sat. $NaHCO_3$ and brine, dried over $MgSO_4$, and concentrated in vacuo to give an oily residue. The residue was chromatographed on a silica-gel column to give **7″** (88 mg, 81% yield) as a crystalline solid: Mp 77—78 °C. ^1H NMR ($CDCl_3$) δ=1.25 (3H, d, J=6 Hz), 1.42 (6H, t, J=6 Hz), 3.41—3.70 (1H, m), 3.84 (1H, dd, J=8, 2 Hz), 4.12 (2H, dq, J=16, 2 Hz), 4.28 (2H, dq, J=16, 2 Hz), 5.26 (2H, s), 7.00 (1H, bs), 7.49—8.35 (4H, A_2B_2-quartet). MS m/z 430 (M^+). Found: C, 47.48; H, 5.27; N, 6.39; P, 7.09%. Calcd for $C_{17}H_{23}N_2O_9P$: C, 47.44; H, 5.35; N, 6.51; P, 7.21%.

(3*S*,4*R*)-4-Diethoxyphosphinyl-3-[(*R*)-1-hydroxyethyl]-2-azetidinone (8). (a) A solution of **7″** (106 mg, 0.246 mmol) in MeOH (5 ml) and 5% Pd-C (100 mg) was stirred for 2 h at room temperature under hydrogen. Filtration, concentration and column chromatography on silica gel (eluted with EtOAc-EtOH=19 : 1) gave **8** (56 mg, 91% yield) as a crystalline solid; mp 70—71 °C (from EtOAc-cyclohexane). $[\alpha]_D^{24}$ —4.9° (*c* 0.59, $CHCl_3$). IR ν_{max}(KBr) cm^{-1}; 3350, 3200, 1750. ^1H NMR δ=1.24 (3H, d, J=6 Hz), 1.32 (6H, t, J=8 Hz), 3.29 (1H, dt, 9, 3 Hz, C_3-H)), 3.61—4.41 (7H, m, containing OH), 7.40 (1H, bs, NH). MS m/z 233 (M^+−18). Found: C, 43.03; H, 7.12; N, 5.67; P, 11.53%. Calcd for $C_9H_{18}NO_5P$: C, 43.02; H, 7.16; N, 5.57; P, 12.34%.

(b) A solution of **7′** (140 mg, 0.383 mmol) in THF (2 ml) and *n*-Bu_4NF (1.0 M solution in THF, 0.6 ml) was allowed to stand overnight at room temperature. The solution was concentrated in vacuo to give an oily mixture which was chromatographed on a silica-gel column. Elution with EtOAc and then 10% EtOH in EtOAc gave **8** (70 mg, 72% yield), which was identical with that obtained from **7″** in procedure (a).

References

1) a) M. M. Campbell and N. Carruthers, *J. Chem. Soc., Chem. Commun.*, **1980**, 730; b) M. M. Campbell, N. I. Carruthers, and S. J. Mickel, *Tetrahedron*, **38**, 2513 (1982).

2) a) M. Shiozaki, N. Ishida, T. Hiraoka, and H. Maruyama, *Chem. Lett.*, **1983**, 169; b) M. Shiozaki, N. Ishida, T. Hiraoka, and M. Maruyama, *Bull. Chem. Soc. Jpn.*, **57**, 2135 (1984); c) M. Shiozaki, N. Ishida, T. Hiraoka, and H. Yanagisawa, *Tetrahedron Lett.*, **22**, 5205 (1981); d) M. Shiozaki, N. Ishida, T. Hiraoka, and H. Maruyama, *Tetrahedron*, **40**, 1795 (1984); e) H. Maruyama, M. Shiozaki, and T. Hiraoka, *Bull. Chem. Soc. Jpn.*, **58**, 3264 (1985); f) H. Yanagisawa, A. Ando, M. Shiozaki, and T. Hiraoka, *Tetrahedron Lett.*, **24**, 1037 (1983); g) M. Shiozaki, H. Maruyama, and N. Ishida, *Heterocycles*, **22**, 1725 (1984); h) M. Shiozaki, N. Ishida, and H. Maruyama, *Agric. Biol. Chem.*, **50**, 2353 (1986) i) M. Shiozaki and H. Masuko, *Heterocycles*, **22**, 1727 (1984); j) H. Maruyama, M. Shiozaki, S. Oida, and T. Hiraoka, *Tetrahedron Lett.*, **26**, 4521 (1985); k) S. Hanessian, A. Bedeshi, C. Battistini, and N. Mongelli, *J. Am. Chem. Soc.*, **107**, 1438 (1985); l) M. Shiozaki, T. Hiraoka, H. Yanagisawa, H. Maruyama, N. Kishi, and O.

Oda, *Heterocycles*, **24**, 1007 (1986).

3) a) A. Yoshida, T. Hayashi, N. Takeda, S. Oida, and E. Ohki, *Chem. Pharm. Bull.*, **29**, 2899 (1981); b) P. J. Reider, R. Rayford, and E. J. J. Grabowski, *Tetrahedron Lett.*, **23**, 379 (1982); c) P. J. Reider and E. J. J. Grabowski, *Tetrahedron Lett.*, **23**, 2293 (1982); d) S. Karady, J. S. Amato, R. A. Reamer, and L. M. Weinstock, *J. Am. Chem. Soc.*, **103**, 6765 (1981).

4) R. W. Ratcliffe and B. G. Christensen, *Tetrahedron Lett.*, **1973**, 4645.

5) Y. Shimohigashi, M. Waki, and N. Izumiya, *Bull. Chem. Soc. Jpn.*, **52**, 949 (1979).

 © 1987 The Chemical Society of Japan Bull. Chem. Soc. Jpn., 60, 649—652 (1987)

The Optical Resolution and Asymmetric Transformation of DL-*p*-Hydroxyphenylglycine with (+)-1-Phenylethanesulfonic Acid

Ryuzo YOSHIOKA,* Masanori TOHYAMA,† Osamu OHTSUKI, Shigeki YAMADA,†† and Ichiro CHIBATA†††
Research Laboratory of Applied Biochemistry, Tanabe Seiyaku Co., Ltd.,
16-89, Kashima 3-Chome, Yodogawa-ku, Osaka 532
(Received July 18, 1986)

Optically active 1-phenylethanesulfonic acid was found to be an efficient resolving agent for the optical resolution and asymmetric transformation of DL-*p*-hydroxyphenylglycine. When DL-*p*-hydroxyphenylglycine was resolved by the fractional crystallization of its diastereomeric salt with (+)-1-phenylethanesulfonic acid, less soluble D-*p*-hydroxyphenylglycine (+)-1-phenylethanesulfonate [D-HPG·(+)-PES] was obtained in a good yield. Soluble L-HPG·(+)-PES was easily epimerized into DL-HPG·(+)-PES by heating it at 100 °C in glacial acetic acid in the presence of a small amount of salicylaldehyde. Under such epimerizing conditions, the asymmetric transformation of DL-HPG·(+)-PES was attempted by simultaneously combining the fractional crystallization of the less soluble D-HPG·(+)-PES and the epimerization of the soluble L-HPG·(+)-PES. This asymmetric transformation was achieved successfully; that is, 80% of the DL-HPG used as the starting material was converted into D-HPG.

D-*p*-Hydroxyphenylglycine is a starting material in the production of β-lactam antibiotics, such as semi-synthetic penicillins or cephalosporins. In order to develop a practical method for the production of this D-*p*-hydroxyphenylglycine (D-HPG), we have been studying the optical resolution of synthetic DL-HPG[1,2] by several techniques, for instance, preferential crystallization,[3] diastereomer salt formation,[4] and asymmetric transformation.

In our recent studies of asymmetric transformation,[5–8] it was reported that D-HPG was successfully prepared by asymmetric transformation combined with preferential crystallization and simultaneous racemization.[8] Besides this convenient procedure, if a suitable resolving agent of DL-HPG through diastereomer salt formation can be found, it will also provide an advantageous resolution method (i.e., asymmetric transformation) for the preparation of D-HPG. In the present work, we could find that optically active 1-phenylethanesulfonic acid was a favorable resolving agent for this purpose. In this paper, we wish to describe particularly a unique method for the preparation of D-HPG by asymmetric transformation between two diastereomeric salts of DL-HPG with (+)-1-phenylethanesulfonic acid.

In general, free neutral amino acids can not form diastereomeric salts directly with ordinary weak basic or weak acidic resolving agents. For the formation of these diastereomeric salts, it has usually employed such strongly acidic resolving agents[9,13] as the camphorsulfonic acids and also, rarely, the terpenesulfonic acids or cholestenonesulfonic acid. However, these chiral sulfonic acids derived from naturally occurring products are not necessarily satisfactory for practical production because they are expensive, are somewhat optically or chemically labile, and are not available in large amounts. Therefore, we have carried out the screening of resolving agents aimed at discovering one without these disadvantages; this led to the finding of 1-phenylethanesulfonic acid.

The synthesis and optical resolution of racemic 1-phenylethanesulfonic acid [(±)-PES] has been fairly well described in the literature.[10] According to the previously reported synthetic method, however, (±)-PES could not be easily prepared.[11] In the course of our further researches, it was found that (±)-PES synthesized by sulfonating (±)-1-phenylethyl bromide[11] could be resolved into the (+)-isomer through its diastereomeric salt with D-HPG in an aqueous solvent. On the contrary, DL-HPG could be easily resolved in the same manner into the D-isomer by using the (+)-PES as the resolving agent. In Table 1, the physical properties of D-*p*-hydroxyphenylglycine (+)-1-phenylethanesulfonate (D-HPG·(+)-PES) and L-HPG·(+)-PES are shown. Since the difference in solubility between the two diastereomeric salts in water (20 °C) was very large, the fractional crystallization of DL-HPG with less than an equivalent amount of (+)-PES in water afforded almost optically pure D-HPG·(+)-PES in a good yield (43.8% based on DL-HPG·(+)-PES).

On the other hand, we previously reported that the racemization of optically active amino acid salts (e.g., achiral sulfonates) was accomplished by heating them in an acetic acid solution in the presence of a catalytic amount of an aldehyde and free DL-amino acid.[6] This racemization method prompted us to study the asymmetric transformation of DL-HPG with (+)-PES.

In order to apply the asymmetric transformation to DL-HPG·(+)-PES, (+)-PES must be chemically and optically stable under the conditions for the above racemization (epimerization for diastereomer). The optical stability of (+)-PES was tested under the pre-

†Present address: Chuoh Sellers Office Osaka Branch, Tanabe Seiyaku Co., Ltd., 5-37, Zuiko 2-Chome, Higashiyodogawa-ku, Osaka 533.
††Present address: Research Planning & Investigation Division, Tanabe Seiyaku Co., Ltd., 16-89, Kashima 3-Chome, Yodogawa-ku, Osaka 532.
†††Present address: Research & Development Headquarters, Tanabe Seiyaku Co., Ltd., 16-89, Kashima 3-Chome, Yodogawa-ku, Osaka 532.

Table 1. Properties of D-HPG·(+)-PES and L-HPG·(+)-PES

		D-HPG·(+)-PES	L-HPG·(+)-PES
Mp (θ_m/°C)		251—252	204—205
$[\alpha]_D^{25}$/° (*c* 1, MeOH)		−78.9	+98.6
Solubility (g/100 ml water)	5°C	0.8	—
	20°C	1.1	77
	40°C	1.7	—
(g/100 ml AcOH)	20°C	0.2	1.0
	70°C	0.2	4.1

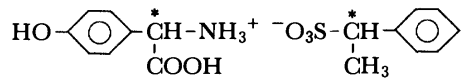

D-*p*-Hydroxyphenylglycine (+)-1-Phenylethanesulfonate
[D-HPG·(+)-PES]

Table 2. Optical Stability of (+)-PES in Various Solvents

Solvent	Racemization degree/%		
	2h	5h	10h
Water	0	0	0
1M-H_2SO_4	0	0	0
AcOH	0	0	0
2M-NaOH	8	17	31

The solutions of (+)-PES (0.2 g) dissolved in solv. (6 ml) were stirred at 100°C for 10 h.

sent heating conditions in various solvents. As shown in Table 2, (+)-PES was quite stable at 100 °C for 10 h in water, 1 M H_2SO_4 (1 M=1 mol dm^{-3}) and in acetic acid, but in 2 M NaOH it was gradually racemized. Since (+)-PES was optically stable in acetic acid, it was preferable to accelerate the epimerization of the soluble L-HPG·(+)-PES (i.e., the racemization of the L-HPG moiety). As can be seen in Fig. 1, L-HPG·(±)-PES was easily epimerized into DL-HPG·(±)-PES by heating it at 100 °C for ca. 4 h in acetic acid containing a 0.2 molar equivalent of salicylaldehyde. In addition, the crystals of D-HPG·(+)-PES were also confirmed to be rather insoluble in acetic acid (Table 1) and to precipitate without changing, even under the above epimerizing conditions.

Thus, the characteristics of the foregoing HPG·(+)-PES satisfied the most essential requirement for the intended asymmetric transformation via diastereomer salt formation. Therefore, using the optical resolution and the epimerization method described above, the asymmetric transformation of DL-HPG·(+)-PES was examined in a system. For instance, a mixture of DL-HPG (10.0 g), (+)-PES (11.2 g), glacial acetic acid (200 ml), and salicylaldehyde (0.63 ml) (added for accelerating the epimerization) was stirred at 100 °C for 5 h. The reaction proceeded continuously in a slurry state of the solid-liquid heterogeneous system. After this reaction mixture had then been cooled at 20 °C, precipitated crystals were collected to give D-HPG·(+)-PES

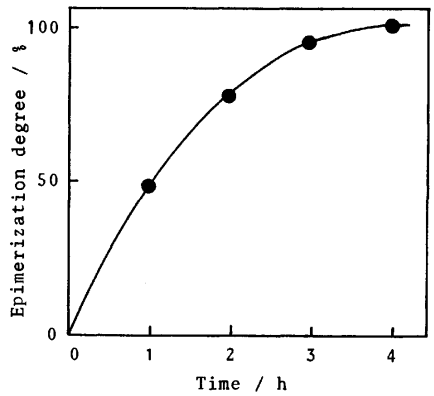

Fig. 1. Time course on epimerization of L-HPG·(±)-PES. The reactions were carried out at 100°C in L-HPG·(±)-PES/AcOH in the presence of salicylaldehyde (0.2 molar equivalent).

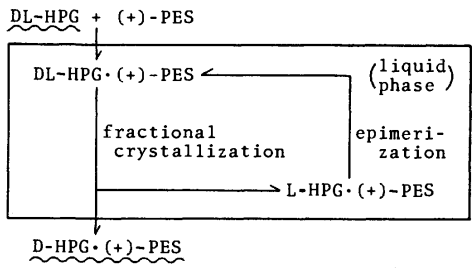

Fig. 2. Asymmetric transformation of DL-HPG with (+)-PES. ~~~, solid state.

(18.0 g); $[\alpha]_D^{25}$ −74.5° (*c* 1, MeOH); optical purity, 95.0%; yield, 85.1% (based on DL-HPG·(+)-PES). The pathway of the asymmetric transformation described here is considered to be that shown in Fig. 2: When the crystals of D-HPG·(+)-PES were fractionally precipitated from a salt solution consisting of DL-HPG and (+)-PES, the epimerization of the soluble L-HPG·(+)-PES proceeded simultaneously in the liquid phase, and D-HPG·(+)-PES was also thereupon immediately precipitated from the epimerizing solution. Since

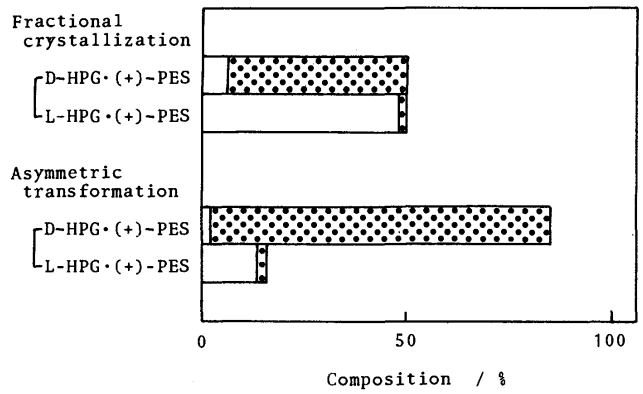

Fig. 3. The change in the composition of D- or L-HPG·(+)-PES by fractional crystallization and asymmetric transformation.
▩: Crystals of (+)-PES salt, □: (+)-PES salt in solution.

these steps were repeated continuously in the reaction system, the equilibrium finally shifted in favor of D-HPG·(+)-PES as a whole. As a result, 80% of the DL-HPG·(+)-PES was transformed into D-HPG·(+)-PES. Figure 3 shows a comparison of the results of the ordinary fractional crystallization and of the asymmetric transformation.

Among the various techniques for optical resolution, the fractional crystallization of the diastereomeric salts with a chiral resolving agent under simultaneous epimerizing conditions is known as an asymmetric transformation of the second order.[12,13] This method is very attractive, particularly when separations for industrial applications are contemplated, because it is possible to transform the racemate to the desired isomer in a nearly quantitative yield through a simple operation. The asymmetric transformation of DL-HPG with (+)-PES is, therefor, expected to be a very promising procedure for the industrial production of D-HPG.

Experimental

Materials and Analyses. D-, L-, and DL-HPG manufactured by our company, Tanabe Seiyaku Co., Ltd. were used. The (±)- and (+)-1-phenylethanesulfonic acids (PES) were prepared by the method shown below. Other chemicals were obtained from Tokyo Kasei Kogyo Co., Ltd. All samples were dried overnight in vacuo at 40 °C. Melting points were measured with a Yamato MP-21 melting point apparatus in an unsealed capillary tube; they are uncorrected. Optical rotations were measured with a Perkin-Elmer 141 automatic polarimeter. IR spectra were recorded on a Shimadzu infrared spectrophotometer, Model IR-420. ^{1}H NMR spectra were obtained using a Hitachi Perkin-Elmer R-40 High Resolution ^{1}H NMR spectrometer, with tetramethylsilane as an internal standard. Elemental analyses were performed with a Perkin-Elmer 240 elemental analyzer. Solubility was determined by approaching saturation equilibrium from both undersaturation and supersaturation. Solute concentration was measured with a Karl Zeiss immersion refractometer.

Preparation of Barium (±)-1-Phenylethanesulfonate. (±)-1-Phenylethanesulfonic acid [(±)-PES] was prepared from commercially available (±)-1-phenylethyl bromide in the manner described by Kharasch et al.[11] That is, a mixture of (±)-1-phenylethyl bromide (70 g), a 50% ammonium hydrogensulfite solution (75 g), and 28% aqueous ammonia (30 ml) was stirred at room temperature overnight. After the oil part of the reaction mixture had been removed, barium hydroxide octahydrate (60 g) was added and the ammonia was boiled out. The aqueous solution was then adjusted to neutrality with sulfuric acid, and the insoluble barium salts were filtered off and washed with water. The filtrates were partly concentrated under reduced pressure, and the precipitated crystals were filtered, washed with cold water, and dried to give (±)-PES·1/2Ba·1/2H_2O (44 g) in a 44% yield; IR (nujol) 3475, 1630, 1185, and 1065 cm^{-1}; ^{1}H NMR (DMSO-d_6) δ=1.48 (3H, d, J=7 Hz, CH_3), 3.72 (1H, q, J=7 Hz, CH), and 7.1—7.4 (5H, m, aromatic).

Optical Resolution of (±)-1-Phenylethanesulfonic Acid. To a solution of (±)-PES·1/2Ba·1/2H_2O (42.1 g) in hot 10% HCl (590 ml) was added D-HPG (26.7 g). After it had then been cooled slowly to room temperature, the mixture was stirred at 25 °C for 2 h. The resulting crystals were filtered, washed with a small amount of cold water, and dried to give crude (+)-PES·D-HPG; $[\alpha]_D^{25}$ −79.5° (*c* 1, MeOH). The crude salt (26.0 g) was recrystallized from 0.1% sulfuric acid (430 ml) to afford the pure (+)-PES·D-HPG (23.0 g); $[\alpha]_D^{25}$ −78.9° (*c* 1, MeOH); mp 262—263 °C (decomp); IR (nujol) 3050, 1740, 1600, and 1140 cm^{-1}; ^{1}H NMR (DMSO-d_6) δ=1.48 (3H, d, J=7 Hz, CH_3), 3.72 (1H, q, J=7 Hz, CH), 4.97 (1H, s, CH), 6.8—7.5 (9H, m, aromatic), and 8.7 (2H, br, NH_2).

Found: C, 54.39; H, 5.51; N, 3.99; S, 8.98%. Calcd for $C_{16}H_{19}NO_6S$: C, 54.38; H, 5.42; N, 3.96; S, 9.07%. This product was optically and chemically pure. The specific rotation of a mixture of (±)-PES and an equivalent amount of D-HPG was $[\alpha]_D^{25}$ −87.1° (*c* 1, MeOH), and that of an authentic (+)-PES·D-HPG was $[\alpha]_D^{25}$ −78.9° (*c* 1, MeOH).

The pure (+)-PES·D-HPG (22.0 g) obtained above was suspended in water (22 ml) at 50—60 °C. The solution was adjusted to pH 5.5 with 6M NaOH (ca. 10.4 ml) and then stirred at 20 °C for 2 h. The crystals thus precipitated were filtered, washed with cold water, and dried to obtain D-HPG (9.5 g). The mother liquor filtered was passed through a column of Amberlite IR-120 (100 ml, H^+ form), after which the column was washed with water. The aqueous solution passed through was treated with activated charcoal and concentrated to dryness in vacuo at 40 °C to give (+)-PES (free acid 11.5 g) as pasty crystals; $[\alpha]_D^{25}$ +21.9° (*c* 3, DMSO); ^{1}H NMR (D_2O) δ=1.71 (3H, d, J=7 Hz, CH_3), 4.24 (1H, q, J=7 Hz, CH), and 7.55 (5H, s, aromatic).

Optical Stability of (+)-1-Phenylethanesulfonic Acid. A solution of (+)-PES (free acid 0.2 g) in various solvents (6 ml) was sealed in a glass tube and shaken at 100 °C for 10 h. After the solution had then been cooled and diluted with water (4 ml), the optical rotation was measured. The racemization degree was calculated from the following formula:

$$\frac{\text{initial optical rotation} - \text{final optical rotation}}{\text{initial optical rotation}} \times 100$$

The optical stability of (+)-PES was judged from the resulting racemization degree in the various solvents shown in Table 2.

Optical Resolution of DL-*p*-Hydroxyphenylglycine. DL-HPG was resolved with (+)-PES in the same manner as in

the optical resolution of (±)-PES described above: A mixture of DL-HPG (10.0 g), (+)-PES (free acid 10.0 g), and water (200 ml) was heated until clear and then allowed to cool to 25 °C with stirring. After 2 h, the product was collected, washed with cold water, and dried to give crude D-HPG·(+)-PES (9.7 g); $[\alpha]_D^{25}$ −74.8° (*c* 1, MeOH); optical purity, 95.4% [based on D-(+) salt $[\alpha]_D^{25}$ −78.9° (*c* 1, MeOH) and DL-(+) salt $[\alpha]_D^{25}$ +9.8° (*c* 1, MeOH)]; yield, 43.8% (based on DL-HPG·(+)-PES). The change in the composition of the diastereomeric salts is shown in Fig. 3.

Epimerization of L-HPG·(+)-PES. The epimerization study of the soluble L-HPG·(+)-PES was carried out by using L-HPG·(±)-PES in order to determine the racemization degree of the L-HPG moiety. A mixture of L-HPG·(±)-PES (0.2 g), a 0.2 molar equivalent of salicylaldehyde (6.8 μl), and glacial acetic acid (6 ml) was heated in a sealed tube at 100 °C for the prescribed time interval. The reaction mixture was then diluted with acetic acid (10 ml), and the optical rotation was measured. The epimerization degree was calculated from the decrease in the optical rotation according to the above-noted formula. The results are shown in Fig. 1.

Asymmetric Transformation of DL-*p*-Hydroxyphenylglycine. A mixture of DL-HPG (10.0 g), (+)-PES (11.2 g), salicylaldehyde (0.63 ml), and glacial acetic acid (200 ml) in a flask fitted with a mechanical stirrer and a condenser was continued at 100 °C for 5 h, during which period the reaction system was heterogeneous. The reaction mixture was cooled to 20 °C, and the precipitated crystals were quickly collected by filtration, washed with a small amount of acetic acid, and dried to give crude D-HPG·(+)-PES (18.0 g); $[\alpha]_D^{25}$ −74.5° (*c* 1, MeOH); optical purity, 95.0%; yield, 85.1% (based on DL-HPG·(+)-PES). This ^{1}H NMR and the IR spectra were in accord with an authentic sample of D-HPG·(+)-PES. The change in the composition of both diastereomeric salts by the present asymmetric transformation is shown in Fig. 3.

Preparation of D-*p*-Hydroxyphenylglycine. The crude D-HPG·(+)-PES (17.0 g) obtained above was recrystallized from hot water (300 ml) to give optically pure D-HPG·(+)-PES (14.5 g); $[\alpha]_D^{25}$ −78.9° (*c* 1, MeOH). The pure salt (14.0 g) was suspended in water (15 ml) at 50—60 °C, and the mixture was adjusted to pH 5.5 by the dropwise addition of 6 M NaOH (ca. 6.6 ml), after which it was stirred at 20 °C for 2 h. The crystals thus precipitated were collected, washed with water, and dried to give D-HPG (6.0 g); $[\alpha]_D^{25}$ −158.4° (*c* 1, 1 mol dm^{-3} HCl).

Found : C, 57.50; H, 5.51; N, 8.33%. Calcd for $C_8H_9NO_3$: 57.48; H, 5.43; N, 8.38%.

References

1) A. A. W. Long, J. H. C. Nayler, H. Smith, T. Taylor, and N. Ward, *J. Chem. Soc. C*, **1971**, 1920.

2) M. J. Elton, J. W. Herrison, and A. Jackson, Ger. offen. 2134251 (1972); *Chem. Abstr.*, **76**, 113526p (1972).

3) S. Yamada, C. Hongo, and I. Chibata, *Agric. Biol. Chem.*, **42**, 1521 (1978).

4) S. Yamada, C. Hongo, R. Yoshioka, and I. Chibata, *Agric. Biol. Chem.*, **43**, 395 (1979).

5) C. Hongo, S. Yamada, and I. Chibata, *Bull. Chem. Soc. Jpn.*, **54**, 3286, 3291 (1981).

6) C. Hongo, R. Yoshioka, M. Tohyama, S. Yamada, and I. Chibata, *Bull. Chem. Soc. Jpn.*, **56**, 3744 (1983).

7) C. Hongo, R. Yoshioka, M. Tohyama, S. Yamada, and I. Chibata, *Bull. Chem. Soc. Jpn.*, **57**, 1328 (1984).

8) C. Hongo, M. Tohyama, R. Yoshioka, S. Yamada, and I. Chibata, *Bull. Chem. Soc. Jpn.*, **58**, 433 (1985).

9) P. Newman, "Optical Resolution Procedures for Chemical Compounds," ed by Optical Resolution Information Center, New York (1978), Vol. 1.

10) E. B. Evans, E. E. Mabbott, and E. E. Turner, *J. Chem. Soc.*, **1927**, 1159.

11) M. S. Karasch, E. M. May, and F. R. Mayo, *J. Org. Chem.*, **3**, 175 (1938).

12) M. M. Harris, "Progress in Stereochemistry," ed by W. Klyne and P. B. D. Mare, Butterworths Scientific Publications, London (1958), Vol. 2, p. 157.

13) J. Jacques, A. Collet, S. H. Wilen, "Enantiomers, Racemates, and Resolutions," ed by John Wiley and Sons, Wiley-Interscience, New York (1981), p. 369.

 © 1987 The Chemical Society of Japan Bull. Chem. Soc. Jpn., 60, 653—659 (1987)

The Effects of Catalysts on the Mean Structure of Solvent-Refined Coal in Coal Liquefaction

Koji CHIBA,* Hideyuki TAGAYA, Shimio SATO, and Shinya OHGI
Department of Chemical Engineering, Faculty of Engineering, Yamagata University, Johnan, Yonezawa 992
(Received July 23, 1986)

The effects of MoO_3, Fe_2O_3, or SnO on the conversion and the solvent-refined coal (SRC) yield of Taiheiyo coal were small, whereas their effects on the structure of SRC were large. SRC was separated into four fractions by successive extraction in order to clarify the differences in SRC's among the catalysts. The formation of SnO_2 after the liquefaction was confirmed. It was considered that the oxygen-abstraction ability and the radical-stabilization ability of SnO prevented the retrogressive reaction of coal, SRC, and model compounds. MoO_3 and Fe_2O_3 have a higher ability to hydrogenate and accelerate the hydrocracking of coal and coal-model compounds than does SnO, but their ability to suppress the retrogressive reaction producing heavier compounds is small.

Although many attempts have been made to find more effective coal-liquefaction catalysts, most of them have been limited to the purpose of increasing the conversion to the liquid products of coal.[1,2] However, in order to evaluate a coal-liquefaction reaction and the use of its products, the difference in the structure of the liquefaction products obtained by the use of the different catalysts needs also to be investigated.

In this paper, three different metal oxides, MoO_3, Fe_2O_3, and SnO, were used as catalysts for Taiheiyo-coal liquefaction in tetralin or decalin under a hydrogen or nitrogen atmosphere. In order to clarify the differences in the structures of the products, solvent-refined coal (SRC) was separated into four fractions by successive extraction and their structural parameters were calculated using the Brown-Ladner method.[3]

SRC was treated in the presence of a catalyst in order to correlate the results with the results of coal liquefaction. Further, the reactions of coal model compounds were also examined in order to obtain information about the roles of the catalysts.

Experimental

Taiheiyo coal-1, -2, and -D (Table 1) were ground, passed through a 100-mesh (149 μm) screen and then dried at 107 °C under a nitrogen atmosphere. Taiheiyo coal-2 was deashed to prepare Taiheiyo coal-D by the method of Fan et al.[4] The ash content decreased from 14.4 to 2.2%. For coal liquefaction, a mixture of coal (5 g), a solvent (15 g), and a catalyst (0.5 g) was placed in a Pyrex glass liner, inserted into a 100-ml magnetdriven autoclave; this autoclave was then pressurized to 5.1 MPa at room temperature with hydrogen or nitrogen. It is well-known that the autoclave wall acts as a catalyst. So a Pyrex glass liner was used. The nominal reaction time was 60 min at 400 °C. The materials remaining in the autoclave after the liquefaction were extracted with benzene. A benzene-insoluble material was weighed after drying and then further extracted with THF. The liquefaction solvent was recovered from the benzene extract by vacuum distillation. The distillation residue was weighed as SRC.[5] The conversions to a benzene-soluble material (BC) and to a THF-soluble material (TC) were calculated according to the following equation:

$$\text{Conversion to BC or TC (wt\% daf coal basis)} = \frac{(\text{Coal-charged} - \text{benzene or THF-insoluble material}) \times 100}{\text{daf coal}}$$

The SRC was separated into four fractions by successive extractions; when benzene 4%–heptane 96% (Solvent 1), benzene 15%–heptane 85% (Solvent 2), benzene 50%–hexane 50% (Solvent 3), benzene 60%–methanol 40% (Solvent 4) were used successively as the extraction solvents, Fractions 1—4 were thus obtained.

The ^{1}H NMR spectra were recorded at 90MHz on a Hitachi R 22 apparatus. The solution for the measurements of the ^{1}H NMR spectra was prepared by dissolving 40 mg of a sample in 0.4 ml of chloroform-*d*, using tetramethylsilane as the internal standard.

Results

The liquefaction reactions of Taiheiyo coal-1, -2, and -D in tetralin under a hydrogen atmosphere using different catalysts at 400 °C are shown in Table 2. When no catalyst was used, the conversions to BC and the SRC yields were in the following order: Taiheiyo-D>Taiheiyo-2>Taiheiyo-1. The same order was observed when MoO_3, Fe_2O_3, or SnO was used as the catalyst. The use of catalysts was effective for coal liquefaction, and the conversions to BC with catalysts were from 12 to 18% higher than those without catalysts, even in tetralin. Although SnO was a more effec-

Table 1. Analysis of Coals (wt%)

Coal	Ultimate analysis				Proximate analysis[a]			
	C	H	N	Odiff	Ash	Mois	V.M.	F.C.
Taiheiyo-1	76.7	5.6	0.7	17.0	13.1	3.9	39.6	43.4
Taiheiyo-2	76.6	6.3	0.9	16.2	14.4	4.7	49.6	31.1
Taiheiyo-D[b]	77.0	6.5	1.2	15.3	2.2	2.2	52.4	43.2

a) Mois: Moisture, V.M.: Volatile matter, F.C.: Fixed carbon. b) Taiheiyo-D is Taiheiyo-2 deashed.

Table 2. Liquefaction of Taiheiyo Coal-1, 2 and D at 400 °C under a Hydrogen Atmosphere for 60 min in Tetralin

Coal	Catalyst	Conversion to		SRC yield	O[a] of SRC	fa[b]
		BC	TC			
Taiheiyo-1	None	55.7	83.0	31.8	6.31	0.615
	MoO_3	61.2	84.9	38.9	4.79	0.619
	Fe_2O_3	61.9	88.1	38.5	6.52	0.605
	SnO	67.7	92.2	44.4	3.43	0.600
Taiheiyo-2	None	58.6	81.7	40.7	5.10	0.564
	MoO_3	69.9	85.5	48.4	4.13	0.581
	Fe_2O_3	68.0	92.3	43.9	5.96	0.578
	SnO	76.2	91.4	51.4	3.70	0.578
Taiheiyo-D	None	74.1	84.7	46.4	4.87	0.577
	MoO_3	76.4	85.6	51.7	4.25	0.564
	Fe_2O_3	76.8	87.2	49.2	4.29	0.584
	SnO	80.5	90.0	55.6	4.33	0.560

a) Oxygen content. b) Carbon aromaticity.

Table 3. Effects of Catalysts, Solvents, and Atmospheres on the Liquefaction of Taiheiyo Coal-1

Catalyst	Solvent		Conversion		SRC yield[a]	Aromaticity (fa)[b]
			to BC[a]	to TC[a]		
None	Tetralin	H_2	55.7	83.0	31.8	0.615
		N_2	52.2	78.5	32.0	0.614
	Decalin	H_2	37.5	48.6	23.9	0.571
		N_2	28.3	34.0	14.3	0.539
MoO_3	Tetralin	H_2	61.2	84.9	38.9	0.619
		N_2	49.7	73.4	30.2	0.599
	Decalin	H_2	40.5	46.8	24.9	0.569
		N_2	24.4	26.3	11.7	0.513
Fe_2O_3	Tetralin	H_2	61.9	88.1	38.5	0.605
		N_2	37.3	61.9	25.6	0.566
	Decalin	H_2	23.5	38.8	18.1	0.559
		N_2	20.5	22.3	13.4	0.496
SnO	Tetralin	H_2	67.7	92.2	44.4	0.600
		N_2	43.0	72.5	26.5	0.589
	Decalin	H_2	44.9	62.3	23.9	0.597
		N_2	31.8	35.4	19.8	0.560

a) Wt% daf basis. b) Carbon aromaticity of SRC calculated using Brown-Ladner method.

tive catalyst than MoO_3 and Fe_2O_3, the differences between them were only from 4 to 6%. The highest conversion to BC was always obtained with Taiheiyo-D, and the tendency of conversion to BC with catalysts was not affected by the removal of coal minerals. On the other hand, the differences in the conversions to TC among the catalysts used were relatively small. This indicated that the interaction between coal minerals of Taiheiyo coal and the added catalyst was small. Taiheiyo coal-1 was exclusively used in the latter part of this study.

Taiheiyo coal-1 was liquefied at 400 °C for 60 min in tetralin or decalin under a hydrogen or nitrogen atmosphere using three different kind of catalysts, as is shown in Table 3. Irrespective of the catalyst, the conversion to BC, the TC, and the SRC yields were in the following order:

in tetralin under hydrogen > in tetralin under nitrogen > in decalin under hydrogen > in decalin under nitrogen.

From Table 3, it may seem that two important factors in the conversion to BC, and to TC, and in the SRC yield were the solvent and the atmosphere. To quantify the effects of the liquefaction conditions, variance analysis[6] was applied to these results. The conversions on repeated runs at 440 °C in tetralin were 64.5 and 66.4% for conversion to BC, and 92.1, and 91.9% for conversion to TC. These runs indicated that the experimental data were applicable to the analysis. In the three-way model, we investigated the effects of sixteen different combinations of four catalysts (none, MoO_3, Fe_2O_3, SnO), two solvents (tetralin, decalin), and two atmospheres (hydrogen, nitrogen). The significance at the α=0.01 level showed that the main effects of the conversion and the SRC yields were due to the solvent and the atmosphere, not to the catalyst. The SRC's were analyzed by the use of ^1H NMR, and the structural parameters of the SRC's were then calculated. The three-way variance analysis was also applied to the structural parameter, fa (aromaticity), of

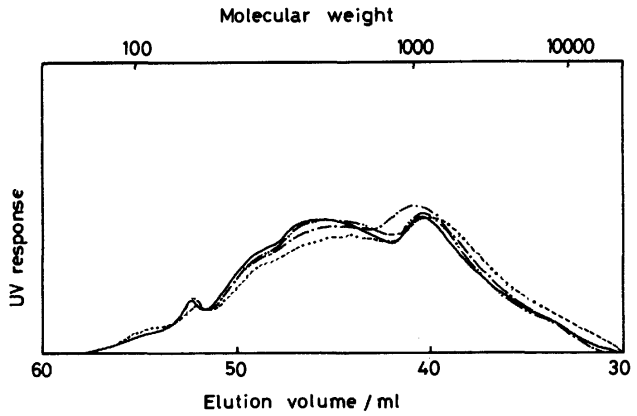

Fig. 1. Molecular weight distributions of SRC's measured by GPC.
Catalyst
None: ——, MoO_3: -·-·-·-, Fe_2O_3: ·····, SnO: -·-·-.

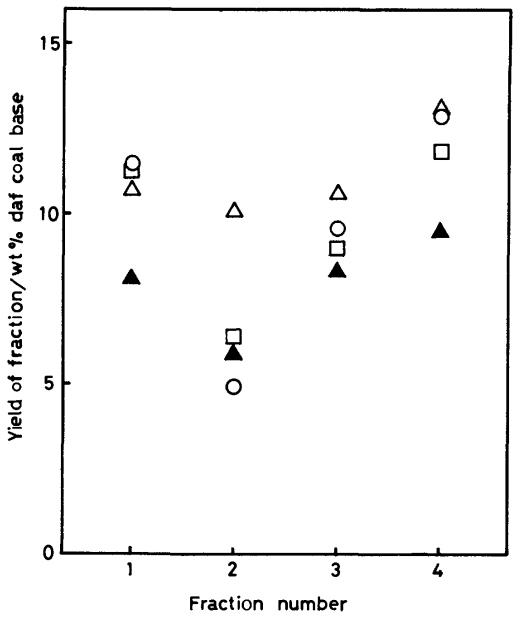

Fig. 2. Yield of fraction 1—4 obtained by successive extraction of SRC. Catalyst None: ▲, MoO_3: ○, Fe_2O_3: □, SnO: △.

SRC. In this case, even with catalysts, a significance at the α=0.01 level was observed. It was concluded that, under these liquefaction conditions, the effects of catalysts on the conversion and the SRC yield were small, whereas the effects of the catalysts on the structure of SRC were large and important.

To obtain information about the difference in the SRC structure, the molecular-weight distributions of the SRC's were measured by means of GPC; the results are shown in Fig. 1. When a catalyst, especially Fe_2O_3, was used, the heavier compounds (with molecular weights of around 10000) were larger than those with no catalyst. Moreover, when SnO was used, the compounds whose molecular weights were around 1000 were larger than those of the SRC with other catalysts. However, we could not clarify the differences in distribution among them and the difference in the role of the catalyst in the course of coal liquefaction, for the SRC contains many compounds. Therefore, the SRC was separated into four fractions by means of successive extractions.

The SRC yields of Taiheiyo coal in tetralin under a hydrogen atmosphere were 39, 39, and 44% with MoO_3, Fe_2O_3, and SnO, respectively. They were extracted successively using Solvents 1—4, whose compositions have already been described in the Experimental section. The fraction yields based on daf coal are shown in Fig. 2.

The SRC yield without a catalyst was 32%, approximately 12% smaller than that with SnO, but the distributions of the SRC without a catalyst were almost identical with those with SnO; the yields were in the following order: Fraction 4>Fraction 3≥Fraction 1> Fraction 2.

When MoO_3 or Fe_2O_3 was used, both the lighter (Fraction 1) and the heavier (Fraction 4) components were larger than those in the SRC with no catalyst.

To compare the structure of the SRC, all fractions were analyzed by means of ^1H NMR. The results of the elemental analysis and their structural parameters are shown in Table 4. The hydrogen/carbon ratio (H/C) decreased, and the oxygen content, the carbon aromaticity (fa), and the number of rings (Ra, Rn, Rt) increased, with an increase in the fraction number, irrespective of the kind of catalyst. The oxygen contents of Fractions 1—4 which were obtained using SnO were smaller than those obtained using no catalyst or Fe_2O_3. When MoO_3 was used, the oxygen contents of Fractions 1 and 2 were smaller than those obtained using SnO, but those of Fractions 3 and 4 were larger. Not only the smallest number of aromatic rings (Ra), but also the smallest number of non-aromatic rings (Rn), of all fractions were obtained when SnO was used. When MoO_3 or Fe_2O_3 was used, the numbers of total rings of Fractions 3 and 4 were 4.94 and 7.01, and 4.98 and 5.39, respectively; these numbers were larger than those when no catalyst or SnO was used. The yield of Fraction 3 was from 8.5 to 10.5 wt%, and the effect of the kind of catalyst used on the yield was relatively small. The mean molecular weight of Fraction 3 was measured by means of VPO. Values of 420 with MoO_3 and 520 with Fe_2O_3 were obtained; these values were larger than those of 320 without a catalyst and 350 with SnO.

In this way, we can clarify the differences among catalysts in the structure of SRC; when SnO was used, lighter compounds than those with other catalysts were obtained, despite the larger SRC yield.

To obtain further information on the liquefaction products, SRC was treated in the presence of a catalyst. The SRC had been obtained by the liquefaction of Taiheiyo coal without a catalyst at 420 °C for 60 min under a hydrogen atmosphere. In the reaction of SRC,

Table 4. Structural Parameters of Fractionated SRC

Catalyst	Fraction No	Extract	O	H/C	fa[a]	Ra[b]	Rn[b]	Rt[b]	Mn[c]
None	All	100	6.31	1.05	0.62	2.62	1.85	4.48	
	1	25.5	3.01	1.31	0.47	1.86	1.53	3.39	
	2	18.4	5.21	1.17	0.78	2.21	1.88	4.09	
	3	26.1	7.05	1.10	0.60	2.22	1.67	3.89	370
	4	29.9	9.66	0.91	0.71	2.95	1.84	4.80	
MoO_3	All	100	4.79	1.09	0.62	2.76	1.93	4.68	
	1	29.5	1.38	1.33	0.47	1.63	1.31	2.95	
	2	12.7	3.38	1.18	0.53	2.11	1.81	3.92	
	3	24.7	5.69	1.06	0.59	2.82	2.12	4.94	420
	4	33.2	7.94	0.93	0.66	4.13	2.87	7.01	
Fe_2O_3	All	100	6.52	1.08	0.61	2.13	1.70	3.83	
	1	29.4	2.55	1.30	0.48	1.73	1.39	3.12	
	2	16.5	4.75	1.12	0.56	2.45	2.00	4.44	
	3	23.3	5.81	1.01	0.63	2.92	2.06	4.98	520
	4	30.9	8.86	0.90	0.69	3.16	2.23	5.39	
SnO	All	100	3.43	1.06	0.60	1.47	1.58	3.05	
	1	24.0	1.89	1.40	0.45	1.04	1.12	2.17	
	2	22.8	3.70	1.16	0.54	2.10	1.88	3.97	
	3	23.9	4.95	1.09	0.56	1.97	1.60	3.57	350
	4	29.3	7.12	0.93	0.69	2.82	1.89	4.71	

a) fa: carbon aromaticity. b) Ra, Rn, Rt: number of aromatic, nonaromatic, and total rings per structural unit. c) Mn: mean molecular weight as measured by vapor-pressure osmometry (VPO).

Table 5. Effects of Treatment[a] of SRC with Catalysts on SRC Structure

Catalyst	fa[b]	σ[c]	n[c]	Ra[b]	Rn[b]	Rt[b]	Mn[b]
Feed SRC	0.57	0.52	3.08	2.61	1.88	4.48	320
None	0.58	0.50	2.58	2.72	2.01	4.73	310
MoO_3	0.55	0.54	2.63	2.92	2.37	5.29	350
Fe_2O_3	0.56	0.49	2.60	3.01	2.26	5.26	340
SnO	0.56	0.54	2.52	1.97	1.80	3.76	250

a) SRC's were treated at 400 °C under a hydrogen atmosphere for 60 min in tetralin. b) Abbreviation as in Table 4. c) σ: degree of substitution for aromatic nucleus, n: number of carbon atoms of side chain.

few gaseous compounds were produced during the treatment, and most of the SRC was recovered as benzene-soluble. The structural parameters are shown in Table 5. Without a catalyst, the H/C ratio of SRC decreased from 1.2 to 1.1, and the chain length decreased from 3.1 to 2.6; this indicates the presence of a slight retrogressive reaction. When MoO_3 or Fe_2O_3 was used, the retrogressive reaction was confirmed by the increases in the total rings per structural unit and in the mean molecular weight. On the other hand, when SnO was used, the mean molecular weight and the total number of rings decreased from 320 to 250, and from 4.48 to 3.76, respectively.

The retrogressive reaction for MoO_3 and Fe_2O_3 was also confirmed from model-compound studies. MoO_3 and Fe_2O_3 were more effective than was SnO for the hydrogenation reaction of naphthalene and benzophenone to tetralin and diphenylmethane. The results were identical with those reported previously.[7] Furthermore, the reactions of dibenzyl ether at 360 °C and of biphenyl at 400 °C were accelerated in the presence of MoO_3 or Fe_2O_3, as is shown in Table 6. However, the yields of unknown compounds were larger with MoO_3 or Fe_2O_3 than with no catalyst or with SnO. For example, although DBE reacted completely in the presence of MoO_3, 78.2% of the products were unknown, and some of them were insoluble to a solvent like acetone. The GPC data showed that most of the unknown products were compounds whose molecular weights were larger than that of DBE, indicating the presence of a retrogressive reaction.

Discussion

It is well-known that coal minerals catalyze liquefaction and hydrogenation in coal-conversion processes.[8-10] Guin et al. reported that certain coal minerals, particularly iron compounds, catalyze hydrogenation.[9] Atomic-absorption analysis has shown that the content of iron in Taiheiyo coal is 0.65 wt%, based on dry coal. The hydrogenation ability of coal minerals was affected by the degree of their dispersion in the coal. Therefore, we could not estimate the degree of

Table 6. Effects of Catalysts on the Decomposition Reaction of Dibenzyl Ether (DBE) at 360°C and Biphenyl (DP) at 400°C

Catalyst	Model compounds	Conversion	Reaction products					
			Benzene	Toluene	Benzaldehyde	Benzylalcohol	Dibenzyl	Others
None	DBE	73.5	3.8	36.4	28.9	—	4.2	0.2
	DP	9.4	1.5					7.9
MoO_3	DBE	100	1.4	13.5	trace	trace	6.9	78.2
	DP	24.8	2.5					22.3
Fe_2O_3	DBE	68.1	3.7	32.8	28.5	3.0	trace	0.1
	DP	26.9	2.4					24.5
SnO	DBE	85.9	3.2	51.5	7.1	13.1	7.5	3.5
	DP	4.3	1.7					2.6

coal-mineral effects only from the content,[11] 0.65 wt%. Conversions to BC and TC with no catalyst in decalin were larger under a hydrogen atmosphere than under a nitrogen atmosphere, as is shown in Table 3. This suggests that the participation of hydrogen molecules in coal liquefaction promotes the coal conversion. Namely, in a non-donor solvent like decalin, organic radicals react directly with hydrogen molecules.[12] Other explanation that coal minerals, the autoclave wall or the blade catalyze the liquefaction is also possible. Wall participation has been called the "memory effect."[13,14] We could not clarify this situation. However, from the liquefaction results of Taiheiyo-D, which consisted of deashed coal of Taiheiyo-2, the interaction between coal minerals and the catalyst added might be small, for the effects of an added catalyst on conversion and on the SRC yields were not affected by the deashing. Therefore, the effects of coal minerals on the following catalyst study were excluded.

The composition of the recycle solvent is an important factor in the liquefaction of coal.[15,16] One of the functions of a liquefaction solvent is to donate hydrogen to the coal.

Under a hydrogen atmosphere, the conversions to TC in the donor solvent, tetralin, were from 30 to 40% larger than those in the non-donor solvent, decalin, irrespective of the kind of catalyst. The contribution of the donor solvent to conversion was large even in the presence of a catalyst. Under a nitrogen atmosphere, the contribution of the donor solvent increased, and the differences in the conversion to TC between solvents were from 40 to 50%. These results indicated that the catalyst suppressed somewhat the contribution of the solvent donor. The structure of Taiheiyo coal SRC was directly affected by coal conversion; we have previously reported that the aromaticity, fa, of SRC tended to increase with an increase in the conversion.[17] Therefore, we could not ascertain the relationship between the solvent used and the structure of SRC.

Variance analysis was very helpful in clarifying the relationship between them. Statistical analysis, such as variance analysis, has been applied to coal chemistry, usually, applying multiple-regression analysis to coal liquefaction.[17-19] Statistical analysis gives quantitative considerations, and intuitive conclusions could be excluded. That the effects of the catalysts on the structure of SRC were large and important was concluded from the variance analysis. In order to evaluate coal liquefaction, information about the effects of catalysts on liquid-product structures was essential. Because SRC contains many compounds,[20] the fractionation of SRC before structure analysis is effective. Figure 3 shows the molecular-weight distribution of Fractions 1—4 of SRC with no catalyst; it indicates that SRC is effectively fractionated. In our fractionation method, heavier compounds were extracted increasingly with the extract solvent numbered from 1 to 4. Although the yields of Fractions 2 and 3 without a catalyst were almost identical with those with MoO_3 or Fe_2O_3, their structures were different, as is shown in Table 4. Such a difference was caused by the difference in the catalytic action of the catalysts.

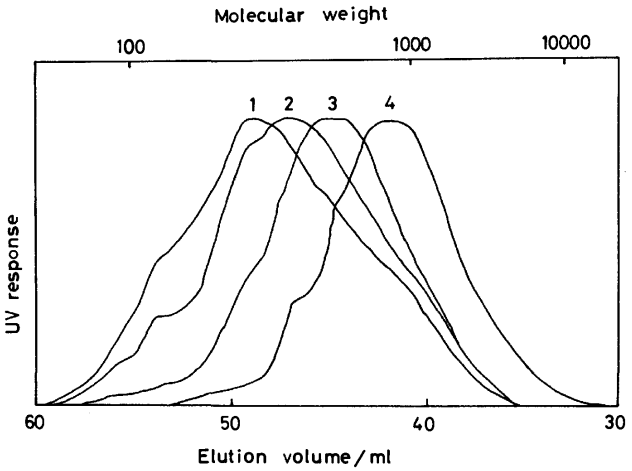

Fig. 3. Molecular weight distribution of Fractions 1—4 of SRC with no catalyst. Number in the Figure shows fraction number.

The oxygen content and ring numbers of the extract were mostly affected by the catalyst used. Lower oxygen contents were obtained with SnO. This indicates the greater ability of SnO to disrupt a linkage such as

ether bonding efficiently. DBE was decomposed more with SnO than with no catalyst, as is shown in Table 6. The yield of toluene was 51.5%, and it was the main product of the reaction. It also showed an imbalance of oxygen content between reactant and products. The oxygen contents of the products were less than that of DBE. The solution of this imbalance was obtained by means of the X-ray diffraction pattern of the liquefaction residue. SnO was oxidized to SnO_2 in the course of liquefaction. The oxygen abstraction of SnO caused the lower oxygen content of the SRC extract. On the other hand, α-Fe_2O_3 (hematite) changed to γ-Fe_2O_3 (maghemite) in the course of liquefaction, but the oxygen content of the catalyst did not change. Although the X-ray diffraction pattern of the residue with MoO_3 was not very clear because of the overlapping of plural compounds, the presence of MoO_2 after the liquefaction was confirmed. Oxygen functional groups related to hydrogen bonding between coal molecules and the extractability of coal was highly affected by the hydrogen bonding.[21] The removal of the oxygen might mean the acceleration of the dissociation of the association molecules. Furthermore, it has been reported that phenolic OH condensed to form an ether linkage, eliminating water.[22] It is possible that the oxygen release of MoO_3 to MoO_2 causes the condensation reaction. The oxygen contents of the extract with MoO_3 were not very large, but the condensation reaction produced an insoluble residue.

SRC was chosen as the more appropriate coal model. It is well-known that the reactivity of liquefaction products like SRC was less than that of coal itself,[23] but it was possible to observe the structure change in the whole compounds. In coal liquefaction, the smallest number of aromatic and nonaromatic rings was obtained with SnO. The ring number of SRC decreased when SnO was used, as is shown in Table 5. The ability of SnO to hydrogenate aromatic rings was less than that of MoO_3; this was confirmed by the hydrogenation of naphthalene.

These results indicate that SnO is effective for the cleavage reaction of a linkage like an ether bond and that, further, it possesses the ability to suppress the condensation reaction. The oxygen-removal reaction relates to the latter ability. Bacand et al. has reported that Al_2O_3 could stabilize free radicals by means of adsorption.[24] SnO could possess such a radical stabilization ability to suppress condensation reactions.

MoO_3 and Fe_2O_3, especially MoO_3, have higher abilities to hydrogenate or accelerate the hydrocracking of coal structures similar to coal-model compounds, as is shown in Table 6. However, they could not prevent the retrogressive reactions of coal, which were confirmed by the structures of the SRC extracts and by model-compound studies.

The difference in SRC structure appears to result from the inherent ability of a catalyst to liquefy coal.

Conclusions

From the three-way variance analysis, it was concluded that the effects of catalysts on conversion and on the SRC yield were small, whereas the effects of catalysts on the structure of SRC were large and important. The fractionation of SRC into four fractions was very effective for comparing the structures of SRC. The oxygen content and ring numbers of the extracts were mostly affected by the catalyst used. The formation of SnO_2 after the liquefaction shows the oxygen-abstraction reaction of SnO, which cause the oxygen content of the extract to be lower. The decomposition of SRC, dibenzyl ether, and biphenyl as coal-model compounds was also accelerated by the catalysts, but retrogressive reactions were observed when MoO_3 or Fe_2O_3 was used.

More effective catalysts for coal liquefaction can be prepared by investigating the structures of liquid products obtained with other catalysts and by selecting combinations of catalysts suitable for producing the desired liquid products. Studies of this point are under way.

The authors are grateful to Mr. Katsumi Watanabe and Mr. Hiroshi Nakamura for their technical assistance, and to Mr. Tohru Suzuki for the analyses of coal and SRC.

References

1) M. R. Hatswell, W. R. Jackson, F. D. Larkins, M. Marshall, D. Rash, and D. E. Rogers, *Fuel*, **62**, 47 (1983).
2) T. Yokono, S. Iyama, and Y. Sanada, *Nenryo Kyokai Shi*, **63**, 298 (1984).
3) J. K. Brown and W. R. Ladner, *Fuel*, **39**, 87 (1960).
4) C. W. Fan, R. Markuzewski, and T. D. Wheelock, *Am. Chem. Soc. Div. Fuel Chem. Preprints*, **29**, 114 (1984).
5) K. Chiba, H. Tagaya, S. Sato, and K. Ito, *Fuel*, **64**, 68 (1985).
6) N. R. Draper and H. Smith, "Applied Regression Analysis," John Wiley and Sons, New York (1965).
7) S. J. Cochran, M. R. Hatswell, W. R. Jackson, and F. D. Larkins, *Fuel*, **61**, 831 (1982).
8) D. D. Mukherjee and P. B. Chowdhury, *Fuel*, **55**, 4 (1976).
9) J. A. Guin, A. R. Tarrer, J. W. Prather, D. R. Johnson, and J. M. Lee, *Ind. Eng. Chem. Process Des. Dev.* **17**, 118 (1978).
10) J. A. Guin, A. R. Tarrer, J. M. Lee, L. Lo, and C. W. Curtis, *Ind. Eng. Chem. Process Des. Dev.* **18**, 371 (1978).
11) H. Tagaya, K. Chiba, S. Sato, K. Ito, and M. Sakurai, *Nippon Kagaku Kaishi*, **1983**, 1172.
12) L. W. Vernon, *Fuel*, **59**, 102 (1980).
13) T. Yoshii, R. Yaginuma, S. Utoh, and H. Yoshikawa, *Fuel*, **62**, 47 (1983).
14) H. W. Slotboom and J. M. L. Penninger, *Ind. Eng. Chem. Process Des. Dev.*, **13**, 296 (1974).
15) D. D. Whitehurst, T. O. Mitchell, and M. Farcasiu, "Coal Liquefaction," Academic Press (1980).

16) K. Chiba, H. Tagaya, S. Sato, and T. Watanabe, *Nenryo Kyokai Shi*, **63**, 195 (1984).
17) H. Tagaya, K. Chiba, S. Sato, K. Miyashita, and M. Sagawa, *Nippon Kagaku Kaishi*, **1983**, 1181.
18) M. B. Abdel-Baset, R. F. Yarzab, and P. H. Given, *Fuel*, **57**, 89 (1978).
19) R. A. Winschel, G. A. Robbins, and F. P. Burke, *Fuel*, **65**, 526 (1986).
20) T. Yao, T. Uchida, H. Sato, and Y. Kamiya, *Nippon Kagaku Kaishi*, **1980**, 327.
21) M. L. Gorbaty, J. W. Larsen, and I. Wender, "Coal Science," Vol. 2, Academic Press (1983).
22) M. L. Poutsuma and C. W. Dyer, *J. Org. Chem.*, **47**, 3367 (1982).
23) Y. T. Shah, "Reaction Engineering in Direct Coal Liquefaction," Addison-Wesley Publishing Company (1981).
24) R. Bacaud, M. Besson, H. Charcosset, M. Oberson, H. V. Tran, and J. Varloud, Proceedings of Symposium on Chemistry of Coal Liquefaction and Catalysts, Sapporo, March, (1985), p. 160.

 © 1987 The Chemical Society of Japan Bull. Chem. Soc. Jpn., 60, 661—666 (1987)

Optical Resolution by Preferential Crystallization of 1,1,3,3-Tetramethylbutylammonium Salt of *N*-Formyl-DL-α-phenylglycine

Tadashi SHIRAIWA,* Hideya MIYAZAKI, Tomoki IMAI, Michio SUNAMI, and Hidemoto KUROKAWA
Faculty of Engineering, Kansai University, Yamate-cho, Suita, Osaka 564
(Received July 29, 1986)

Infrared spectrum, solubility, and ternary phase diagram of solubility indicated that 1,1,3,3-tetramethylbutylammonium salt (DL-TMB salt) of *N*-formyl-DL-α-phenylglycine is a conglomerate. In order to resolve DL-TMB salt efficiently, crystallization of D- and L-TMB salts was examined by free energy of critical nucleation in supersaturated solutions. Successive preferential crystallization of DL-TMB salt was experimented at 10 °C for racemic solution in ethanol with the degree of supersaturation of 130%, and D- and L-α-phenylglycine with 100% optical purity were obtained from pure D- and L-TMB salts.

D-α-Phenylglycine (abbreviated as D-Phg) as a useful material of ampicillin has been chemically synthesyzed,[1] because Phg is not found in natural amino acids. Synthetic DL-Phg is then subjected to optical resolution by preferential crystallization[2-4] and diastereomeric procedures[5-7] to obtain D-Phg. For the optical resolution of DL-amino acids, their *N*-acyl derivatives have been purposely used. In the case of *N*-acetyl- or *N*-benzoyl-DL-α-phenylglycine, the Phg obtained is partially racemized during hydrolysis of the derivatives,[8] because Phg is apt to racemize on heating in an acid solution. It is expected that *N*-formyl-α-phenylglycine (FrPhg) is easier to be hydrolyzed under mild conditions than *N*-acetyl and *N*-benzoyl derivatives. It was attempted, therefore, to resolve organic ammonium salts of DL-FrPhg.

The organic ammonium salts of DL-FrPhg examined are propylammonium, isopropylammonium, butylammonium, *t*-butylammonium, 1,1,3,3-tetramethylbutylammonium (DL-TMB salt), cyclohexylammonium, benzylammonium, and dibenzylammonium salts. The racemic structure of organic ammonium salts of *N*-acyl-DL-amino acids has been determined from calculated values of free energy of formation by enthalpy of fusion and melting point described in our previous papers.[3,4,9] Since the salts of DL- and D-FrPhg decompose on heating, the racemic structure of these compounds was determined by comparing infrared spectra and solubility values of the DL-salts with those of the corresponding D-salts. The TMB salt of DL-FrPhg which seems to be in a conglomerate was subjected to resolution by a preferential crystallization. Conditions of hydrolysis of the D- and L-TMB salts resolved was examined to obtain D- and L-Phg without racemization. The optical resolution by preferential crystallization needs that unseeded enantiomer remains in the solution as a supersaturation state during crystallization. Although Hongo et al. reported on the stability of solution of DL-serine *m*-xylene-4-sulfonate dihydrate,[10] such problem has not been fully studied. Therefore, crystallization of D- and L-TMB salts was examined by free energy of critical nucleation to find appropriate conditions for optical resolution of DL-TMB salt.

Table 1. Preparation of Supersaturated Solutions of 1,1,3,3-Tetramethylbutylammonium Salt of *N*-Formyl-DL-α-phenylglycine[a]

Solvent	Degree of supersaturation[b]/%	Amount/g
Methanol	110	12.855
Methanol	120	14.024
Methanol	130	15.192
Ethanol	110	3.341
Ethanol	120	3.645
Ethanol	130	3.949

a) Solvent: 50 cm³. b) Temperature: 10 °C.

Experimental

Materials. DL- and D-Phg were purchased from Sigma Chemicals Co., and amines from Wako Pure Chemicals Ind.

***N*-Formylation.** DL- and D-FrPhg were prepared by formylating DL- and D-Phg, respectively, as usual as the preparation of ordinary amino acids.[11] DL-FrPhg: Mp 175 °C. D-FrPhg: Mp 178 °C; $[\alpha]_D^{20}$ −252° (*c* 1.00, methanol).

Preparation of Organic Ammonium Salts. A solution of 0.01 mol of DL- or D-FrPhg and equimolar amine in 150 cm³ of acetone was allowed to stand overnight at 5 °C. The salt formed was filtered and recrystallized from ethanol.

D-TMB salt: C, 66.02; H, 9.08; N, 9.08% (Calcd for $C_{17}H_{28}N_2O_3$: C, 66.20; H, 9.15; N, 9.08%); mp 176—179 °C (decomp); $[\alpha]_D^{20}$ −124° (*c* 1.00, water) and $[\alpha]_D^{20}$ −109° (*c* 1.00, ethanol); solubility 14.964 g/(100 cm³ methanol), 3.571 g/(100 cm³ ethanol) at 10 °C. DL-TMB salt: C, 66.21; H, 9.07; N, 9.12%; mp 157—160 °C (decomp); solubility 23.373 g/(100 cm³ methanol), 6.075 g/(100 cm³ ethanol) at 10 °C.

L-TMB salt obtained from mother liquor in the optical resolution of DL-salt was recrystallized twice from ethanol to give L-salt with 100% optical purity; mp 177—179 °C (decomp); $[\alpha]_D^{20}$ +124° (*c* 1.00, water).

Optical Resolution. DL-TMB salt was dissolved in 50 cm³ of ethanol or methanol at approximately 40 °C to give racemic solutions with the degree of supersaturation of 110, 120, and 130% at 10 °C; results of preparation of these supersaturated solutions were summarized in Table 1. The solution was slowly cooled to 10 °C and seeded with 0.050 g of D-TMB salt. After stirring the solution at 30 rpm and 10 °C,

the precipitated salt was collected by filtration, washed with a small amount of diethyl ether, and dried. The optical purity, yield of optically pure modification (YOPM), and degree of resolution of the salt were determined by the equations described in a previous paper.[3]

Successive Preferential Crystallization. DL-TMB salt (3.949 g) was dissolved in 50 cm^3 of ethanol at 40 °C. After being cooled to 10 °C, the solution was seeded with 0.050 g of D-TMB salt and stirred for 15 min. The precipitated salt was collected by filtration, washed with a small amount of diethyl ether, and dried. DL-TMB salt (0.319 g) was dissolved in the filtrate at 40 °C. After being seeded with 0.050 g of the L-TMB salt at 10 °C, the mixture was treated similarly to the case of D-TMB salt. The degree of resolution of D- and L-TMB salts was calculated by

$$\text{Degree of resolution}/\% = [\text{YOPM}/g \times 100]/[(\text{Operation amount of D- or L-salt}/g) - 1.519/g]. \quad (1)$$

Preparation of Optically Active α-Phenylglycine. D- or L-TMB salt (8.00 g) with optical purity of approximately 95% was dissolved in 30 cm^3 of ethanol at an elevated temperature. The solution was allowed to stand overnight at 5 °C. The precipitated salt was collected by filtration to give the D- and L-TMB salts with 100% optical purity in 90% yield.

D- or L-TMB salt (3.08 g) was dissolved in a mixture of 8 cm^3 of 5 mol dm^{-3} hydrochloric acid, 22 cm^3 of water, and 20 cm^3 of ethanol. After being stirred for 2 h at 50 °C, the solution was allowed to stand overnight at room temperature, and dried under reduced pressure at 50 °C. The residue was dissolved in 40 cm^3 of methanol and pH was adjusted to 6 with concentrated aqueous ammonia. Precipitated Phg was filtered, washed with a small amount of each water and methanol, and dried. **D-Phg**: Yield 1.253 g; $[\alpha]_D^{20}$ −158° (*c* 1.00, 1 mol dm^{-3} HCl) (lit,[12] $[\alpha]_D$ −157.8°(dil HCl)). **L-Phg**: Yield 1.249 g; $[\alpha]_D$ +158° (*c* 1.00, 1 mol dm^{-3} HCl).

Measurements. The specific rotation was measured by a Union Giken PM-101 digital polarimeter with a quartz cell of 0.5 dm path length. Infrared spectra were obtained in the range 4000—400 cm^{-1} with a JASCO A-102 infrared spectrophotometer by the KBr disk method.

Saturated methanol or ethanol solutions of DL- and D-TMB salts were prepared at 10 °C and diluted appropriately. The absorbance was measured at 260 nm with a Shimadzu double-beam spectrophotometer UV-150-02 by using a quartz cell of 0.1 dm path length. Solubility values of the salts were determined from calibration curves.

Results and Discussion

Racemic Structure. Infrared spectra of DL-FrPhg ammonium salts were compared with those of the corresponding D-salts. DL-TMB salt shows infrared spectrum identical with that of D-salt, whereas the spectra of other DL-salts are different from those of D-salts. This result indicates that DL-TMB salt is either a conglomerate or a racemic solid solution but other DL-salts form racemic compounds.[13] Further, DL-TMB salt is more soluble than the D-salt as described in the experimental section, and the ternary phase diagram in Fig. 1 illustrates the patterns of a conglomerate.[14]

The above results lead to the conclusion that only DL-TMB salt exists in a conglomerate at room temperature.

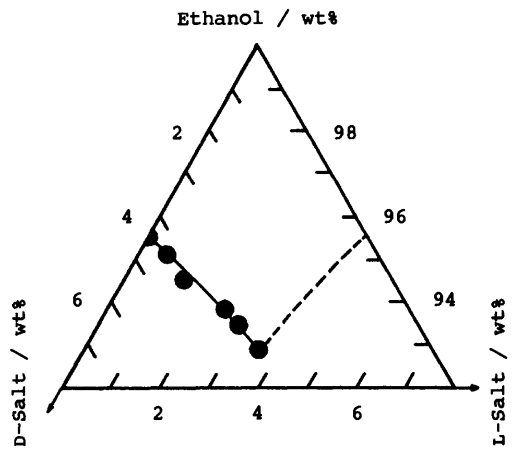

Fig. 1. Ternary phase diagram of solubility of 1,1,3,3-tetramethylbutylammonium salt of *N*-formyl-α-phenylglycine. Solvent: Ethanol. Temperature: 10°C.

Preferential Crystallization and Free Energy of Critical Nucleation. Free Energy of Critical Nucleation: The crystallization of unseeded enantiomer from a supersaturated solution is relevant to the primary nucleation; therefore the crystallization is influenced by a free energy of critical nucleation (Δg_{max}/J nucleus^{-1}).[15-17] On the other hand, the crystallization of seeded enantiomer cannot be elucidated by the Δg_{max}, but is to be related to the secondary nucleation.[17] It is, however, estimated that Δg_{max} has some influence on the crystallization of seeded enantiomer, because the growth of critical nucleus is accelerated by seeding.[17] On the assumptions that no interaction exists between D- and L-TMB salts in a supersaturated solution and that the critical nucleus of TMB salt is spherical, the Δg_{max}[17] is calculated by

$$\Delta g_{max} = 4\pi r_{cr}^2 \sigma_{cr} - (4\pi r_{cr}^3 \kappa T/3V_0) \cdot \ln(C/C^*), \quad (2)$$

where r_{cr}/m is the radius of critical nucleus, σ_{cr}/J m^{-2} the interfacial energy, T/K the temperature, V_0[18]/m^3 the molecular volume of TMB salt, κ the Boltzmann constant, C^* the solubility of TMB salt at temperature T/K, and C the amount of TMB salt in supersaturated solution. The r_{cr} and σ_{cr} were calculated by Eqs. 3 and 4.[17,19]

$$r_{cr} = 2V_0 A/\kappa T \cdot \ln(C/C^*) - 2r_0, \quad (3)$$

$$\sigma_{cr} = r_{cr} A/(r_{cr} + 2r_0), \quad (4)$$

where r_0 is the molecular radius[18] and A is a constant. The constant A was calculated from a relationship between r and σ of nucleus;[19] $\sigma_{cr}(1+2r_0/r_{cr})$=constant $(A)=\sigma_{sa}(1+2r_0/r_{sa})$, where r_{sa} and σ_{sa} are the radius and interfacial energy of embryo in saturated solution, respectively.[20] The r_{cr}, σ_{cr}, and Δg_{max} in methanol and ethanol solutions with degrees of supersaturation of 110, 120, and 130% were calculated, and listed in Table 2. The optical resolution by preferential crystallization of DL-TMB salt was carried out in methanol and

Table 2. Properties of Critical Nucleus in Supersaturated Solutions of 1,1,3,3-Tetramethylbutylammonium Salt of *N*-Formyl-DL-α-phenylglycine[a]

Solvent	Degree of supersaturation/%	r_{cr}[b]	σ_{cr}[c]	Δg_{max}[d]
		$\times 10^{-8}$ m	$\times 10^{-2}$ J m^{-2}	$\times 10^{-17}$ J nucleus^{-1}
Methanol	110	3.64	1.49	8.28
Methanol	120	1.86	1.46	2.11
Methanol	130	1.26	1.43	0.95
Ethanol	110	4.77	1.96	18.7
Ethanol	120	2.45	1.92	4.83
Ethanol	130	1.67	1.89	2.21

a) Temperature: 10°C. b) r_{cr}: Radius of critical nuleus. c) σ_{cr}: Interfacial energy of critical nucleus. d) Δg_{max}: Free energy of critical nucleation.

Table 3. Preferential Crystallization of 1,1,3,3-Tetramethylbutylammonium Salt of *N*-Formyl-DL-α-phenylglycine in Methanol[a]

Degree of supersaturation	Resolution time	Yield	Optical purity	YOPM[b]	Degree of resolution
%	min	g	%	g	%
110	20	0.120	83.3	0.050	8.6
	30	0.149	82.0	0.072	12.3
	40	0.173	84.0	0.095	16.3
	60	0.202	84.3	0.120	20.5
	70	0.263	76.4	0.151	25.9
	80	0.289	66.7	0.143	24.5
120	10	0.168	88.1	0.098	8.4
	15	0.239	89.1	0.163	14.0
	20	0.307	73.9	0.177	15.2
	30	0.463	60.7	0.231	19.8
	45	0.784	55.1	0.382	32.7
	60	1.029	46.2	0.425	36.4
	90	1.677	26.9	0.401	34.4
130	5	0.247	83.8	0.157	9.0
	10	0.573	71.4	0.359	20.5
	15	1.030	20.2	0.158	9.0

a) Solvent: 50 cm^3 of methanol. Seed crystals: 0.050 g of D-salt. Temperature: 10°C. b) YOPM: Yield of optically pure modification.

Table 4. Preferential Crystallization of 1,1,3,3-Tetramethylbutylammonium Salt of *N*-Formyl-DL-α-phenylglycine in Ethanol[a]

Degree of supersaturation	Resolution time	Yield	Optical purity	YOPM[b]	Degree of resolution
%	min	g	%	g	%
110	30	0.071	93.7	0.017	11.2
	60	0.116	95.7	0.061	40.2
	90	0.158	90.1	0.092	60.6
	120	0.177	89.8	0.109	71.8
	130	0.200	75.0	0.100	65.8
	150	0.221	63.8	0.091	59.9
120	15	0.115	91.6	0.055	18.1
	30	0.155	94.8	0.097	31.9
	40	0.209	93.2	0.145	47.7
	60	0.285	95.1	0.221	72.8
	70	0.341	73.6	0.201	66.2
	90	0.519	30.6	0.109	35.9
130	7	0.193	97.4	0.138	30.3
	12	0.326	97.2	0.267	58.6
	17	0.415	96.4	0.350	76.8
	22	0.907	9.1	0.033	7.2

a) Solvent: 50 cm^3 of ethanol. Seed crystals: 0.050 g of D-salt. Temperature: 10°C. b) YOPM: See note b) in Table 3.

Table 5. Retardation Time for Crystallization of L-Salt and Amount of Crystallization per Time for D-Salt[a]

Solvent	Degree of supersaturation	Retardation time[b]	Amount of crystallization per time[c]
	%	min	$\times 10^{-3}$ g min^{-1}
Methanol	110	75	2.07
Methanol	120	18	11.5
Ethanol	110	125	1.12
Ethanol	120	65	3.82
Ethanol	130	20	22.8

a) Salt: 1,1,3,3-Tetramethylbutylammonium salt of *N*-formyl-α-phenylglycine. b) The retardation time for crystallization of L-salt was estimated from Figs. 2 and 3. c) The amount of crystallization per time for D-salt was calculated from linear plots in Figs. 2 and 3.

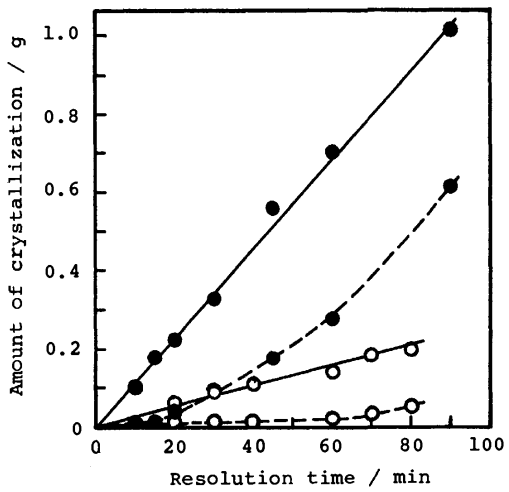

Fig. 2. Relationships between amounts of crystallization and resolution times in methanol. Temperature: 10°C. ——: D-Salt. ----: L-Salt. ○: Degree of supersaturation of 110%. ●: Degree of supersaturation of 120%.

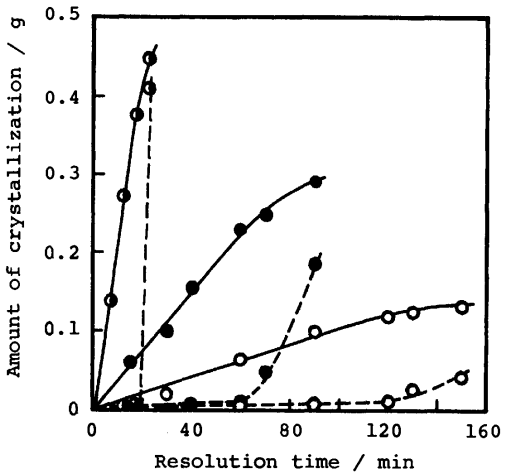

Fig. 3. Relationships between amounts of crystallization and resolution times in ethanol. Temperature: 10°C. ——: D-Salt. ----: L-Salt. ○: Degree of supersaturation of 110%. ●: Degree of supersaturation of 120%. ◑: Degree of supersaturation of 130%.

ethanol with D-salt as seed crystals; results are listed in Tables 3 and 4. From the results, amounts of crystallization[21] of D- and L-TMB salts were calculated, and the relationships between amount and resolution time are shown in Figs. 2 and 3.

Since Δg_{max} is regarded as energy barrier for growth of the primary nucleus, it is predictable that the unseeded enantiomer tends to crystallize with a decrease in Δg_{max}.[17] This is supported by the retardation time for crystallization of L-TMB salt. The retardation time is defined as the resolution time until L-TMB salt begins to crystallize; the results estimated from Figs. 2 and 3 are listed in Table 5. Although Figs. 2 and 3 indicate the presence of L-TMB salt in the D-salt crystallized in short times, it will be due to the DL-salt adhered on filtration. Rapid crystallization of L-TMB salt requires longer retardation time with an increase in Δg_{max} values. The relationship between the retardation time (θ/min) and Δg_{max} was obtained by

$$\log \theta = -0.8913 \log(1/\Delta g_{max}) + 16.18, \quad (5)$$

where the correlation coefficient is 0.972.

Figures 2 and 3 also suggest that seeded D-TMB salt tends to crystallize rapidly with a decrease in Δg_{max}. The amount of crystallization of D-TMB salt per time (R_D/g min^{-1}) listed in Table 5 was calculated from linear plots in Figs. 2 and 3. Since the Δg_{max} values of D-TMB salt are equal to those of L-salt, the relationship between R_D and Δg_{max} was examined and is expressed by

$$\log R_D = 1.275 \log(1/\Delta g_{max}) - 23.09, \quad (6)$$

where the correlation coefficient is 0.959. This result shows that the crystallization of seeded D-TMB salt is strongly influenced by Δg_{max}.

Conditions of Optical Resolution: It is possible to estimate factors on crystallization of D- and L-TMB salts from Eqs. 5 and 6. In the optical resolution for methanol solution with a degree of supersaturation of 130%, the θ and R_D values calculated from Eqs. 5 and 6 are 10.2 min and 4.11×10^{-2} g min^{-1}, respectively. L-TMB salt begins to crystallize rapidly after 10 min, and

Table 6. Optical Resolution by Successive Preferential Crystallization of 1,1,3,3-Tetramethylbutylammonium Salt of *N*-Formyl-DL-α-phenylglycine[a)]

Run	Added amount of DL-salt	Operation amount[b)]/g		Salt obtained			
				Yield	Optical purity	YOPM[c)]	Degree of resolution
	g	D-Salt	L-Salt	g	%	g	%
1	3.949	1.975	1.975	0.369	D 95.5	0.302	66.2
2	0.319	1.823	2.125	0.577	L 95.1	0.499	82.3
3	0.527	2.173	1.876	0.584	D 93.3	0.495	75.7
4	0.534	1.915	2.123	0.495	L 96.7	0.429	71.0

a) Solvent: 50 cm^3 of ethanol. Degree of supersaturation of initial racemic solution: 130%. Seed crystals: 0.050 g of D- or L-salt. Temperature: 10 °C. b) The operation amounts of D- and L-salts in solutions were calculated on the basis of analyses of the salts obtained in runs 1—3. c) YOPM: See note b) in Table 3.

the amount of D-salt crystallized at a resolution time of 10.2 min is 0.419 g; this amount corresponds to 23.5% of theoretical value. This agrees well with the results shown in Table 3; D-salt with optical purity of 71.4% was obtained in degree of resolution of 20.5% at resolution time of 10 min, the amount of crystallization of D-salt was 0.441 g, and further, the optical resolution at 15 min gave D-salt with low optical purity (20.2%). However, the above result suggests that the optical resolution for methanol solution with degree of supersaturation of 130% is not favorable for obtaining D-TMB salt with high optical purity in high degree of resolution.

The optical resolution for ethanol solution with the degree of supersaturation of 130% gave D-TMB salt with optical purity of 96.4% and degree of resolution of 76.8% at the resolution time of 17 min. The resolution for 15 min seems to be more favorable for stable optical resolution than 17 min, because it is estimated by θ values that L-TMB salt begins to crystallize rapidly after 20 min. We can estimate from R_D that 0.342 g of D-TMB salt crystallizes at resolution time of 15 min and the amount corresponds to 75.0% of theoretical value. This optical resolution gives D-TMB salt with high optical purity in relatively high degree of resolution.

Optical Resolution of Successive Preferential Crystallization. Successive Preferential Crystallization: According to the above suggestion, the successive preferential crystallization of DL-TMB salt was carried out at 10 °C at resolution time of 15 min for the ethanol solution with degree of supersaturation of 130%, as shown in Table 6. The D-TMB salt with 95.5% optical purity was obtained in degree of resolution of 66.2% from the initial solution. Since the amount of crystallized D-salt was 0.310 g, this result supports the preceding suggestion.

The successive preferential crystallization gave D- and L-TMB salts with optical purity of approximately 95% in degree of resolution of 66—82%.

Purification of Salt Partially Resolved: The D- and L-TMB slats obtained by successive preferential crystallization were easily purified by recrystallization from ethanol as described in the experimental section. TMB salt with low optical purity was purified to optically pure salt in high yield with the optimum amount of ethanol calculated from the solubility of DL-TMB salt in ethanol.[22,23)] For example, D-TMB salt with optical purity of 40.9% (1.477 g) was recrystallized from 15 cm^3 of ethanol; the optimum amount calculated is 14.37 cm^3. Solution of D-TMB salt dissolved at 40 °C was stirred for 30 min at 10 °C to crystallize 0.548 g of the D-salt with 100% optical purity; the theoretical yield of the optically pure D-salt is 0.604 g.

Hydrolysis of *N*-Formyl-α-phenylglycine: The D- or L-FrPhg with 100% optical purity was hydrolyzed by refluxing in 1 mol dm^{-3} hydrochloric acid for 2 h to give D- and L-Phg with optical purity of approximately 95%. This result indicates that these Phg were partially racemized by refluxing in hydrochloric acid. The hydrolysis of D- and L-salts with 100% optical purities was carried out by the procedure described in the experimental section. The D- and L-Phg were not racemized under these conditions, and obtained in 83% yields. Although the hydrolysis of *N*-acetyl-D-α-phenylglycine (D-AcPhg) was also attempted under similar conditions, D-Phg did not crystallize from a methanol solution at pH 6 adjusted with concentrated aqueous ammonia. AcPhg is not hydrolyzed under such conditions. This result suggests that DL-FrPhg is more favorable for the optical resolution than DL-AcPhg.

The above results indicate suitable conditions for the optical resolution of DL-TMB salt on the basis of Δg_{max} in supersaturated solutions and procedures to give optically pure D- and L-Phg by successive preferential crystallization of DL-TMB salt.

References

1) R.E. Steiger, *Org. Synth.*, Coll. Vol. 3, 84 (1955).
2) J. Santhanam, British Patent, 1210495 (1967); *Chem. Abstr.*, **74**, 42618 (1971).
3) T. Shiraiwa, Y. Ohmichi, K. Iwafuji, and H. Kurokawa, *Nippon Kagaku Kaishi*, **1983**, 1070.
4) T. Shiraiwa, H. Miyazaki, S. Konishi, and H. Kurokawa, *Nippon Kagaku Kaishi*, **1985**, 1577.

5) K. Murakami, N. Katsuta, K. Takano, Y. Yamamoto, T. Kakegawa, K. Saigo, and H. Nohira, *Nippon Kagaku Kaishi*, **1979**, 765.
6) T. Watanabe, S. Hayashi, S. Ouchi, and S. Senoo, Japan Patent, 78137 (1973); *Chem. Abstr.*, **80**, 71099 (1974).
7) T. Shiraiwa, K. Umegaki, and H. Kurokawa, *Nippon Kagaku Kaishi*, **1983**, 1687.
8) K. Suzuki, S. Kiyooka, T. Miyagawa, and A. Kawai, *Nippon Kagaku Kaishi*, **1983**, 1687.
9) T. Shiraiwa, H. Miyazaki, Y. Sakamoto, and H. Kurokawa, *Bull. Chem. Soc. Jpn.*, **59**, 2331 (1986).
10) C. Hongo, S. Yamada, and I. Chibata, *Bull. Chem. Soc. Jpn.*, **54**, 1905 (1981).
11) J. C. Sheehan and D. D. H. Yang, *J. Am. Chem. Soc.*, **80**, 1154 (1958).
12) J.S. Davies, "Amino Acids and Peptides," Chapman and Hall, London, New York (1985), p. 65.
13) J. Jacques, A. Collet, and S. H. Willen, "Enantiomers, Racemates, and Resolutions," John Wiley and Sons, New York, Chichester, Brisbane, Toronto (1981), p. 18.
14) A. Collet, M. J. Brienne, and J. Jacques, *Chem. Rev.*, **80**, 215 (1980).
15) S. C. Furman and C. S. Garner, *J. Am. Chem. Soc.*, **74**, 2333 (1952).
16) Ref. 14, p. 236.
17) T. Nakai, "Shouseki Kougaku," Baifukan, Tokyo (1986), Section 2.
18) The value measured in ethanol at 25 °C (4.53×10^{-28} m^3) was used as V_0 of TMB salt, because this value closely agrees with the value estimated in crystalline state (4.41×10^{-28} m^3); A. Immirzi and B. Perini, *Acta Cryst., Sect. A.* **33**, 216 (1977). The molecular radius (r_0) is calculated to be 4.77×10^{-10} m on the assumption of spherical molecule.
19) T. Nakai, *Bull. Chem. Soc. Jpn.*, **42**, 2143 (1969).
20) The values of r_{sa} (6.14×10^{-10} m in methanol, 6.09×10^{-10} m in ethanol) and σ_{sa} (6.01×10^{-3} $J\,m^{-2}$ in methanol, 7.79×10^{-3} $J\,m^{-2}$ in ethanol) were calculated on the basis of the solubilities of DL-TMB salt according to the procedure reported in Ref. 19; the average number of TMB salt molecule forming the embryo in these solution is approximately 2.1.
21) T. Shiraiwa, Y. Ohmichi, and H. Kurokawa, *Nippon Kagaku Kaishi*, **1983**, 1102.
22) Ref. 14, p. 389.
23) T. Shiraiwa, M. Nakamura, M. Nobeoka, and H. Kurokawa, *Bull. Chem. Soc. Jpn.*, **59**, 2669 (1986).

 © 1987 The Chemical Society of Japan Bull. Chem. Soc. Jpn., 60, 667—672 (1987)

Stereoselective Formation of Allyl Ethers by Reaction of Epoxides with Organic Chlorides under Liquid-Solid Phase-Transfer Catalysis

Xue-Ping Gu, Isao Ikeda, and Mitsuo Okahara*
Department of Applied Chemistry, Faculty of Engineering, Osaka University, Yamadaoka 2-1, Suita, Osaka 565
(Received August 1, 1986)

A series of *trans*-3-chloroallyl ethers and *trans*-3-thioallyl ethers were stereoselectively synthesized in one step by the reaction of 1-chloro-2,3-epoxypropane or 2,3-epoxypropyl sulfides with alkyl chlorides in the presence of solid sodium hydroxide and quaternary ammonium salt as a phase-transfer catalyst. Phase-transfer catalytic hydroxide ion-initiation followed by stereoselective isomerization of the epoxide ring through β-elimination is postulated as the important part of the reaction pathway.

Epoxy compounds have been utilized extensively in organic synthesis and industry as synthetic intermediates because of their facile preparation, and their high chemical reactivity attributable to the ring strain of the small-ring.[1,2] The reactions of various nucleophilic species with these compounds have been developed for synthetic applications.[1,3] Also, the isomerization of epoxides to allylic alcohols under the influence of strong, non-nucleophilic bases such as lithium dialkylamide attracted attention.[4] Since the formation of *trans*-3-chloroallyl alcohol through the stereoselective ring-opening of 1-chloro-2,3-epoxypropane with butyllithium was reported in 1964 (Scheme 1),[5] much work has been reported in this field,[6-9] and the crucial mechanistic point concerning the stereochemistry of β-elimination in the isomerization was indicated by deuterium-labelled experiments.[10]

Phase-transfer (PT) catalytic reaction in organic chemistry has been developed extensively in the last two decades and many synthetic techniques[11-15] have been established, which include hydroxide ion-initiated reactions due to the strong basicity of quaternary ammonium hydroxide under PT catalytic conditions. Recently, during the course of an investigation regarding the reactivity of 1-chloro-2,3-epoxypropane under PT catalytic conditions, we found a simple synthetic method for the preparation of oligoethylene glycol di-2,3-epoxypropyl ethers in good yields.[16] In this reaction, the formation of a small amount of a by-product (compound **1**) was always observed which could be isolated by fractional distillation.

By identifying the compound **1** as *trans*-3-chloroallyl 2,3-epoxypropyl ether, a new reaction of epoxy compounds which can directly and stereoselectively afford *trans*-allyl ethers under PT catalytic conditions was disclosed. Based on the postulated reaction mechanism, we anticipated this new PT catalytic reaction would have utility for the synthesis of various kinds of *trans*-3-substituted allyl ethers.

In this paper, we report the development of this finding to the synthesis of *trans*-3-chloroallyl and *trans*-3-thioallyl ethers under PT catalytic conditions (Scheme 2).

It is reported that 3-chloroallyl ethers are useful materials because of their dual functionality, and accordingly have attracted some attention.[17-22]

Results and Discussion

The structure of compound **1** was ascertained by spectral and elemental analyses. Absorptions due to the carbon-carbon double bond and ether linkages were observed in the infrared spectrum (1640 and 1110 cm^{-1}), and the presence of an epoxy ring and an olefinic moiety in trans form were confirmed from values of chemical shifts and coupling constants in the ^1H NMR. The existence of the *trans*-3-chloroallyloxy moiety was confirmed by ^1H NMR and ^{13}C NMR. Mass spectral and elemental analyses are also consist-

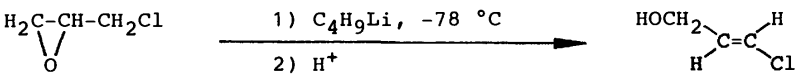

Scheme 1.

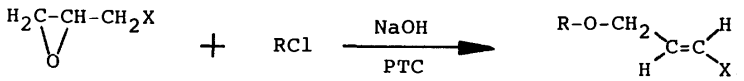

X: Cl-, ⬭-S-, n-C_8H_{17}S- Yield: 22-85%

R: ▽, ⬭-CH_2-, CH_2=C(-CH_3)-CH_2-, n-C_8H_{17}-

Scheme 2.

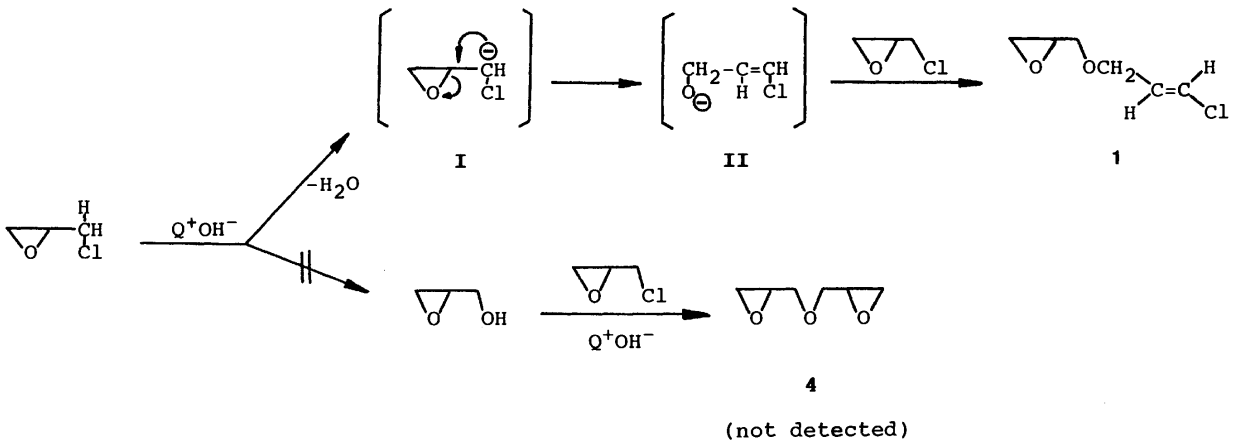

Scheme 3.

ent with this structure. This structure was separately confirmed by the reaction of 1,3-dichloropropene (34% cis, 66% trans) with 2,3-epoxy-1-propanol, which afforded a mixture of about 30% *cis*- and 70% *trans*-3-chloroallyl 2,3-epoxypropyl ethers (**1'**and **1**, respectively) (The cis : trans ratios of raw chlorides and products were estimated by ^{1}H NMR). Compound **1** was synthesized easily in one step from 1-chloro-2,3-epoxypropane in the presence of solid sodium hydroxide under the PT catalytic conditions as described in the experimental section. The proposed mechanism for the formation of **1** is represented in Scheme 3.

It is rational to consider that the reaction is initiated by the abstraction of a proton geminal to the chlorine atom from 1-chloro-2,3-epoxypropane with a hydroxide ion paired with the PT catalyst ammonium ion (Q^+OH^-). The carbanion **I** thus generated rearranges stereoselectively with ring-opening to the more stable and more nucleophilic alkoxide **II**,[4,23] which then reacts with another 1-chloro-2,3-epoxypropane molecule to afford **1**. Of course, the concerted route leading to **II** directly from proton abstraction can not be excluded. In the presence of alcohol, the hydroxide ion of Q^+OH^- gives mainly alkoxide, which further forms the alkyl 2,3-epoxy-1-propyl ethers by the nucleophilic substitution reaction.[16] However, in the absence of alcohol, owing to its poor nucleophilicity, the hydroxide ion acts as a base and gives a 1-chloro-2,3-epoxypropane anion **I** rather than 2,3-epoxy-1-propanol by the nucleophilic substitution reaction. This can be deduced from the fact that di-2,3-epoxypropyl ether was not detected (lower route in Scheme 3).

The above mechanism was supported by the formation of benzyl and 2-methylallyl *trans*-3-chloroallyl ethers (**2** and **3**) via the reaction of 1-chloro-2,3-epoxypropane in the presence of 2-methylallyl chloride or benzyl chloride, respectively (Table 1). The reaction of 1-chloro-2,3-epoxypropane with benzyl chloride (2 : 1 molar ratio) afforded **2** in 50% yield based on benzyl chloride together with **1** (22% based on 1-chloro-2,3-epoxypropane); reaction with 2-methylallyl chloride (2 : 1 molar ratio) gave **3** in 27% yield based on 2-methylallyl chloride together with **1** (15% based on 1-chloro-2,3-epoxypropane). Accordingly, this procedure using liquid-solid PT catalysis may lead to a general synthetic method for the preparation of *trans*-3-chloroallyl ethers.

This reaction did not proceed in the absence of PT catalyst, and the raw material, 1-chloro-2,3-epoxypropane, was recovered almost quantitatively.

In the case of 1-bromo-2,3-epoxypropane, the corresponding *trans*-3-bromoallyl ether was obtained in low yield (about 6%) under the same PT catalytic conditions as those for 1-chloro-2,3-epoxypropane. The major product was light brownish powder which is probably a polymeric substance.

So far as we know, the direct synthesis of *trans*-3-chloroallyl ethers from 1-chloro-2,3-epoxypropane is not recorded in the literature. Although 1-chloro-2,3-epoxypropane is usually reactive to nucleophiles under basic conditions, di-2,3-epoxypropyl ether (**4**) could not be detected in the products of the present reactions. On the other hand, in a separate reaction, it was confirmed that 2,3-epoxy-1-propanol gives di-2,3-epoxypropyl ether (**4**) in 23% yield by the reaction with 1-chloro-2,3-epoxypropane under the same reaction conditions. From these facts, this reaction can be considered to reveal an interesting phenomenon based on the strong basicity and weak nucleophilicity of Q^+OH^-.

This epoxide ring-opening reaction was also applied to 2,3-epoxypropyl sulfide **5**, **13** affording the corresponding *trans*-3-thioallyl ethers. The results of the reaction of phenyl and alkyl 2,3-epoxypropyl sulfide with various chlorides are shown in Table 1.

Although the reaction conditions were not optimized, it is clear that the yield of *trans*-3-thioallyl ethers decreased with less reactive chlorides. The yield of the corresponding octyl ether **10** from octyl chloride was relatively low (22%) compared with more reactive chlorides, such as 2,3-epoxypropyl (**6**, 85%), 2-methylallyl (**9**, 80%) or benzyl chloride (**7**, 73%). Although the reactivity of benzyl chloride toward S_N2 reactions is usually

Table 1. Reactions of Epoxides with Organic Chlorides

Starting Material		Time	Temp	Product	Yield[a]
Epoxide	Chloride	h	°C		%
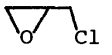	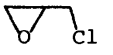	3	70	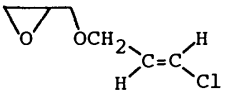 **1**	38
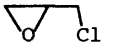	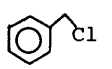	0.75	70	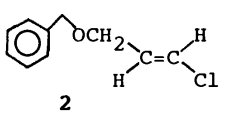 **2**	50
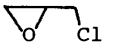	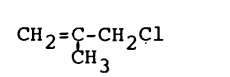	0.75	90	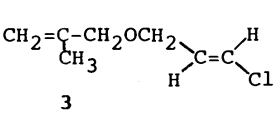 **3**	27
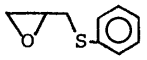 **5**	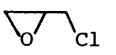	2	70	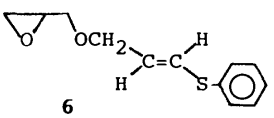 **6**	85
5	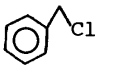	2	90	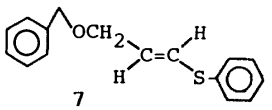 **7**	73
5	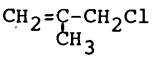	2	90	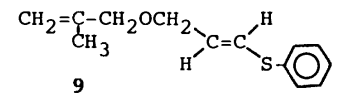 **9**	80
5	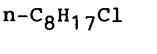	2	100	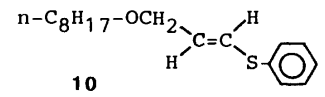 **10**	22
5		2	100	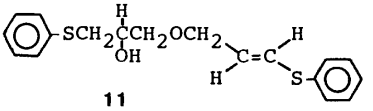 **11**	20
				and 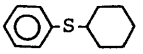 **12**	9
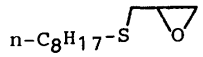 **13**	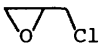	2	90	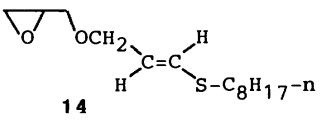 **14**	33

a) Isolated yield.

higher than that of 2-methylallyl chloride, the yield from the former was a little less than that from the latter. Apparently a competitive reaction occurred forming dibenzyl ether by the nucleophilic displacement to form benzyl alcohol under the PT catalytic alkaline conditions in the reaction using benzyl chloride. No noticeable competitive reaction occurred in the case of 2-methylallyl chloride.

In the case of a secondary chloride, cyclohexyl chloride, which has the poorest reactivity among the chlorides used, the major products obtained were *trans*-1,7-bis(phenylthio)-4-oxa-6-hepten-2-ol (**11**) and cyclohexyl phenyl sulfide (**12**) rather than the corresponding cyclohexyl *trans*-3-(octylthio)allyl ether.

It is difficult to deduce the reaction path to **12**, since the formation of the expected oxirane compound **6** or its derivatives has not been confirmed. However, from the fact that the reaction of **11** with cyclohexyl chloride in the presence of solid sodium hydroxide and PT catalyst afforded **12**, it may be reasonable to consider that the nucleophilic attack by certain species (including **III**) on **5** may give rise to the formation of a stable

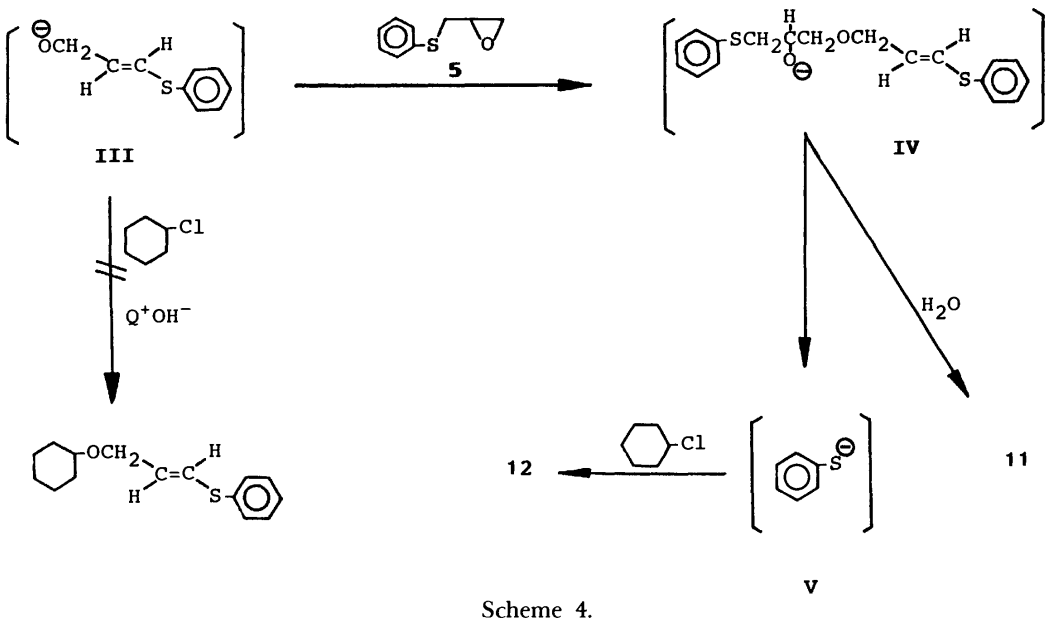

Scheme 4.

benzenethiolate ion (**V**) and **6** (when **III** included) by the intramolecular displacement reaction. The resulting **V** then further reacts with cyclohexyl chloride to produce **12**, as proposed in Scheme 4.

In any reaction of 1-chloro-2,3-epoxypropane with phenyl 2,3-epoxypropyl ether, alkyl 2,3-epoxypropyl ether, 1,2-epoxytetradecane or *N*-benzyl-*N*-methyl-2,3-epoxypropylamine, the corresponding allyl ethers could not be obtained. In these cases, only *trans*-3-chloroallyl 2,3-epoxypropyl ether (**1**) was isolated, and the 2,3-epoxypropyl compounds were recovered almost quantitatively, although it has been reported that 1,2-epoxyalkane afforded the corresponding allylic alcohol by the reaction with butyllithium.[4)]

Experimental

^{1}H NMR spectra were recorded on a JEOL JNM-PS-100 instrument in $CDCl_3$ with Me_4Si as internal standard. ^{13}C NMR spectra were obtained on a JEOL JNM-FX-60S Fourier transform spectrometer operating at 15.04 MHz with $CDCl_3$ as solvent. Mass spectra were measured on a Hitachi RMU-6E spectrometer. Infrared spectra were obtained on a Hitachi 260-10 spectrometer.

The reagents were all of reagent grade and were used without further purification. Evaporative distillation was performed from bulb to bulb using a glass tube oven model GTO-250RS.

Preparation of *trans*-3-Chloroallyl 2,3-Epoxypropyl Ether (1): Into a solution of 1-chloro-2,3-epoxypropane (92.5 g, 1.0 mol) and tetrabutylammonium hydrogensulfate (8.3 g, 0.025 mol) in dioxane (50 ml), sodium hydroxide (32 g, 0.8 mol, pellet) was carefully added maintaining the temperature between 70—80 °C over a period of 30 min with efficient stirring. Stirring was continued for an additional 2.5 h at 70 °C. The solid material was removed by filtration through a short column filled with silica gel. Product **1** was isolated by fractional distillation at reduced pressure as a colorless oil, 28.2 g, yield 38%; bp 110—111 °C/30 Torr (1 Torr= 133.322 Pa). The purity of the product was ascertained by GLC (5% Silicone SE-30 on Celite 545, 1m) as one peak. ^{1}H NMR ($CDCl_3$) δ=2.50—2.70 (m, 1H), 2.70—2.85 (m, 1H), 3.00—3.25 (m, 1H), 3.30—3.50 (m, 1H), 3.64—3.90 (m, 1H), 3.95—4.15 (d, 2H), 5.90—6.15 (m, J=14 Hz, 1H), 6.20—6.40 (m, J=14 Hz, 1H); ^{13}C NMR ($CDCl_3$) δ=43.0, 50.0, 68.4, 70.4, 120.0, 129.5; MS *m/z* (rel intensity) 148 (M^+), 91 (65), 75 (100), 57 (78), 39 (47), 31 (45), 29 (63); IR (liquid film) 2875, 1640, 1110, 930, 800 cm^{-1}. Found: C, 48.51; H, 6.20; Cl, 23.58%. Calcd for $C_6H_9ClO_2$: C, 48.50; H, 6.10; Cl, 23.86%.

Alternative Synthesis of 1 as a Mixture with 1′: Into a Mixture of 1,3-dichloropropene (about 34% cis, 66% trans estimated by ^{1}H NMR) (7.7 g, 0.07 mol), sodium hydroxide (6 g, 0.15 mol, pellet), tetrabutylammonium hydrogensulfate (0.85 g, 0.0025 mol) in dioxane (15 ml), 2,3-epoxy-1-propanol (3.7 g, 0.05 mol) was added dropwise at 30 °C, and stirred at 40 °C for 2 h. After the workup, the mixture of **1** and **1′** was isolated by Kugelrohr distillation at reduced pressure as a colorless oil, 3.9 g, yield 53%; bp 110 °C/30 Torr. The spectral data are the same as **1** expect for ^{1}H NMR ($CDCl_3$) δ=3.90—4.10 (d, 1.2H, *trans*-OCH_2CH=$CHCl$, 70%), 4.10—4.30 (m, 0.8H, *cis*-OCH_2CH=$CHCl$, 30%).

***trans*-3-Chloroallyl Benzyl Ether (2):** A mixture of benzyl chloride (12.7 g, 0.1 mol) and 1-chloro-2,3-epoxypropane (18.4 g, 0.2 mol) was treated with sodium hydroxide under the PT catalytic conditions similar to the procedure for **1**. After the workup, compound **2** was isolated as a colorless oil by distillation at reduced pressure, 9.1 g, yield 50%, together with **1** (3.3 g, 22%); bp 55—56 °C/0.08 Torr. ^{1}H NMR ($CDCl_3$) δ=3.90—4.08 (d, 2H), 4.50 (s, 2H), 5.90—6.20 (m, J=14 Hz, 1H), 6.20—6.36 (d, J=14 Hz, 1H), 7.32 (s, H); MS *m/z* (rel intensity) 182 (M^+), 92 (48), 91 (100), 79 (12), 77 (12), 65 (10); IR (liquid film) 2850, 1640, 1450, 1350, 1110, 930, 800, 730, 700 cm^{-1}. Found: C, 65.72; H, 6.23; Cl, 19,13%. Calcd for $C_{10}H_{11}ClO$: C, 65.78; H, 6.07; Cl, 19.41%.

***trans*-3-Chloroallyl 2-Methylallyl Ether (3):** By the same procedure as used for the benzyl ether **2**, the 2-methylallyl ether **3** was obtained as a colorless oil in 27% yield (4.0 g) together with **1** (2.2 g, 15%) from the reaction of 2-methylallyl chloride (9 g, 0.1 mol) and 1-chloro-2,3-

epoxypropane (18.4 g, 0.2 mol); bp 75—76 °C/30 Torr. ^{1}H NMR ($CDCl_3$) δ=1.74 (s, 3H), 3.85—4.04 (t, 4H), 4.84—5.00 (m, 2H), 5.90—6.15 (m, J=14 Hz, 1H), 6.15—6.35 (d, J=14 Hz, 1H); MS m/z (rel intensity) 146 (M^+), 75 (100), 56 (56), 55 (93), 43 (59), 41 (85), 39 (89); IR (liquid film) 2925, 2860, 1642, 1450, 1120 cm^{-1}. Found: C, 56,98; H, 7.72; Cl, 23.91%. Calcd for $C_7H_{11}ClO$: C, 57.38; H, 7.56; Cl, 24.21%.

Di-2,3-epoxypropyl Ether (4): Into a mixture of 1-chloro-2,3-epoxypropane (13.8 g, 0.15 mol), tetrabutylammonium hydrogensulfate (0.85 g, 5% based on 2,3-epoxy-1-propanol) and potassium hydroxide (5.6 g, 0.1 mol, pellet), 2,3-epoxy-1-propanol (3.7 g, 0.05 mol) was added at 40 °C over 30 min with rapid stirring. Stirring was continued for an additional 30 min at 40 °C. The solid material was removed by filtration. Compound **4** was isolated by Kugelrohr distillation at reduced pressure as a colorless liquid, 1.5 g, yield 23%; bp 100 °C/30 Torr. ^{1}H NMR ($CDCl_3$) δ=2.54—2.70 (m, 2H), 2.70—2.90 (m, 2H), 3.04—3.28 (m, 2H), 3.28—3.60 (m, 2H), 3.70—4.00 (m, 2H); MS m/z (rel intensity) 130 (M^+), 57 (66), 31 (72), 29 (100); IR (liquid film) 2950, 1280, 1120, 940, 880, 780 cm^{-1}.

Phenyl 2,3-Epoxypropyl Sulfide (5): Benzenethiol (11 g, 0.1 mol) in dioxane (50 ml) was added to a suspension of 1-chloro-2,3-epoxypropane (27.7 g, 0.3 mol), sodium hydroxide (12 g, 0.3 mol, pellet) in dioxane (50 ml) at room temperature over 20 min with stirring. Stirring was continued for another 4 h. The solid material was removed by filtration, and compound **5** was isolated by Kugelrohr distillation at reduced pressure as a colorless liquid, 16.2 g, yield 98%; bp 90 °C/0.02 Torr. ^{1}H NMR ($CDCl_3$) δ=2.40—2.56 (m, 1H), 2.65—3.25 (m, 4H), 7.16—7.50 (m, 5H); MS m/z (rel intensity) 166 (M^+), 123 (50), 110 (100). Found: C, 64.66; H, 6.09; S, 19.44%. Calcd for $C_9H_{10}OS$: C, 65.03; H, 6.06; S, 19.28%.

Preparation of *trans*-1-Phenylthio-6,7-epoxy-4-oxahept-1-ene (6): A suspension of phenyl 2,3-epoxypropyl sulfide (**5**) (8.3 g, 0.05 mol), 1-chloro-2,3-epoxypropane (9.2 g, 0.1 mol), sodium hydroxide (6.0 g, 0.15 mol, pellet) and tetrabutylammonium hydrogensulfate (0.85 g, 5% based on **5**) in dioxane (20 ml) was stirred rapidly at 70 °C for 2 h. After separation of the solid material by filtration, compound **6** was isolated by Kugelrohr distillation at reduced pressure as a colorless oil, 9.4 g, yield 85%; bp 100 °C/0.05 Torr. ^{1}H NMR ($CDCl_3$) δ=2.52—2.70 (m, 1H), 2.70—2.85 (m, 1H), 3.00—3.24 (m, 1H), 3.24—3.36 (m, 1H), 3.36—3.88 (m, 1H), 3.88—4.40 (m, 2H), 5.68—6.10 (m, J=15 Hz, 1H), 6.30—6.56 (m, J=15 Hz, 1H), 7.10—7.50 (m, 5H); MS m/z (rel intensity) 222 (M^+), 113 (100), 57 (100); IR (liquid film) 2900, 1650, 1580, 1475, 1430, 1100, 640, 580 cm^{-1}. Found: C, 64.48; H, 6.39; S, 14.17%. Calcd for $C_{12}H_{14}O_2S$: C, 64.84; H, 6.35; S, 14.42%.

Compound **1** was also obtained in yield of 24% (1.7 g).

***trans*-1-Phenyl-5-phenylthio-2-oxapent-4-ene (7):** A mixture of **5** (8.3 g, 0.05 mol) and benzyl chloride (12.6 g, 0.1 mol) was treated with sodium hydroxide under the PT catalytic conditions in dioxane similar to the procedure for **6** at 90 °C for 2 h. After the workup, product **7** was isolated by Kugelrohr distillation at reduced pressure as a colorless liquid, 9.0 g, yield 73%; bp 135 °C/0.03 Torr. ^{1}H NMR ($CDCl_3$) δ=3.95—4.25 (m, 2H), 4.48 (s, 2H), 5.70—6.04 (m, J=15 Hz, 1H), 6.30—6.62 (m, J=15 Hz, 1H), 7.28 (s, 10H); MS m/z (rel intensity) 256 (M^+), 165 (30), 137 (50), 91 (100); IR (liquid film) 3050, 2860, 1600, 1500, 1120, 760, 720 cm^{-1}. Found: C, 74.67; H, 6.55; S, 12.52%. Calcd for $C_{16}H_{16}OS$: C, 74.96; H, 6.29; S, 12.51%.

In this reaction, dibenzyl ether **8** was also obtained as a by-product in 62% yield (6.3 g) based on benzyl chloride (0.1 mol).

***trans*-6-Methyl-1-phenylthio-4-oxahept-1,6-diene (9):** By the same procedure as used for **6**, the corresponding compound **9** was obtained in 80% yield (8.8 g) from phenyl 2,3-epoxypropyl sulfide (8.3 g, 0.05 mol) and 2-methylallyl chloride (9.05 g, 0.1 mol); bp 100 °C/0.02 Torr. ^{1}H NMR ($CDCl_3$) δ=1.76 (s, 3H), 3.60—4.24 (m, 4H), 4.90—5.10 (m, 2H), 5.75—6.10 (m, J=15 Hz, 1H), 6.30—6.56 (m, J=15 Hz, 1H), 7.10—7.50 (m, 5H); MS m/z (rel intensity) 220 (M^+), 111 (42), 109 (33), 55 (100); IR (liquid film) 2900, 1670, 1600, 1120, 910, 750, 700 cm^{-1}. Found: C, 70.62; H, 7.40; S, 14.34%. Calcd for $C_{13}H_{16}OS$: C, 70.87; H, 7.32; S, 14.45%.

***trans*-1-Phenylthio-4-oxadodec-1-ene (10):** By the same procedure as used for **6**, the corresponding compound **10** was obtained in 22% yield (3.1 g) from phenyl 2,3-epoxypropyl sulfide (8.3 g, 0.05 mol) and octyl chloride (14.9 g, 0.1 mol); bp 120 °C/0.05 Torr. ^{1}H NMR ($CDCl_3$) δ=0.80—1.04 (t, 3H), 1.20—1.80 (m, 12H), 3.36—3.60 (m, 2H), 3.95—4.26 (m, 2H), 5.75—6.08 (m, J=15 Hz, 1H), 6.34—6.60 (m, J=15 Hz, 1H), 7.20—7.50 (m, 5H); MS m/z (rel intensity) 278 (M^+), 169 (28), 71 (45), 57 (100); IR (liquid film) 2950, 2875, 1590, 1480, 1100, 740, 700 cm^{-1}.

***trans*-1,7-Bis(phenylthio)-4-oxa-6-hepten-2-ol (11):** After treating phenyl 2,3-epoxypropyl sulfide (8.3 g, 0.05 mol) with cyclohexyl chloride (11.8 g, 0.1 mol) at 100 °C for 2 h under PT catalytic conditions, solid materials were removed by filtration through a short column filled with silica gel, and the reaction mixture was separated by Kugelrohr distillation at reduced pressure. Compound **11** as a colorless oil, 1.7 g, yield 20%; bp 180 °C/0.05 Torr, and phenyl cyclohexyl sulfide (**12**) as a colorless liquid, 0.85 g, yield 9%; bp 60 °C/0.05 Torr, were isolated respectively. Spectral analysis for **11**: ^{1}H NMR ($CDCl_3$) δ=2.80—3.10 (m, 3H), 3.40—3.70 (m, 2H), 3.70—4.10 (m, 2H), 4.10—4.30 (m, 1H), 5.70—6.00 (m, J=15 Hz, 1H), 6.30-6.50 (m, J=15 Hz, 1H), 7.10—7.60 (m, 10H); MS m/z (rel intensity) 332 (M^+), 167 (100), 149 (83), 123 (100); IR (liquid film) 3500, 2900, 1600, 1500, 1460, 1100, 1040, 760, 700 cm^{-1}. Found: C, 64.66; H, 6.09; S, 19.02%. Calcd for $C_{18}H_{20}O_2S_2$: C, 65.03; H, 6.06; S, 19.29%. Spectral analysis for **12**: ^{1}H NMR ($CDCl_3$) δ=1.00—2.10 (m, 10H), 3.00—3.20 (m, 1H), 7.10—7.60 (m, 5H); MS m/z (rel intensity) 192 (M^+), 110 (100), 55 (24). IR (liquid film) 2975, 1600, 1460, 700 cm^{-1}.

Octyl 2,3-Epoxypropyl Sulfide (13): The experimental procedure was similar to the preparation of **5** under the reaction conditions of 50 °C for 3 h. Yield 84%; bp 80 °C/0.03 Torr. ^{1}H NMR ($CDCl_3$) δ=0.80—1.00 (t, 3H), 1.16—1.80 (m, 12H), 2.50—2.90 (m, 6H), 3.00—3.24 (m, 1H); MS m/z (rel intensity) 202 (M^+), 146 (70), 112 (100), 84 (65), 83 (70), 70 (86), 69 (65), 56 (86), 55 (70); IR (liquid film) 2950, 1470, 840 cm^{-1}. Found: C, 65.10; H, 10.94; S, 15.59%. Calcd for $C_{11}H_{22}OS$: C, 65.29; H, 10.96; S, 15.84%.

***trans*-1,2-Epoxy-4-oxa-8-thiohexadec-6-ene (14):** The reaction conditions were similar to those for **6**. Yield 33%; bp 100 °C/0.05 Torr. ^{1}H NMR ($CDCl_3$) δ=0.76—1.04 (t, 3H), 1.16—1.86 (m, 12H), 2.30—2.86 (m, 4H), 3.00—3.80 (m, 3H), 3.96—4.20 (m, 2H), 5.42—5.76 (m, J=15 Hz, 1H), 6.04—6.40 (m, J=15 Hz, 1H); MS m/z (rel intensity) 258 (M^+), 145 (55), 113 (100), 57 (100), 55 (73), 31 (68); IR (liquid film) 2950, 1620, 1470, 1120, 950, 860 cm^{-1}.

Compound **1** was also obtained in 14% yield based on 1-chloro-2,3-epoxypropane.

References

1) A. Rosowsky, "Heterocyclic Compounds with Three- and Four-Membered Rings," ed by A. Weissberger, Wiley-Interscience, New York (1964), Part 1, p. 1.
2) G. Berti, "Topics in Stereochemistry," ed by N. L. Allinger and E. L. Eliel, Wiley-Interscience, New York (1973), Vol. 7, p. 93.
3) J. G. Buchanan and H. Z. Sable, "Selective Organic Transformations," ed by B. S. Thyagarajan, Wiley-Interscience, New York (1972), Vol. 2, p. 1.
4) J. K. Crandall, *Organic Reactions*, **29**, 345 (1983).
5) D. F. Hoeg, J. E. Forrette, and D. I. Lusk, *Tetrahedron Lett.*, **30**, 2059 (1964).
6) J. J. Eisch and J. E. Galle, *J. Am. Chem. Soc.*, **98**, 4646 (1976).
7) R. A. Bartsch and J. Zavada, *Chem. Rev.*, **80**, 453 (1980).
8) R. P. Thummel and B. Rickborn, *J. Org. Chem.*, **36**, 1365 (1971).
9) R. P. Thummel and B. Rickborn, *J. Am. Chem. Soc.*, **92**, 2064 (1970).
10) B. Rickborn and R. P. Thummel, *J. Org. Chem.*, **34**, 3583 (1969).
11) E. V. Dehmlow and S. S. Dehmlow, "Phase Transfer Catalysis," Verlag Chemie GmbH, D-6940 Weinheim (1980), p. 46.
12) "Compendium of Phase-Transfer Reactions and Related Synthetic Methods," ed by W. Keller, Fluka AG. CH-9470 Buchs, Switzerland (1979), p. 1.
13) W. Weber and G. W. Gokel, "Phase Transfer Catalysis in Organic Synthesis," Springer-Verlag, Berlin (1977), p. 1.
14) D. J. Brunelle and A. Singleton, *Tetrahedron Lett.*, **25**, 3383 (1984).
15) L. Lindblom and M. Elander, *Pharmaceutical Technology*, **1980**, 59.
16) X.-P. Gu, I. Ikeda, and M. Okahara, *Synthesis*, **1985**, 649.
17) H. J. Backer, J. S. Strating, and J. F. A. Fazenberg, *Recl. Trav. Chim. Pays-Bas*, **72**, 813 (1953).
18) M. Kotake, "Dai Yuki Kagaku," **2**, Asakura-shoten, Tokyo (1957), p. 114.
19) R. E. Gilbert and N. B., Lorette, U. S. Patent, 3303221; (*Chem. Abstr.*, **67**, 21628j (1967)).
20) S. A. Vertanyan, A. O. Tosunyan, and L. M. Kostochka, *Arm. Khim. Zh.*, **21**, 397 (1968); *Chem. Abstr.*, **70**, 28330b (1969).
21) L. S. Boguslavskaya, A. B. Bulovyatova, A. P. Sineokov, K. V. Yarovykh, and V. S. Etlis, *Zh. Org. Khim.*, **9**, 296 (1973); *Chem. Abstr.*, **78**, 124361y (1973).
22) F. Karrer and S. Farooq, Ger. Offen. 2518018; *Chem. Abstr.*, **84**, 58905z (1976).
23) A. C. Cope and J. K. Heeren. *J. Am. Chem. Soc.*, **87**, 3125 (1965).

 © 1987 The Chemical Society of Japan Bull. Chem. Soc. Jpn., 60, 673—682 (1987)

Reactivities of Stable Rotamers. XIX. Basicities of Rotameric 9-[2-(Dialkylaminomethyl)-6-methylphenyl]fluorenes and Solvent Effects on Them[1,2]

Mikio NAKAMURA and Michinori ŌKI*,†
Department of Chemistry, School of Medicine, Toho University, Ota-ku, Tokyo 143
†Department of Chemistry, Faculty of Science, The University of Tokyo, Bunkyo-ku, Tokyo 113
(Received August 4, 1986)

The pK_a' values of the trifluoroacetate salts of the title compounds were determined in THF–water (3 : 2) solution at 25 °C by potentiometric titration: in every compound examined, basicity of the *ap* rotamer was higher than that of the *sp* rotamer. Differences in pK_a' values (ΔpK_a) between the rotamers are in the range of 0.55 to 1.14 pK_a units, depending upon the substituents on the nitrogen atom. The ΔpK_a values in chloroform-*d* solution at 80.1 °C determined by taking advantage of the equilibrium constants of the salts and the free amines were larger than those obtained in aqueous THF solutions and were nearly independent of the substituents. The results were explained in terms of the intramolecular NH-π interactions in the *ap* salts, which are not possible in the *sp*. ^{1}H and ^{13}C NMR spectral data were in conformity with the presence of the interactions. Examination of the population ratios in various solvents revealed that *sp* conformers of the free amines are generally favored over the *ap* in polar, proton-accepting solvents, but the reverse is true for the trifluoroacetate salts. As the results, ΔpK_a values are large in toluene and chloroform but are rather small in tetrahydrofuran, acetonitrile, and nitromethane. Possible causes for the differences including solvation and hydrogen bond formation are discussed.

Physical properties of an organic compound are often the weighted means of those of several conformers of the molecule, since the interconversion among conformers usually takes place very rapidly. Acidities and basiciteis of organic compounds are examples of those cases. Taking cyclohexylamine, we notice that four processes are involved, as shown in Scheme 1, in the dissociation of this conjugate acid.

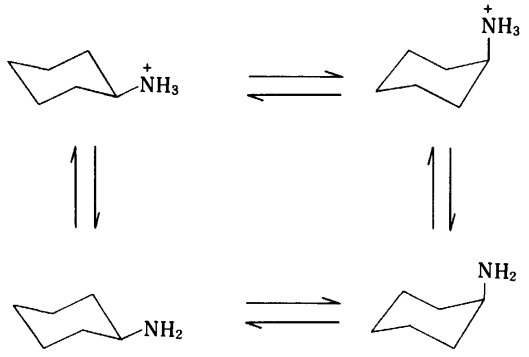

Scheme 1. Equilibria involved in dissociation of the conjugate acid of cyclohexylamine.

A common method of access to the true pK_a values of the equatorial and the axial conformers of the compound is that we use a pair of model compounds in which inversion and consequently the conformational change in the amine moiety is practically prohibited:[3] 4-*t*-Butylcyclohexylamine is a typical example, the cis isomer modelling the axial isomer and the trans the equatorial isomer.[4] Equations to obtain pK_a values of equatorial and axial isomers of the cyclohexane derivative were derived and were used in determining the pK_a values of axial and equatorial cyclohexylamines from those of cis and trans 4-*t*-butylcyclohexylamines.[4] However, such models possess inherent limitations. If we could directly determine acidities and basicities of respective rotamers, the values would be more reliable than those derived from the models.

Since we were able to isolate rotational isomers at room temperature,[5,6] we have been interested in the reactivities of those isomers.[7] The acidity or basicity is one of the examples in which we can see the respective properties of rotational isomers. The understanding of the acid-base properties of rotational isomers should contribute to get further insight into the bulk properties of organic compounds. Thus we launched a project of determining the acid-base properties of rotational isomers. This paper firstly presents some of the results obtained with 9-[2-(dialkylaminomethyl)-6-methylphenyl]fluorene rotamers both in aqueous THF and in chloroform-*d* and discusses the origin for the difference in basicities of the rotameric amines. The second point presented in this paper is the solvent effects on the base properties which can partly be interpreted on the molecular basis.

Syntheses of Amines

General procedure for the syntheses of the rotational isomers of the amines are shown in Scheme 2. The *sp* rotamer or a mixture of *sp* and *ap* rotamers of 9-(2-bromomethyl-6-methylphenyl)fluorene (**1**) was treated with the excess of the corresponding amines in THF solutions to give *sp*-[2-(dialkylaminomethyl)-6-methylphenyl]fluorenes (**2**—**5**) as a sole product after recrystallization. This stereospecific formation of the *sp* rotamer is interesting. There are two possible reasons for this phenomenon.

The first is kinetic control. Deprotonation reactions of 9-(2-methoxy-1-naphthyl)fluorene[8] and 9-(2-methoxymethyl-6-methylphenyl)fluorene and its analogs[9] with butyllithium followed by protonation with water have been known to produce the corresponding *sp* forms only. This phenomenon is attributed to the structure of the intermediate lithio com-

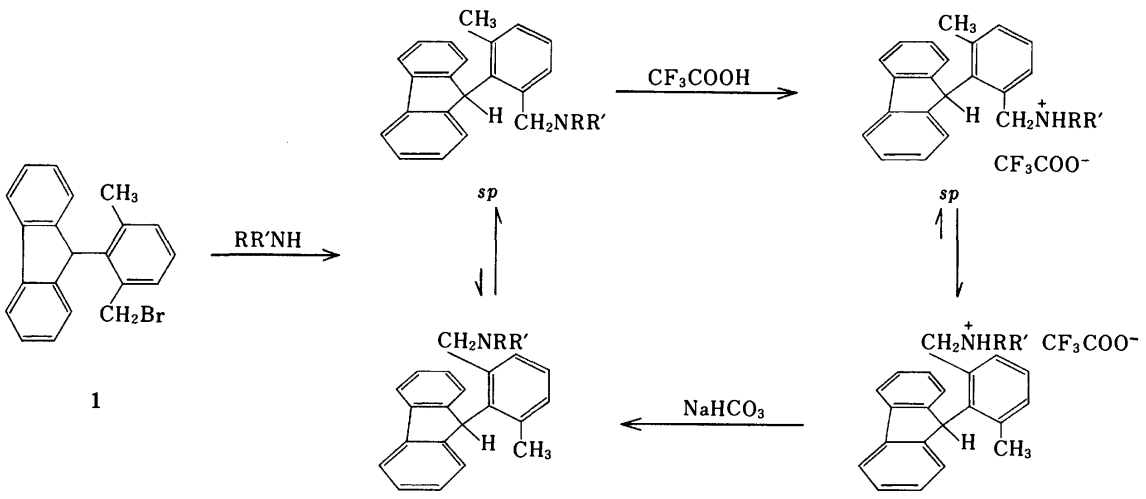

1

	R	R′
2	CH_3	CH_3
3	C_2H_5	C_2H_5
4	C_2H_5	n-C_3H_7
5	n-C_3H_7	n-C_3H_7

	R	R′
6	CH_3	CH_3
7	C_2H_5	C_2H_5
8	C_2H_5	n-C_3H_7
9	n-C_3H_7	n-C_3H_7

Scheme 2. Routes of syntheses of amines (**2**—**5**) and their trifluoroacetates (**6**—**9**).

pound which is stabilized by ligation with the heteroatom in the 2-position of the naphthalene or the phenyl nucleus, and protonation of the lithio compound with retention of configuration.[10] However, it is difficult to find this type of factors for the selectivity of the reaction.

The second is the thermodynamic effect which may favor the *sp* forms. Isomerization of the 9-arylfluorene rotamers takes place when an amine is present:[11] Under the reaction conditions the *sp* and *ap* amines can isomerize and thermal equilibrium may be reached. When we treated a mixture of *sp* and *ap* rotamers of compound **1** (*sp* : *ap*=1 : 2.7) with excess of dimethylamine in a THF solution and quenched with dilute hydrochloric acid after 30 min, we found that *sp* and *ap* amines were obtained in a 6.1 : 1 ratio. This ratio increased to 10 : 1 if the reaction period was lengthened. We conclude from this together with the similar results obtained for the diethylamine and dipropylamine cases that the overwhelming formation of the *sp*-amines is due to thermodynamic control. The equilibrium data obtained here are a little different from those in THF, as discussed later, but the results can be attributed to the presence of excess of amines which are polar and favor the solvation of the *sp* forms.

According to the above results, we have to use another independent way of synthesis to prepare the *ap*-amines. We found, however, that the *ap*-amine trifluoroacetate salts were much more stable than the *sp* in chloroform. Thus heating a chloroform solution of the *sp*-salt at 80.1 °C for 7 d afforded a mixture of rotational isomers, in which the ratio *ap*/*sp* reached nearly 10 or more. The pure *ap* salts were then obtained by recrystallization of the mixture from ether. Treatment of the salts with aqueous sodium hydrogencarbonate produced pure *ap*-amines. The predominance of the *ap* form over the *sp* in chloroform must be derived by the presence of NH-π interactions in the *ap* form, which will be discussed below in more detail.

9-[2-(Dimethylaminomethyl)-6-methylphenyl]fluorene

At the outset of the project, we measured the pK_a' values of rotameric 9-[2-(dimethylaminomethyl)-6-methylphenyl]fluorene trifluoroacetate in 3 : 2 THF-water. The pK_a' values were 5.85 and 6.45 for the *sp* and *ap* forms, respectively. The results were rather unusual in the sense that the amine moiety which is located in a more crowded site is more basic than that in a less crowded site: The general tendency, that is, less crowded amines are more basic than crowded amines, is explained on the basis of the unfavorable solvation of the crowded ammonium moiety.[4,12] There can be various reasons for the anomaly but we wished to focus our attention to the possible presence of the NH-π interactions (**10**), which are possible for

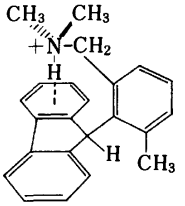

10

the *ap* salt but impossible for the *sp* due to the unfavorable approach of the NH group to the π-system of the fluorene, as the main cause.

Although the OH-π interactions are well documented,[13] the NH-π interactions are rarely reported.[14–16] From the available data, however, the presence of the NH-π interactions is clearly favored when the NH groups becomes electronegative, as is expected from the charge transfer theory. Since the electronegativity of the $^{+}$NH group is very high, it will be reasonable to assume the presence of the NH-π interactions here.

If the NH-π interactions play an important role in stabilizing the *ap* form of the salt relative to the *sp*, then the relative stability should be enhanced in less electron-donating solvents in hydrogen-bond formation, since the competition of the intramolecular NH-π interactions with the hydrogen-bond formation with such solvents will become favorable for the former. Being one of those solvents, chloroform is expected to show a large difference in pK_a values of the rotational isomers of **6**. However, it is very difficult to measure pK_a values in chloroform in the usual sense.

If one is allowed to discuss the difference only, not the absolute values, then there is a trick. The K_a values of the respective rotamers can be expressed by Eqs. 1 and 2.

$$K_a(sp) = \frac{[sp\text{-amine}][CF_3COOH]}{[sp\text{-salt}]} \quad (1)$$

$$K_a(ap) = \frac{[ap\text{-amine}][CF_3COOH]}{[ap\text{-salt}]} \quad (2)$$

Dividing Eq. 1 by Eq. 2, we obtain

$$\frac{K_a(sp)}{K_a(ap)} = \frac{K(\text{salt})}{K(\text{amine})} \quad (3)$$

where K(salt) and K(amine) are equilibrium constants (*ap*/*sp*) of the salt and the free amine, respectively, in chloroform at a given temperature. Then the ΔpK_a values ($\Delta pK_a = pK_a(ap) - pK_a(sp)$) can be obtained by taking the logarithm of Eq. 3, because K(salt) and K(amine) are measurable quantities.

Before getting into discussion of the ratios of the dissociation constants in chloroform, there is one thing which we should not overlook. Due to poor solvation in chloroform, dissociation of trifluoroacetic acid in this solvent should be greatly depressed,[17] or the ammonium salt **6** should be unstable. There is a chance that **6** dissociates into the free amine **2** and trifluoroacetic acid in chloroform to some extent. In order to find out if this is the case, we observed the chemical shifts of the NMR signals due to the benzylic methylene protons and 9-H by gradually adding trifluoroacetic acid to a solution of *sp*-**2** in chloroform-*d*. The results are shown in Fig. 1. As is clear from the Figure, the methylene proton signal at δ 3.69 for the free amine moved to a lower magnetic field on addition of the acid until it reached, on addition of 1.0 equivalent of the acid, at δ 4.63, where it stayed on further addition of the acid. The 9-H signal showed the similar behavior though it moved to a higher magnetic field on protonation of the amine. These clearly indicate that the ammonium salt *sp*-**6** exists without appreciable dissociation into the free amine and the acid under the conditions.

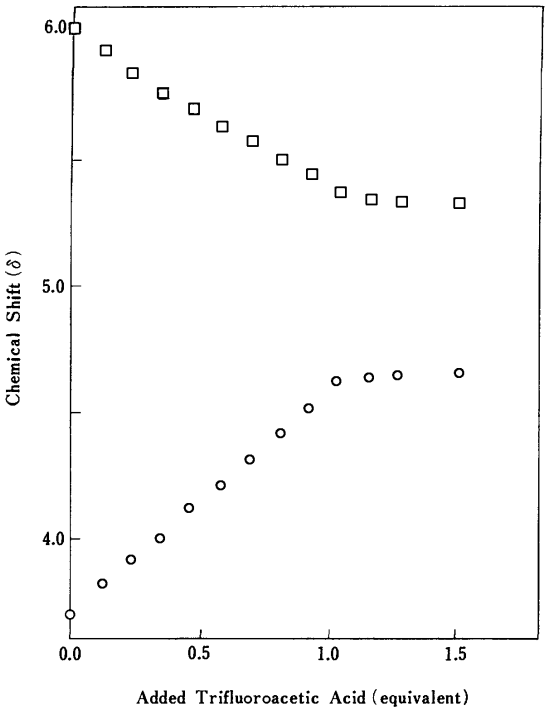

Fig. 1. Dependence of chemical shifts of benzylic protons and 9-H of *sp*-9-[2-(dimethylaminomethyl)-6-methylphenyl]fluorene in $CDCl_3$ on the amount of added trifluoroacetic acid.

In chloroform-*d*, the population ratio (*ap*/*sp*) of the rotamers of the free amine **2** was found to be 1/3.66, whereas that of the ammonium salt **6** was 9.70. Thus the ΔpK_a value in $CDCl_3$ is calculated to be 1.55. This enhancement of the difference in pK_a values of the rotamers in chloroform relative to the value in THF–water supports the idea of the presence of the NH-π interactions in the *ap* form of the salt.

9-[2-(Dialkylaminomethyl)-6-methylphenyl]fluorenes

Since the solvation effects are found to be very important in determining the pK_a values, we have extended the work to see the effects of the alkyl chain length in 9-[2-(dialkylaminomethyl)-6-methylphenyl]fluorenes (**2—5**) and their salts **6—9**. Since the alkyl chain should affect the solvation energy, there should be a chance that enhanced difference in pK_a values is observed. They may as well provide additional evidence for the presence of the NH-π interactions in the *ap* forms, when we compare the data in the series of compounds.

^{1}H and ^{13}C NMR Spectra. The ^{1}H NMR spectral data are given in Table 1. The free amines show fea-

Table 1. ^{1}H NMR Chemical Shift Data (δ) of Amines **2**—**5** and Their Trifluoroacetate Salts **6**—**9** in $CDCl_3$

Compound	Form	CH(α)[a]	CH(β)[a]	CH(γ)[a]	Aromatic CH_3	Benzylic CH_2	9-H
2	*sp*	2.32	—	—	1.10	3.69	6.02
	ap	1.51	—	—	2.70	2.11	5.44
3	*sp*	2.59	0.98	—	1.00	3.83	6.14
	ap	1.86	0.48	—	2.70	2.19	5.50
4	*sp*	2.6 2.5	0.97 1.43	— 0.73	1.10	3.86	6.17
	ap	1.83 1.70	0.57 0.90	— 0.46	2.70	2.17	5.43
5	*sp*	2.43	1.43	0.77	1.09	3.83	6.11
	ap	1.67	0.85	0.53	2.63	2.13	5.48
6	*sp*	2.97	—	—	1.17	4.63	5.33
	ap	1.93	—	—	2.76	2.98	5.53
7	*sp*	3.30	1.40	—	1.16	4.63	5.34
	ap	2.13 2.47	0.66	—	2.75	2.94	5.53
8	*sp*	3.37 3.1	1.40 1.83	— 1.00	1.17	4.70	5.30
	ap	b)	0.6 1.0	— 0.6	2.73	2.9 3.1	5.50
9	*sp*	3.20	1.81	1.00	1.17	4.70	5.29
	ap	1.97 2.24	1.00	0.63	2.73	2.97	5.57

a) α, β, and γ denote the position from the N atom in the alkyl chain. b) Multiplets centering at δ 1.7 (1 H) and 2.3 (3 H) that are not assigned.

tures that are common for the 9-arylfluorene series: The aromatic methyl and benzylic methylene signals are placed at high fields when the groups are located over the fluorene ring. Even the protons involved in the alkyl groups show similar tendency, though the effect becomes smaller as the protons are located remote from the nitrogen atom.

The change in the chemical shifts on protonation is very large especially for the protons of the methylene (methyl) groups which are attached directly to nitrogen. Inspection of the data in detail reveals that the extent of the low field shifts is different in *sp* series from that in the *ap* for some protons. Whereas the benzylic methylene signals of both *sp* and *ap* amines are similarly shifted to a low field by 0.8—0.9 ppm when the amines are protonated, the proton signals ascribable to the methylene (hereafter *N*-methylene) or the methyl group which is directly bonded to the nitrogen are shifted differently in the *sp* form from those in the *ap*. In every compound examined, the change in chemical shifts of the *N*-substituent protons is smaller in the *ap* form than in the *sp* on protonation. The dipropylamino compound **5** and its conjugate acid **9** are typical examples. The difference in the chemical shifts of the *N*-methylene proton signals is 0.77 ppm on protonation of the *sp* rotamer, while that of the *ap* rotamer is 0.44 ppm. These results may be explained on the basis of the freedom of motion of the propyl group. On one hand, the location of the benzylic methylene group is more or less fixed because of the rigidity of the part of the molecule. On the other, the *N*-methylene group can take various positions due to the conformational change in the free amine, while the position is rather fixed in the salt because of the presence of the NH-π interactions. Thus in the *ap* salt, the *N*-methylene protons are placed in the shielding region of the fluorene nucleus to counterbalance the effect of protonation to some extent and to make the smaller shifts to the low field on protonation. A similar tendency is observed in the 2-methylene protons and the methyl protons in the propyl group, though the extent of the difference becomes smaller as the protons become more remote from the nitrogen, the phenomenon being again in conformity with the freedom of motion of the propyl group.

The ammonium NH protons, though not listed in Table 1, show signals at δ ca. 11.5 and 12.5 for the *ap* and the *sp* conformers, respectively. The placement of the NH protons of the *ap* form at a higher magnetic field than that of the *sp* is another support for the presence of the NH-π interactions: The ring current effect of the fluorene ring should bring the chemical

Table 2. ^{13}C NMR Chemical Shift Data (ppm from TMS) of Amines **2**—**5** and Their Trifluoroacetate Salts **6**—**9** in $CDCl_3$

Compound	Form	N-C(α)[a]	N-C(β)[a]	N-CH(γ)[a]	Aromatic CH_3	Benzylic CH_2	9-C
2	*sp*	45.46	—	—	18.54	64.72	49.70
	ap	45.07	—	—	22.05	59.50	49.80
3	*sp*	46.04	11.23	—	18.54	58.57	49.41
	ap	46.38	11.13	—	21.91	53.16	49.80
4	*sp*	46.48	11.08	—	18.59	59.11	49.41
		55.01	19.66	12.01			
	ap	47.16	11.03	—	21.96	53.60	49.80
		54.92	19.66	11.91			
5	*sp*	55.55	19.52	12.06	18.69	59.60	49.41
	ap	55.79	19.71	11.91	21.96	54.14	49.80
6	*sp*	42.48	—	—	19.23	58.09	49.74
	ap	41.95	—	—	22.05	56.48	49.21
7	*sp*	45.94	8.79	—	19.23	53.36	49.70
	ap	45.12	7.57	—	22.05	52.39	49.27
8	*sp*	47.02	8.69	—	19.23	54.14	49.70
		53.06	17.13	11.13			
	ap	46.73	7.28	—	22.05	53.20	49.26
		51.89	16.15	10.93			
9	*sp*	53.45	17.03	11.18	19.23	54.18	49.70
	ap	52.58	15.72	10.99	22.01	53.26	49.21

a) α, β, and γ denote the position from the N atom in the alkyl chain.

shift of the NH protons in the *ap* forms to a high field.

It deserves mention here that the *N*-methylene protons of the *ap* forms of **7** and **9** exhibit AB pattern signals, if we neglect couplings with methylene or methyl protons, at room temperature to indicate that they are diastereotopic. It is also characteristic that the benzylic methylene protons in the *ap* forms give doublet signals. These should mean that the proton attached to the nitrogen atom dissociates slowly on the NMR time scale. Since the *N*-methylene protons of the *sp* forms do not show the diastereotopic nature nor the benzylic protons doublet signals at this temperature, the dissociation of the NH proton must be taking place much faster in the *sp* than in the *ap* form. The slow dissociation of the ammonium proton in the *ap* forms offers additional evidence for the presence of the intramolecular NH-π interactions. The details of the dynamic behavior will be described elsewhere.

The ^{13}C NMR spectral data shown in Table 2 indicate that the difference in chemical shifts between *sp* and *ap* rotamers are in most cases very small, less than 1.5 ppm. The exceptions are the benzylic methylene and aromatic methyl carbons of which differences amounted to 3.5—5.5 ppm in free amines. Although the presence of the ring current effect in ^{13}C NMR spectra is controversial,[18] it is tempting to consider that the ring current effect is operative in this case because of the proximity concerned. The most striking feature of the ^{13}C NMR spectra is the change in chemical shifts of the benzylic methylene carbons when the amine is protonated. In the case of *sp* amines, these carbons moved toward a high magnetic field by at least 5 ppm, while shifts were less than 0.8 ppm except for one case, a pair of **2** and **6**, in the *ap* forms. Since the protonation of amines usually causes a 3—5 ppm high field shift of the carbon signals alpha to the amino group,[19] the change in chemical shifts observed in the *sp* series is normal but that for the *ap* series abnormal. The contrast must be attributed to some effects of the substituents peculiar to the *ap* series.

We wish to attribute again the difference to the conformational change in the salt from that in the free amine. The repulsive interactions between lone-pair electrons and the aromatic π-system seem to be great. For example, the *sp* rotamer of 9-(2-methoxy-1-naphthyl)fluorene predominates over the *ap* form, although the half thickness of a benzo group is larger than the van der Waals radius of the oxygen atom in a methoxyl group.[20] Thus the conformation in which the amino-nitrogen is located closely to the fluorene ring is strongly disfavored. The preferred conformation must be such that the amino moiety takes a position away from the fluorene ring. This will necessarily result in the placement of the benzylic methylene protons, where they face the fluorene ring. This will cause the van der Waals shift for both hydrogens and

Table 3. Equilibrium Constants (*ap*/*sp*) of Amines **2**—**5** and Their Salts **6**—**9** in $CDCl_3$ at 80.1 °C, Ratios of Dissociation Constants, and Differences in pK_a Values

R[a)]	R'[a)]	K_{amine}	K_{salt}	K_{ap}/K_{sp}	ΔpK_a
CH_3	CH_3	1/3.7	9.7	36	1.5_5
C_2H_5	C_2H_5	1/2.8	12	34	1.5_3
C_2H_5	*n*-C_3H_7	1/2.5	14	35	1.5_4
n-C_3H_7	*n*-C_3H_7	1/2.2	22	48	1.6_8

a) R and R' in Scheme 2.

Table 4. Rate Constants of the Internal Rotation about the C_9-C_1' Bond in the Amines **2**—**5** and the Salts **6**—**9** in $CDCl_3$ and Free Energies of Activations at 80.1 °C

Compound	Process *sp*→*ap*		Process *ap*→*sp*	
	k	$\Delta G^{\ddagger}$[a)]	*k*	$\Delta G^{\ddagger}$[a)]
	10^{-6} s^{-1}	kcal mol^{-1}	10^{-6} s^{-1}	kcal mol^{-1}
2	0.85	30.59	3.12	29.68
3	0.61	30.83	1.71	30.10
4	0.69	30.72	1.71	30.10
5	0.48	31.00	1.06	30.44
6	4.73	29.39	0.49	30.99
7	12.6_5	28.70	1.03	30.46
8	9.42	28.80	0.67	30.77
9	7.22	29.10	0.33	31.26

a) 1 cal=4.184 J.

carbons,[21] by which carbon signals are shifted to a high field. In *ap* salts, the conformation is such that the NH-π interactions are possible in it: This requires that at least one of the methylene protons is placed away from the fluorene ring.

Rotational Barriers and Rotamer Populations. Mere consideration of the rotamer populations in equilibrium in discussing the stability of rotamers can lead to an erroneous conclusion, because one rotamer can be rich in population for two reasons; its enhanced stability relative to others and the enhanced instability of the counterparts. In order to diagnose the two possibilities, determination of rotational barriers should lend help, if the transition state for rotation can be assumed nearly equal. Thus we determined the rotational barriers and equilibrium constants in chloroform-*d* at 80.1 °C. The results are shown in Tables 3 and 4.

As is seen in Table 3, the equilibrium constants show a remarkable contrast for every compound examined: In amines, the *sp* forms are favorable species, being consistent with the general tendency that a bulkier substituent takes a position close to the 9-H in 9-(2,6-disubstituted phenyl)fluorenes,[6] while in the salts *ap* forms predominate by a factor of 10—20. The results are in conformity with the presence of the NH-π interactions in the *ap* forms of the salt.

As to the kinetics of internal rotation in amines, the rates of rotation as well as the free energy of activation for rotation are by and large the same irrespective of the alkyl chain, although a slight enhancement of the barrier is observed when one goes from methyl to ethyl and then to propyl (Table 4). This will mean that we may assume that both the ground states and the transition states for rotation are almost the same in their energy in these amines, as far as the molecular interactions are concerned. On protonation of the amine, the transition state energy of rotation will be slightly enhanced, if not the same with the amine, but the degree of the enhancement will be very small. Kinetic data in Table 4 then show that the ground state of the *sp* salt is destabilized to a small extent: This will probably because of the unfavorable steric effects on solvation. In contrast, the barrier to rotation for the process *ap*→*sp* is clearly enhanced in the salt relative to the free amine. If one takes the unfavorable solvation effects seen in the *sp* form of the salt and that the situation is even enhanced in the *ap* salt into consideration, the natural conclusion is that the *ap* form of the salt is stabilized relative to the *sp* forms due to the presence of the NH-π interactions in the former.

Difference in pK_a Values. The ΔpK_a values in chloroform-*d* are given in the last column of Table 3. Generally the difference is invariant. However, if one takes a careful look at the individual data, one notices that both *K*(amine) and *K*(salt) change as the alkyl group changes: Both the *K*(amine) and *K*(salt) values increase as the alkyl chain is lengthened. As a result, the ΔpK_a values appear to be not affected by the chain length. However, the population ratios of the salt change significantly when the alkyl chain becomes long. This is probably because the solvation becomes inefficient for the *sp* forms of the salt as the alkyl chain is lengthened, while the NH-π interactions are still

Table 5. pK_a' Values and Concentrations of the Conjugate Acids **6—9** in 3:2 THF-Water at 25°

Compound	pK_a'	*sp* Concentration / mol L^{-1}	pK_a'	*ap* Concentration / mol L^{-1}	ΔpK_a
6	5.90	0.0071	6.45	0.0059	0.55
7	5.70	0.0059	6.80	0.0072	1.10
8	5.22	0.0059	6.15	0.0059	0.93
9	4.98	0.0059	6.12	0.0077	1.14

efficient in the *ap* salt. In the free amine, the solvation effect is as well important: The solvation energy becomes small as the alkyl chain is lengthened, thus making the unfavorable steric situation for the *ap*-amine less effective.

The pK_a' values of the conjugate acids **6—9** were measured in 3:2 tetrahydrofuran-water. The results are given in Table 5. It is interesting to note that the ΔpK_a value of the methyl compound **6** is now doubled when we go to the ethyl compound **7**, whereas the ΔpK_a values do not change on further lengthening of the alkyl chain. The pK_a' values of the *sp* conjugate acids decrease monotonously when one goes from the short alkyl chains to long alkyl chains, while those of the *ap* forms show a maximum at the ethyl compound. Literature search reveals that the series of *N,N*-dialkylanilines shows the maximum basicity at the ethyl compound,[22] and the diethyl compound is more basic than the dimethyl compound in the series of *N,N*-dialkylbenzylamines,[22] though the exact cause for this phenomenon is not yet identified. It is possible that the monotonous decrease in the pK_a' values in the *sp* series is due to the steric hindrance for solvation, whereas in the *ap* the trend is normal because of the presence of the NH-π interactions. The stable conformation of the dimethylammonio group in the *sp* form of **6** will be such that the dimethylammonio group is perpendicular to the benzene ring of the 2,6-disubstituted phenyl group, as is the case of neopentylbenzene derivatives.[23] In this conformation, a water molecule can approach the ammonio-proton to form a hydrogen bond without much steric hindrance from the direction which is perpendicular to the phenyl ring. By contrast, the conformation of the diethylammonio group in the *sp* form of **7** will be such that the diethylammonio group takes a position in which the group opposes the 3-H of the phenyl ring. This is caused by severe steric interactions of the methyl group in the diethylammonio with the hydrogens at 1 and 8 positions of the fluorene ring. This conformation is unfavorable for solvation due to the steric effect, because the most stable conformation in this frame will be such that the hydrogen on the nitrogen atom of the ammonio group is located closely to the 3-H of the phenyl ring.

The sudden jump in the ΔpK_a value of the diethyl compound from the dimethyl may be ascribed to the NH-π interactions again. Due to the intramolecular interactions, the unfavorable steric effects on solvation are somewhat erased in the *ap* form relative to that of the *sp* form to make the *ap* amine more basic than the *sp*. The same factor operates in compounds with long alkyl chains (**8** and **9**) but the effect of solvation energy must be leveled off to make the apparent ΔpK_a almost the same.

Table 6. Equilibrium Constants (*ap*/*sp*) of Amines **2—5** and Their Salts **6—9** in Various Solvents at 80.1 °C

Compound	Toluene-d_8	THF	CH_3CN	CH_3NO_2
2	1/5.2	1/6.8	1/6.8	1/6.5
3	1/4.5	1/6.5	1/6.4	1/6.1
4	1/4.3	1/5.3	1/5.0	1/5.0
5	1/4.1	1/4.0	/3.9	1/4.0
6	4.1	1.0	1.0	2.2
7	7.4	2.1	1.9	2.5
8	7.9	2.1	3.0	3.4
9	11	2.3	3.4	3.4

Solvent Effects

The discussion presented above emphasizes that the NH-π interactions are important in affecting the difference in basicities of the rotamers in question. Chloroform is a solvent which does not donate electrons in hydrogen bond formation,[24] while the THF-water system may be taken as that NH-O hydrogen bond formation is possible between the solute and the solvent. Thus in THF-water a competition exists between the NH-O hydrogen bond and the NH-π, the former being more favored in terms of enthalpy at least than the latter. Thus it becomes of interest to examine the generality of the effect of hydrogen bond formation on the basicity difference of the rotamers. In this connection, we have examined the pK_a differences in various solvents.

The selected solvents are toluene, tetrahydrofuran, acetonitrile, and nitromethane. Toluene was assumed to be only weakly active in hydrogen bond formation and nonpolar, whereas latter three are capable of hydrogen bonding and polar. The results of the equilibrium constants and $\Delta pK_a'$ s are shown in Tables 6 and 7, respectively.

Table 7. Differences in pK_a Values (ΔpK_a) in Various Solvents at 80.1 °C

R[a)]	R'[a)]	Toluene-d_8	THF	CH_3CN	CH_3NO_2
CH_3	CH_3	1.33	0.83	0.83	1.16
C_2H_5	C_2H_5	1.52	1.14	1.08	1.18
C_2H_5	n-C_3H_7	1.53	1.05	1.18	1.23
n-C_3H_7	n-C_3H_7	1.65	0.96	1.12	1.13

a) R and R' in Scheme 2.

As to the populations of free amines, every solvent used here favors the *sp* forms relative to chloroform. As far as the polar solvents are concerned, the results may be attributed to the favorable steric situation of the *sp* forms for solvation. The population ratios in chloroform and toluene are not explainable in a straightforward manner but they may well be due to the solvation effect again: While toluene is a large molecule which should suffer from the steric effects in solvating the *ap* form, the largest solvation effect by the chloroform molecule should be given by hydrogen-bond formation, where chloroform acts as proton donor[25] and steric requirement is rather small. Close examination of Table 6 reveals that in every solvent examined, the *ap*/*sp* ratios decrease as the chain length of the alkyl group becomes longer. The long alkyl chain seems to disfavor the stabilization due to solvation of the *sp*-amines relative to the *ap*-amines, because intrinsic steric hindrance is larger in the latter than in the former even in the short chain case: The solvation energy becomes relatively less in the *sp* form as the alkyl chain becomes long. Although dielectric constant does not seem to play any role in the population ratio in the proton-accepting solvents, the reason for this phenomenon is not well-understood at the present.

By contrast, the *ap* forms of the amine salts are favored over the *sp* forms except for **5** in THF and acetonitrile, for which the equilibrium constants are 1.0, still a larger value than any of the amines examined. It is reasonable that the equilibrium constants are rather small in polar, hydrogen-bond accepting solvents. Because of the competition between the solute-solvent hydrogen bond and the intramolecular NH-π hydrogen-bond, the former being favored in terms of enthalpy, at least some fractions of the solute molecules will take conformations which are favorable for the intermolecular hydrogen bond but disfavor the intramolecular one. Since the entropic effect is not favorable for the intermolecular hydrogen bond, the intramolecular NH-π bond may still be present in the *ap* form in proton-accepting solvents. It is possible that this effect is partially responsible to the favorable population of the *ap* form relative to the *sp*. The slight increase in the *ap*/*sp* values of every compound in THF, acetonitrile, and nitromethane as the chain is lengthened may be explained similarly as above by the steric effect on solvation.

Toluene gives interesting but puzzling results. If the polarity of the solvent were important in determining the equlibrium constants, this solvent should have given larger *ap*/*sp* values for the salts than chloroform. Since the *ap*/*sp* values of the salts were all smaller in toluene than in chloroform, there must be other factors to be considered. First is the fact that toluene is a π-base. There must be a competition between intramolecular and intermolecular NH-π hydrogen bonds. Even though the entropy effect is not favorable for the intermolecular hydrogen bond, the solute-solvent interaction, such interactions should exist at least to some extent. Second is the fact that chloroform is capable of forming a hydrogen bond. This ability will contribute to stabilizing the *ap* salts by forming a hydrogen bond with the carboxylate anion in addition to the NH-π bond relative to the *sp* salts which exist as tight ion pairs, forming a hydrogen bond between the ammonium ion and the carboxylate anion.

As the results of these factors including the NH-π interaction and the solvation of the free amines and the salts, the differences in pK_a values must be derived (Table 7). It is interesting that in proton accepting solvents the ΔpK_a values are very close to 1.0 pK_a unit, whereas the solvents which cannot form a strong hydrogen bond with the NH group give large differences. The largest ΔpK_a value was obtained for the dipropylamino-compound in $CDCl_3$ with the close second of the same compound in toluene. The results suggest that in nonpolar aprotic solvents, the ΔpK_a values of rotational isomers can be great under certain conditions.

In summary, the results described here clearly demonstrate that the acidity or basicity is different from one rotamer to another and that the solvent effect on the difference is important. The causes for the differences can be the steric effects on solvation and intramolecular interactions such as the NH-π. Although it has not been explicitly discussed in this paper, the steric hindrance to proton abstraction may be a factor to be considered. It is necessary to interpret the pK_a value of a compound by taking the following factors into consideration in addition to the solvation or the intermolecular interactions: The populations and basicities of rotamers concerned which may be affected by intramolecular interactions.

Experimental

Syntheses of Amines 2—5 and Their Trifluoroacetates

Table 8. Melting Points, Yields, and Analytical Data of Amines and Their Trifluoroacetates

Compound	Form	Mp θ_m/°C	Yield/%	Analyses C(%) Found	C(%) Calcd	H(%) Found	H(%) Calcd	N(%) Found	N(%) Calcd
2	*sp*	87—88[a]	82[b]						
	ap	90—91[a]							
3	*sp*	67—68	68	87.79	87.93	7.75	7.97	3.96	4.16
	ap	38—40	85	87.74		7.77		3.94	
4	*sp*	36—38	73	88.10	87.84	7.97	8.22	3.79	3.94
	ap	Oil	76	87.58		8.05		3.86	
5	*sp*	96—97	68	87.58	87.75	8.26	8.46	3.64	3.79
	ap	22—26	84	87.51		8.55		3.65	
6	*sp*[c]	168—170	82	69.11	70.25	5.40	5.66	3.19	3.28
	ap[c]	162—165	71	69.43		5.77		3.44	
7	*sp*	155—157	79	71.17	71.19	6.23	6.20	2.93	3.08
	ap	143—145	70	71.19		6.22		2.89	
8	*sp*[c]	118—120	82	70.70	71.62	6.28	6.44	2.93	2.98
	ap	93—95	76	71.34		6.46		2.78	
9	*sp*	139—142	83	71.94	72.03	6.66	6.67	2.62	2.90
	ap	138—140	72	71.94		6.66		2.72	

a) These compounds had been prepared in alternative ways.[9] b) The yield of the amine prepared by the method described in this paper. c) These compounds seem to contain 0.04—0.09 equivalent excess of trifluoroacetic acid, of which presence was confirmed by ^{19}F NMR spectra. The trifluoroacetic acid could not be removed by heating at 80°C in vacuo for several hours.

6—9. General procedures for the syntheses are described by taking the diethyl compound **3** and **7** as examples. The melting points, yields, and analytical data are given in Table 8.

***sp*-9-[2-(Diethylaminomethyl)-6-methylphenyl]fluorene (*sp*-3).** To a solution of 245 mg (0.70 mmol) of a rotameric mixture of 9-(2-bromomethyl-6-methylphenyl)fluorene (**1**)[26] (*sp*/*ap*=2) in 20 mL of tetrahydrofuran, was added 2.0 g (27.3 mmol) of diethylamine. The solution was stirred at 40 °C for 24 h and then the reaction mixture was poured into 30 mL of water. The mixture was extracted with ether and the ether extracts were dried over sodium sulfate. After evaporation of the solvent, the residue, of which ^1H NMR spectrum showed to be a 10:1 mixture of *sp* and *ap* amines, was submitted to silica-gel TLC. Elution with dichloromethane-ethanol (10:1) afforded 163 mg (68%) of *sp*-**3**. Recrystallization from methanol afforded pure samples.

sp-**3** trifluoroacetate (*sp*-**7**) was prepared by adding 1 mL of trifluoroacetic acid to a solution of 80 mg of *sp*-**3** in 10 mL of ether followed by stirring for 10 min. Evaporation of the solvent together with excess of trifluoroacetic acid in vacuo and then two successive recrystallizations of the residue from ether afforded a pure sample.

ap-**3** trifluoroacetate (*ap*-**7**) was obtained by heating a solution of 30 mg of *sp*-**7** in 0.5 mL of chloroform-*d* in a sealed tube at 80.1 °C by immersing the tube in a boiling benzene bath for 7 d. The ratio *ap*/*sp* of the trifluoroacetate was 12 at this stage. The product was recrystallized from ether to give pure *ap*-**7**.

ap-**3** was obtained by treating a solution of *ap*-**7** in dichloromethane with 3% aqueous sodium hydrogencarbonate. The product was purified by recrystallization from methanol.

Preparation of the dimethylamino compound **2** has been reported[9] but *ap*-**2** was more conveniently prepared by the analogous procedure described above. The results are also included in Table 8.

Some of the *ap* amines had low melting points. In these cases, the free amines were purified by chromatography on silica gel, thoroughly dried in vacuo and submitted to elemental analyses.

pK_a' Measurements. In a typical experiment, 66.9 mg of *sp*-**7** was dissolved in a 25 mL volumetric flask in 3:2 THF-water to make a 0.0059 mol L^{-1} solution. By the use of a pipet, 10 mL of this solution was placed in a two-necked flask and was titrated with a 0.083 mol L^{-1} sodium hydroxide solution in 3:2 THF-water. Evaporation of THF was prevented as much as possible by using small inlets for the buret and for a glass electrode. After a small portion of the sodium hydroxide was added, the pH value of the solution was read by the glass electrode. In one experiment, 20 to 30 points were obtained. The curve which shows the relationship between the added sodium hydroxide and the pH values is simulated by the use of a computer program[27] to get a best fit. The pK_a' values are tabulated in Table 5.

NMR Measurements. ^1H and ^{13}C NMR spectra were recorded on a JEOL FX-90Q spectrometer operating at 89.55 and 22.49 MHz for proton and carbon, respectively. Some of the ^{13}C signals were assigned on the basis of off-resonance experiments and comparison of the peak intensities of the spectra obtained by the gated decoupling mode.

Kinetic Measurements. The rates of isomerization were

determined by monitoring the increase or decrease of the ^{1}H NMR signals due to each isomer in chloroform-*d* solutions. Plots of $\ln[1-(1+1/K)(a/X)]$ vs. time gave a straight line and the first order rate constants were obtained by the conventional method. In some salts in $CDCl_3$, the equilibrium constants seemed too large to afford reliable values by the NMR method. In such cases, the equilibrium constants were determined by treating them as variables starting from the NMR values: They were obtained as values which gave the best straight line in the plots of $\ln[1-(1+1/K)(a/X)]$ vs. time. Agreement between the calculated values and the observed ones by the NMR method was fairly good.

Determination of the Equilibrium Constants in Various Solvents. The amine or the salt was dissolved in a pure solvent under nitrogen and the solution was sealed in a tube, which was immersed in a boiling benzene bath (80.1 °C). It took 7 d to reach equilibrium at that temperature. The sealed tube was opened and the solvent was evaporated in vacuo. The population ratio, *ap*/*sp*, was determined by the integrated intensities in the ^{1}H NMR signals of the product in $CDCl_3$. In the case of salts, a small quantity of trifluoroacetic acid (0.05—0.10 equivalent) was added to avoid the presence of a free amine which would affect the equilibrium constant to a great extent. The effect of the presence of trifluoroacetic acid on the equilibrium was negligible, because changing the quantity of the acid within the range mentioned above did not show any significant difference in the equilibrium constants.

This work was supported by a Grant-in-Aid for Scientific Research administered by the Ministry of Education, Science and Culture, to which our thanks are due.

References

1) For Part XVIII, see M. Ōki, J. Tsukahara, K. Moriyama, and N. Nakamura, *Bull. Chem. Soc. Jpn.*, **60**, 223 (1987).

2) A preliminary note has been published: M. Nakamura and M. Ōki, *Chem. Lett.*, **1985**, 255.

3) S. Winstein and N. J. Holness, *J. Am. Chem. Soc.*, **77**, 5562 (1955); E. L. Eliel and C. A. Lukach, *ibid.*, **79**, 5986 (1957).

4) M. Tichy, J. Jonas, and J. Sicher, *Collection of Czechoslov. Chem. Commun.*, **24**, 3434 (1959); J. Sicher, M. Tichy, F. Sipos, M. Svoboda, and J. Jonas, *ibid.*, **29**, 1561 (1964).

5) M. Ōki, *Angew. Chem. Int. Ed. Engl.*, **15**, 87 (1976).

6) M. Ōki, *Top. Stereochem.*, **14**, 1 (1983).

7) M. Ōki, *Acc. Chem. Res.*, **17**, 154 (1984).

8) M. Nakamura and M. Ōki, *Chem. Lett.*, **1975**, 671.

9) M. Nakamura, Y. Suzuki, and M. Ōki, *Bull. Chem. Soc. Jpn.*, **58**, 2370 (1985).

10) D. Y. Curtin and W. J. Koehl, Jr., *J. Am. Chem. Soc.*, **84**, 1967 (1962).

11) R. Saito and M. Ōki, *Bull. Chem. Soc. Jpn.*, **55**, 3267 (1982).

12) H. C. Brown, D. H. McDaniel, and O. Häflinger, "Determination of Organic Structures by Physical Methods," ed by E. A. Braude and F. C. Nachod, Academic Press, New York (1955), p. 567.

13) M. Ōki and T. Yoshida, *Bull. Chem. Soc. Jpn.*, **44**, 1336 (1971) and earlier papers.

14) M. Ōki and K. Mutai, *Bull. Chem. Soc. Jpn.*, **39**, 809 (1966) and earlier papers.

15) I. Suzuki, M. Tsuboi, and T. Shimanouchi, *Spectrochim. Acta*, **16**, 467 (1960).

16) H. Tukada, M. Iwamura, T. Sugawara, and H. Iwamura, *Org. Magn. Reson.*, **19**, 78 (1982).

17) C. Reichardt, "Solvent Effects in Organic Chemistry," Verlag Chemie, Weinheim (1979), p. 55.

18) K. Sakamoto and M. Ōki, *Chem. Lett.*, **1976**, 257 and references cited therein.

19) T. D. Brown quoted in, W. Horsley and H. Sternlicht, *J. Am. Chem. Soc.*, **90**, 3738 (1968); W. Horsley, H. Sternlicht, and J. S. Cohen, *ibid.*, **92**, 680 (1972).

20) M. Nakamura and M. Ōki, *Bull. Chem. Soc. Jpn.*, **53**, 3248 (1980).

21) A. S. Perlin and B. Casu, *Tetrahedron Lett.*, **1969**, 2921; A. S. Perlin, B. Casu, and H. J. Koch, *Can. J. Chem.*, **48**, 2596 (1970).

22) N. F. Hall and M. R. Sprinkle, *J. Am. Chem. Soc.*, **54**, 3469 (1932).

23) B. Nilsson and T. Drakenberg, *Org. Magn. Reson.*, **6**, 155 (1974) and earlier papers.

24) R. D. Green, "Hydrogen Bonding by C-H Group," John-Wiley, New York (1974), pp. 11—35.

25) R. Mecke, *Discuss. Faraday Soc.*, **9**, 16 (1950); M.-L. Josien and N. Fuson, *J. Chem. Phys.*, **22**, 1169 (1954).

26) S. Murata, S. Kanno, Y. Tanabe, M. Nakamura, and M. Ōki, *Bull. Chem. Soc. Jpn.*, **55**, 1522 (1982).

27) H. Kihara and K. Sukegawa in "Oyo Kagaku Yakugaku Maikon (Microcomputers Applied to Chemistry and Pharmaceutical Sciences)," ed by Y. Tanaka and U. Sankawa, Nankodo, Tokyo (1985), p. 8.

 © 1987 The Chemical Society of Japan Bull. Chem. Soc. Jpn., 60, 683—687 (1987)

Preparation, 1,3-Dipolar Cycloaddition, and Thermal and Photochemical Reactions of 3,5-*exo*- and 3,5-*endo*-7-Methylene-4-azatetracyclo[4.2.1.0.^{2,8}0^{3,5}]nona-9-ones[1]

Nobuhiro KANOMATA, Tadashi KOBAYASHI, Takashi UETAKE, Shuji OKADA, and Makoto NITTA*
Department of Chemistry, School of Science and Engineering, Waseda University, Shinjuku-ku, Tokyo 160
(Received August 6, 1986)

The 1,3-Dipolar cycloaddition of phenyl azide with 1,3,5-trimethyl-6-methylenetricyclo[3.2.1.0^{2,7}]oct-3-en-8-one occurred onto the endocyclic double bond to give the *exo*- and *endo*-adducts (**7** and **8**) in a similar ratio. Upon photoirradiation, **7** and **8** eliminated a nitrogen molecule to give 3,5-*exo*- and 3,5-*endo*-1,3,6-trimethyl-7-methylene-4-azatetracyclo[4.2.1.0.^{2,8}0^{3,5}]nona-9-ones (**9** and **10**) in good yields. The 1,3-Dipolar cycloaddition of 2,4,6-trimethylbenzonitrile oxide with **9** and **10** occurred onto the exocyclic double bond to give two stereoisomers in each case. The stereoselectivity of the reactions is discussed on the basis of the stereoelectronic factor of the aziridine ring. The thermal reaction of **9** and **10** as well as photoirradiation of **9** caused a simple C–N bond cleavage of the aziridine ring. However, photoirradiation of **10** or its dimethyl analogue caused an unusual skeletal rearrangement resulting in the formation of 9-methylene-6-phenyl-6-azatricyclo[3.3.1.0^{2,8}]nona-3-en-7-one ring system. Mechanistic pathways of the rearrangement were postulated.

Previous work in this series has included studies concerning the stereoselectivity and site selectivity of the electrophilic reactions, such as solvomercuration, bromination,[2] 1,3-dipolar cycloaddition,[3] and dichlorocarbene addition[4] of 1,5-diemthyl-6-methylenetricyclo[3.2.1.0^{2,7}]oct-3-en-8-one (**1**)[5] and its related compounds. Among these reactions, the 1,3-dipolar cycloaddition of **1** and 1,3,5-trimethyl-6-methylenetricyclo[3.2.1.0^{2,7}]oct-3-en-8-one (**2**)[5] with 2,4,6-trimethylbenzonitrile oxide (mesitonitrile oxide, MNO) exhibited remarkable stereoselectivity or site selectivity to give cycloadducts **3** and **4**, while **1** with phenyl azide (PA) afforded adduct **5** (Scheme 1). The formation of the *exo*(to the carbonyl group)-adducts **3** and **4** can been explained by the preferential LUMO(MNO)-HOMO(exocyclic double bond of **1** or **2**) interaction. The prohibited endo attack of MNO onto the exocyclic double bond was ascribed to the repulsive orbital interaction, which could be experienced with the endocyclic double bond as depicted in Fig. 1. In the cycloaddition of PA, on the other hand, the LUMO(PA)-HOMO (exocyclic double bond of **1**) interaction to give *endo*- or *exo*- adduct **6** was prohibited by a repulsive orbital interaction or a large van der Waals nonbonded interaction of the phenyl group. Thus, the cycloaddition occurred onto the endocyclic double bond from the endo side to give **5**.

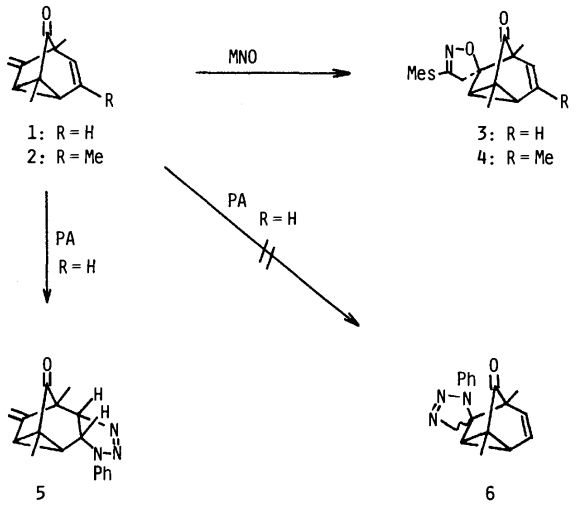

Scheme 1.

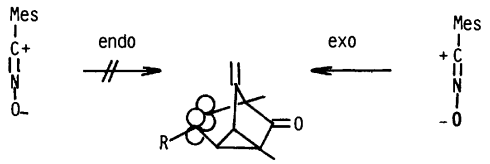

Fig. 1.

In this paper, the 1,3-dipolar cycloaddition of **2** with PA was clarified as occuring onto the endocyclic double bond from the exo and endo sides. These two adducts could eliminate a nitrogen molecule, resulting in the formation of 3,5-*exo*-1,3,5-trimethyl- and 3,5-*endo*-1,3,5-trimethyl-4-azatetracyclo[4.2.1.0.^{3,5}0^{2,8}]nona-9-ones (**9** and **10**) under photoirradiation. The 1,3-dipolar cycloaddition of MNO with the exocyclic double bond of **9** and **10** was interesting from the viewpoint of a comparison of the electronic effect of the aziridine ring of **9** and **10** with that of endocyclic double bond of **1** and **2**, in both of these the endo attack of MNO was completely prohibited (Fig. 1).[3] Furthermore, thermal and photochemical reactions of **9** and **10** were studied in order to clarify the chemical behaviors, which would be affected by stereochemical arrangements of the aziridine ring. The results are described in this paper.

Results and Discussion

The reaction of **2** with PA under reflux in cyclohexane for 50 h gave an *exo*-adduct **7** and an *endo*-adduct **8** in 32 and 31% yields, respectively. The structural proof was based on elemental analyses and spectroscopic data (see Experimental). Especially, the chemical shifts of the protons on the triazoline moieties of **7** (δ 4.12) and **8** (δ 4.14) are suggestive of the assigned

regioselectivity.[6] The stereochemical arrangement of the triazoline moiety of **7** and **8** was deduced from the pseudo-contact NMR spectra observed by using $Eu(fod)_3$.[7] The relative down-field shifts of δ's of typical protons are give in parentheses in the structural formulae **7** and **8** in Scheme 2. The small values of

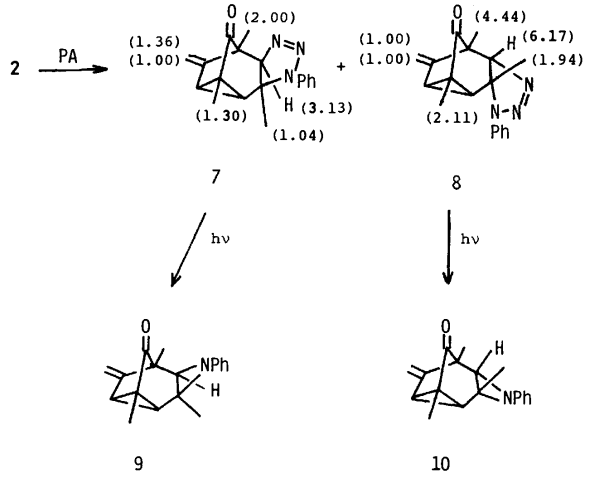

Scheme 2.

3.13 and 1.04 for a proton and a methyl group on the triazoline moiety of **7**, as compared with the corresponding values of 6.17 and 1.94 of **8**, suggest the coordination of $Eu(fod)_3$ occurs on the carbonyl-oxygen and support the structural assignment of **7** and **8**. Since the terminus of the methyl-substituted endocyclic double bond (possibly with a large HOMO coefficient) was bound to a nitrogen atom bearing no phenyl group (large LUMO coefficient), the regioselectivity of the adducts **7** and **8** appears to be controlled by the PA(LUMO)-**3**(HOMO) interaction.[3,8] The carbonyl group and the exocyclic double bond of **1** and **2** exist in a similar stereochemical situation in the molecular framework (as depicted in Fig. 2). In the case of **1**, exo (to the carbonyl group) attack of PA was considered to be prohibited, probably by a steric hindrance between the phenyl group of PA and C_1-methyl group.[3] Thus, an addition occurred from the less-hindered side to give only **5**. Similarly, an exo attack in **2** also expected to be sterically hindered. However, the introduction of a C_3-methyl group in **2** resulted in the competition of exo and endo attack to give **7** and **8**. The effect of the methyl group on the stereoselectivity still remained unclear.

The photoirradiation of **7** and **8** with RPR-350 nm lamps underwent a clear elimination of a nitrogen molecule to give aziridine **9** or **10**, respectively (Scheme 2).[9,10] The structures of **9** and **10** were also confirmed on the basis of the spectral data.

Compounds **9** and **10** contain an aziridine ring instead of a π bond of **2**, the cycloaddition of which occured to give only an *exo*-adduct **4**.[3] Thus, the cycloaddition of MNO with **9** and **10** was investigated in order to gain a further insight into the stereoelectronic control of the aziridine ring, as compared with the endocyclic π bond (Fig. 1). The reaction of **9** with MNO afforded *exo*-adduct **11** and *endo*-adduct **12** in 58 and 23% yields. Similarly, a reaction of **10** afforded two adducts (**13** and **14**) in 79 and 10% yields. The structures of these adducts were deduced from the spectroscopic data. Especially, the chemcial shifts of the

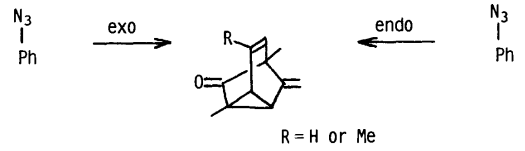

Fig. 2.

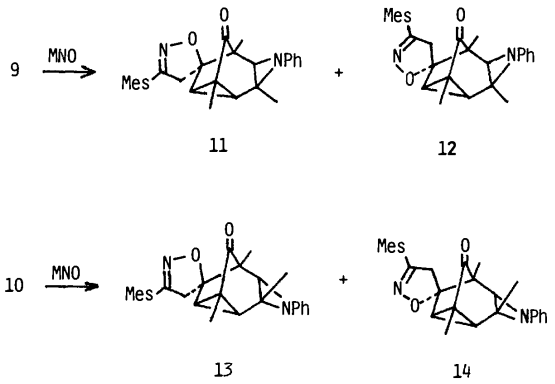

Scheme 3.

methylene group on the isoxazoline moieties were helpful in determining the stereochemistry. In the cases of *endo*-adducts **12** (δ 3.22, 3.29) and **13** (δ 3.03, 3.14), chemical shifts of these protons appeared at higher fields compared with those of *exo*-adducts, **11** (δ 3.24, 3.34) and **13** (δ 3.23, 3.29). This fact could be ascribed to the anisotropy effect of the carbonyl group. Thus, the stereochemical arrangement of the isoxazoline moieties of **11**—**14** were established.

Consequently, in the cycloaddition of MNO with **9**, the stereoelectronic control of the aziridine bent bond seemed to be much reduced compared with that of the endocyclic double bond in **2** (Fig. 1). Thus, the *endo*-adduct **12** was obtained in an appreciable amount. The steric hindrance of the methyl group at C_3 does not seem so significant in the cycloaddition of **9**. The product ratio of **13**/**14** was larger than that of **11**/**12**. This fact is suggestive of a repulsive interaction of MNO with the bent σ (C-N) bonds of the aziridine ring of **10**.

Studies of the thermal reaction[10] of **9** and **10** in 1,2-dimethylbenzene indicated that this fragmentation of the aziridine ring gave the corresponding exo and endo amino compounds **16** and **18** in 15 and 21% yields, leaving unreacted starting materials **9** and **10** in 85 and 79% yields. The structures of products **16** and **18** were unequivocally assigned on the basis of the spectral data. Similarly, a photoirradiation of **9** with RPR-254 nm lamps afforded **16** in a 35% yield. Thus, the reaction seems to proceed via diradical intermediates

15 and **17** formed by homolytic rupture of the C-N bond.[11]

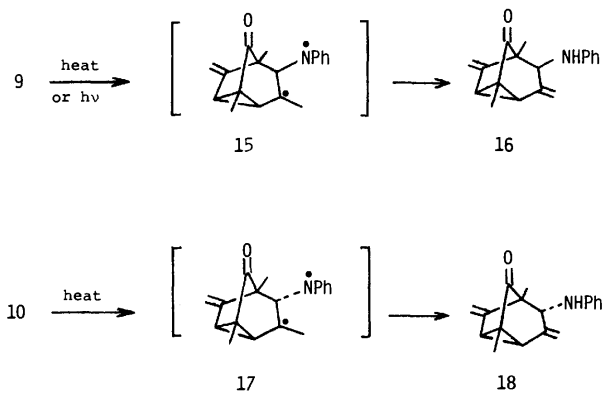

Scheme 4.

However, a similar photoreaction of **10** gave only **19** in an 18% yield, in addition to large amounts of extremely decomposed materials. Similarly, the irradiation of the dimethyl derivative **20**[3] also gave **21** in a 30% yield. The structures of **19** and **21** were assigned on the basis of the spectral data. The ^{1}H NMR spectra of **19** and **21** exhibited typical chemical shifts and coupling patterns of the divinylcyclopropane moiety observed in compounds **1**, **2**,[5] and 5,8-dimethyl-9-methylenetricyclo[3.3.1.0^{2,8}]non-3-en-7-one.[12] The IR spectra suggest the existence of a six-membered amide function. Furthermore, the mass spectra of **19** and **21** exhibited an ion with *m/z* 119 (phenyl isocyanate). Thus, the structures of **19** and **21** could be deduced.

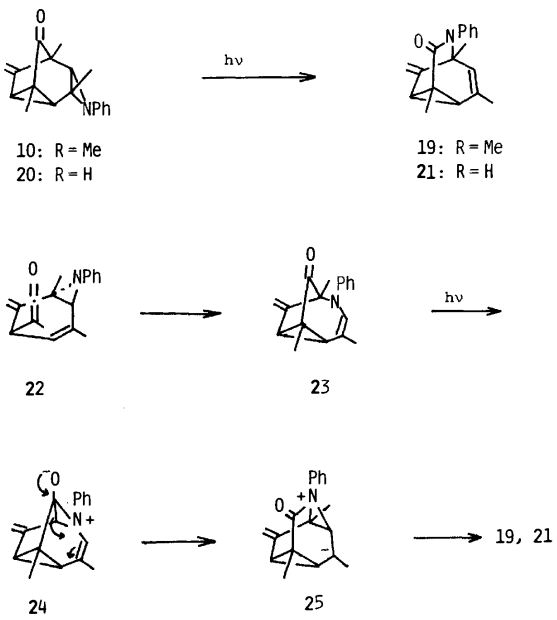

Scheme 5.

Compounds **10** and **20** have a skeleton similar to photolabile tricyclo[3.2.1.0^{2,7}]oct-3-en-8-one derivatives, which have been shown to photoisomerize to ketene derivatives.[13] Therefore, a ketene **22** is postulated to be a possible intermediate. Then, the addition of the ketene to the vinylaziridine moiety gives **23**, the photoreaction of which possibly gives zwitter ion **24**. The photoreaction initiated by the attack of a lone pair electron on nitrogen onto the carbonyl group has been previously reported regarding the rearrangement of the 8-azabicyclo[3.2.1]octa-3,6-dien-2-one ring system.[14] The reaction pathway of **24** may involve a formal intermediate **25** to give **19** and **21**. The reaction sequences postulated above are purely speculative, and evidence has not been obtained. The exo isomer **9** gives only **16** possibly via a diradical intermediate. This fact and the photorearrangement of endo isomers **10** or **20** to give **19** or **21** may stand in contrast to a thermal rearrangement of 3-arylsulfonyl-3-azatricyclo-[3.2.1.0^{2,4}]oct-6-ens.[15]

Experimental

The IR spectra were recorded on a Shimadzu IR-400 spectrometer. The mass spectral studies were conducted using a Shimadzu GCMS-QP1000 and JEOL JMS-DX300 mass spectrometers. The ^{1}H NMR spectra (60 MHz) were recorded on a Hitachi R-24 spectrometer using Me_4Si as internal standard. The photoirradiations were carried out using Rayonet photoreactor fitted with appropriate lamps. All of the thermal and photochemical reactions were carried out under nitrogen atmosphere. Mesitonitrile oxide (MNO)[16] and phenyl azide (PA)[17] were prepared by the standard methods. All of the melting points are uncorrected.

Cycloaddition of 2 with PA. A solution of **2** (2.36 g, 13.6 mmol) and PA (2.78 g, 23.4 mmol) in cyclohexane (12 cm^3) was heated under reflux for 50 h. After the solvent was evaporated, the residue was separated by column chromatography on alumina. The fractions eluted with hexane afforded **2** (377 mg, 16%). The fractions eluted with benzene afforded **7** (1.28 g, 32%). The fractions eluted with dichloromethane afforded **8** (1.25 g, 31%). For **7**: Mp 86—87 °C (from hexane); IR ($CHCl_3$) 1733 cm^{-1}; ^{1}H NMR (CCl_4) δ=1.26 (6H, s), 1.44 (3H, s), 2.10 (1H, d, J=7.2 Hz), 2.37 (1H, d, J=7.2 Hz), 4.12 (1H, s), 4.67 (1H, s), 4.86 (1H, s), 6.80—7.32 (5H, m); MS *m/z* (rel intensity) 265 (M^+-N_2, 9), 77 (100). Found: C, 73.77; H, 6.38; N, 14.41%. Calcd for $C_{18}H_{19}N_3O$: C, 73.69; H, 6.53; N, 14.33%. For **8**: Mp 114—115 °C (from hexane); IR ($CHCl_3$) 1736 cm^{-1}; ^{1}H NMR ($CDCl_3$) δ=1.00 (3H, s), 1.36 (3H, s), 1.52 (3H, s), 2.17 (1H, d, J=7.8 Hz), 2.64 (1H, d, J=7.8 Hz), 4.14 (1H, s), 4.90 (1H, s), 5.03 (1H, s), 6.8—7.5 (5H, m); MS *m/z* (rel intensity) 265 (M^+-N_2, 6), 118 (100). Found: C, 73.84; H, 6.46; N, 14.24%. Calcd for $C_{18}H_{19}N_3O$: C, 73.69; H, 6.53; N, 14.33%.

Photoirradiation of 7. A solution of **7** (2.0 g, 6.83 mmol) in anhydrous acetonitrile (200 cm^3) was irradiated with RPR-350-nm lamps through a Pyrex filter for 5 h. After the solvent was evaporated, the resulting residue was crystallized from ethanol to give colorless crystals of **9** (1.32 g, 73%): Mp 105—106 °C (from EtOH); IR ($CHCl_3$) 1736 cm^{-1}; ^{1}H NMR (CCl_4) δ=1.14 (3H, s), 1.25 (3H, s), 1.27 (3H, s), 1.94 (1H, dXd, J=7.4, 0.8 Hz), 2.04 (1H, d, J=0.8 Hz), 2.40 (1H, d, J=7.4 Hz), 4.53 (1H, s), 4.79 (1H, s), 6.42—7.22 (5H, m); UV (EtOH) 244 (ε 11700) and 291 (2300). Found: *m/z* 265.1472. Calcd for $C_{18}H_{19}NO$: M, 265.1467.

Photoirradiation of 8. A solution of **8** (947 mg, 3.3 mmol) in anhydrous acetonitrile (200 cm^3) was irradiated

with RPR-350 nm lamps through a Pyrex filter. After the solvent was evaporated, the resulting residue was crystallized from hexane to give colorless crystals of **10** (760 mg, 88%): Mp 118—119 °C (from hexane); IR ($CHCl_3$) 1739 cm^{-1}; ^1H NMR (CCl_4) δ=1.19 (3H, s), 1.26 (6H, s), 1.98 (1H, d, J=1.8 Hz), 2.01 (1H, d×d, J=8.0, 1.8 Hz), 2.43 (1H, d, J=8.0 Hz), 4.72 (1H, s), 4.84 (1H, s), 6.54—7.28 (5H, m); UV (EtOH) 236 (ε 14800), 275 (sh, 2120), and 284 (sh, 1480). Found: m/z 265, 1451. Calcd for $C_{18}H_{19}NO$: M, 265.1467.

Cycloaddition of 9 with MNO. A solution of **9** (200 mg, 0.78 mmol) and MNO (122 mg, 0.78 mmol) in anhydrous benzene (5 cm^3) was heated under reflux for 6 h. After the solvent was evaporated, the residue was separated by TLC on silica gel using chloroform-benzene (1/1) as developer. The first band from the TLC plates contained 186 mg (58%) of the adduct **11**. The second band from the TLC plates gave 75 mg (23%) of the adduct **12**. For **11**: Mp 162—163 °C (from EtOH); IR ($CHCl_3$) 1735 cm^{-1}; ^1H NMR ($CDCl_3$) δ=1.18 (3H, s), 1.36 (3H, s), 1.37 (3H, s), 1.50 (1H, s), 2.05 (1H, d, J=2.5 Hz), 2.07 (1H, d, J=2.5 Hz), 2.25 (9H, s), 3.24 (1H, d, J=19.4 Hz), 3.34 (1H, d, J=19.4 Hz), 6.56—7.17 (7H, m); MS m/z (rel intensity) 426 (M^+, 62), 77 (100). Found: C, 78.84; H, 7.04; N, 6.70%. Calcd for $C_{28}H_{30}N_2O_2$: C, 78.84; H, 7.09; N, 6.57%. For **12**: Mp 214—216 °C (from EtOH); IR ($CHCl_3$) 1747 cm^{-1}; ^1H NMR ($CDCl_3$) δ=1.23 (3H, s), 1.34 (3H, s), 1.37 (3H, s), 1.57 (1H, s), 2.08 (1H, d, J=1.8 Hz), 2.17 (1H, d, J=1.8 Hz), 2.32 (9H, s), 3.22 (1H, d, J=17.4 Hz), 3.29 (1H, d, J=17.4 Hz), 6.60—7.24 (7H, m); MS m/z (rel intensity) 426 (M^+, 19), 118 (100). Found: m/z 426. 2338. Calcd for $C_{28}H_{30}N_2O_2$: M, 426.2307.

Cycloaddition of 10 with MNO. A solution of **10** (265 mg, 1 mmol) and MNO (161 mg, 1 mmol) in anhydrous benzene (5 cm^3) was heated under reflux for 5 h. After the solvent was evaporated, the resulting residue was separated by TLC on silica gel using dichloromethane-benzene (2/1) as developer to give the adducts, **13** (323 mg, 76%) and **14** (43 mg, 10%). For **13**: Mp 196—198 °C (from EtOH); IR ($CHCl_3$) 1744 cm^{-1}; ^1H NMR ($CDCl_3$) δ=1.21 (3H, s), 1.34 (3H, s), 1.38 (3H, s), 1.61 (1H, s), 2.09 (1H, d, J=2.0 Hz), 2.17 (1H, d, J=2.0 Hz), 2.32 (9H, s), 3.23 (1H, d, J=17.6 Hz), 3.29 (1H, d, J=17.6 Hz), 6.69—7.42 (7H, m) Found: m/z 426.2314. Calcd for $C_{28}H_{30}N_2O_2$: M, 426.2307. For **14**: Mp 191—192 °C (from EtOH); IR ($CHCl_3$) 1738 cm^{-1}; ^1H NMR ($CDCl_3$) δ=1.28 (3H, s), 1.37 (3H, s), 1.41 (3H, s), 1.69 (1H, s), 2.28 (9H, s), 2.21—2.45 (2H, m), 3.03 (1H, d, J=17.4 Hz), 3.14 (1H, d, J=17.4 Hz), 6.72—7.41 (7H, m). Found: m/z 426.2314. Calcd for $C_{28}H_{30}N_2O_2$: M, 426.2307.

Thermal Reaction of 9. A solution of **9** (100 mg, 0.38 mmol) in 1,2-dimethylbenzene (2 cm^3) was heated under reflux for 20 min. After the solvent was evaporated, the mixture was then separated by TLC on alumina using hexane as developer. The first band from the TLC plates contained **16** (15 mg, 15%). The second band from the TLC plates contained **9** (77 mg, 77%). For **16**: Mp 105—106 °C (from Et_2O); IR (CCl_4) 1742 cm^{-1}; ^1H NMR (CCl_4) δ=1.03 (3H, s), 1.35 (3H, s), 2.33 (1H, d, J=7.3 Hz), 2.71 (1H, d, J=7.3 Hz), 3.51 (1H, d, J=10.3 Hz), 4.12 (1H, d×d×d, J=10.3, 3.2, 2.0 Hz), 4.75 (1H, s), 4.97 (1H, s), 5.06 (1H, d, J=3.2 Hz), 5.10 (1H, d, J=2.0 Hz), 6.35—7.25 (5H, m). Found: m/z 265.1440. Calcd for $C_{18}H_{19}NO$: M, 265.1467.

Thermal Reaction of 10. A solution of **10** (100 mg, 0.38 mmol) in 1,2-dimethylbenzene (1.5 cm^3) was heated under reflux for 2.5 h. After the solvent was evaporated, the residue was separated by TLC on alumina using hexane-benzene (2/1). The first band from the TLC plates gave **18** (21 mg, 21%). The second band from the TLC plates contained **10** (79 mg, 79%). For **18**: Mp 119—120 °C (from Et_2O); IR ($CHCl_3$) 1735 cm^{-1}; ^1H NMR (CCl_4) δ=1.06 (3H, s), 1.36 (3H, s), 2.39 (1H, d, J=7.2 Hz), 2.70 (1H, d, J=7.2 Hz), 3.35 (1H, broad d, J=10.8 Hz), 4.08 (1H, broad d, J=10.8 Hz), 4.79 (1H, s), 4.92 (1H, s), 5.12 (2H, m), 6.34—7.28 (5H, m). Found: m/z 265.1451. Calcd for $C_{18}H_{19}NO$: M, 265.1467.

Photochemical Reaction of 9. A solution of **9** (810 mg, 3.06 mmol) in anhydrous acetonitrile (50 cm^3) was irradiated with RPR-254 nm lamps in a quartz tube for 4 h. After the solvent was evaporated, the residue was separated by TLC on alumina using hexane-dichloromethane (2/1) as developer to give **16** (285 mg, 35%), the spectral data of which was identical with those of the authentic specimen.

Photochemical Reaction of 10. A solution of **10** (62 mg, 0.23 mmol) in anhydrous acetonitrile (10 cm^3) was irradiated with RPR-254 nm lamps in a quartz tube for 3 h. After the solvent was evaporated, the residue was separated by TLC on silica gel using chloroform-ethyl acetate (5/1) as developer to give **19** (11 mg, 18%): Bp 94 °C (bath temp)/93 Pa; IR (CCl_4) 2978, 2926, 1691, 1601, 1503, 1382, 1143, 900, 700 cm^{-1}; ^1H NMR (CCl_4) δ=1.49 (3H, s), 1.51 (3H, s), 1.85 (3H, d, J=1.6 Hz), 1.94—2.10 (2H, m), 5.27—5.50 (3H, m), 6.67—7.74 (5H, m); MS. m/z (rel intensity) 265 (M^+ 12), 250 (14), 146 (22), 119 (15), 77 (100). Found: m/z 265.1491. Calcd for $C_{18}H_{19}NO$: M, 265.1467.

Photochmeical Reaction of 20. A solution of **20** (100 mg, 0.4 mmol) in anhydrous acetonitrile (10 cm^3) was irradiated with RPR-254 nm lamps in a quartz tube for 14 h. After the solvent was evaporated, the residue was separated by TLC on silica gel using benzene-ethyl acetate (2/1) as developer to give **20** (53 mg, 53%) and **21** (30 mg, 30%). For **21**: Bp 110 °C (bath temp)/528 Pa; IR (CCl_4) 3030, 2985, 2915, 1656, 1597, 1492, 1385, 1121, 891 cm^{-1}; ^1H NMR (CCl_4) δ=1.02 (3H, s), 1.33 (3H, s), 1.86—2.13 (1H, m), 2.36 (1H, d, J=6.0 Hz), 4.71 (1H, s), 4.76 (1H, s), 5.54 (1H, d, J=8.0 Hz), 5.70 (1H, d×d, J=8.0, 6.0 Hz), 6.51—7.11 (5H, m); MS, m/z (rel intensity), 251 (M^+, 100), 236 (74), 132 (65), 119 (79). Found: m/z 251.1328. Calcd for $C_{17}H_{16}NO$: M, 251.1310.

References

1) This paper was presented at the National Meeting of Chemical Society of Japan, Tokyo, April 1985, Abstr., No. 4O14.

2) M. Nitta, A. Omata, and H. Sugiyama, *Bull. Chem. Soc. Jpn.*, **55**, 569 (1982).

3) M. Nitta, A. Omata, and S. Okada, *Bull. Chem. Soc. Jpn.*, **57**, 1505 (1984).

4) M. Nitta, S. Okada, and M. Kato, *Bull. Chem. Soc. Jpn.*, **57**, 2463 (1984).

5) J. P-Katalinic, J. Zsindely, and H. Schmid, *Helv. Chim. Acta*, **57**, 223 (1974).

6) R. Huisgen, L. Möbius, G. Müller, H. Stangl, G. Szeimies, and J. M. Vernon, *Chem. Ber.*, **98**, 3992 (1965).

7) The neumerical values presented in parentheses in the structural formulae **7** and **8** are relative down field shifts of δ's obtained by using $Eu(fod)_3$.

8) I. Fleming, "Frontier Orbital and Organic Chemical Reactions," John Wiley and Sons, London (1976).

9) P. Scheiner, *J. Org. Chem.*, **30**, 7 (1965).

10) P. G. Gassman and J. G. Schaffhausen, *J. Org. Chem.*, **43**, 3214 (1978); J. A. Deyrup, "Small Ring Heterocycles Part I," ed by A. Hassner, John Wiley and Sons, New York (1983) and references cited therein.

11) M. J. Haire and G. A. Boswell, Jr., *J. Org. Chem.*, **42**, 4251 (1977).

12) M. Nitta, A. Omata, and H. Sugiyama, *Bull. Sci. Eng. Res. Lab., Waseda Univ.*, **94**, 55 (1981).

13) J. P-Katalinic, J. Zsindely, and H. Schmid, *Helv. Chim. Acta*, **56**, 2796 (1973); M. Nitta, A. Omata, and M. Namiki, *Chem. Lett.*, **1982**, 227; M. Nitta, A. Omata, and H. Nakatani, *Bull. Chem. Soc. Jpn.*, **56**, 2009 (1983).

14) A. Padwa and E. Vega, *J. Org. Chem.*, **40**, 175 (1975).

15) K. Umano, H. Taniguchi, I. Inoue, and E. Imoto, *Tetrahedron Lett.*, **1979**, 247.

16) C. Grundmann and J. M. Dean, *J. Org. Chem.*, **30**, 2809 (1965).

17) R. O. Lindsay and C. F. H. Allen, *Org. Synth. Col. Vol.* III, 710.

A Highly Stereoselective Synthesis of (*E*)-Enol Lactones by the Wittig Reaction of Cyclic Anhydrides with (α-Alkoxycarbonylethylidene)triphenylphosphorane

Sadao Tsuboi, Hirohumi Fukumoto, Hiroshi Wada, Akira Takeda,* and Keiichi Fukuyama†
Department of Synthetic Chemistry, School of Engineering, Okayama University, Tsushima, Okayama 700
†Department of Industrial Chemistry, Faculty of Engineering, Tottori University, Koyama-cho, Tottori 680
(Received August 11, 1986)

Reactions of glutaric anhydride and methyl- or phenyl-substituted ones with (α-alkoxycarbonylethylidene)-triphenylphosphorane (**2a**, ethoxy; **2b**, *t*-butoxy) gave the corresponding 6-alkoxycarbonyl-5-hepten-5-olides (**3**) and 6-alkoxycarbonyl-4-hepten-5-olides in good yields. The reaction proceeded highly stereoselectively to give (*E*)-**3**. The stereochemistry of **3** was determined by an X-ray crystallographic analysis. The reaction of adipic anhydride with **2a** afforded 7-ethoxycarbonyl-5-octen-6-olide, 7-ethoxycarbonyl-5,6-octadienoic acid, and (4*E*, 6*E*)-7-ethoxycarbonyl-4,6-octadienoic acid. A treatment of nonanedioic anhydride with **2a** gave 10-ethoxycarbonyl-8,9-undecadienoic acid, (7*E*,9*E*)-10-ethoxycarbonyl-7,9-undecadienoic acid, and diethyl 2-methyl-2,4-undecadienedioate in low yields.

Enol lactones as well as α-methylene lactones exhibit strong biological activities such as antibiotic activity, carcinogenic properties, and control activity of plant growth.[1] Many naturally occuring enol lactones have been isolated. For example, protoanemonin,[2] tetrenolin,[3] and bovolide[4] are well-known.

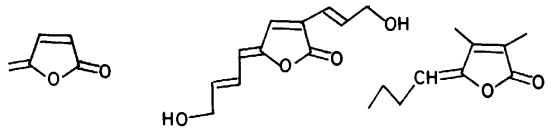

Protoanemonin Tetrenolin Bovolide

Recently, some synthetic methods of enol lactones have been developed.[5-8] We have also reported a facile, highly stereoselective synthesis of (*E*)-enol δ-lactones by the Wittig reaction of glutaric anhydrides (**1**, n=3) with (α-alkoxycarbonylethylidene)triphenylphosphorane (**2**).[9] Here, we report a full description of the previous communication[9] and its further extention to other cyclic anhydrides.

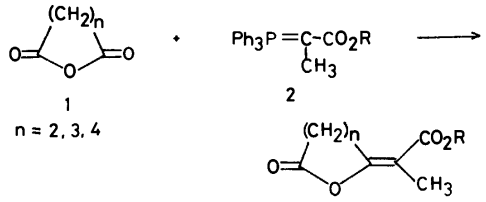

A typical method for the synthesis of enol lactones is the Wittig reaction between stabilized phosphoranes and cyclic anhydrides.[1b] The Wittig reaction of stable phosphoranes with phthalic anhydride or succinic anhydride provides enol γ-lactones in good yield;[1b,10] it has been successfully applied to the syntheses of naturally occuring enol γ-lactones.[11-14] However, Wittig reactions of glutaric anhydrides and acid anhydrides of larger ring with phosphoranes have remained almost uninvestigated. Only Chopard et al. reported that an attempt to prepare enol δ-lactones by the Wittig reaction failed, but resulted in the formation of the ring-opened products.[15]

Recently, we found that a reaction of glutaric anhydride with (α-ethoxycarbonylethylidene)triphenylphosphorane (**2a**) gives 6-ethoxycarbonyl-5-hepten-5-olide (**3a**) (13%) and its *endo*-enol lactone (**4a**) (20%), in contrast to the above result.[15]

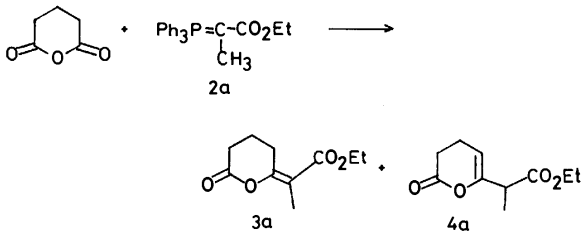

The generality of this Wittig reaction was examined by a reaction of various methyl- or phenyl-substituted glutaric anhydrides with phosphorane **2**; the results are shown in Table 1. Most of the reactions gave mixtures of *exo*-enol δ-lactone **3** and *endo*-enol δ-lactone **4**. The geometry of **3** was tentatively assigned as *E*-configuration by a ^{1}H NMR analysis.[9] Namely, the coupling constant between methylene protons of C_4 and methyl protons of the ethylidene group showed a small value (J=1.5 Hz).[16] The reaction of **2** with β-substituted glutaric anhydrides gave predominantly *exo*-enol δ-lactone **3** in good yields. Especially, the reaction of 3-methylglutaric anhydride (**1e**) with **2b** yielded *exo*-enol δ-lactone **3f** in a high yield (86%) along with *endo*-enol δ-lactone **4f** (6%). On the other hand, a reaction of **2** with glutaric anhydride and α-substituted ones afforded *exo*-enol δ-lactone **4** as the major product (except for the reaction of **1d** with **2b**). Treatments of 2-methylglutaric anhydride with **2** provided (*E*)-6-alkoxycarbonyl-2-methyl-5-hepten-5-olide regioselectively. All of the reactions proceeded highly stereoselectively to give only (*E*)-*exo*-enol δ-lactone **3**. A trace amount of the other stereoisomer, (*Z*)-enol δ-lactone, could not be detected.

In order to definitely determine the stereochemistry of *exo*-enol δ-lactone **3**, an X-ray crystallographic analysis of **3d** was carried out representatively; this

Table 1. Reaction of Glutaric Anhydride **1** with (α-Alkoxycarbonylethylidene)triphenylphosphorane **2**

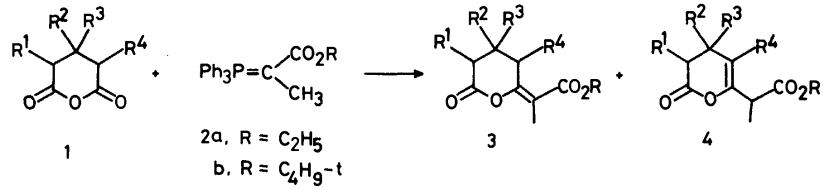

No.	R_1	R_2	R_3	R_4	R	Products (yield/%)[a]	
						3	**4**
a	H	H	H	H	C_2H_5	13[b]	20[b]
b	H	H	H	H	C_4H_9-*t*	0	35
c	CH_3	H	H	H	C_2H_5	12	27
d	CH_3	H	H	H	C_4H_9-*t*	38	33
e	H	CH_3	H	H	C_2H_5	55	12
f	H	CH_3	H	H	C_4H_9-*t*	86	6
g	H	C_6H_5	H	H	C_2H_5	58	13
h	H	CH_3	CH_3	H	C_2H_5	30	0
i	H	CH_3	CH_3	H	C_4H_9-*t*	57	0
j	CH_3	H	H	CH_3	C_2H_5	21[c]	0

a) Isolated yield unless otherwise indicated. b) Estimated by GLC. Analytical sample was purified by preparative GLC (column, 200 °C carrier gas, He, 25 ml min^{-1}): **3a**, R_t 2.6 min; **4a**, R_t 1.6 min. c) Produced together with **5**.

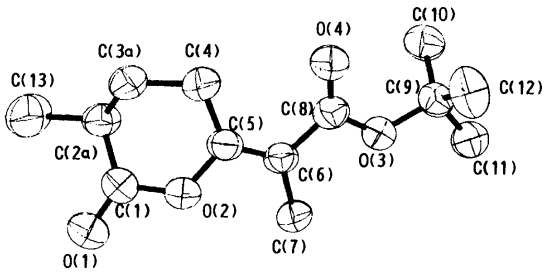

Fig. 1. Perspective view of **3d** drawn by DCMS-3.[17] Only one of the two conformations is shown for the sake of clarity.

revealed that it has an (*E*)-configuration. A perspective view of **3d** drawn by DCMS-3[17] is shown in Fig. 1.

The reaction of *meso*-2,4-dimethylglutaric anhydride (**1j**) with **2a** also afforded a mixture of *exo*-enol δ-lactone **3j** (21%) and 2,6-dioxocyclohexanecarboxylate **5** (7%). The photochemical rearrangement of 1,3-cyclohexanedione to enol δ-lactone is well-known.[18] Irradiation of **5** with a high-pressure Hg lamp in benzene provided **3j** although in a low yield (10%).

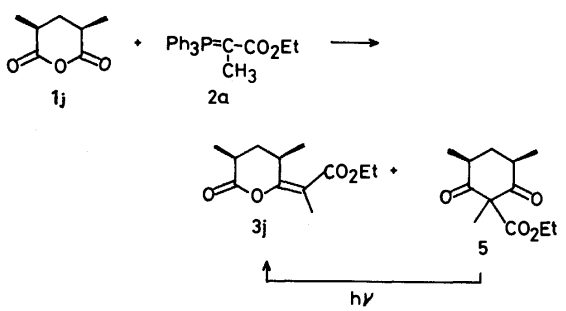

Attempted conversion of **3j** to Prelog-Djerassi lactone or its stereoisomers by hydrogenation resulted in the formation of ring-opened product **6** in 91% yield. ^{13}C NMR analysis revealed that it consists of three stereoisomers. It has been reported that the reduction of β-keto ester **6** affords stereoisomers of the racemic Prelog-Djerassi lactone although the stereochemistry could not be evaluated.[19]

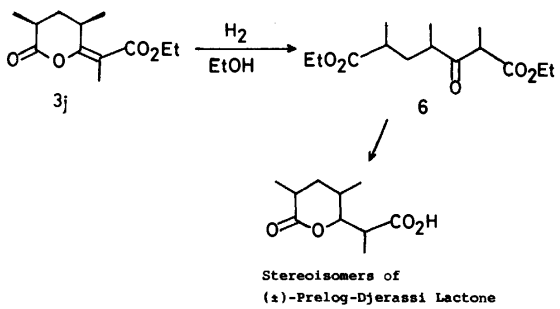

A further extention of the present reaction to other cyclic anhydrides was attempted. The reaction of adipic anhydride with **2a** gave *endo*-enol ε-lactone **7** in 13% yield, accompanied by the formation of ring-opened products, α-allenic ester **8** (4.2% yield) and its isomer **9** (6.3% yield), and ethyl hydrogen adipate (**10**). The structural elucidation of half esters **8** and

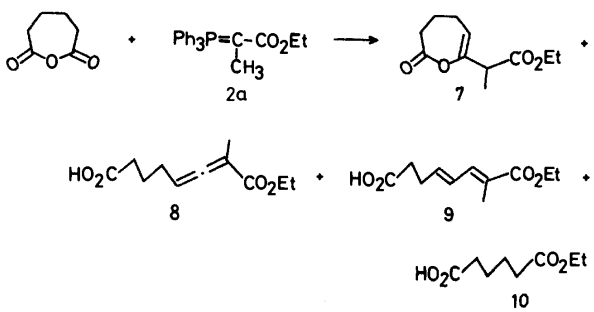

9 was carried out by an analysis of the spectral data of the corresponding methyl ethyl esters. The stereochemistry of **9** was determined by ^{1}H NMR spectral data. Namely, the signal due to C_β H which appeared considerably down field (7.25 ppm) showed α,β-trans geometry.[20] A large coupling constant (J=15.3 Hz) between C_γ H and C_δ H revealed the γ,δ-trans geometry.

A treatment of nonanedioic anhydride with **2a** gave 10-ethoxycarbonyl-8,9-undecadienoic acid (**12**) unexpectedly, although in a low yield. Allene **12** is produced by a prototropic rearrangement of the initially formed *exo*-enol η-lactone **11**. The prolonged reaction gave (7*E*,9*E*)-10-ethoxycarbonyl-7,9-undecadienoic acid (**13**) (20% yield) and its diethyl ester **14** (23% yield), both of which can be produced by a prototropic rearrangement of **12**. The structural assignment of **13** was carried out after a conversion to its methyl ester **15** with diazomethane.

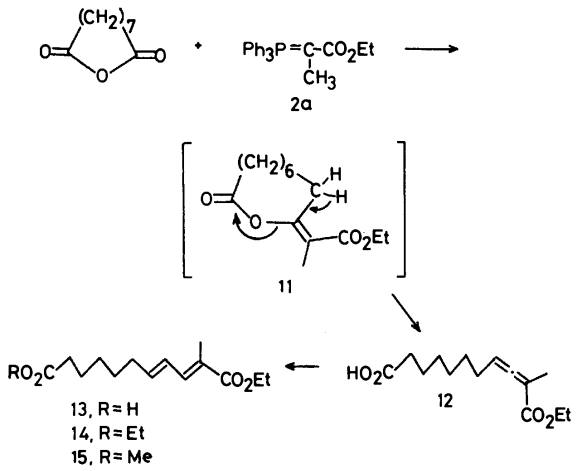

Enol lactones **3** and **4** prepared in this study gradually decomposed with moisture to yield an acid ester. For example, compound **4f** produced 6-*t*-butoxycarbonyl-3,6-dimethyl-5-oxoheptanoic acid (**16**) as a 1 : 1 diastereomeric mixture after 40 days at room temperature.

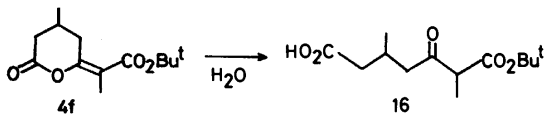

The structural assignment of the products obtained in the present study was made on the basis of IR and NMR data (Tables 2—5). IR absorptions of *exo*-enol δ-lactone **3** at 1770, 1705, and 1640 cm^{-1} indicate the presence of a δ-lactone ring and a α,β-unsaturated ester group. The *exo*-enol lactone skeleton is also supported by the ^{1}H NMR spectra in which a singlet or a triplet (J=1.5 Hz) at 1.80—1.92 ppm due to methyl group attached to the double bond was exhibited. IR absorptions of *endo*-enol δ-lactone **4** at 1770 and 1740 cm^{-1} indicate the presence of a δ-lactone ring and an isolated ester carbonyl group. The structure of **4** was also supported by ^{1}H NMR data, which exhibited a doublet at δ=1.38 due to the methyl group attached to α-carbon of the ester group and a signal at δ=5.23 due to a olefinic proton of endo enol structure. As a part of a continuing ^{13}C NMR study of organic compounds, the ^{13}C NMR spectra of enol δ-lactones **3** and **4** were measured and assigned with the aid of an off-resonance decoupling technique. For the assignment of ^{13}C NMR spectra of **3h**, two peaks due to secondary

Table 2. Spectral and Analytical Data of *exo*-Enol δ-Lactones **3**

Compd	bp[a] (mp) (°C)	IR cm^{-1}	^{1}H NMR (δ)[b]	Found (%) (Calcd) C	Found (%) (Calcd) H
3a		1770, 1705, 1640	1.21 (3H, t, J=7 Hz), 1.90 (3H, t, J=1.5 Hz), 1.59—2.14 (2H, m), 2.63 (2H, t, J=6 Hz), 3.07 (2H, t, J=6 Hz), 4.17 (2H, q, J=7 Hz)	60.39 (60.59)	7.04 (6.97)
3c		1770, 1700, 1640	1.25 (3H, d, J=7 Hz), 1.33 (3H,t, J=7 Hz), 1.83 (3H, t, J=1.5 Hz), 2.0—3.4 (4H, m), 4.08 (2H, q, J=7 Hz)	62.10 (62.25)	7.67 (7.60)
3d	(71—72)	1770, 1700, 1630	1.24 (3H, d, J=7 Hz), 1.45 (9H, s), 1.80 (3H, t, J=1.5 Hz), 2.0—3.5 (4H, m)	64.92 (64.98)	8.34 (8.39)
3e		1770, 1705, 1640	1.08 (3H, d, J=6 Hz), 1.28 (3H, t, J=7 Hz), 1.86 (3H, s), 1.97—3.00 (4H, m), 3.34, 3.59 (1H, 2br. s), 4.14 (2H, q, J=7 Hz)	62.41 (62.25)	7.51 (7.60)
3f		1770, 1700, 1640	1.11 (3H, d, J=6 Hz), 1.48 (9H, s), 1.84 (3H, s), 1.94—2.84 (4H, m), 3.14—3.36 (1H, m)	64.89 (64.98)	8.38 (8.39)
3g	(65—65.5)	1780, 1705, 1640	1.23 (3H, t, J=7 Hz), 1.90 (3H, br. s), 2.21—3.50 (4H, m), 3.63 (1H, br. s), 4.06 (2H, q, J=7 Hz), 7.16 (5H, s)	70.12 (70.06)	6.52 (6.61)
3h		1770, 1710, 1640	1.07 (6H, s), 1.92 (3H, t, J=1.5 Hz), 2.49 (2H, br. s), 2.95 (2H, s), 4.20 (2H, q, J=7 Hz)	63.71 (63.70)	8.18 (8.02)
3i	160/0.25[c]	1770, 1700, 1640	1.24 (6H, s), 1.47 (9H, s), 1.86 (3H, t, J=1.5 Hz), 2.37 (2H, s), 2.87 (2H, s)	66.22 (66.12)	8.75 (8.72)
3j		1780, 1710, 1640	1.15 (3H, d, J=7 Hz), 1.21 (3H, d, J=7 Hz), 1.31 (3H, t, J=7 Hz), 1.86 (3H, s), 2.0—3.0 (3H, m), 4.15 (2H, q, J=7 Hz)	63.72 (63.70)	7.97 (8.02)

a) If not indicated, the boiling point was not measured although the material was an oil. b) Compds **3a**, **3c**, **3d**, **3e**, **3f**, and **3g** were measured in CCl_4 and others in $CDCl_3$. c) Bath temperature on bulb-to-bulb distillation.

Table 3. Spectral and Analytical Data of *endo*-Enol δ-Lactones **4**

Compd[a]	IR (neat) cm^{-1}	^1H NMR (CCl_4, δ)	Found (%) (Calcd) C	H
4a	1770, 1740, 1700	1.21 (3H, t, *J*=7 Hz), 1.30 (3H, d, *J*=7 Hz), 2.04—2.86 (4H, m), 3.24 (1H, q, *J*=7 Hz), 4.10 (2H, q, *J*=7 Hz), 5.23 (1H, t, *J*=4 Hz)	60.54 (60.59)	6.97 (7.12)
4b	1770, 1740, 1690, 1640	1.28 (3H, d, *J*=7 Hz), 1.42 (9H, s), 2.42 (2H, *J*=4 Hz), 2.02—2.72 (2H, m), 2.08 (1H, q, *J*=7 Hz), 5.10 (1H, t, *J*=4 Hz)	63.80 (63.70)	8.06 (8.02)
4c	1770, 1740, 1700, 1640	1.23 (6H, d, *J*=7 Hz), 1.25 (3H, t, *J*=7 Hz), 1.80—2.90 (3H, m), 3.17 (1H, q, *J*=7 Hz), 4.09 (2H, q, *J*=7 Hz), 5.10 (1H, t, *J*=4 Hz)	62.16 (62.25)	7.54 (7.60)
4d	1770, 1740, 1700, 1640	1.26 (3H, d, *J*=7 Hz), 1.31 (3H, d, *J*=7 Hz), 1.40 (9H, s), 1.8—2.9 (2H, m), 3.04 (1H, q, *J*=7 Hz), 5.03 (1H, t, *J*=4 Hz)	64.89 (64.98)	8.33 (8.39)
4e	1770, 1740, 1696	1.16 (3H, t, *J*=7 Hz), 1.32 (6H, 2d, *J*=7 Hz), 1.84—2.89 (3H, m), 3.14 (2H, q, *J*=7 Hz), 5.01 (1H, d, *J*=4 Hz)	62.41 (62.25)	7.51 (7.60)
4f	1770, 1740, 1700	1.12 (3H, d, *J*=6.5 Hz), 1.30 (3H, d, *J*=7 Hz), 1.45 (9H, s), 1.77—2.80 (3H,m), 3.05 (1H, q, *J*=6.5 Hz), 4.98 (1H, d, *J*=4 Hz)	64.79 (64.98)	8.25 (8.39)
4g	1770, 1740, 1690	1.23 (3H, t, *J*=7 Hz), 1.35 (3H, d, *J*=7 Hz), 2.23—2.97 (2H, m), 3.21 (1H, q, *J*=7 Hz), 3.48—3.88 (1H,m), 4.08 (2H, q, *J*=7 Hz), 5.17 (1H, d, *J*=4 Hz), 7.13 (5H, s)	70.08 (70.06)	6.45 (6.61)

a) All compounds are liquid.

Table 4. ^{13}C NMR Data ($CDCl_3$, δ) of *exo*-Enol δ-Lactone **3**

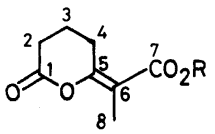

3

Compd	C-1	C-2	C-3	C-4	C-5	C-6	C-7	C-8	Others
3a	168.2	30.8	25.4	18.0	158.8	110.0	167.4	11.8	14.3(q), 60.6 (t)
3c	170.9	36.2[a]	26.0	25.7[a]	158.9	109.0	168.2	11.8	14.3(q), 16.0(q), 60.4(t)
3d	170.9	36.0	26.0	25.7	157.9	111.1	167.4	12.2	28.2(q), 16.0(q), 80.5(s)
3e	167.9	38.3	25.3	33.2	158.7	109.3	166.7	11.8	14.3(q), 20.5(q), 60.4(t)
3f	167.6	38.5	25.2	33.2	156.7	111.6	167.4	12.2	20.6(q), 28.2(q), 80.8(s)
3g	168.0	37.7	35.5	32.8	157.5	110.4	166.8	11.9	14.2(q), 60.5 (t), 126.5(d), 127.4(d), 129.0(d), 141.3 (s)
3h	168.0	44.1[b]	29.5	38.6[b]	157.8	110.4	166.6	11.7	14.2(q), 27.7(q), 60.3(t)
3i	167.5	44.3	29.6	38.6	156.3	112.2	167.1	12.2	28.2(q), 27.9(q), 60.3(t)
3j	172.8	34.9	30.9	34.1	162.3	112.5	167.7	12.3	14.2(q), 15.0(q), 60.6(t)

a), b) Distinguished by selective decoupling technique.

Table 5. ^{13}C NMR Data of *endo*-Enol δ-Lactone **4**

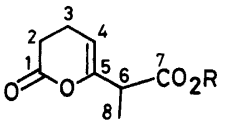

4

Compd	C-1	C-2	C-3	C-4	C-5	C-6	C-7	C-8	Others
4a	172.0	28.3	18.7	101.6	151.4	43.2	168.5	14.5	14.1(q), 61.1 (t)
4b	171.0	28.3	18.6	101.2	151.9	44.0	168.1	14.5	14.5(q), 27.8(q), 80.7(s)
4c	172.7[b]	33.5	26.8	101.2	152.1	43.0	172.3[b]	14.5	14.1(q), 15.4(q), 61.1(t)
						43.2		14.7	
4d[a]	171.0[b]	33.5	26.8	100.8	152.5	43.9	171.1[b]	14.4	15.4(q), 27.9(q), 80.8(s)
	171.4[b]			101.0		44.1			
4e	172.5	36.9	26.1	108.4	151.2	43.5	169.0	14.6	15.1(q), 20.6(q), 61.7(t)
4g	171.8	36.8	36.7	105.5	152.0	43.3	167.4	14.5	14.1(q), 61.3 (t),
								14.7	126.9(d), 127.4(d), 129.1(d), 141.4 (s)

a) Diastereomeric mixture. b) May be interchangeable.

carbon could be assigned using a selective-decoupling technique. The ^{13}C NMR data summarized in Tables 4 and 5 are apparently the first reported for substituted enol δ-lactones, making structural assignments unambiguous.

We briefly discuss the reaction mechanism regarding the present reaction. In contrast to our results, the reaction of (ethoxycarbonylmethylene)triphenylphosphorane (**17**) with glutaric anhydride gave a ring-opened product **18**,[15] which would be stabilized by prototropic rearrangement. Therefore, it would be

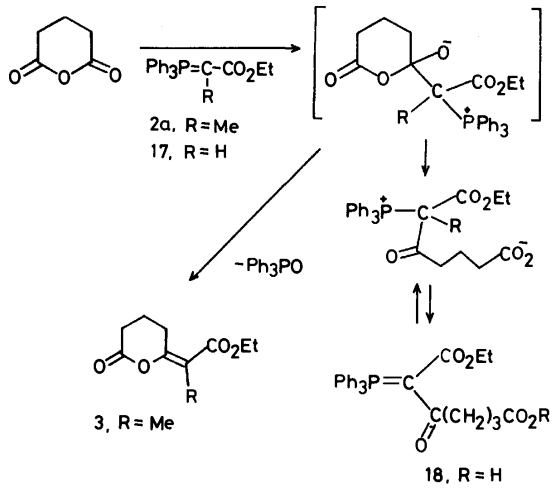

necessary for the formation of the desired enol δ-lactones that an alkylidenephosphorane has no hydrogen atom on the α-position. The present reaction is the first synthesis of enol δ- and ε-lactones, and 2,3- or 2,4-dienedioic esters by the Wittig reaction. It will be useful for the synthesis of these derivatives.

Experimental

The melting and boiling points are uncorrected. Elemental analyses were carried out by Eiichiro Amano of our laboratory. IR spectra were obtained with a JASCO Model A-102 infrared spectrophotometer. ^1H NMR spectra (60 MHz) were recorded with a JEOL JNM-PMX60SI apparatus. ^1H NMR (100 MHz) and ^{13}C NMR spectra (25 MHz) were obtained with a JEOL JNM-FX100 apparatus, with $CDCl_3$ as a solvent. All chemical shifts are reported in δ units downfield from the internal Me_4Si; *J* values are given in hertz. Analytical determinations by GLC were performed on a Hitachi Model 163 gas chromatograph fitted with 10% Apiezone Grease L on Chromosorb W column (3 mm o.d.×1 m). Preparative GLC was performed on a Yanagimoto Model G-80 gas chromatograph fitted with 10% Apiezone Grease L on Chromosorb W column (3 mm o.d.×1 m). Column chromatography was accomplished with a 100—200 mesh Wakogel C-200. Chloroform was dried over $CaCl_2$ and distilled prier to use. The Wittig reaction was carried out under dry conditions.

(α-Ethoxycarbonylethylidene)triphenylphosphorane (**2a**) and (α-*t*-buthoxycarbonylethylidene)triphenylphosphorane (**2b**) were prepared by the method described in the literature.[21] Glutaric anhydride was purchased from Tokyo Kasei Kogyo Co., LTD. Substituted glutaric anhydrides were obtained by the known methods:[22-27] 2-methylglutaric anhydride, bp 130 °C/10 Torr (1 Torr=133.322 Pa) (lit,[24] 180—182 °C/25 Torr); 3,3-dimethylglutaric anhydride, bp 122 °C/12 Torr (lit,[25] 181 °C/25 Torr); 2,4-dimethylglutaric anhydride, bp 117—119 °C/4.5 Torr (lit,[26] 154—158 °C/20 Torr); mp 91—92 °C (lit,[26] 91.5 °C); ^{13}C NMR ($CDCl_3$) δ=15.8 (q), 33.0 (t), 36.8 (d), 170.4 (s); 3-phenylglutaric anhydride, mp 104—105 °C (lit,[27] 105 °C).

Some Wittig reactions were shown representatively.

6-*t*-Butoxycarbonyl-4-hepten-5-olide (4b). To a mixture of glutaric anhydride (0.50 g, 4.39 mmol) and **2b** (2.1 g, 5.49 mmol) was added 4 ml of dry $CHCl_3$ under N_2 and the solution was heated at the reflux temperature for 21 h. After removing the solvent, 30 ml of petroleum ether was added and the mixture was stirred at 40 °C for 3 h and then cooled. After filtration, concentration of the filtrate gave 0.962 g of crude **4b**, which was distilled to give 0.342 g (35%) of **4b**: Bp 135—155 °C/0.22 Torr. Spectral and analytical data are shown in Tables 3 and 5.

(5*E*)-6-*t*-Butoxycarbonyl-2-methyl-5-hepten-5-olide (3c) and 6-*t*-Butoxycarbonyl-2-methyl-4-hepten-5-olide (4c). A solution of 2-methylglutaric anhydride (0.50 g, 3.91 mmol) and **2b** (1.50 g, 3.92 mmol) in 7 ml of dry $CHCl_3$ was heated at the reflux temperatere for 12 h. After concentration, the residue was mixed with petroleum ether. After filtration, the filtrate was concentrated to give 0.938 g of crude product; this was chromatographed on SiO_2 (hexane/ether (20:1—1:1)) to give 0.355 g (38%) of **3c** as crystals (mp 71—72 °C) from the early fraction and 0.307 g (33%) of **4c** as a clean oil from the later fraction. Spectral and analytical data are shown in Tables 2, 3, 4, and 5.

(5*E*)-6-*t*-Butoxycarbonyl-2-methyl-5-hepten-5-olide (3f) and 6-*t*-Butoxycarbonyl-2-methyl-4-hepten-5-olide (4f). A solution of 3-methylglutaric anhydride (0.22 g, 1.72 mmol) and **2b** (0.85 g, 2.18 mmol) in 2 ml of dry $CHCl_3$ was heated at the reflux temperature for 12 h. After concentration, the residue was mixed with petroleum ether and then filtered. After filtration, the filtrate was concentrated and the residue was chromatographed on SiO_2 (hexane/ether (20:1—2:1)) to give 0.354 g (86%) of **3f** from the early fraction and 25 mg (6%) of **4f** from the later fraction. Spectral and analytical data are shown in Tables 2, 3, 4, and 5.

(5*E*)-2,4-Dimethyl-6-ethoxycarbonyl-5-hepten-5-olide (3j) and Ethyl 1,3,5-Trimethyl-2,6-dioxocyclohexanecarboxylate (5). A solution of 2,4-dimethylglutaric anhydride (0.50 g, 3.52 mmol) and **2a** (1.30 g, 3.59 mmol) in 4 ml of $CHCl_3$ was heated at the reflux temperature for 13 h. After removing the solvent, the residue was mixed with petroleum ether and filtered. The filtrate was concentrated to give 0.434 g of the residue. Preparative TLC (SiO_2, hexane/ether (3:1)) gave 0.169 g (21%) of **3j** as an oil at R_f value 0.31. Spectral and analytical data are shown in Tables 2 and 4. The component of R_f value 0.18 gave 53 mg (7%) of **5** as an oil: IR (neat)1760, 1740, 1705 cm^{-1}; ^1H NMR ($CDCl_3$) δ=1.16 (6H, d, *J*=7 Hz), 1.24 (3H, t, *J*=7 Hz), 1.47 (3H, s), 1.62—2.50 (2H, m), 2.5—3.28 (2H, m), and 4.22 (2H, q, *J*=7 Hz); ^{13}C NMR ($CDCl_3$) δ=13.7 (q), 14.2 (q), 14.5 (q), 20.1 (q), 35.1 (t), 43.1 (d), 62.4 (t), 71.0 (s), 168.9 (s), 202.4 (s). Found: C, 63.41; H, 7.78%. Calcd for $C_{12}H_{18}O_4$: C, 63.70; H, 8.02%.

X-Ray Crystallographic Analysis of 3d. The unit-cell constants and intensities were measured at room temperature using Ni-filtered Cu *Kα* radiation on a Rigaku four-circle diffractometer. Crystal data are as follows: $C_{13}H_{20}O_4$, M=

240.3, monoclinic, space group $P2_1/a$, a=24.452(5), b=6.089(2), c=9.206(3) Å, β=99.72(3)°, V=1351.0 Å^3, Z=4, D_c=1.18 g cm^{-3}. Due to broad diffraction profiles ω-scan technique was applied with a scan width of 2.0°+0.15°tanθ. The backgrounds were counted for 4 s at the start and end points of the scan. Of the 2001 independent reflections measured up to 2θ=120°, 1579 reflections with $F>3\sigma$ were used for the structure analysis. The intensities were corrected for the Lorentz and polarization factors. The structure was solved by the direct method,[28] and refined by the block-diagonal least-squares method.[29] Each of the two carbon atoms (C(2) and C(3)) has two sites, and their occupancies were fixed to be 0.5 during the refinement. Most of the hydrogen atoms were located in the difference Fourier synthesis calculated after the refinement with anisotropic temperature factors for the non-hydrogen atoms; the electron density distribution around C(13) was too broad to locate hydrogen atoms. The two positions were calculated for each hydrogen atom bonded to C(2), C(3), and C(4), and their occupancies given 0.5. The contribution of these hydrogen atoms were included in the refinement with their parameters being fixed. The other hydrogen atoms were refined with isotropic temperature factors. The unit weight was given for all reflections. The final R value was 0.066 for 1579 reflections. The atomic-scattering factors were taken from the International Tables for X-ray Crystallography.[30] The final atomic parameters are given in Table 6.[31]

Table 6. Final Atomic Coordinates and Equivalent Temperature Factors

	x	y	z	B_{eq}
C(1)	0.1252(2)	0.2566(8)	0.2937(6)	5.8
C(2a)	0.1130(4)	0.5003(15)	0.2970(10)	5.1
C(2b)	0.1145(4)	0.4735(17)	0.3692(12)	6.6
C(3a)	0.1579(4)	0.5694(15)	0.4402(9)	4.9
C(3b)	0.1558(4)	0.6298(18)	0.3677(13)	7.0
C(4)	0.2146(2)	0.5553(8)	0.3913(6)	5.9
C(5)	0.2212(2)	0.3610(7)	0.2964(5)	4.6
C(6)	0.2640(2)	0.3080(7)	0.2302(5)	4.5
C(7)	0.2635(2)	0.1083(8)	0.1338(6)	5.9
C(8)	0.3147(2)	0.4469(7)	0.2551(5)	5.0
C(9)	0.4071(2)	0.4760(8)	0.1847(5)	5.5
C(10)	0.4026(2)	0.7186(9)	0.1400(7)	7.4
C(11)	0.4321(2)	0.3441(9)	0.0714(6)	7.1
C(12)	0.4395(2)	0.4402(11)	0.3375(6)	7.7
C(13)	0.0533(2)	0.5343(11)	0.3288(8)	8.8
O(1)	0.0924(1)	0.1089(6)	0.2783(4)	7.5
O(2)	0.1782(1)	0.2084(5)	0.2756(4)	5.6
O(3)	0.3515(1)	0.3769(5)	0.1723(3)	5.3
O(4)	0.3230(1)	0.6004(6)	0.3386(4)	6.8

$B_{eq} = \frac{4}{3}\sum_i\sum_j \beta_{ij} a_i a_j$.

Photochemical Rearrangement of 5 to 3j. Following a procedure described in the literature,[18] a solution of **5** (0.20 g, 0.83 mmol) in 10 ml of benzene was irradiated with a 200-W high-pressure Hg lamp (quartz jacket) from a distance of 4 cm under an N_2 atmosphere at room temperature for 65 h. After evaporating the solvent, the residual oil was purified with preparative TLC (SiO_2, hexane/ether (3 : 1)) to give 21 mg (10%) of **3j**: R_f value 0.31. Spectral data were identical with those of an authentic sample. The fraction of R_f value 0—0.2 gave a mixture of unidentified materials.

Preparation of Diethyl 3-Oxo-2,4,6-trimethylheptanedioate (6)[19] by the Hydrogenation of 3j. A mixture of **3j** (0.10 g, 0.42 mmol), dry ethanol (3 ml), Pd/$BaSO_4$ (14 mg),[32] and $FeCl_3$ (60 mg) was stirred under H_2 atmosphere for 8 h at room temperature. After filtration, the organic materials were extracted with ether. The combined extracts were washed with water, and dried over $MgSO_4$. Removal of the solvent gave a pale brown oil, which was purified by preparative TLC (SiO_2, hexane/ethyl acetate (4 : 1), R_f value 0.47) to give 74 mg of **6**:[19] IR (neat) 1740, 1720, 1182, 760 cm^{-1}; ^{1}H NMR (CCl_4) δ=1.1 (9H, m), 1.20 (6H, t, J=7 Hz), 1.5—3.0 (4H, m), 3.6 (1H, q, J=7 Hz), 4.07 (2H, q, J=7 Hz), 4.12 (2H, q, J=7 Hz); ^{13}C NMR ($CDCl_3$) δ=12.8 (q), 13.0 (q), 14.0 (q), 14.2 (q), 15.9 (q), 16.4 (q), 17.2 (q), 17.5 (q), 17.6 (q), 17.8 (q), 17.9 (q), 35.9 (t), 36.1 (t), 36.5 (t), 36.9 (d), 37.1 (d), 37.3 (d), 43.2 (d), 43.5 (d), 43.7 (d), 51.0 (d), 51.3 (d), 52.0 (d), 60.3 (q), 60.4 (q), 170.3 (s), 175.9 (s), 176.1 (s), 176.2 (s). Found: C, 61.47; H, 8.91%. Calcd for $C_{14}H_{24}O_5$: C, 61.74: H, 8.88%.

Reaction of Adipic Anhydride with 2a. Synthesis of 7-Ethoxycarbonyl-5-octen-6-olide (7), 7-Ethoxycarbonyl-5,6-octadienoic Acid (8), and (4*E*,6*E*)-7-Ethoxycarbonyl-4,6-octadienoic Acid (9). A solution of adipic anhydride (0.90 g, 7 mmol) and **2a** (2.69 g, 7.4 mmol) in 7 ml of dry $CHCl_3$ was heated at the reflux temperature for 13 h. After concentration, the residue was chromatographed on SiO_2 (hexane/ethyl acetate (10 : 1–1 : 1)). Concentration of the early fraction gave 0.187 g (13%) of **7**: IR (neat) 1760, 1735, 1680 cm^{-1}; ^{1}H NMR ($CDCl_3$) δ=1.23 (3H, t, J=7 Hz), 1.38 (3H, d, J=6 Hz), 1.6—3.0 (6H, m), 3.25 (1H, q, J=5 Hz), 4.12 (2H, q, J=7 Hz), 5.42 (1H, t, J=6 Hz). Found: C, 62.42; H, 7.46%. Calcd for $C_{11}H_{16}O_4$: C, 62.25; H, 7.60%. Concentration of the second fraction gave 0.246 g of carboxylic acids which were treated with diazomethane. HPLC analysis [SA-I, 6ϕ×250; hexane/ethyl acetate (2 : 1)] of the methylated products showed 4 peaks. The peaks, retention times (min), and integrated percentages are as follow: 1, 12.6, 25%; 2, 13.7, 38%; 3, 15.2, 19%; 4, 16.6, 16%. Each component was collected by preparative HPLC and identified.

1-Ethyl 8-Methyl 2-Methyl-2,3-octadienedioate (Methyl Ester of 8): Peak 1; 4.2% yield; IR (neat) 1961, 1740, 1710, 1270, 1110 cm^{-1}; ^{1}H NMR ($CDCl_3$) δ=1.28 (3H, t, J=7 Hz), 1.86 (3H, d, J=3.5 Hz), 1.60—1.92 (2H, m), 2.12 (2H, t, J=7 Hz), 2.36 (2H, t, J=7 Hz), 3.67 (3H, s), 4.18 (2H, q, J=7 Hz), and 5.40 (1H, m). Found: C, 63.55; H, 7.78%. Calcd for $C_{12}H_{18}O_4$: C, 63.70; H, 8.02%.

(2*E*,4*E*)-1-Ethyl 8-Methyl 2-Methyl-2,4-octadienedioate (Methyl Ester of 9): Peak 2; 6.3% yield; IR (neat) 1740, 1710, 1640, 1240, 760 cm^{-1}; ^{1}H NMR ($CDCl_3$) δ=1.29 (3H, t, J=7 Hz), 1.92 (3H, s), 2.46 (4H, s), 3.67 (3H, s), 4.18 (2H, q, J=7 Hz), 6.0 (1H, m), 6.39 (1H, dd, J=10.6 and 15 Hz), 7.25 (1H, d, J=10.6 Hz). Found: C, 63.64; H, 8.11%. Calcd for $C_{12}H_{18}O_4$: C, 63.70; H, 8.02%.

Peak 3: *N*-Methyl-*N*-nitroso-*p*-toluenesulfonamide (diazomethane source). IR and ^{1}H NMR spectra were identical with those of an authentic sample.

Ethyl Methyl Adipate (Methyl Ester of 10):[33] Peak 4: 3.2% yield: IR and ^{1}H NMR spectra were identical with those of an authentic sample.

10-Ethoxycarbonyl-8,9-undecadienoic Acid (12). A solution of azelaic anhydride (2.26 g, 0.0133 mol) and **2a** (4.88 g, 0.0133 mol) in 14 ml of dry $CHCl_3$ was heated at the reflux temperature for 12 h. After removing the solvent, 40 ml of petroleum ether was added and the mixture was stirred for 3 h and then filtered. The concentration of the filtrate gave an

oil (0.706 g) which was chromatographed on SiO_2 (hexane/ether (20 : 1–1 : 1)). Concentration of the early fraction gave 0.255 g of a mixture of unidentified products. The later fraction gave 0.338 g (10%) of **12** as an oil: IR (neat) 3700—2200, 1960, 1740, 1705 cm^{-1}; ^1H NMR ($CDCl_3$) δ=0.6—1.8 (10H, m), 1.83 (3H, d, J=3 Hz), 2.02—2.60 (4H, m), 4.19 (2H, q, J=7 Hz), 5.40 (1H, m), 10.2 (1H, s); ^{13}C NMR ($CDCl_3$) δ=14.3 (q), 15.2 (q), 24.6 (t), 24.9 (t), 27.9 (t), 28.6 (t), 28.9 (t), 34.0 (t), 60.8 (t), 93.7 (d), 95.7 (s). Found: C, 65.98; H, 8.68%. Calcd for $C_{14}H_{22}O_4$: C, 66.12; H, 8.72%.

(7*E*,9*E*)-10-Ethoxycarbonyl-7,9-undecadienoic Acid (13) and 1-Ethyl 11-Methyl (2*E*,4*E*)-2-Methyl-2,4-undecadienedioate (14). A solution of azelaic anhydride (0.172 g, 1.01 mmol) and **2a** (0.366 g, 1.01 mmol) in 2 ml of dry $CHCl_3$ was heated at the reflux temperature for 21 h. After removing the solvent, 30 ml of petroleum ether was added and the mixture was stirred for 1 h and then filtered. Concentration of the filtrate gave a semisolid (0.445 g) which was separated by preparative TLC [SiO_2, hexane/ethyl acetate (1 : 1)]. **14**: 64 mg (23% yield); R_f 0.90; IR (neat) 1730, 1702, 1640, 1235, 1100 cm^{-1}; ^1H NMR ($CDCl_3$) δ=1.23 (3H, t, J=6 Hz), 1.30 (3H, t, J=6 Hz), 1.2—1.8 (6H, m), 1.92 (3H, s), 2.0—2.5 (4H, m), 4.13 (4H, m), 5.9—6.6 (2H, m), 7.10 (1H, d, J=11 Hz). The component of the carboxylic acid (R_f 0.37—0.63) was treated with diazomethane to give 172 mg of a clean oil which was chromatographed on preparative HPLC [column, SA-I, 6ϕ×250 mm; eluent, hexane/ethyl acetate (5 : 1), 1.3 ml min^{-1}].

(2*E*,4*E*)-1-Ethyl 11-Methyl 2-Methylundeca-2,4-dienedioate (15) (Methyl Ester of 13): R_t 10.0 min; 52 mg (19% yield); IR (neat) 1740, 1703, 1640, 1235, 1102, 970, 750 cm^{-1}; ^1H NMR ($CDCl_3$) δ=1.30 (3H, t, J=7 Hz), 1.58 (6H, s), 2.24 (4H, m), 3.66 (3H, s), 4.18 (2H, q, J=7 Hz), 6.33 (1H, dd, J=11 and 14.7 Hz). Found: C, 67.15; H, 8.81%. Calcd for $C_{15}H_{24}O_4$: C, 67.14; H, 9.01%.

Ethyl Methyl Nonanedioate:[34] R_t 10.5 min; 43 mg; IR (neat) 1740, 1175, 1100, 1035 cm^{-1}; ^1H NMR ($CDCl_3$) δ=1.24 (3H, t, J=6 Hz), 1.60 (10H, m), 2.32 (4H, m), 3.67 (3H, s), 4.12 (2H, q, J=6 Hz). The other component (55 mg, R_t 15 min) was identified as *N*-methyl-*N*-nitroso-*p*-toluenesulfonamide by a comparison of the spectral data with that of an authentic sample.

6-*t*-Butoxycarbonyl-3,6-dimethyl-5-oxoheptanoic Acid (16). Compound **4f** (25 mg) was left at room temperature for 40 days to give 26 mg (97% yield) of **16** as a mixture of two diastereomers: IR (neat) 3500—2500, 1740, 1715 cm^{-1}; ^1H NMR (CCl_4) δ=0.95 (3H, d, J=6 Hz), 1.20 (3H, d, J=7 Hz), 1.42 (9H, s), 1.6—2.6 (5H, m), 3.25 (1H, q, J=6 Hz), 7.40 (1H, s); ^{13}C NMR ($CDCl_3$) δ=12.5 (q), 19.8 (q), 25.7 (d), 27.8 (q), 40.2 (t), 47.3 (t), 53.9 (d), 54.1 (d), 81.8 (s), 169.5 (s), 178.0 (s), 204.9 (s), 205.0 (s). Compound **16** was converted to its methyl ester with diazomethane, purified by preparative TLC [hexane/ethyl acetate (3 : 1), R_f 0.37], and analyzed.

1-*t*-Butyl 7-Methyl 2,5-Dimethyl-3-oxoheptanedioate: IR (neat) 1730, 1705, 1365, 1155, 1010, 845 cm^{-1}; ^1H NMR (CCl_4) δ=0.98 (3H, d, J=6 Hz), 1.19 (3H, d, J=6 Hz), 1.43 (9H, s), 2.06—2.78 (5H, m), 3.30 (1H, q, J=7 Hz), 3.59 (3H, s). Found: C, 61.83; H, 8.96%. Calcd for $C_{14}H_{24}O_5$: C, 61.74; H, 8.88%.

We thank the whole staff of the Crystallographic Research Center of Osaka University for permitting us to use the fourcircle diffractometer.

References

1) For example, see: a) M. Yamamoto, *Yuki Gosei Kagaku Kyokai Shi*, **39**, 25 (1981); b) C. F. Ingham, R. A. Massy-Westropp, G. D. Reynolds, and W. D. Thorpe, *Aust. J. Chem*, **28**, 2499 (1975). Literatures cited therein.

2) B. C. Seegal, M. Holden, *Science*, **101**, 413 (1945).

3) G. G. Gallo, C. Coronelli, A. Vigevani, G. C. Lancini, *Tetrahedron*, **25**, 5677 (1969).

4) G. Lardelli, G. Dijkstra, P. D. Harkes, J. Boldingh, *Rec. Trav. Chim.*, **85**, 43 (1966).

5) D. W. Knight and G. Pattenden, *J. Chem. Soc., Perkin Trans. 1*, **1975**, 635, 641.

6) H. Tomioka, K. Oshima, and H. Nozaki, *Tetrahedron Lett.*, **23**, 99 (1982).

7) J. Eriksen and P. E. Plith, *Tetrahedron Lett.*, **23**, 481 (1982).

8) N. Yanagihara, C. Lambert, K. Iritani, K. Utimoto, and H. Nozaki, *J. Am. Chem. Soc.*, **108**, 2753 (1986).

9) S. Tsuboi, H. Fukumoto, and A. Takeda, *Chem. Lett.*, **1983**, 1219.

10) P. A. Chopard, R. F. Hudson, and R. J. G. Searle, *Tetrahedron Lett.*, **1965**, 2357.

11) C. F. Ingham, R. A. Massy-Westropp, and G. D. Reynolds, *Aust. J. Chem.*, **27**, 1477 (1974).

12) C. F. Ingham and R. A. Massy-Westropp, *Aust. J. Chem.*, **27**, 1491 (1974).

13) M. J. Begley, D. R. Gedge, and G. Pattenden, *J. Chem. Soc., Chem. Commun.*, **1978**, 60.

14) D. R. Gedge and G. Pattenden, *J. Chem. Soc., Chem. Commun.*, **1978**, 880.

15) P. A. Chopard, R. J. G. Searle, and F. H. Devitt, *J. Org. Chem.*, **30**, 1015 (1965).

16) H. O. House and V. Kramas, *J. Org. Chem.*, **28**, 3362 (1963).

17) A. Takenaka, DCMS-3, Tokyo Institute of Technology (1977).

18) H. Nozaki, Z. Yamaguti, T. Okada, R. Noyori, and M. Kawanishi, *Tetrahedron*, **23**, 3993 (1967).

19) a) P. A. Bartlett, *Tetrahedron*, **36**, 54 (1980); b) L. D. Bergel'son and S. G. Batrakov, *Izv. Akad. Nauk SSSR, Ser. Khim.*, **1963**, 1259.

20) a) K. C. Chan, R. A. Jewell, W. H. Nutling, and H. Rapoport, *J. Org. Chem.*, **33**, 3382 (1968); b) S. Tsuboi, T. Masuda, and A. Takeda, *J. Org. Chem.*, **47**, 4478 (1982).

21) O. Tsler and H. Gutmann, *Helv. Chim. Acta*, **40**, 1242 (1957).

22) A. Michael and J. Ross, *J. Am. Chem. Soc.*, **52**, 4598 (1930).

23) Fr.Fichter and A. Beisswenger, *Chem. Ber.*, **36**, 1205 (1903).

24) F. V. Darbishire and J. F. Thorpe, *J. Chem. Soc.*, **87**, 1717 (1905).

25) W. H. Perkin, Jr. and J. F. Thorpe, *J. Chem. Soc.*, **75**, 54 (1899).

26) C. R. Noller and C. E. Pannell, *J. Am. Chem. Soc.*, **77**, 1862 (1955).

27) D. Vorlander and P. Herrmann, *Ann. Chem.*, **320**, 85 (1902).

28) G. Germain, P. Main, and M. M. Woolfson, *Acta Crystallogr., Sect A*, **27**, 368 (1971).

29) T. Ashida, HBLS-V, The Universal Crystallographic

Computing System-Osaka, pp. 55—61. The Computation Center of Osaka University (1973).

30) International Tables for X-ray Crystallography, Vol. IV, Birmingham, Kynoch Press (1974).

31) The atomic parameters of hydrogen atoms, anisotropic temperature factors, bond lengths and angles, and the list of observed and calculated structure factors (×10) are deposited as Document No. 8710 at the Office of the Editor of Bull. Chem. Soc. Jpn.

32) R. Mozingo, *Org. Synth.*, Vol. 26, p. 77 (1964).

33) M. Tokuda, Y. Watanabe, and M. Ito, *Bull. Chem. Soc. Jpn.*, **51**, 905 (1978).

34) C. R. Strauss, *J. Chromatogr.*, **87**, 576 (1973).

 © 1987 The Chemical Society of Japan Bull. Chem. Soc. Jpn., 60, 697—706 (1987)

Design and Synthesis of Amphiphilic Basic Peptides with Antibacterial Activity and Their Interaction with Model Membrane

Hisakazu MIHARA,* Tatsuhiko KANMERA,† Mutsuo YOSHIDA,†† Sannamu LEE, Haruhiko AOYAGI, Tetsuo KATO, and Nobuo IZUMIYA†††
Laboratory of Biochemistry, Faculty of Science, Kyushu University 33, Higashi-ku, Fukuoka 812
(Received August 12, 1986)

Twelve peptides having 4 to 6 basic amino acid residues in the hydrophobic amino acid sequence were designed and synthesized by the solution method to find peptides with potential activity against Gram-positive and -negative bacteria. CD study of the peptides demonstrated that they formed α-helical structures in the presence of phospholipid liposomes consequently to have amphiphilic property along the axis of helix. The peptides also induced the leakage of the dye carboxyfluorescein from phospholipid vesicles, indicating that the peptides possess the ability to perturb the membrane structure. These peptides showed antibacterial activity against Gram-positive bacteria, and some of them were also active against Gram-negative bacteria. Relationships between the structure and antibacterial activity of the synthetic peptides were discussed.

Recently, an amphiphilic α-helical structure, especially that containing basic amino acids, has been found to be a common factor in several biologically active peptides, e.g., plasma apolipoproteins,[1,2] calmodulin-binding peptides,[3,4] bee venom toxins[5,6] and antibacterial peptides.[7-10] Previously, we reported[11,12] that the basic model peptides, e.g., Ac-(Leu-Ala-Lys-Leu)$_{3,4}$-NHCH$_3$ ($\mathbf{4}_3$, $\mathbf{4}_4$), which were designed from the common feature of extension peptides of mitochondrial protein precursors, showed inhibition of import of the precursors to mitochondria, antibacterial activity against Gram-positive bacteria and perturbation of mitochondrial membrane and phospholipid bilayer. Their antibacterial activities were also correlated to the secondary structure of the peptides.[12] Thus, simple model peptides designed can be used as an effective tool to clarify the structure proposed for biological activity.

DeGrado reported[13] that a simple amphiphilic α-helical peptide, Fmoc-(Leu-Lys-Lys-Leu-Leu-Lys-Leu)$_{2\bar{7}}$OH (F),[14] which was designed from cecropin,[7,8] a naturally occurring cationic amphiphilic antibiotic, showed the same strong antibacterial activity as cecropin against Gram-positive and -negative bacteria. Ando et al.[15] reported that an analog of gramicidin S (GS), [D-2,3-diaminopropionic acid (D-Dpr)$^{4,4'}$]GS, had an activity against Gram-positive and -negative bacteria, although GS which has a cationic amphiphilic structure with antiparallel β-sheet and β-turn is only active against Gram-positive bacteria. The reason of the difference in the activity against Gram-negative bacteria between the model peptide $\mathbf{4}_3$ or GS and peptide F or [D-Dpr$^{4,4'}$]GS should be due to the num-

†Present address: Biosciences Laboratory, Research Center, Mitsubishi Chemical Ind. Ltd., Yokohama 227.
††Present address: Dojindo Laboratories, Kumamoto 862.
†††Present address: Kurume Institute of Technology, Kurume 830.

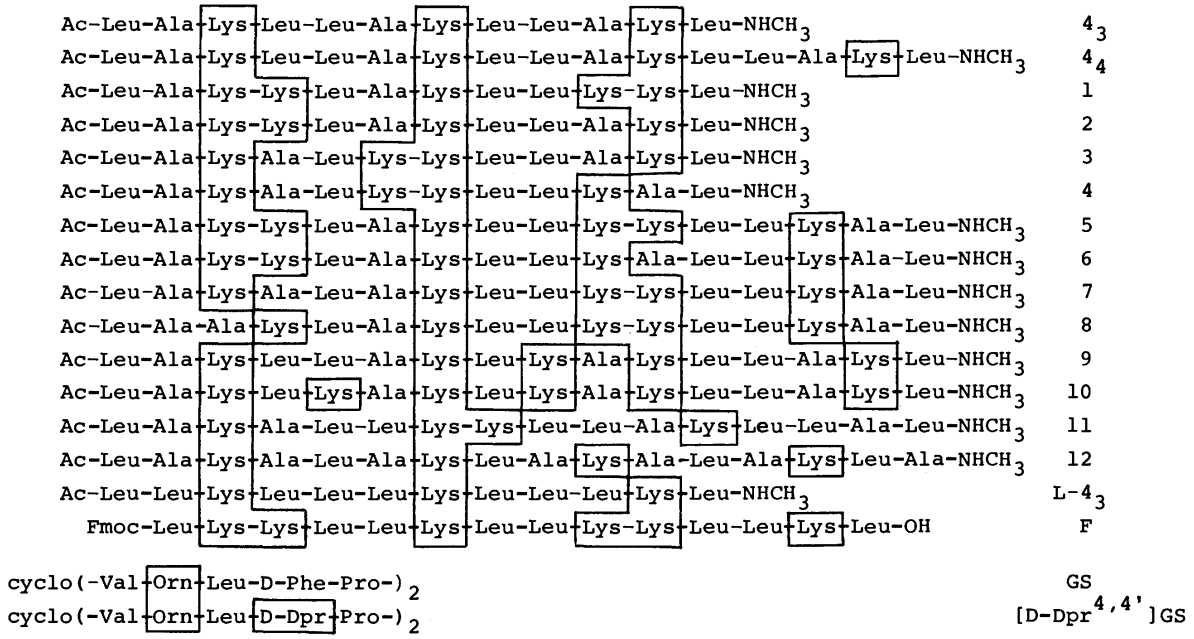

Fig. 1. Synthetic model peptides and gramicidin S. All amino acids are of L-configuration.

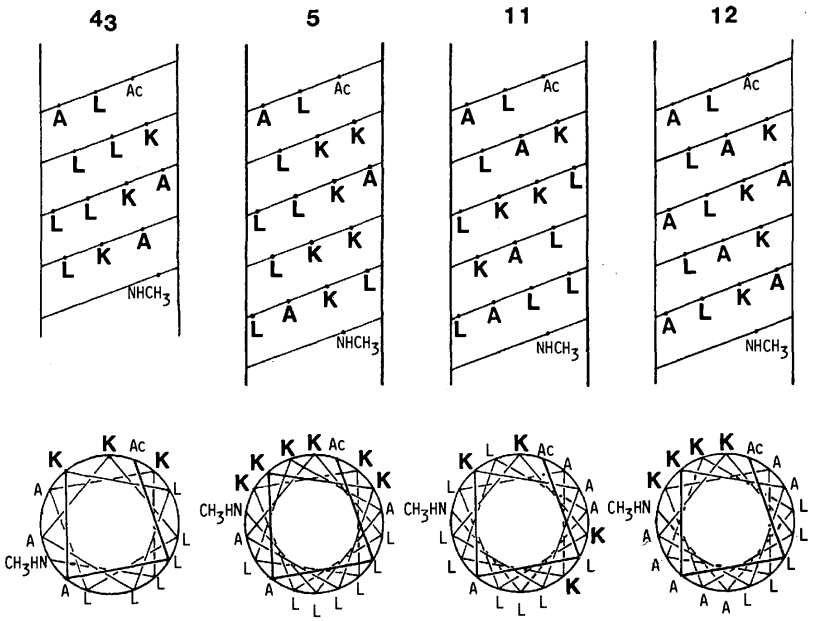

Fig. 2. α-Helical nets and wheels of peptides 4_3, **5**, **11**, and **12**. One-letter symbols of amino acids are used for concise representation: A, alanine; K, lysine; L, leucine.

ber of basic amino acids and the secondary structure, i.e., amphiphilicity. In order to study the relationships between the activity against Gram-positive or -negative bacteria and the property of amphiphilic peptides, we have designed and synthesized several basic peptides as shown in Fig. 1, and examined antibacterial activities of the peptides and their secondary structures by CD measurements. Phase-transition release experiment of carboxyfluorescein from DPPC vesicles using the peptides was also performed in order to examine whether the ability to perturb bacterial membrane relates to the antimicrobial activity.

Results

Design. The model peptides (Fig. 1) were designed on the basis of the structures of 4_3 and 4_4 showing the strongest antimicrobial activity among the previously synthesized model peptides[12] and of peptide F taking amphiphilic α-helical structure and having the activity against Gram-positive and -negative bacteria.[13] The structural differences between 4_4 and F are just the number of basic amino acids and distribution of the Lys residues in hydrophobic sequences. Therefore, to develop peptides active against Gram-negative bacteria, the number and distribution of basic amino acid Lys were altered in the peptides. In compounds **1**—**8**, one or two additional Lys residues are distributed into 4_3 or 4_4 to keep amphiphilicity postulating that these peptides take α-helices. The sequence of **5** is almost the same as that of peptide F except for the acetyl group and the Ala residues in **5** instead of the Fmoc group and the Leu residues in F, respectively. Peptides **9** and **10** were designed to disturb the amphiphilic

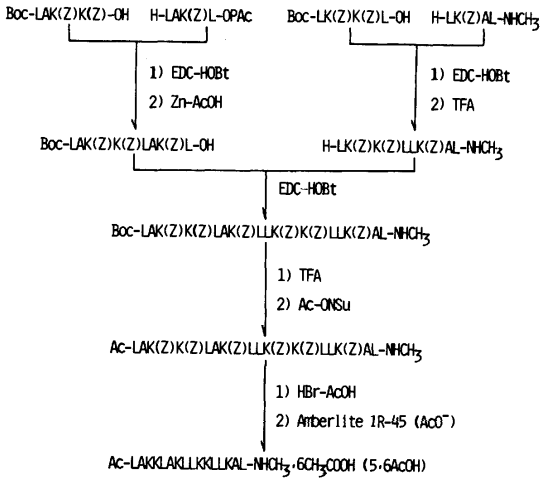

Fig. 3. Synthetic route for Ac-hexadecapeptide-$NHCH_3$ (**5**).

property by the substitution of Lys for the Leu residues in hydrophobic cluster. Orientation of the Lys residues in peptide **11** with α-helical structure is topologically similar to that of four basic amino acid residues in [D-Dpr$^{4,4'}$]GS. α-Helical nets and wheels of representative peptides are shown in Fig. 2. In peptide **12**, the Leu and Lys residues lie straight along the axis of the α-helix. Moreover, peptide L-4_3 containing Leu residues instead of Ala residues in 4_3 and peptide F were also synthesized.

Synthesis. The synthetic route for **5** is shown in Fig. 3. The tetrapeptides were prepared by stepwise elongation of the Boc-amino acid active esters.[16] The Boc-dipeptide-OPac was prepared by the mixed anhydride method.[17] After the cleavage of phenacyl ester

or Boc group, the tetrapeptides were coupled by the EDC-HOBt method[18] to give Boc-octapeptide-OPac or $-NHCH_3$. The phenacyl ester and Boc group were removed with Zn powder in acetic acid and with TFA, respectively. The resulting acid and amine components were coupled by the EDC-HOBt method to give Boc-hexadecapeptide-$NHCH_3$. The Boc group was cleaved with TFA followed by acetylation with Ac-ONSu to give Ac-peptide-$NHCH_3$. The Z groups were removed with 25% HBr in AcOH and peptide hydrobromide obtained was passed through a column of Amberlite IR-45 (acetate form) to give **5** as a tetraacetate. The purity was confirmed by TLC, paper electrophoresis, amino acid analysis and elemental analysis. Other peptides were prepared similarly. Yields and physical constants of protected peptides and final products are shown in Tables 1 and 2.

Antibacterial Activity. Antibacterial assays were

Table 1. Yields and Physical Constants of Protected-Peptides

Peptides	Formula (MW)[a]	Yield %	Mp θ_m/°C	$[\alpha]_D^{20}$[b]	TLC R_f[c]
Boc-AL-OPac (13)	$C_{22}H_{32}O_6N_2$ (420.5)	89	powder	—	0.81
Boc-AK(Z)-OPac (14)	$C_{30}H_{39}O_8N_3$ (569.7)	89	105-110	-19.8	0.68
Boc-K(Z)A-OPac (15)	$C_{30}H_{39}O_8N_3$ (569.7)	82	53-54	-30.1	0.67
Boc-K(Z)K(Z)-OPac (16)	$C_{41}H_{52}O_{10}N_4 \cdot 1/2H_2O$ (769.9)	91	63-64	-36.4	0.70
Boc-AL-$NHCH_3$ (17)	$C_{15}H_{29}O_4N_3$ (315.4)	90	162-165	-33.8	0.64
Boc-LA-$NHCH_3$ (18)	$C_{15}H_{29}O_4N_3$ (315.4)	82	170-171	-18.1	0.66
Boc-AAK(Z)-OPac (19)	$C_{33}H_{44}O_9N_4$ (640.7)	86	119-124	-18.4	0.73
Boc-AK(Z)A-OPac (20)	$C_{33}H_{44}O_9N_4$ (640.7)	90	134-136	-27.5	0.64
Boc-LAK(Z)-OPac (21)	$C_{36}H_{50}O_9N_4$ (682.8)	95	89-92	-21.5	0.76
Boc-K(Z)AL-OPac (22)	$C_{36}H_{50}O_9N_4$ (682.8)	92	83-86	-27.4	0.69
Boc-LK(Z)L-OPac (23)	$C_{39}H_{56}O_9N_4$ (724.9)	91	148-150	-31.8	0.80
Boc-AK(Z)K(Z)-OPac (24)	$C_{44}H_{57}O_{11}N_5$ (832.0)	95	103-105	-17.2	0.75
Boc-LK(Z)K(Z)-OPac (25)	$C_{47}H_{63}O_{11}N_5$ (874.0)	94	116-121	-20.6	0.76
Boc-K(Z)K(Z)L-OPac (26)	$C_{47}H_{63}O_{11}N_5$ (874.0)	87	120-121	-21.9	0.74
Boc-LAL-$NHCH_3$ (27)	$C_{21}H_{40}O_5N_4$ (428.6)	85	220-222	-32.0	0.63
Boc-K(Z)AL-$NHCH_3$ (28)	$C_{29}H_{47}O_7N_5$ (577.7)	97	189-193	-20.2	0.63
Boc-K(Z)LA-$NHCH_3$ (29)	$C_{29}H_{47}O_7N_5$ (577.7)	84	181-183	-21.8	0.62
Boc-LK(Z)L-$NHCH_3$ (30)	$C_{32}H_{53}O_7N_5 \cdot 1/2H_2O$ (628.8)	80	183-187	-27.2	0.68
Boc-K(Z)K(Z)L-$NHCH_3$ (31)	$C_{40}H_{60}O_9N_6$ (769.0)	96	147-150	-16.8	0.65
Boc-LAAK(Z)-OPac (32)	$C_{39}H_{55}O_{10}N_5$ (753.9)	94	117-122	-22.4	0.71
Boc-LAK(Z)A-OPac (33)	$C_{39}H_{55}O_{10}N_5 \cdot 1/2H_2O$ (762.9)	94	168-170	-30.2	0.68
Boc-LLAK(Z)-OPac (34)	$C_{42}H_{61}O_{10}N_5$ (796.0)	95	157-161	-29.5	0.63
Boc-LK(Z)AL-OPac (35)	$C_{42}H_{61}O_{10}N_5 \cdot 1/2H_2O$ (805.0)	97	117-119	-34.2	0.74
Boc-LLK(Z)L-OPac (36)	$C_{45}H_{67}O_{10}N_5$ (838.1)	84	170-173	-36.1	0.75
Boc-LAK(Z)K(Z)-OPac (37)	$C_{50}H_{68}O_{12}N_6 \cdot 1/2H_2O$ (954.1)	86	115-119	-18.7	0.75
Boc-K(Z)AK(Z)L-OPac (38)	$C_{50}H_{68}O_{12}N_6 \cdot 1/2H_2O$ (954.1)	94	151-154	-34.6	0.70
Boc-LLK(Z)K(Z)-OPac (39)	$C_{53}H_{74}O_{12}N_6 \cdot 1/2H_2O$ (996.2)	80	127-129	-24.9	0.69
Boc-LK(Z)K(Z)L-OPac (40)	$C_{53}H_{74}O_{12}N_6 \cdot 1/2H_2O$ (996.2)	93	134-136	-27.2	0.77
Boc-LAAK(Z)-OH (41)	$C_{31}H_{49}O_9N_5$ (635.8)	81	71-78	-14.2	0.59
Boc-LAK(Z)A-OH (42)	$C_{31}H_{49}O_9N_5$ (635.8)	90	131-133	-19.5	0.52
Boc-LLAK(Z)-OH (43)	$C_{34}H_{55}O_9N_5$ (677.8)	87	136-139	-24.2	0.56
Boc-LK(Z)AL-OH (44)	$C_{34}H_{55}O_9N_5$ (677.8)	88	powder	—	0.66
Boc-LLK(Z)L-OH (45)	$C_{37}H_{61}O_9N_5 \cdot 1/2H_2O$ (728.9)	87	108-110	-31.2	0.66
Boc-LAK(Z)K(Z)-OH (46)	$C_{42}H_{62}O_{11}N_6 \cdot 1/2H_2O$ (836.0)	81	124-128	-13.6	0.69
Boc-K(Z)AK(Z)L-OH (47)	$C_{42}H_{62}O_{11}N_6$ (827.0)	93	81-82	-16.0	0.65
Boc-LK(Z)K(Z)L-OH (48)	$C_{45}H_{68}O_{11}N_6$ (869.1)	96	74-76	-22.8	0.67
Boc-LLAL-$NHCH_3$ (49)	$C_{27}H_{51}O_6N_5$ (541.7)	90	257-260	-43.2	0.65
Boc-AK(Z)LA-$NHCH_3$ (50)	$C_{32}H_{52}O_8N_6 \cdot 1/3H_2O$ (654.8)	95	179-181	-23.5	0.66

Table 1. (Continued)

Peptides	Formula (MW)[a]	Yield %	Mp θ_m/°C	$[\alpha]_D^{20}$[b]	TLC R_f[c]
Boc-LK(Z)AL-$NHCH_3$ (51)	$C_{35}H_{58}O_8N_6$ (690.9)	91	186–189	−26.6	0.67
Boc-LLK(Z)L-$NHCH_3$ (52)	$C_{38}H_{64}O_8N_6 \cdot H_2O$ (751.0)	87	190–193	−30.1	0.68
Boc-LK(Z)K(Z)L-$NHCH_3$ (53)	$C_{46}H_{71}O_{10}N_7$ (882.1)	85	207–210	−20.2	0.64
Boc-LAK(Z)LA-$NHCH_3$ (54)	$C_{38}H_{63}O_9N_7$ (762.0)	85	216–219	−24.7	0.65
Boc-LAK(Z)ALAK(Z)-OPac (55)	$C_{62}H_{89}O_{15}N_9$ (1200.4)	95	245–248(d)	−28.5[d]	0.68
Boc-LK(Z)K(Z)LLK(Z)L-OPac (56)	$C_{79}H_{114}O_{17}N_{10} \cdot 3H_2O$ (1529.9)	96	215–224(d)	−23.6	0.67
Boc-LAK(Z)ALAK(Z)-OH (57)	$C_{54}H_{83}O_{14}N_9 \cdot 3/2H_2O$ (1109.3)	95	265–270(d)	−20.9[d]	0.47
Boc-LK(Z)K(Z)LLK(Z)L-OH (58)	$C_{71}H_{108}O_{16}N_{10} \cdot 2H_2O$ (1393.7)	96	240–245(d)	−25.6	0.58
Boc-LAAK(Z)LAK(Z)L-OPac (59)	$C_{68}H_{100}O_{16}N_{10} \cdot H_2O$ (1331.6)	95	181–184(d)	−27.6	0.67
Boc-LAK(Z)ALAK(Z)L-OPac (60)	$C_{68}H_{100}O_{16}N_{10} \cdot 1/2H_2O$ (1322.6)	91	265–267(d)	−30.1	0.62
Boc-LAK(Z)LLAK(Z)L-OPac (61)	$C_{71}H_{106}O_{16}N_{10} \cdot H_2O$ (1373.7)	93	211–216(d)	−28.8	0.64
Boc-LAK(Z)ALLK(Z)K(Z)-OPac (62)	$C_{79}H_{113}O_{18}N_{11} \cdot 1/2H_2O$ (1513.8)	92	225–230(d)	−24.6	0.66
Boc-LAK(Z)ALK(Z)K(Z)L-OPac (63)	$C_{79}H_{113}O_{18}N_{11} \cdot H_2O$ (1522.9)	91	225–228(d)	−25.4	0.68
Boc-LAK(Z)LK(Z)AK(Z)L-OPac (64)	$C_{79}H_{113}O_{18}N_{11} \cdot H_2O$ (1522.9)	96	208–210(d)	−26.0	0.67
Boc-LAK(Z)K(Z)LAK(Z)L-OPac (65)	$C_{79}H_{113}O_{18}N_{11} \cdot H_2O$ (1522.9)	96	245–247(d)	−25.1	0.66
Boc-LAAK(Z)LAK(Z)L-OH (66)	$C_{60}H_{94}O_{15}N_{10} \cdot 3/2H_2O$ (1222.5)	95	230–234(d)	−28.8[d]	0.59
Boc-LAK(Z)ALAK(Z)L-OH (67)	$C_{60}H_{94}O_{15}N_{10} \cdot H_2O$ (1213.5)	95	265–267(d)	−26.8	0.57
Boc-LAK(Z)LLAK(Z)L-OH (68)	$C_{63}H_{100}O_{15}N_{10} \cdot H_2O$ (1255.6)	93	295–300(d)	−29.6[d]	0.56
Boc-LAK(Z)ALLK(Z)K(Z)-OH (69)	$C_{71}H_{107}O_{17}N_{11} \cdot 2H_2O$ (1422.7)	94	227–233(d)	−26.4	0.54
Boc-LAK(Z)ALK(Z)K(Z)L-OH (70)	$C_{71}H_{107}O_{17}N_{11} \cdot 3/2H_2O$ (1413.7)	96	229–234(d)	−22.9	0.52
Boc-LAK(Z)LK(Z)AK(Z)L-OH (71)	$C_{71}H_{107}O_{17}N_{11} \cdot 3/2H_2O$ (1413.7)	94	240–245(d)	−24.4[d]	0.51
Boc-LAK(Z)K(Z)LAK(Z)L-OH (72)	$C_{71}H_{107}O_{17}N_{11} \cdot 3/2H_2O$ (1413.7)	96	264–269(d)	−21.9	0.54
Boc-LLAK(Z)LLAL-$NHCH_3$ (73)	$C_{56}H_{96}O_{12}N_{10} \cdot 1/2H_2O$ (1110.5)	94	257–261(d)	−41.5[d]	0.63
Boc-LK(Z)ALLK(Z)AL-$NHCH_3$ (74)	$C_{64}H_{103}O_{14}N_{11} \cdot 1/2H_2O$ (1259.6)	95	255–258(d)	−21.2	0.58
Boc-LLK(Z)LLLK(Z)L-$NHCH_3$ (75)	$C_{70}H_{115}O_{14}N_{11} \cdot H_2O$ (1352.8)	96	284–287(d)	−41.2[d]	0.64
Boc-K(Z)AK(Z)LLAK(Z)L-$NHCH_3$ (76)	$C_{72}H_{110}O_{16}N_{12} \cdot 1/2H_2O$ (1408.8)	94	267–270(d)	−25.6[d]	0.64
Boc-LK(Z)K(Z)LLK(Z)AL-$NHCH_3$ (77)	$C_{75}H_{116}O_{16}N_{12} \cdot H_2O$ (1459.8)	89	255–260(d)	−17.2	0.55
Boc-LAK(Z)ALAK(Z)LA-$NHCH_3$ (78)	$C_{64}H_{102}O_{15}N_{12} \cdot 1/2H_2O$ (1288.6)	89	276–280(d)	−27.2[d]	0.56
Boc-LAK(Z)K(Z)LAK(Z)LLK(Z)K(Z)L-$NHCH_3$ (79)	$C_{112}H_{168}O_{24}N_{18} \cdot 3/2H_2O$ (2177.7)	96	305–310(d)	−22.0[d]	0.58
Boc-LAK(Z)K(Z)LAK(Z)LLAK(Z)L-$NHCH_3$ (80)	$C_{101}H_{155}O_{22}N_{17} \cdot 3/2H_2O$ (1986.5)	96	296–299(d)	−22.0[d]	0.61
Boc-LAK(Z)ALK(Z)K(Z)LLAK(Z)L-$NHCH_3$ (81)	$C_{101}H_{155}O_{22}N_{17} \cdot 2H_2O$ (1995.5)	95	290–295(d)	−22.6[d]	0.62
Boc-LAK(Z)ALK(Z)K(Z)LLK(Z)AL-$NHCH_3$ (82)	$C_{101}H_{155}O_{22}N_{17} \cdot 2H_2O$ (1995.5)	95	292–297(d)	−25.8[d]	0.62
Boc-LAK(Z)K(Z)LAK(Z)LLK(Z)K(Z)LLK(Z)AL-$NHCH_3$ (83)	$C_{141}H_{213}O_{30}N_{23} \cdot 2H_2O$ (2746.4)	89	295–300(d)	−31.1[d]	0.70
Boc-LAK(Z)K(Z)LAK(Z)LLK(Z)ALLK(Z)AL-$NHCH_3$ (84)	$C_{130}H_{200}O_{28}N_{22} \cdot 2H_2O$ (2555.2)	95	305–310(d)	−17.6[d]	0.68
Boc-LAK(Z)ALAK(Z)LLK(Z)K(Z)LLK(Z)AL-$NHCH_3$ (85)	$C_{130}H_{200}O_{28}N_{22} \cdot 2H_2O$ (2555.2)	95	290–295(d)	−21.4[d]	0.62
Boc-LAAK(Z)LAK(Z)LLK(Z)K(Z)LLK(Z)AL-$NHCH_3$ (86)	$C_{130}H_{200}O_{28}N_{22} \cdot 2H_2O$ (2555.2)	96	295–300(d)	−18.8[d]	0.67
Boc-LAK(Z)LLAK(Z)LK(Z)AK(Z)LLAK(Z)L-$NHCH_3$ (87)	$C_{130}H_{200}O_{28}N_{22} \cdot 5/2H_2O$ (2564.2)	95	275–280(d)	−15.2[d]	0.68
Boc-LAK(Z)LK(Z)AK(Z)LK(Z)AK(Z)LLAK(Z)L-$NHCH_3$ (88)	$C_{138}H_{207}O_{30}N_{23} \cdot 2H_2O$ (2704.3)	92	285–290(d)	−12.8[d]	0.67
Boc-LAK(Z)ALLK(Z)K(Z)LLAK(Z)LLAL-$NHCH_3$ (89)	$C_{122}H_{193}O_{26}N_{21} \cdot 2H_2O$ (2406.0)	95	265–270(d)	−30.0[d]	0.68
Boc-LAK(Z)ALAK(Z)LAK(Z)ALAK(Z)LA-$NHCH_3$ (90)	$C_{113}H_{175}O_{26}N_{21} \cdot 4H_2O$ (2315.8)	96	229–231(d)	−21.4[d]	0.62
Boc-(LLK(Z)L)$_3$-$NHCH_3$ (91)	$C_{102}H_{166}O_{20}N_{16} \cdot H_2O$ (1954.6)	96	305–310(d)	−33.3[d]	0.70
Boc-(LK(Z)K(Z)LLK(Z)L)$_2$-OPac (92)	$C_{145}H_{212}O_{30}N_{20} \cdot 2H_2O$ (2751.4)	92	295–300(d)	−21.6[d]	0.68
Ac-LAK(Z)K(Z)LAK(Z)LLK(Z)K(Z)L-$NHCH_3$ (93)	$C_{109}H_{162}O_{23}N_{18} \cdot 2H_2O$ (2128.6)	95	293–297(d)	−20.4[d]	0.55
Ac-LAK(Z)K(Z)LAK(Z)LLAK(Z)L-$NHCH_3$ (94)	$C_{98}H_{149}O_{21}N_{17} \cdot H_2O$ (1919.4)	96	280–284(d)	−17.2[d]	0.53
Ac-LAK(Z)ALK(Z)K(Z)LLAK(Z)L-$NHCH_3$ (95)	$C_{98}H_{149}O_{21}N_{17} \cdot H_2O$ (1919.4)	86	251–253(d)	−28.9[d]	0.58
Ac-LAK(Z)ALK(Z)K(Z)LLK(Z)AL-$NHCH_3$ (96)	$C_{98}H_{149}O_{21}N_{17} \cdot H_2O$ (1919.4)	93	285–290(d)	−26.3[d]	0.56
Ac-LAK(Z)K(Z)LAK(Z)LLK(Z)K(Z)LLK(Z)AL-$NHCH_3$ (97)	$C_{138}H_{207}O_{29}N_{23} \cdot 2H_2O$ (2688.3)	86	287–292(d)	−12.0[d]	0.60

Table 1. (Continued)

Peptides	Formula (MW)[a]	Yield %	Mp θ_m/°C	$[\alpha]_D^{20}$[b]	TLC R_f[c]
Ac-LAK(Z)K(Z)LAK(Z)LLK(Z)ALLK(Z)AL-$NHCH_3$ (98)	$C_{127}H_{194}O_{27}N_{22}\cdot 2H_2O$ (2497.1)	88	240–245(d)	−16.0[d]	0.68
Ac-LAK(Z)ALAK(Z)LLK(Z)K(Z)LLK(Z)AL-$NHCH_3$ (99)	$C_{127}H_{194}O_{27}N_{22}\cdot H_2O$ (2479.1)	93	240–250(d)	−21.5[d]	0.57
Ac-LAAK(Z)LAK(Z)LLK(Z)K(Z)LLK(Z)AL-$NHCH_3$ (100)	$C_{127}H_{194}O_{27}N_{22}\cdot 3H_2O$ (2515.1)	87	265–270(d)	−16.8[d]	0.64
Ac-LAK(Z)LLAK(Z)LK(Z)AK(Z)LLAK(Z)L-$NHCH_3$ (101)	$C_{127}H_{194}O_{27}N_{22}\cdot 3H_2O$ (2515.1)	95	275–280(d)	−12.0[d]	0.66
Ac-LAK(Z)LK(Z)AK(Z)LK(Z)AK(Z)LLAK(Z)L-$NHCH_3$ (102)	$C_{135}H_{201}O_{29}N_{23}\cdot 2H_2O$ (2646.3)	91	285–290(d)	−11.6[d]	0.65
Ac-LAK(Z)ALLK(Z)K(Z)LLAK(Z)LLAL-$NHCH_3$ (103)	$C_{119}H_{187}O_{25}N_{21}\cdot 4H_2O$ (2384.0)	92	280–285(d)	−22.6[d]	0.59
Ac-LAK(Z)ALAK(Z)LAK(Z)ALAK(Z)LA-$NHCH_3$ (104)	$C_{110}H_{169}O_{25}N_{21}\cdot 4H_2O$ (2257.7)	93	250–255(d)	−17.4[d]	0.51
Ac-$(LLK(Z)L)_3$-$NHCH_3$ (105)	$C_{99}H_{160}O_{19}N_{16}\cdot 3/2H_2O$ (1905.4)	96	305–310(d)	−30.3[d]	0.72
Fmoc-$(LK(Z)K(Z)LLK(Z)L)_2$-OPac (106)	$C_{155}H_{214}O_{30}N_{20}\cdot H_2O$ (2855.5)	81	270–280(d)	−23.2[d]	0.78
Fmoc-$(LK(Z)K(Z)LLK(Z)L)_2$-OH (107)	$C_{147}H_{208}O_{29}N_{20}\cdot 4H_2O$ (2791.5)	88	290–295(d)	−17.6[d]	0.57

a) The results of elemental analysis agreed with calculated values within ±0.3%. b) *c* 1.0, DMF. c) $CHCl_3$–MeOH (5:1, v/v). d) *c* 0.5, DMSO.

Table 2. Yields and Physical Constants of the Model Peptides[a]

Peptide	Formula (MW)[b]	Yield/%	TLC/R_f[c]	Pep(R_{Lys})[d]
Ac-LAKKLAKLLKKL-$NHCH_3\cdot$5AcOH (1·5AcOH)	$C_{69}H_{132}O_{13}N_{18}\cdot 5C_2H_4O_2\cdot 7H_2O$ (1848.3)	88	0.30	0.90
Ac-LAKKLAKLLAKL-$NHCH_3\cdot$4AcOH (2·4AcOH)	$C_{66}H_{125}O_{13}N_{17}\cdot 4C_2H_4O_2\cdot 6H_2O$ (1713.1)	82	0.39	0.80
Ac-LAKALKKLLAKL-$NHCH_3\cdot$4AcOH (3·4AcOH)	$C_{66}H_{125}O_{13}N_{17}\cdot 4C_2H_4O_2\cdot 5H_2O$ (1695.0)	89	0.43	0.79
Ac-LAKALKKLLKAL-$NHCH_3\cdot$4AcOH (4·4AcOH)	$C_{66}H_{125}O_{13}N_{17}\cdot 4C_2H_4O_2\cdot 3H_2O$ (1659.1)	81	0.41	0.81
Ac-LAKKLAKLLKKLLKAL-$NHCH_3\cdot$6AcOH (5·6AcOH)	$C_{90}H_{171}O_{17}N_{23}\cdot 6C_2H_4O_2\cdot 7H_2O$ (2333.9)	84	0.33	0.81
Ac-LAKKLAKLLKALLKAL-$NHCH_3\cdot$5AcOH (6·5AcOH)	$C_{87}H_{164}O_{17}N_{22}\cdot 5C_2H_4O_2\cdot 5H_2O$ (2180.7)	79	0.39	0.77
Ac-LAKALAKLLKKLLKAL-$NHCH_3\cdot$5AcOH (7·5AcOH)	$C_{87}H_{164}O_{17}N_{22}\cdot 5C_2H_4O_2\cdot 6H_2O$ (2198.6)	89	0.45	0.79
Ac-LAAKLAKLLKKLLKAL-$NHCH_3\cdot$5AcOH (8·5AcOH)	$C_{87}H_{164}O_{17}N_{22}\cdot 5C_2H_4O_2\cdot 5H_2O$ (2180.7)	78	0.44	0.75
Ac-LAKLLAKLKAKLLAKL-$NHCH_3\cdot$5AcOH (9·5AcOH)	$C_{87}H_{164}O_{17}N_{22}\cdot 5C_2H_4O_2\cdot 3H_2O$ (2147.7)	73	0.38	0.76
Ac-LAKLKAKLKAKLLAKL-$NHCH_3\cdot$6AcOH (10·6AcOH)	$C_{87}H_{165}O_{17}N_{23}\cdot 6C_2H_4O_2\cdot 5H_2O$ (2255.8)	81	0.36	0.81
Ac-LAKALLKKLLAKLLAL-$NHCH_3\cdot$4AcOH (11·4AcOH)	$C_{87}H_{163}O_{17}N_{21}\cdot 4C_2H_4O_2\cdot 8H_2O$ (2159.7)	84	0.48	0.70
Ac-LAKALAKLAKALAKLA-$NHCH_3\cdot$4AcOH (12·4AcOH)	$C_{78}H_{145}O_{17}N_{21}\cdot 4C_2H_4O_2\cdot 8H_2O$ (2033.5)	94	0.46	0.70
Ac-$(LLKL)_3$-$NHCH_3\cdot$3AcOH (L-$4_3\cdot$3AcOH)	$C_{66}H_{124}O_{13}N_{22}\cdot 3C_2H_4O_2\cdot 3H_2O$ (1688.0)	92	0.48	0.67
Fmoc-$(LKKLLKL)_2$-OH·6AcOH (F·6AcOH)	$C_{99}H_{172}O_{17}N_{20}\cdot 6C_2H_4O_2\cdot 10H_2O$ (2455.1)	90	0.34	0.86

a) Amino acid analysis of the peptides gave satisfactory results of the amino acid components. b) The reasonable compositions were considered from the results of elemental analysis. c) *n*-BuOH–AcOH–pyridine–H_2O (4:1:1:2, v/v). d) Relative value to Lys.

carried out by both agar dilution[19] and serial dilution method in solution medium.[20] The results of antibacterial assay of the peptides are listed in terms of minimum inhibitory concentration of growth (MIC) in Table 3 compared with that of peptide $\mathbf{4}_3$, $\mathbf{4}_4$, GS, [D-Dpr$^{4,4'}$]GS and polymyxin B (PM). In agar dilution method, present model peptides (**1**—**12** and L-$\mathbf{4}_3$) revealed weak activity against Gram-positive bacteria as compared with peptide $\mathbf{4}_3$ and GS. On the other hand, peptides with the increased number of the Lys residues (**1** and **9**) showed weak but substantial activity against Gram-negative bacteria such as *E. coli*. On the contrary, by means of serial dilution method in solution medium, all the peptides examined were active against both Gram-positive and -negative bacteria. Especially peptides **1** and **5** showed stronger activity against *E. coli* than GS did. These results indicate that increase in the number of the Lys residues leads to decrease in the activity against Gram-positive bacteria and increase in that against Gram-negative bacteria. It is noteworthy that the decrease in activity of the peptides against *S. aureus* was more marked than that against *B. subtilis*, this fact being comparable to the result that PM was inactive against *S. aureus* although strongly active against Gram-negative bacteria. Non-amphiphilic peptides (**9** and **10**) showed fairly high activity, suggesting that amphiphilic character is indeed important, but not essential for the activity against Gram-positive bacteria, especially *B. subtilis*. Deviation in distribution of the Lys residues from pep-

Table 3. Antibacterial Activity of the Peptides

Peptide	Minimum inhibitory concentration/μg ml^{-1}			
	S.aureus FDA 209P	*B.subtilis* PCI 219	*E.coli* NIHJ JC-2	*S.flexneri* EW-10
1	100	25 (0.5)[a]	100 (1.25)[a]	6.25
2	100	12.5	>100	12.5
3	50	25	>100	12.5
4	>100	25	>100	25
5	>100	50 (1.25)[a]	>100 (2.5)[a]	50
6	100	50	>100	100
7	100	25	>100	50
8	>100	25	>100	50
9	100	12.5	100	6.25
10	>100	50	>100	12.5
11	25	12.5 (0.5)[a]	>100 (5.0)[a]	12.5
12	>100	50	>100	>100
L-**4**$_3$	25	25	>100	>100
F	>100	100 (2.5)[a]	>100 (5.0)[a]	25
4$_3$	6.25	3.13 (0.5)[a]	>100 (6.0)[a]	6.25
4$_4$	25	12.5	>100	>100
GS	3.13	3.13 (0.5)[a]	>100 (5.0)[a]	6.25
[D-Dpr$^{4,4'}$]GS[b]	100	12.5	25	25
PM	>50	6.25	0.78	0.39

a) Against *B.subtilis* IFO 3007 and *E. coli* B by serial dilution method in solution medium. b) Data are derived from the Ref. 15.

tide **4**$_4$ resulted in decreased activity **12**, indicating that the specific sequence and secondary structure in **4**$_3$ (Figs. 1 and 2) are important to show strong activity against Gram-positive bacteria. It is interesting that the [D-Dpr$^{4,4'}$]GS-resembling peptide (**11**) showed the same activity against Gram-positive and -negative bacteria as peptide **4**$_4$, also indicating the significance of the specific structure. Replacement of the Ala residues in peptide **4**$_3$ by the Leu residues (L-**4**$_3$) caused marked decrease in the activity, indicating that increase of the hydrophobicity in the peptide is not important to show the activity, but the Ala residues are important to show the activity. Generally, the peptides with the length of 12 residues showed higher activity against Gram-positive bacteria than those with 16 residues. This finding is comparable to the fact that peptide **4**$_3$ (n=12) was more active than **4**$_4$ (n=16).[12] The chain length of a peptide is important for its activity as described previously.[12] Peptide F did not show strong activity against Gram-positive and -negative bacteria on our assay systems contrary to DeGrado's results.[13] This might be due to the different bacterial assay systems, e.g., difference in media and conditions of bacteria.

CD Study. CD spectra of peptide **5** in H_2O and in the presence of phospholipid liposomes are shown in Fig. 4, representatively. Although peptide **5** showed the negative band at 200 nm in H_2O attributable to disordered structure, the spectra in the presence of liposomes showed marked increase in ellipticities of the negative bands at 208 and 222 nm, indicating the formation of α-helical structure in the presence of liposomes. A slight difference was observed between the spectra in the presence of neutral DPPC and acidic DPPC-DPPG (3 : 1) liposomes. α-Helicity of the peptides under various conditions was calculated from the ellipticity at 222 nm[21] and is shown in Table 4. All the peptides took the α-helical structure which was amphiphilic (except for peptides **9** and **10**) along the axis of helix in the presence of liposomes in contrast with the disordered structure in H_2O. These findings are similar to those described for peptides **4**$_3$ and **4**$_4$.[12]

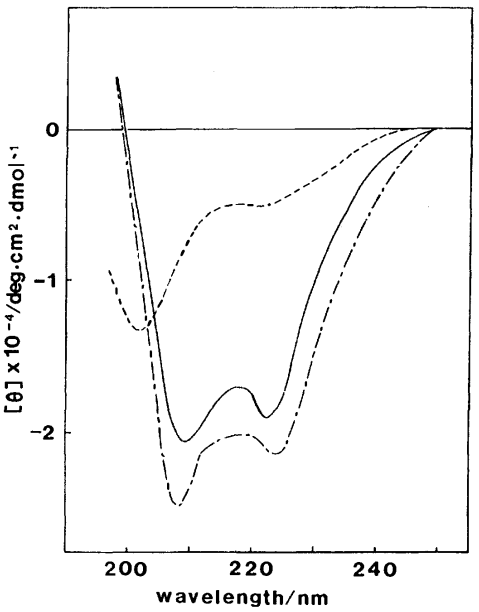

Fig. 4. CD spectra of peptide **5** in H_2O (----) and in the presence of DPPC (——) and DPPC-DPPG (3: 1) (-·-·-) liposomes.

Phase-Transition Release. In order to examine further the interaction of the peptides with model

Table 4. α-Helical Content and Effect on Fluorescein Leakage of the Peptides

Peptide	α-Helical content/%				Fluorescein leakage/%[a]	
	H_2O	TFE	DPPC[b]	DPPC-DPPG[b]	DPPC[b]	DPPC-DPPG[b]
1	R[c]	40	40	55	70	100 (85)
2	R[c]	40	37		85	
3	R[c]	40	45		90	
4	R[c]	37	45		90	
5	R[c]	30	55	63	55	100 (75)
6	20	45	58		55	
7	25	45	60		45	
8	25	40	58		60	
9	28	45	60		60	
10	R[c]	45	40	55	60	100 (100)
11	R[c]	35	50	55	85	100 (65)
12	R[c]	30	40	40	50	100 (65)
L-$\mathbf{4}_3$	25		50	40		60
F	R[c]		30	27		100 (70)
$\mathbf{4}_3$	20	40	60	55	100	100 (50)
$\mathbf{4}_4$	30	40	60		100	
GS	—	—	—	—	[80][d]	25
[D-Dpr$^{4,4'}$]GS	—	—	—	—		25
PM	—	—	—	—	[10][d]	20

a) Values are intensities of fluorescence at scanning time of 5 min (see Fig. 5 and Experimental). Concentrations of peptides are 0.2 μg ml^{-1} (0.1 μg ml^{-1} in parentheses). b) In the presence of DPPC or DPPC-DPPG (3:1). c) Disordered structure. d) Concentrations are 1.0 μg ml^{-1}.

membrane and the ability of the peptides to perturb membrane, the effect on phase-transition release of carboxyfluorescein from phospholipid vesicles was measured.[22,23] Profiles of fluorescence leakage from the DPPC vesicles by the action of peptides are shown in Fig. 5. The degrees of the leakage of the dye by the peptides are listed in terms of a relative value in Table 4. The peptides leaked the dye effectively at the phase-transition temperature of DPPC vesicles, but the degree of the leakage was lower as compared with $\mathbf{4}_3$. These results indicate that the peptides taking the α-helical structure in the presence of the phospholipid have the ability to perturb the phospholipid bilayer structure at the liquid-crystalline state of the membrane. The perturbing effect of the peptides on acidic DPPC-DPPG (3:1) vesicles was larger than that on neutral DPPC vesicles, indicating the electrostatic interaction of the cationic peptides with the acidic vesicles. It should be noted that cyclic peptides GS and PM have only the low degree of the leakage in contrast with the α-helical peptides.

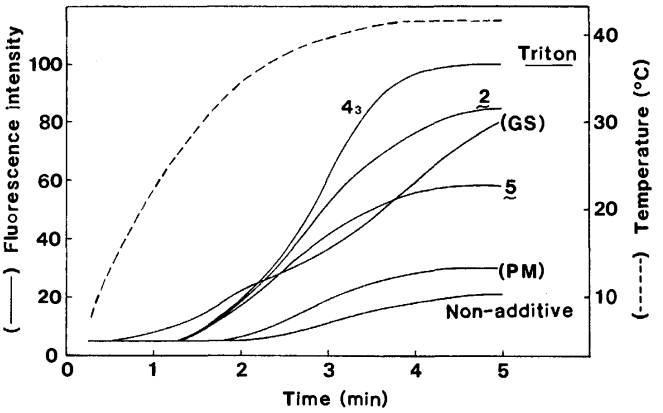

Fig. 5. Profiles of carboxyfluorescein leakage from DPPC vesicles induced by the peptides, GS and PM. Individual peptides were incubated in 2 ml of 0.1 M NaCl/20 mM phosphate buffer (pH 7.4) containing 20 μM DPPC vesicles at temperatures from 0 to 42°C for the indicated scanning time. Peptide concentration: peptide $\mathbf{4}_3$, **2**, and **5** (0.2 μg ml^{-1}); GS and PM (1.0 μg ml^{-1}).

Discussion

Previously,[12] we proposed that α-helical amphiphilicity of the whole peptide molecule, i.e., appropriate positioning of cationic and hydrophobic groups constructed in the stable α-helical structure as shown in the peptides $\mathbf{4}_3$ and $\mathbf{4}_4$, is a significant factor requisite to perturb the membrane of Gram-positive bacteria and to exhibit antibacterial activity against Gram-positive bacteria. We have postulated[12] that the peptide $\mathbf{4}_3$ takes an amphiphilic α-helix on the surface of the membrane of Gram-positive bacteria and the hydrophilic (cationic) side in the helix interacts with the acidic moiety of phospholipid in the membrane and the hydrophobic surface penetrates into the membrane to reveal the antibiosis. Here, the peptides **1**—**12** showed high ability to take α-helical structure in the presence of model membrane (Fig. 4 and Table 4) and to perturb the membrane (Fig. 5 and Table 4), though the abilities were slightly weaker than those of $\mathbf{4}_3$. Antimicrobial activity of the peptides against Gram-positive bacteria was also weaker than that of peptide $\mathbf{4}_3$ (Table 3). The ability of the peptides

and $\mathbf{4}_3$ to interact with model membrane is parallel to the activity against Gram-positive bacteria.

The increase of one or two Lys residues into $\mathbf{4}_3$ and $\mathbf{4}_4$ leads to the increase in the activity against Gram-negative bacteria, and to the decrease in the activity against Gram-positive bacteria, especially against *S. aureus* (Table 3). Polylysine and cecropins are active against both Gram-positive and -negative bacteria.[7,8,24] Polylysine capable to take a helical structure in the presence of phosphatidylserine[25] revealed antimicrobial activity against Gram-negative bacteria, though it has no amphiphilic character. These results indicate that the amphiphilic character of the peptides is not important for the activity against Gram-negative bacteria, but important for the strong activity against Gram-positive bacteria.

The peptide **11** resembling [D-Dpr$^{4,4'}$]GS has four Lys residues in the hexadecapeptide sequence in which distribution of the Lys residues is different from that of peptide $\mathbf{4}_4$ (Fig. 2) and showed the same activity against Gram-positive bacteria as peptide $\mathbf{4}_4$. In view of the low activity of peptide **12** having four Lys residues, the sequence of peptides $\mathbf{4}_3$ and $\mathbf{4}_4$ and another one of peptide **11** are important for the strong activity. However, peptide **11** did not show the activity against Gram-negative bacteria different from [D-Dpr$^{4,4'}$]GS.[15] It is noteworthy that GS has cyclic β-structure which is more rigid than the α-helical structure.

Peptide **12** was designed for the Lys and Leu residues to arrange straight along the axis of helix (Fig. 2) according to repeating heptad sequences $(a\text{-}b\text{-}c\text{-}d\text{-}e\text{-}f\text{-}g)_n$ in which a and e are hydrophobic, and c and g are hydrophilic residues.[26] This peptide showed the low activity against Gram-positive bacteria. Lau et al.[27] reported that the peptides with repeating heptad sequences were inclined to aggregate by forming double-stranded α-helical coiled-coils. The fact that the ability of the fluorescence leakage of peptide **12** was relatively low (Table 4) suggests the presence of such a self-aggregation which weakens the degree of the interaction of the peptide with bacterial membrane resulting in low activity.

It was surprising that replacement of the Ala residues in peptide $\mathbf{4}_3$ by the Leu residue (L-$\mathbf{4}_3$) resulted in 4 and 8 times decrease in activity against *S. aureus* and *B. subtilis*, respectively. This indicates the significance of the Ala residues in the sequence of $\mathbf{4}_3$. α-Helical content also decreased by substituting Leu for Ala (Table 4). These results suggest that the Ala residues in $\mathbf{4}_3$ contribute to the stabilization of α-helix.

It was found that peptide $\mathbf{4}_3$ with specific structure in which the Lys residues twist along the helix (Fig. 2) showed the strongest activity against Gram-positive bacteria, the highest helicity in the presence of liposomes and ability to leak the dye from phospholipid vesicles among the peptides examined.

Experimental

Synthesis of Peptides. TLC was carried out on Merck silica gel G with the following solvent systems: R_f^1, $CHCl_3$-MeOH (5:1); R_f^2, *n*-BuOH-pyridine-AcOH-H_2O (4:1:1:2). Paper electrophoresis was performed on a Toyo Roshi No. 52 paper with the solvent system of HCOOH-AcOH-MeOH-H_2O (1:3:6:10, v/v, pH 1.8) for 3 h at 600 V, the mobility of the peptides being given relative to Lys (R_{Lys}). Optical rotations were measured with a Union high sensitivity polarimeter PM-71. Amino acid analyses were performed on a Hitachi KLA-5 amino acid analyzer after the hydrolysis in 6 M HCl (1 M=1 mol dm^{-3}) in sealed tubes at 110 °C for 24 h.

Representative procedures are described here, and yields and physical constants are summarized in Tables 1 and 2.

Boc-Ala-Lys(Z)-OPac (14). To a mixed anhydride prepared from Boc-Ala-OH (1.52 g, 8.0 mmol), isobutyl chloroformate (1.04 ml, 8.0 mmol) and Et_3N (1.12 ml, 8.0 mmol) in THF (20 ml) was added a solution of H-Lys(Z)-OPac (3.48 g, 8.0 ml) and Et_3N (1.12 ml) in $CHCl_3$ (20 ml) at −10 °C. The mixture was stirred at room temperature for 4 h and evaporated in vacuo. The residue was dissolved in EtOAc, and the solution was washed with 10% citric acid, 4% $NaHCO_3$ and water, and dried over Na_2SO_4. After evaporation, the residue was recrystallized from EtOAc-ether-petroleum ether.

Boc-Ala-Leu-NHCH$_3$ (17). To a chilled solution of H-Leu-NHCH$_3$·HCl (3.05 g, 17 mmol) and Et_3N (2.38 ml, 17 mmol) in DMF (20 ml) was added Boc-Ala-ONSu (4.86 g, 17 mmol). The mixture was stirred at room temperature for 6 h. After evaporation, the residue was dissolved in EtOAc, and washed with 10% citric acid, 4% $NaHCO_3$ and water, and dried over Na_2SO_4. After removal of the solvent, the residue was recrystallized from EtOAc-petroleum ether.

Deprotection of Boc Group in Boc-Ala-Lys(Z)-OPac (14). Compound **14** (5.7 g, 10 mmol) was dissolved in 4 M HCl in dioxane (25 ml) at room temperature for 2 h or in TFA (10 ml) at 0 °C for 30 min. After evaporation, the residue was crystallized by the addition of ether. This was used for the next step without further purification.

Boc-Leu-Ala-Ala-Lys(Z)-OH (41). To a solution of Boc-Leu-Ala-Ala-Lys(Z)-OPac (**32**) (640 mg, 0.85 mmol) in 90% AcOH (10 ml) was added Zn powder (0.6 g) at room temperature. The mixture was stirred at room temperature for 6 h. After filtration, the filtrate was evaporated. To the residue was added 10% citric acid, and the separated oil was extracted with EtOAc and washed with water, and dried over Na_2SO_4. After evaporation, the residue was recrystallized from EtOAc-ether.

Boc-Leu-Ala-Ala-Lys(Z)-Leu-Ala-Lys(Z)-Leu-OPac (59). To a chilled solution of Boc-Leu-Ala-Ala-Lys(Z)-OH (**41**) (636 mg, 1.0 mmol), TFA·H-Leu-Ala-Lys(Z)-Leu-OPac (810 mg, 1.0 mmol), HOBt (270 mg, 2.0 mmol) and Et_3N (0.14 ml, 1.0 mmol) in DMF (10 ml) was added EDC·HCl (288 mg, 1.5 mmol). The mixture was stirred at 0 °C overnight. After evaporation, the residue was solidified by the addition of water. The solid was collected and washed 10% citric acid, 4% $NaHCO_3$ and water, and dried in vacuo.

Ac-Leu-Ala-Lys(Z)-Lys(Z)-Leu-Ala-Lys(Z)-Leu-Leu-Lys(Z)-Lys(Z)-Leu-NHCH$_3$ (93). Boc group in Boc-dodecapeptide-NHCH$_3$ (**79**) (450 mg, 0.21 mmol) was deprotected with TFA (3 ml) at 0 °C for 40 min. To a solution of the TFA salt (430

mg, 0.2 mmol) and Et_3N (0.028 ml, 0.2 mmol) in the mixture of DMF (5 ml) and DMSO (5 ml) was added Ac-ONSu (63 mg, 0.4 mmol) at room temperature. The mixture was stirred at room temperature for 1 d. After removal of the solvent, the residue was solidified by the addition of water. The solid was collected and washed with water, and dried in vacuo.

Ac-Leu-Ala-Lys-Lys-Leu-Ala-Lys-Leu-Leu-Lys-Lys-Leu-$NHCH_3$·5AcOH (1·5AcOH). Compound **93** (300 mg, 0.14 mmol) was dissolved in 25% HBr in AcOH (8 ml) at room temperature. The solution was allowed to stand at room temperature for 4 h. After evaporation, the residue was solidified by the addition of ether and decantated several times with ether. The HBr salt was dissolved in water (5 ml) and passed through a column (0.9×10 cm) of Amberlite IR-45 (AcO^- form), and eluted with water. The fraction was lyophilyzed to give a white powder.

Antimicrobial Assay. Agar dilution method.[19] The minimum inhibitory concentration (MIC) was determined by the standard agar dilution method using Trypticase soy agar. About 5 μl of bacterial suspension containing about 10^7 colony forming units ml^{-1} was inoculated with a multiple inoculator onto agar plates containing twofold serial dilution of each antibiotic. The plates were incubated at 37 °C for 18 h, and the MIC was defined as the lowest concentration of the peptide on which there was either no visible growth or less than four colonies per spot.

Serial dilution method in solution medium.[20] The cell suspension was diluted with the medium to 2×10^6 cells ml^{-1}. Various concentrations of the peptide solution were placed in the test tubes, made up to 1 ml with medium, and the cell suspension (1 ml) was added. After incubation at 30 °C for 17 h, distilled water (1 ml) was added, and the absorbance at 620 nm was measured.

Results of both assays are shown in terms of MIC in Table 3.

Preparation of Phospholipid Liposomes. DPPC and DPPG were purchased from Sigma. Phospholipid (37 mg, 50 μmol) was dissolved in chloroform (2 ml) and dried by breathing of nitrogen in a conical glass tube. The dried lipid was hydrated in 3 ml of 20 mM Tris·HCl buffer (pH 7.4) with repeated vortexed-mixing at 50 °C for 30 min. The suspension was sonicated at 50 °C for 60 min using a TOMY SEIKO ultrasonic disruptor model UR-200P and diluted to 50 ml with the same buffer (lipid concentration, 1.0 mM). The mixture of uni- and multilamellar vesicles was used for the CD measurement without further purification. When the unilamellar vesicles trapping carboxyfluorescein were prepared, the same method as described above was used except that the dried lipid (27 μmol) was hydrated in 2.0 ml of 0.1 M NaCl/20 mM phosphate buffer (pH 7.4) containing 100 mM carboxyfluorescein. The mixture of uni- and multilamellar vesicles trapping carboxyfluorescein was subjected to gel-filtration through a Sephadex 4B column (1×20 cm) in 0.1 M NaCl/20 mM phosphate buffer (pH 7.4). The separated small unilamellar vesicles were utilized in phase-transition release measurements.

CD Measurements. CD spectra were recorded on a JASCO J-40A spectropolarimeter with a JASCO data processor Model J-DPY using quartz cell of 1 mm pathlength. Spectra in water and 2,2,2-trifluoroethanol were measured at a peptide concentration of 100 μM. Spectra in the presence of phospholipid liposomes were measured at a peptide concentration of 10 μM in 20 mM Tris·HCl buffer (pH 7.4) solution containing 0.9 mM vesicles. All the measurements were carried out at 20 °C. The CD data were expressed as mean residue ellipticities as shown in Fig. 3.

Phase-Transition Release. The phase-transition release experiment was carried out according to the procedure of Utsumi et al.[22] Phospholipid vesicles, the peptides and 0.1 M NaCl/20 mM phosphate buffer (pH 7.4) were individually pre-chilled on ice. To 2 ml of phosphate buffer in the cuvette on ice was added 50 μl of the vesicles containing 100 mM carboxyfluorescein to give a final concentration of 20 μM lipid. To the mixture was added 20 μl of an appropriate dilution of the peptide in phosphate buffer. The cuvette was placed in the heated (42 °C) cuvette holder of the fluorometer, and both the fluorescence intensity and the temperature were continuously recorded. For determination of the fluorescence intensity derived from 100% dye-release, 10 μl of Triton X-100 solution (20% in phosphate buffer) was added to dissolve the vesicles. The percentage of dye-release caused by the peptide was evaluated by equation, $100\ (F-F_o)/(F_t-F_o)$, where F is the fluorescence intensity achieved by the peptides, F_o and F_t are intensities of post-transition fluorescence without the peptides and post-Triton X-100 treatment, respectively. Results are shown in Fig. 5 and Table 4.

We thank Prof. Hiroshi Nishikawa of Fukuoka University for CD measurement, and Prof. Nobuyuki Yamasaki of Kyushu University for phase-transition release experiment. We also thank Dr. Hiroo Yonezawa of Kagoshima University and the staff of Takeda Chemical Ind. Ltd. for the microbial assay.

References

1) R. W. Mahley, T. L. Innerarity, S. C. Rall, Jr., and K. H. Weisgraber, *J. Lipid Research*, **25**, 1277 (1984).
2) S. Yokoyama, *Seikagaku*, **58**, 153 (1986).
3) M. Comte, Y. Maulet, and J. A. Cox, *Biochem. J.*, **209**, 269 (1983).
4) D. A. Malencik and S. Anderson, *Biochem. Biophys. Res. Commun.*, **114**, 50 (1983).
5) W. F. DeGrado, F.J. Kézdy, and E. T. Kaiser, *J. Am. Chem. Soc.*, **103**, 679 (1981).
6) T. Higashijima, K. Wakamatsu, M. Takemitsu, M. Fujino, T. Nakajima, and T. Miyazawa, *FEBS Lett.*, **152**, 227 (1983).
7) H. Steiner, D. Hultmark, Å. Engström, H. Bennich, and H. G. Boman, *Nature*, **292**, 246 (1981).
8) H. Steiner, *FEBS Lett.*, **137**, 283 (1982).
9) M. Okada and S. Natori, *J. Biol. Chem.*, **260**, 7174 (1985).
10) T. Teshima, Y. Ueki, T. Nakai, T. Shiba, and M. Kikuchi, *Tetrahedron*, **42**, 829 (1986).
11) A. Ito, T. Ogishima, W. Ou, T. Omura, H. Aoyagi, S. Lee, H. Mihara, and N. Izumiya, *J. Biochem.*, **98**, 1571 (1985).
12) S. Lee, H. Mihara, H. Aoyagi, T. Kato, N. Izumiya, and N. Yamasaki, *Biochim. Biophys. Acta*, **862**, 211 (1986).
13) W. F. DeGrado, "Peptides: Structure and Function," ed. by V. J. Hruby and D. H. Rich, Pierce Chemical Co., Rockford, Illinois (1983), pp. 195—198.
14) Abbreviations used are according to IUPAC-IUB Commissions, *Eur. J. Biochem.*, **138**, 9 (1984). Other abbre-

viations: DPPC, dipalmitoyl-DL-α-phosphatidylcholine; DPPG, dipalmitoyl-DL-α-phosphatidylglycerol; Dpr, 2,3-diaminopropionic acid; EDC, 1-ethyl-3-(3-dimethylaminopropyl)carbodiimide; Fmoc, 9-fluorenylmethyloxycarbonyl; GS, gramicidin S; HOBt, 1-hydroxybenzotriazole; -ONSu, succinimidooxy; Pac, phenacyl; PM, polymyxin B; TFA, trifluoroacetic acid.

15) S. Ando, H. Aoyagi, S. Shinagawa, N. Nishino, M. Waki, T. Kato, and N. Izumiya, *FEBS Lett.*, **161**, 89 (1983).

16) G. W. Anderson, J. E. Zimmerman, and F. M. Callahan, *J. Am. Chem. Soc.*, **86**, 1839 (1964).

17) J. R. Vaugham, Jr. and R. L. Osato, *J. Am. Chem. Soc.*, **88**, 1338 (1966).

18) W. König and R. Geiger, *Chem. Ber.*, **103**, 788 (1970).

19) K. Okonogi, M. Kuno, and E. Higashide, *J. General Microbial.*, **132**, 143 (1986).

20) H. Yonezawa, M. Kaneda, N. Tominaga, S. Higashi, and N. Izumiya, *J. Biochem.*, **90**, 1087 (1981).

21) Y. -H. Chen, J. T. Yang, and K. H. Chan, *Biochemistry*, **13**, 3350 (1974).

22) T. Utsumi, Y. Aizono, and G. Funatsu, *Biochim. Biophys. Acta*, **772**, 202 (1984).

23) J. N. Weinstein, R. D. Klausner, T. Innerarity, E. Ralston, and R. Blumenthal, *Biochim. Biophys. Acta*, **647**, 270 (1981).

24) S. Shima, H. Matsuoka, T. Iwamoto, and H. Sakai, *J. Antibiot.*, **37**, 1449 (1984).

25) G. G. Hammes and S. E. Shullery, *Biochemistry*, **9**, 2555 (1970).

26) J. Sodek, R. S. Hodges, L. B. Smillie, and L. Jurasek, *Proc. Natl. Acad. Sci. U.S.A.*, **69**, 3800 (1972).

27) S. Y. M. Lau, A. K. Taneja, and R. S. Hodges, *J. Biol. Chem.*, **259**, 13253 (1984).

 © 1987 The Chemical Society of Japan Bull. Chem. Soc. Jpn., 60, 707—711 (1987)

Synthesis of 2,6-Dimethyl-6-(8-methyl-4-methylene-7-nonenyl)-2-cyclohexene-1-methanols from α-Santonin[1)]

Hajime NAGANO,* Yukari MASUNAGA (née ISHIKAWA), Yukiko MATSUO, and Michio SHIOTA
Department of Chemistry, Faculty of Science, Ochanomizu University, Otsuka, Bunkyo-ku, Tokyo 112
(Received August 13, 1986)

α-Santonin was converted to 2,6-dimethyl-6-(8-methyl-4-methylene-7-nonenyl)-2-cyclohexene-1-methanols (**1a** and **1b**). Both spectral data of **1a** and **1b** were found to be different from those reported for magydar-2,10(20),13-trien-17-ol, a diterpene isolated from *Magydaris panacifolia* (Vahl) Lange. This indicates that the structure of the natural diterpene should be revised; the structure was later revised to *t*-6-hydroxymethyl-1, *t*-3-dimethyl-*t*-2-(3-methyl-2-butenyl)-3-(4-methyl-3-pentenyl)-*r*-1-cyclohexanol.

In 1978 J. de Pascual Teresa and co-workers reported the isolation and the structural elucidation of three new diterpenes, magydar-2,10(20),13-trien-17-ol(I), its acetate(II), and magydar-2,13-diene-10,17-diol(III), from *Magydaris panacifolia* (Vahl) Lange (Umbelliferae).[2)] The stereochemistry of these diterpenes with a novel carbon skeleton was however left undetermined. With the object of determining the stereochemistry of these diterpenes including the absolute configuration we synthesized a pair of diastereomers of 2,6-dimethyl-6-(8-methyl-4-methylene-7-nonenyl)-2-cyclohexene-1-methanols, (**1a**) and (**1b**), namely the two possible stereoisomers for the structure of magydar-2,10(20), 13-trien-17-ol (I) or its enantiomer.

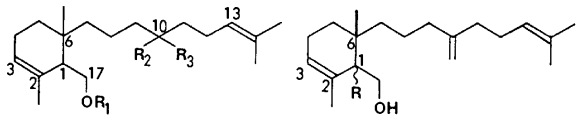

I R_1 = H R_2, R_3 = CH_2
II R_1 = $COCH_3$ R_2, R_3 = CH_2
III R_1 = H R_2 = OH, R_3 = CH_3

1a α-H
1b β-H

In this work we chose α-santonin (**2**), easily available sesquiterpene, as the starting material and converted it into **1a** and **1b** via 6,7-secoeudesmane derivatives. Following the known procedures α-santonin (**2**) was transformed into 5α*H*- (**3a**)[3)] and 5β*H*-eudesmanolide (**3b**),[4)] which have the cyclohexene ring moiety in the diterpene.

In order to convert **3a** into a 6,7-seco derivative functionalization at C-7 was first carried out. Hydroxylation of the enolate of 5α*H*-eudesmanolide (**3a**) with MoO_5·pyridine·HMPT complex[5)] gave the hydroxy lactone **4a**[6)] in 58% yield. The configuration of the hydroxyl group at C-11 was assigned to be β on the basis of the precedents[7)] similar to this case. Reduction of **4a** with lithium aluminium hydride (LAH) in tetrahydrofuran (THF) under reflux afforded the triol **5a** in quantitative yield. Oxidative cleavage of the triol **5a** with sodium periodate in aqueous THF gave the β-hydroxy ketone **6a** in 98% yield. 5β*H*-Eudesmanolide (**3b**) was also converted similarly into the β-hydroxy ketone **6b** in 55% overall yield.

Althogh the Beckmann rearrangement of *O*-mesitylsulfonyloxime **7a**, which was prepared from **6a** and *O*-mesitylsulfonylhydroxylamine, was first attempted using basic alumina (Merck, activity I),[8)] the desired amide **8a** was obtained only in 35% yield together with a less polar product. The latter was assumed to be the oxazoline derivative **9** (27% yield) from its spectral data (ν_{max}. 1643 cm^{-1} (C=N); δ=1.98 (d, *J*=1.5 Hz, Me), 3.17 (m, 7α-H), and 3.26 (dd like, *J*=13 and 11 Hz, 6β-H).[9)] However, treatment of the oximes, **7a** and **7b**, with activated alumina (Wako) gave the amides, **8a** and **8b**, in 80 and 63% yields, respectively.

The hydroxy amides, **8a** and **8b**, were then reduced with LAH to afford hydroxy amines, **10a** (90% yield) and **10b** (88% yield), respectively. Oxidative cleavage of **10a** and **10b** with sodium periodate in aqueous THF followed by reduction with sodium borohydride gave the 6,7-seco derivatives, **11a** (62% yield) and **11b** (74% yield), respectively.

Completion of the side chain transformation was brought as follows. The diol **11a** was transformed into the monoiodide **13a** via the monotosylate **12a** in 46% overall yield. After tetrahydropyranylation of **13a**, the resulting iodide **14a** was treated with 2-lithio-1,3-dithiane at 0 °C to give the dithiane **15a** in 73% yield. The carbanion generated from **15a** with butyllithium was then treated with 4-methyl-3-pentenyl iodide[10)] to give compound **16a** in 60% yield.[11)] Hydrolysis of **16a** with copper(II) chloride-copper(II) oxide in acetone[12)] gave the hydroxy ketone **17a** in 40% yield. Finally the Wittig reaction of **17a** with methylenetriphenylphosphorane ($Ph_3P=CH_2$) afforded **1a** in ca. 30% yield. The ^1H NMR spectral data of **1a** were found to differ from those reported for the diterpene (I) (see Table).

The diol **11b** was converted similarly to the monoiodide **14b** in 26% overall yield. Treatment of **14b** with 2-lithio-2-(4-methyl-3-pentenyl)-1,3 dithiane gave compound **16b** in 52% yield.[11)] Hydrolysis of **16b** gave the hydroxy ketone **17b** in 40% yield.[12)] The Wittig reaction of **17b** with $Ph_3P=CH_2$ gave **1b** in 30% yield. The ^1H NMR spectral data of **1a** were obviously different from those reported for magydar-2,10(20),13-trien-17-ol (I) (see Table).

Since the two stereoisomers, **1a** and **1b**, are found to

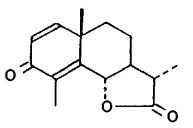

2

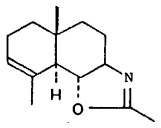

9

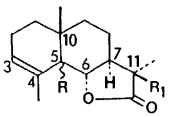

3a, 3b R_1 = H
4a, 4b R_1 = OH

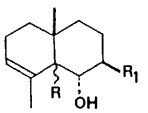

5a, 5b R_1 = C(OH)(Me)CH_2OH
6a, 6b R_1 = COMe
7a, 7b R_1 = C(Me)=$NOSO_2Mst$
8a, 8b R_1 = NHCOMe
10a, 10b R_1 = NHEt

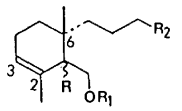

11a, 11b R_1 = H R_2 = OH
12a, 12b R_1 = H R_2 = OTs
13a, 13b R_1 = H R_2 = I
14a, 14b R_1 = THP R_2 = I
15a R_1 = THP R_2 =
16a, 16b R_1 = THP
R_2 =
17a, 17b R_1 = H
R_2 =

3a - 8a, 10a - 17a R = α-H
3b - 8b 10b - 14b, 16b, 17b R = β-H

Table 1. ^{1}H NMR Spectral Data ($CDCl_3$, δ values)

Compounds	6-Me	C=C-Me	CH_2OH	$C=CH_2$	$CH=C(Me)_2$	3-H
I	0.71(s)	1.53(s, 6H), 1.63(s, 3H)	3.65 (ABdq)	4.76(s), 4.62(s)	5.03(m)	5.03(m)
1a	0.99(s)	1.60(s), 1.69(s), 1.74(d, J=1.5 Hz)	3.73(m)	4.70(s)	5.11(m)	5.61(m)
1b	0.85(s)	1.62(s), 1.70(s), 1.74(s)	3.73(m)	4.72(s)	5.16(m)	5.62(m)

differ from magydar-2,10(20),13-trien-17-ol, the structure of the natural diterpene should be revised.

We therefore reinvestigated the structure of magydar-2,13-diene-10,17-diol (II) and established the structure of the diterpene, renamed magydardienediol, to be *t*-6-hydroxymethyl-1,*t*-3-dimethyl-*t*-2-(3-methyl-2-butenyl)-3-(4-methyl-3-pentenyl)-*r*-1-cyclohexanol (**18**) on the basis of the detailed analysis of its 400 MHz ^{1}H NMR spectrum.[13] The structure of the diterpene was also elucidated by J. de Pascual Teresa and co-workers. They proposed the structure **18** including the absolute configuration (1*S*, 2*R*, 3*S*, 6*R*).[14]

M. Bruno et al. have recently reported the isolation and the structure elucidation of a diterpene of *Bonannia graeca* (L.) Halacsy (Umbelliferae).[15] The diterpene, named bonandiol, is identical with magydardienediol (**18**).

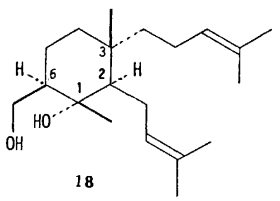

18

Experimental

Melting points were determined on a hot block melting point apparatus and are uncorrected. ^{1}H NMR spectra of all the compounds except for **1a** and **1b** were recorded on a JEOL C-60 (60 MHz) spectrometer and those of **1a** and **1b**

were recorded on a JEOL FX-90Q spectrometer. Chloroform-*d* and tetramethylsilane were used as solvent and internal standard, respectively. IR spectra were taken on a JASCO A-3 spectrometer. Mass spectra were obtained on JEOL DX-300, Hitachi 50-GC, or Hitachi M80-A mass spectrometer using electron impact (70 ev) mode. Optical rotations were determined on a JASCO DIP-181 polarimeter. Pre-coated Merck Kieselgel 60 F_{254} was used for general analytical purposes and silica gel (Wakogel C-200) was used for column chromatography.

Hydroxylation of 3a. To a solution of lithium diisopropylamide, prepared from diisopropylamine (1.5 ml) and butyllithium (1.7 mol dm^{-3} hexane solution, 6.5 ml) in THF (6 ml) under a nitrogen atmosphere, was added a solution of **3a** (2.17 g) in dry tetrahydrofuran (18 ml) at −78 °C. The reaction mixture was stirred for 1 h at this temperature. To the solution was then added Mo_5 · pyridine · HMPT complex (6.0 g) in one portion. The suspension was stirred for 2 h at −78 °C and then warmed to room temperature. Usual work-up gave a yellow residue, which was chromatographed on silica gel (30 g; eluant: hexane–ethyl acetate 10 : 1 v/v) to give 11β-hydroxy-5αH-eudesmanolide (**4a**) (1.36 g) in 58% yield. Recrystallization of the product from diethyl ether gave colorless needles; mp 185.0—186.5 °C; $[\alpha]_D^{34}$ +132°(*c* 0.33, $CHCl_3$); IR (KBr): 3470 and 1755 cm^{-1}; ^1H NMR δ=0.92 (3H, s, 10-Me), 1.44 (3H, s, 11-Me), 1.81 (3H, m, 4-Me), 4.37 (1H, dd, *J*=12 and 9 Hz, 6-H), and 5.37 (1H, m, 3-H); MS: *m/z* 250 (rel intensity 9%, M^+) and 43 (100). Found: *m/z* 250.1555. Calcd for $C_{15}H_{22}O_3$: M, 250.1569.

5βH-Eudesmanolide (**3b**) was similarly hydroxylated to give **4b** in 75% yield. **4b**: colorless needles; mp 131.0—132.5 °C (from diethyl ether); $[\alpha]_D^{34}$ 0° (*c* 0.45, $CHCl_3$); IR: 3430 and 1755 cm^{-1}; ^1H NMR δ=1.11 (3H, s, 10-Me), 1.42 (3H, s, 11-Me), 1.64 (3H, m, 4-Me), 4.73 (1H, dd, *J*=10.5 and 4.5 Hz, 6-H), and 5.45 (1H, broad(br) s, 3-H); MS: *m/z* 250 (4%), 109 (100), and 43 (100). Found: *m/z* 250.1594.

Reduction of 4a with Lithium Aluminium Hydride. To a suspension of lithium aluminium hydride (280 mg) in dry THF (10 ml) was added a solution of **4a** in dry THF (20 ml). The reaction mixture was heated at reflux temperature under a nitrogen atmosphere for 4 h. After work-up as usual the crude product was chromatographed on silica gel (40 g; diethyl ether) to give the triol **5a** (885 mg) together with the partially reduced hemiacetal (545 mg). The hemiacetal was again reduced to **5a** in quantitative yield. **5a**: Colorless viscous oil; $[\alpha]_D^{34}$ +59° (*c* 0.91, $CHCl_3$); IR (neat): 3350 cm^{-1}; ^1H NMR δ=0.76 (3H, s, 10-Me), 1.18 (3H, s, 11-Me), 1.90 (3H, br s, 4-Me), 3.37 (1H, A part of an AB-type quartet, *J*=(−)12 Hz, 12-H), 3.53 (1H, B part of an AB-type quartet, *J*=(−)12 Hz, 12-H), 3.92 (1H, t, *J*=10 Hz, 6-H), and 5.36 (1H, m, 3-H); MS: *m/z* 254 (1%, M^+), 236 (4, M^+-H_2O) 218 (21, M^+-2H_2O), and 43 (100); Found: *m/z* 236.1707. (Calcd for $C_{15}H_{24}O_2$, *m/z* 236.1775).

The hydroxy lactone **4b** was also reduced with lithium aluminium hydride to give the triol **5b** in 75% yield. **5b**: Colorless needles; mp 129.0—129.5 °C (from hexane–diethyl ether); $[\alpha]_D^{34}$ −44° (*c* 0.5, $CHCl_3$); IR (KBr): 3300 cm^{-1}; ^1H NMR δ=0.93 (3H, s, 10-Me), 1.14 (3H, s, 11-Me), 1.80 (3H, br s, 4-Me), 2.60 (3H, br s, OH), 3.37 (1H, A part of an AB-type quartet, *J*=(−)10.5 Hz, 12-H), 3.47 (1H, B part of an AB-type quartet, *J*=(−)10.5 Hz, 12-H), 4.25 (1H, m, 6-H), and 5.55 (1H, m, 3-H); MS: *m/z* 254 (0.1%), 236 (14), 218 (62), and 109 (100).

Oxidative Cleavage of 5a with Sodium Periodate. To a solution of **5a** (615 mg) in THF (30 ml)–H_2O (10 ml) was added dropwise a solution of sodium periodate (623 mg) in water (5 ml). The reaction mixture was stirred for 1.2 h at room temperature. After work-up as usual the crude product was chromatographed (3 g; hexane–ethyl acetate 1 : 1) to give the hydroxy ketone **6a** (527 mg, 98% yield); colorless needles; mp 66.0—67.0 °C (from hexane); $[\alpha]_D^{34}$ +35° (*c* 0.34, $CHCl_3$); IR (KBr): 3420 and 1708 cm^{-1}; ^1H NMR δ=0.82 (3H, s, 10-Me), 1.88 (3H, br s, 4-Me), 2.18 (3H, s, COMe), 4.00 (1H, t, *J*=ca. 10 Hz, 6-H), and 5.35 (1H, m, 3-H); MS: *m/z* 222 (9%, M^+), 204 (10, M^+-H_2O), 189 (15, M^+-H_2O–Me), 161 (62, M^+-H_2O–MeCO), and 43 (100). Found: *m/z* 222.1622. Calcd for $C_{14}H_{22}O_2$: M, 222.1620.

The triol **5b** (201 mg) was also oxidized with sodium periodate (190 mg) to yield the hydroxy ketone **6b** in 98% yield. **5b**: Colorless oil; IR (neat): 3550 and 1710 cm^{-1}; ^1H NMR δ=0.80 (3H, s, 10-Me), 1.74 (3H, d, *J*=1.5 Hz, 4-Me), 2.18 (3H, s, COMe), 2.85 (1H, m, 7-H), 4.20 (1H, t, *J*=3.5 Hz, 6-H), and 5.65 (1H, m, 3-H); MS: *m/z* 222 (0.9%), 204 (68), 189 (30), 161 (100), and 145 (57); Found: *m/z* 204.1542. (Calcd for $C_{14}H_{20}O$, *m/z* 204.1515).

Beckmann Rearrangement of 6a. To a solution of **6a** (485 mg) in dichloromethane (15 ml), stirred at 0 °C, was added *O*-mesitylsulfonylhydroxylamine (813 mg) and the solution was stirred for 30 min at room temperature. The reaction mixture was absorbed on a column of activated alumina (Wako, for column chromatography, 50 g) and allowed to stand for 2 h. The eluate from methanol (200 ml) was evaporated under reduced pressure. Ethyl acetate was added and the resulting suspension was put on a column of silica gel (20 g). Elution with ethyl acetate gave the hydroxy amide **8a** (402 mg, 80% yield). The formation of **9** was not detected. **8a**: Mp 125.0—127.0 °C (from acetone); IR (KBr): 3400, 3330, 1655, and 1545 cm^{-1}; ^1H NMR δ=0.82 (3H, s, 10-Me), 1.78 (3H, br s, 4-Me), 2.01 (3H, s, COMe), 3.0—3.8 (3H, OH, 6-H, and 7-H), 5.34 (1H, m, 3-H), and 6.00 (1H, br s, NH); MS: *m/z* 237 (33%, M), 219 (100, M^+-H_2O), 178 (52), 163 (52), 145 (69), 109 (85). Found: *m/z* 237.1722. Calcd for $C_{14}H_{23}NO_2$: M, 237.1727.

The Beckmann rearrangement of the hydroxy ketone **6b** was similarly performed to yield the hydroxy amide **8b** in 63% yield. The formation of the corresponding oxazoline derivative was not detected. **8b**: Colorless oil; IR (neat): 3320, 1745, 1645, and 1545 cm^{-1}; ^1H NMR δ=0.87 (3H, s, 10-Me), 1.70 (3H, d, *J*=ca. 1 Hz, 4-Me), 2.02 (3H, s, COMe), 3.83 (1H, t, *J*=3.5 Hz, 6-H), 4.23 (1H, m, 7-H), 5.70 (1H, m, 3-H), and 6.00 (1H, br s, NH); MS: *m/z* 237 (0.3%), 219 (6), and 83 (100). Found: *m/z* 237.1797.

The Beckmann rearrangement of **6a** (59 mg) using basic alumina (Merck, activity I, 3 g) gave **8a** (22 mg) together with **9** (16 mg). **9**: Colorless oil; IR (neat): 1643 cm^{-1}; ^1H NMR δ=0.88 (3H, s, 10-Me), 1.78 (3H, m, 4-Me), 1.98 (3H, d, *J*=1.5 Hz, Me), 3.17 (1H, m, 7-H), 3.26 (1H, dd like, *J*=13 and 11 Hz, 6-H), and 5.33 (1H, m, 3-H).

Reduction of 8a with Lithium Aluminium Hydride. A mixture of **8a** (390 mg) and lithium aluminium hydride (470 mg) in dry diethyl ether (30 ml) was heated at reflux temperature for 3 h under a nitrogen atmosphere. Usual work-up gave the hydroxy amine **10a** (90% yield), which was recrystallized to give colorless needles; mp 64.0—65.0 °C; IR (KBr): 3400 cm^{-1}; ^1H NMR δ=0.82 (3H, s, 10-Me), 1.07 (3H, t, *J*=7 Hz, $CH_2C\underline{H}_3$), 1.88 (3H, br s, 4-Me), 2.3—2.9 (3H, m, 7-H and

$C\underline{H}_2CH_3$), 3.24 (1H, dd, J=10 and 8 Hz, 6-H), and 5.31 (1H, br s, 3-H); MS: m/z 223 (2%, M^+), 205 (18, M^+-H_2O), and 84 (100). Found: m/z 223.1910. Calcd for $C_{14}H_{23}NO$: M, 223.1935.

The amide **8b** (93 mg) was similarly reduced with lithium aluminium hydride (177 mg) to yield the hydroxy amine **10b** in 88% yield. Although the product solidified in a refrigerator, its recrystallization was not successful. **10b**: IR (neat): 3400 cm^{-1}; ^1H NMR δ=0.85 (3H, s, 10-Me), 1.12 (3H, t, J=7 Hz, $CH_2C\underline{H}_3$), 1.67 (2H, br s, OH and NH), 1.72 (3H, d, J=1.5 Hz, 4-Me), 2.69 (2H, q, J=7 Hz, $C\underline{H}_2CH_3$), 2.95 (1H, q, J=3 Hz, 7-H), 3.77 (1H, t, J=ca. 3 Hz, 6-H), and 5.68 (1H, br s, 3-H); MS: m/z 223 (M^+).

Conversion of 10a to 11a. To a solution of **10a** (238 mg) in THF (6 ml), stirred at 0 °C, was added a solution of sodium periodate (516 mg) in water (6 ml). The solution was stirred at this temperature for 1 h under a nitrogen atmosphere. A solution of sodium borohydride (371 mg) in water (5 ml) was then added and the resulting solution was stirred for 45 min. The product was extracted with diethyl ether. The ethereal solution was washed successively with water, dilute hydrochloric acid, 5% aqueous sodium hydrogencarbonate, water, and saturated brine, and dried over anhydrous sodium sulfate. Evaporation of the solvent followed by column chromatography (8 g; hexane-ethyl acetate 1:1) gave the diol **11a** (99 mg) and the hydroxy amine **10a** (58 mg). **11a**: Colorless oil; $[\alpha]_D^{34}$ +97° (c 0.86, $CHCl_3$); IR (neat): 3340 cm^{-1}; ^1H NMR δ=1.00 (3H, s, 6-Me), 1.23 (3H, m, 2-Me), 3.5—3.8 (4H, m, two $C\underline{H}_2OH$), and 5.62 (1H, m, 3-H); MS: m/z 198 (nil, M^+), 180 (3%, M^+-H_2O), and 121 (100, $M^+-H_2O-(CH_2)_3OH$); Found: m/z 180.1448. (Calcd for $C_{12}H_{20}O$: m/z 180.1513).

The hydroxy amine **10b** (70 mg) was similarly transformed into the diol **11b** (46 mg; 74% overall yield), colorless oil; IR (neat): 3350 cm^{-1}; ^1H NMR δ=0.85 (3H, s, 6-Me), 1.73 (3H, d, J=1.5 Hz, 2-Me), 2.27 (2H, br s, OH), 3.65 (4H, m, two $C\underline{H}_2OH$), and 5.55 (1H, m, 3-H).

Conversion of 11a to 14a. A solution of **11a** (33 mg) and p-toluenesulfonyl chloride (39 mg) in pyridine (1 ml) was allowed to stand overnight at 4 °C. Then dilute hydrochloric acid was added and the product was extracted with diethyl ether. The crude product (60 mg), containing the monotosylates, the ditosylate, and **11a**, was dissolved in acetone (4 ml). To the solution was added a solution of sodium iodide (34 mg) in acetone (1 ml) and reaction mixture was heated under reflux for 2.2 h. After evaporation of the solvent the residue was chromatographed to yield the monoiodide **13a** (18 mg; 46% yield). The diol **11a** (8.6 mg) was recovered. **13a**: Colorless oil; IR (neat): 3400 cm^{-1}; ^1H NMR δ=1.00 (3H, s, 6-Me), 1.75 (3H, m, 2-Me), 3.13 (2H, t, J=7 Hz, CH_2I), 3.72 (2H, d, J=3 Hz, $C\underline{H}_2OH$), and 5.60 (1H, m, 3-H); MS: m/z 308 (4%, M^+), 290 (8, M^+-H_2O), 277 (51, M^+-CH_2OH), 121 (64), 93 (94), and 81 (100). Found: m/z 308.0541. Calcd for $C_{12}H_{21}IO$: M, 308.0638.

A solution of **13a** (56 mg) and freshly distilled dihydropyran (6 mg) in dry THF (3 ml) was stirred in the presence of a catalytic amount of p-toluenesulfonic acid. Purification of the product using a column of Florisil (10 g; hexane-diethyl ether 80:3) gave **14a** in 82% yield. **14a**: Colorless oil; ^1H NMR δ=0.93 (3H, s, 6-Me), 1.73 (3H, br s, 2-Me), 3.11 (2H, t, J=7 Hz, CH_2I), 3.2—4.0 (4H, m, CH_2OCH_2), 4.52 (1H, m, O-CH-O), and 5.40 (1H, m, 3-H).

Tosylation of the diol **11b** (39 mg) with p-toluenesulfonyl chloride (38 mg) in pyridine (0.5 ml) gave the monotosylate **12b** (22 mg; 31% yield), which was then converted to the monoiodide in quantitative yield. **13b**: Colorless oil; IR (neat): 3420 cm^{-1}; ^1H NMR δ=0.86 (3H, s, 6-Me), 1.75 (3H, br s, 2-Me), 3.19 (2H, t, J=6.5 Hz, CH_2I), 3.72 (2H, d, J=3.5 Hz, $C\underline{H}_2OH$), and 5.61 (1H, m, 3-H). The alcohol **13b** was then treated with dihydropyran in the presence of p-toluenesulfonic acid to give **14b** in 84% yield. **14b**: Colorless oil, MS: m/z 392 (0.1%, M^+), 290 (4), 201 (18), and 85 (100); Found: m/z 290.0501 (Calcd for $C_{12}H_{19}I$: $M^+-C_5H_{10}O_2$, 290.0532).

Treatment of 14a with 2-Lithio-1,3-dithiane. To a solution of **14a** (42 mg; 0.11 mmol) in dry ether (2 ml), stirred at 0 °C, was added a solution of 2-lithio-1,3-dithiane (0.4 mmol) under a nitrogen atmosphere. The crude product was chromatographed on Florisil (4 g; hexane-ether 60:3) to yield the dithiane **15a** (30 mg; 73% yield); colorless oil; ^1H NMR δ=0.94 (3H, s, 6-Me), 2.7—3.0 (4H, m, SCH_2), 3.1—4.2 (6H, m), 4.52 (1H, m, O-CH-O), and 5.39 (1H, m, 3-H); MS: m/z 384 (nil, M^+), 282 (15%, $M^+-C_5H_{10}O_2$), and 85 (100).

4-Methyl-3-pentenylation of 15a. To a solution of **15a** (17 mg; 0.044 mmol) in dry THF (0.8 ml), stirred at −30 °C, was added butyllithium (0.27 mmol) under a nitrogen atmosphere. The solution was stirred for 2 h at this temperature. A solution of 4-methyl-3-pentenyl iodide (57 mg; 0.27 mmol) in dry THF (0.5 ml) was added and the reaction mixture was stirred at 0 °C for 2 h. After work-up as usual, the crude product was passed through a column of Florisil (1 g; hexane-ether 30:1) to yield **16a** (12 mg; 60% yield); colorless oil; ^1H NMR δ=0.95 (3H, s, 6-Me), 1.5—1.8 (9H, m, three olefinic methyls), 2.6—2.9 (4H, m, SCH_2), 3.0—4.1 (4H, m, $C\underline{H}_2O$), 4.55 (1H, m, O-CH-O), 5.10 (1H, m, CH=), and 5.40 (1H, m, 3-H); MS: m/z 466 (0.6%, M), 364 (5, $M^+-C_5H_{10}O_2$), 229 (23), 85 (83), and 71 (100).

Hydrolysis of 16a with Copper(II) Chloride-Copper(II) Oxide. A suspension of **16a** (12 mg) and $CuCl_2\cdot 2H_2O$ (17 mg), and CuO (16 mg) in acetone (4 ml) was heated under reflux for 20 min. The reaction mixture was filtered and the filtrate was evaporated. The residue was chromatographed on silica gel (0.5 g; hexane-ether 10:1) to yield the hydroxy ketone **17a** (3 mg); colorless oil; IR (neat): 3450 and 1710 cm^{-1}; ^1H NMR δ=1.00 (3H, s, 6-Me), 1.5—1.75 (9H, m, three olefinic methyls), 2.34 (4H, m, CH_2COCH_2), 3.72 (2H, d, J=3 Hz, $C\underline{H}_2OH$), 5.05 (1H, m, CH=), and 5.60 (1H, m, 3-H); MS: m/z 292 (nil, M^+), 274 (1.7%, M^+-H_2O), 205 (3), 121 (100), and 69 (82); Found: m/z 205.1676 (Calcd for $C_{14}H_{21}O$: $M^+-H_2O-C_5H_9$, m/z 205.1593).

Treatment of 14b with 2-Lithio-2-(4-methyl-3-pentenyl)-1,3-dithiane. To a solution of 2-lithio-1,3-dithiane (ca. 1 mmol) in dry THF (2.5 ml), stirred at −6 °C under a nitrogen atmosphere, was added a solution of 4-methyl-3-pentenyl iodide (221 mg) in dry THF (0.2 ml). The solution was stirred at 0 °C for 3 h and then cooled to −30 °C. Butyllithium (ca. 1 mmol) was added. A part of the solution (1.5 ml) was added to a solution of **14b** (26 mg) in dry THF (1.5 ml) at −5 °C under a nitrogen atmosphere. The solution was stirred overnight at −5—0 °C. After work-up as usual the crude product was chromatographed on silica gel (2.5 g; hexane-diethyl ether 97:3) to yield the dithiane **16b** (16 mg); colorless oil; MS: m/z 466 (0.6%, M^+), 381 (4), 364 (2, $M^+-C_5H_{10}O_2$), and 69 (100).

Hydrolysis of 16b with Copper(II) Chloride-Copper(II) Oxide. The dithiane **16b** was hydrloyzed with $CuCl_2\cdot$

$2H_2O$-Cu_2O in acetone to give the hydroxy ketone **17b** in 39% yield. **17b**: Colorless oil; IR (neat): 3470 and 1710 cm^{-1}; ^1H NMR δ=0.87 (3H, s, 6 Me), 1.70 (9H, m, three olefinic methyls), 2.38 (4H, m, CH_2COCH_2), 3.73 (2H, d, J=3 Hz, $C\underline{H}_2OH$), 5.08 (1H, m, CH=), and 5.60 (1H, m, 3-H); MS: m/z 292 (nil, M^+), 274 (3%, M^+-H_2O), 109 (100), 107 (46), and 69 (99); Found: m/z 205.1660 (Calcd for $C_{14}H_{21}O$: $M^+-H_2O-C_5H_9$, m/z 205.1593).

Wittig Reaction of 17a with Methylenetriphenylphosphorane. To a solution of methylenetriphenylphosphorane, prepared from methyltriphenylphosphonium bromide (73 mg) and butyllithium (ca. 0.3 mmol) in dry diethyl ether (1 ml), was added a solution of **17a** (3 mg) in dry ether (1 ml) under a nitrogen atmosphere. The reaction mixture was then stirred for 2 h at room temperature. After work-up as usual the product was purified using column chromatography to yield **1a** (ca. 1 mg); colorless oil; IR (neat): 3400 and 890 cm^{-1}; ^1H NMR (90 MHz) δ=0.99 (3H, s, 6-Me), 1.61 (3H, s, Me), 1.69 (3H, s, Me), 1.74 (3H, d, J=1.5 Hz, Me), 3.74 (2H, m, $C\underline{H}_2OH$), 4.71 (2H, br s, $=CH_2$), 5.16 (1H, m, CH=), and 5.62 (1H, m, 3-H); MS: m/z 290 (5%, M^+), 272 (12, M^+-H_2O), 149 (26), 135 (27), 122 (52), 121 (48), 119 (27), 109 (94), 95 (48), 93 (54), 91 (23), 81 (57), 79 (23), and 69 (100). Found: m/z 290.2629. Calcd for $C_{20}H_{34}O$: M, 290.2610.

The hydroxy ketone **17b** (3 mg) was similarly methylenated with $PH_3P=CH_2$ to yield **1b** (ca. 1 mg); colorless oil; IR (neat): 3450 and 885 cm^{-1}; ^1H NMR (90 MHz) δ=0.85 (3H, s, 6-Me), 1.62 (3H, br s, Me), 1.70 (3H, br s, Me), 1.74 (3H, br s, Me), 3.73 (2H, m, $C\underline{H}_2OH$), 4.72 (2H, br s, $=CH_2$), 5.16 (1H, m, CH=), and 5.62 (1H, m, 3-H); MS: 290 (7%, M^+), 272 (8), 135 (23), 123 (20), 122 (38), 121 (38), 110 (24), 109 (83), 107 (54), 95 (37), 93 (46), 81 (46), 79 (20), and 69 (100). Found: m/z 290.2620.

Gas chromatography (20% Carbowax 20M, 3 mm×2 m, N_2 (1.2 kg cm^{-2})) of the final products showed that the contamination due to a more volatile component (t_R=4.5 min) was less than 10%; t_R(**1a**)=9.2 min and t_R(**1b**)=9.0 min.

We wish to thank Professor Akio Kobayashi, Ochanomizu University, for the mass spectral measurements (in part), and Dr. Hiroshi Hirota, The University of Tokyo, for the 90 MHz NMR measurements.

References

1) Preliminary account of this report: H. Nagano, Y. Ishikawa, Y. Matsuo, and M. Shiota, *Chem. Lett.*, **1982**, 1947.

2) J. de Pascual Teresa, C. Grande, and M. Grande, *Tetrahedron Lett.*, **1978**, 4563.

3) W. Cocker and T. B. H. McMurry, *J. Chem. Soc.*, **1956**, 4549.

4) A. E. Greene, *J. Am. Chem. Soc.*, **102**, 5337 (1980).

5) E. Vedejs, *J. Am. Chem. Soc.*, **96**, 5944 (1974); E. Vedejs, D. A. Engler, and J. E. Teleschow, *J. Org. Chem.*, **43**, 188 (1978).

6) Gonzalez et al. reported the hydroxylation of the enolate of **3a** with oxygen. A. G. Gonzalez, J. Bermejo, J. L. Breton, A. Galindo, and G. M. Massanet, *Rev. Latinoam. Quim.*, **9**, 78 (1978); *Chem. Abstr.*, **89**, 180182e (1978).

7) S. Yamada, K. Nakayama, and H. Takayama, *Tetrahedron Lett.*, **1981**, 2591 and references cited therein.

8) Y. Tamura, H. Fujiwara, K. Sumoto, M. Ikeda, and Y. Kita, *Synthesis*, **1973**, 215.

9) L. G. Donaruma and W. Z. Heldt, *Org. React.*, **11**, 1 (1960).

10) W. Biernacki and A. Gdula, *Synthesis*, **1979**, 37.

11) E. J. Corey and D. Seebach, *Angew. Chem. Int. Ed. Engl.*, **4**, 1075 (1965).

12) K. Narasaka, T. Sakashita, and T. Mukaiyama, *Bull. Chem. Soc. Jpn.*, **45**, 3724 (1972).

13) H. Nagano, M. Tori, M. Shiota, and J. de Pascual Teresa, *Bull. Chem. Soc. Jpn.*, **57**, 2971 (1984).

14) J. de Pascual Teresa, C. Grande, J. R. Moran, and M. Grande, *Chem. Lett.*, **1984**, 247.

15) M. Bruno, L. Lamartina, F. Lentini, C. Pascual, and G. Savona, *Tetrahedron Lett.*, **25**, 4287 (1984).

 © 1987 The Chemical Society of Japan Bull. Chem. Soc. Jpn., 60, 713—720 (1987)

Syntheses of 2′,3′-Dideoxykanamycin A, 2′,3′-Dideoxyamikacin and Related Substances

Yoshihiko KOBAYASHI, Tsutomu TSUCHIYA,* Sumio UMEZAWA, Toshio YONETA,†
Shunzo FUKATSU,† and Hamao UMEZAWA††
Institute of Bioorganic Chemistry, 1614 Ida, Nakahara-ku, Kawasaki 211
†Central Research Laboratories, Meiji Seika Co., Ltd., Morooka-cho, Kohoku-ku, Yokohama 222
††Institute of Microbial Chemistry, Kamiosaki, Shinagawa-ku, Tokyo 141
(Received August 19, 1986)

2′,3′-Dideoxykanamycin A has been prepared via two ways. 2″-*O*-Acetyl-4″,6″-*O*-benzylidene-6′-*N*,4′-*O*-carbonyl-1,3,3″-tri-*N*-tosylkanamycin A was converted to a 2′,3′-unsaturated compound by a modified Tipson and Cohen method. Hydrogenation followed by deblocking gave 2′,3′-dideoxykanamycin A (**12**). Another route for **12** was through 2′,3′-anhydro-4′,2″,4″,6″-tetra-*O*-benzoyl-2′-epi-1,3,6′,3″-tetrakis(*N*-ethoxycarbonyl)kanamycin A (**16**). Epoxide-ring opening of **16** with hydrogen iodide gave the 3′,2′-iodohydrin, which, after 2′-*O*-mesylation, led to the 2′,3′-unsaturated compound (**19**). Deblocking and hydrogenation of **19** gave **12**. 2′,3′-Dideoxykanamycin A thus synthesized was led to 2′,3′-dideoxyamikacin and other related compounds by amino protection of **12** other than the 1-amino group by zinc acetate–ethyl trifluoroacetate method followed by 1-*N*-acyl or 1-urethane formation with appropriate reagents. Their antibacterial activities were described.

Due to the lack of the hydroxyl group at C-3′, 3′-deoxykanamycin A[1] inhibits the growth of resistant bacteria producing 3′-*O*-phosphotransferases or 3′-*O*-adenylyltransferases. Attachment of (*S*)-4-amino-2-hydroxybutyryl residue at the 1-amino group of 3′-deoxykanamycin A gave 3′-deoxyamikacin,[2] which was more active than 3′-deoxykanamycin A and amikacin (1-*N*-[(*S*)-4-amino-2-hydroxybutyryl]kanamycin A). 2′-Deoxyamikacin[3] prepared from 2′-deoxykanamycin A[4] had been found more active than amikacin against a variety of resistant bacteria. This suggests the possibility that the lack of 2′-hydroxyl group of kanamycin A may deprive the hydrogen-bond formation between 5- and 2′-hydroxyl groups and cause changes of the angles (ψ and ϕ[5]) between 2-deoxystreptamine and 6-amino-6-deoxy-α-D-glucopyranose moiety to improve the antibacterial activity. The results and the assumption described above let us to prepare 2′,3′-dideoxyamikacin.

2′,3′-Dideoxykanamycin A was prepared by two different ways. 6′-*N*-Benzyloxycarbonyl-1,3,3″-tri-*N*-tosylkanamycin A[6] (**1**) was treated with benzaldehyde dimethyl acetal in an acidic medium to give the 4″,6″-*O*-benzylidene derivative (**2**) in high yield. No benzylidenation of other hydroxyl groups of **1** was observed. Treatment of **2** with sodium hydride[7] in *N*,*N*-dimethylformamide (DMF) gave the 4′,6′-cyclic carbamate (**3**), the structure being confirmed by the IR spectrum (1700 cm^{-1}[7]). Protection of the hydroxyl groups of **3** with 1,1-dimethoxycyclohexane in the presence of trifluoroacetic acid in DMF gave the 2′,3′-*O*-cyclohexylidene derivative (**4**) in high yield. In this reaction, no formation of the 5,2′-*O*-cyclohexylidene derivative as experienced in the isopropylidenation of 6′-*N*,4′-*O*-carbonyl-4″,6″-*O*-cyclohexylidene-1,3,3″-tri-*N*-tosylkanamycin A[6] was observed. Attempts to prepare 2′,3′:4″,6″-di-*O*-cyclohexylidene derivative, instead of **4**, by one-pot cyclohexylidenation of 6′-*N*,4′-*O*-carbonyl-1,3,3″-tri-*N*-tosylkanamycin A gave no desired product in pure state. In the reaction to make **4** from **3**, conversion of the benzylidene to a cyclohexylidene group was not observed, but in strongly acidic conditions some conversion was observed. After acetylation, the 2″-*O*-acetyl derivative (**5**) was hydrolyzed with 80% aqueous acetic acid (40 °C for 3.5 h) to give the decyclohexylidene derivative (**6**) in a moderate yield (57%) with the starting material (**5**) and the debenzylidene-decyclohexylidene derivative (**7**). However, removal of the both protecting groups of **5** (to give **7**) followed by rebenzylidenation gave **6** in high yield (>90%).

Double bond between C-2′ and C-3′ of **6** was created by a modified Tipson-Cohen procedure.[8] Treatment of **6** with trifluoromethanesulfonic anhydride in pyridine gave the bis(trifluoromethanesulfonate) (**8**), that was treated with sodium iodide in DMF in the absence[8] of zinc dust to give the 2′,3′-unsaturated compound **9** almost quantitatively, the yield being unexpectedly high in comparison to the yields for 2,3-unsatunation (≈50%) using other usual 2,3-bis(sulfonic ester). If zinc dust was added in the above reaction, the yield of **9** fairly decreased. In the ^1H NMR spectrum of **9**, resonances of H-2′ and H-3′ appeared at δ 5.93 and 5.80 with the $J_{2',3'}$=10 Hz (see Experimental), the shifts and the coupling being typical for 2,3-unsaturated sugars.[9] From the ^1H-shift-correlated 2-D spectrum of **9**, the sequence of H-1-H-2-H-3 was confirmed. Catalytic hydrogenation of **9** in the presence of platinum oxide gave the 2′,3′-dideoxy derivative (**10**). Alkaline treatment of **10** cleaved the both 4′,6′-carbamate and the 2″-*O*-acetyl groups to give the ninhydrin-positive derivative (**11**), which was treated with sodium in liquid ammonia to cleave the *N*-tosyl and 4″,6″-*O*-benzylidene groups to give the final product, 2′,3′-dideoxykanamycin A (**12**).

Another route for **12** was started from 3′,4′,2″,4″,6″-penta-*O*-benzoyl-1,3,6′,3″-tetrakis(*N*-ethoxycarbonyl)-kanamycin A[4] (**13**). Treatment of **13** with methanesul-

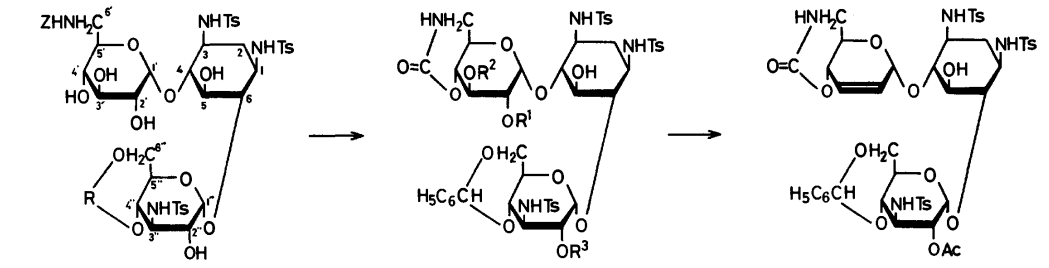

R
1 H, H
2 CHC_6H_5

	R^1	R^2	R^3
3	H	H	H
4	$C(CH_2)_5$		H
5	$C(CH_2)_5$		Ac
6	H	H	Ac
8	SO_2CF_3	SO_2CF_3	Ac

9

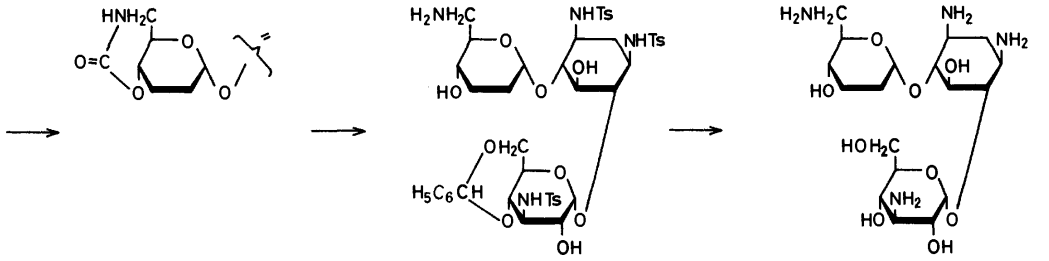

10 11 12
$Z = CO_2CH_2C_6H_5$

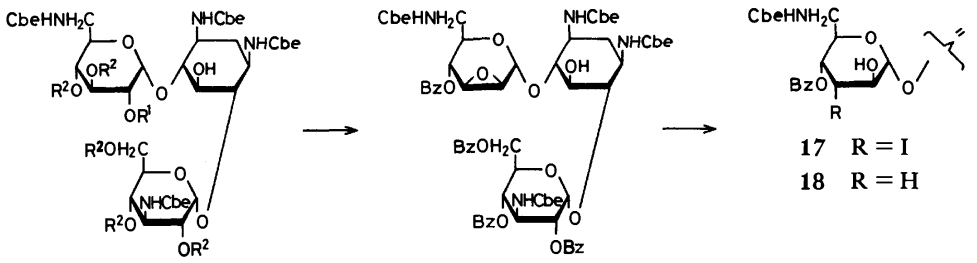

	R^1	R^2
13	H	Bz
14	SO_2CH_3	Bz
15	SO_2CH_3	H

16

17 R = I
18 R = H

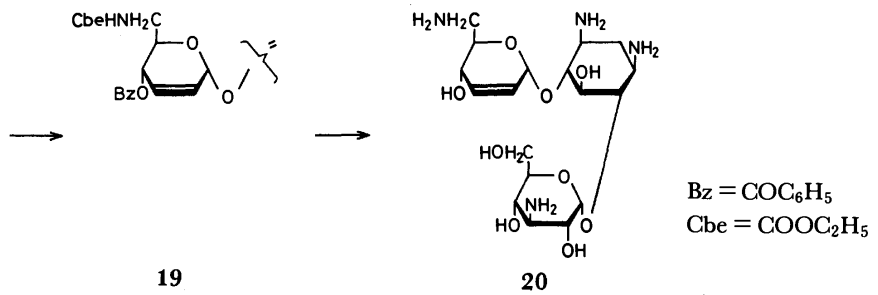

19 20
$Bz = COC_6H_5$
$Cbe = COOC_2H_5$

fonyl chloride in pyridine gave the 2′-*O*-mesylate (**14**). Selective removal of the benzoyl groups of **14** with sodium methoxide in methanol with the mesyloxy group remained intact gave the debenzoyl-2′-*O*-mesylate (**15**). Treatment of **14** with sodium methoxide in 1,4-dioxane-methanol gave the 2′,3′-epoxide, which, without purification, was benzoylated to afford the tetrabenzoate (**16**). Epoxide-ring opening of **16** with sodium iodide in acetone gave the 3′,2′-iodohydrin (**17**). Presence of the 3′-iodo and 2′-hydroxyl (axial) groups were determined by the ^1H NMR spectrum of the reduction product **18** pro-

duced by treating **17** with tributylstannane and 2,2′-azobis(isobutyronitrile) (AIBN). The structure of **18** was further confirmed by giving, after deprotection, 3′-deoxy-2′-epikanamycin A.[10]

Mesylation of **17** with methanesulfonyl chloride in pyridine in the presence of 4-dimethylaminopyridine and triethylamine readily gave the 2′,3′-unsaturated product **19**, possively through the 2′-*O*-mesylate and subsequent 2′,3′-trans-diaxial elimination. It is interesting to note that in the epoxide-ring opening of 3′,4′-anhydro-2′,2″-di-*O*-benzoyl-4″,6″-*O*-cyclohexylidene-4′-epi-tetrakis(*N*-*t*-butoxycarbonyl)kanamycin A,[11] the 4′,3′-diequatorial-iodohydrin was produced, and the iodohydrin gave the 3′,4′-unsaturated compound by a similar procedure as described, but only at an elevated temperature (90 °C). Deblocking of **19** gave 2′,3′-dideoxy-2′-enokanamycin A (**20**). Catalytic hydrogenation of **20** gave 2′,3′-dideoxykanamycin A (**12**) identical with the specimen obtained by the previous route. Total yields of **12** starting from kanamycin A via the former and the latter routes were 17 (12 steps) and 10% (10 steps), respectively.

Couplings of (*S*)-4-amino-2-hydroxybutyric acid and the related acids to the 1-amino group of 2′,3′-dideoxykanamycin A were performed by utilizing zinc acetate-ethyl trifluoroacetate method.[12] Treatment of **12** with *N*-(benzyloxycarbonyloxy)succinimide[13] in dimethyl sulfoxide (DMSO) or DMF-water (10 : 1) in the presence of zinc acetate gave the 3,6′-bis(*N*-benzyloxycarbonyl) derivative (**21**) in 88 and 79% yields, the latter procedure being superior to the former in easy removal of the solvent. After trifluoroacetylation[12] of the 3″-amino group with ethyl trifluoroacetate in DMF (DMSO was used in the original procedure[12]), the free 1-amino group of the resulting product **22** was acylated with the active ester[13] of (*S*)-4-benzyloxycarbonylamino-2-hydroxybutyric acid. Removal of the *N*-trifluoroacetyl group of the coupling product with aqueous ammonia, followed by removal of benzyloxycarbonyl groups by catalytic hydrogenolysis gave the final product 2′,3′-dideoxyamikacin (**23**). Similarly, 1-*N*-[(*S*)-3-amino-2-hydroxypropionyl]- (**24**) and 1-*N*-[(*S*)-4-amino-2-methoxybutyryl]-2′,3′-dideoxykanamycin A (**25**) were prepared, the latter being prepared to check the biological role of the free 2‴-hydroxyl group of **23**. (*S*)-4-Benzyloxycarbonylamino-2-methoxybutyric acid (**28**) required for the synthesis of **25** was prepared from (*S*)-4-benzyloxycarbonylamino-2-hydroxybutyric acid[13] (**26**) by methylation (to give **27**) and hydrolysis.

Since it was reported[14,15] that 1-*N*-(2-aminoethoxycarbonyl)kanamycin A and 1-*N*-(3-aminopropoxycarbonyl)kanamycin A, both prepared readily, showed significant antibacterial activities, 2′,3′-dideoxykanamycin A derivatives having the same 1-*N*-residues were also prepared. Treatment of **22** with *N*-[2-(benzyloxycarbonylamino)ethoxycarbonyloxy]succinimide[14] or *N*-[3-(benzyloxycarbonylamino)propoxycarbonyloxy]succinimde[14] gave the corresponding 1-*N*-alkoxycarbonyl derivatives, which, after deblocking, were led to the 1-*N*-(2-aminoethoxycarbonyl)- (**29**) and 1-*N*-(3-aminopropoxycarbonyl)-2′,3′-dideoxykanamycin A (**30**).

Antibacterial activities of the final products prepared are shown in Table 1. Both 1-*N*-[(*S*)-4-amino-2-hydroxybutyryl]- (**23**) and 1-*N*-[(*S*)-3-amino-2-hydroxypropionyl]-2′,3′-dideoxykanamycin A (**24**) showed slightly enhanced antibacterial activities in comparison to the activity of amikacin, and the two analogues (**29** and **30**) having the urethane residue at C-1 showed slightly decreased activities. The derivative (**25**) having the 2‴-*O*-methyl substituent, however, showed very weak antibacterial activity suggesting the importance of the 2‴-hydroxyl group in terms of antibacterial activity.

Experimental

Melting points were determined with a Kofler block and are uncorrected. Optical rotations were measured with a Perkin-Elmer 241 polarimeter. TLC was carried out on Wakogel B-5 silica gel with detection by spraying with sulfuric acid, followed by slight heating. Column chromatography was performed on Wakogel C-200. IR Spectra were measured with a JASCO A-202 grating spectrophotometer. ^{1}H NMR Spectra were recorded at 250 (unless otherwise

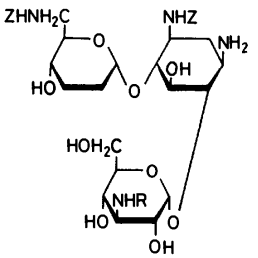

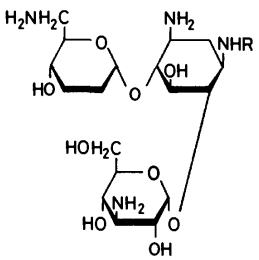

R

21 R = H
22 R = $COCF_3$

23 (*S*)$COCH(OH)CH_2CH_2NH_2$
24 (*S*)$COCH(OH)CH_2NH_2$
25 (*S*)$COCH(OCH_3)CH_2CH_2NH_2$
29 $COOCH_2CH_2NH_2$
30 $COOCH_2CH_2CH_2NH_2$

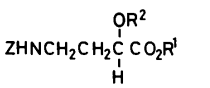

	R^1	R^2
26	H	H
27	CH_3	CH_3
28	H	CH_3

Table 1. Minimal Inhibitory Concentration ($\mu g\,ml^{-1}$) of **12**, **23**, **24**, **29**, and **30** with Kanamycin A (KMA) and Amikacin (AMK)

		KMA	12	AMK	23	24	29	30
S.a.	FDA 209P	1.56	1.56	0.78	0.39	0.78	1.56	0.78
S.a.	Smith	0.39	0.39	0.39	<0.2	<0.2	0.78	0.78
S.a.	Ap01 (C)	25	3.12	3.12	0.78	1.56	3.12	1.56
B.s.	PCI 219	0.78	0.39	0.39	<0.2	0.2	0.39	0.78
E.c.	K-12	0.78	0.78	0.2	0.39	0.39	1.56	0.78
E.c.	K-12 ML1629 (A)	>100	1.56	0.78	0.78	0.78	3.12	3.12
E.c.	K-12 LA290 R55 (D)	50	25	3.12	0.78	0.78	3.12	3.12
E.c.	W677	1.56	0.78	1.56	0.78	1.56	1.56	1.56
E.c.	JR66/W677 (B, D)	>100	50	1.56	3.12	3.12	6.25	3.12
E.c.	JR225 (E)	3.12	3.12	0.39	0.39	0.78	1.56	0.78
M.s.	ATCC 607	6.25	1.56	0.78	0.78	0.78	1.56	1.56
K.p.	PCI 602	1.56	3.12	1.56	1.56	1.56	3.12	3.12
K.p.	22 #3038 (B, D)	>100	50	6.25	3.12	3.12	6.25	6.25
P.v.	OX19	0.78	0.78	0.39	0.78	0.78	1.56	0.78
P.r.	GN311	0.78	0.78	0.78	1.56	1.56	1.56	0.39
S.m.		12.5	6.25	6.25	6.25	6.25	6.25	6.25
Pr. sp.	Pv16 (F)	3.12	3.12	1.56	1.56	3.12	1.56	1.56
P.a.	A3	6.25	1.56	<0.2	0.78	0.78	1.56	1.56
P.a.	TI13 (A)	50	25	1.56	3.12	3.12	12.5	25
P.a.	GN315 (G)	>100	>100	25	25	50	>100	>100

Abbreviations of bacteria: S.a. *Staphylococcus aureus*, B.s. *Bacillus subtilis*, E.c. *Escherichia coli*, M.s. *Mycobacterium smegmatis*, K.p. *Klebsiella pneumoniae*, P.v. *Proteus vulgaris*, P.r. *Proteus rettgeri* S.m. *Serratia marcescens*, Pr. *Providencia*, P.a. *Pseudomonas aeruginosa*. The letters in parenthesis show the resistant bacteria producing 3′-phosphotransferase-I (A), 3′-phosphotransferase-II (B), 4′-adenylyltransferase (C), 2″-adenylyltransferase (D), 3-acetyltransferase (E), 2′-acetyltransferase (F), and 6′-acetyltransferase (G).

stated), 200, and 90 MHz with a Bruker WM 250, JEOL FX200, and Varian EM-390 spectrometers, respectively. The chemical shifts (δ by ppm) of the spectra were measured downfield from internal TMS.

4″,6″-*O*-Benzylidene-6′-*N*-benzyloxycarbonyl-1,3,3″-tri-*N*-tosylkanamycin A (2). A solution of the mixture of **1**[1] (1.58 g), benzaldehyde dimethyl acetal (0.27 ml) and *p*-toluenesulfonic acid (55 mg of monohydrate was dried in vacuo at 100 °C for 1 h) in DMF (8 ml) was kept at room temperature. After 7 h, another acetal (0.13 ml) was added and the solution was kept for further 30 h. The solution was poured into aqueous sodium hydrogencarbonate (saturated, 320 ml) and the precipitates were thoroughly washed with water and ether to give, after drying, a solid of **2**, 1.60 g (94%), $[\alpha]_D^{23}$ −22° (*c* 0.5, oxolane).

Found: C, 55.30; H, 5.49; N, 4.84; S, 8.28%. Calcd for $C_{54}H_{64}N_4O_{19}S_3$: C, 55.47; H, 5.52; N, 4.79; S, 8.23%.

4″,6″-*O*-Benzylidene-6′-*N*,4′-*O*-carbonyl-1,3,3″-tri-*N*-tosylkanamycin A (3). To an ice-cold solution of **2** (4.65 g) in dry DMF (93 ml) was added 50% (in oil) sodium hydride (1.72 g, 9 mol equiv. for **2** as net NaH), and the mixture was vigorously stirred in the cold for 1 h under an atmosphere of nitrogen, and then overnight at room temperature. TLC (chloroform–ethanol=6:1) of the solution showed a single spot (R_f 0.15; cf **2**: 0.5). Addition of 25% acetic acid (15 ml) and evaporation in vacuo, with occasional additions of toluene, gave a residue, that was washed with ether, then thoroughly with water, and dried to give a solid of **3**, 3.97 g (94%), $[\alpha]_D^{22}$ −37° (*c* 1, acetone); IR (KBr): 1700 cm^{-1} (carbamate); ^1H NMR (pyridine-d_5) δ=2.09, 2.27, and 2.35 (each 3H, s, TsX3), 5.48 (1H, s, PhCH), 5.52 (1H, d, *J*=3.5 Hz, H-1′or H-1″), 5.59 (1H, d, *J*=3.5 Hz, H-1″ or H-1′).

Found: C, 52.85; H, 5.39; N, 5.26; S, 8.81%. Calcd for $C_{47}H_{56}N_4O_{18}S_3 \cdot 0.5H_2O$: C, 52.75; H, 5.37; N, 5.24; S, 8.99%.

4″,6″-*O*-Benzylidene-6′-*N*,4′-*O*-carbonyl-2′,3′-*O*-cyclohexylidene-1,3,3″-tri-*N*-tosylkanamycin A (4). A reaction flask containing **3** (3.97 g), 1,1-dimethoxycyclohexane (10.8 ml), trifluoroacetic acid (2.1 ml), dry DMF (20 ml), and dichloromethane (400 ml) was connected to a Soxlhet type of apparatus[2] fitted with a reflux condenser, the Soxhlet extractor being filled with molecular sieves 5A (120 ml, activated at 350 °C under a stream of nitrogen), and the mixture was refluxed for 6 h. Methanol liberated during the reaction was effectively removed by the sieves. TLC (chloroform–ethanol=5:1) of the solution showed a single spot (R_f 0.4; cf **3**: 0.18). The reaction mixture was concentrated to a small volume (≈20 ml), and poured into an ice-cold aqueous sodium hydrogencarbonate solution (saturated). The resulting precipitates were filtered, washed with water and ether alternately several times, to give, after drying, a solid of **4**, 4.15 g (97%), $[\alpha]_D^{23}$ −33° (*c* 0.6, acetone); IR (KBr): 1700 cm^{-1}; ^1H NMR (pyridine-d_5 at 90 MHz) δ=2.12, 2.24, and 2.35 (each 3H, s, TsX3).

Found: C, 55.47; H, 5.77; N, 4.88; S, 8.30%. Calcd for $C_{53}H_{64}N_4O_{18}S_3$: C, 55.78; H, 5.65; N, 4.91; S, 8.43%.

2″-*O*-Acetyl-4″,6″-*O*-benzylidene-6′-*N*,4′-*O*-carbonyl-2′,3′-*O*-cyclohexylidene-1,3,3″-tri-*N*-tosylkanamycin A (5). To an ice-cold solution of **4** (5.26 g) in dry pyridine (105 ml) was added acetic anhydride (4.8 ml) and the solution was kept at room temperature overnight. TLC (chloroform–ethanol=10:1) of the solution showed a main (**5**, R_f 0.25; cf **4**: 0.18) and trace spots (R_f 0.34 and 0.38). The reaction mixture was poured, with vigorous stirring, into an ice-cold aqueous sodium hydrogencarbonate solution (saturated, 1 l). After standing for 1 h, the resulting precipitates were filtered and dried (5.52 g). Column chromatographty of the products with chloroform–acetone (10:7→10:9, gradually changed) gave a glass, 3.15 g (64%), $[\alpha]_D^{22}$ +40° (*c* 1, acetone); IR (KBr):

1730 cm^{-1}; ^1H NMR (pyridine-d_5) δ=2.16, 2.22, and 2.34 (each 3H, s, Ts ×3), 2.52 (3H, s, Ac).

Found: C, 55.47; H, 5.75; N, 4.75; S, 7.92%. Cacld for $C_{55}H_{66}N_4O_{19}S_3 \cdot 0.5H_2O$: C, 55.40; H, 5.66; N, 4.70; S, 8.07%.

2″-*O*-Acetyl-4″,6″-*O*-benzylidene-6′-*N*,4′-*O*-carbonyl-1,3,3″-tri-*N*-tosylkanamycin A (6). A suspension of **5** (1.88 g) in 80% aqueous acetic acid (38 ml) was vigorously stirred at 40 °C for 3.5 h. TLC (chloroform–acetone=1 : 2) of the resulting solution showed spots of R_f 0.44 (**5**, slight), 0.12 (**6**, major), and 0.02 (**7**). The solution was gradually poured into an ice-cold aqueous sodium hydrogencarbonate solution (saturated, 1 l), and the precipitates were filtered, washed with water, and dried (1.44 g). Column chromatography of the products with chroloform–acetone (1 : 1→1 : 2→ acetone, gradually changed) gave a thick syrup of **6**, 0.99 g (57%), recovered **5**, 0.22 g (12%), and a solid of **7**, 0.37 g. Benzylidenation of **7** (0.37 g) in the same manner as described later (see the preparation of **6** from **7**; $C_6H_5CH(OMe)_2$ 66 μl, TosOH 14 mg, and DMF 1.9 ml, room temperature, 40 h) gave another crop of **6**, 0.35 g (totally 77%), $[\alpha]_D^{22}$ −5° (*c* 1, acetone); IR (KBr): 1700 cm^{-1}; ^1H NMR (pyridine-d_5): δ=2.14, 2.26, and 2.30 (each 3H, s, Ts×3), 2.46 (3H, s, Ac), 5.50 (1H, d, *J*=3.5 H, H-1′), 5.55 (1H, s, PhCH), 5.60 (1H, dd, *J*=3.5 and 10 Hz, H-2″), 5.97 (1H, d, *J*=3.5 Hz, H-1″). Irradiation of H-1″ collapsed the doublets of H-2″ to a doublet.

Found: C, 53.34; H, 5.21; N, 5.13; S, 8.66%. Calcd for $C_{49}H_{58}N_4O_{19}S_3$: C, 53.35; H, 5.30; N, 5.08; S, 8.72%.

2″-*O*-Acetyl-6′-*N*,4′-*O*-carbonyl-1,3,3″-tri-*N*-tosylkanamycin A (7). A suspension of **5** (1.70 g) in 80% aqueous acetic acid (34 ml) was vigorously stirred at 80 °C, whereupon clear solution was obtained after ≈5 min. After 1 h (at the same temperature), the solution was concentrated. The residue suspended in toluene was evaporated, and the residual solid was dried (60 °C, 36 h in vacuo) to give **7**, 1.48 g (quant.), $[\alpha]_D^{23}$ 0° (*c* 1, acetone); IR (KBr): 1690 cm^{-1}; ^1H NMR (pyridine-d_5 at 90 MHz) δ=2.16, 2.28, and 2.32 (each 3H, s, Ts×3), 2.51 (3H, s, Ac).

Found: C, 48.81; H, 5.41; N, 5.34%. Calcd for $C_{42}H_{54}N_4O_{19}S_3 \cdot H_2O$: C, 48.83; H, 5.46; N, 5.42%.

Benzylidenation of 7 to Give 6. Compound **7** (2.53 g) was treated with benzaldehyde dimethyl acetal (0.76 ml) in DMF (12.6 ml) in the presence of *p*-toluenesulfonic acid (190 mg) similarly as described for **2** to give a solid of **6**, 2.51 g (91%).

2″-*O*-Acetyl-4″,6″,-*O*-benzylidene-6′-*N*,4′-*O*-carbonyl-1,3,3″-tri-*N*-tosyl-2′,3′-bis(*O*-trifluoromethylsulfonyl)kanamycin A (8). To an ice-cold solution of **6** (887 mg) in dry pyridine (17.7 ml) was added trifluoromethanesulfonic anhydride (1.13 ml) and the solution was kept at the temperature for 4.5 h. TLC (chloroform–acetone=1 : 1) of the solution showed a single spot (R_f 0.25; cf **6**: 0.03). The red solution was poured into excess ice-cold aqueous sodium hydrogencarbonate and the precipitates were filtered, washed thoroughly with water, and dried (in vacuo at room temperature) to give a pale yellow solid of **8**, 1.01 g (quant.); analytical sample was purified by column chromatography with chloroform–acetone (1 : 1), $[\alpha]_D^{23}$ −32° (*c* 1, acetone); IR (KBr): 1730, 1420 cm^{-1}; ^1H NMR (pyridine-d_5) δ=2.15, 2.32, and 2.38 (each 3H, s, Ts ×3), 2.47 (3H, s, Ac).

Found: C, 44.94; H, 4.32; N, 4.21; S, 11.42%. Calcd for $C_{51}H_{56}N_4O_{23}S_5F_6$: C, 44.80; H, 4.13; N, 4.10; S, 11.72%.

2″-*O*-Acetyl-4″,6″-*O*-benzylidene-6′-*N*,4′-*O*-carbonyl-2′,3′-dideoxy-2′-eno-1,3,3″-tri-*N*-tosylkanamycin A (9). A mixture of **8** (60 mg), sodium iodide (600 mg) and imidazole (21 mg) in dry DMF (dried over molecular sieves 3A, 1.2 ml) was stirred at 100 °C for 45 min. TLC (chloroform–acetone=1 : 2) of the resulting deep red solution showed a single spot (**9**, R_f 0.58; cf **8**: 0.7). To the solution, while hot (when cooled, all contents solidified hard), was added hot chloroform (20 ml), and, after shaking for a while, the organic solution isolated was washed successively with water (10 ml×3), 0.1M (1 M= mol dm^{-3}) aqueous sodium thiosulfate (10 ml×2; to remove iodine liberated), and water (10 ml×3), dried (Na_2SO_4) and concentrated to give a glass, 46 mg (98%), $[\alpha]_D^{22}$ −12.5° (*c* 1, acetone); IR (KBr): 1710 cm^{-1}; ^1H NMR (pyridine-d_5 at 70 °C) δ=2.16, 2.25, and 2.30 (each 3H, s, Ts×3), 2.36 (3H, s, Ac), 5.73 (1H, br s, H-1′), 5.80 (1H, dt, *J*=2.5, 2.5, and 10 Hz, H-3′), 5.93 (1H, d, *J*=10 Hz, H-2′).

Found: C, 54.99; H, 5.56; N, 5.15%. Calcd for $C_{49}H_{56}N_4O_{17}S_3$: C, 55.04; H, 5.28; N, 5.24%.

2″-*O*-Acetyl-4″,6″-*O*-benzylidene-6′-*N*,4′-*O*-carbonyl-2′,3′-dideoxy-1,3,3″-tri-*N*-tosylkanamycin A (10). Platinum oxide (PtO_2, 21 mg) in oxolane–water (2 : 1, 2 ml) was activated with hydrogen (3 kg cm^{-2}, 30 min). Compound **9** (100 mg) was added and the mixture was shaken at room temperature under the same hydrogen pressure for 45 min. TLC (chloroform–acetone=1 : 1) of the solution showed a single spot (**10**, R_f 0.24; cf **9**: 0.28). The mixture was filtered and evaporated to give a glass, 97.5 mg (98%), $[\alpha]_D^{23}$ +10° (*c* 1, acetone); IR (KBr); 1700 cm^{-1}; ^1H NMR (pyridine-d_5): δ=1.6—1.85 (4H), 2.04 (1H, m), and 2.50 (1H, m)(H-2_{ax}, 2_{eq}, $2'_{ax}$, $2'_{eq}$, $3'_{ax}$, $3'_{eq}$); 2.17, 2.26, and 2.34 (each 3H, s, Ts×3), 2.51 (3H, s, Ac), 5.57 (1H, s, PhCH), 5.67 (1H, dd, *J*=3.5 and 10 Hz, H-2″), 5.73 (1H, slightly unresolved s, H-1′), 6.28 (1H, d, *J*=3.5 Hz, H-1″).

Found: C, 54.58; H, 5.54; N, 5.02; S, 8.70%. Calcd for $C_{49}H_{58}N_4O_{17}S_3$: C, 54.94; H, 5.46; N, 5.23; S, 8.98%.

2′,3′-Dideoxykanamycin A (12). From 10. To a solution of **10** (178 mg) in oxolane (2.4 ml) was added 3M aqueous sodium hydroxide (1.2 ml), and the mixture was vigorously stirred at 50 °C for 2.5 h. Concentration of the two-phase mixture gave a residue, the methanol solution of which was mixed with Dowex 50W×2 resin (NH_4^+ form, 10 ml, pretreated with methanol–water=2 : 1), and the whole mixture was poured into a column containing the same resin (1 ml). Development of the column with 3M aqueous ammonia–methanol (1 : 2) gave a ninhydrin-positive deacyl product (**11**, 167 mg). The product was purified by passing the solution in acetone through a column of Sephadex LH-20 (16 ml), that was pretreated with acetone to swell and washed with 0.5% hydrochloric acid in acetone and then with acetone. To a solution of the purified product (**11**) in liquid ammonia (≈17 ml) at −50 °C was added sodium metal (≈280 mg), and the deep-blue solution was kept for 1 h at the temperature. Addition of oxolane–water (99 : 1) until the solution became colorless, followed by gradual warming to room temperature, and evaporation under diminished pressure gave a glassy residue. To an aqueous solution of the residue was added Dowex 50W×2 resin (NH_4^+ form, 50 ml), and the mixture, after shaking for a while, was poured into a column containing the same resin (10 ml). The column was washed with water, eluted with 1M aqueous ammonia, and the eluate evaporated to give a residue (63.4 mg). The residue was chromatographed on a column of CM-Sephadex C-25 (NH_4^+ form, 32 ml) with, after washing with water, aqueous ammonia (0.01→0.15M, gradually changed) to give

a solid of **12**, 43.3 mg (51% monocarbonate), $[\alpha]_D^{23}$ +114° (*c* 1, water); $R_{\text{kanamycin A}}$ 2.0 (PPC with 1-butanol-pyridine-water-acetic acid=6:4:3:1, descending), and $R_{\text{kanamycin A}}$ 1.9 (TLC with 1-butanol-ethanol-chloroform-17% aqueous ammonia=4:7:2:7); ^{1}H NMR (20% ND_3 in D_2O) δ=1.23 (1H, q, J=12.5 Hz, H-2_{ax}), 1.6—2.05 (5H, H-2_{eq}, -$2'_{ax}$, -$2'_{eq}$, -$3'_{ax}$, -$3'_{eq}$), 5.02 (1H, d, J=3.5 Hz, H-1''), 5.31 (1H, slightly br s, H-1').

Found: C, 44.08; H, 7.33; N, 10.72%. Calcd for $C_{18}H_{36}N_4O_9 \cdot H_2CO_3$: C, 44.35; H, 7.44; N, 10.89%.

From 20. An aqueous solution (5 ml) of **20** (100 mg, monohydrate) was hydrogenated in the presence of platinum oxide (10 mg) under atmospheric pressure of hydrogen at room temperature for 3 h. After filtration, the product was purified by column chromatography of Amberlite CG-50 (NH_4^+ form, 3 ml) with 0.3M aqueous ammonia to give a solid of **12**, 91 mg (83% monocarbonate).

3',4',2'',4'',6''-Penta-*O*-benzoyl-1,3,6',3''-tetrakis(*N*-ethoxycarbonyl)-2'-*O*-methylsulfonylkanamycin A (14). To a solution of **13**[5] (3.00 g) in pyridine (30 ml) was added methanesulfonyl chloride (0.63 ml) and the solution was kept at room temperature for 1 h. After addition of water (0.2 ml) and standing for 30 min, the solution was concentrated in vacuo to dryness. The solution of the residue in ethyl acetate (100 ml) was washed with aqueous sodium hydrogencarbonate (saturated) and water, dried ($MgSO_4$), and concentrated. The residue was purified by silica-gel column chromatography (60 g) with chloroform-ethanol (50:1) to give a solid of **14**, 2.98 g (94%), $[\alpha]_D^{24}$ +102° (*c* 1, chloroform); ^{1}H NMR ($CDCl_3$ at 200 MHz) δ=2.70 (3H, s, Ms).

Found: C, 57.82; H, 5.44; N, 4.01; S, 2.39%. Calcd for $C_{66}H_{74}N_4O_{26}S$: C, 57.79; H, 5.45; N, 4.09; S, 2.33%.

1,3,6',3''-Tetrakis(*N*-ethoxycarbonyl)-2'-*O*-methylsulfonylkanamycin A (15). To a solution of **14** (137 mg) in dry methanol (5 ml) was added 28% sodium methoxide in methanol (0.1 ml) and the solution was kept at room temperature for 3 d. Resulting precipitates were filtered, washed with methanol, and dried to give a solid of **15**, 69 mg (81%), $[\alpha]_D^{20}$ +79° (*c* 1, DMF); ^{1}H NMR (pyridine-d_5-D_2O=10:1) δ=1.03 (3H), 1.12 (6H), and 1.23 (3H) (each t, $CO_2CH_2CH_3$×4); 3.42 (3H, s, SO_2CH_3), 4.83 (1H, dd, J=3.8 and 10 Hz, H-2'), 5.45 (1H, d, J=3.5 Hz, H-1''), 6.17 (1H, d, H-1'); H-1' and H-2' were confirmed by the shift-correlated 2-D spectrum.

Found: C, 42.99; H, 6.66; N, 6.17%. Calcd for $C_{31}H_{54}N_4O_{21}S \cdot H_2O$: C, 42.85; H, 6.50; N, 6.45%.

2',3'-Anhydro-4',2'',4'',6''-tetra-*O*-benzoyl-2'-epi-1,3,6',3''-tetrakis(*N*-ethoxycarbonyl)kanamycin A (16). To a solution of **14** (2.84 g) in dry 1,4-dioxane-methanol (1:1, 120 ml) was added 28% sodium methoxide in methanol (4 ml) and the solution was kept at room temperature overnight. After neutralization with 1M aqueous hydrochloric acid, the solution was concentrated to dryness. To a solution of the residue in pyridine (100 ml) was added benzoyl chloride (2.5 ml) and the solution was kept at room temperature for 1 h. Successive isolation then followed as described for **14** to give the crude product, that was purified by silica-gel column chromatography (50 g) with chloroform-ethanol (50:1) to give a solid of **16**, 1.98 g (82%), $[\alpha]_D^{20}$ +75° (*c* 1, chloroform).

Found: C, 59.66; H, 5.71; N, 4.56%. Calcd for $C_{58}H_{66}N_4O_{22}$: C, 59.47; H, 5.69; N, 4.78%.

4',2'',4'',6''-Tetra-*O*-benzoyl-3'-deoxy-2',3'-diepi-1,3,6',3''-tetrakis(*N*-ethoxycarbonyl)-3'-iodokanamycin A (17). To a solution of **16** (1.85 g) in acetone (45 ml) were added sodium iodide (1.36 g) and acetic acid (1.26 ml) and the solution was refluxed for 8 h. Concentration of the solution gave a residue, that was extracted with ethyl acetate. The solution was washed with water, dried ($MgSO_4$), and concentrated to dryness. The residue was purified by silica-gel column (50 g) with chloroform-methanol=45:1 to give a solid of **17**, 1.54 g (75%), $[\alpha]_D^{20}$ +33° (*c* 0.8, chloroform).

Found: C, 53.46; H, 5.20; N, 4.23; I, 10.01%. Calcd for $C_{58}H_{67}N_4O_{22}I$: C, 53.61; H, 5.21; N, 4.31; I, 9.78%.

4',2'',4'',6''-Tetra-*O*-benzoyl-3'-deoxy-2'-epi-1,3,6',3''-tetrakis(*N*-ethoxycarbonyl)kanamycin A (18). To a solution of **17** (300 mg) in toluene (10 ml) were added tributylstannane (0.35 ml) and AIBN (10 mg), and the mixture was heated at 70 °C for 30 min under the nitrogen atmosphere. TLC (chloroform-methanol=50:1) of the solution showed a single spot (R_f 0.07; cf **17**: 0.1). Concentration of the solution gave a syrup, that was thoroughly washed with ligroine. The syrup was purified by silica-gel column chromatography with chloroform-methanol (40:1) to give a solid of **18**, 242 mg (90%), $[\alpha]_D^{21}$ +89° (*c* 1, chloroform); ^{1}H NMR (pyridine-d_5) δ=0.75 (3H), 1.04 (6H), and 1.28 (3H) (each t, $CO_2CH_2CH_3$ ×4); 2.45 (1H, m, H-$3'_{ax}$), 2.68 (1H, m, H-$3'_{eq}$), 4.61 (1H, br, s, H-2'), 6.15 (1H, br s, H-1').

Found: C, 59.35; H, 5.96; N, 4.85%. Calcd for $C_{58}H_{68}N_4O_{22}$: C, 59.38; H, 5.84; N, 4.78%.

4',2'',4'',6''-Tetra-*O*-benzoyl-2',3'-dideoxy-2'-eno-1,3,6',3''-tetrakis(*N*-ethoxycarbonyl)kanamycin A (19). To a solution of **17** (1.00 g) in pyridine (20 ml) were added methanesulfonyl chloride (0.3 ml), 4-dimethylaminopyridine (90 mg), and triethylamine (1 ml), and the mixture was stirred at room temperature for 5 h. The mixture was poured into ice-water (50 g) and the precipitates were extracted with ethyl acetate. The organic solution was washed successively with 1M aqueous potassium hydrogensulfate, aqueous sodium hydrogencarbonate (saturated), and water, dried ($MgSO_4$), and concentrated. The residue was purified by silica-gel column chromatography with chloroform-methanol (50:1) to give a solid of **19**, 650 mg (73%), $[\alpha]_D^{22}$ +78° (*c* 0.8, chloroform).

Found: C, 60.11; H, 5.76; N, 4.80%. Calcd for $C_{58}H_{66}N_4O_{21}$: C, 60.30; H, 5.77; N, 4.85%.

2',3'-Dideoxy-2'-enokanamycin A (20). To a solution of **19** (500 mg) in methanol (10 ml) was added 28% sodium methoxide in methanol (0.3 ml) and the solution was kept at room temperature for 30 min. Concentration in vacuo gave a residue, that was dissolved in water (6 ml) containing sodium hydroxide (1.5 g). The alkaline solution was heated at 100 °C for 3 h, then neutralized with aqueous hydrochloric acid. The reaction mixture was poured into a column of Amberlite CG-50 (NH_4^+ form, 20 ml) and, after washing with water, developed with 0.3M aqueous ammonia. Ninhydrin-positive fractions were collected and concentrated to give a solid of **20**, 135 mg (67% hydrate), $[\alpha]_D^{22}$ +106° (*c* 0.7, water); ^{1}H NMR (D_2O at 200 MHz) δ=1.18 (1H, q, J=12.5 Hz, H-2_{ax}), 1.93 (1H, dt, J=4.5, 4.5, and 12.5 Hz, H-2_{eq}), 5.00 (1H, d, J=4 Hz, H-1''), 5.43 (1H, fairly narrow and unresolved m, H-1'), 5.85 (1H, apparently ddd, the lower triplet being intense, J=2.3, 2.3, and 10 Hz, H-3'), 5.98 (1H, d, the high-field signal being intense, J=10 Hz, H-2').

Found: C, 46.25; H, 7.77; N, 11.82%. Calcd for $C_{18}H_{34}N_4O_9 \cdot H_2O$: C, 46.14; H, 7.76; N, 11.96%.

3,6'-Bis(*N*-benzyloxycarbonyl)-2',3'-dideoxykanamycin A (21). Method A. A mixture of **12** (37.7 mg, monocarbo-

nate) and zinc acetate dihydrate (56.3 mg, 3.5 molar equiv for **12**) in dry dimethyl sulfoxide (0.4 ml) was stirred at room temperature overnight. To the resulting clear solution was added *N*-(benzyloxycarbonyloxy)succinimide[13] (40.2 mg, 2.2 molar equiv for **12**) and the solution was kept at room temperature for 40 min. Addition of excess ether gave precipitates, that was filtered and washed thoroughly with ether. A solution of the precipitates in 50% aqueous oxolane was poured into a column of Amberlite CG-50 resin (7 ml, 100—200 mesh, prewashed with 1M aqueous ammonia and water, then with 50% aqueous oxolane). The column was washed with 50% aqueous oxolane (35 ml) and developed with the same solvent mixture containing ammonia (0→1M, gradually changed). The ninhydrin-positive product **21** was eluted by the procedure; zinc ion accompanied remained in the column. The eluate was evaporated to dryness to give a solid of **21**, 47.5 mg (88% hydrate), $[\alpha]_D^{22}$ +76° (*c* 0.7, DMF), R_f 0.3 (TLC with chloroform–methanol–28% aqueous ammonia=1 : 1 : 1, lower layer was used).

Found: C, 55.48; H, 6.61; N, 7.44%. Calcd for $C_{34}H_{48}N_4O_{13}\cdot H_2O$: C, 55.26; H, 6.83; N, 7.58%.

Compound **21** obtained by the above procedure was rather unstable on account of its own basicity and on storage it was liable to change to an undesirable 1,3-ureylene derivative.[16] Therefore when stable **21** was desirable, carbon dioxide was introduced to neutralize the basicity before concentration at the final stage and **21** was isolated as the carbonate salt.

Method B. To an ice-cold solution of **12** (9.84 g, monocabonate) and zinc acetate dihydrate (24.0 g, 5.7 molar equiv for **12**) in DMF–water (10 : 1, 170 ml) was added *N*-(benzyloxycarbonyloxy)succinimide (11.88 g, 2.5 molar equiv for **12**) and the solution was kept at the temperature for 1 h, then at room temperature overnight. Concentration of the solution in vacuo gave a residue, that was chromatographed on a column of Amberlite CG-50 resin (600 ml, pretreated as described for Method A) with, after washing the column with 50% aqueous 1,4-dioxane (2.7 l), 1M ammonia in the same solvent system to give a solid of **21**, 11.20 g (79% hydrate).

3,6′-Bis(*N*-benzyloxycarbonyl)-2′,3′-dideoxy-3″-*N*-trifluoroacetylkanamycin A (22). To a solution of **21** (5.10 g, monohydrate) in DMF (70 ml) was added ethyl trifluoroacetate (2.0 ml) and the solution was kept at room temperature for 20 min. TLC (lower layer of chloroform–methanol–28% aqueous ammonia=1 : 1 : 1) of the solution showed a single spot (R_f 0.5; cf **21**: 0.3). Concentration of the solution gave a syrup, that was washed with ether to give a solid of **22**, 5.9 g.

1-*N*-[(*S*)-4-Amino-2-hydroxybutyryl]-2′,3′-dideoxykanamycin A (2′,3′-Dideoxyamikacin) (23). To a mixture of **22** (5.8 g) and anhydrous sodiom carbonate (0.6 g) in 50% aqueous oxolane (170 ml) was added *N*-[(*S*)-4-benzyloxycarbonylamino-2-hydroxybutyryloxy]succinimide[3] (3.2 g) and the resulting clear solution was kept at room temperature for 2.5 h. TLC (the same solvent system as described above for **22** was used) of the solution showed a single spot (R_f 0.63). Concentration of the solution in vacuo gave a syrup, that was thoroughly washed with water to give a solid. A solution of the solid (6.07 g) in oxolane-2.2M aqueous ammonia (1 : 1, 360 ml) was kept at room temperature overnight. TLC of the solution showed a single spot (R_f 0.43). Concentration gave a residue, that was dissolved in 50% aqueous oxolane (150 ml). After addition of palladium black (360 mg) and acetic acid (6.5 ml), the solution was hydrogenated under atmospheric pressure of hydrogen for 4 h. Filtraion and neutralization of the solution with aqueous sodium hydroxide were followed by chromatography on a column of Amberlite CG-50 resin (NH_4^+ form, 150 ml). Elution with aqueous ammonia (0→0.5M, gradually changed) gave a solid of **23**, 2.89 g (69% based on **21**, monocarbonate), $[\alpha]_D^{22}$ +87° (*c* 0.9, water); IR (KBr): 1650, 950 cm^{-1}; ^1H NMR (20% ND_3 in D_2O) δ=1.43 (1H, q, *J*=12.5 Hz, H-2_{ax}), 1.6—2.05 (7H, H-2_{eq}, -2′$_{ax}$, -2′$_{eq}$, -3′$_{ax}$, -3′$_{eq}$ and COCH(OH)CH_2CH_2–), 4.17 [1H, q, *J*=3.8 and 9.5 Hz, COC*H*(OH)], 5.07 (1H, d, *J*=3.5 Hz, H-1″), 5.30 (1H, slightly br s, H-1′).

Found: C, 44.85; H, 7.43; N, 11.38%. Calcd for $C_{22}H_{43}N_5O_{11}\cdot H_2CO_3$: C, 44.87; H, 7.37; N, 11.38%.

1-*N*-[(*S*)-3-Amino-2-hydroxypropionyl]-2′,3′-dideoxykanamycin A (24). Compound **22** (5.0 g) was treated in the same manner as described for **23** only changing the succinimide reagent to *N*-[(*S*)-3-benzyloxycarbonylamino-2-hydroxypropionyloxy]succinimide (3.6 g) (prepared in a usual manner[15] from (*S*)-3-benzyloxycarbonylamino-2-hydroxypropionic acid,[16] *N*-hydroxysuccinimide, and dicyclohexylcarbodiimide) to give a solid of **24**, 1.30 g (40% based on **21**, hydrate), $[\alpha]_D^{22}$ +97° (*c* 0.7, water); ^1H NMR (D_2O at 200 MHz) δ=1.40 (1H, q, H-2_{ax}), 1.6—2.05 (5H, H-2_{eq}, -2′$_{ax}$, -2′$_{eq}$, -3′$_{ax}$, -3′$_{eq}$), 4.15 [1H, q, *J*=5 and 8 Hz, COC*H*(OH)], 5.04 (1H, d, *J*=3.5 Hz, H-1″), 5.29 (1H, slightly br s, H-1′).

Found: C, 45.44; H, 7.61; N, 12.66%. Calcd for $C_{21}H_{41}N_5O_{11}\cdot H_2O$: C, 45.22; H, 7.79; N, 12.56%.

1-*N*-(2-Aminoethoxycarbonyl)-2′,3′-dideoxykanamycin A (29). To a solution of **22** (100 mg) and anhydrous sodium carbonate (10.5 mg) in 50% aqueous oxolane (3.3 ml) was added *N*-[2-(benzyloxycarbonylamino)ethoxycarbonyloxy]-succinimide[14] (54 mg) in oxolane (1.7 ml) and the mixture was kept at room temperature for 2 h. TLC (chloroform–methanol–28% aqueous ammonia=1 : 1 : 1, lower layer) of the solution showed a single spot (R_f 0.67; cf **22**: 0.52). Evaporation gave a residue, that was washed with water and ether, and dried to give a solid (120 mg). A solution of the solid in 1,4-dioxane–2.5M aqueous ammonia (3 : 2, 6 ml) was kept at room temperature for 30 h. The slightly turbid solution showed, on TLC, a single spot (R_f 0.53). Concentration gave a residue, that was thoroughly washed with water and dried to give a solid (75 mg). A mixture of the solid and palladium black in 1,4-dioxane–water (2 : 1, 15 ml) was hydrogenated under atmospheric pressure of hydrogen for 3 h. The crude product obtained was purified by chromatography of CM-Sephadex C-25 column (NH_4^+ form, 16 ml) with, after washing with water, aqueous ammonia (0.01→0.5M) to give a solid of **29**, 33.0 mg [43% based on **21**, bis(carbonate)], $[\alpha]_D^{21}$ +85° (*c* 1, water); IR (KBr): 1700 cm^{-1}; ^1H NMR (20% ND_3 in D_2O) δ=1.43 (1H, q, *J*=13 Hz, H-2_{ax}), 1.65—2.15 (5H, H-2_{eq}, -2′$_{ax}$, -2′$_{eq}$, -3′$_{ax}$, -3′$_{eq}$), 5.11 (1H, d, *J*=3.8 Hz, H-1″), 5.35 (1H, br s, H-1′).

Found: C, 41.95; H, 7.09; N, 10.48%. Calcd for $C_{21}H_{41}N_5O_{11}\cdot 2H_2CO_3$: C, 41.62; H, 6.84; N, 10.55%.

1-*N*-(3-Aminopropoxycarbonyl)-2′,3′-dideoxykanamycin A (30). A solution of **22** (100 mg) and anhydrous sodium carbonate (10.5 mg) in 50% aqueous oxolane (3.3 ml) was treated with *N*-[3-(benzyloxycarbonylamino)propoxycarbonyloxy]-succinimide[14] (56 mg) in oxolane (1.7 ml) in a manner as described for **29** to give a solid, which was then led to **30**, 32.0 mg [40% based on **21**, bis(carbonate)], $[\alpha]_D^{21}$ +76° (*c* 2.8, water); ^1H NMR (20% ND_3 in D_2O) δ=1.43 (1H, q, *J*=12.5 Hz, H-2_{ax}), 1.65—2.15 (7H, H-2_{eq}, -2′$_{ax}$, -2′$_{eq}$, -3′$_{ax}$, -3′$_{eq}$ and

C(O)OCH$_2$C*H$_2$*CH$_2$NH$_2$), 5.11 (1H, d, J=3.8 Hz, H-1''), 5.35 (1H, br s, H-1').

Found: C, 42.46; H, 7.08; N, 9.94%. Calcd for $C_{22}H_{43}N_5O_{11}\cdot 2H_2CO_3$: C, 42.53; H, 6.99; N, 10.34%.

(*S*)-4-Benzyloxycarbonylamino-2-methoxybutyric Acid Methyl Ester (27). To a solution of (*S*)-4-benzyloxycarbonylamino-2-hydroxybutyric acid[13] (**26**, 2.5 g) in DMF (26 ml) were added silver oxide (4.6 g) and methyl iodide (1.9 ml), and the mixture was stirred in the dark at 5 °C overnight. After addition of methanol (0.5 ml) and ethyl acetate (50 ml), the mixture was filtered, and the filtrate was evaporated. The residue was chromatographed on silica gel with benzene–ethyl acetate (3 : 1) to give an oil of **27**, 1.42 g (51%), $[\alpha]_D^{20}$ −17° (*c* .1, chloroform); ^{1}H NMR ($CDCl_3$) δ=1.75—2.1 (2H, m, CH_2-3), 3.25 (2H, t, J=6 Hz, CH_2-4), 3.35 (3H, s, OCH_3), 3.70 (3H, s, CO_2CH_3), 3.82 (1H, q, J=5 and 7 Hz, H-2), 5.05 (2H, s, $PhCH_2O$), 7.30 (5H, s, C_6H_5).

(*S*)-4-Benzyloxycarbonylamino-2-methoxybutyric Acid (28). To a solution of **27** (1.4 g) in acetone (40 ml) was added 1M aqueous sodium hydroxide (7.5 ml) and the mixture was kept at room temperature for 40 min. After neutralization to pH 9 with aqueous hydrochloric acid, the solution was concentrated. The concentrate was washed with ether and, after addition of aqueous hydrochloric acid (to pH 6), extracted with ethyl acetate. The organic solution was dried (Na_2SO_4) and concentrated to give an oil, that was purified by a charcoal column developed by methanol to give an oil of **28**, 0.85 g (64%), $[\alpha]_D^{22}$ −16° (*c* 1, chloroform); *m/z* 267.11269 (M^+), Calcd for $C_{13}H_{17}NO_5$: 267.11290; ^{1}H NMR ($CDCl_3$) δ=2.00 (2H, m, CH_2-3), 3.27 (2H, t, J=6 Hz, CH_2-4), 3.37 (3H, s, OCH_3), 3.81 (1H, t, J=6 Hz, H-2), 5.07 (2H, s, $PhCH_2O$), 7.30 (5H, s, C_6H_5).

1-*N*-[(*S*)-4-Amino-2-methoxybutyryl]-2',3'-dideoxykanamycin A (25). Compound **22** (360 mg) was treated in a similar manner as described for **23** with *N*-[(*S*)-4-benzyloxycarbonylamino-2-methoxybutyryloxy]succinimide (255 mg), prepared from **28** in a ususl manner, to give a solid of **25**, 100 mg (41% based on **21**), $[\alpha]_D^{22}$ +87° (*c* 0.7, water) and **12**, 105 mg (48%). **25**: ^{1}H NMR (D_2O at 200 MHz) δ=1.40 (1H, q, H-2$_{ax}$), 1.6—2.02 (7H, H-2$_{eq}$, -2'$_{ax}$, -2'$_{eq}$, -3'$_{ax}$, -3'$_{eq}$ and COCH(OCH$_3$)-C*H*$_2$CH$_2$-), 3.37 (3H, s, OCH_3), 5.06 (1H, d, J=3.5 Hz, H-1''), 5.28 (1H, slightly br s, H-1').

Found: C, 47.13; H, 8.00; N, 12.13%. Calcd for $C_{23}H_{45}N_5O_{11}\cdot H_2O$: C, 47.16; H, 8.10; N, 11.96%.

References

1) S. Umezawa, T. Tsuchiya, R. Muto, Y. Nishimura, and H. Umezawa, *J. Antibiot.*, **24**, 274 (1971).

2) T. Tsuchiya, T. Jikihara, T. Miyake, S. Umezawa, M. Hamada, and H. Umezawa, *J. Antibiot.*, **32**, 1351 (1979).

3) S. Fukatsu, T. Yoneta, Unpublished data.

4) N. Sakairi, T. Yoneta, M. D. Rahman, and Y. Ishido, *J. Carbohydr. Chem.*, **3**, 51 (1984).

5) P. Dais, T. K. M. Shing, and A. S. Perlin, *J. Am. Chem. Soc.*, **106**, 3082 (1984); related references are cited therein.

6) T. Jikihara, T. Tsuchiya, H. Umezawa, and S. Umezawa, *Carbohydr. Res.*, **89**, 91 (1981).

7) Y. Takagi, C. Komuro, T. Tsuchiya, and S. Umezawa, *Bull. Chem. Soc. Jpn.*, **54**, 1834 (1981); related references are cited therein.

8) T. Miyake, T. Tsuchiya, S. Umezawa, and H. Umezawa, *Carbohydr. Res.*, **49**, 141 (1976).

9) E. Albano, D. Horton, and T. Tsuchiya, *Carbohydr. Res.*, **2**, 349 (1966).

10) T. Yoneta, T. Matsuno, H. Nanahoshi, and S. Fukatsu, *Nippon Kagaku Kaishi*, **1982**, 1730.

11) T. Yoneta, T. Matsuno, and S. Fukatsu, *Chem. Pharm. Bull.*, **29**, 3464 (1981).

12) T. Tsuchiya, Y. Takagi, and S. Umezawa, *Tetrahedron Lett.*, **1979**, 4951.

13) H. Kawaguchi, T. Naito, S. Nakagawa, and K. Fujisawa, *J. Antibiot.*, **25**, 695 (1972).

14) Y. Takagi, C. Komuro, T. Tsuchiya, S. Umezawa, M. Hamada, and H. Umezawa, *J. Antibiot.*, **34**, 1 (1981).

15) A. K. Mallams, P. Reichert, and J. B. Morton, Current Chemotherapy and Infectious Disease, Proceedings of the 11th International Congress of Chemotherapy and the 19th Interscience Conference on Antimicrobial Agents and Chemotherapy, Boston, Massachusetts, U. S. A., October 1-5, 1979, Vol. 1, p. 406, 1980.

16) T. Yamaguchi, T. Tsuchiya, and S. Umezawa, *J. Antibiot.*, **30**, 71 (1977).

 © 1987 The Chemical Society of Japan Bull. Chem. Soc. Jpn., 60, 721—725 (1987)

Chlorination of Acyclic β-Diketones. Formation and Stability of β-Chloro-β,γ-unsaturated Ketones[1]

Toshio SUGITA,* Hiroshi ITO, Akihiko NAKAJIMA, Motoshi SUNAMI, Atsushi KAWAKATSU, Masakazu SUAMA, and Katsuhiko ICHIKAWA
Department of Hydrocarbon Chemistry, Faculty of Engineering, Kyoto University, Kyoto 606
(Received August 22, 1986)

Chlorination of acyclic β-diketones with triphenylphosphine–carbon tetrachloride and the other chlorinating reagents predominantly afforded β-chloro-β,γ-unsaturated ketones except the cases of the terminal alkyl group of the diketones was methyl or *t*-butyl. In these reactions, the isomerization of the β-chloro-α,β-unsaturated ketones to the β,γ-unsaturated isomers was involved; the isomerization was achieved by triphenylphosphine–carbon tetrachloride as well as by some acid catalysts.

In our series of studies concerning reactions of β-diketones, the chlorination of β-diketones giving β-chloro-α,β-unsaturated ketones has attracted our attention. β-Chloro-α,β-unsaturated carbonyl compounds have become increasingly useful as intermediates in organic syntheses. For example, β-chloro-α,β-unsaturated ketones react with a zinc-silver couple in methanol,[2] active methylene compounds,[3] dimethylsulfoxonium methylide,[4] and a nitrogen compound[5] to produce a series of structurally diverse and potentially fruitful synthetic intermediates.

These β-chloro-α,β-unsaturated ketones were prepared by the chlorination of the corresponding β-diketones. However, the reactions hitherto reported were limited to those of cyclic β-diketones and 2,4-pentanedione.[2-13] Thus, we were prompted to investigate the chlorination of some acyclic β-diketones. As the chlorinating reagents of β-diketones, a variety of reagents, phosphorus trichloride,[6-8] phosgene,[9] acetyl chloride,[10] thionyl chloride,[7] phosphoryl chloride,[6] oxalyl dichloride,[2] and dichlorotriphenylphosphorane,[12] have been employed; however, triphenylphosphine in carbon tetrachloride was advantageously used to substitute the enol-hydroxyl group of β-diketones with a chlorine atom.[13] This procedure is regarded as being superior to the others since the formation of hydrogen chloride is not involved; thus, essentially neutral conditions can be maintained throughout the reaction. We examined the chlorination of several acyclic β-diketones using this procedure with some modification.

Results and Disccusion

The β-diketones were treated with triphenylphosphine and carbon tetrachloride in chloroform or in an excess of carbon tetrachloride to give β-chloro-α,β-unsaturated and/or β-chloro-β,γ-unsaturated ketones (Table 1).

Table 1. Chlorination of β-Diketones

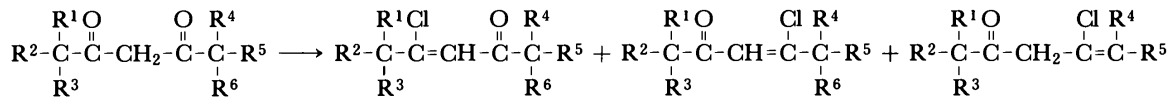

Run	Diketone							Reagent	Solvent	Chloro ketone[a]			
		R^1	R^2	R^3	R^4	R^5	R^6			Yield/%	2	3	4
1	**1a**	H	H	H	H	H	H	Ph_3P-CCl_4	CCl_4	96	100		0
2[b]	**1a**							$(COCl)_2$	$CHCl_3$	50	100		0
3	**1a**							PCl_3	$CHCl_3$	25	100		0
4	**1b**	Me	H	H	Me	H	H	Ph_3P-CCl_4	$CHCl_3$	46(76)	20		80
5	**1b**							Ph_3P-CCl_4	CCl_4	27	17		83
6	**1b**							$(COCl)_2$	C_6H_6	36	27		73
7	**1b**							PCl_3	$CHCl_3$	0[c]			
8	**1b**							$SOCl_2$	$CHCl_3$	0[d]			
9	**1c**	Me	Me	H	Me	Me	H	Ph_3P-CCl_4	$CHCl_3$	45(70)	10		90
10	**1c**							$(COCl)_2$	$CHCl_3$	29	37		63
11	**1d**	Me	Me	Me	Me	Me	Me	Ph_3P-CCl_4	CCl_4	(7)[e,f]	100		0
12	**1e**	H	H	H	Me	H	H	Ph_3P-CCl_4	CCl_4	(54)	35	12	53
13	**1f**	H	H	H	Me	Me	H	Ph_3P-CCl_4	CCl_4	(56)	67	4	29
14	**1g**	H	H	H	Me	Me	Me	Ph_3P-CCl_4	CCl_4	(29)[e,g]	100	0	0

a) Yields are isolated yields, values indicated in parentheses are obtained by GLPC, and the isomer distributions are obtained from the crude products by GLPC. b) Lit.[2] c) Unreacted diketone was recovered. d) Many unidentified products were obtained. e) Refluxed for 7 d. f) 26% of unreacted **1d** was recovered. g) 15% of **1g** was recovered.

Table 2. Isomerization between **2b** and **4b** in Chloroform

Catalyst	Starting material **2b** : **4b**	After 6 h at 60 °C **2b** : **4b**	After standing at room temp. overnight **2b** : **4b**
None	100 : 0	100 : 0	
Ph_3P-CCl_4	89 : 11	23 : 77	17 : 83
Ph_3P-CCl_4	2 : 98	12 : 88	14 : 86
Ph_3P	85 : 15	77 : 23	74 : 26
CF_3COOH	100 : 0	80 : 20	58 : 42
$AlCl_3$	100 : 0		57 : 43

4-Chloro-3-penten-2-one (**2a**) obtained from 2,4-pentanedione (**1a**) was a mixture of geometrical isomers (*E* : *Z*=85 : 15), which was confirmed by comparisons of their ^1H NMR spectra with the reported data.[14] Although β-chloro-α,β-unsaturated ketones were obtained from the corresponding β-diketones when the terminal alkyl group was methyl or *t*-butyl, 3,5-heptanedione (**1b**) and 2,6-dimethyl-3,5-heptanedione (**1c**) predominantly afforded unexpected β-chloro-β,γ-unsaturated ketones, 5-chloro-5-hepten-3-one (**4b**) and 5-chloro-2,6-dimethyl-5-hepten-3-one (**4c**) respectively. These ketones did not show the signal of a vinyl proton of the α,β-unsaturated ketone at around δ=6.5, but a singlet of methylene protons at δ=3.5 in their NMR spectra. These characteristic data, as well as their other NMR signals, indicate that the products are β-chloro-β,γ-unsaturated ketones. The **4b** obtained here was mainly a *Z* isomer, *Z* : *E*=89 : 11; its ^{13}C NMR spectrum indicated central methylene carbon signal at δ=52.60 and the γ-methyl signal at δ=14.27. These chemical shifts of the product were down-field compared with the respective values of its isomer (47.44 and 12.33), a small amount of which was detected in the product mixture in some cases but, unfortunately, could not be isolated. In a preliminary communication, we reported that the β-chloro-β,γ-unsaturated ketones were the exclusive product in these cases;[1] however, we later confirmed the formation of the α,β-unsaturated isomers (even in small amounts). There were some difficulties to separate the α,β-unsaturated isomers from the unreacted β-diketones. On the contrary, the β,γ-unsaturated ketones could be easily separated by column chromatography as well as GLPC. By increasing the steric bulkiness of the terminal alkyl groups of diketones, the reaction became very slow. The chlorination of **1d** resulted in only a product/unreacted diketone=7/12 after refluxing for 7 d.

In order to investigate the regioselectivity of the chlorination, unsymmetrical β-diketones were treated with triphenylphosphine and carbon tetrachloride in the same fashion. 2,4-Hexanedione (**1e**) gave a mixture of 5-chloro-4-hexen-3-one (**2e**), 4-chloro-3-hexen-2-one (**3e**) and 4-chloro-4-hexen-2-one (**4e**) in a ratio of 35 : 12 : 53. **4e** was mainly the *Z* isomer containing small amount of the *E* isomer similarly to **4b**. The chlorination of 5,5-dimethyl-2,4-hexanedione (**1g**) afforded a sole kind of α,β-unsaturated ketone. The ^1H NMR chemical shift of *t*-butyl group of the product (δ=1.14) was the same as that of the starting diketone (δ=1.14), and a long-range coupling (*J*=1.2 Hz) was observed between the methyl and the vinyl protons. Thus, the chlorination product was confirmed to be (*E*)-5-chloro-2,2-dimethyl-4-hexen-3-one (*E*-**2g**). The fact that the chlorination occurred at the acetyl moiety may be due to the steric bulkiness of the *t*-butyl group. The results obtained from these unsymmetrical diketones were comparable in the product distributions to that of symmetrical diketones. The chlorination of acetyl moiety gave only α,β-unsaturated ketones; however, the propionyl and isobutyryl groups were chlorinated, giving a mixtures of α,β- and β,γ-unsaturated isomers. Furthermore, the product ratios of α,β- and β,γ-unsaturated isomers, **3e** : **4e**=18 : 82 for propionyl group and **3f** : **4f**=12 : 88 for isobutyryl group, were quite equal to those obtained from symmetrical diketones, **2b** : **4b**=20 : 80 and **2c** : **4c**=10 : 90.

As control experiments, chlorination with oxalyl dichloride or phosphorus trichloride was pursued in the same way as reported.[2,3,7] The differences on isomeric ratio of the products in each preparation method was not so quite pronounced (Table 1), but triphenylphosphine-carbon tetrachloride system is superior to the other reagents regarding chemical yields.

As the enol form of β-diketones is considered to take an α,β-unsaturated ketone structure, the substitution of enol hydroxyl group of β-diketone by chlorine was expected to afford β-chloro-α,β-unsaturated ketone. In fact, **2b** was predominated over **4b** during an early stage of the chlorination reaction of **1b**; then, **4b** became superior as the reaction progresses. Thus, we undertook to examine the isomerization of the chlorinated products. The results are summarized in Table 2. When **2b** was heated at 60—65 °C in chloroform for 6 h, no isomerization could be observed at all. The isomerization from the α,β-unsaturated ketone **2b** to the β,γ-unsaturated isomer **4b**; however, it readily took place in the presence of triphenylphosphine and carbon tetrachloride, i.e. under the chlorination conditions, giving a mixture of 17% of **2b** and 83% of **4b**. A mixture of 14% of **2b** and 86% of **4b** was also obtained from **4b**. These values were almost identical with the isomeric ratio of the chlorination product. A slow isomerization was also achieved with acid catalysts,

CF_3COOH or $AlCl_3$, and triphenylphosphine alone. As a result of these experiments, it became clear that the β-chloro-β,γ-unsaturated ketone is thermodynamically more stable than its α,β-unsaturated isomer when a methyl group is substituted at the γ-position. The relative stabilities of the α,β- and β,γ-unsaturated carbonyl compounds have been discussed in terms of the conjugative and inductive contributions of substituents located on the three-carbon allylic chain;[15] however, very little is known about β-chloro-β,γ-unsaturated ketones and esters. Martin and Kirschleger indicated that the β-chloro-β,γ-unsaturated ketones preponderated over the α,β-unsaturated isomers in the Friedel-Crafts acylation products of alkylacetylenes with acetyl chloride.[16] Although the equilibrium between the α,β- and β,γ-unsaturated forms of the three-carbon allylic chain is not sensitive to the nature of the adjacent activating group as well as the alkyl substituents at the β-position, the alkyl substitution, particularly methyl substitution, at the γ-position increases the relative thermodynamic stability of the β,γ-unsaturated isomer.[15,17] More recently, Rhoads et al.[18] and Taskinen and Mukkala[19] reported that the introduction of a methoxyl group at the β-position strongly shifted the equilibrium towards the side of β,γ-unsaturated isomers.

In the present case, although the thermodynamic stability of β,γ-unsaturated ketones (**4**) may be primarily due to the γ-methyl substituent,[15] the similar effects to the β-methoxyl substituent would be expected for β-chloro substituent because the equilibration so strongly favored the β,γ-unsaturated isomer that would not have been expected on the basis of earlier analyses.[15] The initially formed β-chloro α,β-unsaturated ketones favored the *E* isomer. This fact may indicate a repulsive *cis* dipole-dipole interaction of the two polar functions, chloride and carbonyl, in the *Z* isomer is quite large. If the *Z* isomer exists in *s-trans* conformation, the repulsive dipole-dipole interaction would be diminished, but the steric repulsion between chlorine and the alkyl group attached to the carbonyl would contrary become prominent. In the *E* isomer of α,β-unsaturated ketones, a large steric repulsion between the ethyl or isopropyl group adjacent to the olefinic linkage and the acyl group destabilizes the *E* isomer. These steric and dipole-dipole interactions are relieved in the β,γ-unsaturated isomer. Thus, the chlorination products of **1b** and **1c** are favored β,γ-unsaturated ketone structures. On the other hand, as **2a** lacks γ-methyl substituent and also as the destabilizing *cis* steric interaction between methyl and acetyl groups would be overcome by the conjugative stabilization of α,β-unsaturated carbonyl system, **1a** gives only α,β-unsaturated **2a**.

Experimental

All bps were uncorrected. ^1H and ^{13}C NMR spectra were taken on JEOL PMX-60 and JNM-FX100 spectrometers respectively in $CDCl_3$ using TMS as an internal standard. IR spectra were measured with a Hitachi EPI-G2 spectrometer. MS spectra were taken on Hitachi M-80 mass spectrometer. GLPC analyses were performed on Hitachi 163 and 263 gas chromatographs using 3 mm×2 m columns packed with Silicone SE-30 30% on Shimalite or PEG-20M 20% on Chromosorb-W. Purifications of products were conducted by medium-pressure column chromatography on silica gel (Merck Kieselgel 60) or by atmospheric-pressure column chromatography on silica gel (Wakogel C-200).

Commercial GR grade 2,4-pentanedione was used after distillation, and the other β-diketones were prepared by reported methods.[20]

General Procedure for the Chlorination of β-Diketones. To a stirred mixture of 3,5-heptanedione (**1b**; 3.85 g, 30 mmol) and triphenylphosphine (15.7 g, 60 mmol), a solution of carbon tetrachloride (7.23 g, 47 mmol) in 55 ml of chloroform was added over a 5-min period. After the addition, the mixture was stirred at 60 °C for 6 h, then allowed to stand overnight at room temperature. The solvent was removed on a rotary evaporator under moderately reduced pressure. The residual viscous matter was extracted four times by grinding with 80 ml of pentane in a mortar finally leaving triphenylphosphine oxide and (dichloromethyl)triphenylphosphonium chloride as white crystalline powder. The extracts were combined and distilled to give a crude product, bp 95—104 °C/50 mmHg (1 mmHg=133.322 Pa), 3.5 g, which was a mixture of **1b** (4.1%), *E*-**2b** (16.3%), **4b** (77.2%), and *Z*-**2b** (2.4%) in order of GLPC retention times. The crude product was purified by moderate pressure column chromatography using hexane and hexane-ethyl acetate (98:2) as the eluent to obtain pure **2b** (0.27 g) and **4b** (1.74 g).

When the chlorination was pursued in excess carbon tetrachloride instead of chloroform solution, the GLPC-determined yields were almost comparable with the reaction in chloroform, however, we suffered some difficulties in the separation of products from the phosphonium salt and triphenylphosphine oxide.

(*Z*)-5-Chloro-5-hepten-3-one (*Z*-4b). Bp 86 °C/19 mmHg; ^1H NMR δ=1.07 (t, *J*=8 Hz, 3H), 1.78 (d, *J*=7 Hz, 1H), 2.57 (q, *J*=8 Hz, 2H), 3.39 (s, 2H), 5.72 (q, *J*=7 Hz, 1H); ^{13}C NMR δ=7.63 (q), 14.27 (q), 35.17 (t), 52.60 (t), 125.05 (s), 127.81 (d), 206.77 (s); IR (neat): 1660, 1720 cm^{-1}; MS: *m/z* 148 (M+2),

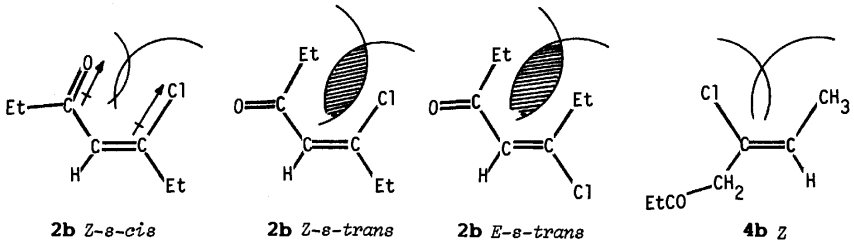

2b *Z-s-cis* **2b** *Z-s-trans* **2b** *E-s-trans* **4b** *Z*

146 (M^+), 117, 91, 89, 57; Found: C, 57.57; H, 7.65; Cl, 23.91%. Calcd for $C_7H_{11}OCl$: C, 57.34; H, 7.56; Cl, 24.18%.

(*E*)-5-Chloro-5-hepten-3-one (*E*-4b). Obtained as a mixture of *E*-**4b** and *Z*-**4b** (12 : 88). Bp 78 °C/20 mmHg; ^{13}C NMR δ=7.63 (q), 12.33 (q), 34.76 (t), 47.44 (t), 126.28 (s), 205.83 (s), a peak derived from C^5 could not be identified; Found: C, 57.54; H, 7.75; Cl, 24.35% (values obtained from the mixture).

(*E*)-5-Chloro-4-hepten-3-one (*E*-2b). ^1H NMR δ=1.06 (t, *J*=7 Hz, 3H), 1.16 (t, *J*=7 Hz, 3H), 2.49 (q, *J*=7 Hz, 2H), 2.96 (q, *J*=7 Hz, 2H), 6.35 (s, 1H); ^{13}C NMR δ=7.87 (q), 12.77 (q), 29.77 (t), 37.70 (t), 124.70 (d), 157.60 (s), 199.32 (s); IR (neat): 1600, 1690 cm^{-1}; Found: C, 57.16; H, 7.60; Cl, 23.99%.

(*Z*)-5-Chloro-4-hepten-3-one (*Z*-2b). ^1H NMR δ=1.20 (t, *J*=7 Hz, 3H), 1.30 (t, *J*=6 Hz, 3H), 2.47 (q, *J*=7 Hz, 2H), 2.60 (q, *J*=6 Hz, 2H), 6.21 (s, 1H); ^{13}C NMR δ=7.81 (q), 12.27 (q), 34.76 (t), 37.22 (t), 123.06 (d), 147.83 (s), 198.40 (s); IR (neat): 1610, 1705 cm^{-1}; Found: C, 57.40; H, 7.73; Cl, 24.29% (values obtained from a mixture of *Z*-**2b** and *Z*-**4b** (33 : 67)).

4-Chloro-3-penten-2-one (2a). Bp 63 °C/170 mmHg; ^1H NMR (*E*) δ=2.21 (s, 3H), 2.56 (d, *J*=1.1 Hz, 3H), 6.48 (q, *J*=1.1 Hz, 1H), (lit,[14] δ=2.20, 2.52, 6.47); (*Z*) δ=2.26 (s, 3H), 2.33 (s, 3H), 6.27 (s, 1H), (lit,[14] δ=2.26, 2.33, 6.27); IR (neat): 1610, 1700 cm^{-1} (lit,[14] 1610, 1705 cm^{-1}). The ratio *E* : *Z*= 85 : 15 was estimated from the peak area of GLPC.

5-Chloro-2,6-dimethyl-5-hepten-3-one (4c). Bp 113 °C/34 mmHg; ^1H NMR δ=1.13 (d, *J*=7 Hz, 6H), 1.71 (s, 3H), 1.84 (s, 3H), 2.64 (m, 1H), 3.57 (s, 2H); ^{13}C NMR δ=18.14 (q), 20.99 (q), 21.72 (q), 39.92 (d), 47.32 (t), 131.57 (s), 152.99 (s), 209.54 (s); Found: C, 61.92; H, 8.65; Cl, 19.82%. Calcd for $C_9H_{15}OCl$: C, 61.89; H, 8.66; Cl, 20.30%.

5-Chloro-2,6-dimethyl-4-hepten-3-one (2c). ^1H NMR δ= 1.25 (d, *J*=8 Hz, 6H), 1.30 (d, *J*=8 Hz, 6H), 2.60 (m, 2H), 2.75 (m, 2H), 6.38 (s, 1H); ^{13}C NMR δ=19.08 (q), 19.32 (q), 36.64 (d), 41.33 (d), 120.41 (d), 202.26 (s), a peak derived from C^5 could not be identified, (values obtained from a mixture with **4c**).

5-Chloro-2,2,6,6-tetramethyl-4-hepten-3-one (2d). ^1H NMR δ=1.17 (s, 9H), 1.26 (s, 9H), 6.57 (s, 1H); IR (neat): 1595, 1695 cm^{-1}; MS: *m/z* 204 (M+2), 202 (M^+), 147, 145, 117, 57.

5-Chloro-4-hexen-3-one (2e). ^1H NMR δ=1.07 (t, *J*=7 Hz, 3H), 2.48 (q, *J*=7 Hz, 2H), 2.54 (s, 3H), 6.39 (s, 1H); ^{13}C NMR δ=7.87 (q), 24.12 (q), 37.75 (t), 125.41 (d), 151.18 (s), 198.50 (s); IR (neat): 1605, 1695 cm^{-1}; Found: C, 54.21; H, 6.88; Cl, 26.87%. Calcd for C_6H_9OCl: C, 54.35; H, 6.84; Cl, 26.74%.

(*E*)-4-Chloro-3-hexen-2-one (*E*-3e). ^1H NMR δ=1.06 (t, *J*=7 Hz, 3H), 2.23 (s, 3H), 2.58 (q, *J*=7 Hz, 2H), 6.27 (s, 1H); ^{13}C NMR δ=7.81 (q), 28.30 (q), 37.10 (t), 124.64 (d), 142.08 (s), 198.85 (s); IR (neat): 1615, 1700 cm^{-1}. Acetyl proton signal, δ=2.23, was observed at almost the same chemical shift with *E*-**2a**, and very weak but clear signals expected to be derived from its *Z* isomer were observed in the ^{13}C NMR spectrum at δ=9.5, 29.2, and 138.4, thus the product was estimated to be *E* isomer.

(*Z*)-4-Chloro-4-hexen-2-one (*Z*-4e). ^1H NMR δ=1.78 (d, *J*=7 Hz, 3H), 2.14 (s, 3H), 3.37 (s, 2H), 5.69 (q, *J*=7 Hz, 1H); ^{13}C NMR δ=14.27 (q), 28.94 (q), 53.66 (t), 125.29 (d), 127.87 (s), 204.08 (s); IR (neat): 1660, 1725 cm^{-1}; Found: C, 54.45; H, 7.00; Cl, 26.51%. Calcd for C_6H_9OCl: C, 54.35; H, 6.84; Cl, 26.74% (values obtained from a mixture of **4e** and **3e** (92 : 8)). The product was almost a single isomer, estimated as a *Z* isomer by compairing its ^1H and ^{13}C NMR spectra with those of **4b**. Weak absorptions at δ=1.64 (d), 2.17 (s), 3.41 (s), 5.87 (s) (^1H NMR) and at δ=37.80, 47.61 (^{13}C NMR) indicated the contamination of small amount of the *E* isomer.

(*E*)-5-Chloro-2-methyl-4-hexen-3-one (*E*-2f). ^1H NMR δ= 1.13 (d, *J*=7 Hz, 6H), 2.28—2.83 (m, 1H), 2.58 (s, 3H), 6.54 (s, 1H); ^{13}C NMR δ=18.02 (q), 24.18 (q), 41.98 (d), 124.58 (d), 151.94 (s), 201.90 (s); IR (neat): 1605, 1695 cm^{-1}; Found: C, 57.55; H, 7.53; Cl, 23.89%. Calcd for $C_7H_{11}OCl$: C, 57.34; H, 7.56; Cl, 24.18%.

(*Z*)-5-Chloro-2-methyl-4-hexen-3-one (*Z*-2f). ^1H NMR δ= 1.13 (d, *J*=7 Hz, 6H), 2.77 (m, 1H), 2.28 (s, 3H), 6.39 (s, 1H); ^{13}C NMR δ=18.02 (q), 28.36 (q), 41.27 (d), 122.88 (d), 142.27 (s), 201.66 (s); IR (neat): 1610, 1695 cm^{-1}; Found: C, 57.29; H, 7.66; Cl, 23.90%.

4-Chloro-5-methyl-4-hexen-2-one (4f). ^1H NMR δ=1.78 (s, 3H), 1.89 (s, 3H), 2.17 (s, 3H), 3.46 (s, 2H); IR (neat): 1670, 1720 cm^{-1}; Found: C, 57.59; H, 7.72; Cl, 23.91%. Calcd for $C_7H_{11}OCl$: C, 57.34; H, 7.56; Cl, 24.18%.

(*E*)-5-Chloro-2,2-dimethyl-4-hexen-3-one (*E*-2g). ^1H NMR δ=1.15 (s, 9H), 2.52 (d, *J*=1.2 Hz, 3H), 6.62 (q, *J*=1.2 Hz, 1H); IR (neat): 1605, 1695 cm^{-1}; Found: C, 59.77; H, 8.22; Cl, 22.02%. Calcd for $C_8H_{13}OCl$: C, 59.81; H, 8.16; Cl, 22.07%.

Isomerization between 2b and 4b. A solution of **2b** (*E* : *Z*=55 : 1; 230 mg, 1.57 mmol), triphenylphosphine (828 mg, 3.14 mmol), carbon tetrachloride (490 mg, 3.14 mmol), tetralin (internal standard, 72 mg) in 5 ml of chloroform was kept at 57—60 °C for 6 h, then at room temperature overnight. The products distribution was analyzed by GLPC, giving the ratio of **2b** : **4b**=17 : 83. **4b** (contained 3% of **2b**, 168 mg, 1.15 mmol) was also treated as same as mentioned above yielding a mixture of **2b** : **4b**=14 : 86.

In the case of trifluoroacetic acid-catalyzed isomerization experiment, *E*-**2b** (147 mg, 1.0 mmol) and trifluoroacetic acid (104 mg, 0.91 mmol) was dissolved in 0.5 ml of $CDCl_3$, the solution in a NMR tube was kept at 53—57 °C for 5 h, and the ratio of **2b** and **4b** was obtained from the peak integrals of δ=6.35 (*E*-**2b**, 1H), 6.21 (*Z*-**2b**, 1H), and 3.39 (**4b**, 2H).

The pertial contribution of Mr. Kazuaki Abe and Mr. Mitsuru Eida to the experimental work is appreciated. The authors are grateful to Dr. Tamio Ueno of the Pesticide Research Institute for measurements of the MS spectra.

References

1) A preliminary communication on part of this work has appeared: M. Suama, A. Nakajima, T. Sugita, and K. Ichikawa, *Chem. Lett.*, **1981**, 1459.

2) R. D. Clark and C. H. Heathcock, *Synthesis*, **1974**, 47; *J. Org. Chem.*, **41**, 636 (1976).

3) J. P. Chorvat, J. R. Palmer, and R. Pappo, *J. Org. Chem.*, **43**, 966 (1978).

4) Y. Tamura, T. Miyamoto, T. Nishimura, J. Eiho, and Y. Kita, *J. Chem. Soc., Parkin Trans. 1*, **1974**, 102; J. P. Marino and T. Kaneko, *J. Org. Chem.*, **39**, 3175 (1974).

5) C. Kashima and T. Tajima, *Synthesis*, **1980**, 880.

6) A. Crossley and H. LeSeur, *J. Chem. Soc.*, **83**, 110 (1903).

7) R. L. Frank and H. K. Hall, Jr., *J. Am. Chem. Soc.*, **72**, 1645 (1950).

8) T. G. Halsall and D. B. Thomas, *J. Chem. Soc.*, **1956**, 2431.

9) M. M. Shemyakin, Yu. A. Arbuzov, M. N. Kolosov, G. A. Shatenshtein, V. V. Onoprienko, and Yu. V. Konnova, *Zh. Obshch. Khim.*, **30**, 542 (1960); *Chem. Abstr.*, **54**, 24575i (1960).
10) W. Hückel and K. Thiele, *Chem. Ber.*, **94**, 96 (1961).
11) W. Pfleiderer and K. Schündehütte, *Justus Liebigs Ann. Chem.*, **612**, 158 (1958).
12) E. Piers and I. Nagakura, *Synth. Commun.*, **5**, 193 (1975).
13) L. Gruber, I. Tömösközi, and L. Radics, *Synthesis*, **1975**, 708; R. Appel, *Angew. Chem.*, **87**, 863 (1975).
14) H. Martens, G. Hoornaert, and S. Toppet, *Tetrahedron*, **29**, 4241 (1973).
15) C. K. Ingold, "Structure and Mechanism in Organic Chemistry," 2nd ed., Cornell Univ. Press, Ithaca, N. Y. (1969), p. 823; P. B. de la Mare, *J. Chem. Soc.*, **1952**, 1602.
16) G. J. Martin and B. Kirschleger, *C. R. Acad. Sci., Ser. C*, **279**, 363 (1974).
17) G. A. R. Kon and K. S. Nargund, *J. Chem. Soc.*, **1934**, 623; E. N. Eccott and R. P. Linstead, *ibid.*, **1930**, 905; and references cited therein.
18) S. J. Rhoads, J. K. Chattopadhyay, and E. E. Waali, *J. Org. Chem.*, **35**, 3352 (1970); S. J. Rhoads and E. E. Waali, *ibid.*, **35**, 3358 (1970); S. J. Rhoads and R. W. Hasbrouck, *Tetrahedron*, **22**, 3557 (1966).
19) E. Taskinen and V.-M. Mukkala, *Tetrahedron*, **38**, 613 (1982).
20) C. R. Hauser, F. W. Swamer, and J. T. Adams, *Org. React.*, **8**, 59 (1954).

 © 1987 The Chemical Society of Japan Bull. Chem. Soc. Jpn., 60, 727—730 (1987)

The Synthesis of 1,3-Dithiolane-2-thione Derivatives

Yoichi TAGUCHI,* Koshin YANAGIYA, Isao SHIBUYA, and Yasuo SUHARA
National Chemical Laboratory for Industry, Higashi 1-1, Yatabe, Tsukuba, Ibaraki 305
(Received August 23, 1986)

The reaction of 2,2-dimethylthiirane with carbon disulfide in the presence of triethylamine was accelerated under high pressure to give 4,4-dimethyl-1,3-dithiolane-2-thione nearly quantitatively. The activation volume of this reaction at 40 °C was estimated to be −41 ml mol^{-1}. The rate of the reaction was proportional to the amount of triethylamine when a limited amount of triethylamine was used. The reaction of 2-methylthiirane, 2-hexylthiirane, 1,2-epithiocyclohexane, and 2-phenylthiirane with carbon disulfide gave the corresponding 1,3-dithiolane-2-thione derivatives in good yields. 2-Chloromethylthiirane was less reactive to carbon disulfide than other thiiranes under high pressure. Tertiary amines such as *N*,*N*-dimethylethylamine, pyridine, and *N*-methylmorpholine were good catalysts of the reaction.

Thiiranes react with various compounds to form the open-ring products.[1,2] It has been known that five-membered heterocyclic compounds are obtained by the reaction of thiiranes with methyl cyanoacetate,[3] malononitrile,[4] acetonitrile,[5] diethyl malonate,[6] and ethyl acetoacetate.[6] Although the reaction of thiirane (**1a**) with carbon disulfide gave 1,3-dithiolane-2-thione in a good yield, the reaction of substituted thiiranes with carbon disulfide showed lower yield.[7] On the other hand, high pressure accelerates many organic reactions[8] including those of carbon disulfide.[9,10] However, there has been no report on the reaction of thiiranes under high pressure.

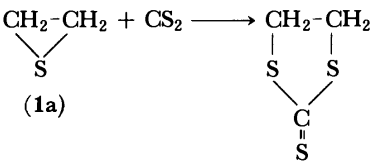

We will report that the reaction of substituted thiiranes with carbon disulfide is accelerated under high pressure to give the corresponding 1,3-dithiolane-2-thione derivatives in good yields. The effects of pressure, reaction temperature, and amount and kind of catalysts on the reaction of 2,2-dimethylthiirane (**1b**) with carbon disulfide were investigated and the reactions of various thiiranes with carbon disulfide attempted.

Results and Discussion

Under 1 kg cm^{-2} pressure, the reaction of **1b** with carbon disulfide at 80—100 °C in the presence of triethylamine as a catalyst gave 4,4-dimethyl-1,3-dithiolane-2-thione (**2**) in 2—12% yield. At a higher temperature (120 °C) the yield was still lower (10%)

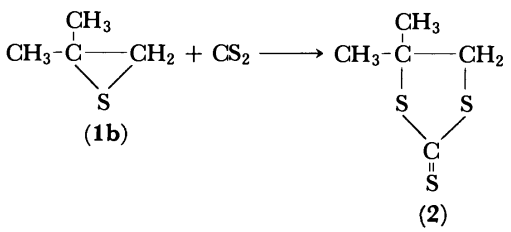

Table 1. Effect of Reaction Conditions on the Reaction of **1b** with CS_2[a]

Run	Temp	Press.[b]	Yield
	°C	kg cm^{-2}	%
1	80	1	2
2	100	1	12
3	120	1	10
4	40	5000	92
5	70	2000	96
6	100	2000	87
7	100	8000	91

a) **1b**: 10 mmol, CS_2: 50 mmol, Et_3N: 0.10 g, reaction time: 20 h. b) 1 kg cm^{-2}=0.9806×10^5 Pa.

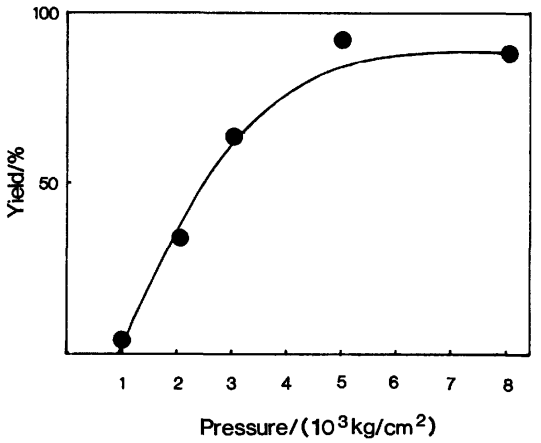

Fig. 1. Effect of pressure on the reaction of **1b** with CS_2; Reaction temperature: 40°C, reaction time: 20 h, **1b**: 10 mmol, CS_2: 50 mmol, Et_3N: 1 mmol.

and various by-products were contained in **2** (Table 1, Runs 1—3). When the reaction was carried out under high pressures (2000—8000 kg cm^{-2}), the yield of **2** increased to over 90% (Runs 4—7). As the pressure was increased to 5000 kg cm^{-2}, the rate of the formation of **2** was enhanced satisfactorily even at 40 °C (Run 4).

The effect of pressure on the reaction of **1b** with carbon disulfide is shown in Fig. 1. The reaction is regarded as a first-order reaction with respect to **1b**, because carbon disulfide is excessive. The reaction-velocity constant k is calculated from the data in Fig. 1.

The activation volume $\Delta V^{\neq}$ at 40 °C estimated by Eq. 1 was −41 ml mol^{-1}. This value suggests that the reaction is considerably accelerated by the pressure.

$$\Delta V^{\neq} = RT(\partial \ln k/\partial P)_T \quad (1)$$

Figure 2 shows that the rate of reaction of **1b** with carbon disulfide is proportional to the amount of triethyamine catalyst when a limited amount of triethylamine is used.

Table 2 shows the products and yields of reactions of various thiiranes with carbon disulfide. The reaction of 2-methylthiirane, 2,2-dimethythiirane, 2-hexylthiirane, 2-phenylthiirane, and 1,2-epithiocyclohexane with carbon disulfide gave the corresponding 1,3-dithiolane-2-thiones in good yields. The yield of the reaction of **1a** with carbon disulfide was 53%. This fact is considered to be due to a tendency of **1a** to polymerize. 2-Chloromethylthiirane showed low reactivity and selectivity toward carbon disulfide in comparison with other thiiranes.

Table 3 shows the effects of various catalysts on the reaction of **1b** with carbon disulfide. *N*,*N*-Dimethylethylamine, triethylamine, *N*-methylmorpholine, and pyridine were good catalysts under high pressure, the catalytic activity decreasing in this order. *N*,*N*-Dimethylaniline had no catalytic activity even under high pressure. The catalytic activity of tertiary amines, therefore, would be influenced by basicity as well as steric factor. Tetramethylammonium bromide, which has been reported to have catalytic activity on the reaction of oxiranes with carbon disulfide,[7] showed low activity under 8000 kg cm^{-2}. Lithium chloride was used as a catalyst of the reaction of thiiranes or oxiranes with various heterocumulenes,[8,11,12] but it had no catalytic activity on the reaction of **1b** with carbon disulfide under 8000 kg cm^{-2} at 100 °C.

The reaction of thiiranes or oxiranes with various heterocumulenes under ordinary pressure has been reported to give five-membered products.[8,11,12] The reactions of **1b** with methyl isothiocyanate, phenyl

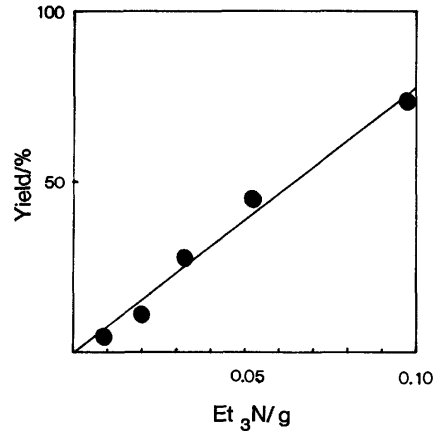

Fig. 2. Effect of amount of Et_3N on the reaction of **1b** with CS_2; Reaction temperature: 40°C, reaction time: 20 h, pressure: 3000 kg cm^{-2}, **1b**: 10 mmol, CS_2: 50 mmol.

Table 2. The Reaction of Various Thiiranes with CS_2[a]

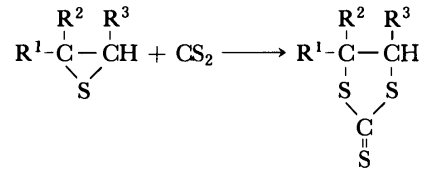

Run	Thiiranes			Temp	Press.	Yield
	R^1	R^2	R^3	°C	kg cm^{-2}	%
1	H	H	H	40	8000	53
2	CH_3	H	H	40	8000	97
3	CH_3	CH_3	H	40	5000	92
4	C_6H_{13}	H	H	40	8000	94
5	C_6H_{13}	H	H	70	2000	94
6	C_6H_5	H	H	100	8000	91
7	$ClCH_2$	H	H	40	8000	6
8	$ClCH_2$	H	H	100	8000	32[b]
9	H	$-(CH_2)_4-$		40	8000	92

a) thiirane: 10 mmol, CS_2: 50 mmol, Et_3N: 0.10 g, reaction time: 20 h. b) 0.30 g of Et_3N was used as catalyst.

Table 3. Effect of Various Catalysts on the Reaction of **1b** with CS_2[a]

Run	Catalyst	Press.	Temp	Yield
		kg cm^{-2}	°C	%
1	Triethylamine	3000	40	74
2	*N*,*N*-Dimethylethylamine	3000	40	83
3	*N*-Methylmorpholine	3000	40	2
4	Pyridine	3000	40	trace
5	*N*,*N*-Dimethylaniline	3000	40	trace
6	*N*-Methylmorpholine	8000	40	100
7	Pyridine	8000	40	99
8	*N*,*N*-Dimethylaniline	8000	40	trace
9	Pyridine	8000	100	100
10	Et_4NBr	8000	40	7
11	Et_4NBr	8000	100	10
12	LiCl	8000	100	trace
13	None	2000	100	trace

a) **1b**: 10 mmol, CS_2: 50 mmol, catalyst: 1 mmol, reaction time: 20 h.

isocyanate, and dicyclohexylcarbodiimide under high pressure were tried, but no effect of the compression appeared in any cases. Accordingly, highly selective reaction of thiiranes under high pressure seems to be characteristic of carbon disulfide; it is carbon disulfide that is activated under high pressure but not **1b**. On the other hand, the reaction of **1b** with carbon disulfide without catalyst under high pressure gave various by-products and only a trace of **2** (Table 3, Run 13). It is well-known that carbon disulfide reacts with amines easily.[14]

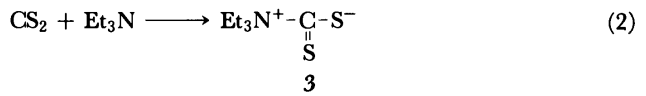

(2)

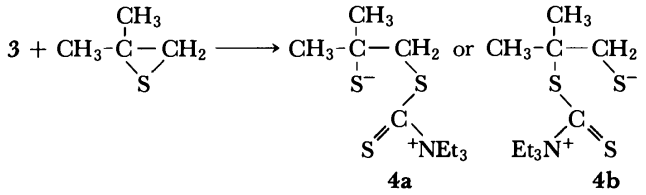

(3)

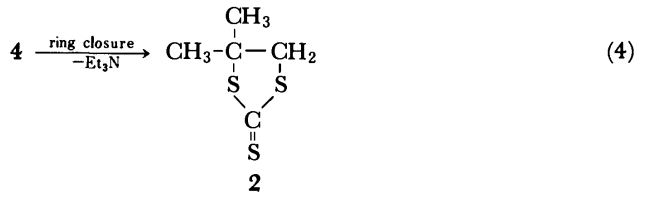

(4)

The reaction of **1b** with carbon disulfide in the presence of triethylamine seems to proceed succesively with the first step of adduct **3** formation from carbon disulfide and triethylamine (Eq. 2), then addition of **3** to **1b** yielding **4** (Eq. 3), and ring closing of **4** (Eq. 4). Whether the structure of **4** is **4a** or **4b** is ambiguous, because both **4a** and **4b** lead to the same product **2** by rapidly succeeding ring closure. But **4a** is more likely, because active methylene compounds[6] and secondary amines[15] are apt to attack the less-hindered carbon atom of thiirane ring. Equation 4 is a reaction in which two molecules (**2** and Et_3N) are formed from one molecule, and it is unlikely that compression accelerates such a reaction. Therefore, the compression seemes to be effective on a step of Eq. 2 or 3.

Experimental

Apparatus. The apparatus used for the reaction under high pressure was the same as that described previousyl.[16]

Measurement. GLC was carried out by a JEOL 20KF chromatograph with 20% SE-30 columns. ^{1}H NMR spectra were measured by a Hitachi R-40 spectrometer. Mass spectra were measured by a JEOL D-300 GC-MS spectrometer using the CI (chemical ion) method with isobutane. IR spectra were obtained by a JASCO A-302 spectrophotometer.

Materials. Thiirane and 2-methylthiirane were purchased from Aldrich Chem. Co. 2,2-Dimethylthiirane, 2-hexylthiirane, 2-phenylthiirane, and 1,2-epithiocyclohexane were prepared as previously described.[6] 2-Chloromethylthiirane was obtained by the method of Culvenor.[17]

Reaction of Thiiranes with Carbon Disulfide. A typical procedure is as follows: A homogeneous mixture of **1b** (10 mmol), carbon disulfide (50 mmol), and triethylamine (1 mmol) in a sealed teflon tube was compressed to 5000 kg cm^{-2}, heated at 40 °C, and maintained for 20 h in a high pressure equipment. The resulting mixture was subjected to evaporation and the residue was purified by distillation with Kugelrohr to give 1.50 g (92%) of **2**. IR: 1054, 1089 cm^{-1}; ^{1}H NMR δ=1.74 (s, 6H, $2CH_3$), 3.76 (s, 2H, CH_2); QM^+: 165.

Thiirane, 2-methylthiirane, 2-hexylthiirane, 1,2-epithiocyclohexane, 2-phenylthiirane, and 2-chloromethylthiirane were treated with carbon disulfide in a similar manner to the reaction of **1b** with carbon disulfide. The spectral data of products of these reactions are as follows:

1,3-dithiolane-2-thione. IR: 1057 cm^{-1}; ^{1}H NMR δ=4.00 (s, 4H, $2CH_2$); QM^+: 137.

4-methyl-1,3-dithiolane-2-thione. IR: 1076, 1050, 1033 cm^{-1}; ^{1}H NMR δ=1.64 (d, 3H, CH_3), 3.55—3.85 (dd, 1H, one proton of CH_2), 3.95—4.20 (dd, 1H, one proton of CH_2), 4.35—4.75 (m, 1H, CH); QM^+: 151.

4-hexyl-1,3-dithiolane-2-thione. IR: 1064 cm^{-1}; ^{1}H NMR δ=0.88 (t, 3H, CH_3), 1.34 (s, 8H, $\{CH_2\}_4$), 1.70—2.10 (m, 2H, CH_2), 4.25—4.60 (m, 1H, CH); QM^+: 221.

4,5-Tetramethylene-1,3-dithiolane-2-thione. IR: 1033, 1058 cm^{-1}; ^{1}H NMR δ=1.00—2.40 (m, 8H, $\{CH_2\}_4$), 3.90—4.40 (m, 2H, CH_2); QM^+: 191.

4-Phenyl-1,3-dithiolane-2-thione. IR: 1047 cm^{-1}; ^{1}H NMR δ=3.90—4.40 (m, 2H, CH_2), 5.55—5.80 (dd, 1H, CH), 7.25—7.70 (m, 5H, C_6H_5); QM^+: 213.

4-Chloromethyl-1,3-dithiolane-2-thione was purified by column chromatography on silica gel using a mixture of hexane and chloroform (7 : 3 v/v) as an eluent. IR: 1067, 1039 cm^{-1}, ^{1}H NMR δ=3.55—4.05 (m, 2H, CH_2), 4.05—4.30 (m, 2H, CH_2), 4.30—4.65 (m, 1H, CH); QM^+: 185.

References

1) M. Sander, *Chem. Revs.*, **66**, 297 (1966).

2) A. V. Fokin and A. F. Kolomiets, *Russ. Chem. Revs.*, **45**, 25 (1967).

3) H. R. Snyder and W. Alexander, *J. Am. Chem. Soc.*, **70**, 217 (1948).

4) Hisamitsu Pharmceutical Co. Ltd., Japan Patent, 13164 (1974).

5) G. K. Helmkamp, D. J. Pettitt, J. R. Lowell, Jr., W. R. Mabey, and R. G. Wolcott, *J. Am. Chem. Soc.*, **88**, 1030 (1966).

6) Y. Taguchi and Y. Suhara, *Bull. Chem. Soc. Jpn.*, **59**, 2321 (1986).

7) G. A. Razuvaev, V. S. Etlis, and L. N. Grovov, *Zh. Obshch. Khim.*, **33**, 1366 (1963); *Chem. Abstr.*, **59**, 9827b (1963).

8) K. Matsumoto and A. Sera, *Synthesis*, **1985**, 999.

9) H. Plieninger and C. C. Heuck, *Tetrahedron*, **28**, 73 (1972).

10) J. Petermann and H. Plieninger, *Tetrahedron*, **31**, 1209 (1975).

11) K. Gulbins, G. Benzing, R. Maysenhölder, and K. Hamann, *Chem. Ber.*, **93**, 1975 (1960).

12) R. Feinauer, M. Jacobi, and K. Hamann, *Chem. Ber.*, **98**, 1782 (1965).

13) Y. Ohshiro, T. Minami, K. Yasuda, T. Agawa,

Tetrahedron Lett., **1969**, 259.
14) T. Takeshima, N. Fukuda, M. Muraoka, and T. Miyauchi, *J. Syn. Org. Chem. Jpn.*, **31**, 808 (1973).
15) Y. Taguchi and Y. Suhara, *Yukagaku*, **33**, 280 (1984).
16) M. Kurabayashi, K. Yanagiya, and M. Yasumoto, *Bull. Chem. Soc. Jpn.*, **44**, 3413 (1971).
17) C. C. J. Culvenor, W. Davies, and K. H. Pausacker, *J. Chem. Soc.*, **1946**, 1050.

 © 1987 The Chemical Society of Japan Bull. Chem. Soc. Jpn., 60, 731—735 (1987)

Synthesis of Imido-Substituted 3,8-Diphenyl-1,2-diazacycloocta-2,4,6,8-tetraenes and Their Thermolysis

Seiichi YOGI,* Kozo HOKAMA, Sadamori TAKAYOSHI, and Otohiko TSUGE†,*
Department of Chemistry, Faculty of Science, Ryukyu University, Nakagami-gun, Okinawa 903-01
†Research Institute of Industrial Science, Kyushu University, Kasugakoen, Kasuga 816
(Received August 23, 1986)

Nucleophilic substitution of 4,7-dichloro-3,8-diphenyl-1,2-diazocine with succinimide, phthalimide, *N*-methyl-*p*-toluenesulfonamide, and *o*-benzosulfimide, in the presence of silver oxide, gave the corresponding 4-mono(imido)- and 4,7-di(imido)-1,2-diazocines. 4-Acetoxy-7-phthalimido- and 4-phenylthio-7-phthalimido-1,2-diazocine were also prepared. Thermolysis of the mono(imido)-1,2-diazocines in xylene under reflux afforded the corresponding di(imido)-1,2-diazocine and/or five pyridine derivatives, whose relative yields depended upon the nature of imido substitutents in the diazocines. However, 4,7-di(imido)-1,2-diazocines did not decompose in xylene under reflux. Thermolysis of 4,7-bis(phthalimido)-1,2-diazocine at 300—310 °C gave 3,6-bis(phthalimido)-2-phenylpyridine with the extrusion of benzonitrile. In the thermolysis of the acetoxy- (230—240 °C) or phenylthio-substituted 1,2-diazocine (240—260 °C), 6-acetoxy- and 6-benzoyl-3-phthalimido-2-phenylpyridine, or 6(and 3)-phenylthio-3(and 6)-phthalimido-2-phenylpyridines were isolated together with benzonitrile, respectively. The feature of thermolysis was also discussed.

Although 1,2-diazacycloocta-2,4,6,8-tetraenes (1,2-diazocines) free of benzo groups were not known until Trost et al.[1] succeeded in an elegant synthesis of the parent 1,2-diazocine (**1**), we have recently reported a convenient method for the synthesis of 4,7-dichloro-3,8-diphenyl-1,2-diazocine (**2**), which is the first example for stable substituted monocyclic 1,2-diazocine.[2] The 1,2-diazocine **2** can be readily converted into other 4,7-disubstituted 1,2-diazocines: Thus, stable acyloxy-,[2] arylthio-,[3] and arylsulfonyl-substituted[4] 1,2-diazocines **3** were prepared by the reaction of **2** with appropriate nucleophiles. It has also been found that in contrast to the parent 1,2-diazocine (**1**), which decomposed slowly in solution at room temperature and rapidly neat to benzene and pyridine with comparable rates,[1] these stable 1,2-diazocines, **2** and **3**, had been pyrolyzed to give only pyridines accompanied by the extrusion of benzonitrile in almost all cases.

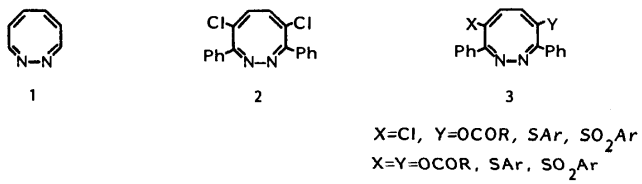

This paper describes the synthesis of stable imido-substituted 1,2-diazocines from **2**, and their thermolysis leading to pyridines. The feature of the thermolysis is also discussed.

Results and Discussion

Synthesis of Imido-Substituted 1,2-Diazocines. Although the dichloro-1,2-diazocine (**2**) did not react with succinimide in benzene under reflux, the reaction of **2** with silver succinimide (5 equiv) in benzene under reflux for 10 h afforded mono(succinimido)- **4a** and bis(succinimido)-1,2-diazocine **5a** in 39 and 34% yields, respectively. However, the succinimido-substituted 1,2-diazocines **4a** and **5a** could be also obtained in 41 and 11% yields respectively, together with unidentified viscous materials, by the reaction of **2** with succinimide (2 equiv) in the presence of silver oxide (2 equiv) in refluxing benzene for 6 h. This procedure was applied to the synthesis of other imido-substituted 1,2-diazocines.

The reaction of **2** with phthalimide, *N*-methyl-*p*-toluenesulfonamide, or *o*-benzosulfimide (saccharin) in the presence of silver oxide under the same conditions gave the corresponding mono(imido)-1,2-diazocines, **4b** (25%), **4c** (47%) or **4d** (47%), and di(imido)-1,2-diazocine, **5b** (36%), **5c** (16%), or **5d** (16%), respectively.

Moreover, in the reaction of mono(phthalimido)-1,2-diazocine (**4b**) with lead acetate or benzenethiol (each 3 equiv) in benzene under reflux for 20 or 10 h, 4-acetoxy-7-phthalimido-(**6**) or 4-phenylthio-7-phthalimido-1,2-diazocine (**7**) was obtained in 47 or 65% yield, respectively (Scheme 1).

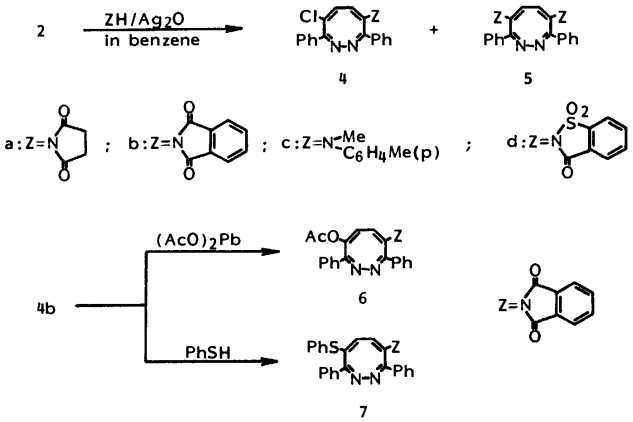

Scheme 1.

Structural elucidation of all the imido-substituted 1,2-diazocines, **4**—**7**, was accomplished on the basis of spectral data.

Thermolysis of Imido-Substituted 1,2-Diazocines. When the mono(succinimido)-1,2-diazocine (**4a**) was heated in dry xylene under reflux for 5 h, the bis-(succinimido)-1,2-diazocine (**5a**), 6-chloro-2-phenyl-

3-succinimidopyridine (**8a**) and 6-benzoyl-2-phenyl-3-succinimidopyridine (**9a**) were isolated in 35, 15, and 8% yields, respectively. The similar thermolysis of the mono(phthalimido)-1,2-diazocine (**4b**) gave 6-chloro-2-phenyl-3-phthalimidopyridine (**8b**) and 6-benzoyl-2-phenyl-3-phthalimidopyridine (**9b**) in 42 and 32% yields, respectively; in this case the bis(phthalimido)-1,2-diazocine (**5b**) was not formed, but benzonitrile was isolated in 17% yield.

The thermolysis of the mono(*N*-methyl-*p*-toluenesulfonamido) (**4c**) and mono(*o*-benzosulfimido)-1,2-diazocine (**4d**) was somewhat complex. The 1,2-diazocine **4c** gave only a complex mixture, from which any identified pyrolysates could not be isolated. In the thermolysis of **4d** under similar conditions, however, the bis(*o*-benzosulfimido)-1,2-diazocine (**5d**), 3-(*o*-benzosulfimido)-6-chloro-2-phenylpyridine (**8d**) and 6-benzoyl-3-(*o*-benzosulfimido)-2-phenylpyridine (**9d**) were isolated in 29, 9, and 11% yields respectively, together with 3,6-dichloro-2-phenylpyridine (**10**)[2] (17%) and 6-benzoyl-3-chloro-2-phenylpyridine (**11**)[2] (5%) (Scheme 2).

The structures of the pyridines, **8** and **9**, were assigned on the basis of spectral data as well as of the chemical conversions.

Treatment of the pyridines **8a** and **8b** with an ethanolic alkali solution under reflux gave the same product, 3-amino-6-chloro-2-phenylpyridine (**12**). The similar treatment of the pyridine **8d** gave an intermediary pyridine **13**, which was then converted into **12** on heating with hydrochloric acid. On the other hand, the treatment of **9b** with an ethanolic alkali solution under reflux afforded 3-amino-6-benzoyl-2-phenylpyridine (**14**), which was then converted, by diazotization, into known 6-benzoyl-3-hydroxy-2-phenylpyridine (**15**)[2] (Scheme 2).

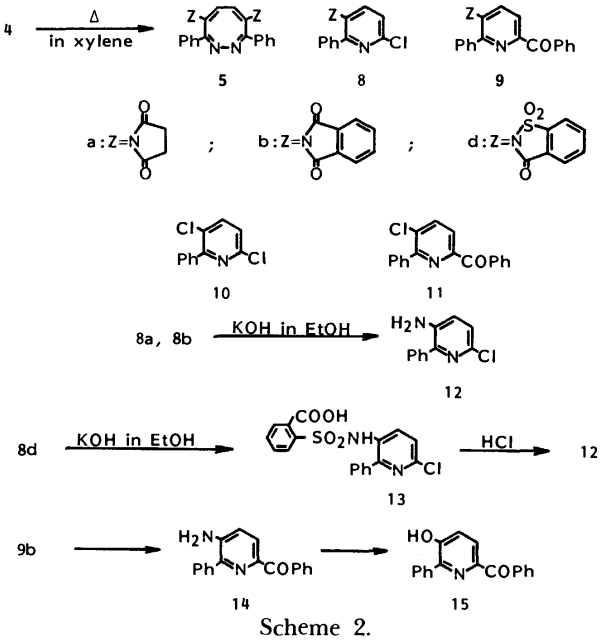

Scheme 2.

As reported previously,[2-4] 4,7-disubstituted 1,2-diazocines, **2** and **3**, thermally isomerize into their valence isomers, diazabicyclooctatrienes, which are in equilibrium with azonia intermediates. Although thermolysis of the mono(imido)-1,2-diazocines (**4**) seemed somewhat more complex than that of the other stable 1,2-diazocines, **2** and **3**, the formation of products, **5** and **8**—**11**, in the thermolysis of **4** can be again explained by the intervention of diazabicyclooctatrienes and azonia intermediates (Scheme 3).

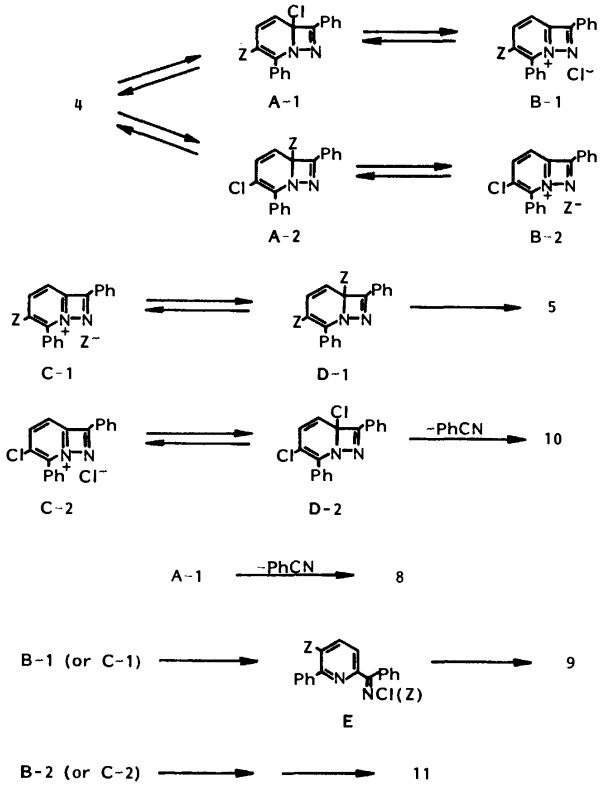

Scheme 3.

The 1,2-diazocine **4** is thermally isomerized into two valence isomers, **A-1** and **A-2**. The valence isomer **A-1** is in equilibrium with the azonia intermediate **B-1**, while **A-2** with **B-2**. The exchange of counter anion between **B-1** and **B-2** yields new azonia intermediates **C-1** and **C-2**, which are, of course, in equilibrium with the diazabicyclooctatrienes **D-1** and **D-2**, respectively. The pyridine **8** is formed from **A-1** with the extrusion of benzonitrile, whereas the ring opening of **B-1** (and/or **C-1**) to an imidoylpyridine **E**, followed by hydrolysis gives the pyridine **9**. The pyridines **10** and **11** are formed from **D-2** and **B-2** (and/or **C-2**) via similar processes, respectively. As mentioned below, di-(imido)-1,2-diazocines (**5**) are stable in xylene under reflux. Thus, **5** formed via a valence isomerization of **D-1** is unchanged under the conditions.

Next, thermolysis of 1,2-diazocines **5**—**7** was investigated. Since the 1,2-diazocines **5**—**7** did not decompose in xylene under reflux, thermolysis was performed without solvent. When the bis(phthalimido)-1,2-diazocine (**5b**) was heated at 300—310 °C (bath temp) for 15 min, benzonitrile and 3,6-bis(phthalimido)-2-phenylpyridine (**16**) were obtained in 43 and 20%

yields, respectively, together with unidentified viscous materials.

Thermolysis of the 4-acetoxy-7-phthalimido-1,2-diazocine (**6**) at 230—240 °C (bath temp) for 15 min gave the benzoylpyridine **9b** and 6-acetoxy-2-phenyl-3-phthalimidopyridine (**17**) in 11 and 10% yields respectively, together with traces of benzonitrile. When 4-phthalimido-7-phenylthio-1,2-diazocine (**7**) was heated at 240—260 °C (bath temp) for 15 min, 2-phenyl-6-phenylthio-3-phthalimidopyridine (**18**) and 2-phenyl-3-phenylthio-6-phthalimidopyridine (**19**) were isolated in 25 and 7% yields respectively, accompanied by benzonitrile (16%) and diphenyl disulfide (trace). Unidentified viscous materials were formed in thermolysis of **6** and **7**.

Structural elucidation of the pyridines **16**—**19** was accomplished on the basis of spectral data. Treatments of the pyridines **18** and **19** with an ethanolic alkali solution under reflux gave 3-amino-2-phenyl-6-phenylthiopyridine (**20**) and 6-amino-2-phenyl-3-phenylthiopyridine (**21**),[3] respectively (Scheme 4). The pathways for the thermolysis of the 1,2-diazocines **5**—**7** can be readily understood.

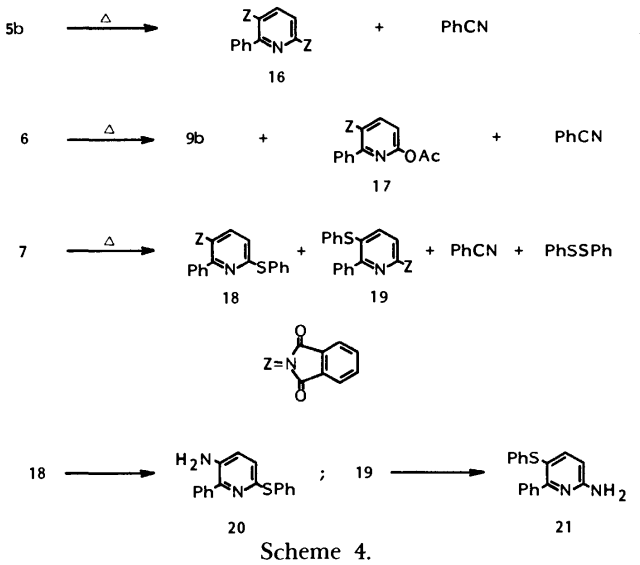

Scheme 4.

Experimental

IR spectra were obtained on a JASCO A-302 spectrometer. ^{1}H NMR spectra were recorded on a Hitachi R-24 or a JEOL FX-100 instrument, and chemical shifts are expressed in parts per million downfield from tetramethylsilane. Mass spectra were taken with a Hitachi RMU-6L spectrometer at 70 eV ionization energy. Elemental analyses were performed on a Yanaco MT 2 CHN corder instrument.

Reaction of the Dichloro-1,2-diazocine (2) with Silver Succinimide. A mixture of **2** (0.65 g, 2.0 mmol) and silver succinimide (2.0 g, 10 mmol) in benzene (50 ml) was refluxed for 10 h. The reaction mixture was filtered, and the precipitate was washed with chloroform (50 ml). The combined filtrate was concentrated in vacuo, and the residue was chromatographed on silica gel to give 0.30 g (39%) of 4-chloro-3,8-diphenyl-7-succinimido-1,2-diazocine (**4a**) (from benzene elution) and 0.30 g (34%) of 4,7-bis(succinimido)-3,8-diphenyl-1,2-diazocine (**5a**) (from chloroform elution).

4a: Mp 179—180 °C (decomp); colorless needles; IR (KBr) 1779, 1703, 1697 cm^{-1}; ^{1}H NMR ($CDCl_3$) δ=2.51 (4H, s, CH_2), 6.68, 6.81 (each 1H, d, =CH, J=4.2 Hz), 7.2—7.6 (4H, m), 7.6—7.9 (4H, m); MS m/z 391, 389 (M^+). Found: C, 67.66; H, 4.01; N, 10.69%. Calcd for $C_{22}H_{16}N_3O_2Cl$: C, 67.78; H, 4.14; N, 10.78%.

5a: Mp 271—273 °C (decomp); colorless prisms; IR (KBr) 1778, 1715 cm^{-1}; ^{1}H NMR ($CDCl_3$) δ=2.56 (8H, s, CH_2), 7.00 (2H, s, =CH), 7.1—7.6 (10 H, m); MS m/z 452 (M^+). Found: C, 69.23; H, 4.35; N, 12.24%. Calcd for $C_{26}H_{20}O_4N_4O_4$: C, 69.02; H, 4.46; N, 12.38%.

Reaction of the Dichloro-1,2-diazocine (2) with Succinimide in the Presence of Silver Oxide. A mixture of **2** (0.65 g, 2.0 mmol), succinimide (0.4 g, 4 mmol) and silver oxide (0.9 g, 4.0 mmol) in benzene (50 ml) was refluxed for 6 h. Similar work-up of the reaction mixture and chromatography of the residue on silica gel gave 0.32 g (41%) of the mono(succinimido)-1,2-diazocine (**4a**) (from benzene elution) and 0.1 g (11%) of the bis(succinimido)-1,2-diazocine (**5a**) (from chloroform elution), together with unidentified viscous materials (0.1 g).

Reaction of the Dichloro-1,2-diazocine (2) with Phthalimide in the Presence of Silver Oxide. A mixture of **2** (0.65 g, 2.0 mmol), phthalimide (0.6 g, 4 mmol) and silver oxide (0.9 g, 4.0 mmol) in benzene (50 ml) was refluxed for 3 h. Similar work-up of the reaction mixture and the residue was chromatographed on silica gel to give 0.19 g (29%) of unchanged **2**, 0.38 g (43%) of 4-chloro-3,8-diphenyl-7-phthalimido-1,2-diazocine (**4b**) (each from benzene elution), and 0.18 g (16%) of 4,7-bis(phthalimido)-3,8-diphenyl-1,2-diazocine (**5b**) (from chloroform elution).

The reaction for 6 h under similar conditions afforded 0.21 g (25%) of **4b** and 0.38 g (36%) of **5b**, together with viscous materials (0.1 g).

4b: Mp 178—180 °C (decomp); colorless needles; IR (KBr) 1787, 1719 cm^{-1}; ^{1}H NMR ($CDCl_3$) δ=6.76, 6.96 (each 1H, d, =CH, J=4.2 Hz), 7.2—7.5 (6H, m), 7.5—7.9 (8H, m); MS m/z 439, 437 (M^+). Found: C, 71.35; H, 3.48; N, 9.57%. Calcd for $C_{26}H_{16}N_3O_2Cl$: C, 71.31; H, 3.68; N, 9.60%.

5b: Mp 285—287 °C (decomp); colorless needles; IR (KBr) 1779, 1713 cm^{-1}; MS m/z 548 (M^+). Found: C, 74.19; H, 3.95; N, 10.33%. Calcd for $C_{34}H_{20}N_4O_4$: C, 74.44; H, 3.68; N, 10.22%.

The ^{1}H NMR spectrum did not measured owing to its insolubility in ordinary solvents.

Reaction of the Dichloro-1,2-diazocine (2) with *N*-Methyl-*p*-toluenesulfonamide in the Presence of Silver Oxide. A mixture of **2** (0.65 g, 2.0 mmol), *N*-methyl-*p*-toluenesulfonamide (0.74 g, 4 mmol) and silver oxide (0.9 g, 4.0 mmol) in benzene (50 ml) was refluxed for 6 h. Similar work-up of the reaction mixture and chromatography of the residue on silica gel gave 0.45 g (47%) of 4-chloro-3,8-diphenyl-7-(*N*-methyl-*p*-toluenesulfonamido)-1,2-diazocine (**4c**) (from benzene elution) and 0.21 g (16%) of 4,7-bis(*N*-methyl-*p*-toluenesulfonamido)-3,8-diphenyl-1,2-diazocine (**5c**) (from chloroform elution), together with viscous materials (60 mg).

4c: Mp 168—170 °C (decomp); colorless prisms; IR (KBr) 1605, 1360, 1345 cm^{-1}; ^{1}H NMR ($CDCl_3$) δ=2.09 (3H, s, CH_3), 2.83 (3H, s, N-CH_3), 5.53, 6.51 (each 1H, d, =CH, J=4.2 Hz), 6.4—7.8 (14H, m); MS m/z 477, 475 (M^+). Found: C, 65.31; H, 4.54; N, 8.99%. Calcd for $C_{26}H_{22}N_3O_2Cl$: C, 65.60; H, 4.66; N, 8.83%.

5c: Mp 244—246 °C (decomp); colorless needles; IR (KBr) 1600, 1355 cm^{-1}; MS m/z 624 (M^+). Found: C, 65.28; H, 5.22; N, 9.06%. Calcd for $C_{34}H_{32}N_4O_4S_2$: C, 65.36; H, 5.16; N, 8.97%.

The ^1H NMR spectrum did not measured owing to its insolubility in ordinary solvents.

Reaction of the Dichloro-1,2-diazocine (2) with *o*-Benzosulfimide in the Presence of Silver Oxide. A mixture of **2** (0.65 g, 2.0 mmol), *o*-benzosulfimide (0.73 g, 4 mmol) and silver oxide (0.9 g, 4.0 mmol) in benzene (50 ml) was refluxed for 6 h. Similar work-up of the reaction mixture and the residue was chromatographed on silica gel to give 0.44 g (47%) of 4-chloro-3,8-diphenyl-7-(*o*-benzosulfimido)-1,2-diazocine (**4d**) (from benzene elution) and 0.20 g (16%) of 4,7-bis(*o*-benzosulfimido)-3,8-diphenyl-1,2-diazocine (**5d**) (from chloroform elution), together with viscous materials (40 mg).

4d: Mp 186—187 °C (decomp); colorless prisms; IR (KBr) 1740, 1350, 1335 cm^{-1}; ^1H NMR ($CDCl_3$) δ=6.74, 6.98 (each 1H, d, =CH, J=4.2 Hz), 7.2—7.6 (8H, m), 7.6—8.0 (6H, m); MS m/z 475, 473 (M^+). Found: C, 63.28; H, 3.51; N, 8.76%. Calcd for $C_{25}H_{16}N_3O_3Cl$: C, 63.35; H, 3.40; N, 8.87%.

5d: Mp 275—277 °C (decomp); colorless needles; IR (KBr) 1740, 1350 cm^{-1}; MS m/z 620 (M^+). Found: C, 61.77; H, 3.51; N, 8.87%. Calcd for $C_{32}H_{20}N_4O_6S_2$: C, 61.92; H, 3.25; N, 9.03%.

4-Acetoxy-3,8-diphenyl-7-phthalimido-1,2-diazocine (6). A mixture of 1.30 g (3.0 mmol) of the chloro-phthalimido-1,2-diazocine (**4b**) and 2.9 g (9 mmol) of lead acetate in benzene (60 ml) was refluxed for 20 h. The reaction mixture was filtered, and the precipitate was washed with chloroform (50 ml). The combined filtrate was concentrated in vacuo, and the residue was chromatographed on silica gel to give 0.20 g (15%) of the unchanged **4b** (from benzene elution) and 0.65 g (47%) of the acetoxy-phthalimido-1,2-diazocine (**6**) (from chloroform elution).

6: Mp 195—196 °C (decomp); colorless prisms; IR (KBr) 1760, 1720 cm^{-1}; ^1H NMR ($CDCl_3$) δ=1.93 (3H, s, CH_3), 6.38, 6.91 (each 1H, d, =CH, δ=4.2 Hz), 7.1—7.4 (6H, m), 7.4—7.8 (8H, m); MS m/z 461 (M^+). Found: C, 72.61; H, 3.91; N, 9.02%. Calcd for $C_{28}H_{19}N_3O_4$: C, 72.87; H, 4.15; N, 9.11%.

3,8-Diphenyl-4-phenylthio-7-phthalimido-1,2-diazocine (7). A mixture of 1.30 g (3.0 mmol) of the chloro-phthalimido-1,2-diazocine (**4b**) and benzenethiol (1.0 ml, 9 mmol) in benzene (60 ml) was refluxed for 10 h. After the reaction mixture was washed with a 10% aqueous sodium hydroxide solution, the benzene solution was concentrated in vacuo to leave a residue. The residue was chromatographed on silica gel to give 70 mg (5%) of the unchanged **4b** (from benzene elution) and 0.98 g (65%) of the phenylthio-phthalimido-1,2-diazocine (**7**) (from chloroform elution).

7: Mp 222—223 °C (decomp); colorless prisms; IR (KBr) 1780, 1720 cm^{-1}; ^1H NMR ($CDCl_3$) δ=6.44, 6.95 (each 1H, d, =CH, J=4.2 Hz), 7.1—7.5 (12H, m), 7.5—7.8 (7H, m); MS m/z 511 (M^+). Found: C, 75.33; H, 4.11; N, 8.29%. Calcd for $C_{32}H_{21}N_3O_2S$: C, 75.12; H, 4.14; N, 8.22%.

Thermolysis of the Mono(succinimido)-1,2-diazocine (4a). A suspension of **4a** (1.0 g, 2.6 mmol) in dry xylene (20 ml) was refluxed for 5 h; the reaction mixture turned to a clear solution after 30 min, and then a precipitate gradually formed. After the reaction mixture had been cooled to room temperature, it was filtered to give 0.41 g (35%) of the bis(succinimido)-1,2-diazocine (**5a**). The filtrate was concentrated in vacuo, and the residue was chromatographed on silica gel to give 0.11 g (15%) of 6-chloro-2-phenyl-3-succinimidopyridine (**8a**) and 70 mg (8%) of 6-benzoyl-2-phenyl-3-succinimidopyridine (**9a**) (each from benzene elution), together with 0.15 g of viscous materials (from chloroform and ethyl acetate elutions).

8a: Mp 187—188 °C; yellow prisms; IR (KBr) 1700 cm^{-1}; ^1H NMR ($CDCl_3$) δ=2.2—2.8 (4H, m, CH_2), 7.40, 7.49 (each 1H, d, PyH, J=8.0 Hz), 7.43 (5H, s); MS m/z 288, 286 (M^+). Found: C, 62.80; H, 3.93; N, 9.86%. Calcd for $C_{15}H_{11}N_2O_2Cl$: C, 62.84; H, 3.87; N, 9.77%.

9a: Mp 140—142 °C; yellow prisms; IR (KBr) 1700, 1650 cm^{-1}; ^1H NMR ($CDCl_3$) δ=2.3—2.9 (4H, m, CH_2), 7.35—7.7 (8H, m), 7.80, 8.16 (each 1H, d, PyH, J=8.2 Hz), 8.0—8.4 (2H, m); MS m/z 356 (M^+). Found: C, 74.29; H, 4.39; N, 7.54%. Calcd for $C_{22}H_{16}N_2O_3$: C, 74.14; H, 4.53; N, 7.86%.

Thermolysis of the Mono(phthalimido)-1,2-diazocine (4b). A suspension of **4b** (1.0 g, 2.3 mmol) in dry xylene (20 ml) was refluxed for 5 h; during which time the reaction mixture turned to a clear solution. The reaction mixture was concentrated in vacuo, and the residue was chromatographed (silica gel, benzene) to give 40 mg (17%) of benzonitrile, 0.32 g (42%) of 6-chloro-2-phenyl-3-phthaliminopyridine (**8b**) and 0.28 g (30%) of 6-benzoyl-2-phenyl-3-phthaliminopyridine (**9b**). In this case, any bis(phthalimido)-1,2-diazocine (**5b**) did not formed.

8b: Mp 139—140 °C; yellow prisms; IR (KBr) 1780, 1720 cm^{-1}; ^1H NMR ($CDCl_3$) δ=7.2—7.7 (7H, m), 7.7—7.9 (4H, m); MS m/z 336, 334 (M^+). Found: C, 68.33; H, 3.21; N, 8.10%. Calcd for $C_{19}H_{11}N_2O_2Cl$: C, 68.17; H, 3.31; N, 8.37%.

9b: Mp 173—174 °C; yellow prisms; IR (KBr) 1780, 1710 cm^{-1}; ^1H NMR ($CDCl_3$) δ=7.2—8.3 (14H, m), 7.87, 8.11 (each 1H, d, PyH, J=8.2 Hz); MS m/z 404 (M^+). Found: C, 77.27; H, 3.45; N, 6.77%. Calcd for $C_{26}H_{16}N_2O_3$: C, 77.21; H, 3.39; N, 6.93%.

Thermolysis of the Mono(*o*-benzosulfimido)-1,2-diazocine (4d). A suspension of **4d** (1.0 g, 2.1 mmol) in dry xylene (20 ml) was refluxed for 5 h; the reaction mixture turned to a clear solution after 30 min, and then a precipitate gradually separated out. After the mixture had been cooled, filtration gave 0.38 g (29%) of the bis(*o*-benzosulfimido)-1,2-diazocine (**5d**). The filtrate was concentrated in vacuo, and the residue was chromatographed on silica gel to give trace amounts of benzonitrile, 70 mg (9%) of 3-(*o*-benzosulfimido)-6-chloro-2-phenylpyridine (**8d**), 0.10 g (11%) of 6-benzoyl-3-(*o*-benzosulfimido)-2-phenylpyridine (**9d**), 80 mg (17%) of 3,6-dichloro-2-phenylpyridine (**10**), mp 100—101 °C (lit,[2] mp 100—101 °C), and 30 mg (5%) of 6-benzoyl-3-chloro-2-phenylpyridine (**11**), mp 119—120 °C (lit,[2] mp 119—120 °C) (each from benzene elution), together with 0.2 g of viscous materials (from chloroform and ethyl acetate elutions).

8d: Mp 196—197 °C; yellow prisms; IR (KBr) 1730, 1340, 1305 cm^{-1}; ^1H NMR ($CDCl_3$) δ=7.1—7.5 (6H, m), 7.5—8.0 (5H, m); MS m/z 372, 370 (M^+). Found: C, 58.11; H, 3.06; N, 7.77%. Calcd for $C_{18}H_{11}N_2O_3SCl$: C, 58.30; H, 2.99; N, 7.56%.

9d: Mp 103—104 °C; yellow prisms; IR (KBr) 1730, 1660 cm^{-1}; ^1H NMR ($CDCl_3$) δ=7.12—7.57 (8H, m), 7.57—7.97 (5H, m), 7.97—8.27 (3H, m); MS m/z 440 (M^+). Found: C, 67.99; H, 3.76; N, 6.57%. Calcd for $C_{25}H_{16}N_2O_4S$: C, 68.17; H, 3.66; N, 6.36%.

3-Amino-6-chloro-2-phenylpyridine (12). i) A solution of 0.1 g of the succinimidopyridine (**8a**) in ethanol (30 ml) containing potassium hydroxide (0.5 g) was refluxed for 3 h.

The reaction mixture was concentrated in vacuo, and water (30 ml) was added to the residue which was extracted with chloroform (50 ml×2). The chloroform extract was concentrated in vacuo, and the residue was chromatographed (silica gel, chloroform) to give 30 mg (42%) of the aminopyridine (**12**).

12: Mp 98—99 °C; yellow prisms; IR (KBr) 3450, 3400, 3350, 3300 cm^{-1}; ^1H NMR ($CDCl_3$) δ=3.7 (2H, broad, NH_2), 7.04 (2H, s, PyH), 7.36—7.76 (5H, m); MS *m/z* 206, 204 (M^+). Found: C, 64.57; H, 4.51; N, 13.77%. Calcd for $C_{11}H_9N_2Cl$: C, 64.55; H, 4.43; N, 13.69%.

ii) A solution of 0.1 g of the *o*-benzosulfimidopyridine (**8d**) in ethanol (30 ml) containing potassium hydroxide (0.5 g) was refluxed for 3 h. The reaction mixture was concentrated in vacuo, and the residue was triturated with water (30 ml) to turn a solution. The aqueous solution was acidified with hydrochloric acid, and then extracted with chloroform (30 ml×2). The extract was concentrated in vacuo to leave 70 mg (67%) of *o*-[(6-chloro-2-phenyl-3-pyridyl)sulfamoyl]benzoic acid (**13**) (mp 184—186 °C; IR (KBr) 2400—3200, 1705, 1340 cm^{-1}; MS *m/z* 390 (M^+)). The pyridine **13** (70 mg) was heated in concd hydrochloric acid (20 ml) under reflux, and then the reaction mixture was concentrated in vacuo. The obtained residue was triturated with a 10% aqueous potassium hydroxide solution (15 ml), and then extracted with chloroform (30 ml×2). The extract was concentrated in vacuo, and the residue was chromatographed (silica gel, benzene) to give 20 mg (54%) of **12**.

Conversion of the Pyridine (9b) into 6-Benzoyl-3-hydroxy-2-phenylpyridine (15). A solution of **9b** (0.8 g) in ethanol (50 ml) containing potassium hydroxide (1.0 g) was refluxed for 4 h. The reaction mixture was poured into water (200 ml), and then extracted with benzene (100 ml×2). The benzene extract was concentrated in vacuo, and the residue was chromatographed (silica gel, chloroform) to give 0.41 g (78%) of 3-amino-6-benzoyl-2-phenylpyridine (**14**).

14: Mp 172—173 °C; yellow prisms; IR (KBr) 3500, 3400, 3350, 1640, 1620 cm^{-1}; ^1H NMR ($CDCl_3$) δ=4.33 (2H, broad, NH_2), 7.10, 7.99 (each 1H, d, PyH, *J*=8.2 Hz), 7.33—7.93 (6H, m), 8.03—8.33 (4H, m); MS *m/z* 274 (M^+). Found: C, 78.90; H, 5.11; N, 10.40%. Calcd for $C_{18}H_{14}N_2O$: C, 78.81; H, 5.15; N, 10.21%.

After diazotization of 0.27 g of the pyridine (**14**) with sodium nitrite in aqueous sufluric acid (concd sufuric acid (4 ml) and water (30 ml)) at 0—5 °C, the reaction mixture was heated at 60 °C for 2 h. The mixture was extracted with chloroform (50 ml×2) and the extract was concentrated in vacuo to leave 0.11 g (41%) of the pyridine (**15**),[2] mp 172—173 °C, which was identical with an authentic sample prepared from hydrolysis of 3-acetoxy-6-benzoyl-2-phenylpyridine.

Thermolysis of the Bis(phthalimido)-1,2-diazocine (5b). The diazocine **5b** (1.0 g) in a test tube was heated at 300—310 °C (bath temp) for 15 min. The pyrolysate was chromatographed on silica gel to give 80 mg (43%) of benzonitrile and 0.16 g (20%) of 3,6-bis(phthalimido)-2-phenylpyridine (**16**) (each from benzene elution), together with 0.5 g of viscous materials (from chloroform and ethyl acetate elution).

16: Mp 303—305 °C; yellow prisms; IR (KBr) 1780, 1720 cm^{-1}; ^1H NMR (DMSO-d_6) δ=7.15—7.35 (5H, m), 7.71, 8.23 (each 1H, d, PyH, *J*=8.2 Hz), 7.8—8.0 (8H, m); MS *m/z* 445 (M^+). Found: C, 72.56; H, 3.54; N, 9.62%. Calcd for $C_{27}H_{15}N_3O_4$: C, 72.80; H, 3.39; N, 9.43%.

Thermolysis of the Acetoxy-phthalimido-1,2-diazocine (6). The diazocine **6** (1.0 g) in test tube was heated at 230—240 °C (bath temp) for 15 min. The pyrolysate was chromatographed on silica gel to give 10 mg of benzonitrile, 0.10 g (11%) of the benzoylpyridine (**9b**) and 80 mg (10%) of 6-acetoxy-2-phenyl-3-phthalimidopyridine (**17**) (each from benzene elution), together with 0.5 g of viscous materials (from chloroform and ethyl acetate elution).

17: Mp 228—230 °C; yellow prisms; IR (KBr) 1780, 1760, 1720 cm^{-1}; ^1H NMR ($CDCl_3$) δ=2.37 (3H, s), 7.1—7.7 (7H, m), 7.7—8.0 (4H, m); MS *m/z* 358 (M^+). Found: C, 70.64; H, 3.83; N, 7.64%. Calcd for $C_{21}H_{14}N_2O_4$: C, 70.38; H, 3.94; N, 7.82%.

Thermolysis of the Phenylthio-1,2-diazocine (7). The diazocine **7** (0.9 g) in a test tube was heated at 240—260 °C (bath temp) for 15 min. Chromatography (silica gel) of the pyrolysate afforded 30 mg (16%) of benzonitrile, trace amounts of diphenyl disulfide, 0.18 g (25%) of 2-phenyl-6-phenylthio-3-phthalimidopyridine (**18**) and 50 mg (7%) of 2-phenyl-3-phenylthio-6-phthalimidopyridine (**19**) (each from benzene elution), together with 0.4 g of viscous materials (from chloroform and ethyl acetate elution).

18: Mp 193—194 °C; colorless needles; IR (KBr) 1780, 1720 cm^{-1}; ^1H NMR ($CDCl_3$) δ=6.87 (1H, d, PyH, *J*=8.2 Hz), 7.0—7.8 (15H, m); MS *m/z* 408 (M^+). Found: C, 73.74; H, 3.69; N, 6.62%. Calcd for $C_{25}H_{16}N_2O_2S$: C, 73.51; H, 3.95; N, 6.86%.

19: Mp 174—176 °C; colorless needles; IR (KBr) 1780, 1720 cm^{-1}; ^1H NMR ($CDCl_3$) δ=7.05—7.65 (10H, m), 7.65—8.0 (6H, m); MS *m/z* 408 (M^+). Found: C, 73.40; H, 3.87; N, 6.66%. Calcd for $C_{25}H_{16}N_2O_2S$: C, 73.51; H, 3.95; N, 6.86%.

Hydrolysis of the Pyridine (18). A solution of **18** (0.15 g) in ethanol (30 ml) containing potassium hydroxide (0.5 g) was refluxed for 3 h. After the reaction mixture was concentrated in vacuo, the residue was triturated with water (50 ml) which was extracted with chloroform (30 ml×2). The extract was concentrated in vacuo, and the residue was chromatographed (silica gel, chloroform) to give 60 mg (60%) of 3-amino-2-phenyl-6-phenylthiopyridine (**20**).

20: Mp 119—120 °C; colorless prisms; IR (KBr) 3460, 3300, 3150, 1635 cm^{-1}; ^1H NMR ($CDCl_3$) δ=2.80 (2H, broad s, NH_2), 6.88 (2H, s, PyH), 7.1—7.7 (10H, m); MS *m/z* 278 (M^+). Found: C, 73.11; H, 5.31; N, 10.22%. Calcd for $C_{17}H_{14}N_2S$: C, 73.35; H, 5.07; N, 10.06%.

Hydrolysis of the Pyridine (19). A solution of **19** (0.1 g) in ethanol (30 ml) containing potassium hydroxide (0.5 g) was refluxed for 3 h. Similar work-up of the reaction mixture, and chromatography (silica gel, chloroform) of the residue gave 40 mg (57%) of 6-amino-2-phenyl-3-phenylthiopyridine (**21**), mp 177—178 °C (lit,[3] mp 177—178 °C).

References

1) B. M. Trost and R. M. Cory, *J. Am. Chem. Soc.*, **93**, 5573 (1971); B. M. Trost, P. H. Schudder, R. M. Cory, N. J. Turro, V. Ramamurthy, and T. J. Katz, *J. Org. Chem.*, **44**, 1264 (1979).

2) S. Yogi, K. Hokama, and O. Tsuge, *Chem. Lett.*, **1982**, 1579; S. Yogi, K. Hokama, K. Ueno, and O. Tsuge, *Bull. Chem. Soc. Jpn.*, **59**, 1087 (1986).

3) S. Yogi, K. Hokama, and O. Tsuge, *Bull. Chem. Soc. Jpn.*, **60**, 335 (1987).

4) S. Yogi, K. Hokama, and O. Tsuge, *Bull. Chem. Soc. Jpn.*, **60**, 343 (1987).

 © 1987 The Chemical Society of Japan Bull. Chem. Soc. Jpn., 60, 737—746 (1987)

In Situ Generation and Synthetic Application of 2-Phenylbenzimidazoline to the Selective Reduction of Carbon-Carbon Double Bonds of Electron-Deficient Olefins

Hidenori CHIKASHITA,* Shuichi NISHIDA, Makoto MIYAZAKI,
Yasuhiro MORITA, and Kazuyoshi ITOH
Department of Applied Chemistry, Faculty of Engineering, Kansai University, Suita, Osaka 564
(Received September 2, 1986)

2-Phenylbenzimidazoline (PBI) as a mild, selective, and convenient reducing agent was efficiently generated in situ from *o*-phenylenediamine and benzaldehyde in alcohols. A generally applicable method for the selective reduction of carbon-carbon double bonds of a variety of electron-deficient olefins with an alcoholic solution of PBI is described. The reduction of α,β-unsaturated ketones to the corresponding saturated ketones could also be accomplished (but, less effectively) with PBI with the aid of a Lewis-acid catalyst. 1-Methyl-2-(*o*-nitrophenyl)benzimidazoline prepared and isolated by the reaction of *o*-nitrobenzaldehyde with *N*-methyl-*o*-phenylenediamine reduced benzylidenemalononitrile to give benzylmalononitrile and 1-methyl-2-(*o*-nitrophenyl)benzimidazole in high yields. This shows the validity of PBI to be the actual reducing species in the present reduction system. From a mechanistic study, the present reductions could be interpreted in terms of a mechanism involving a synchronous transport of a pair of hydrogens or a sequential transfer of a hydride and a proton from PBI to the olefins.

The selective reduction of organic functional groups is an important and frequently encountered synthetic operation in organic syntheses. Many methods have been developed toward this goal and many types of "selective reductions" have been accepted as being synthetically useful. In recent years, heterocyclic compounds having a hydrogen-donating ability, such as dihydrobenzazoles[1,2] or 1,4-dihydropyridines,[3] have been shown to be useful as such selective reducing agents. One such reagent developed in our laboratory is 2-phenylbenzimidazoline (PBI). The development of methods applicable to the selective reductions of carbon-carbon double bonds conjugated with electron-withdrawing groups such as cyano, nitro, or carbonyl group has been a synthetic subject. We have recently indicated the reducing and selective properties of PBI in the reduction of benzylidenemalononitriles and β-nitrostyrenes.[1a] However, the initial reaction mode has been shown to be disadvantageous from a synthetic viewpoint since a half molar amount of the olefins is consumed to form PBI. Due to this disadvantage, a convenient alternative method for in situ generation of PBI has been reported in a previous communication.[1b] This method includes the use of *o*-phenylenediamine (**1**) and benzaldehyde (**2**) in ethanol. In this paper, we report on details regarding the selective reduction of carbon-carbon double bonds of a variety of electron-deficient olefins with a reagent system of diamine (**1**) and aldehyde (**2**); discuss the scope, limitations, and general applicability of this simple reduction method, and show the mechanistic features of these reactions together with evidence that PBI is the actual reducing species (Scheme 1).

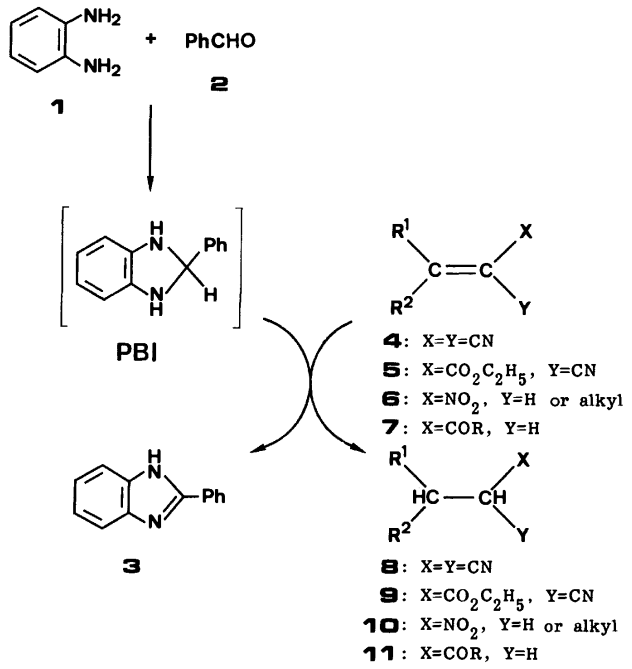

Scheme 1.

In Situ Generation and Properties of PBI. Recently, we have found that benzylmalononitriles or (2-nitroethyl)benzenes were obtained in good yields by a reaction of benzylidenemalononitriles or β-nitrostyrenes with a half molar amount of diamine (**1**); we indicated that the products resulted from a reduction of the olefins by PBI which was formed by the reaction of the olefins with equimolar amount of diamine (**1**).[1a] However, in order to synthetically utilize the reducing ability of PBI to the selective reduction of carbon-carbon double bonds of electron-deficient olefins, PBI should be prepared independently. In our attempts to prepare PBI conveniently, we have found that diamine (**1**) rapidly reacts with aldehyde (**2**) in ethanol at room

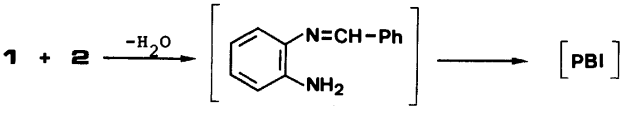

Scheme 2.

temperature to produce a mixture of *N*-benzylidene-*o*-phenylenediamine (**12**) and PBI, expected to be formed through the intramolecular cyclization of **12** (Scheme 2). Although these compounds could not be isolated, the formation of **12** and PBI were indicated by the appearance of signals at 8.57 and 5.74 ppm, assigned to methine protons of **12** and PBI, respectively, in the ^{1}H NMR spectra of an equimolar mixture of diamine (**1**) and aldehyde (**2**) in methanol-d_4 at room temperature. When the reaction mixture was allowed to warm to 50 °C, the complete disappearance of the above mentioned methine signals was observed after 24 h; also 2-phenylbenzimidazole (**3**) was isolated from the reaction mixture in 95% yield. This indicates that PBI is an unstable intermediate and is readily oxidized automatically to benzimidazole (**3**) in the absence of an appropriate hydrogen acceptor. The unstability of PBI is in sharp contrast to the high stability of *N*,*N*′-dimethylated PBI.[1f,h] In addition, Schiff's base (**12**), formed simultaneously, was inert to PBI in this mild reaction system, in contrast to the system reported by Smith et al.[4]

Upon a treatment of diamine (**1**) and aldehyde (**2**) in ethanol at room temperature, when benzylidenemalononitrile (**4a**) coexisted in the reaction system, a mixture of benzylmalononitrile (**8a**) and benzimidazole (**3**) was obtained in high yields (Scheme 3). As shown in

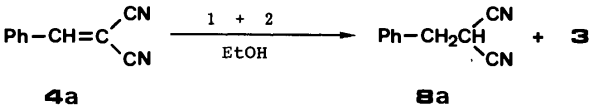

Scheme 3.

Table 1, this reduction also occurred by the treatment of the olefin (**4a**) with diamine (**1**) and other aldehydes under the same reaction conditions to give the same reduced product **8a** in good yields, although it is apparent that aldehyde (**2**) is the most effective among the aldehydes employed. In these reactions, benzimidazolines could not be isolated as well as PBI but the corresponding benzimidazoles were obtained in practically quantitative yields. These results indicate that the olefin (**4a**) was effectively reduced by benzimidazolines produced in situ from diamine (**1**) and aldehydes, and that compensating reactions are oxidations of benzimidazolines to benzimidazoles.

General Applicability of the PBI-Reduction to a Variety of Electron-Deficient Olefins. We have extended this simple reduction technique to a variety of electron-deficient olefins (**4—6**) which have a carbon–carbon double bond conjugated with one or two highly electron-withdrawing groups such as -CN, -NO_2, or -CO_2Et. The results are summarized in Table 2. In general, the yields of products (**8—10**) were consistently high and no other by-products were obtained at all. Benzimidazole (**3**) formed by the reactions is almost insoluble in low-polar organic solvents and could be easily removed from the reaction mixture by simple filtration after removing the solvent. A characteristic feature of the reduction is the steric effect at the β-position on the rate of reduction (Fig. 1). The results obtained by the reduction of a series of α-cyano-β-substituted cinnamonitriles (**4a—d**, **4h**, **4i**) indicate that the reduction was sensitive to a steric hinderance at the β-position associated with group R^1, revealing the following order:

$$R^1 = H > CH_3 > C_2H_5 > n\text{-}C_3H_7 > i\text{-}C_3H_7 \sim t\text{-}C_4H_9 \quad \text{(no reaction)}$$

Table 1. The Reduction of **4a** to **8a** with Diamine (**1**) and Aldehyde[a]

Aldehyde	Yield of **8a**/%[b]
Benzaldehyde (**2**)	96
Acetaldehyde	88
Propionaldehyde	90
Butyraldehyde	89
2-Phenylpropionaldehyde	87
2-Furaldehyde	61

a) All the reactions were carried out in ethanol at room temperature using the reagent system; **4a**: diamine (**1**): aldehyde = 1:1:1 (molar ratio). b) All yields were determined by GLC using benzyl cyanide as an internal standard.

Table 2. Reduction of Electron-Deficient Olefins (**4—6**) with Diamine (**1**) and Aldehyde (**2**)[a]

Product	R^1	R^2	X	Y	Reaction time/h	Yield/%[b]
8b	CH_3	C_6H_5	CN	CN	9	88
8c	C_2H_5	C_6H_5	CN	CN	9.5	88
8d	n-C_3H_7	C_6H_5	CN	CN	12	72
8e	CH_3	CH_3	CN	CN	7	80
8f	CH_3	C_2H_5	CN	CN	8	63
8g	-$(CH_2)_5$-		CN	CN	5	71
9	H	C_6H_5	$CO_2C_2H_5$	CN	11	90
10a	H	C_6H_5	NO_2	H	24	72
10c	H	p-ClC_6H_4	NO_2	H	24	65
10d	H	p-$CH_3C_6H_4$	NO_2	H	24	50
10e	H	p-$CH_3OC_6H_4$	NO_2	H	24	61

a) All the reactions were carried out in ethanol at room temperature using the reagent system; olefin: diamine (**1**): aldehyde (**2**) = 1:1:1 (molar ratio). b) Yield of isolated, pure product.

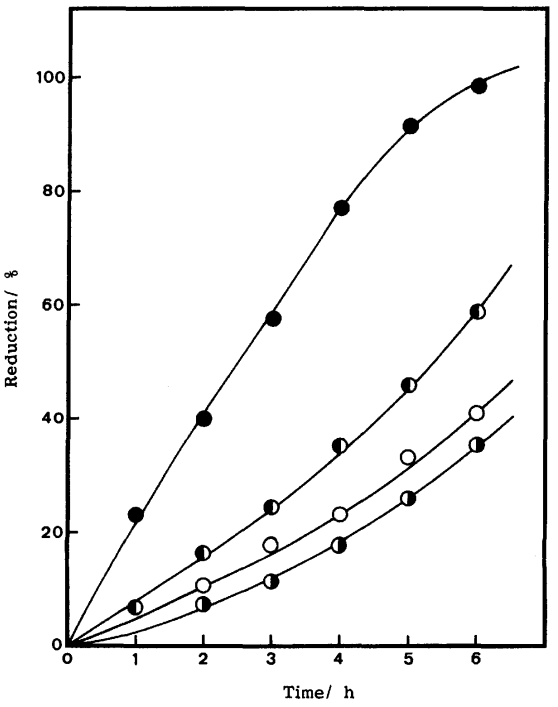

Fig. 1. Rate of reduction of β-substituted benzylidenemalononitriles with **1** and **2** in ethanol at room temperature. Olefins: **4a**(●), **4b**(◐), **4c**(○), and **4d**(◑).

Thus, a highly hindered olefin such as α-cyano-β-isopropylcinnamonitrile (**4h**) or α-cyano-β-(*t*-butyl)-cinnamonitrile (**4i**) could not be reduced at all in the present reduction system. The another feature is the electronic effect of groups X and Y on the reactivity of the olefins. Increasing the sum of the electron-withdrawing abilities of the groups X and Y resulted in a substantial increase in the reactivity of the olefin, revealing the following order:

$$X, Y = CN, CN > CN, CO_2C_2H_5 > NO_2, H > CO_2C_2H_5, CO_2C_2H_5 \text{ (no reaction)}$$

Thus, diethyl benzylidenemalonate (**13**) could not be reduced at all.

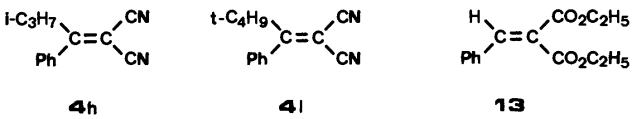

4h **4i** **13**

Scheme 4.

Nitroalkanes have recently been demonstrated to be useful synthetic intermediates for a variety of transformations of the nitro functionality to other functional groups.[5] Especially, aromatic nitroalkanes are of importance in connection with the synthesis of a variety of biochemically and pharmacologically interesting compounds.[6] They also have been used as a synthetically equivalent to enamines and enolates.[7] A combination of preparation of nitroalkenes from aldehydes by the Knoevenagel condensation and subsequent reduction of them to the corresponding nitroalkanes is the most desirable method for the synthesis of nitroalkanes; this is useful in connection with the elongation of aldehydes or the elongating transformation of aldehydes to ketones.[8] A widely employed method[9] for the reduction of nitroalkenes to the corresponding nitroalkanes involves a $NaBH_4$ reduction. Although this type of reduction of nitroalkenes derived from aliphatic aldehydes[9b] or ketones[10] usually proceeds smoothly in good yields, the reduction of aromatic nitroalkenes (**6**) with $NaBH_4$ produces low yields of products due to undesired side reactions such as dimerization.[9] With these considerations in mind, we studied the general applicability of the PBI-reduction method to the selective reduction of a variety of aromatic nitroalkenes (**6**).

Although the reduction of aromatic nitroalkenes (**6**) with diamine (**1**) and aldehyde (**2**) proceeded in ethanol at room temperature (Table 2), it is desirable to optimalize the reaction conditions in order to obtain the products in higher yields. Thus, the reduction of β-nitrostyrene (**6a**) with diamine (**1**) and aldehyde (**2**) was preliminary examined in a variety of solvents. As shown in Table 3, the reduction with PBI could be accelerated by the use of an alcoholic solvent; however, the kind of alcohol used did not influence the rate of reduction at 65 °C. The change in solvent does not change the specificity of the reduction, as no products other than the (2-nitroethyl)benzene (**10a**) was detected. However, the reaction in 1-butanol at reflux temperature gave the best results in terms of rapidity, due to a rise in the reaction temperature. Thus, the reduction of various aromatic nitroalkenes (**6**) were demonstrated with diamine (**1**) and aldehyde (**2**) in 1-butanol at reflux temperature. The results are summarized in Table 4. Although the kind of aromatic substituent in nitroalkenes (**6**) influenced the rate of the reduction, a variety of nitroalkenes employed here were reduced to the corresponding nitroalkanes (**10**) in excellent yields. In particular, the successful conversion of 3-(2-nitrovinyl)indole (**6k**) to the corresponding 3-(2-nitroethyl)indole (**10k**) is of interest in connection with the synthesis of substituted 3-(2-nitroethyl)-indoles which have proven to be valuable as intermediates in the synthesis of functionalized polycyclic indoles and natural products of the ergoline class.[11b] Similarly, β-nitrostyrenes (**6a—h**) without or with a substituent of nitro, chloro, methyl, methoxyl, or hydroxyl group were effectively converted to the corresponding (2-nitroethyl)benzenes (**10a—h**) in high yields by the same method. In addition, the reduction of β-nitrostyrenes (**6m—o**) possessing alkyl substitution at the α-carbon was more sluggish than that of **6a** but afforded high yields of 1-phenyl-2-nitroalkanes (**10m—o**) after the reaction time of 6—9 h. In all cases, carbon-carbon double bonds of nitroalkenes (**6**) were reduced with complete selectivity and no formation of dimer or other by-products could be observed. The use

Table 3. Rates of Reduction of β-Nitrostyrene (**6a**) with Diamine (**1**) and Aldehyde (**2**) in Various Solvents[a,b]

Solvent	Reduction/%[c,d]			
	1 h	3 h	5 h	8 h
1-Butanol	35(100)	57	66	100
1-Propanol	35 (88)	57(100)	65	100
Ethanol	37 (57)	57 (79)	66 (87)	100(100)
Methanol	38 (52)	59 (74)	64 (86)	100(100)
DMF	0	trace	42	76
Acetonitrile	trace	22	30	44

a) In all cases, solutions were 0.20 M (1 M = mol dm^{-3}) in the olefin (**6a**) and 0.24 M in diamine (**1**) and aldehyde (**2**). b) The reactions were carried out at 65 °C. c) All yields were determined by GLC using pentylbenzene as an internal standard. d) The values in parentheses indicate the yields of the reactions at reflux temperature.

Table 4. Reduction of Nitroalkenes (**6**) to Nitroalkanes (**10**) with Diamine (**1**) and Aldehyde (**2**)[a]

Product	R^1	R^2	Y	Reaction time/h	Yield/%[b]
10a	C_6H_5	H	H	1	88
10b	p-$NO_2C_6H_4$	H	H	1	91
10c	p-ClC_6H_4	H	H	1	82
10d	p-$CH_3C_6H_4$	H	H	3	85
10e	p-$CH_3OC_6H_4$	H	H	3	93
10f	p-HOC_6H_4	H	H	6	78
10g	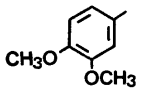	H	H	6	85
10h		H	H	3	82
10i		H	H	2	81
10j		H	H	3	89
10k	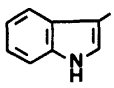	H	H	15	70
10l	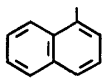	H	H	1	80
10m	C_6H_5	H	CH_3	6	91
10n	C_6H_5	H	C_2H_5	8	87
10o	C_6H_5	H	n-C_3H_7	9	84

a) All the reactions were carried out in 1-butanol at reflux temperature using the reagent system; nitroalkene (**6**): diamine (**1**): aldehyde (**2**) = 1:1.2:1.2 (molar ratio). b) Yield of isolated, pure product.

of 1.2 equivalent of diamine (**1**) and aldehyde (**2**) was sufficient to conduct the reduction, and benzimidazole (**3**) formed by the reaction could be easily removed from the reaction mixture as described previously. Compared with several other methods[11] currently used for the reduction of aromatic nitroalkenes, the present method is advantageous on account of its simplicity and general applicability to a wide range of aromatic nitroalkenes.

Recently, 2-phenylbenzothiazoline has been reported to be a good reducing agent with the aid of $AlCl_3$ for the conjugate reduction of α,β-unsaturated carbonyl compounds.[1c,g] Using this reagent, olefins **4a—c**, **5**, and **6a** could also be reduced to the corresponding reduced products **8a—c**, **9**, and **10a** in 80—98% yields.[1g] However, these reductions with 2-phenylbenzothiazoline were apparently more sluggish than that involving the PBI-reduction method.

Throughout the reductions (Tables 2 and 4), the cyano, nitro, alkoxycarbonyl, hydroxyl, and arylic

chloro groups were inert to the PBI-reduction. In addition, we have found that other functional groups such as carbonyl, unactivated carbon-carbon double bond, carbon-carbon triple bond, and common carbon-halogen bond are inert under the present reduction conditions. These high chemoselectivities are of great importance and enhance the utility of the present reagent.

Lewis Acid-Promoted Conjugate Reduction of α,β-Unsaturated Ketones (7) with PBI. In order to demonstrate the propensity of PBI regarding a reduction of carbon-carbon double bond systems conjugated with electron-withdrawing groups, we finally examined the reduction of α,β-unsaturated ketones (**7**) to the corresponding saturated ketones (**11**). When benzylideneacetone (**7a**) was dissolved in methanol and allowed to react with 2 equivalents of the reagents, **1** and **2**, at 50 °C, no trace of reduction occurred even after 24 h. However, when the same reaction was carried out in the presence of a Lewis acid, the reduction to 4-phenyl-2-butanone (**11a**) proceeded in 6% ($AlCl_3$)—64% ($ZnCl_2$) yields (Table 5). Among the solvent tested, methanol gave the best results while the reduction in acetonitrile, which is recognized as a good medium in the reduction with 1,3-dimethyl-2-phenylbenzimidazoline[1f] or NAD(P)H-model compounds,[3] gave low yield of the product. Thus, although the enone (**7a**) itself should resist a reduction, the increased electron-deficiency of the enone due to the coordination of the carbonyl group with a Lewis acid allowed the reaction to be possible. It should be noted that the catalytic efficiency is not proportional to the efficiency in forming a complex with a carbonyl group, in contrast to the similar Lewis acid-promoted conjugate reduction with 2-phenylbenzothiazoline[1c,g] or 1,3-dimethyl-2-phenylbenzimidazoline.[1f] The latter efficiency denotes the intensity of a Lewis acid and increases in the order $ZnCl_2<FeCl_3<AlCl_3$.[12] This is probably due to the complex action of a Lewis acid on both the producing step of PBI from **1** and **2** and the actual reduction step. To survey the generality, a series of representative enones (**7b—e**) were treated in the same fashion with the reagent system of diamine (**1**), aldehyde (**2**), and $ZnCl_2$. The results are summarized in Table 6. Although conjugate reductions were accomplished in 11—44% yields with complete regiospecificity, these reactions were apparently more sluggish and less effective compared with similar reductions with 2-phenylbenzothiazoline[1c,g] or 1,3-dimethyl-2-phenylbenzimidazoline.[1f] Accordingly, the synthetic utility of PBI in the conjugate reduction of α,β-unsaturated ketones seems to be rather low.

Table 5. Conjugate Reduction of Benzylideneacetone (**7a**) with Diamine (**1**) and Aldehyde (**2**) in the Presence or Absence of Lewis Acid[a]

Lewis acid	Solvent	Yield/%[b]
None	Methanol	0
$AlCl_3$	Methanol	6
$FeCl_3$	Methanol	12
$ZnCl_2$	Methanol	64
$ZnCl_2$	Acetonitrile	10

a) All the reactions were carried out at 50°C for 24 h by using the reagent system; **7a**: Lewis acid: diamine (**1**): aldehyde (**2**)=1:1:2:2 (molar ratio). b) Yield determined by GLC.

Mechanisms. In order to obtain clear evidence of the reducing ability of PBI to electron-deficient olefins, we tried to prepare and isolate the structurally related benzimidazoline (**17**) according to the Scheme 5. When *N*-methyl-*o*-phenylenediamine (**14**) was treated under stirring with the same molar amount of *o*-nitrobenzaldehyde (**15**) in methanol at room temperature, Schiff's base (**16**) could be separated soon from the reaction mixture as orange colored needles. This compound could be directly isolated in high purity by a simple filtration from the reaction mixture; any attempt to purify it was unsuccessful due to its unstability. When **16** was heterogeneously stirred in methanol at room temperature, the orange color of **16** turned to pale brown. This was indicative of the formation of imidazoline (**17**) by the intramolecular cyclization of **16**. This compound, which was isolated by filtration, was also unstable; the continuous stirring of its methanol solution at room temperature led to the formation of a stable benzimidazole (**18**) by autoxida-

Table 6. Conjugate Reduction of α,β-Unsaturated Ketones (**7**) with Diamine (**1**) and Aldehyde (**2**)[a]

	Enone		Product	Yield/%[b]
7b	$C_6H_5CH{=}CHCOC_6H_5$	**11b**	$C_6H_5CH_2CH_2COC_6H_5$	44
7c	$C_6H_5COCH{=}CHCOC_6H_5$	**11c**	$C_6H_5COCH_2CH_2COC_6H_5$	36
7d	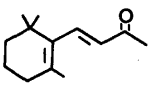	**11d**	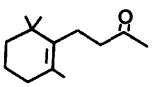	23
7e		**11e**		11

a) All the reactions were carried out at 50°C for 24 h by using the reagent system; enone (**7**): $ZnCl_2$: diamine (**1**): aldehyde (**2**)=1:1:2:2 (molar ratio). b) Yield determined by GLC.

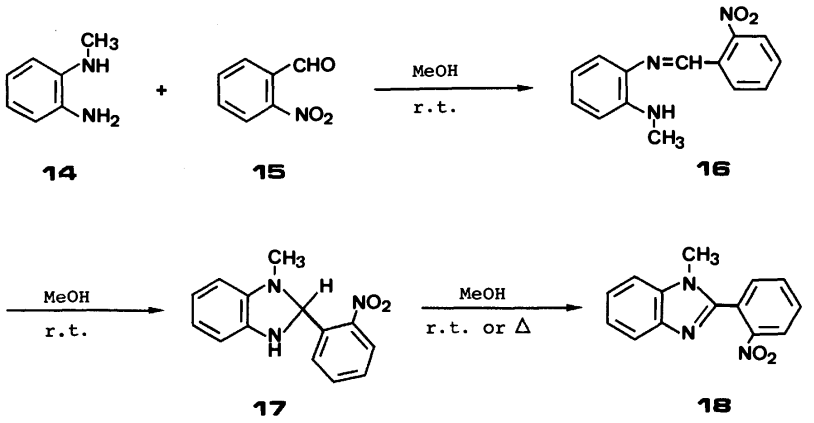

Scheme 5.

tion. The spectral and analytical data of these compounds (**16**—**18**) were entirely consistent with the proposed structures. For an examination of the reducing ability of **17**, a reaction with same molar amount of the olefin (**4a**) was carried out in ethanol at room temperature. Expectedly, the reduced product (**8a**) was obtained in 85% yield together with **18** (97% yield). This result strongly supports the validity of the existence of the reducing ability of PBI to an electron-deficient olefin.

When an ethanol solution of an equimolar mixture of **4a** and **17** was kept standing at room temperature for 12 h, a spectral change gradually occurred in which a new spectrum was reached with four clear isosbestic points at 207, 225, 291, and 331 nm (Fig. 2). The presence of these points indicates that no intermediate is present during a reaction in sufficient concentration for its own spectrum to become apparent, superimposed on those of reactants and products.

In an attempt to determine the destination of a hydrogen atom at the C-2 carbon of PBI, we reduced the olefin **6a** with PBI-2-*d* and PBI-1,3-d_2, which were prepared with the reagent system of diamine (**1**) and benzaldehyde-*d* or *o*-phenylenediamine-d_4 and aldehyde (**2**), respectively (Scheme 6). The product of the

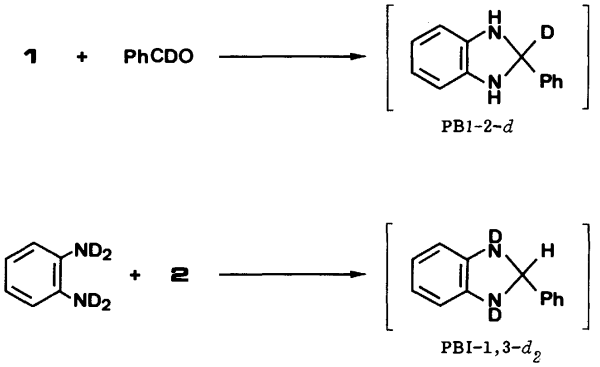

Scheme 6.

reduction with PBI-2-*d* in 1-butanol was found to be (2-nitroethyl)benzene (**19**); it contained one deuterium atom at its β-carbon (Scheme 7). This result shows that the hydrogen atom at the C-2 carbon of PBI surely transfers to the β-carbon of the olefin as a hydride,

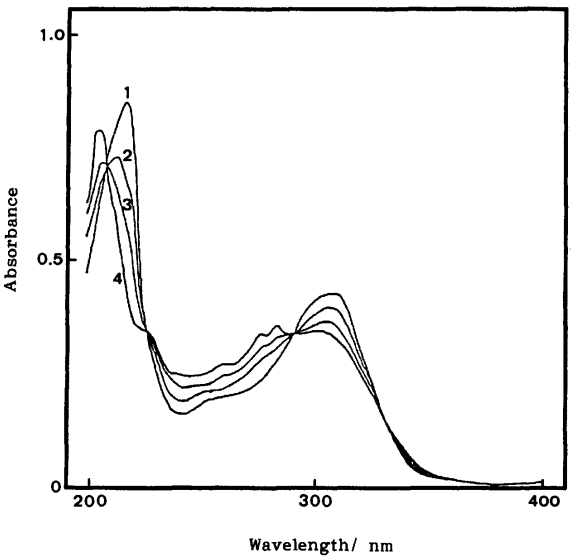

Fig. 2. Spectral change as a function of time for reaction between olefin **4a** and imidazoline **17** in ethanol at 25°C. $[\mathbf{4a}]_0=[\mathbf{17}]_0=2\times10^{-5}$ mol dm^{-3}. Time (h): 1, 0; 2, 4; 3, 8; 4, 12.

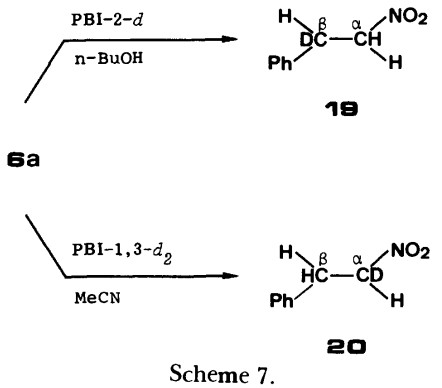

Scheme 7.

since the carbon at the β-position of **6a** is very electrophilic. When the same olefin was reduced in acetonitrile with PBI-1,3-d_2, the α-deuterated product (**20**) was selectively obtained in 83% yield (Scheme 7). This shows that the olefin incorporated the hydrogen atom at the nitrogen of PBI at its α-position probably as a proton.

Table 7. Rates of Reduction of β-Nitrostyrene (**6a**) with diamine (**1**) and *p*-Substituted Benzaldehyde in Refluxing 1-Butanol[a)]

Substituent	Reduction/%[b)]		
	1 h	3 h	5 h
NO_2	63	81	100
Cl	77	100	—
H	100	—	—
CH_3	78	100	—
CH_3O	70	85	100

a) In all cases, solutions were 0.20 M in the substrate and 0.24 M in diamine (**1**) and *p*-substituted benzaldehyde. b) All yields were determined by GLC using pentylbenzene as an internal standard.

The substituent effect on the reduction of the olefin (**6a**) by PBI was studied with the reagent system of diamine (**1**) and *p*-substituted benzaldehyde. Thus, the reaction was monitored by GLC at a reflux temperature of 1-butanol. As shown in Table 7, when the aldehyde (**2**) was substituted by an electron-donating group, the rate of the reduction decreased in proportion to electron-donating ability of the substituent. On the other hand, the rate also decreased with an increase in the electron-withdrawing ability of the substituent. These results well match with a mechanism including a hydride transfer followed by a proton transfer from PBI to the olefin, since the rate of formation of PBI should decrease with an increase in electron-donating ability of the substituent and the rate on the actual reduction stage (hydride transfer) should also decrease with an increase in electron-withdrawing ability of the substituent.

Considering these facts, two possible reaction mechanisms for the present PBI-reduction can be proposed as shown in Scheme 8. They involve the sequential transfer of a pair of hydrogens of PBI (shown as path **a**) and a cyclic addition of two hydrogens of PBI in either exact or nearly exact concurrence (shown as path **b**). We consider that only the stereochemistry of the transfer of a pair of hydrogens of PBI to the carbon-carbon multiple bond of the conjugate olefin system can distinguish between path **a** and **b**. However, all of our attempts to determine such a stereochemical course were unsuccessful. Thus, paths **a** and **b** are, as yet, both candidates for the present PBI-reduction; however, path **b** seems to be more likely in light of the forementioned observation on UV-spectral change in the reduction of **4a** with **17** together with the previous results[1g)] that the hydrogen shift from 2-phenylbenzothiazoline to electron-deficient carbon-carbon double bonds of α,β-unsaturated carbonyl system is a synchronous transport of a pair of hydrogens.

Conclusion. The present study clearly reveals that PBI is a mild, selective and useful reducing agent for the reduction of carbon-carbon double bonds of electron-deficient olefins, and provides a unique and convenient method for this type of reaction. The advantages of the present method are summarized as follows:

(1) Easy preparation (in situ generation) of the reducing agent,

(2) operational simplicity,

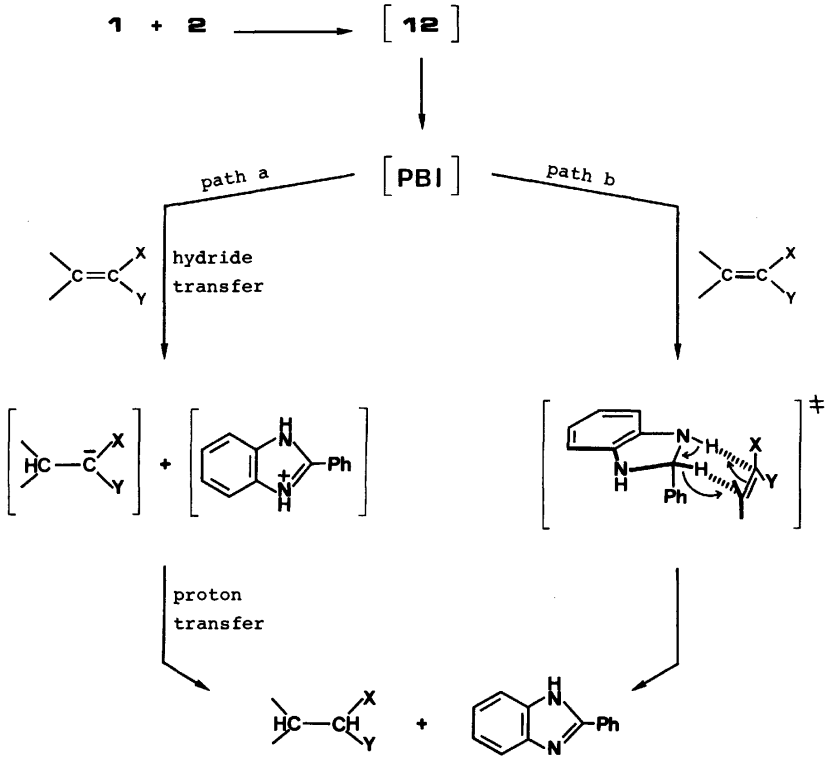

Scheme 8.

(3) mild reaction conditions (moderate temperature, nonbasic, nonacidic, and no active ionic species present),
(4) complete selectivity,
(5) no side reactions,
(6) high chemoselectivity.

Experimental

Melting points were recorded on a Yanagimoto micro melting-point apparatus and are uncorrected. ^{1}H NMR spectra were measured with a JEOL PMX-60 spectrometer at 60 MHz using tetramethylsilane as an internal reference. IR and UV spectra were recorded on a JASCO A-202 and a Simadzu UV-240 spectrophotometers, respectively. Mass spectra were obtained on a JEOL JMS-0lSG mass spectrometer. GLC analyses were carried out on a Shimadzu Gas Chromatograph GC-6AM equipped with a hydrogen flame ionization detector using glass columns (1.5 m) packed with 2% Silicone OV-7 on Uniport HP (60—80 mesh). The yields by quantitative GLC were measured on the same columns by internal standard method. Silica gel (Wakogel C-300) was used for short-column chromatography.

Materials. *o*-Phenylenediamine was purified by recrystallization from ethanol. *o*-Phenylenediamine-d_4 was prepared by continual recrystallization of pure *o*-phenylenediamine from D_2O, that was pure *o*-phenylenediamine-d_4 by ^{1}H NMR; no amino proton absorption was detected. Aldehydes were commercially supplied and purified by distillation or recrystallization. Benzaldehyde-*d* was prepared via deuteration of 2-lithio-2-phenyl-1,3-dithiane with D_2O,[13] that was pure benzaldehyde-*d* by ^{1}H NMR; no aldehyde proton absorption was detected. Commercially available $ZnCl_2$, $FeCl_3$, and $AlCl_3$ were used without purification. Alkylidenemalononitriles,[14] ethyl α-cyanocinnamate,[15] diethyl benzylidenemalonate,[16] and aromatic nitroalkenes[17] were prepared by a Knoevenagel condensation of the corresponding aldehydes or ketones with malononitrile, ethyl cianoacetate, diethyl malonate, or nitroalkanes, respectively. Benzylideneacetone[18] and (*E*)-1,2-dibenzoylethylene[19] were prepared according to methods described in the literature. Other α,β-unsaturated ketones and solvents were commercial materials which were purified by the usual methods.

General Procedure for the Reduction of Electron-Deficient Olefins (4 and 5) with PBI. To a stirred solution of the olefin (2.0 mmol) and benzaldehyde (0.21 g, 2.0 mmol) in ethanol (20 ml) under nitrogen at room temperature, *o*-phenylenediamine (0.22 g, 2.0 mmol) was added. After completion of the reaction (monitored by TLC; see Table 2), the solvent was evaporated under reduced pressure. Dichloromethane was added to the residue and insoluble imidazole (**3**) was filtered off. After removing dichloromethane under reduced pressure, the crude product was purified by short-column chromatography on silica gel to give the pure reduced product (**8** and **9**). In a large-scale synthesis, purification by distillation or recrystallization was also effective. Some physical and spectral data of the products are given as follows: **8a**: Mp 91—92 °C; IR (KBr) 2252 cm^{-1} (CN); ^{1}H NMR (CCl_4) δ=3.16 (d, 2H, CH_2, *J*=7 Hz), 3.70 (t, 1H, CH, *J*=7 Hz), and 7.18 (s, 5H, Ar); MS *m/z* 156 (M^+). **8b**: Bp 117—119 °C/6 mmHg (1 mmHg=133.322 Pa); IR (neat) 2250 cm^{-1} (CN); ^{1}H NMR (CCl_4) δ=1.49 (d, 3H, CH_3, *J*=7 Hz), 3.31 (m, 1H, CH), 3.71 (d, 1H, CH, *J*=6 Hz), and 7.15 (s, 5H, Ar); MS *m/z* 170 (M^+). **8c**: Bp 128—130 °C/5 mmHg; IR (neat) 2250 and 2230 cm^{-1} (CN); ^{1}H NMR (CCl_4) δ=0.83 (t, 3H, CH_3, *J*=6.2 Hz), 1.91 (m, 2H, CH_2), 2.98 (q, 1H, CH), 3.83 (d, 1H, CH, *J*=6 Hz), and 7.15 (s, 5H, Ar); MS *m/z* 184 (M^+). **8d**: Bp 108—111 °C/3 mmHg; IR (neat) 2249 cm^{-1} (CN); ^{1}H NMR (CCl_4) δ=0.88 (t, 3H, CH_3, *J*=5.6 Hz), 1.20 (m, 2H, CH_2), 1.87 (q, 2H, CH_2), 3.07 (q, 1H, CH), 3.73 (d, 1H, CH, *J*=6 Hz), and 7.15 (s, 5H, Ar); MS *m/z* 198 (M^+). **8e**: Bp 85—86 °C/5 mmHg; IR (neat) 2245 cm^{-1} (CN); ^{1}H NMR (CCl_4) δ=1.21 (d, 6H, $2CH_3$, *J*=7 Hz), 2.25 (m, 1H, CH), and 3.62 (d, 1H, CH, *J*=5 Hz); MS *m/z* 107 (M^+−1). **8f**: Bp 77—78 °C/7 mmHg; IR (neat) 2246 cm^{-1} (CN); ^{1}H NMR (CCl_4) δ=0.70—1.24 (m, 6H, $2CH_3$), 1.54 (m, 2H, CH_2), 2.02 (m, 1H, CH), and 3.72 (d, 1H, CH, *J*=4.6 Hz); MS *m/z* 121 (M^+−1). **8g**: Colorless oil; IR (neat) 2251 cm^{-1} (CN); ^{1}H NMR (CCl_4) δ=0.80—2.28 (br, 11H, *c*-C_6H_{11}) and 3.42 (d, 1H, CH, *J*=5.2 Hz); MS *m/z* 147 (M^+−1). **9**: Colorless oil; IR (neat) 2240 (CN) and 1740 (CO) cm^{-1}; ^{1}H NMR (CCl_4) δ=1.14 (t, 3H, CH_3, *J*=7 Hz), 3.10 (d, 2H, CH_2, *J*=6 Hz), 3.48 (t, 1H, CH, *J*=6 Hz), 4.05 (q, 2H, CH_2), and 7.10 (s, 5H, Ar); MS *m/z* 203 (M^+).

General Procedure for the Reduction of Aromatic Nitroalkenes (6) with PBI. To a stirred solution of nitroalkene (**6**) (5.0 mmol) and benzaldehyde (0.64 g, 6.0 mmol) in 1-butanol (25 ml) under nitrogen at room temperature, *o*-phenylenediamine (0.65 g, 6.0 mmol) was added. After refluxing for the appropriate time (monitored by TLC; see Table 4), the solvent was evaporated under reduced pressure. Dichloromethane was added to the residue and insoluble imidazole (**3**) was filtered off. The dichloromethane solution was thoroughly washed with 0.1M HCl, dried with $MgSO_4$, and concentrated to give a crude product. The crude product was purified by short-column chromatography on silica gel to give the pure reduced product (**10**). In a large-scale synthesis, purification by distillation or recrystallization was also effective. Some physical and spectral data of the products are given as follows: **10a**: Bp 78 °C/1 mmHg; ^{1}H NMR ($CDCl_3$) δ=3.00 (t, 2H, β-CH_2, *J*=7 Hz), 4.27 (t, 2H, α-CH_2, *J*=7 Hz), and 6.97 (s, 5H, Ar). **10b**: Mp 96—97 °C; ^{1}H NMR ($CDCl_3$) δ=3.39 (t, 2H, β-CH_2, *J*=7 Hz), 4.63 (t, 2H, α-CH_2, *J*=7 Hz), 7.35 (d, 2H, Ar, *J*=8 Hz), and 8.09 (d, 2H, Ar, *J*=8Hz). **10c**: Bp 136 °C/3 mmHg; ^{1}H NMR ($CDCl_3$) δ=3.17 (t, 2H, β-CH_2, *J*=7 Hz), 4.43 (t, 2H, α-CH_2, *J*=7 Hz), and 7.07 (m, 4H, Ar). **10d**: Bp 96 °C/2 mmHg; ^{1}H NMR ($CDCl_3$) δ=2.25 (s, 3H, CH_3), 3.07 (t, 2H, β-CH_2, *J*=7 Hz), 4.30 (t, 2H, α-CH_2, *J*=7 Hz), and 6.90 (s, 4H, Ar). **10e**: Bp 123 °C/2 mmHg; ^{1}H NMR ($CDCl_3$) δ=3.03 (t, 2H, β-CH_2, *J*=7 Hz), 3.57 (s, 3H, OCH_3), 4.33 (t, 2H, α-CH_2, *J*=7 Hz), 6.93 (d, 4H, Ar). **10f**: Colorless oil; ^{1}H NMR (DMSO-d_6) δ=3.09 (t, 2H, β-CH_2, *J*=7 Hz), 4.43 (t, 2H, α-CH_2, *J*=7 Hz), 6.60 (d, 2H, Ar, *J*=8 Hz), and 6.86 (d, 2H, Ar, *J*=8 Hz). **10g**: Mp 50—51 °C; ^{1}H NMR ($CDCl_3$) δ=3.23 (t, 2H, β-CH_2, *J*=7 Hz), 3.80 (s, 6H, $2OCH_3$), 4.53 (t, 2H, α-CH_2, *J*=7 Hz), and 6.67 (s, 3H, Ar). **10h**: Colorless oil; ^{1}H NMR ($CDCl_3$) δ=3.13 (t, 2H, β-CH_2, *J*=7 Hz), 4.50 (t, 2H, α-CH_2, *J*=7 Hz), 5.80 (s, 2H, OCH_2O), and 6.57 (s, 3H, Ar). **10i**: Bp 61—63 °C/2 mmHg; ^{1}H NMR ($CDCl_3$) δ=3.30 (t, 2H, β-CH_2, *J*=7 Hz), 4.50 (t, 2H, α-CH_2, *J*=7 Hz), 5.97 (m, 2H, Ar), 6.13 (m, 1H, Ar), and 7.17 (s, 1H, Ar). **10j**: Bp 99—101 °C/3 mmHg; ^{1}H NMR ($CDCl_3$) δ=3.33 (t, 2H, β-CH_2, *J*=7 Hz), 4.30 (t, 2H, α-CH_2, *J*=7 Hz), and 6.80—7.03 (m, 3H, Ar). **10k**: Colorless oil; ^{1}H NMR ($CDCl_3$) δ=3.13 (t, 2H, β-CH_2, *J*=7 Hz), 4.30 (t, 2H, α-CH_2, *J*=7 Hz), 6.57 (d, 1H, Ar, *J*=4Hz), 6.97 (m, 3H, Ar), and 7.57 (br, 1H, NH). **10l**: Mp

45—46 °C; ^{1}H NMR ($CDCl_3$) δ=4.43 (t, 2H, β-CH_2, J=7 Hz), 5.30 (t, 2H, α-CH_2, J=7Hz), and 7.80—8.70 (m, 7H, Ar). **10m**: Bp 85 °C/2 mmHg; ^{1}H NMR ($CDCl_3$) δ=1.43 (d, 3H, CH_3, J=7 Hz), 3.00 (m, 2H, β-CH_2), 4.50 (m, 1H, α-CH), and 7.07 (s, 5H, Ar). **10n**: Bp 100 °C/2 mmHg; ^{1}H NMR ($CDCl_3$) δ=0.97 (t, 3H, CH_3, J=7.4 Hz), 1.90 (m, 2H, CH_2), 3.13 (q, 2H, β-CH_2), 4.60 (m, 1H, α-CH), and 7.17 (s, 5H, Ar). **10o**: Bp 81—82 °C/1 mmHg; ^{1}H NMR ($CDCl_3$) δ=0.70—2.20 (m, 7H, C_3H_7), 3.06 (m, 2H, β-CH_2), 4.67 (m, 1H, α-CH), and 7.06 (s, 5H, Ar).

Conjugate Reduction of α,β-Unsaturated Ketones (7) with PBI in the Presence of $ZnCl_2$. A solution of enone (**7**) (1.0 mmol) in dry methanol (3 ml) and $ZnCl_2$ (0.14 g, 1.0 mmol) were mixed in a glass tube under ice-water cooling. After the $ZnCl_2$ was completely dissolved, a solution of *o*-phenylenediamine (0.22 g, 2.0 mmol) and benzaldehyde (0.21 g, 2.0 mmol) in dry methanol (4 ml) was added and the mixture was degassed several times in vacuo. The tube was sealed in vacuo and kept at 50 °C for 24 h. After 0.1M HCl (15 ml) was added to the mixture in the tube under ice-water cooling, the aqueous mixture was extracted with dichloromethane. The dichloromethane solution was thoroughly washed with water, dried with $MgSO_4$, and analyzed by quantitative GLC. The results are given in Table 6. An identification of the products isolated by short-column chromatography on silica gel was performed by spectroscopic (NMR, IR, and MS) methods. These spectral data were in satisfactory agreement with those of the corresponding authentic samples or expected values.

Preparation of 1-Methyl-2-(*o*-nitrophenyl)benzimidazoline (17). A solution of *o*-nitrobenzaldehyde (0.15 g, 1 mmol) and *N*-methyl-*o*-phenylenediamine (0.12 g, 1 mmol) in methanol was stirred at room temperature. After ca. 5 min, precipitated orange-colored needles were separated out, which were collected by filtration, washed with cold methanol, and dried in vacuo to give an almost pure Schiff's base (**16**) (0.22 g, 85%); mp 89—93 °C; IR (KBr) 1590 cm^{-1} (N=C); ^{1}H NMR ($CDCl_3$) δ=2.67 (s, 3H, CH_3), 8.93 (s, 1H, CH), and 7.00—8.00 (m, 8H, Ar).

Found: C, 65.59; H, 5.05; N, 16.41%. Calcd for $C_{14}H_{13}N_3O_2$: C, 65.87; H, 5.13; N, 16.46%.

Without further purification, Schiff's base (**16**) (0.26 g, 1 mmol) was added in methanol and heterogeneously stirred at room temperature for 6 h. During this period, the orange-color of the needles turned to light brown. Filtration, washing with cold methanol, and drying in vacuo gave almost pure benzimidazoline (**17**) as brown needles (0.24 g, 92%); mp 134—136 °C; IR (KBr) 1495 cm^{-1} (NH); ^{1}H NMR ($CDCl_3$) δ=2.97 (s, 3H, CH_3), 6.07 (s, 1H, CH), and 6.20—8.00 (m, 8H, Ar).

Found: C, 65.46; H, 5.06; N, 16.38%. Calcd for $C_{14}H_{13}N_3O_2$: C, 65.87; H, 5.13; N, 16.46%.

Reduction of Benzylidenemalononitrile (4a) with Benzimidazoline (17). The olefin **4a** (0.15 g, 1 mmol) was reduced with benzimidazoline (**17**) (0.26 g, 1 mmol) in ethanol (3 ml) for 12 h according to the general procedure. The usual work-up of the reaction mixture gave benzimidazole (**18**) (0.25 g, 97%). Chromatographic purification of the filtrate gave the pure reduced product (**8a**) (0.13 g, 85%).

Reduction of β-Nitrostyrene (6a) with PBI-2-*d*. Nitrostyrene **6a** (0.45 g, 3.0 mmol) was reduced for 1h with *o*-phenylenediamine and benzaldehyde-*d* according to the general procedure. A chromatographic purification of the crude product gave β-deuterated compound (**19**) as a colorless oil (0.42 g, 91%); ^{1}H NMR (CCl_4) δ=3.00 (t, 1H, β-CDH), 4.27 (d, 2H, α-CH_2), and 6.97 (s, 5H, Ar); MS m/z 152 (M^+).

Reduction of β-Nitrostyrene (6a) with PBI-1,3-d_2. Nitrostyrene **6a** (0.45 g, 3.0 mmol) was reduced with *o*-phenylenediamine-d_4 and benzaldehyde for 24 h according to the general procedure, except that acetonitrile was used in place of 1-butanol. A chromatographic purification of the crude product gave α-deuterated compound (**20**) as a colorless oil (0.38 g, 83%); ^{1}H NMR ($CDCl_3$) δ=3.07 (d, 2H, β-CH_2), 4.30 (t, 1H, α-CDH), and 7.00 (s, 5H, Ar); MS m/z 152 (M^+).

References

1) a) K. Itoh, H. Ishida, and H. Chikashita, *Chem. Lett.*, **1982**, 1117; b) H. Chikashita, S. Nishida, M. Miyazaki, and K. Itoh, *Synth. Commun.*, **13**, 1033 (1983); c) H. Chikashita, M. Miyazaki, and K. Itoh, *Synthesis*, **1984**, 308; d) H. Chikashita, Y. Morita, and K. Itoh, *Synth. Commun.*, **15**, 527 (1985); e) H. Chikashita, and K. Itoh, *Chem. Express*, **1**, 17 (1986); f) H. Chikashita and K. Itoh, *Bull. Chem. Soc. Jpn.*, **59**, 1747 (1986); g) H. Chikashita, M. Miyazaki, and K. Itoh, *J. Chem. Soc., Perkin Trans. 1*, in press; h) H. Chikashita, H. Ide, and K. Itoh, *J. Org. Chem.*, in press.

2) S. H. Mashraqui and M. Kellogg, *Tetrahedron Lett.*, **26**, 1453 (1985).

3) K. Nakamura, A. Ohno, and S. Oka, *Tetrahedron Lett.*, **24**, 3335 (1983); K. Nakamura, M. Fujii, A. Ohno, and S. Oka, *ibid.*, **25**, 3983 (1984); S. Yasui, K. Nakamura, and A. Ohno, *Chem. Lett.*, **1984**, 377; K. Nakamura, M. Fujii, S. Oka, and A. Ohno, *ibid.*, **1985**, 523; K. Nakamura, M. Fujii, H. Mekata, S. Oka, and A. Ohno, *ibid.*, **1986**, 87; S. Yasui, K. Nakamura, M. Fujii, and A. Ohno, *J. Org. Chem.*, **50**, 3283 (1985).

4) J. G. Smith and I. Ho, *Tetrahedron Lett.*, **1971**, 3541.

5) M. R. Galobardes and H. W. Pinnick, *Tetrahedron Lett.*, **22**, 5235 (1981) and references cited therein; C. Grundman and P. Grunanger, "The Nitrile Oxides," Springer-Verlag, New York, 1971, p. 51; O. Von Schickh, G. Apel, H. G. Padeken, H. H. Schwarz, and A. Segnitz, "Houben-Weyl-Muller: Methoden der Organischen Chemie." Vol. X/1, Thieme, Stuttgart, 1971.

6) A. Rotman, J. W. Daly, and C. R. Creveling, *J. Label. Compounds*, **11**, 445 (1975); T. Nagatsu, "Biochemistry of Catecholamines," Univ. of Tokyo Press, 1973.

7) D. Seebach, R. Henning, and J. Gonnerman, *Chem. Ber.*, **112**, 234 (1979).

8) Although the transforming method of aliphatic nitroalkanes into carbonyl compounds has been already established, there is very little data concerning the convertibility of aromatic nitroalkanes into the corresponding carbonyl compounds, probably due to the difficulties involved in the reduction of aromatic nitroalkenes to the corresponding nitroalkanes and the unusual instability of the carbonyl products in acidic solution. However, the latter conversion was effectively accomplished by our improved Nef reaction; H. Chikashita, Y. Marita, amd K. Itoh, *Synth. Commun.*, in press.

9) a) H. Shechter, D. E. Ley, and E. B. Roberson Jr., *J. Am. Chem. Soc.*, **78**, 4984 (1956); b) A. I. Meyers and J. C. Sircar, *J. Org. Chem.*, **32**, 4134 (1967).

10) V. Nair and A. K. Sinhababu, *J. Org. Chem.*, **45**, 1893 (1980); A. Hassner and C. Heathcock, *J. Org. Chem.*, **29**, 1350

(1964).
11) a) A. K. Sinhababu and R. T. Borchardt, *Tetrahedron Lett.*, **24**, 227 (1983); b) L. I. Kruse and E. L. Hilbert, *Heterocycles*, **20**, 1373 (1983).
12) D. Cook, *Can. J. Chem.*, **41**, 522 (1963).
13) D. Seebach, B. W. Erickson, and G. Singh, *J. Org. Chem.*, **31**, 4303 (1966).
14) E. Campaigne, G. F. Bulbenko, W. E. Kreighbaum, and D. R. Maulding, *J. Org. Chem.*, **27**, 4428 (1962).
15) A. C. Cope and E. M. Hancock, *Org. Synth.* Coll., Vol. 3, 399 (1965).
16) C. F. H. Allen and F. W. Spangler, *Org. Synth.* Coll., Vol. 3, 377 (1965).
17) D. E. Worrall, *Org. Synth.* Coll., Vol. 1, 413 (1956); M. Koremura, H. O. Ku, T. Shono, and T. Nakanishi, *Takemine Kenkyusho Nempo*, **13**, 212 (1961): *Chem. Abstr.*, **57**, 16451a (1962).
18) N. L. Drake and P. Allen, Jr., *Org. Synth.* Coll., Vol. 1, 77 (1956).
19) R. E. Lutz, *Org. Synth.* Coll., Vol. 3, 248 (1965).

 © 1987 The Chemical Society of Japan Bull. Chem. Soc. Jpn., 60, 747—752 (1987)

On a Solid-State ECD, WO_3/Solid Electrolyte/Metal

Katsumi KUWABARA,* Shoichi ICHIKAWA, and Kohzo SUGIYAMA
Department of Applied Chemistry, Faculty of Engineering, Nagoya University, Furo-cho, Chikusa-ku, Nagoya 464
(Received October 23, 1986)

Electrochromic display (ECD) was investigated using WO_3 as the electrochromic material and metals as the counter electrode. WO_3 was vacuum-evaporated on a glass substrate coated with indium tin oxide. A film of solid electrolyte, $Sn(HPO_4)_2 \cdot H_2O$, was prepared by means of the spray method on the thin film of WO_3. ECDs with metal electrodes were examined from the points of view of the change in optical density, the current-wave forms, and the response speeds in coloring and bleaching processes. ECD cells with noble metals indicated comparatively high optical density changes on coloration at a constant-voltage operation. The cell with Ag showed a high coloration speed compared with the cells containing graphite and other metals.

Much attention has been paid to the electrochromic display (ECD) since Deb reported on the electrochromic properties of WO_3.[1] The ECDs with WO_3 are classified into the following groups:

WO_3/liquid electrolyte[2,3] (I)

WO_3/dielectric material[4,5] (II)

WO_3/solid electrolyte (super ionic conductor)[6-10] (III)

The first group has been investigated extensively. A few devices in this group have come to practical use because of their excellent performance, especially their distinct image and high response speed, but various problems remain to be solved such as the leakage of liquid electrolytes, the dissolution of the WO_3 film, and the evolution of gases. In the second group, since the dielectric material must adsorb some water in order to have ionic conduction, the performance of the ECD is affected by moisture in the atmosphere. The solid electrolyte in the third group originally contains a mobile ion in its own structure, but the ionic conductivity is not always so high as that of the electrolytic solution. The poor response speed has prevented the ECDs from satisfactory development, although the devices are hopeful because of their stable memory, long life-cycle, and maintenance-free operation.

In previous papers,[11,12] the ECDs were investigated using several inorganic ionexchangers as the solid electrolyte, and an ECD cell with $Sn(HPO_4)_2 \cdot H_2O$ (hereinafter to be referred to as SPA) was found to display the best behavior on coloration. The proton conductivity ($\approx 10^{-5}$ S cm^{-1} at room temperature) of the electrolyte[13] is not high enough for the ECD, but is not affected so much by the temperature as by the humidity in the atmosphere. Therefore, SPA has the possibility of providing an ECD with stable performance.

WO_3 films were studied from various points of view, such as the effect of adsorbed-water, the packing density, and the degree of crystallizatio.[14-16] However, counter electrodes for the ECD had scarcely been examined at all in previous papers. Yoshimura et al. reported that the spontaneous coloration of ECD was suppressed by the use of metal as a counter electrode,[10] and Sakamoto et al. reported the electrochromic behavior to be influenced by the material of the counter electrode.[17] In this paper, we wish to report on solid-state ECDs containing metals as the counter electrode. The performances of the ECDs have been evaluated in comparison with those of the ECD containing graphite as the counter electrode.

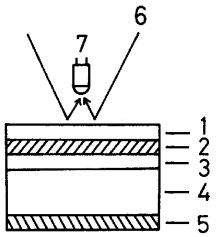

Fig. 1. Schematic diagram of the ECD cell and the experimental set up. 1: glass substrate, 2: ITO electrode, 3: WO_3, 4: $Sn(HPO_4)_2 \cdot H_2O$, 5: counter electrode, 6: tungsten lamp, 7: photo transister.

Experimental

The configuration of the components in the ECD cell is shown in Fig. 1. WO_3 film (450 nm thick) was deposited on an ITO-coated glass substrate by means of vacuum evaporation at a rate of 15 nm s^{-1} and under a vacuum of 2.66×10^{-3} Pa. SPA (Toagosei Chemical Industry Co. Ltd.) was used as the solid electrolyte, and its layer (40—60 μm thick) was formed by spraying the suspension which had beed prepared by mixing SPA fine powder with acetone under ultrasonic vibration.

Metal plates and graphite plate (0.1—0.8 mm thick and 3.29 cm^2) were used as the counter electrode. The metals were Ag, Al, Au, Cu, Fe, Ni, Pt, Pt black, Sn, Ti, Zn, and Zr. The surfaces were polished with tapping film and cleaned with trichloro-ethane before use.

The ITO, the WO_3 film, and the solid-electrolyte layers were sandwiched with the counter electrode in a pile between two bakelite plates (3 mm thick). The bakelite plate facing the glass had a window 10 mm in diameter so as to make it possible to detect the change in color through it.

The change in color was measured in the reflection mode using tungsten lamps and a photo transistor, as is shown in Fig. 2. A d.c. constant current or voltage was supplied to the ECD cell from a d.c. constant-current source (Metronix) and a function generator (Hokuto Denko HB-104). The change in the optical density, $\Delta O.D.$, is defined by the following

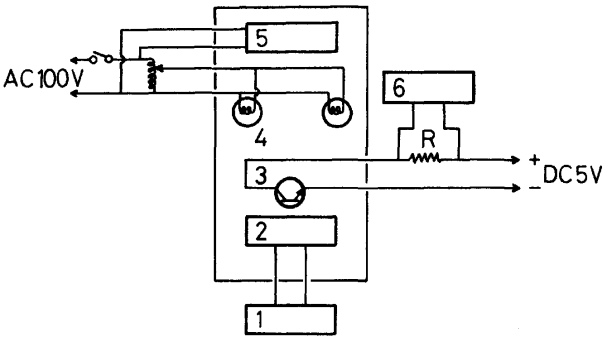

Fig. 2. Schematic diagram for measurement of the optical density changes. 1: d.c. source, 2: ECD cell, 3: photo transistor, 4: tungsten lamp, 5: fan, 6: recorder.

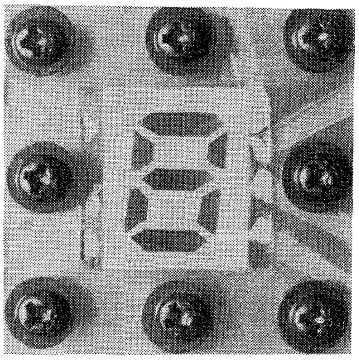

Fig. 3. Demonstration of a seven-segment numeric ECD.

equation:

$$\Delta O.D. = \log CR = \log R_0/R$$

where CR is the contrast ratio and where R_0 and R are the reflection strengths at bleaching and at coloring respectively. In this study, R_0/R was detected in the form of the ratio of the potential drop, V_0/V. V_0 (bleaching) and V (coloring) are the values at a resistor connected in series to the photo transistor. They were recorded by means of a servocoder (Graphtec SR 6341). All the measurements were carried out at room temperature.

Considering the practical ECD cell, a model of the seven-segment numeric ECD was prepared tentatively using WO_3 (EC material), an electrolyte (SPA), graphite (counter electrode), and an acryl plate (package). The appearance is shown in Fig. 3. The white color of SPA can be seen to offer an excellent contrast to the blue color of WO_3.

Results

The optical-density change ($\Delta O.D.$) versus the injected-charge curves at a constant current of 700 μA/cell are shown in Fig. 4. The change in color of the ECD is caused by the double injection of protons and electrons into the WO_3 film (to be described later). Whether or not the distribution of protons in the bulk of the WO_3 film is homogeneous can be considered in principle to influence the $\Delta O.D.$ measured in the reflection mode. In this study, the experimental duration of each run was short, and protons appeared to stay near the surface layer of the WO_3 film on the electrolyte. Therefore, the $\Delta O.D.$ values measured were regarded as not to be influenced by the distribution state of the protons.

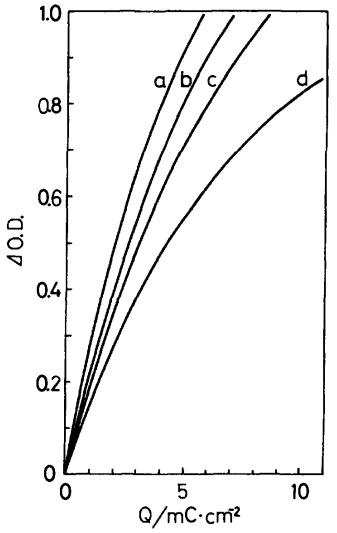

Fig. 4. Optical density changes as a function of injected charge. Counter electrodes a: Au, b: graphite, c: Pt, d: Ag.

Each cell at a certain charge should display a uniform $\Delta O.D.$ value, independent of the material used as the counter electrode. However, as may be seen from Fig. 4, the forms of the curves are different from each other. A high value of the $\Delta O.D.$ at a certain charge means a high current efficiency for coloration, since $\Delta O.D.$ is caused by the concentration change in the color based on an electrochemical reaction. In this experiment, the charge required to achieve $\Delta O.D.$=0.5 was used for the estimation of the current efficiency. The ECDs with Ni, Au, and Cu electrodes colored even in the low-charge region and needed 2.1—2.3 mC cm^{-2} to get $\Delta O.D.$=0.5. The cells with Ag and Pt electrodes indicated efficiencies slightly lower than the efficiency of the cell with graphite as the counter electrode. These data are summarized in Table 1. The three ECDs with Al, Ti, and Zr did not color enough for the $\Delta O.D.$ to be detected.

The current efficiencies shown in Fig. 4 were compared, for reference, with those in the few papers which have described ECDs with a solid-proton conductor. The ECD with antimony (V) oxide as a solid electrolyte and Fe_3O_4 as a counter electrode was reported to require 5 mC cm^{-2} to achieve a $\Delta O.D.$ of 0.5.[18] Similarly, the cell containing *p*-toluenesulfonic acid (TsOH)/urea-glycerol and Pt black was said to need 5 mC cm^{-2}.[9] It can be said from these data that the current efficiencies of ECDs with such counter electrodes as Au and Ag are comparable with, or even higher than, the data previously reported.

In order to examine the coloring-bleaching response to step voltage, the square-wave voltage was applied to

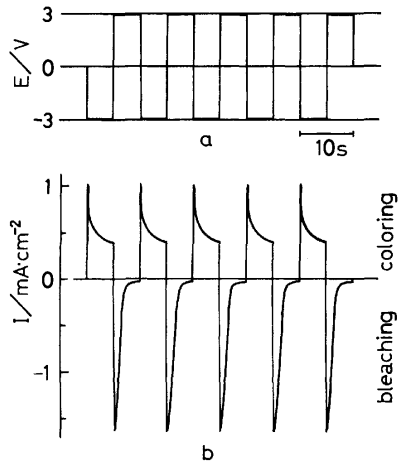

Fig. 5. Current wave form of ECD cell with graphite by applying square-wave voltage (±3 V) to a cell at 0.1 Hz. a: voltage wave form, b: current wave form.

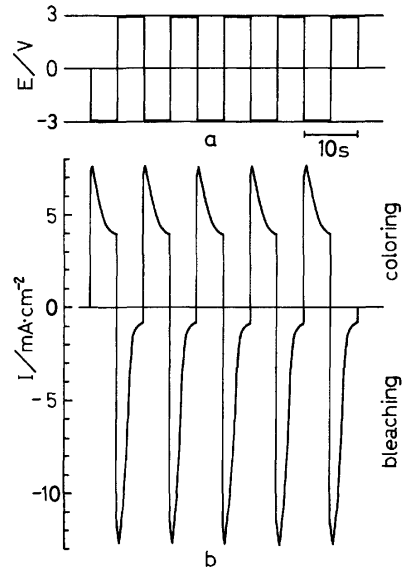

Fig. 6. Current wave form of ECD cell with Ag by applying square-wave voltage (±3 V) to a cell at 0.1 Hz. a: voltage wave form, b: current wave form.

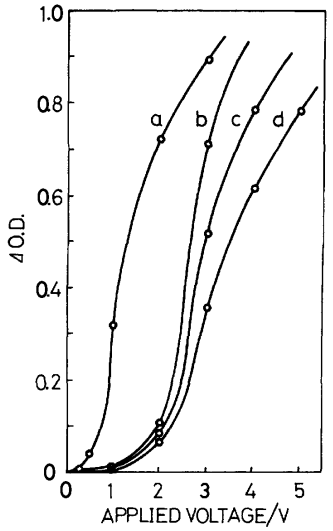

Fig. 7. Optical density changes at various applied voltages. Counter electrodes a: Ag, b: Au, c: graphite, d: Pt.

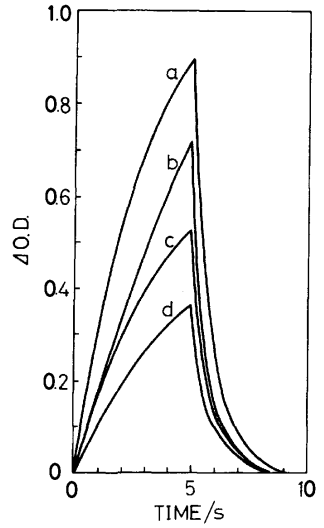

Fig. 8. Response time under an applied voltage of ±3 V. Counter electrodes a: Ag, b: Au, c: graphite, d: Pt.

the ECD and the voltage corresponding to the current was recorded. The current wave form at 0.1 Hz is shown in Fig. 5 on the cell with a graphite electrode, while the current-wave form obtained on the cell with Ag is shown in Fig. 6. In the former case, the current-wave forms differ in their coloring and bleaching processes. The current limit on the coloring process was observed below 1 s. In the latter case, the current was about ten times larger than that in the cell with graphite, and differences in shape in the current-wave forms were observed between the coloring and bleaching processes. The current limit on the coloring process was also observed, but it was slightly more moderate than the current limit shown in Fig. 5.

Figure 7 shows some $\Delta O.D.$ curves obtained at various voltages for a 5-s duration. The cell with Ag colored in the considerably low-voltage region of 1—2 V, while the cell with a graphite electrode did not color so much, even at a voltage higher than 3 V. The ECD with Au exhibited a higher $\Delta O.D.$ value compared with the cell containing graphite. In several papers,[9,19,20] the Pt electrode was used, but in this study the cell set up with Pt did not show so high performance as had been expected.

The minimum voltage at which distinct coloration can be observed is regarded as the threshold voltage for coloration. According to Fig. 7, the threshold voltage can be obtained by a procedure similar to the process of estimating a decomposition voltage on a certain current-voltage curve in an electrolysis. That is, the threshold voltage is found from the point of intersection of two straight lines which are drawn on a $\Delta O.D.$-

Table 1. Characteristic Values of ECDs with Various Electrode Materials. Work Functions of the Materials are Shown for Reference

Material	$Q/\Delta O.D.$ of 0.5	Threshold voltage/V	$\Delta O.D.$ 1 s after start	Work function
	$mC \cdot cm^{-2}$			eV
Ni	2.2	1.7	0.09	4.96
Au	2.1	1.8	0.17	4.83
Graphite	2.6	1.9	0.16	4.83
Cu	2.3	2.0	0.15	4.61
Pt	3.0	2.1	0.09	4.52
Fe	2.7	2.3	0.04	4.40
Sn	4.2	3.5	0.01	4.38
Ag	4.2	0.5	0.28	4.35
Zn	4.4	>5	0.01	4.31
Al	—	—	—	4.25
Zr	—	—	—	4.21
Ti	—	—	—	4.14

voltage curve in a lower $\Delta O.D.$ region ($0 \leqq \Delta O.D. < 0.05$) and in a higher $\Delta O.D.$ region ($0.1 < \Delta O.D. < 0.5$). Most of the cells in this study had the threshold voltage of 1.7—3.5 V. However, the ECD with an Ag electrode had the extremely low value of 0.5 V, as is shown in Table 1.

Figure 8 shows the coloration speed of the ECDs containing four cells with Pt, graphite, Au, and Ag electrodes. Most of the other cells, with various metal electrodes, did not reveal any coloration speed higher than that of the ECD with graphite. The $\Delta O.D.$ values 1 s after the beginning of coloration were 0.28, 0.17, and 0.16 for the Ag, Au, and graphite electrodes respectively. The response speed of the ECD with Ag was proved to be about twice as fast as that of the ECD with graphite. In the same way, the $\Delta O.D.$ values after 5 s were 0.89, 0.72, and 0.53 for Ag, Au, and graphite respectively.

The ECD consisting of Li_2WO_4 and the Au electrode has been reported to take 50 m s to achieve $\Delta O.D.=0.3$ when 3.0 V is applied and the ECD with antimony (V) oxide has been shown to need 500 m s when 1.3 V is applied.[18] In addition, the response speed of the cell of the TsOH/urea-glycerol system was $\Delta O.D.$ of 0.35/s at the applied voltage of 1.5 V.[9] Compared with these values, the coloration speed obtained in this work was not so high.

Discussion

In the ITO/WO_3/SPA/M system (M=metal), the electrochromic reaction on coloration can be written as follows:

$$WO_3 + xH^+ + xe^- \longrightarrow H_xWO_3 \quad (1)$$

where the H^+ ions come to WO_3 from proton-conductive SPA and where, at the same time, the H^+ ions formed at the SPA/M interface move into SPA. The H^+ ions may be formed by the dissociation and/or oxidation of the adsorbed-water at the interface:

$$H_2O \longrightarrow H^+ + OH^- \quad (2)$$

$$H_2O \longrightarrow 2H^+ + 1/2O_2 + 2e^- \quad (3)$$

The $\Delta O.D.$ vs. Q curves obtained at a constant-current operation were not always on a uniform curve, although the deviation was not remarkable; i.e., the charges needed to achieve $\Delta O.D.=0.5$ ranged from 2.1 to 4.4 $mC\,cm^{-2}$, as may be seen in Table 1. Such a difference in Q may be caused by the difference in the voltage applied to the cell to flow the constant current. This was supported by the current behavior obtained at a constant-voltage operation (Figs. 5 and 6).

The voltage applied to the cell during the coloring process will drop first at the SPA/M interface to produce H^+ ions and to make them move into SPA (1st stage), secondly at the SPA layer (2nd stage), and thirdly at the WO_3/SPA interface (3rd stage). In this experiment, the voltage drops at the 2nd and 3rd stages scarcely depend on the material of the counter electrode. Therefore, the 1st stage will dominate the total process. However, the variation in the applied voltage will also have an influence on the behavior of the H^+ ions at the SPA layer and at the WO_3/SPA interface.

Under the application of a d.c. voltage in the coloring process, the density of the H^+ ions in the SPA will vary so as to bring about a concentration gradient which is high at the WO_3/SPA interface and low at the SPA/M interface. When a number of H^+ ions are accumulated at the WO_3/SPA interface under a high voltage, some of them diffuse back to the solid electrolyte and do not always take part in the formation of H_xWO_3.[21] On the other hand, as the voltage increases, the probability of the direct reaction of the H^+ ions with electrons may increase at the WO_3/SPA interface. Such H^+ ions cannot contribute to the formation of H_xWO_3 or in turn, to the coloration of the ECD.

The work functions of the materials[22] used as counter electrodes in this study are summarized for reference in Table 1, together with some numerical values indicating the performances of ECDs. The ECD with electrode material of a large work function seems to have a certain tendency to show a lower threshold

value and a shorter response time on coloration. However, it is not reasonable to analyze the ECD characteristics using only the work function, since there is no distinct difference among the work functions listed in Table 1.

As has been stated above, the current-wave forms (Figs. 5 and 6), threshold voltages, and response times (Table 1) vary with the electrode materials. This suggests that the characteristics of the ECDs in this study are mainly related to the anode reactions. The OH^- ions produced according to Eq. 2 are oxidized to form oxygen gas[5] or metal hydroxide at the counter electrode (anode).

$$2OH^- \longrightarrow H_2O + 1/2O_2 + 2e^- \quad (4)$$

$$M + xOH^- \longrightarrow M(OH)_x + xe^- \quad (5)$$

It may be supposed that materials which bring about the oxidation of OH^- ions at a lower voltage produce H^+ ions with more ease. Furthermore, some materials oxidizing the adsorbed-water at a lower voltage may be supposed to accelerate the production of H^+ ions according to Eq. 3. It is desirable for the oxygen gas produced in Eqs. 3 and 4 to be accommodated by the counter electrode. The surfaces of metals with a strong chemical affinity to oxygen gas, such as Al, will lose their ability as counter electrodes. ECDs using such metals did not show coloration under the present experimental conditions.

The ECD with an Ag electrode showed the lowest threshold voltage and the highest response speed in the coloring process. The reactivity of Ag with the OH^- ion and oxygen gas has to be examined. The OH^- ions produced according to Eq. 2 will react with Ag to form silver (I) hydroxide and silver (I) oxide:[23]

$$2OH^- + 2Ag \longrightarrow 2AgOH + 2e^- \quad (6)$$

$$2AgOH \longrightarrow Ag_2O + H_2O \quad (7)$$

Such redox reactions among Ag, silver (I) oxide, and hydroxide proceed easily. Moreover, Ag can physically take in oxygen gas in the form of lattice oxygen and/or adsorbed oxygen. These reactions will reduce the energy to dissociate the adsorbed-water. According to the equilibrium reactions (2) and (3), the elimination of OH^- ions and oxygen gas leads to the production of H^+ ions. Therefore, the electrochromic reaction in the cell with the Ag electrode may take place at a low-threshold voltage, and the applied voltage may be used effectively to increase the coloration speed.

Besides this explanation, the possibility of the dissolution of Ag into the electrolyte could be considered. If the Ag dissolves to give Ag^+ ions, the Ag^+ ions as well as the H^+ ions will move from the SPA/Ag interface to the electrolyte. In bleaching, some of the Ag^+ ions go back to the SPA/Ag interface with difficulty, since in the coloring process the Ag^+ ions will intercalate in SPA more rigidly than the H^+ ions.[13] However, both the current-wave forms (Fig. 6) and the response feature (Fig. 8) show that the reaction takes place more easily in the bleaching process than in the coloring process. This fact is inconsistent with the assumption mentioned above. Therefore, the possibility of the dissolution of Ag into SPA can be rejected.

Conclusion

All solid-state ECDs, ITO/WO_3/$Sn(HPO_4)_2 \cdot H_2O$ (SPA)/metal or graphite, were examined in the search for good material as counter electrodes. The $\Delta O.D.$-Q curves must be independent of the materials used for the counter electrodes. However, at Q=5 mC cm^{-2} the ECD cells with Au, graphite, Pt, and Ag showed $\Delta O.D.$ values of 0.56—0.93 higher than the cells with other metals. The reason for this phenomenon could not be determined. Asymmetric current-wave forms were, however, observed between the coloring and bleaching processes corresponding to the square-wave voltage (±3 V). The ECD cell with Ag indicated a high $\Delta O.D.$ (0.33), even at 1.0 V, and a high response speed ($\Delta O.D.$=0.28 1 s after the start under 3 V). Such characteristics were discussed with respect to the production of H^+ ions by means of the dissociation and/or oxidation of the adsorbed-water at the SPA/metal interface and the accommodation of OH^- ions and oxygen gas. These anode reactions on coloration will be discussed in a subsequent paper.

The present authors wish to express their sincere thanks to the Research Laboratory, Toagosei Chemical Industry Co., Ltd., for providing an inorganic ion-exchanger and ITO-coated glass.

References

1) S. K. Deb, *Appl. Opt. Suppl.*, **3**, 192 (1969).
2) B. W. Faughnan, R. S. Crandall, and P. M. Heyman, *RCA Rev.*, **36**, 177 (1975).
3) S. K. Mohapatra, *J. Electrochem. Soc.*, **125**, 284 (1978).
4) I. Shimizu, M. Shizukuishi, and E. Inoue, *J. Appl. Phys.*, **50**, 4027 (1979).
5) T. Yoshimura, M. Watanabe, K. Kiyota, and M. Tanaka, *Jpn. J. Appl. Phys.*, **21**, 128 (1982).
6) M. Green and D. Richman, *Thin Solid Films*, **24**, S45 (1974).
7) M. Green and K. S. Kang, *Thin Solid Films.*, **40**, L19 (1977).
8) T. Takahashi, S. Tanase, and O. Yamamoto, *J. Appl. Electrochem.*, **10**, 415 (1980).
9) M. Shizukuishi, E. Kaga, I. Shimizu, H. Kokado, and E. Inoue, *Jpn. J. Appl. Phys.*, **20**, 581 (1981).
10) T. Yoshimura, M. Watanabe, Y. Koike, K. Kiyota, and M. Tanaka, *Jpn. J. Appl. Phys.*, **22**, 152 (1983).
11) K. Kuwabara, A. Sakai, and K. Sugiyama, *Denki Kagaku*, **53**, 243 (1985).
12) K. Kuwabara, H. Nakamura, and K. Sugiyama, *Denki Kagaku.*, **54**, 66 (1986).
13) G. Alberti, M. Casciola, U. Kostantino, G. Levi, and G. Ricciardi, *J. Inorg. Nucl. Chem.*, **40**, 533 (1978).
14) N. Yoshiike and S. Kondo, *J. Electrochem. Soc.*, **130**,

2283 (1983).
15) N. Yoshiike and S. Kondo, *J. Electrochem. Soc.*, **131**, 809 (1984).
16) H. Morita and H. Washida, *Jpn. J. Appl. Phys.*, **23**, 754 (1984).
17) M. Sakamoto, Y. Nakajima, M. Miyajima, and Y. Kihara, Proc. 9th Meeting of Solid State Ionics in Japan, Yokohama (1982), p. 82.
18) N. Matsudaira, K. Fukuyoshi, Y. Yorimoto, Y. Ikeda, and K. Yoshida, "Japan Display '83," Kobe (1983), p. 54.
19) N. Baba, S. Morisaki, and N. Nishiyama, *Jpn. J. Appl. Phys.*, **23**, L638 (1984).
20) J. Nagai and T. Kamimori, *Jpn. J. Appl. Phys.*, **22**, 681 (1983).
21) R. S. Crandall and B. W. Faughnan, *Appl. Phys. Lett.*, **28**, 95 (1976).
22) "Kagaku Binran Kiso-Hen II," ed by Chem. Soc. Japan, Maruzen, Tokyo (1966), p. 1021.
23) C. P. Wales and J. Burbank, *J. Electrochem. Soc.*, **106**, 885 (1959).

 © 1987 The Chemical Society of Japan Bull. Chem. Soc. Jpn., 60, 753—757 (1987)

Synthesis of Sulfoxide-Modified Cellulose Derivatives Designed for the Permselective Membrane of Sulfur Dioxide

Kiyokazu IMAI,* Yasuyuki TEZUKA, Tomoo SHIOMI, and Matsunori TAKADA
Department of Material Science and Technology, Technological University of Nagaoka, Kamitomioka, Nagaoka, Niigata 940-21
(Received September 8, 1986)

The Michael type addition reaction of cellulose with a series of vinyl sulfoxides, namely methyl vinyl sulfoxide, ethyl vinyl sulfoxide, *t*-butyl vinyl sulfoxide, and phenyl vinyl sulfoxide, was performed with NaOH as a catalyst to produce 2-(alkyl- or arylsulfinyl)ethyl cellulose derivatives. The high permselectivity of sulfur dioxide against nitrogen and oxygen was achieved through these sulfoxide modified cellulose membranes.

The increase of the concentration of atmospheric sulfur dioxide(SO_2) caused by anthropogenic sources has been accused of a wide range of environmental dangers, including widely spreading acid rain among industrialized countries. The control techniques for the atmospheric SO_2 concentration are currently carried out in two ways; (1) desulfuration of fuels and (2) desulfuration of combustion gas mixtures. The former system can be applied solely to liquid fuel systems and thus cannot be used for solid fuel systems including widely used coal systems. In the latter system, the technique, which involves alkaline absorption of SO_2 from bulk wasted gas mixtures, requires huge operation facilities, limiting its actual use to big combustion plants. Besides, the disposal of the wasted mass may cause another problem.

The development of the membrane technique which may provide a facile and economic way for a selective accumulation and separation of SO_2, should be of great importance. There have been, however, surprisingly few studies up to now in the search for suitable membrane materials for the selective separation of SO_2.[1-4] We have recently reported that sulfoxide modified poly (vinyl alcohol) can be used as the membrane material for the selective permeation of SO_2.[5] The structure design of this new synthetic membrane was accomplished by taking into account the exceptionally high solubility of SO_2 toward sulfoxides, including dimethyl sulfoxide,[6] since the permeability property of a synthetic membrane is considered to be governed by the solubility and the diffusivity of the gas molecule toward the membrane.

As the continuation and the extension of the previous studies, this paper presents the synthesis of sulfoxide-modified cellulose derivatives and the application to the membrane material for the selective permeation of SO_2. Cellulose, as well as poly (vinyl alcohol), is considered to be another promising candidate for the membrane material for the present purpose due to its good mechanical property and its high gas barrierity. The subsequent modification of cellulose with sulfoxide function is expected to give a membrane material with high permselectivity of SO_2 and good mechanical property.

Experimental

Reagents. A series of vinyl sulfoxides, i.e. methyl vinyl sulfoxide (MVSO), ethyl vinyl sulfoxide (EVSO), *t*-butyl vinyl sulfoxide (BVSO) was prepared by the method described before.[7] Phenyl vinyl sulfoxide (PVSO) was commercially available and was purified by the fractional distillation. Powdery cellulose was supplied from Asahi Chemical Co. (Avicel, PH 101, D.P. 250). Sodium hydroxide was of reagent grade and used without further purification. Water was used after deionization. Ethyl cellulose (from Nakarai Chem., D.S.=2.5, 80—120 cps) was used as received. Other reagents were purified by the conventional procedures.

Synthesis of Sulfoxide-Modified Cellulose Derivatives. A series of sulfoxide modified cellulose derivatives was synthesized through the Michael type addition reaction of cellulose with a series of vinyl sulfoxides. The following example presents the typical reaction procedure. One gram of cellulose powder was slurried and swelled in 20 ml of aqueous NaOH solution at 26—28 °C. A required amount of vinyl sulfoxide was then added and the reaction mixture was stirred for the prescribed period. The reaction solution became gradually less turbid and, in some cases, turned into almost homogeneous. The reaction mixture was then neutralized by acetic acid and poured into an acetone/methanol (7/3 in volume) mixture to isolate the reaction product, which was washed with the above acetone/methanol mixture and finally dried in vacuo at 45 °C for 48 h.

Gas Permeation Measurements. The sample membrane of a series of sulfoxide modified cellulose derivatives was prepared by casting from either 5 wt% water (for MVSO and EVSO adduct) or DMSO (for PVSO adduct) solution on a Teflon-coated plate. MVSO-modified cellulose with low D.S. (0.83 and 0.92), as well as EVSO- and PVSO-modified cellulose samples gave slightly turbid membranes. The casting solvent was evacuated first either in a desiccator containing anhydrous calcium chloride (for water), or in a thermostatic oven at 35 °C (for DMSO) and finally in vacuo at 60 °C for 2 d. An ethyl cellulose membrane was prepared in a similar way from a dichloromethane solution. The gas permeation measurements were carried out by using the volume method apparatus described in the previous report.[5]

Other Measurements. ^{13}C NMR measurements were carried out by a JEOL JNM GX270 apparatus, in which chemical shifts were calibrated either by using cellulose C_1 carbon (103.0 ppm) or DMSO (43.5 ppm) as an internal standard. Sulfur elemental analysis was carried out with a CALRO ERBA Elemental Analyzer MOD 1106. Viscosity measurements were carried out in water at 30 °C with an Ubbelohde

viscometer.

Results and Discussion

1) Synthesis of Sulfoxide-Modified Cellulose Derivatives. The Michael type addition reaction of hydroxyl group to poly (vinyl alcohol), PVA, or cellulose with such vinyl compounds as acrylonitrile, acrylamide, and alkyl vinyl sulfone, has been proved to be a versatile technique to introduce various kinds of functional groups to these polyhydroxy type polymers.[8,9] We have recently adopted this technique to synthesize a series of sulfoxide modified PVA derivatives using a variety of vinyl sulfoxides, i.e. methyl vinyl sulfoxide (MVSO), ethyl vinyl sulfoxide (EVSO) and *t*-butyl vinyl sulfoxide (BVSO).[10]

In the present study, we have carried out the Michael

Table 1. Synthesis of Sulfoxide-Modified Cellulose Derivatives[a]

Run. No.	RVSO	RVSO/Cellulose ratio[b]	React. time	NaOH concn.	Sulfur cont.[c]	D.S.
			h	wt%	wt%	
M-1	MVSO	3.0	1	20	4.60	0.27
M-2	MVSO	3.0	2	20	7.29	0.46
M-3	MVSO	3.0	3	20	9.50	0.66
M-4	MVSO	3.0	5	20	10.45	0.75
M-5	MVSO	3.0	9	20	11.22	0.83
M-6	MVSO	9.0	9	20	14.15	1.19
M-7	MVSO	12.0	9	20	14.50	1.24
M-8	MVSO	9.0	9	15	15.50	1.39
M-9	MVSO	9.0	9	5	13.20	1.06
M-10	MVSO	9.0	9	10	14.20	1.20
M-11[d]	MVSO	9.0+9.0	9+9	10	19.26	2.13
M-12[d]	MVSO	9.0+9.0+9.0	9+9+9	10	20.32	2.40
E-1	EVSO	9.0	9	20	3.45	0.20
E-2	EVSO	27.4	9	20	3.40	0.19
E-3	EVSO	35.7	9	20	2.70	0.14
E-4	EVSO	9.0	9	15	5.79	0.37
E-5	EVSO	9.0	9	10	8.55	0.60
E-6	EVSO	9.0	9	5	4.81	0.29
B-1	BVSO	9.0	9	10	0.54	0.03
P-1	PVSO	9.0	9	10	8.56	0.73
P-2	PVSO	6.0	9	10	6.87	0.51
P-3	PVSO	3.0	9	10	5.40	0.36

a) Reaction conditions: Cellulose 1.0 g, H_2O 20 ml, 26—28 °C. b) Molar ratio between RVSO and hydroxyl group in cellulose. c) Elemental analysis. d) The reaction was continued by adding fresh RVSO repeatedly.

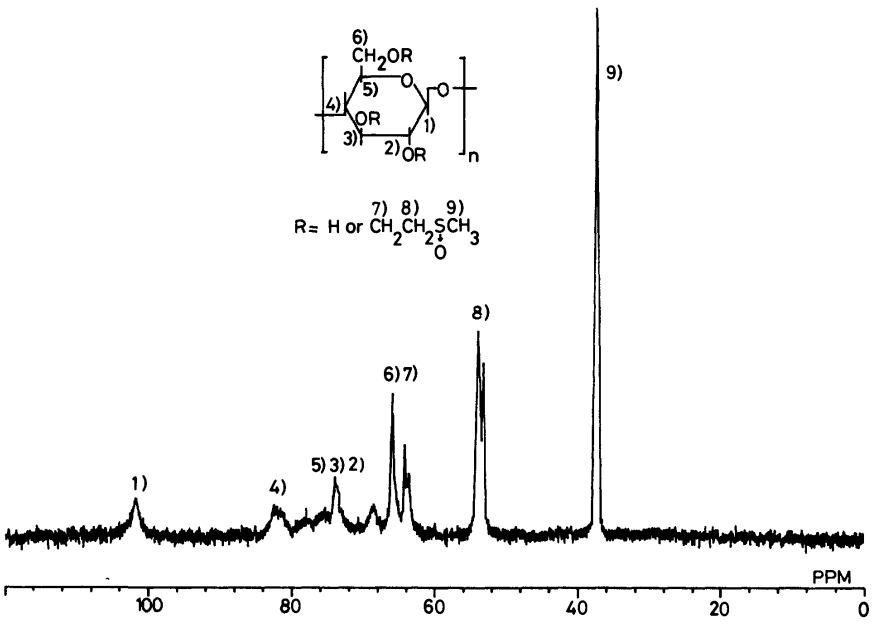

Fig. 1-a. ^{13}C NMR spectrum of MVSO-modified cellulose in D_2O at 40°C (sample M-11 in Table 1).

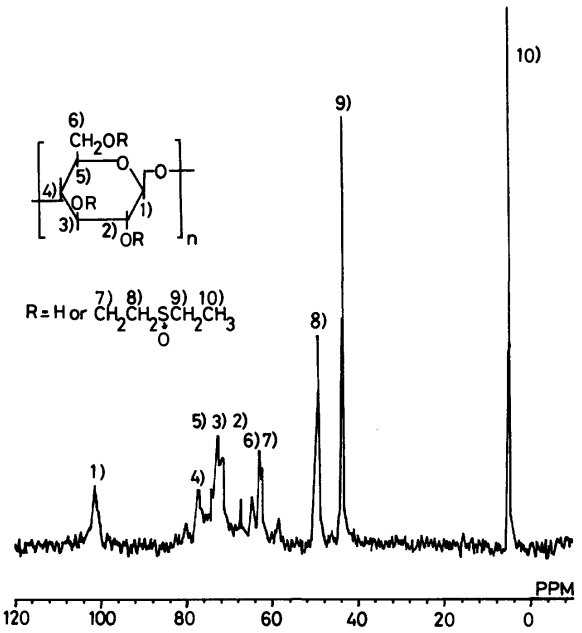

Fig. 1-b. ^{13}C NMR spectrum of EVSO-modified cellulose in D_2O at 40°C (sample E-5 in Table 1).

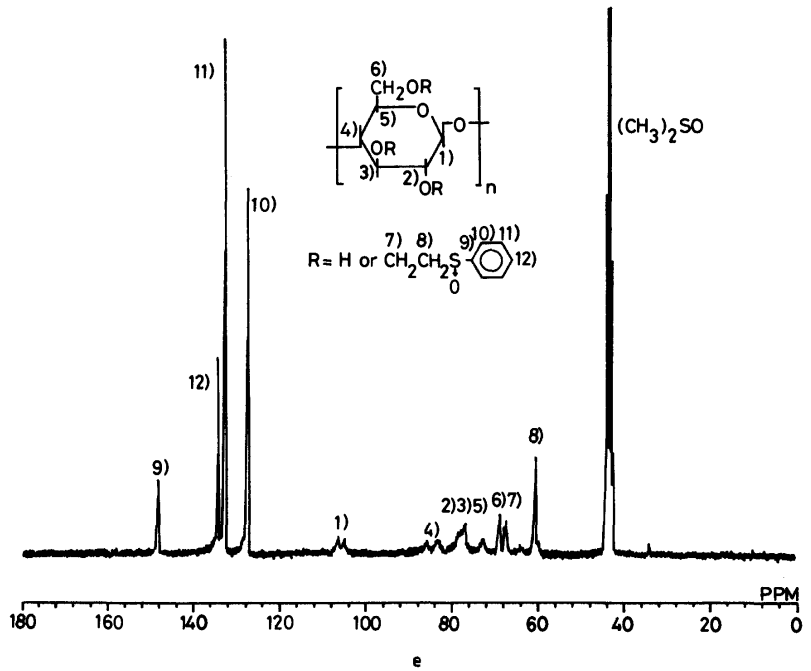

e

Fig. 1-c. ^{13}C NMR spectrum of PVSO-modified cellulose in DMSO-d_6 at 60°C (sample P-1 in Table 1).

type addition reaction of a series of vinyl sulfoxides against another polyhydroxy polymer, cellulose, in the presence of sodium hydroxide, as a catalyst, to produce various sulfoxide modified cellulose derivatives. As is summarized in Table 1, a series of sulfoxide-modified

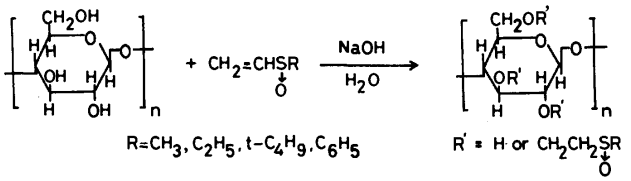

cellulose derivatives with various degrees of sulfoxide contents, i.e. the degree of substitution (D.S.) for the sulfinylethyl function, was obtained in the reaction with MVSO, EVSO, and PVSO, while BVSO was found to be very sluggish to react with cellulose under these reaction conditions. The formation of sulfoxide-modified cellulose derivatives through the Michael type addition reaction was confirmed evidently by ^{13}C NMR spectroscopic analysis given in Fig. 1-a—c, where the peaks assigned for the 2-(alkyl- or phenyl-sulfinyl)ethyl group introduced to cellulose appear to

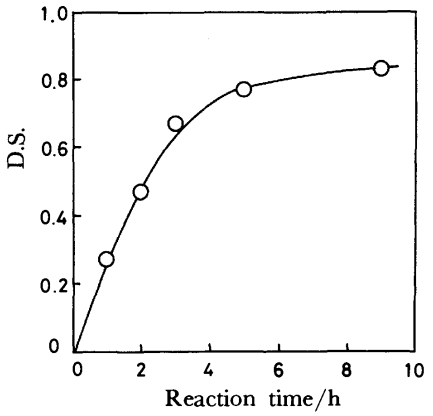

Fig. 2. The degree of substitution of MVSO-modified cellulose at various reaction times. Cellulose 1.0 g(−OH 0.019 mol), MVSO 5.1 g(0.057 mol), NaOH 5.0 g, H_2O 20 ml, 26—28°C.

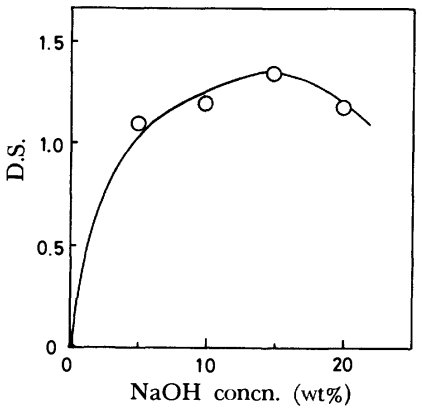

Fig. 3. The degree of substitution of MVSO-modified cellulose at various NaOH concentrations, Cellulose 1.0 g(−OH 0.019 mol), MVSO 15.4 g(0.17 mol), H_2O 20 ml, 9h, 26—28°C.

be present in addition to those for the glucose ring carbon signals.

As is seen in Table 1, the degree of substitution in the cellulose derivatives failed to exceed around 1.4, far less than the total available hydroxyl group in glucose unit 3.0, even when the reaction was performed either with a large excess of vinyl sulfoxide or with a prolonged reaction time (Fig. 2), or with a higher catalyst concentration (Fig. 3). The undesired side reaction, namely the addition reaction of vinyl sulfoxide with water used as the solvent, was observed to give 2-hydroxyethyl sulfoxide in the presence of sodium hydroxide similar to the reaction with poly (vinyl alcohol).[10]

The sulfoxide modified cellulose derivatives with the higher sulfoxide content could be obtained by employing the following reaction technique, where an excess amount of fresh vinyl sulfoxide was repeatedly added to the reaction mixture in an appropriate interval as shown in Table 1 (Runs M-11 and M-12). When such a reaction was repeated three times, sulfoxide-modified cellulose with a D.S. value as high as 2.40 was obtained as listed in Table 1 (Run M-12).

Table 2. Intrinsic Viscosity of MVSO-Modified Cellulose Derivatives with Various Degrees of Substitution[a)]

D.S.	$[\eta]$ (dl g^{-1})
0.83	1.95
1.18	1.81
1.23	1.77
2.01	1.30
2.40	1.25

a) In water at 30°C.

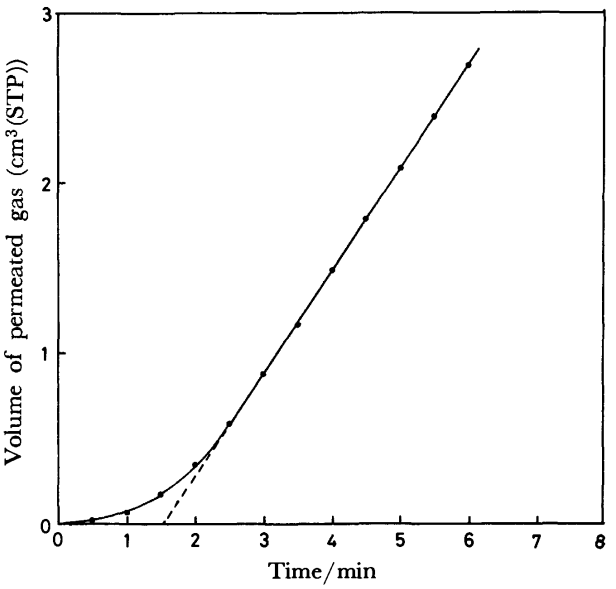

Fig. 4. The permeation measurement of sulfur dioxide through MVSO-modified cellulose membrane (Run 2 in Table 3, 1.0 atm).

The intrinsic viscosity of a series of MVSO-modified cellulose derivatives with various D.S. values was measured as the first-order approximation of the extent of polymer degradation during the sulfoxide-modification reaction. As is summarized in Table 2, MVSO-modified cellulose with the D.S. value of 2.40 was estimated to possess still considerably high molecular weight from its $[\eta]$ value of 1.25, although a slight decrease of $[\eta]$ was actually noticed with the increase in sulfoxide content.

2) Selective Permeation of SO_2 through Sulfoxide-Modified Cellulose Membranes. A series of sulfoxide-modified cellulose derivatives thus obtained was casted to form a membrane and subjected to the gas permeation measurements with such gases as SO_2, N_2, and O_2. The permeation coefficient of each pure gas was obtained through the volume method, where the rate of gas outflow through the sample membrane was measured until a constant flow rate was attained. An example of the permeation experiment for SO_2 by the present system is given in Fig. 4.

Table 3. Gas Permeability of Sulfoxide-Modified Cellulose Derivatives[a)]

Run No.	Modified Cell		Thickness	Temp	P(SO_2)			P(N_2)	P(O_2)	P(SO_2)/P(N_2)
	Type	D.S.	(μm)	°C	1.0atm	1.5atm	2.0atm	2.0atm	2.0atm	2.0atm
1		0.83	81	20	81	155	356	0.16	0.38	2200
2	MMC[b)]	0.92	82	17	553	973	2280	0.40	0.16	5700
3		1.06	55	23	722	2150	4090	0.32	0.37	12800
4		2.13	77	18	—[f)]	—[f)]	—[f)]	0.52	0.73	—
5	EMC[c)]	0.66	66	23	284	1080	2210	0.29	0.48	7600
6	PMC[d)]	0.51	92	19	2790	—[f)]	—[f)]	0.14	0.25	19900[g)]
7	EC[e)]	2.50	127	20	1010	1640	2140	3.10	14.20	690

a) Unit of permeability, P: $(cm^3\ (STP)\cdot cm)/(cm^2\cdot s\cdot cm\ Hg)\times 10^{10}$. b) MVSO-modified cellulose. c) EVSO-modified cellulose. d) PVSO-modified cellulose. e) Ethyl cellulose. f) Too weak to permeability measurements. g) 1.0 atm.

The results of the gas permeation measurements for a series of sulfoxide-modified cellulose membranes were summarized in Table 3, where the result of ethyl cellulose membrane was also listed for comparison. The permeation coefficient of SO_2 was found to increase markedly with the increase of the sulfoxide function content in cellulose, while the permeation coefficients of N_2 and O_2 remained almost unchanged. This leads to the high permselectivity of SO_2 against N_2 and O_2 with these sulfoxide-modified cellulose membranes.

With the increase in applied SO_2 pressure, the permeation coefficient of SO_2 for the sulfoxide modified cellulose membrane was found to increase far more significantly compared to that for ethyl cellulose. At the same time, the notable swelling of the sulfoxide-modified cellulose membrane during the permeation experiment was observed especially in high applied SO_2 pressure, indicating the absorption of SO_2 in the membrane. This, in turn, weakens the membrane at high applied SO_2 pressure, especially in high sulfoxide content membranes.

The type of the substituent in vinyl sulfoxide was also found to exercise a prominent influence on the permeation behavior of SO_2, while little effect on the permeation coefficients of N_2 and O_2. The phenyl substituent was found to be the most remarkable effect on the permeation coefficient and permselectivity of SO_2, compared to methyl and ethyl counterpart, nevertheless the membrane tended to become too weak for the measurement at SO_2 pressures higher than 1 atm, even when the D.S. value of this cellulose derivative is 0.51.

Conclusion

A series of sulfoxide-modified cellulose derivatives was produced through the reaction of cellulose with various substituted vinyl sulfoxides and the obtained sulfoxide-modified cellulose membranes exhibited the high permselectivity of SO_2 against N_2 and O_2.

Financial supports from the Japan Securities Scholarship Foundation to Yasuyuki TEZUKA, and from the Nissan Science Foundation are gratefully acknowledged.

References

1) D. L. Kuehne and S. K. Friedlander, *Ind. Eng. Chem., Process Des. Dev.*, **19**, 609 (1980).
2) D. L. Kuehne and S. K. Friedlander, *Ind. Eng. Chem., Process Des. Dev.*, **19**, 616 (1980).
3) D. R. Seibel and F. P. McCandless, *Ind. Eng. Chem., Process Des. Dev.*, **13**, 76 (1974).
4) R. Zavaleta and F. P. McCandless, *J. Membr. Sci.*, **1**, 333 (1976).
5) K. Imai, T. Shiomi, Y. Tezuka, and M. Satoh, *Makromol. Chem., Rapid Commun.*, **6**, 413 (1985).
6) "Dimethyl Sulfoxide 1, Basic Concept of DMSO," ed by S. W. Jacob, J. Rosenbaum and D. C. Wood, Marcel Dekker Inc., New York (1971).
7) K. Imai, T. Shiomi, Y. Tezuka, and K. Takahashi, *J. Macromol. Sci. -Chem.*, **A22**, 1347 (1985).
8) "Polyvinyl Alcohol, Properties and Application," ed by C. A. Finch, Wiley-Interscience, New York (1973).
9) "Cellulose and Cellulose Derivatives," ed by N. M. Bikales and L. Segal, Wiley-Interscience, New York (1971).
10) K. Imai, T. Shiomi, Y. Tezuka, K. Takahashi and, M. Satoh, *J. Macromol. Sci.-Chem.*, **A22**, 1359 (1985).

Self Regulation in the Cooperative Binding of Small Molecules to Linear Polymers

Takayuki SANO,* Thoru NAKATSUKA, Hirotsugu TSURUTA, and Shoji HARADA
Department of Materials Science, Faculty of Science, Hiroshima University, Hiroshima 730
(Received September 26, 1986)

Synopsis. As for the cooperative binding of small molecules to the linear polymers, including not only synthetic polymers but also biopolymers, an interesting relationship, the so called "self regulation effect" between the isolated binding constant (intrinsic binding constant) and the cooperative binding constant, (binding constant of growth process) can be observed amongst the large amount of data so far reported. The biological significances as well as the possible origin for this "self regulation mechanism" will be discussed.

A number of investigations into the cooperative binding of small molecules to polymers have been undertaken,[1-15] and several theories based on the one dimensional Ising model have been advanced.[6,7,11] For cooperative binding, it has been pointed out that the cooperativity seen in the binding of small dye molecules to counter charged synthetic linear polymers arises from a stacking interaction between bound dyes on polymer.[10,13] However, no systematic investigation of the binding mechanism has been completed. We report here an interesting correlation found between the isolated binding constant and the cooperative interaction parameter obtained for a variety of systems, both synthetic and biological, and propose a "self-regulation" cooperative binding effect in these systems.

Since the theory on the cooperative binding phenomenon was developed, our knowledge of the binding mechanism has been considerably extended. As for the cooperative binding of small molecules to polymers, the following three equations have been independently derived by Scatchard,[1] Schwarz,[7] and McGhee and von Hippel[11] respectively:

$$r/C_f = K_o e^{-2\omega r}(n - r), \tag{1}$$

$$C_f = 1/K_{co} - \{\frac{C_f}{qK_{co}r(n-r)}\}^{1/2}(n - 2r) \tag{2}$$

with

$$K_{co} = q K_o,$$

and

$$r/C_f = K_o(n - r)\{\frac{n - 2r + R}{2(n - r)}\}^2 \tag{3}$$

with

$$R = \{(n - 2r)^2 + 4qr(n - r)\}^{1/2},$$

where r is the ratio of the bound ligand to total polymer concentration, C_f is the concentration of free ligand, K_o is the intrinsic binding constant, ω is the electrostatic force between bound ligands, n is the number of binding sites per residue of polymer, K_{co} is the cooperative binding constant, and q is the cooperative interaction parameter. In these three theories the binding isotherms are described by three parameters, viz., the number of binding sites per residue of polymer, n; the intrinsic binding constant, K_o; and a cooperative interaction parameter, q or ω. The above three equations can be combined as follows through the experimentally measured apparent binding constant, K, determined by the conventional method of using the value of that at the isotherm midpoint;

$$K = \frac{1}{(C_f)_{r=1/2}} = K_o e^{-\omega n} = K_o q = K_{co} \tag{4}$$

The focus of our investigation was to examine the proposed theory and to clarify the origin of the cooperative interaction energy. From the investigations reported so far, it has been found in general that the

Table 1. The Binding Parameters of the Cooperative Binding in Various Systems

	System	T / °C	n	K_0 / M^{-1}	q	pH	c.f.	Ref.
1.	(L-Glu)$_n$[a]+AO[b]	25	1.24	5×10^4	12	7.5	at low P/D[c] } 1 mM	8
2.		25	1.24	3.5×10^2	1700	7.5	at high P/D } Na_2HPO_4/NaH_2PO_4	
3.	(L-Glu)$_n$+PF[d]	25	1.11	6.7×10^2	150	7.5	1 mM Na_2HPO_4/NaH_2PO_4	9
4.	(L-Glu)$_n$+TB[e]	25	0.45	4.7×10^4	3	5	} No added electrolyte	12
5.		25	1.1	$8.6\times10_4$	8	8	}	
6.	(Acry)$_n$[f]+PF	25	0.37	1.1×10^4	90	7.9	high mol. wt. } 1 mM	10
7.		25	0.37	1.4×10^4	180	6.9	low mol. wt. } Na_2HPO_4/NaH_2PO_4	
8.	(Acry)$_n$+TB	20	1.1	2.4×10^4	20	6.5	}	
9.		20	1.2	1.8×10^4	30	8	} No added electrolyte	14
10.		20	1.4	2.1×10^4	80	10	}	
11.	(Phos)$_n$[g]+PF	25	0.8	6.4×10^2	700	6.9	1 mM $Na_2HPO_4/Na_2H_2PO_4$	10
12.	Poly(A)+PF	0	0.9	7×10^3	140	6.8	1 mM cacodylate buffer }	13
13.	DNA+PF	25	1.0	4×10^3	20	6.8	1 mM cacodylate buffer }	
14.	(L-Lys)$_n$[j]+MO[j]	25	1.3	9.2×10^4	2.4	7.0	No added electrolyte	15

a) (L-Glu)$_n$=poly(L-glutamic acid). b) AO=Acridine Orange. c) P/D=polymer to dye ratio. d) PF=Proflavin. e) TB=Toluidine Blue. f) (Acry)$_n$=poly(acrylic acid). g) (Phos)$_n$=poly(phosphoric acid). h) poly(A)=poly(adenylic acid). i) (L-Lys)$_n$=poly(L-lysine). j) MO=Methyl Organge. 1 M=1 mol dm^{-3}.

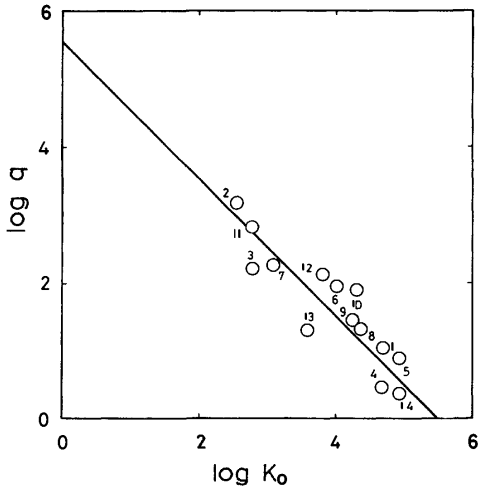

Fig. 1. The logarithmic plots of the cooperative interaction parameter, q against the isolate binding constant, K_o. The numbers on circles correspond to those in Table 1.

binding process of ionic polymers to ionic dye molecules is governed by an electrostatic interaction between bound molecules. The binding parameters obtained by independent workers on various systems at low ionic strength are listed in Table 1. As can be seen from the table there is a systematic trend in the values of q and K_o, i.e., the smaller K_o is, the larger is q. The logarithmic plot of K_o vs. q is shown in Fig. 1 where a general linear correlation was found having a slope equal to -1 regardless of such solution conditions as pH. This new finding between K_o and q has an important meaning with respect to the mechanism of the cooperative binding of small molecules to linear polymers. As described above, the parameter q can be related to K_o by the cooperative binding constant K_{co} or the binding strength K (see, e.g., Eqs. 1—4). Consequently, the obtained linear relationship between K_o and q implies that all the systems listed in Table 1 have essentially the same binding mechanism and also have a single cooperative binding constant, $K_{co}=(2.5\pm 0.5)\times 10^5\ M^{-1}$. In other words, the isolated binding is compensated in strength by the cooperative interaction effect so as to give the same binding strength regardless of the system. We call this effect "self-regulation" in the cooperative binding of small ions to polymers.

It has been reported that the binding mechanisms of the ionic polymer and dye molecules are dependent on the chemical properties of both molecules.[10,13] This is certainly true. However on the basis on the new finding of the linear correlation between K_o and q, it can be pointed out that there must exist a more specific factor in the binding mechanism of small ionic molecules to ionic polymers. At the present time there has still not been enough data reported to clarify what this specific factor is. If, for instance, the electrostatic binding interaction between counter-charged ionic species is the dominant factor in the binding of the systems listed in Table 1, then the state of hydration of the reacting species, especially of the ionic groups of the polymers, may be the most important factor in the "self-regulation" resulting from the cooperative binding interaction.

The "self-regulation" effect has been observed not only for the synthetic polymers but also for biopolymers such as DNA.[13] Therefore it is likely that the effect plays an important role in keeping the in vivo concentration of small ionic molecules at the optimum level. The self-regulation effect proposed here provides motivation for further investigation on the binding of small ligands to polymers, particularly on the role of the state of hydration of the reacting spacies.

References

1) G. Scatchard, Ann. N. W. *Acad. Sci.*, **51**, 660 (1949).
2) D. F. Bradley, and M. K. Wolf, *Proc Natl. Acad. Sci., U. S.*, **45**, 744 (1959).
3) G. G. Hammes, and C. D. Hubbard, *J. Phys. Chem.*, **70**, 165 (1966).
4) D. Crothers, *Biopolymers*, **6**, 575 (1968).
5) W. C. Galley, *Biopolymers*, **6**, 1279 (1968).
6) F. W. Schneider, C.L. Croman, and S.K. Podder, *J. Phys. Chem.*, **72**, 4563 (1968).
7) G. Schwarz, *Eur. J. Biochem.*, **12**, 442 (1970).
8) G. Schwarz, S. Klose, and W. Balthasar, *Eur. J. Biochem.*, **12**, 454 (1070).
9) G. Schwarz and W. Balthasar, *Eur. J. Biochem.*, **12**, 461 (1970).
10) G. Schwarz and S. Klose, *Eur. J. Biochem.*, **29**, 249 (1972).
11) J.D. McGhee and P. H. von Hippel, *J. Mol. Biol.*, **86**, 469 (1974).
12) H. Ushio, T. Yasunaga, T. Sano, and Y. Tsuji, *Biopolymers*, **15**, 187 (1976).
13) M. Dourlent and J. F. Hogrel, *Biopolymers*, **15**, 29 (1976).
14) H. Ushio, H. Nishimura, Y. Tsuji, T. Sano, and T. Yasunaga, *Polymer J.*, **9**, 489 (1977).
15) K. Murakami, T. Sano, K. Ishii, N. Kure, and T. Yasunaga, *Biopolymers*, **22**, 2035 (1983).

^{27}Al High-Resolusion Solid-State NMR Study of Hydration of Ultrafine Powder of Aluminum Nitride

Shigenobu HAYASHI,* Kikuko HAYAMIZU, and Osamu YAMAMOTO
National Chemical Laboratory for Industry, Tsukuba, Ibaraki 305
(Received July 26, 1986)

Synopsis. ^{27}Al NMR spectra of hydrated aluminum nitride ultafine powder, measured using magic angle sample spinning technique, showed two peaks which can be attributed to Al coordinated by four N atoms and to Al coordinated by six O atoms, and the hydration process was discussed.

Aluminum nitride (AlN) is an attractive material as a substrate of electronic devices, since it has high heat-resisting property and large thermal conductivity.[1,2] Since high density is necessary to obtain the large thermal conductivity, ultrafine powder is promising to obtain a homogeneous and dense AlN substrate by sintering, but the powder easily reacts with atmospheric moisture to form a hydrated surface. The adsorbed oxygen-containing species leave their oxygen atoms after sintering, and the thermal conductivity is largely reduced by the oxygen.[2,3]

In the present work we have studied the hydration process of AlN ultrafine powder by means of ^{27}Al high-resolution solid-state NMR.

Experimental

Two kinds of AlN ultrafine powder were supplied by NEC Corporation; they are called Samples A and B, whose particle diameters are 100—1000 and about 2000 Å, respectively.

^{27}Al NMR spectra were obtained using magic angle sample spinning (MAS) technique by a JEOL FX-200 pulsed spectrometer at a resonance frequency of 52.00 MHz. The spinning speed was about 3.6 kHz. An ordinary one-pulse cycle was used with the flip angle of $\pi/6$ and the recycle time of 1 s. The shift values are referred to $AlCl_3$ aqueous solution. ^{1}H NMR spectra were also measured by a Bruker CXP-100 pulsed spectrometer, operating at a resonance frequency of 90.03 MHz, to obtain the hydrogen content. All the NMR measurements were performed at room temperature.

Results

Figure 1a shows an ^{27}Al MAS NMR spectrum of Sample A. Only one signal is observed at a position of 103 ppm with a width of 1.3 kHz. Other peaks are all attributed to spinning sidebands, which was confirmed by changing the spinning speed. ^{1}H NMR spectrum of this sample consists of two components with different linewidth; one is motionally-narrowed, and the other broadened by dipole-dipole interaction, being attributed to spatially fixed hydrogens. Total hydrogen content was estimated to be 0.71 wt%, while the content of the fixed hydrogens was 0.47 wt%

Figure 1b shows a spectrum of a heavily-hydrated sample of A (called AH). The hydration was carried out by exposing Sample A to liquid water at room temperature for 2 d. A new peak appears at −5 ppm with a width of 2.5 kHz, while the peak at 103 ppm slightly shifts to 109 ppm. Other peaks are attributed

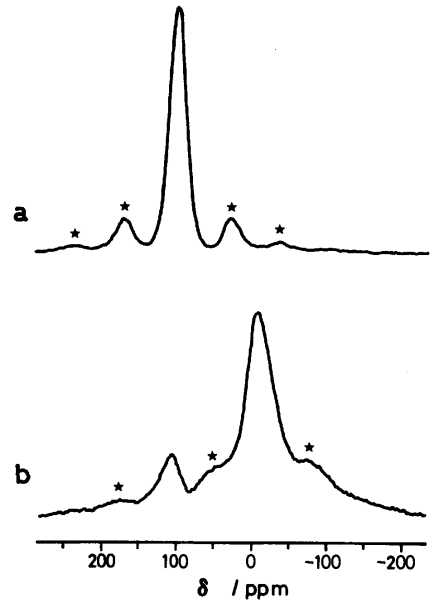

Fig. 1. ^{27}Al MAS NMR spectra of (a) Sample A and (b) Sample AH. The mark ★ denotes spinning sideband.

to spinning sidebands of the above two peaks. The hydrogen content is about 9.0 wt%, and the ^{1}H NMR spectrum shows a very narrow resonance line with a width of 350 Hz and a chemical shift of 5.2 ppm from tetramethylsilane. The shift value agrees with pure H_2O liquid (5.4 ppm),[4] and the line is motionally-narrowed. These facts suggest that most of the hydrogens are contained in the form of physisorbed H_2O left unreacted.

A dehydrated sample of A (Sample AD) was prepared by evacuating Sample A at 250 °C for 1 h. The hydrogen content is reduced to 0.17 wt%, and all hydrogens are spatially fixed. The ^{27}Al MAS NMR spectrum of this sample agrees with that of Sample A.

Sample B has a hydrogen content of 0.028 wt%, much lower than the other samples. The ^{27}Al MAS NMR spectrum agrees with that of Sample A again.

The results of ^{27}Al and ^{1}H NMR are summarized in Table 1.

Discussion

It is well-known that AlN reacts with H_2O in the following way:

$$AlN + 3H_2O \rightarrow Al(OH)_3 + 3NH_3. \quad (1)$$

In the AlN structure an Al atom is coordinated by four N atoms, while an Al atom is coordinated by six O

Table 1. Summary of ^{27}Al and ^{1}H NMR Results

Sample	Treatment	^{27}Al NMR		C_H[c]/wt%	
		Shift[a]/ppm	FWHM[b]/kHz	Total	Fixed
A	as supplied	103	1.3	0.71	0.47
AH	hydrated	−5 109	2.5 2.1	9.0	~0
AD	dehydrated	103	1.3	0.17	0.17
B	as supplied	103	1.3	0.028	0.014

a) Shift from $[Al(H_2O)_6]^{3+}$. b) Full width at half maximum. c) Hydrogen content.

atoms in $Al(OH)_3$. The coordination atom and their number are both changed by the reaction.

In the present work two signals are observed with different chemical shift values; 103 and −5 ppm. Since the hydrogen content is very low in Sample B, the number of Al atoms bonded with H via O is negligible. The signal observed at 103 ppm can therefore be attributed to the Al atom coordinated by four N atoms (abbreviated AlN_4). In the case of Al coordinated by O for aluminates and aluminum oxides, it is established that Al-O tetrahedra (AlO_4) and octahedra (AlO_6) have peaks in the range between 55 and 80 ppm and at about 0 ppm, respectively.[5] Consequently, the −5 ppm line can be assigned to AlO_6 in $Al(OH)_3$.

In a surface region, water reacts with AlN producing NH_3, and leaves surface hydroxyl groups. Some Al atoms may be connected with both N and O atoms. From the viewpoint of the Al coordination the reaction (1) is considered to proceed in the following steps:

$$AlN_4 \xrightarrow{a} AlN_xO_y \xrightarrow{b} AlO_6, \quad (2)$$

where $x+y=4$, 5, or 6. If considerable amounts of AlN_xO_y species were detected, it could be concluded that the reaction (2) proceeds step by step. Experimentally, however, no peaks were observed which can be attributed to AlN_xO_y. Namely, the step b is much faster than the step a.

Heavily hydrated sample, AH, has the two peaks, AlN_4 and AlO_6, indicating that the hydrated sample is a mixture of AlN and $Al(OH)_3$. The slight positive-frequency shift of the AlN_4 peak compared to Sample A is considered to be caused by superposition of the sideband of the AlO_6 peak, and hence it does not mean any structural change.

Samples A and AD have intermediate hydrogen contents between Samples B and AH. If oxygen-containing species such as OH and H_2O are assumed to be distributed homogeneously over all Al atoms, a considerable amount of Al atoms should be bonded to the O atoms. However, the amount of Al atoms bonded to O atoms is less than the detection limit, as shown in Fig. 1a. This fact suggests that oxygen-containing species are distributed over a limited amount of Al atoms.

In summary, the ^{27}Al NMR results demonstrate that the hydration reaction of aluminum nitride takes place quite inhomogeneously. Once an Al atom in AlN reacts with H_2O, the Al atom reacts with H_2O further more easily than the other Al atoms, finally forming $Al(OH)_3$. Consequently, the reaction product is a mixture of $Al(OH)_3$ and unreacted AlN, containing no detectable amounts of intermediate compounds.

The authors acknowledge the supply of materials to NEC Corporation.

References

1) G. A. Slack, *J. Phys. Chem. Solids*, **34**, 321 (1973).
2) A. Abid, R. Bensalem, and B. J. Sealy, *J. Mater. Sci.*, **21**, 1301 (1986).
3) T. Sakai, M. Kuriyama, T. Inukai, and T. Kizima, *Yogyo Kyokai Shi*, **86**, 30 (1978).
4) "Kagaku-Binran, Kisohen," 3rd ed., ed by The Chemical Society of Japan, Maruzen, Tokyo (1984), p. II-526.
5) D. Müller, W. Gessner, H.-J. Behrens, and G. Scheler, *Chem. Phys. Lett.*, **79**, 59 (1981).

Potentiometric Study of Heteropolyanion Formation from Telluric Acid and Molybdate Anion in 1M Na(Cl)

Atsushi YAGASAKI and Yukiyoshi SASAKI*
Department of Chemistry, Faculty of Science, The University of Tokyo, Hongo, Bunkyo-ku, Tokyo 113
(Received July 28, 1986)

Synopsis. The equilibria in the H^+-MoO_4^{2-}-$Te(OH)_6$ system in aqueous solutions were studied potentiometrically at 25.0 °C. The data were expained by (6,6,1), (7,6,1), and (8,6,1) with formation constants log $\beta_{6,6,1}$=50.40±0.02, log $\beta_{7,6,1}$= 53.68±0.07 and log $\beta_{8,6,1}$=55.47±0.07.

Molybdotellurate is one of the best known heteropolyanions. It was first described more than 70 years ago.[1] Morphological and optical measurement of $3Na_2O \cdot TeO_3 \cdot 6MoO_3 \cdot 22H_2O$ were made by Donney and Mélon.[2] The crystal structure of $(NH_4)_6[TeMo_6O_{24}] \cdot 7H_2O$ was reported as early as 1948.[3] However, little work has been done on the molybdotellurate system after Evans reported the crystal structure of the double salt $(NH_4)_6[TeMo_6O_{24}] \cdot Te(OH)_6 \cdot 7H_2O$.[4] Nothing has been reported on the equilibrium conditions of molybdotellurate in aqueous solutions to our knowledge. In the present paper we report the result of our potentiometric investigation of molybdotellurate equilibria in a 1M Na(Cl) (1M=1 mol dm^{-3}) ionic medium. This is the first example of an equilibrium analysis of a heteropolyanion which has an octahedral heteroatom unit.

Experimental

$Te(OH)_6$ was prepared by a standard method.[5] NaCl (Matsunaga, JIS Primary Standard) was heated at 200 °C for ca. 8 h before use. $Na_2MoO_4 \cdot 2H_2O$ (Wako, S) was used without further purification. The same apparatus as in our previous reports was employed.[6,7] Throughout the experiment the temperature was kept constant at 25.0±0.1 °C. Thirteen titrations were performed and 236 data points were collected. The data covered the ranges $7.2 \geqq -\log h \geqq 2.0$, $13.2 \leqq B/\mathrm{mM} \leqq 53.3$, $4.5 \leqq C/\mathrm{mM} \leqq 17.2$ and $1.0 \leqq B/C \leqq 8.0$, where h is the concentration of free hydrogen ion. B stands for the total concentration of molybdate, C that of tellurate.

Stable emf values were obtained within 5 min when $-\log h \leqq 3.5$, although we had to wait more than 2 hr before the readings reached stable values in the range $-\log h \geqq 6$.

The equilibria in solution can generally be written as $pH^+ + qMoO_4^{2-} + rTe(OH)_6 \rightleftarrows (H^+)_p(MoO_4^{2-})_q[Te(OH)_6]_r$. The complex on the right hand side will simply be referred as (p,q,r) and its formation constant β_{pqr}. The search for the best set of (p,q,r) and β_{pqr} was performed with the least squares program LETAGROPVRID version ETITR.[8] The function $U=(H_{calcd}-H)^2$ has been minimized, where H_{calcd} and H stand for calculated and actual total hydrogen concentrations over the zero level (H_2O, MoO_4^{2-}, and $Te(OH)_6$). Separate titrations were carried out to obtain the equilibrium constants of H^+-MoO_4^{2-} system in 1M Na(Cl) medium.[9] For H^+-$Te(OH)_6$ equilibria we used the constants obtained by Kaehler and Brito.[10]

Results and Discussion

Figure 1 shows the result of the initial pqr-analysis.

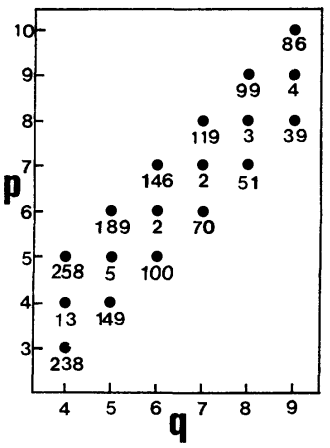

Fig. 1. Result of initial pqr-analysis. Each circle represents a species $(p,q1)$ with obtained U under it in mM^2. 35 points of $-\log h \geq 5$ and $B/C \leq 3$ were employed.

Table 1. Result of the Analysis on High B/C Ratio Points[a]

(p,q,r)	U/mM^2
(5,5,1)	50.1
(6,6,1)	3.4
(7,7,1)	59.7
(8,8,1)	196.0
(9,9,1)	226.8

a) 29 points of $B/C \geqq 6$ and $-\log h \geqq 5$.

The species (6,6,1), (7,7,1), and (8,8,1) gave distinctively low U values.[11] These three species were tested on the data of higher B/C ratios. Figure 1 and Table 1 show that only (6,6,1) can explain both the high and low B/C ratio data. When we tested (6,6,1) on the whole data the residual showed a systematic deviation as h increased. This systematic deviation disappeared after the introduction of (7,6,1) and (8,6,1) to the system. The final model gave U=31.2 mM^2 and $\sigma(H)$=0.37 mM with formation constants log $\beta_{6,6,1}$= 50.40±0.02, log $\beta_{7,6,1}$=53.68±0.07 and log $\beta_{8,6,1}$=55.47± 0.07.[12]

The distribution of molybdate in each species is illustrated in Fig. 2. A notable amount of (6,6,1) is formed even at a high pH of 7. This agrees well with the fact that salts of hexamolybdotellurate crystallize from neutral or slightly basic solutions. Almost all of the molybdate in solution is bound in the molybdotellurate phase in the range $5.0 > -\log h > 2.5$ when the B/C ratio is 6 or lower, which means complex formation between molybdate and tellurate is strong. The composition of the anion (6,6,1) coincides with that of $[TeMo_6O_{24}]^{6-}$, whose structure is shown in Fig. 3.[4] It

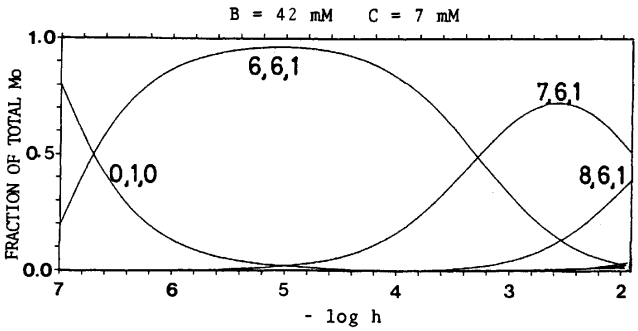

Fig. 2. Distribution diagram of H^+-MoO_4^{2-}-$Te(OH)_6$ system.

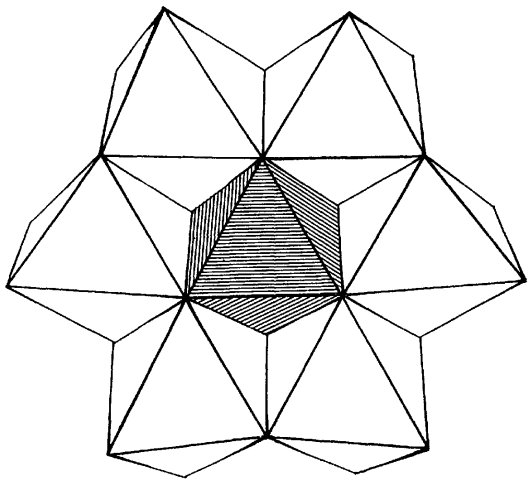

Fig. 3. Structure of $[TeMo_6O_{24}]^{6-}$. Shaded octahedron indicates TeO_6 unit.

is plausible that this structure is also maintained in solution. We presume the protonation of the anion takes place at one of the six oxygen atoms of the central octahedral unit for (7,6,1) case, and two for (8,6,1) case.[13]

The solubility of (6,6,1) seemed to be much lower than those of (7,6,1) and (8,6,1). The sodium salt of $[TeMo_6O_{24}]^{6-}$ sometimes precipitated during titration.[14] The precipitate dissolved when the pH of the solution was lowered to about 3.5.

As we mentioned in the experimental section, the formation of (6,6,1) seemed quite slow. We hope further study of this system will give us some information on the kinetics of polyanion formation.

References

1) A. Miolati, *J. Prakt. Chem.*, **77**, 439 (1908).
2) J. D. H. Donnay and J. Mélon, *Amer. Min.*, **21**, 250 (1936).
3) H. T. Evans, Jr., *J. Am. Chem. Soc.*, **70**, 1291 (1948).
4) a) H. T. Evans, Jr., *Acta Crystallogr., Sect. B*, **30**, 2095 (1974); b) H. T. Evans, Jr., *J. Am. Chem. Soc.*, **90**, 3275 (1968).
5) G. Brauer, "Handbook of Prepartive Inorganic Chemistry," 2nd ed, Academic Press, New York (1963), p. 451.
6) H. Takahama, A. Yagasaki, and Y. Sasaki, *Chem. Lett.*, **1982**, 1953.
7) H. Takahama and Y. Sasaki, *Bull. Chem. Soc. Jpn.*, **56**, 895 (1983).
8) P. Brauner, L. G. Sillén, and R. Whiteker, *Arkiv Kemi*, **31**, 365 (1969).
9) $\log \beta_{1,1}=3.51\pm0.23$, $\log \beta_{2,1}=7.40\pm0.18$, $\log \beta_{8,7}=53.01\pm0.01$, $\log \beta_{9,7}=57.53\pm0.03$, $\log \beta_{10,7}=61.09\pm0.05$ and $\log \beta_{11,7}=63.46\pm0.11$.
10) H. C. Kaehler and F. Brito, *An. Quim.*, **67**, 1185 (1971).
11) Similar analysis was carried out for $r=2$ and 3. The results showed no distinct pits.
12) $\sigma(H)$ is defined $[U/(m-n)]^{1/2}$, where m is the number of data points and n is the number of complexes. Errors given are three times standard deviations. See Ref. 8 for detail.
13) It is known that hexamolybdocromate has 6 protons attached to the CrO_6 unit. See: A. Perloff, *Inorg. Chem.*, **9**, 2228 (1970).
14) Data from these titrations were not used in the calculation.

Double Inclusion of Methylated Cyclodextrin and Sodium Benzenesulfonate by Na-, Ca-, and Cu-Montmorillonites

Tsuyoshi KIJIMA
National Institute for Research in Inorganic Materials, Sakura-mura, Niihari-gun, Ibaraki 305
(Received September 11, 1986)

Synopsis. The uptake of methylated α- and β-cyclodextrins by Na-, Ca-, and Cu-montmorillonites at 25 °C in the presence of sodium benzenesulfonate has been studied. X-Ray diffraction data revealed that the cyclodextrin molecules that embrace benzenesulfonate anion are intercalated as monolayer in the interlayer space of the clay minerals.

Inclusion phenomena have attracted increasing attention in inorganic chemistry. In the recent papers concerning molecular inclusion, we have reported the complexation of layered montmorillonites and α-zirconium phosphate with several cyclodextrins containing a cylindrical cavity capable of including a variety of substances.[1-4] Further inclusion property of the complexes towards any other guest molecules would be intrigued. For the complex of α-zirconium phosphate with an aminated cyclodextrin, we showed that it is similar to zeolites because the water within the cavity of cyclodextrin molecule is released and readsorbed reversibly.[3] No examination, however, has been made for other complexes hitherto obtained.

The montmorillonite intercalates not only positively charged cyclodextrins but also polar but unchargeable ones such as parent and methylated cyclodextrins.[4] This paper reports that molecules of hexakis(2,6-di-*O*-methyl)-α-(denoteded DM-α- for short) and heptakis(2,6-di-*O*-methyl)-β-(DM-β-)-cyclodextrins (CD) accompanied by sodium benzenesulfonate (NaBS) are intercalated by Na-, Ca-, and Cu-montmorillonites.

Experimental

The Na-, Ca-, and Cu-montbmorillonite samples were the same as those used in the preceding work.[4] DM-α- and DM-β-cyclodextrins and sodium benzenesulfonate were of reagent grade and used without further purification.

Each mineral sample (0.1 g) was immersed in 8 cm^3 of a 1:1 (vol.) mixture of 50 mmol dm^{-3} aqueous cyclodextrin and 1 mol dm^{-3} sodium benzenesulfonate solutions at 25 °C for 5 d. Since methylated cyclodextrin taken up by montmorillonite is easily washed away with water,[4] the reaction mixture was centrifuged and rinsed with the starting cyclodextrin solution and then air-dried at 40 °C to give the complex sample. The similar procedure was applied to the system without sodium benzenesulfonate.[4] X-Ray diffraction measurements were made as similarly as in the previous work.[4]

Results and Discussion

Figure 1 compares the X-Ray diffraction patterns of CD-NaBS-montmorillonite with those of CD-montmorillonite. The results suggest that Na-, Ca-, and Cu-montmorillonites form one complex with DM-α-cyclodextrin and a mixture of two complexes with DM-β-cyclodextrin. The X-Ray diffraction profiles of

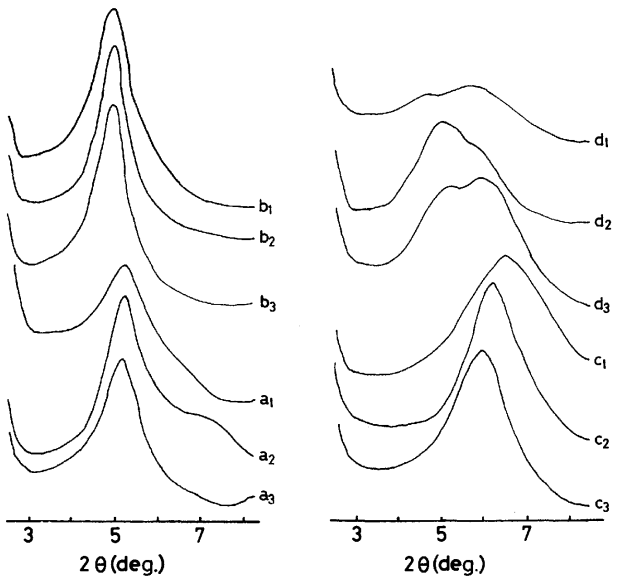

Fig. 1. X-Ray diffraction patterns of (a_i) DM-α-CD-mont, (b_i) DM-α-CD-NaBS-mont, (c_i) DM-β-CD-mont, and (d_i) DM-β-CD-NaBS-mont complexes for Fe*Kα* rays (i=1—3, mont=montmorillonite). Interlayer cations, Na (i=1), Ca (i=2), Cu (i=3).

the clay minerals were not changed by treating with sodium benzenesulfonate solution, indicating that the montmorillonite cannot take up benzenesulfonate anion solely.

The conditions for preparing the complex samples suggest that they contain excess amounts of cyclodextrin and sodium benzenesulfonate. It is, therefore, difficult to determine the equilibrium contents of each compound in the resulting complexes. The complexes were characterized only by their interlayer spacings and change of thickness of intercalated layer (*Δ* value); the obtained values are summarized in Table 1. The *Δ* value was determined by subtracting 9.5 Å for the thickness of the silicate layer[5] from the observed interlayer spacing. The increase of interlayer thickness in the range of 1—5 Å caused by the presence of sodium benzenesulfonate will be attributed to the double inclusion of methylated cyclodextrin and sodium benzenesulfonate by montmorillonite.

The interlayer thickness data in Table 1 also show that the difference of interlayer thickness between CD-NaBS-montmorillonite and CD-montmorillonite complexes with DM-β-cyclodextrin varies from 2.9 to 5.2 Å with the interlayer cation, while the interlayer thickness of complexes with DM-α-cyclodextrin is hardly affected by the variation of interlayer cation. According to the crystal structure analysis of the α-CD-NaBS complex,[6] the benzenesulfonate anion is arranged in the channel which is formed by the stack

Table 1. Characterization of Cyclodextrin-Montmorillonite4) and Cyclodextrin-Sodium Benzenesulfonate-Montmorillonite Complexes with Various Interlayer Cations

Interlayer cation	Cyclodextrin	CD-montmorillonite complex		CD-NaBS-montmorillonite complex[a)]	
		Interlayer spacing/Å	Δ value/Å	Interlayer spacing/Å	Δ value/Å
Na	DM-α-CD	21.4	11.9	22.1	12.6
Ca		21.3	11.8	22.2	12.7
Cu		21.2	11.7	22.4	12.9
Na	DM-β-CD	17.1	7.6	23.3 (19.2)	13.8 (9.7)
Ca		17.9	8.4	22.0 (19.4)	12.5 (9.9)
Cu		18.3	8.8	21.2 (18.6)	11.7 (9.1)

a) Values for the low spacing phases are given in parentheses.

of α-cyclodextrin rings. The benzene ring is located in the cavity, while the sulfonato group is outside the cavity and hydrogen-bonded to the primary hydroxyl groups of the adjacent α-cyclodextrin molecule. The preceding study[4] revealed the following characteristics on the inclusion behavior of methylated cyclodextrins in montmorillonite; (1) the cyclodextrin molecules with cavity axes perpendicular to the silicate layer are intercalated as monolayer with their methylated side chains in fully extended (DM-α-cyclodextrin) and folded (DM-β-cyclodextrin) conformations which give the molecular thickness of 12 and 8 Å, respectively, and (2) the hydrated cations are bound in the intermolecular space within the cyclodextrin layer with hydrophobic methoxyl groups of cyclodextrin molecule. Referring to the structure data in Ref. 5, we assume the length of benzenesulfonate anion to be 9 Å. If we combine the above data and observations with the assumption that the methylated cyclodextrin molecules accompanied by sodium benzenesulfonate are intercalated with the same conformations as in the methylated CD-montmorillonite system, the benzenesulfonate anion would be included completely in the molecular cylinder of fully stretched DM-α-cyclodextrin or partly in the molecular cage of DM-β-cyclodextrin capped by the primary methoxyl groups, as illustrated in Fig. 2. It is also conceivable that the interlayer hydrated cations of DM-α-CD-NaBS-montmorillonite complexes are located in the intermolecular space within the cyclodextrin layer, due to repulsion against the hydrophobic methoxyl groups. As for the high spacing complexes of DM-β-CD, the cations are between the silicate layer and the sulfonato group protruding from the O(2), O(3), side of the cavity, due to the hydrophilic attraction of the sulfonato group. The interlayer thickness of the latter complexes decreases in the order of Na>Ca>Cu. This could be explained by assuming that the interlayer cation with higher polarizing power forms an aqua complex in which all or a part of four coordinating water molecules are located more closely to the sulfonato group, as observed in the case of inclusion of α-cyclodextrin by Na-, Ca-, and Cu-montmorillonites.[4] Furthermore, the interlayer thickness of the low spacing complex of DM-β-CD remains unchanged at 9—10 Å with different interlayer cations. It is likely that the low spacing complex is an intermediate phase whose interlayer space is occupied predominantly by the methylated CD molecules and only partly by those including benzenesulfonate anion.

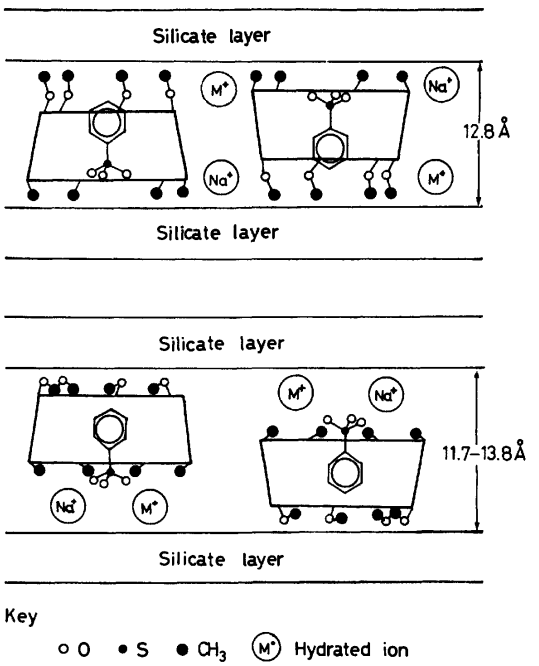

Fig. 2. Models proposed for their probable arrangement of CD molecules, benzenesulfonate anions and interlayer cations in the interlayer space of montmorillonite; (upper) DM-α-CD, (bottom) DM-β-CD (high spacing complex).

We conclude that the methylated cyclodextrin molecules including sodium benzenesulfonate are intercalated as monolayer by Na-, Ca-, and Cu-montmorillonites. The double inclusion method developed in this study may be applied to the micro-encapsulation of various substances such as drugs and dyes for laser.

The author wishes to thank Dr. H. Nakazawa for his encouragement during this work.

References

1) T. Kijima, J. Tanaka, M. Goto, and Y. Matsui, *Nature*, **310**, 45 (1984); *ibid.*, **316**, 280 (1985).
2) T. Kijima, M. Kobayashi, and Y. Matsui, *J. Inclusion Phenom.*, **2**, 807 (1985).
3) T. Kijima and Y. Matsui, *Nature*, **322**, 533 (1986).
4) T. Kijima, *J. Inclusion Phenom.*, in press.
5) B. K. Theng, The Chemistry of Clay-Organic Reactions Adam-Hilger, London (1974), p. 10.
6) K. Harata, *Bull. Chem. Soc. Jpn.*, **49**, 2066 (1976).

(α-Ethoxyvinyl)tributyltin; An Efficient Reagent for the Nucleophilic Acetylation of Organic Halides via Palladium Catalysis

Masanori KOSUGI,* Takashi SUMIYA, Yukimasa OBARA, Motohiro SUZUKI, Hiroshi SANO, and Toshihiko MIGITA*
Department of Chemistry, Faculty of Technology, Gunma University, Kiryu, Gunma 376
(Received September 12, 1986)

Synopsis. (α-Ethoxyvinyl)tributyltin acts as a masked acetylating agent in the palladium catalyzed reaction with various organic halides, such as aryl bromides, vinyl bromides, benzyl chloride, and allyl chloride, giving, after hydrolysis of the resulting reaction mixture, good yields of the corresponding ketone product.

Several reports of ketone syntheses via cross-coupling of organometallics and organic halides have been reported. Palladium catalyzed reactions of organotin compounds with acid chlorides[1] or with organic halides and carbon monoxide[2] are shown to be useful for the preparation of ketone. Recently, palladium catalyzed reaction of α-methoxyvinylzinc compound prepared in situ with organic halides after hydrolytic treatment was reported for the ketone synthesis.[3] Similar reaction of the corresponding tin compound with acid chlorides catalyzed by palladium was reported for the preparation of α-diketones.[4] α-Diketones were also prepared by palladium catalyzed reaction of acid chlorides with acyltin compounds.[5]

In this note, we report the utility of (α-ethoxyvinyl)-tributyltin as a masked acetylating agent in the reactions with organic halides (not only with acid chlorides, but also with aryl and vinyl bromides, benzyl chloride, and allyl chloride). (Eq. 1)

$$n\text{-Bu}_3\text{SnC(OEt)}=\text{CH}_2 + \text{R-X} \xrightarrow{[\text{Pd}]} \xrightarrow{\text{H}^+} \text{R-COCH}_3 \quad (1)$$

As is shown in Table 1, the catalytic efficiency of this reaction, which proceeds smoothly in the presence of only 1 mol% of the catalyst, may be better than that in the reaction of the zinc reagents, which needs 5 mol% of the catalyst.[3] Both of palladium(0) and palladium(II) catalysts gave almost the same results. This implies that palladium(II) complex was reduced by the tin compound under the reaction conditions. The use of nonpolar solvent is recommendable, although the solvent effect was not large. GLC analysis shows that the reaction with bromobenzene proceeds nearly quantitatively. Substituted acetophenones were obtained in good yields from aryl bromides containing a variety of ring functional groups. With β-bromostyrene, the stereochemistry of the substrate was not retained, in contrast to Hegedus's findings for the organozinc compounds.[3]

Experimental

IR spectra were recorded on Jasco A-100 spectrophotometer. ^{1}H NMR spectra were recorded on a Varian EM-360 instrument, using tetramethylsilane as an internal standard. GLC analyses were carried out with Ohkura 802 instrument using columns (1.5 m) packed with 10% Silicone SF-96 and SE-30 on Celite 545.

Materials. (α-Ethoxyvinyl)tributyltin was prepared according to the method described in the literature.[6] Bp.

Table 1. Reaction of (α-Ethoxyvinyl)tributyltin with Organic Halides at 100°C

R-X	Catalyst[a]	Solvent	Yield of R-COMe/%[b]
Ph-Br	None	PhH	0
Ph-Br	A	PhH	(100)
Ph-Br	B	PhH	(100), 80
Ph-Br	C	PhH	(17)
Ph-Br	D	PhH	Trace
Ph-Br	B	DMF	(81)
Ph-Br	B	HMPA	(60)
p-MeC_6H_4-Br	B	PhMe	67
m-MeC_6H_4-Br	B	PhMe	70
o-MeC_6H_4-Br	B	PhMe	78
p-ClC_6H_4-Br	B	PhMe	73
p-$MeOC_6H_4$-Br	B	PhMe	54
p-AcC_6H_4-Br	B	PhMe	89
p-NCC_6H_4-Br	B	PhMe	81
p-$O_2NC_6H_4$-Br	B	PhMe	91
(*E*)PhCH=CH-Br[c]	B	PhMe	63 (E)
(*Z*)PhCH=CH-Br[c]	B	PhMe	73 (E)
$PhCH_2$-Cl[c]	B	PhMe	72
CH_2=$CHCH_2$-Cl[c]	B	PhMe	43
PhCO-Cl	E	PhH	75[d]

a) A: $Pd(PPh_3)_4$, B: $PdCl_2(PPh_3)_2$, C: $PdCl_2[P(o\text{-tolyl})_3]_2$, D: $Pd_2(dba)_3\cdot CHCl_3$,[e] E: $PhCH_2PdCl(PPh_3)_2$. b) Isolated yield based on the halide, in parenthesis GLC yield of α-ethoxystyrene. c) At 80°C. d) Results shown in Ref. 4. e) dba: dibenzylideneacetone.

106/0.4 mmHg (1 mmHg=133.322 Pa). ^{1}H NMR (C_6D_6) δ=0.7—1.8 (m, 30H), 3.60 (q, J=8Hz, 2H), 4.30 (d, J=2Hz, 1H), and 4.83 (d, J=2Hz, 1H). GC-MS m/z 305 (M^+—Bu, 100). Preparation of halides and palladium complexes were already reported.[7]

Reaction Procedures. A mixture of (α-ethoxyvinyl)-tributyltin (5.5 mmol), halide (5.0 mmol), dichlorobis(triphenylphosphine)palladium (0.05 mmol), and toluene (2 cm^3) was heated under argon at 100 °C for 20 h. After hydrolysis of the reaction mixture with 5% hydrochloric acid, the organic layer was extracted with diethyl ether, and dried over sodium sulfate. After evaporation of the solvent, column chromatography of the residue (silica gel; cyclohexane followed by diethyl ether) provided the ketones in the ethereal eluents and the product was isolated by distillation under reduced pressure.

Products. All the products were known and their structures were determined by comparison of their spectroscopic data with the reported values.[3,8,9]

The gift of tributyltin oxide by Hokkoh Kagaku Kogyo Co., Ltd. is gratefully acknowledged. The measurement of GC-MS by Dr. H. Matsuyama of Tokyo Metropolitan University is also acknowledged. The present work was partially supported by a Grant-in-Aid for Scientific Research No. 61225002 from the Ministry of Education, Science and Culture.

References

1) a) M. Kosugi, Y. Shimizu, and T. Migita, *Chem. Lett.*, **1977**, 1423; b) J.W. Labadie, D. Tueting, and J. K. Stille, *J. Org. Chem.*, **48**, 4634 (1983).

2) a) M. Tanaka, *Tetrahedron Lett.*, **1979**, 2061; b) A. N. Bumagin, I. G. Bumagina, A. N. Kashin, and I. P. Beletskaya, *Izv. Akad. Nauk SSSR, Ser. Khim.*, **1981**, 1675; *Chem. Abs.*, **95**, 114980 m (1981); c) V. P. Baillargeon and J. K. Stille, *J. Am. Chem. Soc.*, **105**, 7175 (1983).

3) a) C. E. Russell and L. S. Hegedus, *J. Am. Chem. Soc.*, **105**, 943 (1983); b) E-I. Negishi and F-T. Luo, *J. Org. Chem.*, **48**, 1560 (1983).

4) J. A. Soderquist and W. W. Leong, *Tetrahedron Lett.*, **24**, 2361 (1983)

5) J-B. Verlhac, E. Chanson, B. Jousseaume, and J-P. Quintard, *Tetrahedron Lett.*, **26**, 6075 (1985).

6) J. A. Soderquist and G.I. Hsu, *Organometallics*, **1**, 830 (1982).

7) M. Kosugi, I. Hagiwara, T. Sumiya, and T. Migita. *Bull. Chem. Soc. Jpn.*, **57**, 242 (1984).

8) C. J. Pouchart, "The Aldrich Library of Infrared Spectra," Second Ed., 1975.

9) C. J. Pouchart and J. R. Campbell, "The Aldrich Library of NMR Spectra," 1974

The Ring Opening Reaction of Cyclopolysilanes, $(R_2Si)_n$ (n=3—6), with Iodine. A Kinetic Study

Hamao WATANABE,* Hiromi SHIMOYAMA, Tsutomu MURAOKA, Yuichi KOUGO, Motohiko KATO, and Yoichiro NAGAI*

Department of Chemistry, Faculty of Engineering, Gunma University, Kiryu, Gunma 376

(Received August 16, 1986)

Synopsis. Reactions of a series of peralkylcyclopolysilanes with iodine were found to proceed via second-order kinetics. Rate constants show that, in general, the smaller rings react faster than larger rings. Values of the activation parameters, E_a and $\Delta G^{\ddagger}$, decreased with the decreasing ring size and are parallel with those of the oxidation potentials and of the lowest transition energies.

It is well-known that the Si-Si bond in cyclopolysilanes undergoes electrophilic cleavage reaction by halogens to give the corresponding ring-opening adducts, α,ω-dihalopolysilanes. Although several studies on the halogen-cleavage reactions of cyclopolysilanes have appeared so far,[1] there are no reports on their kinetic behaviors. In our continuing work of polysilanes,[1c,2] we now report a kinetic study on the ring-opening reactions of a series of peralkylcyclopolysilanes with iodine (Eq. 1).

$$[R_2Si]_n + I_2 \rightarrow I(R_2Si)_nI \quad (n = 3 - 6) \qquad (1)$$

Rates were determined by spectroscopic method and the reaction was found to obey typical second-order kinetics within 20% completion. Unfortunately, the reactions of the smallest ring, $[(Bu^tCH_2)_2Si]_3$, was so fast that the rate constant could not be betermined by the present method at any convenient temperatures.

Table 1 shows the absolute rate constants at three different temperatures together with the relative rates of the cyclopolysilanes at 20 °C, that of $Me_3SiSiMe_3$ being taken as standard. The relative rates of the cyclopolysilanes (20 °C) were thus found to fall in the order:

$$[(Bu^tCH_2)_2Si]_3 \gg [Bu^tMeSi]_4\,(241) \approx [Pr^i{}_2Si]_4\,(237) > [Bu^s{}_2Si]_4\,(58) > [Bu^n{}_2Si]_5\,(11) \approx [Pr^n{}_2Si]_5\,(8) > [Me_2Si]_6\,(1) \approx Me_6Si_2\,(1)$$

As might be expected from the intrinsic internal strain, the smaller rings generally react faster than

Table 1. The Rate Constants in the Reactions of Cyclopolysilanes with Iodine in Dichloromethane[3]

Compound	$k_2\times10^2$/dm^3 mol^{-1} s^{-1} [a]			$k_x/k_{Me_6Si_2}$ [b] (293 °K)
	303 °K	293 °K	283 °K	
$[(Bu^tCH_2)_2Si]_3$	—[c]	—[c]	—[c]	5500[d]
$[Bu^tMeSi]_4$	730	563	393	241
$[Pr^i{}_2Si]_4$	817	553	383	237
$[Bu^s{}_2Si]_4$	185	136	92.5	58
$[Bu^n{}_2Si]_5$	42.5	30.9	17.9	11
$[Pr^n{}_2Si]_5$	35.6	23.5	14.7	8
$[Me_2Si]_6$	5.24	3.08	1.64	1
$Me_3SiSiMe_3$	1.00	0.583	0.314	1

a) Average value from three runs. b) Number of the Si-Si bonds in cyclopolysilane was taken into account for the calculations. c) Reaction rate was too fast to be determined. d) Value estimated from the regression line (correlation coefficient, γ=0.94) obtained on the basis of the relative rates in the larger rings, n=4—6.

Table 2. Activation Parameters for the Ring Opening Reactions and Values of Oxidation Potential (E_{pa}) and Longest Absorption Wavelength (λ_{max}) for the Cyclopolysilanes[3,4]

Compound	E_a	$\Delta S^{\ddagger}_{293}$	$\Delta G^{\ddagger}_{293}$	E_{pa} [a]	λ_{max} [b]
	kcal mol^{-1}	cal mol^{-1} K^{-1}	kcal mol^{-1}	V vs. SCE	nm
$[(Bu^tCH_2)_2Si]_3$	—[c]	—[c]	—[c]	+0.44	310sh
$[Bu^tMeSi]_4$	5.29	−34.6	16.1	+0.94	300
$[Pr^i{}_2Si]_4$	6.56	−38.9	16.1	+1.00	290sh
$[Bu^s{}_2Si]_4$	6.00	−39.3	16.9	+1.10	290sh
$[Bu^n{}_2Si]_5$	7.49	−37.4	17.9	+1.40	262
$[Pr^n{}_2Si]_5$	7.69	−37.2	18.0	+1.42	260
$[Me_2Si]_6$	10.0	−33.2	19.1	+1.45	258sh
$Me_3SiSiMe_3$	9.94	−36.8	20.1	—[c]	193.5

a) The first anodic peak potential in MeCN; see Ref. 4. b) The longest-wavelength absorption band in cyclohexane; see Ref. 2b and 2d. c) Not determined.

larger rings. This trend shows that the principal factor in determining the reaction rates is ring strain, although the rates for the cyclotetrasilanes vary in a range of 1—4 times as the steric bulk of the substituents varies.

Table 2 lists the activation parameters, electrochemical oxidation potentials, and the longest-wavelength UV absorptions. Values of activation energy decrease with the decreasing ring size and are parallel with those of the oxidation potentials as well as the lowest transition energies. Thus, the promotion of the HOMO level in smaller rings due to the increasing ring strain can be seen in these energy terms.[3-5] The large negative values of $\Delta S^{\ddagger}$ indicate considerable loss of freedom in the transition states, which are common in bimolecular reactions. In short, the rates and activation parameters for the reactions of the cyclopolysilanes are primarily related to the ring size, although other factors such as steric congestion at the reaction site and the geometrical structures of the ring system[6] have to be also taken into account. Further investigation for such ring opening reactions will be described elsewhere.[7]

Experimental

Materials. All the samples used for the rate study were the cyclopolysilanes reported previously.[2d] The sample of $[Bu^tMeSi]_4$ was a mixture comprising four steroisomers (a—d), the distribution of which was determined by a high-resolution NMR spectrum (400 MHz) (see Ref. 2d):

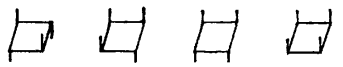

(a) (b) (c) (d)

(a)/(b)/(c)/(d)=13/73/12/2
1: *t*-Butyl group

Measurements of the reaction rates. The CH_2Cl_2-solution of approximately equimolar concentrations of two substrates (a slightly excess in cyclosilanes) ($1—6\times10^{-3}$ mol dm^{-3}) were prepared and kept in a constant temperature bath. Two 2-ml solutions of the substrates were mixed and allowed to react in a spectrometer. The rates were determined by recording concentrations of iodine as a function of time which were monitored by the UV absorption of iodine at λ 555 nm. The rate constant of $[Bu^tMeSi]_4$ sample was determined as a total average of the isomer mixture (see above).

References

1) a) H. Gilman and G. L. Schwebke, "Advances in Organometallic Chemistry," ed by F. G. A. Stone and R. West, Academic Press, New York (1964), Vol. 1, p. 89, and the references cited therein; b) E. Hengge and U. Brychcy, *Monat. Chem.*, **97**, 1309 (1966); c) P. K. Sen, D. Ballard, and H. Gilman, *J. Organomet. Chem.*, **15**, 237 (1968); d) W. Wojnowski, C. J. Hurt, and R. West, *J. Organomet. Chem.*, **124**, 271 (1977); e) H. Watanabe, T. Muraoka, M. Kageyama, and Y. Nagai, *J. Organomet. Chem.*, **216**, C45 (1981); f) C. W. Carlson and R. West, *Organometallics*, **2**, 1801 (1981).

2) a) H. Watanabe, T. Muraoka, Y. Kohara, and Y. Nagai, *Chem. Lett.*, **1980**, 735; b) H. Watanabe, T. Okawa, and Y. Nagai, *J. Chem. Soc., Chem. Commun.*, **1983**, 781; c) H. Watanabe, J. Inose, K. Fukushima, Y. Kougo, and Y. Nagai, *Chem. Lett.*, **1983**, 1711; d) H. Watanabe, T. Muraoka, M. Kageyama, K. Yoshizumi, and Y. Nagai, *Organometallics*, **3**, 141 (1984).

3) H. Watanabe and Y. Nagai, The Proceedings of VIIth International Symposium on Organosilicon Chemistry, Kyoto, Sept. 9-14 (1984); "Organosilicon and Bioorganosilicon Chemistry," ed by H. Sakurai, Ellis Horwood Limited, Chichester, West Sussex, England (1985), Chap. 9, pp. 107—114.

4) H. Watanabe, K. Yoshizumi, T. Muraoka, M. Kato, Y. Nagai, and T. Sato, *Chem. Lett.*, **1985**, 1683.

5) H. Watanabe, H. Shimoyama, T. Muraoka, T. Okawa, M. Kato, and Y. Nagai, *Chem. Lett.*, **1986**, 1057.

6) a) H. Watanabe, M. Kato, T. Okawa, Y. Kougo, Y. Nagai, and M. Goto, 50th Annual Meeting of Chem. Soc. Jpn., Tokyo, April 4 (1985); Abstracts I, 4K27 and 4K28, pp. 539—540; Appl. Organomet. Chem., in press; b) C. L. Wadsworth, R. West, Y. Nagai, H. Watanabe, H. Matsumoto, and T. Muraoka, *Chem. Lett.*, **1985**, 1525; c) C. L. Wadsworth and R. West, *Organometallics*, **4**, 1659 (1985).

7) H. Watanabe, M. Kato, E. Tabei, H. Kuwabara, N. Hirai, T. Sato, and Y. Nagai, *J. Chem. Soc., Chem. Commun.*, **1986**, 1662.

Reduction of Aromatic Nitro Compounds and Thioketones with Sodium Telluride under Aprotic Conditions

Hitomi SUZUKI,* Hajime MANABE, Takashi KAWAGUCHI, and Masahiko INOUYE
Department of Chemistry, Faculty of Science, Ehime University, Bunkyo-cho, Matsuyama 790
(Received August 13, 1986)

Synopsis. Sodium telluride, prepared by heating tellurium and sodium hydride in a 1:2 molar ratio in dry *N,N*-dimethylformamide, reduces aromatic nitro compounds to azo compounds and thioketones to hydrocarbons under mild conditions.

Hydrogen telluride is a weak dibasic Brønsted acid and forms two series of salts known as hydrogentelluride $M^{I}TeH$ and normal telluride M^{I}_2Te. Salts of the former type undergo transformation into those of second type in high pH region. Recently, we reported that aromatic nitro compounds behave differently toward these telluride reagents; sodium telluride easily reduces nitrobenzenes to anilines,[1] while sodium hydrogentelluride does not reduce them beyond the stage of azoxy compounds.[2] Both of these types of reductions proceed cleanly in protic media and are complete within a short reaction time under mild conditions. The reduction with sodium hydrogentelluride is sensitive to steric factor as evidenced by the formation of anilines where nitrobenzenes are hindered.[2]

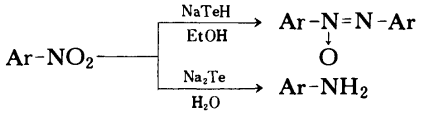

As part of our studies on telluride reduction, we report herein that aromatic nitro compounds undergo another type of reaction with sodium telluride under aprotic conditions, giving not azoxy but azo compounds as the single product. Sodium telluride was also found to effect reductive removal of sulfur atom from aromatic thioketones to yield parent hydrocarbons.

On heating gently with sodium hydride in dry *N,N*-dimethylformamide (DMF) under nitrogen, powdered tellurium dissolved with evolution of hydrogen gas to form a deep red solution of sodium oligotelluride, which on further heating gradually lost color to give sodium telluride as a pale yellow suspension. When a nitroarene (**1**) dissolved in tetrahydrofuran (THF) was added to the suspension and the resulting mixture was heated with stirring at around 70 °C for several hours, smooth reduction took place to give the corresponding azo compound (**3**) in good to moderate yields (Table 1).

$$\underset{\mathbf{1}}{Ar\text{-}NO_2} \xrightarrow[DMF,\ \Delta]{Na_2Te} \underset{\mathbf{2}}{Ar\text{-}\overset{\downarrow}{\underset{O}{N}}\text{=}N\text{-}Ar} \xrightarrow[DMF,\ \Delta]{Na_2Te} \underset{\mathbf{3}}{Ar\text{-}N\text{=}N\text{-}Ar}$$

The reaction proceeded cleanly with nitroarenes **1a—e** and halonitroarenes **1f—g**. The intermediary azoxy compounds (**2**) are too reactive to be isolated under these conditions, although they can be detected in certain cases at an early stage of reduction. A similar reaction of 4-nitrotoluene led to a complex mixture of products arising from abstraction of benzylic hydrogen atom as well as partial reduction of nitro group. Isolation of 1,2-bis(4-nitrophenyl)ethane as one of products revealed the intervention of radical species in the reduction under aprotic conditions. As expected, 3-nitrotoluene **1b** gave azobenzene **3b**. In every case, bis(dimethylcarbamoyl) ditelluride (**4**) was obtained as a common by-product. We attributed the formation of **4** to capture of the initially formed dimethylcarbamoyl radical by telluride anion and subsequent oxidation of the resulting tellurocarbamoyl species. This type of reaction is of interest since it may represent the formal oxidation of DMF to a telluro analog of dimethylcarbamoyl peroxide.

$$(H_3C)_2NCHO \xrightarrow{-H\cdot} (H_3C)_2N\dot{C}(=O) \xrightarrow[-2e]{Te^{2-}}$$
$$(H_3C)_2NC(=O)Te\cdot \longrightarrow \underset{\mathbf{4}}{(H_3C)_2NC(=O)TeTeC(=O)N(CH_3)_2}$$

Table 1. Reduction of Aromatic Nitro Compounds with Sodium Telluride

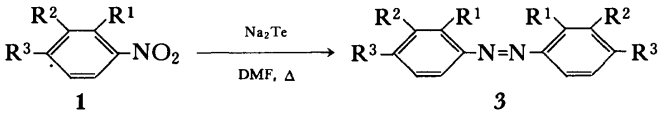

1 **3**

	Nitroarene **1**			Azo compound **3**	
	R^1	R^2	R^3	Mp(θ_m/°C)	Yield/%[a]
a	H	H	H	68—69 (67—68)[6]	97
b	H	CH_3	H	50—52 (54—55)[7]	62
c	C_6H_5	H	H	141—143 (144—145)[8]	75
d	H	H	C_6H_5	245—249 (248—250)[7]	70
e	-(CH=CH)$_2$-		H	194—196 (197—198)[7]	78
f	H	Cl	H	98—101 (103—104)[7]	87
g	H	H	Cl	185—188 (186—188)[6]	67

a) Yields refer to the isolated compounds and are not optimized.

Treatment of aromatic thioketones (**5**) with sodium telluride in aqueous media resulted in the generation of original ketones. Under aprotic conditions, however, the same reagent was found to desulfurize thioketones **5** in a reductive way to afford the corresponding hydrocarbons (**6**). The reaction proceeded slowly and the only predominant product was parent hydrocarbon **6**. Dimerization with loss of sulfur leading to tetraarylethylene (**7**), an important process in the reduction of thioketones with diphosphorus tetraiodide,[3] could not be observed.

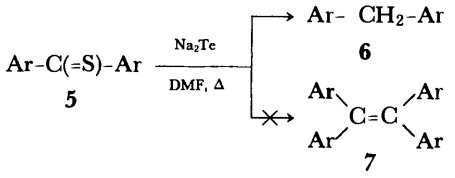

Experimental

Melting points were determined on a hot stage apparatus and are not corrected. Powdered tellurium (99.9% purity) and sodium hydride (60% dispersion in oil) were commercial products and used as received. Thioketones were prepared from the corresponding ketones by known method.[4] Reactions were performed under nitrogen to protect sodium telluride from oxidation. All products except ditelluride **4** are known and identified by direct comparison with authentic samples obtained by other routes.

Preparation of Sodium Telluride. A mixture of powdered tellurium (0.256 g, 2.0 mmol), sodium hydride (0.10 g, 4.2 mmol; washed thoroughly with hexane prior to use), and DMF (3 ml) was stirred at 140 °C for 1 h under nitrogen. As the tellurium went into solution, hydrogen was evolved and a deep red color developed within 10—15 min. After 1 h, the color faded and the mixture turned to a pale yellow suspension of sodium telluride, which was immediately used for reduction. On contact with air, sodium telluride rapidly decomposes with liberation of elemental tellurium.

Reduction of Aromatic Nitro Compound to Azo Compound. To a stirred suspension of sodium telluride (2.0 mmol) in DMF (3 ml), a solution of nitroarene (**1**; 1.0 mmol) in THF (2 ml) was added by cannula at room temperature under nitrogen. The mixture was gently heated to 70 °C and kept at this temperature for 3—5 h. Progress of the reaction was monitored by TLC on silica. The reaction was quenched by bubbling air into the mixture, to which was then added a saturated sodium chloride solution (20 ml) followed by ether (20 ml). The insoluble material was filtered through a thin layer of Celite and the organic phase was separated from the filtrate, washed with 10% hydrochloric acid to remove any DMF, and evaporated to leave a crude azo compound **3**, which was purified by chromatography on silica gel or recrystallization from appropriate solvent.

Isolation of Bis(dimethylcarbamoyl) Ditelluride (4). The reaction mixture was worked up as described above. Without being washed with 10% hydrochloric acid, the ethereal extract was evaporated to a small volume. Hexane was added to the concentrate and the mixture was left to stand in a refrigerator. Ditelluride **4** separated as fine yellow needles, which begins to darken at 118 °C and decomposes at 121—122 °C with liberation of tellurium. Yields were variable, usually in the range of 5—15%. In solid state this compound could be stored for weeks in the dark, but in a solution it readily decomposed. ^{1}H NMR ($CDCl_3$) δ=3.12 (12H, s, CH_3); IR (KBr disk) 1655,1350, 1245, 1075, 870, and 660 cm^{-1}. Found: C, 18.62; H, 3.04; N, 7.02%. Calcd for $C_6H_{12}N_2O_2Te_2$: C, 18.04; H, 3.03; N, 7.02%.

Reductive Desulfurization of Aromatic Thioketones to Parent Hydrocarbons. Typical Procedure: To a suspension of sodium telluride (2.0 mmol) in DMF (3 ml) was added xanthene-9-thione (0.210 g, 1.0 mmol) in THF (5 ml) and the resulting mixture was heated under gentle reflux. The color changed from green to orange to blue, and finally to black. After 2 d excess sodium telluride was destroyed by exposing to air and water (20 ml) followed by dichloromethane (20 ml) was added. The insoluble material was removed by filtration on a thin layer of Celite, and the organic phase was separated from the filtrate, washed with 10% hydrochloric acid, and evaporated. The residue was chromatographed on silica gel to afford xanthene (0. 161 g, 82%). Mp 96—99 °C (lit,[5] 100 °C).

Under similar conditions, thiobenzophenone and 4-bromothiobenzophenone were reduced to diphenylmethane and 4-bromodiphenylmethane, respectively, in 60—70% isolated yields.

References

1) H. Suzuki, H. Manabe, and M. Inouye, *Chem. Lett.*, **1985**, 1671.
2) A. Osuka, H. Shimizu, and H. Suzuki, *Chem. Lett.*, **1983**, 1373.
3) H. Suzuki, H. Tani, and S. Takeuchi, *Bull. Chem. Soc. Jpn.*, **58**, 2421 (1985).
4) J. W. Scheeren, P. H. J. Ooms, and R. J. F. Nivard, *Synthesis*, **1973**, 149.
5) A. Mustafa and M. K. Hilmy, *J. Chem. Soc.*, **1952**, 1343.
6) J. E. Komiecik, *J. Org. Chem.*, **30**, 2014 (1965).
7) K. Tabei and M. Yamaguchi, *Bull. Chem. Soc. Jpn.*, **40**, 1538 (1967).
8) Y. Yost and H. R. Gutman, *J. Chem. Soc. (C)*, **1970**, 2497.

New Birch Type Reduction. Halogen or Halides-Activated Reduction of Disulfides to Thiols with Aluminium in Liquid Ammonia

Ryu SATO,* Ryouichi AKAISHI, Takehiko GOTO, and Minoru SAITO
Department of Resource Chemistry, Faculty of Engineering, Iwate University, Morioka 020
(Received September 11, 1986)

Synopsis. Aromatic and aliphatic disulfides were reduced to the corresponding thiols in high yields by new halogen or halides-activated Birch type reduction with aluminium in liquid ammonia.

In this half century, a great deal of investigations on the Birch type reduction have been reported by many organic and inorganic chemists since the discovery of the reduction with metallic sodium in liquid ammonia by A. J. Birch in 1944.[1] Many improved methods for the Birch reduction have been also developed, for example, use of other metals[2] and amines instead of liquid ammonia,[3] addition of proton sources,[4] and activation of the metals.[5] Recently, Benkeser et al. reported the improved Birch reduction to reveal that a selective reduction of alkynes with metallic calcium in alcohol and amine gave the corresponding alkenes and alkanes in moderate yields.[6] During the course of our investigations on the organic sulfur chemistry in liquid ammonia and amines,[7] we found a new Birch type reduction of disulfides. In this paper, we wish to report this new selective reduction of aromatic and aliphatic disulfides to the corresponding thiols with metallic aluminium, which is activated by halogen or halides in liquid ammonia, as shown in Eq. 1.

$$\underset{\textbf{1a-i}}{R\text{-}S\text{-}S\text{-}R} \xrightarrow[\text{Activator}]{Al/NH_3} \underset{\textbf{2a-i}}{2\ R\text{-}SH} \qquad (1)$$

In initial stage of this investigation, to carry out the reaction at ambient temperature, our efforts were centered on activation of the surface of aluminium, e.g., irradiation of supersonic wave and addition of white sand to the reaction system. Ultimately, the best results were obtained when some halogen or halides were added to the reduction system. Thus, a remarkable acceleration of the reduction was observed by employing iodine and sodium chloride as shown in Table 1 (Runs 2 and 3). In the absence of the halogen or halides, the yield of thiol was only 9% (Run 1). Moreover, we also tested other salts as shown in runs 5 to 9. It should be noted that both halogen (I_2) and halides (NaCl, KCl, KI, and NH_4Cl) exhibited comparable effect (Runs 2 to 7). On the other hand, sulfate and nitrate did not affect this reduction at all (Runs 8 and 9). As shown in Run 4 the sufficient reduction of disulfide to thiol was observed even when a catalytic amount of sodium chloride (0.025 mmol) was used. These results suggest that both the halides and halogen play an important role as activator in this reduction. To our knowledge, there has been no report on the halide or halogen-activated Birch reduction although ammonium sulfate have been used as a proton source.[8] The generality of this method was shown in runs 10 to 17. It is noteworthy that bis(4-chlorophenyl) (**1b**) and bis(2-benzothiazolyl) disulfide (**1i**) could be reduced to give the corresponding thiols in good yields (Runs 10 and 17), since the result implies that only the S-S bond, not C-S, C-Cl, and C=C bond, in the disulfide was reduced selectively.

Table 1. Reduction of Disulfides with Aluminium in Liquid Ammonia

Run[a]	Substrate R-SS-R/R		Catalyst	mmol	React. Time/h	Yield of Thiol	% [b,c]
1	C_6H_5-	**1a**	—	—	8	**2a**	9
2	C_6H_5-	**1a**	I_2	0.15	2	**2a**	93
3	C_6H_5-	**1a**	NaCl	0.3	2	**2a**	93
4	C_6H_5-	**1a**	NaCl	0.025	4	**2a**	100 (98)
5	C_6H_5-	**1a**	KI	0.3	2	**2a**	62
6	C_6H_5-	**1a**	KCl	0.3	2	**2a**	100
7	C_6H_5-	**1a**	NH_4Cl	0.3	2	**2a**	98
8	C_6H_5-	**1a**	$(NH_4)_2SO_4$	0.15	2	**2a**	9
9	C_6H_5-	**1a**	NH_4NO_3	0.3	2	**2a**	0
10	4-Cl-C_6H_4-	**1b**	NaCl	0.3	15(min)	**2b**	89 (71)
11	4-CH_3-C_6H_4-	**1c**	NaCl	0.3	1	**2c**	94 (94)
12	4-CH_3O-C_6H_4-	**1d**	NaCl	0.3	2	**2d**	93 (92)
13	4-CH_3CO-C_6H_4-	**1e**	NaCl	0.3	1	**2e**	(32)
14	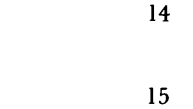	**1f**	NaCl	0.3	12	**2f**	(54)
15	C_6H_5-CH_2-	**1g**	I_2	0.3	4	**2g**	65 (65)
16	CH_3-$(CH_2)_2$-CH_2-	**1h**	I_2	0.3	6	**2h**	45 (45)
17	2-Benzothiazolyl	**1i**	NaCl	0.3	4	**2i**	68 (68)

a) Substrate: 0.5 mmol, Liquid Ammonia: 10 ml, React. Temp: 25°C, Al: 4 mg atom. b) Yield of thiol by iodometry. c) Isolated yields were shown in parenthesis.

Some aliphatic thiols were also obtained upon treating corresponding aliphatic disulfides such as dibenzyl (**1g**) and dibutyl disulfides (**1h**) with aluminium in liquid ammonia at 25 °C (Runs 15 and 16).

In conclusion, aromatic and aliphatic disulfides were reduced by new Birch type reduction, which was activated by halogen (I_2) and halides (NaCl, KCl, KI, and NH_4Cl), with aluminium to afford the corresponding thiols at ambient temperature in good yields. Although, at present stage, the role of the halogen or halides is not necessarily obvious, further applications of this new method to the reduction of other functional groups are expected.

Experimental

Measurements. All melting points were uncorrected. ^1H NMR, IR, and Mass spectra were recorded with HITACHI R-22, HITACHI 295 and HITACHI RMU-6M, respectively. Elemental analyses were determined with YANAGIMOTO MT-3.

Determination of Thiols. The yields of the resulted thiols were determined by the method in the literature.[9]

Materials. Substrates, **1a**, **1b**, **1c**, **1g**, and **1i**, were commercially available and **1d**, **1e**, and **1h** were prepared by the methods in the literature from the corresponding thiols.[10] Bis[4-[1,1-(ethylenedithio)ethyl]phenyl] disulfide (**1f**) was obtained from the corresponding disulfide (**1e**) by the reaction with ethanedithiol in the presence of sodium sulfate and zinc chloride and charaterized as follows. Mp 90 °C; IR (KBr) 2900 and 1480 cm^{-1}; ^1H NMR ($CDCl_3$) δ=2.10 (s, 6H, CH_3), 3.39 (s, 8H, 0.8Hz, $-CH_2CH_2-$), 7.38 (d, 4H, 8 Hz, arom) and 7.66 (d, 4H, 8 Hz, arom); Found: C,52.47; H,4.79%. Calcd for $C_{20}H_{22}S_6$: C, 52.82; H, 4.88%.

Reduction of Disulfides to the Corresponding Thiols with Aluminium Activated by Halide in Liquid Ammonia. General Procedure. Disulfide (0.5 mmol), aluminium (grain, 4 mg atom) and sodium chloride (0.3 mmol) were taken into a stainless steel autoclave. After evacuation, liquid ammonia (10 ml) was charged into the autoclave and the mixture was allowed to react with stirring at 25 °C for 1 h. Water (20 ml) was added to the residue obtained after evaporation of ammonia. A part of the solution was provided for the iodometric titration to determine the yields of the resulting thiols. After acidification with hydrochloric acid, the aqueous solution was extracted with chloroform (5 ml×3). Evaporation of the combined chloroform after drying on sodium sulfate gave desired thiol (**2**). The products obtained (**2a—e** and **2g—i**) were identified by comparing the ^1H NMR, IR, MS, and elemental analysis with those of the authentic samples which were used for preparation of substrate disulfides.

1-Methyl-1-(4-mercaptophenyl)-1,3-dithiolane (2f): Oil; IR (neat) 2950,2550 and 1500 cm^{-1}; ^1H NMR ($CDCl_3$) δ=2.11 (s, 3H, CH_3), 3.23—3.54 (m, 5H, SH and $-CH_2CH_2-$), 7.15 (d, 2H, 9.0 Hz, arom) and 7.58 (d, 2H, 9.0 Hz, arom); MS (70 eV) *m/z* 228 (M^+). Found: C, 53.01; H, 5.46%. Calcd for $C_{10}H_{12}S_3$: C, 52.59; H,5.30%.

References

1) A. J. Birch, *J. Chem. Soc.*, **1944**, 430.

2) For example: C.Ivanov and P. Markov, *Compt. Rend. Acad. Bulgare Sci.*, **15**, 49 (1962); P. Markov and C.Ivanov, *Tetrahedron Lett.*, **1962**, 1139; P. Markov and C. Ivanov, *Naturwissenschafen*, **50**, 688 (1963); P. Markov and C. Ivanov, *C. R. Acad. Sci., Paris, Ser. C*, **264**, 1605 (1966) [*Chem. Abstr.*, **67**, 73636e (1967)]; P. Markov, L. Dimitrova, and K. Ivanoh, *Monatsh Chem.*, **107**, 619 (1976).

3) See review: E. M. Kaiser, *Synthesis*, **1972**, 391.

4) R.G. Schultz, *J. Org. Chem.*, **25**, 1039 (1960).

5) For example: M. G. Veliev, M. M. Guseinov, and S. A. Mamedov, *Synthesis*, **1981**, 400; B. L. Sondengam, G. Charles, and T. M. Akam, *Tetrahedron Lett.*, **22**, 1069 (1981); A. A. P. Screibmann, *Tetrahedron Lett.*, **1970**, 4271; J. H. Stocker and D. J. Walsh, *J. Org. Chem.*, **44**, 3589 (1979).

6) R. A. Benkeser, J. A. Laugal, and A. Rappa, *Tetrahedron Lett.*, **25**, 2089 (1984); R. A. Benkeser and F. G. Belmonte, *J. Org. Chem.*, **49**, 1662 (1984).

7) For example: R. Sato, S. Takizawa, and S. Oae, *Phosphorus and Sulfur*, **7**, 229 (1979); R. Sato, K. Araya, Y. Takikawa, S. Takizawa, and S. Oae, *ibid.*, **7**, 281 (1979); R. Sato, T. Goto, K. Kakuta, Y. Takikawa, S. Takizawa, and S. Oae, *ibid.*, **7**, 289 (1979); R. Sato, T. Goto, Y. Takikawa, and S. Takizawa, *Synthesis*, **1980**, 615; R. Sato, T. Etchu, Y. Takikawa, and M. Saito, *ibid.*, **1981**, 44; R. Sato, T. Senzaki, Y. Shikazaki, T. Goto, and M. Saito, *Chem. Lett.*, **1984**, 1423; R. Sato, K. Itoh, K. Itoh, T. Goto, and M. Saito, *ibid.*, **1984**, 1913; R. Sato, M. Nakayama, Y. Yuzawa, T. Goto, and M. Saito, *ibid.*, **1985**, 1887; A. Sugawara, M. Shirahata, S. Sato, and R. Sato, *Bull. Chem. Soc. Jpn.*, **57**, 3353 (1984).

8) A. L. Henne and K. W. Greenlee, *J. Am. Chem. Soc.*, **65**, 2020 (1943).

9) D. P. Harnish and D. S. Tarbell, *Anal. Chem.*, **21**, 968 (1948); J. H. Karchmer and M. T. Walker, *Anal. Chem.*, **30**, 85 (1958).

10) R. Connor, "Organic Chemistry" ed by H. Gilman, John Wiley & Sons, New York (1949), Vol 1, pp. 55—82 and pp. 861—866, 2nd ed; E. E. Reid, "Organic Chemistry of Bivalent Sulfur," Chemical Publishing Co, New York (1958), Vol 1, pp. 118—126.

Electrogenerated Acid-Assisted Preparation of Ethers from Aldehydes and Ketones

Sigeru TORII,* Sadahito TAKAGISHI, Tsutomu INOKUCHI, and Hiroshi OKUMOTO
Department of Industrial Chemistry, School of Engineering, Okayama University, Tsushima, Okayama 700
(Received July 17, 1986)

Synopsis. Symmetrical and unsymmetrical ethers are prepared from carbonyl compounds and alkoxytrimethylsilanes in the presence of hydrosilane by using an electrogenerated acid catalyst.

Hydrosilane has been investigated as a good reducing agent for the preparation of ethers from carbonyl compounds in the presence of strong acids such as trifluoroacetic acid,[1] trimethylsilyl triflate,[2] and boron trifluoride etherate.[3] However, these acids have their own problems about their preparation and handling in a practical sense. Recently, trityl perchlorate has also been shown to work as an effective catalyst for the same synthetic purpose.[4]

On the other hand, we have reported that electrogenerated acid (EG acid) played a role of catalyst for the acetalization of ketones[5] and the transesterification of glycerides.[6] Now, we found that when a mixture of carbonyl compounds and alkoxytrimethylsilane was treated with EG acid[7] in situ in the presence of hydrosilane (H-Si ≤) in dichloromethane, the corresponding ethers were obtained as a sole product.

All experiments were carried out using platinum electrodes in a simple undivided cell. A mixture of aldehyde and hydrosilane (1.2 equiv.) in dichloromethane containing lithium perchlorate and tetrabutylammonium perchlorate was electrolyzed to give the symmetrical ether only by passing a small quantity of electricity (Eq. 1). Under the same conditions, the electrolysis of the carbonyl compounds with alkoxysilanes afforded the corresponding unsymmetrical ethers (Eq. 2).

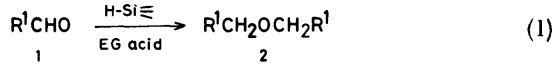

(1)

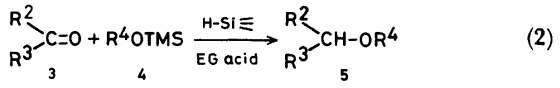

(2)

As shown in Table 1, we have examined the conversion by using triethylsilane and phenyldimethylsilane as reducing agents, but no significant differences were observed. The present procedure is well-suited for the preparation of alkyl and benzyl ethers. Unsymmetrical ethers could be obtained when allyl-, propargyl-, and 3-phenylpropyl-substituted alkoxysilanes were used as nucleophiles. The results are summarized in Table 2. Phenol trimethylsilyl ether, however, did not work in a similar fashion. Activated carbonyl groups such as α,β-enones and β-keto esters can be led to the corresponding ethers. It is interesting to note that unprotected hydroxy ketones did not give any desired ethers, the siloxy ketone **6**, however, undergoes intramolecular version to give the corresponding tetrahydrofuran ring **7** (Eq. 3). Above results reveal that EG

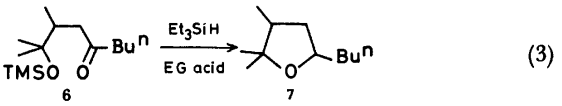

(3)

Table 1. EG Acid-Assisted Preparation of Symmetrical Ethers from Aldehydes

Run	Compound	R^1	H-Si≤[a]	F/mol	Yield/%
1	**2a**	C_6H_5-	A	0.22	91.0
2	**2a**	C_6H_5-	B	0.07	95.7
3	**2b**	4-$CH_3C_6H_4$-	B	0.04	94.5
4	**2c**	4-ClC_6H_4-	B	0.04	86.3
5	**2d**	n-C_6H_{13}-	B	0.15	91.8

a) A: Et_3SiH, B: $PhSi(Me)_2H$.

Table 2. EG Acid-Assisted Preparation of Unsymmetrical Ethers from Aldehydes and Ketones

Run	Compound	R^2	R^3	R^4	H-Si≤[a]	F/mol	Yield/%
6	**5a**	C_6H_5-	H	$C_6H_5(CH_2)_3$-	B	0.06	98.8
7	**5b**	C_6H_5-	H	CH_2=$CHCH_2$-	A	0.20	71.2
8	**5c**	C_6H_5-	H	CH≡CCH_2-	A	0.06	95.0
9	**5d**	C_6H_5-	H	-$(CH_2)_2$-	B	0.34	63.2[b]
10	**5e**	C_6H_5CH=CH-	H	CH_2=$CHCH_2$-	A	0.45	51.1
11	**5f**	C_6H_5CH=CH-	H	CH≡CCH_2-	A	0.30	49.8
12	**5g**	C_6H_5-	CH_3	$C_6H_5(CH_2)_3$-	B	0.15	79.9
13	**5h**	C_2H_5-	CH_3	$C_6H_5(CH_2)_3$-	B	0.30	94.8
14	**5i**	n-C_6H_{13}-	H	$C_6H_5(CH_2)_3$-	B	0.06	81.9
15	**5j**	-CH_2COOMe	CH_3	$C_6H_5(CH_2)_3$-	A	0.20	86.6[c]

a) A: Et_3SiH, B: $PhSi(Me)_2H$. b) Dibenzyl ether was obtained in 27.4% yield. c) The amount of $LiClO_4$ used was 0.3 molar equivalent.

acid is sufficient to activate carbonyl functions for the formation of ether linkages. Furthermore, EG acid can entry in a new class of acid catalyst, because arbitrarily controlable electricity can reflect the nature of EG acid generated in the medium.

Experimental

General Procedure for the Symmetrical Ether 2. A mixture of aldehyde **1** (1.0 mmol), hydrosilane (1.2 mmol), *n*-Bu_4NClO_4 (0.1 mmol), and $LiClO_4$[8] (0.1 mmol) was dissolved in CH_2Cl_2 (3 ml) in an undivided cell. The resulting solution was electrolyzed under constant current (1.67 mA cm^{-2}) with two platinum foil electrodes (1.5 cm^2) at room temperature. After the completion of the reaction, one drop of triethylamine was added and the solution was concentrated. The residue was chromatographed on SiO_2 to give the symmetrical ether.

General Procedure for the Unsymmetrical Ether 5. A mixture of carbonyl compound **3** (1.0 mmol), alkoxysilane **4** (1.2 mmol), *n*-Bu_4NClO_4 (0.1 mmol), and $LiClO_4$ (0.1 mmol) was dissolved in CH_2Cl_2 (3 ml) in an undivided cell. The mixture was electrolyzed under constant current (1.67 mA cm^{-2}) with platinum electrodes at ambient temperature. After 5 min, hydrosilane (1.2 mmol) was added dropwise and the electrolysis was continued. After the completion of the reaction, the same workup and purification as above afforded the corresponding unsymmetrical ether.

Preparation of the Tetrahydrofuran Derivative 7. A mixture of the siloxy ketone **6** (27 mg, 0.1 mmol), triethylsilane (0.12 mmol), $LiClO_4$ (0.03 mmol) and *n*-Bu_4NClO_4 (0.03 mmol) was dissolved in CH_2Cl_2 (3 ml) in an undivided cell. The solution was electrolyzed under constant current (1.33 mA cm^{-2}) with platinum electrodes at ambient temperature. After 20 min, the same workup and purification as above afforded the compound **7** (13 mg) in 71.0% yield.

Spectral and Physical Data. 2a: Bp 125.0—126.5 °C/2.0 mmHg (1 mmHg=133.322 Pa); IR (neat) 2920, 1602, 1090 (C-O-C) cm^{-1}; ^1H NMR ($CDCl_3$) δ=4.52 (s, 4H, CH_2), 7.28 (s, 10H, C_6H_5).

2b: Mp 60—62 °C; IR (Nujol) 2905, 1115 (C-O-C) cm^{-1}; ^1H NMR ($CDCl_3$) δ=2.33 (s, 6H, CH_3), 4.48 (s, 4H, CH_2), 7.16 (s, 10H, C_6H_5).

2c: Mp 44—45 °C; IR (Nujol) 2920, 1600, 1120 (C-O-C) cm^{-1}; ^1H NMR ($CDCl_3$) δ=4.47 (s, 4H, CH_2), 7.24 (s, 8H, C_6H_4).

2d: Bp 82—85 °C/1.5 mmHg; IR (neat) 2945, 2921, 1110 (C-O-C) cm^{-1}; ^1H NMR ($CDCl_3$) δ=0.60—1.05 (m, 6H, CH_3), 1.05—2.00 (broad, 20H, CH_2), 3.38 (m, 4H, CH_2).

5a: Bp 80—83 °C/1—2.0 mmHg; IR (neat) 2920, 2855, 1605, 1100 (C-O-C) cm^{-1}; ^1H NMR ($CDCl_3$) δ=1.60—2.15 (m, 2H, CH_2), 2.45—2.85 (m, 2H, CH_2), 3.42 (t, J=6 Hz, 2H, CH_2O), 4.42 (s, 2H, CH_2O), 7.10 (s, 5H, C_6H_5), 7.22 (s, 5H, C_6H_5).

5b: Bp 80—82 °C/2.0 mmHg; IR (neat) 1640, 1600, 1100 (C-O-C) cm^{-1}; ^1H NMR ($CDCl_3$) δ=3.87—4.08 (m, 2H, CH_2), 4.47 (s, 2H, CH_2), 5.00—5.45 (m, 2H, CH_2=), 5.63—6.27 (m, 1H, CH=), 7.26 (s, 5H, C_6H_5).

5c: Bp 77—80 °C/1.5 mmHg; IR (neat) 3280 (≡C-H), 2845, 2110 (C≡C), 1090 (C-O-C) cm^{-1}; ^1H NMR ($CDCl_3$) δ=2.46 (t, J=2.5 Hz, 1H, ≡C-H), 4.18 (d, J=2.5 Hz, 2H, CH_2), 4.60 (s, 2H, CH_2), 7.34 (s, 5H, C_6H_5).

5d: Bp 118—120 °C/1.5 mmHg; IR (neat) 2920, 2845, 1605, 1100 (C-O-C) cm^{-1}; ^1H NMR ($CDCl_3$) δ=3.17 (s, 4H, CH_2), 4.57 (s, 4H, CH_2), 7.31 (s, 10H, C_6H_5).

5e: Bp 95—97 °C/2.0 mmHg; IR (neat) 2900, 2840, 1640 (C=C), 1110 (C-O-C) cm^{-1}; ^1H NMR ($CDCl_3$) δ=3.90—4.12 (m, 4H, CH_2), 4.91—5.49 (m, 2H, =CH_2), 5.61—6.75 (m, 3H, =C-H), 6.96—7.57 (m, 5H, C_6H_5). Anal. ($C_{12}H_{14}O$) C, H.

5f: Bp 110—120 °C/2.0 mmHg; IR (neat) 3270 (≡C-H), 2100 (C≡C), 1095 (C-O-C) cm^{-1}; ^1H NMR ($CDCl_3$) δ=2.41 (t, J=2.5 Hz, 1H, ≡C-H), 5.95—6.85 (m, 2H, CH=CH), 7.01—7.46 (m, 5H, C_6H_5). Anal. ($C_{12}H_{12}O$) C,H.

5g: Bp 130—132 °C/1—2.0 mmHg; IR (neat) 2965, 2830, 1605, 1105 (C-O-C) cm^{-1}; ^1H NMR ($CDCl_3$) δ=1.45 (d, J=6 Hz, 3H, CH_3), 1.60—2.09 (m, 2H, CH_2), 2.48—2.84 (m, 2H, CH_2), 3.32 (t, J=6 Hz, 2H, CH_2), 4.37 (q, J=6 Hz, 1H, CH), 7.20 (s, 5H, C_6H_5), 7.31 (s, 5H, C_6H_5) ; Anal. ($C_{17}H_{20}O$) C, H.

5h: Bp 96—98 °C/2.0 mmHg; IR (neat) 2970, 2920, 1600, 1090 (C-O-C) cm^{-1}; ^1H NMR ($CDCl_3$) δ=0.90 (t, J=7 Hz, 3H, CH_3), 1.12 (d, J=6 Hz, 3H, CH_3), 1.20—2.12 (m, 4H, CH_2, CH_2), 2.50—2.88 (m, 2H, CH_2), 3.05—3.70 (m, 3H, CH, CH_2), 7.20 (s, 5H, C_6H_5); Anal. ($C_{13}H_{20}O$) C, H.

5i: Bp 80—83 °C/1—2.0 mmHg; IR (neat) 2955, 2925, 1605, 1110 (C-O-C) cm^{-1}; ^1H NMR ($CDCl_3$) δ=0.87 (m, 3H, CH_3), 1.31 (broad, 10H, CH_2), 1.50—2.10 (m, 2H, CH_2), 2.47—2.86 (m, 2H, CH_2), 3.37 (t, J=6 Hz, 2H, CH_2), 7.22 (s, 5H, C_6H_5); Anal. ($C_{16}H_{26}O$) C, H.

5j: Bp 85 °C/1.5 mmHg; IR (neat) 2970, 2940, 1735 (C=O), 1600, 1100 (C-O-C) cm^{-1}; ^1H NMR ($CDCl_3$) δ=1.19 (d, J=6 Hz, 3H, CH_3), 1.64—2.10 (m, 2H, CH_2), 2.45 (d, d, J=6 Hz, 6 Hz, 2H, CH_2), 2.50—2.80 (m, 2H, CH_2), 3.42 (d, t, J=2.5 Hz, 6 Hz, 2H, CH_2), 3.65 (s, 3H, CH_3), 3.50—4.00 (m, 1H, CH), 7.18 (s, 5H, C_6H_5); Anal. ($C_{14}H_{20}O_3$) C, H.

7: IR (neat) 2960, 2940, 2830, 1140, 1070 cm^{-1}; ^1H NMR ($CDCl_3$) δ=0.7—2.5 (m, 21H), 3.7—4.4 (m, 1H).

References

1) a) M. P. Doyle, D. J. DeBruyn, and D. A. Kooistra, *J. Am. Chem. Soc.*, **94**, 3659 (1972); b) M. P. Doyle, D. J. DeBruyn, S. J. Dnnellyl, D. A. Kooistra, A. A. Odubela, C. T. West, and S. M. Zommebelt, *J. Org. Chem.*, **39**, 2740 (1974); c) D. N. Kursanov, Z. N. Parnes, and N. M. Loim, *Synthesis*, **1974**, 633.

2) R. Noyori, S. Murata, and M. Suzuki, *Tetrahedron*, **37**, 3899 (1981).

3) M. P. Doyle, C. T. West, S. T. Donnelly, and C. C. Mcosker, *J. Organomet. Chem.*, **117**, 129 (1976).

4) J. Kato, N. Iwasawa, and T. Mukaiyama, *Chem. Lett.*, **1985**, 1743.

5) S. Torii and T. Inokuchi, *Chem. Lett.*, **1983**, 1349.

6) S. Torii, T. Inokuchi, K. Kondo, and H. Ito, *Bull. Chem. Soc. Jpn*, **58**, 1347 (1985).

7) S. Torii, Electroorganic Syntheses Part I, Oxidations Methods and Applications, Verlag Chemie, Weinheim (1985).

8) Both commercially available and recrystallized $LiClO_4$ and *n*-Bu_4NClO_4 were dried just before use.

Synthesis of (1-Halo-1-alkenyl)trimethylsilanes via *gem*-Trimethylsilylation of Vinyl Halides

Nobujiro SHIMIZU,* Fumihiro SHIBATA, and Yuho TSUNO
Department of Chemistry, Faculty of Science, Kyushu University, Fukuoka 812
(Received July 17, 1986)

Synopsis. Various vinyl halides including enol silyl ethers of α-halo ketones and esters give the corresponding (1-halo-1-alkenyl)trimethylsilanes in fair to good yields on treatment with lithium diisopropylamide at Dry Ice temperature in the presence of chlorotrimethylsilane.

(1-Bromovinyl)trimethylsilane and its homolog are versatile synthetic reagents[1] and obtainable from 1-alkenyl-or 1-alkynyltrimethylsilanes.[2,3] An alternative simple route to (1-halo-1-alkenyl)trimethylsilanes may be provided by *gem*-silylation of vinyl halides which are readily available. Cunico and Han have reported that the treatment of 1-chloro-2-methylpropene with butyllithium below −100 °C, followed by addition of chlorotrimethylsilane (TMS-Cl), gives (1-chloro-2-methyl-1-propenyl)trimethylsilane in 39% yield.[4] The scope of this method, however, would be limited due to the anticipated side reactions including a facile rearrangement of *gem*-haloalkenyllithium species to acetylenic compounds, a metal-halogen exchange reaction, and a coupling reaction between butyllithium and TMS-Cl. For example, we found that under similar metalation conditions to those reported[4] vinyl bromide gave bis(trimethylsilyl)acetylene, while β-bromostyrene afforded β-(trimethylsilyl)-styrene as the major product. This paper deals with the *gem*-trimethylsilylation of various vinyl halides **1a—j** by a modified procedure using lithium diisopropylamide (LDA) in place of butyllithium.

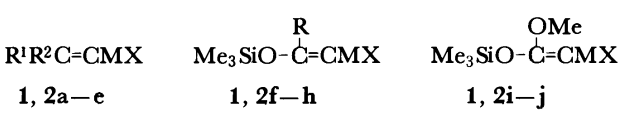

$R^1R^2C{=}CMX$ (1, 2a—e); $Me_3SiO{-}\overset{R}{\overset{|}{C}}{=}CMX$ (1, 2f—h); $Me_3SiO{-}\overset{OMe}{\overset{|}{C}}{=}CMX$ (1, 2i—j)

1; M=H, **2**; M=$SiMe_3$
a; $R^1=R^2=H$, X=Br **b**; $R^1=R^2=Me$, X=Br
c; $R^1=H$, $R^2=Ph$, X=Br **d**; $R^1=H$, $R^2=Me$, X=Cl
e; $R^1=H$, $R^2=CH_2Cl$, X=Cl **f**; R=Me, X=Cl
g; R=Ph, X=Br **h**; $R=CH_2Cl$, X=Cl **i**; X=Cl
j; X=Br

Since LDA is inactive toward TMS-Cl below Dry Ice temperature, the metalation of a vinyl halide can be done in the presence of a trapping agent TMS-Cl. Thus, when a vinyl halide **1** was added to an equimolar mixture of LDA and TMS-Cl in THF/ether (2:1) at −75 °C or below, there was obtained the corresponding (1-halo-1-alkenyl)trimethylsilane **2** in fair to good yields. The results are shown in Table 1.

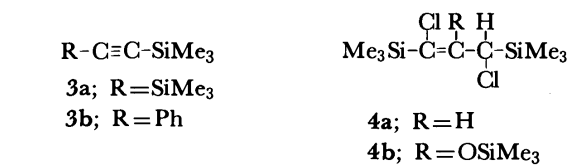

$R{-}C{\equiv}C{-}SiMe_3$
3a; R=$SiMe_3$
3b; R=Ph

4a; R=H
4b; R=$OSiMe_3$

Table 1. *gem*-Trimethylsilylation of Vinyl Halides

Halide	Conditions[a]	Products (Yield/%)[b]
1a	A	**2a** (60) + **3a** (7)[c]
1b	B	**2b** (54)
1c	B	**2c** (55) + **3b** (30)[c]
1d[d]	A	**2d** (23)[d]
1e[d]	B	**2e** (11)[d] + **4a** (58)[d]
1e[d]	B[e]	**2e** (59)[d] + **4a** (5)[c]
1e[d]	B[f]	**4a** (80)[d]
1f[g]	C	**2f** (84)[g]
7a	C[f]	**2f** (67)[h]
1g[i]	C	**2g** (80)[i]
7b	C[f]	**2g** (40)[j]
1h	C	**4b** (74)[k]
1i[d]	C	**2i** (70)[d]
7c	C[f]	**8a** (45)
7b	C[f]	**8b** (45)[l]

a) The silylation was carried out by adding a halide **1** to an equimolar mixture of LDA and TMS-Cl (1—1.2 equiv.) under following conditions: (A) at −100 °C in THF/ether (2:1) for 3 h, (B) at −75 °C in THF/ether (2:1) for 2 h, (C) at −75 °C in THF for 4 h. b) Isolated yield. c) Determined by GLC. d) A mixture of stereoisomers. e) A LDA solution was added to a mixture of **1** and TMS-Cl. f) An excess amount of a LDA/TMS-Cl mixture was used. g) $E/Z<0.05$. h) $E/Z=0.67$. i) $E/Z=0.15$. j) $E/Z=20$. k) Corrected for the recovery of **1**h (49%). l) NMR analysis of a crude product before acidic workup indicated the formation of **2j** ($E/Z=1$) in 58% yield.

The addition of 1,3-dichloropropene **1e** to a LDA/TMS-Cl mixture led to the predominant formation of a doubly silylated product **4a**. Monosilylation at the vinylic site, however, could be effected by inverse addition of a LDA solution to a mixture of **1e** and TMS-Cl. This procedure provides a convenient route to a versatile compound **2e**[5] which otherwise is not readily accessible. **2e** underwent a direct displacement reac-

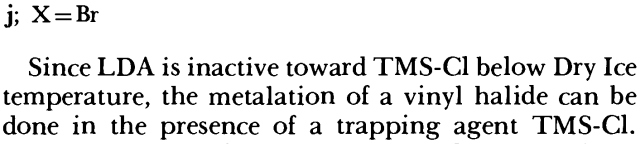

$CH_3(CH_2)_4CH{=}\overset{SiMe_3}{\overset{|}{C}}(CH_2)_3CH_3$ (**6**) $\xleftarrow{ii}$ **2e** $\xrightarrow{i}$ $Cl{-}\overset{SiMe_3}{\overset{|}{C}}{=}CHCH_2Ph$ (**5**)

i; Ph_2CuLi, ii; *n*-BuMgBr/10%CuI

tion with Ph_2CuLi yielding [1-chloro-3-phenyl-1-propenyl)trimethylsilane (**5**, 73%), whereas it reacted with *n*-BuMgBr in the presence of a catalytic amount of cupper (I) iodide to give (1-butyl-1-heptenyl)trimethylsilane (**6**) in 78% yield via a double rearrangement of the allylic double bond.

gem-Silylation was readily accomplished also for vinyl halides bearing an enol ether function. For example, enol silyl ethers (**1f** and **1g**) of α-halo ketones **7a** and **7b** stereoselectively gave **2f** and **2g** in good yields. The use of 2 equiv amounts of a LDA/TMS-Cl

mixture converted these halo ketones directly to **2f** and **2g**, although the concomitant occurrence of the reduction of the carbonyl group with LDA lowered the yield of **2**, especially so in the case of **7b**.[6] Synthesis of α-trimethylsilyl esters **8a** and **8b** was conveniently accomplished by the treatment of halo esters **7c** and **7d** with excess amounts of a LDA/TMS-Cl mixture followed by acidic workup.

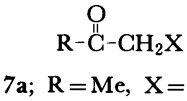

7a; R=Me, X=Cl
7b; R=Ph, X=Br
7c; R=OMe, X=Cl
7d; R=OMe, X=Br

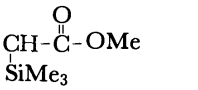

8a; X=Cl
8b; X=Br

Experimental

NMR spectra were recorded on a Hitachi R-20B spectrometer using carbon tetrachloride as solvent. The following examples are representative.

(1-Bromo-2-methyl-1-propenyl)trimethylsilane (2b). A LDA solution prepared from *n*-BuLi (in hexane, 22 mmol) and diisopropylamine (22 mmol) in THF/ether (2:1, 30 cm^3) was cooled to −75 °C and TMS-Cl (22 mmol) was added. To this mixture was added 1-bromo-2-methyl-1-propene (2.3 g) in THF (5 cm^3) over a period of 20 min and the resulting mixture was stirred for 2h at −75 °C. A crude oil obtained after workup was distilled to give **2b** (1.9 g): Bp 124—125 °C (140 Torr: 1 Torr=133.3 Pa); IR 1615 cm^{-1}; ^1H NMR δ=0.26 (9H, s), 1.89 (3H, s), 1.97 (3H, s). Found: C, 40.62; H, 7.35%. Calcd for $C_7H_{15}BrSi$: C, 40.58; H, 7.30%.

(1,3-Dichloro-1-propenyl)trimethylsilane (2e). An ethereal solution (50 cm^3) of LDA (34 mmol) was added to a mixture of 1,3-dichloropropene (3.8 g) and TMS-Cl (3.8 g) in THF (50 cm^3) over a period of 1 h at −75 °C and the resulting mixture was stirred for 1 h at that temperature. Usual workup gave **2e** (3.4 g) as a mixture of stereoisomers (*E*/*Z*=0.48): Bp 65—68 °C (2 Torr) [lit,[5] Bp 25 °C (0.03 Torr)].

1-Chloro-2-trimethylsiloxy-1-trimethylsilylpropene (2f). To a mixture of LDA (18 mmol) and TMS-Cl (18 mmol) in THF (20 cm^3) was added an enol silyl ether **1f** (*E*/*Z*<0.05, 2.4 g) over a period of 10 min at −75 °C and the mixture was stirred at −75 °C for 4h. A crude oil obtained after workup was distilled to give **2f** (2.98 g, *E*/*Z*<0.05): Bp 106—108 °C (29 Torr); IR 1605 cm^{-1}; ^1H NMR δ=0.20 (18H, s), 1.86 (3H, s).

Methyl Chloro(trimethylsilyl)acetate (8a). To a cold (−75 °C) solution of LDA (44 mmol) and TMS-Cl (44 mmol) in THF (25 cm^3) was added a THF solution of methyl chloroacetate (2.16 g) and the mixture was stirred at −75 °C for 4 h. Solvent was removed on a rotary evaporator and the residue was extracted with petroleum ether. The organic layer was washed first with a cold hydrochloric acid (5 M (1 M=1 mol dm^{-3}), 20 cm^3), then with a saturated sodium hydrogencarbonate solution, and dried. A crude oil obtained after workup was distilled to give **8a** (1.63 g): Bp 78—79 °C (20 Torr); IR 1745, 1720 cm^{-1}; ^1H NMR δ=0.18 (9H, s), 3.70 (3H, s), 3.72 (1H, s). Found: C, 39.55; H, 7.28%. Calcd for $C_6H_{13}ClO_2Si$: C, 39.88; H, 7.25%.

Physical and spectral data for other new compounds listed in Table 1 are as follows.

2C: Bp 126—128 °C (16 Torr); IR 1255, 840 cm^{-1}; ^1H NMR δ=0.04 (9H, s), 7.14 (5H, m), 7.84 (1H, s).

2d: Bp 130—135 °C [as a mixture of stereoisomers in the ratio 1:3.3); IR 1610 cm^{-1}; ^1H NMR (Signals of the less abundant isomer were shown in italics.) δ=*0.16* and 0.24 (together 9H, both s), 1.76 (d, *J*=7 Hz) and *1.82* (d, *J*=7 Hz) (together 3H), *6.02* and 6.41 (together 1H, both q, *J*=7 Hz).

***E*-2f**: ^1H NMR δ=0.15 (9H, s), 0.24 (9H, s), 2.03 (3H, s).

2g: Bp 98—100 °C (2 Torr); IR 1605, 1585 cm^{-1}; ^1H NMR δ=−0.09 g (9H, s), 0.06 (9H, s), 7.30 (5H, m); (Found: C, 49.25; H, 6.90%).

2i: Bp 101—103 °C (23 Torr): IR 1615, 1250, 840 cm^{-1}; ^1H NMR δ=0.13 (s), 0.23 (s), 0.28 (s) (1.7:1:1.2, together 18H), 3.49 (s) and 3.78 (s) (1.9:1, together 3H).

2j: 105—108 °C (7 Torr) (*E*/*Z*=1): IR 1610 cm^{-1}; ^1H NMR δ=0.14 (s), 0.24 (s), 0.29 (s) (1.8:1:1, 18H altogether), 3.50 (s) and 3.72 (s) (1:1, together 3H)

4a: Bp 95—98 °C (2 Torr) (*E*/*Z*=0.56). *E*-isomer: IR 1580 cm^{-1}; ^1H NMR δ=0.14 (9H, s), 0.27 (9H, s), 3.89 (1H, d, *J*=13 Hz), 6.36 (1H, d, *J*=13 Hz). *Z*-isomer: IR 1600 cm^{-1}; ^1H NMR δ=0.12 (9H, s), 0.18 (9H, s), 4.40 (1H, d, *J*=10.5 Hz), 5.93 (1H, d, *J*=10.5 Hz); (Found (as a mixture of stereoisomers): C, 42.45; H, 7.80%).

4b: Bp 145—146 °C (35 Torr); IR 1580 cm^{-1}; ^1H NMR δ=0.12 (9H, s), 0.24 (9H, s), 3.95 (1H, s).

8b: Bp 49—50 °C (3 Torr); IR 1745, 1720 cm^{-1}; ^1H NMR δ=0.20 (9H, s), 3.54 (1H, s), 3.70 (3H, s); (Found: C, 31.71; H, 5.60%).

(1-Chloro-3-phenyl-1-propenyl)trimethylsilane (5). **2e** (0.50 g) was added to a solution of lithium diphenylcuprate(I) (12 mmol) in ether (15 cm^3) and the mixture was stirred for 1 h at 0 °C. Bulb-to-bulb distillation of a crude oil gave **5** 450 mg, as a mixture of stereoisomers in the ratio 1:2.6: IR 1615 cm^{-1}; ^1H NMR (Signals of the less abundant isomer were shown in italics.) δ=*0.18* (s) and 0.29 (s) (together 9H), 3.44 (d, *J*=7.8 Hz) and *3.60* (d, *J*=6.6 Hz) (together 2H), *6.08* (t, *J*=6.6 Hz) and 6.51 (t, *J*=7.8 Hz) (together 1H), 7.15 (5H, m); (Found: C, 64.01; H, 7.58%).

(1-Butyl-1-heptenyl)trimethylsilane (6). A solution of butylmagnesium bromide prepared from 2.74 g of butyl bromide in THF (15 cm^3) was added to a mixture of **2e** (930 mg, *E*/*Z*=1.5) and cupper(I) iodide (0.5 g) in THF (15 cm^3) and HMPA (2 cm^3) and the resulting mixture was stirred for 4 h at 0 °C. A crude oil (1.25 g) obtained after workup was distilled to give **6** (880 mg, as a mixture of stereoisomers in the ratio 1:1.9): Bp 108—109 °C (12 Torr); IR 1615 cm^{-1}; ^1H NMR (Signals of the less abundant isomer were shown in italics.) δ=*0.04* (s) and 0.12 (s) (together 9H), 0.75—1.1 (6H, m), 1.1—1.7 (10H, m), 1.8—2.4 (4H, m), *5.64* (t, *J*=7 Hz) and 5.86 (t, *J*=7 Hz) (together 1H); (Found: C, 74.25; H, 13.28%).

References

1) W. P. Weber, "Silicon Reagents for Organic Synthesis," Springer-Verlag, New York (1983), Chap. 7.

2) A. Ottolenghi, M. Fridkin, and A. Zilkha, *Can. J. Chem.*, **41**, 2977 (1963); B. T. Gröbel and D. Seebach, *Chem. Ber.*, **110**, 867 (1977); T. H. Chan, W. Mychajlowskij, B. S. Ong, and D.N. Harpp, *J. Org. Chem.*, **43**, 1526 (1978).

3) G. Zweifel and W. Lewis, *J. Org. Chem.*, **43**, 2739 (1978); H. Westmijze, J. Meijer, and P. Vermeer, *Tetrahedron Lett.*, **1977**, 1823.

4) R. F. Cunico and Y. K. Han, *J. Organomet. Chem.*, **105**, C29 (1978).

5) Alternatively **2e** can be prepared from 3,3-dichloroallyltriphenyllead in two steps: D. Seyferth and R. E. Mammarella, *J. Organomet. Chem.*, **156**, 279 (1978).

6) Enol silylation of halo ketones **7a** and **7b** exclusively gave the *Z*-isomer when the reaction was carried out in ether using triethylamine as base, whereas LDA favored the *E*-isomer.

Microscopic and Dielectric Studies of CH_3NH_3I Crystal

Osamu YAMAMURO, Masaharu OGUNI, and Hiroshi SUGA*
Department of Chemistry and Chemical Thermodynamics Laboratory, Faculty of Science,
Osaka University, Toyonaka, Osaka 560
(Received September 6, 1986)

Synopsis. Observation of CH_3NH_3I crystal under a polarizing microscope showed a rectangular domain structure in the δ phase. Dielectric measurement revealed an antiferroelectric behavior of the same phase. These results indicate that the δ phase has orthorhombic or monoclinic structure with C-N axes of $CH_3NH_3^+$ ions inclining along its a or b axis in an antiferroelectric way.

Methylammonium iodide CH_3NH_3I crystal has the tetragonal structure (α') at room temperature with their C-N axes arranged in the antiparallel way along the c axis of the unit cell ($P4/nmm$, $z=2$). The $CH_3NH_3^+$ ion is orientationally disordered[1-4] with locating its three-fold axis on the four-fold crystallographic axis. The crystal undergoes two different types of transition depending on cooling rate, either discontinuously to the stable β' phase at 220 K or continuously to the metastable δ phase at 166 K. The previous calorimetric study[5] revealed that the $CH_3NH_3^+$ ions were ordered at zero Kelvin in both of the low temperature phases and the higher-order α'-δ transition corresponded to the orientational order-disorder process of the $CH_3NH_3^+$ ions possibly without drastic structural change.

It is the purpose of this paper to report a polarizing microscopic observation of a single crystal and a dielectric measurement of a powdered crystal in order to clarify the nature of the α'-δ phase transition and to discuss a possible structure of the δ phase.

Experimental

A polarizing microscope, Olympus model POM with magnification of 4×10, was used with a home-made cold stage which was designed for the observation of single crystal at liquid N_2 temperature with a rapid cooling. The rapid cooling is important in realizing the full formation of the δ phase. Single crystal was grown by a slow recrystallization from the methanol solution at 5 °C in the dark. The obtained crystal was of a square plate whose side length was about 1 mm.

The complex dielectric permittivity was measured from 80 to 270 K at several frequencies ranging from 50 Hz to 100 kHz with a capacitance bridge, General Radio Co. type 1615A. Powdered crystal was pressed to form a disc, 10 mm in diameter and 1.158 mm in thickness. Circular gold leaves of the size of 60.1 mm^2 in area were stuck with N-Apiezon grease on both faces of the disc as the electrodes.

Results and Discussion

Figure 1(A) shows a room-temperature photograph of the single crystal with its face perpendicular to the c axis, the side lines being parallel to the [110] or its equivalent axis. The equivalent tetragonal axes are shown in the figure. This crystal habit was examined in advance by an X-ray diffraction method. The light passes through the crystal along its c axis. No anomaly was observed by the rotation of polarized light. The observation was obscured around the central part of the specimen owing to the coexistence of adhesively grown powdery crystals, but this did not disturb much the optical features of the following observations. Figure 1(B) and 1(C) show the photographs of the crystal in the δ phase obtained by a rapid cooling down to the liquid N_2 temperature. Dark and bright (green and yellow in the original photograph) bands appeared alternately with the boundaries in parallel to the a axis of the tetragonal phase. The directions of the polarization of light for (B) and (C) were just perpendicular to each other. The alternating colors of the domains were just reversed between (B) and (C), indicating the rectangular domain structure of the crystal. It follows that the two equivalent a axes of the tetragonal structure becomes nonequivalent ($a \neq b$) with keeping γ (the $\angle$ab angle) the same 90° in the δ phase. In other words, the crystal structure of the δ phase belongs to the orthorhombic or monoclinic system. In view of the necessary condition for the formation of rectangular domain structure, the directions of its a and b axes must be inclined by 45° from the original a axis of the tetragonal structure as shown in the figure.

The complex dielectric permittivities of the δ and α' phases were measured in the following way. First, the complex dielectric permittivities were measured at eight frequencies (50, 100, 500, 1 k, 5 k, 10 k, 50 k, and 100 kHz) from 270 to 220 K at 5 K intervals in the cooling direction. After that, the sample was cooled rapidly to the liquid N_2 temperature from 260 K. The cooling rate 10 K min^{-1}, was rapid enough to prevent a possible transformation of the α' to β phase around 200 K. The dielectric constant ε' was then measured at the same frequencies from 77.5 K at 5 K intervals and especially in the δ-α' transition region at 1—2 K intervals in the heating direction. There was no considerable dielectric loss observed in the whole temperature and frequency regions, and the real part ε' was independent of the frequency. Figure 2 shows the temperature dependence of ε' measured at 1 kHz. The data between 190 and 220 K were omitted from the plots because they reflect partial transformation into the β' phase. From the high temperature side, ε' increases gradually and reaches a maximum at about 175 K. After that, it decreases steeply with decreasing temperature. This behavior is quite similar to those of the following antiferroelectric compounds; Pb_4SiO_6,[6] $CsH_3(SeO_3)_2$,[7] and $NH_4PF_6 \cdot NH_4F$.[8] The α'-δ phase transition is thus concluded to be accompanied by the antiparallel arrangement of electric dipoles in the δ phase.

The $CH_3NH_3^+$ ions lie in the (100) plane in an antiparallel arrangement along the c axis in the tetragonal α' phase, and the orientations of the ions around the

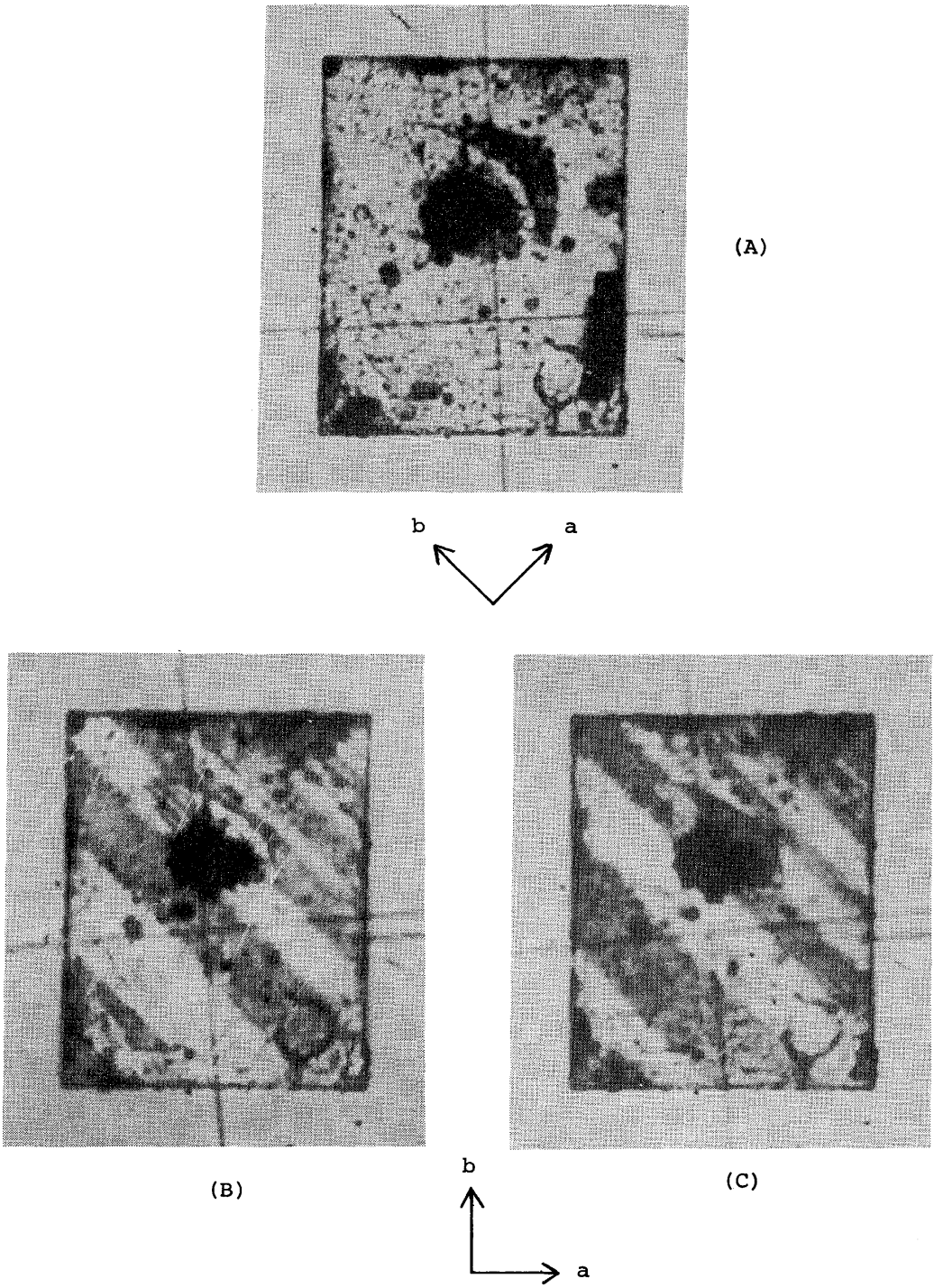

Fig. 1. Microphotographs of the domain structure in CH_3NH_3I single crystal; (A) at room temperature in the α' phase; (B),(C) at the liquid N_2 temperature in the δ phase. (B) and (C) were taken by using the polarized lights whose directions are perpendicular to each other. The crystallographic axes in each phase are shown in the figure.

C-N axes fall into the ordered state through the α'-δ phase transition.[5] The antiferroelectric fluctuation in the phase transition is therefore interpreted to originate from the motion coupled with the orientational ordering; that is, the tilt of the C-N axes from the c axis of the tetragonal structure probably resulting in the strengthening of some hydrogen bonds formed between I^- and $CH_3NH_3^+$ ions. Taking the above microscopic observation into consideration, the tilt would occur either in the (110) or ($1\bar{1}0$) plane in an antiferroelectric way in the δ phase, leading to the loss of the tetragonal symmetry. There are many possible ways of antiferroelectric arrangement of the $CH_3NH_3^+$ ions in space, if we consider larger unit cells than the original one. None of them can be beyond a simple possibility. Direct determination of the low tempera-

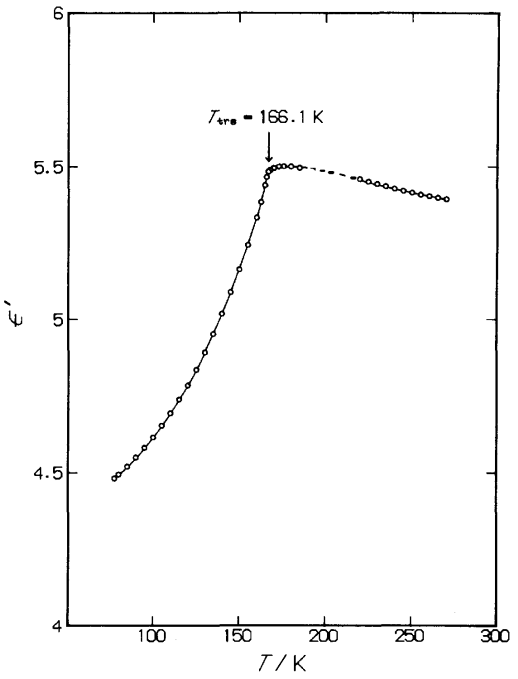

Fig. 2. Dielectric constant of CH_3NH_3I powder crystal measured at 1 kHz.

ture structure by neutron or X-ray diffraction method is highly desiderative.

The authors wish to thank Professor Kazuhide Ogawa and Dr. Hatsuko Tamura of Osaka University for their carrying out the X-ray experiment and allowing us to use the polarizing microscope. Thanks are extended to Mr. K. Mishima of the Workshop Center of Osaka University for constructing the special cold-stage of the microscope.

References

1) S. B. Hendricks, *Z. Kristallogr.*, **67**, 106 (1928).
2) M. Stammler, *J. Inorg. Nucl. Chem.*, **29**, 2203 (1967).
3) E. J. Gabe, *Acta Crystallogr.*, **14**, 1296 (1961).
4) O. Yamamuro, M. Oguni, T. Matsuo, and H. Suga, *Thermochim. Acta*, **98**, 327 (1986).
5) O. Yamamuro, M. Oguni, T. Matsuo, and H. Suga, *J. Chem. Thermodyn.*, **18**, 939 (1986).
6) V. A. Isupov, *Fiz. Tverd. Tela*, **7**, 2221 (1965); *Sov. Phys. Solid State*, **7**, 1789 (1966).
7) Y. Makita, *J. Phys. Soc. Jpn.*, **20**, 1567 (1965).
8) I. Todo and I. Tatsuzaki, *Phys. Status Solidi*, **32**, 263 (1969).

The Crystal Structure of a New Charge-Transfer Complex of Hexamethylenetetrathiafulvalene with Triiodide, HMTTF·I_3[1)]

Kazumasa HONDA,* Midori GOTO, Masayasu KURAHASHI, Hiroyuki ANZAI,† Madoka TOKUMOTO,† Hiroshi BANDO,† and Takehiko ISHIGURO†

National Chemical Laboratory for Industry, Yatabe-machi, Tsukuba-gun, Ibaraki 305
†Electrotechnical Laboratory, Sakura-mura, Niihari-gun, Ibaraki 305

(Received August 4, 1986)

Synopsis. The crystal structure of bis(trimethylene)tetrathiafulvalenium triiodide (hexamethylenetetrathiafulvalenium triiodide) has been determined. The space group is $P\bar{1}$, with a=7.973 (2), b=11.849 (3), c=14.412 (4) Å, α=82.86 (2), β=89.13 (3), γ=95.85 (2)°, and Z=3. The crystal has intermolecular S... S contacts 3.36 and 3.37 Å shorter than the van der Waals distance of 3.7 Å.

Recent attention paid to organic charge-transfer complexes has demonstrated the possibility of their application to new electronic materials because of their large electronic anisotropy and/or conductivity. A series of complexes of bis(trimethylene)tetrathiafulvalene (hexamethylenetetrathiafulvalene[2)]; HMTTF) has been one of the candidates for organic metals since the discovery of HMTTF·TCNQ.[2)] The present authors have attempted the electrocrystallization of HMTTF salts with I_3^-, ClO_4^-, and PF_6^-; they have obtained single crystals of HMTTF·I_3 for the first time. Here, the crystal structure and the electrical properties will be reported.

Experimental

Black plates of HMTTF·I_3 were obtained by electrochemical oxidation (at a constant current of 1 μA under nitrogen at 20 °C) from a 80-ml THF solution containing 0.091 mmol of HMTTF and 0.27 mmol of tetrabutylammonium triiodide.[3)] The electrical resistivity of the single crystal was measured along the long axis (a axis) by the four-terminal method. The cell dimensions and diffraction intensities were measured on a Rigaku AFC-4 four-circle diffractometer by using graphite monochromated Mo$K\alpha$ radiation (λ= 0.71069 Å) at room temperature. 3998 independent reflections with 2θ values from 3° up to 55° ($|F_o| \geqq 3\sigma(|F_o|)$) were used for the analysis.

Crystal Data: $C_{12}H_{12}S_4 \cdot I_3$; FW=665.20; triclinic; space group, $P\bar{1}$; Z=3; a=7.973 (2), b=11.849 (3), c=14.412 (4) Å, α=82.86 (2), β=89.13 (3), γ=95.85 (2)°, U=1343.4 (6) Å^3; D_{obsd}=2.5, D_{calcd}=2.48 gcm^{-3}; μ(Mo $K\alpha$)=55.10 (cm^{-1}). The structure was solved by the use of the *MULTAN* 78 program.[4)] The structural parameters were refined by a block-diagonal least-squares method. The hydrogen atoms were placed at the calculated positions.[5)] All the computations were carried out on a FACOM M-380 computer using the *UNICS* III system.[6)] The final refinement after the absorption correction led to the R value of 0.045. The possibility of another space group, $P1$, was excluded because the I-I bond distance of the I_3 anion on the inversion center was unacceptably prolonged (3.40 Å).

Results and Discussion

The final atomic coordinates of the non-hydrogen atoms are given in Table 1.[7)] An *ORTEP*[8)] projection of the crystal structure along the a axis is shown in Fig. 1. The unit cell contains three HMTTF (A, B, B') and three I_3. One HMTTF (A) and one I_3 have their centers of mass on the crystallographic inversion center. Two I_3 anions are aligned almost parallel to the c axis, and the other one is aligned almost parallel to the b axis. These two types of I_3 anions are alternately stacked along the c axis. The anisotropic temperature factors of the I_3 anion on the inversion center are quite large, indicating that the I_3 anion is probably disordered. Figure 2 shows the bond distances in the HMTTF molecules. In the case of tetrathiafulvalene (TTF) salts,[9)] oxidation is accompanied by a lengthening of

Table 1. Fractional Atomic Coordinates (×10^4) and Equivalent Isotropic Thermal Parameters, with Estimated Standard Deviations in Parentheses

	x	y	z	B_{eq}/Å^2		x	y	z	B_{eq}/Å^2
I1A	814(2)	2451(2)	125(1)	8.67(0.05)	C5A	3192(17)	−599(12)	−1847(8)	4.6(0.4)
I2A	0(0)	0(0)	0(0)	6.94(0.05)	C6A	4001(12)	−418(8)	−2797(6)	2.5(0.2)
I1B	286(1)	1947(1)	7068(1)	3.73(0.02)	C1B	6220(12)	3848(9)	−4432(8)	3.0(0.3)
I2B	378(1)	2249(1)	5010(1)	3.14(0.02)	C2B	6773(13)	3918(10)	−2708(8)	3.4(0.3)
I3B	597(1)	2526(1)	2972(1)	3.70(0.02)	C3B	7412(16)	3979(12)	−1729(10)	4.9(0.4)
S1A	3078(3)	−306(3)	−3882(2)	3.17(0.07)	C4B	6113(19)	3119(15)	−1133(10)	6.0(0.5)
S2A	6763(3)	−41(3)	−3860(2)	3.16(0.07)	C5B	4898(16)	2553(10)	−1785(9)	4.2(0.3)
S1B	4699(4)	2896(2)	−3812(2)	3.52(0.07)	C6B	5445(14)	3134(9)	−2723(8)	3.2(0.3)
S2B	7596(3)	4615(3)	−3768(2)	3.71(0.08)	C7B	6291(12)	4000(9)	−5398(7)	2.9(0.3)
S3B	4885(4)	3249(3)	−6059(2)	3.71(0.08)	C8B	7160(13)	4591(10)	−7126(8)	3.4(0.3)
S4B	7796(3)	4965(3)	−6042(2)	3.63(0.07)	C9B	7956(18)	4979(12)	−8071(9)	4.9(0.4)
C1A	4962(11)	−63(8)	−4510(6)	2.1(0.2)	C10B	6799(20)	4306(15)	−8694(11)	6.5(0.5)
C2A	5681(13)	−290(9)	−2788(6)	2.9(0.3)	C11B	5428(18)	3558(11)	−8081(10)	5.0(0.4)
C3A	6368(16)	−405(12)	−1831(8)	4.4(0.4)	C12B	5837(14)	3813(9)	−7127(8)	3.3(0.3)
C4A	4729(16)	−608(10)	−1200(7)	3.8(0.3)					

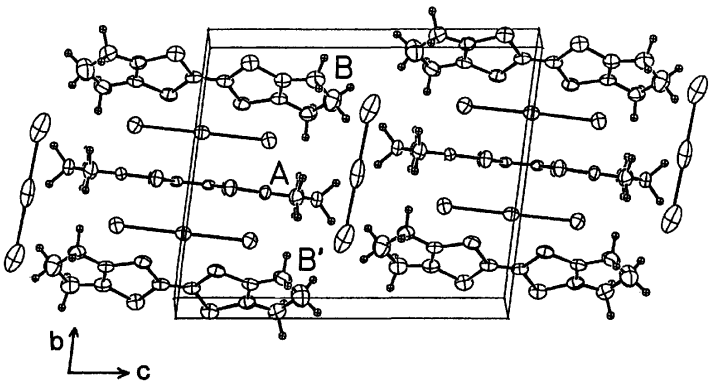

Fig. 1. ORTEP projection of the crystal structure of HMTTF·I_3 on the bc plane. Thermal ellipsoids for non-hydrogen atoms are at 40% probability.

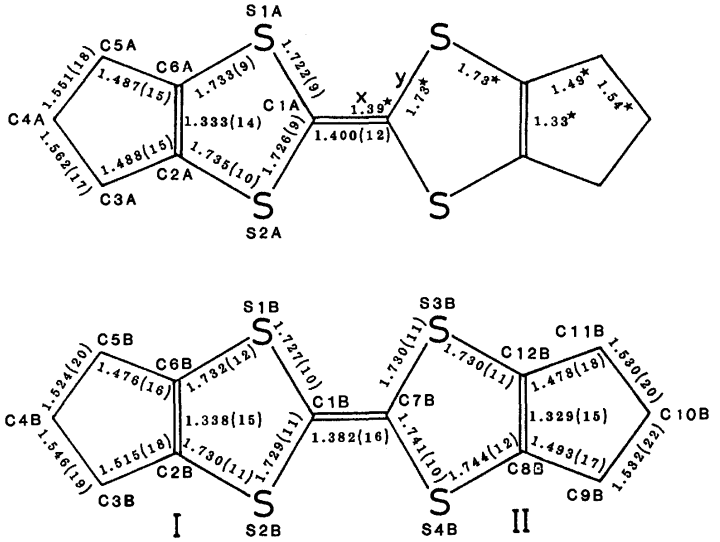

Fig. 2. Numbering system for the non-hydrogen atoms and the bond distances (Å) in the HMTTF molecules. The average distances are indicated at the right side of A with star at shoulder.

the exocyclic double bond (x) and a shortening of the contacts between the two carbon atoms involved in the exocyclic double bond and the sulfur atoms (y). It is impossible to compare the bond distances of HMTTF·I_3 with those of the neutral HMTTF molecule, for the single crystal of the HMTTF has not yet been obtained. The distances of x (1.39 Å) and y (1.73 Å) of HMTTF·I_3, however, agree with the corresponding distances of TTF·I_3 (x, 1.382 (7) Å and y, 1.719 (8) Å). Molecule A is almost planar, within the deviations of 0.05 Å. In Molecule B, both rings I (S1B-C1B-S2-B-C2B-C3B-C4B-C5B-C6B) and II (S3B-C7B-S4B-C8B-C9B-C10B-C11B-C12B) are almost planar, within deviations of 0.08 Å. However, the least-square plane of Molecule B, as a whole, has a deviation of 0.31 Å (C10B); that is, B is slightly folded (8.7°) at the central double bond (C1B—C7B). Figure 3 shows the projection along the c axis. The least-square planes of Molecules A and B have a dihedral angle of 38.0°. The enantiomers B and B′ are parallel and facing to each other, with close S ... S contacts of 3.355 (4) and 3.366

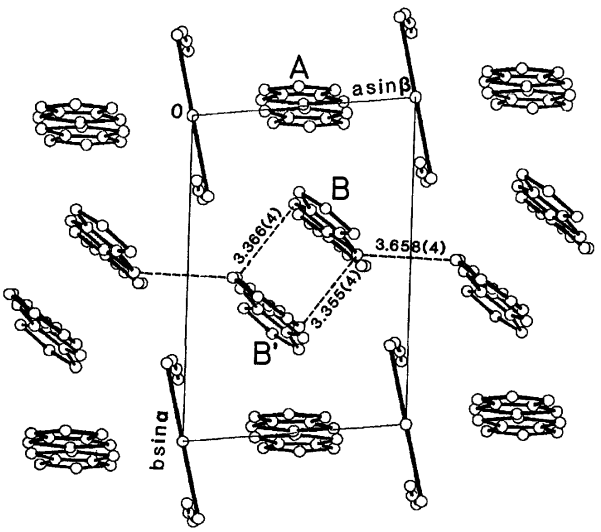

Fig. 3. Crystal structure projected along the c axis. Close intermolecular S···S contacts (Å) are indicated.

(4) Å shorter than the van der Waals distance of 3.7 Å, which may cause the foldings of Molecules B (and B′) described above. A slightly close S ... S contact of 3.658 (4) Å is also found between B and B′ in adjacent cells, but no sufficient overlapping of π-electrons can be expected. No other close S ... S contacts are found around Molecules B and B′ nor around Molecule A.

The temperature dependence of the electrical resistivity along the a axis was also measured. The resistivity increases as the temperature decreases ($\rho=3.7\times10^5$ Ωcm and activation energy $K=0.32$ eV at 300 K);[10] that is, this crystal is semiconductive, which is consistent with the molecular stacking along the a axis.

References

1) Presented in part at the 52nd National Meeting of the Chemical Society of Japan, Kyoto, April 1986; Abstr., No. 2E33.

2) R. L. Greene, J. J. Mayerle, R. Schumaker, G. Castro, P. M. Chaikin, S. Etemad, and S. J. LaPlaca, *Solid State Comm.*, **20**, 943 (1976).

3) H. Anzai, M. Tokumoto, and G. Saito, *Mol. Cryst. Liq. Cryst.*, **125**, 385 (1985).

4) P. Main, S. E. Hull, L. Lessinger, G. Germain, J. P. Declercq, and M. M. Woolfson, *MULTAN* 78, "A System of Computer Programmes for the Automatic Solution of Crystal Structures from X-Ray Diffraction Data," University of York, York, England (1978).

5) The positions of the hydrogen atoms were not refined.

6) T. Sakurai and K. Kobayashi, *Rep. Inst. Phys. Chem. Res.*, **55**, 69 (1978).

7) The lists of observed and calculated structure factors, the atomic parameters for the hydrogen atoms, and the anisotropic thermal parameters for the non-hydrogen atoms are deposited at the Chemical Society of Japan as Document No. 8711.

8) C. K. Johnson, *ORTEP* II, Report ORNL-5138, Oak Ridge National Laboratory, Tennessee, USA (1976).

9) R. C. Teitelbaum, T. J. Marks, and C. K. Johnson, *J. Am. Chem. Soc.*, **102**, 2986 (1980).

10) H. Anzai, M. Tokumoto, H. Bando, and T. Ishiguro, unpublished work.

The ESR Detection of N Atoms in Methane-Air Combustion Flames Doped with Nitrogen Compounds

Masayuki TANIGUCHI, Shoji NODA,† and Hiroshi YOSHIDA*
Faculty of Engineering, Hokkaido University, Kita-ku, Sapporo 060
(Received August 20, 1986)

Synopsis. The ESR spectra of nitrogen atoms were detected for the first time in the combustion flames of methane doped with ammonia. The dependence of the N-atom concentration on the flame conditions was examined. The results were then discussed with reference to the models of the reduction of NH_3, leading to the NO formation.

The elucidation of the mechanism of NO formation in combustion flames is currently one of the most important subjects in combustion-chemical studies. NO is now believed to be formed by three different mechanisms: Thermal NO (from a reaction between N_2 and O_2, the Zeldovich mechanism), prompt NO (originating from reactions between labile intermediates, such as CH or C_2 and N_2), and fuel NO (originating from fuel-bound nitrogen).[1] Nitrogen atoms have been suggested to be of essential importance as the reaction intermediates in the prompt and fuel NO formation. However, there has been very little direct observation of N atoms in combustion flames. Although the paramagnetic intermediates in flames, such as the H and O atoms and the OH radicals, have recently been studied extensively by means of the electron-spin-resonance (ESR) method,[2-4] the ESR detection of N atoms in flames has, as far as the present authors know, not yet been reported.

This note aims to report the first successful ESR detection of N atoms in Bunsen-type flames of methane doped with ammonia under atmospheric pressure. It will also compare the observed dependence of the N-atom yield on the flame conditions with the models of the fuel NO formation reported previously.

Experimental

The Bunsen-type flame was obtained by using a burner composed of three concentric quartz tubes, as has been described in detail previously.[5] Premixed combustible gases, mixtures of methane and air with or without ammonia, were flowed through the innermost tube (4 mm in diameter). The secondary air was supplied through the second tube to support the flame. The outermost tube was used for the flowing of the coolant nitrogen gas, so that the flame was isolated from the surroundings. The flame temperature was measured by using a fine (0.1 mm in diameter) Pt/Pt-Rh thermocouple coated with SiO_2.

The paramagnetic entities were detected by means of the flame-in-cavity method[6] using an X-band spectrometer (Varian, Model E-109) equipped with a TE_{011} large-access cavity (Model E-235). The spectrometer was operated with a 100-kHz field modulation. Because the paramagnetic entities were subjected to ESR measurements under the atmospheric pressure, neither non-S-state atoms nor free radicals could be observed because of the collision broadening. Only H and N atoms with a S-state as the ground electronic state were observed. Another limitation of the flame-in-cavity method is that the paramagnetic entities in a flame are observed as a whole, so that their locations in the flame cannot be determined. This means that neither the concentration distribution in the flame nor the absolute concentration at particular positions in the flame can be determined. Therefore, we are mainly concerned with the relative change in the total amount of the paramagnetic entities dependent on the flame conditions. Occasionally, however, the absolute concentrations of H and N atoms in the flames were estimated from the integrated intensity of the ESR spectra.

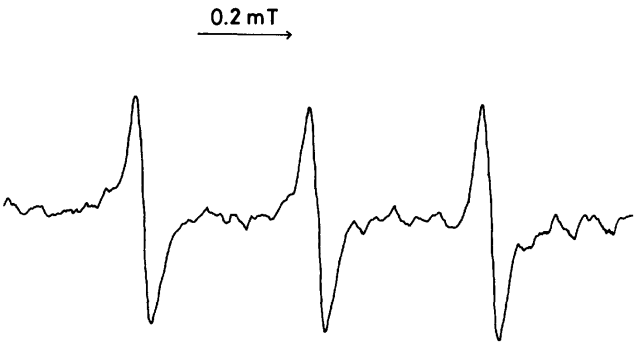

Fig. 1. ESR spectrum of N atoms observed from a Bunsen-type flame of methane-air premixed gas doped with ammonia under atmospheric pressure by the flame-in-cavity method. The flow of premixed gas was 200 cm^3min^{-1} of air, 33 cm^3min^{-1} of methane, and 8 cm^3min^{-1} of ammonia. The flow rate of secondary air was 220 cm^3min^{-1}.

Results and Discussion

The ESR signals observed from the flames of methane-air mixtures doped with ammonia were composed of an intense two-line spectrum with the hyperfine separation of 51.0 mT due to H atoms and a weak three-line spectrum with the hyperfine separation of 0.38 mT at g=2.002. An example of the latter is shown in Fig. 1. This spectrum is attributed to N atoms on the basis of the ESR parameters, which are identical with those of the N atoms studied by the flow-discharge method.[7] The only difference in the spectral features is the much larger linewidth of each hyperfine line in the present study, but this can be attributed to the collision broadening, very probably due to collisions with paramagnetic molecular oxygen[6,8] at high pressures.

When triethylamine was added to the premixed gas instead of ammonia, the ESR spectrum of N atoms was also observed. The premixed gas without nitrogen compounds gave no N-atom spectrum. These observations indicate that the N atoms in the flames come from the added nitrogen compounds and are involved

†Present address: Toyota Central Research and Development Labs., Inc., Nagakute-cho, Aichi 480-11.

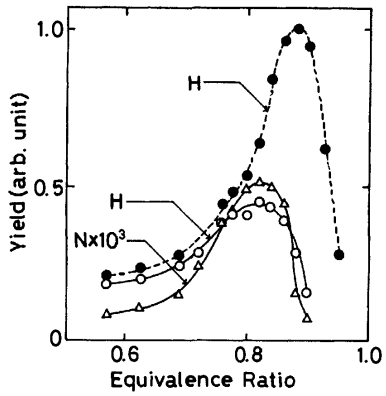

Fig. 2. Dependence of the yield of (circles) H and (triangles) N atoms in Bunsen-type flames of methane-air premixed gas (solid curves) with and (dashed curve) without ammonia on the equivalence ratio of the flame. The equivalence ratio of the flame (calculated by assuming complete mixing of the premixed gas and the secondary air) was changed by changing the flow rate of the secondary air, while the equivalence ratio of the premixed gas was kept constant, 1.71, both in the presence and absence of the added ammonia.

in the fuel-NO mechanism of the NO formation. The yields of N atoms due to the other mechanisms, thermal and prompt NO, are too low to be detected under the present experimental conditions.

The dependence of the ESR intensities of the H- and N-atom spectra on the equivalence ratio (stoichiometric oxygen concentration/actual oxygen concentration) was examined for methane-air flames doped with ammonia by keeping the flow rate of the premixed gas unchanged (33 $cm^3 min^{-1}$ of methane, 200 $cm^3 min^{-1}$ of air, and 8 $cm^3 min^{-1}$ of ammonia) and by changing the flow rate of the secondary air. The composition of the premixed gas corresponds to the equivalence ratio of 1.71, if the combustion of ammonia is expressed as $NH_3+(3/4)O_2 \rightarrow (1/2)N_2+(3/2)H_2O$. The observed dependence is shown in Fig. 2. Both the H and N atoms show their maximum yield at the equivalence ratio of 0.82. The variation in the N-atom yield is found to be parallel with that of the H atom.

For purpose of comparison, the dependence of the H-atom yield for the undoped flame on the equivalence ratio is also shown in Fig. 2. The observed trend of the H-atom yield is essentially the same as has previously been reported and been attributed to the effect of the diffusion of the secondary air (oxygen) into the flame.[5] The composition of the premixed gas was unchanged at the corresponding equivalence ratio of 1.71 here, also. For the undoped flame, the H-atom yield reaches its maximum at the equivalence ratio of 0.88. It should be noted that the H-atom yield is higher in the undoped flame than in the ammonia-doped flame throughout the region of equivalence ratios examined.

The effect of the concentration of added ammonia was also examined at a constant equivalence ratio, 0.88. Qualitatively, the H-atom yield decreases, while the N atom yield increases, with an increase in the concentration of ammonia in the range of the flow rate of ammonia, 0—8 $cm^3 min^{-1}$. The maximum yield of both the H and N atoms appears at a lower equivalence ratio with a higher concentration of added ammonia.

The ESR intensities changed depending on the position of the burner when it was moved along the center axis of the ESR cavity. This is because the H and N atoms are confined in a comparatively narrow region of the flame and because the ESR sensitivity depends on the location of the paramagnetic entities in the cavity (the sensitivity is expressed by the squared sinesoidal function). When the luminous inner cone was at the center of cavity (the position of the highest sensitivity), both the H and N atom signals showed the largest intensity. This indicates that the H and N atoms are located mostly in the inner cone, the height of which is less than 10 mm.

Assuming a uniform distribution of the H atoms in the region within 10 mm from the burner mouth, an assumption based on the concentration profile observed by the probe-sampling-ESR method,[2] the absolute concentration of the H atoms was estimated from the integrated ESR intensity to be 1×10^{15} atoms cm^{-3} (1×10^{-4} mole fraction) for the undoped flame at the concentration maximum shown in Fig. 2. The absolute concentration of N atoms was estimated in the same way to be 5×10^{11} atoms cm^{-3} (5×10^{-8} mole fraction) in the doped flame, also at the concentration maximum in Fig. 2. These estimations were made by calibrating the ESR intensities with reference to the ESR signals of molecular oxygen of known concentrations, and by correcting the temperature effect (the effect of the Boltzman distribution between spin states and of the gas density)[9] on ESR intensities using the highest temperatures actually measured in the luminous cone, 1660 and 1700 K for the doped and undoped flame, respectively.

It has been commonly accepted that the N atoms are generated in the ammonia-doped flame by the successive oxidation of NH_3 with H atoms or OH radicals as $NH_3 \rightarrow NH_2 \rightarrow NH \rightarrow N$. However, the detailed mechanism of the oxidation of ammonia has not been fully elucidated, though it is thought to be dependent on the flame conditions. Miller et al.[10] have studied the reaction mechanism of the ammonia oxidation in one-dimensional flames based on numerical-model calculations. Their conclusion is that NH_i species are oxidized mostly by H atoms or OH radicals, that the increase in the equivalence ratio results in the increase in the mole-fraction ratio of H to O and also in the increase in the N-atom concentration, and that NO is generated not only from N, but also directly from NH_2 by the reaction with the O atom, especially in fuel-lean flames.

The present experimental results may be summarized as: (1) the H and N atoms are observed concomitantly, and (2) the formation of N atoms in the presence of NH_3 accompanies the decrease in the H-atom concentration. Although the present results are still insufficient for the comprehension of the complex reaction mechanism of fuel-NO formation, they seem to be consistent with the view that the N-atom formation by

the fuel-NO mechanism is assisted by the existence of H atoms.[10] The present success in detecting the ESR spectrum of N atoms in combustion flames will encourage the further application of the ESR method to studies of combustion chemistry.

References

1) I. Glassman, "Combustion," Academic Press, New York (1977), p. 213.
2) S. Noda, M. Miura, and H. Yoshida, *J. Phys. Chem.*, **84**, 3143 (1980).
3) J.-F. Pauwels, M. Carlier, and L.-R. Sochet, *J. Phys. Chem.*, **86**, 4330 (1982).
4) S. Noda, H. Demise, O. Claesson, and H. Yoshida, *J. Phys. Chem.*, **88**, 2552 (1984).
5) O. Claesson, S. Noda, and H. Yoshida, *Bull. Chem. Soc. Jpn.*, **56**, 2559 (1983).
6) S. Noda, M. Miura, and H. Yoshida, *Bull. Chem. Soc. Jpn.*, **53**, 841 (1980).
7) C. J. Ultee, *J. Phys. Chem.*, **64**, 1873 (1960).
8) J. E. Benett, B. Mile, and R. Summers, *Nature*, **225**, 932 (1970).
9) A. A. Westenberg and N. de Haas, *J. Chem. Phys.*, **40**, 3087 (1964).
10) J. A. Miller, M. D. Smooke, R. M. Green, and R. J. Kee, *Combust. Sci. Technol.*, **34**, 149 (1983).

Thermal and Photochemical Electron-Transfer Reactions of 4-Chlorobiphenyl with Lithium Diisopropylamides and Diisopropylamine

Yoshio TANAKA,† Kazuo TSUJIMOTO, and Mamoru OHASHI*
†Nisso Master Builders Co., Ltd., 3-16-26, Roppongi, Minato-ku, Tokyo 106
Department of Materials Science, The University of Electro-Communications, Chofu, Tokyo 182
(Received August 13, 1986)

Synopsis. A reaction of 4-chlorobiphenyl with lithium diisopropylamide in a polar solvent gave 3- and 4-(diisopropylamino)biphenyl together with biphenyl, similar to the case of photoinduced reactions of 4-chlorobiphenyl with diisopropylamine. A common electron-transfer mechanism is proposed.

Lithium diisopropylamide(LDA) has been widely used for deprotonation and lithiation as a very strong nucleophile.[1] Recently, Ashby reported that the reaction of an alkyl halide with LDA proceeds through an electron-transfer rather than a lithiation or nucleophilic attack and gives a radical ion pair which collapses via concomitant reactions.[2] If the reaction starts from electron-transfer, the products are expected to be similar to those obtained from the well-known photoinduced electron-transfer reactions of halides with amines.[3-6] In accord with this expectation, comparing the products of reaction between 4-chlorobiphenyl (4-CB, **1**) and LDA with those of the photoinduced reactions of **1** with diisopropylamine (DIA), we found that the products of a thermal reaction in a polar solvent was similar to those of photochemical reactions, and their formation could be accounted for in terms of electron-transfer reactions. However, the features of a thermal reaction in THF at 0 °C were different from those of the photochemical reactions and the product ratios may be explained on the basis of a benzyne intermediate.[7]

We tried thermal reactions under two different reaction conditions; i) 0 °C in tetrahydrofuran(THF) and ii) 0 °C in THF-hexamethylphosphoramide(HMPA) (8:2). The yields of products, 3-and 4-(diisopropylamino)biphenyls (**3** and **4**) and biphenyl (**2**) were calculated by the standard GC analyses. On the other hand, irradiations of **1** in the presence of DIA were carried out in three different solvents, i.e., hexane, THF and acetonitrile. The yields of the products were analyzed in the same way as cases involving thermal reactions. The results are summarized in Table 1.

The major product of photochemical reactions is **2**, in accordance with our previous results.[3] Small amounts of amination products **3** and **4** were also isolated together with **2**. The yields of amination products seem to depend on the solvent polarity, i.e., the relative yield [**3**]/[**4**] is 1.8 in hexane, while 0.04 in acetonitrile. There is ample evidence that photoaddition of aromatics to a primary or secondary amine proceeds through proton-transfer in an exciplex to give a solvent caged radical pair in a nonpolar solvent, while in a polar solvent a solvent separated radical cation-radical anion pair is produced.[8] The solvent depen-

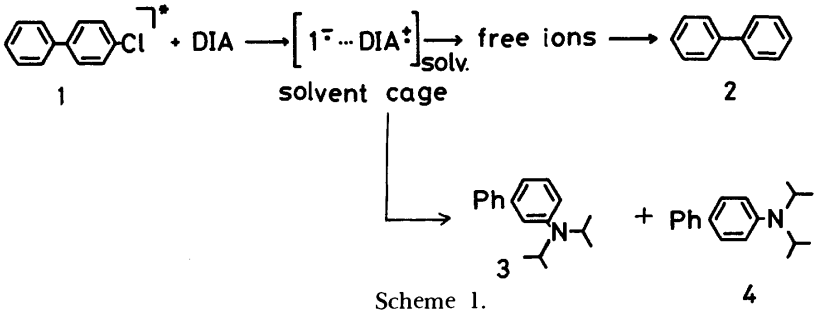

Scheme 1.

Table 1. Yields of Products Obtained from Thermal Reactions of **1** with LDA and from Photochemical Reactions of **1** with DIA[a]

Reagent	Light	Temp °C	Solv.	Time/h	Conv. %	5[b] %	2 %	3 %	4 %	[3]/[4]
LDA	—	0	THF	3	90	0	18	31	21	1.5
LDA	—	0	THF-HMPA[c]	2	100	0	57	18	5.4	3.3
DIA	d)	r.t	Hex	5	38	0	92	1.5	0.8	1.8
DIA	d)	r.t	THF	5	81	1.1	83	1.2	2.4	0.5
DIA	d)	r.t	MeCN	5	100	43	19	0.3	7.8	0.04

a) Yields were calculated based on GC analyses by using 2% OV-17 on Chromosob W NAW. b) 1,4-dihydrobiphenyl which may be produced by further reduction of biphenyl.[10] c) A mixture of THF-HMPA (8:2). d) A 6W low pressure mercury lamp was used.

dency of the product ratio observed in these photochemical reactions may reflect the different behavior of those different intermediate species. However, since the processes leading to the amination products are minor, discussion regarding the reaction mechanism based on the product ratios should be avoided at this stage. We would like to emphasize here that the major product of photoinduced electron-transfer is the reduction product **2**. The mechanism for formation of **2** may be complicate as shown in the case of 1-triethylamine system.[4-6]

The product ratios of thermal reaction of **1** with LDA carried out at 0 °C in THF-HMPA were similar to those of photochemical reactions, i.e., the major product is **2** and small amounts of the amination products **3** and **4** are also produced. Thus, the mechanism of this thermal reaction seems to be similar to that of photochemical reaction. A radical cation radical anion pair formed through thermal electron-transfer may participate in the reaction sequence. We, thus, propose path A in Scheme 2 as the most plausible mechanism for the major reaction between **1** and LDA in the polar solvent.

In sharp contrast with the thermal reaction in a polar solvent, the reaction in THF gave **3** and **4** as the major products and **2** as the minor one. This result is consistent with the case of thermal reaction between 4-bromobiphenyl and lithium piperidide in ether reported previously,[9] where the formation of the major products, 3- and 4-piperidinobiphenyl (47 and 37%), is explained in terms of the well known benzyne intermediate (Scheme 2, path B).[7,9] It is evident that both processes, i.e., electron-transfer and benzyne routes, participate in the thermal reactions aforementioned; however, the former is predominant in a polar solvent, while the latter is the major process in a nonpolar solvent.

In conclusion, on the basis of product analyses of photochemical reactions of **1** with DIA and of thermal reactions of **1** with LDA, we conclude that the reaction of **1** with LDA in a polar solvent proceeds through the electron-transfer mechanism similar to that in the photochemical reactions of **1** with DIA.

Experimental

IR spectra were determined on a JASCO IRA-1 spectrometer. H-and C-13 NMR were taken by using a JEOL GX-270 spectrometer in a $CDCl_3$ solution. UV-VIS spectra were taken on a Hitachi 320 spectrometer. Quantitative GC analyses were conducted with a Shimadzu GC-8 gas chromatograph using Pyrex column (2.5 mm i.d.×2 m) packed with 2% OV-17 on Chromosorb W NAW (80/100) at 130 to 230 °C. **1** and four products showed the following retention times; **1**, 7.5′; **2**, 4′; **3**, 10′; **4**, 10.5′ and 1,4-dihydrobiphenyl (**5**), 3′. GC-MS analyses were carried out on a Hitachi RMU-6MG mass spectrometer (20 eV). High resolution MS were measured with a Hitachi M-80 instrument.

THF was purified by refluxing over and distillation from $LiAlH_4$ under nitrogen. DIA and hexane were distilled from calcium hydride. Acetonitrile was distilled from P_2O_5 before use. *n*-BuLi in hexane was titrated immediately before use.

Typical Thermal Reaction of 1 with LDA. To a solution of LDA (3.13 mmol) prepared from DIA (316 mg, 3.13 mmol) and 1.20 mol dm^{-3} of *n*-BuLi in hexane (2.61 cm^3) was added a solution of **1** (200 mg, 1.06 mmol) in THF (1 cm^3) at 0 °C under nitrogen. The colorless solution gradually turned to deep red (λ_{max}=508 nm). After being allowed to stand for 3 h at 0 °C, the mixture was quenched with methanol, while the color was discharged, and extracted with ether to give 29% of **3**, 19% of **4**, 16% of **2** and 10% of recovered **1**. 1,3-(diisopropylamino)biphenyl (**3**): Bp 170—180 °C/0.5 mmHg* (Kugelrohr) ^1H NMR ($CDCl_3$) δ=7.60—6.85 (9H, m), 3.84 (2H, septet, J=6.8 Hz) and 1.25 (6H, d, J=6.8 Hz); ^{13}C NMR ($CDCl_3$) δ=148.35 (C-1), 118.06 (C-2), 142.21 (C-3), 118.12 (C-4), 117.22 (C-6), 141.57 (C-1′), 47.66 (methine) and 21.42 (methyl); IR (liquid film) 790 cm^{-1}; MS (20 eV) *m/z* (rel intensity) 253 (M^+ 11), 238 (37), 196 (100), 180 (18), 154 (26), 153 (26), and 152 (26): Found; *m/z* 253.1834, Calcd, for $C_{18}H_{23}N$; M^+ 253.1830. 4-(diisopropylamino)biphenyl (**4**): Bp 170—185 °C/0.5 mmHg (kugelrohr); ^1H NMR ($CDCl_3$) δ=7.69—7.20 (5H, m), 6.93 (2H, d, J=8.79 Hz) and 7.45 (2H, d, J=8.79 Hz) ^{13}C NMR ($CDCl_3$) δ=147.44 (C-1), 118.22 (C-2), 129.59 (C-4), 141.18 (C-1′), 47.54 (methine) and 21.32 (methyl); IR (liquid film) 830, 760 and 700 cm^{-1}; MS (20 eV) *m/z* (rel intensity) 253 ((M^+ 16), 239 (18), 238 (46), 223 (8.2), 210 (23), 196 (100), 180 (16), 154 (23), 153 (17) and 152 (16). Found; *m/z* 253.1815, Calcd. for $C_{18}H_{23}N$; M^+ 253.1830.

Alternative Preparation of 4. A suspension of 4-aminobiphenyl (34 mg), KOH (28 mg) and isopropyl iodide (69 mg) in THF (2 cm^3) was refluxed overnight. Extraction with ether gave a crude oil (35 mg). To a solution of the oil in 1,2-dimethoxyethane (2 cm^3) was added 1.20 mol dm^{-3} *n*-BuLi in hexane (0.2 cm^3) at 0 °C under nitrogen. The mixture was refluxed over 2 d and extracted with ether to give 33 mg of a yellow oil in 65% yield.

Typical Photoreaction of 1 with Diisopropylamine. Irradiation of a solution of **1** (20 mg, 0.106 mmol) and diisopropylamine (0.3 cm^3) in acetonitrile (1 cm^3) with a 6 W low-pressure mercury arc for 5 h gave **3** and **4** in 0.30 and 7.8% yields, respectively, in addition to 43% of 1,4-dihydrobiphenyls (**5**)[10] and 19% of **2** as major products.

The present study was partially supported by Grant-in-Aid for Scientific Research from the Ministry of Education, Science and Culture(No. 61123005). Thanks

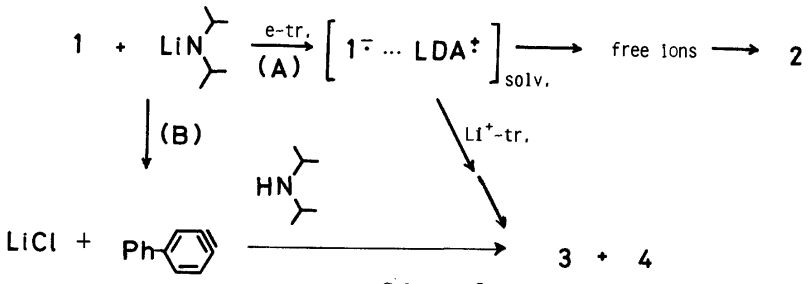

Scheme 2.

are also due to Mr. Shida of Tokyo College of Pharmacy for high-resolution mass spectrometric measurements.

References

1) H. O. House, "Modern Synthetic Reactions" 2nd ed., W. A. Benjamin, Inc., Menlo Park, California (1972), Chaps. 9, 10, and 11.
2) E. C. Ashby and J. N. Argyropoulos, *J. Org. Chem.*, **50**, 3274 (1985).
3) M. Ohashi, K. Tsujimoto, and K. Seki, *J. Chem. Soc., Chem. Commun.*, **1973**, 384.
4) N. J. Bunce, *J. Org. Chem.*, **47**, 1948 (1982).
5) M. Ohashi and K. Tsujimoto, *Chem. Lett.*, **1983**, 423.
6) R. A. Beecroft, R. S. Davidson and D. Goodwin, *Tetrahedron Lett.*, **24**, 5673 (1983).
7) G. B. R. DeGraaff, H. J. DenHertog, and W. Ch. Melger, *Tetrahedron Lett.*, **1965**, 963; Ref. 1, p. 539.
8) M. Bellas, D. Bryce-Smith, M.T. Clarke, A. Gilbert, G. Klunkin, *J. Chem. Soc., Perkin Trans. 1*, **1977**, 2572; D. Bryce-Smith and A. Gilbert, Tetrahedron Report No. 40, "The Organic Photochemistry of Benzene II", Pergamon Press, Oxford (1978); T. Okada, T. Mori, and N. Mataga, *Bull. Chem. Soc. Jpn.*, **49**, 3398 (1976).
9) R. Huisgen and J. Sauer, *Angew. Chem.*, **72**, 91 (1960).
10) J. A. Barltrop, *Pure Appl. Chem.*, **33**, 179 (1973).
#) 1mmHg≈133.322 Pa.

The Steam Stability of H-ZSM-5-Type Zeolites Containing Alkaline Earth Metals

Kazuyoshi FUJISAWA,† Tsuneji SANO,* Kunio SUZUKI, Hideo OKADO,†† Kichinari KAWAMURA,†††
Yasuhiko KOHTOKU,†††† Shigemitsu SHIN, Hiroyuki HAGIWARA, and Haruo TAKAYA
National Chemical Laboratory for Industry, Yatabe, Ibaraki 305
†Nippon Petrochemical Co., Ltd., Uchisaiwai-cho, Chiyoda-ku, Tokyo 100
††Maruzen Petrochemical Co., Ltd., Hatchobori, Chuo-ku, Tokyo 104
†††Idemitsu Petrochemical Co., Ltd., Marunouchi, Chiyoda-ku, Tokyo 100
††††Ube Industries Co., Ltd., Kasumigaseki, Chiyoda-ku, Tokyo 100
(Received June 18, 1986)

Synopsis. The steam stability of H-ZSM-5-type zeolites containing alkaline earth metals was investigated by means of ^{27}Al MASNMR, the TPD of NH_3, and methanol conversion reactions. It was found that the steam stability of the H-ZSM-5-type zeolites is greatly improved by adding alkaline earth metals.

The production of light olefins, such as ethylene and propylene, from methanol with zeolites has been extensively studied. Several patents and articles have claimed that high selectivities to light olefins are attained at high temperatures over highly siliceous zeolites.[1-3] Recently, we have also found that methanol is converted to light olefins with a high selectivity over H-ZSM-5-type zeolites containing alkaline earth metals, especially calcium.[4,5]

It is well-known that many types of zeolites undergo structural degradation when subjected to water vapor at elevated temperatures. Therefore, if the zeolites are used in a moisture-rich atmosphere such as is encountered in the methanol-to-olefin (or gasoline) conversion, their resistance to steaming must be much improved.

From this standpoint, the steam stability of the H-ZSM-5-type zeolites containing alkaline earth metals has been investigated; the results will be described in this paper.

Experimental

The reagents used were aluminium nitrate (Kokusan, guaranteed reagent), colloidal silica (Cataloid SI-30 from Shokubai Kasei, 30—31 wt% SiO_2, 0.36—0.47 wt% Na_2O, 0.03 wt% Al_2O_3), sodium hydroxide (Nakarai, guaranteed reagent), tetrapropylammonium bromide (Tokyo Kasei, guaranteed reagent), and alkaline earth metal acetates (Nakarai, guaranteed reagent). The H-ZSM-5-type zeolites containing alkaline earth metals (M-H-ZSM-5, M=alkaline earth metals) were synthesized as follows. Certain amounts of aluminium nitrate, colloidal silica, and alkaline earth metal acetate were added to a stirred mixture of tetrapropylammonium bromide and sodium hydroxide in a solution. The resultant hydrogel, with the composition of 0.025 M · 0.1 R · 0.052 Na_2O · 0.005 Al_2O_3 · SiO_2 · 40H_2O (M=alkaline earth metal acetates; R=tetrapropylammonium bromide), was then transferred into a 300-ml stainless steel autoclave and stirred at 150—160 °C under an autogeneous pressure for 15—24 h. After the crystallization of the zeolite, the autoclave was rapidly cooled; the precipitated crystals were then filtered off, washed thoroughly with deionized water, dried at 120 °C, and calcined at 500 °C for 16 h in order to remove the organic base occluded in the zeolite framework. The zeolite thus obtained was protonated in a 0.6-M (1M=1 mol dm^{-3}) hydrochloric acid solution and calcined in air at 500 °C for 6 h.

The steaming was carried out using an atmospheric-pressure flow system at 600 °C in 100% steam for 2.5-g of the charged zeolite (14—28 mesh pieces). The rate of the addition of water was 3 ml h^{-1}.

High-resolution ^{27}Al NMR was measured at 51.9 MHz on a JEOL FX-200 Spectrometer equipped with a probe for magic-angle spinning (MAS). The spectra of the various H-ZSM-5-type zeolites were obtained using 0.33-g samples in Delrin bullets spinning at about 3.5 kHz, using 4.6 μs pulses. The chemical shifts in ppm were measured with respect to $Al(OH)_6^{3+}$ as an external reference.

The temperature-programmed desorption (TPD) spectra of the NH_3 adsorbed on the zeolites were obtained using a conventional TPD apparatus. A thermal-conductivity detector was employed for the detection of desorbed NH_3 molecules. The measurement was performed from 100 to 600 °C at a heating rate of 10 °C min^{-1} in helium as the carrier gas (a flow rate, 20 ml min^{-1}) for 0.30-g of the charged zeolite.

Methanol conversion was carried out by the use of an atmospheric-pressure flow reactor at 600 °C and LHSV=4 h^{-1}. The reaction gas was fed in a composition of 50 mol% methanol and 50 mol% argon. The products thus obtained were analyzed by gas chromatography. The methanol conversions and carbon-based selectivities were calculated from the concentration of argon used as the internal standard.

Results and Discussion

The prepared H-ZSM-5-type zeolites containing

Table 1. Characteristics of H-ZSM-5-Type Zeolites Containing Alkaline Earth Metals

	Zeolite	Atomic ratios[a]		BET surface area ($m^2 g^{-1}$)
		Si/Al	Alkaline earth metal/Al	
1.	H-ZSM-5	120		342
2.	Mg-H-ZSM-5	94	0.89	336
3.	Ca-H-ZSM-5	117	1.63	341
4.	Sr-H-ZSM-5	93	1.29	301
5.	Ba-H-ZSM-5	90	1.35	301

a) Determined by X-ray fluoresence spectrometry.

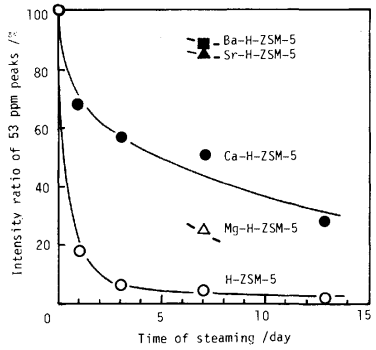

Fig. 1. Relationship between time of steaming and intensity ratio of 53 ppm peaks. Zeolite was subjected to water vapour at 600°C under atmospheric pressure.

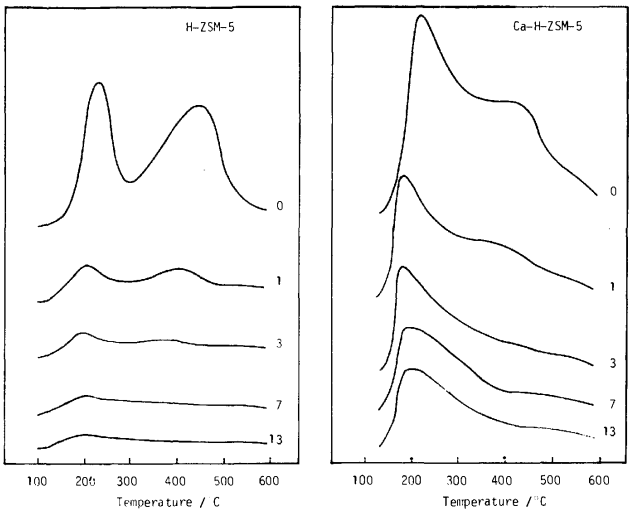

Fig. 2. TPD spectra of NH_3 from steamed zeolites Arabic numbers in Fig. denote a steaming time (day).

alkaline earth metals (M-H-ZSM-5) had a well-defined H-ZSM-5-type structure, as was demonstrated by their X-ray powder diffraction patterns. Some analytical data of the zeolites are given in Table 1. The amounts of alkaline earth metals occluded in the zeolites were more than those of the alkaline earth metals which would be introduced by a conventional ion-exchange method, in which the atomic ratio of alkaline earth metal to aluminium is, at most, 0.5. However, a full explanation of this rare phenomenon will be given in a future study.

As has already been reported, the ^{27}Al MASNMR spectrum of the conventional H-ZSM-5 has one peak, at about 53-ppm, assigned to the framework (tetrahedrally coordinated) aluminiums.[6] The ^{27}Al MASNMR spectra of various M-H-ZSM-5 have the same peak as that of H-ZSM-5. Figure 1 shows the relationship between the time of steaming and the intensity ratio, which means the percentage of a 53-ppm peak intensity of the steamed zeolites relative to that of the corresponding unsteamed zeolites. The rapid decay curve was obtained for H-ZSM-5, whereas the slow decay curves were obtained for M-H-ZSM-5. The intensity ratios of M-H-ZSM-5 decreased in the following order: Ba-H-ZSM-5 > Sr-H-ZSM-5 > Ca-H-ZSM-5 > Mg-H-ZSM-5 > H-ZSM-5, indicating a great stability of Ba- and Sr-H-ZSM-5 for steaming. These results suggest that the release of tetrahedrally coordinated aluminiums from a framework is depressed by the presence of alkaline earth metals to the different degree described above.

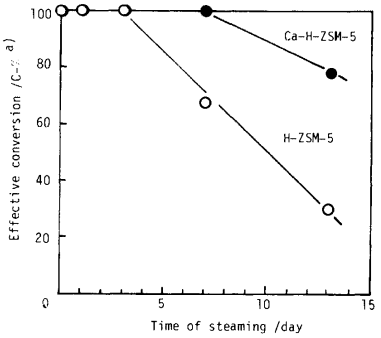

Fig. 3. Effect of steaming on catalytic activity. Reaction conditions: LHSV=4 h^{-1}, T=600°C. a) Effective conversion=100-(Methanol+Dimethyl Ether)-Yield

Some typical TPD spectra of NH_3 for H-ZSM-5 and Ca-H-ZSM-5 before and after the steaming are illustrated in Fig. 2. The TPD spectra from H-ZSM-5 exhibited two fairly sharp peaks at about 220 (l-peak) and 450 °C (h-peak). On the other hand, the two peaks of the TPD spectra from Ca-H-ZSM-5 are broad. The total amount of desorbed NH_3 decreased with an increase in the steaming time for both H-ZSM-5 and Ca-H-ZSM-5, but the amount of desorbed NH_3 of the former was less than that of the latter. As a part of the desorbed NH_3 might originate from physically adsorbed NH_3, the total amount of desorbed NH_3 is not necessarily proportional to the amount of acid sites which would originate from aluminiums in zeolites. Nevertheless, the result of the NH_3 TPD is in accordance with that of ^{27}Al NMR: less desorption for a lower intensity ratio.

Figures 3 and 4 show the results of methanol conversion over various zeolites before and after the steaming. The steaming affected both the catalytic activity and the product distribution. As is shown in Fig. 3, the catalytic activity of H-ZSM-5 decreased markedly with the increase in the steaming time, while that of Ca-H-ZSM-5 decreased slightly. For the steamed zeolites, a remarkable decrease in the selectivities to (C_2H_4+C_3H_6) and (benzen+toluene+xylene) was observed, while those to CH_4 and hydrocarbons with carbons more than six (C_6^+) were increased.

From all of these results, it is concluded that the steam stability of the H-ZSM-5-type zeolites is greatly improved by adding alkaline earth metals. The role of the alkaline earth metals in steam stability is considered to be similar to those of Co or Cu in the previously reported cobalt-ZSM-5 zeolites or cupper-Y-zeolites.[7,8] Although the essential role played by the alkaline earth metals is not very well understood in this work, in any event, the metals seem to prevent the release of aluminium species from the framework during the steaming.

This work is a part of the "C_1 Chemistry Project," a

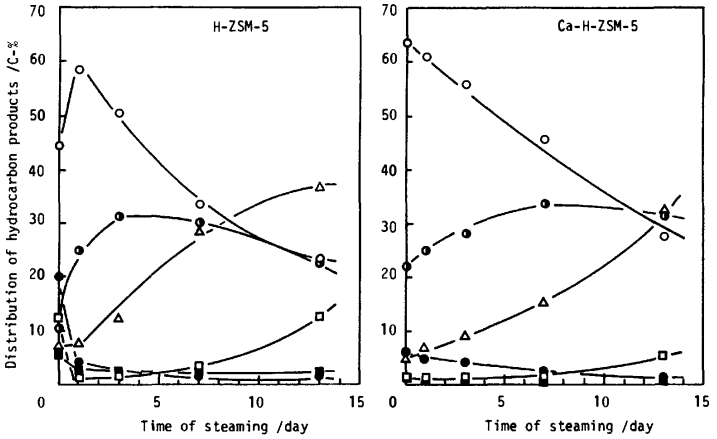

Fig. 4. Effect of steaming on distribution of hydrocarbon products.
○: $C_2H_4+C_3H_6$, ◑: $C_4H_8+C_5H_{10}$, □: CH_4, ■: (C_2–C_5) paraffins, ●: BTX, △: C_6^+.

National Research and Development Program of the Agency of Industrial Science and Technology, Ministry of International Trade and Industry (M.I.T.I.), Japan.

References

1) W. W. Kaeding, and S. A. Butter, *J. Catal.*, **61**, 155 (1980).
2) G. Chen, and J. Ling, China-Japan-U.S. Symposium on Heterogeneous Catalysis, Dalian, China, A010C (1982).
3) D. E. 3304479.
4) U. S. Pat. 4544793.
5) H. Okado, H. Shoji, K. Kawamura, K. Hashimoto, Y. Yamazaki, T. Sano, and H. Takaya, *Nippon Kagaku Kaishi*, **1987**, 25.
6) C. A. Fyfe, J. M. Thomas, J. Klinowski, and G. C. Gobbi, *Angew. Chem. Int. Ed. Engl.*, **22**, 259 (1983).
7) P. A. Jacobs, and H. K. Beyer, *J. Phys. Chem.*, **83**, 1174 (1979).
8) Eur. Pat. Appl. 18117.

Photochromism of Viologen Crystals

Hiroyoshi KAMOGAWA* and Tsuyoshi SUZUKI
Department of Applied Chemistry, Yamanashi University, Takeda 4, Kofu 400
(Received July 8, 1986)

Synopsis. Some viologen crystals bearing a *p*-toluenesulfonate anion as a counter ion were shown to exhibit reversible photoreductions (photochromism) either in air or under vacuum, whereas in a poly(*N*-vinyl-2-pyrrolidone) matrix all investigated viologens indicated reversible photocolor developments. Amphoteric ions such as 1,1′-bis(3-sulfonatopropyl)-4,4′-bipyridinium also developed colors with high stabilities.

It was known that viologens undergo reversible photoreductions in either poly(*N*-vinyl-2-pyrrolidone) (PVP) matrix[1] or in films of the copolymers of *N*-vinyl-2-pyrrolidone (VP) containing viologen units as pendants.[2] Some viologen crystals, on the other hand, have been found to undergo reversible photoreductions accompanied by intense blue or pink color developments.[3]

In this study, various viologen crystals were synthesized and subjected to irradiations of UV light either in air or under vacuum. The resulting color developments were measured to provide preliminary data in order to utilize this phenomenon in the fields of photomemory or control of light quantity.

Results and Discussion

Viologens were synthesized as bromides in acetonitrile as described before.[1] The bromides were converted to *p*-toluenesulfonate (PTS)s either by adding a large excess of *p*-toluenesulfonic acid to precipitate the latters or by passing through an anion-exchange resin (Diaion SA 10) loaded with *p*-toluenesulfonic acid. Amphoteric ions like 1,1′-bis(3-sulfonatopropyl)-4,4′-bipyridinium were synthesized by treating 4,4′-bipyridine with sultones. Analytical data indicated that all viologens were satisfactorily pure. All viologens were soluble in water but amphoteric types provided turbid films when incoporated in a PVP matrix from aqueous solutions. Some viologen crystals afforded (more or less) intense color developments when they were irradiated by near-UV light.[3] Their reflection spectra are shown in Fig. 1 as either absorbance (on a spectrophotometer) or reflectance (on a color sensor). The shapes and positions of the absorption maximum and reflectance minima correspond exactly with those of single radical cations of viologens.[4] The appearance of ESR signals also corresponds to color development, thereby indicating the following generation of radical cation by ilumination:

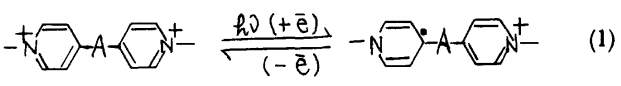

(1)

Here, A denotes -CH=CH- or none.

In Table 1 can be found the results of an investigation of UV irradiation for viologen crystals synthesized in this experiment. It can be recognized in this table

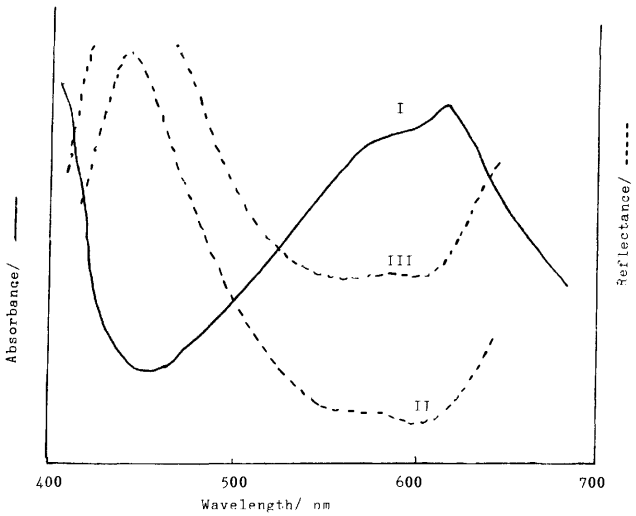

Fig. 1. Reflection curves of the colors developed on viologen crystals with irradiation of near UV light(>350 nm). Curve I: Absorbances for 1,1′-bis-(3-sulfonatopropyl)-4,4′-bipyridinium (**6**). Curves II and III: Reflectances for 1,1′-dibenzyl-4,4′-bipyridinium bis(*p*-toluenesulfonate) (**1a**) under vacuum immediately after 90s irradiation and 10 min after, respectively (color sensor).

that only viologens having PTS as counter anion afford color development in crystals (**1a** and **5a**). In PVP matrix, however, all investigated viologens provided blue (absorption maximum, 610 nm) color developments. Viologen crystals in the form of amphoteric ions also develop colors on UV irradiation (**6**, **7**, and **9**).

Table 2 shows the half recovery times of the color developments in crystals as compared with those in a PVP matrix. It can be seen from this table that the effect of air oxygen is very great for viologens **1a** and **5a**, whereas **6** and **7** are almost insensitive to air oxygen. This fact, together with the very long half recovery times, tells us that amphoteric-type viologens, particularly **6**, afford stable color developments for long times under dry conditions. The developed color disappears quickly upon strong heating. Quantitative data have not yet been taken. The reason why only PTS gives cation radicals discernible even in air is unknown at the present stage. One reason may be that radical anion produced on the part of PTS by a photoelectron transfer from the tosylate anion to viologen dication is relatively stable due to a delocalization of both odd electron and negative charge. The crystal structure, i.e., relative position of an anion against a viologen dication in the crystal lattice, may also make the electron transfer impossible, since the benzenesulfonate (**1b**) does not afford any color development as indicated in Table 1. The effect of air oxygen on both

Table 1. Color Developments of Viologen Crystals with Illumination

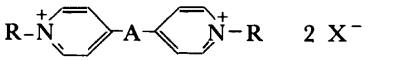

Viologen No.	A	R	X	Color development	
				In air	Under vacuum
1	None	$PhCH_2$	Br	None	None
1a			PTS	Blue (610 nm)[b]	Blue (610 nm)[b]
1b			Benzenesulfonate	None	None
1c			$MeSO_3$	None	None
1d			1-Naphthalenesulfonate	None	None
2	None	*p*-TolylCH_2	Br	None	None
2a			PTS	None	None
3	None	*m*-TolylCH_2	Br	None	None
3a			PTS	None	None
4	None	C_3H_7	Br	None	None
4a			PTS	None	None
5	None	$PhCH_2CH_2$	Br	None	None
5a			PTS	Blue (610 nm)[b]	Blue (610 nm)[b]
6	None	$-(CH_2)_3SO_3^-$	—	Blue (610 nm)[b]	Blue (610 nm)[b]
7	None	$-(CH_2)_4SO_3^-$	—	Blue (610 nm)[b]	Blue (610 nm)[b]
8	-CH=CH-	$PhCH_2$	Br	None	None
8a			PTS	None	Pink (530 nm)[b]
9	-CH=CH-	$-(CH_2)_3SO_3^-$	—	Pink (530 nm)[b]	Pink (530 nm)[b]

a) Irradiation time, 90 s. b) Figures in parentheses indicate absorption maxima or reflection minima.

Table 2. Half Recovery of the Color Developed on Viologen Crystal with Irradiation by UV Light[a]

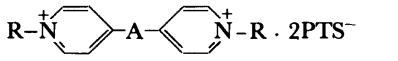

Viologen No.	A	R	Half Recovery/min[b]		
			In air	Under vacuum	In PVP matrix
1a	None	$PhCH_2$	1.1	39.1	2.7
5a	None	$PhCH_2CH_2$	26.1	2136	8.1
6	None	$-(CH_2)_3SO_3^-$[c]	509	542	3698[e]
7	None	$-(CH_2)_4SO_3^-$[c]	364	383	142[e]
9	-CH=CH-	$-(CH_2)_3SO_3^-$[c]	238[d]	380[d]	80.6[d,e]

a) Irradiation time, 90 s. b) At 610 nm except for d (530 nm). c) No PTS. e) Turbid films.

color development and its recovery is significant for some viologen crystals, e.g., viologens **1a** and **5a** in Table 2. Generally, the oxygen accelerates the back oxidations of viologen radical cations to dications. The color developed in the crystal lattice, however, may be more stable to air oxidation than that on a crystal surface. It appears that the rate and extent of the back reaction depend upon the stability of radical ion pair generated in crystal, as shown in pendant copolymers,[5] when the effect of air oxygen, i.e., environmental conditions, is the same.

Experimental

Infrared (IR), ^1H NMR, and elemental analyses were conducted using a Hitachi 215 spectrophotometer, a JNM-PMX 60 spectrometer, and a Perkin-Elmer 240 instrument, respectively. The esr was taken with a JES-FE1XG spectrometer.

1,1′-Dibenzyl-4,4′-Bipyridinium Dibromide(1). This compound was prepared according to a previous report[1] starting with 4,4′-bipyridine (2.00 g, 12.8 mmol) and benzyl bromide (3.91 g, 25.6 mmol) in anhydrous acetonitrile (50 ml) under 6 h refluxing (yield, 93%). Found: C, 57.96; H, 4.33; N, 5.52%. Calcd for $C_{24}H_{22}N_2Br_2$: C, 57.80; H, 4.45; N, 5.62%. IR (KBr) 1630 cm^{-1}; ^1H NMR (D_2O) δ=6.0 (s, 4H, $2CH_2$), 7.7 (s, 10H, ArH), 8.6 (d, 4H, bipyridinium H), 9.3 (d, 4H, bipyridinium H).

All other viologen bromides were prepared in the same manner. Analytical data were all satisfactory.

1,1′-Dibenzyl-4,4′-Bipyridinium Bis(*p*-toluenesulfonate) (1a). To a solution of *p*-toluenesulfonic acid (6.88 g, 40 mmol) in absolute ethanol (50 ml) was added 1,1′-dibenzyl-4,4′-bipyridinium dibromide (**1**; 2.00 g, 4 mmol). To the resulting solution was added anhydrous ether (70 ml) and the mixture was allowed to stand overnight in order to precipitate a crude product, which was recrystallized from methanol-ether to provide white crystalline powder in 56% yield. Found: C, 66.84; H, 5.23; N, 4.12%. Calcd for $C_{38}H_{38}N_2S_2O_6$: C, 67.04; H, 5.33; N, 4.11%. IR (KBr) 1630 cm^{-1}; ^1H NMR (D_2O+DMSO-d_6) δ=2.4 (s, 6H, $2CH_3$), 7.2—7.8 (m, 18H, PTS+ArH), 8.6 (d, 4H, bipyridinium H), 9.3 (d, 4H, bipyridinium H).

1,1′-Dibenzyl-4,4′-bipyridinium bis(benzenesulfonate) (**1b**; yield, 52%), 1,1′-dibenzyl-4,4′-bipyridinium bis(1-naphthalenesulfonate) (**1d**; 79%), and trans-4,4′-vinylenebis[1-benzylpyridinium] bis(*p*-toluenesulfonate) (**8a**; 45%) were prepared in the same manner using benzene- and 1-naphthalenesul-

fonic acids(water as solovent) and *p*-toluenesulfonic acid from respective bromides.

The results of elemental analyses, IR, and NMR were all satisfactory.

1,1'-Diphenethyl-4,4'-bipyridinium Bis(*p*-toluenesulfonate) (5a). A solution of *p*-toluenesulfonic acid (20 g) in water (50 ml) was stirred with an anion-exchange resin (Diaion SA 10A, OH-type, 16 g) overnight. The mixture was then filtered, and the resin was washed thoroughly with distilled water until a neutral to litmus. A solution of 1,1'diphenethyl-4,4'-bipyridinium dibromide (5; 2.00 g) in water (70 ml) was added and the mixture was gently stirred overnight. The ion-exchange resin was filtered off and the filtrate was freeze dried to afford a crude product, which was recrystallized from methanol-ether to give white crystalline powder in 59% yield. Found: C, 67.45; H, 5.79; N, 3.76%. Calcd for $C_{40}H_{40}N_2S_2O_6$: C, 67.70; H, 5.69; N, 3.95%. IR (KBr) 1620 cm^{-1}; ^1H NMR (D_2O) δ=2.3 (s, 6H, $2CH_3$), 3.3 (t, 4H, $2CH_2$), 5.0 (t, 4H, $2CH_2$-$\overset{+}{N}$<), 7.0—7.7 (m, 18H, PTS+ArH), 8.3 (d, 4H, bipyridinium H), 8.7 (d, 4H, bipyridinium H).

1,1'-Dibenzyl-4,4'-bipyridinium bis(methanesulfonate) (**1c**; 53%), 1.1'-bis(*p*- and *m*-methylbenzyl)-4,4'-bipyridinium bis(*p*-toluenesulfonate) (**2a**, **3a**; 76, 71%), and 1,1'-dipropyl-4,4'-bipyridinium bis(*p*-toluenesulfonate) (**4a**; 45%) were prepared in the same manner using methane- and *p*-toluenesulfonic acids from respective bromides. All analytical data were satisfactory.

1,1'-Bis(3-sulfonatopropyl)-4,4'-bipyridinium (6). A solution of 4.4'-bipyridine (2.00 g, 12.8 mmol) and 1,3-propanesultone (7.8 g, 64 mmol) in anhydrous acetonitrile(50 ml) was heated under reflux for 48 h. The resulting mixture was filtered, washed with acetonitrile, and recrystallized from water to give a white crystalline powder in 77% yield. Found: C, 48.22; H, 5.17; N, 6.89%. Calcd for $C_{16}H_{20}N_2S_2O_6$: C, 48.01; H, 5.00; N, 7.00%. IR (KBr) 1640 cm^{-1}; ^1H NMR (D_2O) δ=2.0—3.6 (m, 8H, $2CH_2CH_2$), 5.2 (t, 4H, $2CH_2$-$\overset{+}{N}$<), 8.8 (d, 4H, bipyridinium H), 9.3 (d, 4H, bipyridinium H).

1,1'-Bis(4-sulfonatobutyl)-4,4'-bipyridinium (**7**; DMF, 90—100 °C, yield 78%) and trans-4,4'-vinylenebis[1-(3-sulfonatopropyl)pyridinium] (**9**; 61%) were prepared in similar manners using 1,4-butane- and 1,3-propanesultones, respectively.

Measurements of Photoreductions. Crystals (in air). A Hitachi 200-10 spectrophotometer fitted with a reflection attachment was employed for measurements of reflection spectra in air (20 °C).

Crystals (under vacuum). When measurements in the absence of air oxygen were required, a sample of viologen crystals was sealed in a 5-ml Pyrex glass tube under vacuum (0.1 mmHg) as usual. The sealed tubes were subjected to measurements of reflection spectra on a Hitachi C-120 Color Sensor and spectra ranging from 400 to 700 nm were taken within one second.

In Matrices. Measurements were performed using a Hitachi 200-10 spectrophotometer, as previously described.[1] The irradiation source was Toshiba SHL-100UV (75 W) mercury lamp cut below 350 nm with a glass filter. The irradiation distance was 10 cm.

References

1) H, Kamogawa, T. Masui, and M. Manasawa, *Chem. Lett.*, **1980**, 1145.

2) H. Kamogawa and S. Amemiya, *J. Polym. Sci., Polym. Chem. Ed.*, **23**, 2413 (1985).

3) H. Kamogawa and T. Suzuki, *J. Chem. Soc., Chem. Cmmun.*, **1985**, 525.

4) T. Tamura, M. Kajiwara, and T. Matsuo, *Chem. Lett.*, **1977**, 1199.

5) H. Kamogawa et al., to be published.

Fast Cis-Trans Isomerization of Square-Planar Bis(diethyl sulfide)platinum(II) Complexes. Reaction of *cis*-Dichlorobis(diethyl sulfide)platinum(II) with Mesityllithium

Hiromi TOBITA, Hiroki HABAZAKI, and Hiroshi OGINO*
Department of Chemistry, Faculty of Science, Tohoku University, Aramaki, Sendai 980
(Received September 10, 1986)

Synopsis. Reaction of *cis*-[$PtCl_2(SEt_2)_2$] with a slight excess of mesityllithium in benzene-ether mixture afforded *trans*-[PtCl(Mes)(SEt_2)$_2$] (Mes=2,4,6-trimethylphenyl; SEt_2= diethyl sulfide) as a major product. When mesityllithium reagent containing lithium bromide was used, *trans*-[PtBr(Mes)(SEt_2)$_2$] was obtained. Acceleration of cis-trans isomerization in the presence of mesityllithium was observed.

Arylplatinum(II) complexes having sulfide ligands are useful precursors of various organoplatinum complexes, since the sulfide ligands can be replaced easily by phosphine, pyridine, carbonyl, etc.[1] The reaction of *trans*-[PtX_2L_2] (X=Cl, Br, or I; L=SEt_2 or $SeEt_2$) with phenyl, *o*-tolyl, or mesityllithium has been reported by Sergi et al.[2,3] who found that the trans isomers of [$PtXArL_2$] and/or [$PtAr_2L_2$] were the exclusive products with the exception of the reaction of *trans*-[$PtCl_2(SEt_2)_2$] with phenyllithium. In the latter reaction, the major product was *cis*-[$PtPh_2(SEt_2)_2$] (60%) with 20% of the trans isomer.

The reaction of *cis*-[$PtCl_2(SR_2)_2$] (R=Et, *n*-Pr, or *i*-Pr) with excess phenyl or *p*-tolyllithium has been reported by Steele and Vrieze to give the dimeric [$PtAr_2(SR_2)]_2$ (Ar=Ph or *p*-tolyl).[1] Exceptionally, the reaction of *cis*-[$PtCl_2(SEt_2)_2$] with C_6F_5Li afforded monomeric *cis*-[$Pt(C_6F_5)_2(SEt_2)_2$] in high yield.[1] They also carried out the reaction of *trans*-[$PtCl_2(SEt_2)_2$] with phenyllithium and obtained products which were different from Sergi's, i.e., a dimer [$PtPh_2(SEt_2)]_2$ (55%) and a monomer *cis*-[$PtPh_2(SEt_2)_2$] (20%).

This paper deals with the reaction of *cis*-[$PtCl_2(SEt_2)_2$] with bulky mesityllithium which has not been examined before. When *cis*-[$PtCl_2(SEt_2)_2$] was allowed to react with mesityllithium reagent containing lithium bromide, *trans*-[PtBr(Mes)(SEt_2)$_2$] was obtained. A possible mechanism is proposed for the reaction.

Experimental

Apparatus. ^{1}H NMR spectra were recorded on JEOL FX-90Q and Varian EM-390 spectrometers, and ^{13}C NMR spectra on a JEOL FX-90Q spectrometer. Electronic spectra were measured on a Hitachi 330 spectrophotometer. Mass spectra were obtained on a Hitachi M-52 spectrometer.

Reaction of *cis*-[$PtCl_2(SEt_2)_2$] with Mesityllithium. Reactions were carried out under nitrogen using dried solvents. *cis*-[$PtCl_2(SEt_2)_2$] was prepared according to a literature procedure.[4]

***trans*-[PtBr(Mes)(SEt_2)$_2$] and *trans*-[$PtBr_2(SEt_2)_2$].** A suspension of mesityllithium was prepared by adding 1.5 mol dm^{-3} butyllithium in hexane (10 ml) to an ether solution (40 ml) of bromomesitylene (2.00 g, 10.0 mmol) at room temperature. A 3 ml portion of this suspension (ca. 0.60 mmol) was added to a benzene (20 ml) solution of *cis*-[$PtCl_2(SEt_2)_2$] (200 mg, 0.448 mmol) at 0 °C. After stirring for 15 min, the reaction mixture was allowed to warm to room temperature and stirred for 17 h. The turbid reaction mixture was filtered through a Celite 545 column and the filtrate was evaporated to give a brown crystalline residue. It was then placed on an alumina column (200 mesh) and eluted with benzene. Evaporation of the eluates afforded *trans*-[$PtBr_2(SEt_2)_2$][5] as yellow crystals (12.0 mg, 5%): mp 117—118 °C (lit, mp 129, 124, 118 °C)[5] and *trans*-[PtBr(Mes)(SEt_2)$_2$] as colorless crystals (104 mg, 40%): mp 130—131 °C. Found: C, 35.90; H, 5.57; Br, 14.35%. Calcd for $C_{17}H_{31}BrPtS_2$: C, 35.54; H, 5.44; Br, 13.91%. ^{1}H NMR (90 MHz, C_6D_6) δ=0.95 (12H, t, J_H=7.3 Hz, CH_3 of Et), 2.22 (3H, s, J_{Pt}=5.2 Hz, *p*-CH_3), 2.63 (8H, q, J_H=7.1 Hz, J_{Pt}=42.7 Hz, CH_2 of Et), 2.74 (6H, s, J_{Pt}=8.1 Hz, *o*-CH_3), 6.78 (2H, s, J_{Pt}=8.9 Hz, *m*-H);[6] ^{13}C NMR (22.6 MHz, C_6D_6) δ=13.0 (q, J_{Pt}=42.7 Hz, CH_3 of Et), 20.8 (q, *p*-CH_3), 26.4 (q, J_{Pt}=52.9 Hz, *o*-CH_3), 30.2 (t, J_{Pt}=13.2 Hz, CH_2 of Et), 133.2, 133.4, and 141.3 (aromatic ring carbons);[6] MS *m*/*z* 572 (M^+, based on ^{194}Pt; 6), 482 (1), 403 (10), 392 (1), 374 (42), 362 (7), 346 (21), 281 (9), 120 (96), 105 (83), 90 (100), 75 (73).

***trans*-[PtCl(Mes)(SEt_2)$_2$].** Lithium bromide-free mesityllithium was prepared by removing the supernatant of the reaction mixture by decantation and washing the white, fine crystals of mesityllithium with dry ether several times. This suspension of mesityllithium (0.45 mmol) in ether was added to a solution of *cis*-[$PtCl_2(SEt_2)_2$] (200 mg, 0.448 mmol) in benzene (20 ml) and the mixture was stirred for 2.5 h at room temperature. After removal of the solvent, purification by column chromatography (200 mesh alumina, benzene) followed by recrystallization from hexane gave *trans*-[PtCl(Mes)-(SEt_2)$_2$] as colorless crystals (94 mg, 36%): mp 119 °C. Found: C, 38.81; H, 5.95; S, 12.05; Cl, 7.05%. Calcd for $C_{17}H_{31}ClPtS_2$: C, 38.52; H, 5.89; S, 12.10; Cl, 6.69%. ^{1}H NMR (90 MHz, C_6D_6) δ=0.97 (12H, t, J_H=7.6 Hz, CH_3 of Et), 2.23 (3H, bs, *p*-CH_3), 2.60 (8H, q, J_H=7.9 Hz, J_{Pt}=44.0 Hz, CH_2 of Et), 2.78 (6H, s, J_{Pt}=7.9 Hz, *o*-CH_3), 6.80 (2H, s, J_{Pt}=8.0 Hz, *m*-H);[6] ^{13}C NMR (22.6 MHz, C_6D_6) δ=12.8 (q, J_{Pt}=41.2 Hz, CH_3 of Et), 20.8 (q, *p*-CH_3), 28.8 (q, J_{Pt}=50.9 Hz, *o*-CH_3), 29.1 (t, J_{Pt}=13.4 Hz, CH_2 of Et), 133.1 and 141.6 (aromatic ring carbons);[6] MS *m*/*z* 528 (M^+, based on ^{194}Pt; 6), 438 (1), 403 (2), 374 (41), 346 (24), 318 (8), 282 (6), 120 (81), 105 (77), 90 (100), 75 (97).

***trans*-[Pt(Mes)$_2$(SEt_2)$_2$].** To a solution of *cis*-[$PtCl_2(SEt_2)_2$] (200 mg, 0.448 mmol) in ether (20 ml) was added a suspension of mesityllithium (1.2 mmol) in ether. After stirring for 14 h at room temperature, the solvent was removed in vacuo. The ^{1}H NMR spectrum of the residue in $CDCl_3$ showed both signals of *trans*-[PtBr(Mes)(SEt_2)$_2$] and *trans*-[Pt(Mes)$_2$(SEt_2)$_2$]. The molar ratio of these two products was nearly 1 : 1. Ether and water were added to the residue to remove salt and the ether layer was concentrated. Recrystallization of the residue from methanol yielded *trans*-[Pt(Mes)$_2$(SEt_2)$_2$][3] as colorless crystals (24 mg, 18%): Mp 175—178 °C (decomp) (lit, mp 180 °C (decomp)).[3]

Spectral Measurements. The reactions of *cis*-[$PtCl_2(SEt_2)_2$] with lithium bromide and mesityllithium were followed by monitoring the spectral changes. To a benzene solution of the complex placed in a quartz cell (optical path length=1 cm) was added a solution of slightly excess lithium bromide

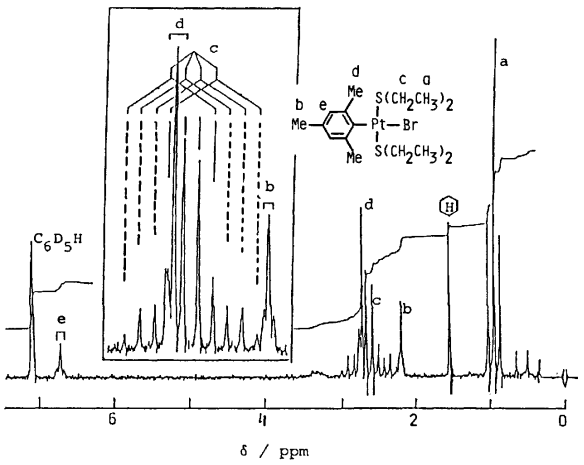

Fig. 1. ^{1}H NMR spectrum of *trans*-[PtBr(Mes)-$(SEt_2)_2$] in C_6D_6 (internal standard, cyclohexane). The inset shows an expanded spectrum in the region of about 2 to 3 ppm.

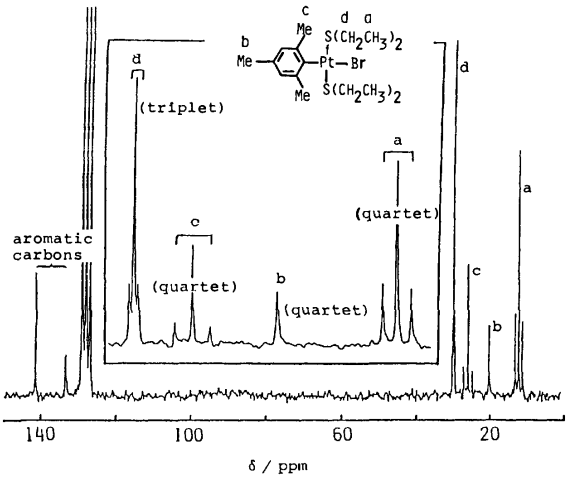

Fig. 2. ^{13}C NMR spectrum of *trans*-[PtBr(Mes)-$(SEt_2)_2$] in C_6D_6. The inset shows an expanded spectrum in the region of the signals of aliphatic carbons. Off resonance patterns are shown in parentheses.

or mesityllithium in ether. Absorption maxima of *cis*-$[PtCl_2(SEt_2)_2]$, *trans*-$[PtBr(Mes)(SEt_2)_2]$, *trans*-$[PtCl_2(SEt_2)_2]$, and *trans*-$[PtBr_2(SEt_2)_2]$ appear at 330, 306 (shoulder), 338, and 357 nm, respectively.

Results and Discussion

Reaction of *cis*-$[PtCl_2(SEt_2)_2]$ with Mesityllithium. When *cis*-$[PtCl_2(SEt_2)_2]$ in benzene was treated with an ether solution of slightly excess mesityllithium prepared from bromomesitylene and butyllithium, two products, *trans*-$[PtBr(Mes)(SEt_2)_2]$ and *trans*-$[PtBr_2(SEt_2)_2]$, were obtained in 40 and 5% yields, respectively, after purification with an alumina column.

$$cis\text{-}[PtCl_2(SEt_2)_2] + MesLi/LiBr \xrightarrow[0\ ^\circ C - r.t.]{\text{ether-benzene}} trans\text{-}[PtBr(Mes)(SEt_2)_2] + trans\text{-}[PtBr_2(SEt_2)_2]$$

The molecular formula of *trans*-$[PtBr(Mes)(SEt_2)_2]$ was determined by elemental analysis and mass spectroscopy. The ^{1}H NMR spectrum of *trans*-$[PtBr(Mes)(SEt_2)_2]$ shows only one set of signals assigned to ethyl groups (Fig. 1) that is consistent with the trans form. The configuration is further confirmed by the ^{13}C NMR spectrum which likewise exhibits a set of ethyl carbon signals (Fig. 2). The known compound *trans*-$[PtBr_2(SEt_2)_2]$ was identified by comparing its melting point (117—118 °C) to the literature value (129, 124, and 118 °C; cf. cis-isomer, mp 93—95 °C)[5] and by measuring mass, ^{1}H NMR, and ^{13}C NMR spectra.

The origin of bromo ligands in *trans*-$[PtBr(Mes)(SEt_2)_2]$ and *trans*-$[PtBr_2(SEt_2)_2]$ is considered to be lithium bromide which was formed as a by-product when mesityllithium was prepared. In fact, when lithium bromide-free mesityllithium was used for the reaction, the major product was *trans*-$[PtCl(Mes)(SEt_2)_2]$ (36%). The reaction of *cis*-$[PtCl_2(SEt_2)_2]$ with ca. 2.5 equivalent of mesityllithium afforded a 1 : 1 mixture of *trans*-$[PtBr(Mes)(SEt_2)_2]$ and *trans*-$[Pt(Mes)_2(SEt_2)_2]$.

Reaction Mechanism. The mechanism of the conversion from *cis*-$[PtCl_2(SEt_2)_2]$ to *trans*-$[PtBr(Mes)(SEt_2)_2]$ should, at least, involve the following three reactions: (a) nucleophilic substitution of halide by mesityl anion, (b) cis-trans isomerization of a square-planar complex, and (c) substitution of chloro ligand by bromo ligand. The ligand substitution reaction of square-planar platinum(II) complexes usually occurs with the retention of geometrical configuration.[7] In other words, the reaction (b) (cis-trans isomerization) is normally much slower than the reactions (a) and (c) (ligand substitutions). However, this empirical rule seems not to apply to the present reaction, since only the isomerized products have been obtained.

The reaction of *cis*-$[PtCl_2(SEt_2)_2]$ in a benzene-ether mixture in the presence of lithium bromide was monitored at 21 °C by periodic measurements of UV-visible spectra, but only a slight change of the spectrum was observed even after two hours. In sharp contrast with this result, when mesityllithium was added to a benzene solution of *cis*-$[PtCl_2(SEt_2)_2]$, this compound disappeared within 30 min and *trans*-$[PtBr(Mes)(SEt_2)_2]$ was formed. These experimental results indicate that mesityllithium accelerates the geometrical isomerization. The formation of *trans*-$[PtBr_2(SEt_2)_2]$ shows that the geometrical isomerization of the platinum(II) complex occurs before the displacement of a coordinated halide ion by a mesityl anion. Low solubility of mesityllithium in ether as well as the bulkiness of mesityl group may significantly contribute to the slow substitution.

From these results, the following mechanism is suggested, where mesityllithium catalyzes the fast cis-trans isomerization followed by the relatively slow substitution by mesityl group (Scheme 1).

$$cis\text{-}[PtCl_2(SEt_2)_2] \xrightarrow{MesLi,\ LiX} trans\text{-}[PtX_2(SEt_2)_2] \quad X = Cl \text{ or } Br$$

$$trans\text{-}[PtX_2(SEt_2)_2] + MesLi \longrightarrow trans\text{-}[PtX(Mes)(SEt_2)_2]$$

Scheme 1.

^{13}C NMR Spectra. The ^{13}C NMR spectrum of *trans*-[PtBr(Mes)(SEt_2)$_2$] shows typical ^{195}Pt couplings on the signals of diethyl sulfide ligands (Fig. 2). A somewhat surprising result is that the methylene carbons show smaller coupling constant ($^2J_{Pt}$=13.2 Hz) than the methyl carbons ($^3J_{Pt}$=42.7 Hz). The spectrum of chloro complex exhibits the same phenomenon ($^2J_{Pt}$=13.4 Hz, $^3J_{Pt}$=41.2 Hz). To our knowledge, there is no report which mentions this phenomenon, but a similar reversal of ^{195}Pt coupling constants can be seen in the ^{13}C NMR spectra of aryl groups in many arylplatinum complexes, where the ^{195}Pt coupling constant on ortho carbon ($^2J_{Pt}$) is smaller than that on meta carbon ($^3J_{Pt}$).[1)]

The present study was supported by Grant-in-Aids for Scientific Research, No.60430011 and 61125007, from the Ministry of Education, Science and Culture.

References

1) B.R. Steele and K. Vrieze, *Transition Met. Chem.*, **2**, 140 (1977).
2) Abbreviations used in this paper: Et=C_2H_5, Pr=C_3H_7, Ph=C_6H_5, Ar=aryl, Mes=mesityl (2,4,6-trimetylphenyl).
3) S. Sergi, V. Marsala, R. Pietropaolo, and F. Faraone, *J. Organomet. Chem.*, **23**, 281 (1970).
4) G. B. Kauffman and D. O. Cowan, *Inorg. Synth.*, **6**, 211 (1960).
5) *Gmelin*, **68**, 302 (1957).
6) J_{Pt} is a coupling constant of ^{195}Pt satellites (the natural abundance of ^{195}Pt=33.7%).
7) S. Kawaguchi, *Kagaku*, **35**, 995 (1980); F. Basolo and R. G. Pearson, "Mechanisms of Inorganic Reactions," 2nd ed, John Wiley and Sons, Inc., New York (1967), Chap. 5.

Conversion of β-Senepoxide to Crotepoxide: Total Synthesis of (+)-Crotepoxide

Seiichiro OGAWA* and Tohei TAKAGAKI
Department of Applied Chemistry, Faculty of Science and Technology, Keio University, Hiyoshi, Yokohama 223
(Received July 26, 1986)

Synopsis. Total synthesis of (+)-crotepoxide has been accomplished by chemical conversion of (+)-β-senepoxide which was prepared from (−)-7-*endo*-oxabicyclo[2.2.1]hept-5-ene-2-carboxylic acid.

Crotepoxide (**1**) was isolated from *Croton macrostachys*[1,2] and *Piper futokadzura*,[3] and has been found to possess significant activity against Lewis lung carcinoma and Walker intramuscular carcinoma. The structure was established by an X-ray crystallographic analysis of the iodohydrin[4] of **1**. Although three total[5-7] and one formal[8] syntheses of the racemic modification of **1** have so far been reported, the optically active natural form (+)-**1** has never been synthesized.

In continuation of our study[9] of highly oxygenated cyclohexane compounds,[10,11] we now describe a total synthesis of (+)-**1** by the chemical conversion of (+)-β-senepoxide[12] [(+)-**6**], the absolute configuration of which has previously been confirmed by a total synthesis.[12,13]

Several attempts to prepare **1** by direct introduction of the *cis*-1,2:3,4-diepoxy functions into *trans*-5,6-diacetoxy-1-benzoyloxymethyl-1,3-cyclohexadiene[14] (**4**) or its *O*-deacetylated derivative[15] using peroxy acid were unsuccessful, and the 4,5-epimer (**5**,[7] epicrotepoxide) of **1** was obtained as a sole diepoxide out of the four possible stereoisomers. Epoxidation of **6**, one of the monoepoxides derived from **4**, also produced **5** exclusively.[14] In this study, epoxidation of **6** to **1** was successfully undertaken through the intermediate bromohydrin **11** prepared from **6**.

Treatment of (±)-**6**[14] with 2 mol equiv *N*-bromoacetamide (NBA) or *N*-bromosuccinimide (NBS) in aqueous dimethyl sulfoxide[16] resulted in the cleavage of the epoxide group to afford the bromohydrin (±)-**7** (49%) and the dihydroxy compound (±)-**8** (21%). The structure of (±)-**7** was confirmed by its conversion to (±)-**6** (63%) with sodium hydrogencarbonate in methanol. A similar treatment of (±)-**6** with NBS in aqueous acetone, ethanol, or dioxane afforded (±)-**7** as the major product. In contrast, when aqueous *N*,*N*-dimethylformamide (DMF) was used as the solvent,[17] (±)-**6** produced two bromo formates [(±)-**9**, 26% and (±)-**10**, 38%], which were obtained by the prefered diaxial opening of the intermediate bromonium ions by an iminium ion. Considering from the product ratio, the formation of the bromonium ion seemed not to be affected by the orientation of the epoxide ring. The structures of (±)-**9** and (±)-**10** were confirmed on the basis of their ^{1}H NMR spectra, which showed the signals due to the ring protons on carbon atoms bearing the bromo atoms as doublets of doublets at δ 4.28 (J=2 and 7.5 Hz) and 4.43 (J=3 and 7.5 Hz), respectively. The former signal did not couple with the epoxide proton, supporting the structure proposed. A treatment of (±)-**9** with methanol at reflux temperature gave the bromohydrin (±)-**11** in good yield. The hydroxy tosylate **12**, prepared by treatment of **1** with *p*-toluenesulfonic acid, was shown to regenerate **1** under the influence of basic alumina.[3] When (±)-**11**, with the same configuration as **12**, was treated in a similar manner, (±)-**11** was recovered unchanged. Finally, it was found that (±)-**11** could be epoxidized only by use of a base strong enough to result in the undesired, partial *O*-deacylation. Thus, (±)-**9** was treated with potassium carbonate in methanol at room temperature for 3 h and the resulting diepoxide (±)-**2** was without isolation acetylated with acetic anhydride in pyridine to give the triacetate (±)-**3** in 60% yield. The ^{1}H NMR spectrum of (±)-**3** was very similar to that of **1**. This is consistent with the proposed structure and excludes a possible migration of the initially formed epoxide group via attack of the vicinal trans hydroxy group. Therefore, the crude (±)-**2** was first selectively benzoylated with benzoyl chloride in pyridine and then acetylated to give rise to a 20% yield[18] of racemic crotepoxide (±)-**1**, which was identified with an authentic sample by comparison of the ^{1}H NMR spectral data.[1]

Likewise, starting from optically active (+)-**6**,[13] (+)-**1** was synthesized. Thus, treatment of (+)-**6** with NBS in aqueous DMF afforded two bromo formates (+)-**9** (22%) and (+)-**10** (30%). The former was converted into (+)-**1** (23%), $[\alpha]_D$ +73° ($CHCl_3$), as described for the preparation of the racemate. The ^{1}H NMR spectrum and the optical rotation were similar with those of an authentic sample.[1]

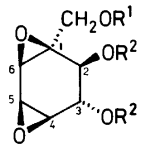

	R^1	R^2
1	Bz	Ac
2	H	H
3	Ac	Ac

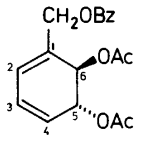

4

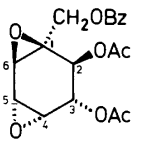

5

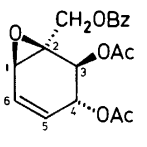

6

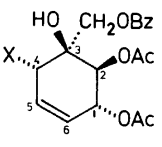

X

	X
7	Br
8	OH

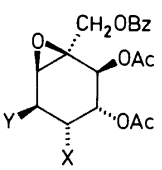

	X	Y
9	Br	OCHO
10	OCHO	Br
11	Br	OH
12	OTs	OH

The absolute structure[4] of (+)-**1** was also supported by the present synthesis and could be correlated to that of (+)-**6**.

Experimental

Melting points were determined in an open capillary tube in a MEL-TEMP melting point apparatus and are uncorrected. ^{1}H NMR spectra were recorded in chloroform-*d* solution[19] with tetramethylsilane as an internal standard. The peak positions are given in δ values. TLC was performed on precoated silica gel 60 F-254 (E. Merck, Darmstadt; 0.2-mm thickness). The silica gel used for column chromatography was Wakogel C-300 (Wako Co., Osaka; 300 mesh). Organic solutions were concentrated below 30 °C under reduced pressure.

(±)-1,2-Di-*O*-acetyl-(1,4/2,3)-3-*C*-benzoyloxymethyl-4-bromo-5-cyclohexene-1,2,3-triol [(±)-7] and (±)-1,2-di-*O*-acetyl-(1,4/2,3)-3-*C*-benzoyloxymethyl-5-cyclohexene-1,2,3,4-tetrol [(±)-8]. A mixture of (±)-β-senepoxide[14] (±)-**6** (200 mg, 0.58 mmol), NBA (160 mg, 1.16 mmol), dimethyl sulfoxide (2 ml), and water (21 µl, 1.17 mmol) was stirred at room temperature for 1 h. TLC (2-butanone-toluene 1 : 5) showed disappearance of (±)-**6** (R_f 0.57) and appearance of two major spots (R_f 0.32 and 0.12). The mixture was diluted with water (5 ml) and extracted with ether (20 ml). The extract was successively washed with aqueous sodium hydrogencarbonate and water, dried, and concentrated. The residue (260 mg) was chromatographed on silica gel (13 g) with 2-butanone-toluene 1 : 4 to give, as the first fraction, (±)-**7** (121 mg, 49%) as needles (from ethanol): Mp 106—107.5 °C. ^{1}H NMR ($CDCl_3$) δ=2.08 (3H, s, OAc), 3.80 (1H, br s, OH), 4.65 (1H, d, J=4.5 Hz, H-6), 4.52 (1H, d) and 4.73 (1H, d) (J=12 Hz, CH_2OBz), 5.57—5.87 (3H, m, H-2, H-3, H-4), 6.01 (1H, ddd, J=1.5, 4.5, and 10.5 Hz, H-5), 7.30—7.67 (3H, m) and 7.98—8.09 (2H, m) (benzoyl).

Found: C, 50.64; H, 4.39%. Calcd for $C_{18}H_{19}BrO_7$: C, 50.60; H, 4.48%.

The second fraction gave (±)-**8** (45 mg, 21%) as a syrup. ^{1}H NMR ($CDCl_3$) δ=1.99 (3H, s) and 2.10 (3H, s) (OAc), 3.26 (2H, br s, OH), 5.42—5.60 (1H, br s, H-4), 5.69 (1H, dd, J=1.5 and 10.5 Hz, H-6), 5.94 (1H, dd, J=3.8 and 10.5 Hz, H-5), 7.30—7.66 (3H, m) and 7.99—8.09 (2H, m) (benzoyl).

Found: C, 56.83; H, 5.40%. Calcd for $C_{18}H_{20}O_8 \cdot H_2O$: C, 56.54; H, 5.76%.

The similar results were obtained when NBS was used instead of NBA.

Conversion of (±)-7 to (±)-6. A solution of (±)-**7** (20 mg, 0.05 mmol) in methanol (20 ml) was slowly evaporated in the presence of large excess of sodium hydrogencarbonate at 40 °C. The residue was extracted with chloroform and the product was purified by chromatography to give (±)-**6** (10 mg, 63%), identical with an authentic sample.[14]

(±)-4,5-Di-*O*-acetyl-2,3-anhydro-1-*O*-formyl-(1,2,3,4/5,6)-3-*C*-benzoyloxymethyl-6-bromocyclohexane-1,2,3,4,5-pentol [(±)-9] and (±)-3,4-Di-*O*-acetyl-1,2-anhydro-5-*O*-formyl-(1,2,3,6/4,5)-2-*C*-benzoyloxymethyl-6-bromocyclohexane-1,2,3,4,5-pentol [(±)-10]. A mixture of (±)-**6** (834 mg, 2.41 mmol), NBS (858 mg, 4.82 mmol), DMF (8.2 ml), and water (87 µl, 4.83 mmmol) was stirred at 30 °C for 4 d. TLC (2-butanone-toluene 1 : 5) showed disappearance of (±)-**6** (R_f 0.57) and appearance of two major spots (R_f 0.62 and 0.54). The mixture was processed as described for preparation of (±)-**7** and (±)-**8**. The products (1.35 g) were chromatographed on a silica-gel column (70 g) with 2-butanone-toluene 1 : 2. The first fraction gave (±)-**9** (292 mg, 26%) as prisms (from ether): Mp 113—114 °C. ^{1}H NMR ($CDCl_3$) δ=1.97 (3H, s) and 2.17 (3H, s) (OAc), 3.69 (1H, d, J=3 Hz, H-2), 4.58 (1H, dd, J=2 and 7.5 Hz, H-6), 5.15 (1H, dd, J=2 and 4.5 Hz, H-5), 5.52 (1H, d, J=4.5 Hz, H-4), 5.60 (1H, dd, J=3 and 4.5 Hz, H-1), 7.33—7.67 (3H, m) and 8.00—8.11 (2H, m) (benzoyl), 8.19 (1H, s, formyl).

Found: C, 48.68; H, 4.00%. Calcd for $C_{19}H_{19}BrO_9$: C, 48.43; H, 4.06%.

The second fraction gave (±)-**10** (431 mg, 38%) as prisms (from ethanol): Mp 85—87 °C. ^{1}H NMR ($CDCl_3$) δ=1.87 (3H, s) and 2.17 (3H, s) (OAc), 3.77 (1H, d, J=3 Hz, H-1), 4.43 (1H, dd, J=3 and 7.5 Hz, H-6), 4.30 (1H, d) and 4.57 (1H, d) (J=11.5 Hz, CH_2OBz), 5.17 (1H, dd, J=2 and 4.5 Hz, H-4), 5.41 (1H, dd, J=2 and 7.5 Hz, H-5), 5.53 (1H, d, J=4.5 Hz, H-3), 7.33—7.67 (3H, m) and 8.00—8.11 (2H, m) (benzoyl), 8.03 (1H, s, formyl).

Found: C, 48.23; H, 3.98%. Calcd for $C_{19}H_{19}BrO_9$: C, 48.43; H, 4.06%.

Similarly, (+)-β-senepoxide[13] (+)-**6** (795 mg, 2.3 mmol) was treated with NBS in aqueous DMF to give, after chromatography, the (1*S*)-enantiomer (+)-**9** (241 mg, 22%), $[\alpha]_D^{21}$ +2.1° (*c* 2.4, $CHCl_3$), and the (3*S*)-enantiomer (+)-**10** (320 mg, 30%), $[\alpha]_D^{21}$ +40° (*c* 1.8, $CHCl_3$). Both compounds were characterized by comparison of their ^{1}H NMR spectral data with those of racemic modification. Mass spectrum, *m/z* (relative intensity); for (+)-**9**, 425.0203 ($M^+ - HCO_2$, 17.7), for (+)-**10**, 425.0215 ($M^+ - HCO_2$, 90.6).

(±)-4,5-Di-*O*-acetyl-2,3-anhydro-(1,2,3,4/5,6)-3-*C*-benzoyloxymethyl-6-bromocyclohexane-1,2,3,4,5-pentol [(±)-11]. A solution of (±)-**9** (110 mg, 0.23 mmol) in methanol (3 ml) was refluxed for 10 min. TLC (2-butanone-toluene 1 : 5) showed disappearance of (±)-**9** (R_f 0.62) and appearance of one major (R_f 0.28) and one minor spots (R_f 0.34). The mixture was concentrated and the residue was eluted from a silica-gel column (5 g) with 2-butanone-toluene 1 : 6 to give (±)-**11** (82 mg, 80%) as a syrup; ^{1}H NMR ($CDCl_3$) δ=1.95 (3H, s) and 2.14 (3H, s) (OAc), 3.00 (1H, br s, OH), 3.69 (1H, d, J=4.1 Hz, H-2), 4.41 (1H, m, H-1), 4.28 (1H, d) and 4.55 (1H, d) (J=11.5 Hz, CH_2OBz), 5.14 (1H, dd, J=2.2 and 5.7 Hz, H-5), 5.62 (1H, d, J=5.7 Hz, H-4), 7.31—7.68 (3H, m) and 8.00—8.10 (2H, m) (benzoyl).

Found: C, 47.78; H, 4.22%. Calcd for $C_{18}H_{19}BrO_8 \cdot 0.5H_2O$: C, 47.84; H, 4.42%.

(±)-2,3-Di-*O*-acetyl-1,6 : 4,5-dianhydro-(1,2,4,5,6/3)-1-*C*-(acetoxymethyl)cyclohexane-1,2,3,4,5,6-hexol [(±)-3]. A mixture of (±)-**9** (30 mg, 0.06 mmol), anhydrous potassium carbonate (12 mg), and methanol (5 ml) was stirred at room temperature overnight. TLC (chloroform-methanol 8 : 1) showed a formation of one major (R_f 0.19) and one minor components (R_f 0.23). The mixture was neutralized with M hydrochloric acid and concentrated, and the residue was acetylated with acetic anhydride and pyridine in the usual way. The product was purified by chromatography on silica gel and crystallized from ethanol to give, as the main product, (±)-**3** (11 mg, 60%) as needles: Mp 70—70.5 °C; ^{1}H NMR ($CDCl_3$) δ=2.06 (6H, s) and 2.09 (3H, s) (OAc), 3.05 (1H, dd, J=1.5 and 3 Hz, H-4), 3.50 (1H, dd, J=2 and 3 Hz, H-5), 3.50 (1H, d, J=2 Hz, H-6), 3.79 (1H, d) and 4.42 (1H, d) (J=11 Hz, CH_2OAc), 4.87 (1H, dd, J=1.5 and 9 Hz, H-3), 5.58 (1H, d, J=9 Hz, H-2).

Found: C, 52.19; H, 5.16%. Calcd for $C_{13}H_{16}O_8$: C, 52.00; H, 5.37%.

Synthesis of Crotepoxide. Compound (±)-**9** (169 mg, 0.36 mmol) was treated with potassium carbonate (75 mg, 0.54 mmol) in methanol (25 ml) as described for the preparation of (±)-**3**. The resulting trihydroxy compound was selectively benzoylated with benzoyl chloride (84 µl, 0.72 mmol) in pyridine (3 ml) at −15 °C for 10 min, and then for 5 h at room temperature. TLC (chloroform-methanol 8 : 1) showed one major spot (R_f 0.54), together with several minor spots. Acetic anhydride (1 ml) was then added to the mixture, and, after 2 h at room temperature, the mixture was

processed in the usual way. The mixture of products was fractionated by a silica-gel column (10 g) with 2-butanone–toluene 1 : 10 to give, as a major product, (±)-**1** (26 mg, 20% based on **9** used) as needles (from ethanol): Mp 109—111 °C (lit,[4] Mp 110—111, 128—129 °C). Crystals show a double melting point (melted at 109—111 °C, resolidified, and then melted again at ca. 128 °C). The ^{1}H NMR ($CDCl_3$) spectral data were shown to be identical with those of an authentic sample.[4,5] (Found: C, 59.67; H, 4.89%).

Likewise, (+)-crotepoxide (+)-**1** was obtained, in 23% yield, by epoxidation of (+)-**9** followed by selective acylation; needles (from methanol): Mp 145—147 °C, $[\alpha]_D^{25}$ +73° (*c* 0.43, $CHCl_3$). lit,[1] Mp 150—151 °C, $[\alpha]_D^{25}$ +74° (*c* 1.7, $CHCl_3$). The ^{1}H NMR spectrum was superimposable on that of a racemic modification. (Found: C, 59.72; H, 4.88%).

We express our sincere thanks to Mr. Akio Takahashi for his elemental analyses. We also thank Dr. Shigeru Nishiyama (Department of Chemistry, Faculty of Science and Technology, Keio University) for measurement of the mass spectra.

References

1) S. M. Kupchan, R. J. Hemingway, P. Coggon, and A. T. Mcphail, *J. Am. Chem. Soc.*, **90**, 2982 (1968).
2) S. M. Kupchan, R. J. Hemingway, and R. M. Smith, *J. Org. Chem.*, **34**, 3898 (1969).
3) S. Takahashi, *Phytochemistry*, **8**, 321 (1969).
4) P. Coggon, A. T. Mcphail, and G. A. Sim, *J. Chem. Soc., (B)*, **1969**, 534.
5) K. Oda, A. Ichihara, and S. Sakamura, *Tetrahedron Lett.*, **1975**, 3187.
6) M. R. Demuth, P. E. Garrett, and J. D. White, *J. Am. Chem. Soc.*, **98**, 634 (1976).
7) M. Matsumoto, S. Dobashi, and K. Kuroda, *Tetrahedron Lett.*, **1977**, 3361.
8) R. H. Schlessinger and A. Lopes, *J. Org. Chem.*, **46**, 5252 (1981).
9) S. Ogawa and T. Takagaki, *J. Org. Chem.*, **50**, 5075 (1985).
10) B. Ganem, *Tetrahedron*, **34**, 3353 (1978).
11) C. Thebtaranonth and Y. Thebtaranonth, *Acc. Chem. Res.*, **19**, 84 (1986).
12) K. Kodpinid, C. Sadavongvivad, C. Thebtaranonth, and Y. Thebtaranonth, *Tetrahedron Lett.*, **24**, 2019 (1983).
13) S. Ogawa and T. Takagaki, *J. Org. Chem.*, **50**, 2356 (1985).
14) S. Ogawa, T. Toyokuni, M. Ara, M. Suetsugu, and T. Suami, *Chem. Lett.*, **1980**, 379; *Bull. Chem. Soc. Jpn.*, **56**, 1710 (1983).
15) S. Ogawa and T. Takagaki; unpublished results. Epoxidation of the 2-*O*-deacetyl derivative of **4** with peroxy acid also gave the diepoxide, the configuration of which was identical to **5**.
16) D. R. Dalton, V. P. Dutta, and D. C. Jones, *J. Am. Chem. Soc.*, **90**, 5498 (1968).
17) D. R. Dalton, R. C. Smith, and D. C. Jones, *Tetrahedron*, **26**, 575 (1970).
18) The reaction was not carried out under the optimum conditions.
19) The spectra were recorded on a Varian EM-390 (90 MHz) spectrometer.

Improvement of Porphyrin Photovoltaic Cells in Panchromaticities and Quantum Yields by Use of Tetrabenzoporphyrin Skeleton

Kazuo YAMASHITA,* Yutaka HARIMA, Hideyuki KUBOTA,† and Hitomi SUZUKI†
Department of Environmental Science, Faculty of Integrated Arts and Sciences, Hiroshima University, Hiroshima 730
†Department of Chemistry, Faculty of Science, Ehime University, Matsuyama 790
(Received August 21, 1986)

Synopsis. Expansion of the porphyrin π electron system by using a tetrabenzoporphyrin (TBP) skeleton leads to better spectral match to the solar spectrum and high quantum yields when the porphyrins are used as sensitizers. Metallotetrabenzoporphyrins such as MgTBP and ZnTBP rank among the most efficient organic photoconducting materials studied so far.

Solar cells that utilize the photoelectric properties of organic materials stand still far from practical use because of conversion efficiencies much lower than those of traditional inorganic solar cells as well as no long-term stability.[1] However, solar cells made from organic compounds have some unique advantages compared with the inorganic devices in respect of low cost, ease of fabrication, flexibleness etc.

Several years ago, we found that the more easily oxidized porphyrins exhibited the higher quantum yields and that peripheral substitution could modulate the oxidation potential of the porphyrin and that long aliphatic chain substituents decreased the quantum yields, presumably by acting as insulators towards electron transport.[2] These results suggest that expansion of the porphyrin π electron system may lead to lower oxidation potentials as well as facilitate energy and electron transfer by increasing π-π interactions between neighbouring molecules and result in the increase of photocurrents and thus the quantum yields.[3]

In the present paper we show evidence that metallotetrabenzoporphyrins such as (tetrabenzoporphyrinato)magnesium (II) (MgTBP) and ZnTBP are indeed oxidized very easily in comparison with other porphyrins studied and act as most efficient sensitizers in simple photovoltaic devices based on Al/porphyrin Schottky barriers and organic *p*-*n* junctions.

Experimental

Porphyrins and metalloporphyrins used were prepared and purified by the methods in references.[4-6] Phthalocyanine (H_2Pc) and (phthalocyaninato)zinc(II) (ZnPc) were purchased from Tokyo Kasei Co. and purified by sublimation before use. Polycarbonate resin Panlite® (Pnl) used as a polymer binder was kindly supplied by Teijin Chemicals Ltd. Dichloromethane and dichloroethane were redistilled after dessication with calcium hydride. An amount of 10 mg of the dye was dispersed in 5 ml of 1 %(W/V) Panlite-dichloroethane solution by using a TomySeiko Handy Sonic UR-20P. A particulate dye film was prepared by casting a suitable amount of the dye-polymer mixture prepared above on an indium-tin oxide(ITO)-coated glass plate. Preparation of an ITO film, fabrication of a M/porphyrin/M′ sandwich-type cell, in which M or M′ denotes an ITO or a metal electrode, and measurements of dark and photoelectric properties of the photovoltaic cells were carried out as described previously.[7,8] Photocurrents were normalized in such a way that the intensity of monochromatic light incident on the interface of the dye film with the illuminated metal was constant at 10 μW cm^{-2} unless otherwise specified.

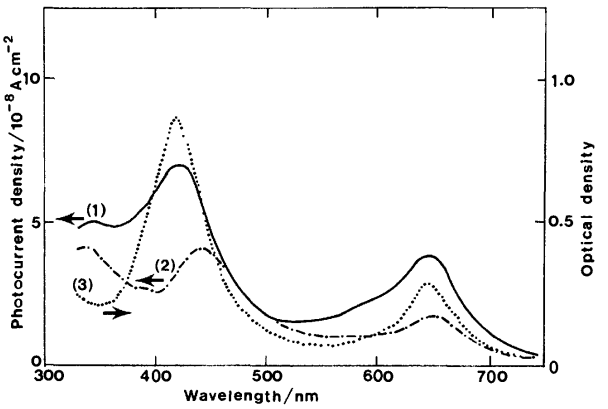

Fig. 1. Action spectra of short-circuit photocurrents for the Schottky barrier cell of Al(8 nm)/CdTBP (60 nm)/Au(9 nm). Curves (1) and (2) are obtained on illumination of the Al and the Au electrodes, respectively. Curve (3) shows the optical absorption spectrum of the CdTBP film used in the sandwich cell.

Results and Discussion

Figure 1 displays short-circuit photocurrent action spectra for the Al/CdTBP/Au Schottky barrier cell with an optical absorption spectrum of the CdTBP film. Currents passing from Al to Au through the cell were taken to be positive. For thin CdTBP films the shapes of the action spectra almost were the same for light incident on both sides. For thick films, however, the action spectra agreed well to the absorption spectrum only when the Al side was illuminated. Similar results were observed with other tetrabenzoporphyrin derivatives and can be explained in terms of an optical filtering effect[9] due to the interposed porphyrin phase on the basis of a band model of *p*-type semiconductors. Namely, only photons absorbed near the Al blocking contact are effective for generation of charge carriers, resulting in the photoresponse, while the Au contact is inert for illumination owing to the ohmic contact.

We further note that the tetrabenzoporphyrins absorb throughout the range of visible light and the light absorbing properties approach those found for chlorophylls in vivo (λ_{max}=680 and 700 nm for Photosystems II and I of green plants, respectively). The maximum fraction of the solar spectrum that can be collected by ZnTBP molecules increases to about 47%,

Table 1. Summary of Photocurrent Quantum Yields of Porphyrin and Metalloporphyrin Films with First Ring Oxidation Potentials

Compound[a]	$E_{1/2}$[b]/V vs. SCE	Cell configuration[c]	Wavelength/nm	Quantum yield[d]	References
MgTBP	0.23	B	445	8.5×10^{-2}	(3)
		C	447	1.5×10^{-1}	(3)
MgOMTBP	0.26	A	390	3.4×10^{-2}	
ZnTBP	0.40	A	390	1.5×10^{-1}	
		B	460	4.5×10^{-2}	(3)
		C	440	1.2×10^{-1}	(3)
CdTBP	0.44	A	402	4.5×10^{-2}	
MgTPP	0.61	B	440	5.2×10^{-2}	(3)
		C	445	9.8×10^{-2}	(2)
MgP	0.68	C	420	2.0×10^{-1}	(2)
ZnTPP	0.78	B	440	3.2×10^{-2}	(3)
		C	440	3.0×10^{-2}	(3)
ZnP	0.80	C	420	9.1×10^{-2}	(2)

a) Abbreviations used; OMTBP 1,4,8,11,15,18,22,25-octamethyltetrabenzo[*b,g,l,q*]porphyrin; P porphyrin; TBP tetrabenzoporphyrin; TPP 5,10,15,20-tetraphenylporphyrin. b) First ring oxidation potentials at Pt in CH_2Cl_2 with 0.1 mol dm^{-3} tetrabutylammonium perchlorate. c) A Al/Porphyrin/Au; B Al/Porphyrin/Ag; C Al/Porphyrin/0.1 mol dm^{-3} $K_3[Fe(CN)_6]$ and 0.1 mol dm^{-3} $K_4[Fe(CN)_6]$/Pt. d) Quantum yield is defined as the number of the electrons produced per photon incident on the dye film at 10 μW cm^{-2}.

which is about 10 or 15% larger than that for (2,3,7,8,12,13,17,18-octaethylporphyrinato)zinc(II) (ZnOEP) or (5,10,15,20-tetraphenylporphyrinato)zinc-(II) (ZnTPP) molecules.[10] Thus the expansion of the porphyrin π electron system by using the TBP skeleton is very effective to improve the panchromaticity of the porphyrin, resulting in the increase of conversion efficiency as shown below.

The first ring oxidation potentials of 0.23 and 0.40 V vs. SCE found for MgTBP and ZnTBP rank these macrocyclic compounds as the easiest to oxidize among a large variety of Mg and Zn porphyrins (Table 1 and see Felton's review[11]). Judging from the oxidation potentials and the exponential correlation previously found between the oxidation potential of the porphyrin and the photocurrent quantum yield, it is expected that both MgTBP and ZnTBP are effective more than MgP. However, the fact is that MgTBP and ZnTBP show photocurrent quantum yields somewhat smaller than MgP. At this time it is necessary to recall the previous finding that for a given porphyrin ligand the quantum yields parallel the first ring oxidation potentials of the porphyrins, but all porphyrins do not fall on the same curve.[2] This might be attributable to a combination of various factors such as the ease of charge carrier formation relating with the oxidation potential of the porphyrin, the packing of porphyrin molecules in solid films and the extent of π-π overlap between the porphyrin rings, which facilitates energy and electron transfer.[12] The quantum yield of MgTBP may be greater than that of MgP under illumination of polychromatic lights such as solar rays, because the maximum fraction of the solar spectrum that can be collected by the tetrabenzo compound is larger than that by MgP. The photocurrent quantum yields for the sandwich-type Schottky barrier cells made from the metallotetrabenzoporphyrins are in the range from 10^{-2} to 10^{-1}. Comparison of the photocurrent quantum yields found here with those obtained for other porphyrins shows distinctly that tetrabenzo compounds fall within the most efficient organic light converters investigated so far.

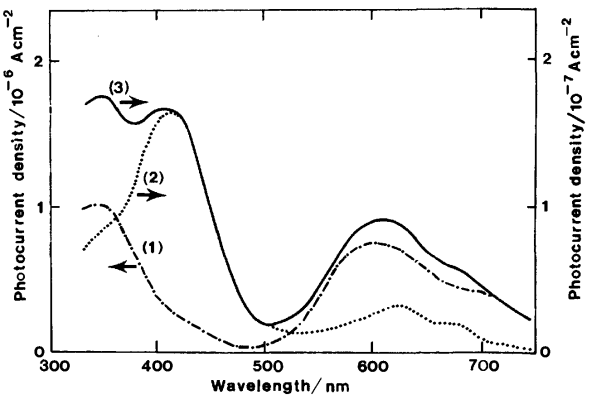

Fig. 2. Action spectra of short-circuit photocurrents for the particulate-type Schottky barrier cells of (1) ITO/H_2Pc-PnI/Al, (2) ITO/TPTBP-PnI/Al and (3) ITO/H_2Pc, TPTBP-PnI/Al. Illumination is made through the Al electrode.

In more recent years photovoltaic cells prepared by dispersing fine particles of pigment in a polymer binder have received much attention as promising devices.[13,14] In particular polar polymers such as poly(vinylidene difluoride) and polyacrylonitrile have been found to give high quantum efficiencies.[15] Up to date, however, there has been no report concerning the particulate-type photovoltaic cells using the porphyrins.

Figure 2 illustrates short-circuit photocurrent action spectra for three kinds of particulate-type Schottky barrier cells. The photocurrents observed with the particulate-type cells are corrected roughly for the reflection and the absorption of light at the Al/dye-PnI interface. Because, it was very hard to measure precisely the intensity of light incident on the dye-polymer film through the Al phase owing to the complex reflection of light, scattering etc. due to the roughness of the Al/dye-polymer interface. The first and the

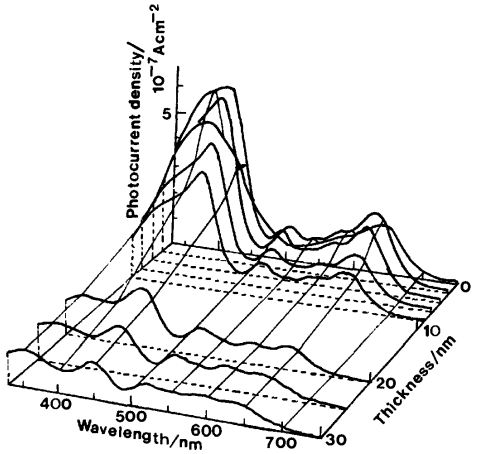

Fig. 3. Dependence of short-circuit photocurrent action spectra for the Au/ZnTBP(40 nm)/T(4-Py)P/Al cells on thickness of the T(4-Py)P film, when illuminated through the Al electrode.

second cells were prepared by dispersing H_2Pc and 5,10,15,20-tetraphenyltetrabenzoporphyrin (TPTBP) in Pnl-dichloroethane solutions, respectively. The third cell was made by dispersing equivalent amounts of H_2Pc and TPTBP in the polymer binder. It is noteworthy that TPTBP is only one sample giving a fairly good photoconducting film with Pnl among porphyrins studied. The shapes of action spectra (1) and (2) resemble those of optical absorption spectra of H_2Pc and TPTBP films. It is clear that combination of TPTBP and H_2Pc brings about the best spectral match to the solar spectrum among them. Unfortunately, however, magnitudes of the photocurrents observed with the third cell are about one tenth as large as those for the ITO/H_2Pc-Pnl/Al cell, though both cells generate photovoltages greater than 1 V.

Figure 3 illustrates short-circuit photocurrent action spectra for the Au/ZnTBP(40 nm thick)/5,10,15,20-tetra(4-pyridyl)porphyrin [T(4-Py)P]/Al *p-n* junction cell with varying thickness of the T(4-Py)P film. The photovoltaic spectral cosensitization effect[16] is clearly observed with the cell having a thin T(4-Py)P film. The optimum thickness of the T(4-Py)P film for the quantum yield seems to be around 2 nm, being somewhat smaller than that (about 7 nm) for the analogue T(3-Py)P in the case of a Au/ZnPc(50 nm thick)/T(3-Py)P/Al cell.[16] Such a thin film of T(4-Py)P may be composed of insular sublimates of the porphyrin. The fraction of the solar spectrum that can be collected by the ZnTBP/T(4-Py)P *p/n* phases becomes 1.3 times as great as that by the ZnTBP phase alone in the Al/ZnTBP Schottky barrier cell. The photocurrent quantum yield and the power conversion efficiency reach about 20 and 2 % respectively for monochromatic incident light (10 μW cm^{-2}) at 430 nm.

Thus the facile, chemical stability (ZnTBP can be heated in air without decomposing), light absorption properties and high quantum yields of the metallotetrabenzoporphyrins suggest that these macrocycles are attractive potential candidates for solar energy conversion devices.

The authors are grateful to the Ministry of Education, Culture and Science for supporting in part this work through the Grant-in-Aid for Energy Research No. 61040040.

References

1) A. J. Nozik, "Photochemical Conversion and Storage of Solar Energy," ed by J. S. Connolly, Academic Press, Inc., New York (1981), p. 288.
2) F. J. Kampas, K. Yamashita, and J. Fajer, *Nature (London)*, **284**, 40 (1980).
3) K. Yamashita, *Chem. Lett.*, **1982**, 1085.
4) A. Volger, B. Rethwisch, H. Kunkely, J. Hutterman and J. O. Besenhard, *Angew. Chem. Int. Ed. Engl.*, **17**, 951 (1978).
5) R. B. M. Koehorst, J. F. Keilbeuke, T. J. Schaafsma, D. A. de Bie, B. Geurtsen, R. N. Henrie and H. C. Van der Plas, *J. Chem. Soc., Perkin Trans. 2*, **1981**, 1005.
6) R. G. Little, J. A. Anton, P. A. Loach and J. A. Ibers, *J. Heterocyclic Chem.*, **12**, 343 (1975).
7) K. Yamashita, Y. Harima, and Y. Matsumura, *Bull. Chem. Soc. Jpn.*, **58**, 1761 (1985).
8) Y. Harima and K. Yamashita, *J. Electroanal. Chem. Interfacial Electrochem.*, **186**, 313 (1985).
9) A. K. Ghosh, D. L. Morel, T. Feng, R. F. Shaw, C. A. Rowe Jr., *J. Appl. Phys.*, **45**, 230 (1974).
10) J. R. Darwent, P. Douglas, A. Harriman, G. Porter and M.-C. Richoux, *Coord. Chem. Rev.*, **44**, 83 (1982).
11) R. H. Felton, "The Porphyrins," ed by D. Dolphin, Academic Press, New York (1978), Vol. V, pp. 53—125.
12) K. Yamashita, N. Kihara, H. Shimidzu, and H. Suzuki, *Photochem. Photobiol.*, **35**, 1 (1982).
13) C. F. Hackett, *J. Chem. Phys.*, **55**, 3178 (1971).
14) R. O. Loutfy and E. R. Menzel, *J. Am. Chem. Soc.*, **102**, 4967 (1980).
15) N. Minami, K. Sasaki, and K. Tsuda, *J. Appl. Phys.*, **54**, 6754 (1984).
16) Y. Harima, K. Yamashita, and H. Suzuki, *Appl. Phys. Lett.*, **45**, 1144 (1984).

Electrochemical Studies of Poly(mercaptohydroquinone) and Poly(mercapto-*p*-benzoquinone) Films Prepared by Electropolymerization. I. Preparation of pH Microsensor and Its Fundamental Characteristics

Gorou ARAI,* Takashi KOIKE, and Iwao YASUMORI
Department of Applied Chemistry, Faculty of Engineering, Kanagawa University, Kanagawa-ku, Yokohama 221
(Received September 3, 1986)

Synopsis. Carbon fibers were electrochemically modified with poly(mercaptohydroquinones). These modified carbon fiber electrodes showed excellent Nernstian response to pH from ca. 2 to 10 and could respond within 2s in the pH range from 3 to 8. These electrodes could work well one month after kept stored in a weak acidic buffer solution and could be easily restored by electroreduction even after their functions had been lowered by successive pH measurements.

In recent years, there has been considerable interest in chemically modified electrodes because of their novel properties such as selective electrolysis,[1] electrocatalysis,[2] and selective ion sensing.[3] Polymeric quinone-hydroquinone systems have been investigated because of their usefulness as specific regenerable redox reagents.[4] Hence, electrodes modified with several poly(benzoquinone) films have been prepared by either the dip-drying or the adsorption method, and their electrochemical behavior and applications in electrocatalysis have been examined by many workers.[5] Recently, we have prepared a poly(mercapto-*p*-benzoquinone) film (PQ) by electrooxidation of mercaptohydroquinone on a glassy carbon electrode[6] and have reported its basic electrochemical behavior.[7] Electrodes modified with PQ thus prepared or poly(mercaptohydroquinone) film (PH_2Q) obtainable by electroreduction of PQ, are expected to possess several novel properties such as mentioned above. More recently, it has been observed that a fine carbon fiber electrode (CFE) modified with PH_2Q (PH_2Q/CFE) is capable of excellent Nernstian response to pH.[8] But its durability was occasionally observed to get lowered after successive pH measurements. In order to reveal the cause for this poor durability, effects of several pretreatments on CFE have been examined by means of a scanning electron microscope. Moreover, three polymer films, namely poly(mercaptomethylhydroquinones)[9] ($PMeH_2Q$), poly(3-mercapto-2,5-dimethylhydroquinone)(PMe_2H_2Q), and PH_2Q films, were prepared on CFE under the same preparation conditions (with respect to, e.g., supporting electrolyte, pH of electrolytic solution, concentration of mercaptohydroquinones, and oxidation potential) and their behavior as pH sensors were investigated in detail. We report here on preferable pretreatment of CFE for the preparation of PH_2Q's/CFE with good durability and their excellent functions as pH microsensors.

Experimental

Mercaptohydroquinones used were synthesized and purified according to the method of Alcolay.[10] Chemicals used for the synthesis of mercaptohydroquinones were of reagent grade. All the other chemicals were of analytical grade and were used without further purification. Electropolymerization of mercaptohydroquinones was performed under potentiostatic conditions with a three-electrode system consisting of a CFE (Torayca T-300, Toray Industries Co., 7 μm in diameter) working electrode, a Pt wire counter electrode, and a saturated calomel electrode (SCE) in a conventional two-compartment glass cell. Potentiostatic electrolysis and cyclic

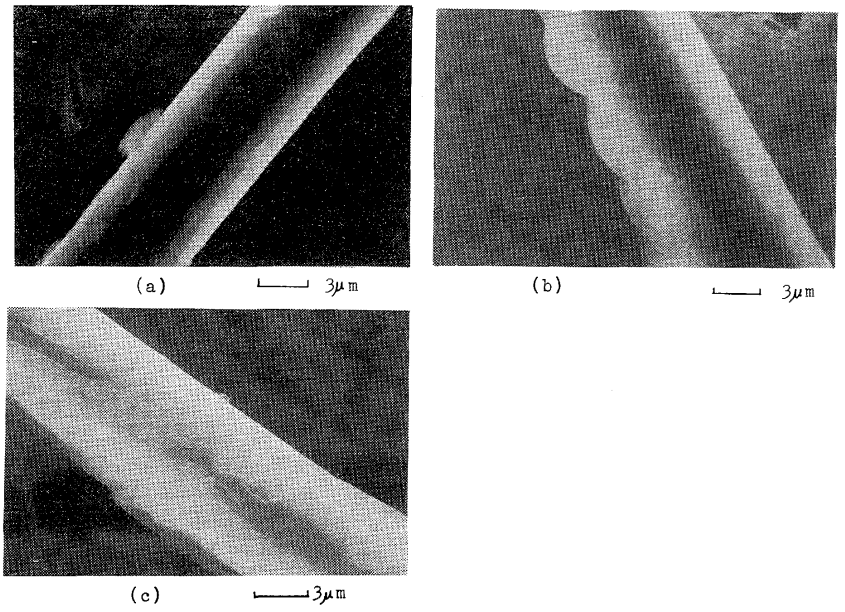

Fig. 1. Scanning electron micrographs of (a) PH_2Q/CFE_0, (b) PH_2Q/CFE_1, and (c) PH_2Q/CFE_2.

voltammetry were performed by using a potentiostat/galvanostat (Model HA-304, Hokuto Denko Co.). PH_2Q/CFE, $PMeH_2Q$/CFE, and PMe_2H_2Q/CFE were attached with Ag paste to an end of a Cu wire which was in a coaxial wire as shown in the previous paper,[8] and their electrode potentials in a buffer solution were measured with an electrometer (Model EM-02, Toho Chemical Research Co.). Scanning electron micrographs were taken on a scanning electron microscope (SEM) (JEOL JSM-35C).

Results and Discussion

Three types of pretreatments were examined on CFE: *Procedure 1* in which a CFE was thoroughly rinsed with deionized water; the CFE thus treated is denoted as CFE_0. *Procedure 2* in which a CFE was thoroughly rinsed with acetone and then washed with deionized water; the CFE thus treated is denoted as CFE_1. *Procedure 3* in which a CFE was rinsed with acetone, then electrochemically cleaned at −1.5 V (vs. SCE), where hydrogen evolution occurs in a Britton-Robinson buffer solution of pH 5.0, for ca. 30 min, and finally washed with deionized water; the CFE thus treated is denoted as CFE_2. CFE_o, CFE_1, and CFE_2 were modified with PQ by potentiostatic electropolymerization using a Britton-Robinson buffer (20 vol% ethanol) solution of pH 6.0 of mercaptohydroquinone (4×10^{-4} mol dm^{-3}) at +0.7 V (vs. SCE) for 30 min under a nitrogen atmosphere at room temperature.

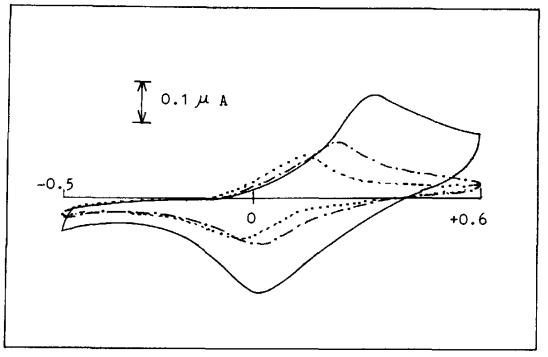

Fig. 2. Cyclic voltammograms of PH_2Q/CFE(——), $PMeH_2Q$/CFE(-·-·-), and PMe_2H_2Q/CFE(·····) in the Britton-Robinson buffer solution of pH 6.0 in an atmosphere of nitrogen at 25°C. Scan rate: 50 mVs^{-1}. Effective lengths of these electrodes dipped into the buffer solution were 3 cm.

Then the PQ's thus prepared were reduced at −0.5 V (vs. SCE) for 30 min in a buffer solution of pH 5.0 to give PH_2Q's. PH_2Q/CFE_0, PH_2Q/CFE_1, and PH_2Q/CFE_2 were stored in a weakly acidic buffer solution and were thoroughly rinsed with deionized water just before SEM measurement. Figure 1 shows scanning electron micrographs of PH_2Q/CFE_0 (a), PH_2Q/CFE_1 (b), and PH_2Q/CFE_2 (c). These micrographs reveal that CFE_2 is uniformly coated over the whole surface with a relatively large amount of PH_2Q, whereas CFE_1 is partially coated with PH_2Q, and that CFE_0 is scarcely coated. Only PH_2Q/CFE_2 displayed good durability. Moreover, PMe_2H_2Q could not be prepared on CFE_1 or CFE_2. These results obtained by SEM indicate that uniform coating of PH_2Q on CFE is required for PH_2Q/CFE to possess good durability as a pH sensor and that the electrochemical cleaning method used here is a preferable pretreatment of the CFE surface. Unless otherwise stated, subsequent examinations were carried out with the CFE_2 prepared as described above. Cyclic voltammograms of CFE's modified with PH_2Q, $PMeH_2Q$, or PMe_2H_2Q are shown in Fig. 2. The anodic and cathodic current integrals of these cyclic voltammograms indicate that the amount of electroactive sites developed on CFE's are in the order: PH_2Q (2.9×10^{-1} mC cm^{-2}) > $PMeH_2Q$ (1.5×10^{-1} mC cm^{-2}) > PMe_2H_2Q (1.1×10^{-1} mC cm^{-2}). The scanning electron micrographs (Fig. 3) of $PMeH_2Q$/CFE and PMe_2H_2Q/CFE surfaces indicate that $PMeH_2Q$ and PMe_2H_2Q, as well as PH_2Q (Fig. 1), are coated uniformly over the whole surfaces of CFE's. Characteristics of their pH responses are summarized in Table 1. Of these three electrodes, only PMe_2H_2Q/CFE could hardly get wetted in an acidic buffer solution having pH lower than 4.5, while in alkaline solution PMe_2H_2Q/CFE was superior to the others in Nernstian response and durability. As seen from Fig. 2, hydroquinone moieties which provide redox sites in PH_2Q, $PMeH_2Q$, and PMe_2H_2Q have an increasing tendency to shift their redox potentials towards negative with increasing number of methyl groups. This tendency is consistent with the fact that redox potentials of hydroquinones are usually shifted more negative with increasing number of electron-releasing substituents such as methyl group.[11] Furthermore, it has been known that acid-base dissociation constants of hydroquinones substituted by electron-releasing groups are smaller than that of unsubstituted hydroquinone

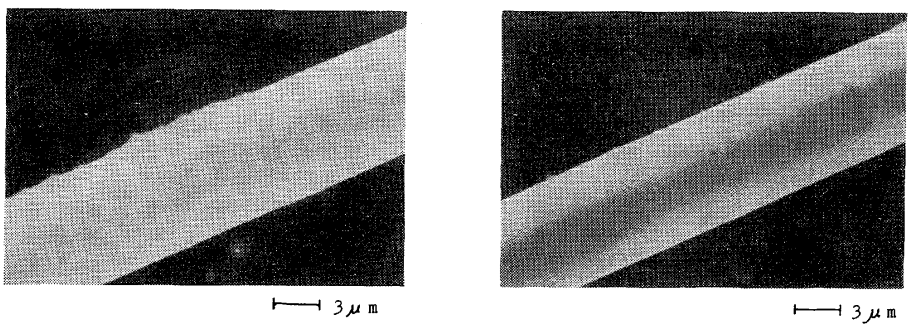

Fig. 3. Scanning electron micrographs of $PMeH_2Q$/CFE (a) and PMe_2H_2Q/CFE (b).

Table 1. pH Response Characteristics of PH_2Q/CFE, $PMeH_2Q$/CFE, and PMe_2H_2Q/CFE at 25 °C[a]

Electrode[b]	Slope	Response range	Response-time pH range (I) within 2s (II) within 10s
	mV/pH	pH	
PH_2Q/CFE	59.0±0.4[c]	1.8—8.5	(I) 3.0—8.0
	30.0±0.8[c]	<10.0	(II) 1.8—3.0, 8.0—9.0
$PMeH_2Q$/CFE	58.9±0.4[c]	2.0—9.0	(I) 3.0—8.0
	30.0±0.8[c]	<10.0	(II) 2.0—3.0, 8.0—9.5
PMe_2H_2Q/CFE	58.9±0.3[c]	4.5—10.0	(I) 4.5—9.0
	30.0±0.7[c]	<11.0	(II) 9.0—10.0

a) Britton-Robinson buffer (2<pH<11) and Clark-Lubs buffer (pH<2) were used as standard pH solutions. b) The effective length immersed into the buffer was ca. 1 mm. c) The standard deviation for slopes obtained with multiple calibrations over 20 times.

in aqueous solution.[12] As can be seen in the response ranges in Table 1, the upper limit of linear response with a slope of ca. 59 mV/pH for each electrode is in the order of PMe_2H_2Q/CFE > $PMeH_2Q$/CFE > PH_2Q/CFE. Consequently, it would be reasonable to judge that the upper limits of linear response (ca. 59 mV/pH) for PH_2Q/CFE, $PMeH_2Q$/CFE, and PMe_2H_2Q/CFE are dependent on the dissociation constants of hydroquinone moieties in PH_2Q, $PMeH_2Q$, and PMe_2H_2Q, respectively. All these electrodes could work well for at least one month when kept stored in a weak acidic buffer solution. But their pH responses gave rise to apparent deviations from the Nernstian behavior after successive measurements in alkaline buffer solution. It is considered that this undesirable behavior results from oxidation of the hydroquinone to quinone moieties in PH_2Q, $PMeH_2Q$, and PMe_2H_2Q by dissolved oxygen gas, because a sufficient deaeration of an alkaline solution by bubbling nitrogen gas could serve to slow down the rate of lowering of their durabilities. Moreover, even after used successively in an alkaline solution, both $PMeH_2Q$/CFE and PMe_2H_2Q/CFE could be practically restored by electroreduction of the resulting quinone moieties to the hydroquinone ones at −0.5 V (vs. SCE) in a weak acidic buffer solution for ca. 30 min in a nitrogen atmosphere. On the other hand, the PH_2Q/CFE whose response function had been lowered could scarcely be restored by the electroreduction. This poor restoration of PH_2Q/CFE may be attributed to the fact that no substituted quinones are more susceptible to aqueous decomposition caused by attack of hydroxide ion than methyl-substituted quinones in alkaline solution.[13] All of PH_2Q/CFE, $PMeH_2Q$/CFE, and PMe_2H_2Q/CFE prepared under the electrolysis conditions of 1×10^{-4} to ca. 1×10^{-3} mol dm^{-3} in concentration, 20 min to ca. one hour in electrolysis time, and +0.5 to +0.7 V (vs. SCE) in electrolysis potential, exhibited similar excellent Nernstian responses to pH as shown in Table 1 and displayed good durabilities. When mercaptohydroquinones were electrooxidized at higher concentrations or for longer period than have been specified above, PH_2Q/CFE, $PMeH_2Q$/CFE, and PMe_2H_2Q/CFE obtained could not respond well to pH. Moreover, when mercaptohydroquinones were oxidized above +0.8 V (vs. SCE) on CFE, the resulting modified CFE's made no response to pH. We have previously reported that mercaptohydroquinone shows an anodic wave which is probably caused by oxidation of a thiol group, at +0.8 V (vs. SCE) on DC polarogram in a Britton-Robinson buffer solution (pH 6.0) using a glassy carbon electrode.[6] Therefore, the no-response behavior observed probably results from oxidation of sulfide linkage in PH_2Q, $PMeH_2Q$, and PMe_2H_2Q.[14] As has been mentioned above, the PH_2Q/CFE, the $PMeH_2Q$/CFE, and the PMe_2H_2Q/CFE are capable of excellent functioning as pH microsensors and will, therefore, be applicable to various microchemical works.

References

1) M. Fujihira, A. Yokozawa, H. Kinoshita, and T. Osa, *Chem. Lett.*, **1982**, 1089; T. Nonaka, S. Abe, and T. Fuchigami, *Bull. Chem. Soc. Jpn.*, **56**, 2778 (1983).

2) W. H. Kao and T. Kuwana, *J. Am. Chem. Soc.*, **106**, 437 (1984); P. G. Pickup, K. N. Kuo, and R. W. Murray, *J. Electrochem. Soc.*, **130**, 2205 (1983).

3) W. R. Heineman, H. J. Wieck, and A. M. Yacynych, *Anal. Chem.*, **52**, 345 (1981); T. Nakamura, K. Ogiwara, K. Izutsu, and G. A. Rechnitz, *Bull. Chem. Soc. Jpn.*, **58**, 3409 (1985).

4) H. G. Cassidy, *J. Polym. Sci.*, D, 1 (1972); G. Manecke, *Pure Appl. Chem.*, **38**, 181 (1974).

5) B. L. Funt and P. M. Hoang, *J. Electroanal. Chem.*, **154**, 229 (1983); C. Degrand and L. L. Miller, *J. Am. Chem. Soc.*, **102**, 5728 (1980).

6) G. Arai and M. Furui, *Nippon Kagaku Kaishi*, **1984**, 673.

7) G. Arai, K. Akiba, K. Yanagisawa, and I. Yasumori, *Nippon Kagaku Kaishi*, **1984**, 1867; G. Arai, A. Fujii, and I. Yasumori, *Chem. Lett.*, **1985**, 1091.

8) G. Arai, T. Koike, and I. Yasumori, *Chem. Lett.*, **1986**, 867.

9) Mercaptomethylhydroquinones synthesized here were a mixture of 2-mercapto-3-methylhydroquinone, 2-mercapto-5-methylhydroquinone, and 2-mercapto-6-methylhydroquinone.

10) W. Alcolay, *Helv. Chim. Acta*, **30**, 578 (1947).

11) P. Zuman, *Collect. Czech. Chem. Commun.*, **27**, 2035 (1962).

12) P. Zuman, "Substituent Effects in Organic Polarography," Plenum Press, New York (1967), Chap. 8.

13) K.T. Finley, "The chemistry of the quinonoid compounds," in "The chemistry of functional groups," ed by S. Patai, John Wiley & Sons, London and New York (1974), pp. 941—947.

14) M. M. Baizer, "Organic Electrochemistry," Marcel Dekker, Inc., New York (1973), pp. 552—554.

Reactions of α,β-Unsaturated Carboxylates, Malonates and Phenylacetates with Manganese(III) Acetate in the Presence of Chloride Ions

Hiroshi YONEMURA, Hiroshi NISHINO, and Kazu KUROSAWA*
Department of Chemistry, Faculty of Science, Kumamoto University, Kurokami 2-39-1, Kumamoto 860
(Received July 26, 1986)

Synopsis. The reaction of alkyl (*E*)-3-phenylpropenoates with manganese(III) acetate in the presence of Cl^- ions gave alkyl (*Z*)-2-chloro-3-phenylpropenoates and alkyl 2,3-dichloro-3-phenylpropanoates. Ethyl (*E*)-2,3-diphenylpropenoate yielded ethyl 2,3-dichloro-2,3-diphenylpropanoate. Alkyl 3,3-diphenylpropenoates gave mainly alkyl 2-chloro-3,3-diphenyl-propenoates. Ethyl 1-cyclohexenecarboxylate gave ethyl 1,2-dichlorocyclohexanecarboxylate. Dimethyl malonate yielded dimethyl dichloromalonate and tetramethyl 1,2-dichloro-1,1,2,2-ethanetetracarboxylate. Substituted malonates resulted in α-chloro derivatives. Methyl phenylacetates gave α-acetoxy derivatives.

Although there have been many investigations into the reaction of manganese(III) acetate,[1] the reaction of this reagent in the presence of the Cl^- ion, which forms a complex, has not been fully examined. In connection with earlier studies of the reactions of aromatic compounds,[2] olefins,[2,3] aryl ketones,[4] and phenyl-substituted propenoic acids,[5] we have now examined the reaction of several kinds of esters with the complex in the hope that this would give chlorinated compounds: we found that α,β-unsaturated esters, malonates, and phenylacetates are reactive towards this complex. We will describe these reactions in this paper.

Results and Discussion

α,β-Unsaturated Esters. The reaction of ethyl (*E*)-3-phenylpropenoate (**1a**) with the manganese(III)-Cl^- complex at a molar ratio of **1a**: Mn(III): Cl^- of 1 : 6 : 12,[6,7] resulted in two products, ethyl 2,3-dichloro-3-phenylpropanoate (**2a**) and ethyl (*Z*)-2-chloro-3-phenylpropenoate (**3a**). The former was the major product. When methyl (*E*)-3-(4-chlorophenyl)propenoate (**1b**) was oxidized with the complex, methyl 2,3-dichloro-3-(4-chlorophenyl)propanoate (**2b**) and methyl (*Z*)-2-chloro-3-(4-chlorophenyl)propenoate (**3b**) were obtained similarly, but in this case **3b** was predominant. Methyl (*E*)-3-(3-nitrophenyl)propenoate (**1c**) and methyl (*E*)-3-(4-methylphenyl)propenoate (**1d**) gave the corresponding 2-chloro derivatives (**3c** and **3d**), while **1d** also yielded **2d** and methyl 3-acetoxy-2-chloro-3-(4-methylphenyl)propanoate (**4d**). When methyl (*E*)-(4-methoxyphenyl)propenoate (**1e**) was oxidized with the complex, methyl (*Z*)-2-chloro-3-(4-methoxyphenyl)propenoate (**3e**), methyl 2-acetoxy-3-chloro-3-(4-methoxyphenyl)propanoate (**4e**) and *p*-anisic acid (**5**) were obtained (Table 1, Entries 1—5).

The reaction of methyl (*E*)-2,3-diphenylpropenoate (**6**) with the manganese(III) acetate-Cl^- complex gave methyl 2,3-dichloro-2,3-diphenylpropanoate (**7**) exclusively (Entry 6).

The reactions of alkyl 3,3-diphenylpropenoates (**8a** and **8b**) gave 2-chloro derivatives (**9a** and **9b**) as the major products, while ethyl 9-fluorenylideneacetate (**8c**) yielded ethyl 9-fluorenylidenechloroacetate (**9c**) and ethyl (9-acetoxy-9-fluorenyl)chloroacetate (**12**) (Entries 7, 8, and 9). The reaction of ethyl 1-cyclohexenecarboxylate (**13**) with the complex yielded only ethyl 1,2-dichloro-1-cyclohexanecarboxylate (**14**) (Entry 10).

Dialkyl Malonates (15a—f). When diethyl methylmalonate (**15a**) was oxidized with the manganese(III) acetate-Cl^- complex, it gave diethyl α-(chloro)-methylmalonate (**16a**) in an excellent yield (Entry 11). Butyl (**15b**) and benzylmalonate (**15c**) yielded monochloro derivatives (**16b** and **16c**) (Entries 12 and 13). Dimethyl chloromalonate (**15d**) gave dimethyl dichloromalonate (**16d**) (Entry 14). Dimethyl malonate (**15e**), on the other hand, yielded two products: dimethyl dichloromalonate (**16d**) and a dimeric compound (**17d**) which was also obtained by the reaction of **15d** with manganese(III) acetate alone (Entries 15 and 16). Dimethyl bromomalonate (**15f**) gave a mixture of various products, from which only tetramethyl 1,2-dibromo-1,1,2,2-ethanetetracarboxylate (**17f**) was isolated and that is in a poor yield (Entry 17). The **15f** yielded tetramethyl ethenetetracarboxylate (**18**) on prolonged heating when the reaction was conducted with manganese(III) acetate alone (Entry 19).

Methyl Phenylacetates (19a and 19b). The reactions of methyl 4-methoxyphenylacetate (**19a**) and methyl 3,4-dimethoxyphenylacetate (**19b**) yielded α-acetoxy derivatives (**20a** and **20b**) in good yields (Entries 20 and 22). When **19a** was oxidized with manganese(III) acetate alone over a prolonged reaction time, methyl 3-(acetoxymethyl)-4-methoxyphenylacetate (**21**) was obtained in a minor quantity, together with **20a** (Entry 21). Unsubstituted ethyl phenylacetate was found to be unreactive towards the manganese(III) acetate-Cl^- complex under the present reaction conditions.

Conclusion. The reaction of methyl (*E*)-3-phenylpropenoate with the manganese(III) acetate-Cl^- was previously briefly reported to give methyl 2,3-dichloro-3-phenylpropanoate and methyl (*E*)-2-chloro-3-phenylpropenoate.[3] However, we found that a substituent on the aromatic ring and an extra phenyl group at the C-2 or C-3 change the product distribution completely. The reaction of methyl (*E*)-3-(4-chlorophenyl)-propenoate (**1b**) gave the 2-chloro derivative (**3b**) as the major product, while methyl (*E*)-3-(4-methoxyphenyl)-propenoate (**1e**) yielded methyl 3-acetoxy-2-chloro-3-(4-methoxyphenyl)propanoate (**4e**). The reaction of **1e** ended in a shorter reaction time compared with the others, whereas **1c**, which has an electron-withdrawing nitro group, was less reactive and 25% of the **1c** was

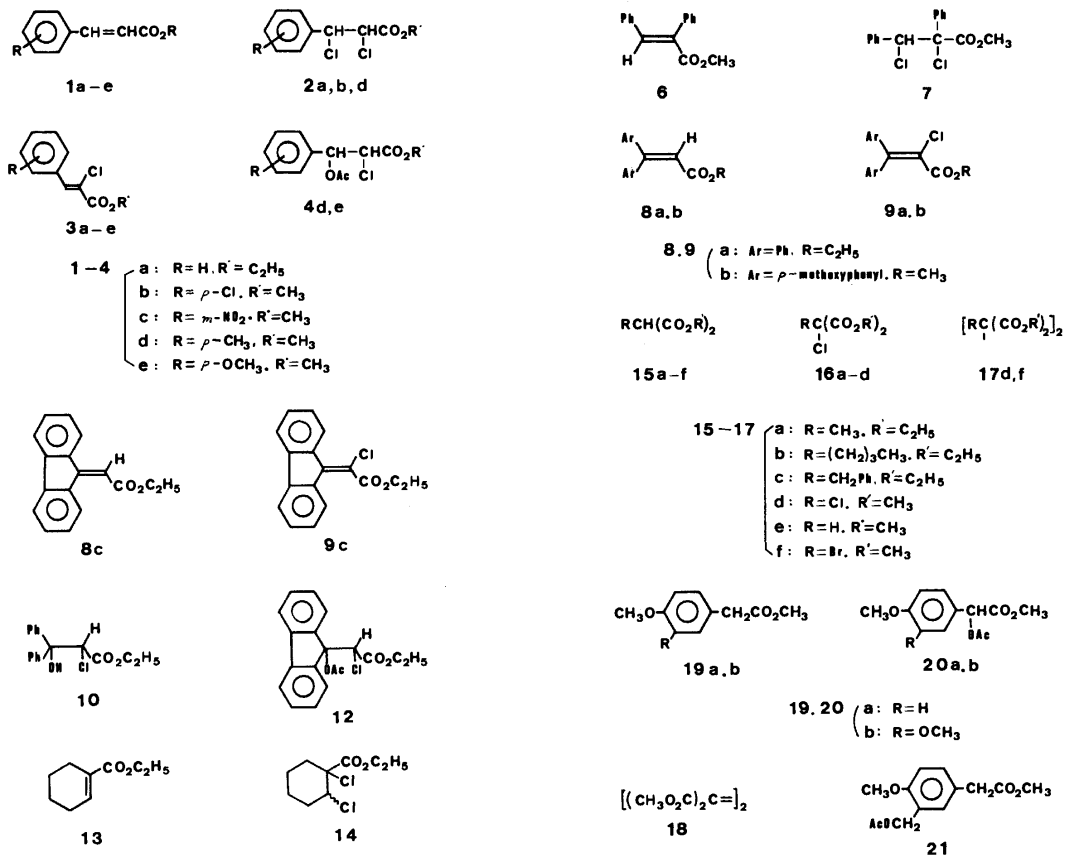

Fig. 1.

Table 1. Reaction of Esters with Manganese(III) Acetate in the Presence of LiCl[a)]

Entry	Substrate	Molar ratio[b)]	Reaction time/min	Product yield[c)]/%
1	**1a**	1 : 6 : 12	310	**2a**[8)](59), **3a**[9)](14)
2	**1b**	1 : 8 : 16	440	**2b**[10)](33), **3b**[11)](49)
3	**1c**	1 : 10 : 15	450	**3c**[11)](35)[d)]
4	**1d**	1 : 8 : 16	410	**2d**[10)](13), **3d**[12)](34), **4d**[11)](21)
5	**1e**	1 : 6 : 12	180	**3e**(17), **4e**[13)](59), **5**(21)
6	**6**	1 : 8 : 24	340	**7**(84)
7	**8a**	1 : 6 : 12	460	**9a**[14)](66), **10**(13)
8	**8b**	1 : 3 : 10	30	**9b**(74), **11**[15)](19)
9	**8c**	1 : 6 : 18	250	**9c**(24), **12**(65)
10	**13**	1 : 6 : 18	310	**14**(83)
11	**15a**	1 : 3 : 10	80	**16a**[16)](88)
12	**15b**	1 : 3 : 10	41	**16b**[17)](90)
13	**15c**	1 : 3 : 10	60	**16c**[18)](95)
14	**15d**	1 : 3 : 10	94	**16d**[19)](69)
15	**15d**	1 : 1.2 : 0	65	**17d**(60)
16	**15e**	1 : 3.4 : 10	16	**16d**(55), **17d**(18)
17	**15f**	1 : 3 : 10	110	**17f**(17)
18	**15f**	1 : 1.2 : 0	60	**17f**(31)
19	**15f**	1 : 3 : 0	215	**18**[20)](76)
20	**19a**	1 : 2.5 : 10	30	**20a**(94)
21	**19a**	1 : 3 : 0	540	**20a**(41), **21**(16)[e)]
22	**19b**	1 : 2.5 : 10	6	**20b**(84)

a) The reaction was carried out at the reflux temperature. b) Substrate: Mn(III): LiCl. c) Isolated yields based on the substrate added. All products were reasonably pure after TLC separation. d) **1c** (25%) was recovered. e) **19a** (39%) was recovered.

recovered even when an excess of the reagent was used. A phenyl group at the C-2 in a propenoate favors the formation of 1,2-dichloro compound **7**, while a phenyl group at the C-3 makes 2-chloro derivatives (**9a** and **9b**) the major products. The reactions of malonic esters and methoxy-substituted phenylacetates with the manganese(III) acetate-Cl^- complex gave α-chloro and α-acetoxy derivatives respectively in excellent yields. These can be useful in organic synthesis.

Table 2. Physical and Spectral Data for the Reaction Products[a)]

Compound	Mp (θ_m/°C) (solvent)[b)]	ν/cm^{-1}[c)]	δ/ppm[d)]
3e	58.8—59.8 (Diethyl ether-Light petroleum)	1717	3.78 (3H, s), 3.82 (3H, s), 6.86 (2H, m), 7.77 (2H, m), 7.79 (1H, s)
7[e)]	Liquid	1735	3.57 (3H, s), 5.79 (1H, s), 6.9—7.5 (10H, m) 3.68 (3H, s), 5.74 (1H, s), 6.9—7.5 (10H, m)
9b	92.8—93.8 (Ethanol)	1719	3.57 (3H, s), 3.75 (6H, s), 6.7—7.3 (8H, m)
9c	72.4—72.6 (Ethanol)	1727	1.39 (3H, t, J=7.2 Hz), 4.42 (2H, q, J=7.2 Hz), 7.1—7.6 (7H, m), 8.2—8.4 (1H, m)
10	122—122.6 (Ethanol)	1725 3500	1.00 (3H, t, J=6.6 Hz), 4.01 (2H, q, J=6.6 Hz), 4.55 (1H, s), 5.17 (1H, s), 7.1—7.6 (10H, m)
12	Liquid	1747	0.72 (3H, t, J=7.2 Hz), 1.90 (3H, s), 3.70 (2H, q, J=7.2 Hz), 5.36 (1H, s), 7.1—7.8 (8H, m)
14	Liquid	1740	1.32 (3H, t, J=7.2 Hz), 1.2—2.7 (8H, m), 4.20 (2H, q, J=7.2 Hz), 4.56 (1H, m)
17d	91—92 (Methanol-Light petroleum)	1745 1760	3.80 (s)
17f	103.5 (Methanol)	1732 1750	3.84 (s)
20a	Liquid	1742	2.09 (3H, s), 3.64 (3H, s), 3.75 (3H, s), 5.79 (1H, s), 6.78 (2H, m), 7.29 (2H, m)
20b	Liquid	1746 1755	2.06 (3H, s), 3.60 (3H, s), 3.72 (3H, s), 3.74 (3H, s), 5.65 (1H, s), 6.6—7.1 (3H, m)
21	Liquid	1732	1.99 (3H, s), 3.41 (2H, s), 3.56 (3H, s), 3.74 (3H, s), 5.00 (2H, s), 6.74 (1H, m), 7.0—7.2 (2H, m)

a) Either the elemental analyses or the high-resolution mass spectra for the new compounds agreed with the calculated values. b) For recrystallization. c) In $CHCl_3$. d) The ^1H NMR spectra were determined in $CDCl_3$ for compounds **3e**, **7**, **9b**, **10**, and in CCl_4 for others. e) A mixture of two diastereoisomers.

Experimental

Oxidation of Propenoates (1a—e, 6 and 8a—c), Malonates (15a—f), and Phenylacetates (19a and 19b) with the Manganese(III) Acetate-Chloride Ions. The general procedure for the oxidation of esters was as follows. A mixture of an ester (1 mmol), manganese(III) acetate,[6)] and chloride ions in the molar ratio shown in Table 1 in acetic acid (30 cm^3) was heated under reflux until the color of the solution had changed from brown to transparent. After the removal of the solvent, 2 M (1 M=1 mol dm^{-3}) hydrochloric acid (40 cm^3) was added to the mixture, which was then extracted with benzene or chloroform (3×30 cm^3). The benzene (or chloroform) solution was evaporated in vacuo, and the products were separated on preparative TLC (Kieselgel 60G or Wakogel B-10), with chloroform or benzene as the developing solvent. The yields are summarized in Table 1. The known compounds were identified by comparing them with the spectral data and/or the melting points in the literature. The physical and spectral data for the new compounds are summarized in Table 2.

We wish to thank Professor Hitoshi Takeshita and Associate Professor Akira Mori of the Research Institute of Industrial Science, Kyushu University, and Mr. Hirohisa Yoshida of JEOL, Ltd., for their kind assistance in obtaining the high-resolution mass spectra.

References

1) R. A. Sheldon and J. K. Kochi, "Metal-catalyzed Oxidations of Organic Compounds," Academic Press (1981).
2) M. Okano, T. Kinoshita, Y. Muramoto, and T. Aratani, *Nippon Kagaku Kaishi*, **1978**, 578.
3) K. D. Donnely, W. E. Fristad, B. J. Gellerman, J. R. Peterson, and B. J. Selle, *Tetrahedron Lett.*, **25**, 607 (1984).
4) T. Tsuruta, T. Harada, H. Nishino, and K. Kurosawa, *Bull. Chem. Soc. Jpn.*, **58**, 142 (1985).
5) H. Yonemura, H. Nishino, and K. Kurosawa, *Bull. Chem. Soc. Jpn.*, **59**, 3153 (1986).
6) Although an oxo-centered structure was assigned to manganese(III) acetate (Ref. 7), we have calculated the molar equivalent for the acetate as $Mn(OAc)_3 \cdot 2H_2O$, according to Dewar et al. (P. J. Andrulis, Jr., M. J. S. Dewar, R. Dietz, and R. L. Hunt, *J. Am. Chem. Soc.*, **88**, 5473 (1966)).
7) W. E. Fristad and J. R. Peterson, *J. Org. Chem.*, **50**, 10 (1985).
8) J. J. Sudborough and T. C. James, *J. Chem. Soc.*, **89**, 105 (1906).
9) E. Walker and T. C. James, *J. Chem. Soc.*, **115**, 1243 (1919).
10) M. D. Johnson and E. N. Trachtenburg, *J. Chem. Soc. (B)*, **1968**, 1018.
11) N. O. Postushak, A. V. Dombrovskii, and A. N. Mukhova, *Zh. Org. Khim.*, **1**, 572 (1965); *Chem. Abstr.*, **63**, 1727c (1965).
12) N. O. Postushak, A. V. Dombrovskii, and A. N. Mukhova, *Zh. Org. Khim.*, **1**, 1875 (1965); *Chem. Abstr.*, **64**, 3403e (1966).
13) P. B. D. de la Mare, M. A. Wilson, and M. J. Rosser, *J. Chem. Soc., Perkin Trans. 2*, **1973**, 1480.
14) G. Koebrich, H. Trapp, K. Flory, and W. Drischel, *Chem. Ber.*, **98**, 3637 (1965).
15) 4,4′-Dimethoxybenzophenone. M. Bösler, *Ber.*, **14**, 323 (1881).
16) O. S. Stepanova, A. S. Yovorskii, and M. T. Proberezhnaya, *Zh. Vses. Khim. Obshchest.*, **15**, 358 (1970); *Chem. Abstr.*, **73**, 65979c (1970).
17) A. S. Yavorskii, G. A. Mazurenko, and O. S. Stepanova, *Mikrobiol. Zh.*, **34**, 509 (1972); *Chem. Abstr.*, **77**, 148358h (1972).
18) M. Conrad, *Ann. Chem.*, **209**, 243 (1881).
19) E. L. Hirst and A. K. Macbeth, *J. Chem. Soc.*, **121**, 2169 (1922).
20) C. A. Bischoff, *Ber.*, **29**, 1280 (1896).

Reaction of Dimethyl 1-Hydroxyalkylphosphonates with Some Chlorides[1)]

Mitsuji YAMASHITA,* Takashi MORIZANE, Keiji FUJITA, Kaname NAKATANI, and Saburo INOKAWA†
Department of Applied Chemistry, Faculty of Engineering, Shizuoka University, Hamamatsu 432
†Department of Chemistry, Faculty of Science, Okayama University, Okayama 700
(Received May 30, 1986)

Synopsis. The reactions of dimethyl 1-hydroxycycloalkylphosphonates having a five- to seven-membered ring with sulfuryl chloride and phosphorus pentachloride afforded olefinic and/or dichloro derivatives of phosphonates. The mechanism of the formation of new dichloro derivatives and the reactions of dimethyl 1-methylethylphosphonate with sulfuryl chloride and phosphorus pentachloride were also investigated.

A carbon–phosphorus bond formation is the key step for the preparation of a phosphorus sugar, a sugar analogue having a phosphorus atom in the hemiacetal ring.[2)] Addition of a P–H group of phosphorus compounds to carbonyl group is well-known to give α-hydroxy phosphorus compounds;[3,4)] the reactivity is dependent on the structures of carbonyl compounds, and α-hydroxy phosphorus compounds from aldehydes and ketones give α-halo- and α,β-unsaturated phosphorus compounds, respectively.[5)] Facile formation of α-carbocations from mesylate derivatives of diethyl 1-hydroxyalkylphosphonates are attributable to the potent electron-withdrawing power of the phosphoryl group.[6)] On the other hand, chloro derivatives of phosphonates such as dimethyl 1-hydroxy-2,2,2-trichloroethylphosphonate are biologically active substances (e.g., insecticides).[7)] This note deals with the reaction of cyclic α-hydroxy phosphonates with sulfuryl chloride and phosphorus pentachloride, known as chlorination or dichlorination reagents,[8–11)] as well as that of an acyclic homologue.

Results and Discussion

Cyclic α-hydroxy phosphonates (**1**—**3**) each having a five to seven-membered ring were prepared by the reaction of cyclic ketones with dimethyl phosphonate in the presence of triethylamine or sodium methoxide.[12)] The reaction of dimethyl 1-hydroxycyclohexylphosphonate (**2**) with sulfuryl chloride in benzene for 8 h at room temperature in the presence of an equivalent amount of pyridine gave dimethyl 1-cyclohexylphosphonate (**4**) in 6% yield and dimethyl 1,2-dichlorocyclohexylphosphonate (**5**) in 58% yield. In the presence of excess amount of pyridine at 50 °C **2** gave 1-cyclohexenylphosphonate **4** in 51% yield, when treated with sulfuryl chloride. Since elimination of chlorine from **5** does not proceed at 50 °C, **4** seems to be formed via **2**, as indicated by the reaction of α-hydroxy phosphonates with thionyl chloride.[5)] In contrast, the reaction of **2** with phosphorus pentachloride gave **4** in quantitative yield.

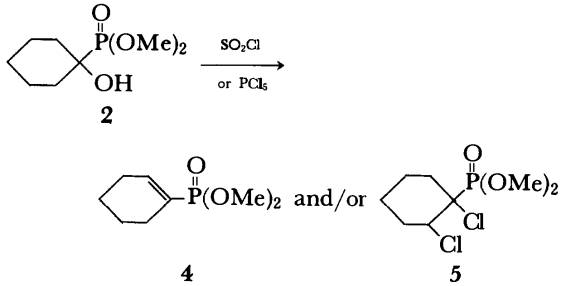

Reaction of dimethyl 1-hydroxycyclopentylphosphonate (**1**) with sulfuryl chloride or phosphorus pentachloride gave the corresponding 1,2-dichloro derivative (**8**) in 58% yield, or the olefin (**9**) in 49% yield. These results together with those for dimethyl 1-hydroxycycloheptyl- and 1-hydroxy-1-methylethylphosphonates (**3** and **12**) are summarized in Table 1. Dichlorination of cyclohexenones and ethylenic compounds and dehydration of sugar derivatives with sulfuryl chloride are known,[9,13,14)] however, the reaction of phosphonates presented here (Table 1) should be attributable to the activation by a phosphoryl group,[15)] whose powerful electron-withdrawing nature is typically shown by the σ_p (0.52) and σ^+ (0.505) values for the diethylphosphoryl group[6,16)] as well as the high reactivity of Horner-Emmons reaction.[17)]

The reaction of **4** with sulfuryl chloride in the presence of excess or equivalent amount of pyridine afforded monochloride **6** or dichloride **5** in 43 or 60% yield, respectively. Compound **6** was also prepared by treatment of **4** with NCS in 93% yield, while the bromo derivative (**7**) was prepared by the analogous reaction with NBS in quantitative yield. With sulfuryl chloride in the presence of equivalent amount of pyridine **6** afforded dichloride **5** in 79% yield. These findings suggest that the formation of dichloride **5** would proceed via intermediates **4** and **6** as shown in Scheme 1. The amount of pyridine suppressed the production of the dichloride, which may presumably be formed by addition of hydrogen chloride to the olefin.

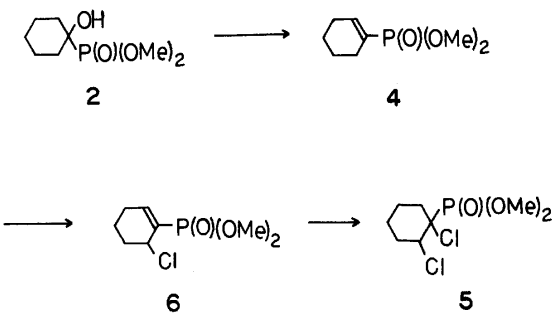

Scheme 1. Plausible mechanism for the reaction of compound **2** with sulfuryl chloride to form dichloro derivative **5**.

Experimental

Measurements. ^{1}H NMR spectra were measured on Hita-

Table 1. Reaction of α-Hydroxy Phosphonates with Some Halogenation Reagents

Substrate	Reaction condition			Product	
	Reagent	Time/h	Temperature/°C		Yield/%
2	SO_2Cl_2/Pyridine (excess)	18	50	**4**	51
	SO_2Cl_2/Pyridine (equivalent)	8	50	**4**	6
				5	58
	PCl_5	0.5	Room temp	**4**	100
4	SO_2Cl_2/Pyridine (excess)	8	50	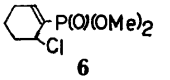 **6**	43
	N-Chlorosuccinimide (NCS)	5	60	**6**	93
	N-Bromosuccinimide (NBS)	5	60	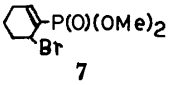 **7**	100
	SO_2Cl_2/Pyridine (equivalent)	8	50	**5**	60
6	SO_2Cl_2/Pyridine (equivalent)	8	50	**5**	79
1	SO_2Cl_2/Pyridine (equivalent)	20	50	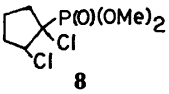 **8**	58
	PCl_5	1	Room temp	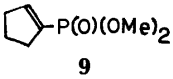 **9**	49
3	SO_2Cl_2/Pyridine (equivalent)	20	50	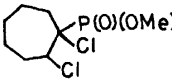 **10**	35
	PCl_5	1	Room temp	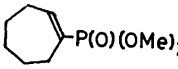 **11**	37
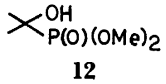 **12**	SO_2Cl_2/Pyridine (equivalent)	8	50	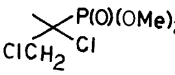 **13**	27
	PCl_5	0.5	Room temp	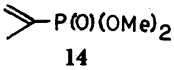 **14**	76

chi R-24 (60 MHz) or R-20 (60 MHz) spectrometer with tetramethylsilane as an internal standard. IR spectra were recorded with Japan Spectroscopic Co., Ltd. A-3 infrared spectrometer. MS spectra were measured by Hitachi RMU 7M GC-MS spectrometer.

Reaction of Dimethyl 1-Hydroxycyclohexylphosphonate (2) with Sulfuryl Chloride. To a solution of compound **2** (4.87 g, 23.4 mmol) in benzene (6 ml) and pyridine (1.85 g) was added sulfuryl chloride (1.89 ml), then the mixture was stirred for 8 h at 50 °C. The product was extracted with diethyl ether and the organic layer was washed with water and dried over anhydrous magnesium sulfate. Evaporation of the solvent in vacuo followed by chromatography on silica gel and recrystallization from carbon tetrachloride gave 1,2-dichlorocyclohexylphosphonate **5** (3.5 g, 58%), mp 76—77 °C, as well as dimethyl 1-cyclohexenylphosphonate (**4**, 0.27 g, 6%). Spectral data for **4**: ^{1}H NMR ($CDCl_3$) δ=1.4—2.5 (m, 8H, C_6H_8), 3.68 (d, 6H, J_{HP}=11.1 Hz, 2OMe), and 6.75 (dt, 1H, J_{HP}=22.2 Hz, J_{HH}=1.2 Hz, CH=CP); IR (neat) 1637 (C=C), 1238 (P=O), and 1180, 1028 cm^{-1} (P-O-C); MS *m/z*, 190 (M^+). Spectral data for **5**: ^{1}H NMR ($CDCl_3$) δ=1.2—2.3 (m, 8H, C_6H_8), 3.82, 3.88 (2d, 6H, J_{HP}=11.1 Hz, 2OMe), and 4.43 (ddd, 1H, J_{PCCH}=3.9 Hz, $J_{H_{ax}CC(Cl)H_{ax}}$=7.8 Hz, $J_{H_{eq}CC(Cl)H_{ax}}$=3.9 Hz, $CH_{ax}Cl$); IR (KBr) 1250 (P=O), 1186, 1015 (P-O-C), and 740, 691 cm^{-1} (C-Cl); MS *m/z*, 260 (M^+, rel intensity 100%), 262 (M^+ + 2, 65%), and 264 (H^+ 4, 9.7%).

Found: C, 36.37; H, 5.91%. Calcd for $C_8H_{15}Cl_2O_3P$: C, 36.80; H, 5.79%.

Reaction of compound **2** (4.00 g) with sulfuryl chloride (1.8 ml) in pyridine (7 ml) for 18 h at 50 °C afforded product **4** (1.86 g, 51%) after work-up and separation by TLC on silica gel.

Reaction of Compound 2 with Phosphorus Pentachloride. To a solution of compound **2** (3.01 g, 14.5 mmol) in benzene (8 ml) was added phosphorus pentachloride (3.50 g, 14.5 mmol) with stirring, and the mixture was then stand for 10 h at room temperature. The reaction mixture was poured into ice-water (50 ml) and extracted with chloroform (total 50 ml). The extract was washed with sodium hydrogencarbonate and water, and dried over anhydrous magnesium sulfate. Removal of the solvent in vacuo gave product **4** (2.75 g, quantitative).

Reaction of Dimethyl 1-Hydroxycyclopenthylphosphonate (1) or Dimethyl 1-Hydroxycycloheptylphosphonate (3) with Sulfuryl Chloride. Reaction of compound **1** or **3** with sulfuryl chloride in the presence of an equivalent amount of pyridine afforded the corresponding dichloride, dimethyl 1,2-dichlorocyclopentylphosphonate (**8**) or dimethyl 1,2-dichlorocycloheptylphosphonate (**10**) in 58 or 35% yield, respectively (Table 1). Spectral data for **8**: ^{1}H NMR ($CDCl_3$) δ=1.9—3.0 (m, 6H, C_5H_6), 3.98, 4.03 (2d, 6H, J_{HP}=10.2 Hz, 2OMe), and 4.4—4.7 (m, 1H, CHCl); MS *m/z*, 246 (M^+), 248

(M^+ +2), and 250 (M^+ +4). Spectral data for **10**: ^{1}H NMR ($CDCl_3$) δ=1.0—3.5 (m, 10H, C_7H_{10}), 3.37, 3.49 (2d, 6H, J_{HP}=10.1 Hz, 2OMe), and 4.4—4.8 (m, 1H, CHCl); MS *m/z*, 278 (M^+), 280 (M^+ +2), and 282 (M^+ +4).

Reaction of Compound 1 or 3 with Phosphorus Pentachloride. Reaction of compound **1** or **3** with phosphorus pentachloride gave the corresponding olefinic product, dimethyl 1-cyclopentenylphosphonate (**9**) or dimethyl 1-cycloheptenylphosphonate (**11**) in 49 or 37% yield, respectively. Spectral data for **9**: ^{1}H NMR ($CDCl_3$) δ=1.3—3.0 (m, 6H, C_5H_6), 3.82 (d, 6H, J_{HP}=15.8 Hz, 2OMe), and 6.75 (dt, 1H, J_{PCCH}=14.3 Hz, J_{HH}=2.0 Hz, CH=CP). Spectral data for **11**: ^{1}H NMR ($CDCl_3$) δ=1.3—2.2 (m, 10H, C_7H_{10}), 3.68 (d, 6H, J_{HP}=10.8 Hz, 2OMe), and 6.98 (dt, 1H, J_{PCCH}=24.3 Hz, J_{HH}=6.5 Hz).

Reaction of Compound 4 with Sulfuryl Chloride. Reaction of compound **4** (0.48 g, 2.5 mmol) with sulfuryl chloride (0.34 g, 2.5 mmol) in pyridine (0.19 ml, equivalent)-benzene (1 ml) or in pyridine (2 ml, excess) for 8 h at 50 °C afforded product **5** or **6** in 60 or 43% yield, respectively. Spectral data for **6**: ^{1}H NMR ($CDCl_3$) δ=1.2—2.4 (m, 6H, ring protons), 3.70 (d, 6H, J_{HP}=10.4 Hz, 2OMe), 4.0—4.6 (m, 1H, CHCl), and 6.67 (dt, 1H, J_{PCCH}=22.7 Hz, J_{HH}=1.7 Hz, CH=CP); IR (neat) 1230 (P=O), 1190, 1018 (P-O-C), and 735, 600 cm^{-1} (C-Cl); MS *m/z*, 224 (M^+, 100%) and 226 (M^+ +2, 29%).

Reaction of Compound 4 with *N*-Chlorosuccinimide (NCS) or *N*-Bromosuccinimide (NBS). Reaction of compound **4** (2.0 mmol) with NCS or NBS (2.0 mmol) was carried out in carbon tetrachloride (2 ml) for 5 h at 60 °C. Usual work-up of the reaction mixture afforded chloride **6** or bromide **7** in 93% or quantitative yield, respectively. Spectral data for **7**: ^{1}H NMR ($CDCl_3$) δ=1.3—2.7 (m, 6H, ring protons), 3.74 (d, 6H, J_{HP}=10.0 Hz, 2OMe), 4.3—5.1 (m, 1H, CHBr), and 6.83 (dt, 1H, J_{PCCH}=20.0 Hz, J_{HH}=1.3 Hz, CH=CP); IR (neat) 1240 (P=O), 1190, 1040 (P-O-C), and 580 cm^{-1} (C-Br); MS *m/z*, 268 (M^+, 100%) and 270 (M^+ +2, 91%).

Reaction of Compound 6 with Sulfuryl Chloride. Reaction of compound **6** (49 mg, 0.22 mmol) with sulfuryl chloride (30 mg, 0.22 mmol) in pyridine (25 μl, equivalent)-benzene (1 ml) for 8 h at 50 °C afforded product **5** (45 mg, 79%).

Reaction of Dimethyl 1-Hydroxy-1-methylethylphosphonate (12). Reaction of compound **12** (0.84 g, 5.0 mmol) with sulfuryl chloride or with phosphorus pentachloride afforded dimethyl 1,2-dichloro-1-methylethylphosphonate (**13**, 0.18 g, 27%) or dimethyl 1-methylvinylphosphonate (**14**, 0.57 g, 76%), respectively. Spectral data for compound **13**: ^{1}H NMR ($CDCl_3$) δ=1.73 (d, 3H, J_{HP}=15.0 Hz, PCMe), 3.69 (d, 2H, J_{HP}=15.0 Hz, $PCCH_2$), and 3.81 (d, 6H, J_{HP}=10.6 Hz, 2POMe); IR (neat) 1260 (P=O), 1040 (P-O-C), and 760, 602 cm^{-1} (C-Cl); MS *m/z*, 220 (M^+, 100%), 222 (M^+ +2, 54%) and 224 (M^+ 4, 19%). Spectral data for compound **14**; ^{1}H NMR ($CDCl_3$) δ=1.95 (ddd, 3H, J_{HP}=14.0 Hz, J_{HH}=1.7 Hz, J_{HH}=1.3 Hz, PCMe), 3.71 (d, 6H, J_{HP}=10.8 Hz, 2POMe), 5.80 (ddq, 1H, J_{HP}=47.0 Hz, J_{HH}=1.7 Hz, J_{HH}=1.3 Hz, $PC=CH_{(trans)}$), 5.97 (ddq, 1H, J_{HP}=22.7 Hz, J_{HH}=1.7 Hz, J_{HH}=1.3 Hz, $PC=CH_{(cis)}$); IR (neat) 1250 (P=O), 1040 cm^{-1} (P-O-C); MS *m/z*, 150 (M^+).

References

1) M. Yamashita, T. Morizane, K. Fujita, K. Nakatani, M. Yamada, H. Yamashita, T. Oshikawa, and S. Inokawa, 13th Annual Meeting of Chubu Kagaku Kankei Gakukyokai Shibu Rengo Shuki Taikai, Tsu, September 1982, Abstr., No. 2G04.

2) M. Yamashita, Y. Nakatsukasa, H. Yoshida, T. Ogata, and S. Inokawa, *Carbohydr. Res.*, **70**, 247 (1979).

3) A. J. Kirby and S. G. Warren, "The Organic Chemistry of Phosphorus," Elsevier, Amsterdam (1967), pp. 54, 57.

4) M. Yamashita, P. T. Long, M. Shibata, and S. Inokawa, *Carbohydr. Res.*, **84**, 35 (1980).

5) K. Gomyo, H. Yoshida, T. Ogata, H. Inokawa, and S. Inokawa, *Nippon Kagaku Kaishi*, **1974**, 1093.

6) X. Creary, C. C. Geiger, and K. Hilton, *J. Am. Chem. Soc.*, **105**, 2851 (1983).

7) J. Emsley and D. Hall, "The Chemistry of Phosphorus," Harper and Row, London (1976), Chap. 12.

8) A. Mooradian and J. B. Cloke, *J. Am. Chem. Soc.*, **68**, 785 (1946).

9) M. S. Kharasch and H. C. Brown, *J. Am. Chem. Soc.*, **61**, 2142 (1939); M. S. Kharasch and H. C. Brown, *ibid.*, **61**, 3432 (1939).

10) D. P. Wyman and P.R. Kaufman, *J. Org. Chem.*, **29**, 1956 (1964).

11) D. P. Wyman, J. Y. C. Wang, and W. R. Freeman, *J. Org. Chem.*, **28**, 3173 (1963).

12) V. S. Abramov, *Dokl. Akad. Nauk SSSR*, **95**, 991 (1954); *Chem. Abstr.*, **49**, 6084d (1955).

13) M. F. Grenier-Loustalot, P. Iratcabal, and F. Metras, *Synthesis*, **1976**, 33.

14) J. Cleophax, J. Leboul, D. Mercier, A. Gaudemer, S. D. Gero, *Bull. Soc. Chim. Fr.*, **1973**, 2992; *Chem. Abstr.*, **80**, 95328b (1974).

15) M. Yamashita, K. Tsunekawa, M. Sugiura, T. Oshikawa, and S. Inokawa, *Chem. Lett.*, **1983**, 1673.

16) E. N. Tsvetkov, D. I. Lobanov, L. A. Isosenkova, and M. I. Kabachnik, *J. Gen. Chem. USSR*, **39**, 2126 (1969).

17) J. C. Stowell, "Carbanions in Organic Synthesis," John Wiley, New York (1979), p. 182.

Deacylation Effect in the Hydrolysis of *p*-Nitrophenyl Esters by Bifunctional Comicelles Containing Imidazolyl and Hydroxyl Groups

Yasuji IHARA,* Mamoru NANGO,† and Joichi KOGA†
Yamaguchi Women's University, 3-2-1 Sakurabatake, Yamaguchi 753
†Department of Applied Chemistry, University of Osaka Prefecture, Sakai, Osaka 591
(Received June 12, 1986)

Synopsis. The rate constants for hydrolysis of *p*-nitrophenyl acetate, hexanoate, and dodecanoate catalyzed by bifunctional catalysts containing the imidazolyl and hydroxyl groups have been determined in the presence of hexadecyltrimethylammonium bromide micelles at 25 °C. The kinetic analysis suggests a nucleophilic mechanism which involves acylation followed by deacylation at the imidazolyl group. Although no appreciable differences in cooperative catalytic efficiencies are observed between the bifunctional groups in the acylation step, it is found that the deacylation rates are accelerated by the hydroxyl group of the catalyst in the presence of micelles.

In the past several years, many micellar enzyme models have been investigated in order to gain further insight into the nature of enzyme reactions[1-5] and, particularly, bifunctional micellar catalysis has been reported as models of esterolytic enzymes for the hydrolysis of *p*-nitrophenyl esters. The catalytic hydrolysis of *p*-nitrophenyl esters by micelles derived from functional surfactants normally occurs by a nucleophilic mechanism with subsequent decomposition of an acylated micellar intermediate.[3a,4,5] We have previously demonstrated the large rate enhancements in deacylation process during the hydrolysis of *p*-nitrophenyl esters by *N*-acylhistidine or dipeptide catalysts in the presence of hydroxyl functionalized surfactant micelles.[6]

The present study describes the results for deacylation effect of bifunctional comicellar catalysts containing the imidazolyl and hydroxyl groups for the hydrolysis of *p*-nitrophenyl acetate (PNPA), hexanoate (PNPH), and dodecanoate (PNPL) in the presence of hexadecyltrimethylammonium bromide (CTAB) micelles. The catalysts used in this experiment are *N*-decanoyl-L-histidine (**1a**) and *N*-benzyloxycarbonyl-L-phenylalanyl-L-histidine (**2a**), both having an imidazolyl group, and *N*-acyl-L-tyrosine (**1b,c**) and *N*-decanoyl-L-serine (**1d**), both having a hydroxyl group, or *N*-benzyloxycarbonyl-L-tyrosyl-L-histidine (**2b**) and *N*-benzyloxycarbonyl-L-histidyl-L-tyrosine (**2d**), both having imidazolyl and hydroxyl groups.

Experimental

Materials. *N*-Decanoyl-L-tyrosine (**1b**), *N*-decanoyl-L-serine (**1d**), and *N*-decanoyl-L-phenylalanine (**1e**) were prepared and purified by standard methods.[7] *N*-Acetyl-L-tyrosine (**1c**), *N*-benzyloxycarbonyl-L-phenylalanyl-L-histidine (**2a**), *N*-benzyloxycarbonyl-L-tyrosyl-L-histidine (**2b**), *N*-benzyloxycarbonyl-L-histidyl-L-phenylalanine (**2c**), and *N*-benzyloxycarbonyl-L-histidyl-L-tyrosine (**2d**) were commercially available and were used without further purification. Other materials have been described elsewhere.[8-11]

Kinetic Measurements. Reactions were generally monitored on a Hitachi 200 spectrophotometer or a Shimadzu 140 spectrophotometer with a thermostated cell holder at 25 °C. In the general procedure, a solution (25 μl) of substrate in acetonitrile was added to a buffer solution (3.00 cm^3) containing the catalyst and surfactant at the desired concentrations. Pseudo-first-order rate constants were obtained from plots of $\log(A_\infty - A_t)$ versus time (t) by use of the least-squares method. Correlation coefficients were >0.999.

Results and Discussion

The catalytic process can be described by Eq. 1, where C_{Im} designates the imidazole catalyst, AcONp is the substrate, Ac–C_{Im} is the acylated intermediate, and k_a and k_d represent the rate constants for acylation and deacylation processes, respectively.

$$C_{Im} + AcONp \xrightarrow{k_a} Ac - C_{Im} \xrightarrow{k_d} C_{Im} + AcOH \quad (1)$$
$$+$$
$$p\text{-nitrophenol}$$

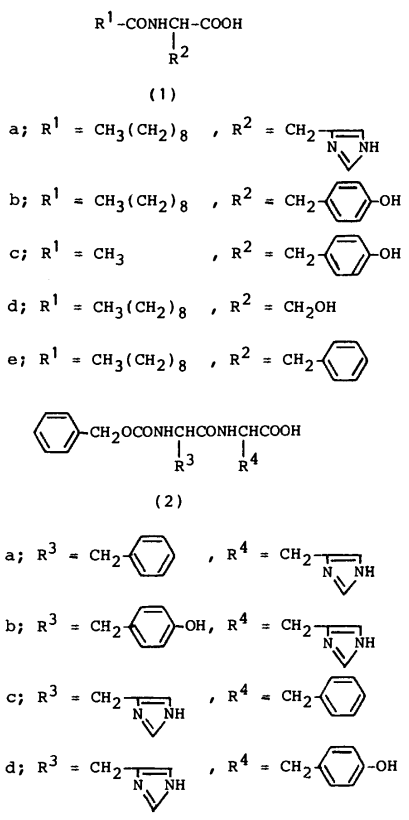

Kinetic studies are carried out at fixed concentration of the catalyst in the presence of CTAB. The hydrolysis of the substrates was examined under single turnover conditions, [surfactant]>[catalyst]>[ester] at pH 7.30, 0.02 mol dm^{-3} phosphate buffer and 25 °C. The pseudo-first-order rate constant k_ψ was determined by monitoring the release of *p*-nitrophenolate ion spectrophotometrically at 410 nm. The acylation rate constant (k_a) was calculated from the following equation, $k_a = k_\psi - k_{CTAB}$, where k_{CTAB} refers the rate con-

Table 1. Rate Constants for the Hydrolysis of Esters by **2a—d** in the Presence of CTAB[a)]

Ester	Catalytic Systems	$10^3 k_a/s^{-1}$	Rel. k_a	$10^4 k_d/s^{-1}$	Rel. k_d
PNPA	**2a**	3.89	1	6.89	1
	2b	3.85	0.99	21.0	3.05
	2c	3.64	1	8.05	1
	2d	3.34	0.92	13.3	1.65
PNPH	**2a**	3.31	1	2.73	1
	2b	3.22	0.97	5.76	2.11
	2c	3.07	1	4.73	1
	2d	3.36	1.09	6.77	1.43
PNPL	**2a**	3.12	1	2.28	1
	2b	2.80	0.90	4.48	1.96
	2c	2.55	1	4.47	1
	2d	2.88	1.13	6.69	1.50

a) At pH 7.30, 0.02 mol dm^{-3} phosphate buffer, and 25 °C, [CTAB]=1.00×10^{-2} mol dm^{-3}, [**2a,b,c,d**]=1.00×10^{-3} mol dm^{-3}, [Ester]=1.0×10^{-4} mol dm^{-3}. From three or more independent experiments, we estimate that the rate constants are reproducible to ±4%.

stant for spontaneous hydrolysis in the presence of CTAB. The deacylation rate constant (k_d) was directly measured spectrophotometrically by following the slow decrease in absorption at 245 nm or at near the isosbestic point[12] for the acylation reactions. In both cases, the kinetics were first order and good rate constants were obtained ($r>0.999$). The deacylation rate constants were calculated from absorbances at 245 nm, near the isosbestic point, and agree with the observed constants within experimental errors. We also carried out some experiments in CTAB under burst conditions, [substrate]≫[catalyst]. The kinetic treatment was that of Bender[13] and has been used by others.[4]

Table 1 summarizes the results for hydrolysis of three esters (PNPA, PNPH, and PNPL) by **2a—d** in the presence of CTAB micelles. The deacylation of the esters by **2b** and **d** which contain both the imidazolyl and hydroxyl functions in the catalysts is 1.4—3.1 times faster than that by **2a** and **c** which contain imidazolyl function alone although the acylation rates are essentially the same. This cooperative effect of the imidazolyl and hydroxyl functions in the catalysts **2b** and **d** for the deacylation process can be visualized in two mechanistic pathways[14] as illustrated in Scheme 1.

In order to obtain more information about the mechanism of deacylation process, the reactions of **2a** and **b** were examined using excess substrate (PNPA) so that there were rapid evolution of *p*-nitrophenol followed by a slow reaction as the acylated intermediates were hydrolyzed to generate the catalyst. The kinetic analysis under burst conditions shows that the deacylation rate enhancement by **2b** is almost similar to that obtained under the single turnover conditions (see Tables 1 and 2). This result suggests that acyl transfer from the imidazolyl to the hydroxyl groups (**ia** or **ib**) is less probable than the general base catalysis by the neighboring phenolic hydroxyl groups (**ii**) as a deacylation mechanism in the present catalytic system (Scheme 1).

The deacylation rate enhancement by **2b** was slightly larger than those by **2d** in all esters used (Table 1). These differences in deacylation process are due to the steric environment of the acylated intermediate in micelles. Thus, these results suggest that the deacylation involves geometrical interactions between the acyl intermediate and the hydroxyl group and that the acyl

Table 2. Kinetic Analysis under Burst Conditions[a)]

Catalytic Systems	k_a / mol^{-1} dm^3 s^{-1}	$10^4 k_d$ / s^{-1}	Rel. k_d
2a	2.38	4.2	1
2b	2.19	11.5	2.74

a) At pH 7.30, 0.02 mol dm^{-3} phosphate buffer, 25 °C, [CTAB]=1.00×10^{-2} mol dm^{-3}, [**2a** or **b**]=1.00—2.50×10^{-5} mol dm^{-3}, [PNPA]=2.50×10^{-3} mol dm^{-3}.

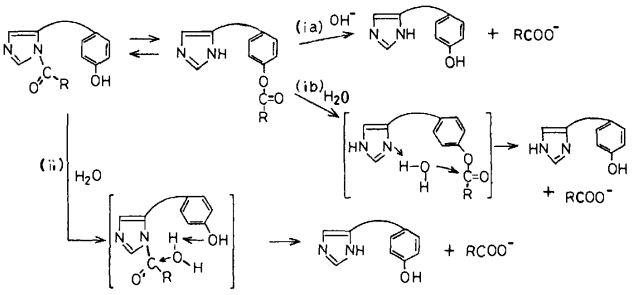

Scheme 1.

intermediate formed from **2b** and PNPA is optimally positioned for reaction by the hydroxyl function of **2b** in micellar phase and results in the largest deacylation rate (3.05).

Tables 3 and 4 summarize the rate constants for acylation and deacylation processes in the hydrolysis of the esters by **1a** and **2a** in four catalytic systems in the presence of micellar CTAB. From Tables 3 and 4, it is apparent that the deacylation is slower than the acylation in all cases. For the acylation process, the catalysis by **1a** was higher than that by **2a** in all esters used. On the other hand, **2a** is more reactive than **1a** in deacylation process. More importantly, PNPA is uniformly most reactive among the esters used in deacylation process. These results indicate that the deacylation process is sensitive to the structures of the catalysts and the esters.

The deacylation rate constants apparently increase in the presence of the catalysts **1b—d** which include the hydroxyl functions, although the acylation rate constants are almost independent of the catalytic systems used. The differences in deacylation rate enhancements suggest that the reaction depends on the catalytic activity of the hydroxyl functions in micelles. This probably reflects the steric environment and acidity of the hydroxyl groups. In our previous papers,[15] we also found the acyl transfer reaction in the hydrolysis of enantiomeric substrates in micelles.

Table 3. Rate Constants for the Hydrolysis of Esters in the Presence of Comicellar Catalytic Systems[a)]

Ester	Catalytic Systems	$10^3 k_a/s^{-1}$	Rel. k_a	$10^4 k_d/s^{-1}$	Rel. k_d
PNPA	**1a**	6.61	1	3.31	1
	1a/1b	6.67	1.01	7.08	2.14
	1a/1c	6.16	0.93	4.41	1.33
	1a/1d	6.28	0.95	4.56	1.38
	1a/1e	6.42	0.97	2.92	0.88
PNPH	**1a**	9.31	1	1.96	1
	1a/1b	9.24	0.99	3.41	1.74
	1a/1c	8.48	0.91	2.35	1.20
	1a/1d	8.38	0.90	2.48	1.27
	1a/1e	9.08	0.98	1.86	0.95
PNPL	**1a**	8.34	1	1.85	1
	1a/1b	8.11	0.97	2.66	1.44
	1a/1c	7.85	0.94	2.46	1.33
	1a/1d	7.33	0.88	2.08	1.12
	1a/1e	7.38	0.88	1.44	0.78

a) At pH 7.30, 0.02 mol dm^{-3} phosphate buffer, and 25°C, [CTAB]$=1.00\times10^{-2}$ mol dm^{-3}, [**1a**]$=1.00\times10^{-3}$ mol dm^{-3}, [**1b**$-$**e**]$=1.00\times10^{-3}$ mol dm^{-3}, [Ester]$=1.0\times10^{-4}$ mol dm^{-3}. From three or more independent experiments, we estimate that the rate constants are reproducible to ±4%.

Table 4. Rate Constants for the Hydrolysis of Esters in the Presence of Comicellar Catalytic Systems[a)]

Ester	Catalytic Systems	$10^3 k_a/s^{-1}$	Rel. k_a	$10^4 k_d/s^{-1}$	Rel. k_d
PNPA	**2a**	3.89	1	6.89	1
	2a/1b	3.49	0.90	8.80	1.28
	2a/1c	3.59	0.92	8.16	1.18
	2a/1d	3.39	0.87	7.24	1.05
	2a/1e	3.38	0.87	6.25	0.91
PNPH	**2a**	3.31	1	2.73	1
	2a/1b	3.32	1.00	4.11	1.51
	2a/1c	3.10	0.94	3.31	1.21
	2a/1d	3.03	0.92	3.56	1.30
	2a/1e	2.68	0.81	2.68	0.98
PNPL	**2a**	3.12	1	2.28	1
	2a/1b	2.68	0.86	5.26	2.31
	2a/1c	3.03	0.97	2.54	1.11
	2a/1d	2.65	0.85	3.00	1.32
	2a/1e	2.18	0.70	1.82	0.80

a) At pH 7.30, 0.02 mol dm^{-3} phosphate buffer, and 25°C, [CTAB]$=1.00\times10^{-2}$ mol dm^{-3}, [**2a**]$=1.00\times10^{-3}$ mol dm^{-3}, [**1b**$-$**e**]$=1.00\times10^{-3}$ mol dm^{-3}, [Ester]$=1.0\times10^{-4}$ mol dm^{-3}. From three or more independent experiments, we estimate that the rate constants are reproducible to ±4%.

Although deacylation enhancements in the present catalytic systems are relatively small, it is clear that these micellar systems cause acylation of the imidazolyl group, followed by the deacylation rate acceleration by the hydroxyl group of the catalyst.

References

1) a) J. H. Fendler and E. J. Fendler, "Catalysis in Micellar and Macromolecular Systems," Academic Press, New York (1975), and references cited therein; b) T. Kunitake and S. Shinkai, *Adv. Phys. Org. Chem.*, **18**, 435 (1980).

2) a) R. A. Moss, R. C. Nahas, and S. Ramaswami, *J. Am. Chem. Soc.*, **99**, 627 (1977); "Micellization, Solubilization, and Microemulsions," ed by K. L. Mittal, Plenum Press, New York (1977), p. 603; b) U. Tonellato, *J. Chem. Soc., Perkin Trans. 2*, **1977**, 821.

3) a) J. Sumamoto, H. Okamoto, H. Kondo, and Y. Murakami, *Tetrahedron Lett.*, **1975**, 2761; b) Y. Murakami, A. Nakano, A. Yoshimatsu, and K. Matsumoto, *J. Am. Chem. Soc.*, **103**, 2750 (1981).

4) T. Kunitake, Y. Okahata, and T. Sakamoto, *Chem. Lett.*, **1975**, 459; *J. Am. Chem. Soc.*, **98**, 7799, (1975).

5) a) W. Tagaki, S. Kobayashi, and D. Fukushima, *J. Chem. Soc., Chem. Commun.*, **1977**, 29; b) W. Tagaki, D. Fukushima, T. Eiki, and Y. Yano, *J. Org. Chem.*, **44**, 555 (1979).

6) a) Y. Ihara, M. Nango, Y. Kimura, and N. Kuroki, *J. Am. Chem. Soc.*, **105**, 1252 (1983); b) Y. Ihara, M. Okamoto, M. Nango, and J. Koga, *Chem. Lett.*, **1985**, 1227.

7) a) T. Inoue, K. Nomura, and H. Kimizuka, *Bull. Chem. Soc., Jpn.*, **49**, 719 (1976); b) P. Heitmann, *Eur. J. Biochem.*, **3**, 346 (1968); c) P. Heitmann, R. Hsung-Bublitz, and H. J. Zunft, *Tetrahedron*, **30**, 4137 (1974).

8) Y. Ihara, *J. Chem. Soc., Chem. Commun.*, **1978**, 984; *J. Chem. Soc., Perkin Trans. 2*, **1980**, 1483.

9) Y. Ihara and R. Hosako, *Bull. Chem. Soc. Jpn.*, **55**, 1979 (1982).

10) Y. Ihara, R. Hosako, M. Nango, and N. Kuroki, *J. Chem. Soc., Chem. Commun.*, **1980**, 393; *J. Chem. Soc., Perkin Trans. 2*, **1983**, 5.

11) a) Y. Ihara, T. Kunikiyo, M. Kunimasa, M. Nango, and N. Kuroki, *Chem. Lett.*, **1981**, 667; b) Y. Ihara, N. Kunikiyo, M. Kunimasa, Y. Kimura, M. Nango, and N. Kuroki, *J. Chem. Soc., Perkin Trans. 2*, **1983**, 1741.

12) An isosbestic point for the acylation reactions was observed at 250—260 nm from repetitive scans and/or successive time scanning with several wavelengths in the kinetic analysis.

13) M. L. Bender and T. H. Marshall, *J. Am. Chem. Soc.*, **90**, 201 (1968).

14) We thank a referee for pointing out these mechanisms.

15) Y. Ihara, Y. Kimura, M. Nango, and N. Kuroki, *Bioorg. Chem.*, **13**, 88 (1985).

Stepwise Oxidation of the Heteroatoms in *O*-Protected Pyridoxine-Like Pyridinophane Containing Thio Groups in the Intramolecular Bridge Chain

Makoto ANDO* and Hiroyoshi KUZUHARA*
RIKEN (The Institute of Physical and Chemical Research), Wako, Saitama 351-01
(Received June 28, 1986)

Synopsis. Racemic 14-Hydroxy-15-hydroxymethyl-*O*,*O*′-isopropylidene-2,8-dithia[9](2,5)pyridinophane, a model compound of our chiral pyridoxamine analogs, was oxidized under various conditions in order to examine the reactivities of the sulfur and the nitrogen atoms. Various degree of oxidized compounds, from monoxide to pentaoxide, including the desired *S*,*S*,*S*′,*S*′-tetraoxide, were obtained.

We have prepared several kinds of novel pyridinophanes with sulfur-containing intramolecular bridge chain as chiral analogs of vitamin B_6,[1,2a,3] **1a**, **1b**, and **1c**, corresponding to the *S*-enantiomers of pyridoxal, pyridoxamine, and pyridoxine analogs, respectively. Combination of **1a** or **1b** with appropriate metal ions has been successfully used for simulating the vitamin B_6-dependent enzymatic reactions with a relatively high enantioface differentiation.[1,2]

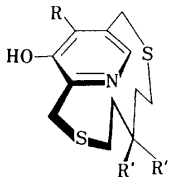

	R	R′
1a:	CHO	H or Me
1b:	CH_2NH_2	H or Me
1c:	CH_2OH	H

A consideration of the mechanism of such enzyme model reactions suggested that the bulkiness of one of the sulfur atoms in vitamin B_6 analogs might play an essential role in the asymmetric induction.[2c] The sulfonyl group is much bulkier than the corresponding thio group and has a very small tendency to chelate to metal ions. These facts suggest that a conversion of the thio group in **1a** or **1b** to the corresponding sulfonyl group might enhance their potency regarding asymmetric induction. An attempt to prepare such new vitamin B_6 analogs from **1a—c**, however, may be hampered by the fact that the oxidation of the sulfur atoms compete with that of the pyridine nitrogen atom to *N*-oxide. This paper describes the selective oxidation of those sulfides to the corresponding sulfones, employing racemic 14-hydroxy-15-hydroxymethyl-*O*,*O*′-isopropylidene-2,8-dithia[9](2,5)pyridinophane (**2**),[1] an *O*-protected pyridoxine analog, as a model substrate.

The oxidation of **2** with *m*-chloroperbenzoic acid (MCPBA) was studied at room temperature in various organic solvents. The employment of 5.5 mole equivalents of MCPBA to **2** in chloroform for 1 d resulted in a mixture of tetraoxide (**3**) of **2** and pentaoxide (**4**) of **2**. Unreacted MCPBA and **3** were still detectable on TLC, even if the reaction period was prolonged. With 7.5 mole equivalents of MCPBA, however, **4** was obtained in quantitative yield. In the UV spectrum of **4**, a blue shift of the absorption maxima was observed when the solvent was changed from acetonitrile to ethanol, whereas this was not observed in that of **3**. Furthermore, the ε-value of the UV absorption of **4** was somewhat larger than that of **3**. These observations elucidated the structures of **3** and **4** as 14-hydroxy-15-hydroxymethyl-*O*,*O*′-isopropylidene-2,8-dithia[9](2,5)-pyridinophane *S*,*S*,*S*′,*S*′-tetraoxide and *N*,*S*,*S*,*S*′,*S*′-pentaoxide, respectively[4] and showed that the oxidation of sulfur proceeded prior to that of nitrogen. However, decreasing the amount of MCPBA to 4.4—1.1 mole equivalents resulted in many products in all cases, indicating that the oxidation of sulfur proceeds without any selectivity. Although the rate of the oxidation was rather slow in dioxane, **4** was obtained in quantitative yield with 7.5 mole equivalents of MCPBA after 3 d. During these oxidation in chloroform or dioxane, we observed that **3** was once precipitated and dissolved again, giving the final product, **4**. In ethanol, **3** could be isolated in 89% yield after 1 d with **4** also obtained in 11% yield from the filtrate.

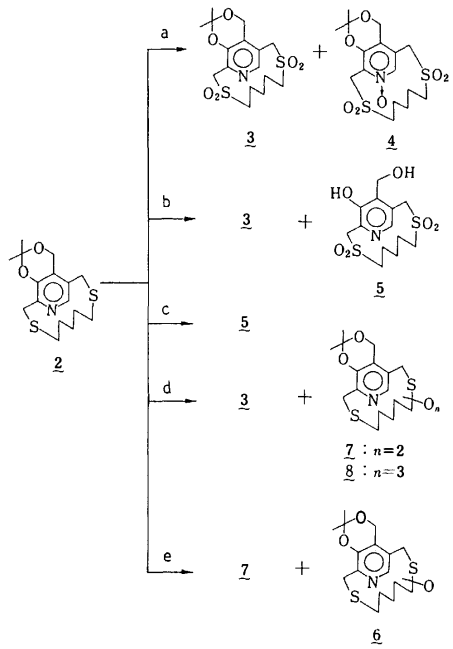

a: MCPBA/$CHCl_3$, dioxane, or ethanol, room temp.
b: catalysts[f]/aq dioxane, 60—85 °C, 3 h.
c: no catalysts/acetic acid, 60—85 °C, 3 h.
d: catalysts[f]/aq dioxane, room temp, 1 d.
e: no catalysts/aq dioxane, room temp, 3 d.
f: AcOH (1.5 wt%) + $Na_2WO_4 \cdot 2H_2O$ (0.5 wt%).

Recently, Giam et al. reported that the selective oxidation of alkyl pyridyl sulfides to the corresponding sulfones without *N*-oxide compounds proceeded in aqueous dioxane at 65—85 °C with hydrogen peroxide

and catalytic amounts of acetic acid and sodium tungustate.[5] This procedure was applied to the oxidation of **2** and found to give satisfactory results. The desired **3** (87%) and its *O,O'*-deprotected compound, 14-hydroxy-15-hydroxymethyl-2,8-dithia[9](2,5)pyridinophane *S,S,S',S'*-tetraoxide (**5**) (5%), were obtained with no *N*-oxide compounds produced. Acidic hydrolysis of **3** gave **5** which precipitated in the form of free base during the reaction. Only **5** was obtained when the oxidation was conducted in acetic acid at 60—85 °C in the absence of sodium tungustate. The hydrogen peroxide oxidation at room temperature gave monoxide (**6**), dioxide (**7**), and trioxide (**8**) of **2** depending on the reaction conditions employed (See experimental). Although **6** and **7** showed the sharp melting points, the NMR signal assignable to the proton attached to the pyridine ring in **6**, **7**, and **8**[6] appeared as 2, 4, and 2 peaks, respectively, suggesting that those compounds were the mixtures of the corresponding *S*-oxides (**6**) (assigned from IR spectrum), *S,S*- and *S,S'*-dioxides (**7**), and *S,S,S'*-trioxides (**8**) of **2**.

In conclusion, the selective oxidation of the sulfides **2** giving the corresponding sulfone derivative **3** was achieved with hydrogen peroxide-acetic acid-sodium tungustate in aqueous dioxane at 60—85 °C or with MCPBA in ethanol at room temperature.

Experimental

General. Melting points are uncorrected. IR and UV-VIS spectra were determined with a Shimadzu IR 27G and a Varian-Cary 2290 spectrometers, respectively. ^{1}H NMR spectra were recorded on a JOEL PS 100 instrument using TMS as an internal standard (100 MHz).[6] Organic extracts were dried over anhydrous magnesium sulfate and evaporated under reduced pressure. TLC was conducted with a precoated silica gel 60F_{254} on aluminium sheet (Merck No. 5554) with chloroform-methanol (50 : 1 or 25 : 1 v/v) as the developing solvent. Column chromatography was performed with a silica gel (Merck No. 7734) column with chloroform-methanol (100 : 1 v/v) as the eluent.

Material. Racemic 14-hydroxy-15-hydroxymethyl-*O,O'*-isopropylidene-2,8-dithia[9](2,5)pyridinophane (**2**) was prepared by the method described in previous papers.[1] Commercially available *m*-chloroperbenzoic acid (MCPBA) (85% purity, Tokyo Kasei) and an aqueous 30% hydrogen peroxide solution (Mitsubishi Gas Chemistry) were used as oxidizing reagents without accurate determination of the contents.

Oxidation of 2 with MCPBA. A typical example is described in the following. A solution of MCPBA (3.43 g, 5.5 mole equivalents to **2**) in chloroform (50 ml) was added to a stirred solution of **2** (1.00 g) in the same solvent (50 ml) cooled in an ice bath over the period of 30 min and the mixture was stirred for 1 d at room temperature. During the addition of MCPBA the precipitate appeared and then gradually dissolved within 5—6 h. After decomposition of the excess MCPBA with an aqueous sodium hydrogensulfite solution, the chloroform solution was washed with a sodium hydrogencarbonate solution and with water, dried, and chromatographed to give **3** (0.25 g, 21%) and **4** (0.91 g, 73%) in this elution order.

Compound **3**: Mp > 280 °C; UV (EtOH) 298 nm (ε 6.2×10^3); (MeCN) 298 nm (ε 6.1×10^3); IR (KBr disk) 1290 and 1100 cm^{-1} (SO_2); ^{1}H NMR ($CDCl_3$) δ=1.65 (6H, s, C-(C$\underline{H}_3$)$_2$), 2.6—3.4 (10H, m), 4.14 (1H, d, J=14 Hz, 2-Py-C$\underline{H}$-S), 4.23 (1H, d, J=14 Hz, 2-Py-C$\underline{H}$-S), 4.28 (1H, d, J=14 Hz, 5-Py-C$\underline{H}$-S), 4.76 (1H, d, J=17 Hz, Py-C$\underline{H}$-O), 4.89 (1H, d, J=13 Hz, 5-Py-C$\underline{H}$-S), 5.31 (1H, d, J=17 Hz, Py-C$\underline{H}$-O), and 8.25 (1H, s, Py-$\underline{H}$). Found: C, 49.31, H, 5.99; N, 3.46; S, 16.50%. Calcd for $C_{16}H_{23}NO_6S_2$: C, 49.34; H, 5.95; N, 3.60; S, 16.47%.

Compound **4**: Mp > 280 °C; UV (EtOH) 279 (ε 7.7×10^3) and 331 nm (ε 3.5×10^3); (MeCN) 282 (ε 7.6×10^3) and 338 nm (ε 2.9×10^3); IR (KBr disk) 1300, 1280 (SO_2 and N→O), and 1120 cm^{-1} (SO_2); ^{1}H NMR ($CDCl_3$) δ=1.72 (6H, s, C-(C$\underline{H}_3$)$_2$), 2.9—3.9 (10H, m), 4.24 (2H, s, 2-Py-C$\underline{H}_2$-S), 4.52 (1H, d, J=13 Hz, 5-Py-C$\underline{H}$-S), 4.80 (1H, d, J=17 Hz, Py-C$\underline{H}$-O), 5.27 (1H, d, J=16 Hz, Py-C$\underline{H}$-O), 5.37 (1H, *d*, J=12 Hz, 5-Py-C$\underline{H}$-S), and 8.25 (1H, s, Py-$\underline{H}$). Found: C, 47.25; H, 5.74; N, 3.31; S, 15.85%. Calcd for $C_{16}H_{23}NO_7S_2$: C, 47.39; H, 5.72; N, 3.45; S, 15.81%.

Oxidation of 2 with Hydrogen Peroxide. a) Reaction at 60—85 °C with Catalysts: Hydrogen peroxide solution (1.5 ml) was added at 60—65 °C over the period of 30 min to a stirred solution of **2** (1.00 g), acetic acid (ca. 15 mg), and sodium tungustate dihydrate (ca. 5 mg) in dioxane (10 ml)-water (10 ml) and the mixture was stirred at 80—85 °C for further 3 h. After the mixture had been cooled, the resulting precipitate of **5** (55 mg, 5%) was filtered off, and the excess hydrogen peroxide was destroyed with an aqueous sodium hydrogensulfite solution. The resulting solution was extracted with chloroform, and the extract was washed with water, dried, and chromatographed to afford **3** (1.04 g, 87%).

Compound **5**: Mp > 280 °C; IR (KBr disk) 3340 (OH), 1290, and 1100 cm^{-1} (SO_2); ^{1}H NMR (DMSO-d_6) δ=2.6—3.4 (10 H, m), 4.40 (1H, d, J=13 Hz, 5-Py-C$\underline{H}$-S), 4.59 (1H, d, J=16 Hz, Py-C$\underline{H}$-O), 4.87 (2H, s, 2-Py-C$\underline{H}_2$-S), 4.89 (1H, s, Py-CH$_2$-O$\underline{H}$), 4.92 (1H, d, J=16 Hz, Py-C$\underline{H}$-O), 5,10 (1H, d, J=13 Hz, 5-Py-C$\underline{H}$-S), 8.43 (1H, s, Py-$\underline{H}$), and 10.09 (1H, s, Py-O$\underline{H}$). Found: C, 44.92; H, 5.48; N, 3.95; S, 18.40%. Calcd for $C_{13}H_{19}NO_6S_2$: C, 44.69; H, 5.48; N, 4.01; S, 18.35%.

b) Reaction in Acetic Acid at 60—85 °C without Catalysts: Hydrogen peroxide solution (1.5 ml) was added to a stirred solution of **2** (1.00 g) in acetic acid (10 ml) at 60—65 °C over the period of 30 min and the mixture was stirred at 80—85 °C for further 3 h. The mixture was cooled and diluted with water and the resulting precipitate of **5** (0.80 g, 75%) was collected.

c) Reaction at Room Temperature with Catalysts: Hydrogen peroxide solution (1.5 ml) was added to a stirred solution of **2** (1.00 g), acetic acid (ca. 15 mg), and sodium tungustate dihydrate (ca. 5 mg) in dioxane (30 ml)-water (10 ml) below room temperature over the period of 30 min, stirred for 1 d at room temperature, and then treated as described in a), giving **3** (0.25 g, 21%), **8** (0.66 g, 58%), and **7** (0.14 g, 13%) in this elution order.

Compound **7**: Mp 201—202 °C dec; IR (KBr disk) 1290, 1090 (SO_2 weak), and 1020 cm^{-1} (SO); ^{1}H NMR ($CDCl_3$) δ=7.91 (0.1H, s, Py-$\underline{H}$), 8.03 (0.2H, s, Py-$\underline{H}$), 8.15 (0.6H, s, Py-$\underline{H}$), and 8.25 (0.1H, Py-$\underline{H}$). Found: C, 53.53; H, 6.46; N, 3.88; S, 17.90%. Calcd for $C_{16}H_{23}NO_4S_2$: C, 53.76; H, 6.49; N, 3.92; S, 17.94%.

Compound **8**: Mp > 280 °C; IR (KBr disk) 1290, 1110 (SO_2), and 1030 cm^{-1} (SO); ^{1}H NMR ($CDCl_3$) δ=8.15 (0.4H, s, Py-$\underline{H}$) and 8.24 (0.6H, s, Py-$\underline{H}$). Found: C, 51.03; H, 6.14; N, 3.78; S, 17.12%. Calcd for $C_{16}H_{23}NO_5S_2$: C, 51.46; H, 6.21; N, 3.75; S, 17.17%.

d) Reaction at Room Temperature without Catalysts: Hydrogen peroxide solution (1.5 ml) was added to a stirred solution of **2** (1.00 g) in dioxane (30 ml)-water (10 ml) below room temperature and the mixture was stirred for 3 d at room temperature. A similar work up gave unreacted **2** (0.25 g, 25%), **6** (0.21 g, 19%), and **7** (0.51 g, 48%) in this elution order.

Compound **6**: Mp 176—177 °C; IR (KBr disk) 1020 cm^{-1} (SO); ^{1}H NMR ($CDCl_3$) δ=7.90 (0.7H, s, Py-$\underline{H}$) and 8.10

(0.3H, s, Py-H). Found: C, 55.97; H, 6.78; N, 3.89; S, 18.78%. Calcd for $C_{16}H_{23}NO_3S_2$: C, 56.27; H, 6.79; N, 4.10; S, 18.78%.

Acidic Hydrolysis of 3. A mixture of **3** (1.00 g), hydrochloric acid (2.5 ml), and water (25 ml) was stirred at 80—85 °C for 2 h and cooled and the resulting precipitate of **5** (0.83 g, 93%) was collected.

The authors wish to express their thanks to the members of the Organic Analysis Center of this Institute for elemental analyses and to Dr. Jun Uzawa and Mrs. Tamiko Chijimatsu for the measurements of ^1H NMR spectra.

This study was performed through Special Coordination Funds of the Science and Technology Agency of the Japanese Government.

References

1) a) H. Kuzuhara, M. Iwata, and S. Emoto, *J. Am. Chem. Soc.*, **99**, 4173 (1977); b) M. Iwata and H. Kuzuhara, *Bull. Chem. Soc. Jpn.*, **58**, 2502 (1985).

2) a) H. Kuzuhara, T. Komatsu, and S. Emoto, *Tetrahedron Lett.*, **1978**, 3563; b) Y. Tachibana, M. Ando, and H. Kuzuhara, *Chem. Lett.*, **1982**, 1765; c) 1769; d) Y. Tachibana, M. Ando, and H. Kuzuhara, *Bull. Chem. Soc. Jpn.*, **56**, 3652 (1983).

3) M. Ando, Y. Tachibana, and H. Kuzuhara, *Bull. Chem. Soc. Jpn.*, **55**, 829 (1982).

4) H. Hirayama and T. Kubota, *Shionogikenkyusho Nenpo*, **2**, 47 (1952).

5) C. S. Giam, K. Kikukawa, and D. A. Trujillo, *Org. Prep. Proced. Int.*, **13**, 137 (1981).

6) Assignments, see Ref. 1b.

Effect of Aryl Substituents on 2-Aryl-1,4,5,6,7,7-hexachloronorbornadiene-Quadricyclane Reversible Isomerization

Hideo TOMIOKA,* Yukinobu HAMANO, and Yasuji IZAWA
Department of Industrial Chemistry, Faculty of Engineering, Mie University, Tsu, Mie 514
(Received July 25, 1986)

Synopsis. 2-Arylhexachloronorbornadiene undergoes photoisomerization to the corresponding quadricyclane, which returns back to the norbornadiene upon heating without catalyst. Effect of aryl substituents on the thermal reversion suggests that both spin delocalization and polar effect equally contribute to the stabilization of the transition state.

The norbornadiene (ND)-quadricyclane (Q) reversible isomerization is an attractive model system for the chemical conversion of light energy.[1] Energy is stored when norbornadiene is converted photochemically to the higher energy quadricyclane. The energy is

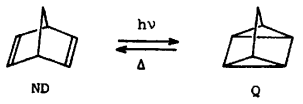

released when quadricyclane is (catalytically) converted back to norbornadiene. Since norbornadiene itself does not undergo efficient valence isomerization upon direct and/or sensitized irradiation, norbornadienes bearing an appropriate chromophore have been synthesized and their photoisomerization has been examined.[2] The properties of quadricyclanes derived from these norbornadienes are also quite important in connection with the design of the system and hence the heat and the rate of the reversion of the quadricyclanes to the starting compounds are measured which provides an important information on the mechanism of the reversion.[3] As a part of such studies we synthesized 2-arylhexachloronorbornadienes and investigated the effect of aryl substituents on the reversible isomerization.

Results and Discussion

The norbornadienes (**3**) were synthesized[4,5] by the Diels-Alder addition between hexachlorocyclopentadiene (**1**) and arylacetylenes (**2**) bearing electron-donating and withdrawing groups in refluxing

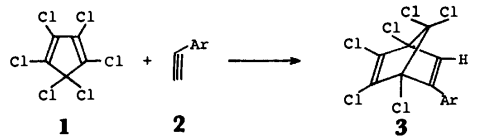

1 **2** **3**

Ar=X- C_6H_4 a: X=4-MeO, b: X=4-Me, c: X=H, d: X=4-Br, e: X=3-Br

toluene. These norbornadienes (**3**) were easily purified by vacuum distillation followed by recrystallization from hexane with exception of the methoxy derivative (**3a**). Irradiation of **3** in Pyrex tube with high-pressure Hg lamp gave the corresponding quardricyclanes (**4**) in quantitative yield. Quantum yield of the photocycloaddition with 313 nm light was 0.42 for **3c**.

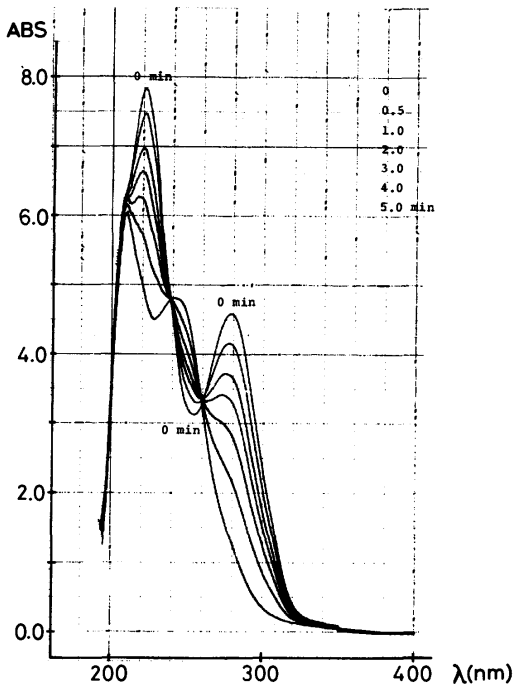

Fig. 1. UV spectra of the photoisomerization of **3c** to **4c**. A carbontetrachloride solution of 1.4×10^{-4} M **3c** was irradiated with 313 nm light.

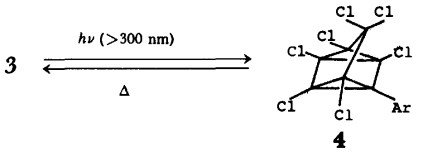

4

Quadricyclanes returned back to the norbornadienes quantitatively upon heating in carbon tetrachloride without catalyst. UV spectra of the photoisomerization of **3c** to **4c** was shown in Fig. 1, which shows the isosbestic point at 238 and 260 nm, indicating the quantitative isomerization of **3c**. UV spectra of the thermal reaction of **4c** to **3c** was superimposable to that of the photoisomerization, again indicating the quantitative isomerization of **4c**. Thus, photoisomerization and thermal back process were completely reversible. The heat of reversion (ΔH) of **4c** to **3c** was 21.6 kcal mol^{-1} (1 cal=4.184 J). The rate constants for the reversion at 60.0 °C were measured by monitoring a ^1H NMR spectra and appear in Table 1 along with Arrhenius parameters.

It has been suggested[3f] that the thermal isomerization of quadricyclanes proceeds via diradical mechanism. While rate constants in Table 1 do not show the wide range distribution that many cationic reactions do, nonetheless there are discernible differences. However, there is no single substituent constant that corre-

Table 1. Rate Constants and Activation Parameters for Thermal Isomerization of **4** to **3**

4	X	k[a)]	E_a[b)]	S[b)]
		$10^3\,s^{-1}$	kJ mol^{-1}	J K^{-1} mol^{-1}
a	4-MeO	58.5	85.8	−20.3
b	4-Me	51.7	91.2	−5.0
c	H	58.8	106.7	42.3
d	4-Br	105.3	98.3	22.4
e	3-Br	73.9	96.2	13.3

a) All rates were measured in CCl_4 at 60 °C. b) These values are each based on 3 runs at temperature between 50 and 60 °C.

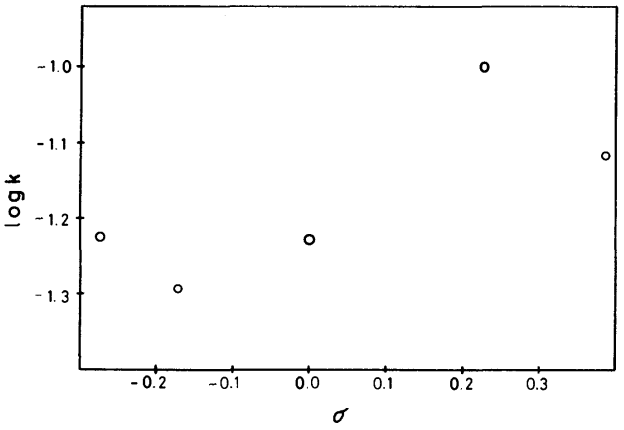

Fig. 2. A plot of relative rate constants for **4**→**3** isomerization at 60.0°C vs. Hammett σ value.

lates all of the data. The effects of substituents on radical stability is not as well understood as in carbocationic reactions. One problem is the separation of true radical-stabilizing effects from polar effects which are known to operate in many radical reactions. Many radical reactions correlate with Hammett σ (σ^+) constants,[6] because of the magnitude of polar effects. No correlation of all the data in Table 1 could be obtained, however, with σ (σ^+) values. On the other hand, various free radical substituent constants ($\sigma\cdot$) have been proposed[7] to separate the polar factors from true free radical stabilizing effects. Attempts to correlate the present data with $\sigma\cdot$ also gave low correlation coefficients.

Recently, a two-parameter Hammett relationship (Eq. 1) has been introduced[7] to evaluate the relative

$$\log k_{rel} = \rho\cdot\sigma\cdot + \rho\sigma \quad (1)$$

importance of radical stabilization vs. polar effects in radical reaction. In this treatment, the data are plotted against two-parameters so as to obtain the best correlation by adjusting the ratio of $\rho\cdot/\rho$ which in turn indicates the relative importance of the radical nature at the transition state. If the value of $\rho\cdot/\rho$ is low, spin delocalization of the intermediates is unimportant and an early transition state, influenced by polar factor, is suggested. If this value is high, the transition state should have radical charactor and polar factors should be relatively unimportant. Using four data available, the best correlation is obtained when the ratio of $\rho\cdot/\rho$

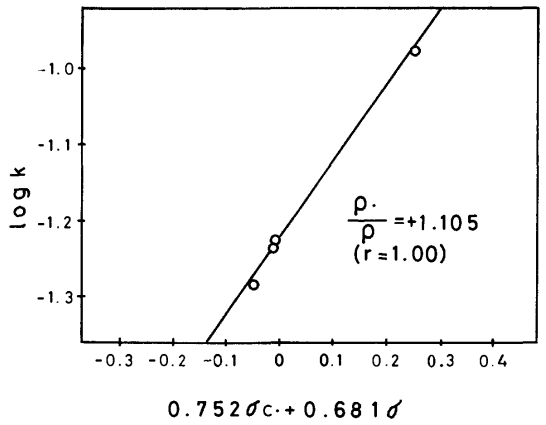

Fig. 3. A plot of relative rate constants for **4**→**3** isomerization vs. two parameters σ and σ_C.

is setted to be 1.105. This indicates that both spin delocalization and polar factors equally contribute to stabilizing the transition state for the thermal isomerization of **4** to **3**.

Thus, the photoisomerization of **3** could be possible with light of wavelength between 300—366 nm, while the heat stored in **4** is as much as that in the parent quadricyclane. Moreover, **4** is fairly stable at room temperature but is easily reverted back to **3** upon heating without catalyst. Finally it should be mentioned that the hexachloro derivatives **3** described in this paper can be prepared much more easily and are much more stable than 2-phenylnorbornadienes, which was synthesized[8] by the Diels-Alder reaction of cyclopentadiene and α-bromostyrene, followed by elimination of HBr by pottasium t-butoxide and decomposed slowly upon standing. Moreover, 2-phenylnorbornadiene-quadricyclane isomerization is not completely reversible.

Experimental

General. All melting and boiling points were uncorrected. UV spectra were recorded on a Hitachi 220-S spectrophotometer. IR spectra were measured on a JASCO IR-G recording spectrometer, and ^{1}H NMR spectra were determined with JEOL JNM-MH-100 NMR spectrometer in CCl_4 with Me_4Si as an internal reference. Mass spectra were recorded on Shimadzu QP-1000 mass spectrometer (70 eV). The heat of isomerization was measured on Rigaku Thermoflex Differential Scanning Calorimeter which was calibrated with KNO_3 standard. Quantum yields were determined using pottasium trioxalatoferrate (III) as an actinometer.

Material. 2-Arylhexachloronorbornadienes were prepared according to the procedure of Fry.[4a] Thus, arylacetylene (0.1 mol) and hexachlorocyclopentadiene (0.1 mol) were dissolved in dry toluene, and the solution refluxed for 3 days. After toluene was removed at the rotary evaporator, the dark brown residue was distilled at reduced pressure to give a viscous oil. A small portion of this oil was triturated with hexane at −10 °C, whereupon it crystallized, with exception of the methoxy derivative (**3a**). The remainder of the adduct was seeded with these crystals, followed by recrystallization from hexane. The data are shown below.

3a: Yield 19%; Bp 123—150 °C/0.4 mmHg (1 mmHg≈ 133.322 Pa); ^{1}H NMR (CCl_4) δ=7.15 (2H, d), 6.80 (2H, d), 6.40 (1H, s), 3.80 (3H, s); MS (70 eV) m/z (rel intensity, %) 401

(M^+, 17.2), 403 (M+2, 33.0), 405 (M+4, 28.9), 407 (M+6, 12.1), 367 (base peak).

3b: Yield 49%; Bp 158—160 °C/0.3 mmHg; Mp 80—81 °C; ^{1}H NMR (CCl_4) δ=7.01 (4H, bs), 6.32 (1H, s), 2.31 (3H, s); MS (70 eV) *m/z* (rel intensity, %) 386 (M^+, 6.3), 388 (M+2, 11.6), 390 (M+4, 9.6), 392 (M+6, 4.1), 317 (base peak).

3c: Yield 25%; Bp 123—124 °C/0.5 mmHg; Mp 94—96 °C; ^{1}H NMR (CCl_4) δ=7.30 (5H, bs), 6.50 (1H, s); MS (70 eV) *m/z* (rel. intensity) 372 (M^+, 7.9), 374 (M+2, 15.2), 376 (M+4, 11.8), 378 (M+6, 5.4), 303 (base peak).

3d: Yield 34%; Bp 60—62 °C/3 mmHg; Mp 76—77 °C; ^{1}H NMR (CCl_4) δ=7.50 (2H, d), 7.15 (2H, d), 6.57 (1H, s); MS (70 eV) *m/z* (rel intensity) 450 (M^+, 5.3), 452 (M+2, 14.5), 454 (M+4, 17.2), 456 (M+6, 11.3), 303 (base peak).

3e: Yield 39%; Bp 150—152 °C/3 mmHg; Mp 93—94 °C, ^{1}H NMR (CCl_4) δ=7.45—7.18 (4H, m), 6.59 (1H, s); MS (70 eV) *m/z* (rel intensity) 450 (M^+, 5.9), 452 (M+2, 15.8), 454 (M+ 4, 17.8), 456 (M+6, 10.4), 303 (base peak).

Photoisomerization of 3 to 4. A solution of **3** (100 mg) in hexane (30 ml) was prepared under an argon atmosphere in Pyrex tubes and was irradiated with a 300-W high-pressure mercury lamp at 10 °C. After irradiation for 5 h, the solvent was evaporated under reduced pressure to leave syrupy oil. Attempts to obtain the quadricyclanes (**4**) in pure forms either by recrystallization or by chromatography were unsuccessful since **4** was always contaminated with **3** due to the thermal back reaction during the work-up even at room temperature. The ^{1}H NMR data of **4** are shown below.

4a: ^{1}H NMR (CCl_4) δ=7.60 (2H, d), 7.18 (2H, d), 3.80 (3H, s), 3.10 (1H, s).

4b: ^{1}H NMR (CCl_4) δ=7.10 (4H, bs), 2.30 (3H, s), 3.08 (1H, s).

4c: ^{1}H NMR (CCl_4) δ=7.27 (5H, bs), 3.02 (1H, s).

4d: ^{1}H NMR (CCl_4) δ=7.53 (2H, d), 7.10 (2H, d), 3.18 (1H, s).

4e: ^{1}H NMR (CCl_4) δ=7.60—7.20 (4H, m), 3.20 (1H, s).

Kinetic Measurement. The rates of thermal back reaction of **4** to **3** were measured in carbon tetrachloride by monitoring ^{1}H NMR spectra. Thus, CCl_4 solution of **3** containing anisole as an internal standard was placed in Pyrex NMR tubes and was irradiated until almost all of **3** were converted to **4**. The tubes were then immersed in a water bath thermostated at a constant temperature (±0.1 °C). The rates were easily measured by monitoring the disappearance of methine proton of **4** at around 2.0 ppm and/or appearance of vinyl proton of **3** at around 6.5 ppm.

The authors gratefully acknowledge a support of this work by the Grant-in-Aid for "Research on Photosynthesis and Photoconversion of Solar Energy" sponsored by the Ministry of Education, Science and Culture. We thank Professor K. Kamiya of this department for measurement of the heat of isomerization.

References

1) R. R. Hautala, R. B. King, and C. Kutal, "Solar Energy: Chemical Conversion and Storage," The Humana Press (1979); W. H. F. Saase "Solar Power and Fuels," ed by J. R. Balton, Acad. Press, New York (1977); K. C. Bishop, III, *Chem. Rev.*, **76**, 461 (1976).

2) See for example, a) K. Hirano, A. Ando, T. Hamada, and O. Yonemitsu, *J. Chem. Soc., Chem. Commun.*, **1984**, 300; b) Z. Yoshida, Japan Patent 57149251 (1982), (*Chem. Abstr.*, **98**, 53253q, 1983); *J. Photochem.*, **29**, 27 (1985), and references cited therein; c) T. Toda, E. Hasegawa, T. Mukai, H. Tsuruta, T. Hagiwara, and T. Yoshida, *Chem. Lett.*, **1982**, 1551; d) K. Maruyama and H. Tamiaki, *Chem. Lett.*, **1982**, 1699.

3) a) S. Miki, T. Ohno, H. Iwasaki, and Z. Yoshida, *Tetrahedron Lett.*, **26**, 3487 (1985); b) T. B. Patrick and D. S. Bechtold, *J. Org. Chem.*, **49**, 1935 (1984); c) K. Maruyama, H. Tamiaki and S. Kawabata, *Chem. Lett.*, **1984**, 743; d) R. W. Hoffmann and W. Barth, *J. Chem. Soc., Chem. Commun.*, **1983**, 345; e) K. Maruyama, K. Terada, and Y. Yamamoto, *J. Org. Chem.*, **46**, 5294 (1981); f) D. S. Kabakoff, J.-C. G. Bünzli, J. F. M. Oth, W. B. Hammond, J. A. Berson, *J. Am. Chem. Soc.*, **97**, 1510 (1975) and references cited therein.

4) a) A. J. Fry, *J. Org. Chem.*, **31**, 1863 (1966); b) E. T. McBee, J. D. Idol, Jr., and C. W. Roberts, *J. Am. Chem. Soc.*, **77**, 6674 (1955).

5) See also C. H. M. Adams, K. Mackenzie, and P. R. Young, *J. Chem. Soc., Perkin Trans. 2*, **1972**, 1856; D. I. Davies, P. Mason, and M. J. Parrott, *J. Chem. Soc., (C)*, **1971**, 3428; D. R. Adams and D. I. Davies, *J. Chem. Soc., Perkin Trans. 1*, **1974**, 246; J. A. Claisse, D. I. Davies, and C. K. Alden, *J. Chem. Soc., (C)*, **1966**, 1498; D. Seyferth and A. B. Evnin, *J. Am. Chem. Soc.*, **89**, 1468 (1967).

6) Classic examples of this are free radical bromination of substituted toluenes; see E. S. Huyser, *J. Am. Chem. Soc.*, **82**, 394 (1960).

7) See for summary, J. M. Dust and D. R. Arnold, *J. Am. Chem. Soc.*, **105**, 1221 (1983).

8) C. W. Jefford and P. T. Huy, paper in preparation. We thank Professor Jefford for sending the preparation method of this norbornadiene before publication.

Optical Resolution of (±)-Phenylsuccinic Acid by Using (−)-Proline as Resolving Agent

Tadashi SHIRAIWA,* Yujin SADO, Shigeru FUJII, Mitsuhiro NAKAMURA, and Hidemoto KUROKAWA
Faculty of Engineering, Kansai University, Yamate-cho, Suita, Osaka 564
(Received August 7, 1986)

Synopsis. A solution of equimolar mixture of (±)-phenylsuccinic acid ((±)-PSA) and (−)-proline ((−)-Pro) in ethanol or its suspension in 2-propanol selectively gave a salt composed of 1-molar amount of PSA and 2-molar amount of (−)-Pro. The salt purified gave (+)-PSA with an optical purity of about 100%. A salt composed of equimolar amounts of PSA and (−)-Pro was obtained from the ethanolic mother liquor, and gave (−)-PSA with an optical purity of 98%.

(±)-Phenylsuccinic acid (abbreviated as (±)-PSA) has been used as an intermediate material for phensuximide.[1,2] (±)-PSA has been optically resolved by the diastereomeric procedure using brucine.[3] However, it is not easy to obtain PSA with high optical purity in high yield, since it is difficult to purify the diastereomeric salts separated by repetition of recrystallization. (±)-Proline ((±)-Pro) has been optically resolved through its diastereomeric salts with an optically active dibasic acid, (+)-tartaric acid.[4] This suggests that (−)-Pro would easily form a salt with a dibasic acid such as PSA. Thus, optical resolution of (±)-PSA was attempted by using (−)-Pro as a resolving agent to find out a more practical procedure. In this note, 1-1 and 1-2 salts represent a salt composed of equimolar amounts of PSA and (−)-Pro and one composed of 1-molar amount of PSA and 2-molar amount of (−)-Pro, respectively; salts which contain the PSA rich in the (+)-enantiomer are represented as (+)-1-1 and (+)-1-2 salts, and those rich in (−)-PSA as (−)-1-1 and (−)-1-2 salts.

Experimental

Materials. (±)-PSA was obtained from Aldrich Chemical Co., Inc., (+)-PSA ($[\alpha]_D^{20}$ +168° (*c* 2.00, acetone); lit,[3] $[\alpha]_D^{20}$ +173.3° (*c* 1.8235, acetone)) from Kanto Chemical Co., Ltd., and (−)-Pro ($[\alpha]_D^{20}$ −84.7° (*c* 1.00, water)) from Wako Pure Chemical Ind., Ltd. (−)-PSA was obtained by optical resolution; $[\alpha]_D^{20}$ −170° (*c* 2.00, acetone).

Preparation of Standard Salts. 1-2 Salts: (+)-PSA (0.01 mol, 1.942 g) and 0.02 mol (2.302 g) of (−)-Pro were dissolved in 80 cm^3 of ethanol. After stirring for 1 h at room temperature, the (+)-1-2 salt formed was collected by filtration and recrystallized from ethanol: yield 3.53 g; mp 160 °C; $[\alpha]_D^{20}$ +13.5° (*c* 1.00, methanol); solubility at 30 °C 1.04 g/(100 cm^3 ethanol).

Found: C, 56.49; H, 6.60; N, 6.57%. Calcd for $C_{20}H_{28}N_2O_8$: C, 56,60; H, 6.65; N, 6.60%.

In the case of (−)-1-2 salt, after stirring a similar initial solution for 30 min at 15 °C, the crude (−)-1-2 salt formed was removed by filtration and the filtrate was stirred for 30 min in an ice bath. The (−)-1-2 salt crystallized was collected by filtration and washed thoroughly with diethyl ether: yield 1.70 g; mp 130 °C; $[\alpha]_D^{20}$ −107°(*c* 1.00, methanol); solubility at 30 °C 3.12 g/(100 cm^3 ethanol).

Found: C, 56.78; H, 6.70; N, 6.62%

1-1 Salts: After dissolving 0.02 mol of (+)- or (−)-PSA and 0.01 mol of (−)-Pro in ethanol, the solution was evaporated to dryness under reduced pressure around 50 °C. The residue was stirred in 200 cm^3 of diethyl ether for 1 h. The salt was collected by filtration and washed with diethyl ether.

(+)-1-1 Salt: Yield 2.92 g; mp 141 °C; $[\alpha]_D^{20}$ +51.4° (*c* 1.00, methanol).

Found: C, 58.09; H, 6.14; N, 4.50%. Calcd for $C_{15}H_{19}NO_6$: C, 58.25; H, 6.19; N, 4.53%

(−)-1-1 Salt: Yield 2.90 g; mp 136 °C; $[\alpha]_D^{20}$ −117° (*c* 1.00 methanol).

Found: C, 57.99; H, 6.18; N, 4.56%

Optical Resolution. Procedure I: (−)-Pro (0.02 mol) was dissolved in 80 cm^3 of ethanol. After cooling to 40 °C, 20 cm^3 of an ethanolic solution of 0.02 mol of (±)-PSA was added, and the solution was stirred for 30 min at 40 °C. The (+)-1-2 salt formed was collected by filtration: yield 2.88 g; $[\alpha]_D^{20}$ +3.8° (*c* 1.00, methanol). After evaporating the filtrate to dryness under reduced pressure around 50 °C, the residure was stirred in 200 cm^3 of diethyl ether for 1 h at room temperature. Then, the (−)-1-1 salt formed was collected by filtration: yield 1.98 g; $[\alpha]_D^{20}$ −115° (*c* 1.00, methanol). PSA (1.23 g, $[\alpha]_D^{20}$ +10.5° (*c* 2.00, acetone)) was recovered from the filtrate and resolved similarly to above. (+)-1-2 Salt ($[\alpha]_D^{20}$ +4.0° (*c* 1.00, methanol)) and (−)-1-1 salt ($[\alpha]_D^{20}$ −115° (*c* 1.00, methanol)) were obtained in 0.91 and 0.66 g yields, respectively, and 0.39 g of PSA was recovered.

Procedure II: (±)-PSA (0.02 mol) was dissolved in 100 cm^3 of 2-propanol, and 0.02 mol of (−)-Pro was added. After refluxing for 30 min followed by stirring for 30 min at 25°C, the (+)-1-2 salt formed was collected by filtration and washed with diethyl ether: yield 4.00 g; $[\alpha]_D^{20}$ +4.0° (*c* 1.00, methanol). After evaporating the filtrate to dryness, the residue and 0.780 g of (−)-Pro were dissolved in ethanol, and the solution was again evaporated to dryness under reduced pressure around 50 °C. After stirring the residue in 200 cm^3 of diethyl ether for 1 h at room temperature, (−)-1-1 salt was collected by filtration and washed with diethyl ether: yield 2.37 g; $[\alpha]_D^{20}$ −114° (*c* 1.00, methanol). PSA (0.35 g) was recovered from the filtrate.

The optical purities of the salts obtained by the procedures I and II were calculated on the basis of the specific rotations of the standard salts.

Preparation of (+)- and (−)-Phenylsuccinic Acids: (+)-1-2 Salt with an optical purity of around 80% was added to ethanol (6 cm^3 g^{-1}). After refluxing for 30 min followed by stirring for 30 min at 30 °C, the (+)-1-2 salt purified was collected by filtration. The (+)-1-2 salt purified or the (−)-1-1 salt obtained was added to concentrated hydrochloric acid (5 cm^3 g^{-1}). After stirring for 1 h in an ice bath, PSA was collected by filtration, washed with a small amount of cooled water, and dried. The PSA was dissolved in diethyl ether, and the solution was filtered. The filtrate was evaporated to dryness to obtain (+)- and (−)-PSAs. For example, 3.23 g of (+)-1-2 salt with an optical purity of 98% gave 1.39 g of (+)-PSA with that of 99.1%; the yields of (+)- and (−)-PSAs were calculated on the basis of the half amount of (±)-PSA consumed by reaction (1.942 g). It is confirmed by ^{1}H NMR spectra in acetone-d_6 that the (+)-and (+)-PSAs obtained are free from (−)-Pro.

Measurements. Specific rotations were measured with a

Table 1. Influence of Temperature on Formation of Diastereomeric Salts[a)]

Temperature °C	Salt or PSA[b)]	Yield g	Specific rotation[c)] ·	Optical purity[d)] %
5	(+)-1-2	1.76	−10.8	56
	(−)-1-1	0.43	−116	99
	PSA	0.74	−42.7	25
20	(+)-1-2	1.61	−2.6	73
	(−)-1-1	0.67	−117	100
	PSA	0.71	−19.9	12
30	(+)-1-2	1.50	+1.5	80
	(−)-1-1	0.76	−115	99
	PSA	0.64	−9.4	5
35	(+)-1-2	1.41	+3.2	83
	(−)-1-1	0.87	−114	97
	PSA	0.61	+2.0	1
40	(+)-1-2	1.36	+3.9	84
	(−)-1-1	0.99	−114	98
	PSA	0.58	+8.1	5

a) (±)-PSA and (−)-Pro: 0.01 mol. Total amount of ethanol: 50 cm³. Stirring time: 30 min. b) PSA: Phenylsuccinic acid. c) (+)-1-2 and (−)-1-1 salts: $[\alpha]_D^{20}$ (*c* 1.00, methanol). PSA: $[\alpha]_D^{20}$ (*c* 2.00, acetone). d) The optical purities of the salts were calculated on the basis of the specific rotations of standard (+)- and (−)-1-1 salts, 1-2 salt, and (+)-PSA ($[\alpha]_D$ +173.3° (*c* 1.8235, acetone)).

Union Giken high sensitivity PM-101 digital polarimeter. The solubilities of the standard (+)- and (−)-1-2 salts and the ternary phase diagram were obtained in a similar manner as described in our previous paper;[5)] (+)- and (−)-1-2 salts have maximal absorptions at 259 nm and molar absorptivities are 152 $cm^3\ mol^{-1}\ cm^{-1}$, ^1H NMR spectra were recorded on a JEOL JNM-PMX 60 NMR spectrometer.

Results and Discussion

Influence of Temperature on Formation of Salts. A separation of the diastereomeric salts was attempted for an ethanolic solution containing 0.01 mol of (±)-PSA and (−)-Pro at 5—40 °C similarly to the optical resolution described in the experimental section. The total amount of ethanol was 50 cm^3. The ^1H NMR spectrum in deuterium oxide and the specific rotation indicated that (+)-1-2 salt deposited selectively from the solution. (−)-1-1 Salt and unreacted PSA were obtained by evaporating the mother liquor to dryness around 50 °C, and the (−)-1-1 salt had an optical purity of about 100%. These results are given in Table 1. The relationship between the degrees of resolution of (+)-1-2 and (−)-1-1 salts and temperature was examined to resolve (±)-PSA efficiently, as shown in Fig. 1. The degrees of resolution were calculated by

$$\text{degree of resolution}/\% = (\text{yield of salt}/g \times \text{optical purity}/\% \times f)/0.971/g, \quad (1)$$

where f is 0.458 for (+)-1-2 salt and 0.628 for (−)-1-1 salt.

The degree of resolution of (+)-1-2 salt is scarcely influenced by temperature, since the optical purity increases with increase in temperature though the yield decreases. On the other hand, the degree of resolution of (−)-1-1 salt linearly increases with increase in temperature. Therefore, it is found that, of the temperatures employed, the separation of (+)-1-2 salt at 40 °C yields (−)-1-1 salt with an optical purity of 98% in the highest yield from the mother liquor.

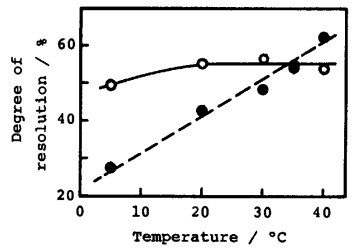

Fig. 1. Relationship between degree of resolution and temperatures. (±)-PSA and (−)-Pro: 0.01 mol. Total amount of ethanol: 50 cm^3.
——○——: (+)-1-2salt, ——●——: (−)-1-1 salt.

A separation of (+)-1-2 salt was attempted at 45 °C with the expectation that (−)-1-1 salt with high optical purity would be obtained in higher yield. However, (+)-1-2 salt did not crystallize under this condition. In the preparation of the standard salts, the salt formation using equimolar amounts of (+)-PSA and (−)-Pro gave (+)-1-2 salt and unreacted (+)-PSA, though (+)-1-1 salt was obtained when (+)-PSA and (−)-Pro were used in the molar ratio of 2 : 1. Moreover, after (+)-1-2 salt was filtered off from a solution of equimolar mixture of (±)-PSA and (−)-Pro, a stirring of the mother liquor in an ice bath or a concentration around 40 °C gave 1-2 salt which was a near racemate. The above results suggest that (+)-1-2 salt tends to form from (±)-PSA and (−)-Pro, and that (−)-1-2 salt forms below 40 °C, whereas (−)-1-1 salt forms above 45 °C.

Optical Resolution by Procedure I. In view of the results in the preceding section, an optical resolution of (±)-PSA was carried out at 40 °C as specified in Table 2. A (+)-1-2 salt with an optical purity of 84% crystallized from the initial solution. A (−)-1-1 salt with an optical purity of 98% and PSA were obtained from the mother liquor. Since the PSA was a near racemate and the yield was about one third of (±)-PSA consumed by reaction, the PSA was again allowed to

Table 2. Optical Resolution of (±)-Phenylsuccinic Acid by Using (−)-Proline[a)]

Procedure	Salts purified				Phenylsuccinic acid		
	Salt	Yield	Specific rotation[b)]	Optical purity[c)]	Yield[d)]	Specific rotation[e)]	Optical purity[f)]
		g	·	%	%	·	%
I[g)]	(+)-1-2	3.23	+12.4	98	71.7	+172	99.1
	(−)-1-1[i)]	2.64	−115	98	80.3	−170	98.1
II[h)]	(+)-1-2	3.58	+12.0	98	83.0	+171	98.7
	(−)-1-1[i)]	2.37	−114	96	70.5	−167	96.6

a) (±)-PSA: 0.02 mol. b) $[\alpha]_D^{20}$ (*c* 1.00, methanol). c) The optical purities were calculated on the basis of the specific rotations of standard (+)- and (−)-1-1 salts and 1-2 salt. d) The yields were calculated on the basis of 1.942 g. e) $[\alpha]_D^{20}$ (*c* 2.00, acetone). f) The optical purities were calculated on the basis of the specific rotation of (+)-PSA: $[\alpha]_D$ +173.3° (*c* 1.8235, acetone). g) PSA (0.39 g) was recovered; $[\alpha]_D^{20}$ +17.1°. (*c* 2.00, acetone). h) PSA (0.35 g) was recovered; $[\alpha]_D^{20}$ +17.8° (*c* 2.00, acetone). i) The salt was not purified.

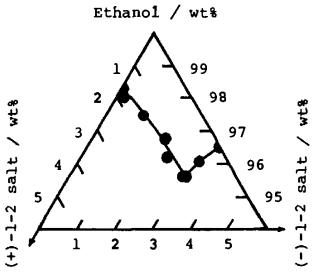

Fig. 2. Ternary phase diagram of solubility of 1-2 salt
Solvent: Ethanol. Temperature: 30°C.

react with an equimolar amount of (−)-Pro. The (±)-1-2 and (−)-1-1 salts obtained in the second run had the same optical purities as the salts obtained in the first run, so that both the salts obtained in the first and second runs were combined. The (−)-1-1 salt was treated with hydrochloric acid without recrystallization, since the salt had an optical purity of about 100%. The salt gave (−)-PSA with an optical purity of 98.1% in 80.3% yield.

For purification of the (+)-1-2 salt, the optimum amount of ethanol was calculated on the basis of the ternary phase diagram of solubility at 30 °C in ethanol shown in Fig. 2;[6)] at the eutectic point, the amount of (+)-1-2 salt is 1.34 wt%, that of (−)-1-2 salt 3.07 wt%, and that of ethanol 95.59 wt%. For 1 g of the (+)-1-2 salt with an optical purity of 80%, the optimum amount of ethanol calculated is 3.99 cm^3. However, 6 cm^3 of ethanol was employed, since 3.99 cm^3 of ethanol was too small to handle. The purification of the crude gave (+)-PSA with an optical purity of 99.1% in 71.7% yield.

Optical Resolution by Procedure II. A suspension of equimolar mixture of (±)-PSA and (−)-Pro in 2-propanol selectively gave (+)-1-2 salt with an optical purity of 84%. The (+)-1-2 salt purified gave (+)-PSA with an optical purity of 98.7% in 83.0% yield. This result is given in Table 2.

It is estimated from the results in ethanol that although equimolar amounts of (+)- and (−)-PSAs in the mother liquor form a racemic compound with each other, the excess of (−)-PSA forms (−)-1-1 salt with an equimolar amount of (−)-Pro. The amounts of (±)-PSA, (−)-PSA, and (−)-Pro in the mother liquor were calculated on the basis of the yield and optical purity of the (+)-1-2 salt obtained: (±)-PSA 0.514 g (0.0026 mol), (−)-PSA 1.540 g (0.0079 mol), and (−)-Pro 0.133 g (0.0011 mol). Therefore, after evaporating the mother liquor to dryness, the residue obtained was allowed to react with 0.780 g (0.0068 mol) of (−)-Pro in ethanol to give (−)-1-1 salt with an optical purity of 96% in 2.37 g yield; the theoretical yield is 2.45 g. (−)-PSA with an optical purity of 96.6% was obtained in 70.5% yield from the (−)-1-1 salt.

The above results indicate that it is possible to resolve (±)-PSA optically by using (−)-Pro as a resolving agent and to obtain (+)- and (−)-PSAs with optical purities of about 100% in 70—83% yield.

References

1) K. Tsuda, S. Yoshida, and A. Kubo, "Iyakuhin Gosei Kagaku," Nankodo, Tokyo (1983), p. 118.
2) C. A. Miller and L. M. Long, *J. Am. Chem. Soc.*, **73**, 4895 (1951).
3) H. Wren and H. Williams, *J. Chem. Soc.*, **109**, 572 (1916).
4) S. Yamada, C. Hongo, and I. Chibata, *Agric. Biol. Chem.*, **41**, 2413 (1977).
5) T. Shiraiwa, H. Miyazaki, A. Ikawa, and H. Kurokawa, *Nippon Kagaku Kaishi*, **1984**, 1425.
6) J. Jacques, A. Collet, and S.H. Wilen, "Enantiomers, Racemates, and Rasolutions," John Wiley & Sons, New York, Chichester, Brisbane, and Toronto (1981), p. 389.

Synthesis and Biological Activity of Substance P Analogs Containing Pyrohomoglutamic Acid and Homoglutamine

Tadashi HASHIMOTO,* Naoki SAKURA, Kyoko HIROSE, Yoshiki UCHIDA, Miwako NISHIJIMA, and Tadashi MORO
School of Pharmacy, Hokuriku University, Ho-3, Kanagawa-machi, Kanazawa 920-11
(Received August 26, 1986)

Synopsis. Eight substance P analogs substituted by L- or D-pyrohomoglutamic acid (6-oxo-2-piperidinecarboxylic acid) and L- or D-homoglutamine at the position 5 and 6 were prepared by the solid phase method. The contractile activities of the analogs were compared with that of SP on isolated guinea-pig organs.

Synthetic study[1] on thyrotropin-releasing hormone [TRH: pGlu-His-Pro-NH_2[2]] revealed that TRH analogs containing pyrohomoglutamic acid (pHgu-OH: 6-oxo-2-piperidinecarboxylic acid) at the N-terminus showed relative selectivity for action in the central nervous system. Therefore, the substitution of pHgu residue for pGlu at N-terminus of a bioactive peptide may be able to provide a new knowledge of the structure-activity relationships.

Up to date, L-pHgu moiety has been incorporated into peptide chain using L-pHgu-OH and the usual peptide bond forming reagent. However, the preparation of L-pHgu-OH involves a troublesome work, that is, generally an enzymatic resolution[3] of N-acetyl-DL-homoglutamic acid (DL-Ac-Hgu-OH) to give L-H-Hgu-OH, followed by cyclization procedure. Our investigation[4] developed a simple method for synthesis of pHgu-peptide that Hgn residue at N-terminus in peptide chain could be cyclized to produce pHgu residue. D-Hgn-peptide is readily converted and yields a new amino acid D-pHgu residue. This conversion reaction was applied to the synthetic study on analogs of substance P (SP) related peptides, pGlu-Gln-Phe-Phe-Gly-Leu-Met-NH_2 (**1**) and pGlu-Phe-Phe-Gly-Leu-Met-NH_2 (**2**), which potencies (Table 1) are higher than the contracting activity of SP itself of guinea-pig ileum.[5]

This paper describes syntheses and biological properties of eight analogs (Fig. 1) of the SP related peptides containing L- or D-pHgu and L- or D-Hgn at position 5 and 6. The contracting activities of the synthetic peptides were compared with that of our synthetic SP in order to examine the biological effects of the substitution of L- or D-pHgu for pGlu moiety and of the replacement of Gln residue by L- or D-Hgn on pGlu-peptides.

The SP analogs were synthesized in the same way with the preparation of SP analogs containing L-Hgn[6] and D-Hgn[7] by the solid phase technique[8] on an automated peptide synthesizer. *t*-Butoxycarbonyl (Boc) protection was used for α-amino function except benzyloxycarbonyl(Z) for pGlu-OH, and the amide nitrogen (N^{ca}) of Hgn. N-Terminal Hgn-peptide was kept at 40 °C for 4 h in aq acetic acid (50%) to produce pHgu moiety. The crude product was purified by preparative reverse-phase high-performance liquid chromatography (HPLC) using aq trifluoroacetic acid (0.1%) in acetonitrile as eluent. Highly purified peptides (Table 2, 3) were obtained after gel filtration on Sephadex G-10 column. The yield was sacrificed for the purity. Homogeneity of the peptides was demonstrated by analytical HPLC and thin-layer chromatography (TLC). When single peaks and single spots were observed for a synthetic peptide in all chromatographic systems, the peptide was considered appropriately pure for bioassay. These chromatographic data were reinforced by the amino acid analytical data.

The results of biological properties of the synthetic analogs are shown in Table 4.

The potency of D-pHgu heptapeptide analog **4** was as high as the contractile activity of **1** and higher than that of L-pHgu-peptide **3** on isolated guinea-pig ileum. The both replacements of pGlu and Gln

Table 1. Relative Contracting Activities of Synthetic Analogs on Guinea-Pig Ileum

Peptide	Amino acid sequence (1 5 6 11)	Relative activity
SP	H-Arg-Pro-Lys-Pro-Gln-Gln-Phe-Phe-Gly-Leu-Met-NH_2	1
1 [pGlu^5]-SP (5—11)	pGlu-Gln-Phe-Phe-Gly-Leu-Met-NH_2	1.7
2 [pGlu^6]-SP (6—11)	pGlu-Phe-Phe-Gly-Leu-Met-NH_2	2.0

	(5 6 11)	
[L-pHgu^5]-SP (5—11)	L-pHgu—Gln-Phe-Phe-Gly-Leu-Met-NH_2	**3**
[D-pHgu^5]-SP (5—11)	D-pHgu—Gln-Phe-Phe-Gly-Leu-Met-NH_2	**4**
[pGlu^5, L-Hgn^6]-SP (5—11)	pGlu-L-Hgn-Phe-Phe-Gly-Leu-Met-NH_2	**5**
[pGlu^5, D-Hgn^6]-SP (5—11)	pGlu-D-Hgn-Phe-Phe-Gly-Leu-Met-NH_2	**6**
[L-pHgu^5, L-Hgn^6]-SP (5—11)	L-pHgu-L-Hgn-Phe-Phe-Gly-Leu-Met-NH_2	**7**
[D-pHgu^5, D-Hgn^6]-SP (5—11)	D-pHgu-D-Hgn-Phe-Phe-Gly-Leu-Met-NH_2	**8**
[L-pHgu^6]-SP (6—11)	L-pHgu-Phe-Phe-Gly-Leu-Met-NH_2	**9**
[D-pHgu^6]-SP (6—11)	D-pHgu-Phe-Phe-Gly-Leu-Met-NH_2	**10**

Fig. 1. Synthetic analogs.

Table 2. Physical Properties and Yields of Synthetic Analogs

Analog	$[\alpha]_D$/°	Retention time[c]	R_f^I	R_f^{II}	Yield/%
3	−25.3 (*c* 0.3)[a]	16.0	0.46	0.81	21.0
4	−42.3 (*c* 0.3)[b]	16.1	0.45	0.84	8.3
5	−34.0 (*c* 0.5)[a]	16.3	0.45	0.81	14.0
6	−42.0 (*c* 0.3)[b]	16.9	0.46	0.83	7.6
7	−28.3 (*c* 0.3)[a]	17.4	0.44	0.82	12.3
8	−43.6 (*c* 0.5)[b]	16.8	0.43	0.83	12.1
9	−37.6 (*c* 0.5)[a]	19.7	0.72	0.87	18.5
10	−56.6 (*c* 0.5)[b]	19.3	0.73	0.87	20.8

a) and b) $[\alpha]_D$ values were measured in DMF at 25 °C and 14 °C respectively. c) Condition of analytical HPLC: column, NOVA-PAK C_{18}; flow rate, 1 ml min^{-1}; Detection, 210 nm; eluent system, linear gradient from 21% to 35% CH_3CN (15 min) in 20 mM phosphate buffer (pH 3.0).

Table 3. Amino Acid Analyses of the Synthetic Peptides

Analog	Found (Calcd)						
	Glu	Gly	Hgu[a]	Met	Leu	Phe	NH_3
3	0.99 (1)	0.95 (1)	1.06 (1)	0.95 (1)	0.98 (1)	2.06 (2)	2.49 (2)
4	0.99 (1)	1.01 (1)	1.04 (1)	0.98 (1)	0.99 (1)	1.99 (2)	2.04 (2)
5	1.01 (1)	0.96 (1)	1.09 (1)	0.97 (1)	0.97 (1)	1.96 (2)	2.92 (2)
6	1.03 (1)	0.99 (1)	1.08 (1)	0.93 (1)	0.99 (1)	1.99 (2)	2.08 (2)
7	—	1.00 (1)	2.10 (2)	0.94 (1)	0.94 (1)	2.01 (2)	2.42 (2)
8	—	1.00 (1)	2.16 (2)	0.88 (1)	0.98 (1)	1.98 (2)	2.47 (2)
9	—	0.96 (1)	1.11 (1)	0.96 (1)	1.00 (1)	1.98 (2)	1.07 (1)
10	—	0.97 (1)	1.03)1)	1.03 (1)	1.04 (1)	1.93 (2)	1.33 (1)

a) Homoglutamic acid.

Table 4. Relative Potencies of Synthetic Analogs on Guinea-Pig Organs

Analog	Relative activity accepted SP as 1	
	Ileum	Trachea
3	0.65	1.10
4	1.76	0.78
5	2.08	3.64
6	0.07	<0.01
7	0.88	1.74
8	0.10	<0.01
9	1.50	3.01
10	0.17	0.14

residues with L- or D-pHgu and L- or D-Hgn brought the decreases of the contracting activities on the ileum assay. Analogs **7** and **8** had 90 and 10% of the activity of SP, and 50 and 6% of that of **1** respectively. pGlu-peptide analogs **5** possessed the highest activities among the eight analogs **3**—**10** on the both assays, while D-Hgn analog **6** showed the lowest potency. Hexapeptide analog **9** was found to be highly active on the both assays, and had 150 and 300% of the activity of SP on the ileum and trachea assays respectively and 75% of that of **2** on the ileum assay. Similarly to SP analogs containing L-Hgn[6] or D-Hgn,[7] the replacement of Gln moiety with L-Hgn on pGlu-peptide enhanced the biological activity, while D-Hgn analog **6** possessed reduced activity. The data indicate that L-pHgu-peptide analogs exert potent agonistic effects and the substitution of D-pHgu for pGlu, except for analog **4**, brings the drastic decrease of the activity. The results also suggest that the L-configuration of the amino acid residue at the position 6 may be more important than that of the residue at the position 5 for the contractile activities of SP related peptides.

Experimental

Amino acid derivatives were purchased from Peptide Institute, Inc., Osaka, and benzhydrylamine (BHA) resin (available amine of the resin: 0.6 mmol g^{-1} of support) from Beckman Inc. Optical rotations were measured in a Nipponbunkoh DIP-4 Polarimeter. Amino acid analyses on samples previously hydrolyzed with 6 M HCl (1 M=1 mol dm^{-3}) (110 °C, 24 h) were performed on a Hitachi KLA-5 Amino Acid Analyzer. TLC were carried out on silica-gel plates (Merck). The following solvent systems were used: R_f^I, *n*-BuOH : AcOH : H_2O (4 : 1 : 5, upper phase); R_f^{II}, *n*-BuOH: pyridine: AcOH: H_2O (30 : 20 : 6 : 24). Analytical HPLC were effected on the following systems: column, NOVA-PAK C_{18} (3.9×150 mm); flow rate, 1 ml min^{-1}; detection, 210 nm; eluent system, linear gradient for 15 min from 21% to 35% CH_3CN in 20 mM phosphate buffer (pH 3.0).

General Procedure for the Preparation of Analogs. The solid phase synthesis was carried out using a Beckman System 990 C Peptide Synthesizer as described previously.[6] Half gram of BHA-resin hydrochloride for each analog served as the solid support. A 2.5 fold excess of amino acid derivative was used for all coupling. The coupling was affected with DCC/HOBt.† The protected peptide resin was treated with anhydrous liquid HF containing 10% anisole. After evaporation of HF in vacuo, the peptide was extracted with 50% AcOH. The extract of N-terminal Hgn-peptide was kept at 40 °C for 4 h to yield pHgu moiety.

Purification of the Peptides. The crude peptide was subjected to HPLC as reported previously.[6] The apparatus was

†DCC=dicyclohexylcarbodiimide, HOBt=1-hydroxybenzotriazole.

composed of a model 590 pump and a U6K injector (Waters) connecting with a column (20×300 mm) of Chemcosorb ODS (Chemco). The eluates were monitored with a UV detector S-310A model-II (Soma) at 210 nm wavelength. CH_3CN–0.1% TFA solvent system was used as eluent at flow rate 10 ml min^{-1}. Each peptide was emerged at 40—60 min by isocratical elution with 27—34% CH_3CN contents of the solvent system. The desired fraction was passed through a Sephadex G-10 column (16×930 mm) eluted with 2 M AcOH. Homogeneity of the peptides was analyzed by analytical HPLC and TLC.

Bioassay. The agonistic activity of the synthetic analog was measured on ileum and trachea taken from guinea-pig, as described before.[6] The contraction was recorded by means of an isotonic transducer (Nippon Kohden, TD-111T) with load of 1 or 2 g (for trachea and ileum respectively) on a Servocorder (Watanabe Instruments, SR6204). Concentration-response curves were obtained using a cumulative dose-assay, and the time between two consecutive dose-response curves was longer than 10 min.

References

1) R. F. Nutt, F. W. Holly, C. Homnick, R. Hirshmann, D. F. Veber, and B. H. Arison, *J. Med. Chem.*, **24**, 692 (1981).

2) Amino acids, peptides and their derivatives mentioned in this paper are of L-configuration. The abbreviations for amino acids and peptides are in accordance with the rules of the IUPAC-IBU Commission on Biochemical Nomenclature in *Eur. J. Biochem.*, **138**, 9 (1984).

3) J. P. Greenstein and M. Winitz, "Chemistry of the Amino Acids," John Wiley and Sons, New York (1961), Vol. 3, p. 2411.

4) K. Hirose, N. Sakura, Y. Uchida, M. Nishijima, and T. Hashimoto, *Chem. Pharm. Bull.*, in press.

5) N. Yanaihara, C. Yanaihara, M. Hirohashi, H. Sato, Y. Iizuka, T. Hashimoto, and M. Sakagami, "Substance P," ed by U. S. von Euler and B. Pernow, Raven Press, New York (1977), p. 27.

6) Y. Uchida, M. Nishijima, T. Moro, N. Sakura, K. Hirose, H. Kontani, and T. Hashimoto, *Bull. Chem. Soc. Jpn.*, **59**, 4003 (1986).

7) T. Hashimoto, Y. Uchida, M. Nishijima, T. Moro, N. Sakura, and K. Hirose, *Bull. Chem. Soc. Jpn.*, **59**, 4009 (1986).

8) R. B. Merrifield, *Adv. Enzymol.*, **32**, 221 (1969).

Electrochemical Reduction of *exo*-5-Acetyl-*endo*-6-trichloromethylbicyclo[2.2.1]hept-2-ene

Sadao TSUBOI, Yasuhiro ISHIGURO, and Akira TAKEDA*
Department of Synthetic Chemistry, School of Engineering, Okayama University, Tsushima, Okayama 700
(Received September 5, 1986)

Synopsis. Electrochemical reduction of exo-5-acetyl-endo-6-trichloromethylbicyclo[2.2.1]hept-2-ene (**2**) using a mercury cathode gave chemoselectively either the corresponding monochloromethyl or dichloromethyl derivatives in high yields by selecting supporting electrolyte. The reduction of **2** using a lead cathode gave 2-acetyl-3-methylbicyclo[2.2.1]-hepta-2,5-diene and *cis*-1-(4-vinyl-2-cyclopentenyl)-2-propanone together with by-products.

As our continuing studies on the chemistry of 5,5,5-trichloro-3-penten-2-one (**1**),[1] we reported that **1** reacted with cyclopentadiene giving stereospecifically exo-5-acetyl-endo-6-trichloromethylbicyclo[2.2.1]hept-2-ene (**2**) in a high yield.[1d] If conversion of the trichloromethyl group of **2** to a chloromethyl or a methyl group could be accomplished, the stereospecific introduction of these groups into the endo position of norbornene will become possible. This conversion was poorly accomplished by conventional reduction of **2** with zinc in acetic acid affording *exo*-5-acetyl-*endo*-6-methylbicyclo[2.2.1]hept-2-ene (**3**) in 13% yield,[1d] which is a minor component of the mixture obtained from the reaction of 3-penten-2-one with cyclopentadiene.[2] As an electrochemical method may be profitable in conversion of compound **2** to **3**, we investigated the cathodic reduction of **2** under various conditions.

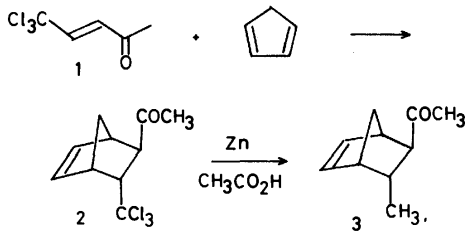

Results and Discussion

Only a few investigations have been made on the electrochemical reduction of trichloromethyl compounds. Nagao, et al.[3] have reported that $\alpha,\alpha,\alpha,\omega$-tetrachloroalkanes can be converted to either α,ω-dichloroalkanes or α,α,ω-trichloroalkanes by selecting cathodic supporting electrolyte. We carried out the reduction of **2** under the similar conditions.

When norbornene **2** was reduced electrolytically at the mercury cathode using tetrabutylammonium bromide as a supporting electrolyte in *N*,*N*-dimethylformamide (DMF), *exo*-5-acetyl-*endo*-6-dichloromethylbicyclo[2.2.1]hept-2-ene (**4**) was obtained in 80% yield. Compound **4** was identical with the major component of the products obtained from the Diels-Alder reaction[1d] of 5,5-dichloro-3-penten-2-one with cyclopentadiene. On the other hand, *exo*-5-acetyl-*endo*-6-chloromethylbicyclo[2.2.1]hept-2-ene (**5**) was formed in 94% yield when tetramethylammonium chloride was used in a 90% methanol solution. It is clear that a supporting electrolyte plays an important role in the present chemoselectivity in the reduction of trichloromethyl group.

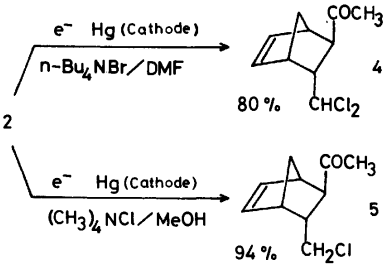

However, the reduction of compound **2** with a lead cathode using tetramethylammonium chloride gave nonchemoselectively 2-acetyl-3-methylbicyclo[2.2.1]-hepta-2,5-diene (**6**) in 44% yield together with **3** (17%), *exo*-5-(1-hydroxyethyl)-*endo*-6-chloromethylbicyclo-[2.2.1]hept-2-ene (**7**) (4.9%) (1 : 1 diastereomeric mixture) and *cis*-1-(4-vinyl-2-cyclopentenyl)-2-propanone (**8**) (18%). The structure of **6** was elucidated by spectral data. Mass spectrum showed a clear peak of molecular ion at m/z 148. The IR bands of **6** at 1665 cm^{-1} are characteristic of the α,β-unsaturated ketone. The structure of **7** was confirmed by the fact that the oxidation with chromium trioxide gave ketone **5**.

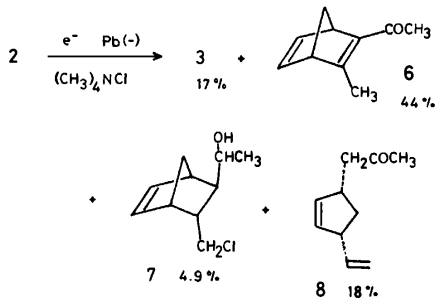

Reduction of **2** with zinc in acetic acid also has afforded cyclopentene **8** as a minor product in addition to **3**, although the structure has not been clarified.[1d] The structure of **8** was determined on the basis of IR, NMR, MS, and elemental analyses. The NMR spectrum of **8** was very similar to that of methyl 4-vinyl-2-cyclopentene-1-acetate with the exception of a singlet (2.15 ppm, $COCH_3$).[4] A signal due to olefin protons of cyclopentene appeared as a singlet at 5.68 ppm along with the disappearence of a signal (ca. 6.2 ppm) due to olefin protons of norbornene. Two multiplets (4.80—5.23 and 5.5—6.1 ppm) due to three olefin protons show the existence of a vinyl group. The unusual high δ value of cis proton of cyclopentene methylene is undoubtedly due to shielding effect of both vinyl and carbonyl groups. In mass spectrum of **8** (MW 150), the

peaks at m/z 107 and 93 show the existence of an acetonyl group. The base peak at m/z 92 must be due to ions of vinylcyclopentadiene.

The following mechanism can be postulated for the formation of **6** and **8**. Compound **6** would be presumably formed from **5** via dehydrochlorination and prototropic shift. Cyclopentene **8** would be produced from **5** via C-C bond cleavage induced by anion. The C-C bond cleavage of norbornene derivatives under

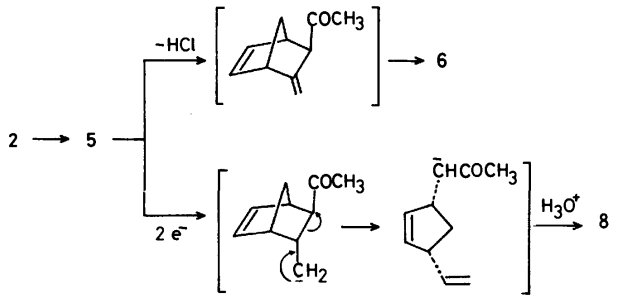

electroreductive conditions is interesting and is similar to a cleavage of diester **9** to produce **10** upon treatment with Na/NH_3.[5,6]

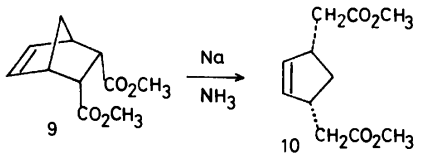

In conclusion, the electrochemical method using mercury cathode could reduce trichloromethyl compound **2** either to dichloromethyl compound **4** or monochloromethyl compound **5** chemoselectively in high yields. In contrast to the conventional method such as the reduction with $Zn-CH_3CO_2H$, the reaction proceeded with no contamination of resinous materials.

Experimental

The melting points and boiling points are uncorrected. Analytical determinations by GLPC were performed on a Hitachi model K-53 gas chromatograph using columns filled with 10% Apiezone Grease L on Chromosorb W (3 mm ϕ×1 m) or 10% polyneopentyl glycol succinate on Chromosorb W (3 mm ϕ×1 m). Preparative GLC was performed on a Yanagimoto model GCG-550 T gas chromatograph. IR spectra were determined on a Hitachi model EPI-S2 spectrometer. ^1H NMR spectra (60 MHz) were obtained with a Hitachi model R-24 apparatus. The mass spectra were measured on a Hitachi model RMS-4 mass spectrometer at 70 ev.

Electrolysis. The electrochemical cell consisted of an anode porcelain cylinder (35 mm in diameter; 150 mm in height) fitted with a calcium chloride tube, and of a cathode glass vessel (80 mm in diameter, ca. 300 ml content) fitted with a gas lead pipe, a thermometer, and a magnetic stirrer. All electrolyses were carried out at room temperature under N_2. Mercury (300 g; surface area, 50 cm^2) or lead (60 mm in diameter; 1.5 mm in thickness; surface area, ca. 58 cm^2) was used as the cathod, while a platinum wire (1.0 mm ϕ×75 mm) was used as an anode.

Material. *exo*-5-Acetyl-*endo*-6-trichloromethylbicyclo-[2.2.1]hept-2-ene (**2**) was prepared from 5,5,5-trichloro-3-penten-2-one (**1**) and cyclopentadiene.[1d]

Reduction of 2 with $Zn-CH_3CO_2H$. This reaction was reported in the previous paper.[1d] The structure of the minor component was newly determined as **8**: 10% yield: IR (neat) 1710 (C=O), 1636 (C=C), 1360, 1160, 910; ^1H NMR ($CDCl_3$) δ=0.8—1.4 (m, 2H, ring CH_2), 2.15 (s, 3H, $COCH_3$), 2.25—2.7 (m, 2H, $C\underline{H}_2COCH_3$), 2.8—3.5 (m, ring methyne), 4.80—5.23 (m, 2H, $CH{=}C\underline{H}_2$), 5.68 (s, 2H, CH=CH), 5.5—6.1 ppm (m, 1H, $C\underline{H}{=}CH_2$); MS (70 ev) m/z (rel intensity) 150 (M^+, 2), 135 (10), 107 (M-$COCH_3$, 38), 93 (56), 92 (100), 91 (86), 79 (58), 77 (60), 66 (58), 43 (72). Found: C, 79.73; H, 9.56%. Calcd for $C_{10}H_{14}O$: C, 79.96; H, 9.39%.

Electrochemical Reduction of 2. (a) Mercury was used as the cathode. A mixture of **2** (2.00 g, 8 mmol), tetrabutylammonium bromide (1.935 g, 6 mmol), and *N,N*-dimethylformamide (100 ml) was charged in a cathode cell. Tetrabutylammonium bromide (0.967 g, 3 mmol) and *N,N*-dimethylformamide (50 ml) was charged in an anode cell. The electrolysis with terminal voltage 27.0 V (current, 40—200 mA) was continued until the starting material **2** was consumed (24 h). The organic materials of the cathode cell were extracted with ether. The combined extracts were washed with water, dried over $MgSO_4$, and concentrated to give 1.43 g (80% yield) of **4** as crystals: 98% pure by GLC analysis (column, polyneopentyl glycol succinate, 150 °C; carrier gas, N_2, 0.5 kg cm^{-2}); mp 68—70 °C (from hexane)(lit,[1d] 66—67.5 °C). IR and ^1H NMR data were identical with those reported previously.[1d] No trace of the isomers was detected by ^1H NMR.

(b) Mercury was used as the cathode. In a cathode cell a mixture of **2** (2.00 g, 8 mmol) tetramethylammonium chloride (2.19 g, 20 mmol), and 90% methanol (100 ml) was charged. In an anode cell a solution of tetramethylammonium chloride (1.10 g, 10 mmol) in 90% methanol (50 ml) was charged. The electrolysis with terminal voltage 27.0 V (44—219 mA) was carried out at room temperature until the starting material **2** was consumed (24 h). The organic materials in the cathode cell were extracted with ether and worked up as described above, giving 1.39 g (94% yield) of **5** as a clean oil: 99% pure by GLC analysis (column, polyneopentyl glycol succinate, 150 °C; carrier gas, N_2, 0.5 kg cm^{-2}); bp 85—87 °C/3 Torr; IR (neat) 1709, 1570 cm^{-1}; MS (70 eV) m/z (rel intensity) 184 (M^+, 7), 149 (M—Cl, 79), 145 (80), 121 (66), 119 (95), 105 (84), 91 (69), 77 (69), 66 (100); ^1H NMR ($CDCl_3$) δ= 1.18—1.74 (m, 2H, C_7-H), 1.87—2.08 (m, 1H, $C\underline{H}COCH_3$), 2.22 (s, 3H, $COCH_3$), 2.5—3.8 (m, 1H, $C\underline{H}CH_2Cl$), 2.85—3.13 (m, 2H, C_1-H, C_4-H), 3.27 (d, 2H, J=6.5 Hz, CH_2Cl), 5.95—6.50 ppm (m, 2H, CH=CH). Found: C, 65.13; H, 7.11%. Calcd for $C_{10}H_{13}ClO$: C, 65.04; H, 7.09%.

(c) Lead was used as the cathode. A mixture of **2** (2.00 g, 8.0 mmol), tetramethylammonium chloride (2.19 g, 20 mmol), and 90% methanol (100 ml) was charged in a cathode cell. A solution of tetramethylammonium chloride (1.10 g, 10 mmol) in 90% methanol was charged in an anode cell. The electrolysis was carried out at terminal voltage 15 V (0.1—0.5 A) at room temperature. Every one hour the reaction mixture was analyzed by GLC. After 10 h, the organic materials in the cathode cell were extracted with ether. The combined extracts were washed with water and dried over $MgSO_4$. Removal of the solvent gave 1.22 g of an oil. GLC (column, Apiezone Grease L, 160 °C; carrier gas N_2, 0.5 kg cm^{-2}) analysis showed five peaks. Peaks, retention times (min), and percentages of peak area are as follows: 1, 1.4, 17%; 2, 1.6, 18%; 3, 2.3, 16%; 4, 3.6, 43%; 5, 7.6, 6%. Each component was separated by preparative GLC and identified. Peak 1: **3**; 17% yield. The retention time, and IR and ^1H NMR data were identical with those of the sample prepared from the reduction of **2** with $Zn-CH_3CO_2H$. Peak 2: **8**; 18% yield. Spectral data were identical with those described above. Peak 3: the structure was unidentified. Peak 4: **6**; 44% yield; IR (neat) 1665 (C=O), 1562 cm^{-1} (C=C); ^1H NMR ($CDCl_3$) δ=1.82 (s,

3H, CH_3), 2.05 (s, 3H, $COCH_3$), 2.12 (m, 2H, CH_2), 2.94 (br. s, 1H, methyne), 3.40 (m, 1H, methyne), 5.92 (m, 2H, CH=CH); MS (70 eV) *m/z* (rel intensity) 148 (M^+, 29), 133 ($M-CH_3$, 27), 105 ($M-COCH_3$, 100), 103 (47), 79 (73), 77 (69), 70 (82). Found: C, 81.05; H, 8.21%. Calcd for $C_{10}H_{12}O$: C, 81.04; H, 8.16%. Peak 5: **7**; 4.9% yield; IR (neat) 3380 (OH), 2960, 1330, 900, 715 cm^{-1}; ^1H NMR ($CDCl_3$) δ=1.29 (d, 3H, J=6 Hz, CH_3), 1.50 (br. s, 1H, ring CH_2), 1.65 (s, 1H, OH), 2.0—4.0 (m, 7H, 5 methyne, CH_2Cl), 6.2 ppm (m, 2H, CH=CH). Found: C, 64.10; H, 8.08%. Calcd for $C_{10}H_{15}ClO$: C, 64.34; H, 8.10%.

Conversion of 7 to 5. To 3 ml of dry pyridine was added CrO_3 (0.31 g, 3.1 mmol) at 15—20 °C with stirring. A solution of **7** (0.199 g, 1.07 mmol) in dry pyridine (3 ml) was added and the mixture was stirred overnight at room temperature, and then poured into cold water. The organic materials were extracted with benzene-ether (1 : 1), washed with water, dried over $MgSO_4$, and concentrated. The residue was chromatographed on SiO_2 (hexane/acetone, 10 : 1), giving 80 mg (40%) of **5**: TLC (SiO_2; hexane/acetone, 3 : 1) R_f 0.54. IR and ^1H NMR spectra were identical with those of the sample prepared above.

We are grateful to Dr. R. D. Miller of International Business Machines Corporation (IBM) for the gift of ^1H NMR spectra of methyl 4-vinyl-2-cyclopentene-1-acetate and for a fruitful suggestion. We also thank Mr. Eiichiro Amano of our laboratory for elemental analyses.

References

1) a) A. Takeda and S. Tsuboi, *J. Org. Chem.*, **35**, 2690 (1970); b) A. Takeda, S. Tsuboi, T. Moriwake, and E. Hirata, *Bull. Chem. Soc. Jpn.*, **45**, 3685 (1972); c) A. Takeda and S. Tsuboi, *J. Org. Chem.*, **38**, 1709 (1973); d) S. Tsuboi, Y. Ishiguro, and A. Takeda, *Bull. Chem. Soc. Jpn.*, **47**, 673 (1974).

2) Y. Kobuke, T. Fueno and J. Furukawa, *J. Am. Chem. Soc.*, **92**, 6548 (1970).

3) M. Nagao, N. Sato, T. Akashi, and T. Yoshida, *J. Am. Chem. Soc.*, **88**, 3447 (1966).

4) R. D. Miller and V. Y. Abraitys, *J. Am. Chem. Soc.*, **94**, 663 (1972).

5) P. G. Gassman and X. Creary, *J. Chem. Soc., Chem. Commun.*, **1972**, 1214.

6) As another example of the formation of cyclopentene from bicyclo[2.2.1]heptene, it is known that the base-catalyzed treatment of dehydronorcamphor gives 2-cyclopentene-1-acetic acid: J. Paasivirta, *Tetrahedron Lett.*, **1968**, 2867.

Asymmetric Synthesis of (2*R*,3*S*)-2,3-Epoxyoctanal, a Key Intermediate of 14,15-Leukotriene A_4

Sadao Tsuboi, Hiroyuki Furutani, and Akira Takeda*
Department of Synthetic Chemistry, School of Engineering, Okayama University, Tsushima, Okayama 700
(Received September 11, 1986)

Synopsis. Asymmetric reduction of ethyl 3-chloro-2-oxooctanoate with baker's yeast gave ethyl 3-chloro-2-hydroxyoctanoate (**3**) [(2*S*,3*R*)/(2*S*,3*S*), 4:1] in 67% yield with >99% e.e. Chlorohydrin (2*S*,3*R*)-**3** was converted to the titled compound in 34% total yield with 80% e.e. via the reduction, dehydrochlorination, and oxidation, successively. (2*R*,3*R*)-2,3-Epoxyoctanal was also prepared from (2*S*,3*S*)-**3** in 33% total yield with 94% e.e.

Samuelsson[1] has reported that (5*Z*,8*Z*,10*E*,12*E*)-icosatetraenoic acid (14,15-LTA_4) is formed by oxidation of arachidonic acid with 15-lipoxygenase and is a key intermediate in further biological transformations. Because of the unavailability of unstable metabolites from natural sources, the synthesis becomes important. Zamboni et al.[2] reported a stereospecific synthesis of 14,15-LTA_4 by using (2*R*,3*S*)-2,3-epoxyoctanal (**1**) as a key intermediate. However, reports on the

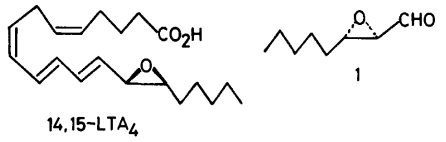

synthesis of **1** are quite few.[3] Here we describe a convenient synthesis of **1** using chiral reduction with fermenting baker's yeast. The reaction sequence is shown in Scheme 1.

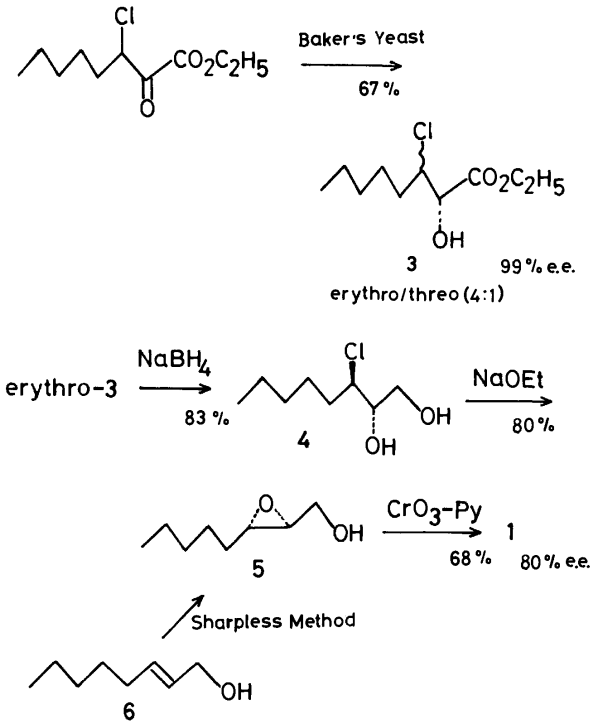

Scheme 1.

The starting material, ethyl 3-chloro-2-oxooctanoate (**2**) is readily available by Darzen type condensation which was developed by us.[4] Treatment of **2** with fermenting baker's yeast gave a 4:1 mixture of ethyl *erythro*(2*S*,3*R*)- and *threo*(2*S*,3*S*)-3-chloro-2-hydroxyoctanoate (**3**) in 67% yield. Each isomer was separated by preparative HPLC. Optical purities of both isomers were estimated as >99% e.e. respectively by ^{1}H NMR analysis in the presence of chiral shift reagent (europium tris[3-(heptafluoropropylhydroxymethylene)-(−)-camphorato] (Eu(hfc)$_3$)) and HPLC analysis of its 3,5-dinitrophenylcarbamate. Reduction of *erythro*-**3** with $NaBH_4$ gave diol **4** in 83% yield. Treatment of **4** with two equivalent of NaOEt yielded (2*S*,3*S*)-2,3-epoxyoctanol (**5**) in 80% yield and the subsequent oxidation of **5** with CrO_3–pyridine afforded aldehyde **1** in 68% yield. Enantiomeric excess was estimated as 80% e.e. by comparison of the optical rotation with that of the literature.[3] Decrease of the optical purity would be attributable to the racemization in the course of the reduction and dehydrochlorination. Furthermore we prepared **5** from *trans*-2-octen-1-ol by Sharpless method[2,5] and confirmed the structure of **5** obtained via baker's yeast reduction. Absolute configuration of α-carbon of **3** was determined to be S from that of **1**.

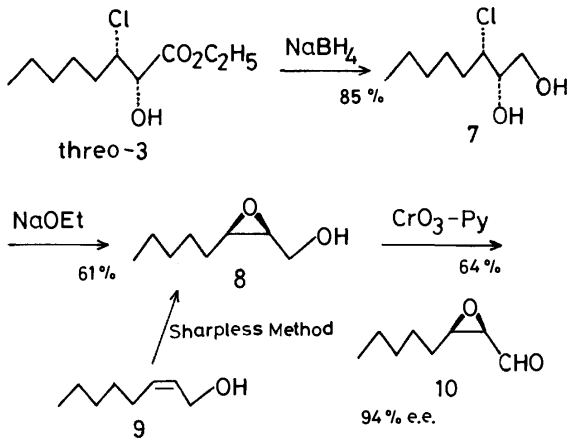

Scheme 2.

Similarly, *threo*-**3**, a minor product by the baker's yeast reduction, was also converted to *cis*-2,3-epoxyoctanol (**8**) via *threo*-diol **7**, as shown in Scheme 2. The spectral data of epoxide **8** was identical with that of the sample prepared by the epoxidation[5] of *cis*-2-octen-1-ol. Oxidation of **8** with CrO_3-pyridine gave (2*R*,3*R*)-2,3-epoxyoctanal (**10**) with 94% e.e. in 64% yield. The coupling constant (5.0 Hz) between two protons of the epoxide ring was a characteristic value for *cis*-epoxide.[6] Compound **10** will be useful for the synthesis of an unnatural form of 14,15-LTA_4.

Our system provides a convenient route to **1**, **8**, and

10 because of availability of the starting material, simplicity of the experiment, and no use of heavy metal.

Experimental

The melting points and boiling points are uncorrected. Elemental analyses were carried out by Eiichiro Amano in our laboratory. Infrared (IR) spectra were obtained with a JASCO Model A-102 infrared spectrophotometer. ^{1}H NMR spectra (60 MHz) were recorded with a JEOL JNM-PMX60SI apparatus. ^{1}H NMR (100 MHz) and ^{13}C NMR spectra (25 MHz) were obtained with a JEOL JNM-FX100 apparatus, using $CDCl_3$ as a solvent. Optical rotations were measured on a JASCO DIP-4 spectrometer. Column chromatography was accomplished with 100—200 mesh Wakogel C-200. High-performance liquid chromatography (HPLC) was obtained with Yanagimoto liquid chromatograph L-2000 fitted with Yanapak SA-I (6 mm o.d.×250 mm) and with Sumipax OA-3000 (4 mm o.d.×250 mm) for the determination of enantioselectivity.

Fermentation was carried out in a thermostat-bath at 31—35 °C, using industrial baker's yeast purchased from Oriental yeast Co. LTD. All glasswares were sterilized by boiling water before use.

Ethyl 3-chloro-2-oxooctanoate (**2**) was obtained by the method described in our previous papers.[4]

Ethyl 3-Chloro-2-hydroxyoctanoate (3). To a mixture of KH_2PO_4 (1 g), $NH_4H_2PO_4$ (1 g), $MgSO_4$ (0.25 g), $CaCO_3$ (2.5 g), glucose (75 g), and boiled water (1 l) was added 8 g of baker's yeast at 35°C. After 20 min, 2.00 g (9.07 mmol) of **2** was added and the mixture was stirred for 4 d at 35 °C. The organic materials were extracted 5 times with ethyl acetate (total 1 l), washed with brine, and dried over $MgSO_4$. Removal of the solvent gave 1.39 g of an oil, which was chromatographed on SiO_2 (hexane/ethyl acetate, 20 : 1—1 : 1) to afford 1.33 g (67%) of **3**. HPLC analysis (SA-I, 6 mm o.d.×250 mm; hexane/ethyl acetate (10 : 1), 1.25 ml min^{-1}) showed two peaks at R_t 16.7 and 22.9 min with the 29 : 71 ratio of the integrated peak area. Each component was separated by preparative HPLC. Peak 1: *threo*(2S,3S)-**3**; R_t 16.7 min; $[\alpha]_D^{25}$ −16.0°(*c* 1.45, $CHCl_3$): IR (neat) 3525, 2950, 1745, 1265 cm^{-1}; ^{1}H NMR (CCl_4) δ=0.90 (t, 3H, *J*=6 Hz), 1.40—2.30 (m, 8H), 1.30 (t, 3H, *J*=6.5 Hz), 4.15 (q, 2H, *J*=6.5 Hz), 4.20 (m, 2H). Found: C, 54.01; H, 8.55%. Calcd for $C_{10}H_{19}ClO_3$: C, 53.93; H, 8.60%. Peak 2: *erythro*(2S,3R)-**3**; R_t 22.9 min; $[\alpha]_D^{25}$ +2.3° (*c* 2.20, $CHCl_3$): IR (neat) 3470, 2975, 1740, 1220 cm^{-1}; ^{1}H NMR (CCl_4) δ=0.90 (t, 3H, *J*=6 Hz), 1.5—2.0 (m, 8H), 1.30 (t, 3H), 4.20 (m, 2H), 4.2 (q, 2H, *J*=6.5 Hz). Found: C, 53.99; H, 8.35%. Calcd for $C_{10}H_{19}ClO_3$: C, 53.93; H, 8.60%.

Determination of Enantiomeric Excess of 3. (A) *threo*-**3**: >95% e.e. by ^{1}H NMR (CCl_4) analysis in the presence of 75% (mol/mol) Eu(hfc)$_3$: one singlet at 2.30 ppm ($CO_2CH_2C\underline{H}_3$) when decoupled with the peak of 6.15 ppm ($CO_2C\underline{H}_2CH_3$). *erythro*-**3**: >95% e.e. by ^{1}H NMR (CCl_4) analysis in the presence of 75% (mol/mol) Eu(hfc)$_3$ in a similar manner as described above. On the other hand, ^{1}H NMR (CCl_4) of (±)-*threo*-**3**[7] in the presence of 75% (mol/mol) Eu(hfc)$_3$ showed two singlets at 2.93 and 2.83 ppm ($CO_2CH_2C\underline{H}_3$) when decoupled with the peak of 7.95 ppm ($CO_2C\underline{H}_2CH_3$). (B) To a mixture of **3** (0.46 mmol), dry toluene (1 ml), and 3,5-dinitrophenyl isocyanate (105 mg, 0.5 mmol) was added 0.5 ml of dry pyridine. The mixture was heated at 80 °C for 1 h and cooled. The precipitate was filtered off and washed with ether. Concentration of the filtrate gave crude 3,5-dinitrophenylcarbamate (DNPC) of **3**, which was analyzed by HPLC [column, Sumipax OA-3000 (4φ×250 mm)].

DNPC of *threo*-**3**: >99% e.e.; HPLC [hexane/ethyl acetate/ethanol (20 : 1 : 0.5), 0.8 ml min^{-1}], a single peak at R_t 4.3 min; ^{1}H NMR (CCl_4) δ=0.86 (t, 3H, *J*=6.5 Hz), 1.30—1.90 (m, 8H), 1.35 (t, 3H, *J*=6.5 Hz), 4.32 (m, 3H), 5.38 (d, 1H, *J*=3.2 Hz), 8.63 (s, 3H). ^{1}H NMR (CCl_4) in the presence of 50% Eu(hfc)$_3$ showed no paired peak.

DNPC of *erythro*-**3**: >99% e.e.; HPLC [hexane/ethyl acetate/ethanol (20 : 1 : 0.5), 0.8 ml min^{-1}], a single peak at R_t 6.0 min; ^{1}H NMR (CCl_4) δ=0.86 (t, 3H, *J*=6.5 Hz), 1.30—1.90 (m, 8H), 1.35 (t, 3H, *J*=6.5 Hz), 4.40 (m, 3H), 5.40 (d, 1H, *J*=3.2 Hz), 8.65 (s, 3H).

(2*S*,3*S*)-3-Chloro-1,2-octanediol (4). To a mixture of $NaBH_4$ (98 mg, 1.54 mmol) and ethanol (3 ml) was added dropwise a solution of *erythro*-**3** (0.342 g, 1.54 mmol) in dry ethanol (2 ml) at 0 °C. The mixture was stirred for 7 h at room temperature, and then poured into ice water. The organic materials were extracted with dichloromethane and the combined extracts were washed with brine, dried over $MgSO_4$, and concentrated. The crude product (290 mg) was chromatographed on SiO_2 (hexane/acetone (10 : 1)) to give 193 mg (83%) of **4**: $[\alpha]_D^{25}$ +18.7° (*c* 1.00, $CHCl_3$): IR (neat) 3400 (OH), 1460, 1075, 790 cm^{-1}; ^{1}H NMR (CCl_4) δ=0.85 (t, 3H, *J*=6 Hz, $C\underline{H}_3(CH_2)_4$), 1.1—2.3 (m, 8H, $CH_3(C\underline{H}_2)_4$-), 3.65 (m, 2H, $C\underline{H}ClC\underline{H}OH$), 4.40 (m, 2H, $C\underline{H}_2OH$). Found: C, 53.07; H, 9.78%. Calcd for $C_8H_{17}ClO_2$: C, 53.18; H, 9.49%.

(2*S*,3*S*)-2,3-Epoxyoctanol (5). Method A: from 4. To a solution of sodium ethoxide (95 mg, 1.4 mmol) in absolute ethanol (4 ml) was added dropwise a solution of **4** (228 mg, 1.27 mmol) in absolute ethanol (3 ml) at 0 °C. The mixture was stirred for 30 min at 0 °C and then for 6.5 h at 25 °C. After the mixture was poured into ice water, the organic materials were extracted with dichloromethane. The combined extracts were washed with water, dried over $MgSO_4$, and concentrated in vacuo. The residual oil (201 mg) was chromatographed on SiO_2 (hexane/acetone (10 : 1)) to give 146 mg (80%) of **5**: HPLC analysis [SA-I, 4.0 o.d.×250 mm; hexane/ethyl acetate (5 : 1), 0.8 ml min^{-1}], a single peak at R_t 24.2 min; $[\alpha]_D^{26}$ −27.2° (*c* 0.75, $CHCl_3$). Recrystallization from pentane gave 91.4 mg of **5**: mp 29.5—30 °C; $[\alpha]_D^{25}$ −36.8° (*c* 0.61, $CHCl_3$) [lit,[2] $[\alpha]_D$ −44° (*c* 1.0, $CHCl_3$)]: IR (neat) 3425 (OH), 2950, 1460, 1030, 885 cm^{-1}; ^{1}H NMR (CCl_4) δ=0.90 (t, 3H, *J*=6.5 Hz, $C\underline{H}_3(CH_2)_4$), 1.45 (m, $CH_3(C\underline{H}_2)_4$), 2.82 (m, 2H, C_2-H, C_3-H), 3.10 (s, 1H, OH), 3.60 (br t, 2H, *J*=4 HZ, $C\underline{H}_2OH$); ^{13}C NMR ($CDCl_3$) δ=13.9 (q,), 22.5 (t), 25.6 (t), 31.5 (t), 56.1 (d), 58.7 (d), 61.9 (t).

Method B: by Sharpless Epoxidation.[5] To a stirred mixture of dry dichloromethane (16 ml), titanium tetraisopropoxide (455 mg, 0.48 ml, 1.60 mmol),diethyl (+)-tartrate (329 mg,1.6 mmol) was added dropwise a solution of trans-2-octen-1-ol[8] (204 mg, 1.6 mmol) in dry dichloromethane (4 ml) at −23 °C. *t*-Butyl hydroperoxide (TBHP) (1 ml, 3.62 mmol), which was extracted from commercial TBHP (70% aqueous solution) with dichloromethane and dried over $MgSO_4$ and 4 A molecular sieves, was added and then the mixture was stirred for 9.3 h at −23 °C. Aqueous tartaric acid (10%, 20 ml) was added and the mixture was stirred for 30 min at −23 °C and then for 1 h at room temperature. The organic materials were extracted with ether, and the ethereal extract was stirred with 1 M NaOH (20 ml) (1M=1 mol dm^{-3}) at 0 °C for 30 min and separated, washed with water, and dried over $MgSO_4$. Removal of the solvent gave 296 mg of an oil which was chromatographed on SiO_2 (hexane/acetone (20 : 1)) to give 151 mg (65.4%) of **5**: HPLC analysis [SA-I, 6.0 o.d.×250 mm; hexane/ethyl acetate (2 : 1), 1.1 ml min^{-1}], a single peak at R_t 21.3 min; $[\alpha]_D^{26}$ −38.1° (*c* 1.48, $CHCl_3$). IR and ^{1}H NMR data were identical with those of the sample prepared in Method A.

(2*R*,3*S*)-2,3-Epoxyoctanal (1).[2,3] To dry chromium oxide (997 mg, 9.97 mmol) was added dropwise a solution of dry pyridine (1.1 ml, 13.7 mmol) in dry dichloromethane (11 ml) at room temperature. After the mixture was stirred for 30 min, a solution of **5** (147 mg, 1.02 mmol) in dry dichlorome-

thane (4 ml) was added. The mixture was stirred for 4 h at 25 °C and the organic materials were extracted with ether. The ethereal extract was washed with 5% NaOH (10 ml), dil HCl (10 ml), saturated $NaHCO_3$, and brine successively, and dried over $MgSO_4$. Removal of the solvent gave the crude product, which was purified by column chromatography (SiO_2, hexane/acetone (15:1)) to afford 91 mg (68%) of **1**: $[\alpha]_D^{25}$ +64.6° (*c* 0.87, $CHCl_3$) [lit,[3] $[\alpha]_D^{25}$ +80.4° (*c* 1.39, $CHCl_3$)], 80% e.e.: IR (neat) 1735 (C=O), 1260, 1020, 805 cm^{-1}; ^1H NMR (CCl_4) δ=0.90 (t, 3H, *J*= 6.5 Hz, $CH_3(CH_2)_4$), 1.40 (m, 8H, $CH_3(CH_2)_4$), 3.00 (m, 2H, C_2-H, C_3-H), 8.85 (d, 1H, *J*=6.4 Hz, CHO).

(2*S*,3*S*)-3-Chloro-1,2-octanediol (7). To a stirred mixture of $NaBH_4$ (52 mg, 0.81 mmol) and ethanol (3 ml) was added *threo*-**3** (180 mg, 0.81 mmol) at 0 °C. The mixture was stirred for 7 h at room temperature, and poured into ice water. The organic materials were extracted with dichloromethane and the combined extracts were washed with brine, dried over $MgSO_4$, and concentrated. The crude product (176 mg) was chromatographed on SiO_2 (hexane/acetone (10:1)) to give 122 mg (85%) of **7**: $[\alpha]_D^{26}$ −23.2 ° (*c* 2.12, $CHCl_3$); IR (neat) 3400 (OH), 1460, 1040, 875 cm^{-1}; ^1H NMR (CCl_4) δ=0.90 (t, 3H, *J*=6 Hz, CH_3), 1.0—2.0 (m, 8H, $(CH_2)_4$), 3.0—4.1 (m, 6H, $CHClCHOHCH_2OH$).

(2*S*,3*R*)-2,3-Epoxyoctanol (8). Method A: from 7. To a solution of sodium ethoxide (54 mg, 0.8 mmol) in absolute ethanol (6 ml) was added dropwise a solution of **7** (116 mg, 0.65 mmol) in absolute ethanol (1 ml) at 0 °C. The mixture was stirred for 9.5 h at 25 °C, and then poured into ice water. The organic materials were extracted with dichloromethane. The combined extracts were washed with water and dried over $MgSO_4$. Removal of the solvent gave an oil (118 mg), which was chromatographed on SiO_2 to give 57 mg (61%) of **8**:[9] $[\alpha]_D^{26}$ −6.12° (*c* 1.42, $CHCl_3$); IR (neat) 3420, 1460, 1030, 880 cm^{-1}; ^1H NMR (CCl_4)δ=0.90 (t, 3H, *J*=6 Hz, CH_3), 1.1—1.8 (m, 8H, $(CH_2)_4$), 2.95 (m, 3H, C_2-H, C_3-H, OH), 3.60 (m, 2H, CH_2OH): ^{13}C NMR ($CDCl_3$) δ=14.0 (q), 22.5 (t), 26.3 (t), 27.9 (t), 31.6 (t), 57.0 (d), 57.2 (d), 60.7 (t).

Method B: by Sharpless Epoxidation.[5] *cis*-2-Octen-1-ol[10] (252 mg, 1.97 mmol) was oxidized at −10 — − 23 °C for 13.5 h by TBHP (1.1 ml, 3.54 mmol) in the presence of titanium tetraisopropoxide (560 mg, 1.97 mmol) and diethyl (+)-tartrate (405 mg, 1.97 mmol), as shown in the preparation of **5**. The crude product was purified by column chromatography (SiO_2, hexane/ethyl acetate (10:1)), giving 206 mg (78%) of **8**: $[\alpha]_D^{26}$ −6.44°(*c* 1.46, $CHCl_3$). IR and ^1H NMR data were identical with those of the sample prepared by method A.

(2*R*,3*R*)-2,3-Epoxyoctanal (10). In the same manner as shown in the preparation of **1**, alcohol **8** (191 mg, 1.33 mmol) was treated with CrO_3 (1.04 g, 10.4 mmol) and pyridine (1.65 g, 20.7 mmol) in dichloromethane (22 ml) at 30 °C for 4.5 h. The same work up as shown in **1** gave 121 mg (64%) of **10**: TLC (hexane/acetone, 3:1), one spot at R_f 0.42. Analytical sample was purified with column chromatography (SiO_2; hexane/acetone, 5:1) to afford 77 mg of pure **10**: $[\alpha]_D^{27}$ +134.6° (*c* 1.47, $CHCl_3$); 94% e.e. by ^1H NMR in the presence of 98% $Eu(hfc)_3$, two paired peaks at 18.0 and 17.6 ppm (intensity ratio of 97:3): IR (neat) 2950, 2840, 1730, 1470, 1050, 835 cm^{-1}; ^1H NMR (CCl_4) δ=0.92 (br. t, 3H, *J*=5 Hz, CH_3), 1.3—1.9 (m, 8H, $(CH_2)_4$), 3.16 (apparent d, 2H, *J*=2.8 Hz, 2 CHO-), 9.35 ppm (d, 1H, *J*=5.8 Hz, CHO); ^1H NMR (CCl_4) in the presence of 13% $Eu(hfc)_3$, δ=1.0 (br. t, 3H, CH_3), 1.2—2.3 (m, 6H, $(CH_2)_3$), 2.56 (m, 2H, C_4-H), 4.35 (m, 1H, C_3-H), 4.76 ppm (t, 1H, *J*=5 Hz, C_2-H).

References

1) B. Samuelsson, *Science*, **220**, 568 (1983).

2) R. Zamboni, S. Milette, and J. Rokach, *Tetrahedron Lett.*, **24**, 4899 (1983).

3) Oral presentation: K. Kobayashi, T. Matsumoto, Y. Kitano, and F. Sato, 52nd National Meeting of the Chemical Society of Japan, Kyoto, April 1986, Abstr. II, p. 1070.

4) a) A. Takeda, S. Wada, and T. Uno, *Mem. School Eng., Okayama Univ.*, **2**, 80 (1967); b) A. Takeda, S. Wada, M. Fujii, and H. Tanaka, *Bull. Chem. Soc. Jpn.*, **43**, 2997 (1970); c) S. Tsuboi, H. Furutani, and A. Takeda, *Synthesis*, in press.

5) B. E. Rossiter, T. Katsuki, and K. B. Sharpless, *J. Am. Chem. Soc.*, **103**, 464 (1981).

6) C. A. Reilly and J. D. Swalen, *J. Chem. Phys.*, **34**, 980 (1961).

7) The racemic compound **3** was prepared by the reduction of **2** with $NaBH_4$ (0.33 equiv) in EtOH at 0 °C for 20 min: 69% yield; erythro/threo (6:94), determined by HPLC.

8) M. Jacobson, *J. Am. Chem. Soc.*, **75**, 2584 (1953).

9) K. C. Nicolaou and S. E. Webber, *J. Chem. Soc., Chem. Commun.*, **1985**, 297. Physical and spectral data are not reported.

10) M. Winter, *Helv. Chim. Acta*, **46**, 1972 (1963).

A Michael Addition-Induced Favorskii Rearrangement

Sadao Tsuboi, Hiroyuki Nagae, Hirofumi Yamato, and Akira Takeda*
Department of Synthetic Chemistry, School of Engineering, Okayama University, Tsushima, Okayama 700
(Received August 26, 1986)

Synopsis. Reaction of 6-chloro-2-vinylidenecyclohexanone with sodium methoxide gave methyl 2-vinylidene-1-cyclopentanecarboxylate and methyl *trans*-2-(1-methoxyalkyl)-1-cyclopentanecarboxylate along with 6-methoxy-2-vinylidenecyclohexanone via a Michael addition-induced Favorskii rearrangement.

The Favorskii rearrangement is the skeletal rearrangement of α-halogenated ketones in the presence of base to give carboxylic acid derivatives.[1] It is useful for organic synthesis, especially for the preparation of highly branched acyclic carboxylic acids.[1] Since the first description of this rearrangement by Favorskii in 1894,[2] various types of the rearrangement have been still reported.[3] In connection with our previous study of Favorskii rearrangement of vinylogs of α-halo ketones,[4] we investigated reactions of 6-chloro-2-vinylidenecyclohexanones (**1**) with sodium methoxide.

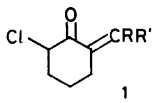

1

Treatment of 6-chloro-2-isopropylidenecyclohexanone (**1a**) with five equivalents of sodium methoxide at 25—50 °C gave a mixture of methyl 2-isopropylidenecyclopentanecarboxylate (**2a**), methyl *trans*-2-(1-methoxy-1-methylethyl)cyclopentanecarboxylate (**3a**),[5] and 2-isopropylidene-6-methoxycyclohexanone (**4a**).

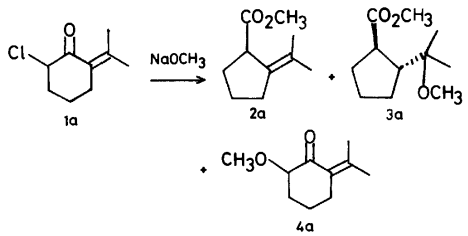

These products were separated by preparative GLC and identified by spectral analysis. To get further support for the structural elucidation, chemical transformations of **2a** were carried out. Hydrogenolysis of **2a** in the presence of palladium-charcoal yielded methyl 2-isopropylcyclopentanecarboxylate (**5**) in 54% yield and oxidation of **2a** with potassium permanganate gave adipic acid which was seemed to be derived from methyl 2-oxocyclopentanecarboxylate.

The formation of **2** and **3** can be explained by Favorskii rearrangement induced by the Michael addition of sodium methoxide to **1**, as shown in Scheme 1. In accordance with the generally accepted mechanism of the Favorskii rearrangement,[1] we suggest three intermediates **A**, **B**, and **C** to account for our results. The elimination of methoxide anion from the intermediate **C** will give vinylidene carboxylate **2** and the protonation of **C** will afford methoxy carboxylate **3**.

Table 1. Reaction of 6-Chloro-2-vinylidenecyclohexanone **1** with $NaOCH_3$

No.	1		Yield/% of Products				
	R	R′	**2**	**3** (erythro/threo)	**4**	**6**	**7**
a	CH_3	CH_3	52	9	4	0	0
b	H	CH_3	0	38 (20/18)	0	24	0
c	H	C_6H_5	0	62 (33/29)	0	0	8

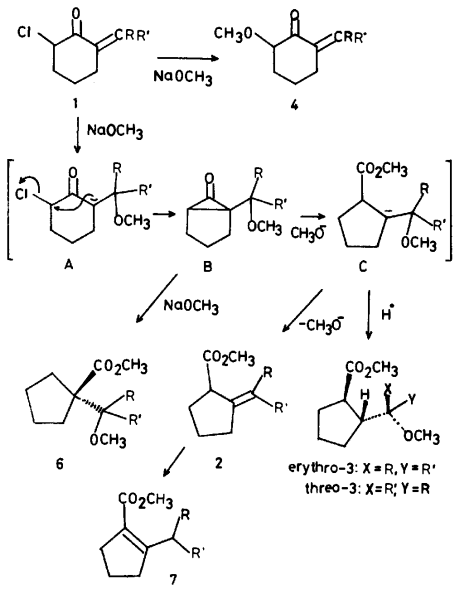

Scheme 1.

We further investigated the reaction of other readily available 6-chloro-2-vinylidenecyclohexanones with sodium methoxide and the results are summarized in Table 1. Treatment of 6-chloro-2-ethylidenecyclohexanone (**1b**) with five equivalents of sodium methoxide at 25—50 °C afforded a mixture of three Favorskii rearrangement product, methyl 1-(1-methoxyethyl)cyclopentanecarboxylate (**6**) (24%) and methyl *trans*-2-(1-methoxyethyl)cyclopentanecarboxylate (**3b**) (erythro/threo, 20:18) (38%). Formation of ester **6** can be explained to be derived from the intermediate **B**, as shown in Scheme 1. Similar treatment of 6-chloro-2-benzylidenecyclohexanone (**1c**) with sodium methoxide gave methyl *trans*-2-(α-methoxybenzyl)methylcyclopentanecarboxylate (**3c**) in 62% yield as a mixture of two stereoisomers (erythro/threo, 33:29) and methyl 2-benzyl-1-cyclopentenecarboxylate (**7c**) in 8% yield. The trans geometry of **3b** and **3c** was determined by comparison of ^{13}C NMR data with those of similar

compounds[6] on the basis of the steric effect.[7] Assignment of erythro and threo between C-2 and C-1′ was made by analyzing the ^{1}H NMR spectra with reference of the literature data.[8] In ^{1}H NMR spectra of *threo*-**3b** and **3c**, signals due to C-2 protons (3.15 and 3.82 ppm) appeared at higher fields than those of erythro-isomers (3.34 and 4.06 ppm, respectively). In the ^{13}C NMR spectrum of *erythro*-**3b**, all signals except those of methyl carbon appeared at higher fields as compared with those of *threo*-**3b**.[9] Similarly, in the spectrum of *erythro*-**3c**, signals due to C-1 (50.6), C-2 (46.5), C=O (176.9), and $\underline{C}HOCH_3$ (86.0) appeared at higher fields than those of *threo*-**3c** (50.8, 47.9, 177.1, and 87.5, respectively).

To our knowledge, the present reaction is a new type of Favorskii rearrangement which includes initiation by the Michael addition of alkoxide and it will be useful for the synthesis of substituted cyclopentane derivatives.

Experimental

The melting points and boiling points are uncorrected. Elemental analyses were carried out by Eiichiro Amano in our laboratory. Analytical determinations by GLC were performed on a Hitachi Model K-53 gas chromatograph fitted with 10% Apiezone Grease L on Chromosorb W column (3 mm o.d.×1 m). Preparative isolations by GLC were performed on a Yanagimoto Model GCG-550T gas chromatograph (3 mm o.d.×1 m, Apiezone Grease L on Chromosorb W).

2-Isopropylidenecyclohexanone (**10**) was prepared from 2-ethoxycarbonylcyclohexanone by the method described in the literature:[10] bp 65 °C/3 Torr (1 Torr=133.322 Pa) (lit,[10] 94—98 °C/14 Torr); 32% yield. 2-Ethylidenecyclohexanone (**11**) was prepared by the reaction of 2-formylcyclohexanone with methylmagnesium iodide:[11] bp 59—61 °C/3 Torr; 55% yield. 2-Benzylidenecyclohexanone (**12**) was obtained by the reaction of *N*-(1-cyclohexenyl)morpholine with benzaldehyde:[12] bp 147 °C/4 Torr (lit,[12] 123—126 °C/0.2 Torr); 52% yield.

6-Chloro-2-isopropylidenecyclohexanone (1a) was prepared by the reaction of **10** with 1.2 equiv of *N*-chlorosuccinimide (NCS) in CCl_4 at the reflux temperature for 20 min:[13] 83% yield; IR (neat) 1680, 1610 cm^{-1}; ^{1}H NMR (CCl_4) δ=1.81 (s, 3H), 1.89 (s, 3H), 2.20 (m, 6H), 4.22 (dd, J=4 and 5 Hz, 1H); MS (70 eV) m/z (rel intensity) 172 (48, 1 Cl, M$^+$), 157 (6), 149 (46), 110 (32), 109 (100), 95 (32), 93 (46), 82 (67), 67 (93). Found: C, 62.31; H, 7.42%. Calcd for $C_9H_{13}ClO$: C, 62.61; H, 7.59%.

6-Chloro-2-ethylidenecyclohexanone (1b) was prepared by the reaction of **11** with 1.2 equiv of NCS in CCl_4 at the reflux temperature:[13] 71% yield; bp 65—70 °C/2.5 Torr; IR (neat) 1700, 1625, 1130, 890, 750 cm^{-1}; ^{1}H NMR (CCl_4) δ=1.75 (dt, J=7.5 and 1.0 Hz, 3), 4.27 (dd, J=4.5 and 6.0 Hz, 1), 6.64 (qt, J=7.5 and 2.5 Hz, 1); MS (70 eV) m/z (rel intensity) 158 (40, 1 Cl, M$^+$), 143 (6), 140 (5), 124 (23), 95 (100), 79 (47), 68 (48), 67 (77), 55 (72). Found: C, 60.63; H, 7.00%. Calcd for $C_8H_{11}OCl$: C, 60.58; H, 6.99%.

6-Chloro-2-benzylidenecyclohexanone (1c) was prepared by the reaction of **12** with 1.2 equiv of NCS in CCl_4 at the reflux temperature:[13] 80% yield; mp 60—62 °C (from hexane); IR (neat) 1680, 1598, 1130, 790 cm^{-1}; ^{1}H NMR ($CDCl_3$) δ=1.5—3.0 (m, 6H), 4.50 (apparent dd, J=5 Hz, 1H), 7.26 (br. s, 6H). It was too labile for elemental analysis.

Reaction of 1a with Sodium Methoxide. To a solution of sodium methoxide (1.76 g, 32.6 mmol) in 20 ml of absolute methanol was added 1.12 g (6.50 mmol) of **1a** at room temperature with stirring. The mixture was stirred for 20 min at 50 °C, and then cooled. It was poured into cold water and acidified with 10% HCl. The organic materials were extracted with ether, washed with water, dried over $MgSO_4$ and concentrated. The resulting residue was purified by short column chromatography (SiO_2, hexane/ethyl acetate (10 : 1)) to give 0.725 g of an oil, which was analyzed by GLC (column: 130 °C, carrier gas: N_2, 0.5 kg cm^{-2}). Peaks, retention times (min), and integrated percentages are as follows: 1, 3.0, 78; 2, 4.5, 6; 3, 6.4, 16. Each component was separated by preparative GLC and identified.

Peak 1: **Methyl 2-Isopropyldenecyclopentanecarboxylate (2a);** 52% yield; IR (neat) 1732, 1430, 1160 cm^{-1}; ^{1}H NMR (CCl_4) δ=1.65 (s, 6H), 1.6—2.5 (m, 6H), 3.3 (m, 1H), 3.59 (s, 3H); MS (70 eV) m/z (rel intensity) 168 (36, M$^+$), 109 (100), 108 (53), 93 (40), 67 (73), 55 (33). Found: C, 71.05; H, 9.44%. Calcd for $C_{10}H_{16}O_2$: C, 71.39; H, 9.59%.

Peak 2: **2-Isopropylidene-6-methoxycyclohexanone (4a);** 4% yield; IR (neat) 1695, 1630, 1450, 1130, 1096 cm^{-1}; ^{1}H NMR (CCl_4) δ=1.78 (s, 3H), 1.88 (s, 3H), 1.5—2.6 (m, 6H), 3.32 (s, 3H), 3.56 (m, 1H). Found: C, 71.25; H, 9.41%. Calcd for $C_{10}H_{16}O_2$: C, 71.39; H, 9.59%.

Peak 3: **Methyl trans-2-(1-Methoxy-1-methylethyl)cyclopentanecarboxylate (3a);** 8.9% yield; IR (neat) 1740, 1450, 1200, 1162 cm^{-1}; ^{1}H NMR (CCl_4) δ=1.06 (s, 6H), 1.4—2.8 (m, 8H), 3,10 (s, 3H), 3.59 (s, 3H). Found: C, 65.82; H, 9.96%. Calcd for $C_{11}H_{20}O_3$: C, 65.97; H, 10.07%.

Methyl 2-Isopropylcyclopentanecarboxylate (5).[14] A mixture of **2a** (0.79 g, 4.70 mmol), 7 ml of methanol and palladium-carbon (4 mg) was stirred for 12 h under an atmosphere of hydrogen. Preparative TLC (SiO_2, hexane/ethyl acetate (3 : 1)) of the crude product gave 0.431 g (54%) of **5**:[14] IR (neat) 1735, 1435, 1367, 1195, 1155 cm^{-1}; ^{1}H NMR (CCl_4) δ=0.88 (d, J=7 Hz, 6H), 1.74 (m, 8H) 2.30 (m, 1H), 3.60 (s, 3H).

Oxidation of 2a with $KMnO_4$. To a mixture of **2a** (0.447 g, 2.66 mmol), $NaHCO_3$ (0.083 g, 1 mmol), and acetone (3 ml) was added powdered $KMnO_4$ (1.46 g, 9.24 mmol) below 7 °C over 1.5 h. The mixture was stirred for 1 h, and then dilute H_2SO_4 and a small amount of $NaHSO_3$ were added alternately until it becomes clear. The mixture was concentrated, washed with ether and acidified with dilute HCl. The organic materials were extracted with ether three times, washed with brine and dried over $MgSO_4$. Removal of the solvent gave 200 mg (52%) of adipic acid: mp 151—152 °C (from benzene)(lit,[15] 151—152 °C).

Reaction of 1b with Sodium Methoxide. To a stirred solution of sodium methoxide (1.51 g, 28 mmol) in 20 ml of absolute methanol was added dropwise 0.888 g (5.60 mmol) of **1b** at 25 °C. The mixture was stirred for 20 min at 50 °C and then cooled, acidified with 10% HCl. The organic layer was extracted with ether and combined extracts were washed with aqueous $NaHCO_3$, brine and water, and then dried over $MgSO_4$. After concentration, the residual oil was distilled with balb-to-balb tube oven to give 0.850 g of a clean oil, which was analyzed by GLC (column, 120 °C; carrier gas, N_2, 0.5 kg cm^{-2}). Peaks, retention times (min), and integrated percentages are as follows: 1, 1.3, 5.0; 2, 2.4, 19; 3, 3.4, 30; 4, 4.3, 24; 5, 4.8, 22. Each component was separated by preparative GLC. Peaks 1 and 2 were not identified. Peaks 3, 4, and 5 were identified as a stereoisomer of **3b**, respectively: total yield, 62%.

Peak 3: **Methyl 1-(1-Methoxyethyl)cyclopentanecarboxylate (6);** 24% yield; IR (neat) 1735, 1165, 1140, 1104, 1006 cm^{-1}; ^{1}H NMR (CCl_4) δ=0.98 (d, J=6 Hz, 3H), 1.3—2.2 (m, 8H), 3.2 (m, 1H), 3.23 (s, 3H), 3.59 (s, 3H); MS (70 eV) m/z (rel intensity) 186 (1, M$^+$), 172 (2), 154 (5), 139 (13), 128 (76), 95 (46), 67 (34), 59 (100); ^{13}C NMR ($CDCl_3$) δ=17.0 (q, $CH\underline{C}H_3$),

25.2 (t, C-4), 27.0 (t, C-3), 31.0 (t, C-5), 45.9 (d, C-2), 49.3 (d, C-1), 51.5 (q, OCH_3), 56.5 (q, $CO_2\underline{C}H_3$), 80.3 (d, $\underline{C}HOCH_3$), 177.2 (s, C=O). Found: C, 64.25; H, 9.80%. Calcd for $C_{10}H_{18}O_3$: C, 64.49; H, 9.74%.

Peak 4: **Methyl *trans-erythro*-2-(1-Methoxyethyl)cyclopentanecarboxylate (3b)**; 20% yield; IR (neat) 1735, 1195, 1160, 1090 cm^{-1}; ^1H NMR (CCl_4) δ=1.06 (d, J=6 Hz, 3H), 1.5—2.8 (m, 8H), 3.31 (s, 3H), 3.34 (dq, J=4 and 7 Hz, 1H), 3.68 (s, 3H); MS (70 eV) m/z (rel intensity) 186 (1, M^+), 171 (6), 155 (4), 149 (11), 111 (33), 95 (50), 67 (34), 59 (100); ^{13}C NMR ($CDCl_3$) δ=17.0 (q, $CH\underline{C}H_3$), 25.3 (t, C-4), 27.1 (t, C-3), 31.1 (t, C-5), 46.1 (d, C-2), 49.4 (d, C-1), 51.5 (q, OCH_3), 56.6 (q, ester CH_3), 78.0 (d, C-1′), 177.1 (s, C=O). Found: C, 64.43; H, 9.73%. Calcd for $C_{10}H_{18}O_3$: C, 64.49; H, 9.74%.

Peak 5: **Methyl *trans-threo*-2-(1-Methoxyethyl)cyclopentanecarboxylate (3b)**; 18% yield; IR (neat) 1736, 1196, 1158, 1092 cm^{-1}; ^1H NMR (CCl_4) δ=1.10 (d, J=6 Hz, 3H), 1.5—2.7 (m, 8H), 3.15 (m, 1H), 3.27 (s, 3H), 3.65 (s, 3H); MS (70 eV) m/z (rel intensity) 186 (3, M^+), 171 (7), 156 (4), 155 (4), 139 (5), 126 (12), 123 (7), 111 (30), 95 (53), 59 (100); ^{13}C NMR ($CDCl_3$) δ=17.0 (q, $CH\underline{C}H_3$), 25.3 (t, C-4), 29.1 (t, C-3), 31.2 (t, C-5), 47.6 (d, C-2), 50.2 (d, C-1), 51.5 (q, OCH_3), 56.3 (q, ester C=O), 80.4 (d, C-1′), 177.4 (s, C=O). Found: C, 64.68; H, 9.75%. Calcd for $C_{10}H_{18}O_3$: C, 64.49; H, 9.74%.

Reaction of 1c with Sodium Methoxide. To a stirred solution of sodium methoxide (2.35 g, 43.5 mmol) in 30 ml of absolute methanol was added dropwise 1.94 g (8.80 mmol) of **1c** at room temperature. The mixture was stirred for 30 min at 50 °C, cooled, and acidified with 10% HCl. The organic materials were extracted with ether and the combined extracts were washed with aqueous $NaHCO_3$, brine and water, and then dried over $MgSO_4$. After concentration, the residual oil (1.68 g) was analyzed by GLC (column, 180 °C; carrier gas, N_2, 0.5 kg cm^{-2}). Peaks, retention times (min), and integrated percentages are as follows: 1, 7.5, 5; 2, 9.3, 43; 3, 10.5, 37; 4, 27.0, 6; 5, 30.0, 9. Each component was separated by preparative GLC (column, Apiezone Grease L, 185 °C; carrier gas, H_2, 27 ml min^{-1}). Components 1 and 5 were not identified. Components 2 and 3 were identified as a stereoisomer of **3c**, respectively: total yield, 67%.

Peak 2: **Methyl *trans-erythro*-2-Methoxyphenylmethylcyclopentanecarboxylate (3c)**; 33% yield: bp 98 °C/0.15 Torr; IR (neat) 1735, 1605, 1494, 768, 705 cm^{-1}; ^1H NMR (CCl_4) δ=1.3—2.15 (m, 6H), 2.2—2.8 (m, 2H), 3.18 (s, 3H), 3.45 (s, 3H), 4.06 (d, J=5 Hz, 1H), 7.20 (s, 5H); MS (70 eV) m/z (rel intensity) 248 (1, M^+), 233 (2), 184 (2), 157 (14), 121 (100), 115 (15), 105 (24), 91 (51). ^{13}C NMR ($CDCl_3$) δ=25.0 (t, C-3), 28.2 (t, C-4), 31.1 (t, C-5), 46.5 (d, C-2), 50.6 (d, C-1), 51.5 (q, OCH_3), 57.1 (q, $CO_2\underline{C}H_3$), 86.0 (d, $\underline{C}HOCH_3$), 127.4, 127.6, and 128.3 (d, phenyl), 140.9 (s, phenyl), 176.9 (s, C=O). Found: C, 72.39; H, 7.91%. Calcd for $C_{15}H_{20}O_3$: C, 72.55; H, 8.12%.

Peak 3: **Methyl *trans-threo*-2-Methoxyphenylmethylcyclopentanecarboxylate (3c)**; 29% yield; bp 98 °C/0.15 Torr; IR (neat) 1735, 1605, 1494, 768, 705 cm^{-1}; ^1H NMR (CCl_4) δ=1.1—2.13 (m, 6H), 2.2—2.9 (m, 2H), 3.10 (s, 3H), 3.52 (s, 3H), 3.82 (d, J=8 Hz, 1H), 7.20 (s, 5H); MS (70 eV) m/z (rel intensity) 248 (1, M^+), 233 (2), 184 (2), 157 (14), 121 (100). ^{13}C NMR ($CDCl_3$) δ=24.7 (t, C-3), 29.1 (t, C-4), 31.1 (t, C-5), 47.9 (d, C-2), 50.8 (d, C-1), 51.4 (q, OCH_3), 56.9 (q, $CO_2\underline{C}H_3$), 87.5 (d, $\underline{C}HOCH_3$), 127.2, 127.6, and 128.1 (d, phenyl), 140.9 (s, phenyl), 177.1 (s, C=O). Found: C, 72.77; H, 8.18%. Calcd for $C_{15}H_{20}O_3$: C, 72.55; H, 8.12%.

Peak 4: **Methyl 2-Benzyl-1-cyclopentenecarboxylate (7c)**: 8.0% yield; IR (neat) 1670, 1630, 1600, 1493, 700 cm^{-1}; ^1H NMR (CCl_4) δ=1.5—2.1 (m, 2H), 2.1—2.6 (m, 4H), 3.56 (s, 2H), 3.70 (s, 3H), 7.17 (s, 5H); MS (70 eV) m/z (rel intensity) 216 (86, M^+), 185 (6), 155 (42), 129 (39), 121 (45), 115 (46), 91 (100). Found: C, 77.62; H, 7.51%. Calcd for $C_{14}H_{16}O_2$: C, 77.75; H, 7.46%.

References

1) See some reviews: a) A. S. Kende, *Org. React.*, **11**, 261 (1960); b) N. J. Turro, *Acc. Chem. Res.*, **2**, 25 (1969); c) K. Sato and M. Oohashi, *Yuki Gosei Kagaku Kyokai Shi*, **32**, 435 (1974); d) A. Baretta and B. Waegill, "Reactive Intermediate," ed by R. A. Abramovitch, Plenum Press, New York (1982), pp. 527—585.

2) A. E. Favorskii, *J. Russ. Phys. Chem. Soc.*, **26**, 559 (1894).

3) For examples, see recent papers: a) P. Martin, *Helv. Chim. Acta*, **66**, 1189 (1983); b) M. Nanasawa and H. Kamogawa, *Bull. Chem. Soc. Jpn.*, **55**, 3655 (1982); c) T. Morimoto and M. Sekiya, *Chem. Pharm. Bull.*, **30**, 3513 (1982); d) N. DeKimpe, R. Verhe, L. DeBuycke, L. Moens, and N. Schamp, *Tetrahedron Lett.*, **22**, 1837 (1981); e) T. Sakai, T. Katayama, and A. Takeda, *J. Org. Chem.*, **46**, 2924 (1981).

4) A. Takeda and S. Tsuboi, *J. Org. Chem.*, **38**, 1709 (1973).

5) Cis-geometry of **3a** would be impossible because of its large steric hindrance. The Favorskii rearrangement of halogenocyclohexanone derivatives usually gives *trans*-cyclopentanecarboxylates as a major product. See (a) E. J. Eisenbraun, P. G. Hanel, K. S. Schorno, F. Dilgen, and J. Osiecki, *J. Org. Chem.*, **32**, 3010 (1967); b) F. G. Bordwell and J. Almy, *J. Org. Chem.*, **38**, 571 (1973).

6) a) D. E. James and J. K. Stille, *J. Org. Chem.*, **41**, 1504 (1976); b) T. Sakai, K. Morita, C. Matsumura, A. Sudo, S. Tsuboi, and A. Takeda, *J. Org. Chem.*, **46**, 4774 (1981).

7) D. E. Dorman, M. Jautelat, and J. D. Roberts, *J. Org. Chem.*, **36**, 2757 (1971).

8) D. A. Evans, J. V. Nelson, E. Vogel, and T. R. Taber, *J. Am. Chem. Soc.*, **103**, 3099 (1981).

9) ^{13}C NMR signals of erythro form appear at higher fields than those of the threo isomer. For example, see: S. Tsuboi, E. Nishiyama, M. Utaka, and A. Takeda, *Tetrahedron Lett.*, **27**, 1915 (1986).

10) F. Nerdel, D. Frank, and H. Marschall, *Chem. Ber.*, **100**, 720 (1967).

11) R. A. J. Smith and T. A. Spencer, *J. Org. Chem.*, **35**, 3220 (1970).

12) L. Birkofer, S. M. Kim, and H. D. Engels, *Chem. Ber.*, **95**, 1495 (1962).

13) The reaction was initiated by the catalytic amount of benzoylperoxide.

14) M. Julia, J. M. Surzur, L. Katz, F. Le Goffic, and C. James, *Bull. Soc. Chim. Fr.*, **1964**, 1106.

15) B. A. Ellis, *Org. Synth.*, Coll. Vol. 1, 18 (1941).

Hydrates of Organic Compounds. XI. Determination of the Melting Point and Hydration Numbers of the Clathrate-Like Hydrate of Tetrabutylammonium Chloride by Differential Scanning Calorimetry

Haruo NAKAYAMA
Department of Chemistry, Faculty of Engineering, Yokohama National University, Tokiwadai, Hodogaya-ku, Yokohama 240
(Received July 19, 1986)

A thermal analytic method using a differential scanning calorimeter has been applied to binary mixtures of water with tetrabutylammonium chloride. It has been found that this method can give the same results concerning the melting point (15.2 °C) and hydration numbers (around 30) of the clathrate-like hydrate of tetrabutylammonium chloride as those determined phase-diagrammatically. The apparent enthalpy of fusion of water which forms hydrogen-bonded water lattice in the clathrate-like hydrate has been observed to be 5.47 kJ mol^{-1}, which is comparable with 5.20 kJ mol^{-1} determined by the direct calorimetric measurements of enthalpy of solution of the hydrate in water. It has been concluded that the proposed method can be applicable to many similar types of systems, including systems forming a hydrate which decomposes incongruently.

In previous papers the formation of clathrate-like hydrates of tetrabutylammonium salts which have various types of anions (inorganic anions,[1,2] saturated and unsaturated carboxylate anions,[3-6] dicarboxylate anions,[7] and alkanesulfonate anions[8]) has been reported. In these investigations the confirmation of the formation of a hydrate and the determination of melting points and of hydration numbers of the hydrates were made by examining a solid-liquid phase diagram of a binary mixture of a tetrabutylammonium salt with water. The phase diagram was obtained by an ampoule method: the temperature at which the solid phase, formed by cooling a sample solution sealed in an ampoule, completely dissolved was measured; and this temperature was plotted against the concentration of the solution. The ampoule method is one of the most suitable methods since the solid-liquid mixture is thermostated at the desired temperature for sufficient time to establish a solid-liquid phase equilibrium. However, this ampoule method cannot be applied to systems either having extremely high viscosities, as in the case of aqueous solutions containing polymeric ions, or being colored.

In this paper a thermal analytic method using a differential scanning calorimeter has been proposed as an alternative way of confirming the formation of a clathrate-like hydrate as well as of determining a melting point and hydration numbers of the hydrate. The validity of the method has been confirmed by comparing the results concerning the properties of the clathrate-like hydrate of tetrabutylammonium chloride with those obtained in previous investigations.[1,9,10]

Experimental

An aqueous solution of tetrabutylammonium chloride was prepared by neutralization of an aqueous solution of tetrabutylammonium hydroxide with an aqueous solution of hydrochloric acid. The tetrabutylammonium hydroxide solution was prepared by the same procedure as mentioned in a previous paper.[8] The concentration of the tetrabutylammonium chloride was determined by measuring the amount of tetrabutylammonium cation by titration with a sodium tetraphenylborate solution which was standardized by pure tetrabutylammonium iodide.

The differential scanning calorimeter used was the model DSC 10 with SSC 580 thermal controller manufactured by Seiko Instruments and Electronics Ltd. Sample solutions (about 15 mg) at various concentrations were sealed in a 15 μl aluminum pan. The enthalpy changes per unit time (DSC signal) were measured either by cooling or by heating the sample as slowly as possible (usually at the rate of 0.5 °C per minute). An empty 15 μl aluminum pan was used as a reference. The observed enthalpy changes were standardized by the enthalpy of fusion of ice, i.e., 6.0095 kJ mol^{-1}.[11]

Results and Discussion

An example of the DSC curves on cooling the tetrabutylammonium chloride aqueous solutions at various concentrations is illustrated in Fig. 1. The DSC curves on heating the same solutions are shown in Fig. 2. The concentration of the tetrabutylammonium chloride is expressed by the mole fraction X. As is seen in Figs. 1 and 2, except for the concentrated solution of X=0.050, two kinds of peaks are observed in both cooling and heating processes: the first-step solidification (shown by h in Fig. 1) occurs at −3—−15 °C depending upon the concentration of the salt and the second-step solidification (shown by i in Fig. 1) at −18—−20 °C; and the first-step melting (shown by i in Fig. 2) occurs at around 0 °C and the second-step melting (shown by h in Fig. 2) at 5—15 °C depending upon the concentration of the salt. From the facts that (1) supercooled pure water usually freezes at around −20 °C, (2) the area of the peak i in Figs. 1 and 2 decreases with increasing the concentration of the salt, and (3), on the contrary,

the area of peak h in both figures increases with increasing the concentration of the salt, it can be concluded that the peaks indicated by i in both figures are related to an ice phase and, therefore, the peaks indicated by h in both figures are related to a hydrate phase. The disappearance of the peak i in the X=0.050 solution indicates that all the water molecules participate in the formation of the hydrate, i.e., the concentration X=0.050 corresponds to the one which is larger than the congruent composition of the hydrate. It is interesting to note that for the X=0.033 solution small peaks i are observed. This suggests that the congruent composition of the hydrate is close to X=0.033. Firstly, the thermal behavior of the solutions of $X \leqq 0.033$ are discussed in the following sections (1) and (2), and those of the solutions of $X>0.033$ are briefly discussed in section (3).

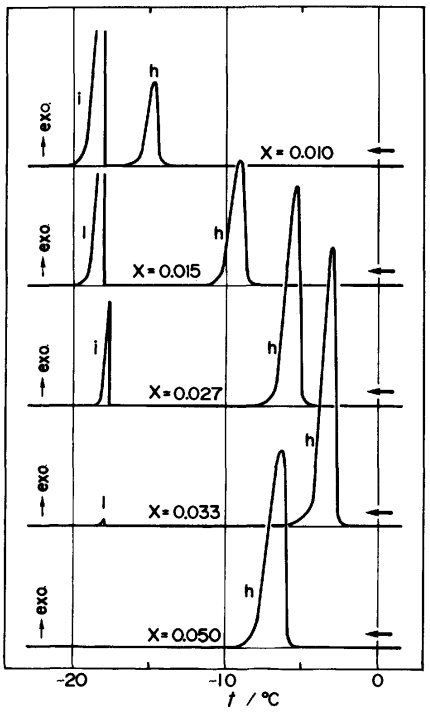

Fig. 1. The DSC curves on cooling for aqueous solutions of tetrabutylammonium chloride at various mole fractions.

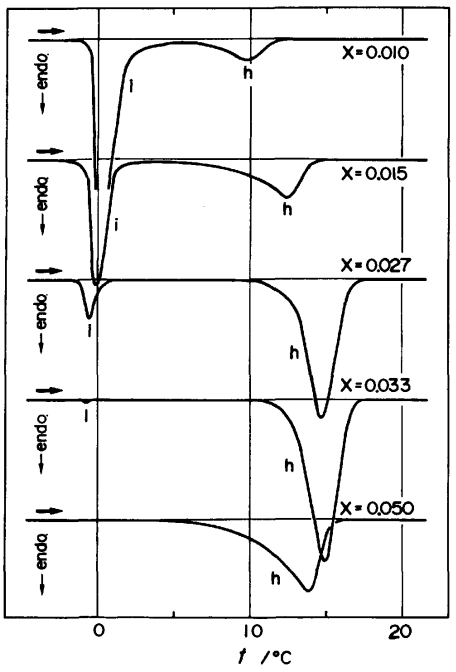

Fig. 2. The DSC curves on heating for the same solutions as shown in Fig. 1.

(1) Determination of the Hydration Numbers of the Clathrate-Like Hydrate of Tetrabutylammonium Chloride. Although two peaks i and h in the cooling processes (Fig. 1) can be completely separated from each other, these two in the heating processes (Fig. 2) cannot always be separated from each other especially in the solutions of $X<0.02$, as is partly seen in Fig. 2. Therefore, in order to know the enthalpy changes due to the melting of ice and of the hydrate separately, the following two enthalpy changes (ΔH_1 and ΔH_2) have been measured by taking advantage of the complete separation of the two peaks (i and h) in the cooling process. These two enthalpy changes are illustrated in Fig. 3 where ΔH_1 is the enthalpy change when heated after the sample solution is completely solidified by cooling below −20 °C (process (a) in Fig. 3). The ΔH_2 is the enthalpy change when heated after the sample solution is partially solidified by cooling the sample down to the temperature at which the hydrate phase is completely solidified but the water which does not participate in the formation of the hydrate remains in a liquid state (process (b) in Fig. 3). The observed values of ΔH_1 and of ΔH_2 are listed in Table 1 together with other data explained below. These values are averages of three to five measurements and the limit of error attached to each value is estimated not only by

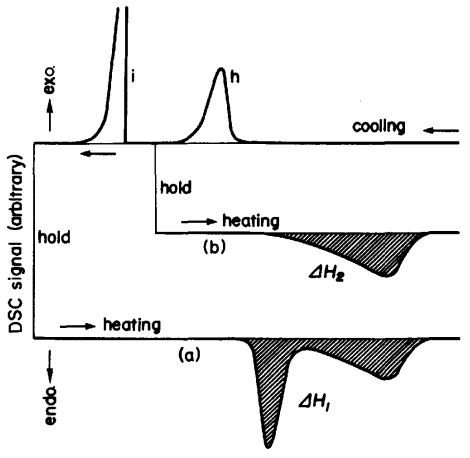

Fig. 3. The measuring processes of the two types of enthalpy changes ΔH_1 and ΔH_2.

the deviations from the mean value but also by the error arising from the procedure of determining the areas of the DSC curves.

The physical meaning of both ΔH_1 and ΔH_2 is not necessarily clear for the following reasons: (1) The composition of the liquid phase co-existing with the hydrate solid which is formed in the first-step cooling (peak h in Fig. 1) is not obvious since this mixture is not in an equilibrium state; and (2) for dilute solutions, especially when X is smaller than 0.005, the observed values of ΔH_2 vary from experiment to experiment, suggesting that the solid phase formed in the first-step cooling has some irregularity. If we neglect all the irregularities concerning the structure and chemical composition of the hydrate solid, ΔH_1 and ΔH_2 can approximately be expressed by the following relations:

$$\Delta H_1 = (n_0 - mn_1)\Delta H_{f,ice} + n_1\Delta H_{f,hyd} + \Delta H_M(n_1), \quad (1)$$

$$\Delta H_2 = n_1'\Delta H_{f,hyd} + \Delta H_M(n_1'), \quad (2)$$

in which n_0 and n_1 are the total number of moles of water and of tetrabutylammonium chloride contained in a sample. $\Delta H_{f,ice}$ and $\Delta H_{f,hyd}$ are the molar enthalpy of fusion of ice and of the hydrate expressed by a formula $(n\text{-}C_4H_9)_4NCl \cdot mH_2O$, in which m is the hydration numbers, and n_1' is the number of moles of the hydrate formed in the first-step cooling. The $\Delta H_M(n_1)$ is the total enthalpy of mixing of $n_0 - mn_1$ moles of water with n_1 moles of the hydrate melt. Similarly $\Delta H_M(n_1')$ is the total enthalpy of mixing of the liquid phase co-existing with the hydrate solid formed in the first-step cooling with n_1' moles of the hydrate melt.

The present results cannot directly be analyzed by these two equations since there is no information about the values of n_1' as well as of the enthalpies of mixing. However, for solutions whose concentration is not extremely low, it can be assumed that n_1' is equal to n_1, at least as a first approximation, since according to the phase-diagrammatic experiment for the same system the eutectic composition of the solution which is in equilibrium with the $(n\text{-}C_4H_9)_4NCl$ hydrate solid+ice mixture is as low as $X=0.002$.[9] This assumption means that the liquid phase which is co-existing with the hydrate solid formed in the first-step cooling is pure water instead of a dilute aqueous solution of $(n\text{-}C_4H_9)_4NCl$. Accordingly it leads to the simple relation that the enthalpy of mixing terms in Eqs. 1 and 2 become identical. Therefore, from Eqs. 1 and 2, the hydration numbers, m, of the hydrate can be expressed by the following relation:

$$m = \frac{1}{n_1}\left\{n_0 - \frac{\Delta H_1 - \Delta H_2}{6.0095 \times 10^3}\right\}, \quad (3)$$

in which both ΔH_1 and ΔH_2 are expressed in J unit and $\Delta H_{f,ice}=6.0095\times10^3$ J is used, which is equal to the molar enthalpy of fusion of ice I at 0 °C.[11]

The calculated values of m, together with the values of n_0 and of n_1 for each sample solution, are listed in Table 1. It is interesting to note that the calculated hydration numbers are around 30, in good agreement with the value 30±1 determined from phase diagrammatic experiments.[9] This suggests that Eq. 3 is appropriate to the determination of the hydration numbers of a clathrate-like hydrate at least as a first approximation. The small value of m obtained for the $X=0.005$ solution indicates that the assumption made to obtain Eq. 3 is not appropriate to such a dilute solution.

It should be noted that the hydration numbers of the hydrate can be determined from the measurements of both ΔH_1 and ΔH_2 for some solutions at any concentrations except for very dilute or very concentrated solutions. Furthermore this method can also be applied to the systems forming a hydrate which decomposes incongruently if the two enthalpy changes, ΔH_1 and ΔH_2, can be measured for the solutions whose concentrations are lower than the composition corresponding to its incongruent melting point.

In Fig. 4, the apparent enthlpy change for one mole of water, $\Delta H_1/n_0$, and the apparent enthalpy change

Table 1. Dissolution Temperature t, Enthalpy Changes ΔH_1 and ΔH_2, and Calculated Hydration Numbers m for the Tetrabutylammonium Chloride Clathrate-Like Hydrate

X[a]	n_0[a] / 10^{-4} mol	n_1[a] / 10^{-5} mol	t / °C	ΔH_1 / J	ΔH_2 / J	m
0.005	7.8712	0.3958	6.4	4.53±0.12	0.43±0.04	26.5±5.3
0.010	7.0441	0.7124	10.2	3.95±0.08	0.98±0.03	29.5±2.0
0.015	7.0666	1.0756	12.5	3.85±0.11	1.66±0.05	31.8±1.9
0.020	6.4807	1.3259	14.3	3.45±0.08	2.11±0.05	32.1±1.2
0.027	5.3167	1.4759	14.8	2.85±0.05	2.39±0.05	30.8±0.8
0.033	5.5761	1.9230	15.2	3.05±0.04	3.05±0.04	29.0±0.5
0.040	5.5580	2.3234	15.0	2.78±0.05	2.78±0.05	—
0.050	4.5064	2.3466	14.2	1.69±0.06	1.69±0.06	—

a) Notations X, n_0, and n_1 are explained in the text.

for one mole of water which forms hydrogen-bonded networks in the hydrate solid, $\Delta H_2/mn_1$, are plotted against X. An exact analysis of both curves is difficult due to the lack of information about the concentration dependence of the enthalpies of dilution and temperature dependence of the enthalpies of fusion and of dilution for both water and the hydrate. However, it is interesting to note that (1) the congruent composition of the hydrate, i.e., the hydration numbers, can also be determined by finding the concentration at which both curves coincide since the relations $\Delta H_1=\Delta H_2$ and $n_0=mn_1$ hold at the congruent composition. It is also notable that the value of $\Delta H_2/mn_1$ (or $\Delta H_1/n_0$) at the congruent composition is equal to 5.47 kJ mol^{-1}, in fair agreement with the value of 5.20 kJ mol^{-1} at 10 °C estimated from direct calorimetric measurements of the enthalpies of solution of the tetrabutylammonium chloride hydrate in water.[10]

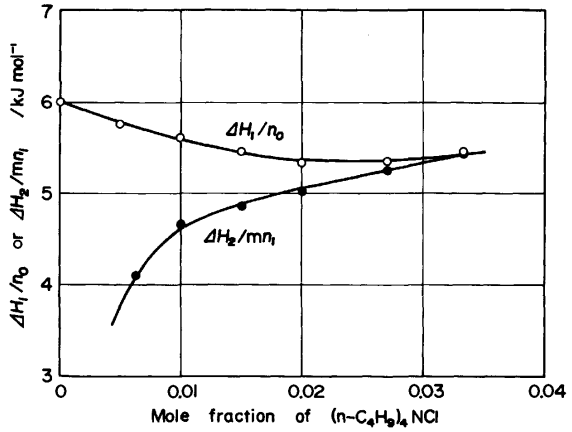

Fig. 4. Concentration dependence of the two apparent enthalpy changes, $\Delta H_1/n_0$ and $\Delta H_2/mn_1$, for tetrabutylammonium chloride–water system. The physical meanings of ΔH_1 and ΔH_2 are shown in Fig. 3, n_0 and n_1 are the total number of moles of water and of the salt contained in a sample solution, and m is the hydration numbers of the hydrate.

(2) Determination of the Melting Point of the Clathrate-Like Hydrate of Tetrabutylammonium Chloride. The melting point of the hydrate can be determined by finding the highest dissolution temperature for solutions at various concentrations. The dissolution temperature is that at which the solid phase completely dissolves when the solidified sample is gradually heated. Although this temperature is measured with the naked eye in an ordinary ampoule method, it can also be determined by the DSC experiments as illustrated in Fig. 5. In the heating process (b) in Fig. 3, the hydrate solid is first heated to a given temperature, t_0 for example, and is held at t_0 for a while. The sample is then further heated to a temperature higher than the presumed melting point. If the dissolution temperature of the sample, t, lies higher than t_0, an additional endothermic enthalpy change can be observed in the reheating process as marked A in Fig. 5. Thus the exact dissolution temperature can be determined by finding the lowest temperature t_0, as t_0'' in Fig. 5, for which no additional enthalpy change (peak A) is observed. It has been found that the dissolution temperature thus determined is practically equal to the temperature at which the heating DSC curves for the hydrate (the (b) process in Fig. 3) show a minimum: i.e., the temperature at which d(DSC signal)/dT=0. The dissolution temperatures so observed are listed in Table 1 for each solution. In Fig. 6, this temperature is compared with that determined by the ampoule method reported earlier.[9] This figure (i.e., a solid-liquid phase diagram) clearly indicates that the dissolution

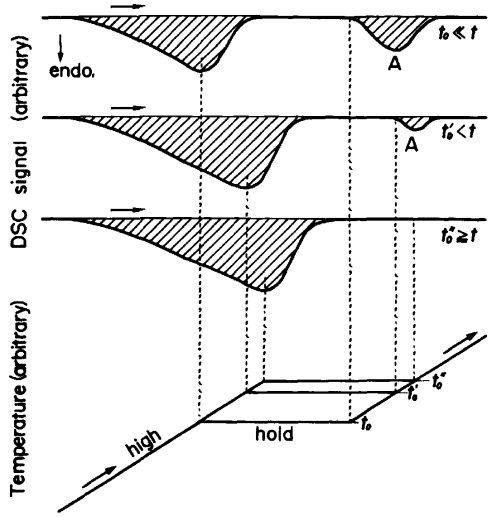

Fig. 5. The measuring process of the dissolution temperature, t, of the hydrate.

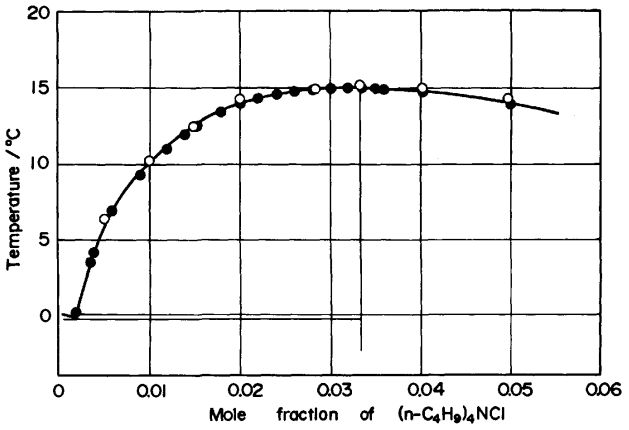

Fig. 6. The solid-liquid phase diagram for tetrabutylammonium chloride–water system determined by the dissolution temperatures. ○: values determined by the present DSC measurements; and ●: values determined by an ampoule method (Ref. 9).

temperature can be exactly determined by the DSC measurements. As is obvious from Table 1 and Fig. 6, a value of X=0.033 gives the maximum dissolution temperature (i.e., the melting point of the hydrate) of 15.2 °C. This indicates not only that this observed melting point is in good agreement with the 15.0 °C, determined phase-diagrammatically[9] but also that X=0.033 corresponds to the hydration numbers of 29, in good agreement with the result obtained in section (1).

In conclusion, through the discussions in the sections (1) and (2), the present thermal analytic method can give the same results concerning the nature of the clathrate-like hydrate of tetrabutylammonium chloride as those obtained phase-diagrammatically. Since the fundamental principle of the present method is not limited to an aqueous solution of the tetrabutylammonium chloride only, this method may be applicable to many similar types of systems, including the systems forming a hydrate which decomposes incongruently, so long as the two enthalpy changes, ΔH_1 and ΔH_2, can be measured.

(3) Thermal Properties of the Solutions at Higher Concentrations Than the Congruent Composition. Finally, the thermal behavior of the solutions above X=0.033 is discussed briefly. The behavior of the DSC signals is exemplified for the solution of X=0.050 in Figs. 1 and 2. The measured enthalpy changes are also listed in Table 1 for two solutions with X=0.040 and 0.050. The two enthalpy changes ΔH_1 and ΔH_2 inevitably become identical since the enthalpy change due to the melting of ice phase is not present for these concentrated solutions (Fig. 1 and 2). If we assume that all the water molecules participate in the formation of the hydrate solid having the hydration numbers around 30 and further that the enthalpy of fusion of these water molecules is equal to 5.47 kJ mol^{-1} estimated in the above discussion, the expected values of ΔH_1 (or ΔH_2) become 3.04 J for the X=0.040 solution and 2.47 J for the X=0.050 solution, respectively. The observed values listed in Table 1, 2.78 J for the X=0.040 solution and 1.69 J for the X=0.050 solution, are apprecially small as compared with those expected values, especially for the X=0.050 solution. At present exact thermal analyses are impossible because of a lack of information concerning the state of the phases existing in such concentrated solutions.

The present work was supported by a Grant-in-Aid for Scientific Research No. 60470006 from the Ministry of Education, Science and Culture.

References

1) H. Nakayama, *Bull. Chem. Soc. Jpn.*, **56**, 877 (1983).
2) R. McMullan and G. A. Jeffrey, *J. Chem. Phys.*, **31**, 1231 (1959).
3) H. Nakayama and S. Torigata, *Bull. Chem. Soc. Jpn.*, **57**, 171 (1984).
4) H. Nakayama and H. Usui, *J. Inclusion Phenomena*, **2**, 249 (1984).
5) M. Bonamico, G. A. Jeffrey, and R. K. McMullan, *J. Chem. Phys.*, **37**, 2219 (1962).
6) Yu. A. Dyadin, L. S. Aladko, L. A. Gaponenko, and T. M. Polyanskaya, *Izv. Sib. Otd. Akad. Nauk SSSR, Ser. Khim. Nauk*, **1981**, 19.
7) H. Nakayama and K. Watanabe, *Bull. Chem. Soc. Jpn.*, **51**, 2518 (1978).
8) H. Nakayama and H. Usui, *Bull. Chem. Soc. Jpn.*, **59**, 833 (1986).
9) H. Nakayama, *Bull. Chem. Soc. Jpn.*, **54**, 3717 (1981).
10) H. Nakayama, *Bull. Chem. Soc. Jpn.*, **55**, 389 (1982).
11) D. Eisenberg and W. Kauzmann, "The Structure and Properties of Water," Oxford Univ. Press, London (1969).

 © 1987 The Chemical Society of Japan Bull. Chem. Soc. Jpn., 60, 845—849 (1987)

Binding Behavior of Metal Cations and Hydrophobic Ions from a Mixed Solution

Kunio Furusawa,* Miyako Iwamoto, and Hideo Matsumura†
Department of Chemistry, The Univesity of Tsukuba, Sakura-mura, Ibaraki 305
†Electrotechnical Laboratory, Sakura-mura, Ibaraki 305
(Received August 7, 1986)

Critical experimental data are presented on the competitive adsorption of metal cations with different ionic valences to phospholipid vesicles, and on the binding of hydrophobic ions from mixed solutions with multivalent metal cations produced under different conditions by means of the Inductively Coupled Argon Plasma. It is apparent that the preferential effect in binding between the metal cations depends not only on their ionic valences but also on the concentrations of each ion at which the corresponding binding is carried out; i.e., the binding strength of the metal cations on the membrane surface increases in the following order: $K^+ < Mg^{2+} < Ca^{2+} < La^{3+} < Th^{4+}$, and this order comes to be more pronounced in the high-concentration region of each component. Furthermore, it is realized that, in binding from mixed solutions of hydrophobic ions and multivalent metal cations (Ca^{2+} or Th^{4+}), a synergistic interaction between these ions occurs; i.e., the binding of hydrophobic anions is promoted by the presence of metal cations, while the binding of hydrophobic cations is hindered by the metal cations.

From a structural point of view, phospholipids are perhaps the most important of all constituents of living systems, for without them a living cell could not exist. Among the various functions of a biological membrane, its permeability property is one of the most interesting points with relation to its interfacial behavior. Many studies[1] of metal-cation binding to phospholipid vesicles in terms of the permeability have indicated that the metal cations, especially the multivalent cations, are bound to the vesicles with a high affinity and that the presence of even small amounts of the cation exerts a profound effect on the vesicle dispersion.[2,3]

On the other hand, some organic ions, such as detergents, antibiotics, and some other lipidsoluble ions, can be bound to the phospholipid vesicles by hydrophobic interaction with the lipid molecules. It is expected, therefore, that the adsorption of these organic ions into the membrane will bring about not only a change in the membrane-surface potential, but also a change in the dipole potential in the membrane arising from the oriented dipoles of the polar-head groups of phospholipid molecules.[4,5]

Biological membranes sometimes operate in a medium containing simultaneously, several kinds of metal cations with different ionic valences and a few hydrophobic ions. For example, some sea plants grow quickly in sea water in which various ionic materials are included. It is assumed that in their growing stage, the permeability of their ionic materials through the cell membrane plays an important role. In such a case, it is important to know the relation between the permeability of the membrane and the composition of the ionic materials included.

In this work, some critical data on the binding character of these metal cations with different ionic valences on the phospholipid vesicles from their mixed systems have been obtained. Further, the binding behavior of hydrophobic ions from the mixed solution with multivalent metal cations has been examined under various component conditions. We believe that these critical data on the binding will provide a crucial illustration of the functionality of phospholipid bilayers.

Experimental

Materials. Bovine brain-phosphatidylethanolamine (PE) and -phosphatidylserine (PS) were used as the membrane-forming lipids; they were purchased from the Sigma Chemical Co., Ltd. (U.S.A.). Sodium tetraphenylborate (TPB) and tetraphenylphosphonium chloride (TPP), which has been obtained from Dojindo Laboratories, were used as a hydrophobic anion and a hydrophobic cation respectively. The other inorganic reagents (metal chlorides) were of an analytical grade. All the solutions of these materials were prepared by dissolving them in deionized (Barnstead, NANO pure system) and doubly distilled water.

Vesicle Preparation. The PE and PS vesicles were prepared by the usual sonication method in a nitrogen atmosphere at 4 °C, without using any buffer to reduce the spurious effects of the buffer ions included.[6] After the removal of the undispersed materials by centrifugation (26000 G, 1 h), the dispersions were filtered through a membrane filter (0.1 μm pore size).

Measurements of Amounts of Binding. The binding strength of each metal cation from a single-component system on the PE (or PS) vesicles has been measured as follows. Ten-ml portions of the vesicle dispersion (0.3 g dm^{-1}) were poured into 10-ml portions of various salt solutions containing different ionic concentrations, after which the mixture was left standing for one night at 25 °C. Only the vesicle particles were then separated from the medium by ultrafiltration (Millipore PTGC), and the concentrations of the metal cations and hydrophobic ions were measured analytically by means of the Inductively Coupled Argon Plasma (ICP) method (Jarrell-Ash 975), which counts the amounts of boronium for TPB and of phosphonium for TPP respectively. By observing the

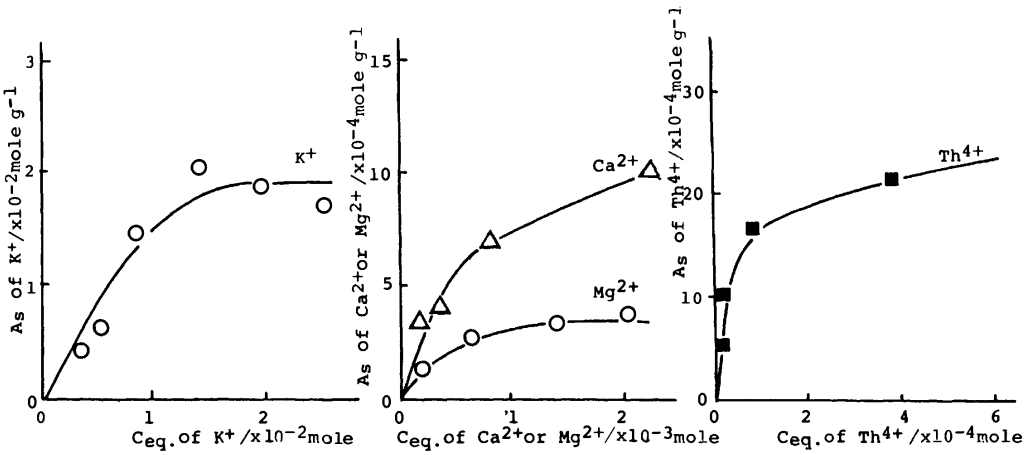

Fig. 1. Binding isotherms of K^+, Ca^{2+}, Mg^{2+}, and Th^{4+} to PE vesicles.

different concentrations in the solutions before and after (C_{eq}) the adsorption process, the amounts of adsorption per unit of vesicle weight (As) were calculated using a calibration curve.

The amounts of binding of each component ion from these mixed solutions of the different ionic species were determined by the same procedure as that used for the singlecomponent system. After a binding period of 24 h, the concentrations of the individual ions remaining in the filtrate as well as in the initial solution were determined simultaneously using the ICP method. By this analysis, the concentrations of many atomic species can be analysed simultaneously from a single liquid solution.

In the simultaneous binding of two ionic species, the effects of the order of addition on their binding are studied as follows. A 5-ml portion of one salt solution is poured into a cylinder with the same volume of the vesicle dispersion, and then the mixture is stored in a thermostat kept at 25 °C for 24 h. After that, a 5-ml portion of another salt solution including the second component ion was added, and the new mixture stored again for 24 h. After the completion of the second binding process, the binding amounts of each component ion were determined in the same analytical way.

Results and Discussion

1) The Binding Behavior of Metal Cations from Single- and Two-Component Systems. Figure 1 presents some typical examples of binding isotherms for metal cations. As may be seen, the affinity of the binding of each cation is much dependent on the ionic valence of the ions, and the affinity increases with an increase in the ionic valence. Especially, the multivalent cations (La^{3+} and Th^{4+}) are bound to the vesicles with very high affinities; even a trace of these ions exerts an important effect on the stability of vesicle dispersion.[2] The present work demonstrated that the binding strength of metal cations to PE and PS vesicles increases in the following order: $K^+ < Mg^{2+} < Ca^{2+} < Mn^{2+} < La^{3+} < Th^{4+}$. Considering their binding order, the competitive (or preferential) binding between the different metal cations has been examined simultaneously in systems including two such species. Figures 2, 3, and 4 show the binding isotherms of K^+ and Ca^{2+}, Ca^{2+} and Mg^{2+}, and Ca^{2+} and Th^{4+}, respectively, as obtained from mixed solutions. It is apparent from Fig. 2 that the preference of Ca^{2+} relative to K^+ can be observed over a wide region except for the lower concentration region of less than 1×10^{-4} mol dm^{-3} $CaCl_2$. It is interesting to notice that the preferential effect of a special ion depends not only on the valence of the ion, but also on the concentration of each ion at which the corresponding binding is carried out. Figure 3 shows the results obtained from the simultaneous binding of Mg^{2+} and Ca^{2+} on the PE vesicles. In the same figure, the isotherms obtained from single-component system are also illustrated by the dotted lines. It follows that

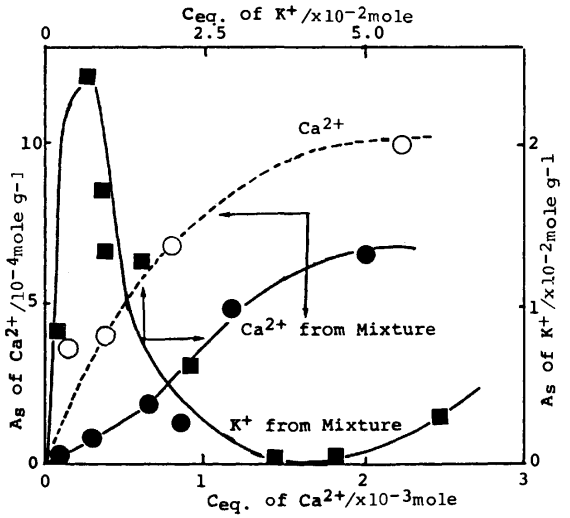

Fig. 2. Binding isotherms of K^+(■) and Ca^{2+}(●) to PE vesicles obtained from their mixed solutions, where the concentration ratio of both the ions is fixed at 30 (K^+) : 1(Ca^{2+}). The dotted line shows the isotherm of Ca^{2+}(○) from the single component system.

the results show a preferential binding of Ca^{2+} in comparison to the binding of Mg^{2+} over the whole concentration region and that the preference of Ca^{2+} depends on the concentration and becomes apparent in concentrations of each ion higher than 1×10^{-3} mol dm^{-3}. As may be seen from Fig. 4, similar results may be found in the simultaneous binding of Ca^{2+} and Th^{4+}, where the concentration of Th^{4+} is fixed at 1×10^{-4} mol dm^{-3}. It is found that the amount of the binding of Th^{4+} is kept constant over the whole concentration region and that only the amount of the adsorption of Ca^{2+} varies with its bulk concentration. All these findings regarding the simultaneous binding between the different metal cations suggest that the binding of metal cations on the membrane surface is influenced by various factors; the ionic species, the ionic valence, the concentration, their ratio in a two-component system and other enviromental factors, and that it is hard to predict the final binding layer from the composition of the equilibrated bulk solution.

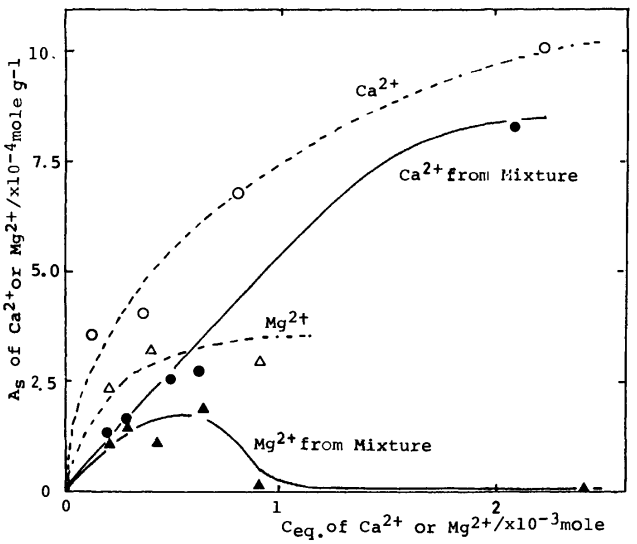

Fig. 3. Binding isotherms of Ca^{2+}(●) and Mg^{2+}(▲) to PE vesicles obtained from their mixed solutions, where the concentration ratio of both the ions is fixed at 1 (Ca^{2+}) : 1(Mg^{2+}). The dotted lines show the isotherms of Ca^{2+}(○) and Mg^{2+}(△) from the single component systems.

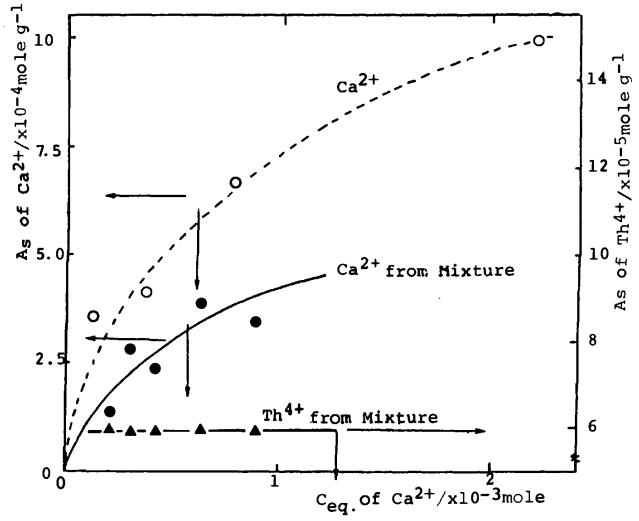

Fig. 4. Binding isotherms of Ca^{2+}(●) and Th^{4+}(▲) to PE vesicles obtained from their mixed solutions, where the concentration of Th^{4+} is kept constant at 1×10^{-4} mol dm^{-3}. The dotted line shows the isotherm of Ca^{2+}(○) obtained from the single component system.

This complexity of the situation in the metal-cation binding from a mixed solution indicates that the binding of their ions will be influenced by the order of the addition of the species. Figure 5 shows some typical results obtained from the two different ways of addition for Ca^{2+} and Th^{4+}, where the concentration of Th^{4+} is fixed at 1×10^{-4} mol dm^{-3}; only the comparison in the binding amounts for Ca^{2+} is indicated for the two mixing methods. As may be seen from the figure, the amounts of bound Ca^{2+} are greatly influenced by the order of addition; the initial addition of Th^{4+} results in decreased amounts of Ca^{2+}. This result indicates that a multivalent cation such as Th^{4+} binds on the membrane surface with an irreversible character and that it is hard to exchange occupied binding-site for other metal cations.

2) Binding Behavior of Hydrophobic Ions from Mixed Solutions with Metal Cations. It has already been reported that there is a great difference between the adsorption behavior of TPB and TPP toward the lipid vesicles from their single-component systems; i.e., the amounts of the binding of TPB are greater than those of TPP, especially at high bulk concentrations.[7] Here, the difference between the binding behavior of the two hydrophobic ions and that of their coexistent systems with the metal cations has been

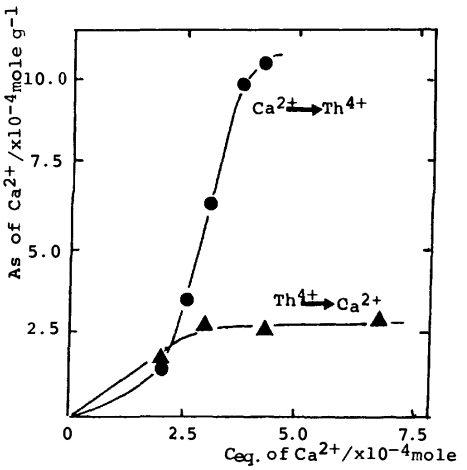

Fig. 5. Binding isotherms of Ca^{2+} to PE vesicles obtained from the two different methods of addition for Ca^{2+}, where the concentration of Th^{4+} is fixed at 1×10^{-4} mol dm^{-3}.

examined using the ICP method. Figures 6 and 7 show the binding isotherms of TPB and Ca^{2+} to the PE and PS vesicles obtained from their mixed solutions with Ca^{2+}. The dotted lines in these figures show the isotherms obtained from the single-component systems of each ion. It is found that the amounts of the binding of TPB are enhanced extensively by the coexistence of Ca^{2+}; a similarly enhanced value is observed in the binding to the PE and PS vesicles. Furthermore, it is apparent that the binding of Ca^{2+} to the PE and PS vesicles is also promoted by the coexistence of TPB. These results indicate that, when the TPB anion and the metal cation are present in the same solution, a synergistic effect by their ions occurs and each ion acts as a cooperator for its binding to the membrane surface.[8]

On the other hand, when the TPP and the metal cations are bound to the vesicles from a mixed solution, very different behavior has been observed. Figures 8 and 9 display the binding isotherms obtained from the mixed solutions of Ca^{2+} plus TPP and of Th^{4+} plus TPP respectively. In Fig. 9, the concentration of Th^{4+} was fixed at 1×10^{-4} mol dm^{-3} and only the binding of TPP is compared. It may be

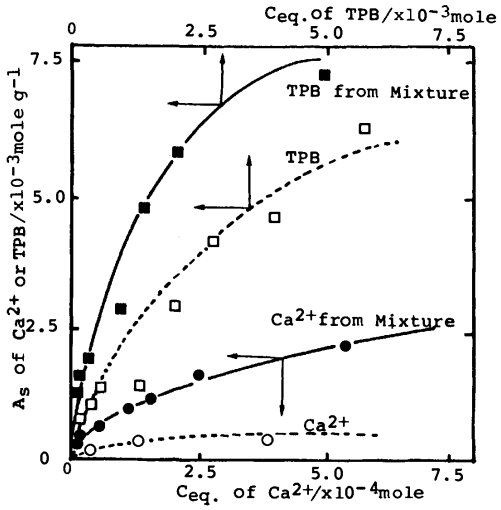

Fig. 6. Binding isotherms of Ca^{2+}(●) and TPB(■) to PE vesicles obtained from their mixed solutions, where the concentration ratio of both the ions is fixed at 1(Ca^{2+}) : 6(TPB). The dotted lines show the isotherms of Ca^{2+}(○) and TPB(□) obtained from the single component systems.

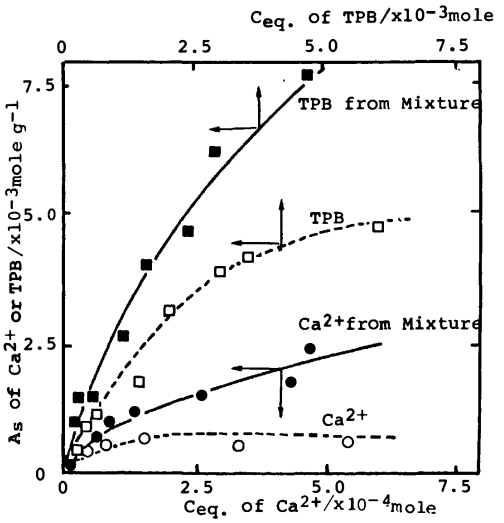

Fig. 7. Binding isotherms of Ca^{2+}(●) and TPB(■) to PS vesicles obtained from their mixed solutions, where the concentration ratio of both the ions is fixed at 1 (Ca^{2+}) : 6(TPB). The dotted lines show the isotherms of Ca^{2+}(○) and TPB(□) obtained from the single components ystems.

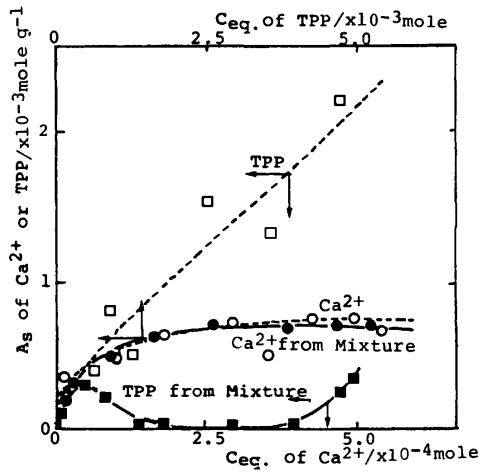

Fig. 8. Binding isotherms of Ca^{2+}(●) and TPP(■) to PE vesicles obtained from their mixed solutions, where the concentration ratio of both the ions is fixed at 1 (Ca^{2+}) : 6(TPP). The dotted lines show the isotherms of Ca^{2+}(○) and TPP(□) obtained from the single component systems.

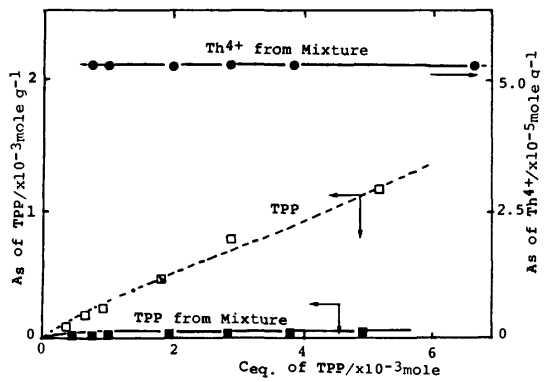

Fig. 9. Binding isotherms of Th^{4+}(●) and TPP(■) to PE vesicles obtained from their mixed solutions, where the concentration of Th^{4+} is fixed at 1×10^{-4} mol dm^{-3}. The dotted line shows the isotherm of TPP (□) obtained from the single component system.

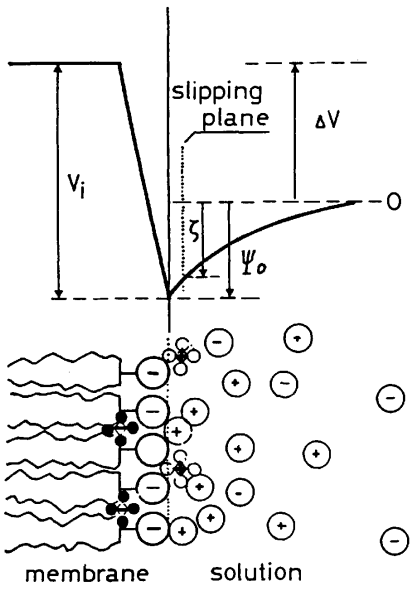

Fig. 10. Schematic picture showing the electrostatic potential through membrane-solution interface and the binding sites on the layer of the lipid membrane (●◇●; TPB, ○⊕○; TPP).

seen from Fig. 8 that the binding of TPP is hindered by Ca^{2+} except in some special concentration regions of TPP. It may be observed by comparison with Fig. 2 that the relations between Ca^{2+} and TPP in their preferential binding resemble those between Ca^{2+} and K^+, suggesting that the binding affinity of TPP results from the same cause as the binding of the metal cation. On the other hand, as may be seen from Fig. 9, the binding of TPP to the vesicles is completely hindered by the coexistence of Th^{4+} because of the strong binding character of Th^{4+} to the membrane surface.

Such a difference in the binding of TPB and TPP to the vesicles from that in mixed solutions with the metal cations may be explained by their different contributions to the electrostatic potential through the membrane-solution interface. Figure 10 shows a schematic picture to elucidate the potential profile near the membrane surface. The membrane potential is described as a combination of potentials arising from the oriented dipoles of polar-head groups of phospholipid molecules and the ionic double-layer potential on their surface.[9] This potential profile can be applied to the PE vesicles under negatively charged conditions.[2] It is usually known that the metal cations bind to the membrane surface and cause the ionic double-layer potential to change. This consideration can be confirmed by measurements of the zeta-potentials of the vesicles (ξ in Fig. 10) and of the surface potentials of the monolayers (ΔV in Fig. 10) in various ionic solutions. On the other hand, the binding of TPB causes a change in both the dipole potential and the double-layer potential as a result of their hydrophobic interaction.[8] According to this concept, if the metal cations and the TPB anions are both present in a solution including PS or PE vesicles, some synergistic interaction in their binding to the vesicles may be expected; some metal cations will initially bind to the negative surface of the vesicles and decrease the negative double-layer potential. This will induce an increase in the binding of some TPB anions by means of their electrostatic forces and again result in a negative surface potential. By repeating the process, a positive cooperative binding between the metal cation and the TPB anion can be observed. On the other hand, when the lipid soluble cations (TPP) are present in a solution with the metal cation, the binding of TPP will be hindered by the positive potential effect induced by the binding of the metal cation to the negative membrane surface. Furthermore, because of the restricted number of binding sites on the outer layer of the lipid membrane which are occupied preferentially by the metal cations, the binding of TPP is extensively hindered by the coexistence of metal cations.

It is clear from the present binding work that the binding sites on the membrane surface for TPP are very different from those for TPB, although they have the same hydrophobic character.

References

1) E.g., D. Papahadjopoulos, *Biochem. Biophys. Acta*, **163**, 240 (1968); S. Ohki and R. Sauve, *Biochem. Biophys. Acta*, **511**, 377 (1978).

2) K. Furusawa, H. Kakoki, and H. Matsumura, *Bull. Chem. Soc. Jpn.*, **57**, 3413 (1984).

3) K. Furusawa, H. Kakoki, and T. Takei, *Nippon Kagaku Kaishi*, **1984**, 992.

4) B. Ketterer, B. Neumcke, and P. Lauger, *J. Membr. Biol.*, **5**, 225 (1971).

5) O. S. Anderesen, S. Feldberg, H. Nakadomari, S. Lery, and S. McLaughlin, *Biophys. J.*, **21**, 35 (1978).

6) K. Furusawa, N. Onda, E. Kokufuda, S. Fujii, and T. Takei, *Nippon Kagaku Kaishi*, **1980**, 506.

7) H. Matsumura and K. Furusawa, *J. Colloid Interface Sci.*, **110**, 137 (1986).

8) H. Matsumura, M. Fukuma, and K. Furusawa, *J. Colloid Interface Sci.*, **103**, 561 (1985).

9) E.g., P. A. Haydon and V. B. Myers, *Biophys. Biochem. Acta*, **307**, 429 (1973).

 © 1987 The Chemical Society of Japan Bull. Chem. Soc. Jpn., 60, 851—855 (1987)

Fast Reactions of Organic Anion Radicals with Organic Halides in Hexamethylphosphoric Triamide Studied by Pulse Radiolysis

Eiji HONDA, Masao TOKUDA, Hiroshi YOSHIDA, and Masaaki OGASAWARA*
Faculty of Engineering, Hokkaido University, Sapporo 060
(Received August 25, 1986)

Fast reactions of diethyl fumarate anion radical (DEF^-) and fluorenone anion radical (Fl^-) with various organic halides (RX) in hexamethylphosphoric triamide have been studied by means of ns pulse radiolysis at room temperature. Reactions of acetophenone anion radical were also studied for comparison. It was found that the reaction rate of Fl^- was subject to the steric and resonance effects of R groups of RX in accord with the classical concept of S_N2 reactions: the rate constant was reduced by 2 orders of magnitude by the steric effect when R was changed from ethyl to bulky isopropyl or *t*-butyl, and it was still large by the resonance effect of R even if R was changed from ethyl to an allyl or a benzyl group. While the reaction rate of DEF^- was not much affected when R was changed to more bulky groups, the rate constant was correlated to the reduction potential of RX. The results were interpreted in terms of a VB correlation diagram approach or rate-equilibrium relationship within a framework of S_N2 reactions.

Most organic anion radicals react efficiently with organic halides, the mechanism being dependent on the kind of anion radical and organic halide. An electron-transfer reaction from radical anions to organic halides accompanied by a dissociation of the electron acceptor into two fragments, organic radical and halide anion, is most commonly observed.[1] Nucleophilic substitution reaction at a saturated carbon atom of the organic halides may also take place. The possibility of an $S_{RN}1$-type substitution reaction,[2] in which the dissociative electron transfer from anion radical to organic halide is followed by addition reaction of the organic radicals to the product neutral molecules, should also be considered.

A few years ago, Satoh et al. studied electrochemical reactions of diethyl fumarate with alkyl halides and confirmed the carbon-carbon bond formation at a saturated carbon atom of the halide.[3] Following nucleophilic substitution reaction of diethyl fumarate anion radical with alkyl halides, RX, was proposed to explain the results.

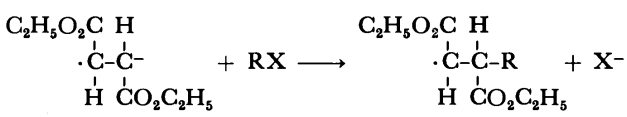

(1)

Similar nucleophilic substitution reactions were found in electrochemical reactions of the fluorenone anion radical.[4]

We report here the pulse radiolysis kinetics of the reactions of the diethyl fumarate anion radical and the fluorenone anion radical with several organic halides, in special reference to free-energy relationship of the reactions, in hexamethylphosphoric triamide (HMPA) at room temperature. Our aim is to attempt to understand the factors which determine the reactivity of these anion radicals toward organic halides.

Experimental

Pulse Radiolysis Apparatus. The source of the electron pulse was the Hokkaido University 45-MeV linear accelerator. The pulse was reducible in its duration down to as short as 10 ns, but only 100 ns pulse with a dose of 140 Gy/pulse was used in the present study. The cells and optical system have been described elsewhere.[5] The electric signals from a Hamamatsu Photonics R446 photomultiplier were digitized by an Iwatsu TS-8123 Storage-scope and the digitized data were processed by a NEC PC-9801 computer.

Materials. HMPA was dried over calcium hydride for 24 h, refluxed with fresh calcium hydride for 2 h, and distilled at reduced pressure before use. 9-Fluorenone (Nakarai Guaranteed Reagent) was used without purification. Ethyl bromide, iso-propyl bromide, *t*-butyl bromide, allyl bromide and ethyl iodide were distilled over calcium chloride before use. Benzyl bromide was distilled over calcium chloride at a reduced pressure before use. The solutions were degassed in vacuum line and sealed into Suprasil cells of the size $1\times1\times4.5$ cm^3.

Cyclic Voltammetry. Cyclic voltammetry was made with Nichia HP-E_{500} potentiostat at a sweep rate of 0.2 V s^{-1} using a platinum disc electrode (1 mm diameter) or hanging mercury drop electrode (HMDE) in solutions of 0.1 mol dm^{-3} *n*-Bu_4NClO_4 in HMPA. The potential was measured in V vs. Ag/AgI.

Results

Diethyl Fumarate Anion Radical. Figure 1 shows the transient absorption spectra observed in the pulse radiolysis of solutions of 4×10^{-3} mol dm^{-3} diethyl fumarate (DEF) in HMPA. The spectrum with an absorption maximum at 340 nm which was observed immediately after a pulse is assigned to the diethyl fumarate anion radical (DEF^-) formed by electron capture by DEF. For comparison, the absorption spectrum of *dimethyl* fumarate anion radical obtained at 77 K in γ-irradiated 2-methyltetrahydrofuran matrix is also shown.[6] Spectra observed with the samples containing a small amount (1×10^{-2} mol dm^{-3}) of ethyl bromide as the second solute are the same as

those observed without ethyl bromide except for the band in the UV region (<320 nm) which is discernible at 250 μs after the pulse. This UV band may be due to the reaction product of DEF^- with the halide.

The time-profile of the absorption monitored at 340 nm consists of a fast-decaying component and a slow-decaying one, although the contribution of the latter component is only one tenth of the initial absorption. It is assumed that only the fast-decaying component which is separable by subtracting the slow-decaying one from the original curve is due to the DEF^-. In the absence of ethyl bromide the decay curve of DEF^- followed a second-order kinetics, suggesting that the DEF^- disappeared via recombination reactions with solvent cations or radicals produced by ionizing radiation. In the presence of ethyl bromide the decays were analyzed as being mixed first- and second-order processes. Evidently, the first-order process is due to a pseudo- first-order reaction of the DEF^- with ethyl bromide. The rate equation therefore is expressed as:

$$-d[DEF^-]/dt = k_1[DEF^-]^2 + k_2[DEF^-]. \quad (2)$$

Where k_1 is the second-order rate constant of the decay reaction of DEF^- in the absence of RX. This was determined empirically as $(1.1\pm0.3)\times10^9$ $OD^{-1}s^{-1}$ under the same experimental conditions. The k_2 infers the rate constant of the pseudo-first-order process which can be rewritten as $k_2=k[RX]$ with the k being the second-order rate constant between DEF^- and RX. With the k as a parameter the decay curves of the DEF^- were simulated, as exemplified in Fig. 2, by the method described elsewhere.[5] The k thus obtained increases linearly with increase of the RX concentration and the second order rate constants, k, are determined from the slope of the straight lines as summarized in Table 1.

Fluorenone Anion Radical. In the pulse radiolysis of solutions of fluorenone in HMPA, transient absorption spectra with a single peak at 570 nm were observed. The spectra are assigned to the fluorenone

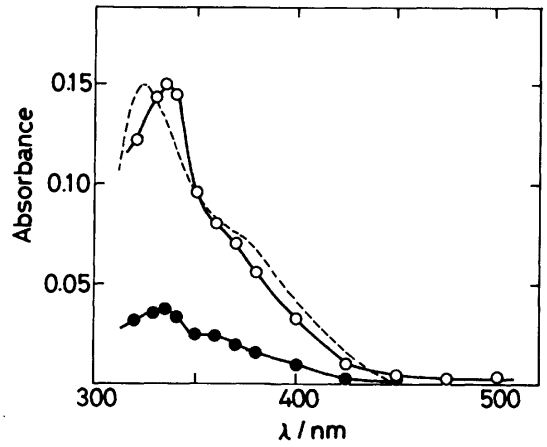

Fig. 1. Transient absorption spectra obtained in the pulse radiolysis of solutions of 4×10^{-3} mol dm^{-3} diethyl fumarate in HMPA: —○— immediately after the pulse, —●— 250 μs after the pulse. The dashed curve indicates the steady state absorption spectrum of dimethyl fumarate anion radical in 2-methyltetrahydrofuran matrix at 77 K.[6]

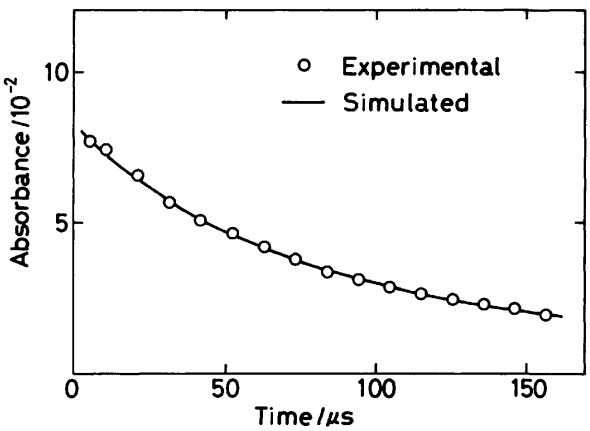

Fig. 2. Decay curve of diethyl fumarate anion radical observed at 340 nm in HMPA solution containing 4×10^{-3} mol dm^{-3} diethyl fumarate and 9×10^{-3} mol dm^{-3} ethyl bromide. The solid line indicates the decay curve simulated on the basis of superimposed first- and second- order kinetics (see the text).

Table 1. Rate Constants of the Reactions between Organic Anion Radicals and Organic Halides

Halogen Compound	Reduction Potential −E/V	DEF^- k/mol^{-1} dm^3 s^{-1}	Fl^- k/mol^{-1} dm^3 s^{-1}	$Acet^-$ [c] k/mol^{-1} dm^3 s^{-1}	Solvent
C_2H_5Br	2.30[a]	$(5.0\pm1.1)\times10^5$	$(3.5\pm0.9)\times10^8$	—	HMPA
$(CH_3)_2CHBr$	2.24[a]	$(8.1\pm1.4)\times10^5$	$(3.1\pm0.9)\times10^6$	$(7.5\pm2.5)\times10^6$	HMPA
ibid.	ibid.	—	$(2.0\pm0.3)\times10^6$	—	CH_3CN
$(CH_3)_3CBr$	2.02[b]	—	$(1.6\pm1.0)\times10^6$	—	HMPA
$CH_2=CHCH_2Br$	1.62[a]	$(1.2\pm0.4)\times10^6$	$(6.3\pm2.8)\times10^8$	—	HMPA
$C_6H_5CH_2Br$	1.47[a]	$(2.6\pm0.9)\times10^6$	$(1.1\pm0.3)\times10^8$	—	HMPA
C_2H_5I	1.84[a]	$(1.6\pm0.4)\times10^6$	—	—	HMPA

a) Determined by CV with Pt disc electrode; V vs. Ag/AgI. b) Determined by CV with a hanging mercury drop electrode; V vs. Ag/AgI. c) Acetophenone anion radical.

anion radical (Fl^-) because of the similarity to those obtained in the pulse radiolysis of ethanol solutions at low temperature and of *N,N*-dimethylformamide solutions at room temperature.[7] In the presence of ethyl bromide essentially the same spectra were observed immediately after the pulse, but a small absorption at ca. 530 nm, probably due to the reaction products of Fl^- with halides, survived for a long time.

The spectra of Fl^- depended markedly on the solvent and the counterion. In acetonitrile solutions the λ_{max} was shifted to ca. 530 nm and a long tail extending on the longer wavelength side was observed. In 2-methyltetrahydrofuran (MTHF) solutions containing sodium tetraphenylborate as *the third solute*, transient spectrum with λ_{max} at 540 nm which was ascribed to ion pair between Fl^- and Na^+ was observed. The shift of λ_{max} in acetonitrile and in MTHF should be due to solvation and coulombic interaction of the counterion, respectively.

The decay kinetics of Fl^- also depended on the solvent. In HMPA, the decay curve monitored at 570 nm arose from a first-order process with a rate constant of $7.3\times10^4\ s^{-1}$. The reaction mechanism of the decay reaction is not known, but the anions may be consumed by reactions with impurities in HMPA. Addition of the second solutes, RX, apparently accelerated the decay rate, indicating efficient reaction of Fl^- with RX. The pseudo-first-order rate constant increased linearly with increase of the RX concentration. Second-order rate constants of Fl^- were determined from the slope of the straight lines for various RX. The reactions of the Fl^- in acetonitrile, which follows a second-order kinetics in the absence of RX, are analyzed by the same method as the case of DEF^-. The results are summarized in Table 1. They showed that the ion pairs, Fl^-Na^+, in MTHF did not react with organic halides in a μs time-domain.

Acetophenone Anion Radical. The absorption spectrum of the acetophenone anion radical in HMPA has a broad band in the visible with double maxima at 460 and 480—490 nm, which disappear following a first-order kinetics. The second-order rate constants k of the reaction between acetophenone anion radical and ethyl bromide are listed in Table 1.

Reduction Potentials of Organic Halides. Reduction potentials (E_{red}) of organic halides in HMPA were determined by cyclic voltammetry. The type of electrode employed in the measurements, Pt or HMDE, did not have much effect, though in general the HMDE electrode gives a little more positive potentials for E_{red}. In Table 1 only the results obtained with the Pt electrode are shown except the one for *t*-butyl bromide.

Figure 3 shows cyclic voltammograms of HMPA solutions containing allyl bromide and n-Bu_4NClO_4. The single peak observed in the cyclic voltammetry

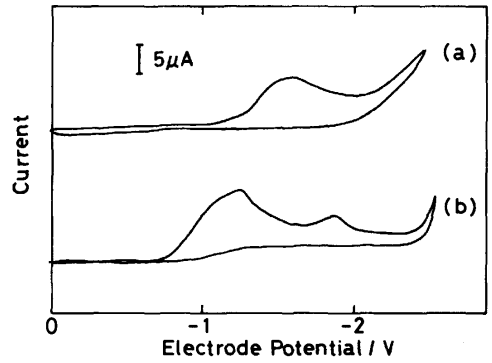

Fig. 3. Cyclic voltammograms of HMPA solutions containing 5×10^{-3} mol dm^{-3} allyl bromide and 0.1 mol dm^{-3} n-Bu_4NClO_4 recorded with Pt electrode (a) and HMDE electrode (b). The electrode potential was measured vs Ag/AgI.

with Pt electrode (Fig. 3(a)) may be ascribed to the following reactions.

$$CH_2{=}CHCH_2Br + e^- \longrightarrow (CH_2{=}CHCH_2Br)^{\cdot-}$$
$$\longrightarrow CH_2{=}CHCH_2\cdot + Br^- \quad (3)$$
$$CH_2{=}CHCH_2\cdot + e^- \longrightarrow CH_2{=}CHCH_2^- \quad (4)$$

The second peak at -1.87 V, which was observed exclusively with HMDE electrode (Fig. 3(b)), can be ascribed to the following reactions.

$$CH_2{=}CHCH_2\cdot + Hg \longrightarrow CH_2{=}CHCH_2Hg\cdot$$
$$\xrightarrow{CH_2=CHCH_2\cdot} (CH_2{=}CHCH_2)_2Hg \quad (5)$$
$$CH_2{=}CHCH_2Hg\cdot + e \longrightarrow CH_2{=}CHCH_2^- + Hg \quad (6)$$

We adopted the value evaluated from the first peak of the cyclic voltammogram shown in Fig. 3(a) as the E_{red} for allyl bromide.

Discussion

The effect of RX on the decay curve of DEF^- clearly indicates that DEF^- reacts with RX very efficiently. In the study of electrochemical reaction of DEF, Satoh et al. concluded that the electron transfer from the electrode to DEF was followed by an S_N2 reaction of the produced DEF^- with RX.[3] Analogously, the most plausible reaction of DEF^- with RX would be an S_N2-type substitution reaction. The resulting radical should be the R-adduct radical of DEF as shown by Eq. 1, although its formation has not yet been confirmed optically. It should be noted that the reaction rate is not much affected when R is changed from ethyl to a bulky isopropyl group. This result is not fully consistent with the classical concept of an S_N2 reaction which is characterized by effective hindrance by the presence of bulky group. Instead, the rate constant is correlated to E_{red} of RX as shown in Fig. 4.

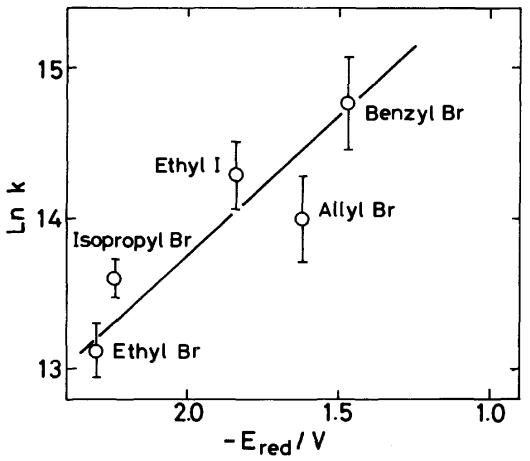

Fig. 4. Second-order rate constant for the reactions at room temperature between diethyl fumarate anion radical and organic halides as a function of the reduction potential of the organic halides.

In S_N2 reactions a nucleophilic reagent forms a new bond to the carbon atom under attack, the old bond breaking. In the transition state the incoming group and the leaving group are both "half-bonded" to the carbon atom. Therefore it had been thought that "crowdedness" in the formation of the activated complex was the most important factor in determining the reaction rate.[8] Actually, in the classical bromide-exchange reaction of alkyl bromide in acetone, the reaction rate changes drastically, by a factor of about 100, when alkyl group of the organic halides is replaced from an ethyl to an isopropyl group.[9] However, recently, some of the theoretical and experimental studies suggested that the difference in the shape or size of the reactant molecules played no obvious part in determining the reaction rate. In some cases those effects can be incorporated into parameters such as proton affinity, ionization potential, or reduction potential of the reactants.[10] The reaction of DEF^- with RX observed in the present study is one of the examples of such cases.

In order to interpret the correlation between the k of the S_N2 reaction and the E_{red} of the reactants, the VB correlation diagram approach can be invoked. The S_N2 reaction is a transformation that involves a synchronous electron shift and a bond interchange as expressed below.

$$N^- + R\text{-}X \longrightarrow N\text{-}R + X^- \qquad (7)$$

In the VB correlation diagram model which was invented and developed by Shaik,[11] four anchor states, i.e. the ground state reactants ($N^-(R\text{-}X)$) and products ($(N\text{-}R)X^-$) and the corresponding valence-charge-transfer forms of the reactants ($N(R\text{-}X)^-$) and products ($(N\text{-}R)^-X$), are correlated with each other.

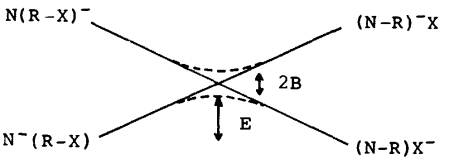

In between these four anchor states a barrier arises owing to avoided crossing of the intersecting curves. The height of the barrier (E) is a fraction (f) of the energy gap separating the anchor states $N(R\text{-}X)^-$ and $N^-(R\text{-}X)$, less the avoided crossing, B, i.e.

$$E = f(I_{N^-} - A_{RX}) - B \qquad (8)$$

I_{N^-} is the vertical ionization potential of the nucleophile, N^-, while A_{RX} is the vertical valence electron affinity of the substrate, RX, that can be related to E_{red}. If constancy of I_{N^-}, f and B for a reaction series is maintained, variation in the activation energy depends only on E_{red}.

Alternatively within a framework of rate-equilibrium relationship originally developed by Marcus,[12] the following elementary steps are assumed.

$$Y^- + RX \rightarrow \underset{\text{I}}{Y^- \; RX} \rightarrow \underset{\text{II}}{YR \; X^-} \rightarrow RY + X^- \qquad (9)$$

Brauman and his co-workers proposed a double minimum potential surface at the first (I) and the second (II) intermediates in Eq. 9.[13] As the reactants approach one another, long-range ion-induced dipole and ion-dipole interactions produce a drop in potential energy. There is then a potential energy increase up to the central transition state between the I and II states which becomes the intrinsic energy barrier of the S_N2 reaction. The difference in the E_{red} of Y and RX may be related to the free energy difference, ΔG, between the I and II states. The ΔG is related, in turn, to the intrinsic energy barrier of the S_N2 reaction by use of the Marcus equation.[10b] Thus, the rate of S_N2 becomes a function of E_{red}. It should be emphasized that the Marcus approach is a very general one and is not limited to electron-transfer reactions, as the parabolic free energy profile arises from summing displacement along many different coodinates.[14]

Another possible reaction mechanism is a dissociative electron-transfer reaction from anion radicals to organic halides. The Marcus quadratic equation for reversible electron-transfer reaction predicts the slope α of the acitivation energy vs. ΔG plot to be >0.5 for positive ΔG. In some systems where the electron-transfer is part of an overall irreversible transformation, such as chemical-bond formation or dissociation into two fragments, the experiments give values for α usually in the ranges 0.2 to 0.5.[15] Actually, α in the present study, which is deduced from the gradient of

the straight line in Fig. 4, is as small as 0.1. This value is not consistent with the prediction or the empirical low of the electron-transfer reaction. Besides, free energy differences of the electron-transfer from DEF^- or FI^- to RX evaluated from the E_{red} of the reactants are very endothermic. The electron-transfer reaction should, even if it occurred, be too slow to be observed by pulse radiolysis in ns or μs time-domains. However, the reaction with benzyl bromide can proceed via an electron-transfer mechanism, since the E_{red} of this halide is only slightly more negative than that of DEF. As it is known that C–C bond formation is accomplished by the reaction of DEF^- with benzyl bromide, so called $S_{RN}1$ mechanism in which the electron transfer occurs prior to C–C bond formation may be applicable.[2]

In the case of the reactions of Fl^-, it is obvious that there is no correlation between the k and the E_{red} of RX. Rather, k is determined by the steric and resonance effect of the R groups as is commonly seen in typical S_N2 reaction. The k is reduced by 2 orders of magnitude by the steric effect when R changes from ethyl to the bulky isopropyl or *t*-butyl groups. However k still remains large because of the resonance effect of R if R changes from ethyl to a bulky allyl or benzyl group. When a benzene ring of the Fl^- is replaced by methyl group, the reaction is accelerated as demonstrated by the rate constant for acetophenone anion radical shown in Table 1. Thus, an S_N2-type substitution reaction between Fl^- and RX is strongly indicated. This conclusion is in accord with the electrochemical study by Lund and Simonet which indicated that Fl^- reacted with RX to form R-adducts.[4] In these substitution reactions,the reaction site of the nucleophilic reagent is supposed to be a negatively charged oxygen atom. The difference between Fl^- and DEF^-, in the hindrance of S_N2 reactions by the presence of a bulky group, may be interpreted as due to the bond length in the transition state between the incoming group and the carbon atom under attacked being shorter as compared with the case of DEF^-, with Fl^- as the nucleophile. The shorter bond length may be caused by the difference in the reaction site, O or C atom, of the substitutions.

The authors would like to express their thanks to Messrs. Hiroaki Tanida and Kohichi Sato for operating the 45-MeV Electron Linear Accelerator of Hokkaido University.

References

1) a) J. F. Garst, *Acc. Chem. Res.*, **4**, 400 (1971); b) B. Bockrath and L. M. Dorfman, *J. Phys. Chem.*, **77**, 2618 (1973); c) S. Takamuku, H. Kigawa, S. Toki, K. Tsumori, and H. Sakurai, *Bull. Chem. Soc. Jpn.*, **54**, 3688 (1981).

2) R. A. Rossi, *Acc. Chem. Res.*, **15**, 164 (1982).

3) a) S. Satoh, T. Taguchi, M. Itoh, and M. Tokuda, *Bull. Chem. Soc. Jpn.*, **52**, 951 (1979); b) S. Satoh, H. Suginome, and M. Tokuda, *ibid.*, **54**, 3456 (1981).

4) H. Lund and J. Simonet, *Bull. Soc. Chim. Fr.*, 1843 (1973).

5) M. Ogasawara, N. Kajimoto, T. Izumida, K. Kotani, and H. Yoshida, *J. Phys. Chem.*, **89**, 1403 (1985).

6) T. Shida, S. Iwata, and M. Imamura, *J. Phys. Chem.*, **78**, 741 (1974).

7) M. Hoshino, S. Arai, and M. Imamura, *J. Phys. Chem.*, **78**, 1473 (1974).

8) E. S. Gould, "Mechanism and Structure in Organic Chemistry," Henry Holt and Co., New York, N. Y. (1959), p. 251.

9) P. B. D. de La Mare, L. Foeden, E. D. Hughes, C. K. Ingold, and J. D. Mackie, *J. Chem. Soc.*, 3200 (1955).

10) a) F. G. Bordwell and D. H. Hughes, *J. Org. Chem.*, **48**, 2206 (1983); b) C. C-. Han, J. A Dodd, and J. I. Brauman, *J. Phys. Chem.*, **90**, 471 (1986).

11) a) S. S. Shaik, *J. Am. Chem. Soc.*, **103**, 3692 (1981); b) S. S. Shaik, *J. Am. Chem. Soc.*, **105**, 4359 (1983); c) S. S. Shaik, *J. Am. Chem. Soc.*, **106**, 1227 (1984).

12) R. A. Marcus, *J. Chem. Phys.*, **24**, 966 (1947).

13) a) M. J. Pellerite and J. I. Brauman, *J. Am. Chem Soc.*, **102**, 5993 (1980); b) M. J. Pellerite and J. I. Brauman, *J. Am. Chem. Soc.*, **105**, 2672 (1983).

14) W. Albery and M. M. Kreevoy, *Adv. Phys. Org. Chem.*, **16**, 87 (1978).

15) F. Scandola, V. Balzani, and G. B. Schuster, *J. Am. Chem. Soc.*, **103**, 2519 (1981).

 © 1987 The Chemical Society of Japan Bull. Chem. Soc. Jpn., 60, 857—861 (1987)

Resonance Raman and ^{129}I Mössbauer Spectroscopic Study of Phenothiazine-Iodine Complexes

Hiroshi SAKAI,* Shu-ichi MURAISHI,† and Yutaka MAEDA
Research Reactor Institute, Kyoto University, Kumatori-cho, Sennan-gun, Osaka 590-04
†Analytical Instrument Division, JEOL, Ltd., Nakagami-cho, Akishima, Tokyo 196
(Received September 5, 1986)

Resonance Raman and ^{129}I Mössbauer spectroscopy have been applied to the phenothiazine-iodine (PT-I_n) complexes, which exhibit relatively low electrical resistivities. It is shown from the resonance Raman spectra that the two iodine species in the PT-I_3 and PT-$I_{2.6}$ complexes are present in essentially the same chemical form, consisting of a distorted I_3^- unit and an I_2 unit strongly coordinated to the I_3^- unit. The ^{129}I Mössbauer spectrum, consistent with the results of the Raman spectra, suggests that the PT-$I_{2.6}$ complex can be approximately formulated as $(PT)_5^{3+}[(I_3)_3(I_2)_2]^{3-}$, in which about three electrons per five PT molecules are transferred to the iodine and the transferred electrons are delocalized on the thirteen iodine atoms. The radical salt is recognized as a partially oxidized mixed-valence compound. The formation of the complex is quite similar to that of the perylene-I_3 complex, which has a low electrical resistivity.

The phenothiazine-iodine (PT-I_n) complex is known to be a typical radical salt, exhibiting a relatively low electrical resistivity.[1] The electrical properties, such as the electrical resistivity, the activation energy, the Seebeck coefficient, and the electromotive force, of the semiconducting complex have been examined in detail as a function of the composition n by Gutmann and Keyzer,[2] Doi et al.,[3] and Matsumoto and Matsunaga.[4] According to their works, anomalous behavior of the electrical properties is observed between n=2.5 and 3: Drastic decreases in the electrical resistivity and in the activation energy, a change in sign of the Seebeck coefficient, and a step-by-step increase in the electromotive force. The vibrational spectrum of the complex at n=3, which exhibits the minimum resistivity of 20 Ωcm at room temperature, indicates that the phenothiazine (PT) exists as a complex radical cation where two PT molecules share a unit positive charge and are equivalent in the time scale of infrared spectroscopy.[1,5] The results of the electrical properties and the vibrational spectrum suggest that the complex with a composition of n=3 is a nonstoichiometric compound, whereas that with the composition of n=2.5 is a stoichiometric one, probably formulated as $(PT)_2^+(I_5)^-$. The latter complex exhibits an electrical resistivity of about 800 Ωcm at room temperature. The crystal structure of the complex has not yet been established because of the difficulty of preparing a good single crystal. Recently, however, Uchida et al.[6,7] have revealed the crystal structures of several phenothiazine complexes with antimony (V) chloride, in which PT forms a segregated stacking column. Generally the structures of iodine complexes with low electrical resistivities consist of stacking columns of partially oxidized donor molecules and reduced iodine acceptor counterions.[8] One might expect the formation of a segregated stacking column of the PT in the present iodine complex because of its low electrical resistivity. However, there is no information on the chemical form and the charge density for the iodine atoms of the complex.

It is important to clarify the chemical form and the electronic structure of iodine in order to understand the electrical properties of the complex. Resonance Raman and ^{129}I Mössbauer spectroscopy are powerful methods for this purpose, and both have been successfully applied to iodine complexes with low electrical resistivities.[9–13] In this paper we wish to report on our resonance Raman and ^{129}I Mössbauer studies of the phenothiazine-iodine complex.

Experimental

Materials. Commercially available phenothiazine was recrystallized from benzene. The PT-I_3 complex was precipitated by mixing PT and I_2, separately dissolved in hot benzene, in a prescribed mole ratio. A complex with a composition of n=2.5 was prepared by the use of a large excess of PT. The iodine contents were determined by elemental analysis and iodometry: Found; C, 24.31; H, 1.55%. Calcd for PT-I_3: C, 24.85; H, 1.56%. Found; C, 26.88, H, 1.72%. Calcd for PT-$I_{2.5}$: C, 27.90; H, 1.76%. By iodometry: Found; I, 65.8%. Calcd for PT-I_3: I, 65.64%. Found; I, 63.9%. Calcd for PT-$I_{2.5}$: I, 61.42%. The elemental analysis and iodometry of the sample prepared by the use of an excess of PT indicated that the composition was approximately PT-$I_{2.6}$. The composition of a precipitate appears to depend on the mole ratio of each component and on the concentration used in the preparation. However, when an excess of PT is used for the preparation, a good crystalline precipitate is obtained with the iodine content of n=2.6. The radioactive ^{129}I-labeled complex used for the measurement of the Mössbauer spectrum was prepared from $Na^{129}I$ in an Na_2SO_3 solution. After the iodide had been oxidized with 3 mol dm^{-3} H_2SO_4 and 10% H_2O_2, the resulting molecular iodine was extracted with benzene. The iodine solution was thoroughly washed with water and passed through a Teflon filter to eliminate any slight amount of water. The hot solution was then added to the hot benzene solution with an excess of PT. The precipitate was identical to that obtained with the natural iodine (PT-$I_{2.6}$). The PT-$^{129}I_3$ complex could not be prepared because of

the uncertainty as to the iodine content in the benzene solution. The sample thickness for the Mössbauer measurement was about 20 mg ^{129}I cm^{-2}.

Measurements. The laser Raman spectra were measured with Ar^+ (514.5 nm) excitation by using a JEOL-JRS-400T triple monochromator. The data were obtained at room temperature with compressed pellets of the powdered complexes (PT-I_3 and PT-$I_{2.6}$) by the front-surface-reflection method, using 60 mW of laser power and a spinning cell. No decomposition was observed with this laser power.

The ^{129}I Mössbauer measurements were carried out in a transmission geometry by cooling the source and the absorber sample (PT-$I_{2.6}$) at 16 K with a closed-cycle helium refrigerator. The Mössbauer source, $^{66}Zn^{129}Te$ ($t_{1/2}$=70 min), was prepared by the neutron irradiation of 140 mg of a $^{66}Zn^{128}Te$ compound at a fluence rate of 2×10^{13} neutrons cm^{-2} s^{-1} for 1 h in the Kyoto University Reactor (KUR). The source activity produced by the $^{128}Te(n,\gamma)^{129}Te$ reaction was initially about 10 mCi. The constant-acceleration Mössbauer drive was calibrated with a six-line spectrum of an Fe foil.

Results and Discussion

Resonance Raman Spectra. In Fig. 1 are presented the resonance Raman spectra of the (a) PT-I_3 and (b) PT-$I_{2.6}$ complexes excited by the Ar^+ 514.5 nm line. Interestingly, the two spectra (107 s, 143 w, 167 m, cm^{-1}) are essentially identical, suggesting that the iodine species exist as an identical chemical form in both complexes. The strong scattering Raman band at 107 cm^{-1} is characteristic of the symmetric stretching vibration of a linear triiodide anion (I_3^-). The isolated and symmetrical I_3^- ions in methanol[14] and $(C_6H_5)_4As^+I_3^-$[9,11] show the strong Raman bands at 112 and 113 cm^{-1} respectively, whereas the corresponding bands are observed at 107—108 cm^{-1} for successive I_3^- chains in (benzamide)$_2H^+I_3^-$[9] and (*N*,*N*′-diphenyl-*p*-phenylenediamine)$(I_3^-)_{0.8}$[13] complexes. In I_3^- units in polyiodides containing I_3^- and I_2, the transition bands are observed in the 105 to 120 cm^{-1} region, depending upon the interaction of the I_3^- and I_2 units.[9,11] The latter distorted I_3^- units give rise to a second, weak Raman band near 145 cm^{-1}; this band has been assigned to the antisymmetric stretching vibration. Therefore, the strong and weak Raman bands at 107 and 143 cm^{-1} observed for the PT-I_n complexes suggest the presence of a distorted I_3^- unit in these complexes.

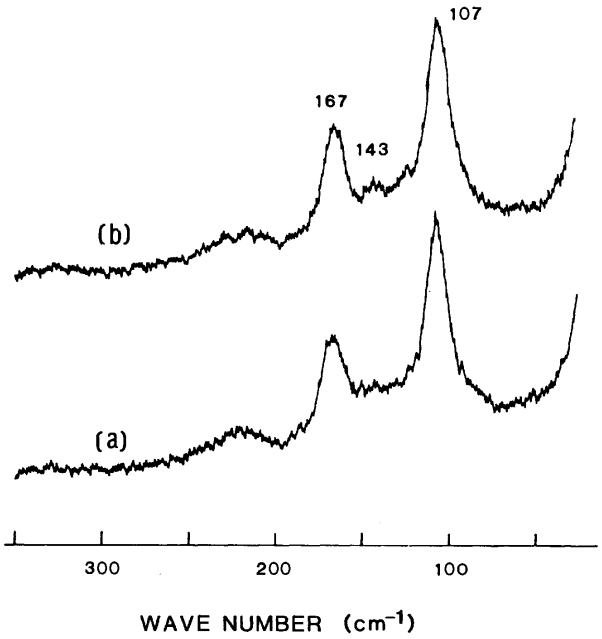

Fig. 1. Resonance Raman spectra excited by the Ar^+ 514.5 nm line of (a) PT-I_3 and (b) PT-$I_{2.6}$ complexes.

On the other hand, the Raman band observed at 167 cm^{-1} can be assigned to a linear pentaiodide anion (I_5^-) or to an I_2 unit coordinated to the I_3^- unit. The resonance Raman spectra of (trimesic acid $H_2O)_{10}H^+I_5^-$ and starch-iodine complexes, in which the iodine atoms exist as linear I_5^- ions, exhibit a strong scattering at 162—163 cm^{-1} and a weaker band at 104—109 cm^{-1}.[9,15] Raman bands for I_2 units in polyiodides are observed at 172—173 cm^{-1} for Cs_2I_8[11] and $(\alpha\text{-CD})_2LiI_5\cdot8H_2O$ (α-CD, α-cyclodextrin).[15] If the I_2 unit strongly coordinates to the I_3^- unit, close to the I_5^- ion, the I-I stretching band shifts to a lower frequency. The band at 167 cm^{-1} observed for the present complexes is just intermediate between those of the I_5^- ion and the I_2 unit coordinated to the I_3^- unit. It may, therefore, be concluded from the resonance Raman spectra that the iodine atoms in the phenothiazine-iodine complexes exist as a polyiodide consisting of a distorted I_3^- unit and an I_2 unit strongly coordinated to the I_3^- unit.

Site 2 1 3 Site 2′ 1′ 3′ 4 5

I—I···I I—I···I···I—I

1: distorted I_3^- unit **2**: I_2 unit coordinated to the I_3^- unit

Undoubtedly resonance Raman spectroscopy is a powerful method for the identification of the chemical form of the iodine species in the iodine complexes, but there is a limitation with respect to the quantification of the relative amounts of iodine species, because the relative intensities of the Raman bands are strongly dependent on the excitation wavelength. The ^{129}I Mössbauer spectroscopy can provide complementary information on the relative amounts of iodine species and the presence of an isolated I^- ion. Furthermore, the electronic structure of each iodine atom (Sites 1 to 5) can be directly derived from the Mössbauer spectrum.

Mössbauer Spectra. The ^{129}I Mössbauer spectrum of the PT-$I_{2.6}$ complex at 16 K is shown in Fig. 2. The spectrum consists of roughly three different quadrupole octets (A, B, and C), indicating the presence of three distinct iodine sites in the complex. In the

analysis of the spectrum, a broadening of the line-width is observed. The line-width of the ^{129}I Mössbauer spectra is usually found with our apparatus to be about 1.0 mm s^{-1}.[13] In particular, the quadrupole octets B and C show considerable line-broadening, enhanced in the higher Doppler-velocity region. This broadening is attributable to an overlap of the spectra originating from iodine atoms with slightly different charge densities. The spectrum clearly rules out the presence of the isolated I^- ion and the molecular iodine (I_2). The former ion, inactive and undetectable by Raman spectroscopy, would show a single absorption peak at -0.5 mm s^{-1} in the spectrum. The latter molecular iodine, which has not been observed in the Raman spectra, would indicate a slightly smaller quadrupole splitting ($e^2Qq=-2255\pm 30$ MHz, $\delta=0.94\times0.05$ mm s^{-1})[16] than that of the quadrupole octet A. The obtained Mössbauer parameters, such as the quadrupole coupling constant (e^2Qq), the asymmetry parameter (η), the isomer shift (δ), the line-width (2Γ), and the relative area, are summarized in Table 1.

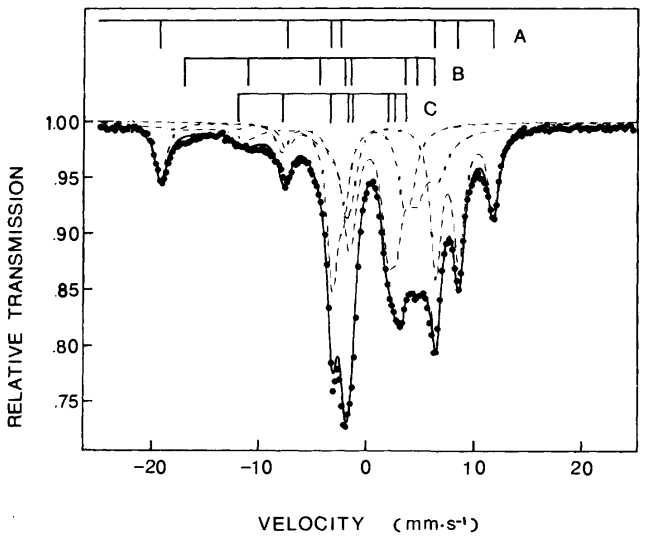

Fig. 2. ^{129}I Mössbauer spectrum at 16 K of the PT-$I_{2.6}$ complex.

The e^2Qq and δ values of the quadrupole octet A, larger than those for the free iodine molecule in inert matrices, indicate that the iodine atom (I_A) corresponding to the octet A has a slightly positive charge density. Such iodine atoms are observed in the central iodine of linear I_3^- ions[12,13] and the intermediate iodines of linear I_5^- ions.[9,15] In addition, when an I_2 unit is strongly coordinated to an I_3^- unit, as is to be expected from the Raman spectra, the iodine atom coordinated to the I_3^- unit has a positive charge density.[11,17] Therefore, it is reasonable to assign the iodine atom I_A to those of Sites 1, 1′, and 4 in the **1** and **2** iodine species. This is the reason for the broadening of the line-width in the sub-spectrum A. Because of the poor resolution of the Mössbauer spectrum of ^{129}I, any distinction among them may be difficult.

The e^2Qq values of the two terminal iodines of the distorted I_3^- ion in CsI_3 are, from the ^{127}I NQR[18] and ^{129}I Mössbauer measurements,[19] found to be about -1440 MHz and -820 MHz. These e^2Qq values are close to those for the quadrupole octets B and C. That is, the iodine atoms, I_B and I_C, corresponding to the B and C octets can be assigned to the iodines of Sites 2 and 3 respectively in the distorted I_3^- species **1**. Since the charge density localized on each iodine of the I_3^- unit is expected to be perturbed by the coordination of the I_2 unit, the e^2Qq and δ values for the iodines of Sites 2′ and 3′ in the **2** species are slightly different from those of Sites 2 and 3 in the **1** species. This difference causes the line-broadening of the quadrupole octets, B and C. The charge density on the iodine of Site 5 may be close to that of Site 2′, because the I_2 unit is strongly coordinated to the I_3^- unit. The spectrum of the iodine Site 5 is included in the broad sub-spectrum B.

The terminal iodine atoms of Sites 2 and 3 in **1** probably interact with the terminal iodines of the other iodine species, **2**. If the interaction is perpendicular to the molecular axis, a large η value must be observed for the iodine atom. The quite large η value observed for the quadrupole octet B suggests that the iodine atoms are, on the average, present in the complex as a polyiodide with the following structure (Fig. 3):

Table 1. Mössbauer Parameters for the Phenothiazine-Iodine (PT-$I_{2.6}$) Complex

		e^2Qq[a] / MHz	η / %	δ[b] / mm s^{-1}	2Γ / mm s^{-1}	Area[c] Ratio	U_p[d]	h_p[e]
PT-$I_{2.6}$	I_A	-2381 ± 25	0	1.34 ± 0.05	1.20 ± 0.10	1.4	1.04	1.25
	I_B	-1414 ± 25	29 ± 10	0.66 ± 0.05	$1.30+\alpha$[f]	1.0	0.62	0.80
	I_C	-918 ± 25	0	0.08 ± 0.05	$1.36+\beta$[f]	1.0	0.40	0.41

a) The e^2Qq values are converted to the ^{127}I nucleus. b) The δ values are relative to the ZnTe source. c) The ratios are normalized with respect to the I_C atom. d) $U_p=-e^2Qq_{obsd}/e^2Qq_{atom}$, $e^2Qq_{atom}=2292.7$ MHz. e) $\delta=1.5\,h_p-0.54$ (mm s^{-1}). f) The values are of the line-widths at zero Doppler velocity. The errors quoted in this work include estimated systematic errors.

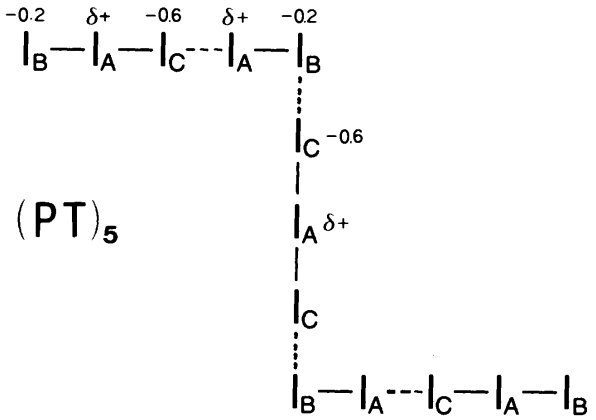

Fig. 3. The speculated structure of the iodine atoms in the PT-$I_{2.6}$ complex.

In Fig. 3 the intermolecular bond (···) between the I_C and I_A atoms implies the strong interaction previously described, whereas the bond (····) between the I_B and I_C atoms indicates a weak intermolecular interaction. The proposed structure with relative populations of 1.25:1.0:1.0 for I_A:I_B:I_C of the iodine species satisfies the relative absorption areas (1.4:1.0:1.0) of the sub-spectra corresponding to I_A, I_B, and I_C. The slight increase in the area of I_A can be explained in terms of the difference in the recoilless fraction. That is, the recoilless fraction of I_A can be expected to be larger than those of I_B and I_C, for the I_A atom is strongly bound to two neighboring atoms. This effect is also found in the other I_3^- ions, where the central atom indicates a stronger absorption intensity than each terminal atom.[12,13]

The charge density localized on each iodine atom is calculated from the values of e^2Qq, η, and δ as follows:[13]

$$U_p = -e^2Qq_{obsd}/e^2Qq_{atom} = -N_z + (N_x+N_y)/2,$$
$$\eta = 3(N_x-N_y)/2U_p,$$
$$\delta = 1.5\,h_p - 0.54 \text{ (mm s}^{-1}\text{, for the ZnTe source)},$$
$$h_p = 6 - (N_x+N_y+N_z),$$

where U_p is the number of unbalanced p-electrons; e^2Qq_{atom}, the atomic iodine quadrupole coupling constant, is equal to 2292.7 MHz for ^{127}I, and h_p is the number of 5p-electrons removed from the $5s^25p^6$ (I^-) configuration. N_x, N_y, and N_z are the populations of 5p-electrons in the x, y, and z directions respectively. When the bonding of iodine is formed by only $5p_\sigma$-electrons, one expects the relationship $U_p=h_p=1\pm i$ to be valid, where i is the ionic character. The U_p and h_p values obtained for each iodine atom are presented in Table 1.

It can be seen that the h_p value is larger than the U_p value for the I_A atom. This phenomenon, also found in the central iodine of linear I_3^- ions,[12,13] can be explained in terms of the contribution of $4d_\sigma$-electrons to the bond formation, in addition to the delocalized three-center four-electron bonding of 5p-electrons.[13] Consequently, the I_A atom has, on the average, a slight positive charge ($\delta+$), less than the $+0.04\,e^-$ obtained from the U_p value. The disagreement of h_p and U_p values for the I_B atom is attributable to the intermolecular interaction in the x or y direction. This result is supported by the large η value of the atom. The charge density localized on the I_B atom is, on the average, estimated from the h_p value to be $-0.2\,e^-$. For the I_C atom, the h_p value is close to the U_p value, suggesting that the bonding of the atom is mainly caused only by $5p_\sigma$-electrons. The charge density on the I_C atom is roughly estimated to be $-0.6\,e^-$ from the h_p and U_p values. The charge densities obtained from the Mössbauer parameters are indicated on the respective iodine atoms in Fig. 3. It should be noted that the charge densities are the averaged values because of the broadening of the line-widths in all sub-spectra.

It is concluded from the results of the resonance Raman and ^{129}I Mössbauer spectra that the present complex with a composition of n=2.6 can be approximately formulated as $(PT)_5^{3+}[(I_3)_3(I_2)_2]^{3-}$. That is, about three electrons per five PT molecules are transferred to a polyiodide, consisting of a distorted I_3^- unit and an I_2 unit strongly coordinated to the I_3^- unit. This complex is apparently not a stoichiometric compound formulated as $(PT)_2^+(I_5)^-$. From the similarity of the resonance Raman spectra, it might be reasonable to speculate that the PT-I_3 complex can be formulated as $(PT)_5^{3+}[(I_3)_3(I_2)_3]^{3-}$ in a manner similar to that used for PT-$I_{2.6}$. The difference in the electrical resistivities of the two complexes is probably the result of a structural factor, such as the stacking of the PT molecules and/or the packing of the polyiodides. These complexes are recognized as partially oxidized mixed-valence compounds. The formation of these complexes is quite similar to that of the perylene-$I_{2.92}$ complex, exhibiting a low electrical resistivity of about 10 Ωcm at 300 K.[11]

The authors wish to express their thanks to Professor Takenobu Higashimura of the Research Reactor Institute, Kyoto University, for his useful discussions and encouragement.

This work was supported by Grants-in-Aid for a special research project on the properties of molecular assemblies (No. 59212018, No. 60104002) from the Ministry of Education, Science and Culture.

References

1) Y. Matsunaga, *Helv. Phys. Acta*, **36**, 800 (1963).
2) F. Gutmann and H. Keyzer, *J. Chem. Phys.*, **46**, 1969

(1967).
3) S. Doi, T. Inabe, and Y. Matsunaga, *Bull. Chem. Soc. Jpn.*, **50**, 837 (1977).
4) T. Matsumoto and Y. Matsunaga, *Bull. Chem. Soc. Jpn.*, **54**, 648 (1981).
5) Y. Matsunaga and K. Shono, *Bull. Chem. Soc. Jpn.*, **43**, 2007 (1970).
6) T. Uchida, M. Ito, and K. Kozawa, *Bull. Chem. Soc. Jpn.*, **56**, 577 (1983).
7) T. Uchida, H. Seki, M. Ito, C. Nakano, T. Hoshizaki, and K. Kozawa, *Chem. Lett.*, **1986**, 999.
8) T. J. Marks and D. W. Kalina, "Extended Linear Chain Compounds," ed by J. S. Miller, Plenum Press, New York (1985), Vol. 1, Chap. 6.
9) M. Cowie, A. Gleizes, G. W. Grynkewich, D. W. Kalina, M. S. McClure, R. P. Scaringe, R. C. Teitelbaum, S. L. Ruby, J. A. Ibers, C. R. Kannewurf, and T. J. Marks, *J. Am. Chem. Soc.*, **101**, 2921 (1979).
10) L. D. Brown, D. W. Kalina, M. S. McClure, S. Schultz, S. L. Ruby, J. A. Ibers, C. R. Kannewurf, and T. J. Marks, *J. Am. Chem. Soc.*, **101**, 2937 (1979).
11) R. C. Teitelbaum, S. L. Ruby, and T. J. Marks, *J. Am. Chem. Soc.*, **101**, 7568 (1979).
12) C. J. Schramm, R. P. Scaringe, D. R. Stojakovic, B. M. Hoffman, J. A. Ibers, and T. J. Marks, *J. Am. Chem. Soc.*, **102**, 6702 (1980).
13) H. Sakai and Y. Maeda, *Bull. Chem. Soc. Jpn.*, **59**. 1311 (1986).
14) K. Kaya, N. Mikami, Y. Udagawa, and M. Ito, *Chem. Phys. Lett.*, **16**, 151 (1972).
15) R. C. Teitelbaum, S. L. Ruby, and T. J. Marks, *J. Am. Chem. Soc.*, **102**, 3322 (1980).
16) S. Bukshpan, C. Goldstein, and T. Sonnino, *J. Chem. Phys.*, **49**, 5477 (1968).
17) H. Sakai, M. Mizota, Y. Maeda, T. Yamamoto, and A. Yamamoto, *Bull. Chem. Soc. Jpn.*, **58**, 926 (1985).
18) A. Sasane, D. Nakamura, and M. Kubo, *J. Phys. Chem.*, **71**, 3249 (1967).
19) B. S. Erhlich and M. Kaplan, *J. Chem. Phys.*, **51**, 603 (1969).

 © 1987 The Chemical Society of Japan Bull. Chem. Soc. Jpn., 60, 863—870 (1987)

The Role of CO_{ad} in the Oxidation of Methanol at a Platinum Electrode in an Acid Solution

Hiroshi MATSUI* and Takeo HISANO†
Department of Applied Chemistry, Faculty of Engineering, The University of Tokushima, Minami-josanjima-cho, Tokushima 770
†Shikoku Women's University, Ojin-cho, Tokushima 771-11
(Received September 5, 1986)

The role of the adsorbate CO_{ad} in the oxidation of methanol was studied under a variety of experimental conditions on the basis of the rate-ratio of the path of CO_2 formation via CO_{ad} to the overall oxidation of methanol at a platinum electrode in 0.5 mol dm^{-3} of H_2SO_4. The results: (a) At potentials below 0.55 V and with a short time of oxidation, CO_{ad} inhibited its own formation; (b) at 0.60—0.75 V and with a long time of oxidation, CO_{ad} was a poison to parallel reactions; (c) at above 0.8 V and at $\theta_1 > 0.15$, the formation of CO_2 via CO_{ad} was predominant, and the CO_{ad} never hindered parallel reactions. There was no difference between the role of the CO_{ad} formed from dissolved CO and that of the CO_{ad} formed from methanol, though, in the absence of dissolved CO, the oxidation of methanol was, for some reason, inhibited at small coverages close to the respective limiting values. When the coverage was larger than about 0.85, CO_{ad} remarkably inhibited all the parallel reactions in the methanol oxidation.

This paper will describe the role of the adsorbate CO_{ad} formed from methanol on a platinum electrode during the anodic oxidation of methanol in 0.5 mol dm^{-3} of H_2SO_4.

Chemical analysis[1] has shown that CO_2 is the final product of the oxidation and that, at high concentrations of methanol, formaldehyde and formic acid are also formed as intermediate products which are soluble in solution and which can be further oxidized to CO_2, depending on circumstances. Several parallel paths producing CO_2 have so far been proposed.[1-3] However, only the following two seem to be based more or less upon experimental facts; the others appear to be rather speculative for the time being: (1) The path via a stably chemisorbed substance (SCS), and (2) the path via formaldehyde and formic acid. The formation of SCS and its oxidation to CO_2 were confirmed by Breiter[4] and Petrii et al[2]. The existence of the latter path was experimentally verified[1] only when the oxidation of methanol was prolonged and the concentration of methanol was high. Any adsorbate in this path is considered[5,6] to be so small in surface concentration that can not yet be experimentally identified. Breiter[7] and Petrii et al.[2] determined the rate-ratio of the production of CO_2 by the path via SCS to the overall oxidation of methanol. From these data, they[2,6] concluded that the SCS 'had the effect of a poison on' (Breiter), or 'passivated' (Petrii), the production of CO_2 by covering the surface of the electrode.

Regardless of a number of such papers,[2,6-9] the present work will also attempt to reexamine the same problem, the role of SCS (CO_{ad}), by a rather similar method. Our main reasons are as follows: (a) Contrary to most previous workers, we consider the SCS to be CO_{ad}.[10,11] Petrii[2] regarded it as COH_{ad}, and Breiter[4], as a mixture of COH_{ad} and $COOH_{ad}$. In their estimation of the rate-ratios stated above, the number of electrons participating in the oxidation of SCS to CO_2 was decisively important. For the oxidation of CO_{ad}, that number is, of course, different. (b) Although many workers[2,6,8-9] have supported the idea that a SCS can be a poison, no detailed study has been published on the oxidation conditions under which a particular SCS passivates a particular parallel reaction. (c) As is well-known,[11-13] the presence of trace amounts of impurities such as a chloride anion in a solution reduces the overall rate of methanol oxidation, while the accumulation of reaction products such as formaldehyde in a solution enhances that rate, because these products are more easily oxidized than methanol. These influences are more or less unavoidable in the case of a prolonged electrolysis of methanol, a method which was adopted in most of the previous works in order to bring a process to the stationary state or to collect a gas sample of the products for analysis. (d) It is also known[14] that the degree of coverage with SCS affects the overall rate of methanol oxidation. On the other hand, previous works[2,7] on the contribution of the path via SCS to the overall oxidation seldom dealt with cases of a low coverage.

In short, the experimental conditions of most previous works seem inadequate or insufficient to clarify the role of SCS. A platinum electrode with a large roughness factor is affected only a little by the presence of impurities, but much by the accumulation of the soluble intermediate products. The reverse is true for an electrode with a small roughness factor. Consequently, we used a platinized platinum electrode with a moderate roughness factor of about 17. In order to minimize the harmful influence of impurities, the time of methanol oxidation was limited to within 400 s, during which period the coverage with impurities never exceeded a few per cent. Consequently, it follows that the present work deals

with the process in which the oxidation of methanol changes from a non-stationary state to an approximately stationary state.

We also assumed that, as have the previous workers,[2,7] that the rates for the path via SCS, which were too hard to measure directly, were equal to the rates of the oxidation of CO_{ad} in the supporting electrolyte containing no methanol. Instead of using these rate values directly, however, we first generalized them in the form of a rate equation. Then, the rates for that path at any set of initial coverages and potentials could be calculated by using the equation.

These improved circumstances led to the following conclusions. At potentials below ca. 0.55 V, the CO_{ad} species were formed rapidly and oxidized slowly. They inhibited mainly their own formation. At 0.6—0.75 V, reactions parallel to the reaction via CO_{ad} became predominant; the CO_{ad} hindered mainly these parallel reactions. At potentials and coverages higher than 0.8 V and 0.15 respectively, the oxidation of CO_{ad} was fast, and no hindrance of any reaction by CO_{ad} was any longer seen.

The adsorbate CO_{ad} is formed also from dissolved carbon monoxide,[2,15] which is well-known[15-18] to be a poison to the oxidation of hydrogen. At first sight, therefore, it is strange that CO_{ad} is not always a poison to the oxidation of methanol, which involves the oxidation of the hydrogen atoms of a methanol molecule. Accordingly, the role of CO_{ad} in the methanol oxidation in the presence of dissolved carbon monoxide was also studied. There was no difference between the role of CO_{ad} formed from dissolved CO and that of the CO_{ad} formed from methanol, though, in the absence of dissolved CO, the oxidation of methanol was, for some reason, inhibited at small coverages that were close to the respective limiting values.

Experimental

The procedures for measuring the overall rate of the methanol oxidation and the coverage with CO_{ad} were almost the same as those described in the previous papers.[11,14]

The formation of CO_{ad} from dissolved CO in a test solution of methanol was very fast.[2,15] Consequently, the duration of Step D for the last cleaning of the electrode in the potential sequence (illustrated in Fig. 1 in Ref. 11) was extremely shortened (to 10 ms) in order to suppress the formation of CO_{ad} at that step to approximately nothing. Otherwise, the electrode surface was almost fully covered with CO_{ad}; i.e., the observation of the methanol oxidation at low coverages became impossible. A trace amount of O_2 present in the commercial CO gas was removed with the aid of an alkaline pyrogallol solution.

The coverages with CO_{ad}, θ_1 and θ_2, were expressed, respectively as:

$$\theta_1 = Q^{ox}/Q^{ox}_{max} \quad (1)$$

$$\theta_2 = (Q^{\circ}_H - Q_H)/Q^{\circ}_H \quad (2)$$

where Q^{ox} was the electric quantity required to oxidize an amount of CO_{ad} to CO_2 and where Q^{ox}_{max} was the maximum Q^{ox}. Q^0_H was the quantity required to cover the electrode surface fully with a monolayer of adsorbed hydrogen atoms in the absence of CO_{ad}, and Q_H was that required to do so in the presence of CO_{ad}.

Proper Use of θ_1 and θ_2. On a particular electrode, the Q^{ox}_{max} for the CO_{ad} formed from methanol differs in value from that for the CO_{ad} formed from dissolved carbon monoxide. The former is always smaller; the cause[14] of this lies in the process of the formation of the CO_{ad} from methanol. A considerable number of single sites remain unoccupied, even at the saturated coverage in the methanol system; these sites can be further occupied by hydrogen atoms or the CO_{ad} molecules from dissolved carbon monoxide. When the original substances are the same as each other, θ_1, unlike θ_2, is proportional to the number of moles of CO_{ad}; hence, the use of θ_1 is reasonable in the case of, e.g., determining the amount of CO_{ad}. However, the use of θ_2 is more reasonable when the roles of the two kinds of CO_{ad}, originating from methanol and carbon monoxide, are compared.

Washing-Electrode Method. The rate of the oxidation of CO_{ad} in a supporting electrolyte solution, 0.5 mol dm^{-3} of H_2SO_4, was measured by means of the washing-electrode method.[2] The apparatus and the pretreatment of the electrode were almost the same as those reported previously.[19] A platinized-platinum electrode with a true surface area of 3.8 m^2 was used. After CO_{ad} had been formed from a methanol solution, the electrode was washed several times with an electrolyte solution containing no methanol, while the potential was kept at about 0.1—0.06 V in order to prevent the oxidation of CO_{ad}. It was confirmed that the height and shape of the oxidation wave of the CO_{ad} were scarcely altered by the washing. After the washing, the adsorbate was potentiodynamically oxidized in the electrolyte solution containing no methanol at a scan rate of

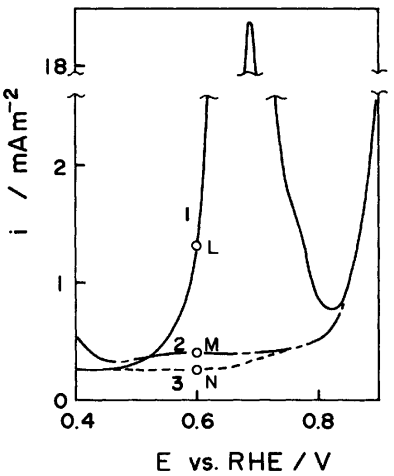

Fig. 1. Potentiodynamic current-potential curve for oxidation of CO_{ad} in 0.5 mol dm^{-3} H_2SO_4, Scan rate= 0.86 mV s^{-1}, CO_{ad} was formed by 10 min-oxidation at 0.6 V in 0.01 mol dm^{-3} CH_3OH+0.5 mol dm^{-3} H_2SO_4:
(1) i''_c at $\theta_1^{t=0} \fallingdotseq 1$; (2) i_{d1} at $\theta_1^{t=0}=0$; (3) i_{d1} calculated.

0.8—4 mV s^{-1}. Neither higher rates nor lower ones were adequate, because both resulted in unreliable data. Figure 1 shows an example of these current -potential curves.

The potentials were quoted with respect to the reversible hydrogen electrode in 0.5 mol dm^{-3} of H_2SO_4. All the measurements were made at 0 °C.

Derivation of Equations

Several reaction paths composing the oxidation of methanol will frequently be referred to hereafter. To avoid misunderstandings caused by the descriptions, the reactions and rates will often be expressed by the symbols shows in Table 1.

Rate of Reaction C′ (i'_C). The net rate of Reaction C′ in the supporting electrolyte containing no methanol, i'_C, was determined by subtracting the double-layer-charging current density, i_{dl}, from the directly measured current density, i''_C:

$$i'_C = i''_C - i_{dl}. \tag{3}$$

According to Frumkin,[16]

$$i_{dl} = i^0_{dl}(1-\theta_1) + i^1_{dl}\theta_1, \tag{4}$$

where i^0_{dl} and i^1_{dl} are i_{dl} values at $\theta_1=0$ and $\theta_1=1$ respectively. To determine the i_{dl} values according to Eq. 4, θ_1 values were needed. These values of i_{dl} and θ_1 were determined by the ordinary trial-and-error method of calculation. An example of the calculation will be shown at the end of this section. In the first calculation, the initial value of i_{dl} at a particular potential was assumed to be i^0_{dl}, i.e., the current density indicated by Curve 2 in Fig. 1, while the Q^{ox} value at the potential was determined by the graphical integration of the following equation:

$$Q^{ox} = v^{-1}\int_E^{0.9}(i''_C - i^0_{dl})dE, \tag{5}$$

where v was the scan rate and where 0.9 was the potential at which the adsorbate was completely removed by oxidation. This Q^{ox} value and Eq. 1 gave a first approximate value of θ_1. When this θ_1 value was substituted in Eq. 4, the second approximate value of i_{dl} at the potential E was obtained. The determination of the i_{dl} values in this way at intervals of 0.025 V gave a plot of i_{dl} against E (Curve 3 in Fig. 1). The higher-order calculations were no longer necessary, because they brought about only a negligibly small change in the i_{dl} value. Thus, the variation in i'_C with the potential and the coverage was determined.

Rates of Reaction A and B. When the oxidation of CO_{ad} is slower than the formation, CO_{ad} is accumulated on the electrode surface; i.e., the coverage with CO_{ad} increases. Taking into account the mass balance for CO_{ad}, the rate of methanol consumption can be approximately represented as i_A+i_B, where i_A is the net rate of CO_{ad} formation when no further oxiation of CO_{ad} is assumed and where i_B is the net rate of Reaction B, which is assumed not to contribute at all to the accumulation of CO_{ad} (Table 1). In other words, the CO_{ad} formed by Reaction B is immediately oxidized to CO_2. In the same way, the whole number of moles of CO_{ad} formed at any given moment can be represented as the sum of the number of moles of CO_{ad} contributing to the increase in the coverage (N_A) and that contributing to the formation of CO_2 (N_B).

The formation of CO_{ad} is written as:

$$CH_3OH = CO_{ad} + 4H^+ + 4e \tag{6}$$

therefore, its net rate i_A is:

$$i_A = 4F\mathrm{d}N_A/\mathrm{d}t. \tag{7}$$

The oxidation of CO_{ad} is expressed as:

$$CO_{ad} + H_2O = CO_2 + 2H^+ + 2e \tag{8}$$

By use of the pulse anodic stripping method, N_A at any instant during the formation of CO_{ad} can be determined. Therefore,

$$N_A = Q^{ox}/2F = (Q^{ox}_{max}/2F)\theta_1. \tag{9}$$

Hence, the time dependence of N_A is:

$$\mathrm{d}N_A/\mathrm{d}t = (Q^{ox}_{max}/2F)\mathrm{d}\theta_1/\mathrm{d}t. \tag{10}$$

From Eqs. 7 and 10, we obtain:

$$i_A = 2Q^{ox}_{max}(\mathrm{d}\theta_1/\mathrm{d}t). \tag{11}$$

Thus, i_A can be determined by using the experimental values of Q^{ox}_{max} and $\mathrm{d}\theta_1/\mathrm{d}t$.

Table 1. Symbols of Reactions and Rate

Symbol of Reaction	Rate	Path	Remark
A	i_A	CH_3OH-CO_{ad}	The CO_{ad} is never oxidized
B	i_B	CH_3OH-CO_{ad}-CO_2	The CO_{ad} never accumulates
C′	$i_{C'}$	CO_{ad}-CO_2	The rate in the absence of methanol
C	i_C	CO_{ad}-CO_2	The rate in the presence of methanol
D	i_D	CH_3OH-HCHO-HCOOH-CO_2	The path suggested by Breiter[7]
	i_T		The overall rate of methanol oxidation

From Eqs. 6 and 8, i_B and i_C are deduced as:

$$i_B = 6F\mathrm{d}N_B/\mathrm{d}t, \quad (12)$$

$$i_c = 2F\mathrm{d}N_c/\mathrm{d}t. \quad (13)$$

From Eqs. 12 and 13, we obtain:

$$i_B = 3i_c, \quad (14)$$

where i_C is the rate of oxidation of CO_{ad} 'in the presence of methanol'. The trouble is that neither N_B nor i_C can be directly measured, because the formation and the oxidation of CO_{ad} occur concurrently in the presence of methanol. Out of necessity, therefore, we assumed, following Petrii et al.[2,7] that i_C is equal to i'_C, the net rate of the oxidation of CO_{ad} in the supporting electrolyte containing no methanol.

Reaction C. As may be seen in Fig. 2, the plot of log (i'_C/θ_1) against E under the same experimental conditions as those in Fig. 1 was a straight line with a slope of 0.073 V/decade over the potential range of about 0.50—0.73 V, i'_C/θ_1 corresponding to the rate of the oxidation of one CO_{ad} molecule. The line was expressed as:

$$E = 0.073 \log (i'_C/\theta_1) + 0.794. \quad (15)$$

The potential range over which Eq. 15 held depended both on the coverage at the beginning of the oxidation, $\theta_1^{t=0}$, and on the scan rate of the potential. However, the equation was valid irrespective of the values of $\theta_1^{t=0}$, provided that the momentary coverage, θ_1, during the oxidation was larger than about 0.15 and that the rate was 0.8—4 mV s^{-1}.

The rearrangement of Eq. 15 gave:

$$i'_C = \theta_1 \exp (31.4E - 24.9) \quad (\theta_1 > \text{ca. } 0.15). \quad (16)$$

The coverage range will soon be discussed. This experimental equation was substantially the same as the equation[20] proposed for an electron-transfer process without reactant transport; i.e., the reactants are preadsorbed species alone.

When θ_1 was smaller than about 0.15, the values of log (i'_C/θ_1) deviated in the direction of the decrease from the straight line (Fig. 3). As is shown in Fig. 4, an approximately linear relationship was found between θ_1 and the magnitude of the deviation, D, which was expressed as:

$$D = \log (i'_C/\theta_1) - (31.4E - 24.9)/2.30. \quad (17)$$

Thus, the linear relationship of Fig. 4 was formulated as:

$$D = 6.95\theta_1 - 0.994 \quad (18)$$

The combination of Eq. 17 with Eq. 18 gave Eq. 19:

$$i'_C = \theta_1 \exp (16\theta_1) \exp (31.4E - 27.2) \quad (\theta_1 < 0.15). \quad (19)$$

Equation 16 or 19 can be used for the estimation of i_C $(=i'_C)$ when the values of E and θ_1 are given.

Example of the Determination of i'_C, i_A, and i_B. (a) i'_C at 0.6 V (see Fig. 1): The value of i''_C at 0.6 V is

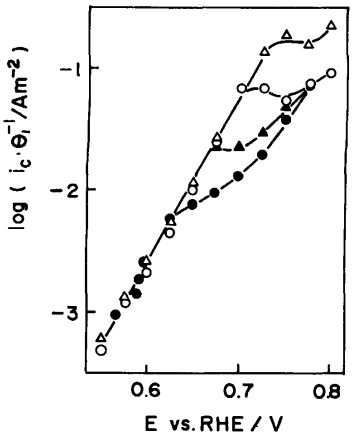

Fig. 3. Relationship between i'_c/θ_1 and potential at different scan rates (mV s^{-1}) and $\theta_1^{t=0}$: △ 2.3, 0.94; ○ 0.86, 1; ▲ 0.86, 0.22; ● galvanostatic oxidation at 0.94 mA m^{-2}, $\theta_1^{t=0}=0.97$.

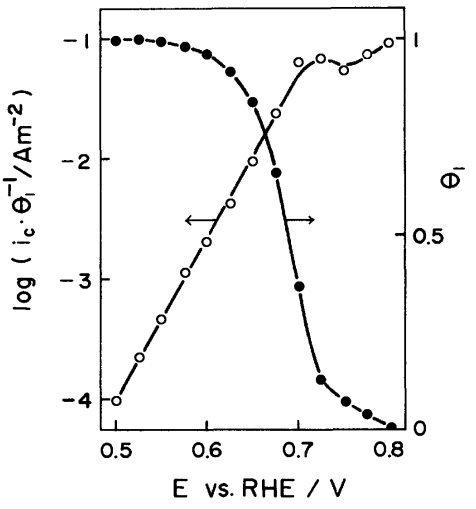

Fig. 2. Relaionship among i'_c/θ_1, potential, and θ_1 (reconstructed curves from Fig. 1.).

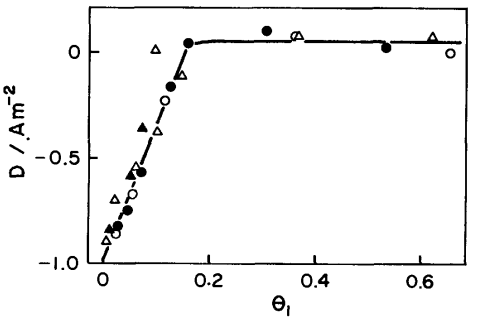

Fig. 4. Relationship between θ_1 and magnitude of deviation, D, from linear line in Fig. 3, $D=\log (i'_c/\theta_1)-13.6E+10.8$, symbols have the same meaning as in Fig. 3.

indicated by Point L, i.e., i''_C=1.35 mA m^{-2}. To determine i'_C, the value of i_{dl} at 0.6 V is necessary (Eq. 3): the i_{dl} can be calculated by the trial-and-error method according to Eq. 4, which requires the values of i^0_{dl}, i^1_{dl}, and θ_1. The i^0_{dl} value at 0.6 V is 0.40 mA m^{-2}, as is indicated by Point M. The θ_1 value at 0.6 V can be obtained if Q^{ox} and Q^{ox}_{max} are given. The graphical determination of the area bounded by Curves 1 and 2 gives the first approximate value of Q^{ox} at 0.6 V, i.e., Q^{ox}=7.65 C. Here, Curve 2, representing i^0_{dl}, is assumed to be the curve of the first approximate values of i_{dl}. The value of Q^{ox}_{max} is measured by an additional experiment at θ_1=1, i.e., Q^{ox}_{max}=7.74 C. Consequently, the substitution of these coverage values into Eq. 1 gives the first approximate value of θ_1 (7.65/7.74=0.988). The value of i^1_{dl} is also found to be 0.23 mA m^{-2} by an additional measurement at θ_1=1 and at 0.4 V. Therefore, by the substitution of the values of θ_1, i^0_{dl}, and i^1_{dl} into Eq. 4 {0.40 (1−0.988)+0.23×0.988=0.23 mA m^{-2}}, the second approximate value of i_{dl} is obtained. The i_{dl} value is represented by Point N on Curve 3. Consequently, the subtraction of the i_{dl} value from the observed i''_C value gives the i'_C value of 1.12 mA m^{-2}. (b) i_A and i_B at 0.55 V, 1 mol dm^{-3} methanol, and 11 s (see Fig. 5): From the curve of θ_1 vs. the time, the $d\theta_1/dt$ value, 0.0076 s^{-1}, at 11 s is obtained. The substitution of this value and Q^{ox}_{max}=2.05 C m^{-2} into Eq. 11 gives the i_A value of 0.031 A m^{-2}. This value is represented by Point F in Fig. 5. At 11 s, the θ_1 value is 0.91, as is indicated by Point G. Consequently, the i'_C value of 0.0020 mA m^{-2} is obtained from Eq. 16, and the i_B value of 0.0059 A m^{-2}, from Eq. 14. The latter is represented by Point H.

Results and Discussion

Effects of Methanol and Its Oxidation Products on i_C. Petrii et al.[2,7] implicitely assumed that the oxidation rate of SCS (COH_{ad}) was not affected by the presence of methanol and its oxidation products, such as hydrogen ions. We consider this assumption to be reasonable, though we differ from them with regard to the kind of SCS. Among the probable products of the oxidation of methanol, the substances not participating in the reaction (Eq. 8) would not affect the rate of the oxidation of CO_{ad} directly. Although some unidentified SCS are formed from formaldehyde and formic acid at low potentials, we found that only very small amount of such SCS was formed at potentials above about 0.5 V in a mixed solution of methanol and formaldehyde or formic acid. The formation of no other influential adsorbate from these two products has ever been reported. According to our test, CO_2 has no effect on the rate so long as the potential is higher than 0.3 V.

Among the products, only the hydrogen ion directly participates in the oxidation of CO_{ad}. However, the effect of the 'increase' in the hydrogen-ion concentration during the oxidation of methanol would be relatively small for the following reasons: (1) The solution originally contains sulfuric acid as the supporting electrolyte at a high concentration of 0.5 mol dm^{-3}. (2) The duration of oxidation is 400 s at the most; hence, the amount of hydrogen ions accumulated on the electrode surface is not very large. (3) The limiting rate of methanol oxidation is relatively small compared with the limiting diffusion rate of methanol; hence, the formation rate for hydrogen ion is relatively small. The amount of hydrogen ions accumulated on a very roughened surface of electrode is larger than that on a smooth surface. However, the roughness factor of the electrode used in the present work is not so large, i.e., 17. Considering this roughness together with the reasons above described, it might safely be said that the effect of hydrogen-ion formation on the rate of CO_{ad} oxidation is relatively small.

Contribution of Reactions A and B to the Overall Oxiation of Methanol. The symbol i_T represents the overall rate of the oxidation of methanol and a quantity directly measured.

As may be seen in Fig. 5, i_B attained a stationary value a short time after the beginning of the oxidation under the conditions described in the figure caption.

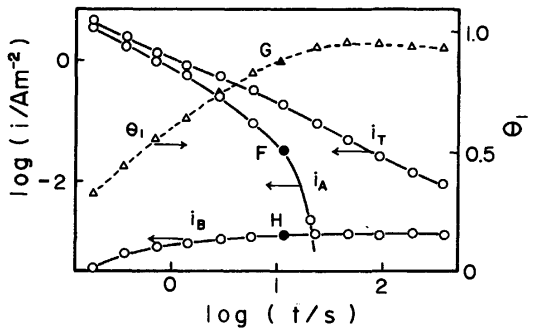

Fig. 5. Variation in i_A, i_R, i_T, and θ_1 with time, 1 mol dm^{-3} CH_3OH+0.5 mol dm^{-3} H_2SO_4, 0.55 V.

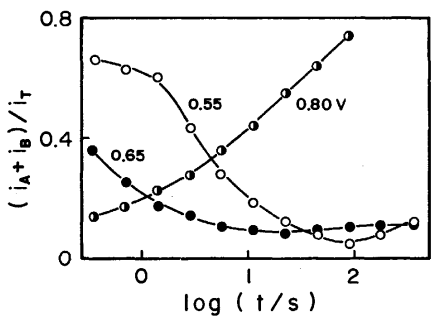

Fig. 6. Variation in $(i_A+i_B)/i_T$ with time, 1 mol dm^{-3} CH_3OH+0.5 mol dm^{-3} H_2SO_4.

On the contrary, i_A and i_T were decreased towards zero and i_B respectively. The $(i_A+i_B)/i_T$ ratio depended upon the potential, the time of oxidation, and the concentration of methanol, as may be seen in Figs. 6 and 7. The essential points about the ratio were as follows:

(1) When the potential was lower than 0.55 V and the time of oxidation was short, e.g., within 2 s, $(i_A+i_B)/i_T>0.5$ (Fig. 6) and $i_A \gg i_B$ (Fig. 5). That is, the formation of CO_{ad} was predominant over Reaction B. Moreover, i_A and i_T decreased with an increase in θ_1. This indicates that molecules of the CO_{ad} hinder their own formation, and hence i_T decreases. As the oxidation time went by, i_A decreased remarkably (Fig. 5) and $(i_A+i_B)/i_T$ became smaller than 0.5 (Fig. 6). Taking into consideration the fact that the yield of CO_2 at low concentrations of methanol was about 100 per cent,[1,21] together with the low value of the i_B/i_T ratio, we must decidedly support the idea of Breiter et al.[2,6] that a parallel reaction D exists, producing CO_2 without going through SCS. It would also exist at high concentrations and high potentials.

(2) When the potential was about 0.6—0.75 V, $(i_A+i_B)/i_T \ll 0.5$ except for the earliest oxidation stage of a few seconds (Figs. 6 and 7). At these potentials, the electrode surface was a quite thoroughly covered with CO_{ad}. Therefore, reactions other than A and B must take place on the surface free from CO_{ad}. Its rate can be expressed by $(i_T-i_A-i_B)/(1-\theta_1)$, i.e., the current density per unit free surface area. This rate did not decrease with an increase in θ_1, as may be seen in Fig. 8, while, on the contrary, $(i_T-i_A-i_B)$ and i_T did decrease. These findings indicate that at least one of the causes of the decreases in the latter two quantities is the occupation of reaction sites by CO_{ad}. θ_1 is generally large at high concentrations of methanol, as is well known,[22] when the other conditions are maintained constant. Consequently, the inhibition by CO_{ad} of parallel reactions such as Reaction D would become remarkable at high concentrations of methanol.

(3) At potentials higher than about 0.8 V and at high concentrations of methanol, i_B increased as the time of oxidation went by (Fig. 9), and $(i_A+i_B)/i_T$ increased beyond 0.5 (Fig. 6). In this case, CO_{ad} was not longer the inhibitor; rather the adsorbate was an intermediate in Reaction B, which was contributing predominantly to the overall oxidation of methanol. Breiter[7] and Pletcher et al.[23] also observed that CO_{ad} was no longer a poison under similar conditions. At low concentrations, however, i_B/i_T $\{\fallingdotseq(i_A+i_B)/i_T\}$ is small even at higher potentials, as is shown in Fig. 10.

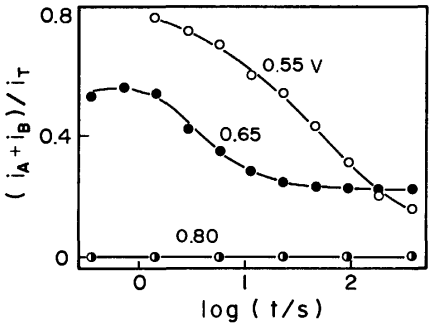

Fig. 7. Variation in $(i_A+i_B)/i_T$ with time, 0.03 mol dm^{-3} CH_3OH+0.5 mol dm^{-3} H_2SO_4.

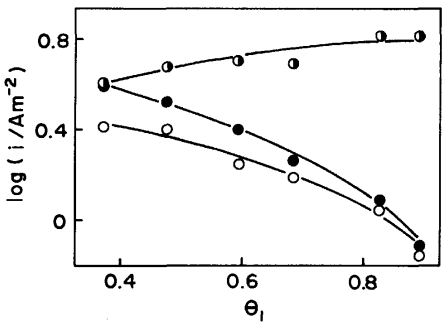

Fig. 8. Variation in i_T[●], $i_T-i_A-i_S$[○], and $(i_T-i_A-i_B)/(1-\theta_1)$[◑] with time, 1 mol dm^{-3} CH_3OH+0.5 mol dm^{-3} H_2SO_4, 0.65 V.

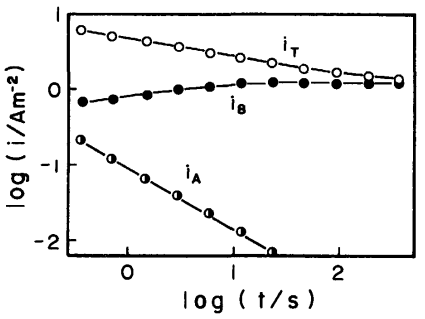

Fig. 9. Variation in i_A, i_B, and i_T with time, 1 mol dm^{-3} CH_3OH+0.5 mol dm^{-3} H_2SO_4, 0.80 V.

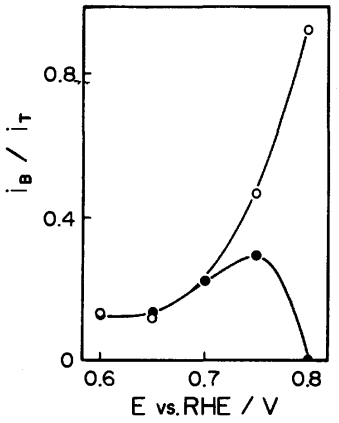

Fig. 10. Variation in i_B/i_T with potential, CH_3OH+0.5 mol dm^{-3} H_2SO_4, concentration of methanol (mol dm^{-3}): ○ 1; ● 0.1, oxidation time=360 s.

In this case, θ_1 was small; therefore, the inhibitory action of CO_{ad} seemed negligibly small. At present it is hard to explain why i_B/i_T decreases towards zero or increases remarkably with an increase in the potential, depending upon the low or high concentrations of methanol respectively.

Oxidation of Methanol in the Presence of Dissolved CO. The adsorbate CO_{ad} is also formed on a Pt electrode from the dissolved CO in a solution. Figure 11 showed potentiodynamic i–E curves taken in the respective solutions of methanol, carbon monoxide, and their mixture. When a solution of methanol was saturated with pure CO, the oxidation of methanol was almost completely inhibited at potentials below about 0.9 V, at which CO began to be oxidized. In this case, the coverage θ_2 with CO_{ad} immediately attained the value of 1 (Fig. 12). The use of a CO gas diluted with N_2 resulted in a slower adsorption of CO, as is indicated by Curve 2 in Fig. 13; that was what made the measurement possible at low coverages in the presence of dissolved CO.

As is indicated by Curve 1 in Fig. 13, the coverage with the CO_{ad} formed from methanol has a limiting value, θ_2^L. It is known[2,22] that this value is less than or equal to about 0.8 at its maximum, depending upon the potential and concentration of methanol. Curve 1 (taken at 0.75 V) in Fig. 14 has about 0.3 as such a limit, while Curve 3 (0.65 V) has about 0.65. As these curves illustrate, a remarkable fall of i_T took place whenever the θ_2 value fell in the narrow range from θ_2^L to (θ_2^L—about 0.1). The fall in a particular case, in which θ_2^L was about 0.8, has been explained[14] by assuming that one CO_{ad} damages a vacant site-aggregate (consisting of two sites) indispensable for the formation of CO_{ad} itself and for the oxidation of methanol to CO_2.

However, the remarkable i_T falls occurring when the θ_2^L values are less than 0.8, e.g., Curves 1 and 3 in Fig. 14, have not yet been explained. Because the falls occur independently of the magnitude of θ_2^L, the CO_{ad} is unlikely to be directly connected. Kita[24] reported an i_T decrease at a small coverage and a high potential in a potentiodynamic oxidation of methanol; he suspected that it was caused by some adsorbate other than CO_{ad}. In any event, further investigations are needed.

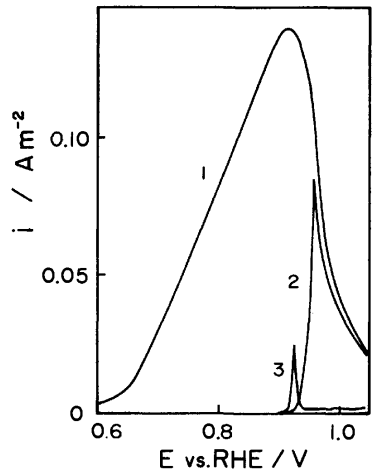

Fig. 11. Potentiodynamic current-potential curve for oxidation of methanol in CH_3OH+0.5 mol dm^{-3} H_2SO_4, concentration of methanol (mol dm^{-3}), staturation gas: (1) 0.3, N_2; (2) 0.3, pure CO; (3) 0, pure CO, scan rate=1 mV/s^{-1}.

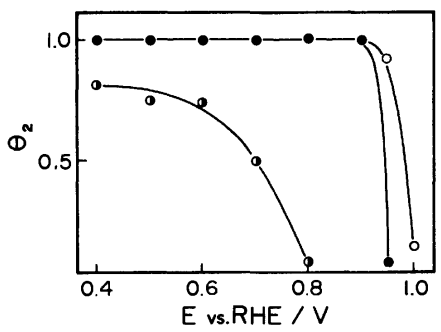

Fig. 12. Variation in θ_2 with potential, methanol was oxidized in CH_3OH+0.5 mol dm^{-3} H_2SO_4, concentration of methanol (mol dm^{-3}), saturation gas: (1) 0.03, N_2; (2) 0, pure CO; (3) 0.03, pure CO, oxidation time=90 s.

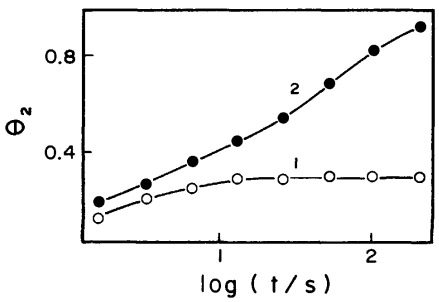

Fig. 13. Variation in θ_2 with time in 0.03 mol dm^{-3} CH_3OH+0.5 mol dm^{-3} H_2SO_4, saturation gas: (1) N_2; (2) CO+N_2 (vol% of CO=20), 0.75 V.

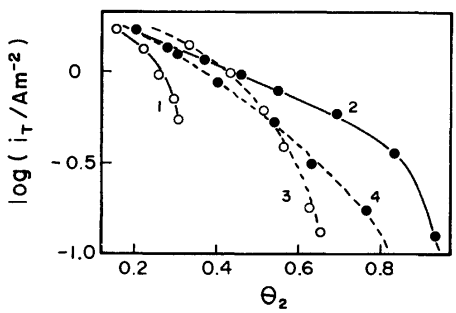

Fig. 14. Variation in i_T with θ_2 in 0.03 mol dm^{-3} CH_3OH+0.5 mol dm^{-3} H_2SO_4, vol% CO in saturation gas (N_2+CO), potential (V): (1) 0, 0.75; (2) 0, 0.65; (3) 20, 0.75; (4) 20, 0.065.

The presence of dissolved CO always increased the limiting coverages up to 1 (Fig. 13), though Curves 2 and 4 in Fig. 14 do not show the whole results. Also, in these cases remarkable i_T falls took place before and after the coverage attained about 0.8. The cause of these falls is the same as those discussed above.

Gently sloping parts preceding the remarkably-falling parts just considered always appeared on the i_T–θ_2 curves, though this part was very short in the case of Curve 1. When the coverage was smaller than (θ_2^L—about 0.1), (e.g., $\theta_2<0.2$ for the pair of curves 1 and 2, $\theta_2<0.55$ for 3 and 4 in Fig. 14), the values of i_T/θ_2 in the presence and absence of dissolved CO were approximately the same. This supports the idea that the roles of the CO adsorbates formed from methanol and dissolved CO are same in the oxidation of methanol. The gentle falls of i_T are attributed to the effect of the site occupation of the effective electrode surface by CO_{ad}.

In short, there is no great difference between the role of CO_{ad} in the presence and absence of dissolved CO, though, in the absence of dissolved CO, the oxidation of methanol is, for some reason, inhibited at small coverages that are close to the respective limiting values. Because the coverage, θ_2 is readily able to attain a value of 1 in the presence of dissolved CO, the steady-state oxidation of methanol is remarkably inhibited by the CO_{ad}, which, at high coverages, makes unavailable the site-aggregates indispensable for the oxidation of methanol.

References

1) K. Ota, Y. Nakagawa, and M. Takahashi, *J. Electroanal. Chem.*, **179**, 179 (1984).

2) O. A. Petrii, "Adsorption of Organic Compounds on Electrodes," ed by B. B. Damaskin, O. A. Petrii, and V. V. Batrakov, Plenum Press, New York (1971), pp. 349, 457.

3) V. S. Bagotzky, Yu. B. Vassilyev, and O. A. Khazova, *J. Electroanal. Chem.*, **81**, 229 (1977).

4) M. W. Breiter, *J. Electroanal. Chem.*, **15**, 221 (1967); *ibid.*, **14**, 407 (1967).

5) C. Lamy, *Electrochim. Acta*, **29**, 1581 (1984).

6) M. W. Breiter, "Modern Aspects of Electrochemistry," ed by J. O'M. Bockris and B. E. Conway, Plenum Press, (1975), Vol. 10, pp. 205.

7) M. W. Breiter, *Discuss. Faraday Soc.*, **45**, 79 (1968).

8) V. B. Hughes and R. Miles, *J. Electroanal. Chem.*, **145**, 87 (1983).

9) B. D. McNicol, *J. Electroanal. Chem.*, **118**, (1981).

10) B. Beden, C. Lamy, A. Bewick, and K. Kunimatsu, *J. Electroanal. Chem.*, **121**, 343 (1981); K. Kunimatsu, *J. Electroanal. Chem.*, **145**, 219 (1985).

11) H. Matsui, T. Hisano, and T. Terazawa, *Bull. Chem. Soc. Jpn.*, **58**, 911 (1985).

12) M. W. Breiter, *Electrochim. Acta*, **9**, 827 (1964).

13) G. Belanger, *Can. J. Chem.*, **50**, 1891 (1972).

14) H. Matsui and T. Hisano, *Bull. Chem. Soc. Jpn.*, **58**, 2298 (1985).

15) B. J. Piersma and E. Gilieadi, "Modern Aspects of Electrochemistry," ed by J. O'M. Bockris, Plenum Press, New York (1966), Vol. 4, pp, 98, 132.

16) P. Delahay, "Double Layer and Electrode Kinetics," translated by K. Kato, Korona Inc. (1970), pp. 97, 276.

17) P. Stonehart and G. Koholmayer, *Electrochim. Acta*, **17**, 369 (1972); W. Vogel, J. Lundquist and P. Stonehart, *ibid.*, **20**, 79 (1975).

18) M. W. Breiter, *J. Electroanal. Chem.*, **115**, 45 (1980).

19) H. Matsui, T. Hisano, and T. Terazawa, *Nippon Kagaku Kaishi*, **1974**, 1861.

20) S. Srinivasan and E. Gileadi, *Electrochim. Acta*, **11**, 321 (1966).

21) H. Matsui, T. Hisano, and T. Terazawa, 50th Meeting of the Electrochemical Society of Japan, Tokyo, May (1983).

22) V. S. Bagotzky and Yu. B. Vassiliev, *Electrochim. Acta*, **11**, 1439 (1966).

23) D. Pletcher and V. Solis, *Electrochim. Acta*, **27**, 775 (1982).

24) H. Kita, 50th Meeting of the Electrochemical Society of Japan, Tokyo, April (1986), Abstr., pp. 134.

Preparation of Nickel(II)-Hydroxide-(Sodium Fluoride Tetrasilicic Mica) Intercalation Complexes and Formation of Ultra Fine Nickel Particles by H_2 Reduction

Kunio OHTSUKA,* Mitsuru SUDA, Mikiya ONO, Minoru TAKAHASHI,†
Minoru SATO,† and Shunji ISHIO†
Research & Development Laboratory, Mitsubishi Mining & Cement Co., Ltd.,
2270 Yokoze, Chichibu-gun, Saitama 368
†Department of Applied Physics, Tohoku University,
Aoba Aza Aramaki, Sendai, Miyagi 980
(Received May 8, 1986)

Nickel(II)-hydroxide-(sodium fluoride tetrasilicic mica) intercalation complexes were prepared by titrating nickel(II) nitrate solutions in the presence of mica with sodium hydroxide. As the degree of interlayering increased, the $I(002)/I(001)$ intensity ratio increased and the specific surface areas decreased. The composition of fully developed nickel(II) hydroxide interlayer, to be exact, hydroxonickel(II) complex was $[Ni_3(OH)_5(H_2O)]^+$ per formula unit. Nickel(II) hydroxide within the interlayers of the silicate was reduced at about 500 °C in H_2 flow and then 5—10 nm ultra fine nickel particles were distributed over the whole surface of mica. With an increase of reducing temperature, the amount of reduced nickel increased and sintering of nickel particles on the surface of mica proceeded.

Intercalation complexes, particularly graphite intercalations, have been one of the most attractive compounds in the study of low dimensional materials. It is well-known that clay minerals have a layered structure like graphite and that intercalation complexes of clay minerals are formed by introduction of organic and inorganic materials within the interlayers of the silicate. In the past several years, extensive studies have been carried out on the formation and properties of aluminium-hydroxide- and magnesium-hydroxide-montmorillonite intercalation complexes in relation to the formation and alteration of clay minerals.[1] The formation of nickel(II)-hydroxide-montmorillonites have been studied as well.[2,3]

The intercalation complexes containing nickel, a typical transition element, must play an important role, particularly on the development of new catalysts and low dimensional magnetic materials. However, the properties and thermal stability of these intercalation complexes have not been fully clarified, especially under reducing conditions.

In the present work, the formation of nickel(II)-hydroxide-(sodium fluoride tetrasilicic mica) and the thermal stability of the complexes in air and in a H_2 flow were investigated.

Sodium fluoride tetrasilicic mica, $NaMg_{2.5}Si_4O_{10}F_2$, used in this study is an artificial compound, which has swelling properties in water similar to natural montmorillonite and also has a large cation exchange capacity. The layer charge of montmorillonite is -0.33 and that of the silicate is -1.

The thermal stability of sodium fluoride tetrasilicic mica is relatively high compared with that of the natural clay minerals, because the OH ions constituting a part of the crystal lattice in natural clay minerals are substituted by F^- ions in the silicate.[4]

Sodium fluoride tetrasilicic mica has also characteristics of high film forming capability because of its flake-like micro particles. Moreover, the silicate differs from natural montmorillonite in having no acidity at all. Thus it receives much attention as an inert support in the study of catalytic reactions.[5]

Experimental

Materials. A 10 wt% sol of sodium fluoride tetrasilicic mica, (supplied by Topy Ind. Co., under the name of Na-TSM) was used. As the silicate sol contains a little α-cristobalite and magnesium fluoride richiterite ($Na_2Mg_6F_2(Si_4O_{11})_2$) as impurities, the sol was diluted with distilled water and most of the impurities were separated by gravimetric sedimentation. Sodium fluoride tetrasilicic mica was finally dried in air at 100 °C.

A diagramatic sketch of the structure of sodium fluoride tetrasilicic mica is shown in Fig. 1.[6] The silicate is

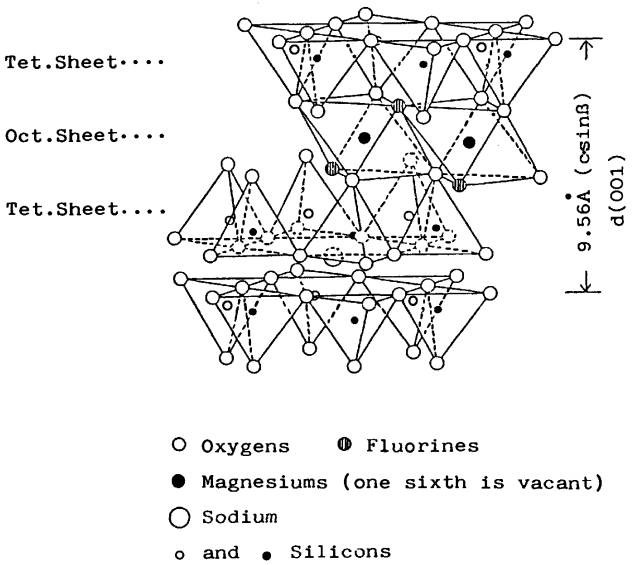

Fig. 1. Diagrammatic sketch of the structure of sodium fluoride tetrasilicic mica ($NaMg_{2.5}Si_4O_{10}F_2$).

composed of units made up of two silicon (Si–O) tetrahedral sheets with a central magnesium (Mg–O,F) octahedral sheet. The unit layers are stacked one above the other. Na^+ ions are located within the interlayers to balance the negative layer charge derived from the vacancies in the octahedral sheets. These Na^+ ions are exchangeable in water and the theoretical cation exchange capacity is 254 meq/100 g·mica.

The crystal structure of sodium fluoride tetrasilicic mica has not been strictly analyzed, only b=9.078 Å and $d(001)=c\cdot\sin\beta$=9.562 Å have been determined.[7] Water molecules can be absorbed within the interlayers. The single water layer hydrated form is stable in air at relative humidities in the range of 40—60% and a double water layer form is stable above that relative humidity.[8] These d-spacings are as follows[7];

$d_1(001)$=12.34 Å (single layer form); $d_2(001)$=15.17 Å (double layer form); $d_3(001)$=18.36 Å (three layer form).

The crystal structure of potassium fluoride tetrasilicic mica ($KMg_{2.5}Si_4O_{10}F_2$), isomorphous substituent of sodium fluoride tetrasilicic mica, was also elucidated[9]; a=5.253 Å, b=9.086 Å, c=10.159 Å, β=99.89.°

Preparation of Nickel(II)-Hydroxide-(Sodium Fluoride Tetrasilicic Mica). Nickel(II)-hydroxide-(sodium fluoride tetrasilicic mica) was prepared by a titration procedure[2] titrating nickel(II) nitrate solution in the presence of the silicate with sodium hydroxide. The preparation procedures are as follows; 10 g samples of the silicate were dispersed in the predetermined amount of 0.1 M (1 M=1 mol dm^{-3}) nickel(II) nitrate solutions. After stirring for 2 d, these suspensions were titrated with a predetermined amount of 0.1 M sodium hydroxide solutions at the rate of 10 ml h^{-1} under vigorous stirring, and stirring was continued for 5 d. Following these treatments, samples were repeatedly washed with distilled water to remove electrolyte and dried at about 100 °C.

Two series of samples were prepared(Table 1); (i) the OH/Ni molar ratio was varied from zero to 1.0 by adding different amounts of 0.1 M sodium hydroxide to 0.1 M nickel(II) nitrate solutions with the sodium fluoride tetrasilicic mica (Ni/mica ratio fixed at 1000 meqNi/100 g·mica). (ii) the Ni/mica ratio was varied from 100 meqNi/100 g·mica to 2000 meqNi/100 g·mica by adding different amounts of 0.1 M nickel (II) nitrate solutions to the silicate (OH/Ni ratio was fixed at 0.5).

Heat Treatment in Air and in H_2 Flow. Since sodium fluoride tetrasilicic mica decomposes at about 800 °C,[10] the thermal stability of the intercalation complexes was studied below 800 °C. The intercalation complexes were heat-treated for 2 h at 100—700 °C in air and at 400—700 °C in H_2 flow (heating rate; 10 °C min^{-1}).

Results and Discussion

Chemical Analyses. Chemical analyses of sodium fluoride tetrasilicic mica and nickel(II)-hydroxide-(sodium fluoride tetrasilicic mica) by atomic absorption analysis are shown in Table 1. The chemical composition of sodium fluoride tetrasilicic mica can be expressed by the formula $Na_{1.00}Mg_{2.63}(Si_{3.98}Al_{0.05}Mg_{0.01}O_{10})O_{0.19}F_{1.81}$,[8] for which the interlayer charge is +1 per formula unit and the interlayer cations are Na^+. Part of interlayer Na^+ cations are displaced by H^+ ions in distilled water when the silicate sol is diluted to eliminate the impurities.

As is shown in Table 1, the amount of nickel taken into the silicate increased with an increase of the OH/Ni ratio or the meqNi/100 g·mica ratio. The highest nickel yields of about 21% were obtained with OH/Ni ratio of 1.0 (No. 8) and meqNi/100 g·mica ratio of 2000 (No. 7). X-Ray diffraction analysis did not detect any free nickel(II) hydroxide in these samples or nickel(II) oxide in the heat-treated ones. Thus, under our experimental conditions, the nickel(II) hydroxide forming reaction took place primarily within the interlayer of the silicate without precipitating free nickel(II) hydroxide.

X-Ray Diffraction. All samples were examined by XRD as thin, oriented films on glass slides. Basal spacings of nickel(II)-hydroxide-(sodium fluoride

Table 1. Conditions of Preparation and Chemical Analyses of Sodium Fluoride Tetrasilicic Mica and Nickel(II)-Hydroxide-(Sodium Fluoride Tetrasilicic Mica)

No.	Conditions of preparation		Chemical analyses (wt%)			Molar ratio (SiO_2=4)		
	OH/Ni	meq Ni/100 g·mica	SiO_2	Na	Ni	SiO_2	Na	Ni
*			55.74	3.84	—	4.00	0.72	—
1	0	1000	54.13	1.63	2.60	4.00	0.32	0.20
2	0.2	1000	51.15	1.48	7.26	4.00	0.30	0.58
3	0.5	100	53.49	1.72	3.20	4.00	0.34	0.24
4	0.5	250	52.91	1.66	5.40	4.00	0.33	0.42
5	0.5	500	49.90	1.57	8.56	4.00	0.33	0.70
6	0.5	1000	46.84	1.34	13.48	4.00	0.30	1.18
7	0.5	2000	40.35	1.08	21.00	4.00	0.28	2.13
8	1.0	1000	40.23	1.22	20.96	4.00	0.32	2.13

*: Initical sodium fluoride tetrasilicic mica ($NaMg_{2.5}Si_4O_{10}F_2$)
Interlayer charge is +1; Interlayer cations are Na^+ and H^+ which replaced the part of Na^+ cations in distilled water.

tetrasilicic mica) are listed in Table 2. These basal spacings are almost constant (ca. 14.7 Å) independent of the amount of the nickel taken into the silicate. Therefore, nickel(II) hydroxide developed onto the horizontal plane within the interlayer of the silicate, forming the brucite like layer. The mechanism of formation of nickel(II) hydroxide interlayers must be the same as in montmorillonite.[2]

X-Ray powder diffraction patterns of nickel(II)-hydroxide-(sodium fluoride tetrasilicic mica) (1000 meq Ni/100 g·mica) are shown in Fig. 2. With an increase of the OH/Ni ratio, the (001) first order reflection decreased in intensity, on the contrary, the (002)—(004) higher order reflections increased in intensities without any changes in basal spacings. With an increase of the meqNi/100 g·mica ratio, the same XRD changes were observed as for samples prepared with an OH/Ni ratio of 0.5. These indicate that the nickel(II) hydroxide forming reaction took place within the interlayer of the silicate, because it is known that the relative intensities of the first and second order reflections are indicative of interlayering and that generally, the $I(002)/I(001)$ intensity ratio increases with an increase of the degree of interlayering.[11]

Table 2. Basal Spacings of Nickel(II)-Hydroxide-(Sodium Fluoride Tetrasilicic Mica)

1000 meq Ni/100 g·mica const.	OH/Ni=0.5 const.
initial mica : 9.6 Å	No. 3 (100 meq Ni/100 g·mica) : 14.3 Å
No. 1 (OH/Ni=0) : 14.3 Å	No. 4 (250 meq Ni/100 g·mica) : 14.6 Å
No. 2 (OH/Ni=0.2) : 14.7 Å	No. 5 (500 meq Ni/100 g·mica) : 14.6 Å
No. 6 (OH/Ni=0.5) : 14.7 Å	No. 6 (1000 meq Ni/100 g·mica) : 14.7 Å
No. 8 (OH/Ni=1.0) : 14.7 Å	No. 7 (2000 meq Ni/100 g·mica) : 14.7 Å

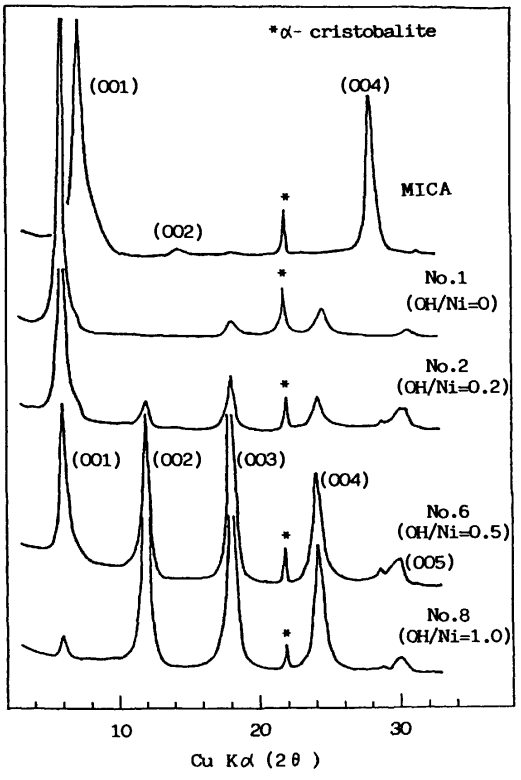

Fig. 2. X-Ray powder diffraction patterns of nickel(II)-hydroxide-(sodium fluoride tetrasilicic mica) (1000 meqNi/100 g·mica).
: Mica; initial mica; single water layer hydrated form.

Thermal Stability of Nickel(II)-Hydroxide-(Sodium Fluoride Tetrasilicic Mica) in Air. Figure 3 shows the DTA and TGA curves for nickel(II)-hydroxide-(sodium fluoride tetrasilicic mica) (No. 2 and No. 8)(the rate of heating was 10 °C min^{-1}). Sample No. 2, which contains a small amount of nickel, showed a single endothermic peak at about 160 °C and a corresponding weight loss. On the other hand, sample No. 8, which contains a large amount of nickel and has a well developed nickel(II) hydroxide interlayer, showed a first endothermic peak at about 120 °C, a second one at about 260 °C, and a third one at about 430 °C with corresponding weight losses. The first endothermic peak corresponds to the loss of absorbed water. The second and the third endothermic peak can be attributed to the dehydration of the nickle(II) hydroxide interlayer, to be exact, hydroxonickel(II) complex $[Ni_m(OH)_{2m-n}\ x(H_2O)]^{n+}$ i.e.; the second one to the loss of coordinated water and the third one to the loss of hydroxo group.

Changes of basal spacings after heat treatment are shown in Fig. 4. With 2 h heat treatment above 200 °C, sample No. 2 collapsed to under 10 Å, while sample No. 8 retained a basal spacing of 14.7 Å up to 300 °C. These results show that nickel(II) hydroxide within the interlayers of the silicate is stable until the loss of hydroxo begins and that samples with fully developed nickel(II) hydroxide interlayer have higher

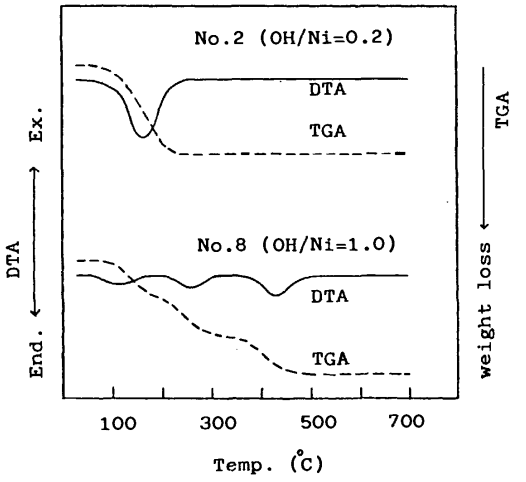

Fig. 3. TGA and DTA curves for nickel(II)-hyroxide-(sodium fluoride tetrasilicic mica) (samles No. 2 and No. 8).

thermal stability. X-Ray diffraction analysis did not detect nickel(II) oxide in these heat-treated samples at 700 °C. Moreover, the (001) mica basal reflection peak of these heat-treated samples broadened with an increase of nickel taken into the interlayer. Therefore, after the nickel(II) hydroxide interlayer has been dehydrated, nickel(II) oxide is present in the interlayers as monomolecules.

The chemical composition of the interlayer material of sample No. 8 was determined by chemical analyses (Table 1) and thermal analyses. From thermal analyses, the amount of coordinated water and hydroxo correspond to the weight loss between 200 and 300 °C, and between 300 and 700 °C respectively. The amounts of dehydration at each temperature are listed in Table 3. Chemical compositions of the interelayer material are calculated to be $Ni_{2.13}(OH)_{3.46}0.61(H_2O)$ per sodium fluoride tetrasilicic mica formula unit. As the ion exchange rate is 68%, this can be rewritten as $[Ni_{3.13}(OH)_{5.09}\text{-}0.90(H_2O)]^{1.17+}_{0.68}$ per formula unit. Therefore, the composition of the fully developed nickel(II) hydroxide interlayer (hydroxonickel(II) complex) must be $[Ni_3(OH)_5(H_2O)]^+$, which balances the negative layer charge of −1, and corresponds to a complete hydroxide interlayer in chlorite. The structure of nickel(II)–hydroxide–(sodium fluoride tetrasilicic mica), shown in Fig. 5, is the same as that of chlorite.[12,13]

Table 3. Chemical Compositions of Nickel(II) Hydroxide Interlayer (Hydroxonickel(II) Complex); $[Ni_m(OH)_{2m-n}xH_2O]^{n+}$ (Sample No. 8)

		Chemical analyses (wt%)	Molar ratio (SiO_2=4)
SiO_2		40.23	4.00
Ni		20.96	2.13
H_2O	R.T−200 °C (1)	3.22	
	R.T−300 °C (2)	5.05	
	R.T−700 °C (3)	10.26	
xH_2O	(2)-(1)	1.83	0.61
$(OH)_{2m-n}$	(3)-(2)	5.21	3.46

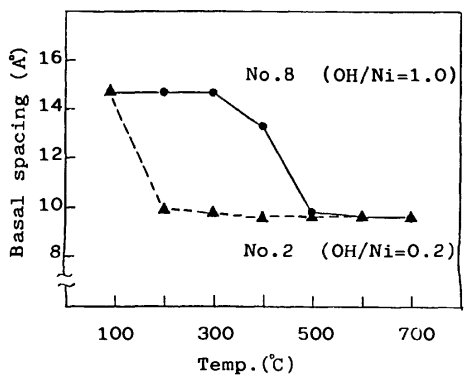

Fig. 4. Changes of basal spacings after heat treatment.

Specific Surface Areas. Specific surface areas of the complexes, measured by the N_2 adsorption method, after heat treatment at 100 and 700 °C are shown in Fig. 6. With an increase of the OH/Ni ratio, the specific surface areas of the complexes heat-treated at

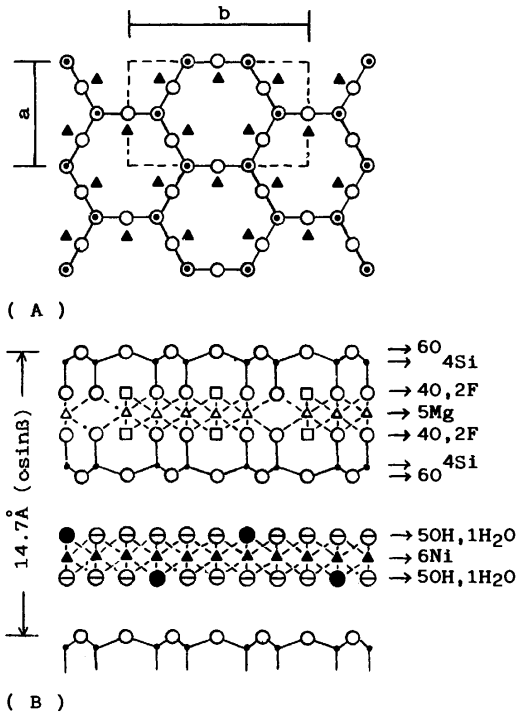

Fig. 5. Structure of nickel(II)–hydroxide–(sodium fluoride tetrasilicic mica).
(A) interlayer Ni cations (▲) onto upper tetrahedral sheet of 2 : 1 layer below.
(B) [100] view of structure.

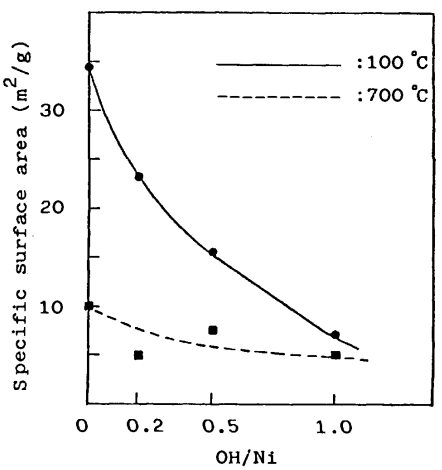

Fig. 6. Specific surface areas of nickel(II)–hydroxide–(sodium fluoride tetrasilicic mica) (1000 meqNi/100 g·mica) heat-treated at 100 °C and 700 °C.

100 °C decreased rapidly. These results correspond to the fact that, according to the development of nickel(II) hydroxide within the interlayers of the silicate, the interlayer space becomes smaller and that finally the internal surfaces are completely covered with nickel(II) hydroxide.

After heat treatment at 700 °C, the specific surface areas were nearly constant, 5—10 $m^2 g^{-1}$, independent of the changes of the OH/Ni ratio, because nickel(II) hydroxide within the interlayers completely dehydrated and collapsed at 700 °C.

The specific surface areas of the sample with an OH/Ni ratio of 1.0 heat-treated at 100 °C is also 5—10 $m^2 g^{-1}$, which is almost equal to that of collapsed sample. This indicates that nickel(II) hydroxide is fully developed within the interlayers of the sample with an OH/Ni ratio of 1.0.

Heat Treatment in H_2 Flow. Nickel(II)-Hydroxide-(sodium fluoride tetrasilicic mica) was heat-treated in H_2 flow at 400, 500, 600, and 700 °C for 2 h. In Fig. 7 are shown the XRD patterns of the H_2 reduced nickel(II)-hydroxide-(sodium fluoride tetrasilicic mica)(sample No. 8). After heat treatment above 500 °C in H_2 flow, sample No. 8 collapsed to a basal spacing of under 10 Å and showed the presence of metallic nickel. With an increase of reducing temperature, the (111) Ni reflection increased in intensity and the (001) mica basal reflection peak became sharper. These results indicate that nickel(II) hydroxide within the interlayer of the silicate decomposed to metallic nickel by H_2 reduction and that reduced nickel atoms migrated from the interlayer of the silicate to its outer surface. This quantity of metallic nickel reduced (shown as relative XRD peak (111) Ni intensity in Fig. 8)increased according to the increase of the OH/Ni ratio, i.e. an increase of nickel(II) hydroxide taken into the silicate interlayer, and an increase of the reducing temperature.

In Fig. 9 are shown the specific surface areas of H_2 reduced nickel(II)-hydroxide-(sodium fluoride tetrasilicic mica). Samples treated above 500 °C in H_2 flow had larger surface areas than those (5—10 $m^2 g^{-1}$) of collapsed samples in air. These increase of specific surface areas are attributed to the reduced nickel

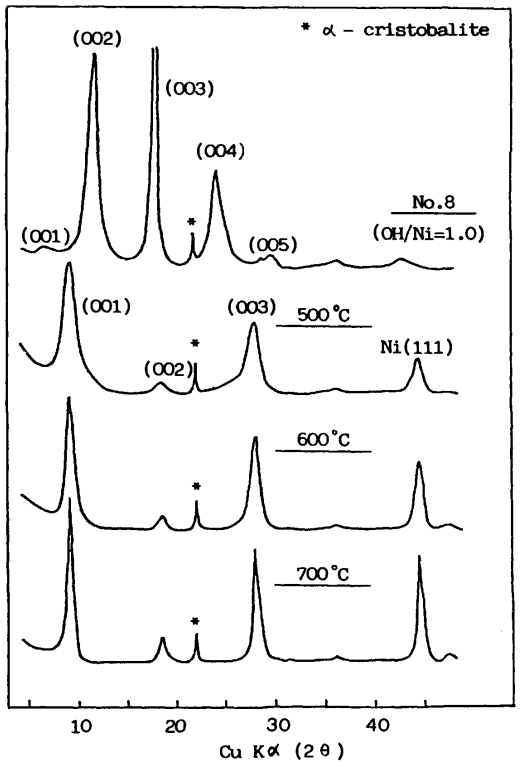

Fig. 7. X-Ray powder diffraction patterns of nickel-(II)-hydroxide-(sodium fluoride tetrasilicic mica) heat-treated in H_2 flow at various temperatures (sample No. 8).

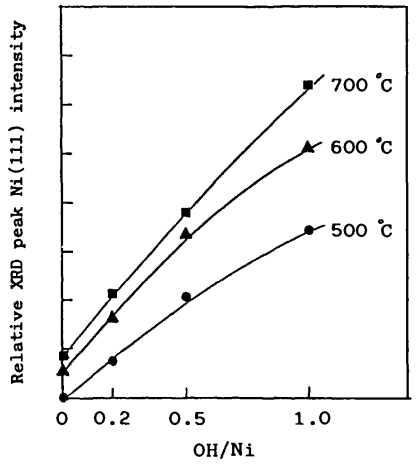

Fig. 8. Quantity of metallic Ni reduced from nickel-(II)-hydroxide-(sodium fluoride tetrasilicic mica)(1000 meqNi/100 g·mica) at various temperatures in H_2 flow.

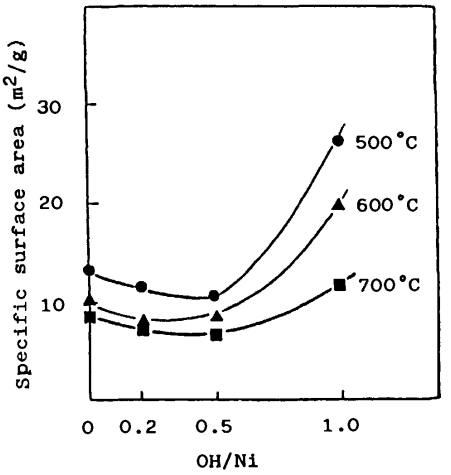

Fig. 9. Specific surface areas of nickel(II)-hydroxide-(sodium fluoride tetrasilicic mica)(1000 meqNi/100 g·mica) heat-treated at various temperatures in H_2 flow.

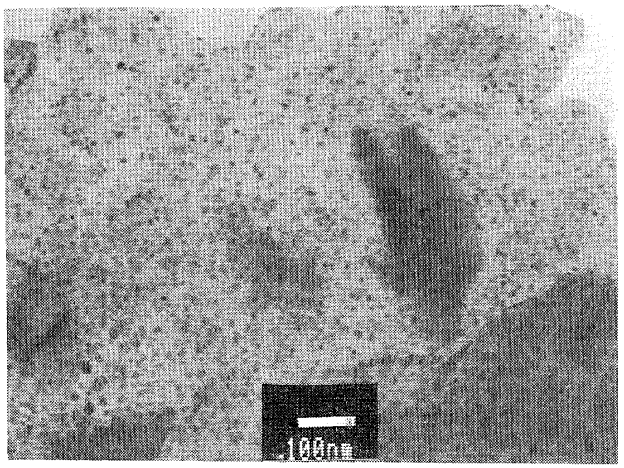

(A)

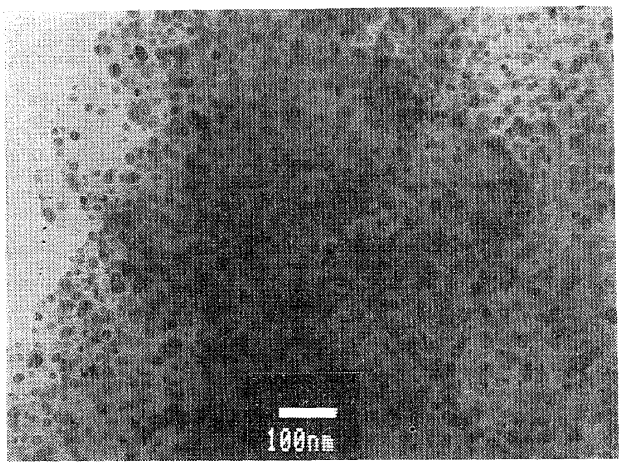

(B)

Fig. 10. Transmission electron micrographs of nickel (II)–hydroxide–(sodium fluoride tetrasilicic mica) heat-treated in H_2 flow.
(A) Nickel(II)–hydroxide–(sodium fluoride tetrasilicic mica) (sample No. 8) heat-treated at 500 °C in H_2 flow.
(B) Nickel(II)–hydroxide–(sodium fluoride tetrasilicic mica)(sample No. 8) heat-treated at 700 °C in H_2 flow.

atoms. Specific surface areas decreased with an increase of reducing temperature, which can be explained by the fact that reduction and sintering of nickel particles on the surface of mica simultaneously proceeded with an increace of reducing temperature.

TEM photographs of sample No. 8 heat-treated at 500 °C and at 700 °C in H_2 flow show that ultra-fine metallic nickel particles with almost the same grain diameter are distributed over the whole surface of the mica (Fig. 10). Grain diameter of metallic nickel reduced is about 5—10 nm at 500 °C and 15—25 nm at 700 °C.

References

1) G. W. Brindley and Chih-chun Kao, *Clays Clay Miner.*, **28**, 435 (1980).
2) S. Yamanaka and G. W. Brindley, *Clays Clay Miner.*, **26**, 21 (1978).
3) G. C. Gupta and W. U. Malik, *Clays Clay Miner.*, **17**, 233 (1969).
4) N. Daimon, *Saiensu*, **8**, No. 3, 9 (1978).
5) Y. Morikawa, K. Takagi, Y. Moro-oka, and T. Ikawa, *J. Chem. Soc., Chem. Commun.*, **1983**, 845.
6) We modified the sketch in "Clay Mineralogy," 2nd ed. R. E. Grim, Mc Graw-Hill, New York (1968), p. 93.
7) K. Kitajima and N. Daimon, *Nippon Kagaku Kaishi*, **1975**, 991.
8) S. Goto, K. Sugimori, T. Hayashi, and R. Kondo, *Nendo Kagaku (J. Clay Sci. Soc. Jpn.)*, **17**, 18 (1977).
9) H. Toraya, S. Iwai, F. Marumo, M. Daimon, and R. Kondo, *Z. Kristallogr.*, **144**, 42 (1977).
10) S. Udagawa, K. Urabe, H. Ikawa and N. Miura, *Nendo Kagaku*, **21**, 46 (1981).
11) C. I. Rich, *Clays Clay Miner.*, **16**, 15 (1968).
12) R. E. Grim, "Clay Mineralogy," 2nd ed. McGraw-Hill, New York (1968), p. 99.
13) S. W. Bailey, "Crystal Structures of Clay Minerals and Their X-Ray Identification," ed by G. W. Brindley, and G. Brown, Mineralogical Society, London (1980), p. 86.

 © 1987 The Chemical Society of Japan Bull. Chem. Soc. Jpn., 60, 877—883 (1987)

A Solvent-Extraction Study of the Hydrolysis of Tracer Concentrations of Bismuth(III) in Chloride Solutions

Hideo SUGANUMA,* Itaru SHIMIZU, and Itsuhachiro HATAYE
Radiochemistry Research Laboratory, Faculty of Science, Shizuoka University,
836, Ooya, Shizuoka 422
(Received July 11, 1986)

The backward solvent extraction with dithizone(H_2dz)–CCl_4 solutions was used to examine the chemical species of bismuth(III) in 1 mol dm^{-3} of a (H,Na)Cl solution. A tracer concentration of bismuth(III) (ca. 10^{-11} mol dm^{-3}) was found to exist mainly in the form of $[BiCl_5]^{2-}$, $[BiCl_5(OH)]^{3-}$, $[BiCl_4(OH)]^{2-}$, and $[BiCl_3(OH)_3]^{3-}$ in the (H,Na)Cl solutions. The constants of the successive hydrolysis, β_1, β_2, and β_3, were calculated by using the distribution data. The resulting $\log\beta_1$, $\log\beta_2$, and $\log\beta_3$ values were 10.9, 17.5, and 30.2 respectively. The chemical composition of the extracted species was most probably $[Bi(Hdz)_3]$.

The hydrolysis of the major concentrations of bismuth(III) in solution has been extensively studied by many investigators. Their works revealed that the chemical species of bismuth(III) exist mainly in polynuclear species in solutions,[1–11] as a result of the hydrolysis of bismuth(III). On the other hand, Bidleman studied the mononuclear species formed in minor concentrations of bismuth(III) (ca. 10^{-5} M; 1 M=1 mol dm^{-3}) in 0.1 M NH_4ClO_4 solutions, based on solvent extraction using dithizone (H_2dz).[12] In his work, the equilibrium constants for the Bi–H_2dz extraction system and the formation constants for the species of $[Bi(OH)]^{2+}$, $[Bi(OH)_3]$, and $[Bi(OH)_4]^-$ have been determined. Furthermore, Hataye et al. studied the mononuclear species formed in more diluted concentrations of bismuth(III) (ca. 10^{-9} M) in 1.0 M (H,Na)ClO_4 and 1.0 M (H,Na)NO_3 solutions, based on the backward solvent extraction with an H_2dz–CCl_4 solution.[13] In their work, they found that chemical species of bismuth exist in the forms of Bi^{3+}, $[Bi(OH)]^{2+}$, $[Bi(OH)_2]^+$, and $[Bi(OH)_3]$ in 1.0 M (H,Na)ClO_4 solutions, and in those of $[Bi(NO_3)_n]^{3-n}$, $[Bi(NO_3)_n(OH)]^{2-n}$, $[Bi(NO_3)_n(OH)_2]^{1-n}$, and $[Bi(NO_3)_n(OH)_3]^{n-}$ in 1.0 M (H,Na)NO_3 solutions, depending on the acidity of the solutions.

In continuation of preceding works on the hydrolysis of tracer concentrations of bismuth(III) in perchlorate and nitrate solutions,[13] we investigated the hydrolysis and chloro complex formation of bismuth(III) in 1.0 M (H,Na)Cl solutions through backward solvent extraction with H_2dz–CCl_4 solutions.

Experimental

Reagents. Water was highly purified with a MILLI-Q reagent-grade water system (MILLIPORE). All the aqueous solutions used were finally purified by extraction with H_2dz–CCl_4 solutions.

Lead (^{210}Pb) containing an equilibrium amount of ^{210}Bi in 3 M HNO_3, imported from the Radiochemical Centre, Amersham, England, was used by diluting it to the appropriate concentration with 3 M HNO_3. A ^{210}Bi tracer solution was prepared by milking with an H_2dz–CCl_4 solution every 4 d from a diluted ^{210}Pb–^{210}Bi solution (pH ≃ca. 1). The ^{210}Bi tracer solution thus prepared was substantially free from any ^{210}Pb and/or ^{210}Po immediately after milking. After the extracted dithizonate (^{210}Bi–H_2dz) has been decomposed with 3 M HNO_3 solution, a portion of the ^{210}Bi tracer solution was transferred into another separatory funnel containing water, and the ^{210}Bi was extracted with an H_2dz–CCl_4 solution of a fixed concentration at $2 \leq pH \leq 3$. The stock solution thus prepared in a lower concentration (less than 10^{-5} M H_2dz) showed practically no change for 3 h after preparation.

Measurements of the Distribution of Bismuth. One ml (1 ml=1 cm^3) of the organic phase containing a given concentration of bismuth was mixed with 10 ml of an aqueous solution (1 M (H,Na)Cl) with a given chemical composition, and the mixture was shaken at room temperature until the partition equilibrium was attained. After the completion of the equilibrium, a 0.5-ml portion of the organic phase was pipetted into a stainless steel planchet, evaporated, and subjected to the measurements of the β-activity (A_{org}) using a G.M. counter with aluminum absorbers against α-particles from ^{210}Po. Because it is difficult to count the activity of the aqueous phase in the same geometrical form as the organic phase in the planchet, it was calculated by using this relation: $A_{aq}=A^{\circ}_{org}-A_{org}$, where A_{aq} is the activity of a 5-ml portion of the aqueous phase and where A°_{org} is the initial activity of a 0.5-ml portion of the organic phase before shaking. Hence, the distribution ratio of bismuth, D, is given by:

$$D = 10 \times A_{org}/(A^{\circ}_{org}-A_{org}).$$

In each case of determining D, the multiple-extraction procedures were repeated under conditions of a definite hydrogen-ion concentration and definite amounts of bismuth in the aqueous phase; the data obtained in the first half were all discarded, and only the reproducible data in the other half were taken.

As for acidic media ($-\log[H^+] \leq 1$), the hydrogen-ion concentration was determined by means of titration with NaOH. In other cases, it was measured with a pH meter (TOA Electronics Ltd, Tokyo), which was adjusted by the use of standard solutions of phthalic acid and oxalate or phosphate at room temperature as soon as possible after shaking.

Results and Discussion

Adsorption of Bismuth onto Vessels Used. To examine the adsorption of bismuth onto glass, the inside surfaces of conical beakers were, in advance, repeatedly and sufficiently equilibrated with respect to the adsorption of bismuth(^{210}Bi) with 30 ml of a 1.0 M (H,Na)Cl solution containing bismuth (ca. 10^{-11} M Bi) at $-\log[H^+]=1.0$. Then, after the conical beaker containing a freshly prepared 1.0 M (H,Na)Cl solution (30 ml, ca. 10^{-11} M Bi), with pH values varying from 0 to 10, has been shaken overnight, the activity of the aqueous phase was measured. The results are shown in Fig. 1. These results indicate that bismuth is leached out from the glass wall in an acidity higher than $-\log[H^+]=1.0$, while on the contrary, it is adsorbed onto it in a lower acidity. Reproducible results of D should, therefore, be obtained in the solvent-extraction study of bismuth only when a distribution equilibrium set up among the aqueous phase, the organic phase, and the glass wall of the vessel used in definite hydrogen-ion and bismuth concentrations.

Dependence of the Distribution Ratio on the Bismuth Concentration. The partition equilibrium of bismuth in a carrier-free state between 1.0 M (H,Na)Cl solutions and the organic phase was reached within 30 min. Accordingly, the partition system involving carrier-free bismuth was shaken for more than 40 min in all the experiments in order to attain a complete equilibrium. On the other hand, in the case of less diluted solutions containing a bismuth carrier, the partition equilibrium of bismuth was not attained within 30 min. Therefore, the shaking time was previously examined in each bismuth concentration. For example, in case of 10^{-7} M Bi, the shaking should be continued for more than 12 h, as is shown in Fig. 2: in addition, it was necessary to take into account the decomposition of the dithizone and dithizonate formed. The higher the carrier concentration, the longer a shaking time was needed. This elongation of the shaking time is thought to be caused by the extreme decrease in the concentration ratio of bismuth to dithizone. However, as far as carrier-free bismuth is concerned, the partition equilibrium of bismuth should be attained within 30 min. Moreover, Fig. 3 shows the variation in the distribution ratios measured as a function of the amounts of the bismuth carrier in minor-to-trace concentrations. No effect of the bismuth concentration was observed for the 1.0 M (H,Na)Cl solutions of $-\log[H^+]=0.83$ and 3.2. These results suggest that there is no difference in the degree of polymerization of bismuth species between aqueous and organic phases. On the other hand, it is impossible for any polymerized species to remain stable in both phases. We may, therefore, safely assume that the monomers are the main species prevailing in the solvent extraction of tracer concentrations of bismuth.

Dependence of Distribution Ratio on the Dithizone Concentration in the Organic Phase. The distribution ratio, D, was plotted as a function of the H_2dz concentration at different hydrogen-ion concentra-

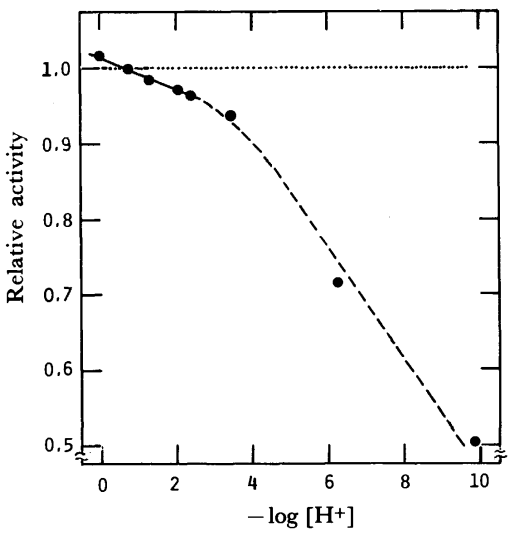

Fig. 1. The adsorption/desorption of bismuth onto/from glass wares (Erlenmeyer flasks). The flasks were in advance equilibrated with 30 ml of ^{210}Bi solution (ca. 10^{-11} M Bi, 1.0 M (H, Na) Cl) at $-\log[H^+]=1.0$.

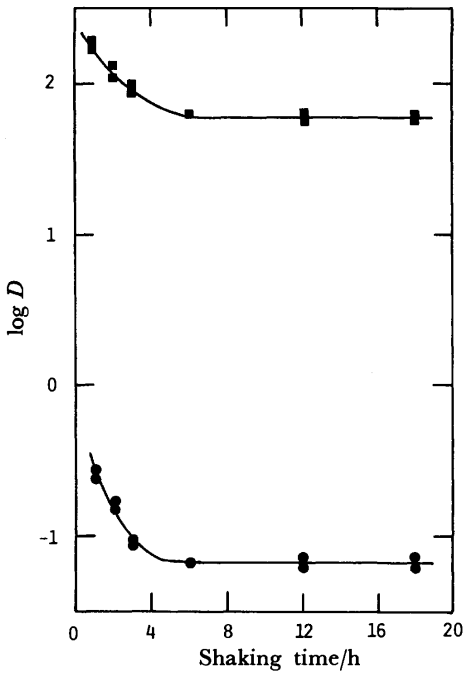

Fig. 2. The effect of shaking time on the distribution ratio in less diluted bismuth concentration (10^{-7} M). ●; $-\log[H^+]=0.83$, $[H_2dz]_{org}=1.9\times10^{-3}$ M. ■; $-\log[H^+]=3.2$, $[H_2dz]_{org}=9.5\times10^{-5}$ M.

tions. Figure 4 shows that the plots of $\log D$ vs. $\log [H_2dz]_{org}$ have the identical slope of +3, independent of the acidity, where H_2dz denotes a neutral dithizone molecule. The narrow range of dithizone concentrations at $-\log [H^+]=0.5$ is attributable to the limited solubility of dithizone in CCl_4, and at the same time the very low values of the distribution ratio might lead to larger experimental errors. In general, the slope of $\log D$ vs. $\log [H_2dz]_{org}$, or $\partial \log D/\partial \log [H_2dz]_{org}$, indicates the difference in the average number of univalent (bidentate) dithizonate ligands (Hdz^-) attached to a bismuth atom between the organic and aqueous phases. It is generally accepted that the coordination number of bismuth(III) is six, so the total number of ligands (as univalent) combined to a bismuth atom can be reasonably assumed not to exceed six; at the same time, the extracted species must be electrically neutral. Since the Hdz^- ion is a bidentate ligand, our results, shown in Fig. 4, lead to the conclusion that bismuth exists in the chemical form of the $[Bi(Hdz)_3]$ in the organic phase. It also means that the concentration of the Bi-Hdz^- complex species is negligibly low in the aqueous phase of 1.0 M (H,Na)Cl solutions.

Dependence of the Distribution Ratio on the Hydrogen-Ion Concentration. The distribution ratio for the extraction system of Bi-H_2dz in chloride solutions, D, is expressed as follows:

$$D = [Bi(Hdz)_3]_{org}/\sum_{x=0}^{6-n}\sum_{n=0}^{6-x}[BiCl_x(OH)_n^{3-x-n}] \quad (1)$$

$$= (K_3[H_2dz]_{org}^3[H^+]^{-3})/(\sum_{x=0}^{6-n}\sum_{n=0}^{6-x}\beta_{x,n}Q_w^n[Cl^-]^x[H^+]^{-n}), \quad (2)$$

where:

$$K_3 = [Bi(Hdz)_3]_{org}/([Bi^{3+}][H_2dz]_{org}^3[H^+]^{-3}), \quad (3)$$

$$\beta_{x,n} = [BiCl_x(OH)_n^{3-x-n}]/([Bi^{3+}][Cl^-]^x[OH^-]^n), \quad (4)$$

$$Q_w = [H^+][OH^-]. \quad (5)$$

D can be rewritten as follows in terms of the hydrolysis of bismuth in the case of $[Cl^-]=1.0$ M:

$$D/[H_2dz]_{org}^3 = K_3/(\sum_{x=0}^{6-n}\sum_{n=0}^{6-x}\beta_{x,n}Q_w^n[H^+]^{3-n}). \quad (6)$$

In the present case, $\sum_{x=0}^{6-n}\sum_{n=0}^{6-x}\beta_{x,n}$ is denoted by $\sum_{n=0}^{6}\beta_n$, because each $\beta_{x,n}$ can not be measured separately, and the $\sum_{x=0}^{6}\beta_{x,0}$ is regarded as unity. Accordingly, Eq. 6 should be rewritten as follows:

$$D/[H_2dz]_{org}^3 = K_3/(\sum_{n=0}^{6}\beta_nQ_w^n[H^+]^{3-n}). \quad (7)$$

In Fig. 5, we plot $\log (D/[H_2dz]_{org}^3)$ as a function of $-\log [H^+]$ in 1.0 M (H,Na)Cl solutions. Since it is difficult to determine the distribution ratio by using only a single solution of a given dithizone concentration in all regions of the hydrogen-ion concentration, $\log (D/[H_2dz]_{org}^3)$ is plotted instead of $\log D$. As is shown in the figure, the slope seems to be nearly +3 at $-\log [H^+]=0$, while it is nearly 0 at $4.5<-\log [H^+]$. Therefore, there exist few chlorohydroxo compounds

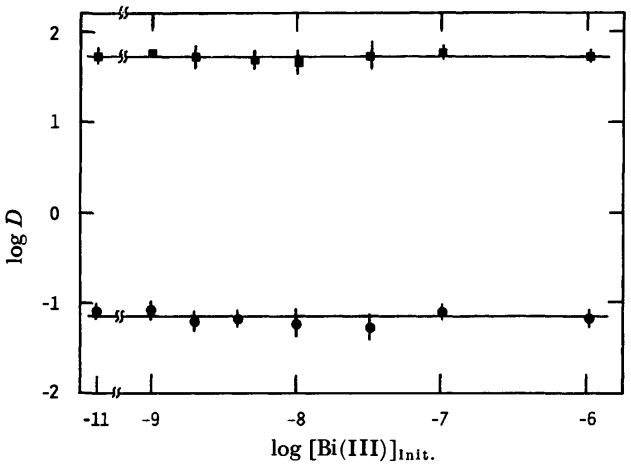

Fig. 3. The dependence of the distribution ratio on the initial concentration of bismuth(III) in 1.0 M (H, Na)Cl solutions.
●; $-\log [H^+]=0.83$, $[H_2dz]_{org}=1.9\times10^{-3}$ M. ■; $-\log [H^+]=3.2$, $[H_2dz]_{org}=9.5\times10^{-5}$ M.

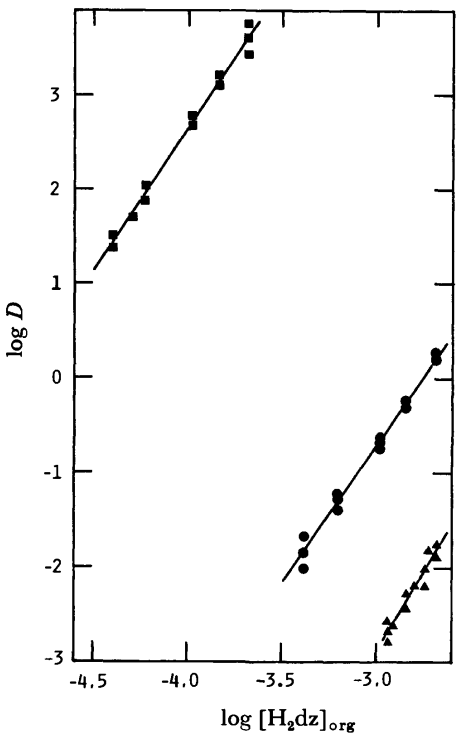

Fig. 4. The dependence of the distribution ratio of bismuth on the dithizone concentration in the organic phase.
▲; $-\log [H^+]=0.5$, ●; $-\log [H^+]=1.38$, ■; $-\log [H^+]=3.7$.

of bismuth in high acidity, while $[BiCl_x(OH)_3]^{x-}$ is predominant in the weakly acidic to neutral solutions. The distribution ratio in Eq. 7 can be expressed in terms of each hydrolysis constant, β_n (n=1, 2, and 3), as follows:

$$D/[H_2dz]^3_{org} = K_3/([H^+]^3 + \beta_1 Q_w[H^+]^2 + \beta_2 Q_w^2[H^+] + \beta_3 Q_w^3), \quad (8)$$

where:

$$\beta_1 = [BiCl_x(OH)^{2-x}]/([Bi^{3+}][Cl^-]^x[OH^-]), \quad (9)$$

$$\beta_2 = [BiCl_x(OH)_2{}^{1-x}]/([Bi^{3+}][Cl^-]^x[OH^-]^2), \quad (10)$$

$$\beta_3 = [BiCl_x(OH)_3{}^{x-}]/([Bi^{3+}][Cl^-]^x[OH^-]^3). \quad (11)$$

Estimation of K_3, $\beta_3 Q_w^3$, $\beta_2 Q_w^2$, and $\beta_1 Q_w$. Figure 5 shows that the slope of $\log(D/[H_2dz]^3_{org})$ vs. $-\log[H^+]$ is nearly 3 at $-\log[H^+]=0$, so Eq. 8 can be simplified to $D/[H_2dz]^3_{org} \simeq K_3$. Consequently, the approximate value of K_3 could be obtained as $(4.27\pm0.24)\times10^4$ from the data in Fig. 5 and the vast number of data on the partition equilibrium at $-\log[H^+]=0$, where the uncertainty is designated by σ. This value is much smaller than the K_3 values in 1.0 M (H,Na)ClO_4 and 1.0 M (H,Na)NO_3, as is shown in Table 1. This fact suggests that the formation of extractable species ([Bi(Hdz)$_3$]) is depressed by forming chloro complexes in trace concentrations of bismuth solutions in the presence of a large amount of chloride ions.

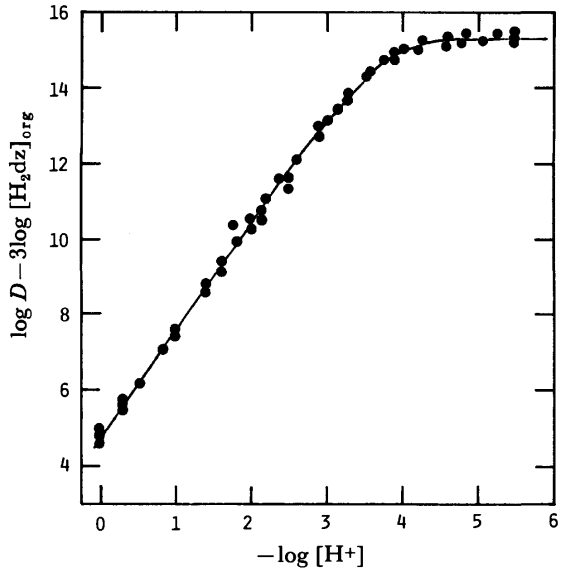

Fig. 5. The dependence of the distribution ratio of bismuth on the hydrogen-ion concentration in 1.0 M (H, Na)Cl solution.

Furthermore, since Fig. 5 shows that the slope of $\log(D/[H_2dz]^3_{org})$ vs. $-\log[H^+]$ ($-\log[H^+]>4.5$) is nearly zero, independent of the acidity, Eq. 8 can be also simplified to $D/[H_2dz]^3_{org} \simeq K_3/(\beta_3 Q_w^3)$. Consequently, the approximate value of $\beta_3 Q_w^3$ was obtained from Fig. 5 ($-\log[H^+]>4.5$) as $(2.04\pm0.13)\times10^{-11}$ for 1.0 M (H,Na)Cl solutions, where the uncertainty is indicated by σ. By using the set of K_3 and $\beta_3 Q_w^3$ values thus obtained, the approximate values of a set of $\beta_1 Q_w$ and $\beta_2 Q_w^2$ were obtained by the least-squares fit from the data in Fig. 5; the results were $\beta_1 Q_w = 1.91\times10^{-3}$ and $\beta_2 Q_w^2 = 2.00\times10^{-10}$ for 1.0 M (H,Na)Cl solutions. Equation 8 is cubic with respect to the hydrogen-ion concentration; therefore, no meaningful error in $\beta_1 Q_w$ and $\beta_2 Q_w^2$ calculations could be obtained. The values obtained for $\log\beta_1$, $\log\beta_2$, and $\log\beta_3$ are 10.9, 17.5, and 30.2 respectively for a 1.0 M (H,Na)Cl solution, when $\log Q_w$ is -13.62.[14] In general, the n-th step-by-step hydrolysis constant gives a lower value than the $(n-1)$ th constant. However, our results for bismuth in this solution exhibit an abnormal sequence, compared with those in 1.0 M (H,Na)ClO_4 and 1.0 M (H,Na)NO_3.[13] For this reason, it is thought that the coordination number of bismuth changes with a variation in the hydrogen-ion concentrations and that, furthermore, the effects of $\Delta H°$ (enthalpy) and/or $\Delta S°$ (entropy) for the formation of the bismuth species in the progressing hydrolysis play an important part. Unfortunately, from the hydrolysis constants alone we can not determine which reason is the dominant factor.

Table 1. Equilibrium Constants on Bismuth Hydrolysis in the Bi-Dithizone Extraction System

Medium	Method[a]	Concentration of Bi [M]	Equilibrium constant[b]					Reference
			$\log\beta_1$	$\log\beta_2$	$\log\beta_3$	$\log\beta_4$	$\log K_3$	
1.0 M (H, Na)Cl	Ex	ca. 10^{-11}	10.9	17.5	30.2	—	4.63	This work
1.0 M (H, Na)ClO_4	Ex	$< 10^{-7}$	12.0	22.9	33.9	—	11.38	13
1.0 M (H, Na)NO_3	Ex	$< 10^{-7}$	11.9	22.7	33.2	—	11.37	13
0.1 M NH_4ClO_4	Ex	$> 10^{-5}$	12.4	—	31.9	32.9	10.9	12
3 M $NaClO_4$	P	10^{-4} −0.05	12.4	—	—	—	—	4

a) Ex; extraction, P; potentiometry. b) $\beta_n = \dfrac{[Bi(OH)_nX_x^{3-n-x}]}{[Bi^{3+}][OH^-]^n[X^-]^x}$, (X; ClO_4, NO_3, or Cl), and $K_3 = \dfrac{[Bi(Hdz)_3]_{org}[H^+]^3}{[Bi^{3+}][H_2dz]^3_{org}}$.

The percentage abundances of the chemical species of bismuth calculated from each β_n value at different hydrogen-ion concentrations in 1.0 M (H,Na)Cl solutions are presented in Fig. 6(a), along with those for 1.0 M (H,Na)ClO_4 (b) and 1.0 M (H,Na)NO_3 (c) solutions.[13] As can be seen from Fig. 6, the hydrolysis of bismuth in the 1.0 M (H,Na)Cl solution (a) is greatly depressed compared with the other two solutions (b and c); this is caused by the strong complexing ability of the chloride ion. Furthermore, it is found that $[BiCl_x(OH)_2]^{1-x}$ in the 1.0 M (H,Na)Cl solution is a minor species; its maximum abundance is estimated to be only ca. 0.05%.

Number of Chloride Ions Coordinated to a Bismuth Atom. As no effect of the perchlorate-ion concentration on the distribution ratios of bismuth in the extraction with dithizone from a 1.0 M (H,Na)ClO_4 solution was observed,[13] the 1.0 M (H,Na)ClO_4 solution was employed as the diluent in order to examine the effect of the chloride ion by varying its mole fractions in the aqueous phase.

In general, the slope of log D vs. log $\{[Cl^-]/([Cl^-]+[ClO_4^-])\}$ in 1.0 M (H,Na)(Cl,ClO_4) solutions at a given hydrogen-ion concentration indicates the difference in the average number of univalent chloride ions attached to a bismuth atom between the organic and aqueous phases, so we determined the slope by varying the mole fractions of chloride ions in 1.0 M (H,Na)(Cl,ClO_4) solutions at a given hydrogen-ion concentration; a typical example is shown in Fig. 7 (lower line). The slope of -5.07 ± 0.07 (σ) indicates the average number of chloride ions coordinated to a bismuth atom in a 1.0 M (H,Na)Cl solution at $-\log[H^+]=1.21$; that is, it can be presumed that, in that solution, bismuth exists mainly as such a chemical species as $[BiCl_5]^{2-}$. Furthermore, the average numbers of chloride ions coordinated to a bismuth atom in 1.0 M (H,Na)Cl at $-\log[H^+]=0.29$, 0.83, 1.85, 2.54, and 3.12 were all determined to be close to five (4.67—5.07; they are plotted in Fig. 8) in a manner similar to that above mentioned. However, as the plots seemed not to be a straight line, but to form a concave curve upward at $-\log[H^+]=3.8$, as is shown in Fig. 7 (upper line), the number of chloride ions was determined from the slope of the tangential line (dotted line) of an approximate quadratic equation at $\log\{[Cl^-]/([Cl^-]+[ClO_4^-])\}=0$ obtained by the least-squares fit to the experimental data.

On the other hand, this method can not be applied to the solutions of $-\log[H^+]\geq4$, because it is difficult to adjust the hydrogen-ion concentration without using any buffer solutions. Instead, in this case, the value of (log $D-3\log[H_2dz]_{org})_{ClO_4}$[13] minus (log $D-3\log[H_2dz]_{org})_{Cl}$ shown in Fig. 5 was plotted as a function of $-\log[H^+]$ (≥4), as is shown in Fig. 8. Nevertheless, these values are not reasonable because

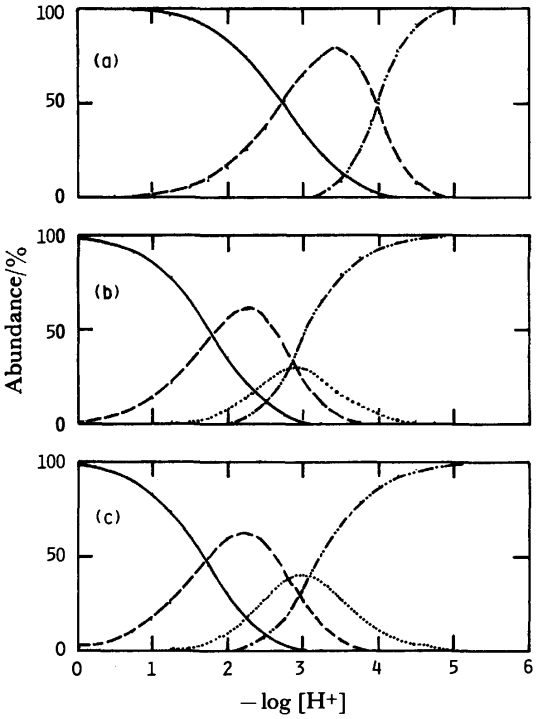

Fig. 6. The abundance of the hydrolyzed chemical species of bismuth(III) in (a) 1.0 M (H, Na)Cl, (b) 1.0 M (H, Na)ClO_4,[13] and (c) 1.0 M (H, Na)NO_3 solutions.[13] (——), (----), (·····), and (—··—) indicate unhydrolyzed, monohydroxide, dihydroxide, and trihydroxide species, respectively.

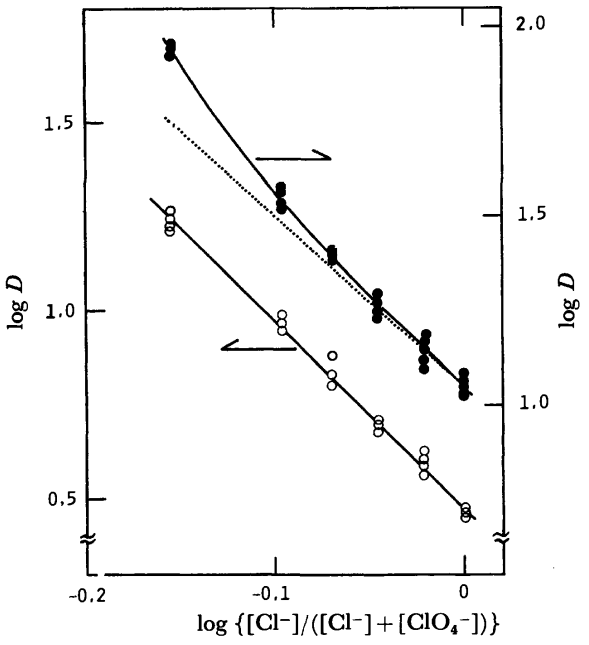

Fig. 7. The dependence of the distribution ratio of bismuth on the chloride ion concentration in 1.0 M (H, Na)(Cl, ClO_4) solutions. ○; $-\log[H^+]=1.21$, $[H_2dz]_{org}=2.6\times10^{-3}$ M, the solid line represents a slope of −5.07. ●; $-\log[H^+]=3.8$, $[H_2dz]_{org}=2.6\times10^{-5}$ M, the dotted line represents a slope of −4.60.

the values were calculated from the inclination of the curve, as is shown in Fig. 9(b), and the total number of ligands (the sum of the chloride and hydroxide ions calculated from the hydrolysis constants) exceeds 6. The reasonable value has to be determined by the method shown in Fig. 9(a) or Fig. 7 (upper line).

The two-dot chain line in Fig. 8 represents a variation in the average number of chloro ligands attached to a bismuth atom, calculated from this relation: (5 minus the average number of hydroxide ligands, as estimated from the hydrolysis constants), by assuming 5 for the coordination number of bismuth (octahedral). In this case, Eqs. 1, 2, 6, and 7 have to be rewritten by using 5 for the coordination number of bismuth, but the original equations remain practically valid to obtain the hydrolysis constants of bismuth. On the other hand, the dash-dotted line was calculated by assuming 6 for the coordination number of bismuth (pentagonal bipyramid), in a way similar to that used for the two-dot chain line. We can assume that the dash-dotted line probably suggests true values at $4 \leq -\log[H^+] < 6$, because the experimental value at $-\log[H^+]=3.8$ is close to the dash-dotted line, while the two-dot chain line is consistent with the experimental results in the region of $-\log[H^+] \leq 1.2$. Moreover, the experimental results in the region of $1.2 < -\log[H^+] < 3.8$ are not consistent with either of the two lines.

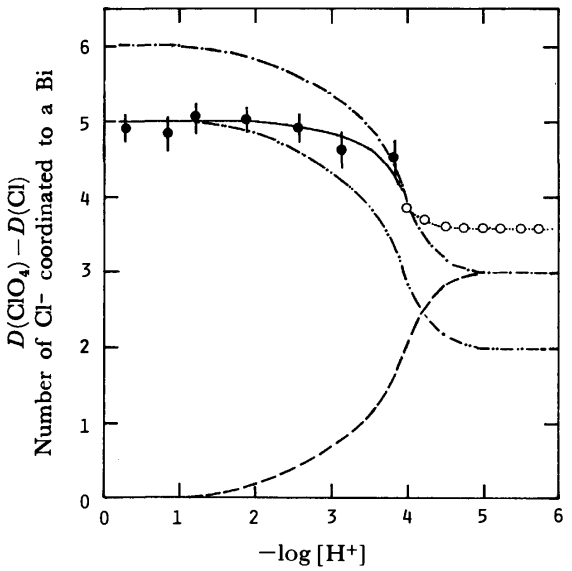

Fig. 8. The number of chloride ions coordinated to a bismuth atom in 1.0 M (H, Na)Cl solutions. ●; experimental values, ○; estimated values from {(log $D-3\log[H_2dz]_{org})_{ClO_4}$[13] − (log $D-3\log[H_2dz]_{org})_{Cl}$}, and (—·—) and (—··—) indicate the values estimated from both formulas; (6 or 5−average number of hydroxide combined to a bismuth atom in 1.0 M (H, Na)Cl), respectively. (----) represents the variation of average number of hydroxide attached to a bismuth atom in 1.0 M (H, Na)Cl.

We are able to make two assumptions on the basis of the above discussion: that the coordination number of bismuth varies from 5 to 6 with a decrease in the hydrogen-ion concentration in 1.0 M (H,Na)Cl, and that the coordination number holds at 6 in all regions of 1.0 M (H,Na)Cl. Unfortunately, we could not determine directly with any experiments on a trace scale of bismuth which assumption should be adopted. Ahrland et al.,[15] Miranov et al.,[16] and Johansson[17] have obtained formation constants for chloro complexes of bismuth (larger concentrations) in 2, 3, and 4 M chloride solutions respectively. Their results revealed the existence of $[BiCl_6]^{3-}$; that is, those results indicated one of the structures of the pentagonal bipyramid by the sp^3d^3 hybridization with a lone pair of electrons. In our results, moreover, the extracted species of bismuth is $[Bi(Hdz)_3]$, as can be seen from Fig. 4. Therefore, it is reasonable to assume 6 for the coordination number of bismuth throughout the pH region of 1.0 M (H,Na)Cl. Accordingly, in our results at $-\log[H^+] < 3.8$, it is necessary to take into account the coordination of water molecules to a

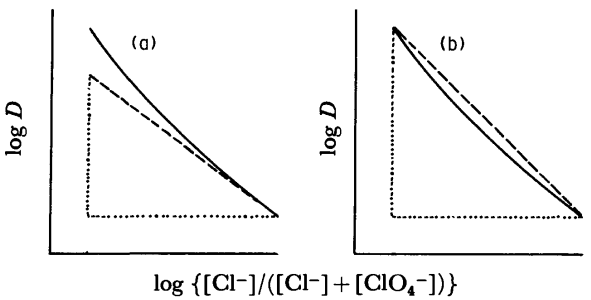

Fig. 9. Estimation of average number of chloride ions attached to a bismuth atom. Tangential broken lines indicate a ture value in (a) and an overestimated value in (b).

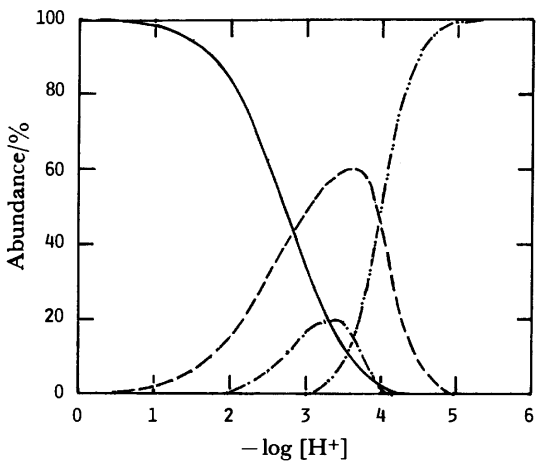

Fig. 10. The abundance of chemical species of Bi(III) in 1.0 M (H, Na)Cl solutions. (——); $[BiCl_5(H_2O)]^{2-}$ (----); $[BiCl_5(OH)]^{3-}$, (—·—); $[BiCl_4(OH)(H_2O)]^{2-}$, (—··—); $[BiCl_3(OH)_3]^{3-}$.

bismuth atom. Hereafter, we will consider the bismuth species in some detail by assuming a pentagonal bipyramid structure.

The average number of chloride ions attached to a bismuth atom in 1.0 M (H,Na)Cl was estimated from a smooth curve combined by the least-squares fit for both the experimental values and the dash-dotted line ($-\log[H^+] \geq 4$) in Fig. 8. In addition, it has been assumed that the only chloride numbers were 3, 4, and 5; that is, 0, 1, 2, and 6 were negligibly low abundances. Consequently, the number of H_2O molecules attached to a bismuth atom was found to be 0 or 1. The average number of hydroxide ions was calculated from the hydrolysis constants, where the second hydrolysis products were neglected because of their very low abundance. Based on the assumptions described above, the following bismuth species can probably be concluded to exist: $[BiCl_5(H_2O)]^{2-}$, $[BiCl_5(OH)]^{3-}$, $[BiCl_4(OH)(H_2O)]^{2-}$, and $[BiCl_3(OH)_3]^{3-}$. In addition, the percentage abundances of the each species were calculated to be as is shown in Fig. 10. The $[BiCl_5(H_2O)]^{2-}$ is present as the main species in a high acidity, while the abundance of $[BiCl_5(OH)]^{3-}$ increases with an increase in $-\log[H^+]$ up to 3.5 and then decreases in the region of further lower acidity. The $[BiCl_4(OH)(H_2O)]^{2-}$ exists in the region of $2 \leq -\log[H^+] \leq 4$. Furthermore, the lower the acidity, the higher the abundance of $[BiCl_3(OH)_3]^{3-}$ in an acidity lower than $-\log[H^+]=3$; its abundance may be nearly 100% at $-\log[H^+]>5$ if our assumption is valid. The abundances of $[BiCl_5(OH)]^{3-}$, $[BiCl_4(OH)(H_2O)]^{2-}$, and $[BiCl_3(OH)_3]^{3-}$ contain some uncertainty at $3.5<-\log[H^+]<4.2$, because the average number of chloride ions attached to a bismuth atom can not be determined exactly.

From the above discussion, it is thought that the abnormal variation in hydrolysis constants is mainly dependent on the effects of $\Delta H°$ and/or $\Delta S°$, which arise from a competition with the chloro ligand; the hydrolysis constants observed are conditional ones.

The authors wish to thank Professor Shunji Utsuno (Shizuoka University) for his valuable discussion.

References

1) F. Graner and L. G. Sillén, *Acta Chem. Scand.*, **1**, 631 (1947).
2) P. Souchay and D. Peschanski, *Bull. Soc. Chim. Fr.*, **1948**, 439.
3) R. W. Holmberg, K. A. Kraus, and J. S. Johnson, *J. Am. Chem. Soc.*, **78**, 5506 (1956).
4) A. Olin, *Acta Chem. Scand.*, **11**, 1445 (1957).
5) A. Olin, *Acta Chem. Scand.*, **13**, 1791 (1959).
6) C. Dragulescu, A. Nimano, and I. Julean, *Rev. Roum. Chim.*, **7**, 1181 (1972).
7) R. S. Tobias, *J. Am. Chem. Soc.*, **82**, 1070 (1960).
8) R. S. Tobias and S. Y. Tyree, Jr., *J. Am. Chem. Soc.*, **82**, 3244 (1960).
9) H. A. Levy, M. D. Danfold, and P. A. Agron, *J. Chem. Phys.*, **31**, 1458 (1959).
10) V. A. Maroni and T. G. Spiro, *J. Am. Chem. Soc.*, **88**, 1410 (1966).
11) V. Frei, G. Mages, and H. Wendt, *Ber. Bunsenges. Phys. Chem.*, **77**, 243 (1973).
12) T. F. Bidleman, *Anal. Chim. Acta*, **56**, 221 (1971).
13) I. Hataye, H. Suganuma, H. Ikegami, and T. Kuchiki, *Bull. Chem. Soc. Jpn.*, **55**, 1475 (1982).
14) A. Ferse, *Z. Phys. Chem.*, **229**, 51 (1965).
15) S. Ahrland and I. Grenthe, *Acta Chem. Scand.*, **11**, 1111 (1957); correction, *ibid.*, **15**, 932 (1961).
16) V. E. Mironov. F. Ya. Kul'ba, V. A. Fedorov, and T. F. Nikitenko, *Zh. Neorg. Khim.*, **8**, 1852 (1963).
17) L. Johansson, *Acta Chem. Scand.*, **23**, 548 (1969).

 © 1987 The Chemical Society of Japan Bull. Chem. Soc. Jpn., 60, 885—890 (1987)

Sulfur Contents of Volcanic Rocks in Japan

Yoshiko ARIKAWA
Department of Chemistry, Faculty of Home Economics, Japan Women's University, Mejiro-dai, Bunkyo-ku, Tokyo 112
(Received July 26, 1986)

The total sulfur content was determined for 140 samples of Japanese volcanic rock by the mercury(II) thiocyanate photometric method of hydrogen sulfide formed by a wet reduction of the sample by tin(II)–strong phosphoric acid. Though determined values are widely scattered from 5390 down to 10 ppm (or less), the cumulative frequency distribution of the sulfur contents shows lognormality. The geometric and arithmetic means are 26 ppm (mg kg^{-1}) and 116 ppm, respectively. The alkaline rocks have high sulfur contents, the geometric mean of which is 62 ppm. Little significant difference was observed among the rhyolitic rock, the andesite and the trachyte, and the basaltic rock. Japanese and foreign standard rock samples were analyzed for sulfur. Almost all results were in good agreement with those obtained by other authors. In this case foreign standard samples also have higher sulfur contents than those of Japanese samples. The fact that the sulfur contents of Japanese volcanic rocks are lower than the previously accepted values seems to be characteristic of the islands arc of volcanism.

From the geochemical point of view sulfur is one of the most interesting and important volatile components of magma and is released as a volcanic gas into the atmosphere in the form of either sulfur dioxide or hydrogen sulfide. However, certain amounts are considered to be fixed in igneous rocks in such a form as sulfate or sulfide during the course of crystallization of magma.

Ever since the first work involving a determination of the sulfur in igneous rocks by Clark and Washington,[1] many authors have reported sulfur contents in igneous rocks. Especially, from numerous samples Goldschmidt[2] has determined the average value of the sulfur contents in igneous rocks to be 520 ppm. However, his data, together with those of others, were widely scattered over more than one order of magnitude; thus, these determination methods seemed to lack reliability.

It was until the late 1950's when standard rock samples were prepared by geological surveys in several countries that the accuracies of individual determination methods could be compared with each other by using these standard samples. As a consequence, the reliability and accuracy of the determination method were much improved.[3–14] Ricke[7] has attempted a separate determination of the sulfate and sulfide sulfur in various kinds of igneous rocks; he found the total sulfur contents to be 300 ppm. From a series of such investigations he concluded that sulfur was generally inclined to be contained in alkaline rocks. He further pointed out that sulfide sulfur was more abundant in alkaline rocks whereas sulfate sulfur was rich in silicic rocks. Moore and Fabbi[8] reported the sulfur contents in deep ocean-floor erupted basalts to be 800±100 ppm. Recently Ueda and Sakai[9] pointed out that the sulfur contents of Quaternary volcanic rocks from the Japanese Islands Arc were less than 40 ppm, much lower than those of ocean-floor basalts.

The total sulfur contents of standard rock samples were summarized in review papers by Fleisher,[15] Abbey,[16] and Flanagan.[17] All of these determined values were not always in good agreement among individual standard samples and fell, as a whole, in the range from several tens to several hundreds ppm. However, the total sulfur contents of the standard samples prepared by the Geological Survey of Japan showed with no doubt lower values by one order of magnitude than those of the foreign standard samples.

To find a reliable and feasible method of determining the total sulfur in rocks, we investigated and established several different methods by means of: (1) the photometric method,[18] (2) the sulfide ion selective electrode method,[19] and (3) the fluorometric method.[20] Each of these are based on a wet reduction of the sample by tin(II)–strong phosphoric acid. A fourth method, the UV-photometric method[21] is used after the combustion of a sample with vanadium pentaoxide. The determined values by these methods showed excellent agreement.

In this paper we present the total sulfur contents mainly determined by the photometric method[18] for 140 volcanic rocks in Japan.

Experimental

Detailed descriptions of each method for the determination of the total sulfur in volcanic rocks can be found in previous papers;[18–21] thus, only brief analytical description of the photometric method will be presented in this section.

Finely powdered rock samples are accurately weighed (100—300 mg) and heated with tin(II)–strong phosphoric acid at 280 °C for 15 min in a flow of carbon dioxide or nitrogen gas. Both the sulfate and sulfide sulfur contained in rock samples are separated from other components in a form of hydrogen sulfide. The hydrogen sulfide, thus formed, is absorbed in a zinc sulfate solution to be fixed as a zinc sulfide. In order to completely separate micro amounts of zinc sulfide by means of a centrifugal separator, a zinc hydroxide is coprecipitated by adding a sodium hydroxide solution to the absorbing solution. After separating the supernatant solution, an acetic acid, a mercury(II) thiocyanate–methyl alcohol solution and iron(III) nitrate–

perchloric acid solution are added to the precipitation. The mixture is shaken and diluted with redistilled water. Then, carbon tetrachloride is added and shaken vigorously to adsorb the suspending mercury(II) sulfide on the surface of small drops of carbon tetrachloride. After centrifugation, the absorbance of the supernatant solution is measured at the wavelength of 460 nm against the redistilled water as a reference. A standard sample to make a calibration curve is prepared as follows. Barium sulfate is mixed in an agate motor with a finely powdered obsidian in which no sulfur is assured to be detected by this method. The mixture is diluted with the obsidian several times until the sulfur content becomes 300 ppm. The lowest detectable limit of this method is 10 ppm for total sulfur. The coefficient of variation for five repeat analysis is 5% for a sulfur content of 200 ppm. The determination of the sulfur was performed in association with the main components and other elements such as halogen[22] and boron[23] for samples which were widely gathered from many locations in Japan by people listed in the acknowledgements.

Results and Discussion

Sulfur Contents of Volcanic Rocks in Japan. The total sulfur contents of volcanic rocks in Japan are summarized in Table 1. As should be apparent from Table 1, the determined values are widely scattered from the maximum value of 5390 ppm to the lowest detectable limit of 10 ppm. The sulfur contents of the volcanic rocks can be fairly well expressed as a log-normal type distribution when they are plotted on a logarithmic scale (log S ppm) on a cumulative frequency diagram (Fig. 1). Strictly, this curve seems to be composed of two straight lines with different slopes having a bend around log S=2.0. This feature can also be observed in other volatile components of volcanic rocks. For example, the cumulative frequency distribution of boron deviates from lognormality and the curve is composed of three straight lines; this is well understood by classifying rocks into three groups: alkaline rocks, glassy rocks and the other rocks.[23] However, in the case of sulfur the bend in the curve could not be explained by such a classification into two groups, i.e., alkaline rocks and the rest other rocks, because both curves also showed a bend around log S=2.0 (Fig. 1). The mean value of log S was estimated to be 1.41. The geometric mean of the total sulfur content is 26 ppm with a standard deviation of 0.64 ppm, while the arithmetic mean is 116 ppm. This does not seem to reflect a good representative value of a statistical measure. It should be noted here that there are considerable numbers of samples that contain a total sulfur content less than this lowest limit. Threrefore, a more sensitive method is required in order to determine the exact distribution and geometric mean of the sulfur contents. Alkaline rocks have high sulfur contents, as pointed out by Ricke,[7] and Ueda and Sakai.[9] Their geometric mean is 62 ppm and can be clearly distinguished from those of other rocks by an inspection at the significant level 0.01. Moreover, the rocks from the Circum-Japan Sea Province have a geometric mean of the sulfur contents of 41 ppm, also showing a significant difference from the geometric mean of other rocks (at the significant level 0.05). In Fig. 2 are given the frequency distributions of each of the sulfur contents of three types of rocks classified by the silica content, i.e., rhyolitic rock, andesite and trachyte, and basaltic rock.

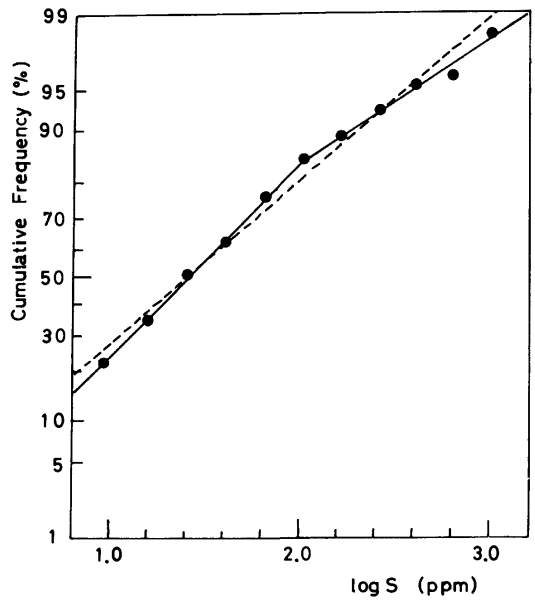

Fig. 1. Cumulative frequency distribution of sulfur contents of volcanic rocks.

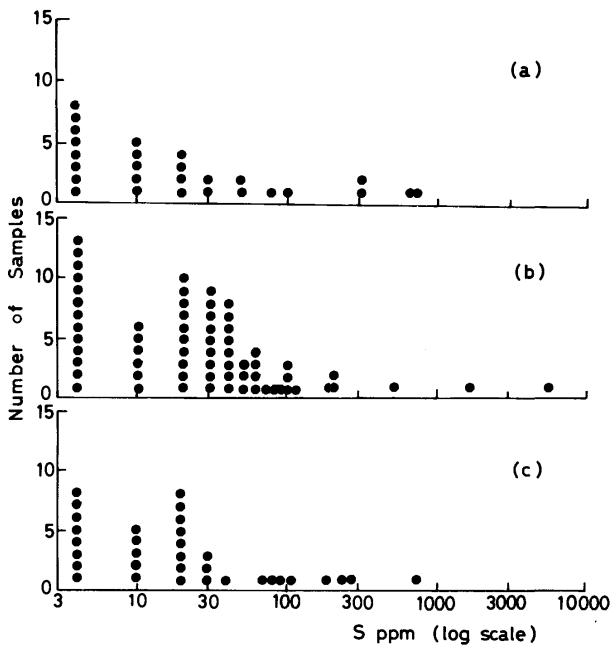

Fig. 2. Frequency distributions of sulfur contents of volcanic rocks.
(a): Rhyolitic rock, (b): andesite and trachyte, (c): basaltic rock.

Table 1. Sulfur Contents of Volcanic Rocks

No.	Sample	*S*/ppm
1	Basalt; Lava of 1950, Mihara-yama, Ō-shima, Tōkyō Metr.	20
2	Basalt; Anei lava, Mihara-yama, Ō-shima	20
3	Basalt; Okata, Ō-shima	40
4	Basalt; Lava of 1962, Miyake-jima, Tōkyō Metr.	10
5	Basalt; Southern coast of Iga-tani, Miyake-jima 660501-9	10
6	Basalt; Southern coast of Iga-tani, Miyake-jima 660501-10	10
7	Basalt; Meiji-lava, Tosa Yuno-hama, Miyake-jima	20
8	Basalt; Kayakuko-ura, Miyake-jima	10
9	Basalt; Oji-ike, Miyake jima	10
10	Basalt; Wall of No. 3 entrance of the crater, Miyake-jima	10
11	Basalt; Northern coast of Ako, Miyake-jima 660501-8-1	20
12	Basalt; Northern coast of Ako, Miyake-jima 660501-8-2	20
13	Basalt; Western foot of Higashi-yama, Hachijō-jima Tōkyō Metr.	30
14	Basalt; Southeastern foot of Nishi-yama, Hachijō-jima	20
15	Basalt; Sakasagawa, Itō. Shizuoka Pref.	10
16	Basalt; Lava of 864, Aokiga-hara, Fuji-san, Yamanashi Pref.; No. 1	<10
17	Basalt; Lava of 864, Aokiga-hara, Fuji-san; No. 2	<10
18	Basalt; Kenmarubi lava, Fuji-yoshida, Fuji-san; No. 3	<10
19	Basalt; Maku-iwa, Fuji-san; No. 4	10
20	Basalt; Shirogane lava, Tokachi-dake, Hokkaidō	20
21	Basalt; Orimoto-tōge lava, Shidara, Aichi Pref.	60
22	Basalt; Orimoto-tōge lava, Shidara	80
23	Basalt; Orimoto-tōge lava, Shidara	210
24	Basalt; Kakuda-yama, Niigata Pref.	10
25	Basalt; Nishimura, Nakamura, Dōgo, Oki, Shimane Pref.	90
26	Basalt; Kuniga, Nishino-shima, Dōdo, Oki	70
27	Basalt; Imazu, Saigō, Oki	30
28	Basalt; Kami-sue, Saigo, Dōgo, Oki	270
29	Basalt; Chika-ishi, Harada, Dōgo, Oki	110
30	Basaltic rock; No. 8 Shimo-motoya, Nakamura, Dōgo, Oki	10
31	Basalt; No. 15 Nishino-shima, Ura-gōri B, Dōgo, Oki	80
32	Basalt; Iwano, Karatsu, Saga Pref.; No. 1	20
33	Basalt; Iwano, Karatsu; No. 2	20
34	Basalt; Taka-shima, Karatsu	20
35	Basalt; Hinode-matsu, Karatsu	<10
36	Basalt; Hanase-zaki Kaimon-dake, Kagoshima Pref.	10
37	Basalt; Trachyandesitic basalt; Intrusive sheet, South of Ōkuwa, Shidara, Aichi Pref.	240
38	Nepheline basalt; Nagahama, Hamada, Shimane Pref.	730
39	Dolerite; Kawai, Shidara, Aichi Pref.	190
40	Basaltic andesite; Dyke, Sukumo-gawa, Hakone, Kanagawa Pref.	<10
41	Chilled margin of dyke No. 31	<10
42	Andesite; Kami-futago-yama, Hakone	60
43	Andesite; Shimo-futago-yama, Hakone	<10
44	Andesite; Nagao-tōge, Hakone	<10
45	Andesite; Southeast of Okimura, Haha-jima, Bonin Islands, Tōkyō Metr.	10
46	Andesite; Kitamuki-kakō lava, Tokachi-dake, Hokkaido	100
47	Andesite; Kami-horokametokku-kabu lava, Tokachi-dake	40
48	Andesite; Kumano-sawa-shita, Tokachi-dake	60
49	Andesite; Lava of parasitic crater (Minami-kakō), Yōtei-zan, Hokkaidō	<10
50	Andesite; Somma lava, Usu, Hokkaidō	<10
51	Andesite; Dome lava, Tarumai-yama, Hokkaidō	30
52	Andesite; Bomb, Tarumai-yama	30
53	Andesite; Eniwa-dake, Hokkaidō	10
54	Andesite; Kenga-mine, Komaga-take, Hokkaidō	20
55	Andesite; Around the crater, Komagatake	20
56	Andesite; Block in a mud flow, Komaga-take	20
57	Andesite; Lava of Yake-yama, Tamagawa Spa, Akita Pref.	40
58	Andesite; Iwaya, Kakuda-yama, Niigata Pref.	20
59	Andesite; Ejecta of Meiji eruption, Azuma-issaikyō-yama, Fukushima Pref.	30
60	Andesite; Lava of 1783, Asama-yama, Gunma Pref.	60
61	Andesite; Dyke, Kuniga, Nishino-shima, Oki, Shimane Pref.	80
62	Andesite; Iimi, Fuse, Dōgo, Oki (epidote, pyrite bearing)	5390
63	Andesite; Chōshi, Harada, Dōgo, Oki	30
64	Andesite; Yunoo, Karatsu, Saga Pref.	<10
65	Andesite; Yakataga-udo, Neko-dake, Aso, Kumamoto Pref.	<10
66	Andesite; South valley of Hinoo-tōge, Neko-dake, Aso	20
67	Andesite; Dyke, Ōshōji-iwa, Yamaguchi-dani, Nekodake, Aso	30
68	Andesite; Chilled margin of dyke, Tengu-iwa, Neko-dake Aso	130
69	Andesite; East valley of Jigoku-dani, Neko-dake, Aso	10
70	Andeside; The 5th valley of western slope of Neko-dake, Aso	10
71	Andesite; Scoria lava of 1958, Neko-dake, Aso	50
72	Andesite; Northern slope of Ōgi-yama, Aso	20
73	Andesite; Sensui-yane, Taka-dake, Aso	30

Table 1. Continued.

No.	Sample	S/ppm	No.	Sample	S/ppm
74	Andesite; Northern slope of Narao-dake, Aso	20	107	Dacite; Usu-dake, Usu	20
75	Andesite; Southern slope of Naka-dake, Aso	30	108	Dacite; Dome lava, Ōusu-dake, Usu	20
76	Andesite; The top of Ōgi-yama, Aso	10	109	Dacite; Komaga-take, Hokkaidō	20
77	Andesite; Southeastern slope of Naka-dake, Aso	10	110	Dacite; Lava of somma, Akagi-yama, Gunma Pref.	10
78	Andesite; Southwestern valley of Naka-dake, Aso	20	111	Dacite; Eboshi-dake, Aso, Kumamoto Pref.	320
79	Andesite; The top of Taka-dake, Aso	90	112	Dacite; Koeboshi, Aso	20
80	Andesite; Eastern slope of Okamado-yama, Aso	10	113	Rhyodacite; Eastern slope of Otogase (Senriga-hama volcano)	30
81	Andesite; Southern slope of Naka-dake, Aso	30	114	Liparite; Tenjō-san, Kōzu-shima, Tōkyō Metr.	10
82	Andesite; Road cutting near the Akamizu station, Aso	20	115	Liparite; Southeastern foot of Tenjō-san, Kōzu-shima	<10
83	Andesite; Kometsuka, Aso	<10	116	Liparite; South of Naga-hama, Kōzu-shima	20
84	Andesite; Bomb, Eastern slope of Ōjō-dake, Aso	30	117	Liparite; Takōdo-yama, Kōzu-shima	<10
85	Andesite; Crater wall of Ōjō-dake, Aso	100	118	Liparite; Mae-hama, Nii-jima, Tōkyō Metr.	10
86	Andesite; Northeastern Eboshi-dake, Shigetama Spa, Aso	50	119	Liparite; Nii-jima	10
87	Andesite; Northern slope of Naka-dake, Aso	10	120	Liparite; Southern coast of Shikine-jima, Tōkyō Metr.	10
88	Andesite; Under the bridge on the Kuro-kawa, Aso	20	121	Liparite; Southeastern coast of Shikine-jima	10
89	Andesite; Lava of 1946, Sakura-jima, Kagoshima Pref.	190	122	Liparite; Nakaya, Fuse, Dōgo, Oki, Shimane Pref.	660
90	Andesite; Lava of 1914, Sakura-jima	200	123	Rhyolitic rock; Nishida, Saigō, Dōgo, Oki	50
91	Andesite; Anei lava, Sakura-jima	110	124	Rhyolitic rock; Igo, Nakamura, Dōgo, Oki; No. 6	10
92	Andesite; Bunmei lava, Sakura-jima	40	125	Potash liparite; Manzō-yama, Shimoda, Shizuoka Pref.	30
93	Andesite; Satsuma-iwō-jima, Kagoshima Pref.	70	126	Alkali rhyolite; Madara-jima, Saga Pref.	100
94	Andesite; Lava of Iwō-dake, inner cliff of Higashi Spa, Satsuma-iwō-jima	100	127	Obsidian; Shirataki, Hokkaidō	<10
95	Andesite; Iwō-dake, Satsuma-iwō-jima	20	128	Obsidian; Wada-tōge (pale part)	<10
96	Andesite; Inamura-dake, Satsuma-iwō-jima	40	129	Obsidian; Koshi-dake, Imari, Saga Pref.	<10
97	Andesite; Yahazu-dake lava, Sakamoto, Satsuma-iwō-jima	50	130	Obsidian; Hime-shima, Ōita Pref.; No. 1	10
98	Andesite; The uppermost lava of Shin-dake, Kuchino-erabu-shima, Kagoshima Pref.	60	131	Obsidian; In a deposit of ejecta of Kikai Caldera, Satsuma-iwō-jima, Kagoshima Pref.	140
99	Glassy andesite; Southern slope of E-san, Hokkaidō	130	132	Obsidian; Mifune	10
100	Glassy andesite; Shōwa-iwō-jima, Satsuma-iwō-jima, Kagoshima Pref.	70	133	Trachyte; Harada, Saigō, Dōgo, Oki, Shimane Pref.	40
101	Glassy andesite; Shōwa-iwō-jima, Satsuma-iwō-jima (pumiceous part)	50	134	Trachyte; Funakoshi, Nishino-shima, Dōgo, Oki	40
102	Dacitic andesite; Sembe-yama, Shimane Pref.	<10	135	Trachyte; Minato, Nakamura, Dōgo, Oki; No. 5	10
103	Trachyandesite; Suribachi-yama, Iwō-jima, Sulfur Islands, Tōkyō Metr.	500	136	Trachyte; Uragōri, Nishino-shima, Dōgo, Oki; No. 14—1	1600
104	Trachyte; Funakoshi, Nishino-shima, Oki, Shimane Pref.	40	137	Trachyte; Uragōri, Nishino-shima, Dōgo, Oki; No. 14—2	200
105	Phonolitic trachyte; Tokage-iwa, Tsuzurao-yama, Dōgo, Oki	30	138	Trachyte; Kojōga-hana, Saigō, Dōgo, Oki; No. 23	40
106	Dacite; Dome lava, Shōwa-shinzan, Usu, Hokkaidō	320	139	Peridotide; Horoman, Hokkaidō	10
			140	Syenite; Oyama, northeastern foot of Takuhi-yama, Nishino-shima, Oki, Shimane Pref.	1550

Each geometric mean is 23 ppm (standard deviation σ=0.72 ppm) for rhyolitic rock, 29 ppm (σ=0.63 ppm) for andesite and trachyte, and 22 ppm (σ=0.61 ppm) for basaltic rock, respectively. No significant difference could be observed among these three types of rocks. Though glassy rocks are enriched in such

Table 2. Comparison of Sulfur Contents of Rock Samples

Sample	Sulfur contents This work a)	b)	c)	d)	ppm References
W-1 Basalt	120				135[7], 124[10], 133[11], 113±2[12] 3[26]
G-1 Granite	40				175[7], 74[10], 65[11], 3[26]
JA-1 Andesite		21.4	22		16[16], 25±5[17]
JB-1 Basalt	20				13.1±2.4[12], 14[16], 50[27]
JB-2 Basalt		17.3	16		19[16], 23±5[17]
JB-3 Basalt		11.1			10±3[17]
JG-1 Granite	20				9.3±0.2[12]
JR-1 Rhyolite		11.7			15±4[17]
JR-2 Rhyolite		11.4			8±2[17]
Andesite-1	200	198	200	200	
Andesite-2	110	103		110	

a) Photometric method.[18] b) Sulfide ion selective electrode method.[19] c) Fluorometric method.[20] d) UV-photometric method.[21]

volatile components as chlorine[22] and boron,[23] the sulfur content of every obsidian, a typical glassy rock, is lower than 10 ppm. This feature is consistent with the experimental result for the sulfur solubility in silicate melts by Katsura and Nagashima,[24] i.e., sulfur has low solubility in silicate melts, especially in silica rich melts. Moreover, sulfur seems to form the heterogeneous phase in silicate rocks even at a fairly low concentration. The sulfur contents of volcanic rocks determined in this study are much lower than those of the igneous rocks reported before. Old data seem to lack reliability concerning the employed determination methods. However, in a recent review by Schneider,[25] the values of the sulfur content of igneous rocks are not so different as the usual values, i.e., about 600 ppm. Samples in his paper are almost entirely from continental, ocean-floor or hot spots; very few are from islands arc. The low sulfur contents of Japanese volcanic rocks may be a characteristic of the islands arc volcanism, as pointed out by Ueda and Sakai.[9] This feature is probably attributed (1) to the extent of an outgassing of sulfur during the course of magmatic emanation and solidification, (2) to the difference of the source magma of the islands arc from those of others, (3) to the isolation of the sulfur containing phase during the fractional crystallization of magma and (4) to the heterogeneous distribution of sulfur in the upper mantle. However, the fact that the sulfur contents of volcanic rocks of the islands arc are low should be discussed more carefully in correlation with the contents of other volatile components.

Comparison of Sulfur Contents of Standard Rock Samples. To confirm the reliability of our determination method, standard rock samples were analyzed by means of three different methods established by the present author;[18-20] the results were compared with those reported by other authors. The sulfur contents of two kinds of andesite were also compared. The results are shown in Table 2. The present three methods (photometric method,[18] sulfide ion selective electrode method,[19] and fluorometric method[20]) are all based on a wet reduction by tin(II)–strong phosphoric acid. These methods together with the UV-photometric method gave good agreeable results for common andesite samples. The results for some standard samples and andesites by the three methods were also in good agreement with each other.

The sulfur content of standard rock sample G-1 (determined by the present author) showed fairly good agreement with those obtained by Frost and Thomas,[10] and Murphy and Sergeant[11] (ranging from 40 to 74 ppm). For the sulfur in W-1, a satisfactory agreement was also obtained between our result and those of Ricke,[7] Frost and Thomas,[10] Murphy and Sergeant,[11] and Ueda and Sakai[12] (showing contents between 120 and 135 ppm). The results of the present author for the standard rock samples of Japan were in good agreement with those by Ueda and Sakai,[12] Terashima,[13] and Terashima et al.[14] (about 20 ppm); this is very close to the geometric mean (26 ppm) of the volcanic rocks in Japan. The sulfur contents of Japanese standard rock samples also show lower values than those of foreign standard rock samples.

The author wishes to express her thanks to emeritus professor Iwaji Iwasaki of Tokyo Institute of Technology for his hearty encouragement throughout this work and professors Takejiro Ozawa of Saitama University and Minoru Yoshida of Tokyo Institute of Technology for their valuable discussions. Thanks are also due to Drs. Ryūji Aoyagi, Shigeo Aramaki, Toshio Ishikawa, Kiyoshi Ishibashi, Jyōyo Ossaka, Takejiro Ozawa, Yoshio Katsui, Takashi Katsura, Masaakira Kamada, the late Isao Kayama and Hisashi

Kuno, Hiroshi Haramura, Hatao Matsumoto, Kenzo Yagi, Masaru Yamaguchi, Kanae Yokoyama and Minoru Yoshida for providing many samples.

References

1) R. W. Clark and H. S. Washington, *U. S. Geol. Surv. Prof. Paper*, **1924**, 127.
2) V. M. Goldschmidt, *Skr. Noeske Videns.-Akad. Oslo, I. Mat.-naturv. Kl.*, No. 4 (1937).
3) M. E. Coller and R. K. Leininger, *Anal. Chem.*, **27**, 949 (1955).
4) R. P. Larsen, L. E. Ross, and N. B. Ingber, *Anal. Chem.*, **31**, 1956 (1959).
5) J. G. Sen Gupta, *Anal. Chem.*, **35**, 1971 (1963).
6) A. D. Wilson, G. A. Sergeant, and L. J. Linnel, *Analyst*, **88**, 138 (1963).
7) W. Ricke, *Geochim. Cosmochim. Acta*, **21**, 35 (1960).
8) J. G. Moore and B. P. Fabbi, *Contrib., Mineral. Petrol.*, **33**, 118 (1971).
9) A. Ueda and H. Sakai, *Geochim., Cosmochim. Acta*, **48**, 1837 (1984).
10) I. C. Frost and J. A. Thomas, cited in M. Fleischer, *Geochim. Cosmochim. Acta*, **29**, 1263 (1965).
11) J. M. Murphy and G. A. Sergeant, *Analyst*, **99**, 515 (1974).
12) A. Ueda and H. Sakai, *Geochemical J.* **17**, 185 (1983).
13) S. Terashima, *Bull. Geol. Surv. Jpn*, **30**, 609 (1979).
14) S. Terashima, T. Yamashige, and A. Ando, *Bull. Geol. Surv. Jpn.*, **35**, 171 (1984).
15) M. Fleischer, *Geochim. Cosmochim. Acta*, **33**, 65, (1969).
16) S. Abbey, *Can. Spectrosc.*, **15**, 10 (1970).
17) F. J. Flanagan, *Geochim. Cosmochim. Acta*, **37**, 1189 (1973).
18) Y. Arikawa, T. Ozawa, and I. Iwasaki, *Bunseki, Kagaku*, **21**, 920 (1972).
19) Y. Arikawa, *Nippon Kagaku Kaishi*, **1986**, 1074.
20) Y. Arikawa and H. Kawai, *Bunseki Kagaku*, **35**, 720 (1986).
21) Y. Arikawa, T. Ozawa, and I. Iwasaki, *Bunseki Kagaku*, **24**, 497 (1975).
22) M. Yoshida, K. Takahashi, N. Yonehara, Y. Ozawa, and I. Iwasaki, *Bull. Chem. Soc. Jpn.*, **44**, 1844 (1971).
23) A. Isozaki, M. Yoshida, S. Utsumi, and I. Iwasaki, *Nippon Kagaku Kaishi*, **1973**, 1896.
24) T. Katsura and S. Nagashima, *Geochim. Cosmochim. Acta*, **38**, 517 (1974).
25) A. Schneider, "Hand Book of Geochemistry," Springer-Verlag, Berlin (1978), Vol. 2, Part 2, 16-E.
26) R. Brown and W. A. Wolstenholme, *Nature*, **201**, 598 (1964).
27) J. L. Bouvier, Private Communication, *Geol. Surv. Canada* (1970).

Studies of the Hydrous Zirconium(IV) Oxide Ion Exchanger. I. Ion-Exchange Properties and Effect of Heat Treatment

Yasushi INOUE* and Hiromichi YAMAZAKI
Department of Nuclear Engineering, Faculty of Engineering, Tohoku University, Aramaki, Sendai 980
(Received August 12, 1986)

A satisfactory method was established for synthesizing a hydrous zirconium(IV) oxide ion exchanger; also, its ion-exchange properties and thermal stability were studied. The exchanger was synthesized reproducibly by hydrolyzing a $ZrOCl_2$ solution at pH 9.3 with the addition of NH_3 aq. This material was an amphoteric ion exchanger possessing an isoelectric point close to pH 6.5. The order of affinity for the cations was, transition metal> alkaline earth metal>alkali metal. Transition metal ions form a coordinate bond with OH groups in the exchanger. The OH groups, which were easily condensed by a heat treatment, were not restored even when the samples subjected to thermal treatment were immersed in water: Thirty percent of the initial ion-exchange capacity was lost when the exchanger was heat-treated at a temperature as low as 70 °C, and the exchange sites were completely destroyed between 400 and 550 °C.

Hydrous oxides based on various polyvalent metal ions have been investigated because of their unique selectivity characteristics and the simplicity of preparation. They have, however, a serious disadvantage in that they give inconsistent results to different workers because of the irreproducibility of the synthesis. To promote a further investigation of this group of ion-exchange materials, it is indispensable to reexamine the synthetic conditions for establishing reproducible methods. With this point in mind, the present authors previously established satisfactory methods for synthesizing such hydrous oxides as $TiO_2 \cdot 2.1\,H_2O$, $SnO_2 \cdot 2.2\,H_2O$, and $Nb_2O_5 \cdot 5.3\,H_2O$; they also studied the ion-exchange selectivity, the thermal stability and other important properties of these materials.[1-3]

Hydrous zirconium(IV) oxide is also an important material of this group of inorganic ion exchangers and there is much left to be studied during a series of these investigations. Since the work of Kraus et al., who first reported that hydrous zirconium(IV) oxide was an amphoteric ion exchanger possessing a large anion-exchange capacity, emphasis has been placed on its anion-exchange property. There are, however, a few reports on the cation-exchange properties of hydrous zirconium(IV) oxide. In addition, the effect of a heat treatment on the ion-exchange properties of the material has not yet been investigated, although inorganic ion exchangers are generally expected to be superior to ion-exchange resins regarding thermal stability.

The present paper deals with a study undertaken to establish a reproducible synthetic method for producing hydrous zirconium(IV) oxide, together with its ion-exchange properties and thermal stability. Among various methods for synthesizing hydrous zirconium-(IV) oxides,[4-9] the hydrolysis of a $ZrOCl_2$ solution by alkaline solutions was adopted, because of its applicability to the synthesis of a large amount of the hydrous zirconium(IV) oxide. A recommended procedure was established after examining the effects of such factors as the concentration of the $ZrOCl_2$ solution, the kind of alkaline solutions used, and the pH value during precipitation on the yield as well as the composition and acid-base property of the product. After the reproducibility of the procedure was confirmed, the distribution coefficients of various cations were measured as functions of the pH and temperature in order to study the cation-exchange mechanism. Furthermore, the thermal stability was studied by examining the effect of a heat treatment on the composition and the ion-exchange property of the material.

Experimental

Reagents and Apparatus. All chemicals were of the highest purity grade supplied by Wako Pure Chemical Industries, Ltd. The specific surface area was determined by the BET method (N_2 adsorption at −196 °C) using a Yanagimoto Surface Area Measuring Apparatus, Model GSA-10. All the other equipment was the same as that described previously.[1-3]

Synthesis. The desired amount of $ZrOCl_2 \cdot 8H_2O$ was dissolved in distilled water to make 1 dm^3. The solution was hydrolyzed by adding (drop by drop) either an NH_3 or an NaOH solution of the molar concentration, 2.5-times that of the zirconium solution, up to a desired molar ratio between hydroxide and zirconium ions. After being separated from the mother liquor by a combination of decantation and filtration through Toyo No. 1 filter paper under suction, the precipitate was uniformly dispersed into 5 dm^3 of distilled water and again filtered after being sedimentated. This procedure was repeated until no chloride ions were detected in the filtrate. Then, the precipitate was air-dried at room temperature. The resulting product was then immersed in water in order to break it down into fine particles, which were subsequently again dried at room temperature. At this stage the yield was calculated based on the zirconium recovery. Particles larger than those desired, if any, were ground in a porcelain mortar and seived in order to obtain the required particle size (−100+200 mesh).

The exchanger was converted to the free acidic form (the H form) by the following column method. In the case of the exchangers precipitated at a pH lower than 7, which may adsorb Cl^- ions, 0.05 mol dm^{-3} NaOH was passed through an exchanger column in order to remove Cl^- ions until the pH of the effluent approached that of the influent. Then, the column was washed with distilled water until no Na^+ ions were detected in the effluent and its pH became nearly constant (pH=6.2—6.5). In the case of the exchangers precipitated in the alkaline region, which may adsorb NH_4^+ or Na^+ ions, 0.05 mol dm^{-3} HCl was passed through the column; the column was then washed until no Cl^- ions were detected in the effluent and its pH became nearly constant (pH=6.2—6.5). As shown in Fig. 1, the constant pH value of the effluent corresponds to the isoelectric point of the exchanger. The exchangers, thus prepared, were air-dried at room temperature and allowed to humidify to a constant weight in a desiccator containing a saturated NH_4Cl solution (relative humidity:79% at 25 °C). Table 1 shows the synthetic conditions, yields and compositions of the exchangers.

Ion-Exchange Capacity. The exchanger (0.20 g) in the H form was immersed in 20 cm^3 of various solutions, prepared by the desired combination of 0.1 mol dm^{-3} NaCl, and 0.1 mol dm^{-3} NaOH or 0.1 mol dm^{-3} HCl, for 6 d at room temperature with intermittent shaking. This was followed by a pH measurement and by a determination of the Na^+ and Cl^- ions. The chloride concentration was determined by the Fajans' method after the solution had been neutralized. The sodium ions were converted to an equivalent amount of sodium chloride and were indirectly determined by titrating the chloride ions. The amount of ions taken up by the exchanger was evaluated from the difference between the initial and the final concentrations of the respective ions present in the solution. The dissolved amount of the exchanger was evaluated from the amount of zircoium in the supernatant solution determined spectrophotometrically by the arsenazo III method.[11] The limit of detection was 0.009 wt% of the exchanger used.

Analysis of Chloride Ions in the Exchanger. A half gram of the sample was dissolved by heating with 100 cm^3 of 9 mol dm^{-3} H_2SO_4 in a 500-cm^3 distilling flask, and the HCl evolving therefrom, carried by steam, was absorbed in a slightly alkaline solution and then determined spectrophotometrically using mercury(II) thiocyanate and ammonium iron(III) sulfate as coloring reagents.[10] The limit of detection was 0.009 wt% of the exchanger used.

Analysis of Sodium Ions in the Exchanger. One tenth gram of the sample was dissolved by heating with 10 cm^3 of 6 mol dm^{-3} HCl. After cooling, 6 mol dm^{-3}, NH_3 aq was added, and the precipitate was filtered and washed with 0.05 mol dm^{-3} HCl. A negligible amount of Na^+ ions was lost by occlusion in the precipitate in this procedure (less than 2 wt% of the Na^+ ion to be determined). The filtrate and the washings were collected in a volumetric flask and then diluted to the mark. The concentration of Na^+ ions in this solution was determined by means of atomic absorption spectrophotometry. The limit of detection was 0.007 wt% of the exchanger used.

Analysis of Water in the Exchanger. A quarter gram of the sample was ignited at 800 °C, and the water content was calculated from the weight loss. The validity of the procedure had been confirmed thermogravimetrically.

Density. The apparent density of the exchangers was measured in the usual manner using a 25-cm^3 pycnometer.

Distribution Coefficients. The distribution coefficients, K_d, were determined in the following way. A 0.12-g portion of the exchanger in the H form was immersed in 7 cm^3 of the solution with a suitable pH value, adjusted by using a desired combination of 0.11 mol dm^{-3} NaCl, and 0.11 mol dm^{-3} HCl or 0.11 mol dm^{-3} NaOH, for 2 d at room temperature. A 1-cm^3 portion of the solution containing the metal ion to be examined was added to the slurry to make the concentration of the cation in the test solution 1×10^{-4} mol dm^{-3} and the ionic strength 0.10 mol dm^{-3}. The mixture was then allowed to stand until the concentration of the cation in the supernatant solution became nearly constant (about 6 to 20 d). The pH and the concentration of the cation in the supernatant solution were then measured. The K_d values were calculated by means of the following equation:

Table 1. Synthetic Conditions and Compositions of the Exchangers

Batch No.	Concn of reagents/mol dm^{-3}			Volume ratio	pH at ppt.	Peptization	Appearence	Yield	Composition
	$ZrOCl_2$	NH_3 aq	NaOH	Alkaline soln. / Zr(IV) soln.					mol H_2O/mol ZrO_2
1	0.2		0.50	0.64	5.22	Yes	Glass	0.48	4.22±0.04
2	0.2		0.50	0.72	7.09	Yes	Glass	0.62	4.16±0.04
3	0.2		0.50	0.80	11.15	Slightly	Glass	0.88	4.10±0.04
4	0.2	0.54		0.59	5.23	Yes	Glass	0.49	4.11±0.04
5	0.2	0.54		0.67	7.16	Yes	Glass	0.69	4.16±0.04
6	0.2	0.54		1.1	9.28	No	Glass	0.93	4.10±0.04
7	0.05	0.10		1.4	9.24	No	Glass	0.93	3.78±0.04
8	1	2.4		1.3	9.31	Slightly	Chalk	0.80	4.04±0.04
9	0.2	0.56		0.96	9.15	No	Glass	0.93	3.78±0.04
10	0.2	0.56		1.1	9.30	No	Glass	0.93	3.89±0.04
11	0.2	0.56		1.4	9.60	No	Glass	0.94	3.99±0.04
12	0.2	0.56[a]		1.1	9.30	No	Glass	0.90	3.97±0.04

a) The rate of addition of alkaline solution: 35 cm^3 min^{-1}, in the other cases 10 cm^3 min^{-1}.

$$K_d = \frac{I-F}{F} \cdot \frac{V}{m} (\mathrm{cm^3\,g^{-1}}),$$

where I and F, respectively, are the initial and final concentrations of the metal ions in the solution, V the volume of the solution in cm^3 and m the weight of the exchanger in grams.

The metal ions were added as their chlorides, except Fe^{3+}, Th^{4+} and UO_2^{2+}, for which the corresponding nitrates were used. The analyses of Cs, Sr, Ba, Mn, Fe, Co, Ce, Eu, and Am were carried out radiometrically using ^{137}Cs, ^{85}Sr, ^{133}Ba, ^{54}Mn, ^{60}Co, ^{144}Ce ^{152}Eu, and ^{241}Am. respectively as tracers. Their radioactive purity was confirmed by means of γ-ray spectrometry. Thorium(IV) and uranium(VI), respectively, were analyzed spectrophotometrically using arsenazo III[11] and 2-(5-Bromo-2-pyridylazo)-5-(diethylamino)phenol[12] as coloring reagents, while the concentrations of the other cations were determined by means of atomic-absorption spectrophotometry.

Heat Treatment. About 5 g of the exchanger in the H form was heated in air to a constant weight at a constant temperature, which was controlled within an accuracy of 1% by using an automatic temperature controller (Chino Workers, Ltd.). After being cooled to room temperature over P_2O_5, the sample was weighed and then immersed in water overnight. The sample was then separated from water and allowed to stand to a constant weight in a desiccator containing a saturated NH_4Cl solution (humidifying operation). The water-recovery of the heat-treated samples was calculated from the difference in water content between samples cooled over P_2O_5 immediately after the heat treatment and subjected to a humidifying operation.

The other experimental procedures were the same as those described previously.[1-3]

Results and Discussion

Synthesis of Hydrous Zirconium(IV) Oxide. It is required for practical purposes that a large amount of pure hydrous zirconium(IV) oxide having reproducible and good ion-exchange properties can be easily prepared; in conformity with this line, we examined the effect of synthetic conditions on the yields and the acid-base properties of the products.

The effect of the pH during precipitation (OH^-/Zr^{4+} molar ratio) and of the kind of alkali used on the uptake curves for Na^+ ions are shown in Fig. 1. This figure indicates that the products are amphoteric ion exchangers possessing larger ion-exchange capacities for anions than for cations and have an isoelectric point close to pH 6.5. The ion-exchange capacity is slightly smaller for the products precipitated from alkaline solutions than for those from acidic or neutral solutions. It is, however, considered that the ion-exchange behavior is not very much affected by the kind of alkali used and the pH during precipitation, since the maximum difference in the ion-exchange capacity is only 0.15 m mol g^{-1}. In contrast, the yield was significantly affected by these factors, as is shown in Table 1. The decrease in the yield is due mainly to the peptization of the precipitate during washing. Only the precipitate formed at around pH 9 by adding NH_3 aq can be washed without sufferings from peptization, and affords an excellent yield exceeding 90%. Efforts were then concentrated on examining the properties of the exchanger precipitated under these conditions.

In order to prepare a large amount of the exchanger in one batch, it is preferred to use a concentration of zirconium during precipitation that is as high as possible. The uptake curves of the exchangers prepared from different concentrations of zirconium (batch (6)—(8)in Table 1) are compared in Fig. 2; this

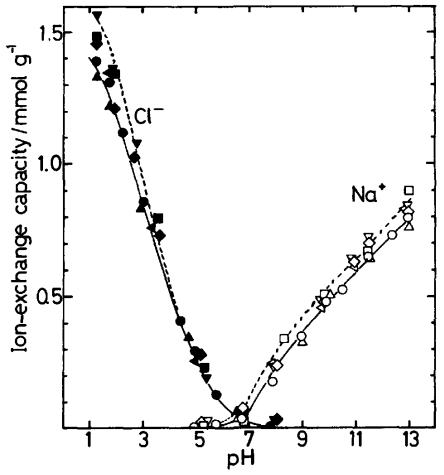

Fig. 1. Uptake curves of various exchangers for Na^+ and Cl^- (Effects of alkali used and pH at precipitation). Exchangers; ◁: No. 1, ◇: No. 2, △: No. 3 (NaOH system). ▽: No. 4, □: No. 5, ○: No. 6(NH_3 system). The numbers are the same as those in Table 1.

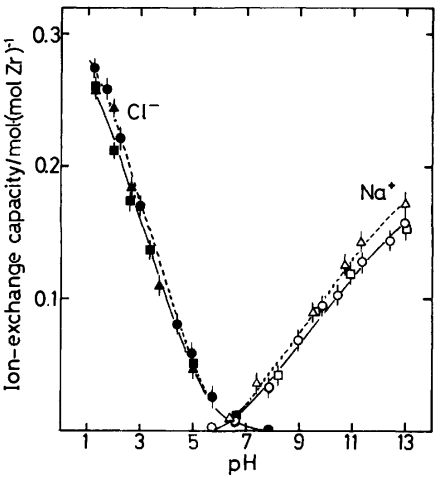

Fig. 2. Uptake curves of various exchangers for Na^+ and Cl^- (Effect of Zr-concentration at precipitation). Exchangers; ○: No. 6, □: No. 7, △: No. 8. The numbers are the same as those in Table 1.

indicates that the concentration did not appreciably affect the ion-exchange property. However, the concentration of zirconium did influence the yield and the physical properties of the product; the exchangers precipitated from the solution with a high concentration of zirconium (1 mol dm^{-3}) had poor physical strength (brittle chalk), while those precipitated from a dilute solution of zirconium had a large, glassy grains. The yield decreased with increasing concentration of zirconium due to the accentuating degree of peptization during washing. Thus, 0.2 mol dm^{-3} of zirconium concentration was selected for preparing the exchanger.

While the water content of the products slightly increased with the volume of NH_3 aq added (less than 5%), the ion-exchange capacity remained unchanged within the limit of the experimental error, as is shown in Table 1 (batch (9)—(11)). Furthermore, the rate of addition of NH_3 aq was not found to affect the composition and ion-exchange properties of the products. Therefore, no exact control of the procedure is necessary; thus, the present method for preparing hydrous zirconium(IV) oxide is considered to be fairly reproducible.

From these results, the synthetic conditions of batch (10) in Table 1 was selected as being the best method for reproducibly synthesizing a hydrous zirconium-(IV) oxide ion exchanger. The contents of both Na^+ and Cl^- ions as impurities were below the limit of detection (0.007 wt%). Thus, the conditioning is effective for converting the exchanger into the H form. The composition of the product was $ZrO_2 \cdot (3.8—4.1)H_2O$, in agreement with that of fully-hydrolyzed zirconium(IV) hydroxide, $Zr_4(OH)_{16}(H_2O)_8$, which was reported by H. Th. Rijnten in the study of the hydrolysis of $ZrOCl_2$ solution.[13] The solubilities of the exchanger in 0.1 mol dm^{-3} NaOH- and HCl solutions were determined to be 0.01 and 0.07 wt%, respectively; this assures the applicability of the exchanger in pH region.

Selectivity for Cations. Figure 3 shows the pH-dependency of the K_d values for the representative elements. As can be seen from this figure, the affinity of the exchanger is much greater for alkaline earth metal ions than for alkali metal ions; this indicates that the electrostatic interaction between counter ions and ion-exchange sites is an important factor in governing the selectivity of the hydrous zirconium(IV) oxide. The higher K_d values for Li^+ than for Cs^+ may suggest that removal of the solvated water molecules from counter ions. However, there is no difference in the affinity between alkaline earth metal ions.

Figure 4 shows the pH-dependency of the K_d values for transition metal ions. The affinity of the exchanger was much greater for the transition metal ions than for the representative elements. The order of selectivity for the transition metals, $Fe^{3+} >> UO_2^{2+} > Th^{4+} >> Am^{3+} > Eu^{3+} > Ce^{3+} > Zn^{2+} > Co^{2+} > Mn^{2+}$, indicates the general trend that the exchanger exhibits a preference for transition metal ions with a larger ionic charge and a smaller crystalline radius. The distribution coefficients for Th^{4+}, which are smaller than would be expected from the ionic charge, are

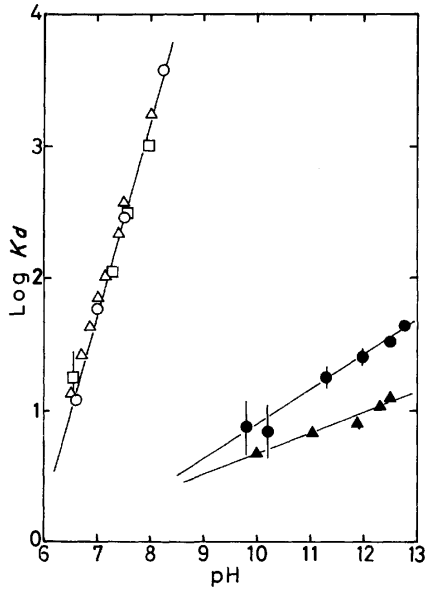

Fig. 3. Log K_d for several representative metal ions. Ionic strength: 0.10 mol dm^{-3} (NaCl-NaOH) at room temperature. Initial concentration of cation: 1×10^{-4} mol dm^{-3}. Cations; ●: Li^+, ▲: Cs^+, □: Mg^{2+}, ○: Sr^{2+}, △: Ba^{2+}.

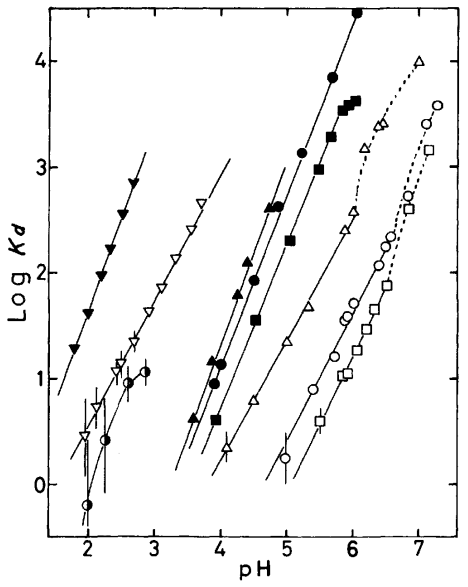

Fig. 4. Log K_d for several transition metal ions. Ionic strength: 0.10 mol dm^{-3} (HCl-NaCl) at room temperature. Initial concentration of cations: 1×10^{-4} mol dm^{-3} (Am^{3+}: Tracer scale). Cations; □: Mn^{2+}, ○: Co^{2+}, △: Zn^{2+}, ▼: Fe^{3+}, ■: Ce^{3+}, ●: Eu^{3+}, ◑: Th^{4+}, ▽: UO_2^{2+}, ▲: Am^{3+}.

attributable to the hydrolysis of ions in the pH region effective for sorption (pH>2). On the other hand, K_d values for UO_2^{2+} ions, which are higher than expected from the ionic charge, may be due to the peculiarity of the structure of UO_2^{2+} ions; the efffective charge on a uranium atom is higher than the formal charge of the ions. With these exceptions, the electrostatic force may be considered as being an important factor in determining the selectivity of the hydrous zirconium(IV) oxide for the transition metals.

In order to obtain further information on the important factors affecting the selectivity for the transition metals, the K_d values at pH 4 were compared with their first hydrolysis constants[14] and the first stability constants of their acetato complexes.[15] The results are shown in Table 2, where the

Table 2. Interaction between Cations and Exchange Sites

Metal ion	Log K_d(at pH 4)	A[1]	B[2]
UO_2^{2+}	2.9	−5.8	2.61
Fe^{3+}	5.1	−2.19	3.36
Eu^{3+}	1.2	−7.8	2.13
Ce^{3+}	0.69	−8.3	1.91
Zn^{2+}	0.22	−9.0	1.3
Co^{2+}	−0.73	−9.7	1.1
Mn^{2+}	−1.2	−10.6	0.8
		R=0.99	
		R=0.98	

1) $A=\log K_{11}(OH^-)$: First hydrolysis constant.[14] 2) $B=\log K_{11}(CH_3COO^-)$: First stability constant(equilibrium quotient at 25 °C and ionic strength 0.1)[15] R: Correlation coefficient.

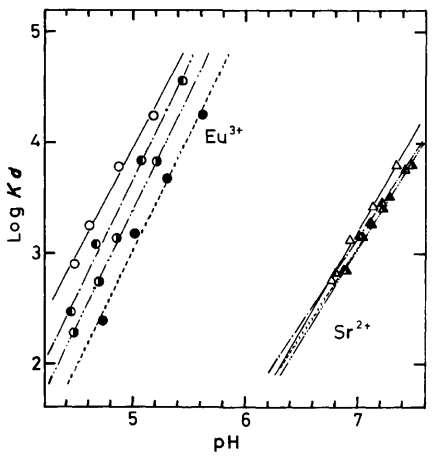

Fig. 5. Temperature dependence of K_d values for Sr^{2+} and Eu^{3+} ions.
Initial concentration of metal ions: 1×10^{-6} mol dm^{-3}. Ionic strength: 0.10 mol dm^{-3} (HCl-NaCl-NaOH). Temperature/°C; ▲●: 14.8, ◭◑: 25.2, ◭◐: 34.5, △○: 44.8.

K_d values which could not be obtained experimentally were estimated from an extrapolation of the log K_d vs. pH plot to pH 4 (Fig. 4). This table indicates that the K_d values is very strongly related to the hydrolysis constants (R=0.99) and the stability constants (R=0.98). Figure 5 shows the temperature-dependence of K_d values for Sr^{2+} and Eu^{3+} ions. The values for Sr^{2+} ions depended little on the temperature, while those for Eu^{3+} ions increase with temperature, indicating an endothermic reaction. From the slope of the linear plot of the logarithm of K_d against $1/T$, the standard enthalpy change of the latter reaction was found from a calculation to be 55±6 kJ mol^{-1}; this is considerably larger than the values (<10 kJ mol^{-1}) associated with the exchange of the dissociated ions in the exchanger and the counter ions in solutions. From these results, we concluded that the formation of a coordination bond between anionic sites in the exchanger and counter cations plays a part in determining the selectivity of the exchanger, along with the remote coulombic interaction. This consideration is in line with the fact that the affinity with the exchanger was greater for transition metals than for representative elements, since the former is stronger than the latter as Lewis acids.

Thermal Stability. Figure 6 shows the effect of a heat treatment of the hydrous zirconium(IV) oxide on the composition and the specific surface area. It should be noted that the water content was normalized to the number of moles of water per 1 mole of ZrO_2. The amount of water contained in the exchanger immediately after the heat treatment at 70 °C was reduced to about 30% of the original value; then, it gradually decreased with temperature, and finally fell to zero at 400 °C. When the exchangers heated at temperatures up to 400 °C were subjected to the humidifying operation, a roughly constant amount of water, viz. 0.85 to 1.4 mole per 1 mole of ZrO_2, was recovered, while the samples heated over 550 °C

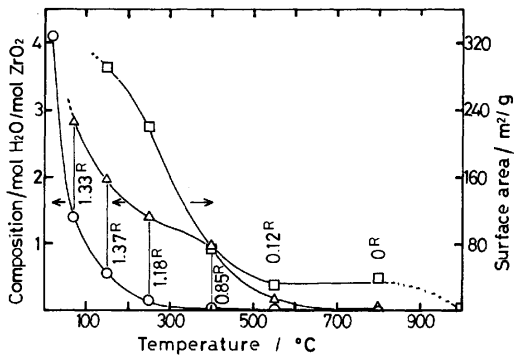

Fig. 6. Change in composition and surface area.
Water content; ○: Immediately after heat treatment, △: Heat-treated, followed by humidifying operation. R: Water recovery. □: Specific surface area of heat-treated sample.

recovered a negligible amount of water. The amount of water recovery as a result of humidifying the exchangers heat-treated even at a temperature as low as 70 °C fell short of the full recovery by 1.4 mole of water per 1 mole of ZrO_2. The surface area decreased sharply with increasing temperature up to 550 °C, where the surface area became nearly constant (40 $m^2 g^{-1}$). As is shown in Table 3, the density of the samples immediately after the heat treatment increased with temperature, approaching to a constant value of 5.53±0.08 g cm^{-3} at 550 °C. This value corresponds to the density of tetragonal ZrO_2, 5.60 g cm^{-3} within the limit of experimental error.

In order to examine the effect of the heat treatment on the acid-base property of the exchanger, the ion-exchange capacities for Na^+ or Cl^- ions were measured as a function of the pH (Fig. 7). The ion-exchange capacities for both ions decreased even at a temperature as low as 70 °C, and were reduced to about 30 % of the original value when the exchanger was heated at 250 °C. The sample heated at 550 °C exhibited a very small exchange capacity for only Cl^- ions. Therefore, the exchange sites of the hydrous zirconium(IV) oxide is susceptible to thermal decomposition.

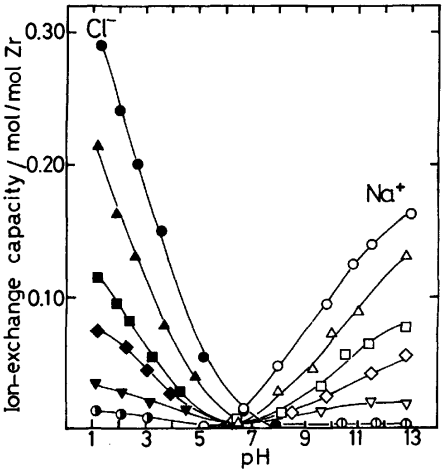

Fig. 7. Uptake curves for Cl^- and Na^+ ions (Effect of thermal treatment).
Temperature of treatment/°C; ○: R. T., △: 70, □: 150, ◇: 250, ▽: 400, ⓓ: 550.

Figure 8 shows DTA curves for the samples subjected to the humidifying operation. The large endothermic peaks appearing in the range lower than 200 °C sharpened and became smaller in area as the temperature of the heat treatment became higher. The position of the peak, observed at 80 °C for the sample without heat treatment, shifted to the lower-temperature side upon increasing the temperature of the heat-treatment (gradually up to 400 °C, and then abruptly). When the exchanger was heat-treated at 550 °C, the peak shifted to 40 °C and developed a very small area. Apparently, this observation is compatible with changes in both the exchange capacity and the degree of water recovery with the heat-treatment temperature, if the peak is considered to correspond mainly to the release of water recoverable by humidifying, that is, a certain kind of zeolitic water. The shoulders observed at the high- and low-

Table 3. Density of the Samples Immediately after the Heat Treatment

Temperature of treatment / °C	Density / g cm^{-3}
150	4.30±0.07
250	5.15±0.06
550	5.53±0.08
700	5.53±0.06

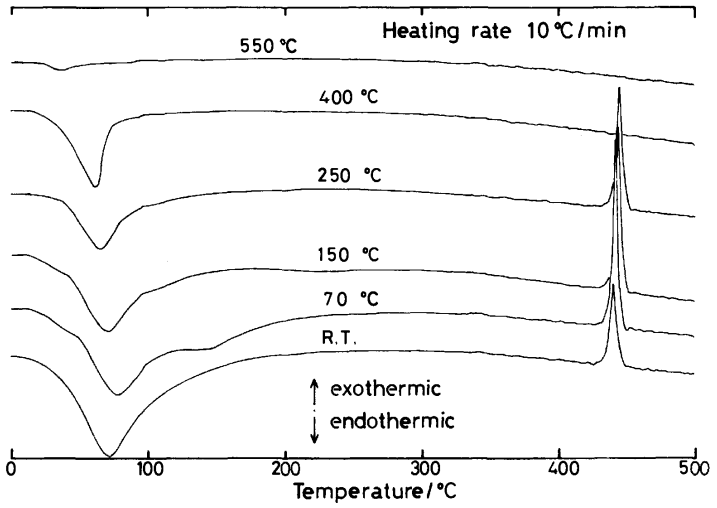

Fig. 8. DTA curves of the samples subjected to the humidification.

temperature sides, respectively, of the peak for the samples heated at temperature below 150 °C are attributable to the bound water liberated by the condensation of the hydroxyl groups and to the adherent water in the exchanger matrix. As the area under the shoulder decreased with increasing temperature of the treatment, both bound and adherent water are considered to be released irreversibly. A large exothermic peak observed at 430 °C for samples heated at a temperature below 400 °C may be assigned to the crystallization of the exchanger as judged from the change in the degree of recovery of water, in the density and in the exchange capacity of the samples. Rijnten obtained a similar thermogram for hydrous zirconium(IV) oxide prepared by a similar method to the present study. In his report, the exothermic peak at 405 °C was attributed to crystallization into monoclinic ZrO_2, which eventually transformed into a mixture of tetragonal and monoclinic ZrO_2 at 800 °C.[13] In the present experiment, however, X-ray studies made on the samples heated at 550 and 800 °C, showed no diffraction peak in spite of prolonged heating for 72 h; a few peaks, indicating the formation of a mixture of tetragonal and monoclinic ZrO_2, appeared only when the sample was heated at 1000 °C for 72 h. With the appearence of such peaks, the surface area of the sample suddenly decreased to about 5 $m^2 g^{-1}$.

From the above observations, the thermal stability of the hydrous zirconium(IV) oxide can be summarized as follows. When the exchanger is heat-treated at a low temperature, a disordered network structure, formed at precipitation, is stabilized by irreversibly releasing adherent water and a portion of structural water. Then, the stabilized matrix can accommodate an approximately constant amount of water which can be recovered by humidification. With the stabilization of the network structure, the water molecules formed by the condensation of a part of the OH groups in the exchanger together with the water molecules bound to these groups are released irreversibly, even at low temperatures, causing a decrease in the ion-exchange capacity. The crystallization occuring at temperatures between 400 to 550 °C brings about densification as well as a decrease in the surface area and in the interstitial space which can accommodate water molecules. Thus, almost all the water is not recovered by the humidifying operation and the ion-exchange capacity completely disappears.

References

1) Y. Inoue and M. Tsuji, *J. Nucl. Sci. Technol.*, **13**, 85 (1976); *Bull. Chem. Soc. Jpn.*, **49**, 111 (1976); **51**, 479, 794 (1978).

2) Y. Inoue and H. Yamazaki, *Bull. Chem. Soc. Jpn.*, **55**, 3782 (1982); **57**, 1534, 3437 (1984); Y. Inoue, H. Yamazaki, and H. Nakamizo, *ibid.*, **58**, 1292 (1985).

3) Y. Inoue, H. Yamazaki, and Y. Kimura, *Bull. Chem. Soc. Jpn.*, **58**, 2481 (1985); Y. Inoue, H. Yamazaki. K. Okada, and K. Morita, *ibid.*, **58**, 2955 (1985); Y. Inoue, H. Yamazaki, and Y. Matsuda, *ibid.*, **58**, 3225 (1985).

4) C. B. Amphlett, L. A. McDonald, and M. J. Redman, *J. Inorg. Nucl. Chem.*, **6**, 236 (1958).

5) K. A. Kraus, H. O. Phillips, T. A. Carlson, and J. S. Johnson, *Proc. Int. Conf. Peaceful Uses Atomic Energy, Geneva*, **28**, 3, United Nations (1959).

6) G. H. Nancollas and R. Paterson, *J. Inorg. Nucl. Chem.*, **29**, 565 (1967).

7) A. Clearfield, *Inorg. Chem.*, **3**, 146 (1964).

8) D. Britz and G. H. Nancollas, *J. Inorg. Nucl. Chem.*, **31**, 3861 (1969).

9) S. Tustanowski, *J. Chromatogr.*, **31**, 268, 270 (1967).

10) A. Tomonari, *Nippon Kagaku Kaishi*, **83**, 693 (1962).

11) H. Onishi, *Japan Analyst*, **12**, 1153 (1963).

12) D. A. Johnson and T. M. Florence, *Anal. Chim. Acta*, **53**, 73 (1971); *Talanta*, **22**, 253 (1975).

13) H. Th. Rijenten, "Formation, Preparation and Properties of Hydrous Zirconia," in "Physical and Chemical Aspects of Adsorbents," ed by B. G. Linsen, Academic Press, London and New York (1970), Chap. 7.

14) C. F. Baes, Jr., and R. E. Mesmer, "The Hydrolysis of Cations," John Wiley and Sons, New York (1976).

15) A. E. Martell and R. M. Smith, "Critical Stability Constants, Volume 3: Other Organic Ligands," Plenum Press, New York (1977), p. 3.

 © 1987 The Chemical Society of Japan Bull. Chem. Soc. Jpn., 60, 899—902 (1987)

Structure of Aquachloro(4-hydroxy-L-prolinato)copper(II)

Shiroo Itoh, Yasuhiko Yukawa,* Yoshie Inomata, and Toshio Takeuchi
Department of Chemistry, Faculty of Science and Technology, Sophia University,
7-1, Kioi-cho, Chiyoda-ku, Tokyo 102
(Received August 13, 1986)

An X-ray diffraction study of the title complex has been carried out. The crystal is monoclinic, with the space group $P2_1$; $Z=2$, $a=8.712(1)$, $b=6.055(1)$, $c=8.187(1)$ Å, $\beta=109.83(1)°$. Block-diagonal least-squares refinements have led to the final R value of 0.052. The structure consists of a one-dimensional polymer chain bridged by only one carboxylato group of a 4-hydroxy-L-prolinato ligand. The chains are parallel to the b axis; each is connected with the neighboring one by hydrogen bonds between water oxygen atoms and chlorine atoms. Thus a sheet forms parallel to the (0 0 1) plane. One carboxylato oxygen atom of the 4-hydroxy-L-prolinato ligand is coordinated to two copper atoms, and the other is coordinated to one of these two copper atoms. The copper atom is surrounded by three carboxylato oxygen atoms, one water oxygen atom, one nitrogen atom in a pyrrolidine ring, and one chlorine atom. Therefore the copper atom has distorted octahedral coordination.

The amino acids having a pyrrolidine ring, 4-hydroxy-L-proline (Hhpro) and L-proline (Hpro), are a little different from other α-amino acids. Some interesting properties of their metal complexes have been reported: for example, the studies of circular dichroism spectra[1,2] and of stereoisomerism.[3] The properties of their complexes are based on the structures. Therefore studies about syntheses, properties, and structures of some metal complexes with Hhpro and Hpro have been carried out in our group.[4–6]

Two copper(II) complexes with hpro has been reported:[5] one is [Cu(hpro)$_2$] and the other is [CuCl(hpro)(H$_2$O)]. The structure of the latter complex was determined by infrared spectra. In the free ligand, Hhpro, there are some peaks assigned to NH_2^+ stretching and bending vibrations. On the other hand, in the complex there are peaks assigned to NH vibrations without any assigned to NH_2^+. The peak assigned to Cu-Cl stretching vibration is observed at about 280 cm^{-1}. This is a rather low frequency, if we assume that the chlorine atom is a terminal one. For example, ν_{CuX}(terminal)=311 cm^{-1}, ν_{CuX}(bridge)=280, 230 cm^{-1} for $(NH_4)_2[Cu_2Cl_6]$, ν_{CuX}(terminal)=301 cm^{-1}, ν_{CuX}(bridge)=278, 236 cm^{-1} for $K_2[Cu_2Cl_6]$.[7] Therefore the peak should be considered to be based on the bridged chlorine atom and the metal bonding. However, it is difficult to determine the structure from the infrared spectra.

In this work, the confirmation of the structure [CuCl(hpro)(H$_2$O)] by an X-ray diffraction study and the interpretation of the properties based on the structure were carried out.

Experimental

Preparation of the Sample. The samples for the X-ray diffraction study were prepared in the following way, modifying the previous method:[5] equimolar amounts of $CuCl_2 \cdot 2H_2O$ and Hhpro were mixed in aqueous solution, then the aqueous solution was condensed at 60—70 °C for several hours. The sample crystals were obtained from the aqueous solution of the complex by keeping it in a desiccator containing acetone for several days.

Table 1. Crystal Data

$CuCl(C_5H_8NO_3)(H_2O)$	$F.W.=247.14$
Monoclinic	Space group $P2_1$
$a=8.712(1)$ Å	
$b=6.055(1)$ Å	$\beta=109.83(1)°$
$c=8.187(1)$ Å	
$Z=2$	$U=406.3(1)$ Å^3
$D_m=2.015(3)$ g cm^{-3}	$D_x=2.020$ g cm^{-3}
μ(Mo $K\alpha$) = 30.9 cm^{-1}	

X-Ray Measurements and Structure Determination. The crystal data are given in Table 1. The reflection intensities were collected by the θ—2θ scan techniqe ($2\theta<76°$) on a Philips PW1100 automated four-circle diffractometer. The 2253 intensities ($|F_o|>3\sigma(|F_o|)$) were corrected for Lorentz and polarization factors, but not for absorption, because of the low magnitude of μr(=0.46). All calculations were carried out on a HITAC M-200H/M-280H computer at the Computer Center of The University of Tokyo, using the local version of the UNICS.[8] The scattering factors were taken from tables.[9] The structure was solved by a heavy-atom method and refined by a block-diagonal least-squares method. The positions of hydrogen atoms, except for hydroxyl and water hydrogen atoms, were obtained by difference-Fourier syntheses. The weighting scheme was $W=1/[\{\sigma(|F_o|)\}^2+(0.02\times|F_o|)^2]$. The final R value[10] was 0.052.

Results and Discussion

The final atomic parameters are listed in Table 2,[11] the interatomic distances in Table 3, and the bond angles in Table 4. The perspective drawing of the complex and the numbering scheme of the atoms are shown in Fig. 1.

The structure of the complex consists of a one-dimensional polymer chain bridged by only one carboxylato group of hpro. One carboxylato oxygen atom of the hpro is coordinated to two copper atoms to form an oxygen bridge, and the other is coordinated to one of these two copper atoms.

The copper atom is surrounded by six atoms: Three carboxylato oxygen atoms, one water oxygen atom, one nitrogen atom in a pyrrolidine ring, and one chlorine atom. Among them, the O(11)^{I} and Cl are at a longer distance from the metal than the others. The angle O(11)^{I}–Cu–O(12)^{I} is 54.4(1)°. Therefore the octahedron surrounding the copper atom is extremely distorted.

The prediction given by the infrared spectra was confirmed: The nitrogen atom in the pyrrolidine ring

Table 2. Final Positional Parameters ($\times 10^4$ for non-hydrogen atoms; $\times 10^3$ for hydrogen atoms) and equivalent isotropic temperature factors (B_{eq}/Å^2),[a] with the estimated standard deviations.

Atom	X	Y	Z	B_{eq}/Å^2
Cu	1873.1(4)	−2500	4807.6(4)	1.42
Cl	3041(1)	−5540(2)	3373(2)	2.45
O(11)	331(3)	−4442(5)	5303(3)	1.87
O(12)	−158(3)	−6389(5)	7344(3)	1.79
O(4)	4170(3)	−1044(6)	11145(3)	2.17
O(W)	3417(3)	−391(5)	4353(4)	2.09
N	3045(3)	−2551(6)	7406(3)	1.41
C(1)	661(4)	−4987(5)	6882(4)	1.35
C(2)	2052(4)	−3832(5)	8241(4)	1.36
C(3)	1430(4)	−2140(7)	9258(5)	2.18
C(4)	2750(4)	−377(6)	9737(4)	1.88
C(5)	3227(5)	−247(7)	8119(4)	2.14
				B_{iso}/Å^2
H(2)[b]	268(5)	−502(10)	904(7)	1.2(8)
H(31)	153(7)	−284(14)	1000(9)	3.6(15)
H(32)	55(8)	−180(19)	852(14)	5.2(20)
H(4)	229(6)	103(12)	991(8)	1.8(10)
H(51)	247(6)	56(11)	725(9)	2.4(12)
H(52)	477(10)	−55(28)	837(16)	8.6(31)
H(N)	390(5)	−330(10)	775(7)	1.2(9)

a) The equivalent isotropic temperature factors for non-hydrogen atoms were computed using the following expression:

$B_{eq}=4/3(B_{11}a^2+B_{22}b^2+B_{33}c^2+B_{13}ac\cos\beta)$.

The B_{ij}'s are in the form:

$\exp\{-(h^2B_{11}+k^2B_{22}+l^2B_{33}+2klB_{23}+2hlB_{13}+2hkB_{12})\}$.

b) The numbering scheme of hydrogen atoms is based on the number of the atom attached to the hydrogen atoms.

Table 3. Interatomic Distances (l/Å), with the Estimated Standard Deviations in Parentheses

Cu–Cl	2.571(2)	C(1)–C(2)	1.510(5)
Cu–O(11)	1.930(4)	C(2)–C(3)	1.530(7)
Cu–O(11)^{I}	2.647(4)	C(3)–C(4)	1.519(5)
Cu–O(12)^{I}	2.001(3)	C(4)–C(5)	1.519(9)
Cu–O(W)	1.980(4)	C(4)–O(4)	1.434(5)
Cu–N	2.024(5)	C(5)–N	1.499(6)
C(1)–O(11)	1.269(7)	N–C(2)	1.490(6)
C(1)–O(12)	1.248(5)		
C(2)–H(2)	1.00(7)	C(5)–H(51)	0.93(8)
C(3)–H(31)	0.73(12)	C(5)–H(52)	1.34(10)
C(3)–H(32)	0.83(10)	N–H(N)	0.84(5)
C(4)–H(4)	0.98(8)		
O(W)–Cl^{II}	3.034(5)	Cl–O(W)^{III}	3.017(3)

Key to symmetry operations: I. $-x$, $0.5+y$, $1.0-z$; II. x, $1+y$, z; III. $1-x$, $-0.5+y$, $1-z$.

Table 4. Bond Angles (ϕ/°), with the Estimated Standard Deviations in Parentheses

Cl–Cu–O(11)	94.1(1)	C(1)^{I}–O(11)^{I}–Cu	76.4(3)
Cl–Cu–O(W)	88.7(1)	C(1)^{I}–O(12)^{I}–Cu	107.2(3)
Cl–Cu–N	109.4(2)	O(11)–C(1)–O(12)	122.1(4)
Cl–Cu–O(11)^{I}	151.6(1)	O(11)–C(1)–C(2)	118.5(4)
Cl–Cu–O(12)^{I}	97.6(1)	O(12)–C(1)–C(2)	119.3(4)
O(11)–Cu–O(W)	177.3(2)	C(1)–C(2)–N	110.4(4)
O(11)–Cu–N	84.7(2)	C(1)–C(2)–C(3)	111.5(3)
O(11)–Cu–O(11)^{I}	83.4(1)	N–C(2)–C(3)	105.6(3)
O(11)–Cu–O(12)^{I}	91.5(1)	C(2)–C(3)–C(4)	103.5(4)
O(W)–Cu–N	94.4(2)	C(3)–C(4)–O(4)	112.3(4)
O(W)–Cu–O(11)^{I}	94.2(1)	O(4)–C(4)–C(5)	107.5(4)
O(W)–Cu–O(12)^{I}	88.2(1)	C(3)–C(4)–C(5)	102.6(4)
N–Cu–O(11)^{I}	98.6(2)	C(4)–C(5)–N	105.5(4)
N–Cu–O(12)^{I}	153.0(2)	Cu–N–C(5)	110.1(3)
O(11)^{I}–Cu–O(12)^{I}	54.4(1)	Cu–N–C(2)	109.1(2)
Cu–O(11)–C(1)	116.1(3)	C(5)–N–C(2)	107.9(4)
Cu–O(11)^{I}–Cu^{I}	165.5(2)		

Key to symmetry operation: I. $-x$, $0.5+y$, $1.0-z$.

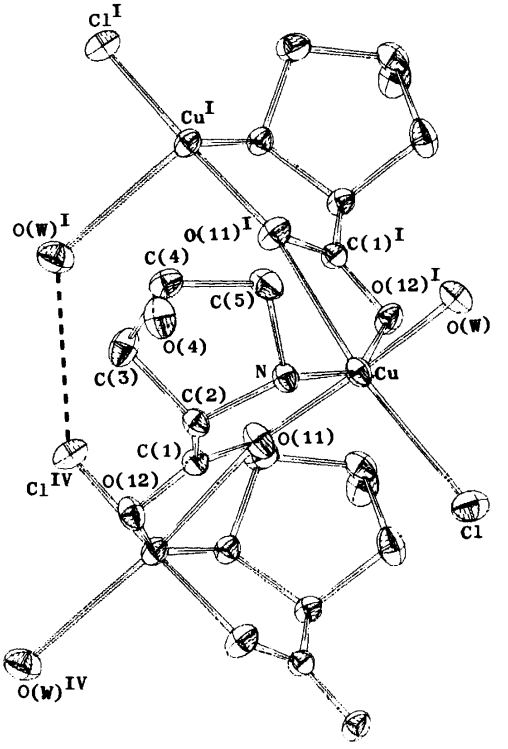

Fig. 1. The perspective drawing of [CuCl(hpro)(H_2O)] and the numbering scheme of the atoms. (----: Hydrogen bonding).
Key to symmetry operations: I. $-x$, $0.5+y$, $1.0-z$; IV. $-x$, $-0.5+y$, $-z$.

is coordinated to the metal. The bond length of Cu–N, 2.024(5) Å, is not very different from that of common amino acid chelate compounds.

The distance of Cu–O(11)^{I}, 2.647(4) Å, is rather longer than the common Cu–O bond. However, this is not so surprising, because similar or more extreme examples have been reported in copper(II) oxalate,[12] bis[(alkylthio)acetato]copper(II)–amine adduct,[13] and mixed amino acid copper complexes.[14,15] The chlorine atom is coordinated to the metal not as a bridging atom, but as a terminal one. In the classification according to bond lengths, the Cu–Cl bond, 2.571(2) Å, however, should belong to Cu–Cl(bridging) rather than of Cu–Cl(terminal). For example, Cu–Cl(bridging): 2.337 Å and 2.769 Å in dichloro(1,2,4-triazole)copper(II),[16] Cu–Cl(terminal): 2.241(6) Å in dichlorobis(tetramethylthiourea)copper-(II).[17]

The bond distances and angles of the binding hpro are not very different from those of the free molecule. In the free molecule the four atoms of a pyrrolidine ring are nearly coplanar, except for the carbon atom carrying a hydroxyl group.[18] On coordination, however, the pyrrolidine ring is bent on the line from N to C(3), and C(4) and C(5) deviate from the plane formed by C(2), N, and C(3) in the direction against the carboxylato group. The deviation is in the opposite direction to that of the Hhpro in [$CdCl_2$-(Hhpro)].[4]

There are two types of chelate rings in this complex. One is the five-membered ring which is formed by Cu, O(11), C(1), C(2), and N, the other is the four-membered ring formed by Cu, O(11)^{I}, C(1)^{I}, and O(12)^{I}. Both chelate rings are fairly flat planes, as shown in Table 5. They neighbor each other between two copper atoms. The dihedral angle of these chelate rings is 172.5°.

Table 5. Least-Squares Planes and the Deviations of Atoms (l/Å)

Plane (1) [Cl, O(11), O(W), O(11)^{I}]
$-0.2465X+0.05472Y-0.9676Z-3.4549=0$
Cl, 0.3355; O(11), −0.3524; O(W), −0.2376; O(11)^{I}, 0.3657; Cu, −0.2839

Plane (2) [O(11), O(W), N, O(12)^{I}]
$0.5469X-0.7554Y-0.3608Z-0.3007=0$
O(11), 0.2149; O(W), 0.2397; N, −0.2594; O(12)^{I}, −0.1281; Cu, 0.2739

Plane (3) [Cl, N, O(11)^{I}, O(12)^{I}]
$0.7260X+0.6777Y-0.1165Z-1.3053=0$
Cl, −0.0299; N, 0.0218; O(11)^{I}, −0.0467; O(12)^{I}, 0.0596; Cu, 0.603

Plane (4) [Cu, O(11), C(1), C(2), N]
$-0.6098X+0.7897Y+0.0676Z-1.1583=0$
Cu, 0.0286; O(11), 0.0285; C(1), −0.0589; C(2), 0.0545; N, −0.0449

Plane (5) [Cu, O(12)^{I}, C(1)^{I}, O(11)^{I}]
Cu, −0.0030; O(12)^{I}, 0.0073; C(1)^{I}, −0.0093; O(11)^{I}, 0.0051

$$\begin{pmatrix} X \\ Y \\ Z \end{pmatrix} = \begin{pmatrix} a & b\cos\gamma & c\cos\beta \\ 0 & b\sin\gamma & -c\cos\alpha^{*}\sin\beta \\ 0 & 0 & c\cos\alpha^{*}\sin\beta \end{pmatrix} \begin{pmatrix} x \\ y \\ z \end{pmatrix}$$

Key to symmetry operation: I. $-x$, $0.5+y$, $1.0-z$.

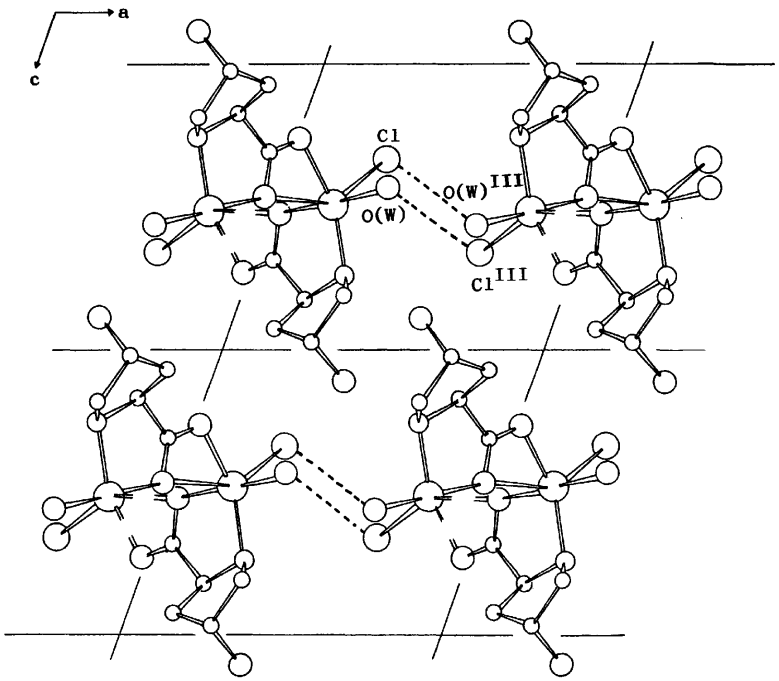

Fig. 2. The projection of the structure along the b axis. (----: Hydrogen bonding).
Key to symmetry operation: III. $1.0-x$, $-0.5+y$, $1.0-z$.

The projection of the structure along the b axis is given in Fig. 2. There are two types of hydrogen bonds between the water oxygen and the chlorine atoms. One is the intra-chain hydrogen bond ($O(W)$-Cl^{II}=3.034(5) Å), shown with broken line, between $O(W)^{I}$ and Cl^{IV}, in Fig. 1. The other is the inter-chain hydrogen bond (Cl-$O(W)^{III}$=3.017(3) Å; see Fig. 2). The rather long bond length of Cu-Cl may be due to the intra- and inter-chain hydrogen bonds. Each chain arranged in parallel with the b axis is linked to the neighboring one, by hydrogen bonds. Thus, a sheet forms parallel to the (001) plane, as shown in Fig. 2. The oxygen atom of the hydroxyl group does not form any hydrogen bonds. On the basis of the structural data, the properties of the complex reported previously[5] are reconsidered.

In the infrared spectra, the peak assigned to Cu-Cl stretching vibration, about 280 cm^{-1}, is a rather low frequency for Cu-Cl(terminal) bonding. In the complex, [CuCl(hpro)(H_2O)], the peaks of carboxylato group stretching vibrations are at 1592 and 1567 cm^{-1} (COO^- antisymmetric) and at 1407 and 1393 cm^{-1} (COO^- symmetric). In the bis-chelate complex, [Cu(hpro)$_2$], the peaks are at 1592 cm^{-1} (COO^- antisymmetric) and 1407 cm^{-1} (COO^- symmetric).[5] The splitting peaks of antisymmetric and symmetric stretching vibrations in the former complex may result from the complicated bridging carboxyl group as mentioned above. The difference between the mean value of COO^- antisymmetric vibrations and that of COO^- symmetric vibrations in [CuCl(hpro)(H_2O)] is smaller than the difference between two peaks of antisymmetric and symmetric vibrations in [Cu(hpro)$_2$] or in free ligand (Hhpro). This fact agrees with the vibrational spectrum patterns of behavior established for the carboxylato ligand:[19,20] in the bidentate (chelate) carboxylato complex, the separation between the COO^- stretching vibrations is smaller than that of the free carboxylate ion or of the unidentate carboxyl complex.

The electronic spectrum of the aqueous solution is different from the powder diffuse reflection one in [CuCl(hpro)(H_2O)]. This indicates that the complex has different coordination types in the aqueous solution and in the crystalline form. In the aqueous solution there is a broad peak at 680 nm, which is characteristic of a six-coordinated Cu^{II} complex. On the other hand, the peak at 769 nm has a shoulder near 900 nm in the powder diffuse reflection:[21] This may result from some extreme distortion of the octahedron surrounding copper(II). This result suggests that the coordination polyhedron changes from its distorted shape into a shape nearer an octahedron, because the polymer chain cleaves and then an octahedron is rebuilt by becoming coordinated to water molecules in the aqueous solution.

The magnetic or thermal properties of this complex are consistent with the structure proposed.

The authors wish to express their thanks to Professor Yoichi Iitaka of The University of Tokyo for X-ray diffractometer measurements. They would also like to thank Dr. F. S. Howell of Sophia University for correcting this manuscript.

References

1) T. Yasui, J. Hidaka, and Y. Shimura, *J. Am. Chem. Soc.*, **87**, 2762 (1965).
2) T. Yasui, *Bull. Chem. Soc. Jpn.*, **38**, 1746 (1965).
3) R. G. Denning and T. S. Piper, *Inorg. Chem.*, **5**, 1056 (1966).
4) Y. Yukawa, Y. Inomata, T. Takeuchi, M. Shimoi, and A. Ouchi, *Bull. Chem. Soc. Jpn.*, **55**, 3135 (1982).
5) Y. Inomata, T. Takeuchi, and T. Moriwaki, *Inorg. Chim. Acta*, **68**, 187 (1983).
6) Y. Yukawa, Y. Inomata, and T. Takeuchi, *Bull. Chem. Soc. Jpn.*, **56**, 2125 (1983).
7) A. Finch, P. N. Gates, L. Radcliffe, F. N. Dickson, and E. F. Bentley, "Chemical Applications of Far Infrared Spectroscopy," Academic Press, London and New York (1970), pp. 145—150.
8) "The Universal Crystallographic Computation Program System (UNICS)," ed by T. Sakurai, Crystallographic Society of Japan, Tokyo (1967).
9) "International Tables for X-Ray Crystallography," Kynoch Press, Birmingham, U. K. (1974), Vol. IV.
10) $R=\Sigma||F_o|-|F_c||/\Sigma|F_o|$.
11) The final thermal parameters and the final F_o-F_c table are deposited as Document No. 8724 at the Office of the Editor of the Bulletin of the Chemical Society of Japan.
12) A. Gleizes, F. Maury, and J. Caly, *Inorg. Chem.*, **19**, 2074 (1980).
13) A. Ouchi, Y. Sato, Y. Yukawa, and T. Takeuchi, *Bull. Chem. Soc. Jpn.*, **56**, 2241 (1983).
14) T. Ono, H. Shimanouchi, Y. Sasada, T. Sakurai, O. Yamauchi, and A. Nakahara, *Bull. Chem. Soc. Jpn.*, **52**, 2229 (1979).
15) Y. Sasada, A. Takenaka, and T. Furuya, *Bull. Chem. Soc. Jpn.*, **56**, 1745 (1983).
16) J. A. J. Jarvis, *Acta Crystallogr.*, **15**, 964 (1962).
17) E. A. H. Griffith, W. A. Spofford, III, and E. L. Amma, *Inorg. Chem.*, **17**, 1913 (1978).
18) T. F. Koetzele, M. S. Lehmann, and W. C. Hamilton, *Acta Crystallogr., Sect. B*, **29**, 231 (1973).
19) K. Nakamoto, "Infrared and Raman Spectra of Inorganic and Coordination Compounds," 3rd ed, John Wiley and Sons, New York (1978), pp. 230—233.
20) R. C. Mehrotra and R. Bohra, "Metal Carboxylates," Academic Press, London (1983), pp. 48—60.
21) The data in Ref. 5 was measured by a Hitachi 624 digital spectrophotometer (190—900 nm). In this work, the data obtained by means of a JASCO UVIDEC-590 NIR spectrophotometer (700—2500 nm) were added. From the data, the shoulder near 900 nm was detected.

A Method of Calculation for d.c. Polarographic Catalytic Wave

Kenji KIKUCHI
Shiga Prefectural Junior College, Hikone, Shiga 522
(Received August 25, 1986)

A new numerical method for theoretical analysis of polarographic catalytic current is proposed and applied to well-studied systems to prove that the method is dependable. In this method, a system of partial differential equations of diffusion is transformed to finite-difference form by using Crank-Nicolson difference scheme, and the latter is solved by using both Gauss-Seidel and successive over relaxation methods. Chemical kinetics terms in the diffusion equations is substituted by ones rewritten by three alternative procedures. The method has been applied to a system of copper(II) and hydrogen peroxide. Resulted rate constant of participating chemical reaction agrees with the rate constant obtained from bulk solution experiments. This and other results show that the method is a useful tool for theoretical analysis of catalytic waves.

Catalytic reaction in polarographic wave has been studied by several methods. The one, which was first used, was a method invented by Bridicka and Wiesner.[1] Although it is simple and appealing, the conception of reaction layer on which the method based is of an approximate nature. Hence numerical values of rate constants of chemical reactions, calculated by this method, are considered unreliable. Kolthoff and Parry found that the rate constant calculated from observed currents was of the order of 10^4 times greater than the one determined from the experiment of bulk solution kinetics in the Fe(III)–hydrogen peroxide system.[2]

Koutecky derived a rigorous solution for a pseudo-first-order reaction at the surface of the expanding sphere electrode.[3] He solved simultaneous differential equations of diffusion, with chemical kinetics terms, using the method of dimensionless parameters. Though it is ingenious, his method can not be applied to reactions of higher orders.

The same kind of simultaneous differential equations are arising in problems of ECE mechanisms. Galvez et al. derived explicit solutions of the simultaneous differential equations without the steady state approximation and obtained current-potential curves of ECE mechanisms.[4–6] However, application of their method is limited to (pseudo-) first-order reactions owing to the common defect of analytic method.

Today numerical method becomes increasingly a popular tool for electrochemists with increasingly easier accessibility to computers. Ruzic et al. solved problems of ECE mechanisms by the method of explicit finite-difference digital simulation, and reported d.c. and a.c. polarographic curves of several ECE mechanisms, calculated by their method.[7–11] However, the method is inherently inflexible with respect to setting boundary conditions, and it is very difficult to apply to more complex systems.

Ultimate aim of this study is to diagnose observed polarograms of catalytic nature by comparing with calculated curves based on several possible mechanisms, and to estimate rate constants. Candidate mechanisms may be of second order or higher. Number of chemical species participated is not necessarily confined to three or four. All methods mentioned above are insufficient to achieve this aim. Another mathematical method is needed in these circumstances.

Winograd used an implicit method of finite-difference to simulate spectro-electrochemical working curves for a diffusion controlled system, and state that the method was much more efficient than explicit method.[12] In this paper the implicit method of Crank–Nicolson is used for calculation of polarograms of a simple system of catalytic current. Before to do this, however, soundness of the method must be established.

Theory

The catalytic current in the Cu^{2+}–H_2O_2 system is well-known through the study of Kolthoff and Woods.[18] This reaction mechanism is given as follows.

$$Cu^{2+} + e^- \rightleftharpoons Cu^+ \quad (1)$$

$$Cu^+ + H_2O_2 \longrightarrow Cu^{2+} + OH^- + OH \quad (2)$$

$$Cu^+ + OH \longrightarrow Cu^{2+} + OH^- \quad (3)$$

To generalize treatment the above reaction scheme is rewritten as

$$O + e^- \rightleftharpoons R, \quad (4)$$

$$R + A \xrightarrow{k} O + B, \quad (5)$$

$$R + B \longrightarrow O, \quad (6)$$

where O represents copper(II) ion, R copper(I) ion, A hydrogen peroxide, and B hydroxyl radical in a scheme of Reactions (1)—(3), and the current is controlled by the rate of Reaction (5). Partial differential equations for concentrations of species in Reactions (4)—(6) are given as follows:

$$\frac{\partial C_O}{\partial t} = D_O\left(\frac{\partial^2 C_O}{\partial r^2}\right) + \left(\frac{2}{r}D_O - u\right)\frac{\partial C_O}{\partial r} + 2kC_AC_R, \quad (7)$$

$$\frac{\partial C_R}{\partial t} = D_R\left(\frac{\partial^2 C_R}{\partial r^2}\right) + \left(\frac{2}{r}D_R - u\right)\frac{\partial C_R}{\partial r} - 2kC_AC_R, \quad (8)$$

and

$$\frac{\partial C_A}{\partial t} = D_A\left(\frac{\partial^2 C_A}{\partial r^2}\right) + \left(\frac{2}{r}D_A - u\right)\frac{\partial C_A}{\partial r} - kC_R C_A, \quad (9)$$

where C_h is the concentration of a species h, C^*_h its value in bulk solution, D_h the diffusion coefficient of the species h, r the distance from the center of the electrode mercury drop, and

$$u = m/(4\pi\rho r^2). \quad (10)$$

Here m is the flow rate of mercury, and ρ the density of mercury. It is assumed that the center of mercury drop remains fixed.

Initial conditions are

$$C_O = C^*_O, \quad C_A = C^*_A, \quad C_R = 0 \quad (t=0,\ r>0), \quad (11)$$

and boundary conditions are

$$C_O = 0,\ D_O\left(\frac{\partial C_O}{\partial r}\right) = -D_R\left(\frac{\partial C_R}{\partial r}\right),\ \left(\frac{\partial C_A}{\partial r}\right) = 0 \quad (t>0,\ r=a), \quad (12)$$

$$C_O = C^*_O,\ C_R = 0,\ C_A = C^*_A \quad (t>0,\ r=\infty). \quad (13)$$

The current, i, is given by

$$i = FD_O S(\partial C_O/\partial r)_{r=a}, \quad (14)$$

where a is the radius of the mercury drop, S the surface area of mercury drop, and F the Faraday constant. To facilitate calculation one introduces following transformations.

$$y_O = C_O/C^*_A,\ y_R = C_R/C^*_A,\ y_A = C_A/C^*_A,$$
$$x = (r-a)/L,\ d_O = D_O/D_A,\ d_R = D_R/D_A,$$
$$u' = m/(4\pi\rho a^2) \quad (15)$$

In the above L is the representative length. With the aid of Eq. 15, Eq. 7 is transformed as follows.

$$\frac{L^2}{D_A}\frac{\partial y_R}{\partial t} = d_R\frac{\partial^2 y_R}{\partial x^2} + \left\{\frac{2d_R}{x+a/L} + \frac{Lx(x+2a/L)u'}{D_A(x+a/L)^2}\right\}\frac{\partial y_R}{\partial x} - \frac{2L^2C^*_A}{D_A}ky_A y_R \quad (16)$$

Because the reaction proceeds in the neighborhood of the electrode surface, numerical results most desired are those in the proximity of the electrode surface. For this end, numerical integration of the differential equations is carried out more efficiently using a network, of which mesh is finer at near the electrode surface and becomes coarser with increasing the distance from the surface. Hence, one introduces a parameter given by

$$s = 1 - 1/(1+Hx), \quad (17)$$

where H is a constant.

Equation 16 is rewritten with the aid of Eq. 17.

$$\frac{\partial y_R}{\partial T} = d_R H^2(1-s)^4\frac{\partial^2 y_R}{\partial s^2} + \left\{\frac{2D_R}{x+a/L} + \frac{x(x+2a/L)}{(x+a/L)^2}U - 2d_R H(1-s)\right\}H(1-s)^2\frac{\partial C^*_A}{\partial s} - 2ky_R y_A, \quad (18)$$

where

$$T = D_A t/L^2,$$
$$K = L^2 C^*_A k/D_A, \quad (19)$$
$$U = Lu/D_A.$$

Equation 18 is solved by an implicit method of finite difference, Crank-Nicolson's method with some modifications.[14-16] If the domains of s and T are divided into equal intervals Δs and ΔT, respectively, the space and time coordinates are expressed as

$$s_i = i\Delta s,\ T_j = j\Delta T \quad (20)$$

$$x_i = i\Delta s/H(1+i\Delta s) \quad (21)$$

and the concentration $y_R(s,T)$ as

$$y_R(s,T) = y_R(i\Delta s, j\Delta T) = y_{R,i,j} \quad (22)$$

A finite-difference equation is derived from Eq. 18.

$$(E_{R,i}+\Delta TKy_{A,i,j+1})y_{R,i,j+1} = F_{R,i}y_{R,i+1,j+1} + G_{R,i}y_{R,i-1,j+1} + D_{R,i} - \Delta TKy_{A,i,j}y_{R,i,j} \quad (23)$$

Where

$$E_{R,i} = 1 + \frac{\Delta T}{\Delta s^2}d_R H^2(1-s_i)^4 \quad (24)$$

$$F_{R,i} = \frac{\Delta T}{2\Delta s}H(1-s_i)^2\left\{\frac{d_R H(1-s_i)^2}{\Delta s} + \frac{d_R}{x_i+a_{j+1}/L} + \frac{x_i(x_i+2a_{j+1}/L)}{2(x_i+a_{j+1}/L)^2}U_{j+1} - d_R H(1-s_i)\right\} \quad (25)$$

$$G_{R,i} = \frac{\Delta T}{2\Delta s}H(1-s_i)^2\left\{\frac{d_R(1-s_i)^2}{\Delta s} - \frac{d_R}{x_i+a_{j+1}/L} - \frac{x_i(x_i+2a_{j+1}/L)}{2(x_i+a_{j+1}/L)^2}U_{j+1} + d_R H(1-s_i)\right\} \quad (26)$$

$$D_{R,i} = F_{R,i}y_{R,i+1,j} + G_{A,i}y_{R,i-1,j} + \left\{1 - \frac{\Delta T}{\Delta s^2}d_R H^2(1-s_i)^4\right\}y_{R,i,j} \quad (27)$$

In much the same way the equations concerning with species A and O are transformed as follows.

$$E_{O,i}y_{O,i,j+1} = F_{O,i}y_{O,i+1,j+1} + G_{O,i}y_{A,i-1,j+1} + D_{O,i} + \Delta TK(y_{A,i,j+1}y_{R,i,j+1} + y_{A,i,j}y_{R,i,j}) \quad (28)$$

$$(E_{A,i}+\Delta TKy_{R,i,j+1}/2)y_{A,i,j+1} = F_{A,i}y_{A,i+1,j+1} + G_{A,i}y_{A,i-1,j+1} + D_{A,i} - \Delta TKy_{A,i,j}y_{R,i,j}/2 \quad (29)$$

Boundary conditions in finite-difference form are expressed in two alternative ways as shown in the following.

(i) The boundary condition $(D_O(\partial C_O/\partial r)_a=-D_R(\partial C_R/\partial r)_a)$ at the current time $(j+1)$ is expressed with concentrations at the nodes $(0,j+1)$, $(1,j+1)$, and $(2,j+1)$, and Eq. 30 is derived after some modifications.

$$y_{R,0,j+1} = -(4y_{R,1,j+1}-y_{R,2,j+1})/3-d_O(4y_{O,1,j+1} -y_{O,2,j+1}-3y_{O,0,j+1})/3d_R \quad (30)$$

The first derivative $(y'_{R,1j+1})$ of $y_{R,1j+1}$ is given as

$$y'_{R,1,j+1} = (y_{R,2,j+1}+4y_{R,1,j+1}-5y_{R,0,j+1} -2\Delta s y'_{R,0,j+1})/8\Delta s + (y_{R,2,j}+4y_{R,1,j} +5y_{R,0,j}-2\Delta s y'_{R,0,j})/8\Delta S, \quad (31)$$

where $y'_{R,0j+1}$ is calculated by

$$y'_{R,0,j+1} = \frac{4y_{R,1,j+1}-y_{R,2,j+1}-3y_{R,0,j+1}}{2\Delta s} = -\frac{d_O}{2\Delta s d_R}(4y_{O,1,j+1}-y_{O,2,j+1}-3y_{O,0,j+1}), \quad (32)$$

the second derivative $(y''_{R,1j+1})$ is written as

$$y''_{R,1,j+1} = (y_{R,2,j+1}-2y_{R,1,j+1}+y_{R,0,j+1})/2(\Delta s)^2 + (y_{R,2,j}-2y_{R,1,j}+y_{R,0,j})/2(\Delta S)^2. \quad (33)$$

Introduction of Eqs. 31—33 to Eq. 18 gives

$$\begin{aligned}(1+E-F+\Delta TKy_{A,1,j+1})y_{R,1,j+1} &= \\ (E/2-F/4)(y_{R,2,j+1}+y_{R,2,j}) &\\ +\ (E/2-5F/4)(y_{R,0,j+1}+y_{R,0,j}) &\\ +\ (1-E+F-\Delta TKy_{A,1,j})y_{R,1,j} &\\ -\ \Delta sF(y'_{R,0,j+1}+y'_{R,0,j})/2, & \quad (34)\end{aligned}$$

where

$$E = \Delta T d_R H^2(1-s_i)^4/(\Delta s)^2 \quad (35)$$

$$F = \frac{\Delta T}{\Delta s}H(1-s_i)^2\left\{\frac{d_R}{x_i+a_{j+1}/L} +\frac{x_i(x_i+2a_{j+1}/L)}{2(x_i+a_{j+1}/L)^2}U_{j+1}-d_RH(1-s_i)\right\}. \quad (36)$$

The value of $y_{R,1j+1}$ is calculated with Eq. 34.

(ii) The boundary conditions $(D_O(\partial C_O/\partial r)_a=-D_R(\partial C_R/\partial r)_a)$ is expressed with concentrations at nodes $(0,j+1)$, $(1,j+1)$, $(2,j+1)$, and $(3,j+1)$, and Eq. 37 is obtained with some modifications.

$$y_{R,0,j+1} = -(2y_{R,3,j+1}-9y_{R,2,j+1}+18y_{R,1,j+1})/11 -d_O(2y_{O,3,j+1}-9y_{O,2,j+1}+18y_{O,1,j+1} -11y_{O,0,j+1})/11d_R \quad (37)$$

The derivatives at $i=1$ are expressed as following equations.

$$y'_{R,1,j+1} = -(y_{R,3,j+1}-9y_{R,2,j+1}-9y_{R,1,j+1}+17y_{R,0,j+1} +6\Delta s y'_{R,0,j+1})/36\Delta s-(y_{R,3,j}-9y_{R,2,j} -9y_{R,1,j}+17y_{R,0,j}+6\Delta s y'_{R,0,j})/36\Delta S, \quad (38)$$

$$y''_{R,1,j+1} = (-2y_{R,3,j+1}+27y_{R,2,j+1}-54y_{R,1,j+1} +29y_{R,0,j+1}+6\Delta s y'_{R,0,j+1})/36(\Delta s)^2 +(-2y_{R,3,j}+27y_{R,2,j}-54y_{R,1,j} +29y_{R,0,j}+6\Delta s y'_{R,0,j})/36(\Delta S)^2, \quad (39)$$

$y'_{R,0j+1}$ in the above is calculated by

$$y'_{R,0,j+1} = (2y_{R,3,j+1}-9y_{R,2,j+1}+18y_{R,1,j+1} -11y_{R,0,j+1})/6\Delta s = -(d_O/6\Delta s d_R)(2y_{O,3,j+1}-9y_{O,2,j+1} +18y_{O,1,j+1}-11y_{O,0,j+1}). \quad (40)$$

Introduction of Eqs. 38—40 to Eq. 18 results

$$\begin{aligned}(1+3E/2-F/2+\Delta TKy_{A,1,j+1})y_{R,1,j+1} &= \\ (-E-F)(y_{R,3,j+1}+y_{R,3,j})/18 &\\ +\ (-3E/4+F/2)(y_{R,2,j+1}+y_{R,2,j}) &\\ +\ (1-3E/2+F/2-\Delta TKy_{A,1,j})y_{R,1,j} &\\ +\ (29E/36-17F/18)(y_{R,0,j+1}+y_{R,0,j}) &\\ +\ (E/6-F/3)\Delta s(y'_{R,0,j+1}+y'_{R,0,j}). & \quad (41)\end{aligned}$$

The value of $y_{R,1j+1}$ is calculated with Eq. 41.

It is, however, not possible to apply the method described above to the case where chemical kinetics terms are written with concentrations of second order or higher.

Morihara and Chen reported a procedure which makes possible to transform a higher order function to a linear function. Application of their procedure to the parenthesis in the right-hand side of Eq. 23 yields Eq. 42.[13]

$$y_{A,i,j+1}y_{R,i,j+1} + y_{A,i,j}y_{R,i,j} = y_{A,i,j+1}y_{R,i,j} + y_{A,i,j}y_{R,i,j+1} \quad (42)$$

Introduction of Eq. 42 to 28 gives

$$(E_{R,i}+\Delta TK_{A,i,j})y_{R,i,j+1} = F_{R,i}y_{R,i+1,j+1} + G_{R,i}y_{R,i-1,j+1} + D_{R,i} - \Delta TKy_{A,i,j+1}y_{R,i,j}. \quad (43)$$

In much the same way as Eq. 43 is derived from Eq. 23, Eq. 44 is resulted from Eq. 29.

$$(E_{A,i}+\Delta TK_{R,i,j}/2)y_{A,i,j+1} = F_{A,i}y_{A,i+1,j+1} + G_{A,i}y_{A,i-1,j+1} + D_{A,i}-\Delta TKy_{A,i,j+1}y_{R,i,j}/2 \quad (44)$$

Although Morihara-Chen's procedure is useful as shown above, it becomes powerless when it is applied to fractional order of reaction. Following two procedures are proposed to replace it in the case of fractional order of reaction.

The first of them is as follows. In this procedure, the value of concentrations in chemical kinetics terms in the $(n+1)$-th iteration are replaced with the values of concentrations resulted by n-th iteration. The concentrations at each successive repetitions are expressed as

$$(y_{A,i,j+1})_{n+1} = (y_{A,i,j+1})_n + \delta_1 \quad (45)$$

$$(y_{R,i,j+1})_{n+1} = (y_{R,i,j+1})_n + \delta_2, \quad (46)$$

where n is the number of iteration, and δ_1 and δ_2 are differences in successive iterations. If the values of δ_1 and δ_2 approach to zero with increasing n, the product of the left-hand sides of Eqs. 45 and 46 becomes

$$(y_{A,i,j+1})_{n+1}(y_{R,i,j+1})_{n+1} = (y_{A,i,j+1})_n(y_{R,i,j+1})_n. \quad (47)$$

Equation 47 shows that the value of left-hand side of Eq. 47 is known at the beginning of the $(n+1)$-th iteration. Introduction of Eq. 47 to Eqs. 23 and 29, and modification give following relations.

$$E_{R,i}(y_{R,i,j+1})_{n+1} = F_{R,i}(y_{R,i+1,j+1})_{n+1} + G_{R,i}(y_{R,i-1,j+1})_{n+1} + D_{R,i} - \Delta TKy_{A,i,j}y_{R,i,j} - \Delta TK(y_{A,i,j+1})_n(y_{R,i,j+1})_n \quad (48)$$

$$E_{A,i}(y_{A,i,j+1})_{n+1} = F_{A,i}(y_{A,i+1,j+1})_{n+1} + G_{A,i}(y_{A,i-1,j+1})_{n+1} + D_{A,i} - \Delta TKy_{A,i,j}y_{R,i,j}/2 - \Delta TK(y_{A,i,j+1})_n(y_{R,i,j+1})_n/2 \quad (49)$$

The second procedure is as follows. The values at $T+\Delta T$ may be replaced by the values at T if the rate constant of chemical reaction is not so large. Hence Eq. 42 is written as

$$y_{A,i,j+1}y_{R,i,j+1} + y_{A,i,j}y_{R,i,j} = 2y_{A,i,j}y_{R,i,j}. \quad (50)$$

Using the above relation Eqs. 23 and 29 are rewritten as

$$E_{R,i}y_{R,i,j+1} = F_{R,i}y_{R,i+1,j+1} + G_{R,i}y_{R,i-1,j+1} + D_{R,i} - 2\Delta TKy_{A,i,j}y_{R,i,j} \quad (51)$$

$$E_{A,i}y_{A,i,j+1} = F_{A,i}y_{A,i+1,j+1} + G_{A,i}y_{A,i-1,j+1} + D_{A,i} - \Delta TKy_{A,i,j}y_{R,i,j} \quad (52)$$

Three sets of equations (i.e. Eqs. 43 and 44, and Eqs. 48 and 49, and Eqs. 51 and 52) are derived in place of Eqs. 23 and 29. The latter two sets of equations are derived by new procedures of which dependability must be tested.

In order to establish the soundness of present numerical method, the method was applied first to reconfirm well-known relationships between the diffusion current and the concentration of depolarizer, and between the diffusion current and the height of mercury column. In this case the value of reaction rate constant is zero, and the boundary conditions are given as follows.

$$C_0 = C_0^* \quad (t=0,\ r>0) \quad (53)$$

$$C_0 = 0 \quad (t>0,\ r=a) \quad (54)$$

$$C_0 = C_0^* \quad (t>0,\ r=\infty) \quad (55)$$

Then the method was applied to a system of copper(II)–hydrogen peroxide system.

Experimental

All chemicals used were of reagent grade. The concentration of hydrogen peroxide in stock solution was determined by iodometry.[19] Stock solutions of cadmium(II) sulfate and copper(II) sulfate were made by dissolving weighed amounts of anhydrous salts. The solution of copper(I) ion was prepared by dissolving copper(I) chloride dissolved in 1.0 M† hydrochloric acid from which dissolved oxygen was expelled with bubbles of pure nitrogen. The concentration of copper(I) ion was determined from the diffusion current of copper(II) ion after the oxidation of copper(I) ion by pure oxygen.

Measurements of catalytic wave were carried out in the solution of 1.0 M HCl and 0.005% gelatin. An electrolysis cell with a hole of 0.5 mm in diameter at bottom of the cell was used to prevent contamination of mercury ions through oxidation of mercury collected on the bottom of the cell. A Hokuto Denko Model HA-104 Potentio-Galvanostat was used for application of potential with three-electrode arrangement. Catalytic currents were measured at the end of life of mercury drop. Measurements were carried out within 70 min after preparation of test solutions, in order to avoid the influence of their composition variation. The oxygen was expelled from test solutions with bubbling pure nitrogen through the solutions for 50 min. The diffusion coefficient of both reactants and products were determined from respective diffusion current. Measurements of diffusion currents were carried out in the same conditions as measurements of the catalytic wave, except the absence of the hydrogen peroxide.

The numerical computation in the present method was programmed with Gauss-Seidel method and succesive over relaxation method by using FORTRAN, and performed on a FACOM M382 computer in DATA PROCESSING CENTER KYOTO UNIVERSITY.

Results and Discussion

In order to confirm that the present method reproduces the relationship between the diffusion current and the concentration of depolarizer, the method was applied to the diffusion current of copper(II) ion in a solution of 1.0 M HCl and 0.005% gelatin. It was confirmed by computation that the diffusion current was proportional to the concentration of copper(II) ion, and that observed values of diffusion currents agreed with calculated ones. The value of diffusion coefficient used in the computation is taken from the Ref. 2.

Table 1 shows relation between the height of mercury column and the diffusion currents of copper(II) ion. Observed data agree with ones calculated.

The instantaneous current was also calculated with this method. The current-time curve of diffusion current is proportional to $t^{1/6}$ according to Ilkovic

† 1 M=1 mol dm^{-3}.

equation, to $t^{1/5.2}$ according to the equation introduced by Koutecky,[3] and to $t^{1/5.3}$ according to the present numerical method.

The soundness and the accuracy of this method was confirmed by above results that the observed relationships between the diffusion currents and the concentration of depolarizer and between the diffusion currents and the height of mercury column were both reproduced by the present method, and that a current-time curve of instantaneous current calculated with this method agrees with one calculated from Koutecky's equation.[3] Therefore it may be concluded that this method can be used for the aim of present study, theoretical analysis of the catalytic currents.

The chemical kinetic terms in finite-difference equations are expressed in four different forms. The first is expressed in Eqs. 23 and 29 which were derived by straight forward way, the second is shown in Eqs. 43—44 which were derived by using the procedure proposed by Morihara and Chen, and the third and fourth are respectively, expressed in Eqs. 48—49 and Eqs. 51—52 which were derived by the procedures proposed in the present paper. It is found that the numerical computation by using the fourth is more efficient than using others (see Appendex). The differences of four corresponding values obtained with using the four procedures were smaller than one per cent. Differences of converged values obtained with using various values of ΔT and ΔS were within the limits considered generally permissible. These facts show that the procedures proposed in the present study are dependable. Besides, it must be noted that proposed two procedures are applicable to chemical kinetics term with fractional orders. The boundary condition $(D_O(\partial C_O/\partial r)_a=-D_R(\partial C_R/\partial r)_a)$ is written in two forms. These are shown in Eqs. 30—34 and Eqs. 35—41. The former expresses the condition with using the values of functions at three nodes near the electrode surface, whereas the latter with using values at four nodes. It is found that the time consumed for numerical computation using the former is about twice as large as one consumed using the latter. Difference of two corresponding values computed by the two procedures are small and below the level of error considered generally permissible. Therefore it is concluded that the proposed numerical method for catalytic currents is dependable.

The values of diffusion coefficients used for numerical computations were chosen as ones which gave smallest differences between calculated currents and with observed ones. This procedure produced a value of 0.750×10^{-5} cm^2 s^{-1} for the diffusion coefficient of cadmium ion. This value agrees well with the value in the Ref. 2. Therefore the procedure is usable.

The method was applied to the catalytic current in the Cu^{2+}–H_2O_2 system. The diffusion currents of species participated in the catalytic current were measured in a solution of 1.0 M HCl and 0.005% gelatin. Table 2 shows values of diffusion coefficients, which were used for computation and gave best agreements of calculated diffusion currents with observed ones.

Table 1. Diffusion Current of 2.03 mM Cu(II) Ion in 1 M HCl and 0.01% Gelatin

Height of mercury column H / cm	Flow rate of mercury m / 10^{-3} g s^{-1}	Diffusion current i_d / μA	
		observed	calculated[a]
50	0.675	10.26	10.08
60	0.831	11.28	11.05
70	0.998	12.08	12.02
80	1.147	12.86	12.79
88	1.268	13.46	13.42

a) Values of parameters used for computation are as follows. $\Delta T=3.69\times10^{-4}$, $\Delta S=0.01$, and $L=0.01$ cm.

Table 2. Diffusion Current and Diffusion Coefficient

	i_d/C / μA mM^{-1}	T[a] / s	D / 10^{-5} cm^2 s^{-1}	D[c] / 10^{-5} cm^2 s^{-1}
Cu^{2+}	6.40	5.62	0.720	0.72
Cu^{+}	4.68	5.14	1.502	—
H_2O_2	8.95[b]	4.68	1.420	—

a) Dropping time at a potential corresponding to the diffusion current plateau. b) The diffusion current was measured in a solution of 1.0 M $NaNO_3$ and 0.005% gelatin, because it was partly obscured by hydrogen discharge wave in a solution of 1.0 M HCl and 0.005 % gelatin. c) These value are quoted from the Ref. 2.

Table 3. Reaction Rate calculated from Koutecky's Method and Numerical Method in 2.03 mM Cu^{2+}, 1.0 M HCl, and 0.01% Gelatin

$[H_2O_2]$ / mM	i_l/i_d	k / l mol^{-1} s^{-1}	
		Koutecky's method	Present method[a]
2.18	1.396	131.8	55.0
5.45	1.986	106.8	55.0
10.9	2.398	77.3	55.0
21.8	3.121	65.9	55.0
43.6	4.236	60.7	55.0
76.3	5.478	58.0	55.0
109.0	6.274	53.3	55.0
141.7	7.197	53.9	55.0

a) Values of parameters used for computation are as follows. $\Delta T=3.69\times10^{-4}$, $\Delta S=0.01$, and $L=0.01$ cm.

Table 3 shows that the catalytic currents and the reaction rate constants, calculated by Kouteckey's method and the present method. The value of reaction rate constant of Reaction (2) was given as 55.0 ± 0.5 l mol^{-1} s by which gave best agreements between calculated catalytic currents and observed ones. The value calculated with Koutecky's method[17] decreases with increasing concentration of hydrogen peroxide.

Table 4 shows that variation of the catalytic current with increase of the height of mercury column. The present method gives the same value of reaction rate constant as ones in Table 3. But the value calculated with Koutecky's method increases with increase of the height of mercury column.

From the numerical computation for the catalytic wave, it was found that the value of the reaction rate constant is 55.0 l mol^{-1} s as shown in Tables 3 and 4. This value differs from one reported by Kolthoff and Woods.[18] But in their paper, the rate constant of oxidation of copper(I) by hydrogen peroxide in chloride medium, was determined by observing increase of the cathodic wave of copper(II) ion with time. They gave a value of 58 l mol^{-1} s which agrees with the result of the present study.

Figure 1 shows that the relation between the ratio of the catalytic current to the diffusion current of copper(II) ion (i_l/i_d) and the concentration of hydrogen peroxide. It shows that the observed point are on the calculated curve.

The relation between the ratio (i_l/i_d) and the height of mercury column is shown in Fig. 2, where observed points are on the calculated curve.

The value of the rate constant calculated by Koutecky's method decreases with increasing concentration of hydrogen peroxide. This is explained as follows. In the Koutecky's method, it is assumed that the concentration of hydrogen peroxide in the reaction layer is same as to that in the bulk solution. However, that is not the case.

On the contrary the present method gives the only one value for reaction rate constant which is consistent with all experimental data.

Conclusion

A new numerical method is proposed for numerical solution of diffusion equations with chemical kinetics

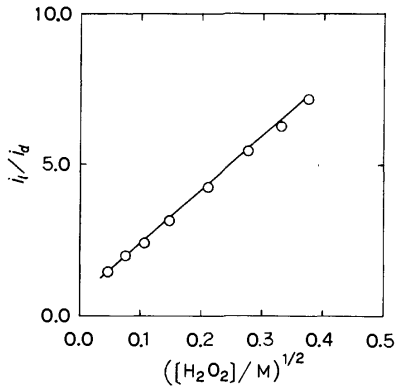

Fig. 1. Plots of i_l/i_d for mixtures of H_2O_2 with 2.03 mM Cu^{2+} in 1 M HCl and 0.01% gelatin. O: Observed data, a solid curve; calculated data.

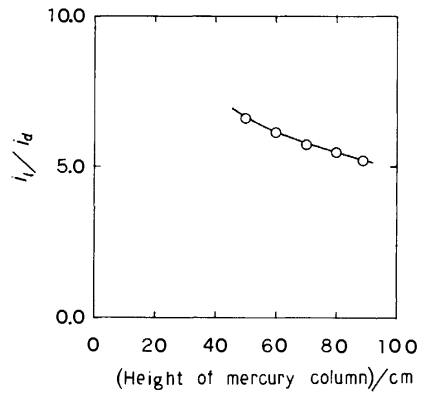

Fig. 2. Effect of the height of mercury column on the catalytic wave. 2.03 mM Cu^{2+}, 76.3 mM, 1 M HCl, and 0.01% gelatin. O: Observed data, a solid curve; calculated data.

Table 4. Reaction Rate Constant Calculated from Koutecky's Method and Numerical Method in 2.03 mM Cu^{2+}, 76.3 mM H_2O_2, 1.0 M HCl, and 0.01% Gelatin

Height of mercury head H / cm	Flow rate of mercury m / 10^{-3} g s^{-1}	i_l/i_d	Dropping time t / s	k / l mol^{-1} s^{-1} Koutecky's method	k / l mol^{-1} s^{-1} Present[a] method
50	0.675	6.55	9.08	47.0	55.0
60	0.831	6.12	7.52	49.5	55.0
70	0.998	5.75	6.44	51.0	55.0
80	1.147	5.46	5.62	52.7	55.0
88	1.268	5.26	5.04	54.6	55.0

a) Values of parameters used for computation are as follows. $\Delta T=3.69\times10^{-4}$, $\Delta S=0.01$, and $L=0.01$ cm.

terms, and is established as a useful tool for theoretical analysis of the catalytic current. Diffusion equations with chemical kinetic terms are transformed to finite-difference equations using the implicit method of Crank-Nicolson. New two procedures are proposed for the purpose of rewriting chemical kinetics terms. These are applicable even to chemical kinetics terms with fractional order. The boundary condition $(D_O(\partial C_O/\partial r)_a=-D_R(\partial C_R/\partial r)_a)$ is written in two forms. The one expresses the boundary condition with the values of functions at three nodes near the electrode surface, whereas the other with the values of four nodes. It is found that the time consumed for numerical computation using former is about twice as large as one consumed using latter. The dependability of these procedures is proved through comparison of values of functions obtained with one obtained using other procedures.

Appendix

Differences between calculated values of the catalytic current were within ±0.3%, irrespective of computational procedures used for chemical kinetics terms, when values of ΔT, ΔS, and L were, respectively, 0.369×10^{-14}, 0.01, and 0.01 cm. Times consumed for computations were 5.01, 5.86, 5.12, and 3.56 s with first, second, third, and fourth procedures, respectively. These values show that the fourth procedure is most efficient.

The author wish to express his thanks to Professor Teisuke Murayama of Faculty of Engineering, Shizuoka University for his helpful discussion.

References

1) R. Bridicka and W. Wiesner, *Collect. Czech. Chem. Commun.*, **12**, 39 (1947); R. Bridicka and K. Wiesner, *Natur.*, **31**, 247 (1943).
2) I. M. Kolthoff and J. J. Lingane, "Polarography," Interscience Publishers (1966).
3) J. Koutecky, *Czech. J. Phys.*, **2**, 50 (1953).
4) J. Galvez and A. Molina, *J. Electroanal. Chem.*, **110**, 49 (1980).
5) J. Galvez and A. Molina, *J. Electroanal. Chem.*, **115**, 15 (1980).
6) J. Galvez, A. Molina, R. Saura, and F. Martinez, *J. Electroanal. Chem.*, **127**, 17 (1981).
7) I. Ruzic and S. Felderg, *J. Electroanal. Chem.*, **50**, 153 (1974).
8) I. Ruzic, D. E. Smith, and S. W. Feldberg, *J. Electroanal. Chem.*, **52**, 157 (1974).
9) I. Ruzic and D. E. Smith, *J. Electroanal. Chem.*, **58**, 145 (1975).
10) I. Ruzic, H. R. Sobel, and D. E. Smith, *J. Electroanal. Chem.*, **65**, 21 (1975).
11) I. Ruzic, R. J. Schwall, and D. E. Smith, *Croat. Chem. Acta*, **48**, 651 (1976).
12) N. Winograd, *J. Electroanal. Chem.*, **43**, 1 (1973).
13) H. Morihara and R. T. Cheng, *J. Compu. Phys.*, **11**, 550 (1973).
14) J. Crank, "The Mathematics of Diffusion," The Clarendon Press Oxford, Chap. 10.
15) J. Crank and P. Nicolson, *Proc. Chembrige Phill. Soc.*, **43**, 50 (1974).
16) P. J. Roache, "Computational Fluid Dynamics," Hermsa Publishers Inc. (1976).
17) J. Koutecky, *Collect. Czech. Chem. Commun.*, **18**, 311 (1953).
18) I. M. Kolthoff and R. Woods, *J. Electroanal. Chem.*, **12**, 385 (1966).
19) E. P. Treadwell, "Analytical Chemistry," John Wiley and Sons, New York (1955), Vol. 2, p. 609.

Mössbauer Spectroscopic Studies of Trialkyl- and Triaryltin Complexes of Transition Metal Cyanides

Motomi KATADA,* Yoshio UCHIDA, Kumiko IWAI, Hirotoshi SANO,
Hiroshi SAKAI,† and Yutaka MAEDA†
Department of Chemistry, Faculty of Science, Tokyo Metropolitan University,
Fukasawa, Setagaya-ku, Tokyo 158
†Research Reactor Institute, Kyoto University, Kumatori-cho, Sennan-gun, Osaka 590-04
(Received August 30, 1986)

The structural diagnosis and lattice dynamics of three complexes, $\{[R_3Sn](\mu\text{-}NC)[Au(\mu\text{-}CN)]\}_x$ (R=Me, Bu(*n*-Bu), or Ph), $\{[R_3Sn]_2[(\mu\text{-}NC)_4Pt]\}_x$ (R=Me, Bu, or Ph), and $\{[R_3Sn]_3[(\mu\text{-}NC)_6Fe]\}_x$ (R=Bu or Ph) have been undertaken by means of ^{57}Fe-, ^{119}Sn-, and ^{197}Au-Mössbauer spectroscopic techniques. The Mössbauer parameters for the complexes indicate that all the tin atoms are coordinated with three alkyl or aryl groups and two cyano groups having a trigonal-bipyramidal structure. The asymmetry of the quadrupole split-peak intensity observed in the ^{119}Sn-Mössbauer spectra for the complexes was attributed to the anisotropic mean square vibrational amplitude with respect to a molecular symmetry axis. The temperature dependence of the recoil-free fraction of the ^{119}Sn-Mössbauer atom shows that the mean-square vibrational amplitude of tin atoms in the complexes falls in the range of values found for a number of one-dimensional organotin polymers. In ^{57}Fe-Mössbauer spectroscopy, the quadrupole splitting for $\{[Bu_3Sn]_3[(\mu\text{-}NC)_6Fe]\}_x$ rapidly decreases with an increase in the temperature, reflecting small separations among the three d_ε levels in energy. The very large ^{197}Au-quadrupole splitting for $\{[R_3Sn](\mu\text{-}NC)[Au(\mu\text{-}CN)]\}_x$ was explained by assuming strong σ-donating and π-accepting properties of the CN ligand.

Recently, Uson et al. synthesized various kinds of trialkyl- and triaryltin complexes of transition metal cyanides by treating the trialkyl- or triaryltin perchlorates with several cyano compounds of transition metals.[1] If the reaction with anionic dicyano compounds, such as $K[Au(CN)_2]$ and $Bu_4N[Ag(CN)_2]$, is carried out, the reaction products can be expected to have an infinite one-dimensional polymeric structure. On the other hand, the reaction with the square-planar coordinated palladium or platinum cyanides can be expected to give polymer complexes which are assumed to have an infinite two-dimensional structure. In the case of the reaction with $K_3[Fe(CN)_6]$, three-dimensional polymer products will be obtained.

On the basis of the IR spectra of those complexes, Uson et al. proposed that, in every case, the tin atoms are five-coordinated with three alkyl or aryl groups in the equatorial position and two cyano groups in the axial position of a trigonal-bipyramidal and that the tin and the transition metal are bridged by a cyano group.

Mössbauer spectroscopy can provide valuable information about the nature of chemical bonding and the structures of compounds containing "Mössbauer-active atoms," such as tin, iron, and gold, because Mössbauer parameters are very sensitive to the number and nature of ligands coordinated to the Mössbauer atoms.[2-4] Especially, ^{197}Au-Mössbauer spectroscopy is one of the most powerful techniques in the structural diagnosis of the gold compounds. In the present study, ^{57}Fe-, ^{119}Sn-, and ^{197}Au-Mössbauer spectroscopic studies have been undertaken in order to examine the coordination for the iron, tin, and gold atoms and to elucidate the lattice dynamical properties of tin and iron sites in the trialkyl- and triaryltin complexes of transition metal cyanides, such as $\{[R_3Sn](\mu\text{-}NC)[Au(\mu\text{-}CN)]\}_x$ and $\{[R_3Sn]_2[(\mu\text{-}NC)_4Pt]\}_x$ (R=Me, Bu, or Ph), and $\{[R_3Sn]_3[(\mu\text{-}NC)_6Fe]\}_x$ (R=Bu or Ph).

Experimental

Materials. All the complexes investigated were prepared by the following method, described in a reference.[1] Organotin perchlorates R_3SnClO_4 (R=Me, Bu, or Ph) were prepared in acetone by treating stoichiometric amounts of the corresponding organotin chloride, R_3SnCl, with $AgClO_4$. The filtrate was used for further reactions without any other treatment. The $\{[R_3Sn](\mu\text{-}NC)[Au(\mu\text{-}CN)]\}_x$ complexes (R=Me, Bu, or Ph) were obtained by treating a solution of $K[Au(CN)_2]$ (3 mmol) in acetone with an equimolar amount of R_3SnClO_4. The precipitates were filtered off and washed with a mixture of water and acetone. The $\{[R_3Sn]_2[(\mu\text{-}NC)_4Pt]\}_x$ (R=Me, Bu, or Ph) complexes were prepared by the same procedure using 3 mmol of $K_2[Pt(CN)_4]$ and 6 mmol of R_3SnClO_4. The precipitates were washed with acetone and then hexane. The $\{[R_3Sn]_3[(\mu\text{-}NC)_6Fe]\}_x$ (R=Bu or Ph) complexes were also prepared as has been described above by treating 3 mmol of $K_3[Fe(CN)_6]$ with 9 mmol of R_3SnClO_4. The products were washed with acetone. The purity of the complexes was confirmed by elemental analyses for C, H, and N.

Mössbauer Spectroscopic Measurements. The temperature-dependent Mössbauer-effect measurements for ^{57}Fe and ^{119}Sn were carried out by using a constant-acceleration-type spectrometer over the temperature range of 78 K$\leq T\leq$300 K. Most of the ^{119}Sn-Mössbauer spectroscopic measurements were carried out from 78 to about 200 K, since the recoil-free fraction of the complexes becomes too small to be measured at high temperatures. The temperature of the absorber was controlled within $\pm$0.5 K. ^{197}Au-Mössbauer spectroscopic measurements were carried out with a source and an

absorber, both cooled to 16 K by using a constant-acceleration-type spectrometer in connection with a pure-Ge diode detector. The details of the ^{197}Au-Mössbauer spectroscopy have been described elsewhere.[5]

The spectra observed were fitted with Lorentian-line shapes by using the least-squares fitting procedure. The velocity scale was calibrated by using a metallic iron-foil spectrum. The isomer shifts of the ^{57}Fe and ^{119}Sn spectra are reported with respect to α-Fe and $BaSnO_3$ resonances respectively at room temperature. All the isomer shifts of the ^{197}Au-Mössbauer spectra are referred to metallic gold at 16 K.

Results and Discussion

^{119}Sn-Mössbauer Spectra. Some typical ^{119}Sn-Mössbauer spectra obtained at 78 K are shown in Fig. 1 for $\{[R_3Sn](\mu\text{-CN})[Au(\mu\text{-CN})]\}_x$ (R=Me, Bu, or Ph), while the Mössbauer parameters, such as the isomer shift (*IS*), the quadrupole splitting (*QS*), and the half-width (Γ_{exp}), derived from the observed spectra are summarized in Table 1. The spectra observed consist of one doublet with relatively large *QS* values, as may be seen in Fig. 1.

In ^{119}Sn-Mössbauer spectroscopy, the major variation in the *QS* values observed can be attributed to the difference in the structural change. The range of *QS* values for organotin compounds can be classified into the following four groups:[6] 1) tetrahedral R_nSnX_{4-n} (n=1—3) [0.00—2.31 mm s^{-1}], 2) octahedral *cis*-R_2SnX_4 [1.63—2.34 mm s^{-1}], 3) trigonal-bipyramidal R_3SnX_2 (X axial) [2.76—3.86 mm s^{-1}], and 4) octahedral *trans*-R_2SnX_4 [3.37—4.32 mm s^{-1}]. On the basis of this criterion, the tin atoms in the complexes under discussion can be concluded to have a five-coordinated structure, in which the tin atom is bridged by a CN group. This result is in good agreement with the hypothetical conclusion proposed by Uson et al.[1] for the coordination state of tin atoms in the same compounds.

The *QS* values for Ph_3Sn derivatives are smaller than those of the corresponding Me_3Sn or Bu_3Sn derivatives. The decrease in the *QS* values for the Ph_3Sn derivatives can be explained by the greater partial *QS* value assigned to the phenyl group compared to that of the alkyl group. The same tendency was observed for various kinds of organotin compounds containing the phenyl group.[6]

The temperature dependence of the quadrupole splitting is negligible in every case, since the *QS* for organotin(IV) compounds arises from mainly an inequality in the nature of the tin-ligand bonds, which is temperature-independent. However, the intensity asymmetry of the quadrupole line and its temperature dependence were observed, as is shown in

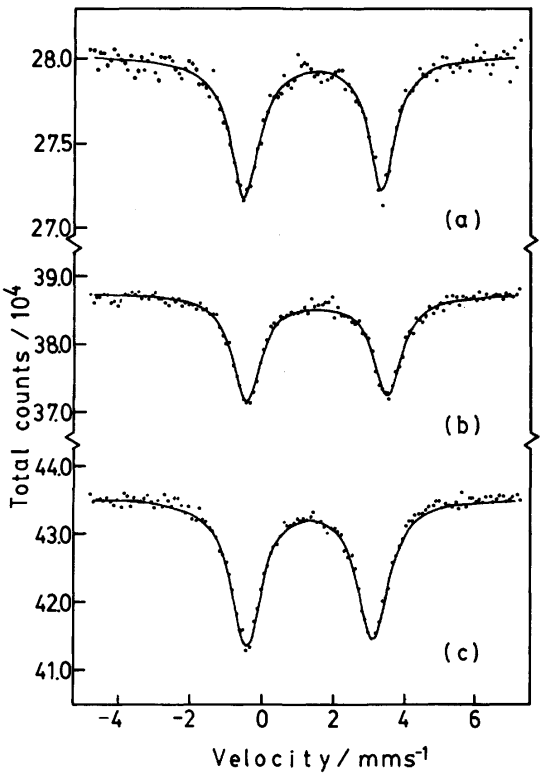

Fig. 1. ^{119}Sn-Mössbauer spectra for (a) $\{[Me_3Sn](\mu\text{-NC})[Au(\mu\text{-CN})]\}_x$, (b) $\{[Bu_3Sn](\mu\text{-NC})[Au(\mu\text{-CN})]\}_x$, and (c) $\{[Ph_3Sn](\mu\text{-NC})[Au(\mu\text{-CN})]\}_x$ at 78 K.

Table 1. ^{119}Sn-Mössbauer Parameters for Trialkyl- and Triaryltin Complexes of Transition Metal Cyanides

Complex	*IS*[a]	*QS*[b]	Γ_{exp}[b]		θ^2M[c]
	mm s^{-1}	mm s^{-1}	mm s^{-1}	mm s^{-1}	$10^6\times$deg^2 amu
$\{[Me_3Sn](\mu\text{-NC})[Au(\mu\text{-CN})]\}_x$	1.43	3.86	1.00	0.87	0.76 (78—157 K)
$\{[Bu_3Sn](\mu\text{-NC})[Au(\mu\text{-CN})]\}_x$	1.54	3.92	0.95	1.00	0.80 (78—133 K)
$\{[Ph_3Sn](\mu\text{-NC})[Au(\mu\text{-CN})]\}_x$	1.33	3.54	0.98	1.04	1.59 (78—219 K)
$\{[Me_3Sn]_2[(\mu\text{-NC})_4Pt]\}_x$	1.33	3.86	0.98	1.07	1.08 (78—179 K)
$\{[Bu_3Sn]_2[(\mu\text{-NC})_4Pt]\}_x$	1.58	4.18	1.07	1.13	1.00 (78—179 K)
$\{[Ph_3Sn]_2[(\mu\text{-NC})_4Pt]\}_x$	1.36	3.90	1.09	1.09	1.25 (78—179 K)
$\{[Bu_3Sn]_3[(\mu\text{-NC})_6Fe]\}_x$	1.49	3.86	0.98	1.16	1.00 (78—145 K)
$\{[Ph_3Sn]_3[(\mu\text{-NC})_6Fe]\}_x$	1.29	3.35	0.99	1.17	1.33 (78—195 K)

a) Relative to $BaSnO_3$; $\pm$0.02 mm s^{-1}. b) $\pm$0.02 mm s^{-1}. c) $\pm$0.05 deg^2 amu.

Fig. 2 for $\{[Bu_3Sn]_2[(\mu\text{-}NC)_4Pt]\}_x$. This asymmetry is commonly found in one- and two-dimensional polymeric compounds.[7] The temperature dependences of intensity asymmetry observed in other complexes are summarized graphically in Fig. 3, where R is the ratio of the areal intensity, A_+, of the resonance peak at the higher velocity to that, A_-, of the peak at the lower velocity.

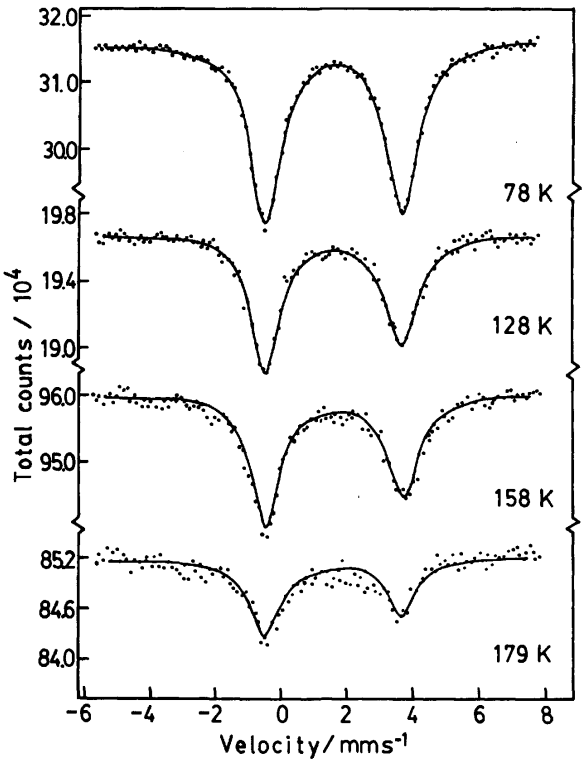

Fig. 2. ^{119}Sn-Mössbauer spectra for $\{[Bu_3Sn]_2[(\mu\text{-}NC)_4\text{-}Pt]\}_x$ at various temperatures.

The intensity asymmetry has been theoretically expressed as a function of the difference in the mean-square vibrational amplitude parallel and perpendicular with respect to the principal axis of the electric-field gradient (EFG) tensor:[8]

$$R' = \frac{I(\pm 1/2 \leftrightarrow \pm 3/2)}{I(\pm 1/2 \leftrightarrow \pm 1/2)} = \frac{\int_0^{\pi} \exp\{-(1/\lambda^2)[\langle z^2\rangle - \langle x^2\rangle]\cos^2\theta\}(1+\cos^2\theta)\sin\theta d\theta}{\int_0^{\pi} \exp\{-(1/\lambda^2)[\langle z^2\rangle - \langle x^2\rangle]\cos^2\theta\}(5/3-\cos^2\theta)\sin\theta d\theta}, \quad (1)$$

where $\langle z^2\rangle$ and $\langle x^2\rangle$ are the mean square vibrational amplitudes parallel and perpendicular respectively to the principal axis of the EFG tensor.

The more intense line can be assigned to the $\pm 1/2 \leftrightarrow \pm 3/2$ transition by assuming that the difference in $[\langle z^2\rangle - \langle x^2\rangle]$ is negative, i.e., that the vibrational motion of the tin atom in the plane of R_3Sn is larger than that along the molecular symmetry axis corresponding to the CN-Sn-NC chain. Thus, the observed intensity asymmetry suggests that the sign of the quadrupole coupling constant, e^2qQ, is negative; that is, the electric-charge distribution around a tin atom can be described as being oblate with respect to the polymer axis. This result is consistent with those for organotin compounds which have tin atoms five-coordinated in a one-dimensional chain structure in a solid.[7,9-11]

The observed intensity asymmetry R shown in Fig.

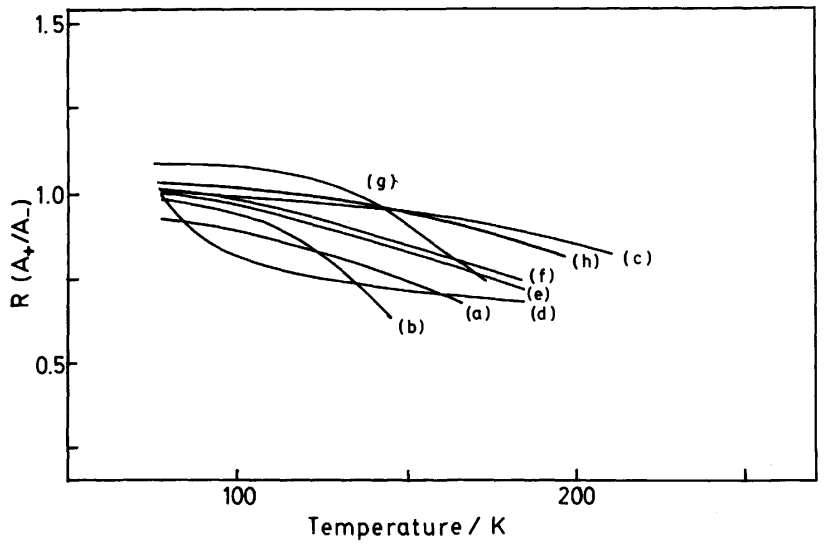

Fig. 3. Temperature dependences of peak intensity ratio for trialkyl- and triaryltin complexes of transition metal cyanides; (a) $\{[Me_3Sn](\mu\text{-}NC)[Au(\mu\text{-}CN)]\}_x$, (b) $\{[Bu_3Sn](\mu\text{-}CN)[Au(\mu\text{-}CN)]\}_x$, (c) $\{[Ph_3Sn](\mu\text{-}NC)[Au(\mu\text{-}CN)]\}_x$, (d) $\{[Me_3Sn]_2[(\mu\text{-}NC)_4Pt]\}_x$, (e) $\{[Bu_3Sn]_2[(\mu\text{-}NC)_4Pt]\}_x$, (f) $\{[Ph_3Sn]_2[(\mu\text{-}NC)_4Pt]\}_x$, (g) $\{[Bu_3Sn]_3[(\mu\text{-}NC)_6Fe]\}_x$, and (h) $\{[Ph_3Sn]_3[(\mu\text{-}NC)_6Fe]\}_x$.

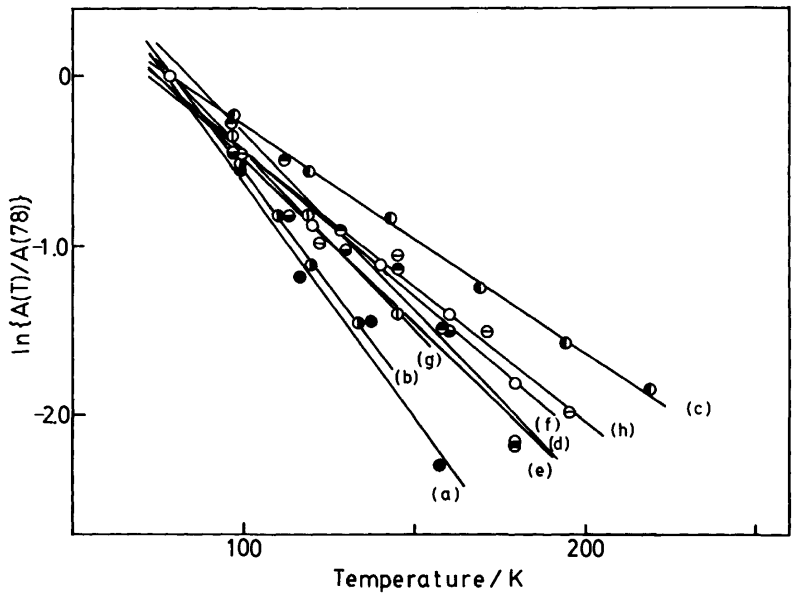

Fig. 4. Temperature dependences of the area under ^{119}Sn-resonance line for (a) $\{[Me_3Sn](\mu\text{-}NC)[Au(\mu\text{-}CN)]\}_x$, (b) $\{[Bu_3Sn](\mu\text{-}NC)[Au(\mu\text{-}CN)]\}_x$, (c) $\{[Ph_3Sn](\mu\text{-}NC)[Au(\mu\text{-}CN)]\}_x$, (d) $\{[Me_3Sn]_2[(\mu\text{-}NC)_4Pt]\}_x$, (e) $\{[Bu_3Sn]_2[(\mu\text{-}NC)_4Pt]\}_x$, (f) $\{[Ph_3Sn]_2[(\mu\text{-}NC)_4Pt]\}_x$, (g) $\{[Bu_3Sn]_3[(\mu\text{-}NC)_6Fe]\}_x$, and (h) $\{[Ph_3Sn]_3[(\mu\text{-}NC)_6Fe]\}_x$.

3 is inversely proportional to the ratio R' in Eq. 1. All the R values decrease with an increase in the temperature. This means that the mean-square vibrational amplitude in the direction perpendicular to the polymer axis depends significantly on the temperature. The temperature dependence of R for Ph_3Sn derivatives is smaller than those for Me_3Sn and Bu_3Sn derivatives. This result can be explained by assuming that the steric effect of the bulky phenyl group restricts the motion of the tin atom.

The recoil-free fraction, f_a, and its temperature dependence provide useful information about the lattice dynamical properties of a solid which are associated with the motion of Mössbauer atoms. The temperature dependences of the area under the resonance line are shown in Fig. 4 for the complexes studied in this work.

According to the Debye approximation at high temperatures, the "relative" values of the recoil-free fraction, f_a, are expressed as:

$$f_a = \exp\left(\frac{-3E_\gamma^2 T}{Mc^2k\theta^2}\right), \tag{2}$$

where E_γ is the energy of the Mössbauer transition, θ is the Debye temperature, M is the effective vibrating mass, and k is the Boltzmann constant. The temperature dependence of the recoil-free fraction, f_a, is given by Eq. 3:

$$\frac{d\ln f_a}{dT} = \frac{-3E_\gamma^2}{Mc^2k\theta^2}. \tag{3}$$

Noting that $k\theta/h=\nu_{max}\propto(\alpha/M)^{1/2}$, the following equation is obtained for the parameter of the intermolecular force constant, α:

$$\alpha \propto \theta^2M = \frac{-3E_\gamma^2}{kc^2}\left[\frac{d\ln f_a}{dT}\right]^{-1}, \tag{4}$$

where ν_{max} is the maximum lattice frequency, which is assumed to be equal to the Debye cut-off frequency, and where h is the Planck constant. The coefficient of the temperature-dependent term, $d\ln f_a/dT$, in Eq. 4 can be replaced for a "thin" absorber by the observed temperature dependence of the areal intensity under the resonance line (normalized to 78 K point).

It was found in our previous study that there was a distribution of the θ^2M values with respect to the state of molecular association in a solid.[12] The values of $\theta^2M/10^6$ deg^2 amu are distributed around unity for a non-polymeric compound, while those of one-dimensional and two-dimensional polymeric compound are distributed around 1.3 and 1.7 respectively. The distribution of the θ^2M values for three-dimensional polymeric compounds may be beyond the value of the two-dimensional polymer. The distribution of the parameters can be used to determine the state of intermolecular association in a solid. Although much overlapping is observed between the non-polymeric compounds and one-dimensional polymeric compounds, and between the one-dimensional and two-dimensional polymers, the discrimination between the nonassociated and one-dimensional polymeric states and between two- and three-dimensional polymeric states can be done by detecting the asymmetric quadrupole split lines, as has been mentioned previously.

The values of θ^2M, as estimated from the data of the

temperature dependence of the area for the complexes, are summarized in Table 1. Although the $\{[R_3Sn]_2[(\mu\text{-}NC)_4Pt]\}$ and $\{[R_3Sn]_3[(\mu\text{-}NC)_6Fe]\}_x$ complexes are considered to be two- or three-dimensional polymer complexes, the values of θ^2M in Table 1 suggest that the state of molecular association for these complexes is close to that of non-polymeric compounds or one-dimensional polymers. The values of θ^2M for Me_3Sn and Bu_3Sn derivatives are smaller than those for Ph_3Sn derivatives in each series. This means that the motion of tin atoms in these complexes depends mainly on the ligands in the first coordination sphere of tin atoms. A large temperature dependence of the mean-square vibrational amplitude perpendicular to the polymer axis strongly affects the values of θ^2M. The relatively large values of θ^2M for Ph_3Sn derivatives presumably reflect the restriction on the motion of tin atoms attributable to the bulky phenyl group, which is packed rigidly in a solid. The same tendency was observed for R_4Sn compounds; e.g., the value of θ^2M for Me_4Sn is 0.77×10^6, while that for Ph_4Sn is 1.28×10^6.[12] Consequently, a comparison of the parameters of the intermolecular force constant, $\alpha \propto \theta^2M$, gives valuable information about the motion of tin atoms associated in a solid.

^{57}Fe-Mössbauer Spectra. The ^{57}Fe-Mössbauer spectra and their temperature dependence for $\{[Bu_3Sn]_3[(\mu\text{-}NC)_6Fe]\}_x$ are shown in Fig. 5, while the Mössbauer parameters derived from the observed spectra are listed in Table 2. The values of *IS* and *QS* and the temperature dependence of *QS* indicate that the iron atom in this complex is at an Fe(III) low-spin state. The temperature dependences of *QS* for $\{[Bu_3Sn]_3[(\mu\text{-}NC)_6Fe]\}_x$ and $\{[Ph_3Sn]_3[(\mu\text{-}NC)_6Fe]\}_x$ are shown in Fig. 6.

A low-spin Fe(III) atom has a nonspheric d shell. The contribution of this configuration to the EFG

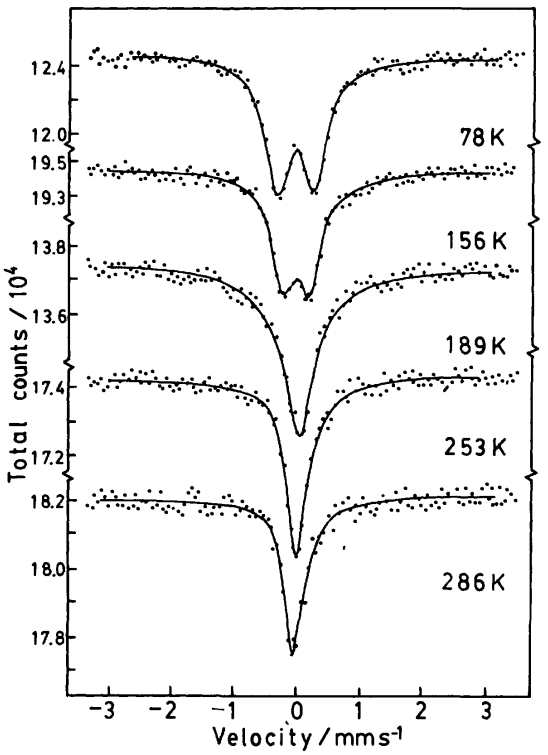

Fig. 5. ^{57}Fe-Mössbauer spectra for $\{[Bu_3Sn]_3[(\mu\text{-}NC)_6\text{-}Fe]\}_x$ at various temperatures.

Table 2. ^{57}Fe-Mössbauer Parameters at 78 *K*

Complex	*IS*[a]	*QS*[b]	Γ_{exp}[b]	
	mm s^{-1}	mm s^{-1}	mm s^{-1}	mm s^{-1}
$\{[Bu_3Sn]_3[(\mu\text{-}NC)_6Fe]\}_x$	−0.05	0.55	0.42	0.47
$\{[Ph_3Sn]_3[(\mu\text{-}NC)_6Fe]\}_x$	−0.07	1.19	0.43	0.45

a) Relative to α-Fe foil; ±0.02 mm s^{-1}. b) ±0.02 mm s^{-1}.

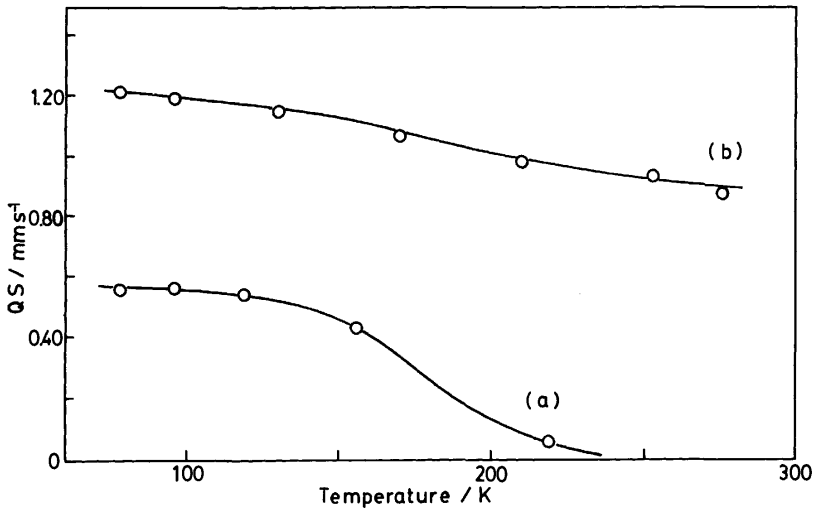

Fig. 6. Temperature dependences of the quadrupole splitting for (a) $\{[Bu_3Sn]_3[(\mu\text{-}NC)_6Fe]\}_x$ and (b) $\{[Ph_3Sn]_3[(\mu\text{-}NC)_6Fe]\}_x$.

Table 3. ^{197}Au-Mössbauer Parameters at 16 *K*

Complex	*IS*[a]	*QS*[b]	Γ_{exp}[b]	
	mm s^{-1}	mm s^{-1}	mm s^{-1}	mm s^{-1}
$\{[Me_3Sn](\mu\text{-NC})[Au(\mu\text{-CN})]\}_x$	4.51	10.45	2.00	2.00
$\{[Bu_3Sn](\mu\text{-NC})[Au(\mu\text{-CN})]\}_x$	4.37	9.99	1.93	2.17
$\{[Ph_3Sn](\mu\text{-NC})[Au(\mu\text{-CN})]\}_x$	4.45	10.08	2.01	2.01

a) Relative to Au foil; ± 0.04 mm s^{-1}. b) ± 0.04 mm s^{-1}.

depends on the symmetry of the external field and the temperature. A large temperature dependence of *QS* for the Bu_3Sn derivative indicates that the three d_ε levels are close to each other in energy. The environment around iron(III) atoms is assumed to be almost cubic. On the other hand, the decrease in the *QS* for the Ph_3Sn derivative is slow. This can be explained by assuming that the three d_ε levels are widely separated as a result of the distortion of $Fe(CN)_6$ octahedra caused by the steric hindrance of bulky phenyl groups.

The values of $\theta^2M/10^6$ for ^{57}Fe estimated by using Eq. 4 are 0.97 and 1.63 for Bu_3Sn and Ph_3Sn derivatives respectively. These values are smaller than those expected for three-dimensional polymeric compounds. This result reflects the linkage of a long CN–Sn–NC chain, which probably reduces the motional rigidity of the iron atoms in these complexes. The fact that the value for the Ph_3Sn derivative is larger than that for the Bu_3Sn derivative can be explained by the same interpretation as has been proposed for the case of ^{119}Sn, that is, the motion of the iron atom is restrained by the steric effect of bulky phenyl groups. The similarity between the values of θ^2M of ^{57}Fe and those of ^{119}Sn for $\{[Bu_3Sn]_3[(\mu\text{-NC})_6Fe]\}_x$ and $\{[Ph_3Sn]_3[(\mu\text{-NC})_6Fe]\}_x$ respectively suggests that the motion of iron atoms depends on that of tin atoms in these complexes.

^{197}Au-Mössbauer Spectroscopy. The ^{197}Au-Mössbauer spectra for the $\{[R_3Sn](\mu\text{-NC})[Au(\mu\text{-CN})]\}_x$ complexes (R=Me, Bu, or Ph) consist of one doublet with quite large *QS* values. The Mössbauer parameters derived from the spectra are summarized in Table 3. The values of *IS* and *QS* for these complexes are very close to those of $K[Au(CN)_2]$.[13]

In linear gold(I) compounds, the $5d_{z^2}$, 6s, and $6p_z$ metal orbitals (the z axis being the molecular axis) are suitable for σ-bonding, while the $5d_{xz,yz}$ and $6p_{x,y}$ orbitals are used in π-bonding to the ligands. The $5d_{xy}$ and $5d_{x^2-y^2}$ orbitals are nonbonding. σ-Donation into the $5d_{z^2}$ and $6p_z$ orbitals is expected to contribute negatively to the quadrupole coupling constant, e^2qQ. The absolute value of e^2qQ might be expected to increase the σ-donor strength of the ligands, assuming that the sign of e^2qQ for the two coordinated gold(I) compounds is negative. The negative e^2qQ has been confirmed experimentally for $K[Au(CN)_2]$.[14] π-Bonding and d_π-back-bonding also affect the e^2qQ, but their contribution is estimated to be smaller than that of σ-donor bonding on the basis of theoretical considerations[15,16] and systematic ^{197}Au-Mössbauer studies of many gold(I) compounds.[17–20] Thus, it is reasonable to conclude that the *QS* values mainly depend on the σ-donating ability of the ligands. On the other hand, it has been known that the *IS* value depends on the s electron density at the gold nucleus. The 6s population directly increases the electron density at the nucleus, while the $5d_{z^2}$ and $6p_z$ populations decrease the electron density because of their shielding effect. The shielding effect of 5d electrons is larger than that of 6p electrons. The d_π-back-bonding reduces the d electrons and then increases the electron density at the ^{197}Au nucleus. Increases in the s electron density at the nucleus lead to the increase in the *IS* value because of the positive $\Delta R/R$ in ^{197}Au-Mössbauer spectroscopy. Hence, both the *QS* and *IS* values depend on the σ-donating and π-accepting ability of the ligands. A linear relationship between the observed *IS* and *QS* values has been established for many gold(I) compounds.[18,20,21]

The values of *IS* and *QS* for the gold(I) compounds with a CN group are expected to be larger than those for other gold(I) compounds. This expectation is confirmed by the observed large *IS* and *QS* values for $\{[R_3Sn](\mu\text{-NC})[Au(\mu\text{-CN})]\}_x$ complexes. It can be concluded that the gold atom in these complexes is coordinated linearly with two cyano groups and forms an infinite one-dimensional polymeric structure.

References

1) R. Uson, J. Fornies, M. A. Uson, and E. Lalinde, *J. Organomet. Chem.*, **185**, 359 (1980).

2) "Mössbauer Isomer Shift," ed by G. K. Shenoy and F. D. Wagner, North-Holland, Amsterdam (1978).

3) P. Gütlich, R. Link, and A. Trautwein, "Mössbauer Spectroscopy and Transition Metal Chemistry," Springer-Verlag, Berlin (1978).

4) "Chemical Mössbauer Spectroscopy," ed by R. H. Herber, Plenum, New York (1985).

5) M. Katada, Y. Uchida, K. Sato, H. Sano, H. Sakai, and Y. Maeda, *Bull. Chem. Soc. Jpn.*, **55**, 444 (1982).

6) G. M. Bancroft and R. H. Platt., *Adv. Inorg. Chem. Radiochem.*, **15**, 59 (1972).

7) H. A. Stöckler and H. Sano, *Phys. Lett.*, **25A**, 550

(1967); *Phys. Rev.*, **165**, 406 (1968); *Chem. Phys. Lett.*, **2**, 448 (1968); *J. Chem. Phys.*, **50**, 3813 (1969); *Polymer Lett.*, **7**, 67 (1969).

8) V. I. Gol'danskii and E. F. Makarov, "Chemical Applications of Mössbauer Spectroscopy," ed by V. I. Gol'danskii and R. H. Herber, Academic Press, New York (1968).

9) R. H. Herber, S. C. Chandra, and Y. Hazony, *J. Chem. Phys.*, **53**, 3330 (1970).

10) R. H. Herber and S. C. Chandra, *J. Chem. Phys.*, **54**, 1847 (1971).

11) R. H. Herber, *J. Chem. Phys.*, **54**, 3755 (1971).

12) S. Matsubara, M. Katada, K. Sato, I. Motoyama, and H. Sano, *J. Phys. Colloq.*, **C2**, 363 (1979).

13) H. D. Bartunik, W. Potzel, R. L. Mössbauer, and G. Kaindl, *Z. Phys.*, **240**, 1 (1970).

14) H. Prosser, F. E. Wagner. G. Wortmann, G. M. Kalvius, and R. Wäppling, *Hyperfine Intr.*, **1**, 25 (1975).

15) D. M. S. Esquivel, D. Guenzburger, and J. Danon, *Phys. Rev., B*, **19**, 1357 (1979).

16) T. K. Sham, R. E. Watson, and M. L. Perlman, *Phys. Rev. B*, **21**, 1457 (1980).

17) C. A. McAuliffe, R. V. Parish, and P. D. Randall, *J. Chem. Soc., Dalton Trans.*, **1977**, 1426.

18) P. G. Jones, A. G. Maddock. M. J. Mays, M. N. Muir, and A. F. Williams, *J. Chem. Soc., Dalton Trans.*, **1977**, 1434.

19) G. C. H. Jones, P. G. Jones, A. G. Maddock, M. J. Mays, P. A. Vergnans, and A. F. Williams, *J. Chem. Soc., Dalton Trans.*, **1977**, 1440.

20) R. V. Parish, *Gold Bull.*, **15**, 51 (1982).

21) Y. Uchida, M. Katada, H. Sano, H. Sakai, and Y. Maeda, *J. Radioanal. Nucl. Chem. Lett.*, **94**, 215 (1985).

Raman Spectra of Tris(bidentate)cobalt(III) Complexes Containing 1,3-Propanediamine and β-Alaninate

Tatsuya KAWAMOTO,* Hisahiko EINAGA,† and Jinsai HIDAKA
Department of Chemistry, University of Tsukuba, Sakura, Ibaraki 305
†Institute of Materials Science, University of Tsukuba, Sakura, Ibaraki 305
(Received September 12, 1986)

The Raman spectra of the tris(bidentate)cobalt(III) complexes containing the six-membered tn and/or β-ala chelate ring, where tn and β-ala denote 1,3-propanediamine and β-alaninate respectively, were measured in order to investigate the relation between the Raman spectra and the structures of the complexes. The Raman bands can be classified into four vibration modes: A totally symmetric stretching vibration mode in the 440—640 cm^{-1} region, a stretching vibration mode excluding the totally symmetric one in the 380—480 cm^{-1} region, a metal-ligand skeletal bending deformation mode in the 260—400 cm^{-1} region, and a chelate ring deformation mode in the 220—290 cm^{-1} region. The present complexes characteristically exhibited more Raman bands than the complexes with the five-membered chelate rings in the totally symmetric stretching vibration mode. For the $[Co(\beta\text{-ala})_2(tn)]^+$ complex, the three geometrical isomers, *trans(O)*, C_2-*cis(O)*, and C_1-*cis(O)*, which were prepared for the first time, each exhibited characteristic Raman spectral features.

Recently, it has been recognized that the configurational structural characteristics of metal complexes are sensitively reflected on the skeletal vibrations rather than on the intra-ligand vibrations of the Raman spectra. For instance, the Raman spectra of the nitro-ammine series of the cobalt(III) complexes, $[Co(NO_2)_n(NH_3)_{6-n}]$-type,[1] have been studied in order to establish the assignments of the skeletal vibrations. Further, the Raman spectra in the skeletal vibration region have been applied successfully to the differentiation of the geometrical isomers of various sorts of cobalt(III) complexes with unidentate ligands and of mixed complexes with unidentate and bidentate ligands.[2,3] In our previous work, the Raman spectra of the $[Co(gly)_x(ox)_y(en)_z]$-type[4] and $[Co(ida)_n(dien)_{2-n}]$-type complexes,[5] where gly, ox, en, ida, and dien denote glycinate, oxalate, 1,2-ethanediamine, iminodiacetate, and diethylenetriamine respectively, have been measured in order to find general information on the relation between the spectra and the structures of these complexes in the skeletal vibration region.

The present work was undertaken on the tris(bidentate)cobalt(III) complexes containing 1,3-propanediamine (tn) and/or β-alaninate (β-ala) in order to investigate the relation between the Raman spectral characteristics in the 200—700 cm^{-1} region and the structures of the complexes.

Experimental

Complexes. The complexes were prepared and characterized according to the literature procedures except for $[Co(\beta\text{-ala})_2(tn)]Cl$ (vide infra): $[Co(en)_2(tn)]Br_3$,[6] $[Co(en)(tn)_2]Br_3$,[6] $[Co(tn)_3]Cl_3$,[7] $[Co(gly)(tn)_2]Cl_2$,[8] $[Co(\beta\text{-ala})(en)_2]Cl_2$,[9] *trans*(O)-$[Co(\beta\text{-ala})_2(en)]Cl$,[9] *fac(N)*-$[Co(\beta\text{-ala})_3]$,[10] and *mer(N)*-$[Co(\beta\text{-ala})_3]$.[10]

$[Co(\beta\text{-ala})_2(tn)]Cl$. This complex was prepared by a procedure similar to that used for $[Co(gly)_2(en)]Cl$.[11] A solution containing 1.7 cm^3 of 1,3-propanediamine and 3.6 g of β-alanine in 15 cm^3 of water was added to a solution containing 5 g of cobalt(II) chloride hexahydrate in 10 cm^3 of water. The solution was oxidized over a steam bath by gradually adding 10 g of lead dioxide for 1 h. After it had then been cooled to room temperature, the mixture was filtered. The filtrate was poured onto a column of SP-Sephadex C-25 (Na^+ form, 3.5 cm×60 cm). After the column had been swept with water, the adsorbed band was eluted with a 0.05 mol dm^{-3} aqueous solution of NaCl. Three colored bands, violet (A-1), pink (A-2), and red-violet (A-3), were eluted in this order; they were present in a ratio of about A-1:A-2:A-3=1.6:1.4:3.5. Each eluate was concentrated to a small volume by the use of a rotary evaporator below 30 °C, and the deposited NaCl was filtered off. The filtrate was passed through a column of Sephadex G-10 (3 cm×50 cm) by means of elution with water. A small amount of ethanol was added to the eluate after its concentration again. The precipitate which appeared was collected by filtration. Found for A-1: C, 28.76; H, 6.51; N, 14.89%. Calcd for $[Co(\beta\text{-ala})_2(tn)]Cl\cdot 5/4H_2O\cdot 1/7NaCl = CoC_9H_{22}N_4O_4Cl\cdot 5/4H_2O\cdot 1/7NaCl$: C, 28.78; H, 6.58; N, 14.92%. Found for A-2: C, 26.24; H, 6.17; N, 13.57%. Calcd for $[Co(\beta\text{-ala})_2(tn)]Cl\cdot 3/2H_2O\cdot 5/8NaCl$: C, 26.48; H, 6.17; N, 13.72%. Found for A-3: C, 29.18; H, 6.45; N, 15.22%. Calcd for $[Co(\beta\text{-ala})_2(tn)]Cl\cdot 1/2H_2O\cdot 1/4NaCl$: C, 29.35; H, 6.30; N, 15.21%. Absorp. max. $10^{-3}\sigma/cm^{-1}$ (log ε): A-1: 18.1 (2.17), 21.5sh (1.88), 27.3 (2.12); A-2: 19.9 (2.07), 27.6 (1.95); A-3: 19.3 (2.17), 27.4 (1.99). ^{13}C NMR: A-2: δ=27.8, 36.0, 40.3, 40.7, 184.8; A-3: δ=28.0, 36.0, 36.2, 40.0, 40.4, 40.6, 182.1, 185.2. On the basis of the absorption spectra of *trans(O)*-, C_2-*cis(O)*-, and C_1-*cis(O)*-$[Co(gly)_2(en)]^+$,[11] it was found from their absorption spectra that the A-1 eluate contained the trans(O) isomer, and the A-2 and A-3 eluates, cis(O) isomers. Further, from the ^{13}C NMR spectral measurements, it was found that A-2 and A-3 eluates contained C_2-cis(O) and C_1-cis(O) isomers respectively.

Measurements. The Raman spectra were recorded on a JASCO Laser Raman Spectrometer, which was constructed specially with a double monochromator, model CT-25, a He–Ne laser, model NEC GLG-8500, and a data processor, model DP-500, as the main components. The sample solution was excited at 632.8 nm, and the Raman spectra were calibrated with indene. The electronic absorption

spectra were recorded with a JASCO UVIDEC-1 spectrophotometer, and the ^1H and ^{13}C NMR spectra were recorded in deuterium oxide on a JEOL JNM-FX-100 NMR spectrometer at the probe temperature. Sodium 2,2-dimethyl-2-silapentane-5-sulfonate (DSS) was used as the internal reference.

Results and Discussion

The Raman spectral data in the skeletal vibration region of the tris(bidentate)cobalt(III) complexes containing the six-membered tn and/or β-ala chelate ring are summarized in Table 1, together with those of $[Co(gly)_n(en)_{3-n}]^{(3-n)+}$ and $[Co(NH_3)_6]^{3+}$. There is a significant distinction between the Raman spectral characteristics of the cobalt(III) complexes containing the six-membered chelate ring and those with the five-membered rings; on going from the latter to the former, the number of the Raman bands is increased, and the bands are shifted to lower frequencies (vide infra). For instance, the Raman spectrum of $[Co(en)_3]^{3+}$ exhibits four major low frequency lines, which were assigned to the stretching and bending deformation modes ($A_{1g}+E_g+T_{2g}$ with the effective symmetry of O_h) and to the chelate ring deformation mode on the basis of a comparison with the skeletal vibrations of $[Co(NH_3)_6]^{3+}$,[4,12] whereas the spectrum of $[Co(tn)_3]^{3+}$ exhibits eight Raman bands. The increase in the number of Raman bands reflects the difference between tn and en chelate rings, and it is expected that the Raman bands of $[Co(tn)_3]^{3+}$ can be treated in terms of a molecular symmetry slightly lower than the true one, $D_3(3A_1+5E)$, which is determined by the configuration of the chelate rings. Above all, the 451 cm^{-1} band (strong and polarized) and the 431 cm^{-1} band (shoulder and depolarized) can be assigned to A_1 (totally symmetric stretching mode) and E (stretching vibration mode excluding the totally symmetric one) respectively. An X-ray structure analysis[13] and model consideration of $[Co(tn)_3]^{3+}$ show that the six-membered rings are more flexible than the five-membered ones and that the distortion of the octahedral coordination[13] makes the former more conformationally labile than the latter. In fact, the CD spectrum of Λ-$(+)_{589}$-$[Co(tn)_3]^{3+}$ indicates a conformational equilibrium in solution between the tris skew-boat and tris chair forms.[14] Accordingly, it may be inferred that the Raman spectrum of $[Co(tn)_3]^{3+}$ reflects the conformational complexity of the six-membered chelate ring. Here, we should refer to the Raman spectra of the $[Co(a)(b)(tn)_2]$-type complexes, where a and b denote unidentate ligands, exhibiting also some Raman bands in the region of 400—550 cm^{-1}.[3] The very strong bands at ca. 450 cm^{-1} and the bands in the region of 480—550 cm^{-1} have been assigned to the Co-N(tn) stretching mode, ν(Co-N(tn)), and the deformation vibration of the chelate ring, δ(CNN), respectively, by considering the Raman spectra of the $[Co(a)(b)(en)_2]$-type complexes and the $[M(en)_2]^{2+}$ (M=Cu, Pd, and Pt) complexes based on the normal coordinate analysis. However, in the case of the $[Co(tn)_3]^{3+}$ complex, it seems reasonable to consider that the bands in the region of 450—530 cm^{-1} can be assigned to the totally symmetric stretching vibration mode, because the bands at 451 and 530 cm^{-1} of $[Co(tn)_3]^{3+}$ are shifted to lower frequencies (ca. 15 cm^{-1}) upon a deuteration of the amino protons of the 1,3-propanediamine ligand, as is to be expected for the bands due to the Co-N stretching vibration. On the basis of the above consideration and the Raman spectral characteristics summarized in Table 1, the Raman spectra of the cobalt(III) complexes containing the six-membered chelate ring can be classified into four vibration modes, like those with the five-membered chelate rings:[4] The totally symmetric stretching vibration mode (440—640 cm^{-1}), the stretching vibration mode excluding the totally symmetric one (380—480 cm^{-1}), the metal-ligand skeletal bending deformation mode (260—400 cm^{-1}), and the chelate ring deformation mode (220—290 cm^{-1}) from the higher frequency region.

A comparison of the Raman spectra in the skeletal vibration region of the four $[Co(en)_n(tn)_{3-n}]^{3+}$($n$=0—3) complexes (Fig. 1 and Table 1) clearly demonstrates

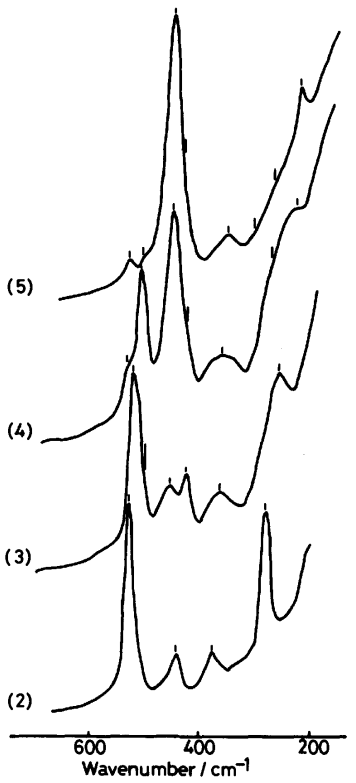

Fig. 1. Raman spectra of $[Co(en)_n(tn)_{3-n}]^{3+}$ (n=0, 1, 2, and 3). Numbers in parentheses correspond to those in Table 1.

Table 1. Raman Spectral Data of Tris(bidentate)cobalt(III) Complexes with Six-Membered Chelate Rings

No.	Complex	Raman frequency/cm^{-1}, a)			
1	$[Co(NH_3)_6]^{3+}$ b)	495 s (p)	440 m (dp)	320 w (dp)	
2	$[Co(en)_3]^{3+}$ b)	525 s (p)	440 w (dp)	378 w (dp)	283 s (p)
3	$[Co(en)_2(tn)]^{3+}$	517 s (p) 502 sh (—) 449 m (p)	423 m (dp)	364 m (dp)	254 m (p)
4	$[Co(en)(tn)_2]^{3+}$	534 vw (—) 506 s (p) 449 s (p)	423 sh (dp)	355 w (dp) 271 vw (dp)	226 w (p)
5	$[Co(tn)_3]^{3+}$	530 w (p) 502 vw (—) 451 s (p)	431 sh (dp)	352 m (dp) 307 vw (—) 269 vw (dp)	222 m (p)
6	$[Co(gly)(en)_2]^{2+}$ b)	584 w (p) 521 s (p)	471 vw (dp) 447 w (dp)	374 w (dp)	279 s (p)
7	$[Co(gly)(tn)_2]^{2+}$	590 w (—) 534 vw (—) 482 m (p) 450 s (p)	380 m (dp)	342 w (dp)	221 w (p)
8	$[Co(\beta\text{-ala})(en)_2]^{2+}$	523 m (p)	439 vw (—)	440 vw (dp)	256 w (p)
9	C_1-*cis*(*O*)-$[Co(gly)_2(en)]^+$ b)	593 m (p) 526 m (p)	494 w (dp) 469 w (dp) 430 vw (dp) 422 vw (dp)	358 w (dp)	276 s (p)
10	C_2-*cis*(*O*)-$[Co(gly)_2(en)]^+$ b)	598 m (p) 538 s (p)	486 w (dp) 433 w (dp)	360 w (dp)	276 s (p)
11	*trans*(*O*)-$[Co(gly)_2(en)]^+$ b)	596 m (p) 523 m (p)	504 sh (dp) 458 w (dp)	368 w (dp)	275 s (p)
12	*trans*(*O*)-$[Co(\beta\text{-ala})_2(en)]^+$	624 w (p) 510 m (p) 493 sh (—)	421 vw (dp)	382 w (p)	
13	C_1-*cis*(*O*)-$[Co(\beta\text{-ala})_2(tn)]^+$	628 vw (p) 534 w (p) 498 m (p) 454 s (p)	402 vw (—)	350 vw (dp)	
14	C_2-*cis*(*O*)-$[Co(\beta\text{-ala})_2(tn)]^+$	633 w (p) 534 vw (p) 486 s (p)	466 sh (dp) 407 m (p)	371 w (dp) 362 w (dp)	
15	*trans*(*O*)-$[Co(\beta\text{-ala})_2(tn)]^+$	634 w (p) 507 m (p) 465 s (p)	479 sh (dp)		
16	*fac*(*N*)-$[Co(gly)_3]$ b)	603 s (p)	487 w (dp) 438 w (dp)	364 w (dp)	270 s (p)
17	*mer*(*N*)-$[Co(gly)_3]$ b)	602 s (p)	540 vw (dp) 496 w (dp) 440 vw (dp)	356 w (dp)	272 s (p)
18	*fac*(*N*)-$[Co(\beta\text{-ala})_3]$	616 vw (p) 531 m (p) 503 w (p)	405 w (p)	378 w (p)	288 vw (—)
19	*mer*(*N*)-$[Co(\beta\text{-ala})_3]$	632 vw (—) 534 w (—) 509 w (—) 485 w (—)	409 vw (—)	381 vw (—)	
	Assignment a)	ν_{ts}(Co-L)	ν(Co-L)	δ_{sbd}(L-Co-L)	$\delta_{crd}\left(\text{Co}\langle^{\text{L}}_{\text{L}}\rangle\right)$

a) The following abbreviations are used: s, strong; m, medium; w, weak; vw, very weak; sh, shoulder; p, polarized; dp, depolarized; ν_{ts}, totally symmetric stretching vibration mode; ν, stretching vibration mode excluding the totally symmetric one; δ_{sbd}, metal-ligand bending deformation mode; δ_{crd}, chelate ring deformation mode. The Raman band intensities (s, m, w, vw, and sh) are classified by a comparison of all the Raman bands among all the complexes. The numerical data in the parentheses are the polarization ratios. b) Ref. 4.

that the number of bands increases with the substitution of the en ligand by the tn one and that the Raman bands of the chelate ring deformation mode are shifted to lower frequencies. Furthermore, $[Co(en)_2(tn)]^{3+}$ and $[Co(en)(tn)_2]^{3+}$ exhibit equally the bands due to the Co-N(en) and Co-N(tn) totally symmetric stretching vibration mode; the bands due to ν_{ts}(Co-N(en)) and ν_{ts}(Co-N(tn)) are observed in the region above 500 cm^{-1} and at ca. 450 cm^{-1} respectively. The shift of the Raman bands due to ν_{ts}(Co-N(en)), 525, 517, and 506 cm^{-1} for the $[Co(en)_n(tn)_{3-n}]$-type complexes may be attributed to the increased relaxation of the Co-N(en) bonds by stepwise substitution of the tn ligand for the en one. That is, there is no appreciable vibrational coupling between ν_{ts}(Co-N(tn)) and ν_{ts}(Co-N(en)). In addition, the intensities of the bands, ν_{ts}(Co-N(tn)) and ν_{ts}(Co-N(en)), of the mixed complexes are proportional to the number of the en ligand and the tn one. Here, it is worthy of note that the ν_{ts}(Co-N) Raman shifts of $[Co(NH_3)_6]^{3+}$, $[Co(en)_3]^{3+}$, and $[Co(tn)_3]^{3+}$ decrease in the following order; ν_{ts}(Co-N(en))>ν_{ts}(Co-N(NH_3))>ν_{ts}(Co-N(tn)). This decreasing order is in line with that for the $^1T_{1g}\leftarrow{}^1A_{1g}(O_h)$ electronic transition energy of the $[Co(N)_6]$ chromophore; 21.30×10^3 cm^{-1}($[Co(en)_3]^{3+}$)[15]>20.96×10^3 cm^{-1}($[Co(NH_3)_6]^{3+}$)[16]>20.49×10^3 cm^{-1}($[Co(tn)_3]^{3+}$).[7] The spectral behavior caused by the substitution of the en ligand by the tn one is also observed for the $[Co(gly)(en)_2]^{2+}$ and $[Co(gly)(tn)_2]^{2+}$ complexes. That is, $[Co(gly)(tn)_2]^{2+}$ shows more Raman bands than does $[Co(gly)(en)_2]^{2+}$, as is to be expected from the results for the $[Co(en)_n(tn)_{3-n}]$-type complexes (Fig. 2). The Raman band due to the chelate ring deformation mode of $[Co(gly)(tn)_2]^{2+}$ is also shifted to a lower frequency. Furthermore, a comparison of the Raman bands in the totally symmetric stretching vibration region of $[Co(tn)_3]^{3+}$ (Fig. 1) and $[Co(gly)(tn)_2]^{2+}$ suggests that the band at 482 cm^{-1} of $[Co(gly)(tn)_2]^{2+}$ is the characteristic band of the coordinated gly ligand, similar to the spectral relation between $[Co(en)_3]^{3+}$ and $[Co(gly)(en)_2]^{2+}$.[4]

The Raman spectra of $[Co(\beta\text{-ala})(en)_2]^{2+}$ and $[Co(en)_3]^{3+}$ reveal that the replacement of the en ligand in $[Co(en)_3]^{3+}$ by the β-ala one causes no changes in the intrinsic spectral features; the four bands of $[Co(\beta\text{-ala})(en)_2]^{2+}$ can be correlated to those of $[Co(en)_3]^{3+}$ (Fig. 3). This spectral behavior is quite in contrast to that resulting from the replacement of the en ligand by the gly one.[4] The good correlation of the Raman spectral features between $[Co(\beta\text{-ala})(en)_2]^{2+}$ and $[Co(en)_3]^{3+}$ may result from the fact that the skeletal vibration behavior of the former is determined by the two en chelate rings because of the conformational restriction due to the five-membered chelate ring and because of the proximity of the reduced mass of the donor atoms. The Raman spectra of $[Co(\beta\text{-ala})(en)_2]^{2+}$ and *trans(O)*-$[Co(\beta\text{-ala})_2(en)]^+$ show that the Raman spectral features are no longer retained upon a structural change from the former to the latter (Fig. 3), whereas a comparison of the spectra of $[Co(gly)(en)_2]^{2+}$ and *trans(O)*-$[Co(gly)_2(en)]^+$ reveals that the spectral features are well retained

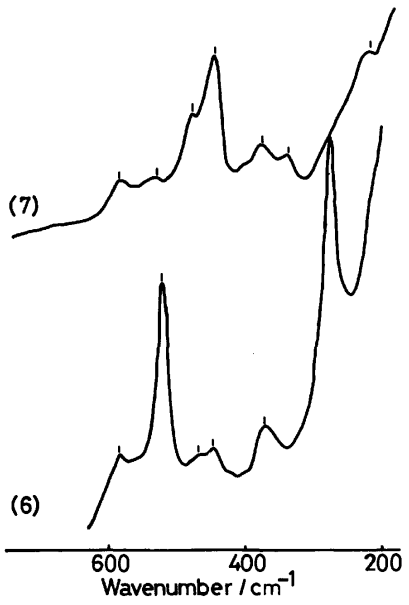

Fig. 2. Raman spectra of $[Co(gly)(tn)_2]^{2+}$ and $[Co(gly)(en)_2]^{2+}$. Numbers in parentheses correspond to those in Table 1.

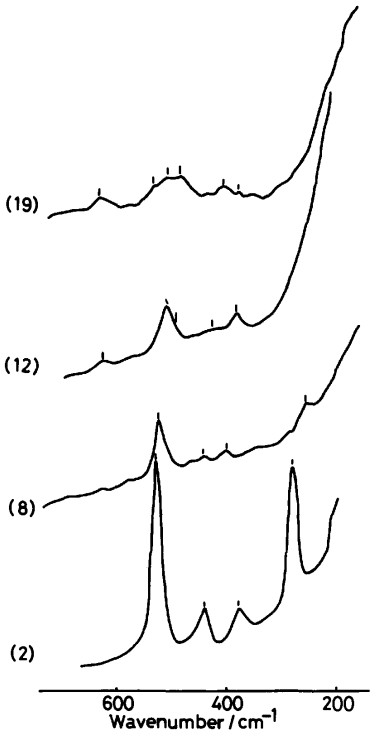

Fig. 3. Raman spectra of *mer(N)*-$[Co(\beta\text{-ala})_3]$, *trans(O)*-$[Co(\beta\text{-ala})_2(en)]^+$, $[Co(\beta\text{-ala})(en)_2]^{2+}$, and $[Co(en)_3]^{3+}$. Numbers in parentheses correspond to those in Table 1.

even after the structural change.[4] This Raman spectral evidence clearly demonstrates that the six-membered β-ala chelate ring is more flexible than the five-membered gly chelate ring, as in the case of the tn and en chelate rings (vide supra).

A conspicuous difference was found in the Raman spectra in the totally symmetric stretching vibration mode of the geometrical isomers, *fac(N)*- and *mer(N)*-[Co(β-ala)$_3$], as is shown in Fig. 4; the mer(N) isomer exhibits a more complicated Raman spectrum than does the fac(N) one. An analogous tendency has been observed for the spectra of *fac(N)*- and *mer(N)*-[Co(gly)$_3$].[4] However, it is interesting that the Raman spectral differences among the geometrical isomers of the cobalt(III) complexes with the six-membered chelate rings are noticed in the totally symmetric stretching vibration mode, whereas those of the complexes with the five-membered chelate rings appear in the stretching vibration mode excluding the totally symmetric one.

As is shown in Fig. 5, the Raman spectral features of the three geometrical isomers, *trans(O)*-, C_2-*cis(O)*-, and C_1-*cis(O)*-[Co(β-ala)$_2$(tn)]$^+$, which have been prepared for the first time in this work are, in a first approximation, similar to each other, as in the case of the geometrical isomers, *trans(O)*-, C_2-*cis(O)*-, and C_1-*cis(O)*-[Co(gly)$_2$(en)]$^+$.[4] On a closer inspection, however, we can find some differences among the Raman spectral features of the three geometrical isomers of [Co(β-ala)$_2$(tn)]$^+$. Firstly, the difference between the trans(O) isomer and the two cis(O) ones can be observed in the skeletal bending deformation region; the trans(O) isomer has no Raman band, but the cis(O) isomers have a few Raman bands.

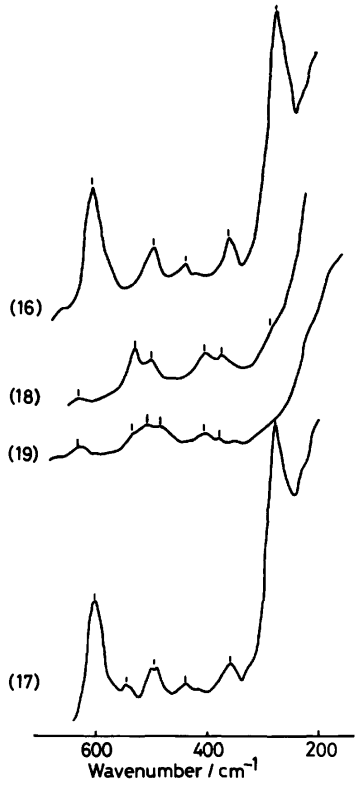

Fig. 4. Ranam spectra of mer(N) and fac(N) isomers of [Co(gly)$_3$] and [Co(β-ala)$_3$]. Numbers in parentheses correspond to those in Table 1.

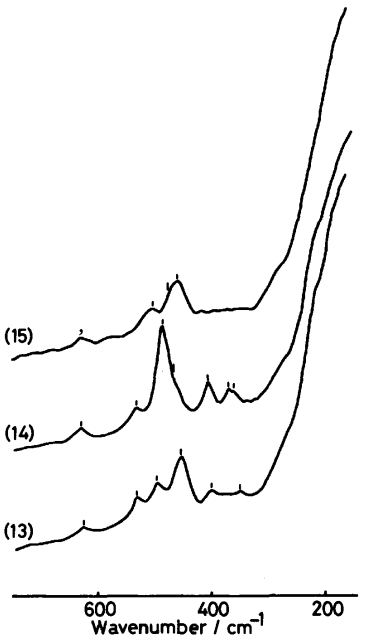

Fig. 5. Raman spectra of three geometrical isomers of [Co(β-ala)$_2$(tn)]$^+$. Numbers in parentheses correspond to those in Table 1.

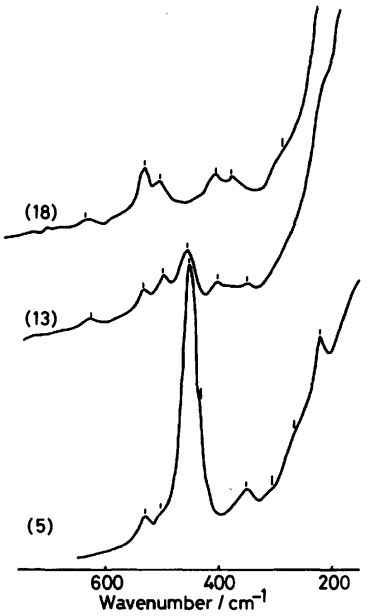

Fig. 6. Raman spectra of *fac(N)*-[Co(β-ala)$_3$], C_1-*cis(O)*-[Co(β-ala)$_2$(tn)]$^+$, and [Co(tn)$_3$]$^{3+}$. Numbers in parentheses correspond to those in Table 1.

Incidentally, the trans(O) isomer exhibits the strong and polarized band (465 cm^{-1}) at a slightly lower frequency than the depolarized one (479 cm^{-1}). Secondly, a difference between the C_2-cis(O) isomer and the C_1-cis(O) one can be observed in the totally symmetric stretching vibration region; the C_2-cis(O) isomer with a higher symmetry exhibits three Raman bands, but the C_1-cis(O) isomer splits into a quartet. This sort of spectral difference has also been observed for the two cis(O) isomers of $[Co(gly)_2(en)]^+$ with five-membered chelate rings[4] in the stretching vibration mode excluding the totally symmetric one (400—520 cm^{-1}). Finally, it should be pointed out that the characteristic feature of the Raman spectrum of C_1-*cis(O)*-$[Co(\beta\text{-ala})_2(tn)]^+$ is considered to be an overlapping with those of *fac(N)*-$[Co(\beta\text{-ala})_3]$ and $[Co(tn)_3]^{3+}$ as is shown in Fig. 6. That is, we can say that the strong and polarized band at 454 cm^{-1} of C_1-*cis(O)*-$[Co(\beta\text{-ala})_2(tn)]^+$ corresponds to the totally symmetric stretching vibration mode, ν_{ts}(Co–N(tn)), and also that the polarized bands in the region above 490 cm^{-1} are principally related to the β-ala ligand. Incidentally, the complexes containing more than one β-ala ligand exhibit their highest frequency polarized bands around 630 cm^{-1}, somewhat higher than those for the complexes containing the gly ligand. It is not certain at present what has brought about this interesting feature, but we can say that it reflects the skeletal vibrational characteristics of the cobalt(III) complexes with six-membered aminocarboxylate chelate rings.

References

1) K. Kanamori, T. Morikawa, and K. Kawai, *Bull. Chem. Soc. Jpn.*, **53**, 2787 (1980).

2) a) K. Kanamori and K. Kawai, *Bull. Chem. Soc. Jpn.*, **53**, 2520 (1980); b) K. Kanamori and K. Kawai, *Bull. Chem. Soc. Jpn.*, **55**, 764 (1982); c) K. Kanamori, Y. Nunomura, M. Takashima, K. Nagata, K. Kawai, and J. Hidaka, *Bull. Chem. Soc. Jpn.*, **58**, 92 (1985); d) K. Kanamori, I. Bansho, K. Kawai, K. Akamatsu, and Y. Shimura, *Bull. Chem. Soc. Jpn.*, **58**, 943 (1985).

3) K. Kanamori, I. Ichinose, and K. Kawai, *Bull. Chem. Soc. Jpn.*, **55**, 1315 (1982).

4) T. F. Maruyama, K. Okamoto, J. Hidaka, and H. Einaga, *Bull. Chem. Soc. Jpn.*, **56**, 2610 (1983).

5) T. Kawamoto, T. F. Maruyama, T. Yasui, K. Okamoto, J. Hidaka, and H. Einaga, *Bull. Chem. Soc. Jpn.*, **59**, 2393 (1986).

6) H. Ogino and J. Fujita, *Bull. Chem. Soc. Jpn.*, **48**, 1836 (1975).

7) J. C. Bailar, Jr. and J. B. Work, *J. Am. Chem. Soc.*, **68**, 232 (1946).

8) G. R. Brubaker and D. P. Schaefer, *Inorg. Chem.*, **10**, 2170 (1971).

9) M. Ogawa, Y. Shimura, and R. Tsuchida, *Nippon Kagaku Zasshi*, **81**, 72 (1960).

10) M. B. Ćelap, S. R. Niketić, T. J. Janjić, and V. N. Nikolić, *Inorg. Chem.*, **6**, 2063 (1967).

11) N. Matsuoka, J. Hidaka, and Y. Shimura, *Bull. Chem. Soc. Jpn.*, **45**, 2491 (1972).

12) P. Stein, V. Mishowski, W. H. Woodruff, J. P. Griffin, K. G. Werner, B. P. Gaber, and T. G. Spiro, *J. Chem. Phys.*, **64**, 2159 (1976).

13) T. Nomura, F. Marumo, and Y. Saito, *Bull. Chem. Soc. Jpn.*, **42**, 1016 (1969).

14) P. G. Beddoe, M. J. Harding, S. F. Mason, and B. J. Peart, *J. Chem. Soc., Chem. Commun.*, **1971**, 1283.

15) J. B. Work, *Inorg. Synth.*, **2**, 221 (1946).

16) J. Bjerrum and J. P. McReynolds, *Inorg. Synth.*, **2**, 216 (1946).

 © 1987 The Chemical Society of Japan Bull. Chem. Soc. Jpn., 60, 925—931 (1987)

Studies on Dissolved Metalloenzymes in Lake Water. III. Correlation between Dissolved Alkaline Phosphatase and Orthophosphate in Lake Water

Kensei KOBAYASHI,[†1] Kimikazu IWASE,[†2] Shinya HASHIMOTO,[†3] Hirotaka UEDA,[†4] Kitao FUJIWARA, Akira OTSUKI,[†] Keiichiro FUWA,[†] and Hiroki HARAGUCHI*
Department of Chemistry, Faculty of Science, The University of Tokyo, Hongo, Bunkyo-ku, Tokyo 113
[†]Division of Chemistry and Physics, National Institute for Environmental Studies, Yatabe, Ibaraki 305
(Received September 12, 1986)

Alkaline phosphatase activity (both dissolved and total) in Lake Kasumigaura was determined periodically together with concentrations of phosphorus compounds therein. Distinct negative correlation was found between the dissolved alkaline phosphatase activity and the orthophosphate concentration during the phosphorus-limited season. The decrease of the concentration of dissolved alkaline phosphatase was observed at the level of 1 ng ml^{-1} of orthophosphate. The present results suggest that both alkaline phosphatase in vivo and dissolved alkaline phosphatase in the lake water play important roles in phosphorus cycles in natural water.

Alkaline phosphatase in natural water was first studied in the context of the phosphorus cycle. In 1938, Steiner first suggested the possibility of the ecological participation of phosphatases in hydrolyzing phosphate esters to orthophosphate for phytoplankton growth in lakes.[1] Since then, several investigations on intercellular alkaline phosphatase have been carried out.[2-4] Alkaline phosphatase activity remaining in filtered water was first reported by Overbeck et al.[5] Not only total (cell-associated plus dissolved) phosphatase activity but also dissolved phosphatase activity per se, have been discussed in relation to their roles in the hydrolysis of phosphatase esters in sea water[6-8] and freshwater.[9-14] The correlation between phosphatase activity and other biological variables such as plankton biomass and chlorophyll *a* were reported as being positive.[15] However, the correlation between phosphatase activity and phosphate concentration has not been clarified. Stevens and Parr concluded that phosphatase activity could not be used as a reliable indicator of algal growth under conditions of phosphorus starvation.[16] Kobori and Taga reported a positive relationship between phosphatase activity and the inorganic phosphorus content of ocean sediment.[17] Berman reported that no correlation was found between them,[10] in spite of the fact that the production of alkaline phosphatase in bacteria is induced by phosphate-deficient media, and suppressed by phosphate-sufficient media.[18]

It has been confirmed in the previous papers[19,20] that dissolved phosphatase activity in sea and lake water is caused by zinc-containing metalloenzyme *alkaline phosphatase*. The seasonal changes in alkaline phosphatases and their sources (algae and bacteria) in Lake Kasumigaura have also been discussed previously.[21] In the present paper, the correlation between phosphatase activity and phosphorus concentration has been studied by using the data obtained through periodic analysis for two years in Lake Kasumigaura. The role of alkaline phosphatase in the phosphorus cycle in the lake is also discussed.

Experimental

Chemicals and Instruments. All the reagents used in the experiments were of analytical reagent grade.

Glassfilter (Whatman GF/C, pore size: 1.0 μm; diameter: 47 mm) was sterilized by heating at 450 °C for 3 h. The membrane filter was purchased from Toyo Kagaku Sangyo Co. (Type TM-4, pore size: 0.20 μm; diameter 47 mm). A Millipore filter holder (Type XX15-046-00) and a Millipore miniature vacuum-press pump Type XX61-000-00) were used for filtration, under mild suction (such that the suction flask pressure was no less than 250 Torr (1 Torr=133.322 Pa)). A thermostatic bath (Hirayama Manufacturing Co., Model TR-900) was used to incubate the sample-substrate mixture.

A Shimadzu UV-210A spectrophotometer with an SFU-6 semi-auto flow cell unit (optical path of the absorption cell: 10 mm) was used to determine phosphatase activity. Concentrations of orthophosphate were determined with a Technicon Autoanalyzer Type II, using the method of Murphy and Riley.[22]

Sampling and Pre-Treatment of Lake Water Samples. Lake water samples were collected with plastic Van Dorn bottles at 10 sampling stations on Lake Kasumigaura (shown in Figs. 2 and 3) once a month from April, 1980 through March, 1982. The sampling depths were: 0.5 m at every station (April, 1980-April, 1981); 1.5 m and 0.5 m at Stations 4 and 9 (April, 1980-April, 1981); and 1.0 m at every station (May, 1981-March, 1982).

[†1] Present address: Laboratory of Chemical Evolution, University of Maryland, College Park, Maryland 20742, U.S.A.
[†2] Present address: Science and Technology Agency, Kasumigaseki, Chiyoda-ku, Tokyo 101.
[†3] Present address: National Research Institute for Metals, Nakameguro, Meguro-ku, Tokyo 153.
[†4] Present address: Sumitomo Metal Mining Co., Ltd., Suehiro-cho, Ome, Tokyo 188.

The samples were cooled in an ice box immediately after being taken. Most of them were then filtered as soon as possible, as shown in Fig. 1. A portion of each sample, to which 2 v/v% of chloroform was added, was kept unfiltered to determine *total phosphatase activity* and *total phosphorus concentration*. A water sample filtered through the 1.0 μm pore size glassfiber membrane filter was used to determine *total dissolved phosphorus concentration* and *orthophosphate concentration*. A sample filtered through the 0.2 μm-membrane filter was used for the determination of *dissolved phosphatase activity*. All the filtered samples were stored at a constant temperature of 0 °C until analyzed.

Determination of Phosphatase Activity and Phosphorus Concentration. Procedures for determination of phosphorus concentration and phosphatase activity are shown in Fig. 1. Total phosphatase activity (TPA) and dissolved phosphatase activity (DPA) were determined by using *p*-nitrophenyl dihydrogen phosphate as a substrate, as described in the previous paper.[21]

Total phosphorus concentration (TP) and total dissolved phosphorus concentration (TDP) were determined with a Technicon Autoanalyzer after peroxodisulfate digestion in an autoclave at 120 °C for 45 min using a culture bottle (50 ml) with a polycarbonate screwcap.[23] Orthophosphate concentration (Pi) was determined with the Autoanalyzer using an unautoclaved filtered sample. The particulate phosphorus concentration (PP) was obtained by subtracting TDP from TP. The dissolved organic phosphorus concentration (DOP) was obtained by subtracting Pi from TDP.

Results and Discussion

Horizontal and Vertical Distribution of Phosphatase Activity and Phosphorus Concentration. Table 1 shows data for phosphatase activity and phosphorus concentrations in Lake Kasumigaura in July, 1980 and January, 1981. TP in Lake Kasumigaura was around 100 μg-P l^{-1} or more, much higher than the eutrophication level of 20 μg-P l^{-1}. No significant change in phosphatase activity and phosphorus concentration vs. vertical position was found, except for the phosphorus concentration at Station 4 in summer, which was higher at a depth of 5 m than at shallower levels. The vertical homogeneity of Lake Kasumigaura is due to the shallowness of the water and the constant agitation of the water by the wind. The increase in phosphorus at the 5.0 m depth at Station 4 in summer may be linked to the release of phosphate into the lake water from the sediments.[24]

Figures 2 and 3 show the horizontal distributions of phosphorus concentration and phosphatase activity,

Table 1. Phosphatase Activity and Phosphate Concentrations in Lake Kasumigaura in July, 1980 and January, 1981

Date	Sta.	depth	DPA	TP	PP	DTP	Pi	DPA/PP
		m	nM min^{-1}	ng ml^{-1}	ng ml^{-1}	ng ml^{-1}	ng ml^{-1}	mmol/g/min
Jun. 21, 1980	1	0.5	3.9	147	121	26	2	0.032
	2	0.5	9.0	155	127	28	2	0.071
	3	0.5	4.9	118	95	23	2	0.052
	4	0.5	1.1	87	68	19	< 2	0.016
		1.5	1.3	81	65	16	< 2	0.020
		5.0	1.1	109	81	28	14	0.014
	6	0.5	2.6	149	128	21	3	0.020
	7	0.5	1.9	97	78	19	2	0.024
	8	0.5	0.9	73	56	17	< 2	0.016
	9	0.5	0.4	64	51	13	< 2	0.008
		1.5	1.5	70	55	15	< 2	0.027
		5.0	1.1	66	53	13	< 2	0.021
Jan. 26, 1981	1	0.5	3.4	77	57	20	6	0.060
	2	0.5	4.7	67	53	14	2	0.089
	3	0.5	3.8	57	47	10	< 2	0.081
	4	0.5	2.2	46	38	8	< 2	0.057
		1.5	2.4	47	38	9	< 2	0.063
		5.0	2.5	47	39	8	< 2	0.065
	6	0.5	0.6	92	80	12	7	0.008
	7	0.5	2.4	39	33	6	2	0.073
	8	0.5	2.5	36	30	6	2	0.085
	9	0.5	2.4	39	33	6	< 2	0.073
		1.5	2.7	38	32	6	< 2	0.083
		5.0	2.4	38	32	6	< 2	0.075

DPA: dissolved phosphatase activity, TP: total phosphorus-P concentration, PP: particulate phosphorus-P concentration, DTP: dissolved total phosphorus-P concentration, Pi: orthophosphate-P concentration.

respectively. Both the concentrations of phosphorus and the phosphatase activity decrease with the horizontal decline of the water stream from the inner part of the two bays, (e.g., Stations 1 and 6), to the center (Station 9) or outlet (Station 12) of the lake. This trend is particularly noticeable in summer. There is known to be a linear relationship between particulate phosphorus concentration (PP) and chlorophyll *a* concentration (which is proportionate to the biomass of photoautotrophs) over the whole area of Lake Kasumigaura.[25] Waters highly mixed with waste-water near urban area (for example, Stations 1 and 6) seem to have a large biomass (which gives high particulate phosphate concentration), and consequently have a high level of phosphatase activity produced by algae and bacteria.[21]

Dissolved phosphatase activity (DPA) was around 10% of total phosphatase activity (TPA), which was about the same ratio as that found in Tokyo Bay[8] and in the Pluss-See.[9]

The correlation factors for phosphatase activity and phosphorus concentration are shown in Table 2. There were positive correlations between the various

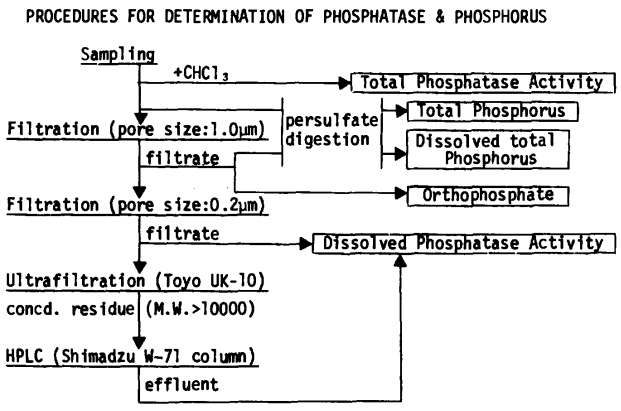

Fig. 1. Procedures for determination of phosphatase activity and phosphorus concentration.

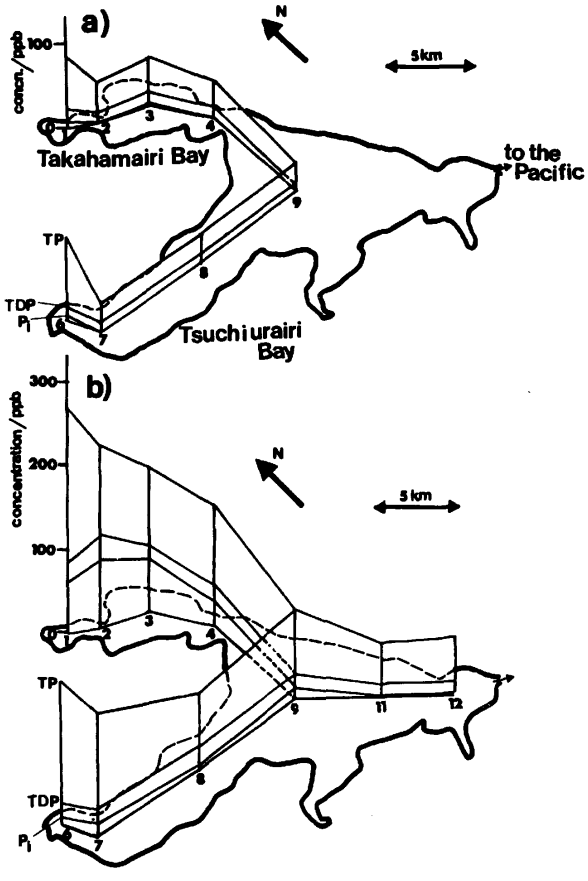

Fig. 2. Horizontal distribution of phosphorus concentration in Lake Kasumigaura.
a) February, 1981; b) August, 1981.
TP: total phosphorus-P concentration; TDP: total dissolved phosphorus-P concentration; Pi: orthophosphate-P concentration.

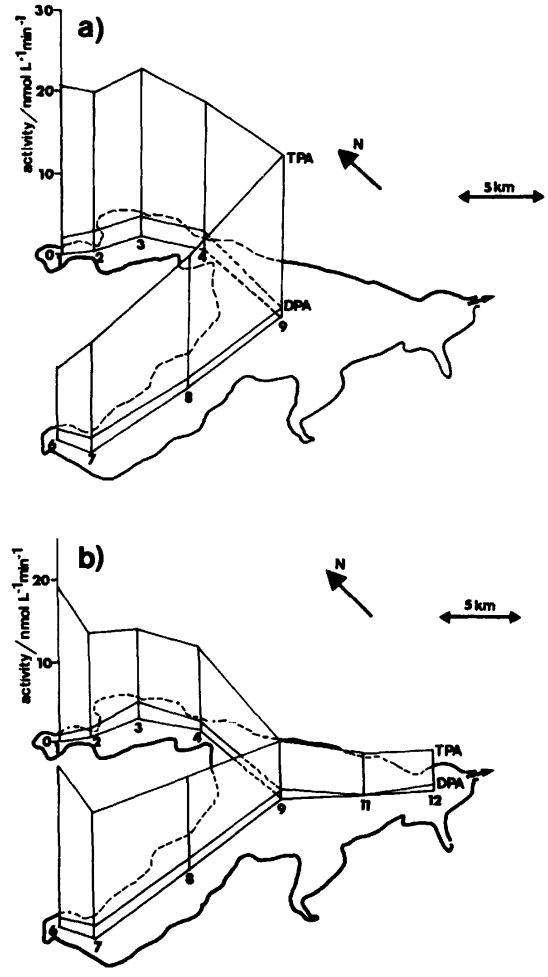

Fig. 3. Horizontal distribution of phosphatase activity in Lake Kasumigaura.
a) February, 1981; b) August, 1981.
TPA: total phosphatase activity; DPA: dissolved phosphatase activity.

phosphorus concentrations (such as TP vs. PP; PP vs. DOP), but there was no apparent correlation between the phosphorus concentrations and phosphatase activity (TPA or DPA). At this point, the value of DPA/PP was seen as being a possible indication of phosphatase activity in lake water normalized by the biomass. As shown in Fig. 4, there was an apparent negative correlation between DPA/PP and Pi (orthophosphate concentration) in May, 1981 (correlation coefficient (r) is −0.72), but no correlation in August, 1981 (r is 0.00).

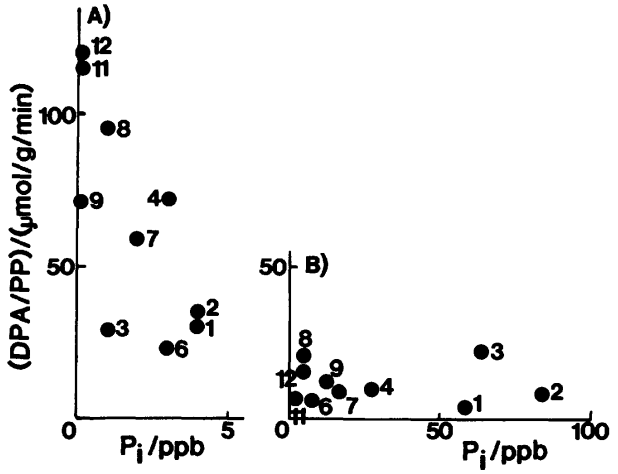

Fig. 4. Correlation between phosphatase activity and orthophosphate concentration.
A) May, 1981; B) August, 1981.
DPA: dissolved phosphatase activity: PP; particulate phosphorus-P concentration; Pi: orthophosphate-P concentration.

Seasonal Variations in Phosphatase Activity and Phosphorus Concentration. The seasonal variations in phosphorus concentrations at Stations 2 and 9 are shown in Fig. 5. In most of the stations, phosphorus increased in summer and decreased in winter, as is seen more markedly in the changes at Station 2. Such phenomena are also characteristic of algal blooms in eutrophic lakes.[26] In Fig. 5, the seasonal changes of phosphorus compounds at Station 9 were quite smaller than those at Station 2. These facts may be ascribed to less eutrophication near the lake center at Station 9 compared to the Takahamairi area at Station 2. In 1980, the summer was cooler than usual, so that the phosphorus peak for summer in 1980 shown in Fig. 5 was somewhat distored. The phenomenal increase in orthophosphate concentration (Pi) during mid-summer is probably caused by the chemical and biological release of phosphate from the sediment.[27]

Figure 6 shows the seasonal variations in dissolved phosphatase activity (DPA) and orthophosphate (Pi) at Station 2. DPA has two peaks a year, one of which would appear to be caused by the heavy blooms of blue-green algae (*Microcystis aeruginosa*) in summer, and the other by blooms of diatoms and flagellates in winter or spring.[28] Figure 6 also shows a negative correlation between DPA and Pi.

Seasonal variations in the correlation coefficients (r) of Pi and DPA/PP at the different stations and in the TP/TPA values are shown in Table 3. TP/TPA, whose dimension is $[\text{time}]^{-1}$, may indicate the

Table 2. Correlation Coefficients among Phosphatase Activity and Phosphorus Concentration

May 25, 1981							
	DPA	TPA	TP	TDP	PP	DOP	Pi
DPA	×	0.67	−0.36	−0.24	−0.38	−0.37	−0.39
TPA		×	−0.10	−0.20	−0.01	0.00	−0.45
TP			×	0.90	1.00	0.99	0.50
TDP				×	0.85	0.83	0.79
PP					×	1.00	0.37
DOP						×	0.73
Pi							×
August 17, 1981							
	DPA	TPA	TP	TDP	PP	DOP	Pi
DPA	×	−0.08	0.01	0.25	−0.20	−0.19	0.29
TPA		×	0.45	0.37	0.91	0.74	0.33
TP			×	0.83	0.89	0.35	0.81
TDP				×	0.50	−0.22	1.00
PP					×	0.73	0.47
DOP						×	−0.26
Pi							×

DPA: dissolved phosphatase activity, TPA: total phosphatase activity, TP: total phosphorus-P concentration, TDP: total dissolved phosphorus-P concentration, PP: particulate phosphorus-P concentration, DOP: dissolved organic phosphorus-P concentration, Pi: orthophosphate-P concentration.

turnover time of phosphorus in lake water. In May, TP/TPA was at its minimum value, and r was at its maximum value. These results suggest that microorganisms produce more alkaline phosphatase than usual in vivo, and that they are forced to use phosphorus in lake water more efficiently than usual in order to bloom in the phosphate-deficient season of May.

Table 3. Seasonal Variations in Correlation between Phosphatase Activity and Phosphorus Concentration

Year	Month	Pi	r(Pi: DPA/PP)	TP/TPA
1980	December	3	−0.72	—
1981	January	2	−0.71	—
	February	< 2	−0.78	2.0±1.7
	March	6	−0.59	5.9±3.2
	April	6	−0.31	3.4±1.4
	May	4	−0.72	1.2±0.7
	June	6	+0.32	2.4±1.3
	July	78	+0.51	4.8±1.7
	August	85	0.00	7.0±1.7
	September	3	+0.26	5.3±1.4
	October	3	+0.14	4.6±1.4
	November	1	−0.48	3.5±2.5
	December	3	−0.57	2.4±1.4
1982	January	3	−0.68	2.8±1.5
	February	4	−0.73	2.7±2.7
	March	11	−0.80	6.4±5.7

Pi: orthophosphate-P concentration at Station 2 [ng/ml], r(Pi: DPA/PP): correlation coefficient between orthophosphate and (dissolved phosphatase activity/particulate phosphorus-P concentration) at all the stations, TP/TPA: (total phosphorus-P concentration/total phosphatase activity.

The Role of Alkaline Phosphatase in the Phosphorus Cycle in Lake Water. Phosphorus is one of the most important nutrient elements. Microorganisms in natural water use phosphorus in the form of orthophosphate. It is recognised that the synthesis of an enzyme in vivo is suppressed by the presence of the

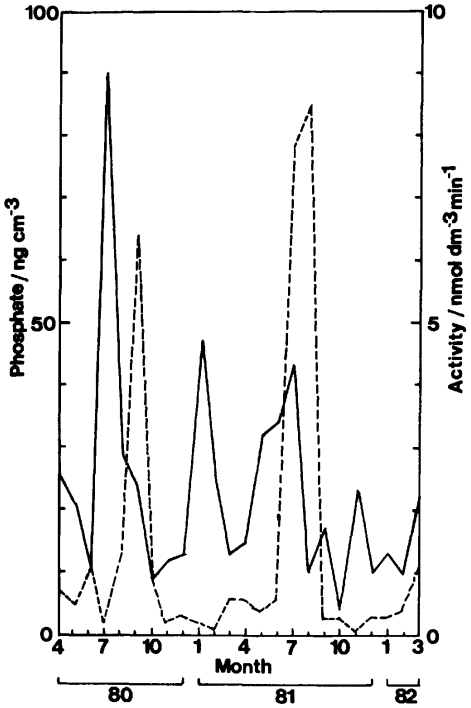

Fig. 6. Seasonal variations in dissolved phosphatase activity and orthophosphate concentration in Lake Kasumigaura (Station 2).
——: Dissolved phosphatase activity; —·—: orthophosphate-P concentration.

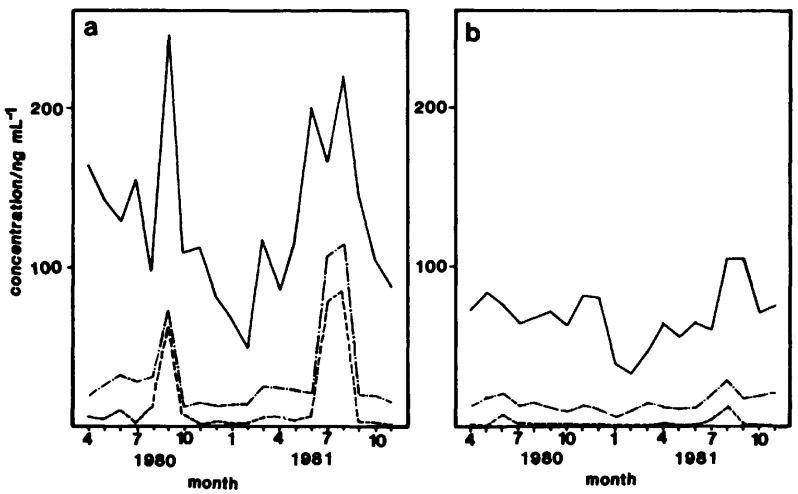

Fig. 5. Seasonal variations in phosphorus concentration in Lake Kasumigaura.
a) Station 2; b) Station 9.
——: Total phosphorus-P concentration; —·—: total dissolved phosphorus-P concentration; ----: orthophosphate-P concentration.

final product of its catalysis in the media.[18] It seems that the same phenomenon occurs in ecological systems, such as lake water. In algae's blooming season, the ecological system has a high requirement for nutrients such as inorganic phosphorus and nitrogen. If there is no sufficient orthophosphate in the lake water for the algae to grow, the algae have to produce more alkaline phosphatase in order to get a quick supply of orthophosphate. On the other hand, when the phosphate concentration is high enough to supply the algae's needs, the key element in the bloom of algae is not phosphorus but other nutrient elements such as nitrogen. When the latter conditions prevail, there is no correlation between DPA/PP and Pi. This hypothesis is supported not only by the clear negative correlation between DPA/PP and Pi, but also by the low apparent turnover time of phosphorus (TP/TPA) in phosphorus-deficient season (such as May, 1981).

In the laboratory incubation experiments of bacteria (*Escherichia coli*)[18] and algae,[29] the depression of the enzyme production can be observed under orthophosphate concentration of 7—10 μg-P ml^{-1}. On the other hand, the decrease in the dissolved alkaline phosphatase in the lake water appears at ca. 1 ng-P ml^{-1}, which means more than three order of magnitude in difference between the lake and experimental laboratory systems. When considering that the surface area of Lake Kasumigaura is 171 km^2, it is important to note that such negative feedback is also maintained between orthophosphate and the release of dissolved phosphatase on the scale of a large lake.

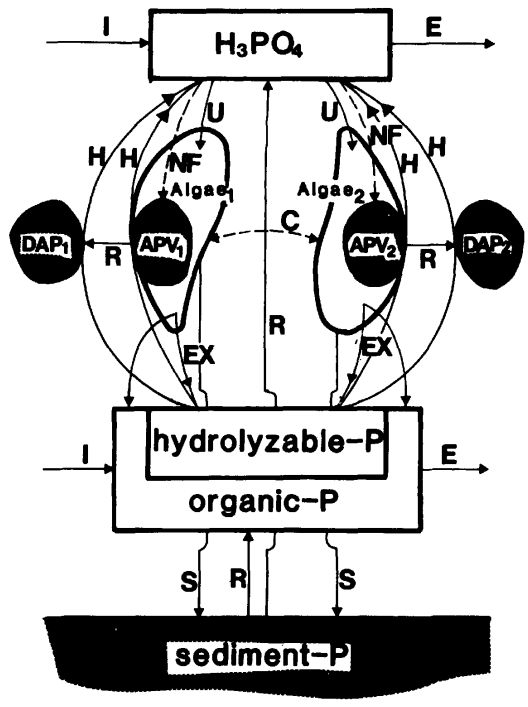

Fig. 7. A schematic diagram of phosphorus cycle in lake water.
DPA: dissolved alkaline phosphatase; APV: alkaline phosphatase in vivo; I: influx; E: efflux; U: uptake; R: release; S: sedimentation; H: hydrolysis; EX: excretion; NF: negative feedback; C: competition.

Conclusion

A simplified representation of the role of alkaline phosphatase in the phosphorus cycle in lake water is illustrated in Fig. 7. As described above, it is suggested that intercellular phosphatase controls the uptake of phosphorus by algae at times when there is a phosphate deficiency, and that dissolved alkaline phosphatase also plays a part in this process. Conversely, an excess of phosphate suppresses the biosynthesis of alkaline phosphatase in vivo, and is followed by a decrease in dissolved alkaline phosphatase.

Various kinds of microorganisms are present in natural water, and each of them produces its own type of alkaline phosphatase.[21] It is known that different types of algae are frequently in competition within any particular ecological systems; for example, blue-green algae inhibit the blooming of other algae such as diatoms in natural water.[28] In order to elucidate further the role of alkaline phosphatase (in vivo and dissolved forms), it will be necessary to determine alkaline phosphatase activity originating from each source.

The present authors thank Dr. Lawrence J. Sacks, Laboratory of Chemical Evolution, Department of Chemistry, University of Maryland, for his kind help in preparation of the manuscript.

This research has been supported by Grant-in-Aid for Environmental Science from the Ministry of Education, Science and Culture.

References

1) M. Steiner, *Naturwissenshaften*, **26**, 723 (1938).
2) R. Y. Morita and R. A. Howe, *Deep-Sea Research*, **4**, 254 (1957).
3) H. Goldschmiedt, M. W. Mettenleiter, and P. R. Borchardt, *Turtox News*, **36**, 269 (1958).
4) J. Overbeck, *Intern. Ver. Theoret. Angew. Limnol. Verhand.*, **14**, 226 (1959).
5) J. Overbeck and H.-D. Babenzien, *Arch. Hydrobiol.*, **60**, 107 (1964).
6) M. J. Perry, *Mar. Biol.*, **15**, 113 (1972).
7) J. Kim and C. E. ZoBell, *Eff. Ocean Environ. Microb. Act., Proc. U.S. Jpn. Conf., 2nd*, **1972**, 369 (Pub. 1974).
8) N. Taga and H. Kobori, *Mar. Biol.*, **49**, 223 (1978).
9) W. Reichardt, J. Overbeck, and L. Steubing, *Nature*, **216**, 1345 (1967).
10) T. Berman, *Limnol. Oceanogr.*, **15**, 663 (1970).
11) W. Reichardt, *Hydrobiologia*, **38**, 377 (1971).

12) T. Berman and G. Moses, *Hydrobiologia*, **40**, 487 (1972).
13) M. Janson, *Hydrobiologia*, **56**, 175 (1977).
14) J. Olah and E. O. Toth, *Aquaculture Hungaria (Szaarbas)*, **1**, 15 (1978).
15) A. Miliuis and M. Pork, *Eesti NSV Tead. Akad. Toim., Biol.*, **26**, 128 (1977).
16) R. J. Stevens and M. P. Parr, *Freshwater Biol.*, **7**, 351 (1977).
17) H. Kobori and N. Taga, *Deep-Sea Res.*, **26A**, 799 (1979).
18) A. Torriani, *Biophys. Biochem. Acta*, **38**, 460 (1960).
19) K. Kobayashi, K. Iwase, M. Matsui, M. Watanabe, H. Ueda, K. Fujiwara, H. Haraguchi, and K. Fuwa, *Bull. Chem. Soc. Jpn.*, **55**, 3459 (1982).
20) K. Kobayashi, M. Matsui, H. Haraguchi, and K. Fuwa, *J. Inorg. Biochem.*, **18**, 41 (1983).
21) K. Kobayashi, S. Hashimoto, A. Otsuki, K. Fujiwara, K. Fuwa, and H. Haraguchi, *Bull. Chem. Soc. Jpn.*, **59**, 3067 (1986).
22) J. Murphy and J. P. Riley, *Anal. Chim. Acta*, **27**, 31 (1962).
23) D. W. Menzel and N. Corwin, *Limnol. Oceanogr.*, **10**, 280 (1965).
24) T. Kawai, A. Otsuki, M. Aizaki, and M. Nishikawa, *Res. Rep. Natl. Inst. Environ. Stud.*, No. 22, 23 (1981).
25) A. Otsuki, S. Kasuga, and T. Kawai, *Verh. Internal. Verein. Limnol.*, **21**, 602 (1981).
26) T. Okino, *Jpn. J. Bol.*, **20**, 381 (1973).
27) A. Otsuki, T. Kawai, and M. Aizaki, *Res. Rep. Natl. Inst. Environ. Stud.*, No. 22, 3 (1981).
28) N. Imamura and M. Yasuno, *Res. Rep. Natl. Inst. Environ. Stud.*, No. 22, 123 (1981).
29) G. P. Fitzgerald and T. C. Nelson, *J. Phycol.*, **11**, 32 (1966).

 © 1987 The Chemical Society of Japan Bull. Chem. Soc. Jpn., 60, 933—939 (1987)

Geochemical Characterization of Geological Standard Rock Samples from Rare Earth Element Distribution Patterns Measured by Inductively Coupled Plasma Atomic Emission Spectrometry

Kazuhiro Toyoda and Hiroki Haraguchi*
Department of Chemistry, Faculty of Science, The University of Tokyo,
7-3-1, Hongo, Bunkyo-ku, Tokyo 113
(Received September 22, 1986)

Rare earth elements (REEs) in twelve standard rock samples have been determined by inductively coupled plasma atomic emission spectrometry after separation of diverse metal ions with cation exchange resin. These rock samples are old six standard rocks (W-1, BCR-1, AGV-1, GSP-1, JB-1, JG-1) and new six standard rocks (JB-2, JB-3, JA-1, JR-1, JR-2, JGb-1) issued from the Geological Survey of Japan. These samples are various types of igneous rocks, which show various shapes of the REE distribution patterns. Geochemical characteristics of these standard rock samples will be discussed from the relationships between rock types and the shapes of the REE pattern.

In recent years, inductively coupled plasma atomic emission spectrometry (ICP-AES) has been extensively used as a convenient and sensitive analytical method for simultaneous multielement determination of geological samples.[1-6] The determination of various elements in the wide range of concentrations can be carried out by ICP-AES without matrix matching of the standard solutions.[1] The analytical sensitivities of REEs have been also improved by ICP-AES.[2-6] Thus, we have tried to perform simultaneous multielement determination of REEs in twelve geological standard rock samples issued from the Geological Survey of Japan.

The determination of rare earth elements have been receiving more attention in geological studies.[7] The behaviors of trace elements such as REEs during the process of genesis and differentiation of magma depend fundamentally on the distribution coefficients between melt and minerals.[8] On the basis of this assumption, for example, mutual genetic relationships of various rock types, such as tholeiitic and alkali rocks, has been studied. Petrogenetic studies of igneous rocks involve the determination of the history of the sources of melts, the conditions of melting, the chemical composition of the sources during melt, melting process and so forth. Since REEs are the most useful elements for such a geochemical study, precise analysis of REEs and trace element modeling using the element distribution coefficients (K_d) in mineral-melt systems have been examined.[7] Then it has been noted that REEs are significantly valuable for placing limits on the applicability of proposed petrogenetic models. Moreover, the REE patterns do not change so significantly through the process of alternation and metamorphism, because REEs belong to the group of chemically resembled elements and are strong to weathering.[9,10] Thus the behaviors of REEs during the melting and differentiation of igneous rock are explained mathematically by the Masuda-Coryell plot REE distribution pattern[11] which is the plot of the REE contents normalized to chondrite abundance.

Genetic classification and characterization of igneous rocks are commonly made by major chemical composition as well as mineral compositions.[13-15] Such classification and characterization, however, are sometimes done by the survey of minor element compositions, for example, first-row transition metal abundance patterns,[16,17] Sr/Ca-Ba/Ca systematics,[18] incompatible element patterns,[19,20] various ratios of two elements[8] and so on. Among the studies of trace elements for geological rock samples, the REE pattern is most popular and useful. Hence, in the present study, the determination of REEs in twelve geological standard rock samples has been performed by ICP-AES; JB-1 (alkali basalt), JB-2 (tholeiitic basalt), JB-3 (high aluminum basalt), BCR-1 (andesine tracky basalt), W-1 (dolelite), JGb-1 (gabbro), AGV-1 (trachy andesite), JA-1 (tholeiitic andesite), JR-1 and JR-2 (rhyolite), JG-1 and GSP-1 (granodiolite). The analytical results have been compared with the literature values,[22,23] which have been mainly determined by isotope dilution mass spectrometry (IDMS) and neutron activation analysis (NAA). Furthermore, the relationship between rock types and the shape of the REE patterns of twelve rock samples will be discussed according to knowledge of REE geochemistry.

Experimental

Instrument. An ICP emission spectrometer used is Jarrell-Ash model 975 Atom Comp MKII with some laboratory modification. The instrumental components and operating parameters for the emission measurements are summarized in Table 1. The analytical lines employed are shown in Table 2. The calibration curves were made by using low (blank) and high standard solutions.

Chemicals and Standard Solution. All the chemicals used were of analytical reagent grade. All the stock solutions (1000 μg ml^{-1}) were prepared from pure metals or oxides, and their concentrations were checked by the EDTA titration method with XO indicator. Working standard solutions for calibration curves were prepared by mixing the

Table 1. Operating Conditions for ICP-AES Measurement

RF power	1.1 kW
Gas flow rate	Coolant Ar gas 18 l min^{-1}
	Auxiliary Ar gas 1 l min^{-1}
	Carrier Ar gas 0.4 l min^{-1}
Observation height	16 mm above load coil
Nebulizer	Cross flow type
Spectrometer focal length	75 cm
Grating	2400 grooves mm^{-1}
Reciprocal linear dispersion	0.53 nm mm^{-1}
Slit width	Entrance slit 25 μm
	Exit slit 50 μm
Integration time	40 s
Internal standard	10 μg of Cd/ml
	[observed at 228.8 nm (2nd order)]

stock solutions into three groups, taking into consideration of minimizing mutual spectral interferences among rare earth elements. The combinations of elements for working standard solutions are summarized in Table 2. Standard IV contains internal standard element (Cd) and interferring elements (Y, Sc, Al, Fe, Zr, Cr), which could not be eliminated by chemical separation mentioned below. The internal standard was used to compensate possible fluctuations in nebulization or droplet transport. In order to minimize the variation of the nebulization efficiency due to the differences of the viscosities of the solutions, the acid content in each standard solution was adjusted to be 3 M (M=mol dm^{-3}) HCl so as to match those in the digested sample solutions.

Sample Digestion and Separation Procedure. Rock samples (0.5 g) were digested by two methods such as HF-HNO_3 acid digestion and Na_2CO_3 alkali fusion.[5] After digestion, the samples were dissolved to 50 ml with 1 M HCl. The solution was loaded onto a 20×1 cm column of 100-200 mesh AG50W-X8 cation exchange resin. The

Table 2. Compositions of Mixed Standard Solutions for Calibration Curves and Analytical Wavelengths

Standard I		Standard II		Standard III		Standard IV	
Concn	Wavelength	Concn	Wavelength	Concn	Wavelength	Concn	Wavelength
μg ml^{-1}	nm	μg ml^{-1}	nm	μg ml^{-1}	nm	μg ml^{-1}	nm
La 10	398.8	Nd 20	430.3	Pr 10	422.2	Cd 100	228.8
Ce 20	418.7	Sm 10	442.2	Eu 10	381.9	Sc 10	361.3
Gd 10	303.2	Tb 10	367.6	Dy 10	340.7	Y 10	377.4
Lu 10	261.5	Ho 10	345.6	Er 10	369.2	Al 100	308.2
		Yb 10	328.9	Tm 10	313.1	Fe 100	238.2
						Zr 10	349.6
						Cr 10	205.5

Table 3. Correction Coefficients for Spectral Interferences[a]

Element	La	Ce	Pr	Nd	Sm	Eu	Gd	Tb	Dy	Ho	Er	Tm	Yb	Lu
La	—	0.9	0.3	0.6	0.8	—	—	0.6	0.2	0.4	—	—	—	1.7
Ce	0.6	—	15.7	1.4	10.9	—	0.7	5.7	1.7	0.6	0.7	1.2	—	—
Pr	4.1	9.9	—	70.3	29.9	0.6	4.1	9.3	3.0	2.4	3.3	2.5	—	—
Nd	6.6	22.7	3.73	—	8.0	4.6	3.8	10.0	4.5	2.4	5.4	19.2	—	—
Sm	1.8	7.2	10.8	1.6	—	0.4	6.3	10.3	12.6	3.1	10.3	14.1	—	—
Eu	3.5	2.7	0.5	2.7	0.9	—	1.9	1.8	1.5	0.6	2.6	3.1	—	—
Gd	0.3	1.6	12.3	4.3	2.5	—	—	1.0	46.7	4.5	1.0	117.0	—	—
Tb	0.6	11.8	12.2	2.0	4.9	0.2	30.0	—	14.9	7.4	5.5	50.1	0.2	0.2
Dy	0.6	129.0	2.0	2.4	1.2	0.1	7.0	80.6	—	0.8	2.7	13.6	0.4	0.2
Ho	0.6	1.0	—	0.3	2.2	—	13.9	3.0	15.8	—	1.0	17.0	0.5	0.5
Er	—	16.0	—	8.9	0.9	—	5.3	34.0	11.0	1.3	—	15.1	—	—
Tm	—	0.9	0.4	—	0.8	—	36.1	0.8	4.7	6.5	0.8	—	0.4	0.2
Yb	6.5	0.8	—	—	—	—	5.7	1.0	0.5	1.6	15.0	44.1	—	0.6
Lu	0.3	0.5	1.8	—	—	—	—	—	0.9	—	—	0.8	—	—
Y	—	2.8	0.7	0.6	1.1	0.1	0.5	1.3	1.2	0.4	2.5	0.7	0.1	—
Sc	1.9	1.4	—	1.0	1.0	—	—	3.2	1.3	0.4	0.7	—	—	—
Al	—	0.7	0.5	—	—	—	—	—	—	—	—	—	0.7	—
Fe	—	0.7	—	—	—	—	—	1.8	1.7	—	—	—	—	42.7
Zr	—	80.0	0.4	0.4	—	—	1.6	1.1	12.2	2.3	0.6	17.8	—	—
Cr	—	0.5	0.4	0.2	1.4	—	13.9	1.4	8.3	—	—	4.6	—	—

a) The correction coefficient is expressed as the analyte concentration (ng ml^{-1}) equivalent to the background emission intensity which is provided with 1 μg ml^{-1} of major element.

column was first eluted with 130 ml of 2 M HNO_3 solution. The REEs on the resin were then eluted with 50 ml of 6 M HNO_3, and the eluent was taken in a Teflon beaker. The eluent was then evaporated to dryness on a hot plate. The residue was dissolved again with 5 ml of 3 M HCl, in which 10 μg ml^{-1} of Cd was added as an internal standard. These procedures were carried out for both acid-digested and alkali-fused samples in the same manner. The solutions were then used for the determination of REEs by ICP-AES. Major elements (Al, Fe, Ca, Mg, Na, and K) and interferring elements (Mn, Ti, V, Be, and Th) could be removed from the sample solutions through the above procedures. When removal of Fe was insufficient, Fe was further removed from eluted solution by solvent extraction with MIBK. Total yield of the whole procedure was 96—98%. Cadmium was chosen as the internal standard, because its emission profile in the plasma was similar to most REE profiles and it had no spectral interferences with the selected REE emission lines. It was also noticed that Cd originally contained in the samples were eliminated during the cation exchange separation.

Correction of Spectral Interferences. The influences of background emission intensities due to major elements were investigated by observing the intensity profiles near analytical lines of minor and trace elements. The profiles were obtained by moving the entrance slit horizontally. The profile measurements allowed to distinguish the emission signals caused by major elements (spectral interferences) or impurities. The spectral interference due to other REEs and interfering elements such as Zr, Sc, and Cr were estimated as the correction coefficient expressed as the analyte concentration (ng ml^{-1}) equivalent to the background emission intensity which was provided with 1 μg ml^{-1} of each major element. The correction coefficients of REEs and other diverse elements for spectral interference correction are summarized in Table 3.

Results

The detection limits in solution by ICP-AES are listed in Table 4, where the detection limits are defined as the analyte concentration corresponding to twice the standard deviation of background emission when the standard solution samples are nebulized into the ICP. The detection limits in rock sample are also listed in Table 4, along with the Leedey normarized values of REEs in Chondorite The detection limits in sample are evaluated from the detection limits in solution in case that 0.5 g of rock sample is digested and diluted to 5 ml. As can be seen in Table 4, the detection limits in sample are below the Leedey Chondrite abundance levels of REEs except Pr and Tb in geological samples. This means that the present experimental method is applicable to the determination of REEs in geological samples. After background correction, blank subtraction and spectral interference correction were carried out to obtain the analytical values for the standard rock samples. All the analytical values for REEs in JG-1, JB-1, AGV-1, BCR-1, W-1, and GSP-1 are summarized in Tables 5 and 6. Good agreement between the acid-digested and alkali-fused samples can be seen in terms of both AGV-1 and JB-1, and also the present data in five standard rocks except JG-1 are almost consistent with the literature values determined by NAA and IDMS. From these results it can be noted that the present method is suitable enough for the simultaneous multielement determination of all REEs except Tb and Tm. The analytical values for Tb and Tm were prone to serious interferences with the coexisting other REEs.

Recently it has been pointed out that the proposed values for heavy rare earth elements in JG-1 are not consistent, depending on the analytical methods. The values for heavy REEs in JG-1 obtained by NAA were about twice as much as the proposed values which were determined by IDMS technique.[23,25]

The present authors also pointed out in the previous paper[5] that the values of heavy REEs in JG-1 did not agree with each other, when the different decomposition methods were employed. As can be seen in Table 5, the values obtained by the alkali fusion preparation are about two times larger compared to those obtained by the acid digestion. The present values of REEs by acid digestion are almost identical with the values[23] formerly certified from GSJ, which were mainly determined by IDMS with acid digestion treatment. On the contrary, the REE values for the alkali fusion are consistent with those obtained by NAA.[25] These facts suggest that heavy REEs are enriched in some minerals which can not be completely decomposed by acid digestion. JG-1 is porphric biotite granodiorite, in which zircon is usually found as an accessory mineral. It is well known that zircon ($ZrSiO_4$) is not easily decomposed by acid digestion[26] and enriches heavy REEs.[7] In fact,

Table 4. Detection Limits (in Solution and in Sample) and Leedey Normalizing Values

Element	Detection limits		Leedey normalizing values
	in solution	in sample	
	ng ml^{-1}	μg g^{-1}	μg g^{-1}
La	4.4	0.044	0.378
Ce	21.2	0.212	0.976
Pr	18.7	0.187	0.136
Nd	15.0	0.150	0.716
Sm	12.4	0.124	0.230
Eu	0.8	0.008	0.0866
Gd	25.6	0.256	0.311
Tb	11.6	0.116	0.0589
Dy	14.2	0.142	0.390
Ho	3.4	0.034	0.0888
Er	3.6	0.036	0.255
Tm	11.0	0.110	0.0385
Yb	0.4	0.004	0.249
Lu	0.9	0.009	0.0387

from the determination of Zr in JG-1 decomposed by two different methods, it was found that Zr contents in JG-1 are 38 μg g^{-1} in acid digestion and 118 μg g^{-1} in alkali fusion, while the recommended value of Zr in JG-1 is 111 μg g^{-1}.[26] The difference of Zr values for JG-1 obtained by two decomposition methods may correspond to mean chemical composition of zircon which can not be dissolved by acid digestion. Then, GSP-1, JR-1, and JR-2, in which zircon is known to exist as an accessory mineral, were also decomposed by alkali-fusion method.

Discussion

The analytical values for 12 standard rock samples are summarized in Tables 5—7. As can be seen from these values, the concentrations of REEs in rock samples are characteristic, depending on the types of rock samples. Thus the geochemical features of standard rock samples will be discussed with emphasis on the REE patterns.

The REE patterns normalized by the Leedey normalizing factors are shown in Figs. 1—6, which were figured from the analytical data in Tables 5—7. Generally the REE patterns provide smooth curves

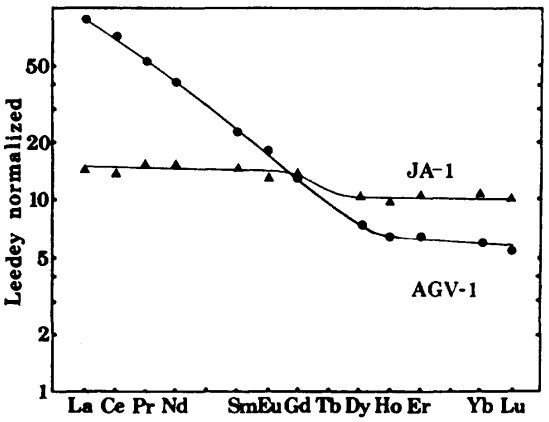

Fig. 3. REE patterns of JA-1 (tholeiitic andesite) and AGV-1 (trachy andesite).

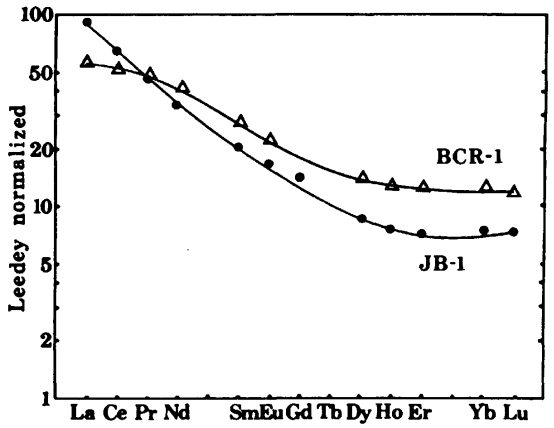

Fig. 1. REE patterns of BCR-1 (andesine tracky basalt) and JB-1 (alkali basalt)

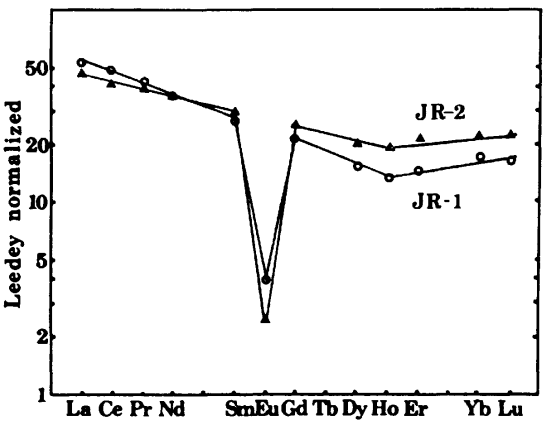

Fig. 4. REE patterns of JR-1 (rhyolite) and JR-2 (rhyolite).

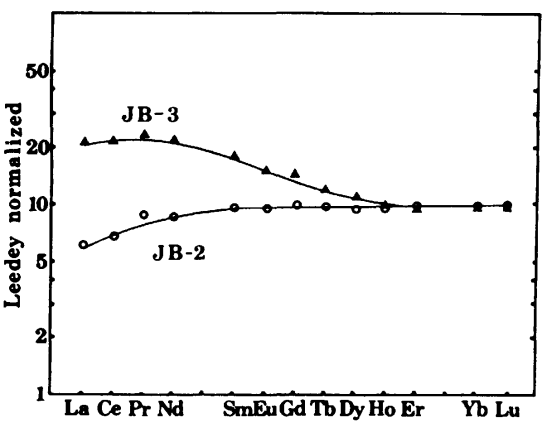

Fig. 2. REE patterns of JB-2 (tholeiitic basalt) and JB-3 (high aluminum basalt).

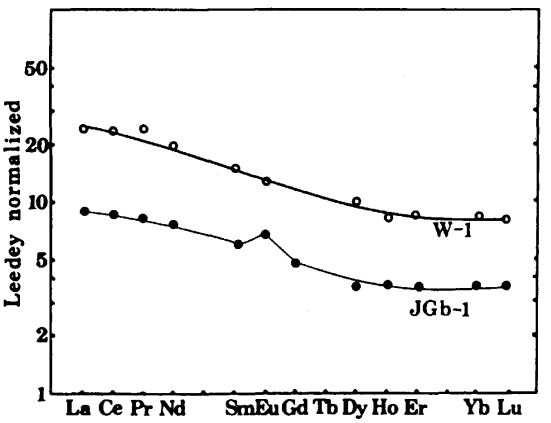

Fig. 5. REE patterns of W-1 (dolelite) and JGb-1 (gabbro).

except for Eu. Since Eu exists as the di- and tri-valent ions, it often shows some anomaly. Thus, these REE distribution patterns including Eu anomaly are useful to discuss some geochemical or geological characteristics of rock samples as well as their origin and classification.

Basalt. Masuda analyzed several basalts from Japan and found that basalts can be classified into three groups, based on general petrographic characteristics and REE patterns[27-29]; alkali basalt, tholeiitic basalt, and high aluminum basalt. Alkali basalt shows the REE pattern, in which light REEs are usually enriched, as is seen for JB-1 shown in Fig. 4. On the other hand, tholeiitic basalt contains less light REEs and show the rather flat pattern through all REE elements, which is seen in JB-2. The difference of these two REE patterns may be interpreted as follows. As has been known,[8] tholeiitic basalt magma and alkali olivine basalt magma have different genesis. The difference of the shapes of REE patterns mainly depends on degree of partial melting of upper mantle, when magma is generated from upper mantle. Already, this assumption has been elucidated by high pressure experiment in laboratory.[8,30,31] Most models for the formation of tholeiites assume about 20—30% melting of upper mantle peridotite with various REE contents, which reasonably explains the REE contents in tholeiites.[32] Tholeiites with low REE contents and flat REE distribution in Leedey-normalized curves are assumed to melt from primitive mantle with little or no

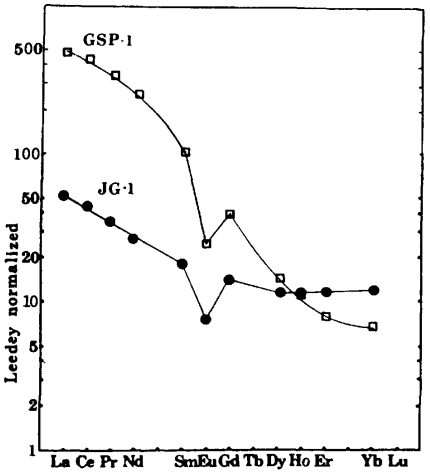

Fig. 6. REE patterns of JG-1 (granodiolite) and GSP-1 (granodiolite).

Table 6. Analytical Results of Standard Rock Samples[a]

	BCR-1		W-1		GSP-1	
	Found[b]	Ref. 22	Found[b]	Ref. 22	Found[c]	Ref. 22
La	22.1	25.0	10.3	10.9	182	183
Ce	50.5	53.7	23.0	23	428	406
Pr	6.7	6.9	3.3	3.2	54.5	51
Nd	29.1	28.7	14.5	15	186	190
Sm	6.4	6.58	3.5	3.5	26.1	26.8
Eu	1.8	1.96	1.1	1.11	2.3	2.36
Gd	—	6.68	—	3.9	12.8	13
Tb	—	1.05	—	0.65	—	1.36
Dy	5.4	6.35	4.2	3.9	5.5	5.4
Ho	1.1	1.25	0.73	0.81	—	1.2
Er	3.3	3.61	2.2	2.3	2.2	2.5
Tm	—	0.59	—	0.34	—	—
Yb	3.1	3.39	2.1	2.12	1.8	1.7
Lu	0.45	0.512	0.31	0.34	—	0.22

a) All values are in $\mu g\,g^{-1}$. b) Acid digestion. c) Alkali fusion.

Table 5. Analytical Results of Standard Rock Samples[a]

	JG-1			JB-1			AGV-1		
	Found[b]	Found[c]	Ref. 23	Found[b]	Found[c]	Ref. 23	Found[b]	Found[c]	Ref. 22
La	20.3	19.9	22	36.7	36.1	36	34.1	35.7	38
Ce	43.6	42.9	43	63.5	63.7	67	71.6	64.9	66
Pr	4.85	4.49	2.3	6.76	6.26	8.7	7.42	7.25	6.5
Nd	18.8	18.1	20.6	25.3	24.6	27	32.0	30.8	34
Sm	4.36	4.38	4.5	4.90	5.04	5.16	5.63	5.93	5.9
Eu	0.66	0.65	0.69	1.54	1.51	1.5	1.56	1.60	1.66
Gd	3.82	4.42	3.9	4.85	4.73	4.80	4.62	4.64	5.2
Tb	—	—	0.63	—	—	0.47	—	—	0.71
Dy	3.20	4.45	3.2	3.96	3.75	4.1	3.36	3.23	3.8
Ho	0.55	0.95	0.57	0.73	0.70	0.7	—	0.55	0.73
Er	1.68	2.96	1.60	2.19	2.15	2.23	1.91	1.67	1.61
Tm	—	—	—	—	—	—	—	—	0.32
Yb	1.63	3.03	1.5	2.00	2.10	2.1	1.96	1.68	1.67
Lu	—	—	0.23	—	—	0.3	—	—	0.28

a) All values are in $\mu g\,g^{-1}$. b) Acid digestion. c) Alkali fusion.

Table 7. Analytical Results of New Standard Rocks from GSJ[a)]

	JB-2[b)]	JB-3[b)]	JR-1[c)]	JR-2[c)]	JA-1[b)]	JGb-1[b)]
La	2.3±0.1	8.0±0.2	19.4±0.6	16.5±0.8	5.3±0.3	3.4±0.1
Ce	6.6±0.1	21.0±0.3	46.9±0.9	41.0±0.7	13.3±0.6	8.6±0.2
Pr	1.2±0.1	3.2±0.1	5.8±0.2	5.5±0.1	2.1±0.1	1.1±0.1
Nd	6.2±0.2	15.4±0.4	24.8±1.0	25.0±0.4	11.0±0.8	5.5±0.3
Sm	2.2±0.1	4.2±0.1	5.7±0.2	6.6±0.2	3.4±0.1	1.4±0.1
Eu	0.82±0.01	1.3±0.1	0.25±0.08	0.20±0.04	1.15±0.06	0.60±0.02
Gd	3.1±0.1	4.6±0.2	6.6±0.2	7.8±0.9	4.6±0.3	1.50±0.05
Tb	0.58±0.06	0.70±0.09	—	1.3±0.2	—	—
Dy	3.7±0.3	4.4±0.2	5.9±0.3	7.7±0.1	4.0±0.2	1.4±0.1
Ho	0.83±0.03	0.84±0.01	1.12±0.02	1.7±0.1	0.88±0.03	0.32±0.02
Er	2.5±0.1	2.5±0.1	3.7±0.1	5.2±0.1	2.7±0.2	0.91±0.02
Tm	—	—	—	—	—	—
Yb	2.5±0.1	2.5±0.1	4.2±0.2	5.3±0.1	2.7±0.1	0.90±0.02
Lu	0.38±0.01	0.37±0.01	0.62±0.06	0.84±0.05	0.40±0.05	0.14±0.02

a) All values are in $\mu g\ g^{-1}$. b) Acid digestion. c) Alkali fusion.

enrichment of the light REEs relative to the heavy REEs.[33)] On the other hand, the model for the formation of alkali basalt assumes about 0.8—2.9% partial melting and 4.5—5% garnet content in residue.[30)] Garnet, with its very large mineral/melt *D* value for heavy REEs,[31)] must also be present in the residue left after partial melting. BCR-1, which also belongs to alkali rock,[22)] have the REE pattern similar to JB-1, as shown in Fig. 1.

High aluminum basalt is aluminum-rich tholeiitic basalts whose composition of Al_2O_3 is over 17%. Generally high aluminum basalt shows chemical characteristics between alkali basalts and tholeiitic basalts.[34)] This can be seen from the slope of the REE pattern of JB-3 which is between those of JB-1 and JB-2, shown in Figs. 1 and 2.

Andesite and Ryolite. Andesitic magma is generally formed by fractional crystallization of plagioclase, amphibole, pyroxene, or magnetite from the more basic melts.[35,36)] Such crystallization models are common to explain tholeiitic trend. Tholeiitic andesites formed by crystallization have trend to show the flat pattern in Leedey-normalized curves. Its abundance of REEs is slightly increased, but the shapes of the REE patterns do not significantly change during forming andesitic magma from basaltic magma by crystallization differentiation. Then, AGV-1 (trachy andesite, in alkali series) shows the light REE-enriched pattern, while JA-1 (tholeiitic andesite) does rather flat REE pattern. This can be seen in the REE patterns shown Fig. 3.

JR-1 and JR-2 were collected from the same sampling location, and so their REE patterns and major chemical compositions should be similar to each other. This trend can be seen in their REE patterns shown in Fig. 4. In addition, negative Eu anomaly is remarkably observed for both JR-1 and JR-2, which are interpretated in terms of Eu^{2+} depletion in the melting process owing to the crystallization of Ca-feldsper. Since oxygen fugasity is very low in magma chamber, some part of Eu exists as Eu^{2+} which has similar ion radius with Ca^{2+}.[37,38)] The *D* values of REEs (except Eu) for plagioclase/melt are low, and then the concentration of REEs (except Eu) in melt slightly increases through crystallization process of plagioclase. In general, Eu is concentrated in plagioclase rather than other REEs when it precipitates from the magma. Thus the differentiated magma may develop larger negative Eu anomalies from original magma that may have little or no Eu anomaly.

Plutonic Rock. Dolerite (W-1) is hypoabyssal basaltic rock and gabbro (JGb-1) is plutonic basaltic rock. W-1 and JGb-1 generally have the properties between alkali and tholeiitic rocks, and they show small slope in the patterns with light REE-enriched abundance. Positive Eu anomaly is clearly seen in JGb-1, while it is not in W-1. It can be explained that magma of W-1 have been mixed with Eu positive substance such as anorthite.[10,39)]

In JG-1 and GSP-1, light REEs are significantly enriched with negative Eu anomaly. As is well noted,[40)] the origin and genesis of granite is very complicated.[41,42)] The range of granitic melts can be determined by melting a variety of sources (mantle basaltic magma, intermediate and felsic magma, sedimentary rocks etc.). Petrography and experimental petrology of granitic rock indicate a wide range of mineral parageneses due to differences in magma compositions, temperature, pressure, and contents of dissolved volatile species. In addition, granitic magma are very viscous, and so the assumption of complete separation of crystals and magma is not realistic. Then, it is still difficult to

propose an exact model using the REE pattern to help explain the petrogenesis of granitic melts. The REE patterns of JG-1 and GSP-1 cannot be well interpreted only by the present REE data.

Conclusion

The concentration of REEs in standard rock samples have been determined by ICP-AES. The REE patterns obtained from the present analytical data are useful to discuss the geological properties of standard rock samples along with the origins and genesis of these rock samples. From these experimental results and discussion it can be concluded that these standard rock samples can be used as the references in analysis as well as in geological or geochemical characterization of rock samples when their REE patterns can be obtained by proper analytical methods.

The present authors express sincere thanks to Hiroshi Shimizu and Kiyoshi Iwasaki for their valuable discussion. This research has been supported by the Grant-in-Aid for Scientific Research (No. 61030026) from the Ministry of Education, Science and Culture.

References

1) H. Tao, Y. Iwata, T. Hasegawa, Y. Nojiri, H. Haraguchi, and K. Fuwa, *Bull. Chem. Soc. Jpn.*, **56**, 1074 (1983).
2) J. G. Crock and F. E. Lichte, *Anal. Chem.*, **54**, 1329 (1982).
3) J. N. Walsh, F. Buckley, and J. Barker, *Chem. Geol.*, **33**, 141 (1981).
4) K. Yoshida and H. Haraguchi, *Anal. Chem.*, **56**, 2580 (1984).
5) K. Iwasaki, K. Fuwa, and H. Haraguchi, *Anal. Chim. Acta*, **183**, 239 (1986).
6) K. Toyoda and H. Haraguchi, *Chem. Lett.*, **1985**, 981.
7) G. N. Hanson, *Ann. Rev. Earth Planet. Sci. Lett.*, **8**, 381 (1980).
8) P. W. Gast, *Geochim. Cosmochim. Acta.*, **32**, 1057 (1968).
9) A. G. Herrmann and K. H. Wedepole, *Contri. Mineral. Petrol.*, **29**, 255 (1970).
10) T. H. Green, A. O. Brunfelt, and K. S. Heier, *Geochim. Cosmochim. Acta*, **36**, 241 (1972).
11) A. Masuda, *J. Earth Sci., Nagoya Univ.*, **10**, 173 (1962).
12) A. Masuda and Y. Matsui, *Geochim. Cosmochim. Acta*, **30**, 239 (1966).
13) E. A. K. Middlemost, *Bull. Volcanol.*, **36**, 382 (1972).
14) H. Kuno, *Bull. Volcanol.*, **219**, 195 (1966).
15) A. Miyashiro, *Am. J. Sci.*, **274**, 321 (1974)
16) J. A. Pearce and J. R. Cann, *Earth Planet. Sci. Lett.*, **19**, 290 (1973).
17) A. E. J. Engel, C. G. Engel, and R. G. Harvens, *Geol. Soc. Am. Bull.*, **76**, 719 (1965).
18) N. Onuma, M. Hirano, and N. Isshiki, *Geochem. J.*, **15**, 315 (1981).
19) J. A. Pearce and M. J. Norry, *Contrib. Mineral. Petrol.*, **69**, 33 (1979).
20) C. J. Hawkesworth, M. J. Norry, J. C. Roddick, and P. E. Baker, *Earth Planet. Sci. Lett.*, **42**, 45 (1979).
21) F. J. Flanagan, *Geochim. Cosmochim. Acta*, **31**, 289 (1967).
22) E. S. Gladney, C. E. Burns, and I. Roelandts, *Geostandards Newsletter*, **7**, 3 (1983).
23) A. Ando, *Bunseki*, **1984**, 597.
24) A. Ando, H. Kurasawa, T. Ohmori, and E. Takeda, *Geochem. J.*, **8**, 175 (1974).
25) M. Ebihara, Y. Minai, M. K. Kubo, T. Tominaga, N. Aota, T. Nikko, K. Sakamoto, and A. Ando, *Anal. Sci.*, **1**, 209 (1985).
26) H. Uchida, K. Iwasaki, and K. Tanaka, *Anal. Chim. Acta*, **134**, 375 (1982).
27) A. Masuda, *Geochem. J.*, **1**, 11 (1966).
28) A. Masuda, *Earth Planet. Sci. Lett.*, **4**, 284 (1968).
29) J. A. Philpotts, W. Martin, and C. C. Schnetzler, *Earth Planet. Sci. Lett.*, **12**, 89 (1971).
30) R. W. Kay and P. W. Gast, *J. Geol.*, **81**, 653 (1973).
31) S. S. Sun and G. N. Hanson, *Geology*, **3**, 297 (1975).
32) D. H. Green, *Earth Planet. Sci. Lett.*, **19**, 37 (1973).
33) Y. Masuda and K. Aoki, *Earth Planet. Sci. Lett.*, **39**, 289 (1978).
34) H. Kuno, *J. Petrogy*, **1**, 121 (1960).
35) S. R. Taylor, "Geochemistry of Andesites," in "Origin and Distribution of the Elements," ed by L. H. Ahrens, Pergamon Press, Oxford (1968), p. 559.
36) Y. Masuda and K. Aoki, *Earth Planet. Sci. Lett.*, **44**, 139 (1979).
37) J. A. Philpotts and C. C. Schnetzler, *Chem. Geol.*, **3**, 5 (1968).
38) J. A. Philpotts and C. C. Schnetzler, *Chem. Geol.* **4**, 464 (1969).
39) T. H. Green, A. O. Brunfelt, and K. S. Heier, *Earth Planet. Sci. Lett.*, **7**, 93 (1969).
40) G. N. Hanson, *Earth Planet. Sci. Lett.*, **38**, 26 (1978).
41) M. Takahashi, *Mem. Geol. Soc. Japan*, **25**, 225 (1985).
42) M. Takahashi, S. Aramaki, and S. Ishihara, *Mining Geol. Special Issue*, **8**, 13 (1980).

 © 1987 The Chemical Society of Japan Bull. Chem. Soc. Jpn., 60, 941—946 (1987)

Mössbauer and DTA Studies of Semiconducting Potassium Vanadate Glasses Containing Iron

Tetsuaki NISHIDA* and Yoshimasa TAKASHIMA
Department of Chemistry, Faculty of Science, Kyushu University
33, Hakozaki, Higashiku, Fukuoka 812
(Received October 15, 1986)

A Mössbauer spectrum of a series of potassium vanadate glasses containing 10 mol% Fe_2O_3 shows a paramagnetic quadrupole doublet, of which isomer shift proves to be smaller than 0.4 mm s^{-1} with respect to metallic iron. This indicates that the individual Fe^{3+} ion is present at the substitutional site of the V^{5+} (and probably V^{4+}) ion constituting a VO_4 tetrahedral unit. An increase in the K_2O content of the potassium vanadate glasses results in a continuous decrease in the glass transition temperature (Tg), ranging from 239 to 200 °C, when the K_2O content is changed from 5 to 30 mol%. This suggests a decrease in the coordination number of the V^{5+} (and V^{4+}) ion from 5 to 4 and a formation of nonbridging oxygen atoms in the VO_4 and FeO_4 tetrahedral units. The formation of nonbridging oxygen atoms in the VO_4 and FeO_4 units is also estimated from a continuous decrease in the quadrupole splitting, suggesting a decrease in the electric field gradient at the iron nucleus and an increase in the symmetry around the Fe^{3+} ion. These results lead to the conclusion that the introduction of the alkali oxide (K_2O) into the V_2O_5 results in a structural change of the V^{5+} (and V^{4+}) ions from VO_5 tetragonal pyramid (or trigonal bipyramid) to VO_4 tetrahedral units.

Electric conducting glasses, i.e., superionic conducting glass and semiconducting glass, have attracted much attention because of the scientific interest in the conduction mechanism as well as the high technological applicability. The electric conductivity of the superionic conducting glasses is known to reach the order of 10^{-2} S cm^{-1},[1-14] which is almost equivalent to that of the crystalline superionic conductor (solid state electrolytes) such as α-AgI and β-Al_2O_3. The high electric conductivity of the superionic conducting glasses is assumed to be due to the "ion migration" of monovalent cations such as Ag^+, Li^+, and Na^+. Comparing the magnitude of the electric conductivity of the superionic conducting glasses to that of the ordinary oxide glasses such as borate and phosphate glasses, which is usually smaller than about 10^{-12} or 10^{-13} S cm^{-1},[15] it is easily understood that the former is extraordinary larger than the latter. Also, the electric conductivity of semiconducting glasses is known to be comparable to that of the superionic conducting glasses.[16-18] The essential difference between the two types of the electric conducting glasses lies in the conduction mechanism. Namely, the electric conductivity of the semiconducting glasses, such as V_2O_5-based glasses studied in the present paper, is known to be due to the electron hopping from the metal ion of lower valence state to the metal ion of higher valence state.[19-21] In the case of the V_2O_5-based glasses, the electric conduction is reported to be performed by a step-by-step electron hopping from the V^{4+} ions, which were produced as a result of thermal decomposition of the V_2O_5 during the sample preparation,[22] to the V^{5+} ions of which number is usually larger than that of the V^{4+}.[19-21] A great number of theoretical treatments of the electric conduction have so far been performed on these semiconducting glasses using a "small polaron hopping theory" proposed by Mott.[23-25] Therefore, it should be noted that the electric conductivity of the semiconducting V_2O_5-based glasses has been studied satisfactorily.

In contrast to the variety of studies performed on the physical properties of vanadate glasses, only a few studies have so far been performed on the structure of the semiconducting V_2O_5-based glasses. Structure of crystalline V_2O_5 has been studied by Byström et al.[26] and by Jansen and Sperlich.[27] They reported that each V^{5+} ion is surrounded by five oxygen atoms making a distorted tetragonal pyramid, which can also be viewed as a distorted trigonal bipyramid, sharing edges and corners to form layers. IR study of several vanadate glasses performed by Dimitriev et al.[28] revealed that the introduction of alkali or alkaline earth oxides, which usually play a role of network modifier, into the V_2O_5 matrix results in a destruction of the vanadate layers followed by a formation of tetrahedral VO_4 units. Dimitriev et al.[28] also elucidated that only the VO_4 units are present in the skeleton of metavanadate glasses, where the molar ratio between the alkali or the alkaline earth oxides and the V_2O_5 is equal to 1. They also revealed that the introduction of other kind of oxides, which play a role of network former, such as SiO_2, B_2O_3, GeO_2, and TiO_2 affects no structural change on the skeleton of the glass matrix originally made of only VO_5 units. In the latter case, the individual network-forming atoms, i.e. Si, B, Ge, and Ti were concluded to be substituted for the fivefold-coordinated V^{5+} (or V^{4+}) ions forming VO_5 units. On the other hand, a neutron diffraction study performed by Wright et al.[29] revealed that the coordination number of vanadium is always 5 in the P_2O_5-, BaO-, and PbO-V_2O_5 glasses irrespective of the glass composition, and that the skeleton of the vanadate glasses is composed of interconnected and distorted VO_5 tetragonal pyramid (or trigonal bipyramid), similarly to the VO_5 units in the crystalline

V_2O_5. Besides the VO_4 and VO_5 units described above, the presence of octahedral VO_6 units has also been proposed, based on the composition dependency of specific gravity.[18,30] Iron-Mössbauer spectroscopy has also been utilized for the structural study of vanadate glasses.[31-34] However, the conclusions obtained so far by the Mössbauer spectroscopy are inconsistent with each other. For example, the coordination number of Fe^{3+} ion is reported to be only six in the case of barium vanadate glass[31] and to be both six and four in the cases of barium or calcium borovanadate[32,33] and sodium vanadate[34] glasses. The conclusions concerning the coordination number of the Fe^{3+} ion reported in those papers seem to be very doubtful because all the isomer shifts, which can be a criterion of octahedral and tetrahedral symmetries, actually indicate the presence of only tetrahedral Fe^{3+} species in those vanadate and borovanadate glasses.[31-34] (All the isomer shifts obtained in those glasses are smaller than 0.4 mm s^{-1} with respect to metallic iron.)

In the light of these reasons, the present Mössbauer and DTA (Differential Thermal Analysis) studies were carried out in order to elucidate the local structure and the structural change, brought about by the introduction of K_2O into the V_2O_5 matrix, of a series of potassium vanadate glasses. Small amounts of Fe_2O_3 were incorporated into the vanadate glasses as a Mössbauer probe. DTA method was utilized in order to know the structural change of the vanadate glasses through the glass transition temperature (T_g), because the T_g is known to reflect the change in the coordination number of network forming atoms and the destruction of the network structure followed by a formation of nonbridging oxygen atoms.[14,35-39]

Experimental

A series of potassium vanadate glasses were prepared by fusing the individual mixtures of commercially available K_2CO_3, V_2O_5, and Fe_2O_3, of a guaranteed reagent grade, at 1000 °C for 1 h in an electric muffle furnace. After the fusion in the ambient atmosphere, each melt in a platinum crucible was immediately quenched with ice-cold water in a beaker. The vanadate glasses were tried to prepare in the compositional ranges of $0 \leqq K_2O \leqq 40$ mol%, 50 mol% $\leqq V_2O_5 \leqq$ 90 mol%, and 5 mol% $\leqq Fe_2O_3 \leqq 20$ mol%. All the glass samples prepared in the present study were almost black in color and completely transparent. Mössbauer and DTA measurements were performed only for the vanadate glasses of which composition is expressed by $xK_2O \cdot (90-x)V_2O_5 \cdot 10Fe_2O_3$ in order to investigate the effect of the alkali oxide (K_2O) content on the structure of the vanadate glasses. Mössbauer measurements were performed by a constant acceleration method at room temperature with a proportional counter and a 1024 channel multichannel analyzer. Cobalt-57 (10 mCi) diffused into a palladium foil was used as the Mössbauer source. As the standard material for the isomer shift, a metallic iron foil enriched with iron-57 was used. The iron foil was also used for the velocity-calibration of the spectrometer. Each Mössbauer spectrum was analyzed into a quadrupole doublet with the same peak intensity and the same linewidth. DTA measurements of the vanadate glasses were performed in the temperature range from room temperature to 550 °C with a heating rate of 5 °C min^{-1}. An Al_2O_3 powder was used as the standard material in the DTA measurements.

Results and Discussion

The glass-forming region for the ternary K_2O-V_2O_5-Fe_2O_3 glass system is shown in Fig. 1, where open and closed circles indicate the formations of glass and non-glassy (devitrified) samples, respectively. It is easily understood from Fig. 1 that the introduction of the Fe_2O_3 into the K_2O-V_2O_5 system results in an extended glass-forming region as compared to the binary K_2O-V_2O_5 system. Extended glass-forming region has also been observed in CuO-V_2O_5-TeO_2 glass system,[18] and in BaO-V_2O_5-TeO_2, P_2O_5-V_2O_5-TeO_2, Fe_2O_3-V_2O_5-TeO_2, and ZnO-V_2O_5-TeO_2 glass systems.[40] On the other hand, reduced glass-forming region has been observed when TiO_2 is introduced into the V_2O_5-TeO_2 system.[40] The change in the glass-forming region will be correlated with the chemical and physical properties of the components, such as nature of the chemical bond, ionic radius, melting point, and viscosity. It is understood from Fig. 1 that the formation of the ternary K_2O-V_2O_5-Fe_2O_3 glasses is limited to a relatively small compositional region. A Mössbauer spectrum of the potassium vanadate glasses measured at room temperature is shown in Fig. 2, which indicates the

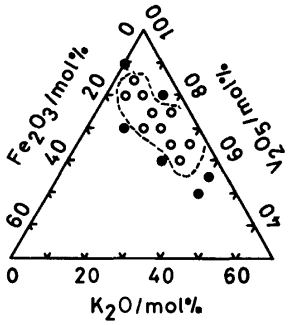

Fig. 1. Glass-forming region for the K_2O-V_2O_5-Fe_2O_3 system.

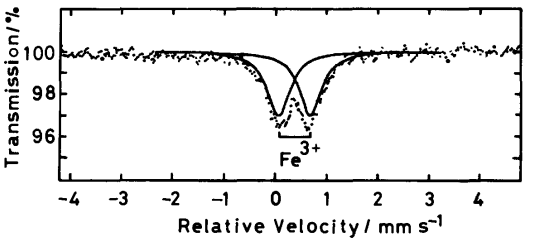

Fig. 2. Mössbauer spectrum of $15K_2O \cdot 75V_2O_5 \cdot 10Fe_2O_3$ glass measured at room temperature.

presence of paramagnetic Fe^{3+} ions of high spin state, since the isomer shift (with respect to metallic iron) of the quadrupole doublet is much larger than 0 mm s^{-1}.[41,42] (In the case of the absorptions due to the Fe^{3+} ions of low spin state, the isomer shift is known to fall to the neighborhood of 0 mm s^{-1}.[41,42]) All the Mössbauer parameters for the vanadate glasses studied in the present paper are summarized in Table 1, from which it is seen that the isomer shifts are located in a small range of 0.35—0.37 mm s^{-1}. As for the coordination number of iron in glasses, earlier works are reviewed by Kurkjian[43] and Coey.[44] Recent works on the structure of glasses are reviewed by Müller-Warmuth and Eckert.[45] Coey suggested that the Fe^{3+} ions are present at the tetrahedral sites in borate and silicate glasses.[44] This is well consistent with the Mössbauer results of a series of borate[14,46-48] and borosilicate[49,50] glasses containing small amounts of Fe_2O_3, performed by the present authors. In those Mössbauer studies,[14,46-50] all the isomer shifts (with respect to metallic iron) proved to lie in a range of 0.22—0.38 mm s^{-1}, and the experimental error for the isomer shift has been estimated to be ±0.01 or 0.02 mm s^{-1}. Judging from the experimental results shown in the reviews on the structure of glasses[43-45] and from the recent Mössbauer results on the structure of glasses performed by the present authors,[14,46-50] the isomer shift of the Fe^{3+} ions is concluded to be smaller than 0.40 mm s^{-1} for the tetrahedral symmetry. On the other hand, octahedrally coordinated Fe^{3+} ions have been observed in several phosphate glasses,[51-53] where all the isomer shifts proved to be larger than 0.42 mm s^{-1}. These experimental results lead to the conclusion that the criterion of the isomer shift for the Fe^{3+} ions with tetrahedral and octahedral symmetries lies at about 0.40 mm s^{-1}. Those symmetries strictly refer to the "distorted" octahedral and "distorted" tetrahedral configurations, since the bond lengths and the bond angles are widely distributed in the amorphous materials such as the glasses. This is well reflected in the magnitude of the linewidth summarized in Table 1, i.e., the linewidth is much larger than that of the ordinary crystalline compounds containing iron.[41,42] Considering all the experimental results described above, the present Mössbauer results, especially the isomer shifts suggest that the Fe^{3+} ions are present at the tetrahedral sites in the alkali vanadate glasses. This conclusion indicates the presence of VO_4 tetrahedral units as well as the FeO_4 units, because all the Mössbauer spectra, e.g. Fig. 2, obtained in the present study indicate the presence of a paramagnetic and homogeneous glass phase. All the Fe^{3+} ions are therefore concluded to be present at the substitutional sites of the V^{5+} (and probably V^{4+}) ions constituting VO_4 tetrahedra, as a constituent of the skeleton of the glass matrix. Similarly to the case of the Fe^{3+} ions incorporated into borate,[14,44,46-48] silicate,[44] and borosilicate[49,50] glasses, it is considered that the Fe^{3+} ions are easily incorporated into the vanadate matrix. The substitution of the iron for the other metal or metalloid ions will easily occur in the high energy and non-equilibrium states where the glass samples are prepared by fusion. It is also concluded that the introduction of the alkali oxide (K_2O in the present study) into the V_2O_5 matrix results in a formation of VO_4 tetrahedral units, instead of the VO_5 tetragonal pyramids (or trigonal bipyramids) which originally constituted the V_2O_5 matrix.[26,27] This conclusion is well consistent with the IR results obtained by Dimitriev et al.[28] They concluded that the introduction of the alkali or alkaline earth oxides into the V_2O_5 matrix results in a formation of VO_4 tetrahedral units. Their conclusion is based on the disappeared vibrational mode, originally observed at 1020 cm^{-1}, of the V=O bond constituting the VO_5 tetragonal pyramid (or trigonal bipyramid).[28] On the other hand, a few Mössbauer studies on the structure of vanadate glasses obtained recently[31-34] suggest that a large number of Fe^{3+} ions are octahedrally present at the interstitial sites, i.e., between the layer structure composed of the VO_5 units. The individual isomer shifts reported in those vanadate glasses are 0.36,[31] 0.35,[34] 0.30,[33] and 0.27—0.29[32] mm s^{-1} with respect to metallic iron. (The isomer shift of 0.36 mm s^{-1} in Ref. 31 was obtained by subtracting 0.26 mm s^{-1} from the isomer shift with respect to sodium nitroprusside.[41,42]) Considering the experimental results obtained in the present study, together with the several Mössbauer results of the structure of several kinds of glasses[14,43-53] and with the reviews on the coordination number of iron in several compounds,[41,42] it should be noted that those isomer shifts[31-34] are actually indicative of the presence of FeO_4 tetrahedral units constituting the skeleton of the glass matrix. Therefore, the conclusion on the structure of the vanadate glasses obtained in those Mössbauer studies,[31-34] i.e. a large number of Fe^{3+} ions are present at the octahedral and interstitial sites (between the layer structure), seems very doubtful.

Table 1. Mössbauer Parameters for K_2O-V_2O_5-Fe_2O_3 Glasses

Composition	δ[a] / mm s^{-1}	Δ[b] / mm s^{-1}	Γ[c] / mm s^{-1}
$5K_2O \cdot 85V_2O_5 \cdot 10Fe_2O_3$	0.37	0.61	0.60
$10K_2O \cdot 80V_2O_5 \cdot 10Fe_2O_3$	0.36	0.63	0.55
$15K_2O \cdot 75V_2O_5 \cdot 10Fe_2O_3$	0.36	0.62	0.53
$20K_2O \cdot 70V_2O_5 \cdot 10Fe_2O_3$	0.37	0.61	0.59
$25K_2O \cdot 65V_2O_5 \cdot 10Fe_2O_3$	0.36	0.59	0.58
$30K_2O \cdot 60V_2O_5 \cdot 10Fe_2O_3$	0.35	0.55	0.67

a) Isomer shift. b) Quadrupole splitting. c) Linewidth.

The composition dependency of the isomer shifts for the Fe^{3+} ions in the vanadate glasses obtained in the present study is shown in Fig. 3. It is seen from Fig. 3 that the isomer shifts are almost constant irrespective of the alkali oxide (K_2O) content, and that the isomer shift shows a slight decrease with the increase in the K_2O content. A drastic decrease in the isomer shifts of the Fe^{3+} ions has already been observed in borate[46-48] and borosilicate[49,50] glasses when the alkali oxide content increases. In those glasses,[46-50] the decrease in the isomer shift of the Fe^{3+} ions, which are present at the substitutional sites of the tetrahedral boron or silicon atoms, was ascribed to the formation of nonbridging oxygen atoms ($-O^-$) in BO_4 and SiO_4 tetrahedral units, because the formation of nonbridging oxygen atoms results in decreased interatomic distances between boron and oxygen or silicon and oxygen atoms. This will cause an increase in the s-electron density at the iron nucleus and the decrease in the isomer shift. The formation of nonbridging oxygen atoms will also affect the degree of the thermal vibration of boron or silicon atoms, and as a result, the increased thermal vibration (second order Doppler effect) will result in the decrease in the isomer shift. In the case of germanate glasses,[37,54] of which network structure is composed of GeO_4 and GeO_6 units, a drastic increase in the isomer shift of Sn^{4+} ions was observed. The increase in the isomer shift of the Sn^{4+} suggests an increased s-electron density at the tin nucleus, brought about by the formation of nonbridging oxygen atoms in GeO_4 tetrahedral units. (In the case of the ^{119}Sn-Mössbauer spectroscopy, an increase in the s-electron density results in the increase in the isomer shift, opposite to the case of the ^{57}Fe-Mössbauer spectroscopy.[41,42]) A slight decrease in the isomer shift shown in Fig. 3 is therefore ascribed to the formation of nonbridging oxygen atoms in the VO_4 tetrahedral units. This conclusion is supported by the remarkable composition dependence of the quadrupole splitting shown in Fig. 4. It is seen from Fig. 4 that the quadrupole splitting shows a distinct decrease when the K_2O content exceeds about 15 mol%. As for the composition dependency of the quadrupole splitting of the Fe^{3+} ions in glasses, distinct decreases in the quadrupole splitting have been observed when the nonbridging oxygen atoms are formed in borate,[46-48] borosilicate,[49,50] and phosphate[52,53] glasses. The decrease in the quadrupole splitting of the Fe^{3+} ions is ascribed to the increased symmetry around the Fe^{3+} ions, because the Fe^{3+} ions of high spin state have a symmetric electron configuration of $3d^5$, and only the electric field gradient brought about by the neighboring atoms or ions primarily affects the quadrupole splitting values. Similar phenomenon has been observed in the germanate glasses containing tin (Sn^{4+}),[37,54] where the nonbridging oxygen atoms are concluded to be formed in GeO_4 tetrahedral units. These considerations lead to the conclusion that the increase in the symmetry around the Fe^{3+} ions constituting the FeO_4 tetrahedral units, observed in the present study, indicates the formation of nonbridging oxygen atoms in the VO_4 tetrahedral units constituting the skeleton of the alkali vanadate glasses, because each Fe^{3+} ion is considered to be present at the substitutional site of the V^{5+} or V^{4+} ion as described above. Therefore, the present Mössbauer results lead to the conclusion that the increase in the K_2O content results in a decrease in the coordination number of vanadium ion from 5 to 4. At the same time, it is also concluded that nonbridging oxygen atoms are formed in some of the VO_4 tetrahedral units. (These Mössbauer results are based on the assumption that the structural change of the V^{5+} or V^{4+} ions, brought about by the introduction of K_2O into the V_2O_5 matrix, is equivalent to that of the Fe^{3+} ions.)

Each DTA curve of the potassium vanadate glasses containing 10 mol% Fe_2O_3 proved to consist of a simple endothermic peak due to glass transition and one or a few exothermic peak(s) due to crystallization. All the glass transition temperatures (T_g) obtained in the present study are shown in Fig. 5, where the T_g values are plotted against the K_2O content of the vanadate glasses. DTA studies on the structure of several glasses have already revealed that

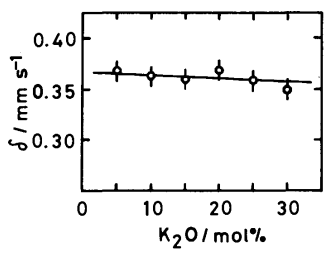

Fig. 3. Composition dependence of the isomer shift (δ) of the Fe^{3+} ions in K_2O–V_2O_5 glasses containing 10 mol% Fe_2O_3.

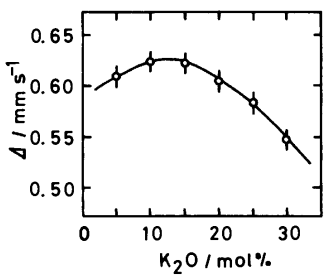

Fig. 4. Composition dependence of the quadrupole splitting ($\triangle$) of the Fe^{3+} ions in K_2O–V_2O_5 glasses containing 10 mol% Fe_2O_3.

T_g shows a close correlation with the change in the coordination number of the network-forming atoms (network former) and with the formation of nonbridging oxygen or fluorine atoms which means a destruction or depolymerization of the network structure.[14,35-38] The T_g, in general, shows a distinct increase when the coordination number of the network former increases. For example, the change in the coordination number of Ge from 4 to 6 is observed as a continuous increase in the T_g in the case of germanate glasses.[35-37] Contrary to this, a formation of nonbridging oxygen is known to cause a decrease in the T_g.[35-37] Considering these results, it is expected that a decrease in the coordination number of the network former, if present, will be observed as a decrease in the T_g. The continuous and distinct decrease in the T_g from 239 to 200 °C observed in the present study, therefore, seems to suggest the gradual decrease in the coordination number of V^{5+} and V^{4+} ions from 5 to 4. This conclusion obtained from the DTA measurements is well consistent with the IR results obtained by Dimitriev et al.[28] All the T_g values obtained in the present study are summarized in Table 2, together with the individual crystallization temperatures (T_c). It is understood from Table 2 that the T_c is higher than the T_g by 20—45 °C. In Table 2, only one crystallization temperature (the lowest one) is given for each glass sample. Considering the Mössbauer results (Figs. 3 and 4) obtained in the present study together with the previous DTA results described above,[35-37] the decrease in the T_g shown in Fig. 5 (and Table 2) is ascribed to the formation of nonbridging oxygen atoms in the VO_4 and FeO_4 tetrahedral units as well as the decrease in the coordination number of the V^{5+} and V^{4+} ions from 5 to 4. The formation of nonbridging oxygen atoms will become pronounced when the alkali oxide content of the vanadate glasses is high.

Table 2. Glass Transition and Crystallization Temperatures of K_2O-V_2O_5-Fe_2O_3 Glasses

Composition	T_g[a]/°C	T_c[b]/°C
$5K_2O \cdot 85V_2O_5 \cdot 10Fe_2O_3$	239	264
$10K_2O \cdot 80V_2O_5 \cdot 10Fe_2O_3$	232	255
$15K_2O \cdot 75V_2O_5 \cdot 10Fe_2O_3$	232	252
$20K_2O \cdot 70V_2O_5 \cdot 10Fe_2O_3$	224	253
$25K_2O \cdot 65V_2O_5 \cdot 10Fe_2O_3$	220	265
$30K_2O \cdot 60V_2O_5 \cdot 10Fe_2O_3$	200	240

a) Glass transition temperature. b) Crystallization temperature.

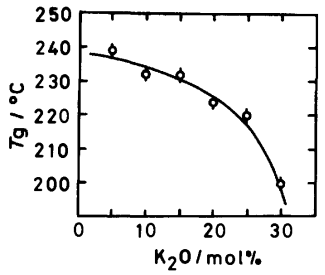

Fig. 5. Composition dependence of the glass transition temperature (T_g) of K_2O-V_2O_5 glasses containing 10 mol% Fe_2O_3.

All the experimental results obtained in the present study suggest that the introduction of alkali oxide into V_2O_5 matrix results in a structural change from VO_5 tetragonal pyramid (or trigonal bipyramid) to VO_4 tetrahedra. In addition to the formation of the VO_4 tetrahedra, a formation of nonbridging oxygen atoms is also concluded in the VO_4 tetrahedral units especially when the alkali oxide content is high. Each Fe^{3+} ion is concluded to be present at the substitutional site of the V^{5+} or V^{4+} ion constituting the VO_4 tetrahedral unit.

The authors are grateful to Dr. Hiroshi Hirashima of Keio University for his useful comments on the structure and physical properties of vanadate glasses. One of the authors (TN) is grateful to the Itoh Science Foundation for the financial support. The present work is partially supported by a Grant-in-Aid for Scientific Research No. 61740350 from the Ministry of Education, Science and Culture.

References

1) T. Minami, Y. Takura, and M. Tanaka, *J. Electrochem. Soc.*, **124**, 1659 (1977).
2) J. P. Malugani, A. Wasniewski, M. Doreau, G. Robert, and A. Rikabi, *Mater. Res. Bull.*, **13**, 427 (1978).
3) T. Minami and M. Tanaka, *Rev. Chim. Miner.*, **16**, 283 (1979).
4) A. Magistris, G. Chiodelli, and A. Schiraldi, *Electrochim. Acta*, **24**, 203 (1979).
5) T. Minami and M. Tanaka, *J. Non-Cryst. Solids*, **38/39**, 289 (1980).
6) T. Minami, K. Imazawa, and M. Tanaka, *J. Non-Cryst. Solids*, **42**, 469 (1980).
7) J. P. Malugani, G. Robert, and R. Mercier, *Mater. Res. Bull.*, **15**, 715 (1980).
8) G. Chiodelli, A. Magistris, M. Villa, and J. L. Bjorkstam, *Mater. Res. Bull.*, **17**, 1 (1982).
9) A. Fontana, G. Mariotto, E. Cazzanelli, G. Carini, M. Cutroni, and M. Federico, *Phys. Lett.*, **93A**, 209 (1983).
10) G. Dalba, A. Fontana, P. Fornasini, G. Mariotto, M. R. Masullo, and F. Rocca, *Solid State Ionics*, **9/10**, 597 (1983).
11) J. P. Malugani, R. Mercier, B. Fahys, and G. Robert, *J. Solid State Chem.*, **45**, 309 (1982).
12) J. P. Malugani and R. Mercier, *Solid State Ionics*, **13**, 293 (1984).
13) G. Chiodelli, G. Camparivigano, G. Flor, A. Magistris, and M. Villa, *Solid State Ionics*, **8**, 311 (1983).
14) T. Nishida, M. Ogata, and Y. Takashima, *Bull. Chem. Soc. Jpn.*, **59**, 2401 (1986).

15) L. Murawski, *J. Mater. Sci.*, **17**, 2155 (1982).
16) H. Hirashima, M. Mitsuhashi, and T. Yoshida, *Yogyo Kyokai Shi*, **90**, 411 (1982).
17) H. Hirashima, K. Nishii, and T. Yoshida, *J. Am. Ceram. Soc.*, **66**, 704 (1983).
18) T. Yoshida, H. Hirashima, and M. Kato, *Yogyo Kyokai Shi*, **93**, 244 (1985).
19) J. H. de Boer and E. J. W. Verway, *Proc. Phys. Soc. (London) Suppl.*, **49**, 59 (1937).
20) G. L. Sewell, *Phys. Rev.*, **129**, 597 (1963).
21) T. Allersma, R. Hakim, and J. D. Mackenzie, *J. Chem. Phys.*, **46**, 154 (1967).
22) E. M. Milan, *J. Phys. Chem.*, **38**, 498 (1929).
23) N. F. Mott, *Adv. Phys.*, **16**, 49 (1967).
24) N. F. Mott, *J. Non-Cryst. Solids*, **1**, 1 (1968).
25) I. G. Austin and N. F. Mott, *Adv. Phys.*, **18**, 41 (1969).
26) A. Byström, K. A. Wilhelmi, and O. Brotzen, *Acta Chem. Scand.*, **4**, 1119 (1950).
27) K. Jansen and G. Sperlich, *Phys. Status Solidi B*, **55**, 495 (1973).
28) Y. Dimitriev, V. Dimitrov, M. Arnaudov, and D. Topalov, *J. Non-Cryst. Solids*, **57**, 147 (1983).
29) A. C. Wright, C. A. Yarker, P. A. V. Johnson, and R. N. Sinclair, *J. Non-Cryst. Solids*, **76**, 333 (1985).
30) T. Yoshida, K. Matsumoto, and H. Hirashima, *Yogyo Kyokai Shi*, **87**, 349 (1979).
31) L. G. Bogomolova, M. P. Glassova, O. E. Budatovko, S. I. Reiman, and S. N. Spasibkina, *J. Non-Cryst. Solids*, **58**, 71 (1983).
32) A. K. Bandyopadhyay, M. Ribes, F. Pernot, and J. Zarzycki, *Phys. Chem. Glasses*, **23**, 31 (1982).
33) T. K. Bansal, N. Kishore, and R. G. Mendiratta, *Phys. Chem. Glasses*, **26**, 94 (1985).
34) D. K. Kanchan, R. K. Puri, and R. G. Mendiratta, *Phys. Chem. Glasses*, **26**, 217 (1985).
35) J. E. Shelby, *J. Am. Ceram. Soc.*, **57**, 436 (1974).
36) J. E. Shelby, *J. Appl. Phys.*, **46**, 193 (1975).
37) T. Nishida, M. Katada, and Y. Takashima, *Bull. Chem. Soc. Jpn.*, **57**, 3566 (1984).
38) T. Nishida, T. Nonaka, and Y. Takashima, *Bull. Chem. Soc. Jpn.*, **58**, 2255 (1985).
39) T. Nishida and Y. Takashima, *Bull. Chem. Soc. Jpn.*, **59**, 2789 (1986).
40) H. Hirashima and T. Yoshida, *Proc. XIV Int. Congr. Glass (India)*, **1986**, 287.
41) N. N. Greenwood and T. C. Gibb, "Mössbauer Spectroscopy," Chapman and Hall Ltd., London (1971), Chap. 3.
42) R. Ingalls, F. Van der Woude, and G. A. Sawatzky, "Iron and Nickel," in "Mössbauer Isomer Shifts," ed by G. K. Shenoy and F. E. Wagner, North-Holland Pub Co., Amsterdam (1978), Chap. 7.
43) C. R. Kurkjian, *J. Non-Cryst. Solids*, **3**, 157 (1970).
44) J. M. D. Coey, *J. Phys.*, **35**, C6-89 (1974).
45) W. Müller-Warmuth and H. Eckert, *Phys. Rep.*, **88**, 91 (1982).
46) T. Nishida and Y. Takashima, *J. Non-Cryst. Solids*, **37**, 37 (1980).
47) T. Nishida, T. Shiotsuki, and Y. Takashima, *J. Non-Cryst. Solids*, **41**, 161 (1980).
48) T. Nishida, T. Hirai, and Y. Takashima, *J. Non-Cryst. Solids*, **43**, 221 (1981).
49) T. Nishida, T. Hirai, and Y. Takashima, *Phys. Chem. Glasses*, **22**, 94 (1981).
50) T. Nishida, T. Hirai, and Y. Takashima, *Bull. Chem. Soc. Jpn.*, **54**, 3735 (1981).
51) M. F. Taragin, J. C. Eisenstein, and W. Heller, *Phys. Chem. Glasses*, **13**, 29 (1972).
52) T. Nishida, T. Shiotsuki, and Y. Takashima, *J. Non-Cryst. Solids*, **43**, 115 (1981).
53) T. Nishida, T. Shiotsuki, and Y. Takashima, *J. Non-Cryst. Solids*, **43**, 123 (1981).
54) T. Nishida, M. Katada, and Y. Takashima, *Bull. Chem. Soc. Jpn.*, **58**, 1745 (1985).

 © 1987 The Chemical Society of Japan Bull. Chem. Soc. Jpn., 60, 947—952 (1987)

Racemic Structures of Organic Ammonium Salts of *N*-Acetyl-DL-2-aminobutyric Acid and *N*-Acetyl-DL-norvaline and Optical Resolution by Preferential Crystallization of DL-Ammonium Salts

Tadashi SHIRAIWA,* Hirokazu YOSHIDA, Makoto TSUDA, and Hidemoto KUROKAWA
Faculty of Engineering, Kansai University, Yamate-cho, Suita, Osaka 564
(Received May 19, 1986)

The racemic structures of the ammonium salts (AM salts) and seven organic ammonium salts of *N*-acetyl-DL-2-aminobutyric acid (DL-AcAbu) and *N*-acetyl-DL-norvaline (DL-AcNva) were studied on the basis of thermodynamic analyses to explore the possibility of optical resolution by preferential crystallization. An empirical equation has been derived from thermodynamic data at melting points of ammonium and organic ammonium salts of *N*-acyl-DL-amino acids to predict racemic structures around room temperature. The AM salts of DL-AcAbu and -AcNva exist in conglomerate around room temperature. It is possible to resolve optically these DL-AM salts by preferential crystallization in ethanol at 10 °C, and the successive preferential crystallization followed by purification gave D- and L-2-aminobutyric acids and -norvalines with optical purities close to 100%.

DL-2-Aminobutyric acid[1] (abbreviated as DL-Abu) and DL-norvaline[2] (DL-Nva) have been optically resolved in the form of the *N*-acetyl derivatives by using the optically active α-methylbenzylamine as a resolving agent. However, no optical resolution by preferential crystallization of DL-Abu or -Nva has been reported though this procedure is considered to be useful for industrial operation. This paper describes an attempt to resolve optically the ammonium salts and organic ammonium salts of *N*-acetyl-DL-2-aminobutyric acid (DL-AcAbu) and *N*-acetyl-DL-norvaline (DL-AcNva) by preferential crystallization. The DL-salts employed are the ammonium (AM), *t*-butylammonium (TBA), pentylammonium (PTA), hexylammonium (HA), and 1,1,3,3-tetramethylbutylammonium (TMB) salts of DL-AcAbu and the AM, ethylammonium (EA), butylammonium (BA), and propylammonium (PA) salts of DL-AcNva.

The racemic structures of these DL-salts were examined, since optical resolution by preferential crystallization requires that a racemic modification exists in conglomerate. A racemic modification existing in conglomerate has a positive free energy of formation of racemate,[3-5] shows an infrared spectrum identical with that of the corresponding optically active one,[6] and is more soluble than the optically active one.[6] In this paper, an empirical equation is also derived on the basis of thermodynamic data at melting points of ammonium and organic ammonium salts of *N*-acyl-DL-amino acids[5,7-11] to predict racemic structures around room temperature. Since it was found that the AM salts of DL-AcAbu and -AcNva exist in conglomerate around room temperature, optical resolution by preferential crystallization of these DL-salts were attempted at 10 °C in ethanol.

Experimental

Materials. DL-Abu and -Nva were purchased from Sigma Chemicals, and (−)-α-methylbenzylamine and amines from Wako Pure Chemicals Ind.

***N*-Acetylation.** DL-AcAbu[12] and -AcNva[2] were obtained, respectively, by acetylating DL-Abu and -Nva in the usual way. The DL-AcAbu obtained was recrystallized from ethanol, and the DL-AcNva from water. DL-AcAbu: Mp 134 °C (lit,[12] 128—130 °C); yield 82.0%. DL-AcNva: Mp 117 °C (lit,[2] 118—119 °C); yield 81.7%.

Preparation of Optically Active *N*-Acetylamino Acids. D- and L-AcAbu's[1] and -AcNva's[2] were obtained, respectively, by optical resolution of DL-AcAbu and -AcNva by using (−)-α-methylbenzylamine as a resolving agent. D-AcAbu: Mp 135 °C (lit,[1] 135 °C); $[\alpha]_D^{20}$ +43.3° (*c* 2.00, water) (lit,[1] $[\alpha]_D^{20}$ +43.6° (*c* 2, water)). L-AcAbu: Mp 135 °C (lit,[1] 135 °C); $[\alpha]_D^{20}$ −43.3° (*c* 2.00, water) (lit,[1] $[\alpha]_D^{20}$ −43.5° (*c* 2, water)). D-AcNva: Mp 105 °C (lit,[12] 100 °C); $[\alpha]_D^{20}$ +34.7° (*c* 2.00, water) (lit,[12] $[\alpha]_D^{25}$ +35.0° (*c* 1—2, water)). L-AcNva: Mp 105 °C; $[\alpha]_D^{20}$ −34.3° (*c* 2.00, water).

Preparation of Salts. DL-, D-, or L-AcAbu (0.01 mol) and 0.01 mol of an amine were dissolved in 50 cm³ of acetone. After stirring for 30 min at 5 °C, the salt formed was collected by filtration. The salt obtained was recrystallized from ethanol. The AM salts of DL-, D-, and L-AcNva's were also prepared in a similar manner.

The AM salt of DL-AcAbu: Mp 170 °C; found C, 44.35; H, 8.67; N, 17.43% (calcd for $C_6H_{14}N_2O_3$: C, 44.43; H, 8.70; N, 17.27%); solubility at 10 °C 2.103 g/(100 cm³ ethanol). The D-salt: Mp 188 °C; found C, 44.35; H, 8.66; N, 17.38%; $[\alpha]_D^{20}$ −20.7° (*c* 0.50, ethanol); solubility at 10 °C 1.319 g/(100 cm³ ethanol). The L-salt: Mp 188 °C; $[\alpha]_D^{20}$ +20.7° (*c* 0.50, ethanol).

The AM salt of DL-AcNva: Mp 150 °C; found C, 47.61; H, 9.11; N, 15.99% (calcd for $C_7H_{16}N_2O_3$: C, 47.71; H, 9.15; N, 15.90%); solubility at 10 °C 4.733 g/(100 cm³ ethanol). The D-salt: Mp 181 °C; found C, 47.57; H, 9.11; N, 16.04%; $[\alpha]_D^{20}$ −19.7° (*c* 0.50, ethanol); solubility at 10 °C 2.269 g/(100 cm³ ethanol). The L-salt: Mp 181 °C; $[\alpha]_D^{20}$ +19.7° (*c* 0.50, ethanol).

Optical Resolution by Successive Preferential Crystallization. Ammonium Salt of *N*-Acetyl-DL-norvaline: The AM salt of DL-AcNva (5.208 g) and 0.050 g of the L-salt were dissolved in 100 cm³ of ethanol around 40 °C. The solution was slowly cooled to 10 °C and seeded with 0.010 g of the L-salt. After stirring for 10 min at 10 °C, the salt that

precipitated was collected by filtration, washed with a small amount of diethyl ether, and dried; yield 0.276 g. The DL-salt (0.277 g) was added to the filtrate, and dissolved in ethanol around 40 °C. The solution was cooled to 10 °C and seeded with 0.010 g of the D-salt. After stirring for 11 min at 10 °C, the salt that precipitated was collected by filtration; yield 0.287 g. The filtrate was treated similarly.

Ammonium Salt of *N*-Acetyl-DL-2-aminobutyric Acid: The AM salt of DL-AcAbu (2.103 g) and 0.050 g of the L-salt were dissolved in 50 cm^3 of ethanol and the solution was seeded with 0.020 g of the L-salt at 10 °C. After stirring for 8 min, the salt precipitated was collected by filtration. The DL-salt (0.218 g) was dissolved in the filtrate. After seeding with 0.020 g of the D-salt and stirring for 8 min at 10 °C, the salt precipitated was collected by filtration. The filtrate was treated similarly.

The degree of resolution of the AM salts of D- and L-AcAbu and -AcNva's obtained was calculated by

$$\text{Degree of resolution/\%} = [\text{YOPM/g} \times 100]/[(\text{Operation amount of D- or L-salt/g}) - \text{M}],$$

where YOPM is the yield of optically pure modification[7] and M is 0.526 for the AM salts of AcAbu, and 2.367 g for the AM salts of AcNva.

Purification of Partially Resolved Ammonium Salts. The AM salt of D-AcAbu with an optical purity of 52.7% (3.78 g) was added to 85 cm^3 of ethanol. After stirring around 40 °C for 30 min, the suspension was further stirred for 1 h at 10 °C. The D-salt was collected by filtration, washed with a small amount of diethyl ether, and dried; yield 1.94 g; $[\alpha]_D^{20}$ −20.7° (*c* 0.50, ethanol).

The partially resolved AM salts of D-AcNva were purified by using ethanol similarly to the AM salt of D-AcAbu. The D-salt with an optical purity of 74.1% (6.96 g) was treated with 39 cm^3 of ethanol to give the D-salt with an optical purity of 100% in 5.07 g yield.

Preparation of Optically Active Amino Acids. The AM salts of D- and L-AcAbu's and -AcNva's obtained by preferential crystallization were purified similarly. The salts purified were treated with hydrochloric acid in the usual way to give the respective optically active amino acids.

The AM salt of D-AcNva with an optical purity of 100% (3.50 g) was dissolved in 4 cm^3 of 6 mol dm^{-3} hydrochloric acid around 50 °C, and the solution was stirred around 5 °C for 1 h. The D-AcNva was collected by filtration, washed with a small amount diethyl ether, and dried; yield 3.03 g; $[\alpha]_D^{20}$ +34.9° (*c* 2.00, water). The D-AcNva (2.90 g) was added to 7 cm^3 of 6 mol dm^{-3} hydrochloric acid. After refluxing for 2.5 h, the solution was evaporated to dryness under reduced pressure around 35 °C and the residue was dissolved in 30 cm^3 of methanol. After adding 2.4 cm^3 of concentrated aqueous ammonia, the solution was stirred for 1 h around 5 °C. The D-Nva that precipitated was collected by filtration, washed with small amounts of cold water and methanol, and dried: yield 1.56 g (total yield 71.1%); $[\alpha]_D^{20}$ −24.0° (*c* 2.00, 5 mol dm^{-3} HCl) (for L-Nva[13] $[\alpha]_D^{20}$ +24.1° (5 mol dm^{-3} HCl)).

The purified AM salts of L-AcNva and D- and D-AcAbu's were treated with hydrochloric acid similarly to the AM salt of D-AcNva. L-Nva: total yield 70.5%; $[\alpha]_D^{20}$ +23.9° (*c* 2.00, 5 mol dm^{-3} HCl). D-Abu: total yield 65.3%; $[\alpha]_D^{20}$ −20.7° (*c* 2.00, 5 mol dm^{-3} HCl). L-Abu: total yield 65.1%; $[\alpha]_D^{20}$ +20.9° (*c* 2.00, 5 mol dm^{-3} HCl) (lit,[13] $[\alpha]_D^{20}$ +20.9° (5 mol dm^{-3}HCl)).

Measurements. Specific rotations were measured with a Union Giken high sensitivity PM-101 digital polarimeter using a quartz cell of 0.5 dm path length. Infrared spectra were obtained in the range 4000—400 cm^{-1} with a JASCO A-102 infrared spectrophotometer by the KBr disk method. Enthalpies of fusion and melting points were determined with a Rigaku Denki differential scanning calorimeter DSC-8230.

Results and Discussion

Racemic Structure. Thermodynamic Data: The formation of a racemate in the solid state corresponds to the reaction between the solid enantiomers. The Gibbs energy of formation at *T* K (ΔG_T^F) is calculated

Table 1. Thermodynamic Data for Ammonium and Organic Ammonium Salts of *N*-Acetyl-2-aminobutyric Acid and *N*-Acetylnorvaline

N-Acetylamino acid	Salt	Mp/K		ΔH^f a)/kJ mol^{-1}		ΔG_T^F b)/kJ mol^{-1}	
		DL-Salt	D-Salt	DL-Salt	D-Salt	ΔG_{mp}^F	ΔG_{283}^F
AcAbu[c]	AM[e]	443	461	33.3	38.7	−1.08	+1.48
	TBA[f]	435	411	38.2	25.2	−4.51	−5.68
	PTA[g]	385	386	33.1	23.1	−2.15	−3.83
	HA[h]	388	388	34.2	25.9	−2.24	−3.43
	TMB[i]	421	434	37.2	37.8	−1.29	−0.43
AcNva[d]	AM[e]	423	454	32.1	36.7	+0.16	+1.15
	EA[j]	397	404	31.9	25.9	−1.84	−2.74
	PA[k]	388	397	28.5	28.1	−0.52	−1.09
	BA[l]	387	398	35.9	28.9	−0.76	−2.82

a) ΔH^f: Enthalpy of fusion. b) ΔG_T^F: Free energy of formation of racemate. The ΔG_T^F's at the melting point (ΔG_{mp}^F) and at 283 K (ΔG_{283}^F) were calculated from equations in Refs. 3—5. c) AcAbu: *N*-Acetyl-2-aminobutyric acid. d) AcNva: *N*-Acetylnorvaline. e) AM: Ammonium salt. f) TBA: *t*-Butylammonium salt. g) PTA: Pentylammonium salt. h) HA: Hexylammonium salt. i) TMB: 1,1,3,3-Tetramethylbutylammonium salt. j) EA: Ethylammonium salt. k) PA: Propylammonium salt. l) BA: Butylammonium salt.

by the following equation which is derived from the equations reported by Jacques et al.[3] by combination:

$$\Delta G_T^F = (\Delta H_A^f - \Delta H_R^f) - T(\Delta S_A^f - \Delta S_R^f) - RT\ln 2 - \Delta C_p(T_A^f - T_R^f + T\ln T_R^f/T_A^f) + (\alpha/2)(T_{R,A}^f - T)^2, \quad (1)$$

where ΔH^f, ΔS^f, and T^f are the enthalpy of fusion, entropy of fusion, and melting point, respectively, R is the gas constant, and ΔC_p is the difference in heat capacity between the liquid and solid states in the vicinity of melting point; subscripts "A" and "R" represent the optically active and racemic modifications, respectively; $T_{R,A}^f$ represents T_R^f when $T_R^f < T_A^f$ and T_A^f when $T_R^f > T_A^f$; α is calculated from $C_A^s - C_R^s = \alpha T_{R,A}^f$ as a first approximation; C^s is the heat capacity in the solid state.[3] The term containing ΔC_p is negligible for the calculation of ΔG_{mp}^F at the melting point because the contribution is very much smaller than that of the sum of the other terms in the right-hand side of Eq. 1;[3] T is equal to $T_{R,A}^f$ at the melting point and hence the last term is zero. In our calculation, ΔC_p was taken as 105 J mol^{-1} K^{-1} and $C_A^s - C_R^s$ as 31.4 J mol^{-1} K^{-1}.[3-5] The ΔG_T^F's at the melting point (ΔG_{mp}^F) and 283 K (ΔG_{283}^F) are given in Table 1.

As found in Table 1, all salts of DL-AcAbu and -AcNva give negative ΔG_{mp}^F values except the AM salt of DL-AcNva. The eutectic temperatures and compositions calculated on the basis of the ΔH^f and melting points[14] are listed in Table 2, together with the observed melting points of mixtures with eutectic compositions. Only the AM salt of AcNva shows the composition of 0.5. These results indicate that only the AM salt of DL-AcNva exists in conglomerate and that the other DL-salts form racemic compounds in the vicinity of the melting points. The above results are supported by the binary phase diagrams of melting points; the phase diagrams of the AM salts of AcAbu and AcNva are shown in Figs. 1 and 2 as examples.

Table 2. Mole Fractions and Temperatures at Eutectic Points

N-Acetyl-amino acid	Salt	Mole fraction of D-salt[a]	Temperature/K	
			Found	Calcd[a]
AcAbu	AM	0.64	442	441
	TBA	0.94	408	407
	PTA	0.82	377	375
	HA	0.82	378	379
	TMB	0.68	419	418
AcNva	AM	0.50	423	424
	EA	0.76	390	390
	PA	0.73	381	383
	BA	0.72	383	384

a) These values were calculated from the Schröder-Van Laar and Prigogine-Defay equations.

The AM salt of DL-AcNva gives a positive ΔG_{283}^F value, whereas negative ΔG_{283}^F values were obtained for the TBA, PTA, HA, and TMB salts of DL-AcAbu and the EA, BA, and PA salts of DL-AcNva. Therefore, the racemic structures of the latter around room temperature may be identical with those in the vicinity of the melting points, respectively. On the other hand, since the AM salts of DL-AcAbu and DL-AcNva give positive ΔG_{283}^F values, it is inferred that the DL-salts do not form racemic compounds around room temperature.

Racemic Structure Around Room Temperature: The relationship among various thermodynamic data at melting points was examined to predict the racemic structures around room temperature for the 41 kinds of AM and organic ammonium salts of DL-AcAbu, DL-AcNva, and *N*-acyl-DL-amino acids, dealt with in our previous paper.[5,7-11] There is an empirical relationship among their ΔG_{mp}^F, ΔT^f ($=T_R^f - T_A^f$), and $\Delta\Delta H^f$

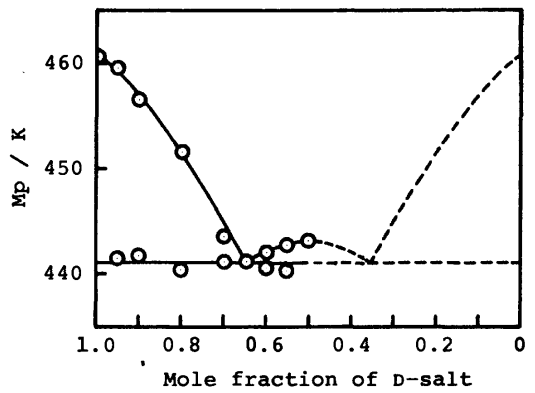

Fig. 1. Binary melting point diagram of ammonium salt of *N*-acetyl-2-aminobutyric acid.

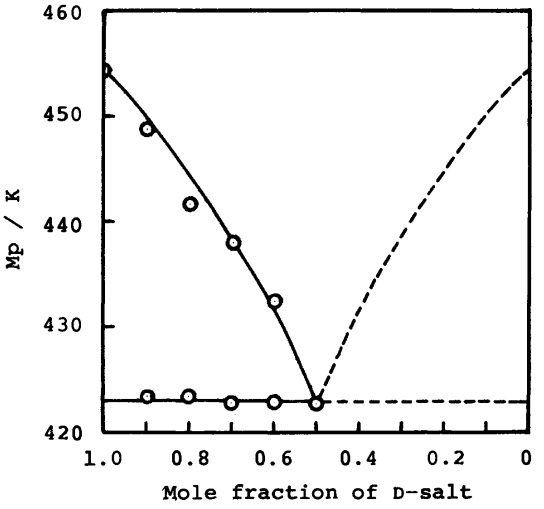

Fig. 2. Binary melting point diagram of ammonium salt of *N*-acetylnorvaline.

$(=H^f_R - \Delta H^f_A)$, which reads

$$\Delta G^F_{mp} = -0.0865\Delta T^f - 0.0223\Delta\Delta H^f - 2.285, \quad (2)$$

where $-0.0865\Delta T^f - 0.0223\Delta\Delta H^f$ $(=\Delta E)$ and 2.285 must be of the same order as ΔG^F_{mp}; the correlation coefficient was 0.958. This empirical equation shows that a DL-salt that exists in conglomerate around room temperature gives ΔE larger than $+1.17$ kJ mol^{-1}, irrespective of whether the DL-salt forms a racemic compound in the vicinity of its melting point, and that a DL-salt forming a racemic compound in the temperature range between room temperature and its melting point gives ΔE smaller than $+1.14$ kJ mol^{-1}. The AM salt of DL-AcAbu gives a ΔE value of $+1.68$, the AM salt of DL-AcNva $+2.87$, and the other DL-salts -2.4—$+1.13$ kJ mol^{-1}. Therefore, the ΔE values may be used to determine if the AM salts of DL-AcAbu and -AcNva exist in conglomerate around room temperature. This is consistent with the conclusion derived from their ΔG^F_{283} values, and is also supported by the infrared spectra and solubilities of these DL- and D-salts; the AM salts of DL-AcAbu and -AcNva show infrared spectra identical with those of the corresponding D-salts, they are more soluble than the D-salts, and the ternary solubility diagram of the AM salt of DL-AcAbu shows what is expected for a conglomerate, as shown in Fig. 3.[15] The above results indicate that the AM salts of DL-AcAbu and -AcNva exist in conglomerate around room temperature though the AM salt of DL-AcAbu forms a racemic compound in the vicinity of the melting point.

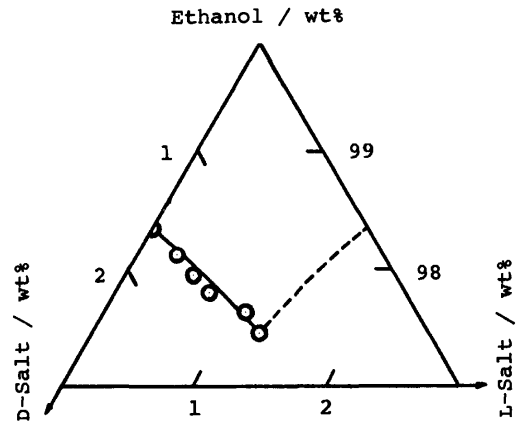

Fig. 3. Ternary solubility diagram of ammonium salt of *N*-acetyl-2-aminobutyric acid.
Solvent: ethanol. Temperature: 10 °C.

The TBA, PTA, HA, and TMB salts of DL-AcAbu and the EA, BA, and PA salts of DL-AcNva probably form racemic compounds around room temperature because their infrared spectra are different from those of the corresponding D-salts and because their ΔG^F_{283} values are negative.

Optical Resolution by Preferential Crystallization. Results of Optical Resolution and Purification of Salts Partially Resolved: Optical resolutions by preferential crystallization of the AM salts of DL-AcAbu and DL-AcNva were attempted at 10 °C in ethanol using a solution of the AM salt of DL-AcAbu with a degree of supersaturation of 200% and a solution of the AM salt of DL-AcNva with 110%, by a procedure similar to that described in our previous paper;[10] the D-salts were used as seed crystals. The results of the optical resolutions are given in Table 3.

The AM salts of D-AcAbu obtained did not have so high optical purities (41—79%) and the degrees of resolution were also low (10—25%); however it was possible to obtain AM salts of D-AcNva with optical purities of 72—95% and degrees of resolution of 40—78%.

The AM salt of D-AcAbu with a low optical purity was easily purified. The AM salt of D-AcAbu with an optical purity of 71.2% (3.00 g) was dissolved in 110 cm^3 of ethanol around 40 °C, and the solution was

Table 3. Optical Resolutions by Preferential Crystallization of Ammonium Salts of *N*-Acetyl-DL-2-aminobutyric Acid[a] and *N*-Acetyl-DL-norvaline[b]

N-Acetyl-amino acid	Resolution time / min	Yield / g	Optical purity / %	YOPM[c] / g	Degree of resolution / %
AcAbu	5	0.096	79.1	0.056	10.7
	10	0.176	74.0	0.110	20.9
	15	0.233	59.7	0.119	22.6
	20	0.362	41.7	0.131	24.9
AcNva	10	0.113	94.8	0.097	40.9
	15	0.205	94.9	0.184	77.7
	20	0.248	72.5	0.170	71.9

a) Solvent: 50 cm^3 of ethanol. Degree of supersaturation of racemic solution: 200%. Seed crystals: 0.020 g of D-salt. Temperature: 10 °C. b) Solvent: 100 cm^3 of ethanol. Degree of supersaturation of racemic solution: 110%. Seed crystals: 0.010 g of D-salt. Temperature: 10 °C. c) YOPM: Yield of optically pure modification.

allowed to stand for a day around 5 °C to give a D-salt with an optical purity of 100%. However, the yield (1.62 g) was 75.7% of the theoretical (2.14 g) and the recrystallization resulted in a loss of about 24%.

The optimum amount of ethanol was estimated on the basis of the solubility at 10 °C of the DL-salt to obtain the maximum yield of the optically pure salt.[16] The AM salt of D-AcAbu with an optical purity of 52.7% was treated with ethanol. Since 3.78 g of the D-salt was not completely dissolved in 85 cm^3 of ethanol around 40 °C, the suspension was treated by the procedure described in the experimental section; the optimum amount of ethanol calculated was 85.1 cm^3. The purification by this procedure gave the D-salt with an optical purity of 100% in 1.84 g yield; the yield was 92.5% of the theoretical (1.99 g).

The AM salt of D-AcNva partially resolved was also easily purified similarly. The D-salt with an optical purity of 74.1% (6.96 g) was treated with 38 cm^3 of ethanol (the optimum amount 38.0 cm^3) to give the D-salt with an optical purity of 100% in 5.07 g yield; the yield was 98.3% of the theoretical (5.16 g).

Successive Preferential Crystallization: The optical resolution by successive preferential crystallization was carried out to obtain the D- and L-Abu's and -Nva's. The results of such optical resolution are given in Tables 4 and 5.

The AM salts of D- and L-AcAbu obtained had optical purities of 72—81%, and the degrees of resolution were 20—28%. On the other hand, the optical resolution of the AM salt of DL-AcNva was found to give better results; D- and L- salts with optical purities of 90—100% were obtained at degrees of resolution of about 80%. These D- and L-salts purified were treated with hydrochloric acid to give D- and L-Abu's and -Nva's with optical purities of 99—100%.

It was found from the above results that the AM salts of DL-AcAbu and -AcNva exist in conglomerate around room temperature though the AM salt of DL-AcAbu forms a racemic compound in the vicinity of the melting point, and that the optical resolution by preferential crystallization followed by purification gives D- and L-Abu's and -Nva's with optical purities of about 100%.

References

1) D. Pitre and S. Boveri, *Farmaco, Ed. Sci.*, **26**, 733 (1971).
2) P. Alaupovic, *Croat. Chem. Acta*, **29**, 131 (1957).
3) M. Leclercq, A. Collet, and J. Jacques, *Tetrahedron*, **32**, 821 (1976); J. Jacques, A. Collet, and S. H. Wilen,

Table 4. Successive Preferential Crystallization of Ammonium Salt of *N*-Acetyl-DL-2-aminobutyric Acid[a]

Run	Added amount of DL-salt / g	Operation amount[b] / g		Resolution time / min	Salt obtained			
		D-Salt	L-Salt		Yield / g	Optical purity / %	YOPM / g	Degree of resolution[c] / %
1	2.103	1.051	1.101	8	0.217	L 73.9	0.140	24.3
2	0.218	1.131	1.041	8	0.233	D 81.2	0.169	27.9
3	0.233	1.056	1.136	10	0.197	L 72.0	0.122	20.0
4	0.198	1.127	1.086	13	0.230	D 72.0	0.146	24.3

a) Solvent: 50 cm^3 of ethanol. Seed crystals: 0.020 g of D- or L-salt. Temperature: 10 °C. This initial solution contains 2.103 g of DL-salt and 0.050 g of L-salt. b) The operation amounts of D- and L-salts in solutions were calculated on the basis of the analyses of the salt obtained in Runs 1—3. c) Degree of resolution/% = [YOPM/g × 100]/[(Operation amount of D- or L-salt/g) − 0.526].

Table 5. Successive Preferential Crystallization of Ammonium Salt of *N*-Acetyl-DL-norvaline[a]

Run	Added amount of DL-salt / g	Operation amount[b] / g		Resolution time / min	Salt obtained			
		D-Salt	L-Salt		Yield / g	Optical purity / %	YOPM / g	Degree of resolution[c] / %
1	5.208	2.604	2.654	10	0.276	L 90.5	0.240	83.6
2	0.277	2.730	2.540	11	0.287	D 100	0.277	76.3
3	0.288	2.597	2.684	11	0.270	L 92.3	0.239	75.4
4	0.271	2.722	2.570	13	0.305	D 97.5	0.287	80.8

a) Solvent: 100 cm^3 of ethanol. Seed crystals: 0.010 g of D- or L-salt. Temperature: 10 °C. This initial solution contains 5.208 g of DL-salt and 0.050 g of L-salt. b) The operation amounts of D- and L-salts in solutions were calculated on the basis of the analyses of the salt obtained in Runs 1—3. c) Degree of resolution/% = [YOPM/g × 100]/[(Operation amount of D- or L-salt/g) − 2.367].

"Enantiomers, Racemates, and Resolutions," John Wiley and Sons, New York, Chichester, Brisbane, and Toronto (1981), pp. 97—99, 140—142.

4) T. Shiraiwa, A. Ikawa, K. Fujimoto, K. Iwafuji, and H. Kurokawa, *Nippon Kagaku Kaishi*, **1984**, 764.

5) T. Shiraiwa, H. Miyazaki, A. Ikawa, and H. Kurokawa, *Nippon Kagaku Kaishi*, **1984**, 1425.

6) S. Yamada, M. Yamamoto, and I. Chibata, *J. Org. Chem.*, **38**, 4408 (1973).

7) T. Shiraiwa, S. Taniguchi, A. Ikawa, K. Iwafuji, and H. Kurokawa, *Nippon Kagaku Kaishi*, **1983**, 1189.

8) T. Shiraiwa, H. Miyazaki, S. Konishi, and H. Kurokawa, *Nippon Kagaku Kaishi*, **1985**, 1577.

9) H. Miyazaki, T. Shiraiwa, and H. Kurokawa, *Nippon Kagaku Kaishi*, **1986**, 87.

10) T. Shiraiwa, H. Yoshida, K. Mashima, and H. Kurokawa, *Nippon Kagaku Kaishi*, **1986**, 177.

11) T. Shiraiwa, H. Miyazaki, Y. Sakamoto, and H. Kurokawa, *Bull. Chem. Soc. Jpn.*, **59**, 2331 (1986).

12) R. Marshall, S. M. Birnbaum, and J. P. Greenstein, *J. Am. Chem. Soc.*, **78**, 4636 (1956).

13) "Seikagaku Data Bukku," ed by the Japanese Biochemical Society, Tokyo Kagaku Dojin, Tokyo (1982), Vol. I, pp. 36, 48.

14) S. H. Wilen, A. Collet, and J. Jacques, *Tetrahedron*, **33**, 2725 (1977).

15) A. Collet, M. J. Brienne, and J. Jacques, *Chem. Rev.*, **80**, 215 (1980).

16) T. Shiraiwa, M. Nakamura, M. Nobeoka, and H. Kurokawa, *Bull. Chem. Soc. Jpn.*, **59**, 2669 (1986).

^{13}C NMR Spectra of Substituted 2-Thiophenecarboxylic Acid Methyl Esters and MNDO Calculations

Hajime SATONAKA,* Kazuhisa ABE,† and Minoru HIROTA†
Industrial Research Institute of Kanagawa Prefecture,
3173, Showa-machi, Kanazawa-ku, Yokohama 236
†Department of Applied Chemistry, Faculty of Engineering, Yokohama National University,
Hodogaya-ku, Yokohama 240
(Received July 4, 1986)

The ^{13}C NMR spectra have been reported on substituted 2-thiophenecarboxylic acid methyl esters. The chemical shift of ring carbons in methyl (4- and 5-substituted 2-thiophenecarboxylate)s was correlated linearly with that of the corresponding carbons in substituted thiophenes. Plots of the ^{13}C-H coupling constants of methyl (substituted 2-thiophenecarboxylate)s against those of substituted thiophenes showed a good linear relation. The ^{13}C NMR data were interpreted by the stable conformation and percent *s* character of C-H bonds obtained by MNDO calculation.

The ^1H NMR spectra of methyl (3-substituted 2-thiophenecarboxylate)s (**1**), methyl (4-substituted 2-thiophenecarboxylate)s (**2**), and methyl (5-substituted 2-thiophenecarboxylate)s (**3**), were reported by one of the present authors,[1] and the effects of the substituents were discussed.[1] The additivity rule for the ^1H chemical shifts of simple substituted thiophenes was applicable to the ring protons in the compounds of series **2** and **3**, but inapplicable to those in the compounds of series **1**. Based on the facts we

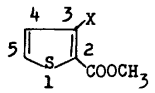

1

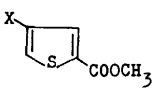

2

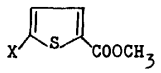

3

examined the ^{13}C NMR spectra of substituted 2-thiophenecarboxylates of these three series. Similar deviation from the additivity rule has also been observed by ^{13}C chemical shift of some 2,3-disubstituted thiophenes by the present authors. The deviation will be due to steric and electronic interaction between the neighboring substituents on thiophene ring. The conformational change may affect on the deviation, because the anisotropy caused by substituents as well as the attractive interaction between substituents considerably perturbs ^{13}C and ^1H chemical shifts. Molecular orbital calculation with geometry optimization has been applied in many investigations as one of the reliable methods for predicting the stable conformer. Among many versions of MO calculation, MNDO[2,3] is known as the most practicable and trustworthy way to estimate the geometry and the energy of conformation of the organic molecule.

We will discuss the relation between observed ^{13}C chemical shift and the stable conformers predicted by MNDO calculation. In addition, this report deals with the correlation between the percent *s* character obtained from $^1J_{C-H}$ and that calculated by MNDO method.

Experimental

The preparation of materials were described previously.[1] ^{13}C NMR spectra were recorded by a JEOL FX-90Q spectrometer. The concentration of sample solutions was adjusted to approximately 0.6 mol dm^{-3}. The chemical shift was measured in an accuracy of ±0.1 ppm with internal TMS reference in a $CDCl_3$ solution at the probe temperature. Data acquisition was done by the following conditions: flip angle of pulse 30°, number of transients 1000, data points 16384, and spectral width 4500 or 5000 Hz. The ^{13}C-H coupling constant in an accuracy of ±0.1 Hz was obtained from proton coupled spectra measured by the normal gated decoupling technique. Data acquisition was done by the following conditions: flip angle of pulse 45°, number of transients 2000, data points 16384, and spectral width 450 Hz.

MNDO Calculation[2,3]

The MNDO (Modified Neglect of Diatomic Overlap) calculation, semiempirical SCF molecular orbital calculation which takes all valence electrons into account, was carried out by MOPAC program[4] on HITACHI M-280H computer at the Computer Center of the University of Tokyo. By the standard MNDO calculation, electronic energy, core-core repulsion energy, ionization potential, heat of formation, density matrix (electron density and bond order), eigenvalue (energy level), and eigenvector of the molecular orbitals can be obtained. The structure of stable conformers of methyl (substituted 2-thiophenecarboxylate)s was estimated by means of XDC data base (Cambridge Crystallographic Data Base) installed at the Computer Center of the University of Tokyo. The structural parameters were used as the input data for the MNDO calculation. The *s* character of the C-H bonds was calculated from the coefficients of the corresponding molecular orbitals.

Results and Discussion

The ^{13}C NMR signals of methyl (3-, 4-, and 5-substituted 2-thiophenecarboxylate)s (**1**—**3**) were as-

signed by the procedures described below. The signals of protonated carbons were assigned from the coupling constants of carbon-proton bonds. Since $J_{C_5H_5}$ in thiophene compounds is larger than $J_{C_3H_3}$ or $J_{C_4H_4}$ by ca. 15 Hz,[5-7] C_5 and C_4 in the compounds of series **1** and C_5 and C_3 in the compounds **2** are easily distinguished from each other by ^{13}C-H one bond coupling constants. The ^{13}C-signals of C_3 and C_4 in the compounds of series **3** were assigned by the comparison with those of substituted thiophenes and partly by the analysis of line splitting due to a long-range coupling.[5,6] The signals of quaternary carbons were assigned by their intensity, and also by the ^{13}C-H long-range couplings. The results are given in Tables 1—3.

The plots of the chemical shift of carbons in methyl (4-substituted 2-thiophenecarboxylate)s against that of the corresponding carbons in 3-substituted thiophenes[8] showed good linear correlations (δC_2 r[9] 0.917, p 1.09, s 0.396; δC_3 r 0.993, p 1.06, s 0.464; δC_4 r 1.000, p 0.981, s 0.621; δC_5 r 0.996, p 0.898, s 0.843). The chemical shift of carbons in methyl (5-substituted 2-thiophenecarboxylate)s also correlates linearly with that of the corresponding carbons in 2-substituted thiophenes. These results suggest that the additivity rule for the ^{13}C chemical shift of simple substituted thiophenes is applicable to the chemical shift of the ring carbons in methyl (4- and 5-substituted 2-thiophenecarboxylate)s in which two substituents are attached to non-adjacent ring-carbon atoms. However, the chemical shift of carbons in methyl (3-substituted 2-thiophenecarboxylate)s and that of the corresponding carbons in 3-substituted thiophenes showed poor correlations. Thus, the interaction among substituents seems to result in deviation from the linear correlation. The interaction will be of steric nature, and the perturbation by neighboring substituent in a conformational preference can cause a considerable change in chemical shift.

In order to investigate the relation between chemical shift and stable conformation, we have estimated the stable conformation of these thiophene derivatives and their populations by MNDO calculation. Methyl 2-thiophenecarboxylate can take any one of the planar conformers **a**—**d**. Our calculations showed, however, that this ester is a mixture of **a** (50%) and **b** (50%) conformers and that other two conformers (**c** and **d**) have considerably higher energy than **a** and **b**. The calculations also showed that all other esters do not exist in the **c** and **d** conformers. It agrees with

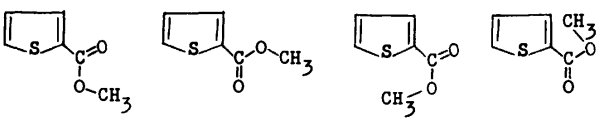

a (50%) (*s-cis*) **b** (50%) (*s-trans*) **c** (0%) **d** (0%)

Table 1. ^{13}C NMR Chemical Shifts and ^{13}C-H Coupling Constants of Methyl (3-Substituted 2-Thiophenecarboxylate)s (Series **1**)

No.	X	Chemical shifts (δ)							Coupling constants/Hz			
		δ_{C_2}	δ_{C_3}	δ_{C_4}	δ_{C_5}	δ_{CO}	δ_{CH_3}	Others	$J_{C_4H_4}$	$J_{C_5H_5}$	$J_{C_4H_5}$	$J_{C_3H_4}$	Others
1	H	133.8	133.4	127.4	132.4	162.6	52.0		170.3	185.9	3.8	7.0	
2	OCH_3	109.6	162.1	116.4	130.6	162.1	51.4	59.0 (OCH_3)	170.4	187.2	3.9	4.3	
3	CH_3	126.7	146.1	131.6	129.9	163.1	51.5	15.8 (CH_3))	167.6	185.0	3.7	6.8	4.6 ($J_{C_4-CH_3}$)
4	Cl	125.9	131.6	130.2	130.4	161.0	52.1		175.9	188.3	3.9	5.8	
5	Br	127.5	117.0	133.0	131.2	161.0	52.1		176.5	188.2	3.8	6.0	
6	I	130.5	86.1	138.6	132.7	161.2	52.1		176.1	187.5	4.1	6.5	
7	CHO	138.5	144.6	127.7	130.6	161.5	52.7	186.3 (CHO)	173.9	187.8	4.0	6.8	3.7 (J_{C_4-CHO})
8	$COCH_3$	131.2	147.3	128.0	130.9	161.7	52.5	198.4 (CO) 30.7 (CH_3)	172.0	187.5	4.1	6.5	
9	$COOCH_3$	134.0	137.2	128.7	130.5	161.5	52.5	164.4 (CO) 52.6 (CH_3)	173.3	188.1	4.1	6.5	
10	NO_2	129.5	148.6	124.1	129.3	159.7	53.3		179.4	192.2	4.1	5.4	

Table 2. ^{13}C NMR Chemical Shifts and ^{13}C-H Coupling Constants of Methyl (4-Substituted 2-Thiophenecarboxylate)s (Series **2**)

No.	X	Chemical shifts(δ)							Coupling constants/Hz				
		δ_{C_2}	δ_{C_3}	δ_{C_4}	δ_{C_5}	δ_{CO}	δ_{CH_3}	Others	$J_{C_3H_3}$	$J_{C_5H_5}$	$J_{C_3H_5}$	$J_{C_5H_3}$	Others
1	H	133.8	133.4	127.4	132.4	162.6	52.0		170.8	185.9	9.0	11.0	
11	OCH_3	132.0	124.3	158.3	105.1	162.4	52.0	57.6(OCH_3)	172.0	184.0	6.6	7.7	
12	CH_3	133.4	135.3	138.4	128.1	162.6	51.9	15.4(CH_3)	167.9	182.4	8.4	10.2	4.2($J_{C_3-CH_3}$) 5.7($J_{C_5-CH_3}$)
13	Cl	134.0	133.0	126.2	126.7	161.5	52.3		176.8	190.3	6.9	8.2	
14	Br	134.6	135.4	110.6	129.5	161.3	52.4		177.3	191.3	7.2	8.7	
15	I	135.4	140.2	77.5	135.2	160.9	52.3		177.2	191.4	7.8	9.6	
16	CHO	135.8	131.2	142.9	140.4	161.7	52.5	184.3(CHO)	174.1	186.5	7.9	9.5	3.0(J_{C_3-CHO})
17	$COCH_3$	134.9	132.5	142.8	137.2	161.9	52.4	191.3(CO) 27.4(CH_3)	173.0	185.9	7.7	9.0	
18	$COOCH_3$	134.6	133.5	134.1	138.0	161.8	52.3	162.3(CO) 52.0(CH_3)	174.9	188.8	7.6	9.2	
19	NO_2	134.9	127.3	148.4	132.1	160.9	52.9		180.8	193.9	6.0	7.4	

Table 3. ^{13}C NMR Chemical Shifts and ^{13}C-H Coupling Constants of Methyl (5-Substituted 2-Thiophenecarboxylate)s (Series **3**)

No.	X	Chemical shifts(δ)							Coupling constants/Hz				
		δ_{C_2}	δ_{C_3}	δ_{C_4}	δ_{C_5}	δ_{CO}	δ_{CH_3}	Others	$J_{C_3H_3}$	$J_{C_4H_4}$	$J_{C_3H_4}$	$J_{C_4H_3}$	Others
1	H	133.8	133.4	127.4	132.4	162.6	52.0		170.8	170.3	5.5	5.0	
20	OCH_3	118.8	133.2	105.6	172.5	162.8	51.7	60.4(OCH_3)	170.3	169.8	4.0	5.4	
21	CH_3	131.2	133.9	126.4	147.9	162.6	51.8	15.6(CH_3)	170.0	167.8	5.2	4.8	4.2($J_{C_4-CH_3}$)
22	Cl	132.0	133.0	127.3	137.4	161.5	52.2		173.3	174.6	4.3	5.0	
23	Br	134.9	133.6	130.9	120.2	161.4	52.2		173.1	175.0	4.5	5.1	
24	I	139.3	134.3	137.7	82.6	161.1	52.2		172.7	174.7	5.1	5.2	
25	CHO	141.0	133.4	135.0	148.0	161.9	52.7	183.2(CHO)	173.8	170.7	4.6	4.6	
26	$COCH_3$	139.7	133.4	131.6	148.9	162.0	52.5	190.5(CO) 26.9(CH_3)	173.1	170.2	4.5	5.1	
27	$COOCH_3$	139.0	133.0	133.0	139.0	162.0	52.5	162.0(CO) 52.5(CH_3)	173.0	173.0	4.9	4.9	
28	NO_2	138.5	131.7	128.0	155.5	161.0	53.0		176.7	178.1	3.6	4.8	

the previous reports informing the predominance of (*Z*)-conformations in alkoxycarbonyl groups.[10-12]

In general, conjugated enones take *s-trans* (**b**) conformation preferentially, while the electrostatic interaction between sulfur and carbonyl dipole repels to each other to make the *s-cis* (**a**) conformer

Table 4. The Stable Conformers and Their Abundance (%) of Methyl (3-Substituted 2-Thiophenecarboxylate)s (Series **2**)

Conformer	Abundance %	Conformer	Abundance %	Conformer	Abundance %	Conformer	Abundance %
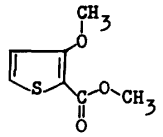	75	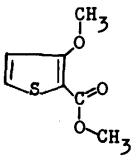	25				
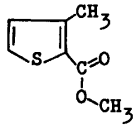	61	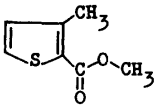	38				
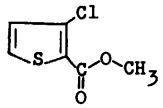	69	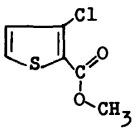	31				
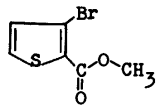	68	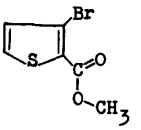	32				
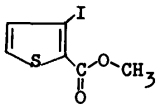	62	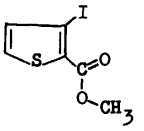	38				
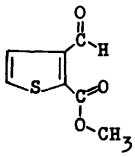	76	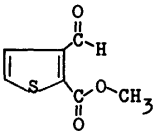	24				
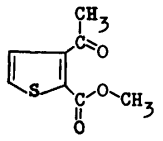	81	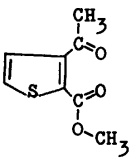	19				
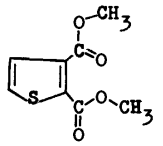	51	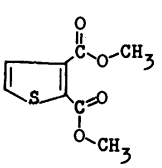	28	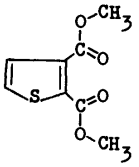	14	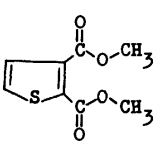	7
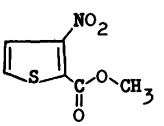	71	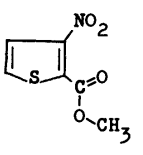	29				

predominant. Thus, the competition of effects of opposite directions controls the equilibrium between the conformers. The stable conformations calculated and their populations for methyl (substituted 2-thiophenecarboxylate)s are shown in Tables 4—6. The two possible rotamers about the methoxycarbonyl group of methyl (4- and 5-substituted 2-thiophenecarboxylate)s are estimated to be nearly

Table 5. The Stable Conformers and Their Abundance (%) of Methyl (4-Substituted 2-Thiophenecarboxylate)s (Series **2**)

Conformer	Abundance %	Conformer	Abundance %	Conformer	Abundance %	Conformer	Abundance %
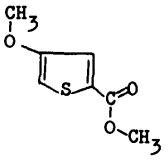	54	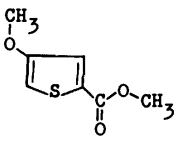	46				
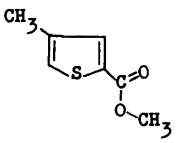	50	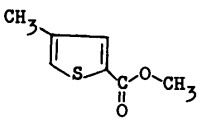	50				
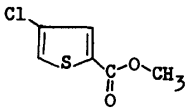	57	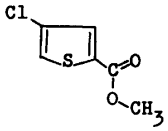	43				
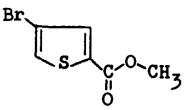	56	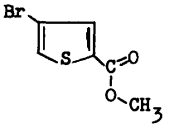	44				
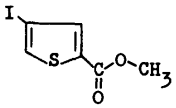	55	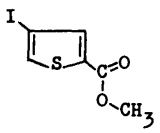	45				
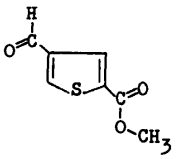	44	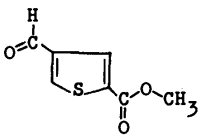	43	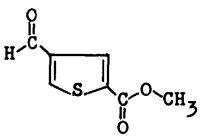	9	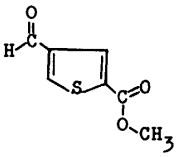	4
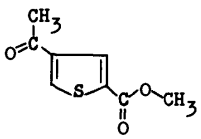	51	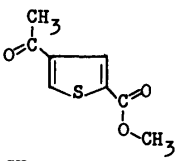	33	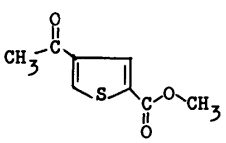	11	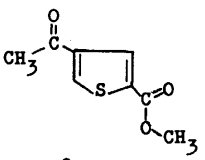	5
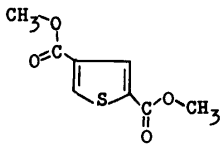	45	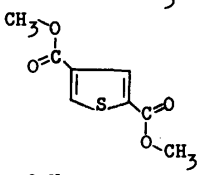	31	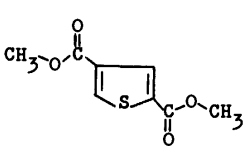	17	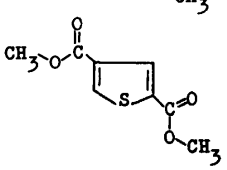	7
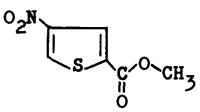	66	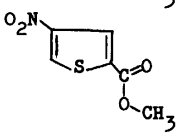	34				

equally populated, because the energy difference between *s-cis* and *s-trans* conformers calculated is small, though the *trans* conformer has a slightly lower energy than the *cis* conformer. This implies that the conformational distribution of these substituted compounds is similar to that of parent methyl 2-thiophenecarboxylate, and, in addition, the four stable conformers exist in a nearly equal population even when the substituent (X) is unsymmetrical with respect to the plane perpendicular to molecular plane

Table 6. The Stable Conformers and Their Abundance (%) of Methyl (5-Substituted 2-Thiophenecarboxylate)s (Series **3**)

Conformer	Abundance %	Conformer	Abundance %	Conformer	Abundance %	Conformer	Abundance %
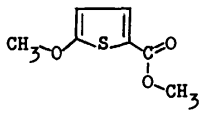	31	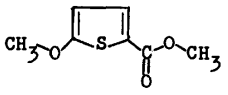	28	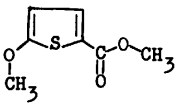	21	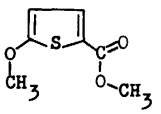	20
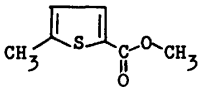	51	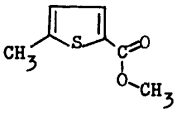	49				
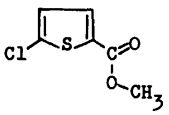	50	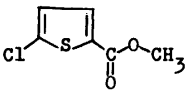	50				
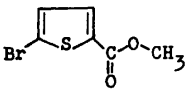	50	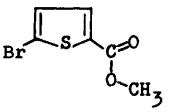	50				
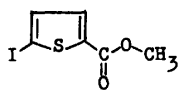	51	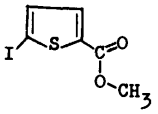	49				
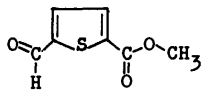	30	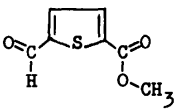	26	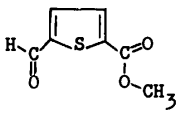	23	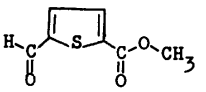	21
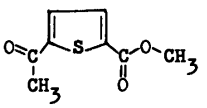	38	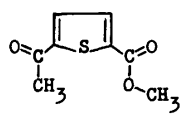	31	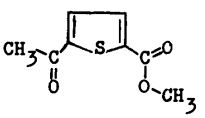	17	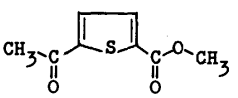	14
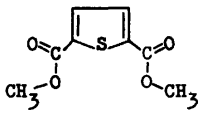	27	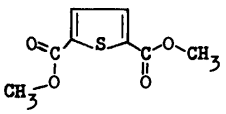	26	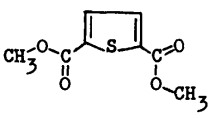	26	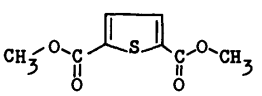	23
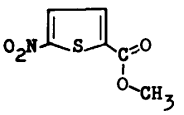	51	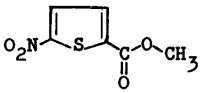	49				

(i.e. when the substituent is methyl, formyl, acetyl, and methoxycarbonyl). In methyl (4- and 5-substituted 2-thiophenecarboxylate)s, methoxycarbonyl group was confirmed to be coplanar with thiophene ring. The additivity rule for the ^{13}C chemical shift of substituted thiophenes should be applicable to explain the chemical shift of ring carbons in the compounds of series of **2** and **3**, because the effect of two dissimilar conformations balances in series **2** and **3**.

In the compounds of series **1**, the conformational equilibrium tends to shift to the most stable conformer, and the population sometimes becomes as high as 80%, generally ca. 70%. As a whole, the neighboring substituent effect seems to be governed by the electrostatic interaction between substituent and 2-methoxycarbonyl group, as revealed by calculated dipole moments of conformers (Table 7). As enone is inclined to take the electrostatically stabilized *s-trans* conformation, *s-trans* conformers of **1** predominate over other conformers. In other words, carbonyl group of 2-methoxycarbonyl tends to lie *anti* to the

Table 7. Calculated Dipole Moments and Populations of the Most and Next Stable Conformers of **1**

X	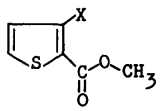		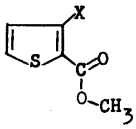	
	Dipole moment/D	Population %	Dipole moment/D	Population %
H	2.58	50	1.65	50
Cl	1.79	69	2.48	31
Br	1.81	68	2.24	32
I	1.66	62	2.25	38
NO_2	2.77	71	5.22	29
CH_3	2.62	38	1.50	62
CH_3CO (*s-cis*)	3.46	81	3.51	19
CHO (*s-trans*)	0.36	24	2.76	76*

a) This conformer is capable of forming CH···O hydrogen bond.

Table 8. Electron Density of Methyl (Substituted 2-Thiophenecarboxylate)s

No.	X	e_{S_1}	e_{C_2}	e_{C_3}	e_{C_4}	e_{C_5}	e_{CO}	e_{CH_3}	Others
					3-Substituted compounds				
1	H	0.157	−0.212	0.014	−0.111	−0.119	0.397	0.187	
2	OCH_3	0.181	−0.250	0.157	−0.160	−0.095	0.406	0.187	0.182(OCH_3)
3	CH_3	0.153	−0.198	−0.027	−0.095	−0.119	0.396	0.187	0.079(CH_3)
4	Cl	0.187	−0.196	0.047	−0.094	−0.118	0.395	0.186	
5	Br	0.185	−0.181	−0.012	−0.086	−0.111	0.354	0.186	
6	I	0.179	−0.162	−0.157	−0.079	−0.122	0.388	0.186	
7	CHO	0.164	−0.159	−0.100	−0.064	−0.127	0.392	0.186	0.305(CHO)
8	$COCH_3$	0.184	−0.131	−0.081	−0.083	−0.128	0.382	0.185	0.231(CO) 0.006(CH_3)
9	$COOCH_3$	0.179	−0.134	−0.049	−0.067	−0.134	0.381	0.185	0.370(CO) 0.186(CH_3)
10	NO_2	0.220	−0.121	−0.033	−0.059	−0.130	0.378	0.184	
					4-Substituted compounds				
11	OCH_3	0.173	−0.196	−0.017	0.036	−0.146	0.396	0.187	0.188(OCH_3)
12	CH_3	0.157	−0.212	0.030	−0.155	−0.101	0.397	0.187	0.093(CH_3)
13	Cl	0.184	−0.207	0.026	−0.065	−0.102	0.396	0.186	
14	Br	0.182	−0.210	0.032	−0.123	−0.087	0.397	0.187	
15	I	0.178	−0.210	0.041	−0.268	−0.068	0.397	0.187	
16	CHO	0.172	−0.215	0.044	−0.231	−0.038	0.397	0.187	0.324(CHO)
17	$COCH_3$	0.177	−0.215	0.038	−0.192	−0.039	0.396	0.187	0.259(CO) 0.002(CH_3)
18	$COOCH_3$	0.180	−0.220	0.050	−0.157	−0.036	0.397	0.187	0.384(CO) 0.187(CH_3)
19	NO_2	0.219	−0.212	0.051	−0.137	−0.028	0.397	0.187	
					5-Substituted compounds				
20	OCH_3	0.178	−0.242	0.051	−0.181	0.030	0.401	0.188	0.178(OCH_3)
21	CH_3	0.169	−0.211	0.012	−0.092	−0.162	0.396	0.187	0.088(CH_3)
22	Cl	0.206	−0.208	0.013	−0.080	−0.098	0.396	0.187	
23	Br	0.209	−0.206	0.009	−0.069	−0.154	0.395	0.187	
24	I	0.207	−0.200	−0.006	−0.047	−0.296	0.394	0.187	
25	CHO	0.213	−0.190	−0.009	−0.030	−0.252	0.393	0.187	0.323(CHO)
26	$COCH_3$	0.188	−0.185	−0.010	−0.018	−0.209	0.392	0.187	0.258(CO) 0.002(CH_3)
27	$COOCH_3$	0.227	−0.195	−0.013	−0.013	−0.195	0.400	0.190	
28	NO_2	0.276	−0.174	−0.020	0.018	−0.197	0.389	0.186	

electronegative group at the 3-position, avoiding close access of two negatively charged atoms. Exceptionally, in methyl 3-formyl-2-thiophenecarboxylate, the *s-cis* conformer which has higher dipole moment is predominant to the *trans* conformer. In the most stable conformer of the formyl derivative, weak intramolecular interaction like hydrogen bonding[13] will occur between formyl proton and carbonyl oxygen of methoxycarbonyl group, because the proton is acidic due to the electron-attracting ability of formyl carbonyl oxygen. The assumption is supported by remarkably large bond population (0.00338) between nonbonded formyl hydrogen and carbonyl oxygen of 2-$COOCH_3$. The bond population between two nonbonded atoms is usually less than 10^{-5}. In respect of this figure, the bond population is exceptionally large and comparable to the value for OH$\cdots\pi$ hydrogen bonded atoms.[14] On the other hand, in acetyl, methoxycarbonyl, and nitro derivatives, methoxycarbonyl group will lose the coplanarity with thiophene ring due to the steric hindrance. Since the alkoxycarbonyl conformation of 3-substituted 2-thiophenecarboxylates is remarkably altered by a neighboring substituent, the magnetic anisotropy and electric field by carbonyl group will affect differently the chemical shift of ring carbons in each compound.[15] The chemical shift of ring carbons of methyl (3-substituted 2-thiophenecarboxylate)s is not correlated linearly with that of substituted thiophenes. However, if various effects by steric and electronic interactions between the neighboring substituents on thiophene ring in the compounds of series **1** are corrected, the ^{13}C chemical shift of compounds of this series will be correlated well with those of substituted thiophenes.

The electron density values derived from MNDO calculation of methyl (substituted 2-thiophenecarboxylate)s are summarized in Table 8. Levy and coworkers have reported that the plot of ^{13}C chemical shift vs. CNDO/2 total charge density for para position of substituted benzene shows fairly good linearity.[16] However, the MNDO electron density on the C_2 of compounds of series **3** which corresponds to *para* position in substituted benzene[17,18] correlates poorly with the ^{13}C chemical shift. For all the compounds studied, plots of the electron density against ^{13}C chemical shift showed poor correlations. As the electron density in MNDO calculation is of the diamagnetic term, the ^{13}C chemical shift in methyl (substituted 2-thiophenecarboxylate)s is considered to be controlled by the paramagnetic contributions as the case of pyridine.[19]

The ^{13}C-H one bond coupling constant of the ring C-H of methyl (substituted 2-thiophenecarboxylate)s is correlated linearly with that of substituted thiophenes [$^1J_{C_4H_4}$ (**1**) r 0.991, p 0.903, s 0.465; $^1J_{C_5H_5}$ (**1**) r 0.975, p 1.04, s 0.442; $^1J_{C_3H_3}$ (**2**) r 0.996, p 0.958, s 0.364; $^1J_{C_5H_5}$ (**2**) r 0.999, p 0.973, s 0.192; $^1J_{C_3H_3}$ (**3**) r 0.990, p 0.854, s 0.301; $^1J_{C_4H_4}$ (**3**) r 0.994, p 0.899, s 0.297]. It is interesting that the relation between the ^{13}C-H one bond coupling constants of methyl (3-substituted 2-thiophenecarboxylate)s and those of 3-substituted thiophenes is linear. Although the substituent effect on the ^{13}C chemical shift of ring carbons is considerably affected by steric and electronic interactions between neighboring substituents, the substituent effect on $^1J_{C_4H_4}$ (**1**) and $^1J_{C_5H_5}$ (**1**) is linear.

Table 9. Comparison of Observed and Calculated Persent s Characters of C-H Bonds for Methyl (Substituted 2-Thiophenecarboxylate)s

No.	X	$\rho_{C_3H_3}$(%)		$\rho_{C_4H_4}$(%)		$\rho_{C_5H_5}$(%)	
		obs	calcd	obs	calcd	obs	calcd
		3-Substituted compounds					
1	H	—	—	34.1	33.5	37.2	36.0
2	OCH_3	—	—	34.1	33.4	37.4	36.0
3	CH_3	—	—	33.5	33.7	37.0	36.0
4	Cl	—	—	35.2	33.8	37.7	36.2
5	Br	—	—	35.3	33.8	37.6	36.2
6	I	—	—	35.2	33.9	37.5	36.2
7	CHO	—	—	34.8	34.0	37.6	36.2
8	$COCH_3$	—	—	34.4	33.6	37.5	36.1
9	$COOCH_3$	—	—	34.7	33.9	37.6	36.1
10	NO_2	—	—	35.9	34.1	38.4	36.4
		4-Substituted compounds					
11	OCH_3	34.4	33.5	—	—	36.8	35.9
12	CH_3	33.6	33.6	—	—	36.5	36.1
13	Cl	35.4	33.8	—	—	38.1	36.2
14	Br	35.5	33.9	—	—	38.3	36.2
15	I	35.4	33.9	—	—	38.3	36.3
16	CHO	34.8	33.7	—	—	37.3	36.3
17	$COCH_3$	34.6	33.6	—	—	37.2	36.3
18	$COOCH_3$	35.0	33.9	—	—	37.8	36.3
19	NO_2	36.2	34.1	—	—	38.8	36.2
		5-Substituted compounds					
20	OCH_3	34.1	33.8	34.0	33.6	—	—
21	CH_3	34.0	33.5	33.6	33.6	—	—
22	Cl	34.7	33.8	34.9	33.8	—	—
23	Br	34.6	33.7	35.0	33.7	—	—
24	I	34.5	33.7	34.9	33.8	—	—
25	CHO	34.8	33.7	34.1	33.9	—	—
26	$COCH_3$	34.6	33.7	34.0	33.8	—	—
27	$COOCH_3$	34.6	33.7	34.6	33.7	—	—
28	NO_2	35.3	34.0	35.6	33.9	—	—

The percent s character (ρ_{C-H}) obtained by an empirical correlation expressed by Eq. 1[20] from $^1J_{C-H}$ of methyl (substituted 2-thiophenecarboxylate)s is given in Table 9 together with the results calculated by MNDO method.

$$\rho_{C-H}=0.2\,{}^1J_{C-H} \quad (1)$$

It was shown in Tables 1 and 2 that $^1J_{C_5H_5}$ is larger than

$^1J_{C_3H_3}$ or $^1J_{C_4H_4}$, and the same tendency also appeared in the results by MNDO calculation. Plots of the percent *s* characters for all 28 compounds from $^1J_{C-H}$ and MNDO method showed a good correlation (*r* 0.940, *p* 0.718, *s* 0.386).

The authors wish to thank Mr. Hitoshi Shimazaki for his assistance in MNDO calculation. The calculation was carried out by HITACHI M-280H computers of the University of Tokyo and Institute for Molecular Science.

References

1) H. Satonaka, *Bull. Chem. Soc. Jpn.*, **56**, 2463 (1983).
2) M. J. S. Dewar and W. Thiel, *J. Am. Chem. Soc.*, **99**, 4899 (1977).
3) M. J. S. Dewar and E. Healy, *J. Comput. Chem.*, **4**, 542 (1983).
4) QCPE Program No. 464, By using this program we can perform MNDO calculations on the molecules which comprise H, B, C, N, O, F, Al, Si, P, S, Cl, Br, and I elements.
5) K. Tori and T. Nakagawa, *J. Phys. Chem.*, **11**, 3163 (1964).
6) K. Takahashi, T. Sone, and K. Fujieda, *J. Phys. Chem.*, **74**, 2765 (1970).
7) S. Gronowitz, I. Johnson, and A. B. Hornfeldt, *Chem. Scr.*, **7**, 76 (1975).
8) Although ^{13}C NMR data for substituted thiophenes in $(CD_3)_2CO$ have been reported in Ref. 6, data for $CDCl_3$ were measured to correlate with the data for methyl (substituted 2-thiophenecarboxylate)s.
9) The authors use the notation *r*, *p*, and *s* for the correlation coefficient, slope, and standard deviation, respectively.
10) P. W. Allen and L. E. Sutton, *Acta Crystallogr*, **3**, 46 (1950).
11) M. Ōki and H. Nakanishi, *Bull. Chem. Soc. Jpn.*, **43**, 2558 (1970).
12) M. Ōki and H. Nakanishi, *Bull. Chem. Soc. Jpn.*, **44**, 3197 (1971).
13) The examples of hydrogen bonding formed by C-H groups are reported in the following references. a) A. Goel, C. N. R. Rao, *Trans. Faraday Soc.*, **67**, 2828 (1971); b) P. L. Olympia Jr., *Chem. Phys. Lett.*, **5**, 593 (1970); c) M. F. Rettig and R. S. Drago, *J. Am. Chem. Soc.*, **88**, 2966 (1966).
14) Respective non-bonded OH···C bond populations in the CH···π hydrogen-bonded conformers (two species) of 1-phenyl-2-propanol were reported to be 4.79×10^{-3} and 7.44×10^{-3}. See: K. Abe, M. Hirota, and K. Morokuma, *Bull. Chem. Soc. Jpn.*, **58**, 2713 (1985).
15) For example, the differences between the observed and the calculated ^{13}C chemical shifts of methyl 3-formyl-2-thiophenecarboxylate were 6.8, 5.1, 1.8, and 4.1 ppm, on C_2, C_3, C_4, and C_5, respectively. The differences on C_3 and C_5 are explained by the change of conformation of methoxycarbonyl group, because the differences in electron density (Δe) between the two conformers of methyl 3-formyl-2-thiophenecarboxylate become in the order $C_3(0.013)>C_5(0.007)>C_2(0.002)$, $C_4(0.002)$. The 3-formyl group is fixed to take the (*E*) conformation with respect to the C_3–C_{formyl} bond in methyl 3-formyl-2-thiophenecarboxylate, while 3-thiophenecarbaldehyde exists as a mixture of the two possible conformers. Thus, the reference chemical shift value of 3-thiophenecarbaldehyde corresponds to the equilibrium mixture of the conformers, and the difference in electron density on C_2 of the two conformers (Δe=0.029) may cause large deviation. Accordingly, it is considered that the chemical shift of β-carbon to carbonyl group changes more than 5 ppm by complete change of the carbonyl conformation.
16) G. L. Nelson, G. C. Levy, and J. D. Cargioli, *J. Am. Chem. Soc.*, **94**, 3089 (1972).
17) E. Imoto, Y. Otsuji, and T. Hirai, *Nippon Kagaku Zasshi*, **77**, 804 (1956).
18) Y. Otsuji, T. Kimura, Y. Sugimoto, E. Imoto, Y. Omori, and T. Okawara, *Nippon Kagaku Zasshi*, **80**, 1021 (1959).
19) T. Tokuhiro, N. K. Wilson, and G. Fraenkel, *J. Am. Chem. Soc.*, **90**, 3622 (1968).
20) N. Muller and D. E. Pritchard, *J. Chem. Phys.*, **31**, 1471 (1959).

NAD(P)$^+$-NAD(P)H Model. 62. The Mechanism of the Silica Gel-Catalyzed Reduction with an NAD(P)H Model

Shinro YASUI,* Masayuki FUJII,† Kaoru NAKAMURA,† and Atsuyoshi OHNO†
Tezukayama College, Gakuen-Minami, Nara 631
†Institute for Chemical Research, Kyoto University, Uji, Kyoto 611
(Received July 23, 1986)

The reduction of diethyl acetylenedicarboxylate, diethyl fumarate, and diethyl maleate as well as several α,β-unsaturated carbonyl compounds by a model of NAD(P)H on silica gel was examined. The order of the reactivity for the reduction was reverse to that of the degree of adsorption of the substrates onto the surface of silica gel. Semiquantitative analysis of the results suggests the possibility that silanol groups on the surface of silica gel act as general acid catalysts in the course of the reduction.

Recently, attentions have been focused on the utility of NAD(P)H models as reducing agents in organic synthesis.[1-5] The advantage of the reduction with an NAD(P)H model relies on its mildness in reducing ability. Thus, the model has a capacity to exert a novel selectivity in the reduction of a particular functional group with the aid of a certain catalyst. We reported previously that an NAD(P)H model selectively gives rise to reductive dehalogenation of an organic halide in the presence of a rhodium complex.[1] Moreover, we found that silica gel is a selective catalyst for the 1,4-reduction of α,β-unsaturated carbonyl compounds by an NAD(P)H model, 3,5-bis(ethoxycarbonyl)-1,4-dihydro-2,6-dimethylpyridine (Hantzsch ester: HEH), in benzene.[4]

Silica gel sometimes seems more useful catalyst in organic synthesis than an organometal complex such as a rhodium complex, since one can easily handle it and can remove it from the reaction mixture by filtration after completion of the reaction. Unfortunately, we have little informations in our hands about the mechanism of catalysis by silica gel. In order to apply the silica gel-catalyzed reduction by an NAD(P)H model to other systems more widely, it may be important to reveal the details as to the role of silica gel.

We studied the mechanism of the reduction by using diethyl acetylenedicarboxylate (**1**), diethyl fumarate (**2**), and diethyl maleate (**3**) as model substrates. These substrates are expected to be adsorbed onto the surface of silica gel in a different manner due to their individual configurations. Through the product analyses for the reduction by HEH as well as the measurements of efficiency of substrate adsorption onto the surface of silica gel, we found several interesting facts. We report in this article the possibility that silanol groups on the surface of silica gel contribute to the reduction of the unsaturated carbon-carbon bonds in **1**, **2**, and **3** through general acid catalysis. We also mention briefly the results for the reduction of several α,β-unsaturated carbonyl compounds.

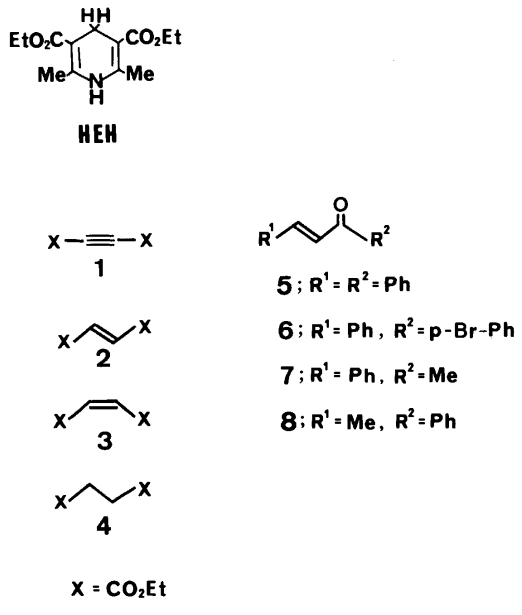

Chart

Results

NAD(P)H Model and Silica Gel. We have found that an NAD(P)H model, Hantzsch ester (HEH), has tolerance against self-decomposition in the presence of silica gel. Furthermore, in polar solvents such as acetonitrile, methanol, and chloroform, the reduction does not take place.[4] Based on these reasons, we employed HEH as an NAD(P)H model and benzene as the solvent in the present studies.

Use of silica gel with a fine mesh (e.g. 200 mesh) afforded scattered results for the yield, probably due to difficulty of complete removal of the materials from the surface of silica gel prior to the product analysis even when the catalyst was washed repeatedly with an appropriate solvent. Moreover, extremely slow rate of sedimentation of silica gel with a fine mesh after the stirring prevented accurate determination of the amount of adsorbed substrate. Then, we utilized silica gel 60 of 35—70 mesh (Nakarai Chem. CO.). The content of water in the silica gel 60 used in this study was measured to be 4.6±0.2 mmol g^{-1} on Kirl-Fisher

moisture content meter. Drying the silica gel over phosphorus pentaoxide in vacuo at 100—120 °C for 7 h removed only ca. 20% of adsorbed water, then causing no appreciable alteration in the yield of the reduction. On the other hand, adsorption of the substrate and HEH as well as the reduction was dramatically suppressed when silica gel contains ca. 12 mmol g^{-1} of water. Water content in the solvent was measured to be negligible relative to that in the silica gel.

Adsorption onto the Surface of Silica Gel. The efficiency of adsorption of diesters **1—3** and HEH as well as diethyl succinate (**4**) onto the surface of silica gel was examined initially. The amount of the substrate as well as HEH in the bulk phase (S_{Bulk}) was determined on vapor phase chromatography (VPC) for **1—4** or high performance liquid chromatography (HPLC) for HEH after stirring an appropriate amount of the substrate (or HEH) and 0.2 g of the silica gel in 1 ml of benzene at 70 °C under nitrogen atmosphere for 30 min.[6] The adsorbed amount of the substrate (or HEH) (S_{Ad}) was given by subtracting S_{Bulk} from the stoichiometric amount of the substrate (or HEH).

In order to analyze the results, we assume a simple equilibrium with respect to the adsorption of substrate (or HEH) onto the surface of silica gel, as is expressed by Eq. 1.

$$S_{Bulk} + Q_{free} \overset{K}{\rightleftharpoons} S_{Ad} \quad (1a)$$

$$Q_{free} = Q_0^{0.2} - S_{Ad} \quad (1b)$$

where S_{Bulk} and S_{Ad} are the amounts (mmol) of the substrate (or HEH) in bulk phase and adsorbed, respectively, and $Q_0^{0.2}$ is the maximum amount (mmol) of substrate being adsorbed onto the surface of 0.2 g of silica gel. Equilibrium constant K in Eq. 1 is given by Eq. 2

$$K = S_{Ad}/(S_{Bulk} \cdot Q_{free}) \quad (2)$$

Note that since these experiments were performed in 1 ml of the solvent, each term with dimension of mmol is equivalent to molarity, and, as a consequent, K has a dimension of M^{-1} (=dm^3/mol). We can readily lead Eq. 2 to Eq. 3.

$$\frac{1}{S_{Ad}} = \frac{1}{K \cdot Q_0^{0.2}} \cdot \frac{1}{S_{Bulk}} + \frac{1}{Q_0^{0.2}} \quad (3)$$

Equation 3 predicts that the plot of $1/S_{Ad}$ vs. $1/S_{Bulk}$ with the amount of the substrate being variable will give a straight line, and each line for different substrates will have a common intercept because the value of $Q_0^{0.2}$ could be reasonably considered to be identical for all substrates. This is indeed the case, and the correlations for diesters **1—4** and HEH are exemplified in Fig. 1. The intercepts for five straight lines are identical within experimental error, affording $Q_0^{0.2}=(7.37\pm0.28)\times10^{-2}$ mmol. Importantly, this value is compatible with the amounts of several types of modifying agents loaded onto the surface of silica gel.[7] Thus, the value elucidated presently designates an "effective" amount of silanol groups on the surface. Dividing the intercept by the slope, we obtain equilibrium constants K for **1—4** and HEH. The values are summarized in Table 1.

Although the plots are scattered a little (correlation coefficient r=0.98—0.998), reinforcement for the validity of this treatment is given by similar examinations for chalcone (**5**), 4′-bromochalcone (**6**), benzylideneacetone (**7**), and crotonophenone (**8**). The relationships between $1/S_{Ad}$ and $1/S_{Bulk}$ for these substrates showed excellent linearity (r>0.9999 except for r=0.9997 for **7**) and from the intercepts of the lines (Fig. 2) the value of $Q_0^{0.2}$ was determined to be $(7.18\pm0.16)\times10^{-2}$ mmol,[8] which is consistent with that obtained from the set shown in Fig. 1. The K values for **5—8** are also summarized in Table 1. The results support our assumption that the ad-

Table 1. Equilibrium Constants K for Adsorption of Diesters, α,β-Unsaturated Carbonyl Compounds, and HEH onto the Surface of Silica Gel[a]

Substrate	K/M^{-1}	Substrate	K/M^{-1}
1	6.49	**5**	6.81
2	8.58	**6**	5.49
3	33.3	**7**	21.3
4	43.1	**8**	10.9
		HEH	51.1

a) At 70 °C.

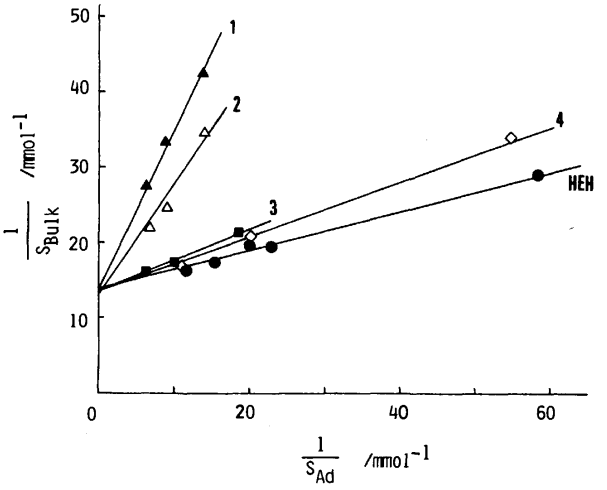

Fig. 1. $1/S_{Ad}$ vs. $1/S_{Bulk}$ plots for diesters and HEH with 0.2 g of the silica gel in 1 ml of benzene.

sorbed and free substrates (and HEH) are in equilibrium in the mixtures.

Silica Gel-Catalyzed Reduction by HEH. The reduction of diesters **1—3** were carried out in the presence of the silica gel in 1 ml of benzene at 70 °C under nitrogen atmosphere in the dark for 18 h. After removal of the silica gel by filtration followed by concentration of the filtrate, the residue was analyzed on VPC, GC/MS, and HPLC (see Experimental Section). It was confirmed that the unsaturated carbon-carbon bonds of the substrates are reduced, ester groups remaining intact. The yields of the reduction product(s) and the recovered starting material are listed in Table 2. Although the yields of the reduction product(s) for each run are not so high, the data listed in Table 2 are suggestive of the role of the silica gel when the K values listed in Table 1 are taken into consideration as well (vide infra).

The reduction of α,β-unsaturated carbonyl compounds **5—8** were also carried out under the same conditions mentioned above. Although these substrates were quantitatively reduced into the corresponding saturated carbonyl compounds, their relative reactivities can be roughly compared on the basis of the yield of reduction product after the reaction period of 4 h (Table 3).

We examined the catalytic abilities of heterogeneous acid catalysts, Amberlyst 15 and Nafion 511, toward the reduction of **3** by HEH. Whereas 27 and 33% of 1.0×10^{-1} mmol of **3** was adsorbed on Amberlyst 15 and Nafion 511, respectively, in 1 ml of benzene at 70 °C, no reduction product was found from these systems. This is mainly due to rapid decomposition of HEH under the catalysis of the strong acids.

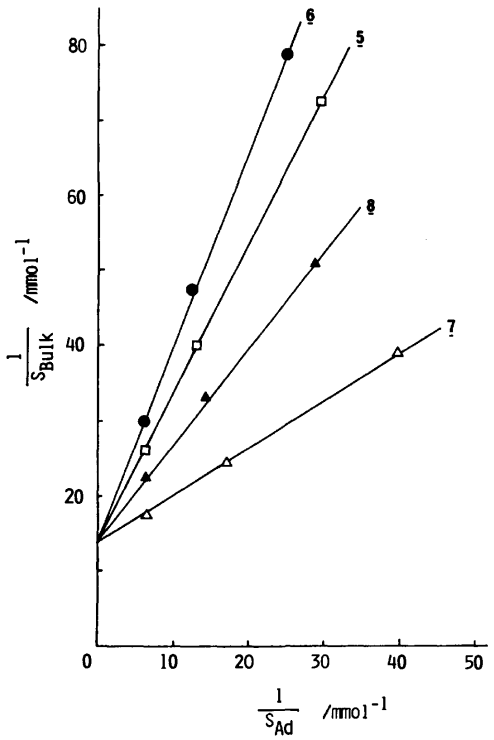

Fig. 2. $1/S_{Ad}$ vs. $1/S_{Bulk}$ plots for α,β-unsaturated carbonyl compounds with 0.2 g of the silica gel in 1 ml of benzene.

Table 2. Reduction of Diesters by HEH in the Presence of the Silica Gel[a]

Substrate	S.G.[c]/g	Yield/%[b]			
		1	**2**	**3**	**4**
1	0.01	49[d]	21	6	N.D.[e]
	0.05	12[d]	38	11	Trace
	0.1	Trace[d]	43	13	4
	0.2	N.D.[d,e]	42	11	8
2	0.01	—	95[d]	—	N.D.[e]
	0.05	—	74[d]	—	15
	0.2	—	53[d]	—	43
3	0.01	—	—	100[d]	N.D.[e]
	0.05	—	—	86[d]	12
	0.2	—	—	57[d]	31

a) 1.0×10^{-1} mmol of a substrate and 1.5×10^{-1} mmol of HEH were used. The reaction was carried out in 1 ml of benzene at 70 °C in the dark under N_2 atmosphere for 18 h. b) The yield determined by VPC analysis based on the amount of the substrate used. c) The amount of silica gel 60. d) The yield of the recovered starting materials. e Not detected.

Table 3. Reduction of α,β-Unsaturated Carbonyl Compounds by HEH in the Presence of the Silica Gel[a]

Substrate	Reaction time/h	Yield/%[b]	
		Recov.[c]	Redn.[d]
5	4	36	60
	18	N.D.[e]	95[f]
6	4	19	76
	18	N.D.[e]	88[f]
7	4	72	28
	18	<2	98
8	4	4	96

a) 1.0×10^{-1} mmol of a substrate, 1.5×10^{-1} mmol of HEH, and 0.2 g of silica gel 60 were used unless otherwise mentioned. The reaction was carried out in 1 ml of benzene at 70 °C in the dark under N_2 atmosphere. b) The yield determined by VPC analysis based on the amount of the substrate used. c) The yield of the recovered starting material. d) The yield of the reduction product, corresponding saturated carbonyl compound. e) Not detected. f) Isolated yield from the reaction of 5.0×10^{-1} mmol of a substrate with 7.5×10^{-1} mmol of HEH in the presence of 1.0 g of silica gel 60 in 5 ml of benzene.

Discussion

The order of K values for diesters is **1**<**2**≪**3**<**4** as shown in Table 1. The examination of CPK models reveals that four oxygen atoms of the two ester groups in **3** and **4** can approach closely, that is, **3**, and **4** are able to have both hydrophilic and hydrophobic faces within one molecule. On the other hand, **1** and **2** cannot assume such a conformation. Therefore, it is reasonably expected that the former substrates are adsorbed onto the surface of silica gel through hydrophilic interaction between the oxygens of the substrate and silanol group(s) on the surface of silica gel. HEH exhibits large K value, to which poor solubility of HEH in benzene may also contribute. The degree of adsorption of α,β-unsaturated carbonyl compounds **5**—**8** seems to depend on the electronegativity of the carbonyl oxygen rather than on the steric factor.

Table 2 shows that the order of reactivity of diesters in the reduction by HEH is **1**>**2**>**3**; the reverse order of the equilibrium constant. The *trans*-alkene **2** is reported to have less negative reduction potential than the *cis*-alkene **3**.[9] Moreover, it is well documented that a carbon-carbon triple bond is more susceptible to a nucleophile than a double bond.[10] Reduction potential and electrophilicity are, of course, predominant factors in determining the reactivity of these reductions. Nevertheless, taking such limited factors alone into consideration, one obtains much less useful informations about the role of the silica gel. Here, it is worthwhile to emphasize that the larger the K value, the lower the reactivity toward the reduction. The reductions of α,β-unsaturated carbonyl compounds **5**—**8** gives similar results. Again, the tendency can be seen that the substrate with a larger K value is less reactive except for **8**. The compound **8** may belong to the category other than that for **5**—**7** because of difference in the structure, i.e., substitution of a methyl group in place of the β-phenyl group.

Now, we can simulate the amounts of the substrate and HEH on the surface of silica gel under the reaction conditions at the incipient stage of the reaction (S_{Ad}). Thus, S_{Ad}'s for two coexisting components are given by resolving Eqs. 4—6, which are derived from Eq. 2, simultaneously.

$$K_A = (S_{Ad})_A/((S_0)_A - (S_{Bulk})_A)Q_{free} \quad (4)$$

$$K_B = (S_{Ad})_B/((S_0)_B - (S_{Bulk})_B)Q_{free} \quad (5)$$

$$Q_{free} = Q_0^{0.2} - (S_{Ad})_A - (S_{Ad})_B, \quad (6)$$

where subscripts A and B denote the parameters referred to components A and B, respectively, and S_0 is the stoichiometric amount of the substrate. Computation without any approximation afforded the S_{Ad} values as listed in Table 4 for each reduction. The validity of this treatment was supported by the excellent agreement between computed and observed S_{Ad} values for the solution containing **5** and **6**, where both values can be directly compared with each other because no reaction takes place in this mixture. The data are also listed in Table 4. Significantly, S_{Ad} values for the substrates to be reduced are not so large; in particular for the reduction of **1** with a small amount of the silica gel, S_{Ad} values for the substrate are nearly two orders less than the total amounts of the products generated. Note that the reduction product(s) is (are) adsorbed onto the surface of silica gel to the extent similar to or larger than that for the starting material as can be seen in Table 1.

Table 4. Calculated S_{Ad} Values[a]

Component ($S_0/\times 10^{-1}$ mmol)[b]		S.G.[c]/g	S_{Ad}(calcd)/$\times 10^{-2}$ mmol	
A	B		$(S_{Ad})_A$	$(S_{Ad})_B$
1(1.00)	HEH (1.50)	0.01	0.0514	0.587
		0.05	0.134	1.45
		0.10	0.289	2.84
		0.20	0.668	5.41
2(1.00)	HEH (1.50)	0.01	0.0663	0.574
		0.05	0.172	1.42
		0.10	0.368	2.78
		0.20	0.836	5.28
3(1.00)	HEH (1.50)	0.01	0.200	0.456
		0.05	0.505	1.13
		0.10	1.02	2.23
		0.20	2.08	4.31
5(1.00)	HEH (1.50)	0.20	0.695	5.39
6(1.00)	HEH (1.50)	0.20	0.581	5.47
7(1.00)	HEH (1.50)	0.20	1.60	4.69
8(1.00)	HEH (1.50)	0.20	1.00	5.15
5(0.504)	**6**(0.508)	0.20	1.25(1.28)[d]	1.07(1.08)[d]
5(1.47)	**6**(0.988)	0.20	2.59(2.73)[d]	1.45(1.48)[d]

a) Based on $Q_0^{0.2} = 7.18\times 10^{-2}$ mmol and the K values listed in Table 1. See text for details. b) The values in parentheses indicate the stoichiometric amount (S_0) of each component. c) The amount of the silica gel. d) The values in parentheses are observed ones.

One possible explanation for the role of silica gel is that it acts as a carrier of a substrate to its surface on which materials are concentrated to facilitate the reaction.[11] Such an effect would be essential in some heterogeneous catalyst-mediated reactions. In fact, the adsorbents other than silica gel, Celite 545 and cellulose, gave rise to no adsorption of **1**—**3** as well as HEH and then no reduction was observed in these systems. Yet, this effect does not appear to explain entirely the role of the silica gel at least in the present study. A perspective of S_{Ad} values in Table 4 suggests, instead, that the species in bulk phase is responsible for the reaction. There are several examples where an organic reagent adsorbed on heterogeneous catalyst

interacts with another organic reagent in bulk phase to afford a product.[12] Although the possibility cannot be excluded that HEH reduces the substrate only when both reagents are adsorbed in the vicinity of the surface of silica gel at the same time during the time course of dynamic equilibrium between the surface and bulk phase, it is safely speculated that the reaction takes place between HEH on the surface of silica gel and the substrate in bulk phase.[13]

This concept is partly supported by the results from the experiments using acetonitrile as a solvent. In acetonitrile, neither the reduction of **3** by HEH nor adsorption of HEH onto the surface of silica gel was observed, while **3** was adsorbed onto the surface with the equilibrium constant of $4\pm1\ M^{-1}$.[14] This indicates the requirement of adsorption of HEH onto the surface of silica gel for the reaction, adsorption of the substrate being dispensable. Less adsorption in acetonitrile than that in benzene is attributable to higher solubility of the components in acetonitrile and/or stronger adsorption of the solvent molecule onto the surface. Interestingly, no reduction of **3** by HEH occur in the presence of active alumina (acidic and basic) in place of silica gel even though the adsorption of **3** onto the aluminas were 18—26% under the conditions where 1.0×10^{-1} mmol of **3** and 0.2 g of alumina were stirred in 1 ml of benzene at 70 °C for 30 min.

It is not probable that the trace amount of alumina in the silica gel plays an important role in the reactions, because no appreciable alteration in the reactivity of the reduction as well as the equilibrium constant K for the adsorption is recognized in the experiments using highly pure silica gel [special silica gel #923 (100—200 mesh) (Fuji Davison Chem. Co.); the content of alumina is 0.04%] in place of the silica gel 60 used in this study: the yield of the product in the reduction of **5** after the reaction period of 4 h is 55%; the K value for **5** is $8.2\ M^{-1}$; and the value of $Q_0^{0.2}$ for the silica gel #923 is 8.5×10^{-2} mmol. These results are comparable to those obtained by using the silica gel 60.

Consider that in the present system the silica gel not only adsorbs reactants on the surface but also plays certainly a more crucial role for the reduction. Consequently, we propose the possibility that the silica gel facilitates the reduction with HEH through general acid catalysis of silanol group(s) on the surface.[11b] The possibility would persist provided that some quantity of silanol groups on the surface remains free.[15] It was also shown in this study that unnecessarily strong acid catalyst is unfavorable for the reduction due to the sensitivity of an NAD(P)H model toward the acid-catalyzed decomposition. Although the evidence obtained presently is not direct for supporting general acid catalysis by silica gel, the concept might be a useful working hypothesis for the study on the role of silica gel.

Experimental

Apparatus. VPC, HPLC, and GC/MS analyses were performed on a Yanaco G-180 gas chromatograph, a Toyo Soda CCPD high-performance liquid chromatograph equipped with a UV-8000 UV-visible detector, and a Hewlett-Packard 5992B GC/MS spectrometer, respectively. ^{1}H NMR and IR spectra were recorded on a JASCO JNM-FX 100FT NMR spectrometer and a Hitachi 260-10 infrared spectrophotometer, respectively. Water content in the solvent and the silica gel was measured on a Kyoto Electronics MFG Karl-Fisher moisture content meter Model MK-AS. Computer-assisted simulations were run on an NEC PC-9801 personal computer VM2 with a N_{88} BASIC program.

Materials. 3,5-Bis(ethoxycarbonyl)-1,4-dihydro-2,6-dimethylpyridine (HEH) was synthesized according to the procedure described in the literature.[16] Diesters **1**—**4** as well as α,β-unsaturated carbonyl compounds **5**, **7**, and **8** were commercially available. 4′-Bromochalcone (**6**) was obtained by condensation of benzaldehyde with 4-bromoacetophenone followed by recrystallization from ethanol (mp 101—104 °C). Spectral data of these compounds were satisfactory. Heterogeneous catalysts, silica gel 60 (35—70 mesh) (Nakarai Chem. Co.), active aluminium oxide (acidic and basic) (Merck & Co. Inc.), Amberlyst 15 (Organo), and Nafion 511 (Toyo Soda),[17] were purchased and, if required, activated with ordinary method prior to the use. Benzene was distilled and deaerated with an inert gas, then the content of water was measured.

Measurement of Adsorption onto the Surface of Silica Gel. In 1 ml of benzene were vigorously stirred an appropriate amount of a substrate and 0.2 g of silica gel 60 (35—70 mesh) at 70 °C under nitrogen atmosphere for 30 min. A 25-μl aliquot from the supernatant was added to 100 μl of benzene containing an internal standard for VPC or HPLC analysis, then the solution was analyzed on VPC (for **1**—**8**; OV-330 column) or HPLC (for HEH; TSKgel ODS-80T$_M$ column, methanol:water=7:3 (v/v) as eluent).

Product Analysis. In the presence of an appropriate amount of silica gel 60, 1.0×10^{-1} mmol of a substrate was allowed to react with 1.5×10^{-1} mmol of HEH at 70 °C in the dark under nitrogen atmosphere with vigorous stirring. After 18 h, the silica gel was filtered off through a glass filter, and washed repeatedly with several portions of 10 ml of benzene. Careful concentration of the filtrate below 40 °C in vacuo to dryness and subsequent addition of 1 ml of methanol to the residue afforded a transparent solution, which was analyzed on VPC, HPLC, and GC/MS. For the isolation of the product, the reaction was performed on the scale five times larger than that mentioned above. Then, the reduction product was isolated on column chromatography (silica gel No. III (200 mesh) (Nakarai Chem. Co.); benzene as eluent), and its ^{1}H NMR and IR spectra were recorded.

References

1) a) S. Yasui, K. Nakamura, and A. Ohno, *Chem. Lett.*, **1984**, 377; b) S. Yasui, K. Nakamura, M. Fujii, and A. Ohno, *J. Org. Chem.*, **50**, 3283 (1985).

2) K. Nakamura, A. Ohno, and S. Oka, *Tetrahedron Lett.*, **24**, 335 (1985).

3) K. Nakamura, M. Fujii, A. Ohno, and S. Oka, *Chem. Lett.*, **1984**, 925.

4) K. Nakamura, M. Fujii, A. Ohno, and S. Oka, *Tetrahedron Lett.*, **25**, 3983 (1984).

5) S. H. Mashraqui and R. M. Kellogg, *J. Am. Chem. Soc.*, **105**, 7792 (1983).

6) Equilibrium appears to be very rapidly established relative to the time scale in the experiments. Incubation for 30 min was required for thermostaticity of the mixture.

7) a) D. M. Sindorf and G. E. Maciel, *J. Am. Chem. Soc.*, **105**, 1848 (1983); b) E. C. Kelusky and C. A. Fyfe, *ibid.*, **108**, 1746 (1986); c) J. F. W. Keana, M. Shimizu, and K. K. Jernstedt, *J. Org. Chem.*, **51**, 1641 (1986); d) T. Iwachido, H. Naito, F. Samukawa, K. Ishimaru, and K. Tôei, *Bull. Chem. Soc. Jpn.*, **59**, 1475 (1986); e) S. Shiraishi, M. Komiyama, and H. Hirai, *ibid.*, **59**, 507 (1986).

8) In the later discussion we utilized this value for $Q_0^{0.2}$ because the value is more reliabile than the former one which was obtained from the experiments with diesters **1**—**4** and HEH.

9) C. Pac, M. Ihama, M. Yasuda, Y. Miyauchi, and H. Sakurai, *J. Am. Chem. Soc.*, **103**, 6495 (1981).

10) Y. Amiel, "The Chemistry of Functional Groups, Supplement C: The Chemistry of Triple-bonded Functional Groups," ed by S. Patai and Z. Rappoport, John Wiley & Sons, New York (1983).

11) a) S. Tamagaki, K. Suzuki, and W. Tagaki, *Chem. Lett.*, **1982**, 1237; b) K. Takahashi, T. Nishizuka, and H. Iida, *Tetrahedron Lett.*, **22**, 2389 (1981).

12) a) T. Chihara, E. Waniguchi, T. Wakabayashi, and K. Taya, *Chem. Lett.*, **1983**, 1647; b) T. Chihara, E. Waniguchi, T. Wakabayashi, and K. Taya, *Bull. Chem. Soc. Jpn.*, **57**, 2479 (1984); b) H. Ogawa, T. Chihara, and K. Taya, *J. Am. Chem. Soc.*, **107**, 1365 (1985).

13) The mechanism may be discussed in terms of Langmuir–Hinshelwood or Rideal mechanisms. Thus, our proposed mechanism could be related to the latter. However, it should be noted that the adsorptions in our system are not chemical but physical ones.

14) It was confirmed that small amount of water in acetonitrile used does not affect both the reduction of **3** by HEH and adsorption of **3** and HEH onto the surface of silica gel.

15) Table 4 shows, for example, that the amount of "free" silanol group on the surface of silica gel is 1.10×10^{-2} mmol in the reaction of 1.0×10^{-1} mmol of **1** with 1.5×10^{-1} mmol of HEH on 0.2 g of the silica gel at the incipient stage.

16) A. Singer and S. M. McElvain, *Org. Synth.* Coll. Vol. **2**, 214 (1966).

17) Nafion 511 was a gift from Toyo Soda Manufacturing Co.

 © 1987 The Chemical Society of Japan Bull. Chem. Soc. Jpn., 60, 969—975 (1987)

Synthesis and Properties of Cyclohepta[*hi*]pyrrolo-[2,1,5-*cd*]indolizines[1)]

Michihiko NOGUCHI,* Ryoichi TAMAI, Noriyuki TANIGAWA, Hiroyuki OKUMURA, and Shoji KAJIGAESHI

Department of Industrial Chemistry, Faculty of Engineering, Yamaguchi University, Tokiwadai, Ube 755

(Received July 23, 1986)

The oxidation of the methylene moiety of 4,5,6,7-tetrahydrocyclohepta[*hi*]pyrrolo[2,1,5-*cd*]indolizines with NBS gave 5-bromo-6,7-dihydro- (**4**) and 5-bromo-cyclohepta[*hi*]pyrrolo[2,1,5-*cd*]indolizines. The dehydrobromination of **4** with DBU afforded cyclohepta[*hi*]pyrrolo[2,1,5-*cd*]indolizines in good yields. The characteristic electronic features of these cycloheptapyrroloindolizines are discussed on the basis of the MO calculations and the spectroscopic properties.

Many investigations on cyclazine systems have been reported from synthetic and physicochemical as well as biological viewpoints.[2)] Among them, the cyclazine systems peri-fused by another ring system have attracted our attention regarding the following three points: i) the development of synthetic strategies, ii) the interest for novel chemical and physical properties, and, especially, iii) the investigation on the perturbation of parent nuclei stemmed from the condensation of another ring system.

Recently, we reported that 4*H*-benzo[*hi*]pyrrolo-[2,1,5-*cd*]indolizin-4-ones were synthesized by the regioselective oxidation of 5,6-dihydro-4*H*-benzo[*hi*]-pyrrolo[2,1,5-*cd*]indolizines with 2,3-dichloro-5,6-dicyano-*p*-benzoquinone (DDQ) and that their spectral data implied the exsistence of a peripheral 12 π electronic system in an acidic medium.[3)] As a continuation of our studies, we investigated the synthesis of cyclohepta[*hi*]pyrrolo[2,1,5-*cd*]indolizine, a novel ring system,[4)] which was expected to have a highly polarized structure as predicted from MO calculations.

We wish to report here the synthesis of some cyclohepta[*hi*]pyrrolo[2,1,5-*cd*]indolizine derivatives by the oxidation of the methylene moiety of 4,5,6,7-tetrahydrocyclohepta[*hi*]pyrrolo[2,1,5-*cd*]indolizines with DDQ or *N*-bromosuccinimide (NBS). The interesting electronic features of the cyclohepta-pyrroloindolizines are also discussed.

Results and Discussion

Synthesis of Cyclohepta[*hi*]pyrrolo[2,1,5-*cd*]indolizines. The dehydrogenation of 4,5,6,7-tetrahydro-1,2-bis(methoxycarbonyl)-3-phenylcyclohepta[*hi*]pyrrolo-[2,1,5-*cd*]indolizine (**1a**) with an equimolar DDQ in dry benzene at 5—10 °C gave the 6,7-dihydro derivative **2**[5)] in 31% yield. However, the sequent dehydrogenation of **2** to the expected 1,2-bis(methoxycarbonyl)-3-phenylcyclohepta[*hi*]pyrrolo[2,1,5-*cd*]indolizine (**3a**) with DDQ or palladium-charcoal under various conditions afforded only unsatisfactory results (see experimental section).

In any event, these findings implied an oxidation of the methylene moiety of **1a** with an appropriate oxidizing agent to provide the full conjugated cyclohepta[*hi*]pyrrolo[2,1,5-*cd*]indolizine system; therefore, we examined the oxidation of **1a** with NBS.

When a solution of **1a** and NBS (2.2 equimolar) in dry carbon tetrachloride was refluxed under irradiation with a tungsten lamp for 6 h, two kinds of colored products, **4a** and **5a**, were obtained in 56 and 33% yields, respectively. The similar oxidation of the pentadeuteriophenyl derivative (**1a**-d_5) with NBS gave

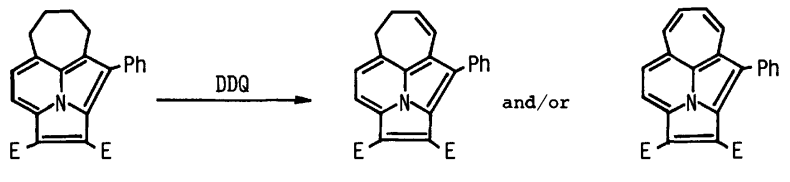

1a **2** **3a**

E: CO_2Me

2 —(Pd/C or DDQ)→ **3a** (poor yield)

Scheme 1.

corresponding pentadeuteriophenyl-type products, **4a**-d_5 and **5a**-d_5. The heating of **4a** with an equimolar NBS in carbon tetrachloride afforded **5a** in 64% yield. This means that **4a** is an intermediary product leading to **5a**.

The yellow crystalline **4a** was assigned to 5-bromo-6,7-dihydro- and the reddish crystalline **5a** to 5-bromo-3-phenylcyclohepta[*hi*]pyrrolo[2,1,5-*cd*]indolizine from the analytical and spectral data in comparison with those of **2** and **3a**.

Especially, the regiochemistry of the bromo substituent of **4a** or **5a** was confirmed by measurements of nuclear Overhauser effect (NOE) of **5a**-d_5. As shown in Fig. 1, the irradiation at δ 7.38 (8-H) resulted in an 11% enhancement in the signals at δ 6.65 (superimposed signals due to 6- and 7-H). On the other hand, the irradiation at δ 8.10 (9-H) resulted in a 4% decrease in the signals due to 6- and 7-H.

Similarly, the reaction of 4,5,6,7-tetrahydrocyclohepta[*hi*]pyrrolo[2,1,5-*cd*]indolizines **1b—d** with NBS gave the corresponding 5-bromo-6,7-dihydro-**4b—d** and 5-bromo-cyclohepta[*hi*]pyrrolo[2,1,5-*cd*]-indolizines **5b—d** in good total yields (Scheme 2). These results as well as electronic spectral data of **4** and **5** are summarized in Tables 1 and 4, respectively.

A reaction of **4a** with an excess of 1,8-diazabicyclo-[5.4.0]undec-7-ene (DBU) in toluene under reflux gave **3a** in 64% yield. The 3-arylcyclohepta[*hi*]pyrrolo-[2,1,5-*cd*]indolizines **3a**-d_5-**3d** were also obtained by a similar dehydrobromination of the 5-bromo-6,7-dihydro derivatives **4a**-d_3-**4d**. These results as well as the electronic spectral data of **3** are summarized in Tables 2 and 4, respectively.

Our attention was then focused on the preparation of 1,2-unsubstituted cyclohepta[*hi*]pyrrolo[2,1,5-*cd*]-indolizines. The saponification of **3a** with 5% methanolic potassium hydroxide followed by acidification afforded the diacid. This was decarboxylated in refluxing quinoline in the presence of copper dust to give the expected 3-phenylcyclohepta[*hi*]pyrrolo-[2,1,5-*cd*]indolizine (**6a**) in 84% yield from **3a**. 3-Pentadeuteriophenyl (**6a**-d_5) and 3-(*p*-bromophenyl)-cyclohepta[*hi*]pyrrolo[2,1,5-*cd*]indolizine (**6d**) as well as 4,5,6,7-tetrahydro-3-phenylcyclohepta[*hi*]pyrrolo[2,1,5-*cd*]indolizine (**7a**) and its pentadeuteriophenyl derivative **7a**-d_5 were obtained by similar saponification and successive decarboxylation (Scheme 3). However, a similar treatment of **5a** afforded an unseparable mixture of the desired 5-bromo-3-phenylcycloheptapyrrolo-indolizine and **6a**, in which a reductive debromination by copper would occur.

As mentioned above, the full conjugated cyclo-

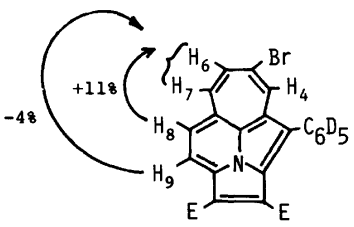

5a-d_5 E: CO_2Me

Fig. 1. NOE Results for **5a**-d_5.
%: Change of signal area.

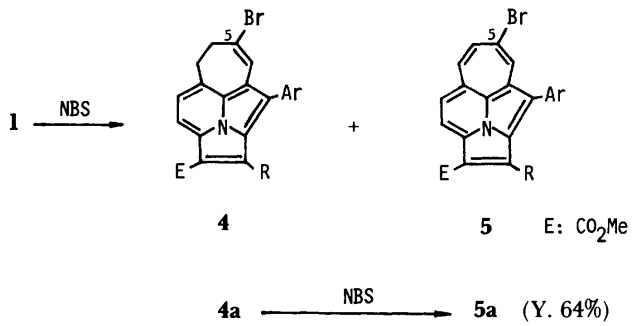

Scheme 2.

Table 1. Reaction of Tetrahydrocycloheptapyrrolo-indolizines **1** with NBS

Substrate	Ar	R[a]	Yield/%	
			4	**5**
1a	C_6H_5	E	56	33
1a-d_5	C_6H_5	E	55	41
1b	C_6H_5	H	72	28
1c		E	68	25
1d		E	55	38

a) E: CO_2Me.

Table 2. Dehydrobromination of **4** Leading to the Cycloheptapyrroloindolizines **3**

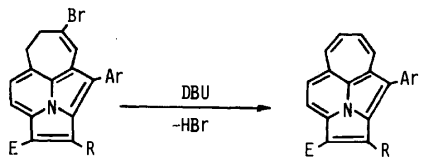

4 **3**

Compd	Ar	R[a]	Yield/%
3a	C_6H_5	E	64
3a-d_5	C_6H_5	E	58
3b	C_6H_5	H	62
3c		E	75
3d	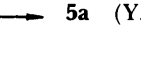	E	60

a) E: CO_2Me.

hepta[*hi*]pyrrolo[2,1,5-*cd*]indolizines **3** and **5** were obtained by the oxidation of the 4,5,6,7-tetrahydro derivative **1** or the dehydrobromination of 5-bromo-6,7-dihydro derivatives **4**. Thus, this oxidation reaction of the methylene moiety turned out to be available for the synthesis of the full conjugated fused [3.2.2]cyclazine systems.

Properties of Cyclohepta[*hi*]pyrrolo[2,1,5-*cd*]indolizines. The Hückel molecular orbital calculations for cyclohepta[*hi*]pyrrolo[2,1,5-*cd*]indolizine (**B**) were carried out using the reported parameters[6] for pyrrolo[2,1,5-*cd*]indolizine (**A**). These results[7] show that the introduction of the cyclohepta moiety into **A** causes a large change in the electronic features of the parent cyclazine nuclei, as follows: The difference of the π-electron densities at the 8- and 9-positions of **B** becomes remarkably large in comparison with that[6] at the 6- and 7-positions of **A**. The π-electron densities at the 1- and 2-positions of **A** are considerably different from one another, while those of **B** are reversed and averaged. As a whole, in cycloheptapyrroloindolizine **B** the seven-membered ring is slightly positively charged and the negative charge is delocalized over the cyclazine system. Therefore, the contribution of the polarized structure, **C** or **D**, to the ground state of **B** is conceivable (Scheme 4).

The electronic spectra of the 6,7-dihydro derivatives of cyclohepta[*hi*]pyrrolo[2,1,5-*cd*]indolizine, **2** and **4**, shift wholly toward longer wavelengths (10—30 nm) compared with that of the tetrahydro derivative **1a** owing to the extention of π-electron system (Table 4). On the other hand, the electronic spectra of 4,5,6,7-tetrahydro-3-phenyl- (**7a**) and 3-phenylcyclohepta-[*hi*]pyrrolo[2,1,5-*cd*]indolizine (**6a**) in chloroform are shown in Fig. 2. Therein, the spectrum of **6a** exhibits fine structures over the range of 490—620 nm; these would be attributed to the proposed dipolar structure.

The ^{1}H NMR spectra of the cycloheptapyrroloindolizines and their dihydro and tetrahydro derivatives were highly dependent on the concentrations of the measuring probes, i.e., the signals of protons of **6a** were observed at higher field as the concentration of the sample is increased. Thus, considerations on the chemical shifts of ring protons are made using a 0.12 M† solution in deuteriochloroform[8] of the corresponding samples. The chemical shifts and coupling constants of the pentadeuteriophenyl derivatives, **6a**-d_5 and **7a**-d_5, are listed in Table 3.

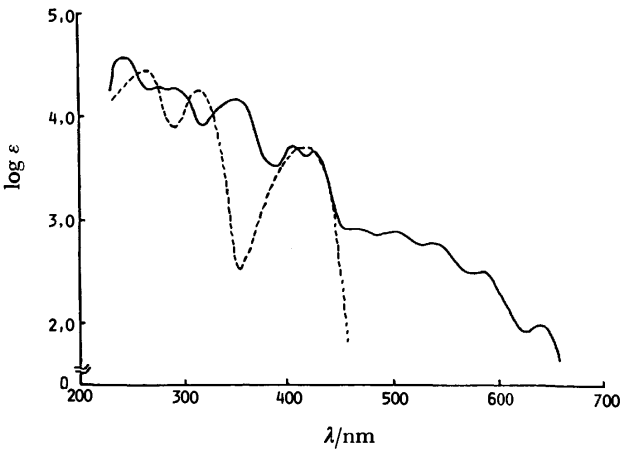

Fig. 2. Electronic spectra of **6a** (——) and **7a** (----) in chloroform.

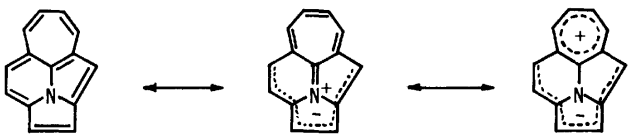

B **C** **D**

Scheme 4.

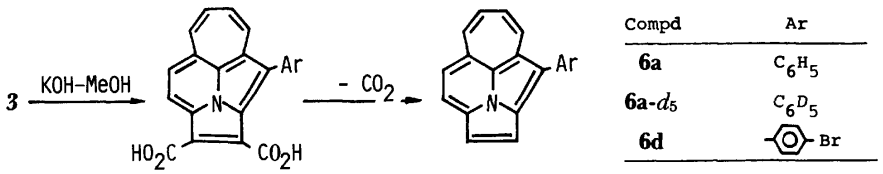

Compd	Ar
6a	C_6H_5
6a-d_5	C_6D_5
6d	

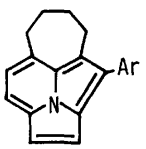

Compd	Ar
7a	C_6H_5
7a-d_5	C_6D_5

Scheme 3.

† 1 M=1 mol dm^{-3}.

The seven-membered ring protons of **6a**-d_5 were observed at a higher field than those of 2-phenylcyclohepta[*hi*]imidazolo[2,3,4-*cd*]indolizine,[9] a 2-aza analog of **6**, and comparable to those of acepleiadiene,[10] tropone,[11] or cycloheptatrienylideneamines.[12] On the other hand, taking the deshielding effect due to the newly-formed polyene system into consideration it is noteworthy that the proton at the 8-position of **6a**-d_5 could be observed at a higher field ($\Delta\delta$=0.26) than that of **7a**-d_5. Probably, the negative charge resulted from a dipolar structure (**C** or **D**) partially located at the carbon atom at the 8-position.

The values of the coupling constants between the protons of seven-membered ring of **6a**-d_5 are almost consistent with those of acepleiadiene,[10] tropone,[11] heptafulvenes,[11] or cycloheptatrienylideneamines.[12] This means an apparent bond-alternation of the seven-membered ring of **6**, while the bond-alternation of the seven-membered ring of 2-phenylcyclohepta-[*hi*]imidazolo[2,3,4-*cd*]indolizine[9] can be scarcely seen.

From these results, we suggest that the resonance for **C** is the most predominant polarized structure contributed to the ground state of cyclohepta[*hi*]-pyrrolo[2,1,5-*cd*]indolizine (**B**).

Further investigations on the properties and chemical reactivities of cyclohepta[*hi*]pyrrolo[2,1,5-*cd*]indolizines are now in progress.

Experimental

General. All melting points are uncorrected. The IR spectra were obtained on a JASCO IRA-1 spectrometer. The ^{1}H NMR spectra were recorded on a JEOL FX-200, FX-100, or JMN-MH-100 spectrometer with tetramethylsilane as an internal standard. The mass spectrometer was equipped with a direct inlet and had at an ionization energy of 75 eV. The elemental analyses were performed on a Hitachi 026 CHN analyzer. For thin-layer and preparative column chromatography, silica gel 60F-254 (Merck) and Wakogel C-300 were used, respectively.

The unknown starting materials **1a**-d_5, **1b**, **1c**, and **1d** were prepared from the reaction of the corresponding cyclohepta-[*hi*]pyrroloindolizines and acetylenes in a similar way to a reported method.[13]

1a-d_5: ^{1}H NMR ($CDCl_3$) δ=2.2 (4H, m, 5- and 6-H), 3.26, 3.46 (2H each, 2t, J=7 Hz each, 4- and 7-H), 3.80, 4.06 (3H each, 2s, $-CH_3$), 7.74 (1H, d, J=8 Hz, 8-H), and 8.34 (1H, d, J=8 Hz, 9-H).

1b: Yellow needles (ethanol); mp 144—146 °C.

Found: C, 80.34; H, 5.78; N, 4.46%. Calcd for $C_{22}H_{19}NO_2$: C, 80.22; H, 5.81; N, 4.25%.

1c: Yellow needles (ethanol); mp 152—153 °C.

Found: C, 71.98; H, 5.59; N, 3.34%. Calcd for $C_{25}H_{23}NO_5$: C, 71.93; H, 5.55; N, 3.36%.

1d: Yellow needles (ethanol); mp 161—162 °C.

Found: C, 61.94; H, 4.28; N, 3.22%. Calcd for $C_{24}H_{20}BrNO_4$: C, 61.81; H, 4.32; N, 3.00%.

Oxidation of 1a with DDQ. A solution of **1a** (500 mg, 1.29 mmol) and DDQ (300 mg, 1.32 mmol) in dry benzene (30 mL) was stirred at 5—10 °C for 24 h under a nitrogen atmosphere. After removing of the resultant hydroquinone by filtration, the filtrate was evaporated to dryness. The residue was subjected to chromatography on silica gel to afforded 155 mg (31%) of **2** together with unreacted **1a** (56%) as chloroform eluents.

The oxidation of **1a** with 6.4 equiv of DDQ under similar conditions gave an unseparable mixture of **3a** (11%), **2** (33%), and **1a** (36%).

2: Yellow needles (ethanol); mp 191—192 °C; IR (KBr) cm^{-1}: 1730 and 1710 (CO); ^{1}H NMR ($CDCl_3$) δ=2.8—2.9 (2H, m, 6-H), 3.3—3.4 (2H, m, 7-H), 3.78, 4.00 (3H each, 2s, $-CH_3$), 6.1—6.2 (1H, m, 5-H), 6.89 (1H, br d, J=11 Hz, 4-H), 7.4—7.7 (6H, m, 8-H and phenyl protons), and 8.28 (1H, d, J=8 Hz, 9-H); MS m/z (rel intensity): 385 (M^+, base peak), 354 (M^+-OCH_3, 16), 326 ($M^+-CO_2CH_3$, 10), 308 (M^+—Ph, 6), and 267 ($M^+-2\times CO_2CH_3$, 27).

Found: C, 74.51; H, 5.04; N, 3.65%. Calcd for $C_{24}H_{19}NO_4$: C, 74.79; H, 4.97; N, 3.63%.

Oxidation of 2 with Pd/C or DDQ to 3a. A solution of **2** (33 mg) in dry toluene (10 mL) in the presence of 20 mg of

Table 3. Chemical Shifts and Coupling Constants of **6a**-d_5 and **7a**-d_5

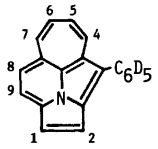

6a-d_5

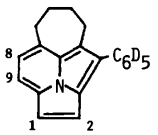

7a-d_5

Compd	Chemical shifts/δ 1-H	2-H	4-H	5-H	6-H	7-H	8-H	9-H
6a-d_5 (δ_1)	7.49	7.74	7.56	6.11	6.38	6.91	7.23	7.89
7a-d_5 (δ_2)	7.24	7.58					7.49	7.81
$\Delta\delta(\delta_1-\delta_2)$	0.25	0.16					−0.26	0.02

Coupling constants for **6a**-d_5 (Hz): $J_{1,2}$=4.2, $J_{4,5}$=11.2, $J_{5,6}$=8.4, $J_{4,6}=J_{5,7}$=1.2, $J_{6,7}$=11.8, $J_{8,9}$=8.4

Coupling constants for **7a**-d_5 (Hz): $J_{1,2}$=4.2, $J_{8,9}$=8.4

10% Pd/C was refluxed for 72 h. After the Pd/C was filtered off, the filtrate was evaporated to dryness. The residue was subjected to column chromatography on silica gel to afford 5 mg (16%) of **3a** as an eluent of chloroform.

Also, the oxidation of **2** with 1.2 equiv of DDQ under similar conditions gave an unseparable mixture of **3a** (24%) and **2** (46%).

3a: Deep red needles (ethanol); mp 189—190 °C; IR (KBr) cm^{-1}: 1740 and 1720 (CO); ^1H NMR ($CDCl_3$) 3.75, 4.04 (3H each, 2s, $-CH_3$), 6.32 (1H, ddd, J=11, 8, and 1 Hz, 5-H), 6.58 (1H, ddd, J=11, 8, and 1 Hz, 6-H), 6.97 (1H, d, J=11 Hz, 4-H), 7.4—7.7 (7H, m, 4- and 8-H and phenyl protons), and 8.36 (1H, d, J=8 Hz, 9-H); MS m/z (rel intensity): 383 (M^+, base peak), 352 (M^+-OCH_3, 24), and 265 ($M^+-2\times CO_2CH_3$, 48).

Found: C, 75.05; H, 4.45; N, 3.74%. Calcd for $C_{24}H_{17}NO_4$: C, 75.18; H, 4.47; N, 3.65%.

Oxidation of 1 with NBS. Typical Procedure: A solution of **1a** (1.00 g, 2.58 mmol) and NBS (1.00 g, 5.62 mmol) in dry carbon tetrachloride (80 mL) was refluxed under the irradiation of a tungsten lamp for 6 h. The resultant succinimide was filtered off and the filtrate was evaporated in vacuo to give a residue. The residue was subjected to column chromatography (silica gel-chloroform) to afford 543 mg (45%) of **4a** and 387 mg (32%) of **5a**. The similar oxidation of **1a**-d_5 with NBS gave the correspoding pentadeuteriophenyl derivatives **4a**-d_5 and **5a**-d_5, respectively.

4a: Yellow needles (ethanol); mp 232—233 °C; IR (KBr) cm^{-1}: 1730 and 1710 (CO); ^1H NMR ($CDCl_3$) δ=3.4 (4H, m, 6- and 7-H), 3.79, 4.00 (3H each, 2s, $-CH_3$), 7.30 (1H, br s, 4-H), 7.4—7.6 (5H, m, phenyl protons), 7.65 (1H, d, J=8 Hz, 8-H), and 8.29 (1H, d, J=8 Hz, 9-H); MS m/z (rel intensity): 465, 463 (M^+, base peak), 434, 432 (M^+-OCH_3), 384 (M^+-Br, 23), 267 (29), 266 (48), and 265 (53).

Found: C, 62.33; H, 4.02; N, 3.23%. Calcd for $C_{24}H_{18}BrNO_4$: C, 62.08; H, 3.90; N, 3.03%.

4a-d_5: ^1H NMR ($CDCl_3$) δ=3.4 (4H, br s, 6- and 7-H), 3.85, 4.05 (3H each, 2s, $-CH_3$), 7.36 (2H, br s, 4-H), 7.68 (1H, d, J=8 Hz, 8-H), and 8.22 (1H, d, J=8 Hz, 9-H).

5a: Deep red needles (ethanol); mp 195.5—197 °C; IR (KBr) cm^{-1}: 1730 and 1710 (CO); ^1H NMR ($CDCl_3$) δ=3.76, 4.04 (3H each, 2s, $-CH_3$), 6.7 (2H, br s, 6- and 7-H), 7.4—7.7 (6H, m, 8-H and phenyl protons), 7.79 (1H, s, 4-H), and 8.28 (1H, d, J=8 Hz, 9-H); MS m/z (rel intensity): 463, 461 (M^+, base peak), 432, 430 (M^+-OCH_3, 17), 282 (M^+-Br, 14), 265, 264, and 263.

Found: C, 62.62; H, 3.54; N, 3.24%. Calcd for $C_{24}H_{16}BrNO_4$: C, 62.35; H, 3.49; N, 3.03%.

5a-d_5: ^1H NMR ($CDCl_3$) δ=3.88, 4.12 (3H each, 2s, $-CH_3$), 6.65 (2H, br s, 6- and 7-H), 7.38 (1H, d, J=8 Hz, 8-H), 7.83 (1H, br s, 4-H), and 8.10 (1H, d, J=8 Hz, 9-H).

A solution of **4a** (100 mg, 0.22 mmol) and NBS (40 mg, 0.22 mmol) in dry carbon tetrachloride (10 mL) was similarly refluxed for 5 h. After a similar work-up, **5a** was obtained in 64% yield together with the unreacted **4a** (22%).

The reaction of **1b**, **1c**, and **1d** with NBS gave the corresponding 6-bromo-6,7-dihydro-**4** and 6-bromo derivatives **5**, respectively. These results are presented in Table 1.

4b: Yellow needles (ethanol); mp 157—159 °C; IR (KBr) cm^{-1}: 1685 (CO), ^1H NMR ($CDCl_3$) δ=3.4 (4H, m, 6- and 7-H), 4.02 (3H, s, $-CH_3$), 7.43 (1H, br s, 4-H), 7.4—7.8 (6H, m, 8-H and phenyl protons), 8.08 (1H, s, 2-H), and 8.25 (1H, d, J=8 Hz, 6-H); MS m/z (rel intensity): 407, 405 (M^+, base peak), 376, 374 (M^+-OCH_3, 12), 326 (M^+-Br, 48), and 267 ($M^+-Br-CO_2CH_3$, 71).

Found: C, 65.11; H, 4.11; N, 3.57%. Calcd for $C_{22}H_{16}BrNO_2$: C, 65.04; H, 3.97; N, 3.45%.

5c: Deep brown needles (ethanol); mp 205—206 °C; IR (KBr) cm^{-1}: 1700 (CO); ^1H NMR ($CDCl_3$) δ=4.05 (3H, s, $-CH_3$), 6.64, 6.75 (1H each, 2d, J=11 Hz each, 6- and 7-H), 7.4—7.7, 7.7—7.8 (7H total, m, 4- and 8-H and phenyl protons), 8.19 (1H, s, 2-H), and 8.31 (1H, d, J=8 Hz, 9-H); MS m/z (rel intensity): 405, 403 (M^+, base peak), 374, 372 (M^+-OCH_3, 9), 346, 344 ($M^+-CO_2CH_3$, 36), and 267 (78).

Found: C, 65.15; H, 3.51; N, 3.78%. Calcd for $C_{22}H_{14}Br_2NO_2$: C, 65.36; H, 3.49; N, 3.47%.

4c: Orange plates (ethanol); mp 221—222 °C; IR (KBr) cm^{-1}: 1720 and 1700 (CO); ^1H NMR ($CDCl_3$) δ=3.4 (4H, br s, 6- and 7-H), 3.84, 3.90, 4.00 (3H each, s, $-CH_3$), 7.04 (2H, br d, J=8.5 Hz, phenyl protons), 7.27 (1H, s, 4-H), 7.53 (2H, br d, J=8.5 Hz, phenyl protons), 7.62 (1H, d, J=8 Hz, 8-H), and 8.23 (1H, d, J=8 Hz, 9-H); MS m/z (rel intensity): 493, 491(M^+, base peak), 478, 476 (M^+-CH_3, 12), and 417 (66).

Found: C, 60.59; H, 4.04; N, 2.74%. Calcd for $C_{25}H_{20}BrNO_5$: C, 60.37; H, 4.07; N, 2.83%.

The recrystallization of **5c** from benzene gave deep red needles, which consisted as 2:1 molecular complex of **5c** and benzene. Mp 204—205 °C; IR (KBr) cm^{-1}: 1730 and 1710 (CO); ^1H NMR ($CDCl_3$) δ=3.82, 3.91, 4.04 (3H each, 3s, $-CH_3$), 6.73 (2H, br s, 6- and 7-H), 7.08 (2H, br d, J=8 Hz, protons), 7.37 (3H, s, benzene), 7.52 (1H, d, J=7.5 Hz, 8-H), 7.58 (2H, br d, J=8 Hz, phenyl protons), 7.76 (1H, br s, 4-H), and 8.33 (1H, d, J=7.5 Hz, 9-H); MS m/z (rel intensity): 493, 491 (M^+, base peak), 478, 476 (M^+-CH_3, 7), 462, 460 (M^+-OCH_3, 12), and 252.

Found: C, 63.31; H, 4.07; N, 2.69%. Calcd for $C_{25}H_{18}BrNO_5 \cdot 1/2\ C_6H_6$: C, 63.31; H, 4.07; N, 2.63%.

4d: Yellow needles (ethanol); mp 191—192 °C; IR (KBr) cm^{-1}: 1740 and 1700 (CO); ^1H NMR ($CDCl_3$) δ=3.4 (4H, m, 6- and 7-H), 3.82, 4.00 (3H each, 2s, $-CH_3$), 7.21 (1H, s, 4-H), 7.4—7.7 (5H, m, 8-H and phenyl protons); MS m/z (rel intensity): 545, 543, 541 (M^+, base peak), 514, 512, 510 (M^+-OCH_3, 14), and 265 (26).

Found: C, 53.29; H, 3.15; N, 2.80%. Calcd for $C_{24}H_{17}Br_2NO_4$: C, 53.06; H, 3.16; N, 2.58%.

5d: Deep brown needles (benzene); mp 177—178 °C; IR (KBr) cm^{-1}: 1730 and 1705 (CO); ^1H NMR ($CDCl_3$) δ=3.81, 4.04 (3H each, 2s, $-CH_3$), 6.8 (2H, br s, 6- and 7-H), 7.4—7.6 (3H, m, 8-H and phenyl protons), 7.68 (2H, br d, J=8.5 Hz, phenyl protons), 7.71 (1H, br s, 4-H), and 8.36 (1H, d, J=8.5 Hz, 9-H); MS m/z (rel intensity): 543, 541, 539 (M^+, 22), 512, 510, 508 (M^+-OCH_3, 5), 463, 461(M^+-Br, base peak), 432, and 430(16).

Found: C, 53.31; H, 3.07; N, 2.70%. Calcd for $C_{24}H_{15}Br_2NO_4$: C, 53.26; H, 2.79; N, 2.59%.

Preparation of 3 by Dehydrobromination of 4 with DBU. Typical Procedure: A solution of **4a** (200 mg, 0.43 mmol) and DBU (300 mg, 2.0 mmol) in dry toluene (30 mL) was heated under reflux for 24 h. The resultant precipitate was filtered off and the filtrate was washed with water (20 mL×3). The toluene layer was dried and evaporated to give a residue. The residue was subjected to column chromatography on silica gel using benzene to afford

159 mg (64%) of **3a**.

Analogously, the dehydrobromination of **4a**-d_5, **4b**, **4c**, and **4d** with DBU gave the corresponding cyclohepta[*hi*]-pyrrolo[2,1,5-*cd*]indolizines **3a**-d_5, **3b**, **3c**, and **3d** in good yields. These results are presented in Table 2.

3a-d_5: Deep brown needles (ethanol); mp 184—186 °C; ^{1}H NMR ($CDCl_3$) δ=3.73, 4.01 (3H each, 2s -CH_3), 6.25 (1H, dd, J=11 and 8 Hz, 5-H), 6.52(1H, dd, J=10 and 8 Hz, 6-H), 6.95 (1H, d, J=10 Hz, 7-H), 7.44(1H, d, J=10 Hz, 4-H), 7.47(1H, d, J=8 Hz, 8-H), and 8.30 (1H, d, J=8 Hz, 9-H).

3b: Red needles (ethanol); mp 170—171.5 °C; IR (KBr) cm^{-1}: 1690 (CO); ^{1}H NMR ($CDCl_3$) δ=4.00 (3H, s, -CH_3), 6.29 (1H, dd, J=11 and 8 Hz, 5-H), 6.44 (1H, dd, J=11 and 8 Hz, 6-H), 6.91 (1H, d, J=11 and 7-H), 7.4—7.6 (5H, m, 4- and 8-H and phenyl protons), 7.85 (2H, m, phenyl protons), 8.13 (1H, s, 2-H), and 8.28 (1H, d, J=8.5 Hz, 9-H); MS m/z (rel intensity): 325 (M^+, base peak), 294 (M^+-OCH_3, 24), and 162.5 ($M^+/2$, 5).

Found: C, 81.44; H, 4.71; N, 4.45%. Calcd for $C_{22}H_{15}NO_2$: C, 81.21; H, 4.65; N, 4.31%.

3c: Deep red needles (benzene); mp 177—178 °C; IR (KBr) cm^{-1}: 1730 and 1710 (CO); ^{1}H NMR ($CDCl_3$) δ=3.82, 3.91, 4.04 (3H each, 3s, -CH_3), 6.27 (1H, dd, J=11 and 8.5 Hz, 5-H), 6.52 (1H, dd, J=11.5 and 8.5 Hz, 6-H), 6.96 (1H, d, J=11.5 Hz, 7-H), 7.02 (2H, br d, J=9 Hz, phenyl protons), 7.41 (1H, d, J=11 Hz, 4-H), 7.54 (1H, d, J=8.5 Hz, 8-H), 7.61 (2H, br d, J=9 Hz, phenyl protons), and 8.33 (1H, d, J=8.5 Hz, 9-H); MS m/z (rel intensity): 413 (M^+, base peak), 398 (M^+-CH_3, 9), 382 (M^+-OCH_3, 11), and 251(15).

Found: C, 72.44; H, 4.68; N, 3.42%. Calcd for $C_{25}H_{19}NO_5$: C, 72.63; H, 4.63; N, 3.39%.

3d: Deep red needles (ethanol); mp 189—190 °C; IR (KBr) cm^{-1}: 1710 and 1690 (CO); ^{1}H NMR ($CDCl_3$) δ=3.81, 4.02 (3H each, 2s, -CH_3), 6.33 (1H, dd, J=11 and 8.5 Hz, 5-H), 6.59 (1H, dd, J=11.5 and 8.5 Hz, 6-H), 7.02 (1H, d, J=11.5 Hz, 7-H), 7.38 (1H, d, J=11 Hz, 4-H), 7.52 (2H, br d, J=9 Hz, phenyl protons), and 8.37 (1H, d, J=8.5 Hz, 9-H); MS m/z (rel intensity): 463, 461 (M^+, base peak), 432, 430 (M^+-OCH_3, 14), 403, 402 ($M^+-CO_2CH_3$, 7), 265, 264, and 263.

Found: C, 62.40; H, 3.51; N, 3.07%. Cacld for $C_{24}H_{16}BrNO_4$: C, 62.35; H, 3.49; N, 3.03%.

Preparation of 1,2-Unsubstituted Cyclohepta[*hi*]pyrolo-[2,1,5-*cd*]indolizines 6 from 3. Typical Procedure: 3a (120 mg, 0.31 mmol) was heated under reflux in 5% methanolic potassium hydroxide (40 mL) for 20 h and the methanol was removed to give a residue. The residue was made acidic with 6 M hydrochloric acid (50 mL). The resultant diacid was filtered, dried and subjected to the next decarboxylation without further purification. A solution of the diacid in quinoline (15 mL) in the presence of copper dust (50 mg) was refluxed for 1 h. The copper dust was filtered off and the filtrate was evaporated to give a residue. The residue was dissolved in dichloromethane and washed with 0.5 M hydrochloric acid (50 mL×3) in order to remove the quinoline completely. The organic layer was evaporated to dryness. The residue was subjected to chromatography on silica gel using hexane–benzene (3:1) to afford 70 mg (84% from **3a**) of the desired **6a**.

6a: Deep red needles (ethanol); mp 79.5—81 °C; IR (KBr) cm^{-1}: 800, 760, and 680; ^{1}H NMR ($CDCl_3$) δ=6.11 (1H, ddd, J=11.2, 8.4, and 1.2 Hz, 5-H), 6.35 (1H, ddd, J=11.8, 8.4, and 1.2 Hz, 6-H), 6.91 (1H, dd, J=11.8 and 1.2 Hz, 7-H), 7.23 (1H, d, J=8.4 Hz, 8-H), 7.4—7.8 (8H, m, 1-, 2-, and 4-H and phenyl protons), and 7.89 (1H, d, J=8.4 Hz, 9-H); MS m/z (rel intensity): 267 (M^+, base peak), 265 (M^+-H_2, 28), 133.5 ($M^+/2$, 10), 132.5 ($M^+-H_2/2$, 17), and 77(7).

Found: C, 89.99; H, 5.04; N, 5.17%. Calcd for $C_{20}H_{13}N$: C, 89.86; H, 4.90; N, 5.24%.

6d: Yield 90% from **3d**; deep brown needles (ethanol); mp 151—153 °C; IR (KBr) cm^{-1}: 1310, 1020, and 800; ^{1}H NMR ($CDCl_3$) δ=6.06 (1H, ddd, J=12, 8, and 1 Hz, 5-H), 6.32 (1H, ddd, J=12, 8, and 1 Hz, 6-H), 6.84 (1H, dd, J=12 and 1 Hz, 7-H), 7.18 (1H, d, J=8 Hz, 8-H), and 7.3—8.0 (9H, m, 1-, 2-, 4-, and 9-H and phenyl protons); MS m/z (rel intensity): 347, 345 (M^+, base peak), 267 (33), 266 (M^+-Br, 31), 265 (M^+-HBr, 88), 173.5, and 172.5 ($M^+/2$, 9).

Found: C, 69.58; H, 3.70; N, 4.24%. Calcd for $C_{20}H_{12}BrN$: C, 69.38; H, 3.49; N, 4.05%.

As referential compounds, **7a** and **7a**-d_5 were obtained similarly from **1a** and **1a**-d_5, respectively.

7a: Yield 78%; orange prisms (ethanol); mp 102—104 °C; IR (KBr) cm^{-1}; 1280, 1020, 790, and 690; ^{1}H NMR ($CDCl_3$) δ=1.7—2.1 (4H, m, 5- and 6-H), 3.1-3.3 (4H, m, 4- and 7-H), and 7.2—8.0 (9H, m, 1-, 2-, 8-, and 9-H and phenyl protons).

Found: C, 88.32; H, 6.36; N, 5.31%. Calcd for $C_{20}H_{17}N$: C, 88.52; H, 6.32; N, 5.16%.

We wish to thank Professors Masashi Tashiro and Hitoshi Takeshita, Institute of Industrial Science, Kyushu University, for the elemental analyses and the measurement of NOE. We are also grateful to Drs.

Table 4. Electronic Spectral Data of Cyclohepta[*hi*]-pyrrolo[2,1,5-*cd*]indolizines and Their Dihydro and Tetrahydro Derivatives

Compd	λ_{nm}^{max} (log ε) in $CHCl_3$
1a	205(4.46), 269(4.45), 319(4.27), 412(3.68), 424(3.71)
2	245(4.42), 271(4.56), 342(4.28), 438(4.12), 450(4.12)
4a	243(4.40), 274(4.40), 344(4.27), 442(4.20), 455(4.21)
4b	246(4.36), 263(4.39), 286(4.46), 343(4.29), 441(4.17), 458(4.17)
3a	241(4.52), 265(4.74), 322(4.25), 345(4.30), 357(4.33), 390(3.75), 412(4.02), 438(4.19), 489(3.40), 524(3.28), 568(2.97), 620(2.33)
5a	246(4.52), 265(4.77), 304(4.42), 324(4.27), 345(4.35), 358(4.37), 392(3.78), 417(4.08), 443(4.21), 537(3.12), 585(2.74), 640(2.07)
5b	245(4.53), 267(4.76), 324(4.28), 349(4.39), 358(4.39), 393(3.76), 417(4.03), 442(4.16), 500(3.03), 539(2.80), 584(2.41), 640(1.81)
6d	249(4.56), 284(4.34), 297(4.32), 356(4.26), 410(3.72), 431(3.72), 467(2.96), 501(2.95), 538(2.83), 582(2.54), 640(1.97)

Shigeki Nagai, Yoshiaki Ishida, and Keiji Saito and Mr. Tsuyoshi Arai, Ube Research Laboratory, Ube Industries LTD, for the measurement of ^{1}H NMR spectra at 200 MHz.

References

1) Studies on Nitrogen-Bridged Heterocycles. IV. Part III in this series: M. Noguchi, N. Tanigawa, T. Yamamoto, and S. Kajigaeshi, *Chem. Lett.*, **1985**, 873.

2) K. Matsumoto, T. Uchida, and J. Yamauchi, *Yuki Gosei Kagaku Kyokai Shi*, **35**, 739 (1977); W. Flitsh and U. Kramer, *Adv. Heterocycl. Chem.*, **22**, 321 (1978).

3) M. Noguchi, N. Tanigawa, T. Yamamoto, and S. Kajigaeshi, *Chem. Lett.*, **1985**, 873.

4) The syntheses and properties of 2-aza and 2,3-diaza analogs of this system were reported.[9]

5) The 4,5-dihydro derivative as another structure for **2** was ruled out from the similarity of its electronic spectrum to those of **4**. Also, the dark-green solution at the initial stage of the DDQ oxidation suggested the formation of the CT complex between benzene ring of **1a** and DDQ similarly to the regioselective oxidation of 5,6-dihydro-4*H*-benzo[*hi*]-pyrrolo[2,1,5-*cd*]indolizines.[3]

6) R. J. Windgassen, Jr., W. H. Saunders, Jr., and V. Boekelheide, *J. Am. Chem. Soc.*, **81**, 1459 (1959).

7) π-Electron density (a) and bond order (b) for cyclohepa[*hi*]pyrrolo[2,1,5-*cd*]indolizine (**B**) by Hückel method are shown.

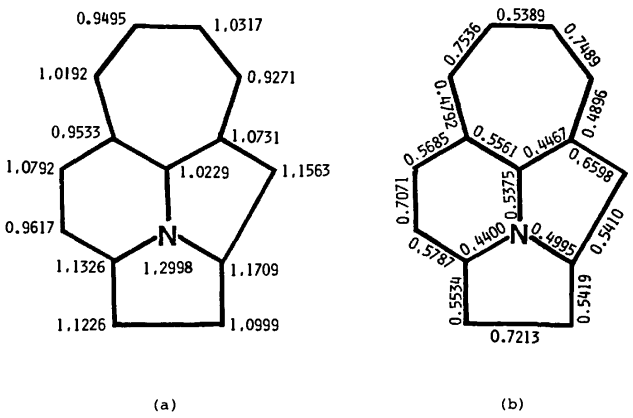

Fig. 3

8) The chemical shifts were almost constant at concentrations below 0.1 M, e.g., the difference of the chemical shifts between 0.12 and 0.06 M deuteriochloroform solution of **6a** was within 0.03 ppm.

9) N. Abe, T. Nishiwaki, H. Yamamoto, and N. Kunishige, *Bull. Chem. Soc. Jpn.*, **56**, 3703 (1983).

10) A. J. Jones, P. D. Gardner, D. M. Grant, W. H. Litchmann, and V. Boekelheide, *J. Am. Chem. Soc.*, **92**, 2395 (1970).

11) D. J. Bertelli and T. G. Andrews, Jr., *J. Am. Chem. Soc.*, **91**, 5286 (1969).

12) N. L. Bauld amd Y. S. Rim, *J. Am. Chem. Soc.*, **89**, 6763 (1967).

13) M. Noguchi, N. Tanigawa, and S. Kajigaeshi, *J. Heterocycl. Chem.*, **22**, 1049 (1985).

High-Pressure Kinetics of the (6+4)π Cycloaddition of Tropone with 2,3-Dimethyl-1,3-butadiene, an Acyclic Diene. The Temperature and Solvent Effects

Shigeru SUGIYAMA and Hitoshi TAKESHITA*
Research Institute of Industrial Science, 86, Kyushu University,
Kasuga-koen, Kasuga, Fukuoka 816
(Received July 30, 1986)

By a high-pressure kinetic analysis in isopropylbenzene, 1,4-dioxane and *N,N*-dimethylformamide, the activation parameters for the (6+4)π cycloaddition reaction of tropone with 2,3-dimethyl-1,3-butadiene were determined. The findings support the concerted nature for the Woodward-Hoffmann rule-allowed thermal addition reaction of tropone. A secondary orbital interaction, which was used to predict the correct stereochemistry of the adducts, exerted no effect on the volume profile.

Previously, we confirmed the concerted nature of the (6+4)π cycloaddition of tropone (**1**) to 1,3-cyclohexadiene (**2**) by a kinetic analysis regarding pressure and temperature effects.[1] The activation enthalpy ($\Delta H^{\neq}$) and activation entropy ($\Delta S^{\neq}$), showing no anomaly, were consistent with those obtained by Tanida and Pfaendler in a reaction of **1** with cyclopentadiene (**3**) under ordinary pressure.[2] Moreover, the activation volume ($\Delta V^{\neq}$) and the volume profile ($\Delta V^{\neq}/\Delta V$, where ΔV represents reaction volume) were also in accord with the concerted cycloadditions.

Herein, we wish to describe the pressure and temperature effects on the cycloaddition of **1** with 2,3-dimethyl-1,3-butadiene (**4**), an acyclic diene, which is conformationally mobile in solutions.[3] The volume profile of the (6+4)π cycloaddition with such a combination has not been investigated; the rate constant showed a little different pressure dependence from our previous combinations.[1,4,5]

Experimental

The purity of **1**[6] was more than 99.0% in respect to a gas-liquid chromatographic analysis. A commercial sample of **4**, from Aldrich Japan Co. Ltd., Tokyo, was purified by distillation over $NaBH_4$ under an N_2 atmosphere. The solvents, isopropylbenzene (cumene), 1,4-dioxane (dioxane) and *N,N*-dimethylformamide (DMF), were purified as stated previously.[1] The adduct (**5**), a pale yellow oil, was purified by repeated silica-gel column chromatography, and showed pertinent figures of elemental analysis. Its IR, NMR, and mass spectra were also consistent with the structure.

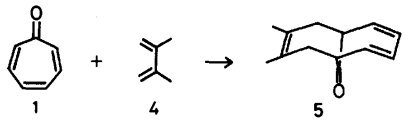

Scheme 1.

The same instruments were used for a density measurement and kinetic experiment as those in previous studies.[1,5] The progress of the reaction was monitored by observing an increase of product (**5**) by means of high-pressure liquid chromatography (Nippon Waters' Model 244 Apparatus).

Results and Discussion

Activation Parameters. Although extensive studies have been carried out concerning both theoretical and synthetic aspects of the (6+4)π cycloaddition of **1**, there have been few kinetic studies, even under atmospheric pressure on the subject (e.g., those by Tanida et al.[2] and ours[1]). This could be due to an instability of the popular cycloaddend, **3**, toward spontaneous dimerization. In this respect, **4** is thermally stable and the present combination is appropriate for a kinetic analysis.

Table 1 shows the second order rate constants (k) in three solvents of different polarities at various temperatures (T) under atmospheric pressure. Within the temperature range studied, there is a good linear relationship between ln k and $1/T$ in each solvent (correlation coefficient: $r>0.999$), as predicted by the Arrhenius equation. The $\Delta H^{\neq}$, $\Delta S^{\neq}$ and the activation free energy ($\Delta G^{\neq}$) at 100 °C are listed in Table 2. There

Table 1. Rate Constants for the Reaction of **1** with **4** at Various Temperatures ($10^6 k$/kg mol^{-1} s^{-1})

Solvent	Temperature/°C			
	80	90 (85)[a]	100 (90)[a]	110 (95)[a]
Cumene	2.16±0.05	3.67±0.02	7.47±0.07	13.6 ±0.1
Dioxane	1.58±0.02	2.22±0.04	3.16±0.08	4.28±0.06
DMF	0.99±0.01	1.81±0.02	3.32±0.04	5.41±0.08

a) Rates in dioxane were measured at the temperatures indicated in parentheses.

were very little solvent effects, and the values of $\Delta S^{\neq}$ were similar to those of a typical Diels-Alder reaction[4,5,7,8] and those of other (6+4)π cycloadditions of **1** with **3**[2] and with **2**.[1] Therefore, this reaction could be interpreted as a concerted electrocyclic reaction. The considerably large negative $\Delta S^{\neq}$ indicates that the pressure effect on the reaction is as large as that on a Diels-Alder reaction, because $\Delta S^{\neq}$ is generally known to be related to $\Delta V^{\neq}$.[9]

The rate constants at various pressures are listed in Table 3. The pressure dependence of the rate constants is expressed by

$$(\partial \ln k/\partial P)_T = -\Delta V^{*}/RT. \quad (1)$$

As illustrated in Fig. 1, in each solvent plots of ln k vs. P showed a more pronounced curvature than those obtained in our previous Diels-Alder reactions and the (6+4)π cycloaddition of **1**,[1,4,5] indicating that $\Delta V^{\neq}$ become less negative with increasing pressure. In this respect, there have been very few theoretical studies; however, it has been stated that the differences in the compression between the ground and the transition states may influence the pressure effect on $\Delta V^{\neq}$. In the present case, one reason for this phenomenon might be the conformational mobility of acyclic diene, **4**. Under the atmospheric pressure, **4** may be sufficiently mobile, but its mobility might be restricted with increasing pressure. This means, the ground state may be less rigid reflecting the flexibility of the cycloaddend, **4**, than the transition state, for which, there would be no objection to conceive a rigidity from the cyclic and product-like structure (see below). On the other hand, under high-pressure conditions, the freedom of the ground state is restricted, but the degree of freedom of the transition state is not appreciably altered. Thus, with increasing pressure, the difference in the degree of freedom between the ground state and the transition state ($\Delta S^{\neq}$) might become less negative. Since $\Delta S^{\neq}$ is known to be related to $\Delta V^{\neq}$, the $\Delta V^{\neq}$ would become less negative at higher pressures and the plot of ln k vs. P would show a curvature. This interpretation might be justified by the observation that an almost linear plot was obtained using a conformationally-rigid, cyclic cycloaddends for **1** in the Diels-Alder and the (6+4)π cycloaddition reactions.[1,4,5] To express the present dependence of ln k, we used the following equation because of its established wide usage:

$$\ln k = a + bP + cP^2. \quad (2)$$

Table 4 shows the partial molar volume of each substance (Vi), given by the density measurement, ΔV at 60 °C, $\Delta V^{\neq}$ at 80 °C under atmospheric pressure, and the volume profile ($\Delta V^{\neq}/\Delta V$). As shown, the $\Delta V^{\neq}$ and $\Delta V^{\neq}/\Delta V$ are in the range of those for the typical Diels-Alder reactions.[10] Moreover, the other reliable data from the (6+4)π cycloaddition of **1** with **2**[1] was similar.

With respect to the solvent effect, $\Delta V^{\neq}$ became slightly less negative upon increasing the polarity of the solvent. This behavior resembled our results regarding the concerted cycloaddition of **1** measured in cumene and DMF.[1,5] Also, this solvent effect was

Table 2. Activation Parameters for the Reaction of **1** with **4** at 100 °C.

Solvent	ΔH^{*}/kJ mol^{-1}	ΔS^{*}/J mol^{-1} K^{-1}	ΔG^{*}/kJ mol^{-1}
Cumene	67±3	−166±9	129±7
Dioxane	69±2	−162±5	130±4
DMF	61±2	−188±5	131±3

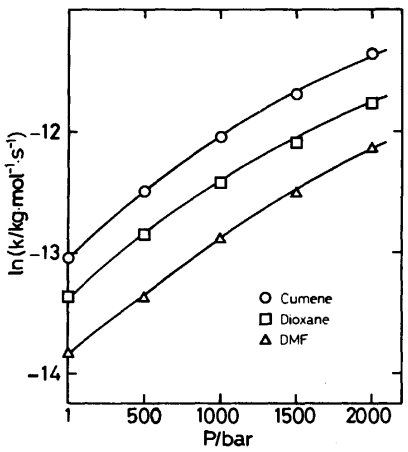

Fig. 1. Pressure dependence of ln k for the reaction of tropone with dimethylbutadiene at 80 °C.

Table 3. Rate Constants for the Reaction of **1** with **4** at Various Pressures at 80 °C ($10^6 k$/kg mol^{-1} s^{-1})

Solvent	Pressure/bar				
	1	500	1000	1500	2000
Cumene	2.16±0.05	3.70±0.04	5.83±0.01	8.29±0.07	11.6 ±0.1
Dioxane	1.58±0.02	2.59±0.06	4.01±0.09	5.57±0.06	7.79±0.05
DMF	0.99±0.01	1.55±0.01	2.57±0.03	3.80±0.01	5.48±0.05

very small and in accord with typical concerted reactions.

Consequently, an effect resulting from the dipolar character of **1** on the volume, pointed out by le Noble and Ojosipe,[11] is insignificant.

Volume Profile. From our previous and the present results, the transition state of the (6+4)π cycloaddition of **1** was found to be very product-like as far as the reaction volume is concerned: that is, $0.87<\Delta V^{\neq}/\Delta V<1.04$.[1] This phenomenon has often been observed in Diels-Alder reactions; in a special case, $\Delta V^{\neq}$ was more negative than ΔV.[12] In view of the secondary orbital interaction by the Woodward-Hoffmann rule for the Diels-Alder reaction,[13] the attractive force between the HOMO of dienes and the LUMO of dienophiles should yield the endo-adducts under kinetically controlled conditions. Accordingly, the transition state could be explained as becoming very product-like, or smaller than the product. On the same grounds, the exemplified exo-orientation for the (6+4)π cycloadducts of **1** has been explained in terms of a repulsive secondary orbital interaction in the endo-transition state.[14]

According to le Noble and Ojosipe,[11] a much larger $\Delta V^{\neq}/\Delta V=1.74$ in the (6+4)π cycloaddition of **1** with **3**, which was invalidated though,[1] was explainable in terms of an attractive, secondary interaction between the HOMO of **1** and the LUMO of **3** in the exo-transition state to make the transition state compressed (Scheme 2: **A**, unfortunately, the illustration contained a false figure).[11] However, an ab initio calculation showed the difference in energy level between the HOMO of **1** and the LUMO of **3** to be ca. 10 eV, and that between the LUMO of **1** and the HOMO of **3** to be ca. 8 eV.[15] Consequently, the former combination is not appropriate; in fact, the (6+4)π cycloaddition of **1** has often been explained[16] on the basis of the latter combination, in which the coefficient of the carbonyl group of **1** in the LUMO is 0 (Scheme 2: **B**).

In such a circumstance, the secondary orbital interaction can not be significant in the exo-(6+4)π cycloaddition of **1**. Moreover, if one considers the contribution of HOMO of **1** and the LUMO of dienes on volume profile, it should at least be discussed on the basis of the correct figure drawn as Scheme 2: **C**.[15] That is, the coefficient of carbon in carbonyl group is 0, and the attractive secondary orbital interaction can not be so strong as mentioned by le Noble. Furthermore, this combination is minor one. Taking these points into accounts, the secondary orbital interaction is concluded to contribute insignificantly to the volume profile of the exo-(6+4)π cycloaddition of **1**. In addition, the comparison on volume profile between (6+4)π cycloaddition of **1** and the Diels-Alder reactions disclosed a remarkable feature; Scheme 3 shows, although (6+4)π cycloaddition and Diels-Alder reaction suffer differently from secondary orbital interaction, very similar volume profiles with illustrations of the HOMO-LUMO combinations for a (6+4)π cycladdition of **1** observed by us[1] and one of the typical Diels-Alder reaction, **3** with methyl acrylate.[17] Therefore, the secondary orbital interaction does not play a significant role on the volume profile, and the often observed $\Delta V^{\neq}/\Delta V>1$ in the Diels-Alder reaction must be explained in terms of another factor, such as a transannular attractive force.[18]

In conclusion, contributions of the dipolar character of **1** and the secondary orbital interaction to the volume profile of the Woodward-Hoffmann rule-allowed thermal (6+4)π electrocyclic reaction of **1** should not be overestimated. Also, the high-pressure cycloadditions of troponoids in organic syntheses are certainly profitable.[19]

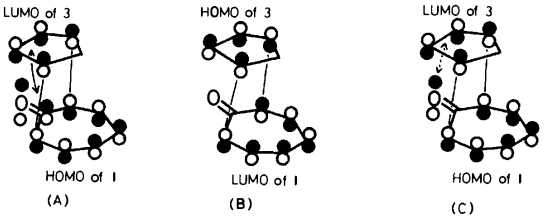

Scheme 2.

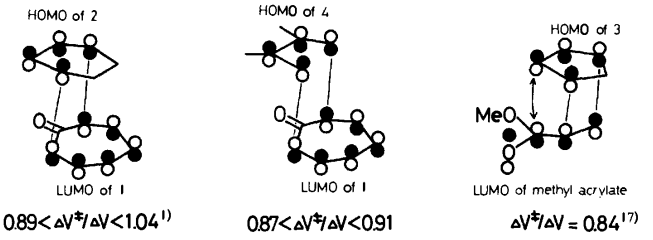

Scheme 3.

Table 4. The Volume Parameters for the Reaction of **1** with **4** ($cm^3\ mol^{-1}$)

Solvent	ΔV_1[a]	ΔV_4[a]	ΔV_5[a]	ΔV[a]	$\Delta V^{\neq}$[b]	$\Delta V^{\neq}/\Delta V$
Cumene	99.8	118.5	183.4	−34.9	−33.1	0.91
Dioxane	99.1	119.4	183.5	−35.0	−30.5	0.87
DMF	97.0	115.8	178.8	−34.0	−30.1	0.89

a) Measured at 60±0.01 °C. b) Measured at 80±0.5 °C.

The authors thank the Ministry of Education, Science and Culture for a Grant-in-Aid for Scientific Research to S. S. (No. 61740294).

References

1) H. Takeshita, S. Sugiyama, and T. Hatsui, *J. Chem. Soc., Perkin Trans. 2.*, **1986**, 1491.

2) H. Tanida and H. R. Pfaendler, *Helv. Chim. Acta*, **55**, 3062 (1972).

3) M. E. Gorst, V. A. Roberts, and C. Prussin, *Tetrahedron*, **39**, 581 (1983).

4) H. Takeshita, S. Sugiyama, and T. Hatsui, *Chem. Lett.*, **1984**, 1855.

5) H. Takeshita, S. Sugiyama, and T. Hatsui, *Bull. Chem. Soc. Jpn.*, **58**, 2490 (1985).

6) T. Ikemi, H. Sugiyama, and T. Nozoe, *Chem. Ind. (London)*, **1960**, 932.

7) J. Sauer, H. Wiest, and A. Mielert, *Chem. Ber.*, **97**, 3183 (1964).

8) S. Itô, A. Mori, Y. Shoji, and H. Takeshita, *Tetrahedron Lett.*, **1972**, 2685.

9) D. Chen, and K. J. Laider, *Trans. Faraday Soc.*, **354**, 1026 (1958); K. J. Laider and D. Chen, *Can. J. Chem.*, **37**, 599 (1959).

10) T. Asano and W. J. le Noble, *Chem. Rev.*, **78**, 407 (1978).

11) W. J. le Noble and B. A. Ojosipe, *J. Am. Chem. Soc.*, **97**, 5939 (1975).

12) R. A. Grieger and G. A. Echert, *J. Am. Chem. Soc.*, **92**, 2918 (1970).

13) R. Woodward and R. Hoffmann, "Conservation of Orbital Symmetry," Verlag Chemie, GmbH, Weinheim/ Bergstr., 1970, pp. 83—84.

14) The (6+4)π cycloaddition of isobenzofuran with 6,6-dimethylfulvene and 6,6-diphenylfulvene gave stereospecifically the endo-adducts. The results have been explained in terms of the cross-conjugated geometry for the 6π system of the fulvenes where the secondary effect is not strong enough to control the stereochemistry. See H. Takeshita, A. Mori, S. Sano, and Y. Fujise, *Bull. Chem. Soc. Jpn.*, **48**, 1661 (1975).

15) D. Mukherjee, C. R. Watts, and K. N. Houk, *J. Org. Chem.*, **43**, 817 (1978).

16) I. Fleming, "Frontier Orbital and Organic Chemical Reactions," John Wiley & Sons, Ltd., New York (1976), Chap. 4; and the references cited therein.

17) K. Seguchi, A. Sera, and K. Maruyama, *Bull. Chem. Soc. Jpn.*, **47**, 2242 (1974).

18) This has been pointed out in the pressure accelerated retro-Diels–Alder reaction. See A. V. George and N. S. Isaacs, *J. Chem. Soc., Perkin Trans., 2*, **1985**, 1845.

19) K. Matsumoto and A. Sera, *Synthesis*, **1985**, 999; S. Sugiyama, T. Tsuda, A. Mori, H. Takeshita, and M. Kodama, *Chem. Lett.*, **1986**, 1315.

 © 1987 The Chemical Society of Japan Bull. Chem. Soc. Jpn., 60, 981—999 (1987)

Glycinoeclepins, Natural Hatching Stimuli for the Soybean Cyst Nematode, *Heterodera Glycines*. I. Isolation

Tadashi MASAMUNE,* Masaki ANETAI, Akio FUKUZAWA, Mitsuo TAKASUGI, Hideki MATSUE, Kiroku KOBAYASHI, Shoji UENO, and Nobukatsu KATSUI
Department of Chemistry, Faculty of Science, Hokkaido University, Sapporo 060
(Received August 7, 1986)

Hatching stimuli, designated as glycinoeclepins, for the soybean cyst nematode (*Heterodera glycines*) have been isolated by repeated chromatography of the aqueous extracts of dried roots of kidney bean (*Phaseolus vulgaris*), one of the host plants of the nematode. One of these compounds, glycinoeclepin A, stimulates the hatching and emergence of larvae in vitro in highly diluted aqueous solutions.

The cyst nematodes (genera *Heterodera, Globodera* and others, ca. 40 species)[1] generally have a limited host range. This specificity arises from the fact that the hatching of dormant second stage larvae from eggs and the emergence of the hatched larvae from cysts occur in response to chemical stimuli in the root diffusates secreted by the host plants.[2-5] This fact was first discovered by Baunacke in 1922 for the potato cyst nematode (*G. rostochiensis*).[6] Since then, much time and effort has been expended in attempts to purify and characterize these stimuli,[2-5] in view of their scientific interest and importance in agriculture. However, success has been limited by the extremely small amounts of active substances available.

The soybean cyst nematode (*H. glycines* Ichinohe) parasitizes a small group of host plants, including soybean (*Glycine max*), kidney bean (*Phaseolus vulgaris*), and adzuki bean (*P. angularis*), and causes "soybean sickness."[7] The life cycle of this nematode is summarized as follows.[7] The female adult, after copulation, is almost completely filled with the ovary and then with the eggs, and dies. Within a few days, the embryo in the egg molts into the first and second stage larva, and enters a domant stage in the dead female called "cyst." Each cyst usually contains about 250 eggs within the body and, without host plants, persists in the soil for many years. In spring, when temperature, moisture, and other factors become desirable, and also when the host plants are cultivated in the soil, the second stage larvae in the eggs hatch, and the hatched larvae emerge out of the cysts. After invading the roots and causing formation of giant cells, the second stage larvae become large and molt into the male and female adults via the third and fourth stage larvae. These larvae feed on the giant cells and hence infect the host plants. This life cycle is completed within 4 weeks, if all the conditions are satisfied. The most interesting stage in this life cycle is hatching and emergence. Various factors affecting the hatching and emergence have been examined in details.[8-13] Of these factors, the most important one is chemical stimuli secreted by the roots of host plants, since these stimuli are connected with the host-parasite specificity. In 1966 Tsutsumi and Sakurai demonstrated[14] that the hatching and the larval emergence of the soybean cyst nematode were stimulated by root diffusates from the host plants. The present investigation was then commenced in 1967 with the purpose of ecological eradication of the nematode, based on these findings, and resulted recently in successful isolation and structure elucidation of the relevant natural hatching stimuli, designated as glycinoeclepins A, B, and C. These results have been reported in preliminary communications.[15-18] In the present article we describe the isolation procedure of these active principles in details.

Bioassay. The method of bioassay for the hatching, required for efficient isolation of the active principles, was carried out as follows. Usually ca. 100 cysts were obtained from ca. 100 g of the nematode-infested soil, which were collected in October at Memuro, Hokkaido, and stored in a refrigerator at 5 °C. The cysts were soaked at 25 °C for 10 d, then dissected in water and sieved through a 325-mesh sieve. The dissected cyst wall fragments remained on the sieve. The eggs and larvae, which had been hatched, were collected on filter papers and transferred to a beaker with water so that 1 ml of the aqueous suspension contained 150—200 eggs. Then 1 ml of this suspension was transferred to a Syracuse watch glass to which 1 ml of the test solution and 8 ml of distilled water were added. The whole suspension was kept at 25 °C, and the number of larvae hatched was counted after 10 d. The per cent hatching rate was expressed as $P=P_t-P_w$, where P_t and P_w denote the per cent hatching observed in the test solution and in distilled water, respectively. The test solution was said to be active, when the hatching rate, P, exceeded 50%. This bioassay is characterized by using the free eggs instead of the cysts, and also by soaking the cysts in water at 25 °C for 10 d before the test. Compared with the bioassays which had been performed with the cyst by most of the previous workers, this bioassay has been found to be simpler and more reproducible.

Preparation of Hatch-Stimulating Concentrates. A large amount of the concentrates, the active raw materials, were prepared from aqueous extracts of the

roots of two subspecies ("Hon-kintoki" and "Beni-kintoki") of kidney bean rather than those from their root diffusates, because the diffusates were highly active, compared with the aqueous extracts, but too unstable for further purification.[19] The two subspecies were cultivated in 1 hectare of the field at Memuro for 3 months (early May to late July). The roots were collected by cutting just before flowering, air-dried for 1—3 months (August to November), and pulverized. The dried and powdered roots (ca. 100 kg) thus obtained were extracted with water (1.5—3 kl) at a temperature below 10 °C for 1 month (November to December). The aqueous suspensions were filtered and concentrated below 30 °C, acidified with concd hydrochloric acid to pH 3, and extracted again with chloroform repeatedly (January to April). The chloroform solution, after concentration, gave the hatch-stimulating concentrates (ca. 100 g) (Chloroform extracts A), which stimulated the hatching and emergence at 10^{-5} g ml^{-1} in water at 25 °C. The dilute (10^{-5} g ml^{-1}) aqueous solution of the concentrates was called "standard solution" and always used for the bioassay for reference.

Isolation. In 1982 we reported[15] the isolation of a natural hatching stimulus, designated as glycinoeclepin A (GEA), for the soybean cyst nematode, as its bis(*p*-bromophenacyl) ester (p-BPE). In 1977, five years before the isolation, we had obtained one fraction [Fraction L (p-BPE)] after repeated chromatography of the hatch-stimulating concentrates according to the procedure shown in Table 1.[20] The fraction had revealed a single peak by analytical high performance liquid chromatography (HPLC) on a variety of columns and showed high activity (active at 10^{-11}—$^{-12}$ g ml^{-1}) for the hatching. However, with a limited amount (ca. 5 μg from ca. 100 g of the concentrates) of the fraction, it had not been feasible in the year of 1977 to obtain any useful MS and ^{1}H NMR spectral data of the fraction, because of unavoidable contamination by impurities of solvent and column origin. Four years later, in 1981, the fraction could be identified as p-BPE of the active principle in question on the basis of the same chromatographic behavior and FD-MS spectrum as those of GEA p-BPE. It implies that the procedure described in Table 1 has resulted in the first isolation

Table 1. Isolation of GEA as its p-BPE

Dried and powdered roots of kidney bean "Beni-kintoki" [135 kg (1 ha)]	
↓ Extraction with water (2 kl) (<10 °C)	
↓ Evaporation (<30 °C) under reduced pressure	
Concentrates	
↓ Continuous extraction with chloroform at pH 2—3	
Chloroform extracts A	(115 g, active at 10^{-5} g ml^{-1})
↓ EtOAc-aq $NaHCO_3$	
Acidic extracts B	(66.5 g, active at 10^{-5}—$^{-6}$ g ml^{-1})
↓ Charcoal-Celite column (aq acetone)	
Fraction C	(5.2 g, active at 10^{-7} g ml^{-1})
↓ Silica-gel column (EtOAc-$CHCl_3$-AcOH, 15:5:1)	
Fraction D	(360 mg, active at 10^{-8} g ml^{-1})
↓ Silica-gel column (Ether-AcOH, 99:1)	
Fraction E	(117 mg, active at 10^{-8} g ml^{-1})
↓ Siliconized Hyflo Super Cel column (MeOH-H_2O-AcOH-$CHCl_3$-$C_8H_{17}OH$, 150:150:2:15:15)	
Fraction F	(25.5 mg, active at 10^{-8}—$^{-9}$ g ml^{-1})
↓ Amberlyst-15 (Ag^+ form) column (EtOH)	
Fraction G	(14.4 mg, active at 10^{-8}—$^{-9}$ g ml^{-1})
↓ Amberlyst XN-1005 (Ag^+ form) column (MeOH)	
Fraction H	(1.53 mg, active at 10^{-9}—$^{-10}$ g ml^{-1})
↓ *p*-Bromophenacylation (*p*-$BrC_6H_4COCH_2Br$, $KHCO_3$, crown ether in MeCN, 80 °C)	
↓ Silica-gel column	
Fraction I (p-BPE)	(0.91 mg, active at 10^{-9}—$^{-10}$ g ml^{-1} after hydrolysis)
↓ Preparative HPLC, MicroPak CN-10 (C_6H_{14}-ether, 45:55)	
Fraction J (p-BPE)	(0.19 mg, active at 10^{-10} g ml^{-1} after hydrolysis)
↓ Preparative HPLC, MicroPak NH_2-10 (C_6H_{14}-CH_2Cl_2-MeCN, 70:18:12)	
Fraction K (p-BPE)	(≈50 μg, active at 10^{-10}—$^{-11}$ g ml^{-1} after hydrolysis)
↓ Preparative HPLC, Hitachi Gel #3011 (MeOH-CH_2Cl_2, 9:1)	
Fraction L (p-BPE) (=GEA p-BPE)	(≈5 μg, active at 10^{-11}—$^{-12}$ g ml^{-1} after hydrolysis)

of GEA.

The isolation procedure summarized in Table 1 will deserve the following comments. a) The hatch-stimulating concentrates were initially fractionated (Fraction A to H) by various types of column chromatography such as adsorption, reversed-phase partition, and ionic exchange chromatography, in the light of the separation procedure of gibberellins[21] and prostaglandins. A number of inactive aliphatic and aromatic acids and abscisic acid-related compounds were isolated and identified during chromatography over Charcoal-Celite (Fig. 1) and silica gel (see Experimental). Usually several active fractions were separated in each of the steps. Fortunately, any special enhancement in the activity was not observed by combination of such active fractions, and only the most active fraction in each step was submitted to the subsequent separation step. The following points are annotated. i) Chromatography over silica gel (Fraction C to E) did not always give satisfactory results in reproducibility; it sometimes resulted in remarkable decrease of the amount without increase or with loss of the activity.[22] ii) Reversed-phase partition chromatography on a siliconized Hyflo Super Cel column (Fraction E to F) led to efficient concentration of active fractions (Fig. 2) under almost the same conditions as those for effective separation of prostaglandins.[23] However, the column was not expected to be suitable for separation of a large amount of the material. iii) Subsequent separation by chromatography over ionic exchange resins (Fraction F to H), Amberlyst-15 (Ag^+ form) and Amberlyst XN-1005 (Ag^+ form) columns, appeared to have been

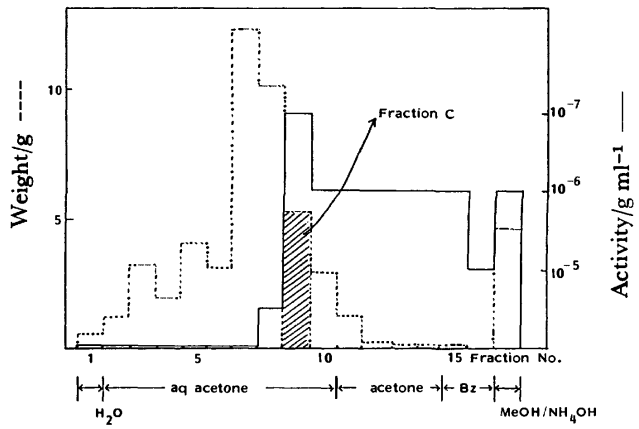

Fig. 1. Column chromatography of Acidic extracts B on the Charcoal-Celite column (Table 1). Eluent: Frs. 1—10, H_2O–acetone (10 : 0, 9 : 1, 8 : 2, 7 : 3, 6 : 4, 3 : 7, 2 : 8, 1 : 9); Frs. 11—14, acetone: Frs. 15—16 (benzene); Fr. 17, (MeOH–concd NH_4OH). The hatching activity was checked with the eggs.

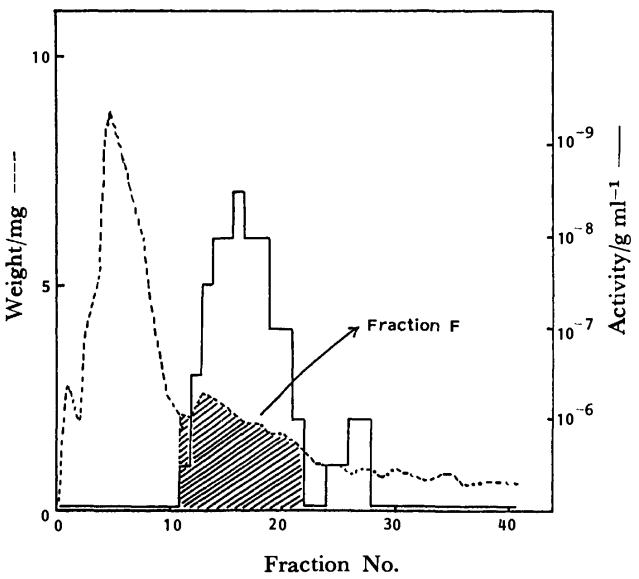

Fig. 2. Reversed-phase partition chromatography of Fraction E on the siliconized Hyflo Super Cel column (Table 1). Moving phase, MeOH–H_2O–AcOH (75 : 75 : 1); stationary phase, $CHCl_3$–2-ethyl-1-hexanol (1 : 1). The hatching activity was checked with the eggs.

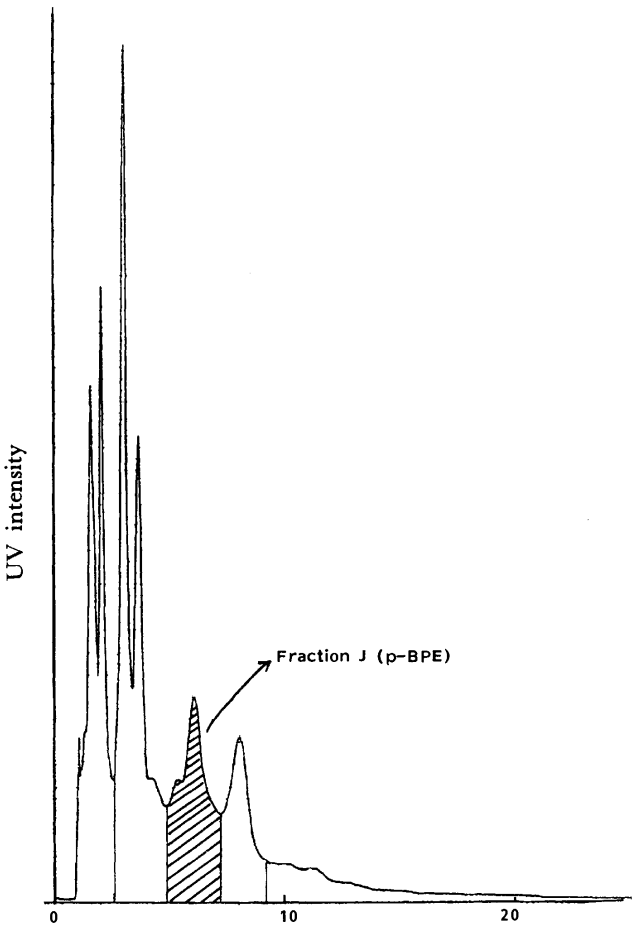

Fig. 3. Preparative HPLC of Fraction I (p-BPE) on the MicroPak CN-10 column (Table 1). Eluent, hexane–ether (45 : 55).

performed efficiently, as had been exemplified by smooth separation of prostaglandins such as PGE_1 and PGE_2.[24,25] However, the silver cations, contaminated in the columns and eluted with solvents, caused serious decrease in the activity of eluates and disturbed the bioassay. It was necessary to wash the columns with distilled water repeatedly (ca. 1 month) in order to remove the silver cations completely and carry out the bioassay in a usual manner. b) *p*-Bromophenacylation of the acid mixture [Fraction H to I (p-BPE)] did not proceed in a satisfactory yield (ca. 30%) by the reported procedure using crown ethers.[26] c) Preparative HPLC on three different types of columns resulted in the effective separation of active fractions, giving only one active fraction in each of the steps without loss of the activity (Figs. 3, 4, and 5). The MicroPak CN-10 column[27] is packed with silica gel (LiChrosorb Si-60) whose surface is bonded chemically with 3-cyanopropylsilyl groups and hence is hydrophobic. The column was found to be superior to silica gel itself (MicroPak Si-10)[20,27] in reproducibility. On the other hand, the MicroPak NH_2-10 column[27] is much polar than the MicroPak CN-10 one, because it is filled up with silica gel (LiChrosorb Si-60) whose surface is modified chemically with 3-aminopropylsilyl groups and interacts with solutes by hydrogen bonding. The Hitachi Gel #3011 column[27b,28] is completely different from these two columns in the separation mode. The packing is a porous polystyrene-divinylbenzene copolymer and the separa-

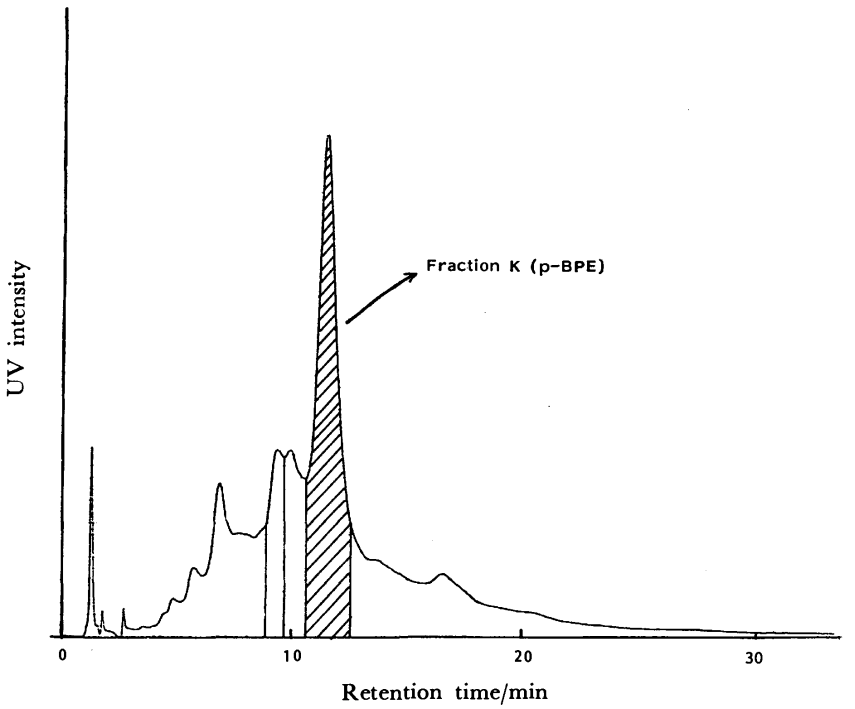

Fig. 4. Preparative HPLC of Fraction J (p-BPE) on the MicroPak NH_2-10 column (Table 1). Eluent, hexane–CH_2Cl_2–MeCN (70 : 18 : 12).

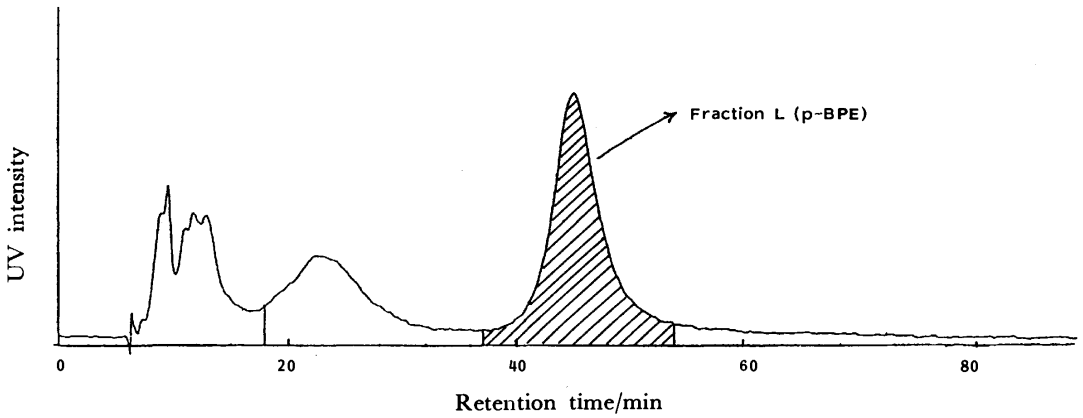

Fig. 5. Preparative HPLC of Fraction K (p-BPE) on the Hitachi Gel #3011 (Table 1). Eluent, MeOH–CH_2Cl_2 (9 : 1).

tion appears to be attributed to a kind of hydrophobic adsorption and/or van der Waals' interaction between the gels and solutes. Examination with p-BPEs of monobasic and dibasic acids suggested that the active principle(s) would probably be dibasic acid(s).[20] All these findings led us to revise the procedure as shown in Table 2 and to obtain a lot of Fraction L (p-BPE) which, if necessary, may be subjected to further purification.

The isolation procedure summarized in Table 2 was improved as follows. a) Initial fractionation of the hatch-stimulating concentrates (Fraction C to F) (Figs. 6 and 7), following the Charcoal-Celite chromatography, proceeded smoothly without loss of the activity and with high recovery of the material by chromatography on columns different from the previous ones; namely, chromatography over silica gel, siliconized Hyflo Super Cel, and ionic exchange resins (Table 1) was replaced by that over Sephadex LH-20 and DEAP-Sephadex LH-20. The Sephadex LH-20 column consists of a kind of methylene-bridged dextran (Sephadex G-25) whose surface (hydroxyl groups) is bonded chemically with 2-hydroxypropyl groups, and is used for gel permeation chromatography as a molecular sieve, including weak interaction (adsorption) between the gels and solutes, and partition chromatography,[29] depending on eluents. The partition chromatography on this column with a 95:5 mixture of dichloromethane and methanol had been used for separation of prostaglandins[29b] as efficiently as that on the siliconized Hyflo Super Cel column. On the other hand, the DEAP-Sephadex LH-20 column[30,31] is packed with Sephadex LH-20 whose surface (hydroxyl groups) is modified chemically by 3-diethylamino-2-hydroxypropyl groups and behaves as a lipophilic anion exchanger. This was effective for group separation of mono-, di-, and polybasic acids as had been shown for separation of fatty acids.[31] b) Efficient *p*-bromophenacylation of the acid mixture [Fraction F to G (p-BPE)] was achieved in the presence of *N,N*-diisopropylethylamine in acetonitrile,[32] giving the corresponding esters in an almost quantitative yield. c) Fractionation of a mixture of the p-BPEs of acids [Fraction G (p-BPE) to I (p-BPE)] was initially performed by preparative HPLC on Hitachi Gel #3019 and then on Bondapak C_{18}/Porasil B columns,[27d] which are recommended for large scale preparative work, because of a large amount (ca. 300 mg) of Fraction G (p-BPE) compared with that (ca. 1 mg) of

Table 2. Isolation of GEA as its p-BPE

Dried and powdered roots of kidney bean "Hon-kintoki" [113 kg (1 ha)]	
↓ Extraction with water (1.5 kl) (<10 °C)	
↓ Evaporation (<30 °C) under reduced pressure	
Concentrates	
↓ Continuous extraction with chloroform at pH 2—3	
Chloroform extracts A	(102 g, active at 10^{-5} g ml^{-1})
↓ EtOAc-aq $NaHCO_3$	
Acidic extracts B	(57 g, active at 10^{-5}--$^{-6}$ g m^{-1})
↓ Charcoal-Celite column (aq acetone)	
Fraction C	(21.5 g, active at 10^{-6} g ml^{-1})
↓ Sephadex LH-20 column (MeOH)	
Fraction D	(10.1 g, active at 10^{-6}--$^{-7}$ g ml^{-1})
↓ DEAP-Sephadex LH-20 column (72% EtOH-AcOH-NH_4OH)	
Fraction E	(2.16 g, active at 10^{-7} g ml^{-1})
↓ Sephadex LH-20 column (CH_2Cl_2-MeOH, 95:5)	
Fraction F	(135 mg, active at 10^{-8} g ml^{-1})
↓ *p*-Bromophenacylation (*p*-$BrC_6H_4COCH_2Br$ and *i*-Pr_2NEt in MeCN, 20 °C)	
↓ Silica-gel column	
Fraction G (p-BPE)	(316 mg, active at 10^{-8} g ml^{-1} after hydrolysis)
↓ Preparative HPLC, Hitachi Gel #3019 (MeOH-CH_2Cl_2, 7:3)	
Fraction H (p-BPE)	(112 mg, active at 10^{-8}--$^{-9}$ g ml^{-1} after hydrolysis)
↓ Preparative HPLC, Bondapak C_{18}/Porasil B (MeOH-H_2O, 8:2)	
Fraction I (p-BPE)	(29 mg, active at 10^{-9} g ml^{-1} after hydrolysis)
↓ Preparative HPLC, μBondapak NH_2 column (C_6H_{14}-CH_2Cl_2-MeCN, 70:18:12)	
Fraction J (p-BPE)	(2.2 mg, active at 10^{-10} g ml^{-1} after hydrolysis)
↓ Preparative HPLC, μBondapak NH_2 column (C_6H_{14}-CH_2Cl_2-MeCN, 80:12:8)	
Fraction K (p-BPE)	(1.2 mg, active at 10^{-10} g ml^{-1} after hydrolysis)
↓ Preparative HPLC, μBondapak NH_2 column (C_6H_{14}-CH_2Cl_2-MeCN, 60:36:4)	
Fraction L (p-BPE) (=GEA p-BPE)	(≈50 μg, active at 10^{-11}--$^{-12}$ g ml^{-1} after hydrolysis)

the corresponding fraction [Fraction I (p-BPE)] in Table 1. These columns, packed with particles of dp ≒50 μm, are similar to Hitachi Gel #3011[27b,28] and μBondapak C_{18}, columns[27b,27c] (dp≒10 μm), respectively, in the chemical constitution and separation selectivity. Of the latter two columns, the μBondapak C_{18} one is packed with silica gel (μPorasil) whose surface is chemically bonded with octadecylsilyl groups and hence hydrophobic, and is useful for high-efficiency reversed-phase partition chromatography, as shown by effective separation of p-BPEs of a variety of fatty acids differing in the number and geometry of double bonds and hydroxyl groups.[33] Thus Fractions G and H (p-BPEs) were separated roughly into several fractions with somewhat loss of active fractions. d) Subsequent preparative HPLC [Fraction I (p-BPE) to L (p-BPE)] on a μBondapak NH_2 column with three different systems of eluents effected smooth separation of active fraction(s), finally giving the relevant fraction, Fraction L (p-BPE). The column[27,34] is packed with silica gel (μPorasil) whose surface is bonded chemically with 3-aminopropylsilyl groups and is used for normal-phase adsorption chromatography. Examination of

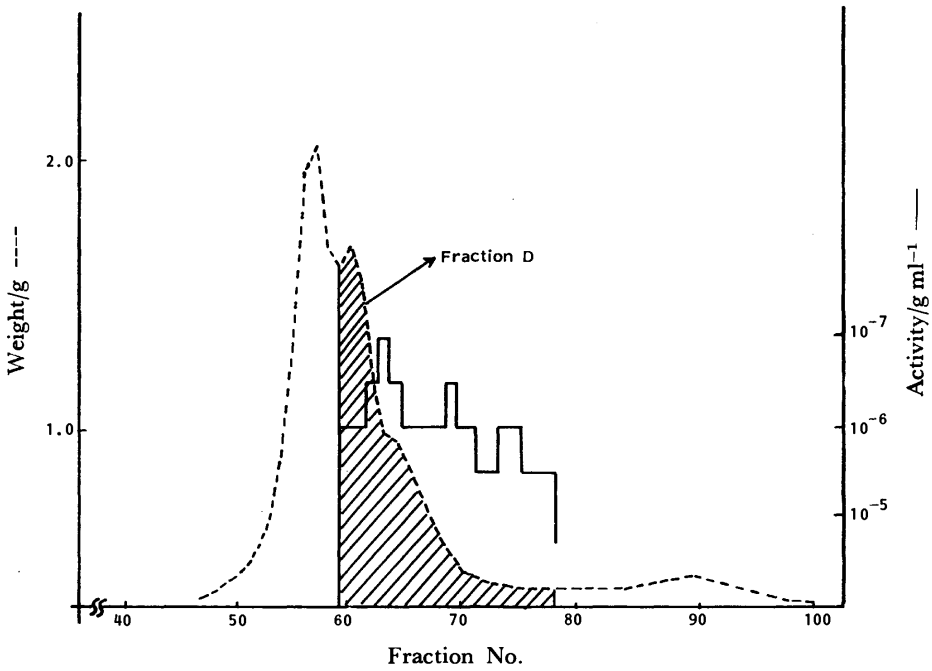

Fig. 6. Column chromatography of Fraction C on the Sephadex LH-20 column (Table 2). Eluent, MeOH. The hatching activity was checked with the eggs.

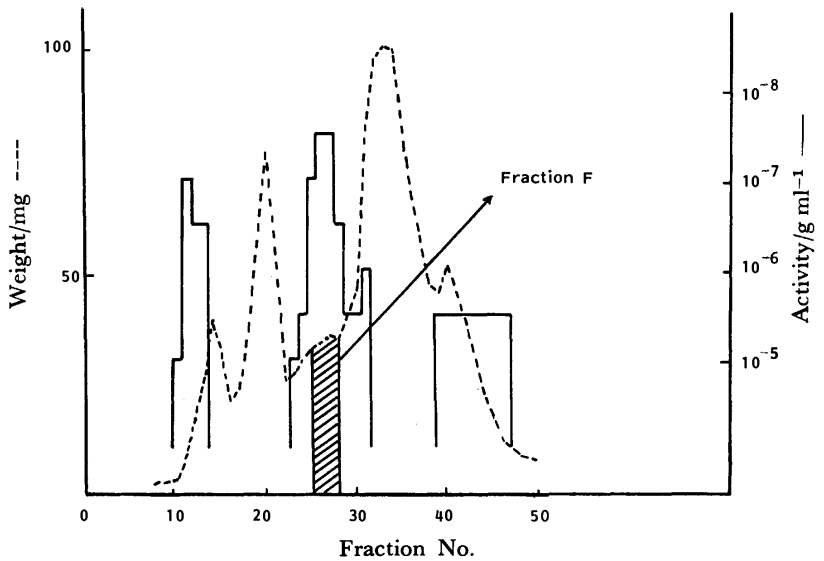

Fig. 7. Column chromatography of Fraction E on the Sephadex LH-20 column (Table 2). Eluent, CH_2Cl_2–MeOH (95 : 5). The hatching activity was checked with the eggs.

model compounds indicated that the separation sequence or selectivity of a series of p-BPEs of fatty acids and their derivatives was influenced remarkably by delicate change of the eluent systems.[20]

In 1981, after the careful chromatographic purification described above, we could achieve the isolation of ca. 50 μg of Fraction L (p-BPE), which showed a single peak by analytical HPLC on μBondapak NH_2, μBondapak C_{18}, and μBondapak/Phenyl columns,[27] and stimulated the hatching at 10^{-11}—$^{-12}$ g ml^{-1} after hydrolysis. With this sample, we could observe a clear triplet, corresponding to the molecular ion peaks, in the FD-MS spectrum[15] and useful signals in the ^{1}H NMR spectrum.[15] These spectral data led us to assign the molecular formula to GEA and to presume the presence of several oxygen functions.[15] These results, coupled with other evidence discussed later, have led us to believe that Fraction L is the p-BPE of an active principle itself, designated as GEA.[15] However, we could not accomplish the elucidation of the whole structure of GEA, owing to the limited amount (ca. 50 μg) of the isolated GEA p-BPE. It was required to isolate a large amount, at least 500 μg, of GEA p-BPE. Thus the starting hatch-stimulating concentrates (ca. 1 kg) were prepared from dried and powdered roots (ca. 1 ton) of kidney bean, which had been collected in 10 hectares of the field at Memuro, and fractionated, according to the procedure shown in Table 3.

The procedure summarized in Table 3 was practically the same as the previous one (Table 2) in the sequence and efficiency. a) In each of the steps, a dozen or several dozens of chromatographic separations were repeated cautiously and laboriously,

Table 3. Isolation of GEA, GEB, and GEC as their p-BPEs

Dried and powdered roots of kidney bean [1058 kg (10 ha)]
↓ Extraction with water (<10 °C, 15 kl)
↓ Evaporation (<30 °C) under reduced pressure
Concentrates
↓ Continuous extraction with chloroform at pH 2—3
Chloroform extracts A (1011 g, active at 10^{-5} g ml^{-1})
↓ EtOAc-aq $NaHCO_3$
Acidic extracts B (636 g, active at 10^{-5}—$^{-6}$ g ml^{-1})
↓ Charcoal-Celite column (aq acetone)
Fraction C (197.3 g, active at 10^{-6} g ml^{-1})
↓ Sephadex LH-20 column (MeOH)
Fraction D (88.9 g, active at 10^{-6}—$^{-7}$ g ml^{-1})
↓ DEAP-Sephadex LH-20 column (72% EtOH-AcOH-NH_4OH)
Fraction E (18.15 g, active at 10^{-7} g ml^{-1})
↓ Sephadex LH-20 column (CH_2Cl_2-MeOH, 95:5)
Fraction F (3.59 g, active at 10^{-7}—$^{-8}$ g ml^{-1})
↓ Sephadex LH-20 column (CH_2Cl_2-MeOH, 97:3)
Fraction G (951 mg, active at 10^{-8} g ml^{-1})
↓ *p*-Bromophenacylation (*p*-$BrC_6H_4COCH_2Br$ and *i*-Pr_2NEt in MeCN, 20 °C)
↓ Silica-gel column
Fraction H (p-BPE) (2057 mg, active at 10^{-8} g ml^{-1} after hydrolysis)
↓ Hitachi Gel #3019 column (MeOH-CH_2Cl_2, 8:2)
Fraction I (p-BPE) (336 mg, active at 10^{-9} g ml^{-1} after hydrolysis)
↓ Preparative HPLC, μBondapak C_{18} (MeOH-H_2O, 8:2)
Fraction J (p-BPE) (79 mg, active at 10^{-10} g ml^{-1} after hydrolysis)
↓ Preparative HPLC, μBondapak NH_2 (C_6H_{14}-CH_2Cl_2-MeCN, 76:14:10)
→ Fraction K′ (p-BPE) (4.9 mg, inactive ? after hydrolysis)
↓ μBondapak NH_2 (C_6H_{14}-CH_2Cl_2-MeCN, 60:36:4)
Fraction K″ (p-BPE) (1.8 mg, inactive at 10^{-8} g ml^{-1} after hydrolysis)
↓ (=GEC p-BPE)
Fraction K (p-BPE) (8.8 mg, active at 10^{-11} g ml^{-1})
↓ Preparative HPLC, μBondapak NH_2 (C_6H_{14}-CH_2Cl_2-MeCN, 63:33:4)
→ Fraction L′ (p-BPE) (2.6 mg, inactive ? after hydrolysis)
↓ Preparative HPLC, μBondapak NH_2 (C_6H_{14}-CH_2Cl_2-MeCN, 68:13.2:8.8)
Fraction L″ (p-BPE) (1.8 mg, inactive at 10^{-8} g ml^{-1} after hydrolysis)
↓ (=GEB p-BPE)
Fraction L (p-BPE) (1.25 mg, active at 10^{-11}—$^{-12}$ g ml^{-1} after hydrolysis)
(=GEA p-BPE)

because of a large amount of the material to be fractionated. b) Two previous large-scale separation steps (Table 2), which had not always given satisfactory results, were revised as follows. i) Chromatography on the Hitachi Gel #3019 column [Fraction H (p-BPE) to I (p-BPE)] was carried out more easily at atmospheric pressure (Fig. 8) (not at high pressure in Table 2), and ii) preparative HPLC of Fraction I (p-BPE), corresponding to Fraction H (p-BPE) in Table 2, was performed more efficiently on the μBondapak C_{18} column (expensive !) for preparative scale work (Fig. 9) (not on the Bondapak C_{18}/Porasil B one). c) Subsequent fractionation of Fraction J (p-BPE) on the μBondapak NH_2 column afforded Fraction K (p-BPE) as the major fraction, which was active at 10^{-11} g ml^{-1} after hydrolysis, along with the minor one [Fraction K′ (p-BPE)] (Fig. 10). The latter was further purified by preparative HPLC on the same column to give Fraction K″ (p-BPE) [=glycinoeclepin C (GEC) p-BPE] (1.8 mg). The major fraction was further purified by preparative HPLC on the same column with a different eluent

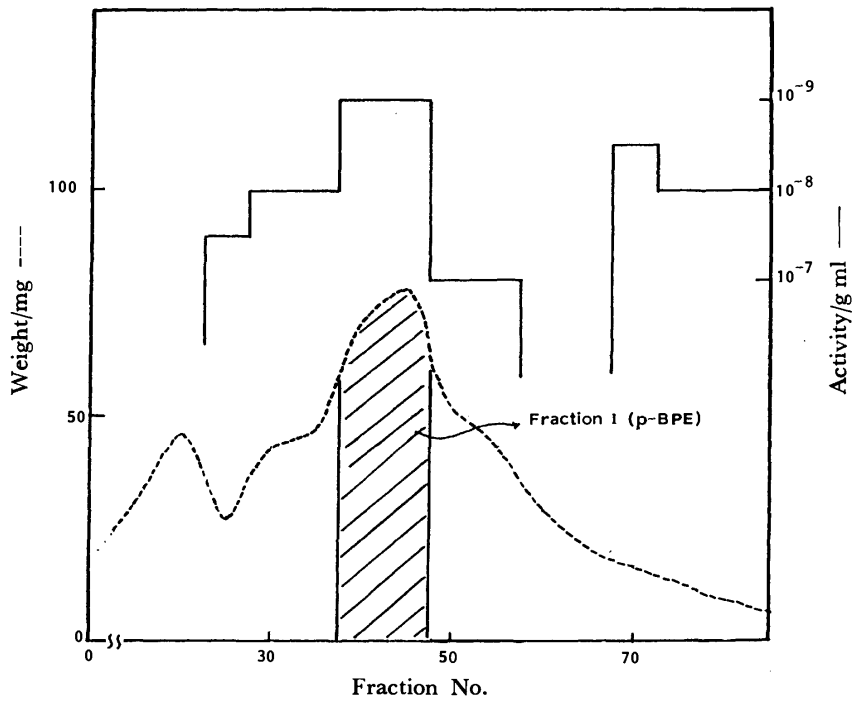

Fig. 8. Column chromatography of Fraction H (p-BPE) on the Hitachi Gel #3019 column (Table 3). Eluent, MeOH–CH_2Cl_2 (8 : 2). The hatching activity was checked with the eggs.

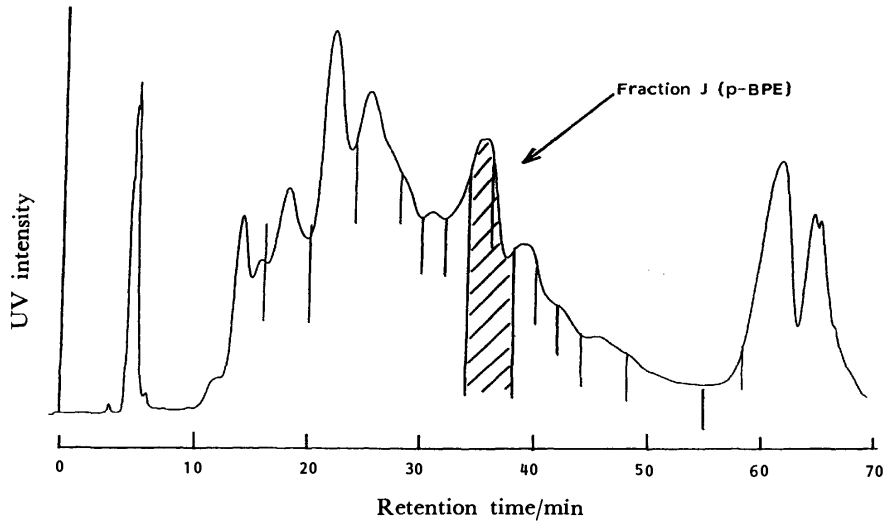

Fig. 9. Preparative HPLC of Fraction I (p-BPE) on the μBondapak C_{18} (Table 3). Eluent: R_t 0—55 min, MeOH–H_2O (8 : 2); R_t 55—70 min, MeOH.

system to give Fraction L (p-BPE) (=GEA p-BPE) (1.25 mg) and Fraction L′ (p-BPE) (Fig. 11). The latter was purified in the same manner to yield Fraction L″ (p-BPE) [=glycinoeclepin B (GEB) p-BPE] (1.8 mg). The p-BPE of GEA was then hydrolyzed with base under mild conditions to give GEA, which, after purification by HPLC on the μBondapak C_{18} column, showed a single peak (Fig. 12) and high activity (active at 10^{-12} g ml^{-1}) for the hatching in water. Likewise, the p-BPEs of GEB and

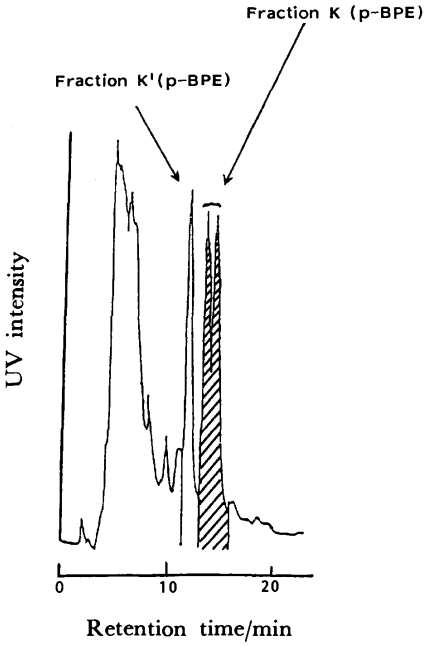

Fig. 10. Preparative HPLC of Fraction J (p-BPE) on the μBondapak NH_2 column (Table 3). Eluent, hexane–CH_2Cl_2–MeCN (76 : 14 : 10).

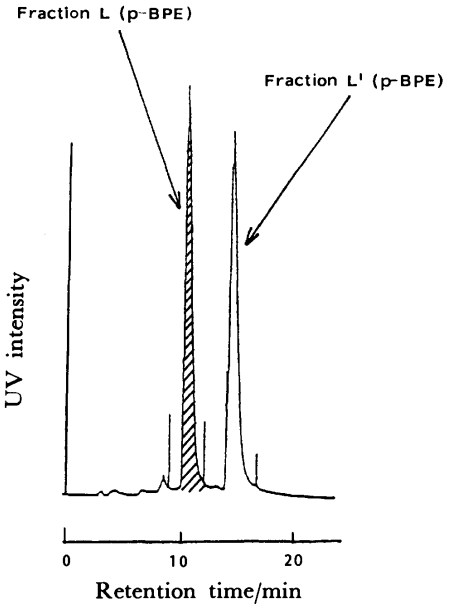

Fig. 11. Preparative HPLC of Fraciton K (p-BPE) on the μBondapak NH_2 column (Table 3). Eluent, hexane–CH_2Cl_2–MeCN (63 : 43 : 3).

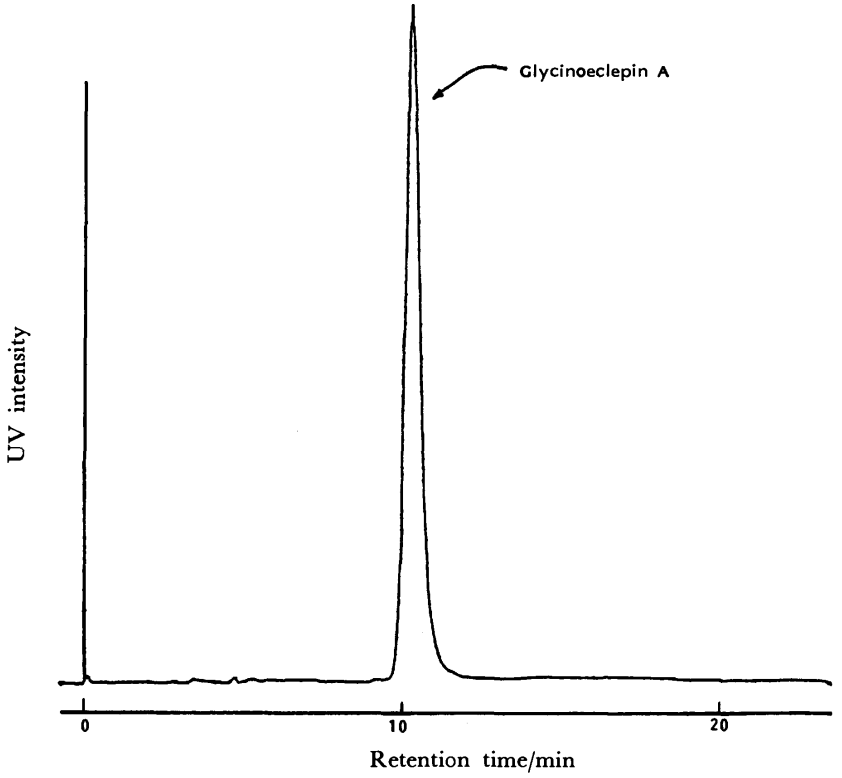

Fig. 12. Analytical HPLC of Glycinoeclepin A on the μBondapak C_{18} column. Eluent, 0.1% AcOH–H_2O and MeOH (35 : 65).

Table 4. Hatching and Larval Emergence of the Soybean Cyst Nematode[a] in an Aqueous Solution of GEA[b]

Test soln	Total eggs	Unhatched eggs	Hatched larvae	
			Unemerged	Emerged
GEA[b]	2158 (8 cysts)	505 (23.4%)[c]	136 (6.3%)	1517 (70.3%)[d]
Water	2875 (9 cysts)	2352 (81.8%)	302 (10.5%)[e]	221 (7.7%)[e]

a) The cysts were soaked at 25 °C and, without dissection, kept in the test soln and in water, respectively, at 25 °C for 10 d. b) A highly dilute soln of GEA (10^{-10} g ml^{-1}) was used. c) Most of the eggs were immature or dead. d) These larvae moved actively. e) These larvae did not move actively, and when kept in the test soln, moved actively.

GEC were converted into the corresponding acids GEB and GEC, which were purified by HPLC on a NOVA-PAK cartridge C_{18}[35] and were not active for the hatching at 10^{-8} g ml^{-1} in water.

Identification of Glycinoeclepin A as the Active Principle. Identification of GEA as the active principle was deduced from the following evidence. i) The fraction isolated always showed a single peak by analytical HPLC over a variety of columns (μBondapak NH_2, MicroPak NH_2-10, μBondapak C_{18}, and μBondapak/Phenyl) with different solvent systems. ii) The fraction was divided into ten fractions by HPLC on a Develosil ODS-5 column. The hatching activity of each divided fraction after hydrolysis paralleled the quantity of the respective fraction, estimated by the UV spectra.[19] iii) The activity (10^{-12} g ml^{-1}) of crystalline GEA p-BPE, obtained by recrystallization from hexane and dichloromethane, was slightly higher than that (10^{-11}—$^{-12}$ g ml^{-1}) of GEA p-BPE contained in the mother liquors after hydrolysis. iv) As described in the preceding section, the fraction was hydrolyzed with base (0.1 M† KOH in MeOH), acidified with acid (0.2 M HCl) to pH 2—3, and extracted with ethyl acetate. The extracts were simply separated by HPLC over μBondapak C_{18} with acidic aqueous methanol to give GEA, which showed a single peak on the column and high activity (10^{-12} g ml^{-1}) (Fig. 12). Surprisingly, the IR spectrum [1572 and 1420 cm^{-1} (KBr)] indicated that GEA was not isolated as the acid itself but as its (potassium) salt. All these facts confirmed that GEA is the active principle itself.

Biological Activity of Glycinoeclepin A. Biological activity of GEA for the hatching and emergence was examined, the result (Table 4) being summarized as follows. The cysts were soaked in water at 25 °C for 10 d, and then kept in a highly dilute solution (10^{-10} g ml^{-1}) of GEA in water at 25 °C for 10 d. In the test solution, ca. 80% of the eggs hatched and most of the hatched larvae emerged out of the cysts, while in water more than 80% of the eggs were not hatched, and less than half (8%) of the hatched larvae emerged out of the cysts. The result indicates that GEA stimulates not only hatching but also emergence of the soybean cyst nematode in a highly dilute solution, and is completely consistent with the Sakurai and Tsutsumi result using the root diffusate of kidney bean.[14] Further examination revealed that (i) most of the unhatched eggs in the test solution were found to be dead or immature under a microscope, and were not hatched by additional addition of the test solution, (ii) the larvae which emerged in the test solution moved actively, while those in water did not move, but moved actively on addition of the test solution, and (iii) naturally, the unhatched eggs in water were hatched when kept in the test solution. These observations imply that the hatching may be only a resultant phenomenon of active motion of the second stage larvae, and GEA may stimulate the motor nervous system of the larvae.

† 1 M=1 mol dm^{-3}.

Experimental

The bioassay was carried out according to the procedure described in the text. The melting points were measured in open capillaries or under a microscope, and uncorrected. Preparative TLC was carried out on silica gel (Wakogel B-5F or Merck Kieselgel 60 F254) and spots were detected by a UV lamp or in iodine vapor unless otherwise stated. The IR and ^{1}H NMR spectra were measured in liquid state and in [^{2}H]chloroform, respectively, unless otherwise stated. Analytical and preparative HPLC were performed at 22 °C with a Varian Aerograph 4200 and a Waters Associates 6000A liquid chromatograph, equipped with a UV monitor (JASCO UVDEC-100), and the chromatograms were recorded on a Unicorder Model-22 M or -225 MB (Nippon Denshi Kagaku Co.). All guranteed solvents (Wako Pure Chemical Ind.) were used as carrier solvents without further purification, unless otherwise stated.

(I) Experimentals Summarized in Table 1. Preparation of Chloroform Extracts A and Acidic Extracts B. Roots of "Beni-kintoki," a subspecies of kidney bean, cultivated in 1 hectare of the field at Memuro, Hokkaido, were collected in late July or in early August just before the flowering time, washed roughly with water, air-dried, and crushed. The powdered roots amounted to 135 kg. A part of the roots (ca. 15 kg) was extracted with water (95 l) below 10 °C for 3 d to be prevented from putrefaction. After being squeezed, the roots were again extracted with water (2×60 l). The combined aqueous (aq) muddy suspension was concentrated

to ca. 10 l below 30 °C by a thin film evaporator (Hitachi Kontro). This process (extraction and concentration) was repeated nine times. All the concentrates (ca. 100 l) were combined and made acidic to pH 2—3 with 6 M hydrochloic acid (HCl). A part of the aq suspension (ca. 40 l) was extracted with chloroform (ca. 60 l) continuously for 50 h by a special Soxhlet apparatus (Shibata Chemical Apparatus Mfg. Co.). This extraction procedure was repeated three times. The combined chloroform solution (soln) was evaporated to leave an oily material (223 g), which was distilled under reduced pressure below 50 °C to remove inactive lower fatty acids, giving Chloroform extracts A (115 g).

The fraction (115 g) was dissolved in ethyl acetate (300 ml) and treated with saturated aq sodium hydrogencarbonate ($NaHCO_3$) (600 ml+4×50 ml). The acetate soln was washed with water (50 ml), dried and evaporated to leave neutral and basic substances, which were not further examined. The combined aq soln (ca. 850 ml) was acidified to pH 2 by addition of 6 M HCl (140 ml) and extracted with ethyl acetate (5×200 ml). The combined acetate soln was washed with water (50 ml) and evaporated to give Acidic extracts B (66.5 g), which was active at 10^{-5}—$^{-6}$g ml^{-1} for the hatching. The acidic aq soln was further extracted with 1-butanol (3×300 ml). The butanol soln was evaporated to leave an acidic oil (7.9 g), which was active at 10^{-5} g ml^{-1} and was not further examined.

Chromatography on a Charcoal-Celite Column (B to C). Charcoal (220 g, Tokusei-Shirasagi Brand, Takeda Chemical Ind.) and Celite-545 (440 g, Johns-Manville) were mixed thoroughly with water and packed in a glass column (7×64 cm). A part (22 g) of Acidic extracts B was dissolved in acetone, mixed with Celite (40 g), evaporated, placed on the top of the column, and then eluted successively with water (2.2 l), water-acetone (9:1, 8:2, 7:3, 6:4, 5:5, 4:6, 3:7, 2:8 and 1:9, v/v, each 2.2 l), acetone (4×2.2 l), benzene (2×2.2 l), and methanol-concd aqueous ammonia (NH_4OH) (21:1, v/v, 4.4 l). This procedure was repeated three times. Each fraction, other than that eluted with ammoniacal methanol, was evaporated to give an oily or solid eluate. The methanol fraction was dissolved in water (100 ml), acidified and extracted with 1-butanol, and the butanol soln was likewise evaporated. The amount and biological activity of each eluate is described in Fig. 1. The 80% aq acetone eluate (5.2 g) (Fraction C), showing the highest activity (active at 10^{-7} g ml^{-1}), was submitted to further separation. Each eluate, even if inactive, was examined in somewhat detail.

i) Eluates with 40% Aqueous Acetone. The oily eluate (950 mg) was separated into 6 fractions by preparative TLC with benzene-1-butanol-acetic acid (16:3:1): Fraction (Fr.) 1, (R_f=0.7) 125 mg: 2, (0.4) 337; 3, (0.3) 253; 4, (0.2) 40; 5, (0.15) 36; 6, (0.05) 29 mg. To an ethanol soln (10 ml) of Fr. 2 (305 mg), adjusted to pH 6.8 with 0.1 M aq potassium hydroxide (KOH) and one drop of 0.1 M HCl, was added *p*-bromophenacyl bromide (1 g) in ethanol (25 ml). The mixture was heated under reflux for 1.5 h,[36] cooled and extracted with chloroform (4×10 ml). The chloroform soln was worked up as usual to give orange crystals (1048 mg), which were roughly separated by column chromatography over silica gel (Merck 120—230 mesh, 10 g, 1.8×9.5 cm) with chloroform into 3 fractions. The third eluate gave a crystalline mixture of p-BPEs (577 mg), from which 2-hydroxy-4-methylpentanoic acid p-BPE (90 mg), mp 86.5—88 °C ($CHCl_3$-hexane), $[\alpha]_D$ −5° ($CHCl_3$), and 2-hydroxy-3-methylpentanoic acid p-BPE (125 mg), mp 35—39 °C ($CHCl_3$), $[\alpha]_D$ −12° ($CHCl_3$), were isolated by twice preparative TLC with chloroform-benzene (9:1, double development). The IR and ^1H NMR spectra of these esters were identical with those of the p-BPEs of the authentic samples, respectively.[37,38] Fr. 4 was purified by chromatography over silica gel with ethyl acetate to give crude vomifoliol (9 mg), which will be described later.

ii) Eluates with 50% Aqueous Acetone. A part (2.05 g) of the solid eluate was separated into 6 fractions by preparative TLC with a 1:4 mixture of ethyl acetate and an upper phase of benzene-propionic acid-water (8:3:5): Fr. 1, (R_f=0.8) 600 mg; 2, (0.6) 327; 3, (0.4) 216; 4, (0.25) 130; 5, (0.2) 161; 6, (0.1) 128. Fr. 1 (25 mg) gave 3- furoic acid (10 mg), mp 120—120.5 °C, on recrystallization from water. Fr. 2 (100 mg) was separated into 3 fractions by preparative TLC with an upper phase of benzene-acetic acid-water (3:3:1). The lst fraction (R_f=0.6) gave a crystalline substance (25 mg), which on recrystallization from water afforded suberic acid (3 mg), mp 135—137°C. The mother liquor (18 mg), after sublimation, gave 2-furoic acid (4 mg), mp 128—129 °C. The 2nd fraction (R_f=0.5) gave a crystalline substance (18 mg), which on recrystallization from water yielded maltol (3 mg), mp 158—159 °C.

Fr. 5 (150 mg) was purified by preparative TLC with ethyl acetate to give a crystalline substance (55 mg), which on recrystallization from benzene gave vomifoliol (i) (24 mg), mp 112—113°C; $[\alpha]_D$ +220° ($CHCl_3$); CD, λ_{max}^{MeOH} ($\Delta\varepsilon$) 318 nm (−0.65) and 240 (+11.9); UV (MeOH), 237 nm (ε 13900); IR (Nujol), 3400, 1662, 1617, and 973 cm^{-1}; ^1H NMR, δ=1.01 and 1.07 (each 3H, s), 1.28 (3H, d, J=6 Hz), 1.88 (3H, d, J=1.5 Hz), 2.07 (2H, 2OH, D_2O-exchangeable), 2.23 and 2.42 (each 1H, ABq, J=17 Hz), 4.38 (1H, dq, J=6 and 3.5 Hz), 5.75 (1H, d, J=16 Hz), 5.83 (1H, dd, J=16 and 3.5 Hz), and 5.88 (1H, q, J=1.5 Hz); MS m/z 206 (M^+ −18), 168, and 124 (base). This was identified by direct comparison with (+)-vomifoliol[39—43] (blumenol A) from *Podocarpus blumei* Endl.[41]

Fr. 3 (130 mg) was purified by preparative TLC with ether-benzene (9:1) and then with ethyl acetate to give dehydrovomifoliol (ii) (11 mg), oil; $[\alpha]_D$ +159°($CHCl_3$); CD, λ_{max}^{EtOH} ($\Delta\varepsilon$) 318 nm (−1.95), 240 (+27.6); UV (EtOH), 237 nm (ε 20000); IR ($CHCl_3$), 3400, 1666, 1626, and 982 cm^{-1}; ^1H NMR, δ=1.01 and 1.09 (each 3H, s), 1.87 (3H, d, J=1.5 Hz), 2.29 (3H, s), 2.34 and 2.48 (each 1H, ABq, J=17 Hz), 5.95 (1H, q, J=1.5 Hz), and 6.45 and 6.83 (each 1H, ABq, J=16 Hz); MS, m/z 166 (M^+ −56) and 124 (base). These spectral data indicated the compound (**ii**) to be a dehydro derivative of vomifoliol (**i**). This was confirmed by conversion of **i** into **ii** as follows. To a soln of **i** (23 mg) in acetone (0.5 ml) was added Jones reagent [CrO_3 (10 mg), H_2SO_4 (0.01 ml), and H_2O (0.03 ml)]. The mixture was stirred for 3 min, diluted with water (2 ml), and extracted with ethyl acetate (3×1 ml). The combined acetate soln was evaporated to leave an oil (22 mg), which was purified by preparative TLC with benzene-ethyl acetate (1:1) to yield **ii**. The compound (**ii**), named (+)-dehydrovomifoliol,[42—46] appeared to be a new compound isolated from natural sources, although its racemate had been prepared by two groups.[39,47,48] (+)-Dehydrovomifoliol (**ii**) was converted

into (+)-abscisic acid in the same manner[47] as the synthetic racemate[47,48] as follows. A mixture of **ii** (18 mg) and (ethoxycarbonylmethylene)triphenylphosphorane (29 mg) in toluene (1 ml) was heated under reflux for 4 h and distilled to remove the toluene. The residue was heated at 150—170 °C for 40 min, cooled, and separated by preparative TLC with benzene–ethyl acetate (1:1) to give a mixture (9 mg) of esters. The mixture (8 mg) was hydrolyzed with 2M methanolic KOH (6 ml) at room temperature (temp) for 23 h. The reaction mixture was evaporated, acidified with 1.5 M HCl (4 ml), and extracted with ether (3×2 ml). The ether soln gave a 1:1 mixture[39] of (+)-abscisic acid[49] and its 2-*trans*-isomer:[47,48] CD, $\lambda_{max}^{0.006\,M\,HCl\,in\,EtOH}$ ($\Delta\varepsilon$) 318 nm (−0.92), 265 (+28.2), and 230 (−21.0); UV (0.006 M HCl in EtOH), 262 nm (ε 21000). These spectral values indicated that (+)-dehydrovomifoliol (**ii**) possessed the same absolute configuration at the carbon atoms corresponding to C-6 of abscisic acid.[39]

Fr. 6 (80 mg) was purified by preparative TLC with benzene-1-butanol-acetic acid (14:5:1) to give dihydrophaseic acid (**iii**) (34 mg), amorphous; CD, λ_{max}^{MeOH} ($\Delta\varepsilon$) 265 nm (−2.8); UV (MeOH), 259 nm (ε 15500); ^{1}H NMR (CD_3COCD_3), δ=0.90 and 1.06 (each 3H, s), 1.80 (4H, br), 1.95 (3H, d, J=1.5 Hz), 3.60 (1H, d, J=7.5 Hz), 3.73 (1H, dd, J=7.5 and 1.5 Hz), 4.10 (1H, br), 5.66 (1H, br s), and 6.54 and 8.06 (each 1H, d, J=16 Hz); MS, m/z 282 (M^+) and 264. The acid (**iii**) was converted with ethereal diazomethane into its methyl ester, amorphous; IR ($CHCl_3$), 3420, 1710, 1674, and 1610 cm^{-1}; ^{1}H NMR, δ=0.95 and 1.17 (each 3H, s), 1.80 (4H, br), 2.05 (3H, d, J=1.5 Hz), 3.72 (3H, s), 3.77 (2H, br), 4.26 (1H, m, W_H=20 Hz), 5.73 (1H, q, J=1.5 Hz), 6.40 and 7.98 (each 1H, d, J=16 Hz); MS, m/z 296 (M^+), 278, 264, 247, 246, 154, 125, 122, 94, and 43 (base). The ester was oxidized with Jones reagent as follows. To a soln of the ester (6 mg) in acetone (0.05 ml) was added Jones reagent [CrO_3 (5 mg), H_2SO_4 (0.005 ml), and H_2O (0.02 ml)] for 3 min. The mixture was diluted with water (0.3 ml) and extracted with ethyl acetate (3×0.3 ml). The acetate soln was dried and evaporated to leave an oil (3 mg), which was separated by preparative TLC with benzene–ethyl acetate (1:1) to give the dehydro ester (1 mg), mp 152—155 °C (benzene); CD, λ_{max}^{MeOH} ($\Delta\varepsilon$) 314 nm (−0.55), 262 (+5.2), and 230 (−4.2); ^{1}H NMR,

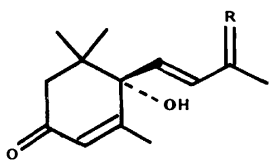

i R=—H, ---OH

ii R==O

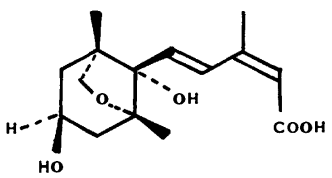

iii

δ=2.50 and 2.64 (each 2H, br s), 3.73 (1H, d, J=8 Hz), and 3.95 (1H, dd, J=8 and 1.5 Hz); MS, m/z 294 (M^+), 276, 121, and 43 (base). The ester was identified as methyl phaseate[49-51] by comparison of the spectral data (MS, IR, and ^{1}H NMR), and hence compound **iii** was named dihydrophaseic acid.[52]

iii) Eluates with 60% Aqueous Acetone. The solid eluate (453 mg) was separated into 6 fractions by preparative TLC with an upper phase of benzene–acetic acid–water (8:3:5): Fr. 1, (R_f=0.4) 178 mg; 2, (0.3) 35; 3, (0.25) 97; 4, (0.15) 28; 5, (0.1) 37; 6, (0.0) 16. Frs. 1 (167 mg) and 2 (30 mg) gave benzoic acid (160 mg) and vanillic acid (19 mg) after sublimation, respectively. Fr. 3 (90 mg) was purified by preparative TLC with ethyl acetate–chloroform–acetic acid (15:5:1) and recrystallized from water to give azelaic acid (46 mg). Fr. 5 (30 mg) was crystallized and recrystallized from chloroform to give *p*-hydroxybenzoic acid (2 mg).

iv) Eluates with 70% Aqueous Acetone. Benzoic, vanillic, and *p*-hydroxybenzoic acids were detected, when the eluate was developed on a silica-gel plate with an upper phase of benzene–acetic acid–water (8:3:5).

v) Eluates with 90% Aqueous Acetone. The solid eluate (2.9 g) was separated by chromatography over silica gel (Merck 120—230 mesh, 300 g, 5×42.5 cm) with ethyl acetate–chloroform–acetic acid (15:5:1). The eluates (each 15 ml) were collected, evaporated and assayed: Frs. 1—36, (537 mg) inactive; 37—41, (506) active at 10^{-6} g ml^{-1}; 42—68, (1033) active at 10^{-7}—$^{-8}$; 69—88, (285) active at 10^{-6}; 89—200, (257), inactive. Fr. 33 (90 mg) was separated into 5 fractions by preparative TLC with an upper phase of benzene–acetic acid–water (8:3:5, developed twice): Fr. 1′, (R_f=0.50) 34 mg; 2′, (0.45) 12; 3′, (0.35), 8; 4′, (0.25) 12; 5′, (0.10) 18. Fr. 1′ (30 mg) gave salicylic acid (8 mg) after sublimation in twice and recrystallization from benzene. Fr. 2′ (10 mg) afforded dodecanedioic acid (4 mg) after recrystallization from chloroform.

vi) Eluates with Acetone, Benzene, and Ammoniacal Methanol. Salicylic acid was detected on a silica-gel plate with ethyl acetate–chloroform–acetic acid (15:5:1).

Chromatography on a Silica-Gel Column (C to D).[53] Fraction C (5.2 g) was separated by chromatography over silica gel (Merck 70—325 mesh, 520 g, 5×66.5 cm) with ethyl acetate–chloroform–acetic acid (15:5:1, v/v/v). The eluates (each 19.5 ml) were collected, evaporated and assayed. The amount and activity of each or collected eluates are summarized as follows: Frs.31—39, (55 mg) inactive; 40—55, (2468) inactive; 56—57, (203) active at 10^{-6} g ml^{-1}; 58—60, (241) active at 10^{-7}; 61—67, (360) active at 10^{-8}; 68—83, (402) active at 10^{-7}; 84—100, (231) active at 10^{-6}; 101—140, (384) active at 10^{-6}; 141—154, (97) inactive; 155—226, (307) inactive. Frs. 61—67 (360 mg) (Fraction D) was the most active and submitted to further separation. Other inactive or less-active fractions were examined in somewhat detail.

i) Fraction 45. The fraction (194 mg) was separated into 5 fractions by preparative TLC with an upper phase of benzene–acetic acid–water (8:3:5): Fr. 1, (R_f=0.45) 53 mg; 2, (0.35) 46; 3, (0.25) 29; 4, (0.10) 28; 5, (0.03) 20. Fr. 2 was treated with ethereal diazomethane and analyzed by GC-MS; column, 5% diethylene glycol adipate polyester on Anakrom Q. Sebacic, undecanedioic acid (ca. 90%), and dodecanedioic acids were identified.

ii) Fraction 53. The fraction (145 mg) was separated into

8 fractions by preparative TLC (twice development) in the same manner as Fr. 45: Fr. 1, (R_f=0.50) 2 mg; 2, (0.45) 2; 3, (0.35) 11; 4, (0.30) 10; 5, (0.25) 35; 6, (0.15) 29; 7, (0.05) 19; 8, (0.00) 19. Fr. 1 gave veratric acid, and Fr. 3 was found to consist of sebacic (trace), undecanedioic (ca. 90%), and dodecanedioic acids by GLC of the trimethylsilyl derivatives (2% OV-17 on Anakrom Q). Fr. 4 gave syringic acid (3 mg) after chromatography over silica gel. Fr. 5, when recrystallized from diisopropyl ether-hexane, gave 4-hydroxydodecanedioic acid γ-lactone (13 mg), mp 48.5—50 °C, which was converted with diazomethane into its methyl ester, mp 20—22 °C: acid, IR ($CHCl_3$), 1760, 1705, and 1170 cm^{-1}: ester, ^1H NMR, δ=1.2—1.9 (14H, br), 2.26 (2H, t, J=7 Hz), 2.5 (2H, m), 3.60 (3H, s), and 4.46 (1H, m, W_H=18 Hz); MS, m/z 242 (M^+), 224, 211, 192, 151, and 85 (base). Frs. 6—8 were found to consist of a mixture of long-chain fatty acids on the basis of their NMR spectra.

iii) Fractions 101—154. The fractions (480 mg) were crystallized from methanol-ethyl acetate and recrystallized from acetic acid to give 9,10,13-trihydroxyoctadecanoic acid (16 mg), mp 139—139.5 °C, which formed its methyl ester, (with diazomethane), mp 117.5—119.5 °C, and trimethylsilyl derivative [with trimethylsilyl *N*-(trimethylsilyl)acetimidate]. The planar structure was elucidated on the basis of the spectral data and chemical reactions.[54] The filtrate (465 mg) was dissolved in ethanol (2 ml). To the soln, adjusted to pH 6.6 with 0.1 M aq KOH and a few drops of 0.1 M HCl, was added *p*-bromophenacyl bromide (607 mg) in ethanol (2 ml). The mixture was heated under reflux for 2.5 h,[36] cooled, concentrated, diluted with water (15 ml), and then extracted with chloroform (2×10 ml). The chloroform soln was worked up as usual to leave an oily residue (1.0 g), which was roughly separated by chromatography over silica gel (Merck 120—230 mesh, 10 g, 2×6.4 cm), with benzene (950 ml), benzene-chloroform (1:1, 600 ml), chloroform (200 ml), and ethyl acetate (200 ml). A fraction eluted with ethyl acetate afforded a mixture of p-BPEs (563 mg), which was further separated into more than 215 fractions [Frs. 1′—137′ (each eluent 9.1 g) and Frs. 138′—215′, (each eluent 14.7 g)] by chromatography over silica gel containing 10% silver nitrate (Merck 120—230 mesh, 70 g, 2×40 cm) with a mixture of chloroform, ethyl acetate, and methanol as eluents.

Frs. 111′—135′ (81 mg), eluted with chloroform-ethyl acetate (2:3), was crystallized and recrystallized from ethyl acetate containing a trace of methanol to give (11*E*)-9,10,13-trihydroxy-11-octadecenoic acid p-BPE (20 mg), mp 127—128 °C. This planar structure was deduced from the following experiment. The ester (7.6 mg) was hydrolyzed with 0.1 M KOH in methanol (2 ml) at room temp for 24 h. The mixture was evaporated, acidified with 3M HCl and extracted with 1-butanol (2×2 ml). The butanol extracts were treated with ethereal diazomethane in methanol to give a mixture of its methyl ester and methyl *p*-bromobenzoate, which was submitted to chromatography over silica gel (Merck 120—230 mesh, 2 g, 1×7 cm) with chloroform and/or ethyl acetate. Eluates with ethyl acetate was evaporated and recrystallized from ethyl acetate to give its methyl ester (3.1 mg), mp 88.5—90.5 °C; IR (KBr), 3270, 1735, and 968 cm^{-1}; ^1H NMR, δ=0.90 (3H, br t, J=7 Hz), 1.2—1.8 (23H, br, 20H on addition of D_2O), 2.30 (2H, t, J=7 Hz), 3.60 (1H, br), 3.66 (3H, s), 4.12 (2H, br), and 5.77 (2H, m, W_H=9 Hz). The methyl ester (0.5 mg) was treated with trimethylsilyl *N*-(trimethylsilyl)acetimidate (40 μl) at 55 °C for 5 min. The mixture was mixed with water (100 μl) and extracted with hexane (2×100 μl). The combined hexane soln was washed with water (30 μl) and evaporated to leave its tris(trimethylsilyl ether), oil, which showed the following MS spectrum: m/z 545 (M^+−15), 460 [$M^+-C_6H_{12}O$ (hexanal)], 455, 439, 399, 387, 301, 297, 259, 227, 173 (base), 155 [$^+O{\equiv}C(CH_2)_7CHO$], 147, 129, 103, 83, 75, and 73.[54] On the other hand, the methyl ester was oxidized with potassium periodate[55] as follows. A soln of the ester (not of the ether) (0.23 mg) in acetic acid (0.5 ml) was combined with 0.02 M aq potassium periodate (0.05 ml) and stirred at room temp for 30 min. To the soln was added ethylene glycol (0.005 ml) in water (0.02 ml) and then 0.4% 2,4-dinitrophenylhydrazine in 4 M HCl (0.5 ml). The mixture was kept at 2 °C for 3 d, and the precipitates (ppts) were collected by filtration, washed with water and dried. The hydrazone mixture was proved to consist of methyl 9-oxononanoate 2,4-dinitrophenylhydrazones by HPLC (TSK-G1000H8) and TLC by comparison of the authentic samples,[56] which were prepared from 9-oxononanoic acid[57] by the known procedure.

Frs. 181′-200′ (65 mg), eluted with chloroform-ethyl acetate (1:4), were crystallized and recrystallized from ethyl acetate to give (15*Z*)-9,10,13-trihydroxy-15-octadecenoic acid p-BPE (21 mg), mp 112—113 °C. ^1H NMR, δ=0.97 (3H, t, J=7 Hz), 1.35—1.64 (16H, br), 2.07 and 2.28 (each 2H, m), 2.48 (2H, t, J=7 Hz), 2.61 (3H, br s, D_2O-exchangeable), 3.62 (3H, br), 5.27 (2H, s), 5.48 (2H, m), and 7.60 and 7.76 (each 2H, d, J=9 Hz). This p-BPE was converted into the corresponding methyl ester, which was further derived into the tris(trimethylsilyl ether): The methyl ester, oil; IR (neat), 3300 and 1735 cm^{-1}: the ether, oil; MS, m/z 529 (M^+−31), 491, 455, 439, 401, 389, 311, 301, 299, 259, 227, 171, 155, 147, 129, 103, 81, 75, and 73 (base).[54]

Fr. 216′ (6 mg), eluted with ethyl acetate, and Fr. 217′ (19 mg), eluted with ethyl acetate and methanol (9:1), were combined, crystallized and recrystallized from ethyl acetate to give (11*E*, 15*Z*)-9,10,13-trihydroxy-11,15-octadecadienoic acid p-BPE (3 mg), mp 114—115 °C; ^1H NMR, δ=0.96 (3H, t, J=7 Hz), 1.35—1.62 (12H, br), 2.07 and 2.28 (each 2H, m), 2.47 (2H, t, J=7 Hz), 2.60 (3H, br, s, D_2O-exchangeable), 3.60 (1H, br), 4.12 (2H, br), 5.27 (2H, s), 5.47 (2H, br), 5.78 (2H, m, W_H=9Hz), and 7.60 and 7.76 (each 2H, d, J=9 Hz). The p-BPE was converted into the corresponding methyl ester, which was further derived into the tris(trimethylsilyl ether): The methyl ester, oil; IR (neat), 3360, 1735, and 973 cm^{-1}; the ether, oil; MS, m/z 543 (M^+−15), 460 [$M^+-C_6H_{10}O$ (hexenal)], 453, 437, 399, 387, 299, 297, 259, 171, 155, 147, 129, 103, 81, 75, and 73 (base).[54]

Chromatography on a Silica-Gel Column (D to E). Fraction D (360 mg) was separated by chromatography over silica gel (Merck 70—325 mesh, 55 g, 2×28.5 cm) with ethyl ether-acetic acid (99:1, v/v). The eluates (each 6 ml) were collected, evaporated, and assayed: Frs. 1—33, (3 mg) inactive; 34—44, (127) inactive; 45—62, (117) active at 10^{-8} g ml^{-1}; 63—74, (28) active at 10^{-7}; 75—120, (12) active at 10^{-6}—$^{-7}$. The fractions 45—62 (Fraction E) was the most active and submitted to further separation.

Reversed-Phase Partition Chromatography on a Siliconized Hyflo Super Cel Column (E to F). Hyflo Super Cel

(Johns-Manville; Nakarai Chemicals) was washed successively with 6 M HCl, distilled water and methanol, dried at 110 °C for 46 h, cooled, and kept in a desiccator containing dimethyldichlorosilane for 10 d. The siliconized Hyflo Super Cel was washed with methanol until the washings became neutral, and dried at 110 °C for 3 h.[58] The hydrophobic Hyflo Super Cel (18 g) thus obtained was mixed with a lower (stationary) phase (16 ml) of methanol-water-acetic acid-chloroform-(2-ethyl-1-hexanol) (150:150:2:15:15, by vol.) for 3 min. To the mixture was added the upper (mobile) phase (50 ml).[59] The slurry mixture was poured into a glass tube (12 mm in diameter), homogenized by rapid up and down movement of a stainless plunger. The resulting fine suspension was then packed in the tube to give a column of 33 cm in length.[58] Fraction E (115 mg) dissolved in the mobile phase (1 ml) was separated by chromatography on the column with the same solvent mixture. The eluates (each 20 ml) were collected, evaporated in vacuo, and assayed. The amount and activity of each or collected eluates are summarized in Fig. 2. As shown in Fig. 2, a large amount of inactive substances were eluted in early fractions (Frs. 1—10), and two groups of active fraction [Frs. 11—22 (23.9 mg) and Frs. 24—28 (4.6 mg)] were then eluted separately. The former active fractions were combined (Fraction F, active at 10^{-8}—$^{-9}$ g ml^{-1}, 23.9 mg) and submitted to further separation. The inactive fractions were examined in somewhat detail.

Fractions 5 and 6. The fractions (16.7 mg) gave a crystalline mixture, which was again purified by chromatography on the hydrophobic Hyflo Super Cel (18 g) under the same conditions described above to yield hydroxy dibasic acid (11.8 mg), mp 149—153 °C. This acid was converted easily into its dimethyl ester, oil; IR ($CHCl_3$), 1726 cm^{-1}; ^{1}H NMR, δ=1.2—1.7 (14H, br), 1.9 (1H, br s, D_2O-exchangeable), 2.32 (2H, t, J=7 Hz), 2.45 (2H, m), 3.69 and 3.73 (each 3H, s), and 3.9 (1H, br); MS, m/z 225 (M^+−31−18), 211 (M^+−31−32), 210 [(OH)CH$(CH_2)_8$COOCH$_3$], 193 (201—18), 172 [$(CH_2)_8$COOCH$_3$+H], 169 (201—32), 151 (193—42), 143, 129, 103 [base, (OH)CHCH_2COOCH$_3$], 87, and 74. The acid was identified as 3-hydroxydodecanedioic acid by comparison with a racemic, synthetic sample,[60] mp 105—107 °C.

Chromatography on an Amberlyst-15 (Ag^+ form) Column (F to G). Amberlyst-15 (Rohm & Haas; Organo Ltd., 9.0 g) was washed with ethanol in a Soxhlet apparatus for 20 h, packed into a glass tube (1.0 cm in diameter), and washed with distilled water. The resin was then converted into the silver form by passing 5% aq silver nitrate ($AgNO_3$), until silver cations were detected in the effluent (ca. 130 ml). The resin was then washed with distilled water thoroughly, when silver ions had not been detected, and then with ethanol.[23] Fraction F (23.1 mg) in ethanol was placed on the column, and eluted with ethanol (total 18 ml) and then with 5% cyclohexene in ethanol (total 50 ml). All eluates were collected in 2 ml portions. The odor of cyclohexene was detected in the fractions after Fr. 19. Frs. 4—10, 11—18, and 19—34 were combined, evaporated and assayed, respectively: Frs. 4—10, (14.4 mg) active at 10^{-8}~$^{-9}$ g ml^{-1}; 11—18, (0.5) active at 10^{-6}; 19—34, (3.0) active at 10^{-6}. The second fraction (Frs. 4—10) (Fraction G) was the most active and submitted to further separation. Less active fractions were examined in somewhat detail.

The Fourth Fraction (Frs. 19—34) gave a crystalline mixture (0.3 mg), which was treated with diazomethane in ether, evaporated, and then treated with trimethylsilyl *N*-(trimethylsilyl)acetimidate (25 μl) for 24 h. The soln was mixed with water (50 μl) and extracted with hexane (2×50 μl). The hexane soln was washed with water (20 μl), evaporated to leave an oily residue, whose MS spectrum [m/z 455 and 453 (M^+−15), 439 and 437 (M^+−31)] indicated that the fraction would contain dihydroxyoctadecadienoic and dihydroxyoctadecatrienoic acids.

Chromatography on an Amberlyst XN-1005 (Ag^+ form) Column (G to H). Amberlyst XN-1005 (Rohm & Haas; Organo Ltd., 100 g) placed in a large column was washed successively with 1 M aq sodium hydroxide (NaOH) (600 ml), distilled water (600 ml), 1 M HCl (1200 ml), distilled water (600 ml), 95% ethanol (600 ml), and distilled water (600 ml). This procedure was repeated three times. The purified resin was converted into the silver form by addition of 5% aq $AgNO_3$ (1200 ml) and washed with distilled water, until silver ions were not detected in the effluent, and then with methanol. The resin thus treated was packed into a long glass column (1.0 cm in diameter) to form a bed of 216 cm in length.[25] Fraction G (14.4 mg) in methanol was placed on the column and eluted with methanol to give 46 fractions (each 5 ml). An aliquot (2 μl) of each fraction was assayed. Active fractions [Frs. 28—33, (0.90 mg) active at 10^{-9}—$^{-10}$ g ml^{-1}, and Frs. 34—39, (0.63) active at 10^{-9}] were combined to amount to 1.53 mg (Fraction H) and submitted to further purification.

***p*-Bromophenacylation [H to I (p-BPE)].** A mixture of Fraction H (1.53 mg), potassium hydrogencarbonate ($KHCO_3$) 2.7 mg, 0.027 mmol), *p*-bromophenacyl bromide (9.4 mg, 0.034 mmol), and dicyclohexano-18-crown-6 (1.31 mg, 0.0035 mmol) in acetonitrile (60 μl) was heated in a sealed tube at 75 °C for 30 min,[26] cooled, and evaporated to remove the acetonitrile. The residue was dissolved in a small volume of benzene, placed on a silica-gel column (Merck 120—230 mesh, 3 g, 1.3×5.5 cm), and then eluted successively with benzene (Fr. 1), chloroform (Fr. 2), chloroform-ethyl acetate (9:1 and 1:1) (Frs. 3 and 4), ethyl acetate (Fr. 5), and ethyl acetate-acetic acid (9:1) (Fr. 6) to give 6 fractions (each 15 ml). An aliquot (3 μg) of each of Frs. 1—5 was hydrolyzed with 0.1 M KOH in methanol (25 μl) at room temp for 15 h, respectively. After removal of the methanol, the reaction mixture was acidified with 0.2 M HCl (25 μl) and extracted with ethyl acetate (3×50 μl). The combined ethyl acetate soln was washed with distilled water (15 μl) and evaporated in vacuo or under flashing argon. The residue and a part (2 μg) of Fr. 6 were dissolved in distilled water (2 ml) and assayed, respectively: Fr. 1, (8.7 mg) inactive; 2, (0.10) active at 10^{-8}—$^{-9}$ g ml^{-1}; 3, (0.91) active at 10^{-10}; 4, (0.55) active at 10^{-9}; 5, (0.11) active at 10^{-8}—$^{-9}$; 6, (0.47) active at 10^{-8}—$^{-9}$. Fr. 3 (0.91 mg) was the most active, named Fraction I (p-BPE), and submitted to further separation.

Preparative HPLC on a MicroPak CN-10 Column [I (p-BPE) to J (p-BPE)]. Fraction I (p-BPE) (0.90 mg) was dissolved in chloroform (100 μl), and the soln was injected in 20 μl portions onto the column (Varian, MicroPak CN-10, 2.2 mm×25 cm)[27c] and separated into 5 fractions, a 45:55 mixture of hexane and diethyl ether being used as an eluent at flow rate of 0.83 ml min^{-1} (Fig. 3). An aliquot (3 μg) of each fraction was hydrolyzed as described above and

assayed, respectively: Fr. 1, (0.225 mg) active at 10^{-8} g ml^{-1}; 2, (0.225), active at 10^{-8}–$^{-9}$; 3, (0.190) active at 10^{-10}–$^{-11}$; 4, (0.170) active at 10^{-7}–$^{-8}$; 5, (0.110) active at 10^{-7}–$^{-8}$. Fr. 3 (0.190 mg) was the most active, named Fraction J (p-BPE), and submitted to further purification.

Preparative HPLC on a MicroPak NH_2-10 Column [J (p-BPE) to K (p-BPE)]. Fraction J (p-BPE) (0.180 mg) was dissolved in chloroform, and the soln was injected onto the column (Varian, MicroPak NH_2-10, 2.0 mm×25 cm),[27c] and separated into 5 fractions, a 70:18:12 mixture of hexane, dichloromethane and acetonitrile being used as an eluent at flow rate of 0.5 ml min^{-1} (Fig. 4). An aliquot (ca. 0.3 μg) of each fraction was hydrolyzed as described above, and then assayed, respectively: Fr. 1, (≈45 μg) inactive; 2, (≈15) inactive; 3, (≈15) inactive; 4, (≈50) active at 10^{-11} g ml^{-1}; 5, (≈55) inactive. Fr. 4 [Fraction K (p-BPE)] (≈50μ g) was the most active and submitted to further purification.

Preparative HPLC on a Hitachi Gel #3011 Column [K (p-BPE) to L (p-BPE) (=GEAp-BPE)]. Fraction K (p-BPE) (≈50 μg) was dissolved in chloroform (5 μl) and separated into 4 fractions by preparative HPLC on a Hitachi Gel #3011 column [Hitachi Ltd., 4 mm×50 cm; eluent, methanol-dichloromethane (9:1); flow rate, 1 ml min^{-1}] (Fig. 5). One-two hundredth of each separated fraction was hydrolyzed as described above, dissolved in water, and assayed. Only Fr. 3 [Fraction L (p-BPE) =GEA p-BPE] 5—10 μg, estimated by the UV intensity of the chromatogram) was active after hydrolysis, and was purified by simple chromatography on the MicroPak NH_2-10 column under the same conditions to remove impurities contaminated from the gels and/or solvents.

The homogeneity of Fraction L (p-BPE) was further checked by analytical HPLC on a MicroPak CH-10 column [Varian, 2.2 mm×25 cm, methanol-water (8:2); flow rate, 0.67 ml min^{-1}], when a single peak (R_t 9 min) was observed on the chromatogram.

(II) Experimentals Summarized in Table 2. Preparation of Chloroform Extracts A and Acidic Extracts B. Roots of "Hon-kintoki," a subspecies of kidney bean, cultivated in 1 hectare of the field at Memuro, were collected in early August, washed roughly with water, dried in the shade and crushed. The dried and powdered roots amounted to 113 kg. A part (41 kg) of the roots was extracted with water (300 l) at 2—8 °C for 4 d. After being squeezed, the roots were further extracted with water (2×200 l). The combined aq muddy suspension (ca. 650 l) was concentrated to 13 l below 30 °C by a thin-film evaporator. This process was repeated three times. All the concentrates (38 l) were combined, made acidic to pH 2—3 with 6 M HCl, and extracted with chloroform (ca. 60 l) continuously for 50 h by a special Soxhlet apparatus. The chloroform soln was evaporated to give an oily material (Chloroform extracts A) (102 g), which was active at 10^{-5} g ml^{-1} for the hatching in water at 25 °C.

The extracts (102 g) was dissolved in ethyl acetate (400 ml) and treated with saturated aq $NaHCO_3$ (500+6×100 ml). The combined aq soln was acidified to pH 2 by addition of 6 M HCl (250 ml) and extracted with ethyl acetate (300+5×200 ml). The combined acetate soln was washed with water (2×50 ml), dried over sodium sulfate, and evaporated to give an acidic oily material (Acidic extracts B) (56.9 g), which was active at 10^{-5}–$^{-6}$ g ml^{-1}.

Chromatography on a Charcoal-Celite Column (B to C). A mixture of Charcoal (500 g) and Celite-545 (1 kg) in water was packed in a glass column (8.4×88 cm). Acidic extracts B (56.5 g) was dissolved in acetone, mixed with Celite (60 g), evaporated, placed on the top of the column, and eluted successively with water (5 l) (Fr. 1), water–acetone (9:1, 8:2, 7:3, 6:4, 5:5, 4:6, 3:7, 2:8, and 1:9, v/v, each 5 l) (Frs. 2—10), and methanol–concd NH_4OH (22:1, v/v, 12 l) (Fr. 11). All the fractions, except the last one, were simply evaporated and assayed, while that (Fr. 11) eluted with ammoniacal methanol, after being evaporated, was dissolved in water (100 ml), acidified with 3 M HCl, and extracted with ethyl acetate (3×100 ml). The acetate solution was then dried, evaporated, and assayed. The hatching activity of each fraction is summarized as follows: Fr. 1, (0.01 g) inactive; 2, (0.07) inactive; 3, (0.53) active at 10^{-6} g ml^{-1}; 4, (0.68) active at 10^{-5}; 5, (2.08) inactive; 6, (5.17) inactive; 7, (7.49) inactive; 8, (8.25) active at 10^{-6}–$^{-7}$ g ml^{-1}; 9, (5.66) active at 10^{-6}; 10, (3.18) active at 10^{-5}; 11, (4.41) active at 10^{-6}. Frs. 8—11 were combined (Fraction C) (21.5 g) and submitted to further separation.

Chromatography on a Sephadex LH-20 Column (C to D). Fraction C (21.5 g) in methanol (50 ml) was separated by chromatography on a Sephadex LH-20 column (Pharmacia, 1013 g) (8.4×74 cm). The column was eluted with methanol (6.5 l), 130 fractions (each 50 ml) being collected. The amount and biological activity of each eluate is summarized in Fig. 6. Fractions 59—78 were active nearly at 10^{-6}–$^{-7}$ g ml^{-1}, combined (Fraction D) (10.1 g), and submitted to further separation.

Chromatography on a DEAP-Sephadex LH-20 Column (D to E). A suspension of DEAP-Sephadex LH-20 (120 g), prepared according to the reported procedure,[30] in 72% aq ethanol was packed in a glass column (3.1×63 cm) and washed successively with 0.5 M aq potassium acetate in 72% aq ethanol (6 l), which had been prepared and adjusted to pH 10 by addition of 1 M aq KOH, 72% aq ethanol (4 l), 0.1 M acetic acid in 72% aq ethanol (4 l), and 72% aq ethanol (4 l), when the packing was converted into the acetate form (3.1×81.5 cm). Fraction D (10.1 g) in 72% aq ethanol (90 ml) was placed on the top of the column and then eluted successively with 72% aq ethanol (4 l) (Fr. 1), 0.1 M acetic acid in 72% aq ethanol (4 l) (Fr. 2), 0.3 M acetic acid in 72% aq ethanol (4 l), which had been adjusted to pH 6.0 by addition of concd NH_4OH (Fr. 3), and 0.3 M acetic acid in 72% aq ethanol (4 l), which had been adjusted to pH 9.0 by addition of concd NH_4OH (Fr. 4).[30,31] Frs. 1 and 2 were evaporated thoroughly to dryness to give inactive oily mixtures (3.18 and 4.87 g) of neutral compounds and monobasic acids, respectively. Fr. 3 was evaporated, dissolved in water (150 ml), acidified with 3 M HCl (130 ml), and extracted with ethyl acetate (4×100 ml). The combined acetate solution was washed with water (3×50 ml), dried, and evaporated to leave an oily mixture of dibasic acids (1.99 g), which was active at 10^{-7} g ml^{-1}. Fr. 4 was treated in the same manner to give an amorphous mixture of polybasic acids (0.17 g) (active at 10^{-6} g ml^{-1}). The mixtures of dibasic and polybasic acid were combined (Fraction E) (2.16 g) and submitted to further separation.

Chromatography on a Sephadex LH-20 Column (E to F). Fraction E (2.12 g) was separated by partition chromatography on a Sephadex LH-20 column (106 g) (2.5×90 cm). The column was eluted with dichloro-

methane–methanol (95:5), 50 fractions (each 30 ml) being collected. The amount and biological activity of each eluate is summarized in Fig. 7. Frs. 25—28 were combined (Fraction F) (135 mg) and submitted to *p*-bromophenacylation.

***p*-Bromophenacylation [F to G (p-BPE)].** A mixture of Fraction F (135 mg), *p*-bromophenacyl bromide (1.70 g), and *N,N*-diisopropylethylamine (0.5 ml) was stirred in dry acetonitrile (15 ml) at room temp for 19 h and then evaporated to leave an oily material. The residue was dissolved in benzene (5 ml) and separated simply by chromatography on a silica-gel column (Wakogel C-200, 20 g) (2.1×21.5 cm) with benzene (Fr. 1), chloroform (Fr. 2), chloroform–ethyl acetate (9:1 and 1:1) (Frs. 3 and 4), ethyl acetate (Fr. 5), and ethyl acetate–acetic acid (99:1) (Fr. 6) (each eluent 100 ml): Fr. 1, (1364 mg); 2, (20.9); 3, (315.7); 4, (27.3); 5, (5.3); 6, (7.7). A part (0.20—0.40 mg) of each eluate was treated with 0.1 M KOH in methanol (50 μl) at room temp for 20 h. The reaction mixture was evaporated, acidified with 0.2 M HCl (50 μl), and extracted with ethyl acetate (3×100μl). The combined acetate solution was washed with water (50 μl) and evaporated under a stream of nitrogen. The residue was dissolved in water (1 ml for 0.02 mg of the initial weight) and assayed: Frs. 1 and 2, both inactive; 3, active at 10^{-8} g ml^{-1}; 4 and 5, both inactive; 6, active at 10^{-6}–$^{-7}$ g ml^{-1}. Fr. 3 [Fraction G (p-BPE)] (315.7 mg) was submitted to further separation.

Preparative HPLC on a Hitachi Gel #3019 Column [G (p-BPE) to H (p-BPE)]. A soln of Fraction G (p-BPE) (316 mg) in chloroform (1.4 ml) was injected in portions of 60—100 μl onto a Hitachi Gel #3019 column (8 mm×50 cm) and separated roughly into 4 fractions, methanol–dichloromethane (7:3) being used as an eluent at flow rate of 4 ml min^{-1}. Each fraction (40 μg) was hydrolyzed as described above and then assayed: Fr. 1, (59.5 mg) inactive; 2, (57.0) active at 10^{-6}–$^{-7}$ g ml^{-1}; 3, (112) active at 10^{-8}–$^{-9}$; 4, (67.7) active at 10^{-8}. Fr. 3 [Fraction H (p-BPE)] (112 mg) was submitted to further separation.

Preparative HPLC on a Bondapak C_{18}/Porasil B Column [H (p-BPE) to I (p-BPE)]. A soln of Fraction H (p-BPE) (112 mg) in a 1:1 mixture (1 ml) of chloroform and methanol was injected onto a Bondapak C_{18}/Porasil B column (7.8 mm×61 cm) and separated into 6 fractions, methanol–water (8:2) being used as an eluent at flow rate of 6 ml min^{-1}. Each fraction (40 μg) was hydrolyzed as described above and assayed: Fr. 1, (9.1 mg) active at 10^{-8} g ml^{-1}; 2, (14.9) active at 10^{-8}; 3, (7.7) active at 10^{-9}; 4, (21.6) active at 10^{-9}; 5, (7.1) active at 10^{-8}; 6, (30.7) active at 10^{-7}–$^{-8}$. Frs. 3 and 4 were combined [Fraction I p-BPE)] (29 mg) and submitted to further separation.

Preparative HPLC on a μBondapak NH_2 Column [I (p-BPE) to J (p-BPE)]. A soln of Fraction I (p-BPE) (29 mg) in chloroform (1.3 ml) was injected in portions of 100—150 μl onto a μBondapak NH_2 column (3.9 mm×30 cm) and separated into 4 fractions, hexane–dichloromethane–acetonitrile (70:18:12) being used as an eluent at flow rate of 1.5 ml min^{-1}. Each fraction (4 μg) was hydrolyzed as described above and then assayed: Fr. 1, (18.18 mg) active at 10^{-6}–$^{-7}$ g ml^{-1}; 2, (0.93) active at 10^{-8}–$^{-9}$; 3, (2.17) active at 10^{-10}; 4, (1.90) active at 10^{-8} g ml^{-1}. Fr. 3 [Fraction J (p-BPE)] (2.17 mg) was submitted to further separation.

Preparative HPLC on a μBondapak NH_2 Column [J (p-BPE) to K (p-BPE)]. A soln of Fraction J (p-BPE) (2.17 mg) in chloroform (0.5 ml) was injected in portions of 100, 200, and 200 μl onto the same column as described above and separated into 4 fractions, hexane–dichloromethane–acetonitrile (80:12:8) being used as an eluent at flow rate of 2.5 ml min^{-1}. Each fraction (0.4 μg) was hydrolyzed and assayed as described before: Fr. 1, (0.28 mg) active at 10^{-8} g ml^{-1}; 2, (0.07) active at 10^{-8}; 3, (0.44) active at 10^{-10}; 4, (0.76) active at 10^{-10}. Frs. 3 and 4 [Fraction K (p-BPE)] (1.20 mg) were submitted to further separation.

Preparative HPLC on a μBondapak NH_2 [K (p-BPE) to L (p-BPE) (=GEA p-BPE)]. A soln of Fraction K (p-BPE) (1.20 mg) in chloroform (120 μl) was injected in portions of 10—25 μl (6 times) onto the aforementioned column and separated into 3 fractions, a 60:36:4 mixture of hexane–dichloromethane–acetonitrile being used as an eluent at flow rate of 1.5 ml min^{-1}. Each fraction (0.4 μg) was hydrolyzed as described above and then assayed: Fr. 1, (0.77 mg) active at 10^{-8}–$^{-9}$ g ml^{-1}; 2, (0.05) active at 10^{-11}–$^{-12}$; 3, (0.07) active at 10^{-10}–$^{-11}$ g ml^{-1}. The second fraction [Fraction L (p-BPE)] showed a single peak by analytical HPLC on the following columns and the highest activity for the hatching after hydrolysis. Analytical HPLC: column, solvent (flow rate), retention time; μBondapak NH_2 (3.9 mm×30 cm), hexane–dichloromethane–acetonitrile (60:36:4) (1.5 ml min^{-1}), 9.5 min; μBondapak C_{18} (3.9 mm×30 cm), methanol–water (8:2) (2.0 ml min^{-1}), 8.5 min; μBondapak/Phenyl (3.9 mm×30 cm), methanol–water (8:2) (2.0 ml min^{-1}), 8.5 min.

(III) Experiments Summarized in Table 3. Preparation of Chloroform Extracts A and Acidic Extracts B. Dried and powdered roots (1058 kg) of "Beni-kintoki" and "Hon-kintoki," subspecies of kidney bean, which had been collected in late July during several years at Memuro (10 hectares) were extracted with water, concentrated and then extracted with chloroform continuously as described above. The total Chloroform extracts A, prepared from all the roots, amounted to 1011 g which stimulated the hatching and emergence at 10^{-5} g ml^{-1} in water at 25 °C.

A part (120 g) of Chloroform extracts A was dissolved in ethyl acetate (500 ml) and treated with saturated aq $NaHCO_3$ (6×200 ml) repeatedly. The aq solns were combined, acidified with 6 M HCl (250 ml) to pH 2—3, and extracted again with ethyl acetate (5×200 ml) and then with chloroform continuously for 18 h. The neutral acetate extracts were dried over anhydrous sodium sulfate and evaporated to leave a dark gum (27.3 g) (inactive), while the acidic acetate extracts were treated in the same manner to give a viscous oil (Acidic extracts B) (84 g) (636 g from total Chloroform extracts A), which was active at 10^{-5}–$^{-6}$ g ml^{-1}. The chloroform extracts also afforded an active oil (4.2 g) (active at 10^{-5}–$^{-6}$ g ml^{-1}).

Chromatography on a Charcoal-Celite Column (B to C). A part (88.2 g) of Acidic extracts B was dissolved in acetone (200 ml) and mixed with Celite-545 (70 g) under vigorous stirring. The mixture, after being evaporated, was placed on the top of a column (11.4×92 cm) prepared from Charcoal (1 kg) and Celite-545 (2 kg) in water, and eluted with water (10 l) (Fr. 1), water–acetone (9:1 to 1:9, each 10 l) (Frs. 2—10), acetone (10 l) (Fr. 11), and methanol–concd NH_4OH (19:1, 20 l) (Fr. 12). The final fraction (Fr. 12) was evaporated, acidified and extracted with ethyl acetate (3×

100 ml), and the acetate extracts were combined with Fr. 11. Frs. 9—11, eluted with 80 and 90% aq acetone and acetone, were more active than other fractions and combined to give a resinous oil (Fraction C) (26.6 g) (197.3 g from total Acidic extracts B), which was active at 10^{-6} g ml^{-1}.

Chromatography on a Sephadex LH-20 Column (C to D). A part (17.57 g) of Fraction C in methanol (40 ml) was separated by chromatography on a Sephadex LH-20 column (1 kg) (8.4×72 cm) in methanol. The column was eluted with methanol (5 l), 180 fractions (each 25—30 ml) being collected. Frs. 76—100 were more active (10^{-6}–$^{-7}$ g ml^{-1}) than those 130—160 (10^{-6} g ml^{-1}), and were combined to give a viscous oil (Fraction D) (7.40 g) (88.9 g from total Fraction C).

Chromatography on a DEAP-Sephadex LH-20 Column (D to E). A part (38.4 g) of Fraction D in 72% aq ethanol (390 ml) was submitted to chromatography on a DEAP-Sephadex LH-20 column[30] (128 g) (3.1×82 cm) packed in 72% aq ethanol (v/v). The column was eluted with 72% aq ethanol (3.9 l) (Fr. 1), 0.1 M acetic acid in 72% aq ethanol (4 l) (pH 4.0) (Fr. 2), and then with 0.3 M acetic acid in 72% aq ethanol (4 l) and concd NH_4OH (127 ml) (pH 9.0) (Fr. 3). Frs. 1 and 2 were evaporated to dryness to give inactive oily residues (20.57 and 9.35 g), respectively. Fr. 3 was evaporated, dissolved in water (100 ml), acidified with 6 M HCl (195 ml) to pH 2, and extracted with ethyl acetate (5×100 ml). The acetate extracts were washed with saturated brine (3×50 ml), dried and evaporated to leave a slightly dark oil (Fraction E) (7.75 g) (18.15 g from total Fraction D), which was active at 10^{-7} g ml^{-1}.

Chromatography on a Sephadex LH-20 Column (E to F and to G). A part (3.21 g) of Fraction E in dichloromethane–methanol (95:5, v/v) (7 ml) was separated by chromatography on a column (2.7×75 cm), which had been packed by Sephadex LH-20 (120 g) with methanol and then with dichloromethane–methanol (95:5). The column was eluted with the same solvent mixture (total 2 l), 60 fractions (each 35 ml) being collected. Most of the fractions were active to some extent. Frs. 19—31 were more active than other fractions and combined to give an oil (Fraction F) (636 mg) (3.59 g from total Fraction E), which was active at 10^{-7}–$^{-8}$ g ml^{-1}.

Fraction F (3.59 g) in dichloromethane–methanol (95:5, v/v) was separated by rechromatography on the same column (2.7×75 cm) packed with Sephadex LH-20 (140 g). The column was eluted with dichloromethane–methanol (97:3) (total 2.5 l), 18 fractions (each ca. 150 ml) being collected. Frs. 9—13 were more active than others and combined to give an oil (Fraction G) (0.95 g), which was active at 10^{-8} g ml^{-1}.

***p*-Bromophenacylation [G to H (p-BPE)].** To a soln of Fraction G (0.95 g) and *p*-bromophenacyl bromide (4.01 g) in acetonitrile (10 ml) was added *N,N*-diisopropylethylamine (2 ml), and the mixture was stirred vigorously at room temp for 19 h, when white ppts appeared. The whole suspension was evaporated to leave a semisolid residue (6.42 g), which was simply purified by chromatography (5.5×26 cm) over silica gel (Wakogel C-200) (250 g). The column was eluted with benzene (1.5 l), chloroform (1 l), chloroform–ethyl acetate (9:1 and 1:1) (each 1 l), ethyl acetate (1 l), and ethyl acetate–methanol (1:1) (1 l). Fracitons eluted with chloroform–ethyl acetate (9:1 and 1:1) were combined to give a gum [Fraction H (p-BPE)] (2.21 g), which was active at 10^{-8} g ml^{-1} after hydrolysis as described below.

A part (0.1 mg) of Fraction H (p-BPE) was treated with 0.1 M KOH in methanol (0.2 ml) at room temp for 4 h. The reaction mixture was evaporated, acidified with 0.2 M HCl (0.4 ml), and extracted with ethyl acetate (3×0.1 ml). The extracts were washed with water (0.1 ml), dried and evaporated to leave a residue, which was dissolved in acetone (one drop) and diluted with water for the bioassay.

Chromatography on a Hitachi Gel #3019 Column [H (p-BPE) to I (p-BPE)]. A part (944 mg) of Fraction H (p-BPE) in dichloromethane–methanol (3:7) (2 ml) was separated by chromatography on a column (2.5×64 cm) packed with Hitachi Gel #3019 (100 g) in dichloromethane–methanol (2:8). The column was eluted with dichloromethane–methanol (2:8) (total 1.6 l), 100 fractions (each 16 ml) being collected (Fig. 8). Frs. 36—50 were more active than others and combined to give a brown oil [Fraction I (p-BPE)] (149 mg) [336 mg from total Fraction H (p-BPE)], which was active at 10^{-9} g ml^{-1} after hydrolysis.

Preparative HPLC on a μBondapak C_{18} Column [I (p-BPE) to J (p-BPE)]. A part (5 mg) of Fraction I (p-BPE) in acetone (0.2 ml) was submitted to preparative HPLC on a μBondapak C_{18} column (7.8 mm×30 cm) and separated into 15 fractions, 80% aq methanol (v/v) (Frs. 1—13) and methanol (Frs. 14 and 15) being used as eluents at flow rate of 2 ml min^{-1} (Fig. 9). The eluents were monitored by the UV spectra and checked by the hatching activity after hydrolysis. Frs. 8 and 9 were more active than others after hydrolysis and combined to give an oil [Fraction J (p-BPE)] (ca. 1.2 mg), which was active at 10^{-9}–$^{-10}$ g ml^{-1} after hydrolysis. This procedure was repeated 70 times to give 79 mg of the Fraction J (p-BPE).

Preparative HPLC on a μBondapak NH_2 Column [J (p-BPE) to K (p-BPE) and K″ (p-BPE)(=GEC p-BPE)]. A part (1.5 mg) of Fraction J (p-BPE) in dichloromethane (0.24 ml) was separated into 6 fractions by preparative HPLC on a μBondapak NH_2 column (7.8 mm×30 cm), hexane–dichloromethane–acetonitrile (76:14:10, v/v/v) being used as an eluent at flow rate of 1.5 ml min^{-1} (Fig. 10). Only Fr. 5 (R_t 13—16 min) was highly active after hydrolysis. This fraction was collected by repeated HPLC (55 times) to amount to 8.8 mg of an oily substance [Fraction K (p-BPE)], which was active at 10^{-10}–$^{-11}$ g ml^{-1} after hydrolysis. On the other hand, Fr. 4 (R_t 11 min) [Fraction K′ (p-BPE)] [4.9 mg from total Fraction J (p-BPE)], showing a practically single peak, was further purified by preparative HPLC on the same column with a mixture of hexane, dichloromethane, and acetonitrile (60:36:4, v/v/v) to give Fraction K″ (p-BPE) (=GEC p-BPE) [1.8 mg from total Fraction J (p-BPE)].

Preparative HPLC on a μBondapak NH_2 Column [K (p-BPE) to L (p-BPE) (=GEA p-BPE) and L″(p-BPE) (=GEB p-BPE). A part (0.50 mg) of Fraction K (p-BPE) in dichloromethane (0.1 ml) was purified by preparative HPLC on a μBondapak NH_2 column (7.8 mm×30 cm), a 63:33:14 (v/v/v) mixture of hexane, dichloromethane, and acetonitrile being used as an eluent at flow rate of 1.5 ml min^{-1}. The eluents were monitored by the UV spectra, when two major fractions with R_t 10.5 and 14.5 min were separated, as shown in Fig. 11. This procedure was repeated 20 times. The former, which was active at 10^{-11}–$^{-12}$

g ml^{-1} in water after hydrolysis, was crystallized on trituration with hexane and dichloromethane to give GEA p-BPE (1.25 mg). On the other hand, the latter [Fraction K' (p-BPE)] [2.6 mg from total Fraction K (p-BPE)] was much less active after hydrolysis and was further purified by preparative HPLC on the same column with a 68:13.2:8.8 (v/v/v) mixture of hexane, dichloromethane, and acetonitrile (flow rate, 3 ml min^{-1}) to give an oil [Fraction L'' (p-BPE)] (=GEB p-BPE)] [1.80 mg from total Fraction K (p-BPE)].

GEA p-BPE (0.1 mg) was treated with 0.1 M KOH in methanol (0.2 ml) at room temp for 4 h. After being evaporated, the soln was acidified with 0.2 M HCl (0.4 ml) to pH 2—3 and extracted with ethyl acetate (3×0.1 ml). The acetate extracts were washed with water (0.1 ml) and purified by preparative HPLC on a μBondapak C_{18} column (7.8 mm×30 cm), 0.1% aq acetic acid–methanol (35:65, v/v) being used as a solvent at flow rate of 2 ml min^{-1} (Fig. 12). The eluent was monitored by the UV spectrum to give an amorphous substance with R_t 10.1 min, GEA (as its potassium salt), which was active at 10^{-12} g ml^{-1}.

The authors are grateful to Mr. Shizuo Sanae for collection of kidney bean, and also to Drs. Minoru Ichinohe, Kazuo Kegasawa, Haruo Inagaki, Masaaki Tsutsumi, and Toshiaki Okada, Hokkaido National Agricultural Experiment Station, for helpful discussion on the bioassay. The research was supported by a Grant-in-Aid for Special Project Research No. 56104009 and Grant-in-Aid for Scientific Research No. 57470022 provided by the Ministry of Education, Science and Culture of Japan, and many other funds.

References

1) A. R. Stone, *Nematologica*, **23**, 273 (1977).
2) A. J. Clarke and R. N. Perry, *Nematologica*, **23**, 350 (1977).
3) A. M. Shepherd and A. J. Clarke, "Plant Parasitic Nematodes," ed by B. M. Zuckerman, W. F. Mai, and R. A. Rohde, Academic Press, New York (1971), Vol. 2, Chap. 25, p. 267.
4) D. L. Lee and H. J. Atkinson, "Physiology of Nematodes," 2nd ed, The MacMillan Press Ltd., London (1976), p. 125.
5) T. Okada, *Jap. J. Nematol.*, **5**, 1 (1975).
6) W. E. Baunacke, *Arb. Biol. Bund Anst. Land-u. Forstw.*, **11**, 185 (1922).
7) M. Ichinohe, *Report of Hokkaido National Agricultural Experiment Station*, **48**, 25 (1955).
8) P. S. Lehman, K. B. Barker, and D. Huisingh, *Nematologica*, **17**, 467 (1971).
9) T. Okada, *Bull. Agric. Chem. Inspect. Stn.*, **10**, 73 (1970); *ibid.*, **11**, 118 (1971).
10) T. Okada, *Jap. J. Appl. Ent. Zool.*, **15**, 215 (1971).
11) T. Okada, *Appl. Ent. Zool.*, **7**, 99, 234 (1972).
12) T. Okada, *Jap. J. Nematol.*, **6**, 1 (1977).
13) C. B. Skotland, *Phytopathology*, **47**, 623 (1957).
14) M. Tsutsumi and K. Sakurai, *Jap. J. Appl. Ent. Zool.*, **10**, 129 (1966).
15) T. Masamune, M. Anetai, M. Takasugi, and N. Katsui, *Nature (London)*, **297**, 495 (1982).
16) A. Fukuzawa, A. Furusaki, M. Ikura, and T. Masamune, *J. Chem. Soc., Chem. Commun.*, **1985**, 222, 748.
17) A. Fukuzawa, H. Matsue, M. Ikura, and T. Masamune, *Tetrahedron Lett.*, **26**, 5539 (1985).
18) T. Masamune, "Natural Products and Biological Activities," ed by H. Imura, T. Goto, T. Murachi, and T. Nakajima, University of Tokyo Press, Tokyo (1985), p. 25.
19) A. Fukuzawa, M. Anetai, and T. Masamune, *Shokubutsu Boeki*, **38**, 116 (1984).
20) M. Anetai, Ph. D. Thesis, Hokkaido University, Sapporo, Japan, 1977; T. Masamune, "Seibutsu no Seigyo-Kiko," ed by M. Nakajima, T. Goto, and N. Takahashi, Kagaku-Dozin, Kyoto (1978), p. 127.
21) N. Takahashi, "Gibberellins," ed by S. Tamura, University of Tokyo Press, Tokyo (1969), pp. 27—54; N. Murofushi, S. Iriuchijima, N. Takahashi, S. Tamura, J. Kato, Y. Wada, E. Watanabe, and T. Aoyama, *Agric. Biol. Chem.*, **30**, 917 (1966).
22) K. Kobayashi, Ph. D. Thesis, Hokkaido University, Sapporo, Japan, 1974.
23) M. Hamberg, *Eur. J. Biochem.*, **6**, 135 (1968); J. E. Shaw and P. W. Ramwell, "Methods of Biochemical Analysis," ed by D. Glick, Wiley-Interscience, New York (1969), Vol. 17, p. 325.
24) G. V. Marinetti, "Lipid Chromatographic Analysis," Marcel Dekker Inc., New York (1968), Vol. 2, p. 313.
25) E. A. Emken, C. R. Scholfield, and H. J. Dutton, *J. Am. Oil Chem. Soc.*, **41**, 388 (1964); E. A. Emken, C. R. Scholfield, V. L. Davison, and E. N. Frankel, *ibid.*, **44**, 373 (1967).
26) H. D. Durst, M. Milano, E. J. Kikta, Jr., S. A. Connelly, and E. Grushka, *Anal. Chem.*, **47**, 1797 (1975); E. Grushka, H. D. Durst, and E. J. Kikta, Jr., *J. Chromatogr.*, **112**, 673 (1975).
27) a) S. R. Abbott, *J. Chromatogr. Sci.*, **18**, 540 (1980); b) For recent reviews, see: R. E. Majors, *J. Chromatogr. Sci.*, **15**, 334 (1977); *ibid.*, **18**, 488 (1980); c) R. V. Vivilecchia, R. J. Cotter, R. J. Limpert, N. Z. Thimot, and J. N. Little, *J. Chromatogr.*, **99**, 407 (1974).
28) H. Takahagi and S. Seno, *J. Chromatogr. Sci.*, **12**, 507 (1974).
29) a) E. Nyström and J. Sjövall, *Anal. Biochem.*, **12**, 235 (1965); *J. Chromatogr.*, **17**, 574 (1965); b) P. Zia and R. Horton, *Prostaglandins*, **4**, 543 (1973).
30) B. Almé, A. Bremmelgaard, J. Sjövall, and P. Thomassen, *J. Lipid Res.*, **18**, 339 (1977); B. Almé and E. Nyström, *J. Chromatogr.*, **59**, 45 (1971).
31) B. Almé and G. Hansson, *Prostaglandins*, **15**, 199 (1978).
32) F. A. Fitzpatrick, *Anal. Chem.*, **48**, 499 (1976); W. Morozowich and S. L. Douglas, *Prostaglandins*, **10**, 19 (1975).
33) R. F. Borch, *Anal. Chem.*, **47**, 2437 (1975).
34) L. R. Snyder and T. C. Schunk, *Anal. Chem.*, **54**, 1764 (1982).
35) The cartridge is packed with silica gel (μPorasil) whose surface is modified chemically with octadecylsilyl groups and then treated with trimethylchlorosilane (for the unmodified part).
36) R. L. Shriner, R. C. Fuson, and D. Y. Curtin, "The Systematic Identification of Organic Compounds," 4th ed, John Wiley, New York (1956), p. 220, 276.
37) Cf., P. A. Levene, T. Mori, and L. A. Mikeska, *J. Biol. Chem.*, **75**, 337 (1927).

38) Cf., H. Scheibler and A. S. Wheeler, *Ber.*, **44**, 2684 (1911).
39) M. Takasugi, M. Anetai, N. Katsui, and T. Masamune, *Chem. Lett.*, **1973**, 245.
40) J. -L. Pousset and J. Poisson, *Tetrahedron Lett.*, **1969**, 1173.
41) M. N. Galbraith and D. H. S. Horn, *J. Chem. Soc., Chem. Commun.*, **1972**, 113; *ibid.*, **1973**, 566.
42) G. Weiss, M. Koreeda, and K. Nakanishi, *J. Chem. Soc., Chem. Commun.*, **1973**, 565.
43) H. Fukui, K. Koshimizu, S. Usuda, and Y. Yamazaki, *Agric. Biol. Chem.*, **41**, 175 (1977).
44) M. Koreeda, G. Weiss, and K. Nakanishi, *J. Am. Chem. Soc.*, **95**, 239 (1973).
45) K. Mori, *Tetrahedron*, **30**, 1065 (1974).
46) T. Kato, M. Tsunakawa, N. Sasaki, H. Aizawa, K. Fujita, Y. Kitahara, and N. Takahashi, *Phytochemistry*, **16**, 45 (1977).
47) D. L. Roberts, R. A. Heckman, B. P. Hege, and S. A. Bellin, *J. Org. Chem.*, **33**, 3566 (1968).
48) S. Isoe, S. B. Hyeon, H. Ichikawa, S. Katsumura, and T. Sakan, *Tetrahedron Lett.*, **1968**, 5561.
49) B. V. Milborrow, "Aspects of Terpenoid Chemistry and Biochemistry," ed by T. W. Goodwin, Academic Press, London and New York (1971), p. 137.
50) B. V. Milborrow, *J. Chem. Soc., Chem. Commun.*, **1969**, 966.
51) J. MacMillan and R. J. Pryce, *Tetrahedron*, **25**, 5893, 5903 (1969).
52) E. T. Tinelli, E. Sondheimer, D. C. Walton, P. Gaskin, and J. MacMillan, *Tetrahedron Lett.*, **1973**, 139; B. V. Milborrow, *Phytochemistry*, **14**, 1045 (1975).
53) M. Takasugi, M. Anetai, and T. Masamune, *Chem. Lett.*, **1974**, 947.
54) M. Takasugi, K. Kobayashi, M. Anetai, S. Ueno, N. Katsui, and T. Masamune, *Chem. Lett.*, **1973**, 445.
55) A. Graveland, *J. Am. Oil Chem. Soc.*, **47**, 352 (1970).
56) L. Crombie and J. L. Tayler, *J. Chem. Soc.*, **1954**, 2816.
57) G. King, *J. Chem. Soc.*, 1826 (1938).
58) G. A. Howard and A. J. P. Martin, *Biochem. J.*, **46**, 532 (1950).
59) J. B. Lee, K. Crowshaw, B. H. Takman, K. A. Attrep, and J. Z. Gougoutas, *Biochem. J.*, **105**, 1251 (1967).
60) P. H. M. Schreurs, P. P. Montijn, and S. Hoff, *Recl. Trav. Chim. Pays-Bas*, **90**, 1331 (1971).

 © 1987 The Chemical Society of Japan Bull. Chem. Soc. Jpn., 60, 1001—1014 (1987)

Glycinoeclepins, Natural Hatching Stimuli for the Soybean Cyst Nematode, *Heterodera Glycines*. II. Structural Elucidation

Tadashi MASAMUNE,* Akio FUKUZAWA, Akio FURUSAKI, Mitsuhiko IKURA, Hideki MATSUE, Tatsuya KANEKO, Atsushi ABIKO, Noriyasu SAKAMOTO, Norihiko TANIMOTO, and Akio MURAI

Department of Chemistry, Faculty of Science, Hokkaido University, Sapporo 060

(Received August 7, 1986)

The structures of three new compounds, glycinoeclepins A, B, and C, isolated from the hatch-stimulating extracts of kidney beans for the soybean cyst nematode, have been determined. The structures were resolved by using spectroscopic methods, especially by the difference NOE techniques, and confirmed by the X-ray diffraction analysis. These structures are characterized by (1) migration of two methyl groups in the C and D rings, (2) oxidative cleavage of the B ring with loss of one carbon atom and (3) presence of the 7-oxabicyclo[2.2.1]heptane system in the A ring, compared with those of cycloartanes, and are regarded as pentanor- (GEA) or nortriterpenes (GEB and GEC).

In the preceding paper[1] we described the isolation of natural hatching stimuli, designated as glycinoeclepins A, B, and C (GEA, GEB, and GEC), for the soybean cyst nematode as their *p*-bromophenacyl esters (p-BPEs). Of these compounds, GEA, identified as an active principle, stimulated the hatching at 10^{-11}—$^{-12}$ g ml^{-1} in water at 25 °C.[2] In preliminary communications,[3,4] we reported the structures of these stimuli. However, it has recently been found that the reported (20*R*, 23*S*, 24*E*) configuration[4,5] of the side chain of GEC should be revised to the (20*R*, 23*R*, 24*E*) one. The present paper describes the details of the structural elucidation of GEs including the structural revision of GEC.

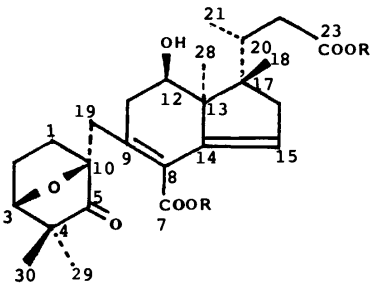

GEA (**1**), R=H
GEA p-BPE (**1a**), R=$CH_2COC_6H_4Br$

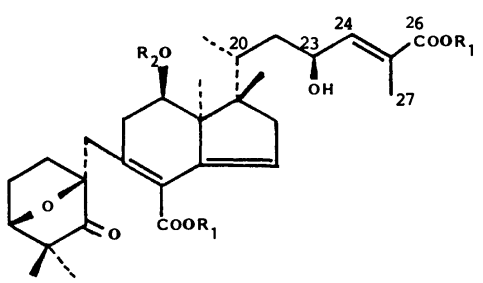

GEB (**2**), R_1=H, R_2=$COCH_3$
GEB p-BPE (**2a**), R_1=$CH_2COC_6H_4Br$, R_2=$COCH_3$
Deacetyl GEB (**2b**), R_1=H, R_2=H

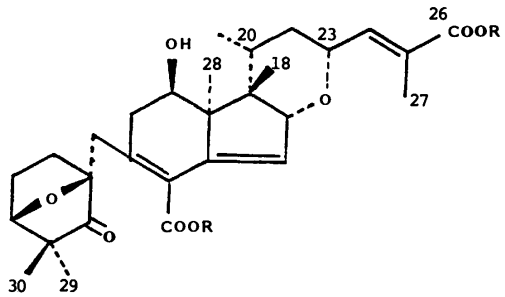

GEC (**3**), R=H
GEC p-BPE (**3a**), R=$CH_2COC_6H_4Br$

Structural Elucidation of GEA on the Basis of the Spectroscopic Evidence. The molecular formula of GEA (**1**) was determined as $C_{25}H_{34}O_7$ on the basis of the FD-MS [*m/z* 838, 840, and 842 (1:2:1)] and CI(NH_3)-MS spectra [*m/z* 856, 858, and 860 (1:2:1)] of GEA p-BPE (**1a**) as well as the ^{1}H NMR spectra of **1a** [$CDCl_3$ (Fig. 1) and C_6D_6]. The ^{13}C NMR spectra of **1a** ($CDCl_3$ and C_6D_6) under completely decoupled (Table 1) and off-resonance conditions, combined with the INEPT studies, indicated the presence of 5 methyl, 6 methylene, 1 methine, and 3 quaternary (■) carbon atoms, 2 methine and 1 quaternary carbon atoms bearing oxygen atoms, 1 trisubstituted and 1 tetrasubstituted double bonds, and 2 carboxyl and 1 carbonyl carbon atoms. These spectral data, coupled with IR spectrum of **1a** (1758 cm^{-1}, sh), revealed the presence of the following oxygen functions: 2 -COOH, 1 -OH, 1 -O-, and 1 -C(=O)- (ketone). Moreover, the ^{1}H NMR spectra of **1a**, combined with the detailed analysis of the COSY spectra (Fig. 2) and extensive decoupling studies, indicated the presence of structural units (i) to (x) as shown in Table 2. However, confirmatory evidence was required for the presence of the units (iii) and (iv), because the coupling constants between vicinal protons in the units [unit (iii), ■-C(12)H(OH)-C(11)H_2-■, $J_{12\alpha,11\beta}$=

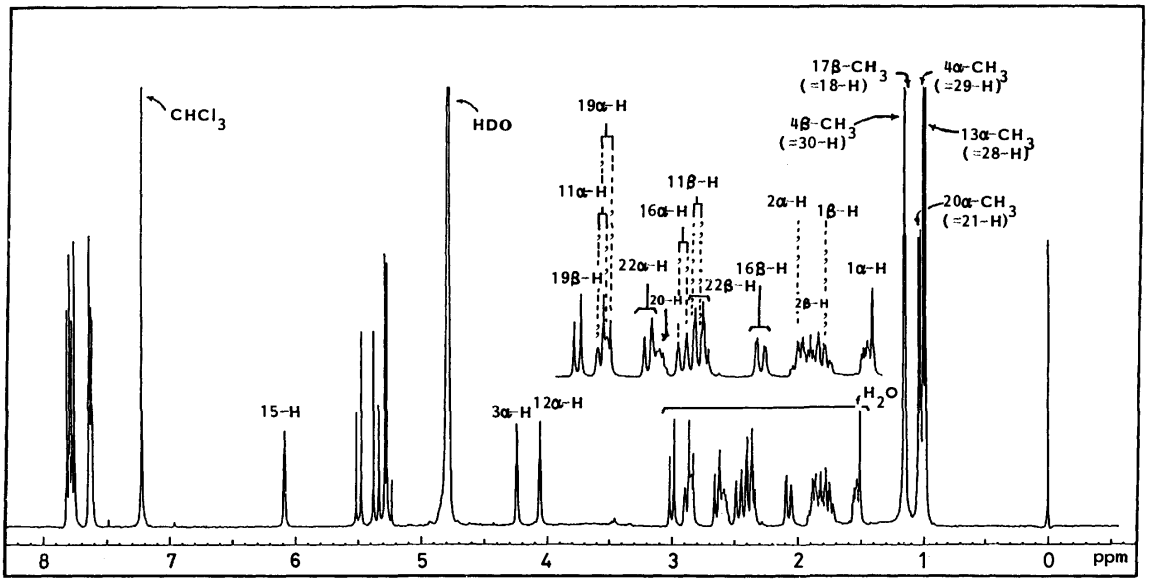

Fig. 1. The ^{1}H NMR spectrum of GEA p-BPE (**1a**) (400 MHz, 0.5 mg in $CDCl_3$ and D_2O).

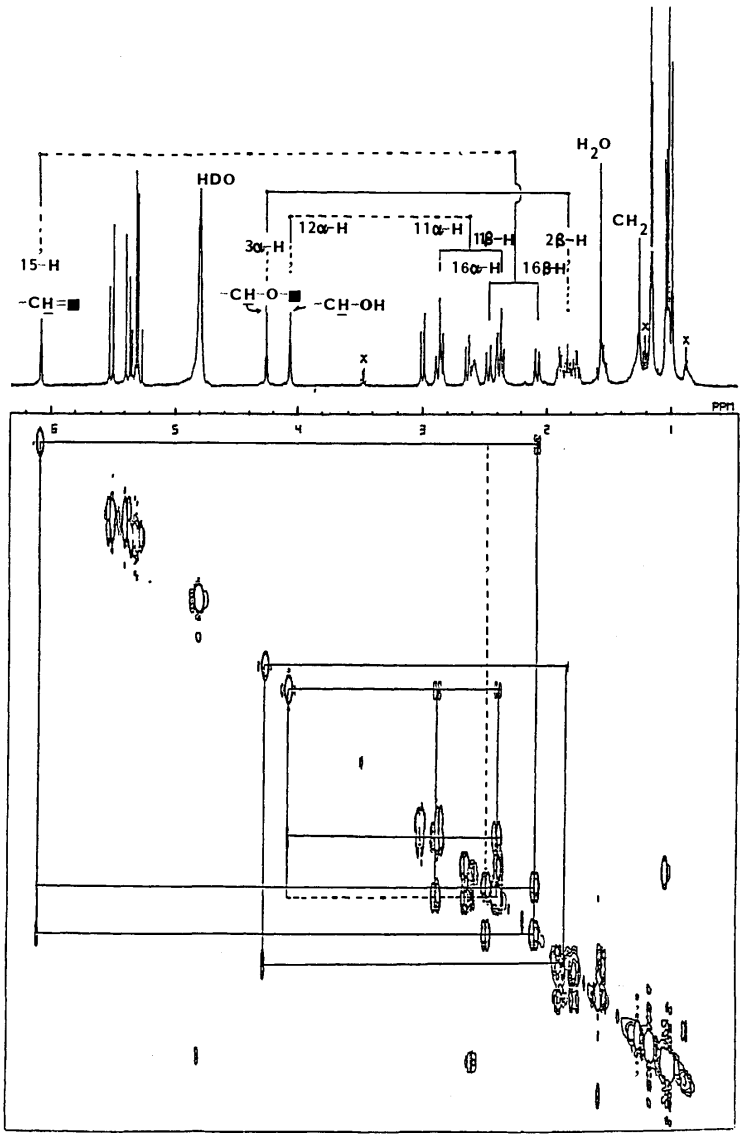

Fig. 2. The COSY spectrum of GEA p-BPE (**1a**) (500 MHz, 1 mg in $CDCl_3$ and D_2O).

1.5 Hz and $J_{12\alpha,11\alpha}$=3 Hz; unit (iv), ■=C(15)H-C(16)H_2-■, $J_{15,16\beta}$=3.5 Hz, $J_{15,16\alpha}$=1.5 Hz] were less than 4 Hz and hence might be attributed to long-range coupling. Thus the NOE difference spectra of these vicinal protons were measured. The result clearly demonstrated that the protons in question in the respective units are situated in a narrow region each other, and the C(11) and C(15) atoms are connected directly to the C(12) and C(16) atoms, respectively.

The following comments are annotated on Tables 1 and 2. (1) The olefinic proton H_{15} in the unit(iv) of **1a** was observed at δ 6.08 (cf., **2a**, δ 6.02; **3a**, δ 6.22), at rather low-field compared with usual olefinic protons. (2) Two *p*-bromophenacyloxycarbonyl carbon atoms in the units(viii) and (ix) of **1a** appeared with clearly different chemical shifts (δ 167.6 and 173.1, $\Delta\delta$ 5—6 ppm) (Table 1), while the corresponding atoms in **2a** and **3a** did at practically the same field (**2a**, δ 167.8 and 167.8; **3a**, δ 167.2 and 167.6) (Table 1). These facts are consistent with that one of the relevant carbon atoms is connected to an sp^3-type carbon atom [unit(ix)] and another to an sp^2-type carbon atom [unit(viii)] in **1**. (3) The chemical shift (δ 216.6) of one carbonyl carbon atom [unit(x)] of **1a** strongly suggested that the carbonyl group would be sterically hindered and/or involved in a strained system (cf., **2a**, δ 216.7; **3a**, 216.3).[6] All these facts will be discussed again.

Table 1. Chemical Shift of the ^{13}C Atoms of GEA (**1**), GEB (**2**), and GEC (**3**) in the ^{13}C NMR Spectra of their p-BPEs

	1 (22.5 and 25 MHz)		**2**(25 MHz)	**3**(125 MHz)
Solvent	$CDCl_3$	C_6D_6	C_6D_6	C_6D_6
CH_3-	16.2	17.0	16.4	16.8
	18.4	19.3	18.9	20.3
	19.1	19.8	19.7	23.3
	19.8	20.3	20.4	24.8
	22.7	23.3	23.5	29.2
			13.4[a],	13.8[a]
			22.0[b]	
-*C*H_2-	25.1	25.8	25.9	25.8
	29.4	29.8	29.5	30.1
	33.5	34.4	34.3	34.8
	38.0	38.9	39.2	36.8
	40.9	42.2	40.8	42.0
	46.0	46.9	47.5	
-*C*H-	35.1	36.0	34.3	40.4
-*C*- (sp^3)	48.7	49.1	49.3	47.5
	51.2	52.2	52.3	49.2
	53.3	54.1	52.3	54.6
-*C*H(OH)-	71.3(d)	71.9(d)	67.4(d)[c]	73.3(d)
-*C*H(O-)-	83.5(d)	84.0(d)	73.3(d)	75.4(d)
-*C*(O-)-	88.4(s)	89.3(s)	84.2(d)	84.1(d)
			89.3(s)	84.1(d)
				91.0(s)
-*C*=*C*H-	126.4(d)	126.7(d)	125.5(d)	126.1(d)
-*C*=*C*-	127.2(s)	126.7(s)	128.8(s)	132.4(d)
	133.6(s)	134.4(s)	129.1(s)	137.9(s)
	138.9(s)	140.8(s)	134.6(s)	144.5(s)
			141.5(s)	144.5(s)
			146.8(d)	147.2(s)
-*C*OO-p-BPE	166.8	167.6	167.8	167.2
	172.7	173.1	167.8	167.6
-*C*(=O)-	216.9	216.6	216.7	216.3

a) -CH(*C*H_3)=CH-. b) -OC(=O)*C*H_3.
c) -*C*H(OCOCH_3)-.

Now we must connect these structural units(i) to (x), which are disconnected by ten quaternary (■) carbon atoms. The NOE difference spectra[7,8] (Fig. 3) between protons of two geminal methyl groups [unit(vii)] and those in the unit(i) indicated that (1) one [■=C(4)] of the terminal quaternary carbon atoms in the unit(i) must be identical with that of the unit(vii), and (2) another terminal quaternary carbon [■=C(10)] of the unit(i) must be identical with that bearing the ether oxygen atom, because (a) neither of the two protons ($H_{1\beta}$ and $H_{1\alpha}$) at the C(1), attached to C(10), is located close to all other protons involved in the units(ii) to (vi), and (b) if the relevant carbon C(10) were identical with the former C(4), forming a four-membered ring, the coupling constants between geminal protons at C(1) and C(2) would be much smaller than those observed ($J_{1\beta,1\alpha}=J_{2\beta,2\alpha}$=12 Hz). Hence the units(i) and (vii) can be extended to a structural moiety (A), in which the coupling constants between protons at C(3) and C(2) were $J_{3\alpha,2\beta}\fallingdotseq$ 5 Hz and $J_{3\alpha,2\alpha}\fallingdotseq$0 Hz. These constants led us to presume that the moiety (A) must be involved in a 7-oxabicyclo[2.2.1]heptane system. This skeletal system indeed exists as the A ring in acerinol[9] (**4**), a triterpene of natural origin. The coupling con-

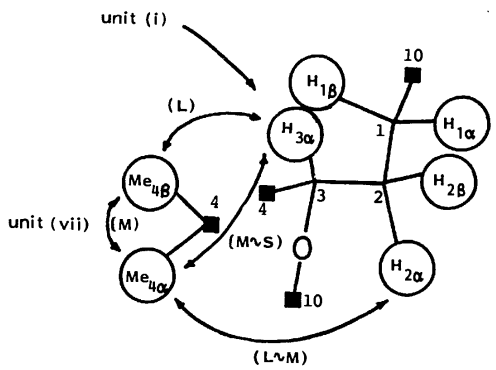

Fig. 3. The difference NOEs (⌒) between the geminal methyl and other protons in GEA p-BPE (**1a**).

stants between protons in the A ring of **4** were readily obtained by measurement of the decoupling difference spectrum (Fig. 4), the result being tabulated in Table 3. Table 3 revealed that these coupling constants were essentially the same as those of the protons in the moiety (A), indicating that the moiety (A) can be extended to a 4,4-dimethyloxabicyclo[2.2.1]heptane moiety[10] (B) with an sp^2-type carbon atom at C-5 (a carbonyl carbon or an olefinic carbon). Then we prepared 1-bromomethyl-3,3-dimethyl-7-oxabicyclo[2.2.1]heptan-2-one (**5**) (Scheme 1) and compared the spectral data with those of **1a**

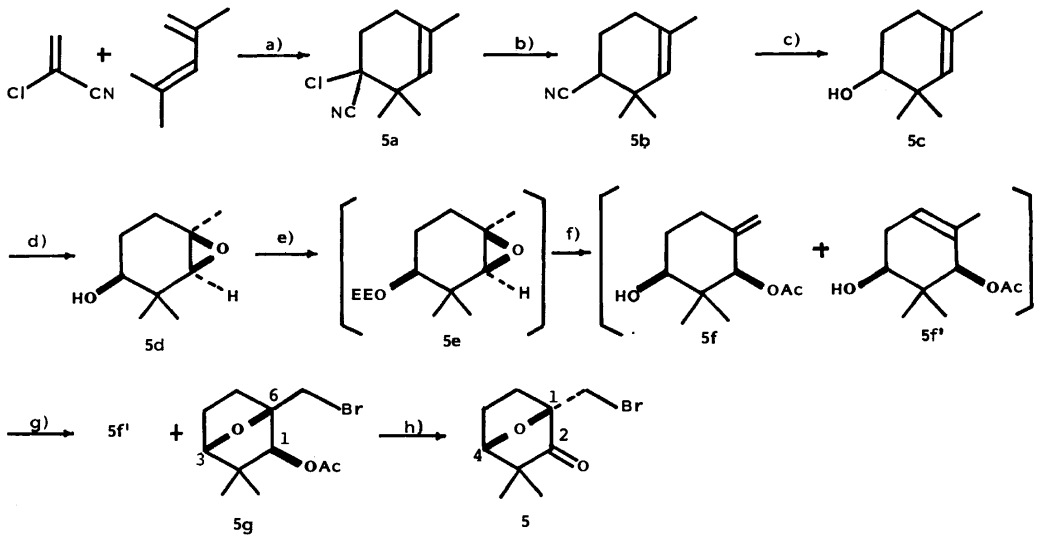

Scheme 1. Preparation of 1-bromomethyl-3,3-dimethyl-7-oxabicyclo[2.2.1]heptan-2-one (**5**). Reagents: a) Δ (80%), b) Zn-Cu (98%), c) LDA, O_2, $P(OEt)_3$; $NaBH_4$ (62%), d) *t*-BuOOH, $VO(acac)_2$ (95%), e) $EtOCH{=}CH_2$, PPTS (94%), f) $LiNEt_2$, HMPA; Ac_2O, Py; HCl (35%), g) NBS (33% and 33%), h) K_2CO_3; CrO_3, H_2SO_4 (99%).

Table 2. Structural Units of GEA (**1**), GEB (**2**), and GEC (**3**)

Unit	GEA ($C_{25}H_{34}O_7$)	GEB ($C_{31}H_{42}O_9$)	GEC ($C_{29}H_{38}O_8$)
(i)	■-CH(O-■)CH_2CH_2-■	■-CH(O-■)CH_2CH_2-■	■-CH(O-■)CH_2CH_2-■
(ii)	■-CH(CH_3)CH_2-■	■-CH(CH_3)CH_2CH(OH)CH=C(CH_3)-■	■-CH(CH_3)CH_2CH(O-)CH=C(CH_3)-■
(iii)	■-CH(OH)CH_2-■	■-CH(OCOCH_3)CH_2-■	■-CH(OH)CH_2-■
(iv)	■=$CHCH_2$-■	■=$CHCH_2$-■	■=CHCH(O-)-■
(v)	■-CH_2-■	■-CH_2-■	■-CH_2-■
(vi)	CH_3-■, CH_3-■	CH_3-■, CH_3-■	CH_3-■, CH_3-■
(vii)	CH_3-■-CH_3	CH_3-■-CH_3	CH_3-■-CH_3
(viii)	■=■-■OOH	■=■-■OOH	■=■-■OOH
(ix)	(C_{sp^3})-■OOH	(C_{sp^2})-■OOH	(C_{sp^2})-■OOH
(x)	■=O	■=O	■=O

Table 3. The Chemical Shifts (δ) and Coupling Constants (*J*) of the Protons in the Structure Moiety (A) of GEA p-BPE (**1a**) and the A ring of Acerinol (**4**)[a]

Protons	GEA p-BPE (moiety A)		Acerinol (A ring)	
	δ	*J* (Hz)[b]	δ	*J* (Hz)[b]
1α-H	1.54	(ddd, J=4, 9, 12)	1.60	(ddd, J=4.5, 9.5, 11.5)
1β-H	1.76	(ddd, J=5, 10, 12)	1.41	(ddd, J=5, 11.5, 11.5)
2α-H	1.90	(ddd, J=5, 9, 12)	1.93	(ddd, J=5, 9, 12.5)
2β-H	1.84	(dddd, J=4, 5, 10, 12)	1.71	(dddd, J=4.5, 5, 11.5, 12.5)
3α-H	4.26	(d, J=5)	3.73	(d, J=5)

a) The spectra were measured in $CDCl_3$. b) The coupling constants were estimated at the 1st order approximation.

[IR (KBr), **1a**, 1760 cm^{-1} (sh) (**1**, 1757 cm^{-1}) (C=O); **5**, 1757 cm^{-1}: ^{13}C NMR ($CDCl_3$), **1a**, δ 216.9 (C=O); **5**, δ 214.6: ^1H NMR ($CDCl_3$ and C_6D_6), **1a**, δ *1.02 and 0.73* (4α-CH_3), and 1.17 and 1.10 (4β-CH_3); **5**, δ *1.06 and 0.66* (3α-CH_3), and 1.23 and 1.04 (3β-CH_3)]. The absorption peaks due to the carbonyl group in the IR (near 1760 cm^{-1}) and ^{13}C NMR spectra (near δ 215 ppm), coupled with the up-field shift ($\Delta\delta \approx 0.4$ ppm) of α-oriented methyl protons in the ^1H NMR spectrum in hexadeuteriobenzene, have established that a 4,4-dimethyl-3,10-epoxy-5-cyclohexanone moiety[10] (C) is involved in GEA (**1**).

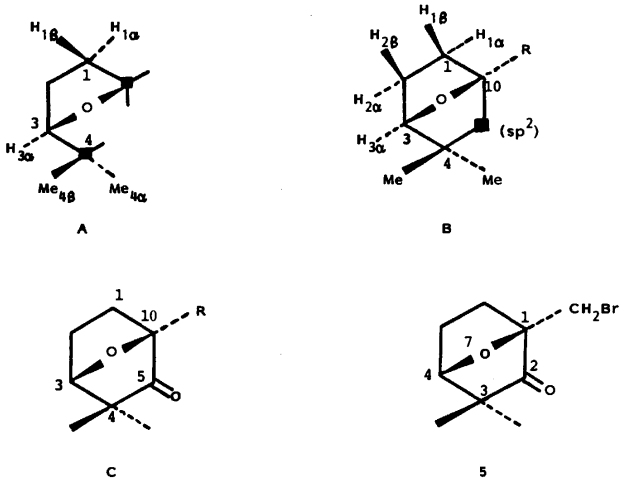

We next discuss on a structural moiety constructed by the units(ii), (iii), (iv), and (vi) in Table 2. The NOE difference spectra[7,8] between the protons of these units of **1a** were measured in details, the result being summarized in Fig. 5. As shown in Fig. 5, the protons of one (17β-CH_3=18-H) of two methyl groups in the unit(vi) were located close to secondary methyl protons (20β-CH_3=21-H)[11] and one proton (22β-H)[11] in the unit(ii), a hydroxyl proton (measured in C_6D_6) in the unit(iii), and two protons (16β-H and 15-H) in the unit(iv), while another methyl protons (13α-CH_3=28-H) were situated close to most of the remaining protons of the units(ii) (20α-H and 22α-H), (iii) (12α-H and 11α-H), and (iv) (16α-H). These findings revealed that (1) three major C–C bonds of the units(ii) to (iv) constitute an almost flat plane, and (2) half (20β-CH_3, 22β-H, OH, and 16β-H) of these protons and one methyl protons (17β-CH_3) are disposed at an upper (or lower) side of the plane, and the remaining protons (20α-H, 22α-H, 12α-H, 11α-H, and 16α-H) and another methyl protons (13α-CH_3) are located at a lower (or upper) side of the plane. It is emphasized that any notable NOE was not observed between these protons of the units(ii), (iii), (iv), and (vi) and other protons of the units(i) and (vii). We had to connect these units so as to form a structural moiety consistent with all the spectral data, although a number of combinations of the units were possible.

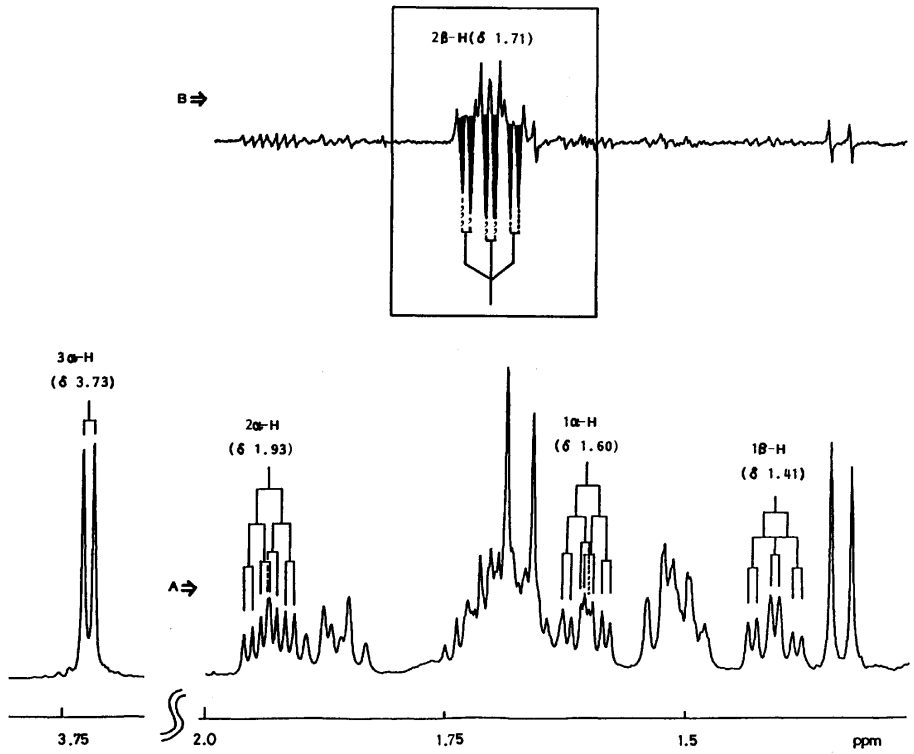

Fig. 4. The ^1H NMR spectrum of the A-ring of acerinol (**4**) (500 MHz, $CDCl_3$).
(A) The normal spectrum: (B) The decoupling difference spectrum on irradiation at δ 3.73 (3α-H).

As indicated in Fig. 5, the secondary methyl protons (20β-CH_3)[11] in the unit(ii) were located near to both two geminal protons (16β-H and 16α-H) in the unit(iv) and the methyl protons (17β-CH_3), attached to a quaternary carbon [C(17)] and disposed at the upper side of the plane. The latter protons (17β-CH_3) were also situated close to one proton (22β-H) in the unit(ii) and one proton (16β-H) in the unit(iv). Thus one terminal quaternary carbon atom of the unit(ii) and that of the unit(iv) must be identical with the quaternary carbon atom C(17), forming a structural moiety (D). The same discussion holds for relation between another methyl protons (13α-CH_3), attached to a quaternary carbon atom [C(13)] and located at the lower side of the plane, two protons (12α-H and 11α-H) in the unit(iii), and half (20α-H, 22α-H, and 16α-H) of the protons in the moiety (D). Hence one terminal quaternary carbon atom of the unit(iii) must be identical with that C(13), which must be connected directly to that C(17) in the moiety (D). It follows that the moiety (D) can be extended to a structural moiety (E).

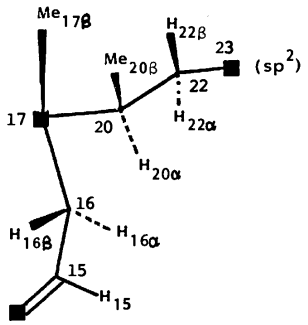

D

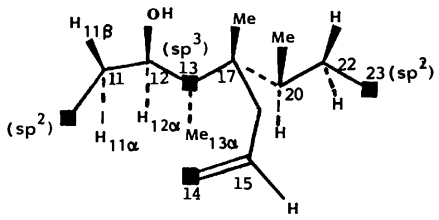

E

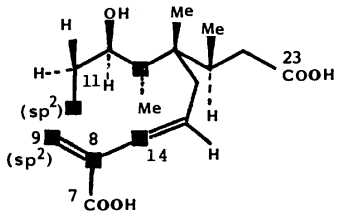

F

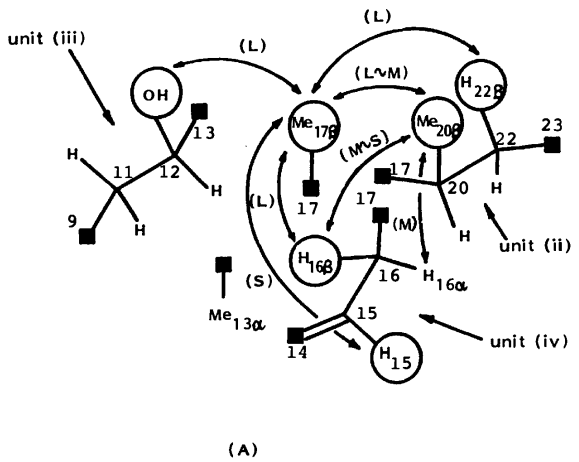

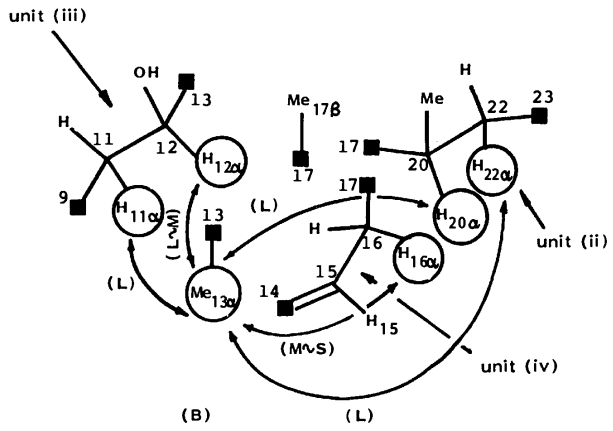

Fig. 5. The difference NOEs (⌒) (A) and (B) between the two methyl (unit vi) and other protons in GEA p-BPE (**1a**).

The moiety (E) is further extended to a structural moiety (F) on the basis of the following reasons. (1) GEA (**1**) showed an absorption maximum at 251.5 nm (ε 8300) in the UV spectrum [cf., **1a**, 254.5 nm (ε 27100)] and a sharp signal (W_H=3 Hz) due to an olefinic proton at δ 5.66 in the ^{1}H NMR spectrum (CD_3OD) [cf., **1a**, δ 6.08 ($CDCl_3$) and 6.54 (C_6D_6)]. These data indicated that two double bonds in the units(iv) [and hence in the moiety (E)] and (viii) are conjugated in a cross-conjugation manner. (2) Two protons (22β-H and 22α-H) in the unit(ii) [hence in the moiety (E)] appeared at δ 2.64 and 2.37 in the ^{1}H NMR spectrum of **1a** ($CDCl_3$) (cf., δ 2.75 and 2.44 in C_6D_6). These chemical shifts indicated that the carbon atom [C(22)] bearing these protons must be attached to an sp^2-type quaternary carbon atom. Examination of Table 2 revealed that the units of **1** seriously differed from those of **2** only in the units(ii) and (ix), indicating the (C_{sp^3}) and (C_{sp^2}) atoms in the unit(ix) of **1** and **2** must be the methylene carbon [C(22)] and methyl-substituted olefinic carbon atoms [C(25)] in the unit(ii) of **1** and **2**, respectively. Thus the moiety (F) can be constructed reasonably by the units(ii), (iii), (iv), (vi), (viii), and (ix). The remaining unit is only that (v).

Careful and repeated measurement of the NOE difference spectra revealed the presence of the small NOEs between one (19β-H)[11] of two geminal protons in the unit(v) and both the protons (1β-H) (Fig. 6) and (11β-H) in the moieties (C) and (F).[12] This finding led us to presume that one of two quaternary carbon atoms of the unit(v) must be identical with the undefined one [C(10)] of the moiety (C), and another with that [C(9)] attached to the carbon bearing the relevant proton (11β-H), respectively. Thus partial structures (C) and (F), and the unit(v) must be connected straightforward as shown in Fig. 7. GEA is therefore represented favorably by formula **1**, in which the absolute configuration remains undetermined.

Structural Elucidation of GEA on the Basis of the X-Ray Diffraction Analysis. A good single crystal of GEA p-BPE (**1a**) was grown by slow evaporation from the solution in hexane and dichloromethane containing a trace amount of methanol. The crystal data follow as: $C_{41}H_{44}O_9Br_2 \cdot 1/2CH_2Cl_2$, monoclinic, space group $P2_1$, a=18.596(6), b=15.010(4), c=16.112(5) Å,

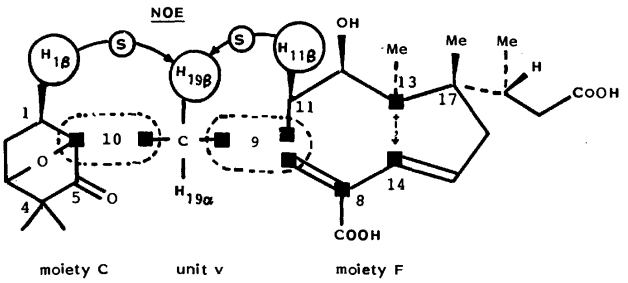

Fig. 7. A combination of the moieties (C) and (F) and the unit (v).

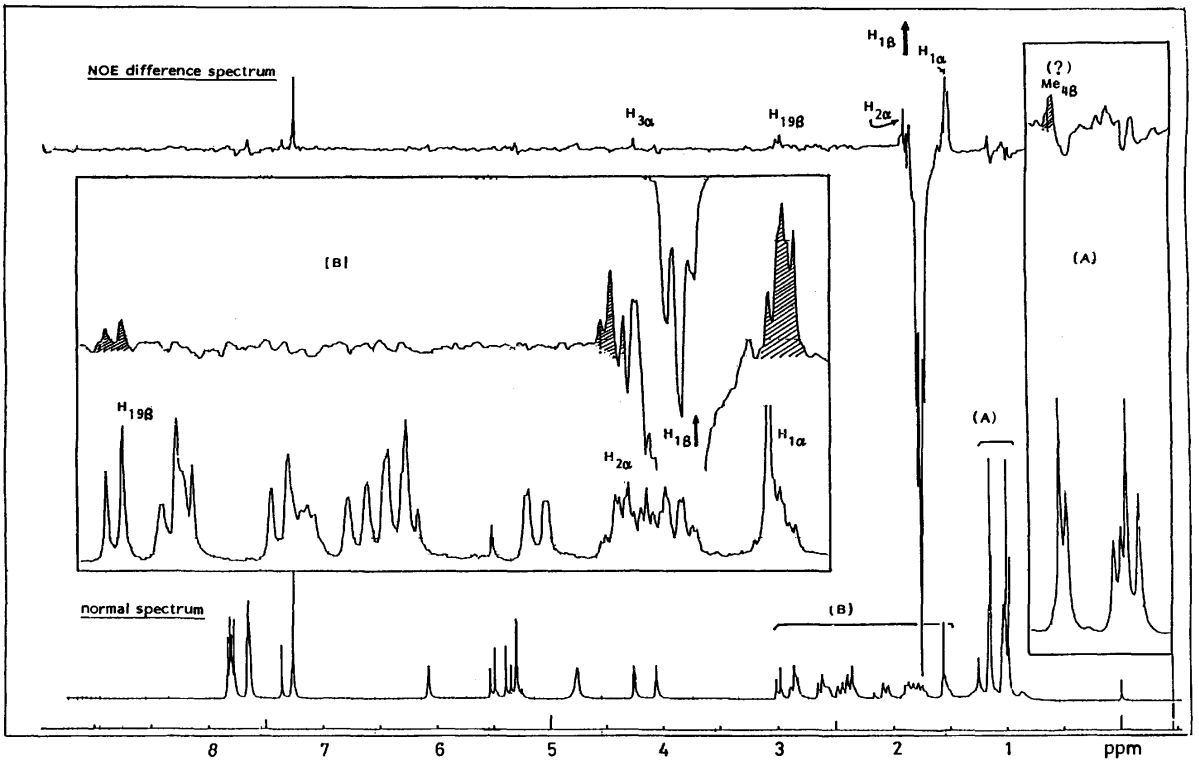

Fig. 6. The NOE difference spectrum of GEA p-BPE (**1a**) on irradiation at δ 1.76 (1β-H) (400 MHz, 0.5 mg in $CDCl_3$ and D_2O).

β=114.41(2)°, Z=4, D_C=1.432 g cm^{-3}, μ(Cu-$K\alpha$)=35.6 cm^{-1}. The intensities of 4725 independent reflections with $2\theta<120°$ were collected on an automatic, four-circle diffractometer with graphite-monochromated Cu-$K\alpha$ radiation using the ω—2θ scanning technique.[13] Since three standard reflections showed a gradual decrease in intensity with the course of data collection, the intensities were corrected for this damage to the sample as well as for the Lorenz and polarization factors. The structure was solved by the Monte Carlo direct method,[14] using the 30 strongest reflections as a starting set. An E-map based on the 58th random phase set afforded all the non-hydrogen atoms in the two ester molecules. The dichloromethane molecule was located in a difference Fourier map. After several cycles of the least-squares refinement had been carried out using the carbon atomic scattering factors for all the light atoms, the oxygen atoms were distinguished from the carbon atoms on the basis of the isotropic temperature factors and the bond distances and angles. The structure was then refined by the block-diagonal least-squares method with anisotropic thermal parameters. The absolute configuration was assigned by taking account of the anomalous dispersion of the halogen atoms for Cu-$K\alpha$ radiation. The R-factor for two enantiomeric structures, 1.106, excluded one of them at the 99.5% confidence level.[15] After the 78 hydrogen atoms had been located in a second difference Fourier map, further least-squares refinement were performed including these hydrogen atoms. The final R-value was 7.8%. These two crystallographically-independent molecules of **1a** had almost the same geometries, and one of the two is depicted in Fig. 8. The molecular structure including the absolute configuration of **1a** has thus been determined, and hence the structure of GEA is represented by formula **1**.[16]

On the basis of the assigned structure, we propose the following biogenesis for formation of GEA, shown in Fig. 9. The biogenesis, including a cycloartane, one of naturally occurring triterpenes such as acerinol[9] (**4**) and cimigenol[9] (**6**), as a

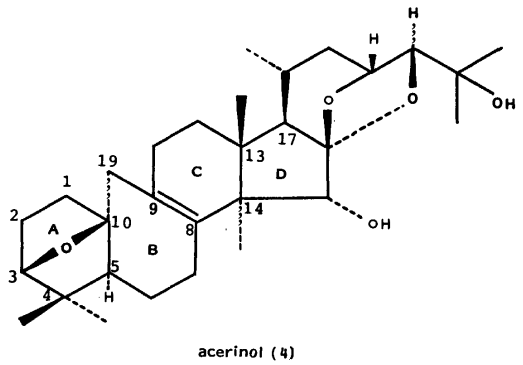

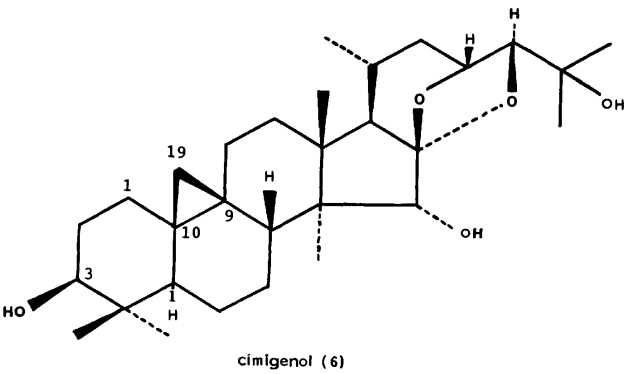

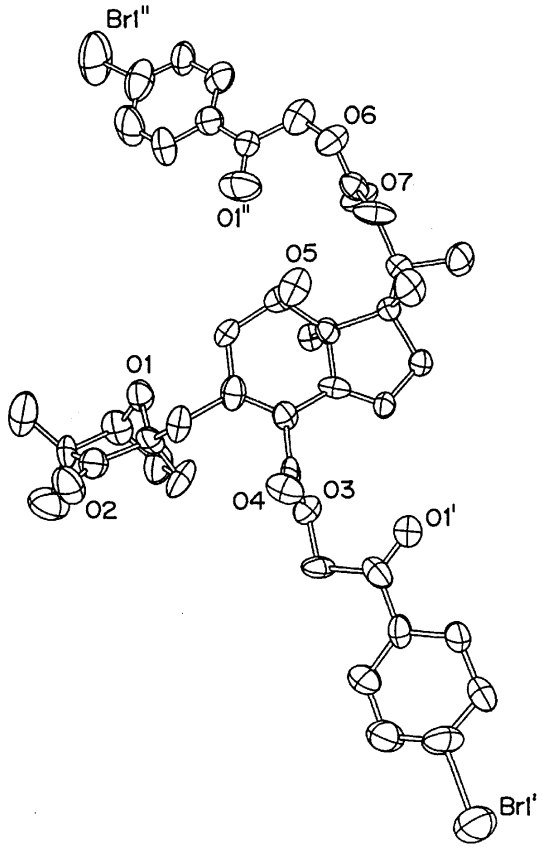

Fig. 8. The X-ray crystal structure of GEA p-BPE (**1a**).

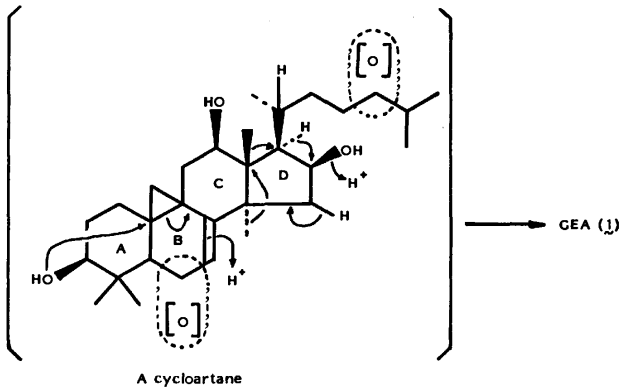

Fig. 9. A plausible biogenesis for formation of GEA (**1**).

precursor, involves (1) migration of two methyl groups in the C and D rings in a back-bone rearrangement manner, (2) cleavage of the C(9)–C(10) bond followed by formation of a 7-oxabicyclo[2.2.1]-heptane system, and (3) oxidative cleavage of the B ring and side chain with loss of one and four carbon atoms. Thus GEA (**1**) is regarded as a pentanortriterpene. These biogenetical characteristics represent the distinctive structural features of GEA. The structure with such characteristics has not been encountered previously. Only recently, isolation of a triterpene, mariesiic acid A, "having a methyl-rearranged skeleton of lanostane" from *Abies mariesii* has been reported by Hasegawa et al.[17]

Structural Elucidation of GEB. The molecular formula of GEB (**2**) was established as $C_{31}H_{42}O_9$ on the basis of the FD-MS spectrum [*m/z* 950, 952, and 954 (1:2:1)] of GEB p-BPE (**2a**) as well as the ^{1}H NMR spectra of **2a** [$CDCl_3$ (Fig. 10) and C_6D_6]. The ^{13}C NMR (Table 1) and ^{1}H NMR spectra of **2a** measured in the same manner as **1a**, indicated the presence of ten structural units(i) to (x) tabulated in Table 2. The ^{1}H NMR spectral properties, especially the difference NOEs[7,8] and coupling constants summarized in Fig. 11, of most of the protons included in these units, were essentially identical with those of the corresponding protons of **1a**. Thus structural moieties (a) including the units(i), (vii), and (x) (**2a**, IR_{max} 1750 cm^{-1}), (b) equivalent to the unit(v), (c) involving the units(iii), (iv), (vi), and (viii) [**2**, UV_{max} 252 nm (ε 9500)], and (d) containing the units(ii) and (ix), must constitute the A, B (cleaved), C and D rings, and the side chain, respectively. In view of the co-occurrence of **1** and **2** in the same plant, GEB

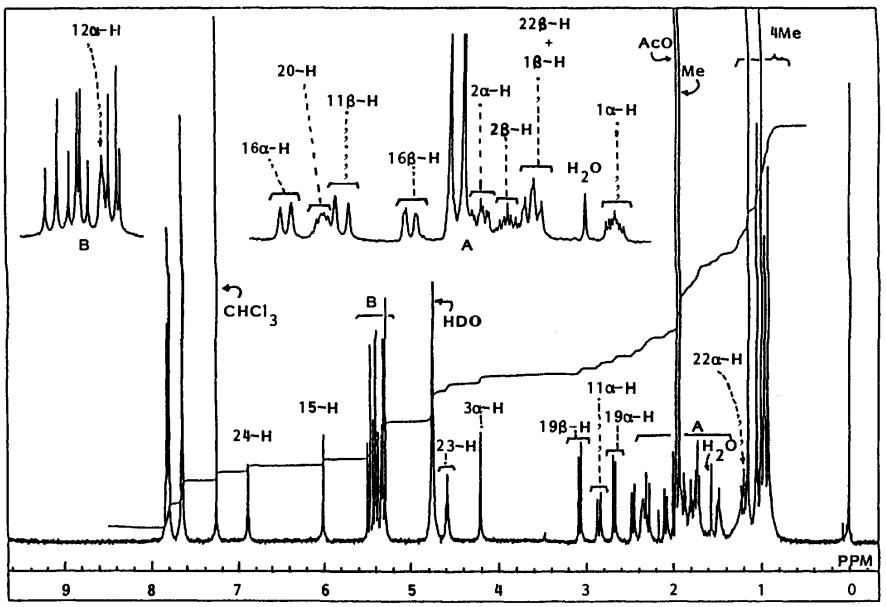

Fig. 10. The ^{1}H NMR spectrum of GEB p-BPE (**2a**) (500 MHz, 1 mg in $CDCl_3$ and D_2O).

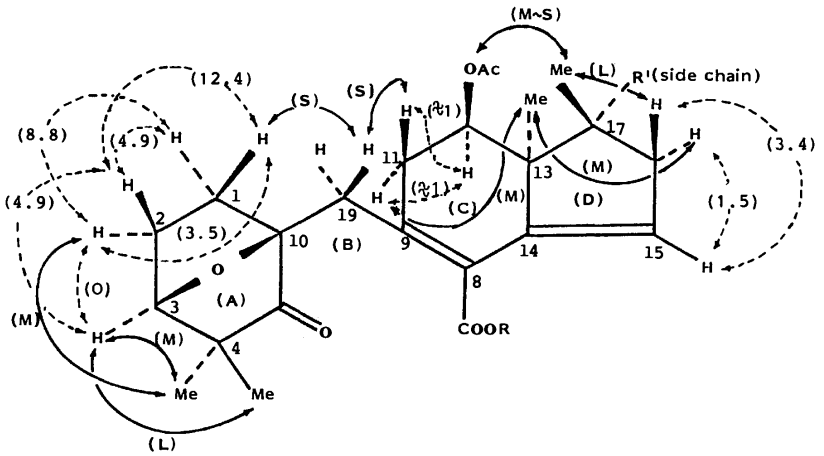

Fig. 11. The NOEs (⌒) and coupling constants (Hz) between the protons in the A→D rings of GEB p-BPE (**2a**) (R=$CH_2COC_6H_4Br$).

must possess the same skeleton and the same absolute configuration as GEA, differing from **1** only in the substituent (OH→OAc) at C(12) and the side chain. The structure of the side chain [the units(ii) and (ix)] was elucidated on the basis of the result of conformational analysis, deduced from the difference NOEs[7,8] (Fig. 12) between the relevant protons. The result was also consistent with the following coupling constants (Hz): $J_{20\alpha,22\beta}$=0 (dihedral angle, $\theta\fallingdotseq$110°); $J_{20\alpha,22\alpha}$=11.1 ($\theta\fallingdotseq$10°); $J_{22\beta,23\alpha}$=12.8 ($\theta\fallingdotseq$160°); $J_{22\alpha,23\alpha}$=2.0 ($\theta\fallingdotseq$80°); $J_{23\alpha,24}$=8.2 ($\theta\fallingdotseq$180°); $J_{24,27}$=1.2. The conformation depicted in Fig. 12 indicates that **2a** possesses the (20*R*, 23*S*, 24*E*) configuration. GEB is therefore represented most favorably by formula **2**.

Structure Elucidation of GEC. The molecular formula of GEC (**3**) was established as $C_{29}H_{38}O_9$ on the basis of the FD-MS spectrum [*m/z* 906, 908, and 910 (1:2:1)] and the ^{1}H NMR spectra of GEC p-BPE (**3a**). The ^{13}C NMR (Table 1) and ^{1}H NMR spectra of **3a** revealed the existence of ten structural units(i) to (x) shown in Table 2. Detailed examination of the NOE difference spectra between the methyl and other protons included in these units indicated that GEC (**3**) must possess the same skeleton as GEA (**1**) with the C(16) atom substituted by an ether oxygen atom, which involves three structural moieties (a) including the units(i), (vii), and (x) (**3a**, IR_{max} 1754 cm^{-1}), (b) the unit(v), and (c) including the units(ii), (iii), (iv), (vi), and (viii) [**3**, UV_{max} 253 nm (ε 9500)], corresponding to the A, B (cleaved), and C and D rings, respectively. The (20*R*, 23*R*, 24*E*) configuration in the D ring and the side chain was deduced mainly from the difference NOEs[7,8] shown in Fig. 13 (cf., Fig. 4 in Ref. 4). The coupling and difference coupling constants (Hz) between the relevant protons were in good accord with the conformation depicted in Fig. 13: $J_{20\beta,22\beta}$=6 (dihedral angle, $\theta\fallingdotseq$35°); $J_{20\beta,22\alpha}$=13 ($\theta\fallingdotseq$155°); $J_{22\beta,22\alpha}$=13; $J_{22\beta,23\beta}$=3 ($\theta\fallingdotseq$40°); $J_{22\alpha,23\beta}$=13 ($\theta\fallingdotseq$160°); $J_{23\beta,24}$=8 ($\theta\fallingdotseq$170°); $J_{24,27}$=1.2. GEC is therefore represented best by formula **3**.

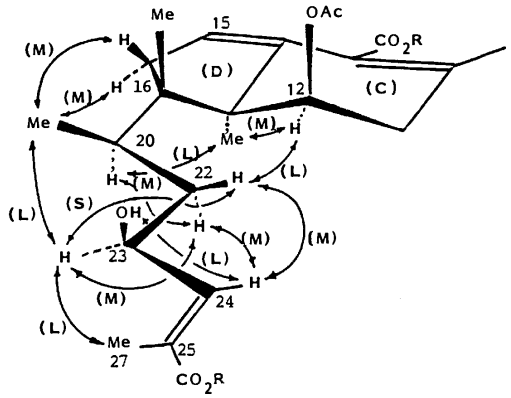

Fig. 12. The difference NOEs (⌒) between the protons in the side chain of GEB p-BPE (**2a**) (R= $CH_2COC_6H_4Br$).

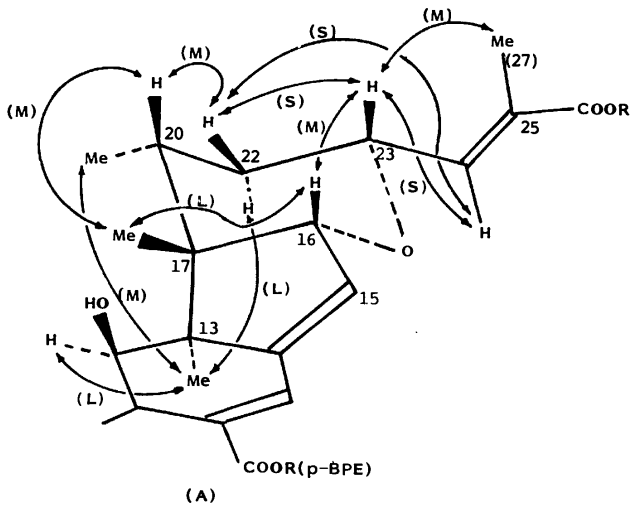

(A)

Fig. 13. The difference NOEs (⌒) between the protons in the side chain of GEC p-BPE (**3a**) (R= $CH_2COC_6H_4Br$).

Experimental

The IR spectra were recorded on KBr disks with JASCO model IRA-810 and/or JEOL model JIR-100 spectrometers, and the UV spectra in methanol with a Hitachi model 124 spectrometer. The MS spectra was measured with JEOL model JMS-D300 and/or JMS-OISG-2 spectrometers. The ^{1}H NMR spectra, COSY spectra, and NOE difference spectra, and decoupling difference spectra were measured in [^{2}H]chloroform, (Merck Co., Inc. and Aldrich Chem. Co., Inc.), [$^2H_6$]benzene, and/or [$^2H_4$]methanol with JEOL model PS-100, FX-400, GX-400 and/or GX-500 spectrometers, TMS (Aldrich Chem. Co., Inc.) being used as an internal standard. The ^{13}C NMR spectra were recorded in [^{2}H]chloroform and/or [$^2H_6$]benzene with JEOL model FX-90, FX-100 and/or GX-500 spectrometers.

GEA p-BPE (1a). CD, λ_{max}^{MeOH} ($\Delta\varepsilon$) 257.5 nm (−5.6), 235.0 (−1.2), 224 (−2.0), and 198.5 (+10.6): UV (MeOH), 254.5 nm (ε 27100): IR (KBr), 1760 (sh), 1738 (s), 1704 (s), 1587 (m), 1543 (w), 1460 (w), 1422, 1377, 1231 (w), 1202, 1171, 1113, 1071 (s), 975 (s), 823 (m), and 761 (m) cm^{-1}: ^{1}H NMR (500 MHz, $CDCl_3$ and D_2O) (Fig. 1), δ=0.99 (3H, br s, 28-H=13α-CH_3), 1.02 (3H, s, 29-H=4α-CH_3), 1.04 (3H, d, *J*=6.5 Hz, 21-H=20α-CH_3), 1.15 (3H, br s, 18-H=17β-CH_3), 1.17 (3H, s, 30-H, 4β-CH_3), 1.54 (1H, ddd, *J*=12, 9, and 4 Hz, 1α-H), 1.76 (1H, ddd, *J*=12, 10, and 5 Hz, 1β-H), 1.84 (1H, dddd, *J*=12, 10, 5, and 4 Hz, 2β-H), 1.90 (1H, ddd, *J*=12, 9 and 5 Hz, 2α-H), 2.08 (1H, dd, *J*=17 and 3.5 Hz, 16β-H), 2.37 (1H, dd, *J*=14.5 and 11.5 Hz, 22β-H), 2.39 (1H, dd, *J*=18 and 1.5 Hz, 11β-H), 2.47 (1H, dd, *J*=17 and 1.5 Hz, 16α-H), 2.58 (1H, dq *J*=11.5 and 6.5 Hz, 20β-H), 2.64 (1H, br d, *J*=14.5 Hz, 22α-H), 2.85 (1H, d, *J*=14.5 Hz, 19α-H), 2.86 (1H, dd, *J*=18 and 3 Hz, 11α-H), 3.00 (1H, d, *J*=14.5 Hz, 19β-H), 4.07 (1H, dd, *J*=3 and 1.5 Hz, 12α-H), 4.26 (1H, d, *J*=5 Hz, 3α-H), and 6.08 (1H, dd, *J*=3.5 and 1.5 Hz, 15-H); p-BPE part, δ=5.28 and 5.33 (each 1H, ABq, *J*=16.5 Hz, $BrC_6H_4COCH_2$), 5.38 and 5.49 (each 1H, ABq, *J*=16.5 Hz, $BrC_6H_4COCH_2$), 7.65 and 7.79 (each 2H, ABq, *J*=8.5 Hz, $BrC_6H_4COCH_2$), 7.65 and 7.83 (each 2H, ABq, *J*=8.5 Hz,

$BrC_6H_4COCH_2$): ^1H NMR (500 MHz, C_6D_6) δ=0.73 (3H, s, 29-H=4α-CH_3), 1.05 (3H, br s, 28-H=13α-CH_3), 1.10 (3H, s, 30-H=4β-CH_3), 1.10 (3H, d, J=6.5 Hz, 21-H=20α-CH_3), 1.24 (3H, br s, 18-H=17β-CH_3), ≈1.43 and ≈1.70 (3H and 1H, each m, 1α-H to 2β-H), 1.97 (1H, dd, J=17 and 3.5 Hz, 16β-H), 2.34 (1H, dd, J=18 and 1.5 Hz, 11β-H), 2.36 (1H, dd, J=17 and 1.5 Hz, 16α-H), 2.44 (1H, dd, J=14.5 and 11.5 Hz, 22β-H), 2.75 (1H, br d, J=14.5, 22α-H), ≈2.75 (1H, br m, 20β-H), 2.87 (1H, dd, J=18 and 3 Hz, 11α-H), 3.06 (1H, d, J=14.5 Hz, 19α-H), 3.22 (1H, d, J=14.5 Hz, 19β-H), 3.78 (1H, d, J=5 Hz, 3α-H), 3.93 (1H, br d, J=7.5 Hz, 12α-H), and 6.54 (1H, br s, 15-H); p-BPE part, δ=4.72 and 4.83 (each 1H, ABq, J=16.5 Hz, $BrC_6H_4COCH_2$), 4.82 and 5.10 (each 1H, ABq, J=16.5 Hz, $BrC_6H_4COCH_2$), ≈7.06 and ≈7.19 (each 4H, m, 2×$BrC_6H_4COCH_2$): ^{13}C NMR (25 MHz, $CDCl_3$) (Table 1), p-BPE part, δ=65.58 (t), 65.93 (t), 129.0 (s), 129.1 (d), 132.0 (d), 132.7 (s), 191.0 (s), and 191.2 (s): ^{13}C NMR (25 MHz, C_6D_6) (Table 1), p-BPE part, δ=66.10 (t), 66.51 (t), 129.0 (s), 129.1 (d), 132.0 (d), 132.9 (s), 191.2 (s), and 191.2 (s): FD-MS, m/z 842, 840 (base), 838 (1:2:1), and 843, 841, 839 (1:2:1): CI(NH_3)-MS, m/z 860, 858, 856 (1:2:1), 662, 660 (1:1), 644, 642 (1:1), 624, 185, 183 (1:1), 138 (base): EI-MS, m/z 598, 596 (1:1) ($C_{32}H_{37}O_6Br$), 557, 555 (1:1), 511, 509 (1:1), 185, 183 (base) (1:1) (C_7H_4OBr).

GEA (1). UV (MeOH), 251.5 nm (ε 8300): IR (KBr), 3438—3380 (m), 1758 (w), 1670 (w), 1575 (vs), 1425 (s), 1411 (s), 1333 (w), 1043 (m), 1012 (m), 924 (w), 837 (w), 650 (m), and 619 (m) cm^{-1}: ^1H NMR (500 MHz, CD_3OD and D_2O), δ=1.01 (3H, d, J=6.7 Hz, 21-H=20α-CH_3), 1.08 and 1.18 (each br s, 28- and 18-H=13α-CH_3 and 17β-CH_3), 1.11 and 1.25 (each s, 29- and 30-H=4α-CH_3 and 4β-CH_3), ≈1.40 (4H, m, 1α-H to 2β-H), ≈2.00 (5H, m, 16β-H, 22β-H, 16α-H, 20β-H, and 22α-H), 2.48 (1H, d, J=14.5 Hz, 19α-H), 2.52 and 2.85 (each 1H, br d, J=18.9 Hz, 11β-H and 11α-H), 3.06 (1H, d, J=14.5 Hz, 19β-H), 4.08 (1H, br s, 12α-H), 4.39 (1H, d, J=4.5 Hz, 3α-H), and 5.66 (1H, br s, 15-H).

GEB p-BPE (2a). IR (KBr), 3200, 1750 (m), 1716 (s), 1579 (m), 1374, 1242 (s), 1210 (s), 1060 (m), 968 (s), 812 (m), and 747 (m) cm^{-1}: ^1H NMR (500 MHz, $CDCl_3$) (Fig. 7), δ=0.93 (3H, br s, 28-H=13α-CH_3), 0.97 (3H, d, J=6.7 Hz, 21-H=20α-CH_3), 1.01 (3H, s, 29-H=4α-CH_3), 1.06 (3H, br s, 18-H=17β-CH_3), 1.15 (3H, s, 30-H=4β-CH_3), 1.20 (1H, ddd, J=12.8, 11.1, and 2.0 Hz, 22α-H), 1.48 (1H, ddd, J=12.4, 8.8, and 4.9 Hz, 1α-H), 1.62 (1H, br d, J=3.7 Hz, D_2O-exchangeable, OH), 1.72 (2H, m, 1β-H and 22β-H), 1.80 (1H, dddd, J=12.4, 12.4, 4.9, and 4.9 Hz, 2β-H), 1.87 (1H, ddd, J=12.4, 8.8, and 3.5 Hz, 2α-H), 1.93 (3H, d, J=1.2 Hz, 27-H=25-CH_3), 1.97 (3H, s, $OCOCH_3$), 2.09 (1H, br dd, J=17.0 and 3.4 Hz, 16β-H), 2.30 (1H, br d, J=19.8 Hz, 11β-H), 2.35 (1H, br dq, J=11.1 and 6.7 Hz, 20α-H), 2.46 (1H, br d, J=17.0 Hz, 16α-H), 2.68 (1H, d, J=14.8 Hz, 19α-H), 2.86 (1H, br d, J=19.8 Hz, 11α-H), 3.08 (1H, d, J=14.8, 19β-H), 4.21 (1H, d, J=4.9 Hz, 3α-H), 4.60 (1H, dddd, J=12.8, 8.2, 3.7, and 2.0, and ddd, J=12.8, 8.2, and 2.0 on addition of D_2O, 23α-H), 5.33 (1H, br s, 12α-H), 6.02 (1H, br s, 15-H), 6.89 (1H, dq, J=8.2 and 1.2 Hz, 24-H); p-BPE part, δ=5.30 and 5.48 (each 1H, ABq, J=16.5 Hz, $BrC_6H_4COCH_2$), 5.40 and 5.42 (each 1H, ABq, J=16.5 Hz, $BrC_6H_4COCH_2$), 7.65 (4H, m, $BrC_6H_4COCH_2Br$), and 7.80 and 7.83 (each 2H, ABq, J=8.5 Hz, $BrC_6H_4COCH_2$): ^1H NMR (400 MHz, C_6D_6), δ=0.75 (3H, s, 29-H=3α-CH_3), 0.83 (3H, d, J=6.8 Hz, 21-H=20α-CH_3), 0.94 (1H, br d, J=4.0 Hz, D_2O-exchangeable, OH), 1.05 (3H, br s, 28-H=13α-CH_3), 1.09 (3H, s, 30-H=4β-CH_3), 1.20 (3H, br s, 18-H=17β-CH_3), 1.20 (1H, m, 22α-H), 1.45 (3H, m, 1α-H, 1β-H, and 2β-H), 1.64 (3H, s, $OCOCH_3$), 1.76 (1H, m, 2α-H), 1.90 (3H, d, J=1.5 Hz, 27-H=25-CH_3), 1.92 (1H, br dd, J=14.0 and 11.0 Hz, 22β-H), 2.06 (1H, br dd, J=16.6 and 3.4, 16β-H), 2.37 (1H, m, 20β-H), 2.43 (1H, br d, J=16.6 Hz, 16α-H), 2.48 (1H, br d, J=19.0 Hz, 11β-H), 2.85 (1H, d, J=14.6 Hz, 19α-H), 3.02 (1H, br d, J=19.0 Hz, 11α-H), 3.41 (1H, d, J=14.6 Hz, 19β-H), 3.79 (1H, br d, J=2.4 Hz, 3α-H), 4.27 (1H, m, 23α-H), 5.70 (1H, br s, 12α-H), 6.59 (1H, br s, 15-H); p-BPE part, δ=4.66 and 4.90 (each 1H, ABq, J=16.5 Hz $BrC_6H_4COCH_2$), 4.79 and 5.01 (each 1H, ABq, J=16.5 Hz, $BrC_6H_4COCH_2$), 7.04 and 7.15 (each 2H, ABq, J=8.5 Hz, $BrC_6H_4COCH_2$), 7.10 and 7.12 (each 2H, ABq, J=8.5 Hz, $BrC_6H_4COCH_2$): ^{13}C NMR (25 MHz, C_6D_6) (Table 1), p-BPE part, δ=66.8 (t), 127.1 (s), 129.9 (d), 132.4 (d), 134.4 (s), 135.6 (s), 191.6 (s), and 192.0 (s): FD-MS, m/z 954, 952 (base), 950 (1:2:1).

GEB (2). A solution (soln) of **2a** (0.3 mg) in 0.1 M† potassium hydroxide (KOH) in methanol (0.1 ml) was stirred at room temperature (temp) for 10 h. After being evaporated, the reaction mixture was mixed with 0.2 M hydrochloric acid (HCl) (0.2 ml) and extracted with ethyl acetate (3×0.1 ml). The ethyl acetate soln was dried and evaporated to leave an morphous residue, which was purified by preparative HPLC on a NOVA-PAK cartridge C_{18} column (8 mm×10 cm) with a UV light (254 nm) monitor, a 4:6 mixture of acetonitrile and 1% aqueous (aq) acetic acid being used as an eluent at a flow rate of 15 ml min^{-1}, giving **2** (0.17 mg), amorphous, UV (MeOH), 245 (sh, ε 8000), 252 (9500), and 260 nm (sh, 7300): IR (KBr), 3417 (m), 1740 (w), 1575 (vs), 1543 (s), 1414 (s), 1016 (w), 651 (m), and 620 (w) cm^{-1}: ^1H NMR (500 MHz, CD_3OD) δ=0.96 (3H, d, J=6.4 Hz, 21-H=20α-CH_3), 0.99 and 1.15 (each 3H, s, 29-H and 30-H=4α-CH_3 and 4β-CH_3), 1.01 and 1.11 (each 3H, br s, 28-H and 18-H=13α-CH_3 and 17β-CH_3), 1.25 (1H, m, 22α-H), 1.37 (1H, m, 1α-H), 1.78 (2H, m, 1β-H and 22β-H), 1.84 (3H, br s, 27-H=25-CH_3), 1.86 (1H, m, 2β-H), 1.88 (3H, s, $OCOCH_3$), 1.93 (1H, ddd, J=9, 9, and 3 Hz, 2β-H), 1.95 (1H, dd, J=18 and 4 Hz, 16β-H), 2.03 (1H, br d, J=19 Hz, 11β-H), 2.32 (1H, d, J=15 Hz, 19α-H), 2.33 (1H, m, 20β-H), 2.42 (1H, d, J=18 Hz, 16α-H), 2.84 (1H, br d, J=19 Hz, 11α-H), 3.03 (1H, d, J=15 Hz, 19β-H), 4.03 (1H, br s, 12α-H), 4.24 (1H, d, J=5 Hz, 3α-H), 4.47 (1H, ddd, J=11, 9, and 2 Hz, 23α-H), 5.58 (1H, br s, 15-H), and 6.43 (1H, m, 24-H).

Deacetylglycinoeclepin B (2b). A soln of **2** (0.1 mg) in 5% sodium methoxide in methanol (0.1 ml) was stirred at 70 °C for 10 h. The mixture was evaporated, acidified with 0.2 M HCl (0.2 ml), and extracted with ethyl acetate (3×0.1 ml). The ethyl acetate soln was dried and evaporated to leave an oily residue, which was purified by preparative HPLC on a NOVA-PAK cartridge C_{18} column (8 mm×10 cm), a 4:6 mixture of acetonitrile and 1% aq acetic acid being used as an eluent at a flow rate of 1.5 ml min^{-1}, to give **2b** (0.1 mg), amorphous. UV (MeOH), 242 (sh, ε 9500), 250 (9900), and 260 nm (sh, 6900): IR (KBr), 3438—3380 (m), 1751 (w), 1576 (vs), 1545 (s), 1414 (vs), 1016 (w), 652 (m), and 621 (w) cm^{-1}: ^1H NMR (500 MHz, CD_3OD), δ=0.92 (3H, d, J=6.8 Hz, 21-H=20α-CH_3), 0.95 and 1.11 (each 3H, s, 29-H and 30-H=4α-

† 1 M=1 mol dm^{-3}.

CH_3 and 4β-CH_3), 0.96 and 1.06 (each 3H, br s, 28-H and 18-H=13α-CH_3 and 17β-CH_3), 1.80 (3H, br s, 27-H=25-CH_3), 1.98 (1H, br d, J=18 Hz, 11β-H), 2.27 (1H, d, J=14 Hz, 19α-H), 2.30 (1H, m, 20β-H), 3.38 (1H, br d, J=16 Hz, 16α-H), 2.80 (1H, br d, J=18 Hz, 11α-H), 2.99 (1H, d, J=14 Hz, 19β-H), 3.99 (1H, m, 12α-H), 4.20 (1H, d, J=5 Hz, 3α-H), 4.43 (1H, m, 23α-H), and 5.54 (1H, br s, 15-H).

GEC p-BPE (3a). ^{1}H NMR (500 MHz, $CDCl_3$ and D_2O), δ=1.01 (3H, s, 29-H=4α-CH_3), 1.16 (3H, s, 30-H=4β-CH_3), 1.25 (3H, br s, 18-H=17β-CH_3), 1.29 (3H, d, J=7 Hz, 21-H=20α-CH_3), 1.37 (3H, br s, 18-H=13α-CH_3), 1.48 (1H, ddd, J=13, 6, and 3 Hz, 22β-H), 1.54 (1H, m, 1α-H), 1.75 (1H, ddd, J=12, 12, and 3.5 Hz, 1β-H), 1.77 (1H, ddd, J=13, 13, and 13 Hz, 22α-H), 1.82 (1H, dddd, J=12, 12, 5, and 5 Hz, 2β-H), 1.90 (1H, ddd, J=12, 9, and 4 Hz, 2α-H), 1.94 (3H, d, J=1.5 Hz, 27-H=25-CH_3), 2.03 (1H, m, 20β-H), 2.40 (1H, dd, J=19 and 1.5 Hz, 11β-H), 2.89 (1H, d, J=14.5 Hz, 19α-H), 2.94 (1H, br d, J=19 Hz, 11α-H), 3.08 (1H, d, J=14.5 Hz, 19β-H), 4.00 (1H, d, J=3.5 Hz, 16β-H), 4.08 (1H, br s, 12α-H), 4.25 (1H, d, J=5 Hz, 3α-H), 4.88 (1H, ddd, J=13, 8, and 3 Hz, 23β-H), 6.22 (1H, d, J=3.5 Hz, 15-H), and 6.88 (1H, dq, J=8 and 1.5 Hz, 24-H); p-BPE part, δ=5.28 and 5.35 (each 1H, ABq, J=16.5 Hz, $BrC_6H_4COCH_2$), 5.36 and 5.51 (each 1H, ABq, J=16.5 Hz, $BrC_6H_4COCH_2$), 7.63 and 7.65 (each 2H, ABq, J=8.5 Hz, $BrC_6H_4COCH_2$), 7.78 and 7.81 (each 2H, ABq, J=8.5 Hz, $BrC_6H_4COCH_2$): ^{1}H NMR (500 MHz, C_6D_6), δ=0.85 and 1.48 (each 3H, s, 29-H and 30-H=4α-CH_3 and 4β-CH_3), 1.19 (3H, d, J=7 Hz, 21-H=20α-CH_3), 1.21 and 1.44 (each 3H, br s, 28-H and 18-H=13α-CH_3 and 17β-CH_3), 1.25 (1H, ddd, J=13, 6, and 3 Hz, 22β-H), 1.39 (1H, d, J=7.5 Hz, OH), ≈1.48 (3H, m, 1α-H, 1β-H, and 2β-H), 1.70 (1H, m, 22α-H), 1.81 (1H, m, 20β-H), 1.85 (1H, m, 2α-H), 2.08 (3H, d, J=1.5 Hz, 27-H=25-CH_3), 2.42 (1H, br d, J=19 Hz, 11β-H), 3.06 (1H, br d, J=19 Hz, 11α-H), 3.18 (1H, d, J=14.5 Hz, 19α-H), 3.44 (1H, d, J=14.5 Hz, 19β-H), 3.90 (1H, d, J=4 Hz, 3α-H), 4.05 (1H, br d, J=7.5 Hz, 12α-H), 4.09 (1H, d, J=3 Hz, 16β-H), 4.24 (1H, ddd, J=13, 8, and 3 Hz, 23β-H), 6.90 (1H, d, J=3 Hz, 15-H), and 7.42 (1H, dq, J=8 and 1.5 Hz, 24-H); p-BPE part, δ=4.89 and 5.17 (each 1H, ABq, J=16.5 Hz, $BrC_6H_4COCH_2$), 4.90 and 4.98 (each 1H, ABq, J=16.5 Hz, $BrC_6H_4COCH_2$), 7.15 and 7.16 (each 2H, ABq, J=8.5 Hz, $BrC_6H_4COCH_2$), 7.26 and 7.28 (each 2H, ABq, J=8.5 Hz, $BrC_6H_4COCH_2$): ^{13}C NMR (125 MHz, C_6D_6), (Table 1), p-BPE part, δ=66.1 (t), 66.2 (t), 129.36 (d), 129.44 (d), 132.0 (d), 133.2 (s), 133.4 (s), 190.77 (s), 190.83 (s): FD-MS, m/z 910, 908 (base), 906 (1:2:1).

GEC (3). Compound **3a** (0.5 mg) was hydrolyzed with 0.1 M KOH in methanol at room temp for 10 h. The reaction mixture was worked up as usual to yield an amorphous residue, which was purified by preparative HPLC as described above to give **3** (0.26 mg), amorphous. UV (MeOH), 253 nm (ε 9500): IR (KBr), 3375 (m), 1761 (m), 1572 (vs), 1414 (vs), 1055 (m), 1018 (m), and 654 (w) cm^{-1}: ^{1}H NMR (400 MHz, CD_3OD), δ=0.99 and 1.15 (each 3H, s, 29-H and 30-H=4α-CH_3 and 4β-CH_3), 1.23 and 1.29 (each 3H, br s, 28-H and 18-H=13α-CH_3 and 17β-CH_3), 1.28 (3H, d, J=6.5 Hz, 21-H=20α-CH_3), 1.89 (3H, br s, 27-H=25-CH_3), 2.01 (1H, m, 20β-H), 2.06 (1H, br d, J=18.5 Hz, 11β-H), 2.33 (1H, br d, J=14 Hz, 19α-H), 2.88 (1H, br d, J=18.5 Hz, 11α-H), 3.05 (1H, br d, J=14 Hz, 19β-H), 3.90 (1H, br s, 16β-H), 3.93 (1H, br s, 12α-H), 4.24 (2H, m, 3α-H and 23β-H), 5.75 (1H, br s, 15-H), and 6.37 (1H, m, 24-H).

1-Bromomethyl-3,3-dimethyl-7-oxabicyclo[2.2.1]heptan-2-one (5). (Scheme 1). a) A soln of α-chloroacrylonitrile (18.5 g, 0.22 mol), 2,4-dimethyl-1,3-pentadiene (10.5 g, 0.11 mol), and 2,6-di-*t*-butyl-4-methylphenol (BHT, 500 mg) in benzene (100 ml) was stirred under reflux for 7 h. The reaction mixture was evaporated and then distilled under reduced pressure to give 1-chloro-2,2,4-trimethyl-3-cyclohexene-1-carbonitrile (**5a**) (12.1 g), bp 108—113 °C (12 Torr) (1 Torr=133.322 Pa). The undistilled residue was submitted to chromatography over silica gel with hexane–benzene (10:1) to afford an additional amount (4.0 g) of **5a**. The total yield of **5a** amounted to 80%. **5a**: ^{1}H NMR (100 MHz, CCl_4), δ=1.17, 1.30, and 1.69 (each 3H, s), and 5.11 (1H, br s): MS, m/z 185 and 183 (1:3, M^+), 132 and 96 (base).

b) To a soln of copper(II) sulfate (68.0 g as $5H_2O$, 0.272 mol) in water (250 ml) was added zinc powder at 0 °C. The mixture was stirred at the temp for 10 min and filtered to give zinc-copper couples (Zn–Cu), which were washed with water and ethanol. To a soln of **5a** (25.0 g, 0.136 mol) in 80% aq ethanol (750 ml) were added the couples. The mixture was stirred under reflux for 15 h, when precipitates (ppts) appeared, and were then collected by filtration and washed with methanol and ethyl acetate repeatedly. All the organic solns were combined, evaporated, diluted with saturated brine, and extracted with ethyl acetate. The ethyl acetate soln was washed with water and brine, dried and evaporated to leave an oily residue, which was distilled under reduced pressure to afford 2,2,4-trimethyl-3-cyclohexene-1-carbonitrile (**5b**) (19.6 g, 97%), bp 122—123 °C (15 Torr): IR (neat), 2220 and 1460 cm^{-1}: ^{1}H NMR (100 MHz, CCl_4), δ=1.11 (6H, s), 1.63 (3H, s), and 5.08 (1H, br s): MS, m/z 149 (M^+), 134, 107, and 96 (base).

c) To a soln of diisopropylamine (12.9 ml, 92 mmol) in tetrahydrofuran (THF, 100 ml) was added butyllithium [BuLi, 1.6 M hexane soln (57.5 ml, 92 mmol)] at 0 °C, and the mixture was stirred for 30 min at 0 °C. To the mixture cooled at −78 °C was added **5b** (12.4 g, 83 mmol) in THF (60 ml) during a period of 1 h, and the mixture was then stirred at the temp for 1 h. Into the mixture was bubbled oxygen gas at −78 °C for 1 h, and was then added triethyl phosphite (15 ml, 87 mmol). The whole mixture was stirred at −78 °C for 15 min and then at 0 °C for 1.5 h. The reaction mixture was diluted with water and extracted with diethyl ether. The ether soln was washed with water and brine, dried, and evaporated to leave an oily residue, which was distilled in vacuo to give 2,2,4-trimethyl-3-cyclohexen-1-one (4.1 g). The undistilled residue was separated by chromatography over silica gel (130 g) with hexane–benzene (1:1) to yield an additional amount of the ketone (3.4 g): ^{1}H NMR (100 MHz, CCl_4), δ=1.07 (6H, s), 1.72 (3H, s), and 5.20 (1H, br s). The combined ketone was reduced without further purification.

A soln of the ketone (7.5 g, 54 mmol) in methanol (100 ml) was stirred with sodium borohydride (2.0 g, 54 mmol) at 0 °C for 1 h. After being quenched with acetic acid and neutralized with saturated aq sodium hydrogencarbonate ($NaHCO_3$), the reaction mixture was concentrated, diluted with water, and extracted with ether and then with ethyl acetate. The combined extracts were washed with saturated brine, dried, and evaporated to leave an oily residue, which was purified by distillation to give 2,2,4-trimethyl-3-cyclohexen-1-ol (**5c**) (7.17 g, 95%), bp 48—49 °C (0.35 Torr):

^{1}H NMR (100 MHz, $CDCl_3$), δ=0.95, 1.00, and 1.62 (each 3H, s), 3.53 (1H, dd, J=7 and 4 Hz), and 5.06 (1H, br s).

d) To a soln of **5c** (4.7 g, 33.6 mmol) and bis(acetylacetonato)oxovanadium(IV) [$VO(acac)_2$, 10 mg, 0.035 mmol] in benzene (100 ml) was added dropwise *t*-butyl hydroperoxide (a 70% soln in water, 8.6 g, 67 mmol), which had been dried azeotropically with benzene, in benzene under stirring. The mixture was stirred at room temp for 10 h, and quenched by addition of aq sodium thiosulfate ($Na_2S_2O_3$). The aq soln was separated and extracted with ether. The benzene and ether solns were combined, washed with aq $NaHCO_3$ and brine, dried, and evaporated to leave an oily residue which was purified by chromatography over silica gel (100 g) with benzene to give 2,2,4-trimethyl-*c*-3,*c*-4-epoxy-*r*-1-cyclohexanol (**5d**) (4.85 g, 93%): ^{1}H NMR (100 MHz, $CDCl_3$), δ=1.04, 1.17, and 1.32 (each 3H, s), 2.73 (1 h, br s), and 3.30 (1H, t, J=4 Hz): MS, m/z 156 (M^+), 138, 123, 100, and 44 (base).

e) A soln of **5d** (400 mg, 2.56 mmol) and ethyl vinyl ether (1 ml, 10.5 mmol) in dichloromethane (20 ml) was stirred with pyridinium *p*-toluenesulfonate (PPTS, 64 mg, 0.26 mmol) at room temp for 15 h. The soln was diluted with ether, washed with aq $NaHCO_3$ and brine, dried, and evaported to leave an oily residue, which was purified by chromatography over silica gel (20 g) with benzene–ethyl acetate (10:1) to give 2-ethoxyethyl ether (**5e**) of **5d** (0.55 g, 94%): IR (neat), 1380, 1135, 1100, 1085, 1060, and 1050 cm^{-1}: ^{1}H NMR (100 MHz CCl_4), δ=0.93—1.24 (15H, m), 2.35 (1H, br s), 3.40 (3H, m), and 4.55 (1H, m). Compound **5e** was a diastereoisomeric mixture and showed complex signals in the NMR spectrum.

f) To a soln of diethylamine (0.1 ml, 1.0 mmol) in ether (2 ml) was added BuLi [1.6 M hexane soln (0.65 ml, 1.0 mmol)] at 0 °C, and the mixture was stirred at the temp for 30 min. To this soln was added hexamethylphosphoric triamide (HMPA, 0.17 ml, 1.0 mmol) and then **5e** (114 mg, 0.5 mmol) in ether. The whole mixture was stirred under reflux for 20 h, cooled, poured into aq ammonium chloride (NH_4Cl), and extracted with ether repeatedly. The ether soln was washed with aq $NaHCO_3$ and brine, dried, and evaporated to leave an oily residue, which was separated by chromatography over silica gel (8 g) with benzene–ethyl acetate (10:1) to give a diastereoisomeric mixture (51 mg, 45%) of 2-ethoxyethyl ethers of 2,2-dimethyl-4-methylene-*c*-3,*r*-1-cyclohexanediol and of 2,2,4-trimethyl-4-cyclohexene-*c*-3,*r*-1-diol: IR (neat), 3490, 3040, 1660, 1450, 1380, 1130, 1095, 1025, 990, and 930 cm^{-1}: ^{1}H NMR (100 MHz, $CDCl_3$), δ=1.82 (3/2H, br s), 4.68 (1H, m), 4.82 (2/2H, br s), and 5.24 (1/2H, m). The mixture was used for the next reaction without further separation.

A soln of the mixture of the olefinic alcohols (45 mg, 0.20 mmol) in pyridine (2 ml) was treated with acetic anhydride (0.2 ml, 2.0 mmol) under stirring at room temp for 15 h. The reaction mixture was diluted with ether, washed with dil HCl, aq $NaHCO_3$ and brine, dried, and evaporated to leave an oily mixture of the acetates. This acetate mixture in THF (2 ml) was treated with 2 M HCl (0.3 ml) under stirring at room temp for 1 h. The mixture was worked up as usual to give an oily residue, which was separated by chromatography over silica gel (3 g) with benzene–ethyl acetate (5:1) to afford a mixture (30 mg, 77%) of 2,2-dimethyl-6-methylene-*c*-3-hydroxy-*r*-1-cyclohexyl acetate (**5f**) and 2,2,6-trimethyl-*c*-3-hydroxy-5-cyclohexane-*r*-1-yl acetate (**5f′**): IR (neat), 3490, 3090, 1740, 1660, 1445, 1370, 1260, 1110, 990, and 920 cm^{-1}: ^{1}H NMR (100 MHz, $CDCl_3$), δ=2.09 and 2.12 (total 3H, each s), and 3.50 (1H, m). The mixture was used for the next reaction without further separation.

g) A soln (30 mg, 0.15 mmol) of **5f** and **5f′** in acetonitrile (5 ml) was treated with N-bromosuccinimide (35 mg, 0.20 mmol) under stirring at room temp for 10 h. The mixture was diluted with ether, washed with aq $NaHCO_3$ and brine, dried, and evaporated to leave a residue, which was submitted to chromatography over silica gel (3 g) with benzene–ethyl acetate (5:1) to give 6-bromomethyl-2,2-dimethyl-*c*-3,*c*-6-epoxy-*r*-1-cyclohexyl acetate (**5g**) (14 mg, 33%) and the unreacted olefin (**5f′**) (10 mg, 33%). **5g**, mp 70—71.5 °C: IR ($CHCl_3$), 1740, 1385, 1260, 1060, and 1020 cm^{-1}; ^{1}H NMR (500 MHz, $CDCl_3$), δ=0.95 and 1.15 (each 3H, s), 2.02 (3H, s), 3.55 and 3.69 (each 1H, ABq, J=10.1 Hz), 4.01 (1H, d, J=4.6 Hz), and 4.61 (1H, s): MS, m/z 278, 276 (M^+), 235, 233, 183, and 154. Found: m/z 278.0262 and 276.0398. Calcd for $C_{11}H_{17}O_3Br$: M, 278.0340 and 276.0362. **5f′**, oil: ^{1}H NMR (100 MHz, $CDCl_3$), δ=0.96 and 0.99 (each 3H, s), 1.63 (3H, d, J=2 Hz), 2.12 (3H, s), 3.54 (1H, t, J=5 Hz), 5.48 (1H, br s), and 5.53 (1H, m).

h) A soln of **5g** (11 mg, 0.04 mmol) in an 8:1 mixture of methanol and water was treated with potassium carbonate (10 mg, 0.06 mmol) at 0 to 15 °C for 12 h. The soln was evaporated, mixed with water, and extracted with ether. The ether soln was worked up as usual to give an oily, crude alcohol, which was dissolved in acetone (4 ml). The acetone soln was treated with Jones' reagent (5 drops) at 0 °C under stirring for 30 min. The reaction mixture was quenched with isopropyl alcohol, diluted with water, and extracted with ether. The ether soln was worked up as usual to leave an oily residue, which was purified by chromatography over silica gel (3 g) with hexane–ethyl acetate (9:1) to give **5** (9.2 mg, 99%), oil: IR (neat), 1760, 1470, 1390, 1245, and 1020 cm^{-1}: ^{1}H NMR (400 MHz, $CDCl_3$), δ=1.06 and 1.23 (each 3H, s), 3.66 and 3.78 (each 1H, ABq, J=11.7 Hz), and 4.34 (1H, d, J=3.9 Hz): ^{13}C NMR (25 MHz, $CDCl_3$), δ=19.73 and 22.43 (each q), 25.83, 28.42, and 28.77 (each t), 49.61 (s), 84.01 (d), 87.30 (s), and 214.65 (s): MS, m/z 234, 232 (M^+), 206, 204, 125 (base), and 107. Found: m/z 234.0060 and 232.0067. Calcd for $C_9H_{13}O_2Br$: M, 234.0077 and 232.0097.

The authors wish to express their sincere thanks to many investigators for measurement of the spectra: Drs. Tetsuo Higuchi (JEOL) of FD-MS, CI-MS, and EI-MS, Kenji Watanabe (Hokkaido Univ.) for FD-MS, and Minoru Isobe (Nagoya Univ.) for FD-MS; Drs. Fumiko Kaneuchi (JASCO) for FT-IR and CD, Shun-ichi Ikawa (Hokkaido Univ.) for FT-IR and Akihiro Shibata (Toray) for FT-IR; Drs. Tsutomu Higashijima (The Univ. of Tokyo) for ^{1}H NMR (270 MHz), Tetsu Hinomoto (JEOL) for ^{13}C NMR (22.5 MHz), and Toshio Inubushi (Kyoto Univ.) for ^{1}H NMR (220 MHz). The research was supported by a Grant-in-Aid for Special Project Research No. 56104009 and a Grant-in-Aid for Scientific Research No. 57470022 provided by the Ministry of Education, Science and Culture of Japan, and many other funds.

References

1) T. Masamune, M. Anetai, A. Fukuzawa, M. Takasugi, H. Matsue, K. Kobayashi, S. Ueno, and N. Katsui, *Bull. Chem. Soc. Jpn.*, **60**, 981 (1987).

2) T. Masamune, M. Anetai, M. Takasugi, and N. Katsui, *Nature (London)*, **297**, 495 (1982).

3) A. Fukuzawa, A. Furusaki, M. Ikura, and T. Masamune, *J. Chem. Soc., Chem. Commun.*, **1985**, 222, 748.

4) A. Fukuzawa, H. Matsue, M. Ikura, and T. Masamune, *Tetrahedron Lett.*, **26**, 5539 (1985).

5) H. Matsue, Ph. D. Thesis, Hokkaido University, Sapporo, Japan, 1986.

6) G. C. Levy, R. L. Lichter, and G. L. Nelson, "Carbon-13 Nuclear Magnetic Resonance Spectroscopy," Wiley-Interscience, New York (1980), p. 136.

7) The exact intensities of NOEs were not measured, and the relative ones were estimated: L (large, 5—15%), 1.8—2.4 Å; M (medium, 3—5%), 2.4—2.8 Å; S (small, 1—3%), 2.8—3.1 Å.

8) Examination of the model of talaromycin A revealed that the intensities of NOEs did not always depend only on the distances ($\propto r^{-6}$) between the protons: cf., D. G. Lynn, N. J. Phillips, W. C. Hutton, J. Shabanowitz, D. I. Fennell, and R. J. Cole, *J. Am. Chem. Soc.*, **104**, 7319 (1982).

9) G. Kusano, F. Uchida, Y. Murakami, N. Sakurai, and T. Takemoto, *Yakugaku Zasshi*, **96**, 321 (1976); T. Takemoto, G. Kusano, and N. Yamamoto, *ibid.*, **87**, 1489 (1967).

10) The numbering is referred to that of GEA (**1**).

11) The methyl groups and hydrogen atoms included in the B ring and side chains of **1a**, **2a**, and **3a** were tentatively assigned α or β on the basis of Figs. 5, 7, 12, and 13.

12) The small NOEs of the proton (19β-H) were observed clearly on irradiation of those (1β-H) and (11β-H), but any NOE of the latter protons (1β-H and 11β-H) was not detected on irradiation of the former (19β-H).

13) Performed at the High Brilliance X-Ray Diffraction Laboratory of Hokkaido University.

14) A. Furusaki, *Acta Crystallogr. (A)*, **35**, 220 (1979).

15) W. C. Hamilton, *Acta Crystallogr.*, **18**, 502 (1965).

16) The atomic coordinates for this work are available on request from the Director of the Cambridge Crystallographic Data Centre, University Chemical Laboratory, Lensfield Road, Cambridge CB2 1EW.

17) S. Hasegawa, T. Miura, Y. Hirose, and Y. Iitaka, *Chem. Lett.*, **1985**, 1589.

 © 1987 The Chemical Society of Japan Bull. Chem. Soc. Jpn., 60, 1015—1019 (1987)

Concentration Quenching of Fluorescence from Bridged Synthetic Porphyrins

Kazuhiro MARUYAMA,* Soichi MORIKAWA, and Atsuhiro OSUKA
Department of Chemistry, Faculty of Science, Kyoto University, Sakyo-ku, Kyoto 606
(Received August 21, 1986)

Concentration quenching phenomena of singly and doubly bridged porphyrins and their zinc and magnesium complexes were studied. Hypothetical nonfluorescent dimer trap was suggested to be not a coplanarly stacked face-to-face dimer but a loosely interacting pair.

In the primary events of green plant photosynthesis, photons are absorbed by the antenna chlorophyll molecules and the resultant singlet excitation is transfered from molecule to molecule and ultimately trapped to the reaction center, where the efficient one-electron transfer from the special chlorophyll dimer to an appropriate acceptor takes place very rapidly. However, in vitro, chlorophylls and/or synthetic porphyrins exhibit the phenomenon of concentration quenching[1] of the excited singlet state whether in fluid solutions,[2,3] or in organized assemblies such as lipid monolayers,[4] multilayers,[5] lipid bilayer vesicles,[6] and detergent micelles,[7] or in a swollen polyethylene phase in the presence of other amphiphilic substances.[8] Whenever chlorophyll concentration is high enough for being comparable with that (ca. 10^{-1} M†) in the chloroplast, the singlet excited state is efficiently quenched, with complete annihilation of its photochemistry and usually that of the triplet also. Since singlet-singlet energy transfer between chlorophyll (or porphyrin) monomers (Eq. 1) has been well-established as a key step in photosynthesis and does not lead to the consumption of the excitation energy, it is reasonable to assume that dimers or aggregated form of chlorophyll or porphyrin is involved in the nonradiative decaying process of the concentration quenching. A possible molecular mechanism for the quenching process in homogeneous solutions has been suggested to involve capture of excitation energy by a nonfluorescent dimer trap[9] (Eq. 2—4).

$$^1P^* + P \xrightarrow{k_1} P + {}^1P^* \quad (1)$$

$$P + P \xrightarrow{K} P{-}P \quad (2)$$

$$^1P^* + P{-}P \xrightarrow{k_2} P + {}^1P{-}P^* \quad (3)$$

$$^1P{-}P^* \xrightarrow{k_d'} P{-}P \quad (4)$$

Although a large number of measurements on fluorescence lifetimes and fluorescence quantum yields have been reported in vivo and in vitro, relatively little is known about the steric effects around the porphyrin macrocycle upon the concentration quenching of fluorescence. Singlet energy transfer of chlorophyll and/or porphyrins may proceed via Förster-type inductive resonance-transfer mechanism (dipole-dipole interaction)[10] and thus may be independent of the steric hindrance around the macrocycles. However, one can expect *the steric effects on the formation of the hypothetical non fluorescent dimer* (Eq. 2). In order to obtain a better understanding of the quenching process and to make a model of an antenna chlorophyll function *in solution*, we have undertaken systematic studies on fluorescence properties of bridged porphyrins **H_2SB** and **H_2DB**.

Results and Discussion

Mesoporphyrin-II dimethyl ester (**1**) was prepared according to Chang's modified procedure.[11] Singly bridged porphyrin **4** (**H_2SB**) was synthesized in 45% yield by the reaction of 1,12-dodecamethylenediamine with mesoporphyrin-II bis(4-nitrophenyl) ester **3**,[12] which, in turn, was prepared by the treatment of mesoporphyrin-II dicarboxylic acid **2** with 4-nitrophenyl trifluoroacetate.[12] Coproporphyrin-I tetramethyl ester **5** (**H_2NB**) was hydrolyzed to the corresponding tetracarboxylic acid **6**, which was converted into tetrakis(4-nitrophenyl) ester **7**. The reaction of **7** with 1,12-dodecamethylenediamine in a dilute pyridine solution gave doubly bridged porphyrin **8** (**H_2DB**) in 8% yield. Dodecamethylene bridged structures of **H_2SB** and **H_2DB** were apparent from their 400 MHz ^{1}H NMR spectra; dodecamethylene protons in **H_2SB** appeared at δ −0.26 (4H, m), −0.12 (4H, m), 0.07 (4H, m), 0.14 (4H, m), 0.53 (4H, m), and 2.80 (4H, m) ppm; those in **H_2DB** appeared at δ −0.22 (8H, m), −0.11 (8H, m), 0.06 (8H, m), 0.18 (8H, m), 0.47 (8H, m), and 2.81 (8H, m) ppm. Almost the same chemical shifts of dodecamethylene protons in **H_2SB** and **H_2DB** indicate that a dodecamethylene bridge has a similar conformation in both porphyrins and thus may provide a similar degree of steric hindrance on one porphyrin side.

The optical absorption spectra and the fluorescence emission spectra of **H_2SB** and **H_2DB**, and their zinc and magnesium complexes were not significantly

† 1 M=1 mol dm^{-3}.

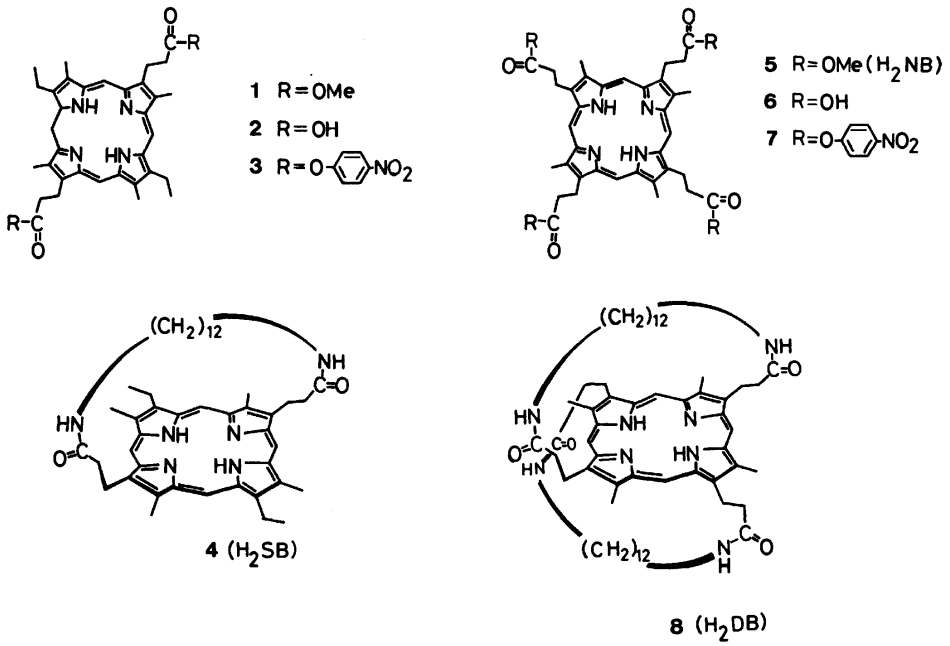

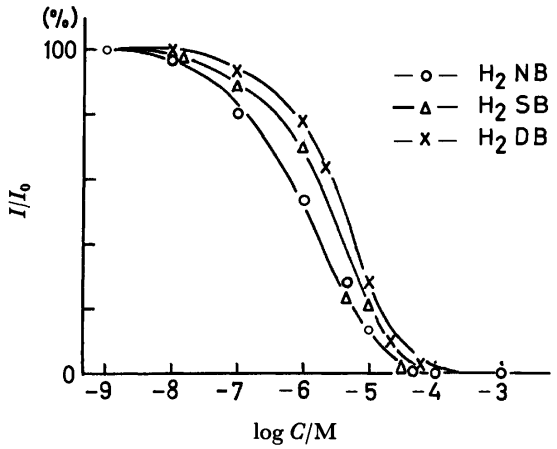

Fig. 1. Relative fluorescence yields of H_2NB, H_2SB, and H_2DB in CH_2Cl_2–CH_3OH (v/v=95/5) at 25 °C as a function of concentration.

altered by introduction of dodecamethylene bridge (Table 1). Relative fluorescence quantum yields were determined in CH_2Cl_2–MeOH (v/v=95/5) or CH_2Cl_2 at various concentration of porphyrins (Figs. 1—4). As shown in Fig. 1, there are small but distinct differences among **H_2NB**, **H_2SB**, and **H_2DB**. Critical concentrations of porphyrins and metalloporphyrins are defined as the concentration where an half of the intrinsic porphyrin fluorescence yields is lost by self-concentration quenching. The critical concentrations of **H_2NB**, **H_2SB**, and **H_2DB** are 1.1×10^{-6} M, 2.8×10^{-6} M, and 5.0×10^{-6} M, respectively (Table 2). Thus, the introduction of a dodecamethylene bridge roughly doubled the critical concentration of free base porphyrins in dichloromethane at room temperature.

Effects of the dodecamethylene bridge were much more pronounced in zinc porphyrins, **ZnNB, ZnSB,** and **ZnDB** (Fig. 2). Fluorescence concentration

Table 1. Absorption and Emission spectra of Nonbridged and Bridged Porphyrins[a)]

Porphyrin	Absorption/nm		Emission/nm	
	Soret band ($\varepsilon\times10^{-5}$)	Q-bands ($\varepsilon\times10^{-3}$)		
H_2NB	398 (1.48)	496 (10.8), 533 (8.8), 570 (5.6), 620 (5.0)	620	686
H_2SB	398 (1.47)	497 (9.7), 534 (7.5), 567 (5.7), 623 (4.7)	622	687
H_2DB	402 (1.48)	500 (11.0), 531 (7.2), 568 (4.3), 622 (3.8)	622	688
ZnNB	406 (4.04)	533 (21), 570 (32)	578	624
ZnSB	404 (3.95)	533 (20), 570 (30)	578	627
ZnDB	404 (4.09)	533 (19), 569 (26)	578	630
MgNB	411 (4.16)	546 (18), 582 (17)	587	627
MgSB	409 (4.17)	545 (19), 582 (23)	587	627
MgDB	408 (4.26)	545 (20), 582 (27)	588	628

a) Measured in CH_2Cl_2 at 10^{-5} M at 25 °C.

quenching of **ZnNB** occurred at more dilute conditions compared with that of **H_2NB** and the critical concentration of **ZnNB** was only 5.2×10^{-8} M. Zinc-complexes of porphyrins have been shown to be five-coordinate in a number of studies,[13] and we expect the same to be true for **ZnNB** and **ZnSB.** Therefore, the concentration quenching of zinc porphyrins may be in part due to the formation of a dimer (or larger aggregate) bridged by coordination of one ester or amide group to other central zinc. The presence of the dodecamethylene bridge over the porphyrin macrocycle must result in retardation of such coordination, thus suppressing the concentration quenching. Accordingly, doubly bridged zinc porphyrin **ZnDB** showed the nearly same critical concentration (2.0×10^{-6} M) as that of the corresponding free base, **H_2DB.**

While effects of the dodecamethylene bridge upon the concentration quenching of Mg-porphyrins were much less than those of Zn-porphyrins in a CH_2Cl_2-MeOH (v/v=95/5) solution (Fig. 3), those became more prominent in an aprotic nonpolar solution (CH_2Cl_2) (Fig. 4). This may be ascribed to a much stronger coordination of methanol to the central magnesium, which leads to monomerization of Mg-porphyrin.

Fluorescence lifetimes of these nonbridged and bridged porphyrins and metalloporphyrins were measured by the time-correlated single-photon-counting technique. For all of the solution studied, the fluorescent decay is a single exponential within experimental error (Table 3). In accordance with the results of the fluorescence quantum yields, fluores-

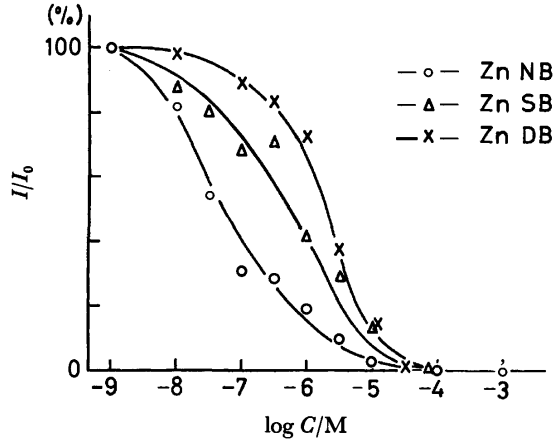

Fig. 2. Relative fluorescence yields of ZnNB, ZnSB, and ZnDB in CH_2Cl_2-CH_3OH (v/v=95/5) at 25 °C as a function of concentration.

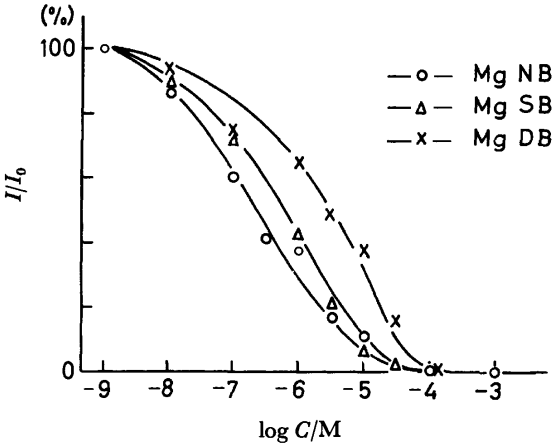

Fig. 3. Relative fluorescence yields of MgNB, MgSB, and MgDB in CH_2Cl_2-CH_3OH (v/v=95/5) at 25 °C as a function of concentration.

Table 2. Critical Concentration[a] of Porphyrin Fluorescence Quenching

Central metal	NB	SB	DB
H_2	1.1×10^{-6}	2.8×10^{-6}	5.0×10^{-6}
Zn	5.2×10^{-8}	5.6×10^{-7}	2.0×10^{-6}
Mg	2.5×10^{-7}	6.3×10^{-7}	3.2×10^{-6}
Mg[b]	7.9×10^{-8}	1.0×10^{-6}	7.1×10^{-6}

a) Defined in the text, M in CH_2Cl_2-MeOH (v/v, 95/5) at 25 °C. b) In CH_2Cl_2 at 25 °C.

Table 3. Fluorescence Lifetimes[a] (ns) of Bridged Porphyrin

Central metal	NB	SB	DB
H_2	11.5	12.4	14.0
Zn	1.69	1.71	2.04
Mg	6.3	6.7	7.2

a) 10^{-5} M in CH_2Cl_2, aerated conditions. Excitation at soret band in Table 1, measured at 620 nm (free base), at 578 nm (Zn complexes), and at 587 nm (Mg complexes), and measured on a HORIBA Model NAES 1100 nanosecond lifetime fluorometer at 25 °C.

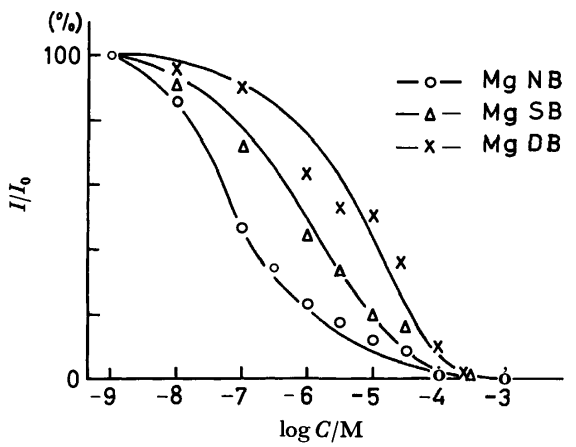

Fig. 4. Relative fluorescence yields of MgNB, MgSB, and MgDB in CH_2Cl_2 at 25 °C as a function of concentration.

Table 4. Relative Fluorescence Quantum Yields[a] in Micellar System

Porphyrin	SDS[b]	CTAB[c]	Brij-58
H_2NB	1.0	1.0	1.0
H_2SB	1.5	1.1	1.07
H_2DB	4.5	1.3	1.12

a) Relative fluorescence quantum yields of **H_2SB** and **H_2DB** to that of **H_2NB** measured at 25 °C. b) Porphyrin concentration was 1×10^{-6} M, and detergent concentration was 6×10^{-2} M. b) Sodium dodecyl sulfate. c) Hexadecyltrimethylammonium bromide.

cence lifetime increased in the order of **H_2NB<H_2SB<H_2DB, ZnNB<ZnSB<ZnDB,** and **MgNB<MgSB<MgDB.** At 10^{-5} M, the introduction of a dodecamethylene bridge increased the singlet lifetimes of **H_2NB** and **H_2SB** by ca. 1.5 ns.

Finally, we examined the relative fluorescence quantum yields of porphyrins in micellar systems such as sodium dodecyl sulfate (SDS), hexadecyltrimethylammonium bromide (CTAB), and Brij-58. It is interesting to note that the fluorescence quantum yield of **H_2DB** was retained 4.5 times as much as that of **H_2NB** in a SDS micelle. This result may suggest the steric hindrance around the porphyrin macrocycles becomes increasingly important in the more ordered and highly viscous environment.

In all the cases examined here, the steric hindrance imposed by the dodecamethylene bridge diminished the concentration quenching phenomena of porphyrin and metalloporphyrin to some extent. However, the concentration quenching was still observed even in the doubly bridged system under much more dilute conditions than those of antenna chlorophyll in chloroplast. Since a stacked face-to-face dimer cannot be formed from **H_2DB** and its metal complexes, it seems unnecessary to form such a compact dimer for the self-concentration quenching. In other words, the hypothetical nonfluorescent dimer may have a very loose structure.

Experimental

Melting points were measured on a Yanagimoto micro melting point apparatus and are uncorrected. Infrared spectra were recorded on a JASCO model 402-G spectrometer. 400 MHz ^{1}H NMR spectra were recorded on a JEOL GX-400, and chemical shifts are reported in parts per million on the δ scale from internal tetramethylsilane. Elemental analyses are performed at the Microanalytical Laboratory of Kyoto University. Preparative separations were usually performed by flash column chromatography on silica gel (Merk, Kieselgel 60 H, Art. 7736). Fluorescence spectra and fluorescence quantum yields were measured under aerobic conditions on a Shimadzu model RF 502 fluorometer. Fluorescence lifetimes were measured by the time-correlating single-photon-counting technique on a HORIBA NAES 1100 model.

1,12-Dodecamethylenediamine, 4-nitrophenyl trifluoroacetate (Aldrich), SDS, CTAB, and Brij-58 were commercially available and were used without further purification. Mesoporphyrin-II dimethyl ester (**H_2NB**),[11] mesoporphyrin-II dicarboxylic acid (**1**),[12] mesoporphyrin-II bis-(4-nitrophenyl) ester (**2**),[12] and coproporphyrin-I tetramethyl ester (**5**)[13] were prepared according to the reported procedures. Coproporphyrin-I tetracarboxylic acid (**6**) was prepared by acid-catalyzed hydrolysis of **5**.[12]

Preparation of Singly-Bridged Porphyrin H_2SB. To 400 mL of dry pyridine (maintained at 65—70 °C) were added six equimolar portions of mesoporphyrin-II bis(4-nitrophenyl) ester (**2**) (646 mg, 0.8 mmol) and 1,12-dodecamethylenediamine (169 mg, 0.8 mmol) under argon atmosphere at 2 h intervals. After completion of the last reagent addition, the reaction mixture was left overnight at 65 °C. The pyridine was removed on the rotary evaporator. The residue was dissolved in CH_2Cl_2-MeOH (v/v=5/1) and filtered through alumina short column. Filtrate was concentrated and then separated on flash column chromatography using CH_2Cl_2-MeOH (v/v=20/1) as the eluant. First porphyrin fraction was singly bridged porphyrin , **5 (H_2SB)**, yield 262 mg, 45%; mp> 300 °C. IR (KBr) 2860 and 1640 cm^{-1}; ^{1}H NMR ($CDCl_3$) δ=10.11 (s, 2H, meso H), 10.07 (s, 2H, meso H), 4.80 (br., 2H, -CONH-), 4.66 (dd, 2H, -CH_2CH_2CO-), 4.11 (dd, 2H, -CH_2CH_2CO-), 4.10 (q, 4H, -CH_2CH_3), 3.25 (dd, 2H, -CH_2CH_2CO-), 3.07 (dd, 2H, -CH_2CH_2CO-), 1.87 (t, 6H, -CH_2CH_3), and -3.78 (br, 2H, NH). Chemical shifts due to the dodecamethylene bridge were discussed in the text.

Coproporphyrin-I Tetrakis(4-nitrophenyl) Ester (7). Coproporphyrin-I tetracarboxylic acid (**6**) (654 mg, 1 mmol) was dissolved in dry pyridine (300 mL) under nitrogen atmosphere. 4-Nitrophenyl trifluoroacetate (3.3 g, 14 mmol) was added to the above solution and the resulting solution was stirred at 50—55 °C for 3 h, and then at 10 °C for 12 h. Microcrystalline solids were precipitated, which were collected and washed with pyridine and hexane, and dried under vacuum to give **7**, (1.49 g, 88%): mp, 204—206 °C; IR (KBr) 1770 (ester C=O), 1500 and 1350 (NO_2) cm^{-1}. ^{1}H NMR δ=10.22 (s, 8H, meso H), 7.94 (d, 8H), 6.88 (d, 8H), 4.62 (t, 8H, CH_2-CH_2CO-), 3.68 (t, 8H, CH_2CH_2CO-), 3.62 (s, 12H, CH_3), 3.65 (br, 2H, NH).

Doubly Bridged Porphyrin, 8 (H_2DB). Doubly bridged porphyrin **8 (H_2DB)** was synthesized in the same fashion with 5 by the reaction of **7** (890 mg, 0.8 mmol) with 1,12-dodecamethylenediamine (320 mg, 1.6 mmol). Separation by flash column chromatography over silica gel using CH_2Cl_2-MeOH (v/v=5/1) gave **8**, (63 mg, 8%) as the first fraction. **8 (H_2DB)**; mp >300 °C; IR (KBr) 2860 and 1640 (amide C=O) cm^{-1}; ^{1}H NMR ($CDCl_3$-CD_3OD, v/v=20/1) δ=10.7 (s, 4H, meso), 4.87 (br., 4H, -CONH-), 4.65 (dd, 4H, -CH_2CH_2CO-), 4.15 (dd, 4H, -CH_2CH_2CO-), 3.62 (s, 12H, -CH_3), 3.19 (dd, 4H, -CH_2CH_2CO-), 3.00 (dd, 4H, -CH_2CH_2CO-), and −3.75 (br, 2H, NH). Chemical shifts due to the dodecamethylene bridge was discussed in the text.

References

1) For review, see: K. Sauer, in "Bioenergetics of Photosynthesis", ed. by Govindjee, Academic Press, New

York (1975).

2) W. F. Watson and R. Livingston, *J. Chem. Phys.*, **18**, 802 (1950).

3) M. J. Yuen, L. L. Shipman, J. J. Katz, and J. C. Hindman, *Photochem. Photobiol.*, **32**, 281 (1980); J. A. Anton, P. A. Loach, and Govindjee, *ibid.*, **28**, 235 (1978).

4) W. D. Bellamy, A. G. Tweet, and G. L. Gaines, *J. Chem. Phys.*, **41**, 2068 (1964); T. Trosper, R. B. Park, and K. Sauer, *Photochem. Photobiol.*, **7**, 451 (1968).

5) A. R. Kelly and G. Porter, *Proc. Roy. Soc.*, **A 315**, 149 (1970); A. R. Kelly and L. K. Paterson, *ibid.*, **A 324**, 117 (1971).

6) G. S. Beddard, S. E. Carlin, and G. Porter, *Chem. Phys. Lett.*, **43**, 27 (1976); A. G. Lee, *Biochemistry*, **14**, 4397 (1975).

7) E. Lehoczki and K. Csatorday, *Biochem. Biophys. Acta*, **396**, 86 (1975).

8) G. R. Seely and V. Senthilarthpan, *J. Phys. Chem.*, **87**, 373 (1983), and references cited therein.

9) G. S. Beddard and G. Porter, *Nature*, **260**, 366 (1976).

10) N. J. Turro, "Modern Molecular Photochemistry," The Benjamin/Cummings Publishing Co. Inc. (1978), Chapt. 9, p. 296.

11) C. K. Chang, *J. Am. Chem. Soc.*, **99**, 2819 (1977).

12) J. P. Collman, F. C. Anson, C. E. Barnes, C. S. Bencosme, T. Geiger, E. R. Evitt, R. P. Kreth, K. Meier, and R. B. Pettman, *J. Am. Chem. Soc.*, **105**, 2694 (1983).

13) A. H. Jackson, G. W. Kenner, and J. Wass, *J. Chem. Soc., Perkin Trans. 1*, **1972**, 1475.

14) J. L. Hoard in K. M. Smith, ed. "Porphyrins and Metalloporphyrins," Elsevier, New York (1975), Chapt. 8, p. 345.

Photochemistry of Epoxynaphthoquinones. 8. Endo-Stereoselective Photocycloaddition of 2,3-Epoxy-2,3-dihydro-2,3-dimethyl-1,4-naphthoquinone to Olefins Containing Amide Group

Kazuhiro MARUYAMA,* Atsuhiro OSUKA, and Katsuhiko NAKAGAWA†
Department of Chemistry, Faculty of Science, Kyoto University, Kyoto 606
†Department of Industrial Chemistry, Niihama National College of Technology, Niihama 792
(Received August 25, 1986)

Irradiation of a benzene solution of 2,3-epoxy-2,3-dihydro-2,3-dimethyl-1,4-naphthoquinone with olefins containing amide group, i.e., *N*-substituted acrylamides and *N*-allylcarboxamides predominantly gave the endo-cycloadducts. Upon further irradiation, the cycloadducts underwent photorearrangement to give spirophthalides and alkylidenephthalides.

Recently, we reported the photochemical generation of the carbonyl ylide **2** or the 1,3-biradical **3** from several epoxynaphthoquinones **1**.[1] These intermediates were trapped by a variety of reagents including olefins,[2] ketones, aldehydes, singlet oxygen, and alcohol.[3] Reaction of **2** or **3** with olefin gave the tricyclic diketone **5**, which, upon further irradiation, underwent the secondary photorearrangement to produce the spirophthalide **6** and the alkylidenephthalides (*Z*)-**7** and (*E*)-**7**. (Scheme 1) The endo-exo stereoselectivity in the formation of the primary adduct **5** has been extensively studied in the photoreaction of 2,3-epoxy-2,3-dihydro-2,3-dimethyl-1,4-naphthoquinone (**1a**; R^1=R^2=Me) with a variety of functionalized olefins, whereby electron-releasing substituents show a endo-orientating tendency and electron-attracting substituents show a exo-orientating tendency.

Among these, cyano group has been found to be quite unique, since it shows remarkable high endo-orientating tendency in spite of its electron-attracting nature. In connection with these studies, we have studied the photoreaction of **1a** with olefins containing amide group, such as acrylamides and *N*-allylcarboxamides, so as to see the effect of nitrogen atom on the endo-exo stereoselectivity of the cycloaddition of **2** or **3**.

Results and Discussion

Photochemical Cycloaddition of 1a with *N*-Substituted Acrylamides. When a benzene solution of **1a** (0.04 M†) containing a high concentration (0.16 M) of *N*-phenylacrylamide (**4a**) was irradiated for 10 h, **1a** was mostly recovered and substantial amounts of polymeric materials derived from **4a** were formed. On the other hand, irradiation of a benzene solution of **1a** (0.04 M) containing a much less concentration (0.048 M) of **4a** for 10 h resulted in a smooth conversion of **1a**, giving the endo cyclodduct **5a**-*endo* (55%) along with the spirophthalide **6a** (25%) and the alkylidenephthalides (*Z*)-**7a** (6%) and (*E*)-**7a** (6%). In the latter photolysate, the amounts of polymeric materials derived from **4a** were greatly reduced.

These photoproducts were separated by column chromatography on silica gel, and their structures were determined on the basis of their spectroscopic properties (see Tables 5 and 6). The endo-

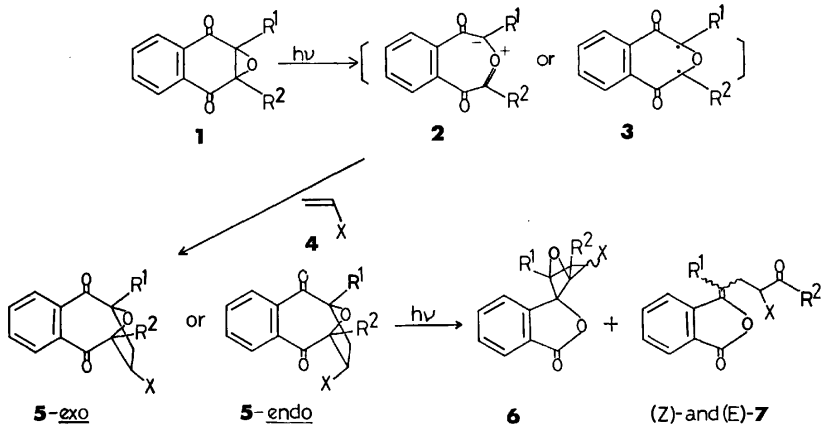

Scheme 1.

† 1 M=1 mol dm^{-3}.

stereochemistry of phenylcarbamoyl group in **5a**-*endo* was unambiguously determined by its independent synthesis from the tetracyclic adducts **8**, whose stereochemistry is apparently endo because of the hemiacetal structure.[2] Jones' oxidation of **8** afforded the corresponding carboxylic acid **5q**-*endo*, which, after treatment with oxalyl dichloride in dichloromethane, was reacted with aniline to give **5a**-*endo* in a 45% overall yield. In order to investigate the substituent effect of *N*-substituted acrylamides on the stereochemistry of the photocycloaddition of **1a**, we examined the photochemical reactions of **1a** with *N*-substituted acrylamides **4b—f**. The results are summarized in Table 1.

In the reaction with *N*-monosubstituted acrylamides **4a—d**, the stereochemistry of the primary adduct **5** is exclusively endo, regardless of the steric hindrance of *N*-substituents in olefins. Under identical conditions, isolated yields of **5c** and **5d** were lower than those of **5a** and **5b**, indicating that the secondary photorearrangements of **5c** and **5d** are faster than **5a** and **5b**. Since the secondary photorearrangement of **5** to **6** or **7** can be considered to proceed via a reversible α-cleavage (Eq. 1), more efficient secondary photoreaction of **5c**-*endo* and **5d**-*endo* may be ascribed to the buttressing effect of bulky substituents st the nitrogen, which may suppress the recombination of biradical **10** to **5**.

In sharp contrast to **4a—d**, the photochemical reaction of **1a** with *N*,*N*-disubstituted acrylamides **4e** and **4f** gave substantial amounts of **5e**-*exo* and **5f**-*exo*, along with **5e**-*endo* and **5f**-*endo*, **6e** and **6f**, and **7e** and **7f**, respectively. Structure determinations of the primary cycloadducts **5e**-*endo* and **5f**-*endo* were based on the independent synthesis of these compounds from **8**. Similary, the isomeric adducts **5e**-*exo* and **5f**-*exo* were independently synthesized from the tricyclic compounds **9**, whose structure had previously been well-established.[2]

Next, we have investigated the photochemical

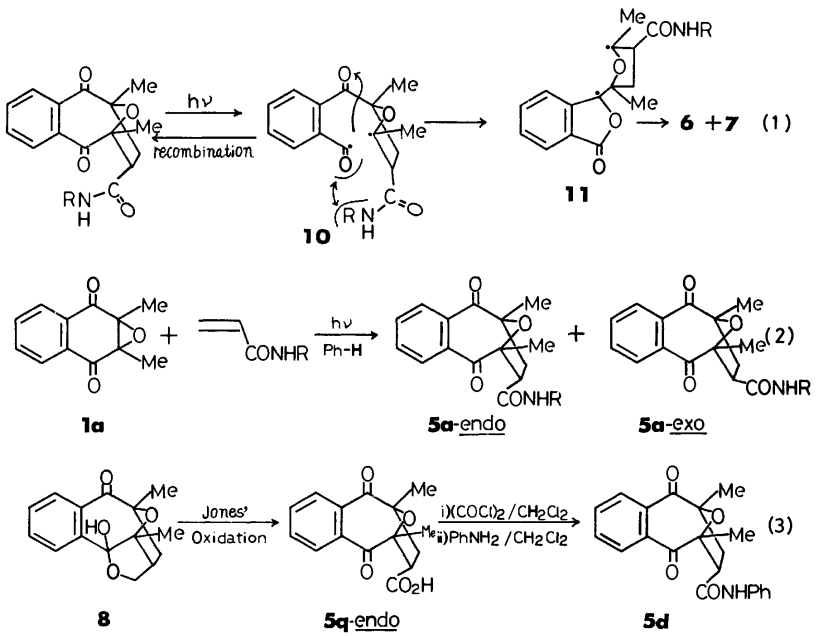

Table 1. Photoinduced Cycloaddition of Epoxynaphthoquinone **1a** to *N*-Substituted Acrylamides[a]

Run	Olefin		Irrad. time/h	Conversion %	Isolated yield[b]/%			
					5		6	7
					endo	exo		(Z)- (E)-
1	CH_2=CH·CONHPh	**4a**	3	61	55	0	25	12
2	CH_2=CH·CONHEt	**4b**	3	60	45	0	20	22
3	CH_2=CH·CONH·*t*-Bu	**4c**	3	90	7	0	32	48
4	CH_2=CH·CONHC_8H_{17}	**4d**	3	70	9	0	67	18
5	CH_2=CH·CONMe$_2$	**4e**	3	78	1	20	42	31
6	CH_2=CH·CONMe(Ph)	**4f**	2	72	0.8	18	29	41

a) A benzene solution of **1a** (0.04 M) and acrylamides (0.048 M) were used. b) Isolated yield based on the consumed amounts of **1a**.

cycloaddition reactions of **1a** with *N*-allylcarboxamides **4g—k**, which can be regarded as electron-rich olefin. Photoreaction of **1a** with **4g—k** proceeded well similarly with **4a—f**, giving **5g—k**-*endo*, **5g—j**-*exo*, **6g—k**, and **7g—k** in moderate to good yields. Isolated yields and physical properties of these photoproducts are listed in Tables 2, 5, and 6.

Photoinduced cycloaddition of **1a** to olefin consists primarily of two processes, namely photochemical oxirane ring opening leading to the formation of **2a** or **3a** and subsequent (presumably thermal) 1,3-dipolar cycloaddition of olefin to **2a** or **3a**. The first step has been well-shown to occur from the lowest triplet state of **1a**. In the previous studies on the photoreaction of **1a** with olefins, there has been also shown to exist a deactivating process for ^{3}(**1a**)* by charge transfer interactions with olefin.

Quantum yields for the disappearance of **1a** (0.04 M) in benzene containing various concentrations of olefins were determined at 313 nm by using valerophenone as the chemical actinometer[4] (Table 3). Quantum yields for the disappearance of **1a** in the reaction with acrylamide **4a**, **4d**, *N*-allylpropion-

Table 3. Quantum Yields for Disappearance of **1a**, Acrylamides, and *N*-Allylcarboxamides[a,b]

Olefin	Concd/M[c]	Φ_d^{1a} [d]	Φ_d^{o} [e]
CH_2=CH·CONHPh (**4a**)	0.04	0.027	0.040
	0.08	$<10^{-3}$	0.112
	0.16	$<10^{-3}$	0.141
CH_2=CH·CONHEt (**4b**)	0.04	0.032	0.037
	0.08	0.012	0.056
	0.20	$<10^{-3}$	0.087
CH_2=CH·CH_2NHCOEt (**4h**)	0.04	0.038	0.044
	0.08	0.008	0.042
	0.32	$<10^{-3}$	0.101
CH_2=CH·CH_2NHCOPh (**4j**)	0.04	0.041	0.053
	0.08	$<10^{-3}$	0.124
	0.16	$<10^{-3}$	0.190

a) Benzene solution of **1a** (0.04 M) were used. b) The conversions of **1a**, acrylamides, and *N*-allylcarboxamides were determined by HPLC. c) Concentration of olefin. d) Quantum yield for disappearance of **1a**. e) Quantum yield for disappearance of olefin.

Table 2. Photoinduced Cycloaddition of Epoxynaphthoquinone **1a** to *N*-allylcaboxamides[a]

Run	Olefin		Irrad. time/h	Conversion %	Isolated yield[b]/%			
					5		**6**	**7**
					endo	exo		(Z)- (E)-
1	CH_2=CH·CH_2NHCOMe	**4g**	3	58	52	6	15	24
2	CH_2=CH·CH_2NHCOEt	**4h**	3	60	60	3	12	21
3	CH_2=CH·CH_2NHCOC_7H_{15}	**4i**	3.5	90	46	4	12	31
4	CH_2=CH·CH_2NHCOPh	**4j**	3.5	85	23	0	25	48
5	CH_2=CH·CH_2N(Me)COMe	**4k**	2.5	88	1	17	15	57

a) A benzene solution of **1a** (0.04 M) and *N*-allylcarboxamides (0.048 M) were used. b) Isolated yields based on the consumed amounts of **1a**.

Table 4. The endo/exo Ratio of the Primary Adducts at an Early Stage[a] of Photochemical Reaction of **1a** with Acrylamides and *N*-Allylcarboxamides

Runs	Olefin		The *endo*/*exo* ratio of the Primary Adducts[b]		
			Ph-H	Ph-H/*t*-BuOH[c]	Ph-H/DMF[c]
1	CH_2=CH·CONHPh	**4a**	99	99	99
2	CH_2=CH·CONHEt	**4b**	99	99	99
3	CH_2=CH·CONH·*t*-Bu	**4c**	99	99	99
4	CH_2=CH·CON(Me)$_2$	**4e**	0.3	0.1	0.1
5	CH_2=CH·CON(Me)Ph	**4f**	0.1	0.06	0.1
6	CH_2=CH·CH_2NHCOEt	**4h**	4	2	3
7	CH_2=CH·CH_2NHCOPh	**4j**	99	99	99
8	CH_2=CH·CH_2N(Me)COMe	**4k**	0.3	0.2	0.2
9	CH_2=CH-CH_2-OH		18	5	3

a) The conversion of **1a** was less than 5%. b) The endo/exo of the primary adducts were determined by use of HPLC in the case of acrylamides and *N*-allylcaboxamides and by use of GC in the case of allyl alcohol. c) The ratio of Ph-H/*t*-BuOH and Ph-H/DMF was 50/50 by the volume.

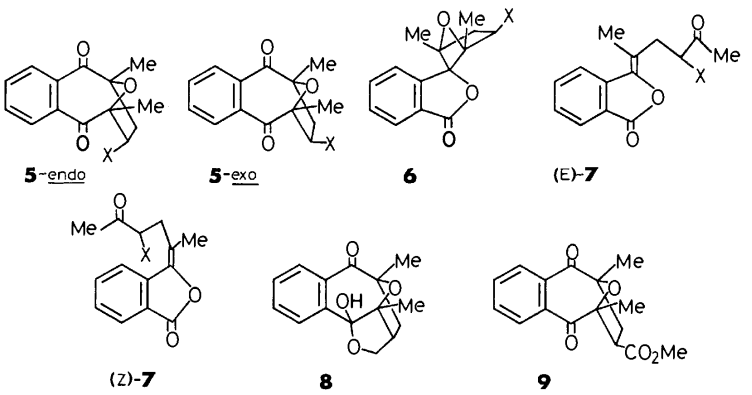

Fig. 1. Photoproducts of **1a** with acrylamides and *N*-allylcarboxamides.
a; X=CONHPh, b; X=CONHEt, c: X=CONH-*t*-Bu, d; X=CONH-*n*-C_8H_{17}, e; X=$CON(Me)_2$, f; X=CON(Me)Ph, g; X=$CH_2NHCOMe$, h; X=$CH_2NHCOEt$, i; X=CH_2NHCO-*n*-C_7H_{15}, j; X=$CH_2NHCOPh$, k; X=$CH_2N(Me)COMe$, q; X=CO_2H.

Table 5. Physical Properties of Primary Adducts **5**

Compound	Mp (θ_m/°C)	Formula	Found(%)	Calcd(%)	ν_{max}/cm^{-1} (KBr)
5a-*endo*	128—130	$C_{21}H_{19}O_4N$	C, 71.90	C, 72.19	2970, 1680, 1645
			H, 5.34	H, 5.48	1600, 1275, 1140
			N, 4.04	N, 4.01	
5b-*endo*	137—139	$C_{17}H_{19}O_4N$	C, 67.71	C, 67.76	2980, 1680, 1650
			H, 6.39	H, 6.35	1270, 1140, 980
			N, 4.81	N, 4.65	
5c-*endo*	199—201	$C_{19}H_{23}O_4N$	C, 69.50	C, 69.28	2980, 1670, 1640
			H, 7.13	H, 7.04	1250, 1145, 975
			N, 4.20	N, 4.25	
5d-*endo*	116—118	$C_{23}H_{31}O_4N$	C, 71.82	C, 71.66	2990, 1670, 1640
			H, 8.18	H, 8.10	1265, 1125, 975
			N, 3.60	N, 3.63	
5e-*exo*	127—129	$C_{17}H_{19}O_4N$	C, 67.60	C, 67.76	2980, 1685, 1640
			H, 6.39	H, 6.35	1270, 1145
			N, 4.80	N, 4.65	
5f-*exo*	134—136	$C_{22}H_{21}O_4N$	C, 72.80	C, 72.71	2980, 1680, 1640
			H, 5.88	H, 5.82	1600, 1275
			N, 3.90	N, 3.85	
5g-*endo*	145—147	$C_{17}H_{19}O_4N$	C, 67.71	C, 67.76	2975, 1680, 1650
			H, 6.25	H, 6.35	1280, 1150
			N, 4.67	N, 4.65	
5h-*endo*	137—139	$C_{18}H_{21}O_4N$	C, 68.45	C, 68.55	2990, 1670, 1640
			H, 6.75	H, 6.71	1280, 1150
			N, 4.52	N, 4.44	
5i-*endo*	149—151	$C_{23}H_{31}O_4N$	C, 71.53	C, 71.66	2950, 1690, 1640
			H, 8.23	H, 8.10	1240, 1170
			N, 3.72	N, 3.63	
5j-*endo*	137—139	$C_{22}H_{21}O_4N$	C, 72.50	C, 72.71	2960, 1680, 1645
			H, 5.79	H, 5.82	1600, 1245
			N, 3.90	N, 3.85	
5k-*exo*	132—134	$C_{18}H_{21}O_4N$	C, 68.33	C, 68.55	2960, 1695, 1645
			H, 6.84	H, 6.71	1275, 1160
			N, 4.49	N, 4.44	

amide (**4h**), *N*-allylbenzamide (**4j**) were one or two orders of magnitude lower compared with other functionalized olefins. Upon increasing the concentration of olefins, quantum yields for the formation of primary cycloadduct **5** decreased, whereas those for the disappearance of the olefin increased. Typically, irradiation of **1a** in the presence of high concentration of **4b** or **4j** (<ca. 0.2 M) merely resulted in the polymerization of the olefin, leaving **1a** almost intact in the reaction mixture. These facts clearly indicate the quenching of ^{3}(**1a**)* by olefins, presumably through the chrarge-transfer interactions.[5]

Since the primary cycloadducts **5** underwent the secondary photoreaction with different efficiencies depending upon their structures, the endo/exo ratios were determined at low conversions (<5%)(Table 4[5]). Results with allyl alcohol were included in Table 4 for the purpose of comparison. The cycloaddition with *N*-monosubstituted acrylamide **4a, 4b,** and **4c** proceeds exclusively with endo stereoselectivity, while *exo*-cycloaddition was favored in the reaction with *N,N*-disubstituted acrylamide. The reaction with *N*-allylpropinamide (**4h**) and *N*-allylbenzamide (**4j**) proceeded also with endo-stereoselectivity, but the selectivity of **4h** was much less than in the reaction with *N*-monosubstituted acrylamide and **4j**. However, as in the reaction with acrylamides, endo-stereoselectivity was inverted from endo to exo in the reaction with *N*-allyl-*N*-methylacetamide (**4k**); the endo/exo=0.3. Remarkably high endo-stereoselectivity observed with **4a—c, 4i,** and **4j** and inversed exo-stereoselectivity with **4e, f,** and **k** suggest the favorable

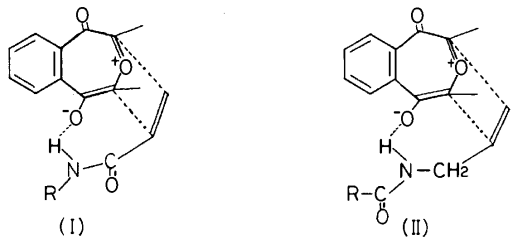

Fig. 2. Photochemical cycloaddition of **1a** with acrylamides and *N*-allylcarboxamides.

Table 6. ^{1}H NMR ($CDCl_3$, δ) of Primary Adducts **5**

Compound	Me[1], Me[2]	H_{arom}	H_{others}
5a-*endo*	1.62	7.3—7.6(m, 5H)	2.39(dd, J=8 and 14Hz, 1H), 2.84(dd, J=8 and 13Hz,
	1.66	7.7—7.9(m, 2H)	1H), 3.30(dd, J=7 and 12Hz, 1H), 6.02(br, 1H)
		7.9—8.2(m, 2H)	
5b-*endo*	1.50	7.5—7.8(m, 2H)	1.18(t, 3H), 2.50(dd, J=8 and 14Hz, 1H), 2.85(dd,
	1.62	7.8—8.1(m, 2H)	J=8 and 15Hz, 1H), 3.35(t, 1H), 5.74(br, 1H)
5c-*endo*	1.67	7.7—7.9(m, 2H)	1.31(s, 9H), 2.23(dd, J=8 and 13Hz, 1H), 2.68(dd,
	1.77	7.9—8.2(m, 2H)	J=6 and 12Hz, 1H), 3.21(dd, J=8 and 12Hz), 6.30
			(br, 1H)
5d-*endo*	1.54	7.6—7.8(m, 2H)	0.90(t, 3H), 1.32(br, 12H), 2.34(dd, J=6 and 12Hz, 1H),
	1.68	7.9—8.2(m, 2H)	2.52(dd, J=7 and 13Hz, 1H), 3.35(m, 2H), 5.75(br, 1H)
5e-*exo*	1.48	7.6—7.8(m, 2H)	2.40(dd, J=7 and 12Hz, 1H), 3.04(s, 3H), 2.80(dd,
	1.72	7.9—8.0(m, 2H)	J=8 and 13Hz, 1H), 3.12 (s, 3H), 3.60 (dd, J=6 and
			8Hz, 1H)
5f-*exo*	1.40	7.2—7.6(m, 4H)	2.24(dd, J=8 and 13Hz, 1H), 2.85(dd, J=8 and 13Hz,
	1.55	7.7—8.1(m, 4H)	1H), 3.08(s, 3H), 3.38(t, 1H)
5g-*endo*	1.56	7.5—7.7(m, 2H)	1.96(s, 3H), 2.34(dd, J=8 and 12Hz, 1H), 2.64(dd,
	1.60	7.7—7.9(m, 2H)	J=6 and 8Hz, 1H), 2.90(dd, J=6 and 8Hz, 1H), 3.58—
			3.88(m, 2H), 6.04(br, 1H)
5h-*endo*	1.58	7.7—7.9(m, 2H)	1.16(t, 3H), 2.24(q, 2H), 2.62(dd, J=6 and 11Hz, 1H),
	1.62	7.9—8.1(m, 2H)	3.48(dd, J=6 and 10Hz, 1H), 3.72(dd, J=6 and 8Hz,
			1H)
5i-*endo*	1.60	7.6—7.8(m, 2H)	0.91(t, 3H), 1.28(br, 8H), 1.66(br, 2H), 2.22(t, 2H),
	1.62	7.9—8.2(m, 2H)	2.64(dd, J=6 and 8Hz, 1H), 2.91(dd, J=6 and 8Hz,
			1H), 3.60(dd, J=6 and 8Hz, 1H), 3.73(dd, J=6 and
			8Hz, 1H), 6.54(br, 1H)
5j-*endo*	1.53	7.2—7.5(m, 4H)	2.14(dd, J=8 and 11Hz, 1H), 2.68(dd, J=8 and 13Hz,
	1.55	7.6—7.9(m, 4H)	1H), 3.60(dd, J=6 and 8Hz, 1H), 3.70—3.96(m, 2H),
			6.05(br, 1H)
5k-*exo*	1.62	7.5—7.7(m, 2H)	2.10(s, 3H), 2.48(dd, J=8 and 13Hz, 1H), 2.67(dd,
	1.74	7.8—8.1(m, 2H)	J=8 and 12Hz, 1H), 2.93(d, 2H), 3.42(dd, J=8 and
			12Hz, 1H), 3.92(t, 2H)

hydrogen-bonding interaction by amide N-H bond in the transition state of the cycloaddition such as I and II in Fig. 2. Similar interaction may explain a relatively high endo-selectivity of allyl alcohol.

Thus, we examined the effects of hydrogen-bond donating or accepting solvent upon the endo-exo stereoselectivity in the formation of **5** (Table 4). Exclusive endo-selective stereochemistry observed with **4a**—**c** and **4j** was not affected by addition of *t*-BuOH or *N*,*N*-dimethylformamide (DMF). However, the endo/exo ratio in the reaction with **4h** decreased by addition of *t*-BuOH and DMF (Run 6, in Table 4). Much more prominent solvent effects are observed in the reaction of **1a** with allyl alcohol (Run 9, in Table 4), indicating that the hydrogen-bonding interaction plays an important role in determination of 1,3-dipolar cycloaddition stereochemistry.

High endo-selective stereoselectivity in the reaction of **1a** with **4a**—**c** and **4j** may be accounted for in terms of the interplay of the strong hydrogen bond and the secondary orbital overlap between the carbonyl ylide and the amide nitrogen lone pair in the olefins. Although we have not succeeded in a quantitative assessment of these interactions, it may be considered that amide N-H bond at an appropriate position can control the stereochemistry of cycloaddition of epoxynaphthoquinone (**1a**).

Experimental

Apparatus. Melting points were measured on Yanagimoto micro-melting points apparatus and are uncorrected. Infrared spectra were taken on a JASCO-IR-1A spectrometer. ^{1}H NMR spectra were recorded on a JEOL GX-400 (400 MHz) and a JEOL FX-90Q (90 MHz) spectrometer with use of tetramethylsilane as an internal standard and the chemical shifts are expressed in δ values. UV spectra were taken by using a Shimadzu UV-200 spectrometer. Elemental analyses were performed at the Microanalytical Laboratory of Kyoto University. Mass spectra were recorded on a JEOL JNM DX-300 spectrometer. High pressure liquid chromatography (HPLC) analyses were performed on a Yanaco LC-2000 equipped with an UV detector (Yanaco M-315). The separations were made on a 250×4 mm stainless-steel column packed with Shodex ODS pack F-411 with a mixture of methanol and water (80/20) as the eluent. GC analyses were performed on a Hitachi Model 163, using a 3 mm i.d., ×2 M stainless-steel column packed with 10% SE-30 on celite 545 AM. Preparative separations were performed by column chromatography over silica gel (Wakogel C-200). UV irradiations were carried out in a Pyrex vessel (Fuji glass) under a nitrogen atmosphere with a Fuji glass 300-W high-pressure mercury lamp.

Materials. 2,3-Epoxy-2,3-dihydro-2,3-dimethyl-1,4-naphthoquinone[2] (**1a**) was prepared by the epoxidation of 2,3-dimethyl-1,4-naphthoquinone with 10% aqueous sodium hypochlorite in pyridine. *N*-Substituted acrylamides **4a**—**f** were prepared by the condensation of acryloyl chloride with the corresponding amines at temperature below 5 °C.[6] *N*-Allyl-carboxamides **4g**—**k** were prepared by condensation of allyl amine with the corresponding acyl chlorides at temperature below 5 °C. *N*,*N*-Dimethylacrylamide **4e** and *N*-Allyl-*N*-methyl-acetamide **4k** were prepared by the alkylation of the corresponding amides with methyl iodide in dimethyl sulfoxide.

General Procedure for the Photochemical Reaction of 1a with Acrylamides and *N*-Allylcarboxamides. A degassed solution of **1a** (1 mmol) and acrylamides or *N*-allylcarboxamides (1.2 mmol) in 25 ml of benzene in a Pyrex tube, using a 300-w high-pressure mercury lamp from outside. The progress of the reaction was followed by thin-layer chromatography (TLC), HPLC or GC. After removal of solvent, the residual oil was separated by chromatography on silica gel with ethyl acetate / hexane as an eluent. Final purification was usually accomplished by preparative TLC and recrystallization. Physical properties of the photoproducts were summarized in Table 5 and 6.

Transformation of 9 into the Primary Adduct (5e-*exo*). A mixture of **9** (100 m), 10 ml of 5% aqueous NaOH, and 10 ml of isopropyl alcohol was heated at 50 °C under a nitrogen atmosphere for 4 h. Then the reaction mixture was acidified with 5% aqueous HCl. The resulting mixture was extracted twice with ether, and the combined extracts were washed with water and dried over Na_2SO_4. Removal of the solvent on a rotary evaporator afforded crude acid (**5q**-*exo*). This was treated with oxalyl dichloride in dry dichloromethane, giving the acid chloride. After dimethylamine hydrochloride was added to the acyl chloride under a nitrogen atmosphere, the reaction mixture was stirred at room temperature for 12 h. Removal of the solvent on a rotar evaporator afforded the crude amide, which was chromatographed on silica gel to yield the primary adduct (**5e**-*exo*) (47 mg, 45%) (mp 128—129 °C).

Measurement of Quantum Yields. Valerophenone actinometry was used for quantum yield determination. The 313-nm line was isolated with a filter solution containing 0.002 M K_2CrO_4 in a 1% aqueous solution of K_2CO_3. The degree of the reaction was determined by HPLC analyses relative to a known concentration of internal standard (naphthalene) in the case of acrylamides and *N*-allylcarboxamides. The standard naphthalene was added after the photoreaction. And in the case of allyl alcohol the degree of the reaction was determined by GC analysis relative to a known concentration of internal standard (dodecane).

References

1) S. Arakawa. *J. Org. Chem.*, **42**, 3800 (1978).

2) A. Osuka, H. Suzuki, and K. Maruyama, *J. Chem. Soc., Perkin. Trans. 1*, **1982**, 2671 and references cited therein.

3) A. Osuka, *J. Org. Chem.*, **48**, 1712 (1983) and references cited therein.

4) The energy (E_T) of the lowest triplet state of **1a** is determined to be 68 kcal mol^{-1} (1 cal=4.184 J) by its phosphorescence spectrum, although E_T of **4a**, **4d**, **4h**, and **4g** is not available.

5) For example, the relative reactivity of **5h**-*endo*/**5h**-*exo* was about 4.

6) R. E. Harm, B. L. Jensen, S. K. Gupta and J. D. Nelson, *J. Org. Chem.*, **35**, 825 (1970).

 © 1987 The Chemical Society of Japan Bull. Chem. Soc. Jpn., 60, 1027—1036 (1987)

A General Synthetic Method of Chiral 2-Arylalkanoic Esters via Thermal 1,2-Rearrangement[1)]

Yutaka HONDA,* Aiichiro ORI, and Gen-ichi TSUCHIHASHI*
Department of Chemistry, Faculty of Science and Technology, Keio University,
3-14-1, Hiyoshi, Kohoku-ku, Yokohama 223
(Received August 27, 1986)

(*S*)-1-Aryl-2-sulfonyloxy-1-alkanone acetals, prepared from natural ethyl (*S*)-lactate or (*S*)-valine (chiral sources) by the use of a Grignard reaction, were rearranged under hydrolytic conditions in the presence of a base to give (*S*)-2-arylalkanoic esters which, in general, showed much higher pharmacological activities than their antipodes.

2-Arylalkanoic acids constitute a group which involves many biologically active compounds. Especially, 2-arylpropanoic acids, such as 2-(6-methoxy-2-naphthyl)propanoic acid (Naproxen, **1**), show potent antiinflammatory activity,[2)] and 2-aryl-3-methylbutanoic acid is known as the acid-moiety of pyrethroid-type insecticides (**2**) (Fig. 1).[3)] These acids have an asymmetric center at C-2, and each (*S*)-enantiomer shows much higher pharmacological activity than its antipode.[4,5)] A typical conventional process for preparing the chiral acid includes an optical resolution of the corresponding racemic derivative using a resolving reagent such as cinchonidine.[6)] However, the optical resolution is disadvantageous from an economical standpoint, since one half of the racemic acid is an unnecessary isomer and complicated racemization steps are required to reuse the antipode.[7)] On the other hand, the process starting from a chiral compound does not require optical resolution as the final step, and is economical compared with the conventional processes.

In these seven years, many investigators have reported syntheses of the racemic 2-arylalkanoic esters by a 1,2-aryl shift. Recently, a general commentary was written by C. Giordano et al.[8)] Previously, we reported that hydrolysis of 1-aryl-2-sulfonyloxy-1-propanone acetals (**3**) afforded 2-arylpropanoic esters (**4**) via 1,2-rearrengement of the aryl group (Eq. 1).[9,10)]

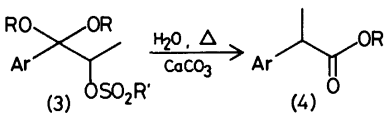

(1)

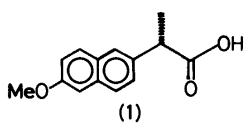

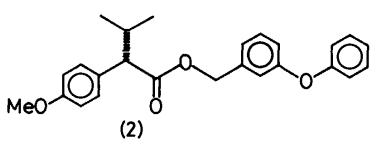

Fig. 1.

Next, optically active (*S*)-sulfonate (**5**), prepared using the optical resolution of (−)-10-camphorsulfonate, afforded (*S*)-2-arylpropanoic esters (**6**) with 100% inversion on the C-2 chiral center (Eq. 2).[11,12)]

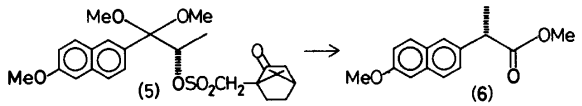

(2)

We assume that this rearrangement proceeds through a concerted process which involves a concominant attack of H_2O, a 1,2-aryl shift, and an elimination of the sulfonyloxy group. Thus, it is regarded as a substitution-type rearrangement (Eq. 3),[13-15)] in contrast to the elimination-type (Eq. 4),[16)]

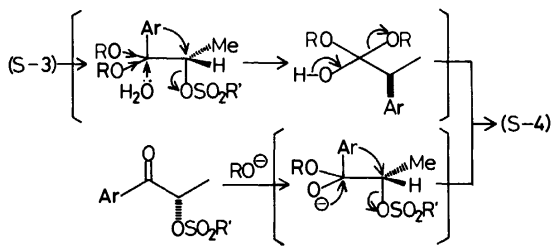

(3)
(4)

such as pinacol, Favorskii, and quasi-Favorskii rearrangements. In the former, one of the driving forces is a push effect by the electron pairs of the oxygen of an acetal oriented antiperiplanar to the migrating group and the attacking nucleophile;[17)] in the latter, an electron pair of oxygen anions plays the role.

Next, we developed a route involving a Friedel-Crafts reaction[1b,13g)] using chiral acyl chlorides (**7**)[18)] and (**8**) derived from (*S*)-lactic acid and ethyl (*S*)-lactate respectively (Fig. 2). In the case of the derivatives which have the aryl group substituted by the alkyl group, (*R*)-α-halogeno ketone (**9**) and (*S*)-α-sulfonyloxy ketone (**10**) were obtained in high yields. However, the regioselectivity of *o*- and *p*-orientation was reduced by electron-donating substituents on the aryl group.[19)] Resulting ketone (**9**) was rearranged by a treatment with silver carbonate and boron trifluoride diethyl etherate in methanol to afford (*R*)-**4**.[13a,k)] On the other hand, ketone (**9**) was treated with sodium

methoxide,[9,20] followed by sulfonylation to afford the partially racemic sulfonate (**3**). Ketone (**10**) was acetalized by a treatment with trimethoxymethane and sulfonic acid, followed by hydrolysis to afford (*S*)-**4**. However, in the case when the β-carbon atom to acetal was secondary, the reaction rate of acetalization was small.[17] Acetalization using trimethylsilyl trifluoromethanesulfonate and 2,2-dimethyl-1,3-bis(trimethylsilyloxy)propane in dichloromethane[21] was accompanied by a little racemization (98% ee).[14b]

Now, we report a general procedure for the synthesis of chiral 2-arylalkanoic esters which overcomes these faults.

Results and Discussion

At first, the synthesis of chiral α-hydroxy ketone was examined by reactions between chiral α-hydroxyalkanoic acid derivatives and organometallic reagents.[22-24] α-Amino acid can be transformed quantitatively into α-hydroxy acid by the Van-Slyke procedure.[25] *O*-Protected alkanamides,[26] for example (*S*)-2-*O*-methoxymethyl- or 2-*O*-(1-ethoxyethyl)-*N*,*N*-dimethyllactamide (**11** or **12**) and (*S*)-2-(1-ethoxyethoxy)-*N*,*N*,3-trimethylbutanamide (**13**), were readily prepared; these were suitable for reactions with organometallic reagents to give the protected α-hydroxy ketones (**14**) in high yields (Fig. 3, Table 1).

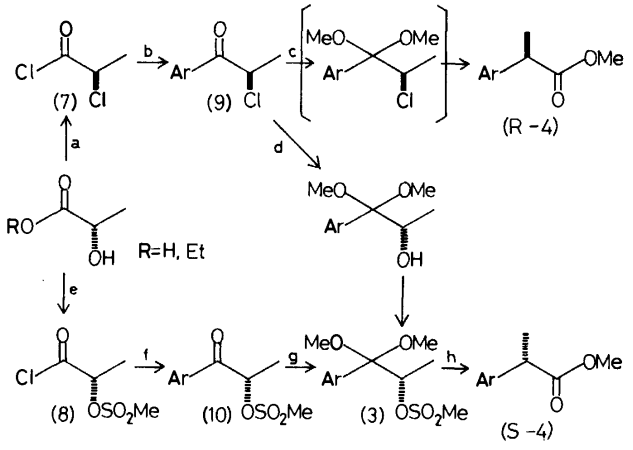

Fig. 2. Friedel-Crafts procedure.
a: 1; $SOCl_2$, pyridine, 2; PhCOCl. b: ArH, $AlCl_3$ in CS_2. c: Ag_2CO_3, BF_3–OEt_2 in MeOH. d: MeONa in MeOH. e: 1; MsCl in pyridine, 2; aq KOH, 3; SO_2Cl_2, pyridine. f: $FeCl_3$ or $FeSO_4$ in $MeNO_2$. h: $CaCO_3$ in MeOH–H_2O.

The ketone (**14**, R=1-ethoxyethyl=EE) was easily deprotected by the treatment with pyridinium *p*-toluenesulfonate (PPTS)[27] in ethanol to give the chiral α-hydroxy ketone (**15**) in a high yield. In the case of the hydrolysis of **14** (R=methoxymethyl=MOM) it was necessary to heat at 60 °C in dilute hydrochloric acid (Fig. 3, Table 1).

The sulfonylation of α-hydroxy ketone (**15**) was easily achieved by the use of methanesulfonyl chloride (MsCl) and triethylamine (Et_3N) at −42 °C[28] to give α-sulfonyloxy ketone (**16**) quantitatively, but the acetalization of **16** was accompanied with the various difficulties described above. Among the number of methods, four procedures were successfully applied

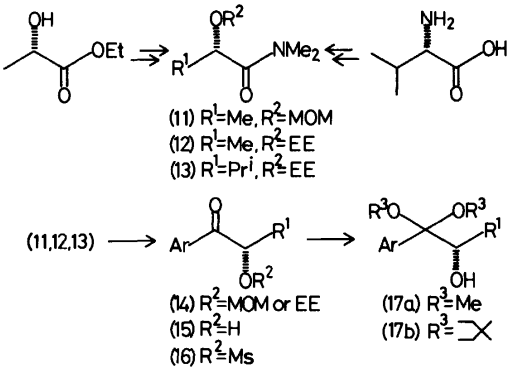

Fig. 3. Synthesis of α-hydroxy acetal (**17**).

Table 1. Synthesis of α-Hydroxy Acetal (**17**)

Run	Ar	R^1	Yield/%							
			14		**15**		**17a**		**17b**	
			R^2=MOM	R^2=EE	from 8 (R^2=MOM)	from 8 (R^2=EE)	Procedure A	Procedure B	Procedure C	Procedure D
1	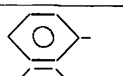	Me	94	98	96	94	95	93	89	—
2	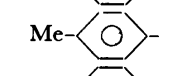	Me	98	95	93	99	82	87	93	93
3	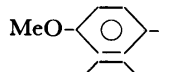	Me	99	98	93	99	85	57	96	93
4	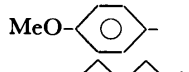	Pr^i	—	85	—	97	72	—	decompd	57
5	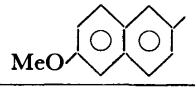	Me	92	99	96	96	96	91	94	100

for the acetalization of **15** without racemization. The α-hydroxy ketone (**15**) was treated with trimethoxymethane (5 equiv) and methanesulfonic acid (1 equiv) in anhydrous methanol[29] at 0 °C to give dimethyl acetal (**17a**) (Procedure A). On the other hand, the ketone (**14**, R=MOM) was treated with the same reagent as in procedure A at 50 °C to give dimethyl acetal (**17a**) in a moderate yield (Procedure B). The α-hydroxy ketone (**15**) was treated with 2,2-dimethyl-1,3-propanediol (10 equiv) and trimethylsilyl chloride (1.5 equiv) in anhydrous methanol[30] to give cyclic acetal (**17b**) in a good yield (Procedure C). Under acidic and dilute conditions in methanol, the reaction proceeded smoothly via internal epoxidation without racemization. Under high-concentration conditions or at high temperature, the dimer (**18** or **18'**) of the epoxide was the major product (Fig. 4). In the presence of a catalytic amount of *p*-toluenesulfonic acid, the reaction using 2,2-dimethyl-1,3-propanediol proceeded with an azeotropic removal of water with benzene under reflux at 50 °C to give cyclic acetal (**17b**) in a high yield (Procedure D). However, in the case when the β-carbon atom to carbonyl was secondary, an elimination of water easily occurred (Table 1, Run 4).

The resulting α-hydroxy acetal (**17**) was sulfonylated by the usual method to give α-sulfonyloxy acetal (**19**) (Fig. 5, Table 2). Since this sulfonate is relatively unstable, it was purified by using short silica-gel column chromatography (dichloromethane).

Sulfonate (**19**) was hydrolyzed by heating in the presence of a base to yield the desired ester (**20**) (Fig. 5, Table 2). The aryl group migrates more preferentially than the alkoxyl group. The cyclic acetal derivative gave a half ester (**20b**) in high yield without any migration of the oxygen of the acetal as the side reaction. This was because the intermediate in migration of the alkoxyl group has a seven-membered ring. The use of sodium acetate increased the reaction rate as compared with the case using calcium carbonate,[8] and enabled the lowering the reaction temperature. As the results, the formation of the by-product, α-methoxy ketone (**21**),[8] decreased in the case of the dimethyl acetal (Table 2, **20a**). The optical purity of the obtained ester was determined to be over 98% by an ^{1}H NMR measurement of methyl ester (**20a**) in the presence of a chiral shift reagent.[31] Half ester (**20b**) was transformed to methyl ester (**20a**) by the acidic ester exchange without racemization.

Consequently, it is concluded that the optical purity of the starting, *N*,*N*-dimethyl amide remained throughout the rearrangement and the following derivation. If ethyl (*S*)-lactate contained a trace amount of (*R*)-isomer,[32] the optical purity can be increased to 100% by the recrystallization of α-hydroxy ketones (**15**) or sulfonates (**19**). In practice, methyl ester (**20a**) and half ester (**20b**) of Naproxen (Table 2, Run 5) were obtained as a pure form by the recrystallization of α-hydroxy ketone (**15**). In our

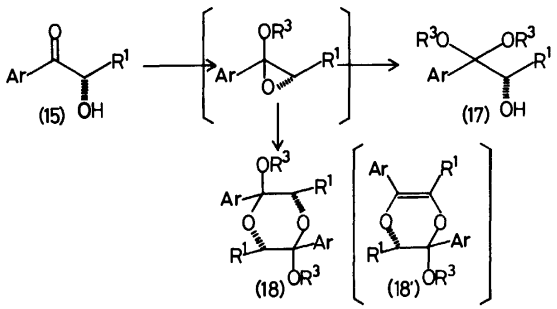

Fig. 4. Acetalization of α-hydroxy ketone (**15**).

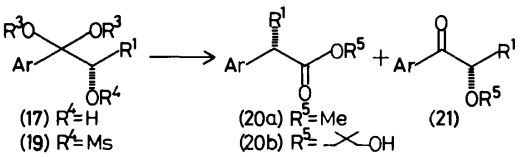

Fig. 5. Thermal 1,2-rearrangement of sulfonate (**19**).

Table 2. Synthesis of α-Aryl Esters (**20**)

Run	Ar	R¹	Yield/%			
			19a	**19b**	**20a**	**20b**
1		Me	88	98	72 (67)[a]	93
2	Me-	Me	100	100	85	93
3	MeO-	Me	100	100	97 (93)[a]	92
4	MeO-	Pr^i	90	94	90	96
5	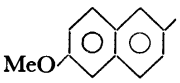	Me	96	100	97 (94,[a] 89[b])	97

a) $CaCO_3$ (2.0 equiv), 110 °C in $MeOH/H_2O=7/3$. b) $CaCO_3$ (2.0 equiv), 130 °C in $DMF/H_2O=4/1$.

laboratory, methods for obtaining the other chiral sources that are difficult to be derived from natural sources have been studied. For example, an asymmetric hydrolysis by using microorganisms to afford the chiral α-hydroxy ketones has been demonstrated.[33]

Experimental

General. Optical rotation was measured with a Japan Spectroscopic DIS-SL Polarimeter. The ^{1}H NMR spectra were recorded with a Varian EM 390 spectrometer at 90 MHz, the peak position being given in δ values. The IR spectra were recorded with a Japan Spectroscopic A-202 spectrophotometer. Kieselgel F_{254} (Merck), Wakogel C-300 (Wako), and Wacogel B-5F (Wako) were used for TLC, column chromatography, and preparative TLC, respectively.

(*S*)-*N*,*N*-Dimethyllactamide. According to the literature,[26] a 150-ml Pyrex heavy-walled pressure bottle was charged with ethyl (*S*)-lactate (Aldrich, 20.0 g, 0.169 mmol) and anhydrous dimethylamine (Kodack, 23.0 g, 0.510 mmol) under ice-salt cooling. The bottle was tightly sealed with a steel cap and heated at 70 °C for 60 h with stirring. After cooling, the reaction mixture was concentrated, followed by distillation under reduced pressure to yield 18.5 g (93%) of (*S*)-*N*,*N*-dimethyllactamide, bp 71—74 °C/0.7 mmHg (1 mmHg=133.322 Pa), $[\alpha]_D^{24}$ +0.85° (*c* 1.01, MeOH), IR (film) 3400, 1660, 1640 cm^{-1}, ^{1}H NMR ($CDCl_3$) δ=1.33 (3H, d, *J*=6.6 Hz, H-3), 3.01 (6H, s, -NMe), 3.8 (1H, broad s, -OH), 4.47 (1H, q, *J*=6.6 Hz, H-2) ppm.

(*S*)-2-*O*-Methoxymethyl-*N*,*N*-dimethyllactamide (11). Into a suspension of sodium hydride (60% oily, 1.02 g, 25.5 mmol) in THF (30 ml) was added a solution of (*S*)-*N*,*N*-dimethyllactamide (2.00 g, 17.1 mmol) in THF (7 ml) at 0 °C. The mixture was stirred for 30 min, and then chloromethyl methyl ether (1.67 ml, 22.2 mmol) was added. After 2 h stirring, water (2 ml) was added to form the precipitate. The pH of the decanted supernatant was adjusted 6.5—7.0 by using Na_2CO_3–aqueous $NaHCO_3$. The mixture was dried over Na_2SO_4, concentrated and distilled to give 3.07 g of **11** (82%), bp 102—103 °C/15 mmHg, $[\alpha]_D^{21}$ −95.3° (*c* 1.03, MeOH), IR (film) 1650 cm^{-1}, ^{1}H NMR ($CDCl_3$) δ=1.39 (3H, d, *J*=6.6 Hz, H-3), 2.97 (3H, s, -NMe), 3.07 (3H, s, -NMe), 3.38 (3H, s, -OMe), 4.55 (1H, q, *J*=6.6 Hz, H-2), 4.63 (2H, s, -OCH_2O-) ppm.

HRMS; Found: *m*/*z* 161.1022. Calcd for $C_7H_{15}O_3N$: M$^+$, *m*/*z* 161.1050.

(*S*)-2-*O*-(1-Ethoxyethyl)-*N*,*N*-dimethyllactamide (12). Into the mixture of (*S*)-*N*,*N*-dimethyllactamide (10.0 g, 85.4 mmol) and ethyl vinyl ether (8.2 ml, 128 mmol) in anhydrous dichloromethane (50 ml) was added PPTS (2.15 g, 8.6 mmol) at 0 °C. The mixture was allowed to warm to room temperature. After stirring overnight, solid $NaHCO_3$ (1.1 g) was added, and the mixture was vigorously stirred for 1 h. The reaction mixture was evaporated and the obtained residual syrup that contained salts was purified by flash column chromatography (Wacogel C-300, 50 g, hexane/ethyl acetate=3/1) to give crude **12** (15.8 g). It was distilled to yield pure **12** (15.3 g, 95%); bp 78—80 °C/0.7 mmHg; IR (film) 1660 cm^{-1}, ^{1}H NMR ($CDCl_3$) δ=1.1—1.5 (9H, m, -CMe), 2.96 (s), 3.09 (s), 3.12 (s) (total 6H, -NMe), 3.3—3.9 (2H, m, -OCH_2C-), 4.4—4.9 (2H, m, -OCHO- and -CHCO-) ppm.

HRMS; Found: *m*/*z* 189.1351. Calcd for $C_9H_{19}O_3N$: M$^+$, *m*/*z* 189.1363.

Methyl (*S*)-2-Hydroxyisovalerate. According to the literature,[25] a solution of sodium nitrite (30 g, 435 mmol) in H_2O (40 ml) was added into a solution of L-valine (25.8 g, 220 mmol) in 2 M† H_2SO_4 (250 ml) over 6 h under ice-cooling. The mixture was stirred for 6 h at 0 °C, and then for 12 h at rt. Furthermore, it was treated with H_2SO_4 (10.6 g, 108 mmol) and sodium nitrite (15 g, 217 mmol) by the above procedure. The reaction mixture was saturated by NaCl, followed by extraction with diethyl ether (100 ml×12). The organic layer was dried over $MgSO_4$ and then concentrated to yield crude (*S*)-2-hydroxyisovaleric acid (25.7 g, 99%) as an oily residue: IR (film) 1730 cm^{-1}, ^{1}H NMR ($CDCl_3$) δ=0.92 (3H, d, *J*=6.9 Hz, H-4), 1.05 (3H, d, *J*=6.9 Hz, H-4′), 1.9—2.3 (1H, m, H-3), 4.11 (1H, d, *J*=3.6 Hz, H-2), 5.77 (2H, broad s, -COOH and -OH) ppm.

The solution of the crude acid (5.00 g, 42.3 mmol) in diethyl ether (10 ml) was treated with diazomethane under ice-cooling to yield methyl (*S*)-2-hydroxyisovalerate (4.50 g, 81%); bp 90—92 °C/70 mmHg, $[\alpha]_D^{32}$ +18.2° (*c* 1.0, $CHCl_3$), IR (film) 3500, 1735 cm^{-1}, ^{1}H NMR ($CDCl_3$) δ=0.86 (3H, d, *J*=6.6 Hz, H-4), 1.01 (3H, d, *J*=6.6 Hz, H-4′), 1.8—2.2 (1H, m, H-3), 2.06 (1H, s, -OH), 3.76 (3H, s, -COOMe), 4.03 (1H, d, *J*=3.6 Hz, H-2) ppm.

HRMS; Found: *m*/*z* 132.0754. Calcd for $C_6H_{12}O_3$: M$^+$, *m*/*z* 132.0758.

(*S*)-2-Hydroxy-*N*,*N*,3-trimethylbutanamide. A 150 ml Pyrex heavy-walled pressure bottle was charged with methyl (*S*)-2-hydroxyisovalerate (4.43 g, 33.5 mmol), 4-dimethylaminopyridine (0.49 g, 3.35 mmol), and anhydrous dimethylamine (6.6 ml, ab. 100 mmol) under ice-salt cooling. The bottle was heated at 70 °C for 110 h, followed by distillation to give (*S*)-2-hydroxy-*N*,*N*,3-trimethlbutanamide (3.87 g, 80%): bp 59—61 °C/2 mmHg, $[\alpha]_D^{25}$ +38.4° (*c* 0.97, MeOH). ^{1}H NMR ($CDCl_3$) δ=0.73 (3H, d, *J*=6.8 Hz, H-4), 0.94 (3H, d, *J*=6.8 Hz, H-4′), 1.6—1.9 (1H, m, H-3), 2.86 (6H, s, -NMe), 3.19 (1H, d, *J*=7.5 Hz, -OH), 3.93 (1H, dd, *J*=7.5 Hz, *J*=2.9 Hz, H-2) ppm.

HRMS; Found: *m*/*z* 128.1098. Calcd for $C_7H_{14}ON$: M$^+$−OH, *m*/*z* 128.1074.

(*S*)-2-(1-Ethoxyethoxy)-*N*,*N*,3-trimethylbutanamide (13). According to the above procedure, (*S*)-2-hydroxy-*N*,*N*,3-trimethylbutanamide (3.87 g, 20.67 mmol) was treated with ethyl vinyl ether (3.85 ml) and PPTS (0.72 g) to give **13** (4.35 g, 88%); bp 82—83 °C/2.2 mmHg; IR (film) 1645 cm^{-1}; ^{1}H NMR ($CDCl_3$) δ=0.8—1.4 (12H, m, CMe), 2.95 (3H, s, NMe), 3.13 (3H, s, -NMe), 3.3—3.8 (2H, m, -OCH_2C-), 3.85 (d, *J*=8.5 Hz), 4.20 (d, *J*=8.5 Hz) (total 1H, -OCHO-), 4.6—4.8 (1H, m, H-2) ppm.

HRMS; Found: *m*/*z* 172.1345. Calcd for $C_9H_{18}O_2N$: M$^+$−OEt, *m*/*z* 172.1337.

General Procedure for a Grignard Reaction with *N*,*N*-Dimethylalkanamide (11—13) [Synthesis of (*S*)-2-*O*-(Protected hydroxy)ketone (14)]. Into a solution of *N*,*N*-dimethylamide (**11**—**13**, 10 mmol) in anhydrous THF (10 ml) under an argon atmosphere, cooled in an ice bath, was added a solution of arylmagnesium halide (0.5—2.0 M,

† 1 M=1 mol dm^{-3}.

12 mmol). After 1 h, the mixture was treated with 1 M aqueous ammonium chloride (30 ml), and extracted with dichloromethane (50 ml×3). The organic layer was dried over $MgSO_4$, concentrated, and purified by silica-gel column chromatography (hexane–ethyl acetate) to give ketone (**14**) as a colorless oil.

(*S*)-2-Methoxymethoxy-1-phenyl-1-propanone (94% from **11**); $[\alpha]_D^{27}$ −91.6° (*c* 1.00, $CHCl_3$); IR (film) 1695, 1595 cm^{-1}; ^1H NMR (CCl_4) δ=1.42 (3H, d, *J*=6.9 Hz, H-3), 3.22 (3H, s, -OMe), 4.51 (1H, d, *J*=7.2 Hz, $-OCH_2O-$), 4.60 (1H, d, *J*=7.2 Hz, $-OCH_2O-$), 4.77 (1H, q, *J*=6.9 Hz, H-2), 7.2—7.6 (3H, m, -Ph), 7.8—8.1 (2H, m, -Ph) ppm.

HRMS; Found: *m/z* 194.0908. Calcd for $C_{11}H_{14}O_3$: M^+, *m/z* 194.0942.

(*S*)-2-(1-Ethoxyethoxy)-1-phenyl-1-propanone (98% from **12**); IR (film) 1697, 1684, 1598 cm^{-1}; ^1H NMR (CCl_4) δ=0.9—1.6 (9H, m, -CMe), 3.2—3.7 (2H, m, $-OCH_2C-$), 4.5—5.1 (2H, m, H-2 and -OCHO-), 7.3—7.7 (3H, m, -Ph), 7.9—8.2 (2H, m, -Ph) ppm.

HRMS; Found: *m/z* 222.1271. Calcd for $C_{13}H_{18}O_3$: M^+, *m/z* 222.1255.

(*S*)-2-Methoxymethoxy-1-(3-methylphenyl)-1-propanone (98% from **11**); $[\alpha]_D^{21}$ −67.2° (*c* 1.00, MeOH); IR (film) 1690, 1605 cm^{-1}; ^1H NMR ($CDCl_3$) δ=1.47 (3H, d, *J*=6.9 Hz, H-3), 2.17 (3H, s, $-C_6H_4$-Me), 3.32 (3H, s, -OMe), 4.63 (1H, d, *J*=6.9 Hz, $-OCH_2O-$), 4.73 (1H, d, *J*=6.9 Hz, $-OCH_2O-$), 5.01 (1H, q, *J*=6.9 Hz, H-2), 7.25 (2H, d, *J*=8.4 Hz, $-C_6H_4-$), 7.91 (2H, d, *J*=8.4 Hz, $-C_6H_4-$) ppm.

HRMS; Found: *m/z* 208.1099. Calcd for $C_{12}H_{16}O_3$: M^+, *m/z* 208.1099.

(*S*)-2-(1-Ethoxyethoxy)-1-(3-methylphenyl)-1-propanone (95% from **12**); IR (film) 1695, 1680, 1610 cm^{-1}; ^1H NMR (CCl_4) δ=0.99 (t, *J*=7.2 Hz), 1.07 (t, *J*=7.2 Hz) (total 3H, $-CH_2Me$), 1.19 (d, *J*=5.4 Hz), 1.21 (d, *J*=5.4 Hz) (total 3H, -CHMe), 1.37 (d, *J*=7.1 Hz), 1.40 (d, *J*=7.1 Hz) (total 3H, H-3), 2.39 (3H, s, $-C_6H_4-$) 3.2—3.6 (2H, m, $-OCH_2O-$), 4.4—5.0 (2H, m, -OCHO- and H-2), 7.15 (2H, d, *J*=8.4 Hz, $-C_6H_4-$), 7.88 (d, *J*=8.4 Hz), 7.93 (d, *J*=8.4 Hz) (total 4H, $-C_6H_4-$) ppm.

HRMS; Found: *m/z* 191.1088. Calcd for $C_{12}H_{15}O_2$: M^+−OEt, *m/z* 191.1072.

(*S*)-2-Methoxymethoxy-1-(4-methoxyphenyl)-1-propanone (99% from **11**); $[\alpha]_D^{21}$ −61.8° (*c* 1.01, MeOH); IR (film) 1690, 1600 cm^{-1}; ^1H NMR ($CDCl_3$) δ=1.48 (3H, d, *J*=7.2 Hz, H-3), 3.32 (3H, s, -OMe), 3.85 (3H, s, $-C_6H_4$-OMe), 4.62 (1H, d, *J*=6.9 Hz, $-OCH_2O-$), 4.72 (1H, d, *J*=6.9 Hz, $-OCH_2O-$), 4.98 (1H, q, *J*=7.2 Hz, H-2), 6.92 (2H, d, *J*=8.7 Hz, $-C_6H_4-$), 7.99 (2H, d, *J*=8.7 Hz, $-C_6H_4-$) ppm.

HRMS; Found: *m/z* 224.1049. Calcd for $C_{12}H_{16}O_4$: M^+, *m/z* 224.1047.

(*S*)-2-(1-Ethoxyethoxy)-1-(4-methoxyphenyl)-1-propanone (98% from **12**); IR (film) 1685, 1595 cm^{-1}; ^1H NMR (CCl_4) δ=1.00 (t, *J*=6.9 Hz), 1.07 (t, *J*=6.9 Hz) (total 3H, $-CH_2Me$), 1.19 (d, *J*=5.4 Hz), 1.21 (d, *J*=5.4 Hz) (total 3H, -CHMe), 1.38 (d, *J*=6.6 Hz), 1.40 (d, *J*=6.6 Hz) (total 3H, H-3), 3.2—3.6 (2H, m, $-OCH_2C-$), 3.83 (3H, s, -OMe), 4.4—4.9 (2H, m, -OCHO- and H-2), 6.83 (2H, d, *J*=8.4 Hz, $-C_6H_4-$), 8.00 (d, *J*=8.4 Hz), 8.03 (d, *J*=8.4 Hz) (total 4H, $-C_6H_4-$) ppm.

HRMS; Found: *m/z* 207.1008. Calcd for $C_{12}H_{15}O_3$: M^+−OEt, *m/z* 207.1020.

(*S*)-2-(1-Ethoxyethoxy)-1-(4-methoxyphenyl)-3-methyl-1-butanone (85% from **13**); IR (film) 1675, 1600 cm^{-1}; ^1H NMR (CCl_4) δ=0.8—1.3 (12H, m, -CMe), 1.9—2.3 (1H, m, H-3), 3.1—3.6 (2H, m, $-OCH_2C-$), 3.86 (3H, s, -OMe), 3.97 (d, *J*=7.5 Hz), 4.34 (d, *J*=7.5 Hz) (total 1H, -OCHO-), 4.61 (1H, m, H-2), 6.87 (2H, d, *J*=9.0 Hz), 8.06 (2H, d, *J*=9.0 Hz) (total 6H, $-C_{10}H_6-$) ppm.

HRMS; Found: *m/z* 280.1672. Calcd for $C_{16}H_{24}O_4$: M^+, *m/z* 280.1672.

(*S*)-2-Methoxymethoxy-1-(6-methoxy-2-naphtyl)-1-propanone (92% from **11**); $[\alpha]_D^{22}$ −53.9° (*c* 1.01, MeOH); IR (film) 1680, 1620 cm^{-1}; ^1H NMR ($CDCl_3$) δ=1.55 (3H, d, *J*=6.9 Hz, H-3), 3.35 (3H, s, -OMe), 3.92 (3H, s, $-C_6H_4-$), 4.69 (1H, d, *J*=6.9 Hz, $-OCH_2O-$), 4.80 (1H, d, *J*=6.9 Hz, $-OCH_2O-$), 5.17 (1H, q, *J*=6.9 Hz, H-2), 7.14 (2H, s), 7.8—8.0 (2H, m), 8.06 (1H, dd, *J*=9.0 Hz), 8.52 (1H, s) (total 6H, $-C_{10}H_6-$) ppm.

HRMS; Found: *m/z* 274.1203. Calcd for $C_{16}H_{18}O_3$: M^+, *m/z* 274.1203.

(*S*)-2-(1-Ethoxyethoxy)-1-(6-methoxy-2-naphtyl)-1-propanone (99% from **12**); IR (film) 1680, 1625, 1590 cm^{-1}; ^1H NMR (CCl_4) δ=0.8—1.4 (6H, m, -CMe), 1.46 (d, *J*=7.2 Hz), 1.49 (d, *J*=7.2 Hz) (total 3H, H-3), 3.2—3.7 (2H, m, $-OCH_2C-$), 3.90 (3H, s, -OMe), 4.6—5.2 (2H, m, -OCHO- and H-2), 7.03 (1H, s), 7.0—7.2 (1H, m), 7.64 (1H, d, *J*=9.0 Hz), 7.78 (1H, d, *J*=9.0 Hz), 7.9—8.2 (1H, m), 8.53 (1H, d, *J*=6.0 Hz) (total 6H, $-C_{10}H_6-$) ppm.

HRMS; Found: *m/z* 302.1491. Calcd for $C_{18}H_{22}O_4$: M^+, *m/z* 302.1516.

General Synthetic Procedure of (*S*)-1-Aryl-2-hydroxyl-1-alkanone (15): 1) From **14** (R′=MOM); Into a solution of **14** (10 mmol) in methanol (80 ml) was added 1 M HCl (30 ml), and then the mixture was stirred at 60 °C for 6 h. Extraction with dichloromethane was repeated three times (50 ml each). The organic layer was washed with water (100 ml), dried over $MgSO_4$, concentrated, and purified by silica-gel column chromatography (hexane-ethyl acetate) to give α-hydroxy ketone (**15**).

2) From **14** (R′=EE); Into a solution of **14** (10 mmol) in ethanol (30 ml) was added PPTS (250 mg, 1 mmol). After 6 h, saturated aq NaCl (50 ml) was added, and then extracted with dichloromethane (50 ml×3). The organic layer was treated by the above procedure to give **15**.

(*S*)-2-Hydroxy-1-phenyl-1-propanone [96% from **14** (R′=MOM), 94% from **14** (R′=EE)]; colorless semicrystaline residue; $[\alpha]_D^{20}$ −48.4° (*c* 1.00, MeOH); IR (film) 3470, 1685, 1595 cm^{-1}; ^1H NMR ($CDCl_3$) δ=1.44 (3H, d, *J*=6.9 Hz, H-3), 3.80 (1H, d, *J*=6.9 Hz, -OH), 5.15 (1H, quintet, *J*=6.9 Hz, H-2), 7.4—7.8 (3H, m, $-C_6H_4-$), 7.9—8.1 (2H, m, $-C_6H_4-$) ppm.

HRMS; Found: *m/z* 150.0685. Calcd for $C_9H_{10}O_2$: M^+, *m/z* 150.0680.

(*S*)-2-Hydroxy-1-(4-methylphenyl)-1-propanone [93% from **14** (R′=MOM), 99% from **14** (R′=EE)]; colorless crystals from hexane-diethyl ether; mp 49.5—50.5 °C; $[\alpha]_D^{21}$ −41.1° (*c* 1.11, MeOH); IR (film) 3430, 1680, 1605 cm^{-1}; ^1H NMR ($CDCl_3$) δ=1.43 (3H, d, *J*=6.5 Hz, H-3), 2.42 (3H, s, $-C_6H_4$-Me), 3.82 (1H, d, *J*=6.5 Hz, -OH), 5.12 (1H, quintet, *J*=6.5 Hz, H-2), 7.29 (2H, d, *J*=8.4 Hz, $-C_6H_4-$), 7.84 (2H, d, *J*=8.4 Hz, $-C_6H_4-$) ppm.

HRMS; Found: *m/z* 164.0857. Calcd for $C_{10}H_{12}O_2$: M^+, *m/z* 164.0837.

(*S*)-2-Hydroxy-1-(4-methoxyphenyl)-1-propanone [93% from **14** (R′=MOM), 99% from **14** (R′=EE)]; colorless oil;

$[\alpha]_D^{21}$ −33.4° (*c* 1.05, MeOH); IR (film) 3475, 1670, 1595 cm^{-1}; ^1H NMR ($CDCl_3$) δ=1.36 (3H, d, *J*=7.0 Hz, H-3), 3.84 (3H, s, -OMe), 3.8 (1H, m, -OH), 5.05 (1H, quintet, *J*=7.0 Hz, H-2), 6.94 (2H, d, *J*=9.1 Hz, $-C_6H_4-$), 7.90 (2H, d, *J*=9.1 Hz, $-C_6H_4-$) ppm.

HRMS; Found: *m/z* 180.0798. Calcd for $C_{10}H_{12}O_3$: M^+, *m/z* 180.0686.

(*S*)-2-Hydroxy-1-(6-methoxy-2-naphtyl)-1-propanone [96% from **14** (R′=MOM), 99% from **14** (R′=EE)]; colorless crystals from diethyl ether; mp 68.6—70.0 °C; $[\alpha]_D^{23}$ −98.4° (*c* 1.01, $CHCl_3$), $[\alpha]_D^{23}$ −59.4° (*c* 1.05, MeOH); IR (film) 3440, 1685, 1625 cm^{-1}; ^1H NMR ($CDCl_3$) δ=1.51 (3H, d, *J*=6.7 Hz, H-3), 3.94 (3H, s, -OMe), 4.30 (1H, q, *J*=6.7 Hz, H-2), 7.17 (1H, s), 7.1—7.3 (1H, m), 7.6—8.0 (3H, m), 8.39 (1H, s) (total 6H, $-C_{10}H_6-$) ppm.

HRMS; Found: *m/z* 230.0943. Calcd for $C_{14}H_{14}O_3$: M^+, *m/z* 230.0943.

(*S*)-2-Hydroxy-1-(4-methoxyphenyl)-3-methyl-1-butanone [97% from **14** (R′=EE)]; colorless oil; $[\alpha]_D^{23}$ +37.5° (*c* 1.00, MeOH); IR (film) 3480, 1665, 1600 cm^{-1}; ^1H NMR (CCl_4) δ=0.61 (3H, d, *J*=6.9 Hz, H-4), 1.12 (3H, d, *J*=6.9 Hz, H-4′), 2.05 (1H, m, *J*=2.4 Hz, *J*=6.9 Hz, H-3), 3.33 (1H, d, *J*=6.3 Hz, -OH), 3.86 (3H, s, -OMe), 4.73 (1H, dd, *J*=6.3 Hz, *J*=2.4 Hz, H-2), 6.89 (2H, d, *J*=9.0 Hz, $-C_6H_4-$), 7.84 (2H, d, *J*=9.0 Hz, $-C_6H_4-$) ppm.

HRMS; Found: *m/z* 208.1127. Calcd for $C_{12}H_{16}O_3$: M^+, *m/z* 208.1099.

General Synthetic Procedure of (*S*)-1-Aryl-2-hydroxy-1-alkanone Dimethyl Acetal (17a): 1) Procedure A [from **14** (R′=MOM)]; Into a solution of **14** (10 mmol) in anhydrous methanol (150 ml) were added trimethoxymethane (5.53 ml, 50 mmol) and methanesulfonic acid (0.65 ml, 10 mmol) under an argon atmosphere. The mixture was heated at 50 °C for 1 h and allowed to cool to rt. The reaction mixture was poured into the vigorously stirred $NaHCO_3$ solution at 0 °C, and then extracted with diethyl ether (100 ml×3). The organic layer was washed with water (50 ml), dried over $MgSO_4$ in the presence of pyridine (1 ml), concentrated, and then purified by column chromatography (Florisil, Waco, hexane-diethyl ether) to give **17a** as a colorless oil.

2) Procedure B (from **15**); Into a solution of **15** (10 mmol) and trimethoxymethane (5.53 g, 50 mmol) in anhydrous methanol (150 ml), cooled in an ice bath, was added methanesulfonic acid (0.65 g, 10 mmol). The reaction mixture was treated by the above procedure to give **17a** (procedure B).

(*S*)-2-Hydroxy-1-phenyl-1-propanone Dimethyl Acetal (93% from **14**, 85% from **15**); $[\alpha]_D^{28}$ −17.7° (*c* 1.11, MeOH); IR (film) 3500 cm^{-1}; ^1H NMR (CCl_4) δ=0.88 (3H, d, *J*=6.9 Hz, H-3), 2.41 (1H, s, -OH), 3.16 (3H, s, -OMe), 3.38 (3H, s, -OMe), 3.98 (1H, q, *J*=6.9 Hz, H-2), 7.2—7.6 (5H, m, -Ph) ppm.

HRMS; Found: *m/z* 179.1035. Calcd for $C_{11}H_{15}O_2$: M^+-OH, *m/z* 179.1071.

(*S*)-2-Hydroxy-1-(4-methylphenyl)-1-propanone Dimethyl Acetal (87% from **14**, 82% from **15**); $[\alpha]_D^{20}$ −15.5° (*c* 1.29 MeOH); IR (film) 3500 cm^{-1}; ^1H NMR ($CDCl_3$) δ=0.95 (3H, d, *J*=6.6 Hz, H-3), 2.34 (3H, s, $-C_6H_4-Me$), 2.40 (1H, d, *J*=3.0 Hz, -OH), 3.21 (3H, s, -OMe), 3.37 (3H, s, -OMe), 4.09 (dq, 1H, *J*=3.0 Hz, *J*=6.6 Hz, H-2), 7.17 (2H, d, *J*=8.1 Hz, $-C_6H_4-$), 7.38 (2H, d, *J*=8.1 Hz, $-C_6H_4-$) ppm.

HRMS; Found: *m/z* 210.1248. Calcd for $C_{12}H_{18}O_3$: M^+, *m/z* 210.1254.

(*S*)-2-Hydroxy-1-(4-methoxyphenyl)-1-propanone Dimethyl Acetal (57% from **14**, 85% from **15**); $[\alpha]_D^{19}$ −13.1° (*c* 0.98, MeOH), IR (film) 3500 cm^{-1}; ^1H NMR ($CDCl_3$) δ=0.95 (3H, d, *J*=6.6 Hz, H-3), 2.34 (1H, d, *J*=3.0 Hz, -OH), 3.21 (3H, s, -OMe), 3.35 (3H, s, -OMe), 3.81 (3H, s, $-C_6H_4-OMe$), 4.09 (1H, dq, *J*=3.0 Hz, *J*=6.6 Hz, H-2), 6.90 (2H, d, *J*=12.0 Hz, $-C_6H_4-$) ppm, 7.39 (2H, d, *J*=12.0 Hz, $-C_6H_4-$) ppm.

HRMS; Found: *m/z* 209.1183. Calcd for $C_{12}H_{17}O_3$: M^+-OH, *m/z* 209.1176.

(*S*)-2-Hydroxy-1-(4-methoxyphenyl)-3-methyl-1-butanone Dimethyl Acetal (72% from **15**); $[\alpha]_D^{24}$ −9.1° (*c* 1.20 MeOH); IR (film) 3550 cm^{-1}; ^1H NMR ($CDCl_3$) δ=0.70 (3H, d, *J*=6.6 Hz, H-4), 0.87 (3H, d, *J*=6.6 Hz, H-4′), 1.2—1.7 (1H, m, H-3), 2.51 (1H, s, *J*=2.1 Hz, -OH), 3.24 (3H, s, -OMe), 3.26 (3H, s, -OMe), 3.7—3.9 (1H, m, H-2), 3.81 (3H, s, $-C_6H_4-OMe$), 6.88 (2H, d, *J*=9.0 Hz, $-C_6H_4-$), 7.78 (2H, d, *J*=9.0 Hz, $-C_6H_4-$) ppm.

HRMS; Found: *m/z* 223.1350. Calcd for $C_{13}H_{19}O_3$: M^+-OMe, *m/z* 233.1333.

(*S*)-2-Hydroxy-1-(6-methoxy-2-naphthyl)-1-propanone Dimethyl Acetal (91% from **14**, 96% from **15**); $[\alpha]_D^{21}$ −13.9° (*c* 0.92, MeOH); IR (film) 3520 cm^{-1}; ^1H NMR ($CDCl_3$) δ=1.00 (3H, d, *J*=6.6 Hz, H-3), 2.60 (1H, broad s, -OH), 3.26 (3H, s, -OMe), 3.43 (3H, s, -OMe), 3.92 (3H, s, $-C_{10}H_6-OMe$), 4.21 (1H, q, *J*=6.6 Hz, H-2), 7.1—7.2 (2H, m), 7.56 (1H, dd, *J*=1.8 Hz, *J*=8.5 Hz), 7.7—7.9 (2H, m), 7.97 (1H, s) (total 6H, $-C_{10}H_6-$) ppm.

HRMS; Found: *m/z* 276.1363. Calcd for $C_{16}H_{20}O_4$: M^+, *m/z* 276.1360.

General Synthetic Procedure of (*S*)-1-Aryl-2-hydroxy-1-alkanone 2,2-Dimethyltrimethylene Acetal (17b): 1) Procedure C (from **15**); Into a solution of **15** (10 mmol) and 2,2-dimethyl-1,3-propanediol (10.42 g, 100 mmol) in anhydrous methanol (150 ml), cooled in an ice bath, was added trimethylchlorosilane (27.16 g, 25 mmol). The mixture was stirred in an ice bath for 2 h. The reaction mixture was poured into the vigorously stirred $NaHCO_3$ solution at 0 °C, and then extracted with ethyl acetate (100 ml×3). The organic layer was dried over magnesium sulfate, concentrated, and then purified by silica-gel column chromatography (hexane/ethyl acetate) to give **17b** as a colorless oil.

2) Procedure D (from **15**); Into a 500 ml flask equipped with a Soxlet's extractor packed by molecular sieves 4A 1/16 was charged **15** (10 mmol), 2,2-dimethyl-1,3-propanediol (1.56 g, 15 mmol), *p*-toluenesulfonic acid (0.34 g, 2 mmol), and benzene (200 ml). The resulting mixture was heated at 50 °C and a vacuum was applied in order to maintain a smooth reflux. After completion, the reaction mixture was cooled and poured into the stirred aqueous $NaHCO_3$, and then extracted with diethyl ether (50 ml×3). The organic layer was treated by the above procedure to give **17b** as a colorless oil.

(*S*)-2-Hydroxy-1-phenyl-1-propanone 2,2-Dimethyl-trimethylene Acetal [89% from **15** (Procedure C)]; $[\alpha]_D^{28}$ −0.7° (*c* 1.12 MeOH); IR (film) 3510 cm^{-1}; ^1H NMR (CCl_4) δ=0.60 (3H, s, -CMe), 0.93 (3H, d, *J*=6.6 Hz, H-3), 1.25 (3H, s, -CMe), 2.24 (1H, d, *J*=3.6 Hz, H-3), 3.39 (4H, s, $-CCH_2C-$), 3.62 (1H, dq, *J*=3.6 Hz, *J*=6.6 Hz, H-2), 7.2—7.5 (5H, m, -Ph) ppm.

HRMS; Found: *m/z* 219.1362. Calcd for $C_{14}H_{19}O_2$: M^+-OH, *m/z* 219.1383.

(*S*)-2-Hydroxy-1-(4-methylphenyl)-1-propanone 2,2-Dimeth-

yl-trimethylene Acetal [93% from **15** (Procedure C), 93% from **15** (procedure D)]; $[\alpha]_D^{19}$ −0.05° (*c* 1.10, MeOH); IR (film) 3510 cm^{-1}; ^1H NMR ($CDCl_3$) δ=0.58 (3H, s, -CMe), 1.03 (3H, d, *J*=6.6 Hz, H-3), 1.27 (3H, s, -CMe), 2.37 (3H, s, $-C_6H_4$-Me), 2.51 (1H, d, *J*=3.6 Hz, -OH), 3.39 (2H, d, *J*=9.3 Hz, $-OCH_2C$-), 3.52 (2H, d, *J*=9.3 Hz, $-OCH_2C$-), 3.73 (1H, dq, *J*=3.6 Hz, *J*=6.6 Hz, H-2), 7.2—7.5 (4H, m, $-C_6H_4$-) ppm.

HRMS; Found: *m/z* 233.1558. Calcd for $C_{15}H_{21}O_2$: M^+−OH, *m/z* 233.1541.

(*S*)-2-Hydroxy-1-(4-methoxyphenyl)-1-propanone 2,2-Dimethyl-trimethylene Acetal [96% from **15** (Procedure C), 93% from **15** (Procedure D)]; $[\alpha]_D^{28}$ −2.0° (*c* 0.99, MeOH); IR (film) 3505 cm^{-1}; ^1H NMR (CCl_4) δ=0.59 (3H, s, -CMe), 0.93 (3H, d, *J*=6.3 Hz, H-3), 1.25 (3H, s, -CMe), 2.13 (1H, broad s, -OH), 3.28 (2H, d, *J*=12.0 Hz, $-OCH_2C$-), 3.42 (2H, d, *J*=12.0 Hz, $-OCH_2C$-), 3.60 (1H, q, *J*=6.3 Hz, H-2), 3.83 (3H, s, -OMe), 6.81 (2H, d, *J*=9.0 Hz, $-C_6H_4$-), 7.21 (2H, d, *J*=9.0 Hz, $-C_6H_4$-) ppm.

HRMS; Found: *m/z* 266.1488. Calcd for $C_{15}H_{22}O_4$: M^+, *m/z* 266.1516.

(*S*)-2-Hydroxy-1-(4-methoxyphenyl)-3-methyl-1-propanone 2,2-Dimethyl-trimethylene Acetal [57% from **15** (Procedure D)]; $[\alpha]_D^{24}$ −8.9° (*c* 1.01, MeOH); IR (film) 3580 cm^{-1}; ^1H NMR ($CDCl_3$) δ=0.58 (3H, s, -CMe), 0.83 (3H, d, *J*=6.6 Hz, H-4), 0.89 (3H, d, *J*=6.6 Hz, H-4′), 1.27 (3H, s, -CMe), 1.66 (1H, double heptet, *J*=6.6 Hz, *J*=2.7 Hz, H-3), 2.38 (1H, d, *J*=5.4 Hz, -OH), 3.4—3.7 (1H, m, H-2), 3.42 (4H, s, $-CCH_2C$-), 6.92 (2H, d, *J*=9.0 Hz, $-C_6H_4$-), 7.32 (2H, d, *J*=9.0 Hz, $-C_6H_4$-) ppm.

HRMS; Found: *m/z* 294.1833. Calcd for $C_{17}H_{26}O_4$: M^+, *m/z* 294.1830.

(*S*)-2-Hydroxy-1-(6-methoxy-2-naphtyl)-1-propanone 2,2-Dimethyltrimethylene Acetal [94% from **15** (Procedure C), 100% from **15** (Procedure D)]; $[\alpha]_D^{22}$ +0.7° (*c* 1.10, MeOH); IR (film) 3520 cm^{-1}; ^1H NMR ($CDCl_3$) δ=0.55 (3H, s, -CMe), 1.07 (3H, d, *J*=6.3 Hz, H-3), 1.30 (3H, s, -CMe), 2.56 (1H, d, *J*=3.9 Hz, -OH), 3.3—3.7 (4H, m, $-OCH_2C$-), 3.83 (1H, dd, *J*=3.9 Hz, *J*=6.3 Hz, H-2), 3.94 (3H, s, -OMe), 7.1—7.3 (2H, m), 7.48 (1H, dd, *J*=1.8 Hz, *J*=9.0 Hz), 7.7—7.9 (3H, m) (total 6H, $-C_{10}H_6$-) ppm.

HRMS; Found: *m/z* 316.1643. Calcd for $C_{19}H_{24}O_4$: M^+, *m/z* 316.1673.

General Synthetic Procedure of (*S*)-1-Aryl-2-methylsulfonyloxy-1-alkanone Acetal (19): Into a solution of **17** (10 mmol) in pyridine (100 ml), cooled in an ice bath, was added methanesulfonyl chloride (1.16 g, 15 mmol). After stirring for 12 h at room temperature, water (300 ml) was added into the mixture, which was then extracted with diethyl ether (50 ml×3), and washed with water (50 ml×2). The organic layer was dried over $MgSO_4$, concentrated, and purified by the short silica-gel column chromatography (dichloromethane) to give **19**.

(*S*)-2-Methylsulfonyloxy-1-phenyl-1-propanone Dimethyl Acetal (95% from **17a**); colorless oil; $[\alpha]_D^{25}$ −14.7° (*c* 1.13, $CHCl_3$); IR (film) 1350, 1170 cm^{-1}; ^1H NMR ($CDCl_3$) δ=1.19 (3H, d, *J*=6.6 Hz, H-3), 3.12 (3H, s, -OMs), 3.25 (3H, s, -OMe), 3.33 (3H, s, -OMe), 5.01 (1H, q, *J*=6.6 Hz, H-2), 7.3—7.7 (5H, m, -Ph) ppm.

HRMS; Found: *m/z* 274.0851. Calcd for $C_{12}H_{18}O_5S$: M^+, *m/z* 274.0873.

(*S*)-2-Methylsulfonyloxy-1-phenyl-1-propanone 2,2-Dimethyl-trimethylene Acetal (98% from **17b**); colorless oil; $[\alpha]_D^{25}$ −2.6° (*c* 0.98, $CHCl_3$); IR (film) 1350, 1170 cm^{-1}; ^1H NMR ($CHCl_3$) δ=0.59 (3H, s, -CMe), 1.28 (3H, s, -CMe), 1.39 (3H, d, *J*=6.6 Hz, H-3), 2.69 (3H, s, -OMs), 3.46 (4H, s, $-CCH_2C$-), 4.60 (1H, q, *J*=6.6 Hz, H-2), 7.45 (s, 5H) ppm.

HRMS; Found: *m/z* 219.1349. Calcd for $C_4H_{19}O_2$: M^+−OMs, *m/z* 219.1383.

(*S*)-2-Methylsulfonyloxy-1-(4-methylphenyl)-1-propanone Dimethyl Acetal (99% from **17a**); colorless oil; $[\alpha]_D^{23}$ −15.0° (*c* 1.20, $CHCl_3$); IR (film) 1350, 1170 cm^{-1}; ^1H NMR ($CDCl_3$) δ=1.18 (3H, d, *J*=6.6 Hz, H-3), 2.35 (3H, s, $-C_6H_4$-Me), 3.11 (3H, s, -OMs), 3.23 (3H, s, -OMe), 3.32 (3H, s, -OMe), 4.99 (1H, q, *J*=6.6 Hz), 7.17 (2H, d, *J*=8.4 Hz, $-C_6H_4$-), 7.36 (2H, d, *J*=8.4 Hz, $-C_6H_4$-) ppm.

HRMS; Found: *m/z* 257.0839. Calcd for $C_{12}H_{17}O_4S$: M^+−OMe, *m/z* 257.0845.

(*S*)-2-Methylsulfonyloxy-1-(4-methylphenyl)-1-propanone 2,2-Dimethyl-trimethylene Acetal (100% from **17b**); colorless oil; $[\alpha]_D^{13}$ −2.0° (*c* 0.98, $CHCl_3$); IR (film) 1360, 1175 cm^{-1}; ^1H NMR ($CDCl_3$) δ=0.59 (3H, s, -CMe), 1.28 (3H, s, -CMe), 1.37 (3H, d, *J*=6.6 Hz, H-3), 2.38 (3H, s, $-C_6H_4$-), 2.73 (3H, s, -OMs), 3.46 (4H, s, $-CCH_2C$-), 4.60 (1H, q, *J*=6.6 Hz, H-2), 7.2—7.5 (4H, m, $-C_6H_4$-) ppm.

HRMS; Found: *m/z* 327.1275. Calcd for $C_{16}H_{23}O_5S$, M^+−1, *m/z* 327.1265.

(*S*)-2-Methylsulfonyloxy-1-(4-methoxyphenyl)-1-propanone Dimethyl Acetal (99% from **17a**); colorless oil; $[\alpha]_D^{22}$ −15.2° (*c* 1.03, $CHCl_3$); IR (film) 1350, 1170 cm^{-1}; ^1H NMR ($CDCl_3$) δ=1.17 (3H, d, *J*=6.6 Hz, H-3), 3.11 (3H, s, -OMs), 3.24 (3H, s, -OMe), 3.31 (3H, s, -OMe), 3.82 (3H, s, $-C_6H_4$-OMe), 4.98 (1H, q, *J*=6.6 Hz, H-2), 6.89 (2H, d, *J*=8.7 Hz, $-C_6H_4$-), 7.39 (2H, d, *J*=8.7 Hz, $-C_6H_4$-) ppm.

HRMS; Found: *m/z* 273.0818. Calcd for $C_{12}H_{17}O_5S$: M^+−OMe, *m/z* 273.0796.

(*S*)-2-Methylsulfonyloxy-1-(4-methoxyphenyl)-1-propanone 2,2-Dimethyl-trimethylene Acetal (95% from **17b**); colorless crystals from diethyl ether; mp 127.0—128.0 °C; $[\alpha]_D^{29}$ −3.7° (*c* 1.00, $CHCl_3$); IR (film) 1360—1330, 1180 cm^{-1}; ^1H NMR ($CDCl_3$) δ=0.59 (3H, s, -CMe) 1.26 (3H, s, -CMe), 1.36 (3H, d, *J*=6.6 Hz, H-3), 2.76 (3H, s, -OMs), 3.85 (3H, s, -OMe), 4.57 (1H, q, *J*=6.6 Hz, H-2), 6.90 (2H, d, *J*=9.0 Hz, $-C_6H_4$-), 7.34 (2H, d, *J*=9.0 Hz, $-C_6H_4$-) ppm.

HRMS; Found: *m/z* 249.1477. Calcd for $C_{15}H_{21}O$: M^+−Ms, *m/z* 249.1489.

(*S*)-2-Methylsulfonyloxy-1-(4-methoxyphenyl)-3-methyl-1-butanone Dimethyl Acetal (90% from **17a**); colorless oil; $[\alpha]_D^{26}$ −4.6° (*c* 1.01, $CHCl_3$); IR (film) 1390, 1170 cm^{-1}; ^1H NMR ($CDCl_3$) δ=0.70 (3H, d, *J*=6.9 Hz, H-4), 0.90 (3H, d, *J*=6.9 Hz, H-4′), 1.6—1.9 (1H, m, H-3), 3.19 (3H, s, -OMs), 3.21 (3H, s, -OMe), 3.26 (3H, s, -OMe), 3.81 (3H, s, $-C_6H_4$-), 4.77 (1H, d, *J*=3.6 Hz, H-2), 6.89 (2H, d, *J*=9.0 Hz, $-C_6H_4$-), 7.43 (2H, d, *J*=9.0 Hz, $-C_6H_4$-) ppm.

HRMS; Found: *m/z* 301.1100. Calcd for $C_{14}H_{21}O_5S$: M^+−OMe, *m/z* 301.1108.

(*S*)-2-Methylsulfonyloxy-1-(4-methoxyphenyl)-3-methyl-1-butanone 2,2-Dimethyl-trimethylene Acetal (94% from **17b**); colorless oil; $[\alpha]_D^{24}$ −10.2° (*c* 0.97, $CHCl_3$); IR (film) 1360, 1170 cm^{-1}; ^1H NMR (CCl_4) δ=0.59 (3H, s, -CMe), 0.83 (3H, d, *J*=7.5 Hz, H-4), 0.91 (3H, d, *J*=7.5 Hz, H-4′), 1.27 (3H, s, -CMe), 1.91 (1H, double septet, *J*=2.1 Hz, *J*=7.5 Hz, H-3), 2.79 (3H, s, -OMs), 3.39 (4H, s, $-OCH_2C$-), 6.87 (2H, d, *J*=9.0 Hz, $-C_6H_4$-), 7.30 (2H, d, *J*=9.0 Hz, $-C_6H_4$-) ppm.

HRMS; Found: *m/z* 372.1600. Calcd for $C_{18}H_{28}O_6S$: M$^+$, *m/z* 372.1604.

(*S*)-2-Methylsulfonyloxy-1-(6-methoxy-2-naphthyl)-1-propanone Dimethyl Acetal (96% from **17a**); colorless oil; $[\alpha]_D^{21}$ −17.3° (*c* 1.01, $CHCl_3$); IR (film) 1385, 1170 cm^{-1}; ^{1}H NMR ($CDCl_3$) δ=1.21 (3H, d, *J*=6.6 Hz, H-3), 3.14 (3H, s, -OMs), 3.28 (3H, s, -OMe), 3.39 (3H, s, -OMe), 3.93 (3H, s, $-C_6H_4-$), 5.12 (1H, q, *J*=6.6 Hz, H-2), 7.1—7.2 (2H, m), 7.55 (1H, dd, *J*=1.8 Hz, *J*=8.5 Hz), 7.7—7.9 (2H, m), 7.98 (1H, s) (total 6H, $-C_{10}H_6-$) ppm.

HRMS; Found: *m/z* 354.1123. Calcd for $C_{17}H_{22}O_6S$: M$^+$, *m/z* 354.1135.

(*S*)-2-Methylsulfonyloxy-1-(6-methoxy-2-naphthyl)-1-propanone 2,2-Dimethyl-trimethylene Acetal (100% from **17b**); colorless oil; $[\alpha]_D^{19}$ +1.5° (*c* 0.98, $CHCl_3$); IR (film) 1390, 1170 cm^{-1}; ^{1}H NMR ($CDCl_3$) δ=0.56 (3H, s, -CMe), 1.30 (3H, s, -CMe), 1.41 (3H, d, *J*=6.6 Hz, H-3), 2.67 (3H, s, -OMs), 3.51 (4H, s, $-OCH_2C-$), 3.94 (3H, s, -OMe), 4.70 (1H, q, *J*=6.6 Hz, H-2), 7.17 (1H, s), 7.1—7.3 (1H, m), 7.51 (1H, dd, *J*=1.8 Hz, *J*=8.4 Hz), 7.7—7.9 (3H, m) (total 6H, $-C_{10}H_6-$) ppm.

HRMS; Found: *m/z* 394.1441. Calcd for $C_{20}H_{26}O_6S$, M$^+$, *m/z* 394.1292.

General Synthetic Procedure of Methyl (*S*)-Alkanoate (20a) or 3-Hydroxy-2,2-dimethylpropyl (*S*)-Alkanoate (20b): A Pyrex pressure bottle was charged with **19** (10 mmol), sodium acetate (984 mg, 12 mmol), and methanol-water (7:3 v/v, 50 ml). The bottle was tightly closed with a cap and heated at 100—110 °C for 6—18 h with stirring. After cooling, the reaction mixture was poured into a stirred ice water (100 ml), which was then extracted with diethyl ether (50 ml×3). The organic layer was dried over $MgSO_4$, concentrated, and purified by silica-gel column chromatography (hexane-ethyl acetate) to give **20**.

Methyl (*S*)-2-Phenylpropionate (72% from **19a**); colorless oil; $[\alpha]_D^{28}$ +93.3° (*c* 0.96, EtOH); IR (film) 1735 cm^{-1}; ^{1}H NMR (CCl_4) δ=1.10 (3H, d, *J*=7.2 Hz, H-3), 3.57 (3H, s, -COOMe), 3.58 (1H, q, *J*=7.2 Hz, H-2), 7.20 (5H, s, -Ph) ppm.

HRMS; Found: *m/z* 164.0838. Calcd for $C_{10}H_{12}O_2$: M$^+$, *m/z* 164.0836.

3-Hydroxy-2,2-dimethylpropyl (*S*)-2-Phenylpropionate (93% from **19b**); colorless oil; $[\alpha]_D^{25}$ +38.3° (*c* 1.00, $CHCl_3$); IR (film) 3470, 1735 cm^{-1}; ^{1}H NMR ($CDCl_3$) δ=0.82 (6H, s, -CMe), 1.52 (3H, d, *J*=7.2 Hz, H-3), 1.99 (1H, broad s, -OH), 3.13 (2H, s, $-OCH_2C-$), 3.74 (1H, q, *J*=7.2 Hz, H-2), 3.82 (1H, d, *J*=11.4 Hz, $-COOCH_2-$), 4.00 (1H, d, *J*=11.4 Hz, $-COOCH_2-$), 7.32 (5H, s, -Ph) ppm.

HRMS; Found: *m/z* 219.1354. Calcd for $C_{14}H_{19}O_2$: M$^+$−OH, *m/z* 219.1383.

Methyl (*S*)-2-(4-Methylphenyl)propionate (85% from **19a**); colorless oil; $[\alpha]_D^{20}$ +84.4° (*c* 0.98, $CHCl_3$); IR (film) 1740 cm^{-1}; ^{1}H NMR (CCl_4) δ=1.39 (3H, d, *J*=7.2 Hz, H-3), 2.26 (3H, s, $-C_6H_4-$Me), 3.53 (1H, q, *J*=7.2 Hz, H-2), 3.55 (3H, s, -COOMe), 6.9—7.2 (4H, m, $-C_6H_4-$) ppm.

HRMS; Found: *m/z* 177.0891. Calcd for $C_{11}H_{13}O_2$: M$^+$−1, *m/z* 177.0914.

3-Hydroxy-2,2-dimethylpropyl (*S*)-2-(4-Methylphenyl)propionate (93% from **19b**); colorless oil; $[\alpha]_D^{20}$ +35.8° (*c* 1.03, $CHCl_3$); IR (film) 3460, 1730 cm^{-1}; ^{1}H NMR ($CDCl_3$) δ=0.83 (6H, s, -CMe-), 1.49 (3H, d, *J*=7.2 Hz, H-3), 2.31 (3H, s, $-C_6H_4-$Me), 2.46 (1H, broad s, -OH), 3.13 (2H, s, $-OCH_2C-$), 3.70 (1H, q, *J*=7.2 Hz, H-2), 3.81 (1H, d, *J*=12.0 Hz, $-COOCH_2-$), 3.99 (1H, d, *J*=12.0 Hz, $-COOCH_2-$), 7.17 (4H, s, $-C_6H_4-$) ppm.

HRMS; Found: *m/z* 250.1554. Calcd for $C_{15}H_{22}O_3$: M$^+$, *m/z* 250.1567.

Methyl (*S*)-2-(4-Methoxyphenyl)propionate (97% from **19a**); colorless oil; $[\alpha]_D^{21}$ +75.3° (*c* 1.02, $CHCl_3$); IR (film) 1735 cm^{-1}; ^{1}H NMR (CCl_4) δ=1.39 (3H, d, *J*=7.2 Hz, H-3), 3.52 (1H, q, *J*=7.2 Hz, H-2), 3.56 (3H, s, -COOMe), 3.70 (3H, s, -OMe), 6.71 (2H, d, *J*=8.7 Hz, $-C_6H_4-$), 7.09 (2H, d, *J*=8.7 Hz, $-C_6H_4-$) ppm.

HRMS; Found: *m/z* 194.0954. Calcd for $C_{11}H_{14}O_3$: M$^+$, *m/z* 194.0942.

3-Hydroxy-2,2-dimethylpropyl (*S*)-2-(4-Methoxyphenyl)-propionate (92% from **19b**); colorless oil; $[\alpha]_D^{30}$ +30.2° (*c* 1.00, $CHCl_3$); IR (film) 3500, 1730 cm^{-1}; ^{1}H NMR ($CDCl_3$) δ=1.47 (3H, d, *J*=7.2 Hz, H-3), 3.67 (2H, s, $-OCH_2C-$), 3.68 (1H, q, *J*=7.2 Hz, H-2), 3.80 (3H, s, -OMe), 6.87 (2H, d, *J*=8.7 Hz, $-C_6H_4-$), 7.24 (2H, d, *J*=8.7 Hz, $-C_6H_4-$) ppm.

HRMS; Found: *m/z* 266.1524. Calcd for $C_{15}H_{22}O_4$: M$^+$, *m/z* 266.1517.

Methyl (*S*)-2-(4-Methoxyphenyl)-3-methylbutanoate (90% from **19a**); colorless oil; $[\alpha]_D^{23}$ +61.6° (*c* 1.01, MeOH); IR (film) 1735 cm^{-1}; ^{1}H NMR (CCl_4) δ=0.70 (3H, d, *J*=6.6 Hz, H-4), 1.00 (3H, d, *J*=6.6 Hz, H-4′), 2.28 (1H, m, *J*=10.5 Hz, *J*=6.6 Hz, H-3), 3.07 (1H, d, *J*=10.5 Hz, H-2), 3.65 (3H, s, -COOMe), 3.79 (3H, s, -OMe), 6.83 (2H, d, *J*=9.0 Hz, $-C_6H_4-$), 7.24 (2H, d, *J*=9.0 Hz, $-C_6H_4-$) ppm.

HRMS; Found: *m/z* 222.1253. Calcd for $C_{13}H_{18}O_3$: M$^+$, *m/z* 222.1254.

3-Hydroxy-2,2-dimethylpropyl (*S*)-2-(4-Methoxyphenyl)-3-methylbutanoate (96% from **19b**); colorless oil; $[\alpha]_D^{24}$ +24.9° (*c* 1.00, $CHCl_3$); IR (film) 3510, 1730 cm^{-1}; ^{1}H NMR ($CDCl_3$) δ=0.71 (3H, d, *J*=6.6 Hz, H-4), 0.85 (6H, s, $-CMe_2C-$), 1.03 (3H, d, *J*=6.6 Hz, H-4′), 2.1—2.5 (2H, m, H-2), 3.0—3.3 (3H, m, $-CCH_2OH$ and -OH), 3.77 (3H, s, -OMe), 3.90 (2H, s, $-COOCH_2C-$), 6.84 (2H, d, *J*=9.0 Hz, $-C_6H_4-$), 7.22 (2H, d, *J*=9.0 Hz, $-C_6H_4-$) ppm.

HRMS; Found: *m/z* 294.1844. Calcd for $C_{17}H_{26}O_4$: M$^+$, *m/z* 294.1830.

Methyl (*S*)-2-(6-Methoxy-2-naphthyl)propionate (97% from **19a**); colorless crystals from hexane-diethyl ether; mp 91.0—92.0 °C; $[\alpha]_D^{21}$ +78.4° (*c* 1.05, $CHCl_3$); IR (film) 1735 cm^{-1}; ^{1}H NMR ($CDCl_3$) δ=1.57 (3H, d, *J*=7.2 Hz, H-3), 3.68 (3H, s, -COOMe), 3.90 (1H, q, *J*=7.2 Hz, H-2), 3.91 (3H, s, -OMe), 7.13 (1H, s), 7.1—7.2 (1H, s), 7.43 (1H, dd, *J*=1.8 Hz, *J*=8.4 Hz), 7.70 (2H, s), 7.79 (1H, s) (total 6H, $-C_{10}H_6-$) ppm.

HRMS; Found: *m/z* 244.1109. Calcd for $C_{15}H_{16}O_3$: M$^+$, *m/z* 244.1099.

3-Hydroxy-2,2-dimethylpropyl (*S*)-2-(6-Methoxy-2-naphthyl)propionate (95% from **19b**); colorless crystals from hexane-diethyl ether; mp 59.0—60.0 °C; $[\alpha]_D^{21}$ +31.2°C (*c* 0.92, $CHCl_3$); IR (film) 3500, 1730 cm^{-1}; ^{1}H NMR ($CDCl_3$) δ=0.84 (6H, s, $-CMe_2C-$), 1.58 (3H, d, *J*=7.2 Hz), 2.17 (1H, s, -OH), 3.12 (2H, s, $-OCH_2C-$), 3.84 (1H, d, *J*=10.5 Hz, $-COOCH_2C-$), 3.87 (1H, q, *J*=7.2 Hz, H-2), 3.91 (3H, s, -OMe), 4.01 (1H, d, *J*=10.5 Hz, $-COOCH_2C-$), 7.12 (1H, s), 7.1—7.3 (1H, m), 7.42 (1H, dd, *J*=1.8 Hz, *J*=8.4 Hz), 7.6—7.8 (3H, m) (total 6H, $-C_{10}H_6-$) ppm.

HRMS; Found: *m/z* 316.1676. Calcd for $C_{19}H_{24}O_4$: M$^+$, *m/z* 316.1656.

Transformation of 3-Hydroxy-2,2-dimethylpropyl Ester

(20b) to Methyl Ester (20a): A Pyrex pressure bottle was charged with **19b** (1 mmol), anhydrous methanol (15 ml), and sulfuric acid (41 mg, 0.7 mmol). The bottle was tightly closed with a cap and heated at 110 °C for 1 d. After cooling in an ice bath, the reaction mixture was powered into a stirred aqueous $NaHCO_3$ solution (100 ml), and extracted with diethyl ether (30 ml×3). The organic layer was concentrated and purified by silica-gel column chromatography to give the corresponding methyl ester (**20a**) quantitatively. Enantiomeric excess was determined to be over 98% by ^1H NMR measurement using $Eu(tfc)_3$.

A part of this research was financially supported by the Asahi Glass Foundation for Industrial Technology.

References

1) a) A part of this work was presented at the 49th National Meeting of the Chemical Society of Japan, April 3, 1984, Abstr. II, 1469; b) G. Tsuchihashi, Reports of the Asahi Glass Foundation for Industry Technology, **46**, 169 (1985).

2) J. H. Fried and I. T. Harrison, U. S. Patent 196707 (1967).

3) N. Ohno, K. Fujimoto, Y. Okuno, T. Mizutani, M. Hirano, N. Itaya, T. Honda, and H. Yoshioka, *Agric. Biol. Chem.*, **38**, 881 (1974).

4) (*S*)-Naproxen is 28 times as active as (*R*)-isomer: I. T. Harrison, B. Lewis, P. Nelson, W. Books, A. Roszkowski, A. Tomalonis, and J. H. Fried, *J. Med. Chem.*, **13**, 203 (1970).

5) (*S*)-(+)-Acid esters are nealy twice as active as those of the racemic esters, while (*R*)-(−)-acid esters are virtually inactive: M. Miyakado, N. Ohno, Y. Okuno, M. Hirano, K. Fujimoto, and H. Yoshioka, *Agric. Biol. Chem.*, **39**, 267 (1975).

6) J. H. Fried, I. T. Harrison, F. Alvarez, P. H. Nelson, M. Marx, and K. G. Untch, DE(West German Patent) 2039602 (1971); JP(Japanese Patent) 14097 (1981).

7) a) N. H. Dyson, U. S. Patent 809957 (1969); JP 31981 (1974); b) Recently the synthetic procedure of the chiral Naproxen by using the preferential crystallization with racemization have been published: K. Arai, Y. O-hara, T. Iizumi, and Y. Takakuwa, 47th Symposium on Organic Synthesis, Japan, June 5, 1985, Abstr., 64.

8) C. Giordano, G. Castaldi, and F. Uggeri, *Angew. Chem. Int. Ed. Engl.*, **23**, 413 (1984).

9) G. Tsuchihashi, K. Kitajima, and S. Mitamura, JP 125355 (1980); EP(European Patent) 48136 (1982); *Tetrahedron Lett.*, **22**, 4305 (1981).

10) Synthesis of chiral 2-methyl-3-alkanoic esters via 1,2-rearrangement of alkenyl group has been also reported: Y. Honda, A. Ori, and G. Tsuchihashi, *Chem. Lett.*, **1986**, 13.

11) S. Ohba, G. Tsuchihashi, Y. Saito, K. Kitajima, and S. Mitamura, *Acta Crystallogr., Sect. C*, **1983**, 1432.

12) G. Tsuchihashi, S. Mitamura, K. Kitajima, and K. Kobayashi, *Tetrahedron Lett.*, **23**, 5427 (1982).

13) Some substitution-type rearrangements which afforded the 2-arylalkanoic esters have been reported in these seven years: a) 1-Aryl-2-halogeno-1-alkanone acetal was treated with silver salts: C. Giordano, G. Castaldi, F. Casagrade, and A. Belli, IT(Italian Patent) 20187 (1980); *J. Chem. Soc., Perkin Trans. 1*, **1982**, 2575; b) 1-Aryl-1-alkanone acetal was treated with iodine monochloride: A. Goosen and C. W. McCleland, *J. Chem. Soc., Chem. Commun.*, **1982**, 1311; c) 1-Aryl-2-halogeno-1-alkanone acetal was treated with zinc alkanoate: J. A. Walker and S. I. Amin, U. S. Patent 396967 (1982); DE 3322459 (1984); d) 1-Aryl-2-halogeno-1-alkanone acetal was treated with Lewis acid: G. Castaldi, A. Belli, F. Vaggeri, and C. Giordano, *J. Org. Chem.*, **48**, 4658 (1983); C. Giordano, G. Castaldi, F. Uggeri, and F. Gurzoni, *Synthesis*, **1985**, 436; e) 1-Aryl-2-iodo-1-alkanone acetal was treated with peroxy acid, chlorine, or iodine–chlorine, and 1-aryl-2-amino-1-alkanone acetal was treated with nitrous acid: S. D. Higgins and C. B. Thomas, *J. Chem. Soc., Perkin Trans. 1*, **1983**, 1483; f) Chiral 1-aryl-2-sulfonyloxy-1-alkanone acetal, which was prepared by Friedel-Crafts reaction, was treated with trimethoxymethane and sulfonic acid: G. Tsuchihashi, K. Kitajima, and S. Mitamura, JP 90978 (1981); EP 67698 (1982); G. Tsuchihashi, S. Mitamura, K. Kitajima, and K. Kobayashi, the 47th National Meeting of the Chemical Society of Japan, April 1, 1983, Abstr. II, 958, 959; U. S. Patent 4539420 (1985); g) Chiral 1-aryl-2-sulfonyloxy-1-alkanone acetal, which was prepared by the use of coupling of α-sulfonyloxypropanoyl chloride (**8**) with organometallic reagent, was treated with potassium acetate (92% ee): G. C. Schloemer, U. S. Patent 329672 (1981); EP 81993 (1983); JP 135833 (1983); h) Chiral 1-aryl-2-amino-1-alkanone acetal was treated with nitrous acid and 1-aryl-2-disulfonamido-1-alkanone acetal was treated with calcium carbonate under reflux: G. Tsuchihashi, S. Mitamura, K. Kitajima, and K. Kobayashi, EP 91575 (1983); i) 1-Aryl-2-hydroxy-1-alkanone acetal was treated with base (or amide) and SO_nXX' (or SO_2–X_2, n=0—1, X, X'=halogen): T. Yamauchi, K. Hattori, S. Ikeda, K. Nakano, and K. Tamaki, JP 75551 (1984); EP 160241 (1985); j) 2-Alkyl-1-aryl-2-halogeno-1-alkanone was treated with trialkoxymethane and methanesulfonic acid in methanol: S. Numata and K. Kitajima, JP 137442 (1985); 50th National Meeting of the Chemical Society of Japan, April 3, 1985, Abstr. II, 1047; k) 1-Aryl-2-phenylseleno- or 2-phenyltelluro-1-alkanone acetal was treated with peracid: S. Umemura, S. Fukuzawa, T. Yamauchi, K. Hattori, S. Mizutani, and K. Tamaki, *J. Chem. Soc., Chem. Commun.*, **1984**, 426; l) 1-Aryl-1-alkanone was treated with $PhI(OAc)_2$, trimethoxymethane in the presence of sulfuric acid: Y. Tamura, Y. Shirouchi, and J. Haruta, *Synthesis*, **1984**, 231; in the presence of $HClO_4$: Y. Tamura, T. Yakura, Y. Shirouchi, and J. Haruta, *Chem. Pharm. Bull.*, **33**, 1097 (1985); m) 1-Aryl-2-halogeno-1-alkanone acetal was treated with base: G. Castaldi, C. Giordano, and F. Uggeri, *Synthesis*, **1985**, 505; G. Castardi and C. Giordano, EP 151817 (1985); C. Giordano, F. Uggeri, and F. Minisci, EP 152003 (1985); n) 1-Aryl-2-halogeno-1-alkanone was treated with Broensted acid: IT 19434 (1984); EP 152004 (1985); o) Chiral 1-aryl-2-halogeno-1-alkanone acetal was treated with base: C. Graziano, V. Fulvio, and C. Giordano, IT 19782 (1984); EP 153701 (1985); G. Castaldi, F. Uggeri, and C. Giordano, IT 19783 (1984); EP 154853 (1985); p) 1-Aryl-1-alkanone was treated with iodine and trimethoxymethane in toluene under reflux: A. Citterio, L. Tinucci, L. Filippin, and A. Belli, IT 21883 (1984); EP 171840 (1986).

14) Some synthetic approach of the chiral 2-arylalkanoic esters by the use of asymmetric syntheses of the intermediates for rearrangement has been reported. a) The acetal of

racemic 2-chloro-1-(6-methoxy-2-naphtyl)-1-propanone with (+)-dimethyl (*R,R*)-tartrate was treated with KH_2PO_4–NaOH to afford (*S*)-Naproxen ester (diastereo selective rearrangement, 62% ee): C. Giordano, G. Castaldi, F. Uggeri, and S. Cavicchioli, EP 158255 (1985); b) Asymmetric bromination of the acetal of 1-(6-methoxy-2-naphtyl)-1-alkanone with (+)-dimethyl (*R,R*)-tartrate, followed by rearrangement, afforded the ester of 5′-bromo-(*S*)-naproxen (97% ee): C. Giordano, G. Castaldi, and F. Uggeri, EP 158913 (1985); c) Asymmetric reduction of 1-aryl-1,1-dimethoxy-2-alkanone with $LiAlH_4$ and the chiral ligand, (*S*)-(+)-2-(anilinomethyl)pyrrolidine[34] or (*S*)-(−)-2,2′-dihydroxy-1,1′-binaphtyl,[35] followed by sulfonylation and rearrangement, afforded (*S*)-2-arylalkanoic ester (69—79% ee): Y. Honda and G. Tsuchihashi, Ref. 1b.

15) On this basis, substitution-type rearrangements accompanied by the introduction of some anions, for example hydride,[a] alkyl, alkynyl,[b] and cyano anion,[c] have been developed. a) Y. Honda, M. Sakai, and G. Tsuchihashi, *Chem. Lett.*, **1985**, 1153; b) Y. Honda, E. Morita, and G. Tsuchihashi, *ibid*, **1986**, 277; c) Y. Honda, M. Sakai, and G. Tsuchihashi, 50th National Meeting of the Chemical Society of Japan, April 2, 1985, Abstr. II, 1023.

16) Some elimination-type rearrangements which afforded 2-arylalkanoic esters have been reported in these seven years; a) Aryl methyl ketone was treated with lead(IV) acetate in the presence of methanol and boron trifluoride diethyl etherate: B. Myrboth, H. Ila, and H. Junjappa, *Synthesis*, **1981**, 126; b) Aryl ethyl ketone was treated with lead acetate in the presence of trialkoxymethane and perchloric acid: K. Fujii, K. Nakao, and T. Yamauchi, *Synthesis*, **1982**, 456; *ibid*, **1983**, 444; c) Chiral 1-aryl-2-sulfonyloxy-1-alkanone acetal was treated with iodotrimethylsilane and Lewis acid, for example aluminum trichloride and titanium tetrachloride: K. Kitajima, S. Mitamura, Y. Honda, and G. Tsuchihashi, unpublished data; G. C. Shloemer, Ref. 13g.

17) P. Deslongchamps, "Stereoelectronic Effects in Organic Chemistry," Pergamon Press (1983), Series Vol. 1.

18) S.-C. J. Fu, S. M. Birnbaum, and J. P. Greenstein, *J. Am. Chem. Soc.*, **76**, 6054 (1954).

19) When isobutylbenzene was treated with (*S*)-2-(methylsulfonyloxy)alkanoyl chloride in the presence of iron(III) chloride in nitromethane, 1-(*p*-isobutylphenyl)-1-propanone was mainly obtained (*p*-/*o*-=37). But when methoxybenzene was treated by the same procedure, 1-(*o*-methoxyphenyl)-1-alkanone was obtained in a half yield of the 1-(*p*-methoxyphenyl)-1-alkanone.[1b,13f]

20) C. L. Stevens, W. Malik, and R. Pratt, *J. Am. Chem. Soc.*, **72**, 4758 (1950).

21) T. Tsunoda, M. Suzuki, and R. Noyori, *Tetrahedron Lett.*, **21**, 1357 (1980).

22) α-Hydroxy amide was reacted with 3 equivalents of Grignard reagent to yield α-hydroxy ketone: S. S. Jenkins, *J. Am. Chem. Soc.*, **56**, 682 (1934).

23) a) Magnesium bromide 2-bromopropionate was treated with arylmagnesium bromide to yield the 2-arylpropanoic acid: G. J. Matthews and R. A. Arnold, U. S. Patent 769070 (1977); JP 111018 (1978); b) Asymmetric coupling of α-metalated propanoic acid derivatives with aryl halide in the presence of the organotransition metal catalyst has been reported: G. W. Erickson, JP 112735 (1985).

24) a) D. Enders and H. Lotter, *Angew. Chem., Int. Ed. Engl.*, **20**, 795 (1981); b) T. F. Buckley and H. Rapoport, *J. Am. Chem. Soc.*, **103**, 6157 (1981).

25) a) A. H. Cook, S. F. Cox, T. H. Farmer, *J. Chem. Soc.*, **1949**, 1022; b) E. Fisher and H. Scheibler, *Chem. Ber.*, **41**, 2897 (1908).

26) K. Feudenberg, W. Kuhn, and I. Bumann, *Chem. Ber.*, **63**, 2380 (1930).

27) N. Miyashita, A. Yoshikoshi, and P. A. Grieco, *J. Org. Chem.*, **42**, 3772 (1977).

28) R. K. Crossland and K. L. Servis, *J. Org. Chem.*, **35**, 3195 (1970).

29) E. Wenkert and T. E. Goodwin, *Synth. Commun.*, **7**, 409 (1977).

30) T. H. Chan, M. A. Brook, and T. Chaly, *Synthesis*, **1983**, 203.

31) Enantiomeric excess of methyl ester (**20a**) was determined to be over 98% by 100 MHz ^1H NMR measurement using $Eu(tfc)_3$. The difference in chemical shift for OMe group of (*R*)- and (*S*)-**20a** was about 0.06 ppm in the presence of 0.4 equivalent of $Eu(tfc)_3$ in CCl_4.

32) Enantiomeric excess of ethyl (*S*)-lactate (Aldrich) was determined to be over 99% by HPLC measurement of the (+)-2-methoxy-2-trifluoromethyl-(*R*)-phenylacetic acid ester[36] of the corresponding alcohol, which was prepared by the treatment with $LiAlH_4$, by using Develosil 60-3 (Nomura Chemical); hexane/dichloromethane/methanol=6/1/0.007 (v/v/v), flow rate 0.5 ml min^{-1}, k'_{SR}=3.24, $\alpha=k'_{RR}/k'_{SR}$=1.21.

33) H. Ohta, M. Ikemoto, H. Ii, Y. Okamoto, and G. Tsuchihashi, *Chem. Lett.*, **1986**, 1169.

34) T. Mukaiyama, M. Asami, J. Hanna, and S. Kobayashi, *Chem. Lett.*, **1977**, 783.

35) R. Noyori, I. Tomino, and Y. Tanimoto, *J. Am. Chem. Soc.*, **101**, 3129 (1979).

36) J. A. Dale, D. L. Dull, and H. Mosher, *J. Org. Chem.*, **34**, 2543 (1969).

 © 1987 The Chemical Society of Japan Bull. Chem. Soc. Jpn., 60, 1037—1040 (1987)

Reactions of 2,4,6-Tri-*t*-butylphenyllithium with Deuterated Formate, Thioformate, and Selenoformate

Akihiko Ishii, Renji Okazaki,* and Naoki Inamoto
Department of Chemistry, Faculty of Science, The University of Tokyo, Hongo, Tokyo 113
(Received September 2, 1986)

O-Cholesteryl chalcogenoformates-*d*, DC(=X)(OR) (**2**: X=O; **3**: X=S; **4**: X=Se; R=3β-cholesteryl), were synthesized and allowed to react with 2,4,6-tri-*t*-butylphenyllithium. 1,3,5-Tri-*t*-butylbenzene was a main product in each reaction. The other products were 2,4,6-tri-*t*-butylbenzaldehyde-*d* (**9**) for **2**, 2,4,6-tri-*t*-butylthiobenzaldehyde-*d* for **3**, and **9**, 6,8-di-*t*-butyl-1-deuterio-3,4-dihydro-4,4-dimethyl-1*H*-2-benzoselenin, bis(2,4,6-tri-*t*-butyl-α-deuteriobenzyl) diselenide, and bis(2,4,6-tri-*t*-butyl-α-deuteriobenzyl) triselenide for **4**. The mechanisms for these reactions have been discussed.

We have previously reported[1] that 2,4,6-tri-*t*-butylphenyllithium (**1**) reacts with selenoformates at three different sites (i.e. the selenoformyl hydrogen, the selenoformyl carbon, and the selenium atoms). We became interested in the hydrogen abstraction from the selenoformyl group and studied similar abstraction reactions of a series of chalcogen analogs **2**—**4** having a deuterated formyl group in order to elucidate the effect of these heteroatoms on the reactivity and the mechanism of these reactions.

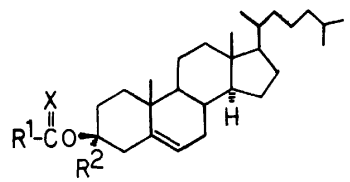

2 X=O; R^1=D, R^2=H
3 X=S; R^1=D, R^2=H
4 X=Se; R^1=D, R^2=H
5 X=Se; R^1=H, R^2=H
6 X=Se; R^1=H, R^2=D

Syntheses of Formate 2 and Thioformate 3. Deuterated compounds **2** and **3** were synthesized by the reaction of iminium salt **7**,[2] prepared from *N*,*N*-dimethylformamide-d_7, with cholesterol followed by treatment with water and hydrogen sulfide, respectively.

$$D\text{-}\overset{Cl}{\overset{|}{C}}{=}\overset{+}{N}(CD_3)_2 \quad \mathbf{7} + ROH \longrightarrow D\text{-}\overset{OR}{\overset{|}{C}}{=}\overset{+}{N}(CD_3)_2 \longrightarrow D\text{-}\overset{OR}{\overset{|}{C}}{=}X$$

H_2X

2: X=O 96%
3: X=S 33%
R=3β-cholesteryl

Reactions with 2,4,6,-Tri-*t*-butylphenyllithium (1). The esters **2**—**4** were allowed to react with **1**, prepared from 1-bromo-2,4,6-tri-*t*-butylbenzene with 2 equiv of *t*-butyllithium, at −78 °C in tetrahydrofuran (THF). The reaction mixtures were allowed to warm to room temperature in the reactions of **2** and **3** or to 60 °C in the reaction with **4**. The results are listed in Table 1.#

The formate **2** afforded mostly 1,3,5-tri-*t*-butylbenzene (**8**) along with a small amount of deuterated 2,4,6-tri-*t*-butylbenzaldehyde (**9**). The thioformate **3** gave rise to similar products (**8** and **10**), but the yield of **8** was decreased when compared with the reaction of **2**. The reaction of **4** resulted in an even smaller amount of **8**; **9** and other four products **11**—**13**, and $(ArSe)_2$[1] being also formed. It has been reported that **11** and **9** are formed by cyclization of 2,4,6-tri-*t*-butylselenobenzaldehyde-*d* (**14**) and hydrolysis of the initial adduct **15** (X=Se), respectively.[1] The mechanism for the formation of **12** and **13** will be discussed later.

$$ArLi + D\text{-}\overset{X}{\overset{\|}{C}}\text{-}OR \longrightarrow ArD\ (\text{or } ArH) + Ar\text{-}\overset{X}{\overset{\|}{C}}\text{-}D + \text{Others}$$

8 **9**: X=O **10**: X=S

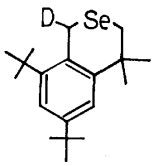

11

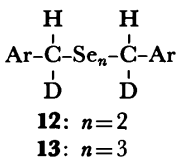

12: n=2
13: n=3

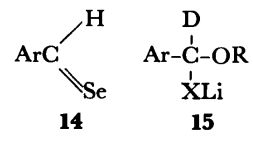

14 **15**

Reaction Mechanism. There are two conceivable mechanisms for the reaction of ArLi with the formates **2**—**4** (Scheme 1); one is an ionic mechanism (Path A) and the other is a homolytic one involving single electron transfer (SET) from ArLi to the formates (Path B)(Scheme 1).[3] The following experiments using THF-d_8 as a solvent clearly show that Path B involving Ar· is operative in these reactions. Thus, the quenching of a THF-d_8 solution of ArLi after 35 min of the preparation gave ArH (88% yield) with no deuterium (by MS), while a similar experiment with the selenoformate **5** (having a HC(=Se) group) added soon after the preparation of ArLi gave ArH (37%) containing 2.6±0.4% deuterium (by MS). The formation of ArD in the latter reaction can be explained only in terms of the abstraction of deuterium from THF-d_8 by 2,4,6-tri-*t*-butylphenyl radical Ar· which is formed by SET from ArLi to **5**, since the former reaction shows that ArLi itself is stable under the reaction conditions and can not react

Throughout this paper, Ar denotes 2,4,6-tri-*t*-butylphenyl.

with THF-d_8 to give ArD. Although the possibility that Path A and Path B are both operative in these reactions can not be excluded, we consider that the formation of all the reaction products can be accounted for in terms of Path B as shown in Scheme 1.

As can be seen from Table 1, the yield and deuterium content of 1,3,5-tri-*t*-butylbenzene show an interesting and systematic change depending on the heteroatoms in the formates **2**—**4**. The results suggest that the relative rate of the reaction of Ar· with anion radical **16** is in the order of O>S>Se for D-attack and O<S<Se for C-attack. This is probably related to the spin density on the duterium and the carbon of the anion radical **16**. ArH is most probably formed from the reactions of Ar· and unreacted ArLi with THF. Actually ArLi was found to react with THF to give ArH at room temperature.

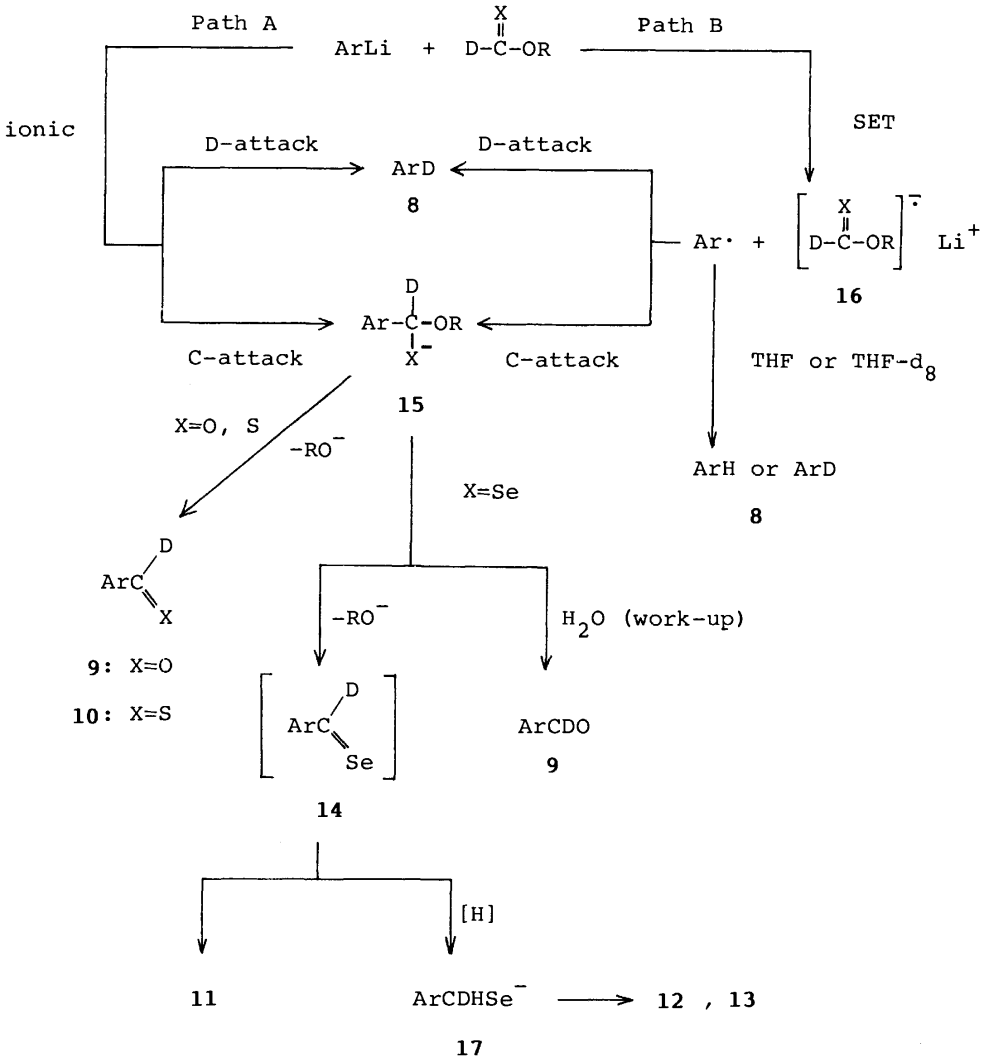

Scheme 1.

Table 1. Products and Yields of the Reactions of **1** with Esters **2**—**4**

Ester	Product Yield/%			
	ArH + ArD(%d) (**8**)	ArCDO (**9**)	ArCDS (**10**)	Others
2	86 (41.0±0.2)	3		
3	51 (21.5±0.9)		37	
4	35 (5.8±0.1)	16		**11**(2), **12**(8) **13**(14), $(ArSe)_2$(trace)

Selenides **12** and **13** are considered to be formed during work-up procedure by the oxidative coupling of selenide ion **17** with another molecule of **17** and $ArCHDSe_2^-$ which is formed from **17** and selenium, respectively. Since **17** is a reduced form of **14**, some attempts to clarify the formation mechanism of **17** were carried out. Since it has been reported that an alkoxide ion derived from an alcohol having α-hydrogen atom can reduce thioketones,[4] one possible reducing agent of selenoaldehyde **14** is a cholesteryloxide anion formed from **15**. To check this possibility, selenoformate **6** was synthesized from the corresponding 3α-deuteriocholesterol and was allowed to react with ArLi under the conditions identical with those for **4**. The products were ArH (38%), ArCHO (2%), 6,8-di-*t*-butyl-3,4-dihydro-4,4-dimethyl-1*H*-2-benzoselenin (9%), and $ArCH_2Se_nCH_2$-Ar (**18**, n=2, 9%; n=3, 9%). Since **18** thus formed contained no deuterium, the above possibility was excluded. The mechanism for the formation of **12** and **13** is not clear at present.

The formation of **8** in a high yield in the reactions with the formate **2** suggests a possibility of the existence of anion $^-C(=O)(OR)$ **19** in solution. The anion **19** is an interesting species since it is an umpolung species of chloroformate ClC(=O)(OR) and enables the synthetically useful process, HC(=O)-(OR)→R′C(=O)(OR), if it is quenched with electrophiles such as aldehydes and alkyl halides.[5] To check this possibility, the reactions of ArLi with some formates HC(=O)(OR) (**20**, R=cholesteryl, *i*-Pr, *t*-Bu) were carried out at low temperatures (−78—−98 °C) and quenched with benzaldehyde, benzophenone, and benzyl chloride. The products, however, were **8** and ArCHO, no trapping of **19** being observed. This is probably due to high instability of **19**, which decomposes into carbon monoxide and an alkoxide ion.[6]

Table 2. Attempted Trapping Experiments of Anion **19**

R of **20**/equiv	Temp/°C	Quencher/equiv
i-Pr (5)	−78	$PhCH_2Cl$ (2)
cholesteryl (1)	−78	$PhCH_2Cl$ (1)
i-Pr (1.6)	−78	PhCHO (1.5)
i-Pr (1.6)	−98	PhCHO (1.5)
i-Pr (1.5)	−78	PhCHO (1.5)[a]
i-Pr (1.5)	−98	PhCHO (1.5)[a]
t-Bu (1.2)	−98	PhCHO (1.5)
i-Pr (2)	−78	Ph_2C=O (5)[b]
i-Pr (2)	−98	Ph_2C=O (5)[b]

a) A mixture of **20** and PhCHO was added to ArLi. b) **20** was added to a mixture of ArLi and Ph_2C=O.

$$HC(=O)(OR) + ArLi \longrightarrow \underset{\mathbf{20}}{}$$

$$ArCHO + ArH + [^-C(=O)(OR)] \longrightarrow CO + RO^- \quad (\mathbf{19})$$

Experimental

Melting points are uncorrected. ^1H NMR spectra were measured in $CDCl_3$ with a JEOL FX-90Q spectrometer at 90 MHz using tetramethylsilane as an internal standard. The mass spectra were recorded with a JEOL JMS-D300 mass spectrometer. Preparative liquid chromatography (PLC) was carried out using JAI Gel 1H column (Japan Analytical Industry) with chloroform as solvent. All reactions were carried out under argon.

The "usual work-up" refers to quenching with aqueous ammonium chloride, extraction with ether, washing with water, drying over anhydrous magnesium sulfate, and evaporation. The "chromatographic purification" refers to separation by column chromatography (silica gel, hexane) and subsequent purification of each fraction by PLC.

***O*-Cholesteryl Chalcogenoformate-*d*.** *O*-Cholesteryl formate-*d* (**2**): Colorless needles (ethanol-methanol), mp 98.3—98.8 °C (lit,[7] mp 97 °C for its protium analog); ^1H NMR δ=0.68—2.46 (43H, m), 4.48—4.96 (1H, m), 5.31—5.48 (1H, br d), and 8.02 (trace, HC(=O)); *O*-cholesteryl thioformate-*d* (**3**): Pale yellow needles (ethanol), mp 132.5—133.5 °C (lit,[2] mp 124—126 °C for its protium analog); ^1H NMR δ=0.69—2.58 (43H, m), and 4.99—5.75 (2H, m); *O*-3α-deuteriocholesteryl selenoformate (**6**) was prepared using 3α-deuteriocholesterol[8,9] by the Barton's method[2]: Orange crystals (hexane), mp 129.5—131.5 °C (lit,[2] mp 126—128 °C for its protium analog).

Reaction of *O*-Cholesteryl Formate-*d* (2) with 2,4,6-Tri-*t*-butylphenyllithium (ArLi). ArLi was prepared from 1-bromo-2,4,6-tri-*t*-butylbenzene[13] (151.4 mg, 0.465 mmol) by treatment with *t*-BuLi (2 equiv) in THF (5 ml) at −78 °C. To this ArLi was added **2** (0.232 g, 0.557 mmol) in THF (2 ml) at −78 °C. The mixture was allowed to warm to room temperature. The usual work-up and chromatographic purification gave ArCDO (**9**, 3.6 mg, 3%) and a mixture of ArD and ArH (98.4 mg, 86%). The ratio of ArD/ArH was (41.0±0.2)/(59.0±0.2) (n=7) as determined by its mass spectra (20 eV). **9**: Colorless crystals (methanol), mp 195.2—197.0 °C; ^1H NMR δ=1.33 (9H, s, *p*-*t*-Bu), 1.37 (18H, s, *o*-*t*-Bu), 7.37 (2H, s, arom.), and 11.13 (trace, CHO); MS m/z (rel intensity) 275 (M^+, 24), 260 (100), 242 (46), 218 (30), and 57 (83).[14]

Reaction of *O*-Cholesteryl Thioformate-*d* (3) with ArLi. ArLi was prepared from ArBr (172.6 mg, 0.531 mmol) by treatment with *t*-BuLi (2 equiv) in THF (5 ml) at −78 °C. To this ArLi was added **3** (273 mg, 0.632 mmol) in THF (2 ml) at −78 °C. The mixture was stirred for 10 min at −78 °C and allowed to warm to room temperature. The usual work-up and chromatographic purification gave ArCDS (**10**, 56.8 mg, 37%) and a mixture of ArD and ArH (66.8 mg, 51%). The ratio of ArD/ArH was (21.5±0.9)/(78.5±0.9) (n=9) by its mass spectra (20 ev). **10**: Purple crystals (methanol under N_2), mp 154.7—155.0 °C; ^1H NMR δ=1.33 (9H, s, *p*-*t*-Bu), 1.37 (18H, s, *o*-*t*-Bu), and 7.38 (2H, s,

arom); MS *m/z* (rel intensity) 291 (M^+, 34), 276 (10), 258 (19), 235 (40), 234 (44), 220 (30), 202 (15), 179 (15), 87 (25), and 57 (100).[15]

Reaction of *O*-Cholesteryl Selenoformate-*d* (4) with ArLi. ArLi was prepared from ArBr (201.4 mg, 0.619 mmol) and *t*-BuLi (2 equiv) at −78 °C. To this ArLi was added **4**[1] in THF (3 ml) at −78 °C. The mixture was allowed to warm to 60 °C and stirred at this temperature for 20 h. The usual work-up and chromatographic purification afforded 6,8-di-*t*-butyl-1-deuterio-3,4-dihydro-4,4-dimethyl-1*H*-2-benzoselenin (**11**, 4.4 mg, 2%), ArCDO (26.5 mg, 16%), $ArCDHSe_nCDHAr$[14] (48.6 mg; **12**, 8% and **13**, 14% from ^1H NMR), $(ArSe)_2$[1] (trace), and a mixture of ArD and ArH (53.7 mg, 35%). The ratio of ArD/ArH was (5.8±0.1)/(94.2±0.1) (n=5) by its mass spectra (20 ev). **11**: ^1H NMR δ=1.32 (9H, s, *t*-Bu), 1.47 (9H, s, *t*-Bu), 1.53 (6H, s, $SeCH_2C(C\underline{H}_3)_2$), 2.76 (2H, s, $SeC\underline{H}_2C(CH_3)_2$), 4.01 (1H, br s, benzyl), and 7.35 (2H, s, arom); MS *m/z* (rel intensity) 339 (M^+, 37), 324 (18), 282 (19), 245 (10), 230 (20), and 57 (100). Found: *m/z* 339.1570. Calcd for $C_{19}H_{29}D^{80}Se$: M, 339.1573.[14]

Reaction of *O*-Cholesteryl Selenoformate (5) with ArLi in THF-d_8. THF-d_8 (Merck, 99%) was dried over sodium-potassium alloy[16] before use. ArLi was prepared from ArBr (81.4 mg, 0.250 mmol) and *n*-BuLi (1.2 equiv.) in THF-d_8 (2 ml) at −78 °C. To this ArLi was added **5**[2] (147.1 mg, 0.308 mmol) at −78 °C. After stirring for 30 min, methanol was added for quenching to the reaction mixture at −78 °C. The usual work-up and chromatographic purification gave a mixture of ArD and ArH (22.7 mg, 37%). The ratio of ArD/ArH was (2.6±0.4)/(97.4±0.4) (n=8) by its mass spectra (20 ev).

Reaction of *O*-3α-Deuteriocholesteryl Selenoformate (6) with ArLi. ArLi was prepared from ArBr (256.6 mg, 0.789 mmol) and *t*-BuLi (2 equiv) in THF (13 ml) at −78° C. To this ArLi was added **6** (413.8 mg, 0.865 mmol) in THF (4 ml) at −78 °C. The mixture was allowed to warm to 60 °C and stirred at this temperature for 20 h. The usual work-up and chromatographic purification gave ArH (73.4 mg, 38%), 2,6-di-*t*-butyl-3,4-dihydro-4,4-dimethyl-1*H*-2-benzoselenin (23.8 mg, 9%),[1] $ArCH_2Se_nCH_2Ar$ (70.0 mg; n=2, 9% and n=3, 9% from ^1H NMR)[1] and ArCHO (4.8 mg, 2%). No deuterium was introduced to the products by their mass and/or ^1H NMR spectra.

Attempted Trapping of Anion 19. ArLi was prepared from ArBr (1 mmol) and *n*-BuLi (1.2 equiv) in THF at −78 °C. To this ArLi was added formate **20** and a quencher under the conditions described in Table 2. The usual work-up gave only a mixture of ArCHO and ArH by its ^1H NMR spectra.

References

1) A. Ishii, R. Okazaki, and N. Inamoto, *Bull. Chem. Soc. Jpn.*, **59**, 2529 (1986).

2) D. H. R. Barton and S. W. McCombie, *J. Chem. Soc., Perkin Trans. 1*, **1975**, 1574; D. H. R. Barton, P.-E. Hansen, and K. Picker, *ibid*, **1977**, 1723.

3) The single electron transfer mechanism has been proposed for the reactions of organometallic reagents with ketones and thioketones. For example, see: E. C. Ashby and A. B. Goel, *J. Am. Chem. Soc.*, **103**, 4983 (1981); A. Ohno, K. Nakamura, Y. Shizume, and S. Oka, *Bull. Chem. Soc. Jpn.*, **50**, 1003 (1977) and references cited in these papers.

4) A. Ohno, K. Nakamura, M. Uohama, S. Oka, T. Yamabe, and S. Nagata, *Bull. Chem. Soc. Jpn.*, **48**, 3718 (1975).

5) Similar conversions were studied for formamide and thioformamide; B. Bánhidai and U. Schöllkopf, *Angew. Chem., Int. Ed. Engl.*, **12**, 836 (1973); R. R. Fraser and P. R. Hubert, *Can. J. Chem.*, **52**, 185 (1974); A. S. Fletcher, K. Smith, and K. Swaminathan, *J. Chem. Soc., Perkin Trans. 1*, **1977**, 1881; D. Seebach, W. Lubosch, and D. Enders, *Chem. Ber.*, **109**, 1309 (1976).

6) F. Adickes and G. Schäfer, *Ber.*, **65B**, 950 (1932); F. Adickes and P. P. Peckelhoff, *Ber.*, **68B**, 1138 (1935).

7) K. Morita, S. Noguchi, and M. Nishikawa, Japan Patent 9859 (1963); *Chem. Abstr.*, **59**, 14079d (1963).

8) a) R. S. Rosenfeld, D. K. Fukushima, L. Hellman, and T. F. Gallagher, *J. Biol. Chem.*, **211**, 301 (1954); b) J. Diekman and C. Djerassi, *J. Org. Chem.*, **32**, 1005 (1967).

9) 3α-Deuteriocholesterol was prepared by the reduction of cholest-5-en-3-one[10] with tri-*t*-butoxyaluminum deuteride[8b,11,12]: Colorless plates (ethanol), mp 149.5—150.0 °C, MS *m/z* 387 (M^+).

10) L. F. Fieser, *Org. Synth.*, Col. Vol. IV, 195 (1963).

11) H. C. Brown and R. F. McFarlin, *J. Am. Chem. Soc.*, **78**, 252 (1956).

12) O. H. Wheeler and J. L. Mateos, *Chem. Ind.*, **1957**, 395.

13) D. E. Pearson, M. G. Frazer, V. S. Frazer, and L. C. Washburn, *Synthesis*, **1976**, 621.

14) See Ref. 1 for its protium analog.

15) For its protium analog: R. Okazaki, A. Ishii, N. Fukuda, H. Oyama, and N. Inamoto, *J. Chem. Soc., Chem. Commun.*, **1982**, 1187.

16) H. Gilman and T. C. Wu, *J. Org. Chem.*, **18**, 753 (1953).

 © 1987 The Chemical Society of Japan Bull. Chem. Soc. Jpn., 60, 1041—1047 (1987)

The Photoreduction Mechanism of 10-Methylacridinium Chloride in Methanol. The Formation of 9,10-Dihydro-9-methoxy-10-methylacridine and Hydride Transfer

Koji KANO,* Bin ZHOU, and Shizunobu HASHIMOTO
Department of Applied Chemistry, Faculty of Engineering, Doshisha University, Kamikyo-ku, Kyoto 602
(Received September 8, 1986)

The photolysis of 9,10-dihydro-9-methoxy-10-methylacridine (MeOA), which is a product of the nucleophilic addition of methanol to 10-methylacridinium chloride, yielded 9,10-dihydro-10-methylacridine (AH_2) and 10,10′-dimethyl-9,9′,10,10′-tetrahydro-9,9′-biacridinyl ($(AH)_2$) in various solvents. The quenching experiment using 1,3-pentadiene indicates that AH_2 and $(AH)_2$ are produced from the photoexcited singlet and triplet states of MeOA respectively. The results on the solvent effects and the photolyses in solvent matrices at 77 K suggest that the photochemical reaction of MeOA yielding AH_2 occurs via hydride transfer from the methoxide anion to the 10-methylacridinium cation, these ions being generated from the heterolysis of MeOA in the photoexcited singlet state.

The photochemical reduction of acridine in alcohols has been a well-studied subject.[1–15] 9,10-Dihydroacridine is a major photoproduct of the dilute alcoholic solutions of acridine ($<10^{-3}$ M, 1 M=1 mol dm^{-3}), while 9,9′,10,10′-tetrahydro-9,9′-biacridinyl is also produced at higher acridine concentrations ($<10^{-1}$ M).[2] Photoexcited acridine (n, π* singlet or triplet states) abstracts a hydrogen atom from a solvent to yield the 9,10-dihydroacridinyl radical, which subsequently gives 9,10-dihydroacridine and 9,9′,10,10′-tetrahydro-9,9′-biacridinyl through disproportionation and coupling reactions respectively (Eqs. 1—3).[16] The photochemical reactions of the 10-methylacridinium ion (A^+) in alcohols are somewhat similar to those of acridine.[2,3,6,17] For example, the photolysis of 1.2×10^{-3} M 10-methylacridinium chloride (A^+Cl^-) in methanol containing trimethylamine gives 9,10-dihydro-10-methylacridine (AH_2) and 9,10-dihydro-9-hydroxymethyl-10-methylacridine in 11 and 28% yields respectively.[6] At higher concentration of A^+Cl^- (2.2×10^{-2} M) in ethanol, 10,10′-dimethyl-9,9′10,10′-tetrahydro-9,9′-biacridinyl ($(AH)_2$, 17%) is formed, together with AH_2 (12.7%) and 9,10-dihydro-9-(1-hydroxyethyl)-10-methylacridine (12.6%). Although the photoreduction mechanism of acridine has been studied in detail,[16] that for the acridinium ion is still unresolved. Zanker et al. have postulated a mechanism for the formation of $(AH)_2$ involving hydrogen abstraction by the photoexcited acridinium ion from ethanol.[17] Such hydrogen abstraction by the photoexcited acridinium ion, however, is hard to accept because the 10-alkylacridinium ion has no odd electrons which can participate in the n–π* transition.

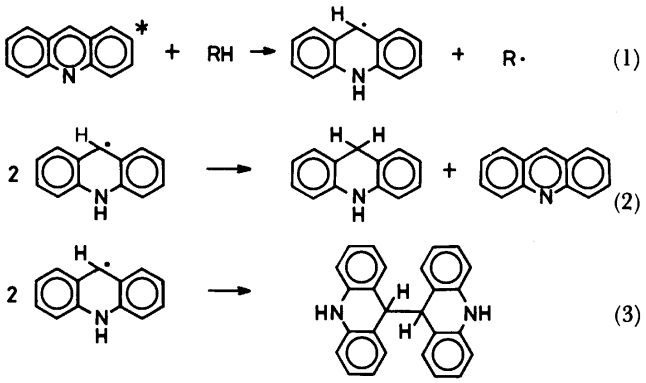

In the present paper, we demonstrate a mechanism of the photoreduction of A^+Cl^- in a methanolic solution which is quite different from those for acridine. In a previous communication, we reported a nucleophilic addition of primary and secondary alcohols to the 9-position of A^+Cl^- in dilute solutions ($[A^+Cl^-]=1\times10^{-5}$ M):[18]

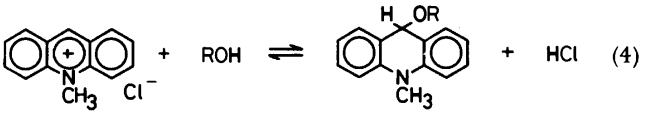

The mechanisms presented herein involve the photoreactions of 9-methoxy-9,10-dihydro-10-methylacridine, a methanol adduct of A^+Cl^-.

Experimental

A^+Cl^- was prepared by passing an aqueous solution of 10-methylacridinium iodide through an ion-exchange column (Dowex-1- X8), the crude A^+Cl^- thus obtained was recrystallized from acetonitrile. 9,10-Dihydro-9-methoxy-10-methylacridine (MeOA),[19] AH_2,[20] and $(AH)_2$[6] were prepared according to the procedures described in the literature. 1,3-Pentadiene was distilled. The analysis by means of HPLC indicated that distilled 1,3-pentadiene was still a mixture of cis and trans isomers. Spectral grades of methanol, ethanol, and 2-propanol were refluxed in the presence of K_2CO_3 and distilled. The other solvents (reagent grades) were used without further purification. All the solvents were dried using molecular sieves. Water was distilled and passed through an ion-exchange column.

The absorption spectra were taken on a Shimadzu UV-200S spectrophotometer. The fluorescence and phosphorescence spectra were measured by means of a Hitachi 650-60

spectrofluorometer. Photolyses were carried out by using an Ushio USH-5000 super-high-pressure Hg lamp (500 W) as the point-light source. The sample, in a Pyrex tube (ϕ=4 mm) or in a quartz cell (1-cm optical length), was placed at a distance of 60 cm from the light source. The deaeration of the sample was performed by five freeze-pump-thaw cycles. For photolyses and/or spectroscopic measurements at 77 K, the sample in the glass tube was placed in a Dewar vessel equipped with a quartz cell. The identification and the quantitative analyses of photoproducts were performed by a Shimadzu LC-5A HPLC apparatus equipped with a column of Shimadzu ZORBAX ODS (46×250 mm). AH_2, $(AH)_2$, and 10-methyl-9(10*H*)-acridinone (A=O) could be analyzed by means of HPLC but not A^+Cl^- and MeOA.

Results and Discussion

Nucleophilic Addition of Alcohols to A^+Cl^-. The absorption spectra of A^+Cl^- in water and alcohols are shown in Figs. 1 and 2. The assignments of the absorption bands of acridinium compounds blended in polymer films have been done by linearly-polarized absorption spectroscopy.[21,22] The shape of the absorption spectrum of A^+Cl^- (1×10^{-5} M) in water (pH 5.5) is essentially the same as that in polymer film. As is shown in Fig. 1, however, the spectrum in methanol is completely different from that in water; i.e., the ^1L_a (440, 415, and 395 nm), ^1L_b (358 and 343 nm) and ^1B_b (258 and 242 nm) bands observed in water disappear in methanol, while new absorption bands appear at 320 and 280 nm. This spectral change of A^+Cl^- in methanol has been ascribed to the formation of MeOA, which is a product of the nucleophilic addition of methanol to A^+Cl^- (Eq. 1).[18] MeOA was not formed in methanol containing small amounts of HCl. Figure 3 shows the absorption spectra of various concentrations of A^+Cl^- in methanol. An increase in the initial concentration of A^+Cl^- causes a decrease in the conversion of A^+Cl^- into MeOA. The addition of triethylamine to the system, containing both MeOA and A^+Cl^-, caused the disappearance of A^+Cl^- and an enhancement of the MeOA formation. These results clearly indicate the equilibrium shown in Eq. 4. Although it is expected that the equilibrium constant (K) can be determined spectroscopically, the poor reproducibility did not allow us to get an accurate K value. The determination of K is now in progress.

As is shown in Fig. 2, ethanol also converts A^+Cl^- to 9,10-dihydro-9-ethoxy-10-methylacridine. The nucleophilic addition of primary alcohols to A^+Cl^- occurs in 1-propanol, 1-butanol, and 1-octanol, but not in grycerol. *t*-Butyl alcohol does not give an alcohol adduct (Fig. 2). In the case of a secondary alcohol, 2-propanol, small amounts of unreacted A^+Cl^- coexist with the corresponding 9-alkoxy-9,10-

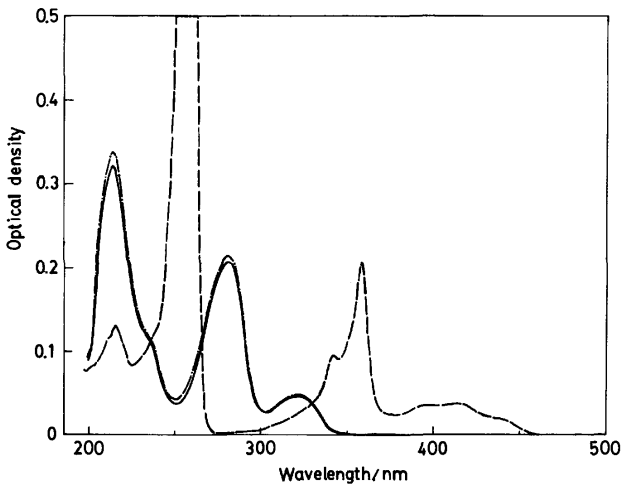

Fig. 1. Absorption spectra of A^+Cl^- (1×10^{-5} M) in water (----) and methanol (——) and authentic MeOA (1×10^{-5} M) in methanol (—·—) at 25 °C.

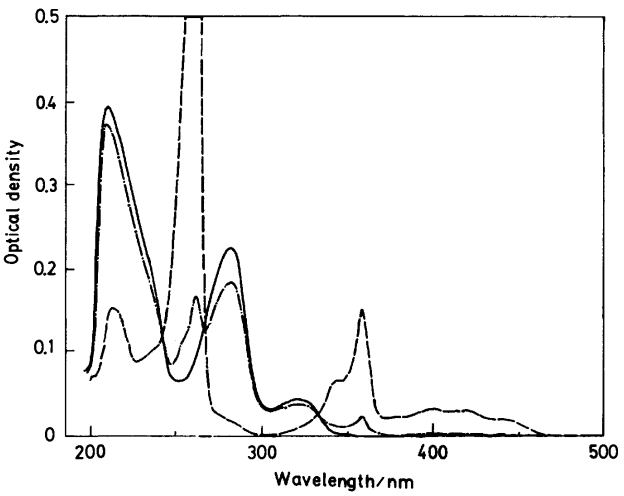

Fig. 2. Absorption spectra of A^+Cl^- (1×10^{-5} M) in ethanol (——), 2-propanol (—·—), and *t*-butyl alcohol (----) at 25 °C.

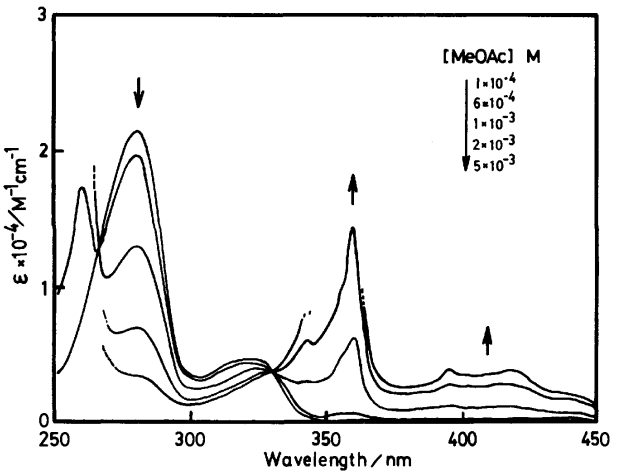

Fig. 3. Concentration effect on the absorption spectrum of A^+Cl^- in methanol at 25 °C.

dihydro-10-methylacridine. These findings reveal that the formation of 9-alkoxy-9,10-dihydro-10- methylacridine is sensitively affected by steric factor(s). Steric hindrance due to the hydrogen atoms at the 1- and 8-positions of the acridinium ring and the thermodynamically unstable structures of the alcohol adducts may inhibit the formation of 9-alkoxy-9,10-dihydro-10-methylacridines in 2-propanol, *t*-butyl alcohol, and glycerol.

It has been known that the 9-position of the 10-methylacridinuim ion (A^+) is so electrophilic that such nucleophiles as hydroxide[20,23-27] and methoxide anions[19,28,29] attack this position, thus yielding 9-hydroxy- and 9-methoxy-9,10-dihydro-10-methylacridines respectively. Our present observation reveals that weaker nucleophiles, the alcohols, also attack the 9-position of A^+. A^+Cl^- acts as a pseudo acid in the primary and secondary alcohols, such as methanol, ethanol, 1-propanol, 1-butanol, 1-octanol, and 2-propanol (Eq. 4).

Photolysis of MeOA. It is reasonable to assume that the primary step in the photoreaction of a dilute methanolic solution of A^+Cl^- is the photoexcitation of MeOA. Therefore, we studied the photochemical reaction of MeOA under various conditions.

Figure 4 shows the progressive absorption spectral changes of MeOA (5×10^{-5} M) in deaerated ethanol upon irradiation at room temperature. The photolyzed solution was analyzed by means of HPLC. $(AH)_2$ was produced as a major photoproduct, along with small amounts of AH_2 and A=O. $(AH)_2$ was isolated from the photolyzed solution of MeOA (5×10^{-4} M) and identified by means of ^1H NMR and elementary analysis. The results of the fluorescence spectral measurment of the photolyzed solution (λ_{ex}=298 nm) support the formation of AH_2 (λ_{em}=360 nm).

The yields of AH_2, $(AH)_2$ and A=O for the photolyses of MeOA in methanol, ethanol, 2-propanol, and acetonitrile under anaerobic and aerobic conditions are summarized in Table 1. Under anaerobic conditions, AH_2, $(AH)_2$, and A=O are formed, and the yields of $(AH)_2$ are higher than those of AH_2 in all the solvents used herein. In air-saturated solutions, however, the formation of $(AH)_2$ was almost completely depressed, and the yields of AH_2 increased remarkably. Prolonged irradiation in aerated solvents, especially in 2-propanol, led to an enhancement of the A=O formation (Fig. 5). In 2-propanol, the rapid formation of AH_2 was followed by the decomposition of AH_2, while the yield of A=O gradually increased. The reaction profile for the photolysis in acetonitrile

Table 1. Photochemical Reactions of MeOA in Deaerated and Aerated Solvents[a]

Solvent	Yield/%[b]		
	A=O	AH_2	$(AH)_2$
Methanol	6 (1)	14 (32)	19 (0)
Ethanol	4 (5)	7 (35)	40 (0)
2-Propanol	2 (31)	5 (20)	19 (1)
Acetonitrile	3 (21)	5 (21)	24 (0)

a) MeOA (5×10^{-5} M) in a solvent was irradiated with a 500 W super-high pressure Hg lamp for 2 min at room temperature. The yields of the photoproducts were determined by means of HPLC. b) The values in parentheses are the yields for the photolyses in air-saturated solvents.

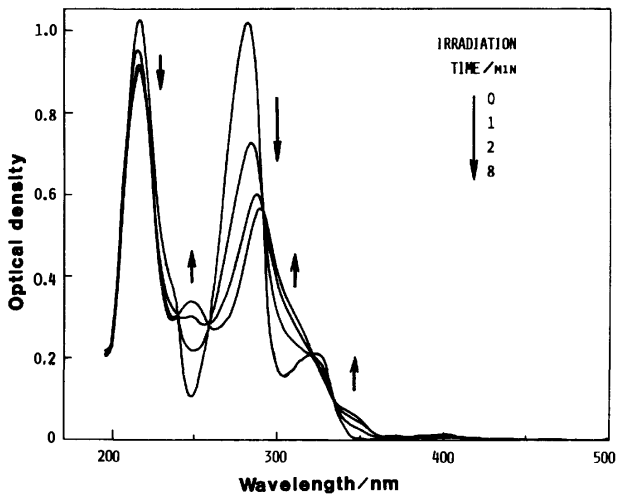

Fig. 4. Progressive absorption spectral changes of MeOA (5×10^{-5} M) in deaerated ethanol upon full irradiation with a 500 W super-high pressure Hg lamp at room temperature.

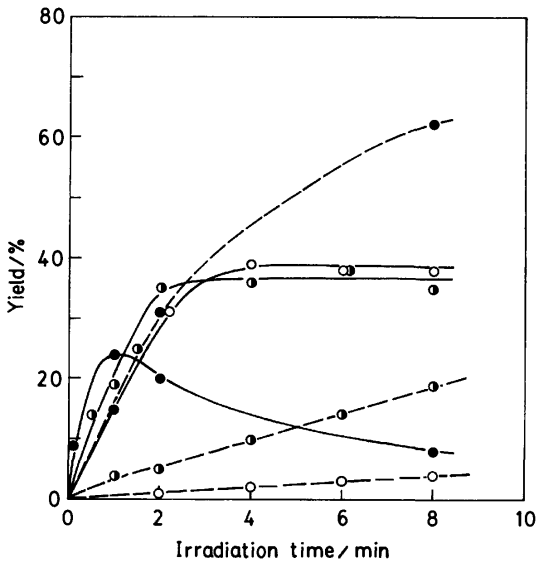

Fig. 5. Plots of the yields of AH_2 (——) and A=O (----) against the irradiation time when MeOA (5×10^{-5} M) in air-saturated methanol (○), ethanol (◑), and 2-propanol (●) was irradiated with a 500 W super-high pressure Hg lamp at room temperature.

was similar to that in 2-propanol (the data are not shown). In the cases of methanol and ethanol, the formation of A=O continued even after the rate of the AH_2 formation has become a plateau. These findings suggest that A=O is formed by the photooxidation of AH_2. Figure 6 shows the progressive absorption-spectral changes, which show the time course of the photoreaction of AH_2 (5×10^{-5} M) in air-saturated acetonitrile. The isosbestic points were observed at 325, 276, and 216 nm. The spectrum of the final photoproduct is completely in agreement with that of authentic A=O. Rapid photooxidation giving A=O was also found for $(AH)_2$ in aerated acetonitrile and 2-propanol (Fig. 7). It can be concluded, therefore, that A=O is produced by the photooxidation of AH_2 and/or $(AH)_2$ in these solvents. In methanol and ethanol, however, there was a very slow photooxidation of AH_2. A 70-min irradiation in methanol gave A=O in only a 30% yield. The reaction profiles for the photolyses of MeOA in methanol and ethanol shown in Fig. 5 can be explained by saying that the rate of AH_2 formation competes with that of the photooxidation of AH_2 to A=O at a longer irradiation time. The photolysis of $(AH)_2$ in methanol did not produce A=O at an initial stage, but a photoproduct with an absorption maximum at 280 nm was formed upon irradiation for 1 min. The HPLC analysis indicated the photoproduct to be AH_2 (40% yield). Under anaerobic conditions, however, no photoinduced conversion of $(AH)_2$ to AH_2 occurred. At the present stage, the solvent effects on the photooxidation of AH_2 and $(AH)_2$ and the effects of oxygen on the photoreaction of $(AH)_2$ are not understood.

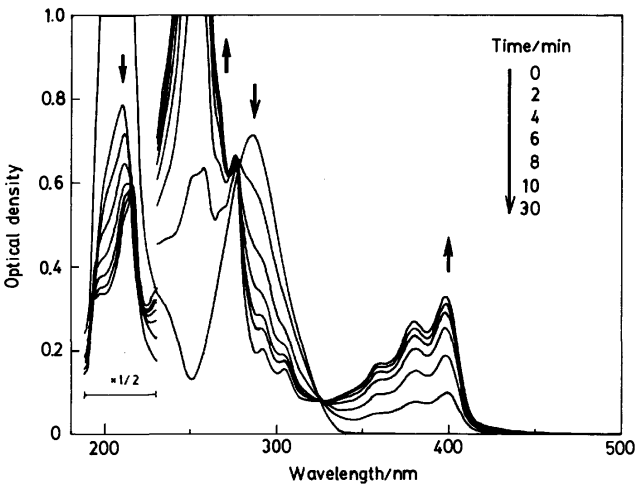

Fig. 6. Progressive absorption spectral changes of AH_2 (5×10^{-5} M) in air-saturated acetonitrile upon irradiation with a 500 W super-high pressure Hg lamp at room temperature.

Effects of 1,3-Pentadiene. The photochemical reaction of MeOA is very sensitive toward oxygen dissolving in solutions (vide supra). Oxygen can be expected to be a triplet-quencher for the photoreactions of MeOA. The photochemical reactions of MeOA under aerobic conditions, however, were so complex that the role of oxygen as a triplet quencher

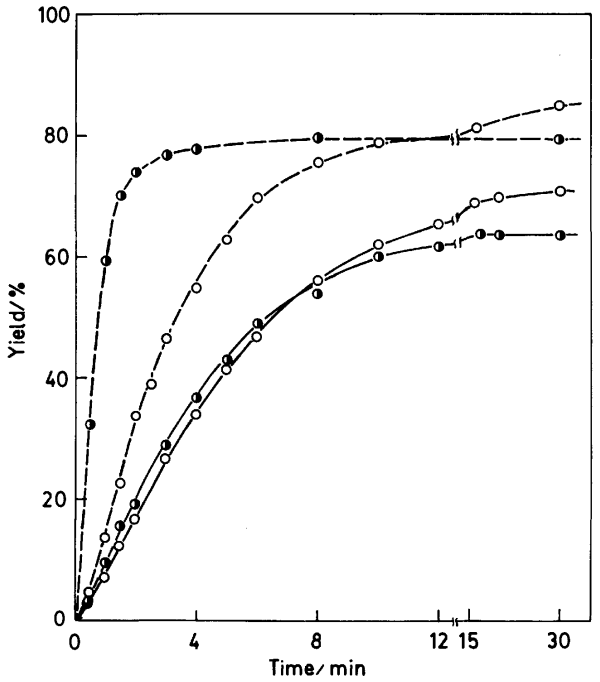

Fig. 7. Plots of the yields of A=O against the irradiation time when AH_2 (——) and $(AH)_2$ (----) in air-saturated 2-propanol (○) and acetonitrile (◑) were irradiated with a 500 W super-high pressure Hg lamp at room temperature.

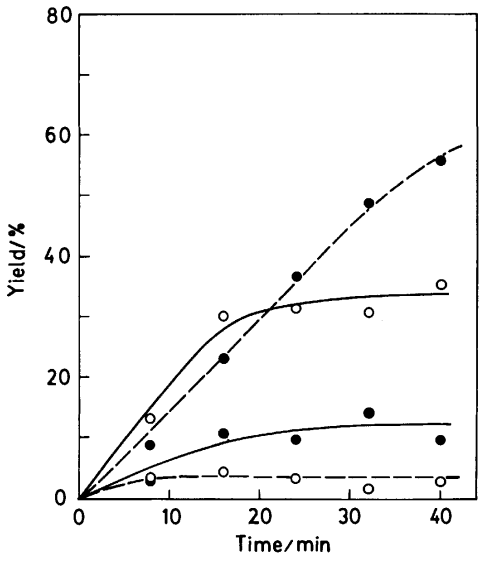

Fig. 8. Plots of the yields of AH_2 (○) and $(AH)_2$ (●) against the irradiation time when MeOA (5×10^{-5} M) in deaerated ethanol was irradiated with a 500 W super high-pressure Hg lamp (>300 nm) in the absence (----) and the presence (——) of 1,3-pentadiene (1×10^{-2} M) at room temperature.

could not be verified from the results presented above. Therefore, we examined the photolysis of MeOA (5×10^{-5} M) in degassed ethanol containing 1,3-pentadiene, which is well-known as an effective triplet quencher.[30]

The effects of 1,3-pentadiene (1×10^{-2} M) on the yields of AH_2 and $(AH)_2$ are shown in Fig. 8. The samples were irradiated by light with wavelengths above 300 nm (glass filter) in order to avoid the excitation of the 1,3-pentadiene. As Fig. 8 clearly shows, 1,3-pentadiene inhibited the formation of $(AH)_2$ and enhanced the yield of AH_2. The effects of 1,3-pentadiene are similar to those of oxygen. $(AH)_2$ did not decompose at all upon irradiation (>300 nm). Judging from these results, it can be concluded that AH_2 and $(AH)_2$ are produced via the lowest excited singlet and triplet states of MeOA respectively.

Photolyses of MeOA in Rigid Matrices and Reaction Mechanisms. In order to detect the reaction intermediate(s) for the photoreaction of MeOA, MeOA (5×10^{-5} M) in ethanol was irradiated at 77 K. In a glassy ethanol matrix, MeOA showed an absorption spectrum similar to that in the liquid phase except for the bands at around 320 nm, a broad absorption band at 320 nm in the fluid medium being split into two bands in the ethanol matrix (Fig. 9). Photoirradiation caused a rapid disappearance of the absorption bands of MeOA and the appearance of the characteristic absorption bands attributable to the 10-methylacridinium cation (A^+) (Fig. 9). The photoproduct should be 10-methylacridinium methoxide (A^+MeO^-). The emission spectra of the photolyzed solution were also measured (Fig. 10). Although MeOA does not fluoresce in ethanol at room temperature, it emits fluorescence with a maximum intensity at 337 nm (λ_{ex}=288 nm) in glassy ethanol at 77 K. Upon irradiation, the fluorescence intensity due to MeOA decreased, while new fluorescence and phosphorescnce bands appeared at 512, 481, and 472 nm (λ_{ex}=358 nm) and 418 nm (λ_{ex}=300 nm). The fluorescence excitation spectrum of the photolyzed solution followed at 481 nm corresponds to the absorption spectrum of A^+MeO^- shown in Fig. 9. The phosphorescence spectrum was completely in agreement with that of the authentic sample of AH_2. After a 13-min irradiation at 77 K, the sample was thawed at room temperature and analyzed by means of HPLC. The formation of AH_2 (ca. 10% yield) was detected. No $(AH)_2$ was measured by means of HPLC.

In place of ethanol, methanol, 1-propanol, and 1-butanol were also useful for the solvents in which MeOA was photoionized to yield A^+MeO^- at 77 K. Meanwhile, the formation of A^+MeO^- was not detectable in the photolyses in 1-octanol, *t*-butyl alcohol, methylcyclohexane, and acetonitrile at 77 K. In smaller alcohols without bulky group(s), the methoxide anion generated photochemically as a counter anion of A^+ may interact with the surrounding alcohol molecules through hydrogen bonding, resulting in the stabilization of the methoxide anion. Since alcohols with long or bulky alkyl chains as well as aprotic solvents could not interact with the methoxide anion at 77 K, a rapid recombination reaction of A^+ and MeO^- may occur to yield original MeOA. In all the media used herein, small amounts of AH_2 (<10%) were formed in the photolyses of MeOA at 77 K.

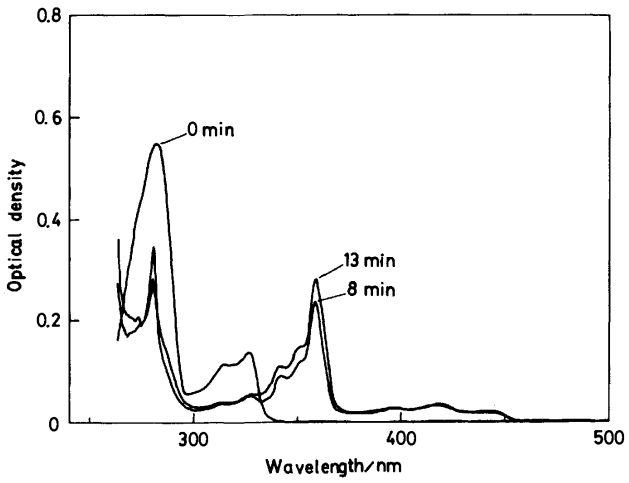

Fig. 9. Progressive absorption spectral changes of MeOA (5×10^{-5} M) in glassy ethanol upon irradiation with a 500 W super-high pressure Hg lamp at 77 K.

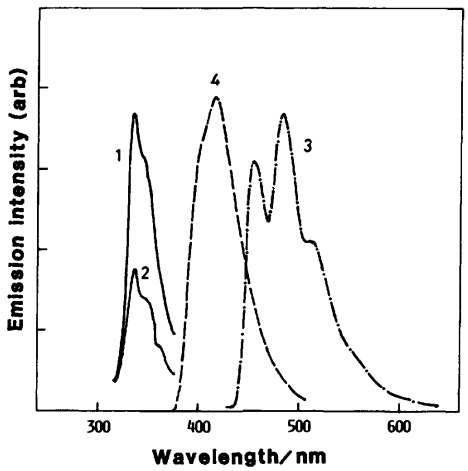

Fig. 10. Emission spectra of MeOA (5×10^{-5} M) and the photolyzed sample of MeOA in glassy ethanol at 77 K: 1 : MeOA before irradiation (λ_{ex}=288 nm), 2: MeOA after irradiation for 13 min (λ_{ex}=288 nm), 3: fluorescence of A^+MeO^- generated by the photolysis of MeOA (λ_{ex}=358 nm), 4: phosphorescence of AH_2 generated by the photolysis of MeOA (λ_{ex}=300 nm).

We can use the information obtained for the photolyses in rigid matrices to elucidate the reaction mechanisms of MeOA in fluid solutions. The heterolysis of MeOA may occur via the photoexcited singlet state of MeOA to give A^+MeO^-. Two competing reactions, the hydride transfer from MeO^- to A^+ forming AH_2 and formaldehyde (a most plausible product from MeO^-), and the recombination of A^+ and MeO^- regenerating MeOA, seem to proceed in fluid solutions:

$$MeOA + h\nu \longrightarrow {}^1MeOA^* \quad (5)$$

$${}^1MeOA^* \longrightarrow A^+ + MeO^- \quad (6)$$

$$A^+ + MeO^- \longrightarrow AH_2 + HCHO \quad (7)$$

$$A^+ + MeO^- \longrightarrow MeOA \quad (8)$$

This mechanism for forming AH_2 can account for the formation of AH_2 in the photolysis of MeOA in acetonitrile (see Table 1). Of course, a two-step mechanism involving electron transfer, followed by hydrogen transfer, may account for the formation of AH_2 from A^+MeO^-:

$$A^+ + MeO^- \longrightarrow AH\cdot + MeO\cdot \quad (9)$$

$$AH\cdot + MeO\cdot \longrightarrow AH_2 + HCHO \quad (10)$$

This mechanism, however, seems inadequate for the reasons to be presentd below.

In the absence of oxygen, the photochemical reaction via the triplet state of MeOA becomes predominant. The major photoproduct of this case is $(AH)_2$. The most plausible precursor of $(AH)_2$ is the 9,10-dihydro-10-methylacridinyl radical (AH·). If the coupling reaction of these radicals provides $(AH)_2$ in the photolysis of MeOA, AH· should have a low ability to abstract a hydrogen atom from MeO· and/or the surrounding solvent molecule. The yield of $(AH)_2$ in 2-propanol is similar to those in methanol and acetonitrile, and no significant difference in the yield of AH_2 was observed between the hydrogen-donative alcohols and acetonitrile (see Table 1). The low ability of the acridinyl radical to abstract a hydrogen atom has also been found in the photolysis of acridine.[11,16] In the case of the photoreduction of acridine in hydrogen donative alcohols, a disproportionation of the 9,10-dihydroacridinyl radicals has been assumed for the mechanism of the 9,10-dihydroacridine formation (Eq. 2).[16] A possible mechanism for the $(AH)_2$ formation can be represented as:

$${}^3MeOA^* \longrightarrow AH\cdot + MeO\cdot \quad (11)$$

$$2AH\cdot \longrightarrow (AH)_2 \quad (12)$$

$$2MeO\cdot \longrightarrow MeOH + HCHO \quad (13)$$

The two-step mechanism, however, may still remain if a contact radical pair of AH· and MeO· is produced by the electron transfer from MeO^- to A^+ (Eq. 9) and if a subsequent hydrogen abstraction by AH· from MeO· (Eq. 10) occurs instantaneously. At the present stage, we cannot distinguish this two-step mechanism (a total hydride transfer mechanism) from the hydride transfer mechanism.

Conclusion

We have pesented mechanisms for the photochemical reactions of MeOA yielding AH_2 and $(AH)_2$. There is no doubt that the photolysis of a dilute methanolic solution of A^+Cl^- occurs via MeOA. The reaction mechanisms can be represented as Eqs. 5—8 and 11—13. At higher concentration of A^+Cl^-, the direct photoreaction of A^+Cl^- with methanol cannot be excluded because A^+Cl^- and MeOA coexist in the system. We found, however, that A^+Cl^- (5×10^{-5} M) in methanol containing 2×10^{-4} M HCl does not show any photochemical reaction. This indicates the absence of any reactivity of the 10-methylacridinium cation toward photolysis in the hydrogen-donative alcohol. The mechanism involving MeOA as an intermediate seems to be reasonable, even for the photolysis of A^+Cl^- at higher concentrations.

References

1) V. Zanker and P. Schmid, *Z. Phys. Chem. (Frankfurt am Main)*, **17**, 11 (1958).
2) V. Zanker and H. Schnith, *Chem. Ber.*, **92**, 2210 (1959).
3) F. Mader and V. Zanker, *Chem. Ber.*, **97**, 2418 (1964).
4) V. Zanker and G. Prell, *Ber. Bunsenges. Phys. Chem.*, **73**, 791 (1969).
5) P. Cerutti and M. Goth, *Angew. Chem.*, **76**, 54 (1964).
6) H. Göth, P. Cerutti, and H. Schmid, *Helv. Chim. Acta*, **48**, 1395 (1965).
7) A. Kellman, *J. Chim. Phys.*, **54**, 468 (1957).
8) A. Kellman, *J. Chim. Phys.*, **57**, 1 (1960).
9) S. Kato, S. Minagawa, and M. Koizumi, *Bull. Chem. Soc. Jpn.*, **34**, 1026 (1961).
10) S. Niizuma and M. Koizumi, *Bull. Chem. Soc. Jpn.*, **36**, 1629 (1963).
11) M. Koizumi, S. Niizuma, and T. Miyashita, *Z. Phys. Chem. (Frankfurt am Main)*, **71**, 165 (1970).
12) M. Hoshino, S. Niizuma, and M. Koizumi, *Bull. Chem. Soc. Jpn.*, **45**, 2988 (1972).
13) A. Kira and M. Koizumi, *Bull. Chem. Soc. Jpn.*, **42**, 625 (1969).
14) A. Kira, Y. Ikeda, and M. Koizumi, *Bull. Chem. Soc. Jpn.*, **39**, 1673 (1966).
15) D. G. Whitten and Y. J. Lee, *J. Am. Chem. Soc.*, **93**, 961 (1971).
16) For example; M. Koizumi, S. Kato, N. Mataga, T. Matsuura, and Y. Usui, "Photosensitized Reactions," Kagaku Dojin, Kyoto (1978), Chap. 4.
17) V. Zanker, E. Erhardt, F. Mader, and J. Z. Thies, *Naturforsch. B*, **21**, 102 (1966).
18) K. Kano, B. Zhou, and S. Hashimoto, *Chem. Lett.*, **1985**, 791.

19) F. Kröhnke and H. L. Honig, *Chem. Ber.*, **90**, 2215 (1957).
20) J. Clark and M. Bakavoli, *J. Chem. Soc., Perkin Trans. 1*, **1977**, 1966.
21) Y. Matsuoka and K. Yamaoka, *Bull. Chem. Soc. Jpn.*, **52**, 3163 (1979).
22) Y. Matsuoka and K. Yamaoka, *Bull. Chem. Soc. Jpn.*, **53**, 2146 (1980).
23) A. Hantzsch and M. Kolb, *Chem. Ber.*, **32**, 3109 (1899).
24) J. J. Dobbie and C. K. Tinkler, *J. Chem. Soc.*, **1905**, 269.
25) J. A. Aston, *J. Am. Chem. Soc.*, **53**, 1448 (1931).
26) J. W. Bunting and G. M. Kauffman, *Can. J. Chem.*, **62**, 729 (1984).
27) S. Shinkai, T. Tsuno, and O. Manabe, *J. Chem. Soc., Perkin Trans. 2*, **1984**, 661.
28) J. W. Bunting and W. G. Meathrel, *Can. J. Chem.*, **52**, 981 (1974).
29) N. Suzuki, Y. Kazui, T. Tsukamoto, M. Kato, and Y. Izawa, *Bull. Chem. Soc. Jpn.*, **56**, 1519 (1983).
30) N. J. Turro, "Modern Molecular Photochemistry," Benjamin/Cummings, Menlo Park, Calif. (1978), Chap. 8.

 © 1987 The Chemical Society of Japan Bull. Chem. Soc. Jpn., 60, 1049—1052 (1987)

Free Radical Addition of 2-Bromoalkanoic Acids to Alkenes

Taichi NAKANO,* Mikio KAYAMA,† and Yoichiro NAGAI*
Department of Chemistry, Faculty of Technology, Gunma University, Tenjin-cho, Kiryu 376
(Received September 9, 1986)

The benzoyl peroxide-catalyzed reaction of 2-bromoalkanoic acids such as bromoacetic, 2-bromopropionic, and 2-bromobutyric acid with 1-alkenes was found to proceed through the addition of the C-Br bond across the double bond followed by cyclization affording 4-alkanolides in good yields.

There has been considerable interest in the construction of γ-butyrolactone skeleton, since γ-butyrolactones act as precursors for biologically active α,β-butenolides[1] or 2-methylene-4-alkanolides,[2] and are sometimes used for flavor and additive for foods.[3]

Although a variety of synthetic methods for the construction of γ-butyrolactone skeleton have been reported,[4] we present in this paper a convenient method for the construction of γ-butyrolactone structure which is easily accomplished by the reaction of a 2-bromoalkanoic acid with simple alkenes in the presence of benzoyl peroxide.[5]

Experimental

Boiling points are uncorrected. GLC analysis was performed on an Ohkura Model 802 instrument equipped with a thermal conductivity detector and 6 mmϕ×1—2 m columns packed with Celite 545AW (60—80 mesh) coated with Silicone DCQF-1 (20%). The yields determined by GLC were corrected with thermal conductivity coefficients. IR spectra were recorded on a Jasco A 102 spectrophotometer, and ^{1}H NMR spectra were obtained on a Varian Associate Model EM-360 spectrometer. Chemical shifts(δ) are given in ppm relative to tetramethylsilane as an internal standard. Abbreviations for multiplicity are t; triplet and m; multiplet. Di-*t*-butyl peroxide[6] and the ruthenium(II) complex[7] were prepared according to literature directions. Benzoyl peroxide (BPO), 2,2′-azobisisobutyronitrile (AIBN), copper(I) chloride, bromoacetic acid, 2-bromopropionic acid, and 2-bromobutyric acid were commercially available and used without further purification. Alkenes were purchased commercially and distilled from calcium hydride prior to use. Known 4-alkanolides obtained in the present work were identified by comparing their physical properties with those of an authentic sample, and for the new compounds, structural determination was made by elementary analysis as well as spectral analysis. All of the physical data for the new compounds are compiled in Table 3.

BPO-, DTBP-, and AIBN-Catalyzed Reactions Were Carried Out as Follows. To a refluxing mixture of bromoacetic acid (12 mmol), 1-octene (10 mmol), and benzene (15 ml) was added with stirring a solution of a catalyst (1—2 mmol) in benzene (15 ml) during 1 h under nitrogen. After the addition was completed, the resulting mixture was refluxed for additional 5—15 h and then subjected to GLC analysis.

CuCl-Catalyzed Reaction. A mixture of bromoacetic acid (12 mmol), 1-octene (10 mmol), acetonitrile (4 ml), and copper(I) chloride (0.6 mmol) was introduced into a glass ampoule. The mixture was degassed through several freeze-evacuate-thaw cycles prior to sealing in vacuo. Then, the sealed ampoule was kept at 80 °C for 12 h. GLC analysis of the resulting mixture disclosed that the expected γ-butyrolactone (**3**) was not produced at all. The starting materials were recovered.

$RuCl_2(PPh_3)_3$-Catalyzed Reaction. A mixture of bromoacetic acid (12 mmol), 1-octene (10 mmol), and the ruthenium(II) complex (0.18 mmol) was heated at reflux for 10 h under argon. GLC analysis of the resulting mixture showed that the alkene was consumed in 41% and the lactone (**3**) was formed in 30% yield.

A Typical Example for the Synthesis of 4-Alkanolides. 2-Methyl-4-nonanolide (7): To a refluxing mixture of 2-bromopropionic acid (19.6 g, 128 mmol), 1-heptene (9.8 g, 100 mmol), and benzene (30 ml) was added with stirring a solution of BPO (3.6 g, 15 mmol) in benzene (45 ml) during 1 h under nitrogen. The reflux was further continued for additional 9 h. The resulting mixture was washed with water and dried with magnesium sulfate. Distillation of the mixture gave 13.0 g (78% yield) of **7**.

Results and Discussion

Initially, catalytic activity of several catalysts such as benzoyl peroxide, di-*t*-butyl peroxide, azobisiso-

Table 1. Comparison of Catalysts for the Construction of γ-Butyrolactone[a]

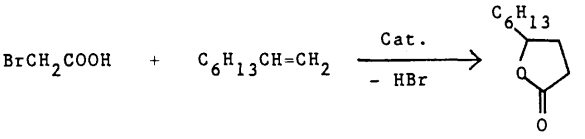

Catalyst/mol%[b]	Conditions	Conv./%[c]	Yield/%[d]
BPO (10)	80 °C, 6 h	77	77
DTBP (20)	130 °C, 16 h	85	29
AIBN (10)	80 °C, 9 h	0	0
CuCl (6)	80 °C, 12 h	0	0
Ru (II)	130 °C, 10 h	41	30

a) A 1.2 : 1 mixture of bromoacetic acid and 1-octene was used. b) Based on the alkene charged. c) Conversion of 1-octene. d) Determined by GLC. Based on the alkene charged.

† Present address: Chemistry Department, Central Research Laboratories, Ajinomoto Co., Inc., 1-1, Suzuki-cho, Kawasaki-ku, Kawasaki 210.

butyronitrile, copper(I) chloride, and dichlorotris-(triphenylphosphine)ruthenium(II) complex toward the reaction of bromoacetic acid with 1-octene was investigated. The results are summarized in Table 1 which shows that benzoyl peroxide is the most favorable catalyst. BPO-catalyzed reactions of 2-bromoalkanoic acids (bromoacetic, 2-bromopropionic, and 2-bromobutyric acid) with some 1-alkenes were carried out, the results being shown in Table 2. As is clearly seen from the Table, the reaction of bromoacetic acid with 1-alkenes afforded the corresponding γ-butyrolactones in 65—77% yields. In each reaction, a small amount of debrominated carboxylic acid (2—3% yield) was produced as a by-product, but γ-butyrolactones could be readily isolated by means of simple fractional distillation. Similarly, the reactions of 2-bromopropionic and 2-bromobutyric acid with 1-alkenes gave the corresponding 2-methyl- or 2-ethyl-4-alkanolides in 50—80% yields.

In these reactions, the Markownikoff-type products, $RCH(OOCHBrR^1)CH_3$, were not detected to any appreciable extent. In all cases the γ-butyrolactones thus obtained possess an alkyl group in the γ-position only (Eq. 1).

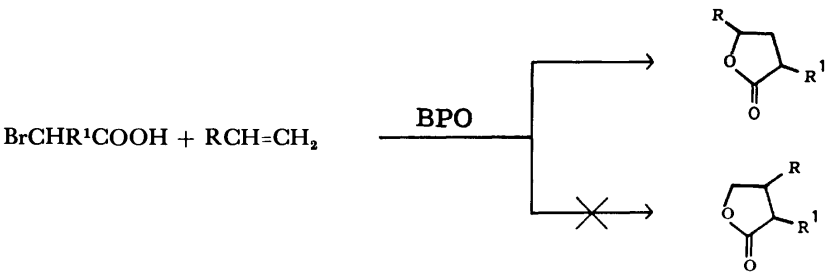

(1)

The observed regioselectivity is in accord with the finding of Kharasch et al. that carbon–carbon bond formation in the reaction of bromoacetic acid with 1-hexene takes place exclusively on the terminal carbon atom of the alkene under free radical conditions (vide post, Eq. 9).[8] In the reaction of 2-bromopropionic and 2-bromobutyric acid with 1-alkenes, the formation of two geometrical isomers (cis

Table 2. Yields and Boiling Points of γ-Butyrolactones[a]

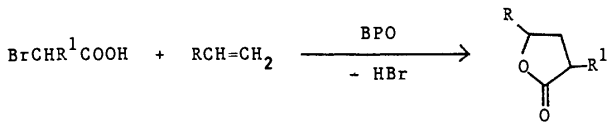

Alkene	Acid[R^1]	Product[R]	Yield/%[b]	Bp(°C/mmHg)	No.
1-Hexene	H	C_4H_9	68 (65)	82/2.5	[1][c]
1-Heptene	H	C_5H_{11}	71 (69)	100/0.12	[2][d]
1-Octene	H	C_6H_{13}	74 (68)	97/0.6	[3][e]
1-Nonene	H	C_7H_{15}	70 (58)	129/3	[4][f]
1-Decene	H	C_8H_{17}	77 (54)	111/0.35	[5][c]
1-Hexene	CH_3	C_4H_9	64	81/0.12	[6][g]
1-Heptene	CH_3	C_5H_{11}	80 (78)	83/0.2	[7][h]
1-Octene	CH_3	C_6H_{13}	79 (45)	100/1	[8][e]
1-Nonene	CH_3	C_7H_{15}	78 (53)	100/0.3	[9]
1-Decene	CH_3	C_8H_{17}	72 (63)	111/0.3	[10][i]
1-Hexene	CH_2CH_3	C_4H_9	60 (54)	107/6	[11]
1-Heptene	CH_2CH_3	C_5H_{11}	72 (50)	90/0.15	[12]
1-Octene	CH_2CH_3	C_6H_{13}	50	109/0.3	[13][e]
1-Nonene	CH_2CH_3	C_7H_{15}	67 (53)	110/0.3	[14]
1-Decene	CH_2CH_3	C_8H_{17}	73 (45)	119/0.3	[15]

a) To a refluxing 1.2 : 1 benzene solution of a 2-bromoalkanoic acid and an alkene was added with stirring a solution of BPO(0.1 equiv) in benzene during 1 h. Then, the mixture was heated for 5—9 h. b) Determined by GLC. In parentheses are shown isolated yields. c) See Ref. 10). d) See Ref. 11). e) See Ref. 12). f) See Ref. 13). g) See Ref. 14). h) See Ref. 15). i) See Ref. 16).

Table 3. Physical Properties of New γ-Butyrolactones

Lactone No.	IR($\nu_{C=O}$)	^{1}H NMR (δ, ppm)	Elemental Analysis[a] C	H
[9]	1775	4.26(m, 1H, -O-C-H), 2.33(m, 3H, =CHH, -COC<u>H</u>(CH_3)-), 1.15(m, 15H, -$(CH_2)_6$-, -COCH(C<u>H</u>$_3$)-), 0.92(t, 3H, -CH_3)	73.11 (72.68	11.29 11.18)
[11]	1770	4.22(m, 1H, -O-C-H), 2.27(m, 3H, =CHH, -COC<u>H</u>(CH_2-CH_3)-), 1.57(m, 8H, -$(CH_2)_3$-, -COCH(C<u>H</u>$_2$$CH_3$)-), 0.87(m, 6H, -$CH_3$, -COCH($CH_2$C<u>H</u>$_3$)-)	70.55 (70.55	10.66 10.66)
[12]	1770	4.17(m, 1H, -O-C-H), 2.25(m, 3H, =CHH, -COC<u>H</u>(CH_2-CH_3)-), 1.54(m, 10H, -$(CH_2)_4$-, -COCH(C<u>H</u>$_2$$CH_3$)-), 0.93(m, 6H, -COCH($CH_2$C<u>H</u>$_3$), -$CH_3$)	71.36 (71.70	11.01 10.94)
[14]	1770	4.34(m, 1H, -O-C-H), 2.33(m, 3H, =CHH, -COC<u>H</u>(CH_2-CH_3)-), 1.62(m, 14H, -$(CH_2)_6$-, -COCH(C<u>H</u>$_2$$CH_3$)-), 1.00(m, 6H, -COCH($CH_2$C<u>H</u>$_3$)-, -$CH_3$)	73.75 (73.54	11.34 11.39)
[15]	1770	4.23(m, 1H, -O-C-H), 2.27(m, 3H, =CHH, -COC<u>H</u>(CH_2-CH_3)-), 1.57(m, 16H, -$(CH_2)_7$-, -COCH(C<u>H</u>$_2$$CH_3$)-), 0.91(m, 6H, -COCH($CH_2$C<u>H</u>$_3$)-, -$CH_3$)	74.05 (74.29	11.54 11.58)

a) In parentheses are shown calculated values.

and trans) is possible. For example, ^{13}C NMR analysis revealed 2-methyl-4-octanolide (**6**) thus obtained to be a mixture of two geometrical isomers,[9] although isomer ratio was not ultimately determined.

A plausible pathway leading to γ-butyrolactone involves the free radical addition of a 2-bromoalkanoic acid to an alkene through the rupture of the C-Br bond to give the expected 1 : 1 adduct followed by subsequent cyclization. Thus, the formation of the 4-bromoalkanoic acid [**C**] is simply explained in terms of a free-radical chain process, involving the two chain-carrying species [**A**] and [**B**] (Eqs. 5 and 6).

$$\text{BPO} \longrightarrow 2\,\text{PhCOO}\cdot \quad (2)$$

$$\text{PhCOO}\cdot \longrightarrow \text{Ph}\cdot + CO_2 \quad (3)$$

$$\text{Ph}\cdot + \text{BrCHR}^1\text{COOH} \longrightarrow \underset{[\mathbf{A}]}{\text{PhBr} + \cdot\text{CHR}^1\text{COOH}} \quad (4)$$

$$[\mathbf{A}] + \text{RCH=CH}_2 \longrightarrow \underset{[\mathbf{B}]}{\text{RCHCH}_2\text{CHR}^1\text{COOH}} \quad (5)$$

$$[\mathbf{B}] + \text{BrCHR}^1\text{COOH} \longrightarrow \underset{[\mathbf{C}]}{\text{RCHBrCH}_2\text{CHR}^1\text{COOH}} + [\mathbf{A}] \quad (6)$$

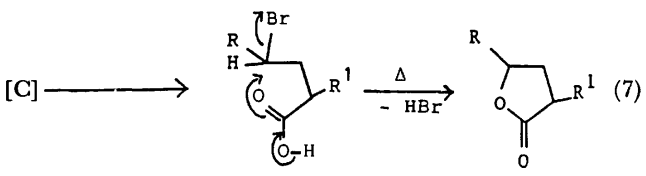

(7)

Ring closure of the adduct [**C**] with liberation of hydrogen bromide can be most conveniently interpreted by the intramolecular nucleophilic substitution (Eq. 7). Formation of the debrominated adducts is elucidated in terms of the attack of [**B**] on the labile allylic hydrogens in 1-alkenes, HS, (Eq. 8).

$$[\mathbf{B}] + \text{HS} \longrightarrow \underset{\text{H}}{\text{RCHCH}_2\text{CHR}^1\text{COOH}} + \cdot\text{S} \quad (8)$$

In fact, Kharasch et al.[8] reported that the photolysis of bromoacetic acid in excess 1-hexene yielded octanoic acid in 80% yield (Eq. 9).

$$\text{BrCH}_2\text{COOH} + \text{C}_4\text{H}_9\text{CH=CH}_2 \xrightarrow{h\nu} \text{C}_7\text{H}_{15}\text{COOH} \quad (9)$$

References

1) Y. S. Rao, *Chem. Rev.*, **76**, 625 (1976).

2) F. A. Grieco, *Synthesis*, **1975**, 67.

3) G. Ohloff, "Fortschritte der Chemie Organischer Naturstoff," **35**, Springer-Verlag, Wein-New York (1978), pp. 431—527.

4) For example, P. Baldt, W. Thielecke, and J. Etzemüller, *Chem. Ber.*, **102**, 4157 (1969); J. B. Bush. Jr. and H. Finkbeiner, *J. Am. Chem. Soc.*, **90**, 5903 (1968): E. I. Heiba, R. M. Dessau, and W. J. Koehl. Jr., *J. Am. Chem. Soc.*, **90**, 5905 (1968); E. I. Heiba and R. M. Dessau, *J. Am. Chem. Soc.*, **93**, 995 (1971); M. Okano, *Chem. Lett.*, **1973**, 165; E. I. Heiba, R. M. Dessau, and P. G. Rodewald, *J. Am. Chem. Soc.*, **96**, 7977 (1974); T. Kishimoto, H. Ishihara, and Y. Matsubara, *Bull. Chem. Soc., Jpn.*, **50**, 1897 (1977); T. Shono, H. Ohmizu, S. Kawakami, and H. Sugiyama, *Tetrahedron Lett.*, **21**, 5029 (1980).

5) T. Nakano, M. Kayama, H. Matsumoto, and Y. Nagai, *Chem. Lett.*, **1981**, 415.

6) N. A. Milas and P. M. Surgenor, *J. Am. Chem. Soc.*, **68**, 205 (1946); *ibid.*, **68**, 643 (1946).

7) P. S. Hallman, T. A. Stephenson, and G. Wilkinson, *Inorg. Chem.*, **12**, 238 (1972).

8) N. Kharasch, P. Lewis, and R. K. Sharma, *J. Chem. Soc., Chem. Commun.*, **1967**, 435.

9) Carbon-13 NMR analysis of (**6**) showed two kind of carbonyl carbons at 179.7 and 179.2.
10) B. Rothstein, *Bull. Soc. Chim. Fr.*, **2**, 1936 (1935).
11) G. I. Nikishin, Yu. N. Ogibin, L. Kh. Rakhmatullina, and N. G. Maksimova, *Bull. Acad. Sci. USSR*, **25**, 103 (1976).
12) M. S. Kharasch, P. S. Skell, and P. Fisher, *J. Am. Chem. Soc.*, **70**, 1055 (1948).
13) F. Richter, "Beilsteins Handbuch," EII, BD XVII, 1952, p. 294.
14) M. Okano, *Chem. Lett.*, **1973**, 165.
15) F. Richter, "Beilsteins Handbuch," EII, BD XVII, 1933, p. 246.
16) A. P. Kozikowski and Y. Y. Chen, *J. Org. Chem.*, **45**, 2236 (1980).

 © 1987 The Chemical Society of Japan Bull. Chem. Soc. Jpn., 60, 1053—1056 (1987)

Syntheses and Some Reactions of 4*H*-Cyclohepta[4,5]-pyrrolo[1,2-*a*]pyrimidin-4-ones

Noritaka Abe
Department of Chemistry, Faculty of Sciences, Yamaguchi University, Yamaguchi 753
(Received September 10, 1986)

The reaction of 2-aminocyclohepta[*b*]pyrroles with ethyl acetoacetate in phoshoryl chloride–polyphosphoric acid gives 2-methyl-4*H*-cyclohepta[4,5]pyrrolo[1,2-*a*]pyrimidin-4-ones. A ring closure of diethyl *N*-(cyclohepta[*b*]pyrrol-2-yl)aminomethylenemalonates gives 4-oxo-4*H*-cyclohepta[4,5]pyrrolo[1,2-*a*]pyrimidine-3-carboxylates (**2**) in phosphoryl chloride–polyphosphoric acid or in hot *t*-butylbenzene, which are deesterified by the treatment with hot hydrobromic acid. Compounds **2** undergo replacement reactions towards some electrophiles at positions C-3, C-11, and C-7 (in that order).

Hetero-annulated azaazulenes are interesting compounds for their physical and chemical properties as well as physiolosical activities. Although some synthetic studies on hetero-annulated azaazulenes are known,[1–4] investigations on azaazulenes fused with a pyrimidine ring are rare,[5,6] in spite of the attractive attention on hetero-annulated pyrimidines.[7,8] In this paper, I wish to report on the syntheses of 4*H*-cyclohepta[4,5]pyrrolo[1,2-*a*]pyrimidin-4-ones by means of the annulation of 2-aminocyclohepta[*b*]-pyrroles (2-amino-1-azaazulenes) in a phosphoryl chloride–polyphosphoric acid mixture ($POCl_3$–PPA), a useful condensing agent.[9]

The treatment of ethyl 2-aminocyclohepta[*b*]pyrrole-3-carboxylate[2,6] (**1a**) with ethyl acetoacetate (EAA) in $POCl_3$–PPA for 1 h at 115 °C yielded ethyl 2-methyl-4-oxo-4*H*-cyclohepta[4,5]pyrrolo[1,2-*a*]pyrimidine-11-carboxylate (**2a**) in 81% yield (which was stimulative). Deesterification of **2a** with hot 48% hydrobromic acid (HBr) gave 2-methyl-4*H*-cyclohepta-[4,5]pyrrolo[1,2-*a*]pyrimidin-4-one (**2b**) in 80% yield together with cyclohepta[*b*]pyrrol-2(1*H*)-one[10] (2%). The structure of **2b** was confirmed from observing the deshielding effects produced by tris(dipivaloylmethanato)europium shift reagent [Eu(dpm)$_3$] on the ^{1}H NMR spectrum. The ^{1}H NMR spectrum of **2b** shows protons at δ 2.45 (s, Me), 6.18 (s, H-3), 6.71 (s, H-11), 6.90—7.35 (m, H-7, 8, and 9), 7.55—7.85 (m, H-10), and 9.50—9.75 (m, H-6). The addition of Eu(dpm)$_3$ produced progressive down-field chemical shifts, and protons were observed at δ 3.47 (s, Me), 7.10—7.60 (m, H-7, 8, and 9), 7.68 (s, H-11), 8.15—8.45 (m, H-10), 9.43 (s, H-3), and 13.85—14.10 (m, H-6). Protons at C-3 and C-6 are most affected, to the extent of 3.25 and 4.35 ppm, respectively; these are much larger than those of H-11 and H-10, 0.97 and 0.60 ppm, respectively. These show that the complexing of the Eu(dpm)$_3$ with amide oxygen at C-4, not at C-2 of **3**, gives rise to a predominant deshilding effect positions C-3 and C-6. If the carbonyl group is present at C-2 as **3**, only the proton of C-3 should be deshilded predominantly.

When 2-aminocyclohepta[*b*]pyrrole[4,11] (**1b**) was treated in a similar manner as for **1a**, the reaction was rather complex and compound **2b** could be isolated only in low yield.

In a similar treatment of **1a** with ethyl benzoate (EBA) in $POCl_3$–PPA, **2c** and **2d** were obtained in moderate yields.

Unsubstituted 4*H*-cyclohepta[4,5]pyrrolo[1,2-*a*]pyrimidin-4-one (**2h**) was synthesized by the reaction of 2-aminocyclohepta[*b*]pyrroles (**1**) with diethyl ethoxymethylenemalonate (DEEM) and a subsequent cyclization and deesterification.

The treatment of **1a—c** with DEEM in hot ethanol or hot 1-butanol gave diethyl *N*-(cyclohepta[*b*]pyrrol-2-yl)aminomethylenemalonates (**4a—c**), respectively, in excellent yields. The ^{1}H NMR spectra of **4a—c** shows low-field resonated olefinic protons at δ 9.1—9.2 which couple (J=13 Hz) with amine protons at δ 11.3—12.5. By adding of D_2O, latter signals were disappeared and former changed to singlets. The results show that the substitution occurred on the amino group at C-2 of **1**, not on the N-1 position. Regarding the reaction of **1b** with DEEM, thermal cyclization partly occurred, and small amount of **2f** was obtained. In the ^{1}H NMR spectrum of **2f**, two signals of singlets can be seen at δ 7.00 (H-11) and 8.97 (H-2), and seven-menbered ring protons at δ 7.25—7.70 (3H, m, H-7, 8, and 9), 7.85—8.20 (1H, m, H-10), and 10.05—10.40 (1H, m, H-6), besides an ethyl ester group. The low-field appearance of the H-6 proton may be due to a shielding effect by the carbonyl group.

Compound **2f** was easily deesterified by the treatment with a hot 48% HBr–PPA mixture to give **2h** in 75% yield. The ^{1}H NMR spectrum of **2h** shows two 1H doublets (J=6.5 Hz) at δ 6.35 (H-3) and 8.15 (H-2) and low-field resonated 1H multiplet at δ 9.60—9.85 (H-6). The results agree with the report that H-2 protons resonate at δ ca. 8.1 and H-6 protons at lowest field in ^{1}H NMR spectra of 4-oxopyrimido[2,1-*b*]-benzazoles.[12]

The treatment of **2e** with 48% HBr or 48%HBr–PPA gave **2h** in low yields together with cyclohepta[*b*]-pyrrol-2(1*H*)-one[10] and **1b** which should be hydrolyzed products.

Cyclizations of **4a—c** were achieved by heating in xylene, *t*-butylbenzene, or tetralin, and yielded **2e—g**,

in moderate to excellent yields. Treatment of **4a** with $POCl_3$–PPA at 120 °C for 1h yielded **2e** in 95% yield. Similar treatment of **4b** with $POCl_3$–PPA resulted in complex mixture. From the mixture, **2f** was isolated in 17% yield together with yellow prisms **5** (48%). Compound **5** was assigned as ethyl 1,4-dihydro-4-oxocyclohepta[4,5]pyrrolo[2,3-*b*]pyridine-3-carboxylate. The IR spectra of **5** exhibits a signal at 3370 cm^{-1} assignable to NH. In its ^1H NMR, no signals are seen around δ 7.0; it does exhibit the signals of seven-membered ring protons at δ 7.75—8.15 (3H, m, H-6, 7, and 8), 8.45—8.75 (1H, m, H-9), and 9.75—10.00 (1H, m, H-9). It is known that ethyl 6-methyl-4-oxo-4*H*-pyrido[1,2-*a*]pyrimidine-3-carboxylate transformed thermally to ethyl 7-methyl-1,4-dihydro-4-oxo-1,8-naphthyridine-3-carboxylate.[13] However, an interconversion of **2f** and **5** was not observed under the conditions of boiling *t*-butylbenzene or hot $POCl_3$–PPA. Therefore, **5** would be directly produced from **4b**.

Electrophilic Replacement of 2. Compound **2h** was deuteriated by a treatment with D_3PO_4 or CF_3CO_2D to give 3,11-dideuteriated product **2i**. Bromination of **2h** gave 3,11-dibrominated compound **2j** in excellent yield. Bromination of **2f** gave **2k** in 82% yield. When the positions (C-3 and 11) were blocked, bromination occurred at C-7 position; thus the brominatin of **2e** afforded **21** in 15% yield. When Vilsmeier-Haak reaction of **2h** was carried out at 65 °C, a 3-formylated product **2m** (24%) and a 3,11-diformylated product **2n** (18%) were obtained. Compound **2f** was formylated at C-11 position to give **2o** in 44% yield, but **2e** was not formylated at all. These results show that compounds **2** were reactive towards some electrophiles at the positions of C-3, C-11, and C-7, in the order.

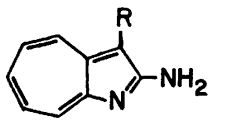

1a: R=CO_2Et
1b: R=H
1c: R=CN

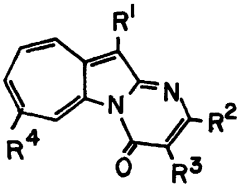

	R¹	R²	R³	R⁴
2a:	CO_2Et	Me	H	H
2b:	H	Me	H	H
2c:	CO_2Et	Ph	H	H
2d:	H	Ph	H	H
2e:	CO_2Et	H	CO_2Et	H
2f:	H	H	CO_2Et	H
2g:	CN	H	CO_2Et	H
2h:	H	H	H	H
2i:	D	H	D	H
2j:	Br	H	Br	H
2k:	Br	H	CO_2Et	H
21:	CO_2Et	H	CO_2Et	Br
2m:	H	H	CHO	H
2n:	CHO	H	CHO	H
2o:	CHO	H	CO_2Et	H

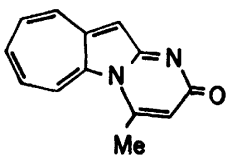

3

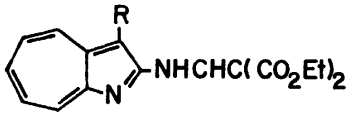

4a: R=CO_2Et
4b: R=H
4c: R=CN

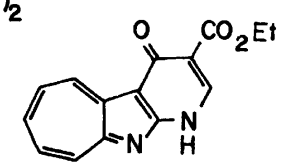

5

Experimental

Melting points were uncorrected. ^1H NMR spectra were recorded on a Hitachi R-24B spectrometer and ^{13}C NMR spectra on a JEOL FX-100 spectrometer using deuteriochloroform as a solvent with tetramethylsilane as an internal standard, unless otherwise stated. IR spectra were recorded on a JASCO IR-G spectrometer for Nujol mulls and electronic spectra on a Hitachi 220A spectrophotometer for ethanol solutions. Kieselgel 60 was used for column chromatography.

Reaction of 1 with EAA. A mixture of **1a** (1.729 g, 8.00 mmol), EAA (4.16 g, 32.0 mmol), $POCl_3$ (4.90 g, 32.0 mmol), and PPA (3.0 g) was stirred for 1 h at 115 °C. After hydrogen chloride evolution has ceased, ethanol (10 ml) was added, and the mixture was heated for 10 min at 100 °C. The reaction mixture was poured into ice-water (200 ml), neutralized with Na_2CO_3, extracted with chloroform, dried (Na_2SO_4), and evaporated to dryness. Chromatography of the residue with chloroform gave **2a** (1.826 g, 81%), which, was crystallized from cyclohexane-dichloromethane to give reddish violet prisms (1.170 g, 52%), mp 176—178 °C; λ_{max} 217 nm (log ε 4.40), 236 (4.38), 268 (4.52), 288 (4.29), 297 (4.28, sh), 431 (4.07), and 490 (3.77, sh); ν_{max} 1675 (ester C=O) and 1665 cm^{-1} (amido C=O); ^1H NMR δ=1.48 (3H, t, J=7 Hz, Me), 2.53 (3H, s, Me), 4.48 (2H, q, J=7 Hz, OCH_2), 6.25 (1H, s, H-3), 7.35—7.70 (3H, m, H-7, 8, and 9), 8.95—9.30 (1H, m, H-10), and 10.05—10.30 (1H, m, H-6). Anal. ($C_{16}H_{14}N_2O_3$) C, H, N. Elution with ethyl acetate gave **1a** (0.178 g, 10%).

In a similar manner, **1b** gave **2b** (14%).

2b: Dark violet needles (from cyclohexane-dichloromethane), mp 196—198 °C; λ_{max} 260 nm (log ε 4.54), 289 (4.14), 299 (4.13, sh), 400 (3.99), 425 (4.01), 479 (3.71), 510 (3.67, sh), 545 (3.50, sh); ν_{max} 1675 (amido C=O); ^1H NMR δ=2.45 (3H, s, Me), 6.18 (1H, s, H-3), 6.71 (1H, s, H-11), 6.90—7.35 (3H, m, H-7, 8, and 9), 7.55—7.85 (1H, m, H-10), and 9.50 (1H, m, H-6), δ[$CDCl_3$-Eu(dpm)$_3$]= 3.47 (3H, s, Me), 7.10—7.60 (3H, m, H-7, 8, and 9), 7.68 (1H, s H-11), 8.15—8.45 (1H, m, H-10), 9.43 (1H, s, H-3), and 13.85—14.10 (1H, m, H-6), δ (CF_3CO_2D)=2.68 (3H, s, Me), 6.48 (1H, s, H-3, exch.), 7.33 (1H, s, H-11, exch.), 8.10—8.50 (3H, m, H-7, 8, and 9), 8.65—8.90 (1H, m, H-10), and 10.35—10.70 (1H, m, H-6). Anal. ($C_{13}H_{10}N_2O$) C, H, N.

Deesterification of 2a. a) A solution of **2a** (0.800 g, 2.83 mmol) in 48% HBr (10 ml) was heated under reflux for 2 h, and poured into water (200 ml). The mixture was neutralized with $NaHCO_3$, extracted with chloroform, dried

(Na_2SO_4), and evaporated to dryness. Chromatography of the residue with chloroform gave **2b** (0.481 g, 80%). Elution with ethyl acetate gave cyclohepta[*b*]pyrrol-2(1*H*)-one[10] (0.010 g, 2%).

b) A mixture of **2a** (0.200 g, 0.71 mmol) and PPA (5.0 g) was heated at 150 °C for 3 h, and worked up as above. Chromatography of the residue with chloroform gave **2a** (0.060 g, 30%) and **2b** (0.084 g, 56%), successively.

Reaction of 1a with EBA. a) A mixture of **1a** (0.432 g, 2.00 mmol), EBA (1.54 g, 8.00 mmol), $POCl_3$ (2.46 g, 16.0 mmol), and PPA (3.0 g) was stirred at 120 °C for 3 h. The reaction mixture was treated as for **1a** with EAA. Chromatography of the residue with chloroform gave **2c** (0.347 g, 50%), which was crystallized from cyclohexane-dichloromethane to give reddish violet needles (0.180 g, 26%), mp 201—203 °C; λ_{max} 212 nm (log ε 4.39), 258 (4.48), 273 (4.42, sh), 297 (4.38), 315 (4.36, sh), 353 (3.87, sh), 435 (3.97), and 495 (3.69, sh); ν_{max} 1675 (ester C=O) and 1655 (amido C=O); ^{1}H NMR δ=1.55 (3H, t, J=7 Hz, Me), 4.49 (2H, q, J=7 Hz, OCH_2), 6.82 (1H, s, H-3), 7.10—7.65 (6H, m, H-7, 8, 9, and *m,p*-phenyl), 8.00—8.25 (2H, m, H-*o*-phenyl), 9.00—9.40 (1H, m, H-10), and 10.00—10.25 (1H, m, H-6). Anal. ($C_{21}H_{16}N_2O_3$) C, H, N.

b) When the above reaction was carried out under reflux for 1 h and worked up, compound **2d** (0.055 g, 10%) was isolated by chromatography with chloroform; this was crystallized from cyclohexane-dichloromethane to give brown needles (0.030 g, 5%), mp 201—203 °C; λ_{max} 261 nm (log ε 4.50), 288 (4.50), 300 (4.44, sh), 345 (3.88, sh), 403 (3.93), 428 (3.99), 486 (3.72), 510 (3.71, sh), 550 (3.56, sh), and 605 (3.09, sh); ν_{max} 1660 cm^{-1} (amido C=O); ^{1}H NMR δ=6.82 (1H, s, H-3), 6.92 (1H, s, H-11), 7.00—7.30 (3H, m, H-7, 8, and 9), 7.35—7.55 (3H, m, H-*m,p*-phenyl), 7.60—7.95 (1H, m, H-10), 8.00-8.20 (2H, m, H-*o*-phenyl), and 9.65—9.90 (1H, m, H-6). Anal. ($C_{18}H_{12}N_2O$), C, H, N.

Reaction of 1 with DEEM. a) A mixture of **1a** (2.60 g, 12.0 mmol) and DEEM (7.80 g, 36.1 mmol) in abs ethanol (100 ml) was heated under reflux for 48 h, then evaporated. Chromatography of the residue with chloroform gave **4a** (4.197 g, 90%), which was crystallized from cyclohexane-dichloromethane to give yellow needles (3.601 g, 77%), mp 158—160 °C; λ_{max} 266 nm (3.96), 311 (4.37), 317 (4.36, sh), 330 (4.31), 386 (4.40), 443 (3.54); ν_{max} 3200 (NH), 1685, 1670, and 1650 cm^{-1} (ester C=O); ^{1}H NMR δ=1.38, 1.41, and 1.53 (each 3H, t, J=7 Hz, Me), 4.28, 4.40, and 4.53 (each 2H, q, J=7 Hz, OCH_2), 7.60—7.95 (3H, m, H-5, 6, and 7), 8.25—8.50 (1H, m, H-8), 9.00—9.30 (1H, m, H-4), 9.20 (1H, d, J=13 Hz, NHC<u>H</u>), 12.53 (1H, bd, J=13 Hz, NH, exch.). Anal. ($C_{20}H_{22}N_2O_6$) C, H, N. Elution with ethyl acetate gave 1a (0.075 g, 3%).

In a similar manner, **1b** gave **4b** (95%) and **2f** (4%).

4b: Reddish orange prisms (from cyclohexane-dichloromethane), mp 129—131 °C; λ_{max} 239 nm (log ε 4.21, sh), 246 (4.22), 253 (4.21), 286 (4.33, sh), 295 (4.41), 328 (4.55), 381 (4.50), 455 (3.89); ν_{max} 3250 (NH), 1690 and 1675 cm^{-1} (ester C=O); ^{1}H NMR δ=1.34 and 1.38 (each 3H, t, J=7 Hz, Me), 4.28 and 4.34 (each 2H, q, J=7 Hz, OCH_2), 6.83 (1H, s, H-3), 7.3—7.85 (3H, m, H-5, 6, and 7), 8.05—8.50 (2H, m, H-4 and 8), 9.10 (1H, d, J=13 Hz, NHC<u>H</u>), 11.35 (1H, bd, J=13 Hz, NH, exch.). Anal. ($C_{17}H_{18}N_2O_4$) C, H, N.

2f: Red needles (from cyclohexane-dichloromethane), mp 179—181 °C; λ_{max} 237 nm (log ε 4.32), 263 (4.48), 305 (4.06), 403 (3.90, sh), 428 (4.04), 480 (3.95, sh), 495 (3.97); ν_{max} 1735 (ester C=O) and 1655 cm^{-1} (amido C=O); ^{1}H NMR δ=1.42 (3H, t, J=7 Hz, Me), 4.40 (2H, q, J=7 Hz, OCH_2), 7.00 (1H, s, H-11), 7.25—7.70 (3H, m, H-7, 8, and 9), 7.85—8.20 (1H, m, H-10), 8.97 (1H, s, H-2), and 10.05—10.40 (1H, m, H-6). Anal. ($C_{15}H_{12}N_2O_3$) C, H, N.

b) When above reaction was carried out in hot 1-butanol, **1a** and **1c** gave **4a** (95%) and **4c** (96%), respectively.

4c: Yellow needles (from cyclohexane-dichloromethane), mp 210—212 °C; λ_{max} 242 nm (log ε 3.94, sh), 262 (4.12), 305 (4.48), 329 (4.48), 382 (4.45), 445 (3.66); ν_{max} 3190 (NH), 2210 (CN), 1700, and 1660 cm^{-1} (ester C=O); ^{1}H NMR δ=1.37 and 1.40 (each 3H, t, J=7 Hz, Me), 4.31 and 4.40 (each 2H, q, J=7 Hz, OCH_2), 7.75—7.95 (3H, m, H-5, 6, and 7), 8.27—8.53 (2H, m, H-4 and 8), 9.10 (1H, d, J=13 Hz, NHC<u>H</u>), and 11.62 (1H, bd, J=13 Hz, exch.). Anal. ($C_{18}H_{17}N_3O_4$) C, H, N.

Cyclization of 4. a) A mixture of **4a** (4.910 g, 12.7 mmol), $POCl_3$(18.0 g), and PPA (4.0 g) was stirred for 1 h at 120 °C. To the mixture, ethanol (20 ml) was added, and the mixture was heated for 10 min at 100 °C. The reaction mixture was poured into ice-water (200 ml), neutralized with Na_2CO_3, extracted with chloroform, dried (Na_2SO_4), and evaporated. Chromatography of the residue with chloroform gave **2e** (4.110 g, 95%), which was crystallized from cyclohexane-dichloromethane to give red needles (3.910 g, 90%), mp 213—215°C; λ_{max} 233 nm (log ε 4.34), 266 (4.50), 299 (4.22), 310 (4.18, sh), 431 (3.98), 475 (4.00); ν_{max} 1725 and 1670 (ester C=O), and 1655 cm^{-1} (amido C=O); ^{1}H NMR δ=1.43, 1.50 (each 3H, t, J=7 Hz, Me) 4.42, 4.55 (each 2H, q, J=7 Hz, OCH_2), 7.65—8.00 (3H, m, H-7, 8, and 9), 9.07(1H, s, H-2), 9.25—9.55 (1H, m, H-10), and 10.35—10.65 (1H, m, H-6). Anal. ($C_{18}H_{16}N_2O_5$) C, H, N.

In a similar treatment, **4b** gave **2f** (17%) and **5** (48%).

5: Yellow prisms (from methanol-ethyl acetate), mp 234—236 °C; λ_{max} 260 nm (log ε 4.12, sh), 282 (4.40), 315 (4.47), 388 (3.89), 435 (2.98, sh); ν_{max}3370 (NH), 1715 (ester C=O), and 1705 (C=O); ^{1}H NMR δ=1.41 (3H, t, J=7 Hz, Me), 4.42 (2H, q, J=7 Hz, OCH_2), 7.75—8.15 (3H, m, H-6, 7, and 8), 8.45—8.75 (1H, m, H-9), 8.4—9.0 (1H, broad, NH), 8.83 (1H, s, H-2), and 9.75—10.00 (1H, m, H-5); MS (70 eV) *m/z* (rel intensity) 268 (M^+; 50), 222 (61), 196 (34), 194 (100), 166 (29), 140 (47), 139 (54), and 113 (21). Anal. ($C_{15}H_{12}N_2O_3$) C, H, N.

b) Solutions of **4a** and **4b** (0.795 mmol) in tetralin (3 ml) were heated under reflux for 1 h and evapolated. Chromatography of the residue with chloroform gave **2e** (46%), and **2f** (46%), respectively.

c) A solution of **4b** (0.300 g, 0.954 mmol) in *t*-butylbenzene (5 ml) was heated under reflux for 12 h and evaporated. Chromatography of the residue with chloroform gave **2f** (0.266 g, 88%).

d) A solution of **4c** (0.150 g, 0.442 mmol) in dry xylene (30 ml) was heated under reflux for 48 h and evaporated. The residue was chromatographed. Elution with chloroform gave **4c** (0.014 g, 9%). Further elution gave **2g** (0.117 g, 90%), mp 240—242 °C (dec); λ_{max} 232 nm (log δ 4.40), 267 (4.57), 297 (4.24), 305 (4.21, sh), 435 (4.06), 475 (4.03); ν_{max} 2230 (CN), 1730 (ester C=O), and 1670 cm^{-1} (amido C=O); ^{1}H NMR δ=1.43, (3H, t, J=7 Hz, Me), 4.38 (2H, q, J=7 Hz, OCH_2), 7.70—8.00 (3H, m, H-7, 8, and 9), 8.30—8.60 (1H, m, H-10), 9.00 (1H, s, H-2), 10.40—10.60 (1H, m, H-6). Anal. ($C_{16}H_{11}N_3O_3$) C, H, N.

Deesterifications of 2. A mixture **2f** (0.300 g, 1.19 mmol), PPA (4.0 g), and 48% HBr (15 ml) was heated under reflux for 1 h, then poured into ice-water (200 ml). The mixture was neutralized with Na_2CO_3, extracted with chloroform, dried (Na_2SO_4), and evaporated. The residue was chromatographed with chloroform to give **2h** (0.210 g, 96%), which was crystallized from cyclohexane-dichloromethane to give dark violet needles (0.167 g, 76%), mp 160—162 °C; λ_{max} 225 nm (log ε 4.19), 256 (4.42), 288 (4.03, sh), 397 (3.93), 425 (3.92), 482 (3.64), 505 (3.62); ν_{max} 1660 (amido C=O); ^{1}H NMR δ=6.35 (1H, d, J=6.5 Hz, H-3), 6.83 (1H, s, H-11), 6.95—7.45 (3H, m, H-7, 8, and 9), 7.55—7.90 (1H, m, H-6), 8.15 (1H, d, J=6.5 Hz, H-2), 9.60—9.85 (1H, m, H-10); ^{13}C NMR δ=106.3 (C-11), 108.2 (C-3), 125.9 (C-9), 131.7 (C-7), 132.0 (C-8), 133.8 (C-10), 135.9 (C-6), 141.9 (C-10a), 144.0 (C-5a), 153.4 (C-2), 157.8 (C-11a), 162.2 (C-4). Anal. ($C_{12}H_8N_2O$) C, H, N.

In a similar manner, **2e** gave **2h** (16%) and cyclohepta[*b*]-pyrrol-2(1*H*)-one[10] (5%).

Deutriation of 2h. Compound **2h** (0.090 g, 0.46 mmol) was dissolved in D_3PO_4(1.0 g) and set for 7 d at ambient temperature. The solution was diluted with water (100 ml), neutralized with $NaHCO_3$, extracted with chloroform, and dried (Na_2SO_4). Evaporation of the solution gave **2i** (0.089 g, 98%), which was crystallized from cyclohexane-dichloromethane to give violet needles (0.060 g, 73%), mp 160—161 °C; ^{1}H NMR δ=6.90—7.35 (3H, m, H-7, 8, and 9), 7.55—7.85 (1H, m, H-10), 8.14 (1H, s, H-2), 9.55—9.75 (1H, m, H-6); MS (70 eV) *m/z* (rel intensity) 198 (M^+; 100), 170 (67) 115 (12).

Bromination of 2. A solution of **2h** (0.150 g, 0.76 mmol) and bromine (0.30 g, 1.87 mmol) in acetic acid (4 ml) was stirred for 24 h at ambient temperature. The reaction mixture was diluted with water (100 ml) and neutralized with $NaHCO_3$. The precipitate formed were collected by filtration and washed with water to give **2j** (0.265 g, 98%), which was crystallized from cyclohexane-dichloromethane to give brown needles, (0.176 g, 65%), mp 223 °C (decomp); λ_{max} 221 nm (log ε 4.43), 270 (4.47), 300 (4.06, sh), 418 (4.09), 445 (4.11), 505 (3.74) 534 (3.71), 575 (3.55, sh); ν_{max} 1680 cm^{-1} (amido C=O); ^{1}H NMR δ=7.20—7.50 (3H, m, H-7, 8, and 9), 7.75—8.00 (1H, m, H-10), 8.52 (1H, s, H-2), 9.70—9.85 (1H, m, H-6). Anal. ($C_{12}H_6Br_2N_2O$) C, H, N.

In a similar manner, **2f** and **2e** gave **2k** (82%) and **21** (15%), respectively.

2k: Violet prisms (from cyclohexane-dichloromethane), mp 204—206 °C; λ_{max} 220 nm (log ε 4.43) 238 (4.35), 269 (4.46), 297 (4.04), 303 (4.03), 420 (3.96), 444 (4.11), 490 (3.90), 513 (3.90); ν_{max} 1735 (ester C=O) and 1660 cm^{-1} (amido C=O); ^{1}H NMR δ=1.43 (3H, t, J=7 Hz, Me), 4.43 (2H, q, J=7 Hz, OCH_2), 7.35—7.70 (3H, m, H-7, 8, and 9), 7.95—8.25 (1H, m, H-10), 9.00 (1H, s, H-2), 10.00—10.25 (1H, m, H-6). Anal. ($C_{15}H_{11}BrN_2O_3$) C, H, N.

21: Red needles (from cyclohexane-dichloromethane), mp 210—212 °C; λ_{max} 222 nm (log ε 4.17), 271 (4.46), 299 (4.15), 309 (4.14), 440 (3.93), 485 (3.84); ν_{max} 1735, 1690 (ester C=O), and 1660 cm^{-1} (amido C=O); ^{1}H NMR δ=1.43, 1.48 (each 3H, t, J=7 Hz, Me), 4.42, 4.53 (each 2H, q, OCH_2), 7.48 (1H, dd, J=10 and 9 Hz, H-9), 8.13 (1H, dd, J=9 and 2 Hz, H-8), 9.06 (1H, s, H-2), 9.25 (1H, d, J=10 Hz, H-10), 10.88 (1H, d, J=2 Hz, H-6). Anal. ($C_{18}H_{15}BrN_2O_5$) C, H, N.

Formylation of 2. To a solution of **2h** (0.150 g, 0.76 mmol) in *N,N*-dimethylformamide (DMF) (2 ml), a mixture of DMF (3 ml) and $POCl_3$ (0.5 g) was added drop by drop. The mixture was stirred for 24 h at 65 °C. After addition of NaOAc (0.300 g), the mixture was stirred for 1 h at 65 °C, then poured into water (100 ml), neutralized with $NaHCO_3$, and extracted with chloroform. The extract was dried (Na_2SO_4) and evaporated. Chromatography of the residue with chroloform gave **2h** (0.015 g 10%), **2n** (0.035 g, 18%), and **2m** (0.041 g, 24%), successively. [**2m:** violet needles from cyclohexane-dichloromethane, mp 230 °C (dec); λ_{max} 219 nm (log ε 4.00), 237 (4.08), 264 (4.32), 305 (3.82), 312 (3.82), 405 (3.66, sh), 433 (3.84), 497 (3.89); ν_{max} 1670 cm^{-1} (C=O); ^{1}H NMR δ=7.12 (1H, s, H-11), 7.45—7.85 (3H, m, H-7, 8, and 9), 8.05—8.40 (1H, m, H-10), 8.85 (1H, s, H-2), 10.10—10.35 (1H, m, H-6), 10.42 (1H, s, CHO). Anal. ($C_{13}H_8N_2O_2$) C, H, N. **2n:** red needles (from cyclohxane-dichloromethane), mp >300 °C; λ_{max} 218 nm (log ε 4.26), 237 (4.33), 265 (4.54), 305 (4.07), 314 (4.07), 407 (3.93, sh), 433 (4.08), and 498 (4.13); ν_{max} 1675 and 1660 cm^{-1} (C=O); ^{1}H NMR (DMSO-d_6) δ=8.30—8.55 (3H, m, H-7 , 8, and 9), 8.76 (1H, s, H-2), 9.60—9.80 (1H, m, H-10), 10.23 and 10.58 (each 1H, s, CHO), 10.50-10.65 (1H, m, H-6). Anal. ($C_{14}H_8N_2O_3$) C, H, N. MS *m/z* 252 (M^+)].

In a similar manner, **2f** gave **2o** (44%).

2o: Red needles (from cyclohexane-dichloromethane), mp 229—231 °C; λ_{max} 223 nm (log ε 4.16), 235 (4.09, sh), 269 (4.22), 303 (4.05, sh), 320 (4.09), 450 (3.87), and 465 (3.87); ν_{max} 1735 (ester C=O) and 1660 cm^{-1} (C=O); ^{1}H NMR δ=1.42 (3H, t, J=7 Hz, Me), 4.40 (2H, q, J=7 Hz, OCH_2), 7.80—8.20 (3H, m, H-7, 8, and 9), 9.00 (1H, s, H-2), 9.60—9.85 (1H, m, H-10), 10.73 (1H, s, CHO), 10.55—10.80 (1H, m, H-6). Anal. ($C_{16}H_{12}N_2O_4$) C, H, N.

I am grateful to Dr. Akira Mori, Kyushu University, for the ^{13}C NMR and Mass spectra.

References

1) T. Nishiwaki and N. Abe, *Heterocycles*, **15**, 547 (1981).
2) N. Abe, T. Nishiwaki, H. Yamamoto, and N, Kunishige, *Bull. Chem. Soc. Jpn.*, **56**, 3703 (1983).
3) K. Yamane, K. Fujimori, and S. Ichikawa, *Chem. Lett.*, **1982**, 707.
4) K. Fujimori, N. Hirako, and K Yamane, *Bull. Chem. Soc. Jpn.*, **56**, 1247 (1983).
5) W. Flitsch and E. Mukidjam, *Chem. Ber.*, **112**, 3577 (1979).
6) T. Nozoe, S. Seto, and T. Toda, *Bull. Chem. Soc. Jpn.*, **41**, 208 (1968).
7) A. Albert, *Adv. Heterocyclic Chem.*, **32**, 1, (1982).
8) I. Hermecz and Z. Meszaros, *Adv. Heterocyclic Chem.*, **33**, 241, (1983).
9) I. Hermecz, A. Horvath, L. Vasvari-Debreczy, and Z. Meszaros, *Synthesis*, **1984**, 152.
10) T. Nozoe, S. Seto, S. Matsumura, and T. Terasawa, *Chem. Ind. (London)*, **1954**, 1356.
11) T. Nozoe, S. Seto, S. Matsumura, and T. Terasawa, *Chem. Ind. (London)*, **1954**, 1357.
12) J. J. Wade, R. F. Hegel, and C. B. Toso, *J. Org. Chem.*, **44**, 1811 (1979).
13) I. Hermecz, Z. Meszaros, L. Vasvari-Debreczy, A. Horvath, G. Horvath, and M. Pongor-Csakvari, *J. Chem. Soc., Perkin Trans. 1*, **1977**, 789.

Synthetic Approach toward Antibiotic Ezomycins. III. Synthesis of a Protected Derivative of the Octose Moiety

Osamu SAKANAKA, Takashi OHMORI, Shuji KOZAKI, and Tetsuo SUAMI*
Department of Applied Chemistry, Faculty of Science and Technology, Keio University, Hiyoshi, Yokohama 223
(Received September 13, 1986)

A protected derivative of the octose moiety of antibiotic ezomycins A_1 and A_2, 4-*N*-benzoyl-1-[methyl 3,7-anhydro-2-*O*-benzoyl-5-(3-*N*-benzoylureido)-6-*O*-benzyl-5-deoxy-β-D-*threo*-D-allooctofuranos-(1,4)-yluronate]-cytosine, has been synthesized from 5-acetamido-6-*O*-benzyl-5-deoxy-1,2-*O*-isopropylidene-3-*O*-methylthiomethyll-β-L-*erythro*-D-allooctofuranose-(1,4) by a series of reactions involving 23 steps.

Antibiotic ezomycins are produced by a fermentation of a very similar strain of Streptomyces Kitazawaensis.[1] They exhibit antimicrobial activity against limited species of phytopathogenic fungi, such as Sclerotinia and Botritis. Their structures were established by a degradation study and a spectroscopic analysis as shown in Scheme 1.[2-4] The unique bicyclic trans-fused 3,7-anhydrooctofuranose-(1,4) skeleton was also found in octosyl acids.[5] Several synthetic approaches toward 3,7-anhydrooctofuranose-(1,4) derivatives have been reported,[6-8] and total syntheses of octosyl acid A_1 were recently published by two groups.[9,10] However, so far any synthesis of the octose moiety of ezomycins has not appeared in the literature.

In the preceding papers,[11,12] a preliminary investigation on the synthesis of 5-acetamido-5-deoxyoctofuranose-(1,4) derivatives and their conversion into 3,7-anhydrides has been described. A potassium fluoride-catalyzed Henry reaction between 5-nitro-D-ribose derivative (**1**) and L-glyceraldehyde derivative (**2**) and a successive hydrogenation followed by *N*-acetylation afforded three diastereomeric isomers (**3a**, **3b** and **3c**). Also their absolute configurations of the newly introduced chiral centers on C-5 and C-6 have been established. The configurations of the major product **3a** were found to be identical with those of the octose moiety of ezomycins. Furthermore, from **3a** and **3b** 3,7-anhydride (**6a** and **6b**) could be successfully synthesized by a series of reactions involving ten and

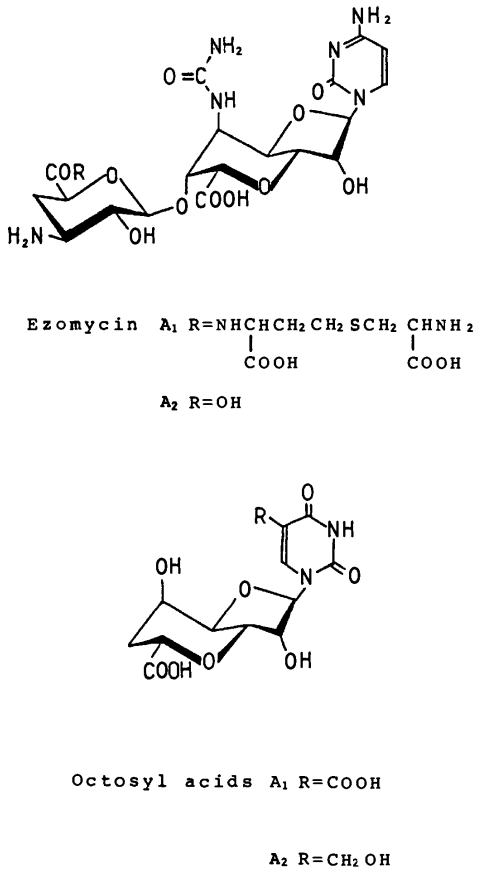

Scheme 1.

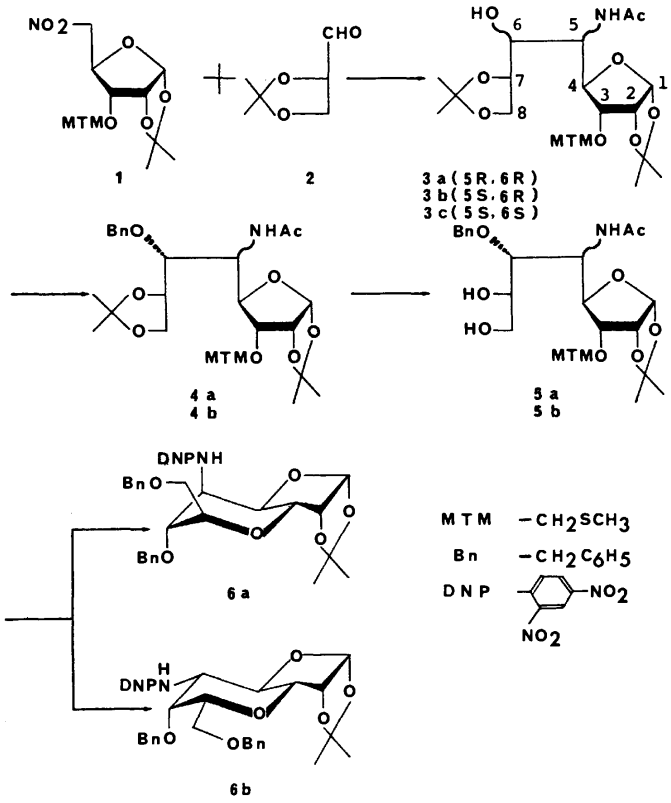

Scheme 2.

eight steps, respectively.

In the present paper, we wish to report a synthesis of the octose moiety of ezomycins A_1 and A_2 as a protected form.

Results

A preparation of **5a** was previously described.[11] *O*-Benzylation of an intact mixture (67% yield from **1**) of **3a** and **3b**, which could not be separated chromatographically, with benzyl bromide and sodium hydride in *N*,*N*-dimethylformamide (DMF) gave the corresponding benzyl ethers (**4a** and **4b**), which could be isolated readily in 49 and 30% yield, respectively. Selective removal of 7,8-*O*-isopropylidene group in **4a** with aqueous acetic acid afforded a diol (**5a**) in 91% yield.

Preferential protection of a primary alcoholic group of **5a** with allyl bromide and sodium hydride in tetrahydrofuran (THF) gave an allyl ether (**7**) in 65% yield. *O*-Mesylation of **7** with methanesulfonyl chloride in pyridine and successive treatment of the resultant mesylate (**8**) with sodium hydride in DMF followed by an acidic workup with silica gel afforded an epimer (**9**) at C-7 in a high yield. An alkaline hydrolysis of **9** with sodium hydroxide in aqueous 2-methoxyethanol and successive treatment of the free amine (**10**) with 2,4-dinitrofluorobenzene and triethylamine in THF gave a reprotected compound **11** in a high yield. Simultaneous removal of 1,2-*O*-isopropylidene and 3-*O*-methylthiomethyl groups of **11** with aqueous trifluoroacetic acid followed by a conventional *O*-acetylation produced an anomeric mixture of tetra-*O*-acetates (**13a** and **13b** 1/2.8) in 82% yield. A glycosidation of the intact mixture with bis(trimethylsilyl)uracil in the presence of trimethylsilyl trifluoromethanesulfonate in acetonitrile[13] afforded only the aimed β-glycoside (**14**) in a high yield. De-*O*-acetylation with methanolic sodium methoxide, *O*-isopropylidenation with 2,2-dimethoxypropane in the presence of *p*-toluenesulfonic acid in DMF, *O*-mesylation with methanesulfonyl chloride in pyridine and removal of isopropylidene group with aqueous trifluoroacetic acid were successively carried out to give a mesylate (**18**) in 82% yield from **14**. Treatment of **18** with sodium hydride in dimethyl sulfoxide (DMSO) afforded the desired 3,7-anhydride (**19**) in 87% yield. *O*-Benzoylation of **19** with benzoyl chloride in pyridine yielded a benzoate (**20**) almost quantitatively. Treatment of **20** with oxalyl dichloride in 1,2-dichloroethane containing a small amount of DMF and successive ammonolysis of the resultant chloropyrimidinone (**21**) with methanolic ammonia gave a cytosine derivative (**22**) in 80% yield. De-*N*-protection of **22** with Amberlite IRA-400 (OH^-) in a mixture of acetone, methanol and water[14] and successive *N*-carbamoylation of the resultant amine (**23**) with

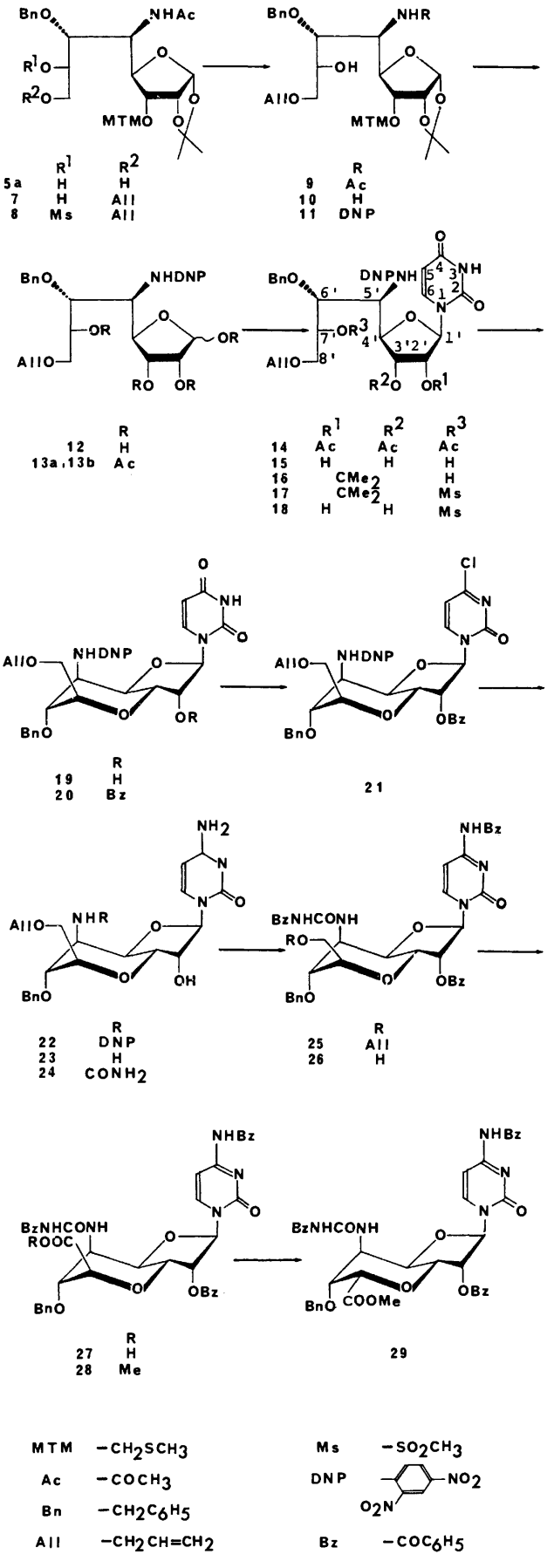

Scheme 3.

sodium cyanate in aqueous acetic acid[15] afforded an ureido derivative (**24**) in 31% yield. Benzoylation of **24** with benzoyl chloride in pyridine gave a tribenzoyl compound **25** in 62% yield. Oxidative cleavage of allyl group of **25** with selenium dioxide in dioxane containing acetic acid[16] afforded a primary alcohol (**26**) in 73% yield. Oxidation of **26** with chromium trioxide in acetone containing sulfuric acid yielded an uronic acid (**27**), which was successively esterified with methanolic hydrogen chloride to give a methyl ester (**28**) in 47% yield. Treatment of **28** with 1,8-diazabicyclo[5.4.0]undec-7-ene (DBU) in DMF resulted in an epimerization at C-7′ as expected to afford an epimer (**29**) in 60% yield. It was confirmed by comparison with the ^{1}H NMR data of the derivatives from natural product that the uronate (**29**) had the identical configurations with those of the octose moiety of ezomycins.[2]

Experimental

Melting points were determined on a Büchi 510 capillary apparatus and are uncorrected. Optical rotations were measured with a Jasco DIP-4 polarimeter. IR spectra were recorded on a Hitachi 225 spectrometer. ^{1}H NMR spectra were recorded on a Varian EM-390 (90 MHz) or a JEOL FX-200 (200 MHz) spectrometer with a reference to tetramethylsilane as an internal standard. Mass spectra were recorded on a Hitachi M-80A or a Hitachi M-80B spectrometer. Solutions were dried over anhydrous sodium sulfate and concentrated under reduced pressure below 40 °C. Column chromatography was performed using Merck Kieselgel 60 F_{254} (Art. 7734) or Wakogel C-200. Preparative TLC was performed on glass plates coated with Merck Kieselgel 60 F_{254} (Art. 5715).

5-Acetamido-8-*O*-allyl-6-*O*-benzyl-5-deoxy-1,2-*O*-isopropylidene-3-*O*-methylthiomethyl-β-L-*erythro*-D-allooctofuranose-(1,4) (7). To a solution of **5a** (2.80 g) in anhydrous THF (28 ml) were added allyl bromide (0.67 ml) and sodium hydride (60% dispersion in mineral oil, 475 mg) under ice cooling, and the mixture was allowed to stand for 40 h in the refrigerator. After addition of cold water (100 ml), the mixture was repeatedly extracted with dichloromethane. The combined extract was dried and concentrated to dryness. The residue was chromatographed on a silica-gel column (toluene–ethyl acetate (v/v) 1:2) to afford 1.96 g (64.5%) of **7** as crystals and 0.35 g (12.5%) of the starting material. Recrystallization from cyclohexane–toluene (2:1 v/v) yielded an analytical sample: Mp 130—131 °C; $[\alpha]_D^{27}$ +8.5° (*c* 1.09, $CHCl_3$); IR (KBr) 3240, 3080, 1635 cm^{-1}; ^{1}H NMR (90 MHz, $CDCl_3$) δ=1.36, 1.54 (3H×2, s×2, CMe_2), 1.99 (3H, s, NHAc), 2.18 (3H, s, SMe), 5.25 (2H, m, $OCH_2CH=C\underline{H}_2$), 5.81 (1H, d, *J*=5 Hz, H-1), 5.69—6.18 (2H, NH and $OCH_2C\underline{H}=CH_2$), 7.35 (5H, s, Ph).

Found: C, 58.77; H, 7.18; N, 2.71%. Calcd for $C_{25}H_{37}O_8NS$: C, 58.69; H, 7.29; N, 2.74%.

5-Acetamido-8-*O*-allyl-6-*O*-benzyl-5-deoxy-1,2-*O*-isopropylidene-3-*O*-methylthiomethyl-α-D-*threo*-D-allooctofuranose-(1,4) (9). To a solution of **7** (2.34 g) in dry pyridine (24 ml) was added methanesulfonyl chloride (1.06 ml) under ice cooling, and the mixture was allowed to stand for 14 h in the refrigerator. After addition of cold water (2 ml) the mixture was concentrated, and the residue was dissolved in ethyl acetate, and the solution was washed with aqueous sodium hydrogencarbonate and water successively, dried and concentrated to dryness. The residue was dissolved in anhydrous DMF (24 ml), and under ice cooling to the solution was added sodium hydride (732 mg). After 90 min at room temperature, the reaction mixture was partitioned between cold water and ethyl acetate. The organic layer was repeatedly washed with water, dried and concentrated to dryness. The residue was dissolved in a small amount of toluene, and a silica-gel column was charged with the solution. After 2 h, elution (toluene–ethyl acetate (v/v) 1:2) gave 2.28 g (97.2%) of **9** as crystals: Mp 91—92 °C; $[\alpha]_D^{25}$ +30.5° (*c* 1.11, $CHCl_3$); IR (KBr) 3410, 3290, 1655 cm^{-1}; ^{1}H NMR (90 MHz, $CDCl_3$) δ=1.34, 1.53 (3H×2, s×2, CMe_2), 1.93 (3H, s, NHAc), 2.19 (3H, s, SMe), 2.59 (1H, d, *J*=4 Hz, OH), 5.24 (2H, m, $OCH_2CH=C\underline{H}_2$), 5.67—6.13 (3H, H-1, NH and $OCH_2C\underline{H}=CH_2$), 7.35 (5H, s, Ph).

Found: C, 58.57; H, 7.13; N, 2.56%. Calcd for $C_{25}H_{37}O_8NS$: C, 58.69; H, 7.29; N, 2.74%.

8-*O*-Allyl-6-*O*-benzyl-5-deoxy-5-(2,4-dinitrophenylamino)-1,2-*O*-isopropylidene-3-*O*-methylthiomethyl-α-D-*threo*-D-allooctofuranose-(1,4) (11). A mixture of **9** (1.38 g), 2-methoxyethanol (19 ml), water (1 ml) and sodium hydroxide (1.6 g) was heated for 90 min under reflux. The mixture was partitioned between cold water and ethyl acetate. The organic layer was repeatedly washed with water, dried and concentrated to dryness. The residue was dissolved in THF (14 ml), and to the solution were added triethylamine (1.13 ml) and 2,4-dinitrofluorobenzene (1.0 g). After 90 min at room temperature, the reaction solution was diluted with ethyl acetate. The mixture was washed with water, dried and concentrated to dryness. The residue was chromatographed on a silica-gel column (toluene–ethyl acetate (v/v) 5:1) to give 1.64 g (95.9%) of **11** as amorphous solids: $[\alpha]_D^{24}$ +17.4° (*c* 1.70, $CHCl_3$); IR (KBr) 3430, 3330, 1525 cm^{-1}; ^{1}H NMR (90 MHz, $CDCl_3$) δ=1.34, 1.53 (3H×2, s×2, CMe_2), 2.09 (3H, s, SMe), 2.55 (1H, d, *J*=5 Hz, OH), 5.16 (2H, m, $OCH_2CH=C\underline{H}_2$), 5.75 (1H, d, *J*=5 Hz, H-1), 5.78 (1H, m, $OCH_2C\underline{H}=CH_2$), 7.16 (1H, d, *J*=10 Hz, H-6′), 7.32 (5H, s, Ph), 8.02 (1H, dd, *J*=3, 10 Hz, H-5′), 9.06—9.28 (2H, NH and H-3′).

Found: C, 54.78; H, 5.90; N, 6.30%. Calcd for $C_{29}H_{37}O_{11}N_3S$: C, 54.79; H, 5.87; N, 6.61%.

1,2,3,7-Tetra-*O*-acetyl-8-*O*-allyl-6-*O*-benzyl-5-deoxy-5-(2,4-dinitrophenylamino)-β(and α)-D-*threo*-D-allooctofuranose-(1,4) (13a and 13b). Compound **11** (2.25 g) was dissolved in 90% aqueous trifluoroacetic acid (45 ml), and the solution was allowed to stand for 75 min at room temperature. After coevaporation with toluene, the residue was dissolved in a mixture of dry pyridine (55 ml) and acetic anhydride (5.4 ml). After 1 h at room temperature, the mixture was coevaporated with toluene to dryness. The residue was chromatographed on a silica-gel column (toluene–ethyl acetate (v/v) 5:1) to afford 0.54 g of **13a** and 1.50 g of **13b** (total 81.9%) as amorphous solids, respectively.

13a: $[\alpha]_D^{24}$ −137° (*c* 1.34, $CHCl_3$); IR (KBr) 3320, 1750, 1535 cm^{-1}; ^{1}H NMR (90 MHz, $CDCl_3$) δ=1.78, 1.93, 1.98, 2.09 (3H×4, s×4, OAc×4), 4.75 (1H, d, *J*=12 Hz, CH_2Ph), 4.92 (1H, d, *J*=12 Hz, CH_2Ph), 5.79 (1H, m, OCH_2-

CH=CH_2), 6.10 (1H, s, H-1), 7.09 (1H, d, J=10 Hz, H-6′), 7.38 (5H, s, Ph), 8.26 (1H, dd, J=3, 10 Hz, H-5′), 8.89—9.26 (2H, NH and H-3′).

Found: C, 54.56; H, 5.36; N, 5.77%. Calcd for $C_{32}H_{37}O_{15}N_3$: C, 54.62; H, 5.30; N, 5.97%.

13b: $[\alpha]_D^{24}$ −51.1° (c 1.00, $CHCl_3$); IR (KBr) 3330, 1750, 1515 cm^{-1}; ^1H NMR (90 MHz, $CDCl_3$) δ=1.93, 1,97, 2.03, 2.09 (3H×4, s×4, OAc×4), 4.73 (1H, d, J=12 Hz, CH_2Ph), 4.89 (1H, d, J=12 Hz, CH_2Ph), 5.82 (1H, m, OCH_2-CH=CH_2), 6.32 (1H, d, J=4 Hz, H-1), 7.39 (5H, s, Ph), 8.27 (1H, dd, J=3, 9 Hz, H-5′), 9.01—9.27 (2H, NH and H-3′).

Found: C, 54.64; H, 5.29; N, 5.91%. Calcd for $C_{32}H_{37}O_{15}N_3$: C, 54.62; H, 5.30; N, 5.97%.

1-[2,3,7-Tri-*O*-acetyl-8-*O*-allyl-6-*O*-benzyl-5-deoxy-5-(2,4-dinitrophenylamino)-β-D-*threo*-D-allooctofuranos-(1,4)-yl]-uracil (14). A suspension of uracil (1.4 g) in 1,1,1,3,3,3-hexamethyldisilazane (14 ml) was heated for 90 min under reflux to become a clear solution, which was concentrated to give 2,4-*O*-bis(trimethylsilyl)uracil quantitatively as a syrup. Without any purification the product was dissolved in dry acetonitrile (5 ml) containing trimethylsilyl trifluoromethanesulfonate (1.04 ml), and the solution was added to a solution of an intact mixture of **13a** and **13b** (2.04 g) in dry acetonitrile (21 ml). The total mixture was heated for 45 min under reflux. The mixture was partitioned between aqueous sodium hydrogencarbonate and ethyl acetate. The organic layer was washed with water, dried and concentrated to dryness. The residue was chromatographed on a silica-gel column (toluene–ethyl acetate (v/v) 2:3) to give 2.01 g (91.8%) of **14** as amorphous solids: $[\alpha]_D^{23}$ −235° (c 3.52, $CHCl_3$); IR (KBr) 3330, 1750, 1700, 1525 cm^{-1}; ^1H NMR (90 MHz, $CDCl_3$) δ=1.86, 1.92, 2.07 (3H×3, s×3, OAc×3), 4.71 (1H, d, J=13 Hz, CH_2Ph), 4.92 (1H, d, J=13 Hz, CH_2Ph), 7.36 (5H, s, Ph), 8.29 (1H, dd, J=3, 9 Hz, H-5″), 8.99 (1H, d, J=9 Hz, NHDNP), 9.11 (1H, d, J=3 Hz, H-3″), 9.74 (1H, s, H-3).

Found: C, 53.88; H, 5.02; N, 9.14%. Calcd for $C_{34}H_{37}O_{15}N_5$: C, 54.04; H, 4.93; N, 9.27%.

1-[8-*O*-Allyl-6-*O*-benzyl-5-deoxy-5-(2,4-dinitrophenylamino)-7-*O*-methylsulfonyl-β-D-*threo*-D-allooctofuranos-(1,4)-yl]uracil (18). A solution of **14** (1.08 g) in 0.1 M methanolic sodium methoxide (20 ml) was stirred for 3 h under ice cooling. The solution was neutralized with Amberlite IR-120 (H^+), and the resin was filtered off. The filtrate was concentrated to dryness, and the residue was dissolved in dry DMF (9 ml). To the solution were added 2,2-dimethoxypropane (3.5 ml) and p-toluenesulfonic acid monohydrate (55 mg), and the mixture was stirred for 10 h at room temperature. The reaction mixture was partitioned between aqueous sodium hydrogencarbonate and ethyl acetate. The organic layer was repeatedly washed with water, dried and concentrated to dryness. The residue was dissolved in dry pyridine (9 ml), and to the solution was added methanesulfonyl chloride (0.33 ml) under ice cooling. The mixture was stirred for 90 min at room temperature, and partitioned between aqueous sodium hydrogencarbonate and ethyl acetate. The organic layer was washed with water, dried and concentrated to dryness. The residue was dissolved in ice-cooled 90% aqueous trifluoroacetic acid (10 ml). After 3 h under ice cooling the solution was concentrated to dryness. The residue was chromatographed on a silica-gel column (toluene–ethyl acetate (v/v) 1:3) to afford 824 mg (81.6% from **14**) of **18** as crystals: Mp 166—167 °C; $[\alpha]_D^{24}$ −134° (c 3.16, $CHCl_3$); IR (KBr) 3280, 1675, 1515, 1175 cm^{-1}; ^1H NMR (90 MHz, CD_3COCD_3) δ=2.98 (3H, s, SO_2Me), 8.30 (1H, dd, J=3, 9 Hz, H-5″), 9.02 (1H, d, J=3 Hz, H-3″), 9.29 (1H, d, J=11 Hz, NHDNP), 10.20 (1H, bs, H-3).

Found: C, 49.36; H, 4.75; N, 9.94%. Calcd for $C_{29}H_{33}O_{14}N_5S$: C, 49.22; H, 4.70; N, 9.90%.

1-[8-*O*-Allyl-3,7-anhydro-6-*O*-benzyl-5-deoxy-5-(2,4-dinitrophenylamino)-α-L-*erythro*-D-allooctofuranos-(1,4)-yl]uracil (19). To a solution of **18** (1.41 g) in anhydrous DMSO (14 ml) was added sodium hydride (0.40 g), and the mixture was stirred for 4 h at 30 °C. The reaction mixture was poured into cold water, and the mixture was extracted with ethyl acetate. The extract was dried and concentrated to dryness, and the residue was chromatographed on a silica-gel column (toluene–ethyl acetate (v/v) 1:5) to give 1.06 g (86.9%) of **19** as amorphous solids: $[\alpha]_D^{23}$ +206° (c 2.17, $CHCl_3$); IR (KBr) 3330, 1730, 1695, 1515 cm^{-1}; ^1H NMR (90 MHz, $CDCl_3$) δ=5.59 (1H, s, H-1′), 6.33 (1H, d, J=10 Hz, H-6″), 7.18 (1H, d, J=8 Hz, H-6), 7.45 (5H, s, Ph), 7.94 (1H, dd, J=3, 9 Hz, H-5″), 8.74 (1H, d, J=5 Hz, NHDNP), 8.98 (1H, d, J=3 Hz, H-3″), 9.92 (1H, bs, H-3).

Found: C, 54.71; H, 4.76; N, 11.09%. Calcd for $C_{28}H_{29}O_{11}N_5$: C, 54.99; H, 4.78; N, 11.45%.

1-[8-*O*-Allyl-3,7-anhydro-2-*O*-benzoyl-6-*O*-benzyl-5-deoxy-5-(2,4-dinitrophenylamino)-α-L-*erythro*-D-allooctofuranos-(1,4)-yl]uracil (20). To a solution of **19** (531 mg) in dry pyridine (5.3 ml) was added benzoyl chloride (0.18 ml), and the mixture was stirred for 1 h under ice cooling. After addition of water (1 ml) the mixture was concentrated. The residue was dissolved in ethyl acetate, and the solution was washed with aqueous sodium hydrogencarbonate and water successively, dried and concentrated to dryness. The residue was chromatographed on a silica-gel column (toluene–ethyl acetate (v/v) 2:1) to afford 610 mg (98.2%) of **20** as amorphous solids: $[\alpha]_D^{22}$ +114° (c 1.20, $CHCl_3$); IR (KBr) 3330, 1720, 1520, 1515 cm^{-1}; ^1H NMR (90 MHz, $CDCl_3$) δ=5.56 (1H, s, H-1′), 6.30 (1H, d, J=10 Hz, H-6″), 7.14 (1H, d, J=8 Hz, H-6), 7.46 (5H, s, CH_2Ph), 7.93 (1H, dd, J=2, 9 Hz, H-5″), 8,77 (1H, d, J=5 Hz, NHDNP), 8.99 (1H, d, J=2 Hz, H-3″), 9.34 (1H, bs, H-3); MS (FD) 716 (M+1).

1-[8-*O*-Allyl-3,7-anhydro-6-*O*-benzyl-5-deoxy-5-(2,4-dinitrophenylamino)-α-L-*erythro*-D-allooctofuranos-(1,4)-yl]cytosine (22). To a solution of **20** (463 mg) in dry 1,2-dichloroethane (25 ml) were added oxalyl dichloride (0.42 ml) and dry DMF (1 drop) under ice cooling, and the mixture was stirred for 36 h at room temperature. The mixture was poured into cold 1% aqueous sodium hydrogencarbonate, and the mixture was extracted with ethyl acetate. The extract was repeatedly washed with water, dried and concentrated to dryness. The residue was dissolved in saturated methanolic ammonia (60 ml), and the solution was allowed to stand for 5 d at ambient temperature. The reaction mixture was concentrated to dryness, and the residue was chromatographed on a silica-gel column (dichloromethane–methanol (v/v) 10:1) to afford 316 mg (80.0%) of **22** as amorphous solids: $[\alpha]_D^{22}$ +173° (c 1.05, MeOH); IR (KBr) 3390, 1650 cm^{-1}; ^1H NMR (90 MHz, CD_3OD) δ=5.65 (1H, d, J=9 Hz, H-5), 5.70 (1H, s, H-1′), 6.84 (1H, d, J=11 Hz, H-6″), 7.40 (5H, s, Ph), 8.08 (1H, dd, J=2, 9 Hz, H-5″), 8.95 (1H, d, J=2 Hz, H-3″); MS (SIMS) 611 (M+1).

1-[8-*O*-Allyl-3,7-anhydro-6-*O*-benzyl-5-deoxy-5-ureido-α-L-*erythro*-D-allooctofuranos-(1,4)-yl]cytosine (24). A mixture of **22** (267 mg), Amberlite IRA-400 (OH^-) (ca. 3 ml), acetone (14 ml), methanol (7 ml) and water (7 ml) was heated for 3 h under reflux. After the resin was filtered off, the filtrate was concentrated to dryness. To a solution of the residue in 30% aqueous acetic acid (15 ml) was added sodium cyanate (270 mg), and the mixture was allowed to stand for 10 h at 50 °C. The reaction mixture was coevaporated with ethanol, and the residue was roughly chromatographed on a silica-gel column (dichloromethane–methanol (v/v) 5:1). Crystallization of the crude product from ethanol gave 66 mg (31%) of **24**: Mp 158—159 °C; $[\alpha]_D^{25}$ +21° (*c* 0.76, $CHCl_3$–MeOH (v/v) 1:1) IR (KBr) 3400, 1670 cm^{-1}; ^1H NMR (90 MHz, $CDCl_3$–CD_3OD (v/v) 1:1) δ=5.30 (1H, s, H-1′), 5.84 (1H, d, *J*=8 Hz, H-5), 7.32 (5H, s, Ph), 7.51 (1H, d, *J*=8 Hz, H-6); MS (SIMS) 488 (M+1).

1-[8-*O*-Allyl-3,7-anhydro-2-*O*-benzoyl-5-(3-benzoylureido)-6-*O*-benzyl-5-deoxy-α-L-*erythro*-D-allooctofuranos-(1,4)-yl]-4-*N*-benzoylcytosine (25). To a solution of **24** (66 mg) in dry pyridine (2 ml) was added benzoyl chloride (145 mg) at −20 °C, and the mixture was stirred for 1 h under ice cooling. The reaction mixture was diluted with ethyl acetate, and the solution was washed with aqueous sodium hydrogencarbonate and water successively, dried and concentrated to dryness. The residue was chromatographed on a silica-gel column (toluene–ethyl acetate (v/v) 2:3) to afford 68 mg (62%) of **25** as crystals. Recrystallization from toluene yielded an analytical sample: mp 200—201 °C (decomp); $[\alpha]_D^{25}$ +42° (*c* 0.65, $CHCl_3$); IR (KBr) 3400, 3250, 1680 cm^{-1}; ^1H NMR (200 MHz, $CDCl_3$) δ=3.65 (1H, dd, *J*=6, 10 Hz, H-8′), 3.76 (1H, dd, *J*=5, 10 Hz, H-8′), 4.60 (1H, d, *J*=12 Hz, CH_2Ph), 4.74 (1H, d, *J*=12 Hz, CH_2Ph), 5.08—5.20 (3H, H-5′ and $OCH_2CH{=}CH_2$), 5.77 (1H, d, *J*=6 Hz, H-2′), 5.80 (1H, m, $OCH_2CH{=}CH_2$), 6.18 (1H, s, H-1′), 7.30 (5H, s, $CH_2\underline{Ph}$).

Found: C, 66.05; H, 5.17; N, 8.60%. Calcd for $C_{44}H_{41}O_{10}N_5$: C, 66.07; H, 5.17; N, 8.76%.

1-[3,7-Anhydro-2-*O*-benzoyl-5-(3-benzoylureido)-6-*O*-benzyl-5-deoxy-α-L-*erythro*-D-allooctofuranos-(1,4)-yl]-4-*N*-benzoylcytosine (26). To a solution of **25** (45 mg) in anhydrous dioxane (4.5 ml) were added selenium dioxide (7.5 mg) and acetic acid (5 μl), and the mixture was vigorously stirred for 45 min under reflux. The reaction mixture was concentrated to dryness, and the residue was chromatographed on a silica-gel column (ethyl acetate) to give 31 mg (73%) of **26** as amorphous solids: $[\alpha]_D^{25}$ +32° (*c* 0.69, $CHCl_3$); IR (chloroform) 3270, 1695 cm^{-1}; ^1H NMR (200 MHz, $CDCl_3$) δ=4.41 (1H, dd, *J*=6, 10 Hz, H-3′), 4.55 (1H, d, *J*=12 Hz, CH_2Ph), 4.67 (1H, d, *J*=12 Hz, CH_2Ph), 4.92 (1H, m, H-5′), 5.95 (1H, d, *J*=6 Hz, H-2′), 6.10 (1H, s, H-1′), 7.25 (5H, s, Ph); MS (FD) 760 (M+1).

4-*N*-Benzoyl-1-[methyl 3,7-anhydro-2-*O*-benzoyl-5-(3-benzoylureido)-6-*O*-benzyl-5-deoxy-α-L-*erythro*-D-allooctofuranos-(1,4)-yluronate]cytosine (28). To a solution of **26** (31 mg) in acetone (4 ml) was added Jones' reagent (0.3 ml, a solution of chromic trioxide (2.67 g) in sulfuric acid (2.3 ml) diluted with water to a volume of 10 ml) under ice cooling, and the mixture was stirred for 1 h under ice cooling. After the reaction mixture was diluted with ethyl acetate the solution was repeatedly washed with water, dried and concentrated to dryness. The residue was dissolved in 5% methanolic hydrogen chloride, and the solution was refluxed for 1 h. The reaction solution was concentrated to dryness, and the residue was dissolved in pyridine (2 ml). To the solution was added benzoyl chloride (30 mg) under ice cooling, and the mixture was stirred for 15 min under ice cooling. The mixture was partitioned between aqueous sodium hydrogencarbonate and ethyl acetate. The organic layer was washed with water, dried and concentrated to dryness. The residue was chromatographed on a silica-gel column (toluene–ethyl acetate (v/v) 1:2) to give 16 mg (47%) of **28** of amorphous solids: $[\alpha]_D^{25}$ +27° (*c* 1.05, $CHCl_3$); IR (KBr) 3400, 1690 cm^{-1}; ^1H NMR (200 MHz, $CDCl_3$) δ=3.70 (3H, s, COOMe), 4.52 (1H, dd, *J*=5, 11 Hz, H-3′), 4.88 (1H, m, H-5′), 5.87 (1H, d, *J*=5 Hz, H-2′), 6.24 (1H, s, H-1′), 7.26 (5H, s, CH_2Ph); MS (FD) 788 (M+1).

4-*N*-Benzoyl-1-[methyl-3,7-anhydro-2-*O*-benzoyl-5-(3-*N*-benzoylureido)-6-*O*-benzyl-5-deoxy-β-D-*threo*-D-allooctofuranos-(1,4)-yluronate]cytosine (29). To a solution of **28** (11.3 mg) in dry DMF (0.5 ml) was added 1,8-diazabicyclo-[5.4.0]undec-7-ene (20 mg), and the mixture was stirred for 2 h at room temperature. After addition of acetic acid (20 mg) the mixture was diluted with ethyl acetate, and the solution was repeatedly washed with water, dried and concentrated to dryness. The residue was chromatographed on a silica-gel preparative plate (toluene–ethyl acetate (v/v) 2:3) to afford 6.8 mg (60%) of **29** as amorphous solids: $[\alpha]_D^{25}$ +5.2° (*c* 0.58, $CHCl_3$); IR ($CHCl_3$) 1695 cm^{-1}; ^1H NMR (200 MHz, $CDCl_3$) δ=3.55 (3H, s, COOMe), 4.33 (1H, dd, *J*=5.5, 11 Hz, H-3′), 4.42 (1H, dd, *J*=2.5, 5.5 Hz, H-6′), 4.61 (1H, d, *J*=2.5 Hz, H-7′), 4.62 (1H, d, *J*=12 Hz, CH_2Ph), 4.66 (1H, dd, *J*=4.5, 11 Hz, H-4′), 4.82 (1H, d, *J*=12 Hz, CH_2Ph), 4.90 (1H, m, H-5′), 5.81 (1H, d, *J*=5.5 Hz, H-2′), 5.95 (1H, s, H-1′), 7.32 (5H, s, CH_2Ph); MS (FD) 788 (M+1).

The authors express their sincere thanks to Miss Shigeko Miki and Mr. Masayuki Ito, Meiji Seika Kaisha, Ltd., for recording the mass spectrum, and to Mr. Akio Takahashi for his elemental analyses.

References

1) K. Takaoka, T. Kuwayama, and A. Aoki, Japanese Patent, 1971, 615332.

2) K. Sakata, A. Sakurai, and S. Tamura, *Agric. Biol. Chem.*, **37**, 697 (1973); *ibid.*, **38**, 1883 (1974); *ibid.*, **39**, 885 (1975); *ibid.*, **40**, 1993 (1976); *Tetrahedron Lett.*, **1974**, 1522; *ibid.*, **1974**, 4327; *ibid.*, **1975**, 3191.

3) K. Sakata and J. Uzawa, *Agric. Biol. Chem.*, **41**, 413 (1977).

4) K. Sakata, *Nippon Nogeikagaku Kaishi*, **49**, R51 (1975).

5) K. Isono, R. F. Crain, and J. A. McKloskey, *J. Am. Chem. Soc.*, **97**, 943 (1975).

6) K. Anzai and T. Saita, *Bull. Chem. Soc. Jpn.*, **50**, 169 (1977).

7) S. Hanessian, T. J. Liak, and D. M. Dixit, *Carbohydr. Res.*, **88**, C14 (1981); *Pure Appl. Chem.*, **53**, 129 (1981).

8) K. S. Kim and W. A. Szarek, *Can. J. Chem.*, **59**, 878 (1981); *Carbohydr. Res.*, **100**, 169 (1982).

9) S. Danishefsky and R. Hungate, *J. Am. Chem. Soc.*, **108**, 2486 (1986).

10) S. Hanessian, J. Kloss, and T. Sugawara, *J. Am. Chem. Soc.*, **108**, 2758 (1986).

11) O. Sakanaka, T. Ohmori, S. Kozaki, T. Suami, T. Ishii, S. Ohba, and Y. Saito, *Bull. Chem. Soc. Jpn.*, **59**, 1753 (1986).
12) O. Sakanaka, T. Ohmori, S. Kozaki, and T. Suami, *Bull. Chem. Soc. Jpn.*, **59**, 3523 (1986).
13) H. Vorbruggen, K. Krolikiewicz, and B. Bennua, *Chem. Ber.*, **114**, 1234 (1981).
14) P. F. Lloyd and M. Stacey, *Tetrahedron*, **9**, 116 (1960).
15) S. R. Sandler and W. Karo, "Organic Functional Group Preparations," II, 134 (1971).
16) K. Kariyone and H. Yazawa, *Tetrahedron Lett.*, **1970**, 2885.

A Convenient Reduction Method of β-Phenyl α,β-Unsaturated Carbonyl Compounds with Me_3SiCl-NaI-ROH Reagent

Takashi SAKAI, Kazuyoshi MIYATA, Masanori UTAKA, and Akira TAKEDA*
Department of Synthetic Chemistry, School of Engineering, Okayama University, Tsushima, Okayama 700
(Received July 23, 1986)

Treatment of β-phenyl α,β-unsaturated ketones, cinnamic acid and its ester with Me_3SiCl-NaI-ROH reagent in hexane at room temperature gave the corresponding saturated carbonyl compounds in good yields. A similar reaction of 2,4-hexadienoic acid afforded 4-hexanolide.

A Me_3SiCl–NaI reagent has been applied to a variety of organic syntheses as a Me_3SiI equivalent,[1] where beside the application to cleavage of ether, ester and amide,[2] it can be used effectively in the deoxygenation of sulfoxide,[3] alcohol,[4] epoxide,[5] and vicinal diol[6] as well as in the dehalogenation of α-halo ketone.[7] The reagent is also effective for the conversion of α,β-unsaturated carbonyl compounds to β-iodo carbonyl compounds. Thus, the reaction of conjugated enones with Me_3SiI gives β-iodo ketones,[8] and a similar treatment of 2-alkenoic acids affords trimethylsilyl 3-iodoalkanoates.[9] Recently, Larson et al.[10] have reported that acrylaldehyde and methyl vinyl ketone were transformed into ethylene acetals of 3-iodopropanal and 4-iodo-2-butanone, respectively, by the action of Me_3SiCl-NaI–ethylene glycol reagent in CH_3CN. However, reduction of carbon-carbon (C-C) double bond of α,β-unsaturated carbonyl compounds with the reagent has not been reported.

In relation to our continuing investigations[11,12] to extend the applicability of the Me_3SiCl-NaI reagent in organic synthesis, we have found that β-phenyl α,β-unsaturated ketones, ester, and acid (**1a—f**) can be reduced to the corresponding saturated carbonyl compounds (**4a—f**) in good yields by using an excess of Me_3SiCl–NaI–ROH reagent in hexane at room temperature (Scheme 1 and Table 1). It is interesting that water or poly alcoholic compounds such as 2,3-butanediol, (*R,R*)-diethyl tartrate, and cellulose are used for ROH as hydrogen sources.

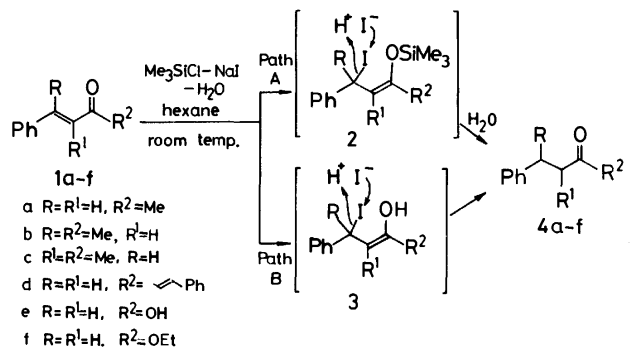

Scheme 1.

Although such transformation can be done by using several known methods, for example, alkali metals in liquid ammonia,[13] amalgamated zinc in hydrochloric acid,[14] Me_3SiH in CF_3CO_2H,[15] combination of $LiAlH_4$ and CuI,[16] 2-phenylbenzothiazoline,[17] Hantzsch ester-silica gel,[18] and so on, the present method offers the significant advantages that the reagent is inexpensive and the reaction can be done conveniently under mild conditions. Furthermore, products obtained after washing with aqueous $Na_2S_2O_3$ have sufficient purity, as checked by using ^1H NMR.

The present reaction was usually carried out by adding Me_3SiCl (6—10 mmol) with stirring to a mixture of substrate 1 (1 mmol), NaI (6—10 mmol), H_2O (6—10 mmol), and hexane (2 ml) as shown in Table 1. Since the amount of water added was equimolar with those of Me_3SiCl and NaI, it would completely be consumed to produce HI. The reaction was retarded by using a large excess of water. When 10 mmol of water and 6 mmol of Me_3SiCl–NaI were used in the reduction of 1 mmol of **1a**, **4a** was obtained still in an 80% yield. However, an increase in the amount of water to 30 mmol (five equivalents of Me_3SiCl-NaI) decreased the yield of **4a** to 23% accompanied by unidentified impurities. A further increase in the amount of water to 60 mmol resulted merely in recovery of **1a**.

Scheme 1 shows a possible mechanism for the reduction which involves two pathways. In path A, the reaction is initiated by 1,4-addition of Me_3SiI generated in situ to **1** to produce β-iodo enol silyl ether intermediate **2**, whose allylic and benzylic iodo substituent would be extremely labile and attacked by an iodide anion existing in excess to generate iodine molecule in parallel with hydrogenation. The compound having the same functionality as that of **2** has been isolated by Miller[8] in the reaction of α,β-unsaturated ketone with Me_3SiI under anhydrous conditions, and identified by using ^1H NMR. In the present reaction, however, the intermediate **2** seems to make relatively small contribution because, as described above, the reaction in the presence of 1.67 equivalent of water to Me_3SiCl-NaI gave **4a** in 80% yield in spite of the fact that Me_3SiCl and Me_3SiI are

readily hydrolysed by water.[19] In path B, HI generated in situ adds to the C-C double bond of **1** to give β-iodo ketone intermediate **3** as reported in the literatures.[9,10] Subsequent reduction of **3** with HI leads to **4** in a manner similar to path A. Path B is supported on the basis of two facts: a) addition of **1a** to a stirred mixture of Me_3SiCl, NaI, H_2O, and hexane also gave **4a** in an 80% yield, and b) the reaction of **1a** with dry HI, generated by adding 55% aqueous HI to phosphorus pentoxide, also afforded **4a** in a 57% yield (Scheme 2). Comparison of the yield between the two methods indicates the obvious advantage of the present method using Me_3SiCl-NaI-H_2O.

Table 1 shows several examples of the reactions by using olefins whose C-C double bond is conjugated with phenyl group and carbonyl moiety. When 2,3-butanediol was employed instead of water for the reduction of **1a**, cyclic acetal **5** was obtained predominantly. The work-up procedure becomes more convenient by using cellulose (absorbent cotton), which is easily removable from the reaction mixture. It is worthy to note here that asymmetric induction

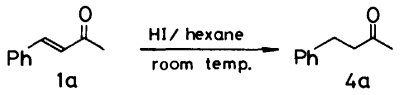

Scheme 2.

Table 1. Reduction of β-Phenyl α,β-Unsaturated Carbonyl Compounds **1a—f** with Me_3SiCl-NaI-ROH Reagent

Substrate[a]	ROH[b] (Molar ratio vs. 1)	Reaction time/h	Product[c] (Yield/%)[d]
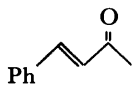 **1a**	A (6)	30	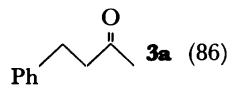 **3a** (86)
1a	A (6)[e]	30	**4a** (95)[f]
1a	B (10)	38	**4a** (29) + 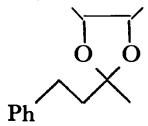 **5** (51)
1a	C[g]	20	**4a** (60)
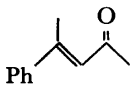 **1b**	A (10)	22	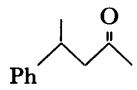 **4b** (52)
1b	C[g]	22	**4b** (70)[h]
1b	D (3)	7	**4b** (81)[i]
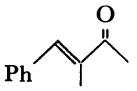 **1c**	A (10)	31	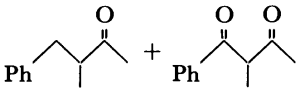 **4c** (42) **6** (31)
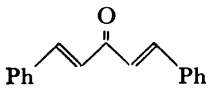 **1d**	A (10)	100	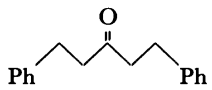 **4d** (75)
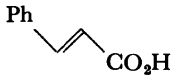 **1e**	A (10)	100	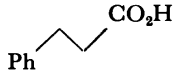 **4e** (90)
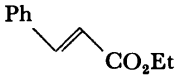 **1f**	A (10)	108	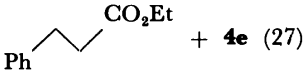 + **4e** (27) **4f** (66)

a) 1 mmol of substrate was generally used. b) A: H_2O; B: 2,3-butanediol; C: cellulose (absorbent cotton); D: (*R,R*)-diethyl tartrate. c) Products obtained are known compounds excepting 5. d) Isolated yield by preparative TLC. e) 10 mmol of substrate was used. f) After purification by distillation. g) Against 1 mmol of **1a** or **1c**, 1.8 g of cellulose (absorbent cotton) was used. h) $[\alpha]_D^{25}$ −1.2° (*c* 3.06, C_6H_6) [maximun rotation, $[\alpha]_D$ −75.5° (*c* 1, C_6H_6) for *R*-(−)-**4b**: F. Leyendercker, F. Jesser, and B. Ruhland, *Tetrahedron Lett.*, **22**, 3601 (1981)]. i) $[\alpha]_D^{21}$ −1.8° (*c* 4.1, C_6H_6).

was observed, though very slight, in the reduction of **1b** by using (*R,R*)-diethyl tartrate or cellulose. Reaction of **1c** with Me_3SiCl–NaI–H_2O reagent afforded **4c** and oxidation product **6**, which may be formed via addition of generated iodine to **1c** and subsequent hydrolysis. The methyl group at C-3 would retard 1,4-addition of iodide anion by the electron donating effect.[20]

Unfortunately, the present reduction method is not applicable to β-alkyl α,β-unsaturated ketone and acid. For example, the reactions with mesityl oxide and crotonic acid gave merely 4-iodo-4-methyl-2-pentanone (**7**) (70% yield) and 3-iodobutanoic acid (**8**) (94% yield), respectively, as expected[8,9,10] (Scheme 3).

The reactions listed in Table 1 were generally done in a small scale by using 1 mmol of substrates. The crude products obtained were therefore purified by preparative TLC. The preparative scale of 10 mmol order was exemplified by employing typical enone **1a**. In this case, vacuum distillation of the crude product gave **4a** with 98% purity (GLPC and ^1H NMR analysis) in a 95% yield.

The Me_3SiCl–NaI–H_2O reagent was also found to be effective for the transformation of 2,4-hexadienoic acid (**9**) to 4-hexanolide (**12**) (54% yield), although it required refluxing. The formation of **12** suggests the occurrence of the reduction of **9** to a mixture of regioisomers of hexenoic acids and/or their trimethylsilyl esters (**10a—c**), addition of HI to **10b, c** to give 4-iodohexanoic acid and/or its trimethylsilyl ester (**11**), and lactonization to **12** in a successive way (Scheme 4). We confirmed that the treatment of 3-hexenoic acid with the reagent at room temperature also gave **12** in a 66% yield.

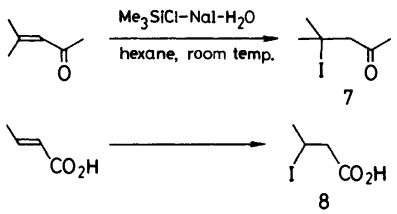

Scheme 3.

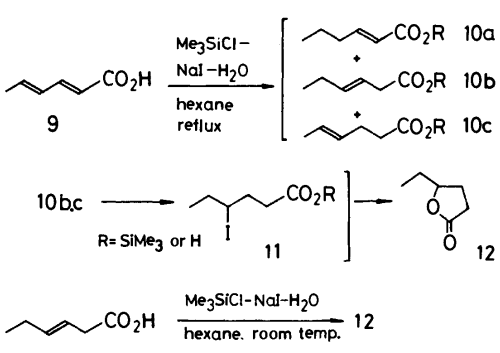

Scheme 4.

Experimental

General. IR spectra were taken on a JASCO Model A-102 spectrometer. ^1H NMR spectra (60 MHz) were measured with a JEOL Model JNM-60 SI spectrometer using Me_4Si as an internal standard. Optical rotation was recorded with a JASCO Model DIP-4 apparatus. GLPC analysis was done with a Hitachi Model 163 gas chromatograph. The preparative TLC was carried out on silica gel (Kieselgel 60 PF_{254}, Merck A. G. Darmstadt). Elemental analysis was performed by Eiichiro Amano of our laboratory. Starting materials **1b**,[21] **1c**,[22] and **1d**[23] were prepared according to the methods reported and **1a**, **1e**, and **1f** are commercially available.

General Procedure for the Reaction of 1a—f with Me_3SiCl–NaI–H_2O Reagent. To a mixture of NaI (1.5 g, 10 mmol), olefin **1** (1 mmol), water (0.18 ml, 10 mmol) and hexane (2 ml), was added Me_3SiCl (1.28 ml, 10 mmol) dropwise with stirring. Then, stirring was continued at room temperature for the time indicated in Table 1. During the course of the reaction, the mixture was colored dark purple gradually due to liberated iodine. After addition of water (3 ml), the ether extract was washed with aqueous $Na_2S_2O_3$ and brine, dried over $MgSO_4$, and concentrated. Purification of the residue by preparative TLC (hexane–ether 3:1) gave product, whose IR and ^1H NMR spectral data were identical with those reported (compounds **4a**,[24] **4b**,[25] **4c**,[24] **4d**,[26] **6**,[27] **7**,[28] and **8**[29]) or with those of authentic samples commercially available (**4e** and **4f**).

Reactions by using 2,3-butanediol, (*R,R*)-diethyl tartrate, or cellulose for ROH were done in a similar way to that described above and the quantities of ROH used are indicated in Table 1.

Reaction of 1a with Me_3SiCl–NaI–2,3-Butanediol. Crude products were fractionated by preparative TLC (hexane–ether, 3:1) to give **4a** (R_f 0.45, 29% yield) and **5** (R_f 0.67, 51% yield). **5**: IR (neat) 1583, 1604 cm^{-1}; ^1H NMR (CCl_4) δ=1.18 (6H, d, *J*=6 Hz), 1.30 (3H, s), 1.84 (2H, m), 2.66 (2H, m), 3.53 (2H, m), 7.08 (5H, s). Anal. ($C_{14}H_{20}O_2$)C, H.

Effects of the Amount of Water on the Yield of 4a. The reaction of **1a** (146 mg, 1 mmol) with Me_3SiCl (0.77 ml, 6 mmol), NaI (900 mg, 6 mmol) and water (0.18 ml, 10 mmol) in hexane (4 ml) was carried out in a manner similar to that described above. The crude product was distilled [bp 105—110 °C (5 mmHg) (1 mmHg=133.322 Pa)] to give **4a** (119 mg, 80% yield).

A similar reaction with an increased amount of water (540 mg, 30 mmol) gave a 88:12 (by ^1H NMR) mixture (38 mg) of **4a** (23% yield) and **1a** (3% recovered) after distillation [bp 110 °C (5 mmHg)]. A considerable amount of tarry material remained as a still residue.

The reaction with a large excess of water (1.1 g, 60 mmol) was done in a similar way and the recovery of the most of **1a** with a small amount of unidentified material was confirmed by using ^1H NMR.

Reduction of 1a by Addition to a Mixture of Me_3SiCl–NaI–H_2O. A mixture of Me_3SiCl (0.77 ml, 6 mmol), NaI (900 mg, 6 mmol), water (0.108 ml, 6 mmol) and hexane (4 ml) was stirred for 1 h at room temperature and then **1a** (146 mg, 1 mmol) was added. The mixture was stirred for

additional 24 h at room temperature and treated in a usual way to give **4a** (120 mg, 80% yield) after distillation.

Reduction of 1a in a Preparative Scale. A similar reaction using **1a** (1.46 g, 10 mmol) and Me_3SiCl-NaI-H_2O each with 60 mmol gave **4a** (1.40 g, 95% yield) after distillation [bp 100—110 °C (5 mmHg)]. GLPC analysis (SE-30, 1.0 m×5 mm o.d., N_2 27 ml min^{-1}, oven temperature 100 °C) of the product showed a peak at the retention time of 4.5 min with an relative intensity of 98%.

Reduction of 1a with Dry HI. To a mixture of **1a** (292 mg, 2 mmol) and hexane (5 ml) was introduced dry HI, which was generated by dropping 55% aqueous HI solution (5 ml, 37 mmol) to phosphorus pentoxide (13 g, 92 mmol).[30] The mixture was stirred for 24 h at room temperature and then poured into aqueous $NaHCO_3$. The organic layer was extracted with ethyl acetate and treated in a usual way to give **4a** (167 mg, 57% yield) after distillation. A tarry material was remained as a still residue.

4-Hexanolide (12) from 2,4-Hexadienoic Acid (9). To a mixture of acid **9** (224 mg, 2 mmol), NaI (3.0 g, 20 mmol), water (0.36 ml, 20 mmol) and hexane (4 ml), was added Me_3SiCl (2.56 ml, 20 mmol) at room temperature. After being stirred under reflux for 18 h, the mixture was washed with aqueous $NaHCO_3$ and treated in a usual way. Kugelrohr distillation [bp 120—130 °C (18 mmHg)] of the residual oil gave **12** (123 mg, 54% yield), whose IR and ^1H NMR spectra were identical with those reported.[31] The aqueous $NaHCO_3$ layer was acidified and the ether extract was treated in a similar way to give 189 mg of a mixture of acidic materials, whose separation and structual identification were unsuccessful.

Lactone 12 from 3-Hexenoic Acid. A mixture of 3-hexenoic acid[32] (228 mg, 2 mmol), Me_3SiCl (2.56 ml, 20 mmol), NaI (3.0 g, 20 mmol), water (360 mmol), and hexane (4 ml) was allowed to react for 44 h at room temperature and treated in a usual way to give **12** (152 mg, 66% yield) after distillation. Attempts to purify the acidic material (87 mg) by preparative TLC was failed.

References

1) Review: G. A. Olah, and S. C. Narang, *Tetrahedron*, **38**, 2225 (1982).

2) G. A. Olah, S. C. Narang, B. G. B. Gupta, and R. Malhotra, *J. Org. Chem.*, **44**, 1247 (1979).

3) G. A. Olah, B. G. B. Gupta, and S. C. Narang, *Synthesis*, **1977**, 583; G. A. Olah, S. C. Narang, B. G. B. Gupta, and R. Malhotra, *Synthesis*, **1979**, 61.

4) W. Ando and M. Ikeno, *Tetrahedron. Lett.*, **1979**, 4941.

5) J. N. Denis, R. Magnane, M. Van Eenoo, and A. Krief, *Nouv. J. Chim.*, **3**, 705 (1979).

6) N. C. Barua, J. C. Sarma, R. P. Sharma, and J. N. Barua, *Chem. Ind.*, **1982**, 956; N. C. Barua and R. P. Sharma, *Tetrahedron Lett.*, **23**, 1365 (1982).

7) G. A. Olah, M. Arvanaghi, and Y. D. Vankar, *J. Org. Chem.*, **45**, 3531 (1980).

8) R. D. Miller and D. R. McKean, *Tetrahedron Lett.*, **1979**, 2305.

9) T. Azuhata and Y. Okamoto, *Synthesis*, **1983**, 461.

10) G. L. Larson and R. Klesse, *J. Org. Chem.*, **50**, 3627 (1985).

11) T. Sakai, K. Miyata, M. Ishikawa, and A. Takeda, *Tetrahedron Lett.*, **26**, 4727 (1985).

12) T. Sakai, K. Miyata, and A. Takeda, *Chem. Lett.*, **1985**, 1137.

13) A. J. Birch, *Quart. Rev. Chem. Soc.*, **4**, 69 (1950).

14) J. G. St. C. Buchanan and P. D. Woodgate, *Quart. Rev. Chem. Soc.*, **23**, 522 (1969).

15) D. N. Kursanov, Z. N. Parnes, and N. M. Loim, *Synthesis*, **1974**, 633.

16) E. C. Ashby, J. J. Lin, and R. Kovar, *J. Org. Chem.*, **41**, 1939 (1976).

17) H. Chikashita, M. Miyazaki, and K. Itoh, *Synthesis*, **1984**, 308.

18) K. Nakamura, M. Fujii, A. Ohno, and S. Oka, *Tetrahedron Lett.*, **25**, 3983 (1984).

19) a) D. A. Armitage, "Comprehensive Organometalic Chemistry," ed by G. Wilkinson, Pergamon Press (Oxford), Vol. 2, p. 155; b) W. Patnode and D. F. Wilcock, *J. Am. Chem. Soc.*, **68**, 358 (1946); c) M. J. Hunter, E. L. Warrick, J. F. Hyde, and C. C. Curre, *ibid.*, **68**, 2284 (1946).

20) For example, the yields of the hydrocyanation of methacryronitrile and methyl methacrylate were greatly reduced as compared with those of acrylonitrile and methyl acrylate: a) W. Nagata and M. Yoshioka, "Organic Reactions," ed by W. G. Dauben, John Wiley & Sons, Inc., New York (1977), Vol. 25, Chap. 3, pp. 300—305; b) P. Kurtz, *Ann. Chem.*, **572**, 23 (1951).

21) S. N. Huckin and L. Weiler, *Can. J. Chem.*, **52**, 2157 (1974).

22) H. Muller, *Chem. Ber.*, **35**, 970 (1902).

23) C. R. Conard and M. A. Polliver, *Org. Synth.*, Coll. Vol. II, 167 (1943).

24) L. E. Hightower, L. R. Glasgow, K. M. Stone, D. A. Albertson, and H. A. Smith, *J. Org. Chem.*, **35**, 1881 (1970).

25) Y. Yamamoto, S. Yamamoto, H. Yatagai, Y. Ishihara, and K. Maruyama, *J. Org. Chem.*, **47**, 119 (1982).

26) D. Sovoia, C. Trombini, and A. Umani-Ronchi, *J. Org. Chem.*, **43**, 2907 (1978).

27) R. Howe and D. Johnson, *J. Chem. Soc., Perkin Trans. 1*, **1972**, 977.

28) J. N. Marx, *Tetrahedron*, **39**, 1529 (1983).

29) G. A. Olah, R. Karpeles, and S. C. Narang, *Synthesis*, **1982**, 963.

30) G. K. Rollefson and J. E. Booher, *J. Am. Chem. Soc.*, **53**, 1728 (1931).

31) W. Sucrow and U. Klein, *Chem. Ber.*, **108**, 48 (1975).

32) S. E. Boxer and R. P. Linstead, *J. Chem. Soc.*, **1932**, 740.

 © 1987 The Chemical Society of Japan Bull. Chem. Soc. Jpn., 60, 1067—1069 (1987)

Novel Type of the Favorskii Rearrangement Combined with Aldol Reaction Leading to γ-Butyrolactone Derivatives

Takashi SAKAI, Akitoshi YAMAWAKI, Tsuyoshi KATAYAMA, Hiroshi OKADA, Masanori UTAKA, and Akira TAKEDA*

Department of Synthetic Chemistry, School of Engineering, Okayama University, Tsushima, Okayama 700

(Received October 9, 1986)

Reaction of Aromatic aldehydes or hetero-aromatic aldehydes with 3-chloro-3-methyl-2-butanone in ethanolic KOH at room temperature gave 3,3-dimethyl-5-aryltetrahydro-2-furanone as a major product. The reaction can be tentatively explained by the combination of Favorskii rearrangement and aldol reaction.

The Favorskii rearrangement has been known as a useful synthetic method of carboxylic acids or their derivatives by the skeletal rearrangement of α-halo ketones with nucleophilic bases.[1] This paper describes a novel type of the Favorskii rearrangement which involves an aldol reaction (KOH/EtOH) of aromatic aldehyde (**1**) with the enolate of 3-chloro-3-methyl-2-butanone (**2**), giving γ-butyrolactone derivative (**3**) as a major product in one-pot reaction (Scheme 1). In order to estimate the synthetic utility of the present reaction, the scope of reaction and the possible mechanism are discussed.

The reaction conditions and the product distribution were examined by the use of typical reaction of benzaldehyde (**1a**) wirh α-halo ketone (**2**) (Table 1). It is well-known that the Favorskii rearrangement is affected by many factors such as base, solvent, halogen, and so on.[1] For example, treatment of **2** with 40% aqueous NaOH gives pivalic acid, while

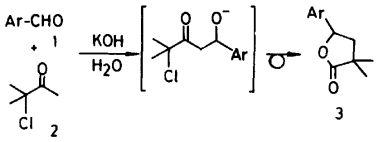

Scheme 1.

Table 1. Reaction of Benzaldehyde (**1a**) with Halo Ketone (**2**)

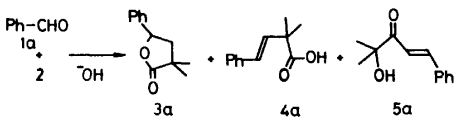

Reaction conditions	Yields/%		
	3a	**4a**	**5a**
40% $NaOH/H_2O$	32[a]	14	3
40% KOH/H_2O	25[a]	14	5
14% KOH/EtOH	50	14	5
14% $NaOH/H_2O$	0	0	80

a) The decreased yield is due to the formation of pivalic acid, which was checked by ^1H NMR.

treatment with weak base such as 20% aqueous Na_2CO_3 affords 3-hydroxy-3-methyl-2-butanone, exclusively.[2] We also confirmed that the reaction of **2** with 14% aqueous or ethanolic KOH also yielded the hydroxy ketone. Thus, a mixture of compounds **1a** and **2** were treated with 40% aqueous NaOH (**1a**:**2**:NaOH=1:3.5:7)[3] at room temperature for 3 h to give 3,3-dimethyl-5-phenyltetrahydro-2-furanone (**3a**)[4] (32% yield), accompanied by 2,2-dimethyl-4-phenyl-3-butenoic acid (**4a**) (14% yield) and 4-hydroxy-4-methyl-1-phenyl-1-penten-3-one (**5a**)[5] (3% yield). It is quite interesting that the yield of lactone **3a** was improved up to 50% in the reaction with 14% ethanolic KOH, in spite of the fact that it is the hydrolytic conditions of **2**.[6] On the contrary, when the reaction was done in 14% aqueous NaOH, **5a**[7] was obtained exclusively in an excellent yield. In aqueous media with weak base, hydrolysis of **2** may occur readily in competition with the aldol reaction. Furthermore, the analogous reaction carried out with NaOEt in ether was found to give a mixture of **3a** (11% yield), **4a** (23% yield), and 1,2-epoxy-4-methyl-1-phenyl-3-pentanone (**6**) (28% yield).

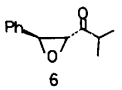

A conceivable mechanism of the present reaction (KOH/EtOH) is shown in Scheme 2, which involves the Favorskii rearrangement of initially formed aldol product **7**. It is possible that the cyclopropanone intermediate **8**[8] is cleaved either by the intramolecular alkoxide ion[9] (route a) or by hydroxide ion (route b). The by-product **5** may be formed either by hydrolysis of **7** or by the Claisen-Schmidt condensation of **1** with 3-hydroxy-3-methyl-2-butanone, which is formed initially in competition with the reaction of **1** with **2**. The present reaction is the first example of the Favorskii rearrangement which undergoes in combination with an aldol reaction.

Table 2 shows that this reaction (KOH/EtOH) can be adapted to a variety of aromatic aldehydes and hetero-aromatic aldehydes,[10] giving γ-butyrolactone derivatives **3b**—**g** as the major product. In addition, a

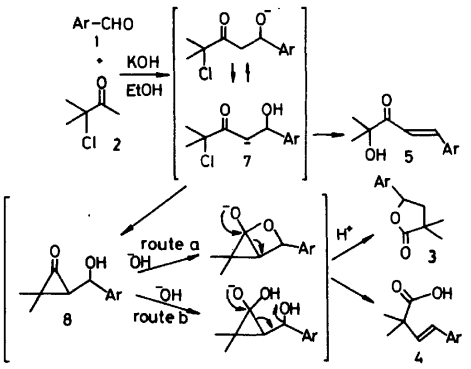

Scheme 2.

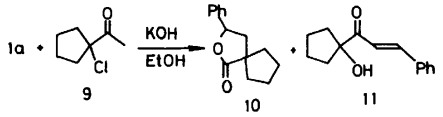

Scheme 3.

Table 2. Yields[a] of Reaction Products **3**, **4**, and **5**

Aldehyde **1** Ar		Products (Yields/%)					
		3		**4**		**5**	
1b	2-Chlorophenyl-	**3b**	(52)			**5b**	(27)
1c	4-Chlorophenyl-	**3c**	(54)	**4c**	(33)		
1d	2,4-Dichlorophenyl-	**3d**	(47)				
1e	3-Nitrophenyl-	**3e**	(42)	**4e**	(20)		
1f	3-Pyridyl-	**3f**	(29)				
1g	2-Furyl-	**3g**	(31)	**4g**	(16)		

a) In the reaction with 14% ethanolic KOH.

similar reaction of 1-(1-chlorocyclopentyl)ethanone (**9**)[11] with **1a** gave 3-phenyl-2-oxaspiro[4.4]nonan-1-one (**10**) (23% yield) and 1-(1-hydroxycyclopentyl)-3-phenyl-2-propen-1-one (**11**) (13% yield) (Scheme 3). Although the yields of the lactones **3a—g** and **10** were moderate to low and they were accompanied by the by-products such as **4**, **5**, or **11**, the present method has the advantage that the reaction can be done in one-pot in a very simple way.

Experimental

Melting points were measured on a Yamato Model MP-21 melting point apparatus and are uncorrected. Evaporative bulb-to-bulb distillation was done using a Büchi Kügelrohrofen. IR spectra were taken on a JASCO Model A-102 spectrometer. ^{1}H NMR spectra (60 MHz) were measured with a JEOL Model JNM-60 SI spectrometer and ^{13}C NMR spectra (25 MHz) were taken on a JEOL Model FX-100 spectrometer using Me_4Si as an internal standard. Analysis and preparative isolation by GLC were done with Hitachi Model 163 (SE-30 5 mmϕ×1.2 m, N_2 27 ml min^{-1}, oven temperature 130 °C) and Yanagimoto Model G-80 (Apiezone Glease L on 10% Chromosorb, N_2 50 ml min^{-1}, oven temperature 200 °C) gas chromatographs, respectively. The preparative TLC was carried out on silica gel (Kieselgel 60 PF_{254}, Merck A. G. Darmstadt). Elemental analysis was performed by Eiichiro Amano of our laboratory.

Typical Reaction of α-Halo Ketones with Aromatic Aldehydes in Ethanolic KOH. 3,3-Dimethyl-5-phenyltetrahydro-2-furanone (3a). To a solution of benzaldehyde (**1a**) (0.53 g, 5.0 mmol) and 3-chloro-3-methyl-2-butanone (**2**)[12] (2.11 g, 17.5 mmol) in ethanol (10 ml), was added a solution of KOH (1.96 g, 35 mmol) in ethanol (10 ml) over a period of 30 min at room temperature. After being stirred for 3 h at room temperature, ethanol was removed under reduced pressure. The residue was acidified with 10% HCl and then stirred for 30 min for completion of lactonization. The resulting organic layer was extracted with ether, washed with aqueous $NaHCO_3$ and then with water, dried ($MgSO_4$), and concentrated under reduced pressure. The residual oil was subjected to vacuum distillation [bp 125—145 °C (2 mmHg) (1 mmHg=133.322 Pa)] to give 504 mg of a mixture of **3a**[4] (50%)[13] and **5a**[5,6] (5%)[13] which were separated by preparative GLC. Structural identification was done by comparison of their spectral data with those reported in the literature. The aqueous $NaHCO_3$ layer was acidified and the ether extract was treated in a similar way as described above to give 2,2-dimethyl-4-phenyl-3-butenoic acid (**4a**) (133 mg, 14%) after purification by preparative TLC (hexane–acetone, 3:1). **4a**: IR (neat) 3600—2300, 1685, 1600, 1580 cm^{-1}; ^{1}H NMR (CCl_4) δ=1.40 (6H, s), 6.40 (2H, s), 7.30 (5H, br s), 10.80 (1H, br s); ^{13}C NMR ($CDCl_3$) δ=24.9 (q), 44.4 (s), 126.6 (d), 127.7 (d), 128.7 (d), 130.3 (d), 133.8 (d), 137.1 (s), 182.7 (s). Anal. ($C_{12}H_{14}O_2$) C, H.

Reaction of 1a with 2 in the Presence of NaOEt in Ether. To a solution of **1a** (382 mg, 3.6 mmol) and **2** (434 mg, 3.6 mmol) in ether (20 ml), was added NaOEt (294 mg, 4.3 mmol) at room temperature. After being stirred for 20 h at room temperature, the mixture was acidified with 10% HCl. The resulting mixture was treated in a manner similar to that described above and the crude products were firstly divided into neutral and acidic portions. The former was fractionated by column chromatography (hexane–ether, 20:1) to give **3a** (76 mg, 11%) and 1,2-epoxy-4-methyl-1-phenyl-3-pentanone (**6**) (192 mg, 28%): IR (neat) 1715 cm^{-1}; ^{1}H NMR (CCl_4) δ=1.10 (3H, d, J=7 Hz), 1.13 (3H, d, J=7 Hz), 2.74 (1H, m), 3.37 (1H, d, J=2 Hz, trans[14]), 3.85 (1H, d, J=2 Hz, trans[14]), 7.27 (5H, br s); ^{13}C NMR ($CDCl_3$) δ=17.3 (q), 18.1 (q), 37.0 (d), 58.4 (d), 61.9 (d), 125.6 (d), 128.6 (d), 128.9 (d), 135.3 (s). Anal. ($C_{12}H_{14}O_2$) C, H. The acidic portion was purified by TLC to give **4a** (156 mg, 23%).

γ-Butyrolactones **3b—g** and **10** were synthesized in the similar way to the typical reaction described above. Procedure for purification of the poroducts, their yields and physical properties are as follows.

5-(2-Chlorophenyl)-3,3-dimethyltetrahydro-2-furanone (3b). A neutral portion was subjected to vacuum distillation [bp 148—152 °C (2 mmHg)] and further purified by preparative TLC (hexane–acetone, 3:1) to give **3b** (R_f 0.50—0.58, 52% yield) and 1-(2-chlorophenyl)-4-hydroxy-4-methyl-1-penten-3-one (**5b**)[5] (R_f 0.25—0.40, 27% yield). **3b**: IR (neat) 1780, 1595, 1577 cm^{-1}; ^{1}H NMR (CCl_4) δ=1.21 (3H, s), 1.33 (3H, s), 1.82 (1H, dd, J=10 Hz and 14 Hz), 2.66 (1H, dd, J=7 Hz and 14 Hz), 5.52 (1H, dd, J=7 Hz and 10 Hz), 7.6—

7.9 (4H, m). Anal. ($C_{12}H_{13}O_2Cl$) C, H.

5-(4-Chlorophenyl)-3,3-dimethyltetrahydro-3-furanone (3c). A neutral portion was purified by vacuum distillation [bp 148—150 °C (3 mmHg)] followed by preparative TLC (hexane-acetone, 3:1, R_f 0.1—0.26) to give **3c**: 54% yield, mp 56—57 °C (hexane-ether, 3:1); IR (KBr) 1780, 1605 cm^{-1}; ^1H NMR (CCl_4) δ=1.24 (3H, s), 1.30 (3H, s), 1.88 (1H, dd, J=7 Hz and 14 Hz), 2.42 (1H, dd, J=7 Hz and 14 Hz), 5.32 (1H, dd, J=7 Hz and 10 Hz), 7.27 (4H, br s). Anal. ($C_{12}H_{13}O_2Cl$) C, H. An acidic portion was purified by TLC (hexane-acetone, 3:1, R_f 0.26—0.37) to obtain 4-(4-chlorophenyl)-2,2-dimethyl-3-butenoic acid (**4c**): 33% yield, mp 145—147 °C (hexane-ether, 3:1); IR (KBr) 1690, 1602 cm^{-1}; ^1H NMR ($CDCl_3$) δ=1.45 (6H, s), 6.42 (2H, s), 7.30 (4H, br s). Anal. ($C_{12}H_{13}O_2Cl$) C, H.

5-(2,4-Dichlorophenyl)-3,3-dimethyltetrahydro-2-furanone (3d). A neutral portion was purified by vacuum distillation [bp 180—200 °C (0.2 mmHg)] and preparative TLC (hexane-acetone, 3:1) to give **3d**: 47% yield, IR (neat) 1785, 1592, 1561 cm^{-1}; ^1H NMR (CCl_4) δ=1.27 (3H, s), 1.32 (3H, s), 1.82 (1H, dd, J=10 Hz and 13 Hz), 2.59 (1H, dd, J=6 Hz and 13 Hz), 5.60 (1 H, dd, J=6 Hz and 10 Hz), 7.1—7.6 (3H, m). Anal. ($C_{12}H_{12}O_2Cl_2$) C, H.

3,3-Dimethyl-5-(3-nitrophenyl)tetrahydro-2-furanone (3e). A neutral portion was purified by preaparative TLC (hexane-acetone, 2:1) to give **3e**: 42% yield; mp 82—84 °C (CCl_4); IR (KBr) 1768, 1535 cm^{-1}; ^1H NMR ($CDCl_3$) δ=1.33 (3H, s), 1.60 (3H, s), 2.05 (1 H, dd, J=10 Hz and 13 Hz), 2.62 (1H, dd, J=6 Hz and 13 Hz), 5.54 (1H, dd, J=6 Hz and 10 Hz), 7.3—8.4 (4 H, m). Anal. ($C_{12}H_{13}O_4N$) C, H. An acidic portion was refined in a similar way to afford **4e**: 20% yield; mp 105—106 °C (hexane-ether, 1:1); IR (KBr) 3720—2300, 1708, 1615, 1528 cm^{-1}; ^1H NMR (CCl_4) δ=1.45 (6H, s), 6.53 (2H, s), 6.7—8.5 (4H, m), 10.10 (1H, br s). Anal. ($C_{12}H_{13}O_4N$) C, H.

3,3-Dimethyl-5-(3-pyridyl)tetrahydro-2-furanone (3f). A neutral portion was purified by vacuum distillation [bp 160-170 °C (2 mmHg)] and preparative TLC (hexane-acetone, 1:1) to give **3f**: 29% yield; mp 78—79 °C (hexane-ether, 2:1); IR (neat) 1770, 1620, 1615 cm^{-1}; ^1H NMR (CCl_4) δ=1.26 (3H, s), 1.8—2.8 (2H, m), 5.40 (1H, dd, J=6 Hz and 9 Hz), 7.1—8.8 (4H, m). Anal. ($C_{11}H_{13}O_2N$) C, H.

5-(2-Furyl)-3,3-dimethyltetrahydro-2-furanone (3g). A neutral portion was distilled under vacuum [bp 130—135 °C (4 mmHg)] and separated by preparative TLC (hexane-acetone, 3:1) to give **3g** (R_f 0.57, 31% yield) and 1-(2-furyl)-4-hydroxy-4-methyl-1-penten-3-one (**5g**)[5] (R_f 0.50, 16% yield). **3g**: IR (neat) 1768, 1604 cm^{-1}; ^1H NMR (CCl_4) δ=1.29 (6H, s), 2.30 (2H, d, J=8 Hz), 5.29 (1H, t, J=8 Hz), 6.33 (2H, br s), 7.35 (1H, br s); ^{13}C NMR ($CDCl_3$) δ=24.4 (q), 24.9 (q), 40.3 (s), 41.2 (t), 71.0 (d), 110.0 (d), 110.7 (d), 143.7 (d), 150.8 (s), 181.1 (s). Anal. ($C_{10}H_{12}O_3$) C, H.

3-Phenyl-2-oxaspiro[4.4]nonan-1-one (10). A neutral portion was fractionated by preparative TLC (hexane-acetone, 3:1, three times developments) to afford **10** (R_f 0.38—0.44, 23% yield) and 1-(1-hydroxycyclopentyl)-3-phenyl-2-penten-1-one (**11**) (R_f 0.44—0.51, 13% yield). **10**: IR (neat) 1770, 1650, 1610 cm^{-1}; ^1H NMR (CCl_4) δ=1.1—1.9 (8 H, m), 1.9—2.7 (2H, m), 5.27 (1H, dd, J=7 Hz and 9 Hz), 7.25 (5H, s). Anal. ($C_{14}H_{16}O_2$) C, H. **11**: IR (neat) 3480, 1680, 1640, 1610, 1575, 1555 cm^{-1}; ^1H NMR (CCl_4) δ=1.3—2.2 (8H, m), 3.7 (1H, br s), 6.87 (1H, d, J=16 Hz), 7.1—7.8 (5H, m), 7.76 (1H, d, J=16 Hz). Anal. ($C_{14}H_{16}O_2$) C, H.

This research was supported in part by a Grant-in Aid for Special Project Research (No. 57218016) from the Ministry of Education, Science and Culture.

References

1) a) A. S. Kende, "Organic Reactions," ed by A. C. Cope, John Wiley & Sons, Inc., London (1960), Vol. 11, Chap. 4; b) N. J. Turro, *Accounts Chem. Res.*, **2**, 25 (1969).

2) P. Delbaere, *Bull. Soc. Chim. Belg.*, **51**, 1 (1942).

3) The ratio was determined so as to consume all aldehyde **1a** used.

4) a) R. N. Johnson, J. B. Lowry, and N. V. Riggs, *Tetrahedron. Lett.*, **1967**, 5113; b) P. L. Creger, *J. Org. Chem.*, **37**, 1907 (1972).

5) G. G. King and J. V. Karabinos, *J. Chem. Eng. Data.*, **13**, 565 (1968).

6) These results suggest that the mechanism which involves cyclopropanolic Favorskii intermediate shown below is unacceptable.

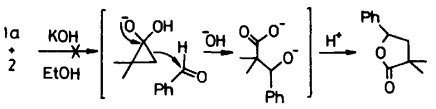

7) Application of compound **5a** to the synthesis of bullatenone [2,2-dimethyl-5-phenyl-3(2*H*)-furanone]: T. Sakai, A. Yamawaki, H. Ito, M. Utaka, and A. Takeda, *J. Heterocycl. Chem.*, in press.

8) The presence of intermediate **8** was not demonstrated.

9) G. W. K. Cavill and C. D. Hall, *Tetrahedron*, **23**, 1119 (1967).

10) The present reaction is not adaptable to aliphtic aldehyde having α-hydrogen and halo ketones such as 2-chloro-2-methyl-3-pentanone, 3-chloro-2-butanone, and 3-bromo-3-methyl-2-butanone, which gave a mixture of complex materials.

11) Y. Josor, M. Gaudry, and A. Marquet, *Bull. Soc. Chim. Fr.*, **1973**, 2732.

12) J. W. Thorpe and J. Warkentin, *Can. J. Chem.*, **51**, 927 (1973).

13) The yield was calculated on the basis of the GLC analysis of the mixture which showed two peaks with retention times (component, relative intensity) of 6.9 min (**3a**, 91%) and 8.6 min (**5a**, 9%).

14) The coupling constant indicates the epoxide to be trans form: A. Gaudener, "Stereochemistry," ed by H. B. Kagan, Georg Thieme Publishers, Stuttgart (1977), Vol. 1, pp. 77—79.

 © 1987 The Chemical Society of Japan Bull. Chem. Soc. Jpn., 60, 1071—1083 (1987)

The Transformation of Cyclic Alcohols into Cyclic Acetals through a New Oxygen Atom Insertion by Photolysis in the Presence of Lead Tetraacetate and Iodine[1)]

Hiroshi SUGINOME,* Haruka WASHIYAMA, and Shinji YAMADA
Organic Synthesis Division, Department of Chemical Process Engineering,
Faculty of Engineering, Hokkaido University, Sapporo 060
(Received October 15, 1986)

Photolysis of the hypoiodites of steroidal cyclic homoallyl alcohols such as cholesterol and of cyclic alcohols such as 5α-androstan-17β-ol generated in situ in benzene with three molar equivalents each of lead tetraacetate and iodine was found generally to result in the unprecedented formation of corresponding lactol acetates in yields up to 66%. The lactol acetates are readily hydrolysed to lactols in most cases during their isolation and lactols are isolated products. Thus, cholesterol gave 4-oxa-*A*-homocholest-5-en-3-ol and its acetate in a 53% yield. The products differ considerably from those reported by us after the photolysis of the hypoiodites by using mercury(II) oxide and iodine as the reagents for generating the hypoiodites; they also differ from those in the oxidation of the steroidal alcohols with lead tetraacetate alone. The photolysis of the hypoiodite of 2,2-dimethyl-5β-cholestan-3-ol was found to lead to the formation of an anomalous lactol, 2α-iodomethyl-2β-methyl-4-oxa-*A*-homo-5α-cholestan-4ξ-ol together with normal lactol. We discuss the paths of the formation of the lactol acetates involving β-scission of the alkoxyl radicals. A new process was found in the photolysis of 2-indanol hypoiodite in the presence of lead tetraacetate and iodine. Our previously suggested pathways to the formation of 3α,5-epoxy-6-iodo-4-oxa-*A*-homo-5α-cholestanes and 3-formyloxy-2-iodo-2,3-seco-*A*-norcholest-5-ene in the photolysis of cholesterol hypoiodite in the presence of mercury(II) oxide and iodine were supported by the results of the photolysis of 4-oxa-*A*-homocholest-5-en-3-ol hypoiodite in the presence of mercury(II) oxide and iodine.

In our previous papers,[2)] we have reported that the photo-induced reaction of the hypoiodites of steroidal cyclic homoallyl alcohols such as cholesterol (**1**) and several methyl-substituted cholest-5-en-3-ols generated in situ in benzene by an excess of mercury(II) oxide and iodine resulted in several typical products arising from the allyl radical intermediates generated by β-scission of the alkoxyl radicals. Typically, the hypoiodite of cholesterol (**1**) in benzene containing an excess of mercury(II) oxide and iodine underwent photoinduced rearrangement to give 3α,5-epoxy-6β- and 6α-iodo-4-oxa-*A*-homo-5α-cholestanes (**2**) and (**3**) together with 3- formyloxy-2-iodo-2,3-seco-*A*-norcholest-5-ene (**4**).[2a)]

^{18}O Labeling studies using $Hg^{18}O$ disclosed that the products such as **2**, **3**, and **4** are formed via new multi-step processes involving the intra- and intermolecular reactions of intermediary allyl radicals, generated by β-scission of the corresponding alkoxyl radicals, with I_2O, as outlined in Scheme 1.[3)]

All alkyl hypoiodites used in these photoinduced reaction were prepared by the reaction of cyclic alcohols with iodine oxide (I_2O) generated in situ from mercury(II) oxide and iodine.[4)] Another reagent which has been proved to be useful for generating alkyl hypoiodites from alcohols is a combination of lead tetraacetate and iodine.[5)] This reagent has been extensively used for the intramolecular functionalization of nonactivated carbons, particularly in the steroid field by a Swiss group.[5,6)]

In this paper, we describe the results of photo-induced reactions of the hypoiodites of steroidal cyclic homoallyl alcohols and cyclic alcohols such as cholesterol (**1**) and 5α-androstan-17β-ol (**40**) generated by lead tetraacetate–iodine reagent. The investigation was aimed at comparing a mercury(II) oxide–iodine reagent and a lead tetraacetate–iodine reagent in the photo-induced reactions of the hypoiodites of cyclic alcohols. These comparisons were thought likely to shed further light on the roles of these reagents in the hypoiodite photolysis.

As we describe below, the products of the photoinduced reactions of the hypoiodites generated by lead tetraacetate–iodine are lactol acetates which are formed in fair to good yields by the hydroxyl oxygen insertion and thus differ considerably from those obtained by using mercury(II) oxide–iodine. The reaction is a new version of the reactions which are performed by the lead tetraacetate–iodine reagent.

Results

Products of the Photoinduced Reactions of Hypoiodites of Steroidal Cyclic Homoallyl Alcohols. We have chosen cholesterol (**1**) and 4,4-dimethylcholesterol (**19**)[7)] as steroidal cyclic homoallyl alcohols. The photoinduced reaction of cholesterol hypoiodite in benzene in the presence of an excess of lead tetraacetate and iodine has already been reported to give a novel ether, cholest-5-en-3β-yl 4-oxa-*A*-homocholest-5-en-3α-yl ether (**11**) in a 23% yield.[8)] We then went on to investigate the reaction in more detail and found that the products of the reaction hinge on the amounts of the lead tetraacetate and iodine used. Irradiation of cholesterol (**1**) in dry benzene containing 3 mol equiv each of lead tetraacetate and

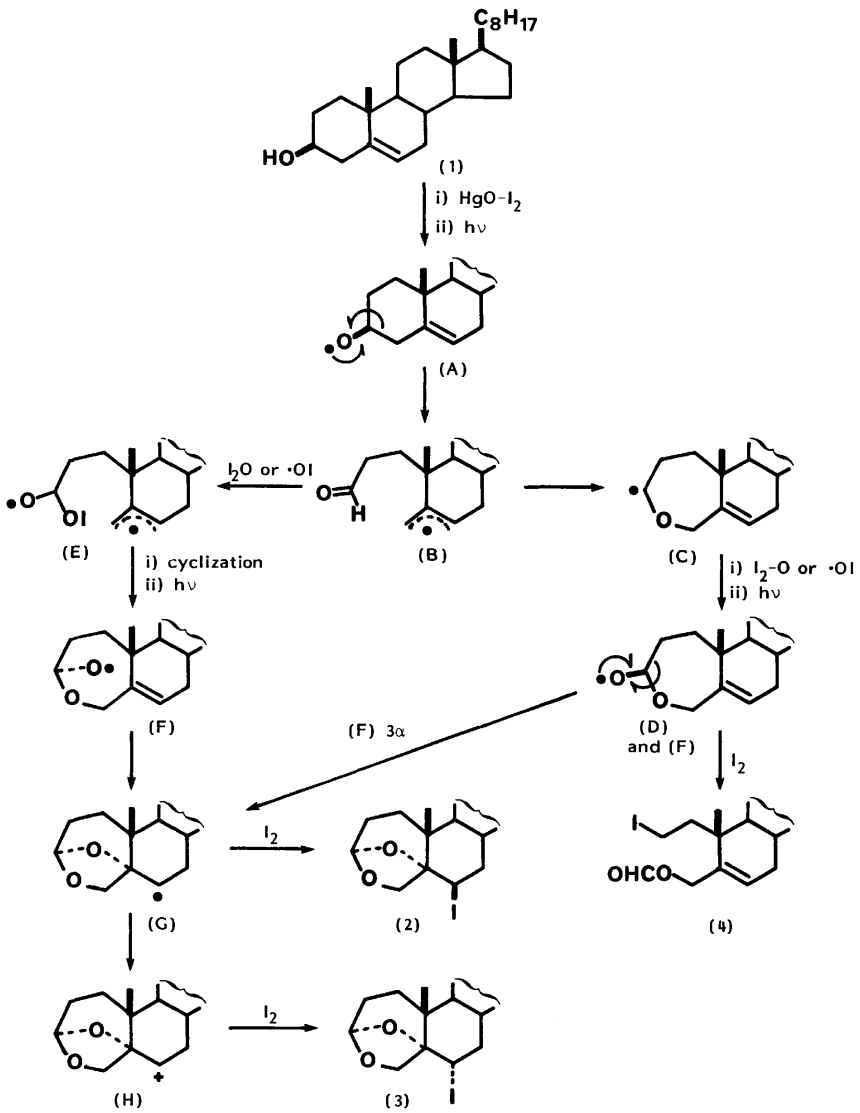

Scheme 1.

iodine in a Pyrex vessel with a light generated by a 100-W high pressure Hg arc lamp for 4.5 h gave a product mixture. Isolation of the products by preparative TLC gave four products [1], [2], [3], and [4] in an order of increasing polarity. The product [1], $C_{29}H_{48}O_3$ (high-resolution mass spectrometry), obtained in a 47% yield showed a band due to an acetoxyl group in the IR spectrum. The ^1H NMR spectrum showed a 3H singlet at δ 2.07, a pair of doublets (2H) at δ 3.70 and 4.41 (J=12.5 Hz), a 1H broad doublet at δ 5.64 and a doublet of doublet (1H) (J=6.84 and 4.41 Hz) at δ 6.00. These signals are assigned to the acetoxyl protons, an isolated methylene group having an oxygen atom, an olefin proton, and a proton attached to the carbon atom carrying two oxygen substituents. Its EIMS showed an ion at m/z 384 as the base peak, a peak derived by the elimination of acetic acid from the molecular ion. These spectral results enabled us to assign the structure of the

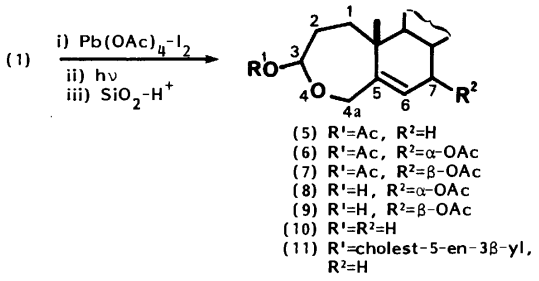

Scheme 2.

product [1] to 4-oxa-*A*-homocholest-5-en-3ξ-ol acetate (**5**) (Scheme 2). This structure was subsequently confirmed by transforming it into the compounds recorded in the literature. Thus, the reduction of acetate **5** with DIBAL (diisobutylaluminium hydride) in toluene afforded two compounds **10** and **12**. The major and more polar product **10** (56%) was identified

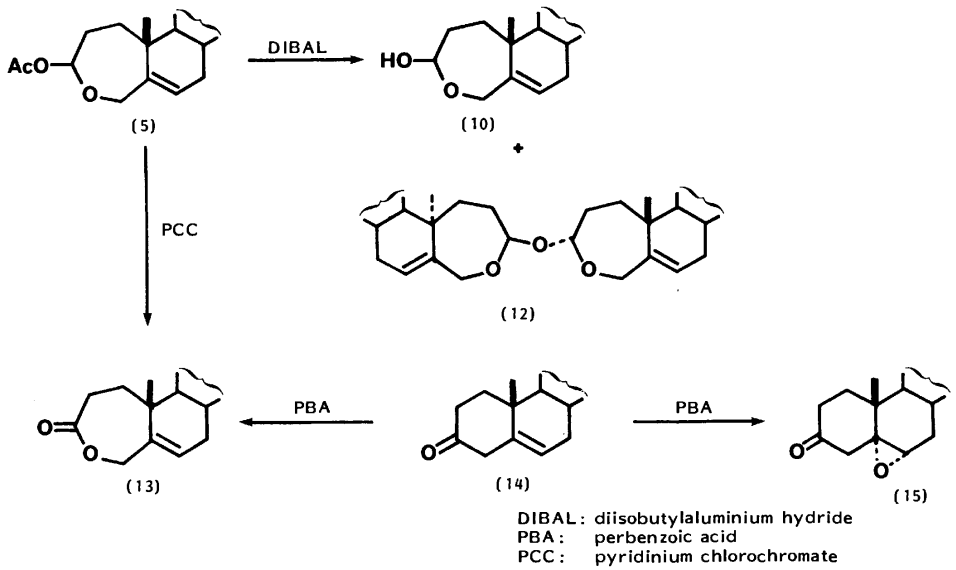

Scheme 3.

as a mixture of 4-oxa-*A*-homocholest-5-en-3α- and 3β-ol,† a product of the acidic hydrolysis[2a] of cholest-5-en-3β-yl 4-oxa-*A*-homocholest-5-en-3α-yl ether (**11**) previously obtained in this photolysis[8] and in the thermolysis of cholesterol hypoiodite in the presence of mercury(II) oxide and iodine in benzene.[2a]

The less polar minor product **12** (8%) proved to be a dimeric acetal. FIMS (field ionization mass spectrometry) showed that the molecular ion at *m/z* 786 corresponded to the molecular formula $C_{54}H_{90}O_3$. The IR spectrum proved the absence of hydroxyl and carbonyl groups. The ^{1}H NMR spectrum was very similar to that of 4-oxa-*A*-homocholest-5-en-3-ol (**10**). These spectral results strongly suggested that product **12** is a dimer of lactol **10**. The assigned structure is also consistent with the spectrum of the EIMS (electron impact mass spectrometry) which showed the base peak at *m/z* 385, attributable to an ion (I) in Scheme 4. A probable genesis of this dimeric acetal involving the reaction of an intermediary oxonium ion (*J*)[9] with lactol **10** is outlined in Scheme 5.

Oxidation of acetate **5** with PCC (pyridinium chlorochromate) gave 4-oxa-*A*-homocholest-5-en-3-one (**13**) which has been obtained together with an epoxide **15** by the oxidation of cholest-5-en-3-one (**14**) with perbenzoic acid[10] (Scheme 3).

† 4-Oxa-*A*-homocholest-5-en-3α-ol reported in the previous paper[2a] may also be a mixture of 3α- and 3β-isomers. Its ^{1}H NMR spectrum (270 MHz) (see Experimental) proved that the chemical shifts of the 3-H, 4a-H, 5-H, and 18-H of 3α- and 3β-isomers are nearly identical but the 19-H of 3α-isomer differs from that of 3β-isomer. The spectrum also proved the presence of a trace of the corresponding ring-opened aldehyde. It is very likely that in solution the 3α- and 3β-isomers and the ring-opened aldehyde are in an equilibrium.

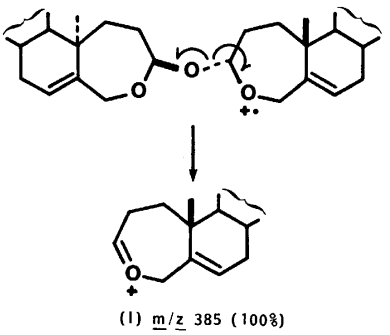

Scheme 4.

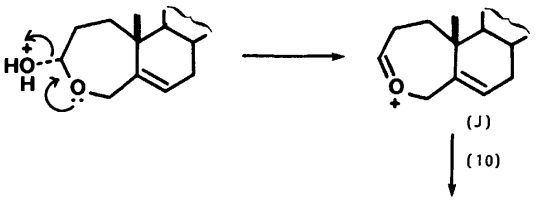

Scheme 5.

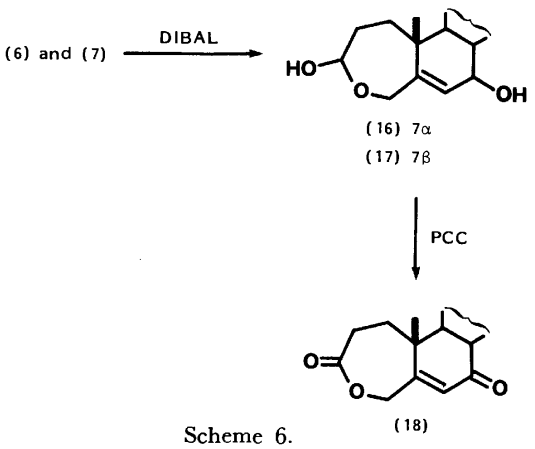

Scheme 6.

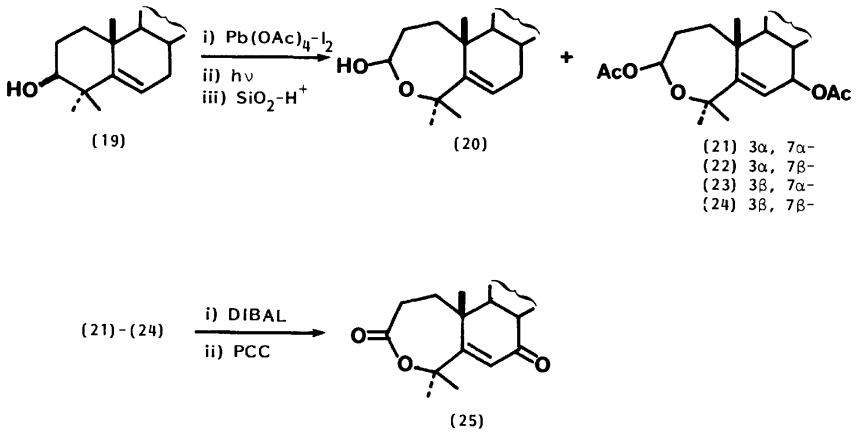

Scheme 7.

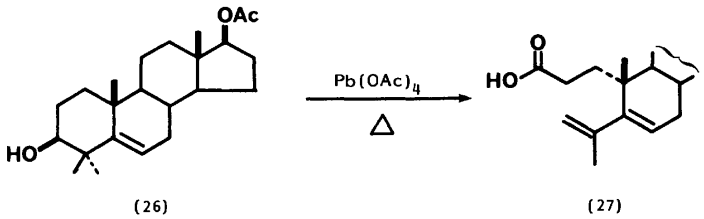

Scheme 8.

The ^{1}H NMR spectrum of the product [2], $C_{31}H_{51}O_5$ (high-resolution mass spectrometry) indicates that it is a stereoisomeric mixture of 4-oxa-*A*-homocholest-5-en-3ξ,7α- (**6**) and 3ξ,7β-diol diacetate (**7**); the IR spectrum indicated a band at 1728 cm^{-1} (OAc). The details of the analysis of the signals in the ^{1}H NMR spectrum of product [2] are recorded in the experimental section. The ratio of diacetates **6** and **7** was found to be 4:1 on the basis of the ratio of the area of the signals due to 7β-H and 7α-H of diacetates **6** and **7**. Their structures were confirmed by further transformations of the mixture. Reduction of the mixture with DIBAL gave a 3:1 mixture of 7α- **16** and 7β-hydroxylactol **17** which was then oxidized with PCC to give a crystalline 4-oxa-*A*-homocholest-5-en-3,7-dione **18** (Scheme 6). The spectroscopic results of dione **18** was fully consistent with the assigned structure (see Experimental).

The product [3] (7% yield) was 4-oxa-*A*-homocholest-5-en-3ξ,7α-diol 7-acetate (**8**) contaminated with its 7β-isomer **9** and their ring-opened aldehydes. The results of the analysis of the ^{1}H NMR spectrum is described in the experimental section.

The product [4] (6%) was identical with the 4-oxa-*A*-homocholest-5-en-3-ols (**10**) obtained by the reduction of lactol acetate **5** with DIBAL. Not a trace of cholest-5-en-3β-yl 4-oxa-*A*-homocholest-5-en-3α-yl ether (**11**), which was reported to be the product in this photoinduced reaction,[8] was found in the products in this experiment.

We then found that cholest-5-en-3β-yl ether **11** is formed at the expense of lactols **5**—**10** if a smaller amount of lead tetraacetate and iodine is used in this reaction. Thus the photolysis of cholesterol hypoiodite prepared by 2 mol equiv of lead tetraacetate and iodine instead of 3 mol. equiv gave cholestenyl ether **11**[2a,8],†† in a 13% yield together with 4-oxa-*A*-homocholest-5-en-3ξ-ol acetate (**5**) (12%), a stereoisomeric mixture of 4-oxa-*A*-homocholest-5-en-3ξ,7β-(**6**) and 3ξ,7β-diol diacetate (**7**) (8%), 4-oxa-*A*-homocholest-5-en-3-ols (**10**)[2a] (11%), and a recovered cholesterol (13%).

A photoinduced reaction of 4,4-dimethylcholest-5-en-3β-ol hypoiodite prepared in situ by the treatment of the 3β-ol **19**,[7] with 3 mol equiv each of lead tetraacetate and iodine was then studied in order to examine the generality of the new reaction found for cholesterol hypoiodite. The irradiation of the hypoiodite in benzene under the conditions as described for the photoreaction of cholesterol gave a mixture of products which were separated by preparative TLC to give products [5] and [6]. The less polar product [5] (4%) was found to be 4a,4a-dimethyl-

†† The formation of cholestenyl ether **11** by using 3 mol equiv each of lead tetraacetate and iodine has been reported in the previous paper.[8] An explanation for this is that while a commercial lead tetraacetate was used in the present experiment, a freshly prepared lead tetraacetate used in the previous experiment was contaminated by some acetic acid.

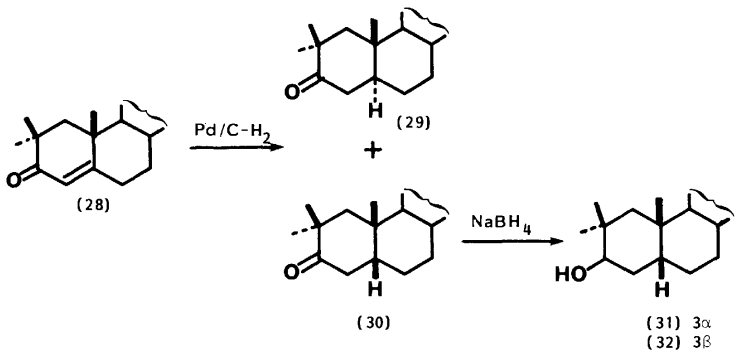

Scheme 9.

4-oxa-*A*-homocholest-5-en-3ξ-ol (**20**) on the basis of the analysis of the ^{1}H NMR which is described in the experimental section. The more polar product [6] was found to be a mixture of the four possible stereoisomers of 4a,4a-dimethyl-4-oxa-*A*-homocholest-5-en-3,7-diol diacetate **21**—**24** by the analysis of the ^{1}H NMR spectrum (see Experimental) (Scheme 7). The assigned structure was further ascertained by transforming it into a crystalline 4a,4a-dimethyl-4-oxa-*A*-homocholest-5-ene-3,7-dione (**25**) by its reduction with DIBAL to 7-hydroxylactols followed by the oxidation with PCC.

The oxidation of 4,4-dimethylandrost-5-ene-3β,17β-diol 17-acetate (**26**) with lead tetraacetate alone has been reported by Amorosa et al.,[11] to give a seco aldehyde **27** in a 28% yield, as outlined in Scheme 8. The different results obtained by the two reagents may thus be apparent.

Products of the Photoinduced Reactions of the Hypoiodites of Steroidal Cyclic Alcohols and 2-Indanol. As was expected, the irradiation of cyclic alcohol hypoiodites under the foregoing conditions similarly gives lactol acetates in better yields in one step if the alkoxyl radicals generated from the hypoiodites are susceptible to β-scission.

We describe the results with steroidal alcohols, i.e. 2,2-dimethyl-5β-cholestan-3α- (**31**) and 3β-ol (**32**), 2,2-dimethyl-5α-cholestan-3β-ol (**33**),[12] 5α-androstan-17β-ol (**40**),[12] and 2-indanol (**45**) below. A mixture of 3-alcohols **31** and **32**, and 3β-alcohol **33** were prepared by reduction of the corresponding ketones with $NaBH_4$ (Scheme 9). Thus, 2,2-dimethylcholest-4-en-3-one (**28**)[13] was hydrogenated in the presence of palladium-charcoal as a catalyst to afford 2,2-dimethyl-5α-cholestan-3-one (**29**) identical with the authentic specimen and its isomer, 2,2-dmethyl-5β-cholestan-3-one (**30**) in a 3:17 ratio. The structure of the latter was apparent from its spectroscopic data (see Experimental). Reduction of 5β-isomer **30** with $NaBH_4$ gave approximately a 1:1 mixture of 2,2-dimethyl-5β-cholestan-3α-ol (**31**) and 3β-ol **32** (Scheme 9). The separatioh of the isomeric alcohols by means of preparative TLC was unsuccessful.

The preparation of the hypoiodite of 3β-alcohol **33** by the reaction with 3 mol equiv each of lead tetraacetate and iodine and irradiation of the solution under the conditions above gave two products **34** and **35**. The molecular formula of the less polar product **34**, which carries an iodine atom, was established to be $C_{28}H_{49}OI$ by an exact mass measurement of the ion due to $(M-CH_3COOH)^+$. The IR spectrum indicated the presence of an acetoxyl group. The ^{1}H NMR spectrum proved that the one of the *gem*-dimethyl of the starting 3β-ol was lost and exhibited only one 3H singlet at δ 1.44 attributable to Me group beside the two singlets due to the 18- and 19-H. It also showed a 3H singlet attributable to an acetoxyl group, and a 2H broad singlet at δ 3.40 assignable to a methylene group having an iodine. Thus, the structure of product **34** should be 2α-iodomethyl-2β-methyl-4-oxa-*A*-homo-5α-cholestan-4ξ-ol which can accommodate all the foregoing spectral results. The iodomethyl group attached to the C-2 of this lactol acetate **34** should be α-oriented since the chemical shift of the signal due to the 19-H (δ 1.03) does not differ appreciably from that of the signal due to the 19-H (δ 1.02) of product **35** for which the structure, 2,2-dimethyl-3-oxa-*A*-homo-5α-cholestan-4ξ-ol, was deduced on the basis of the mass spectrum together with the spectroscopic data (see Experimental).

Similar irradiation of the hypoiodites of 3α- and 3β-ols **31** and **32** in benzene under the conditions as for 3β-ol **33** and the separation of the product by means of preparative TLC gave a 1:1 mixture of 2,2-dimethyl-3-oxa-5β-cholestan-4α-(**37**) and 4β-ols (**38**) in a 66% yield. The structures were deduced by means of the IR, ^{1}H NMR and mass spectra (see Experimental). When this photolysis was carried out by adding a small amount of pyridne, an appreciable amount of a seco-aldehyde **39** (27%) was formed as an accompanying product at the expense of the yields of the lactols.

The irradiation of the hypoiodite of 5α-androstan-17β-ol (**40**),[12] a typical steroidal five-membered cyclic

alcohol, in benzene under the conditions as described above, gave 17a-oxa-D-homo-5α-androstan-17α-ol (**41**) in a 24% yield. The product **41** was identical with the specimen prepared by Baeyer–Villiger oxidation of 5α-androstan-17-one followed by its reduction with DIBAL.[15] The difference in the product **41** with those reported for the oxidation of steroidal 17β-ol **42** with lead tetraacetate alone by Amorosa et al,[11] which is outlined in Scheme 12, is again apparent.

Finally, we undertook the photolysis of 2-indanol hypoiodite which should generate a stabilized benzyl radical by a β-scission of the corresponding alkoxyl radicals. We found that the major product was 2,3-dihydro-1*H*-2-benzopyran-3-ol acetate (**46**) (23% yield),

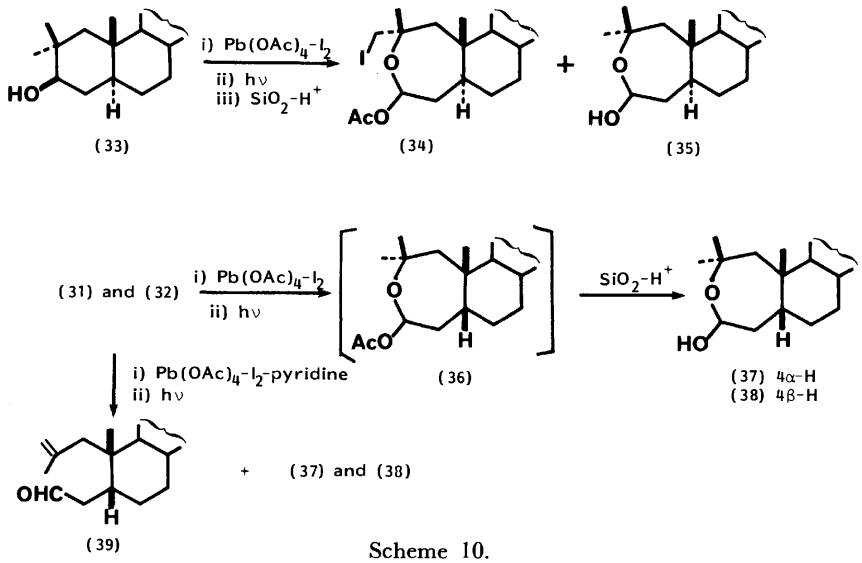

Scheme 10.

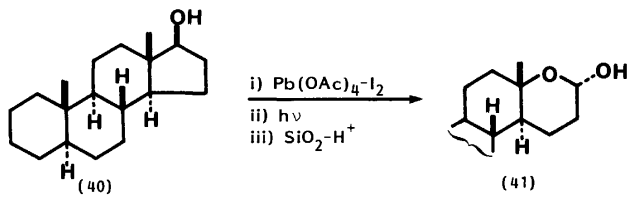

Scheme 11.

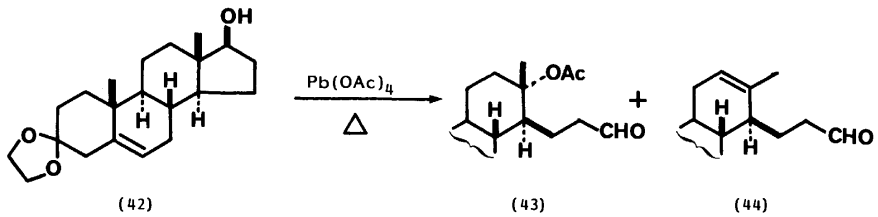

Scheme 12.

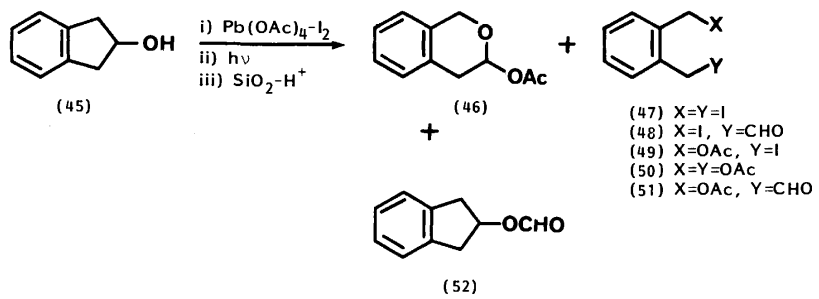

Scheme 13.

while several minor products **47**—**51**, arising from the combinations between the benzyl radical or cation and ·OAc, $^-$OAc, or iodine, as well as 2-indanol formate (**52**), were obtained in low yields (Scheme 13).

Products of the Photoinduced reaction of the Hypoiodite of 4-Oxa-A-homocholest-5-en-3-ols (10) in the Presence of Mercury(II) Oxide and Iodine. As we mentioned at the outset of this paper, the photolysis of hypoiodite of cholesterol (**1**) in benzene containing an excess of mercury(II) oxide and iodine gives 3α,5-epoxy-6β- and 6α-iodo-4-oxa-*A*-homo-5α-cholestanes (**2**) and (**3**) together with iodo formate **4**.[2a,3] It has recently been reported that (diacetoxyiodo) benzene is a good reagent for the production of hypoiodite from alcohols.[16] We therefore prepared cholesterol hypoiodite from (diacetoxyiodo)benzene and cholesterol and subjected it to photolysis. It was found that 3α,5-epoxy-6α-iodo-4-oxa-*A*-homo-5α-cholestane (**3**) and iodo formate **4** are the major products and that no 6β-iodooxasteroid **2** was found in the product. The difference in the products when mercury(II) oxide–iodine and (diacetoxyiodo)benzene are used to generate hypoiodites is interesting.

As outlined in Scheme 1, the paths leading to these products should involve the intermediacy of alkoxyl radicals such as (D) or (F). These species can be generated by the irradiation of the hypoiodites of 3α- and 3β-lactols **10**. In order to ascertain the proposed paths outlined in Scheme 1, the products of the photolysis of the hypoiodites of lactols **10** were studied. Irradiation of lactols **10** in benzene containing 3 mol equiv each of mercury(II) oxide and iodine was found to give oxasteroid **3** (17%) and iodo formate **4** (56%), as otulined in Scheme 14. This photolysis was also carried out in the presence of pyridine. We found

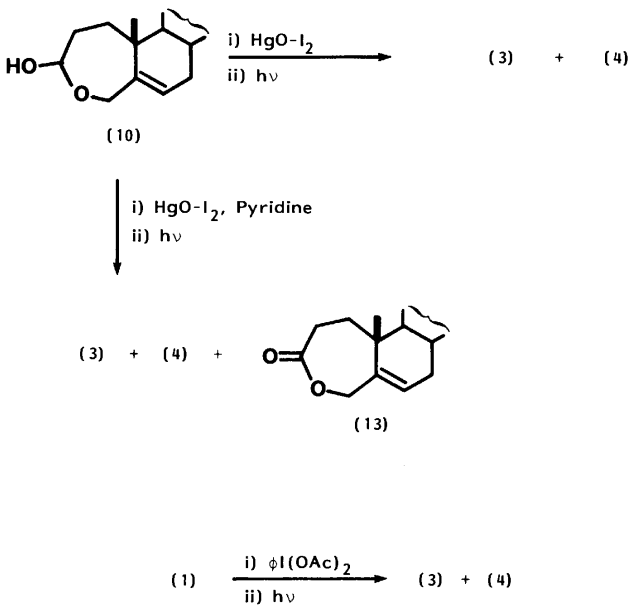

Scheme 14.

that besides oxasteroid **3** (11%) and iodo formate **4** (39%), lactone **13**[10] is formed in a 25% yield. The results can be taken as a further evidence that the immediate forerunners of 3α,5-epoxy-4-oxa-*A*-homosteroids such as **3** and iodo formate **4** in the steroid-5-en-3-ol hypoiodite photolysis are alkoxyl radicals (D) and (F). Pyridine accelerates the formation of lactone **13**. No further experiments have been carried out to clear up the problem as to why radical (G) is more readily oxidized to give cation (H), from which 6α-iodo compound **3** is believed to be formed, in the case of the photolysis of lactol hypoiodite.

Discussion

The foregoing experiments clearly show that the products in the photolysis of the hypoiodites of cyclic alcohols generated in situ in benzene with three molar equivalents each of lead tetraacetate and iodine differ considerably from those in a photolysis using mercury(II) oxide and iodine[2] as the reagent for generating the hypoiodites; the photolysis generally results in the formation of the lactols or their acetates by an oxygen insertion and no 3α,5-epoxy-4-oxa-*A*-homo-5α-cholestanes such as **2** and **3** and iodo formate **4**[2a,3] are formed. The formation of the lactols from the cyclic alcohols in one step is unprecedented.

We confirmed that no reaction took place when the above cyclic alcohols in benzene containing lead tetraacetate alone were irradiated and an intractable mixture resulted when cholesterol in benzene containing lead tetraacetate was heated under reflux.

The probable paths for the formation of the lactols and their acetates in the present study are outlined in Scheme 15. The cyclic alcohols are transformed into the corresponding hypoiodites with CH_3COOI generated in situ by the reaction of lead tetraacetate with iodine.[5,6] The excited hypoiodites generate the corresponding alkoxyl radicals which rearrange to the allyl radicals (B) by β-scission. Its intramolecular combination with the carbonyl oxygen then generates the radicals (C). Thus, the formation of lactol acetates may well follow the same path as that in the photoinduced reaction by using mercury(II) oxide and iodine up to the formation of the intermediate (C). The one-electron oxidation of the radical (C) with lead tetraacetate generates an oxonium ion (I) which traps acetic acid to give lactol acetates (**5**). An alternative formation of lactol **5**, although less likely, by a radical combination between radical (C) and an acetoxyl radical may also be possible. The formation of **5** via a biradical (K) is very unlikely since a β-scission may precede from species (K). The parent cyclic alcohols such as cholesterol can apparently compete with acetic acid in the reaction with the oxonium ion (I) to form an ether such as **11**[8] when a concentration of the lead tetraacetate-iodine reagent is lower. Lactol

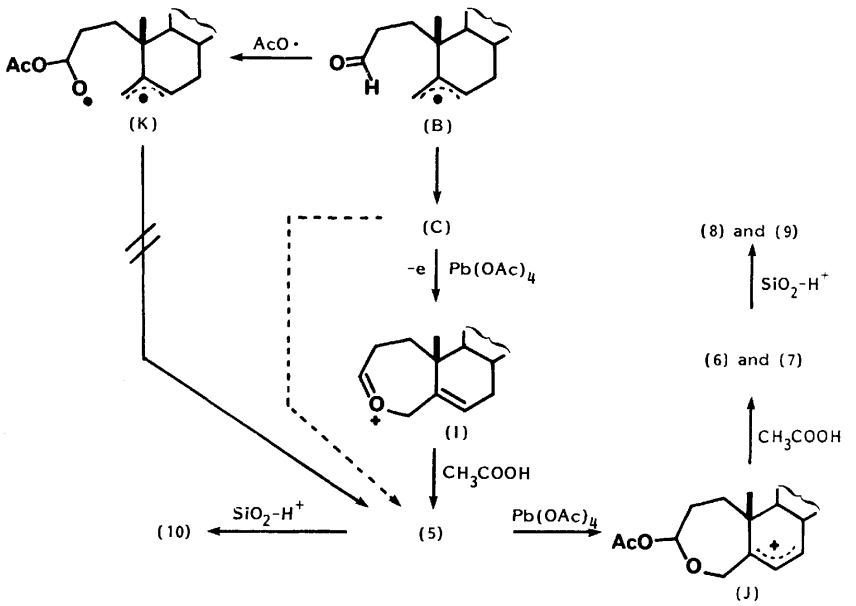

Scheme 15.

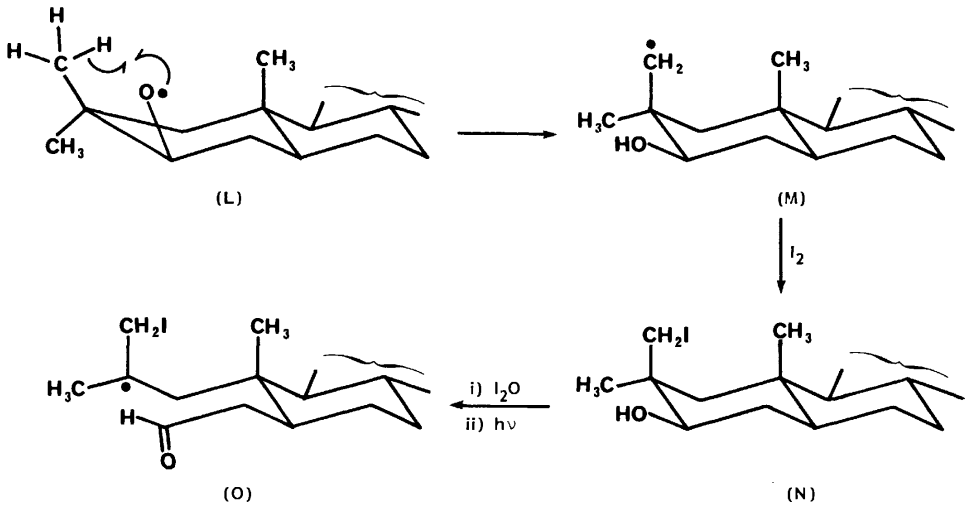

Scheme 16.

acetates **6** and **7** are formed by oxidation of acetates **5** with lead tetraacetate or through a hydrogen abstraction of the allylic hydrogen with acetoxyl radical to form an allyl radical followed by its oxidation to an allyl cation which traps acetic acid. The formation of the lactols alone or with the corresponding acetates have been observed for all the photolysis of the present hypoiodite photolysis. It is clear that these lactols are not the primary products but that they are formed by hydrolysis with silica gel in preparative TLC. The formation of these lactols by preparative TLC of the lactol acetates was in fact confirmed for some of the lactol acetates. It is interesting to note that no lactols corresponding to the lactol acetates **21**—**24** and **34** were found after the treatment with silica gel (preparative TLC), nor were lactol acetates corresponding to lactols **5**, **35**, **37**, **38**, and **41** isolated in preparative TLC with silica gel. These different patterns of behavior of the initially formed lactol acetates are apparently ascribable to hindrance by nearby substituents.

The formation of anomalous lactol acetate **34** which carries an iodine atom (Scheme 10) is interesting. Scheme 16 outlines its formation from the alkoxyl radical (L). The ring A should adopt a somewhat flattened chair conformation owing to the 1,3-diaxial interaction between 2β- and 10β-Me groups. The alkoxyl radical (L), therefore, can abstract a hydrogen of the 2β-Me via a normally incapable five-membered transition state to form a carbon-centred radical (M) which then abstracts an iodine atom to give a new intermediate (N). The path from the intermediate (N) to the lactol acetate **34** via (O) is straightforward.

Finally, all the products with the exception of formate **52** formed in the photolysis of 2-indanol hypoiodite should be derived by a radical (P) arising

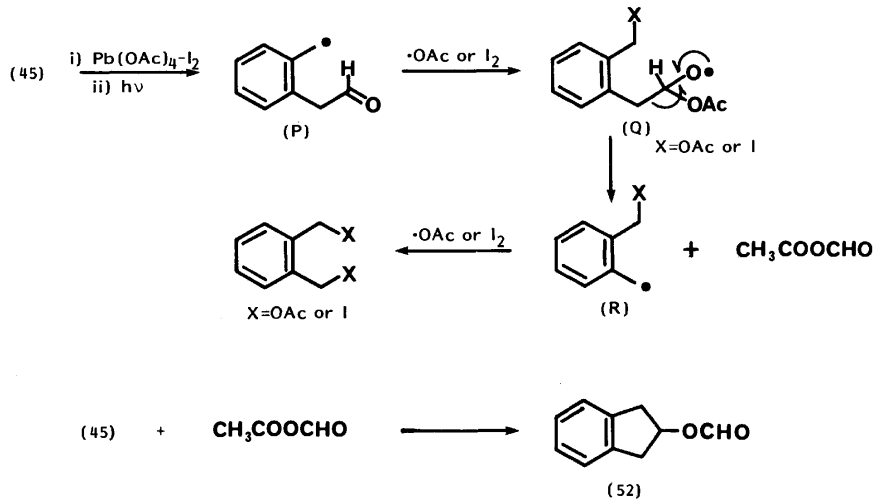

Scheme 17.

from a β-scission of 2-indanyloxy radical as outlined in Scheme 17. The simultaneous formation of formate **52** and products **47**, **49**, and **50** strongly suggests the involvement of an intermediate (Q) which can be generated by the attack of an acetoxyl radical on a formyl group of an intermediary aldehyde. The β-scission of the alkoxyl radical (Q) may give acetic formic anhydride and a new benzyl radical (R). The former then reacts with 2-indanol to give formate **52**[17] while the reaction of the latter with iodine or an acetoxyl radical leads to products **47**, **49**, and **50**.

The present photoinduced reaction can be useful in synthesis since the lactols can be obtained in yields as high as 66% in one step from cyclic alcohols provided the alkoxyl radicals generated from them are susceptible to β-scission. Even the unsaturated lactols such as **5** and **20** which are not easily obtainable by other methods can be obtained in one step from cyclic homoallyl alcohols.

Experimental

Mps were determined with a Yanagimoto micro mp apparatus. IR spectra were determined for Nujol mulls by a Hitachi Model 285 infrared spectrometer unless stated otherwise. ^{1}H NMR spectra was determined by a Hitachi-R-90H spectrometer (90 MHz) or JEOL-JMS-GX-270 spectrometer (270 MHz) (solvent $CDCl_3$: $SiMe_4$ as internal standard). Mass spectra were taken by JEOL JMS-D300 spectrometer (70 eV) (Faculty of Pharmaceutical Sciences of this University). TLC was carried out on Merck Kiesel gel 60 PF_{254}. Elemental analyses were performed by the staff of the Faculty of Pharmaceutical Sciences.

Lead Tetraacetate. A quality of lead tetraacetate was found to affect considerably to the yields of each product. Throughout the present work, a commercial lead tetraacetate was used.

The Photolysis of Cholesterol Hypoiodite in the Presence of Lead Tetraacetate and Iodine. (a) Cholesterol (**1**) (1 g, 2.59 mmol) in benzene (120 mg) containing lead tetraacetate (3.44 g, 7.77 mmol) and iodine (1.97 g, 7.74 mmol) was irradiated under an atmosphere of a nitrogen for 4.5 h. TLC indicated that no starting material remained unchanged. After the removal of the precipitates by filtration, the solution was washed with 5% sodium thiosulfate solution, 5% sodium hydrogencarbonate solution, water and saturated brine successively and dried (Na_2SO_4). After the usual work-up the residue (1.464 g) was subjected to preparative TLC with a benzene–diethyl ether (10:1) to give three fractions. The most mobile fraction (551 mg, 47%) was an oily lactol acetate (**5**). ^{1}H NMR (200 MHz) 0.69 (3H, s, 18-H), 0.98 (3H, s, 19-H), 2.07 (3H, s, OAc), 3.70 (1H, d, J=12.5 Hz, 4a-H), 4.41 (1H, d, J=12.5 Hz, 4a-H), 5.64 (1H, br.d, 6-H), and 6.00 (1H, dd, J=6.84 and 4.41 Hz, 3-H); IR (neat) 1733 (OAc), 1222 (C–O), and 1005 (C–O); MS (70 eV) m/z (rel intensity) 444 (M^+, 0.3), 384 ([M−CH_3COOH]$^+$, 100), 328 (39.9), 247 (36.8), and 215 (42.8). Found: (M−CH_3COOH)$^+$ 384. 33626. Calcd for $C_{27}H_{44}O$: M−CH_3COOH, 384.33916.

The second mobile fraction (233 mg) was a mixture of lactols **8** and **9** and their acetates **6** and **7**. This was again subjected to preparative TLC with benzene and diethyl ether (2:1)to give two fractions A (181 mg) and B (79 mg, 6.6%). The more mobile fraction A was again subjected to preparative TLC with hexane and diethyl ether (1:1) to give an oily mixture of two epimers of lactol acetate **6** and **7** (49 mg, 3.8%). ^{1}H NMR (200 MHz) 0.68 (3H, s, 18-H of two C-7 epimers), 0.98 (3H, s, 19-H) of C-7 epimers), 2.03 (3H, s, Ac), 2.08 (3H, s, Ac), 3.74 (1H, d, J=13.19 Hz, 4a-H of two epimers), 4.40 (0.2H, d, J=13.19 Hz, 4a-H of 7β-acetoxy epimer), 4.44 (0.8H, d, J=13.19 Hz, 4a-H of 7α-acetoxy epimer), 5.00 (0.8H, br.t, J=4.4 Hz, 7β-H of 7α-acetoxy epimer), 5.12 (0.2H, dd, J=2 and 8.6 Hz, 7α-H of 7β-acetoxy epimer), 5.47 (0.8H, d, J=2 Hz, 6-H of 7β-epimer), 5.77 (0.2H, d, J=4.88 Hz, 6-H of 7α-epimer), 6.01—6.41 (1H, m, 3-H of 7α- and 7β-epimers); MS (70 eV) m/z (rel intensity) 502 (M^+, 0.2), 442 ([M−CH_3COOH]$^+$, 23), 400 (30), and 43 (100); IR (neat) 1728 (OAc), 1243 (C–O), and 1020 (C–O). Found: M^+ 502.36289. Calcd for $C_{31}H_{50}O_5$: M, 502.37569. The less mobile fraction B was a gummy 7α-acetoxylactol **8** contaminated with 7β-acetoxylactol **9** and the corresponding ring-opened aldehydes. ^{1}H NMR (90 MHz) 0.66 (s, 18-H

of 7α-acetoxylactol), 0.69 (s, 18-H of 7β-acetoxylactol), 0.94 (s, 19-H of 7α-acetoxylactol), 1.01 (s, 19-H of 7β-acetoxylactol), 2.00 (s, OAc of 7β-acetoxylactol), 2.02 (s, OAc of 7β-acetoxylactol), 3.60 (br.d, J=12 Hz, 4a-H of 7α- and 7β-acetoxylactols), 4.51 (br.d, J=12 Hz, 4a-H of 7α- and 7β-acetoxylactols), 4.06 (br.s, 4a-methylene group of ring-opened aldehyde), 4.95—5.05 (m, 7-H of 7α- and 7β-acetoxylactols and their ring-opened aldehydes), 5.09—5.15 (m, 3-H of 7α- and 7β-acetoxylactols), 5.42 (d, J=2 Hz, 6-H of 7β-acetoxylactol), 5.74 (d, J=5.6 Hz, 6-H of 7α-acetoxylactol), and 9.72 (br.s, CHO of the ring-opened aldehydes); IR 3400 cm^{-1} (OH), 1718 (OAc), 1237 (C-O), and 1020 (C-O); MS (70 eV) m/z (rel intensity) 442 ($[M-H_2O]^+$ of lactols, 3.6%), 400 ($[M-AcOH]^+$ of lactols 47), and 43 (100).

The third fraction (19 mg) was 4-oxa-*A*-homocholest-5-en-3-ol (**10**) which was identical with the authentic specimen.

(b) Cholesterol (100 mg, 0.26 mmol) in benzene (15 ml) containing lead tetraacetate (228 mg, 0.52 mmol) and iodine (131 mg, 0.52 mmol) was irradiated under an atmosphere of a nitrogen for 4 h. TLC of the reaction mixture indicated the presence of some cholesterol. The reaction mixture was worked up as described above. The crude product (153 mg) was subjected to preparative TLC with a benzene–diethyl ether (10:1) to give five fractions a to e. The most mobile fraction a was a mixture and therefore subjected again to preparative TLC with a benzene–hexane (1:1) to give a dimeric acetal **11** (27 mg, 14%) which was identical with the authentic specimen. The next mobile fraction b (14 mg, 12%) was lactol acetate **5**. The fraction c (11 mg, 8%) was a mixture of lactol acetates **6** and **7** judged from the ^1H NMR spectrum. Fraction d (13 mg) was cholesterol. Fraction e was lactols **10**.

Reduction of Lactol Acetate 5 with DIBAL. The lactol acetate **5** (81 mg) in dry toluene (8 ml) was cooled by Dry Ice–methanol. To this solution DIBAL (1 M hexane solution, Ventron) (0.22 ml) was added by means of micro syringe. After the solution was stirred for 2 h, water was added and the reaction mixture was stirred for half an hour. After the precipitates were removed by filtration, the organic layer was washed with brine and dried over anhydrous sodium sulfate. Usual work-up of the solution gave a residue which showed two spots on TLC plate. The product was subjected to preparative TLC with benzene–diethyl ether (5:1) to give two products. The more mobile compound (11 mg, 7.6%) was a dimeric acetal **12** which was recrystallized from dichloromethane. Mp 225—231 °C. FDMS (rel intensity) m/z 786 (M^+, 77%), 768 (40), 385 (100, the ion I in the text). ^1H NMR (200 MHz) 0.68 (6H, s, 18 and 18'-H), 0.89 (6H, s, 19 and 19'-H), 4.30 (2H, d, J=13.3 Hz, 4a- and 4a'-H), 4.95—5.20 (2H, m, 3 and 3'-H), 5.50—5.62 (2H, m, 6- and 6'-H); IR 1257 and 1020 cm^{-1} (C-O). The less mobile compound (41 mg, 56%) was a mixture of 3α- and 3β-lactols **10**. ^1H NMR 0.69 (s, 18-H of 3α- and 3β-isomers), 0.97 (s, 19-H of 3α-isomer), 0.93 (s, 19-H of 3β-isomer), 3.58 (br.d, J=13 Hz, 4a-H of 3α- and 3β-isomers), 4.48 (d, J=13 Hz, 4a-H of 3α- and 3β-isomers), 5.17 (br.t, 3β- and 3α-H of 3α- and 3β-isomers), 5.62 (br.dd, J=2 and 5 Hz; 5-H of 3α- and 3β-isomers), 9.75 (br.t, CHO of the ring opened aldehyde).

Oxidation of Lactol Acetate 5 with Pyridinium Chlorochromate (PCC). To the lactol acetate **5** (41 mg) in dichloromethane (7 ml) containing some Celites, PCC (30 mg) was added and the solution was stirred for 2 h. After the solution was filtered, the filtrate was washed with water and then a brine successively and dried over anhydrous sodium sulfate After the usual work-up, the crude product was purified by means of preparative TLC to give a pure 4-oxa-*A*-homocholest-5-en-3-one (**13**) (30 mg, 70%). Analytical specimen was obtained by recrystallization from methanol. Mp 200—202 °C (lit,[10] 202 °C). ^1H NMR (90 MHz) 0.69 (3H, s, 18-H), 1.07 (3H, s, 19-H), 4.20 (1H, d, J=13.2 Hz, 4a-H), 4.78 (1H, d, J=13.2 Hz, 4a-H), and 5.84 (1H, br.dd, J=6.2 and 2.2 Hz); IR 1733 cm^{-1} (lactonic C=O), 1288, 1155, and 1035; MS (70 eV) m/z (rel intensity) 400 (M^+, 51.6), 385 ($[M-15]^+$, 22.1), 287 (82.3), and 43 (100).

Reduction of Lactol Acetates 6 and 7 with DIBAL. The lactol acetates (63 mg) in dry toluene (6 ml) was reduced with DIBAL (0.26 ml) as described for the reduction of lactol acetate **5**. The product (47 mg) was subjected to preparative TLC with diethyl ether to give a 3:1 mixture of gummy lactols **16** and **17** (24 mg, 61%). ^1H NMR (90 MHz) 0.69 (3H, s, 18-H), 0.96 (3H, s, 19-H), 3.60 (1H, br.d, J=13 Hz, 4a-H), 4.52 (1H, br.d, J=13 Hz, 4a-H), 3.87 (1H, br.s, 7-H), 5.08—5.23 (1H, m, 3-H), 5.53 [0.24H, br.d, J=2 Hz, 6-H of (**14**)], 5.78 (0.75H, br.d, J=5.3 Hz, 6-H of (**13**)]; IR 3340 cm^{-1} (OH) and 1027 (C-O); MS (70 eV) m/z (rel intensity) 418 (M^+, 6.7), 400 ($[M-H_2O]^+$, 23), 353 (57), and 55 (100). Found: M^+ 418.34219. Calcd for $C_{27}H_{46}O_3$: M, 418.34459.

Oxidation of Lactols 16 and 17 with PCC. To the lactols (21 mg) in dichloromethane (5 ml) containing Celite, PCC (33 mg) was added. The reaction mixture was stirred for 4 h and worked up as described for the oxidation of lactol acetate **5**. The curde product (18 mg) was subjected to preparative TLC with a 5:1 benzene–diethyl ether to give a crystalline lactone **18** (7 mg, 34%). The lactone was recrystallized from acetone–methanol. Mp 267—272 °C. ^1H NMR (90 MHz) 0.70 (3H, s, 18-H), 1.28 (3H, s, 19-H), 4.37 (1H, d, J=13.3 Hz, 4a-H), 4.92 (1H, d, J=13.3 Hz, 4a-H), 5.91 (1H, s, 6-H); MS (70 eV) m/z (rel intensity) 414 (M^+, 100), 355 (29.9), and 341 (19.3) and 206 (74.3). Found: m/z 414.31295. Calcd for $C_{27}H_{42}O_3$: M, 414.31335. IR 1719 cm^{-1} (lactonic C=O), and 1652 (α, β-unsaturated C=O).

The Photolysis of the Hypoiodite of 4,4-Dimethylcholest-5-en-3α-ol (19) in the Presence of Lead Tetraacetate and Iodine. The 3β-ol **19** (100 mg, 0.24 mmol) in benzene (15 ml) containing lead tetraacetate (321 mg, 0.73 mmol) and iodine (194 mg, 0.73 mmol) was irradiated for 3.5 h as described above for cholesterol. The reaction mixture was worked up as usual. The product was subjected to preparative TLC with 10:1 benzene–diethyl ether to give two fractions. The more mobile fraction (21 mg) was again subjected to preparative TLC to give a gummy lactol **20** (4 mg). ^1H NMR (90 MHz) 0.69 (3H, s, 18-H), 0.93 (3H, s, 19-H), 1.26 and 1.52 (3H, s, 4a *gem*-dimethyl), 4.87 (1H, br.s, 3-H), 5.39 (1H, m, 6-H); IR 3340 cm^{-1} (OH), and 1042; MS (70 eV) m/z (rel intensity) 412 ($[M-H_2O]^+$, 100), 394 (32.5), and 379 (20.8). Found: m/z 412.36934 $(M-H_2O)^+$. Calcd for $C_{29}H_{48}O$: M, 412.37044.

The less mobile fraction (44 mg) was a mixture of gummy lactol acetates **21—24** which were found to be actually a mixture of four possible stereoisomers by its ^1H NMR spectrum. ^1H NMR (270 MHz) 0.67 an 0.70 (each s, 18-H of

the stereoisomers), 1.20 (s, 19-H), 2.49 and 1.58 (each s, 4a *gem*-dimethyl), 2.038, 2.045, 2.048, 2.065, 2.273, 2.098 (each s, OAc attached to C-3 and C-7 of the stereoisomers), 4.95—5.29 (m, 6-H and 7-H of the stereoisomers), 5.66—6.02 (m, 3-H of the stereoisomers); IR 1733 cm^{-1} (OAc), 1237 and 1011 (-O); MS (70 eV) *m/z* (rel intensity) 515 ($[M-Me]^+$, 1.6), 470 ($[M-AcOH]^+$, 14.7), 428 (33.0), 370 (34.5), and 43 (100).

The Transformation of Lactol Acetates 21—24 into Lactone 25. To lactol acetates (30 mg) in toluene (4 ml) cooled by Dry Ice, DIBAL solution (1 M solution, 0.11 ml, Ventron) was added through micro syringe. The solution was stirred for 2 h and worked up in a usual manner. The crude lactols were dissolved in dichloromethane containing Celite and to this solution PCC (15 mg) was added. The solution was stirred for 2 h at room temperature and filtered. The filtrate was washed with water and then brine and dried over anhydrous sodium sulfate. The usual work-up gave a crude lactone which was purified by means of preparative TLC with 1:1 benzene–diethyl ether to give 4 mg of lactone **25**.

Catalytic Reduction of 2,2-Dimethylcholest-4-en-3-one 28. Enone **28** (280 mg) in ethanol (15 ml) containing Pd-C (30 mg) was placed in a round-bottomed flask and was stirred in an atmosphere of hydrogen for 6 h at room temperature. After the removal of the catalyst and the solvent the residue was recrystallized from methanol–acetone to yield 2,2-dimethyl-5β-cholestan-3-one (**30**), mp 79.5—81.0 °C. ^{1}H NMR (90 MHz) 0.68 (3H, s, 18-H), 0.99 (3H, s, 19-H), 1.05 and 1.19 each 3H, each s, *gem*-dimethyl), 1.97 (1H, dd, J=3.6 and 15.7 Hz, 4β-H), and 2.93 (1H, dd, J=14.3 and 15.7 Hz, 4α-H); IR 1706 cm^{-1} (C=O); MS (70 eV) *m/z* (rel intensity) 414 (M^+, 100), 396 (55.4), 381 (51.4), and 259 (54.0). Found: C, 83.96; H, 12.22%. Calcd for $C_{29}H_{50}O$: C, 83.99; H, 12.15%.

The combined filtrates from the recrystallization was collected and after the removal of the solvent the residue was subjected to preparative TLC to give an isomeric ketone **29** identical with the authentic specimen.[12] The ratio of the yields of ketones **29** and **30** in this catalytic hydrogenation was 3:17.

Reduction of 2,2-Dimethyl-5β-cholestan-3-one (30) with Sodium Borohydride. The 3-ketone **30** (200 mg) in ethanol (20 ml) containing $NaBH_4$ (200 ml) was stirred for 2 h at room temperature. After the addition of water, the solution was extracted with dichloromethane. The solution was washed with water and then brine, and dried over anhydrous sodium sulfate. After the usual work-up, the crude 3-ols **31** and **32** were recrystallized from methanol. Mp 97.5—98.5 °C. ^{1}H NMR (270 MHz) 0.64 (3H, s, 18-H), 0.89 and 0.91 (each s, 19-H of 3α-ol and 3β-ol), 0.95 and 0.99 (each 3H, each s, *gem*-dimethyl), and 3.35—3.41 (1H, m, 3α- and 3β-H); IR 3300 cm^{-1} (OH), 1070, and 1022 cm^{-1}; MS (70 eV) *m/z* (rel intensity) 416 (M^+, 12), 398 ($[M-H_2O]^+$, 100), 383 (41.9), 328 (86.6), 316 (32.5), 243 (50.3), and 95 (15.1). Found: (C, 83.83; H, 12.42%).

The Photolysis of the Hypoiodite of 2,2-Dimethyl-5α-cholestan-3β-ol (32) in the Presence of Lead Tetraacetate and Iodine. The 3β-alcohol (100 mg, 0.24 mmol) in benzene (15 ml) containing lead tetraacetate (321 mg, 0.73 mmol) and iodine (184 mg, 0.73 mmol) was irradiated for 2.5 h as described for the photolysis of cholesterol. After the usual work-up, the product was subjected to preparative TLC with a 10:1 benzene–diethyl ether to give two fractions. The more mobile fraction (31 mg) was gummy lactol acetate **34**. ^{1}H NMR (90 MHz) 0.66 (3H, s, 18-H), 1.03 (3H, s, 19-H), 1.44 (3H, s, 2-Me), 2.06 (3H, s, OAc), 3.40 (2H, br. s, CH_2I), and 5.88 (1H, br.d, J=9.7 Hz, 4-H); MS (70 eV) *m/z* (rel intensity) ($[M-CH_3COOH]^+$, 0.7), 525 ($[M-CH_3COOH-Me]^+$, 1.7), 459 ($[M-CH_2I]^+$, 11), 413 (29.9), 399 (39.4), and 83 (100). Found: *m/z* 540.28212 $(M-CH_3COOH)^+$. Calcd for $C_{29}H_{49}OI$: M, 540.28292.

The less mobile fraction (31 mg) was a gummy lactol **35** which was recrystallized from acetonitrile. Mp 117—119 °C. ^{1}H NMR (90 MHz) 0.65 (3H, s, 18-H), 1.02 (3H, s, 19-H), 1.23 and 1.29 (each 3H, each s, *gem*-dimethyl), and 5.01 (1H, dd, 4-H); IR 3412 cm^{-1}, 1103, 1030, and 1001; MS (70 eV) *m/z* (rel intensity) 414 ($[M-H_2O]^+$, 39), 399 (25.0), 359 (45.2), 314 (44.8), 201 (41.7), and 83 (100). Found: *m/z* 414.38753 $(M-H_2O)^+$. Calcd for $C_{29}H_{50}O$: M, 414.38613.

The Photolysis of the Hypoiodite of 2,2-Dimethyl-5β-cholestan-3α- (31) and 3β-ol (32) in the Presence of Lead Tetraacetate and Iodine. (a) The mixture of 3α- and 3β-alcohols, **31** and **32** (77 mg, 0.19 mmol) in benzene (15 ml) containing lead tetraacetate (245 mg, 0.56 mmol) and iodine (141 mg, 0.56 mmol) was irradiated for 2 h as described for an isomeric 5α-ol hypoiodite above. After the usual work-up the product was subjected to preparative TLC with 5:1 benzene–diethyl ether to give three fractions. The most mobile fraction (18 mg) was an intractable mixture. The second (15 mg) and the third fractions (39 mg) were found to be identical and was a mixture of two lactols **37** and **38**. The second fraction was most probably the corresponding acetate **36** but it was probably hydrolyzed during its extraction from the TLC plates. The mixture of **37** and **38**. ^{1}H NMR (270 MHz) 0.65 (s, 18-H), 0.67 (s, 18-H of C-4 isomer), 0.91 (s, 19-H), 1.02 (s, 19-H of C-4 isomer), 1.15, 1.19, 1.32 and 1.37 (each s, *gem*-dmethyl of two C-4 isomers), 5.11 (dd, J=2.2 and 8.5 Hz, 4-H), 5.21 (dd, J=5.5 and 5.7 Hz, 4-H of C-4 isomer); 414 ($[M-H_2O]^+$, 40.2), 399 (60.3) 314 (41.6), 259 (45.9), and 43 (100); IR 3390 cm^{-1} (OH) and 1042. Found: *m/z* 414.38450 $(M-H_2O)^+$. Calcd for $C_{29}H_{50}O$: M, 414.38610.

(b) In the Presence of Pyridine. The mixture of 3α- and 3β-alcohols, **31** and **32** (112 mg, 0.27 mmol) in benzene (17 ml) containing lead tetraacetate (357 mg, 0.81 mmol), iodine (205 mg, 0.81 mmol) and pyridine (0.1 ml) was irradiated for 4 h as described above. After the work-up of the reaction mixture by the usual method, the product was subjected to preparative TLC to give three fractions. The most mobile fraction was a gummy secoaldehyde **39** (30 mg). ^{1}H NMR (270 MHz), 0.66 (3H, s, 18-H), 1.16 (3H, s, 19-H), 1.80 (3H, s, 2-Me), 2.52—2.81 (2H, m, 4-H), 4.70 and 4.86 (each 1H, each s, 2-methylene), and 9.64 (1H, dd, J=3.3 and 0.7 CHO); IR 2705 cm^{-1} (aldehydic CH), 1720 (CHO), and 890 (C=CH_2); MS (70 eV) *m/z* (rel intensity) 414 (M^+, 4), 399 ($[M-Me]^+$, 4), 359 (51), 341 (44.9), 315 (76.2), and 57 (100). Found: 414.38752 (M^+). Calcd for $C_{29}H_{51}O$: M, 414.38612.

The second fraction (29 mg) was an intractable mixture. The third fraction (27 mg) was lactols **37** and **38**.

The Photolysis of the Hypoiodite of 5α-Androstan-17β-ol (40). The 17β-ol (100 mg, 0.36 mmol) in benzene (20 ml) containing lead tetraacetate (482 mg, 1.09 mmol) and iodine (276 mg, 1.09 mmol) was irradiated under the conditions as

described for cholesterol hypoiodite. The work-up as usual gave a product which was subjected to preparative TLC with a 5:1 benzene–diethyl ether to give three fractions. The most and next mobile fractions were an intractable mixture. The least mobile fraction (25 mg) was lactol **41** which was identical with the authentic specimen.[15]

The Photolysis of the Hypoiodite of Cholesterol in the Presence of (Diacetoxyiodo)benzene. Cholesterol (100 mg) in dry benzene (15 ml) containing (diacetoxyiodo)benzene (166 mg) and iodine (131 mg) was flushed with a nitrogen and irradiated with mercury arc for 4 h. The solution was washed with a 5% aq sodium thiosulfate, aq sodium hydrogencarbonate and water and dried. Evaporation of the solution left a residue which was subjected to preparative TLC with a 4:1 benzene–diethyl ether to give a less polar iodo formate (25 mg, 18%) and a more polar cyclic ether **3** (14 mg, 10%).

Photolysis of the Hypoiodite of 4-Oxa-A-homocholest-5-en-3-ol (10) in the Presence of Mercury(II) Oxide and Iodine. (a) The lactol (238 mg) in dry benzene (35 ml) containing mercury(II) oxide (257 mg), iodine (300 mg) and pyridine (0.3 ml) in a Pyrex vessel was irradiated with a 100-W high pressure mercury arc in an atmosphere of nitrogen for 4.5 h. The photolyzed solution was worked up as described for the photolysis of cholesterol hypoiodite. The crude product (327 mg) was subjected to preparative TLC with 3:1 benzene–hexane to give three fractions. The most mobile fraction (122 mg) was an iodo formate **4** identical with the authentic specimen. The second fraction (35 mg) was identified to be a cyclic ether **3**[2a] by a comparison with the authentic specimen. The third fraction (77 mg) was once purified by preparative TLC to give a pure lactone **13** (60 mg) which was identical with the authentic specimen.

(b) The lactol **10** (41 mg) in dry benzene (5 ml) containing mercury(II) oxide (44 mg) and iodine (52 mg) was subjected to the photolysis under the conditions as described above. The work-up as described above gave iodo formate (30 mg, 56%) and cyclic ether (9 mg, 17%). No lactone **13** was detected in the crude product by TLC.

The Photolysis of the Hypoiodite of 2-Indanol (45) in the Presence of Lead Tetraacetate and Iodine. 2-Indanol **45** (150 mg, 1.11 mmol) in benzene (20 ml) containing lead tetraacetate (1.49 g, 3.35 mmol) and iodine (853 mg, 3.35 mmol) was irradiated for 1.5 h as described for cholesterol. The reaction mixture was worked up as usual. The product was subjected to preparative TLC with 10:1 benzene–diethyl ether to give four fractions. The most mobile fraction (24 mg, 6%) was 1,2-bis[iodomethyl]benzene (**47**) which was recrystallized from hexane. Mp 111—112 °C. IR 1147 and 766 cm^{-1}; ^1H NMR (90 MHz) 4.56 (4H, s, CH_2I) and 7.24 (4H, m, aromatic H); MS (70 eV) *m/z* (rel intensity) 358 (M^+, 3.4%), 231 ($[M-I]^+$ 100), and 104 ($[M-2I]^+$, 85.9).

The next mobile oily fraction (64 mg) was a mixture of 1:5:5 mixture of iodo aldehyde **48**, 2-indanol formate (**52**) and 2-(iodomethyl)benzylacetate (**49**) judged from the ^1H NMR. ^1H NMR (90 MHz) Iodo aldehyde **48**: 3.80 (2H d, *J*=1.8 Hz, CH_2CHO), 4.38 (2H, s, $-CH_2I$), and 9.77 (1H, t, *J*=1.8 Hz, CHO); formate **52**: 3.01 (2H, dd, *J*=6 and 17 Hz, benzylic H), 3.36 (2H, dd, *J*=6 and 17 Hz, benzylic H), 5.5—5.8 (1H, m, CHOCHO), and 7.98 (1H, s, OCHO); Iodide **49**: 2.12 (3H, s, OAc), 4.52 (2H, s, CH_2I), 5.21 (2H, s, CH_2–OAc), and 7.31 (4H, m, aromatic H). This mixture was again subjected to preparative TLC with 5:5:1 mixture of benzene–hexane–diethyl ether to give a 1:1 mixture of 2-indanol formate and 2-(iodomethyl)benzylacetate (4 mg). Further separation could not be achieved.

The next fraction (50 mg, 23%) was an oily 3,4-dihydro-2-benzopyran-3-ol acetate (**46**). ^1H NMR (90 MHz) 2.05 (3H, s, OAc), 2.83 (1H, dd, *J*=4.2 and 16.5 Hz, benzylic H), 3.19 (1H, dd, *J*=3.5 and 16.5 Hz, benzylic H), 4.83 (2H, d, *J*=2.2 Hz), 6.33 (1H, t, *J*=3.5 and 4.2 Hz, acetal-H); IR 1733 cm^{-1} (OAc) and [1220, 1196 and 1131 cm^{-1} (C–O)]; MS (70 eV) *m/z* (rel intensity) ($[M-CH_3COOH]^+$. 93%), and 104 (100 (CH_2-ϕ-CH_2)$^+$). Found: *m/z* 132.05632 ($M-CH_3COOH$)$^+$. Calcd for C_9H_8O: 132.05722.

The most polar fraction (58 mg) was a mixture which was subjected to preparative TLC with a 5:5:1 mixture of ethyl acetate–hexane–diethyl ether to give two fractions. The less polar fraction (11 mg, 4%) was a thick liquid 1,2-bis[acetoxymethyl]benzene **50**.[19]

The more polar fraction (25 mg, 12%) was an aldehyde **51**. IR (neat) 2723 cm^{-1} (CHO), 1724 (CHO), 1222 (OAc), and 1027 (C–O); ^1H NMR (90 MHz) 2.04 (3H, s, OAc), 3.77 (2H, d, *J*=1.8 Hz, CH_2CHO), 5.08 (2H, s, CH_2OAc), 3.35 (4H, m, aromatic H), and 9.72 (1H, t, *J*=1.8 Hz, CHO); *m/z* 191 ($[M-1]^+$, 0.2), 104 ($[M-OAc-CHO]^+$, 100) (Found: C, 68.92; H, 6.35. Calcd for $C_{11}H_{12}O_3$; C, 68.74; H, 6.29).

References

1) Photoinduced Molecular Transformations. Part 84. The general title of this series of papers has been "Photoinduced Transformations." till Part 82. Part 83. H. Suginome, M. Kaji, T. Ohtsuka, S. Yamada, and A. Furusaki, *J. Chem. Soc., Chem. Commun.*, in press.

2) a) H. Suginome, A, Furusaki, K. Kato, N. Maeda, and F. Yonebayashi, *J. Chem. Soc., Perkin Trans. 1*, **1981**, 236; b) H. Suginome and N. Maeda, *Bull. Chem. Soc. Jpn.*, **53**, 2621 (1980); c) H. Suginome and N. Maeda, *Bull. Chem. Soc. Jpn.*, **53**, 2616 (1980); d) H. Suginome, K. Kato, and T. Masamune, *Bull. Chem. Soc, Jpn.*, **54**, 3042 (1981); e) H. Suginome and F. Yonebayashi, *Bull. Chem. Soc. Jpn.* **55**, 517 (1982); f) H. Suginome, N. Maeda, Y. Seki, and K. Orito, *Bull. Chem. Soc. Jpn.*, **55**, 1643 (1982); g) A. Furusaki, C. Katayama, and H. Suginome, *Bull. Chem. Soc. Jpn.*, **55**, 3041 (1982).

3) H. Suginome, Y. Seki, S. Yamada, K. Orito, and N. Miyaura, *J. Chem. Soc., Perkin Trans. 1*, **1985**, 1431.

4) M. Akhtar and D. H. R. Barton, *J. Am. Chem. Soc.*, **86**, 1528 (1964).

5) C. Meystre, K. Heusler, J. Kalvoda, P. Wieland, G. Anner, and A. Wettstein, *Experientia*, **17**, 475 (1961).

6) For reviews. a) K. Heusler and J. Kalvoda, *Angew. Chem. Int. Ed. Engl.*, **3**, 525 (1964); b) J. Kalvoda and K. Heusler, *Synthesis*, **1971**, 501.

7) R. B. Woodward, A. A. Patchett, D. H. R. Barton, D. A. J. Ives, and R. B. Kelly, *J. Chem. Soc.*, **1957**, 1131.

8) H. Suginome and K. Kato, *Bull Chem. Soc. Jpn.*, **54**, 3223 (1981).

9) c. f. J. T. Edward, M. Kaufman, R. K. Wojtowski, D. M. S. Wheeler and T. M. Barrett, *Can. J. Chem.*, **51**, 1610 (1973).

10) L. Ruzicka and W. Bosshard, *Helv. Chim. Acta.*, **20**, 244 (1937); S. Mori and F. Mukawa, *Bull. Chem. Soc. Jpn.*, **27**,

497 (1954).

11) M. Amorosa, L. Caglioti, G. Cainelli, H. Immer, J. Keller, H. Wehri, M. L. Mihailovic, K. Schaffner, D. Arigoni, and O. Jeger, *Helv. Chim. Acta.*, **45**, 2674 (1962).

12) H. Suginome and S. Yamada, *J. Org. Chem.*, **49**, 3753 (1984) J. F. Biellmann and P. Witz, *Bull. Soc. Chim. Fr.*, **1964**, 737.

13) This compound was prepared by the method of Nedelec et al.[14] H. Suginome and M. Kaji, Unpublished results.

14) L. Nedelec, J. C. Gasc, and R. Bucourt, *Tetrahedron*, **30**, 3263 (1974).

15) H. Suginome and S. Yamada, *J. Org. Chem.*, **50**, 2489 (1985).

16) J. I. Concepcion, C. G. Francisco, R. Hernandez, J. A. Salazar, and E. Suarez, *Tetrahedron Lett.*, **25**, 1953 (1984).

17) The formation of several formates in the oxidation of cycloalkanols with lead tetraacetate alone[18] may be explained by assuming the similar mechanism.

18) M. L. Mihailović, Z. Ceković, V. Andrejevic, R. Matić, and D. Jeremić, *Tetrahedron*, **24**, 4947 (1968).

19) J. R. Mahajan and H. Carvalho, *Synthesis*, **1979**, 518.

 © 1987 The Chemical Society of Japan Bull. Chem. Soc. Jpn., 60, 1085—1089 (1987)

Reaction of Aromatic Acyl Chlorides with Potassium or Sodium Cyanide Impregnated onto Amberlite XAD Resins. Efficient Synthesis of Aromatic Acyl Cyanides

Kazuaki SUKATA
Nihon Tokushu Kagaku Kogyo Co., Ltd., 1, Takijiri-aza-hashimoto, Izumi-cho, Iwaki, Fukushima 970-04
(Received October 16, 1986)

The effects of alkali metal cyanide impregnated on Amberlite XAD resins (KCN/XAD, NaCN/XAD) have been examined using the cyanation of benzoyl chloride. In benzene, benzoyl cyanide was obtained in a very high yield with high selectivity under mild conditions. It is proposed that the reaction occurs on the surface of the resin. On the basis of the result obtained in the absence of any solvent, the reactivity of KCN/XAD toward dimerization of benzoyl cyanide has been found to be much poorer than that of KCN in solution. Although the reaction of acyl chlorides with KCN/XAD or NaCN/XAD in benzene gave various acyl cyanides in good to excellent yields, no aliphatic acyl cyanide could be obtained.

Acyl cyanides are versatile and important synthetic intermediates and have classically been prepared by the reaction of acyl chloride (**1**) with mercury(II) cyanide, silver cyanide, or copper(I) cyanide.[1] Subsequently, improved methods have been developed using thallium(I) cyanide,[2] trimethylsilyl cyanide,[3] tributyltin cyanide,[4] or acyl iodide.[5] Although these procedures give good results, the use of them are limited in view of the availability and cost of cyanating agents. Also the liquid–liquid two phase reaction of **1** with NaCN has been reported.[6] This reaction, however, gives substantial quantities of the acyl cyanide dimer (**3**) as well as the acyl cyanide (**2**).

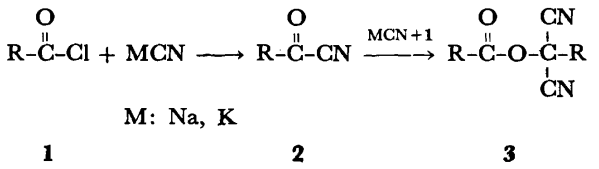

1 **2** **3**

Recently, it has been reported that the reaction of **1** with KCN is remarkably promoted by the addition of a trace amount of water[7] and irradiation with ultrasound[8] giving **2** in good yields. However, the former requires a high reaction temperature and the addition of a crown ether in the case of less reactive *p*-methoxybenzoyl chloride. In the latter, the yield of **3** is still high.

On the other hand, in a previous paper,[9] it has been reported that substitution reactions are accelerated by a simple impregnation of reagents on macroporous polymer resins such as Amberlite XAD-2, XAD-4, and XAD-7. These polymer resins have no ion-exchange capabilities and no phase-transfer catalysis functions. This paper reports that the reaction of aromatic acyl chloride with NaCN or KCN impregnated on XAD-2 or XAD-4 (NaCN/XAD-2,4 or KCN/XAD-2,4) gives **2** in good yields with high selectivities under mild conditions.

Results and Discussion

In order to ascertain the effect of solvents, the reaction of benzoyl chloride (**4**) with KCN/XAD-2 was carried out in various solvents. Table 1 shows the results. The coversion rate of **4** was in the order of acetonitrile $\gg$ benzene$>CH_2Cl_2$, hexane, tetrahydrofuran (THF), dioxane$\approx$no solvent. Although the reaction was extremely fast in acetonitrile, the benzoyl cyanide dimer (**5**) was obtained in very high yield (24%) even for the molar ratio KCN/**4**=1.0. For the molar ratio KCN/**4**=4.0, a large amount of unidentified product was produced. This result contrasts with that of the reaction of **1** with KCN using a trace amount of water or ultrasound in which acetonitrile was effective.[7,8] The yields of benzoyl cyanide (**6**) and **5** in acetonitrile were very similar to those obtained by phase-transfer catalysis.[6] Surprisingly, in the absence of any solvent, the yield of dimer (**5**) was extremely low. This fact indicates that the reactivity of the KCN impregnated on XAD-2 toward the dimerization of **6** is much poorer than that in solution. The yields of **5** in other solvents were very low and quite similar to that in the absence of any solvent. These facts indicate that in acetonitrile the reaction occurs substantially in the bulk organic phase, while in the other solvents, it occurs predominantly on the surface of the resin. Contrary to expectations, the reaction rates in THF and dioxane were similar to those in CH_2Cl_2 and hexane or in the absence of any solvent. Interestingly, when benzene was used as a solvent, **6** was produced in substantial quantities with high selectivity. Also, the reaction rate with benzene was faster than those in other solvents with the exception of acetonitrile.

On the other hand, the importance of a trace amount of water to attack the crystal lattice of the solid in solid-liquid two phase systems is well-known.[7,9,10,11] The same effect was also observed in the present reaction. In the case of THF, CH_2Cl_2, benzene, and hexane, the effect was examined. It was

observed that the addition of a trace amount of water substantially completed the conversion of **4** in 1—2 h. In THF or CH_2Cl_2, however, substantial quantities of benzoic anhydride (**7**) were produced along with **5** as by-products, and in hexane, **5** was produced in a substantial yield as a by-product. On the contrary, in benzene, the yield of by-products such as **5** and **7** was extremely low and was similar to that obtained in the absence of water.

Mass transfer strongly influences the reaction rate in heterogeneous systems.[12] In the present reaction, the mass transfer of substrate **4** from the bulk organic phase to the surface of the resin and the mass transfer of product **6** from the surface of the resin to the bulk organic phase will strongly affect the reaction rate. In the reaction without water, the rates of reaction in the solvents, except benzene and acetonitrile, were quite similar to that in the absence of any solvent. This fact indicates that the mass transfer of **4** from the bulk organic phase to the surface of the resin minimally affects the reaction rate.

At present, although I have no explanation why benzene is the best solvent, I suggest the following interpretation for the specific solvent effect of benzene: It is well-known that XAD-2 and XAD-4 resins can efficiently extract most organic compounds from

Table 1. Reaction of PhCOCl (**4**) with KCN/XAD-2 in Several Solvents[a]

Solvent	H_2O / μl	Time / h	Yield/%[b]			
			4	PhCOCN(**6**),	Dimer(**5**),	$(PhCO)_2O$(**7**)
None	—	2	34	51	1	≈0
Acetonitrile	—	2[c]	10	58	24	≈1
	—	0.5	0	18	0	0
THF	—	2	27	51	≈1	≈1
	10	2	5	67	1	12
Dioxane	—	2	35	45	≈1	≈1
CH_2Cl_2	—	2	26	59	≈1	<1
	10	2	≈0	83	≈2	7
Benzene	—	2	5	85	≈1	0
	10	1	0	89	2	<1
Hexane	—	2	21	54	1	0
	10	2	≈0	68	9	≈0

a) Unless otherwise noted, reactions were carried out with KCN(30 mmol)/XAD-2 (7.5 g), **4** (7.5 mmol), and a solvent (40 ml) at 30 °C. b) Yields were determined by GLC using dodecane for **4** and **6**, and dibenzyl ether for **5** and **7** as internal standards. c) KCN (10 mmol)/XAD-2 (2.5 g) and **4** (10 mmol) were used.

Table 2. Reaction of **4** Using Several Supports in Benzene[a]

Support	H_2O / μl	Temp / °C	Time / h	Yield/%[b]			
				4,	**6**,	**5**,	**7**
Alumina[c]	10	30	3	0	15	0	0
c, d)	10	30	0.5	0	0	0	0
e)	5	30	2	74	3	0	11
e)	—	30	2	77	3	0	6
Silica gel	10	30	2	0	<1	0	0
f)	5	30	2	19	2	0	31
f)	—	30	2	24	2	0	31
Activated C[g]	10	60	2	≈95	0	0	≈0
	—	60	2	≈95	0	0	0
XAD-2	10	30	2	≈0	89	2	<1
h)	10	30	2	≈0	86	2	<1
XAD-4	10	30	2	≈0	90	3	<1
h)	10	30	2	≈0	86	3	<1

a) Unless otherwise noted, reactions were carried out with KCN (30 mmol)/support (7.5 g), **4** (7.5 mmol), and benzene (40 ml). b) Yields were determined by GLC using internal standards. c) KCN (30 mmol)/Al_2O_3 (12.0 g) was used. d) No solvent was used. e) KCN (10 mmol)/Al_2O_3 (4.0 g), **4** (10 mmol), and benzene (20 ml) were used. f) KCN (10 mmol)/silica gel (2.5 g), **4** (10 mmol), and benzene (20 ml) were used. g) Granular activated charcoal was ground in a mortar. KCN (30 mmol)/activated C (12.0 g) was used. h) NaCN was used.

water.[13] Nonpolar compounds are more strongly adsorbed on these resins than polar compounds, and furthermore, aromatic compounds are much more strongly adsorbed on the resin than low-molecular-weight aliphatic compounds.[13] Similarly, in the present system, the XAD resin has such properties as previously described. Since product **6** is an aromatic and relatively polar compound, it must have a stronger affinity to the XAD resin than the solvent with the exception of benzene. Therefore, only in benzene, the cyanide (**6**) produced on the surface migrates much more effectively from the surface of the resin to the bulk organic phase. Consequently, the reaction of **4** with KCN is accelerated and the formation of by-products such as **5** and **7** is suppressed.

Table 2 summarizes the results of cyanation of **4** using several other supports. In the case of alumina, which is effective in the cyanation of alkyl halides,[14] for the molar ratio KCN/**4**=4.0, the conversion of **4** was very fast in the presence of a trace amount of water. The yield of **6**, however, was very poor and a large amount of tarry material was obtained. For the molar ratio KCN/**4**=1.0, the coversion was slow, and the main product was benzoic anhydride (**7**) in both the presence and absence of water. When silica gel was used, for the molar ratio KCN/**4**=1.0, the reaction was faster than that using alumina and gave mainly **7**. A substantial amount of water appeared to remain after drying. For the molar ratio KCN/**4**=4.0, although the conversion of **4** was fast, almost no product was isolated. In the impregnation of KCN onto the silica gel, the evolution of a substantial amount of HCN gas was observed when silica gel was added to an aqueous KCN solution. This HCN must be produced through the reaction of KCN with acidic silica ≡Si–OH.[15]

$$KCN + \equiv Si\text{–}OH \longrightarrow \equiv Si\text{–}OK + HCN$$

For the molar ratio KCN/**4**=4.0, most of **4** would react with ≡SiOK, being trapped on the silica-gel surface as ≡SiOCOPh. When activated charcoal was used as a support, almost all of **4** was recovered. The effect of XAD-4 was similar to that of XAD-2. The reaction using KCN/XAD was slightly faster than that using NaCN/XAD.

Table 3 summarizes the results of the cyanation of the other acyl chlorides using KCN/XAD in benzene. XAD-4 was superior to XAD-2 in reaction rate. This fact may be due to the difference in the surface area.[16] When R in **1** was a strong electron-attracting group such as *p*-chloro- or *p*-bromophenyl, the addition of water increased the yield of by-products such as the acyl cyanide dimer (**3**) and the acid anhydride. In the reaction of **4** in benzene, the increase in the reaction rate by the addition of water was small, though substantially no increase in the yield of by-products was observed (Table 1). These findings suggest that the merit of the addition of water is small with respect to the yield and selectivity.

Table 3. Preparation of Acyl Cyanides Using KCN/XAD in Benzene[a]

Acyl chloride	H_2O / μl	Resin[b]	Time / h	Yield[c] / %	Mp or Bp θ_m/°C (mmHg)	Lit. Mp or Bp θ_b/°C (mmHg)
PhCOCl	10	A	2	81 (89)	30—32	30—32[6]
	10	B	2	83 (90)		
p-MeC_6H_4COCl	10	A	5 (3)	92 (90)[d]	50—51	49.5—50[7]
	10	B	3	95 (98)		
o-MeC_6H_4COCl	0	B	2	82 (91)	76—77 (4)	75—76[8] (4)
p-$MeOC_6H_4COCl$	10	A	6	(80)[d]	57—58	57—58[8]
	10	B	3	87		
p-ClC_6H_4COCl	10	A	6	(58)	40.0—41.5	41.4—42.1[8]
	10	B	3	60 (68)		
	0	B	4	75 (85)		
p-BrC_6H_4COCl	10	B	2	70 (80)	61.5—62.5	62.5—64.0[7]
	0	B	4	84		
PhCH=CHCOCl	10	B	3	(36)	111—113	114.5—115.2[7]
	0	B	4	41		
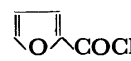	10	B	2	58 (80)	86—87 (15)	86—88[8] (15)
	0	B	2	73 (89)		
	0	A	4	(75)[d]		

a) All reactions were carried out with KCN (30 mmol)/XAD (7.5 g), acyl chloride (7.5 mmol) at 30 °C in benzene (40 ml). b) A: XAD-2; B: XAD-4. c) Isolated yields. Values in parentheses are the yields determined by GLC. d) Conversion percentage of acyl chloride determined by GLC.

Experimental

Materials. Acetonitrile, benzene, and hexane were dried with molecular sieves 3A or 4A. THF and dioxane were passed through an alumina column, distilled, and then dried with molecular sieves 4A. Dichloromethane was washed with aqueous Na_2CO_3, distilled, and then dried with molecular sieves 3A. Benzoyl chloride (**4**) was distilled prior to use. The other acyl chlorides were used as obtained (Tokyo Kasei Kogyo Co.). Authentic samples (benzoyl cyanide (**6**) and benzoyl cyanide dimer (**5**)) were prepared by the literature method,[6] and benzoic anhydride (**7**) was purchased from Wako Chemicals Co. Amberlite XAD resins were purchased from Organo Co., thoroughly washed with methanol, benzene–methanol (1:2 vol), and methanol, and then dried under vacuum. Alumina (Merck 90, neutral, 70—230 mesh, activity I, Art 1077) and silica gel (Merck 60, 70—230 mesh, Art 7734) were used as obtained. Activated charcoal was pulverized in a mortar. KCN/XAD and NaCN/XAD were prepared according to the method previously reported,[9] dried at 90 °C and 0.1 mmHg (1 mmHg=133.322 Pa).

Typical Procedure for the Reaction of Acyl Chloride (1) with KCN or NaCN/Support. In all reactions, **1** was directly added to the flask in which the KCN or NaCN/Support was made and dried. All the products were known compounds.

The Reaction of Benzoyl Chloride (4) with KCN/XAD-2 in Various Solvents. A mixture of KCN/XAD-2 made from KCN (1.95 g, 30 mmol) and XAD-2 (7.5 g) and a solvent (30 ml) with or without water (10 μl) was stirred for 1—2 min. To the mixture was added **4** (1.05 g, 7.5 mmol) in benzene (10 ml) and the resulting mixture was stirred for 2 h at 30 °C. The solid material was filtered off and eluted with benzene (70 ml) and CH_2Cl_2 (30 ml). After removal of most of the solvent under reduced pressure at room temperature, the yields of **4**, **5**, **6**, and **7** were determined by GLC (Silicone OV-17, 10%, 3 m×3 mm, 140 °C for **4** and **6**: Silicone OV-17, 3%, 0.5 m×3 mm, 200 °C for **5** and **7**). Internal standards for **4** and **6**, and **5** and **7** were dodecane and dibenzyl ether, respectively.

Benzoyl Cyanide (6): A solution of **4** (1.05 g, 7.5 mmol) in benzene (10 ml) was added to a mixture of KCN/XAD-4 made from KCN (1.95 g, 30 mmol) and XAD-4 (7.5 g), benzene (30 ml), and water (10 μl). The mixture was stirred for 2 h at 30 °C. The solid material was filtered through Celite and eluted with benzene (70 ml) and CH_2Cl_2 (30 ml). After removal of the solvent, the residue, which solidified immediately at room temperature, was recrystallized from hexane to give 0.81 g (83%) of **6**, mp 30—32 °C (lit,[6] mp 30—32 °C).

***p*-Methylbenzoyl Cyanide:** The reaction was performed with KCN (30 mmol)/XAD-4 (7.5 g), *p*-methylbenzoyl chloride (1.16 g, 7.5 mmol), water (10 μl), and benzene (40 ml) as a solvent for 3 h at 30 °C according to the same method as **6**. Removing the solvent gave 1.04 g (95%) of the cyanide, mp 49—51 °C (lit,[7] mp 49.5—50.0 °C) which was recrystallized from CH_2Cl_2–hexane to give pure *p*-methylbenzoyl cyanide, mp 50—51 °C.

***p*-Chlorobenzoyl Cyanide:** The reaction was performed with KCN (1.95 g, 30 mmol)/XAD-4 (7.5 g), *p*-chlorobenzoyl chloride (1.31 g, 7.5 mmol), and benzene (40 ml) as a solvent for 4 h at 30 °C according to the same method as **6**. Removal of the solvent gave 1.13 g of the crude product. To this product was added CH_2Cl_2 (1 ml) and the insoluble solid was filtered off. The filtrate was passed through a silica-gel column (10 cm) with CH_2Cl_2–hexane (1:4) as an eluent. Removing the solvent gave 0.93 g (75%) of *p*-chlorobenzoyl cyanide, mp 40.0—41.5 °C (lit,[8] mp 41.4—42.1 °C).

***p*-Bromobenzoyl Cyanide:** The reaction was performed with KCN (1.95 g, 30 mmol)/XAD-4 (7.5 g), *p*-bromobenzoyl chloride (1.65 g, 7.5 mmol) and benzene (40 ml) as a solvent for 4 h at 30 °C according to the same method as **6**. Removal of the solvent gave 1.32 g (84%) of *p*-bromobenzoyl cyanide, mp 60.5—62.0 °C (lit,[7] mp 62.5—64.0 °C), recrystallization of which from CH_2Cl_2–hexane gave the pure compound, mp 61.5—62.5 °C.

Cinnamoyl Cyanide: The reaction was performed with KCN (1.95 g, 30 mmol)/XAD-4 (7.5 g), cinnamoyl chloride (1.25 g, 7.5 mmol), and benzene (40 ml) as a solvent at 30 °C for 4 h according to the same method as **6**. Removal of the solvent gave 1.15 g of the residue, which was purified by silica-gel column chromatography (CH_2Cl_2–hexane, 1:3) to give 0.48 g (41%) of cinnamoyl cyanide, mp 111—113 °C (lit,[7] 114.5—115.2 °C).

2-Furoyl Cyanide: The reaction was performed with KCN (1.95 g, 30 mmol)/XAD-4 (7.5 g), 2-furoyl chloride (0.98 g, 7.5 mmol), and benzene (40 ml) as a solvent at 30 °C for 2 h according to the same method as **6**. Removal of the solvent gave 0.81 g (89% yield, 96% purity GLC) of the product, distillation of which gave 0.66 g (73%) of 2-furoyl cyanide, bp 86—87 °C/15 mmHg (lit,[8] bp 86—88 °C/15 mmHg).

I thank Nihon Tokushu Kagaku Kogyo Co., Ltd. for permission to publish this article.

References

1) S. Hünig and R. Schaller, *Angew. Chem., Int. Ed. Engl.*, **21**, 36 (1982); T. S. Oakwood and C. A. Weisgerber, *Org. Synth.*, Coll. Vol. III, 112 (1955).

2) E. C. Taylor, J. G. Andrade, K. C. John, and A. J. Mckillop, *J. Org. Chem.*, **43**, 2280 (1978).

3) K. Herrman and G. Simchen, *Synthesis*, **1979**, 204.

4) G. A. Olah, M. Arvanoghi, and G. K. Suryaprakash, *Synthesis*, **1983**, 636; M. Tanaka, *Tetrahedron Lett.*, **1980**, 2959.

5) K. Haase and H. M. R. Hoffmann, *Angew. Chem., Int. Ed. Engl.*, **21**, 83 (1982).

6) K. E. Koenig and W. P. Weber, *Tetrahedron Lett.*, **1974**, 2275.

7) M. Tanaka and M. Koyanagi, *Synthesis*, **1981**, 973.

8) T. Ando, T. Kawate, J. Yamawaki, and T. Hanafusa, *Synthesis*, **1983**, 637.

9) K. Sukata, *J. Org. Chem.*, **50**, 4388 (1985).

10) T. Ando, T. Kawate, J. Yamawaki, and T. Hanafusa, *Chem. Lett.*, **1982**, 935.

11) W. P. Weber and G. W. Gokel, "Phase Transfer Catalysis in Organic Synthesis," Springer-Verlag, Berlin (1977), p. 15.

12) M. Tomoi and W. T. Ford, *J. Am. Chem. Soc.*, **102**, 714 (1980); M. Tomoi and W. T. Ford, *ibid.*, **103**, 3821 (1981) and references cited therein.

13) A. K. Burnham, G. V. Calder, J. S. Fritz, G. A. Junk, H. J. Svec, and R. Willis, *Anal. Chem.*, **44**, 139 (1972); J. S. Fritz, *Ind. Eng. Chem., Prod. Res. Dev.*, **14**, 94 (1975); R. H. Kopp, *ibid.*, **14**, 96 (1975); E. H. Crook, R. P. McDonnell, and J. T. McNulty, *ibid.*, **14**, 113 (1975) and references cited therein.

14) S. L. Regen, S. Quici, and S.-J. Liaw, *J. Org. Chem.*, **44**, 2029 (1979); G. Bram, T. Filleben-Khan, and N. Geraghty, *Synth. Commun.*, **10**, 279 (1980).

15) Clark and Duke have described that the $(-O)_3SiCN$ species is produced in this impregnation: J. H. Clark and C. V. A. Duke, *J. Org. Chem.*, **50**, 1330 (1985). However, the formation of a Si–CN (hard-soft) bond from a Si–O (hard–hard) bond is difficult to believe. Moreover, if the species of $(-O)_3SiCN$ is present, it would react with acyl chloride to give acyl cyanide.[3] However, no acyl cyanide was actually obtained.

16) XAD-2: Surface area, 300 m^2/g; Av. pore diameter, 90 Å. XAD-4: Surface area, 780 m^2/g; Av. pore diameter, 50 Å.

 © 1987 The Chemical Society of Japan Bull. Chem. Soc. Jpn., 60, 1091—1095 (1987)

Substituent Effects. XVI.[1] Acetolysis of 2-Phenylethyl Tosylates[2]

Mizue Fujio, Kimito Funatsu, Mutsuo Goto, Yoji Seki, Masaaki Mishima, and Yuho Tsuno*
Department of Chemistry, Faculty of Science, Kyushu University, Hakozaki, Higashi-ku, Fukuoka 812
(Received October 16, 1986)

The acetolysis rates of 2-arylethyl tosylates were determined for a series of aryl substituents. The nonlinear substituent effect was reasonably accounted for on the basis of two linear LArSR relationships; one for the aryl-assisted (Fk_Δ) and one for the unassisted (k_s) processes, respectively. A precise dissection of the apparent substituent effect into individual effects for both processes was achieved in this manner. The substituent effect on the k_s process can be described as a linear function of σ° with a small ρ_s of -0.19, and that on the Fk_Δ process in terms of the LArSR Eq., with a $\rho_\Delta=-3.87$ and an $r_\Delta=0.631$. The use of σ^+ for the Fk_Δ process failed to give any reasonable dissection. The r value for this Fk_Δ process is essentially identical to that for the neophyl solvolysis. The unique r value of 0.6 is concluded to be characteristic of β-aryl-assisted ionization processes in general.

Anchimeric assistance in solvolyses has been the subject of a number of investigations.[3] The importance of neighboring phenyl participation can be estimated from the effects of aryl substituents, which have therefore been an important tool for analyzing the exact mechanism.[2-5] Solvolysis of neophyl brosylates (2-methyl-2-phenylpropyl *p*-bromobenzenesulfonates) has often been used as a reference set for the substituent effects on aryl-assisted solvolyses,[4b,6,7] and we have recently reported[8] that the substituent effect on the neophyl acetolysis can be described by a unique r value of 0.56 in our LArSR Eq.[9]

$$\log (k/k_o) = \rho(\sigma^\circ + r\Delta\bar{\sigma}^+_R) \quad (1)$$

This appreciably exalted r value was taken as evidence for a direct π-delocalization interaction between the aryl π-system and the β-carbocation center, i.e., a bridged structure, in the rate-determining transition state.[9,10] The most important conclusion from general LArSR analysis is that the r value can be a unique parameter characteristic of the structure of the transition state.[9] While the r parameter is a sensitive measure of the resonance demands of varying systems, it usually shows little or no variation within a family of essentially the same mechanism. It is therefore expected that the substituent effect for β-aryl-assisted solvolyses can be characterized by such a unique r value, in contrast to the traditional σ^+ characterization.[5] Accordingly, this investigation was undertaken in an attempt to define more precisely the substituent effect for the anchimerically assisted processes of 2-arylalkyl solvolysis systems.

In the acetolysis of 2-arylethyl tosylates chosen for the present study as well as in most such 2-arylalkyl solvolyses, the precise analysis of substituent effects on the rate suffers from the mechanistic complexity caused by the concurring solvent-assisted process.[2-5] The observed solvolysis rate k_t corresponds to a sum of rates, k_s+Fk_Δ, of two competing processes, aryl-assisted (Fk_Δ) and unassisted (k_s) ones. A useful way for the direct analysis of the two substituent effects has been exploited by Schleyer et al.,[4] on the basis of the assumption of a Hammett-type substituent effect correlation for the respective processes. Although this treatment achieved reasonable dissection into k_s and Fk_Δ processes, their data set involving only a few strongly activating substituents is insufficient to define precisely the substituent effect for the anchimerically assisted process. In the present study, we have extended the range of substituents of 2-arylethyl tosylates and analyzed the respective substituent effects on the k_s and Fk_Δ processes, in terms of the LArSR Eq. 1.

Results and Discussion

Rate constants of acetolysis of 2-arylethyl tosylates were determined at 115.00 °C in glacial acetic acid with initial concentrations (0.02 mol dm^{-3}) of tosylates. All runs gave good first order kinetics over more than two half-lives. The rate constants were reproducible to better than ±1% for repeated runs in a single batch of solvent, while they differed sometimes by 5—10% in different solvent batches; thus, the rate data were normalized each time to the rate of a reference substrate. The results are summarized in Table 1. As Schleyer's k_t values were found to be consistently lower than the present data by a factor of 10%, the k_t values for *m*-F, *m*-CF_3, *p*-CF_3, and 3,5-$(CF_3)_2$ derivatives calibrated by this factor were included in the present analysis.

Logarithms of relative rates are plotted against σ° and σ^+ in Fig. 1. The nonlinear behavior of the substituent effect with either set of substituent constants was pointed out earlier for this acetolysis,[3] and was accounted for by varying competition of the two non-crossover processes with the change of aryl

Table 1. Acetolysis Rate Constants of 2-Phenylethyl Tosylates

Substituents	Temp/°C	$10^5 k_t/s^{-1}$ Present study	Lit. values[a]
4-OCH_2CH_2-3[b]	75.00	2.79 ±0.04	
	90.00	13.1 ±0.2	
	100.00	35.3 ±0.4	
	115.00	137[c,d]	
4-MeO-3-Me	75.00	1.96 ±0.03	
	90.00	9.12 ±0.15	
	100.00	23.4 ±0.3	
	115.00	89.3[c,e]	
p-MeO	75.00	0.867±0.001	
	90.00	4.258±0.042	
	100.08	11.22 ±0.08	
	115.00	43.4 ±0.4[f]	40.0
3,4,5-Me_3	115.00	10.26 ±0.03	
p-C_6H_5O	115.00	6.86 ±0.07	6.10
2-Fluorenyl	115.00	6.82 ±0.04	7.00
3,4-Me_2	115.00	6.37 ±0.02	
p-MeS	115.00	5.43 ±0.02	
p-Me	115.00	3.892±0.002	
p-*t*-Bu	115.00	3.56 ±0.006	
4-MeO-3-Cl	115.00	3.275±0.006	
3,5-Me_2	115.00	2.322±0.008	
p-C_6H_5	115.00	1.903±0.005	
m-Me	115.00	1.68 ±0.01	1.62
H	115.00	1.309±0.001	1.27
4-MeS-3-Cl	115.00	1.196±0.005	
p-F	115.00	1.186±0.005	
4-MeO-3-CN	115.00	1.155±0.005	
p-Cl	115.00	0.931±0.002	0.845
p-Br	115.00	0.893±0.003	
4-MeS-3-CN	115.00	0.845±0.003	
m-F	115.00		0.761
m-Cl	115.00	0.790±0.001	0.728
p-CF_3	115.00		0.699
m-CF_3	115.00		0.689
p-NO_2	115.00	0.705±0.002	0.635
3,5-$(CF_3)_2$	115.00		0.584

a) Reference 4. b) 2-(2,3-Dihydrobenzofuran-5-yl)ethyl tosylate. c) Extrapolated from the rate constants at other temperatures. d) $\Delta H^{\ddagger} = 106.3$ kJ mol^{-1}, $\Delta S^{\ddagger} = -28.0$ J K^{-1} mol^{-1}. e) $\Delta H^{\ddagger} = 104.0$ kJ mol^{-1}, $\Delta S^{\ddagger} = -37.6$ J K^{-1} mol^{-1}. f) $\Delta H^{\ddagger} = 106.6$ kJ mol^{-1}, $\Delta S^{\ddagger} = -36.7$ J K^{-1} mol^{-1}.

substituent.[3] When the substituents are sufficiently deactivating, no participation by aryl is observed, and the compounds react exclusively by the unassisted (k_s) process. On the other hand, sufficiently electron-releasing substituents facilitate participation and such compounds react predominantly by the aryl-assisted (Fk_Δ) process.

The substituent effect on k_t ($=Fk_\Delta+k_s$) is given by

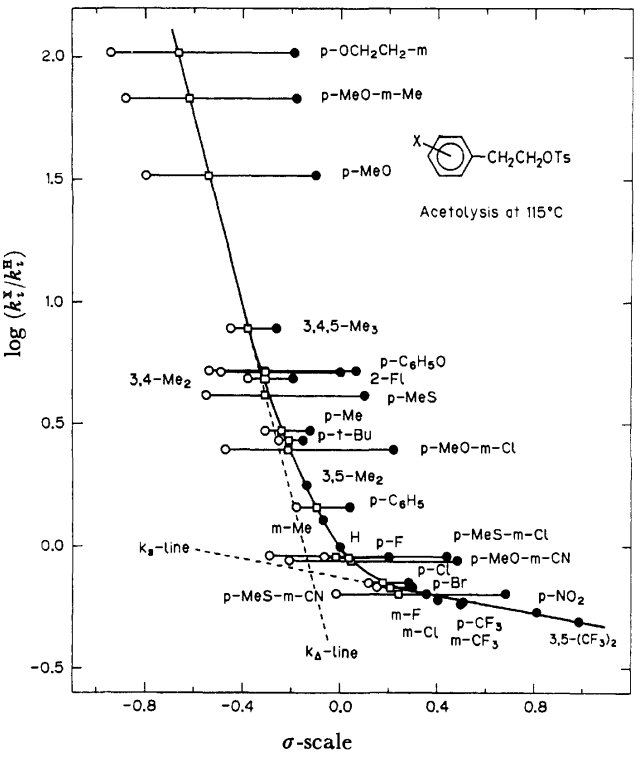

Fig. 1. Plots of log (k_t^X/k_t^H) against σ^+ (open circles), σ° (closed circles), and $\bar{\sigma}$ for $r=0.63$ (squares).

$$\log (k_t^X/k_t^H) = \log (k_s^X/k_s^H) + \log (1+Fk_\Delta^X/k_s^X) + C_s$$

or

$$= \log (Fk_\Delta^X/Fk_\Delta^H) + \log (1+k_s^X/Fk_\Delta^X) + C_\Delta$$

where C_s and C_Δ are constants referred to $\log (k_s^H/k_t^H)$ and $\log (Fk_\Delta^H/k_t^H)$, respectively. When the second terms on the right hand side are neglected, simple Hammett-type relations may be obtained with appropriate sets of substituent constants, $\bar{\sigma}_s$ and $\bar{\sigma}_\Delta$, for the k_s and Fk_Δ processes, respectively,

$$\log (k_t^X/k_t^H) = \rho_s\bar{\sigma}_s + C_s \quad \text{for extreme case of } k_s \gg Fk_\Delta$$

and

$$= \rho_\Delta\bar{\sigma}_\Delta + C_\Delta \quad \text{for the other extreme } Fk_\Delta \gg k_s.$$

The substituent effect on the k_s process may be treated simply with σ°, since the process involves no direct π-interaction between the aryl group and the reaction center. This permits the evaluation of the Fk_Δ values as the residues k_t-k_s for respective substituents and then the Fk_Δ substituent effect may be analyzed in terms of an appropriate $\bar{\sigma}_\Delta$. This is essentially the basis of Schleyer's treatment.[4] The aryl-assisted process is thought to involve a significant direct π-interaction between the aryl and reaction center, and the substituent effect should be described by a set of substituent constants of the σ^+ type. Thus, Schleyer employed σ^+ as an appropriate $\bar{\sigma}_\Delta$ in his original

analysis[4a] but later reported an appreciably improved result by use of the $\bar{\sigma}_\Delta$ from neophyl acetolysis.[4b] Such an appropriate $\bar{\sigma}_\Delta$ set would be described reasonably by the LArSR Eq. 1. Our analysis has therefore been carried out based on the explicit assumption that the LArSR Eq. 1 applies to both the k_Δ and k_s processes of this solvolysis. The best-fit Fk_Δ correlation was given by ρ_Δ=−3.87 and r_Δ=0.631, and the k_s correlation, ρ_s=−0.186 with σ^o (r=0.00).[11] The combined correlation reproduces the $\log(k_t^X/k_t^H)$ values with excellent precision (SD=±0.027), and the fit is distinctly better than the dissection based on σ^+ as the reference $\bar{\sigma}_\Delta$ (SD=±0.10). While a precise LArSR analysis has been achieved statistically,[11] direct graphical analysis in terms of the LArSR Eq. 1 appears to be important in order to verify the LArSR analysis and to understand the nature of the Fk_Δ substituent effects.

Figure 1 is the ordinary LArSR plot for the present system. The line segments between σ^+ and σ^o for the para π-donors represent resonance capabilities, i.e., $\Delta\bar{\sigma}_R^+$ values, of the respective substituents. The LArSR correlation should in general be represented by a single straight line for all substituents, and especially for para π-donors, the line divides all resonance segments at a constant internal ratio corresponding to the r value. For the present system, however, no single straight line correlation was obtained. The nonlinear correlation is of course inevitable because of the mechanistic complexity as described above.

The key principle of this graphical analysis is that only with appropriate $\bar{\sigma}_s$ and $\bar{\sigma}_\Delta$ sets, will the apparent k_t plot result in a single monotonic curvature converging to the theoretical correlation lines at either the activating or deactivating end. All meta substituents as well as para π-acceptors can unequivocally define the k_t correlation, even if nonlinear, in terms of standard σ^o constants, since they are not susceptible to resonance demands (i.e., $\bar{\sigma}_\Delta=\bar{\sigma}_s=\sigma^o$). Such a correlation curve (solid line) ranging from 3,5-Me_2 to 3,5-$(CF_3)_2$ in Fig. 1 should be a rigid reference for analyzing the behavior of the para π-donor substituents susceptible to resonance demands. Clearly the k_t correlation curve can be extrapolated almost linearly toward the activating substrates so as to intersect the resonance segments all at a single point giving a constant ratio of 2:3. This unique ratio refers to the r value of the $\bar{\sigma}_\Delta$ set. Although the plots (squares) in Fig. 1 are shown against the statistically best-fit $\bar{\sigma}_\Delta$ set of r=0.63, there is essentially no difficulty in defining such an intersecting correlation line for p-π-donors even without the aid of the known r value. The LArSR $\bar{\sigma}_\Delta$ plots (squares) all collapse into a single smooth curve determined by r-independent groups. The plot for the activating substrates is sufficiently linear to accurately define the converging Fk_Δ correlation line with a ρ_Δ value of −3.87. The k_s correlation line can also be defined as the tangent line for the k_t curve at the deactivating end, giving a ρ_s value of −0.19. Both correlation (dotted) lines cross at 0.30 log-units below the k_t curve, as required for $k_s=Fk_\Delta=k_t/2$. While the k_t curve intersects the line segments of π-donors at points in between their $\bar{\sigma}_\Delta$ and σ^o values in the crossover section, this is just what is expected for the effective contribution from concurrent k_s process of σ^o-dependence.

On the other hand, neither the σ^o nor the σ^+ plot gives any reasonable single Fk_Δ correlation line connecting smoothly to the k_t-curve. The σ^+ plot splits into three separate curves one each for strong para π-donors, weak ones (alkyl and halogen groups), and resonance-invariant substituents. The σ^+ and LArSR $\bar{\sigma}_\Delta$ correlations are contrasted most sharply by the behavior of the less activating strong π-donors, especially, m-substituted p-MeO and p-MeS derivatives.[12] These disubstituted derivatives have been shown to satisfy the LArSR relationship as united substituents having net $\Delta\bar{\sigma}_R^+$ values comparable to their parent para π-donors.[12] A series of p-π-donors with the same $\Delta\bar{\sigma}_R^+$ should provide a linear plot against σ^+ value with a slope identical to the true ρ value, regardless of the r of the system, since the $r\Delta\bar{\sigma}_R^+$ term in Eq. 1 remains constant for these groups. In fact, the σ^+ plots of strong π-donors with $\Delta\bar{\sigma}_R^+$=−0.6—−0.7 fall on a single line slightly curved at the bottom, covering a reactivity of over 10^2, with an identical slope to the LArSR ρ_Δ value. Similarly, the weak π-donors with $\Delta\bar{\sigma}_R^+$ of −0.15—−0.2 fall on another line with nearly the same slope, lying rather close to reference k_t curve. Note that neither line collapses into the reference k_t correlation curve, and the gap between the lines which should correspond to the $(1-r)\Delta\bar{\sigma}_R^+$ term in LArSR Eq. can be eliminated to coalesce to a single line, by use of $\bar{\sigma}_\Delta$ with an appropriate r value. While there is controversy concerning the real merit of r parameter,[13] it is evident that an intermediate r value is the inevitable requirement in order to account for the substituent effect on the Fk_Δ process of the present reaction.

The above LArSR results are all consistent with the presently accepted mechanism. The complete dissection attained with the k_t substituent effect provides strong support for the accepted competition mechanism, consisting of a non-crossover k_s and a k_Δ processes. The small ρ_s value for the k_s process may be attributed primarily to the relatively long distance between the substituents and the reaction center, as well as the intrinsic S_N2 character of the transition state involving less effective charge separation. The exalted r_Δ value for the assisted process provides evidence for a direct π-delocalization interaction between the aryl π-system and the β-carbocation center in the rate-determining transition state, and further

suggests that the charge delocalization in this aryl-assisted transition state should not be as effective as the benzylic π-delocalization in the 1-methyl-1-phenylethyl solvolysis. The large ρ_Δ value compared with those for the ordinary unassisted β-solvolyses[3] of structurally equivalent systems is also in line with the bridged transition state.

Finally, it should be emphasized that the ρ_Δ and r_Δ values for the present Fk_Δ process are nearly identical with those for the neophyl solvolysis.[8] Furthermore, similar ρ_Δ and r_Δ values have also been obtained for other aryl-assisted processes. It therefore appears likely that the substituent effect for the β-aryl-assisted process can be characterized by this unique r value. An important criticism against our LArSR concept is that the deviation of r from unity or zero may be caused by the mechanistic complexity of the system.[13] The aryl-assisted process of 2-phenylethyl tosylates is indeed a complex one involving significant internal return.[14] On the other hand, neophyl brosylate is thought to solvolyze via a rate-determining aryl-assisted transition state uncomplicated by either internal return or nucleophilic solvent assistance. The essential identity of r_Δ values for both β-aryl-assisted processes indicates that the r value should be determined only by the common rate-determining step, aryl-assisted ionization without return. This fact strongly argues against the interpretation of an intermediate r value in terms of the mechanistic complexity of the reaction.[2,8] As a conclusion, the r value of 0.6 must be characteristic of aryl-assisted ionization process, and the resonance demand of the Fk_Δ process differs intrinsically from the demand r=1.00 defined by the 1-methyl-1-phenylethyl solvolysis. Further discussion will require comparative studies on related systems which involve varying degrees of mechanistic complexity, and also a detailed examination of the results of the statistical analysis.

Experimental

Material. Most of the phenylacetic acids were prepared by the Willgerodt reaction of the appropriate acetophenones. 2-Phenylethyl alcohols were obtained by $LiAlH_4$ reduction of the corresponding acids or esters, as described previously.[2]

2-(3-Cyano-4-methoxyphenyl)ethanol was prepared from *p*-methoxyphenylacetic acid. Bromination of *p*-methoxyphenylacetic acid with Br_2 in acetic acid at 40—45 °C gave 4-MeO-3-Br-phenylacetic acid, mp 116—117 °C, recrystallized from ethanol-water. 4-MeO-3-Br-phenylacetic acid was treated with $LiAlH_4$ and immediately decomposed, since prolonged reaction caused a considerable loss of the bromo group. The crude alcohol, bp 149—151 °C/3 mmHg (1 mmHg=133.322 Pa), containing 5% 2-(*p*-methoxyphenyl)ethanol, was treated with CuCN in DMF and decomposed with $FeCl_3$–HCl, according to the Friedman and Shechter procedure,[15] to give 2-(4-MeO-3-CN-phenyl)ethanol, bp 179—180 °C/3 mmHg, after purification through SiO_2 column.

2-(3-Cyano-4-methylthiophenyl)ethanol was prepared in a similar way as the *p*-MeO derivative. Quick bromination with 2 equiv bromine at 45 °C gave crude acid contaminated with methylsulfoxide derivative which was purified by SiO_2 chromatography, mp 102—103 °C. 2-(4-MeS-3-Br-phenyl)-ethanol and 3-cyano-4-methylthio derivative were purified by chromatography, mp 58—59 °C and mp 40—41 °C.

2-(*p*-Bromophenyl)ethanol was prepared in the usual manner from *p*-bromoacetophenone, via methyl phenylacetate (bp 89—90 °C/0.25 mmHg); bp 103—104.5 °C/2.5 mmHg.

2-(Substituted phenyl)ethyl *p*-toluenesulfonates were synthesized from the corresponding alcohols and tosyl chloride by the Tipson procedure[16] and purified by recrystallization from appropriate solvents. Physical constants of most esters were reported in a previous paper,[2] or are described below.

2-(3-Cyano-4-methoxyphenyl)ethyl tosylate, mp 109.7—110.5 °C. Found: C, 61.57; H, 5.26; N, 4.31%. Calcd for $C_{17}H_{17}NO_4S$: C, 61.61; H, 5.17; N, 4.23%. 4-MeS-3-CN derivative, mp 77—77.5 °C. Found: C, 58.87; H, 4.72; N, 4.19%. Calcd for $C_{17}H_{17}NO_3S_2$: C, 58.77; H, 4.93; N, 4.02%. *p*-Br derivative, mp 91 °C. Found: C, 50.92; H, 4.34%. Calcd for $C_{15}H_{15}O_3SBr$: C, 50.71; H, 4.26%.

Kinetic Measurement. The acetolysis rates were measured by the titrimetric method using the usual ampoule technique. Ten cm^3 (0.02 mol dm^{-3}) aliquots were pipetted into 25 cm^3 of cold acetic acid containing sodium acetate (0.0088 mol dm^{-3}) and titrated with perchloric acid (ca. 0.025 mol dm^{-3}) in acetic acid. The mixture of crystal violet and α-naphtholbenzein was used as indicator.

References

1) For part 15, M. Sawada, M. Ichihara, Y. Yukawa, T. Nakachi, and Y. Tsuno, *Bull. Chem. Soc. Jpn.*, **53**, 2055 (1980).

2) Preliminary report, M. Fujio, K. Funatsu, M. Goto, Y. Seki, M. Mishima, and Y. Tsuno, *Tetrahedron Lett.*, **24**, 2177 (1983); *Mem. Fac. Sci., Kyushu Univ., Ser. C*, **14**, 177 (1983).

3) C. J. Lancelot, D. J. Cram, and P. v. R. Schleyer, "Carbonium Ions," ed by G. A. Olah and P. v. R. Schleyer, Wiley-Interscience, New York (1972), Vol. 3, Chap. 27, p. 1347.

4) a) J. M. Harris, F. L. Schadt, P. v. R. Schleyer, and C. J. Lancelot, *J. Am. Chem. Soc.*, **91**, 7508 (1969); b) F. L. Schadt III, C. J. Lancelot, and P. v. R. Schleyer, *ibid.*, **100**, 228 (1978).

5) C. J. Lancelot and P. v. R. Schleyer, *J. Am. Chem. Soc.*, **91**, 4291 (1969); C. J. Lancelot, J. J. Harper, and P. v. R. Schleyer, *ibid.*, **91**, 4294 (1969); C. J. Lancelot and P. v. R. Schleyer, *ibid.*, **91**, 4296 (1969); H. C. Brown, C. J. Kim, C. J. Lancelot, and P. v. R. Schleyer, *ibid.*, **92**, 5244 (1970); H. C. Brown and C. J. Kim., *ibid.*, **93**, 5765 (1971).

6) R. S. Bly, R. A. Mateer, K. K. Tse, and R. L. Veazey, *J. Org. Chem.*, **38**, 1518 (1973).

7) M. G. Jones and J. L. Coke, *J. Am. Chem. Soc.*, **91**, 4284 (1969).

8) Y. Tsuno, K. Funatsu, Y. Maeda, M. Mishima, and M. Fujio, *Tetrahedron Lett.*, **23**, 2879 (1982); M. Fujio, K. Funatsu, K. Shibata, H. Yoshinaga, Y. Maeda, M. Goto, M.

Mishima, and Y. Tsuno, *Mem. Fac. Sci., Kyushu Univ., Ser. C*, **14**, 319 (1984).

9) a) Y. Yukawa and Y. Tsuno, *Bull. Chem. Soc. Jpn.*, **32**, 971 (1959); b) Y. Yukawa, Y. Tsuno, and M. Sawada, *ibid.*, **39**, 2274 (1966).

10) T. Imamoto, S. G. Kim, Y. Tsuno, and Y. Yukawa, *Bull. Chem. Soc. Jpn.*, **44**, 2776 (1971).

11) Both the iterative least-squares method used by Schleyer[4] and nonlinear least-squares method (Newton method) were applied to the analysis. Identical result was obtained by assuming fixed r_s value at 0, 0.27 for reducing a variable. Use of $\bar{\sigma}_\Delta$ from neophyl solvolysis (r_Δ=0.58 a fixed) gave closely the same correlation; ρ_Δ=−4.04, ρ_s=−0.16 (r_s=0) with a good precision (SD=±0.036). Use of σ^+ for $\bar{\sigma}_\Delta$ (r_Δ=1.00 a fixed) gave a correlation; ρ_Δ=−3.55, ρ_s=−0.58 (r_s=0) with a lower precision (SD=±0.10); unreasonable ρ_s value and the position (k_s^H) may be noticed.

12) The σ^+ used were primarily based on the experimental values for *m,p*-disubstituted derivatives (M. Fujio, T. Adachi, Y. Shibuya, A. Murata, and Y. Tsuno, *Tetrahedron Lett.*, **25**, 4557 (1984)) and the $\Delta\bar{\sigma}_R^+$ values were given to be equal to those of *p*-substituents.

13) C. D. Johnson, *J. Org. Chem.*, **43**, 1814 (1978); C. D. Johnson, "The Hammett Equation," Cambridge University Press London (1973), p. 52.

14) J. L. Coke, F. L. McFarlane, M. C. Mourning, and M. G. Jones, *J. Am. Chem. Soc.*, **91**, 1154 (1969); Y. Tsuno, M. Fujio, Y. Seki, M. Mishima, and S. G. Kim, *Nippon Kagaku Kaishi*, **1977**, 1673; M. Fujio, Y. Seki, M. Mishima, and Y. Tsuno, *Mem. Fac. Sci., Kyushu Univ., Ser. C*, **11**, 119 (1978); Y. Seki, M. Fujio, M. Mishima, and Y. Tsuno, *ibid.*, **12**, 197 (1980); M. Fujio, Y. Seki, R. Fujiyama, M. Mishima, and Y. Tsuno, *ibid.*, **13**, 71 (1981).

15) L. Friedman and H. Shechter, *J. Org. Chem.*, **26**, 2522 (1961).

16) R. P. S. Tipson, *J. Org. Chem.*, **9**, 235 (1944).

 © 1987 The Chemical Society of Japan Bull. Chem. Soc. Jpn., 60, 1097—1101 (1987)

Substituent Effects. XVII.[1] Rearrangement in the Acetolysis of 2-Arylethyl Tosylates[2]

Mizue Fujio, Mutsuo Goto, Yoji Seki, Masaaki Mishima, Yuho Tsuno,*
Masami Sawada,† and Yoshio Takai†
Department of Chemistry, Faculty of Science, Kyushu University,
Hakozaki, Higashi-ku, Fukuoka 812
†The Institute of Scientific and Industrial Research, Osaka University,
Mihogaoka, Ibaraki, Osaka 567
(Received October 16, 1986)

The label scrambling within the ethylene chain of the final acetolysis products was determined for a series of α-D_2 labeled 2-arylethyl tosylates by using proton NMR spectroscopy and the k_Δ/k_s values were derived from the scrambling ratios. For both buffered and unbuffered acetolysis runs $\log(k_\Delta/k_s)$ were not correlated linearly with σ° or σ^+. Application of the LArSR Eq. results in linear correlations with excellent precision, $\log(k_\Delta/k_s)=-3.70\ (\sigma^\circ+0.63\Delta\bar{\sigma}^+_R)+0.152$ for the unbuffered run and $\log(k_\Delta/k_s)=-3.97\ (\sigma^\circ+0.60\Delta\bar{\sigma}^+_R)-0.207$ for the buffered run. The ρ_Δ and r_Δ values for the aryl-assisted pathway are estimated from the above apparent values based on the reasonable assumption of small ρ_s values for the k_s pathway.

The foregoing papers[1,3] described the dissection of the substituent effect on the acetolysis of 2-arylethyl tosylates into the effects on solvent-assisted (k_s) and anchimerically assisted (Fk_Δ) processes.[4] The dissection was based upon an assumption of the LArSR relationship (1)[5]

$$\log(k/k_o) = \rho(\sigma^\circ + r\Delta\bar{\sigma}^+_R) \quad (1)$$

for the respective substituent effects on the two competing processes. While the validity of the individual correlation was supported by the agreement with other experimental facts,[6] convincing evidence would be provided by a direct application of the LArSR relationship to the substituent effect on each process having been separated by a technique independent of the substituent effect analysis.

A kinetic analysis of the respective processes of the acetolysis of 2-arylethyl tosylates was accomplished by using ^{13}C tracer method for typical substituted derivatives.[2,7] Unfortunately, however, the substituents studied are inevitably limited and insufficient to attain a detailed correlation analysis of the substituent effects.

Among the pertinent quantities obtained in these tracer studies, the aryl rearrangement ratio in the product at $t=\infty$ is the useful quantity which can be determined most easily by using the α- or β-methylene-labeled compounds. This can be related directly to the rate ratio k_Δ/k_s by Eq. 2, based on the Winstein-Coke scheme of this reaction,[8a,9] as

$$k_\Delta/k_s = \frac{[\%\text{Rearrangement ROAc } (t=\infty)]}{50-[\%\text{Rearrangement ROAc } (t=\infty)]} \quad (2)$$

The substituent effect on the k_Δ/k_s value may be simply given as the difference of two linear Hammett relations for the k_Δ and k_s processes.

$$\log(k_\Delta/k_s)_X - \log(k_\Delta/k_s)_H = \log(k_X/k_H)_\Delta - \log(k_X/k_H)_s = \rho_\Delta\bar{\sigma}_\Delta - \rho_s\bar{\sigma}_s$$

where $\bar{\sigma}_\Delta$ and $\bar{\sigma}_s$ are the substituent constants appropriate for k_Δ and k_s processes, respectively. Furthermore, from the additivity of the LArSR correlations, the overall substituent effect on the k_Δ/k_s quantity will be treated totally as a single linear LArSR correlation. Thus the k_Δ/k_s substituent effect is quite different from the nonlinear behavior of the k_t substituent effect in the foregoing analysis.[1,3] Nevertheless, both quantities are only different functions of the same rate parameters, and hence a comparative analysis will give further information concerning the intrinsic substituent effect on respective processes.

Results

The label scrambling in the product 2-arylethyl acetate was determined for a series of α-D_2 labeled 2-arylethyl tosylates, by using proton NMR spectroscopy. k_Δ/k_s values were derived from the scrambling ratios based on Eq. 2. The results are listed in Table 1, and compared with the results of previous ^{13}C-tracer studies.[2] The k_Δ/k_s values were determined over a range of 10^4 ranging from the *p*-MeO derivative solvolyzing exclusively through a k_Δ process to the *m*-Cl one reacting primarily through a k_s process. At both extremes of nearly complete and no scrambling, the k_Δ/k_s value should rapidly become less accurate. Thus further extention of the range of substituents was not attempted in this study, but instead, in the present set were included deactivated strong π-donors, such as 3-Cl- or 3-CN-substituted 4-methoxyphenyl and 4-(methylthio)phenyl derivatives, which were found to be particularly effective for defining the *r* value.[10] The addition of sodium acetate lowered the rearrangement ratio for all substrates. The k_s process rather than k_Δ process may be effectively accelerated by the addition of acetate anion, while the substituent change of the ratio remains approximately the same in both buffered and unbuffered acetolyses.

The type of change of k_Δ/k_s with substituents differs

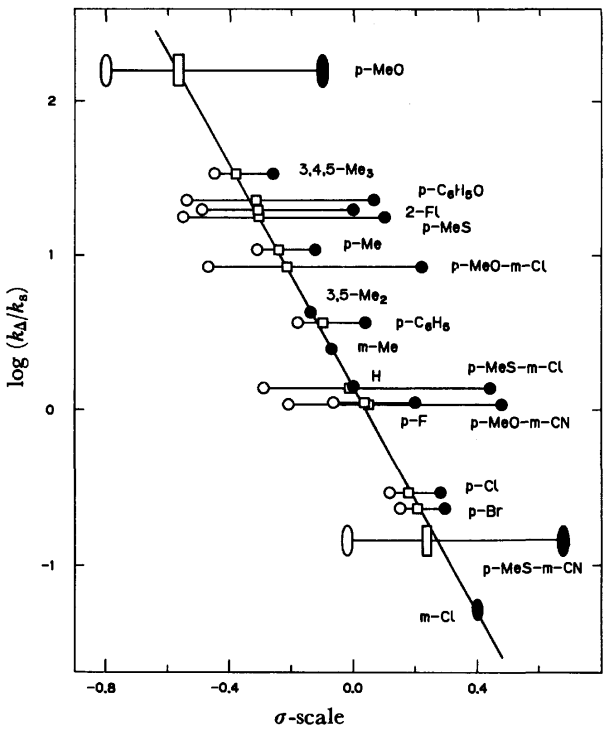

Fig. 1. The LArSR plot of log (k_Δ/k_s) for unbuffered run against σ^+ (open circles), σ° (closed circles), and $\bar{\sigma}$ for $r=0.63$ (squares).

clearly from that of k_t value. There is no simple linear logarithmic relationship between k_Δ/k_s ratios and k_t values. Figure 1 illustrates the substituent effect on log (k_Δ/k_s) quantity for the unbuffered run. Log (k_Δ/k_s) can not be correlated linearly with σ° nor with σ^+, but are linearly described in terms of the LArSR relationship. The line segments between σ° and σ^+ for para π-donors correspond to their $\Delta\bar{\sigma}_R^+$ values, and the LArSR $\bar{\sigma}$ values are represented by the points dividing these resonance segments at a unique internal ratio, which corresponds to the r value. Clearly, we see that such points (squares) with $r=0.63$ all fall on a straight line of a ρ value of -3.70 including m-substituents.

A least-squares application of LArSR Eq. 1 to the unbuffered k_Δ/k_s set results in a linear correlation (Fig. 1),

$$\log (k_\Delta/k_s)_X = -(3.70\pm0.05)(\sigma^\circ + (0.63\pm0.02)\Delta\bar{\sigma}_R^+) + 0.152 \quad (3)$$

with an excellent precision with an R=0.9990 and a SD=±0.042. The substituent parameters used are those employed for the previous analysis.[1] Similarly, the buffered set can also be correlated by (3′)

Table 1. Rearrangement of the Acetolysis Product of 2-(Substituted Phenyl)ethyl Tosylates[a] at 115 °C

Substituent	Without NaOAc		With NaOAc (0.06 mol dm^{-3})	
	%Rearr.[b]	k_Δ/k_s[c,d]	%Rearr.[b]	k_Δ/k_s[c,d]
p-MeO	>49.7[e]	160 (>125[f])	49.4±0.2	82
3,4,5-Me$_3$	48.6±0.1	34	47.3±0.3	17
p-C$_6$H$_5$O	47.9±0.1	23	45.3±0.3	9.6
2-Fluorenyl	47.6±0.2	20	45.0±0.3	9.0
p-MeS	47.4±0.3	18	44.3±0.3	7.8
p-Me	45.8±0.3	11 (11)	41.7±0.3	5.0 (5.8)
4-MeO-3-Cl	44.7±0.3	8.4	38.5±0.2	3.3
3,5-Me$_2$	40.7±0.3	4.4	34.6±0.2	2.2
p-C$_6$H$_5$	39.3±0.2	3.7	30.3±0.3	1.5
m-Me	35.8±0.3	2.5 (2.9)	27.9±0.3	1.3 (1.4)
H	29.2±0.3	1.4 (1.4)	18.7±0.2	0.60 (0.75)
4-MeS-3-Cl	29.0±0.2	1.4	16.9±0.1	0.51
p-F	26.5±0.3	1.1 (1.2)	15.9±0.3	0.47 (0.53)
4-MeO-3-CN	26.2±0.3	1.1	14.5±0.3	0.41
p-Cl	11.4±0.2	0.30 (0.33)	4.9±0.2	0.11 (0.13)
p-Br	9.5±0.1	0.23	4.2±0.1	0.09
4-MeS-3-CN	6.0±0.5	0.14	2.7±0.5	0.06
m-Cl	2.5±0.5	0.05 (0.04)	0	—
p-NO$_2$	0	—	0	—

a) Initial concn of α,α-D$_2$-labeled tosylates, 0.02 mol dm^{-3}; determined by ^{1}H NMR. b) Rearrangement in solvolysis products at complete reaction: 100×[Rearranged acetate]/[Total acetates]. c) Derived from %Rearrangement by Eq. 2. d) Values in the bracket were determined from α-^{13}C labeled tosylates by ^{13}C NMR; Ref. 2. e) At 90 °C. f) At 75 °C.

$$\log (k_\Delta/k_s)_{AcO^-} = (-3.97\pm0.05)(\sigma^\circ + (0.60\pm0.02)\Delta\bar{\sigma}_R^+) - 0.207 \quad (3')$$

with an excellent precision with an R=0.9988 and a SD=±0.045. Both r_Δ values are quite close to the r_Δ obtained for neophyl acetolysis.[10] Both buffered and unbuffered log (k_Δ/k_s) sets in fact give linear plots against log (k_X/k_H) of acetolysis of neophyl brosylates (2-methyl-2-phenylpropyl *p*-bromobenzenesulfonate) with comparable slopes of approximately unity.

Discussion

The linear LArSR correlation with k_Δ/k_s quantities for the entire range of substituents contrasts sharply with the nonlinear behavior observed for the total solvolysis rate of the same reaction. The substituent effects on electrophilic reactions are generally described by the LArSR Eq. 1,[5] in which any sets of apparent substituent constants can be given in a unified manner in terms of varying r characteristic of systems. This unified description of general substituent constants leads to a unique additivity relationship of substituent effects,

$$\Sigma \log (k/k_o)_j = \Sigma \rho_j(\sigma^\circ + r_j\Delta\bar{\sigma}_R^+) = \rho'(\sigma^\circ + r'\Delta\bar{\sigma}_R^+) \quad (4)$$

where $\rho'=\Sigma\rho_j$ and $r'=\Sigma\rho_j r_j/\Sigma\rho_j$. It should be noted that the overall substituent effect can be represented totally as a single linear LArSR correlation with an apparent r'. Mathematically, there is no direct way of differentiating between Eqs. 1 and 4, and of course, the apparent r' for a combined set in itself should have no direct theoretical significance. This is often an important cause of disagreement concerning the real merit of the r parameter,[11-14] as discussed further. The present quantity k_Δ/k_s can be treated, in a similar way, as the difference of the two LArSR correlations again resulting in a single linear LArSR correlation,

$$\log (k_\Delta/k_s)_X - \log (k_\Delta/k_s)_H = \rho_\Delta\bar{\sigma}_\Delta - \rho_s\bar{\sigma}_s = (\rho_\Delta-\rho_s)(\sigma^\circ + ((\rho_\Delta r_\Delta-\rho_s r_s)/(\rho_\Delta-\rho_s))\Delta\bar{\sigma}_R^+) \quad (5)$$

The apparent ρ' and r' values of the correlation (3) should therefore be only the combined values corresponding to $\rho_\Delta-\rho_s$ and $(\rho_\Delta r_\Delta-\rho_s r_s)/(\rho_\Delta-\rho_s)$, respectively. An important key to achieving a reasonable dissection will be provided by the characteristic feature of the k_s substituent effect. From the nature of the k_s reaction, the ρ_s should be small in absolute value and the r_s to be practically unexalted (r=0). A ρ_s value of −0.19±0.04 has been estimated from the k_t effects of sufficiently deactivated derivatives.[1,3] This permits estimation of the ρ_Δ value for the aryl-assisted process to be −3.89, as $\rho_\Delta=\rho'+\rho_s$. Furthermore, because of the small ρ_s value, any conceivable exaltation in r_s does not contribute effectively to the apparent r' value. Thus setting $\rho_s r_s\rightarrow 0$ in Eq. 5 as a reasonable approximation, the r_Δ value can be estimated to be 0.60±0.03. This is essentially the same as the r_Δ value for the Fk_Δ quantity obtained from the k_t analysis.

For the buffered run, acetate ion is known to exert a significant accelerating effect on k_s pathway but no important effect on the rate of aryl-assisted ionization of typical substituted derivatives. Assuming the same ρ_Δ value as for the unbuffered run, the ρ_s can be estimated to be a small positive value of +0.08, and subsequently the r_Δ value is determined to be 0.61±0.02. In fact, a small but positive ρ_s value was observed for the acetolysis rates (k_t) of electron-attracting derivatives in the presence of sodium acetate.[15]

The inherent additivity of LArSR Eq. inevitably causes serious difficulty in dissection of the apparent LArSR correlation (3 or 3'). It should however be noted that the linear analysis applied to the k_Δ/k_s quantity would generally accomplish a correlational result of much higher precision than the nonlinear method applied to the k_t analysis. A precise linear free energy relationship is generally indicative of a fixed mechanism for the reaction. Consequently, the precise conformity to Eqs. 4 or 5 implies that both processes satisfy each individual LArSR correlation for the entire substituent range, providing evidence for the absence of any mechanistic change-over in either process.

The validity of this dissection relies essentially upon the reasonableness of requirement $|\rho_\Delta| \gg |\rho_s|$. As far as this assumption is valid, the apparent r' value of 0.63 in Eq. 3 should not significantly differ from the intrinsic r value for the k_Δ process. Thus the present k_Δ correlation will permit quantitative discussion concerning the substituent effect on the k_Δ quantity as well as on the solvolytic aryl-assisted rate.

The aryl-assisted process of this solvolysis involves significant return from the intermediate, so that the apparent rate constant for this pathway is given as Fk_Δ using a fractionating factor F.[7-9] On the other hand, the present k_Δ quantity based on the product rearrangement is only concerned with the process by which the reactant experiences at least once a symmetrical phenonium intermediate, if any, along the aryl-assisted pathway. It should be emphasized that the k_Δ refers to the relative rate of formation of the first symmetrical intermediate and should be absolutely free from return or any subsequent processes. The identity of both r_Δ values derived from the present k_Δ/k_s and previous k_t analyses evidently indicates that the return process does not cause any significant effect on the ρ and r values for the aryl-assisted pathway. There is independent evidence for the F value of this system being essentially unchanged with substitu-

ents.[7-9] The observed r_Δ value should therefore be characteristic of the aryl-assisted ionization step for the phenonium ion intermediate.

Our results from the present study strongly argue against the contrary view that the deviation of the r value from unity or zero should be attributed for most cases to the complexity of mechanism.[11,12] This view is based exclusively on the use of σ^+ of constant resonance exaltation, termed as $1.00\Delta\bar{\sigma}_R^+$, for conjugative carbocation reactions. According to this traditional treatment, the substituent effect on k_Δ should be described by σ^+ and the effect on k_s by σ° (or σ),[12] and the overall effect on (k_Δ/k_s) quantity can be given as the difference of both effects. The situation is merely a special case $r_\Delta=1.0$ and $r_s=0.0$ of Eq. 5. While the r and ρ are mathematically indefinite in Eqs. 4 or 5, this specification of r enables us to give an unequivocal dissection. From the requirement, $r'=0.63\pm0.02=\rho_\Delta r_\Delta/(\rho_\Delta-\rho_s)$ and $\rho'=-3.70=\rho_\Delta-\rho_s$, this treatment should lead to a definite solution, $\rho_\Delta=-2.3$ and $\rho_s=1.4$. However, this ρ_s value is in serious disagreement with the ρ_s value of -0.19 derived from the k_t dissection. Use of σ (i.e., $r=0.27$) instead of σ° results in an even higher ρ_s value of 1.9. The ρ_s is not negative nor much lower than ρ_Δ in the absolute value when σ^+ is used for $\bar{\sigma}_\Delta$. If the k_s process has such a high, positive ρ_s value, the k_t substituent effect will have to exhibit a curved Hammett plot of significant V shape, which is evidently not the case in the present reaction. While the specification of r values, either 0 or 1, greatly simplifies the way of analysis for any complicated systems apparently satisfying Eq. 1, its definite dissection may not be a reasonable one but often an artifact of the treatment. This obvious conflict invalidates the traditional assumption of a constant resonance demand of $r=1$ generally for electrophilic resonance-exalted processes.

Experimental

Material. Deuterated Compounds. Substituted 2-phenylethan-1,1-d_2-ols were prepared in the usual manner from the corresponding substituted phenylacetic acids by reduction with $LiAlD_4$ (99%D) in ether and were converted into the *p*-toluenesulfonates using the Tipson procedure,[16] followed by recrystallization from appropriate solvents. Physical constants of the deuterated derivatives were generally identical with those of their protio derivatives.

Glacial Acetic Acid. Special grade acetic acid was distilled through a 40 cm glass helixes-packed column and a constant boiling fraction of 0.5 °C range (bp 117—117.5 °C) was collected.

Sodium acetate (special reagent grade) was dried on heating in vacuo immediately before use.

Acetolysis. Acetic acid solution 0.02 mol dm^{-3} of 2-arylethyl-1,1-d_2 tosylates in the absence or the presence of NaOAc (0.06 mol dm^{-3}) were allowed to react for more than 10 half-lives in sealed tubes at 115±0.02 °C. The reaction mixture was concentrated under vacuum at room temperature and extracted with chloroform. The extract was treated with cold water and dil. $NaHCO_3$ solution, and dried over anhydrous magnesium sulfate. The chloroform was removed in vacuo at room temperature and the residue was dissolved in carbon tetrachloride or deuteriochloroform to an appropriate concentration of ca. 1 mol dm^{-3} and was subjected to NMR determination.

Proton NMR Measurement. The ^1H NMR spectrum was obtained at 90 MHz using a Hitachi Perkin-Elmer R-22 Spectrometer. The accumulation method in CW mode was devised to share the data points most effectively into two peak areas of methylene ($\delta \approx 3$ ppm and ≈ 4 ppm) using a Hitac 10 II computer; only two narrow peak areas of the spectrum were accumulated for 100 times or more, sharing 4000 data points for each peak area (sweep width 40 Hz) of α and β-CH_2 signals. These spectral data were further reconfirmed using Brucker AM 360 Spectrometer which was interfaced with an ASPECT 2000 computer (operating at 360.13 MHz, digital resolution of 0.03 Hz/point).

The % rearrangement was calculated as

$$\frac{100\times[\mathrm{ArCD_2CH_2OAc}]}{[\mathrm{ArCH_2CD_2OAc}]+[\mathrm{ArCD_2CH_2OAc}]}$$

from relative peak intensities of α- and β-methylene protons. The NMR intensity determination was repeated more than three times for each run. The reproducibility of % rearrangement value was generally within ±0.3; the *m*-chloro and 4-MeS-3-CN derivatives showed slightly larger deviation of ±0.5. Average % rearrangement values are given in Table 1. In the NMR analysis, any characteristic peak of solvolysis product other than acetate was not detected, especially in the olefin region, for all derivatives.

References

1) For part 16, M. Fujio, K. Funatsu, M. Goto, Y. Seki, M. Mishima, and Y. Tsuno, *Bull. Chem. Soc. Jpn.*, **60**, 1091 (1987).

2) Preliminary report; Y. Tsuno, M. Fujio, Y. Seki, M. Mishima, and S. G. Kim, *Nippon Kagaku Kaishi*, **1977**, 1673; M. Fujio, M. Goto, Y. Seki, and Y. Tsuno, *Mem. Fac. Sci., Kyushu Univ., Ser. C*, **14**, 187 (1983).

3) a) M. Fujio, K. Funatsu, M. Goto, Y. Seki, M. Mishima, and Y. Tsuno, *Tetrahedron Lett.*, **24**, 2177 (1983); b) M. Fujio, K. Funatsu, M. Goto, Y. Seki, M. Mishima, and Y. Tsuno, *Mem. Fac. Sci., Kyushu Univ., Ser. C*, **14**, 177 (1983).

4) J. M. Harris, F. L. Schadt, and P. v. R. Schleyer, *J. Am. Chem. Soc.*, **91**, 7508 (1969).

5) Y. Yukawa and Y. Tsuno, *Bull. Chem. Soc. Jpn.*, **32**, 971 (1959); Y. Yukawa, Y. Tsuno, and M. Sawada, *ibid.*, **39**, 2274 (1966).

6) F. L. Schadt III, C. J. Lancelot, and P. v. R. Schleyer, *J. Am. Chem. Soc.*, **100**, 228 (1978).

7) M. Fujio, Y. Seki, M. Mishima, and Y. Tsuno, *Mem. Fac. Sci., Kyushu Univ., Ser. C*, **11**, 119 (1978); Y. Seki, M. Fujio, M. Mishima, and Y. Tsuno, *ibid.*, **12**, 197 (1980); M. Fujio, Y. Seki, R. Fujiyama, M. Mishima, and Y. Tsuno, *ibid.*, **13**, 71 (1981); Y. Seki, Ph. D. Thesis, Kyushu University, Fukuoka, Japan, 1980.

8) a) J. L. Coke, F. E. McFarlane, M. C. Mourning, and M. G. Jones, *J. Am. Chem. Soc.*, **91**, 1154 (1969); b) M. G. Jones and J. L. Coke, *ibid.*, **91**, 4284 (1969).
9) E. F. Jenny and S. Winstein, *Helv. Chim. Acta*, **41**, 807 (1958).
10) Y. Tsuno, K. Funatsu, Y. Maeda, M. Mishima, and M. Fujio, *Tetrahedron Lett.*, **23**, 2879 (1982).
11) C. D. Johnson, *J. Org. Chem.*, **43**, 1814 (1978).
12) C. D. Johnson, "The Hammett Equation," Cambridge University Press, London (1973), p. 52.
13) C. D. Johnson, *Chem. Rev.*, **75**, 755 (1975).
14) J. Shorter, "Correlation Analysis in Chemistry," ed by N. B. Chapman and J. Shorter, Plenum Press, New York (1978), Chap. 4, p. 119.
15) Unpublished data in this laboratory.
16) R. P. S. Tipson, *J. Org. Chem.*, **9**, 235 (1944).

 © 1987 The Chemical Society of Japan Bull. Chem. Soc. Jpn., 60, 1103—1107 (1987)

Stereoselective Synthesis of Octadecapolyenoic Esters as an Insecticide

Sadao Tsuboi, Xue Han Wu,† Seiji Maeda, Shinichiro Ono, Akihisa Kuroda, Kazuyoshi Kawazu, †† and Akira Takeda*

Department of Synthetic Chemistry, School of Engineering, Okayama University, Tsushima, Okayama 700

††Faculty of Agriculture, Okayama University, Tsushima, Okayama 700

(Received October 24, 1986)

Octadecapolyenoic acid derivatives such as (±)-*t*-butyl coriolate, α-eleostearic acid, *t*-butyl punicate, and *t*-butyl (9*Z*,11*E*)-13-hydroxy-9,11-octadecadien-15-ynoate were synthesized starting from oleic acid with high stereoselectivity and their insecticidal activity was examined.

Hydroxyoctadecapolyenoic acids such as dimorphecolic acid (**1**), coriolic acid (**2**), and (13*S*,9*Z*,11*E*,15*Z*)-13-hydroxy-9,11,15-octadecatrienoic acid (**3**) are self defensive substances in rice plant against rice blast disease, which were isolated by Kato et al.[1] α-Eleostearic acid [(9*Z*,11*E*,13*E*)-9,11,13-octadecatrienoic acid] (**4**) and punicic acid [(9*Z*,11*E*,13*Z*)-9,11,13-octadecatrienoic acid] (**5**) are components in some seed oils,[2] and methyl α-eleostearate is a feeding deterrent for the boll weevil on cotton.[3] Kawazu[4] found that esters of octadecapolyenoic acids such as linoleic acid and linolenic acid possess insecticide activity by preliminary experiments. Recently, we reported the

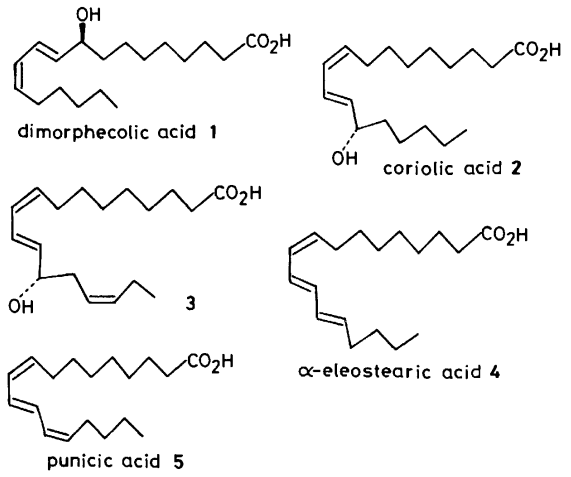

synthesis of **1** and its analogs.[5] As an extention of the previous work,[5] here we report the synthesis of (±)-*t*-butyl coriolate, *t*-butyl punicate, **4**, and an analog of **3**. Furthermore, insecticidal activity of these products was examined.

Coriolic acid (**2**) is a component of plant seed oils[6] and also a self defensive substance in rice plant against rice blast disease.[1] Syntheses of **2** have been reported by some groups.[7] Our synthetic sequence is shown in Scheme 1. Readily available oleic acid was used as a starting material. Ozonolysis of *t*-butyl oleate (**6**) at −20—−30 °C gave *t*-butyl 9-oxononanoate (**7**) in a fair yield. Ethynylation of **7** with ethynylmagnesium bromide yielded *t*-butyl 9-hydroxy-10-undecynoate (**8**) in 79% yield. Ortho-Claisen rearrangement of **8** with an excess of trimethyl orthoacetate gave β-allenic ester **9** quantitatively. Conversion of **9** to 1-methyl 13-*t*-butyl (2*E*,4*Z*)-2,4-tridecadiene-1,13-dioate (**10**) was established by the economical and convenient method which was developed by two of us.[8] Treatment of **9** with alumina at the reflux temperature of benzene gave (2*E*,4*Z*)-dienoic diester **10** in 91% yield with high stereoselectivity. Both proton and carbon-13 NMR analyses showed no presence of stereoisomers.

Regioselective reduction of **10** with various reducing agent was attempted and the results were summarized in Table 1. Reduction of **10** with diisobutylaluminum hydride (DIBAL) gave diol **14** as a major product. Reduction with lithium aluminum hydride (LAH) yielded a mixture of the desired product **11** and diol **14**. Prolonged reaction with LAH

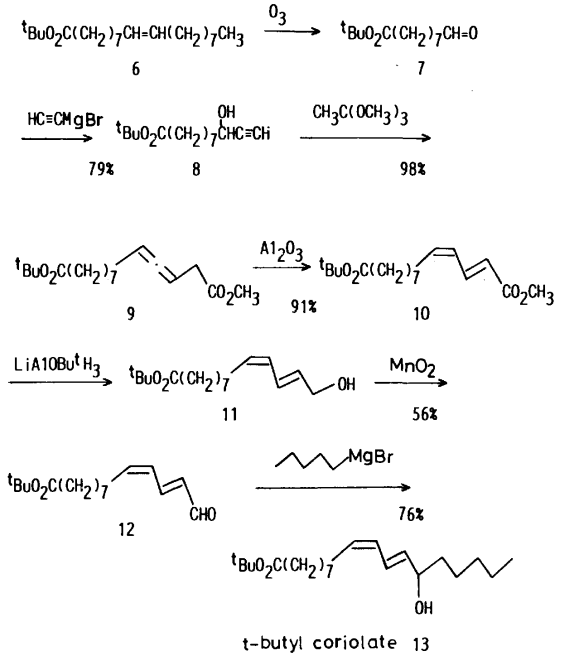

Scheme 1.

† Present address: Institute of Photographic Chemistry, Academia Sinica, Beijing, China.

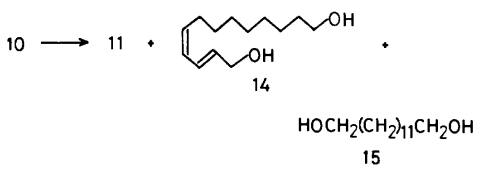

gave a hydrogenated product, 1,13-tridecanediol (**15**) in addition to the reduced products, **11** and **14**. Reduction of **10** with lithium di- or tri-*t*-butoxyaluminum hydride resulted in the formation of *t*-butyl (9*Z*)-13-hydroxy-9-tridecenoate or in the recovery of the starting material. The best result was obtained by the reduction of **10** with lithium *t*-butoxyaluminum hydride at −50 °C to give **11** in 60% yield. Oxidation of the alcohol **11** with active manganese dioxide at room temperature gave *t*-butyl (9*Z*,11*E*)-13-oxo-9,11-tridecadienoate (**12**) in an excellent yield, which is pure by ^{1}H NMR analysis. Reaction of **12** with pentylmagnesium bromide at −15 °C proceeded regioselectively to give (±)-*t*-butyl coriolate **13** in 84% yield as a sole product. The ^{1}H NMR spectrum was identical with that of methyl coriolate[9] except the signal of the ester group. Any 1,4- or 1,6-addition products could not be detected.

Conversion of (±)-*t*-butyl coriolate **13** to naturally occuring carboxylic acid **2** was attempted. However, the hydrolysis of **13** with chlorotrimethylsilane-sodium iodide[10a] at 25 °C afforded α-eleostearic acid (**4**)[11] in 54% yield with simultaneous dehydration. Synthesis of 1,3-diene from cyclic allylic alcohols and from allylic vicinal diols with Me_3SiCl–NaI is known.[10b] However, to our knowledge this type of dehydration for acyclic allylic alcohols has never reported before, and the general applicability is now under an investigation. On the other hand, acid-catalyzed hydrolyses resulted in the formation of polymerized products.

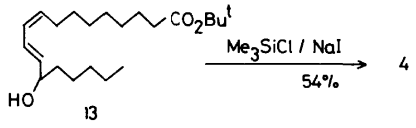

Punicic acid (**5**) is a component of plant seed oils.[2] Conacher and Gunstone[12] reported the synthesis of **5** from linoleic acid. We prepared *t*-butyl ester **16** of **5** by the Wittig reaction of **12** with pentylidenetriphenylphosphorane.

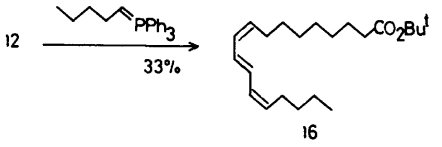

Shimura et al.[13,14] have reported the isolation and structural elucidation of anti-conidial germination substance, (9*Z*,11*E*,15*Z*)-13-hydroxy-9,11,15-octadecatrienoic acid (**3**). The absolute configuration of **3** was determined to be S-configuration by Kato et al.[1] We attempted the synthesis of (±)-**3**. Although it is reported that lithiation of 1-bromo-2-pentyne and the following reaction with a carbonyl compound gave acetylenic alcohol as a major product,[15,16] our attempts on the reaction of 2-pentynyllithium with aldehyde **12** afforded *t*-butyl (9*Z*,11*E*)-13-hydroxy-9,11-octadecadien-15-ynoate (**17**) in low yield along with an allenic compound. Conversion of **17** to *t*-butyl ester of (±)-**3** with stereoselective hydrogenation resulted in the formation of polymerized products.

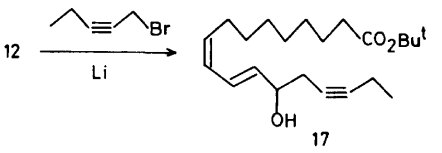

Insecticidal activity of polyenoic esters prepared in the present synthesis and also in the previous paper was examined and the results were shown in Table 2. All of compounds showed fair insecticidal activity (LD_{50}=ca. 25—50 μg/fly) against adults of the fruitfly, *Drosophila melanogaster*. No notable relationship between the molecular structure and the activity was observed.

Table 1. Reduction of **10** with Various Reducing Agents

10 R	Reducing Agent (mol ratio to **10**)	Reaction condition		Yield/% of product[a]		
		Temp/°C	h	**11**	**14**	**15**
Et	DIBAL (2.20)	−15	0.5	2	52	14
Me	$LiAlH_4$ (1.10)	−40—−35	2.5	41	37	
Et	$LiAlH_4$ (1.26)	−50—−40	5.0	39	35	23
Et	$LiAl(OBu^t)_3H$ (3.0)	15	42	b)		
Et	$LiAl(OBu^t)_2H_2$ (2.0)	−20	5.0	c)		
Et	$LiAl(OBu^t)H_3$ (1.3)	−40	3.0	49	21	
		−20	4.0			
Me	$LiAl(OBu^t)H_3$ (1.0)	−50	3.0	60	8	

a) Isolated yield. b) The desired product was not detected. The structure of the product was supposed to be *t*-butyl (9*Z*)-13-hydroxy-9-tridecenoate. c) The starting material **10** was recovered in 91% yield.

Table 2. Insecticidal Activity of Polyenoic Esters against of Drosophilamelanogaster[a)]

Compds	Number of survivors[b)]					
	Dose 0	0.125	0.25	0.50	1.0	2.0 mg
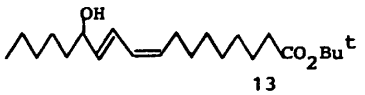 13	10 (8)	8 (0)	7 (0)	4 (0)	2 (0)	2 (0)
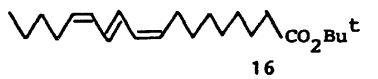 16	9	9	7	6	8	1
17	10	7	6	7	6	0
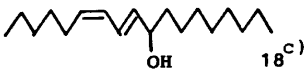 18[c)]	10	8	4	3	0	0
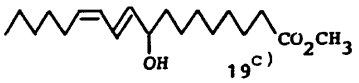 19[c)]	10	7	9	2	0	0

a) Dry film method. b) The number after 24 h. The number in parenthesis is after 48 h. c) The synthesis is reported in the previous paper. See Ref. 5.

Experimental

The melting and boiling points are uncorrected. Infrared (IR) spectra were obtained with a JASCO Model A-102 infrared spectrophotometer. ^{1}H NMR spectra (60 MHz) were recorded with a JEOL JNM-FX100 apparatus, with $CDCl_3$ as a solvent. All chemical shifts are reported in δ units downfield from internal Me_4Si, and J values are given in hertz. Column chromatography was accomplished with 100—200 mesh Wakogel C-200.

Petroleum ether was distilled (bp 40—60 °C) and dried over sodium wire. Tetrahydrofuran (THF) and diethyl ether were dried over sodium benzophenone ketyl and distilled under an atmosphere of nitrogen prior to use. Activated manganese dioxide was prepared according to the procedures in the literature.[17)]

t-Butyl oleate (**6**) was prepared by the reaction of oleoyl chloride with *t*-butyl alcohol in the presence of 2 equivalents of pyridine at 60—80 °C for 3 h: 88% yield.

t-Butyl 9-oxononanoate (**7**) was obtained by the ozonolysis of *t*-butyl oleate according to the procedure of the literature;[18)] bp 85—90 °C/0.08 mmHg (1 mmHg=133.322 Pa); 52.1% yield.

t-Butyl 9-hydroxy-10-undecynoate (**8**) was prepared by following the method described in the preparation of the methyl ester:[19)] 79% yield; IR (neat) 3500, 3300, 2100, 1730 cm^{-1}; ^{1}H NMR ($CDCl_3$) δ=1.30 (m, 10H, $(CH_2)_5$), 1.43 (s, 9H, $C(CH_3)_3$), 2.22 (m, 4H, CH_2CO, $>CHCH_2$), 2.40 (d, 1H, J=2 Hz, HC≡C), 4.35 (m, 1H, >CHOH).

13-*t*-Butyl 1-Methyl 3,4-Tridecadiene-1,13-dioate (9). A mixture of **8** (6.33 g, 0.0249 mol), trimethyl orthoacetate (20.9 g, 0.174 mol), and propionic acid (0.1 g) was heated to the reflux temperature for 24 h with removal of methanol produced by distillation. Removal of volatile materials under reduced pressure gave 7.58 g (98%) of **9**: IR (neat) 1960 (C=C=C), 1730 cm^{-1} (ester C=O); ^{1}H NMR ($CDCl_3$) δ=1.30 (m, 10H, $(CH_2)_5$), 1.45 (s, 9H, $C(CH_3)_3$), 2.12 (m, 4H, $=CHC\underline{H}_2(CH_2)_5$, $C\underline{H}_2CO_2Bu^t$), 3.02 (m, 2H, $C\underline{H}_2CO_2CH_3$), 3.64 (s, 3H, CO_2CH_3), 5.14 (m, 2H, CH=C=CH). Analytical sample was purified by column chromatography (SiO_2, hexane/ethyl acetate (10:1)). Found: C, 69.47; H, 9.50%. Calcd for $C_{18}H_{30}O_4$: C, 69.64; H, 9.74%.

1-Methyl 13-*t*-Butyl (2*E*,4*Z*)-2,4-Tridecadiene-1,13-dioate (10). A mixture of **9** (7.53 g, 0.0243 mol), alumina[8)] (12.4 g), and dry benzene (40 ml) was heated at the reflux temperature for 11 h. After filtration, removal of the solvent gave 6.85 g (91%) of **10** as a clean oil: IR (neat) 1720 (C=O), 1640, 1610 cm^{-1} (C=C); ^{1}H NMR ($CDCl_3$) δ=1.32 (m, 10H, $(CH_2)_5$), 1.41 (s, 9H, $C(CH_3)_3$), 2.17 (m, 4H, $=CHC\underline{H}_2$, $C\underline{H}_2CO_2Bu^t$), 3.66 (s, 3H, CO_2CH_3), 5.50—6.33 (m, 3H, $C\underline{H}$=$C\underline{H}C\underline{H}$=$C\underline{H}CO$), 7.45 (dd, 1H, J=10 and 15.0 Hz, $C\underline{H}$=CHCO). ^{13}C NMR ($CDCl_3$) δ=25.1 (t), 28.1 (s), 29.0 (t), 29.3 (t), 29.5 (t), 29.7 (t), 35.5 (t), 51.4 (q), 79.8 (s), 118.3 (d), 126.5 (d), 139.7 (d), 141.6 (d), 167.6 (s), 173.1 (s). Analytical sample was purified by column chromatography (SiO_2, hexane/ethyl acetate (10:1)). Found: C, 69.41; H, 9.51%. Calcd for $C_{18}H_{30}O_4$: C, 69.64; H, 9.74%.

***t*-Butyl (9*Z*,11*E*)-13-Hydroxy-9,11-tridecadienoate (11).** Lithium aluminum hydride (250 mg, 6.59 mmol) and 10 ml of THF was charged in 60 ml two-necked, round-bottomed flask under an atmosphere of nitrogen. To a stirred mixture was added 0.62 ml (49 mg, 6.58 mmol) of *t*-butyl alcohol at 0 °C. After 10 min, a solution of 2.04 g (6.57 mmol) of **10** in 10 ml of THF was added dropwise at −50 °C. The mixture was stirred for 3 h and then quenched with 1 ml of ethyl acetate and 2.5 ml of 10% HCl. After the mixture was poured into cold water, the organic layer was extracted with

ether. The combined extracts were washed with water and dried over $MgSO_4$. Removal of the solvent gave 1.90 g of a crude product which was purified by column chromatography (SiO_2, hexane/ethyl acetate (9:1—1:1)) to give 1.13 g (60%) of **11** as a clean oil: IR (neat) 3425 (OH), 1735 (ester C=O), 1455, 1365, 1255 cm^{-1}; ^1H NMR δ=1.15—1.75 (m, 10H, $(CH_2)_5$), 1.40 (s, 9H, $C(CH_3)_3$), 1.75—2.40 (m, 4H, $CH_2CH=CH$, $CH_2CO_2Bu^t$), 3.96 (br d, 2H, J=5.6 Hz, CH_2OH), 5.05—6.63 (m, 4H, CH=CHCH=CH). Found: C, 72.32; H, 10.70%. Calcd for $C_{17}H_{30}O_3$: C, 72.30; H, 10.71%. The last fraction gave 110 mg (8%) of **14**: ^1H NMR ($CDCl_3$) δ=1.32 (m, 12H, J=6 Hz, CH_2OH), 4.19 (d, 2H, J=5.5 Hz, $HOCH_2CH=$), 5.17—6.33 (m, 3H, $CH=CHCH=CH$), 6.54 (dd, 1H, J=10 and 15.5 Hz, $HOCH_2CH=CH$). Found: C, 73.67; H, 11.52%. Calcd for $C_{13}H_{24}O_2$: C, 73.54; H, 11.39%.

Reduction of 10 with LiAl(OBu^t)$_3$H. To a stirred mixture of $LiAlH_4$ (120 mg, 3.16 mmol) and THF (3 ml) was added t-butyl alcohol (0.89 ml, 9.44 mmol) at 0 °C. After 10 min a solution of **10** (162 mg, 0.499 mmol) in 5 ml of THF was added dropwise at 15 °C, and the mixture was stirred for 42 h. The work up as described above gave a clean oil (148 mg) or t-butyl (9Z)-13-hydroxy-9-tridecenoate (supposed structure): ^1H NMR (CCl_4) δ=1.03—1.81 (m, 12H), 1.40 (s, 9H), 1.9—2.36 (m, 6H), 2.51 (br s, 1H), 3.50 (t, 2H, J=6 Hz), 5.11—5.52 (m, 2H).

Reduction of 10 with Diisobutylaluminum Hydride (DIBAL). Compound **10** (325 mg, 1 mmol) was reduced in 2 ml of ether with DIBAL (1.0 M in hexane) under the conditions described in Table 1 and worked up as above, giving 63.9 mg of **10**, 30.3 mg (14%) of 1,13-tridecanediol (**15**)[20]: ^1H NMR (CCl_4) δ=1.28 (s, 22H), 1.65 (br s, 2H), 3.40 (t, 4H), 5.9 mg (2%) of **11**, and 110 mg (52%) of **14**.

***t*-Butyl (9*Z*,11*E*)-13-Oxo-9,11-tridecadienoate (12).** (a) To a mixture of 11.0 g of activated manganese dioxide[17] and 100 ml of petroleum ether was added a solution of 1.13 g (4.01 mmol) of **11** in 20 ml of petroleum ether at 5 °C with stirring. The mixture was stirred for 3 h at 25 °C and then filtered off. Concentration of the filtrate gave 0.887 g of an oil which was chromatographed on 10 g of silica gel eluting with hexane/ethyl acetate (10:1) to give 0.624 g (56%) of **12** as a clean oil: IR (neat) 2950, 1725 (ester C=O), 1680 (aldehyde C=O), 1630 (C=C), 1365, 1155, 850 cm^{-1}; ^1H NMR (CCl_4) δ=1.05—1.91 (m, 10H, $(CH_2)_5$), 1.95—2.55 (m, 4H, $CH_2CO_2Bu^t$, $CH_2CH=CH$), 5.69—6.45 (m, 3H, $CH=CHCH=CHCHO$), 7.29 (dd, 1H, J=11 and 15 Hz, $CH=CHCHO$), 9.50 (d, 1H, J=7 Hz, CHO). Found:C, 72.72; H, 10.30%. Calcd for $C_{17}H_{28}O_3$: C, 72.82; H, 10.06%.

^{13}C NMR ($CDCl_3$, δ)

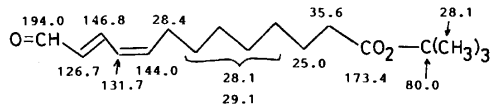

The last fraction eluted with ethyl acetate gave 100 mg of polymerized products.[21]

(b) To a mixture of 0.130 g (1.5 mmol) of activated manganese dioxide and 2 ml of petroleum ether was added a solution of 27 mg (0.096 mmol) of **11** in 0.5 ml of petroleum ether at 25 °C with stirring. The mixture was stirred for 2 h and then filtered off. Concentration of the filtrate gave 25 mg (93%) of **12** as a clean oil. TLC analysis (SiO_2, hexane/ethyl acetate (2:1)) showed one spot at R_f 0.75. IR and ^1H NMR data were identical with those of the authentic sample.

(±)-*t*-Butyl (9*Z*,11*E*)-13-Hydroxy-9,11-octadecadienoate ((±)-*t*-Butyl Coriolate) (13). To a mixture of 18.9 mg (0.778 mmol) of magnesium and 0.3 ml of THF was added dropwise 122 mg (0.808 mmol) of pentyl bromide with stirring. After 2 h, a solution of 96.8 mg (0.345 mmol) of **12** in 3 ml of THF was added dropwise at −15 °C, and then the mixture was stirred for 2 h. The mixture was poured into ice water, and the organic layer was extracted with ether. The combined extracts were washed with water, dried over $MgSO_4$, and concentrated. The resulting residue was chromatographed on 8 g of silica gel eluting with hexane/ethyl acetate (10:1) to give 63.3 mg (76%) of **13**: IR (neat) 3350 (OH), 1730 (C=O); ^1H NMR (CCl_4) δ=0.85 (t, 3H, CH_3), 1.30 (m, 18H, $(CH_2)_5$, $(CH_2)_4$), 1.38 (s, 9H, $C(CH_3)_3$), 2.10 (m, 4H, CH_2CO, $=CHCH_2$), 4.00 (m, 1H, >CHOH), 5.03—6.53 (m, 4H, $(CH=CH)_2$). Found: C, 74.62; H, 11.20%. Calcd for $C_{22}H_{40}O_3$: C, 74.95; H, 11.44%.

^{13}C NMR ($CDCl_3$, δ)

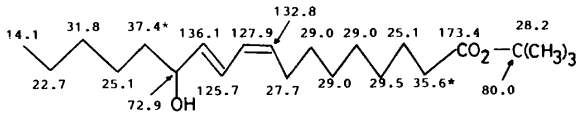

* May be interchangeable.

(9*Z*,11*E*,13*E*)-9,11,13-Octadecatrienoic Acid (α-Eleostearic Acid) (4). To a mixture of 66.3 mg (0.442 mmol) of sodium iodide and 0.5 ml of acetonitrile was added a solution of 82.1 mg (0.233 mmol) of **13** in 1 ml of acetonitrile under an atmosphere of nitrogen. Chlorotrimethylsilane (0.056 ml, 0.44 mmol) was added at 0 °C with stirring and the mixture was stirred for 3 h at 25 °C, and then poured into ice water. The organic layer was extracted with ether, washed with water, dried over $MgSO_4$. After removal of the solvent, the residual oil was chromatographed on silica gel eluting with hexane/ethyl acetate (20:1) to give 35 mg (54%) of **4**. Spectral data were identical with those of the authentic sample.[11]

***t*-Butyl (9*Z*,11*E*,13*Z*)-9,11,13-Octadecatrienoate (*t*-Butyl Punicate) (16).** To a stirred mixture of 143 mg (0.346 mmol) of pentyltriphenylphosphonium bromide and 2 ml of dry THF was added 0.23 ml (0.346 mmol) of 1.65 M butyllithium (1 M=1 mol dm^{-3}) in hexane at −20 °C. After 20 min, a solution of 47 mg (0.168 mmol) of **12** in 1 ml of dry THF was added dropwise. The mixture was stirred for 15 min at −78 °C, then poured into ice water, and neutralized with dilute HCl. The organic materials were extracted with ether, washed with water, and dried over $MgSO_4$. Removal of the solvent gave 71.8 mg of an oil, which was chromatographed (SiO_2, 2.8 g; eluent: hexane/ethyl acetate, 30:1—10:1) to afford 18.6 mg (33%) of **16** as an oil: TLC (hexane/ethyl acetate (1:1)), R_f 0.87. Spectral data were identical with those of the authentic sample[22] except signals due to the ester group. IR (neat) 2950, 1730 (C=O), 1460, 1365, 1255, 1150, 995 cm^{-1}; ^1H NMR (CCl_4) δ=0.90 (br t, 3H, J=6 Hz, CH_3), 1.30 (m, 14H, $7CH_2$), 1.38 (s, 9H, $C(CH_3)_3$), 2.11 (m, 6H, $2CH_2CH=$), 5.00—6.45 (m, 6H, 3CH=CH). ^{13}C NMR ($CDCl_3$) δ=13.9 (q), 22.3 (t), 25.1 (t), 27.8 (t), 28.1 (q), 29.1 (t), 31.8 (t), 35.6 (t), 79.9 (q), 127.9 (d), 128.8 (d), 130.0 (d), 132.7 (d), 173.3 (s). Found: C, 78.83; H,

11.67%. Calcd for $C_{22}H_{38}O_2$: C, 78.99; H, 11.45%.

***t*-Butyl (9*Z*,11*E*)-13-Hydroxy-9,11-octadecadien-15-ynoate (17).** To a stirred mixture of 10 mg (1.44 mmol) of lithium and 1.0 ml of THF was added a solution of 73.5 mg (0.542 mmol) of 1-bromo-2-pentyne and 160 mg (0.571 mmol) of **12** in 1 ml of THF at −40 °C over 1.5 h. Additionally, 73.5 mg (0.542 mmol) of 1-bromo-2-pentyne was added. After being stirred for 4 h at −40 °C, the mixture was poured into ice water. The organic layer was extracted with ether. The combined extracts were washed with water, dried over $MgSO_4$, and concentrated. The residue (178 mg) was purified by column chromatography (SiO_2, hexane/ethyl acetate/methanol (80:9:1), developed twice) to give 47 mg (24%) of **17**: TLC (SiO_2, hexane/ethyl acetate (4:1)), R_f 0.76—0.63; IR (neat) 3450, 2940, 2100 (C≡C), 1730: ^{1}H NMR (CCl_4) δ=0.85—1.86 (m, 13H, $(CH_2)_5$, CH_3), 1.91—2.61 (m, 8H, $CH_2C{\equiv}CCH_2$, $CH_2CH{=}CH$, CH_2CO), 4.20 (br d, 1H, J=5 Hz, CHOH), 5.03—6.89 (m, 4H, olefinic protons); ^{13}C NMR ($CDCl_3$) δ=12.3 (t), 14.0 (q), 24.9 (t), 27.5 (t), 27.9 (t), 27.9 (q), 28.8 (t), 29.3 (t), 35.4 (t), 70.6 (d), 75.0 (s), 79.7 (s), 84.6 (s), 126.3 (d), 217.4 (d), 133.1 (d), 133.4 (d), 173.2 (s). Found: C, 75.55; H, 10.38%. Calcd for $C_{22}H_{36}O_3$: C, 75.82; H, 10.41%. The second fraction gave 35 mg of unidentified compound as an oil. IR (neat) 3450 (OH), 2950, 1950 (C=C=C), 1734 (C=O); ^{1}H NMR (CCl_4) δ=1.0 (t, J=6 Hz), 1.1—1.75 (m), 1.75—2.55 (m), 4.16 (q, 1H, J=6 Hz), 4.80 (t, J=4 Hz), 5.1—6.17 (m), 6.45 (q, J=10 and 15 Hz). The last fraction gave 62 mg of polymerized compounds.

Insecticidal Test (dry film method). The fruitfly, *Drosophila melanogaster*, was reared in the medium described in the literature.[23] An ethyl acetate solution of the test compounds was added to a Petri-dish (ϕ 3 cm). After spontaneous evaporation of the solvent, ten adults of the fruitfly were introduced to the dish and kept at 25 °C for 48 hours. The survivors after 24 or 48 hours were counted and the numbers were shown in Table 2.

We appreciate Dr. Shuhei Nakajima of Department of Agricultural Chemistry, Okayama University for preliminary insecticidal activity test. We also thank Mr. Eiichiro Amano of our laboratory for elemental analysis. The present work was partially supported by a Grant-in-Aid for Developmental Scientific Research No 59850144 from the Ministry of Education, Science and Culture.

References

1) a) T. Kato, Y. Yamaguchi, T. Uyehara, T. Yokoyama, T. Namai, and S. Yamanaka, *Tetrahedron Lett.*, **24**, 4715 (1983); b) T. Kato, Y. Yamaguchi, T. Hirano, T. Yokoyama, T. Uyehara, T. Namai, S. Yamanaka, and N. Harada, *Chem. Lett.*, **1984**, 409.

2) T. Takagi and Y. Itabashi, *Lipids*, **16**, 546 (1981). References cited therein.

3) M. Jacobson, U. S. Patent, 140, 991 (1980); *Chem. Abstr.*, **93**, 232 738v (1980).

4) K. Kawazu, S. Satoh, and S. Nakajima, *J. Agr. Chem. Soc. Jpn.*, **57**, 117 (1983).

5) S. Tsuboi, S. Maeda, and A. Takeda, *Bull. Chem. Soc. Jpn.*, **59**, 2050 (1986).

6) W. H. Tallent, J. Harris, and I. A. Wolff, *Tetrahedron Lett.*, **1960**, 4329.

7) a) H. Suenami, N. Hayashi, K. Funakoshi, H. Akita, T. Oishi, and K. Sakai, *Chem. Pharm. Bull.*, **33**, 2168 (1985); b) A. V. Rama Rao, E. Rajarathnam Reddy, G. V. M. Sharma, P. Yadagiri and J. S. Yadav, *Tetrahedron Lett.*, **26**, 465 (1985); c) C. A. Moustakis, D. K. Weerasinghe, P. Mosset, and J. R. Falck, *Tetrahedron Lett.*, **27**, 303 (1986).

8) S. Tsuboi, T. Masuda, and A. Takeda, *J. Org. Chem.*, **47**, 4478 (1982).

9) B. E. Philips, C. R. Smith, Jr., and L. W. Tjarks, *J. Org. Chem.*, **35**, 1916 (1970).

10) a) G. A. Olah, S. C. Narang, B. G. B. Gupta, and R. Malhotra, *J. Org. Chem.*, **44**, 1247 (1979); b) N. C. Barua, J. C. Sarma, R. P. Sharma, and J. N. Barua, *Chem. Ind.*, **1982**, 956.

11) a) L. Crombie and A. G. Jacklin, *J. Chem. Soc.*, **1957**, 1632; b) O. Suzuki, T. Hashimoto, K. Hayamizu, and O. Yamamoto, *Lipids*, **5**, 457 (1970); c) V. Ratovelomanana and G. Linstrumelle, *Tetrahedron Lett.*, **25**, 6001 (1984).

12) H. B. S. Conacher and F. D. Gunstone, *Chem. Phys. Lipids*, **3**, 191 (1969).

13) M. Shimura, M. Iwata, N. Tashiro, Y. Sekizawa, Y. Suzuki, and T. Watanabe, *Agric. Biol. Chem.*, **45**, 1431 (1981).

14) M. Shimura, S. Mase, M. Iwata, A. Suzuki, T. Watanabe, Y. Sekizawa, T. Sasaki, K. Furihata, H. Seto, and N. Otake, *Agric. Biol. Chem.*, **47**, 1983 (1983).

15) M. Malacria and M. L. Roumestant, *Tetrahedron*, **33**, 2813 (1977).

16) K. Ono, A. Sugie, H. Kawakami, and S. Katsube, Japanese Patent, 18935 (1981).

17) J. Attenburrow, A. F. B. Cameron, J. H. Chapman, R. M. Evans, B. A. Hems, A. B. A. Jansen, T. Walker, *J. Chem. Soc.*, **1952**, 1094.

18) E. H. Pryde, D. E. Anders, H. M. Teeter, and J. C. Cowan, *J. Org. Chem.*, **25**, 618 (1960).

19) T. B. Patrick and G. F. Melm, *J. Org. Chem.*, **44**, 645 (1979).

20) W. H. Carothers and W. L. McEwen, *Org. Synth.*, **14**, 22 (1934).

21) Compound **12** seems to polymerize in part on the treatment of column chromatography.

22) G. Gowrikumar, V. V. S. Mani, T. Chandrasekhara Rao, T. N. B. Kaimal, and G. Lakshminarayana, *Lipids*, **16**, 558 (1981).

23) K. Kawazu, M. Ariwa, Y. Kii, *Agric. Biol. Chem.*, **41**, 223 (1977).

Hydrothermal Growth of Calcite Single Crystal in NaCl Solution

Shin-ichi HIRANO* and Kō-ichi KIKUTA
Department of Applied Chemistry, Faculty of Engineering, Nagoya University,
Furo-cho, Chikusa-ku, Nagoya 464
(Received August 23, 1986)

The hydrothermal synthesis of calcite single crystal was studied by using a NaCl solution as a mineralizer. The solubility of calcite in a 3 mol kg^{-1} NaCl solution was measured by a weight-loss technique to be around 2 g l^{-1} at 500 °C and 100 MPa. An optically clear rhombohedral crystal of up to 1.0 mm could be grown in a hydrothermal NaCl solution. The growth of a homogeneous layer of calcite could be observed on the calcite seed at 400 °C.

A calcite single crystal called Iceland spar has been used for such optical meterials as a Nicol prism. Recently, the demand for the growth of optically clear calcite crystals has been increasing due to a depletion of natural resources.

Many artificial techniques have been employed to grow calcite single crystal.[1-3] The flux method was recognized as being acceptable for growing calcite boule. It, however, encounters some difficulties in producing a high-quality single crystal of calcite owing to CO_2 dissociation, impurity contamination and a large thermal stress.

The hydrothermal method is one of the promissing techniques for growing unstable crystals such as a carbonate compound. The authors had preliminarily reported that calcite single crystals of a euhedral form, bounded by {10$\bar{1}$1}, could be grown spontaneously in hydrothermal NaCl and KCl solutions as the solvent; the kind of anion in the solvent was the most significant factor for controlling the coexisting phase as well as the morphology of the grown crystals.[4] Chloride solutions as a hydrothermal solvent, were first used by N. Yu. Ikornikova and have been examined by some authors.[5,6] Experimental details, however, have not been reported.

In the present work, the solubility of calcite in a 3 mol kg^{-1} hydrothermal NaCl solution was studied as a function of the temperature under 100 MPa; the most appropriate conditions for the growth of a calcite single crystal were elucidated as basic data for the large scale production of calcite single crystals.

Experimental

In this work, highly pure natural Iceland spar was used as a starting material. The hydrothermal run was carried out in a hydrothermal pressure vessel of the cold-seal type (1/4" I. D). The temperature was controlled with a calibrated chromel-alumel thermocouple set in the pressure vessel. The pressure was measured with a calibrated Heise gauge.

The calcite solubility was determined by the weight loss method with a hermetically sealed gold capsule (5.0 mm O. D, 4.7 mm I. D, 50 mm in length) containing cleaved Iceland spar crystals of about 3 mm in size. Crystals and the 3 mol kg^{-1} NaCl solvent solution were sealed in the gold capsule by welding and then set in a pressure vessel.

Solubility measurements were carried out under various conditions for a duration of 3 d; this was previously confirmed to be sufficiently long to achieve equilibrium. After a run, the pressure vessel was quenched into cold water. A stainless filler rod was placed in the space above the capsule so as to suppress any convection and to achieve thermal uniformity along the capsule.

The experimental growth conditions are a temperature of 350—500 °C, a pressure of 100 MPa and a duration of 3—14 d. The morphologies of the grown crystals were observed by optical microscopy. The grown crystals were also characterized by infrared spectroscopy and a back-reflection Laue method.

Results and Discussion

Solubility of Calcite in 3 mol kg^{-1} Hydrothermal NaCl Solution. The solubility of calcite in a 3 mol kg^{-1} hydrothermal NaCl solution was measured as a function of the temperature at 100 MPa by the weight-loss method. The solubility in the 3 mol kg^{-1} NaCl solution increased remarkably with increasing temperature above 400 °C and amounted to 2.0 g l^{-1} at 500 °C (Fig. 1). The value of the solubility is

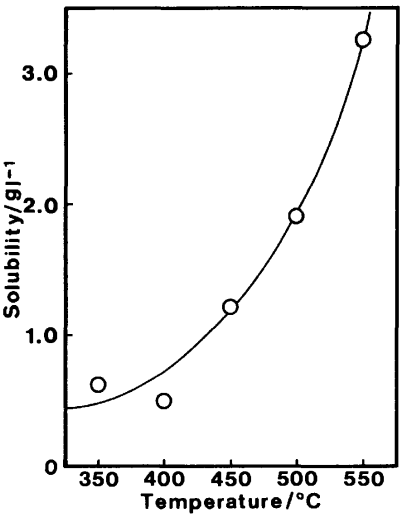

Fig. 1. Solubility of calcite in 3 mol kg^{-1} NaCl solution as a function of temperature.

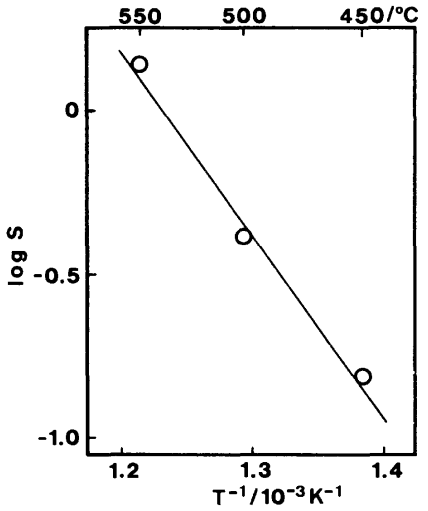

Fig. 2. Log S (solubility) of $CaCO_3$ as a function of $1/T$ in 3 mol kg^{-1} NaCl.

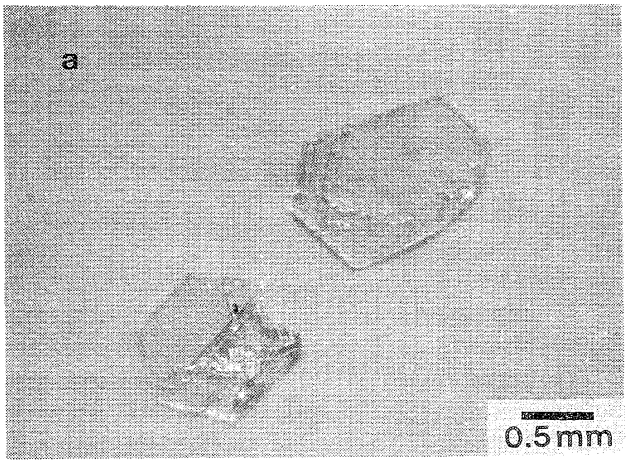

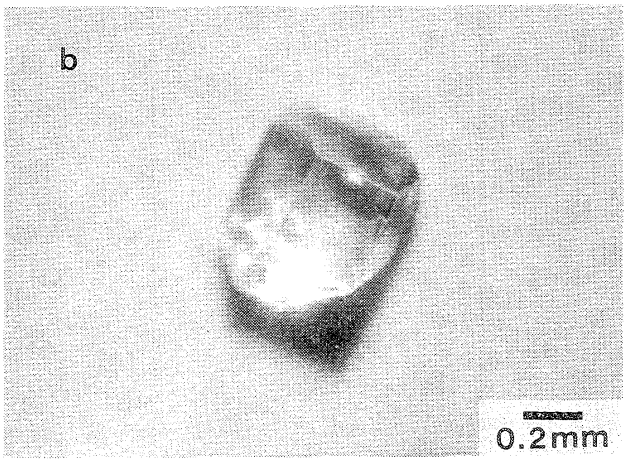

Fig. 3. Photomicrographs of calcite crystals grown in 3 mol kg^{-1} NaCl solution at 500 °C and 100 MPa for 10 d.

acceptable eventually for hydrothermal growth. Thus, all the growth experiments were carried out above 400 °C.

Figure 2 shows a plot of log S (Solubility) vs. $1/T$ in order to investigate the dissolution behavior of calcite in a 3 mol kg^{-1} NaCl solution at 100 MPa. The van't Hoff relation was confirmed to hold. The enthalpy of the solution, ΔH, was calculated to be about 46 kJ mol^{-1}, much larger than $\Delta H°=-12$ kJ mol^{-1} in a $CaCO_3$-H_2O system under ordinal conditions.[7] This fact indicated that the state of dissolved species under hydrothermal conditions was quite different from that under ordinary conditions at atmospheric pressure.

Morphology of Grown Calcite Single Crystal. A few growth runs were carried out with cleaved pure Iceland spar as a starting material of nutrient. Calcite single crystals of sizes up to 1.0 mm were grown spontaneously on the inner wall of the capsule at 500 °C under 100 MPa for 10 d. There were two kinds of crystal habits (Fig. 3). The morphologies of grown crystals were found to be strongly influenced by the growth temperature. Plate-like calcite crystals bounded by well developed {0001} faces could be formed mainly at elevated temperatures (above 500 °C). Associated with the crystals (Fig. 3a), a few polyhedral crystal were grown as shown in Fig. 3b. An identification of the plane is now in progress. The variation of crystal habits showed a good agreement with the occurence of Iceland spar in nature.[8] Euhedral crystals bounded by {10$\bar{1}$1} faces were also prepared at 450 °C and 100 MPa for 10 d (Fig. 4). This fact suggests that the Iceland spar in nature might occur in a hydrothermal solution at a relatively lower temperature.

Figure 5 shows the characteristic IR spectra of a

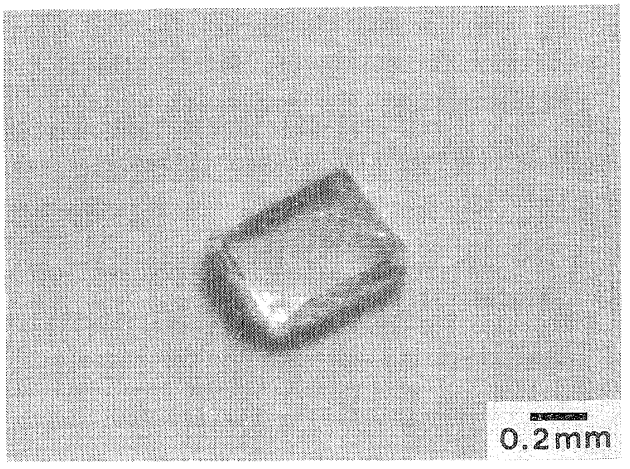

Fig. 4. Photomicrograph of calcite crystal grown in 3 mol kg^{-1} NaCl solution at 450 °C and 100 MPa for 10 d.

grown single crystal of calcite; it is identical to a high-quality natural calcite crystal, even though the crystal includes a stretching vibration due to OH^- around 3500 cm^{-1}. It ensures that the uptake of OH^- in this crystal is comparable to that in a well qualified optical grade of Iceland spar that is used for optical devices.

Growth Experiment with Seed Crystal. On the basis of the preliminary experiments, further growth runs with seed crystals were attempted by using a large pressure vessel (1/2″ I. D) in order to investigate the effect of seed orientation. A gold specimen container was prepared with a lid (10 mm O. D, 9.7 mm I. D, 17 cm in length) instead of a gold capsule. A short stainless filler rod was also placed above a gold container in order to adjust the thermal gradient.

Both spherical and rhombohedral seeds were suspended in the upper portion of the container. The pressure vessel was filled with a 3 mol kg^{-1} NaCl solution, brought up to 400 °C and 100 MPa and maintained for 2 weeks. After a run, it was cooled at a constant rate of 25 °C/hr.

The thickness of the rhombohedral seed increased by 0.087 mm while keeping its appearance. On the other hand, spherical seeds were observed to be completely covered with flat smooth surfaces and the steps of a grown calcite crystal (Fig. 6). The flat plane was identified to be $(10\bar{1}1)$ faces, of which symmetry was confirmed to be two fold by back-reflection Laue photographs. This result revealed that it would be possible to accelerate the growth rate on the seed by a proper selection of the seed orientation, such as $(11\bar{2}0)$.

Conclusion

It is found that the solubility of calcite in a 3 mol kg^{-1} hydrothermal NaCl solution increased remarkably upon increasing the temperature above 400 °C; the enthalpy of the solution, ΔH, was around 46 kJ mol^{-1} at 100 MPa.

Euhedral crystals of calcite could be grown spontaneously in a 3 mol kg^{-1} hydrothermal NaCl solution above 400 °C on the basis of solubility data.

The IR spectra of grown single crystals were found to be identical to high-quality natural Iceland spar with traces of OH^-.

Calcite single crystals could be successfully grown on seed crystals at 400 °C. This result indicates that the growth rate on the $\{10\bar{1}1\}$ plane is too slow for growing a large single crystal; thus, it is necessary to use a seed crystal with the proper orientation for a suitable facet, such as the $(11\bar{2}0)$ face.

References

1) P. M. Gruzensky, *Crystal Growth. Suppl. J. Phys. Chem. Solids*, **1967**, 365.

2) J. F. Balascio and W. B. White, *J. Crystal Growth*, **23**, 101 (1974).

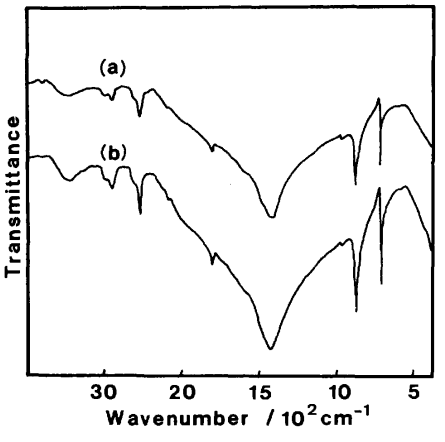

Fig. 5. IR Spectra of calcite single crystals.
(a) Hydrothermally grown crystal in NaCl solution.
(b) Natural Iceland spar crystal.

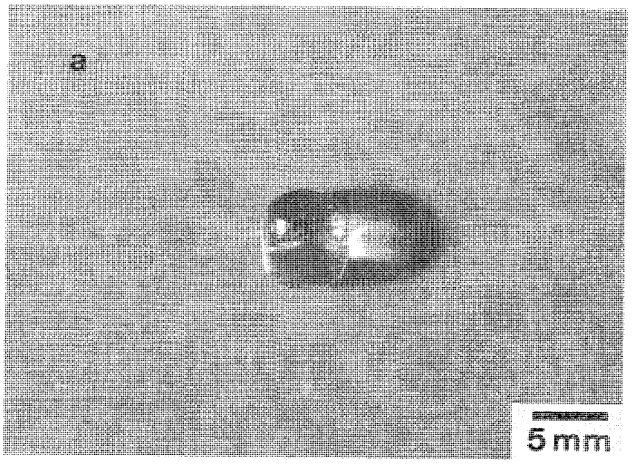

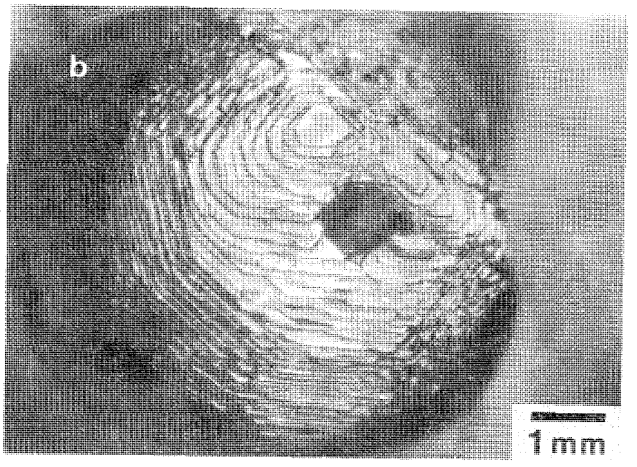

Fig. 6. (a) Spherical seed crystal. (b) Grown layer on the seed.

3) C. Belin, *J. Crystal Growth*, **34**, 341 (1976).
4) S. Hirano and K. Kikuta, *Chem. Lett.*, **1985**, 1613.
5) N. Yu. Ikornikova, *Soviet Phys Cryst.*, **5**, 726 (1961).
6) N. Yu. Ikornikova, *Growth of Crystals*, **3**, 297 (1962).
7) C. F. Bell and K. A. K. Lott, "Modern Approach to Inorganic Chemistry," Butterworth & Co., Ltd., London (1972).
8) I. Sunagawa et al., "Kobutsugaku," Iwanami-shoten, Tokyo (1975).

 © 1987 The Chemical Society of Japan Bull. Chem. Soc. Jpn., 60, 1113—1117 (1987)

A Fast Kinetic Study of Formation and Decay of 2,2′-Azinobis(3-ethylbenzothiazole-6-sulfonate) Radical Cation in Aqueous Solution

Pichai MARUTHAMUTHU,* Lakshmanan VENKATASUBRAMANIAN, and Periasamy DHARMALINGAM
Department of Energy, University of Madras, A. C. College Campus, Madras 600 025, India
(Received November 28, 1985)

The kinetics of oxidation of 2,2′-azinobis(3-ethylbenzothiazole-6-sulfonate) (ABTS) to the radical cation, $ABTS^{\cdot+}$ by $S_2O_8^{2-}$, HSO_5^-, MnO_4^-, $Cr_2O_7^{2-}$, Ce(IV), and molecular Cl_2, Br_2, and I_2 and further oxidation to the dication, $ABTS^{2+}$ by the above oxidants except HSO_5^-, Br_2, and I_2 have been carried out by the stopped-flow spectrophotometric technique. The first-stage oxidation was followed by monitoring the absorption of $ABTS^{\cdot+}$ at 417 nm and the second-stage oxidation, by following the disappearance of $ABTS^{\cdot+}$ or the appearance of $ABTS^{2+}$ at 513 nm. Both the reactions, formation and decay of $ABTS^{\cdot+}$ were found to obey a total second-order kinetics, first-order each with respect to [ABTS] or [$ABTS^{\cdot+}$] and [oxidant]. With I_2, ABTS underwent reversible reaction, the stoichiometry of which being,

$$I_2 + 2ABTS \rightleftharpoons 2ABTS^{\cdot+} + 2I^- \text{ with } K = 142.8,$$

whereas Br_2 generated only the radical cation and Cl_2 gave a decomposed product via radical cation and dication intermediates. $ABTS^{2+}$ formed in presence of excess MnO_4^-, $Cr_2O_7^{2-}$, and Ce(IV) decayed as in the case of Cl_2 reaction but in presence of $S_2O_8^{2-}$ the dication was stable for more than three days. In the absence of excess $S_2O_8^{2-}$, $ABTS^{2+}$ went back to $ABTS^{\cdot+}$, possibly via oxidation of water. The radical cation was converted back to the parent compound ABTS by reducing agents such as dithionite and sulfite ions.

Recently much attention has been focussed on the reactions of radical cations in an aqueous solution to explore the possibility of using them in solar energy conversion processes.[1,2] Würster's salt (TMPD) which forms $TMPD^{\cdot+}$ on one-electron oxidation and Weitz's salt (Methylviologen) which forms a radical cation on one-electron reduction are assessed to be electron-relays in chemical routes to solar energy conversion. We have already reported on the fast kinetics of the formation and decay of *N,N,N′,N′*-tetramethyl-*p*-phenylenediamine raical cation ($TMPD^{\cdot+}$) in aqueous solution by several oxidizing agents.[3] Previous studies on the polarographic oxidation[4,5] of 2,2′-azinobis(3-ethylbenzothiazole) have revealed the formation of a radical cation and a dication. The utility of ABTS as an analytical reagent for colorimetric determination of periodic acid has also been reported.[6] However no kinetic measurements were carried out. Here we present the results of fast kinetics of formation and decay of radical cation, $ABTS^{\cdot+}$ by one-electron as well as multielectron oxidizing agents.

Experimental

All kinetic measurements were made with Applied Photophysics Model-1705 stopped-flow-spectrophotometer. Absorption output was digitised with a Datalab Model-902 Transient recorder equipped with variable input sensitivity and variable sampling interval, and was monitored by Trio Model-CS-1562A Oscilloscope. About 500—700 points were collected for each kinetic measurement and at least six kinetic runs were made for each rate constant measurement. The data were stored and analyzed by CBM-3032 Personal Computer. The kinetic plots were plotted on a Hewlett-Packard graphics plotter. All the measurements were carried out at room temperature (25 °C), with the reagent solutions prepared using doubly distilled water. Cyclic voltammogram studies were carried out with a PAR Model 173/175 electrochemical setup using a platinum wire as the working electrode and KCl as the supporting electrolyte. The chemicals used were of the best research grade commercially available. ABTS was from Boehringer, Mannheim (West Germany) in the form of diammonium salt and was used as such. Peroxomonosulfate (PMS) in the form of a triple salt ($2KHSO_5$–$KHSO_4$–K_2SO_4) with the trade name "OXONE" was obtained from Dupont de Nemours & Co (USA). Other chemicals such as peroxodisulfate (PDS), $KMnO_4$, $K_2Cr_2O_7$, $Ce(NH_4)_2(SO_4)_3$, and molecular I_2, Br_2, and Cl_2 were obtained from Sarabhai M. Chemicals. The reagent solutions were thoroughly degassed by purified nitrogen or argon. The extent of formation and decay of radical cation ($ABTS^{\cdot+}$) were monitored at 417 nm which

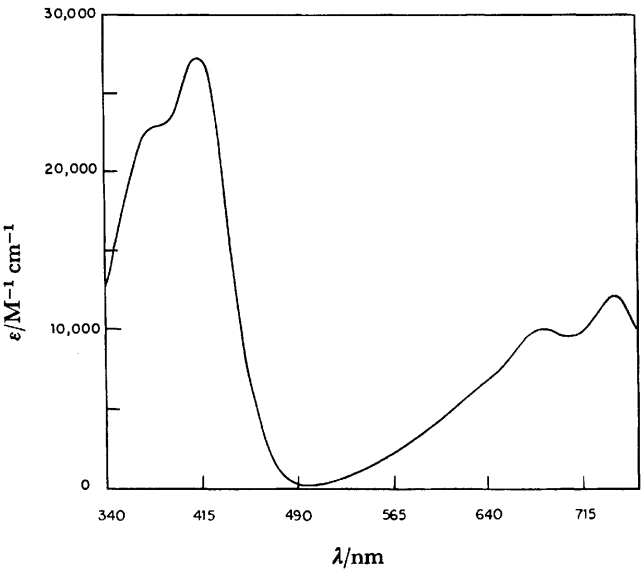

Fig. 1. Molar absorption spectrum of $ABTS^{\cdot+}$.

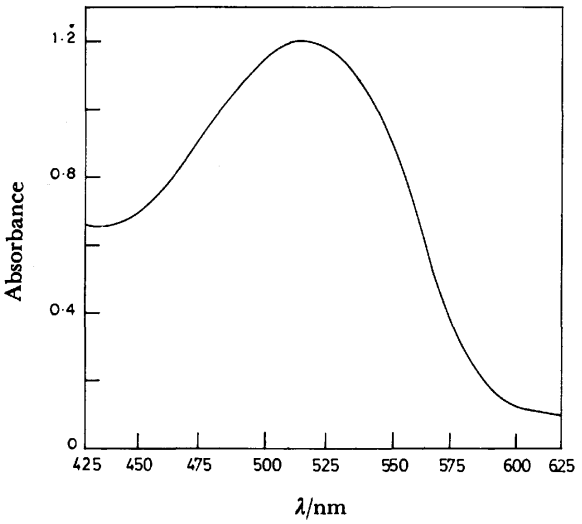

Fig. 2. Transient spectrum of $ABTS^{2+}$.

corresponds to its maximum absorbance ($\varepsilon_{417}=2.70\times10^4\ M^{-1}\ cm^{-1}$ -Fig. 1) (1 M=1 mol dm^{-3}). Formation of dication $ABTS^{2+}$ was monitored by its absorbance maximum at 513 nm (Fig. 2). The radical cation ($ABTS^{\cdot+}$) used was prepared by the reaction of ABTS with PMS (HSO_5^-) in the ratio of 2:1 respectively in deaerated water. The radical cation formed was found to be stable for more than a week.

Results and Discussion

All the kinetic measurements were carried out under pseudo-first order conditions, with the concentration of the oxidant in at least ten times excess over that of ABTS. The changes in the concentration of the transient with time were followed at different time scales depending on the reactivity of the oxidant. Plots of log (absorbance) against time were found to be linear up to ≈70% of the reaction with the correlation coefficient ≥0.99, showing that the reaction is first order with respect to ABTS. Plots of the pseudo first order rate constants k'/s^{-1} against concentrations of oxidant at fixed [ABTS] were found to be linear passing through the origin (Fig. 3), showing the first-order dependence of the rate on the oxidant. From the slopes of the above plots, the second-order rate constants $k_f/M^{-1}\,s^{-1}$ were calculated to be presented in Table 1. The proposed rate law for the formation of radical cation is

$$\frac{d[ABTS^{\cdot+}]}{dt} = k_f[ABTS][Oxidant]. \quad (1)$$

For the determination of the rate constants of the decay of the radical cation either to the dication ($ABTS^{2+}$) or back to ABTS, experiments were carried out with the $ABTS^{\cdot+}$ preprepared as mentioned above. The kinetics were spectrophotometrically followed either at 417 or 513 nm, by varying [$ABTS^{\cdot+}$] as well as [Oxidant] under pseudo-first-order conditions. Rate law analysis similar to the above (Fig. 4)

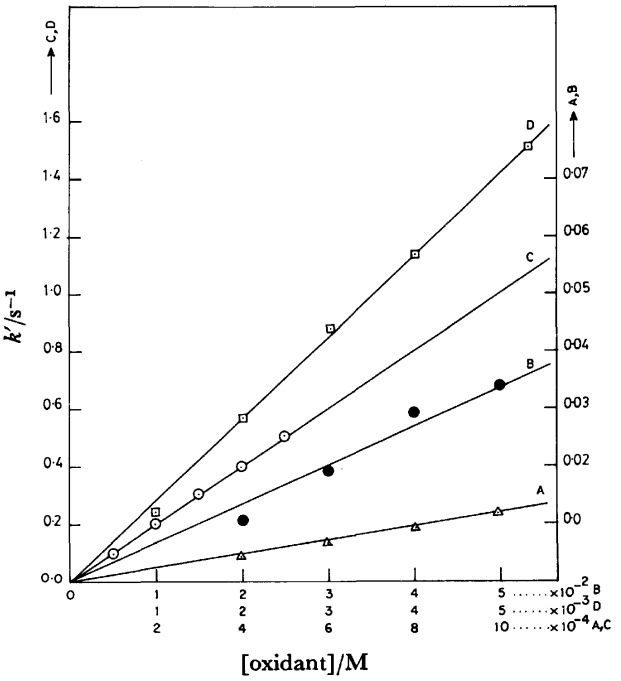

Fig. 3. Evaluation of k_f.
k' vs. [Oxidant]; T=25 °C; A: PMS; B: PDS; C: $Cr_2O_7^{2-}$; D: Ce(IV).

Table 1. Kinetic Data for the Formation and Decay of $ABTS^{\cdot+}$ at 25 °C

Oxidant	$k_f/M^{-1}\,s^{-1}$	$k_d/M^{-1}\,s^{-1}$
PMS	11.16	—
PDS	0.63	0.20
MnO_4^-	2.50×10^4	1.50×10^3
$Cr_2O_7^{2-}$/0.2 M H^+	1.01×10^3	4.00×10^2
Ce(IV)/0.2 M H^+	3.01×10^2	3.00×10^1
I_2	6.28×10^2	—
Br_2	1.00×10^5	—
Cl_2	—	2.40

gave the kinetic rate law for the decay process to be

$$\text{Rate} = -\frac{d[ABTS^{\cdot+}]}{dt} = \frac{d[ABTS^{2+}]}{dt}$$
$$= k_d[ABTS^{\cdot+}][Oxidant]. \quad (2)$$

The calculated rate constants k_d are shown in Table 1.

Reaction with Peroxodisulfate (PDS) and Peroxomonosulfate (PMS). The kinetics of reactions of these two peroxosalts of sulfur with ABTS were found to be first-order each with respect to the oxidant and ABTS. Although these two oxidants are two-electron transferring agents, they behave like a one-electron oxidant in forming the radical cation, $ABTS^{\cdot+}$. On short time scales, (5—20 ms), PDS (1—5×10^{-2} M) and ABTS (1—5×10^{-5} M) generated only the radical cation ($ABTS^{\cdot+}$). However at longer time scales (20—50 ms)

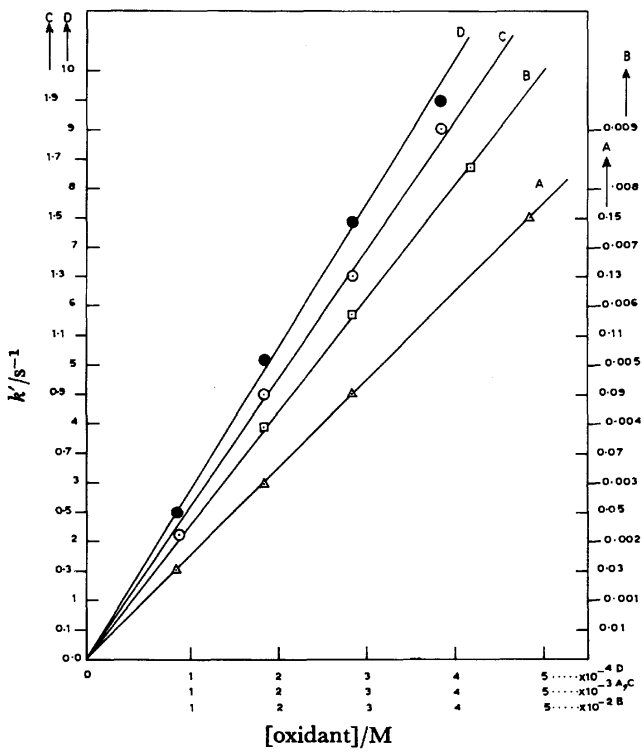

Fig. 4. Evaluation of k_d.
k' vs. [Oxidant]; T=25 °C; A: Ce(IV); B: PDS; C: $Cr_2O_7^{2-}$; D: MnO_4^-.

the radical cation formed decayed to the dication, $ABTS^{2+}$. The rate constant determined for the reaction (3), formation of ABTS$^{\cdot+}$, was 0.63 M^{-1} s^{-1} and that for the second-stage oxidation (4) was 0.20 M^{-1} s^{-1}.

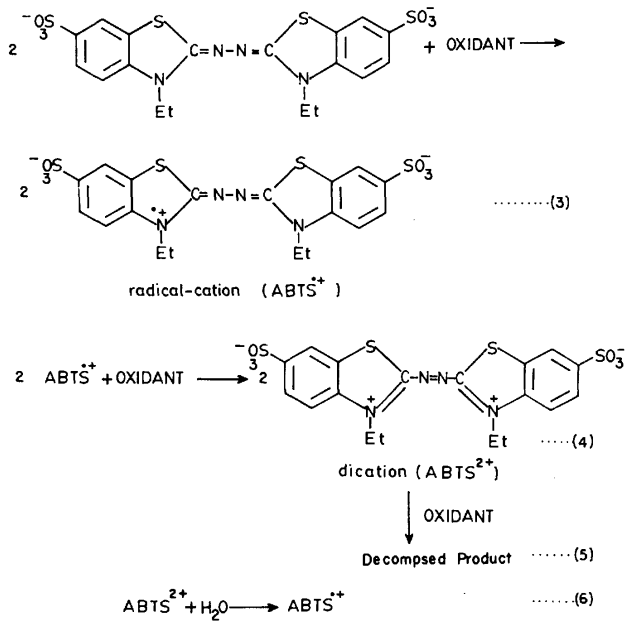

From the magnitudes of the rate constants, it is seen that the oxidation of ABTS$^{\cdot+}$ to $ABTS^{2+}$ is approximately three times slower than that of ABTS to ABTS$^{\cdot+}$. The dication which is pink-red brittle precipitate is stable for more than three days in the presence of excess $S_2O_8^{2-}$. The precipitate, separated and free from $S_2O_8^{2-}$, when dissolved in water turned back into ABTS$^{\cdot+}$ (6). On the other hand, the reaction of HSO_5^- with ABTS, whatever be the concentrations of both of them, stopped with the formation of ABTS$^{\cdot+}$. This unusual stability of the radical cation is explained by strong delocalization of the odd electron into the π-cloud, thus causing a high stability and long wavelength absorption. The rate constant determined for the oxidation of ABTS by PMS is 11.16 M^{-1} s^{-1}. Even though the oxidation potential for PMS (1.81 V) is less than that of PDS (2.01 V), the rate constant for PMS with ABTS is approximately 18 times higher than that of PDS. This observation is similar to the one encountered in many thermal reactions[7] wherein the rate constants for the oxidation by PMS were higher than those of PDS. In some cases, such as oxidation of methoxybenzenes[8] the reaction of PMS took place at measurable rates at 25 °C, whereas PDS reacted only in presence of Ag^+ catalyst. Hence, even though the thermodynamic factor (oxidation potential) is favorable for PDS to react with many substrates, the reactions are kinetically inhibited. This might be true in the present investigation also. However, PMS does not react further with the radical cation unlike $S_2O_8^{2-}$.

Reactions of Halogens. Molecular iodine oxidised ABTS to ABTS$^{\cdot+}$ instantaneously, but I_2 in excess KI (5%) did not bring the reaction instantaneously, suggesting the equilibrium reaction (7),

$$2ABTS + I_2 \underset{k_r}{\overset{k_f}{\rightleftharpoons}} 2ABTS^{\cdot+} + 2I^- \qquad (7)$$

The forward reaction was measured by following the formation of radical cation for various concentrations of ABTS with different amounts of I_2 in water at natural pH (pH=6.9) in 2—10 ms time scale. The second-order rate constant, k_f was calculated to be 628.1 M^{-1} s^{-1}. The reverse process was monitored by following the disappearance of ABTS$^{\cdot+}$ for various concentrations of ABTS$^{\cdot+}$ ($1—5\times10^{-5}$ M) and I^- ($2—8\times10^{-2}$ M). The rate constant for the reverse reaction was, k_r=4.40 M^{-1} s^{-1}, then the equilibrium constant being $K=k_f/k_r$=142.8. The rate constants measured at pH 3—6 did not show any difference from those measured at the near neutral and natural pH. From the equilibrium constant, the change in the Gibbs free energy, $\Delta G°$ at 25 °C for the reaction (7) is calculated to be, $\Delta G°=-RT\ln K$

$$\Delta G° = -8.314 \times 298 \times 2.303 \times 2.155$$
$$\Delta G° = -1.23 \times 10^4 \text{ J mol}^{-1}.$$

The difference in the standard redox potentials between the two one-electron redox couples is $\Delta E° = \Delta G°/F$=−0.127 V. The standard redox potential

$E°$, for $ABTS^{\cdot+}$/ABTS measured in aqueous medium by cyclic voltammetric technique was +0.43 V. Since the $E°$ for I_2/I^- is +0.54 V, theoretical value of the standard electrode potential for the reaction (7) should be −0.11 V which is in good agreement with the one estimated from the equilibrium constant. In the case of the reactions of Br_2 and Cl_2 with ABTS, such equilibrium was not observed. Molecular Br_2 in water or aqueous Br_2/KBr oxidized ABTS to $ABTS^{\cdot+}$ in 0.5—2.0 ms time scale and the rate constant for the reaction (8),

$$ABTS + Br_2 \longrightarrow ABTS^{\cdot+} + Br_2^{\cdot-} \quad (8)$$

was $1.00\times10^5\ M^{-1}\ s^{-1}$. There was no detectable reaction of $ABTS^{\cdot+}$ either with Br_2 or Br^-. No attempt was made to investigate the fate of $Br_2^{\cdot-}$ in the present work since it was postulated to decay by the bimolecular reaction at diffusion controlled rate,[9]

$$2Br_2^{\cdot-} \longrightarrow Br^- + Br_3^- . \quad (9)$$

In the case of Cl_2, the first stage oxidation (3) was very fast and took place within the mixing time of the instrument (dead time 2 ms). The second-stage oxidation resulted in a decomposed product via the dication as the transient even for the lowest concentrations of the reactants $ABTS^{\cdot+}$ and Cl_2. The kinetics of the decay process was also found to be total second-order, first-order each with respect to $[ABTS^{\cdot+}]$ and $[Cl_2]$ and the rate constant was calculated to be $2.40\ M^{-1}\ s^{-1}$.

$$ABTS^{\cdot+} + Cl_2 \longrightarrow ABTS^{2+} \longrightarrow \text{decomposed product} \quad (10)$$

The decomposed product formed in the reaction (10) could not be reverted back to any one of the species, $ABTS^{2+}$, $ABTS^{\cdot+}$, or ABTS by the addition of strong reducing agents such as sulfite or dithionite. Since our interest in this study is centered around the formation and reactivity of radical cations from ABTS, not much attention was paid on the complete identification of the decomposed product. However, IR and UV spectral investigation showed the formation of substituted thiophenol and disulfide depending upon the concentration of Cl_2 used. From the magnitudes of the rate constants (Table 1), the reactivity trend of the halogens with ABTS, $Cl_2>Br_2>I_2$ is similar to the trend of their oxidation potentials and the latter two halogens give only the one-electron oxidation product, $ABTS^{\cdot+}$. In the case of oxidation of $ABTS^{\cdot+}$ to $ABTS^{2+}$, judging from the magnitudes of the oxidation potentials of Cl_2 (1.35 V) and $ABTS^{\cdot+}/ABTS^{2+}$ (0.83 V) and the magnitude of the rate constant for the reaction (10), it is not surprising that Br_2 (oxidation potential 1.06 V) hardly react with $ABTS^{\cdot+}$.

Reaction of MnO_4^-, $Cr_2O_7^{2-}$, and Ce(IV). At low concentrations of the oxidants, ([ABTS]=1—4×10^{-5} M; [oxidant]=1—4×10^{-4} M), both MnO_4^- and $Cr_2O_7^{2-}$ (in 0.2 M H^+) were found to generate only the radical cation. However at higher concentrations of the oxidants and on longer time scales, the radical cation was found to decay at a measurable rate to pink-red dication and then to a decomposed product. In the case of Ce(IV) in 0.2 M H^+, at any concentrations of the reactants, ABTS was oxidized to the dication via the radical cation as a transient. The observed rate constant for both the processes are presented in Table 1. From the magnitudes of the rate constants the reactivity of these oxidants with ABTS as well as $ABTS^{\cdot+}$ is found to be $MnO_4^->Cr_2O_7^{2-}>Ce(IV)$, the second-stage oxidation being one order of magnitude less than that for the radical cation formation in the case of MnO_4^- and Ce(IV). The rate constants estimated are in line with the oxidation potentials[10] of MnO_4^- (1.695 V) and $Cr_2O_7^{2-}$ (1.44 V). In the case of Ce(IV) (1.44 V) on thermodynamic grounds, the reactivity should be comparable to that of $Cr_2O_7^{2-}$. However, it is less reactive than $Cr_2O_7^{2-}$ probably due to its high ability of complexing[11] with groups containing electron donors.

Reduction of Radical Cation. The possibility of the reduction of the radical cation, $ABTS^{\cdot+}$ was tested by using dithionite and sulfite ions as reducing agents. The reaction (11) was brought about, producing the parent compound ABTS,

$$ABTS^{\cdot+} + \text{reductant} \longrightarrow ABTS \cdot \quad (11)$$

The kinetics of the reaction gave the second-order rate constants shown below:

$$ABTS^{\cdot+} + SO_3^{2-} \longrightarrow ABTS,\ k_2 = 1.06\times10^3\ M^{-1}\ s^{-1},$$
$$ABTS^{\cdot+} + S_2O_4^{2-} \longrightarrow ABTS,\ k_2 = 6.30\times10^2\ M^{-1}\ s^{-1}.$$

Other preliminary tests show that the radical cation $ABTS^{\cdot+}$ is capable of oxidizing many organic and inorganic substrates.[12]

The authors are thankful to the Department of Science and Technology, Government of India, New Delhi for financial support.

References

1) M. Grätzel, *Acc. Chem. Res.*, **14**, 376 (1981).
2) G. Levey, A. L. Rieges, and J. O. Edwards, *J. Org. Chem.*, **46**, 1255 (1981).
3) P. Maruthamuthu, L. Venkatasubramanian, and P. Dharmalingam, *J. Chem. Soc., Faraday Trans, 1*, **82**, 359 (1986).
4) S. Hüenig, H. Balli, H. Cornard, and A. Schott, *Justus Liebigs Ann. Chem.*, **676**, 36 (1964).
5) S. Hüenig, *Justus Liebigs Ann. Chem.*, **676**, 32 (1964).
6) G. Mahuzier, B. S. Kirkacharian, and C. Harfouche-obeika, *Anal. Chim. Acta*, **76**, 79 (1975).
7) a) R. Ranganathan and P. Maruthamuthu, *Int. J. Chem. Kinet.*, **18**, 49 (1986); b) R. Ranganathan and P.

Maruthamuthu, *J. Chem. Soc., Perkin Trans. 2*, **1986**, 285.

8) P. Dharmalingam and P. Maruthamuthu, *J. Chem. Soc., Perkin Trans. 2*, submitted for publication.

9) "Rate Constants for Reactions of Inorganic Radicals in Aqueous Solution," ed by A. B. Ross and P. Neta, U. S. Department of Commerce-National Bureau of Standards (1979), p. 38.

10) "Oxidation Potentials," ed by W. M. Latimer, Prentice-Hall Inc., Englewood Cliffs, NJ (1966).

11) J. Handwick and E. Robertson, *Can. J. Chem.*, **29**, 818 (1951).

12) P. Maruthamuthu and L. Venkatasubramanian, unpublished results.

 © 1987 The Chemical Society of Japan Bull. Chem. Soc. Jpn., 60, 1119—1123 (1987)

Ultraviolet Studies and Fluorescence Quenching of Some Aromatic Primary Amines

Samaresh MUKHERJEE
Department of Physical Chemistry, Indian Association for the Cultivation of Science, Jadavpur, Calcutta 700 032, India
(Received January 25, 1986)

The fluorescence quenching of *o*-aminobenzoic acid, 1-naphthylamine, aniline, *p*-toluidine, *m*-toluidine, and *N,N*-dimethylaniline by 2-hydroxy-5-methyl-1,3-benzenedicarbaldehyde (**VII**) was studied. The equilibrium constant of hydrogen bonding in the ground state was evaluated from the absorption spectral change for various donor-acceptor (D-A) pairs. The rate constants of hydrogen-bond formation as well as decomposition in the excited state were evaluated in the case of several donor-acceptor pairs from fluorescence intensity measurements. In addition, the mechanism of fluorescence quenching and absorption spectral shift when **VII** acted as a quencher/proton donor (D) was discussed on the basis of charge-transfer and hydrogen-bond interaction.

Light absorption brings out rather strong change in some molecular properties in the excited state and the proton dissociation, energy transfer or hydrogen-bond formation of aromatic hydroxy and amino compounds occurs far easily in the excited state than in the ground state.[1-5] Apart from spectral shift, hydrogen bonding also causes fluorescence enhancement or quenching. The phenomenon of fluorescence quenching particularly has received wide attention.[6-15] It is known that aromatic amines experience a large change in the excited state[16-18] consequently it will be of interest to investigate the effect of various influences on the ground vis-a-vis excited state properties of aromatic amines. The present investigation dealing with interaction of some aromatic primary amines, viz. *o*-aminobenzoic acid (**I**), 1-naphthylamine (**II**), aniline (**III**), *p*-toluidine (**IV**), *m*-toluidine (**V**), and *N,N*-dimethylaniline (**VI**) with a proton donor (D), viz. 2-hydroxy-5-methyl-1,3-benzenedicarbaldehyde (**VII**) in cyclohexane at 300 K was undertaken with the object to study the spectral changes in relation to hydrogen-bonding properties of the molecules in the ground and excited state and probable reaction processes leading to fluorescence quenching.

Experimental

1-Naphthylamine, *o*-aminobenzoic acid, and *p*/*m*-toluidines were purified by recrystallization followed by vacuum sublimation. Aniline and *N,N*-dimethylaniline were first dried over solid KOH and then distilled over zinc dust. Cyclohexane (Merck, spectroscopic grade) was dried over metallic sodium and distilled fractionally. Proton donor **VII**[19] was received as a gift from department of inorganic chemistry of this institute. All the absorption spectra were recorded with freshly prepared solutions in a Cary 17D spectrophotometer. The fluorescence spectra were recorded in a Perkin-Elmer fluorescence spectrophotometer (Model MP F-44B) using 1 cm stoppered quartz cell at 300 K. Blank runs were made with solvent alone which showed no fluorescence emission at the maximum sensitivity of the instrument in the spectral region of interest.

The fluorescence quantum yield of amines are measured from the corrected area under fluorescence curve relative to that of anthracene[20] in identical conditions. Radiative lifetimes are estimated from integrated absorption spectra using Eq. 1

$$\tau_N = \frac{1.5}{(\bar{\nu}_{max})^2 \times f}, \quad (1)$$

where $f=4.33\times10^{-9}\int\varepsilon\bar{\nu}d\bar{\nu}$, is the oscillator strength of the lowest electronic transition.

Results and Discussion

The change of absorption spectrum caused by hydrogen bonding is shown in Fig. 1 in the case of *o*-aminobenzoic acid (**I**)+2-hydroxy-5-methyl-1,3-benzenedicarbaldehyde (**VII**) system in cyclohexane. Frequency maxima (ν_E in cm^{-1}) and frequency shifts ($\Delta\nu_E$ in cm^{-1}) for the proton acceptor molecules **I** and **II** are given in Table 1. From the observed spectral change, the equilibrium constant K_g of hydrogen-bond formation with proton acceptor molecules for the case **I** and **II** in the ground state can be evaluated by the Ketelaar's method[21] using the Eq. 2.

$$\frac{1}{A_o - A_f} = \frac{1}{[D]} \cdot \frac{1}{A_b - A_f} \cdot \frac{1}{K_g} + \frac{1}{A_b - A_f} \quad (2)$$

In Eq. 2, A_f and A_b denotes the absorbance of free acceptor and the hydrogen-bonded complex respectively and A_o that of a solution of acceptor where the concentration D is [D]. On extrapolating the straightline obtained from $1/(A_o-A_f)$ vs. $1/[D]$ plot to the point where $1/(A_o-A_f)=0$, K is obtained as $K=-1/[D]$. The association equilibrium constants (K_g) evaluated by linear regression analysis are given in Table 2. It is observed that with gradual increase of [D] the position of the absorption maximum shifts gradually (Fig. 1) and then tends to a constant value above a certain concentration indicating that intermolecular hydrogen bond formation is almost complete as such concentration. Another significant observation is that the oscillator strength (f_b) for

Table 1. Frequencies of Fluorescence Maxima (ν_F in cm^{-1}), Excitation Maxima (ν_E in cm^{-1}), and Measured Oscillator Strengths (f) of Free and Hydrogen-Bonded Molecules in Cyclohexane Solvent at 300 K

System	$f_f^* \times 10^3$	$f_b^* \times 10^3$	f_b^*/f_f^*	ν_F	ν_E	$\Delta\nu_F = F^{b*} - F^{f*}$	$\Delta\nu_E = E^{b*} - E^{f*}$	I_P/eV†
I	58.81	—	—	26316	29851			
I+**VII**	—	222.56	3.92	25641	28935	−675	−866	
II	79.21	—	—	27027	31446			
I+**VII**	—	292.33	3.69	26173	30303	−849	−1143	
III				32258	34728			8.64[d]
III+**VII**				32258	34728	0	0	4.34[e]
IV				31250	34247			8.14[d]
IV+**VII**				32051	34247	801	0	3.88[e]
V				32258	34965			8.27[d]
V+**VII**				32787	34965	529	0	3.96[e]
VI				30769	33557			7.14[d]
VI+**VII**				31746	33557	977	0	2.98[e]

* The sub- and superscripts "f" and "b" refer to free and bonded species respectively. † The superscripts "e" and "d" refer to I_p(eV), for acceptor molecules in the ground (obtained from NBS, 34, 1969) and excited (calculated) state, respectively.

Table 2. Equilibrium and Rate Constants of Hydrogen Bonding at 300 K

System	K_1/dm³ mol⁻¹	$\frac{\tau K_1 (= K_Q)}{(1+\tau' K_2)}$	K_g/dm³ mol⁻¹	K_e/dm³ mol⁻¹	K_1/dm³ ml⁻¹ s⁻¹	K_2/s⁻¹
I	3200	1180	265±5	1.74×10^4	2.13×10^{11}	1.22×10^7
II	2000	1106	345±3	8.71×10^4	3.36×10^{11}	0.41×10^7

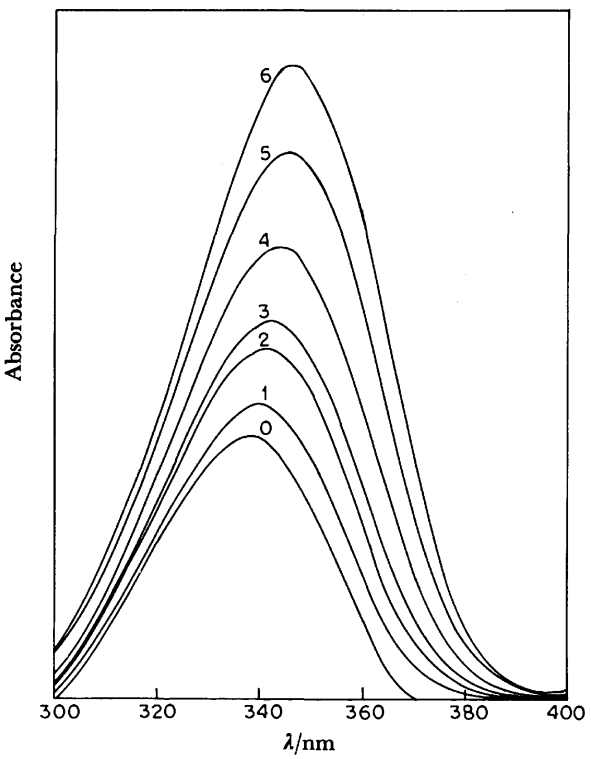

Fig. 1. Absorption spectra of *o*-aminobenzoic acid (**I**)-**VII** (D)-cyclohexane system.
[I] = 4.5×10^{-5} mol dm⁻³; [D]/mol dm⁻³ 0: 0; 1: 2.95×10^{-5}, 2: 5.7×10^{-5} 3: 8.6×10^{-5}, 4: 1.41×10^{-4}, 5: 1.7×10^{-4}, 6: 2.95×10^{-4}.

bonded molecules is always greater than that (f_f) for free molecules in the case of both **I** and **II**. Thus we see from Table 1 that there is a correlation between the hydrogen-bond formation and the increase in f-values of transition.

The change of fluorescence spectrum caused by hydrogen bonding of the proton donor (**VII**) with aniline (**III**) and *N*,*N*-dimethylaniline (**VI**) in cyclohexane is shown in Fig. 2 and the relevant spectral data are set out in Table 1. At low concentration the quenching of fluorescence by a proton donor in solution follows the classic Stern-Volmer relationship (3)

$$f^0/f = 1 + K_Q[D], \quad (3)$$

where K_Q is called the quenching constant, f is the intensity of fluorescence at the proton donor **VII** concentration, [D], and f^0 is its value without D. The K_Q values evaluated graphically (Fig. 3) using the relation (3) are given in Table 3. By equating the bimolecular rate constant for the quenching reaction (K_1) against the rate of emission it can be shown[22] that $K_Q = K_1\tau$ where τ is the actual mean life of the fluorescence i.e., quantum efficiency (ϕ) × radiative life (τ_N) (see Table 3). Detailed quantitative study of the relative fluorescence yield and life time measurements were also carried out for all the systems. The wave number shifts $\Delta\nu_F$ and $\Delta\nu_E$ of the fluorescence

Table 3. Mean Life of the Fluorescence (τ), Radiative Lifetime (τ_N), Quenching Constant (K_Q), Bimolecular Rate Constant (K_1), and Quantum Yield (ϕ and ϕ_A) of Some Aromatic Amines Acting as Proton Acceptor (A) with Donor **VII** in Cyclohexane at 300 K

System	ϕ	ϕ_A	τ_N/s	τ/s	K_Q/dm^3 mol^{-1}	K_1/dm^3 mol^{-1} s^{-1}
I	0.36	—	2.98×10^{-8}	15.0×10^{-9}	—	—
II	0.31	—	1.92×10^{-8}	5.95×10^{-9}	—	—
III	0.12	0.13	4.92×10^{-8}	5.90×10^{-9}	8.3×10^{2}	1.4×10^{11}
IV	0.041	0.039	4.47×10^{-8}	1.83×10^{-9}	7.5×10^{2}	4.1×10^{10}
V	0.029	0.028	3.6×10^{-8}	0.9×10^{-9}	3.75×10^{2}	4.16×10^{11}
VI	0.26	0.24	3.76×10^{-8}	9.78×10^{-9}	1.20×10^{3}	1.22×10^{11}

Range of [A]: 5.7×10^{-5}—9.8×10^{-5} mol dm^{-3} and [D]: 6.1×10^{-5}—8.5×10^{-3} mol dm^{-3}; K_Q: Values are obtain from Stern-Volmer plots (Eq. 2); ϕ_A^a: Limiting quantum yields of photoreactions obtained from the intercepts of the usual Plots of ϕ_A^{-1} vs. [D]$^{-1}$ (in case where K_Q [D]<1) where, ϕ_A is quantum yields for disappearance of amines (see Ref. 11).

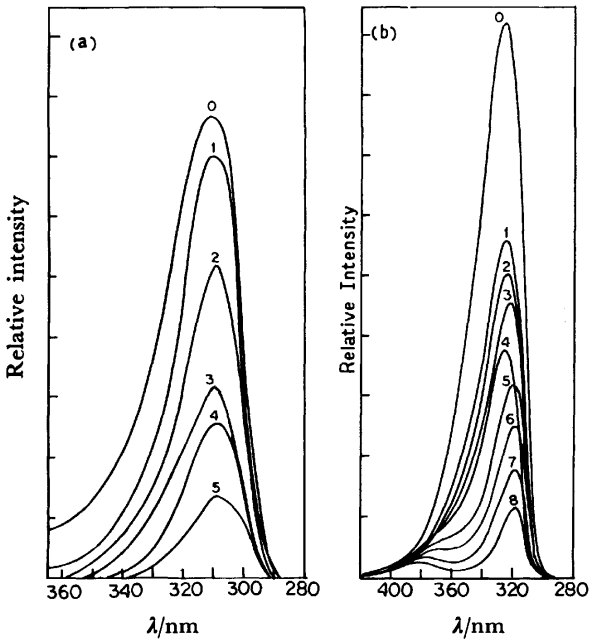

Fig. 2. Fluorescence spectra of (a) aniline (**III**), (b) *N*,*N*-dimethylaniline (**VI**) in mixed **VII** (D)-cyclohexane system.
(a): [**III**] $=1.05\times10^{-4}$ mol dm^{-3}; [D]/mol dm^{-3} 0: 0, 1: 1.14×10^{-4}, 2: 1.71×10^{-4}, 3: 2.28×10^{-4}, 4: 2.85×10^{-4}, 5: 5.02×10^{-4}.
(b): [**VI**] $=1.21\times10^{-4}$ mol dm^{-3}; [D]/mol dm^{-3} 0: 0, 1: 0.65×10^{-4}, 2: 1.06×10^{-4}, 3: 1.48×10^{-4}, 4: 2.13×10^{-4}, 5: 3.19×10^{-4}, 6: 3.48×10^{-4}, 7: 7.5×10^{-4}, 8: 8.5×10^{-4}.

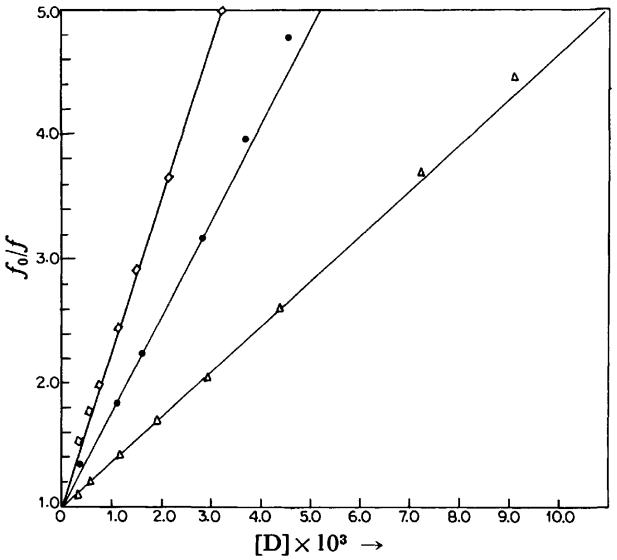

Fig. 3. Stern-Volmer plots for the quenching of acceptor molecules (△) **V**; (●) **IV**; (□) **VI**, by donor **VII**.

and excitation spectrum respectively due to hydrogen-bond formation are given in Table 1. Of all the proton acceptor studied the spectral shift on hydrogen-bond formation in the excited state $\Delta\nu_f=\nu_b-\nu_f$ (b and f referring to bonded and free molecules respectively) is found to be towards longer wavelength for **I** and **II** (i.e., $\Delta\nu<0$) for **IV** to **VI** towards shorter wavelength. For **III**, however, $\Delta\nu=0$.

While K_g is evaluated by Eq. 2 from the absorption spectral change, the corresponding quantity in the excited state, K_e (for **I** and **II**) can be estimated approximately by Eq. 4 assuming the same entropy change due to hydrogen-bond formation in the excited state as well as in the ground state[5]

$$\log K_e = \log K_g + \frac{0.625}{T}\cdot\Delta\nu_a . \quad (4)$$

In Eq. 4 $\Delta\nu_a$ is the limiting wave number shift of the absorption spectrum caused by hydrogen bonding and T is the absolute temperature. The values of K_g and K_e estimated in this way at ≈300 K are given in Table 2. It is important to point out here that in all of the systems under consideration quenching occurred, but the spectral shift observed in the ground state and excited state did not occur in the same way. When **I** and **II** were used as acceptor molecules, spectral shift occurred both in the ground and excited states. On the other hand, in the cases of **IV** and **VI**, spectral shift was observed only in the excited state. However, for **III** no

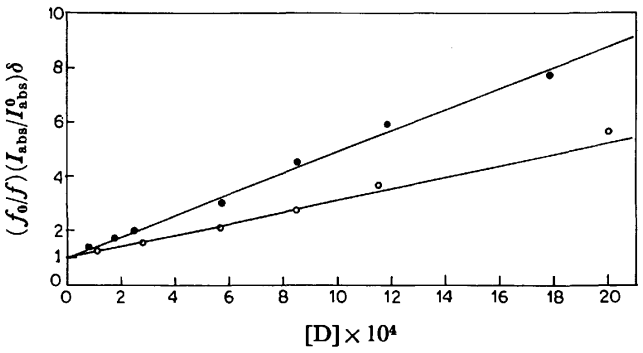

Fig. 4. $(f^0/f)(I^0_{abs})\delta$ vs. [D] relation for (●) **I**—**VII** and (○) **II**—**VII** systems in cyclohexane.

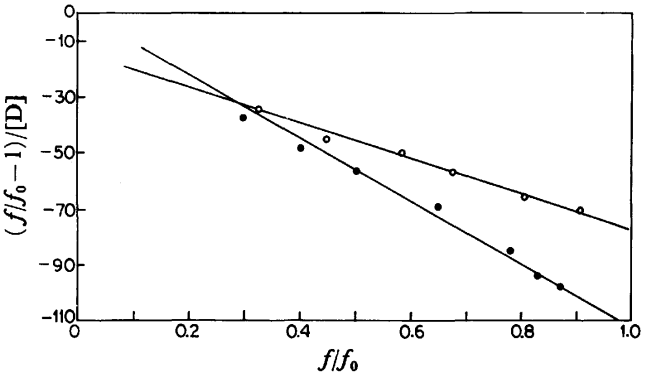

Fig. 5. $(f/f^0-1)/[D]$ vs. (f/f^0) relation for (●) **I**—**VII** and (○) **II**—**VII** systems in cyclohexane.

spectral shift occurred both in ground as well as excited state.

Qualitatively speaking, the observed difference between the hydrogen-bonding effect on the fluorescence and absorption spectrum may indicate that, the equilibrium shifts more or less to the side of hydrogen-bond formation during the life time of fluorescence state. To treat quantitatively the very rapid reaction which occurs during the life time of excited state Mataga et al.[5] has derived the general equation considering the probable reaction scheme and from the general equation they have derived several special cases also assuming the stationary state. For simplicity two approximate relationship can be used here

$$(f_0/f)(I_{abs}/I^0_{abs})\cdot\delta = 1 + K_1\tau[D], \quad (5)$$

$$(f/f_0-1)/[D] = K_f'\tau' K_1/K_f(1+K_2\tau') - [\tau K_1/(1+K_2\tau')]f/f_0 . \quad (6)$$

In these expressions I_{abs} is the total light quanta absorbed by solution when D is present, δ is the fraction of A* and is given by $\delta=1/\{1+(\varepsilon_c/\varepsilon_A)K_g[D]\}$, ε_A and ε_c are the molar extinction coefficients of acceptor (A) and donor acceptor complex (DA) respectively, at the wavelength of exciting light. K_1 is the bimolecular rate constant of hydrogen-bonding reaction and K_2 is the unimolecular rate constant of dissociation of DA*. I^0_{abs} is the total light quanta absorbed by the solution when D is absent and f_0 is the fluorescence intensity in that case. Using Eqs. 5 and 6 one can evaluate $K_1\tau$ and $\tau K_1/(1+K_2\tau')$. Figures 4 and 5 shows that for **I** and **II** these equations are approximately satisfied. The values of τK_1 and $\tau K_1/(1+\tau' K_2)$ obtained in this way are collected in Table 2. Using the values of given in Table 3, K_1 can be easily estimated. From the K_1 values and by means of the relation $K_2=K_1/K_e$, K_2 values may be estimated, if K_e values obtained by Eq. 3 are used. Practically, when no hydrogen-bonded complex exists in the ground state, $\delta=1$. The change of molar extinction coefficient caused by hydrogen-bonding is very small at the wavelengths of exciting light (288, 292, 286, and 298 nm for **III** to **VI** respectively) used, which mean I_{abs} is practically equal to I^0_{abs}. Moreover, because the fluorescence quenching was almost complete in the concentration range studied here, but practically no change in the absorption spectrum was observed, Eq. 6 therefore reduces to $f^0/f=1+K_1\tau[D]$, which incidentally is the simple Stern-Volmer Eq. 3.

One point to note here is that the values of the bimolecular quenching rate constant K_1 given in Tables 2 and 3 are rather high in comparison to diffusion controlled rate constant. A possible explanation may be presumed as follows. As the singlet energy level of **VII** lies below that of the primary aromatic amine, it is quite logical that the observed quenching rate constant K_1 may be composed of two rate constant: viz. (i) for strong hydrogen bond formation by which CT state is produced which may be somewhere below the S_1 state of aromatic amines, and internal conversion (IC) rate from this CT state to the ground state of aromatic amines may be enhanced due to lowering of energy gap between these two states (CT and ground state); (ii) for intermolecular energy transfer from singlet of aromatic amine to singlet of electron acceptor **VII**.

The fluorescence spectral shifts of aniline (**III**), *p*-toluidine (**IV**), *m*-toluidine (**V**), and *N*,*N*-dimethyl-aniline (**VI**) on interaction with **VII** are given in Table 1. It may be noted that in the case of aniline no spectral shift occurs, but the following decreased order of band shift takes place with the other amines: **VI**>**V**>**IV**. This trend is rather expected because the electron density on the nitrogen atom of the substituted anilines have increased by the electron releasing methyl group attached to the nitrogen atom itself or to the aromatic ring. The ionization potentials (I_P) (Table 1) of these compounds (**VI**>**V**>**III**) also clearly indicate that hydrogen bonding of **VII** will occur most easily with **VI** and least readily with **III**. The considerable blue shift of **IV**, **V**, and **VI** in the excited state (Table 1) can be related to the more basic character of these amines in the excited state. This can

be appreciated by taking into consideration the I_P of these molecules in the excited state (Table 1). It may also be noted in Table 2 that $K_e \gg K_g$ which indicates stronger proton acceptor ability (that is more basic character) of the molecules in their electronically excited state. The fluorescence quenching observed in the present study may be interpreted as due to the charge-transfer interaction via hydrogen bonding and seems to be followed by a very rapid nonradiative vibronic interaction process.

Another significant observation is that for certain proton acceptor molecules (**III** to **V**) quenching reaction appears as positive curvature in Stern-Volmer plots at high quencher concentrations.[27-29] Deviations from the Stern-Volmer equation in certain quenching reaction may be explained by a compound formation. In fact it has been observed that proton donor **VII** from Schiff's bases with aniline of the types **VIII** and **IX** at higher concentration of aniline at an elevated temperature.[30]

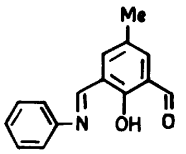

VIII

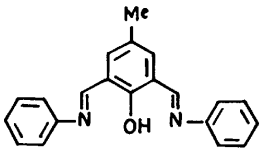

IX

References

1) N. Mataga, Y. Kaifu, and M. Koizumi, *Nature*, **175**, 731 (1955).

2) N. Mataga, Y. Kaifu, and M. Koizumi, *Bull. Chem. Soc. Jpn.*, **29**, 115 (1956).

3) T. Kubota and M. Yamakawa, *Bull. Chem. Soc. Jpn.*, **35**, 555 (1962).

4) B. Ghosh and S. Basu, *J. Chim. Phys. Phys.-Chim. Biol.*, **65**, 1587 (1968).

5) N. Mataga, Y. Torihashi, and Y. Kaifu, *Z. Phys. Chem. NF.*, **34**, 379 (1962).

6) M. H. Niyasaka, A. Karen, and N. Mataga, *J. Phys. Chem.*, **89**, 182 (1985).

7) F. Castro, A. Lazaro, S. Lombrana, and E. Martinez, *Spectrochim. Acta, Part A*, **39**, 33 (1983).

8) R. Ricci and J. Nesta, *J. Phys. Chem.*, **80**, 974 (1976).

9) M. Del, V. Bohorquez, J. J. Cosa, N. A. Garcia, and C. M. Previtati, *Photochem. Photobiol.*, **40**, 701 (1984).

10) C. Quick Jr., J. Tice, J. Preses, and R. Weston, *Chem. Phys. Lett.*, **114**, 371 (1985).

11) C. Pac, M. Yasudu, K. Shima, and H. Sakurai, *Bull. Chem. Soc. Jpn.*, **55**, 1605 (1982).

12) D. Rehm and A. Weller, *Isr. J. Chem.*, **8**, 259 (1970).

13) D. Rehm and A. Weller, *Z. Phys. Chem. NF.*, **69**, 183 (1970).

14) G. G. Aloisi, F. Masetti, and U. Mazzucata, *Chem. Phys. Lett.*, **29**, 502 (1974).

15) N. Mataga and T. Kubota, "Molecular Interaction and Electronic Spectra," Dekker, New York (1970), p. 351.

16) A. Samanta, N. Chattopadhyay, D. Nath, T. Kundu, and M. Chowdhury, *Chem. Phys. Lett.*, **121**, 507 (1985).

17) H. M. Rosenberg and E. Eimutis, *Spectrochim. Acta*, **22**, 1751 (1966).

18) Th. Forster, *Z. Electrochem. Ver. Bunsenges, Phys. Chem.*, **54**, 531 (1950).

19) S. K. Mondal and K. Nag, *J. Chem. Soc., Dalton Trans.*, **1984**, 2141.

20) W. R. Dawson and M. W. Windsor, *J. Phys. Chem.*, **72**, 3251 (1968).

21) J. A. A. Ketelaar, C. Van De Stolpe, A. Goudsmit, and W. Dzcubas, *Recl. Trav. Chim. Pays-Bas*, **71**, 1104 (1952).

22) E. J. Bowen, "Luminescence in Chemistry," D. Van Nostrand (1968), p. 92.

23) M. L. Bhowmik and R. Hardwick, *J. Chem. Phys.*, **39**, 1593 (1963).

24) K. Chatterjee, S. Laha, S. Chakravorti, T. Ganguly, and S. B. Banerjee, *Chem. Phys. Lett.*, **100**, 88 (1983).

25) E. J. Bowen, "Luminescence in Chemistry," Van Nostrand, London (1968), p. 161.

26) K. K. Rohatgi-Mukherjee, "Fundamental of Photochemistry," Wiley Eastern Limited, New Delhi, (1978) P. 191.

27) H. Baba and C. Mugiya, *Bull. Chem. Soc. Jpn.*, **43**, 13 (1970).

28) J. J. Keizer, *J. Am. Chem. Soc.*, **105**, 1494 (1983).

29) A. F. Fuculoro, L. S. Forster, and M. G. Campbell, *Photochem. Photobiol.*, **39**, 503 (1984).

30) B. Adhikary and K. Nag, Private communications, Department of Inorganic Chemistry of this Institute.

 © 1987 The Chemical Society of Japan Bull. Chem. Soc. Jpn., 60, 1125—1128 (1987)

A Molecular Orbital Study of the Electronic Structure of Some 6-Substituted Uracils

Paul George Abdul-Ahad and Graham Alan Webb†,*
Scientific Research Council, Petroleum Research Center, P.O. Box 10039, Baghdad, Iraq
†Department of Chemistry, University of Surrey, Guildford, Surrey, U.K.
(Received March 19, 1986)

Semiempirical molecular orbital calculations are performed on a series of 28 6-[2-(substituted phenyl)-hydrazino]uracils. Approximate ground state electronic properties are obtained for each molecule studied as well as the electrostatic potentials. First and second order interaction energies are calculated for some selected point charges in the vicinity of the parent molecule. The best correlations obtained between the biological activity and the electronic and steric indicies are considered in a mechanistic context.

A number of 6-substituted uracils are reported to be potent inhibitors of *E. coli* thymidine phosphorylase.[1] Some of the 6-[2-(substituted phenyl)hydrazino]uracils are found to inhibit the replication of the specific enzyme DNA polymerase III of *Bacillus subtilis* by forming strong reversible complexes with the template primer DNA and the enzyme. *Bacillus subtilis* has three DNA polymerases. Of these polymerase I is involved in DNA repair, while polymerase III is necessary for DNA replication.[2]

The activity of the 6-(2-Phenylhydrazino)uracils indicates that most of the enzyme-inhibitor binding energy results from an interaction of the enzyme with the phenyl ring.[3] The phenyl ring-enzyme binding may involve van der Waals or possibly charge-transfer interactions with the amino acid. The mechanism of complex formation appears to involve hydrogen bonding of the uracil and its NH moiety with cytosine in the DNA template and binding of the phenyl group with a hydrophobic site on the enzyme.[4]

Table 1. Calculated Indices and Observed Activity of 6-(2-Phenylhydrazino)uracils

No.	Substituent R	pK_{50}[a]	B.E. / eV	m.v. / Å^3	$E_{C_{17}}^{BIND}$ / eV
1	H	5.8538	−373.35	186.86	−95.6866
2	4-OH	6.3979	−383.24	194.82	−95.7966
3	4-Me	6.3010	−407.37	203.37	−95.6514
4	4-F	5.5228	−375.38	191.42	−95.8183
5	4-Cl	6.0457	−372.28	200.39	−95.6941
6	4-NH_2	5.1487	−393.30	198.09	−95.7540
7	4-NO_2	4.5800	−406.62	209.38	−95.7754
8	3-Me	5.6020	−407.38	203.31	−95.2498
9	3-F	6.1549	−375.43	191.43	−95.2096
10	3-Cl	5.9586	−372.25	200.41	−95.1003
11	2-Me	3.6307	−407.41	202.86	−103.352
12	2-Et	3.2502	−423.97	214.09	−102.988
13	3,4-Me_2	5.8538	−441.22	218.70	−95.2252
14	3,4-Cl_2	6.2218	−371.64	213.72	−95.1259
15	3-Cl, 4-Me	6.0969	−406.39	216.36	−95.0642
16	3-Me, 4-OH	4.2907	−417.29	211.19	−95.3437
17	3-Cl, 4-OH	5.0555	−382.45	208.30	−95.1985
18	4-Br	6.1549	−375.61	204.55	−95.6498
19	3-Br	5.8538	−373.59	204.56	−95.4614
20	2-F	5.1426	−373.41	191.27	−102.899
21	4-Et	5.7958	−407.38	203.43	−95.2410
22	2-Me, 4-OH	6.3010	−417.30	211.21	−95.3565
23	3-Me	5.7958	−440.82	218.44	−95.6603
24	3,5-Me_2, 4-OH	3.9065	−451.33	226.94	−95.2773
25	4-CO_2H	4.0087	−416.20	213.44	−95.6931
26	4-SO_2Me	3.6798	−424.19	236.20	−95.6745
27	4-NHAc	3.2518	−459.82	231.66	−95.6889
28	4-*n*-Bu	2.6382	−508.91	252.91	−95.6588

a) pK_{50} is the negative logarithm of the molar concentration required to achieve 50% inhibition of enzyme activity.

The rotation of the phenyl N and hydrazino N-N bons are the basis for the formation of an active inhibitory conformation of the drug molecules. With a view to clarifying some of these assumptions the present work employs semiempirical molecular orbital (MO) methods in an attempt to interpret the mechanism of the action of 6-substituted uracils.

Method

The atom numbering scheme used in the present study is given in Structure I. The series of 28 6-[2-(substituted phenyl)hydrazino]uracils presently considered are given in Table 1 together with their calculated MO indices and observed activity data.[4] They are potent inhibitors of *Bacillus subtilis* DNA polymerase III. The inhibitory activities have been reported elsewhere[4] and are expressed as pK_{50}, which is the negative logarithm of the molar concentration required to achieve 50% inhibition of enzyme activity. Inactive compounds are excluded from the present study.

Two possible rotations about the phenyl N and N-N bonds are expected in the formation of an active inhibitory conformation of the drug molecule. The starting point geometry is obtained from reference.[5] This geometry is optimized using the program "GEOMIN" (QCPE 312), with the CNDO/2 option, to obtain a more reliable estimate of conformation in solution. Standard bond lengths and bond angles[6] are used for the substituent groups in the phenyl ring. The optimized bond lengths and angles are reported in Table 2.

The electrostatic potential (e.p.) of the drug molecule is calculated from the CNDO/2 wave functions using method III of reference,[7] in which monocentric differential overlap is retained. To assist in determining the most favorable binding position in the vicinity of the substrate an in-plane electrostatic contour map is plotted for the 6-(2-Phenylhydrazine)-uracils and given in Fig. 1. The lower the e.p. at a given position, the more energetically favorable is the placement of an electropositive reagent group at that position. The map is obtained using the simple plot program package of the University of Manchester.

First the second order interaction energies with each of five hypothetical point charges, placed at different positions in the molecular plane, are calculated. Positions P_1 and P_2 are chosen to coincide with the e.p. minima at -130 and -124 kcal mol^{-1} in the vicinity of O_7 and O_8, respectively, of the pyrimidine ring as shown in Fig. 1. P_3, P_4, and P_5 are positions which would be occupied by the O_2, N_3, and N_4-H atoms of a receptor cytosine group, assuming that these atoms become linked by hydrogen bonds to

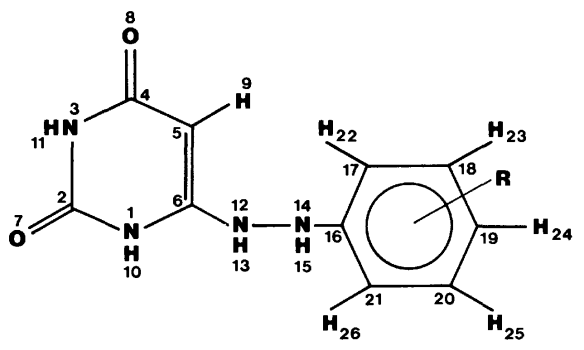

Structure 1

Table 2. Geomin Optimized Bond Lengths, Bond Angles, and Dihedral Angles

Bond lengths/l/Å			
N_1-C_2	1.388	C_2-O_2 =C_4-O_8	1.277
C_2-N_3	1.379	N_1-H_{10} =N_3-H_{11}	1.067
N_3-C_4	1.391	N_{12}-H_{13} =N_{14}-H_{15}	1.077
C_4-C_5	1.435	C_{18}-C_{19} =C_{19}-C_{20}	1.384
C_5-C_6	1.341	C_{20}-C_{21}	1.384
C_5-H_9	1.112	C_{16}-C_{17}	1.397
C_6-N_{12}	1.402	C_{17}-C_{18}	1.382
N_1-N_{14}	1.342		

Bond angles/ϕ/°			
N_3-C_2-N_1	115.6	H_{13}-N_{12}-C_6	108.6
C_4-N_3-C_2	125.6	N_{14}-N_{12}-C_6	112.4
C_5-C_4-N_3	115.4	H_{15}-N_{14}-N_{12}	105.8
C_6-C_5-C_4	119.1	C_{16}-N_{14}-N_{12}	116.1
O_7-C_2-N_3	122.8	C_{17}-C_{16}-N_{14}	119.9
O_8-C_4-C_5	126.5	C_{18}-C_{17}-C_{16}	121.3
H_9-C_5-C_4	118.9	C_{19}-C_{18}-C_{17}	120.3
H_{10}-N_1-C_2	115.3	C_{20}-C_{19}-C_{18}	119.0
H_{11}-N_3-C_4	117.4	C_{21}-C_{20}-C_{19}	120.6
N_{12}-C_6-N_1			

Dihedral angles/ϕ/°	
C_4-N_3-C_2-N_1	346.4
C_5-C_4-N_3-C_2	5.35
C_6-C_5-C_4-N_3	359.2
O_7-C_2-N_3-C_4	169.7
O_8-C_4-C_5-C_6	178.7
H_9-C_5-C_4-N_3	180.7
H_{10}-N_1-C_2-N_3	163.7
H_{11}-N_3-C_4-C_5	171.9
N_{12}-C_6-N_1-C_2	164.0
H_{13}-N_{12}-C_6-N_1	44.9
N_{14}-N_{12}-C_6-N_1	168.2
H_{15}-N_{14}-N_{12}-C_6	131.5
C_{16}-N_{14}-N_{12}-C_6	250.6
C_{17}-C_{16}-N_{14}-N_{12}	210.0
C_{18}-C_{17}-C_{16}-N_{14}	183.7
C_{14}-C_{18}-C_{17}-C_{16}	359.6
C_{20}-C_{19}-C_{18}-C_{17}	359.9
C_{21}-C_{20}-C_{19}-C_{18}	0.27

N_{12}–H_{13}, N_1–H_{10}, and O_7, respectively, of the substrate. These hypothetical hydrogen bonds between substrate and pyrimidine template are shown in Fig. 1 of Ref. 4.

The first order interaction energy, with a point charge of unit magnitude, is simply the electrostatic potential. The second order interaction energy is calculated using uncoupled Hartree-Fock perturbation theory, with retention of monocentric differential overlap.[8]

Experimental

The calculations are performed on the CDC 7600 computer of the University of Manchester, using the "CNDO/2-3R" MO program (QCPE 261). The conformational analyses were performed on an ICL 2903 computer of the Iraqi Science Research Council.

The CNDO/2 wavefunctions are used to calculate all electronic reactivity indices. As well as the first and second order interaction energies, various simple indices are calculated. These may be calculated with a single atomic center, a pair of centers, or the whole molecule.

The first category is represented by the energy of binding of atom A to the rest of the molecule, $E_A^{BIND}=\sum_{B\neq A} E_{A-B}$, where E_{A-B} is the bond energy between centers A and B, calculated using the energy breakdown procedure.[9] E_{A-B} itself is used as an index of bond strength, this being a representative of the second category mentioned above.

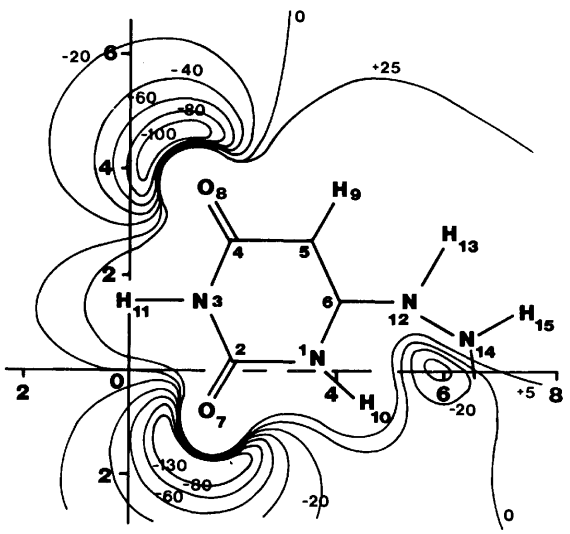

Fig. 1. The CNDO/2 e.p. contour map for 6-(2-phenylhydrazino)uracils (all values are in kcal mol^{-1}).

The following properties of the molecule as a whole are used as indices. The binding energy, B.E. defined as the difference between the CNDO/2 total energy of the molecule and the summed valance electronic energies of the isolated component atoms; the molecular volume, m.v., calculated by numerical integration of the solid produced by centering a sphere of the appropriate van der Waals radius[10] on each atomic center in the molecule. In calculating m.v., a rectangular solid is defined such that all of its faces touch the molecular profile. The solid is segmented into cubes of side 0.1 Å. It is then determined which of these cubes lie within the molecular profile, and a simple counting procedure is used to obtain the molecular volume.

Results and Discussion

The electronic and molecular indices relevant to the best regressions are given in Table 1. The most significant relationships, given in Table 3, have been obtained by searching the regression of inhibitive potency on each single and all pair contributions for eight parameters. The likelihood of random correlation increases with the number of regressions searched, therefore, caution is exercised in the interpretation of the statistical parameters.[11]

The positive coefficient associated with B.E. in regression (1), indicates that the less stable the molecule the higher the drug activity. The negative coefficient of the m.v. indicates that as the molecular size increase, it becomes less active. Since B.E. and m.v. have a substantial negative intercorrelation, it is difficult to decide which, if either, of these is a causal quantity.

The two-variable regressions (3) and (4) each contain an electronic index, as well as a size index. The appearance of the electronic properties of C_{17} tends to confirm the importance of the electronic structure of the phenyl ring. It is possible that there may be a receptor fragment located in this vicinity, in

Table 3. The Best Simple and Two-Variable Regressions Obtained for 6-(2-Phenylhydrazino)uracils

No.	Best simple regressions				No.	Best two variable regressions			
	pK_{50}[a] =	r[b]	s[c]	p[d]/%		pK_{50}[a] =	r[b]	s[c]	p[d]/%
1	0.022(±0.004)B.E. +14.48(±2.01)	0.672	0.85	99.9	3	0.233(±0.05)$E_{C_{17}}^{BIND}$ −0.0541(±0.009)m.v. +39.1(±5.9)	0.807	0.69	>99.9
2	−0.048(±0.01)m.v. +15.41(±2.4)	0.641	0.88	99.9	4	0.190(±0.05)$E_{C_{17}}^{BIND}$ +0.023(±0.004)B.E. +32.95(±5.8)	0.785	0.72	>99.9

a) Negative logarithm of the molar concentration required to achieve 50% inhibition of enzyme activity. b) Correlation coefficient. c) Standard error of estimate. d) Statistical significance determined from an F test.

the drug receptor complex. The positive coefficient associated with $E_{C_{17}}^{BIND}$ which is the only one of the calculated binding energies to enter the regressions, indicates that the more reactive this position the higher the drug activity. It appears that none of the first and second order interaction energies, for the chosen points in the molecular environment, show statistically significant correlations with pK_{50}. Consequently doubt is cast on the possible role of these energies in determining possible receptor binding sites at the chosen positions. Perhaps the electronic structure of the phenyl ring is critical in determining the biological activity of the 6-(2-phenylhydrazino)-uracils studied.

We conclude that, in order to design a more potent compound, with the same basic structure, it is apparently necessary to reduce the substituted molecular size as much as possible, whilst maximizing the reactivity of C_{17}.

References

1) B. R. Baker and W. Rzeszolarski, *J. Med. Chem.*, **10**, 1109 (1967).
2) K. B. Gass and N. R. Cazzarelli, *J. Biol. Chem.*, **248**, 7688 (1973).
3) G. E. Wright and N. C. Brown, *J. Med. Chem.*, **17**, 1277 (1974).
4) G. E. Wright and N. C. Brown, *J. Med. Chem.*, **20**, 1181 (1977).
5) L. L. Coulter and N. R. Cazzarelli, *J. Mol. Biol.*, **91**, 329 (1975).
6) M. S. Gordon and J. A. Pople, *J. Chem. Phys.*, **49**, 4643 (1968).
7) C. Giessner-Prettre and A. Pullman, *Theor. Chim. Acta*, **37**, 335 (1975).
8) P. W. Langhoff, M. Karplus, and R. P. Hurst, *J. Chem. Phys.*, **44**, 565 (1966).
9) J. A. Pople and D. L. Beveridge, "Approximate Molecular Orbital Theory," McGraw-Hill, New York (1970).
10) A. Bondi, *J. Phys. Chem.*, **68**, 44 (1964).
11) J. Topliss, *J. Med. Chem.*, **22**, 1238 (1979).

 © 1987 The Chemical Society of Japan Bull. Chem. Soc. Jpn., 60, 1129—1133 (1987)

Some Properties of Iron(III) Selenite and Its Applications for the Determination of Thorium

Pritam Singh THIND and Jatinder Singh GANDHI*
Department of Chemistry, Guru Nanak Dev University, Amritsar 143 005, India
(Received July 15, 1985)

A new inorganic ion exchanger, iron(III) selenite has been synthesized having an Fe:Se ratio of 2:3 and cation exchange capacity of 0.40 meq g^{-1}. It is fairly stable in water and dilute solutions of acids, bases, and salts. Ion distribution studies on twenty one metal ions have been done in water. Iron(III) selenite granules in H^+-form have also been used as indicators in the determination of thorium in presence of some rare earth cations using hexacyanoferrate(II) as titrant. On the basis of chemical analysis, pH titrations, thermal and infrared analyses the following scheme for the decomposition of iron(III) selenite has been proposed:

$$2Fe_2O_3\cdot 3H_2SeO_3\cdot 2H_2O \xrightarrow{140\,^\circ C} 2Fe_2O_3\cdot 3H_2SeO_3 \xrightarrow{500\,^\circ C} 2Fe_2O_3 .$$

The analytical importance of synthetic inorganic ion exchangers is now firmly established due to their high selectivity, thermal stability and resistance to radiations. There are, however, two fundamental problems which still lack a solution: The ion exchangers, unless crystalline, do not have reproducible properties and they are not chemically stable. It was found that phosphate,[1] arsenate,[2] antimonate,[3] tungstate,[4] and molybdate[5] of iron(III) show interesting properties. Selenites of zirconium,[6] tin,[7] and titanium[8] have been synthesized and used for various separations. A search of literature showed that no such studies have so far been reported on iron(III) selenite. Therefore, a new inorganic ion exchanger, iron(III) selenite has been investigated. The present work describes the synthesis, ion-exchange properties, and analytical applications of iron(III) selenite.

Experimental

Reagents. Sodium selenite (Loba Chemie) and iron(III) nitrate (BDH) were used for the synthesis. All other chemicals used were of AnalaR grade.

Potassium hexacyanoferrate(II): Standard solution of potassium hexacyanoferrate(II) solution (0.025 M)† was prepared by exact weighing and 1.0 g of sodium carbonate was added per liter.

Nitrates of thorium and other metal ions standardized with EDTA were used.

Synthesis of Iron(III) Selenite. The conditions of synthesis are given in Table 1. The iron(III) nitrate solution (0.05 M) was added to a solution of sodium selenite (0.05 M) with constant stirring. The pH of the mother liquor was adjusted to 1.5 (Table 1) by adding either 0.1 M HNO_3 or 0.1 M NaOH. The precipitate so obtained was heated at 60 °C for half an hour and it was allowed to settle for 24 h. Then it was filtered and washed with distilled water till free from nitrate ion. It was heat-treated at 40 °C, converted to H^+-form using 0.1 M HNO_3 and finally washed with demineralized water to remove excess of the acid. Finally it was heat-treated at 40 °C in an electric oven.

Analysis of Metals. Analysis of iron(III) has been done volumetrically using iodometric technique[9] and selenium has been precipitated as selenium metal[10] by passing sulfur dioxide through acidic solution of the material. The red selenium metal separates out. It is then filtered and weighed after heat-treating at 120 °C in an oven to constant weight.

The various cations used for the distribution coefficients determination have been determined by volumetric methods using metal indicators such as Eriochrome Black-T, Xylenol Orange, and PAN and titrating them against standard EDTA solution.

Table 1. Conditions of Synthesis and Properties of Iron(III) Selenites (H^+-form)

Sample No.	Conditions of synthesis		Properties	
	Molarity of reagents(M) Fe : Se	Mixing volume ratio Fe : Se	Color in H^+-form	Ion-exchange capacity/ meq g^{-1}
I	0.05 : 0.05	1 : 3	Brown	0.30
II	0.05 : 0.05	1 : 2	Brown	0.40
III	0.05 : 0.05	1 : 3	Brown	0.35
IV	0.05 : 0.05	2 : 1	No exchanger formed	—
V	0.075 : 0.075	1 : 2	Brown	0.41
VI	0.025 : 0.025	1 : 2	Brown (poor yield)	—
VII	0.10 : 0.10	1 : 2	Brown	0.40

† 1 M=1 mol dm^{-3}.

Instrumentation. The solubility of the meterial has been determined colorimetrically using spectrophoto-colorimeter (DDR). The pH of the solutions during potentiometric titrations was measured using a Toshniwal pH meter (CL-46, India). X-Ray diffractograms were obtained by using a PW 1720 X-ray generator with a Debye-Scherrer camera. Infrared studies were made using a Pye Unicam, SP 300 Philips (England) spectrophotometer.

Adsorption Studies. Adsorption studies were carried out by keeping cation solution in contact with the exchanger. Two hundred mg of the exchanger is added in each container containing cation solution and the volume is made to 20 ml by using the demineralized water. After 24 h cation solution is separated from the exchanger and cation is estimated using standard EDTA solution.

Chemical Composition. One hundred mg of iron(III) selenite sample was dissolved in 10 ml of hydrochloric acid. Iron was determined volumetrically[9] while selenium was determined by reducing it to red metal with sulfur dioxide.[10]

Ion-Exchange Capacity. The ion exchange capacity of the different samples of iron(III) selenite was determined by the column method. One g sample of the exchanger in the H^+-form was placed in the column with glass wool support. Alkali or alkaline earth metal nitrate solution (1.0 M) was used as the eluent. The effluent collected in each case, at the rate of 5—10 drops per min, was about 400 ml. The H^+-ions thus eluted from the column were titrimetrically determined against a 0.1 M standard solution of sodium hydroxide.

Distribution Coefficients. Distribution coefficients (K_d) for some inorganic ions have been determined in water. The K_d values were calculated using the equation

$$K_d = \frac{C_0 - C}{C} \cdot \frac{L}{m} (\text{ml g}^{-1}) ,$$

where C_0 and C are initial and residual concentrations of metal ion solution respectively. L is a solution volume (ml) and m is the amount of ion-exchanger sample taken (g). The cation solution was kept in contact with the exchanger for 24 h.

Effect of Temperature on Ion Exchange Capacity. Sample II in the H^+-form was dried at different temperatures in a muffle furnace for 2 h and the ion exchange capacity for Na^+ (1.0 M) was determined by the column method.

Chemical Stability. Fifty mg of the sample II was shaken with 20 ml of different solvents for 24 h. The supernatant liquid was analysed colorimetrically for selenium[11] and iron.[12]

Potentiometric Titrations. The pH titrations of iron(III) selenite sample II were performed using 0.1 M standard solution of different bases like lithium, sodium, and potassium hydroxide by the method of Topp and Pepper.[13] Five hundred mg of the exchanger was added in each flask and the total volume of the solution was made 50 ml (MOH+MCl).

X-Ray Studies. X-Ray diffraction studies were made on iron(III) selenite by the powder method. The powdered sample was filled in a quartz capillary of 0.5 mm diameter. It was then exposed to X-rays for few hours and its pattern was recorded.

Thermal Analysis and Infrared Studies. Thermal studies were performed on a Paulik Erdey MCM derivatograph (Hungary). The infrared spectra of iron(III) selenite (H^+-form) were obtained in KBr pellet.

Determination of Thorium. To the thorium nitrate solution (3 to 12 mg as thorium) were added 5 ml of 0.1 M HNO_3 so that the pH of the solution becomes 2—3. To this 3—4 granules (<0.1 mg) of iron(III) selenite in H^+-form were added and the titration was conducted by adding potassium hexacyanoferrate(II) (0.025 M) dropwise with vigorous shaking till the granules turn blue in color.

Results and Discussion

The results of the study of synthesis and ion exchange capacity of different samples of iron(III) selenite in H^+-form are presented in Table 1. These results show that ion-exchange capacity is independent of the concentration of reactants. Out of the seven samples prepared, one prepared by mixing 0.05 M solution of iron(III) nitrate and sodium selenite in the volume ratio of 1:2 at pH 1.5 (Table 1) was found to be quite chemically stable and having reasonable ion-exchange capacity. Therefore sample II was selected for detailed studies. Five batches of sample II were prepared under similar conditions and the material was found to be reproducible. A typical analysis for the product heat-treated at 40 °C shows 43% Fe_2O_3, 44.9% SeO_2, and 12.1% H_2O, indicating an empirical fomula $2Fe_2O_3 \cdot 3H_2SeO_3 \cdot 5H_2O$, $2Fe_2O_3 \cdot 3SeO_2 \cdot 5H_2O$. The distribution coefficients of Ce^{3+}, Ba^{2+}, Sr^{2+}, and Pb^{2+} were determined with each sample so as to check its reproducibility.

In order to determine the working capacity of

Table 2. Ion-Exchange Capacity of Iron(III) Selenite (Sample II) for Some Uni- and Bivalent Cations

Metal ion	Salt solution used	Concentration of salt/M	Ion-exchange capacity/meq g^{-1}	Hybrated ionic radii/Å
Li^+	$LiNO_3$	1.0	0.32	3.40
Na^+	$NaNO_3$	1.0	0.32	2.76
K^+	KNO_3	1.0	0.42	2.32
Mg^{2+}	$Mg(NO_3)_2$	0.5	0.25	7.00
Ca^{2+}	$Ca(NO_3)_2$	0.5	0.27	6.30
Sr^{2+}	$Sr(NO_3)_2$	0.5	0.29	—
Ba^{2+}	$Ba(NO_3)_2$	0.5	0.40	5.90

iron(III) selenite (H^+-form) as an ion-exchanger, the ion exchange capacity for sample II was determined for some uni- and bivalent cations (Table 2). The order of exchange capacities for alkali and alkaline earth metal ions respectively is: $K^+>Na^+=Li^+$ and $Ba^{2+}>Sr^{2+}>Ca^{2+}>Mg^{2+}$. These results suggest that the ion exchange capacity decreases from 0.42 to 0.32 and 0.40 to 0.25 meq g^{-1} on going from K^+ to Li^+ and Ba^{2+} to Mg^{2+} respectively. On the basis of the radii of the hydrated ions one would expect the same order.

The analytical significance of iron(III) selenite (H^+-form) can be evaluated from the results of K_d values given in Table 3. These results show that this material has high selectivity to Pb^{2+} in water. This makes it possible to separate Pb^{2+} from a large number of other cations. Sample II was heat-treated at different temperatures for 2 h and the ion exchange capacity for Na^+ was determined (Table 4). These results indicate that as temperature is raised from 40 to 200 °C, a slow decrease in ion exchange capacity is observed. On further raising the temperature there is abrupt decrease in the exchange capacity due to loss of selenium. The results of chemical stability of iron(III) selenite in H^+-form showed that the material was considerably stable in water, acids, bases, and organic solvents (Table 5).

The pH-titration curves of lithium, sodium, and potassium hydroxide for air-dried iron(III) selenite in H^+-form (Fig. 1) show two plateaux each one at pH 7 and the other at pH 9. This bifunctional behavior is similar to both crystalline zirconium phosphate[14] and arsenate[15,16] which also exhibit two pH titration plateaux. All the three curves are very much similar. The initial cation exchange selectivity sequence was $Na^+>K^+>Li^+$. At the first pH plateau, the selectivity was $Na^+>Li^+>K^+$. As exchange progressed the position of Li^+ shifted to give the sequence $Li^+>Na^+>K^+$. The exchange capacity for K^+ changes on heat treatment and it is reduced to about half when heated to 300 °C. When iron(III) selenite in H^+-form is treated at 500 °C to constant weight, the cation exchange capacity is completely lost. The titration

Table 3. Distribution Coefficients (ml g^{-1}) of Some Metal Ions on Iron(III) Selenite Sample II in Water

Metal ion	K_d	Metal ion	K_d
La^{3+}	8	Zn^{2+}	0
Dy^{3+}	5	Mn^{2+}	0
Nd^{3+}	20	Cu^{2+}	17
Gd^{3+}	16	Ni^{2+}	4
Pr^{3+}	10	Mg^{2+}	0
Er^{3+}	2	Cd^{2+}	5
Sm^{3+}	20	Ca^{2+}	0
Ce^{3+}	13	Ba^{2+}	5
Y^{3+}	19	Sr^{2+}	0
Th^{4+}	45	Fe^{3+}	80
Pb^{2+}	132		
Co^{2+}	3		

Amount of ion-exchanger used=200 mg, volume of equilibrated solution=20 ml, initial concentration of metal ion in solution=0.0025 M, concentration of EDTA standard solution=0.025 M

Table 5. Solubility of Iron(III) Selenite in Various Solvents

Solvent	Solubility iron(III)	Se(μg/50 ml)
$NaNO_3$ (1.0 M)	0	81
NH_4NO_3 (1.0 M)	0	155
NaOH (0.1 M)	0	158
HNO_3 (0.1 M)	50	125
HNO_3 (0.075 M)	42	100
HNO_3 (0.05 M)	32	80
HCl (0.075 M)	50	200
H_2SO_4 (0.05 M)	105	275
CH_3COOH (0.1 M)	0	227
Dioxan	0	0
DMF	0	0
DMSO	0	92
C_2H_5OH	0	0

Table 4. Change of Properties of Iron(III) Selenite with Heating Temperature

Drying temp °C	Composition $Fe_2O_3:SeO_2$	Ion-exchange capacity/meq g^{-1}	Colour	IR bands/cm^{-1}
40	1:1.5	0.40	Brown	3360, 1625, 1390, 710, 500
100	1:1.5	0.32	Brown	3400, 1625, 1390, 715, 490
200	1:1.5	0.27	Brown	3400, 1625, 1390, 710, 410
300	1:1.14	0.13	Dark brown	3400, 1625, 710, 475
400	1:0.75	0.10	Dark brown	710, 460
500	1:0.03	0.09	Black	535, 460, 310
600	1:0.00	0.08	Black	525, 455, 310
500[a]	—	—		525, 450, 300

a) $Fe(OH)_3$ dried at 500 °C.

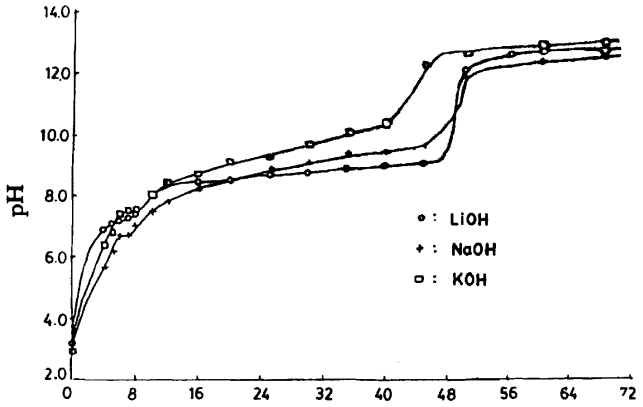

Vol. of 0.1 M standard base added (ml/0.5 g)

Fig. 1. pH-Titrations of iron(III) selenite (H^+-form).

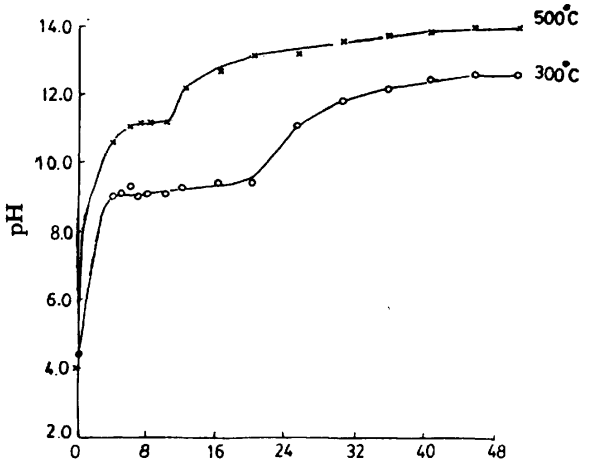

Vol. of 0.1 M standard base added (ml/0.5 g)

Fig. 2. pH-Titrations of iron(III) selenite (H^+-form) heat-treated at different temperatures.

curves obtained for the materials dried at 300 and 500 °C give support to this observation. That is to say, of the most acidic exchange group, the titration curve of iron(III) selenite in H^+-form heat-treated at 300 °C shows a considerable decrease in cation-exchange capacity. At 500 °C, the inflection point originating from the most acidic hydrogen ions completely disappears (Fig. 2).

X-Ray powder diffraction pattern shows that as the drying temperature is increased to 40, 300, and 600 °C, a number of d lines appear. This clearly shows that the material is crystalline at 40 °C as well as at 500 °C.

The infrared studies of iron(III) selenite (Fig. 3) show five absorption peaks with maxima at 3360, 1625, 1390, 710, and 500 cm^{-1}. The band at 3360 cm^{-1} is due to OH stretch of interstitial water, and the band at 1625 cm^{-1} is due to its bending mode. The bands at 1390 and 710 cm^{-1} are due to Se–OH stretching vibrations. The stretching vibration of Fe–O appears at 500 cm^{-1}.

The DTA curve of iron(III) selenite in H^+-form (Fig. 4) shows that there are three endothermic effects (140, 470, and 500 °C). The first endothermic effect (at 140 °C) may be due to the loss of two molecules of water and this is confirmed by analysis and the thermogravimetric analysis. The second endothermic effect (at 470 °C) is accompanied by simultaneous loss of three molecules of water and selenium dioxide (SeO_2). The composition of the product after this endothermic effect at 500 °C corresponds to the formula Fe_2O_3. The infrared spectra show no bands corresponding to stretching or deformation vibration of –OH or $-OH_2$ groups or Se–O groups. A weak band at 3360 cm^{-1} is evidently due to the absorption of moisture on the specimen at the time of recording infrared spectrum. The infrared spectrum of iron(III) selenite dried at 500 °C is very much similar to the

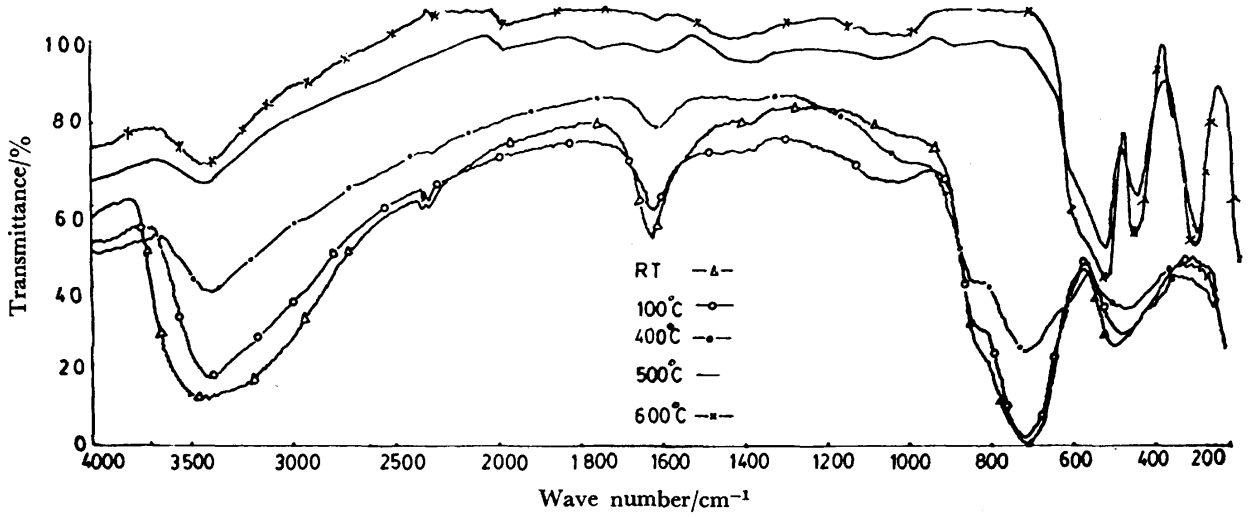

Fig. 3. Infrared spectra of iorn(III) selenite in H^+-form heated to different temperatures.

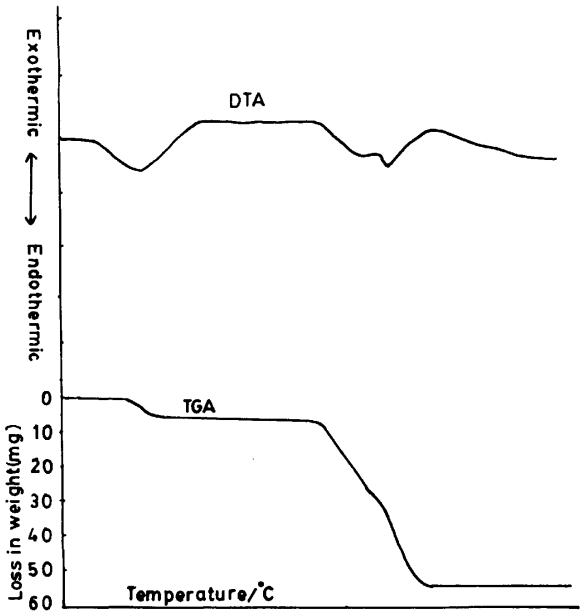

Fig. 4. Simultaneous TGA and DTA of 100 mg of iron-(III) selenite in H^+-form.
Heating rate : 6° min^{-1}.

spectra of iron(III) oxide at 500 °C, indicating that at this temperature the dominant species present is Fe_2O_3.

The following scheme was obtained for the decomposition of iron(III) selenite in H^+-form when it is heated under the conditions for recording DTA curve:

$$2Fe_2O_3 \cdot 3H_2SeO_3 \cdot 2H_2O \xrightarrow{140\,^\circ C} 2Fe_2O_3 \cdot 3H_2SeO_3 \xrightarrow{500\,^\circ C} 2Fe_2O_3$$

Iron(III) selenite granules in H^+-form can also be used as an indicator for the determination of thorium using hexacyanoferrate(II) as titrant. By proposed method 3.02 to 12.06 mg of thorium without and with rare earths can be determined within the conventional error (0.5—1%) for single observation. The amount of the rare earths added as impurities varies from 4.35 to 15.37 mg. This method is superior to other methods involving Th-EDTA. The method is based on the fact that when all the Th(IV) ions are precipitated as $ThFe(CN)_6$ a slight excess of hexacyanoferrate(II) gives a sharp color change to the granules from brown to blue due to the formation of Prussian Blue. As the rare earths used do not form insoluble ferrocyanides under these conditions, they do not interfere.

The method is particularly useful in dilute solution, where the precipitates are not so dense and the color change on the granules can easily be detected at the equivalence point. In more concentrated solutions, the granules are not visible through the thick precipitate, but the color on the solid phase can be seen by raising the beaker above eye level and viewing the granules at the bottom. The titrant solution should not come into direct contact with the indicator granules.

References

1) J. P. Rawat and P. S. Thind, *Can. J. Chem.*, **54**, 1892 (1976).
2) J. P. Rawat and J. P. Singh, *Can. J. Chem.*, **54**, 2534 (1976).
3) J. P. Rawat and D. K. Singh, *Anal. Chim. Acta*, **87**, 157 (1976).
4) J. P. Rawat, T. Khatoon, and H. Shankar, *Ann. Chim.*, **68**, 913 (1978).
5) P. S. Thind, Parveen, and H. Singh, *Bull. Chem. Soc. Jpn.*, **56**, 1536 (1983).
6) P. S. Thind and H. Singh, *Synth. React. Inorg. Met. Org. Chem.*, in press (1985).
7) M. Qureshi and S. A. Nabi, *Talanta*, **19**, 1033 (1972).
8) M. Qureshi, R. Kumar, and H. S. Rathore, *Anal. Chem.*, **44**, 1081 (1972).
9) A. I. Vogel, "Quantitative Inorganic Analysis," 3rd ed, Longman Publications (1975), p. 372.
10) Ref. 9, p. 508.
11) G. E. F. Lundell, H. A. Bright, and J. I. Hoffmann, "Applied Inorganic Analysis," Wiley, New York (1953).
12) Ref. 9, pp. 787, 903.
13) N. E. Topp and K. W. Pepper, *J. Chem. Soc.*, **1949**, 3299.
14) A. Clearfield and J. A. Stynes, *J. Inorg. Nucl. Chem.*, **26**, 117 (1964).
15) E. Torracca, U. Costantino, and M. A. Massucci, *J. Chromatogr.*, **30**, 584 (1967).
16) A. Clearfield, G. D. Smith, and B. Hammond, *J. Inorg. Nucl. Chem.*, **30**, 277 (1968).

 © 1987 The Chemical Society of Japan Bull. Chem. Soc. Jpn., 60, 1135—1139 (1987)

Spectrophotometric Determination of Palladium(II), Osmium(VIII), and Iridium(III) with 2-Methyl-1,4-naphthoquinone 4-Oxime

Kamini SHRAVAH and Sharwan Kumar SINDHWANI*
Department of Chemistry, University of Delhi, Delhi 110 007, India
(Received January 9, 1986)

2-Methyl-1,4-naphthoquinone monoxime (MNQM) forms yellow-colored 1:1 (M:L) complex with palladium(II) and brown-colored 1:2 complex with osmium(VIII) and iridium(III). The complexes are insoluble in water but soluble in 1-butanol. The reagent has been used for the spectrophotometric determination of Pd(II), Os(VIII), and Ir(III). The palladium, osmium, and iridium complexes have maximum absorption at 460, 460, and 450 nm respectively with the sensitivity of 0.012 μg Pd/cm², 0.025 μg Os/cm², and 0.014 μg Ir/cm² for log I_o/I=0.001. The optimum concentration ranges for the determination of Pd(II), Os(VIII), and Ir(III) are 1.58—10.47, 3.02—23.99, and 1.6—11.5 ppm over the pH range 6.5—7.8, 6.5—7.7, and 5.9—7.3 respectively. The determinations have also been carried out in the presence of foreign ions. MNQM reacts with palladium(II) or osmium(VIII) or iridium(III) to form yellow- or brown-colored precipitates which are extractable in 1-butanol. These systems have been studied spectrophotometrically to determine the composition and other physical constants of the complexes. The possibility of determining Pd(II) or Os(VIII) or Ir(III) in presence of diverse ions has also been investigated. Palladium(II) and osmium(VIII) have been successfully determined in synthetic solutions corresponding to the alloys.

Experimental

Reagents and Apparatus. 2-Methyl-1,4-naphthoquinone monoxime (MNQM) was prepared by the method of Veldstra and Wiardi.[1] A 1×10^{-2} M (1 M=1 mol dm^{-3}) solution of the reagent was prepared in ethanol (95%).

1-Butanol (AnalaR) was distilled before use. Buffer solutions were prepared by mixing 0.2 M sodium acetate and 0.2 M acetic acid in requisite proportions. For higher pH, sodium hydroxide was added. Buffer solutions of potassium hydrogen phthalate–sodium hydroxide were prepared from solutions of the corresponding chemicals of reagent grade in doubly distilled water.

Palladium(II) Solution. Standard solution of palladium(II) was prepared by dissolving palladium dichloride (Johnson-Matthey) in dilute hydrochloric acid. The solution was standardized gravimetrically by precipitation with dimethylglyoxime.

Osmium(VIII) Solution. A 1 g ampouls of osmium tetraoxide (Johnson-Matthey) was dissolved in about 100 ml of 0.2 M sodium hydroxide in a glass stoppered flask as described by Ayres and Wells,[2] which was further standardized by the method of Klobbie.[3] Working solutions were prepared by diluting this stock solution, whenever required.

Iridium(III) Solution. A stock solution of iridium was prepared by dissolving iridium(III) chloride (Johnson-Matthey) in doubly distilled water containing 1 M hydrochloric acid. The iridium solution was standardized gravimetrically by precipitating iridium as the hydrated oxide, followed by careful ignition in air and then reduction to the metal in presence of hydrogen and cooling in air atmosphere of carbon dioxide. Subsequent dilutions were made by diluting the stock solution and keeping the acidity at 1 M.

Reagent grade chemicals were used in the study of interferences. Doubly distilled water was used throughout the work.

A Unicam SP 600 spectrophotometer was used for measuring absorbance and an ECIL expanded scale pH meter pH 821A was used for pH measurements.

Absorption Spectra and Effect of pH. Palladium, osmium, and iridium complexes show the maximum absorption at 460, 460, and 450 nm respectively (Figs. 1a, b, and c). This wavelength was chosen for subsequent measurements. A plot of absorbance vs. pH shows that the absorbances remain constant in the pH range 6.5—7.8, 6.5—7.7, and 5.9—7.3 for Pd(II), Os(VIII), and Ir(III), respectively. In subsequent studies the pH of the solutions was adjusted to 7.0, 6.9, and 6.7 for palladium, osmium, and iridium, respectively.

Rate of Color Development and Stability of the Complexes. Complex formation takes place instantaneously after the addition of the reagent to the palladium(II) or osmium(VIII) solution. With iridium(III) it was observed that rate of color development is slow at room temperature, but is accelerated by heating on a water bath. Solutions containing a fixed amount of iridium(III), reagent and buffer was heated on a water bath for different intervals of time and absorbances were measured at 450 nm. Results of this study show that full color development takes place on heating the contents for about 2 h.

The Pd-MNQM, Os-MNQM, and Ir-MNQM complexes were found to be quite stable and absorbances were found to remain unchanged upto 24, 72, and 48 h, respectively after which a slow decrease in absorbance take place.

Effect of Reagent Concentration. A plot of absorbance vs. moles of ligand shows that at least 10, 60, and 30 times molar excess of the reagent is required for maximum complexation for palladium, osmium, and iridium, respectively. In subsequent studies 20, 70, and 40 times molar excess of the reagent was used for Pd, Os, and Ir, respectively.

Adherence to Beer's Law, Optimum Range and Sensitivity. Beer's law is obeyed upto 11.91, 29.48, and 13.7 ppm (1 ppm=1 μg cm^{-1}) and the optimum concentration ranges for accurate determination, as determined from Ringbom plot (Fig. 2), are 1.58—10.47, 3.02—23.99, and 1.6—11.5 ppm for palladium, osmium, and iridium, respectively. The sensitivity, in terms of Sandell's definition, is 0.012 μg Pd/cm², 0.025 μg Os/cm², and 0.014 μg Ir/cm² for log I_o/I= 0.001 with molar absorptivity 8.6×10^3, 7.6×10^3, and 1.26×10^4 l mol^{-1} cm^{-1}, respectively.

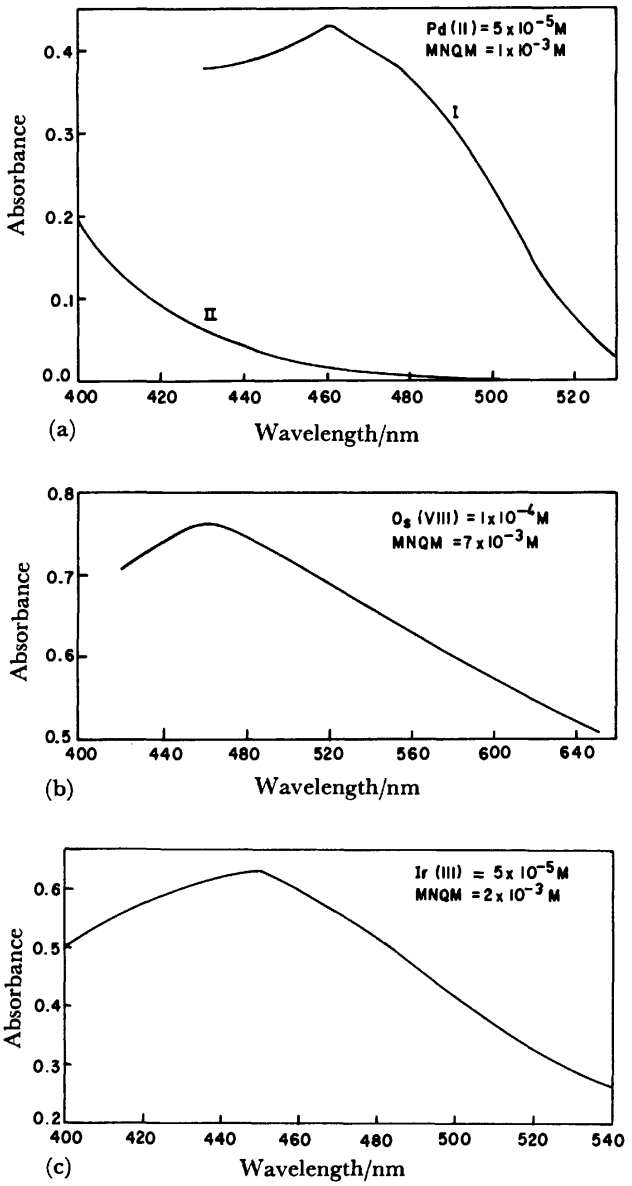

Fig. 1. Absorption spectra of:
(a): I. palladium(II) complex vs. reagent Pd(II), 5×10^{-5} M. II. reagent vs. 1-butanol, MNQM 1×10^{-3} M.
(b): Osmium(VIII) complex vs. reagent, Os(VIII) 1×10^{-4} M.
(c): iridium(III) complex vs. reagent, Ir(III) 5×10^{-5} M.

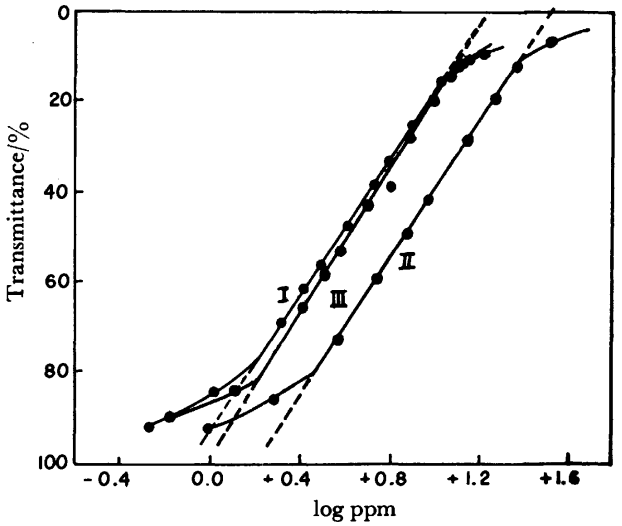

Fig. 2. Ringbom plot for:
I: Pd(II)–MNQM complex.
II: Os(VIII)–MNQM complex.
III: Ir(III)–MNQM complex.

Recommended Procedure. Palladium and Osmium. A suitable aliquot containing 15.8—104.7 μg of palladium(II) or 30.2—239.9 μg of osmium(VIII) is taken and an excess of reagent in ethanol is added. pH is adjusted in the range 6.5—7.8 for palladium with potassium hydrogen phthalate-sodium hydroxide or 6.5—7.7 for osmium with sodium acetate-sodium hydroxide. The volume is made upto 10 ml with doubly distilled water. 10 ml of 1-butanol is added, the contents are shaken on a shaking machine and set aside for equilibration. The nonaqueous layer is separated, centrifuged to remove water droplets and the absorbance is measured against a reagent blank prepared under identical conditions. Knowing the absorbance, the amount of palladium is deduced from the calibration curve.

Iridium(III). To the solution containing 16—115 μg of iridium is added an excess of reagent and pH of the solution is adjusted in the range 5.9—7.3 with acetate buffer and dilute solution of sodium hydroxide. The total volume is made upto 10 ml with doubly distilled water. The contents are heated on a boiling water bath for about 2 h, then cooled to room temperature (30±5 °C) and extracted in 10 ml of 1-butanol. The mixture is shaken on a shaking machine and kept aside for equilibration. The nonaqueous layer is separated, centrifuged and the absorbance is measured at 450 nm. The iridium concentration is then deduced from the calibration curve.

Molar Composition of the Complexes. The composition of the complexes were determined by Job's method of continuous variations,[4,5] which shows that the stoichiometric ratio of metal to MNQM in the complex is 1:1 (Pd:MNQM) or 1:2 (Ir:MNQM) (Figs. 3a and b).

The ratio of osmium to MNQM was determined by logarithmic method of Bent and French,[6] which shows that molar ratio of metal to ligand in the complex is 1:2 (Fig. 3c).

Absorbance Deviations. Measured under optimum conditions, the solutions containing 5.32 ppm of Pd(II) gave absorbance readings with average relative deviation of ±0.46%. The standard deviation was found to be 0.003. 9.51 ppm of Os(VIII) gave an average relative deviation of ±0.44% with standard deviation of 0.0024. 6.4 ppm of iridium the standard deviation comes out to be 0.0024 with an average absorbance of 0.42.

Effect of Diverse Ions. The effect of diverse ions was studied in the determination of palladium, osmium, and iridium following the recommended procedure. The amounts (in ppm) of ions which do not cause any interference with 5.32 ppm of palladium, are given below in parentheses. Masking agents, wherever used, have been mentioned against each:

Chloride or citrate or tartrate (800), bromide or fluoride or

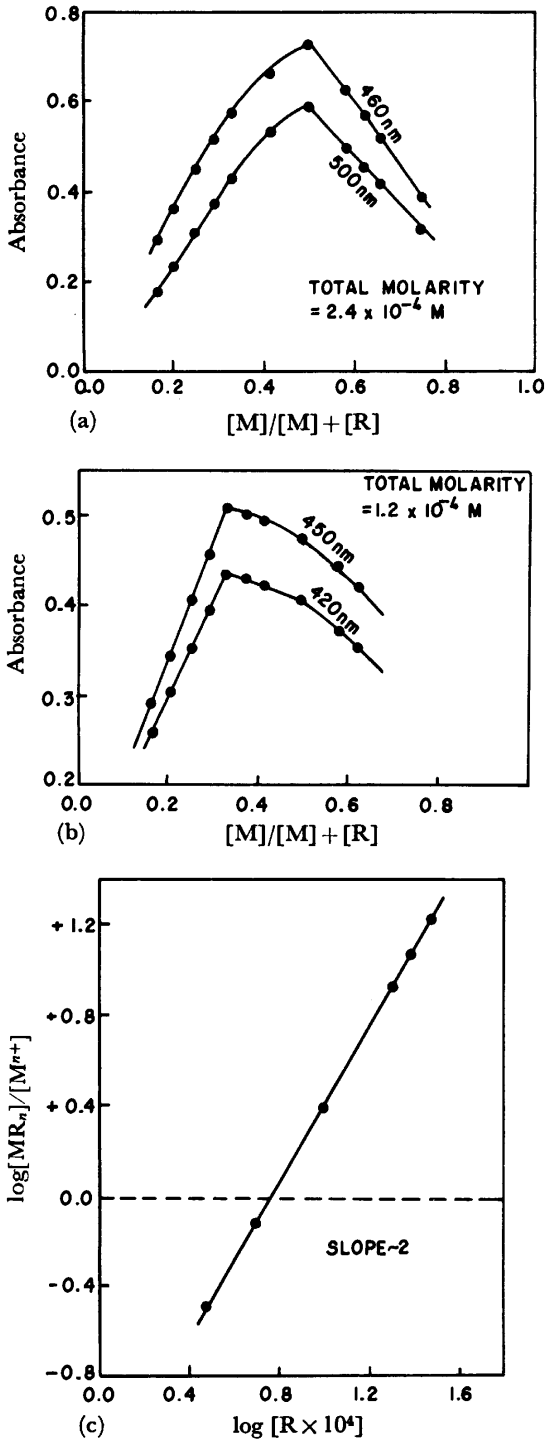

Fig. 3(a). Composition of Pd-MNQM complex by Job's method.
(b): Composition of Ir-MNQM complex by Job's method.
(c): Composition of Os-MNQM complex by Bent and French method.

nitrite (100), nitrate (1500), sulfate or oxalate or phosphate (2500), Ca(II) or Ba(II) or Sr(II) or Cd(II) or La(III) (200), Mg(II) or Ir(III) (20), Al(III) or Sn(II) or Th(IV) (100, F^-), Zn(II) or Hg(II) or Cu(II) or Mo(VI) or U(VI) or V(IV) or Zr(IV) or Li(I) or Y(III) or Pb(II) (100), Fe(II) or Ru(III) (10), Co(II) or Mn(II) (50), Ni(II) or As(III) (70), Cr(III) (50, tar), Ag(I) (70), Rh(III) (8), Pt(IV) (25).

For 9.51 ppm of osmium(VIII), the limits of tolerance are: chloride or bromide or fluoride (250), nitrate (150), nitrite or citrate or sulfide or borate (50), oxalate or thiocyanate (100), phosphate (300), sulfate or sulfite (400), Ca(II) or Hg(II) (100), Ba(II) or Sr(II) or Ni(II) (70), Mg(II) or V(IV) or Pb(II) (40), Al(III) (20, F^-), Mn(II) (10, F^-), Ag*(I) (30, Cl^-), Co(II) or As(III) or Pt(IV) (20), Fe(II) (30), Cu(II) or Ir(III) (10), U(VI) (100, PO_4^{3-}), Ru(III) or Rh(III) (20). Thiosulfate, iodide, and palladium(II) interfere in the determination.

For 6.4 ppm of iridium(III), the limits of tolerance are: chloride (450), bromide or iodide or sulfate or oxalate or tartrate or phosphate (500), nitrate (2500), nitrite or borate or thiocyanate (100), sulfite (1500), citrate (250), fluoride (1000), Ca(II) or Ba(II) (200), Sr(II) (150), Fe(II) or Zn(II) (10), As(III) (70), Mo(VI) (50), Sn(II) (10, F^-), Os(VIII) or Pd(II) (20) (extracted in cold), U(VI) (20, $C_2O_4^{2-}$), Hg(II) (5, I^-), Th(IV) (20, F^-), Cu(II) (5, SCN^-), Al(III) (50, F^-), Mg(II) (20), Ag*(I) (100, Cl^-), Co(II) or Ni(II) (50), Mn(II) (30), V(IV) (60), Pb(II) (80). Ru(III), Rh(III), and Pt(IV) interfere and attempts to mask these cations were unsuccessful.

Table 1. Determination of Pd(II) in Synthetic Solutions

Alloy	Pd present / ppm	Amount of foreign ion taken / ppm	Pd found / ppm	Error/%
1. Pd-Cu (40% Cu, 60% Pd)	6.0	4.0	6.02	+0.33
	6.0	4.0	6.01	+0.16
	6.0	4.0	6.02	+0.33
2. Pd-Ag (40% Ag, 60% Pd)	6.0	4.0	6.01	+0.16
	6.0	4.0	5.99	−0.16
	6.0	4.0	6.03	+0.5
3. Pd-Au (50% Au, 50% Pd)	6.0	6.0	6.0	0.00
	6.0	6.0	6.03	+0.5
	6.0	6.0	6.0	0.00
4. Pd-Ru (Jewellary alloy) (4.5% Ru, 95.5% Pd)	2.00	0.09	1.98	−1.0
	4.24	0.20	4.24	0.00
	3.00	0.14	3.01	+0.33

Determination of Palladium in Synthetic Solutions. To ascertain the selectivity of the reagent the method was successfully used for the determination of palladium in alloys. Synthetic solutions similar to those of the alloys of palladium were prepared and the amount determined following the recommended procedure. Results obtained are summarised in Table 1.

Determination of Osmium in Osmiridium. Osmiridium can be analyzed successfully after decomposition by attack with chlorine and dissolution of platinum metal salts in hydrochloric acid. No distillation is required unless the amounts of interfering elements are above the tolerance

* Removed by centrifugation.

limit. For a synthetic sample of osmiridium results obtained are shown in Table 2.

Discussion

Various chromogenic reagents used for the determination of palladium have been reviewed.[7,8] *N,N*-Dimethyl-*p*-nitrosoaniline[8,9] and *p*-nitrosodiphenylamine[9] have been extensively used for the spectrophotometric determination of palladium. The disadvantage is that both of them cannot be used in presence of large amount of natural salts such as sodium chloride and other platinum metals and several base metals interfere. MNQM is more selective than these methods. As compared to dimethylglyoxime.[8] MNQM is more selective and sensitive. Absorption maximum does not lie in the UV region as in the case of phenyl 2-pyridylketone oxime[10] (340 nm) and triphenylphosphine[11] (346 nm). Methylglyoxime and salicylaldehyde oxime[12] have also been used, but sensitivity of both is low. Palladiazo[13] is less selective than MNQM, since most of the base metals and noble metals interfere. Tropolone[14] method is sensitive but suffers from interference due to many metals. The sensitivity of 2-hydroxy-1-naphthaldehyde oxime[15] is also high but molybdenum(IV) and osmium(III) interfere seriously. The chief advantage of the present method is that palladium can be determined successfully in presence of other metals, especially eighth group metals and platinum metals except osmium.

Out of the several reagents suggested for spectrophotometric determination of osmium, thiourea[16] is one of the most useful and recommended reagent for osmium. Despite the lack of sensitivity, the chief disadvantage is that the quantity of thiourea required for a fixed amount of osmium depends on the volume of the solution. 1,5-Diphenylcarbohydrazide[17,18] is an extremely sensitive reagent for osmium, but the associated platinum metals and base metals (iron, cobalt, nickel, copper) interfere. The color development is dependent on temperature, time of standing in aqueous phase, the period of extraction of the complex into $CHCl_3$ and subsequent absorbance measurement, the concentration of perchloric acid

Table 2. Determination of Osmium(VIII) in Synthetic Mixture Corresponding to Osmiridium

Metals present/ppm				Os Found	Error/%
Os	Ir	Ru	Pt		
6.0	6.0	6.0	2.0	6.01	+0.16
4.0	4.0	4.0	1.0	4.02	+0.5
2.0	0.05	0.3	0.1	1.99	−0.5

Table 3. Sensitivities of Reagents for Pd, Os, and Ir

Reagent	Sensitivity μg Pd/cm²	Reagent	Sensitivity μg Os/cm²	Reagent	Sensitivity μg Ir/cm²
8-Quinolinethiol	0.024/272 nm 0.003/286 nm	1,5-Diphenyl-carbohydrazide	0.00127/560 nm	Leucocrystal violet	0.004/590 nm
N,N-Dimethyl-*p* nitrosoaniline	0.0015/510—525 nm	2-Aminophenol-4-sulfonic acid	0.1/440 nm	4,4′-Bi-*o*-anisidine	0.016/530 nm
Methylglyoxime	3.0/427 nm	Tiron	0.033/470 nm	*N,N*-Dimethyl-*p*-nitroso-aniline	0.010/530 nm
Palladiazo	0.0032/540 nm	7-Amino-1-naphthol-3,6-disulfonic acid	0.2/480 nm	Cerium(IV) sulfate sulfuric acid	0.12/510 nm
Acenaphthene-quinone monoxime	0.0084/385 nm	Acenaphthene-quinone monoxime	0.0323/430 nm	Acenaphthene-quinone monoxime	0.021/385 nm
2-Hydroxy-1-naphthaldehyde oxime	0.0097/402 nm				
2-Methyl-1,4-naphthoquinone 4-oxime (MNQM) (Present method)	0.012/460 nm	2-Methyl-1,4-naphthoquinone 4-oxime (Present method)	0.025/460 nm	2-Methyl-1,4-naphthoquinone 4-oxime (Present method)	0.014/450 nm

and even the order of addition of the reagents. In case of 7-amino-1-naphthol-3,6-disulfonic acid,[19] sensitivity is very low, though the other platinum metals do not interfere. In acenaphthenequinone monoxime[20] 90 min heating of solution is needed and sensitivity is also low. In phenanthrenequinone monosemicarbazone[21] sensitivity is low and 5 min of heating is required.

Very few satisfactory reagents are available for the spectrophotometric determination of iridium. In Leucocrystal Violet[22] method, Rh and Fe(III) interfere seriously and this method depends upon a specific composition of the dissolved iridium salt and aged iridium solutions give green solutions of lower absorbance than those which are freshly prepared. Tin bromide method[23,24] is not selective. This method is sensitive to certain variation in the procedure such as time of contact, temperature, quantity of reagent and hydrobromic acid. In 4,4′-bi-*o*-anisidine[25] method, there is interference from associated metals from oxidants and sulfuric acid solution cannot be used. The absorbance is sensitive to the amount of reagent and to the acidity of the medium. In *N*,*N*-dimethyl-*p*-nitrosoaniline method,[26] composition of the complex is not known and the method offers no specificity among platinum metals and there is interference from nonvolatile acids. The method is sensitive to changes in the conditions. In acenaphthenequinone monoxime method,[27] most of the platinum metals interefere and prior separation of iridium is necessary and sensitivity is also low.

The present method for the determination of Pd(II), Os(VIII), and Ir(III) using 2-methyl-1,4-naphthoquinone 4-oxime, involves simple technique. The method is selective and the complexes are stable for a long time. Effect of pH, buffer, heating time, amount of reagent do not have any effect on the absorbance. Most of the associated metals do not interfere. The sensitivities of the present method are promising and compare well with other known reagents in Table 3.

One of the authors (K.S.) thanks Council of Scientific and Industrial Research, New Delhi for providing financial assistance.

References

1) H. Veldstra and P. W. Wiardi, *Recl. Trav. Chim. Pays-Bas*, **62**, 74 (1943).
2) G. H. Ayres and W. N. Wells, *Anal. Chem.*, **22**, 317 (1950).
3) E. A. Klobbie, *Chem. Zentralbl.*, **11**, 65 (1898).
4) P. Job, *Ann. Chim.*, **9**, 113 (1928).
5) H. Irving and T. B. Pierce, *J. Chem. Soc.*, **1959**, 2565.
6) H. E. Bent and C. L. French, *J. Am. Chem. Soc.*, **63**, 568 (1941).
7) D. F. Boltz and M. G. Mellon, *Anal. Chem.*, **46**, 233R (1974); **44**, 330R (1972); **42**, 152R (1970); **40**, 255R (1968); **38**, 317R (1966); **36**, 256R (1964); **34**, 232R (1962).
8) F. E. Beamish and W. A. E. McBryde, "Analytical Chemistry of Platinum Metals," Pergamon Press, London (1966).
9) J. H. Yoe and L. G. Overhober, *J. Am. Chem. Soc.*, **61**, 2058 (1939).
10) B. Sen, *Anal. Chem.*, **31**, 881 (1959).
11) M. Mojski and M. Plesinska, *Microchem. J.*, **24**, 117 (1979).
12) F. E. Beamish, *Talanta*, **12**, 743 (1965).
13) J. A. Perez-Bustamante, G. C. Morell, and F. Burriel-Marte, *Anal. Chim. Acta*, **44**, 65 (1969).
14) G. H. Rizvi and R. P. Singh, *Indian J. Chem.*, **10**, 273 (1972).
15) K. Uesugi and S. Yamaguchi, *Bunseki Kagaku*, **28**, 268 (1979).
16) S. Kalyanaraman and S. M. Khopkar, *Anal. Chim. Acta*, **78**, 231 (1975).
17) G. Goldstein, *Oak Ridge Natl. Lab., Oak Ridge, Tenn. U. S. Atomic Energy, Comm.*, ORNL 2862, 71 (1961).
18) G. Goldstein, O. L. Manning, O. Menis, and J. A. Dean, *Talanta*, **7**, 301 (1961).
19) B. V. Agarwala and A. K. Ghose, *Talanta*, **20**, 129 (1973).
20) S. K. Sindhwani and R. P. Singh, *Microchem. J.*, **18**, 627 (1973).
21) F. Kamil, S. K. Sindhwani, and R. P. Singh, *Mikrochim. Acta*, **1**, 345 (1980).
22) G. H. Ayres and W. T. Bolleter, *Anal. Chem.*, **29**, 72 (1957).
23) S. S. Berman and W. A. E. McBryde, *Analyst*, **81**, 566 (1956).
24) A. D. Westland and F. E. Beamish, *Mikrochim. Acta*, **1956**, 1974.
25) S. S. Berman, F. E. Beamish, and W. A. E. McBryde, *Anal. Chim. Acta*, **15**, 363 (1956).
26) A. D. Westland and F. E. Beamish, *Anal. Chem.*, **27**, 1776 (1955).
27) S. K. Sindhwani and R. P. Singh, *Z. Anal. Chem.*, **268**, 31 (1974).

 © 1987 The Chemical Society of Japan Bull. Chem. Soc. Jpn., 60, 1141—1143 (1987)

A Structural Model for Octacalcium Phosphate-Succinate Double Salt

Mathai MATHEW* and Walter Eric BROWN
Paffenbarger Research Center, American Dental Association Health Foundation,
National Bureau of Standards, Gaithersburg, MD 20899, U.S.A.
(Received January 20, 1986)

A new structural model for octacalcium hydrogenpentakis(phosphate) succinate pentahydrate, $Ca_8H(PO_4)_5(C_2H_4\cdot(COO)_2)\cdot 5H_2O$, a reaction product of octacalcium dihydrogenhexakis(phosphate) pentahydrate, $Ca_8H_2(PO_4)_6\cdot 5H_2O$, OCP, and succinate ions, is proposed on the basis of similarities in the unit cell dimensions and structures of OCP and calcium succinate trihydrate. This model can be used to develop information on the mode of incorporation of dicarboxylate ions into OCP and hydroxyapatite and its possible effects on biological mineralization processes.

Monma et al.[1,2] have recently made the discovery that saturated aliphatic dicarboxylic acids, $HOOC-(CH_2)_n-COOH$ with n=1 to 6, form a series of double salts with octacalcium dihydrogenhexakis(phosphate) pentahydrate, $Ca_8H_2(PO_4)_6\cdot 5H_2O$; generally referred to as octacalcium phosphate (OCP). They proposed that the double salts are formed by substitution of an HPO_4^{2-} group in OCP by a dicarboxylate ion, with the general formula, $Ca_8(HPO_4)_{2-z}(PO_4)_4\cdot(C_nH_{2n}C_2O_4)_z\cdot mH_2O$, and gave a possible structural model. We propose here a different model for the structure of one of these double salts, octacalcium hydrogenpentakis-(phosphate) succinate pentahydrate, $Ca_8H(PO_4)_5(C_2H_4\cdot(COO)_2)\cdot 5H_2O$, based on the observation that the non-primitive, B-centered cell of calcium succinate trihydrate has b and c dimensions and the angle γ which are very similar to those of OCP[3] and hydroxyapatite (OHAp), $Ca_5(PO_4)_3(OH)$ (Table 1). It was the similarities between the same dimensions of OCP and OHAp that revealed the structural relationship between these two salts which so profoundly affects their physical and chemical properties. At this time, very little is known about the properties of the double salts, but if they form as biominerals, they probably will prove to affect properties such as crystal growth and hydrolysis, morphology, Ca/P ratio and impurity content of hydrolysates.

The structural model for the OCP-dicarboxylate complexes proposed by Monma[2] is based on the structure of OCP[3] and the structures of the corresponding dicarboxylic acids. The model was conceived on the assumption that the [Ca-HPO_4-Ca] pillar in the hydrated layer of OCP (Fig. 1) is substituted by a [Ca-dicarboxylate-Ca] pillar. The [Ca-HPO_4-Ca] pillars implicated in their model are Ca(3)-P(5)'HPO_4-Ca(4)' and Ca(4)-P(5)HPO_4-Ca(3)' (Fig. 1). Based on the structure of OCP, P(5)HPO_4 would be the most likely candidate to be involved in the replacement. Since the projection of the Ca(3)-dicarboxylate-Ca(4) pillar onto the a-b plane is nearly parallel to the a axis, the increase in d_{100} of OCP-dicarboxylate would be proportional to the length of the dicarboxylate ion.

The model proposed by Monma has several drawbacks. The plane of the COO^- group is approximately parallel to the c-axis and the model requires two dicarboxylate ions to be nearly superimposed along the relatively short c-axis (6.88 Å). Furthermore, when the whole unit cell is taken into account, particularly in the a-b plane (001), it becomes obvious from their model that there would be a relatively large volume of empty space in the center of the cell. The increase of d_{100} (e.g. from 18.7 Å in OCP to 21.4 Å in OCP-succinate) would make the apparent volume of this empty space even larger. It is unlikely that this space could be occupied by water molecules or other ions because its major boundaries would be the hydrophobic part (methylene groups) of the dicarboxylate ions. This would be particularly true for the higher members of the series. However, this model may be possible in the case of dicarboxylic acids with additional functional groups (OH, NH_2, COOH) which are more compatible with ions and water molecules.

A New Model. Our model is based on the structure of calcium succinate trihydrate. The structure is reported[4] in the space group $P\bar{1}$ with a=7.937, b=9.450, c=6.688 Å, α=91.47, β=111.80, and γ=71.60°. The transformation matrix ($2\ 0\ \bar{1}/0\ \bar{1}\ 0/0\ 0\ \bar{1}$) converts this primitive cell to a B-centered cell with the dimensions listed in Table 1. The striking similarity of this cell to those of OCP and OHAp is immediately obvious. The cell dimensions b and c and all cell angles of the succinate and OCP are nearly identical.

Table 1. Comparison of Cell Dimensions in OCP, OHAp, and Calcium Succinate Trihydrate

	OCP	OHAp	Ca succinate trihydrate
a/Å	19.692	9.432	14.759
b/Å	9.523	9.432	9.450
c/Å	6.835	6.881	6.688
α/°	90.15	90.0	91.47
β/°	92.54	90.0	93.08
γ/°	108.65	120.0	109.14
Space group	$P\bar{1}$	$P6_3/m$	$B\bar{1}$

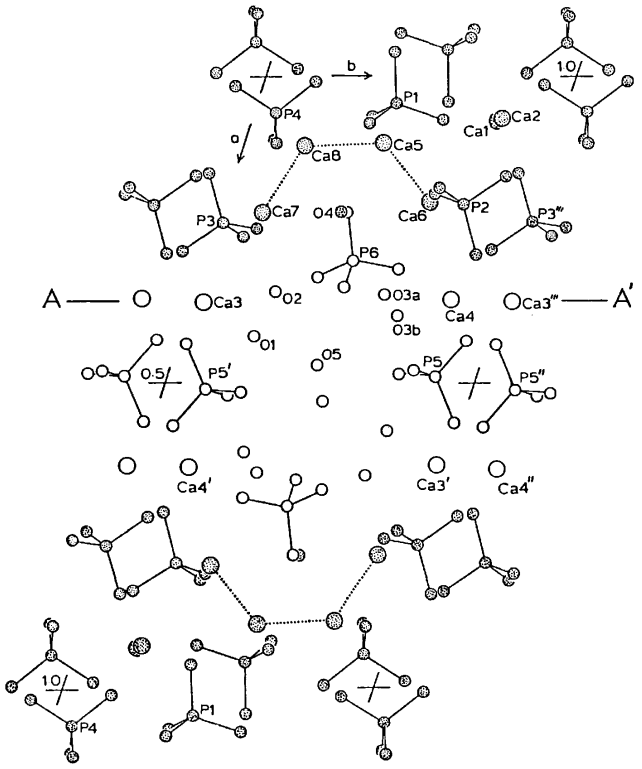

Fig. 1. Structure of OCP projected down the c* axis. The shaded portions correspond to the apatitic layer and the nonshaded atoms correspond to the hydrated layer. Atoms in the asymmetric unit are labelled. Symmetry codes for related atoms are ′ for $(1-x, 1-y, -z)$, ″ for $(1-x, 2-y, -z)$ and ‴ for $(x, 1+y, z)$.

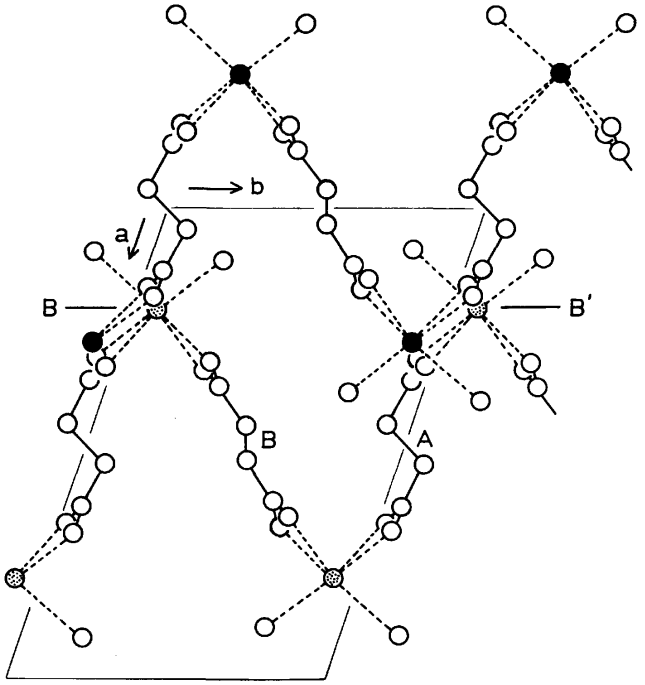

Fig. 2. Structure of calcium succinate trihydrate projected down the c* axis. The filled circles represent Ca atoms at $z=1/2$ and the shaded circles the Ca atoms at $z=0$.

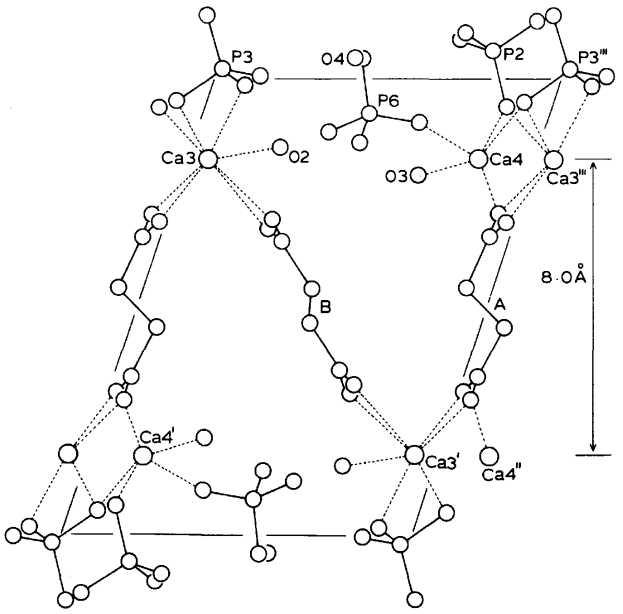

Fig. 3. The proposed model of OCP-succinate, viewed down the c* axis. Only the central portion of the OCP cell ($a=1/4$—$3/4$) showing the incorporated succinate ions is illustrated.

Comparison of the structures of OCP (Fig. 1) and calcium succinate trihydrate (Fig. 2) reveals some important structural similarities. The unit cell dimensions in the (100) planes of the two compounds are nearly the same. The relative positions of the Ca ions in a section of this plane through Ca(3)-Ca(3)‴ in OCP (A-A′ in Fig. 1) are nearly identical to those of a corresponding section, B-B′, in calcium succinate trihydrate (Fig. 2). This implies that epitaxial growth of calcium succinate on the (100) plane of OCP is possible, and that on a sub-unit cell level the OCP structure at A-A′ can be joined to the calcium succinate structure at B-B′ (Fig. 3). A feature of the structure of calcium succinate is that the succinate ions reside on crystallographic centers of symmetry and link pairs of equivalent Ca ions at the same height along c axis in a zigzag way. The succinate ions linking the Ca ions at $z=1/2$ are not on top of those linking the Ca ions at $z=0$, but related by $1/2a+1/2c$ (B-centering). This is to be expected on steric grounds.

The model we propose for the OCP-succinate complex takes into account the structural features of both OCP and calcium succinate trihydrate. Based on the structure of the calcium succinate, it is obvious that the succinate ion, which lies on a center of symmetry, can link only pairs of one type of Ca ion (either Ca(3) or Ca(4)) in the hydrated layer of OCP. On the basis of bond length calculations, Ca(3) appears to be a more probable candidate than Ca(4) for linking succinate ions in the OCP-succinate

complex. It is interesting to note that the position of Ca(3) in OCP corresponds very closely to that of a column calcium in OHAp whereas the Ca(4) position in OCP is shifted by about 1.9 Å along the b axis. Although the Ca(4)-Ca(4)″ (Fig. 1) linkage through a succinate ion is possible, an increase in d_{100} due to the incorporation of this succinate would make the Ca(4)···Ca(4)′ distance considerably longer than that which can be linked by the succinate ion unless there is a corresponding shift of Ca(4) along the b axis.

Our proposed structure contains two types of succinate ions. One succinate ion (A) links Ca(3)‴ and Ca(3)′ of OCP (Fig. 1) primarily along the a axis, thus causing a corresponding increase in d_{100}. In effect, this succinate ion replaces two HPO_4^{2-} ions of OCP. The second succinate ion (B) links Ca(3) and Ca(3)′, without affecting the d_{100} spacing. The succinate ion B is far removed from the HPO_4 ion sites of OCP and fills the void that would otherwise exist in the center of the unit cell.

The proposed model is illustrated in Fig. 3. Most of the structural features of OCP remain intact. The water molecules O(2), O(3), and O(4) in OCP would retain their respective positions in the complex; only O(1) and O(5) need to be relocated if the total amount of water content is to remain the same as in OCP as indicated by the molecular formula proposed by Monma.[2] The proposed structural model implies that at least one of these two water molecules is likely to be coordinated to Ca(4).

The [Ca-succinate-Ca] pillar length down c* in calcium succinate of 8.0 Å (Fig. 2) would make the d_{100} of the OCP-succinate complex 21.6 Å which is in reasonably good agreement with the experimental value[2] of 21.4 Å. Since the dicarboxylate ions are capable of adopting different conformations, the difference may not be significant.

In OCP, both Ca(3) and Ca(4) are coordinated to seven O atoms. In our proposed structure of OCP-succinate, four of these bonds remain intact. In the case of Ca(3), it loses three O neighbors (two from $P(5)HPO_4$ and one from water molecule O(1)), but gains four O from carboxylato groups. Thus the coordination of Ca(3) is 8. However, Ca(4) loses three O neighbors, all from $P(5)HPO_4$ groups, but appears to gain only one O from carboxylato group in succinate A. In calcium succinate, the Ca ion corresponding to Ca(4) is linked to two O atoms of the type A succinate ion, one above and one below the plane of Ca(4). The same configuration of Ca(4) may be achieved in OCP-succinate also, with minor shifts in the positions of Ca(4) and/or with succinate A.

Discussion

When it was first observed that OCP and OHAp had very similar unit-cell parameters *b*, *c*, and angle γ, it was proposed that the two compounds contain a structurally similar layer. This was subsequently established by the determination of the structure of OCP. Nearly identical unit-cell parameters, *b*, *c*, and angle γ, are present in the OCP-succinate salt and in calcium succinate trihydrate. Although this could be a coincidence, it is more likely that the OCP-succinate and the calcium succinate trihydrate contain a common layer which is compatible with the OCP structure. This hypothesis is substantiated by the presence of Ca(3) and Ca(4) in OCP which occupy positions similar to those in calcium succinate trihydrate. Furthermore, when the d_{100} of OCP, 18.7 Å, is increased to that of the OCP-succinate complex, 21.6 Å, the Ca(3)‴-Ca(3)′ and Ca(3)-Ca(3)′ distances (Fig. 1) become such that they can accept succinate bridge coordination similar to those found in calcium succinate trihydrate. We conclude, therefore, that the model proposed in Fig. 3 for OCP-succinate structure is probably a good approximation and that it can be used (i) to visualize the structure of the OCP-succinate complex and (ii) to develop mechanisms for the hydrolysis and growth of OCP-succinate crystals.

Calcium malonate has two crystalline forms, both dihydrates, whose structures are known.[5,6] However, we were not able to transform their unit cells to have *b*, *c*, and γ values compatible with OCP. Examinations of the structures did not reveal compatibilities such as those found in calcium succinate trihydrate. This does not, of course, preclude formation of an OCP-malonate complex detected by Monma,[2] but it suggests that despite the near constancy of the increase in d_{100} with increase in length of the aliphatic carbon chain, there may be substantial differences among the structures of the double salts. Another indication of this is the inability of the dicarboxylate ions with an odd number of carbon atoms to reside on a center of symmetry.

This investigation was supported in part by Grant DE 05030 to the American Dental Association Health Foundation by the National Institutes of Health-National Institute of Dental Research and is part of the Dental Research Program conducted by the National Bureau of Standards in cooperation with the American Dental Association Health Foundation.

References

1) H. Monma and M. Goto, *Bull. Chem. Soc. Jpn.*, **56**, 3843 (1983).
2) H. Monma, *Bull. Chem. Soc. Jpn.*, **57**, 599 (1984).
3) W. E. Brown, *Nature (London)*, **196**, 1048 (1962).
4) A. Karipides and A. T. Reed, *Acta Crystallogr., Sect. B*, **36**, 1377 (1980).
5) B. Briggman and A. Oskarsson, *Acta Crystallogr., Sect. B*, **33**, 1900 (1977).
6) J. Albertsson, A. Oskarsson, and C. Svensson, *Acta Crystallogr., Sect. B*, **34**, 2737 (1978).

Quinoxaline Derivatives. XII. The Reactions of Quinoxaline 1,4-Dioxides with Acetic Anhydride

Yusuf AHMED,* M. Ikram QURESHI, M. Saleem HABIB,† and M. Amir FAROOQI†
Pharmaceutical & Fine Chemicals Research Division, Pakistan Council of Scientific and Industrial Research Laboratories, Karachi 39, Pakistan
†Wellcome Pakistan Ltd., D-43, Textile Avenue, S.I.T.E., Karachi, Pakistan
(Received December 10, 1985)

Quinoxaline 1,4-dioxide (**XIIIa**) with acetic anhydride gave 1-acetoxy-2(1*H*)-quinoxalinone (**XIVa**) which was prone to facile hydrolysis to yield 1-hydroxy-2(1*H*)-quinoxalinone (**XVa**). Both **XIVa** and **XVa** were isolated from the reaction mixture. On prolonged heating with acetic anhydride, **XIIIa**, **XIVa**, and **XVa** were converted slowly to the same end product, 2,3(1*H*,4*H*)-quinoxalinedione (**XXa**). 6-Ethoxy- (**XIIIb**), 6-methoxy- (**XIIIc**), and 6-methylquinoxaline 1,4-dioxide (**XIIId**) behaved similarly, except that the attack of the reagent took place exclusively on *N*-oxide para to the electron-donating substituents, and none of the other expected isomeric compounds **XVIIb—d** were isolated. Whereas 6-chloroquinoxaline 1,4-dioxide (**XIIIe**) bearing an electron-attracting chloro substituent on the benzene ring gave exclusively the other isomers **XVIIe**, **XVIIIe**, and **XXe**. A mechanism for this novel rearrangement is proposed and discussed.

We have reported[1] earlier that 2(1*H*)-quinoxalinone 4-oxides substituted at position 3, on heating under reflux with acetyl chloride, undergo nucleophilic chlorine substitution at C-7 position with simultaneous loss of the oxide function (**I**→**II**). In the absence of carbonyl function at C-2, the chlorine substitution primarily goes to the position adjacent to the *N*-oxide when it is unsubstituted (**III**→**IV**),[2] and in case there be a methyl group at C-3 it undergoes chlorine-substitution (**V**→**VI**);[2] both of these take place at the expense of the oxide function. In the case of 1,4-dioxides of quinoxalines (**VII**) the primary products[3] of the reactions with acetyl chloride were 6-chloroquinoxaline 1-oxides (**VIII**; 60—70%) and 3-chloroquinoxaline 1-oxide (**IX**; 30—40%). On prolonged heating these primary products gave 2,6- and 2,3-dichloroquinoxalines (**X** and **XI**), and all four products (**VIII** to **XI**) were isolated.[3] The presence of electron donating or withdrawing substituent on the benzene ring of the molecule is shown to control the direction of chlorine substitution through the attack of the reagent on one *N*-oxide in preference to the other.

It would be expected that the reaction of acetic anhydride will take place in a similar manner to that of acetyl chloride, resulting in acetoxylation instead of the chlorine nucleophilic substitution (**I**→**II**: AcO for Cl in the above reactions). In a previous paper[4] we have reported that 3-phenyl-2-(1*H*)-quinoxalinone 4-oxides (**I**) gave 1-acetyl-3-benzoyl-1*H*-benzimidazol-2(3*H*)-ones (**XII**) instead of the expected 7-acetoxy-3-phenyl-2(1*H*)-quinoxalinones (**III**; AcO for Cl).[4] However 1-methylated compound **I** gave the normal 7-acetoxy-1-methyl-3-phenyl-2(1*H*)-quinoxalinone[4] (**II**; Me for H and AcO for Cl). These observations prompted us to study the action of acetic anhydride on quinoxaline 1,4-dioxides.

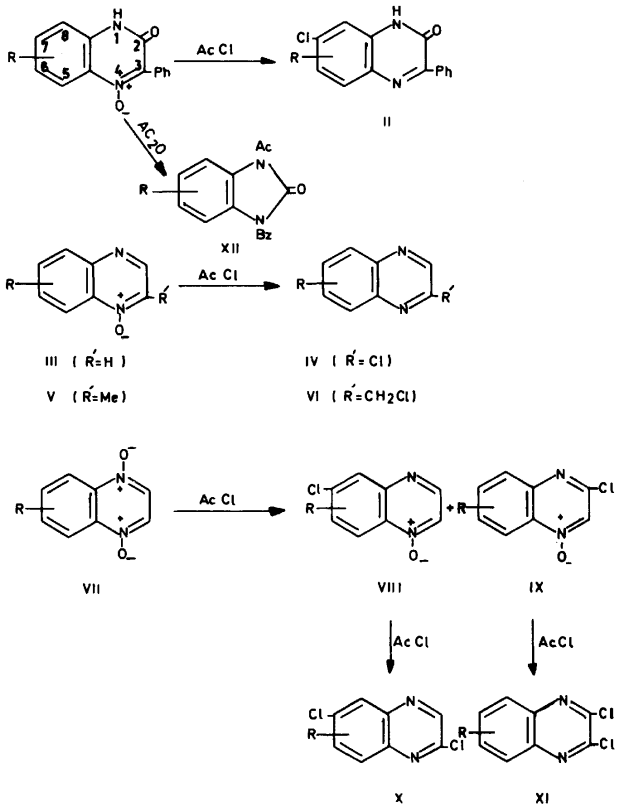

First we reexamined the previous finding[5] that quinoxaline 1,4-dioxide (**XIIIa**), on heating with an excess of acetic anhydride, gave 1-acetoxy-2(1*H*)-quinoxalinone (**XIVa**) in a 30% yield. However the yield was much higher than that reported, and further we observed that **XIVa** was easily hydrolyzed to give 1-hydroxy-2(1*H*)-quinoxalinone (**XVa**) merely on leaving with water. On reduction both **XIVa** and **XVa** afforded 2(1*H*)-quinoxalinone (**XVIa**), which was identical with an authentic sample, establishing the structures of **XIVa** and **XVa**.

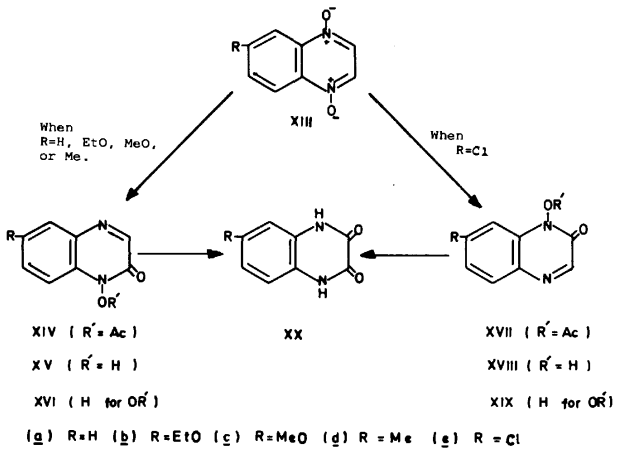

On prolonged heating of **XIIIa** with acetic anhydride, in addition of **XIVa** and **XVa**, a third product, 2,3(1*H*,4*H*)-quinoxalinedione (**XXa**), was also obtained. The amount of **XXa** progressively increased with prolonging the time of heating (9 h and then 16 h), while the amount of **XIVa** and **XVa** decreased, which obviously meant that **XIVa** and **XVa** were slowly converted to the same product **XXa**.

Similarly, 6-ethoxy (**XIIIb**), 6-methoxy (**XIIIc**), and 6-methylquinoxaline 1,4-dioxide (**XIIId**), on heating under reflux for 1 h with acetic anhydride, gave the corresponding 1-acetoxy (**XIVb—d**) and 1-hydroxy-6-substituted-2(1*H*)-quinoxalinone (**XVb—d**). The reduction of **XIVb—d** and **XVb—d** with sodium dithionite in aqueous ethanol gave 6-ethoxy-, 6-methoxy, and 6-methyl-2(1*H*)-quinoxalinones (**XVIb—d**), respectively, which were identical with authentic samples previously prepared and reported by us[6] or synthesized individually in this work (see Experimental). None of the other expected isomers (**XVIIb—d** and **XVIIIb—d**) were formed in these reactions.

On the other hand, the reaction of 6-chloroquinoxaline 1,4-dioxide (**XIIIe**) with acetic anhydride gave 1-acetoxy- and 1-hydroxy-7-chloro-2(1*H*)-quinoxlinone, both of which on reduction with sodium dithionite in aqueous ethanol gave 7-chloro-2(1*H*)-quinoxalinone (**XIXe**); identical with an authentic sample.[7] The other isomers **XIVe** were not formed in this case too. The results are summarized in the table in the experimental section.

To explain the different behavior of quinoxaline 1,4-dioxides, we propose the following mechanism.

The electron-donating substituents (R) on the benzene ring increase the electron density at the oxygen atom of the *N*-oxide para to R, whereby the attack of Ac^+ takes place more favorably to this *N*-oxide than to the other *N*-oxide, resulting in the formation of 1-acetoxy-6-R-2(1*H*)-quinoxalinone as illustrated above. When R is an electron-withdrawing group (viz. chloro, as in **XIIIe**) the electron density is decreased at the oxygen atom of the *N*-oxide para to R, and the attack of Ac^+ therefore takes place to the other *N*-oxide, resulting in the formation of the other isomeric compound 1-acetoxy-7-chloro-2(1*H*)-quinoxalinone (**XVIIe**). The 1-hydroxy derivatives are formed by the facile hydrolysis of the acetoxy compounds.

The formation of the postulated triacetoxy intermediate (see above) has its analogy in the Thiel's reaction[8] of 1,4-naphthoquinone with acetic anhydride to give 1,2,4-triacetoxynaphthalene.

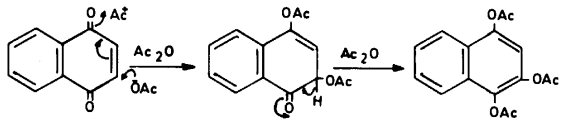

When the time of heating in the reaction of 1,4-dioxides (**XIIIa—e**) with acetic anhydride is prolonged from 1 to 9 h, a third product, the corresponding 2,3(1*H*,4*H*)-quinoxalinedione (**XXa—e**) is formed in addition to the acetoxy and hydroxy compounds, the quantities of which decrease accordingly. On further prolonging the time of heating, the quantities of 2,3(1*H*,4*H*)-quinoxalinediones gradually increase and those of the corresponding acetoxy and hydroxy derivatives decrease. It appears that the postulated triacetoxy intermediate further leads very slowly to the formation of the 2,3(1*H*,4*H*)-quinoxalinediones as shown below.

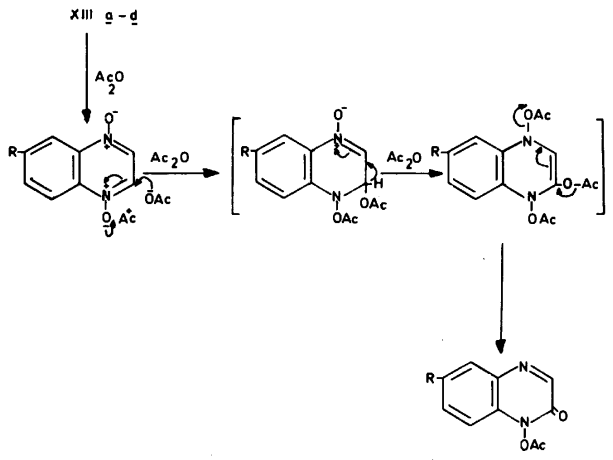

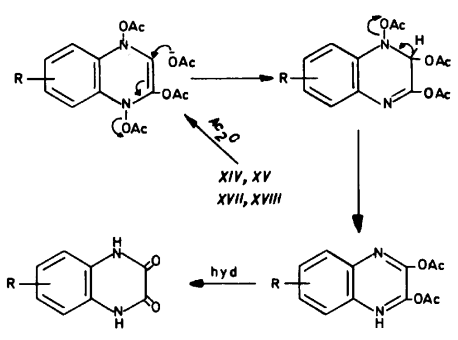

Experimental

Materials. Quinoxaline 1,4-dioxide (**XIIIa**), 6-ethoxyquinoxaline 1,4-dioxide (**XIIIb**), 6-methoxyquinoxaline 1,4-dioxide (**XIIIc**), 6-methylquinoxaline 1,4-dioxide (**XIIId**), and 6-chloroquinoxaline 1,4-dioxide (**XIIIe**) were prepared by the methods already reported.[9] Pet. ether means light petroleum; bp 60—80 °C. Identical structure means undepressed mixed melting point and superimposible IR spectra of the two compounds. All 1-hydroxy-2(1*H*)-quinoxalinones give blood red color on addition of aq iron(III) chloride to their ethanolic solutions (a characteristic of hydroxamic -N(OH)-CO- moiety in a molecule). The solutions were decolorized, whenever necessary, with activated charcoal.

Reaction of Quinoxaline 1,4-Dioxide (XIIIa) with Acetic Anhydride. Procedure A: A mixture of **XIIIa** (2 g) and acetic anhydride (20 ml) was heated under reflux for 1 h. The sticky brown residue, left after removal of acetic anhydride on a vacuum rotary evaporator, was exhaustively extracted with boiling pet. ether. The volume of pet. ether extract was reduced until the crystallization started, whereby small white needles of 1-acetoxy-2(1*H*)-quinoxalinone (**XIVa**); mp 110—111 °C (lit,[5] mp 110.5—111 °C) were obtained (yield 70%). To the residue which could not be extracted with pet. ether, a small amount of water was added and left overnight in a refrigerator. The solidified product, on recrystallization from ethanol gave reddish brown flakes of 1-hydroxy-2(1*H*)-quinoxalinone (**XVa**); mp 210—212 °C (lit,[5] mp 208—209 °C) in a 30% yield.

Both **XIVa** and **XVa**, on treatment with sodium dithionite in 50% aqueous ethanol, gave 2(1*H*)-quinoxalinone (**XVIa**); mp 272 °C (lit,[6] mp 270—272 °C), identical with an authentic sample.[6]

Procedure B: The time of heating was prolonged to 9 h **XIVa** and **XVa** were obtained in 60 and 25% yields, respectively. The extraction of pet. ether insoluble part with ethanol left a residue (13%). The crystallization of the residue from glacial acetic acid gave colorless needles of 2,3(1*H*,4*H*)-quinoxalinedione (**XXa**); mp >360 °C, identical with an authentic sample.[6] **XIVa** and **XVa** afforded three products **XIVa**, **XVa**, and **XXa** in each case when they were treated separately with acetic anhydride under the same conditions.

Procedure C: When the time of heating was further prolonged to 16 h, all three products **XIVa** (55%), **XVa** (20%), and **XXa** (15%) were obtained.

Similarly the results of the reactions of other quinoxaline 1,4-dioxides (**XIIIb—e**) with acetic anhydride are summarized in Table 1.

Table 1.

Starting material	Procedure	Products/%
XIIIb	A	**XIVb** (65) **XVb** (30)
	B	**XIVb** (60) **XVb** (25) **XXb** (10)
	C	**XIVb** (56) **XVb** (20) **XXb** (13)
XIIIc	A	**XIVc** (55) **XVc** (45)
	B	**XIVc** (50) **XVc** (35) **XXc** (10)
	C	**XIVc** (45) **XVc** (30) **XXc** (15)
XIIId	A	**XIVd** (50) **XVd** (40)
	B	**XIVd** (42) **XVd** (36) **XXd** (11)
	C	**XIVd** (36) **XVd** (29) **XXd** (15)
XIIIe	A	**XVIIe** (55) **XVIIIe** (40)
	B	**XVIIe** (50) **XVIIIe** (35) **XXe** (10)
	C	**XVIIe** (43) **XVIIIe** (30) **XXe** (15)

XIVb: Mp 132—133 °C (white needles from pet. ether). Found: C, 58.43; H, 5.02; N, 11.12%. Calcd for $C_{12}H_{12}N_2O_4$: C, 58.06; H, 4.83; N, 11.29%.

XVb: Mp 173—175 °C (needles from ethanol). Found: C, 58.48; H, 5.02; N, 13.58%. Calcd for $C_{10}H_{10}N_2O_3$: C, 58.25; H, 4.85; N, 13.59%.

The reactions of both **XIVb** and **XVb** with sodium dithionite in 50% aqueous ethanol gave 6-ethoxy-2(1*H*)-quinoxalinone (**XVIb**); mp 241—242 °C, identical with an authentic sample.[6]

XXb: Mp >360°, identical with an authentic sample.[6]

XIVc: Mp 115—117 °C (colorless needles from pet. ether). Found: C, 56.72; H, 4.34; N, 12.10%. Calcd for $C_{11}H_{10}N_2O_4$: C, 56.41; H, 4.27; N, 11.96%.

XVc: Mp 190—191 °C (needles from ethanol). Found: C, 56.45; H, 4.09; N, 14.62%. Calcd for $C_9H_8N_2O_2$: C, 56.25; H, 4.16; N, 14.58%.

The reactions of both **XIVc** and **XVc** with sodium dithionite in 50% aqueous ethanol gave the same compound, 6-methoxy-2(1*H*)-quinoxalinone (**XVIc**); mp 271—272 °C, identical with an authentic sample.[6]

XXc: Mp >350 °C, identical with an authentical sample.[6]

XIVd: Mp 104 °C (micro-needles from pet. ether). Found: C, 60.73; H, 4.53; N, 12.90%. Calcd for $C_{11}H_{10}N_2O_3$: C, 60.55; H, 4.59; N, 12.84%.

XVd: Mp 180—182° (ethanol). Found: C, 61.50; H, 4.51; N, 16.00%. Calcd for $C_9H_8N_2O_2$: C, 61.36; H, 4.54; N, 15.90%.

Both **XIVd** and **XVd**, on reduction with sodium dithionite in 50% aqueous ethanol, gave 6-methyl-2(1*H*)-quinoxalinone (**XVId**), mp 248 °C, identical with an authentic sample (the synthesis is described below).

XXd: Mp 345 °C, identical with sample, prepared by the condensation of 4-methyl-*o*-phenylenediamine and diethyl oxalate (yield 85%), and crystallized from ethanol as white needles, mp 345 °C. Found: C, 61.63; H, 4.61; N, 15.82%. Calcd for $C_9H_8N_2O_2$: C, 61.36; H, 4.54; N, 15.90%.

XVIIe: Mp 125—126 °C (white needles from pet. ether). Found: C, 50.42; H, 3.12; N, 11.93%. Calcd for $C_{10}H_7ClN_2O_3$: C, 50.31; H, 2.93; N, 11.74%.

XVIIIe: Mp 260 °C (ethanol). Found: C, 48.67; H, 2.50; Cl, 18.24; N, 14.01%. Calcd for $C_8H_5ClN_2O_2$: C, 48.85; H, 2.54; Cl, 18.07; N, 14.25%.

The reduction of both **XVIIe** and **XVIIIe** with sodium dithionite in 50% aqueous ethanol gave the same product, 7-chloro-2(1*H*)-quinoxalinone, (**XIXe**); mp 251—252 °C, identical with an authentic sample.[7]

XXe: Mp >360 °C, identical with an authentic sample.[6]

Preparation of Authentic 6-Methyl-2(1*H*)-quinoxalinone (XVId). α-Cyano-4-methyl-2-nitroacetanilide was prepared from 4-methyl-2-nitroaniline and ethyl cyanoacetate by the procedure described previously.[6] The anilide (yield 60%) crystallized from benzene as yellowish brown flakes; mp

146—147 °C.

Found: C, 55.20; H, 4.16; N, 19.32%. Calcd for $C_{10}H_9N_3O_3$: C, 54.80; H, 4.11; N, 19.17%.

A solution of the anilide (10 g) in pyridine (50 ml), was shaken with 1 mol dm^{-3} aq NaOH (50 ml) for 1 h. The color of the solution changed to dark red. Neutralization with dil HCl gave a precipitate, which was filtered, washed successively with dil HCl and water, and dried (yield 65%). Crystallization from ethanol gave yellowish brown needles of 3-cyano-6-methyl-2(1*H*)-quinoxalinone 4-oxide; mp 251—253 °C (decomp).

Found: C, 59.50; H, 3.56; N, 21.6%. Calcd for $C_{10}H_7N_3O_2$: C, 59.70; H, 3.48; N, 20.90%.

3-Cyano-6-methyl-2(1*H*)-quinoxalinone 4-oxide treated with sodium dithionite in 50% aqueous ethanol for elimination of the oxide, also lost the nitrile group as observed and reported by us,[6] giving an authentic sample of **XVId**; mp 248 °C.

Found: C, 67.81; H, 4.96; N, 17.63%. Calcd for $C_9H_8N_2O$: C, 67.50; H, 5.00; N, 17.50%.

We wish to thank Wellcome Research Laboratories (U. K.), and the Microanalytical Section of PCSIR Laboratories, Karachi, for the microanalyses reported in this paper.

References

1) Y. Ahmad, M. S. Habib, Ziauddin, and N. Bashir, *Bull. Chem. Soc. Jpn.*, **38**, 1654 (1965).

2) Y. Ahmad, M. S. Habib, Ziauddin, and B. Bakhtiari, *J. Org. Chem.*, **31**, 2613 (1966).

3) Y. Ahmad, M. S. Habib, M. I. Qureshi, and M. A. Farooqui, *J. Org. Chem.*, **38**, 2176 (1973).

4) Y. Ahmad, M. S. Habib, A. Mohammady, B. Bakhtiari, and S. A. Shamsi, *J. Org. Chem.*, **33**, 201 (1968).

5) A. S. Elina, *Zh. Obshch. Khim.*, **32**, 2967 (1962); *Chem. Abstr.*, **55**, 23550i (1961).

6) Y. Ahmad, M. S. Habib, and Ziauddin, *Tetrahedron*, **20**, 1107 (1964).

7) Y. Ahmad, M. S. Habib, M. I. Qureshi, and Ziauddin, *Bull. Chem. Soc. Jpn.*, **38**, 1659 (1965).

8) J. Theile, *Ber.*, **31**, 1247 (1898); S. Goodwin and Witkop, *J. Am. Chem. Soc.*, **79**, 179 (1957); H. Burton and P. F. G. Praill, *J. Chem. Soc.*, **1952**, 755.

9) J. K. Landquist, *J. Chem. Soc.*, **1953**, 2816.

Influence of Pressure on the Menschutkin-Type Reaction of Phenethyl Arenesulfonates with Pyridine

Soo-Dong Yoh,* Jong-Hwan Park, Kyung-A Lee, and In-Sook Han
Department of Chemistry, Teacher's College, Kyungpook National University, Daegu 635, Korea
(Received February 27, 1986)

Kinetic investigation of β-phenylethyl arenesulfonates with pyridine in acetonitrile revealed that the rates of these reactions which were lower than those of the reaction of benzyl benzenesulfonate with pyridine in acetone were increased with raising temperatures and pressures. The activation volumes were comparable to those of benzyl system, but activation entropies were negatively larger than those of benzyl system. From these phenomena it can be deduced that phenethyl system has more S_N2 character in the transition state, comparing with the reaction of benzyl system. With raising pressures the Hammett reaction parameters (ρ) were decreased, indicating that the reaction is probably closer to tight S_N2 character at higher pressures.

Menschutkin reactions—typical S_N2 reactions of alkyl halides with tertiary amine to form quaternary ammonium salts—have been widely investigated for the effects of pressure.[1-5] Recently kinetic studies of Menschutkin type reactions of benzyl benzenesulfonate with pyridine in acetone were carried out by the electric conductivity method under 1 to 2000 bars at 20 to 40 °C.[6] From the enthalpy, entropy, and volume of activation, it was found that this reaction precedes via the S_N2 reaction mechanism in which the rate of the reaction was determined by C–N bond formation in the transition state. In this connection, we studied on pressure dependence of the rate of the reaction of phenethyl arenesulfonates with pyridine which is expected to be more typical S_N2 under high pressure at 40 to 60 °C in acetonitrile to get some detailed information about the transition state.

Experimental

Instruments. Conductivity bridge and conductivity cell. The conductivity bridge is composed of B.N. 532 capacitor, B.N. 332 resistor and B.N. 1212/2 detector made by Rhode Schwarz Co., Germany. The conductivity cell shown in Fig. 1. It is composed of two parts, a glass cylinder of 5 cm^3 in which two Pt circular plate electrodes are sealed, and two-branched teflon tube of 6 cm long and 0.4 cm in diameter. The former acts as a conducting cell and the latter acts as a pressure conductor by pressing. The cell is set in the pressure vessel.

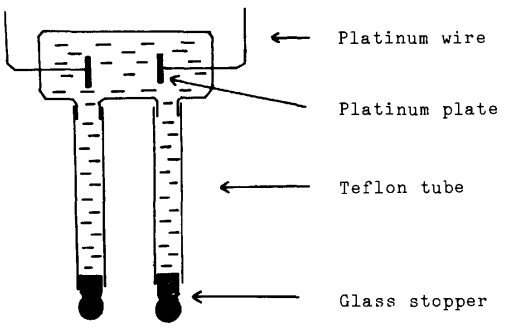

Fig. 1. Schematic drawing of the conductivity cell.

Materials. All materials used throughout were commercially available (Wako, Japan). Acetonitrile was purified by distillation after standing with anhydrous potassium carbonates for three days at room temperature. Pyridine dried over NaOH pellet was fractionated twice, bp 115—115.5 °C and stored in brown ampoule filled with nitrogen gas. IR spectra were recorded on a Hitachi EPI-2G Infrared Grating Spectrophotometer and ^1H NMR spectra were Varian 60 MHz Spectrometer.

The following arenesulfonyl chlorides were synthesized by chlorosulfonation of the corresponding substituted benzenes; *p*-Br derivative,[7] recrystd. from ligroine, (70%), mp 73 °C. Found: C, 38.05; H, 2.14%. Calcd for $C_6H_4BrClO_2S$: C, 38.33; H, 2.14%. *p*-Cl,[8] from ligroine, (58%), mp 52 °C (lit, 53 °C). *p*-MeO,[9] from pet. ether, (60%), mp 41 °C (lit, 41—42 °C). Unsubstituted benzenesulfonyl chloride[7] was obtained by purification of commercial chemicals, bp 137 °C/24 mmHg (1 mmHg=133.322 Pa) (lit, 119—121 °C/15 mmHg, mp 14.5 °C). *m*-Nitrobenzenesulfonyl chloride was prepared by chlorosulfonylation of sodium *m*-nitrobenzenesulfonate with chlorosulfuric acid. Recrystd. from ligroine, (57%), mp 61 °C (lit,[10] 61—62 °C). Found: C, 32.48; H, 1.67; N, 6.40%. Calcd for $C_6H_4ClNO_4S$: C, 32.51; H, 1.81; N, 6.32%. Phenethyl arenesulfonates were prepared from phenethyl alcohol with arenesulfonyl chloride by the Tipson's procedure[11] and purified by recrystallization from appropriate solvents.

N-Phenethylpyridinium *m*-nitrobenzenesulfonate. Pyridine (0.554 g, 0.007 mol) was added in a solution of phenethyl *m*-nitrobenzenesulfonate (2.15 g, 0.007 mol) in anhydrous acetonitrile (80 ml). The reaction mixture was heated under reflux for 4 h and then allowed to stand over night at room temperature. The product obtained was separated from solvent and washed with anhydrous ether. Recrystallization from 2-propanol gave colorless crystals, (40%), mp 122—123 °C, ^1H NMR ($CDCl_3$) δ=3.25 (2H, t, β-H), 5.15 (2H, t, α-H), 9.00 (2H, d, α-H of pyridine), 8.7 (1H, s, γ-H of pyridine); IR (Nujol) 3300, 1600, 1355, 1200, 1050, 835 cm^{-1}. Found: C, 59.52; H, 4.94; N, 7.33%. Calcd for $C_{19}H_{18}N_2O_5S$: C, 59.06; H, 4.70; N, 7.25%.

Kinetics. The reaction of phenethyl arenesulfonates with pyridine at various temperatures and pressures were followed by the conductometric method. As the reaction proceeds, the electric conductance was increased because formation of the salt increases as shown Eq. 1.[12] The conductivity cell was suspended in the high pressure vessel

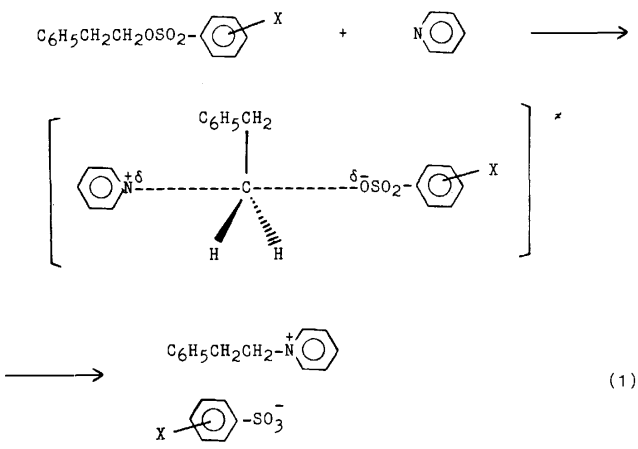

(1)

with electrode leads, and the vessel was set in a thermostat kept at given temperature within ±0.1 °C. All kinetic runs were carried out under pseudo-first-order conditions, being the molar concentration of pyridine more than fifty times of that of phenethyl arenesulfonate. The Guggenheim plots[13] were used for determining the pseudo-first-order rate constant, from which the second-order rate constants were calculated. Rate constants were accurately estimated with the range of ±5% under 1 to 2000 bars and at 40, 50, and 60 °C.

Results and Discussion

Rate constants and thermodynamic parameters. The second-order rate constants for the reaction of phenethyl *p*-bromobenzenesulfonate with pyridine in acetonitrile under various pressures and at various temperatures are summarized in Table 1. As shown in Table 1, the rate constants increase with temperature and pressure and the rate constants are lower than those of the reaction of benzyl benzenesulfonate with pyridine[6] (11.46×10^{-4} dm^3 mol^{-1} s^{-1} at 40 °C, 100 bars). This is probably due to larger stability of benzyl cation.

The activation volumes obtained from the slope in Fig. 1, on the basis of Eq. 2, are shown in Table 2.

$$\left(\frac{\partial \ln k_2}{\partial P}\right)_T = \frac{-\Delta V^{\neq}}{RT} \quad (2)$$

If $\Delta V^{\neq}$ is independent of pressure, Eq. 2 can be integrated as follows

$$k_2 = k_0 \exp\left(\frac{-P\Delta V^{\neq}}{RT}\right), \quad (3)$$

where k_0 is the rate constant under 1 atm. From Table 2, we can see that the activation volumes, $\Delta V^{\neq}$, are all negative at various temperatures and the value of $|\Delta V^{\neq}|$ decrease with increasing temperature. These results are valuable to consider the physical meaning involved in each item for the reaction mechanism.

The $\Delta V^{\neq}$ is equal to $V^{\neq}-V_0$, where $V^{\neq}$ is the volume of the activated complex, and V_0 is the volume of reactants, being composed of the substrate V_m (phenethyl *p*-bromobenzenesulfonate), the nucleophile V_n (pyridine) and the solvent V_s (acetonitrile). But the apparent volume of the activated complex ($V^{\neq}$) is the sum of the volume of the complex ($V_a^{\neq}$) and the solvent $V_s^{\neq}$ (acetonitrile). In particular, $V_s^{\neq}$ is somewhat different from solvent V_s. We can assume that the sum of the volume of V_m and V_n of reactants are not so different from that of activated complex $V_a^{\neq}$ even though the complex is somewhat electronically distorted, but the volume of solvents $V_s^{\neq}$ (acetonitrile) are much different from that of initial state because the charged complex causes more electrostriction than the reactants. As we mentioned above, if the complex is more charged than reactants, it is reasonable that activation volume ($\Delta V^{\neq}$) is negative. From the Eq. 3, we could know that k_2 increase with increasing pressure because of this negative $\Delta V^{\neq}$ value. It is shown in Fig. 2 that the pressure dependence of ln k_2 has a linear relationship. This fact shows that $\Delta V^{\neq}$ is independent of pressure. The temperature dependence of $\Delta V^{\neq}$ can be also explained from the charge separation of the activated complex with the change of temperature. In other words, if temperature is elevated, it is expected that the charge separation of the activated complex is larger and the bond enlargement of the activated complex and so the $|\Delta V^{\neq}|$ value increase with temperature because of the more electrostrict effect at higher temperature.

Generally, a negative $\Delta V^{\neq}$ would be expected for S_N2 reaction where two molecules are brought together in the transition state. $\Delta V^{\neq}$ of S_N2 reaction of benzyl benzenesulfonate with pyridine in acetone at 40 °C at various high pressure was −12.97 cm^3 mol^{-1}, [6] and its negative value was about the same to that of phenethyl

Table 1. Second-Order Rate Constants, $k_2\times10^4$ (dm^3 mol^{-1} s^{-1}), of the Reaction of Phenethyl *p*-Bromobenzenesulfonate with Pyridine in Acetonitrile at Various Temperatures and Under Various Pressures

T/°C	P/bar			
	1	500	1000	1500
40	0.517	0.671	0.823	
50	1.091	1.259	1.607	1.851
60	1.813	2.805	2.671	3.170

Table 2. Activation Volume ($\Delta V^{\neq}$) for the Reaction of Phenethyl *p*-Bromobenzenesulfonate with Pyridine in Acetonitrile at Various Temperatures

T/°C	40	50	60
$\Delta V^{\neq}$/cm^3 mol^{-1}	−12.33	−10.33	−9.56

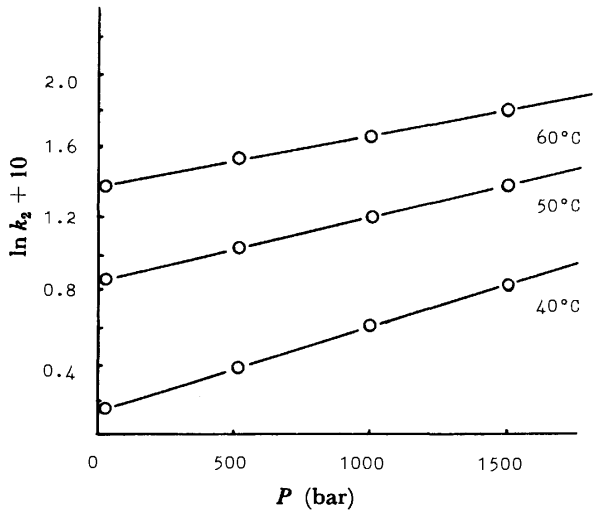

Fig. 2. The plots of ln k_2 vs. pressure at various temperatures.

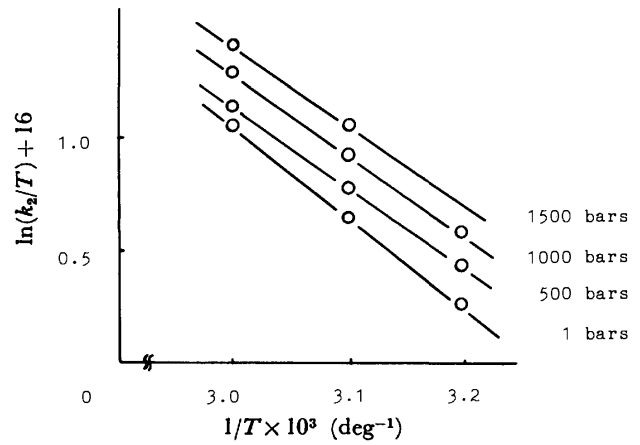

Fig. 3. The plots of ln (k_2/T) vs. $1/T$ at various temperatures.

p-bromobenzenesulfonate, but smaller than that of phenethyl *m*-nitrobenzenesulfonate.[14] This means that the S_N2 character of phenethyl *m*-nitrobenzenesulfonate is more predominant in the reaction of phenethyl *m*-nitrobenzenesulfonate than in that of benzyl benzenesulfonate.

There are other resemblance with the S_N2 Menschutkin reaction for example, of the reaction of EtI with pyridine[15] and that of hexadecyl bromide with pyridine in acetone at 40 °C, in which $\Delta V^{\neq}$ is −15—−20 ml per mole in both case. The activation parameters of the reaction of phenethyl *p*-bromobenzenesulfonate with pyridine are given in Table 4, in which the values of activation enthalpy are calculated from the slopes in Fig. 3. The plots of ln (k_2/T) against $1/T$ at various pressure for the reaction of phenethyl *p*-bromobenzenesulfonate with pyridine exhibit good linearity as shown in Fig. 3.

As shown in Table 4, $\Delta H^{\neq}$ values decrease and $\Delta S^{\neq}$ values increase negatively under higher pressure. These phenomena can be explained by that the S_N2 characters are predominant under higher pressure because the S_N2 mechanism is predominant when $\Delta H^{\neq}$ value is comparatively small and $\Delta S^{\neq}$ values negatively large.[12,16] Comparison of $\Delta S^{\neq}$ values for the reaction of benzyl system with that of phenethyl one shows that the latter is more negative[6] than the former. This result suggests that S_N2 character in the transition state of the phenethyl system is greater than that of the benzyl one, i.e., the former one should be closer to tight S_N2 than that of the latter, in the sense of concerted mechanism that the bond formation with nucleophile cooperates with the fission of leaving group in the transition state.

Table 3. Activation Parameters of the Reaction of Phenethyl *p*-Bromobenzenesulfonate with Pyridine in Acetonitrile at 50 °C

P/bar	1	500	1000	1500
$\Delta H^{\neq}$/kcal mol^{-1}	12.36	11.10	10.91	10.73
$\Delta S^{\neq}$/e.u. mol^{-1}	−38.59	−42.18	−42.30	−42.58
$\Delta G^{\neq}$/kcal mol^{-1}	24.83	24.73	24.58	24.49

Table 4. Second-Order Rate Constants, $k_2 \times 10^4$ (dm^3 mol^{-1} s^{-1}), of the Reaction of Phenethyl Arenesulfonates with Pyridine in Acetonitrile under Various Pressures at 50 °C

Substituents	*P*/bar				
	1	500	1000	1500	2000
m-NO_2	4.264	4.584	4.923	5.313	5.918
p-Cl	1.272	1.458	1.874	2.158	2.459
p-Br	1.091	1.259	1.607	1.851	
H	0.636	0.792	1.053	1.251	1.441
p-CH_3	0.403	0.533	0.728	0.885	1.027

As shown in Table 4, the rate constants increase with increasing both the pressure and the electron-withdrawing power of the substituent, which stabilize the sulfonate anion in the transition state by dispersing the charge. Hammett plots for these reactions at various pressures exhibit good linearity as shown in Fig. 4 and all the results are listed in Table 5. Hammett equation may be written in the form as linear free energy relationship.

$$\Delta\Delta G^{\neq} = -2.303\,RT\,\rho\sigma \tag{4}$$

From Eq. 4, by partial differentiation with respect to pressure *P*,

$$\frac{\partial \rho}{\partial p} = (\partial/\partial p)[-\Delta\Delta G^{\neq}/2.303\,RT\sigma)]$$
$$= (-\Delta\Delta V^{\neq})/2.303RT\sigma\,. \tag{5}$$

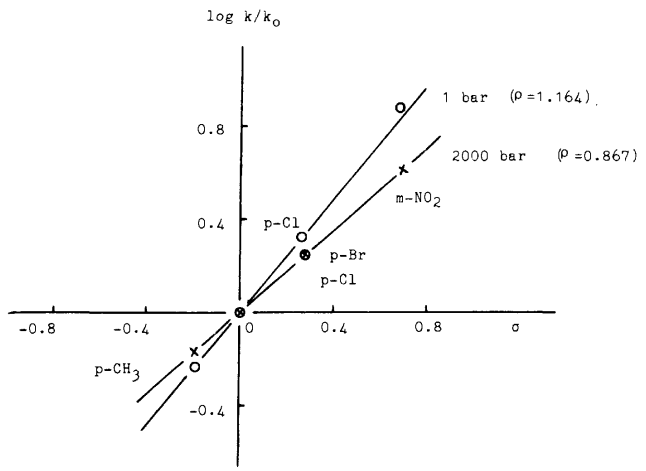

Fig. 4. Hammett plot for the reaction of phenethyl arenesulfonate with pyridine in acetonitrile at 50 °C.

Table 5. Hammett ρ Values for the Reaction of Phenethyl Arenesulfonates with Pyridine at 50 °C and Various Pressures

P/bar	1	500	1000	1500	2000
ρ	1.164	1.063	0.943	0.885	0.867
r	0.998	0.997	0.997	0.997	0.999
n	5	5	5	5	4

When neutral molecules react to produce ions like Menschutkin reaction the Hammett ρ values decrease with increase in pressure (see Table 5). This fact is probably explained by that, when P increases and the solvent becomes more compressed in the solution reaction, the contraction of the solution produced on ionization becomes smaller than the ordinary state. Due to these results, activation volume and, consequently, $|\Delta\Delta V^{*}|$ decrease and from right hand side of Eq. 5, $-\partial\rho/\partial p$ value decreases too; i.e., ρ should be decrease with increase in P. All above results and assumptions are also agreed perfectly with the idea of Fischer and his co-workers.[17]

The Present Studies were supported by the Basic Science Research Institute Program, Ministry of Education, Korea, 1984.

References

1) M. G. Gonikberg and A. L. Kitaigorodsky, *Dokl. Akad. Nauk SSSR.*, **122**, 231 (1958).
2) S. D. Hamann, "High Pressure Physics and Chemistry," ed by R. S. Bradly, Academic Press, New York (1963), Vol. 2, p. 191.
3) W. J. Le Noble, *J. Chem. Educ.*, **44**, 729 (1967).
4) K. Tamura, T. Ogo, and T. Imoto, *Bull. Chem. Soc. Jpn.*, **46**, 2988 (1973).
5) T. Okamoto and K. I. Lee, *J. Am. Chem. Soc.*, **97**, 4015 (1975).
6) J. U. Hwang, S. D. Yoh, and J. G. Jee, *Korean Chem. Soc.*, **24**, 150 (1980).
7) R. L. Shriner, R. C. Fuson, and D. T. Curtin, "The Systematic Identification of Organic Compounds," John Wiley & Sons, New York (1956), p. 331.
8) H. Meerwein, G. Dittmar, R. Göllner, K. Hafner, F. Mensch, and O. Steifort, *Chem. Ber.*, **90**, 841 (1957).
9) M. S. Morgan and L. H. Cretcher, *J. Am. Chem. Soc.*, **70**, 375 (1948).
10) H.-H. Hodgson and J. S. Whitehurst, *J. Chem. Soc.*, **1944**, 482.
11) R. S. Tipson, *J. Org. Chem.*, **9**, 235 (1944).
12) K. A. Lee, K. T. Howang, and S. D. Yoh, *J. Korean Chem. Soc.*, **23**, 243 (1979).
13) E. A. Guggenheim, *Philos. Mag.*, **2**, 538 (1926).
14) S. D. Yoh and J. H. Park, *Rep. Res. Inst. Phys. Chem. Kyungpook Natl. Univ.*, **1985**, 43.
15) R. O. Gibson, E. W. Fawcett, and M. W. Perren, *Proc. R. Soc. London, Ser. A*, **15**, 2223 (1935).
16) D. A. Brown and R. F. Hudson, *J. Chem. Soc.*, **1953**, 3352.
17) A. Fischer, B. R. Mann, and J. Vaughan, *J. Chem. Soc.*, **1961**, 1093.

New Liquid Crystalline Homologous Series Exhibiting the Smectic C Phase

Sakumitsu SAKAGAMI*
National Industrial Research Institute of Kyushu, Tosu, Saga 841
(Received July 4, 1986)

Synopsis. A liguid crystalline homologous series of *N*-[4-(4-alkoxybenzoyloxy)benzylidene]-4-butylanilines and their hydroxyl derivatives at the 2-position were synthesized, and then the liquid-crystalline-phase transitions were determined using a differential scanning calorimeter and a polarizing microscope. All of the members exhibit a nematic phase, and a smectic C phase can be observed for the homologues with a relatively long alkoxyl chain.

It is well-established that smectic liquid crystalline phases can be further subdivided into several modifications, denoted by the letters A through I.[1,2] Among these smectic modifications, the smectic C phase has recently attracted increasing attention because the chiral compound in the smectic C phase can exhibit a spontaneous polarization and because this phase is ferroelectric.[3] The most characteristic feature of the smectic C structure is that the long axes of the molecules are tilted with respect to the planes of the layer.

Much efforts have thus far been made in order to obtain new ferroelectric smectic liquid crystals.[4,7] Unfortunately, the definite relationship between the molecular structure and the smectic C liquid crystal formation has remained unknown, although certain guidelines exist regarding the features of the molecular structure that favor the smectic C-phase formation.[2] Therefore, it is of great importance to synthesize a new liquid crystalline homologous series which exhibits the smectic C phase in connection with an attempt to find a common structural feature for the smectic C formation. In this paper we wish to report two new liquid crystalline homologous series exhibiting the smectic C phase of *N*-[4-(4-alkoxybenzoyloxy)benzylidene]-4-butylanilines and their derivatives, which have a lateral hydroxylsubstituent.

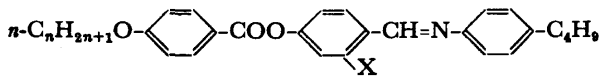

(n=1—8, X=H or OH)

Experimental

Materials. 4-Alkoxybenzoic acids obtained commercially are converted to acid chlorides by treatment with thionyl chloride in a benzene solution as the solvent. After the completion of the reaction, the excess of thionyl chloride and the solvent were removed; then the residue was distilled under reduced pressure. These acid chlorides were esterified by a reaction with 4-hydroxybenzaldehyde(2,4-dihydroxybenzaldehyde) in an ether solution including triethylamine. After they had then stood overnight, the triethylamine hydrochloride formed was removed by filtration, the ether was evaporated, and the solid residue was recrystallized from hexane. Finally, the substituted benzaldehydes thus obtained were coupled with 4-butylaniline by refluxing in an ethanol solution. The crude liquid crystals were purified by successive recrystallizations from ethanol.

Measurements. The liquid crystalline textures and the phase-transition temperatures were determined by means of a Nikon polarizing microscope equipped with a Mettler FP 52 microfurnace for sample temperature control. Checks on the transition temperatures were made using a Rigaku differential scanning calorimeter. Each sample was heated and cooled under a flow of nitrogen gas to prevent the sample from decomposing.

Results and Discussion

The transition temperatures and the liquid crystalline phases of the compounds without the lateral substituent are summarized in Table 1. All the members of this homologous series exhibit a nematic liquid crystal phase. As the length of alkoxyl chain is increased, smectic phases appear. This characteristic that the smectic phase is observed only for the homologues with a relatively long alkoxyl chain is not surprising, for the appearance of the smectic phase is not unusual; it has frequently been observed as the alkoxyl chain length increases in other homologous series of liquid crystalline materials.[8] Furthermore, it is worthwhile to state that, irrespective of the monotropic or enantiotropic transitions, the liquid crystalline phase transitions can be clearly detected by means of both the microscopic texture change and the thermal analysis.

Under polarizing microscopic observation, the smectic I phase of this homologous series exhibits broken fan-shaped or broken polygonal textures when formed on cooling from the nematic phase. These textures can be changed to a smectic schlieren texture by cover-slip displacement. All of the microscopic textures observed in the smectic I phase have been frequently found in the smectic C phase of other liquid

Table 1. Transition Temperatures of Liquid Crystals Without Lateral Hydroxyl Substituent (°C)

n	Smectic II	Smectic I(C)	Nematic	Isotropic
1			110	252
2			128	253
3			125	238
4			116	231
5	(77)	(99)	111	220
6	(76)	93	116	215
7	(77)	86	128	208
8	70	76	141	205

The figures in parentheses show the monotropic transition.

Table 2. Transition Temperatures of Liquid Crystals with Lateral Hydroxyl Substituent (°C)

n	Smectic C	Nematic	Isotropic
1		98	259
2		99	260
3		93	246
4		89	242
5		81	232
6	(77)	80	227
7	76	95	218
8	100	104	214

The figures in parentheses show the monotropic transition.

crystalline compounds and are typical textures of the smectic C phase.[2,9] In addition, it should be stressed that a homeotropic alignment, one of the textures typical of the smectic A phase, can not be observed at all in the smectic I phase. From these characteristic textures, it seems likely that the smectic I phase of this homologous series is the smectic C. On cooling from the smectic I phase to the smectic II phase, the smectic schlieren texture of the smectic C phase distinctly changes to a mosaic texture. However, the exact classification of this smectic II phase remains unclear because several different smectic modifications can exhibit a similar mosaic texture.[9]

Table 2 shows the phase transitions of another homologous series with the lateral substituent of the hydroxyl group. It is evident that, in this series, there also exist liquid crystalline phase transitions quite similar to those described above in the previous series without the lateral hydroxyl substituent. However, it should be kept in mind that the smectic II phase disappears in this homologous series; thus, no smectic polymorphism exists. Furthermore, it should be noted that a longer alkoxyl chain(C_6) is necessary for the smectic C phase to be formed compared with the previous series without the lateral substituent. It is also apparent from a comparison between the Tables 1 and 2 that the lateral hydroxyl substituent lowers the smectic C- nematic transition temperatures. These results indicate that the introduction of the hydroxyl group at the 2-position is unfavorable for the smectic formation and that it thus decreases the smectic C thermal stability. It seems that this behavior can be understood without difficulty by taking account of the change in the molecular structure. In general, it is well recognized that the lateral substituent exerts a full molecular-broadening influence, reducing the lateral intermolecular forces of attraction and thus lowering the smectic thermal stability.[10]

In addition, it is interesting to note the difference in the nematic-isotropic transition temperatures between the two series. The members with the lateral hydroxyl group exhibit higher nematic-isotropic transition temperatures than those without the lateral substituent. This result is quite likely to be associated with the strong intramolecular hydrogen bonding which has been found to occur for certain Schiff bases.[5,11] Such a hydrogen bonding will lead to a reduction in the rotational motions within the molecules and to a decrease in the twist from the noncoplanarity of a skeleton of *N*-(2-hydroxybenzylidene)aniline.[12,13] These effects are obviously favorable for the formation of the nematic structure; thus, they combine to give increased nematic thermal stability, i.e., an enhanced nematic-isotropic transition temperature.

In conclusion, we wish to point out that both the homologous series can exhibit the smectic C phase if the end alkoxyl chain is increased to a certain appropriate length.

References

1) H. Kelker and R. Hatz, "Handbook of Liquid Crystals," Verlag, Leipzig (1980).
2) G. W. Gray and J. W. Goodby, "Smectic Liquid Crystals," Leonard Hill, London (1984).
3) R. B. Meyer, L. Liebert, L. Strzelecki, and P. Keller, *J. Phys. (Paris) Lett.*, **36**, 69 (1975).
4) G. Decobert and J. C. Dubois, *Mol. Cryst. Liq. Cryst.*, **114**, 237 (1984).
5) A. Hallsby, M. Nilsson, and B. Otterholm, *Mol. Cryst. Liq. Cryst. (Lett.)*, **82**, 61 (1982).
6) P. Keller, *Mol. Cryst. Liq. Cryst. (Lett.)*, **102**, 295 (1984).
7) G. Decobert and J. C. Dubois, *Mol. Cryst. Liq. Cryst.*, **114**, 237 (1984).
8) D. Demus, H, Demus, and H. Zaschke, "Fluessige Kristalle in Tabellen," Verlag, Leipzig (1974).
9) H. Sackmann and D. Demus, *Mol. Cryst. Liq. Cryst.*, **21**, 239 (1973).
10) G. W. Gray, "Liquid Crystals and Plastic Crystals," ed by G. W. Gray and P. A. Winsor, Ellis Horwood, Chichester (1974), Vol. 1, p.103.
11) B. I. Ostrovskii, A. Z. Rabinovich, A. S. Sonin, E. L. Sorkin, B. A. Strukov, and S. A. Taraskin, *Ferroelectrics*, **24**, 309 (1980).
12) H. B. Buergi and J. D. Dunitz, *Helv. Chim. Acta*, **53**, 1747 (1970).
13) J. van der Veen and A. H. Grobben, *Mol. Cryst. Liq. Cryst.*, **15**, 239 (1971).

Coordination-Site Exchange of Azaheterocyclic Ligands in Five-Coordinate Palladium(II) Complexes. Bis(4,7-dimethyl-1,10-phenanthroline)(triphenylphosphine)palladium(II) Tetrafluoroborate and the 4,7-Diphenyl Derivative

Shinsaku YAMAZAKI*
Chemistry Laboratory, Kochi Gakuen College,
292 Asahi Tenjin-cho, Kochi 780
(Received September 5, 1986)

Synopsis. Variable-Temperature ^{1}H NMR suggests that the fluxional motion of a potentially five-coordinate complex $[Pd(PPh_3)(4,7\text{-}R_2\text{-}phen)_2][BF_4]_2$ (R=Me, Ph) is frozen at lower temperatures, where the complex is in a rigid configuration (an unusual trigonal bipyramid). The fluxional motion is explained by two synchronous rearrangement systems, and an activation parameter, ΔG^*, for the site exchange is given.

For the ligand rearrangement systems of five-coordinate Pd(II) complexes,[1-6] most of the isolated complexes determined by means of X-ray diffraction and the discernible species in a solution detected by means of the spectra have been found to be in the form of a square pyramid, and their dynamic behavior in solution appears to proceed via the transition state of a trigonal bipyramid.

Previously, the crystal structure of the potentially five-coordinate Pd(II) complex $[PdCl(PPh_3)_2(phen)]^+$ has been described by the present author[6] as a very distorted square pyramid in which one nitrogen atom from the phen occupies the apical position, with a relatively long Pd–N distance (the two phosphines are mutually trans). Its solution structure[7] with a stereochemical non-rigidity, which has been explained by an oscillation of the apical phen, interestingly seems to be rather close to a square planar structure, with an anamalous unidentate phen. It should, however, be noticed that an analogous Pt(II) complex $[PtCl(PEt_3]_2(phen)]^+$,[3] with two phosphines mutually cis displays no dissociation processes in spite of the fact that the phen bite is loosened, in contrast to the Pd(II) complex.

This paper will deal with the dynamic motion of $[Pd(PPh_3)(phen)_2][BF_4]_2$ (R=Me, Ph) as evidenced by variable-temperature ^{1}H NMR spectroscopy.

Experimental

Preparation of Complexes-$[Pd(PPh_3)(4,7\text{-}Me_2\text{-}phen)_2][BF_4]_2$. This complex was prepared by a procedure analogous to that used for the corresponding phen complex.[8] Found: C, 56.93; H, 3.89; N, 5.40%. Calcd for $C_{46}H_{39}N_4B_2F_8PPd$: C, 57.62; H, 4.10; N, 5.84%. Conductance (acetone solution of ca. 10^{-3} M.): Λ_M, 288 Ω^{-1} cm^2 mol^{-1}. ^{1}H NMR ($CDCl_3$). vide infra.

$[Pd(PPh_3)(4,7\text{-}Ph_2\text{-}phen)_2][BF_4]_2$. This complex was prepared as above. Found: C, 64.86; H, 4.16; N, 4.36%. Calcd for $C_{69}H_{53}N_4B_2F_8OPPd$: C, 65.50; H, 4.22; N, 4.42%. IR (nujol mulls): ν(CO)(an acetone of solvation), 1710 cm^{-1}. ^{1}H NMR ($CDCl_3$): vide infra. Conductance (acetone solution of ca. 7.8×10^{-4} M.): Λ_M, 203 Ω^{-1} cm^2 mol^{-1}.

Physical Measurements. The conductivities were measured using a Denki Kagaku Keiki AO-6 instrument in dried acetone solutions. The lower-temperature ^{1}H NMR spectra were recorded, using JEOL FX-90A (89.55 MHz) in the region of 193—303 K in $CDCl_3$, at the NMG Applied Research Center of JEOL Ltd., Akishima, Tokyo.

Results and Discussion

The ^{1}H NMR spectra of $[Pd(PPh_3)(4,7\text{-}R_2\text{-}phen)_2][BF_4]_2$ (R=Me, Ph), which are dependent on the temperature, are shown in Fig. 1.

The lower-temperature ^{1}H NMR of the complex with R=H, as has been described elsewhere,[7] shows that its dynamic motion is not effectively frozen; only resonance broardening and overlapping were observed over a wide range of temperatures (173—303 K). Therefore, 4,7-Me_2 and Ph_2-phen were used as azaheterocyclic ligands, because a relatively simple spectrum with a small number of coupling patterns can then be expected.

At ambient temperatures, $[Pd(PPh_3)(4,7\text{-}R_2\text{-}phen)_2]^{2+}$ is stereochemically non-rigid, but it becomes

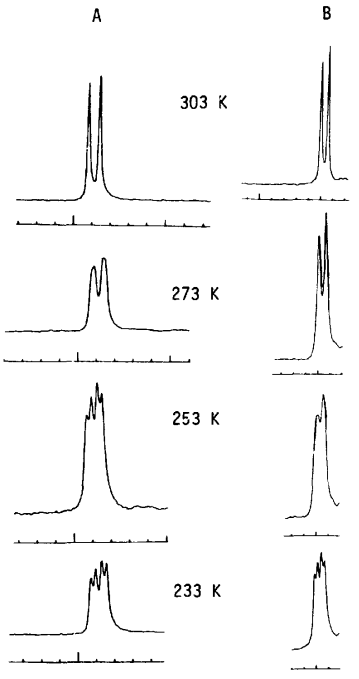

Fig. 1. Variable-temperature ^{1}H NMR (resonances due to 2,9-protons) of: A, $[Pd(PPh_3)(4,7\text{-}Ph_2\text{-}phen)_2][BF_4]_2$ B, $[Pd(PPh_3)(4,7\text{-}Me_2\text{-}phen)_2][BF_4]_2$ in $CDCl_3$.

Table 1. Temperature-Dependent ^{1}H NMR Data of $[Pd(PPh_3)(4,7\text{-}R_2\text{-}phen)_2]^{2+}$ (R=Me, Ph)

Complex	T/°K	δ/ppm[b]	$\delta\nu$[c]	ΔG^*(kcal mol^{-1})[d]
R=Me	303	8.472		
	253(T_c)[a]	8.477		
	233	8.477 8.450	2.415	13.88
R=Ph	303	8.892		
	273(T_c)[a]	8.892		
	253	8.902 8.872	2.635	14.97

a) Coalescence temperature. b) Chemical shifts due to 2,9-protons, which are relative to Me_4Si at δ 0.00. c) Observed spacing between the two resonances due to 2 and 9-H of the azaheterocyclic ligand. d) Calculated by the use of $\Delta G^*/RT_c = 22.96 + \ln(T_c/\delta\nu)$,[10] where ΔG^* is an activation parameter for the site exchange of the azaheterocyclic ligand.

stereochemically rigid at lower temperatures. At 253 K, resonances due to 2,9-H in the 4,7-Ph_2-phen complex (Fig. 1A) were observed as two separate signals, each with coupling with the 3,8-H of the azaheterocyclic rings. The NMR spectrum at this temperature is consistent with the formation of an unsymmetrical structure (stereochemically rigid) in which two 4,7-Ph_2-phen are equivalent, while each azaheterocyclic ligand is unsymmetrically bound to the metal. Only a trigonal bipyramidal structure, with its axial positions occupied with nitrogen atoms, fits this requirement. Above 253 K, the resonance lines due to 2,9-H of the 4,7-Ph_2-phen complex become broadened, and at 273 K they coalesce into one resonance. The lines sharpen with an increase in the temperature. The ^{1}H NMR of the corresponding 4,7-Me_2-phen complex, which is dependent on the temperature, shows a pattern analogous to that observed for the 4,7-Ph_2-phen complex.

Even at lower temperatures, resonance patterns due to the CH_3 group (4,7-Me_2-phen complex) and 5,6-H (both complexes) were observed as a single resonance. These observations may not be unusual, for the 4,7-CH_3 and 5,6-H of the phen derivative may be too distant from the metal to be magnetically influenced.[9]

These NMR data are consistent with a site exchange between two nitrogen atoms of the azaheterocyclic ligand, and the fluxional motion may well be explained by means of two synchronous rearrangement systems: One a twist motion from a trigonal bipyramid to a tetragonal pyramid, and the other a concurrent oscillation of the apical 4,7-R_2-phen, which may average the magnetical environment around its two halves,[11] as is indicated in Scheme 1.

The activation parameters (ΔG^*) for the site exchange were estimated to be 13.9 kcal mol^{-1} for the 4,7-Me_2-phen complex and 15.0 kcal mol^{-1} for the 4,7-Ph_2-phen complex. The other activation parameters could not be obtained because of the relatively large $J/\delta\nu(\approx 2)$ ratio.

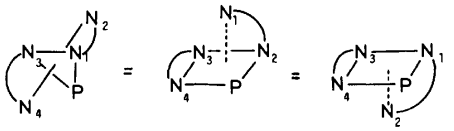

Scheme 1.

Although the conductivity data indicate that the association of the BF_4^- anion does not occur, it is still uncertain whether or not the fluxional motion of the complexes proceeds via dissociation processes. It should, however, be noticed that the fluxional behaviour of an analogous Pt(II) complex $[Pt(PPh_3)(phen)_2][BF_4]_2$ does not proceeds via a dissociation processes; to its ^{13}C NMR spectrum shows ^{195}Pt-C coupling at the 2,9-positions of the azaheterocyclic ligand.[12]

For the fluxional motion of $[Pd(PPh_3)(4,7\text{-}R_2\text{-}phen)_2]^{2+}$, the trigonal bipyramid is unusually the ground state, while the square pyramid is an intermediate. These findings rather resemble the dissociation processes proposed for $[Ni(CN)_2(PMe_3)_3]$,[13] the intermediate of which has been supposed to be square pyramid. In most of the five-coordinate Pt(II) and Pd(II) complexes {i.e. $[PdCl_2(PMe_3)_3]$[4] and $[Pt(CN)(phen)_2][NO_3]$[2]}, the fluxional motion has, on the other hand, been supposed to proceed via the transition state or the intermediate of the trigonal bipyramid.

The author is grateful to Mr. Hiroaki Utsumi (JEOL, LTD.) for obtaining the lower-temperature ^{1}H NMR spectra. This work was partially supported by a Grant-in-Aid for Scientific Research (No. 540402) from the Ministry of Education, Science and Culture.

References

1) W. J. Louw, D. J. A. Waal, and G. J. Kruger, *J. Chem. Soc., Dalton Trans.*, **1976**, 2364.
2) O. Wernberg and A. J. Hazell, *J. Chem. Soc., Dalton Trans.*, **1980**, 973.
3) G. W. Bushnell, K. R. Dixon, and M. A. Khan, *Can. J. Chem.*, **52**, 1367 (1974).
4) R. Favez and R. Roulet, *Inorg. Chem.*, **20**, 1598 (1981).
5) R. Favez, R. Roulet, A. A. Pinkerton, and D. Schwarzenbach, *Inorg. Chem.*, **19**, 1356 (1980).
6) Z. Taira and S. Yamazaki, *Bull. Chem. Soc. Jpn.*, **59**, 649 (1986).
7) S. Yamazaki, *Polyhedron*, **4**, 1915 (1985).
8) S. Yamazaki, *Inorg. Chem.*, **21**, 1638 (1982).
9) S. Yamazaki, *Polyhedron*, **6**, 1183 (1986).
10) R. J. Abraham and P. Loftus, "Proton and Carbon-13 NMR Spectroscopy - An Integrated Approach," Heyden, London (1978), Chap. 7.
11) S. Okeya, T. Miyamoto, S. Ooi, Y. Nakamura, and S. Kawaguchi, *Bull. Chem. Soc. Jpn.*, **57**, 395 (1984).
12) Unpublished results.
13) P. F. Meier, A. E. Merbach, M. Dartiguenava, and Y. Dartiguenava, *Inorg. Chem.*, **18**, 610 (1979).

Bis[perfluoro(1,1-dimethylbutyl)] Trisulfide from the Cesium Fluoride-Assisted Reaction of Hexafluoropropene Dimers with Disulfur Dichloride

Hitomi SUZUKI,* Hiroshi SATAKE, Hidemitsu UNO, and Hiroaki SHIMIZU†
Department of Chemistry, Faculty of Science, Advanced Instrumentation Center for Chemical Analysis, Ehime University, Bunkyo-cho, Matsuyama 790
†Central Research Laboratory, NEOS Company, Ltd., Oike-machi, Kosei-cho, Koga-gun, Shiga 502-32
(Received August 27, 1986)

Synopsis. Perfluoro(1,1-dimethylbutanide) anion generated from hexafluoropropene dimers and cesium fluoride in *N,N*-dimethylformamide, reacts with disulfur dichloride to give the title trisulfide as the predominant product.

Compounds derived from perfluorinated hydrocarbons are characterized by chemical inertness and thermal stability, which justify their wide applications as hydraulic liquids, heat-transfer mediums, lubricants, sealants, protective coatings, etc. As part of our programme to seek perfluoroalkyl compounds of potential uses as dielectric fluids, we attempted to prepare bis[perfluoro(1,1-dimethylbutyl)] disulfide (**2**) by reacting disulfur dichloride with the anion generated from perfluorinated 2-methyl-2-pentene (**1a**) and cesium fluoride in *N,N*-dimethylformamide (*DMF*). Rather surprisingly, the main product was not the expected disulfide but bis[perfluoro(1,1-dimethylbutyl)] trisulfide (**3**) accompanied by small amounts of disulfide **2** and tetrasulfide **4**.

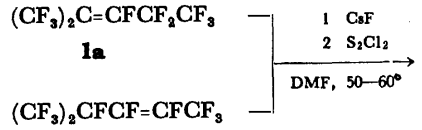

$[CF_3CF_2CF_2(CF_3)_2C]_2S_n$

2: $n=2$; **3**: $n=3$; **4**: $n=4$

Trisulfide **3** was identified by elemental analysis, ^{19}F NMR and high resolution mass spectra. It is a colorless liquid of low viscosity, which can be distilled without decomposition under reduced pressure and lacks unpleasant odor characteristic of organic sulfides. Compound **3** resists oxidation by hydrogen peroxide, potassium permanganate, and sodium periodate, but readily decomposes by the action of hydride reagents to form a complex product mixture. In spite of the difference in structure, perfluoro(4-methyl-2-pentene) (**1b**) afforded the same product, although perfluoro-olefin **1a** reacted more easily to produce **3** in a better yield. Hexafluoropropene dimer **1b** is known to isomerize into the thermodynamically more stable isomer **1a** in the presence of fluoride ion.[1] The reaction should be conducted in the presence of an excess of perfluoro(1,1-dimethylbutanide) anion **5**; otherwise an extensive liberation of sulfur occurs on addition of disulfur dichloride, leading to a poor yield of perfluoroalkyl polysulfides. Sulfur dichloride was not effective as a sulfurizing agent and led to a low yield of trisulfide as the main sulfur-containing product (≈10%). Mass spectral inspection revealed a slight incorporation of chlorine into the product.

Although the reason for preferential formation of trisulfide is not clear at present, a possible reaction passway is shown in Scheme 1.

Cleavage of a disulfide bond of **2** with fluoride ion followed by capture of the anion **6** with disulfur

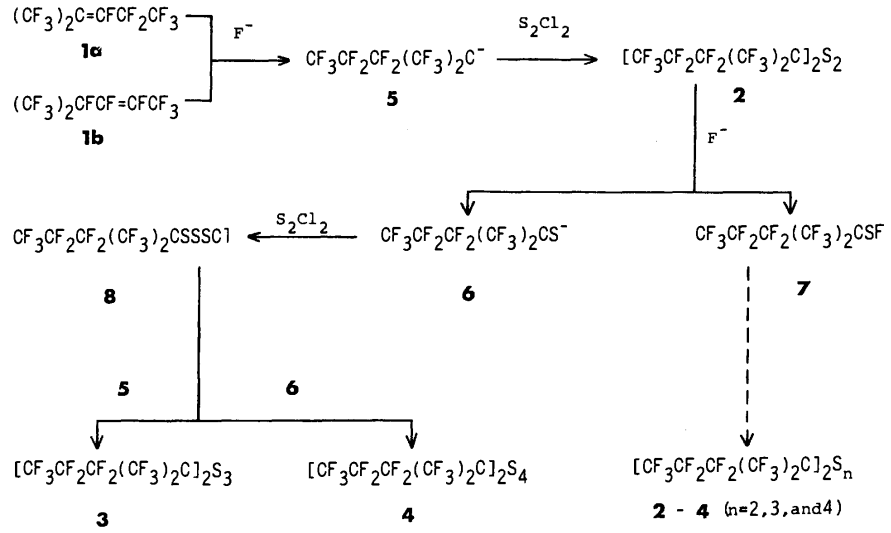

Scheme 1.

dichloride affords **8**, which undergoes nucleophilic attack of anions **5** or **6** on the sulfur atom to yield oligosulfides **3** and **4**. Further fission of a sulfur-sulfur bond of **3** or **4** and subsequent trap of the resulting anionic species with sulfenyl fluoride **7** would lead to the polysulfides **2**—**4**.

Only a few descriptions of the formation of perfluoroalkyl tri- and tetrasulfides have been reported so far. They may be obtained as a by-product when perfluoroalkyl iodides of short chain length are heated with sulfur at 220—310 °C in a sealed tube or when carbon disulfide is treated with iodine pentafluoride at 195 °C in an autoclave.[2,3] Reaction of perfluoro-2-butene with potassium fluoride and elementary sulfur in sulfolane at 180 °C gives a low yield of trisulfide among other products.[4] Decomposition of azoperfluoroalkane or hexafluoroethane in the presence of sulfur vapor also forms trisulfides.[5,6] Reactions of perfluoro-olefins **1a** and **1b** with thiols or thiolate ions are known to lead to a mixture of several vinylic sulfides[7] which, of course, lack chemical inertness necessary for our purposes. Thus, our results present the first example of the preparation of perfluoroalkyl trisulfide from fluoro-olefins under mild liquid phase conditions.

Experimental

Perfluoro(2-methyl-2-pentene) (**1a**) and perfluoro(4-methyl-2-pentene) (**1b**) are commercial products available from NEOS Co. Ltd (Kano-cho, Chuo-ku, Kobe, Japan). Disulfur dichloride was purified by fractional distillation prior to use. Cesium fluoride was used as received.

Reaction of Perfluoro(2-methyl-2-pentene) with Disulfur Dichloride. A mixture of cesium fluoride (3.03 g, 20 mmol), perfluoro(2-methyl-2-pentene) (**1a**; 7.80 g, 26 mmol), and dry *DMF* (4 ml) was stirred at 50—60 °C for 1 h under nitrogen. Color gradually turned deep red. Then disulfur dichloride (1.35 g, 10 mmol; redistilled prior to use) in the same solvent (2 ml) was added dropwise during the course of 0.5 h. After addition, the mixture was kept with stirring at this temperature for 12 h and then diluted with water (15 ml). The resulting cloudy solution was filtered through a thin layer of Celite to remove free sulfur. Insoluble substance was washed with ether and the filtrate was extracted with the same solvent. The extract and washings were combined, dried with sodium sulfate, and evaporated. The residue was distilled in vacuo by Kugelrohr to give crude **3** containing about ten percent of disulfide (*m/z* 702 (M^+), 383 ($M^+-C_6F_{13}$)) and tetrasulfide (*m/z* 766 (M^+), 447 ($M^+-C_6F_{13}$)). Although these impurities tenaciously clung to **3**, they could be mostly removed by repeated chromatography on silica gel (Wako Gel C-200) using hexane as eluent. Further purification of **3** was made on a preparative liquid chromatograph (LC-08 Model, Japan Analytical Industry Co., Ltd). Isolated yield, 3.66 g (50% based on CsF). Bp 42—43 °C/0.08 mmHg (Kugelrohr) (1 mmHg=133.322 Pa). MS (20 eV) *m/z* (rel intensity) 734 (M^+; 40), 415 (100), and 181 (24); ^{19}F NMR ($CFCl_3$) δ=60.1 (12F, quint, CF_3), 80.3 (6F, t, CF_3), 103.7 (4F, m, CF_2), and 121.4 (4F, m, CF_2); IR (neat) 1335, 1200—1260 (vs), 1115, 965, 820, 735, and 710 cm^{-1}. Found: C, 19.66; F, 67.00%. Calcd for $C_{12}F_{26}S_3$: C, 19.63; F, 67.27%.

References

1) N. Ishikawa and A. Nagashima, *Nippon Kagaku Kaishi*, **1975**, 1439.
2) M. Hauptsheim and A. V, Grosse, *J. Am. Chem. Soc.*, **73**, 5461 (1951); G. R. A. Brandt, H. J. Emeléus, and R. N. Haszeldine, *J. Chem. Soc.*, **1952**, 2198.
3) R. N. Haszeldine and J. M. Kidd, *J. Chem. Soc.*, **1953**, 3219; *ibid.*, **1955**, 3871.
4) D. J. Burton and Y. Inouye, *Chem. Lett.*, **1982**, 201.
5) W. J. Chambers, C. W. Tullock, and D. D. Coffman, *J. Am. Chem. Soc.*, **84**, 2337 (1962).
6) T. Yasumura and R. J. Lagow, *Inorg. Chem.*, **17**, 3108 (1978).
7) N. Ishikawa and M. Maruta, *Chem. Lett.*, **1977**, 967.

Synthesis of Bromoacetyl Derivatives by Use of Tetrabutylammonium Tribromide

Shoji KAJIGAESHI,* Takaaki KAKINAMI,† Tsuyoshi OKAMOTO,† and Shizuo FUJISAKI
Department of Industrial Chemistry, Faculty of Engineering, Yamaguchi University, Tokiwadai, Ube 755
†Department of Industrial Chemistry, Ube Technical College, Tokiwadai, Ube 755
(Received October 1, 1986)

Synopsis. Orange crystalline tetrabutylammonium tribromide was prepared using a simple method. The reaction of acetyl derivatives with an equimolar amount of the tribromide in dichloromethane–methanol at room temperature gave bromoacetyl derivatives in fairly good yields.

In general, bromoacetyl derivatives **1** have been synthesized by a reaction of acetyl derivatives **2** with bromine in an appropriate solvent such as water, chloroform, carbon tetrachloride, acetic acid or *N,N*-dimethylformamide.[1] The reagents, copper(II) bromide,[2] 1,4-dioxane bromooxonium bromide,[3] tribromoacetophenone,[4] and *N*-bromosaccharin,[5] have been used as brominating agents instead of bromine for **2** having unsaturated bond or functional groups (hydroxyl group, enol ester, acetal etc.) which should react promptly with bromine or hydrobromic acid. It must be a merit that these reagents can be handled more easily than liquid bromine, because of their solid character.

Furthermore, the solid reagents, organic ammonium tribromides, such as pyridinium tribromide,[6] phenyltrimethylammonium tribromide,[7,8] and tetramethylammonium tribromide,[9] have also been used as selective brominating agents. Recently, Berthelot et al.[10] have shown that tetrabutylammonium tribromide (TBA Br_3) can be used as a brominating agent for the addition of bromine to the double bonds of alkenes and for the selective bromination of acetals. In this paper, we wish to report a facile synthetic procedure of **1** from **2** by the use of TBA Br_3.

Table 1. Bromoacetyl Derivatives **1** from Acetyl Derivatives **2**

	Starting material **2**	Product **1**	Reaction time/h	Yield[a] %	IR(KBr) νCO cm^{-1}	Mp (θm/°C) or Bp (θb/°C)(Torr) found	reported
a	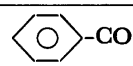	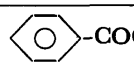	1	78	1695	49—50	50[13]
b	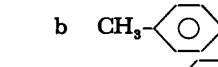	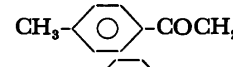	1	83	1695	45—48	48—50[14]
c	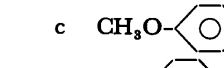	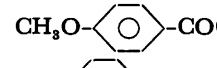	1	79	1695	68—69	73[15]
d	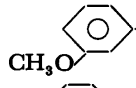	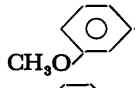	1	80	1700	58—60	62—63[16]
e	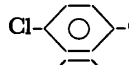	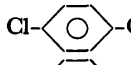	3	85	1700	97—97.5	96—96.5[17]
f	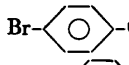	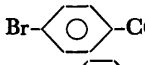	3	86	1700	107.5—108	109—109.5[18]
g	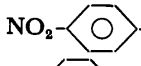	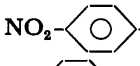	5	75	1705	96—96.5	98[19]
h	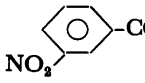	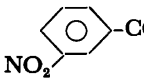	5	71	1705	88—90	96[20]
i	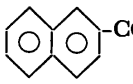		2	75	1700	81—82	82.5—83.5[21]
j	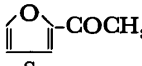	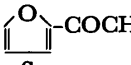	2	85	1675	34.5—36	—
k	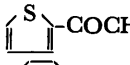	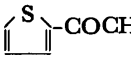	2	80	1665	35—35	—
l	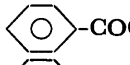	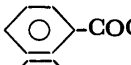	1	99	1695	230—231/760	245—250/[22] 760
m	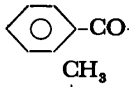	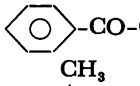	1	88	1695	49—52	54—55[23]
n	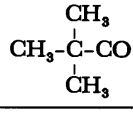	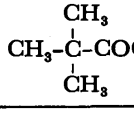	3	90	1725	129—130/760	—

a) Yield of isolated product. 1 Torr = 133.322 Pa.

Results and Discussion

TBA Br_3 have usually been prepared from tetrabutylammonium bromide and bromine in carbon tetrachloride.[11] We readily prepared TBA Br_3 by the addition of hydrobromic acid to an aqueous solution of tetrabutylammonium bromide and sodium bromate at room temperature in quantitative yield.

The reaction of **2** with an equimolecular amount of TBA Br_3 in a dichloromethane–methanol solution for 1—5 h at room temperature readily gave **1** containing a small amount of dibromoacetyl derivatives which could easily be removed by recrystallization. The results are summarized in the Table 1.

$$\underset{\mathbf{2}}{R\text{-}COCH_3} \xrightarrow[\text{in } CH_2Cl_2\text{-}CH_3OH \text{ rt}]{(C_4H_9)_4N^+Br_3^-} \underset{\mathbf{1}}{RCOCH_2Br}$$

These reactions should proceed via an ionic species rather than radical ones. In fact, the bromination of acetophenone with TBA Br_3 in dichloromethane, dichloromethane-containing peroxides, and dichloromethane-containing a free radical inhibitor (*m*-dinitrobenzene) all proceeded at the same rate. As shown by Marquet et al.[12] for the bromination of acetophenone with phenyltrimethylammonium tribromide, the mechanism of bromination of **2** with TBA Br_3, (it is suggested) is also considered to be a slow-stage enolization of the ketone and a fast-stage bromination.

We emphasize that the synthetic procedure for bromoacetyl derivatives will be a highly useful method because of its ease, simplicity, and mildness of conditions.

Experimental

Tetrabutylammonium Tribromide (TBA Br_3). To a solution of tetrabutylammonium bromide (9.7 g, 30 mmol) and sodium bromate (1.50 g, 10 mmol) in water (60 ml) was added dropwise hydrobromic acid (47%, 7 ml) under stirring at room temperature. After the mixture was stirred for a few minutes, the immediate orange precipitate was filtered and recrystallized from ether–dichloromethane (1:1) to give TBA Br_3 as orange crystals; yield 13.7 g (95%); mp 74—75 °C (lit,[11] mp 70—72 °C). Found: Br, 50.08%. Calcd for $C_{16}H_{36}NBr_3$: Br, 49.71%.

Phenacyl Bromide (1a). As a general procedure, the preparation of **1a** was as follows: To a solution of acetophenone (0.5 g, 4.16 mmol) in dichloromethane (50 ml)–methanol (20 ml) was added TBA Br_3 (2.2 g, 4.58 mmol) at room temperature. The mixture was stirred for 1 h until a decoloration of the orange solution took place. The solvent was then distilled and the obtained precipitate was extracted with ether (30 ml×4). The ether layer was dried with magnesium sulfate and evaporated in vacuo to give a residue which was recrystallized from ethanol–water (1:2) affording as colorless needles; yield 0.65 g (78%); mp 49—50 °C (lit,[13] mp 50 °C).

Bromomethyl 2-Furyl Ketone (1j). Compound **1j** was prepared similarly: Yield 85%; colorless crystals; mp 34.5—36 °C; IR (KBr) 1675 cm^{-1}; ^1H NMR ($CDCl_3$) δ=4.30 (2H, s, CH_2Br), 6.53 (1H, dd, J=1.8 and 3.6 Hz, O-CH=C<u>H</u>-CH=), 7.26 (1H, d, J=3.6 Hz, O-CH=CH-C<u>H</u>=), and 7.56 (1H, d, J=1.8 Hz, O-C<u>H</u>=CH-CH=); MS *m/z* 189 and 191 (M^+). Found: Br, 41.88%. Calcd for $C_6H_5O_2Br$: Br, 42.27%.

Bromomethyl Thienyl Ketone (1k). Compound **1k** was prepared similarly: Yield 80%; colorless crystals; mp 33—35 °C; IR (KBr) 1665 cm^{-1}; ^1H NMR ($CDCl_3$) δ=4.40 (2H, s, CH_2Br), 7.13 (1H, dd, J=4.9 and 4.0 Hz, S-CH=C<u>H</u>-CH=), 7.70 (1H, d, J=4.9 Hz, S-C<u>H</u>=CH-CH=), and 7.80 (1H, d, J=4.0 Hz, S-CH=CH-C<u>H</u>=); MS *m/z* 205 and 207 (M^+).

Bromomethyl *t*-Butyl Ketone (1n). Compound **1n** was prepared similarly: Yield 90%; colorless liquid; bp 129—130 °C/760 mmHg (1 mmHg=133.322 Pa); IR (KBr) 1725 cm^{-1}; ^1H NMR ($CDCl_3$) δ=1.23 (9H, s, $C(CH_3)_3$), and 4.17 (2H, s, CH_2Br); MS *m/z* 179 and 181 (M^+). Found: Br, 44.79%. Calcd for $C_6H_{11}OBr$: Br, 44.59%.

References

1) Synthetic examples are illustrated as follows: P. A. Levene, *Org. Synth.*, **II**, 88 (1943); C. Rappe, *ibid.*, **53**, 123 (1973); W. D. Langley, *ibid.*, **I**, 127 (1941); J. J. Klingenberg, *ibid.*, **IV**, 110 (1963); R. M. Cowper and L. H. Davidson, *ibid.*, **II**, 480 (1943); D. E. Pearson, H. W. Pope, and W. W. Hargrove, *ibid.*, **V**, 117 (1973).

2) L. C. King and G. K. Ostrum, *J. Org. Chem.*, **29**, 3459 (1964).

3) L. A. Yanovskaya, A. P. Terentév, and L. I. Belen'kii, *J. Gen. Chem.*, **22**, 1594 (1952); *Chem. Abstr.*, **47**, 8032 (1953).

4) F. Kröhnke and K. Ellegast, *Chem. Ber.*, **86**, 1556 (1953).

5) E. I. Sanchez and M. J. Fumarola, *J. Org. Chem.*, **47**, 1588 (1982).

6) L. F. Fieser and M. Fieser, "Reagents for Organic Synthesis," John Wiley and Sons, New York (1967), Vol. 1, p. 967.

7) A. Marquet and J. Jacques, *Tetrahedron Lett.*, **1959**, 24.

8) S. Visweswariah, G. Prakash, V. Bhushan, and S. Chandrasekaran, *Synthesis*, **1982**, 309.

9) M. Avramoff, J. Weiss, and O. Schachter, *J. Org. Chem.*, **28**, 3256 (1963).

10) M. Fournier, F. Fournier, and J. Berthelot, *Bull. Soc. Chim. Belg.*, **93**, 157 (1984).

11) R. E. Buckles, A. I. Popov, W. F. Zelezny, and R. J. Smith, *J. Am. Chem. Soc.*, **73**, 4525 (1951).

12) A. Marquet, J. Jacques, and B. Tchoubar, *Bull. Soc. Chim. Fr.*, **1965**, 511.

13) J. B. Rather and E. E. Reid, *J. Am. Chem. Soc.*, **41**, 77 (1919).

14) F. Kunckell, *Ber.*, **30**, 577 (1897).

15) F. Kunckell and W. Scheven, *Ber.*, **31**, 173 (1898).

16) R. Fuchs, *J. Am. Chem. Soc.*, **78**, 5612 (1956).

17) A. Collet, *C. R. Acad. Sci.*, **125**, 718 (1897).

18) A. Collet, *Bull. Soc. Chim. Fr.*, [3] **21**, 67 (1899).

19) C. Engler and O. Zielke, *Ber.*, **22**, 204 (1889).

20) H. Hunnius, *Ber.*, **10**, 2008 (1877).

21) I. Rabcewicz-Zubkowski, *Roczniki Chem.*, **9**, 538; *Chem. Abstr.*, **24**, 106 (1930).

22) K. Auwev, *Ber.*, **50**, 1177 (1917).

23) E. Knoevenagel, *Ber.*, **21**, 1355 (1888).

A Convenient Synthesis of Hypotensive (±)-Oudenone

Takashi SAKAI, Kohji IWATA, Masanori UTAKA, and Akira TAKEDA*
Department of Synthetic Chemistry, School of Engineering, Okayama University, Tsushima, Okayama 700
(Received September 22, 1986)

Synopsis. (±)-Oudenone, 2-(tetrahydro-5-propyl-2-furylidene)-1,3-cyclopentanedione, was conveniently synthesized by BF_3-catalyzed acylation of 1,3-cyclopentanedione with 4-chloroheptanoic anhydride and subsequent cyclization with triethylamine in a 36% overall yield.

Oudenone (**1a**) was isolated from a culture filtrate of *Oudemansiella radicata* by the group of Ohno and Umezawa[1] and found to exhibit significant hypotensive effect against spontaneously hypertensive rats due to inhibition of tyrosine hydroxylase.[2] Since it was synthesized initially in relation with the structural

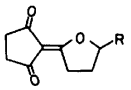

1a R=n-Pr (Oudenone)
1b R=Et

elucidation,[3] several synthetic methods[4-6] have been reported. Recently, Bates et al.[7] have reported a new route to (±)-**1a** which involves the acid-catalyzed C-alkylation of 1,3-cyclopentanedione (**5**) with 5-propyltetrahydro-2-furanol to give dihydrooudenone

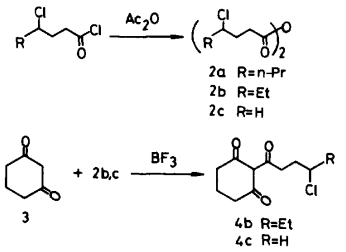

2a R=n-Pr
2b R=Et
2c R=H

3

4b R=Et
4c R=H

Scheme 1.

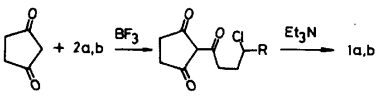

5

6a R=n-Pr
6b R=Et

Scheme 2.

Table 1. Acylation of 1,3-Cyclohexanedione (**3**) with Anhydrides **2b, c**

Entry	Anhydride (R)	Method[a]	Conditions °C/h	Product (Yield/%)
1	**2c** (H)	A	110/12	**4c** (24)
2	**2c** (H)	B	90/12	**4c** (34)
3	**2c** (H)	C	95/12	**4c** (46)
4	**2b** (Et)	B	110/12	**4b** (17)
5	**2b** (Et)	C	95/12	**4b** (36)

a) A: BF_3·OEt_2, B: BF_3 in CH_2Cl_2–AcOEt, C: BF_3.

and subsequent introduction of C–C double bond via phenylselenenylation.

We report here a convenient two-step synthesis of (±)-**1a** which is characterized by boron trifluoride (BF_3)-catalyzed acylation of **5** with 4-chloroheptanoic anhydride (**2a**) to give 2-(4-chloroheptanoyl)-1,3-cyclopentanedione (**6a**). Subsequent cyclization of **6a** by triethylamine gave (±)-**1a** in a 36% overall yield (Scheme 2). While the acylation of **5** would be effective not only for the straightforward synthesis of (±)-**1a** but also for the synthesis of other biologically active compounds,[8] the reaction has not been well established.[9]

Manvik et al.[10] reported that BF_3 was effective for the acylation of carbon atom α to carbonyl group with acid anhydride. Leucht[11] used the procedure for the C-acylation of 3-alkyl-1,2,4-cyclopentanetrione. We applied the method to the present synthesis. In the first place, we examined the reaction conditions for the BF_3-catalyzed acylation of readily available 1,3-cyclohexanedione (**3**) with 4-chloroalkanoic anhydrides **2b, c** as shown in Scheme 1. Anhydrides **2a—c** were easily prepared by heating the corresponding acid chloride[12] in acetic anhydride. As shown in Table 1, the acylation of **3** with **2c** was examined as a typical example by using three conditions: a) use of BF_3·OEt_2 (Entry 1); b) addition of a mixture of **3** and **2c** to CH_2Cl_2–AcOEt after saturation with BF_3[11] (Entry 2), and c) introduction of BF_3 to a mixture of **3** and **2c**,[11] which gave the best result (Entry 3). The use of **2b** slightly decreased the yield of **4b** (Entries 4 and 5).

The BF_3-catalyzed acylation of **5** with **2a** was carried out by using the conditions C of Table 1 to give **6a** in a 74% yield (Scheme 2). Fortunately, the yield was approximately doubled as compared with that of **4b**. Compound **6a** was readily cyclized to (±)-**1a** by the treatment with triethylamine at 0 °C in a 49% yield after recrystallization. In a similar way, oudenone homolog (±)-**1b**[5b] was synthesized via **6b** in a 31% overall yield.

Experimental

Melting points were determined by a Yamato Model MP-21 apparatus and uncorrected. Infrared spectra were taken on a JASCO A-102 spectrometer. ^1H NMR spectra (60 MHz) were measured with a Hitachi R-24 spectrometer. ^{13}C NMR (25 MHz) spectra were taken on a JEOL FX-100 spectrometer. Column chromatography was performed through silica gel (Wakogel C-200). Preparative TLC was done on silica gel (Kieselgel 60 PF_{254}).

Typical Reaction for the Preparation of Anhydrides 2a—c. 4-Chloroheptanoic Anhydride (2a). A mixture of 4-chloroheptanoyl chloride[12] (4.89 g, 26.7 mmol) and acetic anhydride (9 ml, 95.2 mmol) was placed in a reaction vessel

connected with a distillation apparatus and heated at 95 °C for 3 h, removing the resulting acetyl chloride continuously. The reaction mixture was then distilled to give **2a** (2.69 g, 65% yield): bp 120—156 °C (1.0 mmHg) (1 mmHg=133.322 Pa); IR (neat) 1820, 1753, 1045 cm^{-1}; ^1H NMR (CCl_4) δ=0.97 (6H, t, J=8 Hz), 1.20—2.50 (12H, m), 2.65 (4H, t, J=8 Hz), 3.88 (2H, m). Anal. ($C_{14}H_{24}O_3Cl_2$) C, H.

4-Chlorohexanoic Anhydride (2b): Yield 71%; bp 135—143 °C (2 mmHg); IR (neat) 1815, 1745, 1045 cm^{-1}; ^1H NMR (CCl_4) δ=1.07 (6H, t, J=8 Hz), 1.35—2.45 (8H, m), 2.65 (4H, t, J=8 Hz), 3.83 (m, 2H). Anal. ($C_{12}H_{20}O_3Cl_2$) C, H.

4-Chlorobutanoic Anhydride (2c): Yield 88%; bp 120—124 °C (1.5 mmHg); IR (neat) 1815, 1750, 1045 cm^{-1}; ^1H NMR (CCl_4) δ=2.16 (4H, m), 2.64 (4H, t, J=7 Hz), 3.60 (4H, t, J=7 Hz). Anal. ($C_8H_{12}O_3Cl_2$) C, H.

Typical Reactions for Acylation. 2-(4-Chlorobutanoyl)-1,3-cyclohexanedione (4c). a. With BF_3·OEt_2. To a mixture of **3** (275 mg, 2.45 mmol) and BF_3·OEt_2 (2.55 g, 17.7 mmol) was added 4-chlorobutanoic anhydride (**2c**) (640 mg, 2.82 mmol) at room temperature. The mixture was stirred for 12 h at 110 °C. After cooling the mixture, it was poured into water and extracted with ethyl acetate. The extract was washed with water, dried over $MgSO_4$, and concentrated under vacuum. Purification of the residue by preparative TLC (hexane-ethyl acetate, 1:1, R_f=0.68) gave **4c** (112 mg, 23% yield): IR (neat) 3400 (enol OH), 1660, 1550 cm^{-1}; ^1H NMR ($CDCl_3$) δ=1.70—2.90 (8H, m), 3.16 (2H, t, J=7 Hz), 3.58 (2H, t, J=7 Hz), 17.9 (1H, s, enol OH). ^{13}C NMR ($CDCl_3$) δ=19.0 (t), 27.2 (t), 32.8 (t), 38.1 (t), 38.6 (t), 44.3 (t), 112.9 (s), 194.9 (s), 197.5 (s), 204.5 (s). These spectral data implies that **4c** is present in enol form. Anal. ($C_{10}H_{13}O_3Cl$) C, H.

b. With BF_3 in Ethyl Acetate-Dichloromethane. BF_3 generated by using sodium tetrafluoroborate ($NaBF_4$) (60 g, 546 mmol), anhydrous diboron trioxide (B_2O_3) (10 g, 144 mmol), and concd sulfuric acid (60 ml)[13] was introduced into a mixed solvent of ethyl acetate (5 ml) and dichloromethane (8 ml). After cooling the solution in an ice bath, a mixture of **3** (2.2 g, 20 mmol) and **2c** (9.05 g, 40 mmol) was added dropwise. It was stirred for 30 min at 0 °C and for additional 12 h at 90 °C. The mixture was treated in a similar manner to give **4c** (1.46 g, 34% yield) after purification by column chromatography (hexane-ethyl acetate, 5:1).

c. With BF_3. To a cooled (0 °C) mixture of **3** (2.62 g, 23.4 mmol) and **2c** (11.2 g, 49.5 mmol), was introduced BF_3 generated from $NaBF_4$ (60 g, 546 mmol), anhydrous B_2O_3 (10 g, 144 mmol), and concd sulfuric acid (60 ml).[13] The introduction was completed within 15 min. The darkened mixture was stirred for 30 min at 0 °C, for 30 min at room temperature, and for additional 12 h at 95 °C. The reaction mixture was treated in a manner similar to the foregoing experiment to give **4c** (2.31 g, 46% yield).

2-(4-Chlorohexanoyl)-1,3-cyclohexanedione (4b): IR (neat) 3400 (enol OH), 1730, 1662, 1560 cm^{-1}; ^1H NMR ($CDCl_3$) δ=1.04 (3H, t, J=8 Hz), 1.60—2.84 (10H, m), 3.22 (2H, t, J=8 Hz), 3.90 (1H, m), 17.91 (1H, br s, enol OH); ^{13}C NMR ($CDCl_3$) δ=11.0 (q), 19.2 (t), 31.6 (t), 32.5 (t), 32.9 (t), 38.1 (t), 38.8 (t), 64.9 (d), 113.1 (s), 195.3 (s), 197.9 (s), 205.3 (s). Anal. ($C_{12}H_{17}O_3Cl$) C, H.

2-(4-Chloroheptanoyl)-1,3-cyclopentanedione (6a): Yield 74% after purification by column chromatography (hexane-acetone, 8:1); IR (neat) 3420 (enol OH), 1710, 1630, 1585 cm^{-1}; ^1H NMR ($CDCl_3$) δ=0.95 (3H, t, J=7 Hz), 1.20—2.35 (6H, m), 2.35—2.90 (4H, m), 3.15 (2H, t, J=9 Hz), 4.05 (1H, m), 10.90 (1H, br s, enol OH). Anal. ($C_{12}H_{17}O_3Cl$) C, H.

2-(4-Chlorohexanoyl)-1,3-cyclopentanedione (6b): Yield 69% after purification by column chromatography (hexane-acetone, 8:1); IR (neat) 3450 (enol OH), 1710, 1625, 1580 cm^{-1}; ^1H NMR ($CDCl_3$) δ=0.92 (3H, t, J=8 Hz), 1.30—2.20 (4H, m), 2.20—2.80 (4H, m), 3.05 (2H, t, J=9 Hz), 3.86 (1H, m), 11.40 (1H, s, enol OH). Anal. ($C_{11}H_{15}O_3Cl$) C, H.

2-(5-Propyltetrahydro-2-furylidene)-1,3-cyclopentanedione (Oudenone) ((±)-1a). Triethylamine (2 ml) was added to **6a** (90 mg, 0.37 mmol) at 0 °C. After being stirred for 4.5 h at 0 °C, triethylamine unreacted was removed under reduced pressure. The residual oil was extracted with acetone, and purified by column chromatography (hexane-acetone, 1:1) followed by recrystallization from hexane to give (±)-**1a** (37 mg, 49% yield): Mp 81—82 °C (lit.[3a] 77—78 °C); IR (KBr) 3440, 1712, 1660, 1560 cm^{-1}; ^1H NMR ($CDCl_3$) δ=0.92 (3H, t, J=7 Hz), 1.08—1.96 (4H, m), 2.54 (4H, br s), 2.84—3.76 (4H, m), 4.90 (1H, m); ^{13}C NMR ($CDCl_3$) δ=13.9 (q), 18.7 (t), 26.9 (t), 33.8 (t), 34.6 (t), 35.0 (t), 36.8 (t), 90.5 (d), 109.3 (s), 184.6 (s), 200.8 (s), 204.8 (s). These spectral data were consistent with those reported.[3a,7]

2-(5-Ethyltetrahydro-2-furylidene)-1,3-cyclopentanedione ((±)-1b)[5b]: Yield 42%; mp 106—107 °C (hexane-benzene, 2:1); IR (KBr) 3375, 1712, 1660, 1560 cm^{-1}; ^1H NMR ($CDCl_3$) δ=0.97 (3H, t, J=7 Hz), 1.6—2.0 (2H, m), 2.56 (4H, s), 2.92—3.72 (4H, m), 4.84 (1H, m). Anal. ($C_{11}H_{14}O_3$) C, H.

References

1) H. Umezawa, T. Takeuchi, H. Iinuma, K. Suzuki, M. Ito, K. Matsuzaki, T. Nagatsu, and O. Tanabe, *J. Antibiot.*, **23**, 514 (1970).

2) I. Nagatsu, T. Nagatsu, H. Umezawa, M. Matsuzaki, and T. Takeuchi, *Nature*, **230**, 381 (1971).

3) a) M. Ohno, M. Okamoto, M. Kawabe, H. Umezawa, T. Takeuchi, H. Iinuma, and S. Takahashi, *J. Am. Chem. Soc.*, **93**, 1285 (1971); b) M. Ohno, M. Okamoto, and N. Kawabe, Ger. Offen, 2129991. *Chem. Abstr.*, **76**, 113052f (1972); c) M. Ohno, M. Okamoto, N. Kawabe, and M. Kataoka, Ger. Offen, 2141833, *Chem. Abstr.*, **76**, 140489k (1972); d) M. Ohno and K. Hosoi, Japan Patent 7220154, *Chem. Abstr.*, **78**, 3796k (1973); e) M. Ohno and K. Hosoi, Japan Patent 7225157, *Chem. Abstr.*, **78**, 3797 (1973).

4) a) M. Ohno and R. Hosoi, Japan Patent, 7231973, *Chem. Abstr.*, **78**, 29603v (1973); b) M. Ohno and K. Hosoi, Japan Patent, 7230660, *Chem. Abstr.*, **78**, 29605x (1973).

5) a) M. Ohno and K. Kawabe, Japan Patent, 7304460, *Chem. Abstr.*, **78**, 111108w (1973); b) M. Ohno and H. Umezawa, Japan Patent, 7301076, *Chem. Abstr.*, **78**, 147772x (1973).

6) a) T. Tsujikawa, Y. Nakagawa, K. Tsukamura, and K. Masuda, *Heterocycles*, **6**, 261 (1977); b) T. Tsujikawa, T. Hayashi, K. Tsukamura, and K. Masuda, *Chem. Pharm. Bull.*, **25**, 2775 (1977).

7) H. A. Bates and J. Farina, *J. Org. Chem.*, **50**, 3843 (1985).

8) C. A. Henrick, U. S. Patent 4448965, *Chem. Abstr.*, **101**, p72319n.

9) J. B. McIntosh and P. M. Beaumier, *Can. J. Chem.*, **51**, 843 (1973).

10) R. M. Manvik, F. C. Frostick, Jr., J. J. Sanderson, and C. R. Hauser, *J. Am. Chem. Soc.*, **75**, 5030 (1953).

11) E. Leucht and W. Riedl, *Justus Liebigs Ann. Chem.*, **669**, 55 (1963).

12) O. P. Goel and R. E. Seamans, *Synthesis*, **1973**, 538.

13) H. S. Booth and K. S. Willson, "Inorganic Syntheses," McGraw-Hill Book Company, Inc., New York (1939), Vol. 1, p. 21.

Ester Aminolysis in the Presence of Alkylammonium Carboxylate Reversed Micelles. A Mechanistic Study

Omar A. EL SEOUD,*[1a] Rita C. VIEIRA,[1b] and Luzia P. NOVAKI[1b]
Physikalische Chemie I, University Bayreuth, Postfach 3008, D-8580 Bayreuth, West Germany
(Received November 27, 1985)

Synopsis. A study of ester aminolysis in the presence of dodecylammonium carboxylate reversed micelles showed that the catalytic role of the surfactant head-anion (general base) was concentration independent. The presence of co-solubilized water in the micelle did not lead to detectable ester hydrolysis.

Several types of reactions were found to be catalyzed by reversed micelles (RM's).[2,3] Ester aminolysis in the presence of alkylammonium carboxylate RM's has received a fair amount of attention.[4-7] Evidence has been given to show that the carboxylate ion of the surfactant is acting as a general base,[7b] not as a nucleophile.[6] In these reactions the ratio [detergent]/[ester] is usually large (typically ≥ 50). It has been argued, however, that the nucleophilic catalysis pathway can still occur if a much lower [surfactant]/[ester] ratio were used.[8] This implies that a change in the reaction mechanism (from general base to nucleophilic catalysis) can be induced by changing the concentration ratio of the reactants.[9] We checked, therefore, the concentration dependence of the catalytic role of the carboxylate ion of these surfactants and the conditions under which it can act as a nucleophile.

As recently argued,[8] co-solubilization of water in the core of the RM can lead to the occurence of hydrolysis as a competing reaction. This is not in agreement with our study of ester aminolysis in the presence of dodecylammonium diethylarsinate RM's.[7a] Since the carboxylate ion is a much weaker base than the diethylarsinate ion[11] we sought direct evidence for, or against, the occurence of hydrolysis in the case of the present RM's.

Results and Discussion

Consider the aminolysis of *p*-nitrophenyl *p*-nitrobenzoate by dodecylammonium *p*-anisate (DAPA) RM's or by a mixture of DAPA and dodecylamine (DA). The nucleophilic catalysis mechanism should proceed via attack of the *p*-anisoyloxy group on the ester to give the intermediate anhydride $O_2NC_6H_4CO\cdot O\cdot OCC_6H_4OCH_3$ whose aminolysis should yield a mixture of the amides $O_2NC_6H_4CONHC_{12}H_{25}$ and $CH_3OC_6H_4CONHC_{12}H_{25}$.[8] According to the general base catalysis mechanism only one amide, that derived from the ester, i.e., $O_2NC_6H_4CONHC_{12}H_{25}$, should be produced[7b] so that analysis of the products should settle the question. Entries 1—3 of Table 1 show the results for the aminolysis by DAPA and by DAPA+DA using small [detergent]/[ester] ratios. Only *N*-dodecyl-*p*-nitrobenzamide was obtained which clearly shows that the catalytic role of the *p*-anisoyloxy group of DAPA is concentration independent.

The question now arises: Under which conditions will the *p*-anisoyloxy group act as a nucleophile in the micellar core? Recently it has been shown that the acetate ion of $(CH_3)_4N^+{-}O_2CCH_3$ reacts with esters in aprotic solvents producing mixed anhydrides.[13] We decided, therefore, to investigate whether the same result will be obtained in the presence of the surfactant. Entries 4—7 of Table 1 show the results of the reaction of the benzoate ester with DAPA and with DAPA+DA in the presence of tetramethylammonium *p*-anisate (TMA) in CH_3CN and in CH_2Cl_2. The *p*-anisoyloxy group acted as a nucleophile (as shown by the production of amides A,B) only under the condition [TMA]$\geq$[DAPA]. While the formation of RM's in CH_3CN may be dubious[3] the reaction in CH_2Cl_2 is certainly taking place within the micellar domain since TMA is only soluble in the presence of the surfactant.

The preceding results can be rationalized as follows: In the micellar core the *p*-anisoyloxy group can act as a nucleophile only if it is "naked" or desolvated.[10,13] ^1H NMR data demonstrated that the carboxylate ion is strongly hydrogen-bonded to the alkylammonium ion[3] so that it is present in a protic microenvironment. Note that this hydrogen-bonding is an intrinsic property, i.e., it is neither dependent on the presence of the ester nor on the [detergent]/[ester] ratio. Solubilization of TMA in the RM introduces "excess" *p*-anisate ions which are not hydrogen-bonded to their cations (the $(CH_3)_4N^+$ ions) and is thus expected to favor the nucleophilic catalysis mechanism. That the latter took place only at higher [TMA] is understandable in terms of the ability of the alkylammonium

Table 1. Aminolysis of *p*-Nitrophenyl *p*-Nitrobenzoate in the Presence of Dodecylammonium *p*-Anisate Reversed Micelles in Organic Solvents[a]

Reaction	DAPA[b] mmol	DA[b] mmol	TMA[b] mmol	Amides obtained[c]
1	3.0	—	—	A
2	5.0	—	—	A
3	5.0	2.5	—	A
4	5.0	—	2.8	A
5	5.0	2.5	3.2	A
6	5.0	2.5	5.0	A+B
7	5.0	2.5	8.0	A+B

a) At room temperature, ester=0.8 mmol, in 20 ml CH_2Cl_2 (Reactions 1—7) or acetonitrile (Reactions 4—7). b) For abbreviations see text. c) Determined by ^1H NMR. Amide: A=$O_2NC_6H_4CONHC_{12}H_{25}$; B=$CH_3OC_6H_4CONHC_{12}H_{25}$.

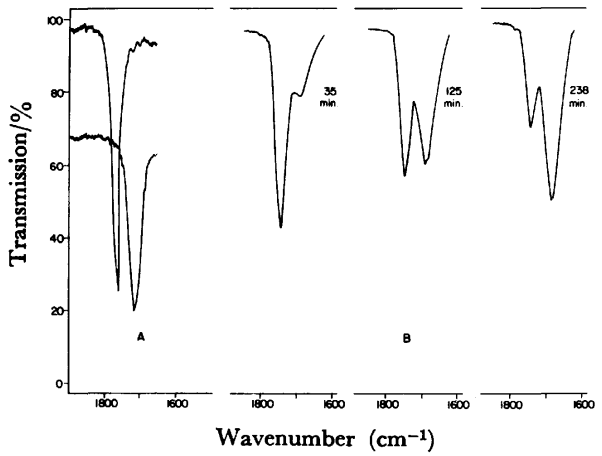

Fig. 1. Part A shows the peaks of the CO groups of methyl *p*-nitrophenyl carbonate and methyl dodecylcarbamate (both 0.05 M) in chloroform. The progress of the reaction of 0.05 M carbonate ester, 0.1 M DAP in the presence of 0.6 M water is shown in part B.

ions to complex more than one carboxylate ion.[14] The relevant point here is that due to the protic nature of the core of alkylammonium carboxylate RM's the possibility that the RCO_2^- group of the surfactant can act as a nucleophile is now essentially excluded.

The aminolysis of methyl *p*-nitrophenyl carbonate in the presence of dodecylammonium propionate (DAP)-solubilized water was studied in chloroform and in toluene. Our choice of this ester was dictated by the favorably large separation between the peaks of the CO groups of the ester (1760 cm^{-1}) and methyl dodecylcarbamate (the product of aminolysis, at 1710 cm^{-1}) as shown in part A of Fig. 1. The reaction progress is shown in part B in which the ester peak gradually disappeared and that due to the aminolysis appeared. Quantitative analysis in both solvents indicated that all the carbonate ester that reacted appeared as amide, i.e., practically no hydrolysis occurred. This is similar to the reaction of alkyl *p*-nitrophenyl carbonates with amines in aqueous solutions where only aminolysis occurs, probably because of the higher reactivity of amines relative to water.[15] Since the head-ions of DAP are strongly hydrogen-bonded it is easy to understand why the carboxylate ion (acting as a general base) accepted a proton from the dodecylammonium ion (leading to aminolysis) rather than from a water molecule (causing hydrolysis).

Experimental

All solvents (Aldrich) were purified and kept on activated 4A molecular sieves. DAP, DAPA, the benzoate, and the carbonate esters, methyl dodecylcarbamate, *N*-dodecyl-*p*-anisamide were obtained as given elsewhere.[5,7] *N*-Dodecyl-*p*-nitrobenzamide was prepared by refluxing DA and benzoyl chloride (molar ratio 2:1) in chloroform and was recrystallized from hexane–chloroform. Mp 96—97 °C. ^1H NMR (Varian T-60 spectrometer, in $CDCl_3$) δ=8.01 (d, 2H), 7.81 (d, 2H), 5.95 (m, 1H), 3.88 (m, 2H), 1.27 (apparent s, 20H), and 0.84 (t, 3H). Found: C, 68.14; H, 8.96; N, 8.29%. Calcd for $C_{19}H_{30}N_2O_3$: C, 68.26; H, 8.98; N, 8.38%. TMA was prepared by carefully neutralizing tetramethylammonium hydroxide with *p*-anisic acid in aqueous methanol. Prolonged drying in vacuo, over P_2O_5 at 70 °C gave the anhydrous salt. ^1H NMR (CD_3CN) δ=7.71 (d, 2H), 6.85 (d, 2H), 3.81 (s, 3H), and 3.21 (s, 12H). This hygroscopic salt was handled in Atomsbag (Aldrich) and was dried to a constant weight before being used. A typical aminolysis reaction in CH_2Cl_2 was as follows: The reactants were stirred overnight under N_2, the organic solution was washed with NaOH (pH=11) until the latter was colorless, with water, dried, and the solvent removed. The solid residue was washed with hexane, dried, then submitted to analysis by ^1H NMR.

IR spectra were obtained with a Perkin-Elmer 238 spectrometer using 0.2 mm CaF_2 cells. Quantitative analysis were carried out using the absorption mode. The concentrations of the reacting ester and of the produced carbamate were determined from the corresponding Beer's law plots (using peak areas and/or weights), and were accurate to ±2%.

We thank the CNPq-PADCT and Pronac-Catalise for support and the following Foundations for fellowships: Alexander von Humboldt (O. A. El Seoud) CNPq (R. C. Vieira) and FAPESP (L. P. Novaki).

References

1) a) On leave from Inst. Química, Univ. São Paulo, S P., Brazil; b) Address: Inst. Quimica, Univ. São Paulo, C. P. 20.780, 01498 São Paulo, S. P., Brazil.

2) Detergent aggregates in organic solvents are termed reversed micelles. Chemical reactions usually take place at the central part, or core, of the RM. This part is surrounded by the surfactant head groups.[3]

3) J. H. Fendler, "Membrane Mimetic Chemistry," Wiley, N. Y. (1982).

4) K. Kon-no, T. Matsuyama, H. Mizuno, and K. Kitahara, *Nippon Kagaku Kaishi*, **1975**, 1857.

5) O. A. El Seoud, A. Martins, L. P. Barbur, M. J. da Silva, and V. Aldrigue, *J. Chem. Soc., Perkin Trans. 2*, **1977**, 1674.

6) C. J. O' Connor and R. E. Ramage, *Aust. J. Chem.*, **33**, 757 (1980).

7) a) M. I. El Seoud and O. A. El Seoud *J. Org. Chem.*, **46**, 2686 (1981); b) M. I. El Seoud, R. C. Vieira, and O. A. El Seoud, *ibid*, **47**, 5137 (1982).

8) C. J. O'Connor, T. D. Lomax, and R. E. Ramage, *Adv. Colloid Interface Sci.*, **20**, 21 (1984).

9) It is possible, however, to change the nature of the rate limiting step by changing the relative concentrations of the reactants.[10]

10) a) F. M. Menger and A. C. Vitale, *J. Am. Chem. Soc.*, **95**, 4931 (1973); b) U. Tonellato, *J. Chem. Soc., Perkin Trans. 2*, **1978**, 307.

11) Compare, e.g., the pK_a of *p*-anisic acid (4.47) with that of diethylarsinic acid (6.42).[12]

12) E. A. Lewis, L. D. Hansen, E. J. Baca, and D. J. Temer, *J. Chem. Soc., Perkin Trans. 2*, **1976**, 125.

13) J. Hajdu and G. M. Smith, *J. Am. Chem. Soc.*, **103**, 6192 (1981).

14) F. Kohler, R. Gopel, G. Götze, H. Atrops, M. A. Demiriz, E. Liebermann, E. Wilhelm, F. Ratkovics, and B. Palagyi, *J. Phys. Chem.*, **85**, 2524 (1981).

15) M. J. Gressner and W. P. Jencks, *J. Am. Chem. Soc.*, **99**, 6963, 6970 (1977).

Anisotropic Rotation of Perylene Studied by Fluorescence Depolarization Method

Takashi SASAKI, Kanji HIROTA, Masahide YAMAMOTO,* and Yasunori NISHIJIMA
Department of Polymer Chemistry, Kyoto University, Kyoto 606
(Received October 20, 1986)

Synopsis. Rotational diffusion coefficients of perylene in solution were determined by a fluorescence depolarization technique. An asymmetric rotor approximation is more appropriate than an oblate approximation for perylene. The ratio of the diffusion coefficients suggests that a partially slipping boundary condition should be taken into account for this system.

The fluorescence depolarization technique has been utilized to study the rotational Brownian motions of various fluorescent molecules.[1-3] We have investigated the anisotropic rotational diffusion of perylene and its derivatives in solution by a time-resolved technique.[4] In the present work, we reinvestigated the rotational motion of perylene with the asymmetric rotor model as well as with the spheroid model, and precisely analyzed the diffusion coefficients.

Theoretical

A theoretical treatment of the rotational relaxation of fluorescence emission anisotropy was performed in the most general manner by Chuang and Eisenthal.[5] Assuming that the transition vector of absorption is parallel to that of the emission, and coincides with one of the principal axes (z-axis in Fig. 1), we can write a reduced expression for the anisotropy ratio, $r(t)$:

$$r(t) = 0.3(\alpha+\beta)\exp[-(6D+2\Delta)t] + 0.3(\beta-\alpha)\exp[-(6D-2\Delta)t], \quad (1)$$

with

$$\alpha = (D_x+D_y-2D_z)/3\Delta, \qquad \beta = 2/3,$$
$$\Delta = (D_x^2+D_y^2+D_z^2-D_xD_y-D_yD_z-D_zD_x)^{1/2},$$

and

$$D = (D_x+D_y+D_z)/3,$$

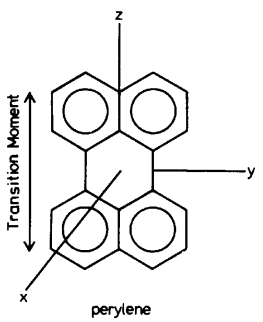

Fig. 1. Molecular fixed coordinate system for perylene.

where D_x, D_y, and D_z are the rotational diffusion coefficients about the corresponding axes. These diffusion coefficients can be related to the molecular shape according to a hydrodynamic assumption. In general, with a sticking boundary condition the rotational diffusion coefficient D_r of a rigid body in a fluid medium obeys the expression

$$1/(6D_r) = \eta\zeta V/kT, \quad (2)$$

where η is the viscosity of the medium, ζ the rotational friction coefficient, V the volume of the body, k the Boltzmann constant, and T the absolute temperature. In the case of a slipping boundary condition, it can be written as

$$1/(6D_r) = \eta\zeta V/kT + \rho_0, \quad (3)$$

where ρ_0 is related to the inertia of the body (order of picoseconds). The rotational friction coefficient for a sphere (radius R) in a fluid medium with the sticking and the slipping boundary conditions are $8\pi\eta R^3$ and zero, respectively; those for a symmetric rotor could be calculated exactly with the sticking boundary condition,[6] and numerically with the slipping boundary condition.[7] If we approximate perylene by a symmetric rotor (an oblate spheroid) with an axial ratio, $r_x:r_y(=r_z)=3:11$, the ratio of the diffusion coefficients predicted by the above theory with the sticking boundary condition is $D_{/\!/}/D_\perp=0.816$, where $D_{/\!/}=D_x$, and $D_\perp=D_y=D_z$. In the case of the slipping boundary condition, the friction coefficient about the symmetric axis (x-axis) is zero; thus $D_{/\!/} \gg D_\perp$ is obtained. On the other hand, the friction coefficients for an asymmetric rotor with the slipping boundary condition have been obtained numerically by Youngren and Acrivos.[8] According to their results, the ratio of the friction coefficients is $\zeta_x:\zeta_y:\zeta_z=1:31:22$, for the ellipsoid with the axial ratio $r_x:r_y:r_z=1:3.2:3.8$, which is estimated by the van der Waals radii of perylene molecule. This is considered to be a more appropriate approximation than the oblate approximation for a perylene molecule. To our knowledge, the friction coefficients for an asymmetric rotor with the sticking boundary condition have not been calculated so far.

Experimental

Perylene was dissolved in propylene glycol. The concentration of this solution was 10^{-5} mol dm^{-3}. The solution was degassed for measurement. A time-resolved fluorescence anisotropy measurement was performed using the nanosecond single-photon counting system in our

laboratory.[9] The data counts were accumulated to 1.3×10^5 counts at the peak of the fluorescence intensity of the parallel component; this was sufficient for ascertaining good precision regarding the data. The data analysis was executed to fit a biexponential function,

$$r(t) = r_0[a_1 \exp(-t/\rho_1) + a_2 \exp(-t/\rho_2)], \quad (4)$$

to experimental points by the method of nonlinear least-squares fitting which involved a deconvolution procedure.[10] Then, we calculated the diffusion coefficient about each axis by Eq. 1 from the obtained values. Further, to test the oblate spheroid model, the ratio a_1/a_2 was fixed at 1/3 (postulated in this case). The same analysis procedure was executed to find $D_{/\!/}$ and $D_\perp$. All these data-analysis procedures were performed on a digital computer FACOM M-382.

Results and Discussion

The results are shown in Tables 1 and 2. As a criteria of the accuracy of the fitting, the reduced sums of the squares of the residuals χ^2 are also shown in Table 1. It can be seen that the ratio $D_{/\!/}/D_\perp$ for perylene agrees neither with the theoretical value for the sticking boundary condition ($D_{/\!/}/D_\perp=0.816$) nor with that for the slipping boundary condition ($D_{/\!/} \gg D_\perp$). Thus, it is considered that the real behavior of perylene is under an intermediate boundary condition between those two ideal boundary conditions. Judging from the values of χ^2, we can say that an approximation with an asymmetric rotor is more appropriate for perylene than that with an oblate spheroid, as might have been expected. This can be clearly seen in Figs. 2 and 3, as the residual plot of the former shows an apparent systematic deviation from the theory. However, as for the values of the diffusion coefficients, it is noticed that a significant discrepancy still exists between theory and experiment, even in the case of an asymmetric rotor approximation. The experimental result is D_x: D_y: D_z=728:1:179 (from Table 2), while the theoretical value (calculated from the ratio of friction coefficients with the slipping boundary condition given in the theoretical section) is 31:1:1.4, provided that the inertia limit ρ_0 is neglected. Thus, the ideal slipping boundary condition seems to be unsatisfactory for perylene; in other words, the 'partially slipping (or sticking)' boundary condition is preferable. In the time region of our experiment, the solvent may not be regarded as a mere continuous medium; also, the discrete chemical structure of the molecules becomes significant: such small-scale molecular motions should be interpreted by jump kinetics[1] rather than by the diffusion model.

Table 1. Best-Fit Parameters for Perylene in Propylene Glycol at 7 °C

Model	r_0	a_1/a_2	ρ_1/ns	ρ_2/ns	χ^2
Oblate	0.290	1/3	6.4	1.0	1.777
Asymmetric	0.303	0.560	4.6	0.74	0.963

Table 2. Diffusion Coefficients Obtained from the Best-Fit Parameters in Table 1

Model	$D_x\times10^{-7}$/s^{-1}	$D_y\times10^{-7}$/s^{-1}	$D_z\times10^{-7}$/s^{-1}	$D_{/\!/}/D_\perp$
Oblate	23.2	2.6		8.9
Asymmetric	31.3	0.043	7.7	

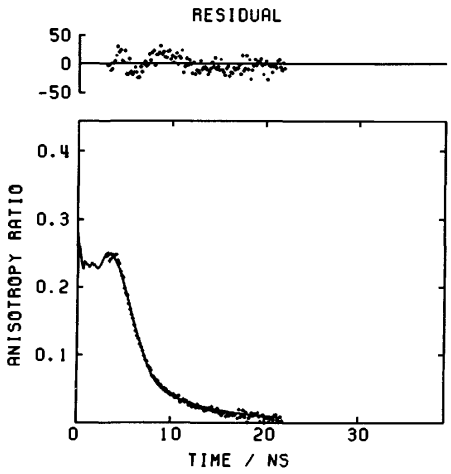

Fig. 2. Anisotropy decay for perylene in propylene glycol at 7 °C. Dots represent experimental data, and a solid curve indicates the theoretical decay convoluted with the best-fit parameters for the oblate model. The weighted residuals are also plotted in an arbitrary scale.

References

1) P. E. Zinsli, *Chem. Phys.*, **20**, 299 (1977).
2) M. D. Barkley, A. A. Kowalczyk, and L. Brand, *J. Chem. Phys.*, **75**, 3581 (1981).
3) J. L. Viovy, *J. Phys. Chem.*, **89**, 5465 (1985).
4) T. Sasaki, M. Yamamoto, Y. Nishijima, *Repts. Progr. Polymer Phys. Jpn.*, **29**, 529 (1986).

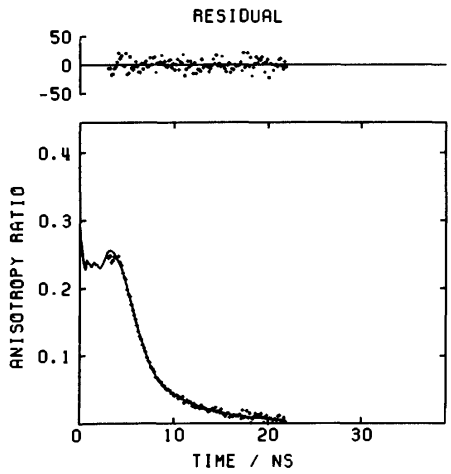

Fig. 3. Anisotropy decay for the sample of Fig. 2. A solid curve indicates the theoretical decay convoluted with the best-fit parameters for the asymmetric rotor model.

5) T. J. Chuang, and K. B. Eisenthal, *J. Chem. Phys.*, **57**, 5094 (1972).
6) F. Perrin, *J. Phys. Radium*, **7**, 1 (1936).
7) C. Hu, and R. Zwanzig, *J. Chem. Phys.*, **60**, 4354 (1974).
8) G. K. Youngren, and A. Acrivos, *J. Chem. Phys.*, **63**, 3846 (1975).
9) T. Sasaki, M. Yamamoto, and Y. Nishijima, *Makromol. Chem., Rapid Commun.*, **7**, 345 (1986).
10) P. Wahl, *Biophys. Chem.*, **10**, 91 (1979).

The Use of End-Loading Technique for the Sample Preparation of Organic Powders in X-Ray Powder Diffractometry

Kazuaki NAKATA* and Yoshito TAKAKI
Department of Physics, Osaka Kyoiku University, Tennoji-ku, Osaka 543
(Received August 14, 1986)

Synopsis. The end-loading technique in preparing samples for X-ray powder diffractometry is found to be an effective method for reducing preferred orientation effects of organic powder samples.

In X-ray powder diffractometry, many attempts have been made to reduce the preferred orientation of mineral powders.[1-5] The end-loading technique has been found to be a simple and effective method for preparing the powder samples.[1] In this paper we report that the end-loading technique is very useful for reducing preferred orientations of organic powders. The powder samples examined in this study are those of benzamide,[6] benzoic acid,[7] α-form of pyrazinecarboxamide (PCA),[8] A-form of DL-2-aminobutyric acid (DL-ABA)[9] and DL-norleucine (DL-NL),[10] in which the latter two samples show marked tendency to orient on the 001 preferred orientation plane. In these samples, a quantitative examination of the preferred orientations in benzamide and PCA powders prepared by the normal (back-loading) technique have been made by Nakata et al.[11] Therefore, it is very interesting to compare the preferred orientations occurring in powders prepared by the normal and the end-loading techniques.

Experimental

The samples used in this study were ground by hand in an agate mortar. The specimen holder was constructed from a usual aluminum-holder by cutting away the end piece, by cementing a ground glass-slide onto the back and by covering the top surface with a glass-slide (see Fig. 2 of Niskanen[1]). The powder sample was then poured and packed in the holder by tapping it at the bottom.

All diffraction patterns taken by the normal and the end-loading techniques were obtained using a Rigaku Geigerflex (CN2013). The experimental conditions were: Cu $K\alpha$ radiation, a nickel filter, 0.5° divergence and 0.15 mm receiving slits, a scintillation detector and a scan speed of $1/2°(2\theta\ \mathrm{min}^{-1})$. Intensity measurements of the diffraction peaks were made by cutting out background-subtracted peak areas from each of the traces and weighing.

Results and Discussion

The degree of randomness of oriented powder particles is given by[11]

$$R_0 = \frac{\Sigma|I_{obs}-I_{ran}|}{\Sigma|I_{ran}|} \quad (1)$$

where I_{obs}'s are the observed intensities and I_{ran}'s, which are calculated from F_o's obtained by single-crystal work, are the intensities from a sample with completely random orientation.

In order to assess the effect of the end-loading technique on the reduction of preferred orientation, we took two diffraction patterns from the same grounded powder using the normal and the end-loading techniques. Table 1 lists the R_0 values for the

Table 1. R_0 Values and Preferred Orientation Parameters in the Powder Samples Prepared by the Normal and the End-Loading Techniques

Sample		R_0	Plane or axis		Orientation parameter					Relative volume			μ[d]/cm^{-1}
			1	2	C_0	C_1	P_1	C_2	P_2	V_0	V_1	V_2	
Benzamide	Normal	0.44	(001)	($\bar{1}$04)	0.02	0.70	6	0.28	5	0.09	0.61	0.30	7.2
	End-	0.20	(100)	($\bar{1}$04)	0.44	0.29	10	0.27	17	0.86	0.09	0.05	
Benzoic acid	Normal	0.43	b-axis	(001)	0.22	0.49	19	0.29	11	0.55	0.35	0.10	8.1
	End-	0.22	(100)	($\bar{1}$02)	0.40	0.46	23	0.14	8	0.87	0.08	0.05	
PCA[a]	Normal	0.47	c-axis	(100)	0.06	0.28	3	0.66	4	0.16	0.42	0.42	9.1
	End-	0.15	(110)	(001)	0.29	0.40	1	0.31	29	0.59	0.37	0.04	
DL-ABA[b]	Normal	1.14	(001)	—	0.01	0.99	35	—	—	0.05	0.95	—	8.2
	End-	0.19	(110)	(100)	0.50	0.37	10	0.13	5	0.85	0.09	0.06	
DL-NL[c]	Normal	0.74	(001)	—	0.01	0.99	27	—	—	0.10	0.90	—	7.2
	End-	0.28	(210)	($\bar{1}$11)	0.16	0.58	11	0.26	63	0.64	0.32	0.04	
Gypsum	Normal	0.81	(010)	(011)	0.00	0.94	31	0.06	50	0.05	0.91	0.04	140
	End-	0.71	(010)	(011)	0.00	0.91	25	0.09	22	0.03	0.88	0.09	
Olivine	Normal	0.36	(010)	(001)	0.02	0.82	10	0.16	15	0.11	0.77	0.12	386
	End-	0.25	(010)	(001)	0.05	0.66	11	0.29	17	0.29	0.54	0.17	

a) α-form of pyrazinecarboxamide. b) A-form of DL-2-aminobutyric acid. c) DL-norleucine. d) Linear absorption coefficients for Cu$K\alpha$ radiation.

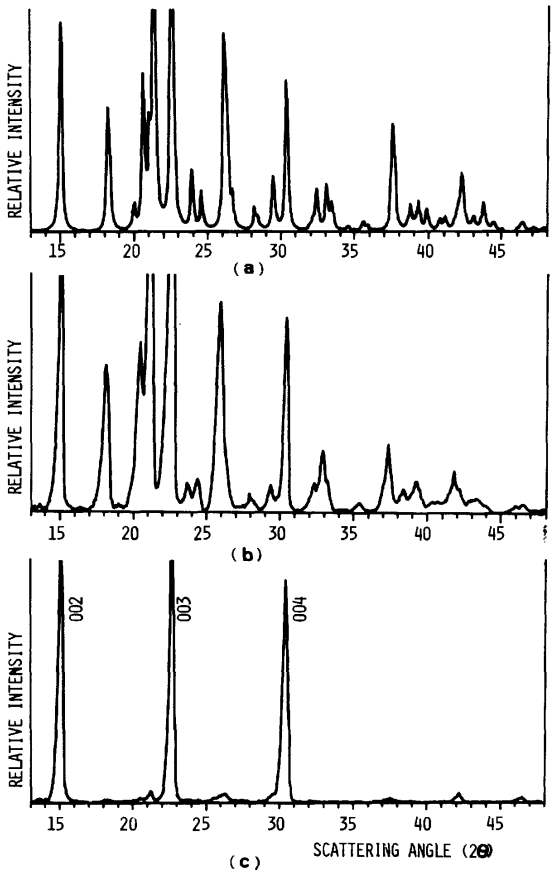

Fig. 1. The observed and calculated diffraction patterns of DL-ABA. a) An "ideal" pattern calculated from I_{ran}.[9] b) The observed pattern taken by the end-loading technique. c) The observed pattern taken by the normal technique.

powder samples of benzamide,[6] benzoic acid[7] and PCA[8] obtained by the two different techniques. Comparing R_0 values in Table 1, it is seen that the end-loading technique effectively reduces the R_0 values to under one-half of the values of the normal technique.

Further, we examined the usefulness of the end-loading technique using the samples of DL-ABA[9] and DL-NL.[10] These powder particles have a habit of thin plate with well developed (001) faces. It therefore show a marked tendency to orient on the 001 preferred orientation plane. Figure 1 shows the observed diffraction patterns of DL-ABA taken by the normal and the end-loading techniques. For comparison, an "ideal" pattern calculated from I_{ran}[9] of DL-ABA[12] is also shown in Fig. 1(a).

As can be seen in Fig. 1, the observed pattern taken by the normal technique yields only the $00l$ diffraction peaks, whereas the pattern taken by the end-loading technique is in good agreement with the "ideal" pattern. The R_0 values obtained by the normal and the end-loading techniques are 1.14 and 0.19, respectively (Table 1). Similarly, a marked decrease of the R_0 value can also be seen in the case of DL-NL; the R_0 values for the powder samples prepared by the normal and the end-loading techniques are 0.74 and 0.28, respectively.

Here, we examine quantitatively the above reduction of preferred orientations using the method of Nakata et al.[11] Table 1 lists the preferred orientation parameters, C_i and P_i, for the powders prepared by the normal and the end-loading techniques. The relative volumes of the domains, V_i, in the powder are also listed in Table 1, where a domain is defined as a collection of particles having the same preferred orientation plane or axis.[11] Comparing V_i values, one can see that the V_0 values of the end-loading technique are much larger than those of the normal technique, indicating that the randomly oriented domains are effectively increased in volume by the use of the end-loading technique. Further it is interesting that most of the preferred orientation planes or axes observed in the powders prepared by the normal technique disappear, and the different planes or axes with small relative volumes appear in the powders prepared by the end-loading technique.

The drastic reduction of preferred orientation effects described above may be explained as follows: Since the end-loading technique applies no pressure normal to the surface of the specimen, the powder particles except for those very near to the surface are not effected by the glass-slide. Furthermore, since organic substances generally have small absorption coefficients for X-rays (Table 1), the organic powder in a holder may allow considerable penetration of the X-ray beam. From the above results, the degree of preferred orientation of powder particles is estimated to be much lower than that of the normal technique.

In order to clarify the effect of absorption, we applied the normal and the end-loading techniques to inorganic powder samples gypsum[13] and olivine[14]; these samples have large absorption coefficients (see Table 1). The preferred orientation parameters, C_i and P_i, and the relative volumes of the domains, V_i, in these powders are listed in Table 1. As expected, no marked decrease in R_0 (and increase in V_0) can be seen in the powders prepared by the end-loading technique. In addition, the same preferred orientation plane or axis is found in both the powders prepared by the two techniques, and that the differences in V_i are rather small.

Consequently, we may say that the end-loading technique effectively minimizes the preferred orientations of organic powder samples, especially for those with low absorption coefficients.

References

1) E. Niskanen, *Am. Mineral.*, **49**, 705 (1964).
2) A. M. Bystrom-Asklund, *Am. Mineral.*, **51**, 1233 (1966).
3) F. D. Bloss, *Am. Mineral.*, **52**, 1243 (1967).
4) R. Hughes and B. Bohor, *Am. Mineral.*, **55**, 1780 (1970).
5) S. T. Smith, R. L. Snyder and W. E. Brownell, *Adv. X-Ray Anal.*, **22**, 77 (1978).
6) C. C. F. Blake and R. W. H. Small, *Acta Crystallogr., Sect. B*, **28**, 2201 (1972).
7) G. Bruno and L. Randaccio, *Acta Crystallogr., Sect. B*, **36**, 1711 (1980).

8) Y. Takaki, Y. Sasada, and T. Watanabè, *Acta Crystallogr.*, **13**, 693 (1960).
9) K. Nakata, Y. Takaki and K. Sakurai, *Mem. Osaka Kyoiku University, Ser. III*, **28**, 73 (1980).
10) A. M. Mathieson, *Acta Crystallogr.*, **6**, 399 (1953).
11) K. Nakata, H. Sugihara, S. Mori, H. Yamaguchi, and Y. Takaki, *Bull. Chem. Soc. Jpn.*, **57**, 3395 (1984).
12) The relative intensity tables (I_{obs} and I_{ran}) of benzamide, benzoic acid, PCA, DL-ABA and DL-NL are kept at the Office of the Chemical Society of Japan (Document No. 8722).
13) W. F. Cole and C. J. Lancucki, *Acta Crstallogr., Sect. B*, **30**, 921 (1974).
14) H. Yamaguchi, K. Akatsuka, A. Kurisu, Y. Takaki, and M. Setoguchi, Annual Meeting of Mineralogical Society of Japan, Tsukuba, June 1982, Abstr., No. 36.

Effects of Alkyl Chain Length on Molecular Interactions. II.[1] Complex Isomerism in the Alkyl *p*-Aminobenzoate–Picric Acid Systems

Atsushi TOGASHI and Yoshio MATSUNAGA*
Department of Chemistry, Faculty of Science, Hokkaido University, Sapporo 060
(Received September 22, 1986)

Synopsis. While a combination of *p*-aminobenzoic acid and picric acid gives a yellow-colored salt by proton transfer, the esterification of the former component compound with methyl to octadecyl groups results in the formation of not only stable salts but also metastable charge-transfer complexes.

We earlier studied the charge-transfer complex formation in pyrene-*N*-alkyl-2,4,6-trinitroaniline systems.[1] The thermal stability of the orange-colored 1:1 complex between the hydrocarbon and unsubstituted 2,4,6-trinitroaniline is drastically decreased by *N*-alkylation. The *N*-octyl derivative and most of the higher homologs produce a single peritectic or a eutectic in the phase diagrams with pyrene, whereas red solids formed on rapid cooling of the melts are progressively stabilized with an increase of the alkyl chain length. Even a stable existence of the red-colored 1:1 complex can be achieved with the *N*-pentadecyl and *N*-heptadecyl derivatives. In the present paper, we compare the effects of alkyl chain length on charge-transfer and proton-transfer interactions operating in solid addition compounds between alkyl *p*-aminobenzoate and picric acid.

Experimental

Materials. Alkyl *p*-aminobenzoates were prepared by reactions between *p*-nitrobenzoyl chloride and appropriate alcohols and then by reduction with iron powder and dilute hydrochloric acid as described by Adams et al.[2] The alkyl groups employed and the melting points of the esters were as follows: methyl, 110.5 °C; ethyl, 89.5 °C; propyl, 76.5 °C; butyl, 59 °C; pentyl, 54.5 °C; hexyl, 62.5 °C; heptyl, 80.5 °C; octyl, 71.5 °C; nonyl, 73 °C; decyl, 79 °C; undecyl, 81 °C; dodecyl, 84.5 °C; tridecyl, 87.5 °C; tetradecyl, 89 °C; pentadecyl, 91 °C; hexadecyl, 89.5 °C; heptadecyl, 95 °C; octadecyl, 96 °C.

Measurements. The phase diagrams were determined using calorimetric curves recorded on a Rigaku Thermoflex differential scanning calorimeter during the process of heating and also by visual examination.[1]

Results and Discussion

The yellow-colored addition compound between *p*-aminobenzoic acid and picric acid has been characterized to be a salt on the basis of its vibrational spectrum according to Issa and El-Essawey.[3] The methyl ester forms only a 1:1 salt when it is combined with picric acid. As is shown in Fig. 1a, the phase diagram is dominated by the freezing point curve of the salt. The melting point is as high as 159 °C. The color changes from yellow to red upon fusion, indicating isomerization into a charge-transfer complex.[4] By rapid cooling solidification occurs without a color change. The melting point of this metastable phase is measurable (see a shaded circle in Fig. 1a). However, it is not clear whether the fusion is congruent or incongruent because the endothermic peak due to the fusion of this charge-transfer complex is followed by an exothermic peak due to the solidification to the stable salt. This temperature is close to the melting point of the corresponding 1,3,5-trinitrobenzene complex, 114—114.5 °C, reported by Sudborough and Beard.[5]

Figure 1b presents the phase diagram of the ethyl ester–picric acid system. This ester forms a congruently melting 1:1 salt and an incongruently melting 2:1 salt. The melting point is located at 128 °C and the peritectic point at 120 °C. The metastable red complex is obtainable by quenching of the melt at 50 mol%. The melting point of this complex is found at 104.5 °C and is significantly higher than that of the corresponding trinitrobenzene complex, 88 °C.[5] The vibrational spectrum of the 2:1 salt shows clearly the presence of both NH_2 and NH_3^+ groups. The color of specimens having the composition of about 2:1 mole ratio is deeper than

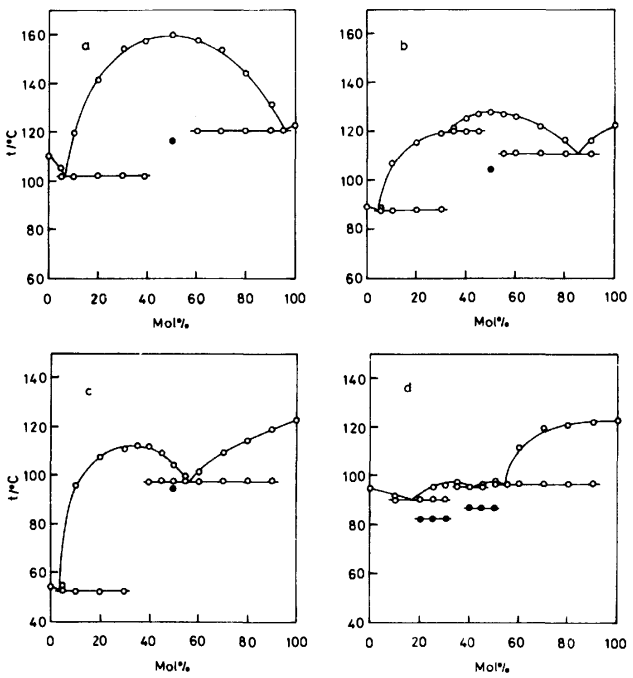

Fig. 1. Phase diagrams of the systems of picric acid with (a) methyl *p*-aminobenzoate, (b) the ethyl ester, (c) the pentyl ester, and (d) the heptadecyl ester. The shaded circles are the melting points of the metastable phase.

that of the 1:1 salt, suggesting a charge-transfer interaction between the donor molecule and the picrate anion.[6] The phase diagram of the propyl ester–picric acid system is of a type similar to that described above. The 1:1 salt melts at 114 °C and the 2:1 salt decomposes at 105.5 °C. The latter temperature is lower by 2 °C than the eutectic on the picric acid-rich side. Molten mixtures in the composition range from 50 to 80 mol% can form red solids on rapid cooling. The metastable phase melts at 89 °C regardless of the composition. The flatness over such a range may be the indication of incongruent melting of the charge-transfer complex. When the butyl ester is employed as a base, the thermal stabilities of the 1:1 and 2:1 salts are reversed. The former salt melts incongruently at 109.5 °C and the latter melts congruently at 112 °C. The charge-transfer complex melting at 97 °C is observed at 45 and 50 mol%.

The phase diagrams obtained empolying the pentyl and hexyl esters show only 2:1 salts. The red complex of the pentyl ester is found only at 50 mol% and melts at 94.5 °C (see Fig. 1c). In the case of the hexyl ester, the 2:1 salt melts at 101.5 °C and the red complex observed in the range from 40 to 50 mol% melts at 90.5 °C. These charge-transfer complexes are possibly of the 1:1 mole ratio.

Simple salts appear again in the systems with the heptyl ester and with the higher homologous members. The octyl, undecyl, and pentadecyl esters are exceptions. The diagrams given by the heptyl, nonyl, decyl, dodecyl, tridecyl, and tetradecyl esters are of the same type as that shown in Fig. 1b. However, the eutectic on the picric acid-rich side is located near 55 mol% because of the low thermal stability of the 1:1 salt. The heptyl ester is unique in the sense that two metastable complexes with distinctly different melting points are formed with picric acid. The one appearing in the range from 10 to 20 mol% melts at 71 °C and the other in the range from 40 to 50 mol% melts at 91 °C. The metastable picric acid complex of the tetradecyl ester is found in an exceptionally wide composition range, namely, from 40 to 80 mol%. The 1:1 salt melts congruently at 99 °C and the charge-transfer complex melts at 90.5 °C. In this combination, the difference in the melting point is the smallest among the similar examined combinations.

The octyl, undecyl, and pentadecyl esters produce phase diagrams which bear a certain similarity to that given in Fig. 1c. The thermal stability of the congruently melting 2:1 salts is lower than that of the salt derived from the pentyl ester. It must be noted that the stability is enhanced by an increase in the alkyl chain length; that is, 92 °C with the octyl ester salt, 95 °C with the undecyl ester salt, and 97.5 °C with the pentadecyl ester salt. The metastable charge-transfer complex is also stabilized in the same order; namely, 67.5 °C in the octyl ester complex, 82.5 °C in the undecyl ester complex, and 88 °C in the pentadecyl ester complex.

The phase diagrams given by the hexadecyl, heptadecyl, and octadecyl esters are exemplified by

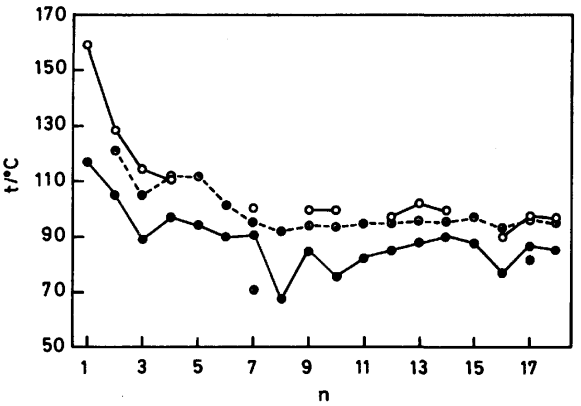

Fig. 2. Congruent or incongruent melting points of the 1 : 1 salt (○), of the 2 : 1 salt (⊙), of the 1 : 1 charge-transfer complex (●), and of the 2 : 1 complex (◑) plotted against the ester alkyl chain length (n).

that of the second member shown in Fig. 1d. Both the 1:1 and 2:1 salts melt congruently. The relative thermal stability of the 1:1 salt is increased by an increase in the alkyl chain length. While the 1:1 salt of the hexadecyl ester melts at 90.5 and the 2:1 salt at 93 °C, the former salt of the octadecyl ester melts at 97 °C and the latter at 95 °C. Note that the two salts in Fig. 1d have approximately the same melting points. Although two metastable charge-transfer complexes melting at 82.5 and 87 °C, respectively, are formed with the heptadecyl ester, the other two esters give only one kind. The hexadecyl ester complex melts at 77.5 °C and the octadecyl ester complex at 85.5 °C. They appear in the composition range covering 50 mol%.

The congruent or incongruent melting points of the 1:1 and 2:1 picrates and also of the 1:1 charge-transfer complex are plotted against the ester alkyl chain length in Fig. 2. The thermal stability of the 1:1 salt represented by open circle diminishes drastically in the first four members. The salt appears intermittently among the higher members. The charge-transfer complex shown by shaded circle is formed with all the esters examined. Contrary to the case of pyrene-*N*-alkyl-2,4,6-trinitroaniline reported earlier,[1] the complexes are similarly colored. Therefore, it is difficult to determine whether the complexes of the lower homologous members are different in the nature from those of the higher members or not. When the 1:1 salt and the 1:1 complex are obtainable with a given ester, the two products may be called isomorphs. The charge-transfer complexes found in the present series are metastable without exception. Nevertheless, one can see that the longer the alkyl group, the thermal stability of the complex comes closer to that of the salt.

The ethyl to octadecyl esters produce 2:1 salts with picric acid. The melting point is least dependent upon the ester alkyl group and is almost constant from the octyl ester to the octadecyl ester. It may be emphasized that complex isomerism is observed even in the 2:1 composition range when the heptyl and heptadecyl esters are the donor compounds.

This work was supported by the Grant-in-Aid of Special Research Project on Properties of Molecular Assemblies (No. 60104002) from the Ministry of Education, Science and Culture.

References

1) A. Togashi and Y. Matsunaga, *Bull. Chem. Soc. Jpn.*, **57**, 1058 (1984).
2) R. A. Adams, E. K. Rideal, W. S. Burnett, R. L. Jenkins, and E. E. Dreger, *J. Am. Chem. Soc.*, **48**, 1758 (1926).
3) R. M. Issa and M. M. El-Essawey, *Z. Phys. Chem. (Leipzig)*, **253**, 96 (1973).
4) G. Saito and Y. Matsunaga, *Bull. Chem. Soc. Jpn.*, **44**, 3328 (1971).
5) J. J. Sudborough and S. H. Beard, *J. Chem. Soc.*, **97**. 773 (1910).
6) Y. Matsunaga and G. Saito, *Bull. Chem. Soc. Jpn.*, **45**, 963 (1972).

Kinetics of the Solubilization of Pinacyanol Chloride into a Complex between Bovine Serum Albumin and Sodium Dodecyl Sulfate

Kunio TAKEDA,* Tohru OHTAWA, Kazuaki HACHIYA, and Koichiro AOKI†
Department of Applied Chemistry, Faculty of Technology, Okayama University of Science, 1-1 Ridai-cho, Okayama 700
(Received July 19, 1986)

Synopsis. The stopped-flow method was applied to the solubilization of pinacyanol chloride into a complex formed by bovine serum albumin and sodium dodecyl sulfate. The rate constant of the solubilization became larger with the step-by-step formation of the complex and finally attained values compatible with those for the pure surfactant micelle.

Various studies have been made of the interaction of bovine serum albumin (BSA) with sodium dodecyl sulfate (SDS).[1-3] However, most attention has been focused on both the binding nature of the surfactant and the conformational change in the protein. Few attempts have been made to find the nature of the bound surfactant ions themselves. The solubilization phenomenon is believed to be convenient for investigating the bound state of the surfactants on the protein. Equilibrium studies have been done on the solubilization of several dyes into the protein-surfactant complex,[4,5] but kinetic studies have not yet been done on this phenomenon.

Pinacyanol chloride is well-known as a useful dye for determining spectrophotometrically the critical micelle concentration (cmc) of anionic surfactants such as SDS.[6,7] In the present study, the solubilization of the pinacyanol chloride into the BSA–SDS complex was studied by the stopped-flow method. This paper shows a kinetic similarity of the complex to the SDS micelle in the solubilization of the dye.

Experimental

The sources of crystalline BSA and SDS have been described elsewhere.[8] The cmc of SDS by the electrical conductance method was 8.3×10^{-3} M at 25 °C (1 M=1 mol dm^{-3}).[8] The BSA concentration was determined spectrophotometrically using $E^{1\%}_{1cm}=6.8$ at 280 nm.[9] The protein concentration was kept at 1.0×10^{-5} M. The pinacyanol chloride was purchased from the Eastman Kodak Co. The absorption coefficient of the dye was assumed to be 88,000 at 600 nm at concentrations around 1.0×10^{-5} M.[7] The dye concentration was kept at 1.0×10^{-5} M. We previously experienced that the presence of an electrolyte accelerated the fading of the dye somewhat.[10-12] Thus, all the measurements were carried out in a non-buffered system, using water prepared by passing redistilled water through a mixed-bed ion-exchange column.[13]

The absorbance measurements were carried out with a Hitachi double-beam spectrophotometer, Model 220. Measurements of stopped-flow and rapid-scanning were made with a stopped-flow apparatus, RA-401, of the Union Giken Co. equipped with a kinetic data processor, RA-415. All the measurements were made at 25 °C.

†Professor Emeritus of Gifu University, Gifu 501-11.

Results and Discussion

The color change of pinacyanol chloride from red to blue occurs in a concentration range not very far from the cmc of the anionic surfactant.[6,7] The blue color above the cmc is characterized by two absorption bands, α- and β-bands at 607 and 562 nm, and the red color below the cmc, by the γ-band around 480 nm. The γ-band is due to the aggregate formed by the dye and the dodecylsulfate ion, while the α- and β-bands are attributable to the solubilization of the dye into the micelle.[6] (In the absence of the surfactant, the α- and β-bands appear at 600 and 550 nm respectively, probably because of the monomer-dimer equilibrium of the dye,[6] while the γ-band does not appear). Figure 1 shows the SDS concentration dependences of the absorbance at these three bands in the absence (dotted curve) and in the presence of BSA. In a SDS solution without the protein, the absorbance at the γ-band disappeared at SDS concentrations higher than 7 mM, which is slightly below the cmc. Simultaneously, the absorbances at α- and β-bands began to increase at this concentration. However, the absorbances at the α- and β-bands began to increase at much lower SDS concentrations in the presence of BSA than in the absence of BSA. This is probably due to the solubilization of the dye into the complex formed by BSA and SDS.[4,5] In the presence of BSA, the

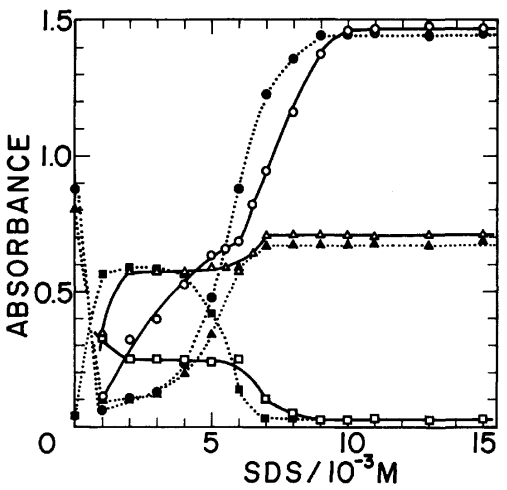

Fig. 1. The SDS concentration dependences of absorbance of pinacyanol chloride at α-(○, ●), β-(△, ▲), and γ-bands (□, ■) in the absence (dotted curve) and the presence (solid curve) of 1.0×10^{-5} M BSA.

absorption at α-band increased step-by-step until 10 mM SDS, making a clear break around 6 mM SDS, as is shown in Fig. 1. The helical structure of BSA is unfolded step-by-step by SDS both in water[13] and in a dilute phosphate buffer.[8] The major structural change is completed at 6 mM SDS in water,[13] where the break of absorbance appears at the α-band in Fig. 1.

Rapid-scanning experiments were made in the wavelength region between 450 and 620 nm, using the stopped-flow mixer to mix the dye solution with the BSA–SDS complex solution. When the pinacyanol was solubilized into the BSA–SDS complex, the absorption increased with time around the α-band in the rapid-scanning measurements, as seen in the inserted figure in Fig. 2. Since the dye has been considered to be solubilized in a state of the dye-surfactant aggregate, the mechanism of the solubilization may be expressed as follows:[12]

$$\mathrm{DS} + \mathrm{M} \longrightarrow \mathrm{MDS}, \quad (1)$$

where DS is an aggregate formed by the dye and SDS and M is one of the solubilizing sites of the micelle or of the surfactant-protein complex. The formation of the DS aggregate has been considered to be very fast compared with the time range of this work.[12] The stopped-flow measurements were made at the α-band in order to follow the solubilization of the DS aggregate. The solubilization of the dye into the SDS micelle has been observed as a pseudo-unimolecular reaction.[12] The first-order plot gave a good linear relationship also in the present kinetic study of the solubilization of the dye into the surfactant-protein complex.[14] These findings suggest that fairly many DS aggregates are solubilized into one micelle or into one surfactant-protein complex. It is generally accepted in the application of the stopped-flow method that only forward reactions can be observed in most of the time range in which the absorbance changes appreciably with the progress of the reaction.[15] Therefore, Reaction (1) can be rewritten as the following pseudo-unimolecular reaction;

$$\mathrm{DS} \xrightarrow{k} \mathrm{MDS} \quad \text{(in excess of M)} \quad (2)$$

where k is the forward rate constant.

The SDS concentration dependence of the rate constant, k_{complex}, of the solubilization of pinacyanol into the complex is shown in Fig. 2, together with the SDS concentration dependence of the rate constant, k_{micelle}, of the solubilization of the dye into the SDS micelle. The rate constant, k_{complex}, increased step-by-step with the increase in the SDS concentration, while k_{micelle} did so gradually and monotonously. On the other hand, since the BSA–SDS complexes are formed in a concentration range of SDS where the concentration of unbound surfactants is lower than the cmc, ordinary micelles do not exist in the total SDS concentrations below about 10.3 mM (=8.3 mM (cmc) of unbound SDS + about 2 mM SDS bound to 1.0×10^{-5} M BSA).[8,13] Therefore, the step-by-step change in k_{complex} below 10 mM SDS must reflect the nature of the BSA–SDS complex. In other words, k_{complex} depends on the binding number of SDS to the protein. After the sudden increase in the k_{complex}, it gave a plateau in spite of the increase in the binding number, as may be seen in Fig. 2. It appears that k_{complex} begins to increase again when a binding of about 120 SDS is attained; this can be said in view of the binding isotherm of the BSA–SDS system in a dilute phosphate buffer of an ionic strength of 0.014[8] and the dependence of the residue ellipticity, $[\theta]_{222}$, on the SDS concentration in the phosphate buffer[8] and in water.[13] Finally, it increased sharply and approached the values of k_{micelle}. However, it is not certain whether the increase in k_{complex} in the narrow concentration range of 8—11 mM SDS means the solubilization of the dye into the complex with a larger number of SDS or into the SDS micelle itself. The present results indicate that the more the surfactants bind to the protein, the faster the solubilization occurs.

Recently, a single relaxation has been found in the same BSA–SDS system by means of the pressure-jump method with conductivity detection.[13] The relaxation time of the BSA–SDS system approaches those in the SDS micelle system, just as the k_{complex} value becomes compatible with the k_{micelle} value with an increase in the SDS concentrations. This relaxation has been considered to be due to the partial breakdown and reformation of the complex.[13] The surfactant monomers participate in the partial breakdown and reformation of the complex, while pinacyanol participates in the present solubilization process.

It is worth noting that a similarity of the protein-surfactant complex to the surfactant micelle also appears in these kinetic phenomena. Both the kinetic phenomena reflect the fact that the bound states of dodecyl sulfate ions on the BSA molecule are very close to those of the SDS micelle.

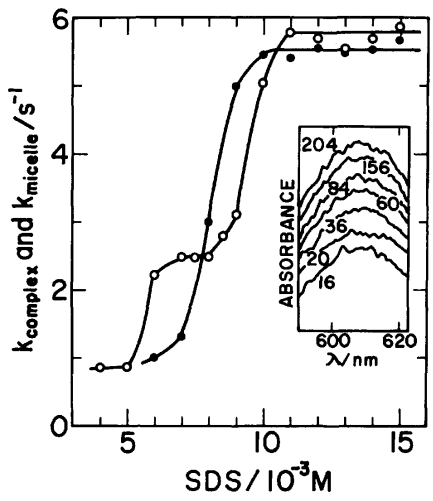

Fig. 2. The SDS concentration dependences of k_{complex} (○) and k_{micelle}(●). The rapid scanning spectra around α-band are inserted in this figure. The numerical values designate time in millisecond unit (including dead time) after mixing dye and complex solutions.

References

1) J. Steinhardt and J. A. Reynolds, "Multiple Equilibria in Proteins," Academic Press, New York (1969), pp. 239—302.
2) M. N. Jones, "Biological Interfaces," Elsevier Scientific Publishing Co., Amsterdam (1975), pp. 101—130.
3) S. Lapanje, "Physicochemical Aspects of Protein Denaturation," John Wiley & Sons, New York (1978), pp. 156—179.
4) J. Steinhardt, N. Stocker, D. Carroll, and K. S. Birdi, *Biochemistry*, **13**, 4461 (1974).
5) J. Steinhardt, J. R. Scott, and K. S. Birdi, *Biochemistry*, **16**, 718 (1977).
6) H. B. Klevens, *Chem. Rev.*, **47**, 1 (1950).
7) P. Mukerjee and K. J. Mysels, *J. Am. Chem. Soc.*, **77**, 2937 (1955).
8) K. Takeda, M. Miura, and T. Takagi, *J. Colloid Interface Sci.*, **82**, 38 (1981).
9) "Handbook of Biochemistry (Selected Data for Molecular Biology)," 2nd ed., ed by H. A. Sober and R. A. Harte, CRC Press, Cleveland, Ohio (1973), p. C-71.
10) T. Yasunaga, K. Takeda, and S. Harada, *J. Colloid Interface Sci.*, **42**, 457 (1973).
11) K. Takeda and T. Yasunaga, *J. Colloid Interface Sci.*, **45**, 406 (1973).
12) K. Takeda, N. Tatsumoto, and T. Yasunaga, *J. Colloid Interface Sci.*, **47**, 128 (1974).
13) K. Takeda, *Bull. Chem. Soc. Jpn.*, **55**, 2547 (1982).
14) For the first-order plot and the determination of the rate constant, see Refs. 10 and 12.
15) B. Chance, "Investigation of Rates and Mechanisms of Reactions (Part II)," ed by G. G. Hammes, John Wiley & Sons, New York (1974), pp. 5—62.

Derivation of the Quantity of Catenanes in Equilibrium Polymeric Mixtures

Kazumi SUEMATSU and Haruo OGURA
Pharmaceutical Science, Kitasato University, Shirogane, 5-9, Minato-ku, Tokyo 108
(Received July 12, 1986)

Synopsis. A theoretical consideration is introduced regarding catenation in an equilibrium mixture. The quantity of catenane from rings i and j is expressed as $[\phi(i, j)]\simeq\Phi PE\ [Ri][Rj]$. The symbols Φ, P, and E denote the catenation probability, the overlapping probability and the penetration probability. At θ points or above a critical monomer concentration C^*, $E\simeq1$. Then, the above equation leads to the analogous form reported previously.[1]

Some theoretical considerations have been reported concerning catenation from two cyclic substances.[1,5] However, there has not been any report that theoretically preestimated the catenane distribution in an equilibrium system; this should be practically important for a characterization of such extensively established industrial materials as polyester, Nylon and polyoxymethylene, or should be one of the guiding principles for challenging a non-bonding polymer gel, one of the most attractive materials that have never been realized. This paper is presented with the aim of preestimating the yields of catenanes in equilibrium, the fundamental idea of which is based on cyclization[2] and entanglement theorems.[3]

Theory

Consider a polymer solution with the Flory distribution D in a volume V and mark half of the randomly chosen molecules red. Then, each will have the equal distribution D and the following equilibria will be established.

A: red.

$$C_{i+x} \rightleftarrows C_i + C_x$$
$$C_i \rightleftarrows R_i$$

B: white.

$$C_{j+y} \rightleftarrows C_j + C_y$$
$$C_j \rightleftarrows R_j$$

Here, C denotes a linear chain, subscripts i, j, x, and y the arbitrary numbers of repeating units and R a cyclic molecule. Then, some ratio of R_i and R_j will encounter and entangle to form a catenane $\phi(i, j)$. Thus, the above equilibria can be rewritten as the following equilibria:

$$C_{i+x} \overset{K_1}{\rightleftarrows} C_i + C_x, \tag{1}$$
$$C_{j+y} \overset{K_2}{\rightleftarrows} C_j + C_y, \tag{2}$$
$$C_i \overset{K_3}{\rightleftarrows} R_i, \tag{3}$$
$$C_j + R_i \overset{K_4}{\rightleftarrows} (C_jR_i), \tag{4}$$
$$(C_jR_i) \overset{K_5}{\rightleftarrows} \phi(i, j), \tag{5}$$

Eqs. 1—5 reduce to

$$C_{i+x} + C_{j+y} \overset{K}{\rightleftarrows} C_x + C_y + \phi(i, j), \tag{6}$$

Equation 1 represents the process in which fragment C_x is released from a permitted angle $\delta\omega$ in a small volume v_s constrained around the terminal atom of fragment C_i to the whole volume V of the system. Assuming that the probabilities of lying in v_s and $\delta\omega$ are independent,† the entropy change of K_1 can be written[2]

$$e^{\Delta S/R} = \left(\frac{1}{\sigma_C}\right)(4\pi V/\delta\omega v_s N_A), \tag{7}$$

where σ_C is the number of the reaction sites of the chain if those have an equal chemical reactivity.

Let ΔH_1 be the enthalpy change of K_1. Then, the equilibrium constant of Eq. 1 is written

$$K_1 = \left(\frac{1}{\sigma_C}\right)(4\pi V/\delta\omega v_s N_A)e^{-\Delta H_1/RT}. \tag{8}$$

Similarly, we have

$$K_2 = \left(\frac{1}{\sigma_C}\right)(4\pi V/\delta\omega v_s N_A)e^{-\Delta H_2/RT}. \tag{9}$$

Equation 3 represents the process that one end of C_i is confined within the angle $\delta\omega$ in volume v_s around another terminal atom to form a new chemical bond. Let σ_{Ri} be the number of the reaction sites of the ring and $W(0)$ the probability that the end-to-end distance is zero. Then, as already pointed out, the equilibrium constant is expressed as

$$K_3 = \left(\frac{\sigma_C}{\sigma_{R_i}}\right)(\delta\omega/4\pi)W_i(0)v_s e^{-\Delta H_3/RT}. \tag{10}$$

Equation 4 represents the process in which C_j and R_i overlap one another under the condition of the phantom molecules. Let this probability be $P(i, j)$. $P(i, j)$ is given

$$P(i, j) = \frac{4\pi S^3 N_A}{3V}, \tag{11}$$

where S is the radius of the overlapping volume.

Now, let $E(i, j)$ be the probability for one molecule

† This is a reasonable assumption since the chain must be sufficiently long (30 bonds or more) for the catenation to occur.[1]

to move into the sphere of another molecule. Then, E should be equal to the ratio of the probability lying inside the sphere to that lying outside the same. If we define ψ as the volume fraction of segments per unit volume, the probaility that all of a given sequence of x lattice sites are available for occupancy by another chain molecule is $(1-\psi)^x$. Then, E is

$$E(i,j) = \left(\frac{1-\psi_i}{1-\psi_o}\right)^x, \tag{12}$$

where subscripts i and o denote the inside of the molecule and the outside, respectively. Note that ψ is not the real volume, but the excluded volume of the segment.[4] Hence, we may let

$$K_4 = P(i,j)\cdot E(i,j) = (4\pi S^3 N_A/3V\cdot[(1-\psi_i)/(1-\psi_o)]^x. \tag{13}$$

Equation 5 represents the process in which the one end of C_j meets the another end, accompanying the interlocking with R_i. If the probability for the interlocking, Φ, is independent of the cyclization probability, applying the expression in K_3 we have

$$K_5 = \Phi\cdot(\sigma_C/\sigma_{R_j})\cdot(\delta\omega/4\pi)\cdot W_j\cdot(0)\cdot v_s\cdot e^{-\Delta H_5/RT} \tag{14}$$

The product of K_1—K_5 gives the equilibrium constant of Eq. 6:

$$K = \prod_k K_k = \Phi\cdot[V^2\cdot P\cdot E/\sigma_{R_i}\cdot\sigma_{R_j}\cdot N_A^2]\cdot W_i(0)\cdot W_j(0)\cdot e^{-\Delta H/RT}, \tag{15}$$

where $\Delta H = \sum_k \Delta H_k$.

Also, the following relationship is established in the solution:

$$K = \frac{[C_x]\cdot[C_y]\cdot[\phi(i,j)]}{[C_{i+x}]\cdot[C_{j+y}]} \tag{16}$$

$$= p^{-(i+j)}[\phi(i,j)]. \tag{17}$$

For a high-molecular-weight mixture, p(the extent of reaction of linear species)$\approx$*1 and* $\Delta H\approx 0$ are approximated. Substituting Eq. 15 to Eq. 17, then we obtain

$$[\phi(i,j)] \approx \Phi\cdot P\cdot E\cdot\{V^2/\sigma_{R_i}\cdot\sigma_{R_j}\cdot N_A^2\}\cdot W_i(0)\cdot W_j(0). \tag{18}$$

Rearranging Eq. 18, we have an expression for the quantity of $\phi(i,j)$:

$$[\phi(i,j)] \approx \Phi\cdot P\cdot E\cdot\{V\cdot W_i(0)/\sigma_{R_i}\cdot N_A\}\times\{V\cdot W_j(0)/\sigma_{R_j}\cdot N_V\} \tag{19}$$

$$\equiv \Phi\cdot P\cdot E\cdot[R_i][R_j] \quad \text{(mole/V)}. \tag{19'}$$

The physical meaning that Eq. 19 suggests is easy to

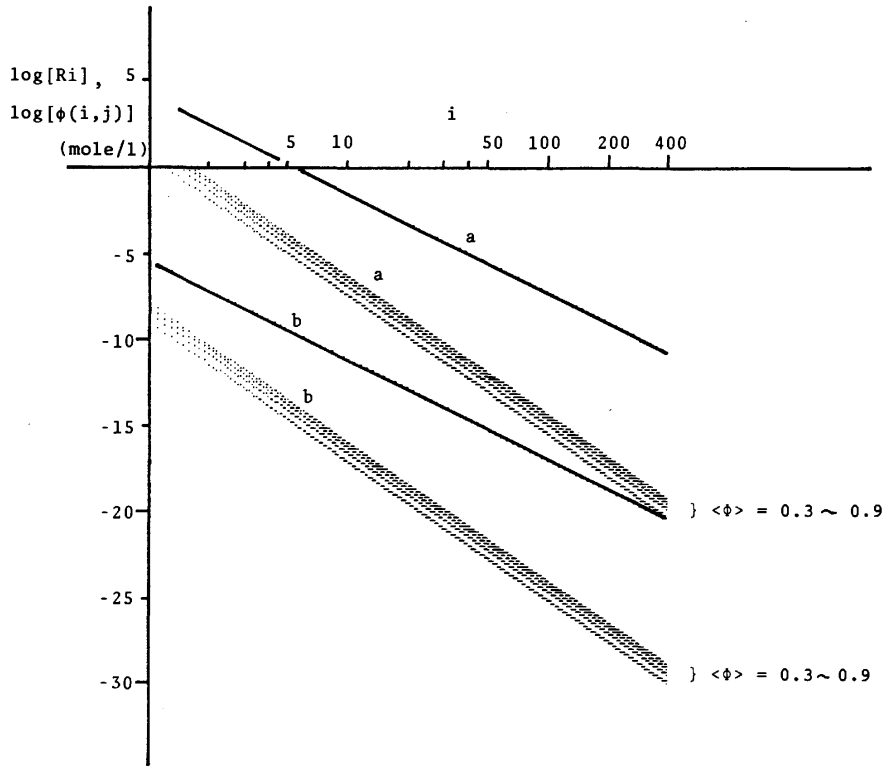

Fig. 1. Catenane distribution (broken lines) from $i=j$ rings compared to ring distribution (solid lines) for Kuhn segment number.
a: Kuhn segment length, $l=2$. b: $l=50$. Each four curves from $\langle\Phi\rangle=0.3$ to 0.9 (step 0.2) are drawn.

Table 1. The Equilibrium Constant of the Catenation between 186 DNA and $\lambda_c I_{857}$DNA

Experimental	Wang & Schwartz	Suematsu & Ogura
$K=2.2\times10^{-13}$ cm^3	7.8×10^{-13}	3.5×10^{-13}

comprehend: i.e., the quantity of the catenane $\phi(i, j)$ is proportional to the product of the concentrations of cyclic i and j-mer, and the probability for the entanglement of both.

In terms of the weight fraction $X_{\phi(i,j)}$, Eq. 19 leads to

$$X_{\phi(i,j)} \simeq \Phi PE\frac{(i+j)}{i\cdot j}C_0X_{Ri}X_{Rj}, \tag{20}$$

where C_0 is the initial monomer concentration.

Discussion

As is clear from Eq. 20, the probability that catenation occurs is proportional to the product of the cyclization probabilities of rings i and j, suggesting that catenanes will be formed only with a very low probability, especially for larger i and j.

Letting n be the segment number, since P varies roughly as $n^{3/2}$ and X_{Rn} as $n^{-3/2}$, $X_{\phi(i,j)}$ must decrease in proportion to $n^{-5/2}$. Thus, the catenane from macrocyclics may be neglected (Fig. 1).

E may be unity in θ points or above the critical concentration C^* defined by $\psi_{in}=\psi_{out}$. Finally, Eq. 19 is reduced to a conclusion analogous to previous reports[1,5]:

$$[\phi(i,j)] \simeq \Phi\left(\frac{4}{3}\pi S^3\frac{N_A}{V}\right)[R_i][R_j]. \tag{21}$$

One credible example has been reported for catenation; i.e., dimeric catenanes between 186 DNA and $\lambda_c I_{857}$DNA are formed to yield $K=2.2\times10^{-13}$ cm^3.[5]

Adopting as a value of s the sum of the radiuses of gyration of the rings and $\langle\Phi\rangle\simeq0.4-0.6$, a better agreement between theory and experiment is found (Table 1) (see Appendix I).

Appendix I

For an extreme rigid(thin) chain, the catenation probability is given by[3]

$$\Phi \cong A\exp(-\alpha s^3).$$

A and α are the constants for the given Kuhn segment number. Then, the average value of Φ may be written

$$\langle\Phi\rangle = \int_0^s 4\pi s^2\Phi ds \Big/ \int_0^s 4\pi s^2 ds.$$

A numerical calculation yields $\langle\Phi\rangle\cong0.33$ for $n=20$, 0.37 for $n=40$, 0.41 for $n=60$ and 0.43 for $n=80$ (increasing slowly with chain length). It seems to be in a rough linear relationship to the logarithm of the segment number in this range, i.e.,

$$\langle\Phi\rangle \sim \mathrm{Log}\, n.$$

Thus, $\langle\Phi\rangle\cong0.4$—0.6 is a good approximation for $n\cong200$ in DNA.

References

1) H. L. Frisch and E. Wasserman, *J. Am. Chem. Soc.*, **83**, 3789 (1961).
2) H. Jacobson and W. H. Stockmayer, *J. Chem. Phys.*, **18**, 1600 (1950).
3) M. D. Frank-Kamenetskii, A. V. Lukashin, and A. V. Vologodskii, *Nature*, **258**, 398 (1975).
4) P. J. Flory, "Principles of Polymer Chemistry," Cornell Univ. Press (1953).
5) J. C. Wang and H. Schwartz, *Biopolymers*, **5**, 953 (1967).

Crystal and Molecular Structure of a Thiolate-Bridged Binuclear Nickel(II) Complex, $[Ni_2\{SCH(CH_2CH_2NH_2)_2\}_2]Br_2$

Masahiro MIKURIYA,* Sigeo KIDA,* and Ichiro MURASE†
Coordination Chemistry Laboratories, Institute for Molecular Science,
Okazaki National Research Institutes, Okazaki 444
†Laboratory of Chemistry, College of General Education, Kyushu University,
01, Ropponmatsu, Chuo-ku, Fukuoka 810
(Received September 26, 1986)

Synopsis. The crystal structure of bis[μ-(1,5-diamino-3-pentanethiolato)-*N*,*N'*, μ-S]-dinickel(II) bromide was determined by the single-crystal X-ray diffraction method. The complex has a thiolate-bridged binuclear structure, with a dihedral angle 145.2° between the two coodination planes.

Recently, 1,5-diamino-3-pentanol (Hdpl) was synthesized by our group,[1] and shown to form essentially planar binuclear complexes with copper(II) and nickel(II), whose skeletal structure illustrated in Fig. 1 was evidenced by X-ray crystal structure analysis for $Cu_2(dpl)_2Cl_2\cdot 3H_2O$[2] and by diamagnetism for the nickel complex.[1] On the analogy of the above examples, 1,5-diamino-3-pentanethiol (Hdpet) is expected to be a planar binucleating ligand. In fact, the nickel complexes formulated as $Ni_2(dpet)_2X_2$ (X=Br, ClO_4, NO_3, BPh_4) were all diamagnetic implying the planar binuclear structure similar to that shown in Fig. 1.[3] However, in thiolate-bridged binuclear nickel(II) complexes so far known, the two coordination planes are all bent at the S–S bond with dihedral angle of 82.3—110.2° and in our knowledge no planar ring has ever been reported.[4-7] Thus, we have determined the crystal structure of $Ni_2(dpet)_2Br_2$ by X-ray analysis to see whether the two coordination planes assume a coplanar or bent structure.

Experimental

Reddish brown crystals of $[Ni_2(dpet)_2]Br_2$ were prepared by the method previously reported.[3] A crystal with dimensions of 0.08×0.38×0.54 mm was used for the X-ray analysis. The unit-cell parameters and intensities were measured on a Rigaku AFC-5 automated four-circle diffractometer with graphite-monochromated Mo $K\alpha$ radiation (λ=0.71073 Å).

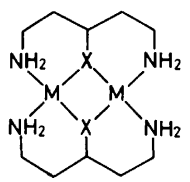

Fig. 1. The binuclear complex cation of dpl or dpet (M=Cu(II) or Ni(II); X=O or S).

Crystal Data: $Ni_2(C_5H_{13}N_2S)_2Br_2$, F.W.=543.65, monoclinic; $P2_1/m$; a=10.072(7), b=18.188(12), and c=5.162(5) Å; β=103.20(7)°; V=920.6(13) Å^3; D_m=1.92, D_c=1.96 g cm^{-3}, Z=2, μ(Mo $K\alpha$)=65.7 cm^{-1}.

The intensity data were collected by the 2θ—ω scan technique with a scan rate of 3° min^{-1}. Three standard reflections were monitored every 50 reflections, and their intensities showed a good stability. A total of 3372 reflections with $2\theta<60°$ were collected. The intensity data were corrected for the Lorentz-polarization effects and for absorption. Independent 1739 reflections with $|F_o|\geq 3\sigma(|F_o|)$ were considered as "observed" and were used for the structure analysis.

The structure was solved by the direct method. Refinement was carried out by the block-diagonal least-squares method. The weighting scheme $w=[\sigma^2_{count}+(0.015|F_o|)^2]^{-1}$ was employed. Hydrogen atoms were inserted in their calculated positions and fixed at the positions. The final discrepancy factors were $R=\Sigma||F_o|-|F_c||/\Sigma|F_o|=0.053$ and $R'=[\Sigma w(|F_o|-|F_c|)^2/\Sigma w|F_o|^2]^{1/2}=0.052$. Final difference Fourier map was featureless. All the calculations were carried out on the HITAC M-680H computer at the Computer Center of the Institute for Molecular Science by the use of the UNICS-III, *MULTAN* 78, and ORTEP programs.[8] The final positional and thermal parameters with their estimated standard deviations are given in Table 1. The coordinates and isotropic temperature factors of the hydrogen atoms, the anisotropic thermal parameters of the non-hydrogen atoms, and the F_o—F_c tables have been deposited as a Document No. 0000 at the Office of the Editor.

Table 1. Fractional Positional Parameters (×10^4) and Thermal Parameters of Non-Hydrogen Atoms with Their Estimated Standard Deviations in Parentheses

Atom	x	y	z	B_{eq}/Å^2
Br	2514(1)	−294(1)	842(1)	3.4
Ni	3080(1)	1638(1)	6191(1)	2.0
S(1)	1848(2)	2500	7413(4)	2.2
S(2)	4607(2)	2500	7007(4)	2.2
N(1)	1659(6)	889(3)	5490(9)	2.8
N(2)	4388(5)	936(3)	5329(9)	2.7
C(1)	129(9)	2500	5135(18)	2.8
C(2)	−115(7)	1806(4)	3466(13)	3.5
C(3)	185(7)	1099(4)	5028(14)	3.7
C(4)	5230(9)	2500	3938(16)	2.4
C(5)	6008(7)	1797(4)	3788(13)	3.3
C(6)	5119(7)	1131(4)	3199(12)	3.2

Results and Discussion

The crystal structure consists of discrete binuclear cations, $[Ni_2(dpet)_2]^{2+}$, and bromide ions. A perspective view of $[Ni_2(dpet)_2]^{2+}$ is shown in Fig. 2. The cation has a symmetry plane along the S(1)-S(2) bond. As has been anticipated, the complex ion has a thiolate-bridged binuclear structure and each nickel ion is in a square-planar N_2S_2 environment. The Ni-S and Ni-Ni distances are normal as Ni(II)-S(thiolate) and Ni(II)-N(amine) bonds.[4-7,9] Each NiS_2N_2 coordination unit is virtually planar, but the two planes are bent at the S(1)-S(2) bond with a dihedral angle of 145.2°, making a contrast with the binuclear metal complexes of dpl.[2] Structural parameters of the present complexes are listed in Table 2 together with those of other thiolate-bridged binuclear nickel(II) complexes.[4-7] As seen in Table 2, the present complex assumes the largest values in the Ni-Ni distance, Ni-S-Ni angle, and the dihedral angle of the two coordination planes, τ. This should be ascribed to the steric requirement of dpet which favors the coplanar structure as supposed from the molecular model study and the planar structure of the analogous complex, $Cu_2(dpl)_2Cl_2 \cdot 3H_2O$. It should be noted here that the dihedral angle, τ, of the present complex is between those of other thiolate-bridged complexes (82.3—110.2°) and 180°. This is understandable as a compromise of the two opposing tendencies, i.e., the steric requirements 1) of the ligand to form a planar structure (τ=180°) and 2) of the thiolate sulfur to form Ni-S bonds with a Ni-S-Ni angle smaller than 90° as observed for several complexes so far reported giving rise to a remarkable bending of the two coordination planes such as τ=82.3—110.2°.

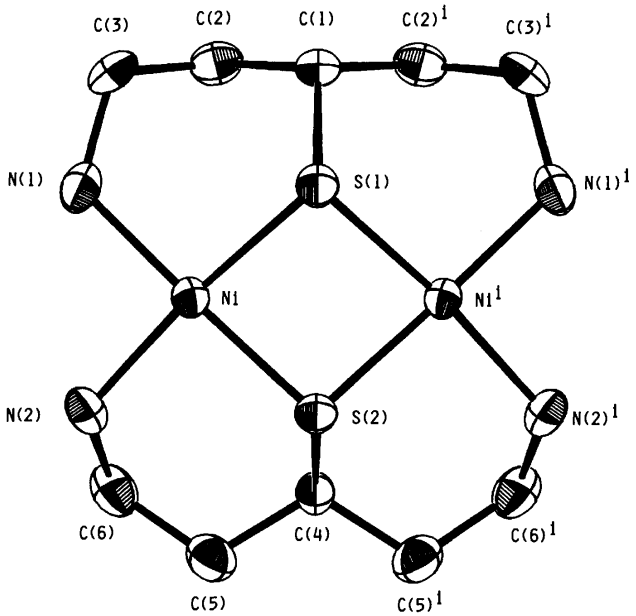

Fig. 2. A perspective view of $[Ni_2(dpet)_2]^{2+}$ ion. Selected bond lengths (l/Å) and angles (ϕ/°) are: Ni-Ni¹ 3.134(2), Ni-S(1) 2.180(2), Ni-S(2) 2.169(2), Ni-N(1) 1.950(6), Ni-N(2) 1.958(6); Ni-S(1)-Ni¹ 91.9(1), Ni-S(2)-Ni¹ 92.5(1), S(1)-Ni-S(2) 81.36(9), S(1)-Ni-N(1) 96.6(2), S(2)-Ni-N(2) 91.8(2), N(1)-Ni-N(2) 90.3(2). Superscript (i) refers to the equivalent position (x, 1/2−y, z).

The six-membered chelate ring, Ni-S(1)-C(1)-C(2)-C(3)-N(1), adopts a boat conformation where Ni and C(2) are −0.76 and −0.64 Å from the least-squares plane of the remaining four atoms, whereas the chelate ring, Ni-S(2)-C(4)-C(5)-C(6)-N(2), adopts a chair form where Ni and C(5) are −1.13 and 0.73 Å from the mean plane of the remaining four atoms.

The bromide ions are placed in the vicinity of the amino groups of dpet forming hydrogen bonds (Br···N(1)(x, y+1, z−1) 3.452(5), Br···N(1)(x, y+1, z) 3.474(6) Å).

The authors wish to express sincere thanks to Dr. Koshiro Toriumi of Institute for Molecular Science for his helpful advices and discussion.

References

1) I. Murase, M. Hatano, M. Tanaka, S. Ueno, H. Okawa, and S. Kida, *Bull. Chem. Soc. Jpn.*, **55**, 2404 (1982).
2) Y. Nishida and S. Kida, *Mem. Fac. Sci., Kyushu Univ., Ser. C*, **13**, 35 (1981).
3) I. Murase, S. Ueno, and S. Kida, *Bull. Chem. Soc. Jpn.*, **56**, 2748 (1983).
4) J. P. Fackler, Jr., *Prog. Inorg. Chem.*, **21**, 55 (1976).

Table 2. Comparison of Some Distances (l/Å) and Angles (ϕ/°) in Ni_2S_2 Rings of Thiolate-Bridged Binuclear Ni(II) Complexes

Complex	Ni-Ni	Ni-S	Ni-S-Ni	S-Ni-S	τ[a]	Ref.
$[Ni_2(SC_2H_5)_2(S_2CSC_2H_5)_2]$	2.76	2.179 −2.196	78.3(1) 78.4(1)	81.6(1) 81.1(1)	110.2	6
$[Ni_2(SCH_2CH_2SCH_2CH_2S)_2]$	2.733(5)	2.144 −2.220	76.7(2) 76.8(2)	82.5(2) 82.6(2)	82.3	7
$[Ni_2(C_5H_4NCH_2CH_2NHCH_2CH_2S)_2](ClO_4)_2$	2.739(1)	2.169(1) 2.186(1)	77.94(5)	79.61(6)	110	5
$[Ni_2(dpet)_2]Br_2$	3.134(2)	2.169(2) 2.180(2)	91.9(1) 92.5(1)	81.36(9)	145.2	This study

a) The dihedral angle between the two coordination planes.

5) T. B. Vance, Jr., L. G. Warner, and K. Seff, *Inorg. Chem.*, **16**, 2106 (1977).

6) A. C. Villa, A. G. Manfredotti, M. Nardelli, and C. Pelizzi, *J. Chem. Soc., Chem., Commun.*, **1970**, 1322.

7) G. A. Barclay, E. M. McPartlin, and N. C. Stephenson, *Inorg. Nucl. Chem. Lett.*, **3**, 397 (1967); *Acta Crystallogr., Sect. B*, **25**, 1262 (1969); D. J. Baker, D. C. Goodall, and D. S. Moss, *J. Chem. Soc., Chem. Commun.*, **1969**, 325.

8) T. Sakurai and K. Kobayashi, *Rikagaku Kenkyusho Hokoku*, **55**, 69 (1979); P. Main, S. E. Hull, L. Lessinger, G. Germain, J-P. Declercq, and M. M. Woolfson, *MULTAN* 78 (1978). A System of Computer Programs for the Automatic Solution of Crystal Structure from X-Ray Diffraction Data. Univ. of York, England and Louvain, Belgium; C. K. Johnson, Report No. 3794, Oak Ridge National Laboratory, Oak Ridge, Tennessee (1965).

9) C. H. Wei and L. F. Dahl, *Inorg. Chem.*, **9**, 1878 (1970).

Preparation and Characterization of the Dicobalt(III) Complexes Containing Bridging Di-μ-hydroxo Ligands

Tomoharu AMA,* Hiroshi KAWAGUCHI, and Takaji YASUI
Department of Chemistry, Faculty of Science, Kochi University,
Akebono-cho, Kochi 780
(Received September 13, 1986)

Synopsis. Three dicobalt(III) complexes, $[(L)Co(\mu\text{-}OH)_2Co(NH_3)_4]^{2+ \text{ or } +}$ (L=edda, $(gly)_2$, or nta), were newly prepared and their structures were assigned on the basis of absorption, ^1H NMR, and CD spectral data. Each of them has a structure in which the chromophores of two different types are bridged with two hydroxo ligands and with two hydrogen bonds between carboxyl and amino groups. These three complexes are stable for several days in aqueous solutions.

Although there have been many reports on the preparation and reactivity of dicobalt(III) complexes containing two bridging hydroxo ligands, only a few studies have reported on complexes in which two different cobalt(III) chromophores were bridged with the two hydroxo.[2,3] Complexes of this type are so important for investigations concerning the interaction between two cobalt atoms that a sure method to prepare a number of complexes of this type is required. In previous work,[4] we succeeded in preparing three isomers of $[(en)(gly)Co(\mu\text{-}OH)_2Co(en)(gly)]^{2+}$[1,4] in aqueous solutions. A modification of the method, which is described below, makes it possible to prepare many dicobalt complexes containing two bridging hydroxo. Two of the newly prepared complexes have chiral structures. The CD spectra of the optically resolved isomers will be reported.

Experimental

Preparation of Complexes. $[(edda)Co(\mu\text{-}OH)_2Co(NH_3)_4]Cl_2$ (1): In 20 cm³ of water, $K[Co(edda)(CO_3)]\cdot H_2O$ (1.7 g)[5] was dissolved and acidified with 60% perchloric acid (2 cm³). Separately, $[Co(NH_3)_4(CO_3)]ClO_4$ (1.5 g) were suspended in 20 cm³ of water and acidified with 60% perchloric acid (2 cm³). The two solutions were mixed with each other. The pH of the mixed solution was adjusted to 8.0 with a 2 mol dm⁻³ NaOH solution and stirred for 40 min in a water bath at 50 °C. The reacted solution was cooled to room temperature and then neutralized using a 2 mol dm⁻³ HCl solution and filtered. The filtrate was chromatographed on an SP-Sephadex column (4.7 cm×50 cm, K^+ form) and the adsorbed band was eluted with a 0.2 mol dm⁻³ KCl solution. The eluate from the dark-red band was evaporated to about 10 cm³ and the KCl deposited was filtered off. To the filtrate, methanol was added in order to eliminate any excess KCl; then, solution was filtered. A crude complex of $[(edda)Co(\mu\text{-}OH)_2Co(NH_3)_4]Cl_2$, obtained by adding ethanol to the filtrate, was optically resolved by the following procedure without further purification.

The crude complex (ca. 100 mg) was dissolved in 20 cm³ of water and the solution was poured onto an SP-Sephadex column (4.7 cm×50 cm, K^+ form). The adsorbed band was developed with a 0.1 mol dm⁻³ $K_2Sb_2(d\text{-tart})_2$ solution. The development was repeated on the same column using a micropump until the adsorbed band completely separated into two dark-red bands. The earlier and later bands denoted (−) and (+) CD signs at 574 nm, respectively. Each band was eluted out with 0.1 mol dm⁻³ $K_2Sb_2(d\text{-tart})_2$; then, each eluate was concentrated to a small volume under reduced pressure. To the concentrated solution, methanol was added to deposit $K_2Sb_2(d\text{-tart})_2$. After the deposited $K_2Sb_2(d\text{-tart})_2$ was filtered off, the filtrate was evaporated almost to dryness in order to exclude methanol. The obtained residue was dissolved in a small amount of water and reloaded on a short QAE-Sephadex column (3 cm×5 cm, Cl^- form). The solution eluted with water was concentrated to a small volume. An optically active isomer was obtained by adding methanol to the concentrated solution, which was recrystallized from water by adding methanol. Found for the $(+)^{CD}_{574}$ isomer: C, 14.84; H, 5.48; N, 17.07%. Calcd for $[(edda)Co(\mu\text{-}OH)_2Co(NH_3)_4]Cl_2\cdot H_2O = C_6H_{26}N_6O_7Cl_2Co_2$: C, 14.92; H, 5.43; N, 17.40%.

$[(gly)_2Co(\mu\text{-}OH)_2Co(NH_3)_4]S_2O_6$ (2): This complex was prepared and resolved by a method similar to that employed for **1**, except for the use of $K[Co(gly)_2(CO_3)]$[6] instead of $K[Co(edda)(CO_3)]$. The dithionate of this complex was obtained by adding a saturated solution of $Na_2S_2O_6$ to the aqueous solution (saturated) of the chloride. Found for the $(+)^{CD}_{572}$ isomer: C, 8.28; H, 4.78; N, 14.39%. Calcd for $[(gly)_2Co(\mu\text{-}OH)_2Co(NH_3)_4]S_2O_6\cdot 3H_2O = C_4H_{28}N_6O_{15}S_2Co_2$: C, 8.25; H, 4.85; N, 14.43%.

$[(nta)Co(\mu\text{-}OH)_2Co(NH_3)_4]Cl$ (3): In 12 cm³ of 15% perchloric acid, $[Co(NH_3)_4(CO_3)]ClO_4$ (1.5 g) was dissolved. Separately, $K_2[Co(nta)(CO_3)]$ (2.0 g) was dissolved in 12 cm³ of perchloric acid. The two solutions were mixed to each other. The pH of the solution was adjusted to 7.5 with a 2 mol dm⁻³ NaOH solution, and heated in a water bath (60 °C) for 30 min. After cooling to room temperature, the solution was diluted to 200 cm³ with water and poured onto an SP-Sephadex column (4.5 cm×50 cm, K^+ form). After the column was swept with 1 dm³ of water, the adsorbed band was developed with a 0.2 mol dm⁻³ KCl solution. A solution eluted from the dark-violet band (major band) was evaporated to about 10 cm³. White precipitates, which became deposited upon the addition of methanol (100 cm³) to the solution, were filtered off. To the filtrate, 100 cm³ of methanol was added once more and the methanolic solution was allowed to stand overnight in a refrigerator in order to obtain crude **3**, which was recrystallized from water by adding methanol. Found: C, 15.08; H, 4.92; N, 14.49%. Calcd for $[(nta)Co(\mu\text{-}OH)_2Co(NH_3)_4]Cl\cdot 2H_2O = C_6H_{24}N_5O_{10}ClCo_2$: C, 15.03; H, 5.04; N, 14.60%.

Results and Discussion

Structural Assignments of the Complexes. On the basis of the following five reasons, **1** was assigned to the structure given in Fig. 1 (A). (1) The column chromatogram gave a single band which was not a mixture of cationic and anionic complexes but was a cationic complex. (2) The elemental analysis data indicates that the NH_3/edda ratio is 4. (3) The absorption spectrum shows a characteristic charge-

transfer band arising from the Co(μ-OH)$_2$Co moiety at ca. 34000 cm^{-1} (Fig. 2), as [Co$_2$(μ-OH)$_2$(en)$_4$]$^{4+}$ and [Co$_2$(μ-OH)$_2$(NH$_3$)$_8$]$^{4+}$[8,9] show. (4) The first absorption band is very broad, suggesting that this complex contains chromophores of two different types. (5) In the ^{1}H NMR spectra (Fig. 3), the methylene protons of two glycinate rings (G-rings) in edda appeared as a quartet signal, suggesting that the two G-rings are equivalent in chemical environments; the edda takes an α-cis chelation form[10] (Fig. 3).

The structure illustrated in Fig. 1 (B) is proposed for the **2** on the basis of an arrangement similar to that described above. The possiblity that the Co(gly)$_2$(μ-OH)$_2$ moiety in this complex has a *trans(N)* structure can be ruled out for the following reasons. (1) The absorption spectrum of **2** is quite similar to that of **1**, having a *cis(N)* structure. (2) If the Co(gly)$_2$(μ-OH)$_2$ moiety has a *trans(N)* structure, it is expected that **2** exhibits a band (shoulder) at ca. 16000 cm^{-1}.[11,12] No such shoulder band appears, as shown in Fig. 2. Therefore, this moiety does not have a *trans(N)*-[Co(N)$_2$(O)$_4$] chromophore but has *cis(N)*. (3) Di(μ-hydroxo)dicobalt(III) complexes prefer a structure that is stabilized by two hydrogen bonds (N-H···OCO-) between the two cobalt chromophores (vide post). These hydrogen bonds can be formed in the proposed *cis(N)* structure but not in a *trans(N)* structure.

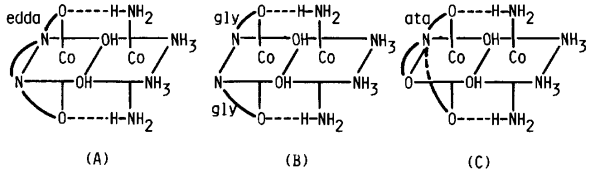

Fig. 1. Structures of the prepared complexes: (A) [(edda)Co(μ-OH)$_2$Co(NH$_3$)$_4$]$^{2+}$ (**1**), (B) [(gly)$_2$Co(μ-OH)$_2$Co(NH$_3$)$_4$]$^{2+}$ (**2**), and (C) [(nta)Co(μ-OH)$_2$Co(NH$_3$)$_4$]$^+$ (**3**).

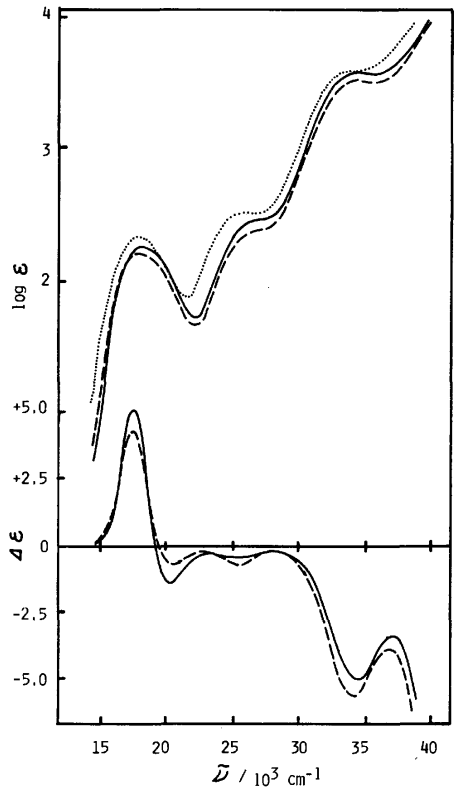

Fig. 2. Absorption and CD curves of the complexes: **1** (——), **2** (----), and **3** (·····).

The structure illustrated in Fig. 1 (C) is proposed for the **3** on the basis of the following: (1) There are three G-rings in the nta. Two of them appear as a quartet signal in the ^{1}H NMR spectra, showing that their chemical environments are equivalent, and one of them appears as a singlet signal. This result shows that there is a symmetrical plane on one of the G-rings and that the nta coordinates to Co(III) as a quadridentate. (2) The elemental analysis data indicates that the NH$_3$/nta ratio is 4. (3) The absorption spectrum of **3** shows a characteristic charge-transfer band at ca. 33900 cm^{-1} with an intensity similar to those of **1** and **2**, suggesting the di-μ-hydroxo structure. Though some geometrical isomers are possible for [(edda)Co(μ-OH)$_2$Co(NH$_3$)$_4$]$^{2+}$ and [(gly)$_2$Co(μ-OH)$_2$Co(NH$_3$)$_4$]$^{2+}$, only one geometrical isomer (achiral) is possible for this [(nta)Co(μ-OH)$_2$Co(NH$_3$)$_4$]$^+$.

CD Spectra. The CD spectra of the optically active complexes are illustrated in Fig. 2. $(+)^{CD}_{574}$ **1** and $(+)^{CD}_{572}$ **2** show quite similar CD patterns to each other. The absolute configuration around Co(gly)$_2$(μ-OH)$_2$ or Co(edda)(μ-OH)$_2$ moiety is assigned to Λ, because their main CD components in the first absorption band region are (+).[13]

A CD band ($|\Delta\varepsilon|$=4—5) was observed in the charge-transfer band region (ca. 34000 cm^{-1}) in each of the resolved complexes. However, the $|\Delta\varepsilon|$ values are about one half of that observed for the optically active isomer of the [(en)(gly)Co(μ-OH)$_2$Co(en)(gly)]$^{2+}$ complex ($|\Delta\varepsilon|$=10.0).

Stability of the Complexes. Absorption spectral changes with time were measured for aqueous solutions of some di-μ-hydroxo complexes at 20 °C. Solutions of the present complexes showed no spectal change for several days, while that of [Co$_2$(μ-OH)$_2$(NH$_3$)$_8$]Br$_4$ showed an obvious change after one day. This result means that the present complexes are more stable than [Co$_2$(μ-OH)$_2$(NH$_3$)$_8$]$^{4+}$, suggesting that some stabilizing factors exist in the present complexes. Regarding an X-ray study of [Cr$_2$(L-

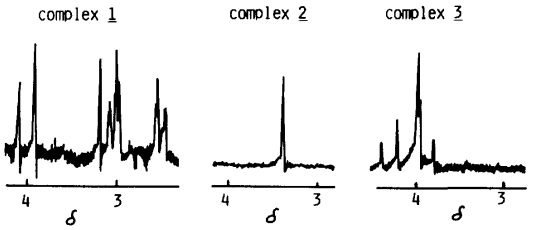

Fig. 3. ^{1}H NMR Spectra of the complexes.

pro)$_4$(μ-OH)$_2$], Oki and Yoneda[14] pointed out that the two intramolecular N–H···O hydrogen bonds (bridging two chromophores) stabilize the di-μ-hydroxo structure. Accordingly, it is reasonable to propose two hydrogen bonds as the stabilizing factor of the present complexes. It was not easy to prepare isomers having one or no hydrogen bonds, but it was easy to prepare some having two hydrogen bonds. This result agrees with that obtained for the isomers of [(en)(gly)Co$_2$(μ-OH)$_2$Co(en)(gly)]$^{2+}$,[4] suggesting that the hydrogen bond is important as one of the stabilizing factors.

References

1) The following abbreviations are used in the present paper: H_2edda=ethylenediamine-*N*,*N*′-diacetic acid; Hgly=glycine; H_3nta=nitrilotriacetic acid; en=ethylenediamine.

2) K. Nakamoto, J. Fujita, and H. Maruta, *J. Am. Chem. Soc.*, **80**, 4817 (1958).

3) W. Hackbusch, H. H. Rupp, and K. Wieghardt, *J. Chem. Soc., Dalton Trans.*, **1975**, 1015.

4) T. Ama, A. Mukai, K. Miyauchi, H. Kawaguchi, and T. Yasui, *Mem. Fac. Sci. Kochi Univ., Ser C*, **7**, 1 (1986).

5) M. Mori, M. Shibata, E. Kyuno, and F. Maruyama, *Bull. Chem. Soc. Jpn.*, **35**, 75 (1962).

6) M. Shibata, H. Nishikawa, and Y. Nishida, *Inorg. Chem.*, **7**, 9 (1968).

7) M. Mori, M. Shibata, E. Kyuno, and Y. Okubo, *Bull. Chem. Soc. Jpn.*, **31**, 940 (1958).

8) H. Kuroya and R. Tsuchida, *Bull. Chem. Soc. Jpn.*, **15**, 427 (1940).

9) J. Springborg and C. E. Schäffer, *Inorg. Synth.*, **18**, 75 (1978).

10) J. I. Legg and D. W. Cooke, *Inorg. Chem.*, **4**, 1576 (1965).

11) H. Yamatera, *Bull. Chem. Soc. Jpn.*, **31**, 95 (1958).

12) N. Matsuoka, J. Hidaka, and Y. Shimura, *Bull. Chem. Soc. Jpn.*, **40**, 1868 (1968).

13) Y. Shimura, Kagaku Sosetsu, No. 13, 83 (1976).

14) H. Oki and H. Yoneda, *Inorg. Chem.*, **20**, 3875 (1981).

Cobalt(III) Complexes with $[N_{6-n}X_n]$-Type Ligands. VI.[1] The Preparation and Properties of Tetraammine-(salicylamidato)cobalt(III) Complexes

Yoshihisa YAMAMOTO* and Noriko SHINYA
Faculty of Pharmaceutical Sciences, Higashi Nippon Gakuen University,
Ishikari-Tobetsu, Hokkaido 061-02
(Received July 10, 1986)

Synopsis. Tetraammine(salicylamidato)cobalt(III) complexes, [Co(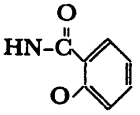)$(NH_3)_4$]X·$n$$H_2O$ (X: Cl, NO_3 and picrate), have been isolated and characterized by means of analytical, spectroscopic, and magnetic methods. The bond between the cobalt atom and the chelated ligand in the complex is expressed in the form of -$\bar{O}$-Co-$\bar{N}$-. The properties of the title complexes are intermediate between those of the tetraammine(salicylideneaminato)cobalt(III) complex, which has the -$\bar{O}$-Co-N- bond, and the tetraammine(salicylato)cobalt(III) complex, which has the -$\bar{O}$-Co-$\bar{O}$- bond.

The previous papers were concerned with the preparation and properties of many mixed-ligand ammine cobalt(III) complexes, such as the tetraammine(salicylideneaminato)cobalt(III) complexes, [Co(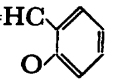)$(NH_3)_4$]X_2 (**A**),[2] the tetraammine-(8-quinolinolato)cobalt(III) complexes, [Co(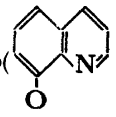)-$(NH_3)_4$]X_2 (**B**),[3-5] the salicylato(triethylenetetramine)-cobalt(III) complexes, [Co(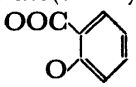)(trien)]X (**C**),[6] and the salicylaldehydato(triethylenetetramine)cobalt-(III) complexes, [Co(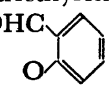)(trien)]X_2 (**D**).[7] The bonds between the cobalt atom and the chelated ligands in the complexes are expressed in the form of -$\bar{O}$-Co-N-, -$\bar{O}$-Co-$\bar{O}$-, and -$\bar{O}$-Co-O-. A few metal complexes for a -$\bar{O}$-Co-$\bar{N}$- bond were isolated, and the structure was confirmed by X-ray diffraction for the bis(glycylglycinato)cobaltate(III) ion, $[Co(gly\text{-}gly)_2]^-$.[8,9] However, no mixed-ligand ammine metal complex for a -$\bar{O}$-M-$\bar{N}$- bond has yet been reported, especially concerning its preparation and properties. The present paper deals with the preparation and properties of tetraammine(salicylamidato)cobalt(III) complexes, [Co(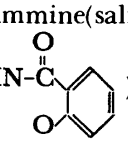)-$(NH_3)_4$]X (X: Cl, NO_3 and picrate); the properties of the complex are compared with those of two related complexes, **A** and **C**.

Experimental

Measurements. The IR spectra were recorded as potassium bromide disks with an IR-27G apparatus (Shimadzu). The visible absorption spectra were recorded with a Shimadzu UV-210 recording spectrophotometer. The electric conductivities of aqueous solutions were determined by the use of a conductometer, CM-30 (Shimadzu), at room temperature. The magnetic susceptibilities were measured by Faraday's method using a magnetic balance (Shimadzu) at room temperature. The NMR spectra were recorded with an R-40 apparatus (Hitachi) for ^1H and with an FX-60 apparatus (JEOL) for ^{13}C.

Preparation of Complexes. Tetraammine(salicylamidato)-cobalt(III) Chloride Hydrate (1): A 28% aqueous ammonia (30 cm^3) was added to an aqueous solution (20 cm^3) of $CoCl_2 \cdot 6H_2O$ (9.52 g, 40.0 mmol), and the mixture was stirred. To the solution was added slowly 6 mol dm^{-3} H_2O_2 solution (11 cm^3) in an ice bath. The color of the solution turned from brown to red. A methanol solution (60 cm^3) of salicylamide (5.48 g, 40.0 mmol) was added to the solution, and the solution was stirred at 55 °C for 22 h. Then, the solution was filtered, and the filtrate was concentrated with a rotary evaporator at 30—40 °C to ca. 50 cm^3. The precipitated salicylamide was filtered off. The filtrate was cooled to 0—5 °C. After 1 or 2 d, the precipitated russet crystals were filtered, washed with ethanol and ether, and recrystallized twice from water. Yield: 3.5 g (27.7%). Found: C, 26.57; H, 6.34; N, 22.13; Cl, 11.18%. Calcd for $CoC_7H_{19}N_5O_3Cl$ (MW 315.65): C, 26.64; H, 6.07; N, 22.19; Cl, 11.23%. Λ=113 S cm^2 mol^{-1} in water. IR spectrum: 850 cm^{-1} ($\rho_r(NH_3)_t$). ^1H NMR spectrum (cf. Fig. 1): δ 3.00 (3H, N(2)H_3), 3.15 (6H, N(1)H_3+N(4)H_3), 3.71 (4H, N(3)H_3+NH proton of salicylamidato), 6.6—7.9 (4H, ring protons of salicylamidato). ^{13}C NMR spectrum[2]: δ 120.0 (C-1), 165.8 (C-2), 117.1 (C-3), 133.2 (C-4), 123.7 (C-5), 130.7 (C-6), 171.7 (C-7). Decomp: 160 °C.

Tetraammine(salicylamidato)cobalt(III) Nitrate Hydrate (2): To an aqueous solution (9 cm^3) of **1** (1.0 g, 3.17 mmol) was added an aqueous solution (2 cm^3) of silver nitrate (0.538 g, 3.17 mmol). The mixture was stirred, and the precipitated silver chloride was filtered off. The filtrate was concentrated with a rotary evaporator at 30 °C to ca. 2 cm^3. The deposit of Complex **2** was filtered and recrystallized from water-methanol-ether (ca. 1:1:2) twice. Yield: 0.31 g (28.6%). Color: russet. Found: C, 24.78; H, 5.82; N, 24.72%. Calcd for $CoC_7H_{19}N_6O_6$ (MW 342.20): C, 24.57; H, 5.60; N, 24.56%. Λ=112 S cm^2 mol^{-1} in water. IR spectrum: 855 cm^{-1} ($\rho_r(NH_3)_t$). ^1H NMR spectrum: δ 2.97 (3H, N(2)H_3), 3.15 (6H, N(1)H_3+N(4)H_3), 3.70 (4H, N(3)H_3+NH proton), 6.6—7.9 (4H, ring protons) in 1.8 mol dm^{-3} D_2SO_4 solution. ^{13}C NMR spectrum: δ 120.0 (C-1), 165.8 (C-2), 117.0 (C-3), 133.2 (C-4), 123.6 (C-5), 130.7 (C-6), 171.7 (C-7) in D_2O. Decomp: 170 °C.

Tetraammine(salicylamidato)cobalt(III) Picrate (3): An aqueous solution of **1** (0.5 g, 1.58 mmol) was added to an

aqueous solution of picric acid (0.363 g, 1.58 mmol), and the mixture was stirred. The precipitated Complex **3** was filtered, washed with water and ethanol, and dried. Yield: 0.76 g (97.4%). Color: yellowish-brown. Found: C, 31.73; H, 4.23; N, 22.60%. Calcd for $CoC_{13}H_{19}N_8O_9$ (MW 490.28): C, 31.85; H, 3.91; N, 22.85%. IR spectrum: 840 cm^{-1} ($\rho_r(NH_3)_r$). ^1H NMR spectrum: δ 2.93 (3H, N(2)H_3), 3.10 (6H, N(1)H_3+N(4)H_3), 3.63 (4H, N(3)H_3+NH proton), 6.3—7.7 (4H, ring proton), 8.53 (2H, picrate proton) in DMSO-d_6. Absorption band in methanol: 550 nm (ε=170). Decomp: 220 °C.

Solubility. Complexes **1** and **2** are soluble in water, 35% hydrochloric acid, acetic acid, and DMSO, and are slightly soluble in methanol, but are insoluble in the common organic solvents. Complex **3** is soluble in tetrahydrofuran, DMSO and DMF, and is slightly soluble in water, alcohols, acetonitrile, and dioxane, but is insoluble in chloroform, dichloromethane, and diethyl ether.

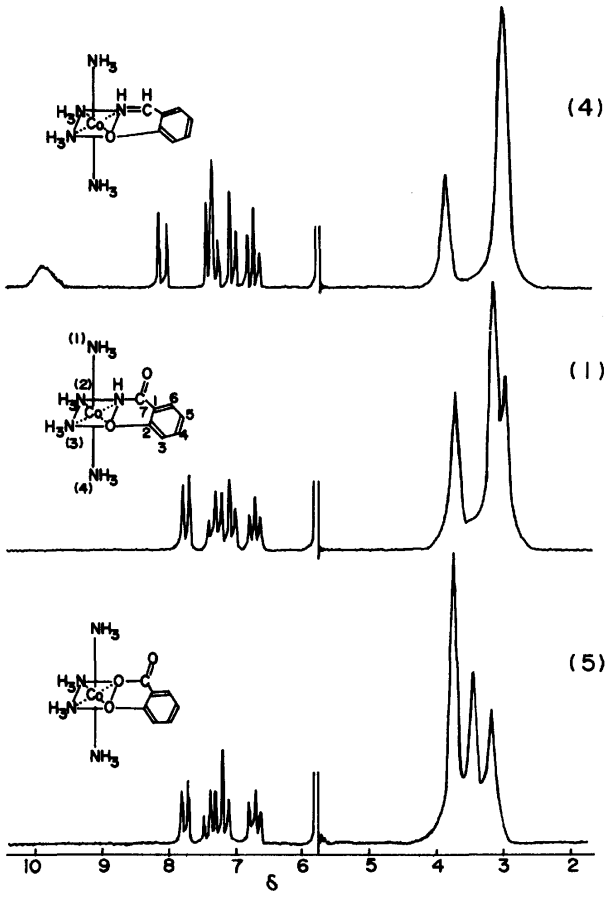

Fig. 1. The ^1H NMR spectra of **1**, **4**, and **5** complexes in 1.8 mol dm^{-3} D_2SO_4, internal DSS (δ=0)

4: $[Co(HN{=}HC\text{-}O)(NH_3)_4]Cl_2 \cdot H_2O$

1: $[Co(HN\text{-}C(=O)\text{-}O)(NH_3)_4]Cl \cdot H_2O$

5: $[Co(OOC\text{-}O)(NH_3)_4]Cl \cdot H_2O$

Results and Discussion

Tetraammine(salicylamidato)cobalt(III) chloride hydrate, (**1**), was isolated from a reaction mixture of $CoCl_2 \cdot 6H_2O$, 28% aqueous ammonia, 6 mol dm^{-3} H_2O_2, and salicylamide. The corresponding nitrate (**2**) and picrate (**3**) were prepared from **1** and silver nitrate or picric acid, respectively.

Complex **1** is a diamagnetic cobalt(III) complex of the low-spin type, judging from the magnetic susceptibility. The aqueous solution was neutral. The absorption spectrum in methanol showed four bands at 328, 378 (shoulder), 512 and 550 nm (Table 1). The absorption band at 378 nm is assigned to the charge-transfer band,[1-3] while the bands at 512 nm and 550 nm are assigned to the split first band.[10,11] In the ^1H NMR spectrum for **1** (Fig. 1), the multiplet signals at 6.6—7.9 ppm (4H) are assigned to the ring protons of the salicylamidato ligand, while the signals at 3.0—3.7 ppm (13H) are assigned to the ammine protons of $(NH_3)_4$ and the NH proton of the salicylamidato ligand. The assignment (cf. the Experimental section) of N(1)H_3, N(2)H_3, N(3)H_3, and N(4)H_3 for ammine protons was attempted by means of a consideration of the assignment of tetraammine(salicylideneaminato)cobalt(III) chloride hydrate, $[Co(HN{=}HC\text{-}O)(NH_3)_4]Cl_2 \cdot H_2O$ (**4**),[2] and tetraammine(salicylato)cobalt(III) chloride hydrate, $[Co(OOC\text{-}O)(NH_3)_4]Cl \cdot H_2O$ (**5**).[12]

The structure of **1** is identified by means of the study of the absorption spectrum, the ^1H NMR spectrum, the IR spectrum, the property of the $-CONH_2$ group of salicylamide, the results of elemental analysis, and electric conductivity in an aqueous solution. The absorption spectrum showed two bands at 512 and 550 nm in the 450—550 nm region. The spectral feature is similar to that (two bands at 475 and 550 nm) for **4**, but is different from that (one band at 532 nm) of **5** (Table 1); i.e., the cobalt atom in **1** may be bonded to the oxygen and nitrogen of the chelated ligand. In the NMR spectrum, the chemical shifts (δ 3.00(3H), 3.15(6H), and 3.71(4H)) for ammine protons are close to those (δ 3.01(9H) and 3.83(3H)) for **4**, but different from those (δ 3.21(3H), 3.48(3H), and 3.78(6H)) for **5** (Fig. 1); i.e., the cobalt atom may also be bonded to the oxygen and nitrogen of the chelated ligand. The signal at 3.71 ppm due to the -NH proton of the

Table 1. Absorption Bands of Complexes **1**, **2**, **4**, and **5**

Complex No.	Absorption bands in methanol λ/nm (ε/cm^{-1} mol^{-1} dm^3)			
1	328 (3020)	378 sh (495)	512 (150)	550 (150)
2	327 (3160)	380 sh (510)	512 (150)	550 (150)
4[a]		378 (2750)	475 sh (185)	550 (110)
5	331 (3200)	380 sh (260)		532 (150)

a) Ref. 2.

salicylamidato ligand is very different from that at 9.91 ppm of **4**; i.e., the electronic state of the -NH proton must be different from that of the =NH proton. Further, the ring-proton signals of the chelated ligand are similar to those of **5** (Fig. 1), and the chemical shift (δ 7.73) for the H_6 proton is very close to that (δ 7.75) for **5**, but different from that (δ 7.35) for **4**; i.e., the electronic and steric effects between the oxygen and H_6 proton of the chelated ligand of **1** may be similar to those of carbonyl oxygen and the H_6 proton for **5**. The IR spectrum of **1** did not show the -C=N stretching signal in the 1620—1630 cm^{-1} region. In addition, the $-CONH_2$ group of salicylamide changes to -CONH because of the electron-attracting of the carbonyl group, such as glycylglycinecobalt(III) complexes.[8,9] Thus, Complex **1** is a tetraammine-(salicylamidato)cobalt(III) chloride hydrate, as is shown in Scheme 1. The structure is supported by the results of the elemental analysis and electric conductivity in an aqueous solution.

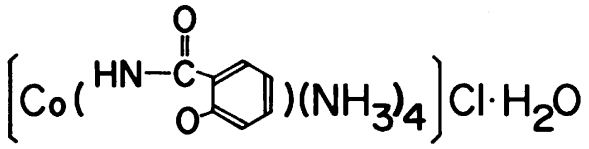

Scheme 1.

The properties of **1** are intermediate between those of Complexes **4** and **5**, judging from the results of ^1H NMR, their absorption spectra, and their stability is solutions. The ammine proton signals for **1** are close to those of **4**, but the ring-proton signals are close to those of **5** (Fig. 1). The spectral features in the 450—550 nm region for **1** are similar to those of **4**, but the ε at 550 nm is similar to that of **5** (Table 1). Complex **1** is more unstable than both Complexes **4** and **5** in a solution such as water and methanol, though the decomposition temperature (160 °C) of **1** is close to that of **4** (163 °C) and **5** (158 °C) in the solid state.

References

1) Part V: Y. Yamamoto and S. Tsukuda, *Bull. Chem. Soc. Jpn.*, **58**, 1509 (1985).
2) Y. Yamamoto and E. Toyota, *Bull. Chem. Soc. Jpn.*, **57**, 2650 (1984).
3) Y. Yamamoto and E. Toyoto, *Bull. Chem. Soc. Jpn.*, **57**, 47 (1984).
4) Y. Yamamoto, E. Toyota, and Y. Yamamoto, *Bull. Chem. Soc. Jpn.*, **56**, 2721 (1983).
5) Y. Yamamoto, *Chem. Lett.*, **1980**, 1555.
6) Y. Yamamoto and E. Toyota, *Bull. Chem. Soc. Jpn.*, **52**, 2540 (1979).
7) Y. Yamamoto, E. Toyota, and S. Tsukuda, *Bull. Chem. Soc. Jpn.*, **58**, 1595 (1985).
8) M. T. Barnet, H. C. Freeman, D. A. Buckingham, I-Nan Hsu, and D. Van Der Helm, *J. Chem. Soc. D.*, **1970**, 367.
9) R. D. Gillard, E. D. Mckenzie, R. Mason, and G. B. Robertson, *Nature*, **209**, 1347 (1966).
10) N. Matsuoka, J. Hidaka, and Y. Shimura, *Bull. Chem. Soc. Jpn.*, **40**, 1868 (1967).
11) H. Yamatera, *Bull. Chem. Soc. Jpn.*, **31**, 95 (1958).
12) Y. Yamamoto, *Bull. Chem. Soc. Jpn.*, **51**, 2894 (1978).

Ylide-Metal Complexes. XII.[1] The Preparation and Properties of Au, Be, Al, Ga, and In Complexes with Dimethylsulfoxonium Methylide

Yoshihisa YAMAMOTO
Faculty of Pharmaceutical Sciences, Higashi Nippon Gakuen University,
Ishikari-Tobetsu, Hokkaido 061-02
(Received August 1, 1986)

Synopsis. The reaction of dimethylsulfoxonium methylide, $(CH_3)_2\overset{+}{S}(O)-\bar{C}H_2$ (**L**), with (triphenylphosphine)gold chloride, $(C_6H_5)_3PAuCl$, yields a new bis(dimethylsulfoxonium methylide)gold(I) chloride, $[(CH_3)_2S(O)CH_2AuCH_2S(O)(CH_3)_2]Cl$. The reaction of the ylide **L** with $BeCl_2$ yields a new compound of tetrakis(dimethylsulfoxonium methylide)beryllium dichloride, $[(CH_3)_2S(O)CH_2]_4BeCl_2$. The reactions of the ylide **L** with $AlCl_3$, $GaCl_3$, and $InCl_3$ yield new dimeric compounds of μ-chloro-bis[tris(dimethylsulfoxonium methylide)metal] pentachloride, $[\{(CH_3)_2S(O)CH_2\}_3M-Cl-M\{CH_2S(O)(CH_3)_2\}_3]Cl_5$ (M: Al, Ga, and In). All complexes are thermally stable.

In this series, we have been concerned with the preparation and properties of the metal complexes[2] with methylenetriphenylphosphorane, $(C_6H_5)_3\overset{+}{P}-\bar{C}H_2$. For the X-ray photoelectron spectroscopy measurements,[3] the phosphorane was an undesirable ylide, i.e., the separation for the carbanion in the coordinated phosphorane was difficult because the intensity ratio between carbanion and phenyl carbons was 1:18. Therefore, we surveyed sulfonium, phosphonium, and arsonium ylides, and found dimethylsulfoxonium methylide, $(CH_3)_2\overset{+}{S}(O)-\bar{C}H_2$ as a suitable one for XPS study. The intensity ratio between carbanion and methyl carbons is 1:2, and the metal complex with the sulfonium ylide has been reported only for a few compounds.[4] Thus, the present paper deals with the preparation and properties of bis(dimethylsulfoxonium methylide)-gold(I) chloride, $[(CH_3)_2S(O)CH_2AuCH_2S(O)(CH_3)_2]Cl$, tetrakis(dimethylsulfoxonium methylide)beryllium dichloride, $[(CH_3)_2S(O)CH_2]_4BeCl_2$, and μ-chloro-bis[tris(dimethylsulfoxonium methylide)metal] pentachloride, $[\{(CH_3)_2S(O)CH_2\}_3M-Cl-M\{CH_2S(O)(CH_3)_2\}_3]Cl_5$ (M: Al, Ga, In).

Experimental

Measurements. The ^1H NMR spectra were measured with R-40 (Hitachi) and XL-200 (Varian) NMR spectrometers. The electric conductivities of solutions were determined using a conductometric meter, CM-30 (Shimadzu).

Preparation of Ylide-Metal Complexes. Bis(dimethylsulfoxonium methylide)gold(I) Chloride (1): Dimethylsulfoxonium methylide[5] (**L**) was prepared by refluxing a mixture of trimethylsulfoxonium bromide (0.73 g, 4.22 mmol) and sodium hydride (0.11 g, 4.58 mmol) in dry tetrahydrofuran (20 cm³) under nitrogen until the evolution of hydrogen ceased. The product was cooled and filtered under nitrogen. To the resulting solution was added triphenylphosphine gold chloride (0.93 g, 1.88 mmol); the mixture was then stirred for 3 h at room temperature. The precipitated yellow complex was filtered, washed with dry pentane and dried under vacuum. Yield: 0.67 g (85.5%). Decomp: 165 °C. Found: C, 16.99; H, 3.70%. Calcd for $C_6H_{16}O_2S_2AuCl$ (MW 416.79) C, 17.29; H, 3.87%. Λ=100 S cm² mol⁻¹ in dry methanol at 20 °C. Λ=113 S cm² mol⁻¹ in water at 4 °C.

Tetrakis(dimethylsulfoxonium methylide)beryllium Dichloride (2): The tetrahydrofuran solution of the ylide was prepared from the mixture of trimethylsulfoxonium bromide (0.80 g, 4.62 mmol) and sodium hydride (0.12 g, 5.00 mmol) in dry tetrahydrofuran (20 cm³). To this solution was added beryllium dichloride (0.08 g, 1.00 mmol). The mixture was stirred for 5 d at room temperature. The precipitated white complex was filtered, washed with pentane and dried under vacuum. Yield: 0.45 g (88.8%). Decomp: 151 °C. Found: C, 31.85; H, 7.20%. Calcd for $C_{12}H_{32}O_4S_4BeCl_2$ (MW 448.59) C, 32.13; H, 7.19%. Λ=71 S cm² mol⁻¹ in dry methanol at −50 °C.

μ-Chloro-bis[tris(dimethylsulfoxonium methylide)aluminium] Pentachloride (3): The tetrahydrofuran solution of the ylide was prepared from the mixture of trimethylsulfoxonium bromide (0.78 g, 4.51 mmol) and sodium hydride (0.13 g, 5.42 mmol) in dry tetrahydrofuran (15 cm³) under nitrogen. Aluminium trichloride (0.15 g, 1.12 mmol) was added to the solution. The mixture was stirred for 3 d at room temperature. The precipitated white complex was filtered under nitrogen, washed with pentane and dried under vacuum. Yield: 0.68 g (61.5%). Decomp: 142 °C. Found: C, 26.11; H, 6.28%. Calcd for $C_{18}H_{48}O_6S_6Al_2Cl_6$ (MW 819.68) C, 26.38; H, 5.90%. Λ=608 S cm² mol⁻¹ in water at 5 °C. Λ=130 S cm² mol⁻¹ in dry methanol at −50 °C.

μ-Chloro-bis[tris(dimethylsulfoxonium methylide)gallium] Pentachloride (4): Gallium trichloride (0.20 g, 1.13 mmol) was added to the tetrahydrofuran solution of the ylide which was prepared from the mixture of trimethylsulfoxonium bromide of 0.78 g (4.51 mmol) and sodium hydride (0.13 g, 5.42 mmol) in dry tetrahydrofuran (15 cm³) under nitrogen. The mixture was stirred for 1 d at room temperature. The precipitated white complex was filtered, washed with pentane under nitrogen, and dried under vacuum. Yield: 0.71 g (57.4%). Decomp: 138 °C. Found: C, 23.68; H, 5.47%. Calcd for $C_{18}H_{48}O_6S_6Ga_2Cl_6$ (MW 905.16) C, 23.89; H, 5.35%. Λ=135 S cm² mol⁻¹ in dry methanol at −50 °C.

μ-Chloro-bis[tris(dimethylsulfoxonium methylide)indium] Pentachloride (5): Complex **5** was prepared from a reaction mixture of indium trichloride (0.16 g, 0.72 mmol) and a tetrahydrofuran solution of the ylide which was prepared from the mixture of trimethylsulfoxonium bromide (0.50 g, 2.89 mmol) and sodium hydride (0.08 g, 3.33 mmol) in dry tetrahydrofuran (15 cm³) under nitrogen. After 3 d at room temperature, the precipitated white complex was filtered, washed with pentane, and dried. Yield: 0.62 g (72.5%). Decomp: 160 °C. Found: C, 21.65; H, 4.86%. Calcd for $C_{18}H_{48}O_6S_6In_2Cl_6$ (MW 995.32) C, 21.72; H, 4.86%. Λ=100 S cm² mol⁻¹ in dry methanol at −50 °C.

Results and Discussion

Gold Complex. Bis(dimethylsulfoxonium methylide)gold(I) chloride (**1**) was prepared from the reaction of dimethylsulfoxonium methylide (**L**) and (triphenylphosphine)gold chloride, $(C_6H_5)_3PAuCl$. Complex **1** is slightly soluble in alcohols, DMSO, and water, but insoluble in common organic solvents such as acetone, benzene, and ether.

The ^1H NMR spectrum of **1** showed a singlet signal for the methylene group at 3.03 ppm and a singlet signal for methyl groups at 3.52 ppm in a ratio of 2:6 in CD_3OD as is shown in Table 1. The chemical shift of the methylene group is at a lower field than that of **L** (Table 1). This property is similar to those of metal complexes[2] with methylenetriphenylphosphorane, e.g. $[(C_6H_5)_3PCH_2\text{-}M\text{-}CH_2P(C_6H_5)_3]Cl_2$, M: IIB group metals.[2c] Thus, the ylide in complex is bonded to the gold atom through the carbanion donor atom.[6] Complex **1** has a free anion according to the molar conductance (cf. Experimental section). Then, the compound is a $[(CH_3)_2S(O)CH_2AuCH_2S(O)(CH_3)_2]Cl$, in which the cation has a linear configuration. The elemental analysis of **1** agreed with the proposed structure.

Beryllium Complex. Tetrakis(dimethylsulfoxonium methylide)beryllium dichloride (**2**) was prepared from a reaction mixture of dimethylsulfoxonium methylide (**L**) and $BeCl_2$. Complex **2** is soluble in methanol and slightly soluble in ethanol, but insoluble in chloroform, dichloromethane, DMSO, DMF, and water. The ylide is bonded to the beryllium atom through the carbanionic donor atom judging from the NMR spectral results (Table 1). Two coordination geometries for the compound are considered to be possible: a tetrahedral configuration of monomeric,[7] dimeric,[8] or polymeric[9] or a trigonal bipyramidal configuration of monomeric,[10] dimeric,[11] or trimeric.[12] The elemental analysis for **2** agreed with the composition of L_4MCl_2, i.e., the structure can not be a tetrahedral of dimeric or polymeric and a trigonal configuration. Complex **2** has free anions according to molar conductance. Thus, we suggest that the structure of **2** is a monomeric tetrahedron:

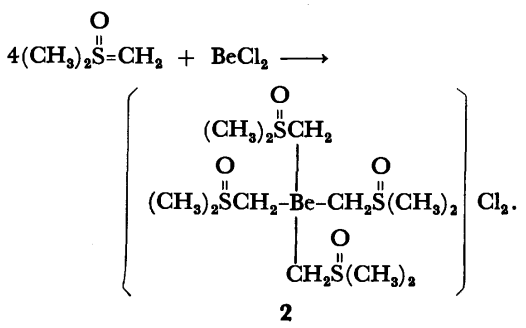

2

Aluminium, Gallium, and Indium Complexes. μ-Chloro-bis(dimethylsulfoxonium methylide)metal(Al (**3**), Ga (**4**), In (**5**)) pentachloride were prepared from a reaction mixture of dimethylsulfoxonium methylide (**L**) and MCl_3 (M: Al, Ga, In), respectively. Complexes **3**—**5** are slightly soluble in DMSO, DMF, methanol and water, but insoluble in chloroform, dichloromethane, and ether. Gallium complex **4** and indium complex **5** are unstable in water at 5 °C, giving the corresponding salt, $[(CH_3)_3S{=}O]Cl$ (**6**). The ylide is bonded to the metal atoms, judging from the NMR spectral results (Table 1). The elemental analysis of **3**—**5** agreed with the composition of L_3MCl_3. From the elemental analysis, four structures for the complexes are considered to be possible: a trigonal planar configuration of monomeric, $[L_3M]Cl_3$, a trigonal bipyramidal configuration of monomeric, $[L_3MCl_2]Cl$, a tetrahedral configuration of monomeric, $[L_3MCl]Cl_2$ and a tetrahedral configuration of dimeric, $[L_6M_2Cl]Cl_5$. The structure of $AlCl_3$, $GaCl_3$ and $InCl_3$ is known to be the bridge structure[13] by chlorines. In addition, the organoaluminium chlorides, bromides and iodides are generally dimeric. The most significant feature of the structure of methylaluminium dichloride, which has been determined by X-ray crystallography,[14] is that the dimer is held together through bridging atoms. Complexes **3**—**5** have free anions according to the molar conductance. Thus, we suggest that the structure of **3**—**5** comprises dimers bridged by chlorine and a metal with a tetrahedral coordination.

Table 1. ^1H NMR Spectra of Complexes, Ylide, and Salt

Complex No.	CH_2 δ/ppm	CH_3 δ/ppm	Solvent	Standard ($\delta=0$)	Temp °C
1	3.08 s (2H)	3.59 s (6H)	D_2O	DSS	5
	3.03 s (2H)	3.52 s (6H)	CD_3OD	TMS	r. t.
2	2.69 s	3.30 s [a]	CD_3OD	TMS	−50
3	2.71 s (2H)	3.83 s (6H)	D_2O	DSS	5
	2.65 s	3.32 s [a]	CD_3OD	TMS	−50
4	2.60 s	3.31 s [a]	CD_3OD	TMS	−50
5	2.63 s	3.28 s [a]	CD_3OD	TMS	−50
6'		3.83 s	D_2O	DSS	r. t.
L[b]	1.92 s (2H)	2.95 s (6H)	C_6D_6	TMS	35

6': $[(CH_3)_3S{=}O]Br$. **L**: $(CH_3)_2S(O){=}CH_2$. a) This signal is overlapped with solvent. b) Ref. 4.

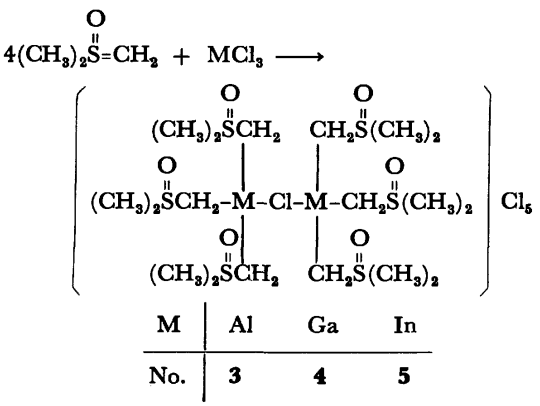

M	Al	Ga	In
No.	3	4	5

References

1) Part XI: Y. Yamamoto, *Bull. Chem. Soc. Jpn.*, **59**, 3053 (1986).

2) a) Y. Yamamoto, *Bull. Chem. Soc. Jpn.*, **56**, 1772 (1983); b) Y. Yamamoto, *Bull. Chem. Soc. Jpn.*, **55**, 3025 (1982); c) Y. Yamamoto and H. Sugimoto, *Bull. Chem. Soc. Jpn.*, **53**, 3176 (1980); d) Y. Yamamoto and Z. Kanda, *Bull. Chem. Soc. Jpn.*, **52**, 2560 (1979).

3) Y. Yamamoto and H. Konno, *Bull. Chem. Soc. Jpn.*, **59**, 1327 (1986).

4) H. Schmidbaur and W. Richter, *Z. Anorg. Allg. Chem.*, **429**, 222 (1977).

5) E. J. Corey and M. Chaykovsky, *J. Am. Chem. Soc.*, **87**, 1333 (1965).

6) Y. Yamamoto and H. Schmidbaur, *J. Organomet. Chem.*, **96**, 133 (1975).

7) V. Amirthalingham, V. M. Padmanabhan, and J. Shanker, *Acta Crystallogr., Sect. B*, **16**, 201 (1960).

8) O. Rahlfs and W. Fischer, *Z. Anorg. Allg. Chem.*, **211**, 349 (1933).

9) a) R. E. Rundle and P. H. Lewis, *J. Chem. Phys.*, **20**, 132 (1952); b) H. Steinfink and G. D. Brunton, *Acta Crystallogr., Sect. B*, **24**, 807 (1968).

10) L. G. Brisseau, M. G. B. Drew, and J. E. Goulter, *J. Chem. Soc., Chem. Commun.*, **1972**, 916.

11) G. E. Coates and F. Glockling, *J. Chem. Soc.*, **1954**, 22.

12) a) J. L. Atwood and G. D. Stucky, *J. Am. Chem. Soc.*, **91**, 4426 (1969); b) J. L. Atwood and G. D. Stucky, *J. Chem. Soc., Chem. Commun.*, **1967**, 1169.

13) a) K. J. Palmer and N. Elliott, *J. Am. Chem. Soc.*, **60**, 1852 (1938); b) S. C. Wallwork and I. J. Worrall, *J. Chem. Soc.*, **1965**, 1816; c) J. D. Forrester, A. Zalkin, and D. H. Templeton, *Inorg. Chem.*, **3**, 63 (1964).

14) G. Allegra, G. Perego, and A. Immirzi, *Makromol. Chem.*, **61**, 69 (1963).

The Crystal and Molecular Structure of Bis(dibenzylamine)bis(thiocyanato)-cadmium(II), $Cd(SCN)_2\{(C_6H_5CH_2)_2NH\}_2$

Masahiro TANIGUCHI* and Akira OUCHI
Department of Chemistry, College of Arts and Sciences, The University of Tokyo, Komaba, Meguro-ku, Tokyo 153
(Received October 2, 1986)

Synopsis. The crystal and molecular structure of the title complex was determined by means of a single-crystal X-ray diffraction technique. A crystal of $CdC_{30}H_{30}N_4S_2$, F. W.=623.13, is triclinic, with a space group $P\bar{1}$, a=11.284(2), b=11.404(2), c=5.974(1) Å, α=93.31(2), β=98.37(1), γ=71.84-(1)°, U=722.6(2) Å^3, Z=1, D_m=1.42(3) D_x=1.43 Mg m^{-3}, and μ(Mo $K\alpha$)=9.17 cm^{-1}. The cadmium(II) atom is hexa-coordinated, being ligated with two thiocyanato(SCN) sulfur atoms as well as two SCN and two dibenzylamine nitrogen atoms, where the respective pairs of the same kinds of atoms are all in a *trans*-configuration. All cadmium(II) atoms are lined along the c-axis and the side-by-side metal atoms are doubly bridged by SCN ions.

It has already been found that many Lewis base(L) adducts of cadmium(II) thiocyanate, $Cd(SCN)_2L_2$ have chain structures in which respective side-by-side metal atoms are bridged by two thiocyanate (SCN) ions. Among them, in the cases of 2-imidazolinethione,[1] 1*H*-1,2,4-triazole,[2] and 3-methylpyridine adducts,[3] the planes of the side-by-side eight-membered rings by two cadmium(II) and six atoms of two SCN ions between them in the chain are parallel. On the other hand, in the cases of 2-methylpyridine,[3] 4-methyl-pyridine,[4] and tri(*p*-tolyl)phosphine adducts,[5] two kinds of planes in different directions appear alternately. Moreover, the coordination positions of the respective ligating atoms around the cadmium(II) atoms are not the same in respective complexes, although all of them, except the tri(*p*-tolyl)phosphine adduct, are in octahedral geometry. In cases of the thiocyanatocadmates(II), it was found that the chain structures bridged by SCN ions change, depending on the kinds of the counter cations. Especially in cases of salts of relatively large cations (such as rubidium and cesium) they are in complicated network structures.[6] Therefore, some special structure complexes may be found if some massive ligands are used as the additional Lewis base. From such an expectation, this time we synthesized the dibenzylamine adduct; its crystal and molecular structures were determined by the single-crystal X-ray diffraction method.

Experimental

Synthesis of Bis(dibenzylamine)bis(thiocyanato)cadmium-(II). Cadmium(II) thiocyanate (1.14 g, 5 mmol) was dissolved into 10 cm^3 of methanol; dibenzylamine (dba) (1.97 g, 10 mmol) dissolved into 10 cm^3 of ethanol was added to it. When the mixed solution was left standing for about one hour at ambient temperature, colorless needle-like crystals were deposited. Yield: 1.7 g (55%). The larger crystals deposited from a more diluted mixed solution (which was left standing several days) were used for an X-ray structure analysis. Anal. Found: Cd, 18.04; C, 57.41; H, 4.84; N, 8.96%. Calcd for ($CdC_{30}H_{30}N_4S_2$), Cd, 18.04; C, 57.82; H, 4.85; N, 8.99%.

Single-Crystal X-Ray Analysis. The crystal used for a structure determination was about 0.3×0.3×0.2 mm^3 in size and was used without shaping. The reflections in the range $3°<2\theta<60°$ (2θ) were collected on a Rigaku AFC-6A automated four-circle X-ray diffractometer using graphite-monochromated Mo $K\alpha$ radiation, by means of a ω—2θ scan technique (scan speed 4° min^{-1}; scan width 1.10+0.5 tanθ° (θ)). The intensities were corrected for Lorentz and polarization factors, but no corrections were made for absorption and extinction. Of 4596 independent reflections collected, 3565 with $|F_o|>3\sigma(|F_o|)$ were used for the structure determination.

All the calculations were carried out on a HITAC M-680H computer at the Computer Center of the University of Tokyo, using UNICS III.[7] The scattering factors were taken from Ref. 8.

The structure was solved by the heavy-atom method. The positions of the cadmium and some sulfur atoms were deduced from a three-dimensional Patterson map; other non-hydrogen atoms were located by means of successive Fourier syntheses. Their positional, isotropic and then anisotropic thermal parameters were refined by a block-diagonal least-squares method. The positions of all hydrogen atoms were obtained by a calculation which assumed C-H bond lengths to be 1.08 Å. They were added to the refinement cycles fixing their positional parameters. The final R value[9] obtained was 0.033.

Results and Discussion

The bond lengths and bond angles are shown in Table 1.[10] A perspective drawing of the complex, together with the numbering scheme of the non-

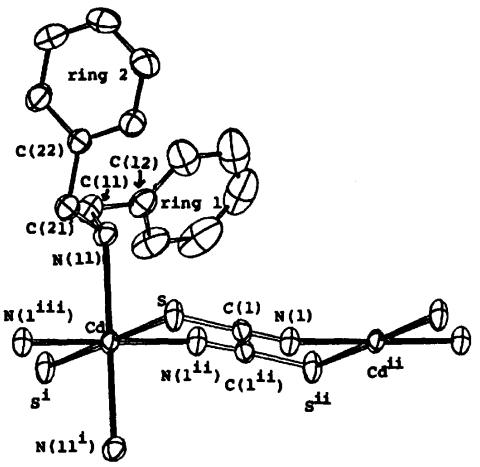

Fig. 1. A perspective drawing of the structure of the title complex with the numbering scheme of the atoms. The key to the symmetry operations; i, $-x$, $-y$, $-z$; ii, $-x$, $-y$, $1-z$; iii, x, y, $-1+z$.

hydrogen atoms, is shown in Fig. 1.[11] Projections of the unit cell along b- and c-axes are shown in Figs. 2 and 3, respectively.

The cadmium(II) atom is at the center of symmetry; it is hexa-coordinated and is in an octahedral geometry. As shown in Fig. 2, the cadmium(II) atoms are lined along the c-axis and the respective pairs of side-by-side metal atoms are bridged by two SCN ions; one of them is *S*-coordinated and the other one is *N*-coordinated to the same side metal atom, thus forming a polymeric linear chain structure.

Around one cadmium(II) atom, two SCN sulfur, two SCN nitrogen, and two dibenzylamine nitrogen atoms are coordinated, where each pair of the same kinds of the ligating atoms are all in a *trans*-configuration. The bond lengths are: Cd-N(SCN), 2.307(3) and Cd-S(SCN), 2.7576(10) Å. Bond angles are: Cd-S-C(1), 99.93(11) and Cd-N(1^{ii})-C(1^{ii}), 161.0-(2)°. These values are all not much different from those of the double SCN ion-bridging type cadmium complexes. The Cd-N(11) (Lewis base) bond length is 2.396(2) Å, longer than that of Cd-N(1^{ii}) (SCN). Moreover, this Cd-N (base) bond length is a little longer than those of the 3- and 4-methylpyridine adducts;[3,4] however, still longer Cd-N (base) bonds were found in 2-methylpyridine and bis(2-amino-methyl) amine adducts.[3,12]

An eight-membered ring, consisting of a pair of side-by-side cadmium(II) atoms and in total six atoms of a pair of SCN ions bridging them, is formed in this complex as in cases of the other cadmium(II) thiocyanate adducts.[1-3] Different from the planes of

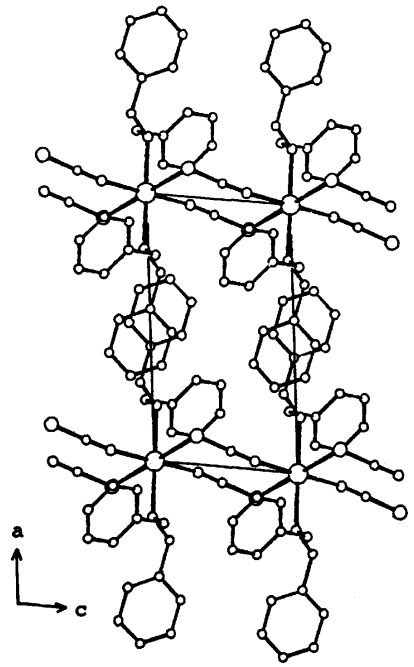

Fig. 2. The projection of the unit-cell along b-axis.

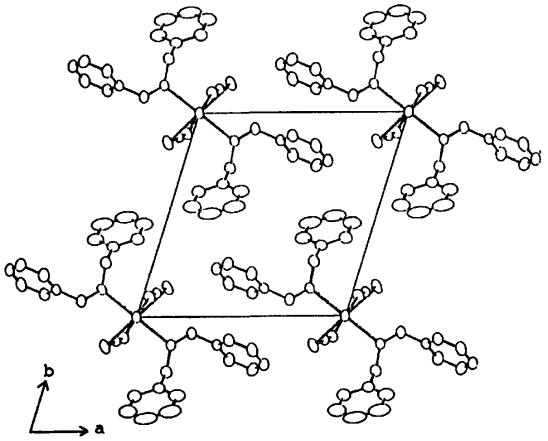

Fig. 3. The projection of the unit-cell along c-axis.

Table 1. Bond Lengths and Bond Angles of the Title Complex with Estimated Standard Deviations in Parentheses

Bond length	(l/Å)	Bond length	(l/Å)	Bond length	(l/Å)
Cd-S	2.7576(10)	Cd^{ii}-N(1)	2.307(3)	Cd-N(11)	2.396(2)
S-C(1)	1.641(3)	C(1)-N(1)	1.142(4)	N(11)-C(11)	1.487(4)
N(11)-C(21)	1.500(5)	C(11)-C(12)	1.491(5)	C(12)-C(13)	1.382(7)
C(13)-C(14)	1.391(9)	C(14)-C(15)	1.365(8)	C(15)-C(16)	1.362(11)
C(16)-C(17)	1·412(8)	C(17)-C(12)	1.373(5)	C(21)-C(22)	1.507(4)
C(22)-C(23)	1.385(4)	C(23)-C(24)	1.377(5)	C(24)-C(25)	1.372(5)
C(25)-C(26)	1.365(6)	C(26)-C(27)	1.396(5)	C(27)-C(22)	1.376(4)
Bond angle	**(ϕ/°)**	**Bond angle**	**(ϕ/°)**	**Bond angle**	**(ϕ/°)**
S-Cd-N(1^{ii})	90.09(7)	S-Cd-N(11)	83.81(6)	N(1^{ii})-Cd-N(11)	91.41(9)
Cd-S-C(1)	99.93(11)	Cd-N(1^{ii})-C(1^{ii})	161.0(2)	S-C(1)-N(1)	178.3(3)
Cd-N(11)-C(11)	118.18(19)	Cd-N(11)-C(21)	110.24(16)	N(11)-C(11)-C(12)	112.1(3)
C(11)-C(12)-C(13)	120.1(3)	C(11)-C(12)-C(17)	119.8(4)	C(12)-C(13)-C(14)	120.0(4)
C(13)-C(14)-C(15)	119.4(6)	C(14)-C(15)-C(16)	121.8(6)	C(15)-C(16)-C(17)	119.0(5)
C(16)-C(17)-C(12)	119.7(5)	N(11)-C(21)-C(22)	113.0(3)	C(21)-C(22)-C(23)	119.9(3)
C(21)-C(22)-C(27)	121.7(3)	C(22)-C(23)-C(24)	121.0(3)	C(23)-C(24)-C(25)	120.1(3)
C(24)-C(25)-C(26)	120.0(3)	C(25)-C(26)-C(27)	120.0(3)	C(26)-C(27)-C(22)	120.5(3)

Key to the symmetry operation: ii, $-x$, $-y$, $1-z$.

the 2-, 3-, and 4-methylpyridine adducts, which are almost in a real plane,[3,4] the ring of this complex is in a chair form; both cadmium(II) atoms are deviated up- and downwards by about 0.5 Å from the average plane of the six atoms of two SCN ions (average deviation of the six atoms from the average plane is 0.003 Å).

As shown in Figs. 2 and 3, the phenyl ring 2 of the dibenzylamine ligand is parallel to the same type ring of the next complex along the a-axis; the distance between the approaching ring planes is about 3.64 Å, and about 13% of the area overlaps each other.[13] On the other hand, as shown in Fig. 3, ring 1 of the ligand takes a position in the wide space between the side-by-side complexes along the b-axis; such an overlapping of rings was not found. This fact should be the cause of the relatively large temperature factors of ring 1 carbon atoms.

The next chains to the a- and b-axis directions are separated by 11.28 and 11.40 Å; these are the respective axis lengths. These values are far longer than those of the other Lewis base adducts of the same type: for example, in the case of 3-methylpyridine adduct, they are 8.77 and 8.33 Å (the latter value is a half of its b-axis length),[3] and the 1*H*-1,2,4-triazol adduct, 7.57 and 7.68 Å.[5] In spite of such a large separation between the polymeric chains, no fundamental discrepancies in the bridging structure were found compared with the other same type complexes, except for the above-mentioned minor differences.

References

1) L. Cavalca, M. Nardelli, and G. Fava, *Acta Crystallogr.*, **13**, 125 (1960).

2) J. G. Haasnoot, G. C. M. de Keyzer, and G. C. Verschoor, *Acta Crystallogr., Sect. C*, **39**, 1207 (1983).

3) M. Taniguchi, Y. Sugita, and A. Ouchi, *Bull. Chem. Soc. Jpn.*, to be published.

4) M. Taniguchi, M. Shimoi, and A. Ouchi, *Bull. Chem. Soc. Jpn.*, **59**, 2299 (1986).

5) R. G. Goel, W. P. Henry, M. J. Oliver, and A. L. Beauchamp, *Inorg. Chem.*, **20**, 3924 (1981).

6) Von G. Thiele and D. Messer, *Z. Anorg. Allgem. Chem.*, **421**, 24 (1976).

7) T. Sakurai and K. Kobayashi, *Rep. Inst. Phys. and Chem. Res.*, **55**, 69 (1979).

8) "International Tables for X-Ray Crystallography," Kynoch Press, Birmingham (1974), Vol. IV, pp. 72, 150.

9) $R=\Sigma||F_o|-|F_c||/\Sigma|F_o|$.

10) The positions of hydrogen atoms, the final thermal parameters, and the final F_o-F_c table are deposited as Document No. 8723 at the Office of the Editor of the Bull. Chem. Soc. Jpn.

11) The numbering of the phenyl carbon atoms are as follows: In the ring 1, the carbon atoms are numbered successively from C(12) to C(17) and the C(17) atom is bonded to C(12) atom. In the ring 2, they are numbered from C(22) to C(27) in the same manner.

12) M. Cannas, G. Carta, A. Cristini, and G. Marongiu, *Inorg. Chem.*, **16**, 228 (1977).

13) Here, the overlapping area was the one between one ring and the projection of the other ring to the former ring plane; the value is shown by the percentage of the overlapping area to one ring area.

Polarographic Determination of Surfactants

Hideaki KINOSHITA,* Mie KOBAYASHI, and Asao MATSUOKA
Kwassui Women's College, Higashiyamate, Nagasaki 850
(Received September 13, 1986)

Synopsis. The suppression of the polarographic oxygen maximum current and the decrease of the differential capacity at a potential of zero charge by surfactants are proportional to the concentration of the surfactants in a dilute solution. Constants representing the abilities for suppressing the maximum current and decreasing the capacity were obtained concerning some thirty surfactants.

Nowadays, surfactants are widely utilized not only as detergent powders and as liquid cleaners, but, also in the preparation of insecticides, polish and cosmetics. The development of a convenient method for the determination of surfactants seems to be very significant. After the separation of a test solution into surfactant solutions by means of a chromatographic method, a determination of surfactants is carried out mainly by the spectrophotometric method, which generally includes many complicated processes.[1] Measurements of the suppression of the polarographic maximum current and of the nonfaradaic admittance based on the adsorption of surfactants to the mercury electrode are very expedient and have been adopted for the determination of surfactants.[2,3] However, up to the present the fundamentals for the determination were not strictly explicated.

This paper tries to describe basic facts regarding the suppression of the oxygen maximum current and the decrease of the differential capacity by some thirty surfactants and to present a convenient method for a determination of surfactants.

Experimental

Chemicals. Reagent-grade chemicals purchased from Nakarai Chemical Co. and Tokyo Kasei Co. were used without further purifications. The water distilled for high-performance liquid chromatography made by Katayama Kagaku Co. was used to prepare the base solution. To prepare an oxygenated test solution this base solution was equilibrated with air by leaving it in air one day or longer.

Instruments. Dc, normal pulse (NP) and phase sensitive ac (psac) polarograms were recorded with a Yanagimoto Polarographic Analyzer P1:00, a Watanabe XY recorder WX4401 and an NF auto-lock-in amplifier LI572B. The amplitude of the superimposed alternating voltage was adjusted to 10 mV (peak to peak) and the frequency to 50 Hz. The open-circuit mercury flow rate at a dropping mercury electrode (DME) was 1.33 mg/s in distilled water at 65 cm of mercury. Usually, the dropping time of DME, t_d, was adjusted to 3 s.

Electrochemical Measurements. Measurements of the oxygen maximum current were carried out at 25 °C in a 10 mM (M=mol dm^{-3}) KCl solution and measurements of the differential capacity were at 20 °C in a 100 mM KCl solution. Potentials were referred to the saturated calomel electrode. To prepare the test solution, aliquots of a surfactant solution, usually containing 1 mg cm^{-3} of surfactant, was injected into 10 cm^3 of the base solution in an H-type cell.

Results

1. Suppression of Oxygen Maximum Current by Surfactant. In the reduction of oxygen dissolved in a KCl solution with a concentration ranging from 1 to 150 mM, a pronounced increase in the current above a limiting value was observed in the potential range between −0.2 and −0.4—−0.6 V on dc, NP, and linear potential sweep polarograms and was considered to be caused by increased transport of oxygen toward the electrode due to streaming motion of the solution.[4] The oxygen maximum current varied with the concentration of KCl and had a maximum value at the concentration of 10 mM. Dc polarograms of the reduction of oxygen in the presence of 0 to 2.5 μg cm^{-3} of sodium dodecyl sulfate (SDS) in 10 mM KCl solution are shown in Fig. 1 and NP polarograms in the presence of 0 to 6 μg cm^{-3} of SDS in Fig. 2. Heights of maximum current obtained by dc method(I) and NP method(I_p) decreased with increasing SDS concentration. These suppressions were proved to be proportional to the amount of surfactant adsorbed on

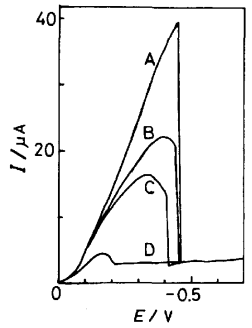

Fig. 1. Dc polarograms of reduction of oxygen in 10 mM KCl in the presence of 0 (A), 0.3 (B), 0.5 (C), and 2.5 (D) μg cm^{-3} of SDS.

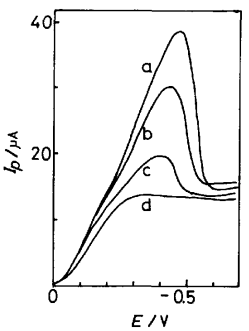

Fig. 2. NP polarograms of reduction of oxygen in 10 mM KCl in the presence of 0 (a), 0.5 (b), 2.5 (c), and 6 (d) μg cm^{-3} of SDS.; initial potential was 0 V, sampling time was 16.6 ms.

the mercury electrode, Γ, by measurements of linear potential sweep polarograms.[5] The net maximum current obtained by the dc method, I^0-I^{lim}, was larger than that obtained by the NP method, $I_p^0-I_p^{lim}$, in the absence of a surfactant. The degree of suppression of the net maximum current by the surfactant obtained by the dc method, $(I^0-I)/(I^0-I^{lim})$, was larger than that by the NP method, $(I_p^0-I_p)/(I_p^0-I_p^{lim})$, at a specific concentration of surfactant. Here I^0 and I_p^0 are the maximum currents in the absence of a surfactant and I^{lim} and I_p^{lim} are the limiting currents. In this NP method the initial potential is held at 0 V, where electrolysis scarcely occurs. Thus, streaming occurs intermittently and the supply of oxygen and surfactant to the electrode is reduced in comparison with the case of the dc method.

Figure 3 shows the dependence of the relative decrease of the oxygen maximum current measured at −0.3 V regarding the concentration of SDS(A, a) hexadecyltrimethylammonium bromide(CTAB)(B, b), and poly(oxyethylene)(20)sorbitan monolaurate-(Tween 20)(C, c) by the dc method(A, B, C) and the NP method(a, b, c). Roughly, linear relationships exist between the relative decrease of the current and the concentration of the surfactant in the range of I/I^0 and $I_p/I_p^0=2/3$ to 1 in the case of some thirty surfactants. Based on such a graph as shown in Fig. 3, the concentration of surfactant could be estimated.

2. Decrease of the Differential Double Layer Capacity by Surfactant. Figure 4 shows the differential capacity vs. potential, C-E, curves in the presence of 0 (A), 20 (B), and 50 (C) μg cm^{-3} of SDS in 0.1 M KCl measured by the psac polarographic method. With the increase in the SDS concentration the differential capacity decreased in the potential range around the potential of zero charge, PZC, which in this case was −0.5 V. For an SDS concentration lower than 20 μg cm^{-3} the relative decrease in capacity, $(C^0-C)/C^0$, was proportional to the square root of the dropping time of DME and the bulk concentration of SDS at −0.5 V, where C^0 is the capacity in the absence of a surfactant and C in the presence of a surfactant.[6]

Figure 5 shows the dependence of the relative decrease in the capacity at −0.5 V on the concentration of SDS (A), CTAB (B), and Tween 20 (C). At a lower surface coverage of the surfactant, an approximately linear relationship exists between the capacity and the bulk concentration of the surfactant. The adsorption of the surfactant at PZC is considered to be controlled by the diffusion, thus, Γ is proportional to $t_d^{1/2}$ and c. For this reason the relative decrease in the capacity might be proportional to the degree of surface coverage of the surfactant, which has a lower dielectric constant than water. The differential capacity at t_d=3 s approached the minimum value, C^m, in the presence of 30 to 40 μg cm^{-3} of water soluble surfactants and did not saturate even in the concentration of 100 μg cm^{-3} of poorly soluble surfactants. The value of the differential capacity obtained in the presence of dissolved oxygen was the same as that obtained in the absence of oxygen at a potential more negative than −0.2 V.

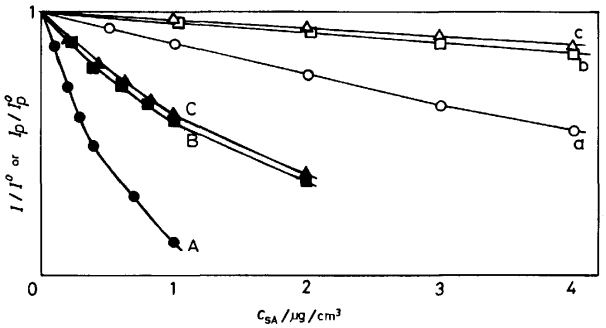

Fig. 3. Dependence of I/I^0 and/or I_p/I_p^0 at −0.3 V on the concn of SDS (A,a) ,CTAB (B,b) and Tween 20 (C,c) by dc (A,B,C) and NP (a,b,c) method.

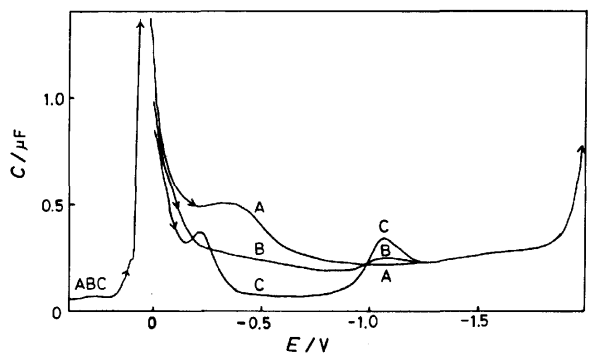

Fig. 4. C-E curves for 0 (A), 20 (B), and 50 (C) μg cm^{-3} of SDS in 100 mM KCl.

Discussion

Measurements of the oxygen maximum current and the differential capacity at a fixed potential are so simple and convenient to take that only one or two minutes are required to determine the concentration of any kind of surfactant ranging from 0.1 to 20 μg cm^{-3}. The presence of amino acids, sugars and non-surfactive fatty acids did not interfere with the measurements up to ten times the quantity of the surfactant. In the presence of any two kinds of surfactants, the total concentration of the two surfactants being lower than 20 μg cm^{-3}, their con-

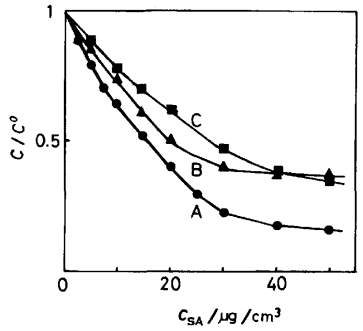

Fig. 5. Dependence of relative decrease of the differential capacity at −0.5 V on the concn of SDS (A), CTAB (B), and Tween 20 (C).

Table 1. Activity of Suppressing the Oxygen Maximum Current at −0.3 V, k, and of decreasing the Differential Capacity at −0.5 V, K

Surfactant	mol mass / g mol^{-1}	k / μg/cm^3	K / μg/cm^3
Na Octanate	166	0.02	0.001
Na Decanoate	194	0.48	0.011
Na Laurate	222	1.70	0.030
Na Myristate	250	1.18	0.026
Na Palmitate	278	0.40	0.014
Na Stearate	306	0.29	—
Na Oleate	304	0.70	0.020
Na Dodecyl sulfate	288	1.40	0.036
Na Hexadecyl sulfate	345	0.60	0.008
Na Dodecanesulfonate	272	1.50	0.036
Na Tetradecanesulfonate	300	1.20	0.028
Na Hexadecanesulfonate	328	0.56	0.016
Na Dodecylbenzenesulfonate	348	1.20	0.025
N-Dodecylpyridinium Cl$^-$	284	0.92	0.031
N-Hexadecylpyridinium Cl$^-$	358	0.65	0.022
Dodecyltrimethylammonium Cl$^-$	264	0.63	0.031
Tetradecyltrimethyl-ammonium Cl$^-$	292	0.61	0.030
Hexadecyltrimethyl-ammonium Br$^-$	365	0.60	0.023
Hexylamine	101	0.00	0.003
Octylamine	129	0.09	0.024
Decylamine	157	0.13	0.022
Dodecylamine	185	0.22	0.021
Tetradecylamine	213	0.07	0.006
poly(oxyethylene)(n) *p*-*t*-octylphenyl ether			
Triton *x*-100 n=9.5	624	0.63	0.030
Triton *x*-305 n=30	1526	0.42	0.018
Triton *x*-405 n=40	1966	0.42	0.017
poly(oxyethylene)(20) sorbitan monoalkanoate			
Tween 20, laurate	1214	0.59	0.020
Tween 40, palmitate	1265	0.57	0.019
Tween 60, stearate	1293	0.54	0.017
Tween 80, oleate	1291	0.54	0.017
Bovine serum albumin	69000	0.11	0.005
Horse cytochrom c	13500	0.14	0.007

tribution in suppressing the maximum current and decreasing the capacity is independent. A rigid control of the temperature (20—30 °C) and the dropping time of DME (3—5 s), which influence the adsorption of surfactant, is desirable for a better analysis. Constants characteristic of the surfactant representing the ability to suppress the oxygen maximum current, k, and to decrease the differential capacity, K, were calculated while assuming that the following empirical equations are valid:

$$I/I^0 = 1 - kc \quad (1)$$

and

$$C/C^0 = 1 - Kc. \quad (2)$$

These concern some thirty surfactants and are summarized in Table 1. This table is useful in a polarographic determination of the surfactants.

We are grateful to Prof. Mitsugi Senda and Dr. Takashi Kakiuchi of Kyoto Univ. for their kind advice.

References

1) M. J. Rosen and H. A. Goldsmith, "Systematic Analysis of Surface-Active Agents," 2nd Ed., John Wiley Sons, Inc (1972).
2) K. Linhart, *Tenside Detergents*, **9**, 241 (1972).
3) H. Jehring, *J. Electroanal. Chem.*, **21**, 77 (1966).
4) J. Heyrovsky and J. Kuta, "Principles of Polarography," Academic Press, New York and London (1966), p. 429.
5) H. Kinoshita, M. Kobayashi, M. Otsuka, and T. Fukamachi, abstract; *Rev. Polarogr. (Kyoto)*, **28**, 84 (1982).
6) H. Kinoshita, M. Kobayashi, abstract; *Rev. Polarogr. (Kyoto)*, **29**, 65 (1983).

Ring Transformation of 1,3-Dinitroquinolizin-4-one with Enolate Anions[1)]

Masahiro ARIGA* and Eizo MATSUMURA
Department of Chemistry, Osaka Kyoiku University,
Minamikawahori-cho, 4-88, Tennoji-ku Osaka 543
(Received September 10, 1986)

Synopsis. The ring transformation of 1,3-dinitroquinolizin-4-one, which is one of the condensed ring compounds of 1-substituted 3,5-dinitro-2-pyridone series, with enolate anions, $R^1CH_2COCHCOR^2$, gave the corresponding 2-COR^2-6-R^1-4-nitrobenzene-1,3-diols. The results show that carbonyl carbon of the quinolizinone behaves as reaction site in the ring transformation.

In a previous paper,[2)] we reported the substituent effects of 4- and 6-methyl or 4-methoxyl groups on the regio-orientation of the nucleophilic ring transformation of 1-substituted 3,5-dinitro-2-pyridones with enolate anions.

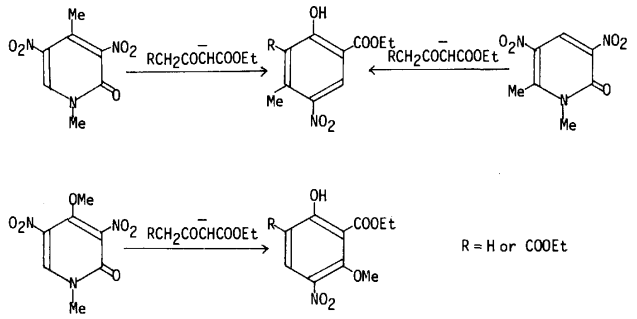

Fig. 1.

We wish to extend examinations to quinolizinone ring in order to investigate the scope and limitation of the reaction. 1,3-Dinitroquinolizin-4-one (**1**) is a 1,6-disubstituted 2-pyridone, of which 1- and 6-positions are linked with conjugated 1,3-butadiene unit, and the conjugation bonds in pyridone ring extend to pyridine unit. These structural features may cause a new type of reaction of electron-deficient 2-pyridone derivatives.

Results and Discussion

1,3-Dinitroquinolizin-4-one (**1**) was obtained by the known procedure.[3)] Treatment of **1** with 3 times equimolar ethyl sodio-3-oxobutanoate in DMF at −15—−10 °C gave colorless needles (**2a**) of mp 112.0—113.0 °C. The ^{1}H NMR spectra of **2a** indicated the presence of two aromatic *ortho*-protons and two hydroxyl protons in addition to methylene and methyl protons of ethoxycarbonyl group. From this result and IR spectra, **2a** was assigned to ethyl 2,6-dihydroxy-3-nitrobenzoate, and identified as that by comparison of spectral data with those of the sample prepared from 2,6-dihydroxy-3-nitrobenzoic acid.[4)]

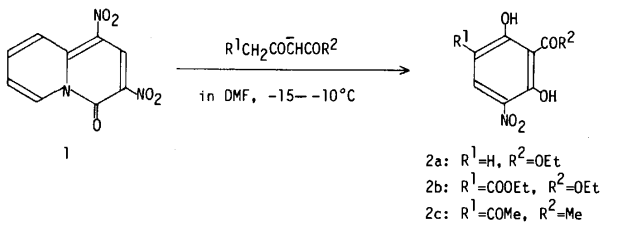

Fig. 2.

Similar reaction of **1** with 1.5 times equimolar diethyl sodio-3-oxopentanedioate gave diethyl 2,4-dihydroxy-5-nitro-1,3-benzenedicarboxylate (**2b**) in a good yield (76%).

Sodium salt of 2,4,6-heptanetrione also reacted in the similar conditions to give 3-acetyl-2,4-dihydroxy-5-nitroacetophenone (**2c**) in a moderate yield (57%).

The reaction of **1** with ethyl sodio-3-oxobutanoate was attempted to reveal appropriate reaction conditions, but no improvement of the yield of **2a** was achieved (Table 1). Diethyl 3-oxopentanedioate and 2,4,6-heptanetrione were sufficiently active to give reasonable yield of the products by using 1.5 mol of each reagent. However, the reaction of 3 molar amounts of ethyl 3-oxobutanoate did not show a good yield probably because the nucleophilic center of the reagent is methyl group which is less reactive than methylene group between two carbonyl groups.

The reaction of sodio-2,4-pentanedione in the conditions similar to those of the reaction of ethyl sodio-3-oxobutanoate gave only an unidentified resinous material.

Our previous results of the ring transformation of 3,5-dinitro-2-pyridones showed that the reaction centers were 4- and 6-positions (vinyl positions of carbonyl carbon) and not 2-position (carbonyl carbon) of 2-pyridone. In the present reaction, however, it is obvious that the product **2** consists of the reagent and C_2–C_3–C_4 part of quinolizinone ring and that carbonyl carbon (C_4 of the substrate **1**, corresponding to the 2-position of 2-pyridone) behaves as reaction site in the ring transformation. The fact is the first example

Table 1. Ring Transformation of 1,3-Dinitroquinolizin-4-one

Reagent[a)]	Reaction conditions		Products (Yields/%)
	mol. ratio	temp/°C	
a	3.0	−15—−10	**2a** (25.6)
b	1.5	−15—−10	**2b** (76.2)
c	1.5	−15—−10	**2c** (56.8)
a	3.0	25	**2a** (trace)
a	1.5	−15—−10	**2a** (trace) **1** (42.5)

a) **a**: ethyl sodio-3-oxobutanoate, **b**: diethyl sodio-3-oxopentanedioate, **c**: sodio-2,4,6-heptanetrione.

in 2-pyridone series.

Another product, 2-(nitromethyl)pyridine, which is supposedly derived from the rest of **1** in the ring transformation was not isolated. With reference to the report that 2-(nitromethyl)pyridine is an acidic and unstable compound,[5] it will give only a resinous material under the conditions of the present work.

From these results, a plausible course of the reaction is suggested as path(b) in the following scheme. The initial attack of enolate anion of β-dicarbonyl compound at the 2-position of substrate **1** (corresponding to the 4-position of 2-pyridone) was followed by the intramolecular nucleophilic attack of another nucleophilic center of introduced reagent at the 4-position of parent quinolizinone unit (carbonyl carbon) to give an intermediate **4**, of which reconstruction leads to the product **2**.

An alternative path(a) may be suggested, where the enolate anion attacks at the electrophilic centers of the quinolizinone in reverse sequence to path(b) to form the same intermediate **4** as is formed in path(b). It is well known that the nucleophilic attack generally occurs at a conjugated position and not at the carbonyl carbon in a conjugated carbonyl system, as the case of path(b). So, we prefer the path(b) as probable reaction course.

In the case of the reaction of ethyl sodio-3-oxobutanoate, a σ-complex, **3d**, may be initially formed, but direct conversion of **3d** to **4d** is unlikely, since it requires abstraction of a proton from less acidic center. Then **3d** is likely to transform to **3a** through equilibrium with **1** in view of easy cyclization to tricyclic intermediate by deprotonation from the most acidic methylene carbon in **3a**, and finally **4a** is given predominantly.[2,6,7]

The results mentioned above suggest that carbony carbon acts as electrophilic center in the intramolecular nucleophilic cyclization step of the ring transformation of 1,3-dinitroquinolizin-4-one. The fact is different from the case of 3,5-dinitro-2-pyridone, and may be explained as follows. If the reaction proceeds in the same way as 3,5-dinitro-2-pyridone,[2,8] an unfavorable crowded tricyclic intermediate, **5**, will be formed through path(c) or (d). Althogh the intermediate **5** appears to be not so unstable to be formed, its reconstruction to stable aromatic product such as **2** in path(b) is impossible. These factors will result in forming the intermediate **4** through path(b).

Experimental

All the melting points were uncorrected. ^{1}H NMR spectra were recorded by a Hitachi R-20B Spectrometer with TMS as the internal standard. IR spectra were obtained by a Hitachi 260-10 Spectrometer.

Reaction of 1 with Ethyl Sodio-3-oxobutanoate. To a solution of 500 mg (2.1 mmol) of **1** in 100 cm^3 of DMF was added dropwise ethyl sodio-3-oxobutanoate sulution, prepared from 150 mg (6.5 mmol) of sodium and 950 mg (7.3 mmol) of ethyl 3-oxobutanoate in 30 cm^3 DMF for 5 h at −15—−10 °C with stirring, and the mixture was allowed to stand at the same temperature overnight. After being quenched by addition of 3.5 cm^3 of 1 mol dm^{-3} HCl, the solvent was evaporated in vacuo, the residual oil was dissolved in 20 cm^3 water, and extracted with chloroform at pH 3.0. After the extract was dried over anhydrous magnesium sulfate chloroform was distilled off, and the residual syrup was column-chromatographed on silica gel (Wakogel C-200). From benzene elute, was obtained 126 mg

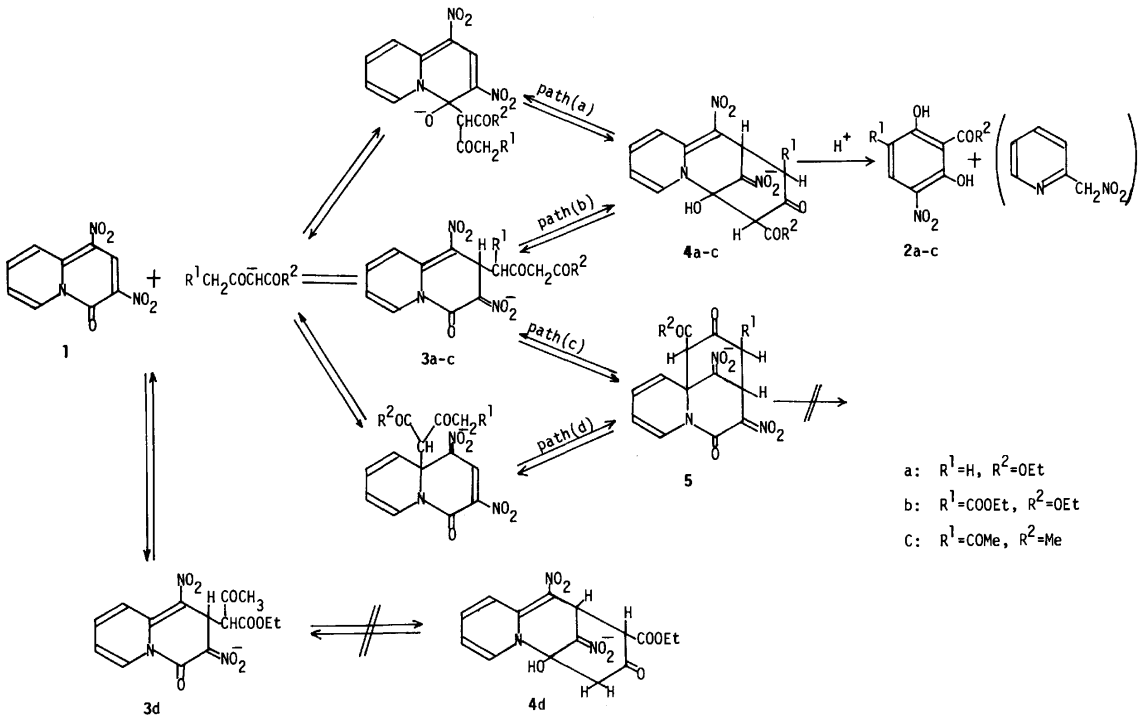

Fig. 3.

(27.7%) of ethyl 2,6-dihydroxy-3-nitrobenzoate (**2a**), which was recrystallized from petroleum benzine of bp 65—75 °C. IR(nujol) ν 3100 (OH), 1750, (C=O), 1540, 1350 (NO_2). ^1H NMR ($CDCl_3$) δ=1.44 (t, J=7.0 Hz, 3H), 4.48 (q, J=7.0 Hz, 2H), 6.52 (d, J=9.0 Hz, 1H), 8.15 (d, J=9.0 Hz, 1H), 12.43 (s, 1H), 12.61 (s, 1H). Found: C, 47.51; H, 3.81; N, 6.08%. Calcd for $C_9H_9NO_6$: C, 47.58; H, 3.99; N, 6.17%.

Reaction of 1 with Diethyl Sodio-3-oxopentanedioate. Treatment of 500 mg (2.1 mmol) of **1** with diethyl sodio-3-oxopentanedioate, prepared from 73 mg (3.2 mmol) of sodium and 720 mg (3.6 mmol) of diethyl 3-oxopentanedioate in the similar procedure as described above, gave 485 mg (76.2%) of diethyl 2,4-dihydroxy-5-nitro-1,3-benzenedicarboxylate (**2b**); colorless plates (petroleum benzine), mp 85.0—86.0 °C. IR(nujol) ν 3200 (OH), 1750 (C=O), 1540, 1350 (NO_2). ^1H NMR ($CDCl_3$) δ=1.40 (t, J=7.0 Hz, 3H), 1.43 (t, J=7.0 Hz, 3H), 4.43 (q, J=7.0 Hz, 2H), 4.44 (q, J=7.0 Hz, 2H), 8.71 (s, 1H), 11.94 (s, 1H), 12.26 (s, 1H). Found: C, 48.31; H, 4.44; N, 4.61%. Calcd for $C_{12}H_{13}NO_8$: C, 48.17; H, 4.38; N, 4.70%.

Reaction of 1 with Sodio-2,4,6-heptanetrione. According to the preliminary expriments, 500 mg (2.1 mmol) of **1** was made to react with sodio-2,4,6-heptanetrione prepared from 73 mg (3.1 mmol) sodium and 500 mg (3.6 mmol) of 2,4,6-heptanetrione to give 290 mg (56.8%) of 3-acetyl-2,4-dihydroxy-5-nitroacetophenone (**2c**); colorless columns (ethanol), mp 142.0—143.0 C. IR(nujol): ν 3100 (OH), 1620 (C=O), 1580 (C=O), 1550, 1345 (NO_2). ^1H NMR ($CDCl_3$) δ=2.69 (s, 3H), 2.82 (s, 3H), 8.73 (s, 1H), 14.94 (s, 2H). Found: C, 50.31; H, 3.89; N, 5.76%. Calcd for $C_{10}H_9NO_6$: C, 50.21; H, 3.79; N, 5.86%.

Referenes

1) Nucleophilic Reaction upon Electron-deficient Pyridone Derivatives. IX. for the preceding paper, *Bull. Chem. Soc. Jpn.*, **60**, 201 (1987).

2) M. Ariga, Y. Tohda, and E. Matsumura, *Bull. Chem. Soc. Jpn.*, **58**, 393 (1985).

3) B. S. Thyagarajan and P. V. Gopalakrishnann, *Tetrahedron*, **20**, 1051 (1964).

4) H. Ruschig and J. Koenig, Ger. Offen., 1930328 (1971).

5) H. Feuer and J. P. Lawrence, *J. Org. Chem.*, **37**, 3662 (1972).

6) M. J. Strauss, T. C. Jensen, H. Schran, and K. O'Conner, *J. Org. Chem.*, **35**, 383 (1970).

7) L. M. Gnanadoss and N. Radha, *J. Org. Chem.*, **78**, 570 (1983).

8) E. Matsumura, M. Ariga, and Y. Tohda, *Bull. Chem. Soc. Jpn.*, **52**, 2413 (1979).

Reactions of 2-Aryl-2*H*-cycloheptathiazoles with Dimethyl Acetylenedicarboxylate

Noritaka ABE,* Satoshi KONDO, and Koichi MORITA
Department of Chemistry, Faculty of Sciences, Yamaguchi University, Yamaguchi 753
(Received September 16, 1986)

Synopsis. Reaction of 2-aryl-2*H*-cycloheptathiazoles with dimethyl acetylenedicarboxylate gave dimethyl 2-aryl-3*H*-1-thia-2a-azacyclopent[*cd*]azulene-3,4-dicarboxylate, tetramethyl 6-phenyl-2,3,4,5-pyridinetetracarboxylate, and tetramethyl 5-[(thioaroyl)iminomethyl]-1,2,3,4-naphthalenetetracarboxylate.

Concerning the cycloaddition reactions of benzothiazoles[1] and azaazulenes,[2] we have reported that the cycloaddition of 2*H*-cycloheptathiazol-2-one with acetylenic esters produced 1:1- and 1:2-cycloadducts via 1,10-dipolar intermediates.[3] Cycloadditions of 8-azaheptafulvene are also known,[4] which proceeded via similar dipolar intermediates. It is interesting to ascertain if 2-aryl-2*H*-cycloheptathiazoles, which are not fully conjugated and would be considered as substituted azaheptafulvenes, undergo a similar cycloaddition or not. We have now carried out the reaction of 2-aryl-2*H*-cycloheptathiazoles with dimethyl acetylenedicarboxylate (DMAD), and found that the reaction gave novel products in addition to the anticipated dipolar cyclization products.

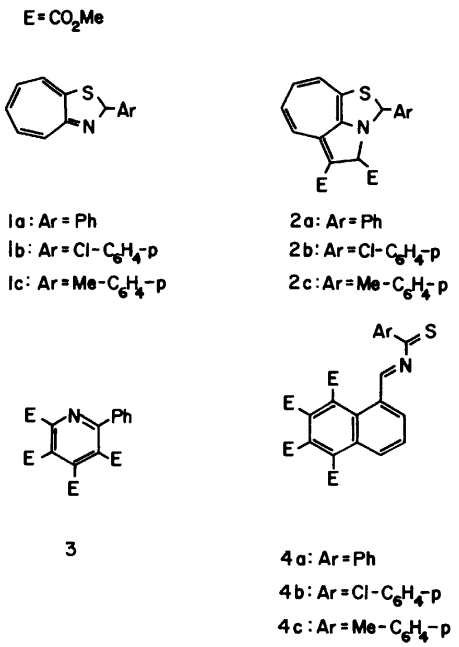

2-Aryl-2*H*-cycloheptathiazoles (**1a—c**) were prepared by the reaction of 2-aminocycloheptatrienethione (2-aminotroponethione)[5] with the corresponding aromatic aldehydes in a similar method as reported[6] for **1b**.

Treatment of **1a** with DMAD in boiling benzene gave a complex mixture, from which four products, **2a** (9%), **3** (8%), **4a** (15%), and **5a** (14%), were isolated by chromatography on silica gel. The structures of these compounds, except **5a**, were elucidated by their spectroscopic data as well as by elemental analyses.

Compound **2a** ($C_{20}H_{17}NO_4S$) was assigned to dimethyl 2-phenyl-3*H*-1-thia-2a-azacyclopent[*cd*]-azulene-3,4-dicarboxylate, which is the corresponding cycloadduct to that described before.[2,3] Its ^{1}H NMR spectrum shows two 1H-singlets at δ 5.08 and 6.10, which should be assigned to H-3 and H-2, respectively. Two ester methyl-singlets are seen at δ 2.98 and 3.72. The relatively high-field appearance of the former may be due to the shielding effect by the phenyl group at C-2. The electronic spectrum of **2a** accords with the structure as a substituted heptafulvene.

Compound **3** was identical with tetramethyl 6-phenyl-2,3,4,5-pyridinetetracarboxylate,[7,8] which was not formed in the reactions of 2*H*-cycloheptathiazol-2-one or azaazulenes.

Compound **4a** ($C_{26}H_{21}NO_8S$) was tentatively assigned to tetramethyl 5-(thiobenzoyliminomethyl)-1,2,3,4-naphthalenetetracarboxylate. In the mass spectrum, a peak at *m/z* 345 (M^+—PhCSNCH) is observed. The electronic spectrum of **1a** has several weak absorption muxima in the visible region; whereas that of **4a** does not. The ^{1}H NMR spectrum of **4a** shows a low-field resonated 1H-singlet at δ 7.67 and a 3H-multiplet at aromatic region (δ 6.85—6.95) together with four ester methyl-singlets and phenyl-multiplets. The IR spectrum of **4a** exhibits a band of medium intensity at 1630 cm^{-1} assignable to C=N in addition to the absorptions of ester carbonyls. These observations suggest that **4a** has a naphthalene nucleus and a C=N group besides four ester groups.

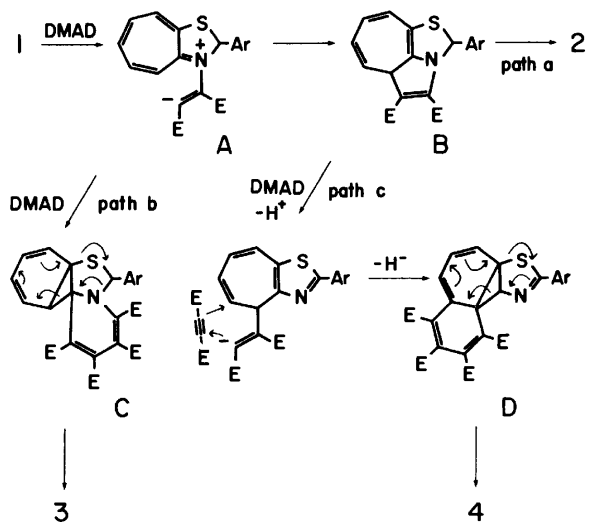

Scheme 1.

A yellow compound **5a** ($C_{26}H_{23}NO_2S$) was a 1:2-adduct, but the structure has not yet been elucidated.

Compounds **1b** and **1c** also reacted with DMAD to give **2b—c**, **3**, **4b—c**, and **5b—c**, respectively. From the results, no particular substituent effect was observed.

A plausible mechanism for the reaction of **1** with DMAD is shown in Scheme 1. Electrophilic attack of DMAD on the nitrogen gives the ylide intermediate **A**. A 1,10-dipolar cyclization of **A** gives **B**, and a subsequent 1,3-hydrogen shift furnishes **2** (path a). Cycloaddition of ylide **A** with DMAD gives **C**. Ring-contraction of **C** accompanied by bond cleavage affords **3** (path b). Cycloaddition of **A** with DMAD and successive rearrangement may lead to **D**, which in turn rearranges to **4** (path c).

Although the dipolar species **A** resembles to that of 2*H*-cycloheptathiazol-2-one, the reaction products differ extremely from each other. This would be associated with the difference of hybridization at C-2 carbon (sp^3 *vs.* sp^2) or the electron-attracting effect of the carbonyl group of 2*H*-cycloheptathiazol-2-one.

Experimental

Melting points are uncorrected. ^1H NMR spectra were taken with a Hitachi R-24B spectrometer (60 MHz) for solutions in $CDCl_3$ with TMS as an internal standard. Electronic spectra were measured for solutions in ethanol and IR spectra for Nujol mulls unless otherwise stated. Mass spectra were determined with a Hitachi M-80 instrument by a field desorption ionization method. Column chromatography was performed on Kieselgel 60.

Syntheses of 2-Arylcycloheptathiazoles. A mixture of 2-aminocycloheptatrienethione[5] (2.74 g, 20 mmol), benzaldehyde (2.12 g, 20 mmol), and concd hydrochloric acid (3.0 ml) in ethanol (40 ml) was refluxed for 4 h. Water (200 ml) was added, and the mixture was extracted with chloroform. The extract was washed, dried (Na_2SO_4), and evaporated. Chromatography of the residue with benzene gave **1a** (2.75 g, 61%) as yellow tar; λ_{max} 248 nm (log ε 4.19), 272 (4.04), 282 (4.03), 290 (4.01), 325 (3.78, sh), 338 (3.80), 354 (3.76), 376 (3.69), 398 (3.26, sh), 419 (3.20), 441 (3.10), 470 (2.82, sh), and 505 (2.17); ν_{max} (neat) 755 and 695 cm^{-1} (phenyl); ^1H NMR δ=6.1—6.8 (5H, m, H-4, 5, 6, 7, and 8), 7.23 (1H, s, H-2), and 7.3—7.55 (5H, m, H-phenyl); Picrate of **1a**: Yellow needles (from ethanol), mp 167—168 °C. Anal. ($C_{20}H_{14}N_4O_7S$) C, H, N.

In a similar manner, we made the following: **1b** [41%, yellow needles (from aq ethanol), mp 80—81 °C (lit,[6] 80.5—81 °C; λ_{max} 219 nm (log ε 4.17), 227 (4.15), 247 (4.15), 270 (3.85), 279 (3.85), 290 (3.84), 342 (3.59, sh), 356 (3.67), 375 (3.59), 397 (3.21), 418 (3.23), 441 (3.15), 468 (2.90), and 500 (2.34, sh); ν_{max} 835 cm^{-1} (phenyl); ^1H NMR δ=6.0—6.8 (5H, m, H-4, 5, 6, 7, and 8), 7.10 (1H, s, H-2), and 7.30 (4H, bs, H-phenyl). Anal. ($C_{14}H_{10}ClNS$) C, H, N.]; **1c** [83%, yellow tar; λ_{max} 252 nm (log ε 4.32), 271 (4.17), 292 (4.16), 342 (3.98), 356 (4.00), 375 (3.89), 395 (3.47, sh), 421 (3.47), 445 (3.38), 471 (3.14, sh), and 503 (2.37, sh); ν_{max} (neat) 820 cm^{-1} (phenyl); ^1H NMR δ=2.33 (3H, s, Me), 6.0—7.0 (5H, m, H-4, 5, 6, 7, and 8), 7.18 (1H, s, H-2), 7.18 (2H, d, J=9 Hz, H-*m*-phenyl), 7.33 (2H, d, J=9 Hz, H-*o*-phenyl). Pycrate of **1c**: Yellow needles (from ethanol), mp 144—146 °C. Anal. ($C_{21}H_{16}N_4O_7S$) C, H, N].

Reaction of 1 with DMAD. A solution of **1a** (3.23 g, 14.4 mmol) and DMAD (6.12 g, 43.1 mmol) in dry benzene (50 ml) was refluxed for 3 h, then evaporated, and the residue chromatographed. Benzene eluted **2a** (0.48 g, 9%), which was crystallized from ethanol as yellow prisms, mp 160—161 °C; λ_{max} 223 nm (log ε 4.52), 275 (3.92), 321 (3.86), and 437 (3.52); ν_{max} 1735 and 1705 cm^{-1} (C=O); 2.90, 3.72 (each 3H, s, OMe), 5.08 (1H, bs, H-4), 6.10 (1H, s, H-2), 6.5—7.1 (3H, m, H-7, 8, and 9), and 7.25—7.7 (6H, m, H-6 and phenyl). Anal. ($C_{20}H_{17}NO_4S$) C, H, N, S. Further elution gave **3** (0.45 g, 8%), which was crystallized from ethanol as colorless prisms, mp 128—129 °C (lit,[7] mp 128—129 °C), Anal. ($C_{19}H_{17}NO_8$) C, H, N. Spectral data were described in lit. 8. Elution with benzene–chloroform (1:1) gave **4a** (1.01 g, 15%), which was crystallized from ethanol as yellow prisms, mp 206—207 °C, λ_{max} 217 nm (log ε 4.66), 321 (3.91), and 390 (3.28); ν_{max} 1750, 1725, 1710, 1700 (C=O), and 1630 cm^{-1} (C=N); ^1H NMR δ=3.02, 3.70, 3.73, 3.84 (each, 3H, s, OMe), 6.85—6.95 (3H, m, H-6, 7, and 8), 7.2—7.4 (3H, m, H-*m,p*-phenyl), 7.6—7.8 (2H, m, H-*o*-phenyl), 7.67 (1H, s, HC=N); MS *m/z* (rel intensity) 507 (M^+, 100), 345 (57). Anal. ($C_{26}H_{21}NO_8S$) C, H, N, S. Further elution gave **5a** (1.06 g, 14%), which was crystallized from ethanol as yellow prisms, mp 147—148 °C; λ_{max} 217 nm (log ε 4.59), 288 (3.83, sh), 313 (3.91), and 369 (3.83); ν_{max} 1735, 1725, 1715, 1695 cm^{-1} (C=O); ^1H NMR δ=3.38, 3.62 (each 3H, s, OMe), 3.67 (6H, s, OMe), 5.00 (1H, dd, J=1.5 and 0.5 Hz), 5.77 (1H, d, J=1.5 Hz), 6.53 (1H, d, J=0.5 Hz), 6.75—6.9 (3H, m), and 7.15—7.4 (5H, m, H-phenyl). Anal. ($C_{26}H_{23}NO_8S$) C, H, N, S.

In a similar manner, **1b** gave **2b** (3%), **3** (28%), **4b** (7%), and **5b** (10%), and **1c** gave **2c** (2%), **3** (23%), **4c** (19%), and **5c** (11%).

2b: Which could not be purified but its structure was elucidated from the ^1H NMR spectrum. ^1H NMR δ=3.03, 3.75 (each 3H, s, OMe), 5.00 (1H, bs, H-4), 6.05 (1H, s, H-2), 6.4—7.0 (3H, m, H-7, 8, and 9), and 7.1—7.5 (5H, m, H-6 and phenyl).

4b: Yellow needles (from cyclohexane–dichloromethane), mp 221—222 °C; λ_{max} 219 nm (log ε 4.58), 321 (3.83), and 392 (3.17); ν_{max} 1750, 1740, 1720, 1705 (C=O), and 1625 cm^{-1} (C=N); ^1H NMR δ=3.10, 3.69, 3.72, 3.83 (each 3H, s, OMe), 6.75—7.0 (3H, m, H-6, 7, and 8), 7.27 (2H, d, J=9 Hz, H-*m*-phenyl), 7.67 (1H, s, HC=N), and 7.70 (2H, d, J=9 Hz, H-*o*-phenyl); MS *m/z* 541 (M^+). Anal. ($C_{26}H_{20}ClNO_8S$) C, H, N, S.

5b: Yellow needles (from ethanol), mp 177—179 °C; λ_{max} 221 nm (log ε 4.52), 282 (3.79), 313 (3.87), and 367 (3.79); ν_{max} 1735, 1720, 1715, and 1685 cm^{-1} (C=O); ^1H NMR δ=3.50, 3.69 (each 3H, s, OMe), 3.72 (6H, s, OMe), 5.03 (1H, dd, J=1.5 and 0.5 Hz), 5.71 (1H, d, J=1.5 Hz), 6.57 (1H, d, J=0.5 Hz), 6.8—7.1 (3H, m), and 7.30 (4H, bs, H-phenyl). Anal. ($C_{26}H_{22}ClNO_8S$) C, H, N, S.

2c: Which could not be purified but its structure was elucidated from the ^1H NMR spectrum. ^1H NMR δ=2.30 (3H, s, Me), 3.00, 3.73 (each 3H, s, OMe), 5.00 (1H, bs, H-4), 6.07 (1H, s, H-2), 6.35—7.0 (3H, m, H-7, 8, and 9), 7.2—7.6 (5H, m, H-6 and phenyl).

4c: Yellow prisms (from ethanol), mp 247—249 °C; λ_{max} 217 nm (log ε 4.70), 322 (3.92), and 395 (3.28); ν_{max} 1755, 1725, 1720, 1705 (C=O), and 1630 cm^{-1} (C=N); ^1H NMR δ=2.33 (3H, s, Me), 3.06, 3.72, 3.75, 3.85 (each 3H, s, OMe), 6.85—7.05 (3H, m, H-6, 7, and 8), 7.12 (2H, d, J=9 Hz, H-*m*-phenyl), 7.67 (2H, d, J=9 Hz, H-*o*-phenyl), and 7.72 (1H, s, HC=N); MS *m/z* (rel intensity) 521 (M^+, 16), 462 (100), 404 (68), 359 (18). Anal. ($C_{27}H_{23}NO_8S$) C, H, N, S.

5c: Yellow needles (from ethanol), mp 125.5—126 °C; λ_{max} 220 nm (log ε 4.55), 288 (3.77, sh), 314 (3.87), and 369 (3.80); ν_{max} 1735, 1725, 1715, and 1690 cm^{-1} (C=O); ^1H NMR δ=2.33 (3H, s, Me), 3.44, 3.66 (each 3H, s, OMe), 3.70 (3H, s, OMe), 5.02 (1H, dd, J=1.5 and 0.5 Hz), 5.80 (1H, d, J=1.5 Hz), 6.58 (1H, d, J=0.5 Hz), 6.8—7.05 (3H, m), and 7.15 (4H, bs, H-phenyl). Anal. ($C_{27}H_{25}NO_8S$) C, H, N.

References

1) R. M. Acheson, *Lect. Heterocyclic Chem.*, **6**, 59 (1982).
2) T. Nishiwaki and N. Abe, *Heterocycles*, **15**, 547 (1981).
3) N. Abe, T. Nishiwaki, and M. Shigematsu, *J. Chem. Soc., Perkin Trans. 1*, **1982**, 2881.
4) T. Iwasaki, S. Kajigaeshi, and S. Kanemasa, *Bull. Chem. Soc. Jpn.*, **51**, 229 (1978).
5) N. Soma, J. Nakazawa, T. Watanabe, Y. Sato, and G. Sunagawa, *Chem. Pharm. Bull.*, **13**, 819 (1965).
6) W. R. Brasen and R. E. Benson, *J. Am. Chem. Soc.*, **83**, 3135 (1961).
7) R. Huisgen and K. Herbig, *Liebigs Ann. Chem.*, **688**, 98 (1965).
8) N. Abe, T. Nishiwaki, and K. Ikeda, *Bull. Chem. Soc. Jpn.*, **55**, 2464 (1982).

Cobaltocene-Catalyzed Reaction of Carbon Dioxide with Propargyl Alcohols

Yoshio INOUE,* Jiro ISHIKAWA, Masaaki TANIGUCHI, and Harukichi HASHIMOTO
Department of Applied Chemistry, Faculty of Engineering, Tohoku University,
Aoba, Aramaki, Sendai 980
(Received September 13, 1986)

Synopsis. The reaction of carbon dioxide with α-ethynyl tertiary alcohols has been catalyzed by cobaltocene to give α-methylene cyclic carbonates in good yields. α-Ethynyl primary or secondary alcohols give noncyclic alkyl carbonates in fair yields.

Considerable attention has been attracted in the fixation of carbon dioxide (CO_2) to organic substrates using transition metals with regard to the use of readily available primary chemicals in organic synthesis.[1] Previously we reported a few examples of cooligomerization of acetylenic compounds with CO_2 catalyzed by nickel(0) complexes to produce α-pyrone derivatives.[2]

In this paper we describe another example of the reaction of CO_2 with acetylenic alcohols catalyzed by cobaltocene ($CoCp_2$; Cp=cyclopentadienyl). α-Ethynyl tertiary alcohols **1** such as 2-methyl-3-butyn-2-ol underwent cycloaddition with CO_2 yielding α-methylene cyclic carbonates **2** in good yield in the presence of $CoCp_2$ and triethylamine.

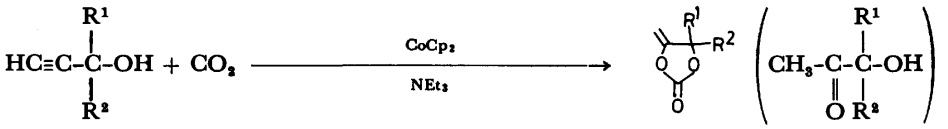

1 **2** **3**

a; $R^1=R^2=CH_3$
b; $R^1=CH_3$, $R^2=C_2H_5$
c; $R^1=CH_3$, $R^2=CH_2CH(CH_3)_2$
d; $R^1=R^2=C_2H_5$

Similar types of reaction are also known to be catalyzed by CuCl[3] or $PdCl_2(MeCN)_2$.[4] Very recently $Ru_3(CO)_{12}$ was shown to catalyze the reaction of CO_2 with α-ethynyl primary or secondary alcohols to afford noncyclic 2-oxoalkyl carbonates.[5]

The cobalt-mediated reaction was performed in an autoclave under the pressure of CO_2 without employing a solvent usually. In addition to the product **2**, a small amount(<9%) of α-hydroxy ketone of the type **3** was also obtained. This may be formed from the reaction of **1** wih the water concomitant with **1**.

Table 1. Reaction of α-Ethynyl Tertiary Alcohols **1** with CO_2[a]

Alcohol 1	Solvent	Reaction temp/°C	Reaction time/h	Product 2	Yield[b] %
1a	—	60	5	**2a**	11
	—	80	0.5		17
	—	80	1		41
	—	80	1.5		83
	—	80	5		87
	—	100	5		87
	—	100	5		84[c]
	Benzene	80	5		3
	THF	80	5		5
	DMF	80	5		28
1b	—	80	5	**2b**	87
1c	—	80	5	**2c**	82
1d	—	80	5	**2d**	52
	—	100	5		83

a) **1**, 50 mmol; solvent, 20 cm^3; $CoCp_2$, 1 mmol; Et_3N, 3.6 mmol; CO_2, 50 kg cm^{-2}. b) GLC yield. c) Without NEt_3.

The results are shown in Table 1. At first, 2-methyl-3-butyn-2-ol (**1a**) was employed as a probe to investigate the reaction conditions. The reaction occurred at the temperature above 60 °C and proceeded smoothly at 80 °C. The reaction terminated almost in 1.5 h at this reaction temperature. Normally triethylamine was added as the co-catalyst. However the reaction took place without adding this amine although the yield of **2a** declined slightly. The employment of a solvent such as benzene, tetrahydrofuran (THF), or *N*,*N*-dimethylformamide (DMF) profoundly diminished the yield of the product **2a**.

The other α-ethynyl tertiary alcohols such as **1b—d** underwent the 1:1 cycloaddition reaction giving **2b—d**, respectively under similar reaction conditions.

3-Butyn-2-ol (**4**), an α-ethynyl secondary alcohol, did not afford the 1:1 cycloaddition product. Instead, a small amount (≈15%) of 1:2 addition product, i.e., 1-methyl-2-oxopropyl 1-methyl-2-propynyl carbonate (**5**) was obtained along with the other minor products.

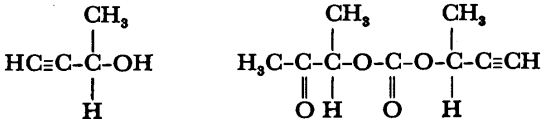

4 **5**

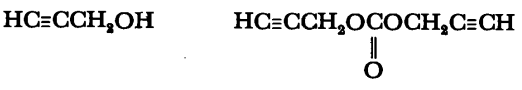

6 7

Propargyl alcohol (**6**), an α-ethynyl primary alcohol, afforded dipropargyl carbonate (**7**) in 6% yield together with a small amount of hydroxyacetone (≈0.2%) after the reaction at 80 °C for 5 h. Addition of an equimolar amount of PPh_3 to the catalyst increased the yield of **7** up to 24%.

α-(1-Alkynyl) tertiary alcohols like **8** or **9** did not react with CO_2. Under forced conditions (110 °C, 5 h), **9** afforded an isomerized product **10** in a moderate yield.

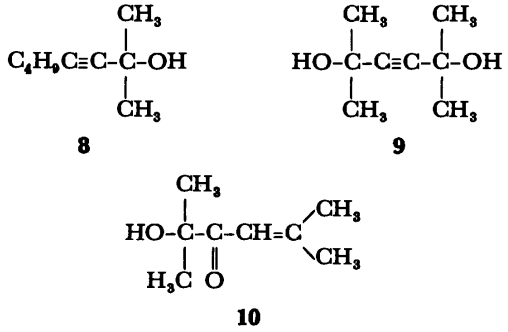

8 9 10

It can be presumed that cobaltocene is oxidized to cobaltocenium ion $[CoCp_2]^+$ in the presence of water or alcohol if the air is present.[6] The possible participation of the ion to the present cyclization reaction has been studied. A solution composed of **1a**, triethylamine, and cobaltocene was stirred in the air at an ambient temperature for 0.5 h and then the mixture was submitted to the reaction with CO_2 (80 °C, 5 h) to yield **2a** in only 5%. Another experiment employing $[CoCp_2]Cl$ as catalyst afforded **2a** from **1a** in 15% yield under the standard reaction conditions. So the participation of cobaltocenium ion to this reaction is partial if any.

Although the mechanism is unknown, one possibility will be mentioned at this time. The first step of the reaction is the formation of monoalkyl carbonate ion from **1a** and CO_2. The presence of triethylamine increases the amount of the ion. Then the monoalkyl carbonate undergoes cyclization under the assist of cobaltocene. It has been reported recently that this type of cyclization occurs in a trans fashion in the palladium-catalyzed reaction.

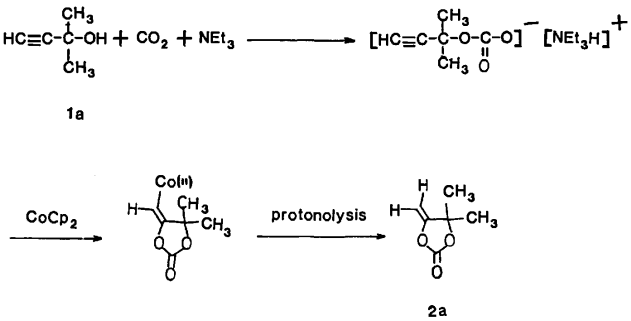

1a 2a

To gain mechanistic information, the deuterio alcohol **1a**-d_1 was employed. This alcohol afforded the cyclic carbonate **2a**-d_1, the deuterium being located almost equally in the exo methylene protons (see the experimental part). This result indicates that exactly the same mechamism as that in the palladium case is not operative.

1a-d_1 **2a**-d_1

Experimental

Materials. Cobaltocene[7] and $[CoCp_2]Cl$[8] were prepared according to the literatures. The alcohols, **1a—d**, **4**, and **6**, were obtained commercially and distilled before use. The alcohol **9** was used as received. The alcohol **8** was synthesized according to the reported method[9] from 1-hexyne and acetone.

Reaction of α-Ethynyl Tertiary Alcohols 1 with CO_2. The reaction of 2-methyl-3-butyn-2-ol (**1a**) with CO_2 is typical. A mixture of **1a** (50 mmol), Et_3N (3.6 mmol), and $CoCp_2$ (1 mmol) was stirred at 80 °C for 5 h under the pressure of CO_2 in an autoclave. GLC analysis (FFAP, 10%, 3 m, 160 °C) showed the formation of 4,4-dimethyl-5-methylene-1,3-dioxolan-2-one (**2a**) and 3-hydroxy-3-methyl-2-butanone (**3a**) in 87 and 9% yield, respectively. The product **2a** was isolated by distillation. Liquid; bp 45 °C/3 mmHg (lit,[3] bp 82 °C/18 mmHg); (1 mmHg= 133.322 Pa). Mp 26.5—27.5 °C.

4-Ethyl-4-methyl-5-methylene-1,3-dioxolan-2-one (2b). Isolated by distillation. Liquid; bp 55 °C/3 mmHg (lit,[3] bp 95 °C/20 mmHg.).

4-Methyl-5-methylene-4-(2-methylpropyl)-1,3-dioxolan-2-one (2c). Isolated by distillation. Liquid; bp 110—125 °C/3 mmHg. Found: C, 63.36; H, 8.65%. Calcd for $C_9H_{14}O_3$: C, 63.51 H, 8.29%. IR (neat) 1820, 1680, 840 cm^{-1}. ^1H NMR ($CDCl_3$) δ=0.89 (d, 6H, J=6 Hz), 1.51 (s, 3H), 2.32—2.60 (m, 1H), 2.60—2.72 (br, 1H), 4.22 (d, 1H, J=4 Hz), 4.72 (d, 1H, J=4 Hz).

4,4-Diethyl-5-methylene-1,3-dioxolan-2-one (2d). Isolated by distilation. Liquid; bp 76 °C/66 mmHg. Found: C, 61.65; H, 7.97%. Calcd for $C_8H_{12}O_3$: C, 61.52; H, 7.74%. IR (neat) 1820, 1680, 845 cm^{-1}. ^1H NMR ($CDCl_3$) δ=0.91 (t, 6H, J=7 Hz), 1.40—2.10 (m, 4H), 4.17 (d, 1H, J=4 Hz), 4.80 (d, 1H, J=4 Hz).

Reaction of 3-Butyn-2-ol (4) with CO_2. The alcohol **4** (64 mmol) was reacted with CO_2 (50 kg cm^{-2}) in the presence of $CoCp_2$ (1 mmol) and Et_3N (3.6 mmol) at 80 °C for 5 h. GLC analysis (Silicone DC-550, 20%, 3 m, 170 °C) showed the formation of 1-methyl-2-oxopropyl 1-methyl-2-propynyl carbonate (**5**)[5] in 15% yield together with several minor products.

Reaction of Propargyl Alcohol (6) with CO_2. The alcohol **6** (86 mmol) was reacted with CO_2 (50 kg cm^{-2}) in the presence of $CoCp_2$ (1 mmol) and NEt_3 (3.6 mmol) at 80 °C for 5 h. GLC analysis (Silicone DC-550, 20%, 3 m, 170 °C) showed the formation of dipropargyl carbonate (**7**) and hydroxyacetone in 6 and 0.2% yield, respectively. Addition of PPh_3 (1 mmol) increased the yield of **7** up to 24%.

Reaction of 2,5-Dimethyl-3-hexyne-2,5-diol (9) with CO_2. The diol **9** (50 mmol) was reacted with CO_2

($50\ kg\ cm^{-2}$) in the presence of $CoCp_2$ (1 mmol) and Et_3N (3.6 mmol) at 110 °C for 5 h. GLC analysis (Silicone GE SE-52, 20%, 2 m, 85 °C) showed the formation of 2-hydroxy-2,5-dimethyl-3-hexanone (**10**) in 53% yield. The product **10** was isolated by distillatiuon. Liquid; bp 44 °C/4 mmHg. Found: C, 67.42; H, 10.25%. Calcd for $C_8H_{14}O_2$: C, 67.57; H, 9.93%. IR (neat) 3440, 1675, 1615, 1440, 1360, 1030, 960 cm^{-1}. ^1H NMR ($CDCl_3$) δ=1.30 (s, 6H), 1.91 (s, 3H), 2.16 (s, 3H), 4.12 (s, 1H), 6.20 (s, 1H).

Reaction of 2-Methyl-3-butyn-2-ol-*d* (1a-d_1) with CO_2. A 50 cm^3 flask was flushed with N_2 and was then charged with 28 cm^3 of diethyl ether, 12 cm^3 of **1a**, and 5 cm^3 of D_2O. The flask was shaken vigorously for 5 min. It was placed in a salt/ice bath, the water layer frozen, then the ethereal layer was transferred by a syringe to another flask containg D_2O. This procedure[10] was repeated for five times in all. The final ethereal solution was dried over K_2CO_3 and distilled to yield ca. 5 cm^3 of **1a**-d_1, which was 76% deuterated (by integration of the NMR). The deuterated alcohol **1a**-d_1 (37 mmol) was reacted with CO_2 ($50\ kg\ cm^{-2}$) in an autoclave in the presence of $CoCp_2$ (1 mmol) without triethylamine at 80 °C for 1 h. After that time, the resulting reaction mixture was analyzed by ^1H NMR. The yield of **2a**-d_1 was 10%. No H–D scrambling between the alcoholic deuterium and the acetylenic proton was observed during the reaction. The ratio of the exo methylene proton in the position cis to the oxidocarbonyloxy group to that in the position trans was 47:53 for the product **2a**-d_1.

References

1) For reviews, see; M. E. Volpin and I. S. Kolomnikov, *Organomet. React.*, **5**, 313 (1975); D. J. Darensbourg and R. A. Kudaroski, *Adv. Organomet. Chem.*, **22**, 129 (1983); S. Inoue, "Organic and Bio-organic Chemistry of Carbon Dioxide," Kodan Sha LTD., Tokyo (1981), Chap. 3.

2) Y. Inoue, Y. Itoh, and H. Hashimoto, *Chem. Lett.*, **1977**, 855; **1978**, 633; Y. Inoue, Y. Itoh, H. Kazama, and H. Hashimoto, *Bull. Chem. Soc. Jpn.*, **53**, 3329 (1980).

3) H. Laas, A. Nissen, and A. Nürrenbach, *Synthesis*, **1981**, 958.

4) N. Yanagihara, K. Iritani, and K. Uchimoto, 52nd National Meeting of the Chemical Society of Japan, Kyoto, April 1986, Abstr., No. 4W15.

5) Y. Sasaki, *Tetrahedron Lett.*, **27**, 1573 (1986).

6) E. O. Fischer and R. Jira, *Z. Naturforsch.*, 8B, 1 (1953); *ibid.*, 8B, 327 (1953).

7) G. Wilkinson, F. A. Cotton, and J. M. Birmingham, *J. Inorg. Nucl. Chem.*, **2**, 96 (1956).

8) D. Hartley and M. J. Ware, *J. Chem. Soc. (A)*, **1969**, 138.

9) B. R. Fleck and J. E. Kmiecik, *J. Org. Chem.*, **22**, 90 (1957).

10) T. F. Murray and J. R. Norton, *J. Am. Chem. Soc.*, **101**, 4107 (1979).

Syntheses and Biological Activities of Substance P Analogs Containing L- and D-Homoglutamine and L- and D-Pyrohomoglutamic Acid at Position 5 and 6

Tadashi HASHIMOTO,* Yoshiki UCHIDA, Miwako NISHIJIMA, Naoki SAKURA, and Kyoko HIROSE
School of Pharmacy, Hokuriku University, Ho-3, Kanagawa-machi, Kanazawa 920-11
(Received October 6, 1986)

Synopsis. Six substance P (SP) analogs substituted by L- and D-homoglutamine and L- and D-pyrohomoglutamic acid (6-oxo-2-piperidinecarboxylic acid) at position 5 and 6 were synthesized by standard solid phase method. The contractile activities of the analogs were compared with that of SP on isolated guinea-pig ileum and trachea.

Substance P[1] (SP), an undecapeptide with the sequence [H-Arg-Pro-Lys-Pro-Gln-Gln-Phe-Phe-Gly-Leu-Met-NH_2[2]], is a putative neurotransmitter or a neuromodulator. Up to date, numerous SP analogs have been synthesized and their structure-activity relationships have been studied. The potencies of SP related peptides, pGlu-Gln-Phe-Phe-Gly-Leu-Met-NH_2 **1** and pGlu-Phe-Phe-Gly-Leu-Met-NH_2 **2**, have been found to be higher than the contracting activity of SP itself on guinea-pig ileum[3] (Table 1).

Our study[4,5] on the structure-activity relationships of SP and the SP related peptide **1** revealed that the elongation of the methylene group of the side chain in the Gln residue(s), that is, the substitution of L-homoglutamine (Hgn) for Gln moiety at position 5 and 6, enhanced the contractile activity on the smooth muscle of isolated guinea-pig ileum, and the replacement of the Gln residue(s) with D-Hgn moiety brought the decrease of the activity on the ileum assay. On pyrohomoglutamic acid (pHgu, 6-oxo-2-piperidinecarboxylic acid) peptide analogs[6] (Table 1) of the SP related peptides, the potency of [pHgu^6]-SP (6—11) **5** was higher than the activity of [D-pHgu^6]-SP (6—11) **6**, while [pHgu^5]-SP (5—11) **3** showed lower activity than that of [D-Hgu^5]-SP (5—11) **4**.

This paper describes syntheses and biological properties of six analogs (Fig. 1) of SP and SP related peptides: [L-Hgn^5, D-Hgn^6]- and [D-Hgn^5, L-Hgn^6]-SP and SP (4—11) and [L-pHgu^5, D-Hgn^6]- and [D-pHgu^5, L-Hgn^6]-SP (5—11). The contracting activities of the synthetic peptides were compared with that of our synthetic SP in order to examine the biological effects of the substitution and confirm the greater importance of the L-configuration of the amino acid residue at the position 6 than that of the residue at the position of 5 for the contractile activities of SP.

The SP analogs were synthesized in the same way with the preparation of L-Hgn analogs[4] by the solid phase technique on an automated peptide synthesizer by standard solid phase method[7] starting from *t*-butoxycarbonyl(Boc)-Met-benzhydrylamine-resin. α-Amino functions were protected by Boc group. The side-chain-protecting groups were benzyloxycarbonyl for Lys, tosyl for Arg and Boc for the amide nitrogen

[Hgn^5, D-Hgn^6]-SP	H-Arg-Pro-Lys-Pro—Hgn-D-Hgn-Phe-Phe-Gly-Leu-Met-NH_2	**7**
[D-Hgn^5, Hgn^6]-SP	H-Arg-Pro-Lys-Pro-D-Hgn—Hgn-Phe-Phe-Gly-Leu-Met-NH_2	**8**
[Hgn^5, D-Hgn^6]-SP (4-11)	H-Pro—Hgn-D-Hgn-Phe-Phe-Gly-Leu-Met-NH_2	**9**
[D-Hgn^5, Hgn^6]-SP (4-11)	H-Pro-D-Hgn—Hgn-Phe-Phe-Gly-Leu-Met-NH_2	**10**
[pHgu^5, D-Hgn^6]-SP (5-11)	pHgu-D-Hgn-Phe-Phe-Gly-Leu-Met-NH_2	**11**
[D-pHgu^5, Hgn^6]-SP (5-11)	D-pHgu—Hgn-Phe-Phe-Gly-Leu-Met-NH_2	**12**

Fig. 1. Synthetic SP analogs.

Table 1. Relative Contracting Activities of Synthetic Analogs on Guinea-Pig Ileum

	Peptide	Amino acid sequence (1 5 6 11)	Relative activity
	SP	H-Arg-Pro-Lys-Pro-Gln-Gln-Phe-Phe-Gly-Leu-Met-NH_2	1
1	[pGlu^5]-SP (5—11)	pGlu-Gln-Phe-Phe-Gly-Leu-Met-NH_2	1.7
2	[pGlu^6]-SP (6—11)	pGlu-Phe-Phe-Gly-Leu-Met-NH_2	2.0
3	[pHgu^5]-SP (5—11)	pHgu-Gln-Phe-Phe-Gly-Leu-Met-NH_2	0.65
4	[D-pHgu^5]-SP (5—11)	D-pHgu-Gln-Phe-Phe-Gly-Leu-Met-NH_2	1.76
5	[pHgu^6]-SP (6—11)	pHgu-Phe-Phe-Gly-Leu-Met-NH_2	1.50
6	[D-pHgu^6]-SP (6—11)	D-pHgu-Phe-Phe-Gly-Leu-Met-NH_2	0.17

(N^{ca}) of Hgn. The Hgn residue can be incorporated into a peptide chain by the usual solid phase technique and solution method using N^{α},N^{ca}-$(Boc)_2$-Hgn-OH[4,8], which is derived from the ester of $(Boc)_2$-Lys-OH by ruthenium tetraoxide oxidation.[9,10] The protecting group Boc on the amide of N^{α},N^{ca}-$(Boc)_2$-Hgn-OH can be removed by the same deblocking reagents as those for the protecting group on the α-amino function to produce the Hgn moiety.[8,10] Our investigation[6,11] developed a simple method for synthesis of pHgu-peptide by cyclization of Hgn residue at N-terminus in peptide chain.

The synthetic products were purified by preparative reverse-phase high-performance liquid chromatography (HPLC) using 0.1% trifluoroacetic acid in acetonitrile as eluent. Highly purified peptides (Tables 2 and 3) were obtained after gel filtration of Sephadex G-10 column. Homogeneity of the peptides was demonstrated by analytical HPLC and thin-layer chromatography (TLC). When single peak and single spot were observed for a peptide in all chromatographic systems used, the peptide was considered appropriately pure for bioassay. These chromatographic data were reinforced by the amino acid analytical data.

The agonistic effects of the synthetic peptides were compared with that of our synthetic SP on the isolated guinea-pig ileum and trachea. The results are presented in Table 4.

Table 2. Physical Properties and Yields of the Synthetic Peptides

Analog	$[\alpha]_D^{14}$ (c 0.5, 3M AcOH)/°	Retention time[a)] / min	R_f^{I}	R_f^{II}	Yield / %
7	−68.0	11.2	0.00	0.58	14.5
8	−53.8	11.3	0.00	0.58	20.6
9	−24.6	14.7	0.13	0.71	11.4
10	−39.4	14.5	0.13	0.71	20.1
11	−35.4[b)]	17.1	0.47	0.85	15.0
12	−46.2[b)]	17.2	0.46	0.85	13.3

a) Condition of analytical HPLC: column, NOVA-PAK C_{18}; flow rate, 1 ml min^{-1}; Detection, 210 nm; eluent system, linear gradient from 21% to 35% CH_3CN (15 min) in 20 mM phosphate buffer (pH 3.0). b) c 0.5, DMF.

The potency of [D-Hgn[5],Hgn[6]]-SP **8** was as high as the activity of SP itself on the guinea-pig ileum assay. The replacements of both Gln residues at the position 5 and 6 with Hgn-D-Hgn sequence brought the drastic decrease of the activities on the both assays. The C-terminal octapeptide analog **10** was found to have about 10% activity of **8** on the ileum assay. D-pHgu-peptide analog **12** possessed the highest potency among the six analogs **7**—**12** on the both assays, while pHgu-peptide analog **11** had little activities. The results indicate that the L-configuration of the amino acid residue at the position 6 may be more important than that of the residue at the position 5 for the contractile activities of SP and SP related peptides.

Experimental

Amino acid derivatives were purchased from Peptide Institute, Inc., Osaka, and benzhydrylamine (BHA) resin (available amine of the resin: 0.6 mmol g^{-1} of support) from Beckman Inc. Optical rotations were measured in a Nipponbunkoh DIP-4 Polarimeter. Amino acid analyses on samples previously hydrolyzed with 6 M HCl (1 M=1 mol dm^{-3}) (110 °C, 24 h) were performed on a Hitachi KLA-5 Amino Acid Analyzer. TLC were carried out on silica-gel plates (Merck). The following solvent systems were used: R_f^{I}, n-BuOH:AcOH:H_2O (4:1:5, upper phase); R_f^{II}, n-BuOH:pyridine:AcOH:H_2O (30:20:6:24). Analytical HPLC were effected on the following systems: column, NOVA-PAK C_{18} (3.9×150 mm); flow rate, 1 ml min^{-1}; detection, 210 nm; eluent system, linear gradient for 15 min from 21% to 35% CH_3CN in 20 mM phosphate buffer (pH 3.0).

Table 4. Biological Activities of the Synthetic SP Analogs on Guinea-Pig Organs

Analog	RA	
	GPI	GPT
7	0.04	0.04
8	1.00	0.17
9	0.01	0.13
10	0.11	0.13
11	0.02	<0.01
12	2.58	0.26

GPI, guinea-pig ileum; GPT, guinea-pig trachea; RA, relative contractile activity to SP=1.

Table 3. Amino Acid Analyses of the Synthetic Peptides

Analog	Found (Calcd)								
	Lys	Arg	Pro	Gly	Hgu[a)]	Met	Leu	Phe	NH_3
7	1.04(1)	1.00(1)	1.93(2)	1.04(1)	2.13(2)	0.98(1)	0.95(1)	1.91(2)	4.04(3)
8	0.87(1)	0.90(1)	2.08(2)	1.20(1)	2.10(2)	1.00(1)	0.96(1)	1.89(2)	3.51(3)
9	—	—	0.89(1)	1.02(1)	2.10(2)	0.98(1)	0.96(1)	2.05(2)	3.13(3)
10	—	—	0.92(1)	1.13(1)	2.12(2)	1.00(1)	0.97(1)	1.86(2)	3.62(3)
11	—	—	—	0.92(1)	2.33(2)	0.93(1)	0.92(1)	1.90(2)	3.20(2)
12	—	—	—	1.02(1)	2.12(2)	0.99(1)	0.97(1)	1.89(2)	2.44(2)

a) Homoglutamic acid.

General Procedure for the Preparation of Analogs. The solid phase synthesis was carried out using a Beckman System 990C Peptide Synthesizer as described previously.[4] Half gram of BHA-resin hydrochloride for each analog served as the solid support. A 2.5 fold excess of amino acid derivative was used for all coupling. The coupling was effected with dicyclohexylcarbodiimide/1-hydroxybenzotriazole. The protected peptide resin was treated with anhydrous liquid HF[12] containing 10% anisole. After evaporation of HF in vacuo, the peptide was extracted with 50% AcOH. The extract of N-terminal Hgn-peptide was kept at 40 °C for 4 h to yield pHgu moiety.

Purification of the Peptides. The crude peptide was subjected to HPLC as reported previously.[4] The apparatus was composed of a model 590 pump and a U6K injector (Waters) connecting with a column (20×300 mm) of Chemcosorb ODS (Chemco). The eluates were monitored with a UV detector S-310A model-II (Soma) at 210 nm wavelength. CH_3CN–0.1% TFA solvent system was used as eluent at flow rate 10 ml min^{-1}. Each peptide was emerged at 40—60 min by isocratical elution with 20—28% CH_3CN contents of the solvent system. The desired fraction was passed through a Sephadex G-10 column (16×930 mm) eluted with 2 M AcOH. Homogeneity of the peptides was analyzed by analytical HPLC and TLC.

Bioassay. The agonistic activity of the synthetic analog was measured on ileum and trachea taken from guinea-pig, as described before.[4] The contraction was recorded by means of an isotonic transducer (Nippon Kohden, TD-111T) with load of 1 or 2 g (for trachea and ileum respectively) on a Servocorder (Watanabe Instruments, SR6204). Concentration-response curves were obtained using a cumulative dose-assay, and the time between two consecutive dose-response curves was longer than 10 min.

References

1) M. M. Chang, S. E. Leeman, and H. D. Niall, *Nature, New Biol.*, **232**, 86 (1971).

2) Amino acids, peptides and their derivatives mentioned in this paper are of L-configuration. The abbreviations for amino acids and peptides are in accordance with the rules of the IUPAC-IBU Commission on Biochemical Nomenclature in *Eur. J. Biochem.*, **138**, 9 (1984).

3) N. Yanaihara, C. Yanaihara, M. Hirohashi, H. Sato, Y. Iizuka, T. Hashimoto, and M. Sakagami, "Substance P," ed. by U. S. von Euler and B. Pernow, Raven Press, New York (1977), p. 27.

4) Y. Uchida, M. Nishijima, T. Moro, N. Sakura, K. Hirose, H. Kontani, and T. Hashimoto, *Bull. Chem. Soc. Jpn.*, **59**, 4003 (1986).

5) T. Hashimoto, Y. Uchida, M. Nishijima, T. Moro, N. Sakura, and K. Hirose, *Bull. Chem. Soc. Jpn.*, **59**, 4009 (1986).

6) T. Hashimoto, N. Sakura, K. Hirose, Y. Uchida, M. Nishijima, and T. Moro, *Bull. Chem. Soc. Jpn.*, **60**, 827 (1987).

7) R. B. Merrifield, *Adv. Enzymol.*, **32**, 221 (1969).

8) Y. Uchida, M. Nishijima, K. Hirose, T. Moro, N. Sakura, and T. Hashimoto, "Peptide Chemistry 1985," ed. by Y. Kiso, Protein Research Foundation, 1986, p. 125.

9) S. Yoshifuji, K. Tanaka, and Y. Nitta, *Chem. Pharm. Bull.*, **33**, 1749 (1985).

10) N. Sakura, K. Hirose, and T. Hashimoto, *Chem. Pharm. Bull.*, **33**, 1752 (1985).

11) N. Sakura, K. Hirose, and T. Hashimoto, *Chem. Pharm. Bull.*, in press.

12) S. Sakakibara, Y. Shimonishi, Y. Kishida, M. Okada, and H. Sugihara, *Bull. Chem. Soc. Jpn.*, **40**, 2164 (1967).

Kinetics of Aquation of Pentaammineglycinerhodium(III) Ion in Acidic Media

Chinmay CHATTERJEE* and Aya Singh BALI
Department of Chemistry, Indian Institute of Technology, Powai, Bombay 400 076, India
(Received February 6, 1986)

Synopsis. Acid-catalyzed aquation of pentaammineglycinerhodium(III) ion has been studied kinetically in aqueous perchloric acid media (0.05—0.45 mol dm^{-3}) over a temperature range of 60—80 °C at an ionic strength of 1.0 mol dm^{-3} adjusted with sodium perchlorate. Under these conditions the reaction occurs by two concurrent paths according to the rate law: Rate=k_o[complex]+k_{H^+}[complex][H$^+$], where k_o and k_{H^+} are the rate constants for the spontaneous and acid-catalyzed pathways, respectively. Analysis of rate data suggests cleavage of metal-oxygen bond in the rate determining step for both the processes.

Kinetics of acid-catalyzed aquation of (carboxylato)- and (aminocarboxylato)pentaamminecobalt(III) complexes have been the subject of several investigations.[1-7] The aquation rates were correlated with the electronic and steric effects of the leaving group. In comparison, limited data[2] is available for the analogous reactions of corresponding rhodium(III) substrate, thus warrants further investigations. An amino acid usually coordinates to a metal ion with its amino and carboxylato group to form a chelate ring. However, in some amino acid cobalt(III) complexes[8,9] glycine has been found to coordinate as an unidentate ligand with its carboxylato end only. Surprisingly, no data is available to date on the nucleophilic substitution reaction of rhodium(III) amino acid complex. This paper reports the results of the kinetics of acid-catalyzed hydrolysis of pentaammineglycinerhodium-(III) ion in which amino acid exists in zwitterionic form and coordinated to the metal ion with its carboxylate end. The influence of the protonated amino group on the catalytic rate constant has been discussed. Based on comparison of rate and activation parameters for the present system with other carboxylato complexes, a plausible mechanism is suggested.

Experimental

Materials and Reagents: Pentaammineaquarhodium(III) perchlorate was prepared according to standard procedures.[10] Chemical analysis confirmed the purity, as did a comparison with the published UV-visible spectral data.[11]

Pentaammineglycinerhodium(III) perchlorate was prepared by digesting an aqueous solution (50 cm^3) of pentaammineaquarhodium(III) perchlorate (5 mmol) with five fold excess of glycine at 90 °C for 3 h followed by the slow evaporation of the reaction mixture to one third of its original volume. The solution on cooling separated white crystals of glycine complex, which were collected on a filter and washed with water–ethanol (1:1) mixture. The complex was recrystallized from cold aqueous solution by the addition of 30% perchloric acid, and washed successively with water–ethanol, ethanol, and finally dried in air. Found: C, 4.35; N, 14.90; H, 3.50%. Calcd for [Rh(NH$_3$)$_5$(glyH)](ClO$_4$)$_3$: C, 4.28; N, 14.96; H, 3.56%. Since the complex has been isolated from acidic solution, the amino acid retains an acidic proton and is coordinated as an unidentate neutral ligand as is evident from the elemental analysis. The positions and intensities of the ligand field bands of the complex (λ_{max} 322 nm, ε=144.0 dm^3 mol^{-1} cm^{-1}; λ_{max} 266 nm, ε=111.0 dm^3 mol^{-1} cm^{-1}) corresponding to $^1A_{1g}\rightarrow{}^1T_{1g}$ and $^1A_{1g}\rightarrow{}^1T_{2g}$ transitions, respectively, match well with those of the pentaamminecarboxylato rhodium(III) ion,[11] in which the ligand undoubtedly coordinates to the metal with its carboxyl group. In accord with the postulate of oxygen-bonded amino acid, IR spectrum of the title complex reveals a strong band at 1630 cm^{-1} assignable to C–O stretching band of the coordinated carboxyl group and the deformation band of $-NH_3^+$ group at 1490 cm^{-1}. ^{1}H NMR spectrum of the complex in DMSO-d_6 exhibits two broad bands at δ=7.5 and 3.75 ppm against TMS as reference with an intensity ratio 1:5 attributable to the $-NH_3^+$ and NH_3 protons. Disappearance of these peaks in D_2O confirms the assignments.

Measurements. A Varian superscan-3 spectrophotometer was used for absorbance measurements. The pH measurements were made using a PHM-64 research pH meter (Radiometer-Copenhagen). ^{1}H NMR spectra were recorded on a Varian XL 100 spectrometer.

Under experimental acidity range glycine complex has been found to aquate quantitatively leading to aqua product. Final concentration of the free glycine was determined by its reaction with ninhydrin as described in the literature.[6] The course of aquation reaction was monitored by measuring the decrease in absorbance at 325 nm, where the extinction coefficients of the glycine complex and aqua product were 143 and 100 dm^3 mol^{-1} cm^{-1}, respectively. The rate studies were made by a batch sampling technique,[12] with the thermostat controlled to ±0.1 °C. All experiments were carried out in excess of perchloric acid and the pseudo-first-order rate constants, k_{obsd}, were computed from the gradients of the linear plots of $\ln(A_t-A_\infty)$ versus time by means of a least-squares program. Under identical conditions k_{obsd} evaluated by the spectrophotometric method agreed well with the value obtained by the ninhydrin method. Acid dissociation constant of [Rh(NH$_3$)$_5$(O$_2$CCH$_2$NH$_3$)]$^{3+}$ at 25 °C and ionic strength 1.0 mol dm^{-3} was determined from conventional pH titrations against carbonate free sodium hydroxide solution. The pK_a value has been estimated as 8.80±0.03. It is thus evident that in the range of acid concentration employed for the reaction, the amino acid exists in zwitterionic form.

Results and Discussion

The observed pseudo-first-order rate constants, k_{obsd}, have been determined at 60.0±0.1, 70.0±0.1, and 80.0±0.1 °C, for perchloric acid concentration 0.05—0.45 mol dm^{-3} at ionic strength 1.0 mol dm^{-3} (NaClO$_4$). The variation of k_{obsd} with [HClO$_4$] under otherwise identical conditions is shown in Fig. 1 and the results suggest the operation of two concurrent paths:

$$-\mathrm{d}\ln[\text{complex}]/\mathrm{d}t = k_{obsd} = k_o + k_{H^+}[H^+], \quad (1)$$

where k_o and k_{H^+} represent the first order rate constant for acid independent and second order rate constant describing the acid-catalyzed pathways, respectively. Their values at different temperatures, as obtained from the intercepts and slopes of the plots shown in Fig. 1 using a linear regression analysis, are summarized in Table 1 along with the activation parameters, ΔH^* and ΔS^* values evaluated using transition state equation,

$$k = (RT/Nh)\exp(-\Delta H^*/RT + \Delta S^*/R). \quad (2)$$

Sequences of changes consistent with kinetic results are depicted below:

$$[(NH_3)_5Rh\text{-}O\overset{O}{\overset{\|}{C}}CH_2NH_3]^{3+} + H_2O \xrightarrow{k_o}$$
$$[Rh(NH_3)_5(OH_2)]^{3+} + \overset{+}{N}H_3CH_2COO^- , \quad (3)$$

$$\overset{+}{N}H_3CH_2COO^- + H^+ \xrightarrow{fast} \overset{+}{N}H_3CH_2COOH , \quad (4)$$

$$[(NH_3)_5Rh\text{-}O\overset{O}{\overset{\|}{C}}CH_2NH_3]^{3+} + H^+ \overset{K}{\rightleftharpoons}$$
$$[(NH_3)_5Rh\text{-}O\overset{H^+\ O}{\overset{\|}{C}}CH_2NH_3]^{3+} , \quad (5)$$

$$[(NH_3)_5Rh\text{-}O\overset{H^+\ O}{\overset{\|}{C}}CH_2NH_3]^{3+} \xrightarrow{k_1}$$
$$[Rh(NH_3)_5(OH_2)]^{3+} + HO_2CCH_2\overset{+}{N}H_3 . \quad (6)$$

The Reaction (3) corresponds to uncatalyzed path involving the attack of solvent molecule in the rate-determining step, while the acid-catalyzed path (5 and 6) involves the fast protonation action of substrate in a pre-equilibrium step followed by the rate-determining loss of glycine from conjugate acid. The catalytic rate constant, k_{H^+} is related to K and k_1 by the relation

$$k_{H^+} = Kk_1/(1+K[H^+]) . \quad (7)$$

The absence of any deviation from linearity for the k_{obsd} vs. $[HClO_4]$ plot even at the highest acid concentration indicates, $K[H^+] \ll 1$ and hence Eq. 7 reduces to $k_{H^+}=Kk_1$. The activation parameters corresponding to k_{H^+} thus involve both rate and equilibrium constants. In conformity with the proposed scheme, the protonated species is found to be more labile than the unprotonated one. This can be ascribed to the fact that the acid catalysis involves protonation of coordinated carboxylate and thereby putting a formal positive charge on ligand oxygen atom. Strong bonding between oxygen atom and H^+ ion in the protonated form of the complex leads to electron withdrawal from Rh-O bond thus facilitating

Table 1. Rate and Activation Parameters for Aquation of Pentaammineglycinerhodium(III) ion. (I=1.0 mol dm^{-3})

Temperature °C	$10^6\,k_o$/s^{-1}	$10^5\,k_{H^+}$/mol^{-1} dm^3 s^{-1}
60.0±0.1	1.5±0.1	5.5±0.1
70.0±0.1	4.5±0.18	18.1±0.2
80.0±0.2	12.4±0.15	55.0±0.2
ΔH^*/kJ mol^{-1}	102.0±1.7	105.8±0.8
ΔS^*/JK^{-1} mol^{-1}	−52.3±9.2	−10.9±6.3

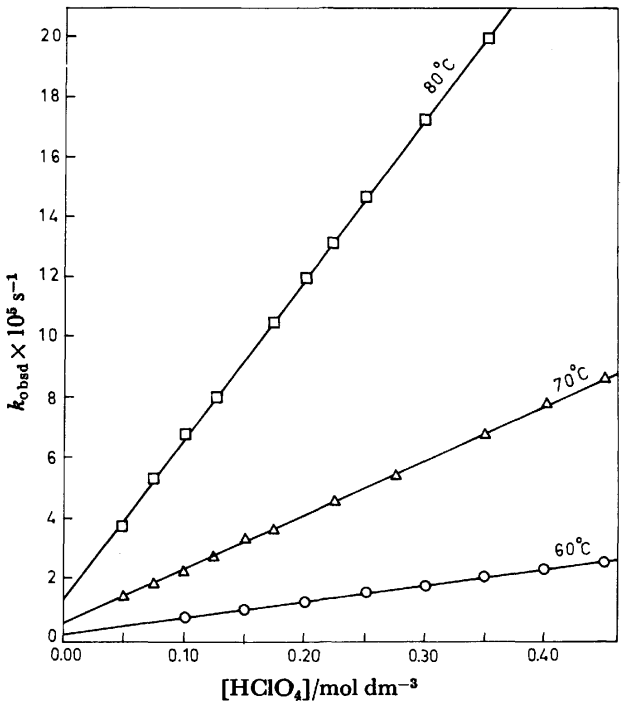

Fig. 1. Effect of acid concentration on k_{obsd} at different temperatures.
[Rh(NH$_3$)$_5$(glyH)]$^{3+}$, 0.002 mol dm^{-3}; I, 1.0 mol dm^{-3}.

Table 2. Rate Parameters for Aquation of Pentaamminecarboxylatorhodium(III) Complexes (I=0.1 mol dm^{-3})

	pK_a of the acid	Temp/°C	k_o/s^{-1}	k_{H^+}/mol dm^3 s^{-1}	Ref.
[Rh(NH$_3$)$_5$CF$_3$COO]$^{2+}$	0.3	78.9	1.5×10^{-4}	1.5×10^{-4}	2
[Rh(NH$_3$)$_5$glyH]$^{3+}$	2.35	80.0	2.0×10^{-5}	0.8×10^{-4}	Present work
[Rh(NH$_3$)$_5$Hmal]$^{2+}$	2.7	80.0	1.8×10^{-5}	3.4×10^{-4}	13
[Rh(NH$_3$)$_5$CH$_3$COO]$^{2+}$	4.75	78.7	4×10^{-6}	26.0×10^{-4}	2
[Rh(NH$_3$)$_5$CH$_3$CH$_2$COO]$^{2+}$	4.87	80.0	4×10^{-6}	30.0×10^{-4}	13
[Rh(NH$_3$)$_5$(CH$_3$)$_3$CCOO]$^{2+}$	5.05	78.6	2×10^{-6}	8.9×10^{-4}	2

the rate of release of glycine. The effect of ionic strength (I) on aquation reaction was examined at 80 °C and the values of the rate constants at I=0.1 mol dm^{-3} have been tabulated in Table 2. The uncatalyzed rate constant tend to decrease slightly whereas acid-catalyzed rate constant, k_{H^+} increases significantly with increase in ionic strength. The equilibrium constant, K, between cations such as that expressed by Eq. 5 generally increases with increasing ionic strength and hence the k_{H^+} value. The rate parameters for the analogous reaction of other pentaamminecarboxylatorhodium(III) complexes have been summarized in Table 2 for comparison. Basolo et al.[2] while studying aquation of carboxylato complexes observed that k_o values tend to decrease with increase in pK_a of the acid. This can be explained due to increase in metal-ligand bond strength with increasing basicity of the carboxylate ligand. k_o value for the title complex nicely fits into the relationship and the reactivity order follows the sequence:

$$CF_3COO^- > \overset{+}{N}H_3CH_2COO^- > CH_2C_2O_4H^- >$$
$$CH_3COO^- \simeq CH_3CH_2COO^- > (CH_3)_3CCOO^-.$$

ΔH^* value for the uncatalyzed path is comparable to that of other carboxylato complexes of rhodium(III). On the basis of comparable ΔH^* values it is reasonable to conclude that the uncatalyzed path proceed by mechanism identical to that operative in other carboxylato complexes where cleavage of metal-oxygen bond is suggested to take place in the rate-determining step.[2]

With the exception of glycine and pentaammine(pivalato)rhodium(III) ion, the acid catalyzed rate constant tend to increase with increasing pK_a of the carboxylic acids. The pK_a affects the magnitude of equilibrium constant K, as expressed by Eq. 5 and hence k_{H^+} value. Low k_{H^+} value for glycine complex can be ascribed to the retardation of protonation arising from an electrostatic effect of the $-\overset{+}{N}H_3$ group present in the neighborhood of carboxyl group, while the impediment of protonation in case of pivalato complex has been explained due to steric factor. The acid hydrolysis of metal carboxylates can proceed either by M–O or C–O bond rupture in the transition state. On the basis of kinetic studies it has been suggested that the cleavage of C–O bond in the transition state leads to a low ΔH^* value (67.0—75.0 kJ mol^{-1}) whereas cleavage of M–O falls in the range of 90—110 kJ mol^{-1} for the aquation of Rh(III) complexes.[14] The enthalpy of activation for the title complex (ΔH^*=105.8±0.8 kJ mol^{-1}) is much higher than that reported for the acid-catalyzed decarboxylation of pentaamminecarbonatorhodium(III) ion (ΔH^*=71.0±2.1 kJ mol^{-1}),[15] for which C–O bond rupture has been proposed to take place in the transition state. Hence Rh–O bond cleavage in the transition state seems to be more plausible for the present system.

References

1) F. Basolo, J. G. Bergmann, and R. G. Pearson, *J. Phys. Chem.*, **56**, 22 (1952).
2) F. Basolo, F. Monacelli, and R. G. Pearson, *J. Inorg. Nucl. Chem.*, **24**, 1241 (1962).
3) C. Andrade and H. Taube, *Inorg. Chem.*, **5**, 1087 (1966).
4) A. C. Dash and R. K. Nanda, *Inorg. Chem.*, **13**, 655 (1974).
5) A. C. Dash and R. K. Nanda, *J. Inorg. Nucl. Chem.*, **38**, 119 (1976).
6) K. Ogino, T. Murakami, and K. Saito, *Bull. Chem. Soc. Jpn.*, **41**, 1615 (1968).
7) R. D. Cannon and J. Gardiner, *Inorg. Chem.*, **13**, 390 (1974).
8) J. Fujita, T. Yasui, and Y. Shimura, *Bull. Chem. Soc. Jpn.*, **38**, 654 (1965).
9) R. T. M. Fraser, *Inorg. Chem.*, **3**, 1561 (1964).
10) G. W. Bushnell, G. C. Lalor, and E. A. Moelwyne-Hughes, *J. Chem. Soc., A*, **1966**, 719.
11) H. H. Schmidtke, *Z. Phys. Chem. (Frankfurt)*, **45**, 307 (1965).
12) C. Chatterjee and A. S. Bali, *J. Coord. Chem.*, **11**, 179 (1981).
13) C. Chatterjee and A. S. Bali, *Indian J. Chem.*, in press.
14) A. Ohyosi, A. Jyo, and N. Shin, *Bull. Chem. Soc. Jpn.*, **45**, 2121 (1972).
15) D. A. Palmer and G. M. Harris, *Inorg. Chem.*, **13**, 965 (1974).

 © 1987 The Chemical Society of Japan Bull. Chem. Soc. Jpn., 60, 1213—1217 (1987)

Application of Pyrrole/*N*-Methylpyrrole Composite Polymer to Cathode Active Material of Lithium Secondary Battery

Katsuhiko NAOI, Takayuki HIRABAYASHI, Ichiro TSUBOTA, and Tetsuya OSAKA*
Department of Applied Chemistry, School of Science and Engineering, Waseda University,
3-4-1 Okubo, Shinjuku-ku, Tokyo 160
(Received May 23, 1986)

An electrochemically prepared polypyrrole(PPy)/poly(*N*-methylpyrrole)(PMPy) composite polymer film-(PPy-PMPy) was used as a cathode active material of a rechargeable lithium battery. The charging-discharging behavior of a Li/$LiClO_4$/(PPy-PMPy) battery was studied and compared with those of Li/$LiClO_4$/PPy and Li/$LiClO_4$/PMPy batteries. In order to rationalize the charging-discharging properties of these batteries, anion doping-undoping processes at PPy, PMPy, and PPy-PMPy electrodes were checked using the usual electrochemical techniques, such as cyclic voltammetry and potential step chronoamperometry. A PPy-PMPy film electrode gave an intermediate conductivity as well as an intermediate redox potential just between those of the PPy and PMPy electrodes. Li/$LiClO_4$/(PPy-PMPy) batteries with thin (0.3 Ccm^{-2}-charged) and thick (10 Ccm^{-2}-charged) PPy-PMPy films were found to show different charging-discharging characteristics, depending on their film thickness. The IR spectra obtained for a PPy-PMPy film showed that the composition of PPy and PMPy in the resulting PPy-PMPy film was different according to its film thickness and that the PPy content in the PPy-PMPy film became higher with an increase in its film thickness.

Electrochemical properties of electro-conductive heterocyclic polymers and their derivatives have recently been studied extensively.[1-13,18,19] Greater attention has been paid to the unique applications of these polymers by many workers.[14-19] These polymers are advantageous because of the ease of formation and strong adhesion to various substrates.[9] PPy and its derivatives are expected to be potential candidates for cathode active materials of polymer batteries.[8] Our research group has been working on the electrochemical properties of several kinds of lithium/polymer batteries, where polymers were used exclusively as cathode active materials. Lithium batteries constructed with these polymers have higher capacities per unit weight than conventional secondary batteries.[8] In our previous study,[20] an excellent PPy film suitable as a rechargeable battery material was successfully obtained by electro-oxidative polymerization in the presence of PF_6^- electrolyte anions. By polymerizing pyrrole in the presence of *N*-methylpyrrole, the resulting PPy-PMPy film showed a somewhat different morphology from a PPy film because of the incorporation of PMPy in a PPy film. Recently, copolymerization of pyrrole and *N*-methylpyrrole was attempted; the resulting composite PPy-PMPy film was applied to a Schottky barrier type diode.[18] It had already been noticed that composite PPy-PMPy films gave various conductivities ranging from 10^{-3} to 10^2 Scm^{-1} at doped states of usual anions,[1] depending on the composition ratio of pyrrole and *N*-methylpyrrole monomers in the electrolyte solution during polymerization.[7] The conductivity of a PPy-PMPy film gradually decreases with an increase in the PMPy content. This fact may indicate that the polymer layer of a PPy-PMPy film lacks planarity and that the polymer chains are more or less separated because of the bulkiness of the methyl group relative to hydrogen. Hence, the copolymerization of PPy and PMPy is expected to yield a practical means of donating a wide range of conductivities and various patterns of charging-discharging properties of Li/$LiClO_4$/(PPy-PMPy) batteries. It is also noteworthy that a PPy film can be highly stabilized in an ambient condition by copolymerizing with PMPy; the reasons for this are as follows. The degradation of a PPy film is rather substantial in the presence of oxygen or vapor. On the other hand, PMPy shows less reactivity with oxygen and water.[7] Therefore, PPy-PMPy must be more stable than a PPy film in an ambient atmosphere and must also be durable for practical use. As for its electrochemical properties, a PPy-PMPy electrode gives an intermediate redox potential in cyclic voltammograms just between those of PPy and PMPy film electrodes. The main purpose of this study was to examine the possibility of using a PPy-PMPy composite film as the positive electrode of a rechargeable lithium battery. In this connection, we examined the charging-discharging properties of a Li/$LiClO_4$/(PPy-PMPy) battery coupled with the basic electrochemical behavior of anion doping-undoping processes at PPy, PMPy, and PPy-PMPy electrodes.

Experimental

Reagent grade $LiClO_4$ and propylene carbonate (PC) were used as the electrolyte salt and the solvent, respectively in our experiment. The PC was used after purification by percolating through activated alumina. The minor water in the PC was removed by adding molecular sieves to it and then letting it stand for a few days until use.[15] All the potentials were in reference to the Ag/Ag^+ (0.01 mol dm^{-3} $AgNO_3$/PC) electrode. Polymer films were formed by electro-oxidative polymerization at a constant current density of 6.5 mA cm^{-2}. PPy and PMPy films were formed in 0.2 mol dm^{-3} $LiClO_4$/PC containing 0.2 mol dm^{-3} pyrrole or *N*-methylpyrrole monomer. A PPy-PMPy composite film was formed in 0.2 mol dm^{-3} $LiClO_4$/PC containing 0.1 mol dm^{-3} pyrrole and 0.1 mol dm^{-3} *N*-methylpyrrole monomers. A platinum plate of 0.25 cm^2 and a platinum wire were used as the deposition of polymers and counter electrodes, respectively. The depos-

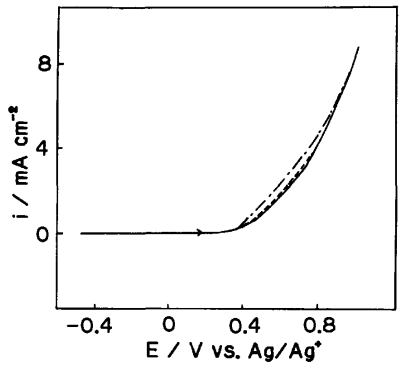

Fig. 1. Current vs. potential curves for Pt electrodes in 0.2 mol dm^{-3} $LiClO_4$/PC containing various monomers (conc.=0.2 mol dm^{-3}) at 50 mV s^{-1}.
——: Pyrrole, ----: pyrrole and *N*-methylpyrrole, -·-·-: *N*-methylpyrrole.

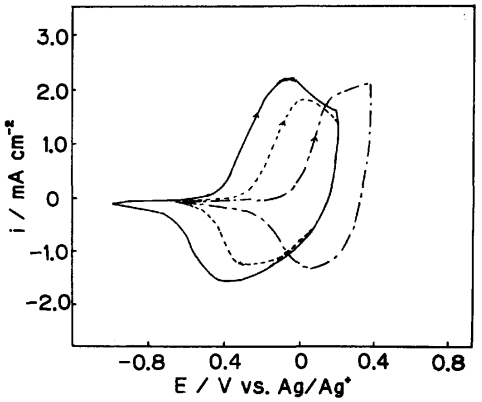

Fig. 2. Cyclic voltammograms of anion doping-undoping process for various polymer electrodes (1.8 C cm^{-2}) in 1.0 mol dm^{-3} $LiClO_4$/PC at 10 mV s^{-1}. ——: Polypyrrole, ----:pyrrole/*N*-methylpyrrole composite polymer, -·-·-: poly(*N*-methylpyrrole).

ited amount of polymers was controlled by monitoring the charge consumed during electropolymerization. Electrochemical measurements were performed in 1.0 mol dm^{-3} $LiClO_4$/PC in an Ar gas atmosphere. A Li/$LiClO_4$-PC/polymer battery was assembled with a polymer cathode and a Li anode pressed onto a Ni expanded mesh; the cell was placed in a small container purged with Ar gas and tightly sealed. Charging-discharging tests were conducted in 1.0 mol dm^{-3} $LiClO_4$/PC at a constant current density of 0.1 or 0.5 mA cm^{-2}. Apparent diffusion coefficients (D_{app}) of dopants within polymer electrodes were determined by potential step chronoamperometry, where the concentrations of dopants in the films (C_o*) were estimated from the anodization charges in cyclic voltammograms measured at 5 mV s^{-1}. Polymer films formed with different formation charges during electropolymerization, viz., 0.3 and 10 C cm^{-2} were characterized by FT-IR spectroscopy, after undoping anions by short-circuiting the cell for a sufficient time.

Results and Discussion

Figure 1 shows polymerization curves at a Pt electrode in electrolyte solutions containing three different monomers. The onset potentials for the three curves show almost the same values (ca. 0.4 V), at which each film begins to grow. As the anodic potential increases, the corresponding currents increase at the same rates, indicating that the polymerization processes for the three monomers occur at the same rate. However, the current efficiencies of the polymerization of these films may not be identical. On the basis of the above results, we formed these films at constant current densities of 6.5 mA cm^{-2}, since a moderate overpotential (ca. 0.49 V) was maintained throughout the formation of each film in order to avoid any decomposition of the films.

In order to survey the electrochemical responses of PPy, PMPy, and their composite PPy-PMPy films, cyclic voltammetry was employed; results are shown in Fig. 2. The anodic and cathodic current peaks for PPy-PMPy composite film are located just between those for PPy and PMPy films. The results suggest that a Li/$LiClO_4$/(PPy-PMPy) battery possesses intermediate charging and discharging voltages between those of a lithium battery assembled with PPy and PMPy films.

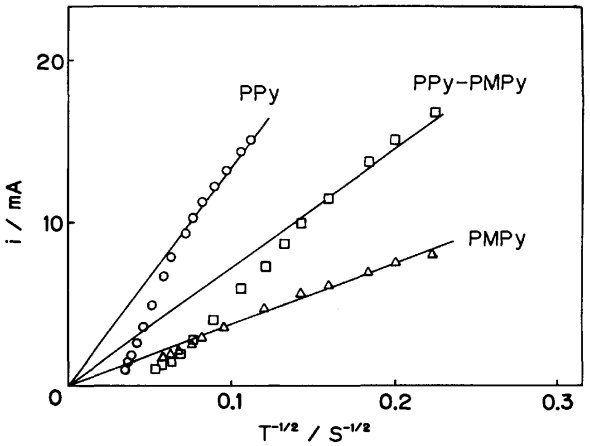

Fig. 3. Typical Cottrell plots for various polymer electrodes formed with 0.3 C cm^{-2}. Potential was stepped from −0.08 V (polypyrrole), 0.0 V (pyrrole/*N*-methylpyrrole composite) and 0.2 V (poly(*N*-methylpyrrole)) to the cathodic direction by 0.8 V.

Figure 3 shows typical Cottrell plots for 0.3 C cm^{-2}-charged films (ca. 0.6 μm) obtained by potential step chronoamperometry. A potential was initially applied at the anodic current peaks (cyclic voltammograms in Fig. 2), in order to oxidize (dope) the films so as to make the surface concentration of dopants (C_o*) in the same orders of magnitude (10^{-2} mol dm^{-3}) as indicated later. Then, the potential was stepped to the cathodic direction by 0.8 V in order to allow the films to reduce (undope). At the same time, the reduction currents of these films were monitored against time. Straight lines were obtained when plotting them against $t^{-1/2}$ (so-called Cottrell plots). Deviations of the plots from linear lines could be observed for larger t values, which

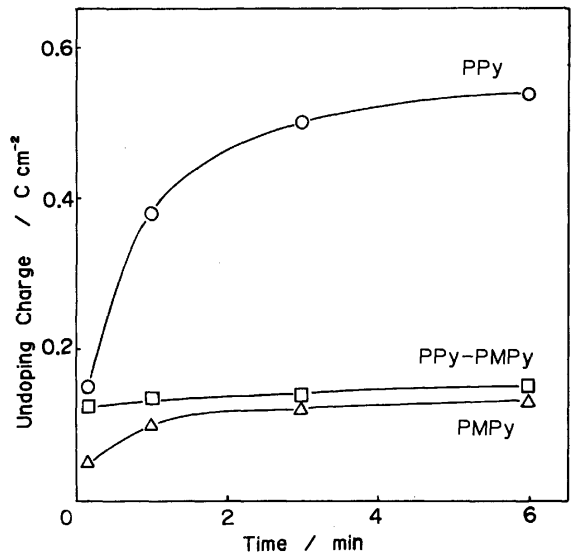

Fig. 4. Time dependence of ClO_4^- undoped charge for various polymer electrodes at −1.0 V, where these films were formed with 1.8 C cm^{-2}.

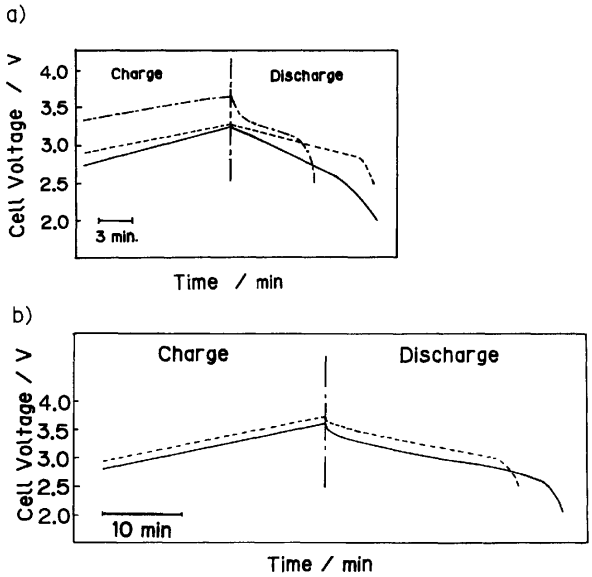

Fig. 5. Charging-discharging curves for Li/polymer batteries at a constant current of a) 0.1 mA cm^{-2} and b) 0.5 mA cm^{-2} in 1.0 mol dm^{-3} $LiClO_4$/PC. These films were polymerized with a) 1.8 C cm^{-2} and b) 10 C cm^{-2}.
——: Polypyrrole, ----: pyrrole/*N*-methylpyrrole composite polymer, -·-·-: poly(*N*-methylpyrrole).

are due to a finite diffusion layer that spread beyond the thickness of the polymer films. The apparent diffusion coefficient of dopants (D_{app}) within these films can be estimated from the slopes of the lines and C_o* by using the Cottrell equation. The D_{app} values obtained for PPy, PPy-PMPy, and PMPy films are 1.28×10^{-8}, 5.38×10^{-9}, and 3.43×10^{-9} cm^2 s^{-1}, respectively, where the C_o* values for the oxidized PPy, PPy-PMPy and PMPy films are 8.71×10^{-2}, 7.06×10^{-2}, and 4.52×10^{-2} mol dm^{-3}, respectively. The PPy-PMPy composite film has an intermediate D_{app} value just between PPy and PMPy films. This fact could be expected from the results in Fig. 2 and may have a close relation to the morphology of films having different composition ratios of PPy and PMPy polymers.

Figure 4 shows the undoping charges from polymer electrodes when the electrodes were polarized at −1.0 V. Although the cathodic current peaks in cyclic voltammograms locate more cathodic in the order of PMPy, PPy-PMPy, and PPy films, the dopants in the PPy electrode show the fastest undoping among other electrodes. The PPy-PMPy and PMPy films show a slower undoping process. The undoping behavior of these polymers can be ascribed to the film morphology and the number of effective reaction sites existing within the polymer matrix. The PPy film is considered to show the roughest morphology; also the number of reaction sites available for doping-undoping is much larger than those in PMPy and PPy-PMPy films. On the other hand, the PPy-PMPy and PMPy films show a surface-localized undoping process owing to the lesser degree of the film roughness and porosity. These facts also suggest that PMPy and PPy-PMPy films are more dense than the PPy film, and that the dopants may be confined tightly within the bulk of polymer layers and can hardly undope in spite of the negative potential step.

Figure 5 shows charging-discharging curves of Li/$LiClO_4$/polymer batteries, where the cathode films were formed with two different formation charges, viz., 1.8 C cm^{-2} for Fig. 5a) and 10 C cm^{-2} for Fig. 5b). By using thin PPy-PMPy films (Fig. 5a)), the Li/$LiClO_4$/(PPy-PMPy) battery gives intermediate curves between lithium batteries assembled with PPy or PMPy. The discharging behavior of the Li/$LiClO_4$/(PPy-PMPy) battery became flatter than those of a lithium battery constructed with PPy and PMPy, indicating better discharging characteristics. The coulombic yields for the lithium batteries constructed with PPy and PPy-PMPy films are both excellent and show almost the same values of 100%. In the case of thick films (10 C cm^{-2}), the Li/$LiClO_4$/(PPy-PMPy) battery gives 80% of coulombic yield, whereas 100% was still attained for the Li/$LiClO_4$/PPy battery. The charging-discharging curve for the Li/$LiClO_4$/PMPy battery is not given here since a 10 C cm^{-2}-charged PMPy film could not be obtained because of its high ohmic resistance. That is, under constant-current anodization, the polymerization potential of PMPy constantly increased, even beyond 5.0 V (at which PMPy film begins to decompose). The average discharge voltages for the lithium cells with the PPy and the PMPy films estimated from the figure are 3.0 and 3.2 V, respectively. The charging-discharging behavior for the lithium cells with PPy and PMPy is slightly different, depending on their film thickness. By increasing the thickness, the coulombic yield of the Li/(PPy-PMPy) battery decreases, indicating that the structure of a composite

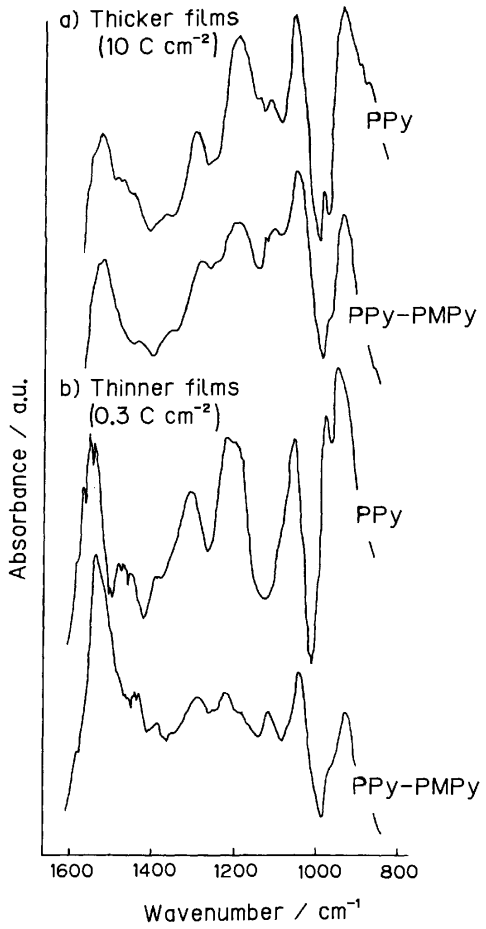

Fig. 6. Infrared spectra of a) thick and b) thin polymer films formed by passing a) 10 C cm^{-2} and b) 0.3 C cm^{-2} at the constant current density of 6.5 mA cm^{-2}.

film is dependent upon the film thickness.

Figure 6 shows the FT-IR spectra of PPy, and PPy-PMPy films of different formation charges. These charts show similar bands due to the pyrrole moiety (1300 cm^{-1}: C-N stretching; 1180, 1045 cm^{-1}: C-H deformation vibration; 965 cm^{-1}: N-H deformation vibration).[21] The IR spectrum of the PPy-PMPy (10 C cm^{-2}) film shown in Fig. 6a) is essentially the same as that of PPy film (10 C cm^{-2}). It is supposed that the PPy-PMPy film has almost the same structure as a PPy film and that the PMPy content is negligibly small in a thick PPy-PMPy film. The peaks due to ClO_4^- anions (1060~1140 cm^{-1}) shown in the two charts for thick films are slightly different. The fact indicates that the number of dopants remaining in the polymer films is different. In a thick PPy-PMPy film, greater amounts of dopants are still confined in the polymer chain than in the PPy film, although dopants have been undoped by short-circuiting the cells for the same duration of time. As for the thin films shown in the lower part of Fig. 6, the PPy-PMPy film shows less similarity to the PPy film than those shown in the thicker films. In the chart of the PPy-PMPy film, several splited peaks can be observed in the region of the C-H or N-H deformation vibration (1000~1300 cm^{-1}). The PMPy content in a PPy-PMPy film of this thickness may be larger than that in a thick PPy-PMPy film.

By comparing the IR charts shown in Figs. 6a) and 6b), the structures of the PPy-PMPy composite films show a strong dependency upon their thickness. It is also deduced from the IR results that each peak in the thick films is broadened because of the poor crystallinity of the polymer layer. Hence, a composite film contains more PMPy at the beginning of film formation. However, as the film grows thicker, the PPy content gradually becomes dominant in the composite film because of an easier growth of a PPy film on thicker polymer films (as is suggested in cyclic voltammograms shown in Fig. 2).

The composition ratio of PPy and PMPy in the PPy-PMPy film offering an optimal charging-discharging curves should await further investigation.

The authors would like to thank Prof. Noboru Oyama and Dr. Takeo Ohsaka, Department of Applied Chemistry for Resources, Tokyo University of Agriculture and Technology, for experimental support. A part of this work was financially supported by a Grant for Scientific Research from the Japanese Ministry of Education.

References

1) K. Kanazawa, A. F. Diaz, W. Will, P. Grant, G. Street, G. Galdini, and G. Kwak, *Synth. Met.*, **1**, 329 (1980).
2) A. F. Diaz, J. V. Vallejo, and A. Duran, *IBM J. Res. Dev.*, **25**, 426 (1981).
3) J. Bargon and A. F. Diaz, *IBM Tech. Disclosure Bull.*, **25**, 2873 (1982).
4) A. F. Diaz, J. I. Castilo, J. A. Logan, and W.-Y. Lee, *J. Electroanal. Chem.*, **129**, 115 (1981).
5) M. Salmon, A. F. Diaz, A. J. Logan, M. Krounbi, and J. Bargon, *Mol. Cryst. Liq. Cryst.*, **83**, 265 (1982).
6) A. F. Diaz and B. Hall, *IBM J. Res. Develp.*, **27**, 342 (1983).
7) K. K. Kanazawa, A. F. Diaz, M. T. Krounbi, and G. B. Street, *Synth. Met.*, **4**, 119 (1981).
8) K. Kaneto, T. Shiraishi, and K. Yoshino, *Jpn. J. Appl. Phys.*, **24**, L107 (1985).
9) J. Prejjza, I. Lundstroem, and T. Skotheim, *J. Electrochem. Soc.*, **129**, 1685 (1982).
10) J. L. Bredas, B. Themans, J. M. Andre, R. R. Chance, and R. Silbley, *Synth. Met.*, **9**, 265 (1984).
11) S. Kuwabata, H. Yoneyama, and H. Tamura, *Bull. Chem. Soc. Jpn.*, **57**, 2247 (1984).
12) M. V. Rozental, T. A. Skotheim, A. Melo, and M. I. Florit, *J. Electroanal. Chem.*, **185**, 297 (1985).
13) T. Yamabe, K. Tanaka, T. Koike, and M. Ueda, *Mol. Cryst. Liq. Cryst.*, **117**, 185 (1985).
14) F. Beniere, D. Boils, H. Canepa, J. Franco, A. LeCorre, and J. P. Louboutin, *J. Electrochem. Soc.*, **132**, 2100 (1985).
15) S. Chen and Y. Chiou, *J. Electrochem. Soc.*, **131**, 1046

(1984).
16) A. Padula, B. Scrosati, M. Schwarz, and U. Pedretti, *J. Electrochem. Soc.*, **131**, 2761 (1984).
17) L. W. Shacklette, J. E. Toth, N. S. Murthy, and R. H. Baughman, *J. Electrochem. Soc.*, **132**, 1529 (1985).
18) H. Koezuka and S. Etoh, *J. Appl. Phys.*, **54**, 2511 (1983).
19) S. Asavapiriyanont, G. K. Chandler, G. A. Gunawardena, and D. Pletcher, *J. Electroanal. Chem.*, **177**, 245 (1984).
20) H. Sakai, K. Naoi, T. Hirabayashi, and T. Osaka, *Denki Kagaku*, **54**, 75 (1985).
21) e.g., G. B. Street, T. C. Clarke, M. Krounbi, K. K. Kanazawa, V. Lee, P. Pfluger, J. C. Scott, and G. Weiser, *Mol. Cryst. Liq. Cryst.*, **83**, 253 (1982).

 © 1987 The Chemical Society of Japan Bull. Chem. Soc. Jpn., 60, 1219—1223 (1987)

Binding and Catalytic Properties of Charged β-Cyclodextrins

Yoshihisa MATSUI,* Kouichi OGAWA, Seiji MIKAMI, Misao YOSHIMOTO, and Kazuo MOCHIDA
Faculty of Agriculture, Shimane University, Nishikawatsu, Matsue 690
(Received July 24, 1986)

The effects of the signs and structures of charged groups in modified β-cyclodextrins on their binding and catalytic properties were examined in aqueous solutions by using ammonium salt of mono(6-sulfonato-6-deoxy)-β-cyclodextrin and hydrogencarbonate salts of mono(6-trimethylammonio-6-deoxy)- and mono[6-(1-pyridinio)-6-deoxy]-β-cyclodextrins as charged hosts. An ionic guest was bound more strongly to an oppositely charged host than to an identically charged host. Binding constants for charged host-guest systems were affected by a change in the ionic strength and by the addition of dimethyl sulfoxide to an aqueous solution. The catalytic effects of the charged hosts on the alkaline hydrolyses of *o*-, *m*-, and *p*-acetoxybenzoic acids were also different from those of the parent β-cyclodextrin. These results could be explained in terms of electrostatic, steric, and hydrophobic interactions between the hosts and guests.

Several intermolecular interactions have been proposed as being responsible for the formation of cyclodextrin (CD) inclusion complexes in aqueous solutions.[1-3] They are hydrophobic interactions, van der Waals interactions, hydrogen bonding, interactions due to the relief of high energy water from the CD cavity upon substrate inclusion, and interactions due to the relief of conformational strain in a CD-water complex upon substrate inclusion. These binding forces also play an important role in the binding processes of enzymes. This is one of reasons why CD has been widely studied as an enzyme model. However, an enzyme is a kind of polyelectrolyte. Electrostatic interactions between charged groups of an enzyme and an ionic substrate often contribute to the specificity of enzyme action.[4] On the other hand, CD is a neutral molecule and no electrostatic interaction can take part in its binding and catalytic processes. In order to enhance the substrate-specificity of CD, it is desirable to build up a molecular system in which a variety of intermolecular interactions, including electrostatic interactions, act simultaneously and cooperatively. Thus far, only a few studies have been reported which dealt with the binding and/or catalytic properties of charged CD's. Tabushi et al.[5] prepared a 1 : 1 complex of Zn(II) with β-CD functionalized by diethylenetriamine and showed that the positively charged host binds a negatively charged substrate, 2-oxo-1-adamantanecarboxylate, 330-times stronger than β-CD. Boger and Knowles[6] prepared positively charged triammonio-per-*O*-methyl-α-CD, which binds benzyl phosphate ca. 1000-times stronger than the corresponding monoammonium host. Matsui and Okimoto[7] examined the binding and catalytic properties of a positively charged CD, mono(6-trimethylammonio-6-deoxy)-β-CD [β-CDtma(+)]. The charged host exhibited abilities to bind an anionic dye more strongly than the parent host and to catalyze the alkaline hydrolyses of negatively charged *o*-, *m*-, and *p*-acetoxybenzoates in a manner significantly different from that of the parent β-CD.

The present investigation was undertaken to examine the effects of the sign and structure of charged groups in modified β-CD's on their binding and catalytic properties. For this purpose, we used the hydrogencarbonate salts of β-CDtma(+) and mono[6-(1-pyridinio)-6-deoxy]-β-CD [β-CDpy(+)] as positively charged CD's and the ammonium salt of mono(6-sulfonato-6-deoxy)-β-CD [β-CDsulf(−)] as a negatively charged CD. Electrostatic interactions are generally affected by such environmental factors as the ionic strength and polarity of the solution. The present study also dealt with the effects of these factors on the action of the charged hosts.

Experimental

Materials. The β-CD of a reagent grade was recrystallized from water and dried overnight in vacuo at 110 °C. Reagent-grade pyridine was dried over calcium hydride and distilled in the presence of fresh calcium hydride just before use. Mono[6-*O*-(*p*-tolylsulfonyl)]-β-CD (β-CDots) was prepared by a reaction of β-CD with *p*-toluenesulfonyl chloride in dry pyridine.[7] The β-CDtma(+) was prepared by a reaction of β-CDots with trimethylamine in *N*,*N*-dimethylformamide and then purified as described previously.[7] Reagent-grade dimethyl sulfoxide (DMSO) was distilled in the presence of calcium hydride in vacuo. Crystal Violet (CV), phenolphthalein (PP), ammonium 8-anilinonaphthalene-1-sulfonate (ANS), Methyl Orange (MO), *p*-nitrophenol (pNP), cyclohexanol (CHX), and *o*-acetoxybenzoic acid (*o*-ABA) were commercially available. The *m*- and *p*-acetoxybenzoic acids (*m*- and *p*-ABA) were prepared by reactions of the corresponding hydroxybenzoic acids with acetic anhydride in dry pyridine and were then recrystallized from chloroform.

Thin-layer chromatography (TLC) was performed on Kieselgel 60F_{254} (Merck) with a mixed solvent of acetic acid–chloroform–water [80 : 10 : 20 (v/v)]. A saturated solution of cerium(IV) sulfate in concentrated sulfuric acid was used as a spray reagent to detect the parent and modified β-CD's. The charged β-CD's were separated from the reaction mixtures by liquid chromatography with a 4.5×43 cm CM-cellulose (Serva) column, a 5×49 cm DEAE-sephadex (Pharmacia) column, and/or a 4×73 cm Sephadex G-15 (Pharmacia) column.

Apparatus. Absorption, fluorescence, and NMR spectra were recorded using a Hitachi Model 220 spectrophotometer, a Hitachi Model 650-10S fluorescence spectrophotometer, and JEOL Model JNM-MH-100 and Nicolet Model NT-300

Table 1. Binding Constants (K_a/mmol^{-1}dm^3) for 1:1 Inclusion Complexes of Parent and Charged β-CDs with Organic Guests at 25 °C

Host	CV(+)[a]	PP(−)[b]	pNP(−)[c]	ANS(−)[d]	MO(±)[e]	CHX(0)[f]	DMSO(0)[g]
β-CD	4.0	29	0.77	0.091	0.30	0.71	0.0018
β-CDsulf(−)	2.6	3.4	0.053	0.037	0.18	0.37	0.0016
β-CDtma(+)	0.43	25	1.37	0.17	0.44	0.34	0.0009
β-CDpy(+)	—	50	1.52	0.26	—	0.43	0.0009

a) Crystal Violet at pH 5.0. b) Phenolphthalein at pH 10.5. c) *p*-Nitrophenolate at pH 10.5. d) 8-Anilinonaphthalene-1-sulfonate at pH 6.8. e) Methyl Orange in 0.1 mol dm^{-3} H_2SO_4. f) Cyclohexanol at pH 10.5. g) Dimethyl sulfoxide at pH 10.5.

NMR spectrometers respectively. The optical rotation was mesured using a Union Giken Model PM-101 polarimeter.

Preparation of β-CDpy(+). A solution of β-CDots (6.00 g, 4.65 mmol) in dry pyridine (120 cm^3) was heated at 100 °C for 12 h. The reaction mixture was evaporated in vacuo at 40 °C to dryness. The residue was dissolved in water, and acetone was added to the solution to give a white precipitate. After being collected, the precipitate was dissolved in water (10 cm^3) and then chromatographed on a CM-cellulose column with 0.05 mol dm^{-3} ammonium hydrogencarbonate as an eluent. Each fraction (10 cm^3) was assayed by UV at 270 nm, polarimetry at 589 nm, and/or TLC. Fractions which gave only one spot with R_f 0.25 (fractions from No. 76 to No. 160) were combined and evaporated to dryness at 40 °C in vacuo. The residue was dissolved in water, and the solution was decolorized by activated charcoal and evaporated to dryness to afford 1.06 g (0.84 mmol; yield, 18% based on β-CDots) of the hydrogencarbonate salt of β-CDpy(+) as a white powder. The ^{1}H NMR spectrum of β-CDpy(+) in D_2O gave peaks due to pyridinium protons at δ=8.07 (t, meta-H), 8.58 (t, para-H), and 8.82 (d, ortho-H) ppm with a ratio in peak area of 2:1:2. The mono-substitution of the CD hydroxyl groups by the 1-pyridinio group was confirmed by a comparison of the peak area of the CD protons with that of the pyridinium protons.

Preparation of β-CDsulf(−). To an aqueous solution (300 cm^3) of sodium sulfite (3.11 g, 24.7 mmol) was added β-CDots (6.03 g, 4.7 mmol); the resulting mixture was heated at 100 °C for 20 h. The reaction mixture was evaporated in vacuo at 40 °C to dryness, and the residue was washed twice with hot ethanol. After being dissolved in water, the residue was chromatographed on a DEAE-sephadex column. Linear gradient elutions were applied with 1.2 dm^3 of 0.02 mol dm^{-3} NH_4HCO_3 and 1.2 dm^3 of 0.1 mol dm^{-3} NH_4HCO_3 and then with 0.3 dm^3 of 0.1 mol dm^{-3} NH_4HCO_3 and 0.3 dm^3 of 0.5 mol dm^{-3} NH_4HCO_3. Each fraction (15 cm^3) were assayed by polarimetry at 405 nm and TLC. Fractions which gave only one spot with R_f 0.10 were combined and evaporated to dryness at 40 °C. The desalting of the resulting residue was carried out with a Sephadex G-15 column to give 2.16 g (1.78 mmol; yield 38% based on β-CDots) of the ammonium salt of β-CDsulf(−). The mono-substitution of the CD hydroxyl groups by the sulfonato group was confirmed by the oxidative degradation of β-CDsulf(−) with hot nitric acid, followed by a turbidimetric determination of the resulting sulfate ion with barium chloride and gelatin.

Determination of Binding Constants for Inclusion Complexes. The charged or parent β-CD was added to an aqueous buffer solution containing 0.008 mmol dm^{-3} CV (pH 5.0, citric acid-Na_2HPO_4), 0.03 mmol dm^{-3} PP (pH 10.5, $NaHCO_3$-NaOH), 0.05 mmol dm^{-3} pNP (pH 10.5, $NaHCO_3$-NaOH), 0.01 mmol dm^{-3} ANS (pH 6.8, NaH_2PO_4-Na_2HPO_4), or 0.02 mmol dm^{-3} MO (0.1 mol dm^{-3} H_2SO_4). After thermal equilibrium at 25 °C had been reached, the UV or fluorescence spectra were recorded. Binding constants (K_a) for 1:1 inclusion complexes of the hosts with the guests were determined by a least-squares curve-fitting analysis of relationships between absorbances and host concentrations with a microcomputer. The K_a values for the DMSO and CHX systems were estimated by a least-squares curve-fitting analysis of the inhibitory effect of the guests on the complexation of the hosts with PP at pH 10.5 in a similar manner described previously.[8]

Kinetics. The rates of the alkaline hydrolyses of *o*-, *m*-, and *p*-ABAs were measured by following the appearance of the absorptions of the corresponding phenoxide anions in the same way as described previously.[7] The K_a values and catalytic rate constants (k_c) for ABA-host systems were also determined in the same way as described previously.[7]

Results and Discussion

Binding Properties of the Charged β-CD's. Table 1 shows the K_a values determined for 1:1 inclusion complexes of the parent and charged hosts with a variety of guests. A positively charged guest, CV(+), was bound more strongly to β-CDsulf(−) than to β-CDtma(+). On the contrary, negatively charged guests, PP(−), pNP(−), and ANS(−), were bound more strongly to β-CDtma(+) and β-CDpy(+) than to β-CDsulf(−). The K_a values for inclusion complexes with amphoteric [MO(±)] and neutral [CHX(0), DMSO(0)] guests were not so much affected by the charges of the hosts. These results indicate that electrostatic attractive interactions do act between an oppositely charged host and its guest, and repulsive interactions between those with charges identical in sign. However, the effect of electrostatic interactions on the binding constants was relatively small. The K_a value for an oppositely charged host-guest system was, at most, 3 times that for a corresponding β-CD system. It seems that the replacement of one of the OH groups of β-CD by a charged group results in a decrease in hydrophobic interactions between the host and a guest. In fact, the K_a value for a β-CD-CHX(0) system, where hydrophobic interactions play an important role in complexation,[8] was decreased by a factor of ca. 2 by the introduction of a charged group to the host.

Among the guests examined, ANS(−) is known to be a fluorescent probe: The wavelength (λ_{max}) of the emis-

Table 2. The Wavelength (λ_{max}) and Relative Intensity (I_{rel}) of the Emission Maximum of Fluorescence for Host-ANS(−) Systems at 25 °C and pH 6.8[a)]

Host	λ_{max}/nm[b)]	I_{rel}[b)]	f[c)]
β-CD	495±1	10.5±0.4	0.48
β-CDsulf(−)	502±2	4.5±0.4	0.27
β-CDtma(+)	487±1	23.1±0.3	0.63
β-CDpy(+)	485±3	2.3±0.1	0.72

a) [Host]=10.0 mmol dm^{-3}, [ANS(−)]=0.010 mmol dm^{-3}. b) The λ_{max} and I_{rel} values for ANS(−) in the absence of a host were 519±1 nm and 1.0 respectively. c) The fraction of ANS(−) bound to each host.

sion maximum decreases and the relative intensity (I_{rel}) of the peak increases with decreasing polarity of microenvironment around the probe[9)] or with decreasing internal rotation of the probe[10,11)] accompanied by an increase in viscosity or by the association with biopolymers. Similar spectral changes have been observed for a β-CD-ANS(−) system, where the hydrophobic nature of the β-CD cavity is responsible for the spectral changes.[12)] Table 2 shows the λ_{max} and I_{rel} values for the emission maxima of ANS(−) in the presence of 10 mmol dm^{-3} neutral and charged β-CD's. The λ_{max} values decreased in the order of β-CDsulf(−)>β-CD>β-CDtma(+)>β-CDpy(+). The I_{rel} values increased in the order of β-CDpy(+)<β-CDsulf(−)<β-CD<β-CDtma(+).[13)] It is unlikey that the significant blue shifts observed for β-CDtma(+) and β-CDpy(+) systems are brought about by a decrease in microenvironmental polarity, since the cavity of the charged β-CD's may be less hydrophobic than that of neutral β-CD. It is more plausible that the internal rotaion of ANS(−) is restricted by the attractive electrostatic interactions between the charged β-CD's and the guest. Similar effects of electrostatic interactions were reported for complexes of ANS(−) with biological membranes and detergent micelles.[14)] The I_{rel} value for a β-CDpy(+) system was unusually low, compared with that for a β-CDtma(+) system. The pyridinio moiety of β-CDpy(+) may interact with the singlet excited species of ANS(−) to accelerate the quenching of the excited species. This presumption was substantiated by the fact that the addition of *N*-ethylpyridinium chloride (Etpy) in place of β-CDpy(+) to an aqueous ANS(−) solution also caused a decrease in I_{rel} (I_{rel}=0.84 at [Etpy]=18 mmol dm^{-3}).

Effects of Ionic Strength and an Organic Solvent on Binding Constants. Thermodynamic stabilities (log K_a) for inclusion complexes of β-CD, β-CDsulf(−), and β-CDtma(+) with CV(+) and PP(−) increased in proportion to the square root of ionic strength (I_c) in a manner similar to that described preveously.[7)] Ionic strength was adjusted by use of potassium sulfate, which does not interact with the cavity of β-CD.[15)] Regression analysis of the relationships between them gave intercepts (A) and slopes (B) (Table 3). It is notable that the B values for identically charged host-guest

Table 3. The Values of Parameter A and B for the Equation; $\log(K_a/\text{mmol}^{-1}\,\text{dm}^3)=A+B\times I_c^{1/2}$

Guest	Host	A	B	n[a)]	r[b)]
CV(+, pH 5.0)	β-CDtma(+)	−0.62	0.54	6	0.972
	β-CD	0.46	0.29	6	0.996
	β-CDsulf(−)	0.26	0.27	6	0.946
PP(−, pH 10.5)	β-CDtma(+)	1.35	0.17	12	0.915
	β-CD	1.41	0.24	6	0.974
	β-CDsulf(−)	0.42	0.50	6	0.988

a) The number of data. b) Correlation coefficient.

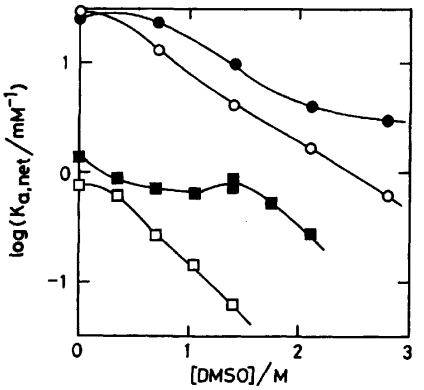

Fig. 1. Changes of log K_a with increasing concentration of DMSO (1 M=1 mol dm^{-3}).
○: β-CD-PP(−) system, ●: β-CDtma(+)-PP(−) system, □: β-CD-pNP(−) system, ■: β-CDtma(+)-pNP(−) system.

systems [β-CDtma(+)-CV(+) and β-CDsulf(−)-PP(−)] are larger than those for oppositely charged host-guest systems. The B values for neutral β-CD systems were intermediate between those for the charged β-CD systems. Hydrophobic interactions are generally strengthened by an increase in I_c (salting-out effect). This may be one reason why the B values for the neutral β-CD systems are positive. Electrostatic interactions are lowered by an increase in I_c (Debye-Hückel theory). In identically charged host-guest systems where electrostatic repulsive interactions as well as hydrophobic interactions are acting between host and guest, an increase in I_c weakens the repulsive interactions and strengthens the hydrophobic interactions. Thus, the B values for these systems become larger than those for the β-CD systems. In oppositely charged host-guest systems, electrostatic attractive interactions are weakened by an increase in I_c, although hydrophobic interactions are strengthened. Then, the B values for these systems become smaller than those for the β-CD systems.

The addition of an organic solvent, DMSO, to the media also changed the log K_a values for β-CD and β-CDtma(+) complexes with PP(−) and pNP(−) (Fig. 1). DMSO is bound to the hosts (Table 1), so that it competitively inhibits the complexation of the hosts with the anionic dyes. In order to shed light on the

Table 4. Kinetic and Equilibrium Parameters for Host-ABA Systems in Alkaline Solutions at 25°C

Host	Substrate	pH	[DMSO] %(v/v)	k_c/k_{un}	K_a mol^{-1}dm^3	$K_a k_c/k_{un}$ mol^{-1}dm^3
β-CD	*o*-ABA	12.0	0	7.7	83	640
	m-ABA	11.9	0	6.3	91	570
		11.8	20	7.4	21	160
		11.9	40	17	16	270
	p-ABA	10.9	0	1.2	710	860
β-CDsulf(−)	*o*-ABA	12.0	0	2.0	830	1700
	m-ABA	11.9	0	0.00	59	0
		11.8	20	0.00	37	0
		12.8	40	0.00	30	0
	p-ABA	10.9	0	0.30	220	67
β-CDtma(+)	*o*-ABA	12.0	0	2.2	430	960
	m-ABA	11.9	0	9.3	290	2700
		11.8	20	9.9	59	580
		11.9	40	43	9.4	410
	p-ABA	10.9	0	1.6	770	1200
β-CDpy(+)	*o*-ABA	12.0	0	0.00	120	0
	m-ABA	11.0	0	5.3	190	980
		11.8	20	3.6	91	330
		11.9	40	11	63	690
	p-ABA	10.9	0	0.32	530	170

solvent effect of DMSO, the net K_a values ($K_{a,net}$) for these systems were calculated from the apparent K_a values by use of Eq. 1, where K_i is the binding constants for the host-DMSO systems:

$$K_{a,net} = K_a(1 + K_i[\text{DMSO}]). \quad (1)$$

This equation can easily be derived on the basis of the law of mass action under conditions that the concentration of DMSO is much larger than that of a host. In neutral β-CD systems where hydrophobic interactions play an important role in complexation, the log $K_{a,net}$ values decreased greatly with increasing [DMSO]. On the other hand, the log $K_{a,net}$ values for the β-CDtma(+) systems were not so much lowered. An addition of DMSO to an aqueous solution results in a decrease in dielectric constant of the solution, which contributes to strengthening electrostatic attractive interactions between the oppositely charged host and guests. However, the attractive interactions were not so large as to overcome an accompanied decrease in hydrophobic interactions.

Effect of the Charged Hosts on the Alkaline Hydrolyses of ABAs. Kinetic parameters determined for the alkaline hydrolyses of ABAs in the presence of the hosts are shown in Table 4, where k_{un} and k_c are the first-order rate constants for free and complexed substrates, respectively. The substrates bear carboxylate anions in alkaline solutions. For *m*-ABA systems where the most remarkable effects of the charged hosts were observed among the substrates examined, kinetic parameters were also determined in the presence of DMSO.

The results were too complicated to be explained simply in terms of electrostatic interactions between hosts and guests in such a manner as described previously.[7] However, a few remarkable features are found among them. The positively charged β-CDtma(+) and the neutral β-CD accelerated, more or less, the hydrolyses of all the substrates examined. The degree of acceleration (k_c/k_{un}) was larger for β-CDtma(+)-*m*- and *p*-ABS systems than for the corresponding β-CD systems, and the reverse was true for *o*-ABA systems. Another cationic host, β-CDpy(+), decelerated the hydrolyses of *o*- and *p*-ABAs, though it accelerated the hydrolysis of *m*-ABA to a lesser extent than β-CDtma(+) or β-CD. The negatively charged β-CDsulf(−) decelerated the hydrolyses of *m*- and *p*-ABAs and accelerated that of *o*-ABA to a lesser extent than β-CD.

It is known that the degree of acceleration is closely related to the distance between the catalytic and reaction sites of the host-guest complex (proximity effect).[1,16] The catalytic site of each host is an alkoxide ion derived by the acid dissociation of a secondary OH group of the host.[1] The reaction site is an ester carbonyl carbon. Thus, the fact that the k_c/k_{un} value for a β-CDtma(+)-*m*- or *p*-ABA system is larger than that for the corresponding β-CD system implies that the reaction site is located more closely to the catalytic site in the former than in the latter. Electrostatic attractive interactions between the host and guest may be responsible, at least in part, for such a change in the geometry of an inclusion complex. Steric interactions between the charged groups of the host and guest may

also contribute to a change in the geometry. It has been reported[17] that the replacement of the primary OH group(s) of β-CD by some bulky group(s) results in significant changes in the rates of the alkaline hydrolyses of phenyl acetates. The trimethylammonio group of β-CDtma(+) is so bulky that it may be advantageous for the acceleration of the hydrolyses.

When the reaction site of a guest is deeply included within the cavity of a host, the site is protected from the nucleophilic attack of either the alkoxide ion of the host or the hydroxide ion in a bulk solution. Then, the hydrolysis of the guest is retarded by complexation. Such non-productive binding is probably brought about in β-CDsulf(−)-*m*- or *p*-ABA and β-CDpy(+)-*o*- or *p*-ABA systems. We could speculate for the case of a β-CDsulf(−) system that *m*- or *p*-ABA is inserted into the cavity of β-CDsulf(−) from the side of the acetyl group to minimize the electrostatic repulsive interactions between the sulfonate anion of the host and the carboxylate anion of the guest. However, it is difficult to reasonably explain at the present stage of investigation why β-CDpy(+) retards the hydrolyses of *o*- and *p*-ABA on one hand and β-CDtma(+) accelerates the reactions on the other hand. Further information on the geometries of the inclusion complexes is necessary in order to solve these problems.

The addition of DMSO to an aqueous solution also caused significant changes in the values of k_c/k_{un} and K_a. Generally, the k_c/k_{un} value increased and the K_a value decreased with increasing DMSO concentration. Similar DMSO effects have been reported by Trainor and Breslow.[18] The addition of DMSO may enhance the dehydration of the alkoxide ion of the hosts to facilitate its nucleophilic attack to the guests. On the other hand, DMSO is competitively bound to the hosts, as was previously described (Table 1), to weaken the binding of hosts to guests. A decrease in the polarity of a solvent with the addition of DMSO also contributes to the weakening of the hydrophobic interactions between the hosts and guests. Thus, the value of a net catalytic parameter, $K_a k_c/k_{un}$, did not always increase with increasing DMSO concentration.

The present work was partially supported by a Grant-in-Aid for Scientific Research (Nos. 59212025 and 60104003) from the Ministry of Education, Science and Culture.

References

1) D. W. Griffiths and M. L. Bender, *Adv. Catal.*, **23**, 209 (1973).
2) W. Saenger, *Angew. Chem., Int. Ed. Engl.*, **19**, 344 (1980).
3) I. Tabushi, *Acc. Chem. Res.*, **15**, 66 (1982).
4) W. P. Jencks, "Catalysis in Chemistry and Enzymology," McGraw-Hill, New York (1969), p. 351.
5) I. Tabushi, N. Shimizu, T. Sugimoto, M. Shiozuka, and K. Yamamura, *J. Am. Chem. Soc.*, **99**, 7100 (1977).
6) J. Boger and J. R. Knowles, *J. Am. Chem. Soc.*, **101**, 7631 (1979).
7) Y. Matsui and A. Okimoto, *Bull. Chem. Soc. Jpn.*, **51**, 3030 (1978).
8) Y. Matsui and K. Mochida, *Bull. Chem. Soc. Jpn.*, **52**, 2808 (1979).
9) G. M. Edelman and W. O. McClure, *Acc. Chem. Res.*, **1**, 65 (1968).
10) a) E. K. Kosower and H. Dodiuk, *J. Am. Chem. Soc.*, **96**, 6195 (1974); b) E. K. Kosower, H. Dodiuk, and H. Kanety, *ibid.*, **100**, 4179 (1978).
11) R. L. Reeves, M. S. Maggio, and L. F. Costa, *J. Am. Chem. Soc.*, **96**, 5917 (1974).
12) F. Cramer, W. Saenger, and H.-Ch. Spatz, *J. Am. Chem. Soc.*, **89**, 14 (1967).
13) Although the guest was not completely bound to the hosts in the present experiments, the orders given were essentially the same as those for completely complexed host-guest systems.
14) B. Rubaleava, D. M. de Munoz, and C. Gitler, *Biochem.*, **8**, 2742 (1969).
15) K. Mochida, A. Kagita, Y. Matsui, and Y. Date, *Bull. Chem. Soc. Jpn.*, **46**, 3703 (1973).
16) Y. Matsui, T. Nishioka, and T. Fujita, "Biomimetic and Bioorganic Chemistry," in "Topics in Current Chemistry," ed by F. L. Boschke, Springer, Berlin, Heidelberg (1985), Vol. 128, pp. 61—89.
17) K. Fujita, A. Shinoda, and T. Imoto, *J. Am. Chem. Soc.*, **102**, 1161 (1980).
18) G. L. Trainor and R. Breslow, *J. Am. Chem. Soc.*, **103**, 154 (1981).

 © 1987 The Chemical Society of Japan Bull. Chem. Soc. Jpn., 60, 1225—1229 (1987)

Solution Properties of Dialkyl Phosphate Salts. Apparent Molar Volumes, Viscosity *B* Coefficients, Heats of Solution, and Osmotic Coefficients

Kunio TAMAKI,* Keita SUGA, and Eiko TANIHARA
Department of Chemistry, Yokohama City University, Kanazawa-ku, Yokohama 236
(Received August 15, 1986)

The apparent molar volumes, viscosity *B* coefficients, and heats of solution of sodium salts of dialkyl phosphates (methyl, ethyl, and butyl) in water were measured. The limiting apparent molar volumes at 25 °C increased with the number of carbon atoms in the alkyl chains. The viscosity *B* coefficients of the salts decreased as the temperature was raised from 25 to 35 °C. The changes in heat capacity for dissolution in water, as calculated from the heats of solution at 15, 25, and 35 °C, were positive for the salts. The osmotic coefficients for lithium, sodium, and potassium salts of dimethyl phosphate were also measured. For a given concentration, the osmotic coefficients decreased in the order: $Li^+ < Na^+ < K^+$. From the results obtained, the $-(-O)_2PO_2^-$ ionic part may be classified as a structure-maker.

The physicochemical properties of organic monovalent anions, such as carboxylates and sulfonates in water, have been studied by many investigators.[1-9] Alkali metal salts of dialkyl phosphates ($(RO)_2PO_2M$) are other organic monovalent electrolytes. It seems that it would be interesting to study the properties of aqueous solutions of dialkyl phosphate anions; and the data would help to elucidate the role of the phosphate group in such a biological substance as nucleic acid. In this paper the experimental results will be reported on the apparent molar volumes, viscosity *B* coefficients, and heats of solution of sodium salts of dimethy, diethyl, and dibutyl phosphates in water. In addition, the osmotic coefficients of lithium, sodium, and potassium salts of dimethyl phosphate have also been measured in order to get information on the ion-solvent interaction of the phosphate anion.

Experimental

$(MeO)_2PO_2M$ (M=Li, Na, and K) was prepared by the reaction of trimethyl phosphate with the corresponding alkali metal iodides in acetone.[10] $(EtO)_2PO_2Na$ and $(n\text{-}BuO)_2PO_2Na$ were prepared by the neutralization of the corresponding dialkyl phosphates with a solution of sodium hydroxide, after which the water was evaporated to dryness; the salts were then extracted with ethanol. Commercial diethyl and dibutyl phosphates were purified before hand by the distribution between water and 1-pentanol according to the method of Stewart and Crandall.[11] The salts were purified by recrystallization from suitable solvents: ethanol-water solutions for $(MeO)_2PO_2Li$ and $(MeO)_2PO_2Na$, and ethanol-ethyl acetate solutions for $(MeO)_2PO_2K$, $(EtO)_2PO_2Na$, and $(n\text{-}BuO)_2PO_2Na$. All the salts were hygroscopic; they were dried in vacuo at 60 °C for several days, and the molecular weights were checked by means of volumetric analysis. A known amount of the sample was dissolved in water and passed through an ion-exchange resin in the hydrogen form; the eluent was titrated with a standard NaOH solution. It was found that the obtained samples were anhydrous. Water was triply distilled. The solutions were made by weight.

The densities were measured using a vibrating-tube densimeter, twin-type SS-D-200, of the Shibayama Scientific Co., Ltd. The viscosities were measured at 25 and 35 °C using an automatic viscometer of the Shibayama Scientific Co., Ltd. The details of the procedure were described in a previous paper.[9] The electric conductivities were measured with an LCR meter, AG-4301B, of the Ando Electric Co., Ltd., using a frequency of 1000 Hz.

The heats of solution were measured at 15, 25, and 35 °C using a twin isoperibol calorimeter, TIC-2C, of the Tokyo Riko Co., Ltd., by a method similar to that described in a previous paper.[9]

The osmotic coefficients were measured at 35 °C using a vapor pressure osmometer of Knauer & Co., Ltd. The resistance difference, ΔR, between matched thermistors, one with a drop of the solution, and the other with a drop of the solvent, was measured on a chart recorder 5 min after the application of the solution. At least 5 readings were made on each solution, and the results were averaged. The osmotic coefficents, ϕ, were calculated from the ΔR values using the relation:[12]

$$\phi = \Delta R/K\nu m, \tag{1}$$

where K is the apparatus constant; ν, the total number of ions produced by the complete dissociation of a molecule; and m, the molal concentration. The apparatus was calibrated with NaCl solutions of known molality and osmotic coefficient.[13]

Results and Discussion

Apparent Molar Volumes. The apparent molar volumes, ϕ_v, in $cm^3\,mol^{-1}$ were calculated from the densities using the following equation:

$$\phi_v = \frac{1000(\rho_0 - \rho)}{m\rho\rho_0} + \frac{M}{\rho}, \tag{2}$$

where M is the molar mass in $g\,mol^{-1}$ and ρ_0 and ρ are the densities in $g\,cm^{-3}$ of water and of a solution respectively. The apparent molar volume of the electrolytes is given by the equation:[14]

$$\phi_v = \phi_v^\circ + A_v c^{1/2} + B_v c, \tag{3}$$

where ϕ_v° is the limitimg value, which is identical with the partial molar volume at infinite dilution; A_v and B_v are the constants. The value of the constant A_v is 1.868 $cm^3\,dm^{3/2}\,mol^{-3/2}$ for water at 25 °C;[14] the rela-

tion $\phi_v - 1.868\,c^{1/2}$ versus c for a series of sodium dialkyl phosphates is shown in Fig. 1. The values of ϕ_v° and B_v are given in Table 1. It is found that the ϕ_v° values increase as the alkyl-chain length increases and that the increments in the ϕ_v° values per methylene group are 14.7 $cm^3\,mol^{-1}$ from dimethyl salt to diethyl salt and 16.1 $cm^3\,mol^{-1}$ from diethyl salt to dibutyl salt. Those results are in accord with Sakurai's opinion[15] that the increments in the ϕ_v° values per methylene group for homologous organic salts approach about 16 $cm^3\,mol^{-1}$ at 25 °C as the chain length increases. The B_v values are found to decrease with an increase in the number of carbon atoms in the alkyl chains, as is shown in Table 1; this fact is in accord with the results for other homologous compounds.[15,16]

The Viscosity *B* Coefficients. The viscosity of an aqueous solution of an electrolyte, η, for concentrations below 0.1 mol dm^{-3} can be represented by the Jones-Dole equation:[17]

$$\eta/\eta_0 = 1 + A_\eta c^{1/2} + B_\eta c, \quad (4)$$

where η_0 is the viscosity of water, and A_η and B_η, the characteristic constants of the solutes. The A_η coefficient was interpreted theoretically by Falkenhagen and Vernon;[18] it can be calculated using the data of the limiting equivalent conductivities of the salt, the cation, and the anion. The B_η coefficient is related to the ion-solvent interaction and to the size and shape of the ion, and it is highly specific for the electrolyte and the temperature. Equation 4 may be converted to:

$$\eta/\eta_0 - 1 - A_\eta c^{1/2} = B_\eta c. \quad (5)$$

When the left-hand side of Eq. 5, using the calculated values of A_η, is plotted against c, the viscosity B coefficient is obtained as the slope of a straight line. Figure 2 shows the results of plotting Eq. 5. The values of A_η and B_η are listed in Table 2.

The B_η values of homologous sodium dialkyl phosphates are found to increase with the chain length. Figure 3 shows the relationship between the B_η values and the number of carbon atoms in the alkyl chains, n, at 25 °C. The B_η values of sodium alkanoates[4,8] as well as sodium alkanesulfonates[8,9] in the literature are also included in Fig. 3. It is found that the B_η values for the three homologous organic electrolytes with the same number of carbon atoms will be in the order: $(RO)_2PO_2Na > RCOONa > RSO_3Na$. In connection with the viscosities of dialkyl and monoalkyl salts in water, it must be pointed out that the B_η values of dialkylam-

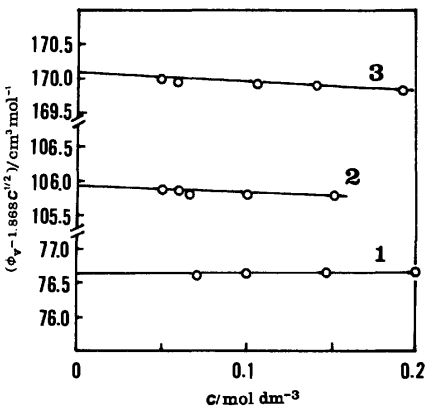

Fig. 1. Apparent molar volumes of $(RO)_2PO_2Na$ at 25 °C. 1: Methyl, 2: ethyl, 3: butyl.

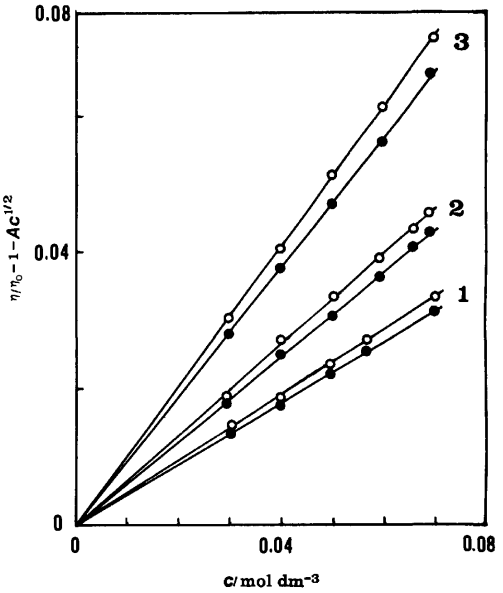

Fig. 2. Plots of $\eta/\eta_0 - 1 - A_\eta c^{1/2}$ against c for $(RO)_2PO_2Na$. 1: Methyl, 2: ethyl, 3: butyl. O: 25 °C, ●: 35 °C.

Table 1. Limiting Apparent Molar Volume of $(RO)_2PO_2Na$ at 25 °C

$(RO)_2PO_2Na$	ϕ_v° / $cm^3\,mol^{-1}$	B_v / $dm\,cm^3\,mol^{-2}$
Methyl	76.64	0
Ethyl	105.95	−1.0
Butyl	170.10	−1.5

Table 2. The Values of A_η, B_η, and ΔB of $(RO)_2PO_2Na$

$(RO)_2PO_2Na$	A_η / $dm^{3/2}\,mol^{-1/2}$		B_η / $dm^3\,mol^{-1}$		ΔB / $dm^3\,mol^{-1}$
	25 °C	35 °C	25 °C	35 °C	
Methyl	0.0088	0.0089	0.479	0.448	−0.031
Ethyl	0.0094	0.0097	0.667	0.618	−0.049
Butyl	0.0105	0.0106	1.030	0.951	−0.079

Table 3. Heats of Solution and Heat-Capacity Changes of $(RO)_2PO_2Na$

$(RO)_2PO_2Na$	$-\Delta H_s°$ / kJ mol^{-1}			$\Delta C_p°$ / JK^{-1} mol^{-1}
	15 °C	25 °C	35 °C	
Methyl	24.52±0.04	24.27±0.04	23.64±0.08	44±7
Ethyl	33.47±0.02	32.01±0.01	30.79±0.03	134±3
Butyl	38.74±0.08	34.77±0.08	30.67±0.04	404±10

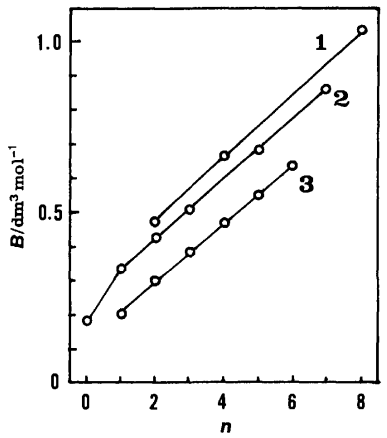

Fig. 3. Plots of viscosity B coefficients for organic salts against number of carbon atoms in the alkyl groups at 25 °C.
1: Sodium dialkyl phosphates, 2: sodium alkanoates,[4,8] 3: sodium alkanesulfonates.[8,9]

monium ions are approximately equal to those of monoalkylammonium ions with the same number of carbon atoms.[19]

The temperature dependence of the B_η values may be regarded as an index of the solute-solvent interaction; the B_η values increase with the temperature for a solvent-structure-breaking salt, while they decrease with temperature for a solvent-structure-making solute.[20] For all three compounds used, as may be seen in Table 2, that the B_η values decrease as the temperature is raised from 25 to 35 °C; these salts may therefore be considered to behave as structure-making salts in the water phase. The changes in the viscosity B coefficients which occur as the temperature is raised from 25 to 35 °C, ΔB, are also listed in Table 2. The ΔB values decrease with the number of carbon atoms in the alkyl chains of the series; this means that the hydrophobic hydration increases with the length of the alkyl chains. The B_η values are naturally made up of the sum of the contributions from both sodium and organic ions. Fortunately, the B_η values of the sodium ion are insensitive to the temperature.[21] Therefore, the temperature dependence of the viscosity B coefficients of sodium dialkyl phosphates discussed above conveniently reflects the nature of the dialkyl phosphate ions.

The solvent structural effect may also be evaluated by using the method of Desnoyers and Perron.[22] The B_η value of the ion is interpreted as consisting of two terms; the first is the effect of the ionic size, B_{size}, and the second is the contribution arising from the ion-solvent interaction, B_{solv}. If we assume that the Einstein equation derived for the case of spherical colloid may be applied approximately to the aqueous electrolyte solutions, B_{size} may be obtained by the use of the equation:

$$B_{size} = 0.0025\,\bar{V}°_{ion}, \tag{6}$$

where $\bar{V}°_{ion}$ is the partial molar volume expressed in cm^3 mol^{-1}. Thus, B_{solv} can be derived by the use of the equation:

$$B_{solv} = B_\eta - 0.0025\,\bar{V}°_{ion}. \tag{7}$$

The B_{solv} value can be used as a criterion for determining the structural effect of an ion. A positive value of B_{solv} will correspond to a structure-maker, while a negative value will indicate a structure-breaker. The B_{solv} values at 25 °C for dimethyl, diethyl, and dibutyl phosphate ions, as calculated from the data in Tables 1 and 2, are 0.187, 0.302, and 0.504 dm^3 mol^{-1} respectively, indicating that the dialkyl phosphate anions studied are all structure-making ions. In this calculation, we adopted the B_η value of sodium ion[21] as 0.084 dm^3 mol^{-1} and the $\bar{V}°_{ion}$ value of sodium ion[23] as −6.6 cm^3 mol^{-1}.

Heats of Solution. Heat-of-solution measurements were carried out in the concentration range of $(0.5-1)\times10^{-3}$ mol dm^{-3}. In this concentration range, any dependence of the heat of solution on the concentration is within the limit of experimental error, so the average of three or more measurements has been taken as the heat of solution at infinite dilution, $\Delta H_s°$. The $\Delta H_s°$ values of sodium dialkyl phosphates in water are listed in Table 3. The $\Delta H_s°$ values were all exothermic, and the results from the $\Delta H_s°$ values were used to calculate the change in the heat capacity for dissolution at infinite dilution, $\Delta C_p°$:

$$\Delta C_p° = d\Delta H_s°/dT, \tag{8}$$

where T is the temperature. The $\Delta C_p°$ values obtained at 25 °C are also listed in Table 3.

The sign and magnitude of $\Delta C_p°$ can be taken as a relative measure of the structural effect upon the solvent water.[24,25] The $\Delta C_p°$ values of simple salts indicate negative values, whereas the $\Delta C_p°$ values of hydrophobic solutes indicate positive values. As may be seen in Table 3, the sign of $\Delta C_p°$ of dimethyl phosphate salt is slightly positive, indicating that dimethyl phosphate salt behaves as a weak structure-maker. The magnitude of $\Delta C_p°$ increase with the number of carbon

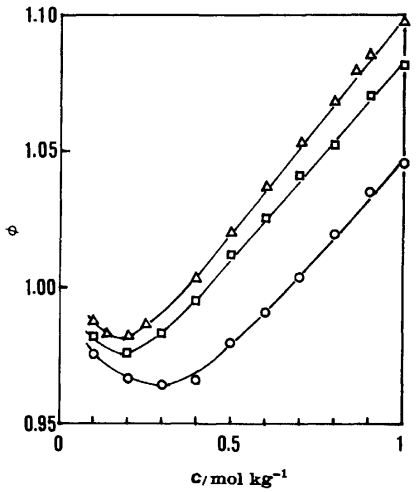

Fig. 4. Plots of osmotic coefficients against molal concentration for $(MeO)_2PO_2M$.
○: Lithium salt, □: sodium salt, △: potassium salt.

atoms in the alkyl chains, and diethyl and dibutyl phosphate salts are excellent structure-makers.

Osmotic Coefficients. Figure 4 indicates the osmotic coefficient versus concentration curves for lithium, sodium, and potassium salts of dimethyl phosphate. It may be seen that for a given concentration the ϕ values decrease in the order: $Li^+ < Na^+ < K^+$. The variation in the order of ion-ion interaction has been discussed by Gurney[26] and by Frank.[27] The rule of Gurney and Frank implied that an anion and a cation with similar structural influences—both being either structure-makers or structure-breakers—will attract each other, whereas if an anion and a cation have different structural tendencies, they will repel each other. Among the cations, Li^+ is a strong, and Na^+, a weak structure-maker, while K^+ is slightly structure-breaking.

As is shown in Fig. 4, the curve for potassium dimethyl phosphate lies at the top, while that for lithium dimethyl phosphate lies at the bottom. Therefore, potassium dimethyl phosphate may be classified as a "breaker-maker" salt, which will give a high-lying osmotic coefficient versus the concentration curve because of the greater escaping tendency between cation and anion. At the opposite extreme, lithium dimethyl phosphate may be classified as a "maker-maker"salt, which will give a lower-lying curve because of the tendency toward more attraction between cation and anion. In this manner, the $-(-O)_2PO_2^-$ ionic part may be classified as a structure-maker.

It must be noted that the acivity coefficients for the alkali metal salts of formic and acetic acids for a given concentration decrease in the order: $Li^+ < N^+ < K^+$.[28] By the application of the rule of Gurney and Frank to this results, formate and acetate ions may be classified as structure-makers. Recently, Miyajima, Sawada, and Nakagaki[4] reported that formate ion is neither a structure-maker nor a structure-breaker, because the viscosity B coefficients of formate ion were practically constant between 15 and 35 °C. However, in view of the sequence of activity coefficients for alkali metal salts of formic acid, formate ion may be considered still to behave as a weak structre-making ion, and it seems that the solvent structural effect of formate ion need to be investigated further.

In addition, the activity coefficients for the salts of *p*-toluenesulfonic acid[29] as well as those for the salts of methane- and ethanesulfonic acid[5] in dilute solutions increase in the order: $Li^+ > Na^+ > K^+$. The application of the rule of Gurney and Frank to these results indicate that these sulfonate ions may be classified as structure-breaking ions. The structure-breaking properties of sulfonate anions have been discussed by Uedaira and Uedaira[6] on the basis of their electric conductivities, and by Katayama et al.[7] on the basis of their partial molar volumes.

Thanks are due to Mr. Takashi Shibui and Mr. Takayoshi Kaneko for the preliminary experiments.

References

1) R. W. Gurney, "Ionic Processes in Solution," McGraw-Hill, New York (1953).
2) R. A. Robinson and R. H. Stokes, "Electrolyte Solutions," Butterworths, London (1968).
3) F. Franks, "Water, A Comprehensive Treatise," Vol. 3, Plenum, New York (1973).
4) K. Miyajima, M. Sawada, and M. Nakagaki, *Bull. Chem. Soc, Jpn.*, **55**, 3101 (1982).
5) H. P. Gregor, M. Rothenberg, and N. Fine, *J. Phys. Chem.*, **67**, 1110 (1963).
6) H. Uedaira and H. Uedaira, *Bull. Chem. Soc. Jpn.*, **37**, 1885 (1964).
7) A. Katayama, T. Matsuura, H. Kuroki, and K. Konishi, *Sen-i Gakkaishi*, **21**, 598 (1965).
8) K. Tamaki, Y. Ōhara, H. Kurachi, M. Akiyama, and H. Odaki, *Bull. Chem. Soc. Jpn.*, **47**, 384 (1974).
9) K. Tamaki, Y. Ōhara, M. Inabe, I. Mori, and F. Numata, *Bull. Chem. Soc, Jpn.*, **56**, 1930 (1983).
10) C. A. Bunton, M. M. Mhala, K. G. Oldham, and C. A. Vernon, *J. Chem. Soc.*, **1960**, 3293.
11) D. C. Stewart and H. W. Crandall, *J. Am. Chem. Soc.*, **73**, 1377 (1951).
12) D. E. Burge, *J. Phys. Chem.*, **67**, 2590 (1963).
13) Ref. 2, p. 481.
14) O. Redlich and D. M. Mayer, *Chem. Rev.*, **64**, 221 (1964).
15) M. Sakurai, *Bull. Chem. Soc. Jpn.*, **46**, 1596 (1973).
16) J. E. Desnoyers and M. Arel, *Can. J. Chem.*, **45**, 359 (1967).
17) G. Jones and M. Dole, *J. Am. Chem. Soc.*, **51**, 2950 (1929).
18) H. Falkenhagen and E. L. Vernon, *Z. Physik.*, **33**, 140 (1932).
19) K. Tamaki, M. Kushida, and Y. Ōhara, *Bull. Chem. Soc. Jpn.*, **49**, 1711 (1976).
20) R. L. Kay, T. Vituccio, C. Zawoyski, and D. F. Evans,

J. Phys. Chem., **70**, 2336 (1966).
21) D. J. P. Out and L. M. Los, *J. Solution Chem.*, **9**, 19 (1980)
22) J. E. Desnoyers and G. Perron, *J. Solution Chem.*, **1**, 199 (1972).
23) F. J. Millero, *Chem. Rev.*, **71**, 147 (1971).
24) E. M. Arnett and J. J. Campion, *J. Am. Chem. Soc.*, **92**, 7097 (1970).
25) T. S. Sarma and J. C. Ahluwalia, *Chem. Soc. Rev.*, **2**, 203 (1973).
26) Ref. 1, p. 256.
27) H. S. Frank, *J. Phys. Chem.*, **67**, 1554 (1963); *Z. Phys. Chem. (Leipzig)*, **228**, 364 (1965).
28) Ref. 2, p. 479.
29) Ref. 2, pp. 492—494.

 © 1987 The Chemical Society of Japan Bull. Chem. Soc. Jpn., 60, 1231—1236 (1987)

Effect of the Electron Correlational Screening upon the Calculated Transition Energies of Aromatic Hydrocarbons

Koichi HIRANO*
Department of Chemistry, Miyagi University of Education, Aramaki-aoba, Sendai 980
(Received September 11, 1986)

A new formalism for two-center repulsion $\Gamma_{\mu\nu}$, including a correlational screening factor, is presented. As a criterion of the screening strength, a parameter ρ (defined by Eq. 13) was introduced. Using $\Gamma_{\mu\nu}$ and ρ, transition energy calculations were performed for aromatic hydrocarbons based on the P.P.P scheme. Calculated transition energies decreases as ρ increases. Adjusting ρ, we can obtain correct values of the transition energies. That optimal ρ values extend over the region 0.3—0.5 indicates the extent of that electron correlation is intermediate. The screening caused by the Ohono-Klopman and Nishimoto-Mataga formulae is very close to that by $\Gamma_{\mu\nu}$'s whose ρ values are 0.2 and 0.6. A linear relationship was found between ρ and n, the number-density of π electrons. Making use of it, a trial calculation of the anthracece transition energies was made and obtained results were quite acceptable.

Electron correlation is very important in many electron systems, such as atoms and molecules.[1] In this regard, Gutefreund and Little have evaluated the effect of electron correlation upon low-lying π-π^* transitions by means of a random-phase approximation (RPA), in the framework of the P.P.P method.[2,3]

Kitaura and Nishimoto[4] also studied this problem using a different RPA formalism, derived by Dunning and Mckoy.[5] Their studies surely improved the calculation of the transition energies for π-conjugated systems.

Here, however, it must be noted that the validity of RPA is restricted to region where the electron density is high, where the inter-electronic spacing is smaller than the Bohr radius. The π electrons in conjugated systems are not so dense in the above sence. Therefore, RPA is rather inappropriate[6-8] for accurately describing the π-electron correlation. Thus, it is worthwhile studying this problem using another model which satisfies the requirement of the short-range behavior of Coulomb repulsion since at lower densities electron correlation due to short-range repulsion becomes very significant.[9] For this purpose we employed a Monte-Carlo screening potential model.[10,11] The reason for this is that this model satisfies the requirement of a radial distribution function of a two-dimensional classical electron fluid whose density is considerably low.[12] In the present paper we derived a new formula for a two-center repulsion based upon a Monte-Carlo screening potential model (MCP) while making use of it in transition energy calculations that were performed for aromatic hydrocarbons. In the following, we briefly describe the most important part of the results:

(1) The new formula for the two-center repulsion.

(2) The correlational effects upon the MO quantities.

(3) The number-density dependence of the correlational parameters.

Model and Method

New Formula for Two-Center Repulsion. According to the physics of strong-coupled classical plasmas,[13,14] let $H(r)$ be the linear screening potential due to the many-particle correlations (defined by DeWitt et al.);[15] then the effective potential between two particles, $V(r)$, in the liquid phase can be expressed in the form

$$V(r) = \frac{(Ze)^2}{r} - H(r), \tag{1}$$

where Ze is the electric charge of a particle and r is the separation between two particles. This potential satisfies the radial distribution function $g(r)$ of the particles:

$$g(r) = \exp[-V(r)/kT]. \tag{2}$$

By analyzing the results of Monte Carlo studies by Brush et al.,[10] Itho and Ichimaru[16] found that apart from the vicinty of $r=0$, $H(r)$ takes a linear form in the interval $1.0 \lesssim r/a \lesssim 2.0$:

$$H(r) = \frac{(Ze)^2}{a}\left(c_0 - \frac{c_1 r}{a}\right), \tag{3}$$

where $a=(3/4\,\pi n)^{1/3}$ is the ion-sphere radius and n the number-density of the particles; c_0 and c_1 satisfy

$$c_1 = \left(\frac{c_0}{2}\right)^2. \tag{4}$$

Here, we notice that by replacing the second term in $H(r)$ by $(c_2 r/a)^2$, we obtain a Salpeter-Horn type screening potential.[14]

Substituting $H(r)$ into Eq. 1 and putting $Z=1$, we obtain the effective potential $V(r)$ for two electrons in the liquid phase:

$$V(r) = \frac{e^2}{r} - \frac{e^2}{a}\left(c_0 - \frac{c_1 r}{a}\right), \tag{5}$$

where a is the Wigner-Seitz sphere radius via $a=(3/4\,\pi n)^{1/3}$ which corresponds to the ion-sphere radius mentioned above. This potential solely holds for two dimensional classical electron liquid.[17]

In obtaining Eq. 5, we assumed that electrons obey classical statics. In the π-electron case, however, special quantum effects must be taken into account, since

the number-densities of π electrons, (Table 1), are higher than those for a classical electron liquid.[18] In spite of this, we assume here that π electrons obey classical statics and that Eq. 5 holds for them. This is very crude; however, we accept it as the zeroth-order approximation. The reason for this is as following: Monte Carlo simulations of fermion systems[18] and analytic calculations on the correlational properties of the degenarate electron fluid have been hitherto made;[19] however, a formalism which can be applied to the π-electron systems has yet not been established. As a consequence, we derived a π-electron two-center repulsion $\Gamma_{\mu\nu}$ from Eq. 5, using a point-charge approximation:[20]

$$\Gamma_{\mu\nu} = \frac{e^2}{R_{\mu\nu}} - \frac{e^2}{d}\left(C_0 - \frac{C_1 R_{\mu\nu}}{d}\right), \quad R_{\mu\nu} < \frac{C_0}{C_1} d$$

and (6)

$$= \frac{e^2}{R_{\mu\nu}}, \qquad R_{\mu\nu} > \frac{C_0}{C_1} d,$$

where $R_{\mu\nu}$ is the internuclear separations, d is the length parameter and C_0 and C_1 are dimensionless constants. Hereafter, we call $\Gamma_{\mu\nu}$ the MCP two-center repulsion; it corresponds to $\gamma_{\mu\nu}$ of the P.P.P scheme.

Next, we consider the physical significance of the new formula $\Gamma_{\mu\nu}$. A qualititatively good description is that $\Gamma_{\mu\nu}$ implies electrostatic interactions due to a potential felt at the center of the Wigner-Seitz sphere of the electrons at the μ core from an electron on the ν-th core as well as its surrounding polarization field. It arises from a charge depletion in the vicinty of the electron by correlation. This interpretation is based on the ion-sphere model provided for the explanation of short-range screening in a strongly coupled classical plasma.[13,14]

Characteristics of $\Gamma_{\mu\nu}$. In this section, we describe a suitable parameter choice and the $R_{\mu\nu}$-dependence of $\Gamma_{\mu\nu}$. As an example, we show the pyrene case. The length parameter was evaluated as d=1.57 Å, based upon two distinct roots: Wigner-Seitz sphere radius a=1.57 Å and radius of Coulomb hole,[21,22] r_{Ch}=1.1 Å. The dimensionless parameters by which correlational screening is chrachterized were determined as C_0=0.95 and C_1=0.50, respectively, by means of a trial- and -error method.

A set of parameters, thus determined , yield

$$\Gamma_{\mu\nu} = \frac{14.398}{R_{\mu\nu}} + 4.607 R_{\mu\nu} - 10.942 \text{ eV} \quad \text{for } R_{\mu\nu} < 2.37 \text{ Å},$$

and (7)

$$= \frac{14.398}{R_{\mu\nu}} \text{ eV} \qquad \text{for } R_{\mu\nu} \geqq 2.37 \text{ Å}.$$

Making use of Eq. 7, we can calculate pyrene transition energies which are in fairly good agreement with the experimental spectra.

Then, we describe the characteristic feature of $\Gamma_{\mu\nu}$. In Fig. 1 , we display the $R_{\mu\nu}$ -dependence of in comparison with those of Ohono-Klopman,[23,24] γ^{OK}, (OK) and Nishimoto-Mataga,[25] $\gamma^{NM}_{\mu\nu}$ (NM) expressions and of the bare Coulomb repulsion:

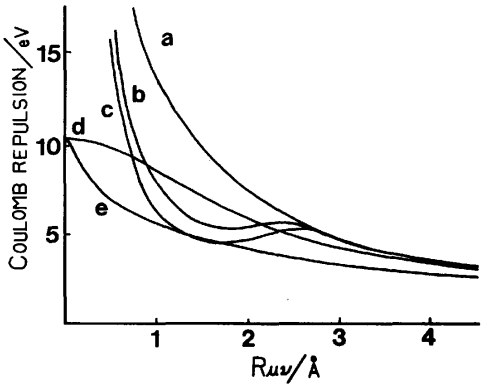

Fig. 1. Comparison of the different forms of effective Coulomb-repulsion:
a): Bare Coulomb potential, b): MCP potential, C_1=0.50, c): MCP potential, C_1=0.45, d): Ohono-Klopmamn potential, e): Nishimoto-Mataga potential.

$$\gamma^{OK}_{\mu\nu} = \frac{e^2}{\sqrt{a^2_{\mu\nu} + R^2_{\mu\nu}}}, \tag{8}$$

and

$$\gamma^{NM}_{\mu\nu} = \frac{e^2}{a_{\mu\nu} + R_{\mu\nu}}, \tag{9}$$

with

$$\frac{1}{a_{\mu\nu}} = \frac{1}{2}\left(\frac{\gamma_{\mu\mu}}{14.398} + \frac{\gamma_{\nu\nu}}{14.398}\right), \tag{10}$$

where $\gamma_{\mu\mu}$ and $\gamma_{\nu\nu}$ denote a one-center repulsion at cores μ and ν. For C-C bonds, we take $a_{\mu\nu}$=1.358 Å.

As Fig. 1 shows, the most striking features of our model potential are: (1) $\Gamma_{\mu\nu}$ has a local minimum at a small distance, $R_{\mu\nu}\approx$1.5 Å; hence, $\Gamma_{12}<\Gamma_{13}$. This result, however, is not so surprising. Since a quite similar result can be seen for the Salpeter-Horn potential[14] for the strong-screening regime. Moreover, a similar structure can also be found in the Jastrow pseudopotential curves of a Lenard-Jones Bose fluid.[26] (2) The rapid decrement of $\Gamma_{\mu\nu}$ at small distances implies a reduction of the bare Coulomb repulsion due to correlational screening; the strength of the screening is strongly parameter sensitive. Therefore, one of the reasons that $\Gamma_{12}<\Gamma_{13}$ may be ascribable to the choice of parameter. (3) By a suitable parameter choice, $\Gamma_{\mu\nu}$ can be determined so as to give the correct values of the MO quantities.

Based on the above, we can perform MO calculations that take the electron-correlation effect into account by using $\Gamma_{\mu\nu}$. This is because, in the study, we employed $\Gamma_{\mu\nu}$ as a two-center repulsion. Hence, the following equality still holds:

$$\gamma_{\mu\nu} = \Gamma_{\mu\nu}. \tag{11}$$

Table 1. Parameters for Aromatic Hydrocarbons

	Benzene	Naphthalene	Anthracene	Pyrene	Coronene
n cm^{-3}[a]	4.0×10^{22}	5.4×10^{22}	5.9×10^{22}	6.1×10^{22}	6.6×10^{22}
a Å[b]	1.69	1.64	1.59	1.58	1.53
d Å[c]	1.25	1.25	1.25	1.25	1.25
C_0	0.95	0.95	0.95	0.95	0.95
C_1	0.61	0.53	0.50[d]	0.50	0.47
ρ	0.30	0.40	0.43[e]	0.43	0.48

a) Number-density of π electrons. b) Radius of Wigner-Seitz sphere. c) Length parameter. d) Estimated from Eq. 14. e) Estimated from Eq. 18.

MO Calculation. P.P.P.-Type SCF-MO calculations were made. In the actual calculations, singly excited configurations higher than 8—10 eV were taken into account. All of the C-C bond lengths and the bond angles were set to 1.39 Å and 120°, respectively. The one-center core integral and the one-center repulsion were evaluated from the valence state ionization potentials and the electron affinities viz. $W_{\mu\mu}$=11.22 and $\gamma_{\mu\mu}$=10.60 eV.[27] A two-center core integral was evaluated by the Wolfsberg-Helmholtz's formula with K=0.96:[28]

$$\beta_{\mu\nu} = \frac{K}{2} S_{\mu\nu}(W_{\mu\mu} + W_{\nu\nu}), \tag{12}$$

where $S_{\mu\nu}$ is the overlap integral between cores μ and ν.

For simplicity, we consider that C_1 alone is variant and that the other parameters are invariant. Then, in the present calculations, we varied $\Gamma_{\mu\nu}$ by changing C_1. In Table 1 the parameters used are listed with other related quantities.

Results and Discussion

Degrees of Screening. As a criterion of electron correlation, we introduced here a new parameter ρ, degrees of screening:

$$\rho = 1 - \frac{\Gamma_0}{U_0}, \tag{13}$$

where Γ_0 and U_0 are, respectivery, the two-center and the bare Coulomb repulsion at the nearest-neighbor distance. It is obvious from the equation that when $\Gamma_0=U_0$, ρ=0, (without screening) and if Γ_0=0, ρ=1, (full screening). For intermediate screening, ρ satisfies $0<\rho<1$.

As a consequence, we can express the relative strength of the electron correlation in terms of ρ. Then, we study the effect of the electron correlation on the transition energies using ρ. For this purpose we derived a parametric formula (14) utilizing Eq. 13 and 6 (where we take a nearest-neighbor distance R_0=1.39 Å):

$$C_1 = 0.854 - 0.809\rho. \tag{14}$$

Making use of this relationship, we can determine a suitable $\Gamma_{\mu\nu}$ for setting the ρ values. This makes it possible to calculate the MO quantities as a function of ρ. Analysing the ρ-dependence of the calculated quantities, we can evaluate the electron correlation effect upon the quantities.

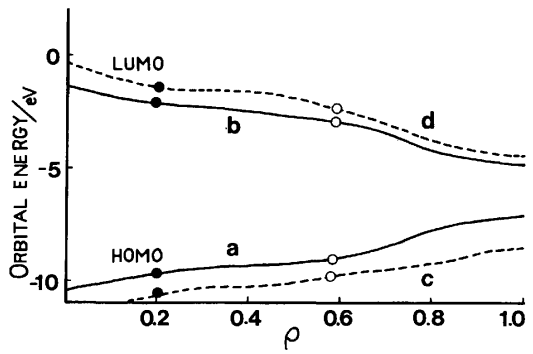

Fig. 2. ρ-Dependence of the orbital energy.
——: Pyrene, a) E_H, b) E_L, ----: Naphthalene, c) E_H, d) E_L, ●: Ohono-Klopman, ○: Nishimoto-Mataga.

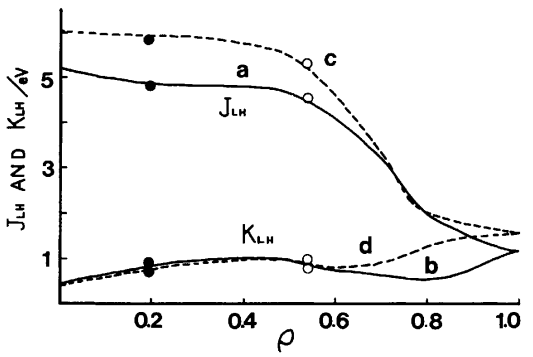

Fig. 3. ρ-Dependence of Coulomb and exchange repulsion.
——: Pyrene, a) J_{LH}, b) K_{LH}, ----: Naphthalene, c) J_{LH}, d) K_{LH}, ●: Ohono-Klopman, ○: Nishimoto-Mataga.

ρ-Dependence of Transition Energies. Here we describe the naphthalene and pylene cases. Figures 2, 3 show the ρ-dependence of the orbital energies as well as the Coulomb and exchange repulsion.

Figure 4 shows the ρ-dependence of the calculated transition energies. As was seen in Fig. 2, the HOMO-levels, E_H's, increase with increasing ρ and the LUMO-levels, E_L's, are lowerd as ρ increases. As a result, the orbital spacing becomes narrow with increasing ρ. This can be explained according to the following interpretation by Hush and Pople.[29] Let ΔE_{LH} be the orbital spacing between LUMO and HOMO; then

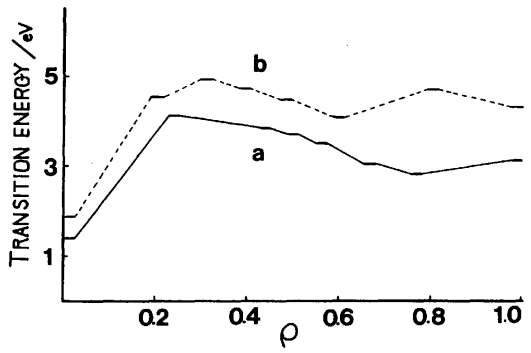

Fig. 4. ρ-Dependence of the transition energies.
a): Pyrene lowest B_{2u}, b): Naphthalene lowest B_{2u}.

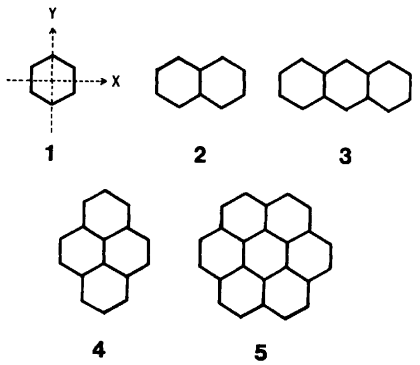

Fig. 5. Coordinate systems and carbon skeltons of the molecules. 1) Benzene, 2) Naphthalene, 3) Anthracene, 4) Pyrene, 5) Coronene.

$$\Delta E_{LH} = E_L - E_H = 2\sum_{\mu<\nu}^{\text{bond}} \beta_{\mu\nu}(C_{L\mu}C_{L\nu} - C_{H\mu}C_{H\nu}) - \sum_{\mu<\nu} P_{\mu\nu}(C_{L\mu}C_{L\nu} - C_{H\mu}C_{H\nu})\Gamma_{\mu\nu}. \quad (15)$$

Here, E_L and E_H are the orbital energies of LUMO and HOMO; $C_{L\mu}$, $C_{H\nu}$, and $P_{\mu\nu}$ are the AO coefficients and the π-bond order between cores μ and ν. To derive the above equation, we used the following approximation:

$$F_{\mu\nu} = \beta_{\mu\nu} - \frac{1}{2}P_{\mu\nu}\Gamma_{\mu\nu}, \quad (16)$$

where $F_{\mu\nu}$ is the off-diagonal elements of the $\boldsymbol{F}$-matrix[30] and $\beta_{\mu\nu}$=0 for non-neighbor μ and ν.

The above equation shows that ΔE_{LH} is reduced when $\Gamma_{\mu\nu}$ decrease; namely, ρ increases since $\Gamma_{\mu\nu}$ is inversely related to ρ and the second summation takes a positive value. This is because, the orbital spacing becomes narrow as ρ increases (Fig. 2). Next, we describe the ρ-dependence of the transition energies. As Fig. 4 shows, for intermediate ρ values (i.e., $0.2<\rho<0.6$) the transition energies decrease as ρ increases. Judging from the ρ-dependence of the ΔE_{LH}'s, this is fairly acceptable. Out of the regions, however, the ΔE's exhibit somewhat irregular changes. This abnormality is probably due to the characteristic ρ-dependence of the Coulomb and exchange repulsion, J_{LH} and K_{LH}, because these quantities are correlated with ΔE through the following formalism:[31]

$$\Delta E = \Delta E_{LH} - J_{LH} + 2K_{LH}. \quad (17)$$

To explain the ΔE vs. ρ curves more exactly, however, the ρ-dependence of the CI matrix elements must be taken into account, since changes in the CI matrix elements strongly alter the transition energies, even if the changes are not so remarkable. This problem will be reported elsewhere.

Here, we direct our attention to a comparison of the new formula $\Gamma_{\mu\nu}$ to that of OK and NM. For this purpose, the calculated results by $\gamma_{\mu\nu}^{OK}$ and $\gamma_{\mu\nu}^{NM}$ are also plotted in Figs. 2, 3. As can be seen from the figures, the values calculated by using OK and NM are in fairly good agreement with those by using $\Gamma_{\mu\nu}$'s (whose values are about 0.2 and 0.6, respectively).

This indicates that the relative values of correlational screening estimated from OK and NM are in the ratio of 1/3. With regard to this, a very similar result has been reported by Fukutome and Sasai[32] while studing the electron correlation in linear polyens. Their proposal can be summarized as follows: The value of $(\gamma_{\mu\mu}-\gamma_0)/|\beta|$ that determines the extent of electron correlation, is about 1 for OK and about 3 for NM. Here, $\gamma_{\mu\mu}$ is the one-center repulsion and γ_0 the nearest-neighbor two-center repulsion. β is the nearest-neighbor two-center core integral. These facts imply that OK is acceptable when the electron correlation is weak, whereas NM is good when the correlation is rather strong.

Transition Energies. Here, we described the transition energies calculated using $\Gamma_{\mu\nu}$. The coordinate systems[33] and carbon skeletons of the molecules are illustrated in Fig. 5. In Tables 2—5 the transition energies, oscillator strength and order of states are given in comparison with other calculated and experimental data. From the tables we can see that MCP gives fairly good results (as compared with the other calculations). In the case of MCP, the optimal ρ values are shown in parenthes, where the ρ values extend over the region 0.3—0.5. This indicates that the degrees of correlation in these molecules is intermediate.

Moreover, a striking feature found in the above tables is that the energy-level spacings and order of states calculated by the MCP are rather close to those by the β-variable method.[39,40] This is probably due to a procedural similarity between the two methods, since for both MCP and β-variable, the off-diagonal elements of $\boldsymbol{F}$-matrix are corrected so as to reproduce the experimental spectra by changing the adjustable parameters of C_1 and β_0.

Next, we describe the number-density dependence of ρ. As can be clearly seen in Table 1, when the molecular size becomes large, ρ increases in parallel with n. This feature suggests that some definite relationship

Table 2. Transition Energies and Intensities of Benzene

State	NM		RPA[34]		MCP (ρ=0.30)		Obsd[35]	
	ΔE/eV	f	ΔE/eV	f	ΔE/eV	f	ΔE/eV	f
B_{2u}	5.48	0.00	4.86	0.00	5.27	0.00	4.71	0.002
B_{1u}	6.66	0.00	4.77	0.00	6.49	0.00	5.96	0.10
E_{1u}	7.48	1.26	6.99	1.537	7.00	1.18	6.76	0.69

Table 3. Transition Energies and Intensities of Naphthalene

State	NM		β-variable[36]		MCP (ρ=0.40)		Obsd[35]	
	ΔE/eV	f	ΔE/eV	f	ΔE/eV	f	ΔE/eV	f
B_{3u}	4.62	0.00	3.98	0.00	4.42	0.00	3.97	0.002
B_{2u}	4.77	0.297	4.51	0.246	4.75	0.51	4.29	0.18
B_{3u}	6.22	2.22	5.54	1.946	5.99	2.05	5.64	1.70
B_{2u}	6.93	0.651	6.07	0.861	6.70	0.65	6.53	0.20

Table 4. Transition Energies and Intensities of Pyrene

State	NM		β-variable[36]		MCP (ρ=0.43)		Obsd[37,38]	
	ΔE/eV	f	ΔE/eV	f	ΔE/eV	f	ΔE/eV	f
B_{3u}	—	—	3.49	0.00	3.79	0.00	3.33	0.002
B_{2u}	3.80	0.972	3.64	0.675	3.81	0.89	3.71	0.33
B_{3u}	5.28	1.17	4.77	0.954	4.98	1.06	4.55	0.35
B_{2u}	6.14	1.59	5.25	1.48	5.86	1.58	5.14	0.85

Table 5. Transition Energies and Intensities of Coronene

State	NM		β-variable[36]		MCP (ρ=0.48)		Obsd[37,38]	
	ΔE/eV	f	ΔE/eV	f	ΔE/eV	f	ΔE/eV	f
B_{2u}	3.43	0.00	3.04	0.00	3.39	0.00	2.91	0.0
B_{1u}	3.83	0.00	3.51	0.00	4.01	0.001	3.66	0.10
E_{1u}	4.67	5.86	4.19	3.89	4.49	3.90	4.18	1.34

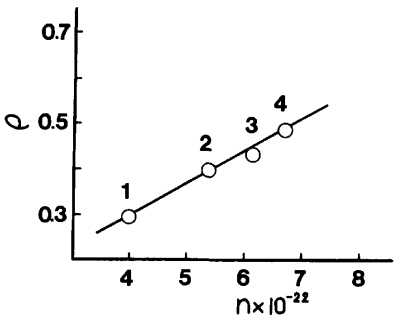

Fig. 6. Relation between ρ and n: ρ is the degrees of screening and n the number-density of π electrons.

exists between them. In fact, plots of ρ against n show the following relationship (displayed in Fig. 6):

$$\rho = 7.00n \times 10^{-24} + 0.02, \tag{18}$$

with

$$n = \frac{\nu DN}{M}. \tag{19}$$

Here, ν is the number of π electrons, D the density of the materials, N Avogadro's number and M the molecular weight. Equation 18 is an empirical formula; therefore, we can not undertake a further analysis. In spite of this, it does a very useful way to perform practical calculations since, by making use of the equation, we can evaluate ρ for an aromatic hydrocarbon when n is given.

For checking the validity of the above relationship, a trial calculation was made for anthracene. In the calculation, we took ρ=0.34 (same as putting n= 5.9×10^{22}). As Table 6 shows, the obtained results are in acceptable agreement with those reported by other authors, except for the appearance of a weak band located above the lowest B_{2u} band. Generally speaking, this band is closely related to the strength of a two-center repulsion $\gamma_{\mu\nu}$. This band appears when $\gamma_{\mu\nu}$ has a simple Coulomb-like form, as a Slater AO-type repulsion.[41] Contrariwise, the band disappeared when $\gamma_{\mu\nu}$ assumed such long-range screened forms as OK,[36] NM[42] and a cusp-like shape interaction.[43] In $\Gamma_{\mu\nu}$ case, screening is restricted within the interval $R_{\mu\nu}< C_0d/C_1$; when $R_{\mu\nu}$ increases beyond this boundary, it

Table 6. Transition Energies and Intensities of Anthracene

State	NM[42]		β-variable[36]		Rudenberg[43]		Pariser[41]		MCP		Obsd[35]	
	ΔE/eV	f	ΔE/eV	f	ΔE/eV	f	ΔE/eV	f	ΔE/eV	f	ΔE/eV	f
B_{3u}	3.989	0.00	3.58	0.00	3.22	0.014	3.715	0.00	4.01	0.00	—	—
B_{2u}	3.279	0.26	3.59	0.313	3.59	0.27	3.645 5.251	0.386 0.091	3.55 5.11	0.329 0.177	3.34	0.1
B_{3u}	5.098	2.74	4.84	2.527	5.26	3.09	5.499	3.229	5.30	2.909	4.84	2.28
B_{2u}	6.648	1.03	5.87	0.604	5.47	0.83	6.686	0.640	6.70	0.903	5.61	0.28

results in a Coulomb-like repulsion (Eq. 6). This indicates that the long-range behavior of $\Gamma_{\mu\nu}$ is very similar to that of a Slater AO-type repulsion when $R_{\mu\nu}$ becomes large. This is because MCP calculates the weak second lowerst B_{2u} band.

From the above results, we then concluded that MCP provides a semiempirical method that is favorable for studying the electron-correlation effect upon a calculation of the transition energies, (and for which Eq. 17 is available). In order to apply this method more extensively, however, the physical concept of the linear screening potential $H(r)$ must be clarified based upon a theoretical consideration.

We wish to express our thanks to Prof. Setsuo Ichimaru of University of Tokyo and Dr. Hiroshi Yasuhara of Tohoku University for sending reprints of their work. We thank Dr. Takeshi Ikeyama of Miyagi University of Education for his helpful discussions. We also thank the Computer Center, Tohoku University, for the use of the ACOS 1000 computer.

References

1) S. Wilson, "Electron Correlation in Molecule," Oxford University Press (1984), p. 43.
2) H. Gutefreund and W. A. Little, *J. Chem. Phys.*, **50**, 4468 (1969).
3) H. Gutefreund and W. A. Little, *Phys. Rev.*, **83**, 68 (1969).
4) K. Kitaura and K. Nishimoto, *Thoret. chim. Acta (Berl.)*, **28**, 111 (1973).
5) H. T. Dunning and V. Mckoy, *J. Chem. Phys.*, **47**, 1735 (1967).
6) D. J. Rowe, *Rev. Mod. Phys.*, **40**, 153 (1968).
7) H. Yasuhara and M. Watanabe, *Phys. Soc. Jpn.*, **33**, 576 (1978).
8) K. Utsumi and S. Ichimaru, *Phys. Soc. Jpn.*, **36**, 504 (1981).
9) H. Yasuhara, *J. Phys. Soc. Jpn.*, **36**, 361 (1974).
10) S. G. Brush, H. L. Sahlin, and E. Teller, *J. Chem. Phys.*, **45**, 2101 (1966).
11) H. Totsuji, *Phys. Rev. A*, **17**, 399 (1978).
12) S. Ichimaru, *Phys.Soc. Jpn.*, **34**, 753 (1979).
13) S. Ichimaru, *Rev. Mod. Phys.*, **54**, 1017 (1982).
14) E. E. Salpeter and H. M. Van Horn, *Astrophys. J.*, **155**, 183 (1969).
15) H. E. DeWitt, H. C. Graboske, and M. S. Cooper, *Astrophys. J.*, **181**, 143 (1973).
16) N. Itoh and S. Ichimaru, *Phys. Rev. A*, **16**, 2178 (1977).
17) N. Itoh, S. Ichimaru, and S. Nagano, *Phys. Rev. B*, **17**, 2862 (1978).
18) M. Imada and M. Takahashi, *J. Phys. Soc. Jpn.*, **53**, 3770 (1984).
19) S. Tanaka and S. Ichimaru, *J. Phys. Soc. Jpn.*, **55**, 2278 (1986).
20) J. A. Pople, *Trans. Faraday Soc.*, **49**, 1357 (1953).
21) B. M. Gimarc, W. A. Coone, and R. G. Parr, *J. Chem. Phys.*, **42**, 21 (1965).
22) C. A. Coulson and A. H. Neilson, *Proc. Phys. Soc.*, **78**, 831 (1961).
23) K. Ohono, *Theoret. chim. Acta*, **2**, 219 (1964).
24) G. Klopman, *J. Am. Chem. Soc.*, **86**, 4550 (1964).
25) K. Nishimoto, and N. Mataga, *Z. Phys. Chem. (N. F)*, **12**, 335 (1957).
26) G. Gaglione, G. L. Masserini, and L. Reatto, *Phys. Rev. B*, **22**, 1237 (1980).
27) K. Hirano, *Bull. Chem. Soc. Jpn.*, **56**, 850 (1983).
28) M. Wolfsberg and L. Helmholtz, *J. Chem. Phys.*, **20**, 837 (1952).
29) N. S. Hush and J. A. Pople, *Trans. Faraday Soc.*, **51**, 600 (1955).
30) C. C. J. Roothaan, *Rev. Mod. Phys.*, **23**, 69 (1951).
31) R. G. Parr and R. S. Mulliken, *J. Chem. Phys.*, **18**, 1338 (1950).
32) H. Fukutome and M. Sasai, *Prog. Theor. Phys.*, **48**, 41 (1982).
33) N. S. Ham and K. Rudenberg, *J. Chem. Phys.*, **25**, 13 (1956).
34) K. Kitaura and K. Nishimoto, *Theoret. chim. Acta (Berl.)*, **31**, 91 (1973).
35) H. B. Klevens and J. R. Platt, *J. Chem. Phys.*, **17**, 470 (1949).
36) K. Nisimoto, *Theoret. chim. Acta (Berl.)*, **7**, 207 (1967).
37) J. Tanaka, *Bull. Chem. Soc. Jpn.*, **38**, 86 (1965).
38) H. Zimmerman and N. Joop, *Zeit. für Electrochem.*, **65**, 138 (1961).
39) K. Nishimoto and L.S. Foster, *Theoret. chim. Acta*, **3**, 407 (1965).
40) K. Tomono and K. Nishimoto, *Bull. Chem. Soc. Jpn.*, **49**, 1179 (1976).
41) R. Pariser, *J. Chem. Phys.*, **24**, 250 (1956).
42) N. Mataga, K. Nishimoto, and S. Mataga, *Bull. Chem. Soc. Jpn.*, **32**, 395 (1959).
43) N. S. Ham and K. Rudenberg, *J. Chem. Phys.*, **25**, 1 (1956).

 © 1987 The Chemical Society of Japan Bull. Chem. Soc. Jpn., 60, 1237—1242 (1987)

Effects of Alkali Metals Added to Silica-Supported Ruthenium Catalysts on Hydrogenation of Carbon Monoxide

Toshiyuki ENOMOTO, Keiichiro KATA,† Toshio OKUHARA,* and Makoto MISONO*
Department of Synthetic Chemistry, Faculty of Engineering, The University of Tokyo, Hongo, Bunkyo-ku, Tokyo 113
(Received September 12, 1986)

The hydrogenation of carbon monoxide to produce hydrocarbons (Fischer-Tropsch synthesis) has been studied over Ru/SiO_2 catalysts to which alkali metals (Li, Na, K, and Cs) were added. The effects of alkalis were compared by varying the amounts added and by varying the support to Al_2O_3. By the alkali addition, the CO conversion and the selectivity to methane decreased but the propagation probability as well as the olefin/paraffin ratio increased. Among the alkali metals, Li least depressed the catalytic activity of Ru/SiO_2, but was most effective for the suppression of methane formation. In contrast to a K-added catalyst, the infrared band of adsorbed carbon monoxide shifted only slightly upon Li addition, showing its small electronic effect. The results in electron microscopy and X-ray diffraction suggested that the Ru particle size remained almost unchanged upon Li addition, although the amounts of adsorbed carbon monoxide and hydrogen significantly decreased. This indicates that Ru particles were partially covered by a compound of Li. On the basis of these results, it was concluded that the suppression of methane formation by Li was due to a geometric or ensemble effect.

Chemical modification of metal catalysts by adding certain metal ions/oxides often brings about a significant increase in the catalytic activity and selectivity, e.g., for the synthesis of methanol or ethanol from CO and H_2.[1-4] Alkali metals have been reported to be effective additives to Fe,[5-7] Ni,[8,9] and Ru[10-12] catalysts for the formation of olefinic hydrocarbons from CO and H_2.

The effects of alkali metals have been attributed to an electronic effect caused by the electron-donating nature of alkali for supported metal catalysts.[8,9,12,13] However, McClory and Gonzalez suggested that the decrease of catalytic activity upon alkali addition was associated with an ensemble effect rather than an electronic effect in the case of silica-supported Ru catalysts,[14] although the changes in the selectivities were rather small.

We previously reported the effects of the dispersion of metal[15] as well as the effects of such additives as K, P, and B,[12] and transition metals[16] on the adsorption and the hydrogenation of CO over alumina-supported Ru catalysts. As an extension of these studies, we have investigated in the present work CO hydrogenation using silica-supported Ru catalysts in which the contents of Li, Na, K, and Cs were widely changed. The catalysts were characterized by infrared spectroscopy of CO chemisorption, electron microscopy, X-ray diffraction, and adsorption stoichiometries of H_2 and CO. The relationship between the catalytic property and the state of Ru particles is discussed while placing emphasis on the peculiar effect of the Li addition.

Experimental

Catalysts. Silica (Aerosil 200) was used as supports after calcination in air at 500 °C for 20 h. Silica-supported Ru catalysts were prepared by incipient-wetness impregnation with an aqueous solution of $RuCl_3$. In the case of alkali-added catalysts, the silica was first impregnated by an incipient-wetness method with an aqueous solution of alkali carbonate. Then, it was dried and calcined at 500 °C prior to impregnation with a $RuCl_3$ solution. All catalysts contained 2.5% Ru by weight. Hereafter, these catalysts will be designated as, e.g., Ru/SiO_2 or $Ru\text{-}Li(1:0.25)/SiO_2$, where the ratios in parentheses are the atomic ratios of Ru to alkali metal. A catalyst ($Li/Ru/SiO_2$) was additionally prepared by impregnating a reduced Ru/SiO_2 catalyst with a Li_2CO_3 solution (Li/Ru=0.25).

Alumina-supported Ru catalysts were also prepared in the same way as Ru/SiO_2 or $Ru\text{-}Li/SiO_2$. γ-Al_2O_3 (Reference Catalyst of Catalysis Society of Japan, ALO-4) was used after calcination in air at 400 °C for 10 h.

Procedure. The hydrogenation of CO was carried out by using conventional flow reactors. After catalysts of 0.2—1.5 g were reduced at 450 °C for 2 h in flowing H_2, a 1 : 2 mixture of CO and H_2 was fed at 260 °C under 1 or 10 atm. The products were analyzed by gas chromatographs, by using a Molecular Sieve 5A, a Porapak Q, a VZ-10 and a Silicone SE-30 column. The formation of methanol, ethanol, and acetaldehyde was checked by a Porapak R column.

Other Measurements. The surface areas of SiO_2 and Li/SiO_2 were measured by N_2 adsorption. The adsorption of CO and H_2 was volumetrically measured at room temperature after the catalysts were reduced by H_2 at 450 °C for 2 h. Infrared spectra (IR) of CO adsorbed were recorded in the same way as described previously.[15] Transmission electron micrographs (EM) were obtained with a JEOL JEM 1250 electron microscope (1000 keV, final magnification: ×150000). The particle-size distributions were calculated by counting 300—400 particles of Ru on several micrographs for each catalyst. Powder X-ray diffraction (XRD) was obtained on an X-ray diffractometer (Rotaflex, Rigaku denki). Mean diameters of Ru particles were estimated from the half width of the main peak of Ru metal (2θ=44.0°).

Results

Hydrogenation of CO. The reaction rates and the

†Present address: Institute of Industrial Science, The University of Tokyo, 7-22-1, Roppongi, Minato-ku, Tokyo 106.

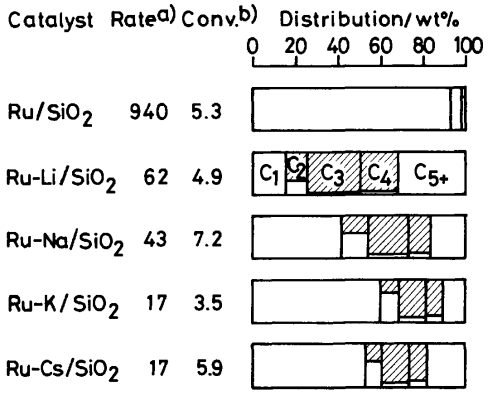

Fig. 1. Effects of alkali addition to Ru/SiO_2 on catalytic activity and product distribution in the CO hydrogenation (260°C, 1 atm, alkali/Ru= 0.25). Shaded parts indicate olefins in C_2–C_4 products. a) Reaction rate/10^{-3} mol g-Ru^{-1} h^{-1}. b) Conversion/%.

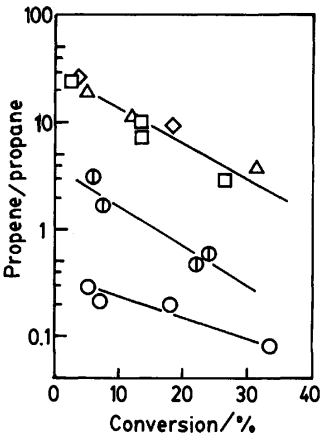

Fig. 2. Propene/propane ratio vs. conversion for the CO hydrogenation on Ru/SiO_2 and Ru-Li/SiO_2 catalysts under 1 atm at 260°C. ○: Ru/SiO_2, ⊕: Ru-Li (1:0.1)/SiO_2, □: Ru-Li (1:0.25)/SiO_2, △: Ru-Li (1:1.5)/SiO_2, ◇: Ru-Li (1:4.5)/SiO_2.

product distributions of CO hydrogenation performed under 1 atm on Ru/SiO_2 and alkali-added Ru/SiO_2 are summarized in Fig. 1. The formation of methanol, ethanol and acetaldehyde was negligible, and the yield of CO_2 was only about 0.1%. In the case of Ru/SiO_2, methane was the main product, and the contents of olefins in C_2–C_4 hydrocarbons were low. When alkali metals were added, the reaction rates decreased by more than a factor of ten. At the same time, the selectivity to methane considerably decreased, and the selectivities to higher hydrocarbons and olefins increased.

As for the relative extents of the effects, the following trends are noted. The reaction rate decreased in the order of none > Li > Na > K≈Cs, while the selectivity to methane was in the order of none > Cs≈K > Na > Li. The turnover frequency (TOF) calculated from H_2 chemisorption varied in the same order as the rate (none > Li > Na > K≈Cs), since the difference in the H/Ru ratio between alkalis was much smaller than the activity change. It is remarkable that Li showed the least suppression of activity, but was most effective for the suppression of methane. The rates of methane formation were 865 and 9.3 mmol g-Ru^{-1} h^{-1} for Ru/SiO_2 and Ru-Li(1 : 0.25)/SiO_2, respectively, exhibiting a decrease of 1/90 by Li addition. On the other hand, the rate of C_{2+} formation decreased only to 70%; 75 and 53 mmol g-Ru^{-1} h^{-1} for Ru/SiO_2 and Ru-Li (1 : 0.25)/SiO_2, respectively. The Li/Ru/SiO_2 catalyst, which was prepared in the reversed order of impregnations, showed the same activity and selectivity as Ru-Li/SiO_2 (reaction rate: 63 vs. 62 mmol g-Ru^{-1} h^{-1}, selectivity to methane: 16 vs. 15%).

The selectivity to methane was almost independent of the extent of conversion. For example, the selectivity was 93±1% for Ru/SiO_2 and 15±2% for Ru-Li (1 : 1.5)/SiO_2, in the conversion range from 3 to 35%. Distributions of the carbon number of hydrocarbons were also independent of the conversion. This fact

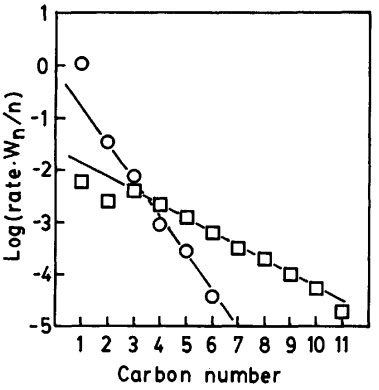

Fig. 3. Schultz-Flory plots (logarithm of (Rate W_n/n), where W_n is weight percentage, and n is carbon number). ○: Ru/SiO_2, □: Ru-Li(1:0.25)/SiO_2.

shows that the distributions of the carbon number are of the primary products. In Fig. 2, the propene/propane ratios in the products are plotted against the % conversion. Most Ru-Li/SiO_2 catalysts showed high propene/propane ratios, but the ratios tended to decrease with an increase in the conversion for both Ru/SiO_2 and Ru-Li/SiO_2. This fact indicates that the hydrogenation of olefins proceeded significantly under the reaction conditions. Li also enhanced the ethylene/ethane and butenes/butane ratios, which similarly decreased with increasing conversion.

The distributions of product hydrocarbons for Ru/SiO_2 and Ru-Li(1 : 0.25)/SiO_2 are shown according to Schultz-Flory plots in Fig. 3. The distributions obeyed the Schultz-Flory distribution for C_{3+} products. The production of C_1 produced on Ru/SiO_2 deviated upward from that predicted by the Schultz-Flory plot, but downward on Ru-Li(1 : 0.25)/SiO_2. This implies that Li addition induced a selective suppression of methane formation.

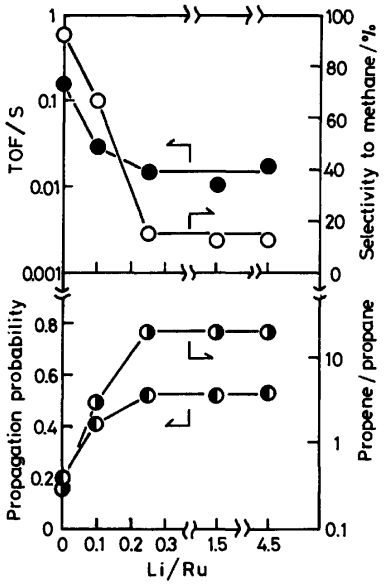

Fig. 4. Effects of the content of Li in $Ru-Li/SiO_2$ on TOF, selectivity to methane, propagation probability, and propene/propane ratio (at 5% conversion) in the CO hydrogenation under 1 atm at 260°C. ●: TOF, ○: selectivity to methane, ◐: propagation probability, ◑: propene/propane ratio.

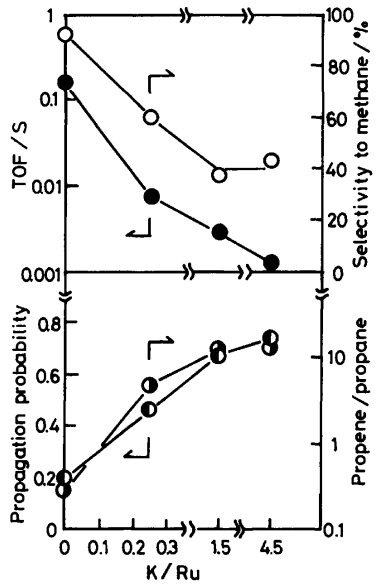

Fig. 5. Effects of the content of K in $Ru-K/SiO_2$ on TOF, selectivity to methane, propagation probability, and propene/propane ratio (at 5% conversion) in the CO hydrogenation under 1 atm at 260°C. ●: TOF, ○: selectivity to methane, ◐: propagation probability, ◑: propene/propane ratio.

In Fig. 4, TOF, selectivity to methane, propagation probability (calculated from Fig. 3), and propene/propane ratio at 5% conversion are plotted against the Li/Ru atomic ratio. In the range of Li/Ru less than 0.25, TOF and the methane formation greatly decreased, while the latter two values increased with an

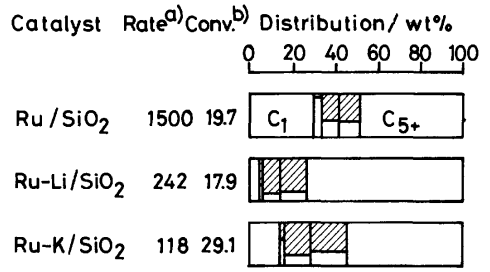

Fig. 6. Effects of alkali addition to Ru/SiO_2 on catalytic activity and product distribution in the CO hydrogenation (260°C, 10 atm, alkali/Ru= 0.25). Shaded parts indicate olefins in C_2–C_4 products. a) Reaction rate/10^{-3} mol g-Ru^{-1} h^{-1}. b) Conversion/%.

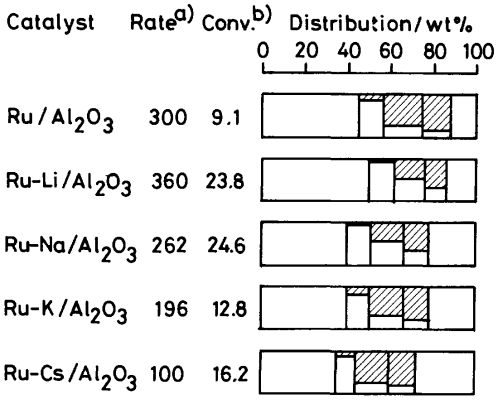

Fig. 7. Effects of alkali addition to Ru/Al_2O_3 on catalytic activity and product distribution in the CO hydrogenation (260°C, 1 atm, alkali/Ru= 3). Shaded parts indicate olefins in C_2–C_4 products. a) Reaction rate/10^{-3} mol g-Ru^{-1} h^{-1}. b) Conversion/%.

increase in Li/Ru. For Li/Ru greater than 0.25, these values were almost independent of Li/Ru.

Figure 5 shows the effect of K. In the case of K, the selectivity to methane decreased only to about 40%, even when the K/Ru atomic ratio was increased to 4.5. The decrease of TOF was greater and TOF continued to decrease with the amounts of K. The propagation probability and the propene/propane ratio increased monotonously with the amount of K.

Figure 6 shows the results of reactions performed under 10 atm. The reaction rates increased and the formation of higher hydrocarbons was promoted for all catalysts, as compared with the results obtained under 1 atm (Fig. 1). Even under 10 atm, the suppression of methane formation by Li was remarkable; the selectivity to methane decreased from 30 to 5% for $Ru-Li(1:0.25)/SiO_2$. The Schultz-Flory plots for Ru/SiO_2 and $Ru-Li/SiO_2$ showed essentially the same trend as in Fig. 3, although the slopes were less steep.

The effects of alkali-addition to Ru/Al_2O_3 are compared in Fig. 7. As already reported, Ru/Al_2O_3 formed less methane than Ru/SiO_2.[12] The extents of methane suppression by alkalis were significantly less than those observed for Ru/SiO_2, although the amounts of

Table 1. BET Surface Areas and Amounts of CO and H_2 Adsorbed on Ru-Li/SiO_2 Catalysts

Li wt%	0	0.018	0.045	0.26	0.77
Li/Ru[a)]	0	0.1	0.25	1.5	4.5
Surface area[b)]	160	152	136	143	88
H/Ru[c)]	0.17	0.15	0.12	0.12	0.06
CO/Ru[d)]	0.14	0.11	0.05	0.06	0.05

a) Atomic ratio. b) Surface areas/m^2g^{-1}; measured before impregnation of Ru. c) Total adsorption at 25 °C. d) Irreversible adsorption at 25 °C.

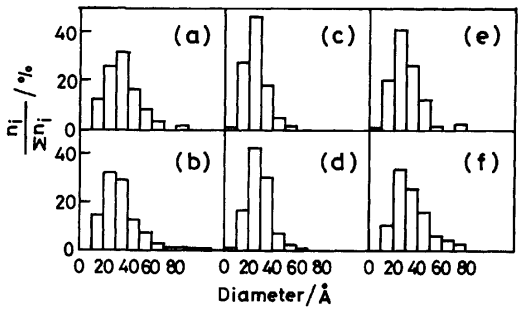

Fig. 8. Distribution of diameters of Ru particles on (a) Ru/SiO_2 after H_2 reduction at 450 °C, (b) Ru/SiO_2 after CO hydrogenation at 260 °C, (c) Ru-Li (1:1.5)/SiO_2 after H_2 reduction at 450 °C, (d) Ru-Li (1:1.5)/SiO_2 after CO hydrogenation at 260 °C, (e) Ru-Li (1:4.5)/SiO_2 after H_2 reduction at 450 °C, and (f) Ru-Li (1:4.5)/SiO_2 after CO hydrogenation at 260 °C.

alkali metals were twelve times greater than that for Ru/SiO_2.

Characterization of Catalysts. Surface areas of SiO_2 and Li-SiO_2 before Ru impregnation are shown in Table 1. The supports containing 0.018, 0.045, 0.26, and 0.77 wt% of Li correspond to atomic ratios of Li to Ru 0.1, 0.25, 1.5, and 4.5, respectively, when 2.5 wt% of Ru is loaded. The decrease in the surface area was not significant when Li was not more than 0.26 wt%. The data of H_2 and CO adsorption are also given in Table 1. The amounts decreased with the Li content. The decrease was a little greater for CO as reported for K-added Ni/SiO_2,[13] but the reason is not clear at present.

Figure 8 shows the size distributions of Ru particles on Ru/SiO_2 and Ru-Li/SiO_2 catalysts measured by EM before and after use for CO hydrogenation. For all catalysts, the distributions little changed by the use for CO hydrogenation. The distributions were centered at ca. 30 Å, and a few Ru particles were present above 60 Å. The distributions for Ru/SiO_2 were slightly wider than those on Ru-Li/SiO_2, but there was no essential difference.

Table 2 summarizes the mean diameters of Ru particles, which were determined by H_2 adsorption, EM, and XRD. The diameters determined by EM decreased upon the addition of Li, but the change was small. Those determined by XRD, which were slightly greater than those by EM, showed no significant change either. On the other hand, the apparent diameter determined by H_2 adsorption definitely increased upon the addition of Li.

Table 2. Mean Diameters of Ru Particles of Ru-Li/SiO_2 Catalysts

Li/Ru[a)]	0	0.1	0.25	1.5	4.5
Mean diameters/Å					
H_2 adsorption	49	57	70	68	131
EM[b)]	35	—	—	25	28
EM[c)]	34	—	—	28	35
XRD	50	45	50	43	45

a) Atomic ratio. b) Diameters measured after H_2 reduction at 450 °C. c) Diameters measured after CO hydrogenation at 260 °C.

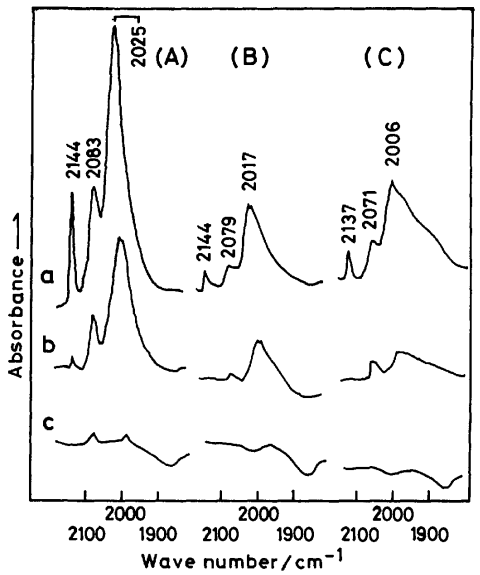

Fig. 9. IR spectra of CO adsorbed on (A) Ru/SiO_2, (B) Ru-Li (1:0.25)/SiO_2, and (C) Ru-K (1:0.25)/SiO_2. The spectra of CO were taken after evacuation at (a) 25 °C, (b) 100 °C, and (c) 200 °C.

Figure 9 shows IR spectra of CO adsorbed on Ru/SiO_2, Ru-Li(1 : 0.25)/SiO_2, and Ru-K(1 : 0.25)/SiO_2. Three peaks at 2025, 2083, and 2144 cm^{-1} were observed for CO on Ru/SiO_2 after evacuation at room temperature. The intensity decreased with an increase in the evacuation temperature, and almost disappeared after evacuation at 200 °C. In the case of Ru-Li/SiO_2, a band was observed at 2017 cm^{-1}, together with two small peaks at 2079 and 2144 cm^{-1}. The relative integrated intensity agreed with the amount of adsorbed CO shown in Table 1. The shift of the main peak was less than about 8 cm^{-1}. On the other hand, the main peak at 2006 cm^{-1} for Ru-K/SiO_2 showed a shift of

about 20 cm^{-1} and the peak envelope extended to the lower wavenumber side. The two peaks at 2083 and 2144 cm^{-1}, which were assigned to CO adsorbed on $Ru^{\delta+}$,[17,18] also shifted but to a lesser extent for $Ru-K/SiO_2$.

Discussion

The principal effects of alkali addition were: (i) a decrease in the catalytic activity, (ii) a suppression of methane formation, (iii) an increased selectivity to higher hydrocarbons, and (iv) an increase in the olefin/paraffin ratio. These effects agreed with those mentioned in the literature.[5-12] As for the kind of alkali metals and the order of catalytic activity: none > Li > Na > K≈Cs, is consistent with those reported for CO hydrogenation on Rh/TiO_2[19] and for methanol formation on Pd/SiO_2.[1] However, it is remarkable that the extent of methane suppression was Li > Na > K≈Cs > none, Li exhibiting the greatest effect. If the suppression of both activity and methane formation was controlled by one common factor like an electronic effect, these effects should show the same orders. In fact, the two orders for Ru/Al_2O_3 were the same. Thus, an additional effect must be considered in the case of $Ru-Li/SiO_2$.

Effects of Alkalis on the Adsorption of H_2 and CO. The possible effects caused by the addition of alkalis are (i) a change of particle size, (ii) an electronic effect on Ru, and (iii) a geometric or ensemble effect.

As shown in Table 2, the particle size calculated from the amounts of adsorbed H_2 (given in Table 1) definitely increased upon Li addition (more than two times), but the particles sizes determined by EM and XRD changed little or slightly decreased. Therefore, the decreases in the amounts of adsorbed CO and H_2 upon Li addition were not ascribable to the increase in the size of Ru particles. One possible explanation may be an electronic effect. Due to a change in the electronic state of Ru caused by Li, a Ru surface might lose the ability to adsorb H_2 and CO. However, the electronic effect was not significant for $Ru-Li/SiO_2$ as inferred from IR of adsorbed CO. The IR band for $Ru-Li/SiO_2$ shifted only by 8 cm^{-1} (Fig. 9), as compared to 20 cm^{-1} for $Ru-K/SiO_2$ and 40 cm^{-1} for $Ru-K/Al_2O_3$.[12]

If one considers the small electronic effect of Li as well as the small change in the particle size, it is more likely that the decreases in the amounts of adsorbed CO and H_2 were due to partial coverage of the Ru surface by Li. This is similar to a "decoration model" proposed for the SMSI effect.[20-22] It is possible that during the preparation and/or activation process of the catalyst, a portion of Li is transported in a form close to Li_2O to the surface of the Ru particles without changing the particle size. The small change observed when the impregnation order was reversed may be consistent with this explanation.

A possible reason for the smaller effects of alkali for Ru/Al_2O_3 (Fig. 7) than for Ru/SiO_2 (Fig. 1) may be that the migration of Li onto the Ru surface was suppressed by the higher affinity of Li to Al_2O_3 support.

Effects of Alkalis on the Catalytic Property in CO Hydrogenation. It has been known for Ru/Al_2O_3 that TOF of CO hydrogenation changes inversely with the particle size of Ru.[15,23,24] In contrast, when Li was added to Ru/SiO_2, although the particle size decreased slightly (Table 2), TOF considerably decreased (Fig. 4). Therefore, the decrease in TOF was not due to the change in the particle size.

We previously reported that the effects of the addition of K, P, and B to Ru/Al_2O_3 were due to an electronic effect. However, the electronic effect of Li seems much smaller than that of K (as discussed above) in spite of the fact that Li was much more effective than K for the suppression of methane. Therefore, the electronic effect is not likely to be the primary function of Li.

We also studied the effect of V addition to Ru/Al_2O_3 and explained the results in terms of a geometric effect that is similar to an ensemble effect.[16] The effects of Li observed in the present study are rather similar to those of V with regard to activity and methane formation. Therefore, a similar geometric effect may be considered to be the primary function of Li in $Ru-Li/SiO_2$. The model proposed in the preceding section, that a Li compound partially covered the Ru surface, is consistent with the presence of a geometric effect.

McClory and Gonzalez reported that the addition of alkali to Ru/SiO_2 decreased the activity, enhanced the selectivities to olefins, and slightly suppressed methane formation.[14] In their study, however, changes in selectivities were much smaller and little difference was observed among the alkali metals. The differences between their and our results are attributable to the amounts of alkalis added. The amounts were 0.1 in atomic ratio to Ru in their study as compared with 0.1—4.5 in the present study. As shown in Fig. 4, the effects became significant when Li/Ru ratio was 0.25.

McClory and Gonzalez explained the above effect of alkali by an ensemble effect which lowered the ability for hydrogenation.[14] The suppression of methane formation and the enhancement of the olefin/paraffin ratio is consistent with the lower ability for hydrogenation. Therefore, the same explanation may be applicable to the effect of alkali observed in the present study. The selective suppression of methane formation, as observed in the present study, indicates that the geometric or ensemble effect was greater for methane formation; methane formation may need larger ensembles or more adjacent sites to supply more hydrogen atoms for the hydrogenation of the CH_x intermediate to methane. Another possibility is that sites which selectively produced methane were present on the Ru surface and Li preferentially poisoned these sites. The fact that methane formation was suppressed by a factor of 90 while the C_{2+} formation decreased only

to 70% favors this explanation. However, there is no direct evidence in the present study to show the presence of those sites.

An increase in the olefin/paraffin ratio was also found in the case of K addition to Ru/Al_2O_3 in our previous study.[12] In the case of Ru/Al_2O_3, the principal effect of K was the suppression of the secondary hydrogenation of olefin due to the increased CO coverage. But, in the case of $Ru\text{-}Li/SiO_2$, secondary hydrogenation was little suppressed. This fact also indicates that the effect is different for K and Li.

We gratefully acknowledge Mr. Hideo Tsunakawa of the Engineering Research Institute of the University of Tokyo for measuring electron micrographs. The present study was supported in part by a Grant-in-Aid for Scientific Research No. 61040012 from the Ministry of Education, Science and Culture.

References

1) Y. Kikuzono, S. Kagami, S. Naito, T. Onishi, and K. Tamaru, *Faraday Discuss. Chem. Soc.*, **72**, 135 (1981).
2) M. Ichikawa, K. Sekizawa, K. Shikakura, and M. Kawai, *J. Mol. Catal.*, **11**, 167 (1981).
3) M. M. Bhasin, W. J. Bartley, P. C. Ellgen, and T. P. Willson, *J. Catal.*, **54**, 120 (1978).
4) P. C. Ellgen, W. J. Bartley, M. M. Bhasin, and T. P. Willson, *Adv. Chem. Ser.*, **178**, 147 (1979).
5) M. E. Dry, "The Fischer-Tropsch Synthesis," in "Catalysis," ed by J. R. Anderson and M. Boudart, Springer-Verlag, Berlin (1981), Vol. 1, Chap. 4.
6) G. B. McVicker and M. A. Vannice, *J. Catal.*, **63**, 25 (1980).
7) R. A. Dictor and A. T. Bell, *J. Catal.*, **97**, 121 (1986).
8) C. T. Campbell and D. W. Goodman, *Surf. Sci.*, **123**, 413 (1982).
9) H. Praliaud, J. A. Dalmon, C. Mirodatos, and G. A. Martin, *J. Catal.*, **97**, 344 (1986).
10) T. Okuhara, K. Kobayashi, T. Kimura, M. Misono, and Y. Yoneda, *J. Chem. Soc., Chem. Commun.*, **1981**, 1114.
11) R. D. Gonzalez and H. Miura, *J. Catal.*, **77**, 338 (1982).
12) T. Okuhara, H. Tamura, and M. Misono, *J. Catal.*, **95**, 41 (1985).
13) H. Praliaud, M. Primet, and G. A. Martin, *Appl. Surf. Sci.*, **17**, 107 (1983).
14) M. M. McClory and R. D. Gonzalez, *J. Catal.*, **89**, 392 (1984).
15) T. Okuhara, T. Kimura, K. Kobayashi, M. Misono, and Y. Yoneda, *Bull. Chem. Soc. Jpn.*, **57**, 938 (1984).
16) T. Enomoto, T. Okuhara, and M. Misono, *Bull. Chem. Soc. Jpn.*, **58**, 1490 (1985).
17) M. F. Brown and R. D. Gonzalez, *J. Phys., Chem.*, **80**, 1731 (1976).
18) H. Chen, Z. Zhong, and J. M. White, *J. Catal.*, **90**, 119 (1984).
19) S. C. Chuang, J. G. Goodwin Jr., and I. Wender, *J. Catal.*, **95**, 435 (1985).
20) A. J. Simoens, R. T. K. Baker, D. J. Dwyer, C. K. F. Lund, and R. J. Madon, *J. Catal.*, **86**, 359 (1984).
21) A. K. Singh, N. K. Pande, and A. T. Bell, *J. Catal.*, **94**, 422 (1985).
22) R. T. K. Baker, K. S. Kim, A. B. Emerson, and J. A. Dumesic, *J. Phys. Chem.*, **90**, 860 (1986).
23) D. L. King, *J. Catal.*, **51**, 386 (1978).
24) C. S. Kellner and A. T. Bell, *J. Catal.*, **75**, 251 (1982).

Photoredox Properties of Viologen Linked Porphyrins

Ichiro OKURA,* Naruhiko KAJI, Shigetoshi AONO, and Tsuyoshi NISHISAKA†
Department of Chemical Engineering, Tokyo Institute of Technology, Meguro-ku, Tokyo 152
†Health Science Center, Tokyo University of Agriculture and Technology, Nakamachi, Koganei, Tokyo 184
(Received September 13, 1986)

Viologen linked water-soluble porphyrins ($ZnP(C_nV)_4$) with different methylene chain lengths (n=2—5) between porphyrin and viologen were synthesized. These compounds were applied to photoinduced hydrogen evolution in a system containing NADPH-$ZnP(C_nV)_4$-hydrogenase under steady state irradiation.

Photoinduced hydrogen evolution systems containing an electron donor (D), a photosensitizer (S), an electron carrier (C), and a catalyst have been studied extensively.[1-3]

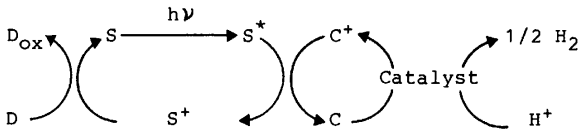

As photosensitizers metallo-porphyrins have been widely used and methyl viologen has been a popular electron carrier. In this work, viologen linked water-soluble zinc porphyrins were synthesized which may act as both a photosensitizer and an electron carrier in the same molecule; these compounds were applied to photoinduced hydrogen evolution.

Experimental

All materials were of analytical grade or the highest grade available.

The structures of viologen linked water-soluble zinc porphyrins are shown in Fig. 1. These compounds were synthesized as follows. The starting material, zinc 5,10,15,20-tetra(4-pyridyl)porphyrin (Zn-TMPyP), was synthesized

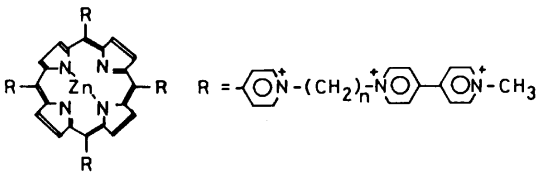

Fig. 1. Structure of viologen linked porphyrins, $ZnP(C_nV)_4$.

according to methods described in the literature.[4,5] Zn-TMPyP was then quaternized with an excess amount of α,ω-dibromoalkane at 130 °C. The quaternized porphyrin and 100—200 fold molar excess amount of 1-methyl-4,4′-bipyridin-1-ium iodide was refluxed in methanol, and the formed precipitate was filtered off and washed with methanol.

Hydrogenase was obtained from Desulfovibrio vulgaris (Miyazaki type, IAM 12604) and purified by Yagi's method.[6] Its concentration is not known, but 1.48×10^{-6} mol of hydrogen was generated by the following reaction system: hydrogenase (0.5 cm^3)-methyl viologen (4.1×10^{-5} mol dm^{-3})-$Na_2S_2O_4$ (5.7×10^{-3} mol dm^{-3}) in 5.0 cm^3 of 0.02 mol dm^{-3} Tris-HCl buffer (pH 7.0) at 30 °C for 10 min.

Electronic and fluorescence spectra were recorded on Shimadzu MPS-5000 and Hitachi model 850 instruments, respectively.

Conventional laser flash photolysis was carried out by using a Nd-YAG laser, model DCR-2A-10 from Quanta-Ray Inc. This generated second-harmonic (532 nm) pulses of 10-ns duration with an energy of 200 mJ per pulse; a repetition rate of 10 Hz was used for the excitation of sample solutions throughout this study. The light beam, after passing through a sample cell, was collimated into the entrance slit of a monochromator (model BM 50/50 from B & M Spectronik Co.). The output signal from a photomultiplier (Hamamatsu Photonics 446) attached to the slit of the monochromator was displayed on a Hitachi oscilloscope, model V-1050F.

For steady state irradiation, a 200 W tungsten lamp was used as the light source. Light of wavelengths less than 390 nm was removed by a Toshiba L-39 filter.

Photoinduced hydrogen evolution was carried out with $ZnP(C_nV)_4$ with n=2—5 under steady state irradiation at 30 °C. A sample solution containing nicotinamide-adenine dinucleotide phosphate (reduced form, NADPH), ZnP-

Table 1. Peak Wavelength of Various Porphyrins

	Soret band/nm		Q band/nm		
ZnTMPyP	438	565	607		
H_2TMPyP	423	516	552	581	627
$ZnP(C_2)_4$*	440	523	537	647	
$ZnP(C_2V)_4$	445	573	625		
$ZnP(C_3)_4$*	433	523	573	647	
$ZnP(C_3V)_4$	442	572			
$ZnP(C_4)_4$*	423	522	563	590	647
$ZnP(C_4V)_4$	436	571			
$ZnP(C_5)_4$*	428	523	593	645	
$ZnP(C_5V)_4$	432	568			

* $ZnP(C_n)_4$ (n=2—5): 5,10,15,20-tetrakis[1-(2-bromoalkyl)pyridinio]porphyrin tetrabromide.

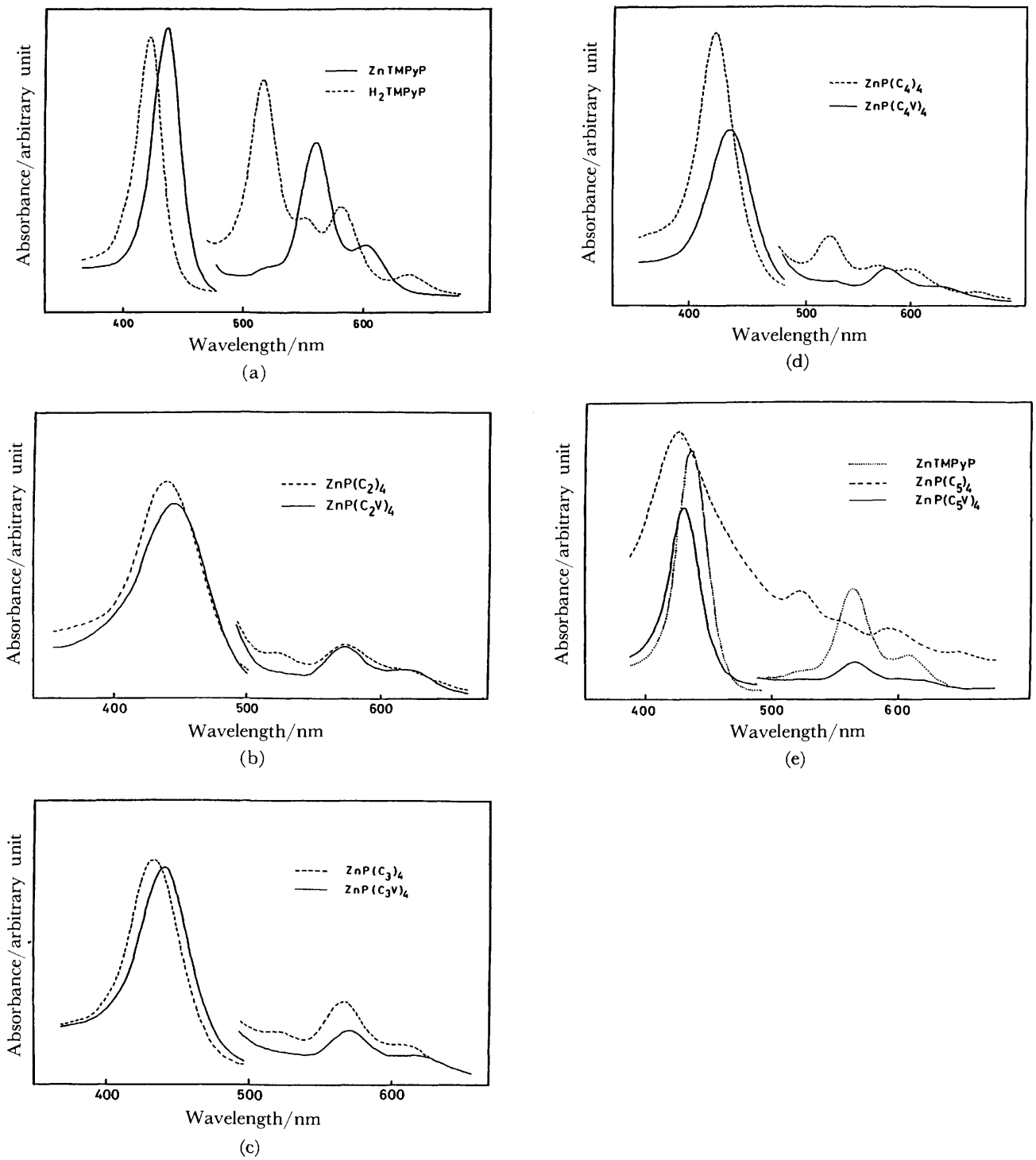

Fig. 2. Absorption spectra of various porphyrins dissolved in water.
(a): ZnTMPyP and H_2TMPyP, (b): ZnP(C_2V)$_4$ and ZnP(C_2)$_4$, (c): ZnP(C_3V)$_4$ and ZnP(C_3)$_4$, (d): ZnP-(C_4V)$_4$ and ZnP(C_4)$_4$, (e): ZnP(C_5V)$_4$ and ZnP(C_5)$_4$.

(C_nV)$_4$, and hydrogenase was deaerated by repeated freeze-pump-thaw cycles.

Results and Discussion

Electronic Spectra of ZnP(C_n)$_4$ and ZnP(C_nV)$_4$. The electronic spectra of the compounds are shown in Fig. 2 (a)—(e) and Table 1. Though ZnP(C_n)$_4$ contain metal ions, the Q band spectra of ZnP(C_n)$_4$ (n=2—5) (shown by dotted lines in Figs. 2 (b)—(e)) are similar to the absorption spectrum of metal-free H_2TMPyP (shown in Fig. 2 (a)). The electrons in the porphyrin ring may be significantly influenced by an interaction between the central metal ion and halogen ions connected at the end of the methylene chain.

Table 2. Relative Emission Intensity of $ZnP(C_n)_4$ and $ZnP(C_nV)_4$

	ZnTMPyP	$ZnP(C_2)_4$	$ZnP(C_3)_4$	$ZnP(C_4)_4$	$ZnP(C_5)_4$
Relative intensity	100	32	79	49	44
		$ZnP(C_2V)_4$	$ZnP(C_3V)_4$	$ZnP(C_4V)_4$	$ZnP(C_5V)_4$
Relative intensity		25	35	32	44

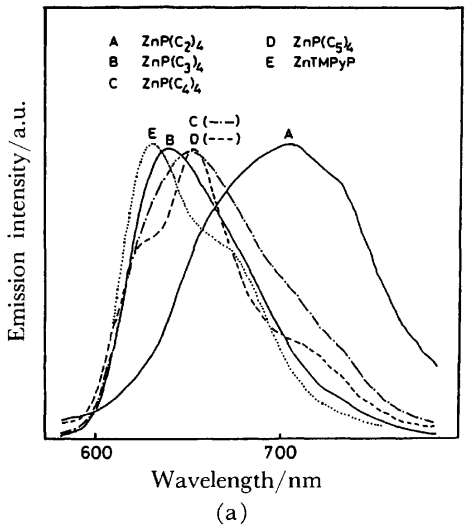

(a)

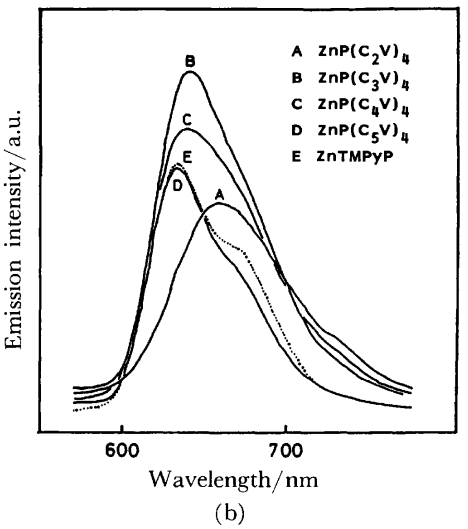

(b)

Fig. 3. Fluorescence spectra of various porphyrins. (a): $ZnP(C_n)_4$, (b): $ZnP(C_nV)_4$.

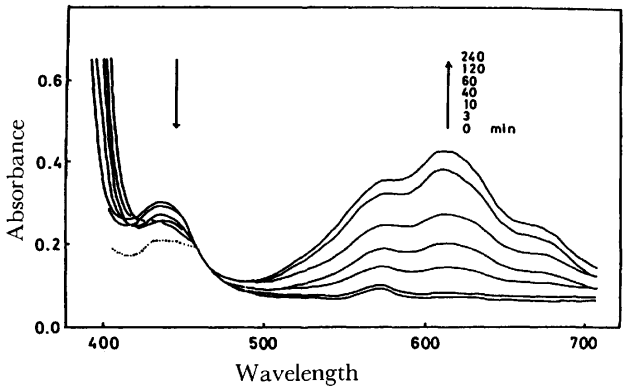

Fig. 4. Absorption spectrum of $ZnP(C_5V)_4$-NADPH system. Sample solution containing $ZnP(C_5V)_4$ (2.0×10^{-6} mol dm^{-3}) and NADPH (1.0×10^{-3} mol dm^{-3}) was irradiated at 30 °C.

The electronic spectra of $ZnP(C_nV)_4$ (shown by solid lines in Figs. 2 (b)—(e)) are similar to the spectrum of ZnTMPyP (Fig. 2 (a)) rather than that of $ZnP(C_n)_4$, showing a smaller interaction between the central metal ion and the viologen connected at the end of the methylene chain. However, there are some interactions between the porphyrin ring and viologen as the absorption spectra of $ZnP(C_nV)_4$ in the Soret region shifts to longer wavelengths.

Fluorescence Spectra $ZnP(C_n)_4$ and $ZnP(C_nV)_4$. The fluorescence spectra of $ZnP(C_n)_4$ and $ZnP(C_nV)_4$ are shown in Figs. 3 (a) and (b). The fluorescence spectra of $ZnP(C_2)_4$ and $ZnP(C_2V)_4$ are broad and the peak wavelengths are at longer wavelengths compared with the other porphyrins shown in Fig. 3. The relative fluorescence intensity obtained by integrating the spectra are shown in Table 2. The relative fluorescence intensity of $ZnP(C_nV)_4$ (n=2—4) are low compared with $ZnP(C_n)_4$. The excited singlet state of the porphyrin with viologen may be quenched by viologen linked with a porphyrin ring.

Photoreduction of Viologen. When a sample solution containing viologen linked porphyrin and NADPH was irradiated, the growth of the reduced form of viologen was observed. Figure 4 shows an example when $ZnP(C_5V)_4$ was used. Since the absorption coefficient of $ZnP(C_5V)_4$ was not known, its concentration was determined by using the absorption coefficient of ZnTMPyP. The concentration of the reduced form of viologen increased with the irradiation time and tended to reach a constant value.

Regarding the exposure of the sample solution to air, an absorption spectrum with λ_{max}=600 nm disappeared, confirming the formation of reduced viologen. The absorption spectrum intensity with λ_{max}=460 nm due to the Soret band of the porphyrin decreased upon irradiation. Owing to the exposure to air, the spectrum returned to the original shape to some extent, but did not completely return to the original shape. This fact indicates that the reduced form of the porphyrin was formed by the irradiation and that an irreversible species was formed at the same time due to the irradiation. The reduced form of the porphyrin may be formed by the reductive quenching of the photoexcited porphyrin by NADPH.

Photoinduced Hydrogen Evolution. Upon irradia-

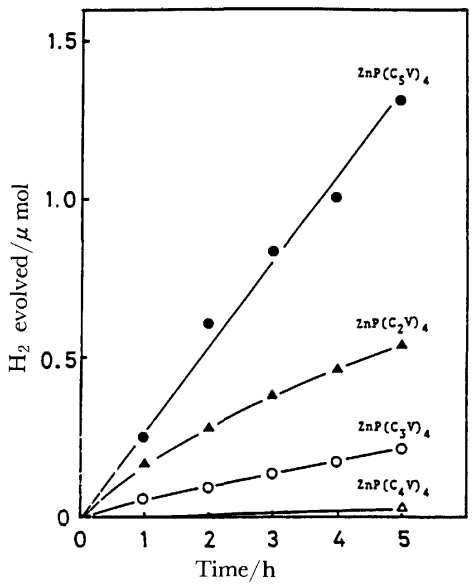

Fig. 5. Time dependence of amount of hydrogen evolved. Sample solution containing $ZnP(C_nV)_4$ (2.0×10^{-6} mol dm^{-3}), NADPH (1.0×10^{-3} mol dm^{-3}) and hydrogenase (0.5 cm^3) was irradiated at 30°C.

tion of the sample solution, hydrogen was generated; the time dependence of the amount of hydrogen evolved is shown in Fig. 5. The concentrations of $ZnP(C_nV)_4$ (n=2—5) were determined by using the absorption coefficient of ZnTMPyP. Thus, it is apparent that every compound, $ZnP(C_nV)_4$ (n=2—5), participates as both a photosensitizer and as an electron carrier in the same molecule. Since the hydrogen evolved almost linearly with irradiation time, an irreversible deactivation of the porphyrin is depressed in these systems. When an intramolecular electron transfer from porphyrin to viologen takes place, the electron can move from the reduced viologen to the catalyst hydrogenase. As shown in Fig. 5, the hydrogen evolution rate strongly depends on the methylene chain length (n) of $ZnP(C_nV)_4$. Within a certain range (n=2—4), the hydrogen evolution rate decreases with increasing chain length. In the case of $ZnP(C_5V)_4$, however, a higher hydrogen evolution rate was observed. The turnover number of hydrogen evolved against $ZnP(C_5V)_4$ was 86 per hour. The activity was at most two-times more active than that of an individual component system containing ZnTMPyP, methyl viologen, NADPH, and hydrogenase. As the chain length is sufficiently long in this case, the porphyrin ring may possibly come close enough to viologen by a conformational change of the molecule, so that the electron can transfer directly from the porphyrin ring to viologen.

Laser Flash Photolysis. Figure 6 shows oscilloscope traces of photoexcited $ZnP(C_nV)_4$ monitored at 500 nm after a laser flash. From these figures the lifetimes of the triplet state of these compounds were obtained (Table 3). There were no remarkable difference between $ZnP(C_n)_4$ and $ZnP(C_nV)_4$, indicating that

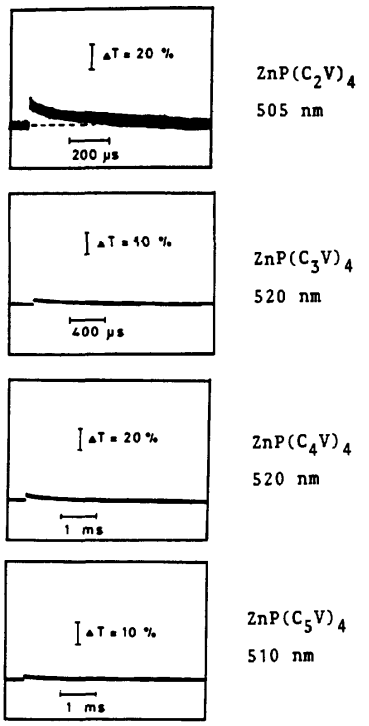

Fig. 6. Typical oscillograms for T–T absorption of $ZnP(C_nV)_4$.

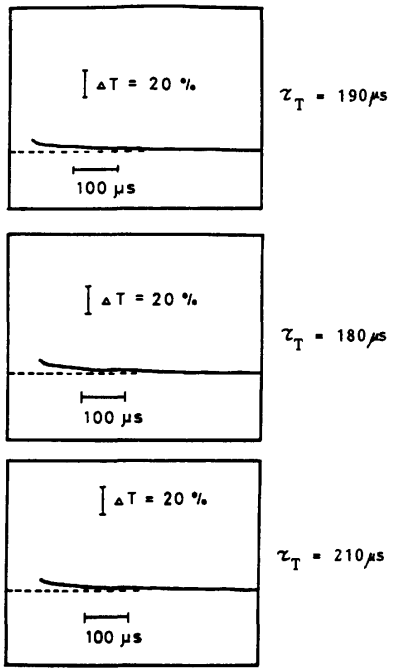

Fig. 7. Typical oscillograms for T–T absorption of $ZnP(C_2V)_4$. laser power (a): 80 mJ pulse^{-1}, (b): 60 mJ pulse^{-1}, (c): 50 mJ pulse^{-1}.

Table 3. Lifetimes of Excited Triplet State of $ZnP(C_n)_4$ and $ZnP(C_nV)_4$

	τ_T/μs		τ_T/μs
$ZnP(C_2)_4$	140	$ZnP(C_2V)_4$	190
$ZnP(C_3)_4$	530	$ZnP(C_3V)_4$	510
$ZnP(C_4)_4$	230	$ZnP(C_4V)_4$	640
$ZnP(C_5)_4$	330	$ZnP(C_5V)_4$	470

the triplet states of these compounds are not quenched by the linked viologen.

Figure 7 shows typical oscillograms for T-T absorption of $ZnP(C_2V)_4$ with different laser powers. Though the intensity of the T-T absorption depends on the laser power, the lifetimes of the triplet state were independent of the laser power, indicating that the triplet state is not quenched by another molecule in the ground state; that is, intermolecular quenching is negligible under these reaction conditions.

From the above results the following reaction mechanism is proposed:

$$^3P^*\text{-}V + D \longrightarrow P^-\text{-}V + D^+,$$

and

$$P^-\text{-}V \longrightarrow P\text{-}V^-.$$

During the first stage of the reaction, the photoexcited triplet state ($^3P^*$-V) is reductively quenched by NADPH and a reduced form of porphyrin (P^--V) is formed; then, the electron transfers from the porphyrin to viologen. This reaction mechanism is based on the fact that both intramolecular and intermolecular quenching of the photoexcited triplet state of the porphyrin did not occur, and that the reductive quenching by NADPH is predominant.

References

1) J. R. Darwent, P. Douglas, A. Harriman, G. Porter, and M.-C. Richoux, *Coord. Chem. Rev.*, **44**, 83 (1982) and the references therein.

2) J. Kiwi, K. Kalyanasundaram, and M. Gratzel, *Struct. Bonding (Berlin)*, **49**, 37 (1982) and the references therein.

3) I. Okura, *Coord. Chem. Rev.*, **68**, 53 (1985) and the references therein.

4) A. D. Adler, *J. Org. Chem.*, **32**, 476 (1967).

5) A. Harriman, G. Porter, and P. Walters, *J. Chem. Soc., Faraday Trans., 1*, **79**, 1335 (1983).

6) T. Yagi, *J. Biochem.*, **68**, 649 (1970).

 © 1987 The Chemical Society of Japan Bull. Chem. Soc. Jpn., 60, 1249—1254 (1987)

ESR and Mass-Spectrometric Studies of Methanol Combustion. I. The Correlation between Labile and Stable Chemical Entities in Free-Burning Methanol-Air Flames under Atmospheric Pressure

Masayuki TANIGUCHI and Hiroshi YOSHIDA*
Faculty of Engineering, Hokkaido University, Kita-ku, Sapporo 060
(Received October 3, 1986)

The concentration profiles of labile (H, O, and OH) and stable chemical entities (CH_3OH, O_2, CH_2O, H_2, H_2O, and CO_2) in premixed methanol-air flames under atmospheric pressure have been studied by the probe-sampling-ESR method combined with mass-spectrometric detection. The concentrations of the labile intermediates have been determined by correcting their destruction in the sampling probe caused by gas-phase reactions, wall reactions, and reactions at the pinhole of the probe. The observed profiles are in good agreement with the numerical model developed previously by Westbrook and Dryer, except that the concentration changes in all the entities are quicker than expected. The dependence of the maximum concentrations of the labile intermediates on the composition of the premixed gas is essentially the same as that observed for the methanol-air flames at low pressure.

The combustion of common fuels consists of chain reactions, with atomic H and O, and the OH radical as principal chain carriers. As these labile intermediates are paramagnetic, the electron spin resonance (ESR) is possibly a useful method for combustion-chemical studies. Actually, since the pioneering work by Westenberg and Fristrom,[1] a combination of the ESR method and the probe-sampling technique has been used for examining the concentration profiles of H and O atoms in combustion flames.[2-4] In 1980, Noda et al.[5] succeeded, as a result of the continual progress in ESR technique, to detect simultaneously all the labile intermediates, H, O, and OH, in a methane-air flame; they thus showed the wide applicability of the ESR method to this research field. Since then, there have appeared extensive studies of the concentration profiles of the unstable intermediates in combustion flames by means of the ESR method.[6-8]

The present investigation concerns the chemical reactions in methanol-air flames under atmospheric pressure. This is an extension of our previous ESR investigation,[7] where only the profiles of the labile intermediates were determined. The purpose of the present investigation was to determine comprehensively both the labile intermediates and the stable entities, including reactants and final products, by combining the mass spectrometric method with the probe-sampling-ESR method.

The combustion chemistry of methanol is attracting interest, because methanol is expected to be one of the future alternatives to petroleum resources. It is one of the simplest model fuels other than hydrocarbons for combustion-chemical studies, and so it has been extensively studied both theoretically and experimentally. Westbrook and Dryer have developed a numerical model for laminar flames of methanol-air mixtures.[9] This model has been substantiated by the agreement between the concentration profiles of the stable entities calculated based on the model and those observed experimentally from low-pressure methanol-air flames by Akrich et al. using the gas-chromatographic method.[10] More recently, Pauwels et al. have determined the concentration profiles of labile intermediates in the low-pressure methanol-air flames by using the ESR method, and have claimed that the observed dependence of the maximum concentration of H, O, and OH on the composition of the premixed gas agrees well with that predicted on the basis of the model.[6] Very recently, Andersson et al.[11] have studied the concentration profiles of both labile intermediates and stable entities in the flame by means of the mass-spectrometric method. They[11,12] have also examined the numerical model on the basis of their experimental data and the rate constants recently proposed for some elementary reactions,[13] and have argued that the diffusion constants of the chemical entities used in the previous model[9] were too large, while the rate constant for the CHO decomposition were too low. In order fully to elucidate the chemical reactions in the methanol combustion, experimental data are still needed on the concentration profiles of both labile intermediates and stable entities simultaneously observed in the methanol-air flame under various conditions. The present investigation was aimed at supplementing the previous experiments on the low-pressure methanol-air flames.[6,10,11]

Experimental

The burner used was made of brass and had a mouth (8 mm in diameter) shaped in such a way that the distribution of the gas-flow velocity in the cross-section area of the mouth was approximately uniform.[7] The secondary air was not allowed to flow through in order to keep the mixing of the surrounding air into the flame as low as possible.[14] A fine stainless steel grid made of 0.3 mm meshes was put on the burner mouth to prevent flash-back. The flow rate of air from a cylinder was controlled with a precision needle valve. Liquid methanol was continuously injected into the air stream, which had been preheated to 403 K.

The reacting gas was continuously sampled from the flame through a pinhole (about 0.1 mm in diameter) of a

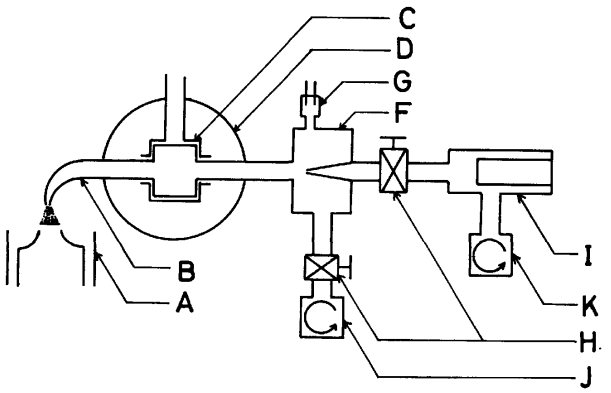

Fig. 1. Schematic view of the experimental set-up. A; burner, B; sampling probe, C; ESR cavity, D; magnet, F; condenser, G; vacuum gauge, H; vacuum valve, I; quadrupole mass spectrometer, J; primary pumping system (mechanical booster and rotary pumps), K; secondary pumping system (diffusion and rotary pumps).

quartz sampling probe, led to an ESR cavity, and subjected to ESR measurements with an X-band spectrometer (Varian, Model E-109) equipped with a large access cavity (TE_{011} mode, Model E-235) at a low pressure (24—80 Pa) in order to examine the concentrations of H, O, OH, and O_2. The calibration of the ESR signal intensities to determine the absolute concentrations within the cavity was made with reference to the intensity of O_2 (for H and O) or NO (for OH) of known concentrations.[15,16] A part of the sampled gas was further led to a quadrupole mass spectrometer (Nihon Shinku, Model MSQ-150A), and the concentrations of stable entity in it were measured at a total pressure of 10^{-3} Pa in the ionization chamber. The whole experimental set-up is shown schematically in Fig. 1. Washing the sampling probe with HF, with NaOH, and then with HNO_3 was found to be the best treatment to prevent the destruction of labile intermediates on the wall during sampling, as has been reported previously.[6]

The gas was sampled at several positions on the center axis of the flame by moving the flame with respect to the sampling probe. The flame temperature was measured with a SiO_2-coated Pt/Pt-Rh thermocouple (0.1 mm in diameter) at the same positions. No correction was made for radiation loss.

Results and Discussion

Flame and Observed Spectra. The flame obtained consisted of a flat, bright, bluish region and a faint, outer, conical region. The former lay 1—2 mm above the burner mouth and was essentially of the premixed-flame nature. The latter had the diffusion-flame nature, and the visible boundary of its top lay 10—18 mm above the burner mouth, depending on the composition of the premixed gas. The flame was found to be axially symmetric both in appearance and in the concentrations of the chemical species. No visual change was observed on inserting the sampling probe. The flow rate of the gas with a different composition was kept constant at 1.0 l min^{-1}. The sampled gas was

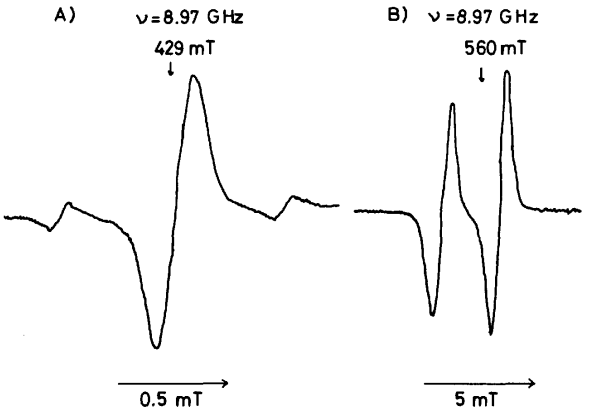

Fig. 2. Typical examples of ESR spectra due to (A) O atoms and (B) OH radicals recorded at 24 Pa.

cooled by adiabatic expansion and showed nearly the ambient temperature.

The ESR spectra due to $H(^2S)$, $O(^3P_2, ^3P_1)$, $OH(^2\Pi_{3/2}, ^2\Pi_{5/2})$, and $O_2(^3\Sigma_g^-)$ were observed from the sampled gas, as in the previous studies of methane-air[5] and methanol-air flames.[6,7] A part of the observed ESR spectra, where the spectral intensity was monitored, attributable to O and OH is shown in Fig. 2. The concentrations of these labile intermediates in the sampled gas within the ESR cavity were determined from the double integration of the observed differential spectral curves after the calibration mentioned in the Experimental section.

Intense mass spectra were detected at m/z=2, 14, 16, 17, 18, 28, 31, 32, and 44 from the sampled gas. The concentration of H_2, H_2O, CH_3OH, and CO_2 were determined directly from the spectral intensities at the mass number of 2, 18, 31, and 44 respectively. Because the peak at m/z=32 due to parent CH_3OH ions overlapped with the peak of the O_2 ions, the CH_3OH concentration was determined from the fragment peak at m/z=31. The concentration of CH_2O was determined by subtracting the contribution of CH_3OH from the spectral intensity at m/z=30. Each spectral intensity was calibrated with reference to the intensity of the corresponding gas of a known concentration. The uncertainty of the concentrations thus determined was less than 10%. The concentration of CO could not be determined because of the overlapping of the N_2 spectrum.

Reactions in the Sampling Probe and Their Correction. A serious problem involved in the probe-sampling procedure is the destruction of labile intermediates in the probe before they can be measured. There are two possible types of processes responsible for the destruction; one is bimolecular gas-phase reactions in the probe such as

$$O + OH \longrightarrow O_2 + H, \quad (1)$$

$$OH + OH \longrightarrow H_2O + O, \quad (2)$$

with a low activation energy, while the other is first-order reactions on the wall.

It was found that the logarithm of the mole fractions of the labile intermediates decreased linearly with the increase in the sampling pressure in the pressure range of 40—80 Pa, and that the gradient of the linear decrease was almost unchanged when the sampling probe was about doubled in length. If the above linear dependence on the sampling pressure is due to the first-order destruction on the wall, the gradient could be expected to be proportional to the length of the probe (residence time in the probe).[6] Therefore, the actual destruction of the labile intermediates in the probe cannot be described simply by the first order wall reaction.

Figure 3 shows the observed concentrations of the labile intermediates in the ESR cavity as a function of their residence time in the probe before reaching the ESR cavity. The residence time was changed by using extension tubes of different lengths. The pressure in the probe was kept constant at 40 Pa. All the H and O atoms and OH radicals appear to follow the first-order decay with different rate constants. However, the extrapolation of the observed straight lines to $t=0$ will not give the actual concentration of the labile intermediates in the flame, for the bimolecular gas-phase reactions become important in the early period.

Using the rate constants, $k_1=1.0\times10^7$ and $k_2=1.5\times10^3T^{1.14}$ $m^3 mol^{-1} s^{-1}$, reported by Warnatz,[17] and also the observed concentrations of all the chemical species involved in Reactions 1 and 2, and assuming a constant temperature, 300 K, of the sampled gas in the probe, the rate constants for the wall reactions were determined by computer simulations to be 1.71×10^2, 1.53×10^2, and 1.07×10^3 s^{-1} for H, O, and OH respectively for the present sampling conditions. The solid curves in Fig. 3 are the best-fitting simulation curves. The destruction caused by the bimolecular gas-phase reactions is significant for O atoms when the OH concentration is high.

Pauwels et al.[6] first reported that the wall reactions are primarily important in the destruction of the labile intermediates at low sampling pressures (5.3—13.3 Pa) and at low temperatures, but they have very recently suggested that the gas-phase reactions should not be ignored.[8] The correction for the destruction of the labile intermediates in the sampling probe made in their recent study is essentially the same as that developed independently in the present study.

Another difficult problem inherent in the probe-sampling is the destruction of labile intermediates caused by reactions at the pinhole and/or at the very end of the probe tip. The temperature and pressure of the sampled gas are necessarily much higher there than in the main body of the sampling probe, where the sampling gas has already been cooled by adiabatic expansion. Biordi et al.[18] have studied the concentration of chemical species in low-pressure CH_4-O_2-Ar flames by using molecular-beam mass spectrometry, and examined the change in the concentration profiles with sampling probes of different cone angles. Their results indicate that the destruction of OH is much more remarkable with small angled cones (smaller than 40°) than with large angled cones. We confirmed the same effect of the cone angle by using two probes, 40°-angled and 15°-angled cones: the observed OH concentrations were higher for the former probe. It should be noted, however, that the observed concentrations of H and O showed almost no difference between these two probes.

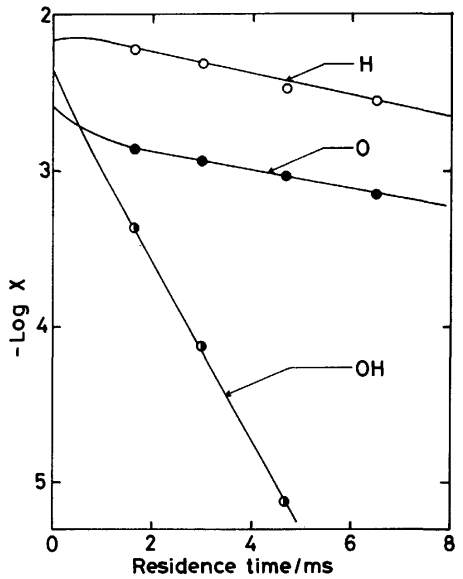

Fig. 3. The dependence of the observed concentrations (X, in mole fraction unit) of the labile intermediates in sampled gas on the residence time of the gas in the sampling probe before reaching at the ESR cavity for the methanol-air flame of stoichiometric composition under the atmospheric pressure. The curves are determined by simulating the destruction of the labile entities due to the gas phase reactions and the wall reactions in the probe (see text for detail).

The effect of the surface treatment of the probe is also significant for the destruction at the pinhole. The observed OH concentrations were found to be three times higher for the 40° cone angle and ten times higher for the 15° cone angle after the HF treatment than before, though the normal wall destruction was not affected by the HF treatment. There is no way at the moment to determine the correction factor for the OH destruction at the pinhole, and so we assumed there to be no destruction at the pinhole for the HF-treated 40°-angled probe. As a whole, the ambiguity in the ESR determination of concentrations is the largest for OH, but it is thought to be within the factor of 2.

Concentration Profiles. The chemical reactions in the outer flame region are strongly dependent on the physical conditions, such as the diffusion of the surrounding air into the flame. The concentration pro-

files of only the labile intermediates, mostly in the down-stream region, have been observed and discussed in previous studies of methane-air[5] and methanol-air[7] flames. In the present study, therefore, we focussed our attention on the concentration profiles in the inner flame region, where the behavior of the profiles shows more inherently the chemical nature of the combustion process. The concentration profiles of both labile intermediates and stable entities in the flame were determined for three different equivalence ratios, defined as $\phi=([\text{fuel}]/[O_2])_{\text{actual}}/([\text{fuel}]/[O_2])_{\text{stoichiometric}}$, of the premixed gas. The results are shown in Figs. 4—6, where all the concentration are expressed in mole fraction units. The concentrations of the labile intermediates are presented after correction for the partial destruction during sampling attributable to the gas-phase and wall reactions. The equivalence ratios examined were in the range of 0.82—1.53, because it was difficult to stabilize the flame in the low-ϕ (fuel-lean) region.

The results obtained from the stoichiometric flame (Fig. 4) show that methanol is totally consumed within the region 1 mm from the burner mouth. Correspondingly, the O_2 concentration also decreases in this region, sharply at first and then slowly. The generation of the final combustion products, CO_2 and H_2O, start at or close to the burner mouth, and their concentrations reach the plateau value when the methanol is completely consumed. The H_2O generation is observed to occur in an earlier region than the CO_2 generation. This observation is consistent with their formation routes: for H_2O, the reaction

$$CH_3OH + OH \longrightarrow CH_2OH + H_2O, \quad (3)$$

occurring in early stage of the combustion is one of the main routes, while CO_2 comes mainly from this reaction;

$$CO + OH \longrightarrow CO_2 + H, \quad (4)$$

which occurs at a later stage of the combustion.

Among the stable intermediate entities, CH_2O appears only in a narrow region and shows a concentration maximum. In contrast, H_2 is distributed over a wide region and shows two concentration maxima. The first H_2 maximum coincides in location in the flame with the CH_2O maximum. The high local concentration of CH_2O is in accord with Bowman's proposal,[19] based on a shock-wave study, that the main oxidation path of methanol at high temperatures is: $CH_3OH \rightarrow CH_2OH \rightarrow CH_2O \rightarrow CHO \rightarrow CO \rightarrow CO_2$.

The concentrations of all the labile intermediates increase sharply, simultaneously with the rapid consumption of CH_3OH and O_2. According to the model of Westbrook and Dryer,[9] the most important reactions for the methanol consumption are:

$$CH_3OH + OH \longrightarrow CH_2OH + H_2O, \quad (3)$$

$$CH_3OH + H \longrightarrow CH_2OH + H_2, \quad (5)$$

$$CH_3OH + H \longrightarrow CH_3 + H_2O, \quad (6)$$

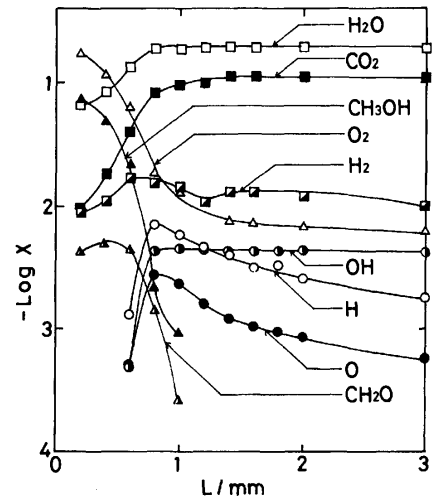

Fig. 4. Concentration profiles of both labile intermediates and stable entities in the methanol-air flame of stoichiometric composition (ϕ=1.0). The concentrations are presented in mole fraction unit (X) in the logarithmic scale. The distance (L) is between the burner mouth and the sampling point on the center axis of the flame.

$$CH_3OH + O \longrightarrow CH_2OH + OH, \quad (7)$$

and the H thus generated reacts with O_2 thus:

$$H + O_2 \longrightarrow O + OH. \quad (8)$$

The observed results agree qualitatively with the model of methanol-air combustion. The concentrations of H and O decrease slowly after passing their maxima, while that of OH remains constant. A closer examination of Fig. 4 may reveal that the sharp increase in the labile intermediates appears to be somewhat later than the rapid drop in the concentrations of CH_3OH and O_2 and the rapid increase in the concentrations of H_2O and CO_2. This apparent delay can be attributed to the effect of the diffusion of the chemical species in the flame; it will be discussed in detail in the following paper of this series.[20]

The peak of the CH_2O concentration appears to be well in advance of the accumulation of the labile intermediates. This may be attributed to its formation by the efficient reaction:

$$CH_2OH + O_2 \longrightarrow CH_2O + HO_2, \quad (9)$$

suggested by Westbrook and Dryer.[9]

Figures 5 and 6 show the effect of the increase in the equivalence ratio. Although the general features of the concentration profiles are the same for all the equivalence ratios examined, the maximum concentrations of the labile and stable intermediates depend on the ϕ value. It may be noted that the OH concentration shows slow decrease after passing through its maximum under fuel-rich conditions.

As the effect of the equivalence ratio was found to be the most noticeable for the maximum concentration of the labile intermediates, it was studied in detail over a

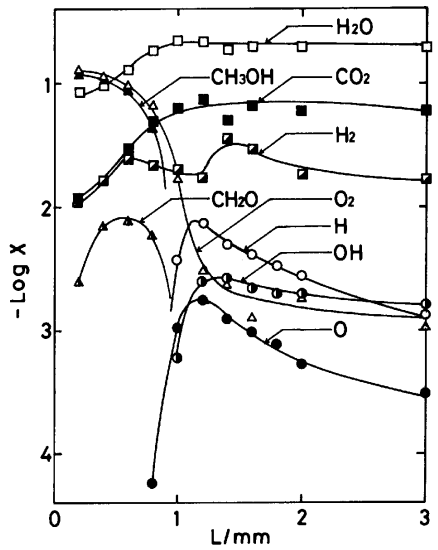

Fig. 5. Concentration profiles for the methanol-air flame of equivalence ratio ϕ=1.2.

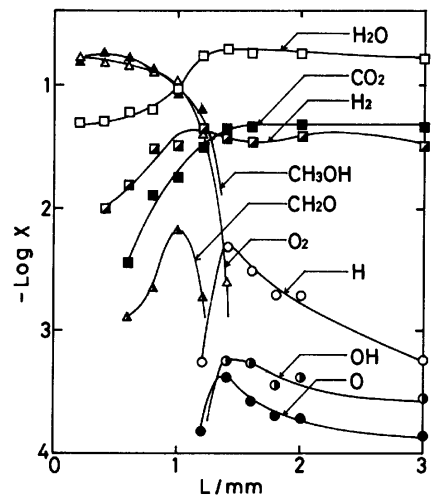

Fig. 6. Concentration profiles for the methanol-air flame of equivalence ratio ϕ=1.5.

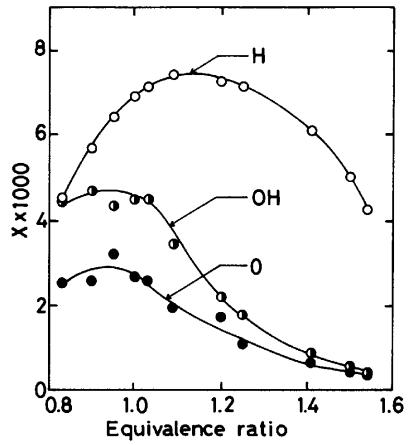

Fig. 7. Dependence of the maximum concentrations of the labile intermediates in the methanol-air flame on the equivalence ratio.

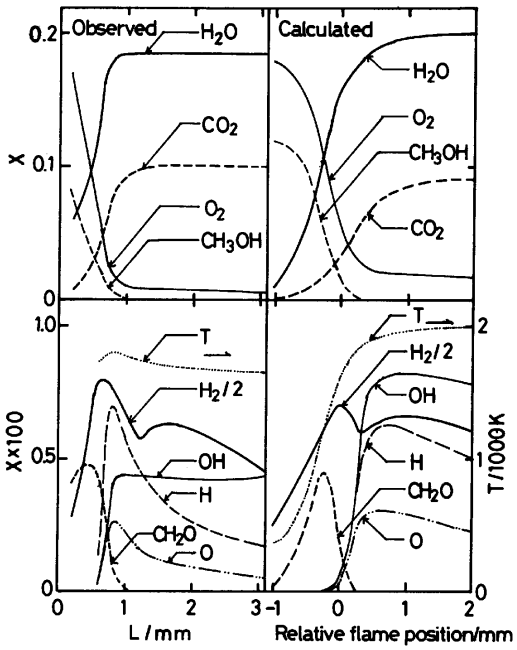

Fig. 8. Comparison of the labile intermediates and stable entities observed by the ESR and mass spectrometric methods and those calculated by Westbrook and Dryer based on the numerical model for the methanol-air flame under atmospheric pressure.

wider range of ϕ, 0.82—1.53, as shown in Fig. 7. H shows a broad maximum around ϕ=1.1. The maxima for O and OH lay at smaller ϕ values. These results, essentially the same as those reported by Pauwels et al.[6] for the low-pressure methanol-air flames, indicate that the dependence of the maximum concentration on the equivalence ratio is little dependent on the pressure.

Comparison with the Numerical Model. Westbrook and Dryer[9] have constructed a comprehensive numerical model of methanol combustion, which includes 26 chemical species and 84 elementary reactions. Based on this model, they have then calculated the concentration profiles by computer-simulation for one-dimensional methanol-air premixed flames under different pressures. Model calculations for methanol combustions have recently been made also by other research group,[11-13] but they have not shown the concentration profiles under atmospheric pressure.

The observed concentration profiles are compared with the calculated ones in Fig. 8 for the flame of ϕ=1.0. One can see suite a good coincidence between the observed and calculated profiles for both stable entities and labile intermediates, though the calculations have made for an ideal adiabatic flame isolated from its surroundings. The observed maximum concentrations of O and H are in good agreement with the calculated values. The decrease in the observed H and O concentrations after the maximum is faster than that

expected from the calculations. This may be attributed to the heat loss to the surroundings, which has not been taken into account in the model calculations. Among the labile intermediates, the concentration of OH shows the poorest agreement in absolute value, but the difference between the observed and the calculated values is within a factor of 2. This difference may be due partly to the actual temperature being lower than the calculated one and partly to the destruction of OH at the pinhole of the probe during sampling.

The calculations[9] have predicted a double-peaked concentration profile for H_2; the first peak is predominantly attributable to Reaction 5, and the second peak, to Reaction 10:

$$CH_3OH + H \longrightarrow CH_2OH + H_2, \quad (5)$$

$$H_2O + H \longrightarrow H_2 + OH. \quad (10)$$

This prediction was satisfactorily proven by the present observation of the two peaks. The observed concentration change in CH_3OH, H, H_2O, and OH is consistent with the predominance of Reactions 5 and 10, leading to the H-generation around the peak positions.

Perhaps the most significant difference between the observation and the calculation is that the transient change in all the observed concentration profiles is quicker than that of the calculated profiles. We examined the perturbation of the flame attributable to the sampling probe in a separate experiment for the methane-air flame and found that the insertion of the sampling probe into the flame caused no serious change in the concentration profiles. The effect of the spatial resolution of the sampling procedure is, if any, to flatten the transient change in the concentration profiles. It can, therefore, be suggested that the calculated concentration change is somewhat too slow. The same difference between calculation and observation has been found for low-pressure methanol-air flames; it has been suggested that it is attributable to too big diffusion coefficients and too small a rate constant for the CHO decomposition used in the calculations.[11,12]

Conclusions

In order to elucidate the chemical reactions involved in the complex combustion process, it is indispensable to determine experimentally the distribution of as many chemical species as possible, both stable and labile, in the combustion system. In the present investigation, the concentration profiles in the methanol-air flame under atmospheric pressure were comprehensively determined by means of ESR measurements combined with mass-spectrometric measurements. The results obtained are totally consistent with the reaction scheme widely accepted, and are in fairly good agreement with the prediction based on the numerical model.[9]

There is no essential difference between the present observations at atmospheric pressure and the previous observations for the stable entities[10,11] and for the labile entities,[6,11] all at low pressures. The experimental conditions of combustion-chemical studies are generally difficult to control; therefore, the results obtained here are not precise enough to check the numerical model in detail. However, it can safely be concluded that the present results give, from the experimental point of view, general support for the previous numerical model and prove that the model can predict the pressure effect properly.

References

1) A. A. Westenberg and R. M. Fristrom, *Symp. (Int.) Combust. [Proc.]*, **10**, 473 (1965).
2) K. H. Eberius, K. Hoyermann, and H. Gg. Wagner, *Symp. (Int.)* Combust. [*Proc.*], **13**, 713 (1971).
3) N. J. Brawn, K. Eberius, R. M. Fristrom, K. H. Hoyermann, and H. Gg. Wagner, *Combust. Flame*, **53**, 151 (1978).
4) T. Miyauchi, M. Miura, and A. Imamura, *Symp. (Int.) Combust. [Proc.]*, **16**, 1073 (1977).
5) S. Noda, M. Miura, and H. Yoshida, *J. Phys. Chem.*, **84**, 3143 (1980).
6) J. F. Pauwels, M. Carlier, and L. R. Sochet, *J. Phys. Chem.*, **86**, 4330 (1982).
7) S. Noda, H. Demise, O. Claesson, and H. Yoshida, *J. Phys. Chem.*, **88**, 2552 (1984).
8) J. F. Pauwels, M. Carlier, P. Devolder, and L. R. Sochet, *J. Phys. Chem.*, **90**, 4377 (1986).
9) C. K. Westbrook and F. L. Dryer, *Combust. Flame*, **37**, 171 (1980).
10) R. Akrich, C. Vovelle, and R. Delbourgo, *Combust. Flame*, **32**, 171 (1978).
11) L. L. Andersson, B. Christenson, A. Höglund, J. O. Olsson, and L. G. Rosengren, *Prog. Astronaut. Aeronaut.*, **95**, 164 (1984).
12) J. O. Olsson, L. S. Karlsson, and L. L. Andersson, *J. Phys. Chem.*, **90**, 1458 (1986).
13) J. E. Dove and J. Warnatz, *Ber. Bunsenges. Phys. Chem.*, **87**, 1040 (1983).
14) O. Claesson, S. Noda, and H. Yoshida, *Bull. Chem. Soc. Jpn.*, **56**, 2559 (1983).
15) A. A. Westenberg and N. de Haas, *J. Chem. Phys.*, **40**, 3087 (1964).
16) A. A. Westenberg, *J. Chem. Phys.*, **43**, 1544 (1965).
17) J. Warnatz, *Symp. (Int.) Combust. [Proc.]*, **18**, 369 (1981).
18) J. C. Biordi, C. P. Lazzara, and J. F. Papp, *Combust. Flame*, **23**, 73 (1974).
19) C. T. Bowman, *Combust. Flame*, **25**, 343 (1975).
20) M. Taniguchi, T. Yoshioka, and H. Yoshida, *Bull. Chem. Soc. Jpn.*, in press (Part II of this series).

 © 1987 The Chemical Society of Japan Bull. Chem. Soc. Jpn., 60, 1255—1259 (1987)

The Crystal and Molecular Structures of 2,4,4,6-Tetraphenyl-1,4-dihydropyridine and 4-Benzyl-1-methyl-2,4,6-triphenyl-1,4-dihydropyridine

Fujiko IWASAKI,* Toshiya WATANABE, and Koko MAEDA†

Department of Materials Science, The University of Electro-Communications, Chofu, Tokyo 182
†Department of Chemistry, Faculty of Science, Ochanomizu University, Bunkyo-ku, Tokyo 112

(Received October 15, 1986)

The crystal structures of 2,4,4,6-Tetraphenyl-1,4-dihydropyridine (**1**) and 4-benzyl-1-methyl-2,4,6-triphenyl-1,4-dihydropyridine (**2**) have been determined by the X-ray method. The crystals of **1** are monoclinic, $P2_1/a$, $a=12.883(1)$, $b=12.953(1)$, $c=12.575(1)$ Å, $\beta=94.95(1)°$, $V=2090.7(2)$ Å^3, $Z=4$, $D_x=1.225$ Mg m^{-3}. **2** is triclinic $P\bar{1}$, $a=7.786(1)$, $b=14.324(1)$, $c=10.759(1)$ Å, $\alpha=90.51(1)$, $\beta=106.89(1)$, $\gamma=92.02(1)°$, $V=1147.2(2)$ Å^3, $Z=2$, $D_x=1.196$ Mg m^{-3}. The final R values are 0.037 and 0.044 for **1** and **2**, respectively. The 1,4-dihydropyridine ring of **1** is a flat twisted boat, while that of **2** has a boat conformation with the apexes at N(1) and C(4). For **1** the dihedral angles of the phenyl rings and the plane of four C atoms, C(2), C(3), C(5), and C(6), of the pyridine ring are 46.6, 106.4, 62.3, and 30.5° for 2-, 4-, 4-, and 6-phenyl rings, respectively. The corresponding angles of **2** are 30.4, 50.2, and 39.1° for 2-, 4-, and 6-phenyl rings. The phenyl ring of benzyl group covers to the pyridine ring making the dihedral angle between these planes of 133.7°. The bond between C(4) and the methylene carbon is 1.576 Å, which is longer than the normal Csp^2–Csp^3 length.

2,4,4,6-Tetraphenyl-1,4-dihydropyridine (**1**) crystallized as colorless needles from an oxygen free benzene solution. The crystals and deaerated solutions of **1** exhibit a violet color on irradiation with UV light. The color of crystals was retained in deaerated media for a long time at room temperature, whereas in deaerated solutions the color was stable at only 77 K but at higher temperatures it gradually faded even under irradiation.[1] In solutions with oxygen the coloration does not occur and oxygenated products, *N*-(2-hydroperoxy-4-oxo-1,3,3-triphenylbutylidene)benzamide and 2,4,4,6-tetraphenyl-3,4-dihydro-3-pyridinol, were produced in benzene whereas 2,4,4,6-tetraphenyl-3-(4*H*)-pyridinone was given in acetone.[2] 4-Benzyl-1-methyl-2,4,6-triphenyl-1,4-dihydropyridine (**2**) also showed change of color from colorless to pale greenish

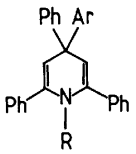

(1) R=H Ar=Ph
(2) R=Me Ar=Ch_2Ph

Table 1. Crystal Data, Experimental Conditions and Details of Refinements

	1 $C_{29}H_{23}N$	**2** $C_{31}H_{27}N$
M_w	385.51	413.56
Crystal system	Monoclinic	Triclinic
Space group	$P2_1/a$	$P\bar{1}$
a/Å	12.883(1)	7.786(1)
b/Å	12.953(1)	14.324(1)
c/Å	12.575(1)	10.759(1)
α/°	90.0	90.51(1)
β/°	94.95(1)	106.89(1)
γ/°	90.0	92.02(2)
V/Å^3	2090.7(2)	1147.2(2)
Z	4	2
D_x/Mgm^{-3}	1.225	1.196
μ(Cu $K\alpha$)/mm^{-1}	0.543	0.526
F(000)	816	440
T/K	293	293
Crystal size/mm	0.20×0.20×0.25	0.2×0.2×0.15
2θ max./°	130	130
Range of h,k,l	$\bar{1}5$—15, 0—15, 0—14	0—9, $\bar{1}6$—16, $\bar{1}2$—12
Scan width $\Delta\omega$/°	1.2+0.5tanθ	1.15+0.4tanθ
Number of reflections		
Measured	3769	4457
Unique	3439	4142
Observed	3138	3222
R	0.037	0.044
R_w	0.036	0.061
S	0.758	1.151
g	9.6×10^{-7}	4.3×10^{-7}

yellow in crystals and in deaerated solutions under irradiation. In order to investigate a relationship between structures and photocoloration structures of **1** and **2** have been determined by the X-ray method.

Experimental

Crystal data and some experimental conditions are listed in Table 1. Intensities were collected on a Rigaku automatic

Table 2. Atomic Coordinates ($\times 10^4$) and Equivalent Isotropic Temperature Factors for Non-H Atoms

Atom	x	y	z	B_{eq}/Å^2	Atom	x	y	z	B_{eq}/Å^2
(a) **1**					(b) **2**				
N(1)	1458(1)	1182(1)	8650(1)	3.5	N(1)	6707(2)	2637(1)	1555(1)	3.0
C(2)	2086(1)	1164(1)	7801(1)	3.1	C(2)	6304(2)	3063(1)	2619(2)	2.9
C(3)	1993(1)	1865(1)	7031(1)	3.6	C(3)	7379(2)	3006(1)	3831(2)	3.1
C(4)	1209(1)	2740(1)	6971(1)	3.3	C(4)	8993(2)	2405(1)	4205(2)	2.8
C(5)	519(1)	2610(1)	7879(1)	3.5	C(5)	9545(2)	2220(1)	2994(2)	2.9
C(6)	622(1)	1870(1)	8615(1)	3.0	C(6)	8444(2)	2299(1)	1792(2)	2.8
C(21)	2876(1)	327(1)	7842(1)	3.3	C(11)	5249(3)	2079(1)	643(2)	4.1
C(22)	3450(1)	75(1)	8792(1)	4.3	C(21)	4698(2)	3647(1)	2277(2)	3.1
C(23)	4173(1)	−725(1)	8810(2)	5.4	C(22)	4198(2)	4112(1)	1103(2)	3.6
C(24)	4322(1)	−1260(1)	7897(2)	5.9	C(23)	2734(3)	4678(1)	793(2)	4.4
C(25)	3757(1)	−1019(1)	6961(1)	5.6	C(24)	1748(3)	4794(2)	1647(2)	4.9
C(26)	3035(1)	−228(1)	6930(1)	4.4	C(25)	2215(3)	4338(2)	2812(2)	5.1
C(411)	481(1)	2698(1)	5933(1)	3.3	C(26)	3680(3)	3767(2)	3126(2)	4.3
C(412)	−124(1)	3548(1)	5610(1)	4.1	C(41)	8495(2)	1468(1)	4800(2)	3.3
C(413)	−846(1)	3492(1)	4736(1)	4.9	C(411)	6966(2)	880(1)	3926(2)	3.1
C(414)	−975(1)	2595(1)	4158(1)	5.0	C(412)	7270(3)	219(1)	3074(2)	4.0
C(415)	−376(1)	1752(1)	4460(1)	5.2	C(413)	5881(3)	−341(2)	2299(2)	5.0
C(416)	342(1)	1803(1)	5345(1)	4.5	C(414)	4150(3)	−248(2)	2368(2)	5.0
C(421)	1808(1)	3769(1)	7042(1)	3.5	C(415)	3825(3)	401(2)	3208(2)	4.8
C(422)	1672(1)	4503(1)	7817(1)	4.6	C(416)	5221(3)	968(1)	3979(2)	3.9
C(423)	2235(1)	5419(1)	7853(1)	5.6	C(421)	10603(2)	2877(1)	5236(2)	3.0
C(424)	2952(1)	5610(1)	7141(1)	5.5	C(422)	12186(2)	2401(1)	5708(2)	3.6
C(425)	3107(1)	4885(1)	6374(2)	5.5	C(423)	13680(3)	2811(2)	6603(2)	4.4
C(426)	2536(1)	3980(1)	6320(1)	4.6	C(424)	13626(3)	3713(2)	7042(2)	5.3
C(61)	−92(1)	1753(1)	9469(1)	3.0	C(425)	12077(3)	4193(2)	6600(2)	5.3
C(62)	241(1)	1346(1)	10458(1)	3.9	C(426)	10576(3)	3785(1)	5698(2)	4.1
C(63)	−429(1)	1284(1)	11260(1)	4.4	C(61)	9046(2)	2111(1)	627(2)	3.0
C(64)	−1440(1)	1624(1)	11087(1)	4.4	C(62)	8619(3)	2706(1)	−424(2)	4.3
C(65)	−1786(1)	2003(1)	10102(1)	4.9	C(63)	9275(3)	2556(2)	−1475(2)	5.1
C(66)	−1127(1)	2058(1)	9297(1)	4.2	C(64)	10353(3)	1817(2)	−1492(2)	4.7
					C(65)	10754(3)	1214(2)	−472(2)	4.4
					C(66)	10097(3)	1361(1)	578(2)	3.8

The e.s.d's in parentheses refer to last digits. $B_{eq}=4/3\sum_i\sum_j\beta_{ij}a_ia_j$.

Table 3. Bond Length and Angles for Non-H Atoms with Estimated Standard Deviations

Distance	**1** l/Å	**2** l/Å	Distance	**1** l/Å	**2** l/Å
N(1)–C(2)	1.394(2)	1.411(2)	C(411)–C(412)	1.390(2)	1.385(3)
N(1)–C(6)	1.396(2)	1.406(2)	C(411)–C(416)	1.378(2)	1.387(3)
N(1)–C(11)		1.471(3)	C(412)–C(413)	1.379(2)	1.383(3)
C(2)–C(3)	1.325(2)	1.334(3)	C(413)–C(414)	1.374(3)	1.383(4)
C(2)–C(21)	1.485(2)	1.487(3)	C(414)–C(415)	1.372(3)	1.370(4)
C(3)–C(4)	1.515(2)	1.507(3)	C(415)–C(416)	1.386(2)	1.390(3)
C(4)–C(5)	1.516(2)	1.510(2)	C(421)–C(422)	1.383(2)	1.394(3)
C(4)–C(41)		1.576(3)	C(421)–C(426)	1.388(2)	1.392(3)
C(4)–C(411)	1.542(2)		C(422)–C(423)	1.390(3)	1.384(3)
C(4)–C(421)	1.539(2)	1.542(3)	C(423)–C(424)	1.363(3)	1.378(3)
C(5)–C(6)	1.332(2)	1.337(2)	C(424)–C(425)	1.373(3)	1.373(4)
C(6)–C(61)	1.481(2)	1.486(3)	C(425)–C(426)	1.383(2)	1.390(3)
C(21)–C(22)	1.389(2)	1.392(3)	C(61)–C(62)	1.385(2)	1.390(3)
C(21)–C(26)	1.385(2)	1.385(3)	C(61)–C(66)	1.390(2)	1.383(3)
C(22)–C(23)	1.392(2)	1.385(3)	C(62)–C(63)	1.384(2)	1.387(4)
C(23)–C(24)	1.369(3)	1.371(3)	C(63)–C(64)	1.375(2)	1.378(4)
C(24)–C(25)	1.366(3)	1.378(4)	C(64)–C(65)	1.370(2)	1.373(3)
C(25)–C(26)	1.382(2)	1.389(3)	C(65)–C(66)	1.377(2)	1.386(3)
C(41)–C(411)		1.508(3)			

Table 3. (Continued)

Angle	θ/°	θ/°	Angle	θ/°	θ/°
C(2)-N(1)-C(6)	118.9(1)	116.5(1)	C(4)-C(41)-C(411)		115.7(2)
C(2)-N(1)-C(11)		116.8(1)	C(4)-C(411)-C(412)	120.3(1)	
C(6)-N(1)-C(11)		116.2(1)	C(4)-C(411)-C(416)	121.7(1)	
N(1)-C(2)-C(3)	121.8(1)	121.9(2)	C(41)-C(411)-C(412)		121.1(2)
N(1)-C(2)-C(21)	115.3(1)	115.2(1)	C(41)-C(411)-C(416)		120.8(2)
C(3)-C(2)-C(21)	122.9(1)	122.6(2)	C(412)-C(411)-C(416)	117.8(1)	118.1(2)
C(2)-C(3)-C(4)	124.5(1)	123.6(2)	C(411)-C(412)-C(413)	121.0(1)	121.3(2)
C(3)-C(4)-C(5)	108.2(1)	107.5(1)	C(412)-C(413)-C(414)	120.6(2)	119.9(2)
C(3)-C(4)-C(41)		109.5(1)	C(413)-C(414)-C(415)	119.2(2)	119.6(2)
C(3)-C(4)-C(411)	111.7(1)		C(414)-C(415)-C(416)	120.3(2)	120.4(2)
C(3)-C(4)-C(421)	108.5(1)	112.8(1)	C(411)-C(416)-C(415)	121.2(1)	120.7(2)
C(5)-C(4)-C(41)		111.5(1)	C(4)-C(421)-C(422)	122.9(1)	119.8(2)
C(5)-C(4)-C(411)	106.3(1)		C(4)-C(421)-C(426)	119.7(1)	122.6(2)
C(5)-C(4)-C(421)	112.1(1)	108.4(1)	C(422)-C(421)-C(426)	117.4(1)	117.5(2)
C(41)-C(4)-C(421)		107.1(1)	C(421)-C(422)-C(423)	120.8(2)	121.6(2)
C(411)-C(4)-C(421)	110.2(1)		C(422)-C(423)-C(424)	121.0(2)	119.9(2)
C(4)-C(5)-C(6)	125.0(1)	123.5(2)	C(423)-C(424)-C(425)	119.0(2)	119.6(2)
N(1)-C(6)-C(5)	120.8(1)	122.1(2)	C(424)-C(425)-C(426)	120.4(2)	120.7(2)
N(1)-C(6)-C(61)	116.0(1)	116.1(1)	C(421)-C(426)-C(425)	121.4(2)	120.7(2)
C(5)-C(6)-C(61)	123.2(1)	121.6(2)	C(6)-C(61)-C(62)	121.8(1)	120.7(2)
C(2)-C(21)-C(22)	120.9(1)	120.8(2)	C(6)-C(61)-C(66)	120.4(1)	121.0(2)
C(2)-C(21)-C(26)	120.1(1)	121.3(2)	C(62)-C(61)-C(66)	117.8(1)	118.3(2)
C(22)-C(21)-C(26)	119.0(1)	117.9(2)	C(61)-C(62)-C(63)	120.8(1)	120.3(2)
C(21)-C(22)-C(23)	119.7(1)	121.1(2)	C(62)-C(63)-C(64)	120.5(1)	120.5(2)
C(22)-C(23)-C(24)	120.3(2)	120.3(2)	C(63)-C(64)-C(65)	119.2(1)	119.7(2)
C(23)-C(24)-C(25)	120.3(2)	119.5(2)	C(64)-C(65)-C(66)	120.6(2)	119.9(2)
C(24)-C(25)-C(26)	120.0(2)	120.4(2)	C(61)-C(66)-C(65)	121.0(1)	121.3(2)
C(21)-C(26)-C(25)	120.7(1)	120.8(2)			

diffractometer with graphite-monochromated Cu $K\alpha_1$ (λ= 1.54051 Å) radiation, using the ω-2θ scan technique with a scanning rate of 4° min^{-1} in 2θ. At both ends of the scan range 10 s background counts were taken for each reflection. Three reflections were monitored for every 50 reflections. Variations of intensities of the monitored reflections were within 3% for both **1** and **2**. Reflections of $|F_o| \geq 3\sigma(F_o)$ were used for structure determination. No absorption correction was applied.

Although the colorless crystals of **1** changed to be blue during an irradiation with X-rays, the intensities of the monitored reflections have not changed. After the intensity measurement a check on the unit cell dimensions and the space group was carried out, but no change was observed. For **2** color change could not be observed.

The structures were solved by the direct method with the program MULTAN 78.[3] All non-hydrogen atoms were refined by the block-diagonal least-squares with anisotropic temperature factors. A difference map showed the all hydrogen atoms. Further refinement with anisotropic temperature factors for non-hydrogen atoms and isotropic ones for H gave the final R values of 0.037 and 0.044 for **1** and **2**, respectively. The quantity minimized was $\sum w(|F_o|-k^{-1}|F_c|)^2$. For **1**, $w=1/(0.8208-0.0710|F_o|+0.002|F_o|^2)$ and for **2**, $w=1/(0.0617+0.0147|F_o|+0.0002|F_o|^2)$. Atomic scattering factors were taken from "International Tables for X-ray Crystallography."[4] All computations were performed on a HITAC M180 Computer of the Data Processing Center of the University of Electro-Communications with the programs UNICS III,[5] MULTAN 78, and ORTEP II.[6] The final atomic parameters are given in Table 2.[7]

Table 4. Torsion Angles

Angle	**1** τ/°	**2** τ/°
C(6)-N(1)-C(2)-C(3)	8.6(2)	−11.5(2)
C(2)-N(1)-C(6)-C(5)	−10.8(2)	12.3(2)
N(1)-C(2)-C(3)-C(4)	−0.7(2)	−6.9(2)
N(1)-C(6)-C(5)-C(4)	5.3(2)	5.3(2)
C(2)-C(3)-C(4)-C(5)	−4.5(2)	21.6(2)
C(3)-C(4)-C(5)-C(6)	2.2(2)	−20.8(2)
N(1)-C(2)-C(21)-C(22)	−42.4(2)	−30.4(2)
N(1)-C(2)-C(21)-C(26)	136.4(1)	151.3(1)
N(1)-C(6)-C(61)-C(62)	27.1(1)	39.0(2)
N(1)-C(6)-C(61)-C(66)	−153.3(1)	−143.3(1)
C(11)-N(1)-C(2)-C(21)		−53.2(2)
C(11)-N(1)-C(6)-C(61)		53.5(2)
H(1)-N(1)-C(2)-C(21)	−25(1)	
H(1)-N(1)-C(6)-C(61)	24(1)	
C(3)-C(4)-C(411)-C(412)	−165.1(1)	
C(3)-C(4)-C(411)-C(416)	20.3(2)	
C(3)-C(4)-C(421)-C(422)	−122.8(1)	178.4(1)
C(3)-C(4)-C(421)-C(426)	55.8(1)	−3.8(2)
C(2)-C(3)-C(4)-C(41)		−99.7(2)
C(2)-C(3)-C(4)-C(421)		141.1(1)
C(4)-C(41)-C(411)-C(412)		88.3(2)
C(4)-C(41)-C(411)-C(416)		−93.6(2)
C(3)-C(4)-C(41)-C(411)		58.8(2)
C(3)-C(4)-C(41)-H(41)		−178(1)
C(3)-C(4)-C(41)-H(42)		62(1)

Discussion

The molecular structures with the atom-numbering are shown in Fig. 1. Bond distances and angles are listed in Table 3. The torsion angles are listed in

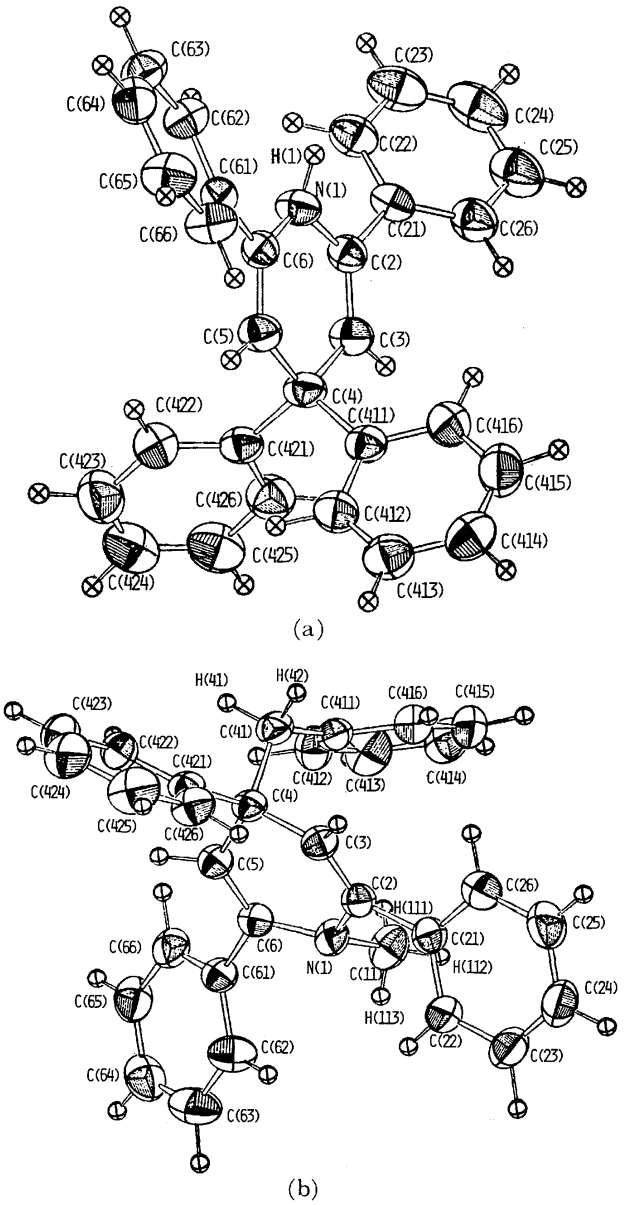

Fig. 1. Atomic numbering of the molecules. (a) **1** and (b) **2**. The thermal ellipsoids for non-H atoms are drawn at 50% probability.

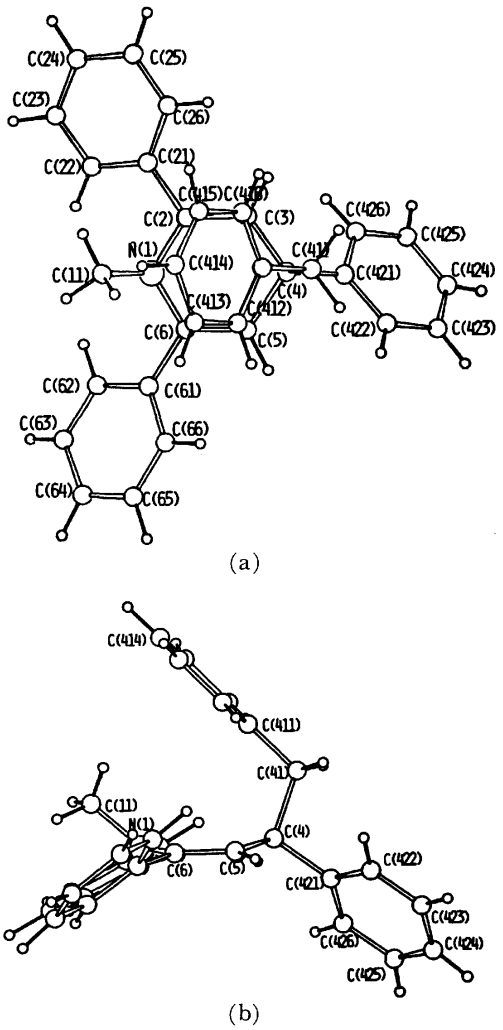

Fig. 2. (a) Projection of the molecule **2** on the dihydropyridine ring. (b) Side view of the molecule **2**.

Table 4. **2** shows a boat conformation with the apexes of C(4) and N(1). The torsion angles about C(4) ring bonds are larger than those about the N(1) bonds. The dihedral angles (boat angles) between the plane **A** defined by four atoms, C(2), C(3), C(5), and C(6), and the planes C(2)-N(1)-C(6) and C(3)-C(4)-C(5) are 10.1 and 17.5°, respectively. The dihedral angle (fold angle) between two N-C=C-C planes is 18.5°. The degree of the ring distorsions at N(1) and C(4) is the same order with those of 4-aryl-3,5-bis(methoxycarbonyl)-2,6-dimethyl-1,4-dihydropyridine.[8] For **1** the torsion angles about the N(1) and C(4) ring bonds are smaller than the corresponding angles of **2** and the other 1,4-dihydropyridines and C(4) is less distorted than N(1).

The lengths of C(2)-C(3) and C(5)-C(6) show the double bond character and are shorter than the corresponding values (1.345—1.369 Å) of the other 1,4-dihydropyridines.[8] The difference of these bond lengths may be attributed to the two methoxycarbonyl groups at 3 and 5 positions. The lengths of N(1)-C(2) and N(1)-C(6) for **2** are slightly longer than those of **1** and the others because of the 1-methyl substituent. The endocyclic angles of **1** and **2** are different from those of the others. The angles C(2)-N(1)-C(6) and C(3)-C(4)-C(5) of **1** and **2** are smaller and the other angles of **1** and **2** are larger than the corresponding angles of 3,5-bis(methoxycarbonyl) derivatives. The lengths of C(2)-C(21) and C(6)-C(61) show typical Csp^2-Csp^2 length while C(4)-C(411) and C(4)-C(421) are longer than the typical Csp^2-Csp^3 length, especially C(4)-C(411) of **2**.

For **1** the dihedral angles between the plane **A** and the four phenyl planes are 46.6, 106.4, 62.3 and 30.5° for 2-, 4-, 4-, and 6-positions, respectively. The corresponding angles of **2** are 30.4, 50.2, and 39.1° for 2-, 4-, and 6-positions, respectively.

The phenyl ring of benzyl group of **2** is trans to the

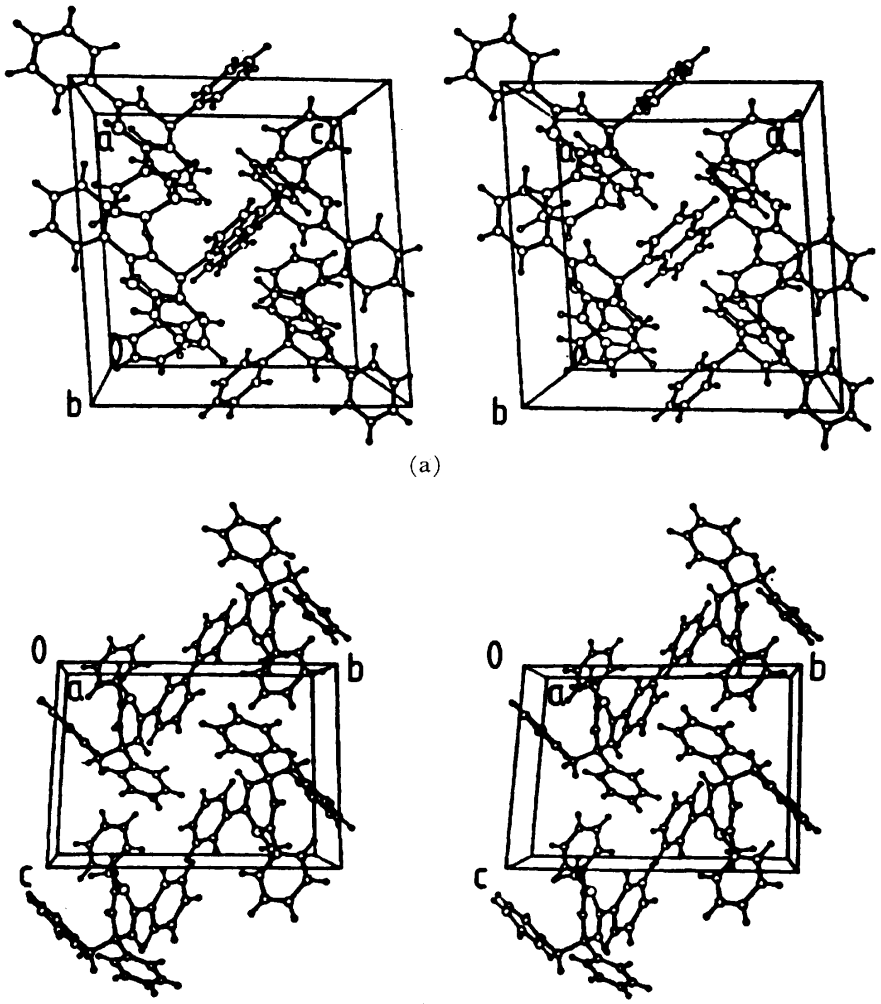

Fig. 3. Stereoscopic view of the crystal structure. (a) **1** and (b) **2**.

4-phenyl ring about the C(4)-C(41) bond and gauche to C(3) and C(5). This conformation of the benzyl group is quite interesting. Figure 2 shows the projection of **2** on the plane of the pyridine ring. The benzyl group covers the pyridine ring far from the phenyl group. The dihedral angles between the phenyl plane (C(411)—C(416)) and the plane **A** is 133.7°. Some intramolecular contacts between the phenyl ring of benzyl group and the pyridine ring, N(1)···C(411), C(2)···C(411), C(6)···C(411), C(3)···C(416), and C(5)···C(412), are 3.569(2), 3.434(3), 3.491(3), 3.344(3), and 3.332(3) Å, respectively.

Figure 3 is the stereoscopic view of the crystal packing. There are no significant contacts shorter than the sum of the van der Waals' radii.

In spite of a color changing of the crystal of **1** during an irradiation with X-rays for intensitiy measurement, the intensities, the dimensions of the unit cell and so the crystal structure have been retained. This result suggests the coloration may be attributed to an electronic effect. A slight difference of photochemical behavior between **1** and **2** may relate to the planality of the 1,4-dihydropyridine and the steric retention of the benzyl group of **2**.

We thank Miss Junko Shibuya for preparing the compounds.

References

1) K. Maeda and M. Nakamura, *J. Photochemistry*, **17**, 87 (1981).

2) K. Maeda, M. Nakamura, and M. Sakai, *J. Chem. Soc., Perkin Trans. 1*, **1983**, 837.

3) P. Main, S. E. Hull, L. Lessinger, G. Germain, J. P. Declercq, and M. M. Woolfson, MULTAN78. A System of Computer Programs for the Automatic Solution of Crystal Structures from X-ray Diffraction Data. Univs. of York, England and Louvain-la-Nerve, Belgium (1978).

4) "International Tables for X-Ray Crystallography," Kynoch Press, Birmingham (1974), Vol. IV.

5) T. Sakurai and K. Kobayashi, *Rikagaku Kenkyusho Hokoku*, **55**, 69 (1979).

6) C. K. Johnson. *ORTEP* II, Report ORNL-5138, Oak Ridge National Laboratory, Tennessee (1971).

7) The tables for the anisotropic temperature factors for non-hydrogen atoms and the F_o—F_c list are deposited as Document No. 8728 at the Office of the Editor of the Bulletin of the Chemical Society of Japan.

8) R. Fossheim, K. Svarteng, A. Mostad, C. Rømming, E. Shefter, and D. J. Triggle, *J. Med. Chem.* **25**, 126 (1982); R. Fossheim, *Acta Chem. Scand., Ser. B*, **39**, 785 (1985).

 © 1987 The Chemical Society of Japan Bull. Chem. Soc. Jpn., 60, 1261—1267 (1987)

Molecular-Weight Dependence of the Polymer Adsorption at Solid-Liquid Interfaces as Studied by ESR Spectroscopy

Harutoshi SAKAI† and Yoshio IMAMURA*
Department of Chemistry, Faculty of Science, Science University of Tokyo, Kagurazaka, Shinjuku-ku, Tokyo 162
(Received October 15, 1986)

The conformation of poly(methyl methacrylate) adsorbed from dilute solution on nonporous silica was investigated by ESR method using three-component spectrum analysis. The fraction of the polymer segments in train, short loop, and long loop or tail, as well as the rotational correlation time for the segments were examined with regard to molecular weight (M=10^3—3×10^6), the degree of adsorption, and the particle size of silica. In CCl_4, the saturation adsorption, A_s, increased from 6 to 16×10^{-8} g cm^{-2}, the fraction of polymer segments in train, p, decreased from 0.9 to 0.4, and the segment mobility reduced with the increase in molecular weight, respectively. Remarkable changes in A_s and p were found in a range of molecular weight of 5×10^4. In benzene, the values of A_s and p were less dependent on molecular weight than the cases of adsorption in CCl_4. Marked effects of intrachain interactions on the conformation were revealed for the adsorption of coiled polymers with high molecular weight from CCl_4 solution at low degrees of adsorption, where the loop formation was observed for polymers of $M>10^4$. The intrachain force was attributed to overlapping among the segments. The difference in the adsorption behavior between the cases in CCl_4 and benzene was interpreted by the difference in the degree of deformation of polymer molecules upon adsorption.

The adsorption of linear macromolecules from solution on solid surfaces is a complicated phenomenon with many problems to be clarified. The cause is mainly due to the constitution of macromolecules with a large number of repeating monomeric units. Among molecular models proposed for characterizing adsorbed and deformed polymer molecules at the interface, the "train-loop" model would be most general and successful.

Many investigations have been published on the adsorption of polymers by the IR method; Fontana and Thomas developed the spectroscopic technique for the quantitative estimation of the segment fraction attached to the surface sites through H-bonding.[1-3] Recently, the ESR method using nitroxide spin labels, developed originally for the study of biopolymers, has been applied to the adsorption of synthetic polymers.[4-7] The ESR measurement supplies unique and important information concerning the molecular dynamics as well as the conformation at solid-liquid interface.

The chain mobility of the adsorbed polymer is different between the anchoring train on solid surface and the detached loop extending into the solution. The correlation time τ_c has the most sensitive range ($10^{-7}<\tau_c<10^{-10}$ s) where the ESR line changes drastically with the time-averaging of anisotropy in hyperfine interaction and g-factor. The ESR spectrum of nitroxide spin labels attached to the polymer chain, therefore, reflects sensitively the difference in the relaxation process between the segments in loop and in train. If any contacts of nitroxide pendant groups with the surface sites can be ignored, the resolution of the ESR spectrum observed for the adsorbed polymer will allow to estimate the average conformation. Thus, the spin-label method seems to be suitable for the polymer adsorption system in which polymer chain has polar functional groups, such as ester, amide, ether, etc.

In our previous studies on the adsorption of spin-labeled PMMA, the ESR spectrum of the adsorbed polymer was resolved into three components: train, short loop, and long loop or tail.[6,7] The three-component analysis of the adsorbed polymer showed a possibility to discuss the conformation and the molecular motion in more detail than the resolution into two components reported by other authors.[4,5] Since the time required for the ESR spectrum analysis has been much saved recently by improving the simulation program using a small computer, it has become possible to treat a lot of spectral data within a short time.

The purpose of this study is to discuss the dependence of adsorption of PMMA on molecular weight over a wide range from 10^3 to 3×10^6, with reference to molecular conformation and molecular motion.

Experimental

Sample Preparation and Measurements. The experimental techniques were basically same as those described in our previous papers.[6,7] The spin-labeled PMMA was prepared by an anionic copolymerization of methyl methacrylate and 4-methacryloyloxy-2,2,6,6-tetramethyl-1-piperidiyloxyl (200—400/1 mol ratios) in toluene at 0 °C using phenylmagnesium bromide catalyst. The polymer was repeatedly fractionated in acetone-water mixture to give narrow molecular weight distributions. The characterization of the polymer samples is listed in Table 1. Each PMMA sample had a highly isotactic microstructure which gave the IR J-value of ca. 26.[8] The spin concentration in the used polymers was in the range of one label per 150 to 450 monomeric residues. The molecular weight was determined by means of viscometry, membrane osmometry, and vapor phase osmometry, and the ratio $\bar{M}_w/\bar{M}_n$ was determined by GPC calibrated with a standard polystyrene.

Two nonporous silica samples, Cabosil M5 (Cabot) and Aerosil OX-50 (Degussa), were used as the adsorbents.

†Present address: Helene Curtis Japan, Inc., Nishishinjuku, Shinjuku-ku, Tokyo 163.

Table 1. Characterization of PMMA Samples Used

No.	$\bar{M}_n$	$\bar{M}_v$	Methods	$\bar{M}_w/\bar{M}_n$
I-1	1370	—	VPO[a]	1.1[d]
I-2	1740	—	VPO	1.1
I-3	2740	—	VPO	1.1
I-4	3770	—	VPO	1.2
I-5	8400	—	VPO	1.4
II-6	16000	—	MO[b]	1.2
II-7	28000	—	MO	1.3
II-8	56000	—	MO	1.3
II-9	76000	—	MO	1.4
II-10	122000	—	MO	1.3
III-11	—	320000	Viscosity[c]	1.4
III-12	—	700000	Viscosity	1.4
III-13	—	1.6×10^6	Viscosity	—
III-14	—	3.3×10^6	Viscosity	—

a) VPO: vapor phase osmometry of $CHCl_3$ at 37 °C. b) MO: membrane osmometry in toluene at 38 °C. c) Viscosity: the intrinsic viscosity in benzene was determined at 30 °C, and $\bar{M}_v$ was calculated by $[\eta]=5.2\times10^{-5}\bar{M}_v^{0.76}$.[14] d) The ratio $\bar{M}_w/\bar{M}_n$ was determined by GPC in THF.

Cabosil M5 had a surface area of 220 m^2g^{-1} by N_2 adsorption, and the average particle size of 14 nm. Aerosil OX-50 had the values of 50 m^2g^{-1} and 40 nm, respectively ($g=10^{-3}$ kg). Reagent grade CCl_4 and benzene were used as the solvents after fractional distillation over a desiccant.

The amount of adsorption, A, was determined by the ESR to measure the decrease of polymer concentration after the adsorption, because the peak-to-peak signal amplitude for the polymer solution was proportional to the concentration. The amplitude was calibrated by simultaneous measurement on an equal volume (0.1 cm^3) of the original solution. The typical adsorption isotherms are shown in Fig. 1. Each adsorption curve shows an initial steep rise followed by the plateau at low equilibrium concentration ($C_e=10^{-4}$ g cm^{-3}). Hence, the saturation adsorption, A_s, was determined by taking the plateau values at $C_e=1\times10^{-3}$—3×10^{-3} g cm^{-3}. The ESR spectrum of the adsorbed polymer was measured in a quartz sample tube which contained ca. 1 cm^3 of silica suspension and sealed under N_2. ESR measurements were made on a JEOL JES FE-3X spectrometer, with a X-band microwave, 100 kHz field modulation, and temperature control of ±1 °C. The g-factor and the sweep width of magnetic field were calibrated by a Mn^{2+} standard.

Analysis of ESR Spectra. The procedures for analyzing ESR spectra are principally same as those described previously with some modifications.[6,7] As shown in Fig. 2, the ESR line shape observed from the adsorption system (spectrum D) was simulated by summation of three model spectra; the triplet line with narrowed width showing high mobility (spectrum A), the intermediately broadened line showing a restricted segment motion (spectrum B), and the powder pattern showing rigid immobilization (spectrum C). The spectrum was normalized by signal intensity obtained from the second integration of first-derivative spectrum. The amplitude of each model spectrum was determined by the least squares method on the multiple regression to fit the summation of the three spectra (spectrum E) with the observed spectrum. The model spectra were selected to make the correlation coefficient close to unity between the observed spectrum and the summation of three model spec-

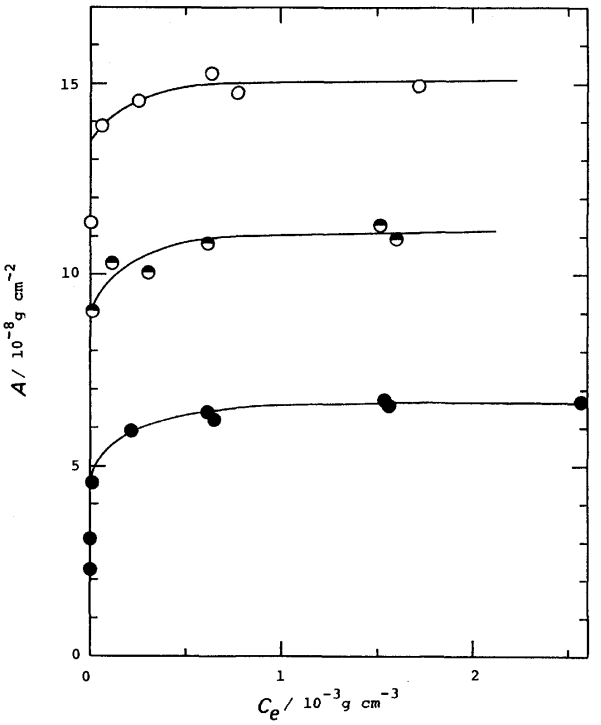

Fig. 1. Adsorption isotherms of PMMA on Cabosil M5 in CCl_4 at 25 °C. ●: M=1370, ◓: 5.6×10^4, ○: 1.22×10^5.

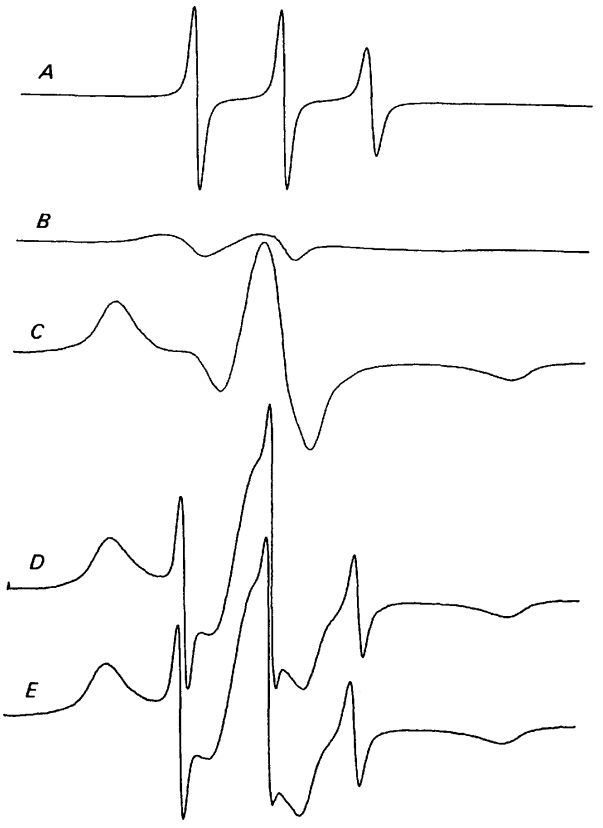

Fig. 2. ESR spectra used for simulation of adsorbed PMMA on Cabosil M5 in CCl_4 at the saturation stage. Spectrum A: model for long loop or tail, B: for short loop, C: for train, D: observed from the adsorption system, and E: synthesized by summation of A, B, and C.

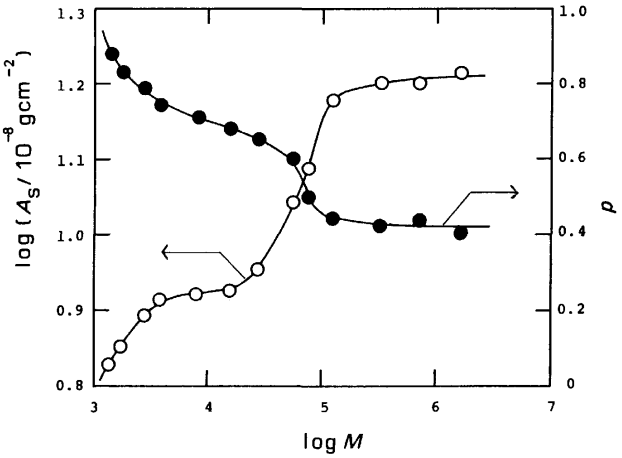

Fig. 3. Plots of logarithm A_s and p-values vs. molecular weight of PMMA adsorbed on Cabosil M5 in CCl_4 at 25 °C.

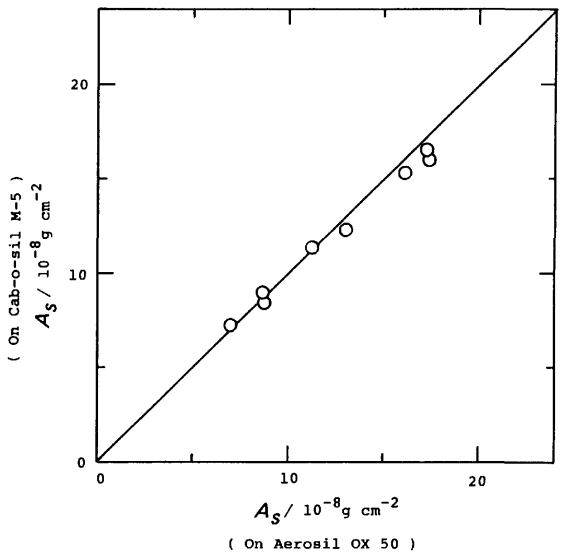

Fig. 4. Correlation diagram between A_s values on two silicas with different particle sizes; Aerosil OX-50 (400 Å) and Cabosil M5 (140 Å).

tra. In the three-component analysis, close curve fitting was found in every case. The intermediate components, however, were not negligible; the content was 10—25% in most cases, and good curve fitting could not be obtained without contribution of the intermediates.

The ESR model spectra of motional-narrowing components were observed at various temperatures, and in some cases calculated by Lorentzian and Gaussian approximation with reference to the temperature changes of the peak-to-peak amplitude ratios and the widths of the triplet lines observed for the polymer solution. The model spectra for the intermediate components were obtained from the amorphous polymers in the rubbery state at 120—160 °C. As for the most restricted segments (train), the model spectra were obtained from the adsorbed oligomer PMMA at a low surface concentration at different temperatures. The line shape was almost similar to that of the powder pattern and remained identical even when the temperature was lowered below 25 °C.

The rotational correlation time was calculated by the equations derived by Kivelson[9] and Goldman et al.,[10] who assumed the isotropic rotational diffusion.

Results and Discussion

1. Amount of Adsorption and the Fraction of Bound Components. The correlation between the saturation adsorption, A_s, and molecular weight of PMMA adsorbed from CCl_4 on Cabosil M5 is illustrated in Fig. 3. The fraction of the bound segments, p-value, is also plotted. The values of A_s increased from 6 to 15×10^{-8} g cm^{-2}, and the p-values decreased from 0.9 to 0.4 with the increase in molecular weight of a lower range from 10^3 to 10^5. Both values approached to constant values, $A_s=16\times10^{-8}$ g cm^{-2} and $p=0.4$, at higher molecular weight range, $M>10^5$. There is a close correlation between the changes in A_s and p; i.e., the loop content increases with the increase in A_s value. The changes in both values with molecular weight, however, were not monotonous but apparent in the molecular weight region of 5×10^4. The feature of the molecular weight dependency was reproducible in the repeated experiments using the polymer samples of different sources.

Similar phenomenon was reported by Kalnin'sh et al.[3] They studied the adsorption of atactic PMMA from several solvents on an Aerosil silica by the IR spectroscopy, and found a rapid drop of p-values with increasing molecular weight near 10^4. They reported a reflection point of p-value at the lower molecular weight region than that in this study. They attributed the rapid drop of p-values to the formation of transitional loops by adsorption of a polymer molecule on several adjacent silica particles, because the size of the polymer coil in solution became commensurate with the adsorbent particle size in the molecular weight region of 10^5.

In order to examine whether or not such a macroscopic interaction effect exists, the adsorption measurements were carried out on Aerosil OX 50 which has larger particle size (average diameter, 400 Å) than that of Cabosil M5 (140 Å) but has similar surface qualities. Figure 4 shows the correlation between the values A_s on Aerosil OX 50 and on Cabosil M5 at various molecular weights in CCl_4 solution. The amounts of polymer adsorbed per unit surface area were almost identical at the same molecular weight for both the adsorbents, yielding the same reflection point as that shown in Fig. 3. The changes of p-values with molecular weight were similar. From these results, a relatively strong molecular weight dependence appeared in the molecular weight region of 5×10^4 can not be explained by the sizes of adsorbent and polymer coil in solution. The effect of simultaneous adsorption seems to be negligible.

2. Dynamic Aspects of Adsorbed Molecule. Figure 5 shows the molecular weight dependence of the rotational correlation time, τ_c, estimated for the seg-

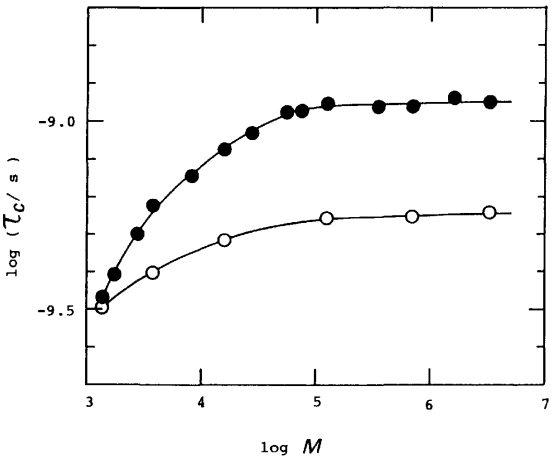

Fig. 5. Double logarithmic plots of rotational correlation time (τ_c) for loop or tail segments vs. molecular weight; ●: in adsorbed polymer, ○: in solution.

ments in long loops or tails, in comparison with that for free segments in CCl_4 solution (C=5×10^{-3} g cm^{-3}) as the reference system. The values of τ_c increase with the molecular weight when $M<10^5$, indicating a decrease of motional freedom in the loop. For $M>10^5$, the values of τ_c approach almost constant values about twice as large as for the free segments in solution. As for extremely short chain molecules, the detached segments appear to have motional freedom which is comparable to that of free segments in solution. This would be due to a contribution of the chain ends in tails.

The reduced degree of the motional freedom for higher molecular weight polymers will be interpreted from the increased segment density in the loop layer, because the A_s values increase and the p-values decrease with molecular weight as illustrated in Fig. 3. The segment motion is restricted by the intra- and interchain interactions in a dense surface layer. Above results will also predict the "compressed conformation" for higher molecular weight polymers at the interface as will be described later.

The values of τ_c of the intermediate components in ESR spectra (short loop) were in the range from 4 to 6×10^{-9} s, and were larger than the values for long loop or tail segment. Those values were less dependent on the molecular weight.

Figure 6 shows the ESR spectra of oligomer molecule (M=1370) adsorbed at a low surface coverage (θ=0.3) on Cabosil M5 in CCl_4 at various temperatures. The line shape of the spectrum at 25 °C is close to the powder pattern which reflects a complete train conformation of the adsorbed molecules. When the temperature was raised, the extreme separation width (W) of the spectrum reduced, indicating a recovery of the segment motion. However, even after keeping the adsorption system at 72 °C for 2 h, the ESR line shape indicated that the adsorbed oligomer molecules

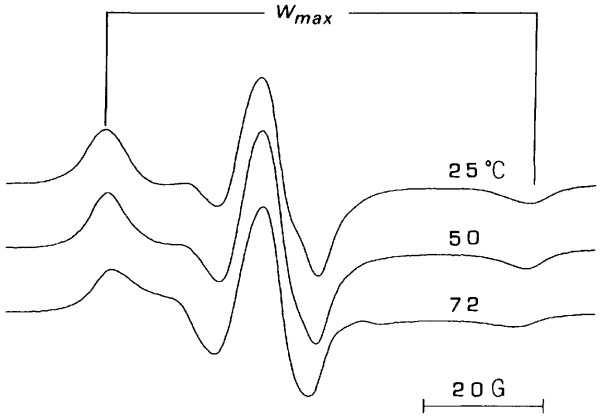

Fig. 6. ESR spectra of adsorbed oligomer molecule, M=1370, at unsaturated stage (θ=0.3) on Cabosil M5 in CCl_4 at various temperatures indicated in right side.

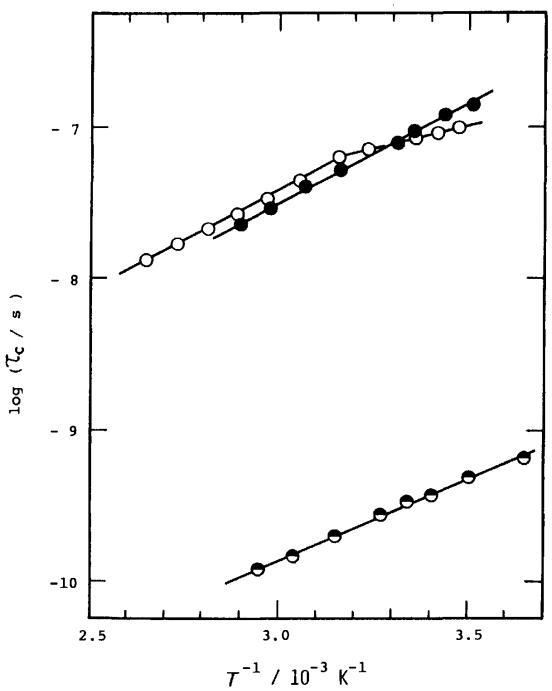

Fig. 7. Arrhenius plots of τ_c for oligomer PMMA (M=1370). ●: For train segments adsorbed on Cabosil M5 in CCl_4, ○: for amorphous solid state polymer, ◒: for free segments in CCl_4 solution (C=5×10^{-3} g cm^{-3}).

remain the deposited conformation. This would be an evidence of persistent adsorption which is characteristic of polymeric chains and different from the case of monomeric molecules.

In Fig. 7, the values of τ_c for the train segments estimated from the changes in W are plotted against the reciprocal of temperature, together with τ_c for solid polymer and free polymer in solution. The τ_c value for the train was estimated to be ca. 1×10^{-7} s at 25 °C. The relaxation time was longer than that estimated for an amorphous polymer in glassy state at 25 °C. The activation energy of rotational diffusion was estimated to

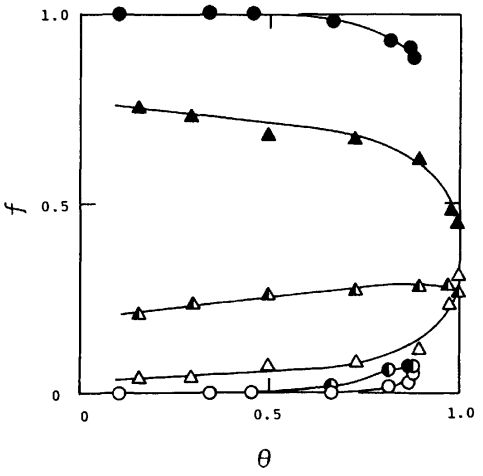

Fig. 8. Plots of the values of p (●,▲), f_{sl} (◐,◭) and f_{ll} (○,△) vs. θ for two polymers adsorbed on Cabosil M5 in CCl_4 at 25 °C. The data are shown with circles for M=1370 and with triangles for M=1.22×10^5.

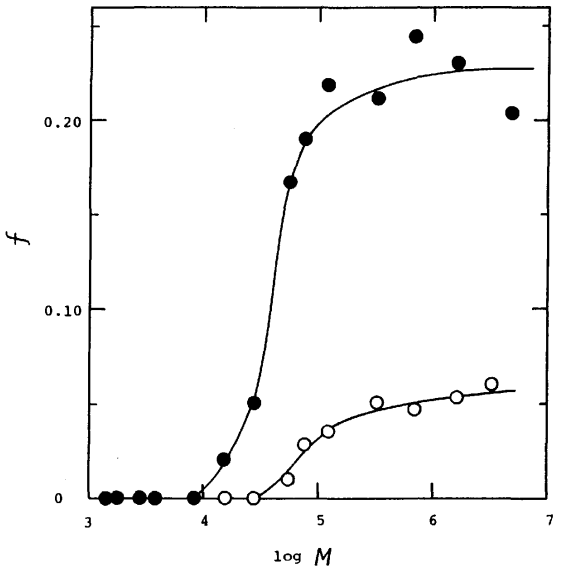

Fig. 9. Plots of values of f_{sl} (●) and f_{ll} (○) vs. logarithms of molecular weight at θ=0.1 on Cabosil M5 in CCl_4 at 25 °C.

be ca. 26 kJ mol^{-1}. This value is eqivalent to that for the rubbery state polymer, but higher than that for free polymer in solution.

In the cases of the molecules with higher molecular weight than 10^5, the values of W were equal to the rigid limit value, and no longer changed over the temperature range of −120 to 70 °C. The values of τ_c for the train segments in polymers with higher molecular weight will exceed 10^{-7} s, because W did not reduce even at ca. 70 °C. In the previous study using an adiabatic rapid passage technique, we revealed that τ_c for the train segment is over 10^{-6} s in a similar adsorption system.[6] These results demonstrate that the train segments in a coiled molecule were immobilized more rigidly than segments of short chain molecule. The stronger restriction of segment motion in higher molecular weight polymers would be caused by a "compression" onto the first layer (train) from the loop layer.

3. Influence of Surface Concentration on the Conformation. The fraction of the segments in train (p), in short loop (f_{sl}), and in long loop or tail (f_{ll}) was examined at various polymer concentrations in the surface layer, in order to elucidate the contribution of intra- and interchain interactions to the conformation. The segment distribution in adsorbed two polymers with different molecular weight is shown in Fig. 8 as a function of θ. The value of θ was determined from the following experimental results: The amount of polymer segments attached directly to the surface ($p \times A_s$) increased slightly (ca. 10%) with increasing molecular weight, and became almost constant at high molecular weight range ($M > 10^5$). The results gave a saturation value $(pA_s)_{max}$ of 6.7×10^{-8} g cm^{-2}. From this value, the surface area occupied per monomer unit in the train was calculated to be 25 Å^2, which is agree with the literature value determined for the case of PVAc adsorbed at a liquid-air interface.[11] The value of θ was obtained by the ratio, $\theta = pA/(pA_s)_{max}$, on an assumption that the surface sites saturate with the polymer segments at the saturation adsorption of high molecular weight polymers.

For the polymer with molecular weight of 1370, the p-values were close to unity (f_{sl}=0 and f_{ll}=0) at unsaturated adsorption stages ($\theta < 0.6$). This means a completely deposited conformation of short chain molecules. When the adsorption approaches the saturation, the p-value reduced to ca. 0.9 with slight increases in f_{sl} and f_{ll}. On the other hand, the higher molecular weight polymers ($M > 10^5$) contain higher amount of looped conformation even at low θ; the content of loop segments is ca. 20—30%. The p-values decreased gradually with increasing θ, and then dropped to ca. 0.4 at the saturation adsorption with relatively rapid increase in f_{ll}.

The dependence of p-value on θ for the high molecular weight polymers was stronger than the published results of other polymers such as poly(alkyl methacrylate), atactic PMMA, etc.[1] The statistical mechanical treatment of polymer adsorption, however, gave evident difference between p-values of saturation adsorption (θ=1) and of an isolated molecule ($\theta \to 0$).[12] The relatively strong dependence of p-value on θ found in this study is in accord qualitatively with the theoretical prediction.

Under the adsorption conditions at low θ, intrachain interaction and interaction between polymer segments and surface sites affect the conformation, whereas interchain forces are weak. The molecular weight dependence of the conformation was examined at low θ of ca. 0.1, in order to elucidate intrachain forces.

Figure 9 illustrates the fractions of the polymer seg-

ments in short loops (f_{s1}) and in long loops or tails (f_{l1}) as a function of molecular weight. The powder pattern of the ESR spectrum was observed for the adsorbed PMMA of lower molecular weight than 10^4. (Consequently, $f_{s1}=0$, $f_{l1}=0$, and $p=1$ for $M<10^4$.) The short chain molecules were completely flattened on the surface at low θ. In the range of higher molecular weight than 10^4, the adsorbed molecules take the looped conformation. The value of f_{s1} and f_{l1} increased with the increase of molecular weight from 10^4 to 10^5, and became constant at $M>10^5$.

These phenomena suggest that there is a difference in the interaction with the surface between the lower ($M<10^4$) and the higher molecular weight polymers. The difference determines whether the molecules behave as coiled chains to the surface or not. The reason why the higher molecular weight polymers are not adsorbed with a flat conformation as the lower molecular weight polymers even at low θ is probably due to intrachain overlapping among the segments. The overlapping in chain polymer reduces the p-value and affects on excluding a volume at the surface. Effects of intrachain interaction on the conformation have been studied by statistical mechanics on the adsorption of macromolecular chain. Several authors reported recently from the computer enumeration a marked reduction in p-value owing to the excluded volume effect.[13]

4. Deformation of Polymer Coil upon Adsorption. Koral et al., studied the adsorption of PVAc, and treated experimental results of the amount of adsorption, A_s, by an adsorption model that adsorbent surface is completely covered by spherical polymer coils.[11] They discussed the deformation of the polymer coil lateral to surface plane, by comparing the experimental values of A_s with the theoretical value expected from the radius of gyration, R, of the polymer in solution. A_s can be related to the surface area (S_s) occupied per polymer coil by

$$A_s = M/S_sN_0 \text{ (g per unit area)},$$

where N_0 is Avogadro's number. If the cross section ($S_b=\pi R^2$) of the polymer coil in solution is estimated, a factor which describes the degree of deformation of polymer coil, β, lateral to the surface when the polymer collapses on the surface can be defined as

$$\beta^2 = S_s/S_b.$$

In the series of adsorption of polymers with different molecular weights, the molecular weight dependence would be more explicitly described by the lateral deformation factor. If one considers important the relative changes of β with molecular weight, the factor β would be a meaningful parameter to describe the behavior of adsorbed polymers at the interfaces.

The dimension of PMMA in a poor solvent, CCl_4, was taken from the published data on the unperturbed chains of isotactic PMMA in a theta solvent.[14] Taking

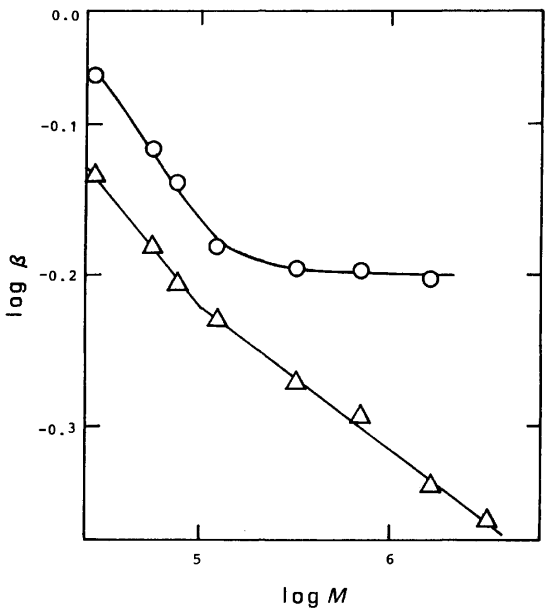

Fig. 10. Double logarithmic plots of β vs. molecular weight for PMMA with high molecular weight adsorbed on Aerosil OX 50 in CCl_4 (O) and in benzene (Δ) at 25°C.

the relationship between the root-mean-square end-to-end distance and molecular weight, $<\bar{r}_0^2>=7\times10^{-9}M^{0.50}$ (cm), the radius of gyration (R) was obtained from the relation, $R_0^2=<\bar{r}_0^2>/6$. In this case, the difference between R and R_0 was ignored in considering relative changes of β with molecular weight. For the cases in benzene, R was estimated from the intrinsic viscosity-molecular weight relationship, assuming $\alpha^{2.43}=[\eta]/[\eta]_\theta$, where α is the expansion factor defined as $\alpha=R/R_0$, and $[\eta]$ and $[\eta]_\theta$ is the intrinsic viscosity in benzene and in a theta solvent, respectively.[14]

Figure 10 illustrates the relation between β for coiled molecules and molecular weight. The logarithm β is a negative function of molecular weight. Namely, the larger the polymer coil in solution is, the smaller the lateral deformation factor upon the adsorption is. The polymer coils seem to be laterally compressed to the surface, occupying narrower space than the cross section of the polymer coil in solution. In CCl_4, the factor β tends to be constant for $M>10^5$. On the other hand, the adsorption data obtained in benzene are expressed by $\beta\propto M^{-0.1}$.

The degree of lateral deformation of the polymer coil is considered to be more significantly influenced by molecular weight in a better solvent than in a poor solvent. It is probably related to higher expansion of the polymer coil in the better solvent. In a poor solvent, the polymer molecule will be in a more compact conformation than in a good solvent, and consequently resistant to the lateral compression when the polymer collapses on the solid surface.

The total number of segments adsorbed per surface site (θ/p) was estimated from the ratio $A_s/(pA_s)_{max}$. This value is a measure of the thickness of adsorbed

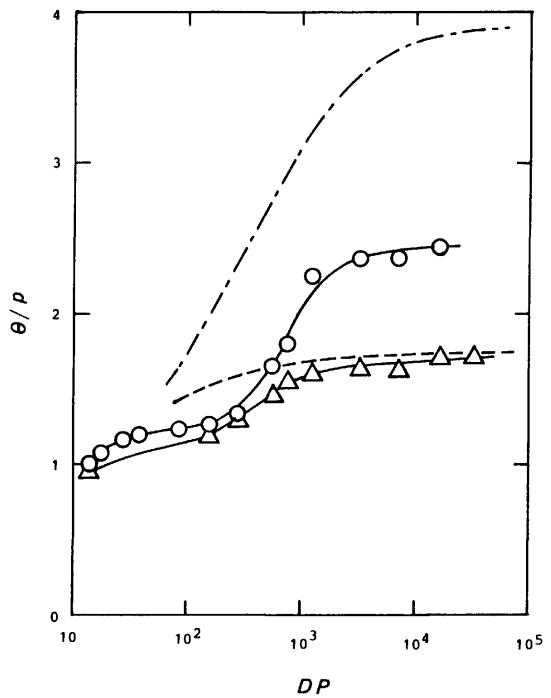

Fig. 11. Plots of θ/p vs. degree of polymerization, DP, O:In CCl_4, Δ:in benzene. Dependence predicted by Silberberg's theory is shown with -·-·- for the case of adsorption from a theta solvent and with ---- for that from an athermal solvent.

polymer layer, and would reflect the feature of the deformation in the axis normal to the surface, as well as the fractions of polymer segments (p, f_{sl}, and f_{ll}) in the surface layer. In Fig. 11, the values of θ/p are plotted against the degree of polymerization (DP). The values predicted by Silberberg's theory are also plotted for the case of adsorption from a theta solvent and an athermal solvent. Here, the values are derived from the given original parameters; $\Phi^*=10^{-4}$, $\gamma_b\gamma_s=0.1$, and $\chi_s=\infty$(namely $\theta=1$).[12]

In the case of short chain molecules ($M<2\times10^4$), the values of θ/p were nearly unity both in CCl_4 and benzene. This means monomolecular layer adsorption. The molecular weight dependence of θ/p in the better solvent (benzene) was weaker than that in the poor solvent (CCl_4), and the larger molecules still remained the flat conformation, within $\theta/p<2$. These data are consistent with the theoretical values predicted for the case of athermal solvent. In CCl_4, the values of θ/p were ca. 2.4 for $M>10^5$, and considerably lower than the predicted values for the adsorption from a theta solvent.

In the case of adsorption from the better solvent, benzene, the degree of deformation of the polymer coils seems to be much higher than the case of adsorption from CCl_4, because the polymer coil is not only flattened but laterally compressed on the surface.

References

1) B. J. Fontana and J. R. Thomas, *J. Phys. Chem.*, **65**, 480 (1961); C. Thies, *ibid*, **70**, 3783 (1966).

2) C. V. Linden and R. V. Leemput, *J. Colloid Interface Sci.*, **67**, 48 (1978); M. Kawaguchi, K. Hayakawa, and A. Takahashi, *Polym. J.*, **12**, 265 (1980); K. I. Brebner, R. S. Chahal and L. E. St-Pierre, *Polymer*, **21**, 533 (1980).

3) K. K. Kalnin'sh, A. N. Krasovskii, B. G. Belen'kii, and G. A. Andreyeva, *Vysokomol. Soedin., Ser. A*, **18**, 2304 (1976).

4) K. K. Fox, I. D. Robb and R. Smith, *J. Chem. Soc., Faraday Trans. 1*, **70**, 1186 (1974); A. T. Clark, I. D. Robb, and R. Smith, *ibid.*, **72**, 1489 (1976); I. D. Robb and R. Smith, *Eur. Polym. J.*, **10**, 1005 (1974); *Polymer*, **18**, 500 (1977).

5) T. M. Liang, P. M. Dickenson, and W. G. Miller, *Am. Chem. Soc. Symp. Series*, **142**, 1 (1980).

6) H. Sakai, T. Fujimori, and Y. Imamura, *Bull. Chem. Soc. Jpn.*, **53**, 3457 (1980).

7) H. Sakai and Y. Imamura, *Bull. Chem. Soc. Jpn.*, **53**, 1749 (1980); H. Sakai, T. Asakura, K. Suzuki, K. Horie, Y. Maeshima, and Y. Imamura, *ibid.*, **54**, 2180 (1981).

8) W. E. Goode, F. H. Owens, R. P. Fellman, W. H. Snyder, and J. E. Moore, *J. Polym. Sci.*, **46**, 317 (1960).

9) D. Kivelson, *J. Chem. Phys.*, **33**, 1094 (1960); T. G. Stone, T. Buckman, P. L. Nordio, and H. M. McConnell, *Proc. Natl. Acad. Sci. U.S.A.*, **54**, 1010 (1965).

10) S. A. Goldman, G. V. Bruno, and J. H. Freed, *J. Phys. Chem.*, **76**, 1858 (1972).

11) J. Koral, R. Ullman, and F. R. Eirich, *J. Phys. Chem.*, **62**, 541 (1958).

12) A. Silberberg, *J. Chem. Phys.*, **48**, 2835 (1968).

13) F. McCrackin, *J. Chem. Phys.*, **47**, 1980 (1967); P. Mark and S. Windwer, *Macromolecules*, **7**, 690 (1974).

14) S. Krause and E. Cohn-Ginsberg, *Polymer*, **3**, 565 (1962); *J. Phys. Chem.*, **67**, 1479 (1963); I. Sakurada, A. Nakajima, O. Yoshizaki, and K. Nakamae, *Kolloid Z. Z. Polym.*, **186**, 41 (1962); H. Morawetz, "Macromolecules in Solution," John Wiley & Sons, New York (1965), p. 276.

 © 1987 The Chemical Society of Japan Bull. Chem. Soc. Jpn., 60, 1269—1275 (1987)

Construction of an Adiabatic High-Pressure Calorimeter Using Helium Gas for Pressurization†

Osamu YAMAMURO, Masaharu OGUNI, Takasuke MATSUO, and Hiroshi SUGA*
Department of Chemistry and Chemical Thermodynamics Laboratory, Faculty of Science, Osaka University, Toyonaka, Osaka 560
(Received October 20, 1986)

A novel adiabatic high-pressure calorimeter was constructed with using helium gas as a pressure transmitting medium. It works under a constant pressure up to 250 MPa in the temperature range from 12 to 370 K. Sample cell is made of Be-Cu alloy and has internal volume of 26 cm^3. The pressure transmitting tube is connected to an external pressure-control system, which enables to keep automatically the inner pressure constant within ±1 kPa over the whole pressure and temperature ranges. Thus the thermodynamic path that any specimen follows during the heat capacity measurement can be described unambiguously. Heat capacities of the sample cells loaded without and with 158.9 MPa He gas were measured in the temperature range from 25 to 370 K. The imprecision of heat capacity data of the compressed He gas was within 0.3%. Thus the present calorimeter enables us to extend the low-temperature thermodynamic study on various kinds of materials to high pressures without a significant loss of the claimed precision.

Stability of states and thermodynamic properties of a substance can be determined from its Gibbs energy as functions of some parameters, temperature and pressure being two of the most important external parameters. The surface of the energy is experimentally obtained by the accurate measurements of heat capacity vs. temperature and volume vs. pressure. Hence calorimetry over wide temperature and pressure ranges is quite important in such studies.

The most accurate calorimetry has been done under adiabatic condition at the normal pressure. There the adiabatic condition is established as closely as possible between a calorimeter cell and its surroundings, and a path of the measurement is unambiguously specified on the p-T surface so that the obtained heat capacity data can be converted correctly to a thermodynamic quantity at constant pressure. However, the extension of this method to the calorimetry under high pressure is not straightforward, owing to many experimental difficulties. Either direct or indirect contact of a pressure transmitting medium with the sample is required for the application of pressure. Since the volume of the pressure transmitting medium as well as that of the sample changes with temperature and pressure, the unambiguous specification of the path of measurement can only be achieved by taking the following two procedures. One is to follow always the pressure change of the calorimeter cell during a series of measurements and then correct the effect of pressure change by using appropriate thermodynamic data as precisely as possible. Such calorimeters, often described as the clamp-bomb type, have been reported by a number of research groups,[1-4] on account of the convenience that an ordinary adiabatic calorimeter can be used without any drastic modification of the apparatus.

The other is to keep the pressure constant by connecting the cell to a pressure control system external to the cryostat through a pressure transmitting tube and permitting the pressure transmitting medium to flow into or out of the cell. The tube must be temperature-regulated to maintain adiabaticity of the calorimeter. Only two groups[5,6] have constructed this type of apparatus with using a liquid as the pressure transmitting medium. The above two methods are both usable only under relatively low pressures, below 1 GPa. This is because, higher the pressure, the cell must be more massive to withstand the pressure, resulting in the decrease in the ratio of the sample heat capacity to the total.

The adiabatic high-pressure calorimeter on which we reported before used liquid 3-methylpentane as the pressure transmitting medium.[5] While being quite effective in that the hydrostatic pressure is easily generated and transmitted to the system, it restricts the substances to be studied to inorganic compounds which are insoluble in the medium and the measurements in the temperature range above 100 K because of the solidification of the pressure transmitting medium itself below 100 K. The former restriction precludes molecular crystals and liquid crystals from the measurements and the latter limits the consideration based on the third law entropy.

The purpose of the present work is to construct a new high-pressure calorimeter which removes these restrictions. The apparatus uses, as a pressure transmitting medium, helium gas which is chemically inert and exists in the gaseous state down to very low temperatures. The use of this apparatus enables calorimetry with high precision up to 250 MPa. The precision of the calorimetry was estimated by measuring the heat capacities of helium gas at 158.9 MPa.

Construction of Apparatus

Principle. The present apparatus employs helium gas as a pressure transmitting medium to pressurize the sample in the cell. The pressure is maintained at a fixed value by permitting the helium gas to flow into

†Contribution No. 114 from Chemical Thermodynamics Laboratory.

or out of the cell through the pressure transmitting tube connected to the high-pressure control system. Heat capacity measurement is performed by the conventional adiabatic method, i.e., by following the temperature increment due to a known quantity of supplied energy under adiabatic condition. Heat flow through helium gas is negligible because the pressure transmitting tube above the cell together with the helium gas contained was maintained the same temperature as the cell. The heat capacity of the sample is obtained by subtracting from the total the contribution of the helium gas in the cell at the average temperature, as described in detail previously.[5] The contribution can be estimated only if the volume of the space occupied by the helium gas and its heat capacity at the confining pressure per unit volume are known.

The total heat capacity C_t obtained experimentally is expressed as

$$C_t(p,T) = nC_s(p,T) + C_e(p,T) + \{V_e(p,T) - nV_s(p,T)\}C_H(p,T). \quad (1)$$

Here, C_s, C_e, and C_H denote the heat capacities at constant pressure of a mole of the sample, empty cell, and helium gas per unit volume, respectively. V_s and V_e are the molar volume of the sample and the volume of the empty cell, respectively, and n the amount of sample. The symbols in the parentheses represent variables; p is the pressure inside the cell and T is the average temperature. Pressure dependence of heat capacity of the empty cell is given by $(\partial C_e/\partial p)_T/C_e \simeq 10^{-5}$ MPa^{-1}. This indicates that the dependence is negligible within the error of measurement in the present pressure range $\approx 10^2$ MPa; i.e.,

$$C_e(p,T) \simeq C_e(T). \quad (2)$$

$C_H(p,T)$ is rewritten as

$$C_H(p,T) = C_H^*(p,T)/V_e(p,T), \quad (3)$$

where $C_H^*(p,T)$ is the heat capacity of the helium gas that occupies the whole space of the cell, and can be determined experimentally. Substituting these two relations into Eq. 1 and rearranging, the molar heat capacity of the sample $C_s(p,T)$ is expressed by

$$C_s(p,T) = [C_t(p,T) - C_e(T) - \{1 - nV_s(p,T)/V_e(p,T)\}C_H^*(p,T)]/n. \quad (4)$$

Here $V_e(p,T)$ is obtained by measuring the total heat capacity $C_t'(p,T)$ containing a standard substance whose heat capacity $C_{st}(p,T)$ and volume $V_{st}(p,T)$ at high pressure are known; *i.e.*,

$$V_e(p,T) = \frac{V_{st}(p,T)\{C_H^*(p,T) - C_e(T)\}}{C_H^*(p,T) + C_{st}(p,T) - C_t'(p,T)} \quad (5)$$

Consequently, the determination of $C_s(p,T)$ requires only the data of $C_t(p,T)$ and $V_s(p,T)$ in Eq. 4. $V_s(p,T)$ must be obtained from other measurements (X-ray diffraction etc.) or by using some reliable equations of state, since it cannot be measured directly with the present calorimeter. When the interest is getting only the anomalous part of the heat capacity, it is not always necessary to know $V_s(p,T)$.

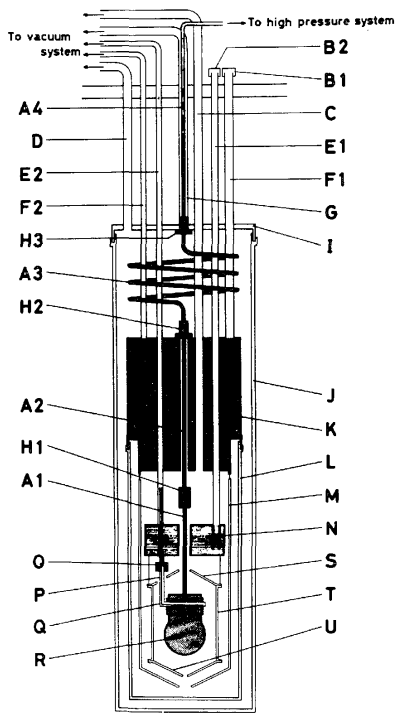

Fig. 1. Schematic drawing of the cryostat.
(A): High pressure transmitting tubes, (B): caps, (C),(D),(G): pumping tubes, (E): liquid nitrogen inlet and outlet, (F): liquid hydrogen inlet and outlet, (H): couplings, (I),(J): outer vacuum jacket, (K): liquid hydrogen tank, (L): inner vacuum jacket, (M): outer adiabatic shield, (N): liquid nitrogen tank, (O): joint,(P): transfer tube, (Q): cooling ring, (R): cell, (S),(T),(U): inner adiabatic shields.

Cryostat and Adiabatic Control. Figure 1 shows a schematic drawing of the cryostat. The pressure transmitting tube, shown in sections by A1, A2, A3, and A4, enters the cell R from the high pressure system through the center of the cryostat. They are made of stainless steel tubes of 0.6 mm I.D. and 3.1 mm O.D. They are connected in series with the couplings H1, H2, and H3. The cell R is dismountable at H1.

Temperatures as low as 12 K can be obtained by the standard cryogenic technique. Normally the cell is cooled from room temperature with the help of He gas of about 10 kPa introduced into the vacuum jackets J and L. However if the sample is volatile, it is possible to cool the cell by introducing liquid nitrogen directly into the cooling ring Q through E1, N, and P without any heat-conduction gas in the jackets. This process of cooling keeps the tubes A1-A4 at higher temperatures than the cell, preventing any volatile sample from condensing on the inner walls of the tubes.

Adiabatic condition between the cell and its envi-

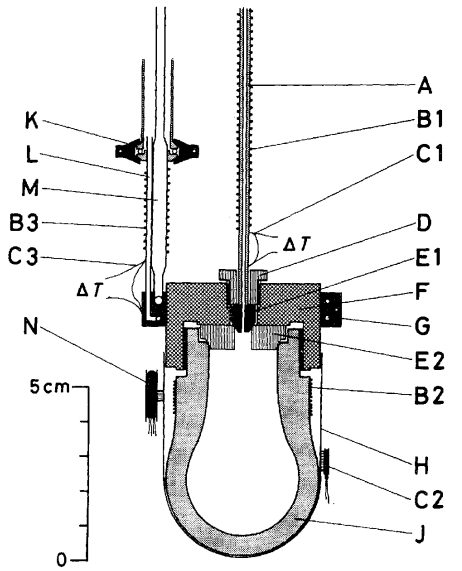

Fig. 2. Sectional drawing of the calorimeter cell. (A): High pressure transmitting tube, (B): heater wire, (C): thermocouples, (D): gland nut, (E): plugs, (F): gland lid, (G): cooling ring, (H): cell cover, (J): body, (K): joint, (L): liquid nitrogen inlet, (M): nitrogen gas outlet.

ronment is achieved during heat capacity measurements by evacuation of the space inside the jacket J and L to 10^{-4} Pa and by temperature-control of the following ten parts surrounding the cell. The inner adiabatic shields S, T, and U, the transmitting tube A1 just above the cell, and the liquid nitrogen transfer tube P are controlled at the same temperature as the cell. The outer shield M and the liquid nitrogen tank N (whose inside space is evacuated) are held a few Kelvins lower than the cell in order to control the inner shields. Furthermore, the tubes A2, A3, and A4 are kept a few Kelvins higher than the cell to prevent the condensation of sample on their inner walls. The temperature control system utilizes the temperature difference signals from the Chromel-P-constantan thermocouples (which are attached to appropriate locations of those parts to be controlled and the respective reference points) and regulates the current passing through the corresponding heaters. The upper temperature limit of the measurement is about 400 K because a low-temperature solder was used in several parts.

Calorimeter Cell. Figure 2 shows the calorimeter cell whose inside volume is 26.271 cm^3 at 30 °C and mass is 622.30 g. The main parts of the cell (J, F, D, E1, and E2) were made of copper-beryllium alloy which has high thermal conductivity and sufficient mechanical strength to withstand the applied pressure. The surface of the cell was gold-plated for reduction of radiative heat transfer and for protection against corrosion. A nearly spherical shape of the body J was devised for the purpose of minimization of the mass of the empty cell and maximization of the inside space. This increased the ratio of the sample heat capacity to the total and contributed to the improvement in the precision of the measurement.

The pressure inside the cell is sealed by two-stage metallic cone connection instead of the traditional Bridgman method. The first plug E2 is pressed down against the tapered top of the inner wall of the body J by driving the screw of the gland lid F and the second plug E1 is pressed against the top of the inside wall of E2 by the gland nut D. The diameter of the contact circle is about 20 mm for the first plug and 5 mm for the second plug, respectively. The sample is introduced through the apertures of E2 and F, after removing plug E1. This sealing method does not require any packing (e.g., tetrafluoroethylene or indium). The packing used in the previous experiments made the pressure and temperature dependence of the cell volume complicated and ambiguous. At present, the maximum pressure that can be applied to the cell without any leak is about 250 MPa.

The cooling ring G, made of copper, serves to cool the cell while the high-pressure tubes are being kept at higher temperatures. Liquid nitrogen is introduced through the inlet L and allowed to vaporize outward through the outlet M. The L and M are controlled during the heat capacity measurement at the same temperature as the cell with the Chromel-P-constantan thermocouple C3 and manganin heater B3. The ring can be removed at the joint K for measurement with nonvolatile samples.

B2 is the manganin heater for supplying electric energy to the cell. The thin cell-cover H made of copper was installed to minimize heat leak by radiation from the heater B2 as well as to fix the thermocouple C2 for the temperature regulation of the inner shields and the copper sheath as a holder for the platinum thermometer N (470 Ω at 273 K, Minco Products, USA).

Calorimetric Measurement. Calorimetric measurement consists of the usual three steps as generally performed: initial temperature measurement, supply of electric energy, and final temperature measurement. The temperature is determined by measuring the resistance of the platinum thermometer with the automatic a.c. resistance bridge (ASL F17, U.K.). The bridge gives a ratio of the thermometer to the standard resistance as a digital output with seven digits and an additional analog output of any umbalance signal. The analog signal is digitalized by the multimeter (Keithley 195, USA), and the resultant resistance readout with eight degits in total is converted to temperature, whose resolution corresponds roughly to 10 μK at temperatures above 50 K. The supplied energy is determined using the digital multimeter (Keithley 195, USA) and the digital clock in the computer.

All operations of the measurement, data processing, and their storage are carried out with the microcomputer (Sharp MZ 2200). The use of the computer contrib-

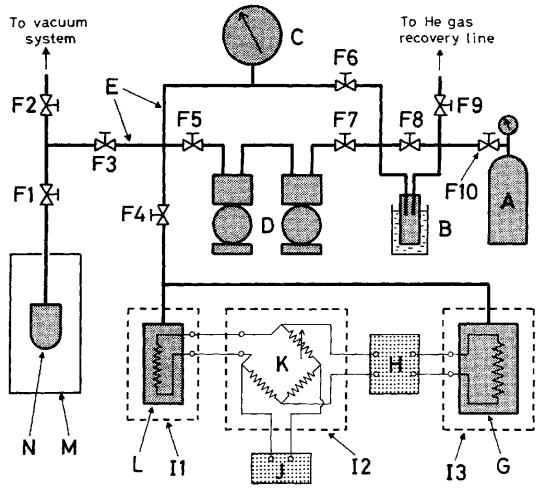

Fig. 3. Block diagram of the high pressure system. (A): Helium tank, (B): trap, (C): Heise gauge, (D): diaphragm compressor, (E): high pressure transmitting tube, (F): valves, (G): helium gas reservoir, (H): PID regulator, (I): thermostats, (J): battery, (K): Wheatstone bridge, (L): manganin wire resistance gauge vessel, (M): cryostat, (N): cell.

utes not only to saving labor but also to improving precision of the thermometry. Usually temperature is read out once in 60 s as the average of 12 readings taken at an interval of 5 s. This procedure of averaging reduces a scattering of data to a large extent, and consequently the precision of the thermometry is estimated to be within 50 μK at temperatures above 50 K. Detailed descriptions of the determination of temperature and input energy were given in the previous articles.[7] The thermometer was calibrated in advance on the IPTS-68.

High-Pressure System. Figure 3 shows the block diagram of the high-pressure system. The system can be divided into three parts; the cryostat in the left portion of the figure, the pressure generation system in the upper right, and the pressure control system in the lower right. Blocks shaded heavily and lightly represent high-pressure parts (A, B, C, D, G, L, and N) and electrical parts (H and J), respectively. Thick and thin solid lines represent high-pressure transmitting tubes and electric wires, respectively. All high-pressure vessels were connected by the transmitting tubes E. Broken lines represent thermostats.

Pressure is generated in the following way. The inner space of the pressure system is first evacuated after opening all valves, except F9 and F10. After closing F2, F6, and F8 and opening F10, helium gas is introduced from tank A into the system to a pressure of about 5 MPa (the specified value for the low pressure side of the compressor). The pressure of the system on the left side of F6 and F7 is increased up to desired value with the double-head model of diaphragm-type compressor D (NOVA SWISS 554.3330-2). While pressurizing, the compressor is supplied with helium gas continuously through the trap B immersed in liquid nitrogen to remove impurities (water etc.). It takes approximately 20 min to pressurize to 200 MPa. After pressurization, pressure generation system is isolated from other parts of the system by closing valve F5. The pressure is read from the Heise gauge C, whose accuracy is within ±0.1 MPa.

The pressure in the cell N is controlled by adjusting the temperature of the helium gas reservoir G, which has about 8 times larger volume than the cell. Pressure change in the cell is detected as the change in resistance of a manganin wire placed in the stainless steel vessel L. This resistance constitutes one arm of the Wheatstone bridge K, and its deviation from the value (corresponding to desired pressure preset with the variable resistance of K) is detected as an electric signal. The signal is amplified with the PID circuit H and utilized to regulate the temperature of the vessel G. Temperatures of the vessel L and of the bridge K are kept constant with air baths thermostatted at 32 °C for I1 and at 35 °C for I2, respectively. This method of pressure control is basically the same as that of the high pressure calorimeter with liquid pressure transmitting medium reported before.[5] The precision of the pressure and the temperature controls of the helium gas reservoir were, however, improved for use of helium gas which has much larger thermal expansivity than the liquid. The detailed description will be given below in separate sections.

Helium Gas Reservoir. Heat capacity measurement is performed at successively increasing temperatures. Consider the process in which the temperature of the cell loaded only with helium gas is increased by ΔT_c from T_c. Correspondingly, the temperature of the reservoir must be decreased from T_r to $T_r-\Delta T_r$ in order to keep the pressure of the system constant. Assuming that the helium behaves as an ideal gas,

$$\Delta T_r = \frac{T_r^2 \Delta T_c}{(V_r/V_c)(T_c+\Delta T_c)T_c + T_r \Delta T_c} \simeq \left(\frac{V_c}{V_r}\right)\left(\frac{T_r}{T_c}\right)^2 \Delta T_c, \quad (6)$$

where V_c and V_r are the volumes of the cell and of the reservoir, respectively. (V_c/V_r) is practically about 1/8. T_r is around room temperature (≈300 K) so that ΔT_r is estimated to be 1/8 K for ΔT_c of ≈1 K, when T_c=300 K; and 4.5 K when T_c=50 K. Since the temperature dependence of thermal expansivity of real high-pressure gas is smaller than that of the ideal gas, the latter value of ΔT_r would have been overestimated. Whatever the real ΔT_r may be, the temperature of the reservoir must be reduced by the same order of magnitude as a rise in temperature of the cell.

The helium gas reservoir and its temperature control system is shown in Fig. 4. The reservoir is made of stainless steel and has the volume of about 200 cm^3. Pressure seal of the upper part was achieved in two stages; at first the plug D2 was Ar-welded to the body J at F and supported by the nut A2, and secondly the

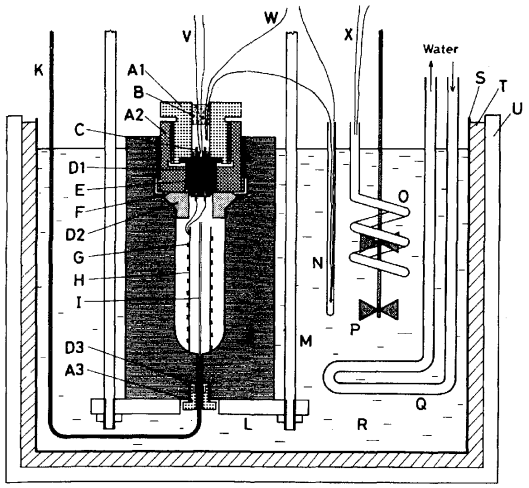

Fig. 4. Schematic drawing of the helium gas reservoir and its temperature control system.
(A): Gland nuts, (B): electric insulator, (C): electrodes, (D): plugs, (E): nylon packing, (F): Ar-welded circle, (G): manganin heater wire, (H): core copper tube, (I): copper capillary, (J): body, (K): high pressure transmitting tube, (L): holder, (M): hanging rods, (N): glass tube, (O): copper tube for heater wire, (P): stirrer, (Q): copper tube for flowing water, (R): silicone oil, (S): stainless steel box, (T): thermal insulator, (U): wooden box, (V): lead wire from PID regulator, (W): Chromel-P-constantan thermocouple, (X): lead wire for heater of oil bath from regulator.

plug D1 was pressed down against the top portion of the inside wall of plug D2 with the nut A1. Pressure seal of the lower part was achieved by the usual metallic cone connection between the plug D3 and the body J. The high pressure transmitting tube K was fixed to plug D3 with silver solder. The helium gas enters or leaves the reservoir through the copper tube I which was also soldered to plug D3. The heater wire G, used to closely control the temperature of the gas in the reservoir, was wound around the copper tube H and connected to the PID circuit through electrodes J and lead wire V. Electric insulation between C and D1 was attained with Nylon packing E.

The reservoir is placed in a variable-temperature thermostatted bath. A Chromel-P-constantan thermocouple W detects the difference in temperature between the space within A1, which reflects the temperature of helium gas in J, and the silicone oil R surrounding the body. Through this signal, the temperature difference is always kept constant by regulating the current passing through the heater installed in the copper tube O. Q is another copper tube in which cold water flows. The temperature of the oil is usually adjusted to be a few Kelvins lower than that of the inside of A1, and should decrease as the temperature of helium gas in the reservoir decreases. The usable temperature of the silicone oil bath is in the range of about 100 to 10 °C. This is broad enough to cover the entire temperature range of the measurement (30—370 K) at 200

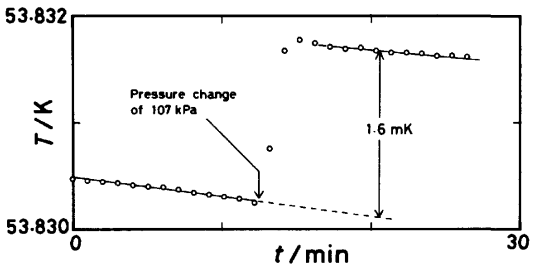

Fig. 5. Temperature response of the calorimeter cell loaded ice specimen to the helium gas pressure change of 107 kPa at 158.9 MPa and 53.83 K.

MPa, even in the case where the cell is completely filled with helium gas.

Precision of Pressure Control. Accurate pressure control is quite important, not only for obtaining the heat capacity of a definite amount of helium gas in the cell at any specified temperature and pressure, but also for attaining adiabataic condition of the cell because the heat of compression of helium gas is considerable. Let us start by deriving the relation according to which the temperature of the cell filled with helium gas is influenced by the change in the pressure within the cell under adiabatic condition. The relation may be regarded as the resultant of two processes through which the temperature of helium gas T_H changes, first by adiabatic compression and next when the gas reaches thermal equilibrium with the cell. Then the following equation is obtained;

$$\left(\frac{\partial T}{\partial p}\right)_S = \left(\frac{C_H}{C_H + C_e}\right)\left(\frac{\partial T_H}{\partial p}\right)_S, \tag{7}$$

where C_e and C_H are the heat capacities at constant pressure of the cell and the helium gas within the cell, respectively. $(\partial T_H/\partial p)_S$, which describes the first process, is given by

$$\left(\frac{\partial T_H}{\partial p}\right)_S = \frac{T_H \alpha_H V_H}{C_H}, \tag{8}$$

so that

$$\left(\frac{\partial T}{\partial p}\right)_S = \frac{T_H \alpha_H V_H}{C_H + C_e}, \tag{9}$$

where α_H and V_H are the thermal expansivity and the volume of the helium gas. If the pressure transmitting medium is liquid (*e.g.*, 3-methylpentane), α_H is of the order of 10^{-4} K^{-1} and changes little with temperature.[5] For helium gas, however, α_H is of the order of 10^{-3} K^{-1} and increases with decreasing temperature.[8] (By way of an example, the assumption of ideal gas results in α_H being proportional to $1/T$. Therefore, $(\partial T_H/\partial p)_S$ becomes large, especially at low temperatures, because both α_H and $1/(C_H+C_e)$ increase more rapidly compared with the decrease in T_H).

Figure 5 shows the observed response of the cell to pressure change of 107 kPa at 53.8 K and 158.9 MPa. The cell contained 18.2 cm^3 of ice sample so that the

volume remaining for the helium gas was about 8.1 cm^3. The temperature of the cell rose by 1.6 mK just after the compression. Substituting T_H=54 K, V_H=8.1 cm^3, C_H+C_c=81 J K^{-1} (experimental value), and α_H= 3.0×10^{-5} K^{-1} (value extrapolated from the data below 100 MPa[8]) into Eq. 9, the temperature change due to the change in pressure of 107 kPa is calculated to be 1.7 mK, which almost agrees with the observed value.

Figure 6 shows the electric signal which corresponds to the fluctuation of pressure from the preset value of 158.9 MPa at 60 K. Half an hour is normally required for one cycle of heat capacity measurement. Stability of the voltage during the measurement cycle is within 20 nV, which corresponds to about 1 kPa on the basis of the calibration in which a pressure change of 4.2 kPa gave rise to the signal of 100 nV. The fluctuation of 1 kPa corresponds roughly to a fluctuation of 15 μK in temperature from the relation shown in Fig. 5. This is small enough since the actual precision of temperature measurements is 50 μK.

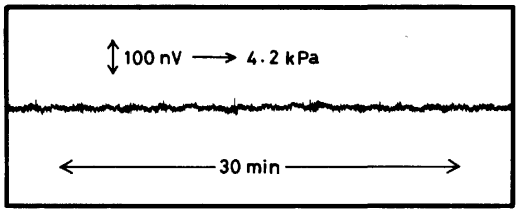

Fig. 6. Electric signal response to the fluctuations of the pressure control system at 158.9 MPa.

Heat Capacity of Helium Gas at 158.9 MPa, and Precision of the Calorimeter

The precision of the present calorimeter was examined by measuring the heat capacity of helium gas at 158.9 MPa in the temperature range between 25 and 370 K. The experimental data are given in Table 1. The starting temperature 25 K is the one below which condensation of the gas is supposed to occur. Plotted in Fig. 7 are the experimental values of the empty cell (○) and the cell fully loaded with helium gas at the constant pressure of 158.9 MPa (●), where the former was measured above 12 K. Reduction of the data to the molar heat capacities of He gas at the high pressure requires the information of equation of state of the gas and volume of the cell as functions of temperature and pressure.

Figure 8 shows the deviations of the experimental

Table 1. Heat Capacities of He Gas in the Sample Cell at 158.9 MPa

T_{av}	C_p	T_{av}	C_p	T_{av}	C_p	T_{av}	C_p	T_{av}	C_p
K	J K^{-1}	K	J K^{-1}	K	J K^{-1}	K	J K^{-1}	K	J K^{-1}
26.52	34.09	70.87	38.61	125.20	33.01	194.96	27.05	275.67	22.33
27.64	34.61	72.30	38.51	127.17	32.76	197.04	26.89	278.52	22.16
28.84	35.10	73.74	38.39	129.15	32.64	199.13	26.62	281.38	21.96
30.11	35.64	75.18	38.28	131.15	32.39	201.25	26.43	284.27	21.89
31.36	36.14	76.63	38.13	133.17	32.15	203.39	26.38	287.18	21.78
32.58	36.60	78.09	37.98	135.22	32.02	205.55	26.26	290.11	21.65
33.83	36.98	79.55	37.78	137.28	31.79	207.74	26.04	293.07	21.56
35.13	37.34	81.02	37.69	139.36	31.65	209.95	25.98	296.05	21.36
36.47	37.69	82.50	37.56	141.47	31.39	212.19	25.83	299.05	21.17
37.82	37.99	83.99	37.35	143.59	31.19	214.45	25.67	302.07	21.10
39.17	38.25	85.49	37.20	145.73	30.93	216.73	25.48	305.12	21.00
40.53	38.47	87.00	37.08	147.90	30.76	219.04	25.27	308.19	20.84
41.88	38.64	88.52	36.89	150.08	30.67	221.37	25.25	311.28	20.65
43.24	38.77	90.07	36.72	152.29	30.47	223.72	25.06	314.40	20.55
44.60	38.99	91.64	36.58	154.51	30.24	226.09	24.93	317.54	20.48
45.96	39.08	93.23	36.42	156.76	29.98	228.50	24.78	320.70	20.38
47.32	39.20	94.84	36.28	159.02	29.76	230.92	24.64	323.88	20.19
48.68	39.28	96.47	36.12	161.31	29.60	233.37	24.48	327.09	20.02
50.05	39.34	98.11	35.89	163.62	29.35	235.84	24.35	330.32	19.95
51.41	39.37	99.78	35.70	165.95	29.19	238.33	24.27	333.57	19.84
52.78	39.47	101.47	35.54	168.30	29.07	240.85	24.15	336.85	19.79
54.15	39.42	103.18	35.34	170.67	28.82	243.39	23.98	340.15	19.73
55.52	39.42	104.91	35.19	173.06	28.62	245.95	23.76	343.47	19.47
56.89	39.50	106.65	35.00	175.22	28.45	248.54	23.74	346.81	19.34
58.27	39.41	108.42	34.71	177.13	28.25	251.15	23.69	350.16	19.25
59.65	39.31	110.21	34.56	179.06	28.10	253.78	23.41	353.54	19.06
61.04	39.23	112.01	34.38	181.00	27.89	256.44	23.16	356.93	18.89
62.43	39.20	113.84	34.22	182.95	27.92	259.11	23.09	360.33	18.76
63.82	39.18	115.68	33.97	184.92	27.74	261.82	23.03	363.75	18.73
65.22	39.02	117.55	33.78	186.91	27.46	264.54	22.77	367.19	18.58
66.63	38.93	119.43	33.66	188.90	27.42	267.29	22.58	370.64	18.44
68.04	38.79	121.33	33.41	190.90	27.28	270.06	22.45		
69.45	38.76	123.26	33.20	192.92	27.04	272.86	22.38		

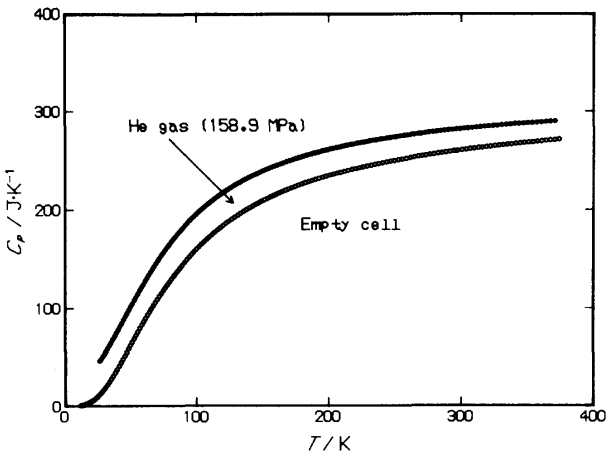

Fig. 7. Heat capacities of the empty cell (○) and of the cell with helium gas at 158.9 MPa (●). The difference between the two curves is equivalent to the heat capacity of the helium gas at 158.9 MPa.

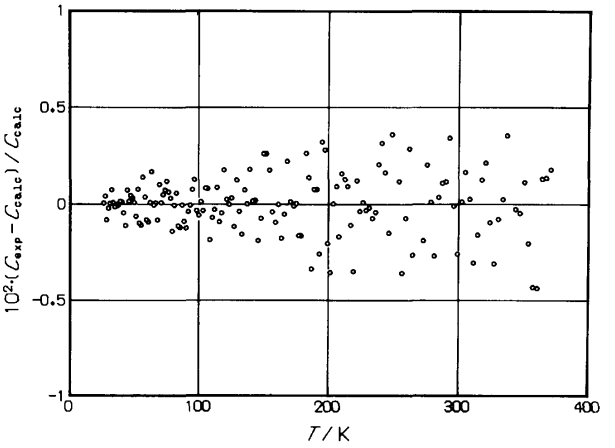

Fig. 8. Deviation plot of the observed heat capacities of helium gas at 158.9 MPa.

values from their smoothed curve. The deviation is within 0.3% over the measured temperature range; remarkably small deviation in the low temperature region is due to the special circumstances that the heat capacity of helium gas is still as large as at higher temperatures while that of the cell decreases rapidly with decreasing temperature. Heat capacities of condensed substances would generally amount only to 50—80% of that of helium gas fully loaded in the cell. The precision of the present calorimeter is therefore estimated to be within 0.5% over the experimental temperature range.

The obtained precision in this instrument is considerably poorer than that of ordinary type of calorimeters, 0.1—0.2%,[7] in the above temperature range at atmospheric pressure. This is attributed to the following two disadvantageous aspects of the present calorimeter. The heat capacity of the empty cell, reaching 270 JK^{-1} at room temperature, is almost ten times larger than that of the ordinary calorimeter. Such a large heat capacity additionally requires a longer period of energy supply for increasing the temperature, yielding the increased ambiguity of the correction for heat leakage. These aspects might have given rise to over ten times larger imprecision than that of the ordinary one unless the thermometry had been improved as described in the previous section. The decreased precision, however, is acceptable as the price for the increased information. Experimental results on some hydrogen bonded crystals will be published in due time.

This work was supported partly by a Grant-in-Aid for Scientific Research No. 57430002 from the Ministry of Education, Science and Culture. Thanks are extended to Mr. Masaharu Morimoto, Mr. Masahiro Shiomi, and Mr. Katsuji Iwamoto of the Workshop Center, Osaka University, for their help in designing and constructing the high pressure calorimeter.

References

1) D. B. McWhan and J. P. Remeika, *Phys. Rev. B*, **7**, 3079 (1973).

2) E. B. Amitin, Yu A. Kovalevskaya, E. G. Lebedeva, and I. E. Paukov, *High Temp. -High Pressures*, **7**, 269 (1975).

3) E. B. Amitin, E. G. Lebedeva, and I. E. Paukov, *Fiz. Tverd. Tela (Leningrad)*, **18**, 614 (1976).

4) J. P. Berton, B. Cornut, J. Odin, J. Paureau, and J. Peyrard, *Cryogenics*, **19**, 543 (1979).

5) M. Oguni, K. Watanabe, T. Matsuo, H. Suga, and S. Seki, *Bull. Chem. Soc. Jpn.*, **55**, 77 (1982).

6) M. A. Anisimov, V. M. Zaprudskii, G. A. Mil'ner, and E. I. Ponomarenko, *Zh. Eksp. Teor. Fiz.*, **80**, 787 (1981).

7) M. Tatsumi, T. Matsuo, H. Suga, and S. Seki, *Bull. Chem. Soc. Jpn.*, **48**, 3060 (1975).

8) R. D. McCarty, *J. Phys. Chem. Ref. Data*, **2**, 923 (1973).

 © 1987 The Chemical Society of Japan Bull. Chem. Soc. Jpn., 60, 1277—1280 (1987)

The Enantioface-Differentiating Hydrogenation of the C=O Double Bond with Asymmetrically Modified Raney Nickel. XXXIX. Repeated Uses of the Catalyst in the Hydrogenation of 2-Alkanones

Tsutomu OSAWA† and Tadao HARADA*
Institute for Protein Research, Osaka University, Yamadaoka, Suita, Osaka 565
(Received October 23, 1986)

The durability of tartaric acid-sodium bromide-modified Raney nickel in the hydrogenation of 2-octanone was investigated. A remarkable lowering of the optical yield was observed in the repeated use of the catalyst. A lack of sodium ions in the reaction system was found to be the origin of this phenomenon. The addition of sodium ions to the reaction mixture was useful for attaining high optical yields in the repeated uses of the catalyst.

The tartaric acid-sodium bromide-modified Raney nickel catalyst(TA-NaBr-MRNi) has been known as an excellent catalyst for the enantioface-differentiating hydrogenation of 2-alkanones[1] as well as β-keto esters,[2] β-diketones,[3] β-keto alcohols,[4] and β-keto sulfones.[5] We have reported regarding the hydrogenation of 2-alkanones over TA-NaBr-MRNi that the addition of a large amount of carboxylic acid to the reaction system is recommended for attaining high optical yields. The addition of pivalic acid was found to be most effective for an improvement in the optical yield. For example, 2-octanone was hydrogenated to 2-octanol in an optical yield of 80% in the presence of pivalic acid, while a negligible optical yield was attained in the absence of pivalic acid.[6]

A weakness of TA-NaBr-MRNi is a lack of durability of its enantioface-differentiating ability under repeated use.[7] On the hydrogenation of methyl acetoacetate (MAA), an optical yield of around 80% in the first use of TA-NaBr-MRNi decreased to around 50% in the fourth use of the catalyst. Since the reaction mixture for the hydrogenation of 2-alkanones contains a large amount of carboxylic acid, the surface components of the catalyst might be removed more readily than during the hydrogenation of MAA. Thus, it can be assumed that a repeated use of the catalyst in the hydrogenation of 2-alkanones would result in remarkable decreases in the optical yields.

This paper describes the results of the repeated use of TA-NaBr-MRNi in the hydrogenation of 2-octanone and our efforts to develop a simple procedure for attaining high optical yields under repeated use.

Experimental

The atomic absorption spectra were recorded on a Shimadzu AA610S atomic absorption spectrophotometer. The optical rotations were measured with a Perkin Elmer 241 polarimeter.

TA-NaBr-MRNi. The Raney nickel catalyst prepared from 3.8 g of the alloy (Ni/Al=42/58) was modified at 100 °C for 1 h, using 200 ml of an aqueous solution of tartaric acid (TA, 2 g) and NaBr (the amount stated in the footnotes of Tables), adjusted to pH 3.2 with 1 mol dm^{-3} NaOH. The modified catalyst, thus obtained, was successively washed with a 20-ml portion of water, two 100-ml portions of methanol, and two 30-ml portions of THF.

Pyridine/MRNi. TA-NaBr-MRNi (prepared as described above) was shaken with pyridine (0.4 ml) in THF (30 ml) for 5 min at room temperature. After removing the supernatant by decantation, the catalyst was washed with two 30-ml portions of THF.

MRNi-T. This was prepared by a similar procedure to that for Pyridine/MRNi. TA-NaBr-MRNi prepared from 3.8 g of the alloy was shaken with a mixture of 2-alkanone (10 ml), pivalic acid (18 ml), and THF (20 ml) for 1 h in a glass flask at room temperature. After the supernatant was removed by decantation, the catalyst was washed with two 30-ml portions of THF.

Hydrogenation of 2-Alkanones. The freshly prepared mixture of 2-alkanone (10 ml), pivalic acid (18 ml), and THF (20 ml) was used as the reaction mixture, unless otherwise stated in the text. Hydrogenation was carried out at 100 or 60 °C under 90 kg cm^{-2} of an initial hydrogen pressure in a 100-ml autoclave.

Repeated Use of TA-NaBr-MRNi. After the reaction was completed, the supernatant was separated from the catalyst by decantation. The catalyst remaining in the autoclave was washed with two 30-ml portions of THF to use the successive hydrogenation. Hydrogenation was carried out under the same conditions as above.

Determination of Optical Yield. After removing the catalyst by decantation and the evaporation of THF, the hydrogenation product was dissolved in 100 ml of ether and washed with a saturated aqueous solution of K_2CO_3. The ether solution was then dried over Na_2SO_4 and concentrated in vacuo. Simple distillation gave the hydrogenation product in a quantitative chemical yield. The optical yields were estimated from the specific rotations of the pure enantiomers: (*S*)-2-octanol, $[\alpha]_D^{20}$+9.76° (neat);[8] (*S*)-3-methyl-2-butanol, $[\alpha]_D^{20}$+4.85° (neat);[9] (*S*)-2-decanol, $[\alpha]_D^{20}$+8.68° (neat).[8]

Determination of Br$^-$ Adsorbed on the Catalyst. The amount of Br$^-$ adsorbed on the catalyst was determined by Volhard's titrimetric method.[10] A 1 g portion of TA-NaBr-MRNi or MRNi-T was decomposed with 15 ml of 60% HNO_3 in the presence of a known amount of $AgNO_3$. The resulting solution was back-titrated with NH_4SCN.

Determination of Na$^+$, Co, and Fe in the Catalyst. A 250 mg portion of TA-NaBr-MRNi or MRNi-T was dissolved in 5 ml of 2 mol dm^{-3} HNO_3. The solution was diluted to

†Present address: IATRON LABORATORIES INC., Yakuendai, Funabashi, Chiba 274.

Table 1. Repeated Uses of TA-NaBr-MRNi and Pyridine/MRNi in Hydrogenation of 2-Octanone

Catalyst[a]	Optical yield/%[b] Repeating number		
	1	2	3
TA-NaBr-MRNi	59	4	0
Pyridine/MRNi	54	6	0

a) Amount of NaBr in the modifying solution: 12g. b) The optical yields attained by the hydrogenation at 100°C.

Table 2. Enantioface-Differentiating Hydrogenation of 2-Octanone over MRNi-T[a,b]

Reaction mixture	Optical yield/%[d]
Freshly prepared	9
Recovered[c]	58

a) Amount of NaBr in the modifying solution: 12g. b) 2-Octanone was used as the 2-alkanone in the mixture for the treatment of TA-NaBr-MRNi. c) The supernatant recovered from the treatment of TA-NaBr-MRNi was used as the reaction mixture. d) The optical yields attained by the hydrogenation at 100°C.

250 ml with deionized water, and subjected to the atomic absorption analyses. The amounts of Na^+, Co^{3+}, and Fe^{3+} in the solution were determined by the calibration curve method.

Results and Discussion

We have developed the amine-treatment procedure for TA-NaBr-MRNi in order to improve the poor durabilities of the optical yields in the repeated use of the catalyst.[7c] The catalyst (Amine/MRNi) prepared by this procedure gave durable optical yields in the hydrogenation of MAA. Optical yields of around 80% were attained even after ten times of its repeated use. However, neither TA-NaBr-MRNi nor Amine/MRNi gave any durable optical yields in the hydrogenation of 2-alkanones. Typical results of the repeated use of the catalysts for the hydrogenation of 2-octanone are listed in Table 1. The optical yields decreased remarkably after the first use of both types of catalysts. In their third use, both gave a 0% optical yield.

In order to determine the origin of the remarkable decrease of the optical yields under repeated use of the catalysts, TA-NaBr-MRNi was treated with a mixture of 2-octanone, pivalic acid, and THF before the catalyst was used for the hydrogenation of 2-octanone. After the treatment, the catalyst (MRNi-T) was separated from the supernatant by decantation. Hydrogenations over MRNi-T were carried out using two kinds of reaction mixtures. One was a freshly prepared mixture of 2-octanone, pivalic acid, and THF. The other was the supernatant recovered from the treatment of TA-NaBr-MRNi. As shown in Table 2, the optical yields are dependent on the kinds of reaction mixtures. The combination of MRNi-T and the freshly prepared mixture gave a poor optical yield. This finding shows that one or more of the constituents (**X**) of the catalyst are extracted from the catalyst surface by contact with the reaction mixture. A lack of **X** in MRNi-T might be the origin of the poor optical yield. On the other hand, when the recovered reaction mixture was employed instead of the freshly prepared one, a high opltical yield was attained on the hydrogenation over MRNi-T. From this fact it is apparent that **X** dissolved in the reaction mixture plays an important role in the improvement of the optical yield. It is noteworthy that the optical yield attained by the use of MRNi-T and the recovered mixture is similar to that attained by the combination of TA-NaBr-MRNi and the freshly prepared reaction mixture (Tables 1 and 2). This similarity of the optical yields is explicable based on the following idea. The surface state of TA-NaBr-MRNi becomes similar to that of MRNi-T by contact of TA-NaBr-MRNi with the freshly prepared reaction mixture prior to the hydrogenation of 2-octanone. The freshly prepared mixture is contaminated with **X** extracted from TA-NaBr-MRNi. If this idea is the case, the poor optical yields in the second and third uses of TA-NaBr-MRNi are expected to be improved by the addition of **X** to the reaction mixture. Thus, the identification of **X** was strongly required in order to demonstrate this idea.

Table 3. Amounts of Inorganic Substances Contained in TA-NaBr-MRNi and MRNi-T

Catalyst[a]	Inorganic Substance/10^{-5} mol·g cat^{-1}			
	Na^+	Co	Fe	Br^-
TA-NaBr-MRNi	2.8	2.0	5.1	3.7
MRNi-T[b]	0.7	2.0	4.8	3.1

a) Amount of NaBr in the modifying solution: 12g. b) 2-Octanone was used as the 2-alkanone in the mixture for the treatment of TA-NaBr-MRNi.

In the course of our survey of extracted substances, several inorganic substances contained in TA-NaBr-MRNi and MRNi-T were determined by the atomic absorption spectra (results are shown in Table 3). It is clear that the treatment of TA-NaBr-MRNi with a freshly prepared reaction mixture resulted in a remarkable decrease in the amount of sodium ions contained in the catalyst. More than 70% of the sodium ions in TA-NaBr-MRNi were extracted by the treatment. The contents of Co, Fe, and Br^- were not decreased by the treatment. These findings show the possibility that the sodium ions are **X** being effective for increasing the optical yields of the hydrogenation of 2-alkanones.

In order to confirm the above possibility, we examined the effects of the sodium ions in a freshly prepared mixture on the optical yields of the hydrogenation of several kinds of 2-alkanones over MRNi-T. The

Table 4. Effects of Added Sodium Ions on Optical Yields of Hydrogenation of 2-Alkanones over MRNi-T

Catalyst[a)]	Substrate	Sodium pivalate/mg	Optical yield/%[e)]
MRNi-T[b)]	2-Octanone	0	9
		0.5	21
		3	61
		20	60
MRNi-T[c)]	3-Methyl-2-butanone	0	3
		20	68
MRNi-T[d)]	2-Decanone	0	13
		20	63

a) Amount of NaBr in the modifying solution: 12g. b, c, d) MRNi-T was prepared by the treatment of TA-NaBr-MRNi with the mixture of 2-octanone(b), 3-methyl-2-butanone(c), or 2-decanone(d), and pivalic acid in THF. e) The optical yields attained by the hydrogenation at 100°C.

Table 5. Relation between Amount of Added Sodium Pivalate and Optical Yield in Repeated Use of TA-NaBr-MRNi

Run	Added sodium pivalate/mg	Optical yield/%[a)] Repeating number					
		1	2	3	4	5	6
1	10	62	61	3	—	—	—
2	20	61	61	25	0	—	—
3	40	59	59	58	17	—	—
4	100	58	58	57	54	47	7
5	10	80	80	6	—	—	—
6	100	74	74	75	73	65	59

a) Runs 1 to 4:
Catalyst: RNi modified with an aqueous solution of TA(2g) and NaBr (12g) at pH 3.2, 100°C.
Hydrogenation temperature: 100°C.
Runs 5 and 6:
Catalyst: RNi modified with an aqueous solution of TA(2g) and NaBr (30g) at pH 3.2, 100°C.
Hydrogenation temperature: 60°C.
a) The optical yields attained by the hydrogenation of 2-octanone.

resulting optical yields are listed in Table 4. The addition of a small amount of sodium pivalate to the reaction mixture remarkably improved the optical yields in the hydrogenation of 2-octanone, 3-methyl-2-butanone, and 2-decanone. The addition of 3 mg of sodium pivalate to the freshly prepared reaction mixture was enough to attain the optical yield around 60% in the hydrogenation of 2-octanone.

We then carried out repeated use of TA-NaBr-MRNi in the hydrogenation of 2-octanone, using freshly prepared reaction mixtures containing various amounts of sodium ions. The optical yields, thus attained, are shown in Table 5. It is evident that the optical yield in the first use of TA-NaBr-MRNi is somewhat decreased with an increase of the amount of the added sodium pivalate, and the durability of the optical yield in the repeated use is remarkably increased with an increase of the amount of sodium pivalate. This tendency was remarkably observed in hydrogenation at 60°C. Upon the addition of 10 mg of sodium pivalate, a high optical yield (80%) was attained and the optical yield in the first use of the catalyst was almost lost in the third use. On the other hand, when 100 mg of sodium pivalate was added, a rather low optical yield (74%) was attained in the first use and an optical yield of around 60% was attained even during the sixth use of the catalyst.

The present investigation clarified the fact that the addition of sodium ions to the reaction mixture improved the durability of the optical yield in the repeated use of TA-NaBr-MRNi for the enantioface-differentiating hydrogenation of 2-alkanones. In order to clarify the origin of the effects of sodium ions, further studies are now in progress.

The authors would like to thank Professor Yoshiharu Izumi of Osakagakuin University, Professor Akira Tai of Himeji Institute of Technology, and Dr. Hiroshi Ozaki of Osaka University for their many helpful discussions and suggestions in the course of this work. The authors also wish to express their thanks to Mr. Hitoshi Yamada of Osaka University for the help in the measurements of the atomic absorption spectra.

References

1) a) T. Osawa and T. Harada, *Chem. Lett.*, **1982**, 315; b) *Bull. Chem. Soc. Jpn.*, **57**, 1518 (1984).

2) T. Harada, M. Yamamoto, S. Onaka, M. Imaida, H. Ozaki, A. Tai, and Y. Izumi, *Bull. Chem. Soc. Jpn.*, **54**, 2323 (1981).
3) K. Ito, T. Harada, and A. Tai, *Bull. Chem. Soc. Jpn.*, **53**, 3367 (1980).
4) S. Murakami, T. Harada, and A. Tai, *Bull. Chem. Soc. Jpn.*, **53**, 1356 (1980).
5) Y. Hiraki, K. Ito, T. Harada, and A. Tai, *Chem. Lett.*, **1981**, 131.
6) T. Osawa, *Chem. Lett.*, **1985**, 1609.
7) a) A. Tai, Y. Imachi, T. Harada, and Y. Izumi, *Chem. Lett.*, **1981**, 1651; b) A. Tai, T. Tsukioka, Y. Inoue, H. Ozaki, T. Harada, and Y. Izumi, *Proc. 8th Int. Congr. Catal.* Berlin (West) (1984), p. V-531; c) A. Tai, K. Tsukioka, H. Ozaki, T. Harada, and Y. Izumi, *Chem. Lett.*, **1984**, 2083.
8) R. H. Pickard and J. Kenyon, *J. Chem. Soc.*, **99**, 45 (1911).
9) R. H. Pickard and J. Kenyon, *J. Chem. Soc.*, **101**, 621 (1912).
10) a) M. B. Stschigol, *Z. Anal. Chem.*, **91**, 182 (1932); b) S. Takagi, "Teiryobunseki No Jikken To Keisan," Kyoritsu Shuppan Co Ltd., Tokyo (1949), Vol. 2, p. 222.

 © 1987 The Chemical Society of Japan Bull. Chem. Soc. Jpn., 60, 1281—1287 (1987)

Self Aggregation of Cationic Porphyrin in Water

Koji KANO,* Takeshi NAKAJIMA, Masao TAKEI, and Shizunobu HASHIMOTO
Department of Applied Chemistry, Faculty of Engineering, Doshisha University, Kamikyo-ku, Kyoto 602
(Received October 28, 1986)

Self aggregation of 4,4′,4″,4‴-(21*H*,23*H*-porphine-5,10,15,20-tetrayl)tetrakis[1-methylpyridinium] cation ($TMPyP^{4+}$) in water has been verified by means of fluorescence and ^1H NMR spectroscopy. The novel fluorescence behavior of TMPyP such as extraordinarily red-shifted Q(0-0) fluorescence band, blue shift of this band upon dilution, effects of added sodium chloride and sodium dodecyl sulfate micelles, and short fluorescence lifetime strongly suggests the formation of a stacking-type dimer of $TMPyP^{4+}$ at the TMPyP concentrations above 1×10^{-6} mol dm^{-3}. The ^1H NMR signal due to the porphyrin ring protons was observed as a broad singlet even though the concentration of TMPyP in D_2O was 1×10^{-5} mol dm^{-3} while the signal in DMSO-d_6 was a sharp singlet, suggesting the spontaneous association of $TMPyP^{4+}$ to form the face-to-face dimer having a considerably loose structure. The π-π interaction has been assumed to be enhanced upon photoexcitation.

It has been known that various anionic porphyrins such as proto-, deutero-, and hematoporphines, and 4,4′,4″-(20-phenyl-21*H*,23*H*-porphine-5,10,15-triyl)-tris[benzenesulfonic acid](TPPS$_3$), and 4,4′,4″,4‴-(21*H*,23*H*-porphine-5,10,15,20-tetrayl)tetrakis[benzenesulfonic acid] (TPPS$_4$) tend to stack spontanously in aqueous solutions to form dimers and/or higher aggregates, the binding constants (K) for dimerization being reported to be 10^4—10^7 mol^{-1} dm^3.[1-12] Well-extended π electron systems of the porphyrins seem to promote the self aggregation which is an opposite process of electron repulsion. In agreement with this assumption, an extremely large equilibrium constant for dimerization has been reported for phthalocyanine-tetrasulfonate ($K=1.48\times10^8$ mol^{-1} dm^3 at 14 °C).[13] On the contrary, Pasternack et al. have demonstrated that a cationic porphyrin, 4,4′,4″,4‴-(21*H*,23*H*-porphine-5,10,15,20-tetrayl)tetrakis[1-methylpyridinium] cation ($TMPyP^{4+}$), and its metal complexes do not aggregate in aqueous solutions.[3,4,14,15] No evidence for self aggregation has been presented from absorption and NMR spectroscopy and temperature-jump relaxation method. In a previous communication, we reported the novel fluorescence behavior of $TMPyP^{4+}$ in water as described below.[16] (1) Although the Q(0-0) and Q(0-1) fluorescence bands of most of porphyrins are well-resolved from each other, the Q(0-0) band of the $TMPyP^{4+}$ fluorescence shifts to longer wavelength to partially overlap with the Q(0-1) band. (2) The fluorescence lifetime of $TMPyP^{4+}$ (4.1 ns) is significantly shorter than those of many other porphyrin free bases (9—14 ns). (3) Addition of methanol or sodium dodecyl sulfate (SDS) micelles causes the blue shift of the Q(0-0) band and the increase in the fluorescence quantum yield and lifetime of $TMPyP^{4+}$. (4) Coalesced Q(0-0) and Q(0-1) bands at low temperature separate each other with increasing temperature. We interpreted these fluorescence results in terms of the monomer-aggregate equilibrium of $TMPyP^{4+}$ in water.[16] Recently, Pasternack et al. criticized our previous assumption on the basis of the results on the absorption and NMR spectroscopy and the complexation of $TMPyP^{4+}$ with nucleosides and nucleotides.[15] Indeed, our previous communication lacks in the discussion about the electronic effects of the peripheral substituents on the $TMPyP^{4+}$ fluorescence. The lower pK_a of $TMPyP^{4+}$[3,17,18] compared with anionic porphyrins suggests the delocalization of positive charge on the peripheral pyridinium cations on the porphyrin ring.

In this work, we reinvestigated the $TMPyP^{4+}$ fluorescence and found that the novel fluorescence behavior cannot be explained only by the electronic effects. All of the fluorescence data could be interpreted in terms of the self association of $TMPyP^{4+}$. ^1H NMR measurements also support the stacking-type interaction of $TMPyP^{4+}$.

Experimental

The tetrakis(*p*-toluenesulfonate) salt of $TMPyP^{4+}$ (TMPyP) was prepared according to the procedures described in a literature[3] and recrystallized from methanol. The tetrachloride salt (TMPyP(Cl)) was also prepared by passing TMPyP through an ion-exchange column. Since the results were essentially the same for these two porphyrins, the former porphyrin was used in this work unless otherwise noted. Sodium dodecyl sulfate (SDS, >99%, Nakarai) was used without further purification.

The absorption spectra were taken on a Shimadzu UV-200S or a Shimadzu MPS-5000 spectrophotometer. The fluorescence spectra were measured by a Shimadzu RF-500 (excitation and emission bandwidths=10 nm) or a Hitachi 650-60 spectrofluorometer (bandwidths=5 nm). In the fluorescence measurements of very diluted sample, a Raman band due to water appeared as a background which was cancelled by using a microcomputer attached to a Hitachi 650-60 spectrofluorometer. The measurements were carried out at 25 °C under aerobic conditions unless otherwise noted. The spectroscopic measurements were done 20 min after each sample was prepared. The fluorescence lifetimes were determined using an Ortec-PRA single-photon counting apparatus. The 400-Mz ^1H NMR spectra in D_2O were obtained on a JEOL GX-400 spectrometer at 23±0.5 °C. Sodium 3-trimethylsilyl-1-propanesulfonate (Merck) was used as an external standard for measurements in D_2O. TMS (Nakarai) was used as an internal standard in DMSO-d_6.

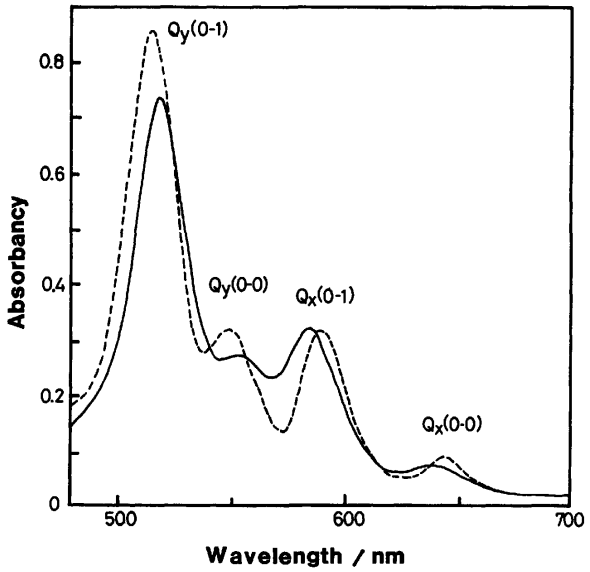

Fig. 1. Absorption spectra of TMPyP (5×10^{-5} M as monomer) in water (——) and methanol (----) at room temperature.

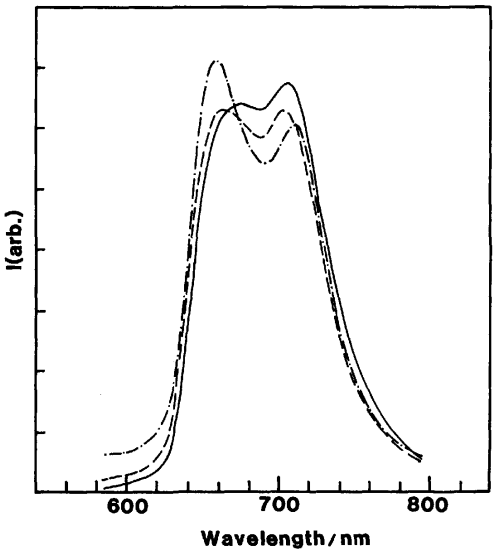

Fig. 2. Fluorescence spectra of 1×10^{-6} (——), 1×10^{-7} (----), and 1×10^{-8} M (-·-·-) TMPyP in water at 25 °C. TMPyP was excited at its Soret band. The concentrations of TMPyP are calculated as the monomer.

Results and Discussion

Electronic Spectra of TMPyP. TMPyP shows novel absorption and fluorescence spectra in aqueous solutions. Most of *meso*-substituted porphyrins show etio-type absorption spectra; i.e., the absorbancies of the Q bands decrease in the order of $Q_y(0\text{-}1)$, $Q_y(0\text{-}0)$, $Q_x(0\text{-}1)$, and $Q_x(0\text{-}0)$ bands. As shown in Fig. 1, however, the absorbancy of $Q_y(0\text{-}0)$ band of TMPyP in water is considerably smaller than that of $Q_x(0\text{-}1)$ band. In methanol, the Q_y bands shift to shorter wavelengths and the Q_x bands move to longer wavelengths compared with those in water and the absorbancy of the $Q_y(0\text{-}0)$ band is restored. The fluorescence emission spectrum of TMPyP in water also differs from those of other porphyrins. In water, the Q(0-0) and Q(0-1) fluorescence bands of 1×10^{-7} M (1 M=1 mol dm^{-3}) TMPyP appeared at 664 and 706 nm (Fig. 2), respectively. The Q(0-0) band shifts to longer wavelength compared with those of other porphyrins and two Q bands partially overlap each other. Upon dilution to 1×10^{-8} M, the Q(0-0) band shifted to shorter wavelength (654 nm) while the shift of the Q(0-1) band was relatively small (708 nm). It was confirmed that the fluorescence spectral change upon high dilution is not due to complexation with trace amounts of metal ions coexisting in the system by using water distilled three times and deionized with an ion-exchange column. The fluorescence excitation spectral maxima were observed at 422 and 430 nm for 1×10^{-7} and 1×10^{-8} M solutions, respectively. These peaks correspond to the Soret bands of the TMPyP absorption spectra.

If the positive charges on the peripheral pyridinium cations perturb the electronic states of TMPyP, the absorption and fluorescence spectra of TMPyP may be affected greatly by the solvent polarity. Table 1 shows the absorption and fluorescence maxima of the Q bands of TMPyP (5×10^{-5} M) in various solvents. We could not recognize any correlation between solvent polarity parameters and the absorption maxima of the $Q_y(0\text{-}1)$ and $Q_y(0\text{-}0)$ bands. Fairly good linear relationships were observed between dielectric constant or Kamlet-Taft's π^* value of solvent and the absorption maxima of the $Q_x(0\text{-}1)$ and $Q_x(0\text{-}0)$ bands.

In analogy with the Q_x absorption bands, both Q(0-0) and Q(0-1) fluorescence maxima shifted to shorter wavelengths with increasing solvent polarity except for the Q(0-0) band in water (Fig. 3). An extremely large red shift of the Q(0-0) fluorescence band in water indicates the stabilization of the lowest excited singlet state of TMPyP by some reason. The dissociation of TMPyP into ions may account for the novel fluorescence behavior in water. It is commonly known that aprotic dipolar solvents such as *N,N*-dimethylformamide (DMF), dimethyl sulfoxide (DMSO), and *N,N*-dimethylacetamide (DMA) can dissolve ions and stabilize cationic species due to strong solvation.[19] As is shown in Fig. 3, however, no deviations were observed for these solvents in the relation between the fluorescence maximum of the Q(0-0) band and the dielectric constant. This supports the contention that the abnormally red-shifted Q(0-0) fluorescence band in water is not due to the dissociation of the *meso*-substituents into ions. The similar red shift of the fluorescence band has been reported for a porphyrin dimer formed by pairing cationic and anionic porphyrins.[20]

The effects of NaCl on organic ions in water may be

Table 1. Absorption and Fluorescence Maxima of Q Bands of TMPyP (5×10^{-5} M) in Various Solvents at 25 °C

Solvent[a]	ε[b]	Absorption maximum/nm				Fluorescence maximum/nm[c]	
		$Q_y(0-1)$	$Q_y(0-0)$	$Q_x(0-1)$	$Q_x(0-0)$	Q(0-0)	Q(0-1)
H_2O	78.5	519	555	585	638	678	706
DMSO	48.9	517	550	588	642	651	712
DMA	37.8	515	549	588	642	650	713
CH_3CN	37.5	516	550	589	643	652	714
DMF	36.7	516	549	589	643	651	713
CH_3OH	32.6	516	550	590	645	655	715
C_2H_5OH	24.3	517	551	591	646	655	716
Acetone	20.5	515	549	589	644	652	714
2-PrOH	18.3	518	552	591	646	655	717
Pyridine	12.3	521	556	593	648	658	719

a) DMSO: dimethyl sulfoxide, DMA: *N,N*-dimethylacetamide, DMF: *N,N*-dimethylformamide. b) Dielectric constant. c) The fluorescence spectra were measured by exciting TMPyP at $Q_x(0-1)$ absorption band.

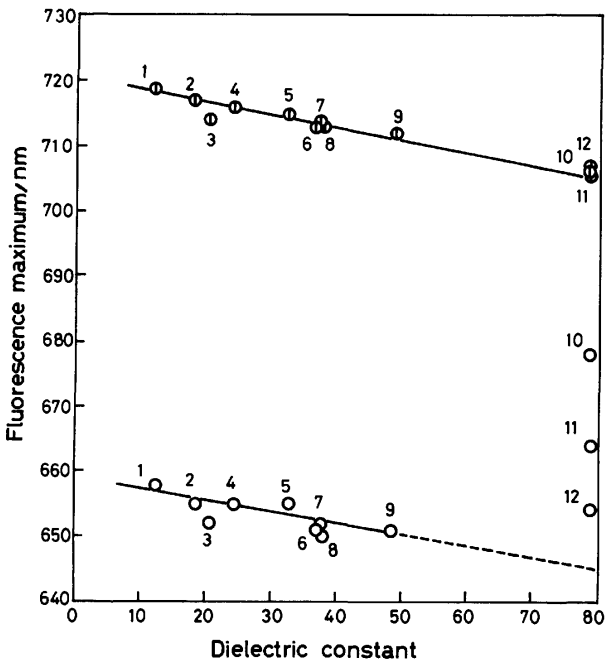

Fig. 3. Fluorescence maxima of the Q(0—0) (○) and Q(0—1) bands (⊕) of TMPyP (5×10^{-5} M as monomer) in various solvents at 25 °C: 1: pyridine, 2: 2-propanol, 3: acetone, 4: ethanol, 5: methanol, 6: *N,N*-dimethylformamide, 7: acetonitrile, 8: *N,N*-dimethylacetamide, 9: dimethyl sulfoxide, 10: water, 11: water ([TMPyP]=1×10^{-7} M as monomer), 12: water ([TMPyP]=1×10^{-8} M as monomer). TMPyP was excited at 583 nm.

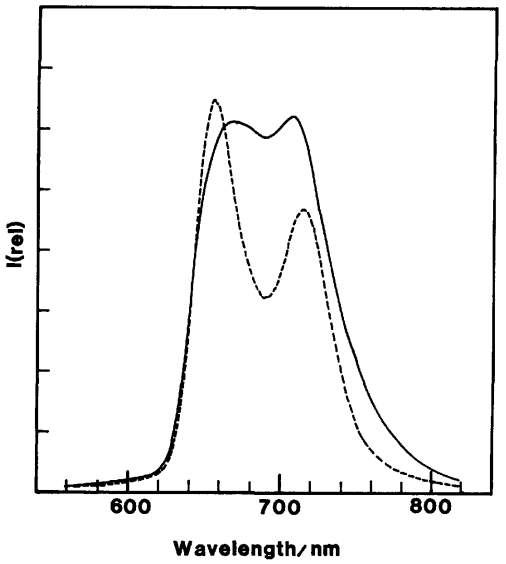

Fig. 4. Fluorescence spectra of TMPyP (1×10^{-7} M as monomer) in water (——) and in water containing 1×10^{-2} M nitrobenzene (----) at 25 °C. TMPyP was excited at 428 nm (bandwidths of spectrofluorometer=5 nm).

somewhat complex. The electrostatic repulsion between the organic ions should be reduced by added NaCl to enhance aggregation of the solute ions. Meanwhile, the dielectric constant of water is lowered upon addition of NaCl. The 1×10^{-6} M aqueous solution of TMPyP showed the fluorescence maxima at 678 and 706 nm (Fig 2). The Q(0-0) fluorescence band shifts to longer wavelength compared with those for the 1×10^{-7} and 1×10^{-8} M solutions. The Q(0-0) band further shifted to longer wavelength upon addition of 1.0 M NaCl and this fluorescence band became a shoulder of the Q(0-1) band, Q(0-0) and Q(0-1) bands being observed at around 680 (sh) and 706 nm, respectively. The shape of the fluorescence spectrum in 4.0 M aqueous NaCl was essentially the same as that in 1.0 M aqueous NaCl, but the fluorescence intensity slightly decreased. If the extraordinary red shift of the Q(0-0) band is due to the effects of the positive charges on the peripheral pyridinio substituents, the neutralization of the charges and the reduction of the dielectric constant caused by added NaCl should provide the blue shift of the Q(0-0) band.

A dramatic fluorescence spectral change was observed when nitrobenzene (1×10^{-2} M) was added to the aqueous TMPyP (1×10^{-7} M) solution without salt, as is shown in Fig. 4. Previously, we have found that nitrobenzene forms a ground-state complex with $TPPS_3$.[21] The result shown in Fig. 4 can be inter-

Table 2. Fluorescence Lifetimes (τ_0) of TMPyP and Other Porphyrins

Porphyrin[a)]	Medium	τ_0/ns[b)]	Ref.
TPP	Methylcyclohexane	13.6 (a)	c
TTP	Acetone	10.7 (a)	d
TTP	Acetone	12.0 (an)	d
$TPPS_3$	pH 8.0	9.2—10.2 (a)	e
$TPPS_4$	pH 5.0	13.6	f
$TPPS_4$	H_2O	14 (an, a)	g
TAPP	H_2O	9.3	h
TMPyP	pH 5.0	5.3	f
TMPyP	H_2O	4.1 (a)	i
TMPyP	CH_3OH	7.2 (a)	i
TMPyP	0.1 M SDS	9.6 (a)	i
TMPyP	Glycerol	10.8 (a)	j
TMPyP	Glycerol (−65°C)	14.5 (a)	j

a) TPP: 5,10,15,20-tetraphenyl-21*H*,23*H*-porphine, TTP: 5,10,15,20-tetrakis(4-methylphenyl)-21*H*,23*H*-porphine, TAPP: 4,4′,4″,4‴-(21*H*,23*H*-porphine-5,10,15,20-tetrayl)tetrakis[trimethylphenylammonium] tetraiodide. b) The anaerobic and aerobic conditions are represented by (an) and (a), respectively. c) A. Harriman, *J. Chem. Soc., Faraday Trans. 1*, **76**, 1978 (1980). d) S. Yamada, T. Sato, K. Kano, and T. Ogawa, *Photochem. Photobiol.*, **37**, 257 (1983). e) Ref. 23. f) K. Kalyanasundaram and M. Neumann-Spallart, *J. Phys. Chem.*, **86**, 5163 (1982). g) A. Harriman, G. Porter, and M.-C. Richoux, *J. Chem. Soc., Faraday Trans. 2*, **77**, 833 (1981). h) K. Kalyanasundaram, *J. Chem. Soc., Faraday Trans. 2*, **79**, 1365 (1983). i) Ref. 16. j) This work.

preted as that nitrobenzene pulls out a TMPyP molecule from the TMPyP dimer or the higher aggregates to form a 1 : 1 complex which shows a fluorescence spectrum similar to those of other porphyrin monomers. We reported the same effects of SDS micelles as that of nitrobenzene.[16] In the case of the SDS micelles, however, the charges of the pyridinium cations of TMPyP are neutralized to some extent by pairing these oppositely charged micelles. The effects of nitrobenzene, a nonionic species, on the TMPyP fluorescence strongly suggest that TMPyP in water is not in monomer form.

All fluorescence data can be explained by the TMPyP dimer (or higher aggregates) formation in water, but not by the electronic effects of the peripheral pyridinio substituents.

Fluorescence Lifetime of TMPyP. The fluorescence lifetime of TMPyP in aqueous solution is about 2-fold smaller than those of other *meso*-substituted porphyrins and of TMPyP in the glycerol and SDS micellar solutions (Table 2). TMPyP is more acidic (pK_a=1—2)[3,17,18,22] than $TPPS_3$ (pK_a=4.8),[3] $TPPS_4$ (pK_a=4.8),[23] and 4,4′,4″,4‴-(21*H*,23*H*-porphine-5,10,15,20-tetrayl)tetrakis[trimethylphenylammonium] salt (TAPP, pK_a=3.6—4.1).[24] Kalyanasundaram measured the pK_a values and the fluorescence of TMPyP and its three isomers.[22] The pK_a value of 2,2′,2″,2‴-(21*H*,23*H*-porphine-5,10,15,20-tetrayl)tetrakis[1-methylpyridinium] tetra-*p*-toluenesulfonate (TMPyP-2) is much smaller (−0.9) than the 3-substituted isomer

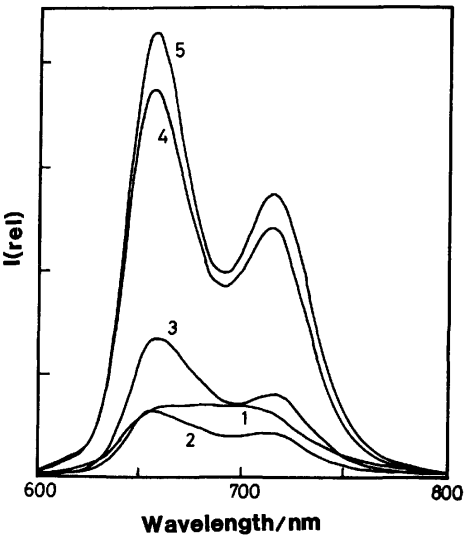

Fig. 5. Fluorescence spectra of TMPyP (1×10^{-6} M as monomer) in water in the presence of SDS at 25°C: 1: [SDS]=0, 2: 1×10^{-4}, 3: 1×10^{-3}, 4: 5×10^{-3}, 5: 1×10^{-2}M. TMPyP was excited at 420 nm.

(TMPyP-3) (1.8) and TMPyP (1.4). Since the free rotation of the peripheral pyridinio substituents of TMPyP-2 is strictly restricted by a steric factor, the positive charges of the pyridinium groups should not delocalize on the π-electron system of the porphyrin ring. In spite of this expectation, pK_a of TMPyP-2 is much smaller than those of TMPyP-3 and TMPyP. Kalyanasundaram explained the difference in the pK_a values by σ charge density in the porphyrin ring.[22] On the other hand, the Q(0-0) fluorescence band and the fluorescence lifetime are sensitive to the pyridinio substituents.[22] Namely, the Q(0-0) fluorescence maxima of TMPyP, TMPyP-3, and TMPyP-2 are 675, 653, and 641 nm, respectively, and the fluorescence lifetimes in water increase in the order of TMPyP (6.0 ns), TMPyP-3 (7.9 ns), and TMPyP-2 (13.8 ns). Such continuous substituent effects on the fluorescence of these cationic porphyrins suggest that the novel fluorescence behavior of TMPyP is ascribed to the delocalization of the positive charges of the peripheral substituents on the porphyrin ring through the π-conjugation system. As is described above, however, the TMPyP-concentration effect as well as the effects of added NaCl and nitrobenzene on the TMPyP fluorescence spectrum cannot be interpreted in terms of the electronic effects of the pyridinio substituents. It is reasonable to assume that, in the case of TMPyP, delocalized positive charges increase the polarizability of TMPyP molecule leading to enhancement of van der Waals interaction between the TMPyP molecules, which may be used as a predominant binding force for forming the TMPyP dimer. The nonradiative transition of the TMPyP dimer may be faster than that of the TMPyP monomer.

Effects of SDS Micelles. Pasternack et al.[15] reexamined our previous experiments of the effects of the SDS

micelles on the TMPyP fluorescence and found that addition of 4×10^{-4} M SDS provides the same effects as does 0.1 M SDS. However, we could not reproduce their result as shown in Fig. 5. The fluorescence yield of TMPyP decreases upon addition of small amounts of SDS (1×10^{-4} M), which may be due to the self quenching occurring in the small aggregates of the association complex of TMPyP and SDS. At near a critical micelle concentration (cmc=9.8×10^{-3} M at 25 °C),[25] the fluorescence yield markedly increased. Above the cmc, the TMPyP dimer seems to dissociate to the monomer which is included within the micelle. The shape of the TMPyP fluorescence spectrum in water containing 1×10^{-3} M SDS was very similar to those in $>5\times10^{-3}$ M SDS solutions, while the fluorescence yield was still small. This may be ascribed to the formation of premicelles which are known to yield in the detergent solutions containing various dyes.[26] The TMPyP molecules are concentrated within the premicelles and both self quenching and energy migration may lead the decrease in the fluorescence yield. The effects of the SDS micelles are also explained by the dimer model.

^{1}H NMR Spectra. The 400-Mz ^{1}H NMR spectra of TMPyP in D_2O and DMSO-d_6 are shown in Fig. 6. For the 1×10^{-2} M D_2O solution of TMPyP, the ring protons of the peripheral pyridinium cations and of the *p*-toluenesulfonate anions, the counter anions of $TMPyP^{4+}$, were observed at 9.20, 8.70, 6.86 and 5.97 ppm, respectively. Interestingly, the porphyrin ring protons appeared at ca. 8.95 ppm as a broad singlet. These signals, especially those of *p*-toluenesulfonate, were shifted to lower magnetic fileds upon dilution. The signal due to the porphyrin ring protons was not sharpened upon dilution up to 1×10^{-4} M, while that in DMSO-d_6 was observed at 9.16 ppm as a sharp singlet. Foster reported that the concentration-dependent chemical shifts of TMPyP are ascribed to a stacking-type interaction between $TMPyP^{4+}$ and its counter anion.[27] Then we measured the ^{1}H NMR spectra of TMPyP(Cl) at various concentrations (5×10^{-2}—1×10^{-5} M) (Fig. 7). At the concentrations below 1×10^{-2} M, the protons of the pyridinium ring were measured at the constant magnetic fields (9.33 and 9.00 ppm). These protons, however, resonanced at higher mag-

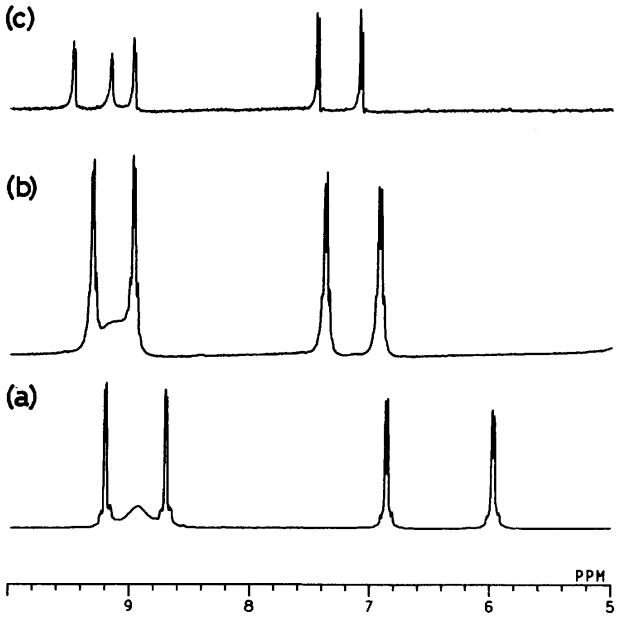

Fig. 6. 400-MHz ^{1}H NMR spectra of (a) 1×10^{-2} and (b) 1×10^{-3} M TMPyP in D_2O and (c) 1×10^{-4} M TMPyP in DMSO-d_6.

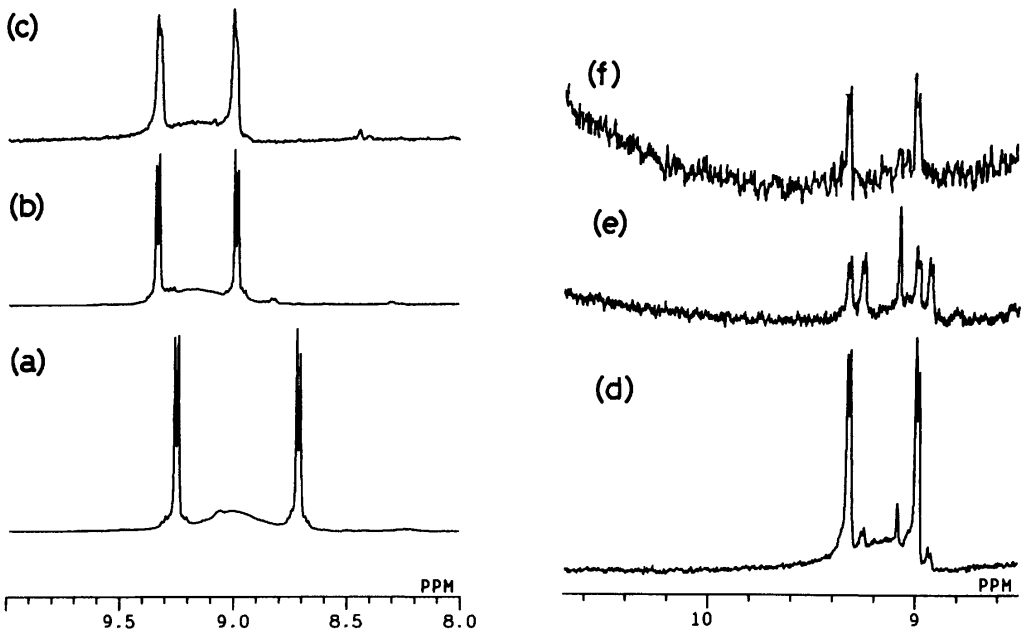

Fig. 7. 400-MHz ^{1}H NMR spectra of (a) 5×10^{-2}, (b) 1×10^{-3}, (c) 1×10^{-4}, and (f) 1×10^{-5} M TMPyP(Cl) in D_2O and of (d) 5×10^{-5} M TMPyP(Cl) in the presence of 1.25×10^{-4} M TMSPS and (e) 1×10^{-5} M TMPyP(Cl) in the presence of 2.5×10^{-5} M TMSPS in D_2O. TMSPS was used as an external standard.

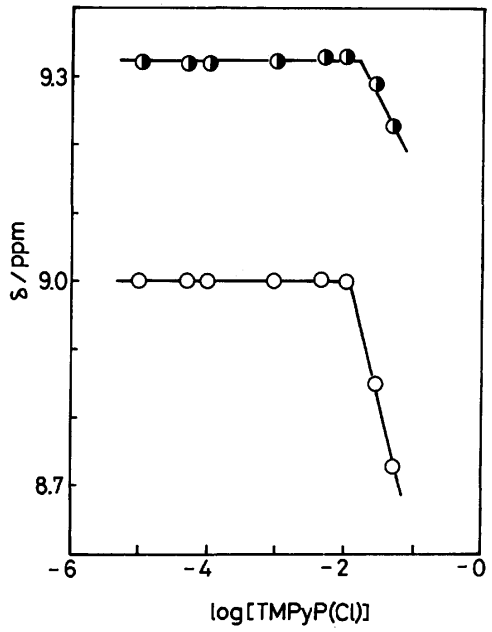

Fig. 8. Plots of the chemical shifts of the protons at the 2 and 6 (◑) and of the 3 and 5 positions (○) of the pyridinium ring of TMPyP(Cl) vs. TMPyP-(Cl) concentration in D_2O.

netic fileds at the TMPyP(Cl) concentrations above 1×10^{-2} M (Fig. 8). Pasternack et al. also studied the concentration effects ($1-50\times10^{-3}$ M) on ^{1}H NMR of TMPyP(Cl) in D_2O at μ=0.3 M and found that the chemical shift of the protons at the 2 and 6 positions of the pyridinium ring moves continuously to higher magnetic field with increasing the TMPyP (Cl) concentration in the presence of inorganic salt.[15] In the absence of inorganic salt, however, the upfield shift was observed only at the concentrations above 1×10^{-2} M. Pasternack et al. did not discuss about the porphyrin ring protons. As Fig. 7 shows, the porphyrin ring protons of TMPyP(Cl) show a very broad signal as in the case of TMPyP. The broadening of the pyrrole protons of TMPyP in ^{1}H NMR, therefore, is not ascribed to the interaction between *p*-toluenesulfonate and the porphyrin ring. It can be concluded that there is an exchange process between the two states of TMPyP in aqueous solution. The monomer-dimer equilibrium is the most plausible process for explaining the broadening of the NMR signal due to the pyrrole protons. In all cases described above, each chemical shift was determined by using 3-trimethylsilyl-1-propanesulfonate (TMSPS) as an external standard. Figure 7 also shows the effect of added TMSPS on the ^{1}H NMR of TMPyP(Cl). Two pairs of the NMR signals due to the pyridinium protons and a sharp singlet due to the porphyrin ring protons were measured clearly for the 1×10^{-5} M D_2O solution of TMPyP(Cl) containing 2.5×10^{-5} M TMSPS. Under the same conditions, we measured the fluorescence spectra, which showed that the fluorescence maximum of the Q(0-0) band at 678 nm in H_2O shifts to 670 nm in the presence

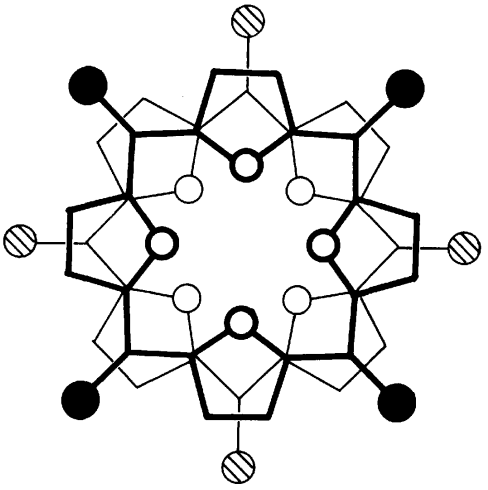

Fig. 9. Plausible structure of the TMPyP dimer in water. ● and ⊘ represent the peripheral pyridinio substituents.

of 2.5×10^{-5} M TMSPS. In the presence of large amounts of TMSPS (1×10^{-2} M) the well-resolved Q(0-0) and Q(0-1) bands of TMPyP(Cl) were observed at 654 and 712 nm, respectively. Both ^{1}H NMR and fluorescence data can be interpreted as that TMSPS binds electrostatically with TMPyP(Cl) leading to the dissociation of the TMPyP(Cl) dimer.

The ^{1}H NMR also suggests the structure of the TMPyP dimer. All of the NMR data can be interpreted in terms of the face-to-face dimer structure, where the peripheral pyridinio substituents of the two TMPyP molecules may be oriented each other to minimize the steric hindrance and the coulombic repulsion (Fig. 9). If the TMPyP dimer is a very tight π complex and the monomer scarecely exists in the system, one should observe a sharp singlet NMR signal due to the porphyrin ring. On the contrary, if the monomer-dimer equilibrium consists of very fast formation and dissociation processes, a sharp singlet signal is also expected. The broadening of the porphyrin ring protons indicates the formation of the TMPyP dimer having an intermediately loose structure. The relatively weak ring current of the pyridinium group, the relative orientation of the adjacent pyridinium groups of the TMPyP dimer (see Fig. 9), the loose structure of the dimer, and the free rotation of the peripheral substituents may account for the sharp AA'XX' multiplet due to the pyridinium ring protons.

On the basis of these results, we concluded that $TMPyP^{4+}$ dimerizes in H_2O in the concentration range, at least, from 1×10^{-2} to 1×10^{-5} M and forms higher aggregates at the concentrations above 1×10^{-2} M. The TMPyP(Cl)-TMSPS complex may include a $TMPyP^{4+}$ ion which shows a NMR spectrum of monomeric $TMPyP^{4+}$.

Dimer Model of TMPyP. As Pasternack et al.[3] indicated, no absorption spectral change was observed for TMPyP in the concentration range from 1×10^{-5} to 1×10^{-3} M.[16] TMPyP obeys Beer's law in this concen-

tration range. The fluorescence behavior is also unchanged at the concentrations above 1×10^{-6} M. These aspects suggest only one species (we assume the dimer) in the aqueous solutions of $>10^{-6}$ M TMPyP. Pasternack et al.[15] also stated that the Soret band of TMPyP does not shift markedly in the SDS solution while that of another cationic porphyrin ($PPIX(en)_4$) aggregates shifts to longer wavelength upon dissociation to the monomer in the SDS micellar solution. A TMPyP molecule has a D_{2h} symmetry. If this symmetry is ruptured by complexation, the Soret band is expected to shift. Indeed, information for the TMPyP-dimer formation could scarecely be obtained from the absorption spectral measurements through the present experiments while all fluorescence behavior can be interpreted in terms of the dimer formation. As the ^1H NMR spectral data suggest, TMPyP may form a considerably loose dimer. The electronic state of the loose dimer may be essentially the same as that of the TMPyP monomer. The intermolecular interaction may be enhanced in the photoexcited singlet state because of the formation of the face-to-face excited dimer (excimer). Pyrene is a typical π-conjugated hydrocarbon which shows excimer fluorescence at high concentration range ($>10^{-3}$ M).[28] No interaction exists between the pyrene molecules in the ground states while pyrene in the excited singlet state associates with another pyrene in the ground state to form the excited dimer (excimer). In the case of TMPyP, however, the excited dimer can be detected by means of the fluorescence spectroscopy even if the TMPyP concentration is 1×10^{-6} M. This should be ascribed to the formation of the loose ground-state dimer of TMPyP as is suggested by ^1H NMR spectroscopy. The exciton-type and charge-exchange interactions may cause stabilization of the lowest singlet state of the TMPyP dimer leading to the red shift of the Q(0-0) band. The similar red shift of porphyrin dimer has been observed for the TAPP-$TPPS_4$ association complex.[19]

Conclusion

In this work, we confirmed that TMPyP in water exists as the dimer having somewhat loose structure at the concentrations above 10^{-6} M and the intermolecular interaction is enhanced upon photoexcitation to the lowest singlet state. The extraordinarily red-shifted Q(0-0) fluorescence band of TMPyP can be explained by the formation of the excimer-like state. The formation of the higher aggregates of TMPyP may be prevented by the electrostatic repulsion between the TMPyP dimer and monomer at the concentrations below 1×10^{-2} M:[29]

$$2TMPyP^{4+} \rightleftharpoons (TMPyP)_2^{8+}, \quad (1)$$

$$(TMPyP)_2^{8+} + TMPyP^{4+} \rightleftharpoons (TMPyP)_3^{12+}, \quad (2)$$

References

1) W. I. White, "The Porphyrins," ed by D. Dolphine, Academic Press, New York (1978), Vol. 5, Chap. 7.

2) R. J. Abraham, P. A. Burbidge, A. H. Jackson, and D. B. Macdonald, *J. Chem. Soc., (B)*, **1966**, 620.

3) R. F. Pasternack, P. R. Huber, P. Boyd, G. Engasser, L. Francesconi, E. Gibbs, P. Fasella, G. C. Venturo, and L. deC. Hinds, *J. Am. Chem. Soc.*, **94**, 4511 (1972).

4) R. F. Pasternack, L. Francesconi, D. Raff, and E. Spiro, *Inorg. Chem.*, **12**, 2606 (1973).

5) M. Krishnamurthy, J. R. Sutter, and P. Hambright, *J. Chem. Soc., Chem. Commun.*, **1975**, 13.

6) S. B. Brown, M. Shillock, and P. Jones, *Biochem. J.*, **153**, 279 (1976).

7) R. J. Abraham, F. E. Eivazi, H. Pearson, and K. M. Smith, *J. Chem. Soc., Chem. Commun.*, **1976**, 698.

8) R. Margalit, N. Shaklai, and S. Cohen, *Biochem. J.*, **209**, 547 (1983).

9) R. Margalit and M. Rotenberg, *Biochem. J.*, **219**, 445 (1984).

10) J. A. Shelnutt, *J. Phys. Chem.*, **88**, 4988 (1984).

11) J. D. Satterlee and J. A. Shelnutt, *J. Phys. Chem.*, **88**, 5487 (1984).

12) T. K. Chandrashekar, H. Van Willigen, and M. H. Ebersole, *J. Phys. Chem.*, **88**, 4326 (1984).

13) K. Bernauer and S. Fallab, *Helv. Chim. Acta*, **45**, 2487 (1962).

14) R. F. Pasternack, E. G. Spiro, and M. Teach, *J. Inorg. Nucl. Chem.*, **36**, 599 (1974).

15) R. F. Pasternack, E. J. Gibbs, A. Gaudemer, A. Antebi, S. Bassner, L. De Poy, D. H. Yurner, A. Williams, F. Laplace, M. H. Lansard, C. Merrience, and M. Perree-Fauvet, *J. Am. Chem. Soc.*, **107**, 8179 (1985).

16) K. Kano, T. Miyake, K. Uomoto, T. Sato, T. Ogawa, and S. Hashimoto, *Chem. Lett.*, **1983**, 1867.

17) E. B. Fleischer and L. E. Webb, *J. Phys. Chem.*, **67**, 1131 (1963).

18) P. Hambright and E. B. Fleischer, *Inorg. Chem.*, **9**, 1757 (1970).

19) E. Kosower, "Introduction to Physical Organic Chemistry," John Wiley & Sons, New York (1968), Chap. 2.

20) E. Ojadi, R. Selzer, H. Linschitz, *J. Am. Chem. Soc.*, **107**, 7783 (1985).

21) T. Sato, T. Ogawa, and K. Kano, *J. Phys. Chem.*, **88**, 3678 (1984).

22) K. Kalyanasundaram, *Inorg. Chem.*, **23**, 2453 (1984).

23) M. Krishnamurthy, *Indian. J. Chem. B*, **15**, 964 (1977).

24) A. N. Thompson and M. Krishnamurthy, *Inorg. Nucl. Chem.*, **41**, 1251 (1979).

25) J. H. Fendler and E. J. Fendler, "Catalysis in Micellar and Macromolecular Systems," Academic Press, New York (1975), Chap. 2.

26) For example: H. Sato, M. Kawasaki, K. Kasatani, Y. Kusumoto, N. Nakashima, and K. Yoshihara, *Chem. Lett.*, **1980**, 1529.

27) N. Foster, *J. Magn. Reson.*, **56**, 140 (1984).

28) For example: Th. Förster and K. Kasper, *Z. Electrochem.*, **59**, 977 (1955).

29) Note added in proof: After this paper was submitted, we were informed that Brookfield et al. have also reexamined our previous study[16] by means of fluorescence spectroscopy and concluded that the TMPyP molecules stack in water to form the face-to-face dimer where the porphyrin-to-porphyrin distance is about 1 nm (R. L. Brookfield, H. Ellul, and A. Harriman, *J. Photochem.*, **31**, 97 (1985).).

 © 1987 The Chemical Society of Japan Bull. Chem. Soc. Jpn., 60, 1289—1293 (1987)

Extraction and Transport of Ions in a Liquid Membrane Containing Crown Ether

Maria SAKIM,† Takashi HAYASHITA, Takeo YAMABE, and Manabu IGAWA*
Department of Applied Chemistry, Faculty of Engineering, Kanagawa University, Rokkakubashi, Kanagawa-ku, Yokohama 221
†Department of Chemistry, Medical College of Shin Jiang, Urumchi, Shin Jiang, China
(Received October 30, 1986)

The ion-transport mechanism through a liquid membrane containing dibenzo-18-crown-6 as a carrier was investigated by measuring the salt flux, the distribution coefficient to the membrane phase, and the membrane potential. The salt flux increased to a great extent with the activity of the source phase solution, but the effect of the activity on the distribution coefficient varied with the membrane solvent. The mobility ratio of cations to anions increased with an increase in the hydrophobicity of the membrane solvent. Although the selectivity of the cation transport is controlled mainly by the size of the crown ring, the hydrophobicity of the cation also influenced the salt flux and the flux of a slightly hydrated large cation, such as cesium ion, was high. The hydration degree of anions influenced the salt flux considerably since the stability constants of the crown ether complexes accompanied by a hydrophobic anions were very high. The salt flux correlated well with the lyotropic number of anions.

Crown ethers complex selectively with cations which have a similar diameter as the size of a crown ring[1] and have been applied for the separation and determination of various cations.[2] Especially in a separation with liquid membranes containing crown ethers as carriers, many reports have been presented up to now. Recently, some interesting applications have been attempted, such as ion transport driven by light energy,[3] by a redox potential,[4] or by a pH gradient.[5]

The basic theory of ion transport through a liquid membrane mediated by a crown ether has been constructed by Reusch and Cussler[6] and Lamb et al.[7] and salt transport equations have been reported. However, the extraction process of the most important process of salt transport has been investigated as solvent extraction separately against the investigation of the salt transport. There have been many reports regarding salt extraction with DB18C6;[8,9] however, extraction coefficients have not been measured in salt transport studies (with some exception).[10]

A membrane potential is also generated specifically during salt transport across the crown ether membrane; its principle is important for a specific determination of ions in ion electrodes.[11-13] However, the relationship between the salt transport and the membrane potential revealed in a liquid membrane containing a crown ether as a carrier has not yet been clarified and investigated.

In this paper, we will simultaneously analyze the extraction, the salt transport, and the membrane potential in a salt transport phenomenon of a liquid membrane containing a typical crown ether (dibenzo-18-crown-6) as the carrier with a flow cell.[14] We will attempt a preliminary clarification of the mutual relationship.

Experimental

Preparation of Membrane Phase and Source Phase Solutions. In this study, dibenzo-18-crown-6 (DB18C6) was used as the carrier of a liquid membrane. DB18C6 was obtained from Nippon Soda Co., as a commercial reagent and was used after recrystalization from benzene. Unless otherwise stated, the liquid membrane was a 0.1 mol dm^{-3} DB18C6 solution of tetrachloroethane and the source phase solution was a 0.1 mol dm^{-3} aqueous solution of KNO_3 (analytical grade reagent). For an investigation of the effect of a membrane solvent on ion transport, some solvents were examined; the solvents used in this study and their dielectric constants[15] were as follows: chloroform, 4.7; Chlorobenzene, 5.6; 1,1,1-Trichloroethane, 7.1; 1,1,2-Trichloroethane, 7.1; 1,1,2,2-tetrachloroethane, 8.0; Dichloromethane, 9.1 and 1,2-Dichloroethane, 10.5.

Measurements of Salt Flux and Distribution Coefficient. The salt flux was measured in a previously reported dialysis cell.[14] The cell comprised 3 compartments separated from each other by a Visking dialysis membrane (the membrane area was 6.6 cm^2, the thickness of each compartment was 3 mm; the source phase solution, membrane phase solution, and pure water of the receiving phase solution were circulated from respective reservoirs by using tubing pumps at a rate of about 15 cm^3 min^{-1}). The receiving phase solution was collected at regular time intervals and its concentration was measured by an atomic absorption spectrophotometer (Shimadzu AA-630-02). The salt flux was calculated from the concentration change with time in the receiving phase and was given in units of mol cm^{-2} min^{-1}. The distribution coefficient was measured with a cell (the same as that of a dialysis cell, except that the cell has only two compartments: a source phase compartment and a membrane phase compartment). A membrane phase solution of 0.10 cm^3 was collected at regular time intervals; each solution was diluted with both 0.9 cm^3 acetonitrile and 0.1 cm^3 pure water, and the metal concentration in it was measured using an atomic absorption spectrophotometer. Standard solutions for this determination were also prepared with the same type acetonitrile-water solution. The distribution coefficient was calculated from the salt activities in the membrane phase and in the salt solution during equilibrium.

Measurement of Membrane Potential. The membrane potential was measured with a cell (the same as that of the dialysis cell, except that both sides of the cell were bored and a salt bridge was set at the vicinity of the each outside surface

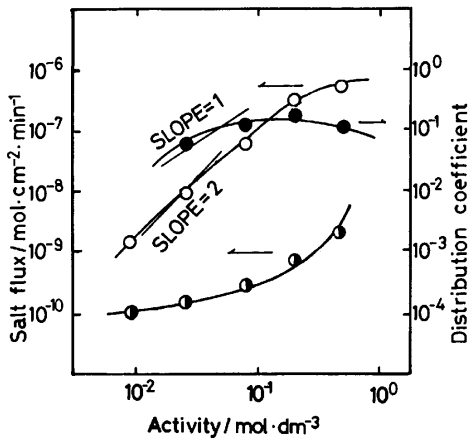

Fig. 1. Salt flux and distribution coefficient vs. KNO_3 activity in carrier-mediated transport in 1,1,2,2-tetrachloroethane solvent.
Source phase:0.1 mol dm^{-3} KNO_3 aq soln. Liquid membranes: 0.1 or 0 mol dm^{-3} dibenzo-18-crown-6(DB18C6) in 1,1,2,2-tetrachloroethane. ●: Distribution coefficient, ○: Salt flux through membrane containing DB18C6, ◑: Salt flux through membrane containing no carrier.

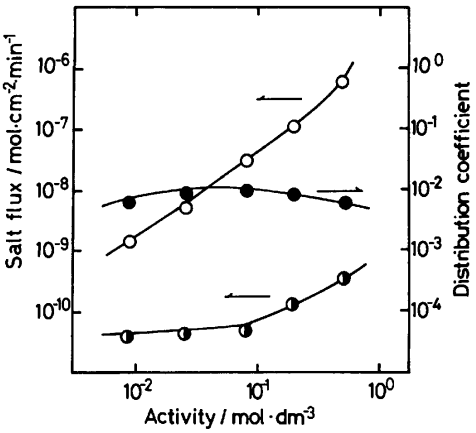

Fig. 2. Salt flux and distribution coefficient vs. KNO_3 activity in carrier-mediated transport in chloroform solvent.
Source phase: 0.1 mol dm^{-3} KNO_3 aq soln. Liquid membranes: 0.1 or 0 mol dm^{-3} DB18C6 in chloroform. ●: Distribution coefficient, ○: Salt flux through membrane containing DB18C6, ◑: Salt flux through membrane containing no carrier.

of the liquid membrane). Circulating the salt solution, the membrane phase solution, and the receiving phase solution with tubing pumps, the membrane potential was measured using a potentiometer (Toa IM-20E) connected to a recorder (Yanagimoto YR-101). The potential changed with time; after an appropriate time it approached a constant value, from which the ion mobility ratio, u_+/u_- or u_-/u_+, was calculated with

$$E = (u_+ - u_-)/(u_+ + u_-) \times RT/F \times \ln a_s/a_r. \quad (1)$$

Here, u_+ and u_- are the mobilities of the cation and anions; R, T, and F are the gas constant, absolute temperature, and the Faraday constant; and a_s and a_r are the salt activities of the source phase solution and the receiving phase solution, respectively.

Results and Discussion

Effects of Salt Activities and Membrane Solvent on Salt Transport. The salt flux depends on the salt activity of the source phase solution. Figures 1 and 2 show the relationship between the permeation characteristics and the salt activity in the cases of liquid membranes of DB18C6 in 1,1,2,2-tetrachloroethane and DB18C6 in chloroform. In the figures, the salt flux, the distribution coefficient, and the salt flux across the liquid membrane containing no carrier are shown together. These permeation characteristics depending on the salt activity can be expressed by the following equations. The distribution coefficient of the salt between the membrane phase and the source or receiving phase, k, is

$$k = a_m/a, \quad (2)$$

where a_m and a are the salt activity in the liquid membrane and that in the source or receiving phase, respectively. The salt flux, J_s, can be expressed by

$$J_s = D_s/l \times (a_{m,s} - a_{m,r}), \quad (3)$$

where D_s is the diffusion coefficient, l is the membrane thickness, and $a_{m,s}$ and $a_{m,r}$ are the activity at the liquid membrane interface adjacent to the source phase solution and that adjacent to the receiving phase solution. If the salt activity of the receiving phase is much lower than that of the feed solution, $a_{m,r}$ becomes much smaller than $a_{m,s}$ and can be ignored. Using Eq. 2, the salt flux in Eq. 3 therefore becomes

$$J_s = D_s/l \times a_{m,s} = D_s ak/l. \quad (4)$$

The crown ether compex is considered to be formed in the liquid membrane phase from the crown ether and the ion pair to be formed in the aqueous phase and distributed to the membrane phase. The formation constant of the ion pair, K_i, is

$$K_i = a_i/a^2, \quad (5)$$

and the distribution coefficient of the ion pair, D_i is

$$D_i = a_{i,m}/a_i. \quad (6)$$

Here, a_i and $a_{i,m}$ are the activity of the ion pair in the aqueous phase and that in the membrane phase, respectively. The salt flux and the distribution coefficient can be correlated with the salt activity in the source phase solution with these equations. For a derivation of the salt flux and the distribution coefficient, the total carrier activity, L_T and the formation constant of the crown ether complex in the liquid membrane phase, K_c can be defined as follows:

$$L_T = L + a_L, \quad (7)$$

and

$$K_c = a_L/(a_{i,m} \times L). \quad (8)$$

Here, L and a_L are the activities of the free crown ether and that of the complex in the liquid membrane phase. Then, a_m is correlated with $a_{i,m}$ and a_L as

$$a_m = a_{i,m} + a_L. \quad (9)$$

If $a_{i,m}$ can be ignored compared to a_L, the distribution coefficient, k, becomes

$$k = a_m/a = a_L/a. \quad (10)$$

From these equations, k can be derived as a function of the salt activity of the source phase solution as

$$k = K_{ex}L_T a/(1 + K_{ex}a^2), \quad (11)$$

where K_{ex} is an extraction coefficient defined by

$$K_{ex} = a_L/(a^2L) = K_c K_i D_i. \quad (12)$$

From Eqs. 4 and 12, the salt flux, J_s, can be derived as

$$J_s = D_s K_{ex} L_T/1 \times a^2/(1 + K_{ex}a^2). \quad (13)$$

This is the same equation reported by Reusch and Cussler.[6] In Fig. 1, both the distribution coefficient and the salt flux increased enormously with the salt activity when the salt activity was lower than 0.1 mol dm^{-3} (while the distribution coefficient was initiated to decrease and the salt flux became constant when the activity was higher than 0.1 mol dm^{-3}). These permeation phenomena can be expected from Eqs. 11 and 13. When the value of $K_{ex}\ a^2$ becomes much lower than 1 (that is, the salt activity becomes very low), Eqs. 11 and 13 can be transformed into

$$k = K_{ex}L_T a, \quad (14)$$

and

$$J_s = D_s K_{ex} L_T a^2/1, \quad (15)$$

where k and J_s are proportional to the first power and the second power of the salt activity, respectively. When the value of $K_{ex}\ a^2$ becomes much higher than 1 (that is, the salt activity becomes very high), Eqs. 11 and 13 can be transformed into

$$k = L_T/a, \quad (16)$$

and

$$J_s = D_s L_T/1, \quad (17)$$

where k is proportional to the reciprocal of the salt activity and J_s is constant.

In the figure, the salt flux through a liquid membrane containing no carrier is also shown. By using Eqs. 2—6, the flux can be expressed as

$$J_s = D_s D_i K_i a^2/1. \quad (18)$$

The salt flux, J_s, is derived to be proportional to the second power of the salt activity in this equation; however, in Fig. 1 this is true only in a high activity range and the J_s becomes a constant with a decrease in the salt activity. The transport of salt in a low-activity range may be mainly caused by leakage through the membrane; This is probably due to the microquantity of the microvolume droplets of water dispersed in the membrane. By comparing Eq. 15 and Eq. 18, the J_s ratio of Eq. 15 to Eq. 18 is found to be $K_c L_T$ when the diffusion coefficient of the crown complex can be assumed to be almost the same to that of the ion pair. As L_T is 0.1 mol dm^{-3}, K_c can be estimated to be about three orders of magnitude from Fig. 1.

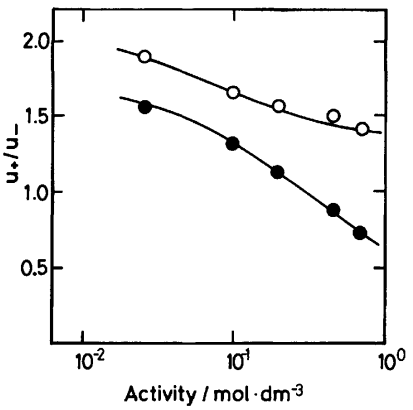

Fig. 3. Effect of salt activity on mobility ratio. Liquid membrane:0.1 mol dm^{-3} DB18C6 in 1,1,2,2-tetrachloroethane (●), chloroform (○). Ratio of salt (KNO_3) concentration: 10 to 1. The abscissa show the activity of the solution of the higher concentration side.

The salt transport characteristics depend not only on the salt activities, but also on many other conditions, such as cation species, anion species, and membrane solvents.[16,17] Figure 2 shows the effect of the salt activity on the salt flux and the distribution coefficient in a different membrane solvent, chloroform membrane containing DB18C6. In this case, the salt fluxes were smaller than those given in Fig. 1 and the dependency of the distribution coefficient on the salt activity was very small; However, the difference between the magnitude of the carrier-mediated transport in this case and that in Fig. 1 was especially small in the range of high salt activity. The independence of the distribution coefficient on the activity can not be explained on the basis of the theory described above. It is reported that in the case of chloroform the solubility of DB18C6 is high but decreases enormously by complexing[1] since the complex is more hydrophilic than DB18C6 alone and chloroform is a hydrophobic solvent. This may be the reason for the low and constant distribution coefficient. Although the distribution coefficient is constant, the ratio of the flux of the complex to that of the ion pair was larger than that in the case of Fig. 1 and must have been caused by a high formation constant of the DB18C6 complex in the hydrophobic solvent, chloroform.

In order to clarify the reason for the effect of the activity on the salt flux and the difference of the effect between the case of 1,1,2,2-tetrachloroethane and the case of chloroform, the mobility ratio of the cation to anion in the liquid membrane phase was measured; values were shown in Fig. 3. When the cation is more

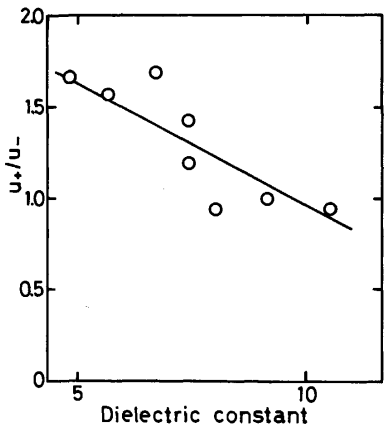

Fig. 4. Mobility ratio vs. dielectric constant of liquid membrane solvent.
Liquid membrane: 0.01 mol dm^{-3} DB18C6 organic soln. Salt concentration: 0.1—0.01 mol dm^{-3}.

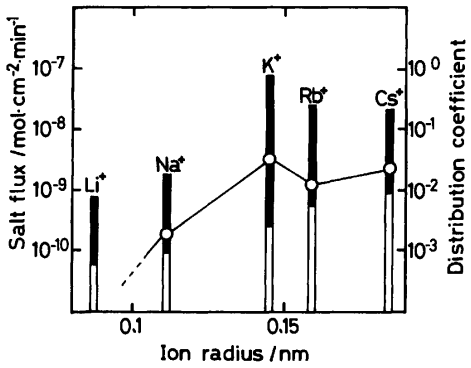

Fig. 5. Effect of cation radius on salt flux and distribution coefficient.
Liquid membrane: 0.1 mol dm^{-3} DB18C6 in 1,1,2,2-tetrachloroethane soln. ○: Distribution coefficient, ■: Salt flux through membrane containing DB18-C6, □: Salt flux through membrane containing no carrier.

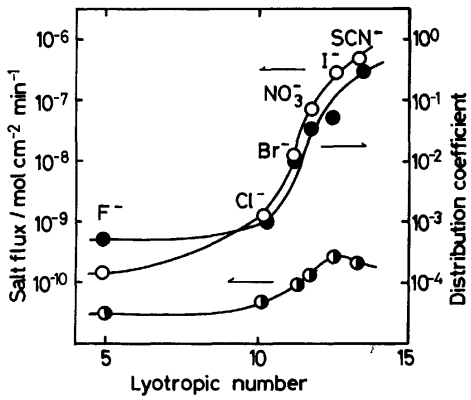

Fig. 6. Effect of lyotropic number of anion on salt flux and distribution coefficient.
Liquid membrane: 0.1 mol dm^{-3} DB18C6 in 1,1,2,2-tetrachloroethane soln. ●: Distribution coefficient, ○: Salt flux through membrane containing DB18-C6, ◑: Salt flux through membrane containing no carrier.

stable than the anion and the permeability of the cation is larger than that of the anion in the membrane phase, the value of u_+/u_- becomes larger than 1. The cations complexed with crown ether, whose hydrophobic group was arranged outside of it, were more stable than naked anions, and the mobility ratio became greater than 1 (with some exceptions). In the case of the 1,1,2,2-tetrachloroethane solution, the values of u_+/u_- decreased with an increase in the salt activity and became smaller than 1 for a high salt activity. In the case of the chloroform solution, the values of u_+/u_- were constant, except within a low salt activity range and were higher than those of a 1,1,2,2-tetrachloroethane solution. These differences between two membrane solvents are considered to be caused by differences in the hydrophobicity of the solvent. The ratio was higher for chloroform than for 1,1,2,2-tetrachloroethane since chloroform is more hydrophobic than 1,1,2,2-tetrachloroethane. In 1,1,2,2-tetrachloroethane, the naked anions were more stable than in chloroform and their stability increased with the ionic strength of the aqueous solution on either side of the membrane.

The relationship between u_+/u_- and the dielectric constant is shown in Fig. 4 in order to investigate the effect of the hydrophobicity of the membrane solvent using chlorinated hydrocarbons for the membrane solvents. As predicted in the prior paragraph, the mobility ratio of the complexed cation to that of the naked anion increased with an increase in the hydrophobicity of the membrane solvent; also, the mobility ratio decreased, on the whole, with an increase in the dielectric constant (an indication of the hydrophilicity of the solvent).

Selective Transport of Salts. The relationship between the salt flux or the distribution coefficient and the ion radius for alkaline cations is shown in Fig. 5 in order to investigate the mechanism of the selective transport. The distribution coefficient is maximum for potassium ions since the stability constant of a DB18C6 complex is maximum for potassium ions in alkaline metal ions.[1] The value of lithium was not plotted in this figure because its concentration in the membrane phase was very low and could not be detected. The salt flux changes with a change in the distribution coefficient and the flux was also maximum for potassium salt. The salt flux through the liquid membrane with no carrier was also measured. This transport was caused by a concentration difference of ion pairs in the membrane without a carrier. Since the hydrophobicity of the ions increases with an increase in the cation radius and hydrophobic ions are easy to be transported in a hydrophobic membrane,[18,19] the flux of ion pairs increased with an increase in the ion radius. The relationship between the salt flux or the distribution coefficient and the lyotropic number[20] of anions is also shown in Fig. 6. The

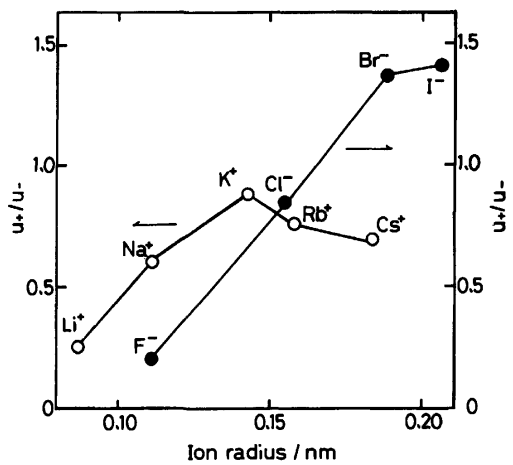

Fig. 7. Mobility ratio vs. ion radius.
Liquid membrane: 0.1 mol dm^{-3} DB18C6 organic soln. Salt concentration: 0.1—0.01 mol dm^{-3}. Counter anion is NO_3^-. Counter cation is K^+.

salt flux through a membrane containing DB18C6 as a carrier can be related well to the lyotropic number (as in the case of anion chromatography on silica gel coated with crown ether polymer;[21] Lamb et al. related the salt transport phenomena to the dehydration energies of anions).[22] The salt flux through a membrane containing no carrier also increased with increasing lyotropic number, but the degree was much smaller for the latter than for the former. The distribution coefficient increased with the salt activity in the same manner as the salt flux. Figure 7 shows the relationship between u_+/u_- and cation radius for the salt of alkaline metal ions and that between u_-/u_+ and anion radius for halogenide ions. The ratio of the mobility of a cation to that of NO_3^- was maximum for potassium ions (all the values were lower than 1). In anions, the mobility ratios increased with an increase in the anion radius and the mobilities of Br^- and I^- were much higher than that of a complexed potassium ion. It is clear that the selectivity for anions was caused by the hydrophobicity of the ions and that for cations was mainly caused by the selective complexation of DB18C6.

References

1) C. J. Pedersen, *J. Am. Chem. Soc.*, **89**, 7017 (1967).
2) M. Igawa, *Kagaku Koujou*, **25**, 49 (1981).
3) S. Shinkai, T. Nakaji, T. Ogata, K. Shigematsu, and O. Manabe, *J. Am. Chem. Soc.*, **103**, 111 (1981).
4) S. Shinkai, K. Inuzuka, K. Hara, T. Sone, and O. Manabe, *Bull. Chem. Soc. Jpn.*, **57**, 2150 (1984).
5) T. M. Fyles, V. A. M. Diemer, and D. M. Whitfield, *Can. J. Chem.*, **59**, 1734 (1981).
6) C. F. Reusch and E. L. Cussler, *AIChE J.*, **19**, 736 (1973).
7) J. D. Lamb, J. J. Christensen, S. R. Izatt, K. Bedke, M. S. Astin, and R. M. Izatt, *J. Am. Chem. Soc.*, **102**, 3399 (1980).
8) H. K. Frensdorf, *J. Am. Chem. Soc.*, **93**, 4684 (1971).
9) Y. Takeda, "Host Guest Complex Chemistry III," Springer-Verlag, (1984), p. 1.
10) S. Yoshida and S. Hayano, *J. Am. Chem. Soc.*, **108**, 3903 (1986).
11) G. A. Rechuitz and E. Eyal, *Anal. Chem.*, **44**, 370 (1972).
12) K. Kimura, T. Maeda, H. Tamura, and T. Shōno, *Anal. Chem.*, **95**, 91 (1979).
13) K. Kimura, K. Kumami, S. Kitazawa, and T. Shōno, *Anal. Chem.*, **56**, 2369 (1984).
14) M. Igawa, K. Saitou, F. Monoe, K. Nishida, M. Tanaka, and T. Yamabe, *Nippon Kagaku Kaishi*, **1985**, 826.
15) "Kagaku-Binran (Kisohen)," ed by Chem. Soc. Jpn., rev. 3, Maruzen (1982).
16) M. Igawa, M. Tanaka, S. Izumi, Y. Kaneko, and T. Yamabe, *Nippon Kagaku Kaishi*, **1980**, 135.
17) M. Igawa, K. Matsumura, M. Tanaka, and T. Yamabe, *Nippon Kagaku Kaishi*, **1981**, 625.
18) I. Satake, H. Nakajima, and H. Noguchi, *Membrane*, **2**, 225 (1977).
19) M. Igawa, K. Torii, M. Tanaka, and M. Senō, *J. Appl. Polym. Sci.*, **29**, 117 (1984).
20) K. Miyajima, Kagaku no Ryoiki, Zokan 106, Nankōdō (1974), p. 83.
21) M. Igawa, K. Saitō, J. Tsukamoto, and M. Tanaka, *Anal. Chem.*, **53**, 1942 (1981).
22) J. D. Lamb, J. J. Christensen, J. L. Oscarson, B. L. Nielsen, B. W. Asay, and R. M. Izatt, *J. Am. Chem. Soc.*, **102**, 6820 (1980).

Nonstoichiometry and Electrical Resistivity in Two Mixed Metal Oxides, La_2NiO_{4-x} and $LaSrNiO_{4-x}$

Kenji Ishikawa,* Shin-ichi Kondo, Hirofumi Okano, Shigenori Suzuki, and Yasuo Suzuki
Department of Industrial Chemistry, Faculty of Engineering, Meiji University, Higashi-mita, Tama-ku, Kawasaki 214
(Received November 7, 1986)

Two mixed oxides, La_2NiO_{4-x} and $LaSrNiO_{4-x}$, had the K_2NiF_4 structure in the oxygen-pressure range from 58000 down to 130 Pa at 1173 K. The oxygen-vacancy concentration, x, in both La_2NiO_{4-x} and in $LaSrNiO_{4-x}$ at 1173 K was determined by thermogravimetric analysis in the oxygen-pressure range from 58000 to 1.3 Pa. The vacancy concentration of $LaSrNiO_{4-x}$ was greater than that of La_2NiO_{4-x} at the same oxygen pressure at 1173 K. The electrical resistivities of La_2NiO_{4-x} and $LaSrNiO_{4-x}$ were measured at 473—1173 K under an oxygen atmosphere at 98—58000 Pa. The density of the state and the drift mobility of oxygen stoichiometric La_2NiO_4 and $LaSrNiO_4$ were estimated from the resistivity data and from the results on the thermogravimetric analysis.

The mixed oxide La_2NiO_4, which was first prepared by Kniga and Zaretskaya,[1] has the very attractive property of a "gradual" semiconductor-metal transition.[2-4] Goodenough et al.[5-7] have previously proposed an invaluable band model which gives the origin of the semiconductor-metal transition of La_2NiO_4. The model, however, does not clearly explain why the transition proceeds "gradually."[8] It seemed that it would be worthwhile from the electrochemical point of view to elucidate the driving force of the "gradual" semiconductor-metal transition of La_2NiO_4.

Recently, Rao et al.[9] have reported on the resistivity and the magnetic susceptibility of a single crystal of La_2NiO_4. They have found a very large positive coefficient of temperature, an irreversible transition, in the resistivity curve of La_2NiO_4 at 550 K. It was presumed that the irreversible transition was attributable to the effect of strain, crystal distortion, charge density waves, or nonstoichiometry. Their finding of the irreversible transition raised the question that the "gradual" semiconductor-metal transition of La_2NiO_4 might be related to the nonstoichiometry, particularly to that of the lattice oxygen.

By the way, the analogous compound, $La_{2-x}Sr_xNiO_4$, has also been reported to exhibit the "gradual" semiconductor-metal transition.[3,10] The temperature dependence of the electrical resistivity and the transport property of $La_{2-x}Sr_xNiO_4$ have previously been measured by the present authors under an inert atmosphere,[8] though the effect of oxygen deficiency on the electrical resistivity was not considered.

In this study, the effect of the oxygen vacancy on the electrical resistivity of $La_{2-x}Sr_xNiO_{4-y}$, especially on the resistivity of La_2NiO_{4-y} (x=0) and on that of $LaSrNiO_{4-y}$(x=1), was investigated at various temperatures and oxygen pressures.

Experimental

Preparation. The two oxides, La_2NiO_{4-x} and $LaSrNiO_{4-x}$, were prepared by heating stoichiometric mixtures of La_2O_3 (Shin-etsu Chem. Ind. Co., Ltd.; 99.9%), $SrCO_3$ (prepared from reagent-grade $Sr(NO_3)_2$), and NiO (Kojundo Kagaku Co., Ltd.; 99.99%) in air at 1433 K for 25 h.

Electrical Resistivity Measurement. A sintered sample, 5 mm^2 in cross section and 5 mm long, was heated in 58000 Pa of oxygen at 1173 K for 2 h in a measurement cell before the resistivity measurements. The electrical resistivity of the sample was immediately measured in the same cell with the four-prove method in 98—58000 Pa of oxygen at 473—1173 K after preheating.

Thermogravimetric Analyses. The oxygen-vacancy concentrations, x, in La_2NiO_{4-x} and in $LaSrNiO_{4-x}$ were determined by thermogravimetric analyses. A powdered sample (about 5 g) was preheated in 58000 Pa of oxygen at 1173 K for 5 h; it was then weighed at room temperature to an accuracy of 0.01 mg. The sample was heated again at the prescribed oxygen pressure at 1173 K for 5 h and then weighed at room temperature. The oxygen vacancy concentration of a sample was evaluated from the weight and the weight loss of the sample. The vacancy content, x, was calculated from this equation:

$$x = \frac{\Delta W \times M(La_2NiO_4 \text{ or } LaSrNiO_4)}{W \times M(O)}, \quad (1)$$

where W was the weight of the sample after preheating, ΔW was the weight loss of the sample during the heating process, $M(La_2NiO_4$ or $LaSrNiO_4)$ was the formula weight of La_2NiO_4 or $LaSrNiO_4$, and $M(O)$ was the atomic weight of oxygen. It was conveniently assumed for the calculation of x that La_2NiO_{4-x} an $LaSrNiO_{4-x}$ have very few oxygen vacancies, x=0, after preheating.

Results and Discussion

The crystal structure and the oxygen vacancy concentration of La_2NiO_{4-x} and $LaSrNiO_{4-x}$ are summarized in Table 1. The La_2NiO_{4-x} oxide was stable in oxygen down to 140 Pa at 1173 K, but was decomposed to some complex materials in vacuo (7 Pa) at the same temperature, while the $LaSrNiO_{4-x}$ oxide was stable to 1 Pa of oxygen at 1173 K.

The electrical resistivities of La_2NiO_{4-x} and $LaSrNiO_{4-x}$ were measured in the oxygen pressure range from 58000 to 100 Pa (Figs. 1 and 2). The resistivities of La_2NiO_{4-x} and $LaSrNiO_{4-x}$ are not oxygen-pressure-dependent below 581 K, but they decrease with an increase in the oxygen pressure over 673 K. The irreversible transition at 550 K found by Rao et al.[9] was not observed in the resistivity curves of La_2NiO_{4-x} in Fig. 1. The resistivity data in Fig. 1 also show that the electrical resistivity of La_2NiO_{4-x} is not

Table 1. Phases and Oxygen-Defect Concentrations of La_2NiO_{4-x} and $LaSrNiO_{4-x}$ at Various Oxygen Pressures at 1173 K

Formula	P/Pa[a]	$\Delta W/W$[b]	x[c]	Phase
La_2NiO_4	58000	0.00000	0.0000	La_2NiO_4
	31100	−0.00002	−0.0005	La_2NiO_4
	13100	0.00023	0.0057	La_2NiO_4
	5870	0.00032	0.0080	La_2NiO_4
	2670	0.00043	0.0107	La_2NiO_4
	400	0.00083	0.0207	La_2NiO_4
	140	0.00090	0.0226	La_2NiO_4
	7	0.00761	0.1905	Decomposed
$LaSrNiO_4$	58000	0.00000	0.0000	$LaSrNiO_4$
	30700	0.00003	0.0007	$LaSrNiO_4$
	10700	0.00043	0.0093	$LaSrNiO_4$
	4930	0.00076	0.0165	$LaSrNiO_4$
	1330	0.00114	0.0250	$LaSrNiO_4$
	430	0.00149	0.0325	$LaSrNiO_4$
	130	0.00532	0.116	$LaSrNiO_4$
	1	0.01035	0.226	$LaSrNiO_4$

a) Oxygen pressure. b) Decrease in weight of the sample during the heating process in oxygen at 1173 K. c) x in La_2NiO_{4-x} or x in $LaSrNiO_{4-x}$ (see. Eq. 1).

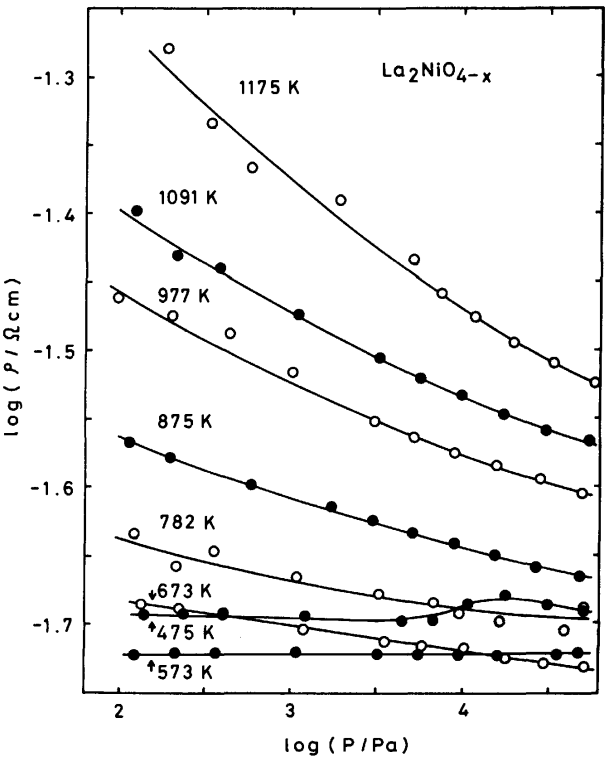

Fig. 1. Oxygen pressure dependence of electrical resistivity for La_2NiO_{4-x}.

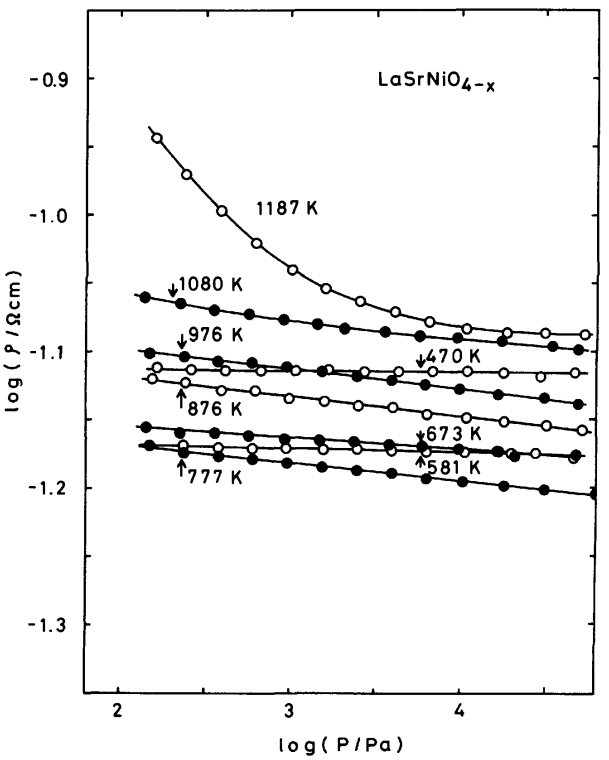

Fig. 2. Oxygen pressure dependence of electrical resistivity for $LaSrNiO_{4-x}$.

oxygen-pressure dependent at 550 K. The irreversible transition by Rao et al. would not be related to the stoichiometry of oxygen of the sample if the resistivity measurements had been performed under an atmosphere containing 100 Pa or more of oxygen.

Figures 1 and 2 show that the slopes in the resistivity curves of La_2NiO_{4-x} and $LaSrNiO_{4-}$ are negative over 673 K. Both La_2NiO_{4-x} and $LaSrNiO_{4-x}$ are p-type conductors in this temperature range. The slope of La_2NiO_{4-x} (Fig. 1) is much larger than that of $LaSrNiO_{4-x}$ (Fig. 2) at the same temperature.

Figure 3 shows the temperature dependence of the electrical resistivities for La_2NiO_{4-x} and $LaSrNiO_{4-x}$ at 316, 3160, and 31600 Pa of oxygen, where the resistivity plots are based on readings of Figs. 1 and 2. A "gradual" semiconductor-metal transition is observed in the resistivity curves of La_2NiO_{4-x} and $LaSrNiO_{4-x}$ at any oxygen pressure. The resistivity curves in Fig. 3 seem to imply that the release of the lattice oxygen is not responsible for the origin of the appearance of the

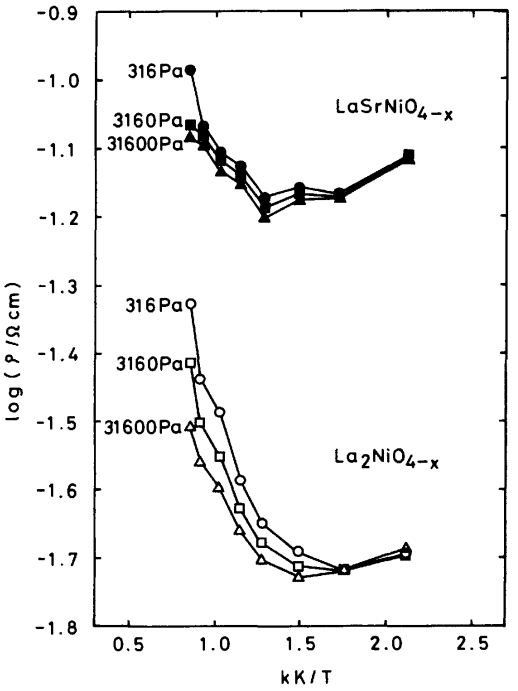

Fig. 3. Temperature dependence of electrical resistivity for La_2NiO_{4-x} and for $LaSrNiO_{4-x}$.

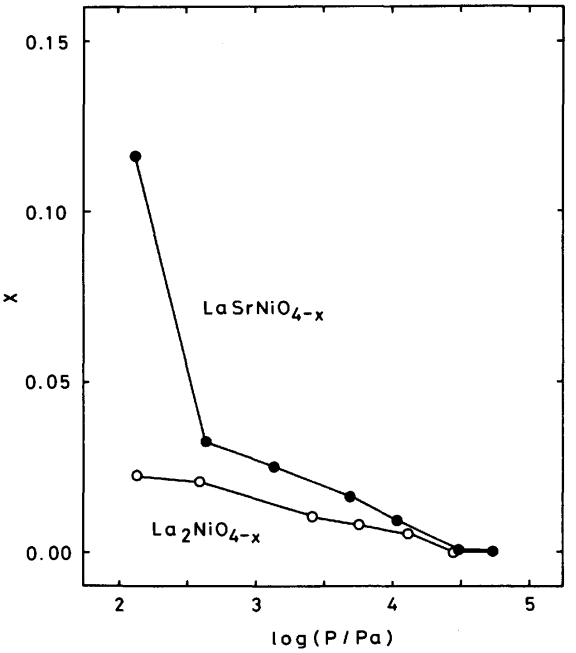

Fig. 4. Oxygen pressure dependence of oxygen content x for La_2NiO_{4-x} and for $LaSrNiO_{4-x}$.

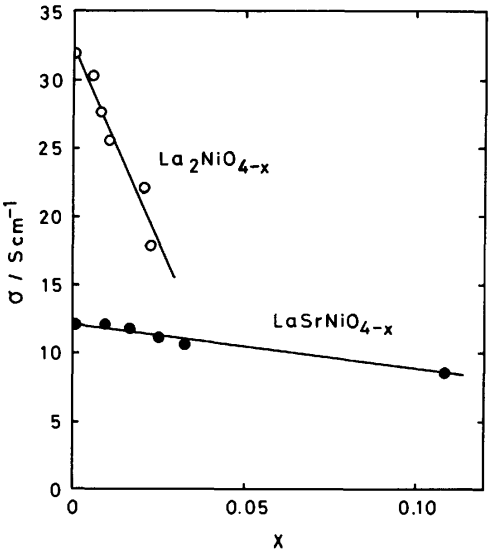

Fig. 5. Oxygen content dependence of electrical conductivity for La_2NiO_{4-x} and for $LaSrNiO_{4-x}$.

"gradual" semiconductor-metal transition. The transition temperature is, however, apparently affected by the atmospheric oxygen pressure, for the transition point is shifted to a higher temperature with the increase in the oxygen pressure.

The oxygen-pressure dependence of the oxygen-vacancy concentration of La_2NiO_{4-x} and $LaSrNiO_{4-x}$ is given in Fig. 4. The x values, the oxygen-vacancy concentration, of La_2NiO_{4-x} and $LaSrNiO_{4-x}$ are almost equal to 0.00 at $\log(P/\mathrm{Pa})=4.5$ and 4.8. The x value of La_2NiO_{4-x} is greater than that of $LaSrNiO_{4-x}$ at the same oxygen pressure at 1173 K. The lattice oxygen of $LaSrNiO_{4-x}$ is much easily released from the bulk than that of La_2NiO_{4-x}.

Figure 5 shows the electrical conductivity vs. the oxygen vacancy concentration plots of La_2NiO_{4-x} and $LaSrNiO_{4-x}$ at 1173 K. The density of the charge carriers of $LaSrNiO_4$ should be larger than that of La_2NiO_4 at 1173 K, as the slope of the conductivity curve of La_2NiO_{4-x} is larger than that of $LaSrNiO_{4-x}$.

For obtaining the density of the charge carriers of oxygenical-stoichiometric La_2NiO_4 and $LaSrNiO_4$, the data were treated as follows. In general, the electrical conductivity, σ, of a compound can be written as:

$$\sigma = ne\mu, \tag{2}$$

where n is the density of the charge carriers and where μ is the drift mobility. If (the density of the charge carriers) n is divided into two densities, that is, the electronic density at the stoichiometric oxygen composition, n_0, and the density produced from the oxygen vacancy, n_v, the electrical conductivity of the compound will be altered thus:

$$\begin{aligned}\sigma &= (n_0 + n_V)e\mu \\ &= (n_0 e\mu) + (e\mu)n_V.\end{aligned} \tag{3}$$

In the case of La_2NiO_{4-x} and $LaSrNiO_{4-x}$, the electronic density, n_v, is written as:

$$\begin{aligned}n_V &= \frac{Ax}{V(La_2NiO_{4-x} \text{ and } LaSrNiO_{4-x})} \\ &= \frac{AZx}{a_0^2 c_0},\end{aligned} \tag{4}$$

where A is a constant of 1 or 2, x is the x in La_2NiO_{4-x} or $LaSrNiO_{4-x}$, $V(La_2NiO_{4-x}$ or $LaSrNiO_{4-x})$ is the lattice volume[10,11], Z is the crystallographic Z value

(which is 2 in the case of La_2NiO_4 and $LaSrNiO_4$), and a_0 and c_0 are the lattice constant at room temperature (a_0=0.38617 nm, c_0=1.2683 nm for La_2NiO_{4-x}[11] and a_0=0.3821 nm, c_0=1.2550 nm for $LaSrNiO_{4-x}$[10]).

In the case of the electron conduction, the A constant is unity when a neutral oxygen vacancy, which is formed by the transfer of an oxygen on a normal site to the gaseous state, donates only one electron to the conduction band:

$$V_O^X \rightleftharpoons V_O^{\cdot} + e'. \quad (5)$$

The A constant is 2 when the vacancy gives two electrons to the band[12]:

$$V_O^X \rightleftharpoons V_O^{\cdot\cdot} + 2e', \quad (6)$$

but A is −1 (Eq. 5) or −2 (Eq. 6) in the case of hole conduction.

The electrical conductivity of La_2NiO_{4-x} or $LaSrNiO_{4-x}$, therefore, can be expressed as:

$$\sigma = (n_0 e\mu) + \frac{AZxe\mu}{a_0^2 c_0}. \quad (7)$$

The electrical conductivity vs. x plot in Fig. 5 show that the conductivities of La_2NiO_{4-x} and $LaSrNiO_{4-x}$ decrease linearly with the increase in x, as is to be expected from Eq. 7. This result supports the validity of the assumption at the induction of Eq. 7 that is, Eqs. 3 and 4. The negative slopes in the conductivity curves imply that the holes are charge carriers of La_2NiO_{4-x} and of $LaSrNiO_{4-x}$ ($A<0$).

The drift mobility, μ, and the density of the holes, n_0, of oxygen stoichiometric La_2NiO_4 or $LaSrNiO_4$ are given from the slope and the intercept of the conductivity line in Fig. 5 by applying Eq. 7. The results are tabulated in Table 2. Unfortunately, the calculated values of n_0 and μ have some equivocality, as it is difficult to determine from the conductivity data where A is −1 or where it is −2. Thus, n_0 and μ were calculated in two ways, namely, in the cases of A=−1 and −2.

The drift mobility of La_2NiO_4 is significantly larger than that of $LaSrNiO_4$. However, the density of the charge carriers of $LaSrNiO_4$ is much greater than that of La_2NiO_4. Table 2 shows that the 0.056—0.112 electron for La_2NiO_4 and the 0.38—0.76 electron for $LaSrNiO_4$ are in a formula.

Goodenough's model for La_2NiO_4[5-7] suggests that the electronic density of a state is not so high at the top of the conduction band of La_2NiO_4 in the metallic state. The observed value of the density, n_0, was 5.9—11.9×10^{20} cm^{-3}, as is shown in Table 2.

The $LaSrNiO_4$ oxide has the same crystal structure as La_2NiO_4. If the band structure of $LaSrNiO_4$ is the same as that of Goodenough's model for La_2NiO_4 and if $LaSrNiO_4$ has fewer conduction electrons than $LaSrNiO_4$ by one electron a formula, one hole must exist in $LaSrNiO_4$. Table 2 indicates that the number of holes in $LaSrNiO_4$ is somewhat smaller than the expected value of one. This result may imply that a few holes are not free in the conduction band of $LaSrNiO_4$.

Table 2. Drift Mobilities and Densities of State for La_2NiO_4 and $LaSrNiO_4$ at 1173 K

Formula	A[a]	μ(drift)[b]	n_0[c]	Electrons
		$cm^2 V^{-1} s^{-1}$	10^{20} cm^{-3}	Formula
La_2NiO_4	−1	0.34	5.9	0.056
	−2	0.17	11.9	0.112
$LaSrNiO_4$	−1	0.018	41.3	0.38
	−2	0.0091	82.6	0.76

a) "A" is a constant in Eq. 7

$$O \rightleftarrows V_O^X + 1/2O_2$$

$$A=\pm 1: V_O^X \rightleftarrows V_O^{\cdot} + e'$$

$$A=\pm 2: V_O^X \rightleftarrows V_O^{\cdot\cdot} + 2e'$$

b) Drift mobility. c) Density of state.

References

1) M. V. Kniga and R. A. Zaretskaya, *Izv. Akad. Nauk SSSR, Neorg. Mater.*, **7**, 464 (1971).

2) P. Ganguly and C. N. R. Rao, *Mat. Res. Bull.*, **8**, 405 (1973).

3) I. F. Kononyuk, N. G. Surmach, and L. V. Makhnach, *Izv. Akad. Nauk SSSR, Neorg. Mater.*, **18**, 1222 (1982).

4) L. F. Kononyuk, N. G. Surmach, and V. Maklnach, *Inorg. Mater.*, **18**, 1029 (1982).

5) J. B. Goodenough, *Mat. Res. Bull.*, **8**, 423 (1973).

6) J. B. Goodenough and S. Ramasesha, *Mat. Res. Bull.*, **17**, 383 (1982).

7) K. K. Singh, P. Ganguly, and J. B. Goodenough, *J. Solid State Chem.*, **52**, 254 (1984).

8) K. Ishikawa, S. Kondo, Y. Suzuki, S. Takayama, K. Shimada, and Y. Suzuki, *Bull. Chem. Soc. Jpn.*, **59**, 703 (1986).

9) C. N. R. Rao, D. J. Buttrey, N. Otsuka, P. Ganguly, H. R. Harrison, C. J. Sandberg, and J. M. Honig, *J. Solid State Chem.*, **51**, 266 (1984).

10) J. Gopalakrishnan, G. Colsmann, and B. Reuter, *J. Solid State Chem.*, **22**, 145 (1977).

11) JCPDS Card 33-712.

12) Per Kofstad, "Nonstoichiometry, Diffusion, and Electrical Conductivity in Binary Metal Oxides," in "Wiley Series on the Science and Technology of Materials," Wiley-Interscience, New York (1972), Chap. 2, pp. 18—19.

 © 1987 The Chemical Society of Japan Bull. Chem. Soc. Jpn., 60, 1299—1302 (1987)

Paramagnetic Cobalt(III) Complexes with Organic Ligands. X.[1] The Preparation and Properties of Radical Diamminebis-(5-nitrosalicylideneaminato)cobalt(III) Complex and Biradical Diamminebis(5-nitrosalicyl-ideneaminato)cobalt(II) Complex

Yoshihisa YAMAMOTO* and Hidetaka KONNO†
Faculty of Pharmaceutical Sciences, Higashi Nippon Gakuen University, Ishikari-Tobetsu, Hokkaido 061-02
†Faculty of Engineering, Hokkaido University, Sapporo 060
(Received July 11, 1986)

From the reaction mixture of diamminebis(salicylideneaminato)cobalt(III) complex, [Co(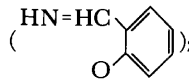)$_2$(NH$_3$)$_2$]Cl·H$_2$O (**1**) and 60% nitric acid, radical diamminebis(5-nitrosalicylideneaminato)-cobalt(III) complex, [Co(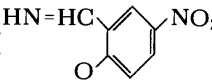)$_2$(NH$_3$)$_2$]Cl·NO$_3$·2H$_2$O (**2**), and biradical diamminebis(5-nitrosalicylideneaminato)cobalt(II) complex, [Co(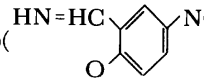)$_2$(NH$_3$)$_2$]Cl·NO$_3$·2H$_2$O (**3**), have been isolated and characterized by analytical, magnetic, spectroscopic, and XPS methods. The effective magnetic moments of **2** and **3** were 1.7 and 5.5 BM, respectively. In the IR spectrum of **2**, a band due to the rocking deformation vibration of NH$_3$ was observed at ca. 840 cm^{-1}. The absorption spectra of **2** and **3** showed a strong absorption peak at ca. 690 nm. In the XPS, Co 2p spectra for **3** showed strong satellites, indicating the oxidation number of the cobalt to be +2, whereas no satellites were observed for the other complexes. In comparison with diamagnetic cobalt(III) complex, [Co(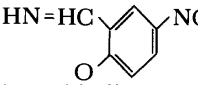)$_2$(NH$_3$)$_2$]NO$_3$·H$_2$O (**4**), C 1s spectra for **2** and **3** showed much larger shoulders on the higher binding energy side due to the electron-poor carbons. It suggests the presence of an unpaired spin on ligands in accordance with paramagnetism of the complexes.

Previous paper of this series was concerned with the preparation, properties and electronic state of radical tetraammine(5-nitrosalicylideneaminato)cobalt(III) complex,[2] [Co(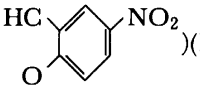)(NH$_3$)$_4$]X$_3$ (X$_3$: Cl$_2$·NO$_3$, (NO$_3$)$_3$). The effective magnetic moment is 1.7 BM, suggesting an unpaired spin. An unpaired spin on the complex is not located on the cobalt atom, but is located over the π-orbitals of the chelated ligand of the complex judging from the physicochemical results.

In the same series of experiments, we have already isolated new paramagnetic cobalt complexes from the reaction mixture of 60% nitric acid and diamminebis(salicylideneaminato)cobalt(III) complex, [Co(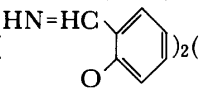)$_2$(NH$_3$)$_2$]Cl·H$_2$O. However, the explanation of the electronic states of the new complexes was deferred, because the magnetic properties and XPS data were not parallel to those of the radical tetraammine(5-nitrosalicylideneaminato)cobalt(III) complex. In the present paper, we present the electronic state and structure of the new paramagnetic complexes as radical diamminebis(5-nitrosalicylideneaminato)cobalt(III) complex, [Co(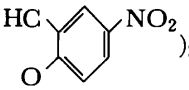)$_2$(NH$_3$)$_2$]Cl·NO$_3$·2H$_2$O, and biradical diamminebis(5-nitrosalicylideneaminato)-cobalt(II) complex, [Co(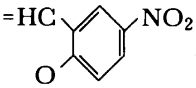)$_2$-(NH$_3$)$_2$]Cl·NO$_3$·2H$_2$O, and report the preparation and properties of them.

Experimental

Measurements. The ^{1}H NMR spectra were recorded with an R-40 apparatus (Hitachi). The IR spectra were recorded in potassium bromide disks with an 270-30 apparatus (Hitachi). The visible absorption spectra were recorded with a Shimadzu UV-210 recording spectrophotometer. The magnetic susceptibilities were measured by the Faraday method using a magnetic balance (Shimadzu) from liq. N$_2$ to room temperature. The electric conductivities of aqueous solutions were determined by the use of a conductometer, CM-30 (Shimadzu) at room temperature. The XPS measurements were carried out in the same manner as described in the previous paper.[2]

Preparation of Complexes. Radical Diamminebis(5-nitrosalicylideneaminato)cobalt(III) Chloride Nitrate Dihydrate (2): Twelve cm^3 of 60% nitric acid were added, drop by drop, to 3 g (7.76 mmol) of trans,trans,trans-diamminebis(salicylideneaminato)cobalt(III) chloride hydrate[5] (**1**). The reaction proceeds with violence. A green crystalline precipitate (complex **2**) was collected by filtration. From the green filtrate, complex **3** (described below) was isolated. The complex **2** on a filter funnel was washed with 60% nitric acid (about 3 cm^3), with acetone and ether, and dried. Yield: 1.42 g (32.9%). Found: C, 30.42; H, 3.43; N, 18.05; Cl, 5.81%. Calcd for CoC$_{14}$H$_{20}$N$_7$O$_{11}$Cl (MW 556.75) C, 30.20; H, 3.62; N, 17.61; Cl, 6.37%. Color: green. D_p=185 °C. Λ=250 S cm^2 mol^{-1} in water. IR spectrum: 1620 cm^{-1} (C=N), 840 cm^{-1}

($\rho_r(NH_3)_r$).

Biradical Diamminebis(5-nitrosalicylideneaminato)cobalt-(II) Chloride Nitrate Dihydrate (3): The green filtrate (described above) was added to acetone-ether (1 : 1) solution and stirred. The green complex **3** thus precipitated was filtered, washed with acetone-ether (1 : 1) solution and with ether, then dried. From the brown filtrate, complex **4** (described below) was isolated. Yield: 1.48 g (34.3%). Found: C, 29.92; H, 3.68; N, 17.23; Cl, 5.08%. Calcd for $CoC_{14}H_{20}N_7O_{11}Cl$ (MW 556.75) C, 30.20; H, 3.62; N, 17.61; Cl, 6.37%. Color: green. D_p=183 °C. Λ=250 S cm^2 mol^{-1} in water. IR spectrum: 1625 cm^{-1} (C=N).

Diamagnetic Diamminebis(5-nitrosalicylideneaminato)-cobalt(III) Nitrate Hydrate (4): The brown colored filtrate (described above) was concentrated and the precipitated brown complex was recrystallized from water. Yield: 0.22 g (5.6%). Found: C, 33.29; H, 3.42; N, 19.65%. Calcd for $CoC_{14}H_{18}N_7O_{10}$ (MW 503.28) C, 33.41; H, 3.61; N, 19.48%. Color: brown. D_p=238 °C. Λ=95 S cm^2 mol^{-1} in water at 50 °C. IR spectrum: 1625 cm^{-1} (C=N), 835 cm^{-1} ($\rho_r(NH_3)_r$). ^{1}H NMR spectrum: The H_5[5] ring proton signal disappeared due to nitration. The H_3, H_4, H_6 ring proton, CH=N and C=NH proton signals were observed at δ 6.79 (d, 2H), 7.96 (dd, 2H), 8.41 (d, 2H), 8.51 (d, 2H), and 11.10 (d, 2H), respectively in DMSO-d_6 solution.

Solubility. Complex **2** is soluble in DMSO, DMF, and slightly soluble in water and 60% nitric acid, but insoluble in the common organic solvents such as alcohols, acetone, and ether. Complex **3** is soluble in DMSO, DMF, water, and 60% nitric acid, and slightly soluble in acetone and methanol, but insoluble in the common organic solvents such as ethanol and ether.

Results and Discussion

Previously, we reported on the preparation, properties, and structure of diamagnetic trans,trans,trans-diamminebis(salicylideneaminato)cobalt(III) chloride hydrate,[5] $[Co(\text{HN=HC-C}_6\text{H}_4\text{-O})_2(NH_3)_2]Cl \cdot H_2O$ (**1**). trans,trans,trans-configuration (abbreviation: t,t,t-) denotes the positions for the two ammine ligands, two phenoxyl groups and two CH=NH groups of the coordinated chelate ligands, respectively.

Radical diamminebis(5-nitrosalicylideneaminato)-cobalt(III) chloride nitrate dihydrate (**2**) and biradical diamminebis(5-nitrosalicylideneaminato)cobalt(II) chloride nitrate dihydrate (**3**) were isolated from a reaction mixture of complex (**1**) and 60% nitric acid.

Radical Diamminebis(5-nitrosalicylideneaminato)-cobalt(III) Chloride Nitrate Dihydrate, $[Co(\text{HN=HC-C}_6\text{H}_3(\text{NO}_2)\text{-O})_2(NH_3)_2]Cl \cdot NO_3 \cdot 2H_2O$ (2): The electric conductivity in an aqueous solution was 250 S cm^2 mol^{-1}. The magnetic susceptibility obeyed the Curie-Weiss law, with effective magnetic moment of 1.7 BM, suggesting the presence of an unpaired spin. A band due to the rocking deformation vibration of the ammine ligand was observed at 840 cm^{-1} in the IR spectrum. This is in the range for Co(III) ammine complexes.[6-10] The ^{1}H NMR spectrum of **2** could not be measured in 1.8 mol dm^{-3} D_2SO_4 solution because of the insolubility.

In the XPS, two N 1s spectra were observed at ca. 400 eV and ca. 406 eV. The lower binding energy peak was separated to two peaks which were assigned to -NH= and NH_3 nitrogens. The higher binding energy peak was also separated into two peaks which were assigned to NO_2 and NO_3 nitrogens[2-4] as shown in Table 1.

Table 1. XPS, Magnetic Moments, and Absorption Spectra of Complexes

Complex No.	Binding energies of electrons, E_B/eV						Magnetic moments μ_{eff}/BM	Curie-Weiss constants θ/K	Absorption bands in 60% nitric acid nm (ε)
	Co 2p$_{3/2}$	Co 2p$_{1/2}$	splitting	C 1s	N 1s	O 1s			
2	782.1 FWHM 2.4 satellites no	797.4	15.3	285.0 (45.2)[a] 286.1 (34.0) 287.4 (16.5) 289.4 (4.3)	399.4 =NH 400.3 NH_3 405.7 NO_2 406.8 NO_3	532.7	1.7	+23	380 (18890) 700 (6600)
3	782.2 FWHM 3.5 satellites very strong	797.3	15.1	285.0 (38.9) 286.3 (27.9) 287.7 (14.5) 289.1 (15.2) 291.2 (3.5)	399.8 =NH 400.2 NH_3 405.8 NO_2 406.9 NO_3	532.4	5.5	+10	363 (13500) 696 (12700)
4	782.1 FWHM 2.5 satellites no	797.0	14.9	285.0 (61.6) 286.3 (33.9) 288.9 (4.5)	399.4 =NH 399.9 NH_3 405.5 NO_2 406.7 NO_3	532.6	dia.		370 (19900)
5[b]	782.5 FWHM 3.0 satellites no	797.5	15.0	285.0 (55) 286.1 (28) 287.1 (11) 288.5 (6)	399.6 =NH 400.6 NH_3 405.8 NO_2 407.4 NO_3	532.4	1.7	+19	363 (5050) 450 (2830) 667 (10060)

a) Relative intensities in % after peak separation. The peak less than 1% was neglected. b) Ref. 2.

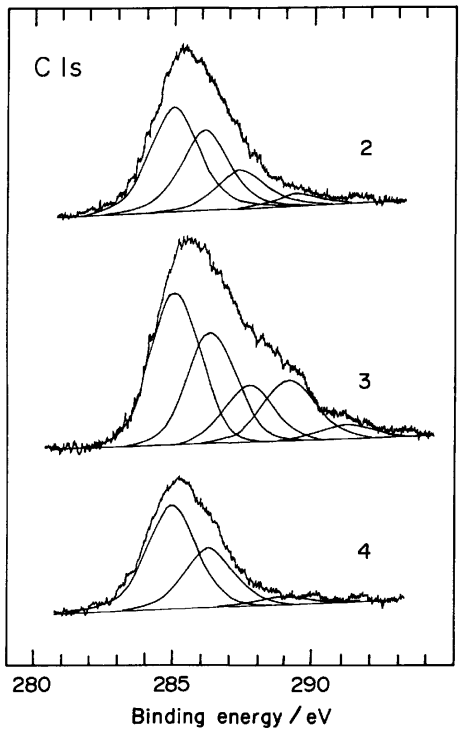

Fig. 1. The XPS in the C 1s region of **2**—**4** complexes.

2: $[Co(\text{HN=HC-C}_6\text{H}_3(\text{NO}_2)\text{-O})_2(NH_3)_2]Cl\cdot NO_3\cdot 2H_2O$,

3: $[Co(\text{HN=HC-C}_6\text{H}_3(\text{NO}_2)\text{-O})_2(NH_3)_2]Cl\cdot NO_3\cdot 2H_2O$,

4: $[Co(\text{HN=HC-C}_6\text{H}_3(\text{NO}_2)\text{-O})_2(NH_3)_2]NO_3\cdot H_2O$.

The C 1s peak was separated into four peaks having a full width at half maximum [FWHM] of 2.1 eV. The peaks that appeared in the higher binding energy region are assigned to electron-poor carbons relative to normal ring carbons at 285.0 eV. As is shown in Fig. 1 and Table 1, the proportion of the electron-poor carbons in the higher binding energy region relative to normal carbons is larger than that of the corresponding diamagnetic cobalt(III) nitrate hydrate, $[Co(\text{HN=HC-C}_6\text{H}_3(\text{NO}_2)\text{-O})_2(NH_3)_2]NO_3\cdot H_2O$ (**4**). The Co $2p_{3/2}$ peak at 782.1 eV in the XPS does not have satellites. The absorption spectrum showed a strong peak at 700 nm. The above results and the magnetic moment are closely similar to those of the green paramagnetic tetraammine(5-nitrosalicylideneaminato)cobalt(III) chloride nitrate, $[Co(\text{HN=HC-C}_6\text{H}_3(\text{NO}_2)\text{-O})(NH_3)_4]Cl_2\cdot NO_3$ (**5**), previously reported.[2] Thus, an unpaired spin on **2** is not located on the cobalt atom but is located over the chelated ligands. Therefore, complex **2** is a radical cobalt(III) complex such as Scheme 1.

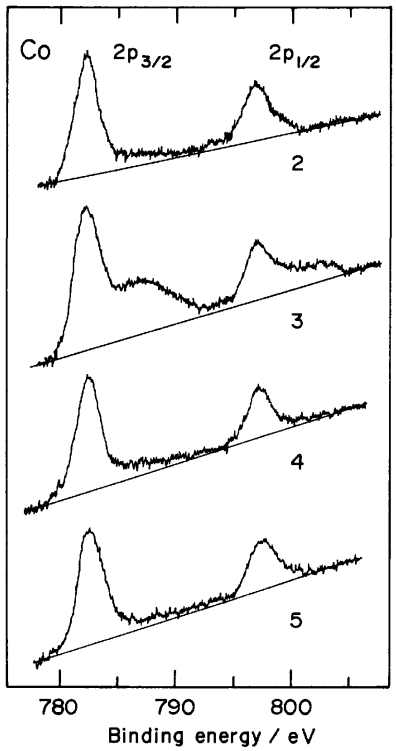

Fig. 2. The XPS in the Co 2p region of **2**—**5** complexes.

2: $[Co(\text{HN=HC-C}_6\text{H}_3(\text{NO}_2)\text{-O})_2(NH_3)_2]Cl\cdot NO_3\cdot 2H_2O$,

3: $[Co(\text{HN=HC-C}_6\text{H}_3(\text{NO}_2)\text{-O})_2(NH_3)_2]Cl\cdot NO_3\cdot 2H_2O$,

4: $[Co(\text{HN=HC-C}_6\text{H}_3(\text{NO}_2)\text{-O})_2(NH_3)_2]NO_3\cdot H_2O$,

5: $[Co(\text{HN=HC-C}_6\text{H}_3(\text{NO}_2)\text{-O})(NH_3)_4]Cl_2\cdot NO_3$.

Biradical Diamminebis(5-nitrosalicylideneaminato)cobalt(II) Chloride Nitrate Dihydrate, $[Co(\text{HN=HC-C}_6\text{H}_3(\text{NO}_2)\text{-O})_2(NH_3)_2]Cl\cdot NO_3\cdot 2H_2O$ (3): The electric conductivity in an aqueous solution and

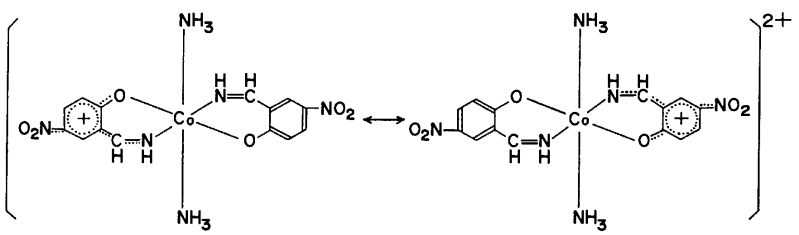

Scheme 1.

the analytical results were both similar to those for **2**. However, the results of the magnetic susceptibility, XPS, and absorption spectra were very different from those of **2**. The ^{1}H NMR spectrum of **3** in 1.8 mol dm^{-3} D_2SO_4 solution did not show the signal because of the paramagnetism. The magnetic susceptibility obeyed the Curie-Weiss low, with effective magnetic moment of 5.5 BM, suggesting the presence of five unpaired spins. The Co 2p peaks in the XPS showed strong satellites. This spectrum is very different from those of **2**, **4**, and **5** as shown in Fig. 2. The strong satellites are due to either Co(II) ions or high spin Co(III) ions. A number of Co(II) compounds are reported to show strong satellites in Co 2p spectra.[11-17] As a high spin Co(III) ion, only CoF_3 is reported to show strong satellites.[11,12] A distinction between Co(II) and high spin Co(III) ions is difficult to evaluate from the Co 2p spectrum alone, however, together with the following experimental results, the cobalt in complex **3** is considered to be Co(II). In the C 1s peak, the proportion of the electron-poor carbons in the higher binding energy region relative to a normal carbon is larger than that of complex **2** as shown in Fig. 1. In addition, the absorption peak (ε=12700) at 696 nm due to the unpaired spin[2] on the complex is much stronger than that (ε=6600) of complex **2**. All these results suggest that two unpaired spins are located over the chelated ligand, and three unpaired spins are located on the cobalt atom. Accordingly, complex **3** is considered to be a biradical diamminebis(5-nitrosalicylideneaminato)cobalt(II) complex such as Scheme 2.

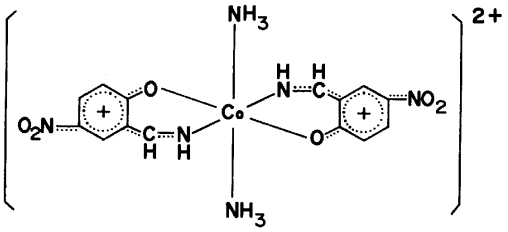

Scheme 2.

The results for complex **4** are collected in Table 1 and in the Experimental section.

In the XPS data, the relative peak intensity of C 1s to N 1s did not show larger scattering than ±10% by complexes and for each measurement, indicating that the level of carbonaceous contamination was almost constant (Note that the atomic ratio between carbon and nitrogen is the same for complex **2**—**4**). Quantitative conclusions, however, were not drawn from the XPS data, as, with our data and a calculation system, E_B assignment for each carbon atom could not be performed. The probability that the higher E_B fraction in C 1s spectra is due to shake up phenomena is very low, since the known shake up satellites are observed at least 6 eV higher than the main peak and the intensity is less than 8% that of the main peak.[18] The higher E_B fraction in C 1s spectra increases in the order of complex **4**<**2**<**3**, as is clearly seen in Fig. 1, and no significant differences were observed for the N 1s spectra. Therefore taken together with the magnetic susceptibility and absorption spectra data, it is definite that one electron is missing per one ligand in complex **3**. Probably, it is on the carbon skeleton, but the location or detailed electronic configulations cannot be specified at present.

References

1) Part IX: Ref. 2.
2) Y. Yamamoto and E. Toyota, *Bull. Chem. Soc. Jpn.*, **59**, 617 (1986).
3) Y. Yamamoto, M. Mori, and H. Konno, *Bull. Chem. Soc. Jpn.*, **54**, 1995 (1981).
4) Y. Yamamoto, H. Kudo, M. Mori, and H. Konno, *Bull. Chem. Soc. Jpn.*, **55**, 136 (1982).
5) Y. Yamamoto and E. Toyota, *Bull. Chem. Soc. Jpn.*, **57**, 2650 (1984).
6) K. Nakamoto, "Infrared Spectra of Inorganic and Coordination Compounds," Wiley-Interscience, New York (1970), p. 150.
7) J. K. Wilmshurst, *Can. J. Chem.*, **38**, 467 (1960).
8) G. F. Svatos, D. M. Sweeny, S. Mizushima, C. Curran, and J. V. Quagliano, *J. Am. Chem. Soc.*, **79**, 3313 (1957).
9) L. Sacconi, A. Sabatini, and P. Gans, *Inorg. Chem.*, **3**, 1772 (1964).
10) D. B. Powell and N. Sheppard, *J. Chem. Soc.*, **1956**, 3108.
11) D. C. Frost, C. A. McDowell, and I. S. Woolsey, *Mol. Phys.*, **27**, 1473 (1974).
12) J. C. Carver, G. K. Schweitzer, and T. A. Carlson, *J. Chem. Phys.*, **57**, 973 (1972).
13) Y. Okamoto, H. Nakano, T. Imanaka, and S. Teranishi, *Bull. Chem. Soc. Jpn.*, **48**, 1163 (1975).
14) M. Oku and K. Hirokawa, *J. Electron Spectrosc. Relat. Phenom.*, **8**, 475 (1976).
15) J. Haber and L. Ungier, *J. Electron Spectrosc. Relat. Phenom.*, **12**, 305 (1977).
16) J. Escard, G. Mavel, J. E. Guerchais, and R. Kergoat, *Inorg. Chem.*, **13**, 695 (1974).
17) J. H. Burness, J. G. Dillard, and L. T. Taylor, *J. Am. Chem. Soc.*, **97**, 6080 (1975).
18) e. g. D. T. Clark, A. Dilks, J. Peeling, and H. R. Thomas, *Faraday Dicuss. Chem. Soc.*, No. 60, 183 (1975).

 © 1987 The Chemical Society of Japan Bull. Chem. Soc. Jpn., 60, 1303—1308 (1987)

The Condensation and Decomposition of Phosphoramidates with Acids

Shoji SATO, Takao TAKAYANAGI, and Makoto WATANABE*
Department of Industrial Chemistry, Chubu University, Matsumoto-cho, Kasugai, Aichi 487
(Received July 21, 1986)

Several phosphoramidates were reacted with dried hydrogen chloride, acetic acid, and oxalic acid. The phosphoramidates reacted with the acids to produce ortho- and polyphosphates, but did not react with them to make polyphosphates containing imino groups, with the elimination of ammonia. The decomposition of the phosphoramidates to orthophosphate by the action of water was considered to be the first step in the production of polyphosphates:

$$MO\text{-}\overset{\overset{O}{\|}}{\underset{\underset{M}{O}}{P}}\text{-}NH_2 + H_2O \longrightarrow MO\text{-}\overset{\overset{O}{\|}}{\underset{\underset{M}{O}}{P}}\text{-}ONH_4,$$

The formation of polyphosphates can be explained, for example, by this equation:

$$MO\text{-}\overset{\overset{O}{\|}}{\underset{\underset{M}{O}}{P}}\text{-}ONH_4 + NH_2\text{-}\overset{\overset{O}{\|}}{\underset{\underset{M}{O}}{P}}\text{-}OM + 2HA \longrightarrow MO\text{-}\overset{\overset{O}{\|}}{\underset{\underset{M}{O}}{P}}\text{-}O\text{-}\overset{\overset{O}{\|}}{\underset{\underset{M}{O}}{P}}\text{-}OM + 2NH_4A,$$

where HA stands for acid.

Among phosphorus-nitrogen compounds, the most outstanding may be phosphazene polymers. Many studies have been made of these compounds, while other phosphorus-nitrogen compounds are not very well-known. We have reported on the syntheses and thermal properties of several phosphoramidates during the last few years.[1-6] The phosphoramidates are thought to be useful as new types of chemical fertilizers containing P-N covalent bonds and as flame-proof materials. These phosphoramidates produce ortho- and polyphosphates, but do not produce polyphosphates containing imino groups, when they are heated in air at a moderately high temperature (100—1000 °C). The chemical reactions of the phosphoramidates with inorganic and organic acids were performed in order to study the condensation and decomposition of the amino groups in the phosphoramidates. To prevent the hydrolysis of the phosphoramidates and the reaction products, hydrogen chloride, acetic acid, and oxalic acid were used.

Experimental

Preparation of Phosphoramidates. The phosphoramidic acid monohydrate, ammonium hydrogenphosphoramidate, sodium hydrogenphosphoramidate, potassium hydrogenphosphoramidate, and disodium phosphoramidate hexahydrate were made by the methods described in Reference 7.

Reaction of Phosphoramidates with Hydrogen Chloride. Hydrogen chloride was prepared by adding concentrated hydrochloric acid to concentrated sulfuric acid, and the HCl gas was dried with concentrated sulfuric acid. The dried HCl gas was introduced to a reaction glass-tube containing about 5 g of a phosphoramidate sample. The product was washed quickly with ethanol to remove the HCl gas adsorbed on the product.

Reaction of Phosphoramidates with Acetic Acid. A phosphoramidate sample (about 2 g) was placed in a mixture of 5 cm^3 of acetic acid and 20 cm^3 of chloroform, and the resulting mixture was reacted at 25 and 60 °C while being stirred. The solid product was filtered off and washed with ethanol. In the case of the reaction of disodium phosphoramidate hexahydrate, the reaction mixture was centrifuged and the solid product was washed with ethanol.

Reaction of Phosphoramidates with Oxalic Acid. Oxalic acid (3 g) was dissolved in 100 cm^3 of ethanol, and then a phosphoramidate sample (about 2 g) was added to the solution. The mixture was heated at 25 and 60 °C while being stirred. The solid product was filtered off and washed with ethanol.

Quantitative Analysis of Nitrogen. The amount of total nitrogen and that of ammonium ions in a sample were measured by the Kjeldahl technique.

Paper Chromatography and Colorimetry of Phosphates. A sample was dissolved in water, and the pH of the solution was adjusted to about 7 with an aqueous sodium hydroxide solution if needed. The one-dimensional paper-chromatographic separation and the colorimetric determination of the phosphate species in the solution were done by the method described in our previous paper.[1]

X-Ray Diffractometry. An X-ray diffraction diagram of a sample was taken with nickel-filtered Cu $K\alpha$ radiation using a Rigaku X-ray diffractometer, RAD-1B.

IR Spectrophotometry. An IR spectrum of a sample was recorded on a JASCO IR spectrophotometer, A-3, using the KBr disc method.

^{31}P NMR Measurement. A sample was dissolved in water and the ^{31}P NMR spectrum of the solution was taken by means of a JNM-GX270 spectrograph. The NMR chemical shifts are reported relative to external 85%-orthophosphoric acid, with the positive shifts being downfield.

Results and Discussion

Reaction with Hydrogen Chloride. The data of the chemical compositions of the products are shown in Table 1, along with the X-ray diffraction data. The chromatographic separation between phosphoramidate and orthophosphate could not be performed with the developing solvents used in this experiment. According to the results listed in Table 1, the phos-

Table 1. Compositions of the Reaction Products of Phosphorammidates with HCl Gas

Phosphoramidates	Reaction time/min	Total N/%	N/% as NH_4^+	X-Ray dif.	Phosphates/P%			
					Amido and Ortho	Di	Tri	Higher
$H_2PO_3NH_2 \cdot H_2O$	60	14.4	1.5	SM	72.0	21.0	4.2	2.8
	180	14.4	2.2	SM	61.4	30.0	6.8	1.5
	300	14.2	2.3	SM	52.9	31.5	9.6	6.0
$NH_4HPO_3NH_2$	60	24.4	11.9	SM, NH_4Cl	70.9	17.3	3.1	8.7
	180	20.1	11.9	SM, UK, NH_4Cl	36.8	30.9	2.1	30.2
	300	16.2	13.7	UK, NH_4Cl	25.4	32.4	3.8	38.4
$NaHPO_3NH_2$	60	11.4	1.1	SM, UK, NH_4Cl	68.3	23.4	8.3	
	180	10.4	3.0	SM, UK, NH_4Cl	60.5	28.9	10.6	
	300	10.6	5.7	SM, UK, NH_4Cl	65.5	22.9	6.6	5.0
$KHPO_3NH_2$	60	10.4	0.2	SM	100	—	—	—
	180	10.3	0.7	SM	86.5	8.3	5.2	
	300	10.2	1.1	SM	83.7	12.1	4.2	
$Na_2PO_3NH_2 \cdot 6H_2O$	60	6.0	5.2	UK, NH_4Cl	92.8	7.2	—	—
	180	6.0	5.2	UK, NH_4Cl	96.3	3.7	—	—
	300	6.0	5.2	UK, NH_4Cl	100	—	—	—

SM and UK stand for the starting materials and an unknown substabce respectively.

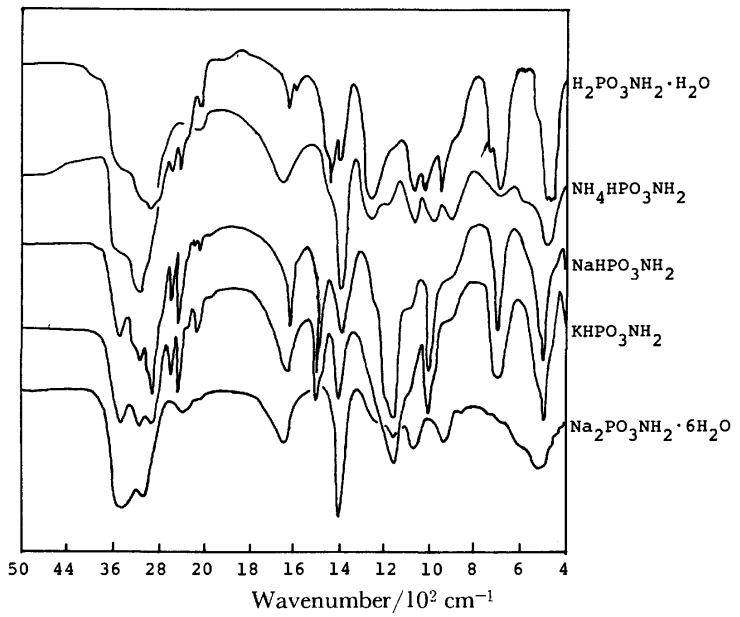

Fig. 1. IR spectra of the reaction products of phosphoramidates with HCl gas for 5 h.

phoramidic acid and phosphoramidates seemed to react with HCl gas to produce ortho- and polyphosphates. The amino group of the phosphoramidates decomposed to ammonia at the same time. The contents of NH_4^+ and polyphosphates increased with the passage of the reaction time in the reactions of $H_2PO_3NH_2 \cdot H_2O$, $NH_4HPO_3NH_2$, and $KHPO_3NH_2$. The IR spectra of the products in Fig. 1 agree well with the results in Table 1. The absorption at 1400 cm^{-1} is due to NH_4^+, while those at about 900 and 700 cm^{-1} are assigned to a P-O-P or a P-N(H)-P linkage respectively. The reaction rate of $KHPO_3NH_2$ was very low; this means that the phosphoramidate is very stable. In the reactions of $NaHPO_3NH_2$ and $Na_2PO_3NH_2 \cdot 6H_2O$, the degradation of polyphosphates to phosphates with shorter chain lengths was observed in addition to the formation of ortho- and polyphosphates. The results in Table 1 and Fig. 1 do

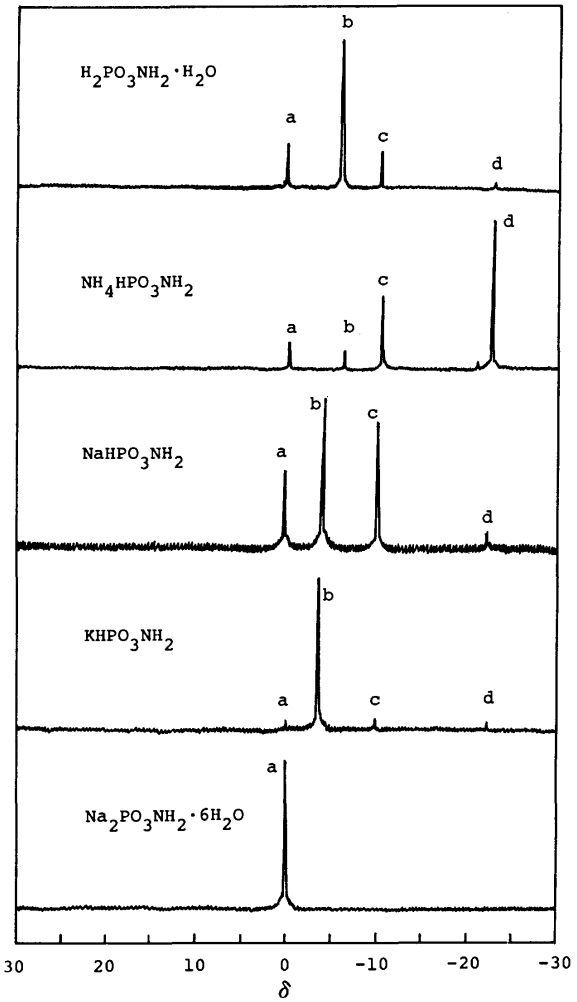

Fig. 2. ^{31}P NMR spectra of the reaction products of phosphoramidates with HCl gas at room temperature for 5 h.
a: Orthophosphate, b: phosphoramidate, c: end-PO_4 group, d: middle-PO_4 group.

not, however, give any information about the formation of a P-N(H)-P linkage. The ^{31}P NMR peaks of the products in Fig. 2 were assigned to phosphoramidate, orthophosphate, and polyphosphates. The NMR data did not give any peak of a compound with a P-N(H)-P linkage. Accordingly, the formation of a P-N(H)-P linkage, with the elimination of ammonia, by the following reaction did not occur in these reaction systems:

$$-\overset{|}{\underset{|}{P}}-NH_2 + NH_2-\overset{|}{\underset{|}{P}}- + HCl \longrightarrow -\overset{|}{\underset{|}{P}}-N(H)-\overset{|}{\underset{|}{P}}- + NH_4Cl. \quad (1)$$

Instead, the reaction processes can be written thus for these reaction systems:

$$MO-\overset{\overset{O}{\|}}{\underset{\underset{M}{O}}{P}}-NH_2 + H_2O \longrightarrow MO-\overset{\overset{O}{\|}}{\underset{\underset{M}{O}}{P}}-ONH_4, \quad (2)$$

$$MO-\overset{\overset{O}{\|}}{\underset{\underset{M}{O}}{P}}-ONH_4 + NH_2-\overset{\overset{O}{\|}}{\underset{\underset{M}{O}}{P}}-OM + 2HCl \longrightarrow$$

$$MO-\overset{\overset{O}{\|}}{\underset{\underset{M}{O}}{P}}-O-\overset{\overset{O}{\|}}{\underset{\underset{M}{O}}{P}}-OM + 2NH_4Cl, \quad (3)$$

$$MO-\overset{\overset{O}{\|}}{\underset{\underset{M}{O}}{P}}-O-\overset{\overset{O}{\|}}{\underset{\underset{M}{O}}{P}}-OM + NH_2-\overset{\overset{O}{\|}}{\underset{\underset{M}{O}}{P}}-OM + 2HCl \longrightarrow$$

$$MO-\overset{\overset{O}{\|}}{\underset{\underset{M}{O}}{P}}-O-\overset{\overset{O}{\|}}{\underset{\underset{M}{O}}{P}}-O-\overset{\overset{O}{\|}}{\underset{\underset{M}{O}}{P}}-OM + MCl + NH_4Cl. \quad (4)$$

The phosphoramidate with an OH group is considered to form a zwitterion:[8]

$$MO-\overset{\overset{O}{\|}}{\underset{\underset{M}{O}}{P}}-NH_2 + H_2O(HCl) \longrightarrow$$

$$HO-\overset{\overset{O}{\|}}{\underset{\underset{M}{O}}{P}}-NH_2 + MOH(MCl), \quad (5)$$

$$HO-\overset{\overset{O}{\|}}{\underset{\underset{M}{O}}{P}}-NH_2 \longrightarrow {}^{-}O-\overset{\overset{O}{\|}}{\underset{\underset{M}{O}}{P}}-NH_3^+. \quad (6)$$

The zwitterion is very active and can react with water and phosphates to form ortho- and polyphosphates respectively:

$$^{-}O-\overset{\overset{O}{\|}}{\underset{\underset{M}{O}}{P}}-NH_3^+ + H_2O \longrightarrow HO-\overset{\overset{O}{\|}}{\underset{\underset{M}{O}}{P}}-ONH_4, \quad (7)$$

$$^{-}O-\overset{\overset{O}{\|}}{\underset{\underset{M}{O}}{P}}-NH_3^+ + HO-\overset{\overset{O}{\|}}{\underset{\underset{M}{O}}{P}}-ONH_4 + HCl \longrightarrow$$

$$HO-\overset{\overset{O}{\|}}{\underset{\underset{M}{O}}{P}}-O-\overset{\overset{O}{\|}}{\underset{\underset{M}{O}}{P}}-ONH_4 + NH_4Cl. \quad (8)$$

It is difficult at present to obtain information about the formation of the zwitterion, so it cannot be determined which process is more reasonable for the reaction system. The water in the reactions can come from the crystal water and/or the adsorbed water of the phosphoramidates and a slight amount of water in the gas in the reaction systems. It was difficult to remove the adsorbed water and the water in the gas completely. In the reactions of $NaHPO_3NH_2$ and $Na_2PO_3NH_2 \cdot 6H_2O$, a degradation of polyphosphates to phosphates with shorter chain lengths was observed. Usually this degradation can not take place in a solid state at room temperature. The water contained in the products may be strongly acidic as a result of the dissolution of HCl gas. The hydrolysis

Table 2. Compositions of the Reaction Products of Phosphoramidates with Acetic Acid at 60 °C for 25 h

Phosphoramidates	Total N/%	N/% as NH_4^+	X-Ray dif.	Phosphates/P%			
				Amido and Ortho	Di	Tri	Higher
$H_2PO_3NH_2 \cdot H_2O$	12.3	10.9	UK	16.9	13.9	7.4	61.8
$NH_4HPO_3NH_2$	22.3	11.9	SM	91.2	5.9	0.2	2.7
$NaHPO_3NH_2$	11.1	0.3	SM	100	—	—	—
$KHPO_3NH_2$	9.9	0.4	SM	96.4	3.6	—	—
$Na_2PO_3NH_2 \cdot 6H_2O$	9.0	0.2	UK	100	—	—	—

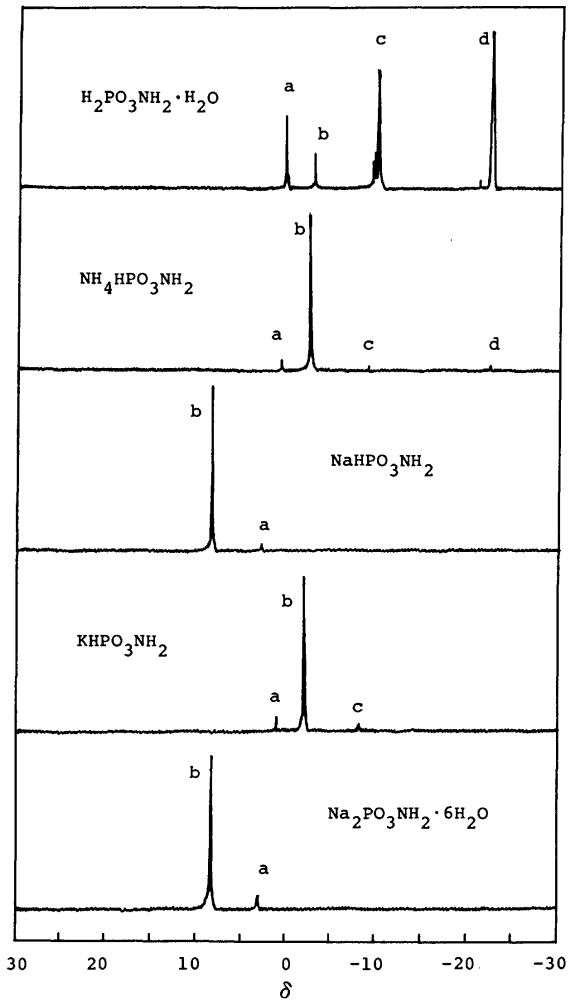

Fig. 3. ^{31}P NMR spectra of the reaction products of phosphoramidates with acetic acid at 60 °C for 25 h. a: Orthophosphate, b: phosphoramidate, c: end-PO_4 group, d: middle-PO_4 group.

of polyphosphates is very much accelerated by an H^+ ion.[9]

Reaction with Acetic Acid. The chemical compositions and X-ray diffraction data of the reaction products at 60 °C are shown in Table 2. The data at 25 °C are not listed because the reaction processes of the phosphoramidates with acetic acid at 25 °C were almost the same as those at 60 °C except for the reaction rates. As Table 2 shows, the reaction rate of the phosphoramidic acid was much faster than those of other phosphoramidates. The ^{31}P NMR spectral data in Fig. 3 support the results in Table 2. The NMR spectra of $NaHPO_3NH_2$ and $Na_2PO_3NH_2 \cdot 6H_2O$ gave a large peak of the amidate and a very small peak of orthophosphate. The NMR spectra of $NH_4HPO_3NH_2$ and $KHPO_3NH_2$ included small peaks of orthophosphate, an end-PO_4 group, and/or a middle-PO_4 group other than the large peak of the phosphoramidate. The NMR spectra of the products of $NaHPO_3NH_2$ and $Na_2PO_3NH_2 \cdot 6H_2O$ were taken by dissolving them in a basic solution (pH 9—10). The peak of phosphoramidate at about −3 — −5 in an acidic solution shifted to about +8.5 in a basic solution. The spectrum of $H_2PO_3NH_2 \cdot H_2O$ exhibited large peaks of orthophosphate, an end-PO_4 group, and a middle-PO_4 group, and a small peak of the phosphoramidic acid. No proof of the presence of imidopolyphosphates was obtained by either the chromatography or the NMR. Therefore, the formation of a P-N(H)-P linkage according to the following reaction did not occur in these systems:

$$\text{-P-NH}_2 + \text{NH}_2\text{-P-} + \text{CH}_3\text{COOH} \longrightarrow \text{-P-N(H)-P-} + \text{CH}_3\text{COONH}_4. \quad (9)$$

Considering the above results, several reaction processes can be written for these systems:

$$\text{MO-P(=O)(O M)-NH}_2 + \text{H}_2\text{O} \longrightarrow \text{MO-P(=O)(O M)-ONH}_4, \quad (10)$$

$$\text{MO-P(=O)(O M)-ONH}_4 + \text{NH}_2\text{-P(=O)(O M)-OM} + 2\text{CH}_3\text{COOH} \longrightarrow \text{MO-P(=O)(O M)-O-P(=O)(O M)-OM} + 2\text{CH}_3\text{COONH}_4, \quad (11)$$

$$\text{MO-P(=O)(O M)-O-P(=O)(O M)-OM} + \text{CH}_3\text{COOH} \longrightarrow \text{MO-P(=O)(O M)-O-P(=O)(O M)-OH} + \text{CH}_3\text{COOM}, \quad (12)$$

Table 3. Compositions of the Reaction Products of Phosphoramidates with Oxalic Acid at 60 °C for 25 h

Phosphoramidates	Total N/%	N/% as NH_4^+	X-Ray dif.	Phosphates/P%			
				Amido and Ortho	Di	Tri	Higher
$H_2PO_3NH_2 \cdot H_2O$	12.3	7.6	SM, UK	22.3	39.0	4.2	34.5
$NH_4HPO_3NH_2$	12.2	12.2	UK	8.8	14.1	4.2	72.9
$NaHPO_3NH_2$	11.6	0.5	SM	100	—	—	—
$KHPO_3NH_2$	5.4	5.2	UK	11.6	8.6	6.2	73.6
$Na_2PO_3NH_2 \cdot 6H_2O$	6.1	0.5	UK	87.0	9.2	3.8	

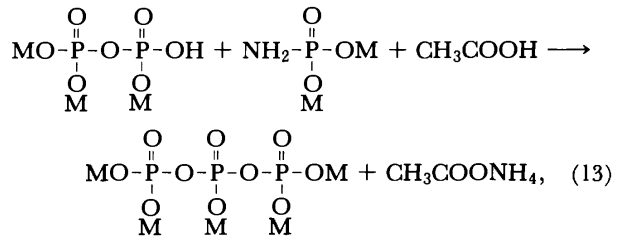

(13)

or

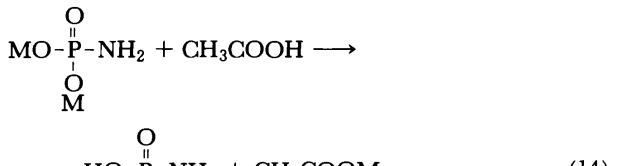

(14)

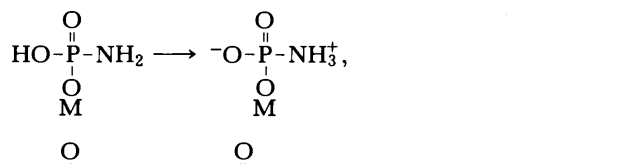

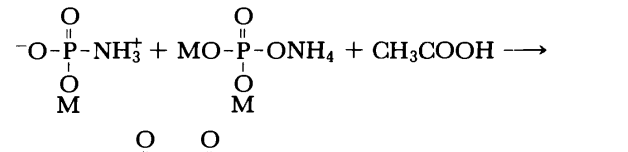

(15)

The water in Eq. 10 can come from crystal water and the adsorbed water of the phosphoramidates. As has been mentioned above, because of the lack of suitable data it is difficult to chose the most reasonable processes for the reaction systems.

Reaction with Oxalic Acid. The data on the chemical composition and the results of the X-ray diffractometry of the products are shown in Table 3, while ^{31}P NMR spectra of the products are presented in Fig. 4. Since the products were ortho- and polyphosphates, while imidopolyphosphates were not produced, the condensation with the elimination of ammonia did not occur in these reaction systems, either:

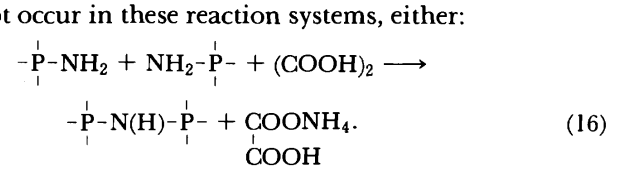

(16)

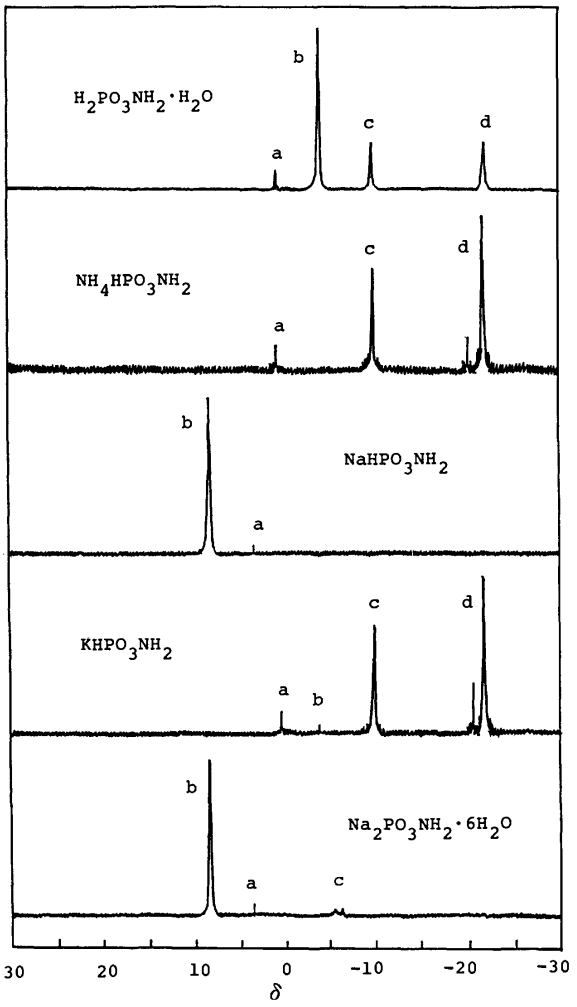

Fig. 4. ^{31}P NMR spectra of the reaction products of phosphoramidates with oxalic acid at 60 °C for 25 h. a: Orthophosphate, b: phosphoramidate, c: end-PO_4 group, d: middle-PO_4 group.

In the reaction with oxalic acid, phosphoramidic acid monohydrate, ammonium hydrogenphosphoramidate, and potassium hydrogenphosphoramidate showed a high reactivity. The reactions of sodium hydrogenphosphoramidate and disodium phosphoramidate hexahydrate were very slow. Accordingly, the reactivity of oxalic acid with the phosphoramidates seemed to be higher than that of acetic acid. As has been described above, since all the products are ortho- and polyphosphates, reaction processes similar to those of acetic

acid must take place in the reaction with oxalic acid, for example, as follows:

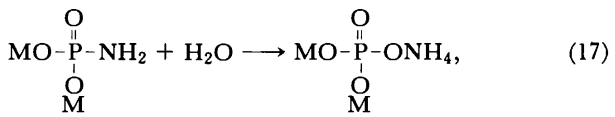

(17)

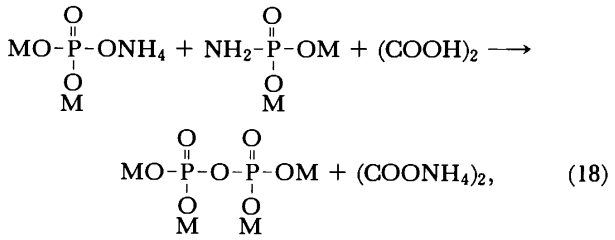

(18)

The water in Eq. 17 can come from the crystal water and/or the adsorbed water of the phosphoramidates. Oxalic acid has a higher reactivity to the phosphoramidates than does acetic acid. This may be explained by, for example, the faster reaction rate of Eq. 18 than that of Eq. 11.

References

1) M. Watanabe, T. Inagaki, and S. Sato, *Bull. Chem. Soc. Jpn.*, **56**, 458 (1983).
2) M. Watanabe, T. Inagaki, Y. Morii, and T. Yamada, *Setsuko To Setsukai*, No. 184, 111 (1983).
3) M. Watanabe, Y. Morii, and S. Sato, *Bull. Chem. Soc. Jpn.*, **57**, 2087 (1984).
4) M. Watanabe, Y. Morii, and S. Sato, *Bull. Chem. Soc. Jpn.*, **57**, 2914 (1984).
5) S. Sato, M. Watanabe, and T. Yamada, *Setsuko To Setsukai*, No. 199, 357 (1985).
6) S. Sato and M. Watanabe, *Bull. Chem. Soc. Jpn.*, **58**, 3513 (1985).
7) A. H. Herzog and M. L. Nielsen, *Anal. Chem.*, **30**, 1490 (1958), and the references cited therein.
8) D. E. C. Corbridge, "Phosphorus," Elsevier, Amsterdam (1980), p. 222.
9) M. Watanabe, *Bull. Chem. Soc. Jpn.*, **47**, 2048 (1974).

 © 1987 The Chemical Society of Japan Bull. Chem. Soc. Jpn., 60, 1309—1320 (1987)

Extraction Equilibria of Hydrochloric Acid by Trioctylamine in Low-Polar Organic Solvents

Takashi KOJIMA* and Hiroshi FUKUTOMI
Research Laboratory for Nuclear Reactors, Tokyo Institute of Technology, O-okayama, Meguro-ku, Tokyo 152
(Received August 20, 1986)

Two-phase emf titrations have been performed for the extraction of hydrochloric acid from aqueous solution containing 1 M NaCl (M=mol dm^{-3}) by trioctylamine (TOA) dissolved in cyclohexane, toluene, benzene, chlorobenzene, nitrobenzene, cyclohexane-benzene mixtures, and benzene-nitrobenzene mixtures. It has been found that the extraction is accompanied with the formation of monomeric trioctylammonium chloride and its successive aggregation from dimer to micell (n-mer) in organic phase: $\overline{\text{TOA}}+\text{H}^+ + \text{Cl}^- = \overline{\text{TOAHCl}}$, K_d; $(\overline{\text{TOAHCl}})_{i-1} + \overline{\text{TOAHCl}} = (\overline{\text{TOAHCl}})_i$, $\overline{K}_i (i=2,3,\cdots,n)$, where the concentration quotients of successive aggregation, $\overline{K}_i$, satisfy the relation $2\overline{K}_2 = 3\overline{K}_3/2 = \cdots = n\overline{K}_n/(n-1)$. The quotients K_d and $\overline{K}_2$ vary with the total volume fraction of TOA in organic phase, $\bar{\psi}_R^\circ$, according to equations, $\ln K_d = \ln K_d^\circ + g\,\bar{\psi}_R^\circ$ and $\ln \overline{K}_2 = \ln \overline{K}_2^\circ + h\,\bar{\psi}_R^\circ$. Diluent effect on the equilibrium constants K_d° and $\overline{K}_2^\circ$ are discussed in detail based on the theory of regular solution.

Long-chain tertiary amines have been well-known as useful extractants of metal ions in acidic aqueous solutions, but detailed extraction mechanisms are not completely elucidated. It has been frequently assumed that the extraction of acid by the amines in water-insoluble organic solvents is accompanied with the formation of salts which exist as an ion pair in organic phase

$$\overline{\text{R}_3\text{N}} + \text{H}^+ + \text{X}^- = \overline{\text{R}_3\text{NH}^+\text{X}^-}, \quad (1)$$

and that the extraction of metal ions is substantially the anion exchange in the salts as follows:

$$\text{M}^{n+} + m\text{X}^- = \text{MX}_m^{(m-n)-}, \quad (2)$$

$$(m-n)\overline{\text{R}_3\text{NH}^+\text{X}^-} + \text{MX}^{(m-n)-} = \overline{(\text{R}_3\text{NH}^+)_{m-n}\text{MX}^{(m-n)-}} + (m-n)\text{X}^-, \quad (3)$$

where a superscript bar on symbols denotes the organic phase. However, several investigations on the extraction equilibrium of acids,[3-12] light scattering,[13] freezing point lowering[14] and vapor pressure lowering[15-19] of organic solutions of long-chain alkylammonium salts have shown that the salts have a strong tendency for electrostatic molecular aggregation into dimer, trimer and higher aggregates in nonpolar organic solvents. Therefore, in order to elucidate the extraction mechanism of metal ions, it is necessary to obtain detailed information on the aggregation equilibrium of the salts in organic solvents.

The most reliable information was given by Högfeldt et al.[3-8] who determined precisely the quantitative relationship between the total concentration of acids extracted by tridodecylamine in organic phase and the hydrogen ion concentration in aqueous phase with a constant ionic strength by using the two-phase emf titration method. They analyzed the extraction data by considering all the possible reactions represented by

$$p\overline{\text{R}_3\text{N}} + q\text{H}^+ + q\text{X}^- = \overline{(\text{R}_3\text{N})_p(\text{HX})_q}, \quad (4)$$
$$(p, q = 1, 2, \cdots)$$

and by assuming the ideal behavior of each species in organic phase, and concluded the presence of aggregates $(\text{R}_3\text{NHX})_p$. The data were best described by assuming the formation of such low aggregates as dimer and trimer, and a high aggregate containing as many as 10—90 monomers, where the aggregation number depends on the nature of amine salts and diluents. For example, tridodecylammonium nitrate forms dimer, trimer and decamer in o-xylene,[3] while tridodecylammonium perchlorate forms dimer, octamer and 90-mer in o-xylene.[8]

Kertes and Markovits[17] studied the aggregation of tridodecylammonium chloride, bromide, nitrate, perchlorate and hydrogensulfate in benzene, carbon tetrachloride and cyclohexane by vapor-pressure lowering, and showed that the salts formed dimer and two higher aggregates, which depend on the kinds of salts and organic solvents, and that the aggregation constants of the dimer in benzene increased in the order, chloride<bromide<nitrate<perchlorate<hydrogensulfate. The values of dimerization constant of the bromide and nitrate in benzene were found to be in fairly good agreement with those in o-xylene, which were obtained by the two-phase emf titration method. This agreement implies that coextracted water does not play a decisive part in determining the extent of aggregation.

Diamond and co-workers[10-12] obtained the following conclusion from the investigation of extraction equilibrium of perchloric acid and hydrohalogenic acids with tridodecylamine. Both the dielectric constant and chemical property of diluents greatly affect the extent of extraction of acids and the degree of aggregation of the resulting salts. In general, the higher the dielectric constant and the stronger the chemical interaction of diluents with one or both of the ions of the salt, the better the extraction and the smaller the degree of aggregation. By examining Diamond's data[12] for the equilibrium constants (K_1) in the extraction of HReO_4 by tridodecylamine in various diluents, Freiser[20] found that there was little correla-

tion between log K_1 and the dielectric constant of organic solvents, but a good linear relation existed between log K_1 and the solubility parameter of organic solvents. He pointed out that the postulation of specific chemical interaction between diluents and the salts might be superfluous and that the diluent effect on the equilibrium constants might be better explained on the theory of regular solution.

Kertes[21] showed that the values of solubility parameter of long-chain primary, secondary and tertiary alkylamines calculated from their solubilities in nonpolar organic solvents, based on the regular solution theory, agreed fairly well with those determined from their heats of vaporization. This agreement was taken as reasonable evidence of the validity of the theory for such binary solutions. Further, he[22] evaluated the values of solubility parameter of primary, secondary and tertiary amine hydrochlorides from their solubilities in low-polar organic solvents, and showed that the solubility parameters decreased markedly from the primary to the tertiary amine salts, and that the values of activity coefficient of these salts in the organic solvents, which were calculated by using the values of solubility parameters, increased sharply in the order of the tertiary to the primary amine salts at a given concentration. The difference in the concentration dependence of the activity coefficients was explained in terms of electrostatic molecular association of these salts. However, this explanation can not be accepted, because it was implicitly assumed in the evaluation of the solubility parameters that these salts are still monomeric in saturated solutions. Nevertheless, the calculated results shown in this investigation seem to indicate that the regular solution theory is also valid for these salt solutions, but the evaluated solubility parameters are the apparent solubility parameters, which are given by a function of the solubility parameters and concentrations of the monomeric salt and its aggregates in saturated solution.

In the present investigation, the extraction equilibria of hydrochloric acid from an aqueous solution containing 1 M NaCl by TOA in cyclohexane, toluene, benzene, chlorobenzene, and nitrobenzene were measured by using the two-phase emf titration method. The experimental results are analyzed by considering the aggregation equilibria from dimer to micelle in organic phase. The analyzed results are discussed in detail based on the regular solution theory.

Experimental

Reagents. Trioctylamine (Tokyo Chemical Industry Co., Ltd.) was distilled three times under reduced pressure, and the fraction in the range of 190—192 °C at 4×10^2 Pa was used. The other chemicals were of analytical grade and used without further purification. Laboratory distilled water was used.

Solutions. Stock solutions containing 8% (v/v) TOA were prepared by weighing appropriate amounts of TOA and diluting with cyclohexane, toluene, benzene, chlorobenzene, and nitrobenzene in measuring flasks at 25±1 °C. Less concentrated TOA solutions were prepared by dilution of the stock solutions. An aqueous solution containing 0.1 M HCl and 1.00 M NaCl was used as a titrant.

Procedure and Analysis. The extraction equilibria of HCl by TOA solutions were measured by the two-phase emf titration method[3] with a Corning digital 112 pH meter and a glass electrode GS-135 (Toa Electronics Co., Ltd.). An appropriate amount of 1.00 M NaCl aqueous solution (usually 50 cm^3) was pippetted into a titration vessel kept in a thermostat at 25±0.1 °C, and carbon dioxide dissolved in the solution was removed by stirring with a magnetic stirrer under an atmosphere of nitrogen introduced through 1.0 M NaCl solution. After the reading of the pH meter settled, a suitable amount of TOA solutions (10—40 cm^3) was pippetted and then appropriate amounts of 0.1 M HCl titrant were added through a buret. The extraction equilibria were reached by rapid stirring (500 rpm) of the organic and aqueous solutions. The equilibration time was 1—2 h for the first point and a few minutes for the last point. The hydrogen ion concentrations in the aqueous phase, $[H^+]$, were evaluated from the electrode potential E measured by the pH meter according to the equation

$$E = E_0 + j[H^+] + 59.16\log[H^+], \tag{5}$$

where E_0 and j are constants. The values of E_0 and j were determined from the titration in the absence of organic solution. The total concentration of HCl extracted into organic phase, $[\overline{HCl}]_T$, was calculated by

$$[\overline{HCl}]_T = C(V/\overline{V}) - h(v + V)/\overline{V}, \tag{6}$$

where C and h are the concentrations of HCl and H^+ in the titrant and aqueous phase, respectively, and v, V, and $\overline{V}$ denote the volumes of the titrant, 1.00 M NaCl aqueous solution, and TOA organic solutions, respectively. The concentrations of TOA in organic solutions were determined by measuring the concentrations of HCl in organic solutions at the extraction equilibrium with 1.0 M HCl aqueous solution. The measurement was carried out by back-titration with a standard base.

Results

Since it has been found that the ionic dissociation of trialkylammonium salts is practically negligible in low dielectric organic solvents,[3,11] the extraction mechanism of HCl by TOA in low-polar organic solvents can be written by

$$\overline{TOA} + H^+ + Cl^- = \overline{TOAHCl}, \tag{7}$$

$$i\,\overline{TOAHCl} = \overline{(TOAHCl)_i}, \quad (i = 2, 3, \cdots) \tag{8}$$

where TOAHCl represents $TOAH^+Cl^-$. The equilibrium constants of Eqs. 7 and 8 are given by

$$^{\circ}K_d = \frac{[\overline{RHCl}]}{[\overline{R}][H^+][Cl^-]} \cdot \frac{\bar{y}_1}{\bar{y}_R y_{H^+} y_{Cl}}, \tag{7'}$$

$$\bar{\beta}_i^{\circ} = \frac{[\overline{(RHCl)_i}]}{[\overline{RHCl}]^i} \cdot \frac{\bar{y}_i}{\bar{y}_1^i}, \tag{8'}$$

where R denotes TOA, a bracket the molarity, and y the molar activity coefficient. $\bar{y}_1$ and $\bar{y}_i$ represent the molar activity coefficients of RHCl and $(RHCl)_i$ in organic phase, respectively. Since the ionic strength in aqueous phase is kept constant (1.00 M NaCl) in this study, it is convenient to introduce another equilibrium constant defined by

$$K_d^\circ = {}^\circ K_d(y_{H^+}y_{Cl^-}) = \frac{[\overline{RHCl}]}{[\overline{R}][H^+][Cl^-]} \cdot \frac{\bar{y}_1}{\bar{y}_R}. \quad (7'')$$

On the other hand, $[\overline{R}]_T$ and $[\overline{HCl}]_T$, the total concentrations of TOA and HCl in organic phase, respectively are given by

$$[\overline{R}]_T = [\overline{R}] + \sum_{i=1} i[\overline{(RHCl)_i}], \quad (9)$$

$$[\overline{HCl}]_T = \sum_{i=1} i[\overline{(RHCl)_i}], \quad (10)$$

where the values of free TOA concentration in organic phase, $[\overline{R}]$, can be easily evaluated from those of $[\overline{R}]_T$ and $[\overline{HCl}]_T$. From Eqs. 9, 10, 7'', and 8', the average number of HCl combined with TOA, Z, is given by

$$Z = \frac{[\overline{HCl}]_T}{[R]_T} = \frac{K_d[H^+][Cl^-] + \sum_{i=2} i\bar{\beta}_i K_d^i [\overline{R}]^{i-1}[H^+]^i[Cl^-]^i}{1 + K_d[H^+][Cl^-] + \sum_{i=1}\sum_{i=2} i\bar{\beta}_i K_d^i [\overline{R}]^{i-1}[H^+]^i[Cl^-]^i}, \quad (11)$$

where K_d and $\bar{\beta}i$ are the equilibrium concentration quotients defined by

$$K_d = K_d^\circ(\bar{y}_R/\bar{y}_1) = [\overline{RHCl}]/[\overline{R}][H^+][Cl^-], \quad (12)$$

$$\bar{\beta}_i = \bar{\beta}_i^\circ(\bar{y}_1^i/\bar{y}_i) = [\overline{(RHCl)_i}]/[\overline{RHCl}]^i. \quad (13)$$

Figure 1 shows the plots of Z vs. $\log[H^+][Cl^-]$ in the extraction with toluene as a diluent. The plots give sigmoidal curves depending on $[\overline{R}]_T$. Plots similar to the plots in Fig. 1 were obtained with respect to cyclohexane, benzene, and chlorobenzene, while the plots with nitrobenzene gave a curve which is nearly independent of $[\overline{R}]_T$. These facts suggest that trioctylammonium chloride is practically monomeric in nitrobenzene, but aggregates in the other solvents. In order to obtain further detailed information on the aggregation equilibria, it is convenient to analyze the experimental data by using Eq. 14 derived from Eqs. 10, 12, and 13.

$$\frac{[\overline{HCl}]_T}{[\overline{R}][H^+][Cl^-]} = K_d + \sum_{i=2} i\bar{\beta}_i K_d^i \{[\overline{R}][H^+][Cl^-]\}^{i-1}. \quad (14)$$

As is seen in Fig. 2, the plots of $[\overline{HCl}]_T/[\overline{R}][H^+][Cl^-]$ vs. $[\overline{R}][H^+][Cl^-]$ give the curves whose intercepts and curvatures depend on $[\overline{R}]_T$. This indicates that the values of K_d and $\bar{\beta}_i$ (i=2,3,$\cdots$,n) change with $[\overline{R}]_T$, i.e. the ratios of actitvity coefficient, $\bar{y}_R/\bar{y}_1$ and $\bar{y}_1^i/\bar{y}_i$, depend on $[\overline{R}]_T$. We tried to determine the values of K_d and $\bar{\beta}_i$ at constant $[\overline{R}]_T$ by the least-squares method,

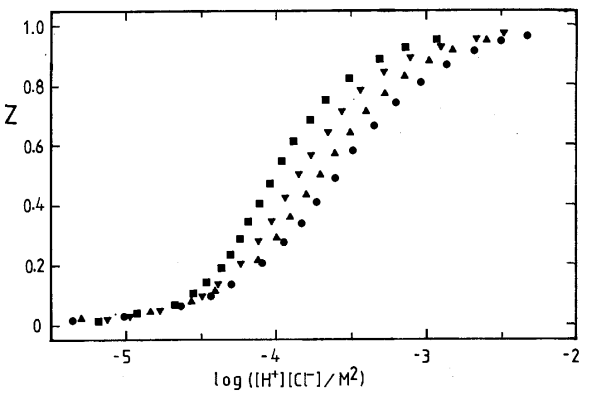

Fig. 1. Plots of Z vs. $\log[H^+][Cl^-]$ in the extraction of HCl by TOA in toluene. ●: 0.0231 M TOA, ▲: 0.0462 M TOA, ▼: 0.0923 M TOA, ■: 0.1843 M TOA.

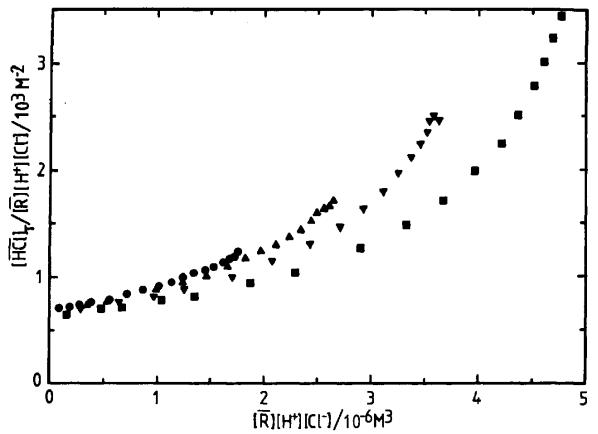

Fig. 2. Plots of $[\overline{HCl}]_T/[\overline{R}][H^+][Cl^-]$ vs. $[\overline{R}][H^+][Cl^-]$ in the extraction of HCl by TOA in benzene. ●: 0.0230 M TOA, ▲: 0.0461 M TOA, ▼: 0.0922 M TOA, ■: 0.1843 M TOA.

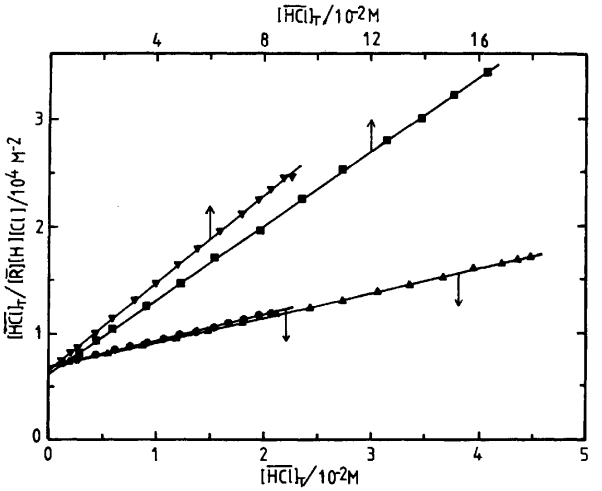

Fig. 3. Plots of $[\overline{HCl}]_T/[\overline{R}][H^+][Cl^-]$ vs. $[\overline{HCl}]_T$ in the extraction of HCl by TOA in benzene. ●: 0.0230 M TOA, ▲: 0.0461 M TOA, ▼: 0.0922 M TOA, ■: 0.1843 M TOA.

Table 1. Values of Intercept A and Slope B in the Plots of $[\overline{HCl}]_T/[\overline{R}][H^+][Cl^-]$ vs. $[\overline{HCl}]_T$

Diluent (S)	δ_S[a] $cal_{th}^{1/2}cm^{-3/2}$	$[\overline{R}]_T$ M $(100\bar{\psi}_R^\circ)$	A M^{-2}	B M^{-3}	B/2A M^{-1}
Cyclohexane	8.20	0.0231 (1.0)	(2.01±0.12)×10	(7.43±0.14)×10³	185±15
		0.0462 (2.0)	(2.37±0.12)×10	(6.90±0.05)×10³	146± 9
		0.0924 (4.0)	(2.83±0.24)×10	(7.27±0.06)×10³	128±12
Toluene	8.91	0.0231 (1.0)	(2.67±0.02)×10³	(1.06±0.01)×10⁵	19.8±0.3
		0.0462 (2.0)	(2.68±0.02)×10³	(1.03±0.01)×10⁵	19.2±0.3
		0.0923 (4.0)	(2.64±0.05)×10³	(9.53±0.09)×10⁴	18.0±0.5
		0.1846 (8.0)	(2.63±0.04)×10³	(8.23±0.03)×10⁴	15.6±0.3
Benzene	9.16	0.0230 (1.0)	(6.84±0.03)×10³	(2.45±0.03)×10⁵	17.9±0.3
		0.0461 (2.0)	(6.74±0.05)×10³	(2.29±0.02)×10⁵	17.0±0.3
		0.0922 (4.0)	(6.55±0.15)×10³	(2.04±0.03)×10⁵	15.6±0.6
		0.1860 (8.0)	(6.28±0.06)×10³	(1.71±0.01)×10⁵	13.6±0.2
Chlorobenzene	9.68	0.0233 (1.0)	(4.75±0.02)×10⁴	(4.58±0.18)×10⁵	4.82±0.21
		0.0465 (2.0)	(4.43±0.04)×10⁴	(4.30±0.18)×10⁵	4.85±0.25
		0.0930 (4.0)	(4.17±0.03)×10⁴	(4.08±0.05)×10⁵	4.89±0.10
		0.1860 (8.0)	(3.65±0.04)×10⁴	(3.58±0.04)×10⁵	4.90±0.11
Nitrobenzene	10.78	0.0230 (1.0)	(2.71±0.01)×10⁶	(6.95±0.16)×10⁶	1.28±0.04
		0.0460 (2.0)	(2.59±0.02)×10⁶	(7.11±0.20)×10⁶	1.37±0.05
		0.0919 (4.0)	(2.39±0.03)×10⁶	(6.66±0.20)×10⁶	1.39±0.06
		0.1838 (8.0)	(1.91±0.02)×10⁶	(6.90±0.12)×10⁶	1.81±0.05

a) The values were determined from the values of heat of vaporization and density listed in Ref. 24. $1\,cal_{th}=4.184\,J$.

Table 2. Values of Intercept A and Slope B in the Plots of $[\overline{HCl}]_T/[\overline{R}][H^+][Cl^-]$ vs. $[\overline{HCl}]_T$[a]

Diluent	Volume% of benzene	A M^{-2}	B M^{-3}	B/2A M^{-1}
Cyclohexane-benzene mixtures	0	(2.01±0.12)×10	(7.43±0.14)×10³	185±15
	12.5	(5.61±0.13)×10	(1.35±0.01)×104	120± 4
	24.0	(1.37±0.02)×10²	(2.13±0.02)×10⁴	77.4±1.9
	49.0	(5.75±0.06)×10²	(5.22±0.06)×10⁴	45.4±1.0
	74.0	(2.02±0.03)×10³	(1.17±0.02)×10⁵	29.0±0.9
	99.0	(6.84±0.03)×10³	(2.45±0.03)×10⁵	17.9±0.3
Benzene-nitrobenzene mixtures	99.0	(6.84±0.03)×10³	(2.45±0.03)×10⁵	17.9±0.3
	87.5	(4.00±0.05)×10⁴	(4.19±0.33)×10⁵	5.24±0.96
	75.0	(1.21±0.01)×10⁵	(7.31±0.33)×10⁵	3.02±0.16
	50.0	(4.85±0.04)×10⁵	(1.71±0.27)×10⁶	1.76±0.29
	25.0	(1.26±0.01)×10⁶	(4.14±0.54)×10⁶	1.64±0.23
	0	(2.71±0.01)×10⁶	(6.95±0.47)×10⁶	1.28±0.09

a) $[\overline{R}]_T=0.0230\,M$ $(\bar{\psi}_R^\circ=0.01)$.

varying n from 2 to 5 in Eq. 14. The calculation yielded fairly good results at $n=3$ for the extraction equilibria with the following solutions: 1, 2, 4, and 8% (v/v) TOA-nitrobenzene, 1, 2, 4, and 8% (v/v) TOA-chlorobenzene, 1 and 2% (v/v) TOA-benzene, 1 and 2% (v/v) TOA-toluene, and 1% (v/v) TOA-benzene-nitrobenzene. On the other hand, the calculation for the extraction equilibria with 4 and 8% (v/v) TOA-benzene, 4 and 8% (v/v) TOA-toluene, 1, 2, and 4% (v/v) TOA-cyclohexane and 1% (v/v) TOA-cyclohexane-benzene showed that the calculated values of $[\overline{HCl}]_T/[\overline{R}][H^+][Cl^-]$ at $n=5$ had still a systematic error for the experimental values. These results suggest that the existence of high aggregates of aggregation number>5 can not be neglected in these extraction equilibria or the values of $\bar{y}_R/\bar{y}_1$ and $\bar{y}_i/\bar{y}_i$ change with varying $[\overline{HCl}]_T$.

As is seen in Fig. 3, the plots of $[\overline{HCl}]_T/[\overline{R}][H^+][Cl^-]$ vs. $[\overline{HCl}]_T$ give good straight lines in all the extraction equilibria studied. This indicates that a quantitative relationship in the extraction equilibria can be represented by

$$\frac{[\overline{HCl}]_T}{[\overline{R}][H^+][Cl^-]} = A + B[\overline{HCl}]_T, \tag{15}$$

where A and B are constants which are independent of $[\overline{HCl}]_T$ at constant $[\overline{R}]_T$. The values of A and B calculated by the least-squares method are given in Tables 1 and 2.

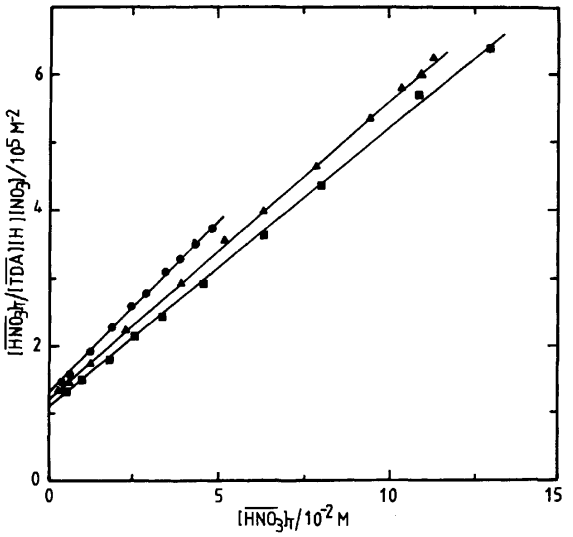

Fig. 4. Plots of $[\overline{HNO_3}]_T/[\overline{TDA}][H^+][NO_3^-]$ vs. $[\overline{HNO_3}]_T$ in the extraction of HNO_3 by TDA in toluene from HNO_3+2.75 M $LiNO_3$ solution (data from Ref. 7). ●: 0.0502 M TDA, ▲: 0.1210 M TDA, ■: 0.2460 M TDA.

Discussion

Equation 15 or a similar equation has not been presented in the literature so far and Eq. 15 can not be derived unconditionally from Eq. 14. Accordingly, we examined whether Eq. 15 is compatible with the experimental results on the extraction of acids by tridodecylamine (TDA) reported by Högfeldt and coworkers.[7,8] Figure 4 shows that Eq. 15 is also applicable to these experimental results. Hence, we sought the conditions to derive Eq. 15 from Eq. 14. Equation 14 can be rewritten as follows:

$$\frac{[\overline{HCl}]_T}{[\overline{R}][H^+][Cl^-]} = K_d + \sum_{i=2} i\left(\prod_{j=2}^{i} \overline{K}_j\right) K_d^i \{[\overline{R}][H^+][Cl^-]\}^{i-1}, \quad (16)$$

$$\overline{K}_j = \overline{\beta}_i/\overline{\beta}_{i-1} = \overline{K}_j^\circ(\bar{\gamma}_{j-1}\bar{\gamma}_1/\bar{\gamma}_j), \quad (17)$$

where $\overline{K}_j$ and $\overline{K}_j^\circ$ are the equilibrium concentration quotient and equilibrium constant, respectively, in the successive aggregation expressed by

$$\overline{(TOAHCl)}_{j-1} + \overline{TOAHCl} = \overline{(TOAHCl)}_j. \quad (18)$$

In the case where the following condition is satisfied,

$$2\overline{K}_2 = \frac{3}{2}\overline{K}_3 = \cdots\cdots = \frac{n}{n-1}\overline{K}_n, \quad (19)$$

Eq. 16 can be transformed to

$$\frac{[\overline{HCl}]_T}{[\overline{R}][H^+][Cl^-]} = K_d\{1 + \sum_{i=2}^{n}(2\overline{K}_2 K_d[\overline{R}][H^+][Cl^-])^{i-1}\}. \quad (20)$$

When n is a large number, i.e. there is a series of aggregates from dimer to micell (n-mer), the following condition

$$2\overline{K}_2 K_d[\overline{R}][H^+][Cl^-] < 1, \quad (21)$$

leads to Eq. 22.

$$\frac{[\overline{HCl}]_T}{[\overline{R}][H^+][Cl^-]} = K_d + 2\overline{K}_2 K_d[\overline{HCl}]_T, \quad (22)$$

A comparison of Eqs. 15 and 22 yields K_d=A and $2\overline{K}_2K_d$=B. Although there is still a question about the validity of an assumption of Eq. 19, we will advance a detailed discussion on K_d and $\overline{K}_2$ determined by Eq. 22, and the physical meaning of Eq. 19 will be mentioned later.

As is seen in Table 1, the values of K_d (=A) and $\overline{K}_2$ (=B/2A) are well correlated with those of total volume fraction of TOA ($\overline{\psi}_R^\circ$) and solubility parameter of diluents (δ_S). This result suggests that the change of K_d and $\overline{K}_2$ with varying $\overline{\psi}_R^\circ$ and diluents may be explained on the basis of the regular solution theory. According to the theory, the activity of components j, a_j, in which a pure liquid is chosen as the reference state, in the solution constituted of m components is given by[23]

$$\ln a_j = \frac{v_j}{RT}\{\sum_{i=1}^{m}(\delta_j - \delta_i)\psi_i\}^2 + \ln\psi_j + \sum_{i=1}^{m}(1 - \frac{v_j}{v_i})\psi_i, \quad (23)$$

where δ_i, v_i, and ψ_i are the solubility parameter, molar volume and volume fraction of component i, respectively. When a total solute concentration is not so high, a molar activity coefficient of solute j, $\dot{y}_j$ ($=\dot{a}_j/c_j$: c_j, molar concentration), may be evaluated approximately by the following equation,

$$\ln\dot{y}_j = \frac{v_j}{RT}(\delta_j - \delta_S)^2(1 - 2\psi_{sol}^\circ) + \ln\frac{v_j}{1000} + (1 - \frac{v_j}{v_S})(1 - \psi_{sol}^\circ), \quad (24)$$

where ψ_{sol}° is the total solute volume fraction, and δ_S and v_S are the solubility parameter and molar volume of solvents S, respectively. Since the molar activity coefficient of solute j, y_j, in which the infinitely dilute solution is chosen as the reference state, is given by

$$y_j = \dot{y}_j/\dot{y}_j(\psi_{sol}^\circ \to 0, \psi_S \to 1), \quad (25)$$

the following equation can be obtained by subtitution of Eq. 24 into Eq. 25.

$$\ln y_j = -\{2v_j(\delta_j - \delta_S)^2/RT + (1 - v_j/v_S)\}\psi_{sol}^\circ, \quad (26)$$

Application of Eq. 26 to $\bar{y}_R$ and $\bar{y}_1$ in Eq. 12 leads to

$$\ln K_d = \ln K_d^\circ + g\overline{\psi}_R^\circ, \quad (27)$$

$$g = (2/RT)\{v_1(\delta_1 - \delta_S)^2 - v_R(\delta_R - \delta_S)^2\} + (v_R - v_1)/v_S, \quad (28)$$

where $\overline{\psi}_R^\circ$ is the total volume fraction of TOA in organic phase, and δ_1 and v_1 denote the solubility parameter and molar volume of TOAHCl, respectively. As is seen from Fig. 5, the plots of $\ln K_d$ vs. $\overline{\psi}_R^\circ$, where the values of A (=K_d) in Table 1 were used, give good straight lines as expected from Eq. 27. The values of $\ln K_d^\circ$ and g calculated by the least-squares method are shown in Table 3. The values of g decrease with increasing the solubility parameter of diluents, and satisfy the relation $\partial g/\partial\delta_S < 0$ which is derived from Eq. 28 by considering that δ_R=7.6 $cal_m^{1/2}$ $cm^{-3/2}$,[21]

Table 3. Values of $\ln K_d^\circ$, g, $\ln \bar{K}_2^\circ$, and h

Diluent (S)	S / $cal^{1/2}cm^{-3/2}$	$\ln K_d^\circ$	g	$\ln \bar{K}_2^\circ$	h
Cyclohexane	8.20	2.90	11.4	5.11	−6.4
Toluene	8.91	7.83	−0.3	3.02	−3.3
Benzene	9.16	8.84	−1.2	2.91	−3.8
Chlorobenzene	9.68	10.79	−3.6	1.58	0.2
Nitrobenzene	10.78	14.78	−5.0	0.19	4.8

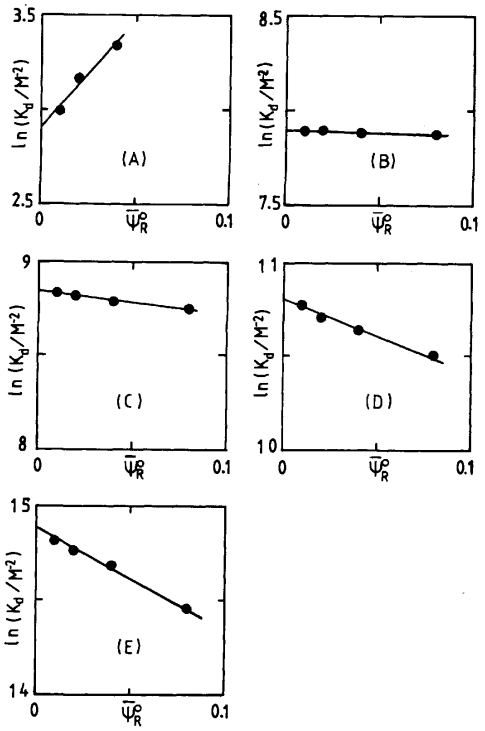

Fig. 5. Plots of $\ln K_d$ vs. $\bar{\psi}_R^\circ$ in the extraction of HCl by TOA in various organic solvents. (A): cyclohexane, (B): toluene, (C): benzene, (D): chlorobenzene, (E): nitrobenzene.

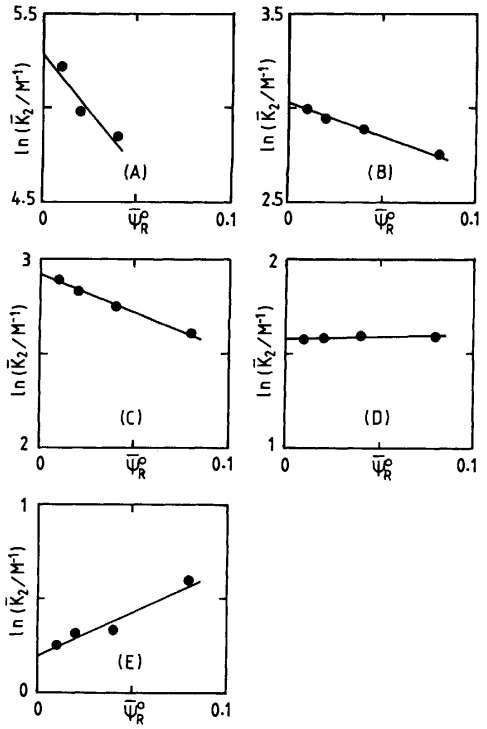

Fig. 6. Plots of $\ln \bar{K}_2$ vs. $\bar{\psi}_R^\circ$ for the aggregation of TOAHCl in various organic solvents. (A): cyclohexane, (B): toluene, (C): benzene, (D): chlorobenzene, (E): nitrobenzene.

δ_1=10.6 $cal_{th}^{1/2}$ $cm^{-3/2}$ [22] and $(v_1-v_R)/v_R \ll 1$.

From Eqs. 17 and 26, the following equation can be obtained by neglecting the volume change in aggregation of TOAHCl,

$$\ln \bar{K}_2 = \ln \bar{K}_2^\circ + h\bar{\psi}_R^\circ, \tag{29}$$

$$h = (4v_1/RT)(\delta_2 - \delta_1)(\delta_1 + \delta_2 - 2\delta_S), \tag{30}$$

where δ_2 denotes the solubility parameter of $(TOAHCl)_2$. Figure 6 shows the plots of $\ln \bar{K}_2$ vs. $\bar{\psi}_R^\circ$, where the values of B/2A (=$\bar{K}_2$) in Table 1 were used. The plots also give fairly good straight lines as expected from Eq. 29. The calculated values of $\ln \bar{K}_2^\circ$ and h are shown in Table 3. The values of h increase with the solubility parameter of diluents, and also satisfy the relation $\partial h/\partial \delta_S > 0$ which is derived from Eq. 30 by assuming that $\delta_1 > \delta_2$.

In order to evaluate the diluent effect on K_d°, it is convenient to introduce another equilibrium constant $K_d^\circ(1)$, where the liquid of TOA and the hypothetical liquid of TOAHCl are chosen as the reference states. The relation between K_d° and $K_d^\circ(1)$ is given by

$$K_d^\circ = K_d^\circ(1)\frac{\bar{\gamma}_R(\bar{\psi}_R \to 0, \bar{\psi}_S \to 1)}{\bar{\gamma}_1(\bar{\psi}_R \to 0, \bar{\psi}_S \to 1)}. \tag{31}$$

Application of Eq. 24 to $\bar{\gamma}_R$ and $\bar{\gamma}_1$ in Eq. 31 leads to

$$\ln K_d^\circ = A_0 + A_1\delta_S + A_2\delta_S^2, \tag{32}$$

$$A_0 = \ln K_d^\circ(1) + (v_R\delta_R^2 - v_1\delta_1^2)/RT + (v_R - v_1)/v_S, \tag{33}$$

$$A_1 = 2(v_1\delta_1 - v_R\delta_R)/RT, \tag{34}$$

$$A_2 = (v_R - v_1)/RT, \tag{35}$$

As is seen in Fig. 7, the plot of $\ln K_d^\circ$ vs. δ_S gives a parabolic curve with upward curvature which satisfies the relations $A_1 > 0$ and $A_2 < 0$ derived from Eqs. 34 and 35 by considering $\delta_1 > \delta_R$ and $v_1 > v_R$. The values of A_0, A_1, and A_2 were determined by the least-squares method as 110.9±2.1, 21.0±0.3 $cal_{th}^{1/2}$ $cm^{3/2}$ and −0.87 ±0.03 cal_{th}^{-1} cm^3, respectively. Equation 35 gives 515

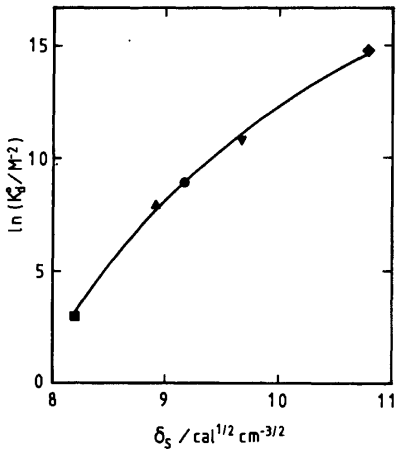

Fig. 7. Plot of ln K_d° vs. δ_s in the extraction of HCl by TOA in various organic solvents. □: Cyclohexane, ▲: toluene, ●: benzene, ▼: chlorobenzene, ◆: nitrobenzene.

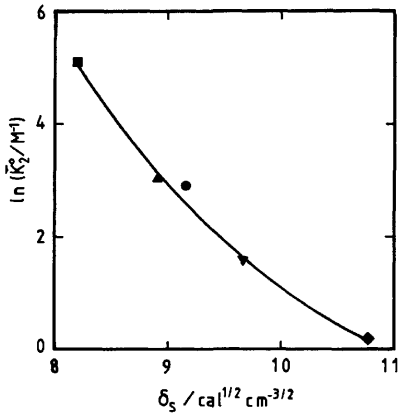

Fig. 8. Plot of ln $\bar{K}_2^\circ$ vs. δ_S for the aggregation of TOAHCl in various organic solvents. ■: Cyclohexane, ▲: toluene, ●: benzene, ▼: chlorobenzene, ◆: nitrobenzene.

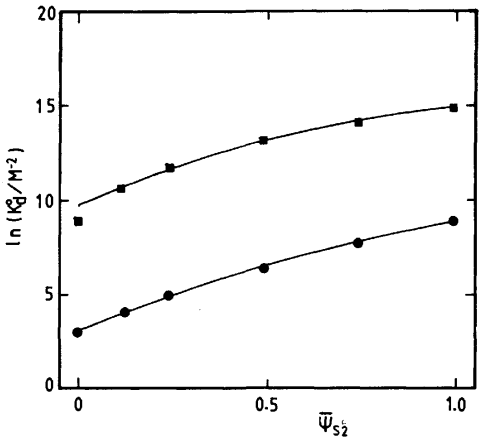

Fig. 9. Plots of ln K_d° vs. $\bar{\psi}_{S2}$ in the extraction of HCl by TOA in mixed solvents. ●: Cyclohexane(S1)-benzene(S2), ■: benzene(S1)-nitrobenzene(S2).

± 18 cm^3 mol^{-1} for $(v_1 - v_R)$ at RT=592 cal$_{th}$ mol^{-1}, but this value is too large for the difference in molar volume of TOA and TOAHCl. Therefore, this result shows that the regular solution theory can not give an exact explanation for the diluent effect of K_d°, but the above equations describe a semiquantitative relationship between ln K_d° and δ_S.

With respect to the diluent effect on the dimerization constant of TOAHCl, the following equations can be obtained in a similar manner to the derivation of Eq. 32 by neglecting the volume change in dimerization,

$$\ln \bar{K}_2^\circ = B_0 + B_1\delta_S, \tag{36}$$

$$B_0 = \ln K_2^\circ(1) + 2v_1(\delta_1^2 - \delta_2^2), \tag{37}$$

$$B_1 = 4v_1(\delta_2 - \delta_1), \tag{38}$$

where $\bar{K}_2^\circ(1)$ is the dimerization constant, and the hypothetical liquids of TOAHCl and $(TOAHCl)_2$ are chosen as the reference states. The plot of ln $\bar{K}_2^\circ$ vs. δ_S gives no straight line, but a parabolic curve with downward curvature as shown in Fig. 8. This fact indicates that ln $\bar{K}_2^\circ$ is expressed by

$$\ln \bar{K}_2^\circ = B_0 + B_1\delta_S + B_2\delta_S^2. \tag{39}$$

The values of B_0, B_1, and B_2 are 55.3±1.2, −9.35±0.18 cal$_{th}^{-1/2}$ cm$^{3/2}$, and 0.393±0.012 cal$_{th}^{-1}$cm^3, respectively. The negative value of B_1 suggests that $\delta_1 > \delta_2$, and is consistent with the presumption that higher aggregates will have lower solubility parameters.

Next we deal with extraction equilibria in mixed solvents. According to Eq. 23, the molar activity coefficient of solute i, $\dot{y}_i$, in the mixed solvents (S1 and S2) containing amall amounts of solutes is given by

$$\ln \dot{y}_j = (v_j/RT)(\delta_j - \delta_{S1})^2 + (\delta_j - \delta_{S2})(\delta_{S1} - \delta_{S2})\bar{\psi}_{S2} + (\delta_{S1} - \delta_{S2})^2\bar{\psi}_{S2}^2 + \ln(v_j/1000) + (1 - v_j/v_{S1}) + v_j(1/v_{S1} - 1/v_{S2})\bar{\psi}_{S2}. \tag{40}$$

The extraction equilibrium constant of HCl by TOA in the mixed organic solvents, K_d°, is correlated to that in S1, K_d°(S1), by

$$K_d^\circ = K_d^\circ(S1)\frac{\bar{y}_R(\bar{\psi}_R \to 0, \bar{\psi}_{S2})\bar{y}_1(\bar{\psi}_R \to 0, \bar{\psi}_{S2} = 0)}{\bar{y}_R(\bar{\psi}_R \to 0, \bar{\psi}_{S2} = 0)\bar{y}_1(\bar{\psi}_R \to 0, \bar{\psi}_{S2})}$$

From Eqs. 40 and 41, the following equations can be derived by neglecting the sixth term in Eq. 40.

$$\ln K_d^\circ = C_0 + C_1\bar{\psi}_{S2} + C_2\bar{\psi}_{S2}^2, \tag{42}$$

$$C_0 = \ln K_d^\circ(S1), \tag{43}$$

$$C_1 = 2\{v_1(\delta_1 - \delta_{S1}) - v_R(\delta_R - \delta_{S1})\}(\delta_{S2} - \delta_{S1})/RT, \tag{44}$$

$$C_2 = (v_R - v_1)(\delta_{S2} - \delta_{S1})^2/RT, \tag{45}$$

When $\delta_{S1} < \delta_{S2}$, it may be expected that $C_1 > 0$ and $C_2 < 0$. Figure 9 shows that the plots of ln K_d° vs. $\bar{\psi}_{S2}$ in the extraction with cyclohexane(S_1)-benzene(S_2) and benzene(S_1)-nitrobenzene(S_2) mixtures give the curves with upward curvatures which are in agreement with the expectation. The calculated values of C_0, C_1, and

Table 4. Values of C_0, C_1, and C_2

Diluent S1	Diluent S2	$\ln K_d^\circ$(S1)	C_0	C_1	C_2
Cyclohexane	Benzene	3.00	3.07±0.09 (3.22±0.09)[a]	7.71±0.09 (7.09±0.15)[a]	−1.96±0.11 (−1.47±0.08)[a]
Benzene	Nitrobenzene	8.83	9.14±0.35 (9.75±0.15)[a]	11.0±0.5 (8.5±0.2)[a]	−5.4±0.4 (−3.4±0.1)[a]

a) The values in parentheses were obtained from the calculation except for the value of $\ln K_d$ at $\bar{\psi}_{S2}=0$.

Table 5. Values of D_0, D_1, and D_2

Diluent S1	Diluent S2	$\ln \bar{K}_2^\circ$(S1)	D_0	D_1	D_2
Cyclohexane	Benzene	5.22	5.19±0.10 (5.10±0.12)[a]	−3.33±0.12 (−2.99±0.12)[a]	1.06±0.08 (0.79±0.08)[a]
Benzene	Nitrobenzene	2.89	2.58±0.53 (1.98±0.27)[a]	−6.2±0.5 (−3.7±0.5)[a]	4.0±1.4 (2.1±0.5)[a]

a) The values in parentheses were obtained from the calculation except for the value of $\ln \bar{K}_2^\circ$ at $\bar{\psi}_{S2}=0$.

C_2 are shown in Table 4. In the extraction with cyclohexane-benzene mixtures, the C_0 value is very close to that of $\ln K_d^\circ$ (cyclohexane), but the agreement between C_0 and $\ln K_d^\circ$ (benzene) is not so good in benzene-nitrobenzene mixtures. Since this difference appears to indicate that there is a specific interaction between TOAHCl and nitrobezene molecules, we carried out the calculation except for the data at $\bar{\psi}_{S2}=0$ in order to make more clear the difference, and the values are given in parentheses in Table 4. Recalculated values in cyclohexane-benzene do not change so much, but those in benzene-nitrobenzene change significantly. These facts strongly suggest that nitrobenzene molecules preferentially solvate to TOAHCl.

In a similar manner to derivation of Eq. 42, the following equations can be obtained for the dependence of $\bar{K}_2^\circ$ on the composition of mixed diluents by neglecting the volume change in the dimerization of TOAHCl,

$$\ln \bar{K}_2^\circ = D_0 + D_1 \bar{\psi}_{S2}, \tag{46}$$

$$D_0 = \ln \bar{K}_2^\circ(\mathrm{S1}), \tag{47}$$

$$D_1 = 4v_1(\delta_1 - \delta_2)(\delta_{S1} - \delta_{S2})/RT, \tag{48}$$

where $\bar{K}_2^\circ$ (S1) denotes the dimerization constant in solvent S1. In the preceding discussion, since it was found that $\delta_1 > \delta_2$, it may be expected that $D_1 < 0$ when $\delta_{S1} < \delta_{S2}$, i.e. the plot of $\ln \bar{K}_2^\circ$ vs. $\bar{\psi}_{S2}$ gives a straight line with a negative slope. However, the plots for mixed diluents do not yield straight lines as shown in Fig. 10. This indicates that the dependence of $\ln \bar{K}_2^\circ$ on the composition of the mixed diluents may be represented as follows:

$$\ln \bar{K}_2^\circ = D_0 + D_1 \bar{\psi}_{S2} + D_2 \bar{\psi}_{S2}^2, \tag{49}$$

where D_1 and D_2 are constants. The calculated values of D_0, D_1, and D_2 are listed in Table 5. The values of

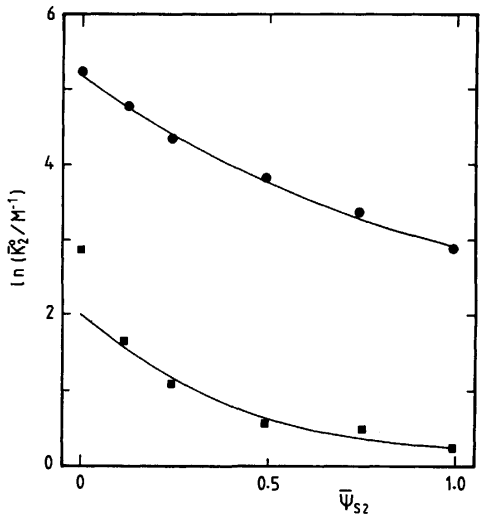

Fig. 10. Plots of $\ln \bar{K}_2^\circ$ vs. $\bar{\psi}_{S2}$ for the aggregation of TOAHCl in mixed solvents. ●: Cyclohexane(S1)-benzene(S2), ■: benzene(S1)-nitrobenzene(S2).

D_0 in cyclohexane-benzene is very close to that of $\bar{K}_2^\circ$ (cyclohexane), but the difference between D_0 in benzene-nitrobenzene and $\bar{K}_2^\circ$ (benzene) is not little. The recalculated values except for the data at $\bar{\psi}_{S2}=0$ are given in parentheses in Table 5. The relationship between the values obtained from the two calculations are similar to that obtained for the values of C_0, C_1, and C_2 as shown in Table 4. The results in Table 5 also suggest that nitrobenzene molecules solvate to TOAHCl and contribute to weaken the aggregation.

From the above discussion, it was found that the experimental results in the present work can be explained fairly well on the assumption of Eqs. 19 and 23.

Estimation of the monomer concentration and mean aggregation number of trioctylammonium chloride in organic phase is carried out by using the total concen-

tration and the dimerization quotient. Since Eq. 22 is rewritten as

$$[\overline{HCl}]_T = [\overline{RHCl}]\{1 + 2\bar{K}_2[\overline{HCl}]_T\},$$

the monomer concentration, $[\overline{RHCl}]$, is given by

$$[\overline{RHCl}] = \frac{[\overline{HCl}]_T}{1 + 2\bar{K}_2[\overline{HCl}]_T}. \quad (50)$$

On the other hand, in order to estimate the mean aggregation number $<i>$ defined by

$$<i> = \frac{\sum_{i=1} i[(\overline{RHCl})_i]}{\sum_{i=1}[(\overline{RHCl})_i]} = \frac{[\overline{HCl}]_T}{[\overline{RHCl}] + \sum_{i=2}\bar{\beta}_i[\overline{RHCl}]^i}, \quad (51)$$

it is necessary to estimate the value of the denominator of Eq. 51. From Eqs. 17 and 19

$$\bar{\beta}_i = \frac{1}{i}(2\bar{K}_2)^{i-1}, \quad (52)$$

and

$$[\overline{RHCl}] + \sum_{i=2}\bar{\beta}_i[\overline{HCl}]^i = -\frac{1}{2\bar{K}_2}\ln(1 - 2\bar{K}_2[\overline{RHCl}]). \quad (53)$$

Substitution of Eqs. 53 and 50 into Eq. 51 yields

$$<i> = \frac{2\bar{K}_2[\overline{HCl}]_T}{\ln(1+2\bar{K}_2[\overline{HCl}]_T)}. \quad (54)$$

Consequently, the values of $<i>$ can be easily calculated by using $[\overline{HCl}]_T$ and $\bar{K}_2$. The calculated values of $<i>$ in several solutions are given in Fig. 11 as a function of $[\overline{HCl}]_T$. Figure. 13 shows that the values of $<i>$ depend markedly on diluents and increase in the order nitrobenzene < chlorobenzene < benzene < toluene < cyclohexane, where $<i>$ values are determined to be 1.04, 1.17, 1.61, 1.70, and 7.82 at $[\overline{HCl}]_T$=0.1 M in 8% (v/v) TOA solutions, respectively.

Finally, we should consider the physical meaning of Eq. 19. The fact that the extraction equilibria are well explained on Eqs. 19 and 23 seems to indicate that the volume fraction is a more reasonable concentration scale than the molarity to describe the extraction equilibria. We introduce a new equilibrium concentration quotient for the successive aggregation, which is defined by

$$\bar{K}_i(\bar{\psi}) = \frac{\bar{\psi}}{\bar{\psi}_{i-1}\bar{\psi}_1}. \quad (55)$$

This quotient can be related to $\bar{K}_i$ by

$$\bar{K}_i(\bar{\psi}) = \frac{1000\,v_i}{v_{i-1}v_1}\bar{K}_i. \quad (56)$$

When the volume change in aggregation is negligible, i.e. $v_i = i\,v_1$, Eq. 56 shows that Eq. 19 is equivalent to

$$\bar{K}_2(\bar{\psi}) = \bar{K}_3(\bar{\psi}) = \cdots\cdots = \bar{K}_n(\bar{\psi}). \quad (57)$$

Equation 57 implies that the binding energy of the aggregate $(TOAHCl)_i$ increases in proportion to the aggregation number, i, and the molar entropy change

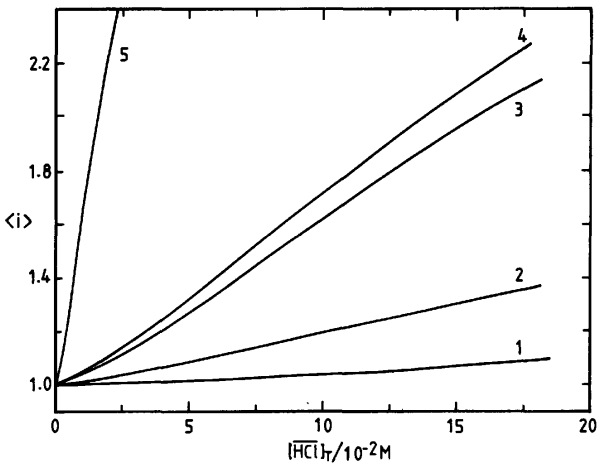

Fig. 11. Mean aggregation numbers of TOAHCl <i> in various organic solvents at 25°C as a function of $[\overline{HCl}]_T$ at 8% (v/v) TOA. 1: Nitrobenzene, 2: chlorobenzene, 3: benzene, 4: toluene, 5: cyclohexane (4% (v/v) TOA).

of each aggregate is proportional to the logarithm of volume fraction of the aggregate. However, we can not answer a question that why the aggregates have such property with respect to the binding energy. In order to make clear the validity of Eq. 19 or Eq. 57, it is instructive to analyze the experimental data so far reported on the aggregation equilibria of trialkylammonium salts by using Eqs. 19 or 57.

As mentioned in the introduction, the most reliable information on the aggregation equilibria was given by the two investigations which were carried out by the two-phase emf titration[3-8] and osmotic measurement.[15-19] The data analysis for the former investigation was carried out based on the following equations assuming the ideal behavior of organic phase,

$$Z = U/W, \quad (58)$$

$$U = \sum_{i=1} i k_i u^i, \quad (59)$$

$$W = w + \sum_{i=1} i k_i u^i, \quad (60)$$

where $u = w\,[H^+][X^-]$, U and W denote the total molar concentrations of acid (HX) and amine, respectively, w is the molar concentration of free amine, and k_i is an equilibrium constant corresponding to $(K_d)^i\bar{\beta}_i$ in the present work. The data of the two-phase emf titration were best described with the formation of monomer, two low aggregates and one high aggregate of the salts in organic phase, i.e. Eqs. 59 and 60 were expressed by

$$U = k_1 u + p k_p u^p + q k_q u^q + r k_r u^r, \quad (59')$$

$$W = w + k_1 u + p k_p u^p + q k_q u^q + r k_r u^r, \quad (60')$$
$$(1 < p < q < r).$$

Values of the aggregation equilibrium constants β_p, β_q, and β_r, where $\beta_i = k_i/k_1^i$, were determined by calcu-

Table 6. Values of $\overline{K}_2$, $\overline{\beta}_i$, and β_i of Tridodecylammonium Salts in Organic Solvents at 25 °C

Salt	Concentration range of salt	Solvent	Measurement	$\log \overline{K}_2$[a]	i	$\log \overline{\beta}_i$[b]	$\log \beta_i$[c]	Ref.
TDAHBr	0.03—0.3 M	*o*-Xylene	Two-phase	1.40—1.06	2	1.40—1.06	1.49±0.3	9
					3	2.93—2.25	3.13±0.3	
					30	47.94—38.12	46.04±1.3	
TDAHBr	0.01—0.1 M	Benzene	Osmotic	1.24	2	1.24	1.34	17
					3	2.61	2.76	
$TDAHNO_3$	0.02—0.25 M	Toluene	Two-phase	1.40—1.28	2	1.40—1.28	1.65±0.3	7
					3	2.93—2.69	3.15±0.3	
					50	81.89—75.82	80.10±2.1	
$TDAHNO_3$	0.01—0.1 M	Benzene	Osmotic	1.26	2	1.26	1.81	15
					3	2.65	2.59	
$TDAHClO_4$	0.04—0.15 M	*o*-Xylene	Two-phase	1.57—1.63	2	1.57—1.63	2.96±0.2	8
					8	12.21—12.64	16.21±0.7	
					90	164.82—170.22	208.09±8.10	
$TDAHClO_4$	0.01—0.1 M	Benzene	Osmotic	1.45	2	1.45	2.41	17
					8	11.38	14.00	
					16	25.11	29.78	

a) The values were determined by using the data in the reference. b) $\overline{\beta}_i=\prod_{j=2}^{i}\overline{K}_j=(1/i)(2\overline{K}_2)^{i-1}$. c) The values in the reference.

lating the values of k_1, k_p, k_q, and k_r, which give the minimum value of the error-square sum $\sum(Z_{exp}-Z_{cal})^2$. The values of β_p, β_q, and β_r of tridodecylammonium bromide perchlorate in *o*-xylene, and tridodecylammonium nitrate in toluene are given in Table 6 together with those of the dimerization concentration quotient $\overline{K}_2$, which were evaluated by assuming the validity of Eq. 19. Values of the aggregation equilibrium concentration quotients $\overline{\beta}_p$, $\overline{\beta}_q$, and $\overline{\beta}_r$, which were evaluated by using the equation $\overline{\beta}_i=(1/i)(2\overline{K}_2)^{i-1}$, corresponding to those of β_p, β_q, and β_r, respectively, are given in Table 6.

In the osmotic measurements, the concentration dependence of osmotic coefficient Φ of the solution containing trialkylammonium salt was analyzed by

$$\Phi = Y/W, \tag{61}$$

$$W = w_1 + \sum_{i=2} i\beta w_1{}^i, \tag{62}$$

$$Y = w_1 + \sum_{i=2} \beta w_1{}^i, \tag{63}$$

where W and w_1 denote the total molar concentration of the salts and the molar concentration of monomer. Kertes and Markovits[17] assumed the formation of three aggregates, which follows the equations

$$W = w_1 + p\beta_p w_1{}^p + q\beta_q w_1{}^q + r\beta_r w_1{}^r, \tag{62'}$$

$$Y = w_1 + \beta_p w_1{}^p + \beta_q w_1{}^q + \beta_r w_1{}^r, \tag{63'}$$

and evaluated the values of β_p, β_q, and β_r, which give the lowest value of the error-square sum $\sum(W_{exp}-W_{cal})^2+\sum(Y_{exp}-Y_{cal})^2$. The values of β_q, β_q, and β_r of tridodecylammonium bromide, nitrate and perchlorate in benzene are also shown in Table 6. In the above report, it was implicitly assumed that the change in activity of solvents resulted from only the change in effective concentration of the solute on the formation of aggregates, but it is found from the present work that this assumption is only applicable to very dilute solutions. Therefore, it is necessary to take into account the change in activity of solvents with varying the total salt concentration and the distribution of aggregates for evaluation of accurate values of aggregation equilibrium concentration quotient from the values of osmotic coefficient. According to Eq. 23, the activity of solvent, a_S, in the solution containing monomer to n-mer of trialkylammonium salt is given by

$$\ln a_S = \frac{v_S}{RT}\left\{\sum_{i=1}^{n}(\delta_S-\delta_i)\psi_i\right\}^2 + \ln \psi_S + \sum_{i=1}^{n}(1-\frac{v_S}{v_i})\psi_i. \tag{64}$$

Equation 64 can be rewritten as

$$-\ln a_S = \sum_{i=1}^{n}\frac{v_S}{v_i}\psi_i + (\frac{1}{2}-\sigma)\psi_T^2 + \frac{1}{3}\psi_T^3 + \cdots, \tag{64'}$$

$$\psi_T = \sum_{i=1}^{n}\psi_i, \tag{65}$$

$$\sigma = (v_S/RT)(<\delta> - \delta_S)^2, \tag{66}$$

$$<\delta> = \sum_{i=1}^{n}\delta_i\psi_i/\sum_{i=1}^{n}\psi_i. \tag{67}$$

Under the condition $\psi_T \ll 1$, Eq. 64′ reduces to

$$-\ln a_S = \frac{v_S}{RT}\sum_{i=1}^{n}w_i + (\frac{1}{2}-\sigma)(\frac{v_S}{1000})^2W^2, \tag{68}$$

where W and w_i are the total molar concentration of the salt and the molar concentration of its i-mer, respectively. Application of Eq. 19 to the successive

Table 7. Values of $\overline{K}_2$ and ρ of Tridodecylammonium Salts in Organic Solvents[a)]

Salt	Solvent (S)	δ_S	t	$\overline{K}_2$	ρ
		$cal_{th}^{1/2}cm^{-3/2}$	°C	M^{-1}	M^{-1}
TDAHCl	Benzene	9.16	25	11.5	1.84
TDAHCl	Benzene	9.16	37	14.8	2.79
TDAHCl	CCl_4	8.6	25	23.1	1.27
TDAHBr	Benzene	9.16	25	17.4	1.58
TDAHBr	Benzene	9.16	37	17.4	2.48
TDAHBr	Cyclohexane	8.20	25	86.2	1.58
TDAHBr	Cyclohexane	8.20	37	72.8	1.77
TDAHBr	Cyclohexane	8.20	50	62.1	1.91
TDAHBr	CCl_4	8.6	25	40.6	0.0
$TDAHNO_3$	Benzene	9.16	25	18.3	1.91
$TDAHNO_3$	Cyclohexane	8.20	25	84.8	1.37
$TDAHNO_3$	CCl_4	8.6	25	44	1.31
$TDAHClO_4$	Benzene	9.16	25	28.4	0.15
$TDAHClO_4$	Cyclohexane	8.20	25	162	0.65
$TDAHClO_4$	Cyclohexane	8.20	37	117	0.62
$TDAGClO_4$	Cyclohexane	8.20	50	109	0.57
$TDAH_2SO_4$	Benzene	9.16	25	60	1.82
$TDAH_2SO_4$	CCl_4	8.6	25	134	0.98

a) The values of $\overline{K}_2$ and ρ were determined by using the data in Ref. 17.

aggregation concentration quotient $\overline{K}_i$, which is defined by $\overline{K}_i=w_i/w_1w_{i-1}$, leads to Eq. 69 under the condition $2\overline{K}_2w_1<1$.

$$-\ln \dot{a}_S = \frac{v_S}{1000}\frac{1}{2\overline{K}_2}\ln(1+2\overline{K}_2W) + (\frac{1}{2}-\sigma)(\frac{v_1}{1000})^2W^2, \quad (69)$$

Substitution of the relation $-\ln \dot{a}_S=(v_S/1000)\,W$[17] into Eq. 69 yields

$$W\Phi = (1/2\overline{K}_2)\ln(1+2\overline{K}_2W) + \rho W^2, \quad (70)$$

$$\rho = (1/2-\rho)(v_1^2/1000v_S). \quad (71)$$

Accordingly, the values of $\overline{K}_2$ and ρ can be determined from Φ and W by the least-squares method. The values of $\overline{K}_2$ and ρ for tridodecylammonium chloride, bromide, nitrate, perchlorate and hydrogensulfate in benzene, carbon tetrachloride and cyclohexane are given in Table 7, where the data of Kertes and Markovits[17] were used. Regardless of the salts, Table 7 shows that the temperature dependences of $\overline{K}_2$ and ρ are as follows: 1) The values of $\overline{K}_2$ in benzene are approximately independent of temperature ($(\partial\overline{K}_2/\partial T)\simeq 0$). 2) The values of $\overline{K}_2$ in cyclohexane decrease with the increase of temperature ($(\partial\overline{K}_2/\partial T)<0$). 3) The values of ρ in benzene increase with temperature ($(\partial\rho/\partial T)>0$). 4) The values of ρ in cyclohexane are nearly independent of temperature ($(\partial\rho/\partial T)\simeq 0$).

The reason why such temperature dependences are obtained is explained mathematically as follows. Equation 67 is rewritten as

$$<\delta> = \frac{1}{2\overline{K}_2W}\sum_{i=1}^{n}\delta_i\{\frac{2\overline{K}_2W}{1+2\overline{K}_2W}\}^i. \quad (72)$$

When $\delta_1<\delta_2<\cdots<\delta_n$, i.e. higher aggregates have lower solubility parameters, Eq. 72 leads to $(\partial<\delta>/\partial\overline{K}_2)<0$. Therefore, it is obvious from the relation $(\partial<\delta>/\partial T)=(\partial<\delta>/\partial\overline{K}_2)(\partial\overline{K}_2/\partial T)$ that $(\partial<\delta>/\partial T)\simeq 0$ at $(\partial\overline{K}_2/\partial T)\simeq 0$ and $(\partial<\delta>/\partial T)>0$ at $(\partial\overline{K}_2/\partial T)<0$. On the other hand, Eq. 73 is derived from Eqs. 71 and 66,

$$\frac{\partial\rho}{\partial T} = \frac{v_1^2(<\delta>-\delta_S)}{1000RT^2}\{(<\delta>-\delta_S) - 2T(\partial<\delta>/\partial T)\}, \quad (73)$$

and this leads to the following relations: $(\partial\rho/\partial T)>0$ at $(\partial<\delta>/\partial T)\simeq 0$ or $(\partial\overline{K}_2/\partial T)\simeq 0$ and $(\partial\rho/\partial T)\simeq 0$ at $(\partial<\delta>/\partial T)\simeq(<\delta>-\delta_S)/2T>0$. The former relation is consistent with the temperature dependences of $\overline{K}_2$ and ρ in benzene, and the latter corresponds to those of $\overline{K}_2$ and ρ in cyclohexane. Accordingly, it is obvious that the values of $\overline{K}_2$ and ρ evaluated based on Eq. 19 have no self-contradiction. This presents suggestive evidence that Eq. 19 is valid, or at least not an unreasonable relationship for the aggregation equilibria of long-chain trialkylammonium salts in low-polar organic solvents.

In order to compare the values of aggregation equilibrium constants (concentration quotients) of tridodecylammonium salts (TDAHX), some values of $\overline{K}_2$ obtained by our analysis are shown in Table 6. As is seen in Table 6, the values of $\overline{\beta}_2$, $\overline{\beta}_3$, and $\overline{\beta}_r$ for TDAHBr and $TDAHNO_3$ having relatively small values of $\overline{K}_2$ are in fairly good agreement with those of β_2, β_3, and β_r, respectively, except for the value of β_2 for $TDAHNO_3$ in benzene obtained by extrapolation from the osmometric data.[15] The values of $\overline{\beta}_2$, $\overline{\beta}_8$, and $\overline{\beta}_r$ for $TDAHClO_4$ with relatively large values of $\overline{K}_2$ are considerably small compared with those of β_2, β_8, and β_r, respectively. The reason for these results can be explained as follows. Since the bromide and nitrate in *o*-xylene, toluene, and benzene have relatively small values of $\overline{\beta}_i$ ($i=2,3,\cdots$), the concentrations of intermediate and high aggregates may be negligibly small

compared with those of such low aggregates as dimer and trimer in the wide range of total concentration of the salts. On the other hand, in *o*-xylene and benzene solutions of the perchlorate with relatively large values of $\overline{\beta}_i$ (i=2,3,$\cdots$), the concentrations of intermediate aggregates may not be neglected compared with those of low aggregates even at the low total concentration of the salt. Accordingly, it seems that the values of β_2, β_8, and β_r for $TDAHClO_4$, which were determined based on Eqs. 59′ and 60′ or Eqs. 62′ and 63′, are not the true values, but the mean values of formation constants of low, intermediate and high aggregates, respectively, i.e. the calculated values of β_2, β_8, and β_r correspond to those of β'_2, β'_8, and β'_r, respectively, which are represented by

$$\beta'_2 = \sum_{i=2}^{s} \beta_i w_1^i / w_1^2, \tag{74}$$

$$\beta'_8 = \sum_{i=s+1}^{t} \beta_i w_1^i / w_1^8, \tag{75}$$

$$\beta'_r = \sum_{i=t+1} \beta_i w_1^i / w_1^r, \tag{76}$$

$$(2 < s < 8 < t < r).$$

From Eqs. 74, 75, and 76, it is estimated that when the values of β_i equal to those of $\overline{\beta}_i$, the values of β'_i become larger than those of $\overline{\beta}_i$ and the ratios of $\beta'_i/\overline{\beta}_i$ increase with the increase of $\overline{\beta}_i$. These relations agreed with those between the calculated values of β_i and $\overline{\beta}_i$ shown in Table 6. This agreement may be taken as additional evidence that Eq. 19 or Eq. 57 is valid not only for the aggregation equilibrium of trioctylammonium chloride, but also for the aggregation equilibria of other long-chain trialkylammonium salts, and the assumption of the formation of at most three aggregates, which was introduced by Högfeldt et al.[3-8] and by Kertes and Markovits,[17] seems to be too simplified, particularly for tridodecylammonium perchlorate in *o*-xylene and benzene.

From the above-mentioned discussion, the following conclusion can be drawn. The extraction of hydrochloric acid by trioctylamine in low-polar organic solvents is accompanied with the formation of trioctylammonium chloride which exists as an ion-pair and of electrostatic molecular aggregates from dimer to micelle. The concentration quotients for the successive aggregation equilibria satisfy Eqs. 19 or 57. Equation 19 is valid also for the aggregation equilibria of other long-chain trialkylammonium salts in the organic solvents. The total solute concentration dependence on the quotients for the extraction equilibrium of hydrochloric acid by trioctylamine and for the successive aggregation of trioctylammonium chloride can be explained reasonably by the theory of regular solution. The diluent effect on the extraction equilibrium constant and on the successive aggregation constant can be also explained reasonably by the theory.

References

1) Y. Marcus and A. S. Kertes, "Ion Exchange and Solvent Extraction of Metal Complexes," John Wiley and Sons, New York (1969), Chapter 10.

2) V. S. Shmidt, "Amine Extraction (Translated from Russian by J. Schmorak)," Israel Program for Scientific Translations, Jerusalem (1971).

3) E. Högfeldt and F. Fredlund, *Trans. Roy. Inst. Tech., Stockholm*, Nos. 226 and 227 (1964).

4) E. Högfeldt and M. de Jesus Tavares, *Trans. Roy. Inst. Tech., Stockholm*, No. 228 (1964).

5) E. Högfeldt, F. Fredlund, and K. Rasmussen, *Trans. Roy. Inst. Tech., Stockholm*, No. 229 (1964).

6) M. A. Lodhi and E. Högfeldt, "Extraction of Hydrobromic Acid by Trilaurylamine Dissolved in *o*-Xylene," in "Solvent Extraction Chemistry," ed by D. Dyrssen, J. O. Liljenzin, and J. Rydberg, North-Holland, Amsterdam (1967), p. 421.

7) L. Kuča and E. Högfeldt, *Acta Chem. Scand.*, **25**, 1261 (1971).

8) E. Högfeldt, P. R. Danesi, and F. Frendlund, *Acta Chem. Scand.*, **25**, 1338 (1971).

9) A. Lodhi, *Arkiv Kemi*, **27**, 309 (1967).

10) J. J. Bucher and R. M. Diamond, *J. Phys. Chem.*, **69**, 1565 (1965).

11) W. Müller and R. M. Diamond, *J. Phys. Chem.*, **70**, 3469 (1966).

12) R. M. Diamond, "Amine Extraction Systems," in Ref. 6, p. 349.

13) K. A. Allen, *J. Phys. Chem.*, **62**, 1119 (1958).

14) V. V. Formin and V. T. Potapova, *Zh. Neorg. Khim.*, **8**, 990 (1963).

15) G. Scibona, S. Basol, P. R. Danesi, and F. Orlandini, *J. Inorg. Nucl. Chem.*, **28**, 1441 (1966).

16) F. Orlandini, P. R. Danesi, S. Basol, and G. Scibona, "Observation on the Aggregation of the Tertiary Alkylammonium Salts," in Ref. 6, p. 408.

17) A. S. Kertes and G. Markovits, *J. Phys. Chem.*, **72**, 4202 (1968), **74**, 3568 (1970).

18) I. J. Gal, I. Paligorić, and V. G. Antonijevic, *J. Inorg. Nucl. Chem.*, **32**, 1645 (1970).

19) I. Paligorić and I. J. Gal, J. *Inorg. Nucl. Chem.*, **38**, 1487 (1976), **40**, 285 (1978).

20) H. Freiser, *Anal. Chem.*, **41**, 1354 (1969).

21) A. S. Kertes, *J. Inorg. Nucl. Chem.*, **24**, 1651 (1962).

22) A. S. Kertes, *J. Inorg. Nucl. Chem.*, **27**, 209 (1965).

23) J. H. Hildebrand and R. L. Scott, "The Solubility of Nonelectrolytes," Reinhold, New York, 3rd ed., (1950).

24) J. A. Riddick and W. B. Bunger, "Organic Solvents," in "Techniques of Chemistry," 3rd ed, ed by A. Weissberger, John Wiley and Sons, New York (1970), Vol. 2, Chap. 3.

 © 1987 The Chemical Society of Japan Bull. Chem. Soc. Jpn., 60, 1321—1326 (1987)

The Crystal and Molecular Structures of Bis(2-methylpyridine)-, and Bis(3-methylpyridine)bis(thiocyanato)cadmium(II) in Polymeric Forms, $[Cd(SCN)_2(CH_3C_5H_4N)_2]_n$

Masahiro TANIGUCHI, Yoshihiko SUGITA, and Akira OUCHI*
Department of Chemistry, College of Arts and Sciences, The University of Tokyo, Komaba, Meguro-ku, Tokyo 153
(Received August 26, 1986)

The crystal and molecular structures of the title complexes were determined by the single-crystal X-ray diffraction method. Both of them are triclinic, with the space group $P\bar{1}$. The crystallographic data: 2-methylpyridine (α-pic) adduct, $a=11.076(3)$, $b=18.478(8)$, $c=9.299(3)$ Å, $\alpha=104.60(3)$, $\beta=114.84(2)$, $\gamma=81.12(3)°$, $Z=4$, final R value is 0.037; 3-methylpyridine (β-pic) adduct, $a=8.7667(16)$, $b=16.655(4)$, $c=5.8447(10)$ Å, $\alpha=91.406(18)$, $\beta=100.571(14)$, $\gamma=92.525(18)°$, $Z=2$, final R value is 0.041. In both complexes, all cadmium atoms are in 4*N*2*S*-hexa-coordination, being in an octahedral geometry; they are oriented as any pair of side-by-side metal atoms being bridged by two thiocyanate ions. In the α-pic adduct, the chain is oriented approximately along the [111] axis. In the chain, the metal atoms in two kinds of orientations appear alternately: Around one kind of the metal atoms three kinds of ligating atoms are all in *trans*-configurations, and around the other kind of the metal atoms the respective pairs of N(base) and S(SCN) atoms are in *cis* and the pair of the N(SCN) atoms in a *trans*-configuration. In the β-pic adduct, the chain is along the [001] axis and pairs of three kinds of ligating atoms are all in *trans*-configurations.

The structures of cadmium(II) thiocyanate and several kinds of its Lewis base adducts have already been elucidated.[1-8] Many of them are in a linear polymeric form having double thiocyanate (SCN) ion bridgings between any pair of adjacent metal atoms.[5-8] Previously, we determined the structure of bis(4-methylpyridine)bis(thiocyanato)cadmium(II), $Cd(SCN)_2(\gamma\text{-pic})_2$ (where γ-pic=γ-picoline=4-methylpyridine).[8] In this complex, there are three kinds of crystallographically independent cadmium atoms. They are oriented approximately along the [111] axis; side-by-side metal atoms are bridged by two SCN ions. This type of the chain structure had not yet been found in the other Lewis base adducts of cadmium(II) thiocyanate. Therefore, it is interesting to make a comparative study of a variety of chain structures caused by differences in the additional Lewis base, especially when the structure of the base molecules are not much different from each other. For this purpose, we determined the structures of the title complexes, $Cd(SCN)_2(\alpha\text{-pic})_2$ (α-pic=α-picoline=2-methylpyridine), and $Cd(SCN)_2(\beta\text{-pic})_2$ (β-pic=β-picoline=3-methylpyridine), by a single-crystal X-ray diffraction method.

Experimental

Synthesis of Bis(2-methylpyridine)bis(thiocyanato)cadmium(II) and Bis(3-methylpyridine)bis(thiocyanato)cadmium(II). These complexes were obtained in almost the same way as that of Ahuja.[9] The crystal used for the X-ray analysis was obtained as follows: crystals of the α-pic adduct were deposited from a mixture of $Cd(SCN)_2$ (0.57 g, 2.5 mmol) in 15 cm^3 of ethanol-water (1 : 1=v/v) and 2-methylpyridine (0.47 g, 5.0 mmol) in 10 cm^3 of ethanol after being left standing at ambient temperature for several hours. The crystals of the β-pic adduct were obtained from a mixed solution of $Cd(SCN)_2$ (0.57 g, 2.5 mmol) and 3-methylpyridine (0.47 g, 5.0 mmol) in 20 and 10 cm^3 methanol, respectively, after being left standing for several hours at ambient temperature. Anal. (for both complexes), ($CdC_{14}H_{14}N_4S_2$), Cd, C, H, N. The wavenumbers of their infrared spectral bands almost coincide with the respective values of the references.[9]

X-Ray Structure Analysis. The crystallographic data, the size of the used crystal, and some experimental conditions to determine intensity data are listed in Table 1. Reflections were collected on a Rigaku AFC-6A automated four-circle X-ray diffractometer with graphite-monochromated Mo$K\alpha$ radiation, the ω—2θ scan technique being employed (scan speed 4° min^{-1} (θ)). The intensities were corrected for Lorentz and polarization factors, but no correction was made for absorption and extinction.

Structure Determination. Their structures were solved by the heavy-atom method. The positions of the cadmium and some sulfur atoms were deduced from a three-dimensional Patterson map; other non-hydrogen atoms were located by successive Fourier syntheses. Their positional, isotropic and then anisotropic thermal parameters were refined by a block-diagonal least-squares method. All the hydrogen atoms of the pyridine rings were at respective calculated positions, assuming their B_{iso}'s to be 8.0 Å^2, and C-H bond lengths to be 1.08 Å. All the calculations were carried out on a HITAC M-680H computer at the computer center of the University of Tokyo using a local version of the UNICS program.[10] The atomic scattering factors were taken from Ref. 11.

Results and Discussion

The final atomic parameters of the non-hydrogen atoms of the complexes are listed in Tables 2 and 3; their selected bond lengths and bond angles are tabulated in Tables 4 and 5.[12] A perspective drawing of the skeleton of the polymeric chain of the α-pic adduct, as well as that around a metal atom of the β-pic complex, together with their numbering scheme of the atoms, are shown in Figs. 1 and 2. Their crystal packing diagrams are given in Figs. 3 and 4.

In the α-pic complex, the arrangement of the cadmium atoms, the coordination geometries of the respective metal atoms, and the bridging modes of the SCN ions resemble those of the γ-pic complex.[8]

There are crystallographically three kinds of cad-

Table 1. Crystallographic Data and Some Experimental Conditions to Obtain the Reflection Intensities of the Complexes; $Cd(SCN)_2(\alpha\text{-pic})_2$ and $Cd(SCN)_2(\beta\text{-pic})_2$

Lewis Base	2-Methylpyridine	3-Methylpyridine
F.W.	414.82	414.82
Crystal System	Triclinic	Triclinic
Space Group	$P\bar{1}$	$P\bar{1}$
$a(l/\text{Å})$	11.076(3)	8.7667(16)
$b(l/\text{Å})$	18.478(8)	16.655(4)
$c(l/\text{Å})$	9.299(3)	5.8447(10)
$\alpha(\phi/°)$	104.60(3)	91.406(18)
$\beta(\phi/°)$	114.84(2)	100.571(14)
$\gamma(\phi/°)$	81.12(3)	92.525(18)
$U(v/\text{Å}^3)$	1668.6(10)	837.6(3)
$D_m(d/\text{Mg m}^{-3})$	1.64(3)	1.65(3)
$D_x(d/\text{Mg m}^{-3})$	1.65	1.65
Z	4	2
$\mu(\text{Mo}K\alpha)(n/\text{mm}^{-1})$	1.54	1.53
Number of Reflections Measured	6233	4920
Reflections used for the Calculation[a]	4413	2756
Measured Range $(2\theta/°)$	3—50	3—60
R[b]	0.037	0.041
R_{weight}[b]	0.048	0.048
S[c]	1.434	1.206
Size of Crystal (v/mm^3)	0.2×0.3×0.1	0.2×0.3×0.1
Scan Width $(\theta/°)$	1.04+0.5tanθ	1.08+0.5tanθ

a) Reflections with $|F_o|>3\sigma(|F_o|)$ were used. b) $R=\sum||F_o|-|F_c||/\sum|F_o|$; $R_{weight}=[\sum(|F_o|-|F_c|)^2/\sum wF_o^2]^{1/2}$, were $w=1/[\{\sigma(|F_o|)\}^2+(F_{weight}\times F_o)^2]$, $F_{weight}=0.020$. c) $S=[\sum w(|F_o|-|F_c|)^2/(N_o-N_p)]^{1/2}$, where N_o=number of reflections, N_p=number of parameters.

Table 2. Final Non-Hydrogen Atomic Coordinates (×10⁴) of $Cd(SCN)_2l(\alpha\text{-pic})_2$ Together with the Equivalent Isotropic Temperature Factors; Estimated Standard Deviations of Them are Shown in Parentheses

Atom	x	y	z	$B_{eq}/\text{Å}^2$[d]	Atom	x	y	z	$B_{eq}/\text{Å}^2$[d]
Cd(1)	0.0	0.0	0.0	3.3_3	N(21)	3562(4)	1666(3)	7039(6)	3.9_8
Cd(2)	5000.0	5000.0	5000.0	3.3_8	C(21)	4869(6)	1487(4)	7305(8)	5.3_1
Cd(3)	2500.4(4)	2499.9(2)	5243.9(5)	3.6_3	C(22)	5681(7)	1041(4)	8328(10)	6.6_6
S(1)	−1216(2)	744(1)	2017(2)	4.2_7	C(23)	5157(7)	753(5)	9137(11)	8.6_0
S(2)	3765(2)	1670(2)	3270(3)	8.4_7	C(24)	3831(7)	917(4)	8885(9)	6.5_8
S(3)	1228(2)	3335(1)	2839(2)	8.1_3	C(25)	3048(6)	1376(3)	7829(7)	4.2_4
S(4)	6216(2)	4256(1)	7491(2)	4.1_7	C(26)	1624(7)	1561(4)	7603(9)	6.3_8
N(1)	578(5)	1854(3)	3828(6)	4.3_8	N(31)	6032(4)	4019(3)	3365(5)	3.5_8
N(2)	1829(5)	673(3)	1219(6)	4.3_0	C(31)	5758(6)	3315(3)	3293(7)	3.9_2
N(3)	3171(5)	4330(3)	3716(6)	4.2_7	C(32)	6202(7)	2683(3)	2467(7)	4.6_9
N(4)	4414(5)	3142(3)	6394(6)	4.3_1	C(33)	6952(7)	2762(4)	1668(8)	5.3_2
C(1)	−157(5)	1400(3)	3091(6)	3.2_9	C(34)	7246(7)	3462(4)	1728(8)	5.1_4
C(2)	2623(5)	1082(3)	2078(6)	3.8_3	C(35)	6778(6)	4089(3)	2579(7)	4.1_7
C(3)	2371(5)	3920(3)	3363(6)	3.7_6	C(36)	7100(8)	4858(4)	2652(10)	7.1_7
C(4)	5158(5)	3599(3)	6849(6)	3.4_3	N(41)	−1039(4)	984(3)	−1689(5)	3.7_5
N(11)	1440(5)	3338(3)	6810(5)	3.7_1	C(41)	−758(6)	1677(3)	−781(7)	4.3_0
C(11)	151(6)	3511(4)	5947(7)	4.4_3	C(42)	−1206(7)	2313(4)	−1429(8)	5.2_3
C(12)	−664(7)	3961(4)	6601(8)	5.9_0	C(43)	−1952(7)	2235(4)	−3051(9)	5.5_4
C(13)	−153(7)	4236(5)	8227(9)	7.3_9	C(44)	−2239(6)	1528(4)	−3976(8)	5.0_3
C(14)	1166(7)	4082(4)	9132(8)	5.7_6	C(45)	−1772(6)	912(3)	−3291(7)	4.0_4
C(15)	1940(6)	3625(3)	8403(6)	3.9_1	C(46)	−2108(8)	142(4)	−4317(8)	6.1_0
C(16)	3367(6)	3432(4)	9406(7)	5.2_1					

d) The equivalent isotropic temperature factors were computed using the following expression;

$$B_{eq}=4/3(B_{11}a^2+B_{22}b^2+B_{33}c^2+B_{12}ab\cos\gamma+B_{13}ac\cos\beta+B_{23}bc\cos\alpha).$$

The B_{ij}'s are defined by;

$$T=\exp[-(h^2B_{11}+k^2B_{22}+l^2B_{33}+2hkB^{12}+2hlB_{13}+2klB_{23})].$$

Table 3. Final Non-Hydrogen Atomic Coordinates ($\times10^4$) of $Cd(SCN)_2(\beta\text{-pic})_2$ Together with the Equivalent Isotropic Temperature Factors; Estimated Standard Deviations of Them are Shown in Parentheses

Atom	x	y	z	B_{eq}/Å$^{2d)}$
Cd	1984.8(5)	2543.9(3)	3864.0(6)	3.1_0
S(1)	955(2)	3829(1)	1288(2)	3.7_8
S(2)	2822(2)	1220(1)	6467(3)	4.5_5
N(1)	1148(6)	3170(3)	−3065(7)	4.0_5
N(2)	2893(5)	1913(3)	10881(7)	3.7_5
C(1)	1087(6)	3440(3)	−1267(9)	3.2_1
C(2)	2853(6)	1633(3)	9046(8)	2.9_9
N(11)	4463(5)	3213(3)	5089(8)	3.5_0
C(11)	5023(6)	3761(4)	3788(9)	3.6_3
C(12)	6422(6)	4190(3)	4442(10)	3.7_8
C(13)	7302(7)	4019(4)	6620(11)	4.5_9
C(14)	6752(7)	3448(4)	7948(10)	4.5_3
C(15)	5339(7)	3059(4)	7145(10)	4.1_1
C(16)	6981(8)	4829(4)	2933(12)	5.2_9
N(21)	−485(5)	1897(3)	2565(8)	3.9_0
C(21)	−759(7)	1370(4)	798(10)	4.3_4
C(22)	−2177(7)	960(4)	−7(11)	4.3_6
C(23)	−3340(7)	1127(4)	1156(14)	5.5_7
C(24)	−3093(8)	1689(5)	2969(15)	6.6_2
C(25)	−1645(7)	2053(4)	3639(12)	5.0_8
C(26)	−2379(10)	337(5)	−2012(14)	6.7_3

d) See below Table 2.

mium atoms; two of them, Cd(1) and Cd(2), are at the centers of symmetry, 0, 0, 0 and 0.5, 0.5, 0.5, while the Cd(3) atom is situated between them. Any pair of adjacent cadmium atoms are bridged by two SCN ions, where one SCN ion is *S*-coordinated, and the other SCN ion is *N*-coordinated to the same side metal atom. The polymeric chain lines approximately along the [111] axis, in the order ···Cd(1)···Cd(3)···Cd(2)···Cd(3^{ii})··· (Key to the symmetry operation: see Fig. 1, caption). All cadmium atoms are 4*N*2*S*-hexa-coordinated, being in an octahedral geometry. Around the Cd(1) and Cd(2) atoms all N(SCN), S(SCN), and N(α-pic) atoms are in *trans*-configurations, while around the Cd(3) atom, N(SCN) atoms are in *trans*; however, the other two kinds of atoms are in *cis*-configurations. Between Cd(1) and Cd(3), as well as Cd(3) and Cd(2) atoms, there are eight-membered rings consisting of the two metal and two SCN ion atoms bridging them. The average positional deviation of the atoms from the average planes of the rings are 0.047 and 0.051 Å, respectively.

On the other hand, there are some differences between the structures of the α-pic and γ-pic adducts, as follows.

The interatomic distances, Cd(1)···Cd(3) and Cd(3)···Cd(2), in the α-pic adduct are 5.834(3) and 5.836(2)

Table 4. Interatomic Distances and Bond Angles of $Cd(SCN)_2(\alpha\text{-pic})_2$ with the Standard Deviations in Parentheses

Bond Length	(l/Å)	Bond Length	(l/Å)
Cd(1)···Cd(3)	5.834(3)	Cd(2)···Cd(3)	5.836(2)
Cd(1)-S(1)	2.734(2)	Cd(2)-S(4)	2.735(2)
Cd(3)-S(2)	2.786(3)	Cd(3)-S(3)	2.792(3)
Cd(1)-N(2)	2.252(5)	Cd(2)-N(3)	2.249(5)
Cd(3)-N(1)	2.308(5)	Cd(3)-N(4)	2.297(5)
Cd(1)-N(41)	2.524(5)	Cd(2)-N(31)	2.517(5)
Cd(3)-N(11)	2.374(5)	Cd(3)-N(21)	2.373(5)
S(1)-C(1)	1.639(5)	S(2)-C(2)	1.627(6)
S(3)-C(3)	1.627(7)	S(4)-C(4)	1.641(6)
N(1)-C(1)	1.135(7)	N(2)-C(2)	1.138(7)
N(3)-C(3)	1.142(8)	N(4)-C(4)	1.145(8)
Bond Angle	**(ϕ/°)**	**Bond Angle**	**(ϕ/°)**
S(1)-Cd(1)-N(2)	96.13(13)	S(1)-Cd(1)-N(41)	88.44(12)
N(2)-Cd(1)-N(41)	86.44(17)	S(4)-Cd(2)-N(3)	96.21(13)
S(4)-Cd(2)-N(31)	88.58(12)	N(3)-Cd(2)-N(31)	86.44(17)
S(2)-Cd(3)-S(3)	86.24(8)	S(2)-Cd(3)-N(1)	93.73(13)
S(2)-Cd(3)-N(4)	81.82(14)	S(2)-Cd(3)-N(21)	88.35(14)
S(3)-Cd(3)-N(1)	81.85(13)	S(3)-Cd(3)-N(4)	93.77(14)
S(3)-Cd(3)-N(11)	87.96(14)	N(1)-Cd(3)-N(11)	89.49(18)
N(1)-Cd(3)-N(21)	94.59(18)	N(4)-Cd(3)-N(11)	94.49(18)
N(4)-Cd(3)-N(21)	89.34(18)	N(11)-Cd(3)-N(21)	97.70(18)
Cd(1)-S(1)-C(1)	98.7(2)	Cd(3)-S(2)-C(2)	99.4(2)
Cd(3)-S(3)-C(3)	99.6(2)	Cd(2)-S(4)-C(4)	98.8(2)
Cd(3)-N(1)-C(1)	163.7(5)	Cd(1)-N(2)-C(2)	164.4(5)
Cd(2)-N(3)-C(3)	164.6(5)	Cd(3)-N(4)-C(4)	163.8(5)
S(1)-C(1)-N(1)	179.6(5)	S(2)-C(2)-N(2)	178.6(5)
S(3)-C(3)-N(3)	179.4(6)	S(4)-C(4)-N(4)	179.6(6)
Cd(3)-N(11)-C(11)	113.6(4)	Cd(3)-N(11)-C(15)	128.7(4)
Cd(3)-N(21)-C(21)	114.1(5)	Cd(3)-N(21)-C(25)	128.3(4)
Cd(2)-N(31)-C(31)	111.9(4)	Cd(2)-N(31)-C(35)	130.5(4)
Cd(1)-N(41)-C(41)	111.4(4)	Cd(1)-N(41)-C(45)	130.4(4)

Table 5. Bond Lengths and Bond Angles of $Cd(SCN)_2(\beta\text{-pic})_2$, with the Standard Deviations in Parentheses

Bond Length	(l/Å)	Bond Length	(l/Å)
Cd-S(1)	2.737(2)	Cd-S(2)	2.759(2)
Cd-N(1^{ii})	2.304(5)	Cd-N(2^{i})	2.296(5)
Cd-N(11)	2.377(4)	Cd-N(21)	2.361(4)
S(1)-C(1)	1.638(6)	S(2)-C(2)	1.637(5)
C(1)-N(1)	1.144(7)	C(2)-N(2)	1.153(7)
Cd···Cd^{i}	5.845(1)		
Bond Angle	**(ϕ/°)**	**Bond Angle**	**(ϕ/°)**
S(1)-Cd-S(2)	176.25(5)	N(11)-Cd-N(21)	178.61(15)
N(1^{ii})-Cd-N(2^{i})	178.15(18)	S(1)-Cd-N(11)	90.82(11)
S(1)-Cd-N(21)	87.95(11)	S(2)-Cd-N(11)	92.64(11)
S(2)-Cd-N(21)	88.60(11)	S(1)-Cd-N(1^{ii})	86.89(13)
S(1)-Cd-N(2^{i})	94.33(13)	S(2)-Cd-N(1^{ii})	91.73(13)
S(2)-Cd-N(2^{i})	87.14(13)	N(11)-Cd-N(1^{ii})	88.92(16)
N(11)-Cd-N(2^{i})	89.68(16)	N(21)-Cd-N(1^{ii})	91.65(17)
N(21)-Cd-N(2^{i})	89.78(16)	Cd-S(1)-C(1)	97.2(2)
Cd-S(2)-C(2)	97.9(2)	Cd-N(1^{ii})-C(1^{ii})	163.3(5)
Cd-N(2^{i})-C(2^{i})	157.4(5)	Cd-N(11)-C(11)	121.8(4)
Cd-N(11)-C(15)	120.6(4)	Cd-N(21)-C(21)	122.4(4)
Cd-N(21)-C(25)	119.8(4)	S(1)-C(1)-N(1)	178.7(5)
S(2)-C(2)-N(2)	178.7(5)		

Key to the symmetry operation: i, x, y, $-1+z$; ii, x, y, $1+z$.

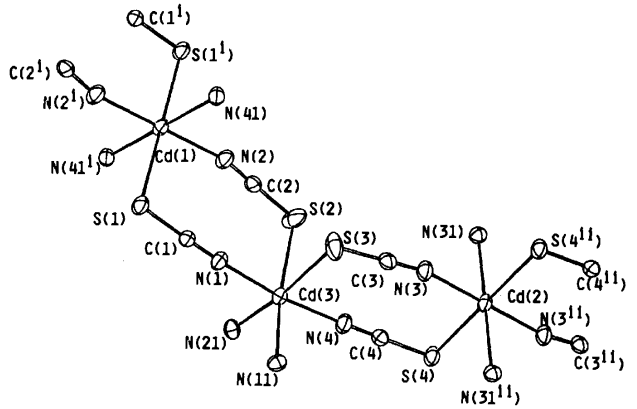

Fig. 1. A perspective drawing of the structure of $Cd(SCN)_2(\alpha\text{-pic})_2$ with the numbering scheme. (Key to the symmetry operation: i, $-x$, $-y$, $-z$; ii, $1-x$, $1-y$, $1-z$.)

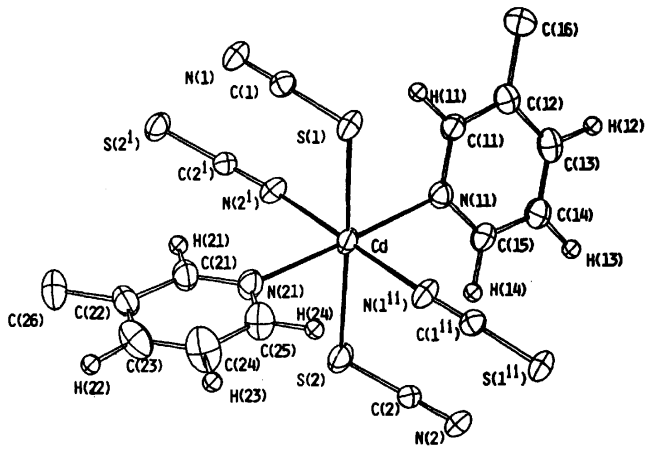

Fig. 2. A perspective drawing of $Cd(SCN)_2(\beta\text{-pic})_2$ around the cadmium atom with the numbering scheme. (Key to the symmetry operation: i, x, y, $1+z$; ii, x, y, $-1+z$.)

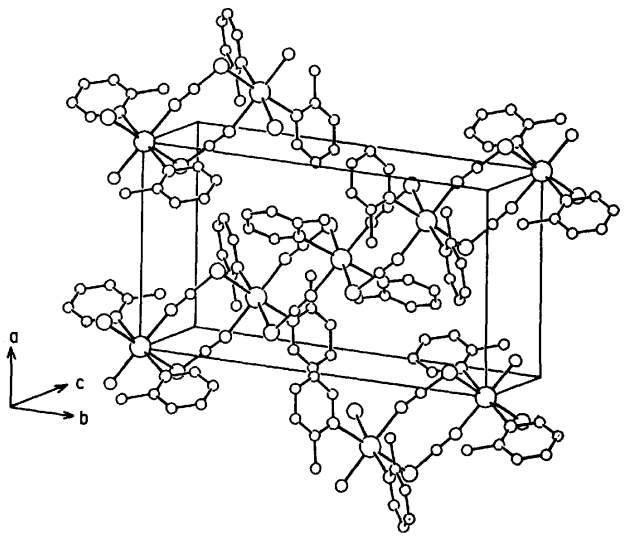

Fig. 3. Crystal packing diagram of $Cd(SCN)_2(\alpha\text{-pic})_2$.

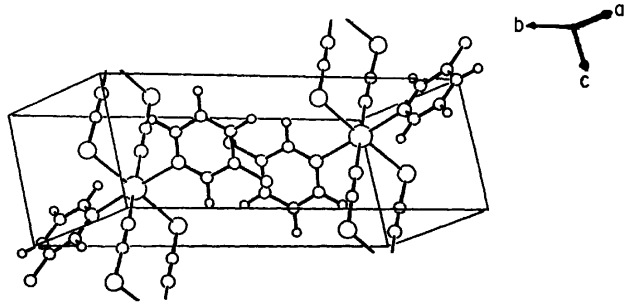

Fig. 4. Crystal packing diagram of $Cd(SCN)_2(\beta\text{-pic})_2$.

Å, respectively, while the corresponding bond lengths in the γ-pic adduct are on the average 5.778 Å. Moreover, the Cd-N(base) bond length of the former, especially those around the Cd(1) and Cd(2) atoms, are longer than the corresponding lengths of the latter complex. These differences are likely caused by a steric effect of the substituted methyl groups on the pyridine rings of the ligands. In the α-pic adduct the methyl groups approach the Cd···Cd chain and prevent the next cadmium, as well as the ligating α-pic nitrogen atoms, from approaching the central metal atom.

The directions of the coordinating ligands in the α- and γ-pic complexes are not the same. As shown in Fig. 3, in the α-pic adduct, the 4-carbon atoms of the pyridine rings of the ligands are directed rather in the c-axis direction, while in the γ-pic adduct, they are directed approximately in the a-axis direction.[8] As a result, the a-axis length of the α-pic adduct (11.076(3) Å) is shorter than that of the γ-pic adduct (11.323(4) Å). This is because in the latter adduct the methyl group of the ligand is directed along the a-axis direction. On the other hand, the b- and c-axis lengths of the α-pic adduct are longer than the respective lengths of the γ-pic adduct; in total, the cell volume of the α-pic adduct (1668.6(10) Å^3) is a little smaller than that of the γ-pic one (1691.7(15) Å^3): the α-pic adduct is a little more closely packed in the crystal.

The crystal structure of the β-pic adduct is drastically different from those of the α- and γ-pic adducts, though the difference between their molecules is only the substituted positions of a methyl group on the Lewis base ligand. In the β-pic adduct, crystallographically, there is only one kind of cadmium atom: 4*N*2*S*-hexa-coordinated with an octahedral geometry, where the respective pairs of N(SCN), S(SCN), and N(β-pic) atoms are ligated in *trans*-configurations. Any pair of adjucent metal atoms is bridged by two SCN ions as in cases of the α- and γ-pic complexes and line along [001] axis. As the intermetallic distance along the line, which is the same as the c-axis length, is 5.8447(10) Å, it is longer than that of the γ-pic adduct; however, it is not much different from that of the α-pic one. The volume per one metal atom is also not much different from those of the α- and γ-pic adducts.

The planarity of the eight-membered ring, comprising two bridging SCN ion atoms and two metal atoms, is not so good as those of the α- and γ-pic adducts; the average deviation of the atoms from the average plane is about twice (0.120 Å) as much. However, the puckering of the ring is not as large as the other complex ones where all eight-membered rings in the chain are parallel.[5,6]

It is interesting to consider the reason why the β-pic adduct takes a different structure. Although an exact quantitative explanation is difficult at this stage (because of the scarcity of available reference data), some considerations will be presentaed from a comparison between the structures of the adducts $Cd(SCN)_2L_2$ (L=Lewis base) where the metal atoms are doubly bridged by SCN ions. In addition to the β-pic adduct, complexes of 1*H*-1,2,4-triazol (trz),[6] dibenzylamine,[14] and imidazolinethione (etu)[5] possess the same type of structure: all have eight-membered rings comprizing the bridging of two SCN ions and two metal atoms. They are parallel in the chain and, crystallographically, only one kind of cadmium atom is in the chain. The anion of the $[(CH_3)_4N]_2[Cd(SCN)_4]$[15] also has the same type of bridge. Therefore, the twisted chains of the α- and γ-pic adducts are rather thought to be exceptional, although the pyridine (py) adduct, $Cd(SCN)_2py_2$, is expected to have a different type of long-period chain.[16]

The volume of the Lewis base is probably not the only factor to determine the type of structure since the massive dibenzylamine as well as the smaller trz adduct have the same type crystal structure as the β-pic adduct.

One probable explanation is that when some interaction between the ligand molecules is dominant, they are regularly laid on a line or accumulated with their planar molecules in parallel. This is because their respective eight-membered rings of the double SCN bridges are in parallel as is found in the β-pic adduct type chain. However, here the interaction means a long-distance type which may be weak in strength.

In trz and etu adducts, the existence of such an interaction between ligands was reported[5,6] and in the dibenzylamine adduct, half of the ligand benzene rings were reported to partially overlap.[14] Also, the unidentate SCN ions in the anion of the $[(CH_3)_4N]_2[Cd(SCN)_4]$ salt have been shown to be electrostatically connected via the cations.[15]

In the case of the α-pic adduct, as the directions of the respective methyl groups of the ligands are quite limited and prevent them from excessively approaching the SCN chain, it is difficult to place the pyridine planes of the ligand in parallel in order to have them overlap in the crystal. In the case of the γ-pic adduct, as the ligand pyridine ring has a methyl group at the 4-position, the next ligand pyridine ring cannot approach or sufficiently overlap, even though they are oriented almost parallel in the crystal.[8] On the other hand, in the case of the β-pic adduct, such obstacles do not exist.

There is another possible explanation regarding the stronger interaction between the pyridine rings of the β-pic adduct. Although the density of the delocalized electrons of the non-substituted pyridine ring is poor, when some electron donating group, such as a methyl group, is introduced as in the case of the β-pic ligand, the electron density of the ring is much increased. It can, thus, form a stronger interaction with the parallel ring of the next ligand than that of the non-substituted pyridine complex. In cases of the α- and γ-pic ligands, although the electrons are similarly supplied from the methyl group, they are absorbed by the ring nitrogen

and/or the ligating metal atom since the methyl group takes the 2- and 4-position of the ring; the increase of the ring electron density is not much. Thus, the interaction of the β-pic ligand is stronger than those of the α- and γ-pic as well as of the py ones.

When such an inter-ligand force is minor, some other type of the chain can be adopted to achieve a closest packing in the crystal. The α- and γ-pic adducts have such twisted chain structures, and they are slightly different from each other and can pack the respective molecules in the most effective way.

As the structure of some methylpyridine adducts of the polymeric metal thiocyanates (Ag(SCN)L (L=α- and β-pic),[17] and Cu(SCN)L_2 (L=α-, β-, and γ-pic))[18] were already elucidated, we can refer to their results and compare them with the results concerning cadmium complexes.

In the case of the Ag(SCN)L type complex,[17] both of the α- and β-pic adducts are in the two-dimensional polymeric structure, where each metal atom is 2S2*N*-tetra-coordinated, and the side-by-side metal atoms are bridged by one SCN ion. Although their space group, as well as their *Z* numbers, are different from each other, the main structural difference between them is some deformation of the Ag(SCN) network. Their best packings are attained mainly by a change in the polymeric network of the complex. As the ligands around the metal atom are not very closely packed, the steric effect of the 2-methyl group of the ligand is not very strong, although the 2,6-dimethylpyridine adduct has a very different skeleton due to the stronger steric effect of the methyl groups.

In cases of the Cu(SCN)L_2 type complex,[18] all of the α-, β-, and γ-pic adducts have one-dimensional polymeric structures, where each metal atom is tetra-coordinated and each pair of the metal atoms are bridged by one SCN ion. Their space groups and the *Z* numbers are different from each other. The polymeric chain of the α-pic adduct is in a zig-zag form, while the chains of the β- and γ-pic adducts have a quasi-mirror plane parallel to the chain line; the structures of the latter two resemble each other. As was discussed by the authors,[18] the steric hindrance of the 2-methyl group is important and, consequently, only the α-pic adduct has a very different type of structure. As the single SCN chain of the type of adduct is easily deformed, the most closely packed, as well as energetically the most stable arrangement, is attained mainly by the deformation of the chain.

On the other hand, in cadmium thiocyanate adducts, the double SCN ion chain is very rigid and is always oriented approximately along one direction. To attain the closest packed and the most stable arrangement, only a deviation of the ligand molecule direction and/or a twisting of the chain are allowed. Therefore, the effect of the interaction between the ligands is rather likely to be dominant, as mentioned in the former part of this paper. The steric effect of the 2-methyl group is not the strongest one, though there is some; this is because the stable double SCN chain is not able to be deformed by the approach of a methyl group.

References

1) M. Cannas, G. Carta, A. Christini, and G. Marongiu, *J. Chem. Soc., Dalton Trans.*, **1976**, 300.

2) Von G. Thiele and D. Messer, *Z. Anorg. Allgem. Chem.*, **421**, 24 (1976).

3) L. R. Groenveld, G. Vos, C. Verschoor, and J. Reedijk, *J. Chem. Soc., Chem. Commun.*, **1982**, 620.

4) M. Cannas, G. Carta, A. Christini, and G. Marongiu, *Inorg. Chem.*, **16**, 228 (1977).

5) L. Cavalca, M. Nardelli, and G. Fava, *Acta Crystallogr.*, **13**, 125 (1960).

6) J. G. Haasnoot, G. C. M. de Keyzer, and G. C. Verschoor, *Acta Crystallogr., Sect. C*, **39**, 1207 (1983).

7) R. G. Goel, W. P. Henry, M. J. Olivier, and A. L. Beauchamp, *Inorg. Chem.*, **20**, 3924 (1981).

8) M. Taniguchi, M. Shimoi, and A. Ouchi, *Bull. Chem. Soc. Jpn.*, **59**, 2299 (1986).

9) I. S. Ahuja and A. Garg, *J. Inorg. Nucl. Chem.*, **34**, 1929 (1972).

10) "Universal Crystallographic Computation Program System (UNICS)," ed by T. Sakurai, Crystallographic Society of Japan, Tokyo (1967).

11) "International Tables for X-Ray Crystallography," Kynoch Press, Birmingham (1974), Vol. IV, pp. 72, 150.

12) The final F_o—F_c tables, the final thermal parameters of the non-hydrogen atoms, and some bond lengths and angles data are deposited as Document No. 8725, at the office of the Editor of Bull. Chem. Soc. Jpn.

13) The numbering scheme of the methylpyridine ligands are as follows: the ring carbon atom next to the N(*n*1) (*n*=1—4) is numbered as C(*n*1), and the other carbon atoms are numbered in succession from n1 to n5 and the C(*n*5) atom is bonded with the N(*n*1) atom. The methyl carbon atom of the ligand is numbered as C(*n*6). Each hydrogen atom is numbered by the same one as the bonded carbon atom.

14) M. Taniguchi and A. Ouchi, *Bull. Chem. Soc. Jpn.*, **60**, 1192 (1987).

15) Y. Kuniyasu, Y. Suzuki, M. Taniguchi, and A. Ouchi, *Bull. Chem. Soc. Jpn.*, **60**, 179 (1987).

16) Unpublished data: $Cd(SCN)_2py_2$ is triclinic, with the space group of $P\bar{1}$, a=9.512(2), b=27.357(10), c=9.515(2) Å^3, α=107.00(3), β=112.47(2), γ=79.19(3)°, U=2180 Å^3, Z=6. The chain is probably laid along the b-axis or some such long axis direction.

17) N. K. Mills and A. H. White, *J. Chem. Soc., Dalton Trans.*, **1984**, 229.

18) P. C. Healy, C. Pakawatchai, R. I. Papasergio, V. A. Patrick, and A. H. White, *Inorg. Chem.*, **23**, 3769 (1984).

 © 1987 The Chemical Society of Japan Bull. Chem. Soc. Jpn., 60, 1327—1332 (1987)

Simultaneous Determinations of Inorganic and Organic Acids by Ion Chromatography

Hisaaki ITOH* and Yoshio SHINBORI
Faculty of Pharmaceutical Sciences, Josai University, Sakado, Saitama 350-02
(Received September 13, 1986)

The elution behavior of seven common inorganic anions (F^-, Cl^-, NO_2^-, Br^-, NO_3^-, SO_4^{2-}, and phosphate) and a large number of organic acids in an AS-5 separator column using a weak carbonate eluent was examined and the possibility of simultaneous determinations of the inorganic and organic acids in a single injection was investigated. For pharmaceutical samples, such as a Ringer's solution which contains some inorganic anions and a single organic anion as anion contents, each anion could be simultaneously analyzed with a relative standard deviation of below 0.6%. Furthermore, it was found that even in a sample such as the liquor of canned goods having a complex matrix, both inorganic and dicarboxylic acid contents could be simultaneously analyzed without any tedious pretreatment, except for a simple dilution with distilled and deionized water. For the liquor samples, the relative standard deviation for five measurments was less than 5.0%.

Ion chromatography, first described in 1975,[1] has become a widely used analytical technique for the determination of ionic species in aqueous samples.[2-14] Today, based on the developments of column technology and a detection system, many separator columns with different selectivities and detection systems have been made available commercially. It should also be noted that with the spread of the application area and an increased need to analyze samples having complex matrices, the key point of success of an analysis primarily depends upon the best selection of a combination of the separator column and the detection mode.

An AS-5 separator column, which was packed with poly(styrene-divinylbenzene) copolymer base pellicular ion exchange resins (particle size: 15 μm), is one type of anion separator column that is commercially available from Dionex (California, USA). It makes it possible to rapidly and sensitively analyze such anions as I^-, SCN^-, and CrO_4^{2-},[15] which have relatively high affinities on the resins, using a mixed solution of *p*-hydroxybenzonitrile, sodium carbonate, and sodium hydrogencarbonate (0.8, 4.4, and 5.4 in mmol dm^{-3}, respectively) as the eluent and conductivity detection. Furthermore, it should be noted that this separator can also be used for the separation of common inorganic anions (except for nitrate and bromide ions) by using a weak eluent such as 2.5 mmol dm^{-3} sodium carbonate/0.25 mmol dm^{-3} sodium hydrogencarbonate.

In previous papers we described both the elution behavior of seven common inorganic anions in AS-1[16] and AS-4[17] separator columns by using carbonate-hydrogencarbonate as the eluent as well as the separation characteristics of many organic acids in an ICE separator column[18,19] using carbonic acid as the eluent and its application to the determination of valproic acid in drugs and patient plasma.[20] The present paper describes the elution behavior of seven common inorganic anions and a large number of organic acids in an AS-5 separator column using a weak carbonate-hydrogencarbonate eluent and its application to simultaneous determinations of inorganic and organic acids in various pharmaceuticals and canned goods.

Experimental

Materials. All reagents used were of reagent grade. All inorganic anion standard solutions were prepared by dissolving the corresponding sodium salts in distilled and deionized water. Organic acid standard solutions were also prepared by dissolving the acid or the corresponding alkali salts in distilled and deionized water, and/or dissolving the acid in aliquots of 1 mol dm^{-3} NaOH solution and then diluting with distilled and deionized water. The active carbon for the chromatograph was from commercial sources and was used after a pretreatment: wash with 1-propanol by means of a Soxhlet extractor for 3 h, filter using suction rinsing with distilled and deionized water, then dry in an electric drier oven at 150 °C for 24 h.

Chromatographic System. A Dionex Model 2000i ion chromatograph equipped with an AG-5 guard column, an AS-5 anion separator column, an AFS-1 anion fiber suppressor, and a conductivity detector was used. In applications to canned-good samples, a UVIDEC-100-VI variable UV-VIS detector (Japan Spectroscopic Co., Ltd.) was also used in series between the separator column and the suppressor. A sample loop with a volume of 50 mm^3 was used. For conductivity suppression, a 0.0125 mol dm^{-3} H_2SO_4 solution was used with a flow rate of c.a. 3 $cm^3 min^{-1}$ for all the eluent solutions used. The column temperature was not regulated but the eluent solution temperature was regulated by immersing the eluent reservoir into a water bath controlled at 25 °C. Chromatograms were recorded by the use of a Pantos U-228 dual-pen recorder.

Results and Discussion

Elution Behavior of Inorganic Anions. Figure 1 exemplifies a chromatogram of seven common anions obtained by using a 2.5 mmol dm^{-3} Na_2CO_3/0.25 mmol dm^{-3} $NaHCO_3$ solution as the eluent. Figure 2 shows the variation in the retention time of seven common anions with a change of the pH of the eluent solution; this was obtained by changing the composition of sodium carbonate/sodium hydrogencarbonate. However, the total concentration of the eluent was held constant at 2.75 mmol dm^{-3}. It can be seen that

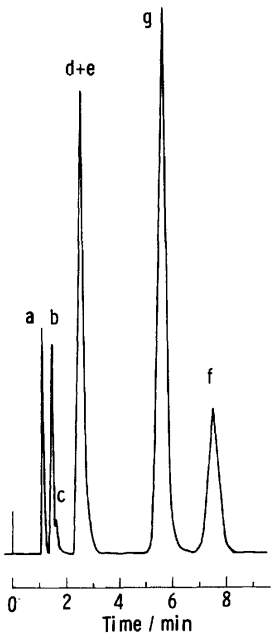

Fig. 1. A typical chromatogram of common seven anions. Column: AS-5 separator column with AG-5 guard column; eluent: 2.5 mmol dm^{-3} Na_2CO_3/0.25 mmol dm^{-3} $NaHCO_3$; flow rate: 2.0 cm^3 min^{-1}; anion fiber suppressor regenerant: 12.5 mmol dm^{-3} H_2SO_4 solution at c.a. 3 cm^3 min^{-1}; detection: conductivity at 30 μS FS; Peak notation: a=fluoride, b=chloride, c=nitrite, d=bromide, e=nitrate, f=phosphate, g=sulfate.

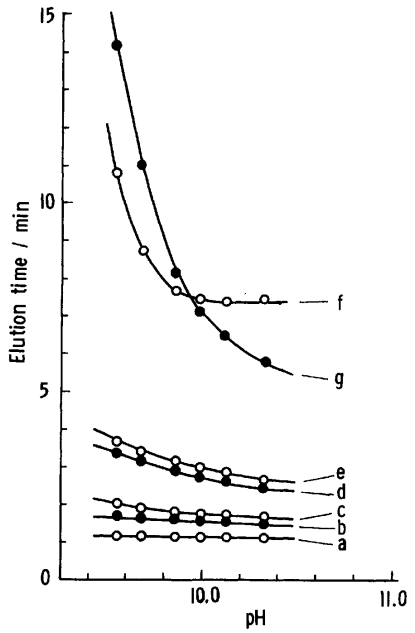

Fig. 2. Variations in the retention time of common seven anions with pH of the eluent solution. All chromatographic conditions except for eluent composition are the same as shown in Fig. 1. The total concentration of the eluent was held constant at 2.75 mmol dm^{-3}.

the effect of the pH of the eluent solution on the retention time of polyvalent ions (SO_4^{2-} and phosphate) is much greater than that of monovalent ions (Cl^-, Br^-, and NO_3^-) and that the difference of the retention time between monovalent and polyvalent ions. Thus, the separation of these ions was very good. It should also be noted that the elution behavior of these ions in an AS-5 separator column is fairly different from that in another previously reported separator columns.[16,17]

Table 1. Carboxylic Acids

Acids	Notation	Acids	Notation
Formic	1	Oxalic	11
Acetic	2	Malonic	12
Propionic	3	Succinic	13
Butyric	4	Glutaric	14
Pivalic	5	Adipic	15
Pyruvic	6	Pimelic	16
Levulinic	7	DL-Malic	17
Lactic	8	(*R*,*R*)-Tartaric	18
Glycolic	9	Maleic	19
Crotonic	10	Fumaric	20
		Itaconic	21

Elution Behavior of Organic Acids. Having noticed the observations described above and directing simultaneous determinations of inorganic and organic acids, the elution characteristics of a large number of organic acids in an AS-5 separator column were investigated.

Table 1 lists the various kinds of carboxylic acids examined. Figure 3 shows the variation in the retention time of carboxylic acids with a change of the pH of the eluent solution. The change of the pH of the eluent solution hardly affected the elution time of the monovalent anions. All of the monocarboxylic acids, regardless of the aliphatic and unsaturated acids (including keto acids), were first eluted for approximately the same elution time as fluoride anion. These results show that since any of the acids examined are fully dissociated in the pH of the eluent solution used, the retention of these ions are based on the eluting power of carbonate ions. Furthermore, these results also imply the possibility of a simultaneous determination of inorganic and carboxylic acids in a single injection.

Applications to the Analysis of Pharmaceuticals. For analytical chemists and analysts who work, especially, in laboratories of pharmaceutical companies and/or in hospitals, measurements of both organic acids and inorganic anions in a single sample solution are among the most frequently encountered determinations from the standpoint quality control. In such case, if possible, it would be the most desirable way for analysts to simultaneously determine both ions in a single measurement without any tedious treatment. The ion chromatography system described in this article offers a simple, rapid, and precise means for such an analysis. The sample preparation required is only a simple dilution with distilled and deionized water.

Figure 4 shows a typical chromatogram of a Rin-

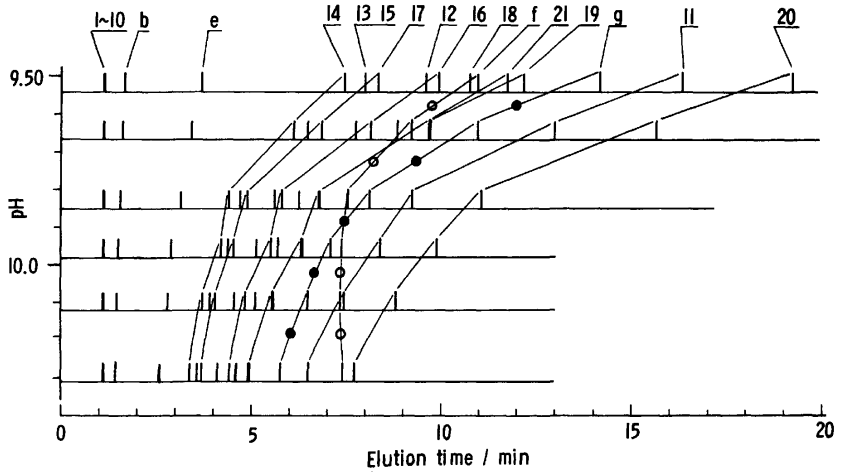

Fig. 3. Variations in the retention time of carboxylic acids with pH of the eluent solution. All chromatographic conditions are the same as shown in Fig. 2. Notations for inorganic and organic anions are the same as shown in Fig. 1 and Table 1, respectively.

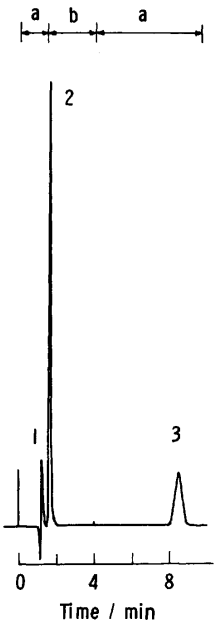

Fig. 4. A chromatogram of a Ringer's solution. All chromatographic conditions except for the eluent composition and the detector range are the same as shown in Fig. 1. Eluent: 1.25 mmol dm^{-3} Na_2CO_3/ 1.50 mmol dm^{-3} $NaHCO_3$ (pH=9.72); detector range: a=10 μS, b=30 μS; peak notation: 1=acetate, 2=chloride, 3=phosphate.

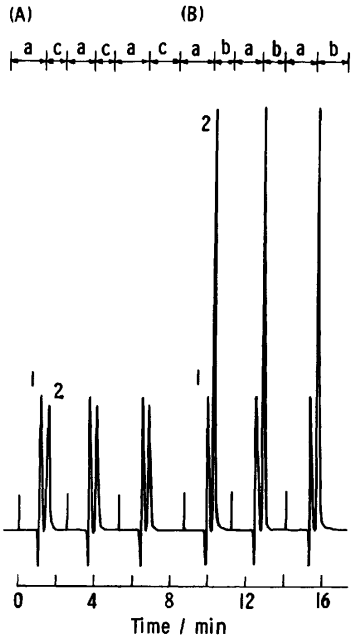

Fig. 5. Chromatograms of a Ringer's solution obtained by the repeated injections. All chromatographic conditions except for the detecor range are the same as shown in Fig. 4. Detector range: a=10 μS; b=30 μS; c=100 μS; Peak notation: 1=lactate, 2=chloride.

ger's solution which contains acetate, chloride, and phosphate as anion components. The detector range was switched from 10 to 30 μS immediately after the elution of an acetate peak and then again to 10 μS at 4 min after injection. Figure 5 also shows chromatograms obtained by repeated injections of a Ringer's solution, which contains lactate and chloride as anion components. In this case, the detector range was also switched from 10 to 100 μS (A) and to 30 μS (B) immediately after the elution of an lactate peak. The analytical results are summarized in Table 2. The determination of each ion was performed by comparing its peak height with that of a standard. The relative standard deviation of all ions in five measurements was less than 0.6%. These results probably indicate that the present system is effectively applicable for a simultaneous determination of organic and inorganic anions in such a routine analysis of pharmaceutical samples as a Ringer's solution.

Applications to the Analysis of the Liquor of Can-

Table 2. Analytical Results for Ringer's Solutions

Sample	Content (mmol dm^{-3})[a] Cl$^-$ (45)		Acetate (20)	$H_2PO_4^-$(10)	Sample	Content (mmol dm^{-3})[a] Cl$^-$ (108)		Lactate (28)
	30 μS[b]	100 μS[b]	10 μS[b]	10 μS[b]		30 μS[b]	100 μS[b]	10 μS[b]
	45.0	45.1	19.7	10.0		108.7	108.5	28.1
	45.0	44.9	19.6	10.0		109.6	108.7	28.0
A[c]	45.3	44.7	19.6	10.1	B[g]	109.3	107.9	28.2
	45.5	44.9	19.8	10.1		109.0	108.5	28.2
	45.1	44.7	19.7	10.0		109.6	108.7	28.4
Mean[d]	45.1_8	44.8_6	19.6_8	10.0_4	Mean[d]	109.2_4	108.4_6	28.1_4
S.D.[e]	0.2_2	0.1_7	0.0_8	0.0_5	S.D.[e]	0.3_9	0.2_8	0.1_7
R.S.D.[f] (%)	0.5	0.4	0.4	0.5	R.S.D.[f] (%)	0.4	0.3	0.6

a) Values indicated in the content table. b) Detector range used. c) ×200 dilution. d) Mean value. e) Standard deviation. f) Relative standard deviation. g) ×500 dilution.

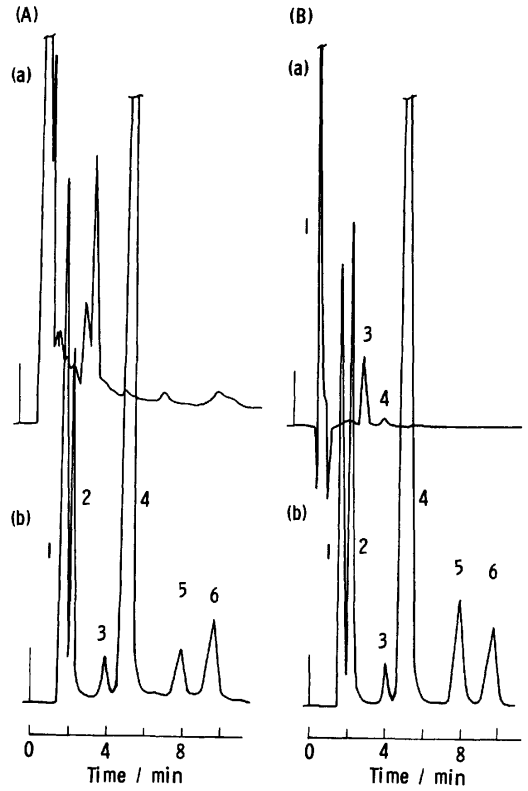

Fig. 6. Chromatograms of the liquor of a canned watermelon. All chromatographic conditions except for the detector range of the conductivity monitor, flow rate, and the use of UV detector are the same as shown in Fig. 1. Detector range of conductivity detector: 10 μS; flow rate: 1.5 cm^3 min^{-1}; UV detector: 235 nm, 0.01 AU. Peak notation: 1=monocarboxylate, 2=chloride, 3=nitrate, 4=malate, 5=sulfate, 6=phosphate.

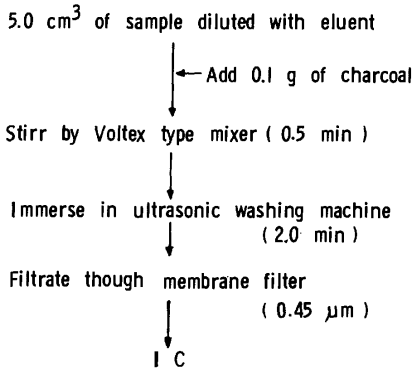

Fig. 7. A sample pretreatment procedure.

ned Goods. A Ringer's solution is a typical example having a clean matrix. However, it is more general for one to have to analyze ionic species in a sample having a complex matrix. In order to estimate the applicability of the present system to an analysis of a sample having a complex matrix, the analysis of anions in the liquor of canned goods was attempted.

Figures 6(A) and 9(A) show typical chromatograms of the liquor of canned watermelons and peachs, respectively, that were diluted with distilled and deionized water and then injected into the sample loop of the chromatograph through a membrane filter (Millipore, HA type, 0.45 μm). In these figures, chromatograms (a) and (b) were obtained by monitoring with a UV detector at 235 nm and a conductivity detector at 10 μS, respectively. In both chromatograms (b) of Figs. 6(A) and 9(A), an identification of each peak is possible by comparing their retention times with those of standard anions (as shown in each figure). However, since both chromatograms (a) in Figs. 6(A) and 9(A) show relatively complex profiles (notably, in the former, the nitrate peak is eluted as an adjacent one to a relatively large unknown one which does not show any clear peak at the corresponding retention time in the chromatogram (b)), a sample pretreatment was attempted in order to confirm the response of each ion in the conductivity detector and the assignment of each peak in chromatogram (b).

After considerable exploratory experiments using Amberlite XAD-2 and XAD-4 resins (Rohm & Haas Co.), Dowex 50W-X8 resin (200—400 mesh, Dow Chemical Co.), SEP-PAK® C_{18} cartridges (Waters Associates), Darco G-60 (active carbon, Darco Dept., Atlas Powder Co.), and active carbon for a chromatograph (Wako Pure Chemical Industries Ltd.), the sample pretreatment procedure using active carbon for a chroma-

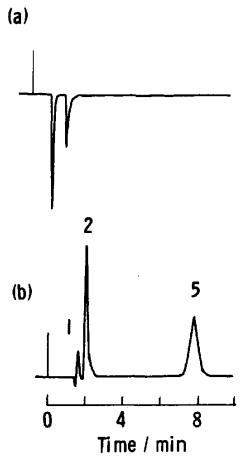

Fig. 8. A typical chromatogram of a blank solution prepared by following the pretreatment procedure using the eluent solution only. All chromatographic conditions and peak notations are the same as shown in Fig. 6.

tograph was determined (Fig. 7).

Although the active carbon was pretreated (described in the experimental section), a blank solution prepared by following a pretreatment procedure using only an eluent solution showed three peaks; this corresponds to the retention time of monocarboxylate, chloride, and sulfate ions (Fig. 8). However, in this experiment, no further pretreatment of the active carbon was performed since the reproducibility of the peak heights of these peaks were extremely good and no other peaks were observed. Furthermore, in this procedure, a liquor of canned goods was diluted with an eluent solution in the place of distilled and deionized water since a decrease of about 30—50% in the peak height of each peak obtained by the conductivity detector before and after the pretreatment procedure was observed when a liquor of canned goods was diluted with distilled and deionized water. However, diluting with an eluent solution resulted in no decrease in the peak height of each peak (as shown below).

Figure 6(B) shows typical chromatograms of liquor of a canned watermelon prepared by following the pretreatment procedure. Chromatogram (a) clearly shows three peaks which can be assigned to monocarboxylate (unidentified), nitrate, and malate ions, respectively. On the other hand, chromatogram (b) shows no changes in the elution profile of nitrate, malate, and phosphate peaks; however, by excluding the first eluted peak, only an increase of the peak heights of the chloride and sulfate peaks (which correspond to the peak height of each ion observed in Fig. 8) can be observed. This means that by the presence of the eluent, any loss of malate and inorganic anions in the sample solution could not be observed before and after the pretreatment procedure. Moreover, it was confirmed that peak 3 of chromatogram (b) in Fig. 6(B) as well as in Fig. 6(A) was based only on a nitrate ion, by

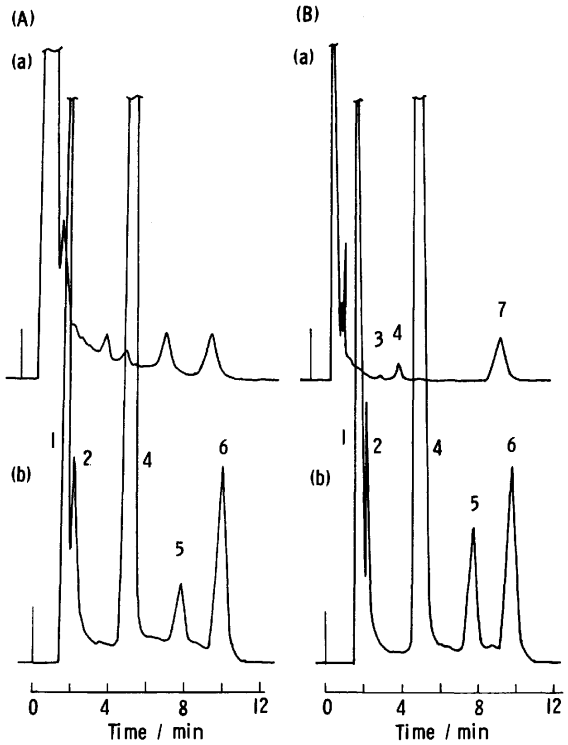

Fig. 9. Chromatograms of the liquor of a canned peach. All chromatographic conditions and peak notations except for fumarate ion are the same as shown in Fig. 6. Peak notation: 7=fumarate.

comparing the response of the sample with that of a standard nitrate ion obtained from both UV and conductivity monitors. Finally, these results indicate that by using a conductivity detector chloride, nitrate, malate, sulfate, and phosphate ions in the liquor of a canned watermelon can be simultaneously analyzed without any tedious pretreatment, except for simple dilution with distilled and deionized water and/or an eluent solution.

Figure 9(B) shows chromatograms of a liquor of canned peachs, prepared by following the pretreatment procedure. In chromatogram (a) obtained from a UV monitor, three peaks can be assigned to nitrate, malate, and fumarate ions, respectively. On the other hand, chromatogram (b), obtained from the conductivity monitor, did not show any changes of the elution profile, except for an increase in the peak heights of chloride and sulfate peaks. In addition, although fumarate and phosphate ions are eluted at the extremely near position, it can be concluded that peak 6 of chromatogram (b) in Fig. 9(B) as well as in Fig. 9(A) is based on only phosphate ions since fumarate ion shows no response for the conductivity detector at 10 μS in the concentration level observed.

The analytical results are summarized in Table 3. The concentration of the fumarate ion in the liquor of canned peach was determined by comparing its peak height with that of standard fumarate ion obtained from the UV monitor. The relative standard deviation

Table 3. Analytical Results for Liquors of Canned Goods[a)]

Ions	Peach[b)]		Watermelon[b)]	
	Mean[c)]±S.D.[d)]	R.S.D.[e)]	Mean[c)]±S.D.[d)]	R.S.D.[e)]
Cl^-	<10[f)]		44.3± 2.2	5.0
NO_3^-	Trace		18.0± 0.2	1.1
Malate	1940 ±51	2.6	1570 ±45	2.8
SO_4^{2-}	38.0± 0.4	1.0	22.4± 0.5	2.2
Phosphate[g)]	244 ± 9	3.7	105 ± 4	3.8
Fumarate[h)]	7.4± 0.3	4.0	—	—

a) In $mg\,dm^{-3}$, the concentration of the original liquor. b) ×20 dilution. c) Mean value. d) Standard deviation. e) Relative standard deviation (%). f) Estimated by assuming the response based on chloride ion only. g) As HPO_4^{2-}. h) Estimated from UV detector response.

of all ions in five measurements was less than 5.0%.

These results indicate that the present system, using a conductivity detector and/or, if necessary, combined with a UV detector, an AS-5 separator column, and a dilute sodium carbonate sodium hydrogencarbonate solution as eluent, is also applicable to a simultaneous determination of dicarboxylic acids and inorganic anions in such samples having complex matrices as the liquor of canned goods. Furthermore, it should be noted that the pretreatment procedure developed in this study is a useful technique for further application studies.

The authors wish to express their thanks to Professor Shigero Ikeda of Osaka University for his helpful discussion.

References

1) H. Small, T. S. Stevens, and W. C. Bauman, *Anal. Chem.*, **47**, 1801 (1975).
2) J. D. Mulik and E. Sawicki, "Ion Chromatographic Analysis of Environmental Pollutants," Ann Arbor Science, Michigan (1979), Vol. 2.
3) G. Muto and K. Oikawa, "Ion Chromatography," Kodansha Scientific, Tokyo (1983), Chap. 6.
4) R. D. Rocklin and E. L. Johnson, *Anal. Chem.*, **55**, 4 (1983).
5) W. F. Koch, *J. Res. of N.B.S.*, **88**, 157 (1983).
6) R. D. Rocklin, *Anal. Chem.*, **56**, 1959 (1984).
7) K. Hasegawa, H. Hiraki, and M. Miyazaki, *Bunseki Kagaku*, **34**, T71 (1985).
8) H. Nagashima, K. Kuboyama, and K. Ono, *Bunseki Kagaku*, **34**, 381 (1985).
9) H. Honma, K. Suzuki, M. Yoshida, and H. Yanashima, *Bunseki Kagaku*, **35**, 536 (1986).
10) K. Fujimura and M. Tsuchiya, *Bunseki Kagaku*, **35**, T50 (1986).
11) M. Yamamoto, H. Yamamoto, Y. Yamamoto, S. Matzushita, N. Baba, and T. Ikushige, *Anal. Chem.*, **56**, 832 (1984).
12) L. K. Tan and J. E. Dutrizac, *Anal. Chem.*, **58**, 1383 (1986).
13) K. Ohsawa, Y. Yoshimura, S. Watanabe, H, Tanaka, A. Yokota, K. Tamura, and K. Imaeda, *Analytical Science*, **2**, 105 (1986).
14) C. D. Chrswell, D. R. Mroch, and R. Markuszewski, *Anal. Chem.*, **58**, 319 (1986).
15) Product information from Dionex, "High Performance Ion Chromatography Anion Selectivity 5 Column," Aug. (1983).
16) H. Itoh and Y. Shinbori, *Bunseki Kagaku*, **29**, 239 (1980).
17) H. Itoh and Y. Shinbori, *Bunseki Kagaku*, **31**, T39 (1982).
18) H. Itoh and Y. Shinbori, *Chem. Lett.*, **1982**, 2001
19) H. Itoh and Y. Shinbori, *Bull Chem. Soc. Jpn.*, **58**, 3244 (1985).
20) H. Itoh, Y. Shinbori, and N. Tamura, *Bull. Chem. Soc. Jpn.*, **59**, 997 (1986).

 © 1987 The Chemical Society of Japan Bull. Chem. Soc. Jpn., 60, 1333—1336 (1987)

Medium Effects on the Redox Properties of 12-Molybdophosphate and 12-Molybdosilicate

Eiki ITABASHI
Miyagi University of Education, Aoba, Aramaki, Sendai 980
(Received September 20, 1986)

The formal redox potentials of 12-molybdophosphate and 12-molybdosilicate up to the twelve-electron reduction per heteropolymolybdate ion were determined by cyclic voltammetry at a glassy carbon electrode in 50% (v/v) water-organic media containing some inorganic acids. These heteropolymolybdates in the presence of 1,4-dioxane (DO) or tetrahydrofuran (THF) display five two-electron reversible cathodic waves, followed by an irreversible two-electron wave, whereas the same heteropolymolybdates in the presence of 1,2-dimethoxyethane, *N*,*N*-dimethylformamide, acetonitrile, ethanol, or acetone yield five successive redox couples of 2, 2, 2, 4, and $2e^-$ (electrons) each. The eight-electron reduction species of 12-heteropolymolybdates are stabilized by cyclic ethers such as DO or THF. The stabilization of the eight-electron reduction species by the addition of a cyclic ether has been explained by taking into account the adduct formation between the molecules of the cyclic ether and 12-heteropolymolybdate.

Many electrochemical studies of 12-molybdophophoric acid (12-MPA) and related 12-heteropolymolybdates have been carried out in order to make clear the redox properties of a series of mixed valence Mo(V, VI) complexes known as a Kiggin structure. The previous voltammetric and polarographic investigations have shown that 12-MPA as well as 12-molybdosilicic acid (12-MSA) in acidic solutions containing some organic solvents undergoes a series of consecutive two-electron reduction to yield various mixed valence Mo(V, VI) complexes.[1] It seems likely that the first three two-electron redox couples of 12-heteropolymolybdates in acidic solutions containing dioxane (DO) or ethanol (EtOH) are remarkably fast and reversible.[2-6] On further reduction above six electrons, however, different results have been reported concerning the fourth and subsequent redox reactions of 12-heteropolymolybdates in acidic solutions containing DO or EtOH.[2,3]

Tsigdinos and Hallada[2] have shown that 12-MSA in 50% (v/v) water-dioxane solutions containing hydrochloric acid exhibited five two-electron reduction waves. Recently, an identical result was reported on the reduction processes of both 12-MPA and 12-MSA in aqueous dioxane media containing sulfuric acid.[5] On the other hand, Souchay and his colleagues[3] have reported that the reduction processes of both 12-MPA and 12-MSA in 50% (v/v) water-ethanol media containing hydrochloric acid displayed three two-electron waves, and 12-heteropoly acids were not further reduced above six electrons in acidic media containing ethanol.

These results suggest that the redox processes of 12-heteropolymolybdates in acidic solutions are influenced by the nature of organic solvent.

This paper presents some unusual solvent effects on the gradual reduction processes of 12-heteropolymolybdates in acidic solutions containing some organic solvents at a glassy carbon electrode.

Experimental

All electrochemical measurements were carried out with a potentiostat (Fuso Co., Model 311) equipped with a function generator (Fuso Co., Model 321) and a recorder (Riken Denshi Co., Model F-43P). A Tokai glassy carbon disc electrode (GCE) with a geometric surface area of 0.071 cm^2 was employed as a working electrode. The counter electrode was a platinum spiral. The potential of the working electrode was measured against a saturated calomel electrode (SCE).

12-Molybdophosphoric acid was purchased from Alfa Chemical Products Co., and was used as received. 12-molybdosilicic acid was obtained from High Purity Chemical Institute (Saitama). Data reported here for both 12-MPA and 12-MSA refer to the stable α-form.[1] All other chemicals were of analytical reagent grade and were used without further purification. All solutions were made up with twice-distilled water and were deaerated with water-pumped nitrogen. All measurements were performed at 25 °C.

Results and Discussion

12-Molybdophosphoric Acid. Figure 1 shows typical cyclic voltammograms of 12-MPA in 50% (v/v) water-dioxane medium containing 0.5 mol dm^{-3} H_2SO_4. The cathodic sweep up to −0.8 V displays six peaks and one flat wave. The first four cathodic waves are reversible. Each step of these waves shows the following characteristics. The cathodic and anodic peak potentials (E_{pc} and E_{pa}) are invariant with scan rate (v) for v between 10 and 200 mV s^{-1}, and the potential difference $\Delta E_p(=E_{pc}-E_{pa})$ is −(29±2) mV. This corresponds closely to the theoretical value of −29 mV for a Nernstian two-electron wave at 25 °C. The fifth cathodic peak is also invariant with scan rate, however, ΔE_p is −(40±2) mV, and the peak height is approximately half of the first cathodic peak. The potential separation between the fifth cathodic peak and the rising potential of the irreversible wave near −0.45 V is about 50 mV. This result suggests that the potential separation on the successive reductions is so small that the fifth peak is distorted by the following wave. It has been pointed out by Polcyn and Shain[7] that the indi-

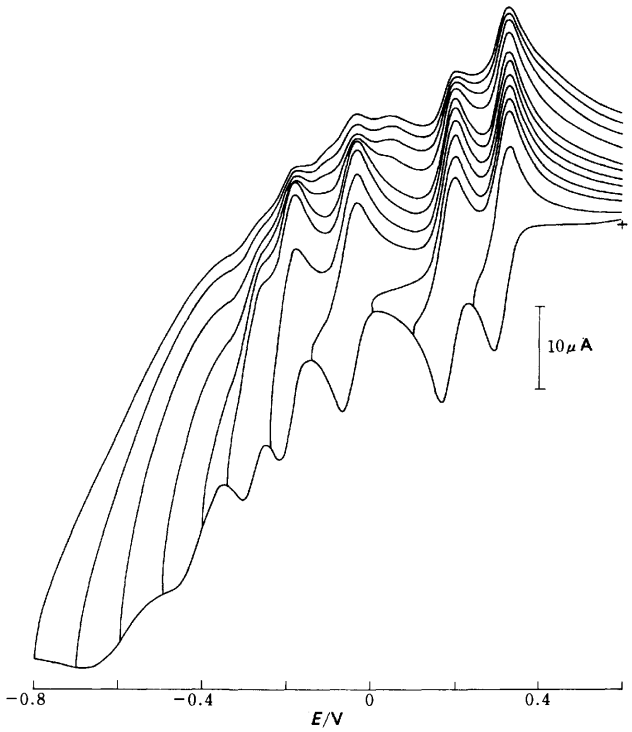

Fig. 1. Cyclic voltammograms of 1×10^{-3} mol dm^{-3} 12-molybdophosphoric acid in 50%(v/v) water-dioxane solution containing 0.5 mol dm^{-3} H_2SO_4 at sweep rate 0.05 V s^{-1}.

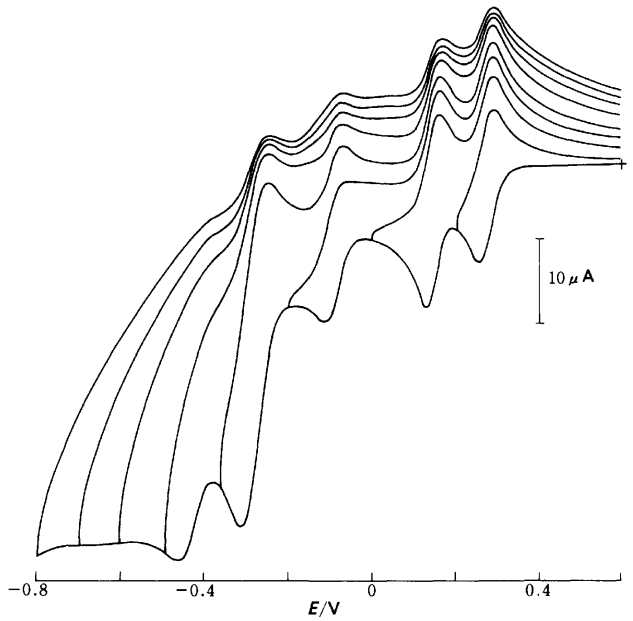

Fig. 2. Cyclic voltammograms of 1×10^{-3} mol dm^{-3} 12-molybdophosphoric acid in 50%(v/v) water-DMF solution containing 0.5 mol dm^{-3} H_2SO_4 at sweep rate 0.05 V s^{-1}.

vidual waves of the stepwise reductions merge into one broad distorted wave whose peak height and shape is no longer characteristic of a reversible wave, as the potential separation between the successive reductions becomes less than about 100 mV n^{-1}, where n is the number of electrons involved in the electrode process. In order that the cyclic voltammograms on the successive reductions behave as independent reversible waves, a certain minimum potential separation of about 118 mV n^{-1} is required.

The first five cathodic waves have been previously assigned to the addition of two electrons for each step.[2,5]

The flat wave near −0.45 V is irreversible. The flat wave increased in height with increase in scan rate, however, it shifted toward more negative potentials, and merged into the broad wave near −0.65 V at scan rates above 200 mV s^{-1}. The height of the flat wave is nearly equal to the first cathodic peak. It is reasonable to infer that the flat wave corresponds to a two-electron process. The broad wave near −0.65 V is also irreversible, and exhibits a plateau current rather than a peak at scan rates above 100 mV s^{-1}. The plot of the current function $i_{pc}v^{-1/2}$ vs. v decreased with increasing scan rate, where i_{pc} was measured from the base current observed in acidic dioxane solution in the absence of 12-MPA. The variation of the current function (i_{pc} $v^{-1/2}$) with scan rate would indicate that the total current function of the broad wave is made up of charge transfer coupled to homogeneous chemical reactions.[8]

A similar cyclic voltammogram with six cathodic peaks and one flat wave was also observed in acidic solutions containing tetrahydrofuran (THF).

On the other hand, 12-MPA in acidic solution containing *N,N*-dimethylformamide (DMF) gives five well-defined cathodic peaks, as shown in Fig. 2. The first three cathodic waves correspond to a two-electron process for each step.[2,5] The fourth step is also reversible, but its peak height is approximately 2.65 times the height of the first cathodic peak. The peak current on the stationary electrode voltammetry is proportional to $n^{3/2}$, where n is the number of electrons involved in the electrode process.[8] If the fourth step corresponds to a four-electron process, the height of the fourth step is $2^{3/2}$ times the height of the first two-electron reversible wave. Accordingly, the fourth step is attributable to a four-electron process. Although the fifth cathodic wave is less reversible than the first cathodic one, the first and fifth cathodic steps have nearly equal height. It is reasonable to assign that the fifth cathodic step slso corresponds to a two-electron process. Similar cyclic voltammograms with five cathodic steps up to −0.80 V were observed in acidified mixed solvents containing 1,2-dimethoxyethane (DME), acetonitrile (MeCN), EtOH, or acetone. A four-electron transfer process on the one-step has been considered to be a phenomenon that appears only rarely, however, the four-electron transfer has been found for the reduction processes of $[X_2Mo_{18}O_{62}]^{6-}$ in acidic solutions, where X is P or As.[1]

The formal redox potential $E_f^{\circ\prime}$ was determined by using the equation $E_f^{\circ\prime}=(E_{pc}+E_{pa})/2$. These data are summarized in Table 1.

Table 1. Voltammetric Characteristics of 12-Molybdophosphoric Acid[a)]

No.	Medium	$E_f^{\circ\prime}$ vs. SCE/V					
		n[b)]=2	4	6	8	10	12
1.	0.5 mol dm^{-3} H_2SO_4, 50%[c)] DO[d)]	+0.315	+0.187	−0.042	−0.189	−0.266	(−0.45s)
2.	0.5 mol dm^{-3} $HClO_4$, 50% DO	+0.317	+0.187	−0.042	−0.191	−0.268	(−0.45s)
3.	0.5 mol dm^{-3} HNO_3, 50% DO	+0.317	+0.187	−0.042	−0.191	−0.267	(−0.46s)
4.	0.5 mol dm^{-3} HCl, 50% DO	+0.304	+0.171	−0.054	−0.200	−0.275	(−0.45s)
5.	0.5 mol dm^{-3} H_2SO_4, 50% THF[e)]	+0.251	+0.173	−0.097	−0.239	−0.285	(−0.44s)
6.	0.5 mol dm^{-3} H_2SO_4, 50% DME[f)]	+0.248	+0.151	−0.096		−0.276	(−0.44)
7.	0.5 mol dm^{-3} H_2SO_4, 50% DMF[g)]	+0.271	+0.144	−0.092		−0.282	(−0.46)
8.	0.5 mol dm^{-3} H_2SO_4, 50% MeCN[h)]	+0.280	+0.168	−0.066		−0.259	(−0.39)
9.	0.5 mol dm^{-3} H_2SO_4, 50% EtOH[i)]	+0.280	+0.174	−0.070		−0.247	(−0.40)
10.	0.5 mol dm^{-3} H_2SO_4, 50% acetone	+0.256	+0.160	−0.082		−0.263	(−0.43)

a) The concentration of 12-MPA was 1×10^{-3} mol dm^{-3}. b) Number of electrons. c) Vol%. d) 1,4-Dioxane. e) Tetrahydrofuran. f) 1,2-Dimethoxyethane. g) *N,N*-Dimethylformamide. h) Acetonitrile. i) Ethanol. s) Flat cathodic wave. Parentheses indicate the cathodic peak potentials.

Table 2. Voltammetric Characteristics of 12-Molybdosilicic Acid[a)]

No.	Medium	$E_f^{\circ\prime}$ vs. SCE/V					
		n=2	4	6	8	10	12
1.	0.5 mol dm^{-3} H_2SO_4, 50% DO	+0.292	+0.175	−0.047	−0.196	−0.272	−0.48
2.	0.5 mol dm^{-3} $HClO_4$, 50% DO	+0.284	+0.176	−0.043	−0.197	−0.270	−0.42
3.	0.5 mol dm^{-3} HNO_3, 50% DO	+0.286	+0.180	−0.041	−0.195	−0.272	−0.43
4.	0.5 mol dm^{-3} HCl, 50% DO	+0.302	+0.187	−0.035	−0.185	−0.266	−0.39
5.	0.5 mol dm^{-3} H_2SO_4, 50% THF	+0.288	+0.175	−0.091	−0.220	−0.288	−0.38
6.	0.5 mol dm^{-3} H_2SO_4, 50% DME	+0.242	+0.155	−0.086		−0.271	−0.41
7.	0.5 mol dm^{-3} H_2SO_4, 50% DMF	+0.198	+0.138	−0.072		−0.301	−0.52
8.	0.5 mol dm^{-3} H_2SO_4, 50% MeCN	+0.240	+0.171	−0.041		−0.249	−0.34
9.	0.5 mol dm^{-3} H_2SO_4, 50% EtOH	+0.235	+0.157	−0.061		−0.245	−0.34
10.	0.5 mol dm^{-3} H_2SO_4, 50% acetone	+0.235	+0.163	−0.067		−0.274	−0.38
11.	0.5 mol dm^{-3} H_2SO_4	+0.271	+0.156	−0.018		−0.215	−0.38
12.	0.5 mol dm^{-3} $HClO_4$	+0.275	+0.159	−0.015		−0.217	−0.41
13.	0.5 mol dm^{-3} HNO_3	+0.268	+0.155	−0.017		−0.227	−0.47
14.	0.5 mol dm^{-3} HCl	+0.275	+0.162	−0.013		−0.219	−0.47

a) The concentration of 12-MSA was 1×10^{-3} mol dm^{-3}. The abbreviation of the organic solvent is the same as that of Table 1.

12-Molybdosilicic Acid. The same set of experiments was performed for 12-MSA. 12-MSA in acidic solutions containing DO or THF is reduced in six steps. Each step appears to correspond to the addition of $2e^-$ (electrons). Whereas, the same heteropoly acids with DME, DMF, MeCN, EtOH, or acetone present give five cathodic peaks of 2, 2, 2, 4, and $2e^-$ each.

12-MSA is moderately stable for the hydrolytic degradation in acidic solutions even though organic solvent is not present in the solution. Some experiments were carried out in acidic solutions in the absence of organic solvent. 12-MSA in aqueous solutions containing H_2SO_4, HNO_3, or HCl is reduced in five steps of 2, 2, 2, 4, and $2e^-$ each, up to −0.80 V. The formal redox potentials of 12-MSA in acidic solutions with and without organic solvent present are listed in Table 2.

Solvent Effect. In acidic solution alone, 12-MPA undergoes hydrolytic degradation, however, it is stabilized by addition of comparatively large amounts of organic solvent. On the other hand, 12-MSA is stable in acidic media with and without organic solvent present. The most striking aspect of the present work is that the eight-electron reduction species of both 12-MPA and 12-MSA are stabilized by cyclic ethers such as DO or THF, however, they are unstable in the presence of DME, DMF, MeCN, EtOH, or acetone. It seems likely that the dielectric constant of the organic solvent plays an important role in the stabilization of the eight-electron reduction species of heteropolymolybdates. A decrease in dielectric constant of the solvent should be accompanied by a decrease in the dissociation of ionic aggregates such as 12-heteropolymolybdates.

Pure DMF, MeCN, EtOH, and acetone have high dielectric constants, ranging from 20 to 50.[9] For ethers such as DO, THF, and DME, the range of the dielectric constants is about 2—8. Consequently, extensive ionic aggregation and a suppression of reorganization are expected for 12-heteropolymolybdates in acidic mixed solvents containing ethers. In spite of the fact that DME and DO have nearly the same dielectric constants, DO rather than DME in acidic mixed solvents is better suited for stabilizing the eight-reduction species

of 12-heteropolymolybdates. This finding raises the question whether the dielectric constant of the solvent serves to any significant extent for stabilizing heteropoly molybdenum blues in acidic solvents. Ethers employed in the present work have low dipole moments, ranging from 0.5 to 1.7.[9] However, the eight-electron reduction species of 12-heteropolymolybdates is not stabilized in acidic solutions containing DME. The possibility can be ruled out that the dipole moment of the organic solvents plays an important role in the stabilization of the eight-electron reduction species of heteropolymolybdates.

12-MSA in sulfuric acid solutions containing DO or THF is reduced at more positive potentials than that in the same electrolyte solution without organic additive present, as is shown in Table 2. The opposite effect was observed in the presence of DME, DMF, MeCN, EtOH, or acetone. The voltammetric behavior of 12-MSA in sulfuric acid solution containing DME is almost identical to that in the same electrolyte solution containing DMF, MeCN, EtOH, or acetone.

The fact that 12-MSA in acidic solutions containing cyclic ethers is reduced at potentials more positive than the hydrated 12-MSA in acidic solutions in the absence of organic solvents suggests that the cyclic ether stimulates the electroreduction of 12-MSA, and that a specific interaction is involved between 12-MSA and the cyclic ether. Such an interaction should be regarded as the coordination of the cyclic ether to the Mo atoms, or the formation of Lewis acid-base adducts between 12-MSA and cyclic ether. It has been shown that the formal redox potentials of the first three redox couples of 12-MPA in sulfuric acid solutions containing DO shift toward more positive potentials with increase in concentration of DO over the concentration range from 10 to 50% in volume.[4] A solid 12-MSA containing 1,4-dioxane molecules instead of water as a crystallization solvent molecule has been prepared.[2] These results further indicate that a strong solvation force is involved between 12-heteropoly acids and 1,4-dioxane. It seems reasonable to suppose that the cyclic ether acts as a Lewis base even in acidic solutions, since large amounts of ether are present in the electrolyte solutions.

The redox behavior of 12-heteropolymolybdates in acidic media is little influenced by the kind of inorganic acid. It has been shown from the conductivity measurements that hydrochloric acid in water-dioxane mixtures behaves as a strong electrolyte, even up to 70% dioxane.[10] Accordingly, it seems likely that various inorganic acids remain unassociated at the concentration employed in the present work.

References

1) M. T. Pope, "Heteropoly and Isopoly Oxometalates," Springer-Verlag, Berlin (1983), Chap. 4.
2) G. A. Tsigdinos and C. J. Hallada, *J. Less-Comm. Met.*, **36**, 79 (1974).
3) J. P. Launay, R. Massart, and P. Souchay, *J. Less-Comm. Met.*, **36**, 139 (1974).
4) N. Tanaka, K. Unoura, and E. Itabashi, *Inorg. Chem.*, **21**, 2087 (1982).
5) C. Rocchiccioli-Deltcheff, M. Fournier, and R. Franck, *Inorg. Chem.*, **22**, 207 (1983).
6) K. Unoura and N. Tanaka, *Inorg. Chem.*, **22**, 2963 (1983).
7) D. S. Polcyn and I. Shain, *Anal. Chem.*, **38**, 370 (1966).
8) A. J. Bard and L. R. Faulkner, "Electrochemical Methods," John Wily & Sons, New York (1980), Chap. 6.
9) C. K. Mann, "Electroanalytical Chemistry," ed. by A. J. Bard, Marcel Dekker, New York (1969), Vol. 3, pp. 128—129.
10) G. A. Tsigdinos and C. J. Hallada, *Inorg. Chem.*, **9**, 2488 (1970).

 © 1987 The Chemical Society of Japan Bull. Chem. Soc. Jpn., 60, 1337—1341 (1987)

The Thermal Decomposition of Lead *cyclo*-Tetraphosphate

Hiroyuki NARIAI,* Itaru MOTOOKA, Yukio KANAJI,† and Mitsutomo TSUHAKO††
Department of Chemistry, Faculty of General Education, Kobe University, Tsurukabuto, Nada-ku, Kobe 657
†Department of Industrial Chemistry, Faculty of Engineering, Kobe University, Rokkodai-cho, Nada-ku, Kobe 657
††Kobe Women's College of Pharmacy, Kitamachi, Motoyama, Higashinada-ku, Kobe 658
(Received September 25, 1986)

The process of the thermal decomposition of lead *cyclo*-tetraphosphate dihydrate (P_{4m}), $Pb_2P_4O_{12}\cdot 2H_2O$, was investigated using X-ray analysis, DTA-TG, HPLC, Isotachophoresis (IP), and IR spectrometry. P_{4m} lost water of crystallization at about 100 °C. In the region of 150—170 °C, P_{4m} decomposed to form oligo phosphates, and at about 190 °C, oligo phosphates changed to a crystalline material which contained ortho- and triphosphate. At about 300 °C, the crystalline material changed to *cyclo*-octaphosphate (P_{8m}) through a new type of *cyclo*-tetraphosphate (P_{4m}*). However, in the presence of a higher water-vapor pressure than the atmospheric one, the crystalline material changed mainly to the new type of P_{4m}* with a little P_{8m}, while at a low water-vapor pressure, the reverse tendency was observed: mainly P_{8m} and a little P_{4m}*.

It is well-known that upon heating condensed phosphates hydrolyse or condense to form various kinds of phosphates.[1-10] The products obtained are pure phosphates or a mixture of linear and/or cyclic phosphates with different numbers of phosphorus atoms. These reactions are affected by the kind of metal, the degree of dryness in the crystal, the atmosphere, the temperature, and the time and rate of heating, thus resulting in the formation of different phosphates. However, these conditions have not yet been comprehensively examined.

In this work, therefore, the effect of water vapor on the thermal decomposition of lead *cyclo*-tetraphosphate (P_{4m}) was investigated in detail. The higher-membered cyclic phosphates, such as six-membered *cyclo*-tri and eight-membered *cyclo*-tetraphosphate, are very important electrolytes because of their high negative charge on a relatively compact structure.[10] Schülke[11] reported in 1968 that P_{4m} decomposed at about 300 °C to form lead *cyclo*-octaphosphate (P_{8m}). Using metals other than lead, such as alkaline earth metals (Mg, Ca, Sr, and Ba), the present authors have investigated the thermal decompositions of *cyclo*-tetraphosphates. P_{8m} could not be obtained. Further, little is known about the detailed formation conditions; i.e., in the synthesis of P_{8m} by the method of Schülke, the product varies with the degree of the dryness of the sample used and with the method of heating. This may be attributable to the effect of water vapor in the reaction process. In this work, therefore, for the purpose of establishing the optimum conditions for the preparation of P_{8m}, the process of the thermal decomposition of P_{4m} was investigated by means of X-ray analysis, thermal analysis (DTA-TG), high-performance liquid chromatography-flow injection analysis (HPLC-FIA), Isotachophoresis (IP), and IR spectrometry.

Experimental

Chemicals. The lead *cyclo*-tetraphosphate (P_{4m}), $Pb_2P_4O_{12}\cdot 2H_2O$, was prepared by the method given in the literature.[11] Unless otherwise stated, guaranteed reagents were used without further purification.

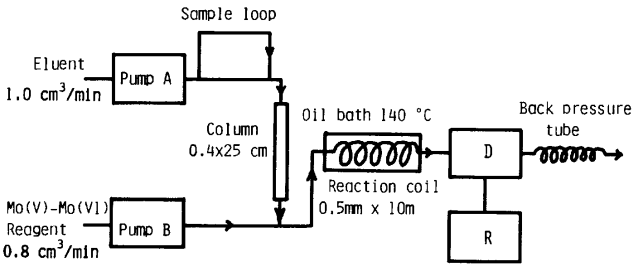

Fig. 1. Flow diagram of chromatograph and detection system. D: detector, R: recorder.

The X-ray diffraction analysis was carried out with a Rigaku Denki Geigerflex diffractometer using nickel-filtered Cu $K\alpha$ radiation. The thermal analysis (DTA-TG) was carried out by means of a Rigaku 8002 SD thermal analyzer. The isotachopherograms were recorded on a Shimadzu IP-2A apparatus equipped with a potential gradient detector (PGD). The operational system and procedure of the isotachophoretic analysis used were as have been described previously.[12-15] The IR spectra were taken by means of a KBr tablet and recorded on a JASCO DS-701G Diffraction Grating Infrared Spectrophotometer.

A diagram of an HPLC-flow injection analysis (FIA) system is shown in Fig. 1. A JASCO TRIROTER V Liquid Chromatograph was used. The sample solution (100 µl) was introduced via a loop-valve sampler onto a separation column and chromatographed at a flow-rate of 1.0 cm^3 min^{-1}. The separations were performed on a column (250×4.0 mm I.D.) packed with a polystyrene-based anion-exchanger (TSK gel SAX, d_p=10 µm, Toyo Soda). The eluents for the chromatographic separation of polyphosphates were comprised of appropriate concentrations of potassium chloride and 0.1% (w/v) Na_4EDTA (pH 10). The Mo(V)-Mo(VI) reagent for the analysis of phosphates was prepared by the method of Lucena-Conde and Prat,[16] and was diluted 10-fold with distilled water. The diluted reagent was merged, at a flow-rate of 0.8 cm^3 min^{-1}, into the stream of the column effluent. The mixed solution was then heated at 140 °C in an oil bath by passing it through 10 m of 2.0×0.5 mm I.D. PTFE tubing. The heteropoly blue complex thus formed was detected at 830 nm in the flow cell. A back-pressure PTFE coil (1.5 m×2.0 mm O.D.×0.25 mm I.D.) was connected to the end coil of the flow-cell outlet to pre-

vent the formation of air bubbles on heating.[17-22]

The sample solutions for HPLC-FIA was prepared as follows. Fifteen-mg portions of samples of phosphates were dissolved in 2 cm^3 of a 1.0 wt% sodium sulfide solution, and the lead sulfide thus precipitated was filtered out. A 1 cm^3 of the filtrate was diluted to 100 cm^3 with distilled water. A 100-μl portions of this solution was used for HPLC-FIA. The insoluble polyphosphate ($P_{high\ poly}$) was determined in the manner described above after decomposition by heating with 3 cm^3 of 1.0 mol dm^{-3} of hydrochloric acid.

The furnace used in the calcination experiments is shown in Fig. 2. The humidity in the furnace was controlled with an Ace Constant-humidity Generator Model AHC-1 (Ace Scientific Laboratory Co., Ltd.) and/or a Heatless Air Drier HF 200-9-30 (Nippon Pure Gas Co., Ltd.). The humidity of the entering air is controlled by passing the air through two water-bubbling towers maintained at the appropriate temperature to give the desired water-vapor pressure. In anhydrous experiments, the air was dried by passage through a molecular-sieve tower. The amounts of water in the dried air detected with a gas detector (GASTEC) were less than 0.1 mg dm^{-3}.

The sample (0.1—0.2 g) was spread on the porcelain boat in a layer less than 1 mm thick to reach, almost instantly, the desired atmosphere.

Results and Discussion

The Thermal Decomposition by DTA-TG at Three Different Atmospheres.

For the purpose of investigating the effect of water vapor upon the thermal-reaction process of P_{4m}, the heating products under atmospheric pressure, reduced pressure, and with a semi-closed cell were compared. Figure 3 shows the DTA-TG curves of P_{4m} at atmospheric pressure. Four endothermic peaks at about 100, 130, 160, and 280 °C, with a weight loss, and two exothermic peaks at about 150 and 190 °C are observed. To clarify these thermal changes at each temperature, the chromatography (HPLC) of the products at 130, 190, 260, and 335 °C, where the thermal changes were completed, was carried out. Figure 4 shows the chromatograms of the products obtained at each temperature. At 130 °C, P_{4m} lost two molecules of water of crystallization. The chromatogram at 190 °C shows that oligo phosphates such as ortho-(P_1), pyro-(P_2), tri-(P_3), and tetraphosphate(P_4) were formed; ring-opening reactions occurred at this temperature, followed by the condensation of these species to form long-chain phosphates. At 260 °C, oligo phosphates were rearranged to P_1 and P_3. Perhaps, they were formed as a double salt. Schülke[11] named the double salt a "crystal compound." The large peak on the chromatogram at about 53 min for the product at 335 °C indicates the formation of P_{8m}. At the same time, the amounts (peak heights) of P_1 and P_3 decreased with the increase in the amount of P_{8m}. The product heated at 600 °C was not dissolved in the sodium sulfide solution, indicating that insoluble polyphosphates ($P_{high\ poly}$) were formed. As is shown in Fig. 5, the rate of the dehydration condensation reaction after ring opening under reduced pressure (about 5 Torr (1 Torr=133.322 Pa)) was faster than that under atmospheric pressure (Fig. 4), with the result that more condensed species, such as penta-(P_5), hexa-(P_6), and heptaphosphate (P_7), was formed in an appreciable abundance. In the 260—335 °C region, P_{4m} formed again; its X-ray pattern was different from that of $Pb_2P_4O_{12}$ prepared by dehydrating $Pb_2P_4O_{12}$.

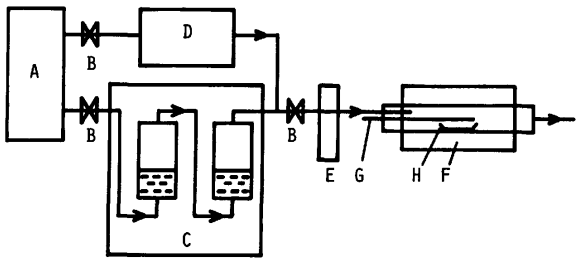

Fig. 2. Diagram of the calcination reactor. A: compressor, B: needle valve, C: constant humidity generator, D: heatless air drier, E: flow meter, F: electric furnace, G: thermocouple, H: sample boat.

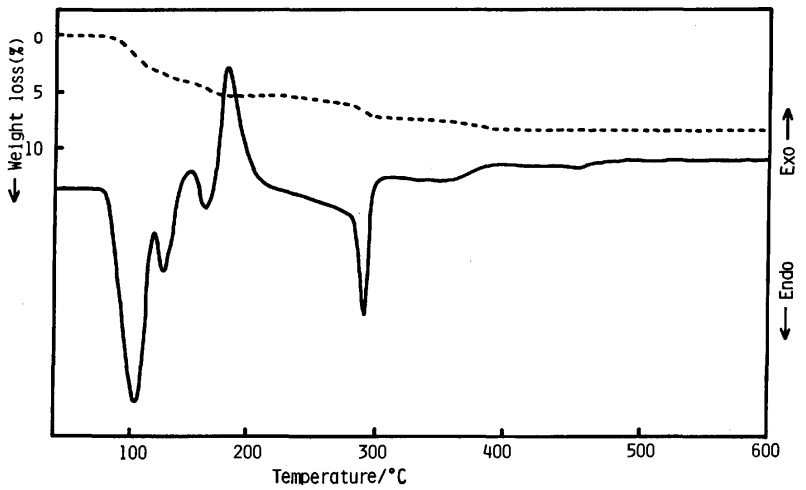

Fig. 3. DTA-TG curves of lead *cyclo*-tetraphosphate. solid line: DTA, dotted line: TG.

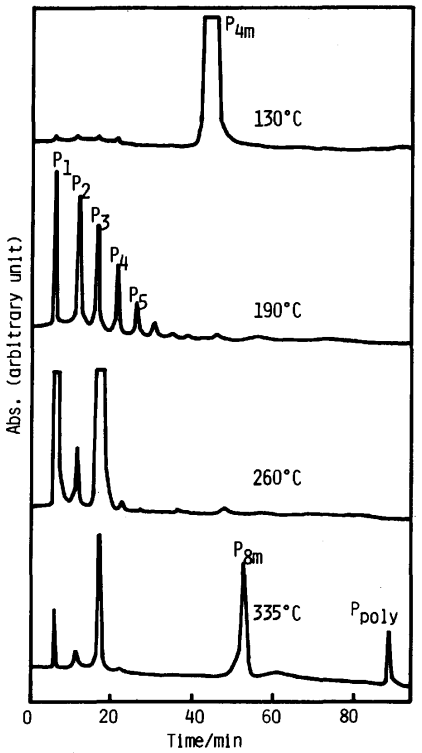

Fig. 4. Chromatograms of the products heated at several temperatures.

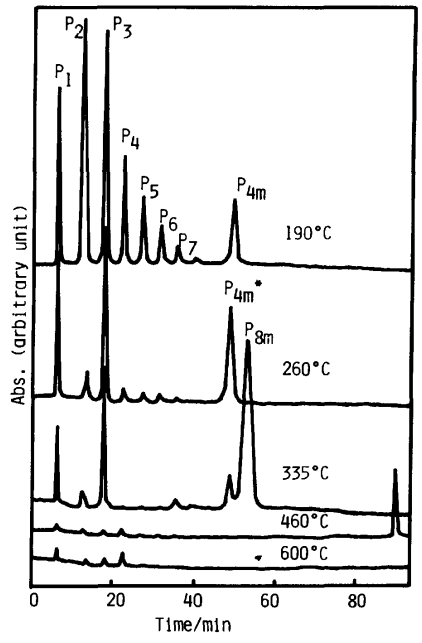

Fig. 5. Chromatograms of the products heated under reduced pressure.

$2H_2O$.

Schülke[11] reported previously that P_{4m} formed again in this temperature range. However, the P_{4m} species formed in the present work had another crystal structure. Further, from the IP[12-15] and IR spectra[23] it was confirmed that the P_{4m} species formed in the present work was cyclic phosphate. This *cyclo*-tetraphosphate is named "high-temperature-type *cyclo*-

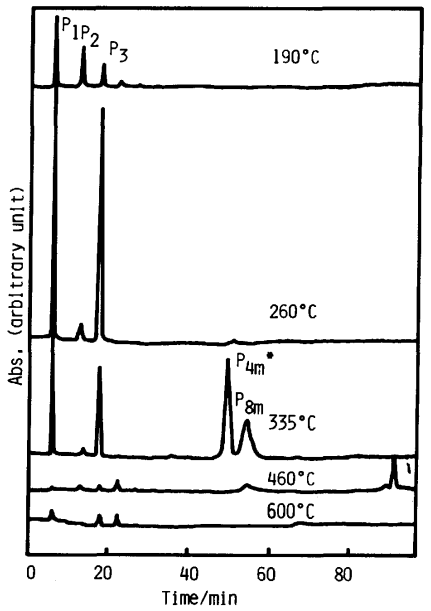

Fig. 6. Chromatograms of the products heated with semi-closed cell.

tetraphosphate (P_{4m}*)." In the case of heating with a semi-closed cell, as is shown in Fig. 6, the hydrolysis proceeded rather faster than the atmospheric pressure. Even at 190 °C, P_{4m} was somewhat changed to P_1, P_2, and P_3. P_{4m} almost entirely turned to P_1 and P_3 at 260 °C. At 335 °C, P_{4m}* was formed, plus a small amount of P_{8m}. Large amounts of the polyphosphates were formed at 460 °C.

Isothermal Change. On the basis of the above results, the effect of water vapor upon the thermal decomposition of P_{4m} was found to be significant; therefore, the influence of water vapor upon thermal decomposition was investigated by means of isothermal heating in an electric furnace at the temperatures of the respective DTA peaks. Figure 7 shows the changes in composition attributable to the calcination time of P_{4m} at 190 °C and at the relative humidities of 0 and 50%. In the case of the relative humidities of 15, 50, and 90%, approximately the same results were obtained. In the 180—200 °C region, a crystalline material containing components of P_1 and P_3 (molar ratio=ca. 1 : 1) was formed under a 15—90% relative humidity (at 25 °C). In a dry-air atmosphere (r.h.=0%), this crystalline material was changed to P_{4m}* (about 45% after 30 min). At 260 °C, as is shown in Fig. 8, the crystalline material changed partially to P_{4m}* (about 45%) at a 50% relative humidity; the same results were obtained in the 15—90% range of relative humidity. However, under the dry-air conditions, both P_{8m} and polyphosphates were produced. Moreover, insoluble polymers were formed in a considerable amount (about 70% at the maximum). This fact indicates that, under dry-air conditions, these condensation reactions proceeded more rapidly than under atmospheric conditions. When $Pb_2P_4O_{12}$ anhydride was used as the

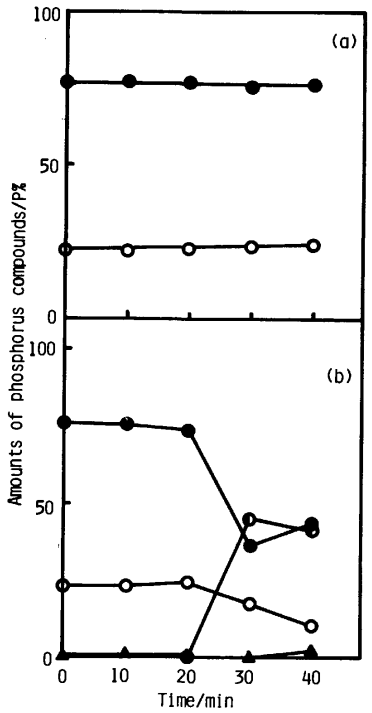

Fig. 7. The changes in composition with calcination time of $Pb_2P_4O_{12}\cdot 2H_2O$ at 190 °C and at various relative humidities. (a): 50%, (b): 0%, —○—: P_1, —△—: P_2, —●—: P_3, —◐—: P_{4m}*.

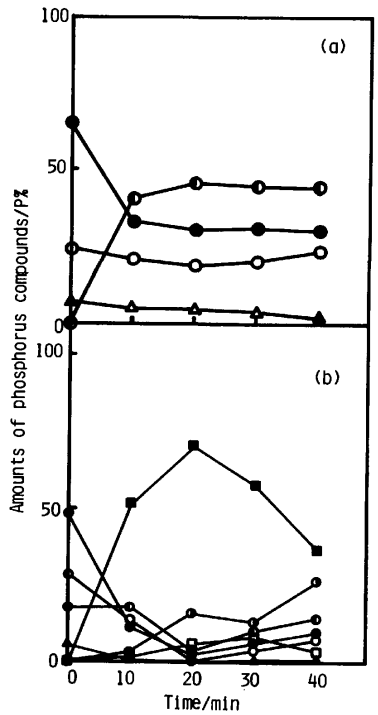

Fig. 8. The changes in composition with calcination time of $Pb_2P_4O_{12}\cdot 2H_2O$ at 260 °C and at various relative humidities. (a): 50%, (b): 0%, —○—: P_1, —△—: P_2, —●—: P_3, —◐—: P_{4m}*, —◑—: P_{8m}, —□—: P_{poly}, —■—: $P_{high\ poly}$.

starting material, similar results were obtained. Therefore, the crystalline material was formed at 260 °C,

Table 1. Changes in the Amounts of Phosphorus Compounds in the Samples Heated at 250 °C at Various Relative Humidities (r.h.) for 40 min (with a crystalline material containing components of P_1 and P_3 as the starting material)

Compound	P_1	P_2	P_3	P_{4m}*	P_{8m}	P_{oligo}
(r.h., %)	%	%	%	%	%	%
0	20.0	4.0	29.4	35.7	10.3	0.6
15	16.0	3.3	37.5	42.8	0	0.4
50	17.3	3.2	37.9	40.6	0	1.0
90	11.9	5.0	52.5	29.0	0	1.6

Table 2. Changes in the Amounts of Phosphorus Compounds in the Samples Heated at 280 °C at Various Relative Humidities (r.h.) for 40 min (with a crystalline material containing components of P_1 and P_3 as the starting material)

Compound	P_1	P_2	P_3	P_{4m}*	P_{8m}	P_{oligo}
(r.h., %)	%	%	%	%	%	%
0	0	0	2.8	5.7	89.3	2.2
15	8.0	1.4	24.2	28.5	37.9	0
50	7.9	0.7	23.9	32.6	34.9	0
90	14.0	3.9	34.0	43.0	4.1	1.0

regardless of the starting material. In the dry-air atmosphere, even at 200 °C, P_{4m}* was already formed in an amount of 46%. As has been mentioned above, a crystalline material containing components of P_1 and P_3 was formed at about 200 °C by means of an exothermic reaction. Whatever the starting material ($Pb_2P_4O_{12}\cdot 2H_2O$ or $Pb_2P_4O_{12}$), the crystalline material was formed. To clarify the effect of the water content in the heating atmosphere at the second endothermic peak, the process of the formation of P_{8m} was investigated using the crystalline material which had been prepared by heating $Pb_2P_4O_{12}\cdot 2H_2O$ at 200 °C for 40 min in an electric furnace. Table 1 shows the changes in the amounts of phosphorus compounds in the samples heated at 250 °C. At 250 °C, a temperature before the endothermic peak (Fig. 3), we expected a remarkable effect of the water vapor upon the formation of P_{8m}. In the dry-air atmosphere (0%), the amounts of P_1 and P_3 decreased, P_{4m}* was formed, and P_{8m} was obtained in about a 10% yield. However, in a 15—90% relative-humidity atmosphere (at 25 °C), P_{4m}* increased with the decrease in P_1 and P_3, while P_{8m} was not formed at all. Further, at 280 °C and at a 0% relative humidity atmosphere, as is shown in Table 2, the amount of P_{8m} reached about 90%, and at a 15—50% relative humidity (at 25 °C), that of P_{8m}, 35—38%. In the dry-air atmosphere, P_1 and P_3 decreased, while, in turn, P_{4m}* was formed, followed by the formation of P_{8m} in fairly large quantities. However, in a 90% relative humidity, P_1 and P_3 remained in fairly large quantities, resulting

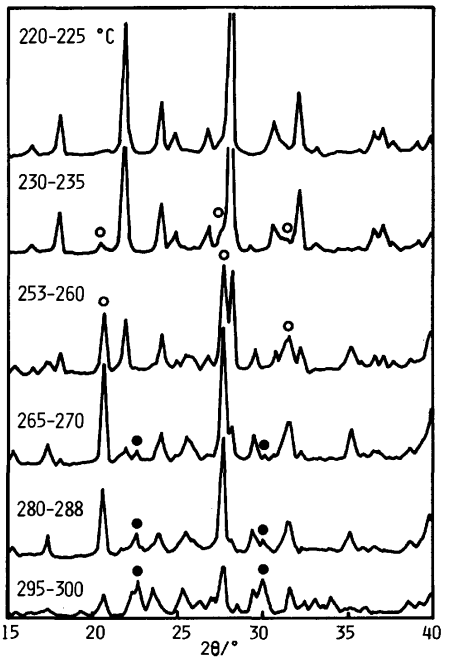

Fig. 9. X-Ray diffraction patterns of products on heating. O: P_{4m}*, ●: P_{8m}.

in the formation of P_{4m}* in a large quantity, and a little P_{8m} was formed.

The process of the thermal decomposition of lead *cyclo*-tetraphosphate under several humid atmospheres may be summarized schematically as follows:

1) $Pb_2P_4O_{12}\cdot 2H_2O$ as the starting material.

$$Pb_2P_4O_{12}\cdot 2H_2O \underset{\text{dry and r.h.}=15-90\%}{\overset{100℃}{\rightleftharpoons}} Pb_2P_4O_{12} \xrightarrow{150-170℃} P_{oligo}$$

$$\xrightarrow[\text{r.h.}=15-90\%]{180-200℃} P_1 + P_3 \xrightarrow{260℃} P_1 + P_3, P_{4m}^*$$

$$\xrightarrow[\text{dry}]{180-200℃} P_1 + P_3 \ll P_{4m}^* \xrightarrow{260℃} P_{8m}, P_{\text{high poly}}$$

2) P_1+P_3 as the starting material.

$$P_1 + P_3 \xrightarrow[\text{r.h.}=90\%]{250℃} P_1 + P_3 > P_{4m}^* \xrightarrow{280℃} P_1 + P_3, P_{4m}^*$$

$$P_1 + P_3 \xrightarrow[\text{r.h.}=15-50\%]{250℃} P_1 + P_3, P_{4m}^* \xrightarrow{280℃} P_1 + P_3, P_{4m}^*, P_{8m}$$

$$P_1 + P_3 \xrightarrow[\text{dry}]{250℃} P_1 + P_3, P_{4m}^* > P_{8m} \xrightarrow{280℃} P_{8m} \gg P_{4m}^*$$

P_1+P_3: crystalline material. The symbols>and≫show the quantitative relations between the products.

X-Ray Analysis on Heating P_{4m}. In order to clarify the facts presented above, X-ray measurements were performed. Figure 9 shows the X-ray diffraction patterns of $Pb_2P_4O_{12}\cdot 2H_2O$ at several stages of heating in an electric furnace attached to the X-ray diffractometer. In the 200—225 °C region, P_1 and P_3 remained unchanged. At 230—235 °C, the characteristic diffraction lines of P_{4m}* at 2θ=20.6 and 27.7° began to appear; they gradually increased with the heating temperature. The X-ray diffraction pattern at 265—270 °C showed P_{4m}*, the diffraction lines of P_1 and P_3 became very small, and small peaks of P_{8m} began to appear. At 280—288 °C, the peaks of P_1 and P_3 disappeared and P_{4m}* began to form (or the peaks of P_{4m}* began to be recognized). At the same time, the peaks of P_{8m} also increased. At 295—300 °C, the peaks of the diffraction pattern are those of P_{4m}* and P_{8m}. The peaks of P_{8m} appeared distinctly with the temperature. These results confirmed that the crystalline material changes to P_{8m} through P_{4m}*. The optimum conditions for preparing P_{8m} are as follows. It is desirable to have a low water-vapor pressure when P_1 and P_3 condense to P_{8m} through a new type, P_{4m}*, at about 300 °C.

The authors wish to thank Mr. Nobuyuki Tada for his helpful work.

References

1) S. L. Friess, *J. Am. Chem. Soc.*, **74**, 4027 (1952).
2) J. D. McGilvery and A. E. Scott, *Can. J. Chem.*, **32**, 1100 (1954).
3) J. R. Van Wazer and E. Karl-Kroupa, *J. Am. Chem. Soc.*, **78**, 1772 (1956).
4) J. F. McCullough, J. R. Van Wazer, and E. J. Griffith, *J. Am. Chem. Soc.*, **78**, 4528 (1956).
5) R. P. Langguth, R. K. Osterheld, and E. Karl-Kroupa, *J. Phys. Chem.*, **60**, 1335 (1956).
6) E. Thilo and U. Schülke, *Z. Anorg. Allg. Chem.*, **341**, 293 (1965).
7) E. J. Griffith and R. L. Buxton, *Inorg. Chem.*, **4**, 549 (1965).
8) M. Watanabe, S. Sato, and H. Saito, *Bull. Chem. Soc. Jpn.*, **48**, 896 (1975).
9) M. Watanabe, M. Matsuura, and T. Yamada, *Bull. Chem. Soc. Jpn.*, **54**, 738 (1981).
10) G. Kura, *Bull. Chem. Soc. Jpn.*, **56**, 3769 (1983).
11) U. Schülke, *Z. Anorg. Allg. Chem.*, **360**, 231 (1968).
12) T. Yagi, K. Kojima, H. Nariai, and I. Motooka, *Bull. Chem. Soc. Jpn.*, **55**, 1831 (1982).
13) H. Nariai, K. Nakazaki, M. Tsuhako, and I. Motooka, *J. Chromatogr.*, **248**, 135 (1982).
14) I. Motooka, H. Nariai, K. Nakazaki, and M. Tsuhako, *J. Chromatogr.*, **260**, 377 (1983).
15) I. Motooka, H. Nariai, K. Nakazaki, and M. Tsuhako, *J. Chromatogr.*, **295**, 533 (1984).
16) F. Lucena-Conde and L. Prat, *Anal. Chim. Acta*, **16**, 473 (1957).
17) Y. Hirai, N. Yoza, and S. Ohashi, *Anal. Chim. Acta*, **115**, 269 (1980).
18) Y. Hirai, N. Yoza, and S. Ohashi, *Bunseki Kagaku*, **30**, 465 (1981).
19) Y. Baba, N. Yoza, and S. Ohashi, *J. Chromatogr.*, **318**, 319 (1985).
20) Y. Baba, N. Yoza, and S. Ohashi, *J. Chromatogr.*, **348**, 27 (1985).
21) Y. Baba, N. Yoza, and S. Ohashi, *J. Chromatogr.*, **350**, 119 (1985).
22) Y. Baba, N. Yoza, and S. Ohashi, *J. Chromatogr.*, **350**, 461 (1985).

 © 1987 The Chemical Society of Japan Bull. Chem. Soc. Jpn., 60, 1343—1347 (1987)

Crystal and Molecular Structures of Two Isomers for Chlorobis-(2-methyl-8-quinolinolato)nitrosylruthenium(III)

Yukiko KAMATA, Takashi KIMURA,† Reiko HIROTA, Eiichi MIKI, Kunihiko MIZUMACHI, and Tatsujiro ISHIMORI*

Department of Chemistry, College of Science, Rikkyo University, Nishi-Ikebukuro, Toshima-ku, Tokyo 171
†The Institute of Physical and Chemical Research, Wako, Saitama 351

(Received October 1, 1986)

Two isomers of [RuCl(2mqn)$_2$(NO)] (2mqn=2-methyl-8-quinolinolate ion) were isolated and their crystal structures were determined by X-ray diffraction. In both the isomers, the Cl atom lies cis to the NO group and the O atom of one of the quinolinolato ligands lies trans to the NO group. One of the two isomers, (**1**), is in cis(O,O) and trans(N,N) configuration for the two quinolinolato ligands, another, (**2**), being in cis(O,O) and cis(N,N). Crystal data: **1**, space group $P2_1/c$ (monoclinic), a=7.412(1), b=27.241(6), c=9.752(1) Å, β=105.49(1)°; **2**, space group $P2_1/c$ (monoclinic), a=7.157(2), b=20.205(4), c=13.359(3) Å, β=107.70(2)°. The final R values for **1** and **2** are 0.044 for non-hydrogen atoms and 0.037 for all the atoms, respectively. The coordination geometries of **1** and **2** are distorted octahedron. The interatomic distances are qualitatively discussed on the basis of π- and σ-bonding abilities of the NO group, the Cl, and the coordinating atoms, N and O, of the quinolinolato ligands.

There has been a report for the solvent extraction of nitrosylruthenium(III) with 8-quinolinol.[1] However, there has been no report on the isolation of nitrosylruthenium(III) complexes with 8-quinolinol or its derivatives. In the reactions of nitrosylruthenium(III) species with 2-methyl-8-quinolinol in ethanol, we isolated two geometrical isomers of [RuCl(2mqn)$_2$(NO)] (2mqn=2-methyl-8-quinolinolate ion). The crystal structures of the isomers were determined by X-ray diffraction. Further, the isomers were characterized by NMR and IR.

Experimental

Materials. Hydrated trichloronitrosylruthenium(III) (Ru=30.8%) was prepared by nitrosylation of commercial $RuCl_3 \cdot 3H_2O$ in a hydrochloric acid solution and evaporation of the solution.[2] The other reagents used were of special grade.

Preparation and Separation of the Isomers of Chlorobis(2-methyl-8-quinolinolato)nitrosylruthenium(III). An ethanol solution of 2-methyl-8-quinolinol (5.4 mmol in 80 cm^3) was added to an ethanol solution of the hydrated trichloronitrosylruthenium(III) (0.90 mmol in 10 cm^3). After the mixture solution had been refluxed for 5 h, it was allowed to stand overnight at room temperature, and evaporated with a rotary evaporator. The dried residue was dissolved in 50 cm^3 of dichloromethane. The dark red solution was added on the silica-gel column (Wakogel C-200, ϕ 3 cm×15 cm). Two red adsorption bands were eluted with dichloromethane. The species in the front and back bands were named **1** and **2**, respectively. The eluates containing **1** and **2** were separately concentrated with a rotary evaporator to a small volume and dried in the open air to obtain reddish brown **1** and dark reddish brown **2**. Yield: 42% for **1** (based on the ruthenium compound); and 9% for **2**. Found: Ru, 21.3; Cl, 7.6; C, 49.6; H, 3.3; N, 8.8% for **1**; Ru, 20.9; Cl, 7.7; C, 49.8; H, 3.2; N, 8.7% for **2**. Calcd for [RuCl($C_{10}H_8NO$)$_2$(NO)]: Ru, 20.9; Cl, 7.3; C, 49.7; H, 3.4; N, 8.7%. The ruthenium was determined by the ruthenate method.[3] The C, H, N, and Cl were analyzed by the Organic Analysis Center of the Institute of Physical and Chemical Research.

X-Ray Crystallographic Analysis. The crystalline samples were prepared by concentrating a dilute CH_2Cl_2-$CH_3COOC_2H_5$ solution of **1**, and a dilute CH_2Cl_2-CH_3CN solution of **2** in the open air. The crystals of **1** with dimensions 0.1×0.15×0.25 mm and **2** with 0.1×0.2×0.55 mm were used for intensity measurements. X-Ray diffraction data were collected on a Rigaku AFC-4 automated four-circle diffractometer at the X-Ray Analysis Center of the Institute of Physical and Chemical Research with graphite-monochromatized Mo $K\alpha$ radiation (λ=0.71073 Å). The space groups were determined with the observed systematic absences, and the lattice parameters were determined by the least-squares refinement using ten high-angle reflections for **1**, and twenty for **2**. The crystal data are shown in Table 1. Intensities were measured by ω—2θ scanning techniques at a ω-scanning speed of 4°/min. The diffraction intensities were monitored by three standard reflections for every 100 reflections recorded. No signs of decomposition of the crystals were observed. The ordinary Lorenz and polarization corrections were applied, but no absorption correction was applied. Independent reflections with $|F_o|>3\sigma(|F_o|)$, 2268 ($2\theta<50°$) and 4702 ($2\theta<70°$) reflections for **1** and **2**, respectively, were used for the structure determinations. Calculations were performed on a FACOM 230-75 computer for **1** and a FACOM M-200 computer for **2** using the UNICS-III Program System.[4] The structures were solved by the heavy atom method,

Table 1. Crystallographic Data for the Complexes **1** and **2**

Complex	**1**	**2**
Formula	$RuClO_3N_3C_{20}H_{16}$	$RuClO_3N_3C_{20}H_{16}$
M_w	482.9	482.9
Crystal system	monoclinic	monoclinic
Space group	$P2_1/c$	$P2_1/c$
a/Å	7.412(1)	7.157(2)
b/Å	27.241(6)	20.205(4)
c/Å	9.752(1)	13.359(3)
β/°	105.49(1)	107.70(2)
V/Å^3	1897.5(5)	1840.3(7)
Z	4	4
D_m/g cm^{-3}	1.68	1.72
D_c/g cm^{-3}	1.691	1.743
R	0.044	0.037

Table 2. Atomic and Thermal Parameters with Their Estimated Standard Deviations in Parentheses

Atom	x	y	z	B_{eq}/Å^2	Atom	x	y	z	B_{eq}/Å^2
	[RuCl(2mqn)$_2$(NO)] (**1**)[a]					[RuCl(2mqn)$_2$(NO)] (**2**)[a]			
Ru	3417(1)	1240(1)	1948(1)	3.0	Ru	1704(0)	2037(0)	1516(0)	2.3
Cl	5717(4)	1126(1)	4149(3)	5.9	Cl	3313(1)	1131(0)	2559(1)	3.4
O(1)	589(11)	1101(3)	3380(8)	8.1	O(1)	−299(5)	2470(2)	2977(3)	5.6
O(2)	1790(7)	1426(2)	24(5)	3.4	O(2)	4050(3)	2618(1)	2113(2)	3.0
O(3)	5494(6)	1256(2)	1040(5)	3.5	O(3)	3015(3)	1857(1)	434(2)	2.8
N(1)	1604(10)	1168(3)	2803(7)	4.8	N(1)	528(4)	2271(1)	2420(2)	3.1
N(2)	2960(8)	527(2)	1072(6)	3.3	N(2)	621(3)	2896(1)	630(2)	2.5
N(3)	4062(8)	1991(2)	2207(6)	3.3	N(3)	−231(3)	1316(1)	616(2)	2.4
C(1)	3471(11)	80(3)	1602(9)	3.7	C(1)	−1149(4)	3059(2)	−8(2)	2.8
C(2)	3194(12)	−340(3)	708(10)	4.3	C(2)	−1461(5)	3674(2)	−531(3)	3.5
C(3)	2344(11)	−301(3)	−698(9)	4.1	C(3)	40(6)	4113(2)	−399(3)	3.8
C(4)	711(12)	238(3)	−2740(9)	4.7	C(4)	3513(6)	4407(2)	522(3)	4.4
C(5)	90(12)	695(4)	−3220(9)	4.8	C(5)	5243(6)	4228(2)	1250(3)	4.4
C(6)	438(11)	1108(3)	−2295(8)	3.9	C(6)	5479(5)	3623(2)	1778(3)	3.5
C(7)	1419(10)	1048(3)	−880(8)	3.2	C(7)	3926(4)	3178(2)	1585(2)	2.8
C(8)	2037(9)	573(3)	−367(8)	3.1	C(8)	2139(4)	3351(2)	812(2)	2.6
C(9)	1691(10)	165(3)	−1299(8)	3.6	C(9)	1905(5)	3966(2)	291(3)	3.3
C(10)	4337(13)	17(3)	3192(9)	4.8	C(10)	−2845(5)	2595(2)	−194(3)	3.7
C(11)	3323(11)	2356(3)	2796(8)	4.4	C(11)	−1775(4)	1015(2)	777(3)	2.9
C(12)	3893(13)	2853(3)	2661(9)	4.8	C(12)	−2872(5)	558(2)	34(3)	3.5
C(13)	5205(14)	2962(3)	1990(10)	5.2	C(13)	−2370(5)	382(2)	−822(3)	3.7
C(14)	7524(12)	2659(4)	717(10)	5.0	C(14)	65(6)	506(2)	−1832(3)	3.5
C(15)	8297(12)	2264(4)	247(10)	5.3	C(15)	1731(6)	810(2)	−1901(3)	3.7
C(16)	7678(11)	1777(3)	370(8)	4.1	C(16)	2750(5)	1276(2)	−1161(3)	3.1
C(17)	6209(10)	1697(2)	978(8)	3.2	C(17)	2088(4)	1438(2)	−319(2)	2.5
C(18)	5442(10)	2102(3)	1533(8)	3.2	C(18)	355(4)	1135(1)	−242(2)	2.4
C(19)	6062(12)	2589(3)	1403(9)	4.3	C(19)	−675(5)	668(2)	−991(2)	2.9
C(20)	1901(13)	2238(4)	3604(10)	5.6	C(20)	−2358(6)	1164(2)	1731(3)	4.0

a) Atomic parameters are multiplied by 10^4.

and refined by standard Patterson, Fourier, and block-diagonal least-squares techniques. The final R values were 0.044 for **1** with anisotropic temperature factors for non-hydrogen atoms, and 0.037 for **2** with anisotropic temperature factors for non-hydrogen atoms and isotropic for hydrogen atoms. The atomic parameters of **1** and **2** are given in Table 2.

The complete F_o—F_c data are deposited as Document No. 8727 at the Office of the Editor of Bull. Chem. Soc. Jpn.

Other Measurements. ^{1}H and ^{13}C NMR spectra were recorded on a JEOL JNM FX-90Q spectrometer. CD_2Cl_2 was used as solvent and the chemical shifts were referred to internal TMS. IR spectra were measured by the Nujol mull method with JASCO A-202 spectrometer. Electronic spectra in dichloromethane were recorded on a HITACHI 340 spectrometer. Conductivities of the dichloromethane solutions were measured at 25.0 °C using a conventional bridge (Model 4225A of Yokogawa-Hewlett-Packard Ltd.).

The UV, IR, conductivity, and NMR data of **1** and **2** are as follows; **1**: UV (CH_2Cl_2) 31300 (log ϵ 3.49) and 25000 cm^{-1} (log ϵ 3.75); IR (Nujol) 1835 cm^{-1} (N-O stretching of the nitrosyl group); Λ_m (CH_2Cl_2, 4.86×10^{-4} mol dm^{-3}, 25 °C) 3.48×10^{-7} S m^{2}mol^{-1}; ^{1}H NMR (CD_2Cl_2) δ=3.06 (3H, s, CH_3), 3.27 (3H, s, CH_3), 6.80—7.48 (8H, m, the hydrogen atoms of the two quinoline rings except the H(3) and the H(13)),[5] 8.18 (1H, d, the H(3) or the H(13)), 8.22 (1H, d, the H(13) or the H(3)); ^{13}C NMR (CD_2Cl_2) δ=27.30 (s, CH_3), 27.63 (s, CH_3), 115—140 (m, the two quinoline rings except the quaternary carbons). **2**: UV(CH_2Cl_2) 31300 (log ϵ 3.45) and 25300 cm^{-1} (log ϵ 3.77); IR (Nujol) 1840 cm^{-1} (N-O stretching of the nitrosyl group); Λ_m (CH_2Cl_2, 5.29×10^{-4} mol dm^{-3}, 25 °C) 11.7×10^{-7} S m^2 mol^{-1}); ^{1}H NMR (CD_2Cl_2) δ=1.83 (3H, s, CH_3), 3.14 (3H, s, CH_3), 6.77—7.55 (8H, m, the

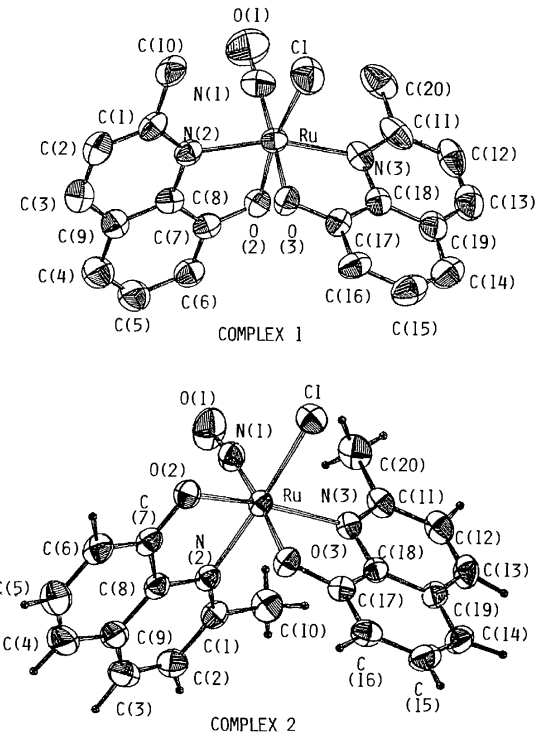

Fig. 1. ORTEP drawing of [RuCl(2mqn)$_2$(NO)] (**1** and **2**) (thermal ellipsoids are drawn at 50% probability).

Table 3. Relevant Interatomic Distances (l/Å) and Bond Angles (ϕ/°) within a Molecule of the Complexes **1** and **2** (Their estimated standard deviations in parentheses)

Complex Distances	**1**	**2**	Complex Angle	**1**	**2**
Ru-Cl	2.378(2)	2.376(1)	Ru-N(1)-O(1)	174.9(7)	174.8(3)
Ru-N(1)	1.772(8)	1.735(3)	N(2)-Ru-O(2)	82.1(2)	82.1(1)
N(1)-O(1)	1.068(12)	1.155(5)	N(3)-Ru-O(3)	81.5(2)	80.4(1)
Ru-N(2)	2.112(6)	2.111(3)	Cl-Ru-N(1)	90.6(2)	93.0(1)
Ru-N(3)	2.100(6)	2.116(2)	Cl-Ru-N(2)	104.1(2)	172.9(1)
Ru-O(2)	2.005(5)	2.005(2)	Cl-Ru-N(3)	86.2(2)	85.4(1)
Ru-O(3)	1.971(6)	1.981(3)	Cl-Ru-O(2)	169.9(2)	91.1(1)
Cl-C(10)	3.245(9)	—	Cl-Ru-O(3)	87.2(2)	92.0(1)
N(1)-C(20)	3.011(13)	2.994(5)	N(3)-Ru-O(2)	85.8(2)	162.6(1)
O(3)-C(10)	—	3.635(5)	N(1)-Ru-N(3)	103.2(3)	102.2(1)
C(10)-C(20)	—	3.814(6)	N(2)-Ru-N(3)	162.0(3)	100.5(1)
			N(2)-Ru-O(3)	84.2(2)	85.2(1)
			O(2)-Ru-O(3)	85.5(2)	82.7(1)

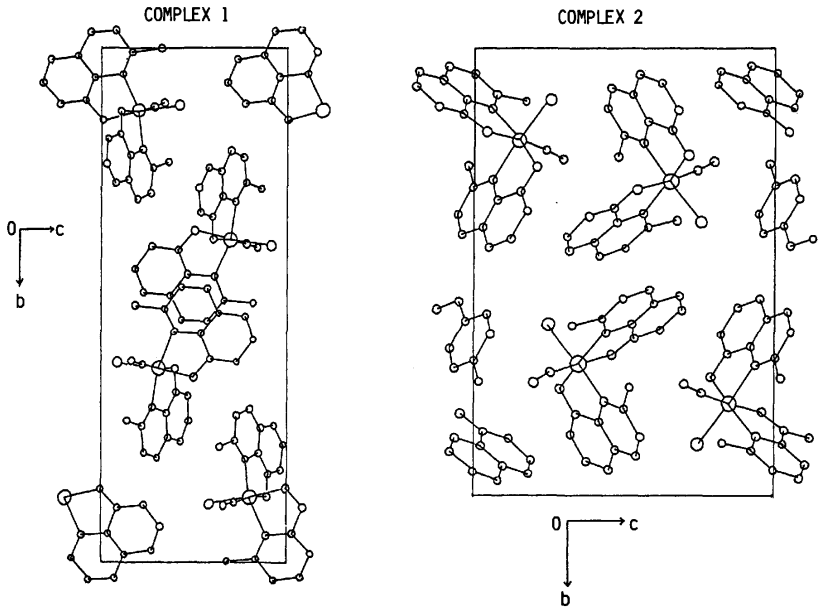

Fig. 2. Crystal structures of [RuCl(2mqn)$_2$(NO)] (**1** and **2**) projected along the a axis.

hydrogen atoms of the two quinoline rings except the H(3) and the H(13)), 8.17 (1H, d, the H(3) or the H(13)), 8.22 (1H, d, the H(13) or the H(3)); ^{13}CNMR (CD_2Cl_2) δ=24.38 (s, CH_3), 27.70 (s, CH_3), 114—141 (m, the two quinoline rings except the quaternary carbons).

Results and Discussion

The wave numbers of the N-O stretching bands[6] and the molar conductivities (Λ_m)[7] of **1** and **2** were consistent with the molecular structures determined as will be mentioned later.

Molecular Structures. The molecular and crystal structures of the two isomers of [RuCl(2mqn)$_2$(NO)], **1** and **2**, are shown in Figs. 1 and 2, respectively. In both isomers, the Cl atom is in cis position to the NO group, the O atom of one of the quinolinolato ligands being in trans to the NO group. On the other hand, the geometry of the N and O atoms of the two quinolinolato ligands is in trans (N,N) and cis (O,O) for **1**, and in cis (N,N) and cis (O,O) for **2**. Hence, in **2**, the methyl group of the C(10) lies under the other quinoline ring.

The bond distances and the angles are shown in Table 3. In **1**, the Cl-C(10) distance is shorter than the sum of the van der Waals radii of methyl group (2.0 Å) and Cl (1.8 Å), and the Cl-Ru-N(2) angle is larger than 100° due to the repulsion between the Cl atom and the methyl group. In **2**, the N(2)-Ru-N(3) angle is about 100° due to the repulsion of the methyl group of the C(10) by the other quinoline ring. The N(1)-Ru-N(3) angle is larger than 100° in both **1** and **2** due to the repulsion between the methyl and the NO groups.

The Ru-N(1) distance in **1** is longer than that in **2**. On the other hand, the N(1)-O(1) distance in **1** is shorter than that in **2** which is about the same with those

in other six-coordinate mononitrosylruthenium complexes with the linear {RuNO}^{6} group, 1.11—1.17 Å.[6,8]

For nitrosyl complexes, the trans-influence of the NO group has been examined on the basis of the accurate X-ray crystal structure analyses[9] and the molecular orbital theory treatment.[10] Relative bond strengths between the metal ion and the donor atoms of the ligands trans to each other depend on the σ- or π-bonding ability of the donor atoms.[10,11] Since the Ru-N(1)-O(1) angles for **1** and **2** are close to 180°, the NO group is formally bound as NO^+.[6] The NO^+ is a strong π-acceptor and weak σ-donor. Chloride ion and the ligating atoms, the N and O atoms, of the quinolinolato ligands seem to be moderate σ-donor, hence are better σ-donor than the NO^+, while these are poor π-acceptor than the NO^+. When the ligand (L) trans to the NO is a good σ-donor and poor π-acceptor, the Ru-NO and Ru-L bond distances are shortened by the mutual reinforcement of the σ- and π-bonding.[10] Thus, in both **1** and **2**, both the σ- and π-electron densities of the O(3) flow into the NO^+ by way of the Ru; the Ru-O(3) bond distances are expected to be shorter than the Ru-O(2). The differences is 0.034 Å for **1** and 0.024 Å for **2** as shown in Table 3. The Ru-Cl bond distances in **1** and **2** are the same as those of the Ru-Cl (cis to NO) in $[RuCl_5(NO)]^{2-}$, av 2.374 Å, but are longer than those of the Ru-Cl (trans to NO), av 2.358 Å,[9] because the ligand trans to the Cl in **1** and **2** does not possess the trans shortening effect. No effects of the methyl group in the quinoline rings on the Ru-Cl bond distance were found.

In addition to the bond angles, the following torsion angles were calculated. Table 4 gives the clockwise torsion of the bond 3—4 with reference to the bond 1—2 when looking the atom-3 from the atom-2. In **2**, the Ru, the N(2), the C(1), and the C(10) are arranged in a plane as well as the Ru, the N(3), the C(11), and the C(20) are. On the other hand, in **1**, the methyl groups undergo considerable torsion; the C(10) and the C(20) are repulsed by the Cl and the NO group, respectively. The two quinoline rings are practically flat in both **1** and **2**.

The NMR spectral data were consistent with the determined molecular structures. The ^1H resonance peaks of the two methyl groups were observed at δ=3.06 and 3.27 for **1**, while at δ=1.83 and 3.14 for **2**. The methyl carbons resonated at δ=27.30 and 27.63 for **1**, while at δ= 24.38 and 27.70 for **2**. According to the molecular structural analysis, the methyl carbon, the C(10), in **2** lies just under the plane of the other quinoline ring. Evidently it causes high field shifts of the methyl carbon, the C(10), and the methyl protons owing to ring-current effect of the quinoline ring. Thus, the resonance peaks at δ=24.38 and 1.83 of **2** can be assigned to the C(10) and the protons attached to it, respectively.

A few six-coordinate metal complexes containing two 2-methyl-8-quinolinolato ligands have been characterized by X-ray structure analysis and NMR measurement. The geometrical arrangement of **1** for the quinolinolato ligands was the same as found for $[Co(2mqn)_2en]$,[12] that of **2** being the same as found for $[TcCl(2mqn)_2O]$.[13] Recently, Bottomley et al. have reported the similar geometrical isomers of *cis*-$[RuCl(pyca)_2(NO)]$ (pyca=2-pyridinecarboxylate ion) as found for the present isomers.[14]

Table 4. The Torsion Angles (ϕ/°)

Atoms 1 2 3 4	Complex **1**	Complex **1**
Ru-N(2)-C(1)-C(10)	10.0(11)[a]	1.1(5)
Ru-N(3)-C(11)-C(20)	8.5(12)	−1.2(5)

a) Parentheses indicate the estimated standard deviations.

The authors with to express their thanks to Professor Makoto Shima (present: Yokohama National University), Professor Toshio Sakurai (present: Shinshu University), and Miss Kimiko Kobayashi of the Institute of Physical and Chemical Research for providing the X-ray facilities and for assisting the calculations of the structural analysis. We also would like to thank Professor Minoru Hirota of Yokohama National University for measuring the NMR spectra. The present work was partially supported by a Grant-in-Aid for Scientific Research No. 58470038 from the Ministry of Education, Science and Culture.

References

1) K. Iwashima and K. Watari, *Koshu-eisei-in Kenkyu Hokoku*, **18**, 72 (1969).

2) M. B. Fairy and R. J. Irving, *J. Chem. Soc., A*, **1966**, 479.

3) E. D. Marshall and R. R. Richard, *Anal. Chem.*, **22**, 795 (1950).

4) T. Sakurai and K. Kobayashi, *Rikagaku Kenkyusho Hokoku*, **55**, 69 (1979).

5) The H(3) and H(13) indicate the hydrogen atoms bound to the C(3) and C(13), respectively. The atomic numbering of carbons are shown in Fig. 1.

6) R. D. Feltham and J. H. Enemark, "Structures of Metal Nitrosyls," in "Topics in Stereochemistry," ed by G. L. Geoffroy, John Wiley & Sons, New York (1981), Vol. 12, pp. 155—215. Mononitrosyl complexes are conveniently described as $\{MNO\}^n$, where n is the number of the d-electrons on the metal when the NO group is formally bound as NO^+.

7) W. L. Geary, *Coord. Chem. Rev.*, **7**, 81 (1971). The molar conductivities in CH_2Cl_2 were much smaller than those of 1 : 1 electrolytes, $(20—50)\times10^{-7}$ S m^2 mol^{-1}, at ca. $10^{-4}—10^{-5}$ mol dm^{-3}.

8) T. Kimura, T. Sakurai, M. Shima, T. Togano, M. Mukaida, and T. Nomura, *Inorg. Chim. Acta*, **69**, 135 (1983).

9) T. Veal and D. J. Hodgson, *Inorg. Chem.*, **11**, 1420 (1972); *idem., Acta Crystallogr., Sect. B*, **28**, 3525 (1972).

10) F. Bottomley, *Coord. Chem. Rev.*, **26**, 7 (1978).

11) S. Pell and J. N. Armor, *Inorg. Chem.*, **12**, 873 (1973);

A. B. Nikol'skii, V. I. Baranovskii, N. V. Ivanova, and O. V. Sizova, *Russ. J. Inorg. Chem.*, **19**, 145 (1974); O. V. Sizova, N. G. Antonov, A. B. Nikol'skii, and V. I. Baranovskii, *Soviet J. Coord. Chem.*, **2**, 853 (1976).

12) Y. Yamamoto and E. Toyota, *Bull. Chem. Soc. Jpn.*, **57**, 47 (1984).

13) B. E. Wilcox, M. J. Heeg, and E. Deutch, *Inorg. Chem.*, **23**, 2962 (1984).

14) F. Bottomley, E. Hahn, J. Pickardt, H. Schumann, M. Mukaida, and H. Kakihana, *J. Chem, Soc., Dalton Trans.*, **1985**, 2427.

Solvatochromism of [Diamine-*N,N'*-polycarboxylato]chromium(III) and -cobalt(III) Complexes

Naoko MIURA, Makoto SHIMURA, and Hiroshi OGINO*
Department of Chemistry, Faculty of Science, Tohoku University, Aramaki, Sendai 980
(Received October 24, 1986)

Visible absorption spectra of [diamine-*N,N'*-polycarboxylato]chromium(III) and -cobalt(III) complexes were measured in twelve different solvents. The diamine-*N,N'*-polycarboxylates used in this work were ethylenediamine-*N,N,N',N'*-tetraacetate ($edta^{4-}$), 1,2-cyclohexanediamine-*N,N,N',N'*-tetraacetate ($cydta^{4-}$), *N'*-(2-hydroxyethyl)ethylenediamine-*N,N,N'*-triacetate ($hedtra^{3-}$), and *N'*-methylethylenediamine-*N,N,N'*-triacetate ($medtra^{3-}$). The first d-d absorption maxima of these complexes depend considerably on the solvents. From the solvatochromic behaviors of these complexes, it was concluded that solid complexes, K[Co(edta)]·$2H_2O$, K[Co(cydta)]·$3H_2O$, [Co(hedtra)(H_2O)], [Co(medtra)(H_2O)]·$3H_2O$, Na[Cr(cydta)]·$4.5H_2O$, and probably K[Cr(edta)]·$2H_2O$, dissolve in the solvents while holding their first coordination sphere intact; in some solvents, however, [Cr(medtra)(H_2O)]·$1.5H_2O$ and [Cr(hedtra)(H_2O)]·$1.5H_2O$ undergo substitutions of the coordinated water molecule to form [Cr(medtra)(solvent)] and [Cr(hedtra)(solvent)], respectively.

It has been known that the metal to ligand or ligand to metal charge-transfer absorption bands of transition metal complexes are solvent-dependent.[1-3] The first d-d absorption bands of the octahedral cobalt(III) or chromium(III) complexes, on the other hand, are generally insensitive to the solvents, and there are only a few reports concerning solvent-dependent d-d absorptions.[4-7] Bjerrum et al. measured the electronic absorption spectra of amine complexes of chromium (III) and cobalt(III) in water, methanol, acetone, and nitromethane, and reported for the first time that the d-d absorption band maxima are practically independent of the solvents.[4] Later, Adamson investigated visible absorption spectra of $K[Cr(NCS)_4(NH_3)_2]$ in eleven different solvents and found that the first ligand field band appears between 518 and 530 nm, depending on the solvents.[5] Nishimura et al. observed rather large solvatochromism for the d-d transition bands of $[CrCl_2(CH_3)(tetrahydrofuran)_3]$.[6] Recently, Taura has reported that the peak position (λ_{max}) for the first d-d absorption band of K[Co(edta)]·$2H_2O$[7,8] changes with solvents and correlates with the acceptor numbers of the solvents which were proposed by Mayer, Gutmann, and Gerger.[9]

In the present paper, solvatochromism of the chromium(III) and cobalt(III) complexes containing diamine-*N,N'*-polycarboxylates was investigated. The ligand, L, used were classified into two types. One is tetraacetates ($edta^{4-}$ and $cydta^{4-}$) to form uninegatively charged complexes and the other is triacetates ($hedtra^{3-}$ and $medtra^{3-}$) to form neutral complexes.

As the Co(III) complexes are substitution inert,[10-12] the incorporation of a solvent molecule into the first coordination sphere does not occur. In fact, the Co(III)-L complexes did not show any spectral change with time in various solvents. Such inertness towards ligand substitution allowed us to measure the absorption spectra of [Co(edta)]$^-$, [Co(cydta)]$^-$, [Co(hedtra)(H_2O)], and [Co(medtra)(H_2O)] in various solvents without incorporating the solvent molecules into their first coordination spheres.

The Cr(III)-L complexes, on the other hand, have variable reactivities towards ligand substitution. Although chromium(III) complexes have been known to be substitution inert, substitutions at the site of the coordinated water molecule in [Cr(edta)(H_2O)]$^-$ and [Cr(hedtra)(H_2O)] proceed very rapidly:[13]

$$[CrL(H_2O)]^{n-} + X^- \rightleftharpoons [CrXL]^{(n+1)-} + H_2O \quad (1)$$

Ligand substitution reactions of [Cr(medtra)(H_2O)] are much slower than those of [Cr(edta)(H_2O)]$^-$ and [Cr(hedtra)(H_2O)], but are still considerably faster than the reactions of ordinary chromium(III) complexes.

An X-ray crystal structure analysis of K[Cr(edta)]·$2H_2O$ has shown that the complex contains sexidentate $edta^{4-}$ and does not contain a water molecule in the first coordination sphere.[14] Although we have formulated the Cr(III)-EDTA complex as [Cr(edta)(H_2O)]$^-$, there is a serious problem concerning the structure of the Cr(III)-EDTA complex in an aqueous solution: whether the $edta^{4-}$ ion acts as a quinquedentate ligand or as a sexidentate ligand.[15-17] Therefore, it is of interest to determine whether the Cr(III)-EDTA complex is present as [Cr(edta)]$^-$, [Cr(edta)(H_2O)]$^-$, or [Cr(edta)(solvent)]$^-$ in various solvents.

The differences in solution behaviors of Co(III)-L and Cr(III)-L complexes should be reflected in the solvatochromism of these complexes, which led us to make the present study.

Experimental

Materials. The chromium(III) and cobalt(III) complexes, K[Cr(edta)]·$2H_2O$,[18] Na[Cr(cydta)]·$4.5H_2O$,[19] [Cr(hedtra)(H_2O)]·$1.5H_2O$,[13] [Cr(medtra)(H_2O)]·$1.5H_2O$,[13] K[Co(edta)]·$2H_2O$,[20,21] K[Co(cydta)]·$3H_2O$,[22] [Co(hedtra)(H_2O)],[11] and [Co(medtra)(H_2O)]·$3H_2O$[23] were prepared by methods described in the literature. Methyltrioctylammonium chloride (Tokyo Kasei), Dicyclohexano-18-crown-6 (Nippon Soda Co.), and dibenzo-18-crown-6 (Aldlich) were used without further purification.

Solvents. Hexamethylphosphoric triamide (HMPA) was

Table 1. Linear Correlations between $\tilde{\nu}_{max}$ Values of the [Diamine-*N,N'*-polycarboxylato]cobalt(III) and -chromium(III) Complexes[a)]

Complex 1	Complex 2	Slope	Intercept / 10^4 cm^{-1}	Correlation coefficient
[Co(cydta)]$^-$	[Co(edta)]$^-$	1.10	−0.197	0.96
[Co(hedtra)(H_2O)]	[Co(edta)]$^-$	0.671	0.572	0.86
[Co(medtra)(H_2O)]	[Co(edta)]$^-$	0.615	0.688	0.96
[Co(hedtra)(H_2O)]	[Co(cydta)]$^-$	0.581	0.746	0.84
[Co(medtra)]H_2O)]	[Co(cydta)]$^-$	0.538	0.838	0.95
[Co(hedtra)(H_2O)]	[Co(medtra)(H_2O)]	0.888	0.193	0.98
[Cr(cydta)]$^-$	[Cr(edta)]$^-$	1.03	−0.066	0.98
[Cr(hedtra)(H_2O)]	[Cr(edta)]$^-$			b)
[Cr(medtra)(H_2O)]	[Cr(edta)]$^-$			b)
[Cr(hedtra)(H_2O)]	[Cr(medtra)(H_2O)]	0.864	0.237	0.95
[Cr(edta)]$^-$	[Co(edta)]$^-$	1.78	−1.46	0.95
[Cr(cydta)]$^-$	[Co(edta)]$^-$	1.86	−1.62	0.95
[Cr(edta)]$^-$	[Co(cydta)]$^-$	1.53	−0.992	0.94
[Cr(cydta)]$^-$	[Co(cydta)]$^-$	1.58	−1.08	0.92

a) The values of the slope and intercept were calculated from the following equation: $\tilde{\nu}_{max}$(complex 1)= intercept+slope$\times\tilde{\nu}_{max}$ (complex 2).
b) Very scattered plots.

purified by distillation over calcium hydride. Other solvents, acetone (AC), acetonitrile (AN), formamide (FA), *N*-methylformamide (NMF), *N,N*-dimethylformamide (DMF), *N,N*-dimethylacetamide (DMA), dimethyl sulfoxide (DMSO), nitromethane (NM), methanol (MA), ethanol (EA), and toluene were of reagent grade, and were used as received.

Spectral Measurements. The visible absorption spectra were recorded on a Hitachi 330 or a Union-Giken SM 401 recording spectrophotometer. Most of the measurements were made at room temperature. Solutions of the complexes were prepared by simply dissolving a complex in solvents. Some anionic complexes with low solubility were dissolved with dibenzo-18-crown-6 or dicyclohexano-18-crown-6. Dissolution rate of the complexes varied depending on the complex and the solvent. In order to achieve sufficient concentrations of the complexes in solution, it was necessary, in some cases, that the mixtures of the complexes and the solvents were shaken vigorously or sonicated for 3—4 h before the spectral measurements. Among the complexes investigated in this study, [Cr(medtra)(H_2O)] and [Cr(eedtra)(H_2O)] revealed spectral changes with times over 1—2 h after dissolution into various solvents. The spectral data for these complexes were those taken after spectral changes came to an end. No spectral changes with time were observed for other complexes examined in this study. Lists of the $\tilde{\nu}_{max}$ values for the complexes measured in this study are deposited at the office of the Chemical Society of Japan (Document No. 8726).

Results and Discussion

Solvatochromism of the Cobalt(III) Complexes Containing Diamine-*N,N'*-polycarboxylate. It is well-established that the edta^{4-} and cydta^{4-} ions act as sexidentate ligands in [Co(edta)]$^-$ and [Co(cydta)]$^-$, respectively.[11,24,25] When the $\tilde{\nu}_{max}$ values for [Co(cydta)]$^-$ in various solvents are plotted against those of the $\tilde{\nu}_{max}$ values for [Co(edta)]$^-$, a linear relation is obtained

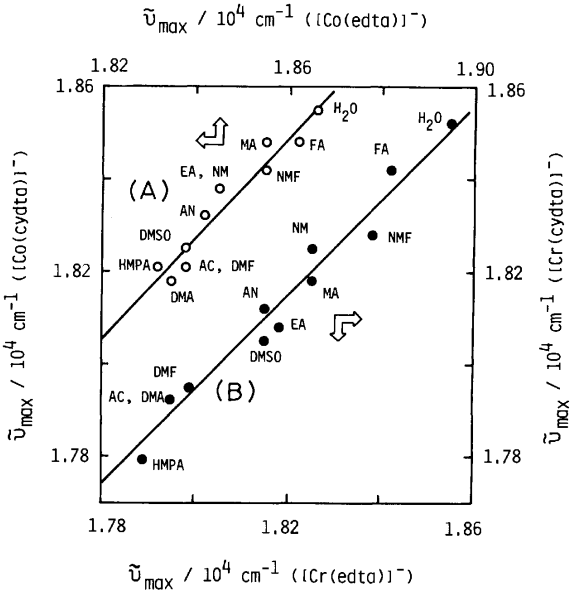

Fig. 1. Linear relationships between $\tilde{\upsilon}_{max}$([Co(cydta)]$^-$) and $\tilde{\upsilon}_{max}$([Co(edta)]$^-$) (A), and between $\tilde{\upsilon}_{max}$([Cr(cydta)]$^-$) and $\tilde{\upsilon}_{max}$([Cr(edta)]$^-$) (B).

as shown in Fig. 1. The slopes of the plots are close to unity (Table 1). Therefore, the solvatochromism of both [Co(cydta)]$^-$ and [Co(edta)]$^-$ arises from common effect(s) which is(are) induced by the solvent molecules surrounding the first coordination sphere.

Good linear correlations between the $\tilde{\nu}_{max}$ values for [Co(edta)]$^-$ (or [Co(cydta)]$^-$) and those for the neutral complexes, [Co(hedtra)(H_2O)] and [Co(medtra)(H_2O)], could also be observed (Fig. 2 and Table 1). These show that the factor(s) governing the solvatochromism of the [Co(edta)]$^-$ and [Co(cydta)]$^-$ complexes is also effective to the solvatochromism of the neutral com-

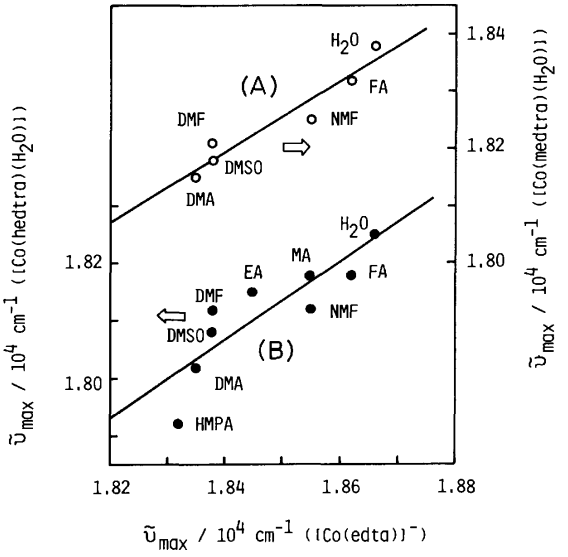

Fig. 2. Plots of $\tilde{\nu}_{max}$([Co(medtra)(H_2O)]) against $\tilde{\nu}_{max}$([Co(edta)]$^-$) (A), and the plots of $\tilde{\nu}_{max}$([Co(hedtra)(H_2O)]) against $\tilde{\nu}_{max}$([Co(edta)]$^-$) (B).

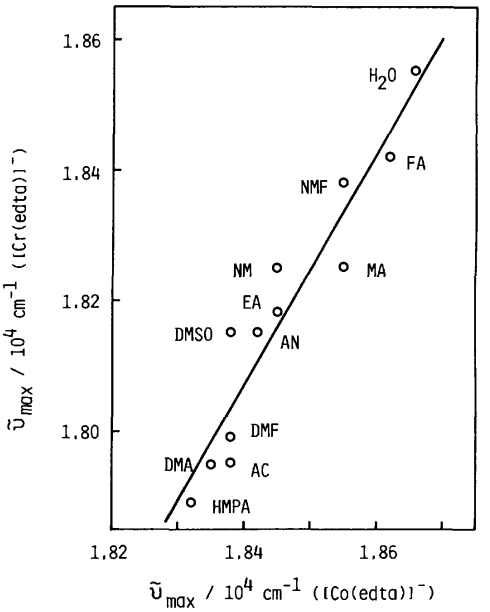

Fig. 3. Plots of $\tilde{\nu}_{max}$([Cr(edta)]$^-$) against $\tilde{\nu}_{max}$([Co(edta)]$^-$).

plexes. However, the degree of the solvent effect is smaller for the neutral complexes than for the [Co(edta)]$^-$ or [Co(cydta)]$^-$: The slopes of the plots in Fig. 2 are only about 0.6.

Solvatochromism of the Chromium(III) Complexes Containing Diamine-*N,N'*-polycarboxylate. The structure of [Cr(edta)]$^-$ in a crystal of K[Cr(edta)]·$2H_2O$ has been determined to be an octahedral coordination with the sexidentate edta^{4-}.[14] Similarly, Na[Cr(cydta)]·$4.5H_2O$ contains the sexidentate cydta^{4-}.[17] However, there have been controversial discussions concerning the structure of the Cr(III)-EDTA complex in an aqueous solution, as to whether it contains a quinquedentate edta^{4-} or a sexidentate one.[15-17] A similar problem may arise when the complex is dissolved in a solvent other than water. If

$$[Cr(edta)]^- + \text{solvent} \rightleftharpoons [Cr(edta)(\text{solvent})]^- \quad (2)$$

takes place in various solvents, the correlation between $\tilde{\nu}_{max}$ values of [Cr(edta)]$^-$ and [Co(edta)]$^-$ is expected to be poor, since the [Co(edta)]$^-$ maintains its strucure in solution. However, plots of the $\tilde{\nu}_{max}$ values of [Cr(edta)]$^-$ against those of [Co(edta)]$^-$ show a good linear relation (Fig. 3 and Table 1). This indicates that [Cr(edta)]$^-$ in K[Cr(edta)]·$2H_2O$ retains its original strucure in most solvents, i.e. octahedral coordination with sexidentate edta^{4-}.[26]

In connection with this, interesting phenomena were found: The Cr(III)-EDTA complex can be extracted from an aqueous solution of K[Cr(edta)]·$2H_2O$ to toluene in the presence of a phase-transfer catalyst, methyltrioctylammonium chloride. The extracted species is reddish violet in a toluene layer and shows visible absorption maximum at 544 nm (only 5 nm longer than the absorption maximum of the aqueous solution (λ_{max}=539 nm)). When solid K[Cr(edta)]·$2H_2O$ is dissolved directly into toluene with methyltrioctylammonium chloride, a bluish violet solution (λ_{max} =554 nm) is obtained, which may indicate that [CrCl(edta)]$^{2-}$ is formed. In the toluene extract from the aqueous solution of K[Cr(edta)]·$2H_2O$, the complex may be present as [Cr(edta)]$^-$ or [Cr(edta)(H_2O)]$^-$. A similar phenomenon was also observed for [Cr(hedtra)(H_2O)].

There is a tendency that the metal complexes containing sexidentate cydta^{4-} are much more stable than corresponding complexes containing both quinquedentate cydta^{4-} and a unidentate ligand: There is no spectral change when an acetate buffer solution is added (up to 1 mol dm^{-3}) to an aqueous solution of Na[Cr(cydta)]·$4.5H_2O$, suggesting that the acetate ions do not coordinate to Cr(III)-CyDTA complex.[27] Although there have been moderately stable cobalt(III) complexes, [CoX(edta)]$^{2-}$ (X=Cl$^-$, Br$^-$, NO_2^-, OH$^-$, NCS$^-$, SCN$^-$)[28-30] and [Co(edta)(H_2O)]$^-$,[31] no cydta^{4-} analogue of this type has been known except [CoCl(cydta)]$^{2-}$.[22] Moreover, [CoCl(cydta)]$^{2-}$ is quite unstable and quickly changes to [Co(cydta)]$^-$ in an aqueous solution. These findings and some other facts[11,19,32] suggest that a Cr(III)-CyDTA complex contains a sexidentate cydta^{4-} ligand in aqueous solution.

The $\tilde{\nu}_{max}$ values of [Cr(cydta)]$^-$ in various solvents correlate linearly well with those of [Cr(edta)]$^-$ and [Co(cydta)]$^-$ as shown in Fig. 1 and Table 1. These facts may indicate that K[Cr(edta)]·$2H_2O$ and Na[Cr(cydta)]·$4.5H_2O$ dissolve in various solvents to form [CrL]$^-$ ions which contain sexidentate L^{4-} without the coordinated solvent molecule. The solvatochromic shifts of [Cr(cydta)]$^-$ and [Cr(edta)]$^-$ observed in this study are larger than those of [Co(edta)]$^-$.

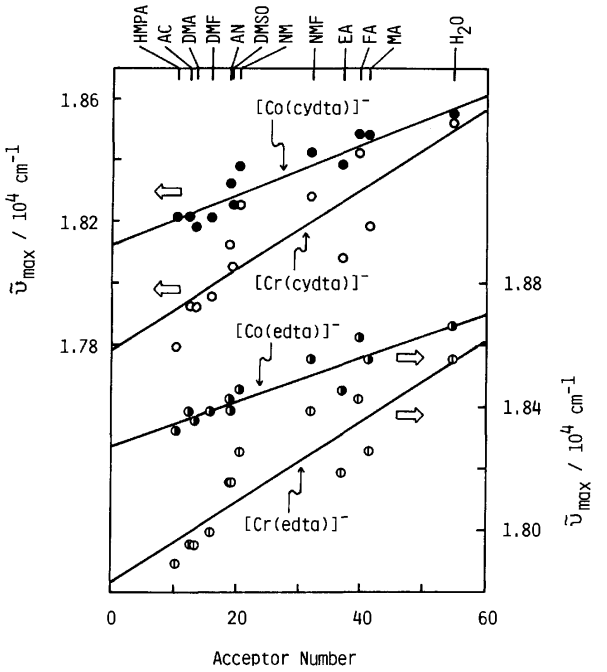

Fig. 4. Relationships between the $\tilde{\nu}_{max}$ values of $[ML]^-$ (M=Cr, Co; L=edta^{4-}, cydta^{4-}) and the acceptor numbers of the solvents. ●: $[Co(cydta)]^-$, ○: $[Cr(cydta)]^-$, ◑: $[Co(edta)]^-$, ⊕: $[Cr(edta)]^-$.

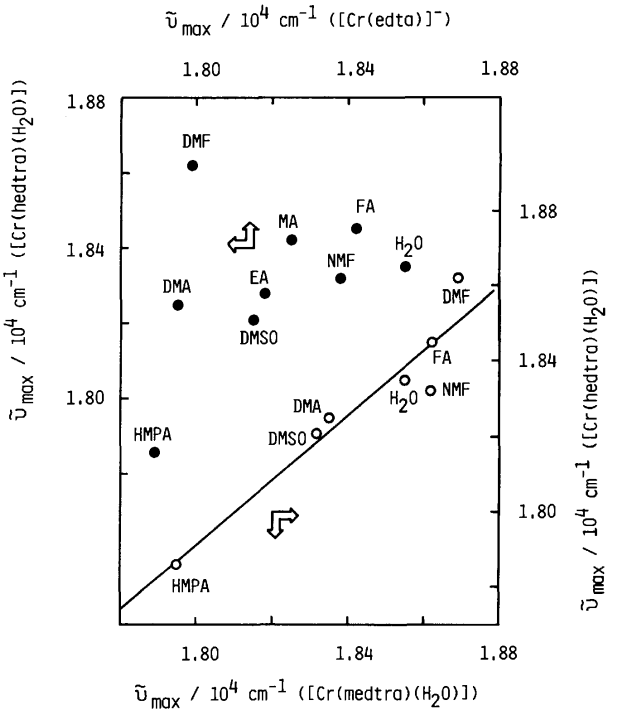

Fig. 5. Plots of $\tilde{\nu}_{max}([Cr(hedtra)(H_2O)])$ against $\tilde{\nu}_{max}([Cr(edta)]^-)$ (●), and linear relationship between $\tilde{\nu}_{max}([Cr(hedtra)(H_2O)])$ and $\tilde{\nu}_{max}([Cr(medtra)(H_2O)])$ (○).

Taura reported that a linear relation could be obtained between the plots of the λ_{max} values of $[Co(edta)]^-$ and the acceptor numbers of the solvents.[7] On the basis of the more extensive measurements in this study, Taura's observation was confirmed, as shown in Fig. 4.[33] It is also shown in Fig. 4 that a linear relation exists between the $\tilde{\nu}_{max}$ values of $[Co(cydta)]^-$, $[Cr(edta)]^-$, or $[Cr(cydta)]^-$ and the accepter numbers. This is quite natural since linear relations exist mutually among the $\tilde{\nu}_{max}$ values of $[Co(edta)]^-$, $[Co(cydta)]^-$, $[Cr(edta)]^-$, and $[Cr(cydta)]^-$ as shown in Figs. 1 and 3 and Table 1.

There is no correlation between $\tilde{\nu}_{max}$ values of $[Cr(hedtra)(H_2O)]$ or $[Cr(medtra)(H_2O)]$ and those of $[Cr(edta)]^-$ or $[Cr(cydta)]^-$ as exemplified in Fig. 5. This is contrasted to the cases of the corresponding cobalt(III) complexes (Fig. 2). A poor correlation (Fig. 5) may be best explained by the occurence of reaction 3, at least in some solvents:

$$[CrL(H_2O)] + \text{solvent} \rightleftharpoons [CrL(\text{solvent})] + H_2O \quad (3)$$
$$(L = \text{hedtra}^{3-}, \text{medtra}^{3-})$$

where the coordinated water molecule is replaced by a solvent molecule.

If the occurrence of reaction 3 is the case, a spectral change with time should be observed in the time scale corresponding to the ligand substitution rates of those chromium(III) complexes. When an aqueous solution of $[Cr(medtra)(H_2O)]$ was mixed with DMF or DMSO, a slow spectral change was observed. The initial λ_{max} value (539 nm) in an aqueous solution shifts to a shorter wavelength in a reaction with DMF, and to a longer wavelength in a reaction with DMSO; the rate of the spectral change is reasonable in view of the kinetic data of the ligand substitution reactions of $[Cr(medtra)(H_2O)]$.[34] When an aqueous solution of $[Cr(eedtra)(H_2O)]$ was mixed with DMF or DMSO, a spectral change similar to the case of $[Cr(medtra)(H_2O)]$ system was observed. These findings are consistent with the occurence of reaction 3. Therefore, the solvatochromism of those complexes such as $[Cr(medtra)(H_2O)]$ contains two factors: The change in chromophore introduced by the formation of [CrL(solvent)], and the solvation at the outer coordination sphere.

The scattered plots in Fig. 5 suggest that $[Cr(hedtra)(H_2O)]$ also undergoes reaction 3. The substitution reaction of the water molecule in $[Cr(hedtra)(H_2O)]$ with a solvent molecule is expected to occur in the stopped-flow time scale.[13,34] However, the stopped-flow experiments were hampered by heat evolving upon mixing, incomplete mixing, and/or cavitation. These unfavorable phenomena are often encountered upon the mixing of different solvents. Therefore, it is impossible to determine whether reaction 3 is completed within the time of mixing or does not take place: in other words, whether the complex exists in the solvents as [Cr(hedtra)(solvent)] or $[Cr(hedtra)(H_2O)]$. However, the $\tilde{\nu}_{max}$ values of $[Cr(hedtra)(H_2O)]$ correlates linearly with those of $[Cr(medtra)(H_2O)]$, as shown in Fig. 5 and Table 1. This may indicate that

[Cr(hedtra)(H_2O)] also undergoes reaction 3.

The formation of [Cr(hedtra)(solvent)] in some solvents raises a question why [Cr(edta)]$^-$ does not accomodate a solvent molecule into the first coordination sphere in most of the solvents, but [Cr(hedtra)(H_2O)] does. The formation of [Cr(edta)(solvent)]$^-$ would be less favorable than that of [Cr(hedtra)(solvent)], since the formation constants of the mixed ligand complexes, [CrX(edta)]$^{2-}$ (X=OAc^-, N_3^-, NCS^-), in aqueous solutions have been known to be 17—28 times smaller than those of the corresponding [CrX(hedtra)]$^-$.[13,34]

References

1) J. C. Curtis, B. P. Sullivan, and T. J. Meyer, *Inorg. Chem.*, **22**, 224 (1983), and references therein.

2) E. M. Kober, B. P. Sullivan, and T. J. Meyer, *Inorg. Chem.*, **23**, 2098 (1984).

3) R. E. Shepherd, M. F. Hoq, N. Hoblack, and C. R. Johnson, *Inorg. Chem.*, **23**, 3249 (1984).

4) J. Bjerrum, A. W. Adamson, and O. Bostrup, *Acta Chem. Scand.*, **10**, 329 (1956).

5) A. W. Adamson, *J. Inorg. Nucl. Chem.*, **28**, 1955 (1966).

6) K. Nishimura, H. Kuribayashi, A. Yamamoto, and S. Ikeda, *J. Organomet. Chem.*, **37**, 317 (1972).

7) T. Taura, *Chem. Lett.*, **1984**, 2011.

8) Abbreviations used in this paper: $edta^{4-}$, ethylenediamine-*N,N,N',N'*-tetraacetate; $cydta^{4-}$, 1,2-cyclohexanediamine-*N,N,N',N'*-tetraacetate; $hedtra^{3-}$, *N'*-(2-hydroxyethyl)-ethylenediamine-*N,N,N'*-triacetate; $edtra^{3-}$, ethylenediamine-*N,N,N'*-triacetate; $medtra^{3-}$, *N'*-methylethylenediamine-*N,N,N'*-triacetate; $eedtra^{3-}$, *N'*-ethylethylenediamine-*N,N,N'*-triacetate; OAc^-, acetate.

9) U. Mayer, V. Gutmann, and W. Gerger, *Monatsh. Chem.*, **106**, 1235 (1975).

10) L. Rosenhein, D. Speiser, and A. Haim, *Inorg. Chem.*, **13**, 1571 (1974).

11) H. Ogino, M. Takahashi, and N. Tanaka, *Bull. Chem. Soc. Jpn.*, **47**, 1426 (1974).

12) J. Phillips and A. Haim, *Inorg. Chem.*, **19**, 1616 (1980).

13) H. Ogino, T. Watanabe, and N. Tanaka, *Inorg. Chem.*, **14**, 2093 (1975).

14) Y. Kushi, K. Morimasa, and H. Yoneda, The 49th National Meeting of the Chemical Society of Japan, Tokyo, April 1984, Abstr., No. 1N31.

15) H. Ogino and M. Shimura, *Adv. Inorg. Bioinorg. Mech.*, **4**, 107 (1986), and references cited therein.

16) W. D. Wheeler and J. I. Legg, *Inorg. Chem.*, **24**, 1292 (1985).

17) S. Kaizaki and H. Mizu-uchi, *Inorg. Chem.*, **25**, 2732 (1986).

18) D. T. Sawyer and J. M. McKinnie, *J. Am. Chem. Soc.*, **82**, 4191 (1960).

19) N. Tanaka, K. Kanno, T. Tomita, and A. Yamada, *Inorg. Nucl. Chem. Lett.*, **7**, 953 (1971).

20) S. Kirschner, *Inorg. Synth.*, **5**, 186 (1957).

21) H. Ogino and K. Ogino, *Inorg. Chem.*, **22**, 2208 (1983).

22) F. P. Dwyer, and F. L. Garvan, *J. Am. Chem. Soc.*, **83**, 2610 (1961).

23) C. W. Van Saun and B. E. Douglas, *Inorg. Chem.*, **7**, 1393 (1968).

24) H. A. Weakliem and J. L. Hoard, *J. Am. Chem. Soc.*, **81**, 549 (1959).

25) R. J. Day and C. N. Reilley, *Anal. Chem.*, **37**, 1326 (1965).

26) The present authors are reluctant to specify whether the formulation of Cr(III)-EDTA in aqueous solution is [Cr(edta)(H_2O)]$^-$ or [Cr(edta)]$^-$. Because both [Cr(edta)(H_2O)]$^-$ and [Cr(edta)]$^-$ have the same chromophore, CrN_2O_4, and there are controversial arguments on the formulation which remain to be settled.[15]

27) H. Ogino and T. Watanabe, unpublished results.

28) G. Schwarzenbach, *Helv. Chim. Acta*, **32**, 839 (1949).

29) M. L. Morris and D. H. Busch, *J. Am. Chem. Soc.*, **78**, 5178 (1956).

30) H. Ogino and H. Isago, *Chem. Lett.*, **1984**, 561.

31) I. A. W. Shimi and W. C. E. Higginson, *J. Chem. Soc.*, **1958**, 260.

32) W. C. E. Higginson, *J. Chem. Soc. A*, **1970**, 1579.

33) In Taura's original paper,[7] the λ_{max} values are plotted against acceptor numbers. However, the λ_{max} values are replaced by the $\tilde{\nu}_{max}$ values ($\tilde{\nu}_{max}=10^2/\lambda_{max}$) in Fig. 4. This change does not influence the linear correlation practically, since the $\tilde{\nu}_{max}$ values lie in a rather narrow range: 1.79×10^4—1.86×10^4 cm^{-1}.

34) H. Ogino, M. Shimura, and N. Tanaka, *Inorg. Chem.*, **18**, 2497 (1979).

 © 1987 The Chemical Society of Japan Bull. Chem. Soc. Jpn., 60, 1355—1359 (1987)

Preparation and Crystal Structures of Binuclear Copper(II) Complexes of *N,N',N'',N'''*-Tetrakis(2-aminoethyl)-1,4,8,11-tetraazacyclotetradecane Containing Azide, Cyanate, or Thiocyanate Ion

Masahiro MIKURIYA,* Sigeo KIDA,*,† and Ichiro MURASE††
Coordination Chemistry Laboratories, Institute for Molecular Science, Myodaiji, Okazaki 444
†Department of Chemistry, Faculty of Science, Kyushu University 33, Hakozaki, Higashi-ku, Fukuoka 812
††Laboratory of Chemistry, College of General Education, Kyushu University 01, Ropponmatsu, Chuo-ku, Fukuoka 810
(Received October 24, 1986)

Three binuclear copper(II) complexes of *N,N',N'',N'''*-tetrakis(2-aminoethyl)-1,4,8,11-tetraazacyclotetradecane (taec), $[Cu_2(taec)N_3](ClO_4)_3$ (**1**), $[Cu_2(taec)(NCO)](ClO_4)_3$ (**2**), and $[Cu_2(taec)(NCS)_2](ClO_4)_2 \cdot H_2O$ (**3**), were prepared and characterized. The crystal structures of these complexes were determined by single-crystal X-ray analysis. In all the complexes taec coordinates to each copper through two ring- and two pendant-nitrogen atoms. Complexes **1** and **2** adopt similar structures, where N_3^- and NCO^- are incorporated into the cavity of taec as a bridging group (end-on fashion). The structure of **3** is substantially different from those of **1** and **2** in that each copper is independently coordinated by NCS^--nitrogen. The spectral and magnetic properties were discussed in relation to the molecular structures.

μ-Azidodicopper(II) complexes have been extensively studied in the last half decade, because of the interest in the fields of molecular magnetism and bioinorganic chemistry.[1-4] It is well-known that azide ion can bridge two copper(II) ions either in end-on fashion I or in end-to-end fashion II.[1] It has been established

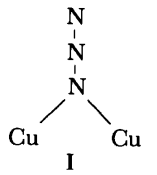

I

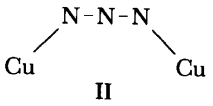

II

that the end-on bridge of azide ion favors the triplet ground state whereas the end-to-end bridge brings about a strong antiferromagnetic interaction.[2] The latter type of μ-azido complexes is of interest as models for azide derivatives of the active site of methemocyanine and met-tyrosinase in which a pair of copper(II) ions are strongly coupled antiferromagnetically.[3]

Recently we have prepared a new octadentate ligand, *N,N',N'',N'''*-tetrakis(2-aminoethyl)-1,4,8,11-tetraazacyclotetradecane (abbreviated as taec) and its metal complexes.[5-7] Interestingly, all the complexes obtained are 2 : 1 (metal : taec) binuclear complexes. So far, two types of coordination modes are known for the taec ligand: one is the trans III form[8] concerning the cyclam ring (chair form, Fig. 1 (A)) as found for $[Cu_2(taec)](ClO_4)_4$[5] and the other is the trans I form[8] (boat form, Fig. 1 (B)) as found for $[Cu_2(taec)Br](ClO_4)_3$.[6] In the latter case, single bromide ion is incorporated into the cavity of the ligand and coordinated to both copper ions. Using this unique property, we have prepared μ-azidocopper(II) complex of taec, $[Cu_2(taec)N_3](ClO_4)_3$, and determined the X-ray crystal structure in order to examine the bridging mode of the azide ion in the cavity of taec. We have also prepared copper(II) complexes with the isoelectronic cyanate and thiocyanate ions, $[Cu_2(taec)(NCO)](ClO_4)_3$ and $[Cu_2(taec)(NCS)_2](ClO_4)_2 \cdot H_2O$. Here, we report the preparation, the crystal structures, and the magnetic and spectral properties of these binuclear copper(II) complexes.

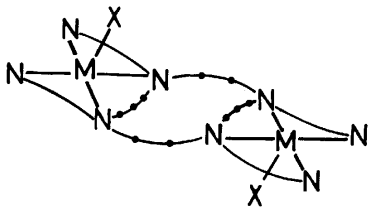

(A)

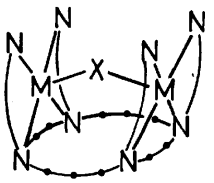

(B)

Fig. 1. Coordination mode of taec.

Experimental

Preparation. The preparative method for taec was already reported in the preceding papers.[5,6]

$[Cu_2(taec)N_3](ClO_4)_3$: To an aqueous solution of $Cu(ClO_4)_2 \cdot 6H_2O$ (185 mg) and taec (93 mg) was added NaN_3 (16 mg), and the mixture was heated at 80 °C for 20 min. The resulting blue solution was filtered. When the filtrate was allowed to stand overnight, blue needles were separated. The crystals were collected and desiccated over P_2O_5. Found: C, 25.64; H, 5.31; N, 18.19%. Calcd for $C_{18}H_{44}Cl_3Cu_2N_{11}O_{12}$: C, 25.74; H, 5.28; N, 18.34%.

$[Cu_2(taec)(NCO)](ClO_4)_3$: The complex was obtained as blue needles in the same way as that of $[Cu_2(taec)N_3](ClO_4)_3$

Table 1. Crystal Data and Data Collection Details[a)]

Complex	$[Cu_2(taec)N_3](ClO_4)_3$	$[Cu_2(taec)(NCO)](ClO_4)_3$	$[Cu_2(taec)(NCS)_2](ClO_4)_2\cdot H_2O$
Formula	$C_{18}H_{44}Cl_3Cu_2N_{11}O_{12}$	$C_{19}H_{44}Cl_3Cu_2N_9O_{13}$	$C_{20}H_{46}Cl_2Cu_2N_{10}O_9S_2$
F. W.	840.06	840.06	832.76
Crystal system	Orthorhombic	Orthorhombic	Orthorhombic
Space group	$Pmn2_1$	$Pmn2_1$	$Pnnm$
a/Å	8.875(4)	8.885(2)	10.926(3)
b/Å	8.076(1)	8.047(1)	16.005(3)
c/Å	21.756(9)	21.847(4)	9.923(2)
V/Å^3	1559.3(9)	1562.0(5)	1735.2(7)
Z	2	2	2
D_c/g cm^{-3}	1.79	1.79	1.56
D_m/g cm^{-3}	1.79	1.78	1.60
$F(000)$	868	868	864
μ(Mo $K\alpha$)/cm^{-1}	17.0	17.0	15.5
Crystal dimensions (mm)	0.35×0.35×0.35	0.20×0.30×0.41	0.28×0.28×0.32
2θ range (°)	1.5—68.0	1.5—68.0	2.0—66.0
Total no. of observed reflections	3613	3622	3696
No. of unique reflections with $\|F_o\|>3\sigma(\|F_o\|)$	2785	2438	2000
Final no. of variables	361	361	203
Final residual R	0.054	0.062	0.066
Final residual R'	0.082	0.089	0.096
Goodness of fit[b)]	0.31	0.34	0.36
Largest peak in final diff Fourier (e/Å^3)	1.07	1.19	1.39

a) Common data: graphite-monochromated Mo $K\alpha$ radiation (λ=0.71073 Å), scan type θ—2θ, scan speed 3 °min^{-1}, scan width $(1.4+0.5\tan\theta)$°. b) GOF=$[\sum w(|F_o|-|F_c|)^2/(N_{observns}-N_{params})]^{1/2}$.

except for using potassium cyanate instead of sodium azide. Found: C, 26.72; H, 5.32; N, 14.83%. Calcd for $C_{19}H_{44}Cl_3Cu_2N_9O_{13}$: C, 27.17; H, 5.28; N, 15.01%.

$[Cu_2(taec)(NCS)_2](ClO_4)_2\cdot H_2O$: The complex was obtained as blue needles in the same way as that of $[Cu_2(taec)N_3](ClO_4)_3$ except for using potassium thiocyanate instead of sodium azide. Found:, C, 29.43; H, 5.75; N, 17.37%. Calcd for $C_{20}H_{46}Cl_2Cu_2N_{10}O_9S_2$: C, 28.85; H, 5.57; N, 16.82%.

Measurements. Carbon, hydrogen, and nitrogen analyses were carried out at the Service Center of Elemental Analysis, Kyushu University. Electronic spectra were measured with a Shimadzu Multipurpose Spectrophotometer Model MSP-5000 at room temperature. Magnetic susceptibility was measured by the Faraday method over the temperature range 80—300 K. The apparatus was calibrated by the use of $[Ni(H_2NCH_2CH_2NH_2)_3]S_2O_3$. The susceptibilities were corrected for the diamagnetism of the constituent atoms by the use of Pascal's constants.[9)] Effective magnetic moments were calculated from the equation, $\mu_{eff}=2.828\sqrt{(\chi_A-N\alpha)T}$, where χ_A is the atomic magnetic susceptibility and $N\alpha$ is the temperature-independent paramagnetism.

X-Ray Crystal Structure Analysis. A Rigaku AFC-5 automated four-circle diffractometer was used for all measurements at 18 °C. Crystal data and details of the data collection are given in Table 1. Lattice constants were determined by least-squares refinement based on 40 reflections with $20<2\theta<30°$. The intensity data were corrected for Lorentz-polarization effects, but not for absorption. The structures were solved by the direct methods. Refinements were carried out by the block-diagonal least-squares methods. In the course of refinement it became apparent that the carbon atom, C(3), is subjected to disorder in $[Cu_2(taec)X](ClO_4)_3$ (X=N_3 and NCO). The carbon atom was divided into two positions with an occupancy factor 0.5 on the basis of a difference Fourier map. Hydrogen atoms were inserted in their calculated positions and included in the refinement. The final discrepancy factors were $R=\sum||F_o|-|F_c||/\sum|F_o|=0.054$, $R'=[\sum w(|F_o|-|F_c|)^2/\sum w|F_o|^2]^{1/2}=0.082$ for $[Cu_2(taec)N_3](ClO_4)_3$, $R=0.062$, $R'=0.089$ for $[Cu_2(taec)(NCO)](ClO_4)_3$, and $R=0.066$, $R'=0.096$ for $[Cu_2(taec)(NCS)_2](ClO_4)_2\cdot H_2O$. The weighting schemes were $w=(6.1+|F_o|+0.010|F_o|^2)^{-1}$ for $[Cu_2(taec)N_3](ClO_4)_3$, $(7.6+|F_o|+0.010|F_o|^2)^{-1}$ for $[Cu_2(taec)(NCO)](ClO_4)_3$, and $(8.0+|F_o|+0.008|F_o|^2)^{-1}$ for $[Cu_2(taec)(NCS)_2](ClO_4)_2\cdot H_2O$.

The atomic scattering factors for Cu, Cl, S, O, N, C, and H and the anomalous dispersion corrections, $\Delta f'$ and $\Delta f''$, for Cu, Cl, S, O, N, and C were taken from Ref. 10. All the calculations were carried out on the FACOM M-200 computer at the Computer Center of Kyushu University using a local version of the MULTAN 78,[11)] UNICS-III,[12)] and ORTEP[13)] programs. The final positional and thermal parameters with their estimated standard deviations are given in Table 2. The coordinates and isotropic temperature factors of hydrogen atoms, the anisotropic thermal parameters of the non-hydrogen atoms, the remaining bond distances and angles, and the F_o—F_c tables have been deposited as a Document No. 8731 at the Office of the Editor.

Results and Discussion

Crystal Structures. $[Cu_2(taec)N_3](ClO_4)_3$: A perspective drawing of the complex cation of $[Cu_2(taec)N_3](ClO_4)_3$ and the numbering system are illustrated in Fig. 2. The complex cation has a mirror plane containing Cu(1), Cu(2), N(5), N(6), and N(7). The cyclam ring assumes the trans I form[8)] and the coordination mode of taec is similar to that of $[Cu_2(taec)Br](ClO_4)_3$.[6)] The taec ligand forms two 5-5-5 fused che-

Table 2. Fractional Positional Parameters ($\times 10^4$) and Thermal Parameters of Non-Hydrogen Atoms with Their Estimated Standard Deviations in Parentheses

Atom	*x*	*y*	*z*	B_{eq}/Å$^{2a)}$	Atom	*x*	*y*	*z*	B_{eq}/Å$^{2a)}$
(1) $[Cu_2(taec)N_3](ClO_4)_3$					O(4)	0	10082(16)	1978(9)	6.9
Cu(1)	0	6434(1)	3330(1)	1.7	O(5)	0	7233(14)	1706(5)	6.5
Cu(2)	0	6417(1)	5312(1)	1.5	O(6)	−1335(10)	9073(13)	1156(6)	6.4
Cl(1)	0	8901(2)	7171(1)	2.4	O(7)	0	9055(20)	−597(18)	13.8
Cl(2)	0	8929(3)	1494(1)	2.5	O(8)	0	11454(31)	−102(8)	15.1
Cl(3)	0	10752(2)	−673(2)	2.8	O(9)	−1107(27)	11183(34)	−934(15)	28.9
O(1)	0	10079(9)	6646(4)	3.9	O(10)	0	10208(11)	4429(9)	5.8
O(2)	0	7295(12)	6901(5)	6.7	N(1)	1589(6)	4579(7)	3216(3)	1.7
O(3)	1301(9)	9159(11)	7552(4)	5.8	N(2)	1607(8)	4579(8)	5421(3)	2.5
O(4)	0	10040(15)	1949(6)	6.4	N(3)	1648(7)	8026(9)	3034(3)	2.6
O(5)	0	7217(10)	1722(4)	5.7	N(4)	1728(7)	7950(8)	5612(4)	2.7
O(6)	−1321(8)	9137(11)	1161(5)	6.2	N(5)	0	7290(10)	4329(8)	2.6
O(7)	0	9058(16)	−638(14)	11.2	C(1)	836(10)	3521(11)	2780(4)	3.1
O(8)	0	11438(24)	−117(6)	15.9	C(2)	2538(9)	4229(11)	3761(4)	2.7
O(9)	−1214(24)	11244(25)	−893(13)	29.5	C(3)	1670(16)	3751(15)	4276(10)	1.8
N(1)	1614(5)	4539(5)	3234(2)	1.9	C(3)'	2623(14)	4418(16)	4387(8)	1.9
N(2)	1574(5)	4598(6)	5442(2)	2.2	C(4)	2139(9)	3480(9)	4909(4)	2.4
N(3)	1680(7)	7990(6)	3029(3)	2.7	C(5)	714(10)	3079(10)	5655(5)	3.0
N(4)	1684(5)	7948(6)	5579(2)	2.2	C(6)	2393(10)	5246(11)	2687(4)	3.0
N(5)	0	7229(6)	4316(5)	2.1	C(7)	2834(11)	6968(13)	2762(6)	4.5
N(6)	0	8708(7)	4344(6)	2.5	C(8)	3020(9)	5356(11)	5697(5)	3.3
N(7)	0	10133(10)	4413(6)	4.8	C(9)	2796(15)	6932(15)	5989(7)	5.1
C(1)	790(8)	3495(9)	2798(4)	3.7	C(10)	0	8748(12)	4357(12)	2.8
C(2)	2544(8)	4200(9)	3759(3)	3.0					
C(3)	1681(12)	3742(12)	4278(8)	1.9	(3) $[Cu_2(taec)(NCS)_2](ClO_4)_2 \cdot H_2O$				
C(3)'	2639(10)	4386(12)	4313(9)	2.1	Cu	2190(1)	5887(1)	0	2.3
C(4)	2151(7)	3452(7)	4907(3)	2.4	Cl	2693(4)	8757(2)	0	7.5
C(5)	767(9)	3073(9)	5662(5)	4.1	S	3914(2)	3012(1)	0	4.4
C(6)	2418(7)	5274(9)	2689(3)	2.7	O(1)	3296(12)	8122(8)	0	12.0
C(7)	2777(8)	6999(9)	2708(5)	4.6	O(2)	3485(19)	9420(9)	0	14.9
C(8)	3035(7)	5344(9)	5680(3)	2.9	O(3)	1324(28)	9023(19)	0	11.8
C(9)	2835(11)	6922(13)	5923(5)	5.2	O(3)'	2267(24)	8719(14)	−1289(21)	16.4
					OW	0	0	2025(11)	8.1
(2) $[Cu_2(taec)(NCO)](ClO_4)_3$					N(1)	892(3)	6031(2)	1541(4)	2.4
Cu(1)	0	6463(1)	3327(1)	1.8	N(2)	3412(4)	6201(3)	1462(5)	3.9
Cu(2)	0	6433(1)	5314(1)	1.6	N(3)	2803(6)	4584(4)	0	4.1
Cl(1)	0	8886(3)	7172(1)	2.3	C(1)	−180(4)	5461(3)	1735(5)	2.8
Cl(2)	0	8934(3)	1485(1)	2.6	C(2)	411(5)	6899(3)	1303(6)	3.1
Cl(3)	0	10734(3)	−664(3)	2.8	C(3)	−291(7)	7021(4)	0	3.2
O(1)	0	10078(13)	6679(4)	4.3	C(4)	1621(5)	6021(3)	2819(5)	3.1
O(2)	0	7281(14)	6881(6)	6.9	C(5)	2790(5)	6497(4)	2678(6)	3.7
O(3)	1256(12)	9167(13)	7560(5)	6.4	C(6)	3302(7)	3933(4)	0	3.1

a) Anisotropically refined atoms are given in the form of the isotropic equivalent thermal parameter defined as $4/3[a^2B(1,1)+b^2B(2,2)+c^2B(3,3)+ab(\cos\gamma)B(1,2)+ac(\cos\beta)B(1,3)+bc(\cos\alpha)B(2,3)]$.

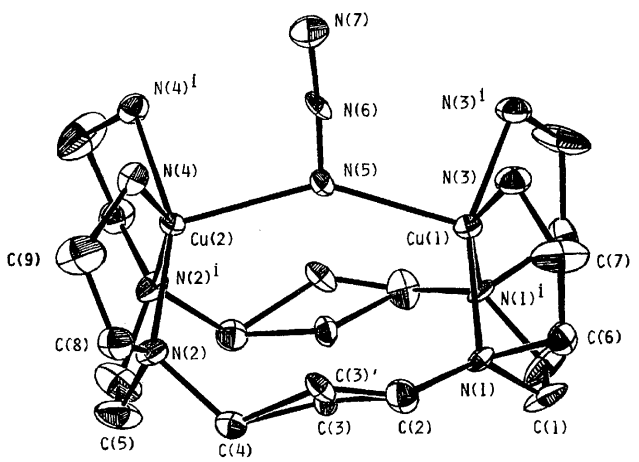

Fig. 2. ORTEP diagram of $[Cu_2(taec)N_3]^{3+}$. Superscript i refers to the equivalent position $(-x, y, z)$.

late rings with two copper ions. The coordination geometry of each copper ion is an elongated square pyramid. The basal plane is formed by two nitrogens of the cyclam ring and two nitrogens of the pendant amino groups. The basal plane is perfectly planar as required from the symmetry (the mirror plane) of the molecule and the copper ion is displaced by 0.45 Å from the plane toward the azide ion. The azide ion lies on the mirror plane and bridges the two copper ions at the apical positions with Cu-N distances of 2.240(12) and 2.263(12) Å. This is the first example of an end-on bridging of azide ion at axial sites of copper(II) ions. The Cu(1)-Cu(2) distance and Cu(1)-N(5)-Cu(2) angle are 4.312(1) Å and 146.5(3)°, respectively.

Of the three perchlorate ions, two are hydrogen bonded to the pendant amino groups (O(1)···N(4) 3.253(9), O(2)···N(4) 3.283(11), O(4)···N(3) 3.238(13),

Table 3. Selected Interatomic Distances (l/Å) and Angles (ϕ/°) with Their Estimated Standard Deviations in Parentheses

(1) $[Cu_2(taec)N_3](ClO_4)_3$[a]			
Cu(1)-N(1)	2.107(5)	Cu(2)-N(2)	2.047(5)
Cu(1)-N(3)	2.057(6)	Cu(2)-N(4)	2.025(5)
Cu(1)-N(5)	2.240(12)	Cu(2)-N(5)	2.263(12)
Cu(1)···Cu(2)	4.312(1)		
N(5)-N(6)	1.196(8)	N(6)-N(7)	1.160(10)
N(1)-Cu(1)-N(1)^i	85.7(2)	N(2)-Cu(2)-N(2)^i	86.0(2)
N(1)-Cu(1)-N(3)	85.4(2)	N(2)-Cu(2)-N(4)	84.0(2)
N(3)-Cu(1)-N(3)^i	92.9(2)	N(4)-Cu(2)-N(4)^i	95.1(2)
N(1)-Cu(1)-N(5)	107.6(2)	N(2)-Cu(2)-N(5)	109.9(2)
N(3)-Cu(1)-N(5)	97.5(2)	N(4)-Cu(2)-N(5)	95.6(2)
Cu(1)-N(5)-Cu(2)	146.5(3)	Cu(2)-N(5)-N(6)	104.0(9)
Cu(1)-N(5)-N(6)	109.5(9)	N(5)-N(6)-N(7)	175.4(15)
(2) $[Cu_2(taec)(NCO)](ClO_4)_3$[b]			
Cu(1)-N(1)	2.085(5)	Cu(2)-N(2)	2.078(7)
Cu(1)-N(3)	2.034(7)	Cu(2)-N(4)	2.066(7)
Cu(1)-N(5)	2.287(17)	Cu(2)-N(5)	2.260(16)
Cu(1)···Cu(2)	4.340(2)		
N(5)-C(10)	1.175(12)	C(10)-O(10)	1.186(14)
N(1)-Cu(1)-N(1)^i	85.2(2)	N(2)-Cu(2)-N(2)^i	86.8(3)
N(1)-Cu(1)-N(3)	85.7(2)	N(2)-Cu(2)-N(4)	83.0(3)
N(3)-Cu(1)-N(3)^i	92.1(3)	N(4)-Cu(2)-N(4)^i	96.0(3)
N(1)-Cu(1)-N(5)	108.8(2)	N(2)-Cu(2)-N(5)	109.0(2)
N(3)-Cu(1)-N(5)	97.0(3)	N(4)-Cu(2)-N(5)	96.9(3)
Cu(1)-N(5)-Cu(2)	145.3(4)	Cu(2)-N(5)-C(10)	104.7(16)
Cu(1)-N(5)-C(10)	109.9(2)	N(5)-C(10)-O(10)	175.4(27)
(3) $[Cu_2(taec)(NCS)_2](ClO_4)_2\cdot H_2O$[c]			
Cu-N(1)	2.098(4)	Cu-N(3)	2.191(7)
Cu-N(2)	2.034(5)	Cu···Cu^{ii}	5.565(1)
N(3)-C(6)	1.176(10)	S-C(6)	1.618(7)
N(1)-Cu-N(2)	84.1(2)	N(2)-Cu-N(3)	92.0(2)
N(1)-Cu-N(1)^i	93.6(2)	Cu-N(3)-C(6)	170.1(6)
N(2)-Cu-N(2)^i	91.0(2)	N(3)-C(6)-S	176.7(7)
N(1)-Cu-N(3)	108.1(2)		

a) Superscript i refers to the equivalent position ($-x$, y, z). b) Superscript i refers to the equivalent position ($-x$, y, z). c) Superscript i and ii refer to the equivalent positions (x, y, $-z$) and ($-x$, $1-y$, z), respectively.

O(5)···N(3) 3.271(11) Å), and one (designated as Cl(3), O(7), O(8), O(9), and O(9)($-x$, y, z)) is not bound to any special atoms.

$[Cu_2(taec)(NCO)](ClO_4)_3$: The crystal of $[Cu_2(taec)(NCO)](ClO_4)_3$ is isomorphous to that of $[Cu_2(taec)N_3](ClO_4)_3$. The complex cation, $[Cu_2(taec)(NCO)]^{3+}$, has a mirror plane containing Cu(1), Cu(2), N(5), C(10), and O(10) (Fig. 3). The nitrogen atom of NCO^- bridges the two copper ions. The Cu(1)-Cu(2) distance and Cu(1)-N(5)-Cu(2) angle are 4.340(2) Å and 145.3(4)°, respectively. This bridging mode of NCO^- was found in $[Cu_2(C_{17}H_{27}N_4O)(CH_3COO)(NCO)][PF_6]$ recently.[4]

$[Cu_2(taec)(NCS)_2](ClO_4)_2\cdot H_2O$: A perspective drawing of the complex cation, $[Cu_2(taec)(NCS)_2]^{2+}$, is shown in Fig. 4. The cation has the center of symmetry and a mirror plane formed by C(3), Cu, N(3), C(6), S, C(3)^{ii}, Cu^{ii}, N(3)^{ii}, C(6)^{ii}, and S^{ii}. Contrary to $[Cu_2(taec)X](ClO_4)_3$ (X=N_3 and NCO), the cyclam ring assumes the trans III form and the coordination mode of taec is the same as that of $[Cu_2(taec)](ClO_4)_4$[5] in which axial coordination sites do not face to each other but face rather opposite directions and are independently coordinated with NCS^-. The coordination geometry of each copper is a square pyramid with a thiocyanate nitrogen at the top (Cu-N(3) 2.191(7) Å).

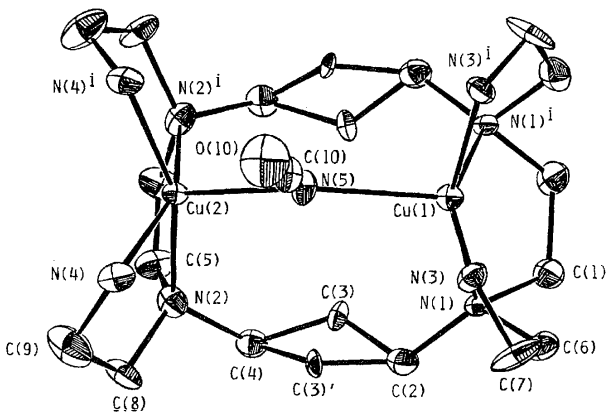

Fig. 3. ORTEP diagram of $[Cu_2(taec)(NCO)]^{3+}$. Superscript i refers to the equivalent position ($-x$, y, z).

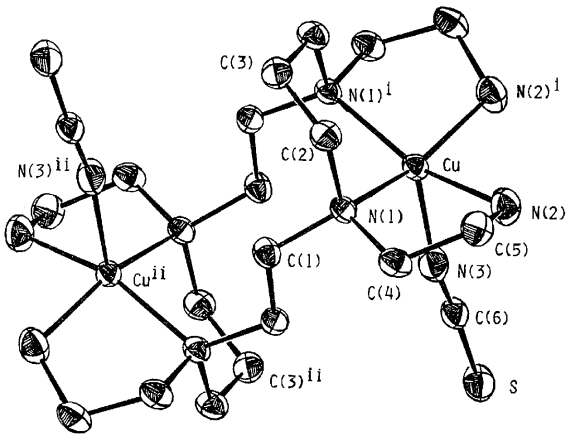

Fig. 4. ORTEP diagram of $[Cu_2(taec)(NCS)_2]^{2+}$. Superscripts i and ii refer to the equivalent positions (x, y, $-z$) and ($-x$, $1-y$, z), respectively.

The basal plane formed by two nitrogens of the cyclam ring and two terminal nitrogens is perfectly planar as required from the symmetry (C_{2h}) of the molecule, and the copper atom deviates by 0.37 Å from the basal plane toward thiocyanate ion.

Each water molecule is located in a vicinity of the pendant amino group of taec forming hydrogen bonds with the amino nitrogen and a perchlorate ion (N(2)$\cdots$OW($1/2+x$, $1/2-y$, $1/2-z$) 2.993(7) Å, O(3)$\cdots$OW(x, $1+y$, z) 2.929(23) Å).

Spectral and Magnetic Properties and Crystal Structures. Nujol mull spectra of $[Cu_2(taec)N_3](ClO_4)_3$, $[Cu_2(taec)(NCO)](ClO_4)_3$, and $[Cu_2(taec)(NCS)_2](ClO_4)_2\cdot H_2O$ each show a d-d band at 15.7, 15.6, and 17.1×10^3 cm^{-1}, respectively. The difference of the wavenumber in these complexes must be mainly due to the degree of the deviation of copper ion from the basal plane, i.e., 0.45, 0.46, and 0.37 Å, respectively. The bands of the azido and cyanato complexes are blue-shifted in aqueous solution relative to those in nujol mull, i.e., 15.7→16.1 (ε=217) and 15.6→15.8×10^3 cm^{-1} (ε=203), indicating the hydrolysis of coordinated anions in aqueous solution in more or less degree (the thiocyanato complex is sparingly soluble in water).[14]

The magnetic moments per copper ion of $[Cu_2(taec)N_3](ClO_4)_3$, $[Cu_2(taec)(NCO)](ClO_4)_3$, and $[Cu_2(taec)(NCS)_2](ClO_4)_2\cdot H_2O$ are 1.82, 1.77, and 1.75 B.M., respectively, at room temperature. All the complexes obey the Curie-Weiss law in the temperature range 80—300 K with the Weiss constants, −1, 0, and −5 K for the azido, cyanato, and thiocyanato complexes, respectively. The very small values indicate that there is no significant magnetic interaction between the copper ions. The result is quite understandable in view of that in these complexes an unpaired electron of a copper(II) ion is localized in the $d_{x^2-y^2}$ orbital of the basal plane of the CuN_5 square-based pyramid so that no overlapping of the magnetic orbitals is feasible.

References

1) Z. Dori and R. Ziolo, *Chem. Rev.*, **73**, 247 (1973).
2) M.-F. Charlot, O. Kahn, M. Chaillet, and C. Larrieu, *J. Am. Chem. Soc.*, **108**, 2574 (1986), and references therein.
3) V. McKee, M. Zvagulis, J. Dadgegian, M. G. Patch, and C. A. Reed, *J. Am. Chem. Soc.*, **106**, 4765 (1984); K. D. Karlin, J. C. Hayes, J. P. Hutchinson, and J. Zubieta, *J. Chem. Soc., Chem. Commun.*, **1983**, 376; Y. Agnus, R. Louis, J.-P. Gisselbrecht, and R. Weiss, *J. Am. Chem. Soc.*, **106**, 93 (1984); T. N. Sorrell, C. J. O'Connor, O. P. Anderson, and J. H. Reibenspies, *J. Am. Chem. Soc.*, **107**, 4199 (1985).
4) M.-L. Boillot, O. Kahn, C. J. O'Connor, J. Gouteron, S. Jeannin, and Y. Jeannin, *J. Chem. Soc., Chem. Commun.*, **1985**, 178.
5) I. Murase, M. Mikuriya, H. Sonoda, and S. Kida, *J. Chem. Soc., Chem. Commun.*, **1984**, 692.
6) I. Murase, M. Mikuriya, H. Sonoda, Y. Fukuda, and S. Kida, *J. Chem. Soc., Dalton Trans.*, **1986**, 953.
7) S. Kida, I. Murase, C. Harada, L. Daizeng, and M. Mikuriya, *Bull. Chem. Soc. Jpn.*, **59**, 2595 (1986).
8) B. Bosnich, C. K. Poon, and M. L. Tobe, *Inorg. Chem.*, **4**, 1102 (1965).
9) P. W. Selwood, "Magnetochemistry," Interscience Publishers, New York (1956), pp. 78, 91.
10) "International Tables for X-Ray Crystallography," Kynoch Press, Birmingham (1974), Vol. 4.
11) P. Main, S. E. Hull, L. Lessinger, G. Germain, J. P. Declercq, and M. M. Woolfson, *MULTAN* **78**, A System of Computer Programs for the Automatic Solution of Crystal Structures from X-Ray Diffraction Data, University of York (1978).
12) T. Sakurai and K. Kobayashi, *Rep. Inst. Phy. Chem. Res. Wako*, **55**, 69 (1979).
13) C. K. Johnson, Report No. ORNL3794, Oak Ridge National Laboratory, Oak Ridge, Tenessee (1965).
14) $[Cu_2(taec)](ClO_4)_4$ shows a d-d band at $17.7\times10^3 cm^{-1}$ in aqueous solution.

 © 1987 The Chemical Society of Japan Bull. Chem. Soc. Jpn., 60, 1361—1365 (1987)

The Identification of Insoluble Adducts of Lewis Acids with Bases by Extension of the Continuous Variation Method to Solid-Liquid Reactions

Goro HIHARA,* Kazuhiro MITANI, Hiroshi MIYAMAE, and Miharu NAGATA
Department of Chemistry, Faculty of Science, Josai University, Keyakidai, Sakado, Saitama 350-02
(Received October 25, 1986)

A method has been developed for identifying occurrence and composition of all the insoluble adducts formed in solid-liquid reactions by extension of the continuous variation method to the heterogeneous systems that were produced by the reactions of PbX_2 (X=Cl, Br, and I) with ethylenediamine(=en) in ethanol solution. Four new adducts, $PbX_2 \cdot i$(en) (i=1/2 and 1; X=Cl and Br), were found. The developed method was effective in identifying formation of the adducts such as $PbCl_2 \cdot 1/2$(en) and $PbBr_2 \cdot 1/2$(en) whose formation is liable to be overlooked in extending the mole ratio method to solid-liquid reactions.

In previous papers,[1-3] we have developed the methods to identify the insoluble adducts formed in solid-liquid reactions by extending either the mole ratio method[4] or the continuous variation method[5] to the heterogeneous reactions. However, the mole ratio method extended to the reactions has a drawback that formation of insoluble adducts is liable to be overlooked when the region of occurrence is narrow as in the cases of $PbI_2 \cdot 2/3$(en)[1] and $PbI_2 \cdot 1/2$(diethylenetriamine)(=dien).[2] The purpose of this psper is to develop theoretically a method for identifying occurrence and composition of insoluble adducts by extending the continuous variation method discussed in the preceding paper[3] to solid-liquid reactions in order to overcome the drawback of the mole ratio method.

Theoretical

Let us assume that an insoluble Lewis acid, A, reacts with a soluble Lewis base, B, in a solution according to Eqs. 1 and 2 to yield two insoluble adducts:

$$\mathrm{A(solid)} + m\mathrm{B(soln.)} = \mathrm{A} \cdot m\mathrm{B(solid)}, \quad (1)$$

$$\mathrm{A} \cdot m\mathrm{B(solid)} + n\mathrm{B(soln.)} = \mathrm{A} \cdot (m+n)\mathrm{B(solid)}. \quad (2)$$

Suppose that A and B react in varying proportions at fixed temperature and pressure in a fixed volume of the reaction solution so that the sum of A and B is kept constant at D mol. Provided that the concentration of B remaining unreacted in solution ([B] mol dm^{-3}) is determined after an equilibrium has been reached, the relation between [B] and B at the beginning of the reaction is depicted by a curve in Fig. 1, which is termed "concentration curve".

As discussed on the basis of the phase rule in a previous paper,[2] the region where [B] increases and the region where [B] becomes constant appear alternately on the concentration curve. Two regions 2 and 4, where the concentration curve is flat, represent two invariant states. Accordingly, A and A·mB coexist in region 2 and A·mB and A·$(m+n)$B, in region 4 in each solid phase. On the other hand, three regions 1, 3, and 5 where the curve has a certain slope represent three monovariant states and correspond to the presence of A, A·mB, and A·$(m+n)$B in the solid phase, respectively.

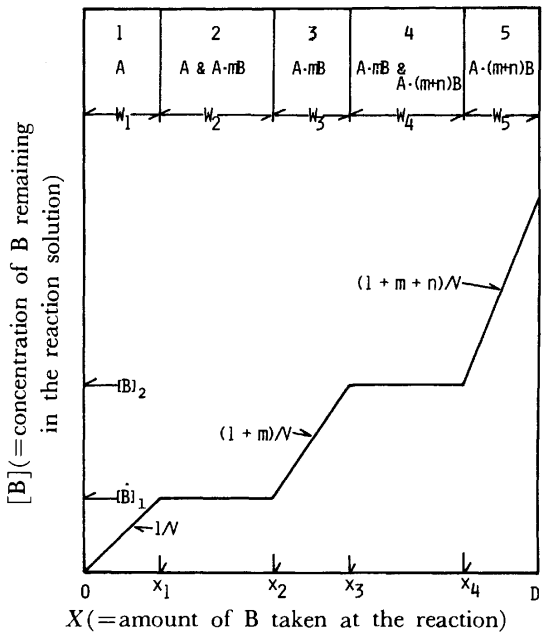

Fig. 1. A typical phase diagram for a ternary system consisting of A, B, and solvent where two insoluble adducts, A·mB and A·$(m+n)$B, form.

Let us consider how the slope on the concentration curve changes in each monovariant region. If the volume of reaction solution (V dm^3) remains unchanged during the reaction and species involving A dissolve sparingly into the solution, [B] is given by:

$$[\mathrm{B}] = (x - yz)/V, \quad (3)$$

where x and z are the amounts of B and A in mol at the beginning of the reaction, respectively, and y is the mole ratio of B/A in the sediment. Since the reaction is carried out under the condition that D is constant,

$$D = x + z = \text{constant}. \quad (4)$$

Equation 5 is obtained from Eqs. 3 and 4 by eliminating z:

$$[\mathrm{B}] = \frac{x - y(D-x)}{V} = \frac{(1+y)}{V}x - \frac{yD}{V}. \quad (5)$$

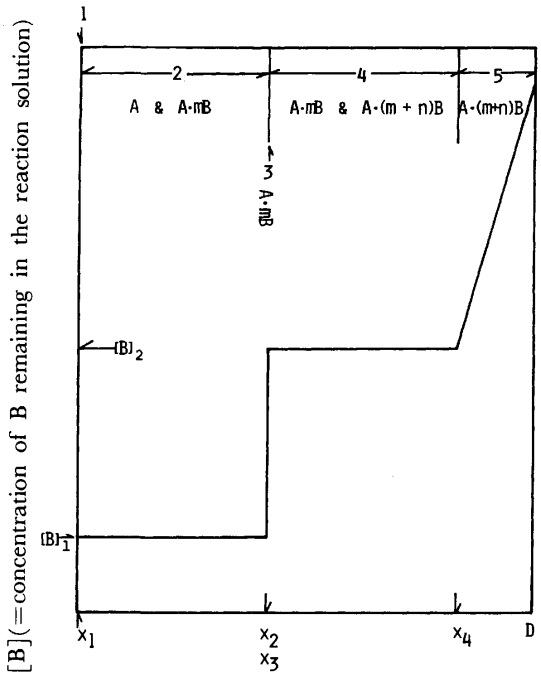

Fig. 2. A typical phase diagram for a ternary system where both $[B]_1$ and $[B]_2$ are very low.

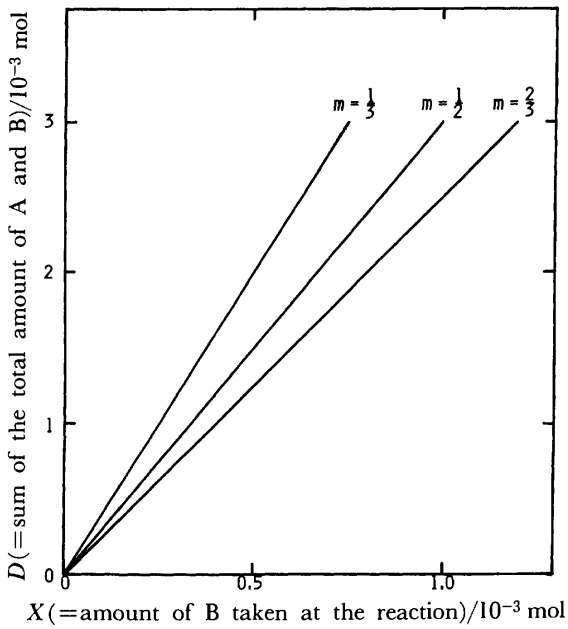

Fig. 3. Relation between the point of phase boundary and D when $[B]_1$ and $[B]_2$ are low.

The value of the slope equals $1/V$ in region 1 where only A is present in the solid phase, because $y=0$. Similarly, the values of the slope are $(1+m)/V$ and $(1+m+n)/V$ in regions 3 and 5, respectively, because $y=m$ and $y=m+n$. Therefore, once the concentration curve is obtained experimentally, the composition of the formed adducts can be determined by the slope of the concentration curve in each monovariant region.

If the equilibrated concentrations of B are $[B]_1$ and $[B]_2$ in the respective invariant regions 2 and 4, the amount of B in the boundary between monovariant and invariant region is given by substituting either $[B]_1$ or $[B]_2$ for [B] in Eq. 5 and solving for x:

$$x_1 = [B]_1V, \tag{6}$$

$$x_2 = (mD + [B]_1V)/(1 + m), \tag{7}$$

$$x_3 = (mD + [B]_2V)/(1 + m), \tag{8}$$

$$x_4 = ((m + n)D + [B]_2V)/(1 + m + n). \tag{9}$$

The width of each region, $W_1, \cdots, W_5$, is given by calculating successively the difference in each x with Eqs. 6—9:

$$W_1 = x_1 - 0 = [B]_1V, \tag{10}$$

$$W_2 = x_2 - x_1 = m(D - [B]_1V)/(1 + m), \tag{11}$$

$$W_3 = x_3 - x_2 = ([B]_2 - [B]_1)V/(1 + m), \tag{12}$$

$$W_4 = x_4 - x_3 = n(D - [B]_2V)/(1 + m + n)(1 + m), \tag{13}$$

$$W_5 = D - x_4 = (D - [B]_2V)/(1 + m + n). \tag{14}$$

Let us consider how each width depends on $[B]_1$ and $[B]_2$ when they are less than 10^{-3} M (1 M=1 mol dm^{-3}). Solid-liquid reactions are usually carried out under the condition that D is 1—2 mmol and V is 10 cm^3. The value of $[B]_1V$ or $[B]_2V$ ($10^{-3}M \times 10^{-2}$ dm^3=10^{-5} mol) is much smaller than mD ($m \times 10^{-3}$ mol). Therefore, both W_1 and W_3 are nearly equal to zero, as is shown in Fig. 2. Hence, Eq. 15 is derived from Eqs. 7 snd 8, because $[B]_1 \approx [B]_2 \approx 0$:

$$x_2 = x_3 = mD/(1 + m). \tag{15}$$

Equation 15 shows that the B value in the boundary between invariant regions 2 and 3, and between 3 and 4, depends on D and composition m. This relation is illustrated in Fig. 3, which shows how the value changes with D. Accordingly, if equilibrated concentration of B is low in invariant regions, the composition of adducts can be determined by Eq. 15.

Experimental

Apparatus. A Toa Denpa HM-18E pH meter was used to determine potentiometrically the concentration of en in equilibrated reaction solutions. Low concentration of en was determined by a Shimazu MPS-2000 double beam spectrophotometer to measure the absorbance at 430 nm. The reactions were carried out in a Taiyo WB-3 incubator with mechanical shaking.

Reagents. The preparation of PbI_2 was described previously.[2] $PbBr_2$ was prepared by mixing a solution of $Pb(NO_3)_2$ with that of KBr in the stoichiometric ratio, the sediment was separated from the solution, dried at 110 °C for about 12 h, and stored in the dark. $PbCl_2$ was purified by recrystallization from distilled water. Ethylenediamine (99.0% pure) purchased from Wako Pure Chemical Co. was used without further purification. Ethanol was dehydrated with molecular sieves (3A1/16) and then distilled.

The Solid-Liquid Reactions of PbX_2 (X=Cl, Br, and I) with en. (1) Extension of the Mole Ratio Method. 0.500 g

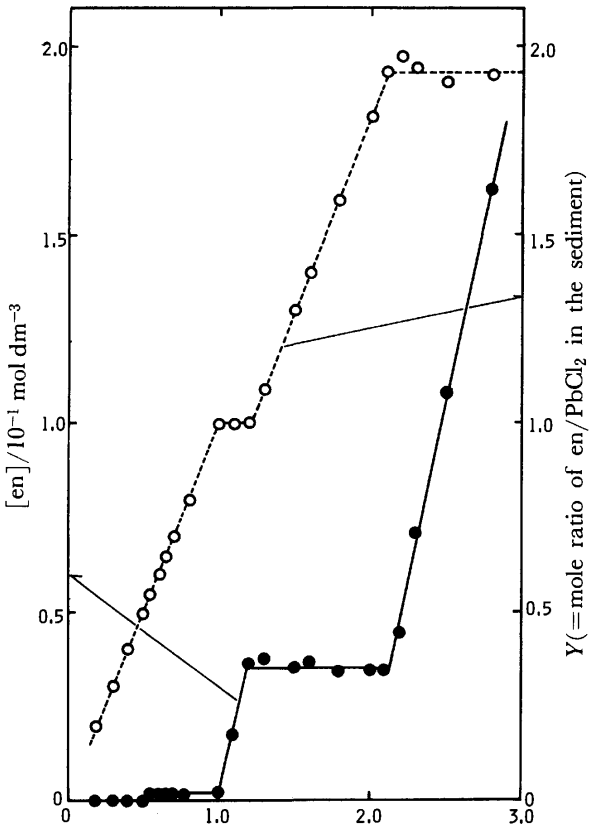

Fig. 4. Relation between the concentration of ethylenediamine remaining in the solution and mole ratio of en/$PbCl_2$ taken at the reaction when the mole ratio method was extended to the reaction of $PbCl_2$ with en: —●—●—, concentration curve; --O--O--, composition curve (definition, see text).

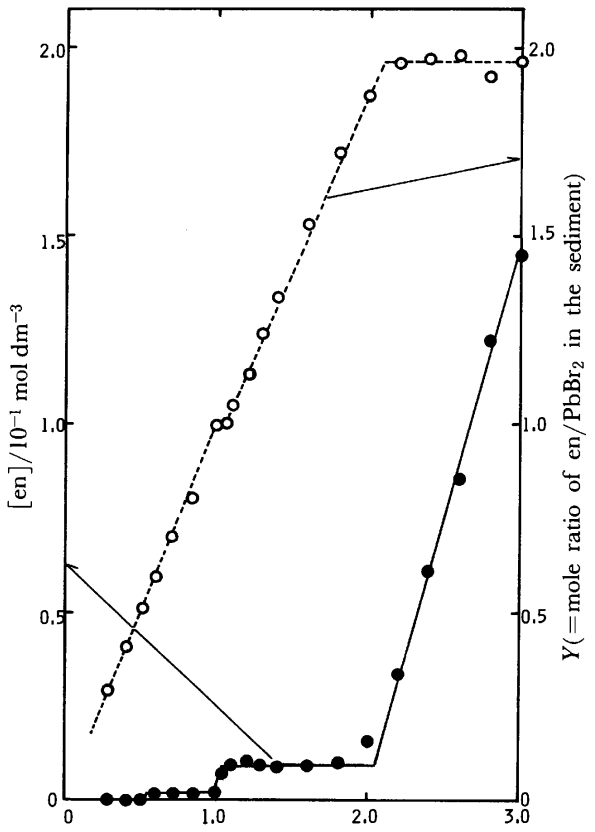

Fig. 5. Relation between the concentration of ethylenediamine remaining in the solution and mole ratio of en/$PbBr_2$ taken at the reaction when the mole ratio method was extended to the reaction of $PbBr_2$ with en: —●—●—, concentration curve; --O--O--, composition curve.

of finely powdered PbX_2 (X=Cl and Br) suspended in 10.0 cm^3 ethanol solution containing various amounts of en was put into ampoule. After several glass beads (about 0.2 cm in diameter) were added, the ampoule was sealed and shaked at 25.0±0.2 °C for about one month in the incubator. The mole ratio of en/PbX_2 at the beginning of reaction varied in the range of 0.3—3.0. Each ampoule was covered with an aluminium film in the case of the reaction of $PbBr_2$ with en to prevent the $PbBr_2$ from turning black owing to exposure to light. Reaction solution was separated from sediment after the reaction reached the equilibrium and then was subjected to chemical analysis.

(2) Extension of the Continuous Variation Method. Various amounts of finely powdered PbX_2 (X=Cl, Br, and I) and 10 cm^3 of ethanol solution containing various amounts of en were mixed in ampoule in varying proportions that the sum of PbX_2 and en is constant. The suspension was then treated as described above. The adopted D was 2.0 mmol for $PbCl_2$, $PbBr_2$, and PbI_2 and 1.5 mmol for $PbCl_2$.

Chemical Analysis of the Equilibrated Reaction Solutions. The concentration of en in the equilibrated reaction solutions was determined either potentiometrically when the concentration is high and spectrophotometrically[6] when low. [Pb^{2+}] was determined complexometrically[7] for some solutions.

Results and Discussion

Preliminary experiments confirmed that PbX_2 (X=Cl, Br, and I) does not react with ethanol and is sparingly soluble in it even in the presence of en.

Wharf et al. prepared $PbX_2 \cdot 2(en)$ (X=Cl, Br, and I).[8] We ascertained, however, the formation of $PbI_2 \cdot 2/3(en)$ and $PbI_2 \cdot en$ in addition to $PbI_2 \cdot 2(en)$.[1] Therefore, solid-liquid reactions of PbX_2 (X=Cl and Br) with en were carried out by extension of the mole ratio method in order to confirm if any other adducts than $PbX_2 \cdot 2(en)$ are formed. Figures 4 and 5 show the results of the reactions of $PbCl_2$ and $PbBr_2$ with en, respectively. The concentration curve of Fig. 4 ascends slightly near 0.5 of x/z and then becomes flat when x/z approaches 1.0. It ascends again at 1.0 of x/z and becomes flat between 1.2 and 2.1 of x/z. Namely, three plateaus appear on the concentration curve in the ranges of x/z of 0.3—0.5, 0.55—1.0, and 1.2—2.1. The concentration curve of Fig. 5 behaves in the same manner as that of Fig. 4 except that the concentration of en in the range of 1.1—2.1 of x/z is lower than that in Fig. 4. According to the phase rule, these facts mean

that three insoluble adducts form in each solid-liquid reaction.

As discussed in Refs. 1 and 2 on extension of the mole ratio method, the slope of monovariant regions on the concentration curve is equal to a certain fixed value depending on the adopted experimental conditions and independent of the composition of the formed adducts. Their compositions can be calculated by Eq. 16, which is converted from Eq. 3:

$$y = (x - [\mathrm{B}]V)/z = (x - [\mathrm{en}]V)/z, \qquad (16)$$

where [en] is the concentration of en in the equilibrated reaction solution. The compositions calculated from Eq. 16 are also shown in open circles in Figs. 4 and 5, where the broken line is termed "composition curve." Two plateaus appear clearly on each composition curve in monovariant regions where each concentration curve has specific slope; nearly equal to 1 and 2 of y in the right ordinate. Two insoluble adducts, $PbX_2 \cdot en$ and $PbX_2 \cdot 2(en)$, seem to correspond to each reaction. On the other hand, each composition curve shows no plateau corresponding to the rise in the concentration curve which occurs near 0.5 of x/z. The occurrence of these adducts is liable to be overlooked because of disappearance of the plateau in the composition curve and slight increase in the concentration curve. This is a drawback in extension of the mole ratio method to solid-liquid reactions. A similar situation was noticed when $PbI_2 \cdot 2/3(en)$[1] and $PbX_2 \cdot 1/2(dien)$[3] are formed. In the case of $PbI_2 \cdot 1/2(dien)$, its formation can be confirmed of not only by a slight concentration rise but also by the powder X-ray diffraction of the solid sediments.

In order to show that extension of the continuous variation method overcomes the drawback of the mole ratio method, the former was applied to the reactions of PbX_2 (X=Cl, Br, and I) with en in ethanol. Figure 6 shows the results of the reactions. When D is 2 mmol, each concentration curve has two plateaus and ascends sharply at 0.7 and 1.0 mmol of x for the reactions of $PbCl_2$ and $PbBr_2$. The reaction of PbI_2 with en also shows two plateaus and ascends at 0.8 mmol of x. When D is 1.5 mmol, the concentration curve ascends at 0.5 mmol of x in the reaction of $PbCl_2$. According to Eq. 15, the value of x where [B] increases sharply is 0.67 mmol for $m=1/2$, 0.8 mmol for $m=2/3$, and 1.0 mmol for $m=1$ when D is 2 mmol, while it is 0.5 mmol for $m=1/2$ when D is 1.5 mmol. Since each value of x found in Fig. 6 is equal to x calculated by Eq. 15, three insoluble adducts, $PbCl_2 \cdot 1/2(en)$, $PbBr_2 \cdot 1/2(en)$, and $PbI_2 \cdot 2/3(en)$, seem to be identified. Similarly, each sharp concentration rise at 1.0 mmol of x in Fig. 6 corresponds to formation of $PbCl_2 \cdot en$ and $PbBr_2 \cdot en$.

In order to prepare adducts with a mole ratio of en/PbX_2 higher than two, suspended PbX_2 powders were made to react with en without solvent. However, resulting adducts were found to be $PbX_2 \cdot 2(en)$ by chemical analysis and powder X-ray diffractometry.

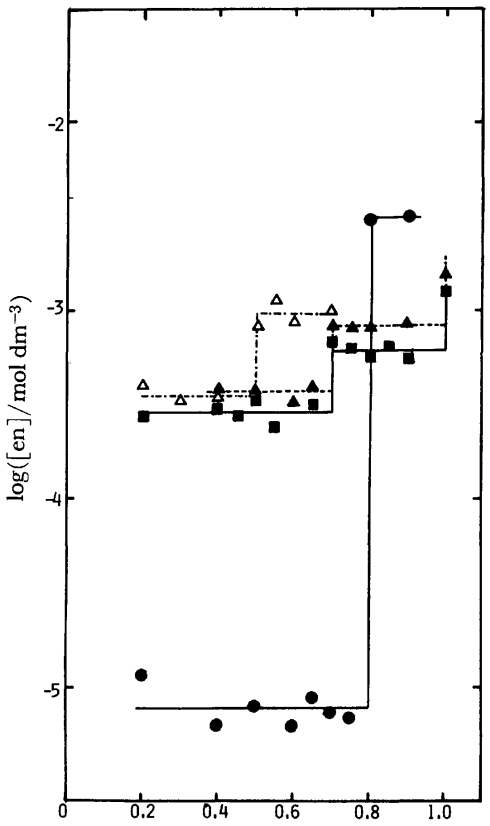

Fig. 6. Relation between the concentration of ethylenediamine remaining in the solution and the amount of en taken at the reaction when the continuous variation method was extended to the reaction of PbX_2 with en: —●—●—, PbI_2, D=2 mmol; —■—■—, $PbBr_2$, D=2 mmol; --▲--▲--, $PbCl_2$, D=2 mmol; -·-Δ-·-Δ-·-, $PbCl_2$, D=1.5 mmol.

When the equilibrated concentration of Lewis bases is high at invariant regions, the composition of formed adducts can be determined by extension of the continuous variation method to the reaction of PbI_2 with pyridine[3] on the basis of the slope at monovariant regions on the concentration curve. In the present work, the extension has been examined in the reactions of PbX_2 (X=Cl, Br, and I) with en where the equilibrated concentration of en is very low at the invariant regions. In this case, their compositions are determined on the basis of the values of sharp rises in the concentration curve. The values are proportional to D, the sum of Lewis acid and base, as shown in Fig. 3. This fact was also demonstrated by the reaction of $PbCl_2$ with en where formation of the same adduct, $PbCl_2 \cdot 1/2(en)$, was confirmed at two different D's, 1.5 and 2.0 mmol. If low concentration of Lewis bases can be accurately determined, the continuous variation method is effective in identifying formation of the adducts such as $PbCl_2 \cdot 1/2(en)$ and $PbBr_2 \cdot 1/2(en)$ whose formation is liable to be overlooked in the mole ratio method, because the composition curve tends to

lose the plateaus corresponding to the rises in the concentration curve.

Formation of $PbX_2 \cdot 2(en)$ (X=Cl, Br, and I) has been reported by Wharf et al.[8] By extension of the mole ratio method, three adducts, $PbI_2 \cdot i(en)$ (i=2/3, 1, and 2), were identified.[1] In the present paper, $PbX_2 \cdot i(en)$ (X=Cl and Br; i=1/2, 1, and 2) were confirmed. The mole ratio method as well as the continuous variation method are necessary to confirm all the adducts formed in solid-liquid reactions. Many adducts have been reported on PbX_2 with monodentate Lewis bases.[8-10] Most of them have the compositions of 1 : 1 and/or 1 : 2 PbX_2: base ratio. $PbCl_2 \cdot 1/2(en)$ and $PbBr_2 \cdot 1/2(en)$ correspond to adducts with PbX_2/base ratio of 1 : 1 and $PbX_2 \cdot en$ with the ratio of 1 : 2, because ethylenediamine is considered to be a bidentate ligand. Therefore, $PbX_2 \cdot 2(en)$ and $PbI_2 \cdot 2/3(en)$ have unusual compositions.

References

1) G. Hihara, H. Miyamae, and M. Nagata, *Chem. Lett.*, **1982**, 647.

2) G. Hihara, T. Shimizu, H. Miyamae, and M. Nagata, *Bull. Chem. Soc. Jpn.*, **58**, 1516 (1985).

3) G. Hihara, H. Miyamae, and M. Nagata, *Chem. Lett.*, **1985**, 1635.

4) J. A. Yoe and A. L. Jones, *Ind. Eng. Chem., Anal. Ed.*, **16**, 11 (1944).

5) Y. Shibata, T. Inoue, and Y. Nakatsuka, *Nippon Kagaku Kaishi*, **42**, 983 (1921); *Chem. Abstr.*, **16**, 2075 (1922); P. Job, *Ann. Chim.*, **9**, 113 (1928).

6) G. Hihara, H. Miyamae, and M. Nagata, *Bull. Chem. Soc. Jpn.*, **54**, 2668 (1981).

7) J. Körbl and R. Pribil, *Chemist-Analyst*, **45**, 102 (1956).

8) I. Wharf, T. Gramstad, R. Makhija, and M. Onyszchuk, *Can. J. Chem.*, **54**, 3430 (1976).

9) M. Glavas, *Therm. Anal., Proc. Int. Conf.*, 3rd **1971** (Pub. 1972), 2, 341.

10) V. M. Koshkin, V. V. Kukol', A. P. Mil'ner, Yu. R. Zabrodskii, and K. A. Katrunov, *Sov. Phys. Solid State*, **19**, 939 (1977).

Preparation and Some Properties of Cobalt(III) Complex with D- and/or L-Selenomethioninates

Hideki UMEHARA,* Takumi KONNO, Ken-ichi OKAMOTO, and Jinsai HIDAKA
Department of Chemistry, University of Tsukuba, Sakura, Ibaraki 305
(Received October 25, 1986)

A novel cobalt(III) complex with D- and/or L-selenomethioninates (D- and/or L-semet) functioning as terdentate-*N,O,Se* ligand was prepared and separated into the five geometrical isomers, trans(N), trans(O), trans(Se), cis,cis,cis, and trans,trans,trans. Of these isomers *trans(N)*- and *trans(O)*-[Co(D- or L-semet)$_2$]$^+$ and *cis,cis,cis*-[Co(D-semet)(L-semet)]$^+$, which were obtained as the crystalline state, were optically resolved by the column chromatographic method. All the isomers were characterized by the electronic absorption, ^{1}H NMR, and CD spectra. The trans(N), trans(O), and cis,cis,cis isomers in the crystalline state take the selective configurations with respect to the absolute configuration, R(Se) or S(Se), of the two coordinated selenium atoms. While, these isomers in an aqueous solution are a mixture of some configurations in the equilibrium state. For the inversion on the asymmetric selenium donor atom of the trans(N) and cis,cis,cis isomers, the rate constants and the ΔG^* values are investigated on the basis of the absorption and ^{1}H NMR spectral changes. The trans(N) and cis,cis,cis isomers showed the characteristic CD spectral behavior in the d-d absorption band region depending on the inversion on the asymmetric selenium donor atoms.

Biochemical roles of selenium-containing amino carboxylates have been remarked in association with transition metals.[1] One of them selenomethioninate (semet) has three donor sites and is potentially terdentate-*N,O,Se* ligand, which has a framework similar to methioninate (met). Accordingly, the stereochemistry of the cobalt(III) complex with semet can be compared effectively with those of the methioninato cobalt(III) complex[2] and its analogues.[3-5] Hence, in order to examine the spectrochemical and stereochemical properties of the coordinated selenium atom, we have undertaken the preparation of the cobalt(III) complex with D- and/or L-selenomethioninates.

In this work, the cobalt(III) complex with D- and/or L-selenomethioninates were prepared and chromatographically separated into the five geometrical isomers: *trans(N)*-, *trans(O)*-, and *trans(Se)*-[Co(D- or L-semet)$_2$]$^+$,[6] and *cis,cis,cis*- and *trans,trans,trans*-[Co(D-semet)(L-semet)]$^+$ (Fig. 1). All isomers were characterized by their electronic absorption spectra in comparison with those of the isomers of the cobalt(III) complex with D- and/or L-methioninates.[2] For the trans(N) and cis,cis,cis isomers which exhibited the electronic absorption, CD, and ^{1}H NMR spectral changes with time in an aqueous solution, an inversion on the asymmetric selenium donor atom is investigated by the spectrophotometric method. The CD spectral behaviors are also discussed in relation to the absolute configuration of the asymmetric selenium donor atom.

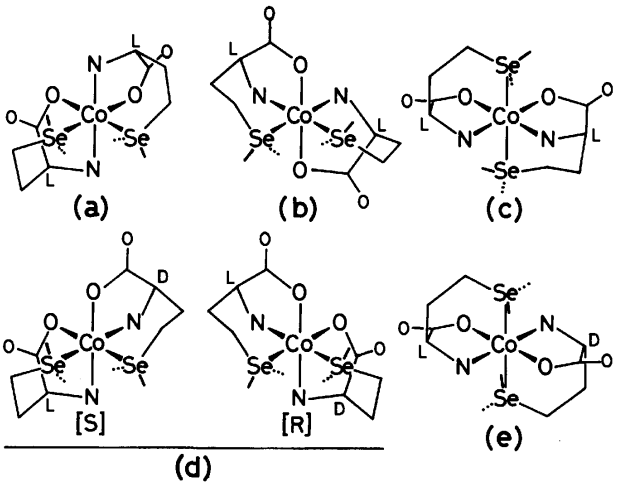

Fig. 1. Possible geometrical isomers of [Co(L-semet)$_2$]$^+$ and [Co(D-semet)(L-semet)]$^+$: (a) trans(N), (b) trans(O), (c) trans(Se), (d) cis,cis,cis, and (e) trans,-trans,trans.

Experimental

Preparation of Complex. A solution containing 1.8 g of $CoCl_2 \cdot 6H_2O$ in 10 cm^3 of water was added to a suspension containing 3.0 g of the racemic Hsemet[7] in 50 cm^3 of water. After the mixture was stirred at 60 °C for 5 min, to this were added 0.5 g of activated charcoal and 8.0 g of PbO_2. The mixture was further stirred at 60 °C for 20 min and then filtered to remove insoluble materials. The dark brown filtrate was poured onto an SP-Sephadex C-25 column (Na^+ form, 4×100 cm). After sweeping the column with water, the adsorbed band was eluted with a 0.015 mol dm^{-3} aqueous solution of Na_2SO_4. A circulating-chromatographic technique was employed for the separation of the isomers. After circulating the eluates in the same column several times, the eluates were separated into the five colored ones, dark violet (A-1), yellow (A-2), violet (A-3), red-violet (A-4), and yellow (A-5) in this order. It was found from the absorption spectral measurements that the eluates A-1, A-4, and A-5 contained *trans(O)*-, *trans(N)*-, and *trans(Se)*-[Co(D- or L-semet)$_2$]$^+$, respectivily, and the eluate A-3 contained *cis,cis,cis*-[Co(D-semet)(L-semet)]$^+$. The formation ratio of the isomers, trans(O): cis,cis,cis: trans(N): trans(Se), was about 1 : 7 : 9 : 1. Each eluate except the eluate A-2 was concentrated with a rotary evaporator below 25 °C and Na_2SO_4 deposited was filtered off. The filtrate was then passed through a QAE-Sephadex A-25 column (ClO_4^- form, 2.5×20 cm) by eluting with water. The eluate was concentrated with a rotary evaporator again and the crystals were collected by filtration. The A-5 isomer could not be obtained as a solid because of

the small amount of the eluate A-5, and then the concentration of the A-5 isomer was evaluated on the basis of the plasma emission spectral analysis. The A-2 isomer, whose formation was very poor, could not be separated as a pure form because of the isomerization during the procedure of the chromatographic separation. Found for A-1: C, 21.18; H, 3.96; N. 4.92%. Calcd for $[Co(semet)_2]ClO_4 \cdot H_2O$=$CoC_{10}H_{20}N_2O_8ClSe_2 \cdot H_2O$: C, 21.20; H, 3.91; N. 4.94%. Found for A-3: C, 22.02; H, 3.66; N, 5.08%. Found for A-4: C, 21.99; H. 3.71; N, 5.09%. Calcd for $[Co(semet)_2]ClO_4$: C, 21.89; H, 3.67; N, 5.11%.

Resolution of Isomers. $(-)^{CD}_{500}$-*trans*(*N*)-[Co(D-semet)$_2$]ClO$_4$ and $(+)^{CD}_{500}$-*trans*(*N*)-[Co(L-semet)$_2$]ClO$_4$. About 0.1 g of *trans*(*N*)-[Co(D- or L-semet)$_2$]ClO$_4$ (A-4) was dissolved in a small amount of water and poured onto an SP-Sephadex C-25 column (Na^+ form, 3.5×100 cm). After sweeping the column with water, the adsorbed band was eluted with a 0.015 mol dm^{-3} aqueous solution of $K_2[Sb_2(d\text{-tart})_2] \cdot H_2O$. After circulating the eluates in the same column twice, the eluates were separated into the two bands and then fractionated. It was found from the CD spectral measurements that the earlier moving band contained $(-)^{CD}_{500}$-*trans*(*N*)-[Co(D-semet)$_2$]$^+$ and the later one contained $(+)^{CD}_{500}$-*trans*(*N*)-[Co(L-semet)$_2$]$^+$. Each of the fractions was concentrated to a small volume with a rotary evaporator below 25 °C and deposited $K_2[Sb_2(d\text{-tart})_2]$ was filtered off. The filtrate was converted into the perchlorate salt using a QAE-Sephadex A-25 column (ClO_4^- form) by eluting with water. The eluate was concentrated to a small volume again and kept in a refrigerator for several days. The resulting crystals were collected by filtration.

$(-)^{CD}_{550}$-[*R*]- and $(+)^{CD}_{550}$-[*S*]-*cis,cis,cis*-[Co(D-semet)(L-semet)]ClO$_4$. *cis,cis,cis*-[Co(D-semet)(L-semet)]ClO$_4$ (A-3) was resolved by a procedure similar to that used for the trans(N) isomer, using the racemic cis,cis,cis isomer (0.1 g) instead of the trans(N) one. The earlier moving adsorbed band contained $(-)^{CD}_{550}$-[*R*]-*cis,cis,cis*-[Co(D-semet)(L-semet)]$^+$ and the later one contained the $(+)^{CD}_{550}$-[*S*] one.

$(-)^{CD}_{600}$-*trans*(*O*)-[Co(D-semet)$_2$]ClO$_4$ and $(+)^{CD}_{600}$-*trans*(*O*)-[Co(L-semet)$_2$]ClO$_4$. *trans*(*O*)-[Co(D- or L-semet)$_2$]ClO$_4 \cdot H_2O$ (A-1) was also resolved by a procedure similar to that used for the trans(N) isomer, except for using about 0.02 g of the trans(O) isomer and an SP-Sephadex C-25 column (Na^+ form, 3.0×40 cm). The earlier moving adsorbed band contained $(+)^{CD}_{600}$-*trans*(*O*)-[Co(L-semet)$_2$]$^+$ and the later one contained $(-)^{CD}_{600}$-*trans*(*O*)-[Co(D-semet)$_2$]$^+$.

The $\Delta\varepsilon$ values of the trans(N), cis,cis,cis, and trans(O) isomers were evaluated from their absorption spectral data.

Kinetic Measurements. The inversion on the asymmetric selenium donor atom of *trans*(*N*)-[Co(D- or L-semet)$_2$]$^+$ and *cis,cis,cis*-[Co(D-semet)(L-semet)]$^+$ in the aqueous solution was monitored spectrophotometrically with a JASCO UVIDEC-1 spectrophotometer equipped with a thermostated cell compartment. The concentrations of the isomers were ca. 1.5×10^{-3} mol dm^{-3}. The temperature of the solutions, T, was in the range of 16.9—25.9 °C and kept constant within ±0.1 °C by use of a temperature-controlled circulating bath, Yamato-Komatsu CTR-220. The absorbance changes with time were followed at 511 nm for the trans(N) isomer and at 556 nm for the cis,cis,cis one, respectively. The first-order rate constant, k, for the trans(N) or cis,cis,cis isomer was determined from the plot of $\ln\{(A_0-A_\infty)/(A_t-A_\infty)\}$ against time, where A_0, A_∞, and A_t stand for absorbances at the initial state, at equilibrium, and at time t, respectively.

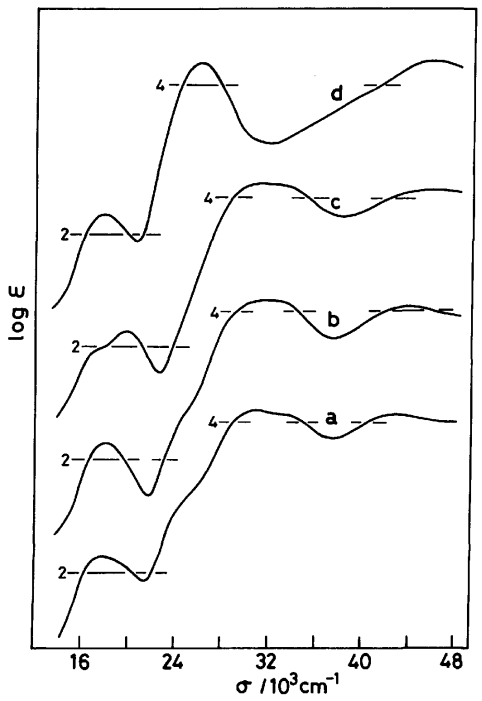

Fig. 2. Absorption spectra of [Co(D- or L-semet)$_2$]$^+$ and [Co(D-semet)(L-semet)]$^+$: (a) trans(O), (b) cis,cis,cis, (c) trans(N), and (d) trans(Se).

The activation parameters were yielded from the Eyring treatment of log (k/T) vs. T^{-1}.

Measurements. The electronic absorption spectra were recorded with JASCO UVIDEC-1 and UVIDEC-610 spectrophotometers and the CD spectra with a JASCO J-20 spectropolarimeter. All measurements were carried out in aqueous solution. The concentration of *trans*(*Se*)-[Co(D- or L-semet)$_2$]$^+$ (A-5 isomer) was determined with a Jarrel-Ash Model 96-975 Plasma Atom Co. The ^{1}H NMR spectra were recorded in deuterium oxide with a JEOL JNM-FX-100 NMR spectrometer at the prove temperature. Sodium 2,2-dimethyl-2-silapentane-5-sulfonate (DSS) was used as an internal reference.

Results and Discussion

Characterization. Five geometrical isomers are possible for the cobalt(III) complex with D- and/or L-selenomethioninates: trans(N), trans(O), and trans(Se) for [Co(D- or L-semet)$_2$]$^+$, and cis,cis,cis and trans,trans,-trans for [Co(D-semet)(L-semet)]$^+$, as in the case of the cobalt(III) complex with D- and/or L-methioninates[2] and its analogues (Fig. 1).[3-5] As shown in Fig. 2 and Table 1, each absorption spectrum of the present five isomers is quite similar to that of the corresponding isomers of [Co(D- or L-met)$_2$]$^+$ and [Co(D-met)(L-met)]$^+$, though the first absorption bands of the selenomethioninato isomers and, especially, the charge-transfer bands due to the selenium to metal (ca. 30—33×10^3 cm^{-1} for A-1, A-3, and A-4, and ca. 26×10^3 cm^{-1} for A-5) shift significantly to lower energy than those of the methioninato isomers.[2] These results are consistent with the absorption behavior observed for the

Table 1. Absorption Spectral Data of Equilibrium State for [Co(D- or L-semet)$_2$]$^+$ and [Co(D-semet)(L-semet)]$^+$

Complex	d–d band	Charge transfer band
trans(*N*)-[Co(D- or L-semet)$_2$]$^+$	17.44 (1.99 sh) 19.49 (2.21)	31.06 (4.18) 32.68 (4.16 sh) 45.66 (4.12)
trans(*O*)-[Co(D- or L-semet)$_2$]$^+$	17.61 (2.21) 19.27 (2.14 sh) 24.88 (3.01 sh)	30.67 (4.16) 32.95 (4.11 sh) 42.74 (4.10)
trans(*Se*)-[Co(D- or L-semet)$_2$]$^+$	17.67 (2.27)	25.97 (4.28) 45.66 (4.30)
cis,cis,cis-[Co(D-semet)(L-semet)]$^+$	17.94 (2.26) 25.07 (2.74 sh)	31.55 (4.20) 43.67 (4.13)

Wavenumbers and log ε values (in parentheses) are given in 10^3cm^{-1} and mol^{-1}dm^{3}cm^{-1}, respectively. sh denotes a shoulder.

[Co(bidentate-*N*,*Se* or -*N*,*S*)(en or tn)$_2$] type complexes.[8,9] Accordingly, the A-1, A-3, A-4, and A-5 isomers are assignable to trans(O), cis,cis,cis, trans(N), and trans(Se), respectively. Hence, it is noted that the selenium to metal charge-transfer bands for the three cis(Se) type selenomethioninato isomers split distinctly in comparison with the sulfur to metal charge-transfer band for the three cis(S) type methioninato isomers (Fig. 2).[2] The absorption spectrum of the A-2 isomer could not be measured because of the its partial isomerization to the cis(Se) type isomer during the chromatographic separation. However, it is probable that the eluate A-2 mainly contains the trans,trans,-trans isomer, because the eluate A-2 exhibits the selenium to metal charge-transfer band in a similar position (ca. 26×10^3 cm^{-1}) to *trans*(*Se*)-[Co(D- or L-semet)$_2$]$^+$, whose band locates at lower energy than those of the cis(Se) type isomers.

Inversion on the Asymmetric Selenium Donor Atom. When the crystals of *trans*(*N*)-[Co(D- or L-semet)$_2$]ClO$_4$ were dissolved in water, the absorption spectral change was observed with time at room temperature and the absorption spectrum exhibited two distinct isosbestic points at 552 and 652 nm (Fig. 3). This spectrum attained equilibrium after 4.5 h, and the absorption spectrum at equilibrium coincided with that of the eluate A-4 obtained by the chromatographic separation. Further, the solution at equilibrium exhibited only the same adsorbed band as that of the eluate A-4 in the rechromatographic separation. Similar trend was also observed for *cis,cis,cis*-[Co(D-semet)(L-semet)]$^+$, namely, the absorption spectrum exhibited the isosbestic points at 463 and 645 nm and attained equilibrium after 6 h. These absorption spectral changes for the trans(N) and cis,cis,cis isomers were simultaneously accompanied by the CD and ^{1}H NMR spectral changes (vide infra). Accordingly, it seems to indicate that the spectral changes for the trans(N) and cis,cis,cis isomers are caused by the inversion on the asymmetric selenium donor atom of the ligand. These are confirmed by the following ^{1}H NMR spectral behaviors.

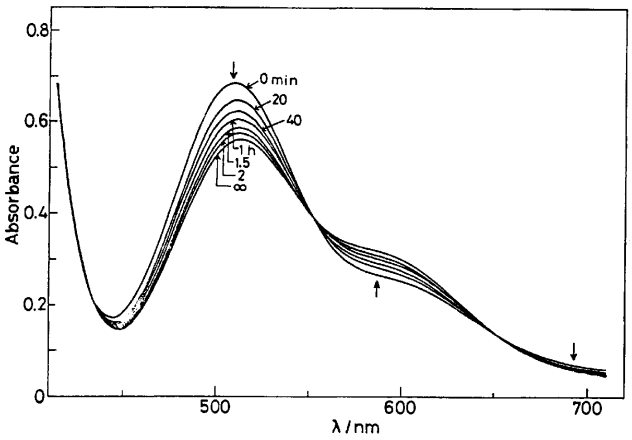

Fig. 3. Change in absorption spectrum with time for *trans*(*N*)-[Co(D- or L-semet)$_2$]$^+$ in water at 25.9°C. The measured times are indicated on the spectral curves. Trends of the spectral change with time are shown by arrows.

Just after *trans*(*N*)-[Co(D- or L-semet)$_2$]ClO$_4$ was dissolved in water, the ^{1}H NMR spectrum exhibited only one resonance line at 2.04 ppm in the *Se*-methyl proton region as shown in Fig. 4-a. Taking the configuration, R(Se) or S(Se), of the asymmetric selenium donor atom into consideration, the ^{1}H NMR spectrum of the R(Se),R(Se) or S(Se),S(Se) isomer having C_2 axis can be expected to exhibit only one resonance line in the corresponding region, while the R(se),S(Se) isomer to exhibit two resonance lines. The present result suggests that the trans(N) isomer in the crystalline state is either R(Se),R(Se) or S(Se),S(Se). The model constructions reveal that the two asymmetric selenium donor atoms take the R(Se)$_D$,R(Se)$_D$ or S(Se)$_L$,S(Se)$_L$ configuration for *trans*(*N*)-[Co(D- or L-semet)$_2$]$^+$, because the S(Se)$_D$,S(Se)$_D$ or R(Se)$_L$,-R(Se)$_L$ configuration has the intramolecular steric interaction between the two *Se*-methyl groups, where

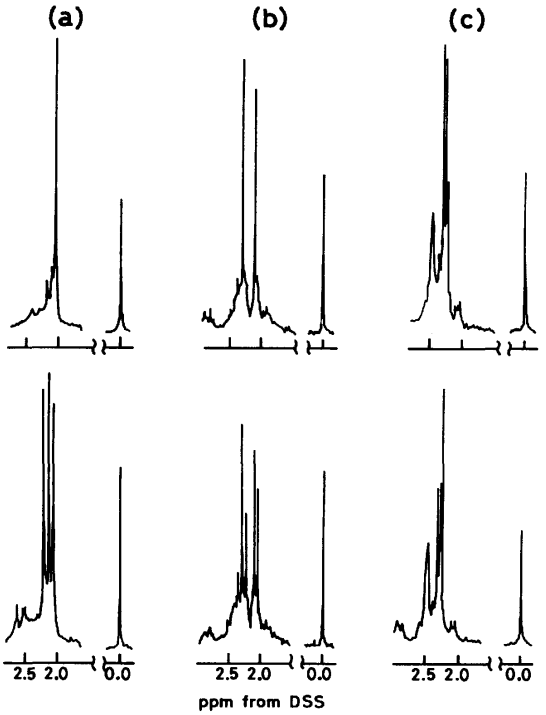

Fig. 4. ^{1}H NMR spectra of [Co(D- or L-semet)$_2$]$^+$ and [Co(D-semet)(L-semet)]$^+$: (a) trans(N), (b) cis,cis,cis, and (c) trans(O); initial state (upper) and equilibrium state (lower).

the subscripts, D and L, correspond to the absolute configurations, R(C) and S(C), for the asymmetric carbon atom of the selenomethioninate. In the aqueous solution, two resonance lines at 2.10 and 2.19 ppm gradually appeared and their intensities increased with time, and finally three resonance lines with the equal intensities were observed at equilibrium (Fig. 4-a). The two resonance lines which newly appeared seems to be due to the R(Se),S(Se) configuration. Accordingly, the ^{1}H NMR spectral behavior suggests that *trans(N)*-[Co(D- or L-semet)$_2$]$^+$ in the aqueous solution at equilibrium is a mixture of the R(Se)$_D$,R(Se)$_D$ and S(Se)$_L$,-S(Se)$_L$ configurations and the R(Se)$_D$,S(Se)$_D$ and R(Se)$_L$,S(Se)$_L$ ones (1 : 2). Namely, the absorption and ^{1}H NMR spectral behaviors of *trans(N)*-[Co(D- or L-semet)$_2$]$^+$ indicate that the inversion on the asymmetric selenium donor atom takes place as follows:

$$R(Se)_D,R(Se)_D \longrightarrow R(Se)_D,S(Se)_D \quad (1a)$$

$$S(Se)_L,S(Se)_L \longrightarrow R(Se)_L,S(Se)_L \quad (1b)$$

Similar trend was also observed for the cis,cis,cis iomer. *cis,cis,cis*-[Co(D-semet)(L-semet)]$^+$ has [R] and [S] configurations based on the chiral arrangement of the coordinated atoms, N, O, and Se.[10] Moreover, four geometrical isomers for each of the [R] and [S] configurations, R(Se)$_D$,R(Se)$_L$, R(Se)$_D$,S(Se)$_L$, S(Se)$_D$,R(Se)$_L$, and S(Se)$_D$,S(Se)$_L$, are possible. Just after the perchlorate salt of the cis,cis,cis isomer was dissolved in water, the ^{1}H NMR spectrum exhibited two resonance lines at 2.11 and 2.30 ppm (Fig. 4-b). This spectrum indicates that the cis,cis,cis isomer in the crystalline state takes only one configuration of the four geometrical isomers. While, in the aqueous solution of this isomers two resonance line at 2.06 and 2.24 ppm gradually appeared and their intensities increased with time, though they were accompanied by the minor two resonance lines at 2.14 and 2.37 ppm (Fig. 4-b). At equilibrium, the intensity ratio of the resonance lines at 2.06, 2.11, 2.24, and 2.30 ppm was about 2 : 3 : 2 : 3 (Fig. 4-b). The model constructions for the cis,cis,cis isomer reveal that the [R]-S(Se)$_D$,R(Se)$_L$ or [S]-R(Se)$_D$,-S(Se)$_L$ isomer has the intramolecular steric interaction between the *Se*-methyl group and the amine protons in the other D- or L-semet ligand. Further, the [R]-S(Se)$_D$,-S(Se)$_L$ or [S]-R(Se)$_D$,R(Se)$_L$ isomer has the interaction between the two *Se*-methyl groups. While, the [R]-R(Se)$_D$,R(Se)$_L$ or [S]-S(Se)$_D$,S(Se)$_L$ isomer and the [R]-R(Se)$_D$,S(Se)$_L$ or [S]-S(Se)$_D$,R(Se)$_L$ one have only a little intramolecular steric interaction. The steric interaction in the cis,cis,cis isomer seems to increase in the order [R]-R(Se)$_D$,R(Se)$_L$ or [S]-S(Se)$_D$,S(Se)$_L$<[R]-R(Se)$_D$,S(Se)$_L$ or [S]-S(Se)$_D$,R(Se)$_L$<[R]-S(Se)$_D$,R(Se)$_L$ or [S]-R(Se)$_D$,S(Se)$_L$<[R]-S(Se)$_D$,S(Se)$_L$ or [S]-R(Se)$_D$,-R(Se)$_L$. Therefore, the ^{1}H NMR spectral behavior suggests that *cis,cis,cis*-[Co(D-semet)(L-semet)]$^+$ in the aqueous solution at equilibrium takes mainly a mixture of the [R]-R(Se)$_D$,R(Se)$_L$ and [S]-S(Se)$_D$,S(Se)$_L$ configurations and the [R]-R(Se)$_D$,S(Se)$_L$ and [S]-S(Se)$_D$,R(Se)$_L$ ones containing the minor [R]-S(Se)$_D$,-R(Se)$_L$ and [S]-R(Se)$_D$,S(Se)$_L$ ones. From these consideration, the cis,cis,cis, isomer in the crystalline state seems to take the [R]-R(Se)$_D$,R(Se)$_L$ and [S]-S(Se)$_D$,-S(Se)$_L$ configurations. The absorption and ^{1}H NMR spectral behaviors for *cis,cis,cis*-[Co(D-semet)(L-semet)]$^+$ indicate the following inversion on the asymmetric selenium donor atom:

$$[R]\text{-}R(Se)_D,R(Se)_L \longrightarrow [R]\text{-}R(Se)_D,S(Se)_L \quad (2a)$$

$$[S]\text{-}S(Se)_D,S(Se)_L \longrightarrow [S]\text{-}S(Se)_D,R(Se)_L \quad (2b)$$

For *trans(O)*-[Co(D- or L-semet)$_2$]$^+$, three isomers, R(Se),R(Se), R(Se),S(Se), and S(Se),S(Se), are possible as well as the trans(N) isomer. In contrast with the trans(N) and cis,cis,cis isomers, the ^{1}H NMR spectral change of the trans(O) isomer could be measured, although the absorption spectral change occurred too fast to be followed. Just after the perchlorate salt of the trans(O) isomer was dissolved in water, the ^{1}H NMR spectrum showed two intense resonance lines at 2.26 and 2.29 ppm and one minor resonance line at 2.23 ppm (Fig. 4-c). This fact suggests that the trans(O) isomer in the crystalline state takes mainly the R(Se),-S(Se) configuration having C_1 symmetry. After 20 min, the inversion reaction attained the equilibrium and the intensities of the two resonance lines at 2.26 and 2.29 ppm are weaker than that at 2.23 ppm (Fig. 4-c). The model constructions reveal that the steric

Table 2. Rate Constants for Inversion on Selenium Atom

Complex	t/°C	k_{obsd}/s^{-1}
trans(*N*)-[Co(D- or L-semet)$_2$]$^+$	16.9	(7.62±0.15)×10^{-5}
	21.7	(1.74±0.08)×10^{-4}
	25.9	(3.34±0.12)×10^{-4}
cis,cis,cis-[Co(D-semet)(L-semet)]$^+$	16.9	(7.50±0.11)×10^{-5}
	21.7	(1.39±0.05)×10^{-4}
	25.9	(2.29±0.09)×10^{-4}

Table 3. Thermodynamic Parameters for Inversion on Selenium Atom

Complex	ΔH^*	ΔS^*	$\Delta G^*_{25°C}$
	kJ mol^{-1}	J mol^{-1} K^{-1}	kJ mol^{-1}
trans(*N*)-[Co(D- or L-semet)$_2$]$^+$	116.1±1.4	76.7±5.0	93.2±0.1
cis,cis,cis-[Co(D-semet)(L-semet)]$^+$	87.2±2.0	−23.1±7.0	94.1±0.1

interaction in the trans(O) isomer increases in the order S(Se)$_D$,S(Se)$_D$ or R(Se)$_L$,R(Se)$_L$<R(Se)$_D$,S(Se)$_D$ or R(Se)$_L$,S(Se)$_L$<R(Se)$_D$,R(Se)$_D$ or S(Se)$_L$,(Se)$_L$. Therefore, in the aqueous solution at equilibrium, the trans(O) isomer seems to take a mixture of the S(Se)$_D$,-S(Se)$_D$ and R(Se)$_L$,R(Se)$_L$ configurations (C_2 symmetry) and the R(Se)$_D$,S(Se)$_D$ and R(Se)$_L$,S(Se)$_L$ ones (C_1 symmetry) (ca. 1 : 1). Accordingly, the ^{1}H NMR spectral behavior seems to indicate the following inversion:

$$R(Se)_D,S(Se)_D \longrightarrow S(Se)_D,S(Se)_D \quad (3a)$$

$$R(Se)_L,S(Se)_L \longrightarrow R(Se)_L,R(Se)_L \quad (3b)$$

Rate constants of the inversion on the asymmetric selenium donor atom for the equations (1) and (2) were determined by monitoring the change in absorbance with time. The absorbance at 511 nm of *trans*(*N*)-[Co(D- or L-semet)$_2$]$^+$ in the aqueous solution at a constant temperature decreased monotonically with time (Fig. 3). The plot of $\ln\{(A_0-A_\infty)/(A_t-A_\infty)\}$ against time gave a straight line, from which the first-order rate constants of the inversion were obtained (Fig. 5-a and Table 2). Similarly, the absorption spectral data for the cis,cis,cis isomer were treated in the same way (Fig. 5-b and Table 2). The rate constant of the trans(N) isomer agreed well with that of the cis,cis,cis one. These rate constants for the inversion are in agreement with those of *t*-[Co(RSeCH$_2$CH$_2$NH$_2$)-(tren)]$^{3+}$ (R=CH$_3$, CH$_3$CH$_2$, and C$_6$H$_5$CH$_2$, and tren=N(CH$_2$CH$_2$NH$_2$)$_3$) and *t*-[Co(CH$_3$SeCH$_2$COO)-(tren)]$^{2+}$.[11] These suggest that the inversion for the present isomers arises from a mechanism similar to that for the tren cobalt(III) complexes with RSeCH$_2$-CH$_2$NH$_2$ (R=CH$_3$, CH$_3$CH$_2$, and C$_6$H$_5$CH$_2$).[11]

Eyring treatments of $\log(k/T)$ vs. T^{-1} yielded activation parameters for the trans(N) and cis,cis,cis isomers (Table 3). Their ΔG^* values at 25 °C resemble each other and agree well with those of the tren cobalt-(III) complexes with RSeCH$_2$CH$_2$NH$_2$ (R=CH$_3$, CH$_3$CH$_2$, and C$_6$H$_5$CH$_2$).[11] Taking account of the stereochemical differences between the trans(O) isomer and the trans(N) or cis,cis,cis one, whose inversion

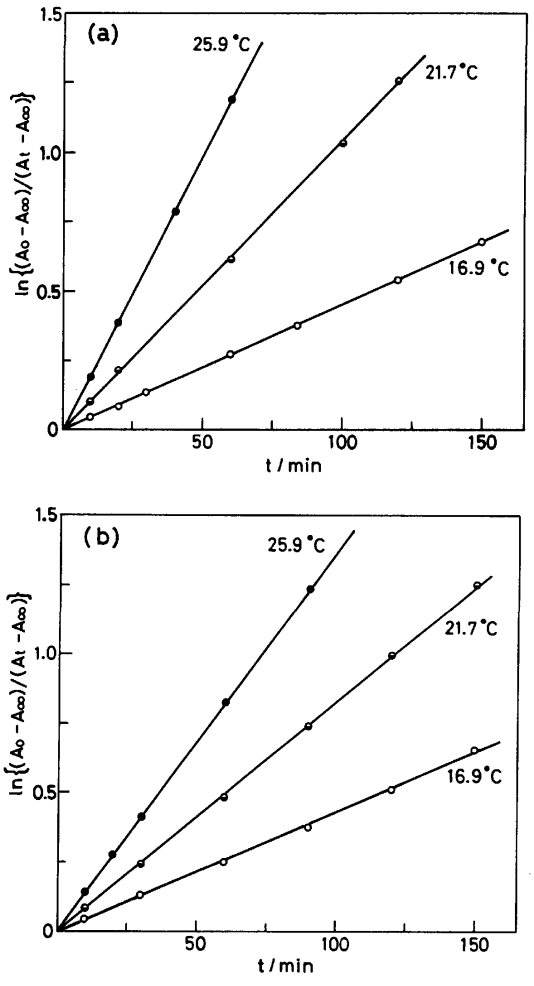

Fig. 5. Plot of $\ln\{(A_0-A_\infty)/(A_t-A_\infty)\}$ against time for (a) *trans*(*N*)-[Co(D- or L-semet)$_2$]$^+$ and (b) *cis,cis,cis*-[Co(D-semet)(L-semet)]$^+$ in water at 16.9, 21.7 and 25.9 °C.

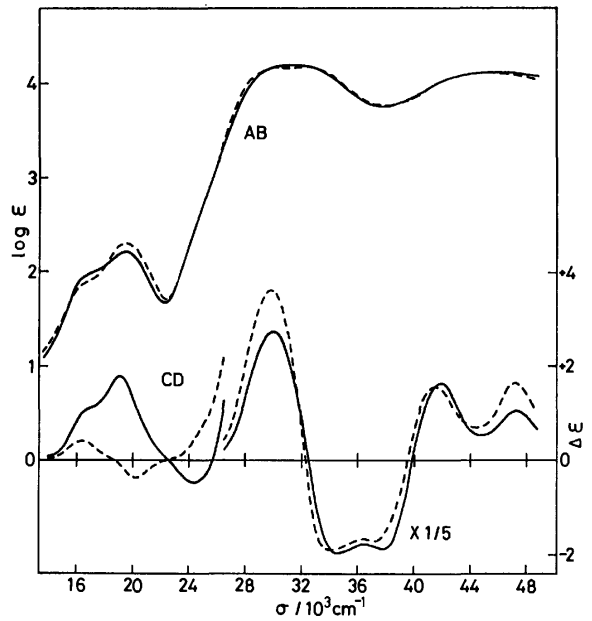

Fig. 6. Absorption and CD spectra of the $(+)^{CD}_{500}$-*trans*(*N*)-[Co(L-semet)$_2$]$^+$: initial state (----) and equilibrium state (——).

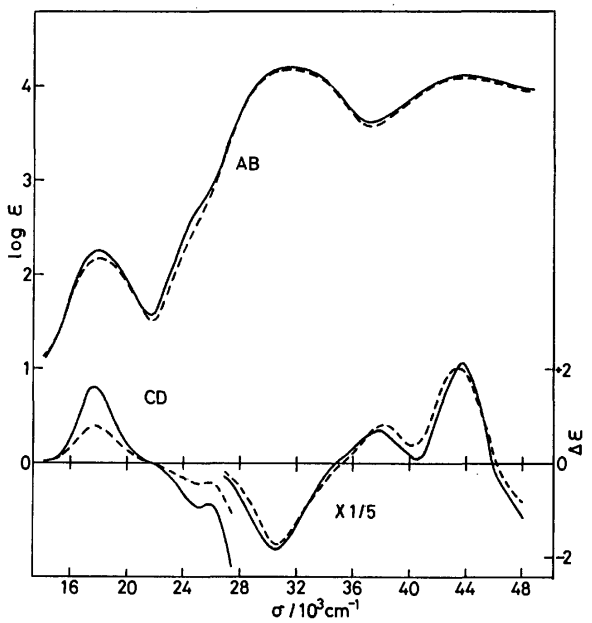

Fig. 7. Absorption and CD spectra of the $(+)^{CD}_{550}$-[*S*]-*cis,cis,cis*-[Co(D-semet)(L-semet)]$^+$: initial state (----) and equilibrium state (——).

mechanism may resemble each other, a somewhat overvalued differences in ΔH^* and ΔS^* between the trans(N) and cis,cis,cis isomers seems to reflect the difference in the stereochemistry around the selenium donor atoms during the kinetic processes, as mentioned about the ^{1}H NMR spectral behavior. Namely, the difference in ΔH^* and ΔS^* seems to associate with the steric effect and rotational freedom for the methyl group on the selenium donor atom on going from the initial to the transitional state.

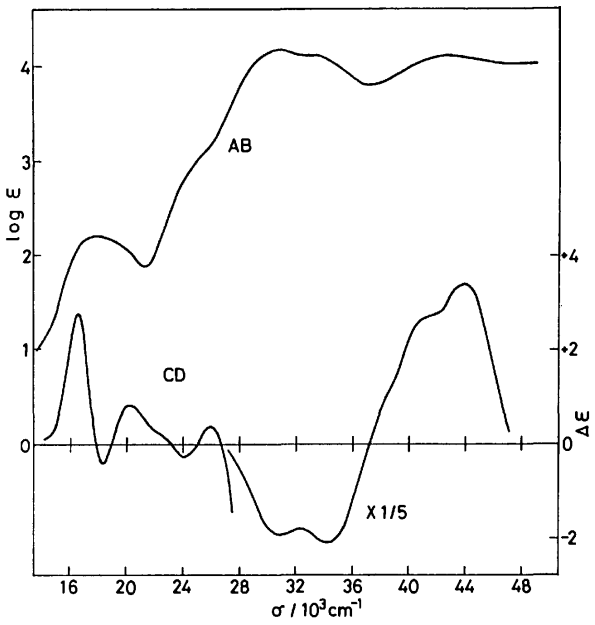

Fig. 8. Absorption and CD spectra of the $(+)^{CD}_{600}$-*trans*(*O*)-[Co(L-semet)$_2$]$^+$.

CD Spectra. The CD spectra at equilibrium of $(+)^{CD}_{600}$-*trans*(*O*)- and $(+)^{CD}_{500}$-*trans*(*N*)-[Co(D- or L-semet)$_2$]$^+$, and $(+)^{CD}_{550}$-*cis,cis,cis*-[Co(D-semet)(L-semet)]$^+$ are shown in Figs. 6—8, together with those of the trans(N) and cis,cis,cis isomers just after dissolved in water, and their spectral data are summarized in Table 4. In the equilibrium state, the $(+)^{CD}_{500}$-trans(N) isomer exhibits a quite similar CD spectral pattern in the whole region to *trans*(*N*)-[Co(L-met)$_2$]$^+$ (Fig. 6),[2] the $(+)^{CD}_{550}$-cis,cis,cis isomer to [*S*]-*cis,cis,cis*-[Co(D-met)(L-met)]$^+$ [12] and -[Co(D-smp)(L-smp)]$^+$ (Fig. 7),[5] and the $(+)^{CD}_{600}$-trans(O) isomer to *trans*(*O*)-[Co(L-met)]$^+$ (Fig. 8).[2] The CD bands of the semet isomers shift to the lower energy in the d-d transition and ligand to metal charge-transfer band regions than those of the corresponding met isomers as in the case of their absorption spectral behavior. These are in line with the fact that the CD spectra of the selenolato, selenenato, and selenoether cobalt(III) complexes shift to a lower energy than those of the corresponding thiolato, sulfenato, and thioether complexes.[8,9] These facts support that the present isomers are assigned to $(+)^{CD}_{500}$-*trans*(*N*)-[Co(L-semet)$_2$]$^+$, $(+)^{CD}_{550}$-[*S*]-*cis,cis,cis*-[Co(D-semet)-(L-semet)]$^+$, and $(+)^{CD}_{600}$-*trans*(*O*)-[Co(L-semet)$_2$]$^+$, respectively.

For $(+)^{CD}_{500}$-*trans*(*N*)-[Co(L-semet)$_2$]$^+$ and $(+)^{CD}_{550}$-[*S*]-*cis,cis,cis*-[Co(D-semet)(L-semet)]$^+$, the CD spectral changes, which are accompanied by their absorption and ^{1}H NMR spectral changes, were observed at room temperature (Figs. 6 and 7). These CD spectral changes seem to correspond with the equations (1b) and (2b). It is noteworthy that the CD pattern of the trans(N) isomer changes drastically with time and the

Table 4. CD Spectral Data of Equilibrium State for $[Co(L\text{-semet})_2]^+$ and $[Co(D\text{-semet})(L\text{-semet})]^+$

Complex	d-d band region	Charge transfer band region
$(+)^{CD}_{500}$-*trans*(*N*)-$[Co(L\text{-semet})_2]^+$	17.15(+1.12 sh) 19.15(+1.80) 24.51(−0.48)	30.12(+13.58) 34.60(−9.92) 38.02(−9.56) 42.02(+8.24) 47.17(+5.29)
$(+)^{CD}_{600}$-*trans*(*O*)-$[Co(L\text{-semet})_2]^+$	16.50(+2.78) 18.32(−0.44) 20.20(+0.84) 24.04(−0.28) 25.91(+0.38)	30.86(−9.72) 34.01 (−10.47) 41.15 (+13.46 sh) 43.86 (+17.05)
$(+)^{CD}_{550}$-[*S*]-*cis,cis,cis*-$[Co(D\text{-semet})(L\text{-semet})]^+$	17.70(+1.60) 25.13(−0.95)	30.49(−9.16) 37.74(+3.45) 43.67 (+10.63)

Wavenumbers and $\Delta\varepsilon$ values (in parentheses) are given in $10^3\,cm^{-1}$ and $mol^{-1}\,dm^3\,cm^{-1}$, respectively. sh denotes a shoulder.

CD spectrum exhibited the isodichroic point at 441.5 nm, without the change in the region of $27—46\times10^3$ cm^{-1} (Fig. 6). A similar CD spectral change was also observed for the cis,cis,cis isomer in the d-d transition band region (the isodichroic point at 458 nm) (Fig. 7). Judging from the investigations of the ^1H NMR and absorption spectral changes mentioned above, the CD spectra of initial state and equilibrium one for *trans*(*N*)-$[Co(L\text{-semet})_2]^+$ suggest the change from the $S(Se)_L,S(Se)_L$ configuration to the mixture of the $R(Se)_L,S(Se)_L$ and $S(Se)_L,S(Se)_L$ configurations, and [*S*]-*cis,cis,cis*-$[Co(D\text{-semet})(L\text{-semet})]^+$ from the $S(Se)_D,S(Se)_L$ configuration to the mixture of $S(Se)_D,R(Se)_L$ and $S(Se)_D,S(Se)_L$ configurations. The results in this work indicate that the change of the configuration of the asymmetric selenium atoms contributes remarkably to the absorption and CD spectra in the d-d transition band region and differs significantly from the stereochemical behavior of the asymmetric sulfur atom in the methioninato complex.[2,13]

The authors wish to express thanks to Mr. Tsutomu Watanabe and Mrs. Yoko Koizumi for their aid in the experiment.

References

1) C. A. Stein, P. E. Ellis. Jr., R. C. Elder, and E. Deutsch, *Inorg. Chem.*, **15**, 1618 (1976).
2) J. Hidaka, S. Yamada, and Y. Shimura, *Chem. Lett.*, **1974**, 1487.
3) T. Konno, K. Okamoto, and J. Hidaka, *Bull. Chem. Soc. Jpn.*, **56**, 2631 (1983).
4) K. Okamoto, K. Wakayama, H. Einaga, S. Yamada, and J. Hidaka, *Bull. Chem. Soc. Jpn.*, **56**, 165 (1983).
5) M. Kanesaka, K. Okamoto, M. Nomoto, and J. Hidaka, *Bull. Chem. Soc. Jpn.*, **57**, 3111 (1984).
6) $[Co(D\text{- or }L\text{-semet})_2]^+$ denotes $[Co(D\text{-semet})_2]^+$ and $[Co(L\text{-semet})_2]^+$ are mixed in equal amount.
7) The racemic selenomethionine was obtained from the Sigma Chemical Company.
8) T. Konno, K. Okamoto, and J. Hidaka, *Bull. Chem. Soc. Jpn.*, **57**, 3104 (1984).
9) T. Konno. K, Okamoto, H. Einaga, and J. Hidaka, *Bull. Chem. Soc. Jpn.*, **58**, 1119 (1985).
10) The symbols, [R] and [S], are denoted by the method of Cahn et al., (R. S. Cahn, C. K. Ingold, and V. Prelog, *Angew. Chem. Int. Ed. Engl.*, **5**, 385 (1966).
11) K. Nakajima, K. Tozaki, M. Kojima, and J. Fujita, *Bull. Chem. Soc. Jpn.*, **58**, 1130 (1985).
12) K. Okamoto and J. Hidaka, Unpublished data.
13) K. Okamoto, H. Maki, and J. Hidaka, *Bull. Chem. Soc. Jpn.*, **57**, 595 (1984).

 © 1987 The Chemical Society of Japan Bull. Chem. Soc. Jpn., 60, 1375—1378 (1987)

Effect of Sodium Dodecyl Sulfate on Spectral Properties of Five- and Six-Coordinate Nitrosyl(protoporphyrin IX dimethyl esterato)iron(II) Complexes

Tetsuhiko YOSHIMURA
The Environmental Science Institute of Hyogo Prefecture, Yukihira-cho, Suma-ku, Kobe 654
(Received October 28, 1986)

EPR and electronic spectra of five- and six-coordinate nitrosyl(protoporphyrin IX dimethyl esterato)iron(II) (Fe(ppixdme)(NO)) complexes as model systems for nitrosylhemoproteins have been investigated in the absence and the presence of sodium dodecyl sulfate (SDS). Dimethyl sulfoxide, an O-donor ligand, is weakly coordinated to iron in an axial vacant position trans to a nitrosyl group in Fe(ppixdme)(NO). Upon addition of SDS to Fe(ppixdme)(NO) in dimethyl sulfoxide, EPR and electronic spectra were changed into five-coordinate type spectra. On the other hand, the addition of SDS to Fe(ppixdme)(NO)(NMeIm) in dimethyl sulfoxide resulted in EPR and electronic spectra arising from a mixture of five- and six-coordinate complexes. Accordingly, sodium dodecyl sulfate was found to hinder the interaction of dimethyl sulfoxide with the sixth axial vacant position of Fe(ppixdme)(NO), and to cleave only partly the iron to imidazole bond in Fe(ppixdme)(NO)(NMeIm) complex.

Sodium dodecyl sulfate (SDS), an anionic detergent, has been known to solubilize insoluble porphyrins and metalloporphyrins in aqueous solution in monomer form.[1,2] Effect of SDS on spectral properties of iron(II) and iron(III) porphyrin complexes with various axial ligands has been investigated.[2] Furthermore, it has been demonstrated that the hydrophobic part of SDS penetrates into the hydrophobic core of the protein to cause a considerable structural change of hemoglobin, myoglobin,[3] and cytochrome c′,[4] and that both the EPR and electronic spectra of NO-hemoglobin[5] and NO-cytochrome c′ modified by SDS[6] resemble those of five-coordinate model nitrosylheme in nonpolar organic solvents in spectral line shape.[7,8]

The clarification of the interaction of SDS and hydrophobic environments around heme in NO-hemoproteins seems to bear a significant implication in understanding the structure of the heme environments of the hemoproteins. In this paper, it is reported that EPR and electronic spectra of five- and six-coordinate nitrosyl(protoporphyrin IX dimethyl esterato)iron(II) (Fe(ppixdme)(NO)) complexes as model systems for NO-hemoproteins are changed upon addition of SDS.

Experimental

Materials and Methods. Fe(ppixdme)Cl and Fe(ppixdme)(NO) were prepared as described before.[7,9] Nitrogen monoxide (99.5% minimum) purchased from Seitetsu Kagaku Co. Ltd. was passed through a KOH column to remove higher nitrogen oxides. ^{15}NO gas was generated by the reaction of $Na^{15}NO_2$ (99.2% enrichment, Prochem) with an aqueous solution of ascorbic acid. 1-Methylimidazole (NMeIm) and dimethyl sulfoxide were distilled by flowing N_2 under reduced pressure and were deoxygenated by bubbling with pure N_2 prior to use. Sodium dodecyl sulfate (Wako chemicals) was purchased and used without further purification. All other chemicals used were obtained as the best available grade and were used without further purification.

EPR and electronic spectral measurements were carried out as described previously.[10]

Sample Preparation. EPR and electronic spectral samples were prepared by following two method. (a) Under N_2 atmosphere, Fe(ppixdme)(NO) was dissolved into dimethyl sulfoxide or NMeIm-dimethyl sulfoxide solution, in the absence or the presence of SDS. (b) The reaction of NO with Fe(ppixdme)Cl in dimethyl sulfoxide or NMeIm-dimethyl sulfoxide solution, in the absence or the presence of SDS was carried out in a Thunberg-type tube with an optical cuvette or with an EPR tube. The solutions were carefully degassed in the Thunberg tube by repeated freezing and thawing in vacuo and then were equilibrated with NO gas at about 1 atm.

Then, the solutions obtained by method (a) or (b) were transferred into an optical cuvette or an EPR tube (or flat cell). Both methods resulted in identical spectral results.

The concentrations of Fe(ppixdme)(NO), NMeIm, and SDS in EPR samples were 0.1—0.6 mM†, 80 mM, and more than 80 mM, respectively; those in electronic spectral samples were 0.016 mM, 0.51—2.03, and 0.10—1.16 M, respectively.

Results and Discussion

It was shown that the N-donor ligands can be coordinated,[8,10-12] both at room temperature and at low temperature, to iron in the axial position trans to a nitrosyl group in Fe(ppixdme)(NO), while the weak ligands such as O- and S-donor ones can be, in general, coordinated only at low temperature.[13] However, the axial coordination of dimethyl sulfoxide, an O-donor ligand, to Fe(ppixdme)(NO) not only at low temperature but also at room temperature has been confirmed by the following findings: EPR g values (g_{iso}), the NO stretching frequencies, and the Soret band maxima of Fe(ppixdme)(NO) in various non-donor solvents at room temperature almost linearly decrease with an increase of a solvent polarity parameter (E_T), and on the other hand, those in dimethyl sulfoxide distinctly deviate from such linear relationships.[8,12]

Addition of Sodium Dodecyl Sulfate to Fe(ppixdme)(NO) in Dimethyl Sulfoxide. In the electronic spec-

† 1 M=1 mol dm^{-3}.

Table 1. Electronic Spectral Data of Nitrosyl(protoporphyrin IX dimethyl esterato)iron(II) Complexes and NO-Hemoproteins with and without Sodium Dodecyl Sulfate at Room Temperature[a]

	Absorpn max/nm (ε/mM^{-1}cm^{-1})				
	γ(Soret)			β	α
Fe(ppixdme)(NO)[b]	405(90.7)		480sh(11)	555(10.8)	
Fe(ppixdme)(NO) in toluene[b]	401(81.2)		480sh(12)	550sh(10)	571(10.9)
Fe(ppixdme)(NO)+SDS[c]	401.5(76.8)		478sh(10.4)	545(10.4)	563.5(10.6)
NO-cyt c′+SDS[d]	395(76.9)		481.5(12.5)	545(9.7)	564(10.0)
Fe(ppixdme)(NO)(NMeIm)		419(115)		545.5(11.4)	576.5(10.7)
Fe(ppixdme)(NO)(NMeIm)+SDS[e]	400sh(67)	417(91.2)	485sh(8.7)	545(11.1)	574(10.3)

a) Abbreviations used: Fe(ppixdme)(NO), nitrosyl(protoporphyrin IX dimethyl esterato)iron(II); NMeIm, 1-methylimidazole; SDS, sodium dodecyl sulfate; cyt c′, cytochrome c′ (*Alcaligenes* sp. NCIB 11015); sh, shoulder. Solvent used for model complexes is dimethyl sulfoxide unless otherwise stated. b) Ref. 8. c) [Fe(ppixdme)(NO)]=0.016 mM, [SDS]=0.1 M. d) Ref. 6. e) [Fe(ppixdme)(NO)]=0.016 mM, [NMeIm]=0.51 M, [SDS]=1.16 M.

Table 2. EPR Parameters of Nitrosyl(protoporphyrin IX dimethyl esterato)iron(II) Complexes and NO-Hemoproteins with and without Sodium Dodecyl Sulfate[a]

	g values					Coupling const/G[b]		
	g_{iso}	g_1	g_2'	g_2[c]	g_3	a_1	a_2'	a_3
Fe(ppixdme)(^{14}NO)[d]	2.048							
Fe(ppixdme)(^{14}NO) in toluene[e]	2.052	2.102	2.058	2.038	2.010	13	16	16.7
Fe(ppixdme)(^{14}NO)+SDS[f]	2.052	2.107	2.059	2.036	2.009_9	13	14	16.6
Fe(ppixdme)(^{15}NO)+SDS[f]	2.052	2.106	2.059	2.032	2.009_7	21	21	22.8
^{14}NO-Hb+SDS[g]		2.094	2.051		2.009			17
^{14}NO-cyt c′+SDS[h]		2.105	2.054	2.035	2.010_2	14	14.2	16.5

a) See footnote a of Table 1 for abbreviations. Solvent used for model complexes is dimethyl sulfoxide unless otherwise stated. g_{iso} is a g values at room temperature and the other parameters are those at 77 K. b) 1T=10^{4}G. c) The g value in lowest field line of g_2 absorption which consists of three (^{14}NO) and two (^{15}NO) lines. d) Ref. 12. e) Ref. 7. f) [Fe(ppixdme)(NO)]=0.6 mM, [SDS]=0.8 M. g) Hb, hemoglobin. Ref. 5. h) Ref. 6.

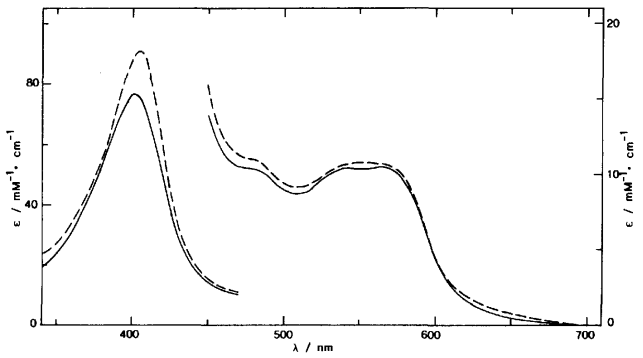

Fig. 1. Electronic spectra of Fe(ppixdme)(NO) (0.016 mM) in dimethyl sulfoxide in the presence (0.1 M) (——) and the absence (----) of sodium dodecyl sulfate at room temperature.

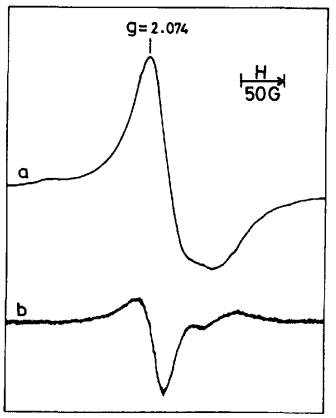

Fig. 2. EPR spectra of Fe(ppixdme)(NO) (0.4 mM) in dimethyl sulfoxide at 77 K; (a) first derivative, (b) second derivative. Instrument settings are given in caption of Fig. 3.

trum of Fe(ppixdme)(NO) in dimethyl sulfoxide (Table 1 and Fig. 1), the Soret band was revealed at 405 nm, which is located at longer wavelength than that (about 396 nm) predicted by λ_{max}(Soret)-E_T relationship,[8] and α- and β-bands were not resolved, suggesting the coordination of a dimethyl sulfoxide to the sixth axial position. On the other hand, the addition of SDS to the dimethyl sulfoxide solution resulted in a spectral change. With an increase in SDS concentration, the Soret band was shifted to shorter wavelength side and the α- and β-bands were resolved. The apparent spectral pattern thus obtained (Fig. 1) resembles those of Fe(ppixdme)(NO) in non-donor solvents such as toluene and benzene[8] and of NO-cytochrome c′ (*Alcaligenes* sp. NCIB 11015) with SDS.[6]

At room temperature, the EPR spectra of Fe(ppixdme)(NO) in organic solvents exhibit a well-resolved triplet.[7] The g_{iso} values at central signal of a triplet in non-donor solvents were in the range of 2.053 to 2.050,[12] while that in dimethyl sulfoxide was 2.048 (Table 2). At 77 K, Fe(ppixdme)(NO) in non-donor

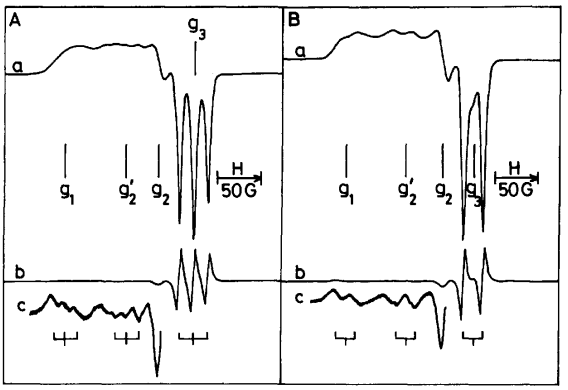

Fig. 3. EPR spectra of (A) Fe(ppixmde)(^{14}NO) and (B) Fe(ppixdme)(^{15}NO) (0.6 mM) in dimethyl sulfoxide in the presence of sodium dodecyl sulfate (0.8 M) at 77 K; (a) first derivative, (b) second derivative, and (c) expansion of the ordinate of (b). Instrument settings: modulation frequency and amplitude, 100 kHz and 2 G; microwave frequency and power, 9.166—9.171 GHz and 10 mW.

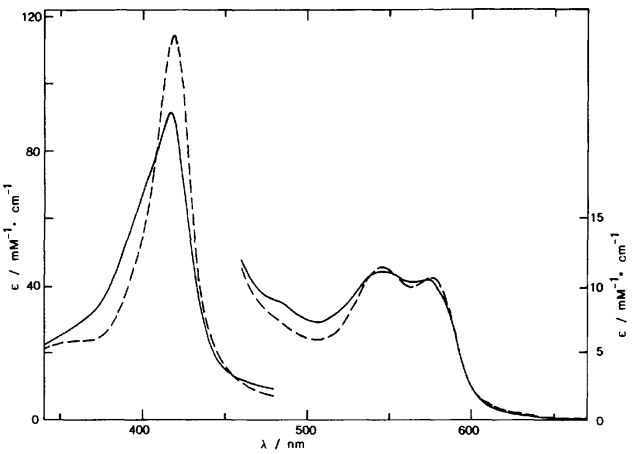

Fig. 4. Electronic spectra of Fe(ppixdme)(NO)(0.016 mM)-NMeIm(0.51 M) in dimethyl sulfoxide in the presence (1.16 M) (——) and the absence (----) of sodium dodecyl sulfate at room temperature.

solvents exhibits characteristic EPR spectra with an intense triplet in g_3 (or g_z) absorption,[7,14] while the spectral line shape in dimethyl sulfoxide was markedly different from such usual ones as shown in Fig. 2. Thus, the EPR spectral results of Fe(ppixdme)-(NO) in dimethyl sulfoxide both at room temperature and at 77 K also suggest the pronounced interaction of a dimethyl sulfoxide with the vacant axial position of Fe(ppixdme)(NO).

The EPR spectrum of Fe(ppixdme)(NO) in dimethyl sulfoxide was markedly changed upon addition of SDS. Both the line shape and the parameters of the spectra thus obtained were quite similar to those of five-coordinate model nitrosylheme,[9,14] of NO-hemoglobin modified by SDS,[5] and of NO-cytochrome c′ (*Alcaligenes* sp. NCIB 11015) with SDS[6] (Table 2 and Fig. 3). Although nitrosylporphyrinatoiron(II) in nonpolar solvents occasionally exhibits complicated EPR spectra arising from a mixture of monomer and dimer below frozen temperature,[12,15,16] the satellite absorptions which are attributable to a dimer were not observed at all in the EPR spectrum of Fe(ppixdme)-(NO) with SDS in dimethyl sulfoxide (Fig. 3).

These results indicate that sodium dodecyl sulfate hinders the interaction of dimethyl sulfoxide, O-donor ligand, with the axial vacant position in Fe(ppixdme)-(NO) and the dimerization of Fe(ppixdme)(NO) molecule.

Both the Soret band maximum and g_{iso} value of Fe(ppixdme)(NO) with SDS in dimethyl sulfoxide were quite similar to those in toluene, a nonpolar solvent (Tables 1 and 2). This suggests that Fe(ppixdme)-(NO) molecule is surrounded by hydrophobic part of SDS and consequently the polarity of molecular environment is decreased locally.

Thus, the nitrosylheme in both NO-hemoproteins modified by SDS and model system with SDS is surrounded by the hydrophobic part of SDS or the environment with a very small polarity.

It has been recently demonstrated from the EPR study on the single crystal of Fe(tpp)(NO) doped in Zn(tpp) (tpp, *m*-tetraphenylporphyrinato) that g_2 (or g_y) value is 2.028.[17] Thus, the 'g_2 absorption' of Fig. 3 and Table 2 can be identified as a lowest field line of triplet or doublet in such a g_2 absorption, which is derived from an ^{14}N nucleus of ^{14}NO or an ^{15}N nucleus of ^{15}NO, respectively. Accordingly, the g_2' absorption of Fig. 3 and Table 2 remains unidentified.

Addition of Sodium Dodecyl Sulfate to Fe(ppixdme)-(NO)(NMeIm) in Dimethyl Sulfoxide. The Soret band in the electronic spectrum of six-coordinate Fe(ppixdme)(NO)(NMeIm) in dimethyl sulfoxide (Fig. 4) was narrower and more intense and was located at longer wavelength side than that of five-coordinate Fe(ppixdme)(NO) in non-donor solvents.[8] Upon addition of SDS to the solution, the Soret band was weakened, the shoulder absorptions was revealed at around 400 and 485 nm, and α- and β-bands were broadened (Fig. 4), which are compatible with the appearance of five-coordinate complex and concomitant decrease in concentration of six-coordinate complex. From the Soret band intensity in the solution with SDS (Fig. 4), the contents of the six- and five-coordinate complexes are estimated to be 60 and 40%, respectively. On freezing the solution with SDS at 77 K, the positions of the band maxima were slightly varied to 400sh, 419.5, 485sh, 542, and 575 nm and the absorptions derived from five-coordinate complex were decreased in intensity. However, the spectrum could not be completely changed to that of five-coordinate complex even in much higher concentration of SDS.

The EPR spectrum of Fe(ppixdme)(NO)(NMeIm) in dimethyl sulfoxide at 77 K exhibited the line shape characteristic of six-coordinate nitrosylheme with

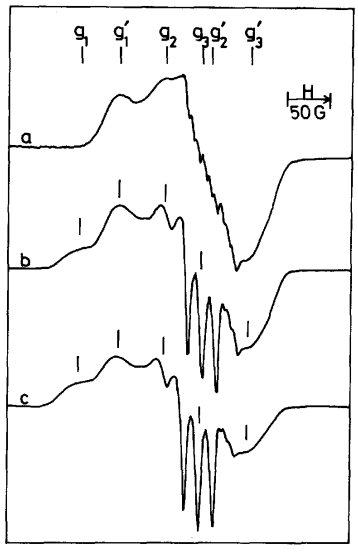

Fig. 5. EPR spectra of Fe(ppixdme)(NO)(0.4 mM)-NMeIm(80 mM) in dimethyl sulfoxide (a) in the absence and (b,c) in the presence of sodium dodecyl sulfate (b, 0.32 M; c, 4 M-almost saturated) at 77 K (g_1=2.10, g_2=2.035, g_3=2.010; g_1'=2.070, g_2'=2.004, g_3'=1.97). Instrument settings are given in caption of Fig. 3.

three g values (g_1', g_2', and g_3' in Fig. 5). Upon addition of SDS, the absorptions (g_1, g_2, and g_3) being attributable to five-coordinate complex were appeared and intensified (Figs. 5-b,c). Even trace amounts of five-coordinate complex were found to be detectable in the EPR spectrum of the sample containing nitrosylheme because the triplet in g_3 absorption of the five-coordinate complex is extremely intense.

Accordingly, the clevage of iron to 1-methylimidazole bond probably results from the interaction of the hydrophobic part of SDS with 6th coordination position or, possibly, from the intercalation of the five-coordinate complex into the micelles of SDS in dimethyl sulfoxide. However, since unhindered N-donor ligands such as imidazoles and pyridines are strongly coordinated to iron in the axial position trans to a nitrosyl group in nitrosylporphyrinatoiron(II),[12] all the iron to nitrogen bond can not be cleaved even in almost saturated solution of SDS.

References

1) J. E. Falk, "Porphyrins and Metalloporphyrins," Elsevier, Amsterdam (1964), p. 117; P. Hambright, "Porphyrins and Metalloporphyrins," ed by K. M. Smith, Elsevier, Amsterdam (1975), p. 233.

2) J. Simplicio, *Biochemistry*, **11**, 2525 (1972); J. Simplicio, *ibid.*, **11**, 2529 (1972); J. Simplicio, K. Schwenzer, and F. Maenpa, *J. Am. Chem. Soc.*, **97**, 7319 (1975).

3) K. Gersonde and H. Netter, *J. Mol. Biol.*, **10**, 475 (1964); K. Kasuga, S. Nakao, T. Kamezawa, K. Tsukahara, and Y. Yamamoto, *Biochim. Biophys. Acta*, **788**, 313 (1984).

4) H. Akutsu, Y. Kyogoku, and T. Horio, *Biochemistry*, **22**, 2055 (1983); T. Yoshimura, S. Suzuki, A. Nakahara, H. Iwasaki, M. Masuko, and T. Matsubara, *Biochim. Biophys. Acta*, **831**, 267 (1985).

5) H. Kon, *J. Biol. Chem.*, **379**, 103 (1975).

6) T. Yoshimura, S. Suzuki, A. Nakahara, H. Iwasaki, T. Matsubara, and M. Iwaizumi, *Inorg. Chim. Acta*, **136**, L17 (1987).

7) T. Yoshimura, *Bull. Chem. Soc. Jpn.*, **51**, 1237 (1978).

8) T. Yoshimura and T. Ozaki, *Arch. Biochem. Biophys.*, **229**, 126 (1984).

9) T. Yoshimura and T. Ozaki, *Bull. Chem. Soc. Jpn.*, **52**, 2268 (1979).

10) T. Yoshimura, *Inorg. Chem.*, **25**, 688 (1986).

11) H. Kon and N. Kataoka, *Biochemistry*, **8**, 4757 (1969); T. Yoshimura, T. Ozaki, Y. Shintani, and H. Watanabe, *Arch. Biochem. Biophys.*, **193**, 301 (1979); T. Yoshimura, *Inorg. Chim. Acta*, **46**, 69 (1980).

12) T. Yoshimura, *Arch. Biochem. Biophys.*, **220**, 167 (1983).

13) T. Yoshimura, *Inorg. Chim. Acta*, **57**, 99 (1982).

14) H. Kon, Biochim. *Biophys. Acta*, **379**, 103 (1975).

15) H. Kon, M. Chikira, and K. M. Smith, *J. Chem. Soc., Dalton Trans.*, **1981**, 1726.

16) T. Yoshimura, *Inorg. Chim. Acta*, **125**, L27 (1986).

17) Y. Ohba, Thesis, Tohoku University, Sendai (1984).

 © 1987 The Chemical Society of Japan Bull. Chem. Soc. Jpn., 60, 1379—1382 (1987)

Mixed Ligand Complexes of Trivalent Metal Ions with an Amine-*N*-polycarboxylate and Fluoride

Akio YUCHI,* Hitoshi HOTTA, Hiroko WADA, and Genkichi NAKAGAWA
Department of Applied Chemistry, Nagoya Institute of Technology, Gokiso-cho, Showa-ku, Nagoya 466
(Received October 28, 1986)

The formation constants of the mixed ligand complexes MLF(M: Al^{3+}, Ga^{3+}, In^{3+}, Fe^{3+}, Sc^{3+}, Y^{3+}, La^{3+}; L: nta^{3-}, $hedta^{3-}$, $edta^{4-}$, $cdta^{4-}$) were determined. Reactivity of a trivalent metal ion with fluoride generally decreases by the coordination of an amine-*N*-polycarboxylate. From the decrease the structures of the parent and mixed ligand complexes are discussed.

Fluoride ion is a unique ligand in that it shows almost pure electrostatic interactions with metal ions in solution. Since the fluoride ion-selective electrode was developed in 1966,[1] the formation constants of nearly every metal fluoro complexes have been determined.[2]

Recently we have found the general presence of the mixed ligand complexes containing fluoride in the equilibrium study on the reaction of aluminum fluoro complexes with masking reagents.[3] Such complexes have never been reported so far as we know. In this paper, the formation constants of a series of the mixed ligand complexes MLF (M: Al^{3+}, Ga^{3+}, In^{3+}, Fe^{3+}, Sc^{3+}, Y^{3+}, La^{3+}; L: nta^{3-}, $hedta^{3-}$, $edta^{4-}$, $cdta^{4-}$; charges of complexes are omitted)[4] are determined.

Experimental

Reagents and Equipments. Aluminum, gallium, lanthanum and iron solutions were prepared by dissolving their nitrates in dilute nitric acid. Indium, scandium, and yttrium solutions were obtained by reacting metallic indium, scandium oxide and yttrium oxide with nitric acid, respectively. All these solutions were standardized against EDTA. Potassium fluoride was dried for 24 h at 110 °C. Fluoride solutions were stored in polyethylene containers. Potassium nitrate was recrystallized twice. Carbonate-free potassium hydroxide solution was prepared as described in the literature.[5] All other chemicals used were of reagent grade.

Throughout this work the ionic strength was adjusted to 0.1 mol dm^{-3} with potassium nitrate. A measuring cell made of polypropylene was placed in a water bath thermostated at 25±0.1 °C. A fluoride ion-selective electrode (Denki Kagaku Keiki Co.; DKK type 7200), a HF-resistant glass electrode (Ohkura electric Co.; GP 1200) and two reference electrodes with a junction made of porous Teflon (DKK type 4400) were soaked in the sample solution, and potentials were measured to 0.1 mV with two potentiometers (DKK IOC-10). The fluoride ion-selective electrode was calibrated with several potassium fluoride solutions between 10^{-2}—10^{-6} mol dm^{-3} made by serial dilution, whereas the glass electrode was calibrated with several nitric acid solutions. Both electrodes gave Nernstian responses. Before and after a series of measurements standard potentials of these electrodes were determined with a 1.00×10^{-2} mol dm^{-3} potassium fluoride solution and a 1.00×10^{-2} mol dm^{-3} nitric acid solution, respectively. The presence of complexing reagents did not affect the standard potential of the fluoride ion-selective electrode.

Procedure. Stability constants of simple metal fluoro complexes and protonation constants of metal amine-*N*-polycarboxylate complexes were determined by the conventional methods.[2] When ternary systems were studied, 10% excess of a ligand against a metal ion was added to suppress the dissociation of an amine-*N*-polycarboxylate complex but not to form a bis complex, ML_2. With a dilute nitric acid or a potassium hydroxide solution, $-\log[H^+]$ was adjusted. This solution being titrated with potassium fluoride solution, $-\log[H^+]$ and $-\log[F^-]$ were measured after each addition. Constant potentials were obtained within 10 min. In the systems containing aluminum, potentials were read after 24 h using a batch method.

Results

Trivalent Metal Fluoro Complexes. The equilibria of reactions between proton and fluoride were first studied at 25 °C and at 0.1 mol dm^{-3} KNO_3. The results were analyzed as described previously,[6] and the following constants were obtained.

$$H^+ + F^- \rightleftharpoons HF: \quad \log K_{HF} = 2.99 \pm 0.03$$

$$HF + F^- \rightleftharpoons HF_2^-: \quad \log K_{HF_2} = 0.38 \pm 0.08$$

The complexation equilibria of trivalent metal ions with fluoride were studied for the comparison described below. The formation functions of metal fluoro complexes

$$\bar{n} = (C_F - [F^-] - [HF] - 2[HF_2^-])/C_M, \qquad (1)$$

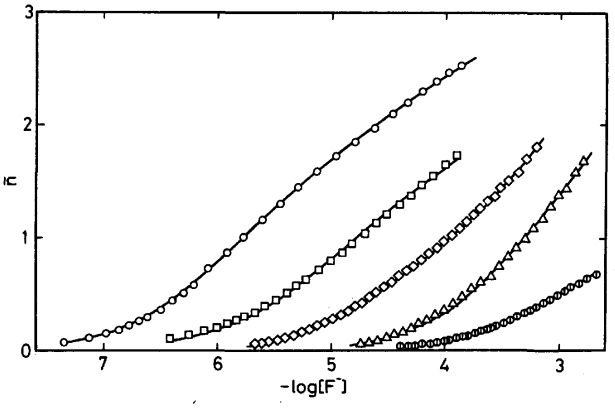

Fig. 1. Plots of $\bar{n}$ vs. $-\log[F^-]$ for trivalent metal fluoro complexes (25 °C, 0.1 mol dm^{-3} KNO_3). Trivalent metal: ○, scandium; □, iron; ◇, gallium; △, indium; ○, proton. Data for aluminum and yttrium complexes are omitted for clarity. The solid curves were calculated with the constants in Table 1.

Table 1. Formation Constants of Trivalent Metal Fluoro Complexes (25 °C; 0.1 mol dm^{-3} KNO_3)

Metal ion	Obtained[a]				Literature				Medium	Ref.
	$\log K_1$	$\log K_2$	$\log K_3$	$\log K_4$	$\log K_1$	$\log K_2$	$\log K_3$	$\log K_4$		
Al^{3+}	6.40(1)	5.24(2)	3.86(3)	2.7(10)	6.40	5.19	3.91	2.42	0.1 mol dm^{-3} NH_4NO_3	b
Ga^{3+}	4.49(2)	3.50(3)			4.40	3.80			1 mol dm^{-3} $NaClO_4$	c
In^{3+}	3.64(3)	2.9(10)			3.69	2.83			1 mol dm^{-3} $NaClO_4$	d
Fe^{3+}	5.30(2)	4.23(2)	3.0(10)		5.16	3.91	2.93		0.5 mol dm^{-3} $NaClO_4$	e
Sc^{3+}	6.22(1)	5.30(2)	3.95(3)		6.22	5.11	3.90		0.5 mol dm^{-3} $NaClO_4$	e
Y^{3+}	3.76(3)				3.91	3.25			0.5 mol dm^{-3} $NaClO_4$	e

a) Numbers in parentheses are estimated errors. b) E. W. Baumann, *J. Inorg. Nucl. Chem.*, **31**, 3155 (1969). c) J. B. Walker, C. R. Twine and G. R. Choppin, *J. Inorg. Nucl. Chem.*, **33**, 1813 (1971). d) T. Ryhl, *Acta Chem. Scand.*, **23**, 2667 (1969). e) A. Aziz and S. J. Lyle, *Anal. Chim. Acta*, **47**, 49 (1969).

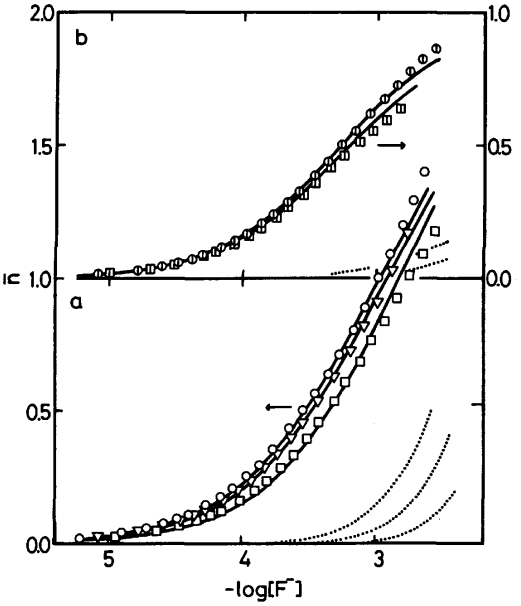

Fig. 2. Plots of $\bar{n}$ vs. $-\log[F^-]$ for Fe-NTA-F and Fe-HEDTA-F systems (25 °C, 0.1 mol dm^{-3} KNO_3). System: a, Fe-NTA-F; b, Fe-HEDTA-F. $-\log[H^+]$: ○, 2.9; ▽, 3.3; □, 3.85;○, 2.9; □, 3.2. The solid curves were calculated with the constants in Table 2. The dotted curves were expected by assuming no mixed ligand complex formation.

are plotted against $-\log[F^-]$ in Fig. 1. The change in the total concentration of a metal ion (from 5×10^{-4} to 2×10^{-3} mol dm^{-3}) or hydrogen ion did not displace the formation functions. Thus neither polymerized fluoro complexes nor hydrolyzed species were formed. The stepwise formation constants of metal fluoro complexes

$$MF_{m-1} + F^- \rightleftharpoons MF_m : K_m,$$

were refined to give a minimum error square sum about $\bar{n}$ (Table 1). Constants smaller than $10^{3.0}$ are less reliable because of low precision of the numerator in Eq. 1. Formation of lanthanum fluoro complexes could not be studied by the same method due to the precipitation of lanthanum trifluoride.

Mixed Ligand Complexes in Fe-NTA-F and Fe-HEDTA-F Systems. Figure 2 shows the formation functions at various $-\log[H^+]$ in Fe-NTA-F and Fe-HEDTA-F systems.

Table 2. Average Deviation of $\bar{n}$ for Various Combinations of Species in Fe-NTA-F and Fe-HEDTA-F Systems[a]

System	No.	Species considered			$\Delta\bar{n}$
		MLF	MLF_2	ML(OH)F	
Fe-NTA-F	1	×	×	×	0.627
	2	○	×	×	0.181
	3	○	○	×	0.042
	4	○	○	○	0.040
Fe-HEDTA-F	1	×	×	×	0.442
	2	○	×	×	0.041
	3	○	○	×	0.040
	4	○	○	○	0.040

a) Numbers of data used for the calculation were 73 for Fe-NTA-F and 67 for Fe-HEDTA-F, respectively.

The parent complex ML hydrolyzes at higher $-\log[H^+]$.

$$ML(OH) + H^+ \rightleftharpoons ML : K^H_{ML}$$

These constants were potentiometrically determined to be $10^{3.96}$ for Fe-NTA and $10^{3.86}$ for Fe-HEDTA. On the other hand, the complex is protonated at lower $-\log[H^+]$.

$$ML + H^+ \rightleftharpoons MHL : K^H_{MHL}$$

Among these species, ML and MHL react with fluoride to form mixed ligand complexes.[3] It was difficult, however, to study the reactivity of MHL, because MHL forms only in strongly acidic solution where on the addition of fluoride the substitution reaction prevails over the formation of the mixed ligand complex. Thus we adopted the data in the $-\log[H^+]$ range where only ML and ML(OH) existed.

Formation of the mixed ligand complex MLF_n is expressed by

$$MLF_{n-1} + F^- \rightleftharpoons MLF_n : K^F_{MLF_n}.$$

For each experimental point, two simultaneous equations in [M] and [L] were solved,

$$C_M = [M] + [ML] + [ML(OH)] + \Sigma[MF_m] + \Sigma[MLF_n], \quad (2)$$

$$C_L = [L]\alpha_{L(H)} + [ML] + [ML(OH)] + \Sigma[MLF_n], \quad (3)$$

Table 3. Total Concentrations of M and F^-, Concentrations of F^- and HF, $-\log[H^+]$, $\bar{n}$ and the Calculated Formation Constants of the Mixed Ligand Complex in Ga-NTA-F System[a)]

	10^4C_M / mol dm^{-3}	10^4C_F / mol dm^{-3}	$10^4[F^-]$ / mol dm^{-3}	$10^4[HF]$ / mol dm^{-3}	$-\log[H^+]$	$\bar{n}$	$\log K^F_{MLF}$[b)]
1	8.963	0.648	0.125	0.272	2.650	0.028	3.365
2	8.960	0.972	0.188	0.405	2.655	0.042	3.373
3	8.957	1.295	0.254	0.542	2.661	0.056	3.366
4	8.954	1.619	0.318	0.674	2.664	0.070	3.373
5	8.951	1.942	0.385	0.806	2.669	0.084	3.376
6	8.948	2.265	0.454	0.938	2.674	0.098	3.377
7	8.945	2.588	0.524	1.074	2.677	0.111	3.375
8	8.939	3.232	0.670	1.352	2.684	0.135	3.368
9	8.933	3.877	0.810	1.617	2.689	0.162	3.377
10	8.924	4.841	1.035	2.019	2.699	0.200	3.382
11	8.915	5.804	1.272	2.425	2.710	0.236	3.385
12	8.904	7.084	1.601	2.957	2.723	0.283	(3.392)
13	8.892	8.361	1.945	3.483	2.737	0.329	(3.402)
14	8.874	10.27	2.496	4.248	2.759	0.397	(3.420)
15	8.857	12.17	3.092	5.022	2.779	0.457	(3.435)
16	8.834	14.69	3.905	5.960	2.806	0.546	(3.487)
17	8.811	17.20	4.744	6.883	2.828	0.631	(3.557)
18	8.782	20.32	5.946	7.857	2.868	0.740	(3.680)
19	8.748	24.04	7.482	8.831	2.918	0.880	(3.992)

a) Formation of HF_2^- is negligible in this system. b) Calculated with Eqs. 2′ and 5.

Table 4. Formation Constants for the Coordination of the First Fluoride to ML

Metal ion	$\log K^F_{MLF}$ for various L[a)]					Ionic radius
	None	nta^{3-}	$hedta^{3-}$	$edta^{4-}$	$cdta^{4-}$	
Al^{3+}	6.40	5.41(2)	5.53(2)	4.95(2)	3.14(2)	0.50
Ga^{3+}	4.49	3.37(2)	3.15(2)	2.3(10)	2.1(10)	0.62
In^{3+}	3.64	2.0(10)	2.0(10)	1.6(10)	2.1(10)	0.81
Fe^{3+}	5.30	3.46(2)	3.31(2)	1.7(10)	1.5(10)	0.64
Sc^{3+}	6.22	3.90(5)	3.62(5)	1.9(10)	2.5(10)	0.81
Y^{3+}	3.76	2.62(5)	1.8(10)	1.5(10)	1.6(10)	0.93
La^{3+}	2.69[b)]	2.0(10)	1.7(10)	1.4(10)	1.8(10)	1.15

a) Numbers in parentheses are estimated errors. b) At ionic strength 0.5 mol dm^{-3} $NaClO_4$. A. Aziz and S. J. Lyle, *J. Inorg. Nucl. Chem.*, **32**, 1925 (1970).

where $\alpha_{L(H)}$ is the side reaction coefficient taking account of the protonation of L. Using [M], [L], $[H^+]$, and $[F^-]$, $\bar{n}$ was calculated.

$$\bar{n}_{cald} = \frac{\sum m[MF_m] + \sum n[MLF_n]}{C_M} \quad (4)$$

Various combinations of the mixed ligand complexes were assumed and $K^F_{MLF_n}$ values in each set were refined to give a minimum error square sum, $\Delta\bar{n}=(\sum(\bar{n}_{obsd}-\bar{n}_{cald})^2/N)^{1/2}$ (Table 2).

When no mixed ligand complex was assumed there were large systematic deviations (dotted curves in Fig. 2 or No.1 in Table 2). By considering the formation of MLF satisfactory agreement between experimental and calculated values was obtained in Fe-HEDTA-F system but not in Fe-NTA-F system (No. 2), where presence of MLF_2 must also be taken into account (No. 3). Further improvement was not obtained by assuming the formation of ML(OH)F (No. 4).

Other Systems. As the K^H_{ML} values of the other complexes are larger than those of Fe(nta) and Fe(hedta),[7] $-\log[H^+]$ can be adjusted so that only ML exists in the solution containing a metal ion and an excess ligand: the concentration of ML(OH) as well as those of MHL and free M is low. When small amounts of fluoride are added to such solutions, formation of MF_m and MLF_n ($n>1$) is negligible. Then Eq. 2 is simplified as

$$C_M = [ML] + [MLF], \quad (2')$$

and [MLF] is obtained by

$$[MLF] = C_F - ([F^-] + [HF] + 2[HF_2^-]). \quad (5)$$

The K^F_{MLF} values can be calculated only with these equations.

Table 3 gives some of the data in Ga-NTA-F system. At lower total concentrations of fluoride (until No. 11) K^F_{MLF} values are constant. On the other hand, $\bar{n}$ and thus K^F_{MLF} abruptly increases at higher C_F because of the dissociation of the ligand from the complex

accompanied by the formation of GaF_m. The K^F_{MLF} values thus obtained are given in Table 4.

Discussion

Metal Fluoro Complexes. Correlation between $\log K_1$ and $Z_+/(r_+ + r_-)$, where Z_+ is the charge of a metal ion and r_+ and r_- are the radii of the metal and fluoride ions, respectively, has been suggested from a simple electrostatic consideration,[8] but it is not satisfactory. For example, Al^{3+} and Sc^{3+} have almost the same formation constants in spite of very different ionic radii. The role of the solvent is completely neglected in this consideration.

As shown in Table 1, the ratio K_2/K_3 is larger than K_1/K_2, and this indicates the irregular change in the solvation during the stepwise complexation,[9] which cannot be quantitatively evaluated at this stage.

M-NTA-F and M-HEDTA-F. Reactivity of a trivalent metal ion with fluoride generally decreases by the coordination of an amine-*N*-polycarboxylate. As NTA and HEDTA complexes hold more than one coordinated water molecules, formation of their mixed ligand complexes corresponds to substitution of water molecules with fluoride ions as in the formation of simple fluoro complexes. The decrease in the reactivity is thus ascribed to the decrease in the statistical factor, the neutralization of the positive charge on the metal ion by the ligand and the decrease in the degree of solvation.

The first effect is not expected to contribute so much but certainly operates so that small decreases in K^F_{MLF} are observed from NTA complexes with tetradentate chelation to HEDTA complexes with pentadentate chelation. The second effect is more decisive but would be relieved for larger ions because positive charges on these ions can only locally be neutralized. This is the case for scandium group and the difference between K^F_{MF} and K^F_{MLF} decreases in the order of $Sc^{3+} > Y^{3+} > La^{3+}$. But the reverse order is found for aluminum group, where again the third effect must prevail.

M-EDTA-F and M-CDTA-F. The K^F_{MLF} values of Ga(edta), Fe(edta), and Sc(edta) are much smaller than those of their HEDTA and NTA complexes, respectively. This suggests that one carboxylato group must become free on the formation of the mixed ligand complex and also that the parent complexes involve the complete hexadentate chelation of EDTA irrespective of the coordination number of metal ions.[10] On the other hand, for aluminum, similar large decrease in K^F_{MLF} is rather found between EDTA and CDTA complexes. This means the weak coordination of one carboxylato group in Al(edta) complex, which agrees with the fact that $K^H_{MH(edta)}$ of aluminum complex ($10^{2.8-3.4}$) is definitely higher than those of other trivalent metal complexes (less than 10^2 except for large metal ion complexes).[7]

If a CDTA complex of a metal also forms the mixed ligand complex with the pentadentate chelation, $K^F_{M(edta)F}$ is expected to be smaller than $K^F_{MH(edta)F}$, because CDTA has a more rigid skeleton and must have more difficulty in detaching one carboxylato group. This is the case for aluminum, gallium, and iron, but the reverse order is found for indium, scandium, yttrium and lanthanum. As these ions have larger ionic radii, fluoride can coordinate to a metal ion with keeping the hexadentate chelation of the ligand as in the reaction of Co(II)(cdta) with cyanide.[16]

The authors wish to thank the Grant-in-Aid for Scientific Research No. 61127007 from the Ministry of Education, Science and Culture.

References

1) M. S. Frant and J. W. Ross, *Science*, **154**, 1553 (1966).
2) A. M. Bond and G. T. Hefter, "Critical Survey of Stability Constants and Related Thermodynamic Data of Fluoride Complexes in Aqueous Solution," IUPAC, Pergamon (1980).
3) A. Yuchi, K. Ueda, H. Wada, and G. Nakagawa, *Anal. Chim. Acta*, **186**, 313 (1986).
4) Ligand abbreviation: NTA, nitrilotriacetic acid (H_3nta); HEDTA, *N'*-(2-hydroxyethyl)ethylenediamine-*N,N,N'*-triacetic acid (H_3hedta); EDTA, ethylenediamine-*N,N,N',N'*-tetraacetic acid (H_4edta); CDTA, 1,2-cyclohexanediamine-*N,N,N',N'*-tetraacetic acid (H_4cdta).
5) J. E. Powell and M. A. Hiller, *J. Chem. Educ.*, **34**, 330 (1957).
6) K. Srinivasan and G. A. Rechnitz, *Anal. Chem.*, **40**, 509 (1968).
7) a) L. G. Sillen and A. E. Martell, "Stability Constants of Metal-Ion Complexes, and Supplement No. 1," The Chemical Society, London (1964 and 1971); b) D. D. Perrin, "Stability Constants of Metal-Ion Complexes Part B," IUPAC, Pergamon (1979).
8) G. Hefter, *Coord. Chem. Rev.*, **12**, 221 (1974).
9) S. Ahrland, *Pure Appl. Chem.*, **51**, 2019 (1979) and references therein; S. Ahrland, *Pure Appl. Chem.*, **54**, 1451 (1982) and references therein.
10) Fe(edta) is seven coordinate both in the solid[11] and in the solution[12] with a coordinated water. But it is ascribed to the unbalanced affinities to amino nitrogen and carboxylate oxygen rather than the size of ionic radius.[13] Once the ligand becomes pentadentate, the metal becomes six coordinate with relaxation of ring constrain as seen in [Fe(hedta)]$_2$O and Fe(Hedta)H_2O.[14,15] This agrees with our observation that the highest species were Fe(nta)F_2 and Fe(hedta)F.
11) M. D. Lind, M. J. Hamor, T. A. Hamor, and J. L. Hoard, *Inorg. Chem.*, **3**, 34 (1964).
12) J. Oakes and E. G. Smith, *J. Chem. Soc., Faraday Trans. 1*, **79**, 543 (1983).
13) J. J. Stezowski, R. Countryman, and J. L. Hoard, *Inorg. Chem.*, **12**, 1749 (1973).
14) S. J. Lippard, H. Schugar, and C. Walling, *Inorg. Chem.*, **6**, 1825 (1967).
15) C. H. L. Kennard, *Inorg. Chim. Acta*, **1**, 347 (1967).
16) J. P. Jones and D. W. Margerum, *Inorg. Chem.*, **8**, 1486 (1969).

 © 1987 The Chemical Society of Japan Bull. Chem. Soc. Jpn., 60, 1383—1389 (1987)

Synthesis of a 24-Epimeric Mixture of 4α,14α,24-Trimethyl-9(11)-cholesten-3-one

Masahiko YAMASHITA, Misuzu NAORA (nee NAMIKAWA), Tatsushi MURAE, Takahiko TSUYUKI,* and Takeyoshi TAKAHASHI*

Department of Chemistry, Faculty of Science, The University of Tokyo, Hongo, Bunkyo-ku, Tokyo 113

(Received July 25, 1986)

A 24-epimeric mixture of 4α,14α,24-trimethyl-9(11)-cholesten-3-one was synthesized from lanosterol through 4α,14α,24-trimethyl-8-cholesten-3β-ol and 4α,14α,24-trimethyl-7,11-dioxocholestan-3β-yl acetate as key intermediates.

A triterpene mixture (ca. 4 mg) was obtained from the plant fossil (ca. 50 g) collected at the Ningyo-toge area on the border between Tottori and Okayama Prefectures.[1] Preparative gas chromatographic separation of the mixture afforded three components, **a** ($C_{29}H_{48}O$), **b** ($C_{29}H_{50}O$), and **c** ($C_{30}H_{50}O$), which weighed about hundreds μg, respectively. Spectral examination suggested that the component **c** is a mixture of two unsaturated tetracyclic triterpene ketone and one of them might be 4α,14α,24ξ-trimethyl-9(11)-cholesten-3-one. However, a paucity of the material prevented us from the further confirmation of the proposed structure. This paper describes a preparation of a 24-epimeric mixture of 4α,14α,24-trimethyl-9(11)-cholesten-3-one (**1**)[2] from lanosterol (**2**) as an authentic sample, whose ^{1}H NMR and mass spectra are compared with those of the natural specimen.

A commercial lanosterol containing ca. 45% dihydrolanosterol (=8-lanosten-3β-ol) (**3**) was acetylated and subjected to hydroboration using diborane in tetrahydrofuran (THF) to afford a mixture of 24-hydroxy-8-lanosten-3β-yl acetate (**4**) and dihydrolanosteryl acetate, the former of which, after separation, was oxidized with Jones reagent to yield 24-oxo-8-lanosten-3β-yl acetate (**5**).

When the hydroboration was effected in situ with diborane generated by sodium borohydride and boron trifluoride etherate in THF, and oxidation with sodium dichromate was followed without isolation of 24-hydroxy-8-lanosten-3β-yl acetate (**4**), the hydroboration-oxidation reaction[3] was found to give a mixture of two ketones, one of which was shown to be identical with **5** by GLC examination and ^{1}H NMR spectrum. The mixture was treated with sodium borohydride to afford a mixture of three hydroxy acetates, one of which was identical with 24-hydroxy-8-lanosten-3β-yl acetate (**4**). The other two showed similar IR, ^{1}H NMR, and MS spectra to those of **4**, and were inferred to be epimeric secondary alcohols (**7** and **7'**), because they gave almost the same ^{1}H NMR spectra each other and the same peak area at δ 3.8 due to *H*-C-OH as that at δ 4.5 due to *H*-C-OAc, respectively. Therefore, the epimeric alcohols (**7** and **7'**) were oxidized with Jones reagent, respectively, to give the same acetoxy ketone (**6**), which showed fragment peaks at *m/z* 369 ([M−Me−100]$^+$) and *m/z* 309 ([M−Me−AcOH−100]$^+$). Since the appearance of these peaks indicates a loss of $C_6H_{12}O$ (*m/z* 100) derived from McLafferty rearrangement,[4] the location of the carbonyl group was deduced to be at C-23 (Scheme 1). This conclusion was confirmed by characteristic fragment peaks at *m/z* 471 and *m/z* 129 observed in the mass specrtum of ethylene acetal (**8**) of the ketone (**6**) (Scheme 2). From these findings, the ketone (**6**) could be formulated as 23-oxo-8-lanosten-3β-yl acetate. Since the absence of 23-ene in the starting material was certified by the ^{1}H NMR examination, the formation of **6** is inexplicable. Further investigation on the formation mechanism is under way.

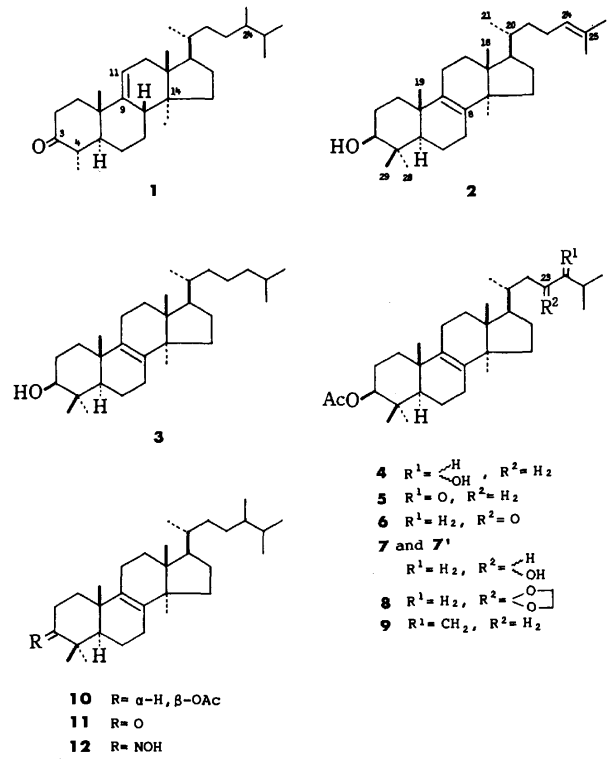

24-Oxo-8-lanosten-3β-yl acetate (**5**) was converted into 24-methylene derivative (**9**) by Wittig reaction, which was subjected to hydrogenation to yield a 24-epimeric mixture of 24-methyl-8-lanosten-3β-yl acetate (**10**)†. 4β-Demethylation of **10** was carried out by

†All 24-methyl derivatives obtained by the preparation described below in this paper are 24-epimeric mixtures, respectively.

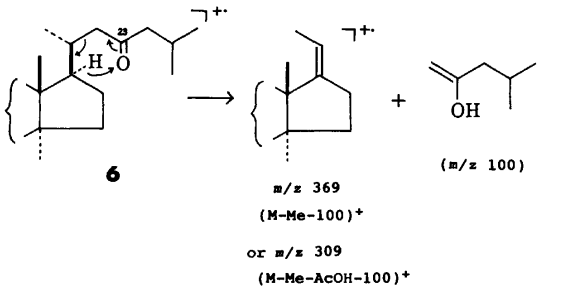

Scheme 1.

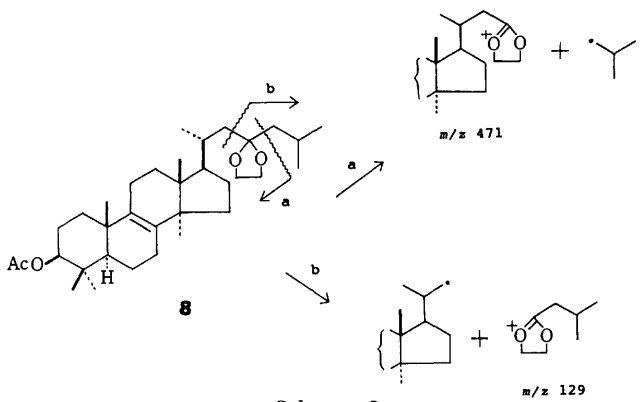

Scheme 2.

the same procedure as described in the previous paper;[1] hydrolysis of 24-methyl-8-lanosten-3β-yl acetate (**10**) followed by Jones oxidation gave a ketone (**11**), which was converted into the corresponding oxime (**12**), a seconitrile (**13**), and then a nitrile epoxide (**14**). On a treatment with boron trifluoride etherate, **14** afforded the demethylation product, 4α,14α,24-trimethyl-8-cholesten-3-one (=24-methyl-29-nor-8-lanosten-3-one) (**15**) in about 6.1% yield from **10**.

4α,14α,24-Trimethyl-8-cholesten-3β-yl acetate (**16**), $C_{32}H_{54}O_2$ [*m/z* 470.4159 determined by high resolution mass spectrometry (HR-MS)] derived from **15** was subjected to an allylic oxidation with chromium trioxide[5] in acetic acid-hexane to afford 4α,14α,24-trimethyl-7,11-dioxo-8-cholesten-3β-yl acetate (**17**), $C_{32}H_{50}O_4$ (*m/z* 498.3709) in 55% yield. An absorption band due to the unsaturated carbonyl group was observed at 1680 cm^{-1} in the IR spectrum. On heating with zinc dust in acetic acid,[5] **17** afforded a saturated dione acetate (**18**), $C_{32}H_{52}O_4$ (*m/z* 500.3896), in 66% yield.

Selective decarbonylation at C-7 was examined using 7,11-dioxolanostan-3β-yl acetate (**19**)[6] as a model compound. Wolff-Kishner reduction of **19** under standard conditions afforded a 7-deoxo derivative (**20**) in 41% yield accompanied with a 7,11-dideoxo derivative, lanostan-3β-ol (**21**), in 18% yield. The formation of **21** was reduced by removing the excess hydrazine at reduced pressure after hydrazone formation.[7] However, this modification could not improve the yield of **20**. Next, the reduction of a tosylhydrazone (**22**) of **19** with sodium (cyano-*C*)trihydroborate[8] was investigated, but the tosylhydrazone (**22**) could not be prepared in a good yield in ethanol nor in acetic acid.[9]

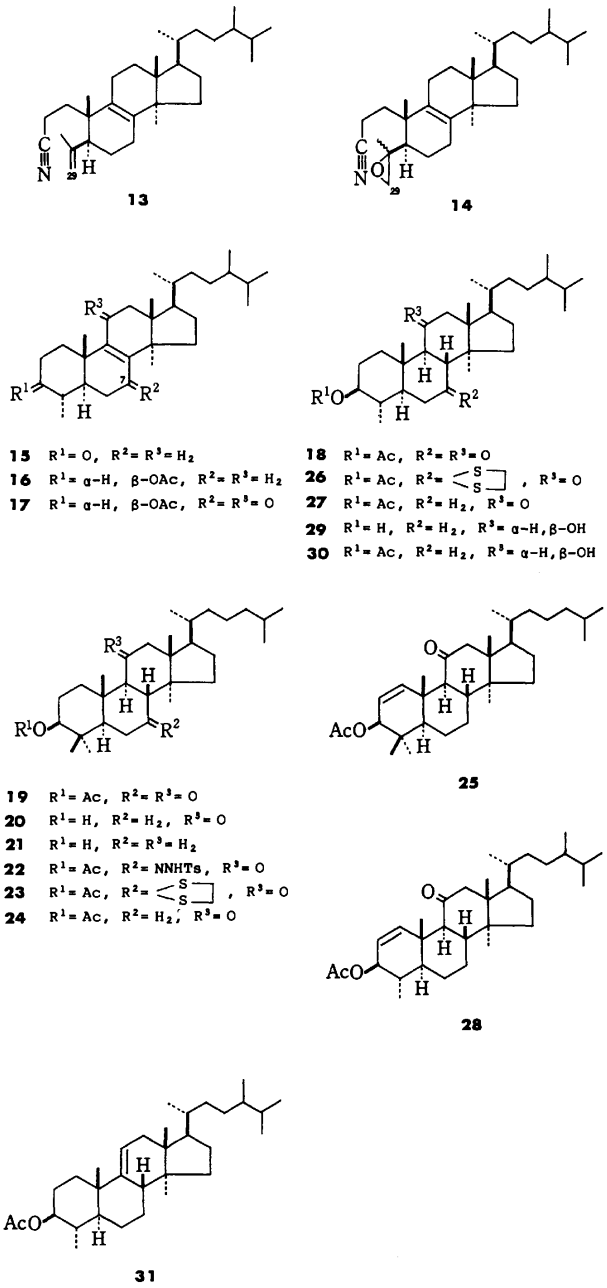

Then the 7,11-dione (**19**) was converted into 7,7-ethylenedithio-11-oxolanostan-3β-yl acetate (**23**), which was treated with Raney nickel W2[10] in dioxane to afford the desired 7-deoxo derivative (**24**) in 86% yield from **19**.[11] Thioacetalization and desulfurization in a large scale, however, afforded a mixture of **24** and an olefin (**25**), latter of which was inferred to be 11-oxo-1-lanosten-3β-yl acetate by ^1H NMR spectrum and GC-MS examination (Scheme 3).[12,13] This was supported by hydrogenation of the mixture (**24** and **25**) giving rise to the single product, **24**.

According to the procedures described above, 4α,14α,24-trimethyl-7,11-dioxocholestan-3β-yl acetate (**18**) was converted into a 7,7-ethylenedithio derivative (**26**), which was treated with Raney nickel W2.[10] The reaction product was also found to consist of two com-

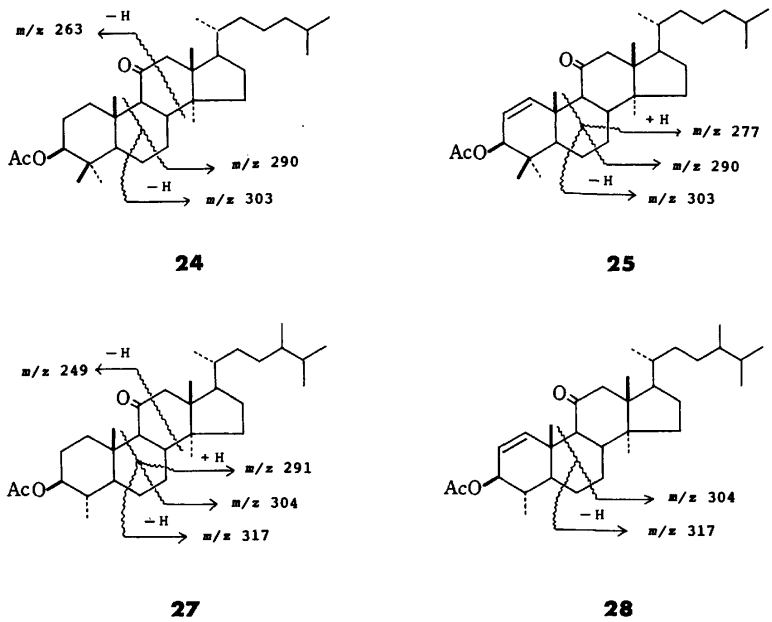

Scheme 3.

pounds by GLC examination. The ^{1}H NMR spectrum of the mixture showed two singlet signals due to acetoxyl groups at δ 2.03 and 2.04 and a couple of doublet signals due to vicinal olefinic protons at δ 5.47 and 5.72, respectively. These findings and the mass spectrum revealed that the mixture consisted of the desired 11-oxo derivative (**27**) together with an olefinic by-product (**28**), whose double bond was confirmed to be 1-ene from the fragment ions at *m/z* 304 and *m/z* 317 (Scheme 3).[12,13] The mixture was hydrogenated to afford the single product, which was identical with **27**. The formation mechanism of **25** and **28** was not made clear yet.

The introduction of a double bond between C-9 and C-11 was achieved by usual manner; 4α,14α,24-trimethyl-11-oxocholestan-3β-yl acetate (**27**) was reduced with lithium aluminium hydride (LAH) to afford a 3β,11β-diol (**29**), which, after a partial acetylation, was treated with phosphoryl chloride, 4α,14α,24-trimethyl-9(11)-cholesten-3β-yl acetate (**31**), mp 119—120 °C (lit,[2] mp 123—125 °C; lit,[14] mp 117.5—118.5 °C), being obtained. Hydrolysis of **31** followed by Jones oxidation gave 4α,14α,24-trimethyl-9(11)-cholesten-3-one (**1**). In the ^{1}H NMR spectrum of **1**, an olefinic proton at C-11 was observed at δ 5.35 and two singlet signals due to C-18 and C-19 methyl groups appeared at δ 0.69 and 1.23, respectively. The ^{1}H NMR spectral data of acetate (**31**) and ketone (**1**) are compatible with 9(11)-ene structure.[1,2,15]

The synthetic 24-epimeric mixture of 4α,14α,24-trimethyl-9(11)-cholesten-3-one (**1**) exhibited the same ^{1}H NMR spectrum at 270 MHz and the same fragment pattern in the mass spectrum as those of the natural specimen obtained from the plant fossil. However, the absolute configuration at C-24 of the natural specimen could not be determined unequivocally from only this finding.

Experimental[16]

24-Oxo-8-lanosten-3β-yl Acetate (5). A mixture (1.0 g) of lanosteryl acetate and dihydrolanosteryl acetate in a ratio of 5:4 was prepared from a commercial lanosterol (**2**) (E. Merck) and dissolved in THF (20 ml). To the solution kept at 1—2 °C, diborane in THF (1.1 mmol ml^{-1}; 1.2 ml) was added with stirring. The stirring was continued for 5.5 h at room temperature, and further for 1.5 h after addition of water (0.13 ml). The solution was cooled to 2—4 °C and 3 M (1 M=1 mol dm^{-3}) sodium hydroxide solution (0.33 ml) and 30% hydrogen peroxide (0.2 ml) were added with stirring. After stirring was continued at room temperature and then at 40—60 °C for 3.5 h, the usual work-up and chromatographic separation on silica gel (12 g) eluted with 10—40% ether in hexane gave dihydrolanosteryl acetate (283 mg) and 24-hydroxy-8-lanosten-3β-yl acetate (**4**; 256 mg).

A cold solution of 24-hydroxy-8-lanosten-3β-yl acetate (**4**; 204 mg) in acetone (15 ml) was treated with Jones reagent (0.25 ml) and the solution was stirred for 5 min. 2-Propanol (0.5 ml) was added and the usual work-up gave a residue, which was crystallized from ether-methanol to afford 24-oxo-8-lanosten-3β-yl acetate (**5**; 118 mg), mp 128—129.5 °C.

23-Oxo-8-lanosten-3β-yl Acetate (6). Sodium borohydride (30 mg) was added to a solution of the mixture (1 g) of lanosteryl acetate and dihydrolanosteryl acetate in THF (5 ml) under a nitrogen atmosphere and the solution was kept at 25—30 °C. Boron trifluoride etherate (0.03 ml) in THF (0.12 ml) was added and the solution was stirred for 6 h. After addition of water (0.15 ml), a solution of sodium dichromate in sulfuric acid [prepared by dissolving $Na_2Cr_2O_7 \cdot 2H_2O$ (0.33 g) in concd sulfuric acid (0.25 ml) and water (ca. 1.2 ml)] was added dropwise. The usual work-up afforded a residue, which was chromatographed on silica gel (55 g). Elution with 10—25% ether in hexane afforded a mixture (224 mg) of 24-one (**5**) and 23-one (**6**), the ratio of which was found to be 2:3 by GLC examination.

The mixture (120 mg) of **5** and **6** in ethanol was reduced with sodium borohydride (22 mg) for 32 h and the usual work-up afforded a residue, which was subjected to separation by preparative TLC developed with 40% ether in hexane twice to afford (23*S* or *R*)-23-hydroxy-8-lanosten-3β-yl acetate (**7**; 28 mg), 24-hydroxy derivative (**4**; 35 mg), and (23*R* or *S*)-23-hydroxy derivative (**7'**; 14 mg). The 24-hydroxy derivative, mp 142—143 °C, was completely identical with the authentic sample (**4**) derived by hydroboration of lanosteryl acetate. **7**: Mp 171—172 °C (colorless needles from ether-methanol); IR (Nujol) 3570, 1730, and 1270 cm^{-1}; ^1H NMR (90 MHz, $CDCl_3$) δ=0.72 (3H, s; 18-Me), 0.88—1.00 (Me's), 2.03 (3H, s; AcO), 3.78 (1H, m; 23-H), and 4.50 (1H, m; 3α-H); MS *m/z* (%) 486 (M^+; 34), 471 (54), 453 (40), 411 (100), 393 (62), 369 (25), 311 (19), and 309 (23). **7'**: Mp 152—153 °C (colorless needles from ether-methanol); IR (Nujol) 3300, 1740, and 1240 cm^{-1}; ^1H NMR (90 MHz, $CDCl_3$) δ=0.70 (3H, s; 18-Me), 0.88—1.00 (Me's), 2.03 (3H, s; AcO), 3.78 (1H, m; 23-H), and 4.49 (1H, m; 3α-H); MS *m/z* (%) 486 (M^+; 19), 471 (33), 453 (32), 411 (100), 393 (60), 369 (18), 311 (25), and 309 (26).

A solution of an epimeric alcohol (**7**; 44 mg) in acetone (3 ml) was treated with Jones reagent (0.05 ml) at 0 °C with stirring for 5 min and 2-propanol (0.3 ml) was added to the reaction mixture. The usual work-up gave a residue, which was separated by silica-gel chromatography (C-200, 2 g). 23-Oxo-8-lanosten-3β-yl acetate (**6**; 31 mg) was eluted with 10—30% ether in hexane, mp 135—136 °C (colorless needles from methanol); IR (Nujol) 1720, 1710, 1265, 1035, and 980 cm^{-1}; ^1H NMR (60 MHz, $CDCl_3$) δ=0.72 (3H, s; 18-Me), 0.84—1.00 (Me's), 2.03 (3H, s; AcO), and 4.50 (1H, m; 3α-H); MS *m/z* (%) 484 (M^+; 31), 469 (76), 424 (8), 409 (100), 369 (48), and 309 (79). The other epimer (**7'**; 17 mg), on oxidation, afforded the same ketone (**6**; 13 mg).

23,23-Ethylenedioxy-8-lanosten-3β-yl Acetate (8). To a solution of a ketone (**6**; 23 mg) in benzene (8 ml), ethylene glycol (0.75 ml) and a small amount of *p*-toluenesulfonic acid were added, and the solution was heated under reflux using a Dean-Stark separator containing Molecular Sieves 4A 1/16 for 10 h. After addition of 10% sodium hydroxide solution, an organic layer was separated and worked up as usual. A residue was purified by silica-gel chromatography (C-200, 3 g, elution with 10—30% ether in hexane) to afford 23,23-ethylenedioxy-8-lanosten-3β-yl acetate (**8**), MS *m/z* 528 (M^+), 513, 471, and 129 (base peak).

24-Methylene-8-lanosten-3β-yl Acetate (9). To the Wittig reagent prepared from methyltriphenylphosphonium bromide (1.41 g) in THF (30 ml) and butyllithium in hexane (10 w/v %, 2.5 ml), a solution of 24-oxo-8-lanosten-3β-yl acetate (**5**; 1.81 g) in THF (7 ml) was added under nitrogen. After reflux for 17 h, solvents were removed and the residue was dissolved in a mixture of ether-water (1 : 1; 60 ml). The ethereal layer was separated and the aqueous layer was extracted with ether three times (each 20 ml). The organic layer and extracts were combined and worked up as usual to afford a residue. Chromatographic separation on silica gel (elution with 2—40% ether in hexane) yielded 24-methylene-8-lanosten-3β-yl acetate (**9**; 1.02 g) together with the starting material (**5**; 197 mg). **9**: Colorless plates (from ether-methanol) sublimes on heating; IR (Nujol) 1720, 1640, 1250, and 890 cm^{-1}; ^1H NMR (90 MHz, $CDCl_3$) δ=0.70 (3H, s), 0.89—1.06 (Me's), 2.04 (3H, s; AcO), ca. 4.4 (1H, m; *H*-C-OAc), 4.67 and 4.72 (each 1H, br s; H_2C=C); MS *m/z* (%) 482 (M^+; 33), 467 (85), 407 (59), and 155 (100).

24-Methyl-8-lanosten-3β-yl Acetate (10). 24-Methylene derivative (**9**; 772 mg) in ether (60 ml) was hydrogenated in the presence of platinum oxide (81 mg) under atmospheric pressure for 48 h to afford 24-methyl-8-lanosten-3β-yl acetate (**10**; 780 mg), mp 127—128.5 °C; IR (Nujol) 1720 and 1245 cm^{-1}; ^1H NMR (90 MHz, $CDCl_3$) δ=0.69 (3H, s), 1.00 (3H, s), 2.03 (3H, s; AcO) and 4.51 (1H, m; *H*-C-OAc); MS *m/z* (%) 484 (M^+; 22), 469 (98), and 409 (100).

24-Methyl-8-lanoten-3-one (11). 24-Methyl-8-lanosten-3β-yl acetate (**10**; 91 mg) was hydrolyzed with potassium hydroxide (0.2 g) in boiling ethanol to afford 24-methyl-8-lanosten-3β-ol (83 mg), mp 156—158 °C (colorless needles from ether-methanol); IR (Nujol) 3300 and 3200 cm^{-1}; ^1H NMR (90 MHz, $CDCl_3$) δ=ca. 3.2 (1H, m; *H*-C-OH); MS *m/z* (%) 442 (M^+; 23), 427 (100), and 409 (48).

24-Methyl-8-lanosten-3β-ol (620 mg) in acetone (70 ml) was oxidized with Jones reagent (2 ml) at 0 °C. The usual work-up and chromatographic separation on silica gel (elution with 5—10% ether in hexane) gave 24-methyl-8-lanosten-3-one (**11**; 350 mg), mp 109—111 °C; IR 1720 cm^{-1}; MS *m/z* (%) 440 (M^+; 18) and 425 (100).

Demethylation of 24-Methyl-8-lanosten-3-one (11). A mixture of ketone (**11**; 1.12 g), potassium acetate (4.9 g), and hydroxylamine hydrochloride (97%, 2.6 g) in methanol (490 ml) was refluxed for 3 h. The reaction product was crystallized from ether-methanol to give the corresponding oxime (**12**; 1.07 g), mp 200—203 °C (colorlsee needles); IR (Nujol) 3270, 950, and 930 cm^{-1}; ^1H NMR (90 MHz, $CDCl_3$) δ=3.03 and 3.20 (total 1H); MS *m/z* (%) 455 (M^+; 13), 440 (90), 424 (23), and 69 (100); Found: *m/z* 455.4116. Calcd for $C_{31}H_{53}NO$: M, 455.4126.

A mixture of oxime (**12**; 1.05 g) and *p*-toluenesulfonyl chloride (recrystallized from hexane; 1.66 g) in pyridine (17 ml) was refluxed for 3 h under nitrogen. Ether (85 ml) was added and the mixture was washed with 2 M hydrochloric acid three times (each 85 ml). The organic layer was washed with a saturated sodium hydrogencarbonate solution and then brine. Chromatographic separation on silica gel (elution with 1—3% ether in hexane) yielded a crude 24-methyl-3,4-seco-4(29),8-lanostadiene-3-nitrile[17] (**13**; 826 mg) as a pale yellow oil, IR (neat) 2250 and 1640 cm^{-1}; ^1H NMR (90 MHz, $CDCl_3$) δ=1.77 (Me), 4.67 (1H), and 4.90 (1H); MS *m/z* (%) 437 (M^+; 82), 422 (83), 394 (22), and 383 (100); Found: *m/z* 437.4003. Calcd for $C_{31}H_{51}N$: M, 437.4020.

m-Chloroperbenzoic acid (80%, 609 mg) was added to a solution of the crude seconitrile (**13**; 732 mg) in dichloromethane (150 ml) kept at 0 °C and the mixture was allowed to stand for 72 h at this temperature. The usual work-up gave a residue, which was subjected to column chromatography on silica gel. Elution with 10—30% ether in hexane yielded 4,29-epoxy-24-methyl-3,4-seco-8-lanostene-3-nitrile[17] (**14**; 359 mg) as a colorless oil, IR (neat) 2250 cm^{-1}; ^1H NMR (60 MHz, $CDCl_3$) δ=2.67 (2H, s; H_2C C); MS *m/z* (%) 453 (M^+; 5), 438 (27), 420 (8), 410 (7), 399 (16), 381 (10), 370 (5), 86 (100); Found: *m/z* 453.3953. Calcd for $C_{31}H_{51}NO$: M, 453.3969.

The epoxy nitrile (**14**; 404 mg) in toluene (47 ml) was heated with boron trifluoride etherate (0.8 ml) for 3 h under nitrogen and the heating was continued for 1 h after addition of 4 M hydrochloric acid (27 ml). The organic layer was separated and worked up as usual. Purification by column

chromatography on silica gel (elution with 5% ether in hexane) followed by crystallization from ether–methanol afforded 4α,14α,24-trimethyl-8-cholesten-3-one (**15**; 113 mg), mp 109—113 °C; IR (Nujol) 1710 cm^{-1}; MS *m/z* (%) 426 (M^+; 17) and 411 (100); Found: *m/z* 426.3783. Calcd for $C_{30}H_{50}O$: M, 426.3860.

4α,14α,24-Trimethyl-8-cholesten-3β-yl Acetate (16). 4α,14α,24-Trimethyl-8-cholesten-3-one (**15**; 113 mg) was treated with LAH (66 mg) in ether to afford a 3β-alcohol, mp 156—158 °C; IR (Nujol) 3350 cm^{-1}; ^1H NMR (90 MHz, $CDCl_3$) δ=ca. 3.1 (1H, m; *H*-C-OH); MS *m/z* (%) 428 (M^+; 17), 413 (100), and 395 (26). This alcohol (70 mg) was acetylated with acetic anhydride (1.4 ml) and pyridine (2.8 ml) to yield 4α,14α,24-trimethyl-8-cholesten-3β-yl acetate (**16**) quantitatively, mp 119—121 °C (colorless needles from methanol); IR (Nujol) 1740 and 1245 cm^{-1}; ^1H NMR (90 MHz, $CDCl_3$) δ=0.70 (3H, s; 18-Me), 0.74—0.98 (Me's), 2.05 (3H, s; AcO), and 4.38 (1H, dt, *J*=5 and 10 Hz; 3α-H); MS *m/z* (%) 470 (M^+; 39), 455 (100), 410 (5), and 395 (51); Found: *m/z* 470.4159. Calcd for $C_{32}H_{54}O_2$: M, 470.4124.

4α,14α,24-Trimethyl-7,11-dioxo-8-cholesten-3β-yl Acetate (17). 4α,14α,24-Trimethyl-8-cholesten-3β-yl acetate (**16**; 80 mg) was dissolved in a mixture of acetic acid (6.5 ml) and hexane (1.3 ml) and chromium trioxide (70 mg) in acetic acid (90%, 1 ml) was added to the solution and then the reaction mixture was refluxed for 3 h. After addition of water, the reaction product was extracted with ether and the ethereal extract was worked up as usual to afford a residue, which was chromatographed on silica gel (C-200, 5 g). Elution with 10% ether in hexane gave 4α,14α,24-trimethyl-7,11-dioxo-8-cholesten-3β-yl acetate (**17**; 47 mg), mp 153—155 °C; IR (Nujol) 1740, 1680, and 1240 cm^{-1}; UV (EtOH) 270 nm (ε 7800); ^1H NMR (90 MHz, $CDCl_3$) δ=0.75—0.91 (18H; Me×6), 1.19 (3H, s; Me), 1.31 (3H, s; Me), 2.05 (3H, s; AcO), and 4.40 (1H, dt, *J*=5 and 10 Hz; 3α-H); MS *m/z* (%) 498 (M^+; 100) and 438 (20); Found: *m/z* 498.3709. Calcd for $C_{32}H_{50}O_4$: M, 498.3709.

4α,14α,24-Trimethyl-7,11-dioxocholestan-3β-yl Acetate (18). Zinc dust (420 mg) was added to a boiling solution of 4α,14α,24-trimethyl-7,11-dioxo-8-cholesten-3β-yl acetate (**17**; 81 mg) in acetic acid (4 ml) portionwise and the reaction mixture was refluxed for 5—6 h. After filtration, the filtrate and the washings were evaporated to afford a residue. Water was added to the residue and the reaction product was extracted with ether. The ethereal extract was worked up as usual and a residue was subjected to separation by chromatography on silica gel (C-200, 7.6 g). Elution with 5—20% ether in hexane gave 4α,14α,24-trimethyl-7,11-dioxocholestan-3β-yl acetate (**18**; 54 mg), mp 203 °C (colorless needles from methanol); IR (Nujol) 1730, 1700, and 1260 cm^{-1}; ^1H NMR (90 MHz, $CDCl_3$) δ=0.72—0.89 (Me's), 1.23 (3H, s; Me), 1.27 (3H, s; Me), 2.05 (3H, s, AcO), and 4.37 (1H, dt, *J*=5 and 10.5 Hz; 3α-H); MS *m/z* (%) 500 (M^+; 100) and 440 (18); Found: *m/z* 500.3896. Calcd for $C_{32}H_{52}O_4$: M, 500.3866.

Wolff-Kishner Reduction of 7,11-Dioxolanostan-3β-yl Acetate (19) under Standard Conditions. A mixture of dioxo acetate (**19**; 77 mg), diethylene glycol (1.5 ml), and hydrazine hydrate (80%, 1 ml) was refluxed for 1.5 h at 135 °C with stirring. After cooling, potassium hydroxide (0.3 g) was added and the mixture was heated. The excess hydrazine was distilled off until the vapor temperature reached to 200 °C, and then the mixture was refluxed for 2 h. The usual work-up and chromatographic separation on silica gel (C-200, 5 g, elution with 10—40% ether in hexane) afforded lanostan-3β-ol (**21**; 12 mg) and 3β-hydroxylanostan-11-one (**20**; 28 mg), mp 164—164.5 °C.

Wolff-Kishner Reduction of 19 under Modified Conditions. A mixture of **19** (50 mg), diethylene glycol (2.5 ml), and hydrazine hydrate (0.5 ml) was refluxed for 1.5 h at 130 °C with stirring, and then the excess hydrazine was removed off at 65 °C under reduced pressure. Potassium hydroxide (0.1 g) was added and the mixture was refluxed for 3 h. The same work-up afforded **20** (26 mg) and **21** (trace).

A Tosylhydrazone (22) of 7,11-Dioxolanostan-3β-yl Acetate (19). A mixture of diketo acetate (**19**; 20 mg) and *p*-tolylsulfonylhydrazine (52 mg) in ethanol (0.7 ml) was refluxed for 2 h. The solvent was removed to give a residue, which was separated by preparative TLC developed with ethyl acetate–hexane. A small amount of mono-*p*-tosylhydrazone (**22**) was obtained together with the starting material (**19**). **22**; IR (Nujol) 1730, 1700, 1330, 1250, 1170, 1150, and 810 cm^{-1}; UV (EtOH) 225 nm (ε 10960); ^1H NMR (90 MHz, $CDCl_3$) δ=0.65 (3H, s; 18-Me), 0.84—0.91 (Me's), 1.11 (3H, s; Me), 2.05 (3H, s; AcO), 2.44 (3H, s; *p*-CH_3-C_6H_4-), 4.40 (1H, m; 3α-H), 7.26, 7.36, 7.79, and 7.89 (each 1H; aromatic proton). The same reaction was examined in acetic acid as a solvent, but the yield of **22** could not be improved.

7,7-Ethylenedithio-11-oxolanostan-3β-yl Acetate (23). 1,2-Ethanedithiol (1.2 ml) was added to 7,11-dioxolanostan-3β-yl acetate (**19**; 44 mg) in chloroform (3 ml), and the solution was stirred with introducing hydrogen chloride at 0 °C for 4 h. The solvent was removed under reduced pressure and a residue was subjected to separation by column chromatography on silica gel (C-200, 5 g). Elution with 10—25% ether in hexane afforded the ethylenedithio derivative (**23**; 46 mg), mp 174.5—175 °C (colorless needles from ether–methanol); IR (Nujol) 1730, 1700, and 1260 cm^{-1}; ^1H NMR (90 MHz, $CDCl_3$) δ=0.83—0.90 (Me's), 1.13 and 1.33 (each 3H, s; Me), 2.04 (3H, s; AcO), 3.26 (4H, s; S-CH_2-CH_2-S), and 4.56 (1H, m; 3α-H); MS *m/z* (%) 576 (M^+; 23), 548 (44), 516 (51), 270 (46), 238 (52), 210 (75), and 185 (100).

11-Oxolanostan-3β-yl Acetate (24). A crude 7,7-ethylenedithio derivative (**23**) prepared from **19** (25 mg) was dissolved in dioxane (10 ml) and the solution was added to Raney nickel W2[10] (ca. 0.4 g) in a flask. The mixture was refluxed for 6 h and filtered. The filtrate and washings were combined and evaporated to afford a residue. Column chromatography on silica gel (C-200, 2.5 g, elution with 10—25% ether in hexane) afforded 11-oxolanostan-3β-yl acetate (**24**; 21 mg), mp 144—145 °C (colorless needles from ether–methanol). When the desulfurization was carried out in a large scale using **23** prepared from **19** (3.5 g), an inseparable mixture (2.94 g) of 11-oxolanostan-3β-yl acetate (**24**) and 11-oxo-1-lanosten-3β-yl acetate (**25**). Gas chromatography (2% Dexsil 300GC) and ^1H NMR examination revealed that the mixture consisted of **24** and **25** in a ratio of 4:1. A mixture of **24** and **25**; ^1H NMR (90 MHz, $CDCl_3$) δ=0.72—0.91 (Me's), 1.08, 1.10 (Me's), 2.03, 2.04 (total 3H, each s; AcO), 4.49 (1H, m), 5.53, and 5.69 (each 0.2H, d, *J*=10.5 Hz); GC-MS **24**; *m/z* (%) 486 (M^+; 13), 426 (31), 411 (14), 383 (46), 303 (100), 290 (38), and 263 (79). **25**; *m/z* (%) 484 (M^+; 13), 424 (60), 409 (35), 303 (100), 290 (32), and 277 (42).

Hydrogenation of the Mixture of 24 and 25. The mixture (39 mg) of **24** and **25** in a ratio of 4:1 was dissolved in ethanol (8 ml) and hydrogenated in the presence of 10% palladium on carbon (25 mg) at room temperature under

atmospheric pressure for 48 h. The usual work-up and chromatography on silica gel (C-200, 3.8 g, elution with 10—15% ether in hexane) afforded the single product, 11-oxolanostan-3β-yl acetate (**24**; 35 mg), mp 144—145 °C (from ether-methanol); IR (Nujol) 1740, 1700, 1245, and 1030 cm^{-1}; ^1H NMR (90 MHz, $CDCl_3$) δ=0.72 (3H, s; Me), 0.83—0.90, 1.07—1.10 (Me's), 2.03 (3H, s; AcO), 2.32, and 2.50 (each 1H, d, J=13.5 Hz; 12-H). ^{13}C NMR (22.5 MHz, $CDCl_3$) δ=14.6, 15.9, 16.8, 17.1, 18.4, 21.1, 21.2, 22.5, 22.8, 24.0, 28.0, 28.2, 28.3, 29.2, 33.0, 36.0, 36.4, 36.6, 37.4, 38.2, 39.5, 40.5, 47.9, 48.7, 49.9, 53.0, 55.1, 61.3, 80.7, 170.8, and 211.5; MS m/z (%) 486 (M^+; 31), 426 (36), 411 (8), 383 (20), 303 (100), 290 (24), and 263 (72); Found: m/z 486.4101. Calcd for $C_{32}H_{54}O_3$: M, 486.4073. HR-MS m/z 303.2676 ($C_{21}H_{35}O$), m/z 290.2615 ($C_{20}H_{34}O$), and m/z 263.1683 ($C_{16}H_{23}O_3$).

4α,14α,24-Trimethyl-7,7-ethylenedithio-11-oxocholestan-3β-yl Acetate (26). 1,2-Ethanedithiol (1.5 ml) was added to a solution of 4α,14α,24-trimethyl-7,11-dioxocholestan-3β-yl acetate (**18**; 54 mg) in chloroform (2 ml). The solution was cooled in an ice bath, and hydrogen chloride was introduced with stirring for 3 h. The same work-up as before afforded a residue, which was purified by column chromatography on silica gel (C-200, 4.8 g). Elution with 10—30% ether in hexane gave 4α,14α,24-trimethyl-7,7-ethylenedithio-11-oxocholestan-3β-yl acetate (**26**; 56 mg), mp 195—196 °C (colorless needles from ether-methanol); IR (Nujol) 1730, 1700, and 1255 cm^{-1}; ^1H NMR (90 MHz, $CDCl_3$) δ=0.75—0.89 (Me's), 1.07 and 1.38 (each 3H, s; Me), 2.04 (3H, s; AcO), 3.26 (4H, s; S-CH_2-CH_2-S), and 4.42 (1H, dt, J=5 and 10 Hz; 3α-H); MS m/z (%) 576 (M^+; 39), 548 (10), 516 (45), and 284 (100); Found: m/z 576.3700. Calcd for $C_{34}H_{56}O_3S_2$: M, 576.3670.

Desulfurization of 4α,14α,24-Trimethyl-7,7-ethylenedithio-11-oxocholestan-3β-yl Acetate (26). A solution of **26** (56 mg) in dioxane (5 ml) was added to Raney nickel W2[10] (ca. 2 g) and the mixture was refluxed for 5—6 h. The same work-up as before and chromatography on silica gel (C-200, 4 g, elution with 2—15% ether in hexane) yielded an inseparable mixture (42 mg) of 4α,14α,24-trimethyl-11-oxocholestan-3β-yl acetate (**27**) and the corresponding 1-ene derivative (**28**), whose ratio was determined to be ca. 1 : 1 by gas chromatography. The mixture of **27** and **28**; ^1H NMR (90 MHz, $CDCl_3$) δ=0.72—0.89 (Me's), 1.02—1.08 (Me's), 2.03 and 2.04 (total 3H, each s; AcO), 4.36 (1H, m; 3α-H), 5.47, and 5.72 (total 1H, d, J=10.5 Hz; CH=CH); GC-MS **27**; m/z (%) 486 (M^+; 19), 426 (34), 411 (7), 317 (66), 304 (35), 291 (8), and 249 (100). **28**; m/z (%) 484 (M^+; 37), 469 (10), 456 (11), 424 (100), 409 (26), 317 (60), 304 (41), and 290 (52).

Hydrogenation of the Mixture of 27 and 28. The mixture (**27** and **28**; 11 mg) in ethanol was hydrogenated in the presence of 10% palladium on carbon (16 mg) for 64 h under the same conditions as before. Crystallization from ether-methanol yielded 4α,14α,24-trimethyl-11-oxocholestan-3β-yl acetate (**27**; 11 mg), mp 141.5—142.5 °C; IR (Nujol) 1730, 1695, 1250, 1020, and 970 cm^{-1}; ^1H NMR (90 MHz, $CDCl_3$) δ=0.72—0.89 (Me's), 1.05 and 1.09 (each 3H, s; Me), 2.04 (3H, s; AcO), 2.32 and 2.52 (each 1H, d, J=13.5 Hz; 12-H), 2.74 (1H, dt, J=3 and 13.5 Hz; 1β-H), and 4.36 (1H, dt, J=6 and 10.5 Hz; 3α-H); MS m/z (%) 486 (M^+; 20), 426 (40), 411 (9), 317 (76), 304 (39), 291 (9), and 249 (100); Found: m/z 486.4080. Calcd for $C_{32}H_{54}O_3$: M, 486.4072.

4α,14α,24-Trimethylcholestane-3β,11β-diol (29). 4α,14α,24-Trimethyl-11-oxocholestan-3β-yl acetate (**27**; 41 mg) in ether (8 ml) was refluxed with LAH (28 mg) for 1.5 h under nitrogen. Ethyl acetate (ca. 2 ml) and 2 M hydrochloric acid (13 ml) were added and the reaction product was extracted with ether. By column chromatography on silica gel (C-200, 4.6 g) eluted with 10—20% ethyl acetate in hexane, 4α,14α,24-trimethylcholestane-3β,11β-diol (**29**; 35 mg) was obtained, mp 206—207 °C (colorless needles from ether-methanol); ^1H NMR (90 MHz, $CDCl_3$) δ=0.75—0.93 (Me's), 1.01 and 1.11 (each 3H, s; Me), 3.07 (1H, dt, J=4.5 and 10 Hz; 3α-H), and 4.22 (1H, m; 11α-H); MS m/z (%) 446 (M^+; 2), 428 (53), 413 (100), 410 (19), and 395 (43).

4α,14α,24-Trimethyl-11β-hydroxycholestan-3β-yl Acetate (30). A solution of diol (**29**; 41 mg) in acetic anhydride (0.5 ml) and pyridine (1 ml) was allowed to stand for 19 h at room temperature and the reaction mixture was worked up as usual. The residue was purified by column chromatography on silica gel eluted with 10—30% ether in hexane to give 4α,14α,24-trimethyl-11β-hydroxycholestan-3β-yl acetate (**30**; 39 mg) as colorless needles after crystallization from ether-methanol; ^1H NMR (90 MHz, $CDCl_3$) δ=0.74—0.88 (Me's), 1.00, and 1.12 (each 3H; Me), 2.03 (3H, s; AcO), 4.22 (1H, m), and 4.37 (1H, dt, J=4.5 and 10.5 Hz; 3α-H); MS m/z (%) 488 (M^+; 3), 470 (60), 455 (100), 410 (27), and 395 (83); HR-MS m/z 470.4187. Calcd for $C_{32}H_{56}O_3$ ($M-H_2O$): m/z 470.4122.

4α,14α,24-Trimethyl-9(11)-cholesten-3β-yl Acetate (31). To a solution of the acetate (**30**; 39 mg) in pyridine (2 ml) was added phosphoryl chloride (0.01 ml) and the mixture was stirred at 90 °C for 3 h. Water was added and the reaction mixture was extracted with ether. The usual work-up gave a residue, which was subjected to column chromatography on silica gel (C-200, 5 g). Elution with 10—20% ether in hexane yielded 4α,14α,24-trimethyl-9(11)-cholesten-3β-yl acetate (**31**; 38 mg) as colorless crystals (from ether-methanol), mp 119—120 °C; ^1H NMR (90 MHz, $CDCl_3$) δ=0.66 (3H, s; Me), 0.76—0.90 (Me's), 1.00 (3H, s; Me), 2.04 (3H, s; AcO), 4.37 (1H, m; 3α-H), and 5.30 (1H, m; 11-H); MS m/z (%) 470 (M^+; 70), 455 (100), 410 (5), and 395 (41); Found: m/z 470.4161. Calcd for $C_{32}H_{54}O_2$: M, 470.4124.

4α,14α,24-Trimethyl-9(11)-cholesten-3-one (1). A solution of the acetate (**31**; 38 mg) in ethanol (5 ml) containing potassium hydroxide (0.1 g) was refluxed for 1.5 h. After the solvent was removed in vacuo, aqueous ammonium chloride solution was added. Extraction with ether and the usual work-up afforded a residue (33 mg), which was purified by crystallization from ether-methanol to give 4α,14α,24-trimethyl-9(11)-cholesten-3β-ol as colorless needles; ^1H NMR (90 MHz, $CDCl_3$) δ=0.66 (3H s; Me), 0.75—1.10 (Me's), 3.07 (1H, m; 3α-H), and 5.28 (1H, m; 11-H); MS m/z (%) 428 (M^+; 3), 413 (14), 410 (41), and 495 (100).

The alcohol (33 mg) above obtained was dissolved in acetone (15 ml) and treated with Jones reagent (3 drops) with stirring at 0 °C. After stirring was continued for 10 min at the same temperature, 2-propanol (10 drops) was added and the reaction mixture was stirred for 10 min. The solvent was evaporated, water (10 ml) was added, and the reaction product was extracted with ether. The extract was washed with a saturated sodium hydrogencarbonate solution and followed by the usual work-up to give a residue, which was chromatographed on silica gel (C-200, 5 g). Elution with 10% ether in hexane afforded 4α,14α,24-trimethyl-9(11)-cholesten-3-one (**1**; 27 mg), mp 143—144 °C (from ether-methanol); $[\alpha]_D^{23}$ 76° (c 0.54, EtOH); IR (Nujol) 1705 cm^{-1}; ^1H NMR (270 MHz, $CDCl_3$) δ=0.69 (3H, s; 18-Me), 0.74 (3H,

s; Me), 0.77—0.90 (Me's), 1.02 (3H, d, J=7.3 Hz; Me), 1.23 (3H, s; 19-Me), and 5.35 (1H, m; 11-H); MS m/z (%) 426 (M^+; 45), 411 (100), 299 (11), 257 (10), 243 (18), and 251 (21); Found: m/z 426.3899. Calcd for $C_{30}H_{50}O$: M, 426.3861.

References

1) M. Naora, T. Murae, T. Tsuyuki, and T. Takahashi, *Bull. Chem. Soc. Jpn.*, **59**, 1767 (1986).

2) The corresponding 3β-alcohol has been obtained from *Lycopersicon esculentum* seeds; T. Itoh, T. Ishii, T. Tamura, and T. Matsumoto, *Phytochemistry*, **17**, 971 (1978).

3) H. C. Brown and C. P. Garg, *J. Am. Chem. Soc.*, **83**, 2951 (1961).

4) M. Namikawa, T. Murae, and T. Takahashi, *Chem. Lett.*, **1981**, 733.

5) C. Dorée, J. F. McGhie, and F. Kurzer, *J. Chem. Soc.*, **1948**, 988.

6) 7,11-Dioxolanostan-3β-yl acetate (**19**) was prepared from dihydrolanosteryl acetate through allylic oxidation followed by a treatment with zinc dust. **19**: Mp 215.5—217 °C (colorless plates from ether-methanol); IR (Nujol) 1740, 1700, and 1260 cm^{-1}; ^1H NMR (90 MHz, $CDCl_3$) δ=0.71 (3H, s; 18-Me), 0.83—0.90 (Me's), 1.22 and 1.31 (each 3H, s; Me), 2.05 (3H, s; AcO), and 4.50 (1H, dd, J=7 and 9 Hz; 3α-H); MS m/z (%) 500 (M^+; 100), 440 (18), 306 (18), and 277 (33); Found: m/z 500.3858. Calcd for $C_{32}H_{52}O_4$: M, 500.3863.

7) D. H. R. Barton, D. A. J. Ives, and B. R. Thomas, *J. Chem. Soc.*, **1955**, 2056.

8) R. O. Hutchins, C. A. Milewski, and B. E. Maryanoff, *J. Am. Chem. Soc.*, **95**, 3662 (1973).

9) D. G. Farnum, *J. Org. Chem.*, **28**, 870 (1963).

10) The Raney nickel W2, stored in ethanol, was washed with dry dioxane and used.

11) M. V. Mijorie, W. Voser, H. Heusser, and O. Jeger, *Helv. Chim. Acta*, **35**, 964 (1952).

12) H. Budzikiewicz, C. Djerassi, and D. H. Williams, "Structure Elucidation of Natural Products by Mass Spectrometry," Vol. 2, Holden-Day Inc., San Francisco (1964), p. 81.

13) R. R. Muccino and C. Djerassi, *J. Am. Chem. Soc.*, **95**, 8726 (1973).

14) A. Rahier, L. Cattel, and P. Benveniste, *Phytochemistry*, **16**, 1187 (1977).

15) L. J. Goad, F. -X. Garneau, J. -L. Simard, J. W. ApSimon, and M. Girard, *Tetrahedron Lett.*, **26**, 3513 (1985).

16) General procedures are the same as those described in Ref. 1.

17) The carbon number at C-29 was given tentatively.

Syntheses and Properties of [1,1′-Bis(α-Aminoisobutyric Acid)]Gramicidin S and [1-α-Aminoisobutyric Acid]Semigramicidin S

Michio KONDO,* Mikio KIMURA, Ken-ichi SATO, and Hideaki HORIMOTO
Department of Chemistry, Faculty of Science and Engineering, Saga University, Honjo-machi, Saga 840
(Received July 28, 1986)

Analogs of gramicidin S, [1,1′-bis(α-aminoisobutyric acid)]gramicidin S (**18**) and [1-α-aminoisobutyric acid] semigramicidin S (**11**), have been synthesized by a conventional solution method. The cyclization reactions of a linear pentapeptide active ester and a linear decapeptide active ester yielded exclusively a protected cyclic pentapeptide and a protected cyclic decapeptide, respectively. After deprotection of these peptides, we obtained the final products (**11** and **18**). The mobility of **18** in paper electrophoresis was the same as that of gramicidin S, however, the CD spectrum of **18** in a methanol solution showed a markedly different pattern from that of gramicidin S. Both analogs (**11** and **18**) are inactive against the Gram-positive microorganisms tested. The results suggest that the positions of the valine residues in gramicidin S require a hydrophobic amino acid having L-configuration to show activity.

Gramicidin S (GS) is a cyclic peptide antibiotic which exhibits a strong activity against Gram-positive bacteria. Its secondary structure is well-known to be an antiparallel β-pleated sheet including four intramolecular hydrogen bonds with C_2 symmetry as shown in Fig. 1.

Regarding the contribution of the side chains of the Val residues in GS to the antibacterial activity, several GS analogs have been synthesized by one of the authors (M.K) and it has been reported that [Ala$^{1,1'}$]GS and [Leu$^{1,1'}$]GS were as active as natural GS toward several microorganisms, whereas [Gly$^{1,1'}$]GS exhibited no antibacterial activity.[1,2] Thus, it is suggested that side chains as bulky or hydrophobic as methyls might be required at positions 1 and 1′ for the interaction between GS and sensitive bacteria.[3] On the other hand, in the syntheses of the above analogs using a dimeric cyclization reaction of the corresponding pentapeptide active esters, the ratio of a cyclic dimer to a cyclic monomer decreases in the order of steric hindrance of an N-terminal amino acid in each pentapeptide active ester substituted with Val,[4] Leu,[2] and Ala.[1] Finally Gly substitution[1] results in only a cyclic monomer as shown in Table 1. From these previous investigations it appears that the steric nature of the side chain of the N-terminal amino acid in a pentapeptide active ester greatly influences the cyclization reaction and consequently induces ring closure to a dimer by dimerization.[5]

In this connection, an analog of GS containing α-aminoisobutyric acid (Aib) in place of Val is of interest in demonstrating the specific contribution of Aib to the activity. This Aib is found in several antibiotics, alamethicin,[6] suzukacillin,[7] antiamebins,[6] emerimicins,[6] trichotoxin A-40,[8] and hypelcins.[9] They are peptide ionophores functioning as transmembrane channels for ion transport.[10] The Aib includes two methyl groups as side chains which have similar bulkiness or hydrophobicity to that of Ala, and is optically inactive as Gly. In addition, the steric hindrance caused by the two methyl groups of Aib sometimes prevents introducing a protecting group, converting to the corresponding active ester, and coupling with other amino acids or peptide.[11-13] Accordingly a moderate yield of a dimer was expected from the cyclization reaction of the pentapeptide active ester containing Aib at the N-terminus. Furthermore, such a synthetic [Aib$^{1,1'}$]GS analog should exhibit biological activity because the side chains of Aib, two methyl

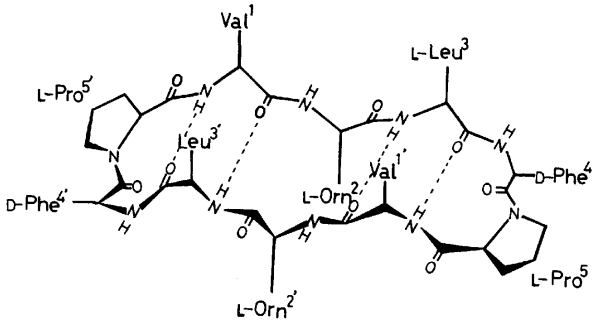

Fig. 1. A model with β-pleated sheet conformation of gramicidin S.

Table 1. Ratio of Protected Monomer and Dimer after Cyclization of Linear Pentapeptide *p*-Nitrophenyl Ester[a]

p-Nitrophenyl ester of pentapeptide					Ratio of compounds in product[b]		Ref.
					Z-cyclic monomer	Z_2-cyclic dimer	
1	2	3	4	5			
Val	Orn(Z)	Leu	D-Phe	Pro	32	68	4
Leu					78	22	2
Ala					91	9	1
Gly					100	0	1

a) The concentration was approximately 3×10^{-3} mol dm^{-3}. b) The ratios shown are weight by weight.

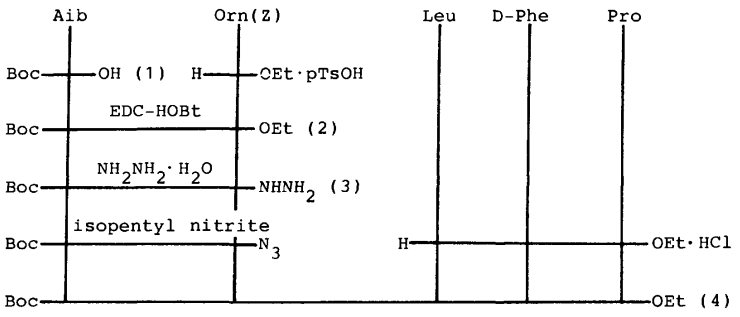

Fig. 2. Synthesis of Boc-pentapeptide.[14]

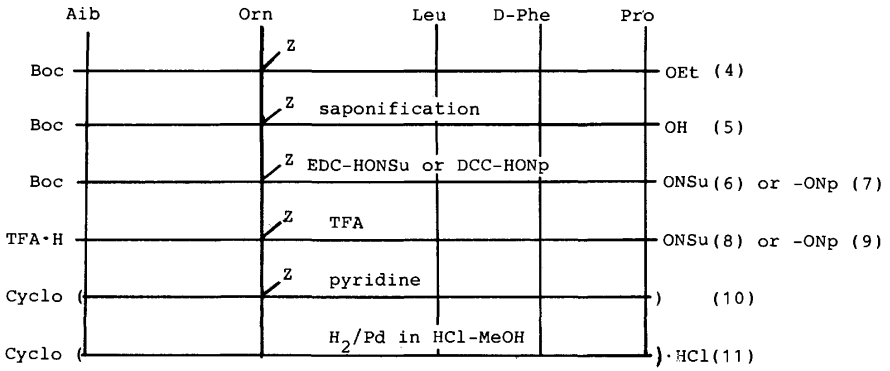

Fig. 3. Cyclization of linear pentepeptide active esters.

groups, in the analog have the same hydrophobicity as that of Ala in [Ala$^{1,1'}$]GS of which the biological activity is as strong as natural GS.[1]

The present paper will describe the syntheses, antibacterial properties, and CD measurements of [Aib$^{1,1'}$]-GS and [Aib^{1}]semiGS.

The route for the synthesis of a protected pentapeptide is indicated in Fig. 2. The dipeptide derivative (**2**) was effectively synthesized by the EDC-HOBt method involving stirring for a long time and extracting with ether, followed by conversion to the hydrazide (**3**). The condensation of the azide derived from **3** with a tripeptide ester gave an acylpentapeptide ester (**4**). The synthetic route for cyclization reactions of two pentapeptide active esters is shown in Fig. 3. The Boc-pentapeptide ester (**4**) was converted to the corresponding Boc-pentapeptide (**5**) by saponification. To investigate the best method for the cyclization reaction, two active esters using *N*-hydroxysuccinimide ester (**6**) and *p*-nitrophenyl ester (**7**) were prepared, and their Boc-groups were removed by the action of TFA at 0 °C. The cyclization of **8** or **9** at a concentration of 3×10^{-3} mol dm^{-3} in pyridine and subsequent purification of the crude cyclopeptide with Dowex 1 and 50 yielded exclusively the Z-substituted cyclic monomer (**10**), instead of the expected bis(Z-substituted) cyclic dimer. Its molecular weight was confirmed by mass spectrometry. The strong tendency of **8** or **9** to ring closure by monomerization indicates that the structural restriction imposed by Aib results in a favorable conformation of the cyclic pentapeptide and in this case of a cyclization of the pentapeptide active ester, L-configuration of the N-terminal amino acid plays basically a more important role than the steric nature in regard to its dimerization reaction. The Z-[Aib^{1}]semiGS (**10**) thus obtained was hydrogenated to afford [Aib^{1}]-semiGS·HCl (**11**) as crystals.

In order to obtain the cyclodecapeptide, a cyclization reaction of a decapeptide active ester was employed for the preparation of Z_2-[Aib$^{1,1'}$]GS. The route outlined in Fig. 4 was employed for synthesis of Z_2-[Aib$^{1,1'}$]GS. The Boc-decapeptide ester (**13**) was synthesized by the EDC-HOBt method from **5** and a pentapeptide ester trifluoroacetate, and **13** was saponified to give the Boc-decapeptide (**14**). The compound **14** was converted to the Boc-decapeptide succinimide ester (**15**). The bis(Z-substituted) cyclodecapeptide (**17**) was obtained through the cyclization reaction at a high dilution in pyridine after treatment of **15** with TFA, and the crude product was then purified with Dowex 1 and 50, gel chromatography on Sephadex LH-20 and silica-gel columns. Its molecular weight determination with a vapor pressure osmometer demonstrated that the molecular size of **17** corresponds to that of the bis(Z-substituted) cyclic decapeptide. The compound **17** was subjected to hydrogenolysis, and the final product **18** was obtained as crystals. Its homogeneity was confirmed by paper and thin-layer chromatographies and paper electrophoresis.

Biological assay of [Aib$^{1,1'}$]GS and [Aib^{1}]semiGS shows no antibiotic activity against all the Gram-positive microorganisms listed in Table 2. The bio-

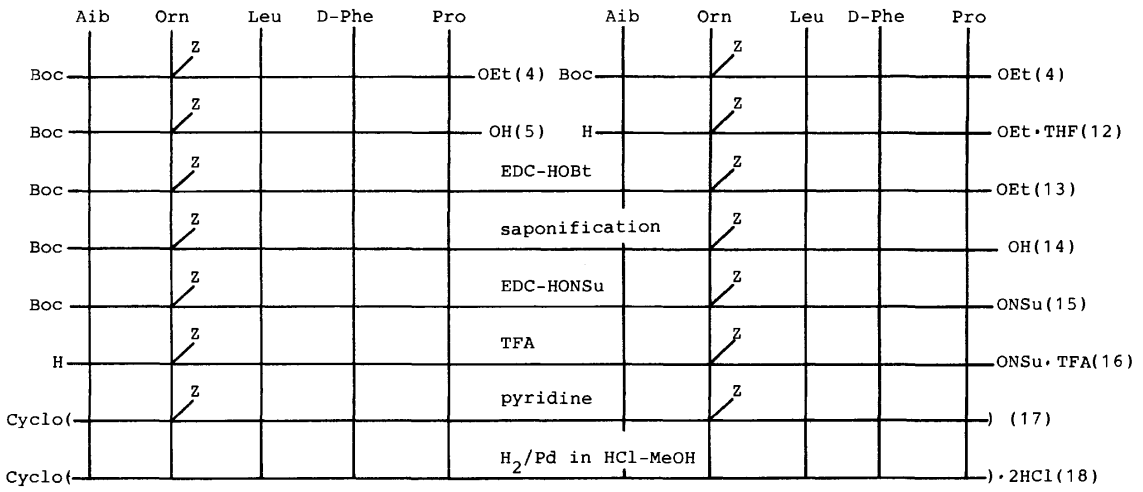

Fig. 4. Synthesis of [Aib$^{1,1'}$] GS·2HCl (**18**).

Table 2. Inhibitory Activity of [Aib^1] semiGS (**11**), [Aib$^{1,1'}$] GS (**18**) and GS on Microorganisms

Test organisms	GS	**11**	**18**
S. Aureus	3	>100	>100
B. subtilis	3	>100	100
E. coli	>100	>100	>100
S. flexneri	6	>100	>100
P. vulgaris	>100	>100	>100
P. aeruginosa	>100	>100	>100

Minimum inhibitory concentration, μg ml^{-1}.

logical data demonstrate that the Val residues in GS can not be substituted by the Aib residues without affecting the biological activity. Further, it has been reported that synthetic GS analogs such as [Aib$^{4,4'}$]GS and [Aib$^{5,5'}$]GS exhibited no antibiotic activity against all the microorganisms tested.[12,13] These results and our study of CPK model indicate that the rigid β-sheet structure of the GS molecule might be destabilized by the steric hindrance of the Aib residue in the GS analog. Hence the loss of sidedness structure affects the biological activity of the analog.[15]

The CD spectra of Boc-pentapeptide-ONSu and the protected cyclopentapeptide were measured to obtain information on a conformational change of the active ester just before ring closure, as shown in Fig. 5. A negative maximum and a shoulder of the protected cyclic pentapeptide (**10**) are about twice as great as those of the protected linear peptide active ester (**6**). Their characteristic shapes resemble each other. This seems to support the view that the conformation of the peptide backbone before ring closure is similar to that after ring formation and the cyclization reaction of the pentapeptide-ONSu afforded a cyclic monomer in good yield (73%) and no cyclic dimer. As shown in Fig. 6, the ellipticities of the negative troughs near 200 nm of three analogs, [Gly^1], [Ala^1], and [Aib^1]semiGS, are considerably smaller than that of GS, and the negative maximum bands of the analogs show blue shifts from that of GS. The shoulder at 218 nm is observed in

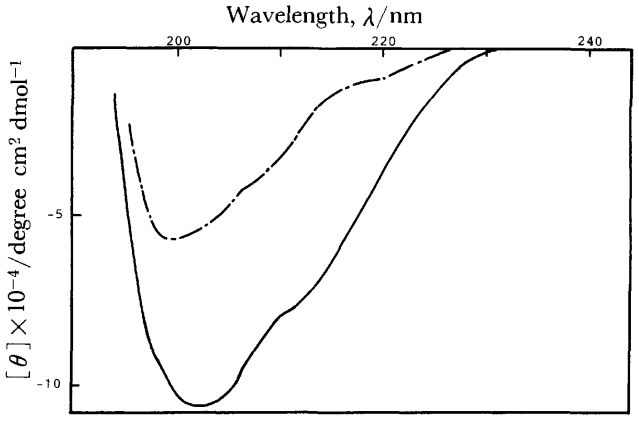

Fig. 5. CD spectra of Boc-pentapeptide-ONSu (**6**) and Z-substituted cyclopentapeptide (**10**) in MeOH. -·-·-: **6**, ——: **10**.

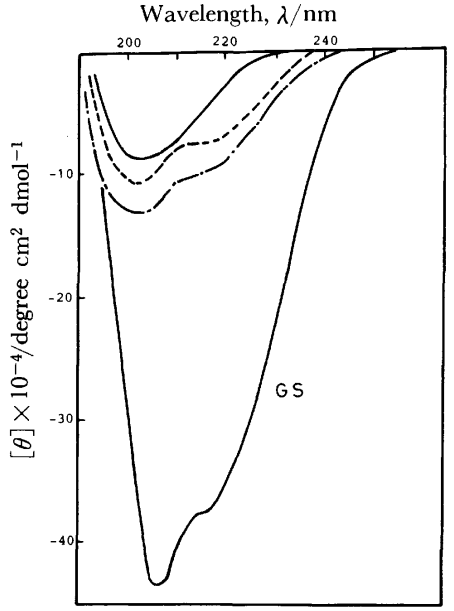

Fig. 6. CD spectra of semiGS analogs and GS. ——: [Aib^1] semiGS, ----: [Gly^1] semiGS, -·-·-: [Ala^1] semiGS.

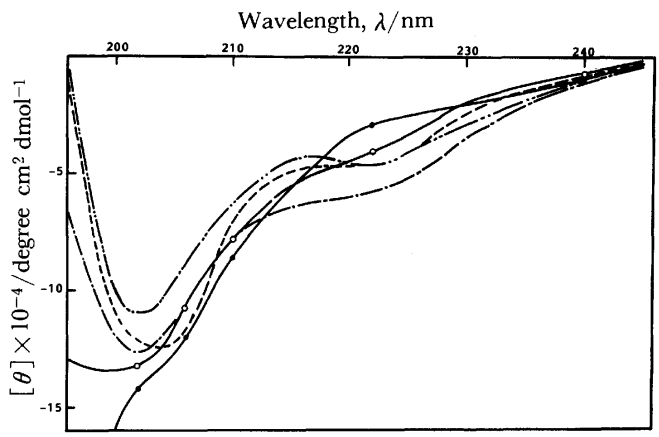

Fig. 7. CD spectra of protected linear **13**, **14**, **15**, **16**, and cyclic decapeptide (**17**) in MeOH. ----: **13**, -·-·-: **14**, -··-··-: **15**, —○—○—: **16**, —●—●—: **17**.

[Gly[1]]semiGS and [Ala[1]]semiGS, but it is not detectable in [Aib[1]]semiGS (**11**). The small and simple Cotton effect of **11** might be due to the influence of the large steric hindrance of Aib residue on the peptide backbone. The CD spectra of the linear decapeptide derivatives before ring closure and the protected cyclic decapeptide in MeOH are shown in Fig. 7. Each of the linear peptides shows a negative trough at 203 nm and a shoulder near 223 nm. However, the spectrum of the cyclic peptide shows only a shoulder instead of a trough at 203 nm, and the trough gives a blue shift from that of the linear decapeptide derivatives. It is obvious that the backbone conformations of the linear peptides and that of the cyclic peptide are different. The CD curves of [Aib[1]]semiGS (**11**) and [Aib[1,1']]GS (**18**) in MeOH as well as that of GS are shown in Fig. 8. The spectral shapes of these compounds indicate that these molecular conformations of **11** and **18** become significantly different from that of GS. The CD pattern of **18** exhibits no characteristic negative Cotton effect shown in GS at 206 and 217 nm, but its CD spectrum is similar to that of [D-Val[1,1']]GS recently synthesized by Tamaki et al.[16] It is also worthy to note that the [D-Val[1,1']]GS has practically no activity. On the basis of these results and observations, several reasonable explanations for the structure-activity relationship of **18** are considered as follows. (a) The Aib residues in **18** behave like D-amino acid residues at positions 1 and 1'. (b) The presence of geminal methyl groups at an α-carbon of Aib greatly restricts the range of accessible conformation for a β-turn of the cyclic peptide containing Aib. (c) This restrictive effect results in a distortion of the molecular conformation of a sidedness feature which is required for exhibiting the activity of antibiotic GS.

Conformational study of the β-turn part in GS analogs containing Gly, Ala, or Aib in place of Val is in progress to elucidate the effect of the amino acid residues at positions 1 and 1' in the peptide backbone on the antibacterial activity.

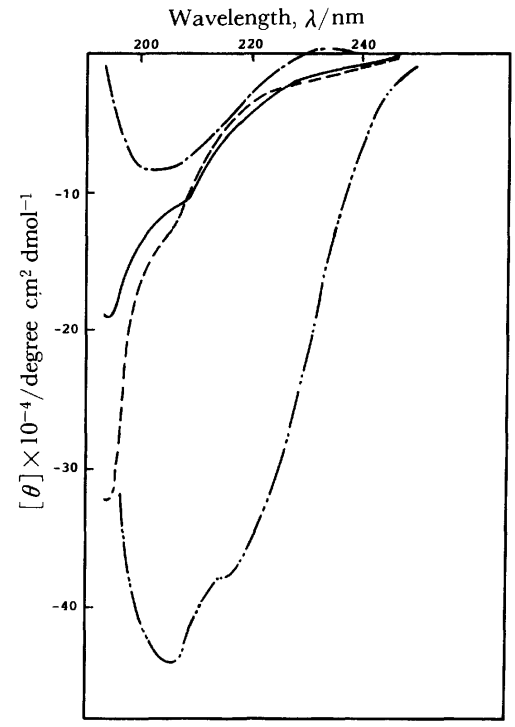

Fig. 8. CD spectra of [Aib[1]] semiGS (**11**), Z_2-[Aib[1,1']] GS (**17**), [Aib[1,1']] GS (**18**), and GS in MeOH. -·-·-: **11**, ----: **17**, ——: **18**, -··-··-: GS.

Experimental

All the melting points are uncorrected. All the $[\alpha]_{589}$ measurements were obtained using a JASCO spectropolarimeter model J-20. The molecular weight of Z-[Aib[1]]semiGS was determined by mass spectrometry using a JMS-D300 mass spectrometer. Amino acid analyses were performed with a Hitachi amino acid analyzer KLA-5. The ratio in parentheses after a solvent system was indicated by volume. Thin-layer chromatography was performed on silica gel (Merck 60 GF_{254}) with the following solvent systems: R_f^1, $CHCl_3$-MeOH (5:1); R_f^2, $CHCl_3$-MeOH (9:1); R_f^3, $CHCl_3$-MeOH-AcOH (8:1:1); R_f^4, $CHCl_3$-MeOH-98% NH_3 (8:4:1); R_f^5, *n*-BuOH-AcOH-H_2O (4:1:2); R_f^6 *n*-BuOH-AcOH-pyridine-H_2O (4:1:1:2).

Boc-Aib-OH (1): To a solution of Aib (3.35 g, 32.5 mmol) in 2 mol dm^{-3} NaOH (15.9 ml, 32.5 mmol) were added Et_3N (4.55 ml, 32.5 mmol) and $(Boc)_2O$ (5.46 g, 25.0 mmol) in dioxane (35 ml). After stirring for 40 h at room temperature, the solution was evaporated in vacuo to remove dioxane and diluted with water (200 ml). After extraction twice with ether (200 ml), the aqueous layer was cooled to 0 °C and adjusted to pH 2.5 with citric acid solution containing NaCl. The reaction product was then extracted twice with EtOAc (200 ml). The combined organic layers were washed twice with water (100 ml), dried over sodium sulfate, and triturated by the addition of petroleum ether. The resulting solid was recrystallized from ether; yield, 4.98 g (98% calculated from $(Boc)_2O$); mp 114—116 °C (lit, 119—120 °C); R_f^1 0.58, R_f^4 0.32.

Found: C, 52.98; H, 8,30; N, 6.93%. Calcd for $C_9H_{17}O_4N$: C, 53.19; H, 8.43; N, 6.89%.

Boc-Aib-Orn(δ-Z)-OEt (2): To a solution of **1** (3.25 g, 15.0 mmol) in DMF (35.0 ml) were added NMM (1.73 g, 15.8

mmol), Orn(δ-Z)-OEt·*p*-TosOH (7.35 g, 15.8 mmol), HOBt (2.43 g, 18.0 mmol), and EDC·HCl (3.22 g, 16.8 mmol) at 0 °C. After stirring for 3 d at room temperature, the reaction mixture was evaporated in vacuo. The residue was dissolved in ether (800 ml). The solution was washed successively with water, 10% citric acid, water, 0.5 mol dm^{-3} $NaHCO_3$ and water, and then dried over sodium sulfate. After removal of the drying agent, the solution was evaporated in vacuo to a small volume. The oily residue was crystallized by letting it stand for 2 h at room temperature. The product was collected by filtration; yield, 6.35 g (88%); mp 87—89 °C; $[\alpha]_{589}$ −7.7°(*c* 2.1, MeOH); R_f^1 0.71, R_f^2 0.58, R_f^4 0.80.

Found: C, 58.87; H, 7.57; N, 8.37%. Calcd for $C_{24}H_{37}N_3O_7 \cdot 1/2H_2O$: C, 59.00; H, 7.84; N, 8.60%.

Boc-Aib-Orn(δ-Z)-NHNH$_2$ (3): A solution of **2** (1.50 g, 3.14 mmol) and hydrazine hydrate (1.57 ml, 31.4 mmol) in MeOH (6.0 ml) was allowed to stand for 16 h at 28 °C. The solution was concentrated in vacuo. The foamy residue was dissolved in CH_2Cl_2 (300 ml), washed with water (200 ml), and then dried over sodium sulfate. After removal of the drying agent, the solution was evaporated in vacuo. The precipitate which formed upon the addition of ether was collected by filtration; yield, 1.34 g (92%); mp 75—76 °C; $[\alpha]_{589}^{22}$ −15.9° (*c* 2.0, MeOH); R_f^1 0.50.

Found: C, 56.64; H, 7.52; N, 15.03%. Calcd for $C_{22}H_{35}N_5O_6$: C, 56.76; H, 7.58; N, 15.04%.

Boc-Aib-Orn(δ-Z)-Leu-D-Phe-Pro-OEt (4): To a solution of **3** (883 mg, 1.90 mmol) in DMF (8.0 ml) were added 4.14 mol dm^{-3} HCl/dioxane (0.916 ml, 3.80 mmol) and isopentyl nitrite (0.290 ml, 2.08 mmol) at −50 °C. After stirring for 10 min at −20 °C, Et_3N (0.531 ml, 3.80 mmol) was added at −50 °C. The reaction mixture was combined with a chilled solution of H-Leu-D-Phe-Pro-OEt·HCl (959 mg, 2.18 mmol)[17] and Et_3N (0.305 ml, 2.18 mmol) in DMF (6.0 ml). The solution was stirred for the 5 d at 0 °C and concentrated to a small volume. The residue was dissolved in EtOAc (300 ml) and it was washed as described for the preparation of **2**. After removal of the drying agent, the solution was evaporated in vacuo. The precipitate which was formed upon the addition of petroleum ether was collected by filtration. The product was recrystallized from EtOAc-petroleum ether; yield, 1.16 g (73%); mp 74—78 °C; $[\alpha]_{589}^{23}$ −43.8°(*c* 2.0, MeOH); R_f^1 0.70, R_f^3 0.91.

Found: C, 62.81; H, 7.79; N, 9.91%. Calcd for $C_{44}H_{64}N_6O_{10}$: C, 63.14; H, 7.71; N, 10.04%.

Boc-Aib-Orn(δ-Z)-Leu-D-Phe-Pro-OH (5): To a solution of **4** (853 mg, 1.02 mmol) in MeOH (5.0 ml) was added 0.94 mol dm^{-3} NaOH (2.17 ml, 2.04 mmol) at 0 °C. The solution was allowed to stand for 5 h at 32 °C, evaporated in vacuo to a small volume, and diluted with water (15 ml). After extraction of the unreacted compound (**4**) with EtOAc (5 ml), the aqueous layer was cooled to 0 °C and adjusted to pH 3 with citric acid, and then extracted twice with CH_2Cl_2 (25 ml). The combined CH_2Cl_2 layers were washed twice with saturated aqueous NaCl (20 ml), dried over sodium sulfate, and then evaporated in vacuo. The precipitate which formed upon the addition of petroleum ether was collected by filtration; yield, 794 mg (96%); mp 103—105 °C; $[\alpha]_{589}^{23}$ −37.6° (*c* 2.0, MeOH); R_f^1 0.47; R_f^3 0.70; R_f^4 0.68.

Found: C, 61.16; H, 7.43; N, 9.85%. Calcd for $C_{42}H_{60}N_6O_{10}\cdot H_2O$: C, 61.00; H, 7.56; N, 10.16%.

Boc-Aib-Orn(δ-Z)-Leu-D-Phe-Pro-ONSu (6): To a solution of **5** (657 mg, 0.812 mmol) in DMF (3.0 ml) were added HONSu (188 mg, 0.812 mmol) and EDC·HCl (315 mg, 1.62 mmol) at 0 °C, and the mixture was then stirred for 26 h at room temperature. The reaction mixture was evaporated in vacuo and diluted with $CHCl_3$ (100 ml). This was washed with 0.5 mol dm^{-3} $NaHCO_3$ and water, and dried over sodium salfate. After removal of the drying agent, the solution was evaporated in vacuo. The residue was solidified with petrolem ether; yield, 599 mg (82%); mp 98—100 °C; $[\alpha]_{589}^{23}$ −40.5° (*c* 1.1, MeOH); R_f^1 0.60.

Found: C, 60.00; H, 7.37; N, 10.18%. Calcd for $C_{46}H_{63}N_7O_{12}\cdot H_2O$: C, 59.79; H, 7.09; N, 10.61%.

Boc-Aib-Orn(δ-Z)-Leu-D-Phe-Pro-ONp (7): To a solution of **5** (649 mg, 0.80 mmol) in pyridine (7.0 ml) were added *p*-nitrophenol (222 mg, 1.60 mmol) and DCC (189 mg, 0.92 mmol) at 0 °C. After stirring for 25 h at room temperature, the precipitated urea was filtered off and the filtrate was concentrated. The residue was worked up as described for the synthesis of **6**; yield, 500 mg (67%); mp 67—70 °C; R_f^1 0.75.

H-Aib-Orn(δ-Z)-Leu-D-Phe-Pro-ONSu·TFA (8): Compound **6** (588 mg, 0.649 mmol) was dissolved in TFA (4.0 ml) at 0 °C. After 30 min, the solution was evaporated, and the residue was triturated with a mixture of ether and petroleum ether. The crystals which remained were collected by filtration; yield, 585 mg (98%); mp 110—112 °C; $[\alpha]_{589}^{23}$ −48.6° (*c* 1.0, MeOH); R_f^1 0.62, R_f^3 0.47, R_f^5 0.57.

Found: C, 54.30; H, 6.20; N, 10.23%. Calcd for $C_{43}H_{56}N_7O_{12}F_3\cdot 2H_2O$: C, 54.02; H, 6.32; N, 10.26%.

H-Aib-Orn(δ-Z)-Leu-D-Phe-Pro-ONp·TFA (9): This compound was prepared from **7** (476 mg, 0.512 mmol) as described for the preparation of **8**; yield, 350 mg (72%); mp 100—103 °C; R_f^1 0.57, R_f^3 0.38.

***Cyclo*[Aib-Orn(δ-Z)-Leu-D-Phe-Pro] (10):** This compound was synthesized by (1) ONSu method and (2) ONp method.

(1) A solution of **8** (374 mg, 0.406 mmol) in DMF (2.6 ml) was added dropwise into pyridine (120 ml) at room temperature. After stirring for 5 d at room temperature, the solution was evaporated in vacuo. The residue was dissolved in a mixture of MeOH and water (2 : 1) and applied to columns (1.8×12 cm) of Dowex 1 and 50. The eluate (ca. 500 ml) was evaporated to dryness. A few mg of the crude product were subjected to hydrogenolysis, and paper electrophoresis of the hydrogenated material showed one spot. The crude product was chromatographed over a silica-gel column (Wako silica gel CQ-3, 2×30 cm) using hexane-$CHCl_3$-MeOH (2 : 3 : 1) as eluent; yield, 204 mg (73%, 59% from **9**); mp 100—102 °C; $[\alpha]_{589}^{23}$−64.8° (*c* 2.0, MeOH); R_f^2 0.50, R_f^3 0.85, R_f^5 0.72, R_f^6 0.78.

Found: C, 63.13; H, 7.39; N, 11.46%; M^+, 690. Calcd for $C_{37}H_{50}N_6O_7\cdot H_2O$: C, 62.69; H, 7.39; N, 11.86%.

(2) A solution of **9** (148 mg, 0.156 mmol) in DMF (5.0 ml) was added dropwise to pyridine (70 ml) heated to 62 °C. After stirring for 6 h at 62 °C and for 10 h at room temperature, the reaction mixture was worked up as described above. The hydrogenated material from a few mg of the crude showed one spot in paper electrophoresis. The crude oily product was crystallized from ether-hexane; yield, 67.0 mg (62%, 30% from **9**); mp 101—103 °C; $[\alpha]_{589}^{23}$ −65.2° (*c* 2.0, MeOH); R_f^3 0.85, R_f^5 0.72, R_f^6 0.78.

Found: C, 62.51; H, 7.30; N, 11.67%; M^+, 690. Calcd for $C_{37}H_{50}N_6O_7\cdot H_2O$: C, 62.69; H, 7.39; N, 11.86%; M^+, 690.

***Cyclo*(Aib-Orn-Leu-D-Phe-Pro)·HCl (11):** A solution of **10** (162 mg, 0.230 mmol) in 1.67 mol dm^{-3} HCl/EtOH

(0.155 ml, 0.250 mmol) and MeOH (10 ml) was subjected to hydrogenolysis in the presence of Pd-black. After 3 h, the catalyst was filtered off and the filtrate was evaporated to dryness; yield, 132 mg (95%); mp 202—206 °C; $[\alpha]_{589}^{23}$ −67.5°(*c* 2.0, MeOH); R_f^1 0.21, R_f^3 0.40, R_f^4 0.94, R_f^5 0.41, R_f^6 0.65.

Found: C, 54.17; H, 7.64; N, 12.59%. Calcd for $C_{29}H_{45}N_6O_5Cl \cdot 3H_2O$: C, 53.82; H, 7.94; N, 12.98%.

Amino acid ratios in acid hydrolyzate of **11**; Aib 1.0, Orn 1.1, Leu 1.0, Phe 1.0, Pro 1.05.

H-Aib-Orn(δ-Z)-Leu-D-Phe-Pro-OEt · TFA (12): This compound was synthesized from **4** (152 mg, 0.169 mmol) as described for the synthesis of **8**; yield, 140 mg (98%); mp 99—106 °C; $[\alpha]_{589}^{23}$ −48.1° (*c* 2.0, MeOH); R_f^1 0.60, R_f^3 0.50, R_f^4 0.75.

Found: C, 56.87; H, 6.76; N, 9.70%. Calcd for $C_{41}H_{57}N_6O_{10}F_3 \cdot H_2O$: C, 56.67; H, 6.84; N, 9.67%.

Boc[-Aib-Orn(δ-Z)-Leu-D-Phe-Pro-]$_2$OEt (13): To a solution of **12** (508 mg, 0.596 mmol) in DMF (4.0 ml) were added Et_3N (0.083 ml, 0.596 mmol), **5** (482 mg, 0.596 mmol), HOBt (96.9 mg, 0.715 mmol), and EDC · HCl (172 mg, 0.896 mmol) at 0 °C. The reaction mixture was stirred for 3 d at room temperature and worked up as described for the synthesis of **4**. The product was recrystallized from EtOAc-ether-petroleum ether; yield, 735 mg (81%); mp 93—96 °C; $[\alpha]_{589}^{23}$ −34.9°(*c* 2.0, MeOH); R_f^1 0.73, R_f^2 0.72, R_f^3 0.90, R_f^4 0.78, R_f^5 0.84, R_f^6 0.81.

Found: C, 62.69; H, 7.53; N, 10.49%. Calcd for $C_{31}H_{114}N_{12}O_{17} \cdot H_2O$: C, 62.93; H, 7.56; N, 10.87%.

Boc[-Aib-Orn(δ-Z)-Leu-D-Phe-Pro-]$_2$OH (14). To a solution of **13** (658 mg, 0.430 mmol) in MeOH (3.0 ml) was added 3.7 mol dm^{-3} NaOH (0.346 ml, 1.29 mmol) at 0 °C. After the solution was allowed to stand for 11 h at 30 °C, 1 mol dm^{-3} HCl (1.29 ml) was added to the solution. Subsequently, the solution was evaporated in vacuo and the oily residue was acidified with 10% citric acid. After the residue had been stored in a refrigerator over night, the precipitate was collected by filtration. The product was recrystallized from EtOAc-ether-petroleum ether; yield, 609 mg (94%); mp 111—112 °C; $[\alpha]_{589}^{23}$ −32.2° (*c* 2.0, MeOH); R_f^4 0.86, R_f^6 0.67.

Found: C, 61.49; H, 7.34; N, 10.66%. Calcd for $C_{79}H_{110}N_{12}O_{17} \cdot 2H_2O$: C, 61.78; H, 7.48; N, 10.94%.

Boc[-Aib-Orn(δ-Z)-Leu-D-Phe-Pro-]$_2$ ONSu (15): This compound was synthesized from **14** (546 mg, 0.346 mmol) as described for the synthesis of **6**; yield, 553 mg (95%); mp 110—111 °C; $[\alpha]_{589}^{22}$ −32.6° (*c* 1.3, MeOH); R_f^1 0.78, R_f^3 0.83, R_f^4 0.96.

Found: C, 60.84; H, 7.10; N, 11.04%. Calcd for $C_{83}H_{113}N_{13}O_{19} \cdot 2H_2O$: C, 61.05; H, 7.22; N, 11.15%.

H[-Aib-Orn(δ-Z)-Leu-D-Phe-Pro-]$_2$ONSu · TFA (16). This compound was synthesized from **15** (526 mg, 0.329 mmol) as described for the synthesis of **8**; yield, 510 mg (96%); mp 123—127 °C; $[\alpha]_{589}^{22}$ −52.6° (*c* 0.63, MeOH); R_f^1 0.78, R_f^3 0.60.

Found: C, 58.95; H, 6.85; N, 10.75%. Calcd for $C_{80}H_{106}N_{13}O_{19}F_3 \cdot H_2O$: C, 58.99; H, 6.68; N, 11.18%.

***Cyclo*[Aib-Orn(δ-Z)-Leu-D-Phe-Pro]$_2$ (17).** Compound **16** (503 mg, 0.312 mmol) was subjected to a cyclization reaction, in a similar manner as described for the preparation of **10**. The crude product was applied to a Sephadex LH-20 column (3.6×114 cm). The column was eluted with MeOH. The main fractions were rechromatographed over a silica-gel column (Wako silica gel CQ-3, 2×30 cm) using a solvent system of EtOAc-$CHCl_3$-MeOH (9:5:1). The purified product was recrystallized from EtOAc-ether-petroleum ether; yield, 208 mg (48%; 44% from **14**); mp 131—134 °C. $[\alpha]_{589}^{23}$ −88.5° (*c* 1.0, MeOH); R_f^1 0.75, R_f^2 0.64, R_f^3 0.82, R_f^4 1.00, R_f^5 0.79, R_f^6 0.83.

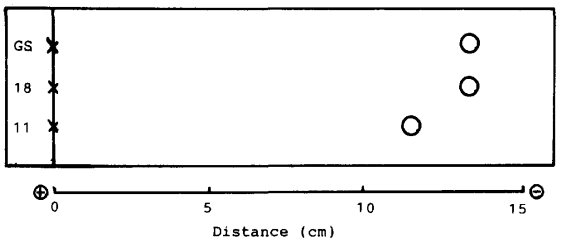

Fig. 9. Paper electrophoresis of [Aib$^{1,1'}$] GS (**18**), and [Aib^1] semiGS (**11**).

Found: C, 63.24; H, 7.37; N, 11.71%. Calcd for $C_{74}H_{100}N_{12}O_{14} \cdot H_2O$: C, 63.50; H, 7.34; N, 12.01%.

The molecular weight was determined by a Hitachi osmometer, type 117 (solvent; MeOH). Found: 1340. Calcd for $C_{74}H_{100}N_{12}O_{14}$: 1381.7.

***Cyclo*(Aib-Orn-Leu-D-Phe-Pro)$_2$ · 2HCl (18).** Compound **17** (52.8 mg, 38.2 mmol) was hydrogenated as described for the preparation of **11**; yield, 43.9 mg, (97%); mp 209—212 °C; $[\alpha]_{589}^{23}$ −76.7° (*c* 0.49, MeOH); R_f^1 0.16, R_f^3 0.37, R_f^4 0.94, R_f^5 0.38, R_f^6 0.65. Amino acid ratios in hydrolysate of **18**; Aib 2.0, Orn 2.03, Leu 2.0, Phe 2.2, Pro 2.1.

Found: C, 53.56; H, 7.84; N, 12.60%. Calcd for $C_{58}H_{90}N_{12}O_{10}Cl_2 \cdot 6H_2O$: C, 53.82; H, 7.94; N, 12.98%.

Paper Electrophoresis. This was carried out on Toyo Roshi No. 51A paper with a HCOOH-AcOH-MeOH-H_2O solvent system (2:9:18:30, pH 1.8) for 3 h at 500 V/30 cm. Each of these analogs showed a single spot. Figure 9 shows that [Aib$^{1,1'}$]GS (**18**) migrates faster toward the cathode than [Aib^1]semiGS (**11**), and that the mobility of **18** is indistinguishable from that of the natural GS.

Microbiological Assay and CD Measurements. The microorganisms employed are listed in Table 2. The minimum amount of the compound necessary for the complete inhibition of growth was determined by a dilution method using a trypticase soy agar. As is shown in Table 2, [Aib$^{1,1'}$]GS (**18**) and [Aib^1]semiGS (**11**) exhibited no antibacterial activity against any of the microorganisms tested. The CD spectra were obtained using a JASCO spectropolarimeter model J-20 in MeOH solution at room temperature.

The authors wish to express their thanks to Dr. Masahiko Fujino of Takeda Chemical Industries, Ltd. for the biological assay. Special thanks are due to Prof. Nobuo Izumiya of Laboratory of Chemistry, Kurume Institute of Technology for his suggestions and a stimulus for our work.

References

1) M. Kondo and N. Izumiya, *Bull. Chem. Soc. Jpn.*, **40**,1975 (1967).

2) M. Kondo and N. Izumiya, *Bull. Chem. Soc. Jpn.*, **43**, 1850 (1970).

3) N. Izumiya, T. Kato, H. Aoyagi, M. Waki, and M. Kondo, "Synthetic Aspects of Biologically Active Cyclic Peptide-Gramicidin S and Tyrocidines," Kodansha, Tokyo, and Halsted Press, New York (1979), pp. 61—62.

4) M. Waki and N. Izumiya, *Bull. Chem. Soc. Jpn.*, **40**,

1687 (1967).
5) Ref. 3, pp. 29—32.
6) R. C. Pandey, H. Meng, J. C. Cook, Jr., and K. L. Rinehart, Jr., *J. Am. Chem. Soc.*, **99**, 5203 (1977).
7) G. Jung, W. A. Konig, D. Liebfritz, T. Ooka, K. Janko, and G. Boheim, *Biochim, Biophys. Acta*, **433**, 164 (1976).
8) H. Bruckner, W. A. Konig, M. Greiner, and G. Jung, *Angew. Chem., Int. Ed. Engl.*, **18**, 476 (1979).
9) T. Fujita, Y. Takaishi, and T. Shiromoto, *J. Chem. Soc., Chem. Commun.*, **1979**, 413.
10) R. Nagaraji and P. Balaram, *Acc. Chem. Res.*, **14**, 356 (1981).
11) K. Inouye, K. Watanabe, K. Namba, and H. Otsuka, *Bull. Chem. Soc. Jpn.*, **43**, 3873 (1970).
12) H. Takiguchi, H. Nishikawa, K. Matsudai, and N. Izumiya, *Fukuoka Univ. Sci. Rep.*, **3**, 31 (1974).
13) M. Kawai and U. Nagai, *Biopolymers*, **17**, 1549 (1978).
14) Amino acid residues with no prefix are of L-configuration. The abbreviations for amino acids and peptides are in accordance with the rules of IUPAC-IBU Commission of Biological Nomenclature [*Eur. J. Biochem.*, **138**, 9 (1984)]. Additional abbreviations used are as follows: DCC, dicyclohexylcarbodiimide; HONSu, *N*-hydroxysuccinimide; NMM, *N*-methylmorpholine; TFA, trifluoroacetic acid; EDC·HCl, 1-ethyl-3-(3-dimethylaminopropyl)carbodiimide hydrochloride.
15) The terms of sidedness was used for a specific conformation of GS molecule in which the charged side chains are on one side and the hydrophobic side chains on the other side. K. Sato, K. Ueda, M. Kondo, H. Aoyagi, and N. Izumiya, *Bull. Chem. Soc. Jpn.*, **51**, 1830 (1978) and references cited herein.
16) M. Tamaki, T. Okitsu, M. Araki, H. Sakamoto, M. Takimoto, and I. Muramatsu, *Bull. Chem. Soc. Jpn.*, **58**, 531 (1985).
17) M. Ohno, T. Kato, S. Makisumi, and N. Izumiya *Bull. Chem. Soc. Jpn.*, **39**, 1738 (1966).

 © 1987 The Chemical Society of Japan Bull. Chem. Soc. Jpn., 60, 1399—1402 (1987)

Action of Serine Carboxypeptidases on Endopeptidase Substrates, *N*-Acyldipeptideamides

Shigeru KUNUGI,* Kazuo TANABE, Kouji YAMASHITA, and Mitsuhiro FUKUDA†
Department of Applied Chemistry, Fukui University, Bunkyo, Fukui 910
†Department of Practical Life Studies, Hyogo University of Teacher Education, Yashiro-cho, Hyogo 673-14
(Received August 9, 1986)

Action patterns of two serine carboxypeptidases, one from yeast (Y) and the other from wheat bran (W), on *N*-[3-(2-furyl)acryloyl]-(Fua-) dipeptideamide substrates were examined by HPLC and amino acid analysis. In the reaction of the wheat enzyme the substrates were hydrolyzed to Fua-amino acid and no sufficient amount of Fua-dipeptides were detected on HPLC in the product mixtures. Very few or no free amino acids were observed by amino acid analysis. This indicates that the wheat enzyme exhibited carboxamidopeptidase activity on these substrates. On the contrary, carboxypeptidase Y gave Fua-amino acids and Fua-dipeptides as products, depending on the structure of the substrates. Accordingly, liberations of free amino acids were detected in some cases. This result shows that the yeast enzyme acts on some of the substrates in a two step manner: First by amidase and second by a carboxypeptidase activity. Based on these results the substrate binding mechanisms of these enzymes are discussed.

Serine carboxypeptidase [EC3.4.16.1] includes cathepsin A, and carboxypeptidases from yeast,[1] molds and plants.[2] They are considerably different from metallo-carboxypeptidases represented by carboxypeptidase A.[3,4] In particular, some of the serine carboxypeptidases show hydrolytic activities towards synthetic chymotrypsin-type substrates, such as Ac-Tyr-OEt and Bz-Tyr-NH-Np.[5-8] Recently, carboxamidopeptidase activities against several peptide hormones have also been reported,[9-12] further, we have found that *N*-substituted peptide amides with such a large 7-amino-4-methyl-2*H*-1-benzopyran-2-one can be hydrolyzed by, for example, an enzyme from yeast (carboxypeptidase Y).[13]

These endopeptidase-like activities of this class of enzyme, especially the esterase activity, have been utilized for peptide synthesis, by aminolysis of the ester or by transpeptidation.[14,15] However, this variety of activities, on the other hand, makes the prediction of the condensation product very complicated. Therefore, we investigate the hydrolysis pattern for the enzymes from yeast and wheat bran (carboxypeptidase W) on *N*-acyldipeptideamides in order to improve the design of the peptide formation by these enzymes. It would also be helpful to obtain an understanding of the substrate binding mechanisms of these enzymes.

Experimental

Materials. Five *N*-acyldipeptideamides (*N*-[3-(2-furyl)-acryloyl]-(Fua-) Gly-Phe-NH_2, Fua-Gly-Leu-NH_2, Fua-Phe-Gly-NH_2, Fua-Phe-Leu-NH_2, and Fua-Phe-Phe-NH_2) and corresponding Fua-dipeptides or Fua-amino acids were prepared as previously reported.[16] Carboxypeptidases Y and W were the same as those used in the previous studies.[13,17,18] The active concentration of the enzyme was determined by a steady state rate constant of the hydrolysis of Fua-Phe-Phe or Fua-Phe-OEt.[19] 2-Morpholinoethanesulfonic acid (Mes) and 2-[4-(2-hydroxyethyl)-1-piperazinyl]-ethanesulfonic acid (Hepes) were from the Dohjindo Laboratories (Kumamoto). Other reagents were of commercial grade and were used without further purifications.

Methods. The absorbance spectrum was measured on a Uvidec 650-C spectrophotometer (Nippon Bunkou Co.; Tokyo). The reaction velocity of the hydrolysis of Fua-substrates at the bond including the carbonyl group of the substituted amino acid was measured by the absorbance decrease at 320—345 nm. The hydrolyzed product was analyzed by the high-pressure liquid chromatography of a Shimadzu LC-5A system attached to a Cosmosil 5C18 reversed-phase column. The absorbance was monitored at 305 nm through a UV-detector (Shimadzu SPD-1) and integrated (Shimadzu CR3A). The release of an amino acid or an amino acid amide was checked by an amino acid analysis on a Shimadzu LC3A-FLD1 system with fluorometric detection by the phthalaldehyde method.

Results and Discussion

The reactivity of carboxypeptidase W towards five Fua-dipeptideamide substrates was measured at pH 5—7.5 and 25 °C. Table 1 shows the amounts of products observed in the reaction mixtures after overnight incubation, relative to the initial amount of the substrate. This pH range was selected since carboxypeptidase W loses its catalytic activity above pH 8.[18] Among the five substrates studied, Fua-Phe-Leu-NH_2 was most susceptible to hydrolysis; only Fua-amino acid was observed as a product in the applied pH range and the pH dependency was not obvious. Fua-Phe-Phe-NH_2 and Fua-Phe-Gly-NH_2 were also susceptible and no sufficient amount of Fua-dipeptide was detected in the reaction mixture. Fua-Gly-Phe-NH_2 and Fua-Gly-Leu-NH_2 were less reactive. The former substrate gave some *N*-Fua dipeptide in the reaction mixture at high pH.

Table 2 shows the result for carboxypeptidase Y catalysis. This enzyme gave a somewhat different pattern from that for carboxypeptidase W. It hydrolyzed Fua-Phe-Leu-NH_2 and Fua-Phe-Phe-NH_2. The degree of hydrolysis was higher at higher pH. In the case of Fua-Phe-Phe-NH_2 nearly half of the product was Fua-dipeptide while in Fua-Phe-Leu-NH_2 only Fua-amino acid was the final product. Fua-Phe-

Table 1. The Product Yields after a Reaction of *N*-Acyldipeptideamides with Carboxypeptidase W at 25°C

Substrate \ pH	4		5		6		7		7.5	
Product[a]	A	D	A	D	A	D	A	D	A	D
Fua-Phe-Gly-NH_2	42	0	49	0	50	0	47	0	18	0
Fua-Phe-Leu-NH_2	76	0	81	0	77	0	91	0	80	0
Fua-Phe-Phe-NH_2	59	0	72	0	60	0	79	0	57	0
Fua-Gly-Leu-NH_2	6	0	3	0	3	0	2	0	0	0
Fua-Gly-Phe-NH_2	4	0	11	0	7	1	6	6	1	10

a) A: Fua-A_1, D: Fua-A_1-A_2; relative (%) to the initial amount of each substrate.

Table 2. The Product Yields after a Reaction of *N*-Acyldipeptideamides with Carboxypeptidase Y at 25°C

Substrate \ pH	4		5		6		7		7.5	
Product[a]	A	D	A	D	A	D	A	D	A	D
Fua-Phe-Gly-NH_2	0	0	5	0	4	0	39	0	25	0
Fua-Phe-Leu-NH_2	39	0	90	0	100	0	100	0	100	0
Fua-Phe-Phe-NH_2	19	0	68	0	65	31	58	42	44	56
Fua-Gly-Leu-NH_2	1	0	2	0	29	1	34	5	19	6
Fua-Gly-Phe-NH_2	1	0	3	4	22	1	32	6	22	6

a) A: Fua-A_1, D: Fua-A_1-A_2, relative (%) to the initial amount of each substrate.

Table 3. The Amount of Liberated Amino Acid Determined by Amino Acid Analysis

Enzyme	Carboxypeptidase Y		Carboxypeptidase W	
Substrate	pH	Amino Acid Fraction/%[a]	pH	Amino Acid Fraction/%[a]
Fua-Phe-Gly-NH_2	5.0	3.1	6.0	0.72
	7.5	0		
Fua-Phe-Leu-NH_2	5.0	55.0	6.0	0.13
	7.5	65.0		
Fua-Phe-Phe-NH_2	5.0	32.0	6.0	4.5
	7.5	38.0		
Fua-Gly-Leu-NH_2	5.0	11.0	6.0	0
	7.5	5.2		
Fua-Gly-Phe-NH_2	5.0	1.3	5.0	0
	7.5	6.4	7.0	0

a) Amount of liberated amino acid relative to the initial amount of each substrate.

Gly-NH_2 fell in the latter category, though its reactivity was not very high and Fua-Gly-Phe-NH_2 and Fua-Gly-Leu-NH_2 showed moderate reactivities and also gave Fua-dipetides as products.

To determine whether the Fua-amino acids observed in these reaction mixtures were produced directly from the substrates by carboxamidopeptidase activity or via Fua-dipeptide, i.e., hydrolyzed first by the amidase activity and successively by carboxypeptidase activity, some of the reaction mixtures were analyzed on an amino acid analysis system. Table 3 shows the detected amount of the corresponding free amino acid, relative to the initial amount of the substrate. In the case of carboxypeptidase W very few or no free amino acid was observed and these substrates were known to be hydrolyzed by this enzyme simply by carboxamidopeptidase activity. On the contrary, a sufficient amount of free amino acid was observed in some of the carboxypeptidase Y catalyzed hydrolyses. As in Table 2, Fua-Phe-Leu-NH_2 was completely hydrolyzed to *N*-Fua amino acid by carboxypeptidase Y at higher pH during the present reaction period; however, a major part of it was produced via two-step hydrolysis. The substrate was hydrolyzed once to Fua-Phe-Leu by amidase activity and then to Fua-Phe and Leu by intrinsic carboxypeptidase activity. Though this activity decreased with increasing pH,[7,20] it was still sufficient to hydrolyze the Fua-dipeptide produced

from the substrate, even at higher pH: at pH 8.0 and 25 °C, k_{cat}/K_m for the carboxypeptidase activity was in the order of 10^5 $M^{-1}s^{-1}$ (1M=1 mol dm^{-3}) for Fua-Phe-Leu.[21]

In the case of Fua-Phe-Phe-NH_2 the reaction proceeded in a similar fashion, but the amidase activity was higher than the carboxypeptidase activity at higher pH, with a considerable amount of the product accumulated at the state of Fua-Phe-Phe. At low pH where the amidase activity decreased,[7,12] a considerable portion of the substrate was left intact after the applied reaction time; only Fua-Phe was observed as a product. Therefore, the relative magnitude of the two activities determined the product distribution. Fua-Phe-Gly-NH_2 is a rather poor substrate of carboxypeptidase Y and was mostly hydrolyzed directly to Fua-Phe by carboxamidopeptidase activity. In Fua-Gly-Phe-NH_2 and Fua-Gly-Leu-NH_2 amidase activity was not very high and the two pathways were more or less concurrent.

The complexity of the hydrolysis of Fua-Phe-Leu-NH_2 by carboxypeptidase Y was reflected in the kinetics of the reaction observed by a change in the UV absorbance. The apparent second-order rate constant of the hydrolysis was obtained from the initial rate divided by both enzyme and substrate concentrations or by a pseudo-first-order analysis at $[E]_0$=50—100 nM and $[S]_0$=10—20 μM. It changed with pH as shown in Fig. 1 (○ and ◐) with an apparent maximum at about pH 7. In the pH range of 6.5—8, however, a semi-logarithmic plot of the absorbance change as a function of time shows a convex shape (insert in Fig. 1); the rate constants given in the figure were evaluated from the later portions of the plots. In contrast to this, the hydrolysis of the same substrate by carboxypeptidase W gave normal pseudo-first-order rate curves (though not shown here); the pH profile of the second-order rate constant (Fig. 1, ●) could be explained by the following simple equation assuming $k_{A(lim)}$=7.96×10^4 $M^{-1}s^{-1}$ and pK_a=6.60 ($k_{A(lim)}$: pH-independent (maximum) value of k_{cat}/K_m):

$$k_{cat}/K_m = k_{A(lim)}/(1 + [H^+]/K_a). \quad (1)$$

For a further consideration of the mechanism of serine carboxypeptidase, we cite here the previously reported change of the reaction parameters with the variation in the side-chain structures of *N*-acyl-dipeptides substrates (*N*-furylacryloyl-substrate for carboxypeptidase W[18] and *N*-benzyloxycarbonyl-substrate for carboxypeptidase Y[7]). Carboxypeptidase W has a relatively broader specificity, compared with carboxypeptidase Y, especially for the k_{cat} parameter. We note that there are some differences in the specificity of the carboxypeptidase activity and the carboxamidopeptidase or amidase activity.

These two carboxypeptidases were shown to exhibit fairly different pK_a values for peptidase activity, sug-

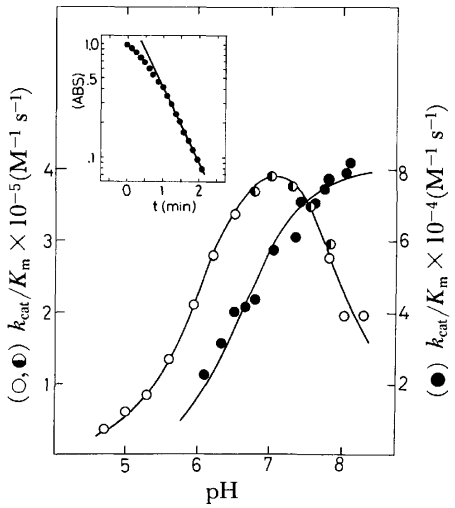

Fig. 1. pH Dependences of k_{cat}/K_m of the hydrolysis of FuaPheLeuNH_2 catalyzed by carboxypeptidase Y (○,◐) and by carboxypeptidase W (●) at 25 °C. [Enzyme]=50—100 nM, [substrate]=5—40 μM, 0.5% *N*,*N*-dimethylformamide, 0.1 M NaCl, 0.1 M Mes or Hepes. Insert; a semi-logarithmic plot of the kinetic data of carboxypeptidase Y at pH 7.0.

Table 4. Change in The Reaction Parameters with The Side Chain Structures of *N*-Acyl-Dipeptide Substrates for The Hydrolysis by Carboxypeptidase W and Carboxypeptidase Y[a]

Dipeptide sequence	Carboxypeptidase W			Carboxypeptidase Y		
	k_{cat}	K_m	k_{cat}/K_m[b]	k_{cat}	K_m	k_{cat}/K_m[b]
	s^{-1}	mM	10^4 $M^{-1}s^{-1}$	s^{-1}	mM	10^4 $M^{-1}s^{-1}$
-Gly-Phe	2.8	0.12	2.3(0.08)	2.2	1.7	0.13(0.04)
-Ala-Phe	39	0.18	22(0.74)	—	—	—
-Leu-Phe	28	0.033	84(2.9)	46	0.1	47(13)
-Phe-Phe	48	0.042	110(3.9)	420	0.5	84(23)
-Phe-Leu	72	0.064	120(4.1)	130	0.1	130(35)
-Phe-Pro	2.9	0.037	7.6(0.26)	23	0.7	3.4(0.93)
-Phe-Gly	93	0.32	29(1.0)	140	4.0	3.7(1.0)
-His-Leu	53	0.91	6.0(0.21)	1.4	1.8	0.078(0.02)

a) The reaction parameters of *N*-Fua-substrates at pH 4.0 and 25 °C (by Fukuda et al.[19]) for carboxypeptidase W and of *N*-CBZ-substrates at pH 6.5 and 25 °C (by Hayashi et al.[7] and Johansen et al. (-His-Leu)[22]) for carboxypeptidase Y. b) In parentheses are k_{cat}/K_m values relative to the value of -Phe-Gly.

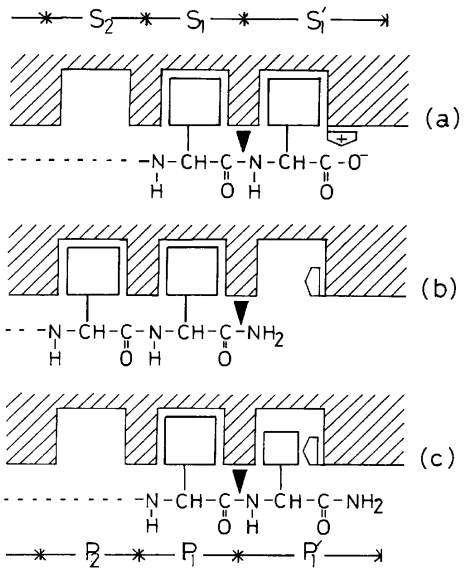

Fig. 2. Scheme of the substrate binding site of carboxypeptidase Y. S_i,S_i': The binding site for the C-terminal amino acid residue of the substrate. P_iP_i': The amino acid residues of the substrate in corresponing binding sites. Dark triangle shows the scissile point. (a) At low pH with a substrate having free carboxylate terminal and bulky amino acid residues. (b) At neutral pH with a substrate having amide end and bulky trerminal amino acid. (c) At neutral pH with a substrate having amide end and a ternial amino acid residue of a smaller size.

gesting that the anion-recognizing residue might be different. Our previous study[18] revealed that the catalytic sites for the carboxypeptidase activity and endopeptidase-like activity of carboxypeptidase W plausibly involved different functional groups. In view of the fact that the catalytic activity of carboxypeptidase Y involves a His residue,[4] and the apparent pK_a value in the substrate binding process[20] implies that this or another protonated His residue can act as an anion-recognition site of carboxypeptidase Y.

These considerations lead to a schematic picture of the substrate binding site of carboxypeptidase Y (Fig. 2): (a) The protonation of a His residue is essential for the binding of substrates having a carboxylate end. (b) At neutral and alkaline pH, the His residue loses its charge and some structural or conformational change might occur in the substrate-binding site. This process limits the size of the S_1' site and prevents the binding of a dipeptideamide substrate which has a bulky residue at P_1'. Therefore, such a substrate is not cleaved at the P_1-P_1' bond but rather at the terminal amide bond. (c) In the case of a dipeptide amide having a smaller residue at P_1', it penetrates into the corresponding position and a carboxamidopeptidase activity occurs. A neutral His residue can also be helpful for the binding of a moderate size residue at P_1'.

The authors gratefully acknowledge the encouragement of Profs. Norio Ise and Yoshiharu Nakamura throughout the work. They also acknowledge the kind advice of Prof. R. Hayashi.

This work was partly supported by a Grant-in-Aid from the Ministry of Education, Science and Culture (No. 60550623).

References

1) R. Hayashi, S. Moore, and W. H. Stein, *J. Biol. Chem.*, **248**, 8366 (1973).
2) D. C. Shaw and J. R. E. Wells, *Biochem. J.*, **128**, 229 (1972).
3) H. Neurath and W. G. Schwert, *Chem. Rev.*, **46**, 69 (1950).
4) R. Hayashi, Y. Bai, and T. Hata, *J. Biol. Chem.*, **250**, 5221 (1975).
5) J. N. Ihle and L. S. Dure, III, *J. Biol. Chem.*, **247**, 5041 (1972).
6) Y. Bai, R. Hayashi, and T. Hata, *J. Biochem.*, **78**, 617 (1975).
7) R. Hayashi, Y. Bai, and T. Hata, *J. Biochem.*, **77**, 69 (1975).
8) T. Hofmann, *Methods Enzymol.*, **45**, 587 (1976).
9) W. H. Simmons and R. Walter, *Biochemistry*, **19**, 39 (1980).
10) F. Widmer, K. Breddam, and J. T. Johansen, *Carlsberg Res. Commun.*, **46**, 97 (1980).
11) K. Breddam and J. T. Johansen, *Carlsberg Res. Commun.*, **49**, 463 (1984).
12) R. Hayashi, in Prospects for Applied Enzymology, the 3rd International Symposium on Life Science, Toyobo Co. Ltd., Japan (1984), pp. 65—68.
13) S. Kunugi, M. Fukuda, and R. Hayashi, *Eur. J. Biochem.*, **153**, 37 (1985).
14) F. Widmer, K. Breddam, and J. T. Johansen, *Carlsberg Res. Commun.*, **45**, 453 (1980).
15) K. Breddam, J. T. Johansen, and M. Ottesen, *Carlsberg Res. Commun.*, **49**, 457 (1984).
16) S. Blumberg and B. L. Vallee, *Biochemistry*, **14**, 2410 (1975).
17) S. Kunugi, K. Tanabe, and M. Fukuda, *Bull. Chem. Soc. Jpn.*, **59**, 2660 (1986).
18) M. Fukuda and S. Kunugi, *J. Biochem.*, **101**, 233 (1987).
19) M. Fukuda, Doctoral Dissertation to Kyoto University (1985).
20) M. Fukuda and S. Kunugi, *Eur. J. Biochem.*, **149**, 657 (1985).
21) H. Shima, Master Thesis for Kyoto University (1986).
22) J. T. Johansen, K. Breddam, and M. Ottesen, *Carlsberg Res. Commun.*, **41**, 1 (1976).

 © 1987 The Chemical Society of Japan Bull. Chem. Soc. Jpn., 60, 1403—1406 (1987)

Wheat Carboxypeptidase-Catalyzed Peptide Synthesis by Aminolysis of *N*-Acyl Amino Acid Ester. Indication of the Acyl-Enzyme Mechanism

Hiroshi SHIMA,† Mitsuhiro FUKUDA,†† Kazuo TANABE, Takanobu ITO, and Shigeru KUNUGI*
Department of Applied Chemistry, Fukui University, Bunkyo, Fukui 910
†Department of Polymer Chemistry, Kyoto University, Sakyo-ku, Kyoto 606
††Department of Practical Life Studies, Hyogo University of Teacher Education, Yashiro-cho, Hyogo 673-14
(Received August 9, 1986)

Dipeptide synthesis from *N*-[3-(2-furyl)acryloyl]-acylated (Fua-) amino acid ethyl ester and amino acid amide catalyzed by wheat bran carboxypeptidase (carboxypeptidase W) was studied. The optimum pH for peptide formation was at pH 8; more than 60% of the initial *N*-Fua-L-phenylalanine ethyl ester was converted to *N*-Fua-L-phenylalanylglycinamide under optimum conditions. The dependence of peptide formation on the concentration of amino acid amide showed an apparent saturation; this could be successfully explained by a reaction scheme which involved an acylated enzyme attacked by an enzyme-bound amine. The results for a reaction in the presence of two different amine components also supported this mechanism. Gly-NH_2 had a better affinity to the acylated carboxypeptidase and the apparent dissociation constant ($K_{N(app)}$) was about 50 mM. These results were compared with those for those reactions catalyzed by carboxypeptidases from yeast and malt.

Serine carboxypeptidases [EC 3.4.16.1] from various origins[1-9] are characterized by the broad substrate specificity and by esterase and/or amidase activity in addition to intrinsic carboxypeptidase.[3,6-11] Some of the enzymes of this group have been successfully utilized for peptide synthesis from *N*-acyl amino acid esters and amino acid amides or esters.[12-14] In addition to these practical aspects, the aminolysis reaction and transpeptidation reactions[15] have been considered as indirect evidence for a reaction mechanism which includes an acylated intermediate. The existence of such an intermediate was observed by a stopped-flow technique in the case of carboxypeptidase Y.[16,17] A carboxypeptidase from wheat bran (carboxypeptidase W)[18] is considered to be a member of this group of enzymes; we have studied the kinetics of its reaction for peptide and ester hydrolyses.[19,20] In due course we found that this carboxypeptidase is useful for peptide synthesis by the aminolysis of an ester substrate. Here, we examine some fundamental points for such a utilization.

Experimental

Materials. Carboxypeptidase W was obtained from Pentel Co. Ltd. (Tokyo, Lot 68305031). Enzyme solutions were prepared by dissolving it in deionized water; it was stored as a concentrated solution (0.05 mM (1M=1 mol dm^{-3})) at 4 °C. The protein concentration was determined from the absorbance at 280 nm using $A1^{\%}_{cm}$=19.6 and Mr=118000.[18] Carboxypeptidase Y was obtained from Oriental Yeast Co. (Osaka) and used as described before.[19] *N*-[3-(2-furyl)acryloyl] amino acids were synthesized by the *N*-hydoxysuccinimide method. Their analytical data have been described previously.[22-24] Other chemicals were of reagent grade and were used without further purifications.

Methods. Reactions were carried out at 37 °C in the presence of 0.2 M NaCl and 15% *N*,*N*-dimethylformamide, unless otherwise mentioned. The pH was adjusted by adding concd HCl or NaOH solutions. After incubation for the indicated time, a portion was taken out, quenched by mixing with a 5-fold volume of acetonitrile, filtered on Millipore FHLP013, and then analyzed on a reversed-phase chromatography (Waters HPLC 6000A-440 with Cosmosil 5C18). The eluent solution contained 45% CH_3CN, 50 mM Na_2SO_4 and approximately 5 mM H_3PO_4.

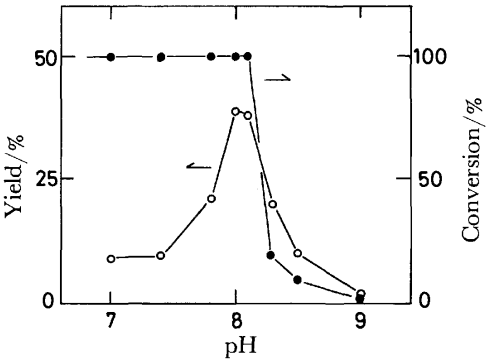

Fig. 1. pH Dependence of the carboxypeptidase W-catalyzed peptide formation from Fua-Phe-OEt and Leu-NH_2 at 37 °C. [enzyme]=0.5μM, [Fua-Phe-OEt]=2 mM, [Leu-NH_2]=0.1 M, [NaCl]=0.2 M, and 15% *N*,*N*-dimethylformamide. ○: Peptide yield, Fraction of product peptide relative to the initial amount of the ester. ●: Ester conversion, Fraction of hydrolyzed ester relative to the initial amount of the ester.

Results and Discussion

Figure 1 shows the pH dependence of the peptide formation from Fua-Phe-OEt and Leu-NH_2 after incubation for 5 h under the indicated conditions. They are given in a form of conversions (=(total consumption of the ester)/(initial amount of the ester)) and yield (=(produced amount of the dipeptide amide)/(initial amount of the ester)). Since the catalytic activity of carboxypeptidase W decreased at a pH above 8,[19] the conversion efficiency decreased above 8 and the maximum yield was obtained at a pH around 8. Similar pH profiles were obtained at different enzyme concentrations. This result is in contrast to

Table 1. Product Distribution in the Aminolysis Reaction of Fua-Phe-OEt Catalyzed by Carboxypeptidases W and Y with Several Nucleophiles at [Fua-Phe-OEt]=2 mM, [Nucleophile]=0.1 M, [enzyme]=0.5 mM, [NaCl]=0.2 M, 15% *N,N*-Dimethylformamide 37 °C and pH 8.0

Nucleophile	pK_a[a]	Carboxypeptidase W					Carboxypeptidase Y		
		Fua-Phe-Xxx-NH_2	Fua-Phe-Xxx	Fua-Phe	f_1/f_0[b]	$K_{N(app)}$(mM)	Fua-Phe-Xxx-NH_2	Fua-Phe-Xxx	Fua-Phe
Phe-NH_2	7.1	23	<1	77	0.30	350	<1	25	75
Leu-NH_2	7.6	38	0	62	0.61	170	19 (66)[c]	16 (15)	65 (19)
Gly-NH_2	7.9	63	0	37	1.7	50	33	0	67
Gly-Gly	8.1	<1	0	100	—	—			

a) from Ref. 25. b) $f_0=v_0/(v_0+v_1)$ as in Eq. 1. Therefore $f_1/f_0=v_1/v_0$. c) Numbers in parentheses were obtained at pH 9.5 in carbonate-hydrogencarbonate buffer (0.1 M).

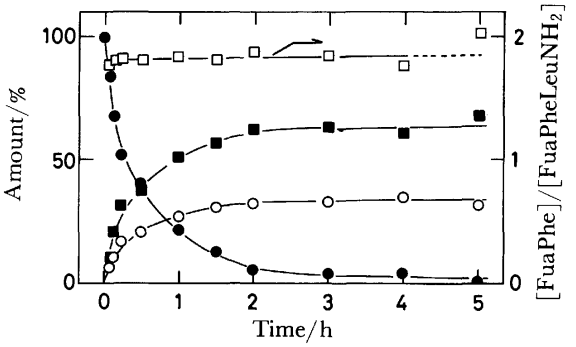

Fig. 2. Time course of the carboxypeptidase W-catalyzed peptide formation from Fua-Phe-OEt and Leu-NH_2 at 37 °C. [Fua-Phe-OEt]=5 mM, [Leu-NH_2]=0.1 M, [enzyme]=0.1 μM, [NaCl]=0.2 M, 15% *N,N*-dimethylformamide and pH 8.0. ●: Fua-Phe-OEt, ■: Fua-Phe, ○: Fua-Phe-Leu-NH_2. □: Ratio of Fua-Phe and Fua-Phe-Leu-NH_2.

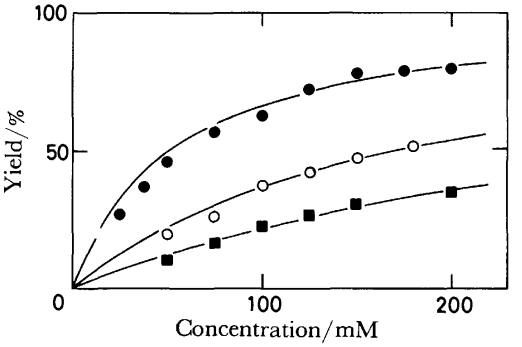

Fig. 3. Amino acid amide concentration dependence of peptide formation at 37 °C. [Fua-Phe-OEt]=2 mM, [enzyme]=0.5 μM, [NaCl]=0.2 M, 15% *N,N*-dimethylformamide and pH 8.0. ●: With Gly-NH_2, ○: with Leu-NH_2, ■: with Phe-NH_2

that for carboxypeptidase Y-catalyzed peptide formation using the same substrates, where the yield increased monotonously (up to pH 10) with an increase in pH (Shima et al. unpublished result). At optimum pH, The time course of the reaction by carboxypeptidase W was as shown in Fig. 2. Under these conditions, the ratio (□) of the hydrolyzate (Fua-Phe) and the aminolysis product (Fua-Phe-Leu-NH_2) was practically constant during the reaction period. Table 1 shows the results for product analyses for reactions with different nucleophiles, together with the results for carboxypeptidase Y under similar conditions. As we have shown in a preceding paper,[20] the amidase activity of carboxypeptidase W is low and the production of *N*-acyldipeptide with carboxylate terminal is practically negligible in the present case. This result is also in contrast to the case of carboxypeptidase Y. Gly-Gly was not an effective nucleophile, while Gly-NH_2 was the best among three amino acid amides used here.

The amide concentration dependency of the peptide yield is shown in Fig. 3 for three amino acid amides. To explain the results we postulate a competition between the hydrolysis and the aminolysis of the acyl-enzyme intermediate, while taking account of a possible inhibitory action of added nucleophile, as shown in Eqs. 1—4:

$$E + S \underset{k_{-1}}{\overset{k_1}{\rightleftharpoons}} E\cdot S \xrightarrow{k_2} EA \quad (1)\ \text{[Acyl-enzyme formation]},$$

$$EA \xrightarrow{k_3} E + P_0 \quad (2)\ \text{[Hydrolysis of acyl-enzyme]},$$

$$EA + N \overset{K_N}{\rightleftharpoons} EA\cdot N \xrightarrow{k_n} E + P_1 \quad (3)\ \text{[Aminolysis]},$$

$$E + N \overset{K_N^i}{\rightleftharpoons} E\cdot N \quad (4)\ \text{[Competitive inhibition]}.$$

Here, the k_i's are the respective rate constants. S, P_i's, E, E·S, and EA are the substrate (ester), products (amino acid and peptide), enzyme, enzyme-substrate complex and acylated enzyme, respectively. EA·N and E·N are a complex formed from the acylated enzyme and the nucleophile and enzyme-nucleophile complex, respectively. K_N and K_N^i are the respective dissociation constants. These expressions are similar to those provided by Bender[26] and by Fastrez and Fersht[27] to explain the partitioning of the acyl-enzyme intermediate of chymotrypsin by water and an acceptor (nucleophile). However, the specific binding of the nucleophile to the enzyme active site is considered in the present case. They are also analogous to expressions given for the reaction of papain by Fink and Bender[28]; here, a reaction path which includes the ternary complex composed of EA and two molecules of N is out of the consideration. In a steady state analysis of the reaction, Eq. 1 is considered to be equivalent to

$$E + S \overset{K_m}{\rightleftharpoons} EA, \quad (5)$$

Table 2. Carboxypeptidase W-Catalyzed Aminolysis of Fua-Phe-OEt with two Amino Acid Amides (Xxx-NH_2 and Yyy-NH_2) at [Fua-Phe-OEt]=2 mM, [Xxx-NH_2]=[Yyy-NH_2]=0.1 M, 15% *N,N*-Dimethylformamide 37 °C and pH 8.0

Xxx-NH_2	Yyy-NH_2	Yield of Fua-Phe-Xxx-NH_2 (f_1) (%)	Yield of Fua-Phe-Yyy-NH_2 (f_1') (%)	f_1/f_1'[a]
Gly-NH_2	Phe-NH_2	61	7.8	7.8 (7.0)
Gly-NH_2	Leu-NH_2	57	14	4.1 (3.4)
Leu-NH_2	Phe-NH_2	29	14	2.1 (7.0)

a) Numbers in parentheses were calculated by Eq. 16.

where $K_m=\{(k_{-1}+k_2)/k_1\}\{k_3^*/(k_2+k_3^*)\}$ and $k_3^*=k_3+k_n[N]/K_N$. Then, we obtain the rates of the formation of two products (P_0 and P_1) as

$$v_0 = dP_0/dt = k_3([S]/K_m)[E]_0 / \{1 + (K_m/[S])(1 + [N]/K_N) + [N]/K_N^i\}, \quad (6)$$

and

$$v_1 = dP_1/dt = k_n([N]/K_N)([S]/K_m)[E]_0 / \{1 + (K_m/[S])(1 + [N]/K_N) + [N]/K_N^i\}. \quad (7)$$

Since [N] is in great excess to the enzyme in each case and there are no cross terms in Eqs. 6 and 7, the ratio of two reaction rates is constant during the reaction period (the case in Fig. 3). Therefore, these equations, though originally written for the initial state of the reaction, can be related to the fraction (f_1) of the aminolysis product over the total consumption of the ester substrate:

$$f_1 = v_1/(v_0 + v_1) = k_n([N]/K_N)/\{k_3 + k_n([N]/K_N)\} = 1/\{1 + (k_3/k_n)(K_N/[N])\}. \quad (8)$$

Equation 8 predicts that an apparent saturation is observed in the concentration dependence of the peptide yield and that the apparent saturation parameter ($K_{N(app)}$) ($=(k_3/k_n)K_N$) shows a total affinity of aminolysis. The observed concentration dependency was analyzed by a least-square method and $K_{N(app)}$ was evaluated (Table 1). Since the nucleophilicity of Gly-NH_2 is weakest, the smallest $K_{N(app)}$ value observed for this amide is due to the smallest K_N value, i.e., the affinity of Gly-NH_2 to the acylated enzyme is best among the three. This is in contrast to the fact that in the hydrolysis reaction K_m values of Fua-Phe-Leu and Fua-Phe-Phe are five- to seven-fold smaller than that of Fua-Phe-Gly at low pH.[19]

When two kinds of amino acid amides are present in a reaction mixture, the product distributions (fractions of two peptide products; f_1 and f_1') are listed in Table 2. For such systems we have to add two equations concerning the second amine component (N'):

$$EA + N' \overset{K_{N'}}{\rightleftharpoons} EA\cdot N' \xrightarrow{k_n'} E + P_1', \quad (9)$$

and

$$E + N' \overset{K_{N'}^i}{\rightleftharpoons} E\cdot N'. \quad (10)$$

In these equations $K_{N'}$, k_n', and $K_{N'}^i$ have similar meanings as K_N, k_n, and K_N^i, respectively.

Then, v_1, v_1', and v_0 are

$$v_0 = k_3([S]/K_m)[E]_0 / \{1 + (K_m/[S])(1 + [N]/K_N + [N']/K_{N'}) + [N]/K_N^i + [N']/K_{N'}^i\}, \quad (11)$$

$$v_1 = k_n([N]/K_N)([S]/K_m)[E]_0 / \{1 + (K_m/[S])(1 + [N]/K_N + [N']/K_{N'}) + [N]/K_N^i + [N']/K_{N'}^i\}, \quad (12)$$

and

$$v_1' = k_n'([N']/K_{N'})([S]/K_m)[E]_0 / \{1 + (K_m/[S])(1 + [N]/K_N + [N']/K_{N'}) + [N]/K_N^i + [N']/K_{N'}^i\}. \quad (13)$$

Also,

$$f_1 = k_n([N]/K_N)/\{k_3 + k_n([N]/K_N + k_n'([N']/K_{N'})\}, \quad (14)$$

and

$$f_1' = k_n'([N']/K_{N'})/\{k_3 + k_n([N]/K_N + k_n'([N']/K_{N'})\}. \quad (15)$$

This means that the ratio of the fractions for two amino acid amides is

$$f_1/f_1' = \{k_n([N]/K_N)\}/\{k_n'([N']/K_{N'})\}. \quad (16)$$

Where [N]=[N'], f_1/f_1' can be calculated from $K_{N(app)}$; the results are listed in parentheses. They are comparable to the experimental values. This supports the scheme presently considered for the reaction of carboxypeptidase W. Under similar conditions, carboxypeptidase Y gave more complex results: Fua-Phe-Phe was 37%, Fua-Phe-Gly-NH_2 18%, and Fua-Phe 45% at [Phe-NH_2]=[Gly-NH_2]=0.1 M. In this case an apparent "activation" of the amidase action on the once produced Fua-Phe-Phe-NH_2[20] was observed in the

presence of the second nucleophile (Gly-NH_2) (compare with the result listed in Table 1) and the present mechanism for carboxypeptidase W was not sufficient for explaining these results.

Thus, carboxypeptidase W was shown to have an efficient activity for a peptide synthesis from *N*-acyl amino acid ester and amino acid amide by an aminolysis of the acylated enzyme intermediate.

We gratefully acknowledge the advice and encouragement of Professor Norio Ise of Kyoto University.

References

1) R. Hayashi, S. Moore, and W. H. Stein, *J. Biol. Chem.*, **247**, 2296 (1973).
2) E. Ichishima and K. Yomogida, *Agr. Biol. Chem.*, **37**, 693 (1973).
3) T. Hofmann, *Methods Enzymol.*, **45**, 587 (1976).
4) H. Zuber, *Hoppe-Seyler's Z. Physiol. Chem.*, **349**, 1337 (1968).
5) J. R. E. Wells, *Biochem. J.*, **97**, 228 (1965).
6) J. Mikola and K. Pietila, *Phytochemistry*, **11**, 2977 (1972).
7) J. N. Ihle and L. S. Dure, *J. Biol.Chem.*, **247**, 5041 (1972).
8) T. Matoba and E. Doi, *J. Biochem.*, **77**, 1297 (1975).
9) K. Breddam, S. B. Sorensen, and M. Ottesen, *Carlsberg Res. Commun.*, **48**, 217 (1983).
10) R. Hayashi, Y. Bai, and T. Hata, *J. Biochem.*, **77**, 69 (1975).
11) S. Kunugi, M. Fukuda, and R. Hayashi, *Eur. J. Biochem.*, **153**, 37 (1985).
12) F. Widmer, K. Breddam, and J. T. Johansen, *Carlsberg Res. Commun.*, **45**, 453 (1980).
13) K. Breddam, F. Widmer, and J. T. Johansen, *Carlsberg Res. Commun.*, **48**, 231 (1983).
14) K. Breddam and M. Ottesen, *Carlsberg Res. Commun.*, **49**, 473 (1984).
15) K. Breddam, F. Widmer, and J. T. Johansen, *Carlsberg Res. Commun.*, **45**, 237 (1980).
16) K. T. Douglas, Y. Nakagawa, and E. T. Kaiser, *J. Am. Chem. Soc.*, **98**, 8231 (1976).
17) S. Kunugi and M. Fukuda, 30th IUPAC Congress (Manchester), 5p—55, Sep. (1985).
18) H. Umetsu, M. Abe, Y. Sugawara, T. Nakai, S. Watanabe, and E. Ichishima, *Food Chem.*, **7**, 125 (1981).
19) M. Fukuda and S. Kunugi, *J. Biochem.*, **101**, 233 (1987).
20) S. Kunugi, K. Tanabe, K. Yamashita, and M. Fukuda, the preceeding paper to this.
21) M. Fukuda and S. Kunugi, *Eur. J. Biochem.*, **142**, 565 (1984).
22) M. Fukuda, S. Kunugi, and N. Ise, *Bull. Chem. Soc. Jpn.*, **56**, 3308 (1983).
23) M. Fukuda, H. Shima, and S. Kunugi, *J. Biochem.*, **98**, 517 (1985).
24) M. Fukuda and S. Kunugi, *Eur. J. Biochem.*, **147**, 657 (1985).
25) "The Merck Index," 10th ed., ed by M. Windholz, Merck & Co., Inc. (1983).
26) M. L. Bender, *J. Am. Chem. Soc.*, **86**, 3697 (1964).
27) J. Fastrez and A. Fersht, *Biochemistry*, **12**, 2025 (1973).
28) A. L. Fink and M. L. Bender, *Biochemistry*, **8**, 5109 (1969).

Solid Phase Synthesis of Oligodeoxyribonucleotides Utilizing the Phenylthio Group as a Phosphate Protecting Group

Jun-ichi MATSUZAKI, Kyoko KOHNO, Shin-ichiro TAHARA, Mitsuo SEKINE, and Tsujiaki HATA*
Department of Life Chemistry, Tokyo Institute of Technology, Nagatsuta, Midori-ku, Yokohama 227
(Received September 6, 1986)

Oligodeoxyribonucleotide synthesis utilizing the phenylthio group as a phosphate protecting group was applied to the solid phase method. The base residues of deoxyguanosine and deoxyadenosine were protected with bis(isobutyryloxy)ethylene (Bibe) and phthaloyl groups to avoid the base modification and depurination, respectively. A key synthetic intermediate of N^2-isobutyryl-N^1,N^2-bis(isobutyryloxy)ethylenedeoxyguanosine was prepared in high yield by four-step reaction from deoxyguanosine and used for preparation of the building blocks of deoxyguanosine required for the polymer support synthesis. Two kinds of polymer supports, i.e., 1% cross-linked polystyrene and controlled pore glass were chosen. The latter was employed for the synthesis of dodecadeoxyribonucleotides by using an automated DNA synthesizer.

In chemical synthesis of oligodeoxyribonucleotides, application of the phosphotriester[1] and phosphoramidite[2] methods to the solid phase synthesis has enabled us to prepare rapidly and practically DNA fragments of defined sequences.[3] Although the latter approach became accessible more successfully to molecular biologists, the former has recently been remarkably improved by introduction of new condensing agents and protecting groups.[4] Especially, we have also developed our own triester approach utilizing the phenylthio group as a phosphate protecting group.[5] In this paper, we wish to report application of our approach to the solid phase method.

Results and Discussion

Partially protected nucleosides (**1a—e**) were prepared by the literature method.[6,7] The amino goup of deoxyadenosine was protected with the benzoyl or phthaloyl group. Our recent study showed that the latter protecting group had considerable retarding effects on the depurination.[7]

Reese[8] and we[9] originally reported side reactions at the O^6-position of guanine residues when the remaining reactive site was not protected during condensations. To avoid such undesired reactions a number of new protecting groups have been proposed showing remarkable improvements.[10-15] In a previous paper,[12] we demonstrated the utility of the bis(isobutyryloxy)ethylene (Bibe) group as the so-called protected protecting group for the guanine base. This protecting group was readily removed under the same conditions as used for removal of the usual *N*-acyl protecting groups. However, the Bibe group has been introduced into the guanine residue only at the last stage of the synthesis of the deoxyguanosine monomer unit.[11] This is a drawback of the Bibe group although its introduction to the guanine base could be very easily performed by simple addition of glyoxal followed by acylation without coloration. Therefore, we searched for synthetic routes to N^2-isobutyryl-N^1,N^2-bis(isobutyryloxy)ethylenedeoxyguanosine (**1f**) which was a versatile synthetic intermediate for synthesis of

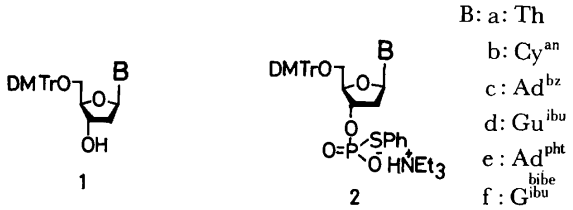

Fig. 1. Nucleoside and nucleotide units for the synthesis.

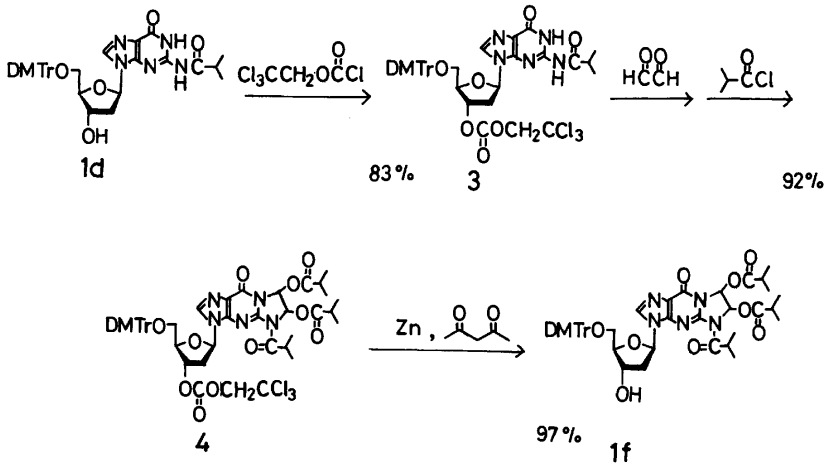

Fig. 2. Introduction of the bibe group into guanosine.

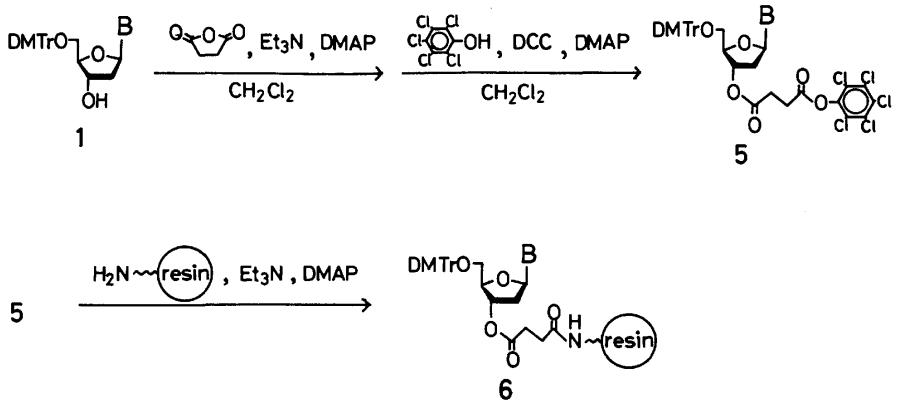

Fig. 3. Immobilization of the nucleosides onto resins.

appropriately protected deoxyguanosine derivatives (**5**, B=G^{ibu} and **2f**). For this purpose, the use of the transient protection procedure using trimethylsilyl chloride seemed to be difficult since the glyoxalation required a large excess of glyoxal which might work as a nucleophile toward the silyl group. Therefore, we chose a more stable protecting group as the 3′,5′-diol protecting group, i.e., the 2,2,2-trichloroethoxycarbonyl (TCECb)group.[7] As s hown in Fig. 2, deoxyguanosine was allowed to react with 2,2,2-trichloroethyl chloroformate and then the Bibe group was introduced to the guanine moiety. Finally, the fully protected nucleoside (**4**) was converted by treatment with zinc-acetylacetone to the desired compound (**1f**) in a 74% overall yield from **1d**.

Solid supports chosen in this study were controlled pore glass (CPG)[17] as an unswellable inorganic resin and 1% cross-linked polystyrene (P.S.)[18] as a swellable organic resin. The 3′-free nucleosides (**1**) were immobilized to the polymer supports according to the modified method of Itakura[19] (Fig. 3). Succinylation of **1** was performed by treatment with succinic anhydride in the presence of triethylamine and a catalytic amount of 4-dimethylaminopyridine (DMAP) in CH_2Cl_2 followed by esterification of the resulting carboxylic acid with pentachlorophenol by dicyclohexylcarbodiimide (DCC) and DMAP in CH_2Cl_2 after extraction. The activated nucleosides (**5**) were immobilized to the 3-aminopropyl group on the resin. The amounts of the nucleosides loaded on the supports were determined by spectroscopic estimation of DMTrOH released by the acid treatment and summarized in Table 2.

Oligomer Synthesis on Polystyrene. One % cross-linked polystyrene has been known to be one of suitable supports for the synthesis of oligonucleotides as reported by Itakura[18a] and Ohtsuka.[18b] We chose this support to prepare oligothymidylates by the use of the phenylthio group and bifunctional condensing reagents.[20] The phosphodiester (**2a**) of thymidylic acid was condensed to the thymidine resin (**6a**) by isodurenedisulfonyl chloride (DDS)[4a] and 3-nitro-1,2,4-triazole (NT)[21] for 1 h. For the detritylation, 1% trifluoroacetic acid (TFA) was used and the capping reaction was performed in the usual way. Reasonable results were obtained (Table 3) but not yet satisfactory. To realize a more smooth reaction on the swellable support, solvents capable of increasing the swellability in the reaction should be chosen. Therefore, dichloromethane was used in the condensation reaction and a few drops of pyridine was added to dissolve the catalyst, NT. A pentathymidylate was synthesized by using this solvent system under the same conditions as used in the above experiment but the reaction required 30 min. Better yields were obtained and the first coupling was optimized (Table 4). The capping reaction was performed by the use of acetic anhydride-triethylamine in dichloromethane in the presence of 0.1 M† DMAP for 5 min.

Table 1. Yields of the Activated Ester (**5**)

B	Succinylation/h	Esterification/h	Yield/%
Th	3	2	81
Cy^{an}	4	1	92
Ad^{bz}	4	1	87
Gu^{ibu}	4	2	96
Gu^{bibe}_{ibu}	4	2	88

Deprotection of the fully protected pentathymidylate was performed in two ways: A) 1) 0.1 M NaOH, pyridine-H_2O (1 : 1, v/v), 3 h 2) 80% AcOH, 15 min. B) 1) 2-pyridinecarbaldehyde oxime-tetramethylguanidine (TMG), pyridine-H_2O (9 : 1, v/v), 22 h 2) 80% AcOH, 15 min.

Isolation of the oligomer was performed by ion exchange HPLC (Partisil 10 SAX) and the yields of $T(Tp)_3T$ were 22 and 43% for methods A and B, respectively. These results would be ascribed to the swellability of the resin in the solvent used in the deprotection (step 1). Even in step 1 of method A, the resin was less swelled than in the condensation reaction where CH_2Cl_2 was used. After removal of the oligomer by filtration and washing with pyridine-H_2O (9 : 1, v/v),

† 1 M=1 mol dm^{-3}.

Table 2. Immoblization of Nucleosides on Resins

1% Cross linked polystyrene		Controlled pore glass (mesh 120/200)		
B	Nucleoside	B	Pore size	Nucleoside
	$\mu mol\ g^{-1}$		A	$mmol\ g^{-1}$
Th	100	Cy^{an}	171	118
Cy^{an}	83	Th	569	24
Ad^{bz}	109	Cy^{an}	569	32
Gu^{bibe}_{ibu}	108	Cy^{an}	547[a]	32
		Ad^{bz}	569	42
		Gu^{bibe}_{ibu}	569	27
		Cy^{an}	1489	24

a) Mesh 200/400 was used.

Table 3. Synthesis of Oligothymmidylate on Polystyrene in Pyridine

Condensation	7th	6th	5th	4th	3rd	2nd	1st
Yield/%	79	87	100	25	101	100	70
	43	53	60	86	77	91	73
	66	64	68	79	74	73	84
	80	83	86	84	94	97	66

Condensation: Tymidine P.S. (50 mg, 5 μmole), phosphodiester (T, 50 μmole), DDS (100 μmole), NT (200 μmole), pyridine (500 μl), r.t., 1 h. Capping: Acetic anhydride-pyridine (1:9, v/v, 1 ml), DMAP (0.1 mmole), r.t., 5 min.

Table 4. Synthesis of Oligothymidylate on Polystyrene in CH_2Cl_2

Condensation	4th	3rd	2nd	1st
Yield/%	91	91	89	92
	91	92	90	100

Condensation: Tymidine P.S. (50 mg, 5 μmole), phosphodiester (T, 50 μmole), DDS (100 μmole), NT (200 μmole), CH_2Cl_2-pyridine (50:3, v/v, 500 μl), r.t., 30 min. Capping; Acetic anhydride-triethylamine-CH_2Cl_2 (2:3:16, v/v/v, 1 ml), DMAP (0.1 mmole), r.t., 5 min.

TFA treatment of the resulting resin indicated that some amounts of oligomers remained in the cage of the resin. This phenomenon was not observed in the case of the CPG described below.

Oligomer Synthesis on the Glass Support. Controlled pore glass (CPG) has been reported as a suitable support for the synthesis of oligodeoxyribonucleotides in the phosphotriester[22] and the phosphoramidite[17] approaches. The thymidylic acid unit was condensed to deoxyribonucleosides on three kinds of CPG (Funakoshi) having the pore sizes of 170, 560, and 1500 A. The yields were essentially dependent on the pore size of resin and the reaction on 560 A CPG gave good results (Table 5). A similar result was obtained by Köster[17b] in his eary study on polymer supported synthesis. In this study, a rapid method for condensation reported by Effimov[23] was introduced to the present system by use of CPG. The sequence of dGpTpApC

Table 5. First Coupling Yields on CPGs

Pore size/A	Mesh	Coupling time/h	Yield/%
171	120—200	1	63
559	120—200	1	80
547	200—400	1	89
1489	120—200	1	11

Condensation: Cytidine CPG (100 mg, 3.2 μmole), phosphodiester (T, 32 μmole), DDS (64 μmole), NT (96 μmole), pyridine (320 μl), r.t., 1 h. Capping: The same conditions described as in Table 3.

was synthesized to search for a suitable condensation system. A phosphodiester (20 equiv), a condensing agent (20 equiv), and *N*-methylimidazole (MeIm) (30 equiv) were used in CH_3CN and the reaction was performed for 40 min. The bifunctional condensing reagent of DDS was not suitable because of its low solubilities compared with monofunctional reagents. A better result was obtained by using mesitylenesulfonyl chloride (MS) as the condensing reagent (Table 6). 2,4,6-Triisopropylbenzenesulfonyl chloride (TPS) gave relatively low yields. The yield, however, slightly increased with an increase of MeIm (100 equiv). Low viscosity of CH_3CN and rigidity of CPG were suitable for synthesis of oligomers by the use of a fully automated DNA synthesizer. To ascertain the coupling efficiency of the MS-MeIm system on CPG, we tried to prepare three kinds of fully protected sequences of dodecadeoxyribonucleotides involving $dT(pT)_{11}$ (**7**), dCpApTpTpApTpTpApApTpApC (**8**), and dGpTpApTpTpApApTpApApTpG (**9**). The latter two sequences were corresponding to a DNA analog of the 5′-terminus of brome mosaic virus (BMV) mRNA No. 4 filament[24] and its complementary sequence (Fig. 4), respectively. In the case of **8**, both the stepwise condensation and the block condensation were tried. The elongation program of DNA synthesizer (SAM 1, Biosearch) is presented in Table 7 and the yields of the condensation reactions are summarized in Fig 5. Among the fully protected dodecadeoxyribonucleotides synthesized on CPG, the protected dodecamers **8b** and **9** were deprotected according to the following conditions: 1) 0.1 M NaOH, pyridine-H_2O

Table 6. Synthesis of dGTAC on CPG

Condensing reagent	Azole	Coupling time	Yield/%			
equiv	equiv	min	1st	2nd	3rd	Average
DDS (20)	NT (30)	60	85	68	76	44
MS (20)	MeIm (30)	30	70	96	98	88
TPS (20)	MeIm (30)	30	80	86	83	83
TPS (20)	MeIm	30	82	91	88	87

Condensation: Cytidine CPG (100 mg, 3.2 μmole), phosphodiester (32 μmole), condensing reagent (64 μmole), azole (96 mg, 320 μmole), CH_3CN (320 μl), r.t., 30 h. Capping: The same conditions described as in Table 4.

Table 7. Elongation Cycle of the Automated Synthesizer

Function	Reagent or/and solvent	Time
Wash	CH_2Cl_2	2:00
Deblock	1% TFA-CH_2Cl_2	1:30
Wash	CH_2Cl_2	3:00
Wash	CH_3CN	2:00
Wash	dry CH_3CN	2:00
Coupling	phosphodiester (10 eequiv)	
	MS (93 equiv)	
	MeIm (450 equiv)	40:00
Wash	CH_3CN	2:00
Capping	Ac_2O/DMAP/pyridine/THF	5:00
Wash	CH_3CN	3:00

m^7GpppGpUpApUpUpApApUpApApUpGp------ BMV mRNA No. 4

$5'$GPTPAPTPTPAPAPTPAPAPTPG$^{3'}$

$3'$CPAPTPAPAPTPTPAPTPTPAPC$_5$'

Fig. 4. DNA analogue of 5′-teminus of BMV mRNA No.4 and its complementary sequence.

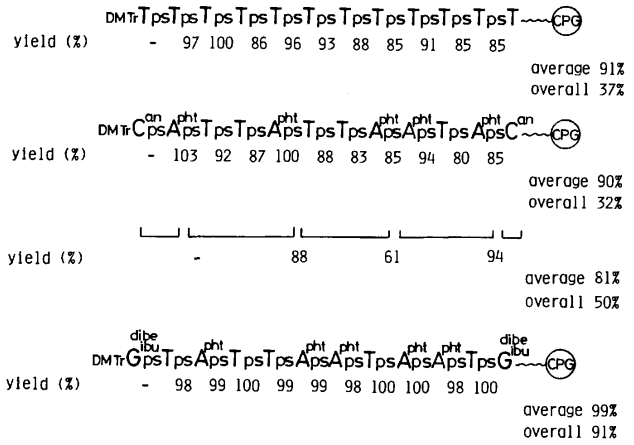

Fig. 5. Results of the automated synthesis of dodecamers.

(1 : 1, v/v), 0 °C, 1 h, 2) concd NH_4OH, r.t. for 30 h, 50 °C for 1 h, 3) 80% AcOH, r.t., 15 min.

Isolation of the unprotected oligomer **8b** and **9** was performed by reversed phase HPLC (μBondapak C_{18}) in the usual manner. A typical example is shown in Fig. 6a. This standard separation procedure gave finally the pure 12 mers **8b** and **9** in 18 and 4% yields. An alternative procedure for isolation of the 12 mer **9**

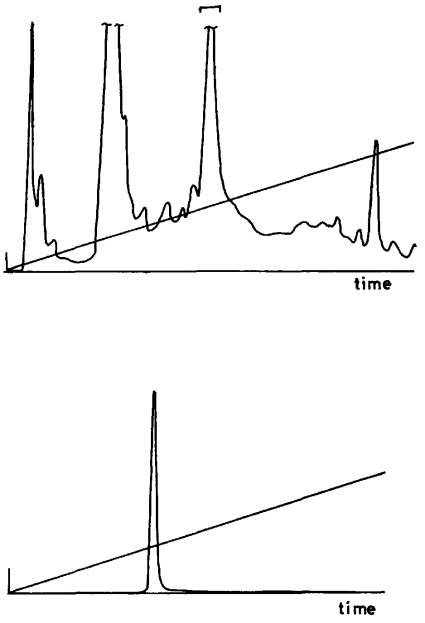

Fig. 6a. Chromatograms of dGTATTAATAATG on μBondapak C_{18}. Upper: After ammonia treatment, lower: Finally purified product.

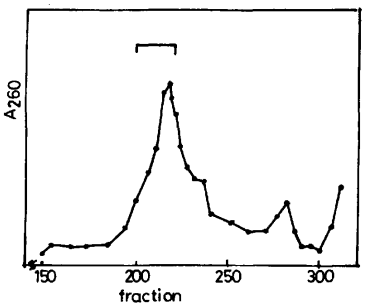

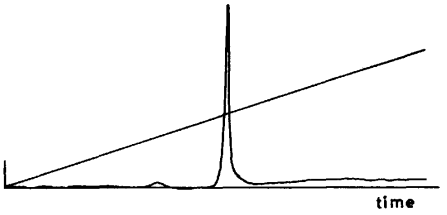

Fig. 6b. Chromatograms of dGTATTAATAATG on Sephadex G50 column (upper) and purified product on μBondapak C_{18} (lower).

was also conducted by using gel permeation column chromatography (Sephadex G 50). This gave an improved yield (12%) of the 12 mer. The separation profiles of the 12 mer are shown in Fig. 6b. The oligomers obtained were characterized by polyacrylamide gel electrophoresis (PAGE) and a modified Maxam-Gilbert sequencing method.[25]

Experimental

General Remarks. ^{1}H NMR spectra were recorded at 100 MHz on a JNM-PS-100 spectrometer using ppm according to tetramethylsilane as an internal reference. UV spectra were obtained on a Hitachi 124 spectrophotometer. Column chromatography was performed with silica gel C-200 purchased from Wako Co., Ltd. Thin-layer chromatography was performed on precoated TLC plates, silica gel 60 F-254 (Merck). Reagent grade pyridine was distilled twice from *p*-toluenesulfonyl chloride and CaH_2 and then stored over molecular sieves 4A. Dichloromethane was dried over phosphorus pentoxide overnight, decanted, distilled from potassium carbonate and then stored over molecular sieves 4A. Acetonitrile was distilled from calcium hydride and stored over molecular sieves 4A. 3-Aminopropyl polystyrene (1% cross linked) was purchased from Peptide Laboratory and aminopropyl CPGs from Electro Nucleonics Inc.. Deoxynucleosides were purchased from Yoshitomi-Seiyaku Co., and properly protected according to the literature.[4,5] The phosphodiester units were prepared according to our previous paper.[4] Ion-exchange HPLC was performed on a Partisil 10 SAX (Whatman) column using a linear gradient of 0.05 M KH_2PO_4 (pH 6.4), 20% CH_3CN to 0.5 M KH_2PO_4 (pH 6.5), 20% CH_3CN for 32 min at a flow rate of 1.5 ml ml^{-1}. Reversed phase HPLC was performed on a μBondapak C_{18} (Waters) using a liner gradient of 0.1 M NH_4OAc to 40% CH_3CN in the same buffer for 40 min at a flow rate of 2 ml at 50 °C. Elemental analysis was performed by the Microanalytical Laboratory, Tokyo Institute of Technology, at Nagatsuta.

5′-*O*-(4,4′-Dimethoxytrityl)-3′-*O*-(2,2,2-trichloroethoxycarbonyl)-N^2-isobutyryldeoxyguanosine (3). 5′-*O*-(4,4′-Dimethoxytrityl)-N^2-isobutyryldeoxyguanosine (3.2 g, 2 mmol) was rendered anhydrous by repeated coevaporation with dry pyridine and dissolved in dry pyridine (30 ml). 2,2,2-Trichloroethyl chloroformate (865 µl, 6 mmol) was added dropwise and the solution was stirred at room temperature for 2 h. Then the mixture was transferred into a separatory funnel with $CHCl_3$ and washed twice with 5% $NaHCO_3$. The aqueous layers were back-extracted with $CHCl_3$ and the combined organic layers were dried over Na_2SO_4. The solvent was removed under reduced pressure and the last traces of pyridine were coevaporated with toluene. The resulting foam was applied to a column of silica gel and eluted with CH_2Cl_2 containing methanol (0—1%, v/v) to give the title compound (3.24 g, 83%); mp 135 °C (decomp); ^{1}H NMR ($CDCl_3$) δ=0.98 (m, 12 H, $CH(CH_3)_2$), 2.69 (m, 2H, 2′H), 3.42 (m, 4H, 5′H, and $CH(CH_3)_2$), 3.80 (s, 6H, CH_3), 4.35 (m, 1H, 4′H), 4.79 (s, 2H, CH_2CCl_3), 5.58 (m, 1H, 3′H), 6.24 (m, 1H, 1′H), 6.82 (m, 4H, DMTr), 7.22—7.56 (m, 9H, ArH), 7.84 (s, 1H, 8).

Found: C, 55.62; H, 4.88; N, 8.33%. Calcd for $C_{38}H_{38}N_5O_9Cl_3$: C, 55.99; H, 4.70; N, 8.59%.

5′-*O*-(4,4′-Dimethoxytrityl)-N^2-isobutyryl-N^1,N^2-bis(isobutyryloxy)ethylenedoxyguanosine (4). Introduction of the Bibe group to **3** was performed according to our previous paper[6] in 92% yield. The fully protected guanosine derivative (2.2 g, 2 mmol) was coevaporated with dry pyridine (3×3 ml) and dissolved in dry pyridine (30 ml). To the solution, activated zinc powder (2.6 g, 40 mmol) and acetylacetone (4.1 ml, 40 mmol) was added and the suspension was stirred at room temperature. After 1 h, the solid material was filtered off and washed with pyridine. The filtrate and the washings were concentrated to one half the volume, transferred into a separatory funnel with $CHCl_3$, and washed three times with phosphate buffer (pH 6.0). The aqueous layers were back-extracted with $CHCl_3$ and the organic layer was washed with water. The organic layers were combined and dried over Na_2SO_4 and the solvent was removed under reduced pressure. Silica-gel column chromatography gave the desired compound in 97% yield (1.6 g); mp 123 °C (decomp); ^{1}H NMR ($CDCl_3$) δ=1.20 (m, 18H, $CH(CH_3)_2$), 2.60 (m, 5H, 2′H, and $CH(CH_3)_2$), 3.43 (m, 2H, 5′H), 3.82 (s, 6H, CH_3O), 4.18 (m, 1H, 4′H), 4.61 (m, 1H, 3′H), 6.32 (t, J=6 Hz, 1H, 1′H), 6.86 (m, 5H, 2,6-ArH of DMTr and one of OCH-CHO), 7.23—7.38 (m, 10H, ArH and one of OCH-CHO), 7.88 (s, 1H, 8H).

Found: C, 64.75; H, 6.54; N, 7.75%. Calcd for $C_{45}H_{51}N_5O_{11}$: C, 64.50; H, 6.14; N, 8.36%.

Pentachlorophenyl Nucleoside-3′-*O*-succinate (5). Typical procedure: 5′-*O*-DMTr-N^4-anisoyldeoxycytidine (680 mg, 1 mmol) was coevaporated with dry pyridine several times and dissolved in dry dichloromethane (10 ml). To the solution were added succinic anhydride (120 mg, 1.2 mmol), DMAP (12 mg, 0.1 mmol), and triethylamine (168 µl, 1.2 mmol). The reaction was performed at room temperature for 4 h. Then the mixture was transferred into a separatory funnel with dichloromethane (50 ml), and washed with an aqueous solution of citric acid (0.9%, 50 ml×2). The aqueous layers were back-extracted with CH_2Cl_2 (50 ml) and the organic layer was washed with water. These organic layers were combined and dried over Na_2SO_4. The solvent was removed under reduced pressure and pentachlorophenol (300 mg, 1.1 mmol) was added to the resulting foam. The mixture was rendered anhydrous by repeated coevaporation with dry pyridine and dissolved with dry CH_2Cl_2 (10 ml). DMAP (12 mg, 0.1 mmol) and DCC (310 mg, 1.5 mmol) were added to the solution and the mixture was stirred at room temperature for 1 h. Then the solid material was removed by filtration and washed with benzene. The filtrate and the washings were mixed and the solvent was removed under reduced pressure. Benzene (5 ml) was added and the resulting solid was filtered and washed with benzene (3 ml×3). The same procedure for removal of *N*,*N*′-dicyclohexylurea (evaporation, addition of benzene and filtration) was repeated one more time. The final filtrate and washings were evaporated and dissolved in CH_2Cl_2 (2 ml) and dropped into hexane–ether (7 : 1, v/v, 300 ml) with continuous stirring. The white precipitate was collected by filtration and dried in a desiccator (946 mg, 92%). This compound was characterized by comparison of its NMR spectrum with that of an authentic material.

Immobilization of Deoxyribonucleosides on Resins. General Procedure: A 3-aminopropyl resin (1 g) was rendered anhydrous by coevaporation with dry pyridine. An activated nucleoside (**5**) (0.1 mmol) and DMAP (0.01 mmol) dissolved in dry CH_2Cl_2 (10 ml) were added to the resin. Triethylamine (0.1 mmol) was added dropwise to the mix-

ture and the resulting suspension was slowly rotated for 1 h by the use of an evaporator. The resin was filtered and washed with CH_2Cl_2 and the unreacted amino group was blocked by the acetyl group by the reaction with acetic anhydride and DMAP in dry pyridine for 1 h. Finally, the nucleoside resin was obtained by filtration, washing with pyridine and CH_2Cl_2, and drying in vacuo. The loading amounts of nucleosides on the resin are listed in the text.

Synthesis of Oligomers on Resins. In the mannual preparation, the synthetic reactions were most conveniently carried out in a glass column with a sintered glass filter and a two way value which end was connected with a collection tube. During the drying step, the top of the column was joined to a vacuum pump and rotated by a rotary evaporator.

A reaction cycle consisted of the following steps: 1) A nucleoside resin in the column was treated with 1% TFA for 30 seconds repeatedly until the color of DMTr cation had disappeared, and the resin was washed with $CHCl_3$ (3 ml) three times. 2) The resin was rendered anhydrous by coevaporation with dry pyridine and mixed with a phosphodiester previously dried by coevaporation with dry pyridine. A condensing reagent was added to the mixture and the final concentration of the phosphodiester was about 0.1 M. The reaction was performed at room temperature with gentle rotation in the case of the CPG or with standing in the case of the polystyrene. 3) After the condensing reaction, all soluble reagents were washed out with pyridine several times, and the remaining 5′-hydroxyl group was blocked by the usual capping reaction, 4) The resin was washed with pyridine and then with $CHCl_3$ several times. Return to step 1, for the next cycle.

In the case of using the automated synthesizer, the resin was packed in a mini column and the reactions were carried out by continuous flow by a solvent pump. All reagents and solvents were delivered from reagent bottles being confirmed with the cycle program listed in the Table 7.

Yields of the condensing reactions were determined by estimation of released DMTr cation with a value of ε_{498}= 71700 (60% $HClO_4$: EtOH=3 : 2, v/v).

Deprotection of Oligomers by NaOH Method. The synthetic oligomer immobilized to a resin was treated with 0.1 M NaOH in pyridine-water (1 : 1, v/v) at room temperature for 1 h. The heterogeneous reaction mixture was applied to a mini column of Dowex 50 W×2 (pyridinium form, 1.5 ml of wet volume) and eluted with pyridine-water (1 : 1, v/v, 10 ml). All the eluent was collected and concentrated in vacuo and treated with concd aqueous ammonia at room temperature for 30 h and then at 50 °C for 1 h. The solution was carefully evaporated under reduced pressure, and in the case of the purification procedure by reversed phase HPLC, the resulting mixture was chromatographed on a μBondapak C_{18} (Waters) column and the desired fraction was collected and lyophilized to the solid. Then 5′ DMTr group was removed by treatment with 80% acetic acid for 15 min and concentrated by evaporation in vacuo. The oligomer was finally purified by rechromatography on a reversed phase HPLC column or by gel filtration chromatography with Shephadex G50 (2×150 cm, 0.05 M HCO_3^-). Purities of the oligomers obtained were analyzed by the HPLC or polyacrylamide gel electrophoresis (UV illumination) and the sequences were determined by the modified Maxam-Gilbert method.[15]

We thank Dr. Akiko Kume, Mr. Yasuo Ohta, Mr. Hitoshi Hotoda for their technical assistance and also thank Mrs. Chieko Sugimura for preparation of this manuscript. This work was supported by a Grant-in-Aid from the Ministry of Education, Science and Culture.

References

1) V. Amarnath and A. D. Broom, *Chem. Rev.*, **77**, 183 (1977); C. B. Reese, *Tetrahedron*, **34**, 3143 (1978); S. A. Narang, *ibid.*, **39**, 3 (1983).

2) M. D. Matteucci and M. H. Caruthers, *J. Am. Chem. Soc.*, **103**, 3185 (1981); S. L. Beaucage and M. H. Caruthers, *Tetrahedron Lett.*, **22**, 1859 (1981).

3) "Oligonucleotide Synthesis," ed by M. J. Gait, IRL Press, Oxford (1984).

4) T. Hata and J. Matsuzaki, *Yuki Gosei Kagaku Kyokai Shi*, **42**, 429 (1984).

5) M. Sekine and T. Hata, *Yuki Gosei Kagaku Kyokai Shi*, **44**, 229 (1986).

6) G. S. Ti, B. L. Gaffney, and R. A. Jones, *J. Am. Chem. Soc.*, **104**, 1316 (1982).

7) a) A. Kume, M. Sekine, and T. Hata, *Tetrahedron Lett.*, **23**, 4365 (1982); b) A. Kume, R. Iwase, M. Sekine, and T. Hata, *Nucleic Acids Res.*, **12**, 8525 (1984).

8) P. K. Bridson, W. Markiewicz, and C. B. Reese, *Chem. Commun.*, **1977**, 447; **1977**, 791; C. B. Reese and A. Ubasawa, *Nucleic Acids Res., Symp. Ser.*, **7**, 5 (1980).

9) P. H. Daskalov, M. Sekine, and T. Hata, *Tetrahedron Lett.*, **21**, 3899 (1980); *Bull. Chem. Soc. Jpn.*, **54**, 3076 (1981)

10) S. S. Jones, C. B. Reese, S. Sibanda, and A. Ubasawa, *Tetrahedron Lett.*, **22**, 4755 (1981).

11) B. L. Gaffney and R. A. Jones, *Tetrahedron Lett.*, **23**, 2257 (1982).

12) M. Sekine, J. Matsuzaki, and T. Hata, *Tetrahedron Lett.*, **23**, 5287 (1982).

13) T. Trichtinger, R. Charubala, and W. Pfleiderer, *Tetrahedron Lett.*, **24**, 711 (1983).

14) B. L. Gaffney, L. A. Marky, and R. A. Jones, *Tetrahedtron*, **40**, 3, (1984).

15) C. B. Reese and P. A. Skone, *J. Chem. Soc., Perkin Trans. 1*, **1984**, 1263.

16) T. B. Windholz and D. B. R. Johnston, *Tetrahedron Lett.*, 2555 (1967); R. W. Adamiak, E. B. K. Grezeskowiak, R. Kierzek, A. Kraszewski, W. T. Markiewica, J. Stawinski, and M. Wiewiorowski, *Nucleic Acids Res.*, **4**, 2321 (1977).

17) a) G. R. Gough, M. J. Brunden, and P. T. Gilham, *Tetrahedron Lett.*, **22**, 4177 (1981); b) H. Köster, A. Stump, and A. Wolter, *ibid.*, **24**, 747 (1983); c) S. P. Adams, K. S. Kavka, E. J. Wykes, S. B. Holder, and G. R. Gallupi, *J. Am. Chem. Soc.*, **105**, 661 (1983).

18) a) H. Ito, Y. Ike, S. Ikuta, and K. Itakura, *Nucleic Acids Res.*, **10**, 1755 (1982); b) M. Ikehara, E. Ohtsuka, T. Tokunaga, Y. Taniyama, S. Iwai, K. Kitano, S. Miyamoto, T. Ohgi, Y. Sakuragawa, K. Fujiyama, T. Ikari, M. Kobayashi, T. Miyake, S. Shibahara, A. Ono, T. Ueda, T. Tanaka, H. Baba, T. Miki, A. Sakurai, T. Oishi, O. Chisaka, and K. Matsubara, *Proc. Natl. Acad. Sci. U.S.A*, **81**, 5956 (1984).

19) K. Miyoshi, T. Miyake, T. Hozumi, and K. Itakura, *Nucleic Acids Res.*, **8**, 5473 (1980); K. Miyoshi, T. Huang, and K. Itakura, *ibid.*, **8**, 5491 (1980).

20) M. Sekine, J. Matsuzaki, and T. Hata, *Tetrahedron Lett.*, **22**, 3209 (1981); *Tetrahedron*, **41**, 5279 (1985).
21) C. B. Reese, R. C. Titmas, and L. Yau, *Tetrahedron Lett.*, **1978**, 2727.
22) B. S. Sproat and W. Bannwarth, *Tetrahedron Lett.*, **24**, 5771 (1983); V. A. Effimov, A. A. Buryakova, S. V. Reverdatto, O. G. Chakhmakhcheva, and Yu. A. Ovchinnikov, *Nucleic Acids Res.*, **11**, 8369 (1983); H. Köster, J. Biernat, J. McManus, A. Wolter, A. Stumps, C. K. Narang, and N. D. Shinha, *Tetrahedron*, **40**, 103 (1984).
23) V. A. Effimov, S. V. Reverdatto, and O. G. Chakhmakhcheva, *Tetrahedron Lett.*, **23**, 961 (1982); *Idem.*, *Nucleic Acids Res.*, **10**, 6675 (1982).
24) D. Dasguta, D. S. Shin, C. Saris, and P. Kaesberg, *Nature*, **256**, 624 (1975).
25) A. N. Banaszuk, K. V. Deugan, D. J. Sherwood, M. Michalak, and B. Glick, *Anal. Biochem.*, **128**, 281 (1983).

 © 1987 The Chemical Society of Japan Bull. Chem. Soc. Jpn., 60, 1415—1428 (1987)

Autoxidation of Guaiazulene and 4,6,8-Trimethylazulene in Polar Aprotic Solvent: Structural Proof for Products[1)]

Yoshiharu MATSUBARA,* Shin-ichi TAKEKUMA, Katsumi YOKOI, Hiroshi YAMAMOTO,*,† and Tetsuo NOZOE*,††

Department of Applied Chemistry, Faculty of Science and Technology, Kinki University, Kowakae, Higashi-Osaka 577

†Department of Chemistry, Okayama University, Okayama 700

††Tokyo Research Laboratories, Takasago Corporation, 5-36-31 Kamata, Ohta-ku, Tokyo 144

(Received September 16, 1986)

Autoxidation of guaiazulene and 4,6,8-trimethylazulene at 100—120 °C in DMF (or HMPA) respectively yielded 25 and 17 separable products, including several known compounds. Most of these new compounds were derivatives of 1,5- and 1,7-azulenequinone, 1*H*-inden-1-one, naphthoquinone, and benzenoid, or dimeric and trimeric forms; structures of these products were established on the basis of spectroscopic (NMR, UV, IR, and MS) and half-wave potential ($E_{1/2}$) data. ^{1}H NMR (200-MHz) parameters of various azulene derivatives are given for comparative study. Possible reaction pathways are suggested for the formation of such a wide variety of interesting products.

Azulene and its derivatives constitute a highly interesting class of compounds due to the fused five-seven bicyclic aromatic ring system. Thus azulenes have been regarded as one of the representative examples of nonbenzenoid aromatic hydrocarbons, which usually do not undergo Diels-Alder-type addition reactions but are easily susceptible to many electrophilic substitution reactions (most easily at the 1 and/or 3 position).[2)]

It has been long-known that some azulenes gradually suffer oxidation even on exposure to air at room temperature and this air oxidation is facilitated by light. Pailer and Lobenwein[3)] have found that, when adsorbed on the surface of silic gel and exposed to air, naturally originating guaiazulene (**1**) gave three major products: 3,3′-biguaiazulene (**1B**, see below) and two guaiazulenylindenones for which the 5*H*-inden-5-one structures (**4**, **5**) were presented. Precise studies on the facile autoxidation of azulenes (especially **1**) are exceedingly of interest in view of preparation of a number of pharmacologically important azulenes because of the fact that a clinically used anti-inflammatory sodium guaiazulene-3-sulfonate (**3**), for example, gradually decomposes on standing but is stabilized by the presence of oxygen-absorbers in the tablet package.[4)] Moreover, information on a general aspect of the reaction mechanism of oxidation of azulenes would be important in exploiting an expedient conversion of azulenes directly to many valuable compounds such as polyazulenes[5)] and azulenequinones,[6)] syntheses of which are currently drawing an increasing interest because of the potential utility of their physicochemical properties as well as biological activity. In this paper, by employing two trialkylazulenes [**1** and 4,6,8-trimethylazulene[7)] (**2**)] as model compounds, we wish to describe the first detailed study on autoxidation of azulenes, together with presumable reaction pathways for the formation of a wide variety of the products, most of which possess highly interesting structures.

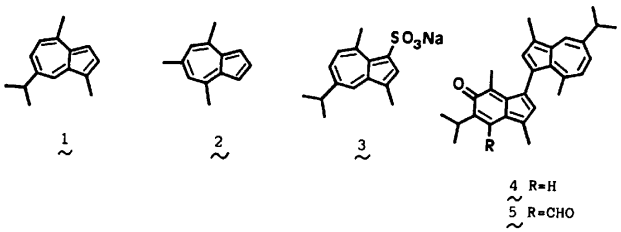

Results and Discussion

Autoxidation of Guaiazulene (1). The oxidation was carried out by passing finely bubbling oxygen into a solution of the substrate **1** in DMF (or HMPA) at 100 °C. When the reaction was monitored by the use of silica-gel TLC and the reversed phase high-pressured liquid chromatography (HPLC), simultaneous formation of more than twenty kinds of products was observed over a period of 24 h (see Fig. 1). In order to examine an earlier stage of the oxidation, the reaction products were separated into each component by using chromatography, when about a half of the starting material was consumed. The products thus obtained as pure components (25 altogether besides the recovered starting material **1**) are referred to as Compounds **1A—S** according to their decreasing R_f values on silica-gel TLC (developed with 15 : 85 AcOEt–hexane); when more than two products are separated from the same fraction by using a different kind of solvent system, they are further distinguished by a subscript number (see Fig. 1).

In Chart I are summarized structures of these products which were established by UV-visible, IR, high-resolution mass (MS), and ^{1}H NMR (and ^{13}C NMR for some compounds) spectroscopy as will be explained below. The theoretical yields of these isolated products (see Experimental Section) totaled to 54%; besides these, there still remained ca. 34% (w/w) yield of unidentified resinous polar products of rather high molecular weights.

Compound $\mathbf{1A}_1$ was the unreacted starting material **1** from the spectroscopic and chromatographic data.

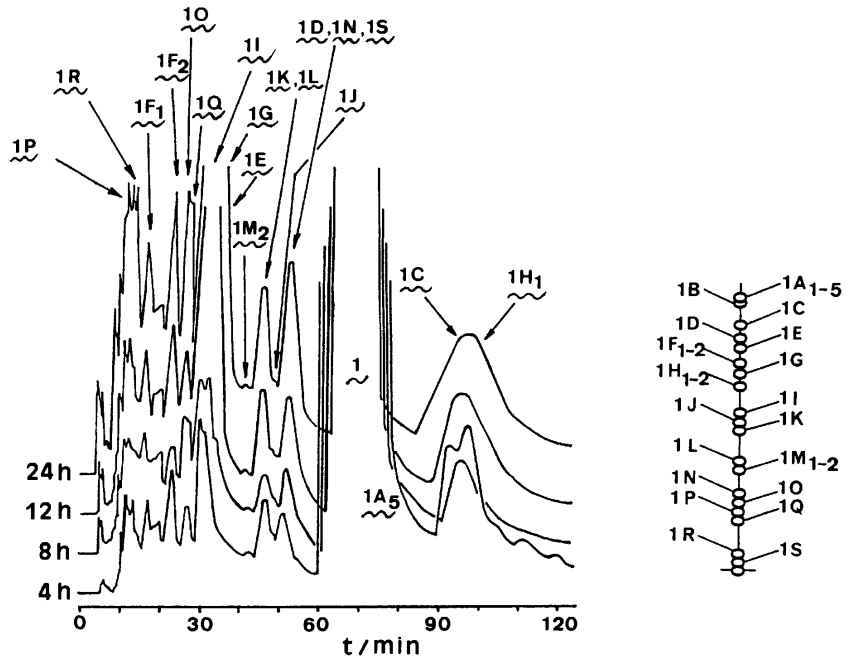

Fig. 1. Time-dependent HPLC diagram of autoxidation of **1** in DMF at 100 °C and TLC diagram of the oxidation products from **1**.

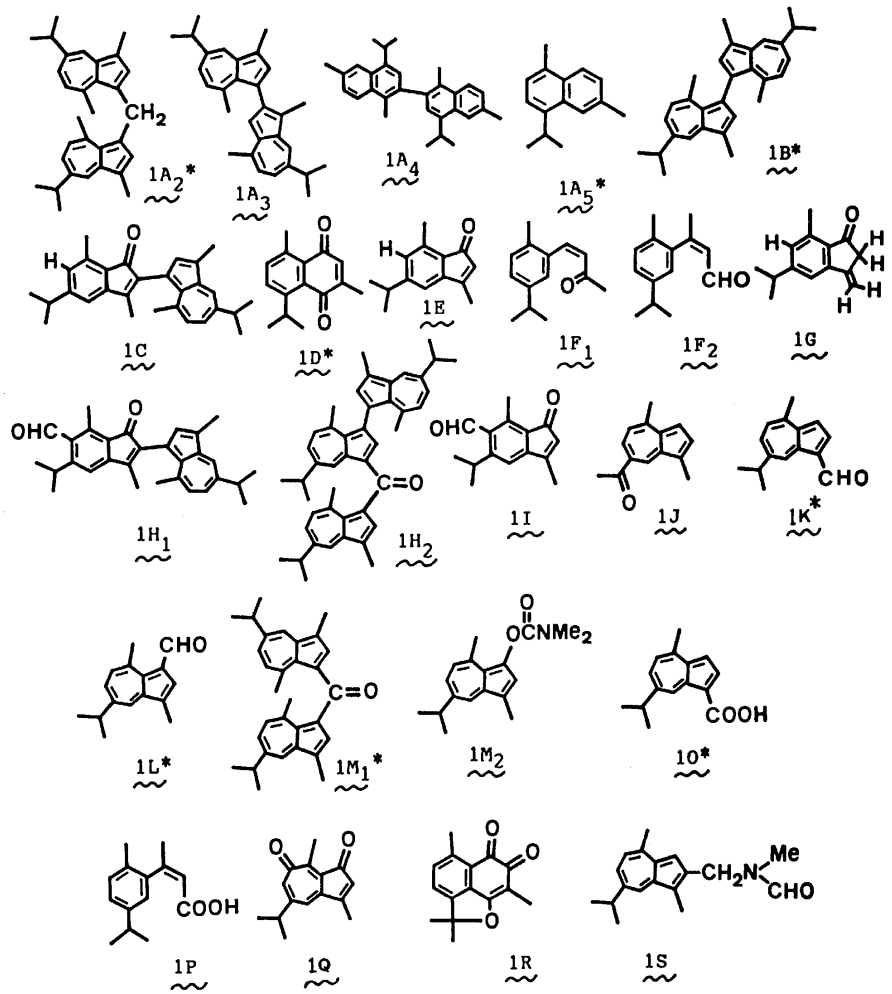

Chart 1. Structures of autoxidation products of guaiazulene (**1**); *Previously known compounds.

Table 1. ^{1}H NMR (200 MHz) Parameters for Azulene Derivatives[a]

Compd	H-1 (H-1′)	H-2 (H-2′)	H-3 (H-3′)	Me-4 (Me-4′)	H-5 (H-5′)	H-6 (H-6′)	H-7 (H-7′)	H-8 (H-8′)	J (J)
1	2.66[b]	7.61	7.21	2.83	7.00	7.41	1.36, 3.08[c]	8.19	d, e, f)
1A$_2$	2.52[b]	7.10	5.21[g]	2.93	6.78	7.24	1.34, 3.01[c]	8.05	e, f)
1A$_3$	2.35[b]	—	7.35	2.81	7.04	7.36	1.38, 3.08[c]	8.20	e, f)
	(2.70)[b]	(7.56)	—	(2.48)	(6.89)	(7.35)	(1.38, 3.10)[c]	(8.18)	(e, f)
1B	2.68[b]	7.46	—	2.18	6.78	7.29	1.39, 3.07[c]	8.18	e, f)
1J	2.74[b]	7.66	7.50	2.87	7.04	8.18	2.74[h]	8.98	d, e, f)
1K	10.32[i]	8.17	7.26	2.93	7.49	7.72	1.41, 3.24[c]	9.72	d, e, f)
1L[j]	2.56[b]	8.19	10.56[i]	3.13	7.38	7.55	1.38, 3.15[c]	8.25	e, f)
1M$_1$[j]	2.56[b]	7.73	—	2.92	7.29	7.56	1.39, 3.14[c]	8.28	e, f)
1M$_2$[j]	2.60[d]	7.35	k)	2.82	6.70	7.21	1.32, 2.98[c]	8.03	e, f)
1O	1.59[l]	8.39	7.25	2.94	7.45	7.70	1.42, 3.25[c]	9.81	d, e, f)
1Q[j]	2.29[b]	6.23	—	2.64	—	6.76	1.26, 2.76[c]	6.63	f, m, n)
1S	2.55[b]	o)	7.38	2.88	6.86	7.29	1.32, 3.02[c]	8.05	e, f)
2	7.34	7.64	7.34	2.88	7.05	2.62[b]	7.05	2.88[b]	d)
2A$_2$	5.16[g]	7.14	7.03	2.77	6.83	2.52[b]	6.80	2.93[b]	d, p)
2F	7.50	7.92	7.50	3.02	7.64	10.06[i]	7.64	3.02[b]	d)
2G	6.67[q]	7.27	7.22	2.82	6.91	2.55[b]	6.97	2.95[b]	d, p)
2I	—	6.38	8.06	2.33	7.09	2.27[b]	—	2.65[b]	d, r)
2J	—	6.25	7.94	2.31	—	2.24[b]	7.04	2.60[b]	d)
2K$_1$	10.64[i]	8.28	7.30	2.92	7.38	2.68[b]	7.40	3.18[b]	d, p)
2K$_3$	—	7.96	7.16	2.90	7.38	2.71[b]	7.47	3.18[b]	d, p)
2L	s)	7.13	7.09	2.74	6.72	2.52[b]	6.77	2.94[b]	d, p)
2M (a)	7.29	t)	7.45	2.84	7.00	2.60[b]	7.00	2.96[b]	
2M (b)	7.31	t)	7.49	2.84	7.02	2.59[b]	7.02	2.95[b]	

a) Chemical shifts (δ) are parts per million from Me_4Si measured in $CDCl_3$ (concn <ca. 0.5% v/v). Coupling constants (J, Hz) were confirmed by double resonance. b) Me. c) *i*-Pr; J=7.0 Hz. d) $J_{2,3}$=4.0 Hz. e) $J_{5,6}$=11.0 Hz. f) $J_{6,8}$=2.0 Hz. g) CH_2. h) Ac. i) CHO. j) For the purpose of comparison, the numbering of this compound corresponds to that of the starting material. k) δ 3.05 and 3.17 (both 3H, s, Me_2NCOO-3). l) COOH. m) $J_{2,8}$=0.5 Hz. n) $J_{Me(1),2}$=1.5 Hz. o) There exist a set of three singlets (3:2:1) due to (-CH_2NMeCHO) at (**a**) δ 2.82, 5.00 and 8.13, (**b**) δ 2.72, 5.11 and 8.13, **a** and **b** being a 3:2 mixture due to restricted rotation of the C-N bond in the amide group; a large number of similar patterns are observed for many amide, e.g., see A. Mannschreck, *Tetrahedron Lett.* **1965**, 1341. p) $J_{5,7}$= 0.5 Hz. q) OHCCH-1; also present is a doublet at δ 10.06 (1H, J=2.3 Hz, CHO). r) $J_{5,Me(6)}$=1.5 Hz. s) There singlets (3:2:1) due to (-CH_2NMeCHO) at δ 3.08, 5.25, and 8.23. t) A set of there singlets (3:2:1) due to (-CH_2NMeCHO) at (**a**) δ 2.88, 5.07, and 8.21, (**b**) 2.77, 5.16 and 8.21, **a** and **b** being a 3:2 mixture; see Ref. in o).

For the purpose of comparison in determining the structures of the oxidation products, the 200-MHz ^{1}H NMR parameters for **1** and other important azulene derivatives obtained in the present study are summarized in Table 1, although slightly different values have been reported for a few of these azulenes (mostly measured at 60-MHz in much concentrated CCl_4 or CH_2Cl_2 solutions).[3,8] Compound **1A$_2$**, one of the major products of this oxidation, was spectroscopically (MS and ^{1}H NMR) identical with known 3,3′-methylenebisguaiazulene.[9] While the chemical shifts of other signals of **1A$_2$** closely resembled those of **1**, an appreciable upfield shift (δ ca. 0.5) was observed for the H-2 signal (see Table 1) presumably due to an electronic as well as an anisotropic effect by a nonplanar conformation of the two azulene nuclei owing to the steric repulsion.

Compound **1A$_3$** was shown to have a composition of $C_{30}H_{34}$ by MS and the structure of 2,3′-biguaiazulene was assigned to this minor product by the careful comparison of the ^{1}H NMR spectral data (see Table 1), as well as their melting points, with those of the reported 2,2′- and 3,3′-biguaiazulenes.[10] Compound **1B** was confirmed by spectroscopy to be identical with 3,3′-biguaiazulene;[3,10] an appreciable upfield shift (δ ca. 0.65) for Me-4 signal in the ^{1}H NMR spectrum (see Table 1) by the same reason as described for **1A$_2$** should be noticed.

Compounds **1A$_5$** ($C_{15}H_{18}$) and **1A$_4$** ($C_{30}H_{34}$ by MS) were shown spectroscopically to be 4-isopropyl-1,6-dimethylnaphthalene (cadalene) and its 2,2′-dehydro dimer, respectively. The assignment of the oxidative coupling position of the new naphthalene dimer **1A$_4$** was based on the ^{1}H NMR data (see the Experimental Section). Compounds **1D** and **1R** were identified by MS, IR, UV, and NMR spectroscopy to be 8-isopropyl-2,5-dimethyl-1,4-naphthoquinone[11] and the 1,2-naphthoquinone derivative,[11b] respectively, both of which had been obtained by autoxidation of **1A$_5$** under the same conditions.[11b]

Compound **1C** ($C_{29}H_{32}O$) and **1H$_1$** ($C_{30}H_{32}O_2$ by MS) appeared to be identical (by ^{1}H NMR) with the autoxidation products which had been obtained[3] from **1** by autoxidation on the surface of silica gel and respectively assigned to be the 3-guaiazulenyl-5*H*-inden-5-one derivatives **4** and **5**. The 1*H*-inden-1-one structures **1C** and **1H$_1$**, however, were apparently more compatible with the observed spectral data, taking into account the spectral parameters for the related 1*H*-inden-1-one derivatives **1E** and **1I**, as well as consider-

ing the mode of formation of these products from **1** (see later); the corrected assignments of the 200-MHz ^{1}H NMR data of **1C** and **1H$_1$** are shown in the Experimental Section.

Compounds **1E** and **1G** (both $C_{14}H_{16}O$ by MS) turned out to be non-azulenic compounds (by UV) but contained a conjugated carbonyl group (IR). Structures of 1*H*-inden-1-one (**1E**) and the prototropic isomer 2,3-dihydro-3-methylene-1*H*-inden-1-one (**1G**) were assigned to these products by taking into consideration the reported ^{1}H NMR data of structurally related parent 1*H*-inden-1-one[12] and 2,3-dihydro-3-alkylidene-1*H*-inden-1-ones.[13] It has been noted that 1*H*-inden-1-one (**1E**) was converted to **1G** gradually on standing (or more quickly when dissolved in $CDCl_3$) at 25 °C, and then slowly gave four kinds (by TLC and GC-MS) of colorless dimers.[14] The lability of these indenones **1E** and **1G** are in analogy with the case of the parent 1*H*-inden-1-one which has been recorded to dimerize quickly at room temperature.[12] Compound **1I** ($C_{15}H_{16}O_2$ by MS) were assigned to the 6-formyl derivative of **1E** on the basis of IR and ^{1}H NMR spectra. Interestingly, this monoformyl compound has been found, on standing at 25 °C, to rearrange to the diformyl compound **1N** (see below). The assignments of the NMR data, which are in good agreement with the proposed structures **1E**, **1G**, and **1I**, are recorded in the Experimental Section.

Compounds **1F$_1$** and **1F$_2$** (both $C_{14}H_{18}O$ by MS) were found spectroscopically to be both benzenoid derivatives, namely (*Z*)-4-(5-isopropyl-2-methylphenyl)-3-buten-2-one and (*Z*)-3-(5-isopropyl-2-methylphenyl)-2-butenal, respectively. Compound **1P** was the corresponding carboxylic acid of **1F$_2$** on the evidences of the MS, UV, IR, and NMR spectra (Experimental Section). The (*Z*) configuration of **1F$_1$** was derived from the magnitude of the medium $J_{3,4}$ value (11.0 Hz), while the same (*Z*) configuration of **1F$_2$** and **1P** were decided on the basis of the close similarity in the UV absorption maximums (and the δ values of H-2 and H-6′) between **1F$_1$** and **1F$_2$**/**1P**.

Compound **1H$_2$** was an extremely minor product which possessed a trimeric composition of $C_{45}H_{48}O$ (by MS) and a carbonyl group (1720 cm^{-1}) attached to C-1 of a guaiazulene nucleus (UV λ_{max} 538 nm). Although its NMR data were not available because of the limited amount of the material, the structure of **1H$_2$** shown in Chart 1 is proposed for this compound from the above spectral data and also by considering the most favorable mode of oxidative trimerization of guaiazulene.

Compound **1J** possessed an acetyl group (instead of an isopropyl) conjugated to the azulene nucleus (by UV, IR, and ^{1}H NMR). Structure of 7-acetyl-1,4-dimethylazulene was therefore assigned to this extremely minor product; see Table 1 for the NMR parameters for **1J**. Compounds **1K** and **1O** were indentified spectroscopically as 7-isopropyl-4-methyl-1-azulenecarbaldehyde and the corresponding carboxylic acid derivative, respectively.[15] Compound **1L** was found to be also the known 3-formyl derivative[15,16] of **1** on the basis of spectral data. The 200-MHz ^{1}H NMR parameters for these compounds are given in Table 1.

Compound **1M$_1$** was spectroscopically identical with bis(3,3′-guaiazulenyl) ketone;[17] although Fry et al.[18] have reported 60-MHz ^{1}H NMR data, more precise 200-MHz parameters for this compound are given in Table 1. Compound **1M$_2$** ($C_{18}H_{23}NO_2$ by MS) contained a dimethylcarbamoyloxy group attaching to guaiazulene nucleus on the evidence of the UV, IR, and ^{1}H NMR data (Table 1). The position (C-3) of the carbamoyl group on the guaiazulene nucleus was derived from the close resemblance of the visible absorption maximums (634 and 654 nm) with those of structurally similar 1-azulenyl benzoate (610 and 644 nm),[19] as well as by judging from the appearance of H-2 signal at relatively low field (7.35) in the NMR spectrum.

Compound **1N**, which is a structural isomer (by MS) of **1I** (see above), contained two formyl groups (1715 and 1700 cm^{-1}; δ 10.56 and 10.68, both singlets) and only one aromatic proton (δ 7.02, singlet), in addition to two methyl (δ 2.68 and 2.90, singlets) and an isopropyl (δ 1.28 and 3.65) groups. The UV spectra (λ_{max} 269, 317, 344, and 418 nm) suggested no azulenyl structure in the molecule. This compound was stable even in air when kept as solid at below 5 °C, but in a $CHCl_3$ solution at 25 °C **1N** gradually gave four kinds (by TLC and GC) of colorless dimers.[14],*

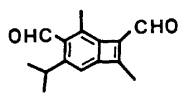

6

Compound **1Q** ($C_{15}H_{16}O_2$ by MS) was assigned to 5-isopropyl-3,8-dimethyl-1,7-azulenequinone on the evidences of UV, IR, NMR spectral data which were in conformity with the reported values of parent 1,7-azulenequinone;[6d] the assignments of the ^{1}H and ^{13}C NMR data are shown in Table 1 and Experimental Section, respectively. This compound is stable on standing at room temperature as in the case of the parent 1,7-azulenequinone.[6d] The quinone structure was confirmed by rather low values of the two half-wave potentials (E_1=−1.13 and E_2=−1.52 V) of **1Q** obtained by cyclic voltammetry.[20]

Compound **1S** was found to be a condensation product of **1** with a molecule of DMF; the position of the substitution at C-2 was derived by comparison of the ^{1}H NMR data (Table 1) with those of **2L** and **2M** (see later).

*For a possible structure of **1N** we tentatively suggested[1] 4-isopropyl-2,6-dimethylbenzocyclobutene-1,5-dicarbaldehyde (**6**). However, the precise structure for **1N** is currently under investigation in relation to those of the dimeric products.[14]

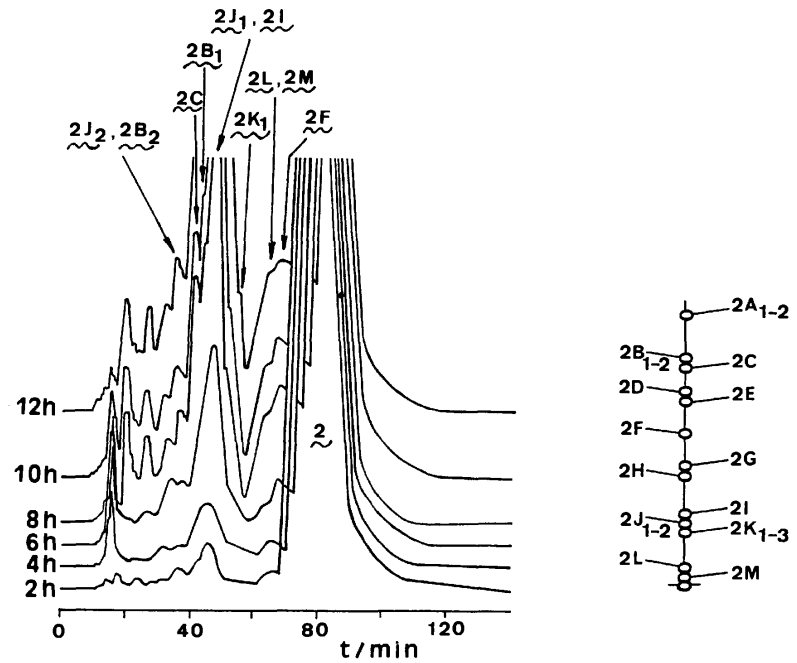

Fig. 2. Time-dependent HPLC diagram of autoxidation of **2** in DMF at 120°C and TLC diagram of the oxidation products from **2**.

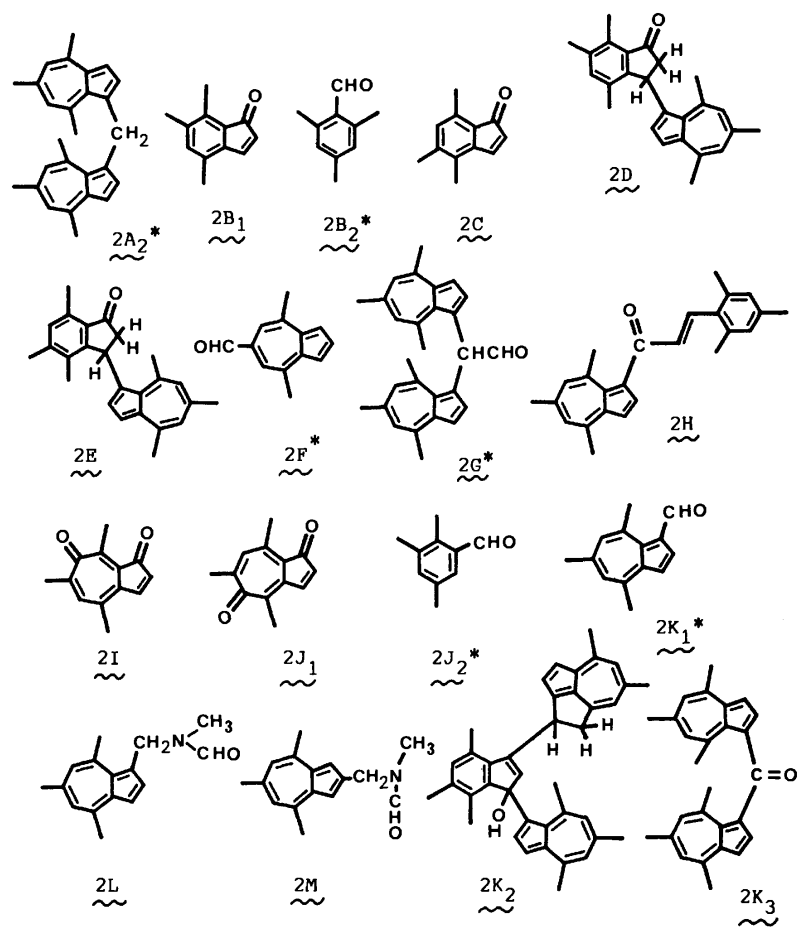

Chart 2. Structures of autoxidation products of 4,6,8-trimethylazulene (**2**); *Previously known compounds.

Autoxidation of 4,6,8-Trimethylazulene (2). The oxidation was carried out in DMF or HMPA at 120 °C for 12 h in a manner similar to that described for **1** and a complex HPLC diagram (Fig. 2) was also obtained, when the reaction was monitored by HPLC; in contrast to that of **1**, the oxidation of **2** took place very slow by at 100 °C. The resulting mixture (see TLC in Fig. 2) was carefully separated by using chromatography, and 17 products (**2A—M**) were obtained as pure components besides the recovered starting material **2** (**2A**$_1$). Structures of these products which have been established as follows are shown in Chart 2. The total theoretical yields of these isolated products were 28%, although there still remained a large amount (59% w/w) of unidentified polar products of relatively high molecular weights as well as a certain amount of inseparable **2**.

Compounds **2A**$_2$ ($C_{27}H_{28}$) and **2K**$_3$ ($C_{27}H_{26}O$ by MS) were readily found to possess structures 1,1′-methylenebis(4,6,8-trimethylazulene) and bis(4,6,8-trimethyl-1-azulenyl) ketone on the basis of their ^{1}H NMR data which closely resembled those of **1A**$_2$ and **1M**$_1$, respectively. The NMR parameters for these new compounds are summarized in Table 1.

Compounds **2B**$_1$ and **2C** (both $C_{12}H_{12}O$ by MS) were spectroscopically assignable to two isomers of 1*H*-inden-1-one having three methyl substituents on the six-membered ring: The structures were presumed to be 4,6,7-trimethyl- and 4,5,7-trimethyl-1*H*-inden-1-one, respectively, when the chemical shifts of the concomitant methyl and ring proton signals (δ 2.22 and 6.88 for **2B**$_1$ vs. δ 2.15 and 6.76 for **2C**) were compared in view of an electronic and anisotropic shift exerted by the carbonyl group on the five-membered ring. Assignments of the NMR data are given in the Experimental Section. Indenones **2B**$_1$ and **2C** both yielded three kinds of dimers[14] on standing at 20 °C.

Compounds **2B**$_2$ and **2J**$_2$ were identified as 2,4,6-[21] and 2,3,5-trimethylbenzaldehyde,[22] respectively, by spectroscopy (MS and NMR).

Compounds **2D** and **2E** (both $C_{25}H_{26}O$ by MS) consisted of a 4,6,8-trimethyl-1-azulenyl group and a 2,3-dihydro-1*H*-inden-1-one moiety having three methyl groups on the six-membered ring. The presence of ABX proton signals (at δ 2.7, 3.3, and 5.4—5.5) as well as a considerable upfield shift (δ ca. 1.0) of the Me-4 signal of the 1-azulenyl moiety indicated that the azulenyl group was linked to C-3 of the indenone moiety for both **2D** and **2E**. The chemical shifts of the singlets at δ 7.14 and 7.00 due to the aromatic six-membered ring proton of **2D** and **2E** suggested the structures of 4,6,7-trimethyl- and 4,5,7-trimethylindenone, respectively, for these products. The assignments of the NMR signals are recorded in the Experimental Section.

Compounds **2F**, **2G**, and **2K**$_1$ were identified by spectroscopy to be all known compounds, namely 4,8-dimethyl-6-azulenecarbaldehyde,[23] bis(4,6,8-trimethyl-1-azulenyl)acetaldehyde,[24] and 4,6,8-trimethyl-1-azulenecarbaldehyde,[16a] respectively; the 200-MHz ^{1}H NMR parameters for these products are summarized in Table 1. Compound **2H** ($C_{25}H_{26}$ by MS) contained a carbonyl group (1710 cm^{-1}) attached to C-1 of the 4,6,8-trimethylazulene moiety (from UV and ^{1}H NMR data). In addition, **2H** possessed a unique (*E*)-(2,4,6-trimethyl)styryl group linked to the carbonyl group on the ground of the NMR data; the (*E*) configuration was derived from the large *J* value (16 Hz) of the vinyl proton coupling; see Experimental Section for assignments of the NMR data.

Compounds **2I** and **2J**$_1$ (both $C_{13}H_{12}O_2$ by MS) were shown by the analysis of their spectroscopic data to be 4,6,8-trimethyl-1,7-azulenequinone and the corresponding 1,5-quinone, respectively. All data were in accord with those of the reported parent 1,7- and 1,5-azulenequinone[6d] as well as that of the trialkyl derivative **1Q**; see Table 1 and Experimental Section for the assignments of ^{1}H and ^{13}C NMR data. These trimethylazulenequinones are stable on standing at room temperature as in the case of **1Q**. The two half-wave potential values[20] (E_1/E_2) obtained for **2I** and **2J**$_1$ were −1.05/−1.5 and −1.05/−1.46 V, respectively, which are slightly higher than those of **1Q** (see above).

Compound **2K**$_2$ ($C_{39}H_{38}O$ by MS) contained a hydroxyl group (3750—3150 cm^{-1}) and a 4,6,8-trimethyl-1-azulenyl group (UV and ^{1}H NMR). Furthermore, the careful analysis of the NMR data obtained by a decoupling technique indicated the presence of 1,3-disubstituted 1*H*-inden-1-ol having three methyl groups on the six-membered ring. The rest of the molecule constituted of 1,8-disubstituted 4,6-dimethylazulene that exhibited ABX proton signals at δ 4.10, 4.39, and 5.40 (J_{AB}=4.0, J_{AX}=7.5, and J_{BX}=0.5 Hz). Combination of these spectral data led to 3-(1,2-dihydro-5,7-dimethylcyclopenta[*c*,*d*]azulen-2-yl)-4,6,7-trimethyl-1-(4,6,8-trimethyl-1-azulenyl)-1*H*-inden-1-ol as the most probable structure for **2K**$_2$.

Compounds **2L** and **2M** (both $C_{16}H_{19}NO$ by MS) were shown by UV, IR, and ^{1}H NMR data to be 4,6,8-trimethylazulene having an *N*-formyl-*N*-methylaminomethyl group at C-1 and C-2, respectively; see Table 1 for assignments of the NMR data of these compounds.

Possible Reaction Pathways for the Formation of Autoxidation Products of 1 and 2. The findings that the present autoxidation of the trialkylazulenes **1** and **2** has resulted in the simultaneous formation of many kinds of products even at an early stage are strongly indicative of the presence of a large number of highly competitive processes during the oxidation obviously initiated by attack of oxygen diradical[25] (or various other free radical species) on several sites of the azulene nucleus. Although electrophilic substitution reactions of azulenes are well-known to take place most easily at the 1 position,[2] no detailed study on radical reactions of azulenes has been made thus far, except for a few, brief descriptions on radical methylation,[26] benzyla-

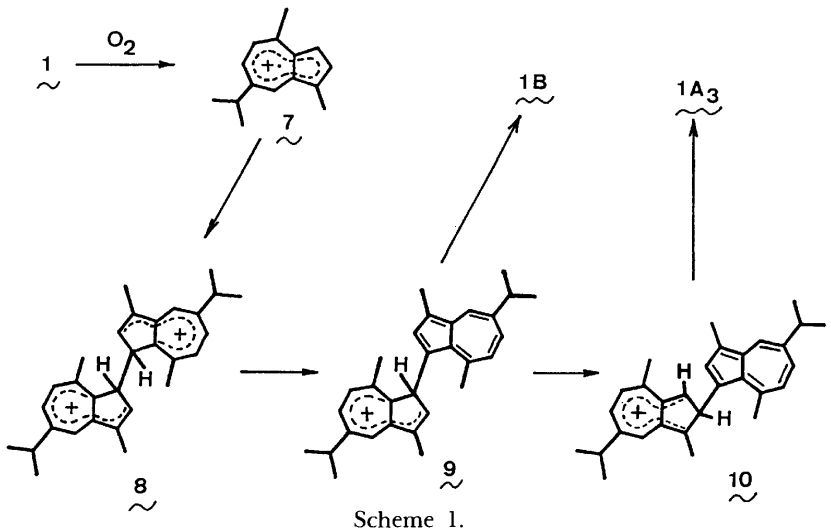

Scheme 1.

tion,[27] and bezoyloxylation,[19] all of which yield the corresponding substitution products preferentially at C-1. Nevertheless, since an unprecedented large number of products have been isolated in a high total, reproducible yield by noncatalyzed autoxidation of the two trialkylazulenes and most of their structures have been established in the present study, an attempt will now be made to suggest presumable reaction pathways for the formation of such a variety of products for the purpose of further detailed investigations of oxidation reactions of azulenes. For convenience, mechanistic considerations on the products from both **1** and **2** are concurrently made after having been divided into several groups according to the site of the oxidation on the azulene nucleus and the type of the products, as illustrated in the following Schemes 1—7.

Oxidative Dimerization. Because of the relatively high reduction potential (E_{pa} 0.71 V vs. SCE),[5] guaiazulene **1** is expected to be very easily oxidized by molecular oxygen, giving the radical cation **7** (see Scheme 1). This in turn undergoes a radical dimerization with a second molecule of **7** to give **8**. Subsequent proton loss from this dimeric cation would lead to the intermediate **9**, which then yields a major product 3,3′-biguaiazulene (**1B**) and a smaller proportion of the 2,3′-isomer (**1A**$_3$) (most likely through the isomerized intermediate **10**). It is assumed that the linkage of the coupling takes place between the sites (C-3) of the highest spin density in the cation radical **7** in the above radical dimerization. At present stage, we consider that such a pathway as described here is the most favorable for this dimerization on the grounds of (a) a preliminary theoretical calculation of the π-electron density in **1** and **7** in connection with the problem of the linkage[28a] and (b) isolation of a high yield of a 2 : 1 mixture of **1B** and **1A**$_3$ by the anodic oxidation of **1** which apparently proceeds through condensation of the radical cation **7**.[28b]

Both dimers **1B** and **1A**$_3$ have remained virtually unchanged on heating in DMF at 100 °C for 24 h in the absence of oxygen. Therefore, once these products are formed, no radical-catalyzed, thermal interconversion would exist between these two products through an equilibrium intermediate **11** analogous to the one proposed for the thermal conversion of 1-phenylazulene to the 2-phenyl isomer.[29]

No such 1,1′- or 1,2′-dimer was isolated among the products from 4,6,8-trimethylazulene **2** under these autoxidation conditions apparently due to further polymerization at 1,3-positions, whereas an appreciable amount of a 2 : 1 mixture of such 1,1′-dimer and a trimer containing 1,2′-linkage were obtained by the anodic oxidation of **2**.[28b]

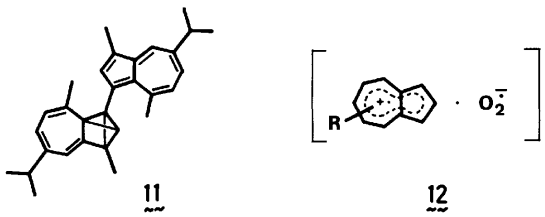

11 **12**

Although such oxidative dimerization described above takes place as one of the major pathways, other products are derived by oxidation of the starting azulenes with oxygen molecule ($^3O_2$), apparently proceeding through a complex shown as formula **12** by an electron transfer.[30] This complex is then expected to lead to a covalent linkage between the azulene nucleus and active radical species such as $^{\cdot}OO^-$, $^{\cdot}OOH$, and $^{\cdot}OH$ (or even $^1O_2$ produced during the oxidation) at various positions according to the ease of their affinity and steric requirement, thus providing several kinds of key intermediates for the formation of a wide variety of other products as outlined in Schemes 2—7.

Oxidation of Side Chain. Scheme 2 illustrates the proposed reaction pathways for the products formed by oxidation of the side chains. One of the major product **1K** is considered to be derived by the attack of

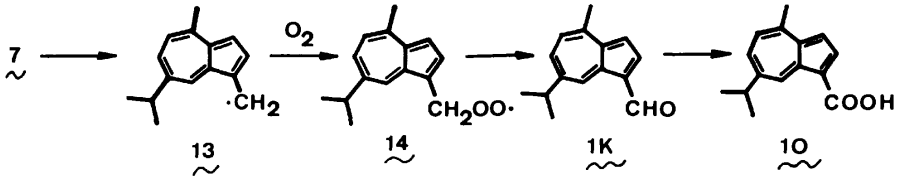

Scheme 2.

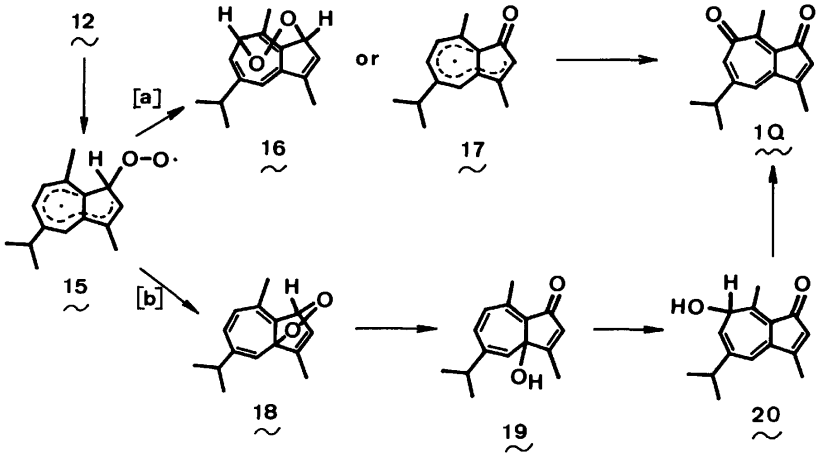

Scheme 3.

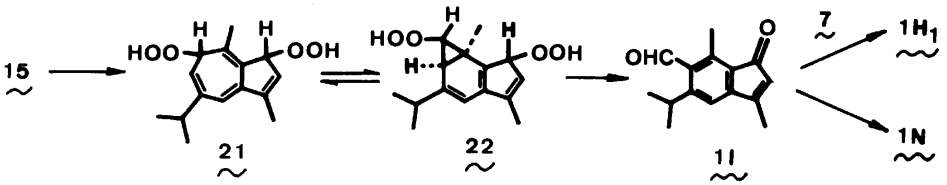

Scheme 4.

an oxygen molecule upon the alkyl side chain of the radical intermediate **13** (derived from **7**) to form the primary peroxyl radical **14** in a manner similar to the well-accepted mechanism for the autoxidation of side chains of alkylbenzenes and naphtalenes.[31] Further autoxidation of the aldehyde **1K** in the usual way gives the carboxylic acid **1O**. The oxidation of the side chain on the 1 position constitutes one of the major pathways in the autoxidation of **1** under the present conditions. The 7-acetylazulene **1J** is available only in an extremely samll amount by oxidation of the isopropyl group of **1**. These facts contrast with the efficient preparation of acetophenone derivatives from isopropylbenzenes by the same autoxidation in DMF.[32] Only an extremely small extent of the side chain oxidation is observed for **2**, affording 6-formyl derivative **2F**. Both **1J** and **2F** are obviously formed via pathways through the radical intermediates similar to those for **1K** outlined in Scheme 2.

Azulenequinones. Scheme 3 illustrates a major reaction pathway when the azulene-oxygen complex **12** from **1** is transformed into the 3-guaiazulenylperoxyl diradical **15**.[33] As in the case of oxidation with singlet oxygen in protic solvent, a stepwise transformation of **15** into a precursor **20** via endo-peroxide **18** and hydroxy ketone **19** by a thermal [1,5] shift of the OH group on the seven-membered ring (path-b) may not be excluded for the formation of **1Q**. However, the fact that 1,7-guaiazulenequinone **1Q** has also been obtained on standing **1** in the dark even at 25 °C for a prolonged period (in as high as 15% yield)[34] suggests to us the transient formation of a highly strained, cross-linked endo-peroxide like **16** (or of a radical ketone **17**) (path-a), as a more likely pathway.

The same type of oxidative pathways for **2** would account for the formation of two azulenequinones $\mathbf{2J}_1$ and **2I**.

6-Formyl-1*H*-inden-1-ones and Related Compounds. Possible reaction pathways for the formation of these compounds are illustrated in Scheme 4. Addition of hydroperoxyl radical to the 5 position of **15** is considered to give an intermediate such as hydroperoxide **21** that would be converted into the 6-formylindenone **1I** most likely through the equilibrated norcaradiene form[35] (e.g. **22**). The formation of no such 6-formylindenone from **2** is obviously due to the presence of the three methyl groups at such positions as to suppress the transformation of the corresponding norcaradiene

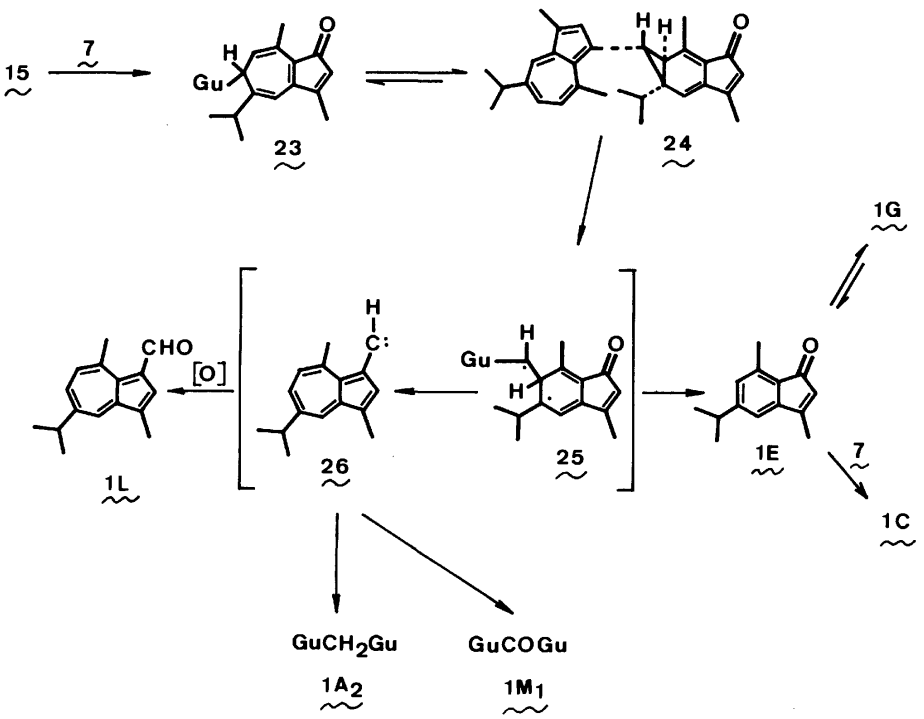

Scheme 5.

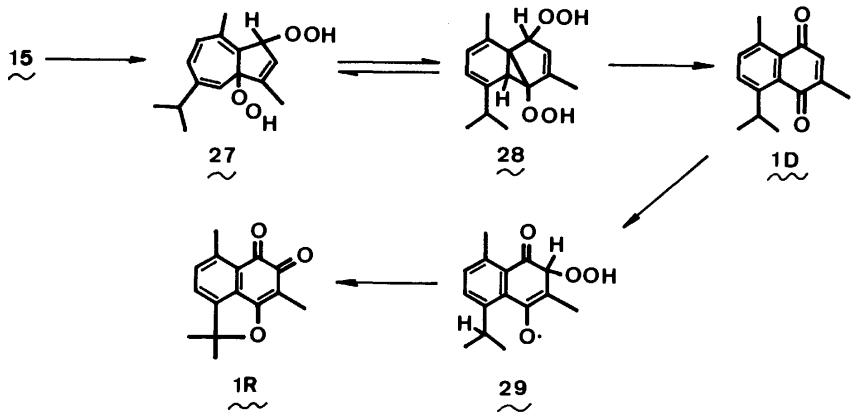

Scheme 6.

form (cf. **22**) into the formyl-substituted six-membered ring.

From indenones **1I** and **1E** (which has liberated one carbon by the rearrangement, see Scheme 5) several secondary products are derived: (i) oxidative coupling of **1I** and **1E** with the 2 position of the unreacted starting material **1** (or more probably **7**) to afford 2-(3-guaiazulenyl)indenones $\mathbf{1H_1}$ and **1C**, respectively, (ii) isomerization to **1N**, and (iii) transformation of **1E** into the thermodynamically more stable prototropic isomer **1G**.

Compounds Formed by Intermolecular One-Carbon Transfer. It should be particularly noticed in the present autoxidation of the trialkylazulenes **1** and **2** that compounds having extra-carbon(s) such as 3-formylguaiazulene (**1L**), 3,3′-methylenebisguaiazulene ($\mathbf{1A_2}$), and related compounds ($\mathbf{1M_1}$, $\mathbf{2A_2}$, $\mathbf{2G_1}$, **2K**) have always been obtained in relatively high yields.

The facts that compound **24**[36] has recently been proved to degrade to **1E** and **1L** on standing in air and the reaction of **24** with an equivalent of guaiazulene **1** under nitrogen in DMF at 100 °C has given $\mathbf{1A_2}$ as one of the major products strongly suggest that this dimeric norcaradiene **24** (formed through **23**) is the most likely key intermediate (Scheme 5). Compound **24**, which is expected to be thermodynamically more stable than **23** due to the absence of a cyclpentadienone form, would then undergo fragmentation (through diradical **25**) to give 1*H*-inden-1-one **1E** and a certain intermediate having a reactive extra-carbon side chain (such as a carbene species **26**). Then, a condensation reaction of the latter with the starting material **1** would afford $\mathbf{1A_2}$, whereas oxidation with $^3O_2$ is considered to give 3-formylguaiazulene **1L**.

Similar pathways for **2** involving intermediates illustrated for **1** would account for the formation of the

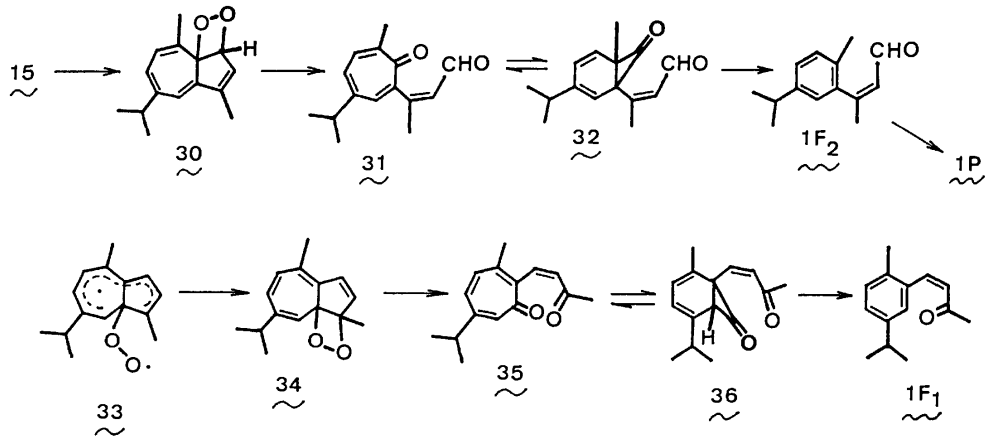

Scheme 7.

bis-trimethylazulenyl derivative **2A**$_2$ and indenones **2B**$_1$ and **2C**, as well as the 1-formyltrimethylazulene **2K**$_1$.

Naphthalenoid Compounds. Proposed pathways for these products are outlined in Scheme 6. Among these products, the formation of the naphthoquinones **1D** and **1R** constitute one of the major reaction pathways from **1**. Taking into account the results of an independent model study,[11b] this transformation may be explained in terms of the process through the intermediates **15** (Scheme 3) and then **27** formed by the addition of the second molecule of oxygen to C-8a of guaiazulene nucleus, followed by the rearrangement involving the norcaradiene intermediate **28** and loss of two hydroxyl radicals. An addition of hydroperoxyl radical at C-2 of **1D** to give an intermediate **29**, and subsequent loss of hydroxyl and H radicals would afford **1R**.

Benzenoid Compounds. The formation of a number of further degraded benzenoid derivatives (**1F**$_2$, **1P**, and **1F**$_1$) from **1** is most likely explained by the intramolecular radical cyclization of **15** at C-3a and of **33** at C-1 to give the dioxetane intermediates **30** and **34** which subsequently yield the benzenoid products through the ring-opened tropone-norcaradiene dicarbonyl compounds **31**, **32** and **35**, **36**, respectively, followed by facile decarbonylation, as illustrated in Scheme 7. The benzenoid compounds (**2B**$_2$, **2H**, and **2J**$_2$) from **2** are derived via essentially similar ring-opening schemes as those described for the benzenoid products from **1**.

The detailed mechanistic consideration for the formation of other minor compounds, however, is not made here because of the limited evidences at this stage with regard to the reaction pathways. Besides these isolated compounds described so far, considerable amounts (34 and 57%) of intractable resinous substances are accompanied by the autoxidation (of **1** and **2**, respectively). Of particular, it is noted that the latter substrate (**2**) bearing no substituents at the most reactive sites C-1 and C-3 tends to give a larger proportion of the polymerized products.

It has now become apparent that the autoxidation of the trialkylazulenes is extraordinarily complex and highly competitive involving oxidation of the nucleus (at various positions), substitutions, ring contraction, and other reactions such as the rearrangement to naphthalenes, although the exact mechanism is under further investigation in detail by employing azulene itself and various other alkylazulenes under various reaction conditions. Nevertheless, the present findings are believed to provide valuable information on exploitation of a convenient preparative route for some useful azulenoid compounds.[37] It is further of interest in relation to the recent isolation, from the polyps of a deep sea gorgonian (at −350 m), of a number of azulene derivatives, including 3,3′-methylenebisguaiazulene[38a] (**1A**$_2$) and 1,7-guaiazulenequinone[38b] (**1Q**) which coincide with the autoxidation products described in this paper.

Experimental

Melting points were determined with a Yanagimoto MP-S3 instrument and are uncorrected. Column chromatography was performed with Wako C-300 silica gel. TLC was conducted on plates precoated with silica gel 60F (0.25 mm, Merck) by using 15 : 85 AcOEt–hexane as eluant. HPLC was carried out with Hitachi gel #3011 with methanol as solvent.

UV (in MeOH) and IR (as KBr disk, unless otherwise stated) spectra were taken on Hitachi 323 and a Nihonbunko IR-A-202 Grating spectrometer, respectively. NMR spectra were recorded in $CDCl_3$ with a JEOL-FX200 cryospectrometer (200-MHz for ^1H and 50 MHz for ^{13}C) at 27 °C. Chemical shifts are reported as δ values in parts per million relative to tetramethylsilane (δ 0.0) as the internal standard. The assignments of all signals were made by employing a first-order analysis with the aid of decoupling technique and the parameters were confirmed by a computer-assisted simulation analysis; those values for simple azulene derivatives are summarized in Table 1. Mass spectra were taken on a Shimadzu LKB-9000 (with a Shimadzu PAC 90 mass data system) low resolution or a JEOL JMS-HX100 (with a JEOL JMA-DA5000 mass data system) high-resolution instrument (for chemical ionization with isobutane), and are given in terms of m/z (rel. intensity) compared with the base peak.

Oxidation of Guaiazulene (1) in DMF. A solution of **1**[39]

(1.00 g) in freshly distilled DMF (20 cm^3) was placed in a Pyrex flask (ϕ 1.8 cm, 60 cm height) and subjected to autoxidation by allowing finely bubbling oxygen to pass through the solution (from the bottom of the flask) for 24 h at 100±5 °C. After cooling, the mixture was diluted with water (200 cm^3) and extracted with AcOEt (4×50 cm^3). The combined organic layers were washed with water, dried (Na_2SO_4), and evaporated in vacuo, giving a brown oil (0.98 g); the HPLC and TLC diagrams of this crude mixture are given in Fig. 1. This residue was preliminarily separated into five fractions by means of preparative HPLC with Hitachi gel #3019 (100 g) using methanol as eluant. Then each fraction was carefully separated by silica-gel column or thin layer with AcOEt–hexane; when necessary, this chromatographic procedure was repeated. Thus, the following 25 products were obtained as pure substances, besides the recovered starting material **1** (**1A**$_1$: 0.41 g; R_f=0.95; ^{1}H NMR, see Table 1) and polar resinous substances [0.20 g, 34% (w/w); R_f=0.0]. The yield of each product is based on the consumed starting material (0.59 g).

3,3′-Methylenebisguaiazulene[9] **(1A$_2$):** Dark blue prisms; 50 mg (8.2% yield); mp 188 °C (Ref. 9a, 187—189 °C); R_f=0.95; ^{1}H NMR, see Table 1. (Found: *m/z* 408.2883).

2,3′-Biguaiazulene (1A$_3$): Dark green prisms; 5 mg (0.9%); mp 149 °C; R_f=0.95; UV ($CHCl_3$) 250, 299, 311, 353, 368,^{sh} 446, and 610 nm (log ε 4.42, 4.46, 4.47, 4.20, 4.07, 3.94, and 2.91); ^{1}H NMR, see Table 1; EI MS, *m/z* 394 (M^+; 56), 379 (100), 336 (19), 321 (20), and 198 (17).

Found: *m/z* 349.2654. Calcd for $C_{30}H_{34}$: M, 394.2660.

4,4′-Diisopropyl-1,1′,6,6′-tetramethyl-2,2′-binaphthalene (1A$_4$): Pale yellow-green oil; 2 mg (0.4%); R_f=0.95; UV 231, 291, 326, and 441 nm (log ε 4.82, 3.82, 2.45, and 2.50); ^{1}H NMR 1.38 (12H, d, *J*=7.0 Hz, 2 *i*-Pr-4), 2.55 (6H, s, 2Me-6), 2.64 (6H, s, 2Me-1), 3.72 (2H, sept, 2CH-4), 7.22 (2H, s, 2H-3), 7.34 (2H, dd, $J_{7,8}$=9.0, $J_{5,7}$=1.7 Hz, 2H-7), 7.90 (2H, d, 2H-5), and 7.91 (2H, d, 2H-8); EI MS, *m/z* 394 (M^+; 100), 379 (30), 351 (35), and 197 (30).

Found: *m/z* 394.2666. Calcd for $C_{30}H_{34}$: M, 394.2661.

4-Isopropyl-1,6-dimethylnaphthalene (Cadalene)[40] **(1A$_5$):** Colorless oil; 5 mg (0.9%); R_f=0.95; ^{1}H NMR 1.32 (6H, d, *J*=7.0 Hz, *i*-Pr-4), 2.49 (3H, s, Me-6), 2.58 (3H, s, Me-1), 3.68 (1H, sept, CH-4), 7.13 (1H, d, *J*=7.0 Hz, H-2), 7.22 (1H, d, H-3), 7.26 (1H, dd, *J*=8.0, 1.0 Hz, H-7), 7.85 (1H, d, H-8), and 7.89 (1H, d, H-5); EI MS, *m/z* 198 (M^+; 100).

3,3′-Biguaiazulene[3,10] **(1B):** Greenish blue prisms; 40 mg (6.8%); mp 144 °C (Ref. 15, 142 °C); R_f=0.93; ^{1}H NMR, see Table 1; EI MS, *m/z* 394 (M^+; 100).

2-(3-Guaiazulenyl)-5-isopropyl-3,7-dimethyl-1*H*-inden-1-one (1C): Dark red prisms; 13 mg (2.2%); R_f=0.86; UV 252, 293, 305,^{sh} 352, 370,^{sh} and 500 nm (log ε 4.59, 4.66, 4.60 4.06, 4.00, and 3.51); IR (CCl_4) 1690 (C=O) cm^{-1}; ^{1}H NMR 1.28 (6H, d, *J*=7.0 Hz, *i*-Pr-5), 1.34 (6H, d, *J*=7.0 Hz, *i*-Pr-7′), 2.08 (3H, s, Me-3), 2.52 (3H, s, Me-7), 2.62 (3H, s, Me-4′), 2.64 (3H, s, Me-1′), 2.89 (1H, sept, CH-5), 3.04 (1H, sept, CH-7′), 6.83 (2H, bs, H-4,6), 6.90 (1H, d, $J_{5',6'}$=11.0 Hz, H-5′), 7.32 (1H, dd, $J_{6',8'}$=2.0 Hz, H-6′), 7.36 (1H, s, H-2′), and 8.12 (1H, d, H-8′); CI MS, *m/z* 397 (M+1; 100).

Found; *m/z* 396.2438. Calcd for $C_{29}H_{32}O$: M, 396.2453.

8-Isopropyl-2,5-dimethyl-1,4-naphthoquinone[11] **(1D):** Yellow oil; 35 mg (5.1%); R_f=0.81; CI MS, *m/z* 229 (M+1; 100).

5-Isoproply-3,7-dimethyl-1*H*-inden-1-one (1E): Pale yellow oil; 10 mg (1.7%); R_f=0.78; UV ($CHCl_3$) 250, 331, 341,^{sh} and 370^{sh} nm (log ε 4.33, 3.73, 3.69, and 3.05); IR (neat) 1680 (C=O) cm^{-1}; ^{1}H NMR 1.23 (6H, d, *J*=7.0 Hz, *i*-Pr-5), 2.20 (3H, d, $J_{2,Me}$=1.5 Hz, Me-3), 2.44 (3H, s, Me-7), 2.88 (1H, sept, CH-5), 5.61 (1H, q, H-2), 6.79 (1H, bs, H-4*), and 6.83 (1H, bs, H-6*), *the assignments may have to be interchanged; ^{13}C NMR 198.79 (C-1), 160.24, 154.11, 146.75, 136.65, 129.64, 124.45, 115.92, 34.45, 23.59, 17.11, and 13.72; CI MS, *m/z* 201 (M+1; 100).

Found: *m/z* 200.1140. Calcd for $C_{14}H_{16}O$: M, 200.1201.

(*Z*)-4-(5-Isopropyl-2-methylphenyl)-3-buten-2-one (1F$_1$): Colorless oil; 10 mg (1.7%); R_f=0.72; UV 279 nm (log ε 4.36); IR (neat) 1680 (C=O) cm^{-1}; ^{1}H NMR 1.21 (6H, d, *J*=7.0 Hz, *i*-Pr-5′), 1.92 (3H, s, H_3-1), 2.26 (3H, s, Me-2′), 2.85 (1H, sept, CH-5′), 6.16 (1H, d, *J*=11.0 Hz, H-3), 7.03 (1H, bs, H-6′), 7.09 (1H, bd, $J_{3',4'}$=8.0 Hz, H-4′), 7.13 (1H, d, H-3′), and 7.15 (1H, d, H-4); EI MS, *m/z* 202 (M^+; 100).

Found: *m/z* 202.1264. Calcd for $C_{14}H_{18}O$: M, 202.1357.

(*Z*)-3-(5-Isopropyl-2-methylphenyl)-2-butenal (1F$_2$): Colorless oil; 10 mg (1.7%); R_f=0.72; ^{1}H NMR 1.24 (6H, d, *J*=7.0 Hz, *i*-Pr-5′), 2.22 (3H, s, Me-2′), 2.24 (3H, d, $J_{2,4}$=1.5 Hz, H_3-4), 2.88 (1H, sept, CH-5′), 6.14 (1H, dq, $J_{1,2}$=8.0 Hz, H-2), 6.92 (1H, bd, $J_{4',6'}$=1.0 Hz, H-6′), 7.10 (1H, dd, $J_{3',4'}$=8.0 Hz, H-4′), 7.16 (1H, d, H-3′), and 9.20 (1H, d, H-1); EI MS, *m/z* 202 (M^+; 100).

Found: *m/z* 202.1295. Calcd for $C_{14}H_{18}O$: M, 202.1357.

2,3-Dihydro-5-isopropyl-7-methyl-3-methylene-1*H*-inden-1-one (1G): Colorless needles; 5 mg (0.8%); mp 84 °C; R_f=0.69; UV 245, 265,^{sh} and 330 nm (log ε 4.32, 4.17, and 3.79); IR (CCl_4) 1720 (C=O) cm^{-1}; ^{1}H NMR 1.29 (6H, d, *J*=7.0 Hz, *i*-Pr-5), 2.62 (3H, s, Me-7), 2.96 (1H, sept, CH-5), 3.25 (2H, dd, 2H-2), 5.24 [1H, t, $J_{2,HC(3)}$=1.8 Hz, (*E*)-H-C-3], 5.78 [1H, t, $J_{2,HC(3)}$=2.0 Hz, (*Z*)-H-C-3), 7.02 (1H, d, $J_{4,6}$=1.0 Hz, H-6], and 7.43 (1H, d, H-6).

Found: *m/z* 200.1205. Calcd for $C_{14}H_{16}O$: M, 200.1202.

2-(3-Guaiazulenyl)-5-isopropyl-3,7-dimethyl-1-oxo-1*H*-indene-6-carbaldehyde (1H$_1$): Reddish brown prisms; 13 mg (2.1%); mp 147 °C (decomp); R_f=0.64; UV 225,^{sh} 256, 293, 307,^{sh} 353, 369, and 537 nm (log ε 4.43, 4.53, 4.60, 4.53, 4.00, 3.93, and 3.50); IR (CCl_4) 1690 and 1680 (C=O) cm^{-1}; ^{1}H NMR 1.33 (6H, d, *J*=7.0 Hz, *i*-Pr-7′), 1.37 (6H, d, *J*=7.0 Hz, *i*-Pr-5), 2.14 (3H, s, Me-3), 2.64 (6H, s, Me-1′, 4′), 2.80 (3H, s, Me-7), 3.01 (1H, sept, CH-7′), 3.79 (1H, sept, CH-5), 6.95 (1H, d, $J_{5',6'}$=11.0 Hz, H-5′), 7.08 (1H, s, H-4), 7.36 (1H, dd, $J_{6',8'}$=2.0 Hz, H-6′), 7.39 (1H, s, H-2′), 8.16 (1H, d, H-8′), and 10.60 (1H, s, OHC-6); CI MS, *m/z* 425 (M+1; 100).

Found: *m/z* 424.2444. Calcd for $C_{30}H_{32}O_2$: M, 424,2404.

3-Guaiazulenyl 3-(3-Guaiazulenyl)-7-isopropyl-4-methyl-1-azulenyl Ketone (1H$_2$): Reddish brown paste; 1 mg (0.2%); R_f=0.64; UV ($CHCl_3$) 248, 290, 394, and 538 nm (log ε 4.70, 4.70, 3.24, and 3.34); IR 1720 (C=O) cm^{-1}; EI MS, *m/z* 604 (M^+; 100), 589 (7), 561 (4), 408 (17), 393 (5), 198 (20), and 183 (19).

Found: *m/z* 604.3670. Calcd for $C_{45}H_{48}O$: M, 604.3704.

5-Isopropyl-3,7-dimethyl-1-oxo-1*H*-indene-6-carbaldehyde (1I): Yellow needles; 20 mg (2.9%); mp 87 °C; R_f=0.55; UV ($CHCl_3$) 268, 342, and 374^{sh} nm (log ε 4.27, 3.96, and 3.66); IR 1700 and 1695 (C=O) cm^{-1}; ^{1}H NMR 1.32 (6H, d, *J*=6.9 Hz, *i*-Pr-5), 2.26 (3H, d, $J_{2,Me}$=1.4 Hz, Me-3), 2.76 (3 H, s, Me-7), 3.72 (1H, sept, HC-5), 5.80 (1H, q, H-2), 7.04 (1H, s, H-4), and 10.58 (1H, s, CHO); ^{13}C NMR 197.56, 193.41, 159.19, 157.44, 149.91, 138.40, 134.26, 129.70, 127.13, 115.28, 29.02, 23.59, 13.67, and 13.37; EI MS, *m/z* 228 (M^+; 100), 213 (47), 199 (23), and 185 (32).

Found: m/z 228.1132. Calcd for $C_{15}H_{16}O_2$: M, 228.1150.

7-Acetyl-1,4-dimethylazulene (1J): Violet bule prisms; 2 mg (0.3%); mp 55 °C; R_f=0.52; UV 245, 304, 396, and 575 nm (log ε 4.47, 4.68, 3.76, and 2.72); IR 1670 (C=O) cm^{-1}; ^1H NMR, see Table 1; EI MS, m/z 198 (M^+; 100), 183 (75), and 155 (52).

Found: m/z 198.1014. Calcd for $C_{14}H_{14}O$: M, 198,1045.

7-Isopropyl-4-methyl-1-azulenecarbaldehyde[15] (1K): Red prisms; 50 mg (7.9%); mp 61 °C (Ref. 15, 61 °C); R_f=0.49; ^1H NMR, see Table 1; EI MS, m/z 212 (M^+; 100).

3-Guaiazulenecarbaldehyde[16] (1L): Brownish red needles; 10 mg (1.5%); mp 86 °C (Ref. 16, 85—86 °C); R_f=0.38; ^1H NMR, see Table 1; EI MS, m/z 226 (M^+; 100).

Bis(3,3′-guaiazulenyl) Ketone[17] ($1M_1$): Dark green prisms; 10 mg (1.6%); mp 191 °C (Ref. 17, 189—190 °C); R_f=0.35; ^1H NMR, see Table 1; EI MS, m/z 422 (M^+; 17), 407 (69), 331 (20), 198 (16), 169 (81), 109 (50), and 43 (100).

3-Guaiazulenyl Dimethylcarbamate ($1M_2$): Dark blue paste; 5 mg (0.6%); R_f=0.35; UV ($CHCl_3$) 249, 290, 352, 368, 634, and 654^{sh} nm (log ε 4.20, 4.26, 3.78, 3.75, 2.67, and 2.63); IR (CCl_4) 1705 (C=O) cm^{-1}; ^1H NMR, see Table 1; EI MS, m/z 285 (M^+; 10), 213 (58), 72 (100), and 42 (12).

Found: m/z 285.1733. Calcd for $C_{18}H_{23}NO_2$: M, 285.1728.

Compound 1N: Pale yellow crystals; 2 mg (0.3%); R_f=0.26; UV 229,^{sh} 242,^{sh} 254,^{sh} 269, 317, 344, and 418 nm; IR (CCl_4) 1715 and 1700 (C=O) cm^{-1}; ^1H NMR* 1.28 (6H, d, J=7.0 Hz, *i*-Pr-4), 2.68 (3H, s, Me-7), 2.90 (3H, s, Me-2), 3.65 (1H, sept, HC-4), 7.02 (1H, s, H-5), 10.56 (1H, s, OHC-8), and 10.68 (1H, s, OHC-3), *the assignments were made for the tentative structure **6** (see the footnote on p. 1418); CI MS, m/z 229 (M+1; 100).

7-Isopropyl-4-methyl-1-azulenecarboxylic Acid[15] (1O): Red-violet needles; 10 mg (1.5%); mp 169 °C (Ref. 15, 169 °C); R_f=0.23; ^1H NMR see Table 1; EI MS, m/z 228 (M^+; 100).

(*Z*)-3-(5-Isopropyl-2-methylphenyl)-2-butenoic Acid (1P): Colorless needles; 15 mg (2.3%); mp 128 °C; R_f=0.20; UV 269 and 278 nm (log ε 4.31 and 4.23); IR 3200—2300, 1680—1660 (COOH) cm^{-1}; ^1H NMR 1.21 (6H, d, J=7.0 Hz, *i*-Pr-5′), 2.12 (3H, d, $J_{2,4}$=1.5 Hz, H_3-4), 2.14 (3H, s, Me-2′), 2.84 (1H, sept, HC-5′), 4.16 (1H, m, COOH; D_2O exchangeable), 5.92 (1H, q, H-2), 6.78 (1H, dd, $J_{4',6'}$=2.0, $J_{3',6'}$=0.5 Hz, H-6′), 7.05 (1H, $J_{3',4'}$=8.0 Hz, H-4′), and 7.08 (1H, dd, H-3′); ^{13}C NMR 169.47 (C-1), 159.02, 146.11, 140.27, 130.58, 129.82, 125.38, 124.15, 118.02, 33.64, 27.45, 24.00, and 18.57.

Found: m/z 218.1308. Calcd for $C_{14}H_{18}O_2$: M, 218.1307.

5-Isopropyl-3,8-dimethyl-1,7-azulenequinone (1Q): Yellow needles; 10 mg (1.5%); mp 94 °C; R_f=0.18; $E_{1/2}$ −1.13 and −1.52 V (vs. SCE); UV ($CHCl_3$) 232, 252, 288,^{sh} 310,^{sh} 386, 394,^{sh} and 420^{sh} nm (log ε 4.14, 4.14, 3.95, 3.92, 3.74, 3.73, and 3.53); IR 1680 and 1590 (C=O) cm^{-1}; ^1H NMR, see Table 1; ^{13}C NMR 196.57 (C-1), 189.38 (C-7), 164.16 (C-3), 154.99 (C-5), 148.91 (C-8), 144.53 (C-3a), 133.09 (C-6), 133.04 (C-8a), 131.45 (C-4), 124.10 (C-2), 37.84 (Me-8), 29.67 (Me_2CH-5), 22.54 (Me_2CH-5), and 14.25 (Me-3); EI MS, m/z 228 (M^+; 100), 213 (80), 199 (16), 195 (12), 185 (26), and 171 (16).

Found: m/z 228.1138. Calcd for $C_{15}H_{16}O_2$: M, 228.1150

2,2,5,8-Tetramethyl-2*H*-naphtho[1,8-*bc*]furan-6,7-dione[11b] (1R): Orange needles; 5 mg (0.7%); mp 220 °C (Ref. 11b, mp 220 °C); R_f=0.05; EI MS, m/z 242 (M^+; 54) and 171 (100).

***N*-(2-Guaiazulenylmethyl)-*N*-methylformamide (1S):** Blue paste; 5 mg (0.6%); R_f=0.02; UV 245, 285, 349, and 608 nm (log ε 4.38, 4.60, 3.68, and 2.64); IR (CCl_4) 1665 (C=O) cm^{-1}, ^1H NMR, see Table 1; EI MS, m/z 269 (M^+; 27), 254 (25), 226 (26), 213 (100), and 198 (23).

Oxdation of 1 in HMPA. The same oxidation procedure was employed, and virtually the same products were obtained except for certain compounds in which fragments from the solvent are incorporated (e.g., $1M_2$ and **1S**).

Oxidation of 4,6,8-Trimethylazulene (2) in DMF. Autoxidation **2**[39] (1.00 g) in DMF (20 cm^3) was carried out for 12 h at 120±5 °C in a manner similar to that described for **1**, thus affording, after the careful chromatographic separation, 17 products as pure compounds (**2A—M**; see Fig. 2 for HPLC and TLC), besides the recovered starting material **2** ($2A_1$, 0.45 g, R_f=0.94; ^1H NMR, see Table 1) and polar resinous substances [0.324 g, 59% (w/w); R_f=0.0]. They yield of each product is based on the consumed starting material (0.55 g).

1,1′-Methylenebis(4,6,8-trimethylazulene) ($2A_2$): Dark violet prisms; 10 mg (1.8%); mp 205 °C; R_f=0.94; UV ($CHCl_3$) 249, 306, 356, and 570 nm (log ε 4.80, 4.89, 4.27, and 2.97); ^1H NMR, see Table 1; EI MS m/z 352 (M^+; 68), 182 (100), and 170 (84).

Found: m/z 352.2176. Calcd for $C_{27}H_{28}$: M, 352.2190.

4,6,7-Trimethyl-1*H*-inden-1-one ($2B_1$): Yellow needles; 30 mg (5.4%); mp 38 °C; R_f=0.79; UV 249, 313, and 400 nm (log ε 3.87, 3.50, and 3.02); IR 1700 (C=O) cm^{-1}; ^1H NMR 2.20 (3H, s, Me-4), 2.22 (3H, s, Me-6), 2.43 (3H, s, Me-7), 5.74 (1H, d, $J_{2,3}$=6.0 Hz, H-2), 6.88 (1H, s, H-5), and 7.58 (1H, d, H-3); EI MS, m/z 172 (M^+; 100) and 129 (20).

Found: m/z 172.0888. Calcd for $C_{12}H_{12}O$: M, 172.0888.

2,4,6-Trimethylbenzaldehyde[21] ($2B_2$): Colorless oil; 2 mg (0.4%); R_f=0.79; ^1H NMR 2.31 (3H, s, Me-4), 2.56 (6H, s, Me-2,6), 6.90 (2H, s, H-3,5), and 10.56 (1H, s, CHO): EI MS, m/z 148 (M^+; 100).

4,5,7-Trimethyl-1*H*-inden-1-one (2C): Yellow needles; 30 mg (5.4%); mp 64 °C; R_f=0.78; UV 247, 349, and 400^{sh} nm (log ε 3.88, 3.52, and 3.25); IR 1695 (C=O) cm^{-1}; ^1H NMR 2.15 (3H, s, Me-5), 2.20 (3H, s, Me-4), 2.42 (3H, s, Me-7), 5.78 (1H, d, $J_{2,3}$=6.0 Hz, H-2), 6.76 (1H, s, H-6), and 7.62 (1H, d, H-3); ^{13}C NMR 200.01, 146.81, 143.31, 143.13, 135.19, 132.91, 131.75, 128.59, 127.13, 19.97, 16.76, and 13.78; EI MS, m/z 172 (M^+; 100) and 129 (22).

Found: m/z 172.0880. Calcd for $C_{12}H_{12}O$: M, 172.0888.

2,3-Dihydro-4,6,7-trimethyl-3-(4,6,8-trimethyl-1-azulenyl)-1*H*-inden-1-one (2D): Violet prisms; 10 mg (1.8%); mp 145 °C; R_f=0.69; UV 266, 297, 359, 563, and 600^{sh} nm (log ε 3.66, 4.30, 3.49, 2.67, and 2.61); IR 1695 (C=O) cm^{-1}; ^1H NMR 1.82 (3H, s, Me-4), 2.32 (2H, s, Me-6), 2.58 (2H, s, Me-6′), 2.64 (3H, s, Me-4′), 2.67 (1H, dd, $J_{2,2}$=18.0, $J_{2,3}$=3.0 Hz, H-2), 2.78 (3H, s, Me-8′), 3.14 (3H, s, Me-7), 3.26 (1H, dd, $J_{2,3}$=8.0 Hz, H-2), 5.42 (1H, dd, H-3), 6.75 (1H, d, $J_{2',3'}$=4.0 Hz, H-2′), 6.94 (1H, s, H-5′), 6.96 (1H, s, H-7′), 7.12 (1H, d, H-3′), and 7.14 (1H, s, H-5); EI MS, m/z 342 (M^+; 10) and 170 (100).

Found: m/z 342.1969. Calcd for $C_{25}H_{26}O$: M, 342.1984.

2,3-Dihydro-4,5,7-trimethyl-3-(4,6,8-trimethyl-1-azulenyl)-1*H*-inden-1-one (2E): Violet prisms; 10 mg (1.8%); mp 145 °C; R_f=0.63; UV 266, 297, 359, 563, and 600^{sh} nm (log ε 3.59, 4.30 3.44, 2.62, and 2.56); IR 1695 (C=O) cm^{-1}; ^1H NMR 1.80 (3H, s, Me-4), 2.28, (3H, s, Me-5), 2.60 (3H, s, Me-6′), 2.64 (3H, s, Me-4′), 2.65 (1H, dd, $J_{2,2}$=18, $J_{2,3}$=3.0 Hz, H-2), 2.78 (3H, s, Me-8′), 3.16 (3H, s, Me-7), 3.26 (1H, dd, $J_{2,3}$=8.0 Hz, H-2), 5.49 (1H, dd, H-3), 6.71 (1H, d, $J_{2',3'}$=4.0 Hz, H-2′), 6.95 (1H, s, H-5′), 6.97 (1H, s, H-7′), 7.00 (1H, s, H-6), and 7.11 (1H, d, H-3′); EI MS, m/z 342 (M^+; 22) and 170 (100).

Found: m/z 342.1979. Calcd for $C_{25}H_{26}O$: M, 342.1984.

4,8-Dimethyl-6-azulenecarbaldehyde[23] (2F): Dark green

prisms; 3 mg (0.5%); mp 98 °C (Ref. 23, 98 °C); R_f=0.57; ^{1}H NMR, see Table 1; EI MS, m/z 184 (M^+; 100).

Bis(4,6,8-trimethyl-1-azulenyl)acetaldehyde[24] (2G): Dark violet prisms; 3 mg (0.5%); mp 167 °C (Ref. 24, mp 177 °C); R_f=0.41; UV ($CHCl_3$) 249, 298,^{sh} 308, 355, 560, and 640^{sh} nm (log ε 4.63, 4.63, 4.63, 4.45, 2.79, and 2.61): IR 2810 and 1720 (CHO) cm^{-1}; ^{1}H NMR, see Table 1; EI MS, m/z 380 (M^+; 8), 351 (100), 321 (35), 183 (25), and 170 (32).

Found: m/z 380.2108. Calcd for $C_{28}H_{28}O$: M, 380.2140.

4,6,8-Trimethyl-1-azulenyl-(*E*)-2,4,6-Trimethylstyryl Ketone (2H): Dark orange prisms; 3 mg (0.5%); mp 132 °C; R_f=0.37; UV ($CHCl_3$) 244, 298, 340, 428, and 530^{sh} nm (log ε 4.52, 4.40 4.22, 4.21, and 2.99); IR (CCl_4) 1710 (C=O) cm^{-1}; ^{1}H NMR 2.22 (6H, s, Me-2′, 6′), 2.30, (3H, s, Me-4′), 2.56 (3H, s, Me-6), 2.69 (3H, s, Me-4), 2.82 (3H, s, Me-8), 6.79 (1H, d, J=16 Hz, CH-CO), 6.84 (2H, s, H-3′,5′), 7.01 (1H, d, $J_{5',7'}$=1.0 Hz, H-5), 7.08 (1H, d, H-7), 7.29 (1H, d, $J_{2',3'}$=4.0 Hz, H-3), 7.94 (1H, d, H-2), and 8.14 (1H, d, CH=C-CO); EI MS, m/z 342 (M^+; 25), 327 (100), 196 (25), 181 (73), 165, (43), 147 (85), 119 (38), and 91 (24).

Found: m/z 342.1946. Calcd for $C_{25}H_{26}O$: M, 342.1984.

4,6,8-Trimethyl-1,7-azulenequinone (2I): Yellow needles; 15 mg (2.3%); mp 118 °C decomp; $E_{1/2}$ −1.05 and −1.5 V (vs. SCE); R_f=0.25; UV 260, 307, 370, 386, and 404^{sh} nm (log ε 4.35, 4.19, 3.95, 3.95, and 3.87); IR 1695 and 1580 (C=O) cm^{-1}; ^{1}H NMR, see Table 1; ^{13}C NMR 197.21 (C-1), 187.28 (C-7), 150.84 (C-3), 148.16 (C-6), 143.95 (C-8), 143.54 (C-3a), 140.56 (C-5), 138.17 (C-8a), 137.70 (C-4), 133.61 (C-2), 23.94 (Me-8), 21.67 (Me-4), and 16.12 (Me-6); EI MS, m/z 200 (M^+; 100), 172 (8), 149 (10), 128 (8), 80 (12), 57 (10), and 43 (10).

Found: m/z 200.0833. Calcd for $C_{13}H_{12}O_2$: M, 200.0837.

4,6,8-Trimethyl-1,5-azulenequinone ($2J_1$): Yellow needles; 15 mg (2.3%); mp 120 °C (decomp); R_f=0.23; $E_{1/2}$ −1.05 and −1.46 V (vs. SCE); UV 245, 318, 380,^{sh} and 400^{sh} nm (log ε 4.17, 3.83, 3.75, and 3.65); IR 1695 and 1575 (C=O) cm^{-1}; ^{1}H NMR, see Table 1; ^{13}C NMR 198.67 (C-1), 189.97 (C-5), 151.25 (C-3), 145.99 (C-6), 144.30 (C-4), 139.10 (C-8), 138.99 (C-7), 138.87 (C-3a), 133.67 (C-8a), 130.81 (C-2), 23.53 (Me-8), 21.55 (Me-4), and 14.72 (Me-6); EI MS, m/z 200 (M^+; 100), 172 (57), 157 (16), 144 (16), 129 (68), 115 (20), 91 (10), 77 (16), and 51 (20).

Found: m/z 200.0829. Calcd for $C_{13}H_{12}O_2$: M, 200.0837.

2,3,5-Trimethylbenzaldehyde[22] ($2J_2$): Colorless needles; 2 mg (0.4%): R_f=0.23; ^{1}H NMR 2.29 (3H, s, Me-5), 2.32 (3H, s, Me-4), 2.47 (3H, s, Me-2), 6.72 (1H, s, H-3), 7.08 (1H, s, H-6), and 9.98 (1H, s, CHO); EI MS, m/z 148 (M^+; 100).

4,6,8-Trimethyl-1-azulenecarbaldehyde[16a] ($2K_1$): Red prisms; 5 mg (0.8%); mp 107 °C (Ref. 16a, 107 °C): R_f=0.18; ^{1}H NMR, see Table 1; EI MS, m/z 198 (M^+; 100).

3-[1,2-Dihydro-5,7-dimethyl-cyclopenta[*c*,*d*]azulen-2-yl]-4,6,7-trimethyl-1-(4,6,8-trimethyl-1-azulenyl)-1*H*-inden-1-ol ($2K_2$): Dark violet prisms; 1 mg (0.2%); mp 202 °C (decomp); R_f=0.18; UV ($CHCl_3$) 247, 306, 340, 566, and 652^{sh} nm (log ε 4.46, 4.45, 4.13, 2.80, and 2.46); IR (CCl_4) 3750—3150 (OH) cm^{-1}; ^{1}H NMR 1.56 (1H, m, OH), 2.14 (3H, s, Me-7), 2.22 (3H, s, Me-6), 2.48 (3H, s, Me-6″), 2.53 (3H, s, Me-7′), 2.69 (3H, s, Me-8″), 2.73 (3 H, s, Me-4″), 2.80 (3H, s, Me-5′), 2.97 (3H, s, Me-4), 4.10 (1H, $J_{1',2'}$=7.5, $J_{1',1'}$=4.0 Hz, H-1′), 4.39 (1H, $J_{1',2'}$=0.5 Hz, H-1′), 5.40 (1H, H-2′), 6.36 (1H, s, H-2), 6.59 (1H, d, $J_{6',8'}$=0.5 Hz, H-8′), 6.64 (1H, d, $J_{5'',7''}$=0.5 Hz, H-7″), 6.82 (1H, d, H-5″), 6.86 (1H, d, H-6′), 6.86 (1H, s, H-5), 7.11 (1H, d, $J_{2'',3''}$=4.0 Hz, H-3″), 7.32 (1H, d, $J_{3',4'}$=4.0 Hz, H-4′), 7.43 (1H, d, H-2″), and 7.85 (1H, d, H-3′); EI MS, m/z 522 (M^+; 9), 364 (53), 350 (43), 335 (100), 180 (36), 170 (85), and 155 (38).

Found: m/z 522.2932. Calcd for $C_{39}H_{38}O$: M, 522.2922.

Bis(4,6,8-trimethyl-1-azulenyl) Ketone ($2K_3$): Orange prisms; 1 mg (0.2%); mp 171 °C; R_f=0.18; UV ($CHCl_3$) 249, 329, 404, and 480^{sh} nm (log ε 4.55, 4.53, 4.25 and 3.59); IR 1635 (C=O) cm^{-1}; ^{1}H NMR, see Table 1; EI MS, m/z 366 (M^+; 0.8), 351 (3), 331 (3), 197 (100), 169 (14), 153 (11), and 43 (25).

***N*-Methyl-*N*-[(4,6,8-trimethyl-1-azulenyl)methyl]formamide (2L):** Blue paste; 6 mg (0.8%); R_f=0.06; UV 247, 294, 358, 600, 625,^{sh} and 650^{sh} nm; IR (CCl_4) 1690 (C=O) cm^{-1}; ^{1}H NMR, see Table 1; EI MS, m/z 241 (M^+; 66), 226 (27), 198 (22), 183 (100), 167 (38), 153 (34), 141 (20), 128 (24), and 42 (62).

***N*-Methyl-*N*-[(4,6,8-trimethyl-2-azulenyl)methyl]formamide (2M):** Violet needles 20 mg (2.6%); mp 90 °C; R_f=0.02; UV 251, 292, 354, and 550 nm (log ε 4.60, 4.66, 4.17, and 2.78); IR 1655 (C=O) cm^{-1}: ^{1}H NMR, see Table 1; EI MS, m/z 241 (M^+; 100), 226 (41), 198 (24), 183 (83), 167 (29), and 153 (19).

Found: m/z 241.1471. Calcd for $C_{16}H_{19}NO$: M, 241,1467.

Oxidation of 2 in HMPA. The same procedures as those for **2** were employed, and virtually the same products were obtained except for certain compounds in which fragments from the solvent are incorporated (e.g., **2L** and **2M**).

We wish to thank Professors Kahei Takase (Tohoku Univ), Ichiro Murata (Osaka Univ), Teruo Matsuura (Kyoto Univ), Wataru Ando (Tsukuba Univ) and Lawrence T. Scott (Nevada Univ) for valuable discussions.

References

1) A part of the results have been preliminarily reported as communications: T. Nozoe, S. Takekuma, M. Doi, Y. Matsubara, and H. Yamamoto, *Chem. Lett.*, **1984**, 627. Y. Matsubara, S. Takekuma, K. Yokoi, H. Yamamoto, and T. Nozoe, *ibid.*, **1984**, 631.

2) For reviews and monographs, see K. Hafner, *Angew. Chem.* **70**, 419 (1958); *Angew. Chem. Int. Ed. Engl.*, **3**, 167 (1964); E. Heilbronner, "Non-benzenoid Aromatic Compounds," ed by D. Ginsburg, Interscience, New York, N. Y. (1959), pp. 171—276, see also W. Keller-Schierlein and E. Heilbronner, *ibid.*, pp. 277—338. T. Nozoe and T. Asao, in "Comprehensive Organic Chemistry," ed by M. Kotake, Asakura, Tokyo (1960), Vol. 13, pp, 439—534; T. Nozoe and S. Ito, *Fortschr. Chem. Org. Naturst.*, **19**, 33 (1961); A. G. Angerson and R. G. Anderson, *J. Org. Chem.*, **27**, 3578 (1962), and references cited therein. K. Takase and M. Yasunami, *Yuki Gosei Kagaku Kyokai Shi.*, **39**, 1172 (1981); D. Lloyd, "Non-Benzenoid Conjugated Carbocyclic Compounds," Elsevier, Amsterdam (1984), pp. 351—377.

3) M. Pailer and H. Lobenwein, *Monatsh. Chem.*, **102**, 1558 (1971).

4) e.g. See Taiyo Yakuhin Kogyo KK. Jpn. Japanese Patent 59176248 [84176247] 1984; *Chem. Abstr.*, **102**, 50897t (1985).

5) J. Bargon, S. Mohmand, and R. J. Waltman, *Mol. Cryst. Liq. Cryst.*, **93**, 279 (1983); *IBM J. Res. Develop.*, **27**, 330 (1983); R. J. Waltman and J. Bargon, *Can. J. Chem.*, **64**, 76 (1986); K. Katagiri, Y. Oguchi, and Y. Takasu, Ger. Offen DE 3320674, 1983; *Chem. Abstr.*, **101**, 31122z (1984).

6) a) L. T. Scott, M. D. Rozeboom, K. N. Houk, T.

Fukunaga, H. J. Lindner, and K. Hafner, *J. Am. Chem. Soc.*, **102**, 5169 (1980), and references cited therein; b) L. T. Scott, *Pure Appl. Chem.*, **1983**, 363; c) L. T. Scott, P. Grutter, and R. Chamberlain, III, *J. Am. Chem. Soc.*, **106**, 4852 (1984); d) L. T. Scott and C. M. Adams, *ibid.*, **106**, 4857 (1984); e) T. Morita, M. Karasawa, and K. Takase, *Chem. Lett.*, **1980**, 197; f) T. Morita, F. Ise, and K. Takase, *ibid.*, **1982**, 1303.

7) K. Hafner, *Angew. Chem.*, **69**, 393 (1957); K. Hafner and H. Kaiser, *Justus Liebigs Ann. Chem.*, **618**, 140 (1958); *Org. Synth.* Coll. Vol. V, **1973**, 1088.

8) S. S. Danyluk and W. G. Schneider, *Can. J. Chem.*, **40**, 1777 (1962).

9) a) W. Treibs, *Chem. Ber.*, **92**, 2152 (1959); b) K. Kohara, Y. Otani, and N. Sakota, *Nippon Kagaku Kaishi*, **1975**, 139; c) K. Sato, I. Ogura, and M. Yamaguchi, *ibid.*, **1982**, 1206.

10) R. Hagen, E. Heilbronner, and P. A. Straub, *Helv. Chim. Acta*, **51**, 45 (1968).

11) a) L. Ruzicka, J. Meyer, and M. Mingazzini, *Helv. Chim. Acta*, **5**, 345 (1922); b) S. Takekuma, Y. Matsubara, H. Yamamoto, and T. Nozoe, *Yukagaku*, **34**, 1026 (1985).

12) C. S. Marvel and C. W. Hinman, *J. Am. Chem. Soc.*, **76**, 5435 (1954); M. B. Floyd and G. R. Allen, *J. Org. Chem.*, **35**, 2647 (1970); D. C. C. Smith and P. H. Lacy, *J. Chem. Soc. C*, **1971**, 41.

13) J. DeLaunary, M. A. Orliac-Le Moning, and J. Simonet, *J. Chem. Soc., Chem. Commun.*, **1983**, 820; L. Jalander and M. Broms, *Acta Chem. Scand. Ser. B.*, **36**, 371 (1982).

14) Compositions of the dimers from **1G** (all $C_{28}H_{32}O_2$, m/z 400), those from **1N** (all $C_{30}H_{32}O_4$, m/z 456), and those from $\mathbf{2B_1}$ and **2C** (all $C_{24}H_{24}O_2$, m/z 344) were confirmed by MS. However, purification and structural determination of these rather unstable dimers are currently under investigation.

15) W. Treibs, *Chem. Ber.*, **90**, 761 (1957); K. Kohara, *Bull. Chem. Soc. Jpn.*, **42**, 3229 (1969).

16) a) K. Hafner and C. Bernhard, *Angew, Chem.*, **69**, 533 (1957); *Justus Liebigs Ann. Chem.*, **625**, 108 (1959); b) M. Miyazaki, M. Hashi, and C. Ukita, *Chem. Pharm. Bull. (Tokyo)*, **8**, 140 (1960).

17) D. H. Reid, W. H. Stafford, and W. L. Stafford, *J. Chem. Soc.*, **1958**, 1118; W. Treibs, C. Vollrad, and M. Reimann, *Justus Liebigs Ann. Chem.*, **648**, 164 (1961).

18) A. J. Fry, B. W. Bowen, and P. A. Leermakers, *J. Org. Chem.*, **32**, 1970 (1967).

19) A. Anderson, Jr. and G. M. C. Chang, *J. Org. Chem.*, **23**, 1512 (1958).

20) In anhydrous acetonitrile at 25 °C [platinum electrode, vs. standard sodium calomel electrode (SCE); supporting electrolyte, 0.1 M Et_4NClO_4 (1 M=1 mol dm^{-3})]. We thank Professor Ichiro Murata (Osaka University) for the measurement of the half-wave potential data. The detailed discussion on the electrochemical data in relation to LUMO energy levels of these azulenequinones and other analogues will be reported later.

21) G. Hafelinger, F. Hack, and G. Westermayer, *Chem. Ber.*, **109**, 833 (1976).

22) E. Niedzielski and F. F. Nord, *J. Org. Chem.*, **8**, 147 (1943); J. Wiemann and P. Lacroix, *Bull. Soc. Chim. Fr.*, **1961**, 2257.

23) H. Arnold and K. Pahls, *Chem. Ber.*, **87**, 257 (1954).

24) Structure **2G** has been briefly described for a product obtained by condensation of **2** with glyoxal: K. Kohara, H. Tachibana, and Y. Ohtani, 23rd Symposium on the Chemistry of Terpenes, Essential Oils, and Aromatics, Tokyo, October 1979, Abstr. p. 102.

25) J. Betts, *Quart. Rev.*, **1971**, 165.

26) R. W. Adler and G. Whittacker, *J. Chem. Soc., Perkin Trans., 2*, **1975**, 1464.

27) J. F. Tilney-Bassett and W. A. Waters, *J. Chem. Soc.*, **1959**, 3123.

28) a) T. Kurihara, S. Ishikawa, and T. Nozoe, 52nd National Meeting of the Chemical Society of Japan, Kyoto, April 1986, Abstr. No. 2V26; b) S. Takekuma, K. Ihara, T. Uchida, Y. Matsubara, and T. Nozoe, 27th Symposium on the Chemistry of Terpenes, Essential Oils, and Aromatics, Nagasaki, October 1983, Abstr. No. 1B-53.

29) K.-P. Zeller, Angew. *Chem. Int. Edtn. Engl.*, **21**, 441 (1982); *Angew. Chem. Suppl.*, **1982**, 1016, and references cited therein.

30) T. Matsuura, "Aerobic Oxidation," Maruzen, Tokyo (1977); W. S. Trahanovski, "Oxidation in Organic Chemistry," Academic Press, New York (1978); M. Matsumoto, *Yoki Gosei Kagaku Kyokai Shi*, **43**, 753 (1985).

31) e.g. See J. Santamaria, *Tetrahedron Lett.*, **22**, 4511 (1981).

32) H. Iwamoto, M. Kanehiro, and Y. Matsubara, *Yukagaku*, **31**, 222 (1982).

33) A preliminary theoretical calculation has indicated that, when steric effect for the approach of oxygen molecule is taken into consideration, the facility of the radical attack on guaiazulene (**1**) is in the order of C-3>C-1>>C-5>C-8a>C-6 position on the nucleus, whereas that on 4,6,8-trimethylazulene (**2**) is C-1,3>>C-6>C-4,8>C-5,7; see Ref. 28a.

34) Y. Matsubara, S. Takekuma, K. Ueno, H. Yamamoto, and T. Nozoe, 52nd National Meeting of the Chemical Society of Japan, Kyoto, April 1986, Abstr. No. 2V27: the detailed mechanistic consideration of the products will be published in due time.

35) By the action of hydrogen peroxide, several examples of oxidative ring contraction of cycloheptatriene derivatives to benzenoid compounds (apparently through norcaradiene intermediates) have been reported: e.g., M. E. Vol'pin and D. N. Kursanov, *Doklady Akad. Nauk S.S.S.R.*, **126**, 780 (1959); M. E. Vol'pin, D. N. Kursanov, and V. G. Dulov, *Tetrahedron*, **8**, 33 (1960); H. Yamamoto, M. Sc. Thesis, Tohoku Univ., Sendai, Japan, 1965.

36) By autoxidation of solid **1** at 25 °C, we have isolated the dimeric norcaradiene **24** (green prisms, mp 155 °C) as a minor product; **24** is also produced when the autoxidation of **1** is performed in DMF in the presence of a small amount of 1 M sulfuric acid: see Ref. 34.

37) Studies on more selective, aerobic, as well as anodic, oxidation of azulenes at lower temperatures or under more dilute conditions are in progress.

38) a) R. K. Okuda, D. Klein, R. B. Kinnel, M. Li, and P. J. Scheuer, *Pure Appl. Chem.* **54**, 1907 (1982); b) P. J. Scheuer, Private communication.

39) We are grateful to Konan Kako Co. (Osaka) for a generous gift of guaiazulene and 4,6,8-trimethylazulene.

40) L. Ruzicka and J. Meyer, *Helv. Chim. Acta*, **5**, 505 (1921).

 © 1987 The Chemical Society of Japan Bull. Chem. Soc. Jpn., 60, 1429—1432 (1987)

Novel Base-Promoted Rearrangement of 2-(4-Cyano-, 2-Nitro-, and 4-Nitrobenzyloxy)tropones and 2-(2-Oxo-2-phenethyloxy)tropone to 2-[(4-Cyano-, 2-Nitro-, and 4-Nitrophenyl)hydroxymethyl]-tropones and 2-(1-Hydroxy-2-oxo-2-phenethyl)tropone

Hitoshi TAKESHITA,* Akira MORI, and Hiroshi SUIZU†
Research Institute of Industrial Science, 86, Kyushu University, Kasuga-koen, Kasuga, Fukuoka 816
†Graduate School of Engineering Sciences, 39, Kyushu University, Kasuga-koen, Kasuga, Fukuoka 816
(Received October 2, 1986)

The base-catalyzed rearrangement of 2-(2-nitro-, 4-nitro-, and 4-cyanobenzyloxy)tropones smoothly yielded corresponding 2-[(aryl)hydroxymethyl]tropones, while their thermolysis gave 3-(arylmethyl)tropolones. This reaction has no precedent analogy in troponoid chemistry, and this rearrangement is widely applicable to the 2-troponyl ethers of alcohols carrying an electron-attractive substituent on the α-position, as was verified by the occurrence of 2-(1-hydroxy-2-oxo-2-phenethyl)tropone from 2-(2-oxo-2-phenethyloxy)tropone.

Among the chemical properties of troponoids, base-promoted ring-contraction to benzenoid derivatives from various functionalized tropone derivatives has been one of the most outstanding features.[1] However, to overcome this disadvantage has been a synthetic problem. In the course of our study on the thermal reaction of troponoids, we have found a new radical reaction of 2-troponyl benzyl ethers to the 3- and 5-(arylmethyl)tropolones.[2] The rearrangement mechanism could be clarified by a kinetic analysis and isotope-labelling experiments. Similar rearrangements also occurred when 2-(2-furyl- and 2-thienylmethoxy)tropones were heated in decalin; i.e., 2-(2-furylmethoxy)tropone gave 3- and 5-(2-furylmethyl)-tropolones and 3- and 5-(5-methyl-2-furyl)tropolones,[3] and 2-(2-thienylmethoxy)tropones gave 3- and 5-(2-thienylmethyl)tropolones.[4] During the preparation of 2-(2- and 4-nitrobenzyloxy)tropones from tropolone and nitrobenzyl halides under basic conditions, we found an unprecedented rearrangement in the troponoid chemistry to form a C-C bond. We will, herein, describe this novel base-catalyzed reaction of 2-troponyl ethers of alcohols having an electron-attractive substituent on their α-position, such as 2-(2- and 4-nitrobenzyloxy)tropones and 2-(2-oxo-2-phenethyloxy)tropone (2-phenacyloxytropone).

Results and Discussion

When a hexamethylphosphoric triamide (HMPA) solution of potassium tropolonate (**1**) and 4-nitrobenzyl chloride (**2a**) was stirred at 50 °C for 10 h, three products (**3a**, **4a**, and **5a**) were isolated by silica-gel column chromatography in 69, 0.3, and 8% yields, respectively. The structures of **3a** and **4a** were identified to be 2-(4-nitrobenzyloxy)tropone and 3-(4-nitrobenzyl)tropolone; i.e., the ^{1}H NMR of **3a** revealed a methylene signal at a lower field, δ=5.24, and nine aromatic protons, while the ^{1}H NMR spectrum of **4a**, showed a methylene signal at a higher field, δ=4.21, and eight aromatic protons. The ^{13}C NMR spectral comparison of **3a** and **4a** with a series of previously prepared derivatives[2] supported this conclusion.

The third product, **5a**, had a secondary hydroxyl group and the tropone ring was retained. In the ^{1}H NMR, a singlet signal ascribable to the newly-formed methine proton appeared at δ=5.86. It was further noticed that its ^{13}C NMR spectrum closely resembled, except for an sp^3-carbon, those of 2-benzyltropones.[5] Following our previous method, the model compounds, 2-(4-nitrobenzyl)tropone (**6**) and 4-(4-nitrobenzyl)tropone (**7**), could be prepared by a thermolysis of 2-(4-nitrobenzylsulfonyl)tropone (**8**).[5,6] The chemical shift differences, $\Delta\delta$(**5a**−**6**), between **5a** and **6**, thus prepared, showed a good correlation: For the seven-membered ring carbons, they were 1.4 (C-1), 0.6 (C-2), 1.3 (C-3), 1.8 (C-4), 1.0 (C-5), 1.0 (C-6), and 0.2 (C-7). In addition, the benzoyl derivative **9a**, a pyridinium dichromate(PDC)-oxidation product of **5a**, showed no singlet proton signal in the region of δ=7 to 7.5. This eliminated the alternative 3-substituted tropone structures;[7] therefore, **5a** must be the α-hydroxylated derivative of **6**, 2-[hydroxy(4-nitrophenyl)methyl]tropone.

When **3a** was kept at room temperature in HMPA, no reaction occurred after 5 h; but when **3a** was refluxed in 1,2-dichlorobenzene (DCB), **4a** was formed in good yield. Furthermore, when **3a** was added to an HMPA solution of sodium hydride, the mixture instantly caused a change in color to yield **5a** in 72%, but no **4a**. Therefore, **3a** is not the precursor of **4a** already formed during preparation, and **4a** is likely to be formed by a direct C-attack. Clearly, the base was responsible for the formation of **5a**. For the rearrangement, the presence of an electron-attractive substituent, such as a nitro group, might be essential in order to generate a delocalized benzyl anion, since the unsubstituted 2-benzyloxytropone (**3d**)[2] gave no rearrangement product under comparable conditions. Such a stable anion (**A**) can be converted to the epoxide (**B**) by the assistance of a coordination with alkali metal ions to the carbonyl group. The following C-O bond cleavage should give **5** by another electrocyclic recombination.

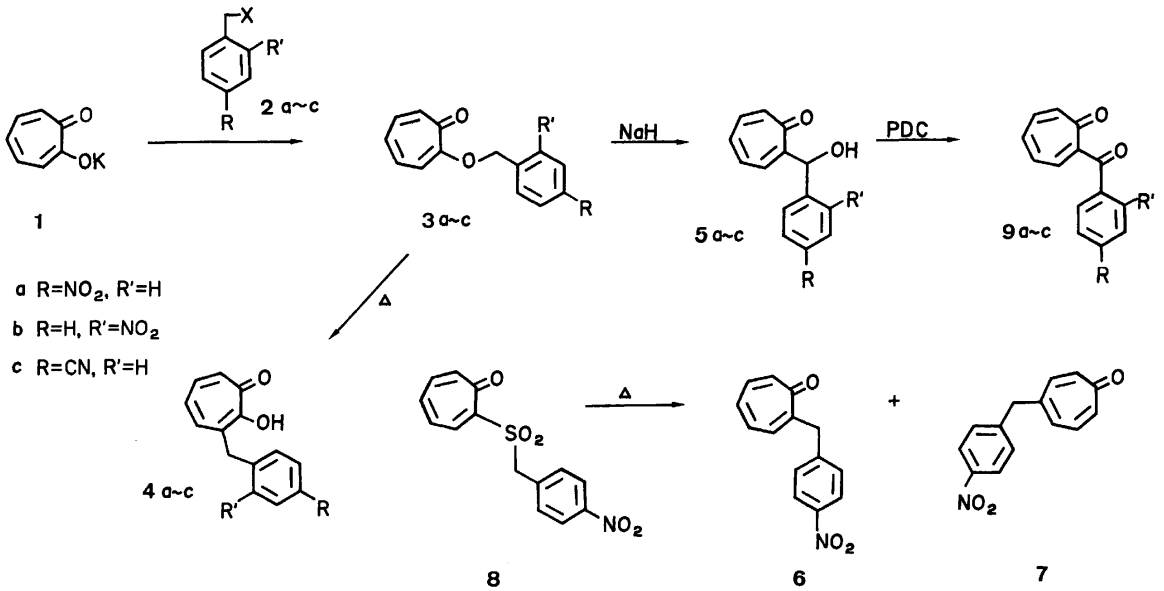

Scheme 1.

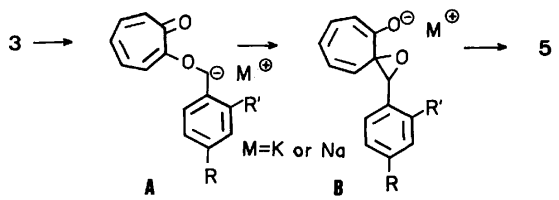

Scheme 2.

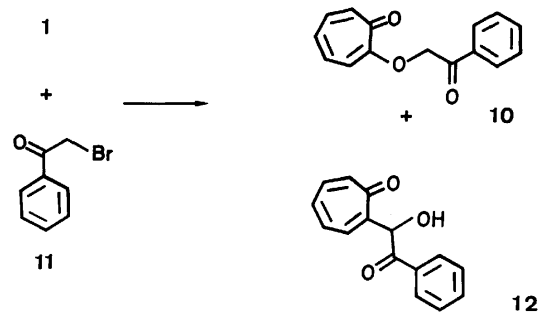

Scheme 3.

This base-promoted reaction was also applicable to the corresponding 2-isomer, **3b**: By a reaction of **1** with 2-nitrobenzyl chloride (**2b**) in HMPA, 2-(2-nitrobenzyloxy)tropone (**3b**) was obtained in 88% yield together with 2-[hydroxy(2-nitrophenyl)methyl]tropone (**5b**). An alkali treatment of **3b** with sodium hydride in HMPA afforded **5b** in 95% yield, but the thermolysis of **3b** in DCB slowly produced **4b**; its yield was ca. 44% at 32% conversion after 13-h period. This low reactivity of thermolysis might be attributable to a steric hindrance of the bulky 2-nitro group. An attempted purification of **4b** resulted in an extensive decomposition of the material. The PDC-oxidation of **5b** yielded 2-(2-nitrobenzoyl)tropone (**9b**).

The rearrangement must be applicable to other derivatives whose ethereal carbon can generate a stable carbanion. This was verified when 2-(4-cyanobenzyloxy)tropone (**3c**), prepared from **1** and 4-cyanobenzyl bromide (**2c**), was converted to 2-[(4-cyanophenyl)-hydroxymethyl]tropone (**5c**). Furthermore, **3c** was thermolyzed to 3-(4-cyanobenzyl)tropolone (**4c**) in good yield.

Moreover, 2-(2-oxo-2-phenethyloxy)tropone (**10**), prepared similarly by condensation of **1** with phenacyl bromide (**11**, ω-bromoacetophenone), disclosed similar features. Thus, the attempted preparation of **10** resulted in a rearrangement product, 2-(1-hydroxy-2-oxo-2-phenethyl)tropone (**12**) in 59% yield; the isolated yield of **10** was only 17%.

Therefore, this base-promoted rearrangement has a considerable utility for introducing functionalized carbon side chains into the tropone system; particularly, there is no versatile method of C-C bond formation on the tropone system. Namely, a Grignard reaction has been generally employed to prepare 2-substituted tropones,[8] but its utility was severely restricted by the low yields of the desired products and a formation of ring-contracted phenyl derivatives; e.g., triphenylmethanol formation from phenylmagnesium bromide and 2-methoxytropone is inevitable.[9] It is also well known that 2-alkoxytropones are unstable under basic conditions and cause a ring-contraction to benzenoids.[1] The sole occurrence of substitution without ring-contraction under the present conditions is rather surprising. The marked difference should primarily be attributed to the different nature of the solvent used; one for protic solvents, such as alcohols which are sufficiently nucleophilic, and another for a bulky and polar-aprotic HMPA, being weakly nucleophilic. This newly-recognized property of 2-alkoxytropones[10] will make various reactions under basic conditions promising.

Experimental

The elemental analyses were performed by Miss S. Hirashima, the Research Institute of Industrial Science, Kyushu University. The mps were measured with a Yanagimoto Micro mp Apparatus and are uncorrected. The NMR spectra were measured with a JEOL FX 100 Spectrometer in $CDCl_3$ solution, and the chemical shifts expressed were in δ units. The mass spectra were measured with a JEOL 01SG-2 Spectrometer. The IR spectra were taken as KBr disks using a Jasco IR-A 102 Spectrometer. The UV spectra were taken with a Hitachi 124 Model Spectrophotometer.

Condensation Reactions of Potassium Tropolonate with Benzyl Halides under Basic Conditions. Following our previous method,[2] to anhydrous HMPA (2 cm^3) of **1** (ca. 1 mmol), an HMPA solution (2 cm^3) of **2a—c** (ca. 1 mmol) was added dropwise at room temperature and kept at 50—100 °C under an N_2 atmosphere. The mixture was then diluted with water, acidified with dil HCl, and extracted with ether. Silica-gel column chromatography of the extracts afforded **3a—c**, **4a**, and **5a**, **b**.

3a: Colorless plates, mp 164—166 °C, 69%. Found: C, 65.25; H, 4.30; N, 5.61%. Calcd for $C_{14}H_{11}O_4N$: C, 65.36; H, 4.31; N, 5.45%. ^1H NMR δ=5.24 (2H, s), 6.6—7.0 (3H, m), 7.1—7.2 (2H, m), 7.60 (2H, d, J=9 Hz), and 8.19 (2H, d, J=9 Hz). ^{13}C NMR δ=69.7, 115.5, 124.1 (2C), 127.8 (2C), 129.3, 132.5, 136.8, 138.0, 141.3, 148.0, 164.1, and 180.8. IR ν: 1620, 1600, 1570, and 1510 cm^{-1}. UV λ_{max}^{MeOH}: 265 nm (ε=11000) and 317 (9900).

4a: Yellow crystals, mp 167—169 °C, 0.3%. Found: C, 65.26; H, 4.29; N, 5.87%. ^1H NMR δ=4.21 (2H, s), 6.99 (1H, ddd, J=9.5, 6, 5 Hz), 7.2—7.6 (3H, m), 7.38 (2H, d, J=9 Hz), and 8.08 (2H, d, J=9 Hz). ^{13}C NMR δ=40.9, 120.5, 123.9 (2C), 127.7, 130.0 (2C), 136.9, 139.5, 140.1, 147.0, 147.3, 167.9, and 173.6. IR ν: 1600, 1545, and 1340 cm^{-1}. UV λ_{max}^{MeOH}: 244 nm (ε=24000), 269 (11600), 322 (7400), 356 (6200), 372 (5900), and 401 (1700).

5a: Yellow crystals, mp 170—172 °C, 8%. Found: C, 65.48; H, 4.37; N, 5.73%. ^1H NMR δ=3.40 (1H, br s, OH), 5.86 (1H, s), 6.9—7.2 (4H , m), 7.46 (1H, d, J=5.5 Hz), 7.58 (2H, d, J=9 Hz), and 8.12 (2H, d, J=9 Hz). ^{13}C NMR δ=75.2, 123.7 (2C), 127.5 (2C), 134.4, 135.4, 135.9, 137.0, 142.2, 147.5, 149.5, 153.3, and 187.5. IR ν: 3250, 1620 and 1595 cm^{-1}. UV λ_{max}^{MeOH}: 275 nm (ε=14000) and 315 (10500).

3b: Yellow needles, mp 151—153 °C, 88%. Found: C, 65.26; H, 4.29; N, 5.87%. Calcd for $C_{14}H_{11}O_4N$: C, 65.36; H, 4.31; N, 5.45%. ^1H NMR δ=5.55 (2H, s), 6.7—7.3 (5H, m), 7.4—7.8 (2H, m), and 8.0—8.2 (2H, m). ^{13}C NMR δ=67.7, 114.9, 125.2, 128.5, 128.8 (2C), 132.7, 134.8, 136.8 (2C), 137.9, 146.7, 164.2, and 180.8. IR ν: 1622, 1590, 1565, and 1515 cm^{-1}. UV λ_{max}^{MeOH}: 237 nm (ε=28600), 319 (9800), 347 (7300), and 362 (4400).

5b: Brown crystals, mp 165—167 °C, 5%. Found: C, 65.12; H, 4.46; N, 5.88%. ^1H NMR δ=6.36 (1H, s) and 6.9—8.0 (9H, m). ^{13}C NMR δ=70.4, 124.8, 128.8, 129.2, 133.5, 134.2, 134.5, 134.9, 136.7, 141.7, 148.9, 153.0 (2C), and 187.4. IR ν: 3250 and 1620 cm^{-1}. UV λ_{max}^{MeOH}: 227 nm (ε=27800) and 306 (8900).

3c: Colorless plates, mp 144—145 °C, 75%. Found: C, 75.95; H, 4.70; N, 5.98%. Calcd for $C_{15}H_{11}O_2N$: C, 75.93; H, 4.67; N, 5.90%. ^1H NMR δ=5.24 (2H, s), 6.6—7.1 (3H, m), 7.1—7.3 (2H, m), 7.53 (2H, d, J=8.5 Hz), and 7.66 (2H, d, J=8.5 Hz). ^{13}C NMR δ=69.8, 112.1, 115.4, 118.7, 127.7 (2C), 129.1, 132.5, 132.7 (2C), 136.7, 137.9, 141.1, 164.1, and 180.7. IR ν: 2225, 1615, 1595, 1565, 1490, 1465, and 1400 cm^{-1}. UV λ_{max}^{MeOH}: 237 nm (ε=40000), 320 (8900), and 345 (6900).

Base-Promoted Rearrangement of 3a. An anhydrous HMPA solution (2 cm^3) of **3a** (49 mg) was treated with NaH (4 mg) at room temperature for 5 min. Silica-gel column chromatography of the mixture gave **5a**, 35.3 mg (72%), which was identical with the sample prepared as described above.

Thermolysis of 3a. A DCB solution (17.5 cm^3) of **3a** (202 mg) was heated in a sealed tube at 180 °C for 12 h. Column chromatography of the mixture afforded **4a**, 161 mg (80%), which was identical with the sample described above.

Preparation of 6 and 7 from 2-(4-Nitrobenzylsulfonyl)-tropone (8) by Thermolysis.[6] A decalin solution (20 cm^3) of **8** (157 mg) [colorless crystals, mp 162—163.5 °C. Found: m/z, 305.0365. Calcd for $C_{14}H_{11}O_4NS$: M, 305.0358. ^1H NMR δ=4.94 (2H, s), 6.8—7.3 (4H, m), 7.52 (2H, m), 7.86 (1H, dd, J=8, 1 Hz), and 8.14 (2H, m). ^{13}C NMR δ=60.5, 123.6 (2C), 131.3, 131.6 (2C), 134.8, 135.8, 139.5, 140.3, 143.9, 145.9, 160.1, and 182.3], prepared from an oxidation of the corresponding sulfinyl derivative by m-chloroperbenzoic acid,[5] was heated at 205 °C for 2 h. The mixture was then chromatographed on a silica-gel column to give a colorless oil, **6**, 28 mg (23%) [Found: m/z, 241.0740. Calcd for $C_{14}H_{11}O_3N$: M, 241.0740. ^1H NMR δ=4.03 (2H, s), 6.9—7.3 (5H, m), 7.40 (2H, d, J=9 Hz), and 8.09 (2H, d, J=9 Hz). ^{13}C NMR δ=40.9, 123.6 (2C), 129.9 (2C), 133.4, 133.6, 135.7 (2C), 136.1, 141.0, 147.0, 152.7, and 186.1], and a colorless oil, **7**, 7 mg (6%) [Found: m/z, 241.0739. ^1H NMR δ=3.93 (2H, s), 6.8—7.1 (5H, m), 7.30 (2H, m), and 8.16 (2H, m)].

PDC-Oxidation of 5a. Formation of 9a. To a CH_2Cl_2 suspension (10 cm^3) of PDC (440 mg) and Celite (1.5 g), a CH_2Cl_2 solution of **5a** (100.4 mg) was added and stirred at room temperature for 5 h. The mixture was then purified by chromatography with Florisil column to give pale yellow crystals, mp 174—176 °C, 72 mg (72%), **9a** [Found: C, 65.77; H, 3.63; N, 5.64%. Calcd for $C_{14}H_9O_4N$: C, 65.88; H, 3.55; N, 5.49%. ^1H NMR δ=7.0—7.5 (5H, m), 7.91 (2H, d, J=9 Hz), and 8.23 (2H, d, J=9 Hz). ^{13}C NMR δ=124.1 (2C), 130.0 (2C), 134.2, 136.8, 137.0, 137.5, 141.0, 143.9, 150.1, 150.5, 186.2, and 195.1. IR ν: 1675, 1625, and 1603 cm^{-1}. UV λ_{max}^{MeOH}: 228 nm (ε=20000), 265 (16000), and 305 (9400)].

Thermolysis of 3b. Similarly, a DCB solution (2 cm^3) of **3b** (100 mg) was heated in a sealed tube at 180 °C for 13 h. The chromatography of the mixture afforded **4b**, 14.3 mg (44%) [Found: m/z, 257.0663. Calcd for $C_{14}H_{11}O_4N$: M, 257.0686. ^1H NMR δ=4.41 (2H, s), 7.2—7.5 (7H, m), and 7.94 (1H, dd, J=9, 2 Hz)], along with unchanged **3b** (67.6 mg; 68%).

Base-Promoted Rearrangement of 3b. An anhydrous HMPA solution (1.5 cm^3) of **3b** (150 mg) was treated with NaH (12.5 mg) at room temperature to give **5b**, 142 mg (95%).

Base-Promoted Rearrangement of 3c. An anhydrous HMPA solution (2.5 cm^3) of **3c** (121.8 mg) was treated with NaH (55%, 6 mg) at 0 °C for 5 min. The mixture was then diluted with water, and extracted with AcOEt. Silica-gel column chromatography of the extract yielded yellow brown crystals, mp 131—133 °C, **5c**, 40.4 mg (62%) [Found: C, 76.00; H, 4.74; N, 5.96%. Calcd for $C_{15}H_{11}O_2N$: C, 75.93; H, 4.67; N, 5.90%. ^1H NMR δ=5.83 (1H, s), 6.9—7.3 (4H, m), 7.45 (1H, d, J=5 Hz), and 7.51 (4H, s). ^{13}C NMR δ=74.9, 111.3, 127.2

(2C), 132.1 (2C), 134.2, 135.1, 135.7, 136.8, 142.0 (2C), 147.4, 153.3, and 187.2. IR ν: 3350, 2240, 1630, 1605, 1575, and 1400 cm^{-1}. UV λ_{max}^{MeOH}: 235 nm (ε=31000) and 314 (7800)], and the recovered **3c** (56.7 mg; 47%).

Thermolysis of 3c. A DCB solution (1.5 cm^3) of **3c** (55.7 mg) was heated at 180 °C for 9 h. Silica-gel column chromatography of the resultant mixture afforded colorless needles, mp 116—118 °C, **4c**, 21.5 mg (55%) [Found: C, 75.76; H, 4.61; N, 5.88%. Calcd for $C_{15}H_{11}O_2N$: C, 75.93; H, 4.67; N, 5.90%. ^1H NMR δ=4.18 (2H, s) and 6.8—7.6 (8H, m), ^{13}C NMR δ=41.4, 110.7, 119.1, 120.7, 127.6, 129.9 (2C), 132.5 (2C), 136.8, 139.5, 140.0, 145.1, 168.1, and 173.5. IR ν: 3200, 2240, 1605, 1550, 1485, 1415, and 1385 cm^{-1}. UV λ_{max}^{MeOH}: 236 nm (ε=30300), 324 (7400), 372 (5500), and 400 (2500)], and **3c** (16.9 mg; 30%).

PDC-Oxidation of 5b. Formation of 9b. To a CH_2Cl_2 suspension (10 cm^3) of PDC (133 mg) and Celite (500 mg), a CH_2Cl_2 solution (10 cm^3) of **5b** (30.1 mg) was added and stirred at room temperature for 5 h. The mixture was worked up in a manner similar to the case of **5a** and afforded yellow crystals, mp 131—133 °C, 15 mg (50%), **9b** [Found: C, 65.72; H, 3.67; N, 5.78%. Calcd for $C_{14}H_9O_4N$: C, 65.88; H, 3.55; N, 5.49%. ^1H NMR δ=6.9—7.3 (4H, m), 7.4—7.8 (3H, m), and 8.0—8.2 (2H, m). ^{13}C NMR δ=123.9, 124.8, 129.0, 130.3, 133.4, 134.1, 135.6, 137.8, 138.5, 140.1, 144.3, 146.5, 185.6, and 193.7. IR ν: 1670, 1620, 1570, 1515, and 1340 cm^{-1}. UV λ_{max}^{MeOH}: 237 nm (ε=28600), 319 (9800), 347 (7300), and 362 (4400, sh)].

PDC-Oxidation of 5c. Formation of 9c. To a CH_2Cl_2 suspension (5 cm^3) of PDC (122.6 mg) and Celite (500 mg), a CH_2Cl_2 solution (5 cm^3) of **5c** (25.1 mg) was added and similarly oxidized to give a light yellow crystals, mp 166—168 °C, 18.5 mg (74%), **9c** [Found: C, 76.44; H, 3.91; N, 5.97%. Calcd for $C_{15}H_9O_2N$: C, 76.58; H, 3.86; N, 5.96%. ^1H NMR δ=7.0—7.5 (5H, m), 7.67 (2H, d, J=8.5 Hz), and 7.87 (2H, d, J=8.5 Hz). ^{13}C NMR δ=116.6, 127.4, 129.5 (2C), 132.7 (2C), 134.2, 136.6, 136.9, 137.3, 139.4, 143.8, 150.2, 186.1, and 195.2. IR ν: 3050, 2220, 1670, 1620, 1560, 1460, and 1395 cm^{-1}. UV λ_{max}^{MeOH}: 233 nm (ε=24500) and 313 (7200)].

Condensation of 1 with 11. Formation of 10 and 12. An anhydrous HMPA solution (3 cm^3) of **1** (300.6 mg) and **11** (305 mg) was stirred at 50 °C for 2.5 h. The mixture was then acidified with dil HCl and extracted with AcOEt. The AcOEt extract was, after drying on $MgSO_4$, chromatographed on a silica-gel column to afford **10** [light brown crystals, mp 132—133 °C, 63.5 mg; 17%. Found: C, 74.97; H, 5.04%. Calcd for $C_{15}H_{12}O_3$: C, 74.99; H, 5.03%. ^1H NMR δ=5.52 (2H, s) and 6.7—8.1 (10H, m). ^{13}C NMR δ=71.7, 117.8, 128.4 (2C), 129.1 (3C), 129.7, 132.7, 134.3, 136.8, 138.4 (2C), 164.3, and 193.6. IR ν: 1685, 1625, 1590, 1565, 1495, 1470, 1450, 1430, 1405, 1395, 1375, and 1300 cm^{-1}. λ_{max}^{MeOH}: 241 nm (ε=31000), 321 (8800), 346 (7300, sh), and 361 (4700, sh)], **12** [colorless crystals, mp 118—120 °C, 222 mg; 59%. Found: C, 75.15; H, 5.08%. ^1H NMR δ=4.4—4.8 (1H, br), 6.19 (1H, s), 6.8—7.2 (4H, m), 7.2—7.6 (4H, m), and 7.8—8.1 (2H, m). ^{13}C NMR δ=73.9, 128.9 (2C), 129.0 (3C), 134.1 (2C), 135.4, 136.4, 137.2, 142.4, 151.4, 185.7, and 199.1. IR ν: 3300, 1670, 1620, 1590, 1535, 1515, 1465, 1445, 1405, and 1330 cm^{-1}. λ_{max}^{MeOH}: 233 nm (ε=25000) and 307 (7900)], and unreacted tropolone [36.8 mg; 16%].

Conversion of 10 to 12. An HMPA solution (1 cm^3) of NaH (trace) and **10** (25.1 mg) was stirred at room temperature for 10 min. After acidification with dil HCl, the mixture was extracted with AcOEt and chromatographed on a silica-gel column to give **12**, 11.1 mg (44%).

Attempted Base-Treatment of 2-Benzyloxytropone (3d). An anhydrous HMPA solution (1.5 cm^3) of NaH (6.8 mg) and **3d**[2] (60 mg) was kept at room temperature for 1.5 h. Thin-layer chromatograms of the mixture gave the recovered **3d** [44 mg; 74%] as the sole identifiable compound.

The authors wish to thank the Ministry of Education, Science and Culture for a financial support through a Grant-in-Aid for Scientific Research to A. M. (No. 60470025).

References

1) T. Nozoe, K. Takase, and H. Matsumura, "Non-Benzenoid Aromatic Compounds," Vol. 13 of "Dai Yuki Kagaku (Comprehensive Organic Chemistry) (ed. M. Kotake)," Asakura Shoten, Tokyo (1960), pp. 181—191.

2) H. Takeshita, H. Mametsuka, A. Chisaka, and N. Matsuo, *Chem. Lett.*, **1981**, 73.

3) H. Takeshita and H. Mametsuka, *Heterocycles*, **22**, 663 (1984).

4) H. Takeshita, H. Mametsuka, and H. Motomura, *J. Heterocyclic Chem.*, **23**, 1211 (1986).

5) H. Takeshita, N. Matsuo, and H. Mametsuka, *Bull. Chem. Soc. Jpn.*, **57**, 2321 (1984).

6) We thank Mr. Norihide Matsuo, M. Eng., for this experiment.

7) On the basis of a mechanistic ground, a formation of 3-substituted tropone derivatives via a less-strained oxetane intermediate than the oxirane intermediate, **B**, as depicted in Scheme 2 may be equally probable.

8) T. Nozoe, T. Mukai, and J. Minegishi, *Proc. Jpn. Acad.*, **27**, 419 (1951); W. von E. Doering and C. F. Haskey, *J. Am. Chem. Soc.*, **74**, 5688 (1952).

9) T. Nozoe, T. Mukai, J. Minegishi, and T. Fujisawa, *Sci. Repts. Tohoku Univ., Ser. I*, **37**, 388 (1953); T. Mukai, *Bull. Chem. Soc. Jpn.*, **31**, 852 (1958).

10) Benzenoid analogs, salicylaldehyde or other phenolic compounds carrying electron-attractive substituents, seem to be worth trying, but at least to date every attempt was unsuccessful.

 © 1987 The Chemical Society of Japan Bull. Chem. Soc. Jpn., 60, 1433—1439 (1987)

Synthesis of 2,2-Di-*C*-methyl-2-deoxy- and 4,4-Di-*C*-methyl-4-deoxypyranosides via Michael Addition of Conjugated Enopyranosiduloses

Nobuya KAWAUCHI, Ken-ichi SATO, Juji YOSHIMURA, and Hironobu HASHIMOTO*
Laboratory of Chemistry of Natural Products, Faculty of Science, Tokyo Institute of Technology, Nagatsuta, Midori-ku, Yokohama 227
(Received October 7, 1986)

Three hexopyranosides having *gem*-di-*C*-methyl group at 2- or 4-positions were synthesized by Michael addition to 2-enopyranosid-4-ulose and 3-enopyranosid-2-ulose derivatives, respectively, followed by hydroboration. A heptopyranosid-6-ulose having *gem*-di-*C*-methyl group at C-4 was also synthesized from 4-enopyranosid-6-ulose derivative in a similar way.

In recent years, carbohydrates have been used widely as chiral sources for synthesis of natural products.[1] *gem*-Dialkylation of carbohydrates has progressed on this utilization. For example, the following *gem*-dialkyl groups have been constructed: a) *C*-cyano-*C*-nitromethyl as well as *C*-methyl-*C*-nitromethyl group from the *C*-nitromethylene group by Michael addition,[2] b) *C*-(ethoxycarbonylmethyl)-*C*-methyl group by enolate alkylation of the ulose derivative,[3] c) *C*-formylmethyl-*C*-vinyl group from *C*-[2-(vinyloxy)ethylidene] group by Claisen rearrangement.[4] On the other hand, introduction of *gem*-dimethyl group into the carbohydrate skeleton has not yet been reported except a recently published paper[5] and our preliminary one,[6] although *gem*-dimethylation has been achieved for non-carbohydrate compounds by several methods.[7-11] In this paper we should like to report on the synthesis of *gem*-di-*C*-methylpyranosides by Michael addition of methylcuprates(I) to conjugated enopyranosiduloses. This method has been proved to be useful for construction of *gem*-dimethyl function at C-2 and C-4 positions of hexopyranosides, while the method by hydrogenolytic cleavage of spirocyclopropane ring for that at C-3 position.[6]

Results and Discussion

Four kinds of conjugated enopyranosiduloses **2**—**5** were used for this study. The first two branched-chain enopyranosiduloses **2** and **3** were derived from a common starting compound, i.e., methyl 6-*O*-trityl-α-D-*glycero*-2-enopyranosid-4-ulose (**6**).[12] Conjugate 1,4-addition of a lithium (cyano)dimethylcuprate(I), $Me_2Cu(CN)Li_2$, to **6** followed by treatment with chlorotrimethylsilane, gave the corresponding enol trimethylsilyl ether **7**. Dehydrosilylation of **7** with *p*-benzoquinone in the presence of palladium(II) acetate[13] afforded **2** in 55% yield from **6**. Alternatively, the enone **2** was prepared from methyl 4,6-*O*-benzylidene-2-deoxy-2-*C*-methyl-α-D-altropyranoside (**9**) via the 3-enopyranoside **8**, which was formed selectively by treatment of the 3-mesylate **10** of **9** with potassium *t*-butoxide. Palladium-catalyzed enone formation[14] was proved to be effective for the enolate **8** to give enone **1**, which was converted into **2** by a conventional tritylation. The total yield of **2** from **9** was 11.4%. The latter route proved to be rather convenient than the previous one[15] in the steps of elimination and enone formation.

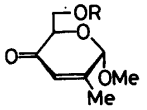

1 R=H
2 R=Tr

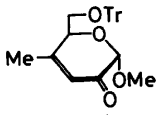

3

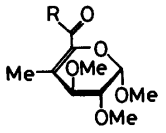

4 R=H
5 R=Me

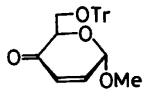

6

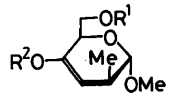

7 R^1=Tr, R^2=TMS
8 R^1, R^2=PhCH

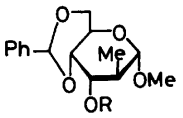

9 R=H
10 R=Ms

On the other hand, the enone **3** was already prepared[16] by pyridinium chlorochromate oxidation of 1,2-adduct **11** obtained by treatment of **6** with methyllithium. In the addition reaction the ratio of **11** and its 4-epimer was proved to be 4 : 3, while with methylcerium(III) reagent[17] instead of methyllithium **11** was obtained exclusively in a quantitative yield. Thus it is noteworthy that the methylcerium reagent tends to facilitate axial attack of carbanion, which was also observed in the reaction of methyl 3,4-dideoxy-6-*O*-trityl-α-D-*glycero*-3-enopyranosid-2-ulose.[18] Furthermore, oxidation of **11** with pyridinium fluoroformate[19] instead of chloroformate gave **3** in a higher yield (86%), indicating that this less acidic oxidant are convenient and effective for allylic alcohol.

The enone **4** was derived from methyl 6-*O*-benzyl-2,3-di-*O*-methyl-α-D-glucopyranoside (**12**)[20] according to a similar strategy to Hanessian et al.[21] Swern oxidation of **12** gave the corresponding 4-ulose, which was converted stereoselectively with methylmagnesium iodide into the 4-*C*-methyl derivative **13** of D-*galacto* configuration in 77% yield in two steps. Methylation of **13** followed by hydrogenolytic removal of 6-*O*-benzyl group and Swern oxidation gave a dialdose **14** in 79% yield. Then, **4** was obtained in 65% yield by treatment of **14** with calcium hydroxide. As shown in

Table 1 the reaction of **4** with various methylcuprates(I) gave in good yields the 1,2-adduct **15**, from which the enone **5** was derived quantitatively by Swern oxidation.

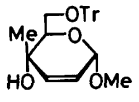

11

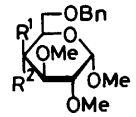

12 $R^1=H$, $R^2=OH$
13 $R^1=OH$, $R^2=Me$

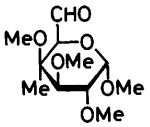

14

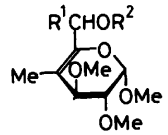

15 $R^1=Me$, $R^2=H$
16 $R^1=Me$, $R^2=Ac$
17 $R^1=R^2=H$

The reaction of these enones **2**, **3**, and **5** with lithium (cyano)dimethylcuprate(I), $Me_2Cu(CN)Li_2$, gave preferentially 1,4-adducts, *gem*-di-*C*-methyl-pyranosiduloses **18**, **19**, and **20**, respectively, in high yields as shown in Table 1. In the case of **3** very small amount of by-product, the *β*-anomer of **19**, was isolated. On the other hand, the reaction of the enal **4** afforded an epimeric mixture of 1,2-adduct **15** together with small amount of reduced product **17**. The distinct difference of regioselectivity in the addition reactions between **4** and **5** coincide with the fact that aldehydes react easily with lithium organocuprates, while ketones not.[22]

Table 1. Reaction of Methyl Branched Enones **2**—**5** with Lithium Methylcuprates (I)

Enone	Product	Yield/%	
		Me_2CuLi	$Me_2Cu(CN)Li_2$
2	**18**	72	77
	5-epimer of **18**	8.4	3.1
3	**19**	82	93
	β-anomer of **19**	6.9	4.1
4[a]	**15**	62	90
	17	12	trace
5	**20**	83	89

a) With $Me_5Cu_2Li_3$ the yield of **15** was 93%.

Thus, it was turned out that *gem*-dimethylation in hexopyranoside ring could be performed very easily using conjugate addition to the enopyranosiduloses. Furthermore, in the cases of **18** and **19** asymmetric carbons lost during the enone formation was also recovered by hydroboration of the silyl enolates[23] e.g., **18** → **21** → **24** or **19** → **23** → **26**. The enolates **21** and **23** were obtained by quenching the above mentioned Michael addition with chlorotrimethylsilane in good yields. Hydroborations of **21** and **23** were examined using various reagents and the products were analyzed after hydrolysis and acetylation. As summarized in Table 2, hydroboration with 3 equivalents of diborane gave the best results. In the case of **21**, only 2-deoxy-2,2-di-*C*-methyl-hexopyranoside derivative **24** was obtained as hydroboration product, where a small amount of 3-deoxy-D-*erythro*-hexopyranoside **25** and 3-enopyranoside **22** were also formed. In the case of **23**, 4-deoxy-4,4-di-*C*-methyl-D-*xylo*- **26** and D-*arabino*-hexopyranoside derivatives **28** were obtained in a ratio of 3 to 1, and 3-deoxy-D-*erythro*-hexopyranoside **27** was also formed. Hydroboration with borane formed in situ from sodium borohydride and Lewis acids such as titanium(III) chloride[24] and cobalt(II) chloride[25] gave also the desired products in moderate yields, although recovery of the uloses were increased. On the other hand, hydroboration with disiamylborane and 9-borabicyclo[3.3.1]nonane (9-BBN) gave small amount of the reduced by-products, **25** and **27**, while the uloses were recovered in high yield. Only in the case of **23** hydroboration with disiamylborane afforded **26**, albeit in 17% yield, stereoselectively. The structures of **24**, **26**, and **28** were confirmed on the basis of two acetyl signals and the coupling constants of methine protons

Table 2. Hydroboration[a] of **21** and **23**

Enolate	Reagent	Product[b] and Yield/%						Recovered ulose/%	
21	Borane (1.1 equiv)	**24**	Trace					**18**	70
21	Borane (3.0 equiv)	**24**	43	**25**	6.4	**22**	5.8		
21	Borane (9.0 equiv)	**24**	44	**25**	8.6	**22**	4.6		
21	$NaBH_4$, $TiCl_3$	**24**	12.5	**25**	12.5	**22**	10	**18**	30
21	$NaBH_4$, $CoCl_2$	**24**	26	**25**	Trace	**22**	2.0	**18**	51
21	Disiamylborane	**24**	Trace	**25**	14			**18**	76
21	9-BBN[c]	**24**	Trace	**25**	7.8			**18**	70
23	Borane (1.1 equiv)	**26**	26	**28**	5.3	**27**	9.0		
23	Borane (3.0 equiv)	**26**	29	**28**	9.7	**27**	13		
23	Borane (9.0 equiv)	**26**	22	**28**	6.3	**27**	13.5		
23	$NaBH_4$, $CoCl_2$	**26**	24	**28**	12	**27**	Trace		
23	$NaBH_4$, $TiCl_3$	**26**	27	**28**	9.1	**27**	16		
23	Disiamylborane	**26**	17			**27**	13	**19**	43
23	9-BBN[c]	**26**	Trace			**27**	7.9	**19**	57

a) Followed by treatment with alkaline hydrogen peroxide. b) Isolated after acetylation with acetic anhydride and pyridine. c) 9-Borabicyco[3.3.1]nonane.

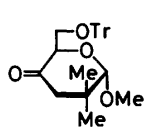

18

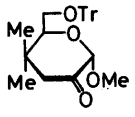

19

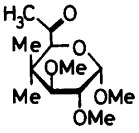

20

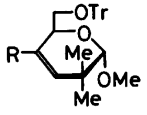

21 R = OTMS
22 R = H

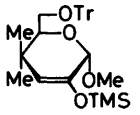

23

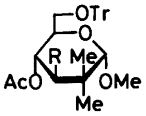

24 R = OAc
25 R = H

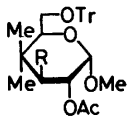

26 R = OAc
27 R = H

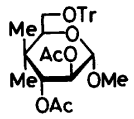

28

with acetoxyl groups, i.e., $J_{3,4}$=8.0 Hz, $J_{2,3}$=7.8 Hz, and $J_{2,3}$=4.0 Hz, respectively. While those of **25** and **27** by one acetyl signal and the coupling constants of methine protons with acetoxyl group, i.e., $J_{3ax,4}$=7.8 Hz and $J_{2,3ax}$=13.3 Hz, respectively.

The formation of the deoxygenated derivatives, **25** and **27**, may be rationalized by trans β-elimination[26] of trimethylsiloxyborane from the hydroboration products, giving the corresponding de(trimethylsilyloxy) derivative. Actually in the reaction of **21**, the de(trimethylsilyloxy) intermediate **22** was isolated. Further hydroboration of **22** followed by oxidation may give **25**, where the stereoselectivity was well-explained by a half-chair conformation as depicted in the following scheme.

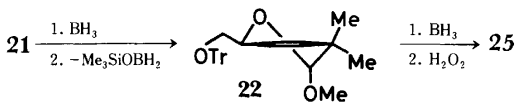

Thus, Michael addition of lithium methylcuprate to 2-enopyranosid-4-ulose and 3-enopyranosid-2-ulose derivatives, followed by hydroboration-oxidation, opened the synthetic routes of hexopyranosides having *gem*-di-*C*-methyl group at 2- and 4-positions, respectively.

Experimental

General Methods. Melting points determined with a Yanagimoto micro melting point apparatus, were uncorrected. Optical rotations were measured in chloroform, by using a 0.5-dm tube with a Carl Zeiss LEP-Al polarimeter. Infrared spectra were recorded on a Hitachi EPI-G2 grating spectrometer. ^{1}H and ^{13}C NMR spectra were recorded at 100 MHz with a JEOL JMN PS-100 spectrometer and at 22.5 MHz with a JEOL FX-90Q spectrometer, respectively, in $CDCl_3$ with tetramethylsilane as internal standard. Column chromatography was performed on silica gel (Wakogel C-300: Wako Pure Chemical Industries, Ltd.) ^{1}H and ^{13}C NMR data of pyranosides having *gem*-di-*C*-methyl group are summarized in Table 3.

Methyl 2,3-Dideoxy-2-*C*-methyl-6-*O*-trityl-α-D-*glycero*-hex-2-enopyranosid-4-ulose (2). To a mixture of palladium(II) acetate (112 mg, 0.5 mmol) and *p*-benzoquinone (54 mg, 0.5 mmol) was added under argon a solution of **7** (460 mg, 0.95 mmol), whose preparation is described below, in acetonitrile (4 ml). The mixture was stirred at 50 °C for 6 h, and fractionated directly on a silica-gel column with benzene-acetone (15 : 1) to give **2** (241 mg, 62%). IR and NMR data of **2** coincided with the reported data.[15]

Methyl 3,4-Dideoxy-4-*C*-methyl-6-*O*-trityl-α-D-*glycero*-hex-3-enopyranosid-2-ulose (3). A solution of pyridinium fluorochromate (2.36 g, 11.9 mmol) and **11** (2.72 g, 6.6 mmol) in dichloromethane (84 ml) was stirred at room temperature for 6 h. The undissolved materials were filtered off, and the filtrate was washed with 2.5% aqueous sodium hydroxide and water, and dried with potassium carbonate. Evaporation of the filtrate gave a syrup, which was purified on a short column of silica gel with hexane-ethyl acetate (18 : 1) to afford **3** (2.33 g, 86%) as a colorless syrup. ^{1}H NMR data was identical with those reported.[16]

Methyl 4-Deoxy-2,3-di-*O*-methyl-4-*C*-methyl-β-L-*threo*-hexodialdo-4-enopyranoside-(1,5) (4). To a solution of **14** (500 mg, 2.0 mmol) in tetrahydrofuran (5 ml) and water (5 ml), was added 0.5 M (1 M=1 mol dm^{-3}) aqueous solution of barium hydroxide (4 ml). The mixture was kept at room temperature for 6 h, then saturated with ammonium chloride and extracted with chloroform. The extract was washed with aqueous sodium chloride, dried over magnesium sulfate, and evaporated to give a crude mixture of products, which was fractionated on a column of silica gel with hexane-acetone (5 : 1) to give **4** (284 mg, 65%), methyl 2,3-di-*O*-methyl-4-*C*-methylene-β-L-*threo*-hexodialdo-4-enopyranoside-(1,5) (17 mg, 3.9%), and starting material (29 mg, 5.8%).

4: Mp 148—150 °C, $[\alpha]_D^{20}$ +31.2° (*c* 0.7, $CHCl_3$). IR (KBr) 1680 (CO) and 1640 cm^{-1} (C=C), ^{1}H NMR δ=5.06 (1H, d, H-1), 3.92 (1H, dd, $J_{1,2}$=2.2 Hz, H-2), 3.60 (1H, d, $J_{2,3}$=7.8 Hz, H-3), 9.76 (1H, s, H-6), 2.12 (3H, s, C-Me), 3.44 (3H, s, OMe) and 3.52 (6H, s, OMe).

Found: C, 55.38; H, 7.48%. Calcd for $C_{10}H_{16}O_5$: C, 55.54; H, 7.46%.

The *exo*-methylene compound was a syrup, and had $[\alpha]_D^{20}$ +10.1° (*c* 0.88, $CHCl_3$). ^{1}H NMR δ=4.96 (1H, d, $J_{1,2}$=3.0 Hz, H-1), 3.6—3.7 (2H, m, H-2 and H-3), 3.98 (1H, bs, H-5), 9.54 (1H, bs, H-6), 3.52 (3H, s, OMe), and 3.56 (6H, s, OMe).

Found: C, 55.41: H, 7.60%. Calcd for $C_{10}H_{16}O_5$: C, 55.54; H, 7.46%.

Methyl 4,7-Dideoxy-4-*C*-methyl-2,3-di-*O*-methyl-β-L-*threo*-hept-4-enopyranosid-6-ulose (5). To a suspension of cerium(III) chloride (318 mg, 1.3 mmol) in tetrahydrofuran (5 ml), was added an ethereal solution of methyllithium (1.2 M solution, 1.1 ml, 1.3 mmol) at −78 °C, and then after 1 h a solution of **4** (260 mg, 1.1 mmol) in tetrahydrofuran (5 ml). The mixture was kept at −78 °C for 4 h and poured into a saturated ammonium chloride solution and extracted with dich-

Table 3. ^1H and ^{13}C NMR Data of Pyranosides Having *gem*-Di-*C*-methyl Group

Compound	1	2	3	4	5	6	C-Me	OMe	Others
18(^1H)	4.36s		2.08, 2.50d (J=15.4)		4.02dd ($J_{5,6}$=4.2)	3.30dd, 3.42t ($J_{5,6'}=J_{6,6'}$=8.8)	0.94s 1.18s	3.44s	7.1—7.5m (Tr)
18(^{13}C)	103.08d	37.39s	47.24t	205.51s	73.16	61.64t	25.23q 25.82q	54.57q	a)
19(^1H)	4.58s		1.96dd (J=1.0), 2.64d (J=14.2)		4.16dd ($J_{5,6}$=7.4)	3.20t, 3.18dd ($J_{5,6'}=J_{6,6'}$=3.8)	1.76bs 1.78s	3.60s	7.1—7.6m (Tr)
19(^{13}C)	100.24	202.58	51.04	39.88	75.53	63.07	20.43 26.82	54.94	b)
24(^1H)	5.16s		5.22d ($J_{3,4}=J_{4,5}$=8.0)	5.08t	3.86m	3.12dd, 3.20t	0.96s 1.12s	3.38s	1.86s, 2.00s (OAc) 7.2—7.6m (Tr)
24(^{13}C)	105.52	40.80	68.28	69.74	75.06	62.86	19.93 20.60	55.00	22.16, 20.74 (Me) 170.48, 169.55 (C=O)[c]
			1.62bt ($J_{3',4}=J_{3',3}$=7.8)						
25(^1H)	4.20s		1.44dd ($J_{3,4}$=4.4)	5.00ddd ($J_{4,5}$=6.6)	3.96ddd ($J_{5,6}$=4.0)	3.16dd, 3.24t ($J_{6,6'}=J_{5,6'}$=8.0)	0.92s 1.04s	3.32s	2.02s (OAc) 7.2—7.6m (Tr)
25(^{13}C)	99.66	35.34	43.99	70.28	71.69	62.28	19.86 21.13	57.20	21.33, 164.62 (OAc)[d]
26(^1H)	4.42d ($J_{1,2}$=4.0)	4.56dd ($J_{2,3}$=7.8)	4.72bd		3.2—3.6m (2H)	3.12dd ($J_{5,6}$=4.0, $J_{6,6'}$=6.8)	0.88s 0.90s	3.60s	2.08s, 2.12s (OAc) 7.2—7.6m (Tr)
26(^{13}C)	98.76	69.45	81.75	38.70	75.88	64.14	20.67 23.43	53.12	24.10, 24.75 (Me) 167.38, 168.94 (C=O)[e]
28(^1H)	4.60d ($J_{1,2}$=1.2)	4.22bdd ($J_{2,3}$=4.0)	4.26bd		3.2—3.5m (2H)	3.14dd ($J_{5,6}$=2.8, $J_{6,6'}$=5.4)	0.82s 0.86s	3.64s	2.02bs (6H) (OAc) 7.2—7.6m (Tr)
28(^{13}C)	100.12	73.16	78.77	39.02	77.51	65.98	19.72 22.80	55.69	27.38, 22.94 (Me) 166.23, 178. 46 (C=O)[f]

a) 85.85 (Ph_3C), 125.87, 126.65, 127.77, and 142.91 (Ph). b) 87.01 (Ph_3C), 127.00, 127.81, 128.68, and 144.06 (Ph). c) 86.63 (Ph_3C), 126.90, 127.72, 128.75, and 143.78 (Ph). d) 85.62 (Ph_3C), 126.43, 127.53, 128.23, and 143.66 (Ph). e) 81.94 (Ph_3C), 127.37, 127.49, 128.68, and 144.06(Ph). f) 85.45 (Ph_3C), 127.26, 127.92, 128.39, and 144.14 (Ph).

loromethane. The extract was washed with aqueous sodium chloride, dried with sodium sulfate, and evaporated to give crude 1,2-adduct as a syrup. The syrup was oxidized with dimethyl sulfoxide (0.3 ml) and oxalyl dichloride (0.2 ml) in dichloromethane (4.5 ml) in the same manner as described for compound **14**. Crude **5** was purified on a column of silica gel with hexane-ether (3:1), yield, 206 mg (82%); syrup, IR (NaCl) 1700 (C=O) and 1660 cm^{-1} (C=C). ^1H NMR δ=4.96 (1H, d, $J_{1,2}$=3.6 Hz, H-1), 3.44 (1H, dd, $J_{2,3}$=6.4 Hz, H-2), 3.72 (1H, d, H-3), 1.88 and 1.96 (each 3H, each s, CMe), 3.50 (3H, s, OMe) and 3.58 (6H, s, OMe).

Found: C, 57.66; H, 8.17%. Calcd for $C_{11}H_{18}O_5$: C, 57.38; H, 7.88%.

Preparation of Enol Trimethylsilyl Ethers 7, 21, and 23 from Enones 6, 2, and 3. To a reaction mixture of an enone with lithium (cyano)dimethylcuprate(I) as described latter, was added after 4 h at −78 °C triethylamine (1.7 ml per 1.0 mmol of enone), hexamethylphosphoric triamide (0.3 ml per 1.0 mmol of enone), and chlorotrimethylsilane (1.7 ml per 1.0 mmol of enone). Being kept at 0 °C for 1 h, the mixture was processed in the same manner as described for **13**. The enol ethers were used for further reaction without purification.

Methyl 2,3-Dideoxy-2-*C*-methyl-4-*O*-trimethylsilyl-6-*O*-trityl-α-D-*threo*-hex-3-enopyranoside (7). Treatment of **6**[12] as described above gave **7** quantitatively, which was characterized only by ^1H NMR δ=4.72 (1H, d, $J_{1,2}$=4.8 Hz, H-1), 2.54 (1H, dq, $J_{2,Me}$=6.8 Hz, H-2), 4.66 (1H, bs, H-3), 4.22 (1H, dd, $J_{5,6}$=4.4 Hz, $J_{6,6'}$=8.0 Hz, H-5), 3.40 (1H, t, $J_{5,6'}$=8.0 Hz, H-6), 3.52 (1H, dd, H-6'), 0.12 (9H, s, SiMe), 1.02 (3H, d, C-Me), 3.62 (3H, s, OMe) and 7.2—7.6 (15H, m, Tr).

Methyl 2,3-Dideoxy-2,2-di-*C*-methyl-4-*O*-trimethylsilyl-α-D-*glycero*-hex-3-enopyranoside (21). Treatment of **2** as described above gave **21** quantitatively, which was characterized only by ^1H NMR δ=4.62 (1H, s, H-1), 4.68 (1H, bs, H-3), 3.0—3.4 (2H, m, H-5 and H-6'), 3.84 (1H, dd, $J_{5,6}$=4.0 Hz, $J_{6,6'}$=6.6 Hz, H-6), 0.18 (9H, s, SiMe), 0.98 and 1.00 (each 3H, each s, C-Me), 3.56 (3H, s, OMe), and 7.2—7.6 (15H, m, Tr).

Methyl 3,4-Dideoxy-4,4-di-*C*-methyl-2-*O*-trimethylsilyl-6-*O*-trityl-α-D-*glycero*-hex-2-enopyranoside (23). Treatment of **3**[16] as described above gave **23** quantitatively, which was characterized only by ^1H NMR δ=4.70 (1H, s, H-1), 4.94 (1H, s, H-3), 3.92 (1H, dd, $J_{5,6}$=3.8 Hz, $J_{5,6'}$=6.2 Hz, H-5), 3.36 (1H, dd, $J_{6,6'}$=7.0 Hz, H-6), 3.28 (1H, dd, H-6'), 0.18 (9H, s, SiMe), 0.76 and 0.84 (each 3H, each s, C-Me), 3.66 (3H, s, OMe) and 7.2—7.6 (15H, m, Tr).

Methyl 6-*O*-Benzyl-2,3-di-*O*-methyl-4-*C*-methyl-α-D-galactopyranoside (13). Swern oxidation of **12**,[20] as described for **14**, gave the corresponding 4-ulose in 84% yield. To a solution of methylmagnesium iodide (2.17 mmol) in ether (5 ml) was added the ulose (227 mg, 0.72 mmol) at 0 °C. After 12 h at the same temperature, the solution was mixed with saturated aqueous ammonium chloride and extracted with dichloromethane. The extract was washed with aqueous sodium chloride, dried over magnesium sulfate, and evaporated. The crude mixture of products was fractionated on a column of silica gel with hexane-ethanol (18:1) to give **13** (187 mg, 81%) and its 4-epimer (23 mg, 10%).

13: Syrup, $[\alpha]_D^{20}$ +62.5° (*c* 0.86, $CHCl_3$); ^1H NMR δ=4.96 (1H, d, $J_{1,2}$=3.6 Hz, H-1), 3.24 (1H, dd, H-2), 3.6—3.8 (4H, m, H-3, H-5, H-6 and H-6'), 1.06 (3H, s, C-Me), 3.44, 3.52, and 3.60 (each 3H, each s, OMe), 4.64 (2H, bs, $CH_2C_6H_5$) and 7.44 (5H, bs, C_6H_5).

Found: C, 63.08; H, 7.56%. Calcd for $C_{17}H_{24}O_6$: C, 62.95; H, 7.46%.

4-Epimer of **13**: Syrup $[\alpha]_D^{20}$ +43.1° (*c* 0.81, $CHCl_3$);

^{1}H NMR δ=5.02 (1H, d, $J_{1,2}$=3.6 Hz, H-1), 3.26 (1H, dd, $J_{2,3}$=6.6 Hz, H-2), 3.6—3.8 (4H, m, H-3, H-5, H-6, and H-6'), 1.32 (3H, s, C-Me), 3.68 (6H, s, OMe), 4.62 (2H, bs, $CH_2C_6H_5$) and 7.44 (5H, bs, C_6H_5).

Found: C, 62.66; H, 7.28%. Calcd for $C_{17}H_{24}O_6$: C, 62.95%; H, 7.46%.

When this reaction was performed at −78 °C, only **13** was obtained in 90% yield. Furthermore, treatment of the ulose with methyllithium in ether at −78 °C for 5 h and at room temperature overnight, gave **13** and its 4-epimer 42 and 36% yields, respectively.

Methyl 2,3,4-Tri-*O*-methyl-4-*C*-methyl-α-D-*galacto*-hexodialdo-pyranoside-(1,5) (14). Treatment of **13** with sodium hydride in *N*,*N*-dimethylformamide for 4 h and then with methyl iodide at 0 °C, gave the 4-*O*-methyl derivative in 94% yield, which was hydrogenolyzed under 3 atm (1 atm=1.01×10^5 Pa) in the presence of 10% palladium on carbon in methanol and water (10 : 1) at room temperature overnight to give the *O*-debenzylated derivative in 93% yield.

To a solution of oxalyl dichloride (0.92 ml, 10.8 mmol) in dichloromethane (30 ml) was added a solution of dimethyl sulfoxide (0.94 ml, 12.9 mmol) in dichloromethane (10 ml) at −78 °C and then the *O*-debenzylated derivative (2.1 g, 8.5 mmol) at −78 °C. The reaction mixture was kept at −78 °C for 30 min, quenched with triethylamine, poured into water, and extracted with chloroform. The extract was washed with water, dried over magnesium sulfate, and evaporated to give **14** (1.87 g, 90%) as colorless syrup, $[\alpha]_D^{20}$ +41.6° (*c* 1.30, $CHCl_3$); ^{1}H NMR δ=5.02 (1H, d, $J_{1,2}$=3.0 Hz, H-1), 3.28 (1H, dd, $J_{2,3}$=8.0 Hz, H-2), 3.62 (1H, d, H-3), 3.88 (1H, bs, H-5), 9.62 (1H, bs, H-6), 1.40 (3H, s, C-Me) and 3.38, 3.42, 3.48, and 3.54 (each 3H, each s, OMe).

Found: C, 53.45; H, 8.27%. Calcd for $C_{11}H_{20}O_6$: C, 53.22; H, 8.12%.

Reaction of Enones 2—5 with Lithium Dimethylcuprate-(I). To a suspension of copper(I) iodide (0.68 g, 3.6 mmol) in ether (10 ml) was added methyllithium (6 ml of 1.2 M ethereal solution, 7.2 mmol) at 0 °C under an atmosphere of argon, and then a solution of an enone (1.2 mmol) in ether (5 ml). The reaction mixture was kept at 0 °C for 4 h and processed in the same manner as described for **13** to give a mixture of products, which was fractionated on a column of silica gel with the solvent system given below in individual cases.

Reaction of Enones 2—5 with Lithium (Cyano)dimethylcuprate(I). To a suspension of copper(I) cyanide (424 mg, 4.73 mmol) in ether (13 ml), was added methyllithium (12.9 ml of 1.2 M ethereal solution, 9.5 mmol) at −78 °C. When the solution became clear, a solution of an enone (1.58 mmol) in ether (6.5 ml) was added, and the same temperature was kept for 4 h. The reaction mixture was processed in the same manner as described above and the results are summarized in Table 1.

A Mixture 15 of Methyl 4,7-Dideoxy-2,3-di-*O*-methyl-4-*C*-methyl-α-D-*xylo*-hept-4-enopyranoside and Its 6-Epimer. The reactions of **4** as described above gave a mixture of unseparable two epimers **15** and methyl 4-deoxy-2,3-di-*O*-methyl-4-*C*-methyl-β-L-*threo*-hex-4-enopyranoside (**17**), which were separated on a silica gel column with hexane-ethyl acetate (3 : 1). The epimeric mixture **15** was only characterized by ^{1}H NMR.

15: Syrup, ^{1}H NMR (major): δ=4.80 (d, $J_{1,2}$=2.0 Hz, H-1), 3.46 (H-2), 3.62 (bd, $J_{2,3}$=6.6 Hz, H-3), 4.54 (bq, $J_{6,7}$=6.4 Hz, H-6), 1.36 (d, H-7), 1.58 (bs, C-Me) and 3.46 (s, OMe), (minor): δ=4.76 (d, $J_{1,2}$=2.0 Hz, H-1), 1.34 (d, H-7) and 3.38 (s, OMe).

Furthermore, conventional acetylation of **15** with acetic anhydride and pyridine gave **16** as colorless syrup, **16**: ^{1}H NMR (major) δ=4.96 (d, H-1), 3.56 (H-2), 3.74 (d, $J_{2,3}$=8.8 Hz, H-3), 5.76 (q, H-6), 1.74 (bs, C-Me), 1.42 (d, H-7), 2.08 (s, OAc) and 3.56 (bs, OMe), (minor) δ=4.94 (d, $J_{1,2}$=2.2 Hz, H-1), 3.78 (d, H-3), 5.76 (q, $J_{6,7}$=6.2 Hz, H-6), 1.40 (d, H-7) and 3.50 (s, OMe).

17: Syrup, $[\alpha]_D^{23}$ +28.5° (*c* 0.43, $CHCl_3$), IR (NaCl) 3500 (OH) and 1610 cm^{-1} (C=C); ^{1}H NMR δ=4.76 (1H, d, $J_{1,2}$=3.6 Hz, H-1), 3.22 (1H, dd, $J_{2,3}$=5.8 Hz, H-2), 3.68 (1H, d, H-3), 3.38 (2H, bs, H-6), 1.74 (3H, bs, C-Me) and 3.42, 3.44, and 3.50 (each 3H, each s, OMe).

Found: C, 54.88; H, 8.27%. Calcd for $C_{10}H_{18}O_5$: C, 55.03; H, 8.31%.

Methyl 2,3-Dideoxy-2,2-di-*C*-methyl-6-*O*-trityl-α-D-*glycero*-hexopyranosid-4-ulose (18). The reactions of **2** with lithium methylcuprates(I) as described above gave a mixture of **18** and its 5-epimer, methyl 2,3-dideoxy-2,2-di-*C*-methyl-6-*O*-trityl-β-L-*glycero*-hexopyranosid-4-ulose, which were separated on a column of silica gel with hexane-ethyl acetate (15 : 1).

18: Syrup, $[\alpha]_D^{23}$ +104.1° (*c* 2.2, $CHCl_3$); IR (NaCl) 1740 cm^{-1} (C=O). The ^{1}H and ^{13}C NMR data are given in Table 3.

Found: C, 78.25; H, 7.09%. Calcd for $C_{28}H_{30}O_4$: C, 78.11; H, 7.02%.

5-Epimer of **18**: Syrup, $[\alpha]_D^{23}$ +38.6° (*c* 1.41, $CHCl_3$); IR (NaCl) 1740 cm^{-1} (C=O), ^{1}H NMR δ=4.36 (1H, s, H-1), 2.12, and 2.48 (each 1H, each d, J=16.0 Hz, H-3 and H-3'), 4.12 (1H, dd, $J_{5,6}$=3.6 Hz, $J_{5,6'}$=5.4 Hz, H-5), 3.4—3.6 (2H, m, H-6), 1.02 and 1.00 (each 3H, each s, C_2-Me), 3.38 (3H, s, OMe) and 7.1—7.5 (m, Tr).

Found: C, 78.05; H, 7.02%. Calcd for $C_{28}H_{30}O_4$: C, 78.11; H, 7.02%.

Methyl 3,4-Dideoxy-4,4-di-*C*-methyl-6-*O*-trityl-α-D-*glycero*-hexopyranosid-2-ulose (19). The reaction of **3** with lithium methylcuprates(I) as described above gave crude **19**, which was purified on a column of silica gel with hexane-ethyl acetate (10 : 1), syrup, $[\alpha]_D^{23}$ +27.1° (*c* 1.5, $CHCl_3$), IR (NaCl) 1740 cm^{-1} (C=O). The ^{1}H and ^{13}C NMR data are given in Table 3.

Found: C, 77.93; H, 7.24%. Calcd for $C_{28}H_{30}O_4$: C, 78.11; H, 7.02%.

Methyl 4,7-Dideoxy-2,3-di-*O*-methyl-4,4-di-*C*-methyl-α-D-*xylo*-heptopyranosid-6-ulose (20). The reactions of **5** with lithium methylcuprates(I) as described above gave crude **20**, which was purified on a column of silica gel with hexane-ethyl acetate (4 : 1), syrup, $[\alpha]_D^{23}$ +55.2° (*c* 0.44, $CHCl_3$), ^{1}H NMR δ=4.68 (1H, d, $J_{1,2}$=3.2 Hz, H-1), 3.4—3.6 (2H, m, H-2), 1.36 and 1.56 (each 3H, each s, C_4-Me), 1.82 (3H, s, C_6-Me), 3.52 (6H, s, OMe) and 3.46 (3H, s, OMe).

Found: C, 58.29; H, 9.20%. Calcd for $C_{12}H_{22}O_5$: C, 58.51; H, 9.00%.

Hydroborations of 21 and 23. (i) With Borane in Tetrahydrofuran. To a solution of a enol trimethylsilyl ether (503 mg, 1.0 mmol) in tetrahydrofuran (6.5 ml), was added calculated amount of borane (the amount given in Table 2, 1 M solution in tetrahydrofuran) at 0 °C under an atmosphere of argon. Being kept at room temperature for 6 h, the reaction mixture was poured into water (10 ml). To a separated organic layer was added, at 0 °C with vigorous stirring, 10%

aqueous sodium hydroxide (5 ml) and hydrogen peroxide (30%, 5 ml) and the stirring was continued at 45 °C for 30 min. The reaction mixture was extracted with chloroform and the extract was washed with aqueous sodium chloride, dried over magnesium sulfate, and evaporated to give a mixture of products as a colorless syrup. The mixture was acetylated conventionally with acetic anhydride (2 ml) and pyridine (3 ml). In the case of **21**, fractionation of the products on a column of silica gel with hexane-ethyl acetate (15 : 1) afforded **22**, **24**, and **25** in the yields given in Table 2, while in the case of **23** with hexane-ethyl acetate (25 : 1) **26**, **27**, and **28**.

(ii) With Sodium Borohydride and Titanium(III) Chloride. To a mixture of sodium borohydride (100 mg, 2.6 mmol) and 18-crown-6 (132 mg, 0.5 mmol) in tetrahydrofuran (10 ml) was added titanium(III) chloride (85 mg, 0.55 mmol), and the mixture was stirred at 30 °C for 1 h under argon. After the color of the solution turned to be dark violet, a solution of enol silyl ether (503 mg, 1.0 mmol) in tetrahydrofuran (5.5 ml) was added, and the mixture was stirred at the same temperature for 8 h. To the mixture was added methanolic sodium methoxide (3 ml of 3 M solution) and then 30% aqueous H_2O_2 (5 ml). Being kept at 40 °C for 1 h, the reaction mixture was processed in the same manner as described above.

(iii) With Sodium Borohydride and Cobalt(II) Chloride. To a suspension of cobalt(II) chloride (325 mg, 2.5 mmol) in tetrahydrofuran (8 ml), was added with stirring at 0 °C under argon sodium borohydride (195 mg, 5 mmol). After 1 h a solution of enol silyl ether (0.66 mmol) in tetrahydrofuran (3 ml) was added after stirring at room temperature for 1.5 h, and the mixture was stirred at room temperature for 8 h. The successive oxidation was performed as described for hydroboration with titanium(III) chloride and sodium borohydride.

(iv) With Disiamylborane. To a 0.6 M solution of disiamylborane (2 ml) in tetrahydrofuran was added a solution of enol silyl ether (503 mg, 1.0 mmol) in tetrahydrofuran (6 ml) at room temperature, and the mixture was stirred at room temperature for 8 h. The oxidation was performed in the same manner as described above.

(v) With 9-Borabicyclo[3.3.1]nonane (9-BBN). To a 0.5 M solution of 9-borabicyclo[3.3.1]nonane (2.4 ml) in tetrahydrofuran was added a solution of enol silyl ether (503 mg, 1.0 mmol) in tetrahydrofuran (5.5 ml). The mixture was heated under reflux for 6 h. The oxidation was performed in the same manner as described above.

Methyl 3,4-Di-*O*-acetyl-2-deoxy-2,2-di-*C*-methyl-6-*O*-trityl-α-D-*arabino*-hexopyranoside (24). Hydroboration of **21** with 3 equivalents of diborane in the same manner as described above gave a mixture of **24**, methyl 4-*O*-acetyl-2,3-dideoxy-2,2-di-*C*-methyl-6-*O*-trityl-α-D-*erythro*-hexopyranoside (**25**), and methyl 2,3,4-trideoxy-2,2-di-*C*-methyl-6-*O*-trityl-α-D-*glycero*-hex-3-enopyranoside (**22**).

24: Syrup, $[\alpha]_D^{23}$ +150.6° (*c* 1.2, $CHCl_3$), IR (NaCl) 1720 cm^{-1} (C=O). The ^1H and ^{13}C NMR data are given in Table 3.

Found: C, 72.11; H, 6.85%. Calcd for $C_{32}H_{36}O_7$: C, 72.16; H, 6.81%.

25: Syrup, $[\alpha]_D^{23}$ +13.7° (*c* 0.97, $CHCl_3$), IR (NaCl) 1720 cm^{-1} (C=O). The ^1H and ^{13}C NMR data are given in Table 3.

Found: C, 75.68; H, 7.50%. Calcd for $C_{30}H_{34}O_5$: C, 75.92; H, 7.22%.

22: Syrup, $[\alpha]_D^{23}$ +12.0° (*c* 1.14, $CHCl_3$), IR (NaCl) 1680 cm^{-1} (C=C), ^1H NMR δ=4.44 (1H, s, H-1), 5.62 (1H, bd, $J_{3,4}$=9.2 Hz, H-3), 5.58 (1H, bdd, $J_{4,5}$=4.6 Hz, H-4), 3.82 (1H, bdd, $J_{5,6}$=4.0 Hz, $J_{5,6'}$=6.8 Hz, H-5), 3.12 (2H, m, H-6), 1.02 and 1.10 (each 3H, each s, C_2-Me), 3.52 (3H, s, OMe) and 7.2—7.6 (15H, m, Tr).

Found: C, 80.96; H, 7.43%. Calcd for $C_{28}H_{30}O_3$: C, 81.13; H, 7.29%.

Methyl 2,3-Di-*O*-acetyl-4-deoxy-4,4-di-*C*-methyl-6-*O*-trityl-α-D-*xylo*-hexopyranoside (26) and Methyl 2,3-Di-*O*-acetyl-4-deoxy-4,4-di-*C*-methyl-6-*O*-trityl-α-D-*arabino*-hexpyranoside (28). Hydroboration of **23** in the same manner as described above gave **26**, **28**, and methyl 2-*O*-acetyl-3,4-dideoxy-4,4-di-*C*-methyl-6-*O*-trityl-α-D-*erythro*-hexopyranoside (**27**).

26: Syrup, $[\alpha]_D^{23}$ +91.5° (*c* 0.89, $CHCl_3$), IR (NaCl) 1700 and 1710 cm^{-1} (C=O). The ^1H and ^{13}C NMR data are given in Table 3.

Found: C, 72.02; H, 6.92%. Calcd for $C_{32}H_{36}O_7$: C, 72.16; H, 6.81%.

28: Syrup, $[\alpha]_D^{23}$ +113.1° (*c* 1.3, $CHCl_3$), IR (NaCl) 1720 cm^{-1} (C=O). The ^1H and ^{13}C NMR data are given in Table 3.

Found: C, 71.96; H, 6.79%. Calcd for $C_{32}H_{36}O_7$: C, 72.16; H, 6.81%.

27: Mp 128—130 °C, $[\alpha]_D^{23}$ +51.2° (*c* 1.2, $CHCl_3$), IR (NaCl) 1710 cm^{-1} (C=O), ^1H NMR δ=4.87 (1H, dd, $J_{1,2}$=3.4 Hz, $J_{1,3}$=0.6 Hz, H-1), 4.89 (1H, ddd, $J_{2,3}$=5.3 Hz, $J_{2,3'}$=13.3 Hz, H-2), 1.42 and 1.76 (each 1H, each dd, $J_{3,3'}$=11.5 Hz, H-3 and H-3'), 3.74 (1H, dd, $J_{5,6}$=3.8 Hz, $J_{5,6'}$=9.8 Hz, H-5), 3.10 (1H, dd, $J_{6,6'}$=9.8 Hz, H-6), 3.22 (1H, t, H-6'), 0.78 and 0.82 (each 3H, each s, C-Me), 2.16 (3H, s, OAc), 3.58 (3H, s, OMe) and 7.2—7.6 (m, Tr). The data for H-1, H-2, H-3, and H-3', were obtained by simulation.

Found: C, 75.63; H, 6.95%. Calcd for $C_{30}H_{34}O_5$: C, 75.92; H, 7.22%.

^1H NMR data of deacetylated **27**: δ=4.86 (1H, d, $J_{1,2}$=3.8 Hz, H-1), 3.58 (1H, dt, $J_{2,3}$=3.8 Hz, $J_{2,3'}$=6.2 Hz, H-2), 1.44 and 1.64 (each 1H, each dd, $J_{3,3'}$=12.0 Hz, H-3 and H-3'), 3.59 (1H, dd, $J_{5,6}$=4.0 Hz, $J_{5,6'}$=7.6 Hz, H-5), 3.14 (1H, dd, $J_{6,6'}$=7.6 Hz, H-6), 3.28 (1H, t, H-6'), 0.72 and 0.80 (each 3H, each s, C-Me), 3.60 (3H, s, OMe) and 7.2—7.6 (m, Tr).

References

1) S. Hanessian, "Total Synthesis of Natural Products: The 'Chiron' Approach," Pergamon Press, Oxford (1983).

2) Y. Ali and W. A. Szarek, *Carbohydr. Res.*, **67**, C17 (1978).

3) Y. Chapleur, *J. Chem. Soc., Chem. Commun.*, **1983**, 141.

4) B. Fraser-Reid, H. Tsang, D. B. Tulshian, and K. M. Sun, *J. Org. Chem.*, **46**, 3764 (1981).

5) S. Nagarajan and K. L. Rinehardt, Jr., *J. Org. Chem.*, **50**, 380 (1985).

6) H. Hashimoto, N. Kawauchi, and J. Yoshimura, *Chem Lett.*, **1985**, 965.

7) E. A. Jeffery, A. Meisters, and T. Mole, *Aust. J. Chem.*, **27**, 2569 (1974).

8) M. T. Reetz J. Westermann, and R. Steinbach, *J, Chem. Soc., Chem. Commun.*, **1981**, 237.

9) G. H. Posner and D. J. Brunelle, *J. Org. Chem.*, **38**, 2747 (1973).

10) a) W. Oppolzer and T. Godel, *J. Am. Chem. Soc.*, **100**, 2583 (1978); b) K. Yamada, Y. Kyotani, S. Manabe, and H. Suzuki, *Tetrahedron*, **35**, 293 (1979).

11) G. Bianchetti, A. Maccioni, and M. Secci, *Ann. Chem. (Rome)*, **60**, 483 (1970).
12) B. Fraser-Reid, A. McLean, E. W. Usherwood, M. Yunker, *Can. J. Chem.*, **48**, 2877 (1970).
13) Y. Ito, T. Hirano, and T. Saegusa, *J. Org. Chem.*, **43**, 1011 (1978).
14) J. Tsuji, I. Minami, I. Shimizu, and H. Kataoka, *Chem. Lett.*, **1984**, 1133.
15) D. R. Hicks and B. Fraser-Reid, *Can. J. Chem.*, **53**, 2017 (1975).
16) B. J. Fizsimmons, D. E. Plaumann, B. Fraser-Reid, *Tetrahedron Lett.*, **1979**, 3925.
17) T. Imamoto, T. Kusumoto, Y. Tawarayama, T. Sugiura, T. Mita, Y. Hatanaka, and M. Yokoyama, *J. Org. Chem.*, **49**, 3904 (1984).
18) These addition reactions are described in the succeeding paper: N. Kawauchi and H. Hashimoto, *Bull. Chem. Soc. Jpn* (In contribution).
19) M. N. Bhattacharjea, M. K. Chaudhuri, H. S. Dasgupat, N. Roi, and D.T. Khathing, *Synthesis*, **1982**, 588.
20) D. J. Garegg and H. Hultberg, *Carbohydr. Res.*, **108**, 97 (1982).
21) S. Hanessian, G. Rancourt, and Y. Guindon, *Can. J. Chem.*, **56**, 1843 (1978).
22) W. Carruthers, "Compounds of Zinc, Cadmium and Mercury, and of Copper, Silver and Gold in Organic Synthesis" in "Comprehensive Organometallic Chemistry," ed by G. Wilkinson, F. G. A. Stone, and E. W. Abel, Pergamon Press (1982), Vol 7, p. 685.
23) a) G. L. Larson, D. Hernandex, and A. Hernandex, *J. Organomet. Chem.*, **76**, 9 (1974); b) J.-P. Lepoittevin and C. Benezra, *Tetrahedron Lett.*, **25**, 2505 (1984).
24) H. S. Lee, K. Isagawa, H. Toyoda, and Y. Otsuji, *Chem. Lett.*, **1984**, 673.
25) N. Satyanarayana and M. Periasamy, *Tetrahedron Lett.*, **25**, 2501 (1984).
26) G. L. Larson and A. Hernandex, *J. Organomet. Chem.*, **102**, 123 (1975).

 © 1987 The Chemical Society of Japan Bull. Chem. Soc. Jpn., 60, 1441—1447 (1987)

Reaction of Enohexopyranoside Acetates with Lithium Dimethylcuprate(I) and Its Application to Synthesis of Prelog-Djerassi Lactone

Nobuya KAWAUCHI and Hironobu HASHIMOTO*
Department of Life Science, Faculty of Science, Tokyo Institute of Technology, Nagatsuta, Midori-ku, Yokohama 227
(Received October 7, 1986)

In the reaction of two 2-*O*-acetyl-3-enohexopyranosides and four 4-*O*-acetyl-2-enohexopyranosides including 2-*C*-methyl and 4-*C*-methyl derivatives, respectively, with lithium dimethylcuprate(I), anti S_N2' substitution was proved to be preferential, giving the corresponding *C*-methylated derivatives. On the other hand, S_N2 substitution occurred in the reaction of the 2-enopyranoside without methyl branch and D-glucal triacetate.

Allylic structure is readily introduced into hexopyranoside ring by elimination of vicinal diol among three consecutive hydroxyl groups.[1] Alkylation of allylic ester with lithium organocuprates[2] have been widely used for synthesis of such natural products as prostaglandin D_2.[3] In this paper, the reaction of unsaturated sugars having allylic acetate structure in the hexopyranoside ring with lithium dimethylcuprate(I) was studied in order to develop a new method for preparation of *C*-methylated chiral synthons, one of which was used for synthesis of Prelog-Djerassi lactone.

Results and Discussion

Because preliminary studies on reactions of such allylic alcohols as **1** and **2** with $MeCu \cdot BF_3$[4] or with methylmagnesium bromide in the presence of bis(triphenylphosphine)nickel(II) chloride[5] did not give promising results,[6] the reaction of allylic acetate with lithium dimethylcuprate(I) was examined. Nine pyranosides having allylic acetate structure (**3**, **4**, **6**, **9**, **10**, **12**, and **15**—**17**) and one glycal acetate (**20**) were subjected for this reaction. The syntheses of **3**,[9] **9**,[10] and **16**[11] were reported by Fraser-Reid et al., while that of **15** by Ferrier and Prasad.[12] 2-*C*-Methyl-branched (**4** and **6**) and 4-*C*-methyl-branched (**10** and **12**) allylic acetates were prepared by 1,2-addition reaction of the corresponding enone **21**[9] and **23**,[13] respectively, with methyllithium or methylcerium(III) dichloride,[14] followed by acetylation. It was noteworthy that the reactions with the latter reagent gave almost exclusively axially attacked products **4** and **10**, while those with the former reagent afforded the same epimers a little preferentially, as shown in Table 1. 4-*C*-Methyl allylic acetate **17** was prepared by 1,2-reduction of the 4-*C*-methyl enone **22**[15] with sodium borohydride and cerium(III) chloride,[16] also followed by acetylation. The

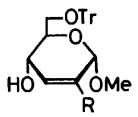

1 R = H
2 R = Me

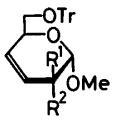

3 R^1 = H, R^2 = OAc
4 R^1 = Me, R^2 = OAc
5 R^1 = Me, R^2 = OH
6 R^1 = OAc, R^2 = Me
7 R^1 = OH, R^2 = Me
8 R^1 = Me, R^2 = H

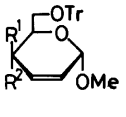

9 R^1 = H, R^2 = OAc
10 R^1 = Me, R^2 = OAc
11 R^1 = Me, R^2 = OH
12 R^1 = OAc, R^2 = Me
13 R^1 = OH, R^2 = Me
14 R^1 = Me, R^2 = H

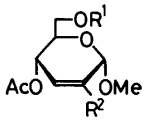

15 R^1 = Ac, R^2 = H
16 R^1 = Tr, R^2 = Me

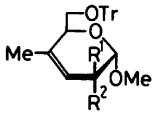

17 R^1 = H, R^2 = OAc
18 R^1 = Me, R^2 = H
19 R^1 = H, R^2 = Me

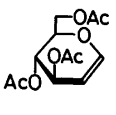

20

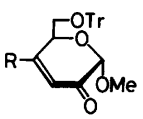

21 R = H
22 R = Me

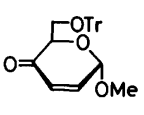

23

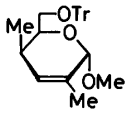

24

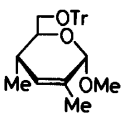

25

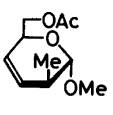

26

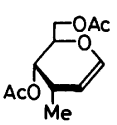

27

Table 1. 1,2-Addition Reaction of **21** and **23** with MeLi or $MeCeCl_2$

Enone	Reagent	Product[a]			Yield
		ax-attack	eq-attack	ax/eq	%
21	MeLi	**4**	**6**	5:2	82.8
21	$MeCeCl_2$	**4**	**6**	10:1	85.9
23	MeLi	**10**	**12**	4:3	96.8
23	$MeCeCl_2$	**10**	**12**	1:0	quant.

a) Isolated as acetates.

Table 2. Reaction of Enohexopyranoside Acetates with Lithium Dimethylcuprate(I) in Diethyl Ether

Allylic acetate	Condition		Product/%	Recovered Starting Material/% (deacetylated)
	Temperature/°C	Time/h		
3	−30	4	**8** 52.9	38.7(38.7)
3	0	4	**8** 79.2	17.1(17.1)
3[a]	0	4	**8** 52.1	40.8 (6.3)
4	−40	4	**24** 69.2	13.9 (5.9)
6	−40	4	**25** 82.6	10.0(trace)
9	−30	6	**8** 28.6	64.9(10.4)
9	−10	4	**8** 48.9	32.1(17.7)
9	0	4	**8** 50.9	35.2(23.0)
10	−30	6	**18** 80.3	8.5(trace)
12	−30	6	**19** trace	82.7 (4.4)
12	0	4	**19** 15.7	67.3 (7.2)
15	−10	4	**26** 54.6[b]	39.5(39.5)[c]
20	−30	4	**27** 35.0	12.7 (−)

a) THF was used as a solvent. b) Isolated as acetate. c) 4-*O*-Deacetylated (25.8%)+6-*O*-deacetylated (13.7%).

structures of these methyl-branched enopyranosides were ascertained by ^{1}H NMR data shown in Table 3, while the configurations at the branched carbon were determined by NOE. The *C*-methyl signal of **6** showed clear NOE when H-5 or *O*-methyl protons were irradiated, while that of **4** not. Further, the *C*-methyl signal of **12** was slightly enhanced when H-5 was irradiated. These configurational assignment was supported also by stereochemical course of reactions, i.e., above-mentioned selectivity of 1,2-addition reaction and the anti S_N2' substitution mechanisms which was observed in cyclohexenyl system.[17]

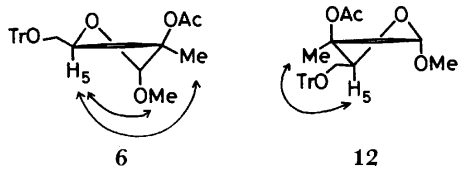

6 12

The reaction of the above-described nine allylic acetates with lithium dimethylcuprate(I) were performed in ether and the results were summarized in Table 2. The configurations of methyl-branching carbons in the products were determined by $J_{4,5}$ (the coupling constant between H-4 and H-5 in ^{1}H NMR) for the 2-enopyranosides such as **24** and **25** and by $J_{1,2}$ and $J_{2,3}$ (allylic geminal coupling)[7] for 3-enopyranosides such as **18**, **19**, and **26** (Table 3). Four enopyranosides having tertiary acetoxyl group at the branching carbon (**4**, **6**, **10**, and **12**) gave stereoselectively *C*-methylated derivatives (**24**, **25**, **18**, and **19**, respectively) in good yields except the last one. The anti S_N2' type reaction may be predominant as reported for cyclohexene derivatives.[18] On the other hand, unbranched 3-eno-**3** and 2-enopyranoside **9** gave the same 2-*C*-methyl derivative **8**, and another unbranched 2-enopyranoside **15** gave, after acetylation, the corresponding 2-*C*-methyl derivative **26**, in each case stereoselectively. The structure of **26** was confirmed by chemical conversion into **8** by deacetylation and tritylation. Because the possibility of 2-enopyranoside **14** could not be excluded completely from the ^{1}H NMR spectrum, compound **8** was further converted, by oxidation with osmium tetroxide and acetylation, into the corresponding 3,4-diacetoxy derivative **28**. Its ^{1}H NMR data analyzed by decoupling technique confirm the 2-*C*-methyl structure. This indicates the reaction of **3** proceeded via S_N2 type mechanism. The result may be attributed to the higher reactivity of the 2-acetoxyl group which lies between olefinic and electron-withdrawing anomeric center. However, introduction of methyl group into the acetoxyl group-bearing carbon reduces the reactivity of S_N2 reaction to prefer rather normal S_N2' reaction as shown in the case of 4. Furthermore, introduction of methyl group into the olefin moiety showed a limitation of this reaction, that is, **16** and **17** did not react at all and the expected *gem*-di-*C*-methyl derivative could not obtained. In the case

Table 3. ^{1}H NMR Data of Starting Allylic Acetates and *C*-Methylated Products

Compound	H-1 ($J_{1,2}$)	H-2 ($J_{2,3}$)	H-3 ($J_{3,4}$)	H-4 ($J_{4,5}$)	H-5 ($J_{5,6}$)	H-6,6′ ($J_{5,6'}$)	($J_{6,6'}$)	OMe	C_2-Me	C_4-Me	Others
4	4.76s	—	6.26d (10.4)	5.88dd (4.8)	4.24m (3.0)	3.18dd, (2.6)	3.42dd (10.0)	3.52s	1.74	—	2.22s(Ac), 7.2—7.6m(Ph)
5	4.48s	—	5.72bs(2H)		4.20t (6.0)	3.18d(2H)		3.44s	1.18s	—	7.2—7.6m(Ph)
6	4.74s	—	5.86bs(2H)		4.20m (3.0)	3.06dd, (2.4)	3.28dd (10.4)	3.40s	1.62s	—	2.06s(Ac), 7.2—7.6m(Ph)
7	4.62s	—	5.64bs(2H)		4.12t (6.4)	**3.34d(2H)**		3.38s	1.42s	—	7.2—7.6m(Ph)
8	4.56bs	2.14m	5.69s(2H)		4.30m	3.17dd,	3.25dd	3.46s	1.06d ($J_{2,Me}$ 7.1)		7.1—7.6m(Ph)
10	4.90d (1.8)	5.64dd (10.8)	6.38d	—	4.10t (5.6)	3.42d(2H)		3.58s	—	1.40s	1.92s(Ac), 7.2—7.6m(Ph)
11	4.92bs	5.76bs(2H)		—	4.00t (6.2)	3.44d(2H)		3.52s	—	1.00s	7.1—7.6m(Ph)
12	4.76bs (1.0)	5.84dd (11.6)	6.22dd ($J_{3,Me}$ 0.8)	—	4.22t (4.8)	3.26d(2H)		3.46s	—	1.74bs	1.96s(Ac), 7.2—7.6m(Ph)
13	4.78d (1.2)	5.54dd (10.2)	5.76bd	—	4.06dd (5.8)	3.30dd, (10.6)	3.52t (10.6)	3.46s	—	1.00s	7.2—7.6m(Ph)
18	4.62d (0.8)	2.12m (4.6)	5.44m ($J_{3,4\text{-}Me}$ 0.8)	—	4.12m (4.4)	3.10ddd, (3.8)	3.40dd (10.4)	3.44s	1.12d ($J_{2,Me}$ 7.4)	1.40bs ($J_{5,4\text{-}Me}$ 1.0)	7.1—7.6m(Ph)
19	4.70d (3.8)	2.42m (2.8)	5.40m	—	4.06m	3.12—3.36m(2H)		3.38s	1.08d ($J_{2,Me}$ 7.0)	1.50bs ($J_{4,Me}$ 1.0)	7.2—7.6m(Ph)
24	4.76s	—	5.52dd (3.8)	2.14ddq (4.4)	3.7m (7.8)	3.06dd, (4.0)	3.38dd (10.2)	3.60s	1.80bs ($J_{3,Me}$ 0.6)	0.76d ($J_{4,Me}$ 9.6)	7.2—7.6m(Ph)
25	4.58bs	—	5.56dd (6.2)	2.04ddq (8.2)	4.00m (6.6)	3.30dd, (4.0)	3.44dd (8.4)	3.44s	1.70bs ($J_{3,Me}$ 0.6)	0.66d ($J_{4,Me}$ 7.8)	7.2—7.6m(Ph)
26	4.82d (1.0)	2.14m	5.80dd (11.6)	5.60dd (2.2)	3.8—4.1m(3H)			3.44s	1.08d ($J_{2,Me}$ 6.0)	—	2.06s(Ac)
27	6.24dd (6.0) ($J_{1,3}$ 1.8)	4.66dd (4.2)	2.64dddq (5.8)	5.02dd (7.4)	4.0—4.2m(3H)			—	1.08d ($J_{3,Me}$ 7.2)	—	2.06s(Ac)

of a glycal **20** only S_N2 substitution was observed to give a 3-*C*-methyl derivative **27**. These results indicate the predominance of anti S_N2' mechanism except the cases of **3** and **20**. The result of **15** is consistent with that of the corresponding ethyl glycoside, reaction of which with several organolithium derivatives including lithium dimethylcuprate(I) was reported very recently to give 2-*C*-substituted derivatives.[18]

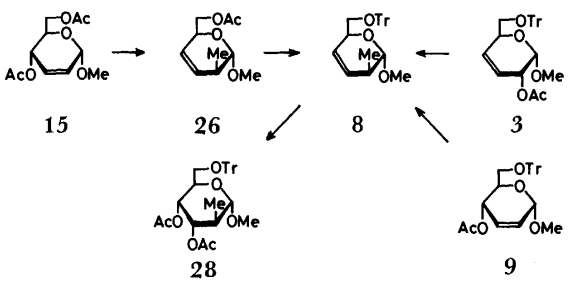

Prelog-Djerassi lactone (**35**) has been one of the key compounds for macrolide construction since synthesis of methymycin[20] and was also synthesized from D-glucose by a few groups.[21] As described above a convenient method for preparation of **25** was developed and then its utilization for synthesis of **35** was undertaken. Hydrogenation of **25** in the presence of palladium(II) hydroxide gave **29** preferentially in 43% yield. This yield seems to be fairly good in comparison with its preparation from the 4-*C*-methyl enone **22** via the corresponding 2-*C*-methylene derivative, where the yield for the latter step were not reported.[21a] Although the synthetic route from **29** to **35** has been already reported,[21a] the following alternative route was also developed.

Swern oxidation of **29** afforded a dialdopyranoside **30** in 75% yield. Treatment of **30** with nitromethane in the presence of sodium methoxide in methanol gave an epimeric mixture of condensation product **31**, which was converted into a nitro olefin **32** with acetic anhydride and pyridine in dichloromethane in 84% yield in two steps. For the last step a conventional treatment with methanesulfonyl chloride and triethylamine gave only poor results. Addition reaction of **32** with $MeCu \cdot BF_3$ in ether gave 6-*C*-methylated product **33** as an epimeric mixture with a ratio of 3 to 2 in 54% yield. On the other hand, the same reactions with lithium dimethylcuprate(I) or $Me_2Cu(CN)Li_2$ proved to give **33** trace and in 26% yield, respectively. Oxidation of **33** with potassium permanganate followed by treatment with acetic acid gave an uronic acid **34**, which was further oxidized with chromium trioxide afforded a mixture of **35** and its 6-epimer. Pure **35** was obtained as crystal from pentane–ether in 7% yield from **33**.

Table 4. ^{13}C NMR Data of *C*-Methylated Products

Compound	C-1	C-2	C-3	C-4	C-5	C-6	O-Me	C-Me
8	102.35d	34.13d	125.43d[a)]	124.18d[a)]	68.22d	66.32t	55.32q	18.58q
18	102.35d	34.49d	124.56d	131.44s	72.44d	64.42t	55.43q	18.91q, 18.46q
19	99.20d	34.60d	129.62d	130.92s	71.95d	64.83t	55.16q	18.95q, 13.06q
24	98.55d	131.55s	129.82d	30.94d	72.71d	64.75t	55.21q	18.75q, 16.80q
25	101.15d	131.29s	129.49d	30.88d	68.48d	64.42t	55.10q	18.85q, 12.57q
26	101.91d	32.31d	125.83d[a)]	123.35d[a)]	70.31d	66.61t	56.97q	19.11q
27	141.46d	104.46d	27.69d	70.98d	68.70d	62.74t	—	16.15q

a) These signals are interchangable.

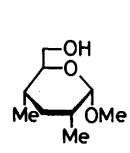
29

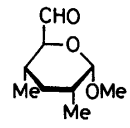
30

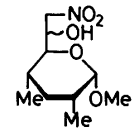
31

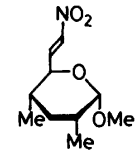
32

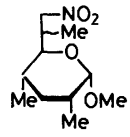
33

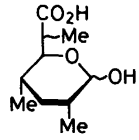
34

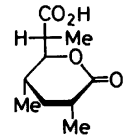
35

Experimental

General Methods. Melting points determined with a Yanagimoto micro melting point apparatus, were uncorrected. Optical rotations were measured in chloroform, by using a 0.5-dm tube with a Carl Zeiss LEP-Al polarimeter. Infrared spectra were recorded on a Hitachi EPI-G2 grating spectrometer. ^1H and ^{13}C NMR spectra were recorded at 100 MHz with a JEOL JMN PS-100 spectrometer and at 22.5 MHz with a JEOL FX-90Q spectrometer, respectively, in $CDCl_3$ with tetramethylsilane as internal standard. Column chromatography was performed on silica gel (Wakogel C-300: Wako Pure Chemical Industries, Ltd.).

Reaction of Allylic Alcohols 1 and 2 with MeCu · BF_3. To a suspension of copper(I) iodide (0.22 g, 1.2 mmol) in ether (35 ml) were added 1.2 M (1 M=1 mol dm^{-3}) ethereal solution of methyllithium (1 ml, 1.2 mmol) at −30 °C, and then after 30 min boron trifluoride etherate (0.14 ml, 1.2 mmol) at −78 °C. After 30 min, to this mixture was added a solution of **1** (380 mg, 0.94 mmol) in ether (2 ml) at 0 °C. Being stood at this temperature for 24 h, the reaction mixture was stirred with saturated ammonium chloride solution and extracted with dichloromethane. The extract was washed with water, dried over sodium sulfate, and evaporated to a syrupy mixture of a few components, which was fractionated on a column with hexane-ethyl acetate (50 : 1). The products, whose yields are give in references,[6] were characterized only by ^1H NMR.

(*S*)-2-[1-Hydroxy-2-(trityloxy)ethyl]furan (36): Mp 89—91 °C (decomp); ^1H NMR δ=6.32 (2H, bs, H-3 and H-5), 7.10 (1H, bs, H-4), 4.68 (1H, bdd, $J_{1',2'a}$=4.4 Hz, $J_{1',2'b}$=6.8 Hz, H-1'), 3.34 (1H, dd, $J_{2'a,2'b}$=8.0 Hz, H-2'a), 3.58 (1H, dd, H-2'b), and 7.2—7.6 (15H, m, Ph).

Reaction of Allylic Alcohol 2 with Methylcopper(I) Trifluoroborate. The reaction was performed in the same manner as described above using **2** instead of **1**. The products[6] were characterized only by ^1H NMR.

(*S*)-2-[1-Hydroxy-2-(trityloxy)ethyl]-4-methylfuran (37): ^1H NMR δ=7.66 (1H, m, H-5), 6.24 (1H, m, H-3), 4.72 (1H, bt, H-1'), 3.90 (2H, bd, CH_2OTr), 2.06 (3H, m, C-Me), and 7.2—7.6 (15H, m, Ph).

(*S*)-3,5-Dimethyl-2-trityloxymethyl-2*H*-pyran (38): ^1H NMR δ=7.78 (1H, m, H-6), 6.14 (1H, m, H-4), 3.84 (1H, bt, H-2), 3.66 (2H, bd, CH_2OTr), 2.12 (3H, bs, CMe), 1.98 (3H, m, CMe), and 7.2—7.6 (15H, m, Ph).

Reaction of Allylic Alcohol 1 with Methylmagnesium Bromide in the Presence of Bis(triphenylphosphine)nickel-(II) Chloride. To bis(triphenylphosphine)nickel(II) chloride (131 mg, 0.2 mmol) was added under argon a solution of **1** (2 mmol) in THF (8 ml), and the mixture was stirred at room temprature for 5 min. Then, to this solution was added 1 M tetrahydrofuran solution of methylmagnesium bromide (8 ml, 8 mmol). Being kept at room temperature for 24 h, the mixture was quenched with aqueous ammonium chloride, and extracted with dichloromethane. The extract was washed with water, dried over sodium sulfate, and evaporated to give a mixture of **39** and **1**, which was fractionated on a column with hexane-ethyl acetate (50 : 1). The compound **39** was characterized only by ^1H NMR data.

Methyl 2,3,4-Trideoxy-6-*O*-trityl-2,4-dienopyranoside (39): ^1H NMR δ= 4.84 (1H, d, $J_{1,2}$=1.4 Hz, H-1), 5.08 (2H, bs, H-2 and H-4), 6.22 (1H, bs, H-3), 3.82 and 3.90 (2H, ABq, J=10.4 Hz, H-6 and H-6'), 3.26 (3H, s, OMe), and 7.2—7.6 (15H, m, Ph).

Reaction of Enones 21 and 23 with Methyllithium. To a solution of the enone (582 mg, 1.45 mmol) in ether (60 ml), was added 0.8 M ethereal solution of methyllithium (7.3 ml, 5.8 mmol) at −78 °C. Being kept at the same temperature for 4 h, the reaction mixture was poured into water and extracted with ethyl acetate. The extract was washed with water, dried over magnesium sulfate, and evaporated to give a crude epimeric mixture of 1,2-addition product, whose separation was described in the following paragraph.

Methyl 2-*O*-Acetyl-3,4-dideoxy-2-*C*-methyl-6-*O*-trityl-α-D-*erythro*-hex-3-enopyranoside (4) and Methyl 2-*O*-Acetyl-3,4-

dideoxy-2-*C*-methyl-6-*O*-trityl-α-D-*threo*-hex-3-enopyranoside (6). The reaction of **21** with methyllithium as described above gave a mixture of **5** and **7**, which was separated on a column with hexane-ethyl acetate (12 : 1).

5: Syrup, $[\alpha]_D$ −13.7° (*c* 0.9, $CHCl_3$); IR (NaCl) 3400 (OH) and 1610 cm^{-1} (C=C).

Found: C, 77.52; H, 6.83%. Calcd for $C_{27}H_{28}O_4$: C, 77.86; H, 6.78%.

7: Syrup, $[\alpha]_D$ +173.5° (*c* 1.9, $CHCl_3$); IR (NaCl) 3400 (OH) and 1610 cm^{-1} (C=C).

Found: C, 77.90; H, 6.48%. Calcd for $C_{27}H_{28}O_4$: C, 77.86; H, 6.78%.

Acetylation of **5** and **7** with acetic anhydride and pyridine in the presence of 4-(dimethylamino)pyridine geve **4** and **6**, respectively, which were purified on a column with hexane-ethyl acetate (15 : 1).

4: Syrup $[\alpha]_D$ +44.7° (*c* 0.9, $CHCl_3$); IR (NaCl) 1730 (C=O) and 1600 cm^{-1} (C=C).

Found: C, 75.80; H, 6.33%. Calcd for $C_{29}H_{30}O_5$: C, 75.96; H, 6.59%.

6: Syrup, $[\alpha]_D$ +38.9° (*c* 5.1, $CHCl_3$); IR (NaCl) 1730 (C=O) and 1600 cm^{-1} (C=C).

Found: C, 75.53; H, 6.28%. Calcd for $C_{29}H_{30}O_5$: C, 75.96; H, 6.59%.

The ^1H NMR data for compounds **4**—**7** are given in Table 3.

Methyl 4-*O*-Acetyl-2,3-dideoxy-4-*C*-methyl-6-*O*-trityl-α-D-*erythro*-hex-2-enopyranoside (10) and Methyl 4-*O*-Acetyl-2,3-dideoxy-4-*C*-methyl-6-*O*-trityl-α-D-*threo*-hex-2-enopyranoside (12). The reaction of **23** with methyllithium as described above gave a mixture of **11** and **13**, which were separated on a column with hexane-ethyl acetate (14 : 1).

11: Syrup, $[\alpha]_D$ −11.8° (*c* 0.6, $CHCl_3$); IR (NaCl) 3400 (OH) and 1600 cm^{-1} (C=C).

Found: C, 77.94; H, 6.58%. Calcd for $C_{27}H_{28}O_4$: C, 77.86; H, 6.78%.

13: Syrup, $[\alpha]_D$ +17.5° (*c* 0.93, $CHCl_3$); IR (NaCl) 3400 (OH) and 1600 cm^{-1} (C=C).

Found: C, 77.95; H, 7.04%. Calcd for $C_{27}H_{28}O_4$: C, 77.86; H, 6.78%.

Acetylation of **11** and **13** with acetic anhydride and pyridine in the presence of 4-(dimethylamino)pyridine gave **10** and **12**, respectively, which were purified on a column with hexane-ethyl acetate (18 : 1).

10: Syrup, $[\alpha]_D$ +56.9° (*c* 2.3, $CHCl_3$); IR (NaCl) 1740 (C=O) and 1610 cm^{-1} (C=C).

Found: C, 76.04; H, 6.74%. Calcd for $C_{29}H_{30}O_5$: C, 75.96; H, 6.59%.

12: Syrup, $[\alpha]_D$ −25.5° (*c* 1.5, $CHCl_3$); IR (NaCl) 1740 (C=O) and 1610 cm^{-1} (C=C).

Found: C, 76.11; H, 6.41%. Calcd for $C_{29}H_{30}O_5$: C, 75.96; H, 6.59%.

The ^1H NMR data for compounds **10**—**13** are given in Table 3.

Reaction of Enones 21 and 23 with Methylcerium(III) Dichloride. To a suspension of finely powdered and dried cerium(III) chloride (740 mg, 3 mmol) in tetrahydrofuran (15 ml), was added with stirring 1.2 M ethereal solution of methyllithium (2.5 ml, 3 mmol) at 0 °C under argon. To this suspension was added a solution of enone (400 mg, 1 mmol) in tetrahydrofuran (3 ml) at −78 °C. The stirring was continued for 7 h at −78 °C, and the mixture was processed as in the same manner described for **4** and **6** or **10** and **12**. The results are summarized in Table 1.

Methyl 2-*O*-Acetyl-3,4-dideoxy-4-*C*-methyl-6-*O*-trityl-α-D-*erythro*-hex-3-enopyranoside (17). To a solution of **22**[15] (414 mg, 1 mmol) in ethanol (1 ml), was added with stirring cerium(III) chloride (490 mg, 2 mmol) and then sodium borohydride (75 mg, 2 mmol) at 0 °C. The stirring was continued for 3 h until gas evolution ceased. The reaction mixture was then poured into aqueous sodium chloride and extracted with dichloromethane. The extract was washed with aqueous sodium chloride, dried over magnesium sulfate, and evaporated to give a crude allylic alcohol as syrup, which was acetylated with acetic anhydride (3 ml) and pyridine (5 ml). The 2-acetate **17** was purified on a column with hexane-ethyl acetate (15 : 1). Yield, 348 mg (76%).

17: Syrup, $[\alpha]_D$ −24.7° (*c* 0.9, $CHCl_3$); IR (NaCl) 1730 (C=O) and 1600 cm^{-1} (C=C); ^1H NMR δ=5.16 (1H, bd, $J_{1,2}$=4.2 Hz, H-1), 5.54 (1H, m, H-2), 5.88 (1H, m, H-3), 4.32 (1H, bt, H-5), 3.36 (2H, bd, $J_{5,6}$=7.8 Hz, H-6 and H-6′), 1.98 (3H, bs, CMe), 2.00 (3H, s, OAc), 3.42 (3H, s, OMe), and 7.2—7.6 (15H, m, Ph).

Found: C, 75.92; H, 6.41%. Calcd for $C_{29}H_{30}O_5$: C, 75.96; H, 6.59%.

Reaction of Allylic Acetates with Lithium Dimethylcuprate-(I). To a suspension of CuI (3 equiv) in ether were added 1.2 M ethereal solution of methyllithium (6 equiv) at 0 °C, and then, after 5 min, a solution of an allylic acetate (1 equiv) in ether. The reaction mixture was poured into saturated aqueous ammonium chloride, and extracted with dichloromethane. The extract was evaporated to give residue, which was purified on a column with a solvent system given in each case. In the reaction of **15** the product was acetylated in usual manner. The yields, ^1H NMR and ^{13}C NMR data of the products (**8**, **18**, **19**, **24**, **25**, **26**, and **27**) are given in Table 2, 3, and 4, respectively.

Methyl 2,3,4-Trideoxy-2-*C*-methyl-6-*O*-tirtyl-α-D-*threo*-hex-3-enopyranoside (8). (a) From 3 or 9. The reaction of **3** or **9** with lithium dimethylcuprate(I) as described above gave crude **8**, which was purified on a column with hexane-ethyl acetate (15 : 1).

8: $[\alpha]_D$ −19.3° (*c* 2.1, $CHCl_3$); IR (NaCl) 1610 cm^{-1} (C=C).

Found: C, 81.27; H, 6.92%. Calcd for $C_{27}H_{28}O_3$: C, 80.97; H, 7.05%.

(b) From 26. To a solution of **26** (25.6 mg, 0.13 mmol) in methanol (1 ml) was added a drop of 1 M sodium methoxide and after 5 min the mixture was neutralized with IR-120 (H^+). The residue obtained by evaporation of the filtrate was treated with trityl chloride (55.8 mg, 0.2 mmol) in pyridine (0.5 ml) in a conventional manner. The crude product was purified on a column with hexane-ethyl acetate (25 : 1) to give **8** (49.9 mg, 88%), which was identified by ^1H NMR spectrum.

Methyl 2,3,4-Tridexoy-2,4-di-*C*-methyl-6-*O*-trityl-α-D-*threo*-hex-3-enopyranoside (18). The reaction of **10** with lithium dimethylcuprate(I) as described above gave crude **18**, which was purified on a column with hexane-ethyl acetate (20 : 1).

18: Syrup, $[\alpha]_D$ +47.5° (*c* 1.4, $CHCl_3$); IR (NaCl) 1610 cm^{-1} (C=C).

Found: C, 81.23; H, 7.51%. Calcd for $C_{28}H_{30}O_3$: C, 81.13; H, 7.29%.

Methyl 2,3,4-Trideoxy-2,4-di-*C*-methyl-6-*O*-trityl-α-D-*erythro*-hex-3-enopyranoside (19). The reaction of **12** with lithium dimethylcuprate(I) as described above gave crude **19**, which was purified on a column with hexane-ethyl acetate

(20 : 1).

19: Syrup, $[\alpha]_D$ −34.0° (*c* 1.0, $CHCl_3$); IR (NaCl) 1610 cm^{-1} (C=C).

Found: C, 81.12; H, 7.07%. Calcd for $C_{28}H_{30}O_3$: C, 81.13; H, 7.29%.

Methyl 2,3,4-Trideoxy-2,4-di-*C*-methyl-6-*O*-trityl-α-D-*threo*-hex-2-enopyranoside (24). The reaction of **4** with lithium dimethylcuprate(I) as described above gave crude **24**, which was purified on a column with hexane-ethyl acetate (15 : 1).

24: Syrup, $[\alpha]_D$ −18.3° (*c* 0.7, $CHCl_3$); IR (NaCl) 1600 cm^{-1} (C=C).

Found: C, 81.01; H, 7.01%. Calcd for $C_{28}H_{30}O_3$: C, 81.13; H, 7.29%.

Methyl 2,3,4-Trideoxy-2,4-di-*C*-methyl-6-*O*-trityl-α-D-*erythro*-hex-2-enopyranoside (25). The reaction of **6** with lithium dimethylcuprate(I) as described above gave crude **24**, which was purified on a column with hexane-ethyl acetate (20 : 1).

25: Syrup, $[\alpha]_D$ +6.5° (*c* 0.8, $CHCl_3$); IR (NaCl) 1600 cm^{-1} (C=C).

Found: C, 80.95; H, 7.38%. Calcd for $C_{28}H_{30}O_3$: C, 81.13; H, 7.29%.

Methyl 6-*O*-Acetyl-2,3,4-trideoxy-2-*C*-methyl-α-D-*threo*-hex-3-enopyranoside (26). The reaction of **15** with lithium dimethylcuprate(I) as described above, followed by a conventional acetylation with acetic anhydride in pyridine, gave crude **26**, which was purified on a column with hexane-acetone (7 : 1).

26: Syrup, $[\alpha]_D$ −19.3° (*c* 2.1, $CHCl_3$); IR (NaCl) 1730 (C=O) and 1610 cm^{-1} (C=C).

Found: C, 60.02; H, 8.14%. Calcd for $C_{10}H_{16}O_4$: C, 59.98; H, 8.05%.

4.6-Di-*O*-acetyl-1,5-anhydro-2,3-dideoxy-3-*C*-methyl-D-*ribo*-hex-1-enitol (27). The reaction of **20** with lithium dimethylcuprate(I) as described above gave crude **27**, which was purified on a column with hexane-acetone (3 : 1).

27: Syrup, $[\alpha]_D$ +3.7° (*c* 0.8, $CHCl_3$); IR (NaCl) 1740, 1720 (C=O) and 1620 cm^{-1} (C=C).

Found: C, 58.19; H, 6.21%. Calcd for $C_{11}H_{14}O_5$: C, 58.40; H, 6.24%.

Methyl 3,4-Di-*O*-acetyl-2-deoxy-2-*C*-methyl-6-*O*-trityl-α-D-altropyranoside (28). To a solution of **8** (120 mg, 0.29 mmol) in oxolane (1.5 ml)-acetone (1.5 ml)-water (1.5 ml) was added *N*-methylmorpholine *N*-oxide (50 mg, 0.43 mmol) and osmium tetroxide (3.3 mg). Being stood at room temperature for 2 d, the reaction mixture was poured into water and extracted with chloroform. A conventional processing of the extract gave a syrupy residue, which was acetylated in a conventional manner with acetic anhydride (3 ml) and pyridine (4 ml). A syrup obtained by usual processing was purified on a column with hexane-ethyl acetate (13 : 2) to give **28**, 87.2 mg (58%), mp 136—139.5 °C (white needles), $[\alpha]_D$ +51.5° (*c* 1.0, $CHCl_3$); ^1H NMR δ=4.45 (1H, d, $J_{1,2}$=3.0 Hz, H-1), 2.15 (H-2), 5.00 (1H, dd, $J_{2,3}$=5.6 Hz, $J_{3,4}$=3.6 Hz, H-3), 5.14 (1H, dd, $J_{4,5}$=8.0 Hz, H-4), 4.12 (1H, ddd, $J_{5,6}$=3.0 Hz, $J_{5,6'}$=4.5 Hz, H-5), 3.25 (2H, m, H-6 and H-6'), 1.14 (3H, d, $J_{2,Me}$=7.5 Hz, CMe), 1.81 and 2.02 (each 3H, each s, OAc), 3.40 (3H, s, OMe), and 7.1—7.5 (15H, m, Ph).

Found: C, 71.64; H, 6.55%. Calcd for $C_{31}H_{34}O_7$: C, 71.80; H, 6.61%.

Methyl 2,3,4,6,7-Pentadeoxy-2,4-di-*C*-methyl-7-nitro-α-D-*ribo*-hept-6-enopyranoside (32). Compound **25** (3.7 g, 8.9 mmol) was hydrogenolyzed (1 atm) in ethanol (200 ml) in the presence of $Pd(OH)_2$-carbon (20%, 0.3 g) at room temperature for 1 week. Undissolved materials were filtered off, and the filtrate was evaporated and then distilled (86 °C/20 mmHg (1 mmHg=133.322 Pa)) to give acolorless oil **29**, (667 mg, 43%), whose NMR data was identical with those reported.[21a] Then, **29** (500 mg, 2.9 mmol) was oxidized with DMSO (0.29 ml, 3.4 mmol) and oxalyl dichloride (0.27 ml, 3.4 mmol) in dichloromethane (50 ml) at −78 °C for 1 h. The reaction mixture was quenched with triethylamine, poured into water and extracted with dichloromethane. Evaporation of the extract gave **30** (363 mg, 75%).

To a solution of nitromethane (1.4 ml) in methanol (2.5 ml), were added 2 M sodium methoxide (0.22 ml) and then a solution of **30** (530 mg, 3.0 mmol) in methanol (2 ml) at 0 °C. Being kept at 0 °C for 3 h, the reaction mixture was acidified with 10% acetic acid and extracted with chloroform. The extract was washed with water, dried over magnesium sulfate and evaporated to give a crude **31** as a mixture of 6-epimers.

To a solution of crude **31** in pyridine (6 ml), was added acetic anhydride (3 ml) and the mixture was kept at room temperature overnight. A usual processing gave crude **32**, which was purified on a column with hexane-ethyl acetate (3 : 1). Yield, 611 mg (84%).

32: Syrup, $[\alpha]_D$ +103° (*c* 0.9, $CHCl_3$); IR (NaCl) 1360, 1530 (NO_2) and 1655 cm^{-1} (C=C). ^1H NMR δ=5.22 (1H, d, $J_{1,2}$=3.4 Hz, H-1), 4.24 (1H, bd, $J_{4,5}$=6.6 Hz, H-5), 7.28 (2H, bs, H-6 and H-7), 1.16 and 1.30 (each 3H, d, C-Me), 1.8—2.3 (4H, m, H-2, H-3,3', and H-4), 3.48 (3H, s, OMe).

Found: C, 55.83; H, 7.67: N, 6.84%. Calcd for $C_{10}H_{17}NO_4$: C, 55.80; H, 7.96; N, 6.51%.

Prelog-Djerassi Lactone (35). To a suspension of copper(I) iodide (162 mg, 0.85 mmol) in ether (10 ml), were added methyllithium (1.2 M in ether, 0.71 ml, 0.85 mmol) at −10 °C, and then after cooling to −30 °C a solution of boron trifluoride etherate (0.11 ml, 0.85 mmol) in ether (10 ml). The mixture was stirred for 20 min at −30 °C, then cooled to −78 °C, and to this mixture was added a solution of **32** (60.3 mg, 0.28 mmol) in ether 5 ml. The stirring was continued for 4 h at −30 °C and, the reaction mixture was poured into water, extracted with dichloromethane, dried over magnesium sulfate, and evaporated. Purification of the residue on a column with hexane-ethyl acetate (2 : 1) gave **33** as a mixture of 6-epimers (35 mg, 54%).

To a suspension of **33** (163 mg, 0.71 mmol) in water (5 ml) was added 0.1 M potassium hydroxide (0.76 mmol) and then, after 20 min, 2 M aqueous manganese(II) sulfate (1 ml) and potassium permanganate (266 mg, 1.5 mmol) in two portions. The reaction mixture was stirred for 6 h at room temperature, and to this mixture was added aqueous sodium thiosulfate. After removal of the precipitated manganese dioxide by filtration, the filtrate was adjusted at pH 2—3 with 10% acetic acid, stood at room temperature for 1 h and then extracted with chloroform-1-butanol. The extract was dried over magnesium sulfate, and evaporated to give crude **34**. To a solution of **34** in acetic acid (15 ml) and water (5 ml) was added chromium trioxide (90 mg, 0.9 mmol) at 0 °C. Being kept at 0 °C for 6 h, the reaction mixture was extracted with chloroform-DMF. The extract was washed with saturated aqueous sodium thiosulfate, and evaporated. Crude product was passed through a short column with chloroform -methanol-acetic acid (5 : 1 : 0.1) to give white syrup (32 mg, 22%) which was crystallized from pentane-ether to give pure **35** (10 mg, 7% from **33**). The data of **35** were identical to

the reported ones. Mp 125—126 °C; lit, mp 124—125 °C;[22] mp 126—128 °C,[23] $[\alpha]_D$ +37.2° (*c* 1.0, $CHCl_3$), lit,[23] $[\alpha]_D$ +38.0° (*c* 1.9, $CHCl_3$). ^{13}C NMR ($CDCl_3$) δ=8.5 (α-CH_3), 16.6 and 17.1 (C_3-CH_3 and C_5-CH_3), 30.6 (C_4), 36.2 and 37.0 (C_3 and C_5), 41.2 (C_α), 86.1 (C_2), 174.4 and 174.9 (HO_2C and C_6), lit,[17b] δ=8.4 (α-CH_3), 16.8 and 17.2 (C_3-CH_3 and C_5-CH_3), 30.8 (C_4), 36.2 and 37.1 (C_3 and C_5), 41.0 (C_α), 86.4 (C_2), 174.7 and 177.6 (HO_2C and C_6).

Found: C, 59.76; H, 8.24%. Calcd for $C_{10}H_{16}O_4$; C, 59.98; H, 8.05%.

References

1) E. Block, "Olefin Synthesis by Deoxygenation of Vicinal Diols," in "Organic Reactions," John Wiley & Sons, New York (1984), Vol. 30, p. 457.

2) R. J. Anderson, C. A. Henrick, and J. B. Siddall, *J. Am Chem. Soc.*, **92**, 735 (1970).

3) S. M. Ali, M. A. W. Finch, S. M. Roberts, and R. F. Newton, *J. Chem. Soc., Chem. Commun.*, **1979**, 679.

4) Y. Yamamoto, S. Yamamoto, H. Yatagai, Y. Ishihara, and K. Maruyama, *J. Org. Chem.*, **47**, 119 (1982).

5) H. Felkin, E. Jampel-Costa, and G. Swierczewski, *J. Organomet. Chem.*, **134**, 265 (1977).

6) The reaction of **1** with methylcopper(I) trifluoroborate in ether at 0 °C for 24 h gave 2-*C*-methyl-substituted derivative **8** and (*S*)-2-[1-hydroxy-2-(trityloxy)ethyl]furan derivative[7] **36** in 19% and 26% yields, respectively (recovered **1**, 49%). At room temperature the yield of **36** increased to 66% (**8**, 14% and **1**, 9%). The same reaction of **2** at 0 °C for 24 h gave the corresponding dimethyl derivative (**24**), 4-methylfuran (**37**) and 3,5-dimethyl-2*H*-pyran (**38**) derivatives, in 15, 7, and 59% yields, respectively. On the other hand, the reaction of **1** with methylmagnesium bromide in the presence of bis(triphenylphosphine)nickel(II) chloride in tetrahydrofuran at room temperature for 24 h gave dienopyranoside[8] (**39**) in only 16% yield (recovered **1**, 79%).

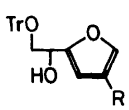

36 R=H
37 R=Me

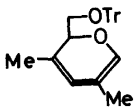

38

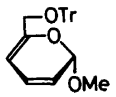

39

7) *O*-Detritylated derivative of **36**: E. Albano, D. Horton, and T. Tsuchiya, *Carbohydr. Res.*, **2**, 349 (1966).

8) H. H. Bear and Z. S. Hanna, *Can. J. Chem.*, **59**, 889 (1981).

9) N. L. Holder and B. Fraser-Reid, *Can. J. Chem.*, **51**, 3357 (1973).

10) B. Fraser-Reid, A. Mclean, E. W. Usherwood and M. Yunker, *Can. J. Chem.*, **48**, 2877 (1970).

11) D. R. Hicks and B. Fraser-Reid, *Can. J. Chem.* **53**, 2017 (1975).

12) R. J. Ferrier and N. Prasad, *J. Chem. Soc. (C)*, **1969**, 570.

13) M. B. Yunker, D. E. Plaumann, B. Fraser-Reid, *Can. J. Chem.*, **55**, 4002 (1977).

14) T. Imamoto, T. Kusumoto, Y. Tawarayama, Y. Sugiura, T. Mita, Y. Hatanaka, and M. Yokoyama, *J. Org. Chem.*, **49**, 3904 (1984).

15) This enone was already reported,[21a] but only the corresponding ethyl glycoside was described in the paper cited therein.

16) J.-L. Luche and A. L. Gemal, *J. Am. Chem. Soc.*, **101**, 5848 (1979).

17) H. L. Goering and V. D. Singleton, Jr., *J. Org. Chem.*, **48**, 1531 (1983).

18) C. Gallina and P. G. Ciattinei, *J. Am. Chem. Soc.*, **101**, 1035 (1979).

19) Y. Chapleur and Y. Grapsas, *Carbohydr. Res.*, **141**, 153 (1985).

20) a) S. Masamune, C. U. Kim, K. E. Wilson, G. O. Spessard, P.E. Georghiou, and G. S. Bates, *J. Am. Chem. Soc.*, **97**, 3512 (1975); b) S. Masamune, H. Yamamoto, S. Kamata, and A. Fukazawa, *J. Am. Chem. Soc.*, **97**, 3513 (1975).

21) a) S. Jarosz and B. Fraser-Reid, *Tetrahedron Lett.*, **22**, 2533, (1981); b) R. E. Ireland and J. P. Daub, *J. Org. Chem.*, **46**, 479 (1981); c) S. Hannesian, "Total Synthesis of Natural Products: The 'Chiron' Approach," Pergamon Press, Oxford (1983), p. 130 and the literatures cited therein.

22) R. Anliker, D. Dvornik, K. Gubler, H. Heusser, and V. Prelog, *Helv. Chim. Acta*, **39**, 1985 (1956).

23) C. Djerassi and J. A. Zderic, *J. Am. Chem. Soc.*, **78**, 6390 (1956).

 © 1987 The Chemical Society of Japan Bull. Chem. Soc. Jpn., 60, 1449—1455 (1987)

Asymmetric Hydrogenation of *N,N'*-Dimethyl-5-alkylidene- and arylmethylenehydantoins Catalyzed by (Achiral Base)bis(dimethylglyoximato)cobalt(II)-Chiral Cocatalyst System[1)]

Seiji TAKEUCHI* and Yoshiaki OHGO
Niigata College of Pharmacy, 5-13-2 Kamishin'ei-cho, Niigata 950-21
(Received October 16, 1986)

Asymmetric hydrogenation of *N,N'*-dimethyl-5-alkylidene- and arylmethylenehydantoins catalyzed by an achiral base coordinated bis(dimethylglyoximato)cobalt(II)-chiral 2-quinuclidinecarboxamide was examined. Attempts resulted in a maximum optical yield in this system (82.1% ee), strongly supporting a proposed asymmetric hydrogenation mechanism in which the chiral base acts as a proton donor, namely, a cocatalyst.

The authors have previously reported the asymmetric hydrogenation of activated ketones and olefins catalyzed by an achiral base coordinated bis(dimethylglyoximato)cobalt(II)-chiral base system (abbreviated as $Co(Hdmg)_2 \cdot B\text{-}B^*$; B and B* are achiral and chiral bases, respectively).[2)] For example, $Co(Hdmg)_2 \cdot B$-quinine catalyzes the hydrogenation of benzil to benzoin with 78% ee[3)] and $Co(Hdmg)_2 \cdot B$-(*S*)-*N*[(*R*)-1-phenylethyl]-2-quinuclidinecarboxamide catalyzes the hydrogenation of *N,N'*-dimethyl-5-benzylidenehydantoin with 79.1% ee.[4)] In the course of our study regarding asymmetric hydrogenation, we proposed an asymmetric hydrogenation mechanism in which $Co(Hdmg)_2 \cdot B$ acts as an electron donor to the substrate or intermediate and a protonated chiral base acts as a chirality-recognizing proton donor to the intermediate carbanion.[3)]

Here, we wish to describe our attempts to obtain a higher optical yield and to find supporting evidence for the proposed asymmetric hydrogenation mechanism.

Table 1. Structures and Abbreviations of Chiral Cocatalysts

B*	X	Abbreviation
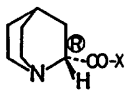	OC_2H_5	QC-(*R*)-OEt
	$NHCH_3$	QC-(*R*)-$NHCH_3$
	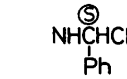	QC-(*R*)*S*
	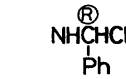	QC-(*R*)*R*
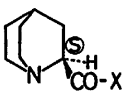	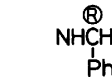	QC-(*S*)*R*
	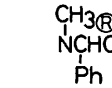	QC-(*S*)*R*-NCH_3
	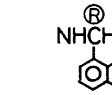	QC-(*S*)*R*-Naph

Results and Discussion

The preparation method for chiral 2-quinuclidinecarboxamides are described in the Experimental section. Structures and their abbreviations are summarized in Table 1.

An asymmetric hydrogenation of *N,N'*-dimethyl-5-alkylidene- and arylmethylenehydantoins with $Co(Hdmg)_2 \cdot B\text{-}B^*$ was examined under various conditions (Scheme 1). The enantioselectivity was affected by the structure of B*, the structure of the substrate, the molar ratio of B* to the cobalt complex, the character of the axial base, the reaction temperature and the basicity of B*.

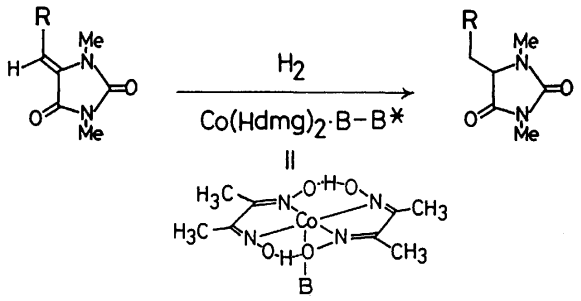

Scheme 1. Asymmetric hydrogenation of *N,N'*-dimethyl-5-alkylidene- and arylmethylenehydantoins with $Co(Hdmg)_2 \cdot B\text{-}B^*$.

Effect of Structure of B*. Hydrogenation of *N,N'*-dimethyl-5-benzylidenehydantoin was carried out using the chiral 2-quinuclidinecarboxamides as B*. The results are shown in Table 2.

The configuration of the predominant enantiomer of the hydrogenated product in every case is determined with that of the chiral center of the 2-quinuclidinecarboxylic acid moiety (Runs 1—7) and in the case of using the chiral secondary amides, the enantioselectivity is little affected by the structure of the amine moiety (Runs 1—5) (QC-(*S*)*R* is the most effective cocatalyst). However, the lack of N-H of amide group causes a remarkable decrease in the enantioselectivity (Runs 6 and 7). Accordingly, a structure excluding the alkyl group of the amine moiety mainly determines the enantioselectivity; also, the presence of N-H of amide group is extremely important.

These indicate the importance of the hydrogen bond

Table 2. Effect of Structure of B* on the Asymmetric Hydrogenation of *N,N'*-Dimethyl-5-benzylidenehydantoin[a)]

Run	B	B*	*N,N'*-Dimethyl-5-benzylhydantoin			
			Yield/%	$[\alpha]_D$/°	Conf.[b)]	%ee[c)]
1	PPh_3	QC-(*S*)*R*	93.0	−68.0	*S*	79.1
2	PPh_3	QC-(*R*)*R*	96.5	+60.7	*R*	70.6
3	$P(Bu^n)_3$	QC-(*R*)*S*	96.0	+63.2	*R*	73.5
4	$P(Bu^n)_3$	QC-(*S*)*R*-Naph	95.0	−58.0	*S*	67.7
5	$P(Bu^n)_3$	QC-(*R*)-$NHCH_3$	94.0	+56.7	*R*	65.9
6	$P(Bu^n)_3$	QC-(*S*)*R*-NCH_3	95.0	−15.0	*S*	17.4
7	$P(Bu^n)_3$	QC-(*R*)-OEt	95.0	+4.3	*R*	5.0

a) The molar ratio of substrate to cobalt was 10:1, while those of triphenylphosphine (PPh_3), tributylphosphine ($P(Bu^n)_3$), chiral cocatalysts and their hydrochlorides to cobalt were all 1:1. Solvent was benzene. b) Configuration. c) Optically pure *S* enantiomer: $[\alpha]_D^{24.0}$ −86.0° (*c* 1.018, $CHCl_3$).

Table 3. Effect of Substituent of *N,N'*-Dimethyl-5-alkylidene- and Arylmethylenehydantoins on the Asymmetric Hydrogenation[a)]

Run	R	B	B*	5-Substituted *N,N'*-dimethylhydantoin				
				Yield/%	$[\alpha]_D$/°	Conf.[b)]	%ee	V[c)]
1	Isopropyl	$P(Bu^n)_3$	QC-(*R*)*S*	84.6	+8.2	*R*	43.8	2.5
2	1-Naphthyl	$P(Bu^n)_3$	QC-(*R*)*S*	95.0	+15.0	*R*	69.3	1.1
3	*p*-NC-C_6H_4[d)]	$P(Bu^n)_3$	QC-(*R*)*S*	95.3	+39.0	*R*	74.0	2.5
4	*p*-Br-C_6H_4[e)]	$P(Bu^n)_3$	QC-(*R*)*S*	96.0	+37.4	*R*	67.6	2.5
5	*p*-F_3C-C_6H_4[f)]	$P(Bu^n)_3$	QC-(*R*)*S*	97.5	+34.9	*R*	69.6	2.1
6	*p*-H_3CO-C_6H_4[g)]	$P(Bu^n)_3$	QC-(*R*)*S*	95.0	+54.8	*R*	72.2	2.1
7	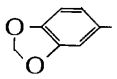	$P(Bu^n)_3$	QC-(*R*)*S*	98.0	+48.5	*R*	66.7	2.1
8	Ph	$P(Bu^n)_3$	QC-(*R*)*S*	96.0	+63.2	*R*	73.5	2.5

a) The molar ratios of substrates to cobalt were 6—10:1, while those of $P(Bu^n)_3$, QC-(*R*)*S* and QC-(*R*)*S*·HCl to cobalt were all 1:1. Solvent was benzene. b) Configuration. c) Maximum velocity (H_2 moles consumed/s/mol of catalyst: $10^{-3}s^{-1}$). d) *p*-Cyanophenyl. e) *p*-Bromophenyl. f) *p*-Trifluoromethylphenyl. g) *p*-Methoxyphenyl.

between N-H of the chiral cocatalysts and the carbonyl group of the substrates.[4)]

Effect of Substituent of Substrate. The results of the hydrogenation of *N,N'*-dimethyl-5-alkylidene- and arylmethylenehydantoins are shown in Table 3.

Enantiomeric excesses of the hydrogenated products (except for *N,N'*-dimethyl-5-benzylhydantoin) were determined by ^1H NMR spectra in the presence of a chiral lanthanoid shift reagent.

Enantioselectivity for 5-(arylmethylene)hydantoins was higher than that of 5-isobutylidenehydantoin. Among the 5-(arylmethylene)hydantoins there is little difference in the enantioselectivity. The difference between 5-(arylmethylene)- and 5-isobutylidenehydantoin can be explained by a conformation of their intermediate carbanion[4)] (depicted in Fig. 1).

Conformation A is preferred to B for 5-(arylmethyl)-hydantoin carbanion because of an electrostatic repulsion between a lone pair on the asymmetric carbon atom and the π-electron on the aromatic ring. However, conformation B is rather preferred to A for 5-isobutylhydantoin carbanion because of a steric repulsion between the isobutyl group and the hydantoin ring and of a decrease in the electrostatic repulsion. One of the two enantiomers in conformation A is smoothly protonated by protonated QC-(*R*)*S* (abbreviated as QC-(*R*)*S*·H^+) to give (*R*)-5-(arylmethyl)hydantoin predominantly via a transition state having a hydrogen bond between N-H of QC-(*R*)*S*·H^+ and C=O of the carbanion of 5-(arylmethyl)hydantoin (CPK model C in Fig. 1). On the other hand, such hydrogen bonding is impossible in conformation B; this should cause a decrease in the enantioselectivity.

Effect of Molar Ratio of B* to the Cobalt Complex. Hydrogenation of *N,N'*-dimethyl-5-benzylidenehydantoin was carried out in various molar ratios of QC-(*R*)*S* (or QC-(*S*)*R*) to the cobalt complex (abbreviated as QC-(*R*)*S*/Co). The results are shown in Table 4.

The optical yield increases with increasing ratio QC-(*R*)*S*/Co and reaches a maximum value (82.1% ee) when the ratio is 7 (Run 5). This can be explained as follows.

A simplified catalytic cycle of this hydrogenation is shown in Fig. 2.[5)]

The point of contact of reaction ② and cycle ④ is the enantioselectivity-determining step: protonation to the intermediate carbanion. Although the electron-

Table 4. Effect of the Molar Ratio of B* to Cobalt Complex on the Asymmetric Hydrogenation of *N,N'*-Dimethyl-5-benzylidenehydantoin[a)]

Run	B	B* (B*/Co)[b)]	*N,N'*-Dimethyl-5-benzylhydantoin				
			Yield/%	$[\alpha]_D$/°	Conf.[d)]	%ee	V[c)]
1	$P(Bu^n)_3$	QC-(*R*)*S* (1)	96.0	+63.0	*R*	73.5	2.2
2	$P(Bu^n)_3$	QC-(*R*)*S* (7)	94.0	+67.0	*R*	77.9	2.6
3	PPh_3	QC-(*S*)*R* (1)	93.0	−68.0	*S*	79.1	0.49
4	PPh_3	QC-(*R*)*S* (2)	92.5	+68.2	*R*	79.3	
5	PPh_3	QC-(*R*)*S* (7)	94.0	+70.6	*R*	82.1	0.27
6	PPh_3	QC-(*R*)*S* (14)	94.5	+70.4	*R*	81.9	0.17

a) The molar ratio of substrate to cobalt was 10:1, while those of PPh_3, $P(Bu^n)_3$, and QC-(*R*)*S*·HCl (or QC-(*R*)*S*·HCl) to cobalt were all 1:1. Solvent was benzene. b) Values in parentheses represent the molar ratio of B* to cobalt. c) Maximum velocity: $10^{-3}s^{-1}$. d) Configuration.

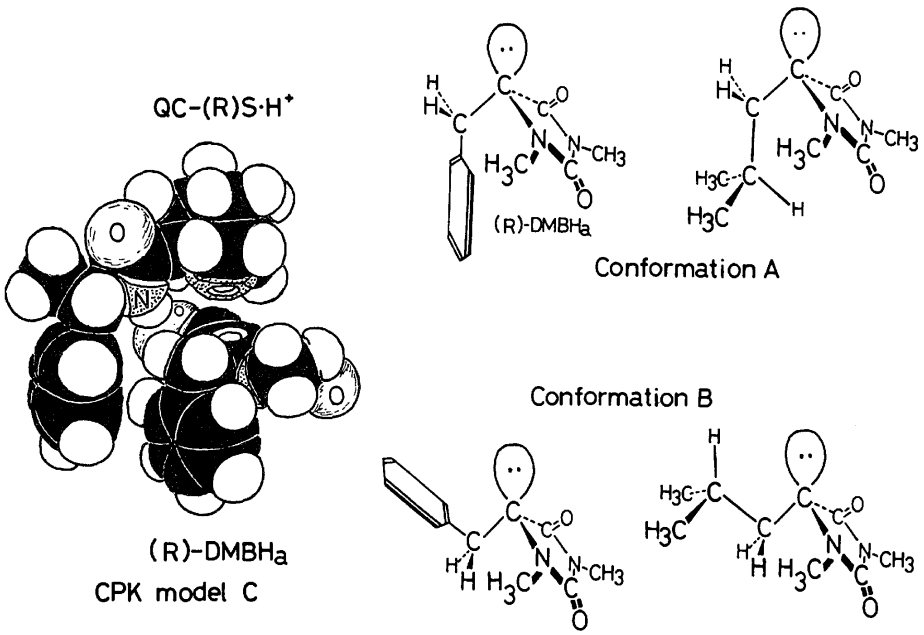

Fig. 1. Conformations of isobutyl- and benzylhydantoin (as representative of 5-(arylmethyl)hydantoin), and CPK model of the chirality-recognizing transition state (the hydrogen atom attached on the nitrogen atom of quinuclidine and the lone pair on the asymmetric carbon atom of (*R*)-*N,N'*-dimethyl-5-benzylhydantoin carbanion, (*R*)-$DMBH_a$, are not depicted).

donating cycle ③ and the proton-donating cycle ④ are independently conjugated with the reductive alkylation ① and the reduction of the alkyl complex ②, the two cycles ③ and ④ are joined by the following equilibrium. QC-(*R*)*S*·HCl in the reaction

$$H\cdot Co(Hdmg)_2\cdot B + QC\text{-}(R)S \rightleftharpoons \bar{C}o(Hdmg)_2\cdot B + QC\text{-}(R)S\cdot H^+$$

solution is included in the equilibrium as QC-(*R*)*S*·H^+. The equilibrium remains constant under a stationary state and, therefore, the optical yield is determined by the ratio of QC-(*R*)*S*·H^+ to H·Co(Hdmg)$_2$·B and other protonated achiral base (B·H^+) in the reaction system. If the ratio has reached a value near the maximum, even in QC-(*R*)*S*/Co=1, the increasing degree of the optical yield should be small and the optical yield should readily reach a maximum even though the ratio QC-(*R*)*S*/Co increases to a great extent.

Effect of σ-Donor Character of Axial Base. Hydrogenation of *N,N'*-dimethyl-5-benzylidenehydantoin was carried out using benzylamine (BA), $P(Bu^n)_3$ and PPh_3 as B. The results are shown in Table 5.

As outlined above, QC-(*R*)*S*·H^+ acts as a chirality-recognizing proton donor. On the other hand, H·Co(Hdmg)$_2$·B or B·H^+ can also act as a proton donor; hence, they competitively disturb the enantioselective proton-donation reaction by QC-(*R*)*S*·H^+ to decrease the optical yield. Since BA is a stronger base than QC-(*R*)*S*, the enantioselective protonation is strongly disturbed by BA·H^+ and decreases the optical yield (Run 1). PPh_3 and $P(Bu^n)_3$ can scarcely act as a proton acceptor since they are considerably weaker and more soft base than QC-(*R*)*S*. The lower optical yield in

Table 5. Effect of σ-Donor Character of Axial Base on the Asymmetric Hydrogenation of *N,N'*-Dimethyl-5-benzylidenehydantoin[a]

Run	B	B* (B*/Co)[b]	*N,N'*-Dimethyl-5-benzylhydantoin				
			Yield/%	$[\alpha]_D$/°	Conf.[c]	%ee	V[d]
1	BA	QC-(*S*)*R* (1)	98.0	−15.6	*S*	18.1	2.6
2	$P(Bu^n)_3$	QC-(*R*)*S* (1)	96.0	+63.0	*R*	73.5	2.5
3	PPh_3	QC-(*S*)*R* (1)	93.0	−68.0	*S*	79.1	0.49
4	PPh_3	QC-(*R*)*S* (7)	94.0	+70.6	*R*	82.1	0.27
5	—[e]	QC-(*S*)*R* (2)	93.5	−58.7	*S*	68.2	0.19
6	—	QC-(*S*)*R* (7)	94.5	−55.4	*S*	64.4	0.52
7	PPh_3 (4)[f]	QC-(*S*)*R* (7)	91.0	−69.4	*S*	80.7	0.09

a) The molar ratio of substrate to cobalt was 10:1, while those of PPh_3, $P(Bu^n)_3$, BA and QC-(*S*)*R*·HCl (or QC-(*R*)*S*·HCl) to cobalt were all 1:1 except for Run 7. Solvent was benzene. b) Values in parentheses represent the molar ratio of B* to cobalt. c) Configuration. d) Maximum velocity: $10^{-3}s^{-1}$. e) No base other than QC-(*S*)*R* was used. f) The molar ratio of PPh_3 to cobalt was 4.

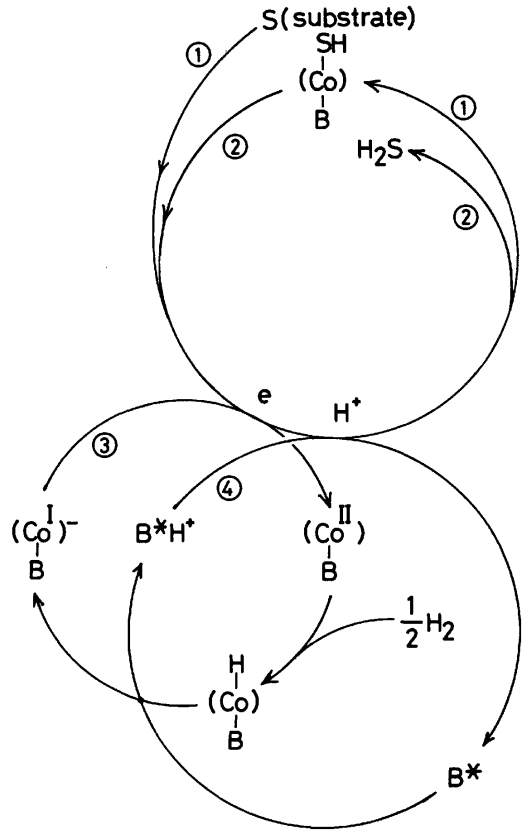

Fig. 2. Simplified catalytic cycle: S= R Me

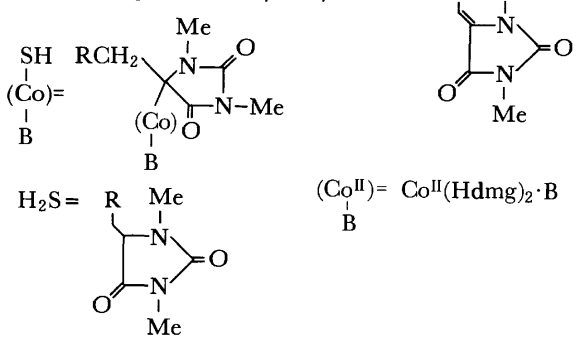

Run 2 than that in Run 3 should be due to the stronger basicity of $P(Bu^n)_3$ than PPh_3. Needless to say, QC-(*R*)*S*·H^+ can not disturb the enantioselective protonation of itself and, hence, the low optical yield in Run 5 compared with those in Runs 2 and 3 must be due to a disturbance by H·Co(Hdmg)$_2$·QC-(*R*)*S*. A comparison of the results in Runs 3 and 4 with those in 5 and 6, respectively, clarifies the role of QC-(*R*)*S*. The optical yield increases in Run 4 but decreases in Run 6 with increasing ratio QC-(*R*)*S*/Co. The axial ligand of the cobalt complex is chiefly PPh_3 in Runs 3 and 4, whereas it is QC-(*R*)*S* in Runs 5 and 6. Consequently, it is clear that coordination of QC-(*R*)*S* to the cobalt complex decreases the optical yield.

Effect of Reaction Temperature. Hydrogenation of *N,N'*-dimethyl-5-benzylidenehydantoin was carried out at room temperature and at −10 °C in benzene and in mesitylene, respectively. The results are shown in Table 6.

The optical yield increases upon using quinine as a cocatalyst (Run 2) but decreases upon using QC-(*R*)*S* as a cocatalyst (Run 4) with decreasing reaction temperature. This should be due to the solubility of QC-(*R*)*S*·HCl in mesitylene, since the optical yield increases upon using only QC-(*R*)*S* (Run 6), but decreases upon using only QC-(*R*)*S*·HCl (Run 8) with decreasing reaction temperature. Since QC-(*R*)*S*·HCl is slightly soluble in such a nonpolar solvent as benzene and mesitylene (even at room temperature), it becomes much less soluble at −10 °C. Such a decreased solubility should result in a decreasing optical yield, since both the chiral base and its hydrochloride are required to obtain a maximum optical yield in this system.[3]

If this deduction is correct, it is possible to attain a much higher optical yield in nonpolar and aprotic solvent systems which easily dissolve QC-(*R*)*S*·HCl, even at low temperatures.

Effect of Basicity of B*. Hydrogenation of *N,N'*-dimethyl-5-benzylidenehydantoin was carried out using quinine and/or QC-(*R*)*S* as cocatalyst. The results are shown in Table 7.

(*S*)-Configuration product with 51.4%ee was obtained upon using a system mixed with quinine, QC-(*R*)*S* and their hydrochlorides (Run 3) although an opposite configuration and a higher optical yield

Table 6. Effect of Reaction Temperature on the Asymmetric Hydrogenation of *N,N'*-Dimethyl-5-benzylidenehydantoin[a]

Run	Temp[b]	Solvent	B	B*	B*·HCl	*N,N'*-Dimethyl-5-benzylhydantoin			
						Yield/%	$[\alpha]_D$/°	Conf.[c]	%ee
1	RT[d]	Benzene	$P(Bu^n)_3$	Quinine (1)	Quinine (1)[e]	91.0	−47.4	*S*	54.7
2	−10°C	Mesitylene	$P(Bu^n)_3$	Quinine (1)	Quinine (1)	90.0	−52.8	*S*	61.4
3	RT	Benzene	$P(Bu^n)_3$	QC-(*R*)*S* (1)	QC-(*R*)*S* (1)	96.0	+63.0	*R*	73.5
4	−10°C	Mesitylene	$P(Bu^n)_3$	QC-(*R*)*S* (1)	QC-(*R*)*S* (1)	97.5	+54.6	*R*	63.5
5	RT	Benzene	$P(Bu^n)_3$	QC-(*R*)*S* (1)	—[f]	94.5	+41.6	*R*	48.4
6	−10°C	Mesitylene	$P(Bu^n)_3$	QC-(*R*)*S* (2)	—	93.5	+49.0	*R*	57.0
7	RT	Benzene	$P(Bu^n)_3$	—[f]	QC-(*R*)*S* (1)	93.0	+42.8	*R*	49.8
8	−10°C	Mesitylene	$P(Bu^n)_3$	—	QC-(*R*)*S* (1)	92.0	+28.9	*R*	33.6

a) The molar ratio of substrate to cobalt was 10:1, while that of $P(Bu^n)_3$ to the cobalt was 1:1. b) Reaction temperature. c) Configuration. d) Room temperature. e) Values in the parentheses represent the molar ratio of B* or B*·HCl to cobalt. f) B*·HCl or B* were not used.

Table 7. Effect of Basicity of B* on the Asymmetric Hydrogenation of *N,N'*-Dimethyl-5-benzylidenehydantoin[a]

Run	B	B*	B*·HCl	*N,N'*-Dimethyl-5-benzylhydantoin				
				Yield/%	$[\alpha]_D$/°	Conf.[b]	%ee	V[c]
1	$P(Bu^n)_3$	Quinine (1)	Quinine (1)[d]	91.0	−47.4	*S*	54.7	1.9
2	$P(Bu^n)_3$	QC-(*R*)*S* (1)	QC-(*R*)*S* (1)	96.0	+63.2	*R*	73.5	2.2
3	$P(Bu^n)_3$	Quinine (1) QC-(*R*)*S* (1)	Quinine (1) QC-(*R*)*S* (1)	94.5	−44.2	*S*	51.4	2.1
4	$P(Bu^n)_3$	Quinine (1)	—[e]	93.5	−23.0	*S*	26.7	2.1
5	$P(Bu^n)_3$	QC-(*R*)*S* (1)	—	94.5	+41.6	*R*	48.4	2.5
6	$P(Bu^n)_3$	Quinine (1) QC-(*R*)*S* (1)	— —	95.0	−31.8	*S*	37.0	2.1

a) The molar ratio of substrate to cobalt was 10:1, while that of $P(Bu^n)_3$ to cobalt was 1:1. Solvent was benzene. b) Configuration. c) Maximum velocity: $10^{-3}\,s^{-1}$. d) Values in the parentheses represent the molar ratio of B* or B*·HCl to cobalt. e) B*·HCl was not used.

were obtained in Run 2 compared with those in Run 1. A similar tendency was observed in the absence of the hydrochlorides, except for a higher optical yield upon using a system mixed with quinine and QC-(*R*)*S* (Run 6) than that using only quinine (Run 4). Thus, the enantioselectivity of QC-(*R*)*S* is masked and that of quinine predominates in a mixed system. Since QC-(*R*)*S* is a weaker base (namely, a weaker proton acceptor than quinine), it should hardly act as a proton acceptor in mixed systems.

This can be demonstrated by the ^{13}C NMR spectra of a mixed system in $CDCl_3$. The ^{13}C NMR spectra of quinine·HCl(I), quinine(II), QC-(*R*)*S*·HCl(III), QC-(*R*)*S*(IV) and their mixture (V and VI) are shown in Fig. 3.

The values near the peaks represent the chemical shift (ppm) of C-9 in quinine or quinine·HCl and that of carbonyl carbon in QC-(*R*)*S* or QC-(*R*)*S*·HCl. From these data the ratio of the components in the solution was estimated. For example, quinine exists almost as hydrochloride (96.9%) in a solution of QC-(*R*)*S*·HCl (3.56×10^{-5} mol) and quinine (3.545×10^{-5} mol) (V); and QC-(*R*)*S* exists completely as free base in that of QC-(*R*)*S*·HCl (1.70×10^{-5} mol), QC-(*R*)*S* (1.66×10^{-5} mol) and quinine (3.45×10^{-5} mol) (VI).[6] These results demonstrate that quinine is a much stronger proton acceptor than QC-(*R*)*S*.

Conclusion

The main problem regarding the mechanism of this asymmetric hydrogenation is what role the chiral base performs. Since the chiral base can coordinate to the cobalt complex, one may think that the chiral cobalt complex is a chirality-recognizing species itself. However, we have proposed another unique asymmetric hydrogenation mechanism (described above). Although the possibility of an enantioselective reaction by the chiral cobalt complex[7] can not be completely excluded, the results obtained above strongly support the proposed asymmetric hydrogenation mechanism. These are summarized as follows: (1) The optical yield increases with increasing ratio QC-(*R*)*S*/Co and reaches a maximum value, (2) coordination of QC-(*R*)*S* to the cobalt complex decreases the optical yield, and (3) the enantioselectivity for a stronger proton acceptor (quinine) predominates in a system mixed with quinine and QC-(*R*)*S*.

Experimental

The melting points were determined by a Yanagimoto micro-melting point apparatus and were uncorrected. The IR spectra were recorded on a JASCO A-3 spectrometer. The ^1H and ^{13}C NMR spectra were obtained on a JEOL-FX 200 spectrometer. The optical rotations were measured with a

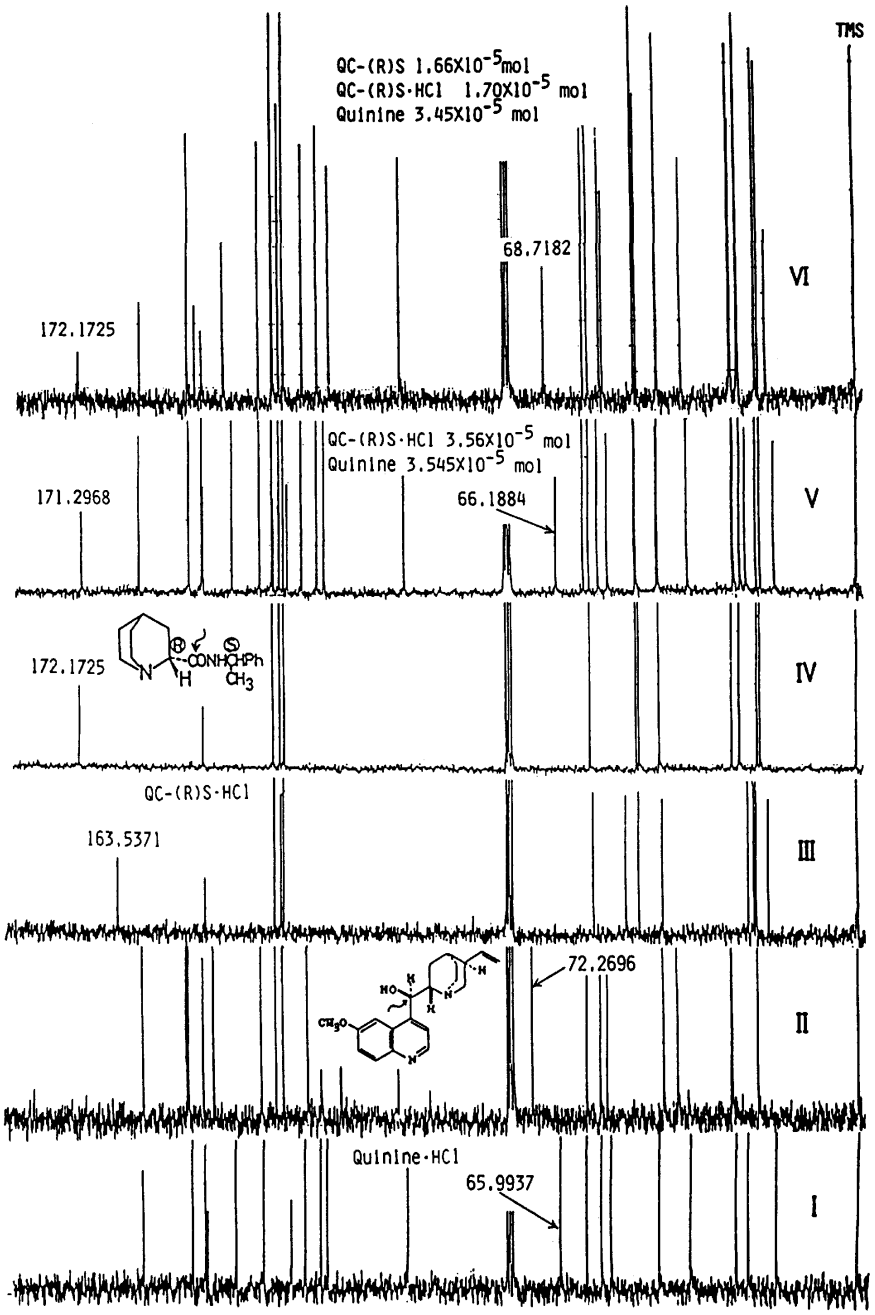

Fig. 3. ^{13}C NMR spectra in $CDCl_3$(0.6 ml).

Perkin Elmer 241 polarimeter.

Preparation of Cocatalyst. As the preparation of QC-(*R*)S and its enantiomer were described in a previous paper,[4] only those of QC-(*S*)*R*-NCH_3, QC-(*S*)*R*-Naph and QC-(*R*)-$NHCH_3$ are described below.

(*S*)-*N*-Methyl-*N*-[(*R*)-1-phenylethyl]-2-quinuclidinecarboxamide (QC-(*S*)*R*-NCH_3). Thionyl chloride (25 g) and (*S*)-2-quinuclidinecarboxylic acid hydrochloride (1.5 g, 7.8 mmol; $[\alpha]_D^{20.1}$ −96.8° (*c* 1.022, H_2O), lit,[8] $[\alpha]_D$ −96.2° (*c* 1, H_2O)) were refluxed for 20 min and the homogeneous solution was concentrated *in vacuo* to remove excess thionyl chloride. To the residue was added dry benzene and concentrated to dryness (repeated twice). To the crystalline residue dry ether was added and then (*R*)-*N*-methyl-1-phenylethylamine (3.6 g, 26.6 mmol) were added on ice cooling with stirring.[9] Stirring was continued for 3 d at room temperature and then to the solution was added a 50% aqueous potassium carbonate solution until the water layer became basic. The ether layer was decanted and the water layer was extracted twice with ether (200 ml×2) and the ether layers were combined and dried (Na_2SO_4). The ether solution was concentrated in order to also remove any excess (*R*)-*N*-methyl-1-phenylethylamine to give oil (1.73 g, 6.3 mmol). The oil and *p*-toluenesulfonic acid monohydrate (1.2 g, 6.3 mmol) were dissolved in methanol and concentrated to dryness. The residue was gradually solidified in ether. After standing overnight the ether was decanted and the residual solid was recrystallized from ethyl acetate to give prisms. The prisms were dissolved in water and the solution was made basic with a 50% aqueous potassium carbonate solution. The solution

was extracted twice with ether (200 ml×2) and then dried (Na_2SO_4). The concentration of the ether solution gave oil (0.79 g).

The oil (0.13 g, 0.48 mmol) was dissolved in methanol and to the solution was added 0.04 ml of concentrated hydrochloric acid. The solvent was removed and the residue was dried by evaporation with dry benzene to give crystals. These were recrystallized from ethanol-ether to give needles (0.1 g): mp>250 °C (sublimed from ca. 220 °C); $[\alpha]_D^{22.0}$ +45.0° (*c* 0.511, CH_3OH); IR (KBr) 2300—2500 (N^+H) and 1640 cm^{-1} (amide C=O); ^1H NMR ($CDCl_3$ and DMSO-d_6) δ=1.50 (2.3H,[10] d, *J*=7.34 Hz, $C\underline{H}_3$-CH), 1.60 (0.7H, d, *J*=6.60 Hz, $C\underline{H}_3$-CH), 1.76 (5H, m), 2.12 and 2.36 (2H, m), 2.63 (0.7H, s, N-$C\underline{H}_3$), 2.73 (2.3H, s, N-$C\underline{H}_3$), 3.28 (3H, m), 4.81 (1H, t, *J*=9.6 Hz, C-2 methine proton), 5.17 (0.23H, q, *J*=6.60 Hz, CH_3-$C\underline{H}$), 5.80 (0.77H, q, *J*=7.34 Hz, CH_3-$C\underline{H}$) and 7.24 (5H, m, Ph). Found: C, 66.11; H, 8.16; N, 9.09. Calcd for $C_{17}H_{25}ClN_2O$: C, 65.77; H, 8.26; N, 8.93.

(*S*)-*N*-[(*R*)-1-(1-naphthyl)ethyl]-2-quinuclidinecarboxamide (QC-(*S*)*R*-Naph). Thionyl chloride (25 g) and (*S*)-2-quinuclidinecarboxylic acid hydrochloride (2.0 g, 10.4 mmol; $[\alpha]_D^{18.2}$ −90.0° (*c* 1.026, H_2O)) were treated as described above. The crystalline residue were suspended in dry ether (200 ml) and to the solution (*R*)-1-(1-naphthyl)ethylamine (1.79 g, 10.5 mmol) and triethylamine (3.3 g, 32.6 mmol) were added on ice cooling with stirring. Stirring was continued for 6 d at room temperature and followed a similar procedure as that for QC-(*S*)*R*-NCH_3 to give syrup (2.84 g, 9.2 mmol). The syrup was reacted with *p*-toluenesulfonic acid monohydrate (1.87 g, 9.8 mmol) and treated similarly as QC-(*S*)*R*-NCH_3 to give crystals (0.92 g). These were recrystallized from petroleum ether to give large columns (0.7 g): mp 134.0—136.0 °C; $[\alpha]_D^{22.4}$ −43.4° (*c* 1.008, $CHCl_3$); IR (KBr) 3370 (NH) and 1662 cm^{-1} (amide C=O); ^1H NMR ($CDCl_3$) δ=1.28 (2H, m), 1.44 (2H, m), 1.64 (3H, d, *J*=6.85 Hz, $C\underline{H}_3$-CH), 1.84 (3H, m), 2.42 (2H, t), 2.83 (2H, m), 3.34 (1H, t, *J*=9.17 Hz, C-2 methine proton), 5.96 (1H, quintet, *J*=6.85 Hz, CH_3-$C\underline{H}$), 7.44 (5H, m, naphthyl and NH), 7.76 (2H, m, naphthyl) and 8.08 (1H, d, naphthyl). Anal. ($C_{20}H_{24}N_2O$)-C,H,O.

(*R*)-*N*-Methyl-2-quinuclidinecarboxamide (QC-(*R*)-$NHCH_3$). Ethyl (*R*)-2-quinuclidinecarboxylate (1.0 g; $[\alpha]_D^{24.6}$ +89.4° (*c* 1.013, ethanol), lit,[8] $[\alpha]_D^{22}$ −88.4° (*c* 1, abs ethanol)) was dissolved in an aqueous 35-41% methylamine solution (150 ml); the solution was allowed to react overnight. The solution was concentrated and the residue was extracted with ether (200 ml). The ether solution was dried (Na_2SO_4) and concentrated to give crystals (0.66 g). These were recrystallized from petroleum ether to give large needles (0.47 g): mp 85.0—87.0 °C; $[\alpha]_D^{24.5}$ +117.1° (*c* 1.008, $CHCl_3$); IR (KBr) 3350 (NH) and 1660 cm^{-1} (amide C=O); ^1H NMR ($CDCl_3$) δ=1.48 (4H, m), 1.87 (3H, d), 2.71 (2H, t), 2.82 (3H, d, *J*=4.9 Hz, $C\underline{H}_3$-NH), 2.89 (2H, m), 3.28 (1H, t, *J*=9.3 Hz, C-2 methine proton), 6.96 (1H, broad s, NH). Anal. ($C_9H_{16}N_2O$)C,H,O.

Asymmetric Hydrogenation of *N,N'*-Dimethyl-5-alkylidene- and Arylmethylenehydantoins with $Co(Hdmg)_2$·B-B*. The hydrogenation (under 1 atm of H_2) and the isolation of the hydrogenated product were carried out according to the procedure described in a previous paper,[4] except for the following case. When a cocatalyst with more than an equimolar amount of the cobalt complex was used, it was dissolved in a solution of the substrate to be injected into the reaction vessel[4] together with the substrate. When PPh_3 and $P(Bu^n)_3$ are not used as B, the purification by column chromatography was not carried out.[11]

Determinations of enantiomeric excesses of the hydrogenated products were similarly performed as that described in a previous paper using tris(3-trifluoroacetyl-*d*-camphorato)-europium(III).[4]

The authors wish to express their thanks to Professor Chung-gi Shin and Assistant Professor Yasuchika Yonezawa, Kanagawa University, for their valuable discussions and generous gift of samples; and to Miss Tatsuko Sakai, Meijho University, for her elemental analyses. We would also like to thank Mr. Masakazu Yamaguchi, Mr. Noriyuki Kameda, Mr. Koji Yamada, and Mr. Takefumi Momose for the preparation of substrates and chiral 2-quinuclidinecarboxamides.

References

1) Asymmetric Reactions XIV.

2) Y. Ohgo, S. Takeuchi, and J. Yoshimura, *Bull. Chem. Soc. Jpn.*, **44**, 583(1971); S. Takeuchi, Y. Ohgo, and J. Yoshimura, *Chem. Lett.*, **1973**, 265; Y. Ohgo, S. Takeuchi, Y. Natori, and J. Yoshimura, *ibid*, **1974**, 33; Y. Ohgo, Y. Natori, S. Takeuchi, and J. Yoshimura, *ibid*, **1974**, 709 and 1327.

3) Y. Ohgo, S. Takeuchi, Y. Natori, and J. Yoshimura, *Bull. Chem. Soc. Jpn.*, **54**, 2124 (1981); Y. Ohgo, Y. Tashiro, and S. Takeuchi, *ibid*, 1549 in this issue.

4) S. Takeuchi, and Y. Ohgo, *Bull. Chem. Soc. Jpn.*, **54**, 2136 (1981) and **57**, 1920 (1984).

5) As this scheme is too simplified, see reference 3) where the detailed asymmetric hydrogenation mechanism is described.

6) Since proton exchange is rapid on the NMR time scale, the observed chemical shift of C-9 or carbonyl carbon should be that in a weighted average of free base and its hydrochloride. Accordingly, the percentage of quinine·HCl in the mixed system (V) can be evaluated by the equation:

$$\frac{72.2696-66.1884}{72.2696-65.9937}\times 100 = 96.9(\%).$$

7) S. Tyrlik, M. M. Kucharska, and I. Wolochowiz, *J. Mol. Cat.*, **6**, 393 (1979).

8) H. Pracejus and G. Kohl, *Ann.*, **722**, 1 (1969).

9) H. Pracejus, F. W. Wilke, and K. Hanemann, *J. Prak. Chem.*, **319**, 219 (1977).

10) The separation of signals ($C\underline{H}_3$-CH, $C\underline{H}_3$-N and CH_3-$C\underline{H}$) is due to rotational isomerization of QC-(*S*)*R*-NCH_3·HCl, which is confirmed by comparison of the ^1H NMR spectrum with that of QC-(*R,S*)*R*-NCH_3·HCl (QC-(*R,S*) represents racemate). Thus the ratio of the number of protons (2.3 : 0.7) represents that of the rotational isomers in the solution. The similar phenomenon was observed for QC-(*R*)*S*-NCH_3 and the ratio was 2.1 : 0.9 in $CDCl_3$.

11) The purification resulted in little change of optical rotation in this case. For example, 1.64 g of *N,N'*-dimethyl-5-benzylhydantoin (in Run 6 of Table 5) whose optical rotation is −55.4° was purified by the column chromatography to give 1.62 g of $[\alpha]_D$ −56.0°. This also indicates that enantiomeric enrichment does not occur in the purification procedure.

 © 1987 The Chemical Society of Japan Bull. Chem. Soc. Jpn., 60, 1457—1464 (1987)

Selective 1,4-Chiral Induction in the Reaction of Enolates Generated from *t*-Butyl δ-Hydroxy Carboxylates

Koichi NARASAKA,* Yutaka UKAJI, and Kazutoshi WATANABE
Department of Chemistry, Faculty of Science, The University of Tokyo, Hongo, Bunkyo-ku, Tokyo 113
(Received October 20, 1986)

Lithium enolates generated from *t*-butyl esters of δ-hydroxy carboxylic acids with lithium dialkylamides in THF-HMPA were alkylated stereoselectively to give the corresponding *syn*-α-alkylated δ-hydroxy esters. The generation of the enolates was accelerated by the addition of lithium trifluoromethanesulfonate, and the successive aldol and hydroxylation reactions of the enolates also proceeded in a stereoselective manner.

In recent years a number of efforts have been devoted on the exploration of stereoselective reactions in acyclic precursors, and various excellent methods have been developed toward the diastereoselection between adjacent carbon atoms (1,2-relationships).[1] However, general approaches to the construction of remote chiral relationships in acyclic systems are rare, and such a control of the diastereoselectivity between remote carbons has still been a challenging problem in organic synthesis.

Concerning 1,3-chiral induction[1b,2] we have reported the stereoselective preparations of *syn*-1,3-diols and *syn*-β-amino alcohols from β-hydroxy ketones.[3] In this paper, we describe the rusults of a study on 1,4-chiral induction[2b,4] directed by a hydroxyl group in the reaction of lithium enolates derived from δ-hydroxy esters.[5]

Results and Discussion

The formation of 6-membered chelate is known to well regulate the 1,2-chiral induction in the reaction of dilithio derivatives generated from β-hydroxy esters.[6] It was considered that the lithium enolate dianion **2** prepared from δ-hydroxy esters would also form even a strained 8-membered chelate by the strong interaction between lithium and the oxygen of the alkoxide group. Hence the successive reaction of **2** with electrophiles would proceed in a stereoselective manner.

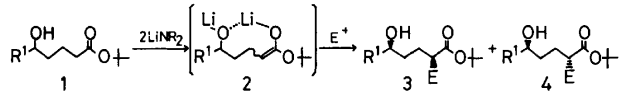

By the above hypothesis, the alkylation reaction of ester enolates generated from **1** was firstly examined. *t*-Butyl 5-hydroxyhexanoate (**1A**) was treated with 2 molar amounts of lithium diisopropylamide (LDA) in THF at −78 °C and the resulting enolate was alkylated with methyl iodide, however, a ca. 1 : 1 mixture of **5a** and **6a** was obtained. When the formation of the enolate from **1A** and the successive alkylation were carried out using hexamethylphosphoric triamide (HMPA) as a co-solvent with THF, the remarkable stereoselectivity was observed to give a *syn*[7]-α-alkylated product **5a** and an *anti*-product **6a** in a ratio of 86 : 14. It was also observed that the enolization of *t*-butyl 5-hydroxynonanoate (**1B**) with LDA in THF or in THF-HMPA at −78 °C was followed by the addition of butyl iodide to furnish **5b** and **6b** in a ratio of 52 : 48 or 88 : 12, respectively.

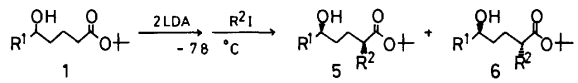

Table 1. Alkylation Reaction of **1** (2 equiv LDA, −78 °C)

	R^1	R^2	Solvent	**5**:**6**[a]
a	Me	Me	THF	56:44
			THF-HMPA	86:14
b	*n*-Bu	*n*-Bu	THF	52:48
			THF-HMPA	88:12

a) The ratios were determined by capillary gas chromatography (PEG-HT).

The geometry of the enolates generated from **1B** in THF and THF-HMPA was studied by trapping the enolates with *t*-butyldimethylsilyl chloride according to the Ireland's procedure,[8] and in each case, the silyl enol ether of the different configuration was formed predominantly. Based on the Ireland's study, lithiation in THF and THF-HMPA was considered to mainly afford the *trans*[9]-enolate *trans*-**2B** and the *cis*-enolate *cis*-**2B**, respectively. Furthermore, the observation that the vinylic proton of the silyl enol ether of the enolate generated in THF-HMPA appears at 0.03 ppm lower field than the corresponding resonance for that generated in THF supported the above stereochemical assignment.[8]

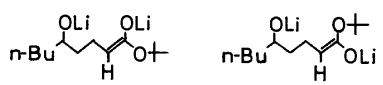

cis-2B trans-2B

We supposed that the enhanced selectivity by the addition of HMPA may be due to the formation of an 8-membered chelate of a *cis*-enolate. In the 8-membered chelate of the *cis*-enolate, the attack of an electrophile would be expected to proceed from the less hindered side in the preferable conformations such as T_1 (no-symmetry) or T_2 (twist chair)[10a] to result in the formation of the *syn*-alkylated product **5**. On the con-

Table 2. Effect of Lithium Dialkylamides on the Methylation Reaction of **1A**

$LiNR_2$	Temp of enolization/°C	MeX	**5a**:**6a**
LDA	−78	MeI	86:14[a]
	−100→−78	MeI	87:13
	−100→−78	Me_2SO_4	90:10
LTMP	−100→−78	Me_2SO_4	90:10
$LiNEt_2$	−100→−78	Me_2SO_4	92: 8
	−100	Me_2SO_4	95: 5
$LiNMe_2$	−100	Me_2SO_4	94: 6
LiN⟨ ⟩	−100	Me_2SO_4	95: 5

a) The alkylation reaction was performed at −78°C.

trary, the formation of a chelate T_3 should be difficult for the *trans*-enolate because of the severe steric strain,[10] therefore any stereoselection was not observed in the alkylation reaction.

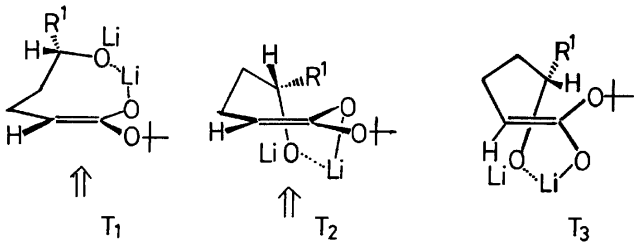

Our initial report that the *syn*-stereoselection is controlled by the addition of HMPA without regard to the configuration of the generating lithium enolate was noted to be incorrect. By the experiments of the reproducibility, it was found that the addition of HMPA after the generation of the enolate (in THF at −78°C) little changed the selectivity of the successive alkylation.

In order to improve the selectivity toward *syn*-alkylated products, the enolate formation was examined using various lithium amides. It is noteworthy that the treatment of the *t*-butyl ester **1A** with less hindered lithium amides such as lithium diethylamide, lithium dimethylamide, or lithium pyrrolidinide in THF-HMPA at lower temperature (−100°C) realized the significant stereoselectivity (Table 2).

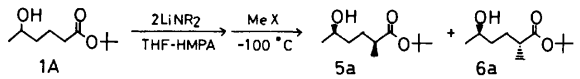

Based on these preliminary investigations, the lithium enolates generated from δ-hydroxy esters (**1A** and **1B**) with 3 molar amounts of lithium dimethylamide in THF-HMPA at −100°C were treated with alkylating reagents. The corresponding *syn*-α-alkylated δ-hydroxy esters **5** were found to be obtained in excellent stereoselectivity (Table 3).

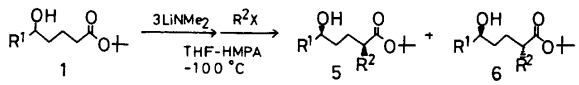

The stereochemistry of **5a** and **5b** was confirmed by the following results. Acid treatment of the *syn*-

Table 3. Stereoselective Alkylation Reaction of **1**

	R^1	R^2X	**5**:**6**[a]	Total yield/%
a	Me	Me_2SO_4	94:6	87
			95:5	81[b]
			95:5	50[c]
b	*n*-Bu	*n*-BuI[d]	94:6	84
c	Me	*n*-BuI[d]	92:8	82
d	*n*-Bu	Me_2SO_4	94:6	92

a) The ratios were determined by capillary gas chromatography (PEG-HT). b) Instead of lithium dimethylamide, lithium pyrrolidinide was used. c) Instead of lithium dimethylamide, lithium diethylamide was used. d) After the addition of *n*-BuI, the reaction mixture was stirred for 1 h at −100°C and gradually warmed to −78°C.

alkylated ester **5a** readily afforded the sex pheromone of the carpenter bee, (±)-*cis*-2-methyl-5-hexanolide (**7**).[11,12]

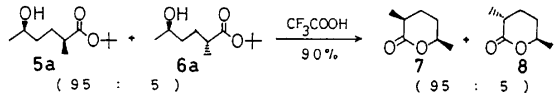

The *syn*-alkylated ester **5b** was also transformed to *cis*-2-butyl-5-nonanolide, which was identical with the authentic *cis*-lactone derived from *cis*-2,5-dibutylcyclopentanone by the Bayer-Villiger reaction.

To confirm the influence of a hydroxyl group on the stereoselection, we examined the alkylation of *t*-butyl 5-hydroxynonanoate (**1B**) after the protection of the hydroxyl group as a *t*-butyldimethylsilyl ether. Although the alkylation reaction of the silyl ether **9** proceeded smoothly, the ratio of the products **10** and **11** was almost 1:1 even when a mixture of THF-HMPA was employed as a solvent. Accordingly, the transformation of a hydroxyl group to lithium alkoxide should be indispensable for the present chiral 1,4-induction.

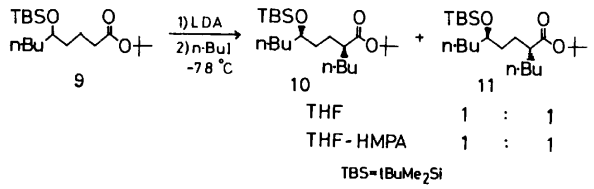

Due to the demonstrated efficiency for the stereoselection in the alkylation of δ-hydroxy carboxylic acid esters, we next investigated the 1,4-chiral induction in the aldol reaction of δ-hydroxy esters with acetone and cyclohexanone.

Hydroxy ester **1A** was lithiated under the same reaction conditions as the alkylation reaction (3 molar amounts of lithium pyrrolidinide, −100 °C), and the successive treatment with acetone was firstly examined. The aldol adducts **12a** and **13a** were obtained in a moderate (81 : 19) ratio, however, the total yield of the products was only 33%. When 3 molar amounts of lithium diethylamide was employed in the above reaction, the yield of the aldol products was not also sufficient (53%). On the other hand, as can be seen in Table 3, the alkylation reaction proceeded smoothly in over 80% yield in the same reaction conditions. By comparison of these results, it was noted that the enolization of δ-hydroxy esters **1** was not sufficient in the first lithiation stage (at −100 °C for 1 h) and that the enolization proceeds furthermore after the addition of an alkylating reagent. The presence of an alkylating reagent or a lithium salt genarated during alkylation reaction would be considered to accelerate the lithiation of δ-hydroxy esters, and the lithiation of **1** was examined in the presence of various lithium salts. Finally lithium trifluoromethanesulfonate (LiOTf) or lithium iodide was found to enhance the lithiation.[13] Thus the hydroxy ester **1A** was smoothly converted to the enolate **2A** with 3 molar amounts of lithium diethylamide in the presence of 3 molar amounts of LiOTf even at −100 °C in THF-HMPA, and the reaction with acetone gave the aldol adducts **12a** and **13a** in 92% yield (Table 4). Furthermore, the high stereoselectivity toward the *syn*-aldol product was also achieved by the addition of LiOTf (**12a** : **13a**=91 : 9). When LiOTf and then acetone were added succesively after the enolate formation at −100 °C, the yield of the aldol products was lower (74%). These observations suggested that LiOTf is not effective to promote the aldol reaction, but accelerates the enolization.

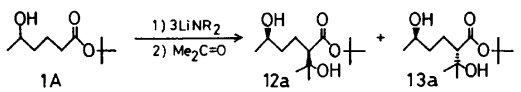

The aldol reaction of **1A** and **1B** with acetone and cyclohexanone was conducted by the combined use of LiOTf and lithium diethylamide with the results shown in Table 5. In all cases, the *syn*-aldol products **12** were obtained in high yield with high stereoselectivity.

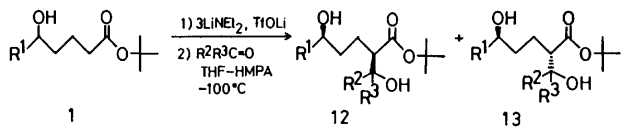

The confirmation of the relative stereochemistry of **12a** was carried out by the transformation of **12a** to **17**,

Table 4. Aldol Reaction of **1A** with Acetone in the Presence of Lithium Halides

$LiNR_2$	Additive[a]	**12a**:**13a**[b]	Total yield/%
$LiNMe_2$		c	24
LiN⟨⟩		81:19	33
	LiI	86:14	64
	LiOTf	89:11	66
$LiNEt_2$		86:14	53
		82:18	78[d]
	LiI	88:12	79
	LiOTf	91: 9	92
	LiOTf[e]	85:15	74
	LiOTf	87:13	82[f]

a) 3 molar amounts of additive were used. b) The ratios were determined by ^{13}C NMR spectra. c) The ratio was not determined. d) Lithiation was performed at −100 °C for 1 h, then warmed to −78 °C. e) 1 molar amount of LiOTf was used. f) 2.2 molar amounts of lithium diethylamide were used.

Table 5. Stereoselective Aldol Reaction of **1** in the Presence of LiOTf

	R^1	R^2 R^3	**12**:**13**[a]	Total yield/%
a	Me	Me Me	91: 9	92
b	Me	$-(CH_2)_5-$	86:14	99
c	*n*-Bu	Me Me	91: 9	99
d	*n*-Bu	$-(CH_2)_5-$	93: 7	97

a) The ratios were determined by ^{13}C NMR spectra.

which was compared with the authentic **17** derived from **6a**. That is, a ca. 4 : 1 mixture of **12a** and **13a** was converted to **17** and **18** as shown in Scheme 1. The authentic samples **18** and **17** were obtained from a ca. 4 : 1 mixture of **5a** and **6a** (Scheme 2). The ^{13}C NMR spectra of the main product **17** obtained from a mixture of **12a** and **13a** and the minor product **17** derived from a mixture of **5a** and **6a** were identical with each other. The ^{13}C NMR spectrum of the minor product **18** produced from a mixture of **12a** and **13a** also agreed with that of the major product **18** from a mixture of **14** and **15**. Furthermore, in ^{13}C NMR spectra, all the chemical shifts of α-carbons (-CH(COO^{t}Bu)-) and δ-

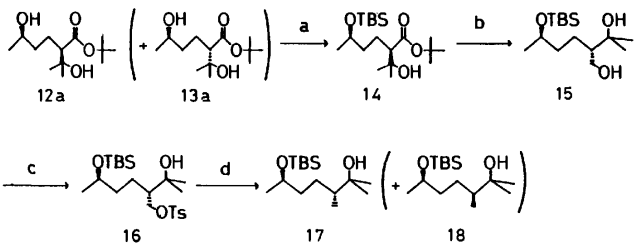

Scheme 1. (a): TBSCl, Et_3N; 90% (b): $LiAlH_4$; 76%, (c): *p*-TsCl, pyridine; 94%, (d): $LiAlH_4$; 69%.

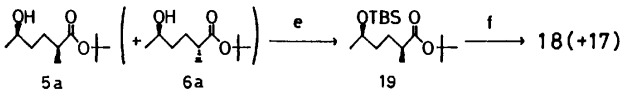

Scheme 2. (e): TBSCl, Et_3N; 90%, (f): MeLi; 89%.

Table 6. Hydroxylation of **1**

	R^1	Temp of lithiation/°C	Oxaziridines	**20**:**21**[a]	Total yield/%
a	Me	−100→−78	**22**	92: 8	40
		−78	**23**	89:11	48[b]
		−78	**24**	88:12	34
		−100→−78	**25**	90:10	70
		−100	**25**	92: 8	83[c]
b	*n*-Bu	−100	**25**	92: 8	82[c,d]

a) The ratios of **20a** to **21a** were determined by capillary gas chromatography (OV-101) and the ratio of **20b** to **21b** was measured by ^{13}C NMR spectrum of the corresponding acetates. b) Instead of lithium diethylamide, LDA was used. c) 3 molar amounts of LiOTf were present during the reaction. d) Diols were isolated as the corresponding diacetates.

carbons (-CH(OH)-) of the *syn*-isomers **12** appear at lower fields about 0.4—0.7 ppm and 0.5—1.0 ppm than those of the *anti*-isomers **13**, respectively.

As the significant effect for the acceleration of the enolate formation was observed by the addition of LiOTf, the alkylation reaction was reexamined in the presence of LiOTf. The enolate formation of **1A** (3 $LiNEt_2$, 3LiOTf in THF-HMPA, −100 °C, 2 h) and the successive alkylation with dimethyl sulfate was carried out at −100 °C. The alkylated products **5a** and **6a** were however obtained in low yield (20%). This result means that LiOTf accelerates the formation of the ester enolate but disturbs the reaction with alkylation reagents.

Next, we have used the lithium enolates of δ-hydroxy esters **1** in the stereoselective preparation of *syn*-1,4-diols by the direct oxidation of the enolates. And it has been found that the α-hydroxylation reaction of this system proceeded with an oxidant, oxaziridine.[14,15] The δ-hydroxy ester **1A** was transformed into the lithium enolate (3 equiv $LiNEt_2$, THF-HMPA, −100→−78 °C) and treated with an excess amount of the oxaziridine **22**. After an immediate reaction, the *syn*-α,δ-dihydroxy ester **20a** and the *anti*-isomer **21a** were obtained in high selectivity (**20a**:**21a**=92:8). It was evident that the sense of chiral induction in this hydroxylation paralleled the observation made in the alkylation and aldol reactions. However, the yield of the diols was modest. As a reaction of the enolate with the generated sulfonylimine was considered to be accompanied, we modified the hydroxylation reaction by means of an employment of more sterically hindered oxaziridines. When a newly synthesized oxaziridine **25** was utilized to the hydroxylation, the yield of diols consequently improved up to 70%. Moreover, the enolate formation at −100 °C in the presence of LiOTf and the treatment of the resulting enolates with **25** afforded the corresponding diols **20** and **21** in superior yield and stereoselectivity (Table 6).

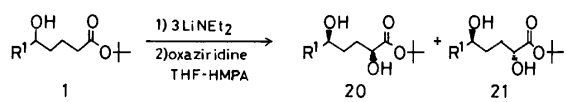

1 20 21

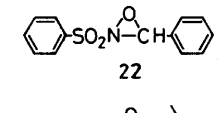

22

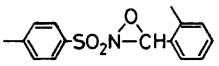

23

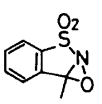

24

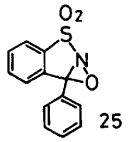

25

The relative stereochemistry of diols was determined by transformation of **21a** and **22a** to silyl ethers **30** and **31** (Scheme 3), which were identified by comparing the ^{13}C NMR spectra with the spectrum of the authentic silyl ether derived from *dl*-2,5-hexanediol.[16]

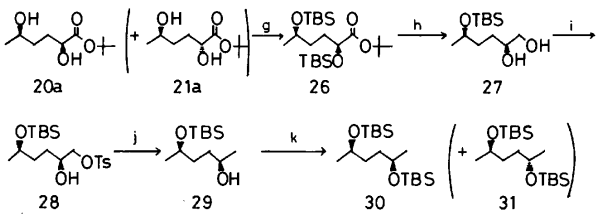

20a 21a 26 27

28 29 30 31

Scheme 3. (g): TBSCl, Et_3N; 99%, (h): $LiAlH_4$; 78%, (i): *p*-TsCl, pyridine, (j): 1) NaOMe, 2) $LiAlH_4$; 50% from **27**, k) TBSCl, Et_3N; 93%.

Experimental

All the boiling points and the melting points are uncorrected. The IR spectra were determined on a Hitachi Model 260-30 spectrometer. The ^1H NMR spectra were recorded with a Hitachi R-24B, a Varian EM-390, and a JEOL GX-400 spectrometers, and ^{13}C NMR spectra were measured with a JEOL FX-90Q spectrometer with tetramethylsilane as an internal standard. Tetrahydrofuran (THF) and diethyl ether were freshly distilled from sodium benzophenone ketyl. Dichloromethane, hexamethylphosphoric triamide (HMPA) and pyridine were distilled from CaH_2 and stored over Molecular Sieves. Purification of products was performed by column chromatography on silica gel (Wakogel C-200 or C-300), preparative TLC on silica gel (Wakogel B-5F).

Preparation of *t*-Butyl 5-Hydroxyhexanoate (1A). 5-Oxohexanoic acid[17] (6.09 g, 47 mmol) was treated with an excess amount of 2-methylpropene and three drops of concd H_2SO_4 in autoclave and was stirred at room temperature overnight.[18] The reaction mixture was quenched with triethylamine and was extracted with CH_2Cl_2. The combined extracts were washed with brine, dried over Na_2SO_4,

and condensed under reduced pressure. Purification by column chromatography (hexane:ethyl acetate=2:1, v/v) gave *t*-butyl 5-oxohexanoate (8.72 g, 74%). IR (neat) 1720 cm^{-1}. ^1H NMR ($CDCl_3$) δ=1.43 (9H, s), 1.73—2.29 (4H, m), 2.13 (3H, s), 2.29—2.67 (2H, m). Next, to a solution of *t*-butyl 5-oxohexanoate (2.15 g, 11.5 mmol) in CH_2Cl_2 (50 mL) and methanol (10 mL) was added sodium borohydride (1.31 g, 34.6 mmol) at 0 °C, and stirred for 15 min at room temperature. The mixture was quenched with sat. aqueous NH_4Cl and extracted with CH_2Cl_2. The separated organic layer was dried over Na_2SO_4 and was condensed under reduced pressure. Purification by column chromatography on silica gel (hexane:ethyl acetate=3:1, v/v) gave *t*-butyl 5-hydroxyhexanoate (**1A**) (2.09 g, 96%). Bp 80 °C/0.15 mmHg (1 mmHg=133.322 Pa). IR (neat) 3430, 1720 cm^{-1}. ^1H NMR ($CDCl_3$) δ=1.13 (3H, d, J=6.0 Hz), 1.45 (9H, s), 1.23—1.90 (4H, m), 1.90—2.53 (2H, m), 3.36—3.98 (2H, m). Found: C, 63.51; H, 10.98%. Calcd for $C_{10}H_{20}O_3$: C, 63.79; H, 10.71%.

Preparation of *t*-Butyl 5-Hydroxynonanoate (1B). To a CH_2Cl_2 (20 mL) solution of 5-oxononanoic acid[19] (5.61 g, 33 mmol) was added concd H_2SO_4 (2 mL). Into the resulting mixture was bubbled 2-methylpropene for 1 h.[20] The reaction was quenched with water and extracted with CH_2Cl_2, then washed with water and brine. The organic layer was dried over Na_2SO_4 and condensed in vacuo. The residue was purified by column chromatography on silica gel (hexane: ethyl acetate=9:1, v/v) to give *t*-butyl 5-oxononanoate (5.10 g, 69%). IR (neat) 1720 cm^{-1}. ^1H NMR (CCl_4) δ=0.62—2.43 (15H, m), 1.29 (9H, s). Reduction of *t*-butyl 5-oxononanoate with $NaBH_4$ as described for **1A** gave *t*-butyl 5-hydroxynonanoate (**1B**) in 92% yield. Bp 135 °C (bath temp)/4 mmHg. IR (neat) 3440, 1735 cm^{-1}. ^1H NMR ($CDCl_3$) δ=0.55—1.83 (14H, m), 1.35 (9H, s), 1.97—2.28 (2H, m), 3.07—3.62 (1H, m). Found: C, 67.65; H, 11.61%. Calcd for $C_{13}H_{26}O_3$: C, 67.78; H, 11.38%.

Stereoselective Alkylation Reaction of 1A with Dimethyl Sulfate. To a THF (7 mL) solution of lithium dimethylamide (2.37 mmol), which was prepared from an excess amount of dimethylamine (ca. 0.5 mL) and butyllithium (2.37 mmol), was added a THF (1 mL) solution of HMPA (0.83 mL, 4.77 mmol) at −78 °C under an argon atmosphere, and cooled to −100 °C. A THF (2 mL) solution of *t*-butyl 5-hydroxyhexanoate (**1A**) (149 mg, 0.79 mmol) was added to the mixture and stirred for 1 h at that temperature. Then a THF (2 mL) solution of dimethyl sulfate (316 mg, 2.51 mmol) was added to the mixture. After being stirred for 1 h at −100 °C, the reaction was quenched with sat. aqueous NH_4Cl and extracted with ether. The combined ether extracts were washed with water and brine, dried over Na_2SO_4, and condensed under reduced pressure. Purification by column chromatography (hexane: ethyl acetate=8:1, v/v) gave *t*-butyl *syn*-5-hydroxy-2-methylhexanoate (**5a**) and the *anti*-isomer **6a** (total 140 mg, 87%) in the ratio of 94:6, respectively.

The stereoselective preparations of **5b—d** were carried out by the same procedure. All the alkylated products were obtained as a mixture of *syn*- and *anti*-isomers **5** and **6**, which were not able to be separated by column chromatography or TLC. Each pair of isomers was indistinguishable by ^1H NMR (90 MHz) spectra, and the following spectral and analytical data were for a mixture of *syn*- and *anti*-isomers (90:10—95:5), respectively.

t-Butyl *syn*-5-hydroxy-2-methylhexanoate (**5a**) and the *anti* isomer **6a**: IR (neat) 3425, 1725 cm^{-1}. ^1H NMR ($CDCl_3$) δ=1.00 (3H, d, J=5.6 Hz), 1.06 (3H, d, J=6.4 Hz), 1.20—1.80 (4H, m), 1.31 (9H, s), 1.92—2.42 (1H, m), 2.67 (1H, br s), 3.38—3.92 (1H, m). Found: C, 65.19; H, 11.25%. Calcd for $C_{11}H_{22}O_3$: C, 65.31; H, 10.96%.

t-Butyl *syn*-2-butyl-5-hydroxynonanoate (**5b**) and the *anti* isomer **6b**: IR (neat) 3450, 1725 cm^{-1}. ^1H NMR ($CDCl_3$) δ= 0.53—2.39 (24H, m), 1.32 (9H, s), 3.17—3.59 (1H, m). Found: C, 71.55; H, 12.18%. Calcd for $C_{17}H_{34}O_3$: C, 71.28; H, 11.96%.

t-Butyl *syn*-2-butyl-5-hydroxyhexanoate (**5c**) and the *anti* isomer **6c**: IR (neat) 3430, 1725 cm^{-1}. ^1H NMR (CCl_4) δ= 0.53—2.24 (14H, m), 0.98 (3H, d, J=5.8 Hz), 1.31 (9H, s), 2.90 (1H, br s), 3.23—3.79 (1H, m). Found: C, 68.60; H, 11.84%. Calcd for $C_{14}H_{28}O_3$: C, 68.81; H, 11.55%.

t-Butyl *syn*-5-hydroxy-2-methylnonanoate (**5d**) and the *anti* isomer **6d**: IR (neat) 3430, 1730 cm^{-1}. ^1H NMR (CCl_4) δ=0.63—1.87 (14H, m), 1.07 (3H, d, J=6.8 Hz), 1.42 (9H, s), 1.90—2.47 (1H, m), 3.18—3.63 (1H, m). Found: C, 68.58; H, 11.49%. Calcd for $C_{14}H_{28}O_3$: C, 68.81; H, 11.55%.

Transformation of a Mixture of 5a and 6a to the Lactones. A 95:5 mixture of **5a** and **6a** (total 140 mg, 0.69 mmol) was dissolved in trifluoroacetic acid (2mL), and stirred for 2 h. After evaporation of the excess trifluoroacetic acid in vacuo, the residue was purified by preparative TLC on silica gel (hexane:ethyl acetate=1:1, v/v) to afford *cis*-2-methyl-5-hexanolide (**7**) and the *trans*-isomer **8** (total 80 mg, 90%) in the ratio of 95:5, respectively. Isomeric ratio was determined by capillary gas chromatography (OV-101, 95 °C).

cis-2-Methyl-5-hexanolide (**7**) and the *trans* isomer **8**: IR (neat) 1720 cm^{-1}. ^1H NMR (400 MHz) ($CDCl_3$) δ=1.23 (2.85H, d, J=6.8 Hz, *cis*), 1.31 (0.15H, d, J=6.4 Hz, *trans*), 1.36 (2.85H, d, J=6.4 Hz, *cis*), 1.37 (0.15H, d, J=6.4 Hz, *trans*), 1.50—1.68 (2H, m), 1.90—2.13 (2H, m), 2.41—2.48 (0.05H, m, *trans*), 2.55—2.64 (0.95H, m, *cis*), 4.43—4.51 (1H, m).

cis-2-Butyl-5-nonanolide. A solution of *cis*-2,5-dibutylcyclopentanone[21] (126 mg, 0.64 mmol) in acetic acid (3 mL) was mixed with 30% hydrogen peroxide (1 mL) and stirred at 50 °C for 3 d.[22] The reaction mixture was poured into water, extracted with ether and washed with aqueous $NaHCO_3$ and brine, dried over Na_2SO_4, and condensed in vacuo. Purification by preparative TLC on silica gel (hexane:ethyl acetate=6:1, v/v) to give *cis*-2-butyl-5-nonanolide (41 mg, 30%). IR (neat) 1740 cm^{-1}. ^1H NMR ($CDCl_3$) δ=0.53—2.59 (23H, m), 3.83—4.42 (1H, m). Found: C, 73.55; H, 11.59%. Calcd for $C_{13}H_{24}O_2$: C, 73.53; H, 11.39%.

By capillary gas chromatography (OV-101, 135 °C), the authentic lactone was identical with the major isomer of the lactones derived from **5b** and **6b**.

Stereoselective Aldol Reaction of 1A with Acetone. To a THF (5 mL) solution of LiOTf (323 mg, 2.07 mmol) was added a THF (5 mL) solution of diethylamine (179 mg, 2.44 mmol) under an argon atmosphere, and cooled to −78 °C. Butyllithium (1.25 mL of a 1.54 M solution in hexane (1 M=1 mol dm^{-3})) was added and the solution was stirred at that temperature for 15 min followed by the addition of a THF (1 mL) solution of HMPA (0.66 mL, 3.79 mmol) and then cooled to −100 °C. A THF (4 mL) solution of **1A** (119 mg, 0.63 mmol) was added to the mixture and stirred for 2 h at that temperature, and then a THF (4 mL) solution of acetone (91 mg, 1.57 mmol) was added. After being stirred for 30 min at −100 °C, the reaction was quenched with sat. aqueous NH_4Cl and extracted with ether. The ethereal

extracts were washed with water and brine, dried over Na_2SO_4, and condensed in vacuo. Purification by preparative TLC on silica gel (hexane : ethyl acetate=1 : 2, v/v) to give *t*-butyl *syn*-5-hydroxy-2-(1-hydroxy-1-methylethyl)-hexanoate (**12a**) and the *anti*-isomer **13a** (total 142 mg, 92%) in a ratio of 91 : 9, respectively.

Stereoselective syntheses of **12b—d** were carried out by the same procedure. All the *syn*- and *anti*-isomers of the aldol products **12** and **13** were not separable by column or thin-layer chromatography. In the ^1H NMR spectra (90 MHz), each isomer was not distinguished.

t-Butyl *syn*-5-hydroxy-2-(1-hydroxy-1-methylethyl)-hexanoate (**12a**) and the *anti* isomer **13a**: IR (neat) 3400, 1725 cm^{-1}. ^1H NMR ($CDCl_3$) δ=1.18 (3H, d, J=6.0 Hz), 1.22 (6H, s), 1.33—1.97 (4H, m), 1.45 (9H, s), 2.10—2.41 (1H, m), 3.03 (2H, br s), 3.37—3.97 (1H, m). ^{13}C NMR ($CDCl_3$) δ=56.20 (Cα, *anti*), 56.66 (Cα, *syn*), 66.90 (Cδ, *anti*), 67.63 (Cδ, *syn*). Analytical data for the corresponding 5-*O*-acetate; Found: C, 62.22; H, 10.13%. Calcd for $C_{15}H_{28}O_5$: C, 62.47; H, 9.79%.

t-Butyl *syn*-5-hydroxy-2-(1-hydroxycylohexyl)hexanoate (**12b**) and the *anti* isomer **13b**: Mp 90.1—90.2 °C (hexane). IR (KBr) 3400, 1715 cm^{-1}. ^1H NMR ($CDCl_3$) δ=1.17 (3H, d, J=5.4 Hz), 1.28—1.97 (14H, m), 1.47 (9H, s), 2.10—2.57 (1H, m), 2.94 (1H, br s), 3.10 (1H, br s), 3.47—4.17 (1H, m). ^{13}C NMR ($CDCl_3$) δ=55.01 (Cα, *anti*), 55.42 (Cα, *syn*), 67.39 (Cδ, *anti*), 67.93 (Cδ, *syn*). Found: C, 67.17; H, 10.84%. Calcd for $C_{16}H_{30}O_4$: C, 67.09; H, 10.56%.

t-Butyl *syn*-5-hydroxy-2-(1-hydroxy-1-methylethyl)-nonanoate (**12c**) and the *anti* isomer **13a**: IR (neat) 3390, 1725 cm^{-1}. ^1H NMR ($CDCl_3$) δ=0.60—1.88 (13H, m), 1.08 (3H, s), 1.12 (3H, s), 1.35 (9H, s), 1.97—2.27 (1H, m), 2.53 (2H, br s), 3.20—3.63 (1H, m). ^{13}C NMR ($CDCl_3$) δ=56.34 (Cα, *anti*), 57.01 (Cα, *syn*), 70.91 (Cδ, *anti*), 71.86 (Cδ, *syn*). Analytical data for the corresponding 5-*O*-acetate; Found: C, 65.45; H, 10.56%. Calcd for $C_{18}H_{34}O_5$: C, 65.42; H, 10.37%.

t-Butyl *syn*-5-hydroxy-2-(1-hydroxycyclohexyl)nonanoate (**12d**) and the *anti* isomer **13d**: Mp 58.0—60.5 °C (2-propanol-H_2O). IR (KBr) 3480, 1695 cm^{-1}. ^1H NMR ($CDCl_3$) δ=0.68—2.70 (25H, m), 1.48 (9H, s), 2.84—3.19 (1H, m), 3.30—3.77 (1H, m). ^{13}C NMR ($CDCl_3$) δ=54.88 (Cα, *anti*), 55.47 (Cα, *syn*), 71.02 (Cδ, *anti*), 71.89 (Cδ, *syn*). Found: C, 69.19; H, 11.33%. Calcd for $C_{19}H_{36}O_4$: C, 69.47; H, 11.05%.

Transformation of 12a and 13a to 17 and 18. a) *t*-Butyl 5-*t*-butyldimethylsilyloxy-2-(1-hydroxy-1-methylethyl)-hexanoate (**14**). A 4 : 1 mixture of **12a** and **13a** (total 531 mg, 2.15 mmol), *t*-butyldimethylsilyl chloride (395 mg, 2.63 mmol), triethylamine (328 mg, 3.24 mmol), and a catalytic amount of 4-dimethylaminopyridine in DMF (6 mL) was stirred for 15 h at room temperature under an argon atmosphere.[23] Then the reaction was quenched with ice and the mixture was extracted with ether. The ether extracts were washed with water and brine and dried over Na_2SO_4. The ether solution was concentrated and the residue was purified by column chromatography on silica gel (hexane: ethyl acetate=10 : 1, v/v) to give the silylated ester **14** (698 mg, 90%). IR (neat) 3450, 1725 cm^{-1}. ^1H NMR (CCl_4) δ=0.03 (6H, s), 0.81 (9H, s), 1.01 (6H, s), 1.01 (3H, d, J=6.0 Hz), 1.25—2.25 (6H, m), 1.40 (9H, s), 2.55 (1H, br s), 3.50—4.00 (1H, m). b) 3-hydroxymethyl-2-methyl-6-*t*-butyldimethylsilyloxy-2-heptanol (**15**). To an ether (5 mL) solution of **14** (698 mg, 1.94 mmol) was added an ether (2.5 mL) solution of lithium aluminum hydride (3.88 mmol) at 0 °C under an argon atmosphere, and stirred for 16 h at that temperature. The mixture was quenched with sat. aqueous Na_2SO_4 (1.8 mL) and the resulting precipitate was filtered off. The condensed filtrate was purified by column chromatography on silica gel (hexane: ethyl acetate=4 : 1, v/v) to furnish the diol **15** (430 mg, 76%). IR (neat) 3340 cm^{-1}. ^1H NMR ($CDCl_3$) δ=0.06 (6H, s), 0.90 (9H, s), 1.11 (3H, d, J=6.0 Hz), 1.18 (3H, s), 1.29 (3H, s), 3.33—4.04 (3H, m), 3.73 (2H, d, J=5.0 Hz). c) 6-(*t*-Butyldimethylsilyloxy)-2-methyl-3-(*p*-tolylsulfonyloxymethyl)-2-heptanol (**16**). A mixture of **15** (430 mg, 1.48 mmol), *p*-toluenesulfonyl chloride (427 mg, 2.24 mmol), and a catalytic amount of 4-dimethylaminopyridine in pyridine (2 mL) was stirred for 2 h at room temperature under an argon atmosphere. After evaporation of the excess pyridine in vacuo, the residue was purified by column chromatography on silica gel (hexane : ethyl acetate=4 : 1, v/v) to afford the corresponding tosylate **16** (621 mg, 94%). IR (neat) 3550, 1365 cm^{-1}. ^1H NMR ($CDCl_3$) δ=0.06 (6H, s), 0.72 (9H, s), 0.91 (3H, d, J=6.0 Hz), 0.92—1.81 (5H, m), 1.00 (3H, s), 1.04 (3H, s), 3.20—3.80 (1H, m), 3.27 (3H, s), 3.98 (2H, d, J=5.4 Hz), 7.13—7.71 (4H, m). d) 6-*O*-(*t*-Butyldimethylsilyl)-2,3-dimethyl-2,6-heptanediol **17** and **18**. Under an argon atmosphere, an ether (1.83 mL) solution of lithium aluminum hydride (2.82 mmol) was added to an ether (20 mL) solution of **16** (621 mg, 1.41 mmol) at room temperature, and stirred for 30 min. The mixture was quenched with sat. aqueous Na_2SO_4 (0.8 mL) and the resulting precipitate was filtered off. The condensed filtrate was purifued by column chromatography on silica gel (hexane : ethyl acetate=4 : 1, v/v) to give **17** and **18** (268 mg, 69%). IR (neat) 3375 cm^{-1}. ^1H NMR (CCl_4) δ=0.02 (6H, s), 0.53—0.88 (3H, m), 0.75 (9H, s), 0.88—1.86 (5H, m), 0.95 (3H, d, J=6.0 Hz), 0.96 (6H, s), 3.28—3.80 (1H, m). ^{13}C NMR ($CDCl_3$) δ=0.81, 14.29, 17.90, 23.53 (**17**), 23.72 (**18**), 25.75 (**17**), 26.21 (**18**), 26.43 (**17**), 26.65 (**17**), 26.81 (**18**), 27.51 (**18**), 38.46, 44.33, 68.79, 73.07.

Transformation of 5a and 6a to 18 and 17. e) *t*-Butyl 5-(*t*-butyldimethylsilyloxy)-2-methylhexanoate (**19**). A 4 : 1 mixture of α-methylated ester **5a** and **6a** (total 299 mg, 1.48 mmol) and triethylamine (222 mg, 2.19 mmol), *t*-butyldimethylsilyl chloride (275 mg, 1.83 mmol), and a catalytic amount of 4-dimethylaminopyridine in DMF (6 mL) was stirred for 18 h at room temperature under an argon atmosphere. The reaction was quenched with ice, and the mixture was extracted with ether. The ether extracts were washed with water and brine and dried over Na_2SO_4. The ether solution was condensed and the residue was purified by column chromatography on silica gel (hexane : ethyl acetate=15 : 1, v/v) to give the silylated ester **19** (419 mg, 90%). IR (neat) 1725 cm^{-1}. ^1H NMR (CCl_4) δ=0.03 (6H, s), 0.87 (9H, s), 1.02 (3H, d, J=6.6 Hz), 1.05 (3H, d, J=6.0 Hz), 1.22—1.76 (4H, m), 1.40 (9H, s), 1.80—2.57 (1H, m), 3.43—4.00 (1H, m). f) 6-*O*-(*t*-Butyldimethylsilyl)-2,3-dimethyl-2,6-heptanediol **18** and **17**. To an ether (5 mL) solution of **19** (92 mg, 0.92 mmol) was added methyllithium (0.49 mL of a 1.29 M solution in ether) at 0 °C under an argon atmosphere, and stirred for 30 min at that temperature. To the mixture was added sat. aqueous NH_4Cl and the organic layer was extracted with CH_2Cl_2. The separated organic layer was dried over Na_2SO_4 and was condensed under reduced pressure. Purification by preparative TLC (hexane: ethyl acetate=5 : 1, v/v) to give **18** and **17** (total 71 mg, 89%).

7*b*-Phenyl-7*bH*-oxazirino[2,3-*b*][1,2]benzisothiazole 3,3-dioxide (**25**). A mixture of 3-phenyl-1,2-benzisothiazole 1,1-

dioxide[24] (1.00 g, 4.1 mmol) in $CHCl_3$ (16 mL) and $NaHCO_3$ (1.05 g, 13 mmol) in water (12 mL) was cooled to 0 °C and rapidly stirred and *m*-chloroperbonzoic acid (2.20 g, 13 mmol) in $CHCl_3$ (30 mL) was added dropwise.[14] After the addition was complete, the solution was stirred overnight and the $CHCl_3$ solution was washed with 10% Na_2SO_3 and 10% $NaHCO_3$. After the solution was dried over K_2CO_3 at 0 °C, the solvent was removed. The residue was dissolved in a small amount of ethyl acetate and precipitated by slow addition of pentane with stirring to give the oxaziridine **25** (0.95 g, 89%). Mp 123 °C. IR (KBr) 1325 cm^{-1}. ^1H NMR ($CDCl_3$) δ=7.42 (5H, s), 7.53—7.68 (4H, m). Found: C, 59.94; H, 3.38; N, 5.26; S, 12.14%. Calcd for $C_{13}H_9NO_3S$: C, 60.22; H, 3.50; N, 5.40; S, 12.37%.

Stereoselective Preparation of 1,4-Diols 20a. To a THF (5 mL) solution of LiOTf (303 mg, 1.94 mmol) was added a THF (4 mL) solution of diethylamine (134 mg, 1.83 mmol) under an argon atmosphere, and cooled to −78 °C. Butyllithium (1.16 mL of a 1.54 M solution in hexane) was added and the solution was stirred at that temperature for 15 min followed by the addition of a THF (1 mL) solution of HMPA (0.62 mL, 3.56 mmol) and then cooled to −100 °C. A THF (4 mL) solution of **1A** (112 mg, 0.59 mmol) was added to the mixture and stirred for 2 h at that temperature, and then a THF (5 mL) solution of the oxaziridine **25** (465 mg, 1.79 mmol) was added. After being stirred for 30 min at −100 °C, the reaction was quenched with sat. NH_4Cl and extracted with ether. The combined extracts were washed with water and brine, dried over Na_2SO_4, and condensed under reduced pressure. Purification by column chromatography on silica gel (hexane: ethyl acetate=4 : 1, v/v) to give *t*-butyl *syn*-2,5-dihydroxyhexanoate (**20a**) and the *anti*-isomer **21a** (total 101 mg, 83%) in a ratio 92 : 8, respectively. The *syn*-and *anti*-isomers **20a** and **21a** could not be separated, and in ^1H NMR (90 MHz) spectrum, two isomers were indistinguishable. IR (neat) 3380, 1725 cm^{-1}. ^1H NMR ($CDCl_3$) δ=1.18 (3H, d, J=6.0 Hz), 1.35—1.99 (4H, m), 1.47 (9H, s), 2.16—2.68 (2H, m), 3.62—4.03 (1H, m), 4.21—4.41 (1H, m). Analytical data for the corresponding diacetate; Found: C, 58.07; H, 8.36%. Calcd for $C_{14}H_{24}O_6$: C, 58.31; H, 8.39%.

Stereoselective preparation of **20b** was carried out by the same procedure. The resulting diols **20b** and **21b** were isolated as corresponding diacetates by the treatment with acetic anhydride, pyridine and a catalytic amount of 4-dimethylaminopyridine because the diols **20b** and **21b** were not separable from generated sulfonyl imine.

t-Butyl *syn*-2,5-diacetoxyhexanoate and *anti*-isomer: IR (neat) 1735 cm^{-1}. ^1H NMR ($CDCl_3$) δ=0.63—2.32 (13H, m), 1.47 (9H, s), 2.02 (3H, s), 2.09 (3H, s), 4.64—5.06 (2H, m). ^{13}C NMR ($CDCl_3$) δ=13.90, 20.53, 21.02, 22.56, 27.06, 27.52, 28.06, 29.63, 33.83, 72.51, 73.51 (*syn*), 73.70 (*anti*), 82.02, 169.02, 170.13, 170.48. Found: C, 61.65; H, 9.21%. Calcd for $C_{17}H_{30}O_6$: C, 61.79; H, 9.15%.

Conversion of 20a and 21a to 30 and 31. g) *t*-Butyl 2,5-bis(*t*-butyldimethylsilyloxy)hexanoate (**26**). A 3 : 1 mixture of dihydroxy esters **20a** and **21a** (total 291 mg, 1.42 mmol), triethylamine (446 mg, 4.41 mmol), *t*-butyldimethylsilyl chloride (572 mg, 3.80 mmol), and a catalytic amount of 4-dimethylaminopyridine in DMF (10 mL) was stirred for 2 d at room temperature under an argon atmosphere. The reaction was quenched with ice, and extracted with ether. The ethereal extracts were washed with water and brine, dried over Na_2SO_4, and condensed in vacuo. Purification by column chromatography on silica gel (hexane: ethyl acetate=15 : 1, v/v) afforded **26** (613 mg, 99%). IR (neat) 1745 cm^{-1}. ^1H NMR ($CDCl_3$) δ=0.01 (3H, s), 0.04 (6H, s), 0.07 (3H, s), 0.88 (9H, s), 0.89 (9H, s), 1.08 (3H, d, J=6.0 Hz), 1.26—1.96 (4H, m), 1.43 (9H, s), 3.48—4.14 (2H, m). h) 5-*t*-Butyldimethylsilyloxy-1,2-hexanediol (**27**). To a THF (10 mL) solution of **26** (613 mg, 1.42 mmol) was added lithium aluminum hydride (125 mg, 3.30 mmol) under an argon atmosphere, and stirred overnight. The mixture was quenched with sat. aqueous Na_2SO_4 (3 mL) and the resulting precipitate was filtered off. The condensed filtrate was purified by TLC on silica gel (ethyl acetate) to give the monosilylated **27** (274 mg, 78%). IR (neat) 3350 cm^{-1}. ^1H NMR ($CDCl_3$) δ=0.07 (6H, s), 0.88 (9H, s), 1.12 (3H, d, J=6.0 Hz), 1.27—1.60 (4H, m), 3.13—4.03 (4H, m), 3.37 (2H, br s). i,j) 5-*O*-(*t*-Butyldimethylsilyl)-2,6-hexanediol (**29**). A mixture of **27** (55 mg, 0.22 mmol) and *p*-toluenesulfonyl chloride (67 mg, 0.36 mmol) in pyridine (3 mL) was stirred at −10 °C for 6 h, then 0 °C overnight under an argon atmosphere. The reaction mixture was quenched with ice, extracted with CH_2Cl_2, dried over Na_2SO_4, and condensed under reduced pressure. Purification by preparative TLC on silica gel (hexane: ethyl acetate=3 : 1, v/v) gave **28** (51 mg). Then to a MeOH (3 mL) solution of **28** was added sodium methoxide (1.15 mL of a 0.12 M solution in MeOH) under an argon atmosphere, and was stirred at room temperature overnight. After the addition of sat. aqueous NH_4Cl the mixture was extracted with CH_2Cl_2, dried over Na_2SO_4, and condensed in vacuo to give a crude epoxide. Next, the crude epoxide was dissolved in THF (5 mL) and cooled to 0 °C. To the solution was added lithium aluminum hydride (0.25 mL of a 1.54 M solution in ether), and stirred at room temperature overnight. After the addition of sat. aqueous Na_2SO_4 (0.1 mL), the resulting precipitate was filtered off and the filtrate was condensed. Purification by preparative TLC on silica gel (hexane: ethyl acetate=4 : 1, v/v) furnished **29** (26 mg, 50% from **27**). IR (neat) 3350 cm^{-1}. ^1H NMR (CCl_4) δ=0.03 (6H, s), 0.87 (9H, s), 1.10 (3H, d, J=6.4 Hz), 1.28—1.65 (4H, m), 1.83—2.28 (1H, m), 3.35—3.98 (1H, m). k) *O*-Bis(*t*-butyldimethylsilyl)-2,5-hexanediol (**30** and **31**). **29** (25 mg, 0.11 mmol) was silylated as described above to give bis(silyl) ether **30** and **31** (35 mg, 93%). ^1H NMR ($CDCl_3$) δ=0.05 (12H, s), 0.88 (18H, s), 1.08 (6H, d, J=6.0 Hz), 1.16—1.52 (4H, m), 3.30—3.90 (2H, m). ^{13}C NMR ($CDCl_3$) δ=−4.65, −4.32, 18.23, 23.86, 25.98, 35.80 (**30**), 35.89 (**31**), 68.68 (**30**), 68.99 (**31**). The ^{13}C NMR spectrum of the major isomer **30** was agreed with that of the authentic sample derived from *dl*-2,5-hexanediol.[16]

The authors are grateful to Professor Teruaki Mukaiyama for valuable discussion during this work.

References

1) a) P. A. Bartlett, *Tetrahedron*, **36**, 2 (1980); b) M. T. Reetz, *Angew. Chem., Int. Ed. Engl.*, **23**, 556 (1984); c) "Asymmetric Synthesis," ed by J. D. Morrison, Academic Press, Inc., New York (1984), Vol. 3.

2) a) P. A. Bartlett and K. K. Jernstedt, *J. Am. Chem. Soc.*, **99**, 4829 (1977); b) T. Fukuyama, B. Vranesic, D. P. Negri, and Y. Kishi, *Tetrahderon Lett.*, **1978**, 2741; c) D. A. Evans, J. Bartroli, and T. Godel, *ibid.*, **23**, 4577 (1982); d) M. Hirama and M. Uer, *ibid.*, **23**, 5307 (1982); e) Y. F. Wang, T. Izawa, S. Kobayashi, and M. Ohno, *J. Am. Chem. Soc.*, **104**,

6465 (1982); f) Y. Matsumura, J. Fujiwara, K. Maruoka, and H. Yamamoto, *ibid.*, **105**, 6312 (1983); g) M. Hirama, T. Shigemoto, Y. Yamazaki, and S. Ito, *ibid.*, **107**, 1797 (1985); h) Y. Yamamoto, T. Komatsu, and K. Maruyama, *J. Chem. Soc., Chem. Commun.*, **1985**, 814.

3) K. Narasaka and F. C. Pai, *Tetrahedron*, **40**, 2233 (1984); K. Narasaka, Y. Ukaji, and S. Yamazaki, *Bull. Chem. Soc. Jpn.*, **59**, 525 (1986).

4) M. T. Reetz, K. Kesseler, S. Schmidtberger, B. Wenderoth, and R. Steinbach, *Angew. Chem., Int. Ed. Engl.*, **22**, 989 (1983); S. R. Wilson and M. F. Price, *Tetrahedron Lett.*, **24**, 569 (1983); J. E. Bäckball, J. E. Nyström, and R. E. Nordberg, *J. Am. Chem. Soc.*, **107**, 3676 (1985) and the references cited therein.

5) Preliminary work of the stereoselective alkylation reaction and aldol reaction of δ-hydroxy esters has been briefly reported as communications; K. Narasaka and Y. Ukaji, Chem. Lett., **1986**, 81: K. Narasaka, Y. Ukaji, and K. Watanabe, *ibid.*, **1986**, 1755.

6) G. Fráter, U. Muller, and W. Gunter, *Tetrahedron*, **40**, 1269 (1984) and the references cited therein; D. Seebach, H. F. Chow, R. F. W. Jackson, K. Lawson, M. A. Sutter, S. Thaisrivongs, and J. Zimmermann, *J. Am. Chem. Soc.*, **107**, 5292 (1985).

7) The relative stereochemistry of δ-hydroxy-α-substituted esters is presented according to the Masamune's nomenclature using *syn* and *anti* terms; S. Masamune, S. A. Ali, D. L. Snitman, and D. S. Garvey, *Angew. Chem., Int. Ed. Engl.*, **19**, 557 (1980).

8) R. E. Ireland, R. H. Mueller, and A. K. Willard, *J. Am. Chem. Soc.*, **98**, 2868 (1976).

9) The geometry of the ester enolates is referred using *cis* and *trans* terms; C. H. Heathcock, C. T. Buse, W. A. Kleschick, M. C. Pirrung, J. E. Sohn, and J. Lampe, *J. Org. Chem.*, **45**, 1066 (1980).

10) a) G. Favini, C. Rubino, and R. Todeschini, *J. Mol. Struct.*, **41**, 305 (1977); b) N. L. Allinger and J. T. Sprague, *J. Am. Chem. Soc.*, **94**, 5734 (1972).

11) Alkylation reaction of 5-hexanolide with methyl iodide gave 1:1 mixture of *cis*- and *trans*-2-methyl-5-hexanolide, see: W. H. Pirkle and P. E. Adams, *J. Org. Chem.*, **44**, 2169 (1979).

12) Recent stereoselective syntheses of *cis*-2-methyl-5-hexanolide, see: K. Mori and S. Senda, *Tetrahedron*, **41**, 541 (1985); J. E. Bäckvall, S. E. Byström, and J. E. Nystrom, *ibid.*, **41**, 5761 (1985).

13) Recently Masamune, Roush, and Rathke reported that lithium halides are effective for the generation of carbanions in Horner-Wadsworth-Emmons reaction using weak bases such as amines; M. A. Blanchette, W. Choy, J. T. Davis, A. P. Essenfeld, S. Masamune, W. R. Roush, and T. Sakai, *Tetrahedron Lett.*, **25**, 2183 (1984); M. W. Rathke and M. Nowak, *J. Org. Chem.*, **50**, 2624 (1985).

14) F. A. Davis, J. Lamendola, Jr., U. Nadir, E. W. Kluger, T. C. Sedergran, T. W. Panunto, R. Billmers, R. Jenkins, Jr., I. J. Turchi, W. H. Watson, J. S. Chen, and M. Kimura, *J. Am. Chem. Soc.*, **102**, 2000 (1980).

15) In contrast to oxaziridines, we found MoOPH to be none stereoselective, and O_2 to be far less reactive.

16) R. M. Dodson and V. C. Nelson, *J. Org. Chem.*, **33**, 3966 (1968).

17) R. Chong and P. S. Clezy, *Aust. J. Chem.*, **20**, 123 (1967).

18) A. L. McCloskey, G. S. Fonken, R. W. Kluiber, and W. S. Johnson, *Org. Synth.*, Coll. Vol. IV, 261 (1963).

19) H. Stetter and W. Dieirchs, *Chem. Ber.*, **85**, 61 (1952).

20) B. Anilin and S. Fabrik, *Chem. Abstr.*, **54**, 16387b (1960).

21) Two isomers of 2,5-dibutylcyclopentanone were separated by column chromatography and the geometry was determined by Irvine's procedure; J. L. Irvine, I. H. Hall, G. L. Carlson, and C. Piantadosi, *J. Org. Chem.*, **37**, 2033 (1972).

22) G. Mehta and P. N. Pandey, *Synthesis*, **1975**, 404.

23) S. K. Chaudhary and O. Hernandez, *Tetrahedron Lett.*, **1979**, 99.

24) R. A. Abramovitch, E. M. Smith, M. Humber, B. Purtschert, P. C. Srinivasan, and G. M. Singer., *J. Chem. Soc., Perkin Trans., 1*, **1974**, 2589.

Racemic Structure and Optical Resolution by Preferential Crystallization of Organic Ammonium Salts of *N*-Formyl-DL-tyrosine

Tadashi SHIRAIWA,* Hideya MIYAZAKI, Atsushi URAMOTO, Michio SUNAMI, and Hidemoto KUROKAWA
Faculty of Engineering, Kansai University, Yamate-cho, Suita, Osaka 564
(Received October 23, 1986)

The Gibbs energy of formation of racemate, binary melting point diagram, and ternary solubility diagram indicated that dicyclohexylammonium salt of *N*-formyl-DL-tyrosine (DL-DCH salt) forms a racemic compound at melting point, but is a conglomerate at room temperature. The optical resolution of the DL-DCH salt was successfully performed by preferential crystallization. A successive preferential crystallization in methanol at 10 °C followed by purification gave D- and L-tyrosines with 100% optical purity.

L-Tyrosine (abbreviated as L-Tyr) as an important substance in vivo has been obtained by hydrolysis of proteins, because no industrially efficient synthesis has been established.[1] Optical resolution by preferential crystallization of DL-Tyr, therefore, has not been reported,[1,2] though DL-Tyr can be optically resolved by the diastereomeric procedure.[3,4] If DL-Tyr is synthesized in an industrial scale, the optical resolution is needed to obtain optically active tyrosines. It was attempted in this study to resolve organic ammonium salts of *N*-formyl-DL-tyrosine (DL-FrTyr) by preferential crystallization.

In the 16 ammonium salts, the salts showing respective melting points are pentylammonium (PTA), 1,1,3,3-tetramethylbutylammonium (TMB), dibutylammonium (DBA), dicyclohexylammonium (DCH), dibenzylammonium (DBZ), and 4-methylpiperidinium (4-MP) salts. The racemic structure of these DL-salts was determined by thermodynamic analysis.[5-7] As for other salts that decompose on heating, the racemic structure was examined by comparing infrared spectra of the DL-salt with those of the corresponding L-salt or ternary solubility diagram; these are propylammonium, isopropylammonium, butylammonium, isobutylammonium, *t*-butylammonium, cyclohexylammonium, benzylammonium, diisopropylammonium, diisobutylammonium, and *N*-methylcyclohexylammonium salts. The DL-DCH salt which seemed to be a conglomerate at room temperature was subjected to optical resolution by preferential crystallization.

Experimental

Materials. DL- and L-Tyrosine were purchased from Sigma Chemicals Co., and amines from Wako Pure Chemicals Ind. or Kanto Chemical Co., Ltd.

***N*-Formylation.** *N*-Formyl-DL- and -L-tyrosine were prepared by formylating each tyrosine similarly to the preparation of ordinary amino acids;[8] specific rotation of L-FrTyr $[\alpha]_D^{20}$ +84.4° (*c* 0.50, ethanol) (lit,[9] $[\alpha]_D$ +84.8° (ethanol)).

Preparation of Organic Ammonium Salts. A mixture of 0.01 mol of DL- or L-FrTyr and equimolar amine in 80 cm^3 of acetone was stirred for 30 min at room temperature. The formed salt was filtered and recrystallized from methanol.

L-DCH salt: Found C, 67.57; H, 8.76; N, 7.11% (calcd for $C_{22}H_{34}N_2O_4$: C, 67.66; H, 8.78; N, 7.17%); $[\alpha]_D^{20}$ +35.1° (*c* 0.50, water), $[\alpha]_D^{20}$ +43.1° (*c* 0.50, ethanol); solubility 3.660 g/(100 cm^3 methanol), 0.504 g/(100 cm^3 ethanol) at 10 °C. DL-DCH salt: Found C, 67.40; H, 8.78; N, 7.13%; solubility 7.181 g/(100 cm^3 methanol), 1.090 g/(100 cm^3 ethanol) at 10 °C.

D-DCH salt obtained from mother liquor in the optical resolution of DL-salt was recrystallized twice from ethanol to give D-salt with 100% optical purity; mp 232 °C; $[\alpha]_D^{20}$ −35.1° (*c* 0.50, water).

Optical Resolution. Preferential Crystallization: DL-DCH salt was dissolved in methanol or ethanol at 40 °C; 2.154 g in 25 cm^3 of methanol, 1.370 g in 100 cm^3 of ethanol. The solution was slowly cooled to 10 °C and seeded with L-salt; 0.050 g for methanol solution, 0.100 g for ethanol solution. After stirring the mixture at 10 °C, the precipitated salt was filtered, washed with a small amount of diethyl ether, and dried. The optical purity, yield of optically pure modification (YOPM), and degree of resolution of the salt were determined by the equations described in our previous paper.[10]

Successive Preferential Crystallization: DL-DCH salt (2.154 g) was dissolved in 25 cm^3 of methanol at 40 °C. After being cooled to 10 °C, the solution was seeded with 0.050 g of L-salt and stirred for 130 min. The precipitated salt was collected by filtration, and DL-DCH salt (0.122 g) was dissolved in the filtrate at 40 °C. After being seeded with 0.050 g of D-salt at 10 °C, the mixture was treated similarly. The degree of resolution of D- and L-DCH salts was calculated by

$$\text{Degree of resolution}/\% = [\text{YOPM}/\text{g} \times 100]/[(\text{Operation amount of D- or L-salt}/\text{g}) - 0.898].$$

Preparation of Optically Active Tyrosine. D- or L-DCH salt (4.00 g) with optical purity of about 93% was dissolved in ethanol at an elevated temperature. After concentrating the solution to 100 cm^3 under reduced pressure at 40 °C, the resulting solution was allowed to stand for 2 d at 5 °C. The precipitated salt was collected by filtration to give about 3.5 g each of optically pure D- and L-salts.

D- or L-DCH salt (3.90 g) was dissolved in a mixture of 10 cm^3 of 1 mol dm^{-3} aqueous sodium hydroxide and 100 cm^3 of water. After removing the liberated dicyclohexylamine by extracting with diethyl ether, 10 cm^3 of 1 mol dm^{-3} hydrochloric acid was added to the aqueous solution. The solution was dried under reduced pressure at 50 °C. After being added 20 cm^3 of methanol to the residue, the mixture was filtered. To the filtrate was added 10 cm^3 of 1 mol dm^{-3} hydrochloric acid. After refluxing the solution for 2 h, the pH was adjusted to 6 with concentrated aqueous ammonia. Precipitated Tyr was filtered, washed with a small amount of cold water and methanol, and dried to give about 1.70 g each of D- and L-Tyr's. D-Tyr: $[\alpha]_D^{20}$ +11.8° (*c* 4.00, 5 mol dm^{-3} HCl).

Table 1. Thermodynamic Data for Organic Ammonium Salts of *N*-Formyltyrosine

Salt	Mp/K		ΔH^{f}[a]/kJ mol^{-1}		ΔG^{F}_{mp}[b]
	DL-Salt	L-Salt	DL-Salt	L-Salt	kJ mol^{-1}
PTA[c]	405	411	35.2	29.0	−1.91
TMB[d]	429	440	36.9	38.0	−1.52
DBA[e]	412	425	34.1	32.8	−1.37
DCH[f]	501	505	39.1	51.7	−2.48
DBZ[g]	437	442	45.4	46.7	−1.99
4-MP[h]	430	443	35.2	31.2	−1.56

a) ΔH^{f}: Enthalpy of fusion. b) ΔG^{F}_{mp}: Gibbs energy of formation of racemate at melting point. c) PTA: Pentylammonium salt. d) TMB: 1,1,3,3-Tetramethylbutylammonium salt. e) DBA: Dibutylammonium salt. f) DCH: Dicyclohexylammonium salt. g) DBZ: Dibenzylammonium salt. h) 4-MP: 4-Methylpiperidinium salt.

L-Tyr: $[\alpha]_D^{20}$ −11.8° (*c* 4.00, 5 mol dm^{-3} HCl) (lit,[11] $[\alpha]_D^{20}$ −11.8° (5 mol dm^{-3} HCl)).

Measurements. The specific rotation was measured by a Union Giken PM-101 digital polarimeter with a quartz cell of 0.5 dm path length. Infrared spectra were obtained in the range 4000—400 cm^{-1} by a JASCO A-102 infrared spectrophotometer by the KBr disk method.

Saturated methanol or ethanol solutions of DL- and L-DCH salts were prepared at 10 °C and diluted in appropriate concentrations when used. The absorbance was measured at 279 nm with a Shimadzu double-beam spectrophotometer UV-150-02 with a quartz cell of 0.1 dm path length. The solubility of the salts was determined from calibration curves.

Results and Discussion

Racemic Structure. Racemic Structure at Melting Point: The Gibbs energy of formation of racemate in the solid state at *T* K (ΔG^{F}_{T}) is calculated by the following equation:[5]

$$\Delta G^{F}_{T} = -\Delta\Delta H^{f} + T\Delta\Delta S^{f} - RT\ln 2 + \Delta C_p(\Delta T^{f} - T\ln T^{f}_{R}/T^{f}_{A}) + (\Delta C^{s}/2T^{f})(T^{f} - T)^2, \quad (1)$$

where subscripts "A" and "R" represent the optically active and racemic modifications, respectively, *R* is the gas constant, ΔC_P is the difference in heat capacity between the liquid and solid states in the vicinity of melting point, and ΔC^{s} is that in solid state between racemic and optically active modifications; $\Delta\Delta H^{f} = \Delta H^{f}_{R} - \Delta H^{f}_{A}$ (ΔH^{f}, enthalpy of fusion), $\Delta\Delta S^{f} = \Delta S^{f}_{R} - \Delta S^{f}_{A}$ (ΔS^{f}, entropy of fusion), and $\Delta T^{f} = T^{f}_{R} - T^{f}_{A}$ (T^{f}, melting point); T^{f} represents T^{f}_{A} when $T^{f}_{R} > T^{f}_{A}$ and T^{f}_{R} when $T^{f}_{R} < T^{f}_{A}$. The term containing ΔC_p is ignored for the calculation of ΔG^{F}_{mp} at melting point, because the contribution is obviously smaller than that of the sum of the other terms in the right-hand side of Eq. 1.[5] The ΔG^{F}_{mp} of the salts of DL-FrTyr having melting points were calculated by Eq. 1 using ΔH^{f} and T^{f}.[5-7] Thermodynamic data of *N*-formyltyrosine salts are listed in Table 1. The values of ΔG^{F}_{mp} are negative, and further, these salts have eutectic points; the mole fractions of L-salt at eutectic point are 0.70—0.77 as listed in Table 2, and the binary melting point diagram of DCH salt is illustrated in Fig. 1. The above results indicate that these DL-salts form racemic compounds at melting point.

Table 2. Data at Eutectic Point for Organic Ammonium Salts of *N*-Formyltyrosine

Salt[a]	Mole fraction of L-salt[b]	Temperature/K	
		Found	Calcd[b]
PTA	0.77	398	399
TMB	0.70	424	425
DBA	0.70	411	410
DCH	0.75	494	493
DBZ	0.75	433	432
4-MP	0.71	425	426

a) See notes in Table 1. b) These values were calculated from Schröder-Van Laar and Prigogine-Defay equations.

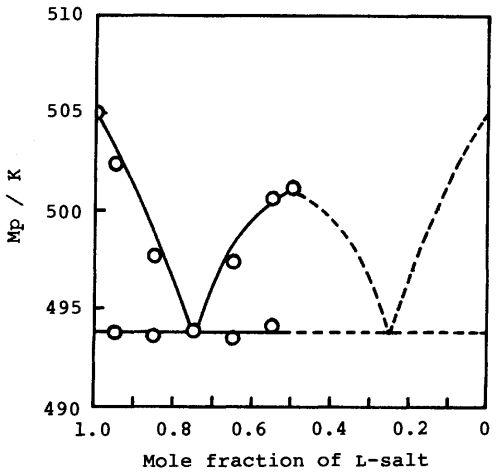

Fig. 1. Binary melting point diagram of dicyclohexylammonium salt of *N*-formyltyrosine.

Racemic Structure at Room Temperature: The ΔG^{F}_{283} at 283 K was also calculated by Eq. 1; in the calculation, ΔC_p was taken as 105 J mol^{-1} K^{-1} and ΔC^{s} as 31.4 J mol^{-1} K^{-1}.[5-7] Only the DL-DCH salt gives a positive ΔG^{F}_{283} value (+5.39 kJ mol^{-1}). This value suggests that the DL-salt does not form a racemic compound at 283 K. DL-DCH salt shows infrared spectrum identical with that of the L-salt and is more soluble than the L-salt as described in the experimental section.

Table 3. Preferential Crystallization of Dicyclohexylammonium Salts of *N*-Formyl-DL-tyrosine[a)]

Solvent	Resolution time	Yield	Optical purity	YOPM[b)]	Degree of resolution
	min	g	%	g	%
Methanol[c)]	60	0.111	97.1	0.058	32.3
	90	0.141	95.7	0.085	47.3
	120	0.154	93.4	0.094	52.4
	175	0.185	87.9	0.113	63.0
	240	0.200	86.4	0.123	68.5
Ethanol[d)]	45	0.141	96.0	0.035	25.0
	90	0.168	95.7	0.061	43.6
	120	0.179	97.7	0.075	53.6
	210	0.183	95.3	0.075	53.6
	300	0.188	91.7	0.072	51.4

a) Temperature: 10°C. b) YOPM: Yield of optically pure modification. c) Methanol: 25 cm³. Degree of supersaturation: 120%. Seed Crystals: 0.050 g of L-salt. d) Ethanol: 100 cm³. Degree of supersaturation: 126%. Seed crystals: 0.100 g of L-salt.

Table 4. Successive Preferential Crystallization of Dicyclohexylammonium Salt of *N*-Formyl-DL-tyrosine[a)]

Run	Added amount of DL-salt	Operation amount[b)]/g		Resolution time	Salt obtained			
					Yield	Optical purity	YOPM	Degree of resolution
	g	D-Salt	L-Salt	min	g	%	g	%
1	2.154	1.077	1.077	130	0.172	L 92.2	0.109	60.9
2	0.122	1.131	1.022	60	0.219	D 94.0	0.156	67.0
3	0.169	1.053	1.100	60	0.195	L 93.7	0.133	65.8
4	0.145	1.120	1.034	100	0.202	D 94.6	0.141	63.5

a) Solvent: 25 cm³ of methanol. Degree of supersaturation of initial solution: 120%. Seed crystals: 0.050 g of D- or L-salt. Temperature: 10°C. b) Operation amounts of D- and L-salts in solution were calculated from analyses of the salts obtained in Runs 1—3.

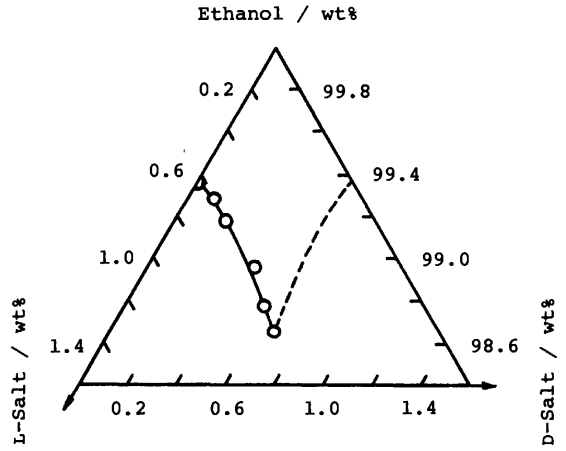

Fig. 2. Ternary solubility diagram of dicyclohexylammonium salt of *N*-formyltyrosine. Solvent: Ethanol. Temperature: 10°C.

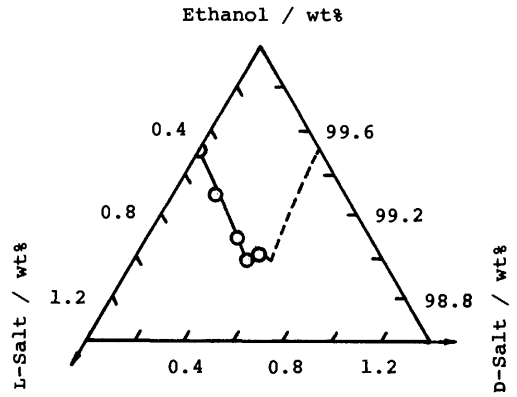

Fig. 3. Ternary solubility diagram of *t*-butylammonium salt of *N*-formyltyrosine. Solvent: Ethanol. Temperature: 10°C.

The ternary solubility diagram shows what is expected for a conglomerate as shown in Fig. 2.[2)]

For other DL-salts, the values of ΔG^{F}_{283} are negative, and the infrared spectra are different from those of the corresponding L-salts. These results indicate that DL-DCH salt exists in a conglomerate at room temperature, whereas other DL-salts form racemic compounds.

In the salts that decompose on heating, DL-*t*-butylammonium salt (DL-TBA salt) shows infrared spectrum excellently identical with that of L-salt, whereas the spectra of other DL-salts are different from those of the corresponding L-salts. DL-TBA salt is more soluble than the L-salt; DL-TBA salt 0.764 g/(100 cm³ ethanol), L-TBA salt 0.423 g/(100 cm³ ethanol) at 10°C. The ternary solubility diagram, however, suggests that DL-TBA salt is an unstable racemic com-

pound at room temperature as shown in Fig. 3,[2] because the mole fraction of L-salt at eutectic point is 0.55. This instability of DL-TBA salt may give infrared spectrum excellently identical with that of L-salt.

The above results lead to the conclusion that only the DL-DCH salt exists in a conglomerate at room temperature though the salt forms a racemic compound at melting point.

Optical Resolution of DL-Dicyclohexylammonium Salt. Preferential crystallization of DL-DCH salt is listed in Table 3; L-DCH salt was used as seed crystals.

It was possible to obtain L-DCH salt with optical purity of over 90%. Since the yield in methanol was nearly equal to that in ethanol, it is expected that the optical resolution from methanol solution in the same scale as that from ethanol solution gives L-DCH salt in about 4 times higher yield from ethanol. The optical resolution by a successive preferential crystallization for methanol solution was found to give D- and L-DCH salts with optical purity of 92—95% in degree of resolution of 60—67% as shown in Table 4. Optically pure D- and L-Tyr's were obtained from purified D- and L-DCH salts, respectively.

References

1) T. Kaneko, Y. Izumi, I. Chibata, and T. Ito, "Amino-san Kogyo," Koudansha, Tokyo (1973), p, 229.
2) A. Collet, M. J. Brienne, and J. Jacques, *Chem. Rev.*, **80**, 215 (1980).
3) R. R. Sealock, *J. Biol. Chem.*, **166**, 1 (1946).
4) G. Losse, *J. Pract. Chem.*, **7**, 141 (1958).
5) M. Leclercq, A. Collet, and J. Jacques, *Tetrahedron*, **32**, 821 (1976).
6) T. Shiraiwa, A. Ikawa, K. Fujimoto, K. Iwafuji, and H. Kurokawa, *Nippon Kagaku Kaishi*, **1984**, 765.
7) T. Shiraiwa, H. Miyazaki, A. Ikawa, and H. Kurokawa, *Nippon Kagaku Kaishi*, **1984**, 1425.
8) J. C. Sheehan and D. D. H. Yang, *J. Am. Chem. Soc.*, **80**, 1154 (1958).
9) E. Abderhalden and H. Sickel, *Z. Physiol. Chem.*, **131**, 277 (1923).
10) T. Shiraiwa, Y. Ohmichi, K. Ikawa, K. Iwafuji, and H. Kurokawa, *Nippon Kagaku Kaishi*, **1983**, 1070.
11) "Seikagaku Data Book [1]," ed by Jpn. Biochem. Soc., Tokyo Kagaku Dojin, Tokyo (1982), p. 31.

 © 1987 The Chemical Society of Japan Bull. Chem. Soc. Jpn., 60, 1469—1479 (1987)

Aggregate Morphology of Peptide Lipids Having Hydroxyl Groups: Molecular Basis for Formation of Inverted Hexagonal, Inverted Cubic, Bilayer, and Micellar Phases

Yukito MURAKAMI,* Jun-ichi KIKUCHI, Toshihiko TAKAKI, and Katsuya UCHIMURA
Department of Organic Synthesis, Faculty of Engineering, Kyushu University, Hakozaki, Higashi-ku, Fukuoka 812
(Received October 24, 1986)

Three types of peptide lipids having different numbers of hydroxyl groups in their head moieties, $(HO)C_5Ala2C_n$, QC_5Ala2C_n, and $Q_2LysC_5Ala2C_n$ (n=14, 16), were prepared, and their morphological behavior was investigated by various physical techniques: negative staining and freeze-fracture electron microscopy, low-angle X-ray diffraction, selected area electron diffraction, fluorescence polarization spectroscopy, and differential scanning calorimetry. QC_5Ala2C_n, having four hydroxyl groups in the head moiety, underwent aggregation in the aqueous dispersion state to afford the nonbilayer phase, which was constituted with highly developed globular domains with face-centered cubic (C_{II}) lattice, above the phase transition temperature (T_m). This C_{II} phase was transformed into the bilayer one below T_m. On the other hand, $Q_2LysC_5Ala2C_n$, having eight hydroxyl groups in the head moiety, formed bilayer aggregates in a whole temperature range, above and below T_m. Deprotonation of the hydroxyl groups of QC_5Ala2C_n and $Q_2LysC_5Ala2C_n$ resulted in morphological changes to afford the bilayer and micellar phases, respectively. Two-component lipid systems composed of $(HO)C_5Ala2C_{14}$ and $Q_2LysC_5Ala2C_{14}$ at appropriate molar ratios afforded the inverted hexagonal (H_{II}) phase in the aqueous dispersion state; the first example of the H_{II} phase formed with artificial double-chain amphiphiles. The aggregate morphology was discussed on the basis of the critical packing mode of lipid molecules.

Extensive studies on structures and functions of biomembranes gave an impetus to rapid growth of *membrane mimetic chemistry*.[1] While synthetic lipids having a wide variety of molecular structures have been demonstrated to afford bilayer aggregates, structural limitations of such lipids in morphological behavior have not been unveiled up to the present time. Nonbilayer structures, such as inverted hexagonal and inverted cubic ones, have often been observed with natural lipid systems,[2] and some useful concepts have been proposed to explain the molecular basis for the formation of such aggregates.[3,4] However, feedback of these concepts to the development of artificial lipids requires the guidepost for molecular design of lipids, which adopt desired aggregate structures, and such attempts have encountered some difficulties.[5] In other words, appropriate structural modifications must be systematically exercised in designing artificial lipids, so that changes in their morphological behavior are significantly amplified. The *peptide lipids* are suitable candidates for such purposes, since amino acid residues involved in aggregates of these lipids form the tight hydrogen-belt domain which acts to separate two intramembrane domains, the surface domain composed of polar head moieties and the hydrophobic interior domain formed with double-chain segments, so that direct structural interactions between the latter two domains tend to be minimized.[6] Thus, only the size of double-chain segments of the lipid molecules primarily controls the phase transition behavior.[6c,7] On these grounds, we can exactly evaluate the effects of structural modifications of lipid molecules on aggregate morphology. In the present work, we investigated the aggregate morphology of individual and mixed lipid systems of the following three types of peptide lipids having different numbers of hydroxyl groups in their head moieties; $(HO)C_5Ala2C_n$, QC_5Ala2C_n, and $Q_2LysC_5Ala2C_n$ (n=14, 16). Four different types of aggregate morphology, inverted hexagonal, inverted cubic, bilayer, and micellar phases, were systematically created for the first time with these artificial lipids by controlling the packing mode of lipid molecules in the aggregate state.

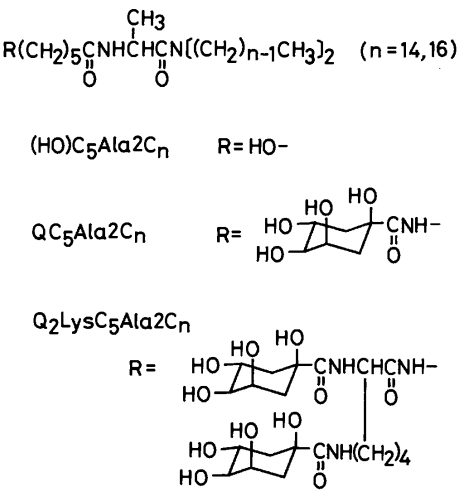

Experimental

Materials. 1,6-Diphenyl-1,3,5-hexatriene (DPH) was obtained from Nakarai Chemicals as a guaranteed reagent and used without further purification. Trisodium 8-hydroxy-1,3,6-pyrenetrisulfonate (pyranine) was purchased from Tokyo Kasei Kogyo Co. and purified after the method reported by Kano and Fendler.[8] Hexadecyltrimethylammonium bromide (CTAB) from Nakarai Chemicals was recrystallized from ethanol, mp 237—239 °C (decomp). Preparation of nonionic peptide lipids having the 1,3,4,5-tetrahydroxy-[1*R*-(1α,3α,4α,5β)]cyclohexylcarbonyl (quinoyl) moiety has been reported previously: *N*,*N*-dihexadecyl-N^{α}-[6-(quinoylamino)hexanoyl]-L-alaninamide (QC_5Ala2C_{16})[7] and *N*,*N*-ditetradecyl-N^{α}-[6-(quinoylamino)hexanoyl]-L-alaninamide

(QC_5Ala2C_{14}).[9]

***N,N*-Dihexadecyl-N^{α}-(6-hydroxyhexanoyl)-L-alaninamide [(HO)C_5Ala2C_{16}].** A mixture of *N,N*-dihexadecyl-N^{α}-(6-bromohexanoyl)-L-alaninamide[7] (1.0 g, 1.6 mmol), formamide (2.5 g, 86 mmol), and water (60 mg, 3.2 mmol) was stirred for 3 h at 140—150 °C and cooled to room temperature. Water (4 mL) was added to the mixture, which was subsequently extracted with dichloromethane (3×10 mL). The solvent was removed in vacuo, and the residue was dissolved in ethanol (20 mL). Aqueous NaOH (2 mol dm^{-3}, 3 mL) was added to the ethanol solution, and the resulting solution was refluxed for 3 h. After addition of water (10 mL), the mixture was acidified with hydrochloric acid and extracted with chloroform (3×15 mL). The extract was washed with water, dried over sodium sulfate, and evaporated to dryness in vacuo. The residue was purified by gel-filtration chromatography on a column of Sephadex LH-20 with methanol as an eluant: a colorless solid, yield 110 mg (11%); mp 44.8—45.2 °C; IR (KBr) 3440 (OH), 3280 (NH), 2920 and 2845 (CH), and 1635 cm^{-1} (C=O); ^1H NMR ($CDCl_3$, Me_4Si) δ=0.87 [6H, t, $(CH_2)_{15}C\underline{H}_3$], 1.25 [65H, m, $CH_2(C\underline{H}_2)_{14}CH_3$, $CH(C\underline{H}_3)$, and $HOCH_2(C\underline{H}_2)_3CH_2$], 2.20 [2H, t, $HO(CH_2)_4C\underline{H}_2$], 3.2 [4H, m, $C\underline{H}_2(CH_2)_{14}CH_3$], 3.60 [2H, t, $HOC\underline{H}_2$], 4.83 [1H, m, $C\underline{H}(CH_3)$], and 6.60 [1H, d, CONH].

Found: C, 74.55; H, 12.50; N, 4.33%. Calcd for $C_{41}H_{82}N_2O_3 \cdot 1/2\ H_2O$: C, 74.60; H, 12.67; N, 4.24%.

***N,N*-Ditetradecyl-N^{α}-(6-hydroxyhexanoyl)-L-alaninamide [(HO)C_5Ala2C_{14}].** This was prepared from *N,N*-ditetradecyl-N^{α}-(6-bromohexanoyl)-L-alaninamide[7] in a manner similar to that stated above: a colorless solid, yield 18%; mp 48.5—49.0 °C; IR (KBr) 3440 (OH), 3280 (NH), 2920 and 2845 (CH), and 1635 cm^{-1} (C=O); ^1H NMR ($CDCl_3$, Me_4Si) δ=0.88 [6H, t, $(CH_2)_{13}C\underline{H}_3$], 1.25 [57H, m, $CH_2(C\underline{H}_2)_{12}CH_3$, $CH(C\underline{H}_3)$, and $HOCH_2(C\underline{H}_2)_3CH_2$], 2.20 [2H, t, $HO(CH_2)_4C\underline{H}_2$], 3.2 [4H, m, $C\underline{H}_2(CH_2)_{12}CH_3$], 3.59 [2H, t, $HOC\underline{H}_2$], 4.84 [1H, m, $C\underline{H}(CH_3)$], and 6.60 [1H, d, CONH].

Found: C, 74.34; H, 12.39; N, 4.75%. Calcd for $C_{37}H_{74}N_2O_3$: C, 74.69; H, 12.54; N, 4.71%.

***N,N*-Dihexadecyl-N^{α}-[6-[[N^{α},N^{ε}-bis(*t*-butoxycarbonyl)-L-lysyl]amino]hexanoyl]-L-alaninamide [(Boc)$_2$LysC_5Ala2C_{16}].** Trifluoroacetic acid (25 g, 220 mmol) was added to a dry dichloromethane solution (20 mL) of *N,N*-dihexadecyl-N^{α}-[6-(*t*-butoxycarbonylamino)hexanoyl]-L-alaninamide[7] (5.0 g, 6.7 mmol), and the mixture was stirred for 4.5 h at room temperature. An excess amount of trifluoroacetic acid and the solvent were evaporated off in vacuo. The residue was dissolved in chloroform (50 mL) and then washed with 5% aqueous sodium hydrogencarbonate (3×30 mL). After being dried over sodium sulfate, the solution was evaporated to dryness in vacuo to give a pale yellow solid (3.0 g). Elimination of the *t*-butoxycarbonyl group was confirmed by IR and ^1H NMR spectroscopy. Dicyclohexylcarbodiimide (0.93 g, 4.5 mmol) was added to a dry dichloromethane solution (20 mL) of the N^{α},N^{ε}-bis(*t*-butoxycarbonyl)-L-lysine dicyclohexylamine salt (2.3 g, 4.5 mmol) and *p*-toluenesulfonic acid (0.77 g, 4.5 mmol) at 0 °C. After the mixture being stirred for 15 min at 0 °C, a dry dichloromethane solution (10 mL) of the amine was added to it at the same temperature. The mixture was stirred for 3 h at 0 °C and overnight at room temperature. The resulting precipitate (*N,N'*-dicyclohexylurea) was removed by filtration, the filtrate was evaporated to dryness in vacuo, and the residue was dissolved in ethyl acetate (100 mL). The ethyl acetate solution was then washed with 10% aqueous citric acid (2×50 mL), water (50 mL), 4% aqueous sodium hydrogencarbonate (2×50 mL), and water (50 mL) in this sequence. After being dried over sodium sulfate, the solution was evaporated to dryness in vacuo. The residue was chromatographed on a column of silica gel (Wako Gel C-100) with chloroform as an eluant: a pale yellow solid, yield 1.7 g (22%); IR (KBr) 3320 (NH), 2920 and 2850 (CH), and 1770 and 1660 cm^{-1} (C=O); ^1H NMR ($CDCl_3$, Me_4Si) δ=0.87 [6H, t, $(CH_2)_{15}C\underline{H}_3$], 1.25 [71H, m, $CH_2(C\underline{H}_2)_{14}CH_3$, $CH(C\underline{H}_3)$, $CONHCH_2(C\underline{H}_2)_3CH$, and $CONHCH_2(C\underline{H}_2)_3CH_2$], 1.42 [18H, s, $OC(CH_3)_3$], 2.3 [2H, m, $CONH(CH_2)_4C\underline{H}_2$], 3.14 [8H, m, $CONHC\underline{H}_2$ and $C\underline{H}_2(CH_2)_{14}CH_3$], 4.27 [3H, m, $C\underline{H}(CH_2)_3$ and $CONHC\underline{H}_2$], 4.80 [1H, m, $C\underline{H}(CH_3)$], 5.12 [1H, d, $OCONH\underline{C}H$], and 7.60 [1H, d, $CONH\underline{C}H$].

***N,N*-Dihexadecyl-N^{α}-[6-[[N^{α},N^{ε}-bis(tetraacetylquinoyl)-L-lysyl]amino]hexanoyl]-L-alaninamide [(AcQ)$_2$LysC_5Ala2C_{16}].** Trifluoroacetic acid (25 g, 220 mmol) was added to a dry dichloromethane solution (20 mL) of (Boc)$_2$LysC_5Ala2C_{16} (1.1 g, 1.1 mmol), and the mixture was stirred for 2 h at room temperature. Evaporation of an excess amount of trifluoroacetic acid and the solvent gave a pale yellow oil (1.2 g). Elimination of the *t*-butoxycarbonyl group was confirmed by ^1H NMR spectroscopy. The amine was dissolved in dry dichloromethane (20 mL), and the solution was cooled to 0 °C. Triethylamine (2.3 g, 22 mmol) was added to the solution, and then (−)-tetraacetylquinoyl chloride[10] (1.7 g, 4.5 mmol) dissolved in dry dichloromethane (20 mL) was added dropwise to the mixture at 0 °C with stirring. The resulting mixture was stirred for 1 h at 0 °C and for 2 h at room temperature, and then dichloromethane (100 mL) was added to it. The mixture was washed with saturated aqueous sodium chloride (2×50 mL), 5% aqueous citric acid (2×50 mL), saturated aqueous sodium chloride (2×50 mL), 5% aqueous sodium hydrogencarbonate (2×50 mL), and saturated aqueous sodium chloride (2×50 mL) in this sequence. After being dried over sodium sulfate, the solution was evaporated to dryness in vacuo. The residue was chromatographed on a column of silica gel (Wako Gel C-100) with ethyl acetate as an eluant. The product was further purified by gel-filtration chromatography on a column of Sephadex LH-20 with methanol as an eluant: a colorless solid, yield 0.32 g (20%); mp 75.0—76.5 °C; IR (KBr) 2920 and 2850 (CH), and 1740 and 1650 cm^{-1} (C=O).

***N,N*-Dihexadecyl-N^{α}-[6-[(N^{α},N^{ε}-diquinoyl-L-lysyl)amino]-hexanoyl]-L-alaninamide [Q_2LysC_5Ala2C_{16}].** After addition of hydrazine monohydrate (700 mg, 14 mmol) to a solution of (AcQ)$_2$LysC_5Ala2C_{16} (270 mg, 0.19 mmol) in 85% aqueous ethanol (3 mL), the mixture was refluxed for 1 h, cooled to room temperature, and poured into cold water (20 mL). Chloroform (30 mL) was added to the mixture, and the organic layer was separated by centrifugation. After being dried over sodium sulfate, the organic layer was evaporated to dryness in vacuo. The residue was purified by gel-filtration chromatography on a column of Sephadex LH-20 with methanol as an eluant: a colorless solid, yield 120 mg (59%); final mp 227 °C; IR (KBr) 3350 (OH), 2920 and 2850 (CH), and 1640 cm^{-1} (C=O).

Found: C, 64.07; H, 10.26; N, 6.20%. Calcd for $C_{61}H_{115}N_5O_{13} \cdot H_2O$: C, 64.01; H, 10.30, N, 6.12%.

***N,N*-Ditetradecyl-N^{α}-[6-[(N^{α},N^{ε}-diquinoyl-L-lysyl)amino]-hexanoyl]-L-alaninamide [Q_2LysC_5Ala2C_{14}].** This was prepared from *N,N*-ditetradecyl-N^{α}-[6-(*t*-butoxycarbonyl-

amino)hexanoyl]-L-alaninamide[7] in a manner similar to that stated above: a colorless solid; final mp 173 °C; IR (KBr) 3350 (OH), 2920 and 2850 (CH), and 1640 cm^{-1} (C=O).

Found: C, 62.93; H, 10.32; N, 6.45%. Calcd for $C_{57}H_{107}N_5O_{13}\cdot H_2O$: C, 62.89; H, 10.09; N, 6.43%.

Analyses and Measurements. Elemental analyses were performed at the Microanalysis Center of Kyushu University. Melting points were measured with a Yanagimoto MP-S1 apparatus (hot-plate type). ^1H NMR spectra were taken on a Hitachi R-24B spectrometer. IR spectra were recorded on a JASCO IR-810 spectrophotometer. pH Measurements were carried out with a Beckman Φ71 pH meter equipped with a Beckman 39505 combined electrode after calibration with a combination of appropriate standard aqueous buffers. A JASCO UVIDEC-100 UV spectrophotometer was used as a detector for gel-filtration chromatography. Fluorescence spectra were recorded on a Hitachi 650-60 spectrofluorometer. A Daini Seikosha SSC-560U calorimeter was used for differential scanning calorimetry (DSC). The phase-transition temperature (T_m, temperature at a peak maximum of DSC thermogram) and the enthalpy change for phase transition (ΔH) were determined in a manner as reported previously.[7]

Electron micrographs were taken on a JEOL JEM-2000FX electron microscope installed at the Research Laboratory for High Voltage Electron Microscopy of Kyushu University. Negatively stained and freeze-fractured samples for the measurements were prepared in a manner as described previously.[7] Selected area electron diffraction measurements were carried out by using the same electron microscope, electron wavelength being adjusted at 100 kV (λ=0.037 Å). The camera length (2870 mm) was calibrated on the basis of diffractions from (111) and (200) planes of the face-centered cubic lattice of single crystalline gold.

The fluorescence polarization measurements were carried out on a Union Giken FS-501A fluorescence polarization spectrophotometer equipped with a Sord microcomputer M200 Mark II; emission at 450 nm originated from DPH was monitored upon excitation at 358 nm with a slit width of 3.5 nm for both excitation and emission sides. The steady-state fluorescence anisotropy (r_S) was calculated by Eq. 1, where I is the fluorescence intensity, and the subscripts v and h refer to the orientations, vertical and horizontal, respectively, for the excitation and analyzer polarizers in this sequence. C_f is the grating correction factor, given by I_{hv}/I_{hh}.

$$r_S = (I_{vv} - C_f I_{vh})/(I_{vv} + 2C_f I_{vh}), \quad (1)$$

The nickel-filtered Cu $K\alpha$ radiation (λ=1.542 Å) from a Rigaku Rotaflex RU-200 X-ray generator was used for X-ray diffraction measurements. Each sample was sealed up in a specimen holder equipped with mica windows, and a low-angle diffraction pattern was recorded on a Fuji X-ray film 150; a sample-film distance being set at 200 mm.

Results and Discussion

Molecular Design of Nonionic Peptide Lipids. Ionic peptide lipids having an α-amino acid residue interposed between a polar head moiety and a hydrophobic double-chain segment generally form bilayer aggregates in an aqueous dispersion state.[6] On the other hand, we have recently found that nonlamellar aggregates appear in the aqueous dispersions of cationic and anionic lipids, *N,N*-dialkyl-N^{α}-[6-(trimethylammonio)hexanoyl]-L-alaninamide bromide [N^+C_5Ala2C_n] and sodium *N,N*-dialkyl-N^{α}-(6-sulfonatohexanoyl)-L-alaninamide [$(SO_3^-)C_5$Ala2C_n], respectively, mixed at the 1:1 molar ratio above the phase-transition temperature (T_m).[11] This nonlamellar phase is

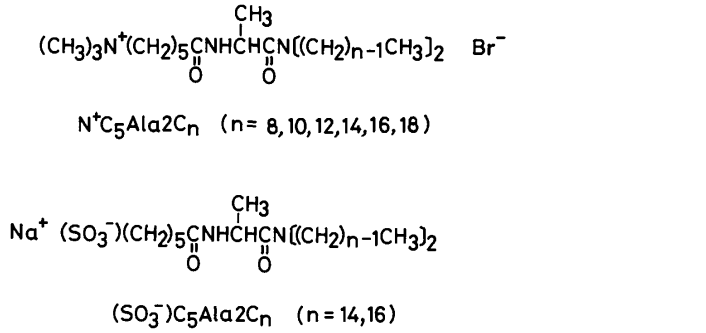

referred to the inverted cubic (C_{II}) one composed of three-dimensional network of globular aggregates with small internal aqueous compartments.[12] The following two effects control the packing mode of lipid molecules to adopt the C_{II} phase in aqueous media: (i) intramembrane electrostatic interactions between cationic and anionic head moieties to form highly developed ion-pair clusters in the membrane surface, and (ii) recovery of the rotational and bending motions of hydrophobic double-chain segments above T_m. As a result, these lipid molecules are allowed to retain the *inverted truncated cone* shape[4a] in their aggregates above T_m, and the critical packing mode under such conditions favors the formation of inverted micellar aggregates. We have also found that the nonlamellar phase was formed with nonionic peptide lipids having the quinoyl moiety, QC_5Ala2C_n, through the hydrogen-bonding interaction among the polar head moieties. These observations imply that the peptide lipids tend to construct various aggregate structures, which have been demonstrated so far with naturally occurring lipid systems, in aqueous media by manipulating steric bulkiness of their polar head moieties so that specific packing modes are attained in their aggregates.

A useful concept has been proposed on the self-assembling behavior of lipid molecules in dilute aqueous solutions, based on the critical packing parameter, v/a_0l_c, where v, a_0, and l_c are the hydrocarbon volume, the optimal surface area, and the critical chain length of lipid molecules, respectively.[4] The following guidepost for the formation of specific aggregate structures has been postulated on the basis of the dynamic packing mode: $v/a_0l_c < 1/3$ for spherical micelles, $1/3 < v/a_0l_c < 1/2$ for cylindrical micelles, $1/2 < v/a_0l_c < 1$ for bilayers, and $v/a_0l_c > 1$ for inverted micelles.[4] However, there are few successful explanations to distinguish between structural factors for the formation of the two kinds of nonlamellar phases; a hexagonally

packed array of inverted cylindrical micelles (H_{II} phase), and a closely packed cubic array of inverted spherical micelles (C_{II} phase).[13] Recently, Verkleij mentioned in his review article that lipidic particles are found in a variety of lipid mixtures and in total lipid extracts under physiological conditions in excess water, and that lipidic particles are only found in mixed systems of natural lipids, in which one component or more of the lipids prefer to adopt the H_{II} phase in their individual states.[2a] Since the C_{II} phase is considered to be the principal morphology pertaining to lipidic particles, the C_{II} aggregate is granted to be the intermediary form lying between bilayer and H_{II} ones. Thus, the critical packing parameter for the H_{II} forming lipid seems to be larger than that for the C_{II} forming lipid.

As for the peptide lipids, the critical packing parameter is primarily controlled by the a_0 value if only the polar head moiety undergoes structural variation and the rest of the molecule remains the same. As one of such purposive series of lipid molecules, we prepared three types of nonionic peptide lipids having various numbers of hydroxyl groups in their head moieties; (HO)C_5Ala2C_n, QC_5Ala2C_n, and Q_2LysC_5-Ala2C_n (n=14, 16). The CPK molecular models of these lipids are shown in Fig. 1. Since the four hydroxyl groups of the quinoyl moiety are located on one side of the cyclohexane ring with chair-type conformation, the head moieties of QC_5Ala2C_n and Q_2LysC_5Ala2C_n seem to hold configurations paralled to the membrane surface. In addition, the extent of solvation of the head moieties of the present lipids mainly depends on a number of the hydroxyl groups in the presence of excess water. Thus, the a_0 value for the present peptide lipids decreases in the following order: Q_2LysC_5Ala2C_n > QC_5Ala2C_n > (HO)C_5Ala2C_n. Now, correlations between aggregate morphology and lipid structure are described below on the basis of the critical packing concept.

Inverted Cubic Phase. Recently, we have found that QC_5Ala2C_n having four hydroxyl groups in the head moiety form nonlamellar aggregates in the aqueous dispersion state by means of negative staining electron microscopy.[9] The low-angle X-ray diffraction technique was applied to these aggregates in this work. Four diffractions with the spacing ratio, $1:\sqrt{3}/2:\sqrt{3}/\sqrt{8}:1/2$, were observed for QC_5Ala2C_n (n=14, 16) at pH 7 above T_m (Table 1). This spacing ratio is in conformity with diffractions from (111), (200), (220), and (222) planes of the face-centered cubic (fcc) lattice with lattice constant a (Fig. 2). We have obtained similar diffraction patterns for aggregates formed with equimolar mixtures of cationic and anionic lipids.[12] It has been claimed that an apparent cubic phase observed in the 1-oleoylglycerol-water system actually consists of a lipid bilayer forming a tetrahedral periodic minimal surface which separates two water channel networks.[14] The existence of such continuous

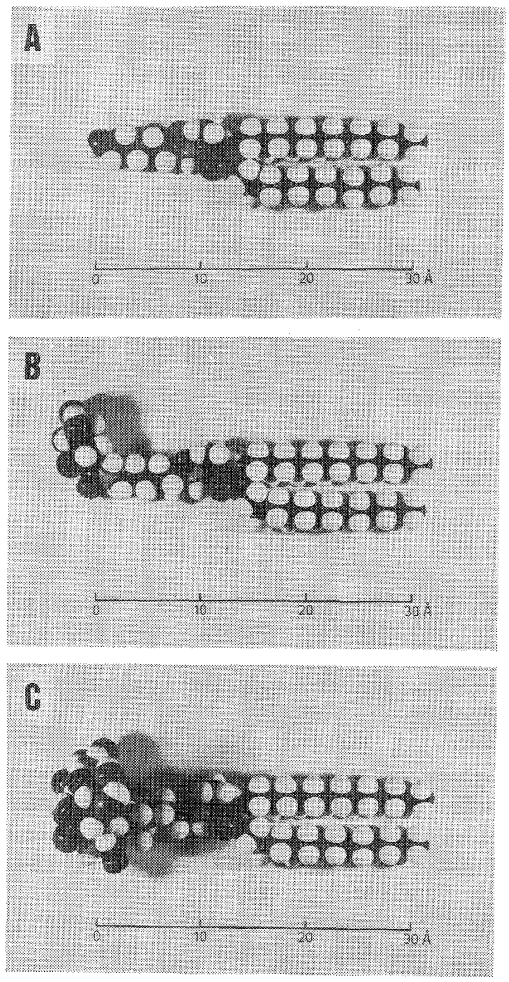

Fig. 1. CPK molecular models of (HO)C_5Ala2C_{14} (A), QC_5Ala2C_{14} (B), Q_2LysC_5Ala2C_{14} (C).

water channels in our peptide lipid systems, however, can be ruled out in the light of the electron microscopic measurements.[9,11,12] The (111) plane of the fcc lattice is the closest packed one, and the distance between the nearest neighbors in the plane ($a/\sqrt{2}$) is referred to the repeating distance of internal aqueous compartments. When the weight fraction of QC_5-Ala2C_{14} in water was increased from 0.22 to 0.28, the $a/\sqrt{2}$ value was reduced by 9 Å. In addition, the $a/\sqrt{2}$ value as observed by negative staining electron microscopy, for which water was completely removed during the sample preparation, was 70 Å.[9] Such large dependence of the $a/\sqrt{2}$ value on the lipid concentration seems to be originated from the fact that the hydrogen-bonding interaction among polar head moieties of the lipid molecules predominantly controls the critical packing mode to give thermodynamically stable aggregates and water molecules solvated onto the head moieties also take part in the hydrogen-bonding interaction. In dilute aqueous solutions, on the other hand, the $a/\sqrt{2}$ value seems to approach to a limiting value (ca. 110 Å) in a manner as observed for an equimolar mixture of N^+C_5Ala2C_{14} and (SO_3^-)-C_5Ala2C_{14} by means of freeze-fracture electron micros-

Table 1. Low-Angle X-Ray Diffraction Data for QC_5Ala2C_n–Water Systems

n[a]	Lipid concn w/w%	pH	Temp °C	Spacing[b] Å	Relative intensity[c]	Lattice plane (hkl)	Lattice constant (a)/Å	$a/\sqrt{2}$ Å
14	22	7	25	83 (82)	s	(111)	142	100
				71 (71)	m	(200)		
				50 (50)	w	(220)		
				41 (41)	w	(222)		
14	28	7	25	75 (74)	s	(111)	128	91
				63 (64)	m	(200)		
				45 (45)	w	(220)		
				37 (37)	w	(222)		
14	22	14	25	59				
16	29	7	40	77 (77)	s	(111)	133	94
				66 (67)	m	(200)		
				47 (47)	w	(220)		
				38 (38)	w	(222)		
16	29	7	10	77	w			
				55	s			

a) A number of carbon atoms in the double-chain segment of QC_5Ala2C_n. b) Calculated values are given in parentheses. c) s, strong; m, medium; w, weak.

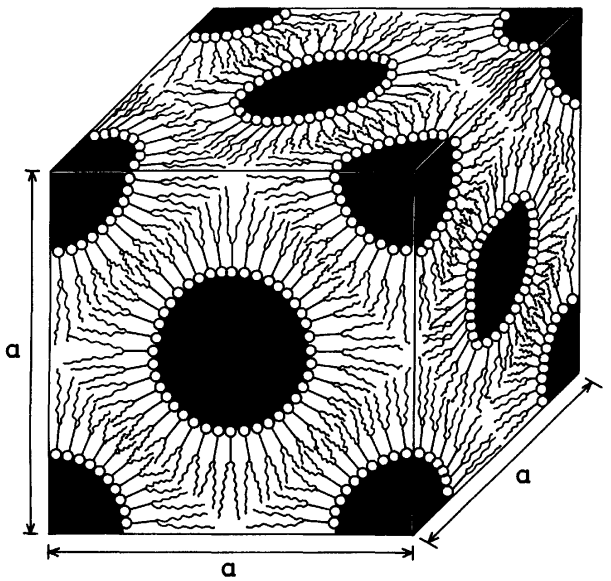

Fig. 2. Schematic representation of the inverted cubic phase formed with QC_5Ala2C_n; a, lattice constant.

copy.[11] It is noteworthy, however, that the $a/\sqrt{2}$ value is not so sensitively dependent on the lipid concentration for the cationic and anionic lipid system as observed for the QC_5Ala2C_{14} system in the light of observations by negative staining and freeze-fracture electron microscopy[11] and low-angle X-ray diffraction measurements.[12] The tight ion-pair cluster formed with cationic and anionic head moieties of the mixed lipid system seems to minimize hydration in the surface domain, while such an effect is not operative for QC_5Ala2C_n. These hydration effects must be reflected on the correlations between $a/\sqrt{2}$ and lipid concentration, and the $a/\sqrt{2}$ value is more strongly dependent on the lipid concentration in the case of the latter lipid system. The $a/\sqrt{2}$ value for the QC_5Ala2C_{16} aggregate (94 Å) is slightly larger than that for the QC_5Ala2C_{14} aggregate (91 Å) at a comparable concentration; mole fraction, 0.009.

Bilayer Phase. We have previously reported that the C_{II} phase formed with QC_5Ala2C_{14} was transformed into the bilayer phase upon deprotonation of the polar head moiety as confirmed by freeze-fracture electron microscopy, differential scanning calorimetry (DSC), and turbidity measurements.[7] This behavior was further evidenced by low-angle X-ray diffraction measurements in this work. As listed in Table 1, the diffractions from the C_{II} lattice at pH 7 completely disappeared at pH 14 to give a single diffraction with a spacing of 59 Å, which corresponds to the bilayer thickness evaluated by the CPK molecular model (Fig. 1B).

The diffraction patterns originating from the C_{II} phase formed with QC_5Ala2C_{16} disappeared below T_m even at pH 7 and were replaced with two diffractions (Table 1). The stronger diffraction with a spacing of 55 Å and the relatively weak one with a spacing of 77 Å presumably correspond to the thickness of the lipid bilayer and that of the bilayer plus water layer, respectively. Formation of the bilayer phase below T_m was also confirmed by negative staining electron microscopy applied to the specimen prepared at 5 °C. We have previously suspected that QC_5Ala2C_{16} would form the nonlamellar phase even below T_m on the basis of its smaller phase transition enthalpy and a lower value of steady-state fluorescence anisotropy for DPH embedded in the aggregate below T_m as compared with the corresponding values for bilayer-forming lipids having an analogous molecular structure.[7] Now, it is concluded that the C_{II} phase formed with QC_5Ala2C_{16} above T_m is transformed through phase transition into the bilayer phase accompanied with relatively loose packing of the hydrocarbon chains in comparison with those of bilayer-forming

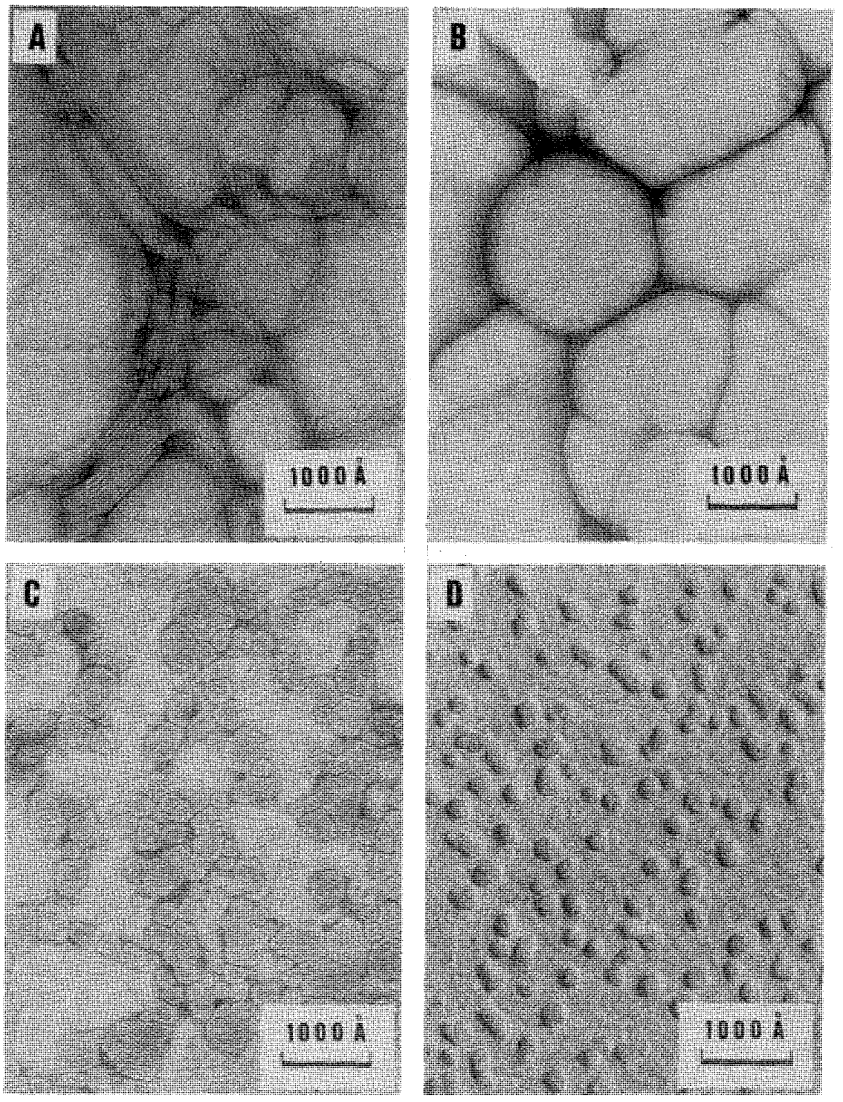

Fig. 3. Electron micrographs for $Q_2LysC_5Ala2C_n$: A, 5 mmol dm^{-3} aqueous dispersion of $Q_2LysC_5Ala2C_{16}$ negatively stained with uranyl acetate; B, 2.5 mmol dm^{-3} aqueous dispersion of $Q_2LysC_5Ala2C_{14}$ negatively stained with uranyl acetate; C, 2.5 mmol dm^{-3} aqueous solution of $Q_2LysC_5Ala2C_{14}$ sonicated for 2 min at 30 W, negatively stained with uranyl acetate; D, 1.5 mmol dm^{-3} aqueous solution of $Q_2LysC_5Ala2C_{14}$ sonicated for 3 min at 30 W, freeze-fractured.

ionic peptide lipids.

The phase transition parameters (T_m; enthalpy change, ΔH) for the aggegates of $Q_2LysC_5Ala2C_n$ having two quinoyl moieties are 1.7 °C and 17.1 kJ mol^{-1} for n=14 and 24.9 °C and 28.0 kJ mol^{-1} for n=16, respectively, at pH 7 as evaluated by DSC. These values are comparable to those observed for other bilayer aggregates having the same double-chain segments.[6c,7] The bilayer aggregates were formed both above and below T_m as observed by electron microscopy. As shown in Figs. 3A and 3B, multiwalled bilayer aggregates are observed in the specimens of $Q_2LysC_5Ala2C_{16}$ and $Q_2LysC_5Ala2C_{14}$, respectively, which were negatively stained at 20 °C in the aqueous dispersion state. Upon sonication of these dispersions with a probe-type sonicator, single-walled bilayer vesicles in the diameter range of 200—500 Å were obtained, as confirmed by negative staining and freeze-fracture electron microscopy (Figs. 3C and 3D). The steady-state fluorescence anisotropy (r_S) of DPH embedded in the $Q_2LysC_5Ala2C_{16}$ membrane is shown in Fig. 4 (curve A) as a function of temperature. The T_m value obtained from the inflection range (24.5 °C) is in good agreement with that evaluated by DSC. When homogeneous mixtures of QC_5Ala2C_n and $Q_2LysC_5Ala2C_n$ (n=14, 16) at the 1:1 and 2:1 molar ratios were dispersed in water, formation of multiwalled bilayer aggregates was detected by negative staining electron microscopy. Thus, it became apparent that transformation of the C_{II} phase formed with QC_5Ala2C_n above T_m into the bilayer phase can be achieved by the following perturbations to reduce the v/a_0l_c value: (i)

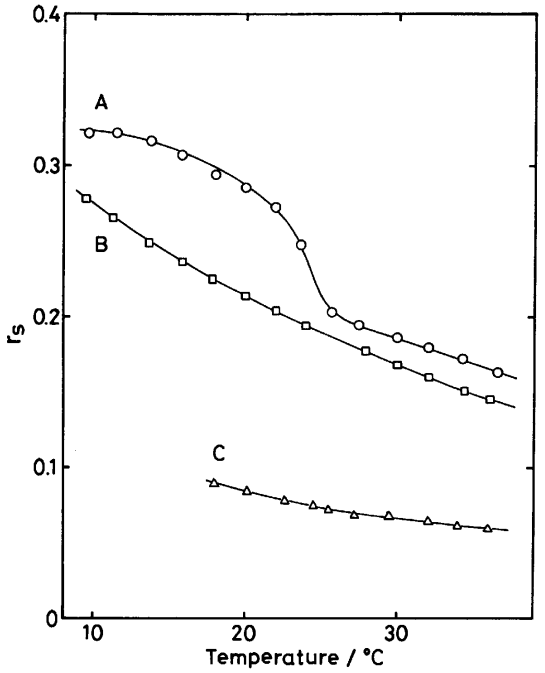

Fig. 4. Correlations of steady-state fluorescence anisotropy (r_S) with temperature for DPH (1.0×10^{-7} mol dm^{-3}) embedded in the following aggregates: A, 0.10 mmol dm^{-3} $Q_2LysC_5Ala2C_{16}$ at pH 7; B, 0.10 mmol dm^{-3} $Q_2LysC_5Ala2C_{16}$ at pH 14; C, 3.0 mmol dm^{-3} CTAB at pH 7.

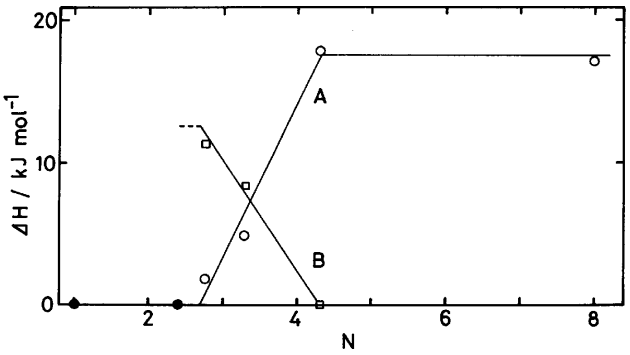

Fig. 5. Correlations of phase transition enthalpy (ΔH) with a number of hydroxyl groups per lipid molecule (N) for the aggregates formed with $(HO)C_5Ala2C_{14}$ and $Q_2LysC_5Ala2C_{14}$; total lipid concentration, 5.0 mmol dm^{-3}: A, for the phase transition peak at 1.8 °C; B, for the phase transition peak at 4.6 °C; closed circles for lipid mixtures which were not dispersed in water. The ΔH value is given for unit mol of the total lipid, regardless of morphology.

freezing of the rotational motion of the hydrophobic double-chain segment by a phase transition from the liquid-crystalline state to the gel state (decrease in v); (ii) a volume increase in the hydration shell around the polar head moiety of the lipid molecule upon deprotonation of the four hydroxyl groups (increase in a_0); and (iii) an increase in average bulkiness of the polar head moiety by incorporation of another bilayer-forming lipid (increase in a_0). In addition, it may be predicted that an increase in l_c, e.g. introduction of a longer hydrocarbon connector in between the quinoyl moiety and an amino acid residue, also causes a morphological change from C_{II} to bilayer.

Inverted Hexagonal Phase. As mentioned above, the H_{II} forming lipids may have v/a_0l_c values greater than those for the C_{II} forming lipids. We examined this criterion in this work by using the three types of nonionic peptide lipids. Since QC_5Ala2C_n forms the C_{II} phase above T_m, the individual or mixed lipid systems having a_0 values smaller than that of QC_5Ala2C_n are the candidates to form the H_{II} phase. Although accurate evaluation of the a_0 values for these peptide lipids is much difficult due to hydration of the polar head moieties, the effective bulkiness of these head moieties can be reasonably correlated with the average number of hydroxyl groups per lipid molecule (N): the N values for $(HO)C_5Ala2C_n$, QC_5Ala2C_n, and $Q_2LysC_5Ala2C_n$ are apparently 1, 4, and 8, respectively. $(HO)C_5Ala2C_n$ was not dispersed in water without coexisting lipid(s). When $(HO)C_5Ala2C_n$ and QC_5Ala2C_n were mixed at the 1 : 1, 1 : 2, and 1 : 4 molar ratios (N values are 2.5, 3.0, and 3.4, respectively), stable aqueous dispersions were not obtained even by prolonged vortex mixing.

Mixtures of $(HO)C_5Ala2C_{14}$ and $Q_2LysC_5Ala2C_{14}$ at the 1 : 1, 2 : 1, and 3 : 1 molar ratios (N values are 4.5, 3.3, and 2.8, respectively) were readily dispersed in water by vortex mixing, and turbidity of the aqueous dispersions remained unchanged at least over a week. The aggregates formed with $(HO)C_5Ala2C_{14}$ and $Q_2LysC_5Ala2C_{14}$ at the equimolar ratio showed a single phase transition at 1.8 °C, and the ΔH value was comparable to that observed for the bilayer aggregates formed with $Q_2LysC_5Ala2C_{14}$ alone (Fig. 5). The negatively stained electron micrograph showed the formation of multiwalled bilayer membranes. On the other hand, the DSC thermograms for the aggregates formed with $(HO)C_5Ala2C_{14}$ and $Q_2LysC_5Ala2C_{14}$ at the 2 : 1 and 3 : 1 molar ratios showed two phase transition peaks at 1.8 and 4.6 °C. The ΔH value for the latter peak increased as the N value was reduced, and the ΔH value for the former peak decreased concomitantly (Fig. 5). In the light of the correlations given in Fig. 5, the aggregate having T_m at 4.6 °C is referred to the H_{II} phase (above T_m) while that having T_m at 1.8 °C to the bilayer phase. In the negatively stained electron micrographs for these aggregates, three types of images, which are typical of the H_{II} phase, were observed: two kinds of striped patterns with different layer thickness and a network array of small internal aqueous compartments were observed in different areas of the specimen (Fig. 6). We evaluated these repeating distances by means of electron diffraction measurements applied to selected areas of the electron micrographs;[15] 52 and 31 Å of the repeating distances of layers (ratio, $\sqrt{3}$: 1) and 62 Å of the repeating dis-

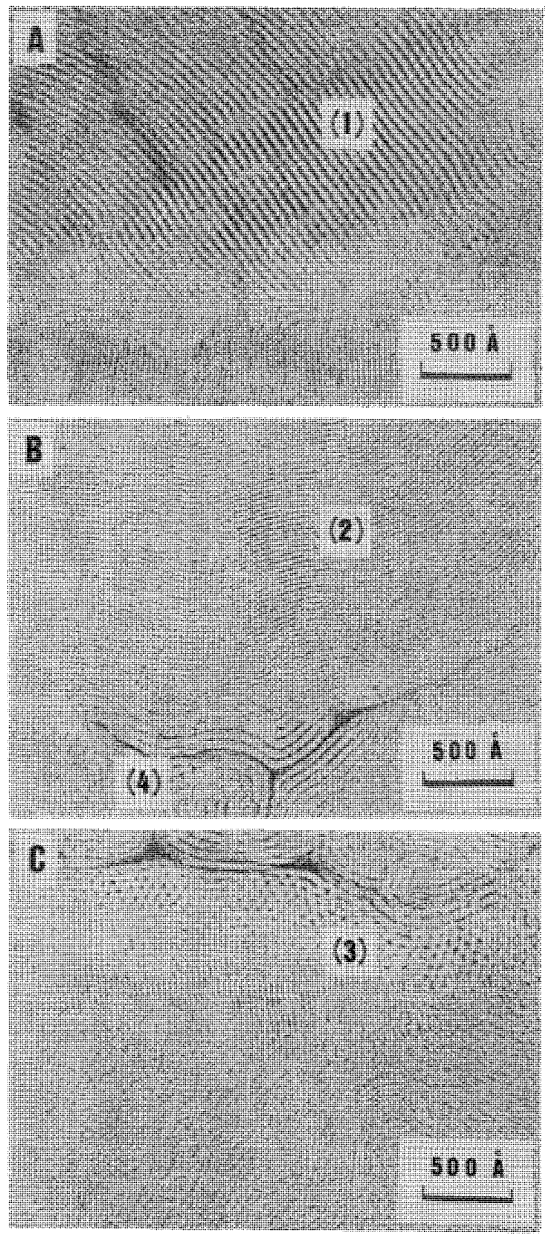

Fig. 6. Electron micrographs for a mixture of $(HO)C_5Ala2C_{14}$ (3.33 mmol dm^{-3}) and $Q_2LysC_5Ala2C_{14}$ (1.67 mmol dm^{-3}) in the aqueous dispersion state at room temperature, negatively stained with uranyl acetate. The images shown in A, B, and C were observed in different areas of the specimen. Numerals **1**, **2**, and **3** refer to three different cross sectional views of the H_{II} tubes, and **4** is attributed to the bilayer phase.

tance of aqueous compartments.[16] On these grounds, the aggregation status, which is referred to the H_{II} phase, is schematically illustrated in Fig. 7. The electron micrographic pattern, which presumably corresponds to the bilayer aggregate, was also observed in a limited area of the electron micrographs. However, it is rather difficult to distinguish between the image due to bilayer aggregates and that due to thicker layers of the H_{II} phase, since these show comparable layer thicknesses. The distinction between these aggregation states became possible by tilting the specimen in the electron microscope, as mentioned in our preliminary communication.[16] That is, the image and the corresponding electron diffraction pattern originating from one of the layers of the H_{II} phase were converted into those from the other type of layers by 30° rotation of the specimen (Fig. 8). The electron micrographic pattern showing a network array of internal aqueous compartments for the H_{II} phase resembles that for the C_{II} phase. However, the domain for the former phase is rather limited relative to that for the latter phase and surrounded by domains of the two types of layers attributable to the H_{II} phase. Fractions of the H_{II} phase in the overall aggregates were evaluated from the phase transition enthalpy; 0.7 and 0.9 for the $(HO)C_5Ala2C_{14}$-$Q_2LysC_5Ala2C_{14}$ system at the molar ratios of 2 : 1 and 3 : 1, respectively. These lipid mixtures were not dispersed in water at the N value smaller than 2.4. However, the H_{II} phase seems to be exclusively obtained at the N value below 2.7 in the light of the correlations given in Fig. 5. The mixed lipid system composed of $(HO)C_5Ala2C_{16}$ and $Q_2LysC_5Ala2C_{16}$ did not give stable aqueous dispersions at the N value smaller than 4, so that the aggregate morphology was not critically characterized.

Micellar Phase. Multiple ionization of the polar head moiety of $Q_2LysC_5Ala2C_n$ tends to expand the hydration shell around the quinoyl moieties to give an increase in a_0. As a result, the bilayer phase may be converted into the micellar one. The multiwalled bilayer aggregates formed with $Q_2LysC_5Ala2C_n$ exhibited relatively large turbidity in aqueous media, presumably due to extended aggregation of the membranes, in comparison with those formed with cationic or anionic peptide lipids. Deprotonation of the hydroxyl groups of the lipids caused turbidity decrease above pH 13. We characterized the aggregates formed at pH 14 by means of DSC, gel-filtration treatments, and fluorescence polarization measurements. The phase transition peak observed for $Q_2LysC_5Ala2C_n$ (n=14, 16) at pH 7 disappeared completely at pH 14 in the temperature range of 0—60 °C. Both dispersed and sonicated (with a probe-type sonicator at 30 W for 3 min) samples of $Q_2LysC_5Ala2C_{16}$ at pH 14 were completely eluted at the void volume on a column of Sephadex G-50 with aqueous 1 mol dm^{-3} KOH as an eluant, as monitored by a UV detector at 254 nm. Then, we adopted experiments entrapping fluorescent probes into the aggregates. When DPH (1.0×10^{-5} mol dm^{-3}) was added to the aqueous dispersion of $Q_2LysC_5Ala2C_{16}$ (1.0 mmol dm^{-3}), this hydrophobic probe was quantitatively incorporated into and remained in the aggregates even by gel-filtration treatments as confirmed by fluorescence spectroscopy. On the other hand, pyranine (1.0 mmol dm^{-3}) as a hydrophilic probe[8,17] was not incorporated at all into the aggregates of $Q_2LysC_5Ala2C_{16}$ (1.0 mmol dm^{-3}) as confirmed by gel-filtration treatments at pH 14,

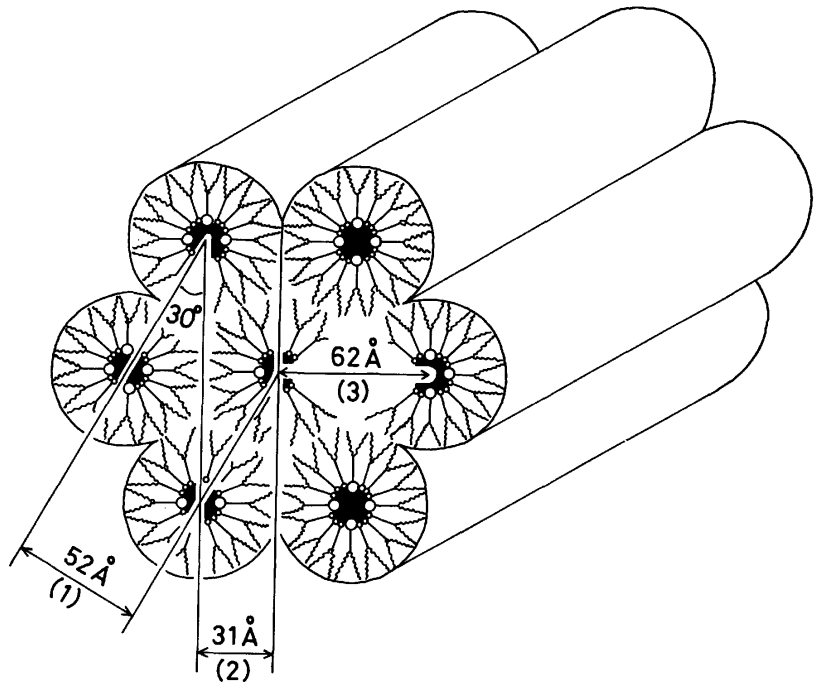

Fig. 7. Schematic representation of the inverted hexagonal phase formed with (HO)C_5Ala2C_{14} and Q_2LysC_5Ala2C_{14}; for numerals 1, 2, and 3, refer to Fig. 6.

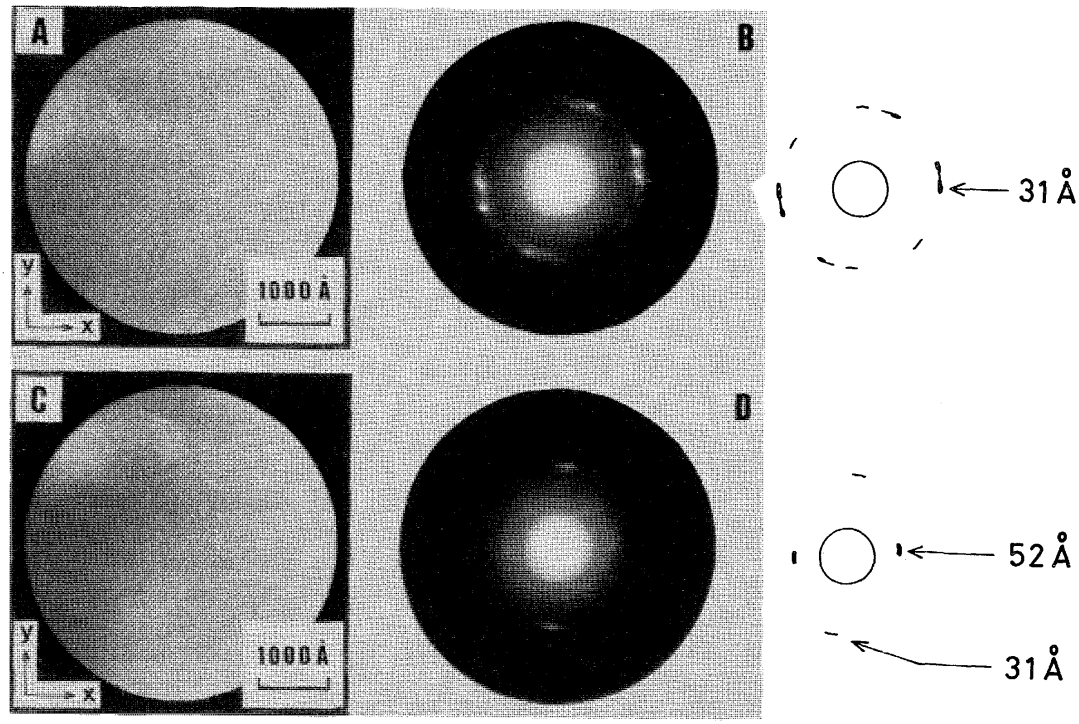

Fig. 8. Electron micrographs for a mixture of (HO)C_5Ala2C_{14} (3.33 mmol dm^{-3}) and Q_2LysC_5Ala2C_{14} (1.67 mmol dm^{-3}) in the aqueous dispersion state at room temperature, as negatively stained with uranyl acetate (A and C); their selected area electron diffraction patterns (B for A and D for C, respectively). Image A and diffraction pattern B were converted into C and D, respectively, by 30° rotation of the specimen around the y-axis.

regardless of the sample conditions, sonicated or dispersed. The results apparently indicate that these aggregates do not hold inner aqueous compartments.

A correlation of the r_S value due to DPH embedded in the aggregates with temperature at pH 14 is shown in Fig. 4 (curve B). Apparently, any inflection region is

Table 2. Aggregate Morphology for Synthetic Peptide Lipids in Aqueous Media

Lipid system	Aggregate morphology	N[a]	N'[b]
$(HO)C_5Ala2C_{14}$-$Q_2LysC_5Ala2C_{14}$	H_{II}[c]	2.7[d]	
QC_5Ala2C_n (n=14, 16)	C_{II}[c]	4	
QC_5Ala2C_n-$Q_2LysC_5Ala2C_n$ (n=14, 16)	Bilayer	5.3—6	
$Q_2LysC_5Ala2C_n$ (n=14, 16)	Bilayer	8	
$(Q^{4-})C_5Ala2C_n$ (n=14, 16)[e]	Bilayer		4
$(Q^{4-})_2LysC_5Ala2C_n$ (n=14, 16)[f]	Micelle		8

a) A number of OH groups per molecule. b) A number of O^- groups per molecule. c) Formed above T_m. d) An estimated value from Fig. 5. e) Anionic form of QC_5Ala2C_n. f) Anionic form of $Q_2LysC_5Ala2C_n$.

not observed. This is consistent with the formation of micelles and in good agreement with the result obtained from DSC. The critical aggregate concentration was evaluated from a correlation of the r_S value due to DPH embedded in the aggregate with the lipid concentration; 3.0×10^{-5} mol dm^{-3} for $Q_2LysC_5Ala2C_{16}$ at pH 14. It should be noted that the r_S values for the aggregates formed with $Q_2LysC_5Ala2C_{16}$ at pH 14 are much larger than those for the normal micelles composed of CTAB at various temperatures (Fig. 4, curve C) and comparable to those for the bilayer aggregates of the same lipid in the liquid crystalline state. Thus, this lipid undoubtedly forms rigid micelles in its polyanionic form. We have previously clarified that monocationic peptide amphiphiles having a hydrophobic single-chain segment form rigid cylindrical micelles by means of negative staining electron microscopy, ESR, and low-angle light scattering measurements.[18] We have also observed similar cylindrical micelles in the aqueous dispersion of $N^+C_5Ala2C_8$, having a double-chain segment shorter than those of the corresponding bilayer-forming lipids, $N^+C_5Ala2C_n$ (n=10—18).[6c] In the latter case, the aggregate morphology is controlled by modifying the v and l_c values but not the a_0 value. The aggregate structures of these various peptide amphiphiles seem to be tightened due to the intermolecular hydrogen-bonding interactions among the amino acid moieties within each aggregate.

Concluding Remarks. It became apparent that a series of synthetic peptide lipids having various numbers of hydroxyl groups in their head moieties, $(HO)C_5Ala2C_n$, QC_5Ala2C_n, and $Q_2LysC_5Ala2C_n$, adopt four kinds of aggregate morphology in aqueous media; H_{II}, C_{II}, bilayer, and micellar phases (Table 2). The difference in aggregate morphology can be well correlated with the critical packing parameter, v/a_0l_c, and the a_0 value is cited as a primary factor for controlling the morphology in the present case. The v/a_0l_c value increases in the order: micelle, bilayer, C_{II}, and H_{II} forming lipids. The a_0 value is reasonably correlated with the average number of hydroxyl groups per lipid molecule involved in the head moieties of the individual or mixed nonionic lipids. Although the polar head moieties of these nonionic lipids in the aggregated state are hydrated to a certain extent, the hydration shells of these moieties become much expanded upon deprotonation of the hydroxyl groups. The a_0 value becomes significantly larger under such conditions, and the aggregate morphology undergoes relevant transformations as a consequence. Recent rapid growth of the membrane mimetic chemistry has yielded a large number of bilayer-forming synthetic lipids. On the other hand, relevant nonbilayer-forming lipids have not been explored up to the present time, even though important aspects of such morphological status in the biomembrane fusion have been emphasized.[2] We believe that the present study provides useful molecular criteria for designing nonbilayer-forming lipids.

We are grateful to Professor Tisato Kajiyama and Dr. Kenji Yamada of Kyushu University for the X-ray diffraction measurements and Professor Toyoki Kunitake of Kyushu University for the use of a freeze-fracture device. We also thank Dr. Yoshitsugu Tomokiyo, Mr. Takeshi Manabe, and Mr. Eiji Tanaka of Kyushu University for their comments and expert technical assistance in the electron diffraction measurements. The present work was supported in part by a Grant-in-Aid for Scientific Research No. 58430016 from the Ministry of Education, Science, and Culture.

References

1) J. H. Fendler, "Membrane Mimetic Chemistry," John Wiley, New York (1982), Chap. 6 and 12.

2) a) A. J. Verkleij, *Biochim. Biophys. Acta*, **779**, 43 (1984), and references cited therein; b) P. J. Quinn and W. P. Williams, *ibid.*, **737**, 223 (1983); c) K. Larsson, K. Fontell, and N. Krog, *Chem. Phys. Lipids*, **27**, 321 (1980); d) P. R. Cullis and B. De Kruijff, *Biochim. Biophys. Acta*, **559**, 399 (1979).

3) C. Tanford, "The Hydrophobic Effect: Formation of Micelles and Biological Membranes," John Wiley, New York (1973), Chap. 12.

4) a) J. N. Israelachvili, S. Marčelja, and R. G. Horn, *Quart. Rev. Biophys.*, **13**, 121 (1980); b) D. J. Mitchell and B. W. Ninham, *J. Chem. Soc., Faraday Trans. 2*, **77**, 601 (1981).

5) For an example of morphological transformation between bilayer and micellar aggregates formed with synthetic lipids, see: J.-H. Fuhrhop, D. Fritsch, B. Tesche, and H. Schmiady, *J. Am. Chem. Soc.*, **106**, 1998 (1984).

6) a) Y. Murakami, A. Nakano, and K. Fukuya, *J. Am. Chem. Soc.*, **102**, 4253 (1980); b) Y. Murakami, A. Nakano, and H. Ikeda, *J. Org. Chem.*, **47**, 2137 (1982); c) Y. Murakami, A.

Nakano, A. Yoshimatsu, K. Uchitomi, and Y. Matsuda, *J. Am. Chem. Soc.*, **104**, 3613 (1984).

7) Y. Murakami, J. Kikuchi, T. Takaki, K. Uchimura, and A. Nakano, *J. Am. Chem. Soc.*, **107**, 2161 (1985).

8) K. Kano and J. H. Fendler, *Biochim. Biophys. Acta*, **509**, 289 (1978).

9) Y. Murakami, A. Nakano, J. Kikuchi, T. Takaki, and K. Uchimura, *Chem. Lett.*, **1983**, 1891.

10) R. Grewe and H. Haendler, *Justus Liebigs Ann. Chem.*, **658**, 113 (1962).

11) Y. Murakami, J. Kikuchi, T. Takaki, and K. Uchimura, *J. Am. Chem. Soc.*, **107**, 3373 (1985).

12) Y. Murakami, J. Kikuchi, T. Takaki, and K. Uchimura, *Bull. Chem. Soc. Jpn.*, **59**, 515 (1986).

13) G. L. Kirk, S. M. Gruner, and D. L. Stein, *Biochemistry*, **23**, 1093 (1984).

14) G. Lindblom, K. Larsson, L. Johansson, K. Fontell, and S. Forsén, *J. Am. Chem. Soc.*, **101**, 5465 (1979); W. Longley and T. J. McIntosh, *Nature (London)*, **303**, 612 (1983); K. Larsson, *ibid.*, **304**, 664 (1983).

15) P. Hirsh, A. Howie, R. B. Nicholson, D. W. Pashley, and M. J. Whelan, "Electron Microscopy of Thin Crystals," 2nd ed, R. E. Krieger, New York (1977), pp. 3—6.

16) Y. Murakami, J. Kikuchi, T. Takaki, and K. Uchimura, *Chem. Lett.*, **1986**, 325.

17) N. R. Clement and J. M. Gould, *Biochemistry*, **20**, 1534 (1981).

18) Y. Murakami, A. Nakano, K. Iwamoto, and A. Yoshimatsu, *Chem. Lett.*, **1979**, 951; Y. Murakami, A. Nakano, K. Iwamoto, and A. Yoshimatsu, *J. Chem. Soc., Perkin Trans. 2*, **1980**, 1809.

 © 1987 The Chemical Society of Japan Bull. Chem. Soc. Jpn., 60, 1481—1488 (1987)

Synthesis of (14*R*)- and (14*S*)-14-De(hydroxymethyl)-14-hydroxymycaminosyl Tylonolides

Shuichi SAKAMOTO, Tsutomu TSUCHIYA,* Sumio UMEZAWA, and Hamao UMEZAWA
Institute of Bioorganic Chemistry, 1614 Ida, Nakahara-ku, Kawasaki 211
(Received October 28, 1986)

The title compounds **29** and **19** have been prepared from mycaminosyl tylonolide 9,20-bis(ethylene acetal) via 9 (for **19**) and 13 steps (for **29**). The key step in the synthesis of **19** is Baeyer-Villiger reaction applied to 2′,4′-di-*O*-acetyl-3-*O*-*t*-butyldimethylsilyl-23-deoxy-23-oxomycaminosyl tylonolide 9,20-bis(ethylene acetal), and the desired 14-*O*-formyl derivative is obtained with other products including 12,13-epoxy and 14-*C*-carboxylic acid. The key step in the synthesis of **29** is Mitsunobu reaction applied to (14*S*)-2′,4′-di-*O*-acetyl-3-*O*-*t*-butyldimethylsilyl-14-de(hydroxymethyl)-14-hydroxymycaminosyl tylonolide 9,20-bis(ethylene acetal), and the desired (14*R*)-acyloxy product is obtained by inversion at C-14, with other compounds including 10(11), 12(22),13(14)-triene and 12-acyloxy-10(11),13(14)-diene.

Several derivatives substituted at C-23 of mycaminosyl tylonolide (MT), a macrolide antibiotic, had been prepared in our laboratory; these include 23-*O*-acyl,[1] 23-deoxy-23-halo,[1] 23-dialkylamino-23-deoxy,[2,3] and 23-acylamido-23-deoxy[4] derivatives. Recently we also prepared 23-C-alkyl[3] and 23-C-alkylidene-23-deoxy derivatives[6] from a 14-C-aldehyde,[5] a key synthetic intermediate, by the reaction using Grignard and Wittig reagents. Some of these synthesized compounds showed marked antibacterial activities against Gram-negative bacteria, to which usual macrolide antibiotics have almost no activity.

Since the above derivatives were all concerned with the substitutions at C-23, we changed our attention to attach functional groups directly at C-14 with cleavage of the C(14)–C(23) bond. One reason for this transformation is that the replacement of the projecting hydroxymethyl group at C-14 with a small functional group will result in a fundamental change in antibacterial activity. In this paper we describe the syntheses of two 14-de(hydroxymethyl)-14-hydroxy derivatives (**19**, **29**) of mycaminosyl tylonolide.

Results and Discussion

Treatment of mycaminosyl tylonolide diethyl acetal[7] (**1**) with ethylene glycol in the conditions described in the Experimental section gave the 9,20-bis(ethylene acetal) **2**. Presence of a ethylene acetal fragment at C-9 was confirmed indirectly by the shift values of H-10 (δ 5.75) and H-11 (δ 6.36), which differ, respectively, from those of usual 9-keto derivatives (δ ≈6.3 and ≈7.3). Acetylation of **2** with acetic anhydride in acetonitrile[8] gave the 2′,4′-di-*O*-acetyl derivative (**3**). Treatment of **3** with *t*-butylchlorodimethylsilane in the conditions reported[5,9] gave the 3,23-bis(*O*-*t*-butyldimethylsilyl) derivative (**4**). The 23-*O*-silyl group was then selectively removed with use of limited amount of tetrabutylammonium fluoride in oxolane to afford the 3-*O*-silyl derivative (**5**). Oxidation of **5** with dimethyl sulfoxide in the presence of pyridinium trifluoroacetate and dicyclohexylcarbodiimide in a manner as reported[5,9] gave the 14-C-aldehyde (**6**).

In order to introduce an oxygen atom at C-14 with splitting of the 14-C-aldehyde group, Baeyer-Villiger reaction was examined for **6** after several kinds of unsuccessful reactions were tested. In **6**, the two carbonyl groups at C-9 and C-20 are protected and the carbonyl at C-23 remains free. For such a C-aldehyde fragment, however, successful application of Baeyer-Villiger reaction has not been described yet to our knowledge. When **6** was treated with 3 molar equivalents of *m*-chloroperbenzoic acid in chloroform, an unstable compound supposed the *N*-oxide (**7**) of **6** was first produced, then four products [**8**, **9**(trace), **10**(trace), and **11**; in the order of mobility] followed. Presence of the 3′-dimethylamino *N*-oxide group in **7** (for the isolation: see the Experimental section for **12**)

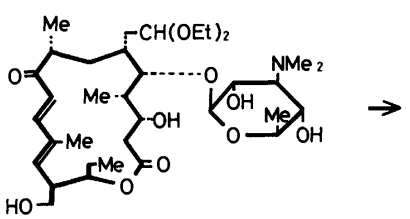

1

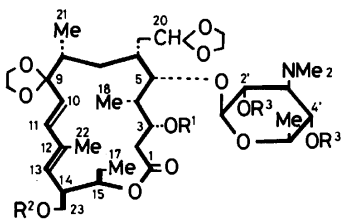

	R^1	R^2	R^3
2	H	H	H
3	H	H	Ac
4	TBS	TBS	Ac
5	TBS	H	Ac

TBS: $SiMe_2Bu^t$

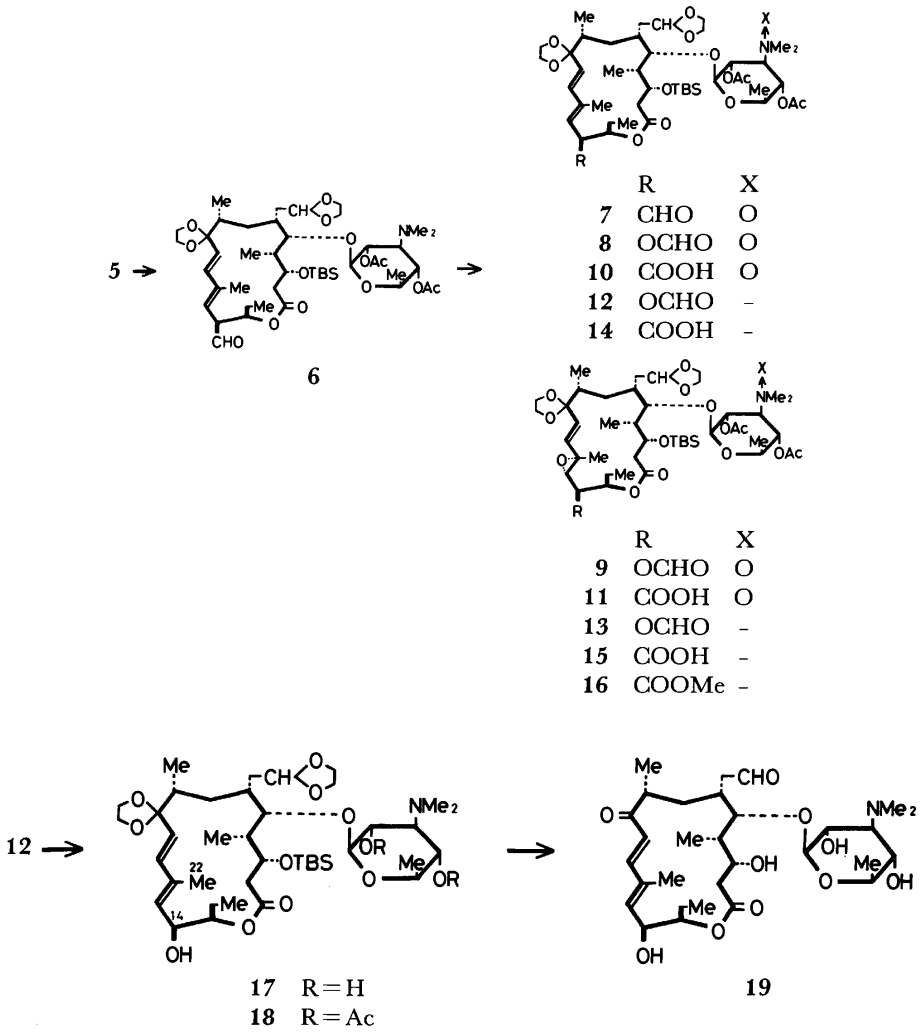

was supported by the shift value of the methyl protons of dimethylamino group (δ 3.23[10]) in the ^{1}H NMR spectrum. The minor product **8**, was presumed, according to its ^{1}H NMR spectrum, the desired product having a formyl ester at C-14 and 3′-dimethylamino *N*-oxide group. As these products were all unstable and considered to have the *N*-oxide structure, de(*N*-oxid)ation was immediately carried out. When, however, triphenylphosphine was used in the presence of acetic acid, a typical procedure for de(*N*-oxid)ation, 9-acetal group was simultaneously hydrolyzed. Thus triphenyl phosphite [$(PhO)_3P$] was attempted as the reducing agent in an inert solvent to successfully give a reaction mixture. Column chromatography of the mixture gave the desired protected 14-formyloxy derivative (**12**) in 24% yield from **5** through **6** and **8**, together with **13** (from **9**), **14** (from **10**), and **15** (from **11**). The structure of **14** is thought to be, from the nature of the reagent, the 14-C-carboxylic acid derivative formed by oxidation of **7**, but the structure remains to be studied.

The structure of **12** was determined by the ^{1}H NMR spectrum; signals for a *t*-butyldimethylsilyl, two acetyls, and two ethylene acetal groups (estimated by the signal integration between δ 3.8—4.0) were observed. The low shift value of H-14 (δ 5.49), and the accordance of $J_{13,14}$(=10 Hz) and $J_{14,15}$(=10 Hz) values with those of other MT derivatives[9,11] including **6** indicate that the aldehyde group at C-14 of **6** was replaced by a formyloxy group with retention of the configuration at C-14. Presence of the formyl group was also supported by appearance of a singlet at low field (δ 8.03).

The structure of **13** was concluded to be the 12,13-epoxy analog of **12**. In its ^{1}H NMR spectrum, H-11, H-14, Me-22, and especially H-13 (δ 3.15) showed marked upfield shifts, in comparison with those of **12**, indicating the disappearance of the double bond between C(12)-C(13). Other proton resonances showed approximate accordance with those of **12** in shift and *J* value. Considering from the reaction reagent, it is clear that the double bond was oxidized to the epoxide, with the C(10)-C(11) double bond remained intact. The structure of **13** was also supported by the UV spectrum[12] and TLC detection [**13** was inert under UV lamp (2536 Å)]. The absolute configurations around the epoxide ring could not be decided, but if the reagent approaches from the less-hindered side, 12*S*,13*S* structure is expected. This assumption was sustained by similarity of the ^{1}H NMR spectra (δ and *J* values,

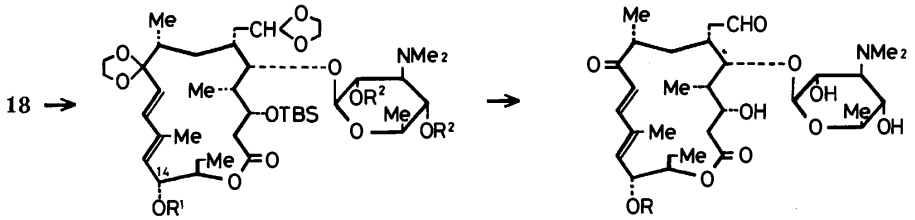

	R^1	R^2
20	CHO	Ac
23	H	H
25	H	Ac
26	Ac	Ac

28 R=Ac
29 R=H

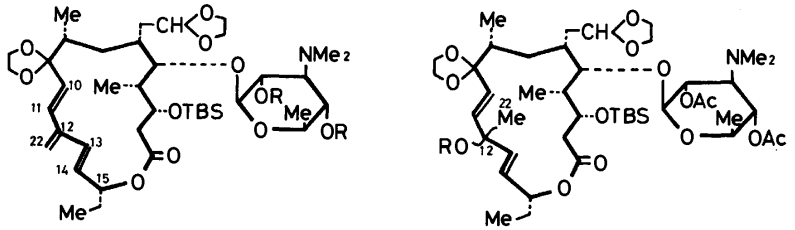

21 R=Ac
24 R=H

22 R=CHO
27 R=Ac

especially $J_{13,14}$) between **13** and rosaramicin, a 16-membered macrolide antibiotic, which contains (12*S*, 13*S*)-12,13-epoxy structure.[13,14]

The structure of another product **15** was determined to be 12,13-epoxy-14-C-carboxylic acid by methylation with diazomethane to give the corresponding methyl ester (**16**), and the similarity of the ^{1}H NMR spectrum with that of **13** with only lacking the formyl proton signal ($\delta \approx 8$). In conclusion, on oxidation with *m*-chloroperbenzoic acid, the 14-C-aldehyde (**6**) was majorly converted to the 12,13-epoxy-14-C-carboxylic acid (**15**), but Baeyer-Villiger reaction also did occur to give the desired 14-*O*-formyl product **12**.

Treatment of **12** in hot methanol removed the acetyl and formyl groups to give **17**, which, on acetylation with acetic anhydride in acetonitrile, gave the 2′,4′-di-*O*-acetyl derivative (**18**). The configuration at C-14 of **18** was determined by the NOE experiment, in that 10% enhancement of H-14 was observed[11] on irradiation of Me-22. This result also supported the structure of **12**.

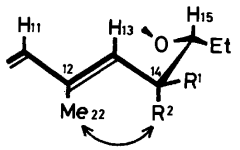

	R^1	R^2
12	OCHO	H
18	OH	H
20	H	OCHO
25	H	OH

Removal of the silyl and acetal groups of **17** with tetrabutylammonium fluoride in oxolane, and acidic treatment followed gave the desired (14*S*)-14-hydroxy compound (**19**). It is noteworthy that **19** was stably obtained under acidic conditions but the corresponding (14*R*)-14-hydroxy compound (**29**) later mentioned was unstable and converted into several products by the same treatment.

Next, inversion of configuration of the hydroxyl group at C-14 of **19** was attempted to obtain the 14*R* isomer **29**. At first, several substitution reactions were tried for the 14-*O*-sulfonyl derivatives of **18**, but only fruitless results were obtained. Attempt to oxidize **18** to the 14-carbonyl derivative, followed by reduction with sodium borohydride to obtain the 14*R* alcohol, also failed only giving **21** (see later). When, however, Mitsunobu reaction[15] was appled to **18** in benzene in the presence of formic acid, the (14*R*)-formyloxy derivative (**20**) was obtained in a moderate yield (≈50%) with other products (**21** and **22**). Comparison of the ^{1}H NMR spectra of **20** and **12** (14*S* isomer of **20**) showed that there were marked differences in the shift and *J* values between them in relation to H-14 (**20**: δ 5.82, $J_{13,14}$=6, $J_{14,15}$=2.5 Hz; **12**: δ 5.49, $J_{13,14}$=$J_{14,15}$=10 Hz). The lower shift of H-14 of **20** indicates that the H-14 is pseudoequatorial for the average macrolactone plane, and this is in accord with the small *J* values showing the gauche relationships between H-14 and H-13, and H-14 and H-15.

In the ^{1}H NMR spectrum of the by-product **21**, the signal of Me-22 (δ 1.73) of **18** disappeared, and, instead, a pair of small doublet (H-22a,b), typical for a terminal methylene, appeared at low field (δ 5.00 and 5.07). The proton of H-14 also resonated at low field (δ 5.57) and coupled with H-13 (δ 6.34, $J_{13,14}$=15.5 Hz) and H-15 ($J_{14,15}$=7.5 Hz). These results indicate that **21** has a *trans, trans*-10,11 : 13,14-dieno-12-C-methylene struc-

ture. The structure of **21** was also confirmed by the ^{1}H NMR spectrum (and the ^{1}H shift-correlated 2D spectrum) of the deacetyl derivative (**24**).

The second by-product **22** in Mitsunobu reaction seems to have a similar structure with that of **21**, because both compounds had almost the same J values relating to $J_{10,11}$, $J_{13,14}$, and $J_{14,15}$. However, in **22**, Me-22 appeared as a singlet at δ 1.62 (**21** has a 22-methylene), the shift being different from the usual value ($\delta \approx 1.8$), and a formyl proton (δ 8.05) was observed. These results indicate that compound **22** is 12-formyloxy-10,11 : 13,14-diene. The reaction mechanism will be that the 14-*O*-phosphonic intermediate[15] (A) of **18** born during Mitsunobu reaction detaches the phosphoniooxy portion to give the intermediate (B) and it

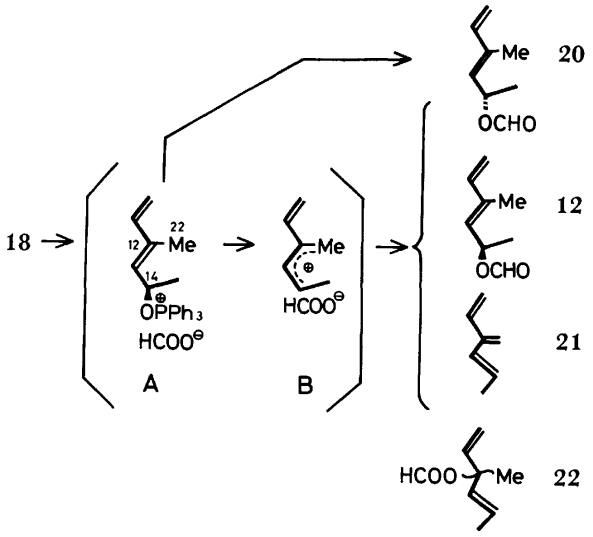

was converted to **20** (and **12**), **21**, and **22** by the action of the formate anion attacked at C-14, H-22, and C-12, respectively. Direct pathway from A to **20** is also considered. The absolute configuration at C-12 of **22**, however, remained undetermined. Disappointingly treatment of **22** and **24** with methanol or 0.1 mol dm^{-3} hydrochloric acid in water-acetonitrile (10 : 1) gave, respectively, a complex mixture indicating there is no hope to obtain the corresponding deblocked derivatives. Deacylation of **20** with methanol (to give **23**) followed by 2′,4′-di-*O*-acetylation gave **25**. In the ^{1}H NMR experiment, no NOE between H-14 and Me-22 was observed supporting indirectly the strucure of **25** and therefore **20**. Unexpectedly deblocking of **23** in an acidic medium to obtain **29** gave a complex mixture. This suggests that the presence of the (14*R*)-hydroxyl group of **23**, unlike the (14*S*)-hydroxyl, make the compound labile against acid. Therefore we intended to change the unstable 14-*O*-formyl group of **20** into an acid-stable *O*-acetyl group. Thus Mitsunobu reaction was carried out on **18** in the presence of acetic acid, whereupon the (14*R*)-acetoxy derivative (**26**) was obtained with **21** and the acetyl congener (**27**) of **22**. Successive treatment of **26** with methanol (to give the 2′,4′-diol derivative), tetrabutylammonium fluoride in oxolane (to remove the silyl group), and hydrochloric acid in aqueous acetonitrile (to remove acetal groups) gave the 14-*O*-acetyl derivative (**28**), all other protecting groups being removed. Finally, basic treatment (NH_3 in aq acetonitrile) of **28** gave the desired product (**29**).

The compound **19** exhibited almost the same or slightly better antibacterial activity in comparison with that of MT, whereas **29** had much weaker activity (see Experimental). Although these two compounds showed no characteristic antibacterial activity, some of the derivatives prepared from them showed remarkable antibacterial activity, which will be reported in another paper.[16] Therefore **19** and **29** will serve as useful compounds, instead of MT, for preparation of new types of macrolides.

Experimental

General. Optical rotations were measured with a Perkin-Elmer 241 polarimeter. Thin-layer chromatography (TLC) was carried out on Kieselgel 60 F-254 (E. Merck) silica gel with detection by spraying with sulfuric acid, followed by slight heating. Column chromatography was performed on Wakogel C-200 or Kieselgel 60, 230—400 mesh (E. Merck). ^{1}H NMR spectra were recorded at 250 MHz with a Bruker WM 250 spectometer.

Mycaminosyl Tylonolide 9,20-Bis(ethylene acetal) (2). A flask containing **1**[11] (38.5 g), ethylene glycol (37 ml), pyridinium *p*-toluenesulfonate (18 g), *p*-toluenesulfonic acid (5.7 g of monohydrate was dried at 100 °C in vacuo for 1 h), sulfolane (200 ml), and benzene (800 ml) was connected to a Soxhlet-type extractor[17] filled with molecular sieves 4A (250 ml, activated at 220 °C under a stream of nitrogen) with a reflux condenser, and the mixture was refluxed for 48 h. On TLC with chloroform-methanol-28% aqueous ammonia (10 : 1 : 0.1), the solution showed spots at R_f 0.3 (**2**, major) and R_f 0.25 (trace; cf. **1**: R_f 0.3). The mixture was poured into an ice-cold, half-saturated aqueous sodium hydrogencarbonate solution (1 L), and extracted with chloroform (1 L×3). The organic solution was washed with aqueous sodium sulfate (saturated, 1 L), dried (Na_2SO_4), and concentrated. The residue was again extracted with benzene (2 L) and the organic solution was washed with aqueous sodium sulfate (saturated, 0.7 L×3), dried (Na_2SO_4), and concentrated. The residue was chromatographed on a silica-gel column with chloroform-methanol-28% aqueous ammonia (25 : 1 : 0.1) to give a solid of **2**, 24.4 g (62%), $[\alpha]_D^{20}$ +13° (*c* 1, chloroform); ^{1}H NMR ($CDCl_3$) δ=2.50 (6H, s, NMe_2), 4.31 (1H, d, $J_{1',2'}$=7.5 Hz, H-1′), 5.30 (1H, d, H-13), 5.75 (1H, d, H-10), 6.36 (1H, d, H-11).

Found: C, 60.48; H, 8.46; N, 1.88%. Calcd for $C_{35}H_{59}NO_{12} \cdot 1/2H_2O$: C, 60.52; H, 8.65; N, 2.02%.

2′,4′-Di-*O*-acetylmycaminosyl Tylonolide 9,20-Bis(ethylene acetal) (3). A solution of **2** (17.2 g) and acetic anhydride (5.6 g) in acetonitrile (172 ml) was kept at room temperature overnight. Evaporation with several additions of toluene gave a residue, that was extracted with benzene, and the organic solution was washed with aqueous sodium hydrogencarbonate (saturated), dried (Na_2SO_4), and concentrated to give a solid of **3**, 17.4 g (90%), $[\alpha]_D^{20}$ -17° (*c* 1, chloroform);

^{1}H NMR ($CDCl_3$) δ=2.01 and 2.05 (each 3H, s, Ac ×2), 2.34 (6H, s, NMe_2), 2.77 (1H, t, $J_{2',3'}=J_{3',4'}$=10 Hz, H-3'), 4.65 (1H, d, $J_{1',2'}$=7.5 Hz, H-1'), 4.76 (1H, t, H-4'), 4.95 (1H, dd, H-2'), 5.34 (1H, d, $J_{13,14}$=10 Hz, H-13), 5.70 (1H, d, $J_{10,11}$=16 Hz, H-10), 6.39 (1H, d, H-11).

Found: C, 60.69; H, 8.02; N, 1.94%. Calcd for $C_{39}H_{63}NO_{14}$: C, 60.86; H, 8.19; N, 1.82%.

2',4'-Di-*O*-acetyl-3,23-bis(*O*-*t*-butyldimethylsilyl)mycaminosyl Tylonolide 9,20-Bis(ethylene acetal) (4). A mixture of **3** (17.4 g), imidazole (9.2 g), and *t*-butylchlorodimethylsilane (17 g) in *N*,*N*-dimethylformamide (140 ml) was heated at 80 °C for 9 h. Evaporation with several additions of xylene gave a residue, that was extracted with benzene. The solution was washed with aqueous sodium hydrogencarbonate (saturated), aqueous sodium sulfate (saturated), dried (Na_2SO_4), and concentrated to give a solid of **4**, 22 g (97%). An analytical sample was obtained by column chromatography with toluene-ethyl acetate (4:1), $[\alpha]_D^{20}$ −58° (*c* 1, chloroform); ^{1}H NMR ($CDCl_3$) δ=0.01, 0.02, 0.03, and 0.13 (each 3H, s, $SiMe_2$×2), 0.87 and 0.89 (each 9H, s, Si-Bu^t ×2), 1.71 (3H, s, Me-22), 2.05 and 2.06 (each 3H, s, Ac ×2), 2.35 (6H, s, NMe_2), 2.72 (1H, t, H-3'), 4.45 (1H, d, H-1'), 4.76 (1H, t, H-4'), 4.90 (2H, H-2',15), 5.37 (1H, d, H-13), 5.55 (1H, d, H-10), 6.34 (1H, d, H-11).

Found: C, 61.55; H, 8.88; N, 1.66%. Calcd for $C_{51}H_{91}NO_{14}Si_2$: C, 61.38; H, 9.13; N, 1.40%.

2',4'-Di-*O*-acetyl-3-*O*-(*t*-butyldimethylsilyl)mycaminosyl Tylonolide 9,20-Bis(ethylene acetal) (5). To an ice-cold solution of **4** (22 g) in oxolane (220 ml) was added a 1 mol dm^{-3} solution (20 ml) of tetrabutylammonium fluoride (1 molar equivalent for **4**) in oxolane, and the solution was kept at room temperature for 2 h. On checking by TLC with toluene-ethyl acetate (2:1), the solution showed a major spot at R_f 0.27. Evaporation gave a residue, that was extracted with benzene. The organic solution was then treated in a manner as described for **4**, to give, after column chromatography with toluene-ethyl acetate (1:1→1:2, gradually changed), a solid of **5**, 16 g (82%), $[\alpha]_D^{20}$ −54° (*c* 1, chloroform); ^{1}H NMR ($CDCl_3$): δ=0.02 and 0.15 (each 3H, s, $SiMe_2$), 0.89 (9H, s, Si-Bu^t), 0.94 (3H, t, Me-17), 1.75 (3H, s, Me-22), 2.05 and 2.06 (each 3H, s, Ac ×2), 2.34 (6H, s, NMe_2), 2.74 (1H, t, H-3'), 2.79 (1H, m, H-14), 4.44 (1H, d, H-1'), 4.76 (1H, t, H-4'), 4.87 (1H, dt, $J_{14,15}=J_{15,16a}$=10, $J_{15,16b}$=3 Hz, H-15), 4.90 (1H, dd, H-2'), 5.36 (1H, d, $J_{13,14}$=10 Hz, H-13), 5.60 (1H, d, H-10), 6.39 (1H, d, H-11).

Found: C, 60.76; H, 8.58; N, 1.57%. Calcd for $C_{45}H_{77}NO_{14}Si$: C, 61.15; H, 8.72; N, 1.58%.

(14*S*)-2',4'-Di-*O*-acetyl-3-*O*-(*t*-butyldimethylsilyl)-14-de(hydroxymethyl)-14-(formyloxy)mycaminosyl Tylonolide 9,20-Bis(ethylene acetal) (12). A solution of **5** (5.02 g), pyridinium trifluoroacetate (1.67 g), and dicyclohexylcarbodiimide (2.37 g) in dry DMSO-benzene (1:1, 50 ml) was stirred at room temperature overnight, then poured into 1,4-dioxane (20 ml) containing oxalic acid dihydrate (1 g). Precipitates occured were filtered off with aid of benzene. The filtered solutions were concentrated, and the residue was extracted with benzene. The extracts were washed as described for **4**, and concentrated. The residual syrup, that showed on TLC with toluene-ethyl acetate (2:1) a single spot at R_f 0.42, was passed through a short column with toluene-ethyl acetate (3:1) to give an unstable solid of **6**, 4.7g. ^{1}H NMR ($CDCl_3$ at 90 MHz) δ=0.90 (9H, s, Si-Bu^t), 1.80 (3H, s, Me-22), 2.07 (6H, s, Ac ×2), 2.38 (6H, s, NMe_2), 3.65 (1H, dt, $J_{13,14}=J_{14,15}$=10 Hz, H-14), 4.47 (1H, d, H-1'), 5.40 (1H, d, H-13), 5.72 (1H, d, H-10), 6.43 (1H, d, H-11), 9.67 (1H, d, $J_{14,23}$=2.8 Hz, H-23).

To a solution of the solid in chloroform (90 ml) were added powdered sodium hydrogencarbonate (1.4 g) and *m*-chloroperbenzoic acid (3.01 g), and the mixture was stirred at room temperature for 3 h. On checking by TLC with chloroform-methanol (5:1), the solution just after the reaction started showed a single spot at R_f 0.46 (**7**; cf. **6**: R_f 0.91; **7** could be isolated by stopping the reaction within 5 min and succeeding prompt purification), and after 3 h, four spots at R_f 0.2 (major, non-sensitive to UV light, **11**), 0.35 (trace, **10**), 0.45 (trace, non-sensitive to UV light, **9**), and 0.53 (minor, **8**). After addition of chloroform (500 ml), the organic solution was washed with aqueous sodium sulfate (saturated), dried (Na_2SO_4), and concentrated to give an unstable mixture of products (≈4.6 g). In a run, **8** was isolated, though in a poor yield, by column chromatography with chloroform-methanol (9:1); ^{1}H NMR ($CDCl_3$) δ=0.04 and 0.12 (each 3H, s, $SiMe_2$), 0.86 (9H, s, Si-Bu^t), 1.87 (3H, s, Me-22), 2.09 and 2.12 (each 3H, s, Ac ×2), 3.23 (6H, s, N(O)Me_2), ≈5.02 (H-15), 5.37 (1H, d, $J_{13,14}$=10 Hz, H-13), ≈5.48 (1H, t, $J_{14,15}$=10 Hz, H-14), ≈5.69 (1H, d, $J_{10,11}$=16 Hz, H-10), 6.27 (1H, d, H-11), 8.04 (1H, s, OCHO).

To an ice-cold solution of the product mixture in toluene (46 ml) was added triphenyl phosphite (4.2 ml) and the solution kept at room temperature overnight. On checking by TLC with previous developing system, all the spots of the starting products disappeared with appearance of spots with larger R_f values, respectively, and with toluene-ethyl acetate (1:1), well-separated four spots of R_f 0.05 (major, **15**), 0.13 (trace, **14**), 0.55 (trace, **13**), and 0.68 (minor, **12**) appeared. Concentration of the reaction mixture gave a product mixture, that was separated by column chromatography with toluene-ethyl acetate (3:1→2:1) to give solids of **12**, 1.22 g (24%) and **13**, 0.28 g (5%). On subsequent change of the developing systems to chloroform-acetone (3:1) and then chloroform-methanol (5:1), solids of **14**, 0.28 g (5.5%) and **15**, 2.15 g (41%) were obtained, respectively.

12: $[\alpha]_D^{20}$ −35° (*c* 2, chloroform); UV_{max} (CH_3OH) 233 nm (ε 21,000); ^{1}H NMR ($CDCl_3$) δ=0.04 and 0.15 (each 3H, s, $SiMe_2$), 0.84 (3H, d, Me-21), 0.90 (9H, s, Si-Bu^t), 0.94 (3H, t, Me-17), 1.04 (3H, d, Me-18), 1.15 (3H, d, Me-6'), 1.86 (3H, s, Me-22), 2.04 and 2.05 (each 3H, s, Ac ×2), 2.34 (6H, s, NMe_2), 2.72 (1H, t, H-3'), 4.42 (1H, d, H-1'), 4.76 (1H, t, H-4'), 4.90 (1H, dd, H-2'), 5.03 (1H, dt, H-15), 5.34 (1H, d, H-13), 5.49 (1H, t, $J_{13,14}=J_{14,15}$=10 Hz, H-14), 5.70 (1H, d, $J_{10,11}$=16 Hz, H-10), 6.30 (1H, d, H-11), 8.03 (1H, s, OCHO).

Found: C, 60.03; H, 8.08; N, 1.66%. Calcd for $C_{45}H_{75}NO_{15}Si$: C, 60.20; H, 8.36; N, 1.56%.

(12*S*,13*S*)-2',4'-Di-*O*-acetyl-3-*O*-(*t*-butyldimethylsilyl)-12,13-epoxy-12,13-dihydro-14-de(hydroxymethyl)-14-(formyloxy)-mycaminosyl Tylonolide 9,20-Bis(ethylene acetal) (13): $[\alpha]_D^{20}$ −18° (*c* 1, chloroform); UV_{max} (CH_3OH) 213 nm (ε 3,000); ^{1}H NMR ($CDCl_3$) δ=0.04 and 0.13 (each 3H, s, $SiMe_2$), 0.89 (9H, s, Si-Bu^t), 0.92 (3H, t, Me-17), 1.01 (3H, d, Me-18), 1.16 (3H, d, Me-6'), 1.47 (3H, s, Me-22), 2.06 and 2.07 (each 3H, s, Ac ×2), 2.34 (6H, s, NMe_2), 2.74 (1H, t, H-3'), 3.15 (1H, d, $J_{13,14}$=9.3 Hz, H-13), 4.41 (1H, d, H-1'), 4.77 (1H, t, H-4'), 4.91 (1H, dd, H-2'), ≈4.97 (2H, H-14,20), 5.13 (1H, dt, H-15), 5.67 (1H, d, $J_{10,11}$=16 Hz, H-10), 5.77 (1H, d, H-11), 8.14 (1H, s, OCHO).

Found: C, 59.30; H, 8.01; N, 1.76%. Calcd for $C_{45}H_{75}NO_{16}Si$: C, 59.15; H, 8.21; N, 1.53%.

(12*S*,13*S*)-2′,4′-Di-*O*-acetyl-3-*O*-(*t*-butyldimethylsilyl)-14-de(hydroxymethyl)-14-carboxy-12,13-epoxy-12,13-dihydromycaminosyl Tylonolide 9,20-Bis(ethylene acetal) (15): $[\alpha]_D^{20}$ −31° (*c* 1, chloroform); UV_{max} (CH_3OH) 213 nm (ε 4,300); ^1H NMR ($CDCl_3$) δ=0.02 and 0.13 (each 3H, s, $SiMe_2$), 0.89 (9H, s, Si-Bu^t), 0.93 (3H, t, Me-17), 1.00 (3H, d, Me-18), 1.17 (3H, d, Me-6′), 1.41 (3H, s, Me-22), 2.07 and 2.09 (each 3H, s, Ac ×2), 2.38 (6H, s, NMe_2), 2.84 (1H, t, H-3′), 3.28 (1H, d, $J_{13,14}$=9.3 Hz, H-13), 4.43 (1H, d, H-1′), 4.80 (1H, t, H-4′), ≈4.95 (2H, H-2′, 20), 5.31 (1H, m, H-15), 5.65 (1H, d, $J_{10,11}$=16 Hz, H-10), 5.79 (1H, d, H-11).

Found: C, 58.82; H, 7.96; N, 1.66%. Calcd for $C_{45}H_{75}NO_{16}Si$: C, 59.15; H, 8.21; N, 1.53%.

(12*S*,13*S*)-2′,4′-Di-*O*-acetyl-3-*O*-(*t*-butyldimethylsilyl)-12,13-epoxy-12,13-dihydro-14-de(hydroxymethyl)-14-(methoxycarbonyl)mycaminosyl Tylonolide 9,20-Bis(ethylene acetal) (16). To a solution of **15** (62 mg) in chloroform (0.6 ml) was added diazomethane in ether and the solution was kept at room temperature for 1 h. The solution showed, on TLC with toluene-ethyl acetate (2:1), a single spot at R_f 0.37 (cf. **15**: R_f 0). Evaporation gave a residue, that was subjected to column chromatography with toluene-ethyl acetate (2:1) to give a solid of **16**, 55 mg (87%). $[\alpha]_D^{20}$ −38° (*c* 1, chloroform); *m/z* 927 (M^+); ^1H NMR ($CDCl_3$) δ=0.90 (9H, s, Si-Bu^t), 1.41 (3H, s, Me-22), 2.05 and 2.07 (each 3H, s, Ac ×2), 2.37 (6H, s, NMe_2), 3.78 (3H, s, COOMe), 4.41 (1H, d, H-1′), 5.30 (1H, m, H-15), 5.62 (1H, d, H-10), 5.80 (1H, d, H-11).

Found: C, 59.37; H, 8.34; N, 1.47%. Calcd for $C_{46}H_{77}NO_{16}Si$: C, 59.52; H, 8.36; N, 1.51%.

(14*S*)-2′,4′-Di-*O*-acetyl-3-*O*-*t*-butyldimethylsilyl-14-de(hydroxymethyl)-14-hydroxymycaminosyl Tylonolide 9,20-Bis(ethylene acetal) (18). A solution of **12** (1.2 g) in methanol (24 ml) was heated at 50 °C overnight. Evaporation gave a solid, that was purified by column chromatography with chloroform-methanol-28% aqueous ammonia (30:1:0.1 → 10:1:0.1) to give a solid of **17**. A solution of the solid and acetic anhydride (0.3 ml) in acetonitrile (11 ml) was treated similarly as described for **3** to give a solid of **18**, 1.04 g (89% based on **12**), TLC: R_f 0.46 with toluene-ethyl acetate=1:1 (cf. **12**: R_f 0.68), $[\alpha]_D^{20}$ −61° (*c* 2, chloroform); ^1H NMR ($CDCl_3$) δ=0.04 and 0.15 (each 3H, s, $SiMe_2$), 0.83 (3H, d, Me-21), 0.90 (9H, s, Si-Bu^t), 0.96 (3H, t, Me-17), 1.04 (3H, d, Me-18), 1.14 (3H, d, Me-6′), 1.73 (3H, s, Me-22), 2.04 and 2.06 (each 3H, s, Ac ×2), 2.34 (6H, s, NMe_2), 2.72 (1H, t, H-3′), 4.30 (1H, dt, $J_{13,14}$=$J_{14,15}$=10 Hz, $J_{14,OH}$=4 Hz, H-14), 4.43 (1H, d, H-1′), 4.76 (1H, t, H-4′), 4.80 (1H, m, H-15), 4.90 (1H, dd, H-2′), 5.43 (1H, d, H-13), 5.68 (1H, d, H-10), 6.33 (1H, d, H-11).

Found: C, 61.05; H, 8.61; N, 1.51%. Calcd for $C_{44}H_{75}NO_{14}Si$: C, 60.76; H, 8.63; N, 1.61%.

(14*S*)-14-De(hydroxymethyl)-14-hydroxymycaminosyl Tylonolide (19). To a solution of **17** (57.8 mg) in oxolane (1 ml) was added a 1 mol dm^{-3} oxolane solution (0.22 ml) of tetrabutylammonium fluoride, and the solution was kept at room temperature overnight. Concentration gave a residue, that was extracted with chloroform. The organic solution was washed with aqueous sodium sulfate (saturated), dried (Na_2SO_4), and concentrated. To the residual syrup in acetonitrile (0.3 ml) was added 0.1 mol dm^{-3} aqueous hydrochloric acid (2.9 ml) and the solution was kept at room temperature overnight. TLC of the solution with chloroform-methanol-28% aqueous ammonia (10:1:0.1) showed a single spot at R_f 0.25 (**19**). After neutralization with excess sodium hydrogencarbonate, the reaction mixture was extracted with chloroform. The obtained product was purified by a short column with chloroform-methanol-28% aqueous ammonia (15:1:0.1) to give a solid of **19**, 35.7 mg (83%), $[\alpha]_D^{20}$ −24° (*c* 1, chloroform); ^1H NMR ($CDCl_3$) δ=0.97 (3H, t, Me-17), 1.02 (3H, d, Me-18), 1.22 (3H, d, Me-21), 1.27 (3H, d, Me-6′), 1.83 (3H, s, Me-22), 2.36 (1H, t, $J_{2',3'}$=$J_{3',4'}$=10 Hz, H-3′), 2.50 (6H, s, NMe_2), 3.06 (1H, t, H-4′), 3.48 (1H, dd, H-2′), 4.25 (1H, d, H-1′), 4.45 (1H, t, $J_{13,14}$=$J_{14,15}$=9 Hz, H-14), 4.84 (1H, dt, $J_{15,16a}$=9, $J_{15,16b}$=3 Hz, H-15), 5.83 (1H, d, H-13), 6.34 (1H, d, H-10), 7.30 (1H, d, H-11), 9.70 (1l, s, H-20).

Found: C, 60.81; H, 8.15; N, 2.62%. Calcd for $C_{30}H_{49}NO_{10}\cdot 1/2H_2O$: C, 60.81; H, 8.44; N, 2.36%.

(14*R*)-2′,4′-Di-*O*-acetyl-3-*O*-*t*-butyldimethylsilyl-14-de(hydroxymethyl)-14-(formyloxy)mycaminosyl Tylonolide 9,20-Bis(ethylene acetal) (20). To a cold (5—6 °C) solution of **18** (436 mg) and triphenylphosphine (300 mg) in benzene (4.4 ml) were added diethyl azodicarboxylate (0.17 ml) and formic acid (42 μl, distilled from 99% commercial formic acid) and the solution was stirred at room temperature for 1 h. TLC of the resulting solution with toluene-ethyl acetate (2:1) showed three spots (except for those of the reagents) at R_f 0.5 (**21**), 0.45 (major, **20**), and 0.36 (**22**). Benzene (30 ml) was added, and the solution was washed with aqueous sodium hydrogencarbonate (saturated), aqueous sodium sulfate (saturated), dried (Na_2SO_4), and concentrated. The residue was chromatographed on a column with hexane-ethyl acetate (3:1, 80 ml), and then toluene-ethyl acetate (3:1) to give solids of **21**, 57 mg (13%), **20**, 240 mg (54%; contaminated by 10% of **12**), and **22**, 87 mg (19%).

20: ^1H NMR ($CDCl_3$; the signals for **12** were not recorded) δ=0.08 and 0.11 (each 3H, s, $SiMe_2$), 0.85 (3H, d, Me-21), 0.91 (3H, t, Me-17), 0.92 (3H, d, Me-18), 0.94 (9H, s, Si-Bu^t), 1.14 (3H, d, Me-6′), 1.82 (3H, s, Me-22), 2.03 and 2.06 (each 3H, s, Ac ×2), 2.34 (6H, s, NMe_2), 2.69 (1H, t, H-3′), 4.46 (1H, d, H-1′), 4.76 (1H, t, H-4′), 4.90 (1H, dd, H-2′), 5.20 (1H, d, $J_{13,14}$=6 Hz, H-13), 5.25 (1H, ddd, H-15), 5.46 (1H, d, $J_{10,11}$=15 Hz, H-10), 5.82 (1H, dd, $J_{14,15}$=2.5 Hz, H-14), 6.15 (1H, d, H-11), 8.15 (1H, s, OCHO).

2′,4′-Di-*O*-acetyl-3-*O*-*t*-butyldimethylsilyl-14-de(hydroxymethyl)-12(22),13-dieno-12,13-dihydromycaminosyl Tylonolide 9,20-Bis(ethylene acetal) (21): $[\alpha]_D^{20}$ −59° (*c* 1, chloroform); ^1H NMR ($CDCl_3$) δ=0.14 and 0.17 (each 3H, s, $SiMe_2$), 0.84 (3H, d, Me-21), 0.94 (3H, d, Me-18), 0.95 (9H, s, Si-Bu^t). 0.96 (3H, t, Me-17), 1.14 (3H, d, Me-6′), 2.00 and 2.05 (each 3H, s, Ac ×2), 2.34 (6H, s, NMe_2), 2.69 (1H, t, H-3′), 4.45 (1H, d, H-1′), 4.75 (1H, t, H-4′), 4.91 (1H, dd, H-2′), 5.00 and 5.07 (each 1H, d, *J*≈2 Hz, H-22a, b), ≈5.05 (1H, H-15), 5.50 (1H, d, $J_{10,11}$=16 Hz, H-10), 5.57 (1H, dd, $J_{13,14}$=15.5, $J_{14,15}$=7.5 Hz, H-14), 6.30 (1H, d, H-11), 6.34 (1H, d, H-13).

Found: C, 61.99; H, 8.29; N, 1.64%. Calcd for $C_{44}H_{73}NO_{13}Si$: C, 62.04; H, 8.58; N, 1.65%.

2′,4′-Di-*O*-acetyl-3-*O*-*t*-butyldimethylsilyl-14-de(hydroxymethyl)-12-formyloxy-13-eno-12,13-dihydromycaminosyl Tylonolide 9,20-Bis(ethylene acetal) (22): $[\alpha]_D^{20}$ −50° (*c* 1, chloroform); *m/z* 897 (M^+): ^1H NMR ($CDCl_3$) δ=0.12 and 0.13 (each 3H, s, $SiMe_2$), 0.89 (3H, d, Me-21), 0.92 (3H, d, Me-18), 0.93 (9H, s, Si-Bu^t), 0.94 (3H, t, Me-17), 1.13 (3H, d, Me-6′), 1.62 (3H, s, Me-22), 2.03 and 2.04 (each 3H, s, Ac ×2), 2.33 (6H, s, NMe_2), 2.70 (1H, t, $J_{2',3'}$=$J_{3',4'}$=10 Hz, H-3′), 4.40 (1H, d, H-1′), 4.74 (1H, t, H-4′), 4.89 (1H, dd, H-2′), 4.96 (1H, t, $J_{15,16a}$=6.5, $J_{15,16b}$=0 Hz, H-15), 5.00 (1H, dd, H-20), 5.52 (1H, dd, $J_{13,14}$=16, $J_{14,15}$=6.5 Hz, H-14), 5.53 (1H, d, $J_{10,11}$=16

Hz, H-10), 5.72 (1H, d, H-13), 6.02 (1H, d, H-11), 8.05 (1H, s, OCHO).

Found: C, 60.29; H, 8.57; N, 1.32%. Calcd for $C_{45}H_{75}NO_{15}Si$: C, 60.20; H, 8.36; N, 1.56%.

(14*R*)-3-*O*-*t*-Butyldimethylsilyl-14-de(hydroxymethyl)-14-hydroxymycaminosyl Tylonolide 9,20-Bis(ethylene acetal) (23). A solution of **20** (200 mg) in methanol (2 ml) was heated at 50 °C overnight. Evaporation gave a residue, that was chromatographed on a column with chloroform–methanol–28% aqueous ammonia (30 : 1 : 0.1 → 20 : 1 : 0.1) to give a solid of **23**, 163 mg (92%), $[\alpha]_D^{20}$ −76° (*c* 1, chloroform); ^{1}H NMR ($CDCl_3$) δ=0.09 and 0.11 (each 3H, s, $SiMe_2$), 0.91 (9H, s, Si-Bu^t), 1.78 (3H, s, Me-22), 2.50 (6H, s, NMe_2), 3.55 (1H, dd, $J_{1',2'}$=7.5, $J_{2',3'}$=10 Hz, H-2'), 4.34 (1H, d, H-1'), 5.12 (1H, ddd, $J_{14,15}$=2, $J_{15,16a}$=6, $J_{15,16b}$=8.5 Hz, H-15), 5.31 (1H, d, $J_{13,14}$=6 Hz, H-13), 5.41 (1H, d, $J_{10,11}$=16 Hz, H-10), 6.18 (1H, d, H-11).

Found: C, 61.30; H, 9.17; N, 1.82%. Calcd for $C_{40}H_{71}NO_{12}Si$: C, 61.15; H, 9.04; N, 1.78%.

3-*O*-*t*-Butyldimethylsilyl-14-de(hydroxymethyl)-12(22),13-dieno-12,13-dihydromycaminosyl Tylonolide 9,20-Bis(ethylene acetal) (24). Compound **21** (58 mg) was treated similarly as described for **23** to give a solid of **24**, 40 mg (76%), $[\alpha]_D^{20}$ −64° (*c* 1, chloroform); *m/z*767 (M^+); ^{1}H NMR (C_6D_6) δ=0.10 and 0.24 (each 3H, s, $SiMe_2$), 0.80 (3H, t, Me-17), 1.03 (9H, s, Si-Bu^t), 2.32 (6H, s, NMe_2), 4.53 (1H, d, H-1'), 4.91 (1H, d, $J_{22a,22b}$=2 Hz, H-22a), 5.02 (1H, t, $J_{14,15}$=$J_{15,16a}$=7.5, $J_{15,16b}$=0 Hz, H-15), 5.04 (1H, d, H-22b), 5.30 (1H, dd, H-20), 5.58 (1H, dd, $J_{13,14}$=15 Hz, H-14), 5.99 (1H, d, $J_{10,11}$=16 Hz, H-10), 6.52 (1H, d, H-13), 6.56 (1H, d, H-11).

Found: C, 62.57; H, 8.80; N, 1.95%. Calcd for $C_{40}H_{69}NO_{11}Si$: C, 62.58; H, 9.00; N, 1.83%.

(14*R*)-2',4'-Di-*O*-acetyl-3-*O*-*t*-butyldimethylsilyl-14-de(hydroxymethyl)-14-hydroxymycaminosyl Tylonolide 9,20-Bis(ethylene acetal) (25). Compound **23** (190 mg) was treated with acetic anhydride (54 μl) in acetonitrile (2 ml) in a manner as described for **3** to give a solid of **25**, 193 mg (92%), $[\alpha]_D^{20}$ −63° (*c* 1, chloroform); ^{1}H NMR ($CDCl_3$) δ=0.09 and 0.11 (each 3H, s, $SiMe_2$), 0.94 (9H, s, Si-Bu^t), 1.76 (3H, s, Me-22), 2.04 and 2.06 (each 3H, s, Ac ×2), 2.35 (6H, s, NMe_2), 2.68 (1H, t, H-3'), 4.46 (1H, d, H-1'), 4.54 (1H, dt, $J_{13,14}$=6, $J_{14,15}$=2, $J_{14,OH}$=6 Hz, H-14), 4.75 (1H, t, H-4'), 4.90 (1H, dd, H-2'), 5.12 (1H, dq, $J_{15,16a}$=6, $J_{15,16b}$=6 Hz, H-15), 5.30 (1H, d, H-13), 5.42 (1H, d, H-10), 6.17 (1H, d, H-11).

Found: C, 60.50; H, 8.46; N, 1.77%. Calcd for $C_{44}H_{75}NO_{14}Si$: C, 60.76; H, 8.63; N, 1.61%.

(14*R*)-14-Acetoxy-2',4'-di-*O*-acetyl-3-*O*-*t*-butyldimethylsilyl-14-de(hydroxymethyl)mycaminosyl Tylonolide 9,20-Bis(ethylene acetal) (26). To a cold (5 °C) solution of **18** (100 mg) and triphenylphosphine (70 mg) in benzene (1 ml) were added diethyl azodicarboxylate (41 μl) and acetic acid (16 μl) and the solution was stirred at room temperature for 1 h. TLC of the resulting solution with toluene–ethyl acetate (2 : 1) showed three spots at R_f 0.52 (**21**), 0.44 (**26**), and 0.34 (**27**). Work-up as described for **20** gave **26**, 72 mg (65%), $[\alpha]_D^{23}$ −38° (*c* 1, chloroform); ^{1}H NMR ($CDCl_3$) δ=0.96 (9H, s, Si-Bu^t), 1.83 (3H, s, Me-22), 2.05 and 2.06 (each 3H, s, Ac ×2), 2.15 (3H, s, AcO-14), 2.35 (6H, s, NMe_2), 4.50 (1H, d, H-1'), 4.80 (1H, t, H-4'), 4.93 (1H, dd, H-2'), 5.23 (1H, d, $J_{13,14}$=6 Hz, H-13), 5.26 (1H, dq, $J_{14,15}$=2.5, $J_{15,16a}$=6, $J_{15,16b}$=9 Hz, H-15), 5.48 (1H, d, H-10), 5.75 (1H, dd, H-14), 6.26 (1H, d, H-11).

Found: C, 60.84; H, 8.36; N, 1.33%. Calcd for $C_{46}H_{77}NO_{15}Si$: C, 60.59; H, 8.45; N, 1.54%.

(14*R*)-14-Acetoxy-14-de(hydroxymethyl)mycaminosyl Tylonolide (28). A solution of **26** (61 mg) in methanol (1 ml) was heated at 37 °C overnight. Evaporation gave a residue, that was chromatographed on a column with chloroform–methanol–28% aqueous ammonia (30 : 1 : 0.1) to give a solid. A solution of the solid and a 1 mol dm^{-3} oxolane solution (0.2 ml) of tetrabutylammonium fluoride in oxolane (1 ml) was kept at room temperature for 3 h. Usual work-up gave a syrup, that was dissolved in acetonitrile (0.25 ml). After addition of 0.1 mol dm^{-3} hydrochloric acid (1 ml), the solution was kept at room temperature for 6 h. After usual work-up, the syrup obtained was chromatographed on a column with chloroform–methanol–28% aqueous ammonia (25 : 1 : 0.1) to give a solid of **28**, 23 mg (41%). $[\alpha]_D^{20}$ −64° (*c* 1, chloroform); ^{1}H NMR ($CDCl_3$) δ=0.92 (3H, t, Me-17), 1.05 (3H, d, Me-18), 1.21 (3H, d, Me-21), 1.26 (3H, d, Me-6'), 1.93 (3H, s, Me-22), 2.16 (3H, s, AcO-14), 2.35 (1H, t, H-3'), 2.50 (6H, s, NMe_2), 3.06 (1H, t, H-4'), 3.51 (1H, dd, H-2'), 4.26 (1H, d, H-1'), 5.21 (1H, dq, $J_{14,15}$=2.5, $J_{15,16a}$=6, $J_{15,16b}$=9 Hz, H-15), 5.67 (1H, dd, $J_{13,14}$=6.5 Hz, H-14), 5.75 (1H, d, H-13), 6.34 (1H, d, $J_{10,11}$=16 Hz, H-10), 7.16 (1H, d, H-11), 9.71 (1H, s, H-20).

Found: C, 61.19; H, 8.11; N, 2.36%. Calcd for $C_{32}H_{51}NO_{11}$: C, 61.44; H, 8.16; N, 2.24%.

(14*R*)-14-De(hydroxymethyl)-14-hydroxymycaminosyl Tylonolide (29). A solution of **28** (167 mg) in 28% aqueous ammonia–methanol (1 : 10, 3 ml) was kept at room temperature for 4 h. TLC (chloroform–methanol–28% aqueous ammonia 10 : 1 : 0.1) of the solution showed spots at R_f 0.28 (**28**), R_f 0.25 (**29**) and R_f 0. Evaporation gave a residue, that was chromatographed on a column with chloroform–methanol–28% aqueous ammonia (15 : 1 : 0.1) to give solids of **29**, 49 mg (38%) and **28** recovered (30 mg). $[\alpha]_D^{20}$ −21° (*c* 1, chloroform); ^{1}H NMR ($CDCl_3$) δ=0.99 (3H, t, Me-17), 1.04 (3H, d, Me-18), 1.21 (3H, d, Me-21), 1.28 (3H, d, Me-6'), 1.98 (3H, s, Me-22), 2.36 (1H, t, H-3'), 2.52 (6H, s, NMe_2), 3.06 (1H, t, H-4'), 3.50 (1H, dd, H-2'), 4.28 (1H, d, H-1'), 4.63 (1H, dt, $J_{13,14}$=6, $J_{14,15}$=$J_{14,OH}$=2.5 Hz, H-14), 5.10 (1H, ddd, $J_{15,16a}$=6, $J_{15,16b}$=8.5 Hz, H-15), 5.80 (1H, d, H-13), 6.35 (1H, d, $J_{10,11}$=16 Hz, H-10), 7.18 (1H, d, H-11), 9.72 (1H, s, H-20).

Found: C, 60.52; H, 8.23; N, 2.17%. Calcd for $C_{30}H_{49}NO_{10}\cdot 1/2H_2O$: C, 60.81; H, 8.44; N, 2.36%.

Antibacterial Activity of 19, 29, and MT (MIC, μg/ml). *Staphylococcus aureus* 209 P: 0.78 (**19**), 6.25 (**29**), 0.78 (MT); *Staphylococcus aureus* Smith: 0.78, 6.25, 0.78; *Bacillus subtilis* NRRL B-558: 3.12, 25, 3.12; *Escherichia coli* NIHJ: 3.12, 25, 6.25; *Klebsiella pneumoniae* PCI 602: 1.56, 6.25, 3.12; *Shigella dysenteriae* JS 11910: 0.39, 1.56, 0.78; *Serratia marcescens*: 12.5, 100, 25; *Pseudomonas aeruginosa* A3: 6.25, 50, 12.5.

We are grateful to Dr. Masa Hamada of Institute of Microbial chemistry for bioassay, to Mr. Saburo Nakada of Keio University for elemental analysis, and to Miss Yoshiko Koyama and Miss Sawa Shirai of our Institute for measurements of the ^{1}H NMR spectra and preparation of the manuscript, respectively.

References

1) A. Tanaka, T. Tsuchiya, S. Umezawa, M. Hamada, and H. Umezawa, *J. Antibiot.*, **34**, 1377 (1981).

2) A. Tanaka, T. Tsuchiya, Y. Okada, S. Umezawa, M. Hamada, and H. Umezawa, *J. Antibiot.*, **35**, 113 (1982).
3) S. Sakamoto, T. Tsuchiya, A. Tanaka, S. Umezawa, M. Hamada, and H. Umezawa, *J. Antibiot.*, **37**, 1628 (1984).
4) S. Sakamoto, T. Tsuchiya, A. Tanaka, S. Umezawa, M. Hamada, and H. Umezawa, *J. Antibiot.*, **38**, 477 (1985).
5) T. Tsuchiya, S. Sakamoto, N. Kajikawa, S. Umezawa, M. Hamada, and H. Umezawa, *J. Antibiot.*, **39**, 1021 (1986).
6) N. Kajikawa, T. Tsuchiya, S. Umezawa, and H. Umezawa, *J. Antibiot.*, **40**, 476 (1987).
7) A. Tanaka, A. Watanabe, R. Kobayashi, T. Tsuchiya, and S. Umezawa, *Bull. Chem. Soc. Jpn.*, **54**, 3837 (1981).
8) A. Tanaka, T. Tsuchiya, S. Umezawa, and H. Umezawa, *J. Antibiot.*, **34**, 1374 (1981).
9) S. Sakamoto, N. Kajikawa, T. Tsuchiya, and S. Umezawa, *Bull. Chem. Soc. Jpn.*, **60**, 355 (1987).
10) A. Nakagawa, K. Suzuki, K. Iwasaki, K. Kaji, S. Ōmura, A. Jakubowski, and M. Tishler, *Chem. Pharm. Bull.*, **24**, 1749 (1976).
11) S. Sakamoto, T. Tsuchiya, T. Miyake, A. Tanaka, and S. Umezawa, *Bull. Chem. Soc. Jpn.*, **57**, 3536 (1984).
12) A. I. Scott, Interpretation of the Ultraviolet Spectra of Natural Products, Pergamon Press, New York (1964).
13) A. K. Ganguly, Y-T. Liu, O. Sarre, R. S. Jaret, A. T. McPhail, and K. K. Onan, *Tetrahedron Lett.* **21**, 4699 (1980).
14) R. W. Vaughan, J. Lotvin, M. S. Puar, M. Patel, A. Kershner, M. G. Kalyanpur, J. Marquez, and J. A. Waitz, *J. Antibiot.*, **35**, 251 (1982).
15) O. Mitsunobu, *Synthesis*, **1981**, 1 (1981); related references are cited therein.
16) S. Sakamoto, T. Tsuchiya, S. Umezawa, and H. Umezawa, under preparation.
17) T. Tsuchiya, *Jap. J. Antibiot.* **32** (Suppl.), S-129 (1979).

 © 1987 The Chemical Society of Japan Bull. Chem. Soc. Jpn., 60, 1489—1495 (1987)

Cycloaddition of Pyridinium Methylides with Electron-Deficient Olefins and Silica-Gel Mediated Elimination of Pyridines from the Cycloadducts: A New Method of Alkylation or Hydroalkylidenation of Olefins

Otohiko TSUGE,* Shuji KANEMASA, and Shigeori TAKENAKA
Research Institute of Industrial Science, and Department of Molecular Science and Technology, Interdisciplinary Graduate School of Engineering Sciences, Kyushu University, Kasugakoen, Kasuga 816
(Received October 28, 1986)

Pyridinium methylides bearing an anion-stabilizing substituent at the ylide carbon react with a variety of olefins carrying two electron-withdrawing groups at the both carbons such as *N*-substituted maleimides, a citraconimide, dimethyl maleate, dimethyl fumarate, and 1,2-dibenzoylethene. The cycloadducts thus formed undergo a ready elimination of pyridines when treated with silica gel. This sequence is a new method for alkylation or hydroalkylidenation of olefins.

Heteroaromatic nitrogen ylides are readily accessible by the general procedure of *N*-alkylation of nitrogen-containing aromatic heterocycles and subsequent deprotonation with a base.[1] These ylides show high reactivity to a wide variety of olefins which are activated by electron-withdrawing substituents.[2] As a result, a fused pyrrolidine ring is added to the heterocycles and this cycloaddition reaction takes place in a highly stereo-, regioselective, and stereospecific manner.[2]

In the cycloaddition step, heteroaromatic ring of the ylides loses its aromaticity. Accordingly, the cycloadducts produced are often rather labile so as to undergo either a thermal retro cycloaddition going back to the ylides and olefins or a carbon-carbon bond cleavage into betaines.[2a,b] These reversible processes become visible only when they are accompanied by some further conversions leading to thermodynamically more stable compounds. A novel fragmentation reaction of the cycloadducts of pyridinium methylides via such betaine intermediates has been recently demonstrated.[3,4]

The present paper describes silica-gel mediated elimination reaction of pyridines from the olefin cycloadducts of pyridinium methylides. Part of the present results was previously reported as a preliminary communication.[4]

Results and Discussion

Pyridinium methylides bearing an anion-stabilizing group W such as benzoyl, 2-furoyl, acetyl, methoxy- and ethoxycarbonyl, cyano, or *p*-nitrophenyl moiety are easily generated in situ by treatment of the corresponding 1-alkylpyridinium halides with such a weak base as triethylamine. If a maleimide as a reactive olefinic dipolarophile is present, the pyridinium methylides are captured by the maleimide as soon as they are generated to give stereoselective cycloadducts **1**—**9** all in quantitative yields (Scheme 1).[2a]

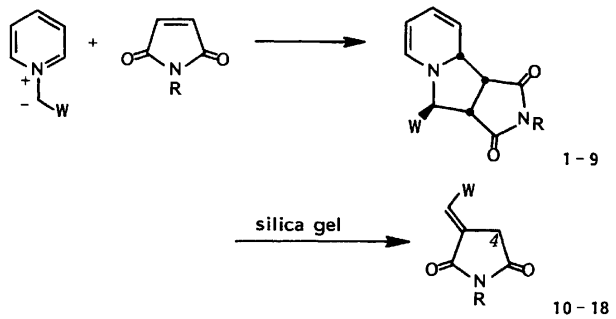

1, 10: W=COPh, R=Me
2, 11: W=COPh, R=Ph
3, 12: W=COPh, R=p-tolyl
4, 13: W=2-furoyl, R=p-tolyl
5, 14: W=COMe, R=p-tolyl
6, 15: W=COOMe, R=p-tolyl
7, 16: W=COOEt, R=p-tolyl
8, 17: W=CN, R=p-tolyl
9, 18: W=p-$NO_2C_6H_4$, R=p-tolyl

Scheme 1.

These cycloadducts have quite different stability in an aprotic and a protic solvent. At room temperature in dry aprotic solvents such as benzene, toluene, dichloromethane, chloroform, tetrahydrofuran, and dimethyl sulfoxide, they stay stable. When warmed at 50—60 °C, they started to decompose slowly and changed into a mixture of complex and unidentified products after a long heating.[5] On the other hand, when heated under reflux in ethanol or treated with a catalytic amount of acetic acid in chloroform at room temperature, **1** underwent a clean decomposition leading to **10**. Use of strong acids such as hydrogen chloride, *p*-toluenesulfonic acid, trifluoroacetic acid, and titanium(IV) chloride, however, led to complex mixture of products. The most effective method of all employed so far is to treat the crude cycloadduct of **1** with silica gel in a glass column.

The procedure is very simple as shown below: A mixture of 1-phenacylpyridinium bromide and *N*-methylmaleimide in chloroform was treated with triethylamine (each 1 equivalent). After 10 min at room temperature, the mixture was poured into ice water and extracted in dichloromethane. The crude cycloadduct **1** thus obtained was charged in a silica-gel

Table 1. Cycloaddition of Pyridinium Methylides to Maleimides and Subsequent Elimination of Pyridines Leading to Itaconimides **10—18**

Ylide $Py^+-\bar{C}H_2-W$ W	Maleimide $(=CHCO)_2NR$ R	Reaction conditions: Cycloaddition[c]	Reaction conditions: Elimination[d]	Cycloadduct[a]	yield/%	Itaconimide[b]	yield/%
COPh	Me	rt, 10 min, CF	S	**1**	100	**10**	86
COPh	Ph	rt, 10 min, CF	S	**2**	100	**11**	85
COPh	*p*-Tolyl	rt, 10 min, DCM	S	**3**	100	**12**	82
2-Furoyl	*p*-Tolyl	rt, 10 min, CF	S	**4**	100	**13**	32
COMe	*p*-Tolyl	rt, 1 h, CF	S	**5**	93	**14**	46
COOMe	*p*-Tolyl	rt, 10 min, CF	S	**6**	100	**15**	87
COOEt	*p*-Tolyl	rt, 10 min, CF	S	**7**	100	**16**	72
CN	*p*-Tolyl	rt, 20 min, CF	S	**8**	87	**17**	51
p-$NO_2C_6H_4$	*p*-Tolyl	rt, 12 h, DMSO	S	**9**	100	**18**	59
		rt, 12 h, DMSO	A	**9**	100	**18**	52
3,5-Dimethylpyridinium phenacylide	*p*-Tolyl	rt, 10 min, DCM	S	**19**	100	**12**	100

a) These cycloadducts were isolated when crude mixture from the cycloaddition was washed with water and then the dried solvent was evaporated in vacuo. b) These products were obtained when the crude cycloaddition product was subjected to a silica-gel chromatography or treated with acetic acid. The yields are all based on maleimides. c) CF: chloroform; DCM: dichloromethane; DMSO: dimethyl sulfoxide. d) S: silica-gel chromatography; A: treatment with acetic acid.

column and then eluted with chloroform to give a single product **10** in 86% yield.

The product **10** was assigned as (*E*)-3-benzoylmethylene-1-methyl-2,5-pyrrolidinedione on the basis of spectral data as well as elemental analysis. The E-geometry of olefin part of **10** was based on low chemical shifts of both the 4-methylene hydrogens (3.76 ppm) and the olefinic hydrogen (7.94 ppm), compared with those (4-H: 3.47 ppm; $=CH_2$: 5.70 and 6.43 ppm) of 3-methylene-1-(*p*-tolyl)-2,5-pyrrolidinedione (*N*-(*p*-tolyl)itaconimide).[3a]

The other cycloadducts **2—9** underwent similar silica gel-mediated elimination of pyridine to afford derivatives of itaconimides **11—18** (Scheme 1 and Table 1).

Scheme 2 illustrates a possible mechanism: The cycloadduct **3** as an example undergoes a reversible cleavage at the 9a,9b-bond into betaine intermediate **A**. This transformation is driven by the recovery of aromaticity. A 1,2-proton migration into **B** is followed by the β-elimination of pyridine to give itaconimide **12**.

The exclusive formation of (*E*)-itaconimide **12** was previously explained by a stereoselective elimination route from the sterically defined cycloadduct **3**.[4] However, this mechanism should be now renewed on the basis of the following observations: 1) 3-Methylene-1-(*p*-tolyl)pyrrolidine-2,5-dione (*N*-(*p*-tolyl)-itaconimide) readily isomerizes into 3-methyl-1-(*p*-tolyl)-3-pyrroline-2,5-dione (*N*-(*p*-tolyl)citraconimide) on treatment with triethylamine;[3a] 2) 4-Methyl derivative of **12** (or **12'**) is so unstable that it is isolated in a structure of 3,4-disubstituted 3-pyrroline-2,5-dione (see compound **39** in Scheme 5); 3) No isomerization occurs on treatment of **12** with butyllithium in THF.[6] Thus, the selective formation of (*E*)-itaconimide **12** has presumably resulted from the thermodynamic stability of

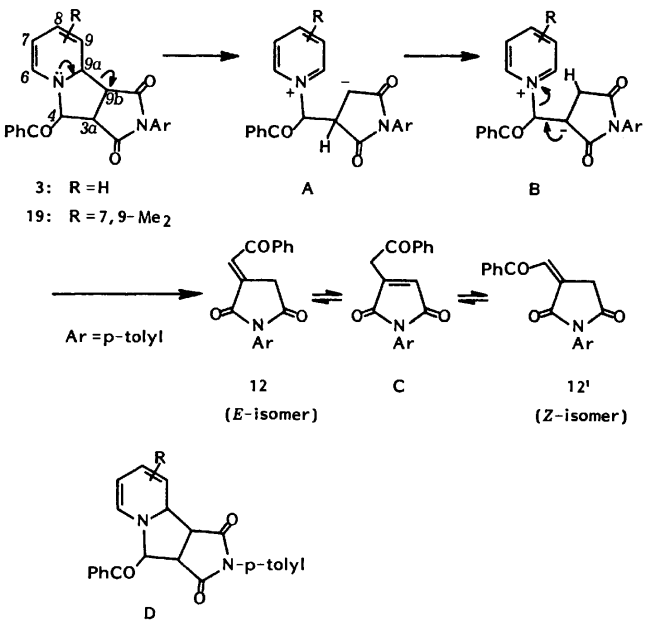

Scheme 2.

12 over either of its *Z*-isomer **12'** or citraconimide **C** (Scheme 2).[7]

Electron-donating substituents on the pyridine nucleus of cycloadducts were found to facilitate the elimination reaction of pyridines. For example, cycloadduct **19** bearing two methyls at the 7- and 9-positions underwent a quick elimination leading to **12** when chromatographed over silica gel.[8] However, cycloadducts **D** bearing an electron-withdrawing substituent (R is 8-CN, 7- or 9-CF_3, and 7- or 9-COOMe) were recovered unchanged under similar conditions. Presumably, the reversible 9a,9b-bond cleavage into betaine **A** was facilitated by the electron-donating substituents (Scheme 2).

Table 2. Reaction of Pyridinium Methylides with Acyclic Olefinic Dipolarophiles Leading to **20**—**23**[a)]

Pyridinium methylide $Py^{+}-\bar{C}H_2-W$ W	Olefin	Reaction conditions	Product	Yield/%[b)]
COPh	PhCOCH=CHCOPh (*Z*)	rt, 10 min, DCM	**20**	61
	PhCOCH=CHCOPh (*E*)	rt, 20 min, DCM		100
COOMe	PhCOCH=CHCOPh (*E*)	rt, 1 h, CF	**21**	62
CN	PhCOCH=CHCOPh (*E*)	rt, 1 h, CF	**22**	38
	MeOOCCH=CHCOOMe (*Z*)	reflux, 3 h, CF	**23**	50
	MeOOCCH=CHCOOMe (*E*)	reflux, 22 h, CF		65

a) After the cycloaddition was over, the crude reaction mixture was chromatographed over silica gel by using chloroform or benzene as an eluent. b) All isolated yields based on the olefin.

Reactions of pyridinium methylides with acyclic olefins such as (*E*)- and (*Z*)-1,2-dibenzoylethene and dimethyl fumarate and maleate formed unstable cycloadducts **E** which could not be isolated in pure forms. During the usual work-up or chromatographic operation on silica gel, the cycloadducts **E** eliminated pyridine to give olefins **20**—**23** (Scheme 3 and Table 2).

These products **20**—**22** were not single isomers but mixtures of several isomers and/or tautomers. As **20**—**22** belong to allyl systems bearing strongly electron-withdrawing substituents at every carbon, the stable structure of **20**—**22** depends upon the polarity of solvent in which they are dissolved. For example, **20** mainly takes propene structures (mixture of *E*- and *Z*-isomers) in chloroform, while 1,3-butadien-1-ol structure as an enol form is a major contributor in dimethyl sulfoxide. When electron-withdrawing property of the substituents is decreased, isomeric purity is increased as seen in the case of **23** which exclusively exists in one isomer form of propene structure, dimethyl 3-cyanopropene-1,2-dicarboxylate, in its chloroform solution.

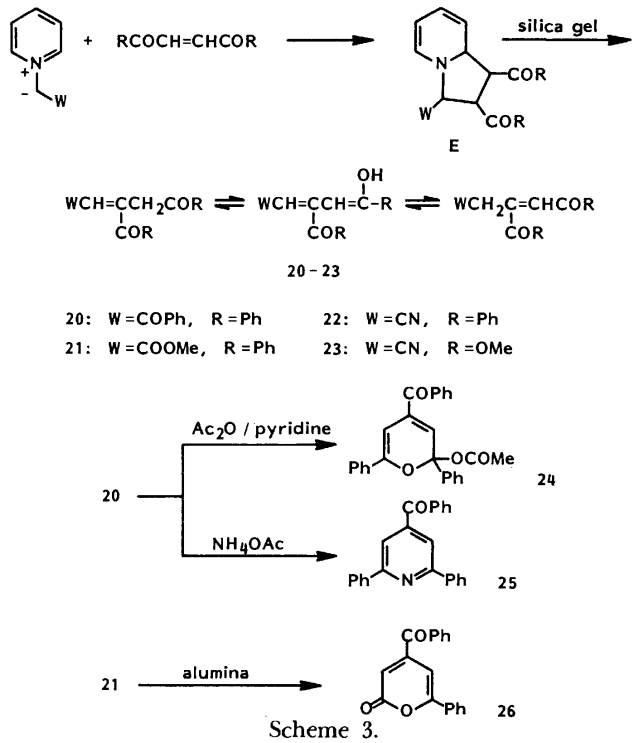

Scheme 3.

Treatment of **20** with acetic anhydride in the presence of a catalytic amount of pyridine gave 2-acetoxy-4-benzoyl-2,6-diphenyl-2*H*-pyran (**24**) (Scheme 3). With ammonium acetate at room temperature, 4-benzoyl-2,6-diphenylpyridine (**25**) was obtained. The latter pyridine formation foregone by the ylide cycloaddition and the pyridine elimination presumably corresponds to a sequence of reactions which are involved in the pyridine synthesis discovered by Kröhnke.[9] The ester group of **21** participated in a lactonization leading to 4-benzoyl-6-phenyl-2*H*-pyran-2-one (**26**) on its chromatography on alumina.

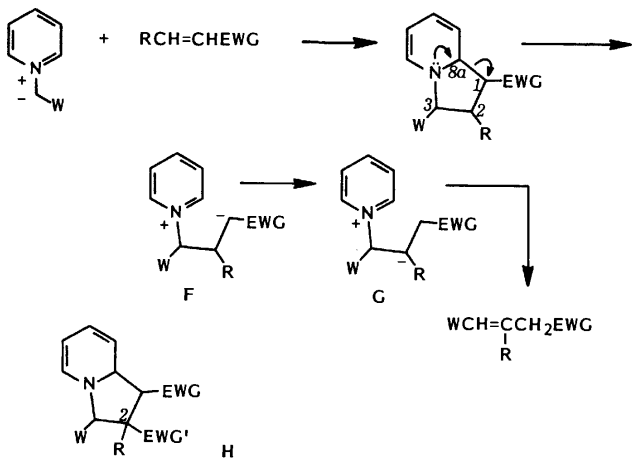

Scheme 4.

Since only olefins activated by electron-withdrawing moiety (EWG) can be successfully employed in the cycloaddition with pyridinium methylides, the cycloadducts carry an EWG at the 1-position (Scheme 4). Accordingly, every cycloadduct has a chance to undergo the 1,9a-bond cleavage leading to betaine **F**. When R is an anion-stabilizing moiety, 1,2-proton migration of **F** occurs to form another betaine **G** which is an inevitable intermediate in the pyridine elimination reaction. This means that the cycloaddition and pyridine elimination sequence can be performed only by use of the olefins in which the both olefinic carbons are attached by electron-withdrawing substituents. If

Table 3. Cycloaddition of Pyridinium Methylides to *N*-(*p*-Tolyl)citraconimide and Subsequent Elimination of Pyridines Leading to **39—42**

Pyridinium methylides W	R	Reaction conditions[a]	Cycloadduct	yield/%	Product[b]	Yield/%[c]
COPh	H	rt, 11 h, DCM	**27**	100	**39**	82
COPh	3,5-diMe	rt, 2 h, DCM	**28**	100	**39**	80
COMe	H	rt, 13 h, CF	**29**	94	**40**	37
COOEt	H	rt, 3 d, CF	**30**	d)	**41**	51
CN	H	rt, 24 h, CF	**31**+**35** (1:2)	100		
CN	2-Me	rt, 3 h, CF	**32**+**36** (1:3)	100		
CN	4-Me	rt, 5 h, CF	**33**+**37** (1:3)	100		
CN	3,5-diMe	rt, 19 h, CF	**34**+**38** (1:3)	100	**42**	20 (79)[e]

a) CF: chloroform; DCM: dichloromethane. b) Obtained after the crude cycloadduct was chromatographed over silica gel by using chloroform as an eluent. c) All isolated yields based on the citraconimide. d) Not isolated. e) Based on **34**.

the 2-position of cycloadduct is occupied by two substituents EWG′ and R as shown in **H**, such elimination should become impossible.

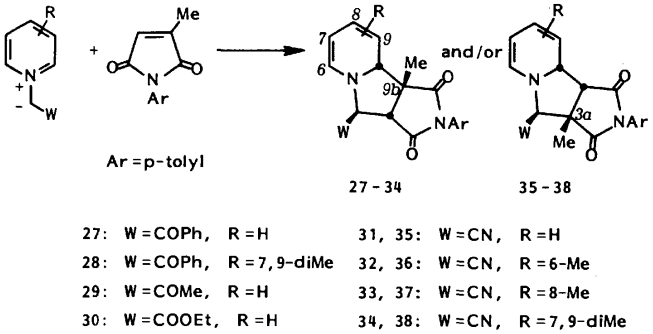

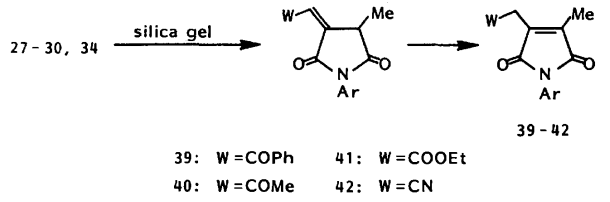

Scheme 5.

N-(*p*-Tolyl)citraconimide was allowed to react with a variety of pyridinium methylides (Scheme 5). When W is a bulky electron-withdrawing substituent such as benzoyl, acetyl, or methoxycarbonyl, single isomers of cycloadducts **27—30** were only produced. They were assigned as endo cycloadducts to the anti form of ylides with the methyl moiety at the 9b-position.[2b] On the other hand, when W is sterically small in size (W is CN), mixtures of two regioisomeric cycloadducts **31—34**+**35—38** were formed. Major regioisomers **35—38** carry the methyl moiety at the 3a-exo position.

The regioisomers with 9b-methyl were found to undergo a similar pyridine elimination when treated with silica gel. Thus, **27—30** and **34** were passed through a silica-gel column to give 3-methyl-4-(substituted methyl)-1-(*p*-tolyl)-3-pyrroline-2,5-diones **34—42**, respectively (Scheme 5 and Table 3). Exclusive isolation of **39—42** was presumably due to the ready isomerization of the intermediary 3-alkylidenepyrrolidine-2,5-diones under the reaction or work-up conditions.

As expected, such pyridine elimination reaction did not occur on the other regioisomers **35—38** bearing 3a-methyl. Instead, they decomposed into complex mixture of unidentified products when treated with silica gel. This instability was surprising. It is probable that cycloadducts **35—38** have taken an unassigned decomposition route via the corresponding betaine intermediates.

Experimental

General. Melting points were determined on a Yanagimoto melting point apparatus and are uncorrected. IR spectra were taken with a JASCO IRA-1 or a JASCO A-702 spectrometer. ^{1}H NMR spectra were recorded on a Hitachi R-40 (90 MHz) or a JEOL FX-100 instrument (100 MHz) and ^{13}C NMR on a JEOL FX-100 spectrometer at 25.05 MHz. Chemical shifts are expressed in parts per million downfield from tetramethylsilane as an internal standard. Mass spectra were measured with a JEOL-01SG-2 spectrometer at 70 eV of ionization energy. GC-Mass spectra as well as high-resolution mass spectra were also obtained on the same instrument. Elemental analyses were performed on a Hitachi 026 CHN analyzer. Thin-layer chromatography (TLC) was accomplished on 0.2 mm precoated plates of silica gel 60 F-254 (Merck) or of aluminum oxide 60 F-254 type-E (Merck). Visualization was made with ultraviolet light (254 and 365 nm), iodine, molybdophosphoric acid (5% in ethanol), or *p*-anisaldehyde (5% in ethanol containing 5% of sulfuric acid). For preparative column chromatography, Wakogel C-200, C-300 (Wako), and Silicagel 60 (Merck) were employed. Flash chromatography was carried out on an EYELA EF-10 apparatus using a column (20×180 mm) packed with Silicagel 60 (Merck, size: 0.04—0.063 mm). Preparative high-performance liquid chromatography (HPLC) was performed on a Kusano KHLC-201 apparatus with a UV-detector Uvilog-III using a column (22×300 mm)

packed with silica gel (Wakogel LC-50H). Gas liquid chromatography (GLC) was accomplished on a Yanaco G-2800 gas chromatograph (Yanagimoto) with an ionization flame detector using a glass column (SE-30, 3×2000 mm) or a glass capillary column (Silicone GE, SE-30, 0.25×5000 mm). Micro vacuum distillation was carried out on a Sibata GTO-250R Kugelrohr distilling apparatus. Solvents were evaporated with a Tokyo Rikakikai rotary evaporator type-V at about 50 °C unless otherwise stated.

General Procedure for the Silica-Gel Mediated Pyridine Elimination from the Cycloadducts 1—9 and 19 Leading to 10—18. The reactions of pyridinium methylides with maleimides were carried out under the conditions previously reported[2a] giving quantitative yields of 1 : 1 cycloadducts **1**—**9** and **19**. The pyridine elimination was performed according to the following two methods: 1) The crude cycloadducts **1**—**9** were chromatographed over silica gel (Wako C-300) by using chloroform as an eluent to furnish the pyridine-eliminated products **10**—**18**. 2) The crude cycloadduct **9** was stirred in chloroform (20 ml/1 mmol) at room temperature for 24 h in the presence of a catalytic amount of acetic acid. The mixture was washed with water several times and then dried over anhydrous magnesium sulfate. The chloroform was evaporated in vacuo to give solid which was washed with a small amount of diethyl ether to afford **18** (52%). The results are summarized in Table 1.

10: Colorless needles (diethyl ether-petr. ether); mp 144 °C; IR (KBr) 1760, 1690, and 1650 cm^{-1}; ^1H NMR ($CDCl_3$) δ=3.13 (3H, s, NMe), 3.76 (2H, d, J=3.0 Hz, 4-H), 7.3—7.7 (3H, m, Ph), 7.83 (1H, t, J=3.0 Hz, =CH-), and 7.9—8.1 (2H, m, Ph); ^{13}C NMR ($CDCl_3$) δ=24.95 (q, NMe), 34.65 (t, 4-C), 122.75 (d, =CH-), 128.45, 128.89, 133.86 (each d), 136.17, 139.76 (s, 3-C), 169.72, 174.01 (each s, 2- and 5-C), and 189.41 (s, CO); MS m/z (rel intensity, %) 229 (M^+, 45), 144 (18), 105 (base peak), 77 (69), and 51 (25). Found: C, 67.92; H, 4.80; N, 6.14%. Calcd for $C_{13}H_{11}NO_3$: C, 68.11; H, 4.84; N, 6.11%.

11: Pale yellow needles (cyclohexane); mp 176 °C; IR (KBr) 1770, 1700, and 1660 cm^{-1}; ^1H NMR ($CDCl_3$) δ=3.93 (2H, d, J=3.0 Hz, 4-H), 7.2—7.6 (6H, m, ph), 7.37 (1H, t, J=3.0 Hz, =CH-), and 7.9—8.1 (4H, m, Ph); ^{13}C NMR ($CDCl_3$) δ=34.94 (t, 4-C), 124.13 (d, =CH-), 126.48, 128.54, 128.77, 129.01, 129.19, 129.36, 134.25 (each d), 137.42, 139.60 (each s), 172.07, 173.25 (each s, 2- and 5-C), and 189.83 (s, CO); MS m/z (rel intensity, %) 291 (M^+, 5), 105 (74), 91 (15), 77 (base peak), 67 (20), and 51 (41). Found: C, 74.04; H, 4.58; N, 4.97%. Calcd for $C_{18}H_{13}NO_3$: C, 74.21; H, 4.50; N, 4.81%.

12: Pale yellow prisms (cyclohexane); mp 180—181 °C; IR (KBr) 1770, 1700, 1660, and 1620 cm^{-1}; ^1H NMR ($CDCl_3$) δ=2.38 (3H, s, p-Me), 3.92 (2H, d, J=2.8 Hz, 4-H), 7.0—7.4 (4H, m, Ar), 7.4—7.7 (3H, m, Ph), 7.8—8.1 (2H, m, Ph), and 7.94 (1H, t, J=2.8 Hz, =CH-); ^{13}C NMR ($CDCl_3$) δ=21.19 (q, p-Me), 34.87 (t, 4-C), 123.70 (d, =CH-), 125.99, 128.51, 128.93, 129.75, 133.98 (each d), 137.20, 138.85, 139.50 (each s), 168.79, 173.08 (each s, 2-and 5-C), and 189.52 (s, CO); MS m/z (rel intensity, %) 305 (M^+, 58), 199 (31), 105 (base peak), and 76 (43). Found: C, 74.55; H, 5.05; N, 4.77%. Calcd for $C_{19}H_{15}NO_3$: C, 74.74; H, 4.95; N, 4.59%.

13: Colorless needles (diethyl ether-petr. ether); mp 172 °C; IR (KBr) 1780, 1710, and 1670 cm^{-1}; ^1H NMR ($CDCl_3$) δ=2.37 (3H, s, p-Me), 3.93 (2H, d, J=3.0 Hz, 4-H), 6.58 (1H, dd, J=4.0 and 1.8 Hz, 4-H of furyl), 7.20 (4H, br s, Ar), 7.34 (1H, dd, J=4.0 and 1.0 Hz, 5-H of furyl), 7.62 (1H, dd, J=1.8 and 1.0 Hz, 3-H of furyl), and 7.72 (1H, t, J=3.0 Hz, =CH-); MS m/z (rel intensity, %) 295 (M^+, 43), 189 (17), and 89 (base peak). Found: C, 69.14; H, 4.45; N, 4.81%. Calcd for $C_{17}H_{13}NO_4$: C, 69.14; H, 4.44; N, 4.74%.

14: Colorless needles (diethyl ether-petr. ether); mp 128 °C; IR (KBr) 1780, 1710, and 1698 cm^{-1}; ^1H NMR ($CDCl_3$) δ=2.37 (3H, s, p-Me), 2.40 (3H, s, COMe), 3.78 (2H, d, J=2.8 Hz, 4-H), 7.1—7.4 (4H, m, Ar), and 7.14 (1H, t, J=2.8 Hz, =CH-); MS m/z (rel intensity, %) 243 (M^+, base peak), 201 (29), 173 (20), 172 (14), 143 (23), 101 (16), 99 (38), 67 (15), and 43 (74). Found: C, 69.11; H, 5.42; N, 5.75%. Calcd for $C_{14}H_{13}NO_3$: C 69.12; H, 5.39; N, 5.76%.

15: Colorless needles (chloroform-diethyl ether); mp 146—147 °C; IR (KBr) 1776, 1720, and 1710 cm^{-1}; ^1H NMR ($CDCl_3$) δ=2.37 (3H, s, p-Me), 3.80 (3H, s, COOMe), 3.80 (2H, d, J=3.0 Hz, 4-H), 6.86 (1H, t, J=3.0 Hz, =CH-), and 7.1—7.3 (4H, m, Ar); ^{13}C NMR ($CDCl_3$) δ=21.24 (q, p-Me), 34.52 (t, 4-C), 52.34 (q, COOMe), 122.46 (d, =CH-), 126.22, 129.10 (each d), 139.11, 140.67 (each s), 165.48, 168.26 (each s, 2- and 5-C), and 172.80 (s, COOMe); MS m/z (rel intensity, %) 259 (M^+, 91), 228 (19), 227 (72), 167 (33), 149 (base peak), 129 (38), 114 (25), 72 (25), 71 (28), 67 (22), and 57 (60). Found: C, 64.87; H, 5.08; N, 5.57%. Calcd for $C_{14}H_{13}NO_4$: C, 64.86; H, 5.05; N, 5.40%.

16: Colorless needles (diethyl ether); mp 121—122 °C; IR (KBr) 1777, 1700, and 1690 cm^{-1}; ^1H NMR ($CDCl_3$) δ=1.34 (3H, t, J=7.0 Hz, Me of Et), 2.37 (3H, s, p-Me), 3.81 (2H, d, J=3.0 Hz, 4-H), 4.26 (2H, q, J=7.0 Hz, CH_2 of Et), 6.85 (1H, t, J=3.0 Hz, =CH-), and 7.2—7.4 (4H, m, Ar); MS m/z (rel intensity, %) 273 (M^+, base peak), 228 (26), 227 (85), and 67 (25). Found: C, 66.04; H, 5.56; N, 5.01%. Calcd for $C_{15}H_{15}NO_4$: C, 65.92; H, 5.53; N, 5.13%.

17: Colorless needles (chloroform-diethyl ether); mp 147 °C; IR (KBr) 2202, 1780, 1705, and 1660 cm^{-1}; ^1H NMR ($CDCl_3$) δ=2.37 (3H, s, p-Me), 3.66 (2H, d, J=3.0 Hz, 4-H), 6.43 (1H, t, J=3.0 Hz, =CH-), and 7.1—7.4 (4H, m, Ar); MS m/z (rel intensity, %) 226 (M^+, base peak), 198 (19), 87 (33), and 65 (40). Found: C, 68.97; H, 4.55; N, 12.38%. Calcd for $C_{13}H_{10}N_2O_2$: C, 69.01; H, 4.46; N, 12.38%.

18: Pale yellow leaflets (chloroform-diethyl ether); mp 220—221 °C; IR (KBr) 1770, 1694; 1649, and 1598 cm^{-1}; ^1H NMR ($CDCl_3$) δ=2.38 (3H, s, p-Me), 3.72 (2H, d, J=2.6 Hz, 4-H), 7.1—7.8 (2H, m, ArH), 7.61 (1H, t, J=2.6 Hz, =CH-), 7.76 (2H, d, ArH), and 8.23 (2H, d, ArH); ^{13}C NMR ($CDCl_3$) δ=21.29 (p-Me), 34.13 (4-C), 125.41 (=CH-), 126.32, 127.73, 129.24, 130.12, 130.86, 132.52, 139.21, 140.33, 148.38, and 172.51 (2- and 5-C); MS m/z (rel intensity, %) 322 (M^+, base peak), 161 (85), 115 (32), and 76 (14). Found: C, 66.82; H, 4.38; N, 9.02%. Calcd for $C_{18}H_{14}N_2O_4$: C, 67.07; H, 4.38; N, 8.69%.

General Procedure for the Reaction of Pyridinium Methylides with Acyclic Olefins Leading to 20—23. To the mixture of a 1-alkylpyridinium bromide (1 mmol) and an olefin (1 mmol) in dichloromethane or chloroform was added triethylamine (1 mmol) at room temperature. The mixture was allowed to react under the conditions listed in Table 2, and then poured in ice water. The organic layer separated was dried over anhydrous magnesium sulfate and evaporated in vacuo. The residue was chromatographed over silica gel (Wako C-300) to give **20**—**23** (eluent for the chromatography: **20**: chloroform; **21**, **22**, and **23**: benzene). Only **23** could be purified by vacuum distilation. The results are summarized in Table 2.

20: (Mixture of several tautomers in solution): Orange

needles (acetone); mp 125—127 °C (lit,[10] mp 121—123 °C); IR (KBr) 3200, 1630, 1600, 1530, and 1530 cm^{-1}; ^1H NMR ($CDCl_3$) δ=4.22 (4/11H, d, J=0.8 Hz, CH_2 of minor isomer), 4.88 (18/11H, d, J=1.4 Hz, CH_2 of major isomer), and 7.1—8.1 (16H, m, Ph); ^1H NMR (DMSO-d_6) δ=4.45, 4.65 (2/9H, each br s, CH_2 of two minor isomers), 6.56 (8/9H, br s, exchanged with D_2O, =CH- of major isomer), 7.2—8.0 (16H, m, Ph and =CH-), and 8.50 (8/9H, br s, exchanged with D_2O, OH of major isomer); ^{13}C NMR (DMSO-d_6) δ=99.86, 108.91 (each d), 110.85 (s), 124.94, 126.81, 127.46, 128.46, 128.75, 129.18 (each d), 131.75, 132.22, 138.91, 140.61 (each s), 164.15, 169.73, and 188.17 (each s); MS m/z (rel intensity, %) 354 (M^+, 14), 105 (base peak), 82 (26), 79 (32), and 78 (52). Found: C, 81.13; H, 5.13%. Calcd for $C_{24}H_{18}O_3$: C, 81.34; H, 5.12%.

This compound **20** was also available in 75% yield from a similar procedure using 3,5-dimethyl-1-phenacylpyridinium bromide (306 mg, 1 mmol), (*E*)-1,2-dibenzoylethene (236 mg, 1 mmol), and triethylamine (0.14 ml, 1 mmol) in dichloromethane (20 ml) at room temperature for 5 min.

21: (Mixture of several tautomers in solution): Yellow liquid; IR (neat) 1720, 1680, and 1600 cm^{-1}; ^1H NMR ($CDCl_3$) δ=3.60, 3.65, 3.70 (each s, COOMe, integration area 18 (1 : 3 : 2)), 3.37 (s, area 1.2), 4.00 (br s, area 5.4), 4.15 (br s, area 0.7), 4.89 (br s, area 3.2), 6.35 (br s, area 1.7), 7.22 (br s, area 4.8), and 7.3—8.0 (area 72); ^{13}C NMR ($CDCl_3$) δ=50.73, 51.78 (each q, COOMe), 98.46, 104.91 (each d), 109.85 (s), 124.82, 126.58, 128.31, 128.63, 128.87, 128.98 (each d), 140.84 (s), 163.69, 166.50, 166.97 (each s). MS m/z (rel intensity, %) 308 (M^+, 33), 249 (18), 105 (base peak), and 77 (77). When chromatographed over alumina, this compound **21** changed into **26** which provided satisfactory elemental analysis as described below.

22: (Mixture of several tautomers in solution): Pale yellow liquid; IR (neat) 2250, 2200, 1740, 1680, 1660, 1600, and 1580 cm^{-1}; ^1H NMR ($CDCl_3$) δ=3.32 (br s, integration area 5), 4.54 (br s, area 14), 5.80 (br s, area 7), and 7.0—8.2 (m, area 150); ^{13}C NMR ($CDCl_3$) δ=32.47, 41.98 (each t), 108.97 (d), 114.96 (s), 128.05, 128.22, 128.52, 128.69, 130.04 (each d), 133.33, 133.74, 135.27, 135.56 (each s), 155.17 (s), 189.34, 194.04, and 194.62 (each s); MS m/z (rel intensity, %) 167 (M^+ −108, 36), 127 (51), 105 (88), 79 (base peak), 78 (89), 92 (29), 51 (55), and 50 (37). This compound **22** was too labile to be purified as an authentic sample for elemental analysis.

23: Pale yellow liquid; IR (neat) 2220, 1750, 1740, 1720, and 1630 cm^{-1}; ^1H NMR ($CDCl_3$) δ=3.66 (2H, d, J=0.8 Hz, CH_2), 3.72, 3.83 (each 3H, s, COOMe), and 6.48 (1H, d, J=0.8 Hz, =CH-); ^{13}C NMR ($CDCl_3$) δ=35.92 (t, CH_2), 52.48, 53.16 (each q, COOMe), 110.76 (d, =CH-), 114.81 (s, CN), 146.04 (s), 164.17, and 168.61 (each s, COOMe); MS m/z (rel intensity, %) 183 (M^+, 12), 152 (79), 139 (33), 124 (29), 113 (base peak), 82 (29), 81 (60), 59 (93), and 39 (22). Found: C, 52.33; H, 4.90; N, 7.57%. Calcd for $C_8H_9NO_4$: C, 52.46; H, 4.95; N, 7.65%.

2-Acetoxy-4-benzoyl-2,6-diphenyl-2*H*-pyran (24): A solution of **20** (100 mg, 0.3 mmol) in acetic anhydride (6 ml) was heated at 50—60 °C under stirring for 1 h in the presence of a catalytic amount of pyridine. The mixture was poured into ice water (200 ml) and sodium hydrogencarbonate was added. After allowed to stand for 2 h, the mixture was extracted with chloroform (30 ml×2). The combined extracts were dried over magnesium sulfate and evaporated in vacuo. The residue was chromatographed over silica gel by using chloroform as an eluent to give **24** (78 mg, 66%): Pale yellow prisms (diethyl ether-petr. ether); mp 153—155 °C; IR (KBr) 1760, 1670, 1640, and 1040 cm^{-1}; ^1H NMR ($CDCl_3$) δ=1.76 (3H, s, COMe), 6.70 (1H, s, 5-H), 7.2—7.7 (10H, m, 3-H and Ph), and 7.8—8.2 (6H, m, Ph); ^{13}C NMR ($CDCl_3$) δ=19.83 (COMe), 115.78 (5-C), 125.28, 129.96, 133.03, 134.11, 136.10, 137.17, 151.11, 153.06, 167.88 (COMe), and 187.96 (COPh); MS m/z (rel intensity, %) 396 (M^+, 9), 337 (22), 250 (18), 249 (93), 105 (base peak), and 77 (78). Found: C, 78.77; H, 5.47%. Calcd for $C_{26}H_{20}O_4$: C, 78.77; H, 5.09%.

4-Benzoyl-2,6-diphenylpyridine (25). A mixture of **20** (187 mg, 0.5 mmol) and ammonium acetate (0.5 g, 0.5 mmol) in ethanol (20 ml) was allowed to stand at room temperature for a week. The precipitate was collected on a filter and washed with hexane to give **25** (141 mg, 84%): Beige leaflets (ethanol); mp 127—129 °C (lit,[9] mp125 °C); IR (KBr) 1660 cm^{-1}; ^1H NMR ($CDCl_3$) δ=7.2—7.7 (9H, m, Ar), 7.8—8.0 (2H, m, Ar), 7.90 (2H, br s, 3- and 5-H), and 8.0—8.3 (4H, m, Ar); MS m/z (rel intensity, %) 336 (M^+ +1, 25), 335 (M^+, base peak), 334 (27), 306 (41), 127 (25), 105 (37), and 77 (49).

4-Benzoyl-6-phenyl-2*H*-pyran-2-one (26): The benzene solution of ester **21** (308 mg, 1 mmol in 0.5 ml) was charged in a column packed with activated alumina (Wako, 300 mesh) and eluted with benzene to give **26** (143 mg, 52%): Yellow prisms (diethyl ether); mp 135—137 °C; IR (KBr) 1720 and 1660 cm^{-1}; ^1H NMR ($CDCl_3$) δ=6.40 (1H, d, J=1.0 Hz, 5-H), 6.90 (1H, d, J=1.0 Hz, 3-H), and 7.3—8.1 (10H, m, Ph); ^{13}C NMR ($CDCl_3$) δ=99.75 (5-C), 114.72 (3-C), 125.70, 128.81, 128.93, 129.87, 131.22, 134.10, 134.62, 150.92 (6-C), 161.34 (2-C), and 192.92 (COPh); MS m/z (rel intensity, %), 276 (M^+, 19), 248 (19), 238 (17), 105 (base peak), and 77 (55). Found: C, 78.21; H, 4.43%. Calcd for $C_{18}H_{12}O_3$: C, 78.25; H, 4.38%.

General Procedure for the Cycloaddition of Pyridinium Methylides with *N*-(*p*-Tolyl)citraconimide Leading to 27—38. To a mixture of pyridinium halide and *N*-(*p*-tolyl)-citraconimide (each 1 mmol) in dry dichloromethane or chloroform (20—30 ml) was added triethylamine (1.1 mmol) at room temperature. The mixture was stirred at room temperature, poured into ice water, and extracted with dichloromethane (20 ml×2). The combined extracts were dried over magnesium sulfate and evaporated in vacuo below room temperature to give **27—38** as unstable products. As cycloadducts **27—29**, **31+35**, and **34+38** are all known, they were prepared under the reported reaction conditions.[2b] The results are summarized in Table 3. Purification of these cycloadducts was unsuccessful because of their lability. The ^1H NMR spectra of regioisomeric mixture are separatedly assigned to each isomer as shown below.

32+36 (Inseparable mixture in a ratio of 1 : 3): Colorless solid; IR (KBr) 2220, 1780, 1720, 1705 and 1510 cm^{-1}; ^1H NMR ($CDCl_3$) **32**: δ=1.60 (3H, s, 9b-Me), 1.93 (3H, s, 6-Me), 2.37 (3H, s, *p*-Me), 3.20 (1H, d, J=0.6 Hz, 3a-H), 4.43 (t, J=2.0 Hz, 9a-H), 4.7—4.9 (1H, m, 7-H), 5.08 (d, 1H, J=0.6 Hz, 4-H), 5.52 (1H, br d, 9-H), 5.88 (1H, m, 8-H), and 6.9—7.3 (4H, m, Ar). **36**: δ=1.69 (3H, s, 3a-Me), 1.93 (3H, s, 6-Me), 2.37 (3H, s, *p*-Me), 3.10 (1H, d, J=8.2 Hz, 9b-H), 4.7—4.9 (2H, m, 7- and 9a-H), 5.00 (1H, s, 4-H), 5.52 (1H, br d, 9-H), 5.88 (1H, m, 8-H), and 6.9—7.3 (4H, m, Ar).

33+37 (Inseparable mixture in a ratio of 1 : 3): Colorless solid; IR (KBr) 2250, 2200, 1780, 1720, 1705, and 1515 cm^{-1}; ^1H NMR ($CDCl_3$) **33**: δ=1.59 (3H, s, 1.72 (3H, br s, 8-Me), 2.34 (3H, s, *p*-Me), 3.23 (1H, s, 3a-H), 4.38 (1H, m, 9a-H), 4.6—5.0 (1H, m, 7-H), 5.30 (1H, m, 9-H), 6.28 (1H, br d,

6-H), and 6.9—7.3 (4H, m, Ar). **37**: δ=1.67 (3H, s, 3a-Me), 1.72 (3H, br s, 8-Me), 2.34 (3H, s, *p*-Me), 3.06 (1H, d, J=8.2 Hz, 9b-H), 4.76 (1H, s, 4-H), 4.6—5.0 (2H, m, 7- and 9a-H), 5.30 (1H, br s, 9-H), 5.94 (1H, br d, 6-H), and 6.9—7.3 (4H, m, Ar).

General Procedure for the Silica-Gel Mediated Elimination of Pyridines from the Citraconimide Cycloadducts 27—30 and 34 Leading to 39—42. The solution of cycloadducts **27—30** and **34** in chloroform (1 mmol in 0.5 ml) was charged in a column packed with silica gel (Wako C-300) and eluted with another portion of chloroform to give pyridine-eliminated products **39—42**. The results are summarized in Table 3.

39: Beige prisms (diethyl ether-petr. ether); mp 99—101 °C; IR (KBr) 1780, 1710, and 1690 cm^{-1}; ^1H NMR ($CDCl_3$) δ=2.02 (3H, s, 4-Me), 2.34 (3H, s, *p*-Me), 4.13 (2H, s, CH_2), and 7.0—8.1 (9H, m, Ar); ^{13}C NMR ($CDCl_3$) δ=9.22 (q, 4-Me), 20.96 (q, *p*-Me), 33.17 (t, CH_2), 125.52, 128.22, 128.65 (each d), 129.28 (s), 129.40, 133.63 (each d), 134.27, 135.80, 137.15, 140.91 (each s), 170.03, 170.32 (each s, 2- and 5-C), and 193.81 (s, COPh); MS *m/z* (rel intensity, %) 319 (M^+, 36), 105 (base peak), 77 (33), 74 (19), and 59 (37). Found: C, 75.06; H, 5.38; N, 4.46%. Calcd for $C_{20}H_{17}NO_3$: C, 75.22; H, 5.37; N, 4.39%.

40: Pale yellow needles (diethyl ether-petr. ether); mp 68 °C; IR (KBr) 1720, 1700, 1520, and 1390 cm^{-1}. ^1H NMR ($CDCl_3$) δ=2.00 (3H, s, 4-Me), 2.25 (3H, s, COMe), 2.34 (3H, s, *p*-Me), 3.56 (2H, s, CH_2), and 7.18 (4H, br s, Ar); ^{13}C NMR ($CDCl_3$) δ=9.28 (q, 4-Me), 21.08 (q, *p*-Me), 30.12 (q, COMe), 37.81 (t, CH_2), 125.64 (d), 129.05 (s), 129.52 (d), 133.68, 137.44, 140.73 (each s), 170.03, 170.32 (each s, 2- and 5-C), and 201.90 (s, COMe); MS *m/z* (rel intensity, %) 257 (M^+, 63), 216 (15), 215 (base peak), 53 (24), and 43 (55). Found: C, 69.84; H, 5.75; N, 5.35%. Calcd for $C_{15}H_{15}NO_3$: C, 70.02; H, 5.88; N, 5.44%.

41: Colorless liquid; IR (neat) 1770, 1740, 1710, 1510, and 1400 cm^{-1}; ^1H NMR ($CDCl_3$) δ=1.33 (3H, t, J=7.0 Hz, Me of Et), 2.12 (3H, s, 4-Me), 2.40 (3H, s, *p*-Me), 3.52 (2H, s, CH_2), 4.20 (2H, q, J=7.0 Hz, CH_2 of Et), and 7.19 (4H, br s, Ar); MS *m/z* (rel intensity, %) 287 (M^+, 37), 202 (14), 201 (base peak), 157 (10), 132 (10), 117 (11), and 68 (12). HRMS Found: *m/z* 287.1130. Calcd for $C_{16}H_{17}NO_4$: M, 287.1156.

42: Pale yellow needles (diethyl ether-petr. ether); mp 106—107 °C; IR (KBr) 2250, 1710, 1520, and 1400 cm^{-1}; ^1H NMR ($CDCl_3$) δ=2.20 (3H, s, 4-Me), 2.35 (3H, s, p-Me), 3.51 (2H, s, CH_2), and 7.19 (4H, br s, Ar); MS *m/z* (rel intensity, %) 240 (M^+, base peak), 213 (11), 169 (11), 156 (20), 132 (17), 104 (13), 91 (13), 79 (12), 78 (17), 77 (15), and 52 (28). Found: C, 69.25; H, 5.09; N, 11.43%. Calcd for $C_{14}H_{12}N_2O_2$: C, 69.99; H, 5.03; N, 11.66%.

References

1) As a review: I. Zugrăvescu and M. Petrovanu, "*N*-Ylid Chemistry," McGraw-Hill Internatl., New York (1976).

2) a) O. Tsuge, S. Kanemasa, and S. Takenaka, *Bull. Chem. Soc. Jpn.*, **58**, 3137 (1986); b) O. Tsuge, S. Kanemasa, and S. Takenaka, *ibid.*, **58**, 3320 (1986); c) The references cited in the above two papers.

3) a) O. Tsuge, S. Kanemasa, S. Kuraoka, and S. Takenaka, *Chem. Lett.*, **1984**, 281; b) Y. Miki, H. Hachiken, and S. Takemura, *Heterocycles*, **22**, 701 (1984).

4) O. Tsuge, S. Kanemasa, and S. Takenaka, *Chem. Lett.*, **1984**, 465.

5) Heating the cycloadducts at about 110 °C in the presence of a dipolarophile gives stereo- and regioselective biscycloadducts in fair yields (unpublished results).

6) When **12** was treated with an equimolar amount of butyllithium in THF at −78 °C, the mixture turned deep red. Quenching the anionic species with water, benzaldehyde, or iodomethane gave unchanged **12**.

7) The double bond of **12** is stabilized by conjugation with the benzoyl moiety. In addition, the benzoyl substituent of **12** is less sterically crowded than that of **12'**.

8) Cycloadducts **D** carrying one methyl (R is 6-Me, 8-Me, and 7- or 9-Me) undergo smooth elimination of pyridines as well.

9) As a review: F. Kröhnke, *Synthesis*, **1976**, 1 and references cited therein.

10) C. A. Henrick, E. Ritchie, and C. Taylor, *Aust. J. Chem.*, **20**, 2441 (1967).

 © 1987 The Chemical Society of Japan Bull. Chem. Soc. Jpn., 60, 1497—1504 (1987)

Reactions of 1,4-Bis(trimethylsilyl)-1,4-dihydropyridines with Carbonyl Compounds: A New Method for Regioselective Synthesis of 3-Alkylpyridines

Otohiko Tsuge,* Shuji Kanemasa, Toshio Naritomi, and Junji Tanaka
Research Institute of Industrial Science, and Department of Molecular Science and Technology, Interdisciplinary Graduate School of Engineering Sciences, Kyushu University, Kasugakoen, Kasuga 816
(Received October 31, 1986)

A new method for the alkyl group introduction at the 3-position of pyridienes is described: Reductive disilylation of pyridine, its 2-methyl, 3-methyl, and 4-methyl derivatives affords the corresponding 1,4-disilyl-1,4-dihydropyridines. In the presence of a catalytic amount of tetrabutylammonium fluoride, these dihydropyridines smoothly react with a variety of aldehydes and ketones to give 3-alkylpyridines.

Although direct substitution at the carbon atom of pyridine has been an attracting theme for a long time, no effective method was reported until a recent year. Compared with benzene as an isoelectronic hydrocarbon counterpart, electrophilic substitution at the ring of pyridine is awfully sluggish.[1] Especially so if a carbon electrophile is used. Quaterization occurs at the ring nitrogen, under the reaction conditions, so that the nucleophilicity of pyridine ring is lowered. Substituted pyridines have been mostly synthesized according to the conventional methods such as a ring synthesis[1,2] and a chain elongation at the preexisting functional groups.[3]

Two new methods have merged recently: One is the reaction of lithiopyridines with an electrophile, which can be generated in a regioselective manner by the aid of a directing group.[4] The other is the nucleophilic addition of organometallics with pyridines in the presence or absence of a pyridine-activating agent.[5] These reactions are performed on the aromatic ring of pyridines, and the pyridines substituted only at the 3-position are hardly accessible.

When the aromatic ring of pyridine is formally reduced by a metal hydride or its equivalent, *N*-metalated dihydropyridines are formed.[6] 1,4-Bis(trimethylsilyl)-1,4-dihydropyridine (**1**), which is available by a reductive disilylation of pyridine and is not so unstable as to exclude its isolation,[7] belongs to this family. So far no synthetic application of **1** has been reported. Since **1** carries an *N*-silylated cyclic enamine moiety,[8] its reaction with electrophiles is expected to occur regioselectively at the 3-position of pyridine.

The present article describes a new synthetic method of 3-alkylpyridines from pyridines.[9] Fluoride-catalyzed reactions of 1,4-bis(trimethylsilyl)-1,4-dihydropyridine (**1**) with a variety of carbonyl compounds produce 3-alkylpyridine derivatives. This method can be extended to several alkyl-substituted pyridines.

Results and Discussion

1,4-Disilyl-1,4-dihydropyridine **1** was synthesized by the known method starting with pyridine, chlorotrimethylsilane, and lithium powder in dry THF.[7] Though isolable by distillation under vacuum, **1** was found extremely air-sensitive. Oxidation starts once **1** is exposed to air, and it becomes contaminated by 4-trimethylsilylpyridine (**5**). The purification by distillation caused its partial oxidation, and the purity of **1** was only slightly higher than 90%. For its safety use, **1** may be stored in a bottle which is capped with a rubber septum and filled with dry nitrogen. A syringe is used to take **1** out of the bottle.

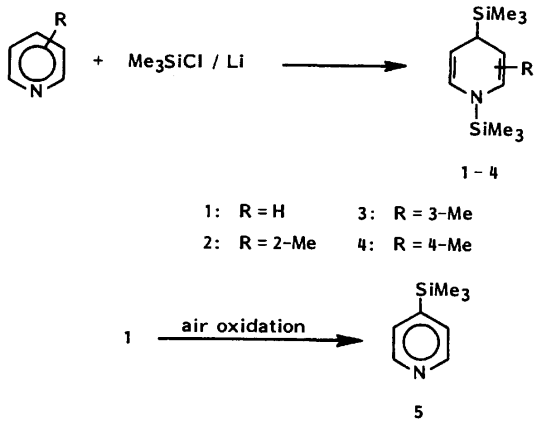

Scheme 1.

This preparation method was successfully applied to 2-methyl-, 3-methyl-, and 4-methylpyridines to give the corresponding 1,4-bis(trimethylsilyl)-1,4-dihydropyridines **2**—**4** in fair yields (Scheme 1). Again they are all air-sensitive.

An equimolar mixture of **1** and benzaldehyde in dry THF was treated, at room temperature and under an inert atmosphere, with a catalytic amount (10 mol%) of tetrabutylammonium fluoride (TBAF). After usual hydrolytic work-up and column chromatography over silica gel, 3-benzylpyridine (**6**) was obtained in 72% yield (Scheme 2). The fluoride catalyst could not be replaced by a Lewis acid, titanium(IV) chloride, most of the benzaldehyde being recovered (1 h at room temperature in dry dichloromethane).

The Friedel-Crafts acylation of benzene with 3-pyridinecarbonyl chloride followed by the carbonyl reduction is the major route for preparing **6**.[10] However, the Friedel-Crafts reaction can not be an effective preparation method for 3-benzylpyridines bearing an *o*- or *m*-substituent. Accordingly, benzaldehydes hav-

Table 1. Reaction of **1** with Aromatic Aldehydes Leading to 3-Substituted Pyridines **6—13**[a]

Ar-CHO	Time/h	Product		Yield/%[b]
PhCHO	15	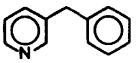	**6**	72
p-MeC_6H_4CHO	14	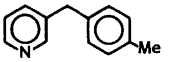	**7**	64[c]
p-ClC_6H_4CHO	15	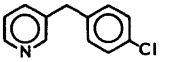	**8**	62
m-MeC_6H_4CHO	18	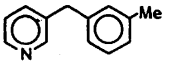	**9**	75
o-MeC_6H_4CHO	12	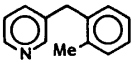	**10**	70
o-FC_6H_4CHO	17	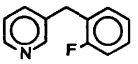	**11**	53
2-Furyl-CHO	13	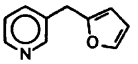	**12**	53
2-Thienyl-CHO	16	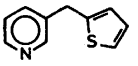	**13**	58[d]

a) All the reactions were carried out at room temperature in dry THF under argon. b) Isolated yield based on the aldehydes. c) Accompanied by 34% of **14**. d) Accompanied by 28% of **15**.

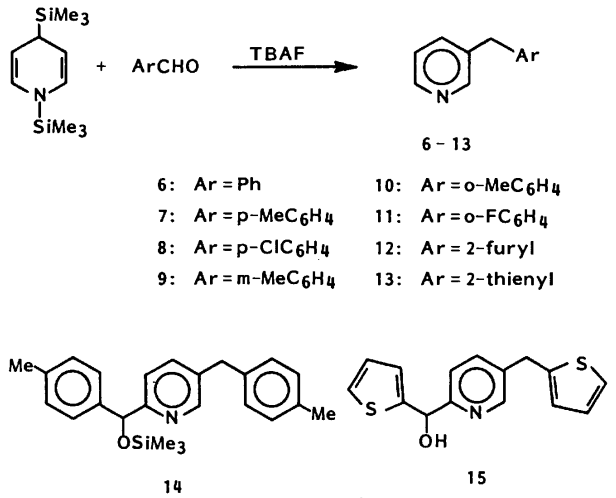

Scheme 2.

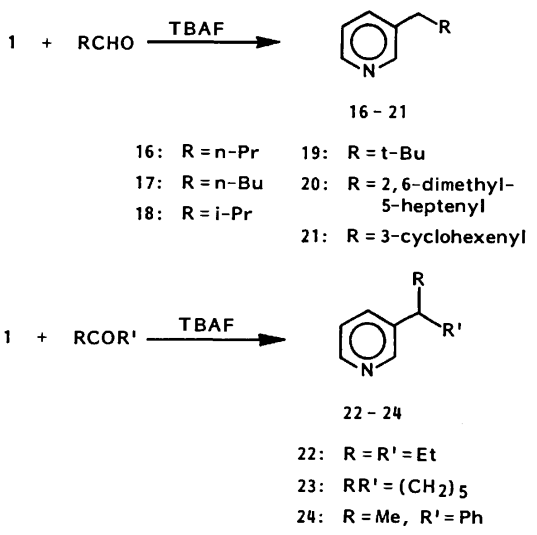

Scheme 3.

ing a variety of substitution patterns were employed to the reaction, and 3-(substituted benzyl)pyridines **7—11** were obtained in good yields (Scheme 2 and Table 1). Heteroaromatic aldehydes such as 2-furan- and 2-thiophenecarbaldehydes also reacted with **1** as well to produce **12** and **13**.

In most cases, 3-alkylpyridines **6—13** were the sole products. However in the reactions with *p*-methylbenzaldehyde and 2-thiophenecarbaldehyde, the major products **7** and **13** were accompanied by minor products **14** and **15**, respectively. They were assigned to be 2,5-disubstituted pyridine structures in which two molelules of the aldehydes had been incorporated at the 2- and 5-positions. Their formation indicates that not only the *N*-silyl group but also the 4-silyl moiety has participated in the reaction. This will be discussed later.

Similar reactions of **1** with aliphatic aldehydes required an elevated reaction temperature. Thus, **1** reacted with aldehydes carrying a primary, secondary, and tertiary alkyl group, under reflux in dry THF, to afford 3-alkylpyridines **16—19** (Scheme 3 and Table 2). Aldehydes bearing a carbon-carbon double bond could be employed without any trouble. The corresponding 3-alkylpyridines **20** and **21** were obtained. Further applications to the reactions with ketones were also successful to giving **22—24**.

The site of substitution was clearly determined to be the 3-position on the basis of spectral data. As an example, **18** shows an unsymmetrical substitution pattern with two vacant α-positions in the ^1H NMR spectrum: δ 7.06 (1H, dd, 5-H), 7.31 (1H, dt, 4-H), and

Table 2. Reaction of **1** with Aliphatic Aldehydes or Ketones Leading to 3-Substituted Pyridines **16—24**[a)]

Aldehyde or ketone	Time/h	Product		Yield/%[b)]
n-PrCHO	10	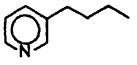	**16**	26
n-BuCHO	6	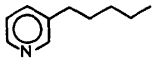	**17**	39
i-PrCHO	7	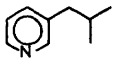	**18**	77
t-BuCHO	8	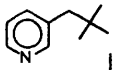	**19**	62
3,7-Dimethyl-6-octenal	10	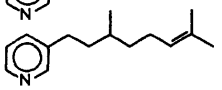	**20**	61
3-Cyclohexene-1-carbardehyde	10	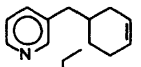	**21**	54
3-Pentanone	10	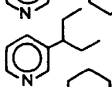	**22**	37
Cyclohexanone	5	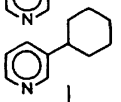	**23**	71
Acetophenone	5	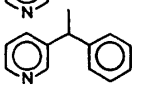	**24**	15

a) All the reactions were carried out under reflux in dry THF under argon. b) Isolated yield based on the carbonyl compounds.

8.2—8.4 (2H, m, 2- and 6-H). Its ^{13}CNMR spectrum confirmed the 3-substitution, in which a singlet signal appeared at δ 136.64 (3-C) and two doublets at 147.11 and 150.38 (2- and 6-C).[11)]

The most practical route to 3-alkylpyridines available so far is a chain elongation of 3-methyl- or 3-ethylpyridines via α-metalated intermediates.[12)] Our present method implies even more important synthetic values since 3-alkylpyridines substituted by a variety of alkyl groups are readily accessible, in a simple procedure under mild conditions, by the employment of appropriate carbonyl compounds.

Figure 1 illustrates a possible mechanism for the reaction of **1** with *p*-methylbenzaldehyde. The silyl moiety on the nitrogen is selectively eliminated by an attack of fluoride anion to form 3-azapentadienyl anion intermediate **A**. This anion adds to the aldehyde at the 3-position to form adduct **B**. The other addition onto the nitrogen might occur as well. Even if so, the resulting adduct would not find any stabilization path, undergoing a reversible retro addition going back to the starting **A**. The elimination of silanol from **B** leads to **C**. Subsequent fluoride-induced desilylation of **C** forms the methanide **D** stabilized by two aryls. **D** is then quenched with water to give 3-(*p*-methylbenzyl)-pyridine (**7**). If the desilylation of **C** is immediately followed by attack of the second molecule of the aldehyde, the 2,5-disubstituted pyridine **14** is produced as a side-product.

Similar reactions of other 1,4-disilyl-1,4-dihydropyridines **2—4** were next examined. In these cases,

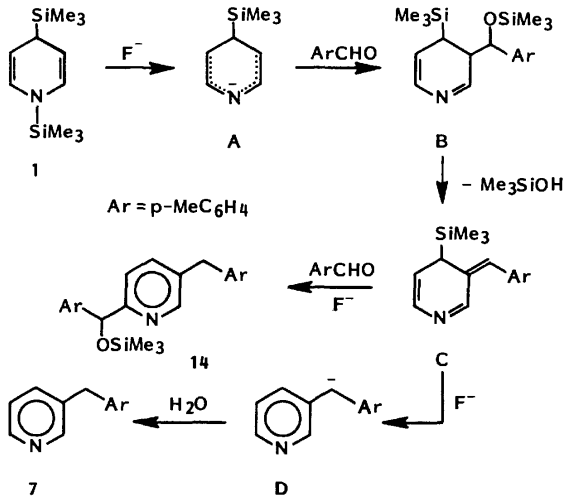

Fig. 1. A mechanism for the reaction of **1** with *p*-methylbenzaldehyde.

benzaldehyde and 2-methylpropanal were employed as representatives of aromatic and aliphatic aldehydes, respectively. The results are summarized in Table 3.

2-Methyl-1,4-disilylpyridine **2** furnished mixtures of 2,5-and 2,3-disubstituted pyridines **25—26** and **25′—26′**, respectively (Scheme 4 and Table 3). Although the 2,5-disubstituted regioisomers **25—26** were major products, their preference over the others was not so big as expected (**25** : **25′**=**6** : 4; **26** : **26′**=6 : 4 (by ^{1}H and/or ^{13}CNMR)). No persuasive explanation for the comparable regioisomeric ratio is available. It is readily understood on the basis of steric demand that only the

Table 3. Reaction of Dihydropyridines **2**—**4** with Aldehydes Leading to **25**—**32**

Dihydropyridine	Aldehyde	Reaction conditions	Time/h	Product	Yield/%[a]
2	PhCHO	room temp. in THF	14	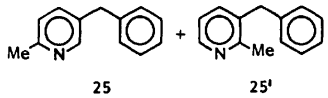 **25** + **25'**	45[b] (**25**:**25'**=6:4)
2	*i*-PrCHO	reflux in THF	10	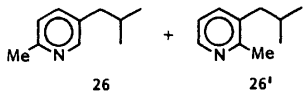 **26** + **26'**	77 (**26**:**26'**=6:4)
3	PhCHO	room temp. in THF	16	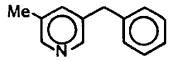 **28**	67[c]
3	*i*-PrCHO	reflux in THF	10	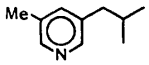 **29**	77
4	PhCHO	room temp. in THF	15	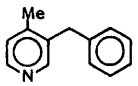 **31**	31
4	*i*-PrCHO	reflux in THF	10	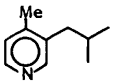 **32**	37

a) All isolated yields based on the aldehydes. b) Accompanied by 22% of **27**. c) Accompanied by 17% of **30**.

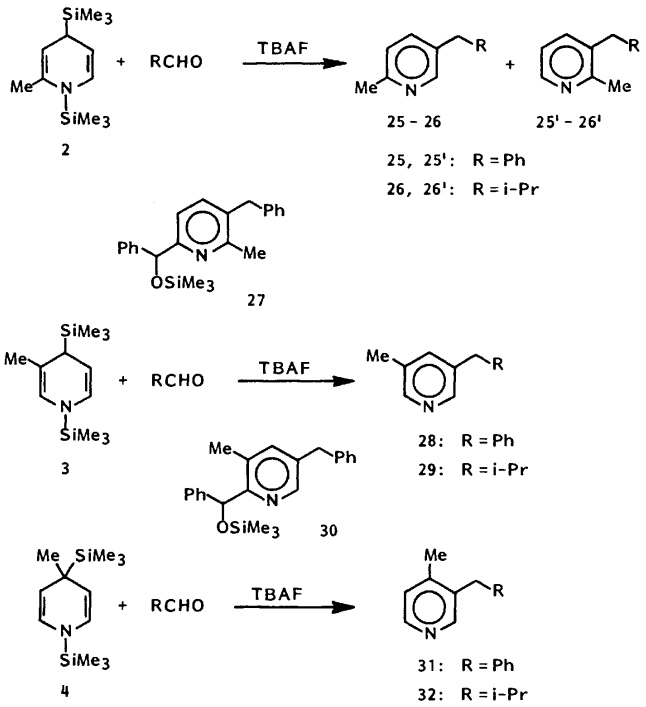

Scheme 4.

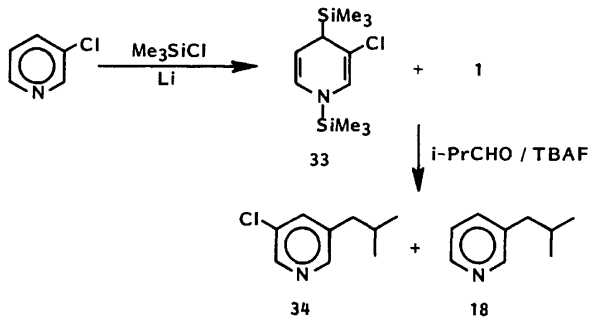

Scheme 5.

intermediate leading to **25'** could further react with the second molecule of benzaldehyde to give **27**.

In the reactions of 3-methyl-1,4-disilylpyridine (**3**), the 5-position is the only place where the nucleophilic addition can occur. For example, 3,5-disubstituted pyridines **28** and **29** were obtained as single isomers in excellent yields. As anticipated, the second addition took place at the place adjacent to the sterically less bulky 3-methyl moiety to give **30**.

4-Methyl-1,4-disilylpyridine (**4**) also demonstrated the 3-substitution providing **31** and **32**, but the yields were relatively diminished (Scheme 4 and Table 3).

Thus, these facile methods of alkyl group introduction could be successfully applied to methylpyridines with all possible substitution patterns. Pyridines with other alkyl group(s) will be utilized as well if the corresponding 1,4-dihydropyridines are obtainable.

Reductive disilylation of 3-chloropyridine was carried out under similar conditions (Scheme 5). The product isolated by vacuum distillation was found to be a mixture of 3-chloro-1,4-bis(trimethylsilyl)-1,4-dihydropyridine (**33**) and **1** (by ^{1}H NMR). As their separation was rather difficult, this mixture was subjected to the reaction with 2-methylpropanal in the presence of TBAF. A mixture of 3-chloro-5-(2-methylpropyl)pyridine (**34**) and 3-(2-methylpropyl)pyridine (**18**) was obtained, indicating that the alkyl group introduction via the disilylation method seems not so fruitful for halogen-substituted pyridines.

Experimental

General. Meting points were determined on a Yanagimoto melting point apparatus and are uncorrected. IR spectra were taken with a JASCO IRA-1 or a JASCO A-702 spectrometer. ^{1}H NMR spectra were recorded on a Hitachi R-40

(90 MHz) or a JEOL FX-100 instrument (100 MHz) and ^{13}C NMR on a JEOL FX-100 spectrometer at 25.05 MHz. Chemical shifts are expressed in parts per million downfield from tetramethylsilane as an internal standard. Mass spectra were measured with a JEOL-01SG-2 spectrometer at 70 eV of ionization energy. GC-Mass spectra as well as high resolution mass spectra were also obtained on the same instrument. Elemental analyses were performed on a Hitachi 026 CHN analyzer. Thin-layer chromatography (TLC) was accomplished on 0.2 mm precoated plates of silica gel 60 F-254 (Merck) or of aluminum oxide 60 F-254 type-E (Merck). Visualization was made with ultraviolet light (254 and 365 nm), iodine, molybdophosphoric acid (5% in ethanol), or *p*-anisaldehyde (5% in ethanol containing 5% of sulfuric acid). For preparative column chromatography, Wakogel C-200, C-300 (Wako), and Silicagel 60 (Merck) were employed. Flash chromatography was carried out on an EYELA EF-10 apparatus using a column (20×180 mm) packed with Silicagel 60 (Merck, size: 0.04—0.063 mm). Preparative high-performance liquid chromatography(HPLC) was performed on a Kusano KHLC-201 apparatus with a UV-detector Uvilog-III using a column (22×300 mm) packed with silica gel (Wakogel LC-50H). Gas liquid chromatography (GLC) was accomplished on a Yanaco G-2800 gas chromatograph (Yanagimoto) with an ionization flame detector using a glass column (SE-30, 3×2000 mm) or a glass capillary column (Silicone GE, SE-30, 0.25×50000 mm). Micro vacuum distillation was carried out on a Sibata GTO-250R Kugelrohr distilling apparatus. Solvents were evaporated with a Tokyo Rikakikai rotary evaporator type-V at about 50 °C unless otherwise stated.

General Procedure for Reductive Disilylation of Pyridines Leading to 1,4-Bis(trimethylsilyl)-1,4-dihydropyridines 1—4. The Sulzbach's method[7] was applied with a minor modification. All the procedure has to be carried out in an inert atmosphere, or air-sensitive dihydropyridines **1—4** are readily oxidized into 4-trimethylsilylpyridines. Detail of the reductive disilylation of pyridine is described below as a typical procedure: To a suspension of lithium powder (2.08 g, 300 mmol) in freshly distilled dry THF (30 ml) was added chlorotrimethylsilane (38.1 ml, 300 mmol) at −10 °C. Pyridine (100 mmol) in dry THF (25 ml) was added dropwise by use of a syringe in a period 30 min. After the completion of addition, the mixture was allowed to stir at 0 °C for 1 h. The precipitate was filtered off by the aid of the pressure of dry nitrogen. The filtrate was condensed in vacuo and then distilled under a reduced pressure to give **1** (7.64 g, 34%) which was contaminated by a small amount of **5** (purity 90%). The receiver flask containing distilled **1** was filled with dry nitrogen and capped with a rubber septum. To the septum was attached a needle which was connected to a balloon filled with dry nitrogen. In this way, **1** can be safely stored at room temperature at least for a week. A syringe may be used in order to take **1** out of the flask.

Similar procedures were applied to 2-methyl-, 3-methyl-, and 4-methylpyridine to give the corresponding dihydropyridines **2—4**. When **1** was exposed to dry air and chromatographed over silica gel with hexane-diethyl ether (10 : 1 vol/vol), 4-trimethylsilyl-pyridine (**5**) was obtained.

1,4-Bis(trimethylsilyl)-1,4-dihydropyridine (1): Yield 34%; colorless air-sensitive liquid; bp 45—50 °C/33 Pa; ^1H NMR ($CDCl_3$) δ=−0.11 (9H, s, 4-Me_3Si), 0.11 (9H, s, 1-Me_3Si), 2.25 (1H, t, J=6.9 Hz, 4-H), 4.35 (2H, dd, J=9.0 and 6.9 Hz, 3- and 5-H), and 5.70 (2H, d, J=9.0 Hz, 2- and 6-H).

2-Methyl-1,4-bis(trimethylsilyl)-1,4-dihydropyridine (2): Yield 27%; colorless air-sensitive liquid; bp 70—75 °C/320 Pa; ^1H NMR ($CDCl_3$) δ=− 0.11 (9H, s, 4-Me_3Si), 0.08 (9H, s, 1-Me_3Si), 1.62 (3H, s, 2-Me), 1.89 (1H, t, J=6.9 Hz, 4-H), 4.0—4.3 (2H, m, 3- and 5-H), and 5.61 (1H, d, J=9.0 Hz, 6-H).

3-Methyl-1,4-bis(trimethylsilyl)-1,4-dihydropyridine (3): Yield 37%; colorless air-sensitive liquid; bp 74—77 °C/200 Pa; ^1H NMR ($CDCl_3$) δ=0.08 (9H, s, 4-Me_3Si), 0.17 (9H, s, 1-Me_3Si), 1.53 (3H, s, 3-Me), 2.07 (1H, d, J=6.9 Hz, 4-H), 4.30 (1H, dd, J=9.0 and 6.9 Hz, 5-H), 5.52 (1H, s, 2-H), and 5.72 (1H, d, J=9.0 Hz, 6-H).

4-Methyl-1,4-bis(trimethylsilyl)-1,4-dihydropyridine (4): Yield 25%; colorless air-sensitive liquid; bp 70—75 °C/333 Pa; ^1H NMR ($CDCl_3$) δ=−0.12 (9H, s, 4-Me_3Si), 0.06 (9H, s, 1-Me_3Si), 1.86 (3H, s, 4-Me), 3.87 (2H, d, J=9.0 Hz, 3- and 5-H), and 5.53 (2H, d, J=9.0 Hz, 2- and 6-H).

4-Trimethylsilylpyridine (5): Pale yellow liquid; IR (neat) 1250 and 840 cm^{-1}; ^1H NMR ($CDCl_3$) δ=0.07 (9H, s, Me_3Si), 7.05 (2H, d, J=6.5 Hz, 3- and 5-H), and 8.55 (2H, d, J=6.5 Hz, 2- and 6-H); ^{13}C NMR ($CDCl_3$) δ=1.82 (q, Me_3Si), 128.05 (d, 3- and, 5-C), 148.54 (d, 2- and 6-C), and 150.18 (s, 4-C); MS *m/z* (rel intensity, %) 151, (M^+, 36), 137 (13), 136 (base peak), 83 (11), and 73 (10). HRMS Found: *m/z* 151.0796. Calcd for $C_8H_{13}NSi$: M, 151.0817.

General Procedure for Fluoride-Catalyzed Reaction of 1 with Aromatic Aldehydes Leading to 6—13. The reaction of **1** with benzaldehyde is described below as a typical procedure: Under an argon atmosphere, **1** (purity 90%, 0.287 g, 1.15 mmol) was added, by use of a syringe, to the solution of benzaldehyde (0.117 g, 1.1 mmol) in dry THF (5 ml). A solution of TBAF in THF (1M solution, 0.1 ml, 0.1 mmol) was slowly added also by the aid of a syringe. The mixture was stirred at room temperature under argon for 15 h and poured into saturated sodium hydrogencarbonate solution. The product was extracted with diethyl ether (20 ml), the ether washed with brine, dried over magnesium sulfate, and then evaporated in vacuo. The residue was chromatographed over silica gel (10 g) by using hexane-diethyl ether (5 : 1 vol/vol) to give **6** (0.134 g, 72%) as a pale yellow liquid.

Other seven aromatic aldehydes were treated in a similar way. The reaction times and the yields of 3-alkylpyridines **6—13** are listed in Table 1.

3-Benzylpyridine (6): Pale yellow liquid; mp (picrate) 100—101 °C; IR (neat) 1600, 1575, 1495, 1480, 1450, 1420, and 1025 cm^{-1}; ^1H NMR ($CDCl_3$) δ=3.92 (2H, s, CH_2), 7.0—7.5 (7H, m, ArH), and 8.3—8.5 (2H, m, 2- and 6-H); ^{13}C NMR ($CDCl_3$) δ=28.65 (t, CH_2), 123.34, 126.41, 127.53, 128.35, 128.59, 128.74, 136.25 (d), 139.66, 147.46 (d, 6-C), and 149.99 (d, 2-C); MS *m/z* (rel intensity, %) 169 (M^+, base peak), 168 (77), 167 (20), 91 (20), 83 (11), and 65 (16). Found (picrate): C, 54.44; H, 3.62; N, 14.27%. Calcd for $C_{18}H_{14}N_4O_7$: C, 54.28; H, 3.54; N, 14.07%.

3-(*p*-Methylbenzyl)pyridine (7): Yellow liquid; mp (picrate) 111—114 °C; ^1H NMR ($CDCl_3$) δ=2.26 (3H, s, *p*-Me), 3.86 (2H, s, CH_2), 6.9—7.2 (5H, m, ArH), 7.35 (1H, m, ArH), and 8.3—8.5 (2H, m, 2- and 6-H); MS *m/z* (rel intensity, %) 183 (M^+, base peak), 182 (46), 168 (34), 167 (13), 105 (15), 91 (12), and 77 (14). Found (picrate): C, 55.40; H, 3.84; N, 13.77%. Calcd for $C_{19}H_{16}N_4O_7$: C, 55.34; H, 3.91; N, 13.59%.

After the first fraction affording **7** was eluted with hexa-

ne-diethyl ether (10:1 vol/vol), the second fraction was followed (5:1 vol/vol) giving **14** in 34% yield. **14**: Pale yellow liquid; IR (neat) 1245, 1080, 880, and 840 cm^{-1}. ^1H NMR ($CDCl_3$) δ=0.16 (9H, s, Me_3Si), 2.34 (6H, s, *p*-Me), 3.89 (2H, s, CH_2), 5.89 (1H, s, CH), 7.0—7.6 (10H, m, ArH), and 8.37 (1H, s, 2-H), MS *m/z* (rel intensity, %) 375 (M^+, base peak), 360 (30), 286 (12), 254 (14), 193 (44), 147 (14), 142 (18), 75 (17), and 73 (43). HRMS Found: *m/z* 375.2008. Calcd for $C_{24}H_{29}NOSi$: M, 375.2017.

3-(*p*-Chlorobenzyl)pyridine (8): Pale yellow liquid; mp (picrate) 107—110 °C; IR (neat) 1570, 1515, 1480, 1420, and 1025 cm^{-1}. ^1H NMR ($CDCl_3$) δ=3.83 (2H, s, CH_2), 6.8—7.5 (6H, m, ArH), and 8.2—8.4 (2H, m, 2- and 6-H); MS *m/z* (rel intensity, %) 205, 208 (M^+, 26 and 78), 168 (base peak), 153 (21), and 80 (13). Found (picrate): C, 49.66; H, 3.21; N, 12.83%. Calcd for $C_{18}H_{13}N_4O_7$: C, 49.96; H, 3.03; N, 12.95%.

3-(*m*-Methylbenzyl)pyridine (9): Yellow liquid; mp (picrate) 142—144 °C; IR (neat) 1610, 1575, 1480, 1420, and 1030 cm^{-1}; ^1H NMR ($CDCl_3$) δ=2.26 (3H, s, *m*-Me), 3.85 (2H, s, CH_2), 6.8—7.5 (6H, m, ArH), and 8.3—8.5 (2H, m, 2- and 6-H); MS *m/z* (rel intensity, %) 183 (M^+, base peak), 182 (55), 169 (13), 168 (94), 167 (44), 128 (11), 115 (17), 105 (14), 91 (16), 80 (16), 77 (19), and 65 (25). Found (picrate): C, 54.95, H, 3.95; N, 13.67%. Calcd for $C_{19}H_{16}N_4O_7$: C, 55.34; H, 3.91; N, 13.59%.

3-(*o*-Methylbenzyl)pyridine (10): Yellow liquid; mp (picrate) 130—132 °C; IR (neat) 1575, 1480, 1455, 1420, and 1025 cm^{-1}; ^1H NMR ($CDCl_3$) δ=2.17 (3H, s, *o*-Me), 3.88 (2H, s, CH_2), 6.9—7.4 (6H, m, ArH), and 8.2—8.5 (2H, m, 2- and 6-H); MS *m/z* (rel intensity, %) 183 (M^+, base peak), 182 (38), 169 (11), 168 (77), 167 (25), and 104 (14). Found (picrate): C, 55.40; H, 4.00; N, 13.61%. Calcd for $C_{19}H_{16}N_4O_7$: C, 55.34, H, 3.91; N, 13.59%.

3-(*o*-Fluorobenzyl)pyridine (11): Yellow liquid; mp (picrate) 97—98 °C; IR (neat) 1590, 1495, 1480, 1450, 1420, 1230, and 1025 cm^{-1}. ^1H NMR ($CDCl_3$) δ=3.92 (2H, s, CH_2), 6.8—7.5 (6H, m, ArH), and 8.2—8.5 (2H, m, 2- and 6-H); MS *m/z* (rel intensity, %) 187 (M^+, base peak), 186 (54), 185 (16), 168 (17), 167 (12), 133 (12), and 109 (18). Found (picrate): C, 52.07; H, 3.23; N, 13.66%. Calcd for $C_{18}H_{13}N_4O_7F$: C, 51.93; H, 3.15; N, 13.46%.

3-(2-Furylmethyl)pyridine (12): Yellow liquid; mp (picrate) 123—125 °C; IR (neat) 1600, 1580, 1500, 1480, 1425, 1250, 1150, 1070, and 1010 cm^{-1}; ^1H NMR ($CDCl_3$) δ=3.90 (2H, s, CH_2), 5.97, 6.23 (each 1H, each m, 3- and 4-H of furyl), 7.1—7.5 (3H, m, ArH), and 8.4—8.5 (2H, m, 2- and 6-H); MS *m/z* (rel intensity, %) 159 (M^+, base peak), 158 (16), 131, (11), 130 (76), 81 (20), and 51 (11). Found (picrate): C, 49.56; H, 3.27; N, 14.44%. Calcd for $C_{16}H_{12}N_4O_8$: C, 49.49; H, 3.11; N, 14.43%.

3-(2-Thienylmethyl)pyridine (13): Yellow liquid; mp (picrate) 104—105 °C; IR (neat) 1570, 1480, 1420, 1030, and 700 cm^{-1}; ^1H NMR ($CDCl_3$) δ=4.09 (2H, s, CH_2), 6.83, 6.98 (each 1H, each m, 3- and 4-H of thienyl), 7.1—7.6 (3H, m, ArH), and 8.3—8.5 (2H, m, 2- and 6-H); MS *m/z* (rel intensity, %) 175 (M^+, base peak), 174 (49), 130 (12), and 97 (46). Found (picrate): C, 47.65; H, 3.24; N, 13.77%. Calcd for $C_{16}H_{12}N_4O_7S$: C, 47.53; H, 2.99; N, 13.86%.

After the first fraction giving **13** was eluted with hexane-diethyl ether (2:1 vol/vol), the second fraction was followed with the same eluent. This fraction afforded **15** (0.127 g, 28%) after treatment with methanol and crystallization from diethyl ether. **15**: Colorless prisms (diethyl ether); mp 98—100 °C; IR (KBr) 3080, 1470, 1430, 1145, 1050, 1030, and 680 cm^{-1}; ^1H NMR ($CDCl_3$) δ=4.10 (2H, s, CH_2), 4.85 (1H, br, OH), 5.94 (1H, s, CH), 6.6—7.3 (7H, m, ArH), 7.45 (1H, m, ArH), and 8.38 (1H, br s, 2-H); MS *m/z* (rel intensity, %) 287 (M^+, 85), 204 (10), 203 (11), 176 (21), 175 (base peak), 174 (22), 173 (11), 149 (28), 147 (11), 113 (19), 111 (11), 97 (71), 85 (33), and 57 (16). Found: C, 52.45; H, 4.61; N, 5.09%. Calcd for $C_{15}H_{13}NOS_2$: C, 62.69; H, 4.56; N, 4.87%.

General Procedure for Fluoride-Catalyzed Reaction of 1 with Aliphatic Aldehydes or Ketones Leading to 16—24. As a typical procedure, the reaction of **1** with 2-methylpropanal is described below: Under argon, **1** (purity 90%, 0.817 g, 3.26 mmol) was added to a solution of 2-methylpropanal (0.35 ml, 3.8 mmol) in dry THF (8 ml). After TBAF (1 M solution in THF, 0.38 ml, 0.38 mmol) was added, the mixture was heated under reflux for 7 h and then poured into saturated sodium hydrogencarbonate. The product was extracted with diethyl ether (30 ml), the ether washed with brine, dried over magnesium sulfate, and finally evaporated in vacuo. The residue was chromatographed over silica gel (20 g) with hexane-diethyl ether (10:1 vol/vol) to give **18** (0.34 g, 77%). Other aliphatic aldehydes and ketones were similarly treated. The results are summarized in Table 2.

3-Butylpyridine (16): Pale yellow liquid; IR (neat) 2800—3000, 1470, 1420, 1360, and 1020 cm^{-1}, ^1H NMR ($CDCl_3$) δ=0.8—2.6 (9H, m, butyl), 7.14 (1H, dd, *J*=8.1 and 5.0 Hz, 5-H), 7.43 (1H, dt, *J*=8.1, 2.1, and 2.1 Hz, 4-H), and 8.3—8.5 (2H, m, 2- and 6-H).

3-Pentylpyridine (17): Pale yellow liquid; IR (neat) 2800—3000, 1570, 1455, 1420, 1370, and 1020^{-1} cm^{-1}; ^1H NMR ($CDCl_3$) δ=0.7—2.6 (11H, m, pentyl), 7.10 (1H, dd, *J*=8.1 and 5.0 Hz, 5-H), 7.38 (1H, dt, *J*=8.1, 2.1, and 2.1 Hz, 4-H), and 8.2—8.4 (2H, m, 2- and 6-H).

3-(2-Methylpropyl)pyridine (18): Pale yellow liquid; mp (picrate) 111—113 °C; IR (neat) 2800—3000, 1570, 1470, 1420, 1030, and 730 cm^{-1}; ^1H NMR ($CDCl_3$) δ=0.82 (6H, d, *J*=7.2 Hz,Me), 1.81 (1H, m, CH), 2.39 (2H, d, *J*=7.2 Hz, CH_2), 7.06 (1H, dd, *J*=8.1 and 4.5 Hz, 5-H), 7.31 (1H, dt, *J*=8.1, 2.1, and 2.1 Hz, 4-H), and 8.2—8.4 (2H, m, 2- and 6-H); ^{13}C NMR ($CDCl_3$) δ=22.17 (q, Me), 29.97 (d, CH), 42.30 (t, CH_2), 123.04 (d, 5-C), 136.34 (d, 4-C), 136.64 (s, 3-C), 147.11 (d, 6-C), and 150.38 (d, 2-C). Found (picrate) C, 49.44; H, 4.46; N, 15.35%. Calcd for $C_{15}H_{16}N_4O_7$: C, 49.45; H, 4.43; N, 15.38%.

3-(2,2-Dimethylpropyl)pyridine (19): Pale yellow liquid; mp (picrate) 125—127 °C; ^1H NMR ($CDCl_3$) δ=0.89 (9H, s, *t*-Bu), 2.46 (2H, s, CH_2), 7.16 (1H, dd, *J*=8.1 and 5.0 Hz, 5-H), 7.38 (1H, dt, *J*=8.1, 2.0, and 2.0 Hz, 4-H), and 8.3—8.5 (2H, m, 2- and 6-H); ^{13}C NMR ($CDCl_3$) δ=29.06 (q, *t*-Bu), 31.59 (s, *t*-Bu), 47.09 (t, CH_2), 122.59 (d, 5-C), 137.44 (d, 4-C), 137.74 (s, 3-C), 147.13 (d, 6-C), and 151.18 (d, 2-C). Found (picrate) C, 50.64; H, 4.91; N, 14.65%. Calcd for $C_{16}H_{18}N_4O_7$: C, 50.79; H, 4.80; N, 14.81%.

3-(3,7-Dimethyl-6-octenyl)pyridine (20): Yellow liquid; IR (neat) 2850—3000, 1580, 1490, 1460, 1430, 1380, 1020, and 720 cm^{-1}; ^1H NMR ($CDCl_3$) δ=0.8—2.7 (12H, m, Me, CH_2, and CH), 1.60, 1.68 (each 3H, s, $=C(Me)_2$), 5.02 (1H, br t, olefinic), 7.08 (1H, dd, *J*=8.0 and 5.0 Hz, 5-H), 7.37 (1H, dt, *J*=8.0, 2.0, and 2.0 Hz, 4-H), and 8.3—8.5 (2H, m, 2- and 6-H); MS *m/z* (rel intensity, %) 217 (M^+, 17), 149 (13), 134 (12), 107 (19), 106 (base peak), 93 (48), 92 (45), 69 (26), and 66 (27).

3-(3-Cyclohexenylmethyl)pyridine (21): Pale yellow liquid; mp (picrate) 101—103 °C; IR (neat) 2850—3030, 1580, 1480, 1425, 1030, 730, and 715 cm^{-1}; ^1H NMR ($CDCl_3$)

δ=0.8—2.1 (7H, m, cyclohexenyl), 2.51 (2H, d, J=7.0 Hz, CH_2), 5.53 (2H, br s, olefinic), 7.08 (1H, dd, J=8.1 and 4.5 Hz, 5-H), 7.35 (1H, dt, J=8.1, 2.0, and 2.0 Hz, 4-H), and 8.2—8.5 (2H, m, 2- and 5-H); MS m/z (rel intensity, %) 173 (M^+, 55), 130 (19), 118 (25), 117 (16), 94 (20), 93 (base peak), 92 (33), 91 (16), 81 (97), 80 (13), 79 (49), 78 (11), 77 (25), and 66 (54). Found (picrate): 53.97; H, 4.60; N, 14.07%. Calcd for $C_{18}H_{18}N_4O_7$: C, 53.73; H, 4.51; N, 13.91%.

3-(1-Ethylpropyl)pyridine (22): Pale yellow liquid; mp (picrate) 112—113 °C; ^{1}H NMR ($CDCl_3$) δ=0.83 (6H, t, Me), 1.57 (4H, m, CH_2), 2.32 (1H, m, CH), 7.13 (1H, dd, J=8.1 and 4.5 Hz, 5-H), 7.32 (1H, dt, J=8.1, 2.1, and 2.1 Hz, 4-H), and 8.3—8.6 (2H, m, 2- and 6-H). Found (picrate) C, 50.63; H, 4.80; N, 14.81%. Calcd for $C_{16}H_{18}N_4O_7$: C, 50.79; H, 4.80; N, 14.81%.

3-Cyclohexylpyridine (23): Pale yellow liquid; mp (picrate) 130—131 °C; IR (neat) 2950, 2850, 1580, 1480, 1450, 1425, 1025, 810 and 720 cm^{-1}. ^{1}H NMR ($CDCl_3$) δ=1.0—2.6 (11H, m, cyclohexyl), 7.09 (1H, dd, J=8.1 and 4.5 Hz, 5-H), 7.41 (1H, dt, J=8.1, 2.0, and 2.0 Hz, 4-H), and 8.3—8.5 (2H, m, 2- and 6-H); MS m/z (rel intensity, %) 161 (M^+, base peak), 160 (18), 133 (41), 132 (24), 130 (10), 119 (13), 118 (59), 117 (25), 107 (12), 106 (40), 105 (96), 104 (20), 93 (26), 92 (38), 91 (13), 80 (15), 78 (15), 77 (13), and 65 (20). Found (picrate): C, 52.31; H, 4.65; N, 14.35%. Calcd for $C_{17}H_{18}N_4O_7$: C, 52.31; H, 4.65; N, 14.35%.

3-(1-Phenylethyl)pyridine (24): Pale yellow liquid; mp (picrate) 138—141 °C; IR (neat) 2900—3100, 1570, 1495, 1480, 1445, 1420, 1020, 710, and 700 cm^{-1}; ^{1}H NMR ($CDCl_3$) δ=1.63 (3H, d, J=6.3 Hz, Me), 4.12 (1H, q, J=6.3 Hz, CH), 7.0—7.5 (7H, m, ArH), and 8.3—8.5 (2H, m, 2- and 6-H); MS m/z (rel intensity, %) 183 (M^+, 47), 169 (14), 168 (base peak), 167 (33), 115 (10), 77 (11), and 51 (12). Found (picrate): C, 54.88; H, 4.01; N, 13.43%. Calcd for $C_{19}H_{16}N_4O_7$: C, 55.34; H, 3.91; H, 13.59%.

Reactions of 2—4 with Benzaldehyde or 2-Methylpropanal Leading to 25—32. The procedures are essentially the same to those described above: The reactions with benzaldehyde was carried out at room temperature and with 2-methylpropanal under reflux. All the results are listed in Table 3.

2-Methyl-5-benzylpyridine (25) + 2-Methyl-3-benzylpyridine (25′): Inseparable mixture (6:4 by ^{1}H NMR and ^{13}C NMR); Pale yellow liquid; ^{1}H NMR ($CDCl_3$) δ=2.43 (3H, s, 2-Me), 3.80, 3.85 (2H, 4:6, each s, CH_2), 6.8—7.4 (7H, m, ArH), and 8.2—8.3 (1H, m, 6-H); ^{13}C NMR ($CDCl_3$) δ=22.08, 23.48 (each q, 6:4, 2-Me), 38.34 (t, CH_2), 120.93 (d), 122.70 (s), 125.99, 128.22, 128.34, 136.32, 136.85 (each d), 146.48, 148.77 (each d, 6-C), 155.58, 156.70 (each s, 2-C); MS m/z 183 (M^+). Found (picrate, mp 143—146 °C): C, 55.22; H, 4.02; N, 13.77%. Calcd for $C_{19}H_{16}N_4O_7$: C, 55.34; H, 3.91; N, 13.59%.

The first fraction affording **25+25′** (hexane-diethyl ether (5:1 vol/vol)) was followed by the second fraction which gave **27** (0.145 g, 22%): Colorless liquid; IR (neat) 2900—3100, 1570, 1490, 1445, 1400, 1245, 1090, 1060, 890, and 840 cm^{-1}; ^{1}H NMR ($CDCl_3$) δ=0.06 (9H, s, Me_3Si), 2.30 (3H, s, 2-Me), 3.83 (2H, s, CH_2), 5.77 (1H, s, CH), 6.9—7.4 (12H, m, ArH); MS m/z (rel intensity, %) 361 (M^+, 36), 281 (10), 179 (29), 91 (12), 77 (15), 75 (24), 73 (38), and 43 (base peak).

2-Methyl-5-(2-methylpropyl)pyridine (26) + 2-Methyl-3-(2-methylpropyl)pyridine (26′): Inseparable mixture (6:4 by ^{13}C NMR); Pale yellow liquid; ^{1}H NMR ($CDCl_3$) δ=0.88 (6H, d, Me), 1.82 (1H, m, CH), 2.3—2.5 (5H, m, 2-Me and CH_2), 6.9, 7.2, and 8.2 (each 1H, m, ArH); ^{13}C NMR ($CDCl_3$) δ=21.72, 22.02 (each q, 2-Me and Me), 28.42, 29.59 (d, 6:4, CH), 41.57 (t, CH_2), 120.41, 122.11 (each d), 124.21 (s), 136.27, 136.73 (each d), 146.07, 149.18 (each d, 6-C), 155.05, and 156.23 (each s, 2-C). Found (picrate, mp 114—116 °C): C, 50.74, H, 4.75; N, 15.25%. Calcd for $C_{16}H_{18}N_4O_7$: C, 50.79; H, 4.80; N, 14.81%.

3-Benzyl-5-methylpyridine (28): Pale yellow liquid; mp (picrate) mp 149—151 °C; IR (neat) 2950—3100, 1605, 1580, 1505, 1460, 1450, 1040, 730, and 710 cm^{-1}; ^{1}H NMR ($CDCl_3$) δ=2.15 (3H, s, 5-Me), 3.79 (2H, s, CH_2), 6.9—7.3 (6H, m, ArH), and 8.13 (2H, br s, 2- and 6-H); MS m/z (rel intensity, %) 183 (M^+, 57), 182 (48), 168 (20), 167 (16), 128 (21), 115 (49), 91 (51), 89 (27), 78 (22), 77 (45), 65 (73), and 39 (base peak). Found (picrate): C, 55.22; H, 3.94; N, 13.66%. Calcd for $C_{19}H_{16}N_4O_7$: C, 55.34; H; 3.91; N, 13.59%.

The first farction containing **28** was followed by the second fraction (both eluted with hexane-diethyl ether (5:1 vol/vol)) which gave **30** (0.074 g, 17%): Pale yellow liquid; IR (neat) 2900—3100, 1600, 1500, 1450, 1410, 1255, 1090, 1060, 890, 840, and 730 cm^{-1}; ^{1}H NMR ($CDCl_3$) δ=0.06 (9H, s, Me_3Si), 2.19 (3H, s, 3-Me), 3.83 (2H, s, CH_2), 5.98 (1H, s, CH), 6.9—7.4 (11H, m, ArH), and 8.17 (1H, br s, 6-H); MS m/z (rel intensity, %) 361 (M^+, 41), 346 (15), 272 (14), 270 (14), 181 (15), 180 (18), 179 (43), 115 (15), 91 (36), and 73 (base peak).

3-Methyl-5-(2-methylpropyl)pyridine (29): Pale yellow liquid; mp (picrate) 140—142 °C; IR (neat) 2900—3050, 1580, 1470, 1440, 1390, 1370, 740, and 720 cm^{-1}; ^{1}H NMR ($CDCl_3$) δ=0.85 (6H, d, J=8.0 Hz, Me), 1.81 (1H, m, CH), 2.23 (3H, s, 5-Me), 2.37 (2H, d, J=8.0 Hz, CH_2), 7.11 (1H, br s, 4-H), and 8.09 (2H, br s, 2- and 6-H); ^{13}C NMR ($CDCl_3$) δ=18.27 (q, 5-Me), 22.22 (q, Me), 30.02 (d, CH), 42.20 (t, CH_2), 132.30 (s, 3-C), 136.00 (s, 5-C), 136.93 (d, 4-C), and 147.60 (d, 2- and 6-C); MS m/z (rel intensity, %) 149 (M^+, 31), 107 (base peak), 106 (70), 92 (11), 86 (11), 84 (17), 79 (29), 78 (26), and 77 (59). Found (picrate): C, 50.57; H, 4.77; N, 15.03%. Calcd for $C_{16}H_{18}N_{N4}O_7$: C, 50.57; H, 4.80; N, 14.81%.

3-Benzyl-4-methylpyridine (31): Yellow liquid; ^{1}H NMR ($CDCl_3$) δ=2.15 (3H, s, 4-Me), 3.91 (2H, s, CH_2), 6.9—7.3 (6H, m, ArH), and 8.2—8.4 (2H, m, 2- and 6-H); MS m/z (rel intensity, %) 183 (M^+, base peak), 182 (81), 168 (40), 167 (27), 128 (17), 115 (31), 105 (45), 91 (37), 78 (22), and 77 (35). HRMS Found: m/z 183.1055. Calcd for $C_{13}H_{13}N$: M, 183.1047.

4-Methyl-3-(2-methylpropyl)pyridine (32): Yellow liquid; mp (picrate) 106—108 °C; IR (neat) 2900—3000, 1600, 1460, and 1410 cm^{-1}; ^{1}H NMR ($CDCl_3$) δ=0.75 (6H, d, J=8.0 Hz, Me), 1.64 (1H, m, CH), 2.06 (3H, s, 4-Me), 2.24 (2H, d, J=8.0 Hz, CH_2), 6.75 (1H, d, J=5.0 Hz, 5-H), and 7.96 (2H, m, 2- and 6-H); MS m/z (rel intensity, %) 149 (M^+, 30), 135 (35), 107 (base peak), 106 (72), 79 (32), 78 (21), 77 (54), and 53 (25). Found (picrate): C, 50.66; H, 4.77; N, 14.99%. Calcd for $C_{16}H_{18}N_4O_7$: C, 50.79; H, 4.80; N, 14.81%.

3-Chloro-1,4-bis(trimethylsilyl)-1,4-dihydropyridine (33) and 3-Chloro-5-(2-methylpropyl)pyridine (34). A similar procedure as mentioned above was performed by employing 3-chloropyridine (3.0 ml, 31 mmol) in dry THF (6 ml), chlorotrimethylsilane (19 ml, 150 mmol), and lithium powder (1.04 g, 150 mmol) in dry THF (40 ml) to give a mixture of **33** and **1** (1.52 g, bp 65—70 °C/146 Pa, yellow liquid): ^{1}H NMR ($CDCl_3$, the signals of **1** were excluded) δ=—0.08 (9H, s, 4-Me_3Si), 0.10 (9H, s, 1-Me_3Si), 2.26 (1H, d, J=7.5 Hz, 4-H), 4.38 (1H, dd, J=10.5 and 7.5 Hz, 5-H), 5.66 (1H, d, J=10.5 Hz, 6-H), and 5.87 (1H, s, 2-H).

To a solution of thus prepared **33** (0.63 g) and 2-methylpropanal (0.22 ml, 2.43 mmol) in dry THF (5 ml) was added slowly TBAF (1M in THF, 0.22 ml, 0.22 mmol). The mixture was refluxed for 10 h under argon. A similar hydrolytic work-up was followed by a column chromatography over silica gel with hexane-diethyl ether (5 : 1 vol/vol) to give **18** (0.112 g, 34% base on the aldehyde) and then **34** (0.086 g, 21% based on the aldehyde). **34**: Pale yellow liquid; ^{1}H NMR ($CDCl_3$) δ=0.88 (6H, d, J=7.5 Hz, Me), 1.77 (1H, m, CH), 2.35 (2H, d, J=7.5 Hz, CH_2), 7.38 (1H, br s, 4-H), 8.19 (1H, br s, 6-H), and 8.32 (1H, br s, 2-H).

References

1) As reviews: A. J. Boulton and A. McKillop, "Six-membered Rings with One Nitrogen Atom," as Vol. 2A of "Comprehensive Heterocyclic Chemistry," ed by A. R. Katritzky and C. W. Rees, Pergamon Press, Oxford, New York, Toronto, Sydney, Paris, and Frankfurt (1984); P. G. Sammes, "Heterocyclic Compounds," as Vol. 4 of "Comprehensive Organic Chemistry," ed by Sir D. Barton and W. D. Ollis, Pergamon Press, Oxford, New York, Toronto, Sydney, paris, and Frankfurt (1979), pp. 1—84.

2) R. A. Abramovitch and J. G. Saha, *Adv. Heterocycl. Chem.*, **6**, 229 (1966); A. R. Katritzky, "Handbook of Heterocyclic Chemistry," Pergamon Press, Oxford, New York, Toronto, Sydney, Paris, and Frankfurt (1985), pp. 379.

3) P. Doyle and R. R. J. Yates, *Tetrahedron Lett.*, **1970**, 3371; Y. Tamaru, Y. Yamada, and Z. Yoshida, *J. Org. Chem.*, **43**, 3396 (1978); D. L. Comins and N. B. Mantlo, *Tetrahedron Lett.*, **24**, 3683 (1983).

4) A. I. Meyers and R. A. Gabel, *Tetrahedron Lett.*, **1978**, 227; G. W. Gribble and M. G. Saulnier, *ibid.*, **21**, 4137 (1980); J. Epsztajn, Z. Berski, J. Z. Brzezinski, and A. Jozwiak, *ibid.*, **21**, 4739 (1980); F. Marsais, G. L. Nard, and G. Quéguiner, *Synthesis*, **1982**, 235; T. Güngör, F. Marsais, and G. Quéguiner, *ibid.*, **1982**, 499; A. I. Meyers and R. A. Gabel, *J. Org. Chem.*, **47**, 2633 (1982).

5) E. Piers and M. Soucy, *Can. J. Chem.*, **52**, 3563 (1974); C. S. Giam, E. E. Knaus, and F. M. Pasutto, *J. Org. Chem.*, **39**, 3565 (1974); C. S. Giam and K. Ueno, *J. Am. Chem. Soc.*, **99**, 3166 (1977); A. R. Katrizky, J. G. Keay, D. N. Rogers, M. P. Sammes, C. W. F. Leung, and C. M. Lee, *Angew. Chem. Int. Ed. Engl.*, **18**, 792 (1979); K. Akiba, H. Matsuoka, and M. Wada, *Tetrahedron Lett.*, **22**, 4093 (1981); K. Akiba, Y. Iseki, and M. Wada, *ibid.*, **23**, 429 and 3935 (1982); D. L. Comins and A. H. Abdullah, *J. Org. Chem.*, **47**, 4315 (1982); D. L. Comins, *Tetrahedron Lett.*, **23**, 2807 (1983); D. L. Comins and N. B. Mantlo, *ibid.*, **24**, 3683 (1983); K. Akiba, Y. Nishihara, and M. Wada, *ibid.*, **24**, 5269 (1983).

6) C. S. Giam and S. D. Abbott, *J. Am. Chem. Soc.*, **93**, 1294 (1971).

7) R. A. Sulzbach, *J. Organomet. Chem.*, **24**, 307 (1970).

8) W. Ando and H. Tsumaki, *Tetrahedron Lett.*, **22**, 3073 (1982); R. J. P. Corriu, V. Huynh, J. J. E. Moreau, and M. Pataud-Sat, *ibid.*, **23**, 3257 (1982).

9) A part of the present work has been reported as a preliminary communication (O. Tsuge, S. Kanemasa, T. Naritomi, and J. Tanaka, *Chem. Lett.*, **1984**, 1255).

10) F. B. LaForge, *J. Am. Chem. Soc.*, **50**, 2484 (1928); F. J. Villani and M. S. King, *Org. Synth.*, **37**, 6 (1957).

11) The ^{13}C chemical shifts of pyridine is referred to p. 33 of "Handbook of Heterocyclic Chemistry" cited in Ref. 2.

12) E. M. Kaiser and J. D. Petty, *Synthesis*, **1975**, 705; S. V. Kannan and H. Pines, *J. Org. Chem.*, **36**, 2304 (1971).

 © 1987 The Chemical Society of Japan Bull. Chem. Soc. Jpn., 60, 1505—1514 (1987)

Thermoelectric Conversion by Thin-Layer Thermogalvanic Cells with Soluble Redox Couples

Tamio IKESHOJI
Government Industrial Research Institute, Tohoku, Nigatake 4-2-1, Sendai 983
(Received September 26, 1986)

Thermogalvanic cells containing a redox couple of $[Fe(CN)_6]^{4-/3-}$ or $Fe^{2+/3+}$ as an electroactive species were built for thermoelectric conversion from low-grade heat with a temperature less than 100 °C. The distance between high- and low-temperature electrodes was set to 1 mm in order to produce a high power density. Thermoelectric powers, inner resistances, and heat fluxes of the cells, which were placed horizontally (i.e. in which the temperature gradient was vertical) were measured under steady state conditions. Natural convection, which was induced by a temperature difference and current flowing in appropriate directions, produced lower inner resistances than those with no convection by several times. It had only a small effect on thermoelectric powers and heat-transfer coefficients. Thus, both the power densities and the thermal efficiencies increased by nearly one order of magnitude due to the convection. A power density of 2.6 W m^{-2} was obtained during steady state using a cell containing an aqueous solution of 0.13 mol dm^{-3} $K_4[Fe(CN)_6]$ and 0.85 mol dm^{-3} $K_3[Fe(CN)_6]$ at a temperature difference of 72 K and a thermal efficiency of 6.7×10^{-5}; the upper electrode was kept at a lower temperature.

The direct energy conversion of heat to electricity is a very attractive technique. Although a successful effort using an electrochemical system has not been presented yet, it has a higher thermoelectric power than that of metal thermocouples by nearly two orders of magnitude. It is of the order of 1 mV K^{-1}, which is as large as that of semiconductor thermocouples.

Several electrochemical systems for thermoelectric conversion appeared in the 1950s—60s and some of them were patented.[1,2] The systems of this period were mainly designed for high-temperature heat from the nuclear reactors in space crafts. In recent years two new systems have been proposed. One is called AMTEC (alkali metal thermoelectric converter), which is for high-temperature heat.[3] The other is a thermogalvanic cell using an aqueous electrolyte solution in order to convert low-grade heat (for instance, waste heat, geothermal heat, ocean thermal energy, etc).[4-6] Such thermoelectric conversions by electrochemical systems, sometimes called "thermally regenerative electrochemical system," have been reviewed in recent papers.[1,2,7] This paper is concerned with the aqueous thermogalvanic cells for energy conversion from heat sources of less than 100 °C.

A basic electrochemical cell for thermoelectric conversion is a thermogalvanic cell in which two electrodes of an identical type are maintained at a high temperature (T_H) and a low temperature (T_L) as

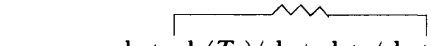

where "electrolyte" means an electrolyte solution such as molten salt, solid solution, or any other ionic conductors. A big difference in the thermoelectric conversion system using a thermogalvanic cell from that using a semiconductor or metal thermocouple concerns the type of charged species that move in the respective closed circuit. Only electrons move in the latter case, while ions and electrons move in the former thermogalvanic cell. A compound is, thus, accumulated at one of the two electrodes, where a charge-transfer reaction between ions and electrons takes place during operation. At the other electrode this same compound is consumed. These accumulated species must be returned to the latter electrode from the former one in order to continuously produce electricity from the cells. In many cases pumps are used to transfer the accumulated species through an outer circuit of the cells. This method, however, results in the losing of a major merit in that there are no moving parts in the direct thermoelectric conversion system. Another way for continuous operation is to periodically reverse the temperatures of the electrodes.[8]

It was suggested by Burrows that it is possible to return the accumulated species without using a pump if a soluble redox couple is used as the electroactive species with innert electrodes.[5,6] The electroactive species, i.e. the redox couple, are transferred by diffusion or convection in the electrolyte solution. As shown in a schematic diagram of the thermogalvanic cell with a soluble redox couple, $M^{m+/n+}$, in Fig. 1, M^{m+} is reduced to M^{n+} at the electrode of T_H, and the opposite reaction takes place at the electrode of T_L, as

$$M^{m+} + (m-n)e^- \longrightarrow M^{n+} \quad (T_H),$$

and

$$M^{n+} \longrightarrow M^{m+} + (m-n)e^- \quad (T_L),$$

where the thermoelectric power of this cell is assumed to be positive, i.e. the potential of the higher temperature electrode is positive against the lower temperature one. The counter ion, X^-, migrates from the higher-temperature electrode to the lower-temperature one in order to maintain the electroneutrality of the solution. At the T_H electrode, MX_m is consumed and MX_n is accumulated. At the T_L electrode, the opposite species are consumed and accumulated. A concentration polarization, then, arises in the thermogalvanic cell. If MX_n and MX_m are not transferred from one electrode

to the other, the potential difference due to this concentration polarization will increase until it becomes equal to the potential difference produced by the thermoelectric power; eventually, current will cease to flow.[8]

Since there is neither a diaphragm nor a membrane in the cell, the accumulated species can diffuse to the opposite electrode. A current corresponding to the amount of the species returned to the electrodes by the diffusion will continue to flow. The amount, however, is usually very small. In Burrows' cell rotating electrodes were used to obtain a higher current than that by diffusion only.[5] In this cell the consumed species is supplied by forced convection. Having a moter to rotate the electrode, the cell unfortunately again loses the big advantage of the direct thermoelectric conversion sysytem. Consequently, a short distance electrode cell, i.e. a thin-layer cell,[9] has been investigated in this study in order to obtain a high power density. Since the thermal efficiency of thermoelectric converters in which heat and electricity pass through the same part in the same direction is not fundamentally changed by their structures,[10] the thin-layer cell is expected to have a high power density without lowering the thermal efficiency.

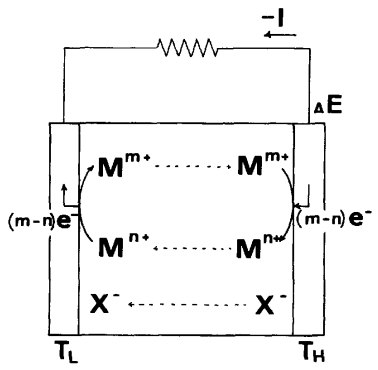

Fig. 1. A schematic diagram of a thermogalvanic cell with a soluble redox couple, $M^{m+/n+}$. T_H And T_L: Temperatures of electrodes ($T_H > T_L$), E: potential at T_H against that at T_L, I: current.

The current at a steady state in a thin-layer cell is, primarily, proportional to the speed of the diffusion determined by the concentration gradient induced by the flowing current. This means that the observed inner resistance of this cell increases from the solution resistance measured by the normal method. If the concentration gradient of the redox species can be diminished by homogenizing, the inner resistance will decrease. This would be possible by a natural convection induced by a temperature and/or concentration gradient in the cell without a motor. However, the convection in the cell has a possibility of enhancing the heat transfer through the cells, which may cause a low thermal efficiency. In this paper some effects to homoginize the redox couple on power densities, thermal efficiencies, etc. in the thin-layer thermogalvanic cells are described. The redox couple of $[Fe(CN)_6]^{4-/3-}$ was used in dilute and saturated solutions. Since a more concentrated solution results in a higher power density,[6] a redox couple of $Fe^{2+/3+}$ was used in a more concentrated solution than the saturated solution of $[Fe(CN)_6]^{4-/3-}$.

Experimental

The thin-layer thermogalvanic cell used in this study is illustrated in Fig. 2. The distance between two platinum plates (ca. 120×120×0.05 in mm) was kept at 1 mm with a byton rubber spacer, which had many holes of ca. 9 mm in diameter. The platinum electrodes were in contact with two heat transfer-plates of copper, of which temperature was kept constant by flowing water from thermostats. The two heat transfer-plates were tightened by electrically insulated bolts. Each hole of a spacer was filled with an aqueous electrolyte solution containing a redox couple ($[Fe(CN_6]^{4-/3-}$ or $Fe^{2+/3+}$). This thermogalvanic cell was horizontally placed and covered with a thermal insulator of polystyrene and polyurethane foams. Since the inner resistance of the cell was very small (<1Ω), a potentiostat or a power supply was used as an electrical load instead of a resistance. The cell voltage was measured through two leads independent of current leads, i.e. 4-probe method.

Three types of aqueous electrolyte solutions were used: a: a dilute solution of mixture of 0.010 mol dm^{-3} $K_4[Fe(CN)_6]$

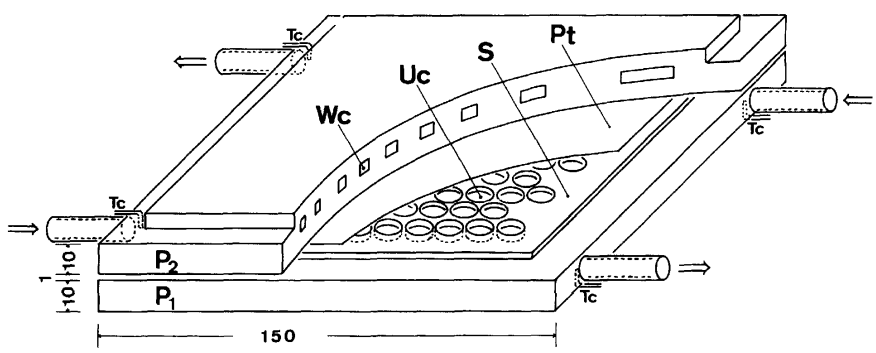

Fig. 2. Thin layer thermogalvanic cell. (Numbers in the illustration is in a unit of mm.) P_1 And P_2: Heat transfer plates, Pt: platinum plate, S: spacer, Tc: thermocouple, Uc: a unit cell, Wc: water channel, ⇨⇦: water inlet and outlet.

and 0.010 mol dm^{-3} $K_3[Fe(CN)_6]$, b: a concentrated solution of mixture of 0.13 mol dm^{-3} $K_4[Fe(CN)_6]$ and 0.85 mol dm^{-3} $K_3[Fe(CN)_6]$, which was made as a saturated solution at 0 °C of their mixture solution, c: a solution of 1.0 mol dm^{-3} $FeCl_2$ and 1.0 mol dm^{-3} $FeCl_3$ in pH 0.6 adjusted by hydrochloric acid. Every chemical used was guaranteed grade.

Notations and Definitions: The potential difference (ΔE) between two electrodes of a cell is defined here as the potential measured for the upper side electrode (temperature T_2) of two horizontal electrodes against the lower one (temperature T_1). The direction of the positive current (I) is defined here from the upper electrode to the lower one through the cell. The temperature difference (ΔT) is defined as T_2-T_1. The thermoelectric power (ε) of the cell is calculated from $\varepsilon=\Delta E/\Delta T$. T_1 and T_2 are the mean values of the temperatures measured by thermocouples placed at the water inlet and outlet in the respective heat-transfer plates, P_1 and P_2. The temperature differences between the inlet and outlet were less than 3 K. Heat transferred through the cell was calculated from a temperature decrease or increase of the flowing water (rates of ca. 15 ml s^{-1}). Heat transfer to the surroundings from the cell was so small that it could be neglected. The current density (i), resistance (R), power density (w), heat flux through the cell (q), and heat transfer coefficient (h) were calculated on a basis of the surface area (A=68.1 cm^2) of the platinum electrodes in contact with the solution as follows (units are shown in parentheses):

i = current through the cell/A (A m^{-2}),

R = cell resistance × A (Ω m^2),

$w = i \times \Delta E$ (W m^{-2}),

q = (heat transferred through the platinum electrode in contact with the solution)/A (W m^{-2}), and

$h = q/\Delta T$ (W K m^{-2}).

Results and Discussion

Thermoelectric Powers. When the temperature of one electrode was increased by changing the water source from a thermostat at ca. 5 °C to another at ca. 40 °C, the potential differences of the cells increased with time (t) as shown in Figs. 3-a, b, and c. In Fig. 3-d, a typical change in the temperature difference with time is shown. It is well known that species in the cell move to the higher or lower temperature electrodes due to Soret diffusion.[11,12] During steady state the Soret diffusion is in equilibrium with the diffusion due to a concentration difference built up by the Soret diffusion. The observed thermoelectric power is, therefore, changed by the potential difference due to this concentration polarization.[11,12] Then, there are two kinds of thermoelectric powers: an initial type (ε_i) defined as the thermoelectric power under the condition of uniform concentration in the cell, i.e. just after the temperature is changed, and a final type (ε_f) at a steady state under no convection, i.e. at time=∞.[11,12] The decreases in $|\Delta E|$ after maximum peaks in case of the cells with the $[Fe(CN)_6]^{4-/3-}$ redox couple (Fig. 3-a(−) and b(−)) are, thus, considered to be due to the Soret diffusion. The first increase in $|\Delta E|$ is toward

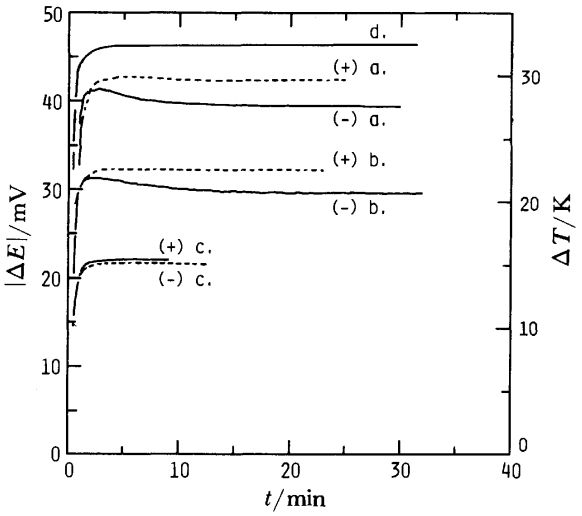

Fig. 3. Variations of potential (a, b, and c) and temperature (d) differences with time. (+): $\Delta E>0$, (−): $\Delta E<0$, min(T_1, T_2)=6.5—6.9 °C, a: cell with dilute $[Fe(CN)_6]^{4-/3-}$ solution, b: cell with concentrated $[Fe(CN)_6]^{4-/3-}$ solution, c: cell with concentrated $Fe^{2+/3+}$ solution, d: a typical temperature difference during the measurement of curve (−)a, ——: changes at $\Delta T>0$, ----: changes at $\Delta T<0$.

$\varepsilon_i\Delta T$, and the decrease of $|\Delta E|$ is toward $\varepsilon_f\Delta T$. The fact that there was no decrease of $|\Delta E|$ in Figs. 3-a(+), b(+), and c will be explained later.

In many measurements of the thermoelectric power reported so far, only initial thermoelectric powers have been presented,[13] since it generally takes a long time to attain Soret equilibrium. It is not surprising that Soret equilibrium was attained within a few minutes in the cells used here. This was because of the short distance between the two electrodes. The speed of the Soret diffusion can be evaluated by a characteristic time, τ, calculated from

$$\tau = \frac{d^2}{\pi^2 D},$$

where d is the distance between the electrodes, and D is the diffusion coefficient of the species in the cell.[13] For instance, from $D(K_4[Fe(CN)_6])=1.183\times10^{-9}$ m^2 s^{-1} (0.01 mol dm^{-3}, 25 °C)[15] and d=1 mm τ is about 1.5 min, which is corresponding to the observed speed.

In Fig. 4 thermoelectric powers under steady state conditions in these cells are shown as a function of the temperature differences with initial thermoelectric powers measured using an anti U-shaped cell shown in Ref. 16. Since the steady state thermoelectric powers were larger than $|\varepsilon_i|$ in cells with $[Fe(CN)_6]^{4-/3-}$, $[Fe(CN)_6]^{3-}$ migrates to the higher-temperature electrode and/or $[Fe(CN)_6]^{4-}$ to the lower-temperature one. In the cell with $Fe^{2+/3+}$, Fe^{2+} migrates to the higher-temperature electrode and/or Fe^{3+} to the lower-temperature one.

There is some evidence for natural convection arising in the cell with $[Fe(CN)_6]^{4-/3-}$, which could make

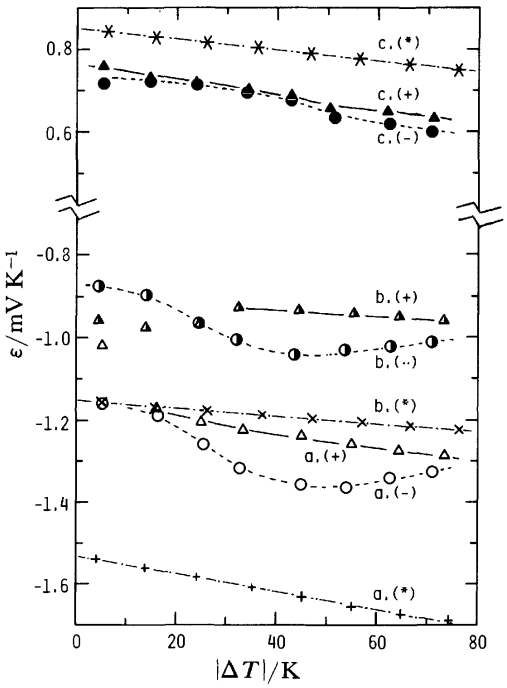

Fig. 4. Initial and steady state thermoelectric powers as a function of temperature difference. Min(T_1, T_2)=4.0—8.0 °C, (+): steady state ε at $\Delta T>0$, (−): steady state ε at $\Delta T<0$, (*): ε_i, a, b, and c: see Fig. 3.

the concentration uniform. They were observations that the steady state thermoelectric powers at $\Delta T<0$ shifted toward ε_i from ε_f (as can be seen in Figs. 4-a and b) and that the potential difference at $\Delta T<0$ achieved a steady state with no maximum (Fig. 3). The cause of the convection is considered to be explained as follows.

Natural convection in a pure solvent occurs when the temperature difference in a vertical direction exceeds a point (ΔT_{cr}) calculated from the critical Rayleigh number (Ra_{cr}) as[17]

$$Ra_{cr} = \frac{g\alpha|\Delta T_{cr}|d^4}{a\nu} = 1708,$$

where g, α, a, and ν are the accelation of gravity, the coefficient of volume expansion, the thermal diffusivity, and the kinematic viscosity of the solvent, respectively, and d is the distance of two plates of different temperature, i.e. the distance between the two electrodes. If $|\Delta T|<|\Delta T_{cr}|$, no convection occurs, even when the lower electrode is hotter. The critical temperature difference calculated is ca. −120 K at d=1 mm for pure water. Since the physical constants in this equation do not change much, even for the electrolyte solutions, ΔT_{cr} will not be so different from −120 K in the thermogalvanic cells. However, convection took place from $\Delta T\approx$−20 K in the cell with $[Fe(CN)_6]^{4-/3-}$ (as can be seen in Figs. 4-a and b, in which ε at $\Delta T<0$ was observed to shift toward ε_i, even at ΔT=−20 K. This suggests that the main cause of the convection is not due to a thermal expansion of the solution but, rather, it comes from the electrolyte, since the critical temperature difference may move close to 0 or convection takes place even at $\Delta T>0$ in two-component fluids.[18] The observed small critical temperature difference would, thus, be due to this special convection in the electrolyte solution.

In the case of $Fe^{2+/3+}$, at ε at $\Delta T>0$ is observed to shift toward ε_i as can be seen in Fig. 4-c. As pointed out in the above, convection could abnormally take place at this temperature difference, in which the lower electrode is hotter. Changes of the potential difference with time by increasing of the temperature (see Fig. 3-c), however, didn't show a distinguishable difference between the $\Delta E-t$ curves at $\Delta T>0$ and $\Delta T<0$. Clearer experimental evidence concerning the convection at $\Delta T>0$ will be given in the next section.

Inner Resistances. Resistances at $T_1=T_2$: When a small potential difference (=10 mV) was applied to cells at $T_1=T_2$, the current densities (i) through the cells decreased with time in different ways depending on the direction of the currents as shown in Fig. 5. The positive i for the cells with $[Fe(CN)_6]^{4-/3-}$ and the negative i for the cells with $Fe^{2+/3+}$ decreased like an exponential curve to steady state currents. Currents in the opposite direction decreased with oscillation to bigger steady state currents. In the latter case $K_4[Fe(CN)_6]$ and $FeCl_3$ were generated at the electrode of the upper side. The density of the solutions containing these compounds was higher than that of $K_3[Fe(CN)_6]$ or $FeCl_2$ solutions in the same molar concentration, respectively. A natural convection, then, could take place in the cells. It produces a smaller inner resistance during steady state than that of the former case in which the currents were controlled by the diffusion. The convection in the cell with a dilute solution seems to be weak (Fig. 5-a); it took a longer time for the oscillation of the current to start and its steady state current was not so large as that by diffusion. The reason is that the concentration difference induced in the dilute solution by the same applied voltage, which corresponds to the ratio of the concentrations of the oxidized and reduced species of the redox couple, is smaller than that in the cell with a concentrated solution.

Relations between the applied potential difference (ΔE) and the steady state current are shown in Fig. 6, wherein the measurements were performed from +500 mV to −500 mV in ΔE for Fig. 6-a and b and from +500 mV to −500 mV for Fig. 6-c, i.e. from the diffusion state to the convection one. The currents approached limiting values at a large potential difference, in which the concentration of one species of the redox couple was almost zero at one electrode. The currents will not increase beyond the limiting currents, unless another charge-transfer reaction or the stronger convection takes place. At a small potential difference (about less than 50 mV) currents were linearly proportional to ΔE in each side of $\Delta E>0$ and $\Delta E<0$ with different proportional ratios, i.e. different resistances, except at ΔE very close to 0, in which the concentra-

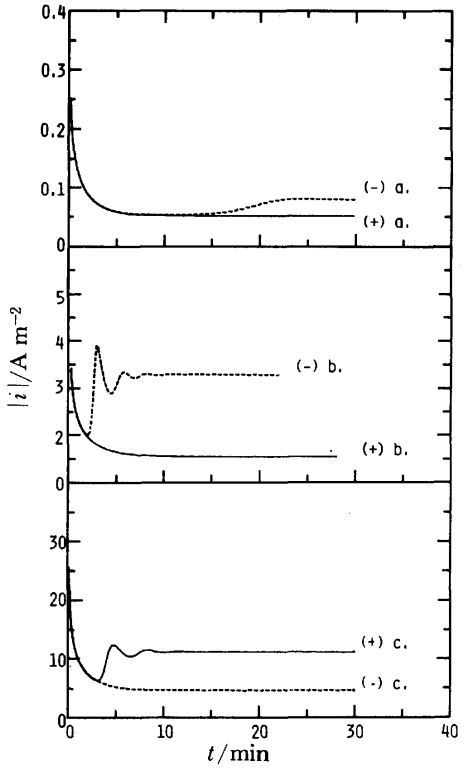

Fig. 5. Current variations with time by applying ±10 mV. (+): $\Delta E>0$ And $i>0$, (−): $\Delta E<0$ and $i<0$, a and b: $T_1=T_2=4.9\,°C$, c: $T_1=T_2=40.6\,°C$, a, b, and c: see also Fig. 3.

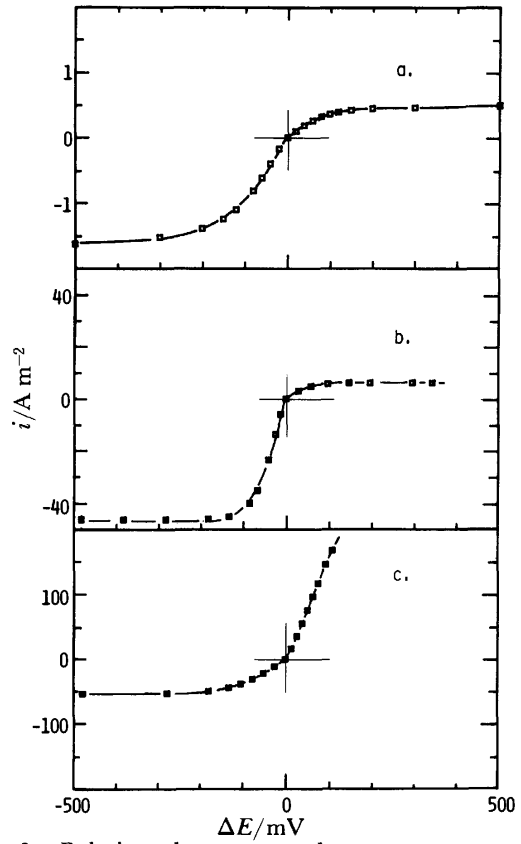

Fig. 6. Relations between steady state current and potential difference applied at $T_1=T_2$. a And b: $T_1=T_2=4.9$—$5.0\,°C$, c: $T_1=T_2=40.6\,°C$, a, b, and c: see also Fig. 3.

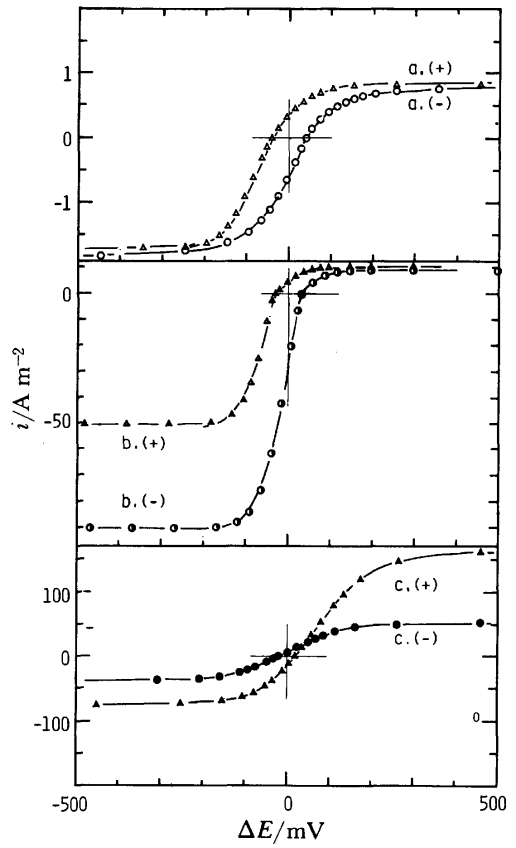

Fig. 7. Relations between steady state current and potential difference applied at $T_1 \neq T_2$. (+): $\Delta T>0$, (−): $\Delta T<0$, a and b: $T_H=39.2\,°C$ and $T_L=6.9\,°C$, c.(+): $T_1=39.1\,°C$ and $T_2=7.6\,°C$, c.(−): $T_1=4.3\,°C$ and $T_2=38.9\,°C$, a, b, and c: see also Fig. 3.

tion difference is so small that no convection arises. Detailed features of $i-\Delta E$ curves and resistances at $T_1=T_2$ are shown in Appendix 1.

Resistances at $T_1 \neq T_2$: In case of $T_1 \neq T_2$ i-ΔE relations can be divided into four regions, due to the signs of ΔT and i, i.e. due to how the convection arises. The results are shown in Fig. 7, wherein the measurements were performed in the same direction for applying ΔE (as in Fig. 6). It is noted here that an observation of the greater current at $\Delta T>0$ than at $\Delta T<0$ in the cell with $Fe^{2+/3+}$ (Fig. 7-c) confirms the previous argument that the convection is induced by $\Delta T>0$.

As already described, it is obvious that there are two causes (the temperature difference and the current) for the onset of convection. Those condisions are summarized as follows.

solutions	ΔT	i
$[Fe(CN)_6]^{4-/3-}$	−	−
$Fe^{2+/3+}$	+	+

When these two causes for the convection were superimposed positively, the biggest currents flowed (i.e. in cases of $\Delta T<0$ and $i<0$ for the cells with $[Fe(CN)_6]^{4-/3-}$ and in case of $\Delta T>0$ and $i>0$ for the cell with $Fe^{2+/3+}$). Under the conditions of the opposite

signs in ΔT and i, the smallest currents controlled by the diffusion were observed (i.e. in cases of $\Delta T>0$ and $i>0$ for the cells with $[Fe(CN)_6]^{4-/3-}$ and in case of $\Delta T<0$ and $i<0$ for the cell with $Fe^{2+/3+}$. When the two causes for convection are competitive, the following three states are possible: convection arises, it is diminished, or no convection arises. In cells with $[Fe(CN)_6]^{4-/3-}$, convection became completely diminished at $i\gg 0$, even at $\Delta T<0$. The limiting currents under these conditions were observed to be equal to those controlled by the diffusion. In the same cells at $\Delta T>0$, convection arose at $i\gg 0$. From these relations it is concluded that the condition $i<0$ is more predominant for convection to arise than that of $\Delta T<0$ in these cells. This is especially evident in a cell with a dilute solution as the almost equal negative limiting currents under the convection were observed at both $\Delta T<0$ and $\Delta T>0$. In cells with $Fe^{2+/3+}$ the condition $\Delta T>0$ was more predominant than that of $i>0$. This can be seen in curves at $\Delta T>0$, in which the currents of either $i\gg 0$ or $i\ll 0$ are bigger than those at $\Delta T<0$. More detailed descriptions for $i-\Delta E$ relations are given in Appendix 1.

The resistance during the generation of the electric power, where $i\Delta E<0$, is dependent on which region the $i-\Delta E$ relation belongs to during this condition. In cells with $[Fe(CN)_6]^{4-/3-}$ a negative current flows when a negative temperature difference is applied, i.e. $\Delta T<0$ and $i<0$. These two conditions are positive for convection to arise (as already described). Therefore, in this case the resistance was much smaller than that obtained under the opposite conditions ($\Delta T>$, $i>0$). In the cell with $Fe^{2+/3+}$ a negative current flowed when a positive temperature difference was applied, i.e. $\Delta T>0$ and $i<0$. Since only one of these two conditions ($\Delta T>0$) is positive for the convection, the resistances were not so small in comparison with that obtained under the opposite conditions ($\Delta T<0$, $i>0$).

The resistances measured by applying half of $\varepsilon\Delta T$, at which maximum power densities were obtained, are shown as a function of ΔT in Fig. 8. A typical change in the resistances with ΔT was observed in the cell with a dilute $[Fe(CN)_6]^{4-/3-}$ solution, in which the difference between the resistances at $\Delta T<0$ and $\Delta T>0$ increased with increasing $|\Delta T|$. This would be a reflection of a stronger convection at a bigger $|\Delta T|$.

Power Densities. Effects of Convection: In the region of $i\Delta E<0$ (Fig. 7) where the cells have electrical works to the surroundings, currents changed linearly with ΔE, i.e. the resistances were constant. Since the maximum power density (w) is obtained when the electrical load is equal to the inner resistance (R), it can be expressed as

$$w=\frac{\varepsilon^2\Delta T^2}{4R}, \qquad (1)$$

where R is assumed to be independent on the potential differences. The power densities obtained by applying $\varepsilon\Delta T/2$, which corresponds to the electrical load=R, are shown in Fig. 9. Those of the convection cells were larger than those of the diffusion cells at equal temperature differences due mainly to $1/R$ rather than ε. The differences between convection and diffusion cells are within 10% in ε, but is 4-times

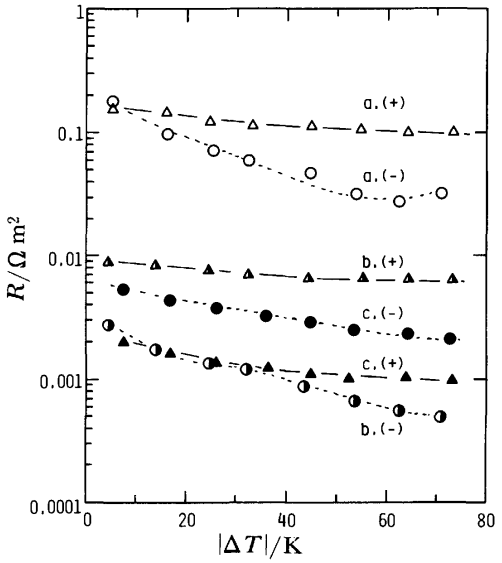

Fig. 8. Steady state resistances as a function of temperature difference. (+) And (−): see Fig. 7, a, b, and c: see Fig. 3.

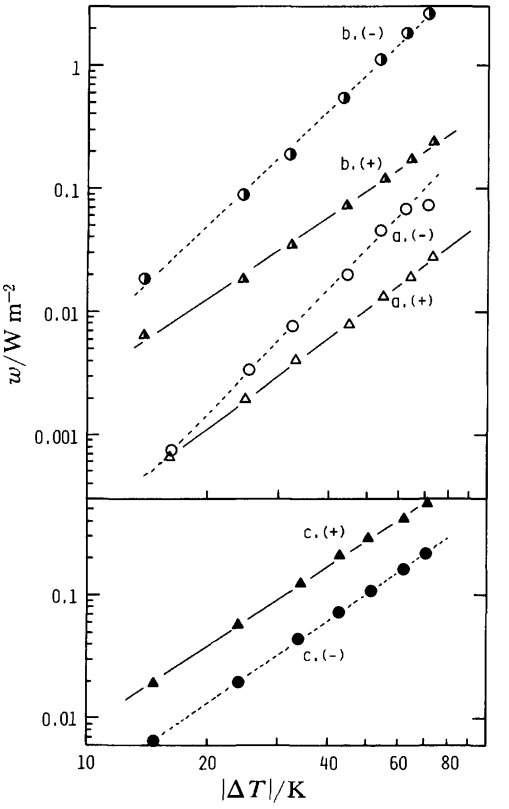

Fig. 9. Maximum power densities as a function of temperature difference. (+): $\Delta T>0$, (−): $\Delta T<0$, a, b, and c: see Fig. 3.

greater in $1/R$ for convection cells. The biggest power density obtained in these measurements was 2.6 W m^{-2} by a cell with a concentrated $[Fe(CN)_6]^{4-/3-}$ solution at ΔT=−72 K. A greater power density might be possible at greater temperature differences; however, it would become difficult to apply a temperature differences of nearly 100 °C or more than 100 °C. The biggest power density obtained in these measurements by a cell with $Fe^{2+/3+}$ was 0.56 W m^{-2} (at ΔT=71 K), less than the above cell because of a smaller $|\varepsilon|$, though the concentration was higher than the former cell and the inner resistance was of the same order.

It is possible to imagine an ideal state in which the inner resistnace is equal to the AC resistance (R_{AC}). This state can be achieved by a strong convection, which would also make the thermoelectric power close to ε_i. The ideal power density (w_{id}) is, then, calculated by inserting ε_i and R_{AC} instead of ε and R, respectively, into Eq. 1. At this ideal state, where the current does not decrease from the initial current, the power density in cells with $[Fe(CN)_6]^{4-/3-}$ can increase up to 40 W m^{-2}, which is higher than the observed power density (by 20 times). These estimations are summarized in Table 1. It is necessary to consider the size of ε_f and ε_i to conclude that convection always makes the power density bigger. In all the cells measured here $|\varepsilon_f|$ was smaller than $|\varepsilon_i|$; however, this relation can not be extended to all kinds of thermogalvanic cells. Some cases of $|\varepsilon_f|>|\varepsilon_i|$ were reported, but the difference between them was negligibly small: usually ca. 0.1—0.5 mV/K.[11] Therefore, it can be stated in a practical sense that convection can produce a higher power density in any type of thermogalvanic cell.

ΔT Dependence: If ε and R were not dependent on ΔT, the power densities should increase by a power of two from Eq. 1. However, the observed power densities fit lines with slopes of 2—3 in log-log plots of w and $|\Delta T|$ (Fig. 9). In the whole region of ΔT used here, $1/R$ increased by ca. 3—4 times in convection cells but only by ca. twice in diffusion cells. In the same region of ΔT the changes of ε were as small as ca. 20% in convection cells and ca. 10% in diffusion cells. The increase of $1/R$ with $|\Delta T|$, therefore, has greater affects on the power densities than on the changes of ε with $|\Delta T|$.

Heat Transfer. In thermoelectric converters the heat supplied to the high-temperature electrode is different from that taken away from the low-temperature electrode. The difference between two thermal energies is converted into electrical work. In the case of thermogalvanic cells, the heat flux supplied to the electrode at T_H is the sum of a heat flux (q_c) transferred by conduction and convection through the cell and that ($q_{e,H}$) transported by electrolyte and electrochemical reactions. The two heat fluxes can be expressed as[10]

$$q_c = h\Delta T, \tag{2}$$

and

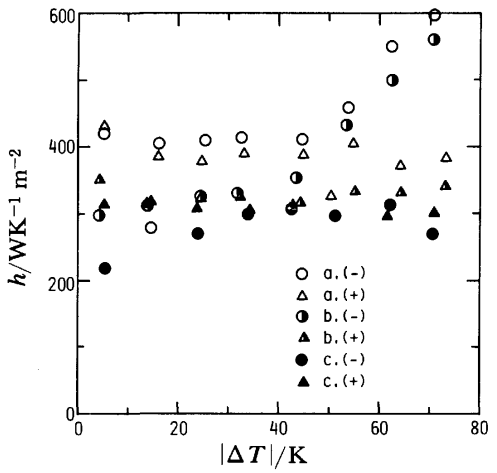

Fig. 10. Heat transfer coefficients as a function of temperature difference at no current. (+) and (−): see Fig. 9, a, b, and c: see Fig. 3.

$$q_{e,H} = -T_H i, \tag{3}$$

where h is the heat-transfer coefficient through the cell. The heat taken away from the cell at the low-temperature electrode is also the sum of q_c and the heat flux ($q_{e,L}=-T_L i$) transported by electrochemical processes. The difference between two heat fluxes, $q_{e,H}$ and $q_{e,L}$, is equal to the electrical work of this cell, $-\varepsilon\Delta T i$. A part of this work is converted into Joule heat in the cell.

Heat fluxes q_c and $q_{e,H}$ passing through a distance of 1 mm are estimated as q_c=609 W m^{-2} and $q_{e,H}$=0.3 W m^{-2} from $h=k$(the thermal conductivity of pure water)=0.609 W K^{-1} m, ε=1 mV K^{-1} the solution resistivity=1 Ωm, ΔT=1 K, and T_H=300 K. From $q_{e,H} \ll q_c$, the heat flux, q, transferred from the high-temperature electrode to the low one will be

$$q \approx q_c = h\Delta T.$$

Heat transfer coefficients obtained from $h=q/\Delta T$ in case of no current are shown as a function of the temperature difference in Fig. 10. In the cells with $[Fe(CN)_6]^{4-/3-}$, the heat-transfer coefficient started to increase at $\Delta T \approx -50$ K owing to the convection due to the temperature difference. In cells with $Fe^{2+/3+}$ it did not increase at both regions of $\Delta T>0$ and $\Delta T<0$. Although there was a possibility for the heat flux to increase by convection due to the current, no increase was observed within the experimental error (less than 40 W m^{-2} in q corresponding to 0.5—20 W K m^{-2} in h) during the measurement of Fig. 7.

Thermal Efficiencies. The thermal efficiency (η) at the maximum power of this cell can be calculated from Eqs. 1, 2, and 3 as

$$\eta = \frac{w}{q_c + q_{e,H}} = \frac{T_H - T_L}{T_H}\frac{1}{2}\left(\frac{1}{1+2/ZT_H}\right),$$

Table 1. Observed and Ideal Characteristics of the Thin-Layer Thermogalvanic Cells

	T_L	$\|\Delta T\|$	ε_d	ε_c	ε_i	R_d	R_c	R_{AC}[d]	w_d	w_c	w_{id}	h_d	h_c	η_d	η_c	η_{id}	Z_d	Z_c	Z_{id}
	°C		mV K^{-1}			$10^{-3}\,\Omega m^2$			W m^{-2}			W K^{-1} m^{-2}		10^{-6}			10^{-6}/K		
a. Dilute[a] $[Fe(CN)_6]^{4-/3-}$	5.5	72	−1.29	−1.33	−1.69	81	30	1.6	0.028	0.074	2.2	383	596	0.98	1.8	82	0.054	0.099	4.7
b. Cocentrated[b] $[Fe(CN)_6]^{4-/3-}$	5.4	72	−0.96	−1.01	−1.22	5.2	0.49	0.046	0.24	2.6	40	340	560	9.6	670	1660	0.053	3.7	95
c. Concentrated[c] $Fe^{3+/2+}$	6.3	71	0.60	0.63	0.75	2.1	0.97	0.18	0.22	0.56	3.9	269	300	11	26	205	0.63	1.4	12

a), b), and c): See Fig. 3-a, b, and c, respectively, d): Measured at 40°C. Meanings of suffixes; AC: measured by alternating current, c: measured under convection, d: measured under diffusion (or weak convection in the cell with $Fe^{2+/3+}$), i: initial, id: ideal.

and

$$Z = \varepsilon^2/hR,$$

where the term, $(T_H-T_L)/T_H$, is the thermal efficiency of the Carnot cycle, and Z is called a figure of merit.[10] Under the condition $q=q_c$, η will be

$$\eta = \frac{w}{q} = \frac{T_H - T_L}{T_H}\frac{ZT_H}{4}. \quad (4)$$

The highest thermal efficiency obtained in these measurements was 6.7×10^{-5} by the cell with the concentrated $[Fe(CN)_6]^{4-/3-}$ solution at $\Delta T=-72$ K (i.e. under the convection) with the biggest figure of merit, 3.7×10^{-6} K^{-1} (Table 1). In any cell a higher η and a bigger Z were obtained by convection cells than those by the diffusion cells. Though the heat-transfer coefficient increased with $|\Delta T|$ in the range of $\Delta T<-50$ K, the thermal efficiencies did not decrease except at one point, since increase in the electric work compensates for the heat leak across the cells. This can be proved generally, as described in Appendix 2.

The thermal efficiencies calculated from the measured power densities and heat fluxes are shown in Fig. 11 as a function of the temperature difference. From Eq. 4, they should increase linearly in the first order with the temperature difference, if the three constants, h, R, and ε, were not dependent on the temperature difference of the cell. The observed thermal efficiencies are on straight lines of slope greater than 1 in $\log(\eta)$-$\log(|\Delta T|)$ plots. This means that the higher thermal efficiencies (than those expected from the small temperature difference) were obtained at a greater temperature difference. This is mainly because of the lower resistance among the three factors (h, R, and ε) at large temperature differences.

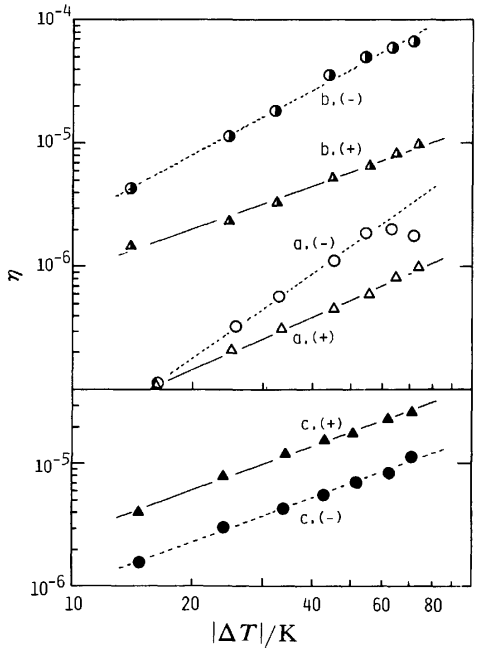

Fig. 11. Thermal efficiencies measured for the cell operating at temperature difference ΔT. (+) And (−): see Fig. 9, a, b, and c: see Fig. 3.

Conclusion

It was confirmed that in thin-layer thermogalvanic cells with soluble redox couples a natural convection induced by a temperature difference and by a concentration change due to current produces a small inner resistance under steady state conditions without sacrificing the thermal efficiency. An $[Fe(CN)_6]^{4-/3-}$ couple with K^+ is more suitable than an $Fe^{2+/3+}$ couple with Cl^-, since the convection induced by two causes is superimposed positively in the former case but it is reciprocal in the latter case. In addition, the former cell exhibits a bigger thermoelectric power than the latter. Minimizing the inner resistance during steady state conditions close to the AC resistance as possible is important for obtaining a high performance thermogalvanic cell. It is also necessary to find a redox couple with a higher thermoelectric power.

Appendix 1

$i-\Delta E$ Relations at Small $|\Delta E|$ and Isothermal Resistances. The $i-\Delta E$ curves measured by small potenital differences at $T_1=T_2$ are shown in Fig. 12, in which the transition points from the diffusion states to the convection states can be clearly seen as inflection points (ΔE_{in}) in those curves; $\Delta E_{in}=-6$ mV for the cell with the dilute $[Fe(CN)_6]^{4-/3-}$ solu-

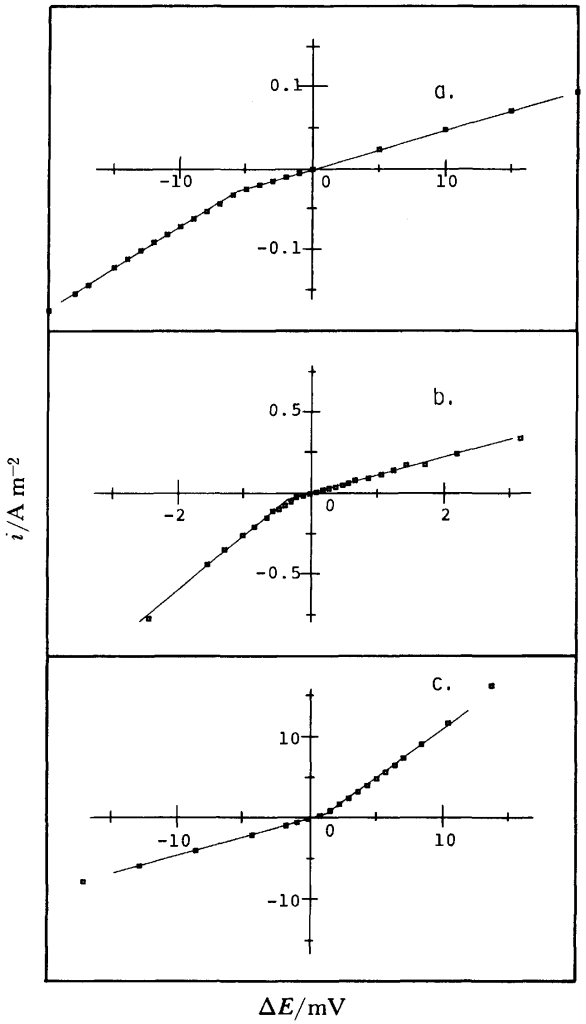

Fig. 12. Relations between steady state current and small potential difference applied at $T_1=T_2$. See Fig.6.

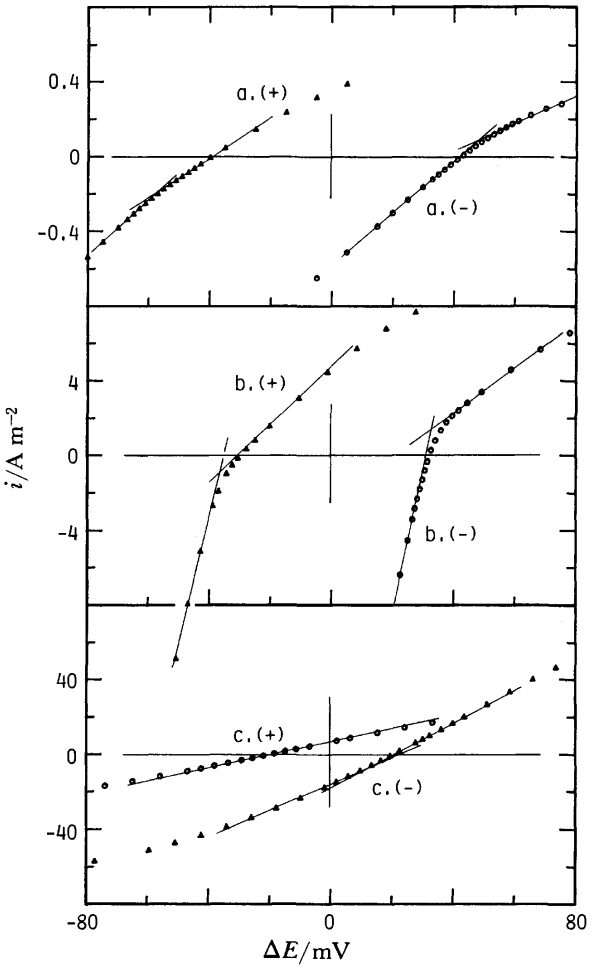

Fig. 13. Relations between steady state current and small potential difference applied at $T_1 \neq T_2$. See Fig. 7.

tion, ΔE_{in}=−0.3 mV for the concentrated $[Fe(CN)_6]^{4-/3-}$ one, and ΔE_{in}=2 mV for the concentrated $Fe^{2+/3+}$ one. In case of low concentration, this inflection point was farther from ΔE=0 than that of the concentrated solutilon, for the same reason as described for weak convection in a cell with a dilute solution.

The $i-\Delta E$ curves measured by small potential differences at $T_1 \neq T_2$ are shown in Fig. 13. The inflection points near i=0 in the $i-\Delta E$ curves (Fig. 13-c) of the cell with $Fe^{2+/3+}$ were not observed clearly. The reason for this may be due to the fact that a change of ΔE from − to + produces a small change in the state of this cell, such as from diffusion to weak convection or from weak convection to strong convection. In cells with $[Fe(CN)_6]^{4-/3-}$ a change of ΔE from + to makes it from diffusion to convection at the both directions of the temperature difference. Therefore, the clearer inflection points were observed in the latter cells. They moved to a somewhat more positive or negative potential difference than $\varepsilon_f \Delta T + \Delta E_{in}$, which is an expected inflection point by assuming no convection due to the temperature difference.

In Fig. 14 three kinds of resistances at $T(=T_1=T_2)$, the steady state resistances under diffusion with no convection (R_d), those under the convection (R_c), and AC resistances measured at 1 or 5 kHz (R_{AC}), are shown. The steady state resistances were calculated from changes in the steady state currents at $|\Delta E|$=5→10 mV. The AC resistances had a small frequency dispersion. Since both resistances (R_d and R_{AC}) are related to the diffusion coefficients, they decreased with an increase in the temperature with almost the same slope in log(R) vs. $1/T$ curves; 0.66±0.04, 0.72±0.09, and 1.1±0.1 $\times 10^3$ K for Fig. 14-a(+, *), b(+, *), and c(−, *), respectively. Since the resistances under convection (R_c) are related not only to R_d and R_{AC}, but also to the convection speeds, there is a possibility of having different features in log(R) vs. $1/T$ curves. However, they exhibited similar slopes in log(R) vs. $1/T$ curves; 0.55, 0.58, and 1.0×10^3 K for Fig. 14-a(−), b(−), and c(+), respectively.

Appendix 2

Thermal Efficiency in the Convection Cells. It is first assumed that a volume, V, of the solution in contact with the electrode at T_H is moved to the electrode at T_L within time Δt; heat flux under this condition can increase by

$$\Delta q_{convection} = V\rho c(T_H - T_L)/\Delta t,$$

where ρ and c are the density and the heat content of the solution, respectively. If all electroactive species transferred

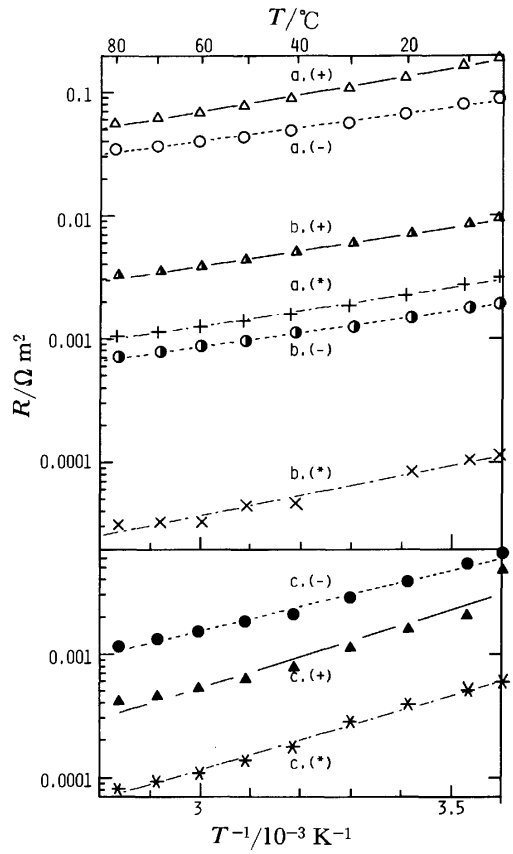

Fig. 14. Steady state and AC resistances as a function of temperature. (T_1=T_2) (+): Steady state R at $\Delta E>0$, (−): steady state R at $\Delta E<0$, (*): R_{AC} at 1 kHz (a and b) or 5 kHz (c), a, b, and c: see Fig. 3.

by this movement have a one-electron charge-transfer reaction with the electrodes, it can result in a current increase

$$\Delta i = FCV/\Delta t \quad (F\text{: Faraday constant}),$$

where C is the concentration of the electroactive species. The efficiency of increased work against the increased heat flux due to the convection is

$$\eta_{convection} = \frac{\varepsilon \Delta T \Delta i}{\Delta q_{convection}} = \frac{F\varepsilon C}{\rho c}.$$

If the efficiency of cells without convection (η_d), which can be roughly estimated as

$$\eta_d = \frac{(\varepsilon \Delta T)(FDC/d)}{k\Delta T/d} = \frac{F\varepsilon DC}{k} \quad (k\text{: thermal conductivity of the solution}),$$

assuming that the current is equal to the limiting current, FDC/d, is larger than $\eta_{convection}$, i.e. if

$$\frac{\eta_{convection}}{\eta_d} = \frac{a}{D} > 1,$$

where $a=k/\rho c$ (thermal diffusivity), the convection will make the thermal efficiency higher than that by the diffusion cell. Since the thermal diffusivity of the pure water is 1.45×10^{-7} $m^2 s^{-1}$ and the diffusion coefficients of many ions in water are in range of 10^{-10}—10^{-8} $m^2 s^{-1}$,[15] it is concluded that the convection always improves the thermal efficiency. If the convection is very strong, however, improvement may be impaired, since the current is limited by $\varepsilon_i \Delta T/R_{AC}$ under this condition. It is necessary to more rigorously determine how convection effects the heat transfer and the electrical resistance. This might be a new type of Benard problem[18] having not only the temperature difference but also the concentration difference induced by the current.

The author wishes to thank Dr. Shigeo Kimura of our Research Institute for his critical reading of the manuscript.

References

1) H. L. Chum and R. A. Osteryoung, *US DOE Rep.*, SERI-TR-332-416-VOL-1 (1980) and -VOL-2 (1981).
2) T. Ikeshoji, *Rept. Governm. Ind. Res. Inst., Tohoku*, **1984**, 39.
3) T. Cole, *Science*, **221**, 915 (1983) and Refs. therein.
4) B. Burrows, *Proc. Inters. Energy Convers. Eng. Conf.*, **10**, 821 (1975).
5) B. Burrows, *J. Electrochem. Soc.*, **123**, 154 (1976).
6) H. L. Chum, *Proc. Inters. Energy Convers. Eng. Conf.*, **15**, 1603 (1980).
7) H. L. Chum ed., *US DOE Rept*, SERI/CP-234-1577 (1981).
8) T. I. Quickenden and C. F. Vernon, *Solar Energy*, **36**, 63 (1986).
9) T. Ikeshoji, *Denki Kagaku*, **54**, 616 (1986).
10) e.g., S. W. Angrist, "Direct Energy Conversion," Allyn and Bacon (1965).
11) R. Haase, "Thermodynamics of Irreversible Processes," Addison-Wesley (1962).
12) J. N. Agar, "Advances in Electrochemistry and Electrochemical Engineering," ed by P. Delahay, Wiley (1961), Vol. 3.
13) J. N. Agar and J. C. R. Turnar, *Proc. Royal Soc.*, **1960**, 307 and refs. therein.
14) J. N. Agar and W. G. Breck, *Trans. Faraday Soc.*, **53**, 167 (1957).
15) "Handbook of Chemistry and Physics," CRC press (1979).
16) T. Ikeshoji and S. K. Ratkje, *J. Electrochem. Soc.*, **133**, 1107 (1986).
17) e.g., S. Chandrasekhar, "Hydrodynamic and Hydromagnetic Stability," Clarendon Press (1979).
18) P. Glansdorff and I. Prigogine, "Thermodynamic Theory of Structure, Stability and Fluctuations," Wiley-Interscience (1971).

Photo-Excitable Membranes. Effects of Nonactin as a Membrane Additive on the Photoresponse of Poly(vinyl chloride)/ Spirobenzopyran Membrane

Jun-ichi ANZAI, Yasushi HASEBE, Akihiko UENO, and Tetsuo OSA*
Pharmaceutical Institute, Tohoku University, Aobayama, Sendai 980
(Received September 11, 1986)

Synopsis. The magnitude of the photoinduced membrane potential across the poly(vinyl chloride)/spirobenzopyran/nonactin composite membrane depends considerably on the concentration of ammonium ion in the aqueous solution. The results are explained in terms of the charge density on the membrane surface.

Several groups have reported that the membrane potential across the polymer membranes doped with spirobenzopyran derivatives changes reversibly upon photoirradiation.[1-7] We have found that the photoinduced potential changes of more than 100 mV can be attained with rapid response time by the use of plasticized poly(vinyl chloride) (PVC) as a membrane matrix.[5-7] The low density of the fixed charge in the membrane and/or on the membrane surface may be favorable for the enhanced photoresponse. To verify the effects of the charge density on the photoresponse, a macrocyclic ionophore, nonactin, is immobilized in the membrane together with spirobenzopyran derivative (**1**). Since nonactin is an ionophore selective for NH_4^+ ion, it is possible to regulate the charge density on the membrane surface by varying the NH_4Cl concentration in the solution. This paper describes the effects of nonactin as a membrane additive on the photoresponse of the PVC/**1** membrane.

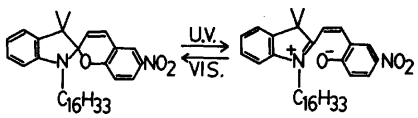

Closed-(1) Open-(1)

Experimental

Materials. PVC (molecular weight of ca. 70000) was obtained from Wako Co. Ltd. and used without further purification. Dibutyl phthalate (DBP), tetrahydrofuran (THF), and ammonium chloride (NH_4Cl) are of extra pure reagent grade. Nonactin was purchased from Fluka Co. The synthetic procedure and analytical data of **1** were reported previously.[7]

Membrane preparation. PVC/**1**/nonactin membrane of ca. 0.15 mm thickness was prepared by pouring the mixture of 250 mg of PVC, 0.5 ml of DBP, 20 mg (0.038 mmol) of **1**, 5 mg (0.007 mmol) of nonactin, and 20 ml of THF onto a flat Petri dish (8.5 cm diameter), and allowing the solvent to evaporate at room temperature. The membrane was conditioned by soaking it in 0.1 mM (M=mol dm^{-3}) NH_4Cl solution before use.

Membrane Potential Measurement. All measurements were conducted at 25 °C using a U-shaped glass cell. The composition of the electrochemical cell for the membrane potential measurements was as follows; Ag/AgCl| 0.1 M $(CH_3)_4NCl$| buffer solution (C_1)| PVC/**1**/nonactin membrane| NH_4Cl solution (C_2)| 0.1 M $(CH_3)_4NCl$| Ag/AgCl. The electrode in the C_1 compartment was earthed. All solutions were prepared using 5 mM Britton-Robinson buffer (pH 5.1). Photoirradiation was carried out from the C_2 side with a 500 W xenon lamp using cut-off filters to isolate UV (320 nm$<\lambda<$400 nm) and visible ($\lambda>$490 nm) light. Noise level in the potential was within 1 mV under the present experimental conditions.

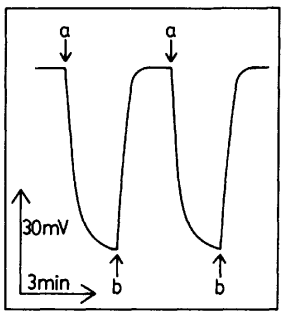

Fig. 1. Photoresponse of the membrane potential across the PVC/**1**/nonactin membrane. The C_2 side solution contained 10^{-5} M NH_4Cl. (a); UV light irradiation and (b); visible light irradiation.

Results and Discussion

A typical photoresponse of the membrane potential across the PVC/**1**/nonactin membrane is depicted in Fig. 1. When the membrane was exposed to UV light, the membrane potential shifted in the negative direction rapidly and, then, the original value of the potential was recovered by the subsequent visible light irradiation. The photoresponse of the membrane potential stems from the photochemical reaction of **1** accompanied with the generation of the fixed charge in the membrane, as was discussed for the PVC/**1** membrane previously.[5-7]

Figure 2 illustrates the membrane potential ($\Delta\phi$) across the PVC/**1**/nonactin membrane in the presence 1×10^{-7}—1×10^{-2} M of NH_4Cl in the C_2 side solution. In the dark, the $\Delta\phi$ values depend linearly on the concentration of NH_4^+ ion in the solution over the range of 1×10^{-5}—1×10^{-2}M, showing that NH_4^+ ions are adsorbed on the membrane surface by forming complexes with nonactin. In other words, the charge density on the membrane surface is determined by the concentration of NH_4^+ ion in the aqueous solution adjacent to the membrane surface. The $\Delta\phi$ values measured under UV light irradiation are also affected by the concentration of NH_4^+ ion in the range of 1×10^{-4}—1×10^{-2} M.

The photoinduced membrane potential ($\Delta(\Delta\phi)$), the difference between the $\Delta\phi$ value under UV light irra-

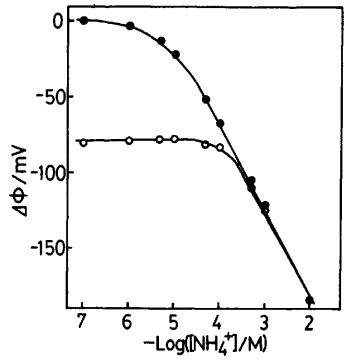

Fig. 2. The membrane potential across the PVC/1/nonactin membrane in the presence of NH_4Cl under UV light irradaition (—○—) and in the dark (—●—). The concentration of NH_4Cl in the C_1 side solution is zero.

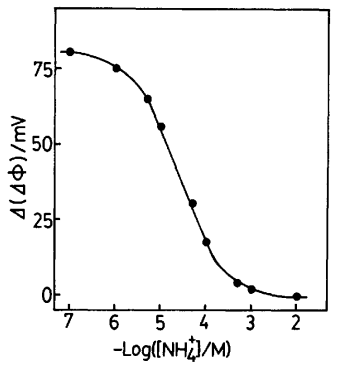

Fig. 3. The effects of the NH_4Cl concentration on the $\Delta(\Delta\phi)$ value.

diation and the one in the dark, is shown in Fig. 3. An approximately linear relationship exists between the $\Delta(\Delta\phi)$ values and the concentration of NH_4^+ ion over the range of 5×10^{-6}—1×10^{-4} M. It is clear that the photoresponse is enhanced in the lower concentration region of NH_4^+ ion. In the case of NH_4^+ ion concentration over 5×10^{-4} M, the photoresponse of the membrane potential is severely suppressed, being only 5 mV or less. This implys that the higher charge density on the membrane surface is not favorable for the enhanced photoresponse.

It is worth noting that these membranes can be applied to the sensitive layer of a novel class of ion sensors which change the $\Delta(\Delta\phi)$ value in response to the concentration of NH_4^+ ion. Furthermore, the membrane may be used for constructing the biosensors by coupling it with microorganisms and enzyme reactions that consume or produce NH_4^+ ion. The development of such biosensors is now in progress in this laboratory.

The authors are grateful to the Ministry of Education, Science and Culture of Japan for support of this work through a Grant-in-Aid for Special Project Research (No.61127003).

References.

1) S. Kato, M. Aizawa, and S. Suzuki, *J. Membr. Sci.*, **1**, 289 (1976).
2) S. Kato, M. Aizawa, and S. Suzuki, *J. Membr. Sci.*, **2**, 39 (1977).
3) I. R. Bellobono, B. Marcandalli, E. Selli, and S. Calgari, *Photogr. Sci. Eng.*, **28**, 162 (1984).
4) M. Irie, A. Menju, and K. Hayashi, *Nippon Kagaku Kaishi*, **1984**, 227.
5) J. Anzai, A. Ueno, and T. Osa, *J. Chem. Soc., Chem. Commun.*, **1984**, 688.
6) J. Anzai, H. Sasaki, A. Ueno, and T. Osa, *Chem. Lett.*, **1985**, 1443.
7) J. Anzai, Y. Hasebe, A. Ueno, and T. Osa, *Kobunshi Ronbunshu*, **43**, 683 (1986).

Liquid Crystal Formation in Binary Systems. XI.[1] Effects of Branching of Ester Alkyl Group on the Induction of Liquid Crystals in the *N,N,N',N'*-Tetramethylbenzidine-Alkyl 4-(4-Nitrobenzylideneamino)benzoate Systems

Yoshio MATSUNAGA* and Yurie NIKI
Department of Chemistry, Faculty of Science, Hokkaido University, Sapporo 060
(Received September 22, 1986)

Synopsis. Smectic A liquid crystals are induced in binary mixtures with normal alkyl esters as well as with esters of branched alkyl groups.

In our previous work,[2] the effects of branching of terminal alkyl groups on the liquid crystal induction in electron-donor-acceptor systems were studied employing nonmesogenic alkyl 4-[4-(dimethylamino)benzylideneamino]benzoates and 4,4'-dinitroazoxybenzene. Smectic A liquid crystals were found not only in the systems with the normal alkyl esters but also with the esters of branched alkyl groups such as *t*-butyl, 1,2-dimethylpropyl, and 1-ethylpropyl. These observations are in contrast with what are known for single mesogenic compounds. According to our study on alkyl 4-(4-phenylbenzylideneamino)benzoates, the *t*-butyl and 1-ethylpropyl esters are nonmesogenic.[3] While the thermally stable nematic and smectic A phases in the propyl ester are eliminated by the introduction of methyl groups to the 1- and 2-carbons, the monotropic smectic B phase is stabilized by 4 °C by the substitution. In order to confirm that methyl branching of the alkyl chains of acceptor molecules does result in the same behavioral trends in binary mixtures, a further study was made on the systems composed of nonmesogenic *N,N,N',N'*-tetramethylbenzidine (TMB) and alkyl 4-(4-nitrobenzylideneamino)-benzoates. TMB is known to produce liquid crystals when it is mixed with 4-alkoxy-4-nitro derivatives of *N*-benzylideneaniline.[4]

Experimental

Materials. *N,N,N',N'*-Tetramethylbenzidine was obtained from Aldrich Chemical Co. and was recrystallized from benzene. The acceptor compounds were prepared by the condensation reaction between *p*-nitrobenzaldehyde and appropriate alkyl *p*-aminobenzoate and purified by repeated recrystallization from ethanol.

Measurements. The calorimetric measurements and visual examinations were carried out as described in our earlier papers.[2,4]

Results and Discussion

The combination of TMB and the ethyl ester gives a phase diagram of the simple eutectic type. The smectic A phase induced in the composition range from 45 to 65 mol% of TMB is stable in a small area as the smectic-isotropic (S-I) transition point curve meets both the freezing point curves of the component compounds near the eutectic point, which is located at 53 mol% and 147 °C. The maximum lies at 152 °C and around 55 mol%. The isopropyl ester forms a 1:1 complex melting incongruently at 144 °C. Metastable smectic A phase appears in the range from 30 to 60 mol%, the maximum temperature being about 148 °C. The *t*-butyl ester complex also produces a peritectic at 151 °C. The maximum of the metastable S-I transition point curve is located at 147 °C. Thus, the branching methyl groups in these two cases enhance the thermal stability of the solid complex but diminish slightly that of the induced smectic A phase.

Figure 1a presents the phase diagram of the propyl ester-TMB system. Unlike the ethyl ester, this ester gives a 1:1 solid complex which decomposes to its component compounds at 104 °C. The induced smectic A phase is stable in the range from 25 to 50 mol%; however, it is metastable at the maximum located at about 138 °C and 55 mol%. No solid complex is produced by the *s*-butyl ester (see Fig. 1b). The smectic A phase is formed entirely beneath the freezing point curve of TMB. Although the maximum of the clearing point curve is not well defined, it is certain that the effect of the branching methyl group on the thermal stability of the mesophase is small.

The phase behavior of the isobutyl ester-TMB system shown in Fig. 1c bears a close similarity to that of the propy ester-TMB system. The peritectic is located at 102 °C and the maximum temperature of the induced mesophase is 133 °C. The latter temperature is lower by 5 °C than the corresponding one found for the *s*-butyl ester. Contrary to these findings, it is generally known for single mesogenic compounds that 1-methylation produces the largest decrease in the thermal stability of the smectic A phase and that as the methyl group is moved to the end of the chain, the effect becomes less marked.[5,6] The stabilization of the solid complex by the methyl groups at both the 1- and 2-carbons is significant (see Fig. 1d). The striking feature is nearly the same maximum S-I transition temperature observed for the 1,2-dimethylpropyl ester- and isobutyl ester-TMB systems.

We examined the effect of a branching methyl group introduced to the 1-, 2-, and 3-carbons respectively on the mesophase induced in the butyl ester-TMB system. The butyl and 1-methylbutyl esters yield diagrams of the peritectic type. The smectic A phase is enantiotropic in the former system and is monotropic in the latter. The whole S-I transition point curve is below the freezing point curve of TMB in the diagrams of the simple eutectic type given by the other two esters. Although the clearing point curve is traceable up to 55 mol% of TMB, the maximum appears to be located at a composition a little higher than this. The highest observable temperature is 149 °C for the liquid crystal

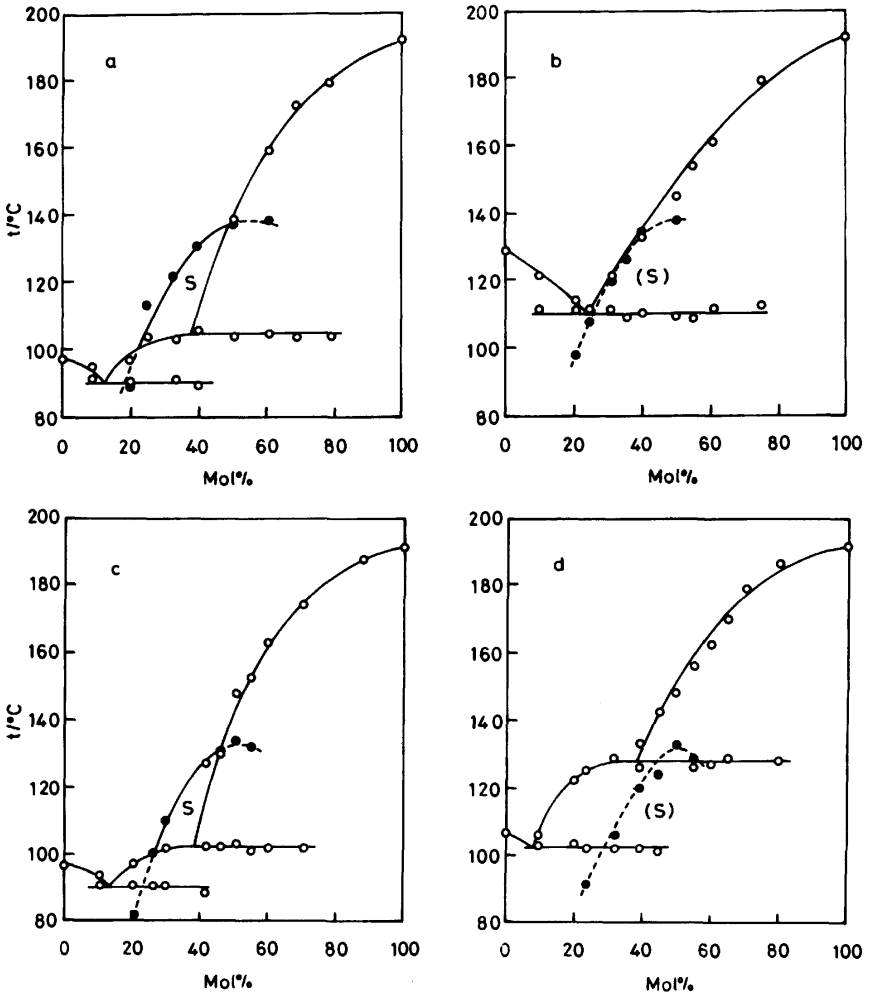

Fig. 1. Phase diagrams of the systems of TMB with (a) the propyl ester, (b) the *s*-butyl ester, (c) the isobutyl ester, and (d) the 1,2-dimethylpropyl ester. The open and shaded circles are transitions observed in the processes of heating and cooling respectively.

given by the butyl ester. It is depressed to 140 °C by 1-methylation, to 134 °C by 2-methylation, and to 138 °C by 3-methylation. The degree of depression by 1- and 2-methyl groups is consistent not only with the tendency found with the propyl ester but also with that reported for the alkyl 4-[4-(dimethylamino)benzylideneamino]benzoate-4,4′-dinitroazoxybenzene system.[2] Thus, the anomalously small effects of 1-methylation of terminal alkyl groups appear to be common to binary liquid crystals and the arguments proposed in the previous paper may also be advanced for them. The 1-methyl group may be accommodated readily within room made available by shorter molecules and cause no serious steric effects when molecules of different lengths are aligned side by side.

This work was supported by the Grant-in-Aid of Special Research Project on Properties of Molecular Assemblies (No. 60104002) from the Ministry of Education, Science and Culture.

References

1) Part X. E. Chino, Y. Matsunaga, and M. Suzuki, *Bull. Chem. Soc. Jpn.*, **57**, 2371 (1984).
2) Y. Matsunaga and I. Suzuki, *Bull. Chem. Soc. Jpn.*, **57**, 1411 (1984).
3) Y. Matsunaga and N. Miyajima, *Mol. Cryst. Liq. Cryst.*, **104**, 353 (1984).
4) M. Fukui and Y. Matsunaga, *Bull. Chem. Soc. Jpn.*, **55**, 3707 (1982).
5) G. W. Gray and K. J. Harrison, *Mol. Cryst. Liq. Cryst.*, **13**, 37 (1971).
6) G. W. Gray and S. M. Kelly, *Mol. Cryst. Liq. Cryst.*, **104**, 335 (1984).

Electrocrystallization of Phenothiazine

Kyuya YAKUSHI,* Michiko YOSHITAKE, and Haruo KURODA
Department of Chemistry, Faculty of Science, The University of Tokyo, Hongo, Tokyo 113
(Received October 1, 1986)

Synopsis. New cation radical salts of phenothiazine with (1:1), (3:2), and (2:1) compositions were prepared by the method of electrochemical oxidation. The electrical resistivities measured on the compaction of crystalline powder were 10^3—10^5 Ω cm at room temperature in the case of the complex salts. The powder absorption spectra in IR and Visible regions were also studied.

Phenothiazine (PTZ) is an electron donor with relatively low oxidation potentials, 0.58 volt vs. SCE, in acetonitrile solution.[1] The electron donor-acceptor compounds and the cation radical salts of PTZ have been studied by several groups,[2-9] but little is known about the behaviors of the complex salts: Only the bromine and iodine complexes prepared by the solid state reaction[10-13] are the complex salts of PTZ which have been studied so far. In addition to the property as an electron donor, PTZ is expected to behave as a proton donor as well as proton acceptor. This could provide a possibility to prepare a new type electronic conductor in which the coupling between the conduction electrons and proton plays an important role. From this point of view, we synthesized several complex salts of PTZ by means of the electrochemical method.

Experimental

The PTZ were recrystallized twice from its benzene solution. As the solvent of elctrochemical reaction, we used 1,2-dichloroethane which were purified by distillation with CaH_2 in nitrogen atmosphere. The materials for the counter anions, $(n\text{-Bu})_4NX$, (X=BF_4, ClO_4, ReO_4, $FeCl_4$, PF_6, AsF_6) were recrystallized for 2 or 3 times from methanol or ethanol. The electrochemical preparation of PTZ salts were carried out by using a U-shape electrochemical cell, in which the anode and the cathod compartments are separated by glass filters. Platinum plates were used as the electrodes. The concentrations of PTZ and supporting electrolyte were 2×10^{-2} mol dm^{-3} and 3×10^{-2} mol dm^{-3}, respectively. The electrochemical preparation were conducted in the galvanostatic mode with a current of 100 μA for 2 d. Since the solubility of PTZ salt is very high, the electrochemical cell were cooled down to −35 °C. The salt crystals deposited on the anode were washed by cooled 1,2-dichloroethane. The results of the chemical analysis are as follows; $(PTZ)FeCl_4$, Found/Calcd: C, 36.50/36.31; H, 2.75/2.29; N, 3.65/3.53; S, 7.80/8.08; Cl, 32.78/35.73.[14] $(PTZ)_2BF_4$, Found/Calcd: C, 57.87/59.39; H, 3.79/3.74; N, 5.62/5.77; S, 12.92/13.21. $(PTZ)_2ClO_4$, Found/Calcd: C, 57.76/57.88; H, 3.65/3.64; N, 5.70/5.63; S, 13.21/12.88; Cl, 7.39/7.12. $(PTZ)_2PF_6$,[15] C, 52.07/53.04; H, 3.30/3.34; N, 5.08/5.15. $(PTZ)_2AsF_6$, C, 48.91/49.07; H, 3.06/3.09; N, 4.79/4.77; S, 11.37/10.91. $(PTZ)_3(ReO_4)_2$, C, 39.42/39.37; H, 2.70/2.48; N, 3.76/3.83; S, 8.56/8.76.

The powder absorption spectra of PTZ salts were measured with HITACHI 260-30 for the infrared region and HITACHI 340 for the Near IR and visible region by use of the KBr disk method.

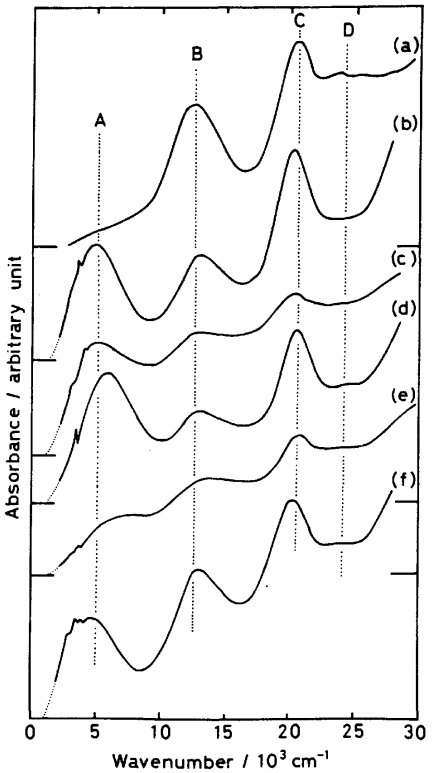

Fig. 1. Absorption spectra of phenothiazine (PTZ) radical salts. (a) $(PTZ)FeCl_4$, (b) $(PTZ)_2BF_4$, (c) $(PTZ)_2ClO_4$, (d) $(PTZ)_2PF_6$, (e) $(PTZ)_2AsF_6$. (f) $(PTZ)_3(ReO_4)_2$.

Results and Discussion

All PTZ complexes were obtained as black crystalline powders. Hexagonal prism were sometimes obtained in the case of $(PTZ)_2ClO_4$ when acetonitrile was used as a solvent, but they were found to be not a single crystal but polycrystalline by X-ray diffraction. PTZ is known to have many oxidation stages in solution including the transfer of hydrogen atom.[16] In this electrochemical cell, the solution always had an orange color at low temperature, which is the typical color of a PTZ radical cation. However, the color of the solution rapidly changed to deep green on mixing of the solutions in the anode and the cathod compartments. The UV-Visible absorption spectrum of the 1,2-dichloroethane solution of each PTZ salt exhibited the spectrum characteristic of PTZ cation radical, which has a weak absorption band around 13.5×10^3 cm^{-1} accompanied by several vibrational structures, a strong band at 19.3×10^3 cm^{-1} with vibrational progressions and a band at 22.5×10^3 cm^{-1}.[7] The absorption bands, B, C, and D of the solid PTZ complexes shown in Fig. 1 correspond to each of these character-

istic absorption bands of PTZ cation radical, providing an evidence for the formation of the PTZ cation radical salt.

The absorption spectrum of solid (PTZ)$FeCl_4$ is quite similar to the polarized absorption spectrum of the single crystal of the PTZ simple salt, (PTZ)$SbCl_6$,[8] in which the PTZ cation is isolated without charge-transfer interaction. Therefore, solid (PTZ)$FeCl_4$ is likely to be composed of an isolated PTZ cation radical. The spectra of $(PTZ)_2BF_4$, $(PTZ)_2ClO_4$, $(PTZ)_2PF_6$, and $(PTZ)_2AsF_6$ are quite similar to each other. They exhibit an absorption band, A, around 5×10^3 cm^{-1}, in addition to bands associated with the intramolecular transitions of PTZ cation radical, B, C, and D. These salts involve formally PTZ^+ and PTZ^0 according to their chemical composition. We can assign the new absorption band, A, to the charge-transfer(CT) transition from PTZ^0 to PTZ^+, since this type of CT band usually appears in the near infrared or infrared region in the case of the organic charge-transfer salts with a mixed valence molecular column. The CT transition of the same type were observed at about 4×10^3 cm^{-1} in TCNQ complex salt[17] and around 2×10^3 cm^{-1} in (2:1) TMTTF salt.[18] Very similar spectra were observed by Doi and Matsunaga in $(PTZ)_2Br$, which were synthesized by the solid state reaction between (PTZ)Br and PTZ.[10] The absorption band corresponding to A was also observed in (PTZ)Br by Iida who attributed it $(PTZ^0)(PTZ^+)(Br_3^-)$ contained by a small amount in the sample of (PTZ)Br.[7] Matsunaga and Shono found that the intensity of the above-mentioned band significantly increased by the addition of iodine to (PTZ)Br,[11] and suggested the formation of a complex cation salt, $(PTZ^0)(PTZ^+)(IBr_2^-)$. All these PTZ complex salts hitherto investigated were prepared by means of the solid state reaction, and are not stoichiometric compounds. In contrast, the PTZ complex salts obtained in the present study were prepared by the electrochemical oxidation and have a definite composition. To the best of our knowledge, these are the first stoichiometric complex salts of PTZ ever made. Among the complex salts prepared here, $(PTZ)_3(ReO_4)_2$ has a stoichiometry different from other salts, but the absorption spectrum of this material was almost the same as the (2:1) complex salts except that the CT band is slightly shifted to the low-wavenumber side.

Finally we listed in Table 1 the electrical resistivities measured on the compaction of powder sample. Unfortunately, none of them exhibits a metallic low resistivity, although the resistivities of the complex salts are found to be smaller by a factor of 10^2—10^3 than that of the simple salt, (PTZ)$FeCl_4$.

Table 1. Electrical Resistivity and the Position of the CT Band of PTZ Cation Radical Salts

Salts	ρ/Ωcm	$\nu_{max}/10^3$ cm^{-1}
(PTZ)$FeCl_4$	2×10^7	—
$(PTZ)_2BF_4$	4×10^4	4.8
$(PTZ)_2ClO_4$	1×10^5	5.0
$(PTZ)_2PF_6$	7×10^5	5.9
$(PTZ)_2AsF_6$	2×10^5	7.6
$(PTZ)_3(ReO_4)_2$	4×10^3	4.5

References

1) R. C. Wheland and J. L. Gillson, *J. Am. Chem. Soc.*, **98**, 3916 (1976).
2) C. J. Fritchie, Jr. and B. L. Trus, *J. Chem Soc., Chem. Commun.*, **1968**, 833.
3) C. J. Fritchie, Jr., *J. Chem. Soc.*, (A) **1969**, 1328.
4) H. Kobayashi, *Acta Crystallogr., Sect. B*, **30**, 1010 (1974).
5) R. Anthonj. N. Karl, B. E. Robertson, and J. J. Stezowski, *J. Chem. Phys.*, **72**, 1244 (1980).
6) A. Singhabhandhu, P. D. Robinson, J. H. Fang, and W. E. Geiger, Jr., *Inorg. Chem.*, **14**, 318 (1975).
7) Y. Iida, *Bull. Chem. Soc. Jpn.*, **44**, 663 (1971), and references therein.
8) T. Uchida, M. Ito, and K. Kozawa, *Bull. Chem. Soc. Jpn.*, **56**, 577 (1983).
9) T. Uchida, H. Seki, M. Ito, K. Nakano, T. Hoshizaki, and K. Kozawa, *Chem. Lett.*, **1986**, 999.
10) S. Doi and Y. Matsunaga, *Bull. Chem. Soc. Jpn.*, **48**, 3747 (1975).
11) Y. Matsunaga and K. Shono, *Bull. Chem. Soc. Jpn.*, **43**, 2997 (1970).
12) S. Doi, T. Inabe, and Y. Matsunaga, *Bull. Chem. Soc. Jpn.*, **50**, 8370 (1977).
13) T. Matsumoto and Y. Matsunaga, *Bull. Chem. Soc. Jpn.*, **54**, 648 (1981).
14) The disagreement of the content of the chlorine atom is probably due to the interference with the ferric ion.
15) The content of the sulfur atom was not determined because of the disturbance of the phosphine atom.
16) P. Hanson and R. O. C. Norman, *J. Chem. Soc., Perkin Trans. 2*, **1973**, 264.
17) M. J. Rice, V. M. Yartsev, and C. S. Jacobsen, *Phys. Rev. B*, **21**, 3437 (1980).
18) C. S. Jacobsen, D. B. Tanner, and K. Bechgard, *Phys. Rev. B*, **28**, 7019 (1983); K. Yakushi, S. Aratani, K. Kikuchi, H. Tajima, and H. Kuroda, *Bull. Chem. Soc. Jpn.*, **59**, 363 (1986).

Partition Parameters for Three Redox Forms of Viologen in a Nonionic Micellar Solution

Katsuyoshi HOSHINO, Hiroaki SASAKI, Kosaku SUGA, and Tetsuo SAJI*
Department of Chemical Engineering, Tokyo Institute of Technology, Ohokayama, Meguro-ku, Tokyo 152
(Received October 24, 1986)

Synopsis. The partition parameters of 1,1′-dimethyl-4,4′-bipyridinium (**1**), 1-decyl-1′-methyl-4,4′-bipyridinium (**2**), and 1-dodecyl-1′-methyl-4,4′-bipyridinium (**3**) between the micellar and water phases were determined by electrochemical methods. It was shown that $\mathbf{1}^0$, $\mathbf{2}^{+}$, $\mathbf{2}^0$, and $\mathbf{3}^{2+}$ are almost completely solubilized in the micellar phase and that $\mathbf{1}^{2+}$, $\mathbf{1}^{+}$ and $\mathbf{2}^{2+}$ are partitioned into two phases.

In relation to photochemical splitting of water, the reduction of 1,1′-dimethyl-4,4′-bipyridinium (methyl violigen) and its surfactant derivatives with photoexcited sensitizers has been investigated in micellar systems.[1] In order to interpret quantitatively the efficiency and kinetics of this process, we must know partition parameters (K) of the viologens between micellar and water phases, because the reaction rate of micelle-solubilized substance is a function of K for both the reactants and the products.[2,3]

No report, however, has dealt with the change in partition of viologens in redox states of bipyridinium group. The purpose of this paper is to estimate the values of K for divalent, mono-reduced, and fully reduced viologens in a nonionic micellar system by means of electrochemical methods.

The viologen derivatives studied are 1,1′-dimethyl-4,4′-bipyridinium dichloride (**1**), 1-decyl-1′-methyl-4,4′-bipyridinium dibromide (**2**), and 1-dodecyl-1′-methyl-4,4′-bipyridinium dibromide (**3**).

Experimental

3 was prepared by the method described in the literature[4] and identified by elemental analysis and melting point. The synthesis of **2** was similar to that of **3**: Mp 266—267 °C; Found: C, 52.85; H, 6.84; N, 5.73%. Calcd for $C_{21}H_{32}N_2Br_2$: C, 53.52; H, 6.63; N, 5.94%. **1** was used as supplied by Tokyo Kasei Co.

Electrochemical measurements were carried out at 25 °C under a nitrogen atmosphere for test solutions containing 0.1 M (1 M=1 mol dm^{-3}) NaCl as a supporting electrolyte. A glassy-carbon disk electrode and a saturated calomel electrode (SCE) were used respectively as working and reference electrodes in cyclic voltammetry and potential-step chronoamperometry. Controlled potential bulk electrolysis was performed with a Hg working electrode.

The host surfactant used is α-[*p*-(1,1,3,3-tetramethylbutyl)-phenyl]-ω-hydroxypoly(oxyethylene), Triton X-100, (TX-100, Wako Pure Chemicals Co.) and used as supplied. The concentration of TX-100 was kept constant at 0.1 M throughout the experiments. The concentration of **1**, **2**, and **3** in 0.1 M TX-100 micellar solution was ajusted to the condition that one micelle contains not more than one molecule of **1**, **2**, and **3** on average. All of the solutions were prepared with twice-distilled water.

Results and Discussion

Figure 1 shows cyclic voltammograms for solutions of 0.62 mM $\mathbf{1}^{n+}$ (n=2, 1, and 0) containining 0.1 M TX-100 and 0.1 M NaCl. The solutions of $\mathbf{1}^{+}$ and $\mathbf{1}^0$ were prepared by controlled-potential bulk reduction of $\mathbf{1}^{2+}$ at −0.84 and −1.3 V vs. SCE, respectively. The color of the solution of $\mathbf{1}^{+}$ was intense blue, while that of $\mathbf{1}^0$ was brownish yellow.

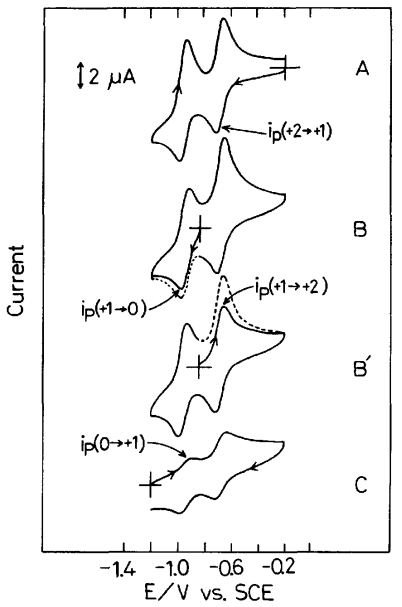

Fig. 1. Cyclic voltammograms for (A) a solution of 0.62 mM $\mathbf{1}^{2+}$, (B) and (B′) a solution of 0.62 mM $\mathbf{1}^{+}$, and (C) a solution of 0.62 mM $\mathbf{1}^0$ containing 0.1 M TX-100 and 0.1 M NaCl at 25 °C. Sweep rate: 12 mV s^{-1}. Working electrode area: 0.071 cm^2.

The first and the second reduction steps seem to be reversible one-electron processes judging from the value of peak separation, i.e., the difference between cathodic and anodic peak potentials.[5] The half-wave potentials were −0.69 and −0.96 V vs. SCE for the first and the second reduction steps, respectively. These values agreed well with those described in the literature.[6] The peak current for the first reduction step of $\mathbf{1}^{2+}$, $i_p(+2\rightarrow+1)$, in Fig. 1A is nearly equal to that for the first reduction step of $\mathbf{1}^{+}$, $i_p(+1\rightarrow0)$, in Fig. 1B and that for the first oxidation step of $\mathbf{1}^{+}$, $i_p(+1\rightarrow+2)$, in Fig. 1B′. On the other hand, the peak current for the first oxidation step of $\mathbf{1}^0$, $i_p(0\rightarrow+1)$, in Fig. 1C is much smaller than $i_p(+2\rightarrow+1)$, $i_p(+1\rightarrow0)$, and $i_p(+1\rightarrow+2)$.

Table 1 shows the apparent diffusion coefficients (D_{app}) for $\mathbf{1}^{2+}$, $\mathbf{1}^{+}$, and $\mathbf{1}^0$ in a solution containing 0.1 M TX-100 and 0.1 M NaCl. D_{app} was determined from inclination of the current vs. (time)$^{-1/2}$ plot in potential-step chrono-amperometry.[5]

According to the electrochemistry of micelle-solubilized substances,[3,7] D_{app} for the solubilizate (S) partitioning into micellar and aqueous phases gives the partition parameter (K) defined as the ratio of concentration of S in aqueous phase, [S]$_w$, to that in

Table 1. Apparent Diffusion Coefficient (D_{app}), Partition Parameter (K), and Mole Fraction in the Micellar Phase (x) of **1**, **2**, and **3** in 0.1 M NaCl with and without 0.1 M TX-100 at 25 °C

Solubilizate	Surfactant	$D_{app}\times10^6$ / $cm^2\,s^{-1}$	K	x
$\mathbf{1}^{2+}$	—	14	—	—
$\mathbf{1}^{2+}$	0.1 M TX-100	7.4	1.0	0.50
$\mathbf{1}^{+}$	0.1 M TX-100	7.4	1.0	0.50
$\mathbf{1}^{0}$	0.1 M TX-100	0.73	0.01	0.99
$\mathbf{2}^{2+}$	—	8.0	—	—
$\mathbf{2}^{2+}$	0.1 M TX-100	3.1	0.50	0.67
$\mathbf{2}^{+}$	0.1 M TX-100	1.4	0.11	0.90
$\mathbf{2}^{0}$	0.1 M TX-100	0.71	0.01	0.99
$\mathbf{3}^{2+}$	—	8.0	—	—
$\mathbf{3}^{2+}$	0.1 M TX-100	0.87	0.03	0.97

micellar phase, $[S]_M$:

$$D_{app} = ([S]_W D_W + [S]_M D_M)/([S]_W + [S]_M), \quad (1)$$

$$K = [S]_W/[S]_M = (D_{app} - D_M)/(D_W - D_{app}), \quad (2)$$

where D_M is the diffusion coefficient of micelles and D_W, the diffusion coefficient of the monomeric S measured in an aqueous solution without micelle. These equations are based on the assumption that the solubilization equilibrium of S is established in the diffusion process of S toward the electrode.

$$S + \text{micelle} \rightleftarrows S(\text{in micelles}), \quad (3)$$

This assumption is valid for $\mathbf{1}^{n+}$ (n=2, 1, and 0), $\mathbf{2}^{n+}$ (n=2, 1, and 0), and $\mathbf{3}^{2+}$ because the electrode reactions were diffusion-controlled, i.e., the current vs. $(\text{time})^{-1/2}$ plots in potential-step chronoamperometry gave straight lines.[8] D_M for TX-100 micelle in the presence of 0.1 M NaCl was 6.5×10^{-7} $cm^2\,s^{-1}$ determined by the method described in the literature.[3] D_W for $\mathbf{1}^{2+}$ in 0.1 M NaCl aqueous solution was 1.4×10^{-5} $cm^2\,s^{-1}$. The values of K for $\mathbf{1}^{2+}$, $\mathbf{1}^{+}$, and $\mathbf{1}^{0}$ were determined by Eq. 2 on the assumption that the values of D_W for $\mathbf{1}^{+}$ and $\mathbf{1}^{0}$ are equal to D_W for $\mathbf{1}^{2+}$ (Table 1). Table 1 also lists the mole fraction (x) of $\mathbf{1}^{n+}$ (n=2, 1, and 0) solubilized in the micellar phase, which can be derived from the respective K value.

$$x = [\mathbf{1}^{n+}]_M/([\mathbf{1}^{n+}]_M + [\mathbf{1}^{n+}]_W),$$

$\mathbf{1}^{2+}$ and $\mathbf{1}^{+}$ are partitioned equally into two phases, and $\mathbf{1}^{0}$ is almost completely solubilized in the micellar phase.

Figure 2 shows cyclic voltammograms for solutions of 0.62 mM $\mathbf{2}^{n+}$ (n=2, 1, and 0) containing 0.1 M TX-100 and 0.1 M NaCl. At a relatively slow sweep rate, both the first and the second reduction steps were electrochemically reversible one-electron steps. The half-wave potentials were −0.56 and −0.84 V vs. SCE for the first and the second reduction steps, respectively.

The peak current is in order of $i_p(+2\rightarrow+1)>i_p(+1\rightarrow0)=i_p(+1\rightarrow+2)>i_p(0\rightarrow+1)$, suggesting that the value of D_{app} is in order of $\mathbf{2}^{2+}>\mathbf{2}^{+}>\mathbf{2}^{0}$. The values of D_{app}, K, and x for $\mathbf{2}^{2+}$, $\mathbf{2}^{+}$, and $\mathbf{2}^{0}$ determined by potential-step chronoamperometry are listed in Table 1. K and x show that the proportion of the solutes in the micellar phase is in order of $\mathbf{2}^{2+}<\mathbf{2}^{+}<\mathbf{2}^{0}$, and that $\mathbf{2}^{+}$ is more hydrophobic than $\mathbf{2}^{2+}$. This result is different from the case of methyl viologen.

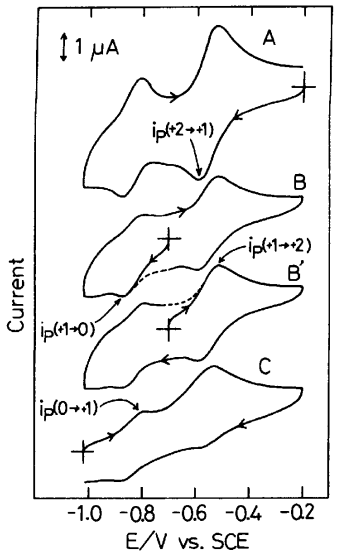

Fig. 2. Cyclic voltammograms for (A) a solution of 0.62 mM $\mathbf{2}^{2+}$, (B) and (B') a solution of 0.62 mM $\mathbf{2}^{+}$, and (C) a solution of 0.62 mM $\mathbf{2}^{0}$ containing 0.1 M TX-100 and 0.1 M NaCl at 25 °C. Sweep rate: 12 mV s^{-1}. Working electrode area: 0.071 cm^2.

D_{app}, K, and x for $\mathbf{3}^{2+}$ are also shown in Table 1. The values of x mean that $\mathbf{3}^{2+}$ is completely solubilized in the micellar phase irrespective of its highly hydrophilic character of bipyridinium group. D_{app} values for $\mathbf{3}^{+}$ and $\mathbf{3}^{0}$ were not obtained, because their electrochemical behavior was complicated due to the adsorption on electrode surface.

The results described in this paper and particularly the suggestion of hydrophobic nature of viologen derivatives with different redox states will be useful for designing a redox system with viologen and for predicting reaction mechanism of chemical conversion of light energy.

References

1) J. H. Fendler, "Membrane Mimetic Chemistry," John Wiley & Sons, New York (1982), pp. 410—417.

2) K. Martinek, A. K. Yatsimirski, A. V. Levashov, and I. V. Berezin, "Micellization, Solubilization, and Microemulsions," ed by K. L. Mittal, Plenum Press, New York (1977), Vol. 2, Part IV, pp. 489—508.

3) Y. Ohsawa and S. Aoyagui, *J. Electroanal. Chem.*, **136**, 353 (1982).

4) M. P. Pileni, A. M. Brown, and M. Grätzel, *Photochem. Photobiol.*, **31**, 423 (1980).

5) A. J. Bard and L. R. Faulkner, "Electrochemical Methods," John Wiley & Sons, New York (1980), pp. 229, 143.

6) A. E. Kaifer and A. J. Bard, *J. Phys. Chem.*, **89**, 4876 (1985).

7) S. Hayano and M. Fujihira, *Rev. Polarogr.*, **21**, 148 (1975); P. Stilbs, *J. Colloid Interface Sci.*, **80**, 608 (1981); J. Georges and S. Desmett, *Electrochim. Acta.*, **29**, 521 (1984); K. Hoshino, T. Saji, Y. Ohsawa, and S. Aoyagui, *Bull. Chem. Soc. Jpn.*, **57**, 1685 (1984).

8) As to the electrochemical behavior of S under conditions of slow exchange of S between the micellar phase and the aqueous phase, see Y. Ohsawa and S. Aoyagui, *J. Electroanal. Chem.*, **145**, 109 (1983).

Lithio Styryl Sulfone as an Acyl Anion Synthon

Makoto YAMAMOTO,* Kazuya SUZUKI, Seiji TANAKA, and Kazutoshi YAMADA
Department of Industrial Chemistry, Faculty of Engineering, Chiba University, 1-33 Yayoi-cho, Chiba 260
(Received October 11, 1986)

Synopsis. Lithio styryl sulfone, which was shown to be an acyl anion synthon, reacted with various electrophiles; the products were rearranged by treatments with *m*-chloroperbenzoic acid to give acyl benzyl sulfones in good yields.

Recents reports concerning reactions of vinyl anions (especially α-vinyl anions activated with such heteroatoms as oxygen,[1] sulfur,[2] nitrogen,[3] silicon,[4] halogen,[5] or selenium[6]) showed that these anions serve as useful synthons for organic syntheses.

Here, we wish to report on a method for the formation and the reaction of lithio styryl sulfone and alkylated products (after epoxidation with *m*-chloroperbenzoic acid (*m*-CPBA)) rearranged to acyl benzyl sulfones in good yields.

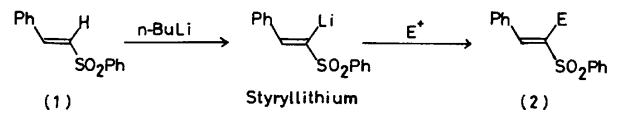

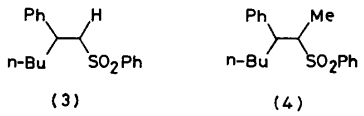

Scheme 1.

(*E*)-Phenyl styryl sulfone (**1**) was lithiated at the β-styryl position regioselectively with butyllithium in tetrahydrofuran (THF) at −78 °C under nitrogen. Styryllithium is stable below −50 °C for several hours, but above −15 °C it gradually decomposes. Styryllithium reacted smoothly with methyl iodide between −78 and −50 °C to give (*E*)-1-phenyl-2-phenylsulfonyl-1-propene (**2a**), mp 91—92 °C (lit,[7] mp 90—93.5 °C) in 92% yield. The reaction was highly regioselective and only the β-methylated product **2a** was obtained. Although this styryl sulfone system has the property that it tends to serve as a Michael acceptor for bases[8] and organometallics,[9] none of **3** or **4** could be detected in a reaction of styryllithium with methyl iodide.[2b]

Styryllithium was allowed to react with various electrophiles to give the corresponding products in good yields (Table 1).

Alkylated styryl sulfone (**2a**) was treated with 3 equivalents of *m*-CPBA in refluxing carbon tetrachloride for 48 h to give 1-phenyl-1-phenylsulfonyl-2-propanone (**5a**), mp 120—122 °C (lit,[10] mp 122—123 °C) in 82% yield. In this reaction none of the Baeyer-Villiger oxidation product (**6** or **7**) was detected.

In the mechanism for the formation of **5a** from **2a**, it is considered that upon a treatment of **2a** with *m*-CPBA, epoxy sulfone (**8**) is initially formed as an unstable intermediate and then rearranged to an acyl compound **5a**, as illustrated in Scheme 2.[11,12]

Table 1. The reaction of Styryllithium with Various Electrophiles

Entry	Electrophile	Yield/%
a	MeI	92
b	$PhCH_2Br$	90[a]
c	*n*-BuI	88[a]
d	PhCOCl	89[a]
e	$(n\text{-Bu})_3SnCl$	85[b]

a) Same reaction condition as general procedure A. b) In addition to the reaction condition of general procedure A, 10 mmol of tetramethylethylenediamine (TMEDA) was used as a stabilizer of styryllithium.

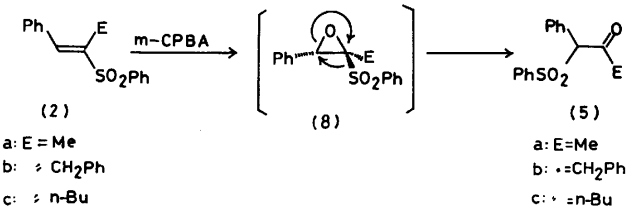

Scheme 2.

Scheme 3.

Styryl sulfones **2b** and **2c** were also allowed to become oxidatively rearranged to the corresponding products: **5b** (75%) and **5c** (72%).

By combining this regioselective alkylation and oxidative rearrangement, it is obvious that lithio phenyl styryl sulfone is a masked acyl anion synthon (Scheme 3). Furthermore, the sulfonyl group can be easily removed from the sulfone (**5**) to obtain an olefin; it can also be reductively removed to form a saturated acyl compound, indicating that this method is useful in organic syntheses.

Experimental

(*E*)-Phenyl Styryl Sulfone (1): Compound **1** was synthesized from methyl phenyl sulfone with benzaldehyde in the presence of a base and a phase-transfer catalyst.[13]

Formation and Reaction of Lithio Styryl Sulfone: General Procedure A: To a stirred solution of **1** (2.44 g, 10 mmol) in 60 ml of dry THF, 6.3 ml (10 mmol) of *n*-BuLi (1.6 mol solution in hexane) was added dropwise within 5 min at −78 °C under a nitrogen atmosphere. After 30 min styryllithium was formed as a red solution.

To this red solution 1.42 g (10 mmol) of methyl iodide in dry THF (5 ml) was added dropwise, continuously stirred at −78—−50 °C for 1 h and then warmed to room temperature within 30 min. The reaction mixture was quenched with water and neutralized with diluted hydrochloric acid. The organic layer was separated and the aqueous layer was extracted with ethyl acetate. The combined organic layer was dried over anhydrous magnesium sulfate and concentrated. The crude product was purified by silica-gel column chromatography with benzene to give a crystalline product **2a** (2.37 g, 92%), mp 91—92 °C (lit,[7] mp 90—93.5 °C). ^{1}H NMR (CCl_4) δ=2.04 (d, 3H), 7.30 (s, 5H), 7.50 (m, 3H), 7.8—8.0 (m, 3H). MS *m/z* 258 (M^+).

Test of the Stability of Styryllithium: The lithio compound was formed by the general procedure A; then, the solution was warmed to −15 °C in an ice-salt bath. After 15 min stirring at −15 °C an equimolar amount of methyl iodide was added dropwise and the reaction mixture was treated by general procedure A. Only 24% of **2a** was detected.

Compound **2b—e** was synthesized by general procedure A.

2b: Mp 143.5—145.5 °C (from EtOH). ^{1}H NMR ($CDCl_3$) δ=4.05 (s, 2H), 7.06 (s, 5H), 7.38 (m, 8H), 7.74 (m, 2H), 8.13 (s, 1H). Found: C; 75.43, H; 5.46% Calcd for $C_{21}H_{18}O_2S$; C; 75.42, H; 5.42%.

2c: Oil ^{1}H NMR (CCl_4) δ=0.68—1.60 (m, 7H), 2.32 (m, 2H), 6.90—7.90 (m, 11H).

2d: Mp 136—137 °C (from EtOH) (Lit,[14] mp 137—138 °C). IR (neat) 1670 (C=O), 1310 and 1150 cm^{-1} (SO_2).

2e: Oil NMR (CCl_4) 0.62—1.60 (m, 27H), 7.28 (s, 5H), 7.51 (m, 3H), 7.85 (m, 2H), 7.83 (s, 1H).

1-Phenyl-1-phenylsulfonyl-2-propanone (5a): General Procedure B: The mixture of **2a** (318 mg, 1.16 mmol) and *m*-CPBA (600 mg, 3.48 mmol) in CCl_4 (10 ml) was refluxed for 48 h under nitrogen. The reaction mixture was then washed with a diluted sodium hydrogencarbonate solution three times and with a diluted sodium hydrogensulfite solution. The organic layer was separated and the aqueous layer was extracted with chloroform. The combined organic layer was worked up as usual and the obtained residue was purified by silica gel column chromatography with benzene-ethyl acetate (19:1) to give crystalline product **5a** in 82% (260 mg) yield. Mp 120—122 °C (lit,[10] mp 122—123 °C). ^{1}H NMR ($CDCl_3$) δ=2.30 (s, 3H), 5.29 (s, 1H), 7.19 (s, 5H), 7.3—7.7 (m, 5H). IR ($CHCl_3$) 1730 (C=O), 1310 and 1150 cm^{-1} (SO_2). MS *m/z* 274 (M^+, 25), 232 (M^+-CH_2CO, 100).

According to general procedure B, compound **5b** and **5c** were synthesized.

5b: Mp 145—145.5 °C (from benzene). ^{1}H NMR ($CDCl_3$) δ=4.00 (s, 1H), 7.00 (s, 5H), 7.1—7.5 (m, 8H), 7.70 (m, 2H), 8.10 (s, 1H). MS *m/z* 192 ($M-PhSO_3H$, 100), 91 ($PhCH_2^+$, 72). Found: C; 71.86, H; 5.15%. Calcd for $C_{21}H_{18}O_3S$: C; 71.98, H; 5.18%.

5c: Oil ^{1}H NMR ($CDCl_3$) δ=0.85 (m, 3H), 1.00—1.60 (m, 4H), 2.65 (t, 2H), 5.24 (s, 1H), 7.3—8.2 (M, 10H). IR ($CHCl_3$) 1730 cm^{-1} (C=O)

Oxidation of 2d: Compound (**2d**) (500 mg, 1.44 mmol) and *m*-CPBA (496 mg, 2.88 mmol) in 15 ml of CCl_4 were refluxed for 24 h. The reaction mixture was then treated as general procedure B. Benzoic acid (81 mg), mp 120—122 °C (lit,[15] mp 122.4 °C) was obtained and the starting material **2d** (308 mg, 62%) was recovered. Both compounds could be identified by their NMR spectra, compared with those of known samples.

Oxidation of 2e: Compound **2e** (250 mg, 0.47 mmol) and *m*-CPBA (162 mg, 0.94 mmol) in 7 ml of CCl_4 were refluxed for 24 h. The reaction mixture was treated by general procedure B. Phenyl styryl sulfone (**1**) (61 mg, 53%) and an unknown product (92 mg) (NMR spectrum of this product in CCl_4 showed at 0.7—1.8 ppm.) were obtained. In this reaction the starting material (**2e**) was not recovered.

References

1) a) R. K. Boeckman Jr. and K. J. Bruza, *Tetrahedron*, **37**, 3997 (1981); b) J. E. Baldwin, G. A. Holfe, and O. W. Lever Jr., *J. Am. Chem. Soc.*, **96**, 7125 (1974); c) J. C. Clinet and G. Linstrumelle, *Tetrahedron Lett.*, **1978**, 137.

2) a) B.-T. Gröbel and D. Seebach, *Synthesis*, **1977**, 357 and references therein; b) B. M. Trost and A. C. Lavoie, *J. Am. Chem. Soc.*, **105**, 5075 (1983) and references therein; c) G. H. Posner, P.-W. Tang, and J. P. Mallamo, *Tetrahedron Lett.*, **1978**, 3995 and references therein; d) J. J. Eisch reported that (1′) was formed by adding methyl lithium to a THF solution of (1) at −95 °C. J. J. Eisch and J. E. Galle, *J. Org. Chem.*, **44**, 3279 (1979).

3) M. P. Periasamy and H. M. Walborsky, *J. Org. Chem.*, **39**, 611 (1974) and references therein.

4) a) B. -T. Gröbel and D. Seebach, *Angew. Chem. Intern. E. Engl.*, **13**, 83 (1974) and references therin; b) T. H. Chan and W. Mychajlowskij, *Tetrahedron Lett.*, **1974**, 171 and references therein; c) M. E. Jung and J. P. Hudspeth, *J. Am. Chem. Soc.*, **102**, 2463 (1980).

5) G. Köbrich, *Angew. Chem. Intern. E. Engl.*, **6**, 41 (1967), **11**, 473 (1972).

6) H. J. Reich, W. W. Willis, Jr., and P. D. Clark, *J. Org. Chem.*, **46**, 2775 (1981) and references therein.

7) W. E. Truce and C. T. Goralski, *J. Org. Chem.*, **36**, 2536 (1971).

8) L. I. Smith and H. R. Davis Jr., *J. Org. Chem.*, **15**, 824 (1950).

9) G. H. Posner and D. J. Brunnelle, *J. Org. Chem.*, **38**, 2747 (1973).

10) W. D. McPhee and E. Klingsberg, *J. Am. Chem. Soc.*, **66**, 1132 (1944).

11) a) T. Durst and K.-C. Tin, *Tetrahedron Lett.*, **1970**, 2369; b) D. F. Taveres, R. E. Estep and M. Blezard, *ibid.*, **1970**, 2373.

12) K. Yamakawa et. al., reported that α,β-epoxy sulfoxides were also rearranged to the corresponding acyl compounds. T. Satoh, T. Kumagawa, and K. Yamakawa, *Bull. Chem. Soc. Jpn.*, **58**, 2849 (1985); T. Satoh, S. Motohashi and K. Yamakawa, *Tetrahedron Lett.*, **1986**, 2889, and references therein.

13) M. Yamamoto, *Nippon Kagaku Kaishi*, **1978**, 771.

14) M. Balasubramanian and V. Baliah, *J. Indian Chem. Soc.*, **32**, 493 (1955).

15) M. Windholz, S. Budavari, R. F. Blumetti and E. S. Otterbein, *The Merck Index, Tenth Ed.*, **1983**, Rahway, p. 155.

Hexacarbonylmolybdenum(0)-Catalyzed Reaction of Allylic Carbonates with Arylsulfonyl-Stabilized Carbanions

Yoshiro MASUYAMA,* Hidenori HIRAI, Yasuhiko KURUSU, and Koh-ichi SEGAWA
Department of Chemistry, Faculty of Science and Technology, Sophia University, 7-1, Kioicho, Chiyoda-ku, Tokyo 102
(Received October 23, 1986)

Synopsis. *p*-Tolylsulfonylacetonitrile reacted with allylic carbonates in the presence of a catalytic amount of hexacarbonylmolybdenum(0) to give monoallylated derivatives. Using sodium hydride as a base, methyl *p*-tolylsulfonylacetate reacted with those to give mixtures of mono- and di-allylated derivatives. No nucleophilic attack of bulky bis-(phenylsulfonyl)methane occurred, whether sodium hydride was present or absent.

Hexacarbonylmolybdenum(0), which is available and stable to oxygen and moisture, is a convenient catalyst for allylic alkylation of carbon nucleophiles with allylic acetates and carbonates.[1] However, sulfones, which stabilize an adjacent carbanion and are easily transformed into other functional groups,[2,3] can not be applied as a carbon nucleophile in this catalytic allylic alkylation yet. If sulfones could be used, the molybdenum-catalyzed allylic alkylation would increase significance as a synthetic tool for the formation of carbon framework in organic synthesis.[4] Here, we wish to report that sulfones, especially *p*-tolylsulfonylacetonitrile reacts with allylic carbonates in the presence of a catalytic amount of $Mo(CO)_6$ to give monoallylated products.

Using methyl *p*-tolylsulfonylacetate (**1**),[5] *p*-tolylsulfonylacetonitrile (**2**),[6] and bis(phenylsulfonyl)methane (**3**)[7] as carbon nucleophile, reactivity of allyl acetate and allyl carbonate for $Mo(CO)_6$-catalyzed reaction was investigated under various conditions. In the case of allyl acetate, neither of carbanions, derived from **1** and **2** with sodium hydride, reacted under the conditions similar to those in the reaction of dimethyl malonate.[1] In refluxing dioxane containing 2,2′-bipyridyl (bpy), a trace of likely product could be detected by thin-layer chromatography. Consequently, investigation of allyl carbonate was attempted using bpy in dioxane, as summarized in Table. **1** did not react under neutral conditions, namely without a base (Entry 1).[8] The use of sodium hydride for the abstraction of proton from **1** caused allylation. However, no selectivity of monoallylation was exhibited, and a mixture of mono- (**4**, 36%) and di-allylated product (40%) was found (Entry 2). On the other hand, the reaction of **2** under neutral conditions provided only monoallylated product in 64% yield (Entry 4). In refluxing THF, the yield was lowered to 16% (Entry 5). Unfortunately, even allyl carbonate did not react with **3**. It seems that steric hindrance of two bulky phenylsulfonyl groups disturbs nucleophilic attack of **3** to π-allylmolybdenum complex.[9] Addition of PPh_3 and *N,N,N′,N′*-tetramethylethylenediamine instead of bpy did not promote the reaction.

The reactions of several allylic carbonates were carried out under the same conditions as Entries 2 and 4 in Table. The results are also summarized in the Table. In the case of crotyl carbonate as well as allyl carbonate, selectivity of **1** to monoallylation was low, while **2** showed high selectivity (Entries 6—8). The reactivity of **2** to α,γ-disubstituted allyl carbonate (2-cyclohexenyl carbonate) was low (Entry 11). Further, geranyl carbonate did not react with **2**. This reaction should be limited by steric demand of both the α-sulfonyl carbanion and the allylic carbonate. At all events, it became possible to employ available *p*-tolylsulfonylacetonitrile (**2**) as the α-sulfonyl carbanion source in the chemistry of π-allylmolybdenum complex.

Experimental

Reaction of Allylic Carbonates with Carbon Nucleophiles. 5: To a solution of **2** (0.20 g, 1.0 mmol), allyl methyl carbonate (0.12 g, 1.0 mmol), and bpy (31 mg, 0.20 mmol) in dioxane (10 ml) was added $Mo(CO)_6$ (53 mg, 0.20 mmol) under argon atmosphere. The mixture was refluxed for 48 h. The reaction mixture was diluted with ether (50 ml), washed

Table. Reaction of Allylic Carbonates with **1** and **2**

Entry	Allylic carbonate		NuH	NaH	bpy	Solvent	Reaction	Product	Yield[a]	Ratio[b]
	R^1	R^2		/mmol	/mol%		time/h		/%	**a**:**b**
1	H	H	**1**	—	20	dioxane	48	—	0	—
2	H	H	**1**	1.1	20	dioxane	48	**4**	36(40)	—
3	H	H	**2**	—	—	dioxane	48	**5**	trace	—
4	H	H	**2**	—	20	dioxane	48	**5**	64	—
5	H	H	**2**	—	20	THF	48	**5**	16	—
6	CH_3	H	**1**	1.1	20	THF	70	**6**	19(53)	33 67
7	CH_3	H	**1**	1.1	20	dioxane	47	**6**	15(44)	40 60
8	CH_3	H	**2**	—	20	dioxane	30	**7**	69	22 78
9	Ph	H	**2**	—	20	dioxane	72	**8**	60	15 85
10	H	C_7H_{15}	**2**	—	20	dioxane	73	**9**	55	40 60
11	$-(CH_2)_3-$		**2**	—	20	dioxane	43	**10**	24	—

a) Isolated yields. Figures in parentheses are yields of diallylated products. b) The ratio was determined by ^1H NMR (Jeolco FX-200). Diastereomer ratios; **6b** (43/57), **7b** (45/55), **8b** (32/68), and **10** (50/50).

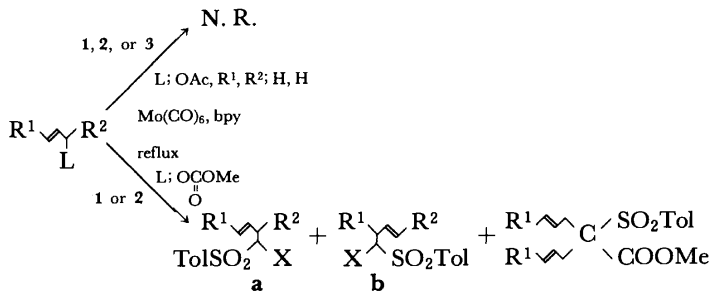

$TolSO_2CH_2COOMe$ **1** **4** and **6**; X = COOMe

$TolSO_2CH_2CN$ **2** **5** and **7**—**10**; X = CN

$PhSO_2CH_2SO_2Ph$ **3**

with 10% aq HCl soln (20 ml) followed by water (2×20 ml), and dried over $MgSO_4$. Evaporation of ether and column chromatography on silica gel using hexane/EtOAc (2/1) as eluent gave monoallylated product **5** as a colorless oil in 64% yield (0.15 g). IR (neat) 2240 (C≡N) and 1320, 1140 cm^{-1} (SO_2); ^1H NMR ($CDCl_3$) δ=2.48 (s, 3H), 2.41—3.03 (m, 2H), 3.82 (dd, J=11, 4 Hz, 1H), 5.20 (d, J=10 Hz, 1H), 5.26 (d, J=16 Hz, 1H), 5.51—6.05 (m, 1H), 7.38 (d, J=8 Hz, 2H), and 7.83 (d, J=8 Hz, 2H); MS (70 eV) m/z (rel intensity) 235 (M^+, 8), 155 (71), and 91 (100). Found: m/z 235.0668. Calcd for $C_{12}H_{13}NO_2S$: 235.0666.

4: The structure was confirmed by comparison with ^1H NMR of the reported one.[10]

6: An oil; IR(neat) 1735 (C=O) and 1320, 1140 cm^{-1} (SO_2); ^1H NMR ($CDCl_3$) δ=1.10 (d, J=6.8 Hz, 0.9H), 1.35 (d, J=6.8 Hz, 1.2H), 1.61 (d, J=6.4 Hz, 0.9H), 2.45 (s, 3H), 2.50—2.88 (m, 0.6H), 2.92—3.15 (m, 0.7 H), 3.51 (s, 1.2H), 3.64 (s, 0.9H), 3.67 (s, 0.9H), 3.98 (d, J=9.1 Hz, 0.4H), 3.94 (d, J=8.4 Hz, 0.3H), 3.90—3.99 (m, 0.3H), 4.93—5.17 (m, 1.4H), 5.17—5.33 (m, 0.3H), 5.43—5.58 (m, 0.3H), 5.58—5.93 (m, 0.7H), 7.28—7.42 (m, 2H), and 7.69—7.83 (m, 2H); MS (70 eV) m/z (rel intensity) 282 (M^+, 0.3), 155 (12), 127 (100), 95 (41), and 91 (44). Found: m/z 282.0930. Calcd for $C_{14}H_{18}O_4S$: 282.0925.

7: An oil; IR (neat) 2240 (C≡N) and 1320, 1140 cm^{-1} (SO_2); ^1H NMR ($CDCl_3$) δ=1.29 (d, J=6.8 Hz, 1H), 1.38 (d, J=6.8 Hz, 1.4H), 1.68 (d, J=6.1 Hz, 0.6H), 2.47 (s, 3H), 2.76—2.92 (m, 0.4H), 3.13—3.33 (m, 0.8H), 3.91—4.02 (m, 1H), 5.13—5.32 (m, 1.6H), 5.32—5.47 (m, 0.2H), 5.60—6.00 (m, 1H), 7.36—7.48 (m, 2 H), and 7.82—7.93 (m, 2H); MS (70 eV) m/z (rel intensity) 249 (M^+, 8), 155 (75), 94 (34), and 91 (100). Found: m/z 249.0824. Calcd for $C_{13}H_{15}NO_2S$: 249.0823.

8: An oil; IR (neat) 2240 (C≡N) and 1340, 1140 cm^{-1} (SO_2); ^1H NMR ($CDCl_3$) δ=2.42 (s, 0.85H), 2.46 (s, 1.7H), 2.47 (s, 0.45H), 2.70—2.86 (m, 0.15 H), 3.00—3.16 (m, 0.15H), 4.01 (dd, J=10.4, 4.5 Hz,0.15H), 4.14 (d, J=3.2 Hz, 0.57H), 4.22 (br. t, J=6.6 Hz, 0.28H), 4.33 (d, J=6.6 Hz, 0.28H), 4.38 (dd, J=8.1, 3.2 Hz, 0.57H), 5.14—5.36 (m, 1.7H), 6.00—6.33 (m, 1H), 6.57 (d, J=15.4 Hz, 0.15H), 7.30 (s, 5 H), 7.24—7.46 (m, 2H), 7.70 (d, J=8.3 Hz, 0.57H), 7.85 (d, J=8.3 Hz, 1.14H), and 7.89 (d, J=8.3 Hz, 0.3 H); MS (70 eV) m/z (rel intensity) 311 (M^+, 0.1), 155 (100), 154 (67), 128 (57), 127 (40), and 115 (54). Found: m/z 311.0985. Calcd for $C_{18}H_{17}NO_2S$: 311.0979.

9: An oil; IR (neat) 2240 (C≡N) and 1320, 1140 cm^{-1} (SO_2) ^1H NMR ($CDCl_3$) δ=0.87 (m, 3H), 1.25 (br, 10.8H), 1.92—2.08 (m, 1.2H), 2.48 (s, 3H), 2.40—2.58 (m, 0.6H), 2.76—2.93 (m, 0.6H), 2.93—3.07 (m, 0.4H), 3.91 (dd, J=11.1, 4.3 Hz, 0.6H), 3.84—3.95 (m, 0.4H), 5.15—5.43 (m, 1.4 H), 5.56—5.78 (m, 1H), 7.42 (d, J=8.2 Hz, 2H), and 7.86 (d, J=8.2 Hz, 2H); MS (70 eV) m/z (rel intensity) 333 (M^+, 4), 178 (91), 155 (81), and 91 (100). Found: m/z 333.1760. Calcd for $C_{19}H_{27}NO_2S$: 333.1761.

10: mp 92—94 °C; IR (KBr) 2240 (C≡N) and 1320, 1140 cm^{-1} (SO_2); ^1H NMR ($CDCl_3$) δ=1.41—2.24 (m, 6H), 2.47 (s, 3H), 2.91—3.22 (m, 1H), 3.67 (d, J=4.5 Hz, 0.5 H), 3.76 (d, J=5.0 Hz, 0.5 H), 5.27—6.02 (m, 2 H), 7.37 (d, J=8 Hz, 2H), and 7.81 (d, J=8 Hz, 2 H); MS (70 eV) m/z (rel intensity) 275 (M^+, 0.5), 157 (44), 120 (100), and 91 (100). Found: C, 65.92; H, 6.31; N, 4.92%. Calcd for $C_{15}H_{17}NO_2S$: C, 65.42; H, 6.22; N, 5.08%.

References

1) B. M. Trost and M. Lautens, *J. Am. Chem. Soc.*, **104**, 5543 (1982); *idem, ibid.*, **105**, 3343 (1983); I. Minami, I. Shimizu, and J. Tsuji, *J. Organomet. Chem.*, **296**, 269 (1985); J. Tsuji, I. Shimizu, I. Minami, Y. Ohashi, T. Sugiura, and K. Takahashi, *J. Org. Chem.*, **50**, 1523 (1985).

2) P. D. Magnus, *Tetrahedron*, **33**, 2019 (1977); T. Durst, *Compr. Org. Chem.*, **3**, 171 (1979).

3) B. M. Trost and M. R. Ghadiri, *J. Am. Chem. Soc.*, **108**, 1098 (1986) and references cited therein.

4) B. M. Trost and T. R. Verhoeven, in "Comprehensive Organometallic Chemistry," ed by G. Wilkinson, Pergamon Press, Oxford (1982), Vol. 8, p. 825; L. S. Hegedus, in "Comprehensive Carbanion Chemistry," ed by E. Buncel and T. Durst, Elsevier, Amsterdam (1984), p. 30; R. F. Heck, "Palladium Reagents in Organic Syntheses," Academic Press, London (1985), p. 130.

5) G. Beck and D. Gunther, *Chem. Ber.*, **106**, 2758 (1973).

6) J. Troger and W. Hille, *J. Prakt. Chem.*, [2], **71**, 226 (1905).

7) H. Stetter and K. Steinbeck, *Justus Liebigs Ann. Chem.*, **1974**, 1315.

8) J. Tsuji, I. Shimizu, I. Minami, and Y. Ohashi, *Tetrahedron Lett.*, **23**, 4809 (1982).

9) B. M. Trost, T. R. Verhoeven, and J. M. Fortunak, *Tetrahedron Lett.*, **1979**, 2301.

10) N. Ono, T. Yoshimura, T. Saito, R. Tamura, R. Tanikaga, and A. Kaji, *Bull. Chem. Soc. Jpn.*, **52**, 1716 (1979).

Hexacarbonylmolybdenum(0)-Catalyzed Reductive Coupling of Allylic Acetates

Yoshiro MASUYAMA,* Kiyotaka OTAKE, and Yasuhiko KURUSU
Department of Chemistry, Faculty of Science and Technology, Sophia University, 7-1 Kioicho, Chiyoda-ku, Tokyo 102
(Received November 20, 1986)

Synopsis. The reaction of allylic acetates with zinc in the presence of a catalytic amount of hexacarbonylmolybdenum(0) led to reductive coupling for the formation of a 1,5-diene framework. Reductive coupling of nerolidyl acetate provided squalene and its isomers in high yield.

Allylic halides have been generally employed in reductive coupling for the formation of 1,5-diene frameworks.[1] Recently, instead of the unstable allylic halides, allylic acetates which are easier to prepare and store than the halides have been applied in the palladium-catalyzed reductive coupling via π-allylpalladium complex with zinc.[2] On the other hand, hexacarbonylmolybdenum(0), which is relatively inexpensive and is stable against oxygen and moisture, reacts with allylic acetates to form π-allylmolybdenum complexes.[3] Hexacarbonylmolybdenum(0) is likely to become a convenient catalyst for the reductive coupling of allylic acetates with zinc.

The molybdenum-catalyzed reductive coupling of cinnamyl acetate was carried out under various reaction conditions, as summarized in Table 1. The coupling reaction did not occur in refluxing toluene, which had been effective in hexacarbonylmolybdenum (0)-catalyzed reactions of the allylic acetates with carbon nucleophiles, and did not also occur in refluxing dioxane or in DMF at 110 °C (Entries 1—3). Next, the effect of ligands was investigated. The addition of 10 mol% of 2,2′-bipyridyl (bpy) accelerated the reaction in refluxing dioxane and THF (Entries 4 and 5). Ligands such as *N,N,N′,N′*-tetramethyl-1,2-ethanediamine, *N,N,N′,N′*-tetramethyl-1,3-propanediamine, and triphenylphosphine were not effective under the same conditions. Accordingly, the reductive coupling of various allylic acetates was carried out in refluxing dioxane containing 10 mol% of bpy. The reaction of 3-acetoxy-1-octene produced 6,10-hexadecadiene (48%)[4] and 9-vinyl-6-tetradecene (52%)[4] in 54% yield. The reaction of (*E*)-3-acetoxy-1-phenyl-1-butene also provided (1*E*,5*E*)-3,4-dimethyl-1,6-diphenyl-1,5-hexadiene (42%), 4,5-diphenyl-2,6-octadiene (8%),[4] and 1,4-diphenyl-3-methyl-1,5-heptadiene (50%)[4] in 37% yield. However, 3-acetoxy-1-cyclohexene did not cause the reductive coupling.

Reactivity and regio- and stereoselectivity were investigated in the reductive coupling of terpenoid allylic acetates such as linalyl, neryl, geranyl, nerolidyl, and farnesyl acetate. The results are summarized in Table 2. Zn-Cu couple as a reducing agent, compared with zinc powder, accelerated the reaction of linalyl acetate (Entries 1 and 2). The difference in the reactivity between linalyl acetate and neryl and geranyl acetate may be due to the difference in the rate of the formation of π-allylmolybdenum complexes (Entries 2—4).[3] In every case (Entries 1—4), the ratios of regioisomers (**I**/**II**) are similar, about 25/75. Being distinct from palladium-catalyzed reductive coupling,[2] stereoselectivities did not depend on the substrates (**a** : **b**=ca. 30 : 70, **c** : **d** : **e**=ca. 10 : 50 : 40). It is presumed from the results that the reductive couplings proceed after syn/anti isomerization of the π-allylmolybdenum complexes occurs to reach the equilibrium,[3] in contrast with the π-allylpalladium complexes which do not cause the syn/anti isomerization.[5] Using this method, nerolidyl acetate, which was more reactive than farnesyl acetate, was reduced to give squalene and its isomers as coupling products (Entries 5 and 6).

As mentioned above, hexacarbonylmolybdenum(0) proved to be a good catalyst for the reductive coupling of allylic acetates.

Experimental

General Procedure of Hexacarbonylmolybdenum(0)-Catalyzed Reductive Coupling of Allylic Acetates. To a solution of allylic acetate (2 mmol), zinc powder (0.39 g, 6

Table 1. Reductive Coupling of Cinnamyl Acetate

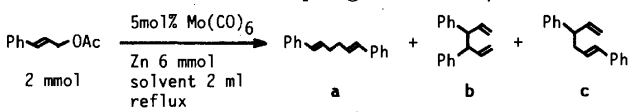

Entry	Solvent	bpy/mol%	Reaction time/h	Yield[a]/%	Ratio[b] a : b : c
1	toluene	—	50	0	——
2	DMF[c]	—	68	9	34 0 66
3	dioxane	—	52	8	39 0 61
4	dioxane	10	10	77	47 4 49
5	THF	10	20	79	47 5 48
6	benzene	10	70	13	49 7 44

a) Isolated yields. b) The isomer ratios were determined by GLPC [5% OV-17/Chromosorb W (AW-DMCS), 60—80 mesh, 2 m, 230 °C] and 200 MHz ^{1}H NMR (Jeolco FX-200). c) Reaction temp 100 °C.

Table 2. Reductive Coupling of Terpenoid Allylic Acetates

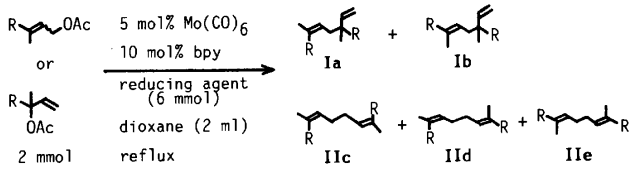

Entry	Allylic acetate	Reducing agent	Reaction time/h	Yield[a]/%	Ratio[b] I : II (a : b) (c : d : e)
1	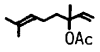	Zn	27	55	27 : 73 (30:70) (11:49:40)
2		Zn–Cu	8	85	23 : 77 (29:71) (10:48:42)
3	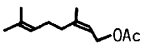	Zn–Cu	66	57	27 : 73 (31:69) (10:50:40)
4	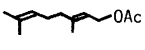	Zn–Cu	96	15	27 : 73 (32:68) (12:50:38)
5	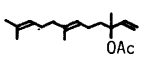	Zn	72	75	25 : 75 (31:69) (14:47:39)
6		Zn–Cu	115	20	20 : 80 (30:70) (10:48:42)

a) Isolated yields. b) The isomer ratios were determined by GLPC [5% OV-17/Chromosorb W (AW-DMCS), 60—80 mesh, 2 m, He, 160 °C (Entries 1—4), 200 °C (Entries 5 and 6).

mmol), and bpy (31 mg, 0.2 mmol) in dioxane (2 ml) was added hexacarbonylmolybdenum(0) (26 mg, 0.1 mmol). The mixture was refluxed for 8—115 h under a nitrogen atmosphere. The reaction mixture was diluted with ether (50 ml), washed with 10% HCl soln (20 ml) followed by water (2×20 ml), and dried over $MgSO_4$. Evaporation of ether and column chromatography on silica gel (Wakogel C-200) using hexane or hexane/EtOAc as the eluent gave coupling products. The structures and isomer ratios were determined by comparison with GLPC and ^1H NMR results of the samples prepared by the alternative method.[2]

References

1) E. J. Corey, M. F. Semmelhack, and L. S. Hegedus, *J. Am. Chem. Soc.*, **90**, 2416 (1968); Y. Kitagawa, K. Oshima, H. Yamamoto, and H. Nozaki, *Tetrahedron Lett.*, **1975**, 1859; Y. Okude, T. Hiyama, and H. Nozaki, *ibid.*, **1977**, 3829; R. D. Rieke, A. V. Kavaliunas, L. D. Rhyne, and D. J. J. Fraser, *J. Am. Chem. Soc.*, **101**, 246 (1979); D. Momose, K. Iguchi, T. Sugiyama, and Y. Yamada, *Tetrahedron Lett.*, **24**, 921 (1983), and references cited therein.

2) S. Sasaoka, T. Yamamoto, H. Kinoshita, K. Inomata, and H. Kotake, *Chem. Lett.*, **1985**, 315 and references cited therein.

3) B. M. Trost and M. Lautens, *J. Am. Chem. Soc.*, **104**, 5543 (1982); *idem, ibid.*, **105**, 3343 (1983).

4) The stereochemistry was not confirmed by GLPC and ^1H NMR.

5) B. M. Trost and T. R. Verhoeven, *J. Am. Chem. Soc.*, **102**, 4730 (1980).

Synthesis on 1,4-Diaminocyclitol Antibiotics. III. Synthesis of 4-Hydroxypurpurosamine B Derivatives

Kazuaki KANAI, Itsuki SAKAMOTO, Seiichiro OGAWA,* and Tetsuo SUAMI†
Department of Applied Chemistry, Faculty of Science and Technology, Keio University, Hiyoshi, Yokohama 223
(Received September 13, 1986)

Synopsis. Methyl 2,6-di-*N*-acetyl-4-hydroxy-6-epi-α-purpurosaminide B and -4-hydroxy-α-purpurosaminide B have been prepared from D-glucosamine by sequence of reactions including stereoselective nitro aldol reaction.

In connection with synthetic studies on 4′-hydroxyfortimicins,[1] synthesis of 4-hydroxy-6-epipurpurosamine B has been carried out.

One of the authors reported that nitro aldol reaction of methyl 2-acetamido-2,3,4-trideoxy-α-*erythro*-hexodialdo-1,5-pyranoside with nitromethane gave the heptose derivative with D-ribo configuration in 52% yield.[2] In contrast the present work has shown that similar reaction of the corresponding 4-*O*-benzyl compound **5** gives selectively single condensate **6** with L-talo configuration in good yield. The C-4 benzyloxy group seems to control the direction of nucleophilic attack of aci-nitronium salt. We now describe syntheses of 4-hydroxypurpurosamine derivatives (**10**) and (**17**) starting from **6**.

Methyl 2-acetamido-2,3-dideoxy-α-D-*ribo*-hexopyranoside (**1**)[3] was converted into the 4-*O*-benzyl derivative (**4**) (84% in three steps). Oxidation of **4** with dimethyl sulfoxide and dicyclohexylcarbodiimide in the presence of pyridinium phosphate gave aldehyde **5**, which reacted with nitromethane in the presence of sodium methoxide to give the nitro compound **6** (84% based on **4**). The stereochemistry of **6** was determined finally by converting it to the known α-purpurosamine B derivative (**11**).[4] Catalytic hydrogenation of **6** in the presence of Raney nickel, followed by *N*-benzyloxycarbonylation, gave **7** in 86% yield. Treatment of **7** with methanesulfonyl chloride in pyridine afforded **8** in 95% yield. Treatment of **8** with sodium isopropoxide in 1,4-dioxane gave an epimino intermediate, which was hydrogenated in the presence of Raney nickel, followed by *N*-acetylation, to give 60% yield of **9**. The ^{1}H NMR spectrum of **9** revealed the presence of a terminal methyl group. Catalytic hydrogenation of **9** in the presence of 10% palladium on charcoal gave **10** in a quantitative yield. Deoxygenation at C-4 was carried out by Barton's method[5] to give **11** identical to an authentic sample[4] in all respects.

Inversion of the 6-hydroxyl group of **6** was attempted in order to obtain the 4-hydroxy-6-epipurpurosamine B derivative. Catalytic hydrogenation of **6** in the presence of Raney nickel, followed by *N*-acetylation, gave the 2,7-di-*N*-acetyl derivative (**12**) in 83% yield. Compound **12** was converted to the mesylate (**13**, 96%), which was then treated with sodium acetate in water, followed by *N*-acetylation, to give 83% yield of the D-allo derivative (**14**). This compound was similarly transformed into **17**. The proposed structure of **17** was determined by converting it to the 6-epipurpurosamine B derivative (**18**)[2,4] as described for the preparation of **11**.

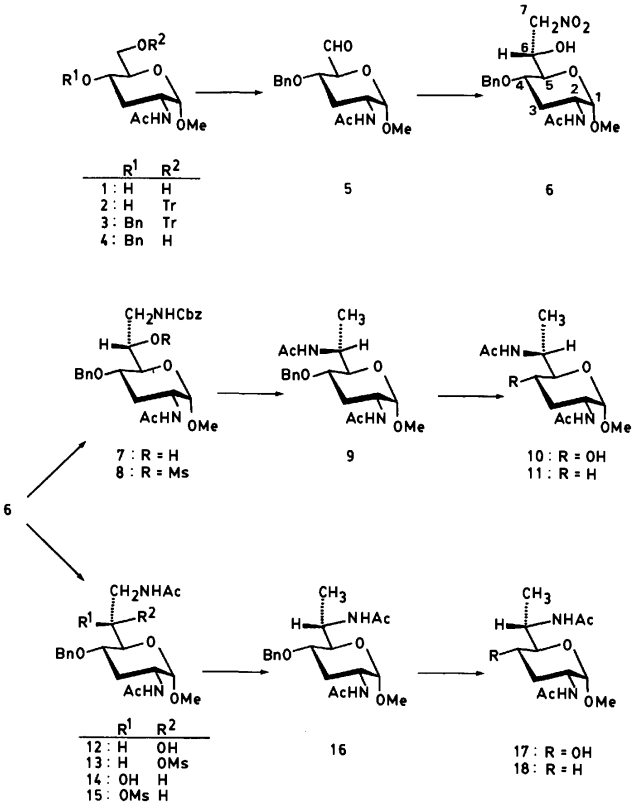

Experimental[6]

Methyl 2-Acetamido-2,3-dideoxy-6-*O*-trityl-α-D-*ribo*-hexopyranoside (2). Compound **1**[3] (6.0 g) was treated with trityl chloride (19.1 g) and 4-dimethylaminopyridine (1.10 g) in pyridine (120 ml) at 60 °C overnight. The mixture was concentrated after addition of triethylamine (1.2 ml). The residue was chromatographed on silica gel with toluene-ethanol (10 : 1) to give **2** (12.6 g, quant.): mp 162—163.5 °C; $[\alpha]_D^{24}$ +35.1° (*c* 1.06, $CHCl_3$).

Found: C, 72.61; H, 6.99; N, 2.88%. Calcd for $C_{28}H_{31}NO_5$: C, 72.86; H, 6.77; N, 3.03%.

Methyl 2-Acetamido-4-*O*-benzyl-2,3-dideoxy-6-*O*-trityl-α-D-*ribo*-hexopyranoside (3). Compound **2** (12.1 g) in *N*,*N*-dimethylformamide (200 ml) was treated with 60% sodium hydride (1.32 g), benzyl bromide (6.44 ml) and tetrabutylammonium iodide (0.11 g) for 1.5 h at room temperature. The product was purified by chromatography on silica gel with toluene-ethanol (20 : 1) to give **3** (14.0 g, 99%): mp 70—76 °C; $[\alpha]_D^{24}$ +39.4° (*c* 0.64, $CHCl_3$).

Found: C, 76.03; H, 6.79; N, 2.46%. Calcd for $C_{35}H_{37}NO_5$: C, 76.20; H, 6.76; N, 2.54%.

Methyl 2-Acetamido-4-*O*-benzyl-2,3-dideoxy-α-D-*ribo*-

†Present address: Department of Chemistry, Faculty of Science and Technology, Meisei University, Hodokubo, Hino, Tokyo 191.

hexopyranoside (4). Compound **3** (14.0 g) was treated with *p*-toluenesulfonic acid monohydrate (9.97 g) in methanol (300 ml). After stirring for 1 h, the mixture was neutralized with $NaHCO_3$ and concentrated. The residue was chromatographed on silica gel with toluene–ethanol (8 : 1) to give **4** (6.90 g, 85%): mp 167—168 °C; $[\alpha]_D^{24}$ +111° (*c* 0.92, MeOH).

Found: C, 62.35; H, 7.38; N, 4.30%. Calcd for $C_{16}H_{23}NO_5$: C, 62.12; H, 7.49; N, 4.53%.

Methyl 2-Acetamido-4-*O*-benzyl-7-nitro-2,3,7-trideoxy-β-L-*talo*-hexopyranoside (6). To a stirred solution of **4** (1.84 g) in dimethyl sulfoxide (8 ml) and benzene (3.4 ml), pyridine (0.47 ml), phosphoric acid (0.16 ml) and dicyclohexylcarbodiimide (3.67 g) were added successively under ice cooling. The stirring was continued for 2 h at room temperature and then oxalic acid (2.20 g) in methanol (20 ml) was added. Dicyclohexylurea precipitated was removed by filtration and the filtrate was extracted with ethyl acetate (200 ml). The extract was successively washed with saturated aqueous $NaHCO_3$ and water, dried, and evaporated to give aldehyde **5**. It was dissolved in methanol (7.4 ml), and nitromethane (6.0 ml) and methanolic 1M sodium methoxide (7.4 ml) were then added under ice cooling. After stirring overnight in a refregirator, the mixture was acidified with Amberlite IR-120 (H^+) resin and concentrated. The product was purified by chromatography on silica gel with toluene–ethanol (14 : 1), and recrystallized from ethanol to give **6** (1.54 g, 84%): mp 150—151 °C; $[\alpha]_D^{26}$ +87.8° (*c* 1.19, MeOH); IR (KBr) 1550, 1370 (NO_2) cm^{-1}.

Found: C, 63.54; H, 6.83; N, 5.93%. Calcd for $C_{25}H_{32}N_2O_7$: C, 63.27; H, 6.72; N, 5.74%.

Methyl 2-Acetamido-4-*O*-benzyl-7-benzyloxycarbonylamino-2,3,7-trideoxy-β-L-*talo*-heptopyranoside (7). Compound **6** (288 mg) was hydrogenated in methanol (3 ml) in the presence of Raney nickel in an initial hydrogen pressure of 3.4 kg cm^{-2} overnight to give the corresponding 7-amino derivative (351 mg). To a solution of the amino-derivative in methanol (6 ml) and water (2 ml), *N*-(benzyloxycarbonyloxy)succinimide (195 mg) and triethylamine (0.06 ml) were added. After stirring for 0.5 h, the mixture was extracted, dried, and concentrated. The residue was chromatographed on silica gel with toluene–ethanol (15 : 1) to give **7** (318 mg, 86%): mp 156—157 °C; $[\alpha]_D^{22}$ +70.9° (*c* 0.17, $CHCl_3$).

Found: C, 63.54; H, 6.83; N, 5.93%. Calcd for $C_{25}H_{32}N_2O_7$: C, 63.27; H, 6.72; N, 5.74%.

Methyl 2-Acetamido-4-*O*-benzyl-7-benzyloxycarbonylamino-2,3,7-trideoxy-6-*O*-mesyl-β-L-*talo*-heptopyranoside (8). Compound **7** (33 mg) was treated with methanesulfonyl chloride (0.01 ml) in pyridine (1 ml) at 0 °C for 1.5 h. The product was purified by chromatography on silica gel with toluene–ethanol (10 : 1) to give **8** as a solid (37 mg, 95%): $[\alpha]_D^{23}$ +29.8° (*c* 1.79, $CHCl_3$).

Found: C, 56.44; H, 6.19; N, 4.90%. Calcd for $C_{26}H_{34}N_2O_9S$: C, 56.72; H, 6.22; N, 5.09%.

Methyl 2,6-Diacetamido-4-*O*-benzyl-2,3,6,7-tetradeoxy-α-D-*allo*-heptopyranoside (9). To a solution of **8** (331 mg) in dioxane (3 ml), a solution of sodium (35 mg) in isopropyl alcohol (6 ml) was added at 95 °C. After stirring for 1 h, an insoluble material was filtered and the filtrate was concentrated to give the epimino derivative, which was hydrogenated as described for the preparation of **7** and then *N*-acetylated with acetic anhydride (0.5 ml) in methanol (5 ml). The product was purified by chromatography on silica gel with toluene–ethanol (10 : 1) to give **9** (132 mg, 60%): mp 196—197 °C; $[\alpha]_D^{22}$ +118° (*c* 1.3, $CHCl_3$); ^1H NMR ($CDCl_3$), δ=0.94 (3H, d, *J*=8 Hz, H-7), 1.89, 1.95 (each 3H, s, NAc), 3.37 (3H, s, OMe), 4.27—4.70 (3H, m, H-1 and benzyl), 7.29 (5H, s, phenyl).

Found: C, 62.35; H, 7.60; N, 7.43%. Calcd for $C_{19}H_{28}N_2O_5$: C, 62.62; H, 7.74; N, 7.69%.

Methyl 2,6-Di-*N*-acetyl-4-hydroxy-α-purpurosaminide B (10). Compound **9** (105 mg) was hydrogenated in ethanol (10 ml) containing 1M hydrochloric acid (0.5 ml) (1 M=1 mol dm^{-3}) in the presence of 10% palladium on charcoal (50 mg) in an initial hydrogen pressure of 3.4 kg cm^{-2} overnight. The product was purified by chromatography on silica gel with toluene–ethanol (3 : 1) to give **10** (90 mg, quant.): mp gradually melt over than 135 °C; $[\alpha]_D^{26}$ +159° (*c* 1.0, MeOH); ^1H NMR (CD_3OD) δ=1.14 (3H, d, *J*=7 Hz, H-7), 1.95 (6H, s, NAcX2), 3.40 (3H, s, OMe), 4.60 (1H, d, *J*=3.8 Hz, H-1).

Found: *m/z*, 275.1622. Calcd for $C_{12}H_{23}N_2O_5$: M+1, 275.1606.

Methyl 2,6-Di-*N*-acetyl-α-purpurosaminide B (11). Compound **10** (50 mg) was converted into the xanthate derivative (44 mg), which was treated with *n*-Bu_3SnH (0.1 ml) and α,α′-azobisisobutyronitrile in toluene (4 ml) to give **11** (17 mg, 56%) by the method described in the preceding paper:[1] mp 256—257 °C; $[\alpha]_D^{19}$ +178° (*c* 0.48, MeOH). Lit,[4] mp 261—262 °C, $[\alpha]_D^{20}$ +185.7° (*c* 0.7, MeOH). ^1H NMR and IR spectra were superimposable on those of an authentic sample.[4]

Methyl 2,7-Diacetamido-4-*O*-benzyl-2,3,7-trideoxy-β-L-*talo*-heptopyranoside (12). Compound **6** (1.54 g) in methanol (10 ml) was hydrogenated as described for the preparation of **7**. The amine was *N*-acetylated and the product was crystallized from ethanol to give **12** (1.37 g, 83%): mp 233—234 °C; $[\alpha]_D^{17}$ +62.4° (*c* 1.0, MeOH).

Found: C, 59.76; H, 7.38; N, 7.31%. Calcd for $C_{19}H_{28}N_2O_6$: C, 59.99; H, 7.41; N, 7.36%.

Methyl 2,7-Diacetamido-4-*O*-benzyl-2,3,7-trideoxy-6-*O*-mesyl-β-L-*talo*-heptopyranoside (13). Compound **12** (916 mg) was treated with methanesulfonyl chloride in pyridine, and the product was purified as described for the preparation of **8** to give **13** (1.01 g, 96%): $[\alpha]_D^{26}$ +25.8° (*c* 0.95, $CHCl_3$); IR (KBr) 1370, 1195 (SO_2) cm^{-1}.

Methyl 2,7-Diacetamido-4-*O*-benzyl-2,3,7-trideoxy-α-D-*allo*-heptopyranoside (14). A suspension of **13** (6.5 g) and sodium acetate (1.2 g) in water (200 mg) was refluxed for 15 h, and then concentrated. The residue was treated with acetic anhydride (1.0 ml) in methanol (10 ml) for 1 h. The product was purified by chromatography on silica gel with toluene–ethanol (5 : 1) and crystallized from methanol–ethyl acetate to give **14** (4.47 g, 83%): mp 173—174 °C; $[\alpha]_D^{20}$ +119° (*c* 1.0, MeOH).

Found: C, 60.25; H, 7.51; N, 7.20%.

Methyl 2,7-Diacetamido-4-*O*-benzyl-2,3,7-trideoxy-6-*O*-mesyl-α-D-*allo*-heptopyranoside (15). Compound **14** (3.92 g) was treated with methanesulfonyl chloride in pyridine, and the product was purified as described for the preparation of **8** to give **15** (4.26 g, 90%): $[\alpha]_D^{26}$ +104° (*c* 0.88, $CHCl_3$); IR (KBr) 1370, 1195 (SO_2) cm^{-1}.

Methyl 2,6-Diacetamido-4-*O*-benzyl-2,3,6,7-tetradeoxy-β-L-*talo*-heptopyranoside (16). Compound **15** (1.60 g) was converted into the epimino derivative, which was hydrogenated, and then acetylated as described for the preparation of **9** to give **16** (698 mg, 55%): mp 144—145 °C; $[\alpha]_D^{18}$ +83.3° (*c* 0.78, $CHCl_3$); ^1H NMR ($CDCl_3$) δ=1.18 (3H, d, *J*=6 Hz, H-7), 1.95, 1.99 (each 3H, s, NAc), 3.38 (3H, s, OMe), 4.59 (1H, d, *J*=3 Hz, H-1), 5.81 (2H, d, *J*=9 Hz, NH-2,6), 7.34 (5H, s, phenyl).

Found: C, 62.76; H, 7.70; N, 7.80%.

Methyl 2,6-Di-*N*-acetyl-4-hydroxy-6-epi-α-purpurosaminide B (17). Compound **16** (50 mg) was hydrogenated as described for the preparation of **10** to give **17** (37 mg, 99%): mp 221—222 °C; $[\alpha]_D^{19}$ +42.3° (*c* 0.70, MeOH); ^1H NMR δ=1.26 (3H, d, *J*=6.5 Hz, H-7), 1.99, 2.11 (each 3H, s, NAc), 3.34 (3H, s, OMe), 4.57 (1H, d, *J*=3 Hz, H-1).

Found: C, 52.44; H, 7.95; N, 10.02%. Calcd for $C_{12}H_{22}N_2O_5$: C, 52.54; H, 8.08; N, 10.21%.

Methyl 2,6-Di-*N*-acetyl-6-epi-α-purpurosaminide B (18).

Compound **17** (75 mg) was converted into the xanthate derivative (97 mg, 97%), which was treated *n*-Bu_3SnH (0.2 ml) and α,α'-azobisisobutyronitrile as described for the preparation of **11** to give **18** (24 mg, 34%): mp 208—209 °C; $[\alpha]_D^{19}$ +70.3° (*c* 0.45, MeOH). Lit,[2] mp 212—213 °C, $[\alpha]_D^{20}$ +63.3° (*c* 1.0, MeOH). ^1H NMR and IR spectra were superimposable on those of an authentic sample.[2]

The authors wish to thank Mr. Saburo Nakada for elemental analyses.

References

1) K. Kanai, I. Sakamoto, Y. Miyamoto, S. Ogawa, and T. Suami, *Bull. Chem. Soc. Jpn.*, **60**, 255 (1987).

2) T. Suami, Y. Honda, T. Kato, M. Masu, and K. Matsuzawa, *Bull. Chem. Soc. Jpn.*, **53**, 1373 (1980).

3) Compound **1** was accessible from methyl 2-acetamido-4,6-*O*-benzylidene-2,3-dideoxy-α-D-*ribo*-hexopyranoside[1] in 99% yield by acid hydrolysis; see also, T. F. Gallagher, and D. Horton, *Carbohydr. Res.*, **116**, 227 (1983).

4) Y. Honda and T. Suami, *Bull. Chem. Soc. Jpn.*, **54**, 2825 (1981).

5) D. H. Barton, and W. B. Motherwell, "Organic Synthesis Today and Tomorrow" ed by B. M. Trost and C. R. Hutchinson, Pergamon Press, (1981), pp. 1—7.

6) The general methods used in the present work have been described in the preceding paper.[1]

Synthesis on 1,4-Diaminocyclitol Antibiotics. V. Synthesis of 3′-Enofortimicin D

Kazuaki KANAI, Shigeki YOKOI, Seiichiro OGAWA,* and Tetsuo SUAMI†
Department of Applied Chemistry, Faculty of Science and Technology, Keio University, Hiyoshi, Yokohama 223
(Received October 7, 1986)

Synopsis. 3′-Enofortimicin D has been prepared by condensation of 1-*O*-acetyl-2,6-bis(2,4-dinitrophenylamino)-2,3,4,6-tetradeoxy-D-*erythro*-hex-3-enopyranose with 2,5-di-*O*-benzoyl-1,4-bis-*N*-(methoxycarbonyl)fortamine B, followed by deprotection.

In the preceding paper,[1] we have reported the synthesis and antibacterial assay of 4′-hydroxyfortimicin D. In continuation of our study on modification of the amino sugar moiety of antibiotic fortimicins, introduction of a double bond into the diamino sugar moiety of fortimicins would be of interest in connection with elucidation of a role of its conformation. We now describe the synthesis and biological activity of 3′-enofortimicin D.

Methyl 2,6-diamino-2,3,4,6-tetradeoxy-α-D-*erythro*-hex-3-enopyranoside sulfate (**1**),[2] was first converted to the bis[*N*-(2,4-dinitrophenyl)] derivative (**2**) in 79% yield. Hydrolysis of **2** with acetic acid containing 2M hydrochloric acid (1 M=1 mol dm^{-3}), followed by acetylation, gave the acetate (**3**) in 64% yield.

Condensation of **3** with 2,5-di-*O*-benzoyl-1,4-bis[*N*-(methoxycarbonyl)] fortamine B (**4**)[3] was carried out in 1,2-dichloroethane in the presence of trimethylsilyl trifluoromethanesulfonate under argon to give sole condensate **5** in 36% yield.

Deprotection of **5** with barium hydroxide in boiling aqueous dioxane in the usual way resulted in further hydrolysis of the glycosidic bond to give mainly fortamine B (**7**) (71%), together with a small amount (11%) of desired 3′-enofortamine KE (**6**). The ^{1}H NMR spectrum of **6** revealed a doublet (δ 5.26, $J_{1',2'}$=3 Hz) due to C-1′ α-anomeric proton. The ready cleavage of the α-glycosidic bond might be attributable to the presence of a double bond between C-3′ and C-4′. Similar results have been observed by Fukatsu[5] in the case of 3′-enokanamycin derivative. Several attempts to increase the yield of **6** failed.

Compound **6** was treated with 2-(*t*-butoxycarbonyloxyimino)-2-phenylacetonitrile (BocON)[6] in aqueous dioxane to give 1,2′,6′-tris[*N*-(*t*-butoxycarbonyl)] derivative (**8**) in 65% yield. The 4-[*N*-(*N*-*t*-butoxycarbonyl)glycyl] derivative (**9**) was obtained in 66% yield by treatment of **8** with activated ester of *N*-(*t*-butoxycarbonyl)glycine[7] in tetrahydrofuran. Finally, treatment of **9** with trifluoroacetic acid in chloroform gave 3′-enofortimicin D (**10**) as the trifluoroacetate.

The minimum inhibitory concentration of **10** is listed together with those of fortimicin A (Table 1). 3′-Enofortimicin D (**10**) exhibited weak activity compared to that of fortimicin A against many organisms.

Table 1. Antimicrobial Activity of **10** and Fortimicin A[a]

Test Organisms	**10**	FM A
Streptococcus faecalis KY4280	100	6.3
Pseudomonas aeruginosa KY4276	50	6.3
Staphyllococcus aureus KY4279	1.6	0.2
Escherichia coli KY4271	12.5	0.78
Bacillus subtilis KY4273	0.78	0.1
Shigela sonnei KY4281	25	1.6
Klebsiella pneumoniae KY4275	3.1	0.2

a) Minimum inhibitory concentration in μg ml^{-1}.

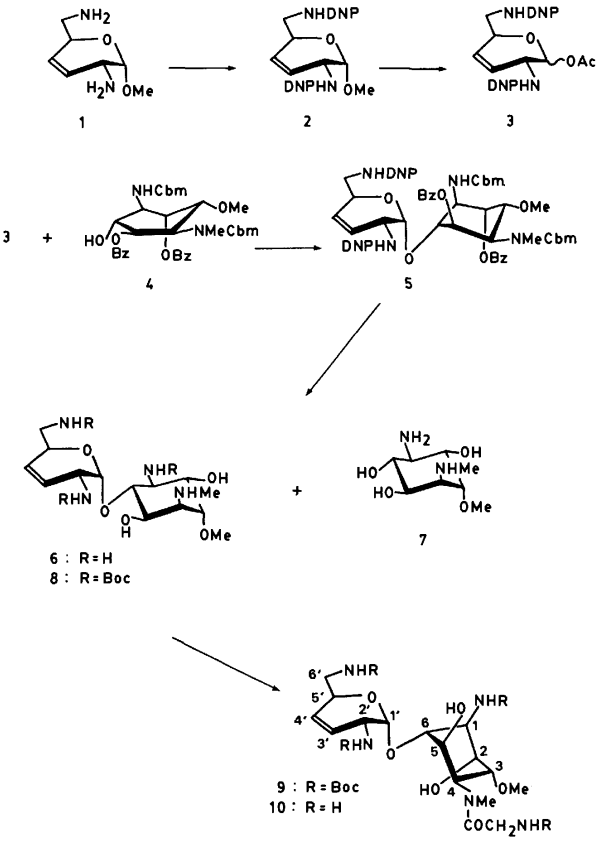

Experimental[8]

Methyl 2,6-Bis(2,4-dinitrophenylamino)-2,3,4,6-tetradeoxy-α-D-*erythro*-3-enopyranoside (2). A solution of methyl 2,6-diamino-2,3,4,6-tetradeoxy-α-D-*erythro*-hex-3-enopyranoside sulfate (**1**)[2] (500 mg) in 85% aqueous methanol (10 ml) containing 1-fluoro-2,4-dinitrobenzene (0.51 ml) and triethylamine (1.1 ml) was stirred at 0 °C for 1 h, and stirring was continued at room temperature overnight. The product was purified by chromatography on silica gel with toluene–acetone (20 : 1) and crystallization from acetone–petroleum ether gave **2** (754 mg, 79%): mp 150—152 °C; $[\alpha]_D^{23}$ −143° (*c* 1.08, $CHCl_3$).

†Present address: Department of Chemistry, Faculty of Science and Technology, Meisei University, Hodokubo, Hino, Tokyo 191.

Found: C, 46.48; H, 3.76; N, 17.04%. Calcd for $C_{19}H_{18}N_6O_{10}$: C, 46.54; H, 3.70; N, 17.14%.

1-*O*-Acetyl-2,6-bis(2,4-dinitrophenylamino)-2,3,4,6-tetradeoxy-D-*erythro*-hex-3-enopyranose (3). A solution of **2** (400 mg) in acetic acid (20 ml) containing 2M hydrochloric acid (2 ml) was stirred at 80 °C for 7 h. The mixture was extracted with chloroform (50 ml) and the extract was dried. After concentration, the residue was treated with acetic anhydride (4 ml) in pyridine (10 ml) for 12 h. The product was purified by chromatography on silica gel and crystallization from acetone-2-propanol gave **3** (273 mg, 64%): mp 92—102 °C; $[\alpha]_D^{24}$ −226° (*c* 1.07, $CHCl_3$).

Found: C, 46.28; H, 3.58; N, 16.34%. Calcd for $C_{20}H_{18}N_6O_{11}$: C, 46.34; H, 3.50; N, 16.21%.

2,5-Di-*O*-benzoyl-2′,6′-bis[*N*-(2,4-dinitrophenyl)]-1,4-bis[*N*-(methoxycarbonyl)]-3′-enofortimicin KE (5). To a solution of **3** (249 mg) and **4**[3] (271 mg) in 1,2-dichloroethane (5 ml) in the presence of powdered molecular sieve 4A (230 mg) was added trimethylsilyl trifluoromethanesulfonate (0.07 ml), and the mixture was stirred for 3.5 h under argon at room temperature. The product was purified by chromatography on silica gel with toluene-2-butanone (30 : 1) and crystallization from acetone-2-propanol gave **5** (166 mg, 36%): mp 134—140 °C; $[\alpha]_D^{20}$ −97.5° (*c* 1.02, $CHCl_3$).

Found: C, 53.22; H, 4.46; N, 11.27%. Calcd for $C_{44}H_{44}N_8O_{19}$: C, 53.44; H, 4.48; N, 11.33%.

3′-Enofortimicin KE (6). A solution of **5** (135 mg) in aqueous dioxane (2 : 1, 9 ml) in the presence of barium hydroxide octahydrate (3.0 g) was refluxed for 12 h. After cooling, carbon dioxide was introduced to the mixture, and an insoluble material was filtered. After concentration, the residue was eluted from a column of Amberlite CG-50 (NH_4^+) resin with aqueous ammonia (0—0.20 M) to give, first, fortamine B (**7**) (20 mg, 71%), the ^1H NMR spectrum of which was superimposable on that of an authentic sample.[4] The fraction eluted second contained compound **6** as a solid (5 mg, 11%): $[\alpha]_D^{25}$ −47.2° (*c* 0.23, MeOH); ^1H NMR (CD_3OD) δ=2.40 (3H, s, NMe), 3.45 (3H, s, OMe), 5.26 (1H, d, *J*=3 Hz, H-1′), 5.71 (2H, bs, H-3′, 4′); MS (SIMS) Found: *m/z*, 333. Calcd for $C_{14}H_{29}N_4O_5$: M+1, 333.

1,2′,6′-Tris[*N*-(*t*-butoxycarbonyl)]-3′-enofortimicin KE (8). To a solution of **7** (7.9 mg) in 50% aqueous dioxane (0.5 ml) was added Boc-ON (29.3 mg), and the mixture was stirred for 6 h. Triethylamine (0.03 ml) was added to it and stirring was continued overnight. The product was purified by chromatography on silica gel with chloroform-methanol (30 : 1) to give **8** as a solid (8.7 mg, 65%): $[\alpha]_D^{23}$ −32.9° (*c* 1.02 . $CHCl_3$); ^1H NMR ($CDCl_3$) δ=1.43 (27H, bs, Boc×3), 2.40 (3H, s, NMe), 3.46 (3H, s, OMe).

1,2′,6′-Tris[*N*-(*t*-butoxycarbonyl)]-4-[*N*-[*N*-(*t*-butoxycarbonyl)-glycyl]]-3′-enofortimicin KE (9). To a mixture of *N*-(*t*-butoxycarbonyl)glycine (3 mg), 1-hydroxybenzotriazole (2.4 mg) and dicyclohexylcarbodiimide (4.3 mg) in tetrahydrofuran (0.5 ml) was added a solution of **8** (8.7 mg) in tetrahydrofuran (0.5 ml), and the mixture was stirred for 3 d. The product was purified by chromatography on silica gel with chloroform-methanol (97 : 3) to give **9** as a solid (7.2 mg, 66%): $[\alpha]_D^{27}$ −6.0° (*c* 0.55, $CHCl_3$); ^1H NMR ($CDCl_3$) δ=1.41, 1.43 (36H in total, each s, Boc×4), 3.14 (3H, s, NMe), 3.46 (3H, s, OMe); MS (SIMS) Found: *m/z*, 790. Calcd for $C_{36}H_{64}N_5O_{14}$: M+1, 790.

3′-Enofortimicin D (10). To a solution of **9** (7.2 mg) in chloroform (0.5 ml) was added trifluoroacetic acid (0.1 ml), and the mixture was stirred for 1.5 h. After concentration, the residue was washed with ether to give a solid of **10** (7.2 mg) as the trifluoroacetate: $[\alpha]_D^{26}$ −5.5° (*c* 0.44, water); ^1H NMR (200 MHz, D_2O) δ=3.12 (1H, s, NMe), 3.22 (1H, dd, *J*=6 Hz, 14 Hz, H-6′a), 3.36 (1H, dd, *J*=3.5 Hz, 14 Hz, H-6′b), 3.46 (3H, s, OMe), 5.46 (1H, d, *J*=4 Hz, H-1′), 5.92 and 6.18 (each 1H, bd, *J*=11 Hz, H-3′ and 4′); MS (SIMS) Found: *m/z*, 390. Calcd for $C_{16}H_{32}N_5O_6$: M+1, 390.

The authors wish to thank Drs. Kunikatsu Shirahata and Hiroshi Sano of Kyowa Hakko Co. for antibacterial assay. We also thank Mr. Akio Takahashi of the University for elemental analyses.

References

1) K. Kanai, I. Sakamoto, Y. Miyamoto, S. Ogawa, and T. Suami, *Bull. Chem. Soc. Jpn.*, **60**, 225 (1987).

2) S. Umezawa, Y. Okazaki, and T. Tsuchiya, *Bull. Chem. Soc. Jpn.*, **45**, 3691 (1972).

3) K. Kanai, J. Nishigaki, S. Ogawa, and T. Suami, *Bull. Chem. Soc. Jpn*, **60**, 261 (1987).

4) H. Sano, T. Sakaguchi, and Y. Mori, *Bull. Chem. Soc. Jpn.*, **52**, 2727 (1979).

5) S. Fukatsu, *Yuki Gosei Kagaku Kyokai Shi.*, **40**, 188 (1982).

6) Boc-ON; M. Itoh, D. Hasegawa, and T. Kamiya, *Bull. Chem. Soc. Jpn.*, **50**, 718 (1977).

7) The activated ester was prepared by the method of M. Sato, K. Mochida, Y. Mori, and K. Shirahata, *J. Antibiot.*, **34**, 513 (1981).

8) The general procedures used in the present work have been described in the preceding paper.[3]

Determination of the Intrinsic Reaction Coordinate in the 2H+O(^{1}D) System Near the Equilibrium H_2O

Seikichi CHO
Department of Chemistry, Faculty of Education, Gunma University, Aramakicho 4-2, Maebashi, Gunma 371
(Received July 23, 1986)

Synopsis. A normal coordinate analysis was applied to the 2H+O(^{1}D) three atomic system, using the Schinke-Lester analytic expression for the adiabatic potential energy. Defining the reaction coordinates as the "infinitely slow motion trajectories," the reaction coordinate of the heavy oxygen atom was calculated easily, while that of the light hydrogen atom was obtained with some difficulty. Several repeated corrections were needed to converge the reaction coordinates to the "intrinsic" reaction coordinate. The intrinsic reaction coordinate of a hydogen atom to the uphill side of H_2O was found to be very difficult to follow. This fact might help to explain the low frequency factor of the decomposition reaction of H_2O.

A chemical reaction arises from a relative motion of nuclei in a system composed of atoms. When the adiabatic potential energy surface of the system is extensively calculated by quantum mechanics, determination of the reaction coordinates turn into a problem of classical mechanics. In a preceding paper,[1] we have defined the reaction coordinates as the infinitely slow motion trajectory,[2] and proved the reaction coordinates to coincide with the normal coordinates.[3] The HNC-to-HCN isomerization reaction was treated by normal coordinate analysis using the STO-3G potential surface, and the intrinsic reaction coordinate[4] was easily calculated. As might be expected, the extension of this work to the reaction of H_2CO was not so easy as the case of HNC. In this paper we treat the 2H+O(^{1}D) three atomic system. For this system contour maps of the potential energy surface could be drawn and the reaction coordinates could be shown explicitly. Schinke and Lester[5] fitted the extensive first-order configuration interaction energies of Howard et al.[6] with an analytic expression, and carried out trajectory calculations.

At first we briefly review the normal coordinate analysis of reaction coordinates. The potential energy V of a system can be expanded in a Taylor series in terms of the normal coordinates Q_i,

$$V = V_0 + \sum_i g_i Q_i + \frac{1}{2}\sum_i \lambda_i Q_i^2, \quad (1)$$

where the expansion is truncated to the second-order. The Lagrange equations of motion are set up and solved by assuming the infinitely slow motions of nuclei. The solutions are given by

$$Q_i = -\tau^2 g_i/(1+\tau^2\lambda_i), \quad (i = 1, 2, \cdots, f) \quad (2)$$

where τ^2 is a constant. Equations 2 imply that the nuclei move along Q_i infinitely slowly, vibrating simple-harmonically along the same Q_i. The magnitude of Q_i is greater the greater the absolute value of g_i and the smaller the absolute value of λ_i. In an equilibrium state the first-order gradients g_i and the reaction coordinates Q_i are all vanishing. The first-order gradients are, however, not always vanishing in any non-equilibrium states and a few or several reaction coordinates are possible. If one of the non-zero reaction coordinates is chosen to be the "intrinsic," the other reaction coordinates should be corrected to zero. The corrections can be easily calculated to

$$d_i = -g_i/\lambda_i, \quad (i = 1, 2, \cdots, f) \quad (3)$$

Equations 3 are consequences of Eq. 1. Once the corrections are made by Eqs. 3, the intrinsic reaction coordinate can be followed step by step uphill or downhill by taking care of the sign of the gradient along the intrinsic reaction coordinate.

If O(^{1}D) aproaches the H_2 molecule colinearly, a small barrier of about 1 kcal mol^{-1} (1 cal=4.184 J) is found at O-H distance about 1.8 Å, as described by Schinke and Lester.[5] Passing through the barrier, the H-H distance increases rapidly and an equilibrium state is attained. In the equilibrium state, the geometry of R(OH)=0.99 Å and R(HH)=2.86 Å is calculated. The Van der Waals complex has three vibrational modes. ν_1=206 cm^{-1} (doubly degenerate), ν_2=396 cm^{-1}, and ν_3=3737 cm^{-1} (the vibrational modes are numbered in an increasing order of wavenumber for convenience sake.) We decided to set up this state as a starting point.

The ν_3 mode is the OH stretching, and the ν_2 mode is an H ··· HO vibration. The motion along Q_2 leads to a further separation of H ··· H or backwards to the H_2+O state. The lowest wavenumber mode is a bending one, along which one is led to a saddle point and further to the equilibrium state of H_2O. The normal coordinate Q_1 is then chosen as the "intrinsic" reaction coordinate of this system. To ascend the potential energy valley to the saddle point, a constant step width (0.05 Å) was used in spite of Eqs. 2. Corrections expressed by Eqs. 3 were made at each step. These movements are illustrated graphically in Fig. 1 and Fig. 2. Figure 1 shows the motion of the oxygen nucleus along the "intrinsic" reaction coordinate, which is plotted in a potential energy contour map. One of the hydrogen atoms is fixed at the origin and the other is floating on the left side of the abscissa. The oxygen atom goes round the hydrogen atom at the origin and no irregularities occur. The saddle point is located at R(OH)=0.99 Å, R(OH′)=3.22 Å, and ∠HOH′=50.0°, and the energy is 1.8 kcal mol^{-1} above the H ··· HO or 112.0 kcal mol^{-1} above the H_2O states. The valley of the potential energy surface is well-defined in Fig. 1.

On the other hand, Fig. 2 shows the motion of one hydrogen nucleus plotted in a contour map, in which the oxygen atom is fixed at the origin and the second hydrogen atom is slightly floating on the right side of

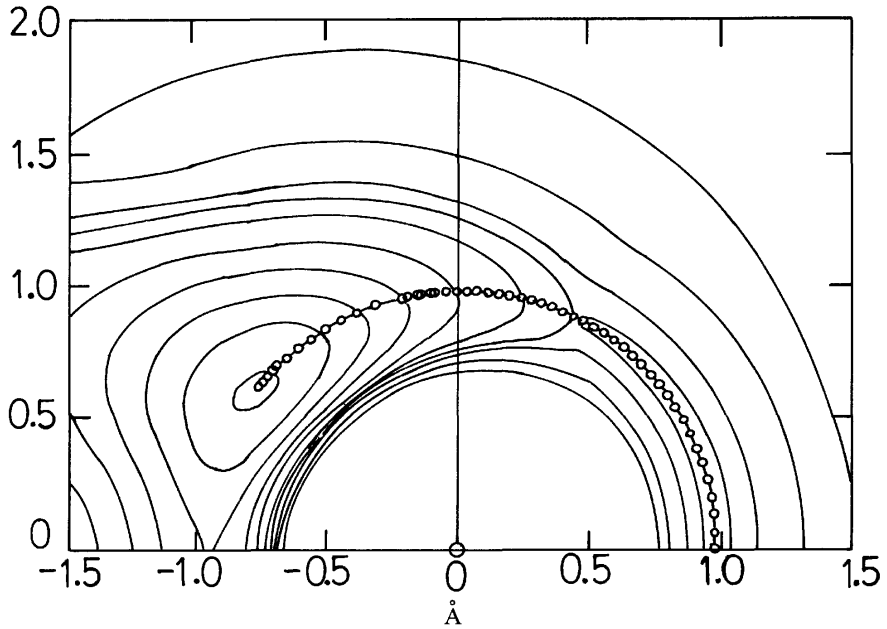

Fig. 1. Contour map of O-motion in the 2H+O(^{1}D) system near the equilibrium H_2O, using the Schinke-Lester analytical expression of energy. One hydrogen atom is located at the origin and the other is floating on the left side of the abscissa. The energies are 2, 20, 40, 60, 80, 100, 112, 120, 140, and 160 kcal mol^{-1} above the equilibrium H_2O. The points denoted by —O— are the calculated intrinsic reaction trajectories of the oxygen atom.

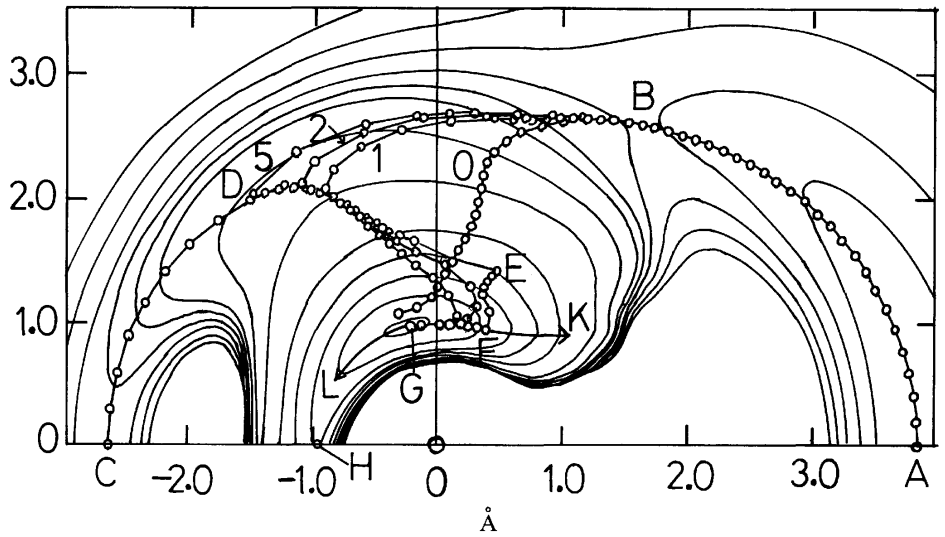

Fig. 2. Contour map of H-motion in the 2H+O(^{1}D) system near the equilibrium H_2O, using the Schinke-Lester analytical expression of energy. The oxygen atom is fixed at the origin and the second hydrogen atom is slightly floating on the right side of the abscissa. The energies are 2, 20, 40, 60, 80, 100, 107, 110, 111, 112, 113, 114, and 115 kcal mol^{-1} above the equilibrium H_2O. The points denoted by —O— are the calculated reaction trajectories of the hydrogen atom.

the abscissa. The intrinsic reaction trajectory of the hydrogen atom is well-defined from the H···HO equilibrium state (denoted by A in the figure) to the saddle point (denoted by B). Passing through the saddle point, the points become scattered. This results from the fact that the corrections given by Eqs. 3 become large and several repeated applications of Eqs. 3 are required. A few of these calculations are also plotted in Fig. 2. The points denoted by 0 describe the calculations with no correction, the points denoted by 1 the calculations with up to one correction at each cycle, and so on. The curve 0 means a "least-motion"

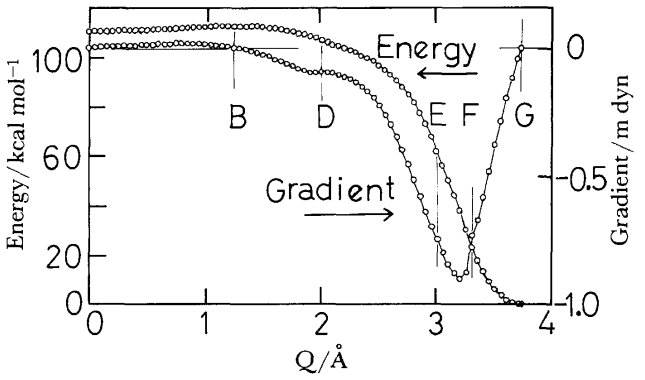

Fig. 3. Variations of the potential energy and the gradient along the intrinsic reaction coordinate of the 2H+O(¹D) system near the equilibrium H_2O. The point where the gradient is vanishing corresponds to the saddle point.

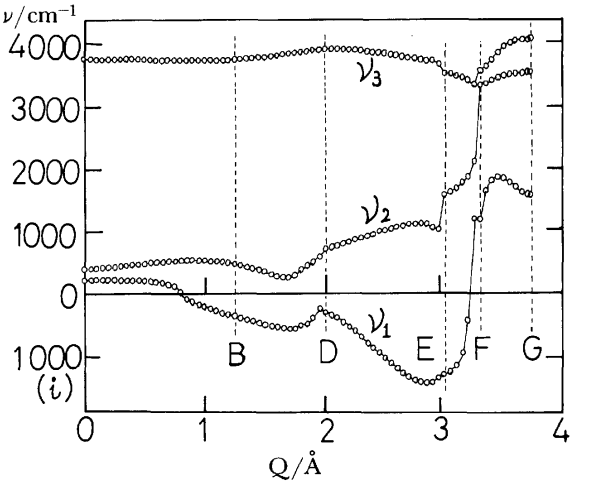

Fig. 4. Variations of the vibrational wavenumber along the intrinsic reaction coordinate of the 2H+O(¹D) system near the equilibrium H_2O. The points were calculated on the Schinke-Lester analytical expression of the potential energy surface.

reaction coordinate. It closely resembles to the "steepest-descent" reaction coordinate, as can be seen from the figure. Once corrections are made, the curves are remote from the "least-motion" reaction coordinate. With up to fivefold correction iteration, the curves converge to the "intrinsic" reaction coordinate. The points C to D denote the descending pathway from a saddle point expressed as H··· O-H (the point C in Fig. 2). The intrinsic reaction coordinate merges in the descending pathway at the point D. Descending the potential energy valley, the curve turns at E and F. The curve F-G is along the bending mode of the vibrations of the equilibrium H_2O.

The reason for this complicated behavior of the hydrogen atom is not yet clear. It is difficult to reverse the intrinsic reaction coordinate from the equilibrium H_2O to the H··· H-O state. The equilibrium H_2O state is calculated to have three vibrational modes, a doubly degenerate bending (ν_1=1568 cm^{-1}), a symmetrical stretching (ν_2=3527 cm^{-1}),and an antisymmetric stretching (ν_3=4037 cm^{-1}) vibrations. If one follows the lowest wavenumber mode Q_1, it leads to the direction of K or L in Fig. 2, which results in the inversion of H_2O. The C_{2v} symmetry of equilibrium H_2O is retained in the inversion pathway. To ascend the "intrinsic" reaction coordinate, one should move along Q_3 (the antisymmetric stretching mode) at the point F. Then the path turns at the point E, and at the point D. Although the intrinsic reaction coordinate does not correspond to any actual trajectory, it is considered to give a path along which many actual trajectories, especially those of low energy, are likely to travel.[4] These facts might be helpful to explain the low frequency factor of the decomposition reaction of H_2O.

Despite the complexity of the H-motion, energies and gradients along the intrinsic reaction coordinate vary smoothly, as is seen in Fig. 3. Variations of the vibratinal wavenumber along the pathway were, however, remarkable as is shown in Fig. 4. The saddle point was of little significance in this case. Discontinuous changes of wavenumber occur at points D,E, and F, where the hydrogen atom comes in another valley on the potential surface. Again, the wavenumbers along the reaction coordinate were imaginary over a wide range of the reaction process.

In conclusion, the determination of an intrinsic reaction coordinate was difficult, especially for the light hydrogen atom. Nevertheless it provides an insight into the detailed mechanism of the chemical reactions.

The whole calculations, including the contour mapping, were carried out with a NEC PC-9801 personal computer in our laboratory.

References

1) S. Cho, *Bull. Chem. Soc. Jpn.*, **58**, 3405 (1985).
2) K. Fukui, S. Kato, and H. Fujimoto, *J. Am. Chem. Soc.*, **97**, 1 (1975).
3) E. B. Wilson, Jr., *J. Chem. Phys.*, **7**, 1047 (1939); **9**, 76 (1941).
4) K. Ishida, K. Morokuma, and A. Komornicki, *J. Chem. Phys.*, **66**, 2153 (1977).
5) R. Schinke and W. A. Lester, *J. Chem. Phys.*, **72**, 3754 (1980).
6) R. E. Howard, A. D. McLean, and W. A. Lester, *J. Chem. Phys.*, **71**, 2412 (1979).

The Determination of a Small Amount of a Biological Constituent by the Use of Chemiluminescence. X. The Determination of Protein Using a 1,10-Phenanthroline-Hydrogen Peroxide-Ruthenium(III) System

Tadashi HARA,* Kazuhiko TSUKAGOSHI, and Masakatsu IMAKI†
Department of Chemical Engineering, Faculty of Engineering, Doshisha University, Karasuma Imadegawa, Kamigyo-ku, Kyoto 602
†Horiba Ltd., Kisshoin, Minami-ku, Kyoto 601
(Received October 2, 1986)

Synopsis. The catalytic activity of ruthenium(III) chloride in a chemiluminescence reaction with 1,10-phenanthroline-hydrogen peroxide has been found to decrease in the presence of protein. On the basis of this phenomenon, bovine serum albumin as a model protein was determined within the concentration range of 5×10^{-5}—1×10^{-1} g dm^{-3} and a detection limit of about 1 ng.

Several new methods for the determination of protein by the use of a chemiluminescence(CL) reaction between 5-amino-2,3-dihydro-1,4-phthalazinedione or 1,10-phenanthroline(phen) and hydrogen peroxide(H_2O_2) have been reported by the present authors in previous papers.[1-4] The methods are based on the measurement of the decreasing catalytic activity of copper(II), the iron(III) complex, or the cobalt(III) complex for a CL reaction in the presence of protein. According to Suzuki et al.,[5,6] CL emission from phen in the presence of H_2O_2 was markedly enhanced by a copper(II) catalyst, but not another catalyst, such as Cd(II), Co(II), Hg(II), Zn(II), Pb(II), or Ni(II). They used this phenomenon in determining a small amount of copper(II). It has now been found by the present authors that the ruthenium(III) chloride acts as a catalyst for a CL reaction between phen and H_2O_2 and that, moreover, its catalytic activity decreases in the presence of protein. As bovine serum albumin(BSA), human serum albumin(HSA), bovine serum α-globulin, and human serum γ-globulin show similar CL responses, BSA was selected as the model protein for their determination. A new procedure for the determination of protein has been established on the basis of the above-mentioned phenomenon. The present method is 10^2—10^3 times as sensitive as the conventional method[7] for the determination of protein and is no less sensitive than the most sensitive other method[4] in the present series of reports by the present authors.

Experimental

All the reagents were of a commercially available special grade. The ion-exchange water was distilled for use. A phen solution, a H_2O_2 solution, and a buffer solution were prepared as in the previous paper.[8] A 1.0×10^{-3} mol dm^{-3} ruthenium(III) catalyst solution was prepared as a stock solution by dissolving ruthenium(III) chloride hydrate(NAKARAI CHEMICAL, LTD.) in 0.36 N HCl; it was then diluted to the desired concentration with a buffer solution. BSA and HSA from NAKARAI CHEMICAL, LTD., bovine serum α-globulin from ICN Pharmaceuticals, Inc., and human serum γ-globulin from the SIGMA CHEMICAL COMPANY were prepared by diluting them with the above-mentioned buffer solution.

The experiment was carried out using the apparatus described in a previous paper.[8] The optimum flow rates and the optimum distance between the point where a phen-H_2O_2 mixture solution and a buffer solution were mixed and a certain cell were decided by the experiment. A definite volume of the ruthenium(III) solution was added to a sample solution containing protein, and the resulting solution was heated for a definite period. After the solution had then cooled to room temperature, an aliquot of the solution (50 mm^3) was injected into the flow-through system and the CL intensity was measured.

Results and Discussion

The CL intensity of the 1.0×10^{-6} mol dm^{-3} ruthenium(III) catalyst solution was measured by the use of 3-, 90-, 180-, and 270-cm portions of the tube, portions which corresponded to the distance between the point where a phen-H_2O_2 mixture solution and a buffer solution were mixed and a certain cell. The maximum CL intensity was observed by the use of a 90-cm tube. Both the flow rate of a phen solution and that of a H_2O_2 solution were chosen simultaneously at the following rates: 0.5, 0.7, 1.0, and 1.3 ml min^{-1}; the CL intensity of a 1.0×10^{-6} mol dm^{-3} ruthenium(III) catalyst solution was also measured. The maximum CL intensity was observed at 0.7 ml min^{-1}. The flow rate of a buffer solution was always set at 2.3 ml min^{-1}, the maximum capacity of the pump, so as to deal with as many samples as possible in a definite time. On the basis of the experimental results, the optimum conditions were established as follows: tube length: 90 cm; flow rates of a phen, a H_2O_2, and a buffer solution: 0.7, 0.7, and 2.3 ml min^{-1} respectively.

The calibration curve for the ruthenium(III) catalyst solution is shown in Fig. 1; it was almost linear for 1.0×10^{-7}—1.0×10^{-5} mol dm^{-3} ruthenium(III).

The relationships between the CL intensity and the reaction time at 20, 60, and 95 °C are shown in Fig. 2. On the basis of the results pertaining to the decrease in the CL intensity and the reaction time, the CL intensity of a protein sample solution was examined after it had been treated for 45 min at 95 °C in all the following experiments.

The CL responses of a sample solution containing 3×10^{-3} g dm^{-3} each of BSA, HSA, bovine serum α-globulin, and human serum γ-globulin were examined (Table 1). As they showed similar responses, BSA was selected as the model protein in the following experiment.

Figure 3 shows the calibration curve for BSA. As

Table 1. The CL Responses of Various Proteins

Protein	Experimental CL intensity/kcps	Relative CL intensity
(Protein-free)	3.44	1.00
BSA	1.68	0.49
HSA	1.80	0.52
Bovine serum α-globulin	1.84	0.53
Human serum γ-globulin	1.74	0.51

a) Conditions: 1.2×10^{-4} mol dm^{-3} phen, 5.0 wt% H_2O_2, 3.0×10^{-6} mol dm^{-3} Ru(III), and 3.0×10^{-3} g dm^{-3} protein.

Table 2. The Apparent Coupling Ratio and Coupling Constant When a Ru(III) or Cu(II) Catalyst is Used

Catalyst	Detection limit of BSA/ng	Catalyst concn used for BSA determination/mol dm^{-3}	Coupling ratio (Metal:Protein)	Coupling constant
Ru(III)	1	3.0×10^{-6}	6.0 : 1	3.5×10^{35} (mol^{-1} dm^3)$^{6.0}$
Cu(II)	5[a)]	5.0×10^{-8}	2.3 : 1	1.9×10^{18} (mol^{-1} dm^3)$^{2.3}$

Conditions: 6.1×10^{-7} mol dm^{-3} BSA against 2.0×10^{-6}—5.0×10^{-6} mol dm^{-3} Ru(III), 6.1×10^{-8} mol dm^{-3} BSA against 7.5×10^{-8}—1.5×10^{-7} mol dm^{-3} Cu(II), ionic strength $\fallingdotseq$0.1 mol dm^{-3}, and reaction temperature=95 °C. The molecular weight of BSA was regarded as being 66000 for purposes of calculation. a) Estimated using the apparatus described in a previous paper.[8)]

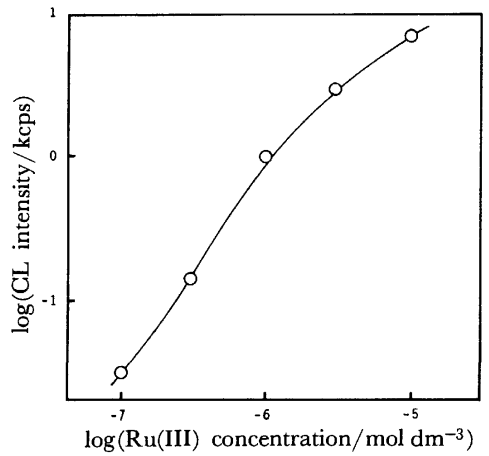

Fig. 1. Calibration curve of Ru(III) catalyst solution. Conditions: 1.2×10^{-4} mol dm^{-3} phen and 5.0 wt% H_2O_2.

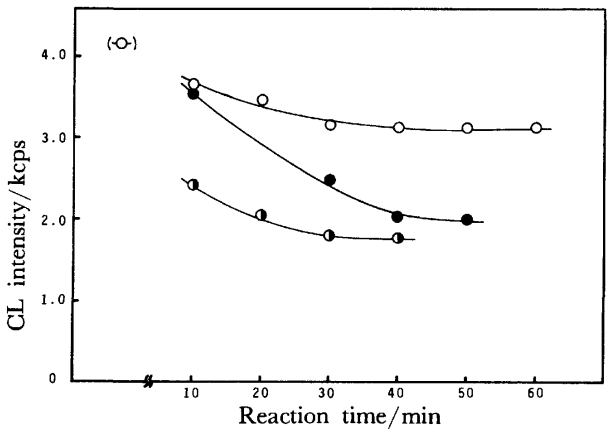

Fig. 2. Relationship between CL intensity and reaction time. Reaction temperature O: 20 °C, ●: 60 °C, and ◑: 95 °C. (-O-): BSA free. Conditions: 1.2×10^{-4} mol dm^{-3} phen, 5.0 wt% H_2O_2, 3.0×10^{-6} mol dm^{-3} Ru(III), and 5.0×10^{-3} mol dm^{-3} BSA.

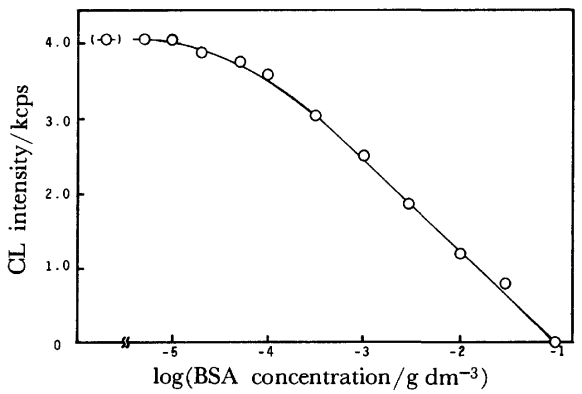

Fig. 3. Calibration curve of BSA. (-O-): BSA free. Conditions: 1.2×10^{-4} mol dm^{-3} phen, 5.0 wt% H_2O_2, and 3.0×10^{-6} mol dm^{-3} Ru(III).

can be seen from Fig. 3, BSA in the concentration range of 5×10^{-5}—1×10^{-1} g dm^{-3} could be determined within a detection limit of about 1 ng. The coefficients of variation for 10 analyses of 1×10^{-3} g dm^{-3} BSA and protein-free sample solutions by the present method were 1.27 and 2.03% respectively. The lowering of the CL activity of the ruthenium(III) catalyst solution in the presence of 5.0×10^{-3} g dm^{-3} glycylglycine and 5.0×10^{-3} g dm^{-3} glycylglycylglycine was examined; their relative CL intensities were 0.88 and 0.79 respectively. The lowering of the CL activity of the ruthenium(III) catalyst solution in the presence of protein seems to be caused by the formation of a ruthenium-polypeptide linkage. The results suggest that the present method can be applied to the determination of biological constituents containing a peptide linkage, such as albumin and globulin as well as an enzyme.

The apparent ratios of ruthenium(III) to a protein and the coupling constant of a ruthenium(III)-protein complex were estimated in a way similar to that de-

scribed in a previous paper.[8] These value were then compared with those of a copper(II)-protein complex in the previous paper;[8] they are shown in Table 2, together with the detection limit of BSA. The apparent coupling ratio and coupling constant of a ruthenium(III) complex were larger than those of a copper(II) complex. It was difficult to compare these values exactly because they were obtained under quite different conditions. However, the data suggest that BSA can be estimated with a detection limit of about 1 ng even though a ruthenium(III) catalyst with a concentration 60 times as high as that of a copper(II) catalyst is used. The reaction mechanism between the metal and the protein still remains unknown.

References

1) T. Hara, M. Toriyama, and K. Tsukagoshi, *Bull. Chem. Soc. Jpn.*, **56**, 1382 (1983).
2) T. Hara, M. Toriyama, and K. Tsukagoshi, *Bull. Chem. Soc. Jpn.*, **57**, 289 (1984).
3) T. Hara, M. Toriyama, K. Kitamura, and M. Imaki, *Bull. Chem. Soc. Jpn.*, **58**, 2135 (1985).
4) T. Hara, T. Ebuchi, A. Arai, and M. Imaki, *Bull. Chem. Soc. Jpn.*, **59**, 1833 (1986).
5) M. Yamada and S. Suzuki, *Anal. Lett.*, **17**, 251 (1984).
6) M. Ishii, M. Yamada, and S. Suzuki, *Bunseki Kagaku*, **35**, 373 (1986).
7) K. Sugawara and M. Soejima, "Seibutsu Kagaku Jikken-hō 7 Tanpakushitsu No Teiryo-hō," Japan Scientific Societies Press, Tokyo (1981).
8) T. Hara, K. Tsukagoshi, A. Arai, and T. Iharada, *Bull. Chem. Soc. Jpn.*, **59**, 3681 (1986).

Vertical Profiles of CCl_3F, CCl_2F_2, and CH_4 in the Stratosphere and Troposphere over Japan as Observed by Balloon Grab-Sampling and by Gas-Chromatographic Analysis

Yoshihiro MAKIDE,* Akihito YOKOHATA, Takeshi TOMINAGA,
Hideyuki HONDA,† Haruya KUBO,† and Tomizo ITOH†

Department of Chemistry, Faculty of Science, The University of Tokyo, Hongo, Bunkyo-ku, Tokyo 113
†The Institute of Space and Astronautical Science, Komaba, Meguro-ku, Tokyo 153
(Received October 7, 1986)

Synopsis. Stratospheric and tropospheric air samples were collected by means of a balloon-borne grab-sampler launched from Sanriku (39°N, 142°E) in the late summers of 1981, 1983, and 1984. The mixing ratios of CCl_3F and CCl_2F_2 were determined precisely by using gas chromatography with ECD, and that of CH_4, by gas chromatography with FID. The vertical profiles of these compounds are presented and compared with the model calculations.

Large amounts of chemical species have been released into the atmosphere from human activities; their atmospheric concentrations increase depending on the released amounts and tropospheric lifetimes. Among them, entirely man-made chlorofluoromethanes, CCl_3F and CCl_2F_2, both with extremely long lifetimes, are believed to have a severe impact on the Earth's environment; the stratospheric ozone is depleted by chlorine atoms released from these compounds in the stratosphere.[1-3] In this connection, we have been measuring the background concentrations of several halocarbons in the atmosphere in Hokkaido since 1979 and have observed that the CCl_3F and CCl_2F_2 concentrations increase by 4—6% a year.[4]

We have also observed that the atmospheric concentration of methane increases gradually as well (about 1% a year); in the troposphere, it will cause an elevation of the surface temperature (i.e., a "greenhouse effect"),[5] and a depletion of the tropospheric OH radical concentration leading to prolonged lifetimes of many air pollutants susceptible to OH attack.[6]

In this paper we report the vertical profiles of CCl_3F, CCl_2F_2, and CH_4 over Japan obtained by the analysis of air samples collected by means of a balloon-borne large-volume grab-sampler. While the vertical distributions of these compounds have often been observed in the USA[7,8] and southern France,[9] no systematic measurements have been attempted to date in Asia.

Experimental

Stratospheric Air Sampling. A balloon-borne grab-sampling system for collecting stratospheric whole air samples was developed; the details have been described elsewhere.[10]

Six 30-l sample cylinders were installed in a sealed large aluminum container called a "scientific gondola" (0.9 m in diameter, 1.3 m in height, and weighing 150 kg), together with a sampling manifold, a monitor circuit, and a valve-controller. A motor-driven stainless-steel bellows valve was installed between each sample cylinder and the sampling manifold; it was operated at the desired altitude by command signal from the ground station. The sampling manifold was connected to an outside air-intake tube (4-m-long flexible tubing equipped with a glass-sealed end for ensuring a high vacuum and extremely clean conditions).

In order to avoid contamination by halocarbons from the components (cylinder, valve, manifold, etc.), all parts were cleaned thoroughly before they were assembled. The inside of the electropolished sample-cylinder was further passivated by silanization with hexamethyldisilazane, and then evacuated for several hours at 150 °C.

After launching, the scientific gondola was reeled down to 100 m below the control gondola/15000 m^3 balloon in order to avoid contamination from these systems and from the helium gas to be released from the balloon. Then, the end glass-seal was cut off and the 4-m intake tubing was extended downward. Sampling was performed when the balloon system was descending, and the inlet port was continuously flushed with ambient air. The sampling system was launched in the early morning on September 2nd, 1981, on August 28th, 1983, and on September 7th, 1984, from the Sanriku Balloon Center on the Pacific coast (39.16°N, 141.83°E). In the beginning, it flew east over the Pacific Ocean while ascending (at 300 m min^{-1}) on the west wind in the troposphere; it then returned to the west at an altitude of about 28 km on the weak east wind in the stratosphere. After 2—4 h flight for degassing and returning to over Sanriku, it was made to descend at 50—100 m min^{-1}; five stratospheric samples were collected in the meantime. Then the balloon was cut off, and one tropospheric sample was collected during descent by parachute. The scientific gondola alighted on the sea near Sanriku and was recovered within an hour.

Analysis. The sample cylinders were returned to the laboratory, and an aliquot of the atmospheric sample was introduced into an extremely clean, evacuated sample loop for precise and accurate analysis with the gas chromatographic system we had developed.[11,12] The halocarbons were determined with an ECD (electron capture detector), while methane was determined with an FID (flame ionization detector).

Results and Discussion

Since the atmospheric pressure decreases with the altitude, the concentration is expressed in terms of the volume mixing ratio (molar ratio of each component to dry air, in units of pptv=10^{-12} v/v or ppmv=10^{-6} v/v).

The observed mixing ratios of CCl_3F and CCl_2F_2 (1981, 1983, and 1984), and CH_4 (1983 and 1984) are shown in Fig. 1, together with the observed concentrations on the surface (background concentrations observed in Hokkaido in August).[4]

While these compounds were distributed uniformly in the troposphere, the mixing ratios of halocarbons decreased rapidly in the stratosphere because of the slow transport into the stratosphere and the photodissociation by intense solar radiation with short wave-

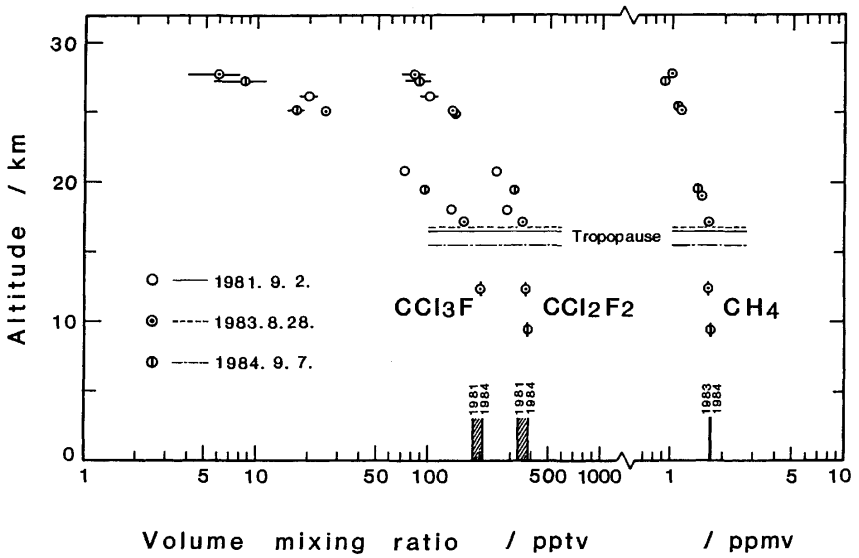

Fig. 1. Observed vertical distribution of halocarbons and methane in the stratosphere and troposphere over Sanriku (39°N, 142°E) in summers of 1981, 1983, and 1984.

lengths (190—220 nm). As compared with CCl_2F_2, CCl_3F, with a larger photodissociation cross-section, indicated a quicker decrease in the mixing ratio.

Since no removal process (sink) for CCl_3F and CCl_2F_2 has been found in the troposphere (i.e., no photodissociation with sunlight (>280 nm), no reaction with OH, no dissolution into rain or sea water, etc.), their tropospheric lifetimes have been confirmed to be extremely long, more than several hundred years.[13] In the stratosphere, however, ultraviolet solar radiation not absorbed by stratospheric ozone can decompose CCl_3F (at about <230 nm) and CCl_2F_2 (at about <220 nm) effectively, with maximum dissociation at altitudes of about 25 and 30 km respectively. The photodissociation of CCl_3F and CCl_2F_2 ($CCl_3F+h\nu\rightarrow Cl+CCl_2F$, and $CCl_2F_2+h\nu\rightarrow Cl+CClF_2$) is followed by the release of all the Cl atoms in the molecule, and the released Cl joins the ClO_x-catalyzed decomposition of ozone ($Cl+O_3\rightarrow ClO+O_2$, and $ClO+O\rightarrow Cl+O_2$), leading to the depletion of the stratospheric ozone.[1-3]

By contrast, methane is decomposed mainly in the troposphere by the reaction with the OH radical ($CH_4+OH\rightarrow H_2O+CH_3$), with a tropospheric lifetime of about 10 years.[6] In the lower stratosphere, the observed mixing ratio of CH_4 decreases only slowly due to the low OH and $O(^1D)$ concentrations, the small photodissociation cross-section with UV, and the upward diffusion to the upper stratosphere. As compared with the CH_4 profile, it is obvious that CCl_3F and CCl_2F_2 are decomposed effectively in the lower and mid stratospheres.

The vertical profiles of the stratospheric mixing ratios observed in this work (Fig. 1) agree reasonably well with those calculated on the basis of recent atmospheric models.[14-17] A two-dimensional (2-D) atmospheric model calculation[14] suggests, for summer at latitude 38°N, that the CCl_3F mixing ratio will drop to 1/10 and 1/100 (of the tropospheric value) at altitudes of about 25 and 28 km respectively, while the CCl_2F_2 mixing ratio will fall to 1/10 at about 31 km. Our measurements at 39°N in summer indicate that the CCl_3F mixing ratio fell to 1/10 and 1/100 at altitudes of 25—26 km and 28—29 km, while that of CCl_2F_2 fell to 1/10 at 30—31 km. The 2-D model calculation[14] similarly suggests that the CH_4 mixing ratio decreases to 1/2 (of the tropospheric value) at about 30 km; this is also in agreement with the value of 29—30 km in the observed profile (Fig. 1).

Meteorological conditions should be taken into consideration for a closer examination of the vertical distribution of these compounds in the stratosphere. The heights of the tropopause were about 16.5, 16.8, and 15.5 km respectively at the time of the flights in 1981, 1983, and 1984. The flights were made in more or less similar seasons and under similar weather conditions, because these factors were chosen to ensure the recovery of the sampler on the sea off Sanriku; the stable combination of a tropospheric west wind and a stratospheric east wind is possible only in early and late summer.

Since the tropopause moves upward or downward with the air, the observed mixing ratios were plotted against the height above the tropopause in Fig. 2; the tropopause height was normalized to 16.5 km. With such normalization, less scattered and more reasonable plots were obtained. The atmospheric pressure-temperature curves on the sampling day were very similar in 1981 and 1983, and a clear turning point corresponding to the tropopause was observed, whereas there was a gradual change in the temperature around the tropopause in 1984, indicating that the profile around the tropopause was affected by air mass motions. Our data are less scattered and indicate a slower fall-off in the lower stratosphere than those reported over the USA (41°N)[7] or southern France (44°N).[9] Such a discrepancy of vertical profiles may be attributed to the difference in the dynamic processes in this altitude region (lower stratosphere) depending on

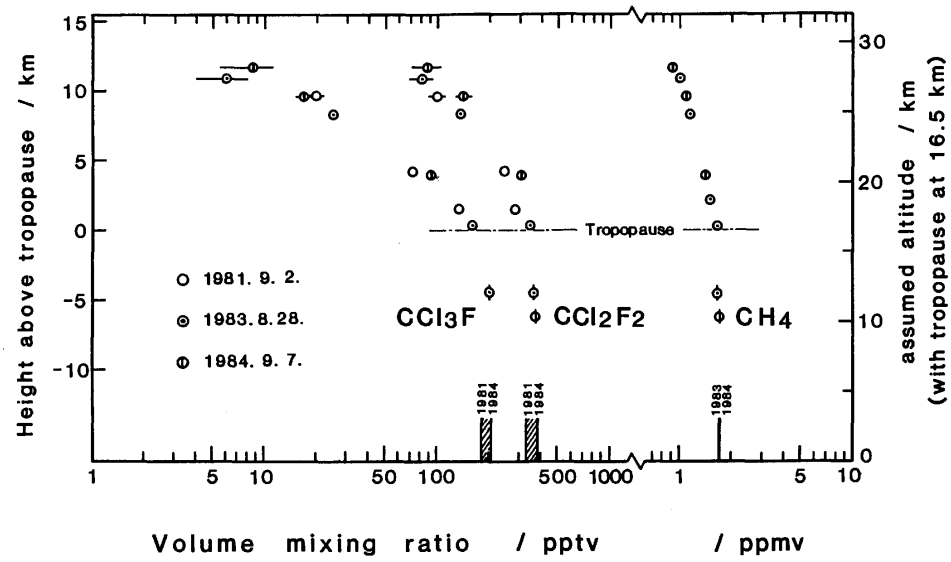

Fig. 2. Vertical distribution of halocarbons and methane vs. height above tropopause.

the latitude, season, and meteorological conditions.

The observed atmospheric concentrations of CCl_3F and CCl_2F_2 on the surface increased by about 12 and 15% respectively in these 3 years (1981—1984).[4] While the mixing ratios of these halocarbons in the stratosphere may also tend to increase slightly (Fig. 2), it is still difficult, in view of variable meteorological conditions, to indicate the trend in the stratosphere quantitatively on the basis of 3 years' data. A long-term monitoring is needed to determine unequivocally the trend of their stratospheric concentrations. Since stratospheric air samples from higher altitudes should be analyzed for a more detailed comparison with models, a balloon-borne liquid-helium-cooled cryogenic-sampler has been developed to collect sufficient amounts of samples at lower-pressure altitudes.[18]

Conclusion

The vertical profiles of CCl_3F, CCl_2F_2, and CH_4 were determined by the analysis of the air samples collected by means of a balloon-borne grab-sampler. The mixing ratios of halocarbons decreased sharply in the stratosphere, indicating the emission of large amounts of Cl atoms, which in turn cause the depletion of stratospheric ozone: this situation will persist for several tens to hundreds of years in view of the increasing tropospheric concentrations of halocarbons with extremely long lifetimes.

References

1) M. J. Molina and F. S. Rowland, *Nature*, **249**, 810 (1974).

2) "The Stratosphere 1981: Theory and Measurements," World Meteorological Organization (WMO Global Ozone Research and Monitoring Project Report No. 11), Geneva (1982).

3) "Causes and Effects of Changes in Stratospheric Ozone: Update 1983," National Academy of Sciences, Washington, D.C., 1984.

4) Y. Makide, A. Yokohata, Y. Kubo, and T. Tominaga, *Bull. Chem. Soc. Jpn.*, **60**, 571 (1987).

5) V. Ramanathan, R. J. Cicerone, H. B. Singh, and J. T. Kiehl, *J. Geophys. Res.*, **90**, 5547 (1985).

6) Y. Makide and F. S. Rowland, *Proc. Natl. Acad. Sci. U.S.A.*, **78**, 5933 (1981).

7) P. D. Goldan, W. C. Kuster, D. L. Albritton, and A. L. Schmeltekopf, *J. Geophys. Res.*, **85**, 413 (1980).

8) C. C. Gallagher, C. A. Forsberg, and R. V. Pieri, *J. Geophys. Res.*, **88**, 3798 (1983).

9) P. Fabian, R. Borchers, G. Flentje, W. A. Matthews, W. Seiler, H. Giehl, K. Bunse, F. Müller, U. Schmidt, A. Volz, A. Khedim, and F. J. Johnen, *J. Geophys. Res.*, **86**, 5179 (1981).

10) T. Itoh, H. Kubo, H. Honda, T. Tominaga, Y. Makide, A. Yokohata, and H. Sakai, *Uchuken Hokoku, Spec. Issue*, No. 11, 59 (1984); *MAP Handbook*, **18**, 431 (1985).

11) Y. Makide, Y. Kanai, and T. Tominaga, *Nippon Kagaku Kaishi*, **1981**, 133.

12) Y. Makide, A. Yokohata, and T. Tominaga, *J. Trace Microprobe Techniques*, **1**, 265 (1983).

13) D. M. Cunnold, R. G. Prinn, R. A. Rasmussen, P. G. Simmonds, F. N. Alyea, C. A. Cardelino, A. J. Crawford, P. J. Fraser, and R. D. Rosen, *J. Geophys. Res.*, **88**, 8379 (1983).

14) M. K. W. Ko, N. D. Sze, M. Livshits, M. B. McElroy, and J. A. Pyle, *J. Atmos. Sci.*, **41**, 2381 (1984).

15) P. Fabian, R. Borchers, D. Gömer, B. C. Krüger, S. Lal, and S. A. Penkett, in "Atmospheric Ozone," ed by C. S. Zerefos and A. Ghazi, D. Reidel Publ. Co., Dordrecht (1985), p. 129.

16) A. Golombek and R. G. Prinn, *J. Geophys. Res.*, **91**, 3985 (1986).

17) "Atmospheric Ozone 1985," World Meteorological Organization (WMO Global Ozone Research and Monitoring Project Report No. 16), Geneva (1986).

18) T. Itoh, H. Honda, H. Kubo, H. Minagawa, T. Tominaga, Y. Makide, Y. Kubo, H. Sakai, M. Tsutsumi, T. Gamo, and T. Nakazawa, Balloon Symposium (1985) at The Institute of Space and Astronautical Science (Tokyo), Abstract, p. 110 (1986).

Synthesis, and Crystal and Molecular Structure of Heptaaquabis (1-hydroxy-2-naphthoato)lanthanum(III) 1-Hydroxy-2-naphthoate Hydrate and the Isomorphous Neodymium(III) Salt, $[M\{C_{10}H_6(OH)CO_2\}_2(H_2O)_7][C_{10}H_6(OH)CO_2]\cdot H_2O$ (M=La, Nd)

Yoshiyuki OHKI,† Yasuo SUZUKI,† and Akira OUCHI*
Department of Chemistry, College of Arts and Sciences, The University of Tokyo, Komaba, Meguro-ku, Tokyo 153
†Department of Industrial Chemistry, Faculty of Engineering, Meiji University, Higashi-Mita, Tama-ku, Kawasaki, Kanagawa 214
(Received November 11, 1986)

Synopsis. The light lanthanoid(III) (La or Nd) 1-hydroxy-2-naphthoate crystals indicated in the title were obtained and their structures were determined by the X-ray diffraction method using their single crystals. They are orthorhombic with the space group $P2_12_12_1$, Z=4. The unit-cell axis lengths of the lanthanum(III) complex are: a=11.985(4), b=40.21(5), and c=7.017(1) Å. The central metal atom is ennea-coordinated and is in a tricapped trigonal-prism geometry, where two carboxylate ions act as the unidentates, and the other coordinating positions are occupied by water oxygen atoms. The non-coordinated carboxylate ion is hydrogen-bonded to two ligated water oxygen atoms with its respective carboxylato oxygen atoms. The complex molecules are not directly bridged by the carboxylate ions, but the complexes are linked by hydrogen-bondings in the a- and c-axis directions. Such hydrophilic and the hydrophobic layers of the naphthalene rings, both of them being parallel to the ac-plane, are laid alternately in the crystal.

It has been already reported that many lanthanoid carboxylates have high coordination-number metal atoms and are almost always in dimeric or polymeric structures in their crystals.[1-6] We previously reported two types of neodymium(III) 1-hydroxy-2-naphthoates: one in a dimer form including water and ethanol, $[NdL_3(H_2O)(C_2H_5OH)]_2\cdot 2H_2O\cdot 2C_2H_5OH$ (**1**),[7] and the other is a monomeric type one, $[NdL_2(H_2O)_5]L\cdot 2H_2O$ (**2**) (HL=1-hydroxy-2-naphthoic acid).[8] The metal atoms of both complexes are ennea-coordinated and are in a tricapped trigonal-prism geometry. This time we could obtain other types of the salts (isomorphous lanthanum(III) and neodymium(III) salts), which include eight molecules of water per one metal atom. It is interesting to compare their structures with those of **1** and **2**; we examined their crystal and molecular structure by the single-crystal X-ray diffraction method.

Experimental

Synthesis of [Heptaaquabis(1-hydroxy-2-naphthoato)-lanthanum(III)] (1-hydroxy-2-naphthoate) Hydrate. The lanthanum hydroxide was obtained by mixing aqueous solutions of lanthanum(III) chloride heptahydrate (0.38 g, 1.0 mmol) and an excess sodium hydroxide. The precipitate was separated, washed with water, and dissolved into 30 cm^3 of a warmed 2-propanol-water mixed solvent (2:1=v/v), including 1-hydroxy-2-naphthoic acid (0.56 g, 3.0 mmol). The solution was filtered and the filtrate was left standing for several days at room temperature; and the crystals of the title complex were precipitated. Yield: 0.37 g (43%). Anal ($LaC_{33}H_{37}O_{17}$), La, C, H. A pure lanthanum complex was thus obtained; however, when the same process was applied to the neodymium salt, the product also contained some crystals of **2**. Therefore, from the mixture we picked up the title complex crystals, which were spatula-like thin-plate types that could be clearly distinguished from those of **2**.

Single-Crystal X-Ray Analysis. Crystallographic data and various experimental conditions for collecting intensity data are summarized in Table 1. Reflections were collected on a Rigaku AFC-6A automated four-circle X-ray diffractometer with graphite-monochromated Mo $K\alpha$ radiation, by means of a ω-scan technique (scan speed=4° min^{-1} (θ)). Reflections with $|F_o|>3\sigma(|F_o|)$ were used for a structure determination. All calculations were carried out on a HITAC M-680H computer at the Computer Center of the

Table 1. Crystallographic Data and Some Experimental Conditions of the Complexes $MC_{33}H_{37}O_{17}$

M=	La	Nd
F. W.	844.55	849.89
a (l/Å)	11.985(4)	11.928(10)
b (l/Å)	40.21(5)	40.22(4)
c (l/Å)	7.017(1)	6.996(1)
U (v/Å^3)	3382(4)	3356(5)
D_m (d/Mg m^{-3})	1.65(3)	1.68(3)
D_x (d/Mg m^{-3})	1.66	1.68
μ (Mo $K\alpha$) (n/mm^{-1})	1.38	1.65
Final R[9]	0.054	0.085
R of the Reversed Structure	0.059	0.082
Reflections Measured	5627	4398
Reflections Used for Calculation	4036	2454
Used Crystal (v/mm^{-3})	0.40×0.12×0.10	0.30×0.15×0.10
Scan Width (θ/°)	1.04	1.10
Scanned Range (2θ/°)	3—60	3.5—55

Table 2. Selected Bond Lengths and Bond Angles of the Complexes $MC_{33}H_{37}O_{17}$ (M=La, Nd)

M=	La	Nd	M=	La	Nd
	Bond Lengths (l/Å)			Bond Angles (ϕ/°)	
M-O(1)	2.447(7)	2.415(14)	O(1)-M-O(W2)	78.3(2)	79.1(4)
M-O(3)	2.521(7)	2.473(16)	O(W2)-M-O(W5)	77.54(19)	77.9(4)
M-O(W1)	2.548(7)	2.512(14)	O(W5)-M-O(1)	70.0(2)	70.9(4)
M-O(W2)	2.531(6)	2.475(13)	O(1)-M-O(W1)	71.0(2)	70.0(5)
M-O(W3)	2.589(7)	2.548(14)	O(1)-M-O(3)	131.2(2)	131.5(5)
M-O(W4)	2.575(7)	2.526(15)	O(1)-M-O(W6)	70.4(2)	70.0(5)
M-O(W5)	2.583(6)	2.584(14)	O(W1)-M-O(3)	113.0(2)	112.4(5)
M-O(W6)	2.578(7)	2.562(15)	O(3)-M-O(W6)	128.6(2)	130.9(5)
M-O(W7)	2.637(7)	2.615(16)	O(W6)-M-O(W1)	118.4(2)	116.7(5)
O(1)-C(C1)	1.235(11)	1.20(2)	O(W3)-M-O(W4)	77.3(2)	77.1(5)
O(2)-C(C1)	1.275(12)	1.23(3)	O(W4)-M-O(W7)	68.0(2)	68.8(5)
C(C1)-C(2)	1.497(13)	1.46(3)	O(W7)-M-O(W3)	76.0(2)	77.3(5)
C(1)-O(C1)	1.349(13)	1.40(3)	O(W3)-M-O(3)	67.7(2)	68.4(5)
O(3)-C(C2)	1.282(10)	1.28(2)	O(W3)-M-O(W1)	144.4(2)	143.7(5)
O(4)-C(C2)	1.244(10)	1.28(2)	O(W3)-M-O(W6)	70.1(2)	71.6(5)
C(C2)-C(12)	1.467(11)	1.48(3)	M-O(1)-C(C1)	165.7(6)	166.8(14)
C(11)-O(C11)	1.361(11)	1.37(2)	O(1)-C(C1)-O(2)	122.7(9)	121(2)
O(5)-C(C3)	1.255(11)	1.26(2)	O(1)-C(C1)-C(2)	119.9(9)	121.6(18)
O(6)-C(C3)	1.271(12)	1.22(2)	O(2)-C(C1)-C(2)	117.4(8)	116.8(18)
C(C3)-C(22)	1.492(11)	1.49(3)	M-O(3)-C(C2)	144.6(5)	143.3(14)
C(21)-O(C21)	1.380(10)	1.36(2)	O(3)-C(C2)-O(4)	122.1(7)	122.9(18)
O(W3)···O(6)	2.659(9)	2.65(2)	O(3)-C(C2)-C(12)	117.8(7)	118.7(17)
O(W4)···O(5)	2.784(10)	2.77(2)	O(4)-C(C2)-C(12)	120.1(7)	118.4(17)
O(W6)···O(W8)	2.901(11)	2.91(2)	M-O(W3)···O(6)	120.1(3)	119.7(6)
			M-O(W4)···O(5)	120.1(3)	121.0(6)
			M-O(W6)···O(W8)	109.9(3)	109.5(6)

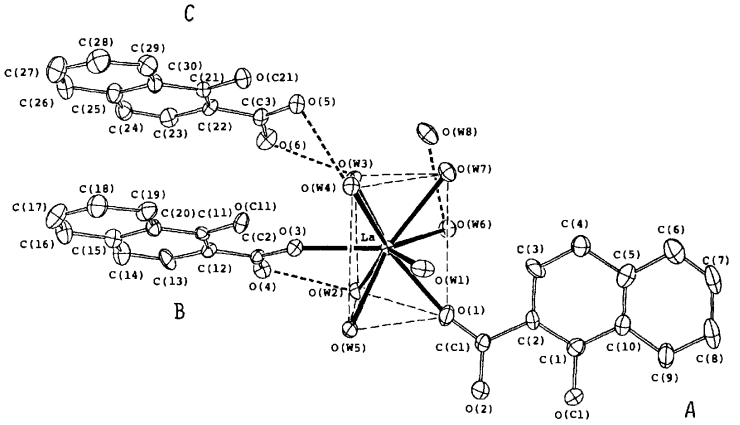

Fig. 1. A perspective drawing around the metal atom with the numbering scheme of the atoms and the notation of the naphthalene rings.

University of Tokyo, using the local version of UNICS.[10] The scattering factors were taken from Ref. 11.

The structure of the lanthanum(III) complex was solved by common heavy-atom method. Refinements of the parameters of the neodymium(III) complex were started from the final parameters of the isomorphous lanthanum(III) salt, and was refined as usual. Their final R values are shown in Table 1, together with those of the reversed structures. As the R value of the reversed structure was larger in the case of the lanthanum complex, it was rejected; however, that of the neodymium complex was a little smaller and should be adopted for the salt.

Results and Discussion

The selected bond lengths and bond angles are shown in Table 2.[12] A perspective drawing of the complex together with a carboxylate ion and a water molecule near it is shown in Fig. 1; the numbering scheme of the atoms as well as the notation of the naphthalene rings are also given. A projection of the unit cell is shown in Fig. 2.

No carboxylato bridgings were found between the metal atoms, although some hydrogen bondings link those complexes in a- and c-axis directions.

The metal atom is ennea-coordinated and is in a tricapped trigonal-prism geometry. Two carboxylate ions are coordinated as unidentates with each carboxyl oxygen atom at one apex of the prism and one cap position; the other seven positions are occupied by the water oxygen atoms. Compared with **2**, where both of

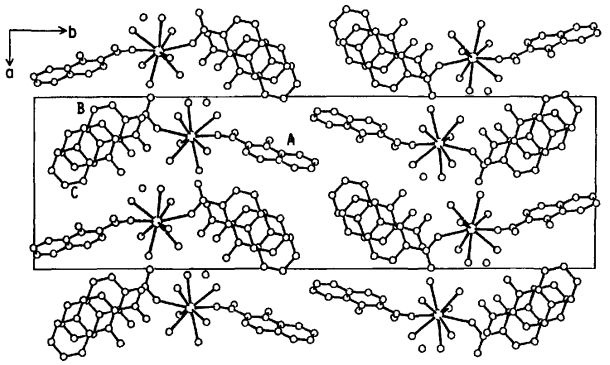

Fig. 2. Crystal packing diagram.

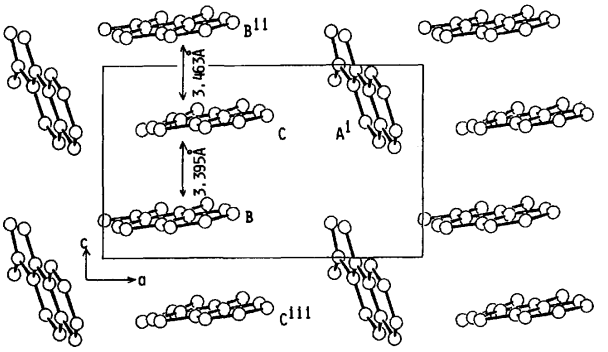

Fig. 3. A projection of the naphthalene rings to the ac-plane. Key to the symmetry operations; i, 0.5+x, 0.5−y, 1−z; ii, x, y, 1+z; iii, x, y, −1+z.

the carboxylate ions form four-membered chelate rings, this compound is regarded as being one in which each carboxyl oxygen atom of the ligands of the former complex is substituted by a water oxygen atom.

The non-coordinated carboxylato oxygen atoms of the coordinated ligands, O(4) and O(2), are hydrogen-bonded with O(W2) and O(W7^{iii}) (Key to the symmetry operation: iii, x, y, −1+z). The carboxylato oxygen atoms of the non-coordinated carboxylate ion, O(5) and O(6), atoms are hydrogen bonded with O(W4) and O(W3) atoms, respectively. These water oxygen atoms, O(W2,) O(W7^{iii}), O(W4), and O(W3) atoms are all ligated to respective metal atoms. The crystalline water oxygen, O(W8), and the hydroxyl oxygen atoms of the carboxylate ions also join the hydrogen-bonding network formation, which is spread approximately parallel to the ac-plane.

In this type complex, the M-O(carboxylate) lengths are shorter than those of M-O(water), though in **2**, on the contrary, the average of the former bond lengths is slightly longer than that of the latter ones. Probably the chelate-ring formation in **2** gives some steric effect to lengthen the former bond lengths.

The lanthanum and neodymium complexes are isomorphous with each other, and the respective La-O bond lengths are longer than the corresponding Nd-O ones, except M-O(W5), which are about the same in length in both complexes. Except for these discrepancies, there are no fundamental differences between the corresponding bond lengths and angles of both complexes, respectively.

The arrangement of naphthalene rings of the ligands and the metal core parts resembles that of **2**. The naphthalene ring parts are intercalated between the hydrophilic sheets of the hydrogen bonded metal core layers. As shown in Fig. 3, **B** and **C** naphthalene rings are almost parallel (dihedral angle=0.8°) and, as written in the figure, the inter-layer distances are approximately the thickness of an aromatic ring. The overlapping area[13] of **B** and **C**, and **C** and **B**^{ii} rings are about 26 and 58%, respectively. The respective dihedral angles between **B** and **A**^{i}, and **C** and **A**^{i} rings are 81.7° and 81.0°.

The hydroxyl groups of the parallel **B** and **C** naphthalene rings direct themselves to the same side in these complexes, while those of **2** to opposite sides from each other.

The authors wish to thank the Shin-Etsu Chemical Ind. Co., Ltd., for the highly pure neodymium(III) oxide.

References

1) G. G. Sadikov, G. A. Kukina, and M. A. Porai-Koshits, *Zh. Strukt. Khim.*, **8**, 551 (1967).
2) L. A. Aslanov, V. M. Ionov, and I. D. Kiekbaev, *Koord. Khim.*, **2**, 1674 (1976).
3) S. Kondo, M. Shimoi, A. Ouchi, and T. Takeuchi, *Bull. Chem. Soc. Jpn.*, **55**, 2840 (1982).
4) Y. Koizumi, H. Sawase, Y. Suzuki, T. Takeuchi, M. Shimoi, and A. Ouchi, *Bull. Chem. Soc. Jpn.*, **57**, 1809 (1984).
5) M. C. Favas, D. L. Kepert, B. W. Skelton, and A. H. White, *J. Chem. Soc., Dalton Trans.*, **1980**, 454.
6) M. S. Khiyalov, I. R. Amiraslanov, Kh. S. Mamedov, and E. M. Movsumov, *Dokl. Akad. Nauk Az. SSR*, **37**, 42 (1981).
7) Y. Ohki, Y. Suzuki, T. Takeuchi, M. Shimoi, and A. Ouchi, *Bull. Chem. Soc. Jpn.*, **59**, 1015 (1986).
8) Y. Ohki, Y. Suzuki, M. Shimoi, and A. Ouchi, *Bull. Chem. Soc. Jpn.*, **60**, 551 (1987).
9) $R=\Sigma||F_o|-|F_c||/\Sigma|F_o|$
10) "The Universal Crystallographic Computation Program System (UNICS)," ed by T. Sakurai, Crystallographic Society of Jpn., Tokyo (1967).
11) "International Tables for X-Ray Crystallography," Kynoch Press, Birmingham (1974), Vol. IV, pp.72, 149.
12) The final atomic and thermal parameters, the final F_o—F_c table, and some additional data about the bond lengths and bond angles are deposited as Document No. 8729 at the Office of the Editor of Bull. Chem. Soc. Jpn.
13) The former ring is projected to the latter ring plane, and the percentage of the overlapping area of the both rings to the whole ring area was calculated.

Template Synthesis of Binuclear Lanthanoid Complexes with Macrocyclic Schiff Base Constituted of 2,6-Diacetylpyridine and 1,3-Diamino-2-propanol

Masatomi SAKAMOTO
Department of Industrial Chemistry, Faculty of Engineering, Ehime University, Bunkyo-cho, Matsuyama 790
(Received November 29, 1986)

Synopsis. Reaction of 2,6-diacetylpyridine with 1,3-diamino-2-propanol in the presence of lanthanoid(III) ions gave complexes of (2+2) macrocyclic tetraimine ligand, H_2apdapy. Complexes synthesized have the composition of $Ln_2(apdapy)(NO_3)_4(H_2O)_5$ (Ln=La or Pr) or $Ln_2(apdapy)(NCS)_4(H_2O)_4$ (Ln=La, Pr, Nd, Sm, or Eu). It is suggested that the complexes are considerably stable and maintain the binuclear structure in dimethylsulfoxide solution.

It is well known that some metal ions function as effective templating agents in the syntheses of macrocyclic Schiff bases constituted of 2,6-diacetylpyridine or 2,6-diformylpyridine and a primary diamine.[1-5] The success in such template syntheses depends upon the conformity in shape and size between the templating ions and the macrocycles thus formed. In this point of view lanthanoid ions have been used for the systematic investigations on template syntheses of macrocyclic complexes.[6-10] The lanthanoid complexes so far characterized, however, are almost limited to those of mononucleating macrocycles, and lanthanoid complexes of binucleating macrocycles have been only reported by Kahwa et al.,[11] in spite of much interest in physicochemical properties[12] and quantum efficiency of luminescence in the condensed systems of f-block elements.[13]

Recently, Bailey et al. have reported that a template reaction of 2,6-diacetylpyridine and 1,3-diamino-2-propanol in the presence of barium perchlorate forms a macrocyclic complex, $Ba(H_2apdapy)(ClO_4)_2 \cdot 2H_2O$ (see Fig. 1).[14,15] This complex was then used for the synthesis of a binuclear copper(II) complex, $Cu_2(Hapdapy)(ClO_4)_3 \cdot 2H_2O$, by the transmetallation.[14,15] X-ray crystal analysis[15] for the dicopper(II) complex demonstrates a relatively large internal cavity size of H_2apdapy and significant flexibility of propanol site, suggesting that the macrocycle, H_2apdapy, can also function as a binucleating ligand toward lanthanoid(III)ions. Therefore, it was attempted in this study to synthesize binuclear lanthanoid complexes of H_2apdapy by template reaction. This paper deals with the synthesis and characterization of $Ln_2(apdapy)(NO_3)_4(H_2O)_5$ and $Ln_2(apdapy)(NCS)_4(H_2O)_4$.

Experimental

Preparations of Complexes. Nitrate complexes were synthesized as follows: Lanthanum(III) nitrate or praseodymium(III) nitrate hydrate (1.2 mmol) and 2,6-diacetylpyridine (1.2 mmol) were dissolved in methanol (20 cm^3). To this solution was added a methanolic solution (10 cm^3) of 1,3-diamino-2-propanol (1.2 mmol) with stirring. After the mixture was refluxed for 2—3 h with stirring, the precipitate thus formed was filtered, washed with methanol, then with diethyl ether, and dried in the open air.

Thiocyanate complexes were prepared as follows: Potassium thiocyanate(33 mmol) was added with stirring to a methanolic solution(50 cm^3) of lanthanoid chloride hydrate (10 mmol) (Ln=La, Pr, Nd, Sm, or Eu). Potassium chloride precipitated was removed by filtration and washed with methanol (50 cm^3). The filtrate and the washings were combined, and to this solution was added 2,6-diacetylpyridine(10 mmol) and then a methanolic solution (25 cm^3) of 1,3-diamino-2-propanol (10 mmol) with stirring. After the mixture was refluxed with stirring for 2—3 h, the precipitate thus obtained was filtered, washed with methanol, then with diethyl ether, and dried in the open air.

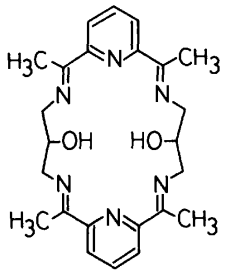

Fig. 1. Chemical structure of H_2 apdapy.

Results of elemental analyses for the complexes are given in Table 1.

Measurements. Infrared spectra were measured with a JASCO IR-G Spectrometer on KBr disks. Magnetic measurements were carried out by the Gouy method at room temperature. The apparatus was calibrated by the use of $HgCo(NCS)_4$. ^{13}CNMR spectra were recorded on a JEOL FX-100 Spectrometer in dimethylsulfoxide-d_6 (DMSO-d_6) at 30 °C.

Results and Discussion

Analytical results summarized in Table 1 demonstrate the composition of the complexes obtained to be $Ln_2(apdapy)(NO_3)_4(H_2O)_5$(Ln=La or Pr) for the nitrate complexes and $Ln_2(apdapy)(NCS)_4(H_2O)_4$ (Ln=La, Pr, Nd, Sm, or Eu) for the thiocyanate complexes, respectively, where the hydroxyl groups of the ligand are presumed to be deprotonated. Infrared spectra of both the nitrate and thiocyanate complexes are essentially similar to each other, except for the IR bands associated with the anions (NO_3^-, NCS^-). For both types of the complexes, the in-plane ring deformation band due to the coordination of pyridine nitrogen is observed at 630—640 cm^{-1}.[1,17] Absorption in the region of 1630—1645 cm^{-1} is attributable to the C=N stretching mode. As described in a previous paper,[17] azomethine nitrogen is probably coordinated to the metal, since Schiff bases of the present type are thermally stabilized only when the azomethine nitrogen is coordinated to a metal ion.[18] In fact, it was impossible to isolate H_2apdapy in the metal free state, as was the case of 1,3-bis(2-pyridylmethyleneamino)-2-prop-

Table 1. Analytical and Magnetic Data of Complexes

	Found(%) (Calcd(%)[a])				μ_{eff}
	Ln	C	H	N	(B.M.)
Nitrate complex					
La	26.38	27.70	3.77	13.05	dia.
	(26.50)	(27.49)	(3.65)	(13.36)	
Pr	27.23	26.65	3.43	12.91	3.42
	(26.78)	(27.39)	(3.64)	(13.31)	
Thiocyanate complex					
La	27.08	32.98	3.28	12.93	dia.
	(27.38)	(33.14)	(3.58)	(13.80)	
Pr	27.33	32.81	3.41	12.91	3.43
	(27.66)	(33.01)	(3.56)	(13.75)	
Nd	28.41	33.18	3.34	13.08	3.49
	(28.13)	(32.80)	(3.54)	(13.66)	
Sm	28.85	32.82	3.14	13.22	1.60
	(28.98)	(32.41)	(3.50)	(13.50)	
Eu	29.18	33.08	3.28	12.85	3.41
	(29.20)	(32.31)	(3.49)	(13.46)	

a) Values for $Ln_2(apdapy)(NO_3)_4(H_2O)_5$ or $Ln_2(apdapy)(NCS)_4(H_2O)_4$.

Table 2. ^{13}CNMR Spectral Data of Complexes

Complex	Chemical shift (ppm)					
	Azomethine carbon[a]	Pyridine carbon[a]	Thiocyanate carbon	Methine carbon	Methylene carbon	Methyl carbon
$La_2(apdapy)(NO_3)_4(H_2O)_5$	168.55, 166.67 167.56	154.87, 125.76 141.67, 125.23	—	75.68 74.39	60.00, 58.42 59.24	16.50, 16.03 16.26, 15.85
$La_2(apdapy)(NCS)_4(H_2O)_4$	169.67, 168.44 168.79, 167.32	154.76, 141.49 154.64, 125.99 154.35, 125.46 141.90	131.10	75.85 74.50	59.83, 58.95 59.24, 58.77	16.97, 16.38 16.50, 16.09
$Ba(H_2apdapy)(ClO_4)_2(H_2O)_2$[b]	165.86	155.05, 123.88 139.67	—	68.69	57.47	16.09

a) Ref. 8 and 22. b) Values measured in this work in order to compare with the present La complexes.

anol.[17]

For the nitrate complexes, the bands assignable to bidentate nitrate ion appear at 1450, 1300, 1030—1035, and 815 cm^{-1}.[19] The frequencies of the nitrate bands are very similar to those of hexaazamacrocyclic lanthanum(III) complex, in which all the nitrate ions are revealed to be bidentate.[6] Based on this fact, it may be concluded that all of the nitrate ions of $Ln_2(apdapy)(NO_3)_4(H_2O)_5$ function as bidentate ligands. This is also supported by the splitting of the combination bands in the 1700—1800 cm^{-1} region;[20] the separation for the La and Pr complexes is 25 and 29 cm^{-1}, respectively.

For the thiocyanate complexes, a sharp singlet band appears at 2050 cm^{-1}, suggesting that the thiocyanate ions are coordinated to the metal at the nitrogen.[21]

Magnetic moments of the complexes at room temperature are common for the tervalent lanthanoid ions and no significant magnetic interaction was inferred between a pair of metal ions, for the reason that 4f-electrons are shielded by outer-shell electrons.

It seems that the binuclear structure of the macrocycle is maintained even in solutions because each complex gave no precipitate when treated with KOH in DMSO or DMSO-H_2O.[6]

The ^{13}CNMR spectral data of $La_2(apdapy)(NO_3)_4(H_2O)_5$ and $La_2(apdapy)(NCS)_4(H_2O)_4$ in DMSO-d_6 are summarized in Table 2. These complexes give no signal at about 200 ppm, whereas the signal due to carbonyl carbon is observed at 198.68 or 200.09 ppm for the DMSO-d_6 solution of 2,6-diacetylpyridine or of lanthanum(III) nitrate and 2,6-diacetylpyridine, respectively, suggesting that apdapy does not dissociate into its components in DMSO. Signals due to the methine carbon atoms of the La complex shift downfield compared with those of complex reported by Fenton et al.,[14] implying that the hydroxyl groups are deprotonated and coordinated to the metal. Furthermore, it is seen that each signal for the La complexes is composed of two or more components. This fact suggests that (1) the symmetry of the binuclear structure is low or (2) the complex is a mixture of some geometrical isomers. All efforts to obtain single crystals of the lanthanoid complexes suitable for X-ray analysis are in vain at this moment.

Though the detailed structure of the complexes is

still unknown, it is evident from the above discussion that the lanthanoid ions function as the template for the 2:2 condensation of 2,6-diacetylpyridine and 1,3-diamino-2-propanol to form binucleating macrocycle H_2apdapy.

The author is greatly thankful to Prof. Tomitaro Ishimori of Ehime University for his helpful discussion and encouragement throughout this work.

References

1) S. M. Nelson, *Pure Appl. Chem.*, **52**, 2461 (1980).
2) S. M. Nelson, C. V. Knox, M. McCann, and M. G. B. Drew, *J. Chem. Soc., Dalton Trans.*, **1981**, 1669.
3) M. G. B. Drew, J. Nelson, and S. M. Nelson, *J. Chem. Soc., Dalton Trans.*, **1981**, 1678.
4) S. M. Nelson, F. S. Esho, and M. G. B. Drew, *J. Chem. Soc., Dalton Trans.*, **1982**, 407.
5) M. G. B. Drew, J. Nelson, F. S. Esho, V. Mckee, and S. M. Nelson, *J. Chem, Soc., Dalton Trans.*, **1982**, 1837.
6) J. D. J. Backer-Dirks, C. J. Gray, F. A. Hart, M. B. Hursthouse, and B. C. Schoop, *J. Chem, Soc., Chem. Commun.*, **1979**, 774.
7) W. Radecka-Paryzek, *Inorg. Chim. Acta*, **45**, L147 (1980); **52**, 261 (1981).
8) K. K. Abid and D. E. Fenton, *Inorg. Chim. Acta*, **95**, 119 (1984).
9) K. K. Abid, D. E. Fenton, U. Casellato, P. A. Vigato, and R. Graziani, *J. Chem. Soc., Dalton Trans.*, **1984**, 351.
10) L. D. Cola, D. L. Smailes, and L. M. Vallarino, *Inorg. Chem.*, **25**, 1729 (1986).
11) I. A. Kahwa, J. Selbin, T. C. Hsieh, and R. A. Laine, *Inorg. Chim. Acta*, **118**, 179 (1986).
12) H. Sugimoto, T. Higashi, A. Maeda, Y. Hirai, J. Teraoka, and M. Mori, *J. Less-Common Met.*, **112**, 387 (1985).
13) M. Nakamura, H. Ōkawa, S. Kida, and S. Misumi, *Bull. Chem. Soc. Jpn.*, **57**, 3147 (1984).
14) N. A. Bailey, D. E. Fenton, I. T. Jackson, R. Moody, and C. R. de Barbarin, *J. Chem. Soc., Chem. Commun.*, **1983**, 1463.
15) V. Mckee and J. Smith, *J. Chem. Soc., Chem. Commun.*, **1983**, 1465.
16) K. Nakamoto, "Infrared and Raman Spectra of Inorganic and Coordination Compounds," 3rd ed., Wiley-Interscience, New York (1978), pp. 211—213.
17) M. Sakamoto, *Bull. Chem. Soc. Jpn.*, **59**, 1273 (1986).
18) M. M. Jones, "Ligand Reactivity and Catalysis," Academic Press, New York (1968), Chap. 2.
19) R. B. King and P. R. Heckley, *J. Am. Chem. Soc.*, **96**, 3118 (1974).
20) A. B. P. Lever, E. Mantovani, and B. S. Ramaswany, *Can. J. Chem.*, **49**, 1957 (1971).
21) K. Nakamoto, "Infrared and Raman Spectra of Inorganic and Coordination Compounds," 3rd ed., Wiley-Interscience, New York (1978), p. 270.
22) D. E. Fenton and M. Vidali, *Inorg. Chim. Acta*, **95**, 187 (1984).

Asymmetric Hydrogenation Catalyzed by Bis(disubstituted glyoximato)-cobalt(II)(L)-Chiral Cocatalyst System. Effect of Structural Variation of Ligands and Hydrogen Pressure[1)]

Yoshiaki OHGO,* Yasuhisa TASHIRO,† and Seiji TAKEUCHI
Niigata College of Pharmacy, 5829 Kamishin'ei-cho, Niigata 950-21
(Received August 25, 1986)

Synopsis. The reaction rate was extremely enhanced by increasing the basicity of the axial ligand of [Co(dmgH)$_2$(L)] and by increasing the hydrogen pressure without decreasing the enantioselectivity. Substituting one and two methyl groups of the dimethylglyoxime ligand in [Co(dmgH)$_2$(L)] with a phenyl group enhanced and retarded the reaction rate, respectively. The chirality at the cobalt did not affect the enantioselectivity.

The authors have reported asymmetric hydrogenations of diketones, α-ketocarboxylates and olefinic compounds[2-6)] catalyzed by bis(dimethylglyoximato)-cobalt(axial ligand)-chiral cocatalyst systems and have proposed a mechanism for the catalysis of the asymmetric hydrogenations.[4,5)] The proposed mechanism involves an electron-donating site and an enantiodifferentiating site that are separated in these systems (Fig. 1).

We examined the effects of a structural variation of inplane and axial ligands as well as hydrogen pressure in order to determine a guideline for finding a better catalyst and to provide further support regarding the mechanism.

Results and Discussion

Effect of Structural Variation of Inplane and Axial Ligands. In Table 1 are summarized the results for asymmetric hydrogenations of benzil that were catalyzed by several catalyst systems in which inplane and axial ligands were varied (Eq. 1 and Fig. 2).

$$\mathrm{PhCOCOPh} \xrightarrow[\mathrm{Co(PL)_2L\text{-}B^*}]{\mathrm{H_2}} \mathrm{Ph\overset{*}{C}HCOPh} \quad (1)$$
$$\qquad\qquad\qquad\qquad\qquad\qquad\quad \mathrm{OH}$$

The chemical yields were almost quantitative. An increase in the sigma-donor character of an axial ligand accelerates the reaction rate (as already reported in part);[5)] an increase in the steric bulkiness decreases it. A steric hinderance of the inplane ligand is considered to decrease the rate, but the electronic effect of an inplane substituent is somewhat complicated. Since the plane of a phenyl group is oriented almost perpendicular to the glyoxime plane,[7)] the electronic influence of the phenyl group is considered to be inductive rather than resonance; thus, the phenyl group will act as an electron-withdrawing group, which can bring about a decrease in the electron density of cobalt atoms. In fact, the Co-CH_3 proton signal in the series of complexes shifts to a lower field (^{1}H NMR spectrum) with an increase in the phenyl substituent (Table 1). The fact that the substitution of one of the two methyl groups of the dimethylglyoxime ligand in Co(dmgH)$_2$L with a phenyl group causes some rate enhancement seems to be incompatible with the fact that the sigma-donor character of the axial ligand enhances the reaction rate. The reason has not yet been clarified.

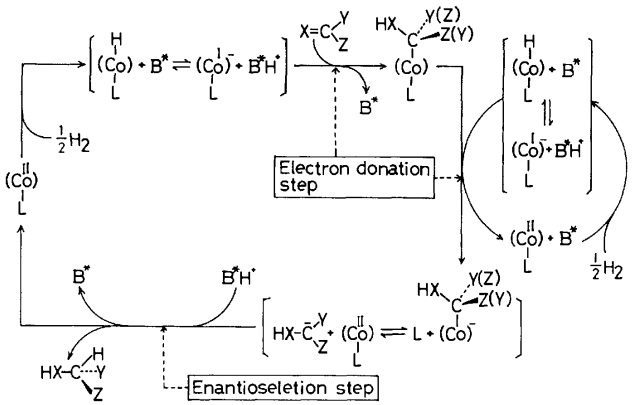

Fig. 1. Catalytic cycle.

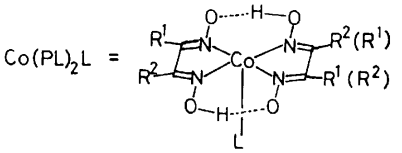

Fig. 2. Structures of Catalysts.

Planar Ligand (PL)	Substituent	
	R^1	R^2
dmgH	CH_3	CH_3
chdH	$-CH_2CH_2CH_2CH_2-$	
mpgH	CH_3(Ph)	Ph (CH_3)
dpgH	Ph	Ph

We have shown that chiral amine coordinates preferentially to one of the two prochiral faces of bis[(*E,E*)-1-phenyl-1,2-propanedione dioximato]cobalt-(I).[8)] If a cobalt complex is involved in the enantiodifferentiating transition state, the enantioselectivities should vary by changing an achiral axial ligand to a chiral one. The results showed that a chiral axial ligand did not alter the enantioselectivity. This provides further support for the proposed mechanism regarding the enantioselection described in previous papers.[4,5)]

Effect of Pressure. Asymmetric hydrogenation catalyzed by chiral rhodium complexes are sensitive to the hydrogen pressure: a high hydrogen pressure decreases the enantioselectivity remarkably.[9,10)] The hydrogen

†Present address: Tokyo Plant, Nippon Kayaku Co., Shimo 3-31-12, Kita-ku, Tokyo 115.

Table 1. Effect of Structural Variation of Inplane and Axial Ligands on the Asymmetric Hydrogenation of Benzil Catalyzed by Bis(glyoximato)cobalt(II)(L)-Quinine System At 30°C[a]

Planar ligand (PL)	Axial ligand[h] (L)	$CH_3(PL)_2Co(L)$ chem. shift (δ/ppm)	V[b] 10^{-3} s^{-1}	(S)-(+)-benzoin Enantioselectivity/%ee[c]
dmgH[d]	Ph_3P	1.19	0.3#	61#
	Py	0.84	2.5#	57#
	$PhCH_2NH_2$	0.74	13.6#	61.5#
	(*R*)-PEA	0.68	11.5	61.5
	(*S*)-PEA		11.5	61.5
chdH[e]	$PhCH_2NH_2$	0.75	10.0	61
mpgH[f]	Bu_3P		1.17	56
	Ph_3P		0.07	53
	Py	1.14 (achiral) [i] 1.15 (chiral)	9.8	60.5
	$PhCH_2NH_2$	1.06 (achiral) [i] 1.07 (chiral)	18.0	62
	(R)-PEA		8.1	62
	(S)-PEA		8.5	62
dpgH[g]	Py	1.44	2.5	59
	$PhCH_2NH_2$	1.33	2.8	57

See Ref. 5).

a) Catalytic hydrogenation was carried out in benzene under atmospheric pressure of hydrogen. In every experiment, equimolar amounts of quinine (Q*) and its HCl salt (Q*HCl) were used (Q*/Co=Q*HCl/Co=1) as the chiral cocatalyst. b) V: initial rate (H_2 moles consumed/s/mol of catalyst). c) The enantioselectivity (%ee: % enantiomeric excess) in every reaction was calculated from the specific rotation of the product based on the specific rotation of pure *S*(+)-benzoin, $[\alpha]_D$ +118.5° (*c* 1, acetone).[5] d) dmgH: dimethylglyoxime monoanion. e) chdH: cyclohexanedione dioxime monoanion. f) mpgH: methylphenylglyoxime monoanion=(*E*,*E*)-1-phenyl-1,2-propanedione dioxime monoanion. g) dpgH: diphenylglyoxime monoanion. h) Ph_3P: triphenylphosphine. Py: pyridine. (*R*)-PEA: (*R*)-1-phenylethylamine. Bu_3P: tributylphosphine. i) Achiral and chiral complexes are formed in the ratio of 1 (achiral): 1.2—1.4 (chiral) when methyl iodide is added to the catalyst solution prepared according to the usual method. Methyl signals (^{1}H NMR) of achiral complexes appear at a higher field than those of corresponding chiral complexes.

Table 2. Pressure Effect on Asymmetric Hydrogenation of Ethyl 2-(Acetylamino)propenoate Catalyzed by Bis(dimethylglyoxomato)cobalt(II)-Quinine[a]

Entry	Pressure Kg/cm^2	S/Co[b]	Solvent	React. temp.	React. time	%ee[c]
1	atm.	10	Benzene	RT[d]	10 h	18.0
2	20	10	Benzene	RT	17 min	17.7
3	40	10	Benzene	RT	12 min	19.7
4	60	10	Benzene	RT	5 min	18.4
5	60	6.8	THF	−14°C	1.5 h	16.0

a) Catalytic hydrogenation was carried out in a 100 ml autoclave. In every experiment, equimolar amounts of quinine (Q*) and its HCl salt were used (Q*/Co=Q*HCl/Co=1) as the chiral cocatalyst. b) S/Co: molar ratio of substrate to cobalt. c) Enantioselectivity (% enantiomeric excess) in every experiment was calculated from the specific rotation of the product based on that of the optically pure (*S*)-(−)-ethyl *N*-acetylalaninate, $[\alpha]_{578}^{20}=-66.4°$ (*c* 6, ethanol).[11] d) RT: Room temperature.

pressure effect was ascribed to a difference in the reactivity of the two diastereomeric complexes (leading to the two enantiomeric products) toward hydrogen.[10] However, our catalyst systems are completely different from the chiral ligand-coordinated rhodium complexes. Mechanistic studies on our systems revealed that the electron-donating site and the enantiodifferentiating site are separated:[4,5] this suggested that a higher hydrogen pressure should accelerate the reaction rate without any decrease in the enantioselectivity. When an easily ligating amine, $PhCH_2NH_2$, was used, the reaction rate was too rapid for a measurement, even at a 20 kg/cm^2 pressure of hydrogen. Consequently, experiments on pressure effect were examined in the asymmetric hydrogenation of ethyl 2-(acetylamino)propenoate by using bis(dimethylglyoximato)cobalt(II)-quinine without the addition of a simple axial base (Eq. 2).

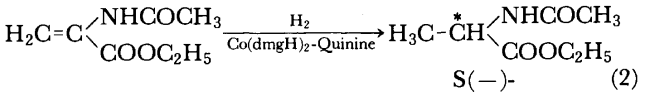

S(−)- (2)

As expected, the reaction rate was extremely enhanced with increasing hydrogen pressure, while the enantioselectivities were almost constant within the experi-

mental error (Table 2). The reaction rate under a 60 $kg\,cm^{-2}$ initial pressure of hydrogen became roughly 100 times that under an atmospheric pressure of hydrogen.

Experimental

Effect of Inplane and Axial Ligands on the Catalytic Asymmetric Hydrogenation of Benzil. Catalytic asymmetric hydrogenation of benzil was carried out in benzene under an atmospheric pressure of hydrogen according to the procedure described in previous papers,[5,6] except for using the inplane and axial ligands specified in Table 1. The reaction temperature was maintained at 30±0.2 °C.

Pressure Effect. The catalyst solution was prepared according to the procedure described in previous papers[5,6] under a nitrogen atmosphere. Methanol was evaporated in vacuo to give a wet paste which was dissolved in 25 ml of a degassed benzene solution of 2-(acetylamino)propenoate. The solution was transferred under a nitrogen atmosphere to a 100-ml autoclave. The nitrogen atmosphere was replaced with hydrogen. Asymmetric hydrogenation was performed in the initial pressure of hydrogen specified in Table 2. The time required to complete the reaction was determined by a pressure gauge. After carrying out the usual workup,[6] an oily product was obtained which was purified on silica gel (Kiesel gel-60) column chromatography using benzene/acetone (3/1) as an eluent. The eluate was concentrated under a reduced pressure to give a syrup whose optical rotation was measured. The enantioselectivities were calculated from the specific rotations. The results are shown in Table 2.

References

1) Asymmetric Reactions. XIII.
2) Y. Ohgo, S. Takeuchi, and J. Yoshimura, *Bull. Chem. Soc. Jpn.*, **44**, 583 (1971).
3) S. Takeuchi, Y. Ohgo, and J. Yoshimura, *Chem. Lett.*, **1973**, 265.
4) Y. Ohgo, Y. Natori, S. Takeuchi, and J. Yoshimura, *Chem. Lett.*, **1974**, 1327.
5) Y. Ohgo, S. Takeuchi, Y. Natori, and J. Yoshimura, *Bull. Chem. Soc. Jpn.*, **54**, 2124 (1981) and references cited therein.
6) S. Takeuchi and Y. Ohgo, *Bull. Chem. Soc.*, **54**, 2136 (1981); *ibid.*, **57**, 1920 (1984).
7) A. Uchida, Y. Ohashi, Y. Sasada, and Y. Ohgo, *Acta Crystallogr., Sect. C*, **41**, 25 (1985).
8) Y. Ohgo and S. Takeuchi, *Chem. Lett.*, **1985**, 407.
9) W. S. Knowles, M. J. Sabacky, and B. D. Vineyard, *Adv. Chem. Ser.*, **132**, 274 (1974); B. D. Vineyard, W. S. Knowles, M. J. Sabacky, G. L. Backman, and D. J. Weinkauff, *J. Am. Chem. Soc.*, **99**, 5946 (1977).
10) A. S. C. Chan, J. J. Pluth, and J. Halpern, *J. Am. Chem. Soc.*, **102**, 5952 (1980); J. Halpern, "Asymmetric Synthesis," ed by J. D. Morrison, Academic Press, Inc. (1985), Vol. 5, pp. 41—70 and references therein.
11) K. Freudenberg and F. Rhino, *Chem. Ber.*, **57B**, 1547 (1924).

Carbonate Formation from Oxiranes and Carbon Dioxide Catalyzed by Organotin Halide-Tetraalkylphosphonium Halide Complexes

Akio BABA,* Takashi NOZAKI, and Haruo MATSUDA
Department of Applied Chemistry, Faculty of Engineering, Osaka University, 2-1, Yamadaoka, Suita, Osaka 565
(Received September 11, 1986)

Synopsis. Cycloaddition of carbon dioxide to oxiranes was excellently promoted by the complexes of organotin halides and tetraalkylonium halides, while either components of the complexes had no catalytic activity individually. Particularly, the complex composed of Bu_3SnI-Bu_4PI was the most favorable catalyst, yielding a variety of five-membered cyclic carbonates under neutral and mild conditions.

Among many studies on carbon dioxide (CO_2) fixation, the reaction of oxiranes with CO_2 has received attention, yielding poly- or cyclic carbonates in the presence of many kinds of catalysts.[1] In particular, the synthesis of five-membered cyclic carbonates has been ardently investigated, and for example, a devised catalytic reactions using γ-butyrolactones and oxiranes was recently reported.[2] However, some inactive or acid sensitive oxiranes were hardly converted to the corresponding cyclic carbonates by these methods. We recently reported that the complexes composed of organotin halides and Lewis bases showed a catalytic activity toward the addition of CO_2 to oxiranes.[3] In this system, it was proposed that the coordinated Lewis bases activated the tin-halogen bond. It is well known that onium haides also readily complexate with organotin halides in a different mode to form a salt complex.[4] Its synthetic use, however, has been scarcely reported.

We wish to report herein a method using a 1 : 1 complex of Bu_3SnI and Bu_4PI as a catalyst(**3**),[5] which permitted inactive or acid sensitive oxiranes to react with CO_2 to produce the corresponding carbonates in good yields. This is probably due to the neutrality and high activity of the catalyst **3**.

The effects of combinations of organotin halides with onium halides on the product yield of the addition of CO_2 to 2-ethyloxirane were shown in Table 1, which shows the following notable features. (1) Tetrabutylphosphonium iodide was more suitable than Bu_4NI (Entries 1, 12). (2) The activity order of Bu_4PX (X=halogen) is X=I>Br>Cl (Entries 1—3). (3) The activities of organotin halides decrease as the following orders; Bu_3SnI, Me_3SnI, Ph_3SnI (Entries 1, 4, 5), Bu_3SnI, Bu_3SnBr, Bu_3SnCl (Entries 1, 6, 7), and Me_3SnI, Me_2SnI_2 (Entries 4, 8). All these orders were reverse to the order of acidity of organotin halides.[6] Thus, the lowest acidic complex **3** was the most efficient catalyst among the complexes examined. This was an interesting result, since even acid sensitive oxiranes were hoped to be beautifully converted to the corresponding carbonates by this almost neutral catalyst.[7] (4) The formation of 1 : 1 complex was strongly suggested by the comparison of the results of Entries 1, 10, and 11. In addition, the complex formation was also confirmed by ^{119}Sn NMR. The upfield shift values by complexations suggest that a five coordinated tin complex is formed,[8] although a six coordinated one, [Me_3SnBr-Et_4NBr], is proposed by Seyferth et al.[4b]

The above tendencies (1)—(4) were distinctly different from the case of ZnX_2-Bu_4NI systems reported quite recently by Kisch et al.,[9] in which $ZnCl_2$ being a stronger acid is more active than ZnI_2, and an ammonium halide is preferred to a phosphonium halide. Furthermore, use of excess amounts of Bu_4NI (4 equiv) is required for the formation of carbonates in high yields.

In the complex Bu_3SnI-Bu_4PI, the iodide anion in Bu_4PI is thought to be transfered on the tin atom,[4] and this iodide anion may play an effective role for a nucleophilic cleavage of oxirane rings, although a detailed mechanism can not be proposed because of the indefinite configuration of the complex.

Table 2 exemplifies the results of the synthesis of

Table 1. Reaction of **1b** with CO_2 (Atmospheric Pressure)[a]

Entry	Sn compd	Onium halide	Yield/% of **2b**[b]		
			2 h	3 h	5 h
1	*n*-Bu_3SnI	*n*-Bu_4PI	60	84	100
2	*n*-Bu_3SnI	*n*-Bu_4PBr	18	41	87
3	*n*-Bu_3SnI	*n*-Bu_4PCl	13	34	65
4	Me_3SnI	*n*-Bu_4PI	42	75	91
5	Ph_3SnI	*n*-Bu_4PI	39	58	84
6	*n*-Bu_3SnBr	*n*-Bu_4PI	41	58	84
7	*n*-Bu_3SnCl	*n*-Bu_4PI	31	53	77
8	Me_2SnI_2	*n*-Bu_4PI	11	39	75
9	*n*-Bu_3SnCl	*n*-Bu_4PCl	13	18	30
10[c]	*n*-Bu_3SnI	*n*-Bu_4PI	19	50	75
11[d]	*n*-Bu_3SnI	*n*-Bu_4PI	74	87	100
12	*n*-Bu_3SnI	*n*-Bu_4NI	16	50	93

a) 2-Ethyloxirane/Sn compd/onium halide=50/1/1 mmol, 60 °C. b) Monitored by GC. c) *n*-Bu_4PI 0.5 mmol. d) *n*-Bu_4PI 2 mmol.

Table 2. Reaction of Oxiranes with CO_2 by n-Bu_3SnI-n-Bu_4PI[a)]

Entry	Oxirane	Temp/°C	Time/h	Carbonate	Yield of 2[b)]/%
i	**1a**	40	1	**2a**	100
ii	**1b**	40	1	**2b**	95 (76)[c)]
iii[d)]	**1b**	40	1	**2b**	16
iv	**1c**	40	1	**2c**	83
v	**1d**	40	3	**2d**	88
vi	**1e**	40	3	**2e**	97
vii	**1f**	40	3	**2f**	86
viii	**1g**	40	1	**2g**	80
ix[e]	**1h**	100	5	**2h**	85

a) Oxirane/n-Bu_3SnI/n-Bu_4PI=50/1/1 mmol, CO_2=50 kg cm^{-2}. b) Determined by GC.. c) Benzene (5 cm^3) solvent, 3 h. d) SnI_2 was used instead of n-Bu_3SnI. e) n-Bu_3SnI-n-Bu_4PI 0.1 eq mol.

various carbonates **2** in the presence of the catalyst **3**. The complexation was essential, since neither Bu_3SnI nor Bu_4PI individually showed any catalytic activity, giving **2b** less than 2% yields under similar conditions. This catalyst was very effective for the reaction of monosubstituted oxiranes. For example, 2-methyloxirane gave propylene carbonate quantitatively at 40 °C for 1 h. Moreover, even in the reaction of acid sensitive monosubstituted oxiranes such as allyl glycidyl ether and glycidyl methacrylate, the corresponding carbonates could be isolated in high yields without polymerization or decomposition (Entries vi, vii). Although the reactivity of oxiranes bearing electron-withdrawing substituents was somewhat lower, satisfactory yields of **2** were effected by the prolonged reaction times. Some vigorous conditions, 100 °C, 5h, were required for the addition of CO_2 to 2,2-dimethyloxirane (85% yield, Entry ix).

An additional advantage of the complex **3** was its high solubility in organic solvents, thus carbonate **2b** was easily obtained from the reaction using benzene as a solvent as well as without solvent (Entry ii). On the contrary, the SnI_2-Bu_4PI system was inefficient probably due to a poor solubility of SnI_2, giving **2b** in only 16% yield (Entry iii).

The complex catalyst, Bu_3SnI-Bu_4PI, provides a method for carboxylation of unreative or acid sensitive oxiranes, extending the scope of a carbonate synthesis under mild conditions.

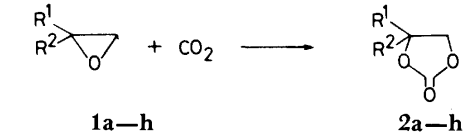

1a—h **2a—h**

	R^1	R^2
a	CH_3	H
b	CH_3CH_2	H
c	C_6H_5	H
d	CH_3OCH_2	H
e		H

	R^1	R^2
f		H
g	$ClCH_2$	H
h	CH_3	CH_3

Experimental

The following instruments were used: Melting points, Yanagimoto micro melting point apparatus; IR spectra, Hitachi 260-10; Mass spectra, Hitachi RMU-6E; GC, Shimadzu 8A (FID, 5% FFAP or 2% OV-17 on Chromosorb WAW); ^{1}H NMR and ^{13}C NMR spectra, Hitachi R-90H.

Tin compounds[10)] and onium halides[11)] were prepared according to the known methods. All oxiranes were available commercially, and were used after distillation on CaH_2.

Values of the boiling points of the compounds are given as °C/mmHg (1 mmHg=133.322Pa).

Reaction of 2-Ethyloxirane and CO_2 under Atmospheric Pressure (Table 1). In a typical procedure, a mixture of organotin compound (1 mmol) and onium halide (1 mmol) and 2-ethyloxirane (50 mmol) was placed in a 30 cm^3 three necked flask, and was heated at 60 °C under the slow stream of CO_2 gas. The amounts of 4-ethyl-1,3-dioxolan-2-one (**2b**) were monitored by GC.

Reaction of Oxiranes and CO_2 under Pressurized Conditions (Table 2). An oxirane (50 mmol), Bu_3SnI (1 mmol), Bu_4PI (1 mmol) and a magnetic bar were placed in a 50 cm^3 stainless steel autoclave, then CO_2 gas was pressurized up to 50 kg cm^{-2}. The vessel was heated with stirring at an appropriate temperature. After cooling, the yields of carbonates were determined by GC. All carbonates were isolated by distillation or recrystalization, and **2a**, **2b**, **2c**, **2d**, and **2g** were characterized by spectral data and bps.[2)]

4-Allyoxymethyl-1,3-dioxolan-2-one (2e): Bp 108 °C/2 mmHg (lit,[2)] 92—94 °C/0.1 mmHg); IR (neat) 1800 (C=O), 1645 cm^{-1} (C=C); MS m/z 158 (M^+); ^{1}H NMR ($CDCl_3$) δ=3.4—4.1 (4H, m), 4.1—4.6 (2H, m), 4.7—5.0 (1H, m), 5.1—5.4 (2H, m), 5.7—6.1 (1H, m).

4-Methacryloyloxymethyl-1,3-dioxolan-2-one (2f): Bp 123 °C/2 mmHg (lit,[2)] 72—73 °C/0.1 mmHg); IR (neat) 1800 (C=O), 1735 (C=O), 1640 cm^{-1} (C=C); MS m/z 186 (M^+); ^{1}H NMR ($CDCl_3$) δ=2.0—2.2 (3H, s), 4.3—4.9 (4H, m), 4.9—5.4 (1H, m), 5.7 (1H, s), 6.2 (1H, s); ^{13}C NMR ($CDCl_3$) δ=17.6, 63.2, 65.9, 73.8, 126.3, 134.9, 154.4, 166.0.

4,4-Dimethyl-1,3-dioxolan-2-one (2h): Bp 57 °C/2 mmHg (lit,[12)] 224 °C/760 mmHg); IR (neat) 1800 cm^{-1} (C=O); MS m/z 116 (M^+); ^{1}H NMR ($CDCl_3$) δ=2.2 (6H, s), 4.8 (2H, s).

This work was supported by Grant-in-Aid for Scientific Research No. 61850152 from the Ministry of Education, Science and Culture.

References

1) S. Inoue, H. Koinuma, and T. Tsuruta, *Polymer Lett.*, **7**, 287, (1969); K. Soga, E. Imai, and I. Hattori, *Poly. J.*, **13**, 407 (1981); M. Ratzenhofer and H. Kisch, *Angew. Chem.*, **92**, 303 (1980); R. Nomura, A. Ninagawa, and H. Matsuda, *J. Org. Chem.*, **45**, 3735 (1980); R. J. De Pasquale, *J. Chem. Soc., Chem. Commun.*, **1973**, 157.

2) T. Nishikubo, T. Iizawa, M. Iida, and N. Isobe, *Tetrahedron Lett.*, **27**, 3741 (1986).

3) R. Nomura, M. Kimura, S. Teshima, A. Ninagawa, and H. Matsuda, *Bull. Chem. Soc. Jpn.*, **55**, 3200 (1980); A.

Baba, H. Meishou, and H. Matsuda, *Makromol. Chem. Rapid Commun.*, **5**, 665 (1984).

4) a) J. W. Nicholson and J. A. Douek, *J. Organomet. Chem.*, **219**, 309 (1981); b) D. Seyferth and S. A. Grim, *J. Am. Chem. Soc.*, **83**, 1610 (1961).

5) A part of this result was already reported: A. Baba, T. Nozaki, H. Matsuda, The 52th Spring Meeting of the Chem. Soc. of Jpn. Kyoto, April 1986, Abstr. No. 2W04.

6) A. G. Davies, P. J. Smith, "Comprehensive Organometallic Chemistry," ed by G. Wilkinson, F. G. A. Stone, W. Abel, Pergamon Press, New York (1982), Vol 2, p. 562.

7) J. Furukawa, T. Saegusa, "Polymerization of Aldehyde and Oxide," John Willy & Sons, New York (1963), p. 155.

8) ^{119}Sn NMR ($CDCl_3$, external standerd Me_4Sn) ppm= Bu_3SnI-Bu_4PI, 61 (Bu_3SnI, 83): Bu_3SnBr-Bu_4PBr, 18 (Bu_3SnBr, 136). These values are similar to ones of five coordinated tri-*n*-butyltin(IV) compounds reported by Nadvornik, and for example, the chemical shift of the Bu_3SnBr coordinated by pyridine is 5.6 ppm: M. Nadvornik, J. Holecek, and K. Handlir, *J. Organomet. Chem.*, **275**, 43 (1984).

9) H. Kisch, R. Millini, and I-J. Wang, *Chem. Ber.*, **119**, 1090 (1986).

10) R. K. Ingham, S. D. Rosenberg, and H. Gilman, *Chem, Rev.*, **60**, 459 (1960).

11) H. A. Laitinen and S. Wawzonek, *J. Am. Chem. Soc.*, **64**, 1765 (1942).

12) M. S. Newman and R. A. Markle, *J. Am. Chem. Soc.*, **94**, 2733 (1972).

An Estimation of the Configurational Stability of Diaryl Selenoxides by Means of ^{77}Se NMR Spectroscopy

Toshio SHIMIZU, Masato YOSHIDA, and Michio KOBAYASHI*
Department of Chemistry, Faculty of Science, Tokyo Metropolitan University, Fukazawa, Setagaya-ku, Tokyo 158
(Received September 25, 1986)

Synopsis. The activation energies for the racemization of the optically active diaryl selenoxides were estimated by the use of the ^{77}Se NMR spectra of the diastereomeric diaryl selenoxides.

Many optically active sulfoxides have been prepared. On the contrary, though, despite repeated attempts,[1] there has been no example of the isolation of the enantiomerically pure selenoxide until recently. The difficulty of the optical resolution of selenoxide has been attributed to its facile racemization through an achiral hydrate ($RSe(OH)_2R'$) formed by the addition of water to seleninyl group.[2] A few years ago, the synthesis of the partly optically active alkyl aryl selenoxides was reported by Davis et al.[3,4] In these alkyl aryl selenoxides, bulky ortho substituents were found to be effective for retarding the racemization via an achiral hydrate.[3] We succeeded previously in preparing the optically active diaryl selenoxides, which had bulky ortho substituents by using asymmetric oxidation[5] or optical resolution.[6] The attempt to resolve optically the diaryl selenoxides which did not possess bulky ortho substituents was unsuccessful as well as in the case of the alkyl aryl selenoxides. Therefore, it seemed that it would be very interesting to study the configurational stabilities of the diaryl selenoxides which have ortho substituents with different bulkiness. The activation energies for the racemization of the optically active diaryl selenoxides have not been studied. When we measured the selenium-77 NMR spectra of diastereomeric mixture of the diaryl selenoxides with the *p*-(*l*-menthoxycarbonyl) group, we noticed the existence of two signals of ^{77}Se assignable to each isomers.

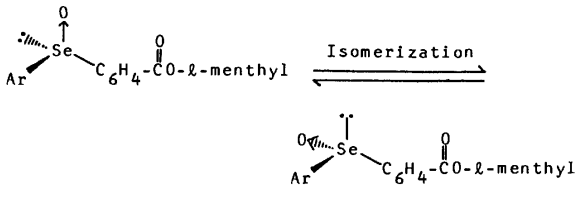

This finding suggested that the measurement of selenium-77 resonance at various temperatures may make it possible to estimate Gibbs' free energies of activation for the racemization of optically active diaryl selenoxides. We will report here the results of one study of the racemization of diastereomeric diaryl selenoxides obtained from selenium-77 NMR.

Results and Discussion

Firstly, the ^{77}Se NMR spectrum of 2,4,6-tri-*t*-butylphenyl 4′-(*l*-menthoxycarbonyl)phenyl selenoxide (**5**) was observed in $CDCl_3$; Compound **5** is a mixture of the diastereomers of d,l- and l,l-form. The chemical shifts of ^{77}Se NMR for organic selenium compounds spread over a range of the order of 3000 ppm, and the half widths of the signals are usually narrow ($\Delta\nu_{1/2} \lesssim 1$ Hz).[7] These features of ^{77}Se resonance allow us to expect that a small difference between two diastereomers may give two well-resolved signals. In fact, the two selenium atoms of the diastereomers of **5** resonated at different frequencies in ^{77}Se NMR; $\Delta\nu_{ab}$=8.79 Hz (Fig. 1). In the ^{1}H NMR (60 MHz) and ^{13}C NMR (22.5 MHz) spectra of **5**, the assignment of signals to each diastereomer was difficult because of their complexity. Similarly, other diastereomeric selenoxides (**1**—**4**), which had less bulky ortho substituents than the *t*-butyl group, were subjected to ^{77}Se NMR measurements. The results are summarized in Table 1. Two signals for the diastereomeric selenoxides were observed for **2**, **3**, and **4**. In the case of **1**, which had no ortho substituent, only one signal was observed at 20 °C; at −40 °C, however, the signals were separated.

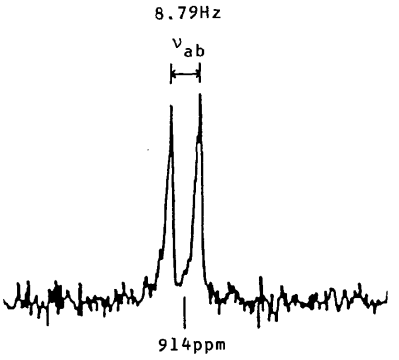

Fig. 1. Resolution of ^{77}Se signals for diastereomeric selenoxide (**5**) in $CDCl_3$ at room temperature.

Table 1. ^{77}Se NMR Chemical Shifts and Separations of Signals for Diastereomeric Selenoxides (**1**—**5**)[a]

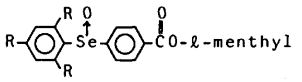

	R	Chemical shift[b] ppm	ν_{ab} Hz
1	H	873	—[c]
2	Me	888	7.08
3	Et	886, 891 d)	6.10, 13.67 d)
4	*i*-Pr	881	4.15
5	*t*-Bu	914	8.79

a) The spectra were measured in $CDCl_3$ at 20 °C. b) The chemical shifts from MeSeMe were calculated based on PhSeSePh[8] as the external standard. c) The signals for this selenoxide could not be separated at 20 °C. d) In C_6D_6.

Table 2. Coalescence Temperatures (T_c) and Gibbs' Free Energies of Activation (ΔG^*) for Isomerization of Diastereomeric Selenoxides (**1**—**5**)

Selenoxide	Solvent	Chemical shift[a]	νab[a]	T_c	ΔG^*
		ppm	Hz	K	(kJ mol^{-1})
1	$CDCl_3$	873	11.35[b]	283	61.6
2	$CHCl_2CHCl_2$	892	5.86	333	74.8
3	$CHCl_2CHCl_2$	929	5.62	343	77.2
4	$CHCl_2CHCl_2$	886	3.42[c]	>373	>85.8
5	$CHCl_2CHCl_2$	919	12.70	>353[d]	>77.1

a) At 20 °C. b) At −40 °C. c) At 70 °C. d) This selenoxide decomposed slowly during the measurement at 80 °C to give di-[4-(*l*-menthoxycarbonyl)phenyl] diselenide as the major decomposition product.

This observation suggested that the isomerization between two diastereomers of **1** is too fast compared to the ^{77}Se NMR time scale at 20 °C. The signals of selenoxide (**1**) coalesced at 10 °C. Gibbs' free energy of the activation for the isomerization of diastereomeric **1** was estimated to be 61.6 kJ mol^{-1} in chloroform-*d* from the following equation[9]:

$$\pi\nu_{ab}/\sqrt{2} = (kT/h)\exp(-\Delta G^{\ddagger}/RT).$$

The two signals for **2**—**5** showed little indication to coalesce at 40 °C in the same solvent. Therefore, in the cases of **2**—**5**, the ^{77}Se NMR were examined in high-boiling solvents such as *p*-xylene (in the case of **5**), chlorobenzene (in the cases of **2** and **5**), or 1,1,2,2-tetrachloroethane. Interestingly, the isomers of **2**—**5** resonated at the same frequencies in the aromatic solvents, even at 20 °C (in the case of chlorobenzene) or at 20—60 °C (in the case of *p*-xylene). The lack of the separation of the ^{77}Se signals may be attributed to the specific aromatic solvent-induced shifts, not to the rapid racemization. The measurement of the coalescence temperature was successful in 1,1,2,2-tetrachloroethane. The coalescence temperatures and the free energies of activation for the isomerization are summarized in Table 2. These results indicate that the rate of the isomerization of the selenoxides is strongly dependent on the bulkiness of the ortho substituents. The free energy of the activation for the isomerization obtained from the coalescence temperature of ^{77}Se signals is, because of the inversion of the configuration around selenium atom in the optically active selenoxides, considered to correspond to the free energy of activation for the racemization. The above results suggest that the optical resolution of the diaryl selenoxides which possess no ortho substituent may be difficult at room temperature because of the facile racemization. For the racemization of the optically active selenoxide, there are two plausible mechanisms. One is the racemization through the formation of the achiral hydrate, and the other is the pyramidal inversion of the configuration around the selenium atom. The values of Gibbs' free energies of activation for the racemization obtained in the present study can reasonably be explained by the pyramidal inversion.

Experimental

All the melting points were determined on a Yamato MP-21 apparatus. The IR spectra were recorded on a Hitachi 260-10 Spectrometer, the ^{1}H NMR spectra, with TMS as an internal standard, on a JEOL-JNM-PMX 60SI apparatus, and the mass spectra, on a JEOL JMS-DX300 Mass Spectrometer. The optical rotations were measured on a JASCO DIP-140 digital polarimeter.

Measurement of ^{77}Se NMR spectra. The ^{77}Se NMR spectra were recorded at 17.03 MHz on a JEOL FX90Q NMR instrument. About 0.2 mol dm^{-3} solutions of the selenoxides were prepared in solvents well-dried with molecular sieves. The external rocks with DMSO-d_6 were used except in the cases using $CDCl_3$ and C_6D_6 as solvents. The chemical shifts were measured with complete proton decoupling at room temperature. The separations of the two signals were observed with 0.24 Hz per data point (data points: 8192, sampling time: 4.09s, pulse-flipping angle: 45°).

Materials. The diastereomeric 2,4,6-trisubstituted-phenyl 4′-(*l*-menthoxycarbonyl)phenyl selenoxides (**1**—**5**) were synthesized by means of the oxidation[5] of the corresponding selenides, which themselves been prepared by the esterification of 2,4,6-trisubstituted phenyl 4′-carboxyphenyl selenides.[6] For the preparation of latter, two synthetic routes were possible. The phenyl and triisopropylphenyl derivatives were prepared by means of reactions of potassium areneselenolates with 4-iodobenzoic acid in the presence of copper powder.[10] For the preparation of mesityl, triethylphenyl, and tri-*t*-butylphenyl derivatives, the reactions[11] of aryllithiums with *p*-ethoxycarbonylphenyl selenocyanate,[12] followed by hydrolysis, were applied. The physical properties of the selenoxides (**1**—**5**) were measured as a mixture of the diastereomeric isomers. The preparation of **4** was previously reported.[6]

Phenyl 4-(*l*-Menthoxycarbonyl)phenyl Selenoxide (1): Mp 164—170 °C; $[\alpha]_D^{24}$−41.1°(*c* 1.12, $CHCl_3$); IR (KBr) ν=825 (Se=O) and 1700 (C=O) cm^{-1}; ^{1}H NMR ($CDCl_3$) δ=0.6—2.3 (18H, m, *l*-menthyl except O-methine H), 4.91 (1H, dt, *J*=5.6, 9.8 Hz, O-methine), 7.3—7.9 (5H, m, aromatic protons of phenyl), 7.73 and 8.09 (4H, ABq, *J*=8.0 Hz, aromatic protons of *p*-substituted phenyl); Exact Mass. Found: *m/z* 432.1146 (^{80}Se), Calcd for $C_{23}H_{28}O_3Se$: 432.1204.

Mesityl 4-(*l*-Menthoxycarbonyl)phenyl Selenoxide (2): Mp 49.5—53 °C; $[\alpha]_D^{24}$−36.9° (*c* 1.03, $CHCl_3$); IR (KBr) ν=825 (Se=O) and 1710 (C=O) cm^{-1}; ^{1}H NMR ($CDCl_3$) δ=0.6—2.2 (18 H, m, *l*-menthyl except O-methine H), 2.24 (3H, s, para methyl), 2.43 (6H, s, ortho methyl), 4.91 (1H, dt, *J*=4.4, 10.0 Hz, O-methine), 6.79 (2H, s, aromatic protons of mesityl), 7.59 and 8.04 (4H, ABq, *J*=8.0 Hz, aromatic protons of *p*-substituted phenyl); Exact Mass. Found: *m/z* 474.1638 (^{80}Se), Calcd for $C_{26}H_{34}O_3Se$: 474.1673.

2,4,6-Triethylphenyl 4′-(*l*-Menthoxycarbonyl)phenyl Selenoxide (3): Viscous oil; $[\alpha]_D^{24}$−32.0° (*c* 1.06, $CHCl_3$); IR (liquid film) ν=820 (Se=O) and 1705 (C=O) cm^{-1}; ^{1}H NMR ($CDCl_3$) δ=0.6—2.3 (27H, m, methyl of triethylphenyl and *l*-menthyl except O-methine H), 2.4—3.2 (6H, m, methylene of triethylphenyl), 4.93 (1H, dt, *J*=4.2, 9.9 Hz, O-methine),

6.93 (2H, s, aromatic protons of triethylphenyl), 7.63 and 8.07 (4H, ABq, J=8.6 Hz, aromatic protons of *p*-substituted phenyl); Mass: 516 (^{80}Se) (M^+). Exact Mass. Found: m/z 500.2228 (^{80}Se) (lack of one oxygen), Calcd for $C_{29}H_{40}O_2Se$: 500.2193.

2,4,6-Tri-*t*-butylphenyl 4′-(*l*-Menthoxycarbonyl)phenyl Selenoxide (5): Mp 145—146 °C; $[\alpha]_D^{21}$−23.2° (*c* 1.25, $CHCl_3$); IR (KBr) ν=830 (Se=O) and 1710 (C=O) cm^{-1}; ^1H NMR ($CDCl_3$) δ=0.6—2.4 (18H, m, *l*-menthyl except O-methine H), 1.37 (9H, s, methyl of para *t*-butyl), 1.48 (18H, s, methyl of ortho *t*-butyl), 4.89 (1H, dt, J=5.6, 10.0 Hz, O-methine), 7.52 (2H, s, aromatic protons of tri-*t*-butylphenyl), 7.01 and 7.91 (4H, ABq, J=8.0 Hz, aromatic protons of *p*-substituted phenyl); Mass: 600 (^{80}Se) (M^+); Exact Mass. Found: m/z 584.3182 (^{80}Se) (lack of one oxygen), Calcd for $C_{35}H_{52}O_2Se$: 584.3133.

References

1) For example: W. R. Gaythewaite, J. Kenyon, and H. Phillips, *J. Chem. Soc.*, **1928**, 2280, 2287.
2) M. Oki and H. Iwamura, *Tetrahedron Lett.*, **1966**, 2917; K. B. Sharpless, M. W. Young, and R. F. Lauer, *ibid.*, **1973**, 1979.
3) F. A. Davis, J. M. Billmers, and O. D. Stringer, *Tetrahedron Lett.*, **24**, 3191 (1983).
4) F. A. Davis, O. D. Stringer, and J. P. McCauley, Jr., *Tetrahedron*, **41**, 4747 (1985).
5) M. Kobayashi, H. Ohkubo, and T. Shimizu, *Bull. Chem. Soc. Jpn.*, **59**, 503 (1986).
6) T. Shimizu and M. Kobayashi, *Chem. Lett.*, **1986**, 161.
7) I. Johannsen, L. Henriksen, and H. Eggert, *J. Org. Chem.*, **51**, 1657 (1986).
8) J. D. Odom, W. H. Dawson, and P. D. Ellis, *J. Am. Chem. Soc.*, **101**, 5815 (1979).
9) D. K. Dalling, D. M. Grant, and L. F. Johnson, *J. Am. Chem. Soc.*, **93**, 3678 (1971).
10) K. Šindelář, E. Svátek, J. Metyšová, J. Metyš, and M. Protiva, *Collect. Czech. Chem. Commun.*, **34**, 3792 (1969).
11) B. Greenberg, E. S. Gould, and W. Burlant, *J. Am. Chem. Soc.*, **78**, 4028 (1956).
12) H. Bauer, *Ber.*, **46**, 92 (1913).

Generation and Reactions of Phosphorin 1-Sulfides

Hideyuki TANAKA and Shinichi MOTOKI*
Department of Chemistry, Faculty of Science, Science University of Tokyo, Kagurazaka, Shinjuku-ku, Tokyo 162
(Received September 26, 1986)

Synopsis. Phosphorin 1-sulfides generated by the thermolysis of 1-phospha-2-thiabicyclo[4.4.0]deca-3,7,9-triene 1-sulfides reacted with triphenylphosphine, dienophiles, or nucleophiles to give the corresponding phosphorins, 1-phosphabicyclo[2.2.0]octa-2,5-diene 1-sulfide, or 1,2-dihydrophosphorin 1-sulfide derivatives, respectively.

Previously, we reported that 2,9-dithia-1-phosphabicyclo-[4.3.0]nona-3,7-diene 1-sulfides (**2**)[1] derived from α,β-unsaturated ketones **1** reacted with phenylacetylene to afford 1-phospha-2-thiabicyclo[4.4.0]deca-3,7,9-triene 1-sulfides (**3**).[2] From the mass spectral fragments, it is expected that thermolysis of **3** generates phosphorin 1-sulfides (**4**) along with α,β-unsaturated thiones (**5**)[3] in the manner of the retro-Diels-Alder reaction.

Recently, Mathey et al. reported that 4,5-dimethyl-2-phenylphosphorin 1-sulfide formed by the treatment of the corresponding phosphorin with sulfur in boiling xylene was trapped by 2,3-dimethylbutadiene or dimethyl acetylenedicarboxylate.[4] However, no other papers on the synthesis or reactions of phosphorin 1-sulfides have been presented.

In this paper, we wish to describe some reactions of phosphorin 1-sulfides **4** generated by the thermolysis of the precursors **3**.

Results and Discussion

Treatment of **3** with triphenylphosphine in refluxing toluene produced phosphorins **6** and triphenylphosphine sulfide (Table 1). Another component, thiones **5** were decomposed by triphenylphosphine. The phosphorins **6** were easily identified by comparison of the ^{1}H NMR spectral data with those of **6a** in the literature.[5] The ^{13}C NMR spectra of **6** were assigned as shown in Table 2.[6]

Phosphorins were synthesized by Märkl et al. by the

Table 1. Reaction of **3** with Various Reagents

Material	Reagent	Reaction time/h	Product from **4**			Product from **5**	
				Mp θ_m/°C	Yield/%[a]	Yield/%[a]	
3a	Ph_3P	3	**6a**	170—172[b]	60	—	
3b	Ph_3P	3	**6b**	173—175	59	—	
3a	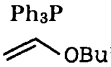	5	**7a**	134—136	13	**8a**	56
3b	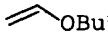	5	**7b**	113—116	31	**8b**	77
3a	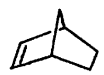	2	**9a** **10a**	187—189 186—188	47 48	**11a**	94
3b	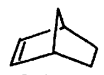	2	**9b** **10b**	128—130 171—173	45 46	**11b**	95
3a	$PhCH_2OH$	1	**12a**[c]	113—115	96	**14a**	98
3b	$PhCH_2OH$	1	**12b**[c]	152—154	95	**14b**	95
3a	PhSH	2.5	**13a**[c]	210—212	48	**14a**	60
3b	PhSH	2.5	**13b**[c]	196—198	44	**14b**	56

a) The yield of the products was based on **3**. b) Lit,[5] 164—166°C. c) Yellow crystals.

Table 2. ^{13}C NMR Spectral Data of the Products [$\delta(J_{CP}$/Hz)]

Product	C(2)	C(3)	C(4)	C(5)	C(6)	$J_{C(2)P}$	$^2J_{C(3)P}$	$^3J_{C(4)P}$	$^2J_{C(5)P}$	$J_{C(6)P}$
6a	169.5	136.6	142.7	141.1	156.4	48.8	11.0	3.7	17.1	52.5
6b	169.4	136.3	142.7	141.1	156.4	48.8	12.2	3.7	17.1	53.7
7a	141.4	147.0	59.6	164.7	127.0	61.0	2.4	31.7	2.4	69.6
7b	141.5	147.0	59.8	165.0	127.0	61.0	2.4	31.7	2.5	69.6
9a	140.5	151.7	57.4	164.2	128.3	61.0	0	36.6	2.4	67.1
9b	140.3	150.9	57.3	164.2	128.3	61.0	0	36.6	2.4	67.1
10a	139.4	148.4	57.6	166.9	128.0	58.6	0	36.6	3.7	69.6
10b	139.2	147.5	57.5	166.9	128.1	58.6	0	35.4	2.4	67.1
12a	135.5	141.1	a)	a)	42.2	61.0	6.1	a)	a)	73.2
12b	134.3	140.5	a)	a)	42.1	61.0	6.1	a)	a)	72.0
13a	139.6	141.4	a)	a)	44.2	56.2	3.7	a)	a)	53.7
13b	139.6	141.1	a)	a)	44.0	56.2	3.7	a)	a)	52.5

a) These signals were not confirmed.

reaction of the corresponding pyrylium salts with $P(CH_2OH)_3$ or $P(SiMe_3)_3$.[7] By our method, **6** can be readily obtained from α,β-unsaturated ketones **1** by three step reactions.

Phosphorin sulfides **4** reacted as heterodienes at their 1, 4 positions with some dienophiles to give the corresponding cycloadducts.[1,4] When the reaction of **3** with butyl vinyl ether was carried out in refluxing toluene, the cycloadducts **7** were obtained along with **8** (Table 1). The cycloadducts **8** were easily identified by comparison with the authentic compounds reported previously.[3] In the ^{13}C NMR spectra of the cycloadducts **7**, the signals for the methine carbons [δ=77.6 (J_{CP}=8.5 Hz)] and the methylene carbons [δ=37.5 (J_{CP}=47.6 Hz)] indicated that butoxyl groups were linked to C(β) carbons,[1] but the cofiguration of the C(β) carbons could not be determined. The signals for the C(2)-(6) carbons in **7** were assigned as shown in Table 2.[2,4]

The reaction of **3** with norbornene gave the cycloadducts **9**, **10**, and **11** in high yields (Table 1). The thione(**5**)-norbornene cycloadducts (**11**) were identified by comparing the spectral data with those for the authentic compounds.[3] The elemental analyses and mass spectra indicated that both **9** and **10** were 1 : 1 adducts of **4** with norbornene. In the ^{13}C NMR spectra of these adducts, seven signals due to the norbornane ring system were observed and the C(α), C(β) methine carbons showed C-P coupling [C(α), δ=52.2—53.2 (J_{CP}=46.4 Hz); C(β), δ=51.1—53.7 ($^2J_{CP}$=8.5—9.8 Hz)]. The signals for the C(2)-C(6) carbons in 1,4-dihydrophosphorin 1-sulfide ring system were assigned by comparison with those for phosphabarrelene derivatives[2,4] (Table 2). The chemical shifts for the C(2), C(3), and C(5) carbons gave the information on the configuration of **9** and **10**. The cycloadducts **10** showed the resonance for C(2) and C(3) carbons shifted upfield by 1.1 and 3.4 ppm, respectively, compared with those for **9**, whereas **9** showed that the resonance for C(5) carbon shifted upfield by 2.7 ppm compared with that for **10**. On the basis of these shifts, the norbornyl skeleton is considered to be situated on the side of the C(5) and C(6) carbons in **9** and on the side of the C(2) and C(3) carbons in **10**.[1,8] The signals for the bridged methylene carbons (C*) in **9** and **10** shifted upfield by 4.8—4.6 ppm compared with that in unsubstituted norbornane and appeared at δ=33.9 and 34.1, respectively. This suggested that the configuration of these isomers would be *exo* with respect to the norbornyl ring.[1,8]

The reactions of **3** with styrene or acrylonitrile were unsuccessful.

Finally, we examined the reaction of **3** with nucleophiles.[9] Treatment of **3** with benzyl alcohol in boiling toluene gave **12** in high yields. The products showed strong IR absorptions due to the P-O bonding at about 1000 cm^{-1}. In the ^1H NMR spectra, the multiplets of two protons at δ=3.33—3.67 were assigned to the H(6) AB protons. The signals for the C(6) methylene carbon showed large C-P coupling constant (Table 2).

Similarly, the reaction of **3** with benzenethiol gave the expected adducts **13**. The structure of **13** was confirmed by comparison of the spectral data with those for **12**.

In these reactions, addition of the hydrogen of the nucleophiles Nu-H to the C(6) carbons took place preferentially. These adducts **12** and **13** seem to be more stable than their isomeric 1,2- or 1,4-dihydrophosphorin 1-sulfides due to the effective conjugation of the double bond in dihydrophosphorin ring with three aryl groups at the 2-, 4-, and 5-positions. In both cases thiones **5** did not react with the nucleophiles, and were recovered as their dimers **14**.[3]

Reaction of **3** with amines was complicated and no identified product was isolated.

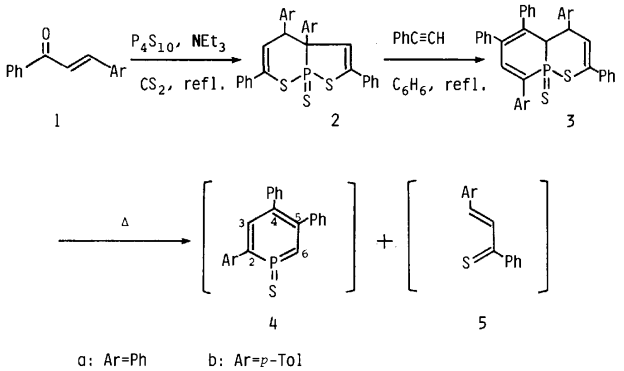

1 2 3 4 5

a: Ar=Ph b: Ar=*p*-Tol

Scheme 1.

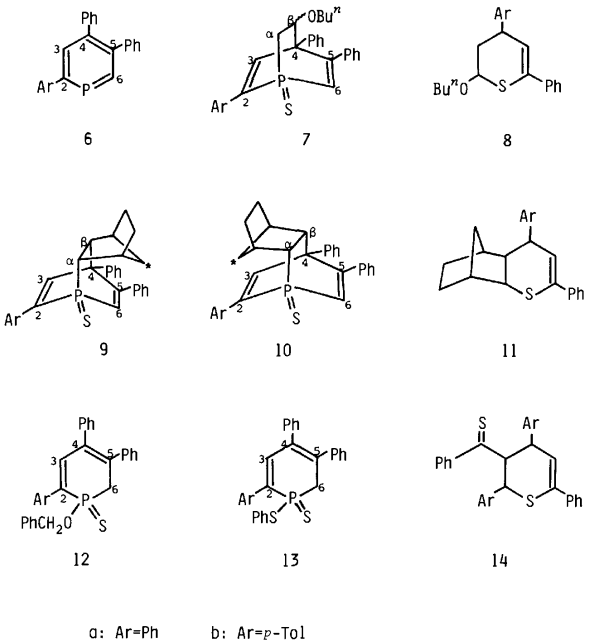

6 7 8 9 10 11 12 13 14

a: Ar=Ph b: Ar=*p*-Tol

Experimental

All melting points are uncorrected. IR spectra were recorded on a Hitachi Model 260-10 spectrometer. ^1H and ^{13}C NMR spectra were measured in $CDCl_3$ solution using Me_4Si as an internal standard [spectrometer: ^1H; JEOL JNM-PMX60SI (60 MHz), ^{13}C; JEOL JNM-FX 100 (25.05 MHz)]. Mass spectra were recorded on a Hitachi M-80 spectrometer or a JEOL JMS-D300 spectrometer, operating at an ionizing potential of 70 eV. Elemental analyses were performed using a Yanaco Model MT-3 CHN corder. 1-Phospha-2-thiabicyclo[4.4.0]deca-3,7,9-triene 1-sulfides

(**3**) were prepared according to the method previously described.[1)]

General Procedure for the Reaction of 3 with Triphenylphosphine: A solution of **3** (1.0 mmol) and triphenylphosphine (1.2 mmol) in dry toluene (5.0 cm^3) was refluxed under a nitrogen atmosphere for 3 h. The toluene was removed, and the residue was chromatographed on Wakogel C-200 with benzene-hexane (1 : 3) as an eluent. The solvent was evaporated, and the residue was recrystallized from hexane to give **6**.

2,4,5-Triphenylphosphorin (6a): ^{1}H NMR δ=6.93—7.87 (m, 15H, Ar-H), 8.08 [d, 1H, J_{HP}=6.0 Hz, H(3)], and 8.73 [d, 1H, J_{HP}=38.0 Hz, H(6)]; MS *m/z* 324 (M^+, 100). Found: C, 84.99; H, 5.23%. Calcd for $C_{23}H_{17}P$: C, 85.17; H, 5.28%. The ^{1}H NMR spectrum is identical with that reported by Märkl et al.[5)]

4,5-Diphenyl-2-*p*-tolylphosphorin (6b): ^{1}H NMR δ=2.43 (s, 3H, CH_3), 6.97—7.90 (m, 14H, Ar-H), 8.08 [d, 1H, J_{HP}=6.0 Hz, H(3)], and 8.73 [d, 1H, J_{HP}=38.0 Hz, H(6)]; MS *m/z* 338 (M^+, 100). Found: C, 85.14; H, 5.62%. Calcd for $C_{24}H_{19}P$: C, 85.19; H, 5.66%.

General Procedure for the Reaction of 3 with Dienophiles or Nucleophiles: A solution of **3** (1.0 mmol) and large excess of dienophile or nucleophile (10.0 mmol) in dry toluene (2.5 cm^3) was refluxed under a nitrogen atmosphere until **3** was consumed, as indicated by TLC. After evaporation of the solvent, the residue was chromatographed on Wakogel C-200 with benzene-hexane (2 : 1—3 : 1) as an eluent. The products were recrystallized from ethanol or ligroine.

8-Butoxy-2,4,5-triphenyl-1-phosphabicyclo[2.2.2]octa-2,5-diene 1-Sulfide (7a): IR(KBr) 1085 cm^{-1} (C-O); ^{1}H NMR δ=0.67—2.67 (m, 9H), 3.33—4.83 (m, 3H), 6.53 [d, 1H, J_{HP}=20.0 Hz, H(3)], and 6.83—7.67 (m, 16H); MS *m/z* 456 (M^+, 1), 356 (**4a**, 72), 324 (**6a**, 50), 254 (**4a**-PhC≡CH, 100), and 100(CH_2=CHOBu^n, 75). Found: C, 76.37; H, 6.45%. Calcd for $C_{29}H_{29}OPS$: C,76.29; H, 6.40%.

8-Butoxy-4,5-diphenyl-2-*p*-tolyl-1-phosphabicyclo[2.2.2]-octa-2,5-diene 1-Sulfide (7b): IR(KBr) 1085 cm^{-1}(C-O); ^{1}H NMR δ=0.67—2.27 (m, 9H), 2.33 (s, 3H, *p*-Tol-CH_3), 3.33—4.00(m, 3H), 6.52 [d, 1H, J_{HP}=20.0 Hz, H(3)], and 6.93—7.67 (m, 15H); MS *m/z* 470 (M^+, 1), 370 (**4b**, 94), 338 (**6b**, 100), 268 (**4b**-PhC≡CH, 82), and 100 (CH_2=CHOBu^n, 76). Found: C, 76.50; H, 6.66%. Calcd for $C_{30}H_{31}OPS$: C, 76.57; H, 6.64%.

8,10,12-Triphenyl-1-phosphatetracyclo[6.2.2.1^{3,6}.0^{2,7}]trideca-9,11-diene 1-Sulfide (9a): ^{1}H NMR δ=0.75—3.17 (m, 9H), 3.67—3.83 (m, 1H), 6.45 [d, 1H, J_{HP}=20.0 Hz, H(3)], and 6.67—7.75 (m, 16H); MS *m/z* 450 (M^+, 3), 356 (**4a**, 100), 324 (**6a**, 65), 254 (**4a**-PhC≡CH, 68), 121 (39), 94 (13), and 66 (81). Found: C, 79.99; H,5.92%. Calcd for $C_{30}H_{27}PS$: C, 79.97; H, 6.04%.

10a: ^{1}H NMR δ=0.67—3.17 (m, 10H), 6.37 [d, 1H, J_{HP}=19.0 Hz, H(3)], and 6.50—7.67 (m, 16H); MS *m/z* 450 (M^+, 2), 356 (**4a**, 100), 324 (**6a**, 42), 254 (**4a**-PhC≡CH, 69), 121 (22), 94 (4), and 66 (31). Found: C, 79.74; H, 6.04%. Calcd for $C_{30}H_{27}PS$: C, 79.97; H, 6.04%.

8,12-Diphenyl-10-*p*-tolyl-1-phosphatetracyclo[6.2.2.1^{3,6}.0^{2,7}]-trideca-9,11-diene 1-Sulfide (9b): ^{1}H NMR δ=0.75—3.17 (m, 9H), 2.35 (s, 3H, CH_3), 3.67—3.83 (m, 1H), 6.45 [d, 1H, J_{HP}=18.0 Hz, H(3)], 6.67—7.50 (m, 13H), and 7.50 (d, 2H, J_{HH}=8.0 Hz, *p*-Tol-H); MS *m/z* 464(M^+, 1), 370 (**4b**, 100), 338 (**6b**, 36), 268 (**4b**-PhC≡CH, 80), 135 (38), 94 (10), and 66 (69). Found: C, 79.81; H, 5.99%. Calcd for $C_{31}H_{29}PS$: C, 80.14; H, 6.29%.

10b: ^{1}H NMR δ=0.67—3.17 (m, 10H), 2.40 (s, 3H, CH_3), 6.35 [d, 1H, J_{HP}=20.0 Hz, H(3)], 6.50—7.50 (m, 13H), and 7.62 (d, 2H, J_{HH}=8.0 Hz, *p*-Tol-H); MS *m/z* 464 (M^+, 2), 370 (**4b**, 100), 338 (**6b**, 63), 268 (**4b**-PhC≡CH, 80), 135 (28), 94 (7), and 66 (47). Found: C, 80.28; H, 6.17; S, 6.96%. Calcd for $C_{31}H_{29}PS$: C, 80.14; H, 6.29; S, 6.90%.

1-Benzyloxy-3,4,6-triphenyl-1,2-dihydrophosphorin 1-Sulfide (12a): IR(KBr) 1000, 970 cm^{-1} (P-O); ^{1}H NMR δ=3.33—3.67 [m, 2H, H(6)], 4.75—5.50 (m, 2H, $PhCH_2O$), 6.82 [d, 1H, J_{HP}=22.0 Hz, H(3)], and 6.67—7.83 (m, 20H, Ar-H); MS *m/z* 464 (M^+, 72), 356 (**4a**, 22), 340 (75), 324 (**6a**, 10), 293 (66), 254 (**4a**-PhC≡CH, 23), 215 (44), and 91 (100). Found: C, 77.58; H, 5.44%. Calcd for $C_{30}H_{25}PS$: 77.56; H, 5.42%.

1-Benzyloxy-3,4-diphenyl-6-*p*-tolyl-1,2-dihydrophosphorin 1-Sulfide (12b): IR(KBr) 980, 960 cm^{-1} (P-O); ^{1}H NMR δ=2.38 (s, 3H, CH_3), 3.33—3.67 [m, 2H, H(6)], 4.75—5.50(m, 2H, $PhCH_2O$), 6.77 [d, 1H, J_{HP}=20.0 Hz, H(3)], 6.60—7.57 (m, 17H, Ar-H), and 7.57 (d, 2H, J_{HH}=8.0 Hz, *p*-Tol-H); MS *m/z* 478 (M^+, 67), 370 (**4b**, 11), 354 (59), 338 (**6b**, 22), 307 (100), 268 (**4b**-PhC≡CH, 15), 215 (33), and 91 (74). Found: C, 77.54; H, 5.57; S, 6.66%. Calcd for $C_{31}H_{27}OPS$: C, 77.80; H, 5.69; S, 6.70%.

1-(Phenylthio)-3,4,6-triphenyl-1,2-dihydrophosphorin 1-Sulfide (13a): ^{1}H NMR δ=3.50—4.00 [m, 2H, H(6)], 6.68 [d, 1H, J_{HP}=18.0 Hz, H(3)], and 6.68—7.83 (m, 20H, Ar-H); MS *m/z* 466 (M^+, 10), 356 (**4a**, 100), 324 (**6a**, 69), 254 (**4a**-PhC≡CH, 87), 121 (36), and 110 (46). Found: C, 74.40; H, 4.88%. Calcd for $C_{29}H_{23}S_2P$: C, 74.65; H, 4.97%.

3,4-Diphenyl-1-(phenylthio)-6-*p*-tolyl-1,2-dihydrophosphorin 1-Sulfide (13b): ^{1}H NMR δ=2.37 (s, 3H, CH_3), 3.50—4.00 [m, 2H, H(6)], 6.68 [d, 1H, J_{HP}=19.0 Hz, H(3)], 6.67—7.50 (m, 17H, Ar-H), and 7.65 (d, 2H, J_{HH}=8.0 Hz, *p*-Tol-H); MS *m/z* 480 (M^+, 3), 370 (**4b**, 87), 338 (**6b**, 100), 268 (**4b**-PhC≡CH, 80), 135 (40), 110 (78), and 66 (17). Found: C, 75.03; H, 5.21%. Calcd for $C_{30}H_{25}S_2P$: C, 74.97; H, 5.24%.

References

1) H. Tanaka, S. Kametani, T. Saito, and S. Motoki, *Bull. Chem. Soc. Jpn.*, **58**, 667 (1985).

2) H. Tanaka and S. Motoki, *Bull. Chem. Soc. Jpn.*, **59**, 2047 (1986).

3) T. Karakasa and S. Motoki, *J. Org. Chem.*, **43**, 4147 (1978); **44**, 4151 (1979).

4) J. -M. Alcaraz and F. Mathey, *J. Chem. Soc., Chem. Commun.*, **1984**, 508.

5) G. Märkl, G. Y. Jin, and E. Silbereisen, *Angew. Chem., Int. Ed. Engl.*, **21**, 370 (1982).

6) G. Märkl, H. Baier, and R. Liebl, *Justus Liebigs Ann. Chem.*, **1981**, 919.

7) G. Märkl, *Angew. Chem., Int. Ed. Engl.*, **5**, 846 (1966) and later papers.

8) J. B. Stothers, "Carbon-13 NMR Sperctroscopy," Academic Press, New York (1972), pp. 68, 414; G. C. Levy, R. L. Lichter, and G. L. Nelson, "Carbon-13 Nuclear Magnetic Resonance for Organic Chemists," Wiley, New York (1972), p. 61.

9) H. Tanaka, T. Saito, and S. Motoki, *Bull. Chem. Soc. Jpn.*, **59**, 59 (1986).

Syntheses and Biological Activities of Neurokinin B Analogs Modified at Positions 2, 3, and 6

Yoshiki UCHIDA, Keiko OKIMURA, Katsuro KUROSAWA, Naoki SAKURA, Kyoko HIROSE, and Tadashi HASHIMOTO*

School of Pharmacy, Hokuriku University, Ho-3, Kanagawa-machi, Kanazawa 920-11

(Received October 28, 1986)

Synopsis. Nine neurokinin B [NKB] related octa- and nona-peptides containing Arg and *N*-methylglycine, D-Ala, D-Phe, D-Trp, D-α-aminophenylacetic acid, D-Arg, D-Pro, D-homoglutamine, or D-homoglutamic acid instead of Met[2] or His[3], and Phe[6], respectively, in the original sequences were synthesized by standard solid phase method. The biological activities of the analogs were assayed on isolated guinea-pig ileum. [Arg[3], D-Ala[6]]-NKB (3—10) was found to act as an antagonist of NKB.

Neurokinin B[1,2] (NKB) is a novel neuropeptide isolated from porcine spinal cord and sequenced as decapeptide amide (Fig. 1). NKB has close structural homology, particularly in the C-terminal sequence, with tachykinin such as substance P (SP).

The relationship study[3] between chain length and activity indicated that the contractile potency of NKB on guinea-pig ileum, rat vas deferens and rat duodenum remained nearly complete after removal of N-terminal tripeptide portion from the native peptide.

Our recent study[4] on the structure activity relationship of NKB revealed that the replacement of Phe[6] or Val[7] residue with Gly moiety brings drastic decrease of the contractile activities on isolated guinea-pig ileum and rat vas deferens, while the substitution of Gly for Phe[5] enhances their activities. Octapeptide analogs, [Gly[6]]-NKB (3—10) **1** and [Gly[7]]-NKB (3—10) **2**, have no agonistic activity on both assays.

Since our synthetic study on the structure activity relationship of NKB aimed the development of a specific and potent antagonist, the analogs **1** and **2** were examined for their antagonistic effects against NKB. The analog **1** was found to exert potent antagonistic effect, but analog **2** was not an antagonist. Based on this observation, a new series of octa-and nona-peptide analogs containing unusual amino acid at position 6 (Fig. 1) was designed in order to obtain more potent antagonist. *N*-methylglycine (sarcosine, Sar), D-Ala, D-Phe, D-Trp, D-α-aminophenylacetic acid (D-α-phenylglycine, Phg), D-Arg, D-Pro, D-homoglutamine (Hgn),[5] or D-homoglutamic acid (Hgu) residue was substituted for Phe[6]. It has been observed that the replacement of natural residue with unusual amino acid in SP[6,7] changes the pharmacological spectrum of SP from that of an agonist to that of an antagonist. Arg moiety was incorporated into peptide chain to improve the solubility of the peptides in water according to SP antagonists.[7]

This paper describes the first application of a new amino acid D-Hgu to the synthetic study of bioactive peptide analogs. D-Hgu residue was incorporated into a peptide chain by the usual solid phase technique using Boc-D-Hgu(OBzl)-OH,[5] which was derived from the N^{α},N^{ca}-(Boc)$_2$-D-Hgn-OH[5,6] by the reaction with anhydrous sodium benzylate in benzyl alcohol.

The new NKB analogs were synthesized in the same way with the preparation of NKB analogs[4] on an automated peptide synthesizer by standard solid phase method[8] starting from *t*-butoxycarbonyl(Boc)-Met-benzhydrylamine-resin. Boc protection was used for α-amino function. The side-chain protective groups used were cyclohexyl for Asp, benzyl for D-Hgu, *p*-tolylsulfonyl for Arg and His, and Boc for the amide nitrogen (N^{ca}) of D-Hgn. After the completion of the chain elongation, the peptide resin was treated with liquid hydrogen fluoride[9] in the presence of anisole to cleave the peptide from the resin with simultaneous removal of the protecting groups and formation of the carboxyl terminal amide. The synthetic products were purified by preparative reverse-phase high-performance liquid chromatography (HPLC) using 0.1% trifluoroacetic acid in acetonitrile as eluent. Highly purified peptides (Table 1) were obtained after gel filtration on Sephadex LH-20 column. Homogeneity of the peptides was demonstrated by analytical HPLC

		1 2 3 6 7 10
	NKB	H-Asp-Met-His-Asp-Phe — Phe-Val-Gly-Leu-Met-NH_2
1	[Gly[6]]-NKB (3—10)	H-His-Asp-Phe — Gly-Val-Gly-Leu-Met-NH_2
2	[Gly[7]]-NKB (3—10)	H-His-Asp-Phe — Phe-Gly-Gly-Leu-Met-NH_2
3	[Arg[3], Sar[6]]-NKB (3—10)	H-Arg-Asp-Phe — Sar-Val-Gly-Leu-Met-NH_2
4	[Arg[3], D-Ala[6]]-NKB (3—10)	H-Arg-Asp-Phe-D-Ala-Val-Gly-Leu-Met-NH_2
5	[Arg[3], D-Phe[6]]-NKB (3—10)	H-Arg-Asp-Phe-D-Phe-Val-Gly-Leu-Met-NH_2
6	[Arg[3], D-Trp[6]]-NKB (3—10)	H-Arg-Asp-Phe-D-Trp-Val-Gly-Leu-Met-NH_2
7	[Arg[3], D-Phg[6]]-NKB (3—10)	H-Arg-Asp-Phe-D-Phg-Val-Gly-Leu-Met-NH_2
8	[Arg[2], D-Arg[6]]-NKB (2—10)	H-Arg-His-Asp-Phe-D-Arg-Val-Gly-Leu-Met-NH_2
9	[Arg[2], D-Pro[6]]-NKB (2—10)	H-Arg-His-Asp-Phe-D-Pro-Val-Gly-Leu-Met-NH_2
10	[Arg[2], D-Hgn[6]]-NKB (2—10)	H-Arg-His-Asp-Phe-D-Hgn-Val-Gly-Leu-Met-NH_2
11	[Arg[2], D-Hgu[6]]-NKB (2—10)	H-Arg-His-Asp-Phe-D-Hgu-Val-Gly-Leu-Met-NH_2

Fig. 1. NKB and its analogs.

Table 1. Physical Properties and Yield of the Synthetic Analogs

Analog	$[\alpha]_D^{18}$/° (*c* 0.1, DMF)	Retention time[a]/min	R_f^1	R_f^2	Yield/%
3	−13	14.0	0.09	0.62	22.9
4	−10	13.8	0.11	0.64	12.6
5	−11	18.4	0.14	0.67	15.9
6	+3	18.0	0.14	0.66	11.2
7	−28	17.8	0.14	0.68	15.3
8	+6	12.7	0.03	0.62	17.7
9	+7	16.7	0.06	0.64	29.5
10	−16	12.8	0.04	0.61	23.4
11	−1	13.9	0.05	0.61	20.6

a) Condition of analytical HPLC: column, Chemcosorb ODS; flow rate, 1 ml min^{-1}; Detection, 210 nm; eluent system, linear gradient from 14% to 35% CH_3CN (15 min) in 20 mM phosphate buffer (pH 3.0).

and thin-layer chromatography (TLC). When single peak and single spot were observed for a peptide in all chromatographic systems, the peptide was considered appropriately pure for bioassay. The chromatographic data were reinforced by the amino acid analytical data.

Biological properties of the synthetic peptides were examined on contractile activities of isolated guinea-pig ileum. The agonistic effects of analogs **3**—**11** were compared with that of our synthetic NKB. Analogs **1**—**11** were tested for their antagonistic effects against NKB. The antagonistic activities of the analogs were evaluated in terms of pA_2 (negative concentration of antagonist that reduces the contractile response to a double dose of agonist in the presence of antagonist to that of a single dose without it), according to Schild.[10] The results are presented in Table 2.

Analogs **3**, **4**, **5**, **7**, **8**, **9**, and **11**, in which Phe[6] was replaced by Sar, D-Ala, D-Phe, D-Phg, D-Arg, D-Pro, or D-Hgu, had no agonistic activity on the ileum assay, and [Arg[3], D-Trp[6]]-NKB (3—10) **6** and [Arg[2], D-Hgn[6]]-NKB (2—10) **10** possessed a little contractile activity. It was observed that the replacement of Phe[6] with Gly or D-Ala changed the pharmacological spectrum of NKB from that of an agonist to that of an antagonist and the substitution by the unusual amino acide except D-Ala was unfavorable for antagonism to NKB. Analogs **1** and **4** exerted antagonistic effects against NKB showing similar pA_2 values. The results reveal that **1** and **4** are the first NKB analogs to act as fairly potent antagonists against NKB.

Table 2. Biological Activities of the Synthetic Analogs on Isolated Guinea-Pig Ileum

Analog[a]	RA[b]	pA_2
1	0[c]	5.82
2	0[c]	—[d]
4	0	5.69
6	<0.01	—
10	<0.01	—

a) **3**, **5**, **7**, **8**, **9**, and **11** showed no agonistic and antagonistic activity. b) Relative contractile activity to NKB=1. c) Data from Ref. 4. d) —, no antagonistic activity.

Experimental

Amino acid derivatives were purchased from Peptide Institute, Inc., Osaka, Japan and benzhydrylamine (BHA) resin (available amine of the resin: 0.6 mmol g^{-1} of support) from Beckman Inc., Palo Alto, Calif. Optical rotations were measured in a 1 dm tube using a Nipponbunkoh DIP-4 Polarimeter. Amino acid analyses on samples previously hydrolyzed with 6 M HCl (1 M=1 mol dm^{-3}) (110 °C, 24 h) or on analog **6** with 4 M methanesulfonic acid containing 0.2% 3-(2-aminoethyl)indole (115 °C, 24 h) were performed on a Beckman System 7300 Amino Acid Analyzer. TLC were carried out on silica-gel plates (Merck). The following solvent systems were used and allowed to ascend for 10 cm: R_f^1, *n*-BuOH: AcOH: H_2O (4:1:5, upper phase); R_f^2, *n*-BuOH: pyridine: AcOH: H_2O (30:20:6:24). Analytical HPLC were effected on the following systems: column, Chemcosorb ODS (Chemco, 3.9×300 mm); flow rate, 1 ml min^{-1}; detection, 210 nm; eluent system, linear gradient for 15 min from 14% to 35% CH_3CN in 20 mM phosphate buffer (pH 3.0).

General Procedure for the Preparation of Analogs. The solid phase synthesis was carried out using a Beckman System 990C Peptide Synthesizer as described previously.[4] Half gram of BHA-resin hydrochloride for each analog served as the solid support. A 2.5 fold excess of the amino acid derivative was used for all coupling. The coupling was affected with dicyclohexylcarbodiimide/1-hydroxybenzotriazole. The protected peptide resin was treated with anhydrous liquid HF containing 10% anisole. After evaporation of HF in vacuo under ice-cooling, the residue was washed with AcOEt and the peptide was extracted with 50% AcOH.

Purification of the Peptides. The crude peptide was subjected to HPLC as reported previously.[4] The apparatus was composed of a model 590 pump and a U6K injector (Waters) connecting with a column of Chemcosorb ODS (Chemco, 20×300 mm) or μ-Bondasphere C_{18} (Waters, 19×150 mm). The eluates were monitored with a UV detector S-310A model-II (Soma) at 210 nm wavelength. CH_3CN-0.1% TFA solvent system was used as eluent at flow rate 10 or 7 ml min^{-1}. Each peptide was emerged at 40-60 min by isocratical elution with 15—26% CH_3CN contents of the solvent system. The desired fraction was passed through a Sephadex LH-20 column (16×500 mm) eluted with aqueous DMF (90%) containing 0.02% 1,2-ethanedithiol. Homogeneity of the peptides was analyzed by analytical HPLC and TLC. Amino acid compositions of the acid hydrolysates of the synthetic peptides were consistent with the calculated values.

Bioassay. The agonistic activity of the synthetic analog was measured on ileum taken from guinea-pig, as described before.[4] The contraction was recorded by means of an isotonic transducer (Nippon Kohden, TD-111T) with load of 2 g on a Servocorder (Watanabe Instruments, SR6204). Concentration-response curves were obtained using a

cumulative dose-assay, and the time between two consecutive dose-response curves was longer than 10 min. Though NKB at concentration 10^{-7} M induced maximal response, all of analogs were applied up to 10^{-6} M. In the tests for antagonistic activity on guinea-pig ileum, analog was added 10 min before NKB was added. The cumulative dose-response curve of NKB in the presence or the absence of the analog was obtained. In the presence of analogs at concentration 2×10^{-6} M, the maximal response induced by NKB was almost the same response without analogs.

References

1) S. Kimura, M. Okada, Y. Sugita, I. Kanazawa, and E. Munekata, *Proc. Jpn. Acad.*, **59B**, 101 (1983); H. Kangawa, N. Minamino, A. Fukuda, and H. Matsuo, *Biochem. Biophys. Res. Commun.*, **114**, 533 (1983).

2) Amino acids, peptides and their derivatives mentioned in this paper are of L-configuration. The abbreviations for amino acids and peptides are in accordance with the rules of the IUPAC-IBU Commission on Biochemical Nomenclature in *Eur. J. Biochem.*, **138**, 9 (1984).

3) F. Osakada, K. Kubo, K. Goto, I. Kanazawa, and E. Munekata, *Eur. J. Pharmacol.*, **120**, 201 (1986).

4) T. Hashimoto, T. Moro, and Y. Uchida, *Bull. Chem. Soc. Jpn.*, **59**, 4006 (1986).

5) N. Sakura, K. Hirose, and T. Hashimoto, *Chem. Pharm. Bull.*, **34**, 3506 (1986).

6) T. Hashimoto, Y. Uchida, M. Nishijima, T. Moro, N. Sakura, and K. Hirose, *Bull. Chem. Soc. Jpn.*, **59**, 4009 (1986).

7) D. Regoli, E. Escher, and J. Mizrahi, *Pharmacology*, **28**, 301 (1984).

8) R. B. Merrifield, *Adv. Enzymol.*, **32**, 221 (1969).

9) S. Sakakibara, Y. Shimonishi, Y. Kishida, M. Okada, and H. Sugihara, *Bull. Chem. Soc. Jpn.*, **40**, 2164 (1967).

10) H. O. Schild, *Br. J. Pharmacol.*, **4**, 277 (1949).

Insertion of Ketene and Diphenylketene to the Pnictogen-Heteroatom Bonds

Fumio ANDO,* Yoshihiko KOHMURA, and Jugo KOKETSU
Department of Industrial Chemistry, College of Engineering, Chubu University, Matsumoto-cho, Kasugai, Aichi 487
(Received November 12, 1986)

Synopsis. Ketene and diphenylketene insert across the heteroatom-metal bond of amino-, alkoxy-, and alkylthiopnictogens, $R_{3-n}MX_n$, to give the corresponding α-metallated acetamides, esters, and thioesters, $R_{3-n}M(CH_2COX)_n$ and $R_{3-n}M(CPh_2COX)_n$ (M=As, Sb, Bi; X=NR_2, OR, SR; n=1,3), respectively.

Ketene has been known to react with various organometallic compounds, especially with the compounds containing the group 3B and 4B elements.[1] However, the reactions of ketene with analogous arsenic, antimony, and bismuth compounds have been received scarce attention so for. Lustenko et al.[2] reported that alkoxyarsines and -stibines react with ketene to give alkoxycarbonylmethylarsines and -stibines. However, there is no report dealing with the reaction of ketene with group 5B metal amides and thiolates. As a part of our continuing work[3] on the reaction of group 5B metal compounds with multiply bonded reagents, the reactions of ketene and diphenylketene with amides, alkoxides, and alkanethiolates of arsenic, antimony, or bismuth have been investigated.

Ketene, generated by the pyrolysis of diketene, reacted with dialkylaminodialkylarsines in ether at about −20 °C to give *N,N*-dialkyl(dialkylarsino)-acetamides. The reaction of dialkylaminodimethylstibines with ketene proceeded more readily to yield *N,N*-dialkyl(dimethylstibino)acetamides (Table 1).

$$R_2M\text{-}NR'_2 + CH_2{=}C{=}O \longrightarrow R_2MCH_2CONR'_2$$
(M = As, Sb; R = Me, Ph; R' = Me, Et)

These insertion products were obtained as thermally stable (up to ca. 200 °C) and distillable liquids. The structure of the products was determined on the basis of IR, NMR, and mass spectra and elemental analyses. The IR spectra of the arsinoacetamides show a strong C=O stretching vibration at 1630—1622 cm^{-1}. The corresponding C=O stretching band of antimony analogues is located at a lower frequency (1620—1613 cm^{-1}). This may be explained by increased electron density on the α-methylene carbon and intramolecular coordination of carbonyl oxygen to antimony. The ^1H NMR spectra of these adducts contain a singlet peak of the methylene protons attached directly to the metal atoms at δ=2.5—3.1 and also characteristic peaks due to magnetically nonequivalent two alkyl groups on the nitrogen atom of amide groups, namely, two singlets at δ=2.7—3.1 for the dimethylamides and two quartets at δ=3.0—3.5 and two triplets at δ=0.9—1.2 for the diethylamides.

Tris(dialkylamino)bismuthines readily reacted with ketene at −50 °C with liberation of heat, and three moleclues of ketene inserted into the Bi-N bonds to give tris(dialkylcarbamoylmethyl)bismuthines. On the treatments of ketene with tris(dialkylamino)arsines at 0 °C or with tris(dialkylamino)stibines at −20 °C, the corresponding addition products containing arsenic or antimony were obtained.

$$M(NR_2)_3 + 3CH_2{=}C{=}O \longrightarrow M(CH_2CONR_2)_3$$
(M = As, Sb, Bi; R = Me, Et)

These adducts are reddish brown viscous liquids or waxy solid which, on attempted vacuum (ca. 10^{-2} Pa) distillation by heating up to 250 °C, decomposed to *N,N*-dialkylacetamides (70—80%) and unidentified black residues containing metals. Nevertheless, the formation of adducts was confirmed by ^1H NMR, ^{13}C NMR and IR spectra. In the ^1H and ^{13}C NMR spectra of the adducts, the methylene groups attached to the metals, in general, appeared at somewhat lower

Table 1. Preparative, Analytical, and Mass Spectral Data for the α-Metallated Acetamides

Compound	Bp/°C(Pa)	Yield/%	Calcd(Found)/%			MS, *m/z* (rel intensity)[a]
			C	H	N	
$Me_2AsCH_2CONEt_2$	60—61(4.0)	81	42.27 (43.84)	8.13 (8.28)	6.47 (6.39)	219(M^+, 10), 204(100), 162(62), 119(10), 114(9), 105(16), 100(21), 72(68)
$Ph_2AsCH_2CONMe_2$	170—173(1.3×10^{-2})	86	60.51 (60.96)	5.88 (5.76)	4.32 (4.44)	315(M^+, 13), 238(43), 229(83), 227(67), 161(4), 86(14), 72(26), 44(100)
$Ph_2AsCH_2CONEt_2$	167—171(1.3×10^{-2})	89	63.28 (62.97)	6.68 (6.48)	3.91 (4.08)	343(M^+, 9), 243(6), 229(10), 227(13), 115(17), 100(9), 72)38), 58(100)
$Me_2SbCH_2CONMe_2$	71—72(26)	75	28.92 (30.29)	6.25 (5.93)	5.75 (5.58)	237(M^+, 2), 222(40), 207(5), 193(3), 165(10), 151(13), 86(3), 72(12), 44(100)
$Me_2SbCH_2CONEt_2$	81—86(4.0)	88	35.54 (36.12)	6.93 (6.82)	5.37 (5.27)	265(M^+, 3), 259(22), 208(18), 193(14), 165(11), 151(35), 115(13), 72(36), 43(100)

a) Masses refer to ^{121}Sb for the antimony compounds.

field compared with those of the corresponding *N,N*-dialkyl(dialkylmetal)acetamides, probably due to additional two electron-withdrawing $NCOCH_3$ groups. The α-methylene groups shift towards higher field with the central metal going from As to Sb and Bi, due to increasing electron density of the neighboring methylene groups in this order.

Diphenylketene, in which the methylene carbon is more sterically crowded than ketene, reacted slowly with aminoarsines and aminostibines, leading to the corresponding insertion products.

$$R_2M\text{-}NR'_2 + Ph_2C{=}C{=}O \longrightarrow R_2MCPh_2CONR'_2$$
$$M(NR'_2)_3 + 3Ph_2C{=}C{=}O \longrightarrow M(CPh_2CONR'_2)_3$$
$$(M = As, Sb;\ R = Me, Ph;\ R' = Me, Et)$$

Reaction of trimethoxyarsine with ketene proceeded very slowly in boiling benzene to give mono-insertion product, dimethoxy(methoxycarbonylmethyl)arsine, in quite low yield (24%), but ethoxy and higher alkoxyarsines did not react under the same conditions. On the other hand, tris(alkoxycarbonylmethyl)stibines were easily obtained in high yield by the reaction of ketene with trialkoxystibines in ether at room temperature, as reported by Lutsenko et al.[2a,b] Tris(ethylthio)stibine also reacted slowly with ketene to afford tris[(ethylthio)-carbonylmethyl)]stibine in 50% yield under refluxing benzene, whereas tris(ethylthio)arsine did not react under the analogous reaction conditions.

$$As(OMe)_3 + CH_2{=}C{=}O \longrightarrow (MeO)_2AsCH_2COOMe$$
$$Sb(OR)_3 + 3CH_2{=}C{=}O \longrightarrow Sb(CH_2COOR)_3$$
$$Sb(SEt)_3 + 3CH_2{=}C{=}O \longrightarrow Sb(CH_2COSEt)_3$$

Thus, the reactivity of tervalent group 5B compounds, =M-X, toward ketene increases in the order As<Sb<Bi for the metal (M), and SR<OR<NR_2 for the functional group(X). The highest reactivity of $Bi(NR_2)_3$ may be attributed to the enhanced nucleophilicity of the nitrogen caused by the weak and highly polar Bi-N bonds.

Experimental

Materials and General Procedures. The compounds Me_2AsNEt_2,[4] Ph_2AsNMe_2,[4] Ph_2AsNEt_2,[4] Me_2SbNMe_2,[5] Me_2SbNEt_2,[5] $As(NMe_2)_3$,[4] $As(NEt_2)_3$,[4] $Sb(NMe_2)_3$,[6] $Sb(NEt_2)_3$,[6] $Bi(NMe_2)_3$,[3c] $Bi(NEt_2)_3$,[3c] $As(OMe)_3$,[7] $Sb(OR)_3$ (R=Et, *n*-Pr, *i*-Pr, *n*-Bu),[7] and $Sb(SEt)_3$[7] were synthesized according to the published procedures. Ketene[8] was generated by the pyrolysis of diketene at 550 °C, and was purified through two traps cooled to −20 °C. Diphenylketene[9] was prepared by dehydrochlorination of diphenylacetyl chloride with triethylamine. All reactions were performed under an atmosphere of nitrogen or argon. ^1H (60 MHz) and ^{13}C (15.04 MHz) NMR spectra were measured in $CDCl_3$ with JEOL C-60 HL and JNM FX-60 FT instruments, respectively. IR spectra were recorded on a Shimadzu IR-430 spectrometer. Mass spectra (70 eV) were measured with a Hitachi RMU-6L spectrometer.

Reaction of Dialkylaminodialkylarsines or -stibines with Ketene. An excess of ketene was passed through a stirred solution of diethylaminodimethylarsine (6.52 g, 36.8 mmol) in 20 ml of ether at about −20 °C during 10 min. Solvent removal under vacuum left a yellow liquid residue. From the residue, *N,N*-diethyl(dimethylarsino)acetamide (6.49 g, 81%) was obtained by fractional distillation as a yellowish liquid. In a similar way, reactions of ketene with dimethylaminodiphenylarsine at room temperature, with dimethyl aminodimethylstibine at −50 °C, and with diethylamino dimethylstibine at −50 °C gave the corresponding insertion products. Bp, yield, analytical, and mass spectral data of these products are shown in Table 1. The NMR and IR spectra of these metallated acetamides are summarized in Table 2.

Reaction of Tris(dialkylamino)arsines, -stibines, and -bismuthines with Ketene. Ketene was passed into an ethereal (20 ml) solution of tris(dimethylamino)arsine (3.89 g, 18.8 mmol) at room temperature. After removal of the solvent, the residue was dried under reduced pressure (ca. 10^{-2} Pa) for 4 h, leaving a reddish brown liquid (5.61 g), and whose ^1H and ^{13}C NMR and IR spectra were measured without further purification because of difficulties encountered during distillation or recrystallization: ^1H NMR δ=2.84 (s, 2H), 2.95 (s, 3H), and 3.11 (s, 3H); ^{13}C NMR δ=29.82, 35.22, 38.27, and 171.20; IR (neat) 1627 cm^{-1}. These spectra proved the product to be tris(dimethylcarbamoylmethyl)arsine (90%). A similar treatment of ketene with tris(diethylamino)-arsine at 0 °C, tris(dimethylamino)stibine at −20 °C, tris(diethylamino)stibine at −20 °C, tris(dimethylamino)bismuthine at −50 °C, or tris(diethylamino)bismuthine at −50 °C gave the corresponding insertion products. $As(CH_2CONEt_2)_3$: Red oil (84%); ^1H NMR δ=1.13, 1.19 (each t, 3H),

Table 2. NMR and IR Spectroscopic Data for the α-Metallated Acetamides, $R_2MCH_2CONR'_2$

Compound	^1H NMR(δ)			^{13}C NMR(δ)				IR
	R_2M	MCH_2	NR'_2	R_2M	MCH_2	CO	NR'_2	ν(CO) cm^{-1}
$Me_2AsCH_2CONEt_2$	1.09(s)	2.53(s)	3.39(q) 1.10(t) 3.50(q) 1.20(t)	9.55	30.99	170.16	38.89 13.38 42.82 14.42	1622
$Ph_2AsCH_2CONMe_2$	7.30(m)	3.05(s)	2.78(s) 2.83(s)	128.52 132.94 139.95	32.62	170.68	35.28 37.94	1630
$Ph_2AsCH_2CONEt_2$	7.27(m)	3.00(s)	3.09(q) 0.98(t) 3.25(q) 1.01(t)	128.52 133.65 140.28	32.88	169.84	40.22 13.06 42.82 14.36	1625
$Me_2SbCH_2CONMe_2$	0.88(s)	2.52(s)	2.94(s) 3.06(s)	−3.95	18.20	171.61	34.25 37.44	1620
$Me_2SbCH_2CONEt_2$	0.89(s)	2.52(s)	3.39(q) 1.11(t) 3.50(q) 1.19(t)	−2.79	18.91	171.53	39.83 13.71 43.01 14.42	1613

3.09 (s, 1H, $AsCH_2$), 3.29 and 3.39 (each q, 2H); ^{13}C NMR δ=13.25, 14.49, 30.08 (AsC), 40.22, 43.08, and 170.68; IR (neat) 1625 cm^{-1} (C=O). Sb $(CH_2CONMe_2)_3$: Red oil (98%); ^1H NMR δ=2.76 (s, 2H, $SbCH_2$), 2.95 (s, 3H), and 3.10 (s, 3H); ^{13}C NMR δ=22.16 (SbC), 35.35, 38.66, and 172.76; IR (neat) 1618 cm^{-1} (C=O). Sb $(CH_2CONEt_2)_3$: Red oil (100%); ^1H NMR δ=1.11, 1.20 (each t, 3H), 2.78 (s, 1H, $SbCH_2$), 3.40 (q, 2H); ^{13}C NMR δ=13.51, 14.49, 22.29 (SbC), 40.28, 43.40, and 172.05; IR (neat) 1610 cm^{-1}. Bi $(CH_2CONMe_2)_3$: Red solid (97%); ^1H NMR δ=2.03 (s, 2H, $BiCH_2$), 2.89 (s, 3H), and 2.99 (s, 3H); ^{13}C NMR δ=21.38(BiC), 34.89, 37.88, and 173.54; IR (nujol) 1640 cm^{-1} (C=O). Bi $(CH_2CONEt_2)_3$: Red oil (100%); ^1H NMR δ=1.12, 1.18 (each t, 3H), 2.08 (s, 1H, $BiCH_2$), 3.22, and 3.38 (each q, 2H); ^{13}C NMR δ=13.12, 14.23, 21.38 (BiC), 40.28, 43.60, and 172.94; IR (neat) 1640 cm^{-1} (C=O).

Reaction of Diphenylketene with Aminoarsines or Aminostibines. Diphenylketene (1.88 g, 9.68 mmol) was added dropwise to a solution of diethylaminodimethylarsine (1.71 g, 9.66 mmol) in 20 ml of ether at room temperature. The mixture was heated under reflux for 30 min. After removal of the solvent, the residue was distilled under vacuum to afford *N,N*-diethyl(dimethylarsino)diphenylacetamide (1.62 g, 45%) as an orange liquid, bp 180—187 °C/1.3×10^{-2} Pa: ^1H NMR δ=0.91 (s, 3H, CH_3As), 1.11, 1.12 (each t, 3H), 3.26, 3.38 (each q, 2H), and 7.22 (m, 5H); ^{13}CNMR δ=6.04 (CH_3As), 12.86, 14.62 (NCC), 40.67, 42.17 (NC), 54.58 (q-C), 126.89 (p), 128.45 (m), 129.04 (o), 140.02 (i), and 170.68 (CO); IR (neat) 1658 cm^{-1} (C=O); MS *m/z* (rel intensity) 371 (M^+; 8), 105 (100), 100 (82), 77 (88). Similarly, the following diphenylketene insertion products were obtained by the reaction of 3 molar equivalent of diphenylketene with dimethylaminodiphenylarsine, diethylaminodiphenylarsine, dimethylaminodimethylstibine, diethylaminodimethylstibine, tris(dimethylamino)arsine, tris(diethylamino)arsine, tris(dimethylamino)stibine, and tris(diethylamino)stibine. *N,N*-Dimethyl(diphenylarsino)diphenylacetamide: Yield 41%; bp 146—151 °C/5.3×10^{-3} Pa; ^1H NMR δ=2.94 (s, 3H), 2.98 (s, 3H), and 7.30 (m, 20H); ^{13}CNMR δ=36.13, 37.55, 54.90 126.96, 128.52, 129.04, 129.17, 131.05, 133.78, 139.63, 146.32, and 179.30; IR ($CHCl_3$) 1645 cm^{-1} (C=O). *N,N*-Diethyl(diphenylarsino)diphenylacetamide: Yield 68%, bp 140—150 °C/5.3×10^{-3} Pa; ^1H NMR δ=1.09, 1.10 (each t, 3H), 3.28, 3.39 (each q, 2H), and 7.27 (m, 10H); ^{13}CNMR δ=12.80, 14.62, 40.61, 42.10, 54.51, 126.83, 128.45, 128.97, 129.17, 130.99, 134.37, 139.95, 146.19, and 173.02; IR ($CHCl_3$) 1640 cm^{-1}. *N,N*-Dimethyl(dimethylstibino)diphenylacetamide: Yield 23%; bp 137—144 °C/1.3×10^{-2} Pa; ^1H NMR δ=0.97 (s, 6H), 2.94 (s, 3H), 2.97 (s, 3H), and 7.32 (m, 10H); ^{13}CNMR δ=4.09, 36.06, 37.55, 54.77, 126.89, 128.52, 129.04, 139.70, and 175.75; IR ($CHCl_3$) 1640 cm^{-1} (C=O). *N,N*-Diethyl(dimethylstibino)diphenylacetamide: Yield 25%; bp 110—111 °C/1.3×10^{-2} Pa; ^1H NMR δ=1.03 (s, 3H), 1.09 (t, 3H), 3.27, 3.39 (each q, 2H), and 7.28 (m, 5H); ^{13}CNMR δ=3.96, 12.86, 14.62, 40.67, 43.17, 54.51, 126.89, 128.26, 128.97, 138.85, and 172.49; IR (neat) 1656 cm^{-1} (C=O). Tris(dimethylcarbamoyldiphenylmethyl)arsine: Yield 41%; bp 114—126 °C/1.3×10^{-2} Pa; ^1H NMR δ=2.92 (s, 3H), 2.95 (s, 3H), and 7.26 (m, 10H); ^{13}CNMR δ=36.00, 37.49, 54.77, 126.89, 128.45, 128.97, 139.63, and 171.72; IR ($CHCl_3$) 1643 cm^{-1} (C=O). Tris(diethylcarbamoyldiphenylmethyl)arsine: Yield 56%; bp 136—141 °C/1.3×10^{-2} Pa; ^1H NMR δ=1.13 (t, 3H), 3.32, 3.44 (each q, 2H), and 7.33 (m, 5H); ^{13}CNMR δ=12.80, 14.62, 40.61, 42.17, 54.51, 126.89, 128.45, 128.97, 139.95, and 170.68; IR ($CHCl_3$) 1630 cm^{-1}. Tris(dimethylcarbamoyldiphenylmethyl)stibine: Yield 23%; bp 158—160 °C/1.3×10^{-2} Pa; ^1H NMR δ=2.98 (s, 3H), 3.00 (s, 3H), and 7.28 (m, 10H); ^{13}CNMR δ=36.06, 37.55, 54.84, 126.96, 128.52, 129.04, 139.63, and 171.72; IR ($CHCl_3$) 1639 cm^{-1} (C=O). Tris(diethylcarbamoyldiphenylmethyl)stibine: Yield 23%; bp 111—112 °C/1.3×10^{-2} Pa; ^1H NMR δ=1.07, 1.10 (each t, 3H), 3.28, 3.40 (each q, 2H), and 7.30 (m, 5H); ^{13}CNMR δ=12.80, 14.55, 40.61, 42.10, 54.44, 126.83, 128.38, 128.97, 139.95, and 170.68; IR ($CHCl_3$) 1625 cm^{-1} (C=O).

Reaction of Trimethoxyarsine and Trialkoxystibines with Ketene. A large excess ketene was bublled into a solution of trimethoxyarsine (4.66 g, 27.7 mmol) in boiling benzene (10 ml). After removal of the solvent, dimethoxy(methoxycarbonylmethyl)arsine (1.37 g, 24%) was obtained by distillation: Bp 58—59 °C/5.3 Pa; ^1H NMR δ=3.13 (s, 2H), 3.55 (s, 6H), and 3.74 (s, 3H); ^{13}CNMR δ=37.88 (AsC), 48.93 (MeOAs), 52.63 (COOMe), and 168.41; IR (neat) 1718 cm^{-1}. Reaction of trialkoxystibines with ketene was carried out in ether at room temperature. The following tris(alkoxycarbonylmethyl)stibines were obtained. $Sb(CH_2COOR)_3$: R=Et (yield 77%): Bp 134—138 °C/0.47 Pa; ^1H NMR δ=1.26 (t, 3H), 2.53 (s, 2H), 4.08 (q, 2H); ^{13}CNMR δ=14.42, 21.77 (SbC), 60.49, and 172.24; IR (neat) 1710 cm^{-1} (C=O). R=*n*-Pr (85%): Bp 150—151 °C/1.3×10^{-2} Pa; ^1H NMR δ=0.95 (t, 3H), 1.66 (m, 2H), 2.52 (s, 2H), and 3.98 (t, 2H); ^{13}C NMR δ=10.46, 21.83 (SbC), 22.16, 66.14 and 172.24; IR (neat) 1709 cm^{-1} (C=O). R=*i*-Pr (85%): Bp 122—123 °C/6.7×10^{-2} Pa; ^1H NMR δ=1.23 (d, 6H), 2.50 (s, 2H), and 4.91 (m, 1H); ^{13}CNMR δ=21.50 (SbC), 22.03, 67.12, and 171.72; IR (neat) 1708 cm^{-1} (C=O). R=*n*-Bu (74%): Bp 161—162 °C/1.2×10^{-2} Pa; ^1H NMR δ=0.95 (t, 3H), 1.13—1.78 (m, 4H), 2.50 (s, 2H), and 4.05 (t, 2H); ^{13}CNMR δ=13.71, 19.17, 21.83 (SbC), 30.86, 64.58, and 172.37; IR (neat) 1700 cm^{-1} (C=O).

Reaction of Tris(ethylthio)stibine with Ketene. Ketene was bubbled through a boiling benzene (20 ml) solution of tris(ethylthio)stibine (3.70 g, 12.2 mmol). Distillation afforded tris[(ethylthio)carbonylmethyl]stibine (2.80 g, 53%) as a yellow liquid: Bp 150—154 °C/1.3×10^{-1} Pa; ^1H NMR δ=1.26 (t, 3H), 2.90 (q, 2H), and 3.06 (s, 2H); ^{13}CNMR δ=19.17, 21.05 (SbC), 24.69, and 178.29; IR (neat) 1662 cm^{-1} (C=O).

References

1) For example, a) T. A. George, K. Jones, and M. F. Lappert, *J. Chem. Soc.*, **1965**, 2157; b) I. F. Lutsenko, Yu. I. Baukov, A. S. Kostyuk, N. I. Savelyeva, and V. K. Krysina, *J. Organomet. Chem.*, **17**, 241 (1969), c) T. Mukaiyama, K. Inomata, and M. Muraki, *J. Am. Chem. Soc.*, **95**, 967 (1973).

2) a) V. L. Foss, E. A. Besolova, and I. F. Lutsenko, *Zh. Obshch. Khim.*, **35**, 759 (1965); b) E. A. Besolova, V. L. Foss, and I. F. Lutsenko, *Zh. Obshch. Khim.*, **38**, 267 (1968); c) V. V. Kudinova, V. V. Grinevich, V. L. Foss, and I. F. Lutsenko, *Zh. Obshch. Khim.*, **39**, 376 (1969).

3) For example, a) J. Koketsu and Y. Ishii, *J. Chem. Soc., (C)*, **1971**, 511; b) J. Koketsu, M. Okamura, and Y. Ishii, *Bull. Chem. Soc. Jpn.*, **44**, 1155 (1971); c) F. Ando, T. Hayashi, K. Ohashi, and J. Koketsu, *J. Inorg. Nucl. Chem.*, **37**, 2011 (1975); d) F. Ando, J. Koketsu, Y. Ishii, *Bull. Chem. Soc. Jpn.*, **54**, 2728 (1981).

4) K. Moedritzer, *Chem. Ber.*, **92**, 2637 (1963).

5) H. A. Meinema and J. G. Noltes, *Inorg. Nucl. Chem. Lett.*, **6**, 241 (1970).

6) K. Moedritzer, *Inorg. Chem.*, **3**, 609 (1964); A. Keinnemann, G. Levy, F. Schue, and C. Tanielan, *J. Organomet. Chem.*, **35**, 143 (1973).

7) T. B. Brill and N. C. Cambell, *Inorg. Chem.*, **12**, 1884 (1973).

8) S. Andreades and H. D. Carlson, *Org. Synth.*, **45**, 50 (1965).

9) E. C. Taylor, A. McKillop, and G. H. Hawks, *Org. Synth.*, **52**, 36 (1972).

The Oxidation of $PbSO_4$ to PbO_2 in Sulfuric Acid Solution

Zen-ichiro TAKEHARA* and Kiyoshi KANAMURA
Department of Industrial Chemistry, Faculty of Engineering, Kyoto University, Yoshida-honmachi, Sakyoku, Kyoto 606
(Received December 24, 1985)

The interface between PbO_2 and $PbSO_4$ was considered to be the reaction site of the oxidation of $PbSO_4$ to PbO_2. The area of this site depended on the changing crystal size of $PbSO_4$ with the discharge conditions. The oxidation rate of $PbSO_4$ to PbO_2 increased with a decrease in the crystal size of $PbSO_4$ since the reaction site area per unit volume increased with a decrease in the crystal size of $PbSO_4$. The oxidation of $PbSO_4$ to PbO_2 depended on the discharge current, the sulfuric acid concentration and the rest time after a discharge.

$PbSO_4$ is deposited on the electrode surface during discharging of the positive active material of a lead-acid battery. The charge reaction of the positive active material is a conversion from $PbSO_4$ by anodic oxidation at the electrode surface. This reaction has been studied by many workers.[1-8] They potentiostatically investigated the oxidation of $PbSO_4$ formed by the anodic polarization of lead in the $PbSO_4$ potential region and suggested that the formation process of PbO_2 involved the nucleation and three-dimensional crystal growth. Casson et al. used an electrodeposited PbO_2 electrode to show that there is no evidence for nucleation and crystal growth.[9] Pohl measured different current-time curves at a lead electrode in a sulfuric acid solution during anodic polarization. He used an anodic current preimpulse before potentiostatic oxidation. The current-time curves measured after an anodic current preimpulse did not have any peaks. From this result, he suggested that the charge reaction did not proceed through nucleation and crystal growth.[2]

$PbSO_4$ is a nonconducting ionic crystal that becomes depodited on an electrode surface as a thin dense film.[9] Its solubility is very small in a sulfuric acid solution.[11] Therefore, only a special site can sustain a sufficient reaction rate to oxidize $PbSO_4$ to PbO_2. In this study, the effect of the size of $PbSO_4$ on the oxidation of $PbSO_4$ to PbO_2 was investigated.

Experimental

A lead rod mounted in a teflon tube was used as the working electrode (purity:99.9%). This electrode was polished with emery paper and etched with dilute nitric acid. The lead electrode surface was oxidized to PbO_2 in 0.5 M† H_2SO_4 at 1 mA cm^{-2} for about 24 h, and then galvanostatically discharged at 1 mA cm^{-2} in 0.5 M H_2SO_4. The discharge-charge cycle was continued until the capacity of the PbO_2 electrode increased to 40 mA min.

Figure 1 shows the experimental cell used in this study. The PbO_2 electrode placed in it and discharged at a constant current. $PbSO_4$ crystals became deposited on its surface during the discharge. The surface $PbSO_4$ was oxidized to PbO_2 by utilizing the potential sweep method. Anodic sweeps from the rest potential after discharging toward the anodic direction at various sweep rates were carried out using a potentiostat (HOKUTO HA-301) and a function-generator (HOKUTO HB-104). The anodic currents were recorded with an X-Y recorder (WATANABE). A Hg/Hg_2SO_4 electrode was used as a reference electrode and a Pt wire was used as a counter electrode. All experiments were performed at 30 °C.

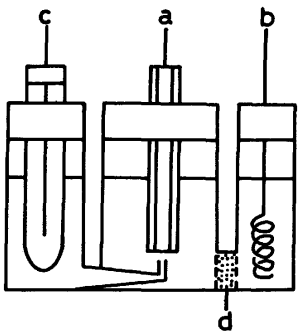

Fig. 1. Schematic representation of cell, a: working electrode (Pb; diameter=0.4 cm), b: counter electrode(Pt), c: reference electrode(Hg/Hg_2SO_4), d: fritted glass.

Results and Discussion

Figure 2 shows a potentiodynamic current-voltage curve for the oxidation of $PbSO_4$ to PbO_2 by the potential sweep method in 5.0 M H_2SO_4. $PbSO_4$ was formed by a potentiostatic discharge at 0.8 V vs. Hg/Hg_2SO_4 in 5.0 M H_2SO_4 until the cathodic current decreased to 0 mA. Two anodic peaks were observed at 1.0 and 1.43 V. The peak at 1.0 V corresponded to the oxidation of PbO to PbO_2.[12] The recovered electrode potential after the potentiostatic discharge was more cathodic than the redox potential of the $PbO_2/PbSO_4$ couple. The PbO_2/PbO redox potential was more cathodic than the $PbO_2/PbSO_4$ redox potential. The recovered redox potential may have been due to the mixed potential of the $PbO_2/PbSO_4$ and PbO_2/PbO

† 1 M=1 mol dm^{-3}.

couples. PbO is not thermodynamically stable in an acidic media. The local pH at the interior of the film formed by the potentiostatic discharge increased, since PbO is thermodynamically stable in the film. The PbO_2/PbO electrode potential at pH=9.34 was about 0.5 V vs. Hg/Hg_2SO_4. The electrode potential of the $PbO_2/PbSO_4$ couple was about 1.0 V vs. Hg/Hg_2SO_4 at pH=0.48.[13] Therefore, the recovered electrode potential was due to a mixed potential of the $PbO_2/PbSO_4$ and PbO_2/PbO couples. The peak at 1.43 V corresponded to the oxidation of $PbSO_4$ to PbO_2. The formation of PbO depended on the discharge conditions. PbO was formed by a deep discharge at a slow rate. In order to avoid the formation of PbO at the interior of $PbSO_4$, the electrode was discharged at a high rate, but not deeply. The potential after such a discharge recovered to the redox potential of the $PbO_2/PbSO_4$ couple. This fact indicates that PbO was not formed at the interior of the film. The oxygen evolution current was observed at 1.5 V and superimposed to the anodic current for the oxidation of $PbSO_4$ to PbO_2. In order to achieve clear curves for the oxidation of $PbSO_4$ to PbO_2, the current for the oxygen evolution was subtracted from the whole anodic current. The oxygen evolution current was determined from the potentiodynamic current-voltage curve by use of a fully charged electrode. Figure 3 shows potentiodynamic current-voltage curves which were obtained after the subtraction of the oxygen evolution current from the

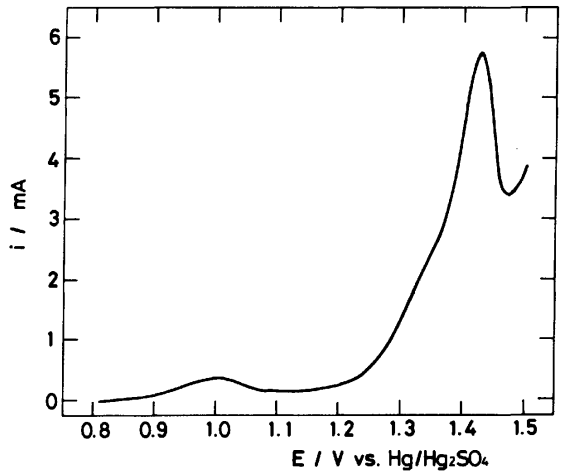

Fig. 2. Potentiodynamic current-voltage curve in 5.0 M H_2SO_4 of PbO_2 electrode discharged at 0.8 V vs. Hg/Hg_2SO_4 in 5.0 M H_2SO_4.

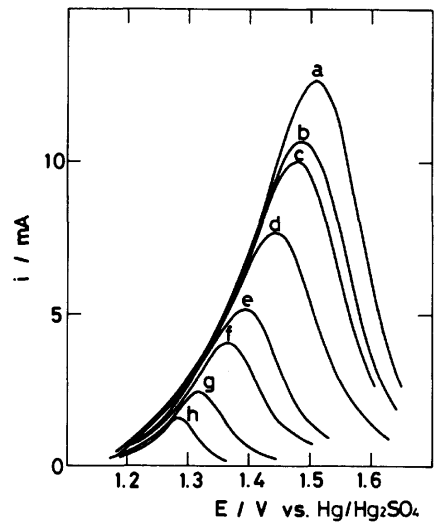

Fig. 3. Potentiodynamic current-voltage curves in 5.0 M H_2SO_4 of PbO_2 electrode discharged at 10 mA cm^{-2} in 5.0 M H_2SO_4, sweep rate a: 10, b: 8, c: 7, e: 3, f: 2, g: 1, h: 0.5 mV s^{-1}.

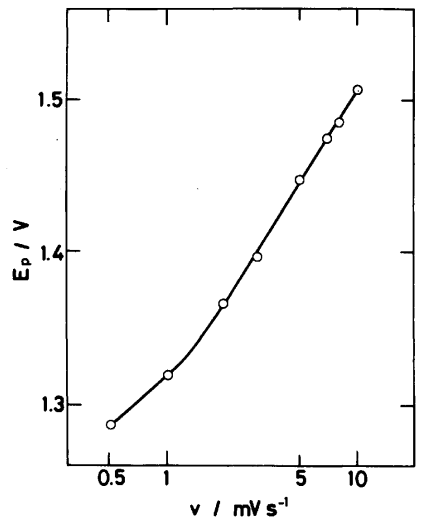

Fig. 4. Dependence of peak potential on sweep rate obtained from Fig. 3.

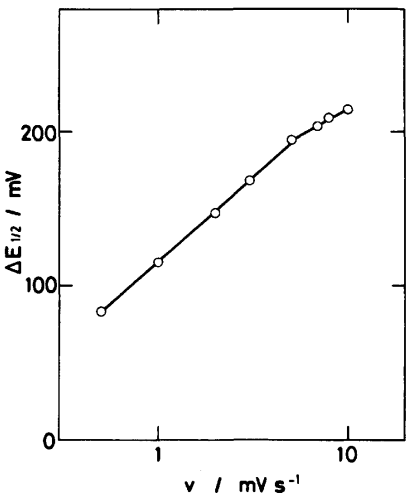

Fig. 5. Dependence of half-wave width on sweep rate obtained from Fig. 3.

whole anodic current. Symmetric current-potential curves were observed. Such curves are similar to those for a surface reaction rather than a diffusion-controlled electrode reaction.[14] Figure 4 shows the dependence of the peak potential on the sweep rate obtained from Fig. 3. The peak potential shifted to a more anodic potential upon increasing the sweep rate. Figure 5 shows the dependence of the half-wave width on the sweep rate (obtained from Fig. 3). The width became larger with increasing sweep rate. These results indicate that the charge-transfer process of the oxidation of $PbSO_4$ to PbO_2 is very slow. These dependences are very similar to those obtained for the irreversible electrode reaction of an adsorbed species on the electrode surface. Figure 6 shows the dependence of the peak current on the sweep rate (obtained from Fig. 3). The peak current was proportional to $v^{0.73}$. Such behavior regarding the oxidation of $PbSO_4$ to PbO_2 may be understood in terms of the electrochemistry of the adsorbed species on the electrode surface, if the $PbSO_4$ deposited on the electrode surface is a monolayer. $PbSO_4$ was deposited on the electrode surface as small ionic crystals. Therefore, it is very difficult to treat the oxidation of $PbSO_4$ to PbO_2 quantitatively in terms of the electrochemistry of adsorbed species, though the results shown in Figures 4, 5, and 6 were very similar to the irreversible electrode reaction of an adsorbed species on the electrode surface. In this study the electrode reaction of the conversion of $PbSO_4$ to PbO_2 was determined by an assumption regarding the reaction site (discussed below).

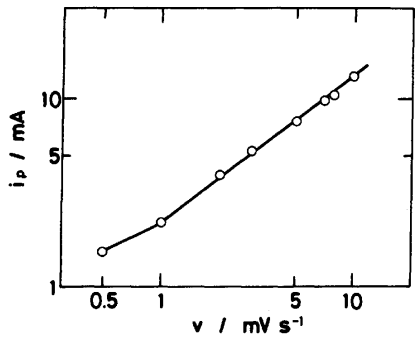

Fig. 6. Dependence of peak current on sweep rate obtained from Fig. 3.

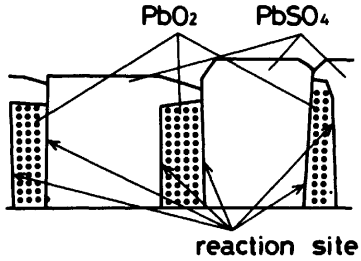

Fig. 7. Schematic representation of reaction site for charging reaction of $PbO_2/PbSO_4$ electrode.

A large ionic crystal without electronic and ionic conductivities would not be able to oxidize in the same way as soluble species. In the case of the oxidation of $PbSO_4$, the soluble species would be Pb^{2+} ions. The dissolving Pb^{2+} ions from a $PbSO_4$ crystal are oxidized to Pb^{4+} ions and react with H_2O to precipitate on the electrode surface as PbO_2:

$$Pb^{2+} + 2H_2O \longrightarrow PbO_2 + 2e^- + 4H^+. \quad (1)$$

Conditions for the oxidation of $PbSO_4$ are not equal over the electrode surface, causing the distribution of the oxidation rate of $PbSO_4$ to PbO_2. The high oxidation rate is sustained by the high concentration of Pb^{2+} ions on the PbO_2 surface. In this study, it is assumed that the interface between PbO_2 and $PbSO_4$ is the reaction site (Fig. 7). At such an interface, Pb^{2+} ions can be adequately supplied from the $PbSO_4$ crystal; also, a charge-transfer reaction can occur on PbO_2. The peak current was larger than that estimated from the solubility of Pb^{2+} ions and the diffusion coefficient in the electrodeposition layer of PbO_2 on a planar electrode in a sulfuric acid solution. If the oxidation of $PbSO_4$ occurs at the interface between $PbSO_4$ and PbO_2, the diffusion path is so short that the mass-transport process hardly influences the oxidation of $PbSO_4$. The potentiodynamic current-voltage curve in Fig. 3 can be explained as follows. As the electrode potential becomes more positive, the charge-transfer reaction rate increases, while the reaction site area decreases. The reaction rate depends on both the charge-transfer reaction rate and the reaction site area. If the oxidation of $PbSO_4$ proceeds with an increase and a decrease of the interface area between PbO_2 and $PbSO_4$, which corresponds to the reaction site area,[15] such a simple anodic peak could not be obtained. The reaction site area seems to decrease monotonously. Therefore, the maximum rate is obtained at the peak. The reaction-site area depends on the size of the $PbSO_4$ crystal since the interface area between PbO_2 and $PbSO_4$ per unit volume of $PbSO_4$ changes with this value. If the discharge capacity is the same, the surface area of $PbSO_4$ increases upon decreasing of the crystal size. As a result, the interface area between PbO_2 and $PbSO_4$ also increases upon decreasing the crystal size of $PbSO_4$.

Figure 8 shows electronmicrographs of $PbSO_4$ precipitated by galvanostatic discharges in 5.0 M H_2SO_4 at 0.5, 1.0, 5.0 and 10.0 mA cm^{-2}. The discharge was continued until it reached 600 mC cm^{-2}. The size of $PbSO_4$ decreased with increasing discharge current. The surface concentration of Pb^{2+} ions during the galvanostatic discharge depended on the discharge current. A large discharge current resulted

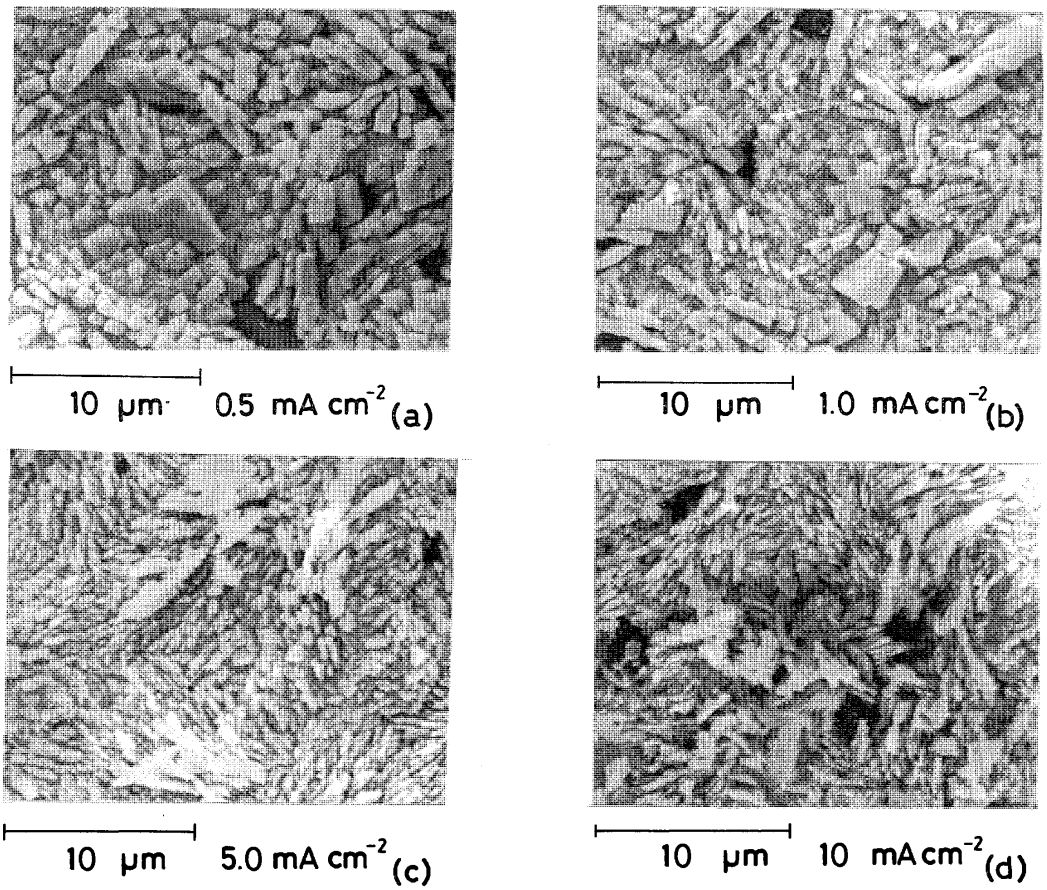

Fig. 8. Electronmicrographs of $PbSO_4$ precipitated by galvanostatic discharge at (a): 0.5 mA cm^{-2}, (b): 1.0 mA cm^{-2}, (c): 5.0 mA cm^{-2}, (d): 10.00 mA cm^{-2} in 5.0 M H_2SO_4, sweep rate 1 mV s^{-1}.

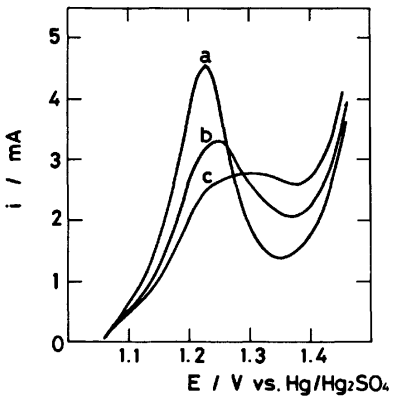

Fig. 9. Potentiodynamic current-voltage curves for the oxidation of $PbSO_4$ formed by galvanostatic discharge at 0.5, 1.0, and 10.0 mA cm^{-2} in 5.0 M H_2SO_4, sweep rate 1 mV s^{-1}.

in a large supersaturation of Pb^{2+} ions on the electrode surface and caused the formation of a lot of $PbSO_4$ nuclei. On the other hand, the large supersaturation of Pb^{2+} ions could not be caused by a small current discharge. Therefore, the crystal size of $PbSO_4$ increases with a decreasing discharge current.

Figure 9 shows potentiodynamic current-voltage curves for the oxidation of $PbSO_4$ formed by galvanostatic discharges at 0.5, 1.0 and 10.0 mA cm^{-2} in 5.0 M H_2SO_4. These discharges were continued until the current reached 1200 mC cm^{-2}. The anodic peak potential shifted to a more positive value upon decreasing the discharge current. This result indicates that the oxidation of $PbSO_4$ formed under a low discharge current is more difficult than that formed at a high discharge current. The size of $PbSO_4$ formed at a low discharge current was very large (Fig. 8). Increasing the size of $PbSO_4$ resulted in a decrease in the reaction-site area (as discussed above). Therefore, increasing the $PbSO_4$ crystal size caused difficulty regarding the oxidation of $PbSO_4$; also, the anodic peak potential shifted to more positive potentials. The shape of the anodic current peak obtained at a low current discharge was broad and nonsymmetrical. $PbSO_4$ may be oxidized with an increase and a decrease in the reaction-site area.[15] The oxidation of the very large $PbSO_4$ formed at a low discharge rate seems to be different from that of a small $PbSO_4$ crystal under high discharge rate.

Figure 10 shows electronmicrograhs of $PbSO_4$ crystals which were immersed in 5.0 M H_2SO_4 for a

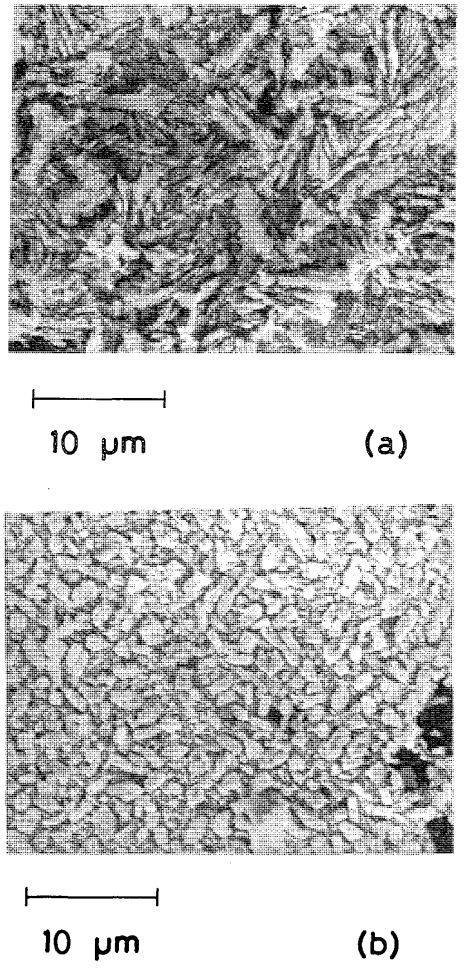

Fig. 10. Electronmicrographs of $PbSO_4$ precipitated by galvanostatic discharge at 1.0 mA cm^{-2} in 5.0 M H_2SO_4, immersion time (a): a few minutes (b): 60 min.

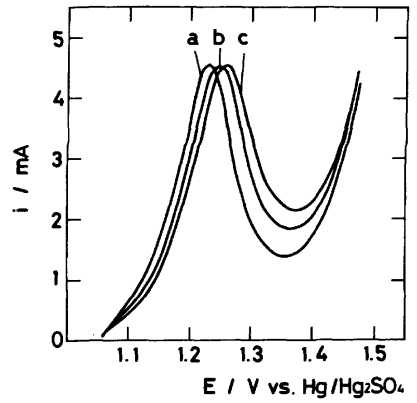

Fig. 11. Potentiodynamic current-voltage curves for the oxidation of $PbSO_4$ formed by galvanostatic discharge at 1.0 mA cm^{-2} in H_2SO_4 after immersion in 5.0 M H_2SO_4 for (a): a few minutes (b): 30 minutes (c): 60 minutes.

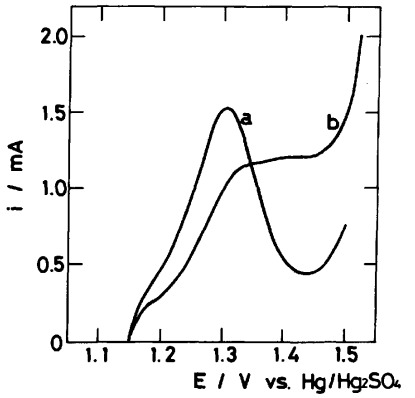

Fig. 12. Potentiodynamic current-voltage curves for the oxidation of $PbSO_4$ formed by galvanostatic discharge at 1.0 mA cm^{-2} for 60 s in 5.0 M and 0.5 M H_2SO_4, in 5.0 M H_2SO_4 at 1 mV s^{-1}.

few minutes or one hour after a discharge at 10 mA cm^{-2} in 5.0 M H_2SO_4. The electronmicrographs show that immersion after a discharge results in an increased size of a $PbSO_4$ crystal as the result of an aging process which involves a mass transfer from small crystals to large crystals by way of the solution. A high stability and a reduction of the surface area and energy were obtained by this aging process. The difference in crystal size between (a) and (b) was smaller than that shown in Fig. 8.

Figure 11 shows potentiodynamic current-voltage curves for the oxidation of $PbSO_4$ in Fig. 10. The anodic current peak for the oxidation of $PbSO_4$ after a one-hour immersion appeared at a more positive potential than that after a few minutes. The amount of $PbSO_4$ increased as the result of immersion in a sulfuric acid solution (Fig. 10). Increasing the crystal size resulted in a shift of the current peak shown in Fig. 11, since the reaction site per unit volume of the $PbSO_4$ crystal decreased.

Figure 12 shows potentiodynamic current-voltage curves for the oxidation of the $PbSO_4$ precipitated during a galvanostatic discharge at 10 mA cm^{-2} in 5.0 M and 0.5 M H_2SO_4 for 60 s. Both electrodes were oxidized in 5.0 M H_2SO_4 by a potential sweep method. The oxidation rate of $PbSO_4$ formed in 5.0 M H_2SO_4 was larger than that in 0.5 M H_2SO_4. The size of $PbSO_4$ depends on the concentration of the sulfuric acid solution (as discussed in previous paper [11]). In this case, the size of $PbSO_4$ formed in 5.0 M H_2SO_4 was less than that in 0.5 M H_2SO_4.

Thus, the reaction rate of the oxidation of $PbSO_4$ depends on the crystal size of $PbSO_4$ precipitated on the electrode surface during a discharge. The crystal size of $PbSO_4$ is very important for the oxidation of $PbSO_4$ to PbO_2. This fact indicates that the reaction site is the interface between $PbSO_4$ and PbO_2, at which a high reaction rate is sustained while allowing the oxidation of $PbSO_4$ to PbO_2.

References

1) P. Casson and N. A. Hampson, *J. Electroanal. Chem.*, **83**, 87 (1977).
2) S. G. Cangarayna, P. Casson, N. A. Hampson and K. Peters, *J. Electroanal. Chem.*, **79**, 281 (1977).
3) C. Lazarides, N. A. Hampson, and M. Henderson, *J. Appl. Electrochem.*, **11**, 605 (1981).
4) N. A. Hampson, S.Kelly, and K. Peters, *J. Appl. Electrochem.*, **10**, 261 (1981).
5) M. Fleischmann and H. R. Thirsk, *Trans. Faraday Soc.*, **151**, 1955 (1954).
6) M. Fleischmann and H. R. Thirsk, *Electrochimica Acta*, **1**, 146 (1959).
7) E. M. L. Valeriote and C. D. Gallop, *J. Electrochem. Soc.*, **124**, 370 (1977).
8) N. A. Hampson and J. B. Lakeman, *J. Electroanal. Chem.*, **107**, 177 (1980).
9) S. Webster, P. J. Mitchell, and N. A. Hampson, *Surface Technology*, **23**, 105 (1984).
10) P. Casson, S. G. Canagratna, N. A. Hampson and K. Peters, *J. Electroanal. Chem.*, **79**, 281 (1981).
11) Z. Takehara and K. Kanamura, *Electrochimica Acta*, **29**, 1643 (1984).
12) C. Lazarides and N. A. Hampson, *J. Power Sources*, **6**, 83 (1981).
13) P. Ruetschi, *J. Electrδchem. Soc.*, **120**, 331 (1973).
14) E. Laviron, "Electroanalytical Chemistry," ed by A. J. Bard, Marcel Dekker, New York (1982), Vol. 22, pp. 53—157.
15) Z. Takehara and K. Kanamura, *J. Electrchem. Soc.*, in press.

The Mechanism of Electron Transfer Reaction for Xanthene Dye-Sensitized Formation of Methyl Viologen Radical

Yoshiharu Usui,* Hiroaki Misawa,† Hirochika Sakuragi,† and Katsumi Tokumaru†
*Department of Chemistry, Faculty of Science, Ibaraki University, Mito 310
†Department of Chemistry, University of Tsukuba, Sakura-mura, Ibaraki 305
(Received June 5, 1986)

Sensitized reduction of methyl viologen, MV^{2+}, occurs efficiently through electron transfer from triplet xanthene dyes to MV^{2+} followed by electron transfer to the resulting semioxidized dyes from a reductant like triethanolamine. Unreactive ion pair complexes between these dyes and MV^{2+} are formed (formation constant: $1.2\times10^3\ M^{-1}$ for Eosine Y and MV^{2+} in 50% aqueous ethanol solution). The quantum yield for the reduced methyl viologen radical depends on the concentrations of MV^{2+} and the amine and on the ionic strength of solution. The efficiency of the electron transfer from triplet dyes to MV^{2+} is increased by addition of alcohol, and solvent effects on the reaction mechanism are discussed.

Active efforts have recently been devoted to the hydrogen liberation from water through visible light irradiation on an appropriate sensitizer in a suitable electron transferring system comprising an electron donor like amine, a mediator like methyl viologen, and a redox catalyst like colloidal platinum or hydrogenase.[1-5]

Although various sensitizers of ruthenium complexes have been well studied, only a few reports have appeared on utilization of organic dyes, and mechanistic studies on such reaction systems are required to increase the reaction yield.[6-16]

We reported that a photosensitized reaction of Eosine Y (EY^{2-}) induced hydrogen evolution from water under the irradiation of visible light on a mixed solution of methyl viologen (MV^{2+}), triethanolamine (TEOA), and colloidal platinum. The maximum quantum yield for the formation of semireduced radical ($MV^{+}\cdot$) was measured to be ca. 0.3.[17] For the three-component system, the yield of $MV^{+}\cdot$ is dependent on such a mechanism as may be switched over from an initial process of electron transfer from $^3EY^{2-}$ to MV^{2+} to that from TEOA to $^3EY^{2-}$. Further it has been observed that an ion pair complex is formed between xanthene dye and MV^{2+}, and that the complex formation is sensitive to the composition of solution.

In the present paper, attention is focused on determination of the efficiency of electron transfer processes from triplet dye to MV^{2+} and on the solvent effect in aqueous alcohol solution, in order to increase the yield of $MV^{+}\cdot$. To elucidate the reaction mechanism, we have mainly investigated effects of the concentrations of TEOA and MV^{2+} and the ionic strength and solvent composition of alcohol–water mixtures on the yield of $MV^{+}\cdot$ by kinetic analysis.

Experimental

Materials. Fluorescein, Eosine Y (2′,4′,5′,7′-tetrabromofluorescein), and Erythrosine (2′,4′,5′,7′-tetraiodofluorescein) were recrystallized three times from ethanol. Methyl viologen (1,1′-dimethyl-4,4′-bipyridinium dichloride, Nakarai, G. R.) and triethanolamine (Tokyo Kasei, G. R.) were used as received. Methanol, ethanol, and 2-propanol (Kanto, G. R.) were used without further purification. Phosphate and borate buffer solutions were prepared by dissolving the respective salts (Kanto, G. R.) in redistilled water. Sodium perchlorate (Kanto, G. R.) was used to control the ionic strength of sample solutions. Each sample was deaerated by bublling argon gas (99.9%) for at least 30 min or by repeating freezing and evacuation 5—7 times under vacuum before irradiation.

Procedures. A degassed sample in a cell (1 cm×1 cm×4 cm) was irradiated at 25 °C in a steady-light illumination apparatus with a 300 W tungsten lamp. The experimental procedure used to determine the quantum yield of $MV^{+}\cdot$ formation was similar to that previously described.[18,19] Laser flash photolysis was carried out by using a pulsed dye laser (Phase R, 2100B; dye, G4; excitation, 500 nm; FWHM of pulse, 500 ns) and a usual monitoring system composed of a light source, a monochromator, and a transient recorder. For the ns-laser excitation, pulsed nitrogen laser was used (excitation; 337 nm FWHM of pulse, 7 ns). The yield of $MV^{+}\cdot$ for the dye-laser flash excitation was determined by the conventional actinometry using Reinecke's salt.

Results and Discussion

Formation of Ionic Complex between EY^{2-} and MV^{2+} in the Ground State. It was observed that the absorption spectrum of EY^{2-} changed with an isosbestic point at 537 nm by addition of MV^{2+} in 50 v/v% aqueous ethanol solution, in such a manner that the maximum wavelength (λ_{max}) of EY^{2-} was shifted from 526 to 528 nm with the maximum extinction coefficient at λ_{max} decreased to 7.6×10^4 from 9.4×10^4 $M^{-1}\,cm^{-1}$ (1 M=1 mol dm^{-3}).[17] Also, the fluorescence of EY^{2-} was remarkably quenched by addition of 1.0×10^{-3} M MV^{2+}, but the fluorescence lifetime in solution was not affected at all. Increasing the alcohol content (95%) in the mixture made the fluorescence from EY^{2-} hardly observable. The degree of the change in absorption spectra and fluorescence intensities depended on the ionic strength, (μ) of solution and the solvent composition of alcohol–

Table 1. Formation Constants of the Ion-Pair Complex, $EY^{2-}\cdots MV^{2+}$ in 50 v/v% Ethanol

μ	K/M^{-1}
0.005	1.5×10^3
0.020	1.0×10^3
0.050	6.0×10^2
0.090	2.1×10^2

water mixture. In a mixed solvent with a molar fraction of ethanol (χ_{EtOH}) of 0.80, the maximum absorption and fluorescence intensities of EY^{2-} with 0.05 mM MV^{2+} were increased by the factors of 1.5 and 50, respectively, with increase in μ from 0 to 0.05. These phenomena mean that EY^{2-} forms a non fluorescent ionic complex with MV^{2+} and that the equilibrium, Eq. 1 is shifted to the right by increase in the molar fraction of ethanol or decrease in the ionic strength:

$$EY^{2-} + MV^{2+} \rightleftharpoons EY^{2-}\cdots MV^{2+} \quad (1)$$

From an analysis of the results of absorption and fluorescence spectra, values of the formation constant (K) for the complex were estimated at several values of ionic strength, as shown in Table 1.

Effects of MV^{2+} Concentration and Ionic Strength on the Quantum Yield of $MV^{+}\cdot$ Formation. For the three-component system of $EY^{2-}/MV^{2+}/TEOA$, either the initial electron transfer from triplet eosine Y ($^3EY^{2-}$) to MV^{2+} or that from TEOA to $^3EY^{2-}$ needs to be considered. The competitive reactions can be switched over between each other depending on the rate constants and the concentrations of TEOA and MV^{2+}.[20] The rate constant of the $^3EY^{2-}$ quenching with MV^{2+} or with TEOA was obtained as 3.2×10^9 (k_Q) or $3.0\times10^6\ M^{-1}\ s^{-1}$ in a laser-flash experiment, respectively ([EY^{2-}]=10 μM, μ=0.05, 50 v/v% ethanol-water mixture). The rate constant of the $MV^{+}\cdot$ formation was also obtained as $3\times10^9\ M^{-1}\ s^{-1}$ (k'_Q) in the $^3EY^{2-}$ reaction with MV^{2+} and was approximately the same as the quenching rate constant. Thus, at an MV^{2+} concentration of about 1 mM and a TEOA concentration of 10 mM, the photosensitized reduction of MV^{2+} is to be initiated by the efficient electron transfer from $^3EY^{2-}$ to MV^{2+}, which leads to formation of $EY^{-}\cdot$ followed by the electron transfer from TEOA.

In the laser flash experiment with an aerated solution of EY^{2-} and MV^{2+} where $MV^{+}\cdot$ was scavenged by oxygen, only transient absorption of $EY^{-}\cdot$ was observed after about 30 μs. The decay rate of free radical $EY^{-}\cdot$ (λ_{max}=462 nm) was increased by the addition of TEOA, and the rate constant (k) of the electron transfer from TEOA to $EY^{-}\cdot$ was obtained as $k=1.5\times10^7\ M^{-1}\ s^{-1}$.

For a steady light irradiation, the dependence of the quantum yield for $MV^{+}\cdot$ radical formation (Φ_{mv}) on the MV^{2+} concentration showed a maximum of 0.2 at an MV^{2+} concentration of ca. 1 mM in aqueous ethanol with a constant ionic strength and a fixed concentration of TEOA (Fig. 1). The concentration of the EY^{2-} complexed with MV^{2+} noted on the upper abscissa in Fig. 1 was calculated from the K values in Table 1. It can be considered that the decreasing tendency of Φ_{mv} values at higher concentrations of MV^{2+} (> ca. 3 mM) is due to the fact that EY^{2-} forms an ion-pair complex with MV^{2+} and that this complex is unreactive. Actually, the transient absorption of $MV^{+}\cdot$ was scarcely observed by the μs-laser flash excitation of the complex.

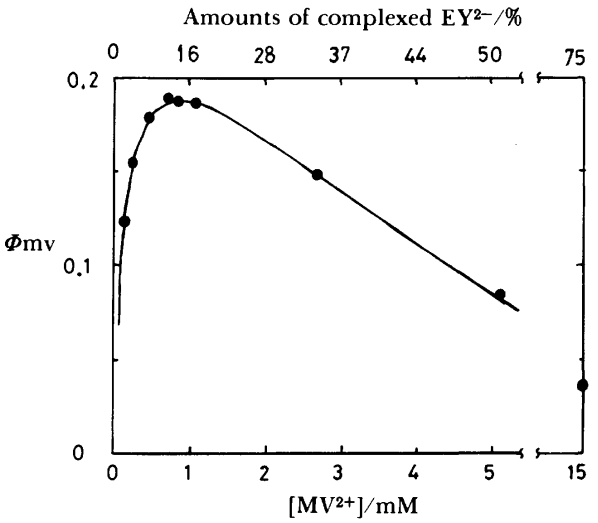

Fig. 1. Effect of MV^{2+} concentration on the quantum yield of $MV^{+}\cdot$ formation. [EY^{2-}]=17 μM, [TEOA]= 10 mM, μ=0.08, pH=11.7, in 40% Ethanol-water mixture.

In an air saturated solution of EY^{2-} and MV^{2+} ([EY^{2-}]=4.85 μM, [MV^{2+}]=0—5 mM, [O_2]=220 μM, pH=5, μ=0.004, 50 v/v% ethanol-water mixture), the photobleaching of EY^{2-} was accelerated by the addition of MV^{2+}. Considering that the $MV^{+}\cdot$ radical produced by the electron transfer from $^3EY^{2-}$ is fairly reactive to the dissolved oxygen ($MV^{+}\cdot + O_2 \rightarrow MV^{2+} + O_2^{-}\cdot$; $k'=6\times10^8\ M^{-1}\ s^{-1}$),[21] the reverse electron transfer to the resulting $EY^{-}\cdot$ from $MV^{+}\cdot$ can be taken to be prohibited. Thus, it is supposed that the acceleration of EY^{2-} bleaching is attributed to the irreversible decomposition of semioxidized radical, $EY^{-}\cdot$.[20] The dependence of the bleaching yield on the MV^{2+} concentration was the same as that shown in Fig. 1, and the contribution of the unreactive ionic pair complex is supposed similar. Figure 2 shows the pH effect on Φ_{mv} which is enhanced in alkaline solution. The production yield of $^3EY^{2-}$ does not seem to undergo a significant change in the pH region.[20] We also confirmed that the equilibrium of

the ionic complex of Eq. 1 was not affected by the change in pH because similar K values were obtained in the pH region from 5.4 to 11.4 (μ=0.05, 50 v/v% ethanol-water mixture). Judging from the property of TEOA that electron donation is effective in its basic form (pK_a (protonated TEOA)=7.76), the curve in Fig. 2 seems to match the result on the dissociation of protonated TEOA.

Figure 3 shows the effect of ionic strength, μ, on Φ_{mv} at two MV^{2+} concentrations. In the case where EY^{2-} and MV^{2+} exist free at the lower concentration of MV^{2+} (0.2 mM), the decrease in Φ_{mv} in Fig. 3 is due to a neutral salt effect on the competetive reactions between $^3EY^{2-}$ and MV^{2+} since the rate constant decreases with increasing μ.[22] At the higher concentration of MV_2^+ (5.7 mM) where 50% of EY^{2-} forms the ion-pair complex, it was suspected that the Φ_{mv} value increased as a result of the dissociation of the unreactive complex to the free EY^{2-} and MV^{2+} caused by increase in μ as shown in Table 1. Considering both of the opposite effects, i.e., the neutral salt effect and the dissociation of the ion-pair complex, the small effect observed at the MV^{2+} concentration of 5.7 mM can be interpreted in terms of the mutual compensation of these effects.

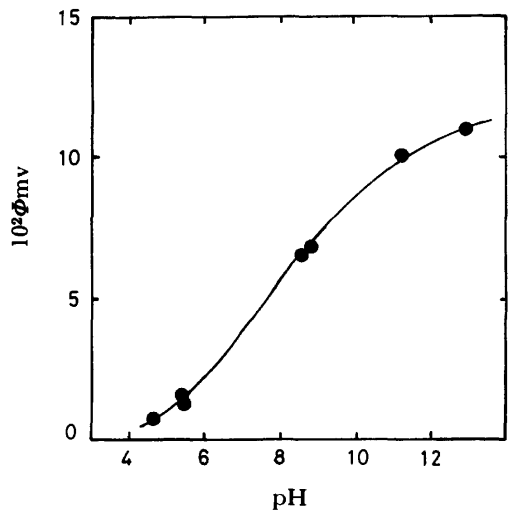

Fig. 2. Effect of pH on the quantum yield of $MV^{+}\cdot$ formation. [EY^{2-}]=17 μM, [MV^{2+}]=5.7 mM, [TEOA]= 10 mM, in 40% Ethanol-water mixture.

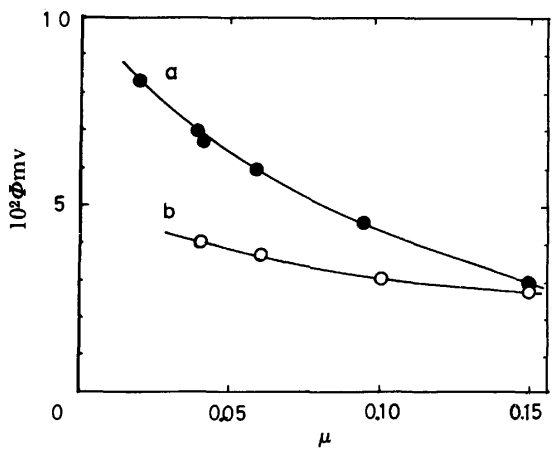

Fig. 3. Effect of ionic strength on the quantum yield of $MV^{+}\cdot$ formation. (a) [MV^{2+}]=0.2 mM, (b) [MV^{2+}]=5.7 mM. [EY^{2-}]=17 μM, [TEOA]=10 mM, in 40% Ethanol-water mixture.

Efficiency of Electron Transfer from Triplet Eosine Y to Methyl Viologen. Kinetic investigations for the efficiency of the initial electron transfer from $^3EY^{2-}$ to MV^{2+} existing in the free form were carried out to increase the sensitization yield. Scheme 1 shows the electron-transfer mechanism proposed as applicable to the present system by reference to the investigations reported by Harriman et al.[12,22-25]

$$^3EY^{2-} + MV^{2+} \underset{k_{DS}}{\overset{k_{DF}}{\rightleftharpoons}} (^3EY^{2-}\ MV^{2+})$$

$$\downarrow k_A$$

$$EY^{-}\cdot + MV^{+}\cdot \underset{k_C}{\overset{k_{-C}}{\rightleftharpoons}} {}^{1,3}(EY^{-}\cdot\ MV^{+}\cdot) \xrightarrow{k_B} EY^{2-} + MV^{2+}$$

$$k_Q{}^r = \frac{k_{DF}k_A}{k_A + k_{DS}} \quad (2)$$

$$k_b = \frac{k_{-C}k_B}{k_B + k_C} \quad (3)$$

Scheme 1.

The formation of an encounter complex ($^3EY^{2-}$ MV^{2+}) is to be a diffusion controlled process (k_{DF}), which is reversible (k_{DS}). The complex undergoes an electron transfer to form a geminate radical pair of $^{1,3}(EY^{-}\cdot\ MV^{+}\cdot)$, which can be regarded as an exciplex with a radical-pair-like electronic structure.[24,25] This complex may collapse either to give the radical ions through a separation (k_C) followed by a recombination (k_{-C}), or to reform the ground states of EY^{2-} and MV^{2+} (k_B). The yield of free radical $MV^{+}\cdot$ or $EY^{-}\cdot$ (ϕ_{mv}) is given by[23,24]

$$\phi_{mv} = \phi_{st}\phi_Q\phi_S \quad (4)$$

where ϕ_{st}, ϕ_Q, and ϕ_s refer to the probabilities of the intersystem crossing to $^3EY^{2-}$ (0.64),[26,27] the quenching of $^3EY^{2-}$ by MV^{2+} to give the geminate radical pair with $\phi_Q = k_Q^r[MV^{2+}]/(k_Q[MV^{2+}]+\tau_T^{-1})$, and the formation of the free radicals from $^{1,3}(EY^{-}\cdot MV^{+}\cdot)$ with $\phi_s = k_C/(k_C+k_B)$, respectively. The lifetime of $^3EY^{2-}$(τ_T) is equal to 220 μs at [EY^{2-}]=10 μM. On the assumption that the rate constant $k_Q{}^r$ ($=k_{DF}k_A/(k_A+k_{DS})=3.0\times10^9\ M^{-1}\ s^{-1}$) as obtained from the ns laser experiment corresponds to the process of $^{1,3}(EY^{-}\cdot MV^{+}\cdot)$ formation, ϕ_Q can be estimated to be 0.94 for the present condition ([MV^{2+}]=0.05 mM) from the observed values of k_Q^r, k_Q, and τ_T, where k_Q^r and k_Q

are the rate constants for the genuine and total reactions between $^3EY^{2-}$ and MV^{2+}, respectively. These rate constants are numerically almost equal to each other as described in a previous section (i.e., $k_Q^r \approx k_Q$). The absorption by $MV^{+}\cdot$ observed in the μs and ms time regions will arise from the free species of $MV^{+}\cdot$ dissociated from $^{1,3}(EY^{-}\cdot\ MV^{+}\cdot)$. Since $EY^{-}\cdot$ is completely reduced by the addition of 10 mM TEOA and $MV^{+}\cdot$ does not decrease, ϕ_{mv} can be obtained from the concentration of $MV^{+}\cdot$ produced per laser pulse. Thus, we can estimate the value of ϕ_s (=0.53) from Eq. 4 and the ratio of k_C/k_B(=1.1) by using the value of the maximum yield of the sensitized $MV^{+}\cdot$ formation (0.32) in 50 v/v% ethanol and water mixture. On the other hand, assuming the diffusion controlled process with k_{-C}(=1.2×10^{10} M^{-1} s^{-1}) and substituting the rate constant k_b (=2.9×10^9 M^{-1} s^{-1}) from the recombination kinetics of the free $EY^{-}\cdot$ and $MV^{+}\cdot$ radicals into the equation of $k_b=k_{-C}/(1+(k_C/k_B))$ we obtain a similar value for the ratio of k_C/k_B(=1—3). These results mean that $^{1,3}(EY^{-}\cdot\ MV^{+}\cdot)$ complex dissociates to the free radicals or to the molecules of ground state to a comparable extent.

The decay processes through the recombination of the free radical ions $EY^{-}\cdot$ (λ_{max}=462 nm, $\varepsilon_{max}=5.5\times10^4$ M^{-1} cm^{-1})[28] and $MV^{+}\cdot$ (λ_{max}=395 nm, $\varepsilon_{max}=4.2\times10^4$ M^{-1} cm^{-1})[29] followed by the dissociation of $^{1,3}(EY^{-}\cdot\ MV^{+}\cdot)$ complex, were monitored under various reaction conditions in a laser flash experiment in the μs region and analyzed in terms of the second-order reaction kinetics to evaluate k_b for the $EY^{-}\cdot$ decay as 4.7×10^9 M^{-1} s^{-1} and that for the $MV^{+}\cdot$ decay as 5.1×10^9 M^{-1} s^{-1} (in 60 v/v% CH_3OH-H_2O, μ=0.02). There was no permanent production of $MV^{+}\cdot$ or $EY^{-}\cdot$ radical in the EY^{2-}/MV^{2+} system by irradiation. Incidentally, it was ascertained that the observed decay process did not correspond to the recombination to the geminate radical pair $^3(EY^{-}\cdot\ MV^{+}\cdot)$, because the decay data hardly satisfy the root equation for the kinetical treatment on the geminate pair in the μs-region.[30]

Values of k_b depend on the solvent composition of binary mixtures of methanol-water, ethanol-water, 2-propanol-water, and ethylene glycol-water, in such a manner that the k_b values decrease initially in regard to the molar fraction of alcohol and then increase gradually. As shown in Fig. 4, the plot of k_b against the reciprocal of solvent viscosity (η) satisfies a linear relationship. Even if the processes designated the rate constants of k_B and k_C result from the local diffusion of each paired radical in a cage to the bulky phase, this viscosity effect will be cancelled out in the expression of Eq. 3 so as to be negligible for the k_b value itself. On the other hand, the polarity effect of solvent is supposed to be in corporated in the k_B value, which will be discussed in a later section. It is known that there is no considerable change in the solvent polarity

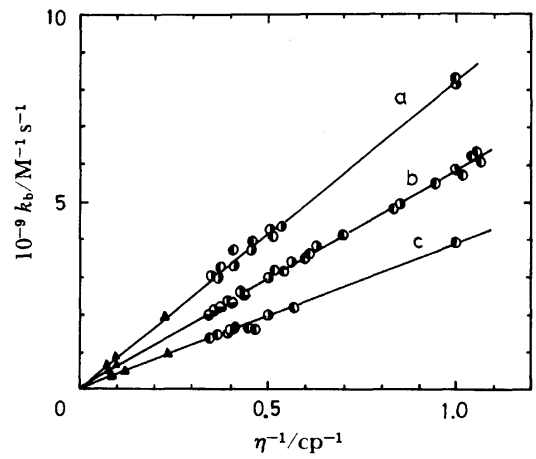

Fig. 4. Solvent viscosity effect on k_b values. (a): Erythrosine/MV^{2+} system, (b): Eosine Y/MV^{2+} system, (c): Fluorescein/MV^{2+} system([NaOH]=0.5 mM). [Dye]=10 μM, [MV^{2+}]=0.05 mM, μ=0.02; Methanol-water mixture(◑), Ethanol-water mixture(◐), 2-Propanol-water mixture(◒), Ethylene glycol-methanol mixture(▲).

of dielectric constant or in the empirical solvent parameters such as Kosowar's Z-value for such a mixture of methanol and ethylene glycol. However, since the linear relationship between k_b and η^{-1} in the methanol and ethylene glycol mixture is the same as that for the alcohol and water mixture, and since the polarity change in the latter mixture is not so large in the region $\chi_{alc}<0.7$, it is considered that the diffusional recombination process between $EY^{-}\cdot$ and $MV^{+}\cdot$ with k_{-C} (=$8RT/3000\eta$) will reflect the viscosity effect on k_b values in the expression of $k_b=k_{-C}/(1+(k_C/k_B))$. Such linear relationships were observed with the Eosine Y-MV^{2+}, Erythrosine-MV^{2+}, and fluorescein-MV^{2+} systems. This result seems to confirm that the observed decay processes correspond to the diffusional recombinations between the free radical ions.

Solvent Effect on ϕ_{mv} Values. Since the quantum yield of hydrogen evolution for the three-component system with a catalyst was increased by the addition of methanol or ethanol, the dependence of ϕ_{mv} after the laser excitation (about 30 μs) on the concentration of methanol, ethanol, or 2-propanol was investigated. ϕ_{mv} values are increased by the addition of each alcohol as shown in Figs. 5a and 5b. The yield for $EY^{-}\cdot$ increased in a similar manner.

The results shown in Figs. 5a—c refer to the solvent effect on ϕ_{mv} and the second shows the difference in ϕ_{mv} among the dye sensitizers. On the basis of the fact that the effect of alcohol addition on ϕ_{st} is negligible[20,26,27] and on the assumption that the effect on ϕ_Q is negligible, the first effect could result from the ϕ_s in Eq. 4. From the view point that the free radicals are produced by the separation of the

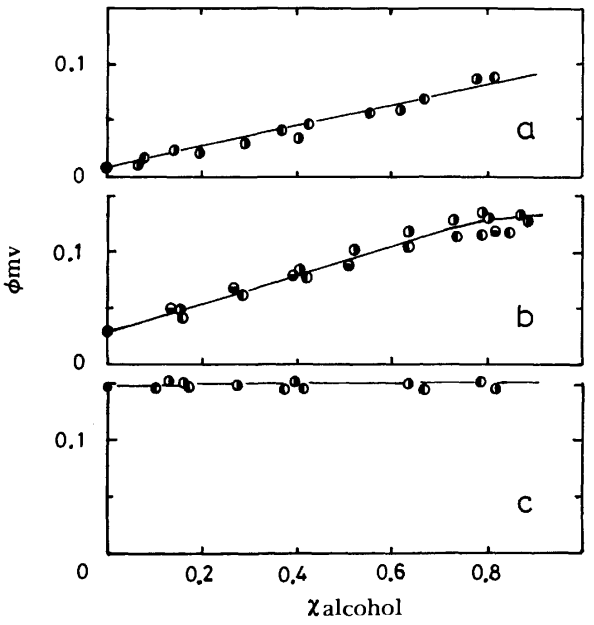

Fig. 5. Effect of molar fraction (χ) of alcohol on the yield of $MV^{+}\cdot$, ϕ_{mv}. (a) Erythrosine/MV^{2+} system, (b) Eosine Y/MV^{2+} system, (c) Fluorescein/MV^{2+} system([NaOH]=0.5 mM). [Dye]=10 μM, [MV^{2+}]= 0.05 mM, μ=0.02; Methanol-water mixture (◑), Ethanol-water mixture(◐), 2-Propanol-water mixture(◒).

geminate radical pair in competition with the decay process as discussed in respect of Scheme 1, a similar explanation as reported by Winter and Steiner can be applied in terms of the solvent polarity dependence of the energy gap between the exciplex and the corresponding Franck-Condon ground state.[32] Thus, the observed effect on ϕ_{mv} is determined by two decay constants for the exciplex as

$$\phi_{mv} = \phi_{st}\phi_Q \frac{k_C}{k_B + k_C} \quad (5)$$

$$= \phi_{st}\phi_Q \left(1 + \frac{F_{el}F_{FC}}{k_C}\right)^{-1} \quad (6)$$

where k_b is a product of a factor F_{el} (the electronic coupling strength) and a factor F_{FC} which is determined mainly by the Franck-Condon weighted density of vibrationally excited ground state levels isoenergitic with the exciplex; $k_B = F_{el}F_{FC}$. If the analysis for ϕ_{mv} discloses no significant influence of solvent on k_C, the radical yield ϕ_{mv} may be concluded to be determined mostly by the factor F_{FC}.

Since the explanation for the polarity dependence in the presence of alcohol added calls for F_{FC} or k_B to be small, it may be expected that ϕ_{mv} becomes large because of the lesser polarity of alcohol. As shown in Fig. 5, such solvent effects are found in the systems of EY^{2-} and MV^{2+} and of Erythrosine and MV^{2+}. In the system of fluoresceine and MV^{2+} shown in Fig. 5c, the solvent effect is little observed and ϕ_{mv} value are larger than those in the other systems.

In the systems of EY^{2-}/MV^{2+} and Ery^{2-}/MV^{2+}, the correlations of ϕ_{mv} with the solvent parameter of Kosowar's Z are similar to each other in both the methanol-water and ethanol-water mixtures. In relation to the solvent dependence on the ionic photodissociation yield in the singlet exciplex state (for example, pyrene and *N,N*-dimethylaniline), the radical yield increased with the solvent dielectric constant (ε) and a quantitative analysis for the mechanism was carried out.[33] In the present case, ϕ_{mv} decreases with ε values of alcohol-water mixtures and the mechanism differs from the case involving the singlet excited state. From a variation of solvent viscosity in the range 1—3 cp effected by mixing methanol, ethanol, or 2-propanol with water, the viscosity dependence may be expected to appear on k_C and accordingly on ϕ_{mv}. However, the effect of viscosity was observed as a decrease in ϕ_{mv} beyond ca. 4 cp.

A second effect on ϕ_{mv} values in Fig. 5 may be derived by making a comparison between the heavy-atom-substituted sensitizers (Br, I). A similar heavy atom effect was reported with thiopyronine reduction by substituted electron donors (Br, I).[32] In the present case, ϕ_{mv} values are 0.12 for fluorescein, 0.090 for Eosine Y, and 0.055 for Erythrosine ([MV^{2+}]=0.05 mM, μ=0.02, χ_{MeOH}=0.5). It is known that ϕ_{st} values of dyes increase in the order: $\phi_{st}(Ery^{2-}) > \phi_{st}(EY^{2-}) > \phi_{st}(Fl^{2-})$.[20] To interpret the order: ϕ_{mv} (Ery^{2-})< $\phi_{mv}(EY^{2-}) < \phi_{mv}(Fl^{2-})$ as obtained from Figs.5a—c at a given molar fraction of alcohol on the basis of Eq. 2, ϕ_s values of dyes must taken to be in the same order with more decrease than the change in the respective ϕ_{st} values: $\phi_S(Ery^{2-}) < \phi_s(EY^{2-}) < \phi_s(Fl^{2-})$. Since the k_b values for the Ery^{2-}/MV^{2+}, EY^{2-}/MV^{2+}, and Fl^{2-}/MV^{2+} systems decrease in the order listed, k_C/k_B and then ϕ_{mv} values should increase in the same order, in conformity with the above results on ϕ_{mv} values. However, further investigations for the effects of solvent viscosity and polarity and the heavy atom associated with spin conversion on the dissociation of $^{1,3}(Dye^{-}\cdot\ MV^{+}\cdot)$ are required for quantitative interpretation.

Electron Donation to Semioxidized Eosine. In an alkaline deaerated aqueous solution of EY^{2-} and MV^{2+} without TEOA, sensitized production of $MV^{+}\cdot$ was observed by means of stationary illumination, although the yield was very low as shown in Table 2. The electron donative reaction from OH^{-} ion to $EY^{-}\cdot$ may be possible to produce an adduct $EYOH^{2-}\cdot$ from $OH\cdot$ and EY^{2-}, since $EY^{-}\cdot$ is a strong oxidant ($E^0(EY^{-}\cdot/EY^{2-}) = 1.1$ V NHE).[34-37] The possibility of the above process is experimentally suggested from: (i) the decay rate of $EY^{-}\cdot$ is enhanced by the addition of OH^{-} ion and the rate constant is about 10^5 M^{-1} s^{-1}; (ii)

Table 2. Quantum Yield of $MV^{+}\cdot$ Formation in Alkaline Solution[a)]

[NaOH]/mM	χ_{CH_3OH}	Φ_{mv}
10	0	0.0021
10	0.23	0.0058
50	0.40	0.042
100	0.51	0.067

a) $[EY^{2-}]=10\,\mu M$ and $[MV^{2+}]=0.05$ mM. χ_{CH_3OH}: mole fraction of methanol.

a transient spectrum (λ_{max}=600 nm, $\tau_{1/2}$=4.4 ms) is observed which is similar to that of $EYOH^{2-}\cdot$ reported by Grossweiner et al. as a result of pulse radiolysis experiment;[38] (iii) the spectrum of $EYOH^{2-}\cdot$ disappeared after reaction with methanol, with simultaneous increase in the permanent yield of $MV^{+}\cdot$, Φ_{mv}. The above phenomenon (iii) suggests that the competetive recombination between $EYOH^{2-}\cdot$ and $MV^{+}\cdot$ is prohibited by the addition of methanol, and thus that the reaction process of $EYOH^{2-}\cdot$ with methanol causes the yield to increase as shown in Table 2.

The authors wish to express their thanks to Mr. Yoshio Takada for his contribution to the work. This work was supported by a Grant-in-Aid for Special Project Research (No. 61123001) from the Ministry of Education, Science and Culture.

References

1) N. Sutin and C. Creutz, *Pure Appl. Chem.*, **52**, 2717 (1980).
2) D. G. Whitten, *Acc. Chem. Res.*, **13**, 83 (1980).
3) M. Grätzel, *Acc. Chem. Res.*, **14**, 376 (1981).
4) M. Rougee, T. Ebbesen, F. Ghetti, and V. Besasson, *J. Phys. Chem.*, **86**, 4404 (1982).
5) J. K. Fendler, *J. Phys. Chem.*, **89**, 2730 (1985).
6) N. Kamiya and M. Okawara, *Kogyo Kagaku Zasshi*, **72**, 96 (1969).
7) J. S. Bellin, R. Alexander, and R. D. Mahoney, *Photochem. Photobiol.*, **17**, 17 (1973).
8) K. Kalyanasundaram and M. Grätzel, *J. Chem. Soc., Chem. Commun.*, **1979**, 1137.
9) A. I. Krasna, *Photochem. Photobiol.*, **29**, 267 (1979); **31**, 75 (1980).
10) K. Kalyanasundaram and D. Dung, *J. Phys. Chem.*, **84**, 2551 (1980).
11) M. S. Chan and J. R. Bolton, *Photochem. Photobiol.*, **34**, 537 (1981).
12) A. Harriman, G. Porter, and M-C. Richoux, *J. Chem. Soc., Faraday Trans. 2*, **77**, 833 (1981).
13) D. L. Roux, J-C. Mialoco, O. Anitoff, and G. Folcher, *J. Chem. Soc., Faraday Trans. 2*, **80**, 909 (1984).
14) I. Tabushi and A. Yazaki, *J. Org. Chem.*, **46**, 1899 (1981).
15) K. Hashimoto, T. Kawai, and T. Sakata, *Chem. Lett.*, **1983**, 709.
16) A. W-H. Mau, O. Johansen, and W. H. F. Sasse, *Photochem. Photobiol.*, **41**, 503 (1983).
17) H. Misawa, H. Sakuragi, Y. Usui, and K. Tokumaru, *Chem. Lett.*, **1983**, 1021.
18) Y. Usui and K. Saga, *Bull. Chem. Soc. Jpn.*, **55**, 3302 (1982).
19) Y. Usui, *Bull. Chem. Soc. Jpn.*, **38**, 206 (1965).
20) M. Koizumi, S. Kato, T. Matsuura, N. Mataga, and Y. Usui, "Photosensitized Reduction," Kagaku Dojin, Kyoto (1978).
21) T. W. Ebbesen, B. L. Tembe, and J. J. Kozak, *J. Phys. Chem.*, **88**, 683 (1984).
22) M-C. Richoux ans A. Harriman, *J. Chem. Soc., Faraday Trans. 1*, **78**, 1873 (1982).
23) A. Harriman, G. Porter, and A. Wilowska, *J. Chem. Soc., Faraday Trans. 2*, **79**, 807 (1983).
24) A. Harriman, G. Porter, and A. Wilowska, *J. Chem. Soc., Faraday Trans. 2*, **80**, 191 (1984).
25) T. Ohno and N. N. Lichtin, *J. Phys. Chem.*, **86**, 354 (1982).
26) N. Nemoto, K. Kokubun, and M. Koizumi, *Bull. Chem. Soc. Jpn.*, **42**, 2464 (1969).
27) S. Gohda, H. Yamazaki, K. Morishige, F. Kitade, and Y. Nishikawa, *Nippon Kagaku Kaishi*, **1984**, 1383.
28) V. Kashe and L. Lindqvist, *Photochem. Photobiol.*, **4**, 923 (1965).
29) T. Watanabe and K. Honda, *J. Phys. Chem.*, **86**, 2617 (1982).
30) H. Sano and M. Tachiya, *J. Chem. Phys.*, **71**, 1276 (1979).
31) H. Misawa, Ph. D. Thesis in Univ. of Tsukuba, Chap. 3 (1984).
32) G. Winter and U. Steiner, *Ber. Bunsenges. Phys. Chem.*, **84**, 1203 (1980).
33) H. Masuhara and N. Mataga, *Acc. Chem. Res.*, **14**, 312 (1981).
34) R. O. Loutfy and J. H. Sharp, *Photogr. Sci. Eng.*, **20**, 165 (1976).
35) J. Moser and M. Grätzel, *J. Am. Chem. Soc.*, **106**, 6577 (1984).
36) W. H. Koppenol and J. F. Liebman, *J. Phys. Chem.*, **88**, 99 (1984).
37) I. S. Schegoleva and T. S. Glikman, *High Energy Chem.*, **7**, 392 (1973).
38) J. Chrysochoos, J. Ovadia, and L. I. Grossweiner, *J. Phys. Chem.*, **71**, 1629 (1967).

 © 1987 The Chemical Society of Japan Bull. Chem. Soc. Jpn., 60, 1579—1583 (1987)

Liquid-Phase Hydration of Acrylonitrile to Acrylamide over the Copper-Nickel Alloy Catalysts

Kazuo SUGIYAMA,* Hiroshi MIURA, Yoshichika WATANABE, Yasunori UKAI, and Tsuneo MATSUDA
Department of Applied Chemistry, Faculty of Engineering, Saitama University, Shimo-okubo, Urawa 338
(Received September 6, 1986)

The liquid-phase hydration of acrylonitrile to acrylamide has been examined over various metal catalysts at 75 °C. Five metal elements-Cu, Ag, Fe, Co, and Ni-showed the catalytic conversion of acrylonitrile. The Cu and Ag catalysts gave the acrylamide with a 100% selectivity, while the other metals, Fe, Co, and Ni, yielded three products: acrylamide, ethylene cyanohydrin, and bis(2-cyanoethyl) ether. The alloying of Cu and Ni led to an increase in the formation of acrylamide with keeping the high selectivity to acrylamide. Especially, Cu-Ni alloys, with a range of 20—70% Cu in their bulk composition, were much more active catalysts than Cu. The maximum yield of acrylamide was obtained on the Cu-Ni alloy catalysts was observed, although such a retardation occurred on the Cu catalyst surface. The maximum synergistic effect was observed over the alloy with the surface component ratio of Cu to Ni of 4; this effect was discussed.

In relation to the liquid-phase hydration of acrylonitrile(AN) over various metal oxides or metals, it has been found that acrylamide(AA), ethylene cyanohydrin(ECH), and bis(2-cyanoethyl) ether(BCE) are chiefly produced.[1] Commercially available AA, which is used as paper-strengthening agents and flocculants etc., can be obtained by the selective hydration of the cyano group in an AN molecule. This hydration is effectively catalyzed by a metallic Cu such as the Cu prepared by reduction with H_2, Raney and Ullmann Cu.[2-4]

It is known that the catalytic hydration processes using metallic Cu catalysts have a number of excellent characteristics, such as simplicity of outline, easy handling, and the absence of any by-product formation.[5] A modification of the catalysts is rather effective if one aims to study the improvement of the hydration process. In the investigation of the basic design of highly active catalysts on AA production, as has been reported in a previous paper,[6] we recently found out that Ni-enriched Cu-Ni alloys had more ability for the AA formation than did the Cu catalysts in the liquid-phase hydration of AN. In this paper, the synergistic effect of Cu and Ni on the AA formation will be reported.

Experimental

Catalyst Preparation: The Cu-Ni alloys employed in this work were prepared by the reduction of the oxides obtained by the thermal decomposition, in air, of the Cu-Ni carbonates coprecipitated from their nitrates in aqueous solutions; this was done in the manner described by a number of workers.[7-11] In a typical preparation of the present investigation, a 5 wt% Na_2CO_3 aqueous solution was slowly added to a 0.5 M solution of mixed nitrates (Kanto Chemicals), keeping it at 32 °C, until the pH value of 9.5 was reached; and the suspension was then stirred for 1 h and left to stand overnight. After the resulting slurry has been filtered, the precipitate was washed with a large amount of ion-exchanged water until the pH value of the filtrate attained 8.0. The mixed carbonate was dried overnight at 120 °C and then calcined in air for 3 h at 300 °C. The resulting oxide powder was sieved from 20 to 60 mesh. The oxide was then reduced in a Pyrex tube with deoxygenated hydrogen-first at a flow rate of 10 ml min^{-1} for 1 h at 150 °C and then at 100 ml min^{-1} for 1.5 h at 300 °C. The reduced metal catalyst was kept in a deoxygenated nitrogen atmosphere.

Pure Cu, Ni, and other metals were prepared by similar procedures. Five wt% Rh, Pd, and Pt, supported on silica, were prepared by the manner described by Benesi et al.[12]

Activity Measurements: The hydration of AN was carried out in a conventional batch reactor equipped with a reflux condenser. After the air in the reactor had been replaced with deoxygenated nitrogen, pure water (100 ml) and purified AN (8.5 ml) were introduced into the reactor, and the mixture was kept at 75 °C. A prereduced catalyst (2.5 g) was transferred from the tube to the reactor in a stream of nitrogen for further reduction. The reaction products were analyzed by the use of a FID gas chromatograph. The detailed procedure was described in a previous paper.[13]

Adsorption Measurements: The chemisorption measurements were carried out in a pulse system with the apparatus described in detail elsewhere.[14] The absorption measurements were done as follows: the samples in the adsorption-tube, connected with a vacuum line, were reduced in the same manner as in the catalyst reduction described above, and then evacuated to 1×10^{-5} Torr (1 Torr=133.322 Pa). The amount of hydrogen chemisorbed on the Ni surface of the catalyst was measured by the pulse chemisorption method. The total surface area of the catalysts was determined by the BET method using N_2 physisorption.

TPD and XRD Analysis: In order to examine the materials, such as AN and AA, adsorbed on the metal-catalyst surface, the TPD experiments were performed. Desorbed molecules were analyzed by means of a quadrupole gas analyzer(ANERVA: NAG-110). The temperature was increased from room temperature to 400 °C at a rate of 5 °C min^{-1}. The crystal structures of the metal

catalysts used were identified by X-ray-diffraction measurements.

Results and Discussion

Activity and Selectivity of Metal Catalysts: As shown in Table 1, the selectivity of the catalysts differed entirely between the Group IB and Group VIII metals. AA was selectively formed on the metallic Cu and Ag catalysts, while AA, ECH, and BCE were produced on the Fe, Co, and Ni catalysts. The other metals, such as Rh, Pd, and Pt supported on silica were inactive.

In order to improve the catalytic activity of metallic Cu, various Cu-based binary metals, such as Cu-Ni, -Co, and -Fe, were prepared. As shown in Table 1, it has been found that the combination of Cu and Ni leads to an increase in the AA formation while keeping a high selectivity to AA. Even in the case of a comparison of the catalytic activity per specific surface area, the amount of AA obtained on the Cu-Ni binary metal was greater than that of the Cu catalyst. Binary metal catalysts combined with Cu and Fe or Co exhibited a low selectivity to AA. When the crystal structures of the binary metals were identified by means of the X-ray-diffraction method, it was observed that a single-phase alloy of Cu and Ni was formed, but in the case of Cu-Fe and -Co no such phase could be detected.

Catalytic Properties of Cu-Ni Alloys: Figure 1 shows the catalytic activity and AA selectivity as a function of the bulk composition of Cu in the Cu-Ni alloys. The catalytic activity of Cu-Ni alloys was greater than that of Cu over a wide range of Cu bulk compositions. Especially, Cu-Ni alloys, having 20—70% Cu in their bulk composition, were much more active catalysts than was neat Cu. The maximum conversion of AN was obtained on the Cu-Ni alloy catalyst containing 35% of Cu in the bulk phase.

It is known that Cu is concentrated on the surface of the alloy; [15] this finding is in agreement with the results of this study, as shown in Table 2. By alloying Ni with a small amount of Cu (e.g., only 3% of Cu), the Cu was concentrated on the surface of the alloy to a value of more than 10 times. Especially, when the content of Cu increased over 20% in the bulk composition, the concentration of Cu on the surface attained 70 to 90%, which agreed with the results reported in the literature.[9-11,16] It seems reasonable that the Cu atom on the alloy surface is the active site for the hydration of AN to AA, because Ni shows a poor catalytic activity.

Figure 2 illustrates the change in turnover frequency (TOF) at the initial stage, i.e., the number of reacted molecules of AN per minute per number of surface Cu or Ni atoms of the alloys. The TOF based on the Cu atom of the alloys increased with an increase in the surface concentration of Cu and attained its maximum at 80% Cu. The TOF based on the Ni atoms was negligibly small in comparison with

Table 1. Catalytic Activity and Selectivity over Various Metals on Liquid-Phase Hydration of Acrylonitrile at 75 °C

Catalyst	Reduction temperature/°C	Conversion of AN/%	Selectivity to AA/%	Yield of AA/%
Cu	300	29.5	100	29.5
Ag	120	1.5	100	1.5
Fe	400	3.1	<20[c]	<0.6
Co	300	18.1	32.8	5.9
Ni	300	1.6	19.1	0.3
Rh[a]	300	0	—	—
Pd[a]	300	0	—	—
Pt[a]	300	0	—	—
Cu-Fe (1:1)[b]	300	18.3	71.3	13.0
Cu-Co (1:1)[b]	300	53.7	57.0	30.6
Cu-Ni (1:1)[b]	300	38.0	100	38.0

a) 5 wt% M/SiO_2. b) Atomic ratio of Cu/M. c) The coexistence of polymers of the unidentified structure was observed.

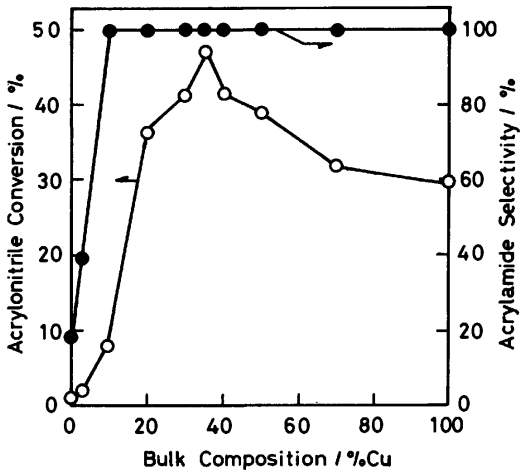

Fig. 1. Catalytic activity and selectivity on the liquid-phase hydration of acrylonitrile to acrylamide at 75 °C by Cu-Ni alloy catalysts.

Table 2. Charcateristics of Cu-Ni Alloy Catalysts

Cu bulk atomic fraction	BET surface area / $m^2 g^{-1}$	H_2 chemisorption / $\times 10^{19}$ atoms m^{-2}	Surface Cu atomic fraction
0	6.5	1.51	0
0.03	3.1	0.99	0.34
0.20	5.0	0.41	0.73
0.35	5.2	0.32	0.79
0.40	4.5	0.27	0.82
0.50	4.1	0.30	0.80
0.70	5.5	0.12	0.92
1.0	5.8	0.00	1.0

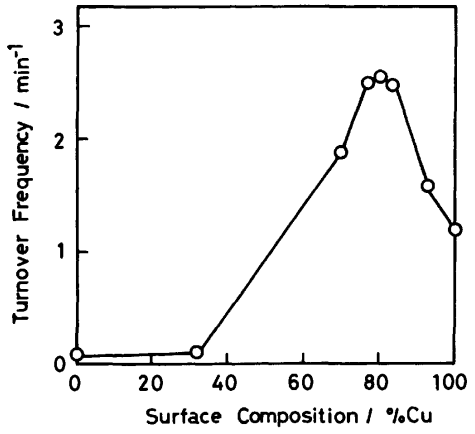

Fig. 2. Relation between turnover frequency and surface composition of Cu-Ni alloy catalysts.

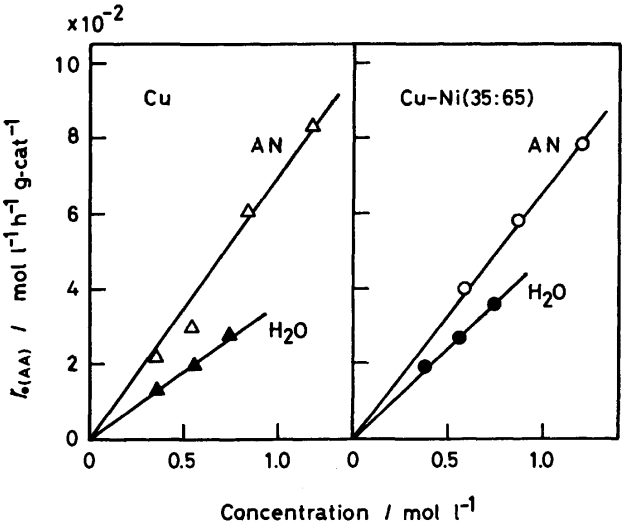

Fig. 3. Reaction order of Cu and Cu-Ni (35:65) catalysts.

that of Cu.

Kinetic Parameters at the Initial Stage of the Reaction: The initial rate of AA formation on Cu-Ni and Cu catalysts was examined in various concentrations of AN and water. On the Cu-Ni (35:65) and Cu catalysts, a first-order concentration dependency of both AN and water was obtained, as shown in Fig. 3. In addition, the values of the apparent activation energy of the Cu-Ni (35:65) and Cu catalysts were 10.9 and 12.1 kcal mol^{-1} (1 cal=4.184 J) respectively. These results indicate that the hydration on the Cu-Ni (35:65) and Cu catalysts proceeds according to the same mechanism at the initial state of the reaction.

Effect of Product Retardation: Differences in the catalytic activity between the Cu and Cu-Ni (35:65) catalysts were observed a few hours after the start of the reaction. Deviations from the first-order plots were observed on the Cu catalyst at a higher

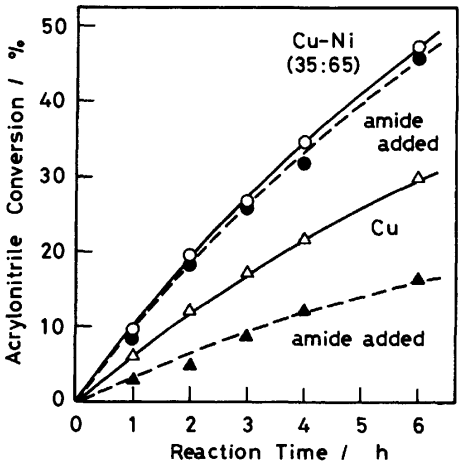

Fig. 4. Addition effect of acrylamide; amount of AA added is 1 g.

conversion of AN, while in the case of the Cu-Ni (35:65) alloy catalyst no deviation was observed.

Hayashi et al.[17] have proved that the catalytic activity of Cu supported on $MgO-SiO_2$ is depressed by the accumulation of AA on the catalyst surface. It is predictable that the retardation on the support-free Cu catalyst in this study is also caused by AA. Therefore, the effect of the addition of AA on the reaction was investigated.

Figure 4 shows the plots of the time course of the hydration in the existence and in the absence of AA. In the case of the Cu catalyst, the activity dropped to 55% of its original value upon the addition of AA. On the other hand, the catalytic activity of the Cu-Ni (35:65) alloy was not affected at all by the AA addition. It can be thought that AA is not liable to adsorb on the Cu-Ni catalyst surface.

In order to further ascertain the effect of AA on the Cu and Cu-Ni catalysts, the solution in the reactor, after the reaction had finished, was removed by means of a syringe equipped with a long needle in a N_2 atmosphere, leaving the catalyst in the reactor. After the catalyst had then been washed with pure water a few times, the reaction was started again by charging AN and water into the reactor. The relations of AN conversion to the reaction time were shown by exactly the same dotted lines as those shown in Fig. 4. Thus, the retardation was observed on Cu, and not on Cu-Ni, catalysts. Therefore, it is necessary also to examine the absorption behavior of AA and AN on the Cu and Cu-Ni catalysts.

By assuming the pseudo-first-order kinetics from the reaction conditions being rich in water, the hydration rate of AN may be expressed as:

$$r_{AN} = k\theta_{AN} \quad (1)$$

where k represents the rate constant and where θ is the surface coverage of AN.

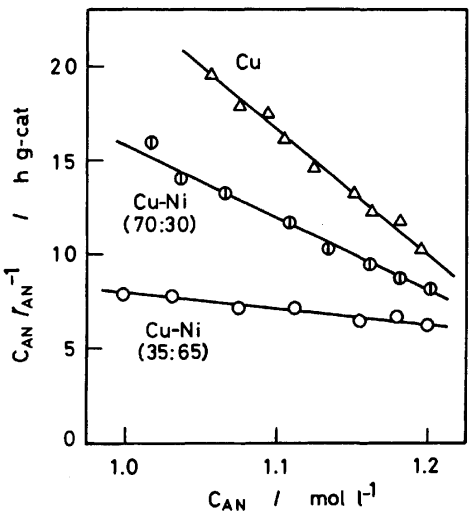

Fig. 5. Verification of Eq. 4.

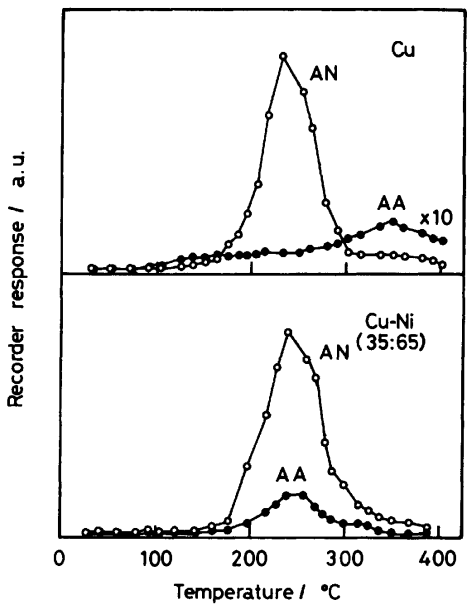

Fig. 6. TPD profiles of Cu and Cu-Ni (35:65) alloy.

Table 3. Adsorption Equilibrium Constants of Acrylonitrile and Acrylamide on Cu and Cu-Ni Alloy Surface

Catalyst	Cu atomic fraction		K_{AN} / l mol^{-1}	K_{AA} / l mol^{-1}
	Bulk	Surface		
Cu	1.0	1.0	1.6	20.5
Cu-Ni	0.70	0.92	0.7	11.4
Cu-Ni	0.35	0.79	0.3	2.1

In the case of the competitive adsorption of AN and AA, the surface coverage of AN can be expressed as:

$$\theta_{AN} = \frac{K_{AN}C_{AN}}{1+K_{AN}C_{AN}+K_{AA}C_{AA}} \quad (2)$$

where K_{AN} and K_{AA} represent the adsorption equilibrium constants of AN and AA respectively. In Eq. 2, the adsorption term of water is neglected, for scarcely water is absorbed on the Cu catalysts.[18-20]

As the hydration product is AA alone:

$$C_{AA} = C_{AN_0} - C_{AN} \quad (3)$$

By substituting Eqs. 2 and 3 into Eq. 1, we obtain:

$$\frac{C_{AN}}{r_{AN}} = \frac{1+K_{AA}C_{AN_0}}{kK_{AN}} + \left(\frac{K_{AN}-K_{AA}}{kK_{AN}}\right)C_{AN} \quad (4)$$

Figure 5 shows excellent fits of the data with Eq. 4. The negative slopes indicate that K_{AA} is greater than K_{AN}. The adsorption constants in Eq. 4 were calculated to be as shown in Table 3. These results indicate that AA is rather more strongly adsorbed on the Cu surface than is AN. The values of K_{AA} decreased with the increase in the concentration of Ni atoms on the Cu-Ni alloy surface. This suggests that the coexistence of Cu and Ni on the alloy surface leads to the smooth desorption of AA from that surface.

TPD Profiles: The TPD profiles of Cu and Cu-Ni (35:65) catalysts after a 6-h reaction are shown in Fig. 6. On the Cu surface, a small amount of AA desorption at a higher temperature (ca. 350 °C) and a large amount of the desorption of AN at a lower temperature (ca. 250 °C) were observed. On the other hand, on the Cu-Ni alloy catalyst the desorption peak of AA shifted to a lower temperature. Thus, it seems clear that AA can easily desorb from the catalyst surface as a result of the functioning of Ni in Cu-Ni alloy. Consequently, it can be concluded that the deactivation of the Cu catalyst by product retardation can be prevented by alloying Cu and Ni, thus leading to the improvement of the hydration catalyst to a more active one.

Conclusion

The results of the liquid-phase hydration of AN to AA over the metal catalysts can be summarized as follows:

1) Cu and Ag in Group IB selectively produced AA, while Fe, Co, and Ni in Group VIII yielded AA, ECH, and BCE.

2) The Cu-Ni alloy with the surface concentration of 80% Cu was the best catalyst for the AA formation.

3) The Ni in the Cu-Ni alloy contributes to the smooth desorption of AA from the catalyst surface, preventing the retardation of AA; a high activity can thus be preserved.

References

1) D. C. MacWilliams, "Kirk-Othmer; Encyclopedia of

Chemical Technology," 3rd ed, Wiley (1978), Vol. 1, p. 298.
2) F. Matsuda and J. Hashimoto, *Shokubai*, **17**, 192 (1975).
3) F. Matsuda, *CHEMTECH*, May 306 (1977).
4) E. N. Zil'bermann, *Russian Chemical Reviews*, **53**, 900 (1984).
5) F. Matsuda, *Yuki, Gosei Kagaku Kyokai Shi*, **35**, 212 (1977).
6) K. Sugiyama, H. Miura, Y. Watanabe, Y. Ukai, and T. Matsuda, *Chem. Lett.*, **1986**, 47.
7) R. J. Best and W. W. Russel, *J. Am. Chem. Soc.*, **76**, 838 (1954).
8) T. Takeuchi and M. Sakaguchi, *Bull. Chem. Soc. Jpn.*, **30**, 177 (1957).
9) J. H. Sinfelt; J. L. Carter, and D. J. C. Yates, *J. Catal.*, **24**, 283 (1972).
10) E. Igresia and M. Boudart, *J. Catal.* **81**, 204 (1983).
11) M. Chen, C. Cheng, and C. Teh, *J. Catal.*, **95**, 346 (1985).
12) H. A. Benesi, R. M. Cartis, and H. P. Studer, *J. Catal.*, **10**, 328 (1968).
13) K. Sugiyama, H. Miura, Y. Nakano, H. Sekiwa, and T. Matsuda, *Bull. Chem. Soc. Jpn.*, **59**, 2983 (1986).
14) H. Miura, T. Narita, M. Haruta, K. Sugiyama, and T. Matsuda, *Bull. Chem. Soc. Jpn.*, **58**, 1043 (1985).
15) a) T. Takeuchi, *Shokubai*, **22**, 373 (1980). b) B. C. Gates, J. R. Katzer, and G. C. A. Shuit, "Chemistry of Catalytic Processes," McGraw-Hill, New York (1979), p. 213.
16) K. Watanabe, M. Hashiba, and T. Yamashita, *Surface Sci.*, **61**, 483 (1976).
17) H. Hayashi, H. Nishi, Y. Watanabe, and T. Okazaki, *J. Catal.*, **69**, 44 (1981).
18) A. Spitzer and H. Luth, *Surface Sci.*, **120**, 376 (1982).
19) A. Spitzer and H. Luth, *Surface Sci.*, **160**, 353 (1985).
20) A. Spitzer, A. Ritz, and H. Luth, *Surface Sci.*, **152/153**, 543 (1985).

Hydrates of Organic Compounds. XII. Intercalation of Methyl and Ethyl Alcohols within the Clathrate-Like Hydrates of Tetrabutylammonium Fluoride and of Tetrabutylammonium Propionate

Haruo NAKAYAMA,* Kiyoshi TSUNAKAWA, Mizue KANŌ, and Hiroshi MATSUI†
Department of Chemistry, Faculty of Engineering, Yokohama National University, Tokiwadai, Hodogaya-ku, Yokohama 240
†The Radio Isotope Center, Yokohama National University, Tokiwadai, Hodogaya-ku, Yokohama 240
(Received October 2, 1986)

The amount of either methyl or ethyl alcohol intercalated within clathrate-like hydrates of tetrabutylammonium fluoride and of tetrabutylammonium propionate has been determined using ^{14}C-labeled alcohols. It was found that (1) methyl alcohol could be intercalated within the tetrabutylammonium fluoride hydrate but not within the tetrabutylammonium propionate hydrate; (2) ethyl alcohol could be intercalated within both the tetrabutylammonium fluoride and tetrabutylammonium propionate hydrates; and (3) the amount of the alcohol intercalated increased with increasing concentration of alcohol in the initial solutions. These results were interpreted by taking into consideration the states of vacant pentagonal dodecahedra formed by hydrogen-bonded water networks.

As a way of examining the ability of an organic substance to form a clathrate-like hydrate, we have proposed a new method.[1,2] It is based upon the examination of the formation of either double or mixed hydrates in a ternary system consisting of the substance under consideration, water, and a third component which is clearly known to form a clathrate-like hydrate by itself. In an earlier experiment[2] for ternary systems of methyl (or ethyl) alcohol–water–tetrahydrofuran(THF), it was found that (1) both methyl and ethyl alcohols were intercalated within the THF clathrate hydrate, (2) ethyl alcohol could form a mixed hydrate with THF, and (3) the amount of methyl alcohol intercalated within the THF hydrate increased with increasing the concentration of methyl alcohol, indicating that methyl alcohol formed a double hydrate with THF, presumably by being intercalated in a vacant pentagonal dodecahedron. These results suggest that the state of vacant polyhedra, especially of vacant pentagonal dodecahedra, plays an important role for the intercalation of such alcohols into a clathrate-like hydrate.

On the other hand, according to the single-crystal X-ray examination for a clathrate-like hydrate of tetrabutylammonium fluoride, $(n\text{-}C_4H_9)_4NF$, by Jeffrey et al.,[3] vacant pentagonal dodecahedra coexist with large polyhedra (such as tetrakaidecahedra and pentakaidecahedra) which accommodate one of the butyl groups of a tetrabutylammonium cation, and five pentagonal dodecahedra face-share with each other and form a part of anionic host structure together with the fluoride ions. It is of interest to examine the capability of these pentagonal dodecahedra to intercalate such small organic molecules as methyl and ethyl alcohols.

Furthermore, it has recently been known that various tetrabutylammonium carboxylates, $(n\text{-}C_4H_9)_4NOOCC_2H_5$ for example, can also form a clathrate-like hydrate having the same hydration numbers as that of the tetrabutylammonium fluoride hydrate (around 30).[4–6] It has been presumed that (1) these carboxylate hydrates are iso-structural with the $(n\text{-}C_4H_9)_4NF$ hydrate and (2) an alkyl group of the carboxylate anion occupies one pentagonal dodecahedron which is located in the nearest position to the tetrabutylammonium cation. If this speculation is correct, there may be some difference in the states of the pentagonal dodecahedra between the $(n\text{-}C_4H_9)_4NF$ hydrate and the tetrabutylammonium carboxylate hydrates, i.e., all the pentagonal dodecahedra are vacant in the former, whereas some of them are already occupied by the alkyl group of the carboxylate anion in the latter.

In this investigation, the enclathration of methyl and ethyl alcohols within the clathrate-like hydrates of $(n\text{-}C_4H_9)_4NF$ and $(n\text{-}C_4H_9)_4NOOCC_2H_5$ has been investigated in order to see if (1) such alcohols can actually be intercalated in vacant pentagonal dodecahedra existing in these tetrabutylammonium salt hydrates and (2) there exists some difference in the intercalation abilities between the two hydrates.

Experimental

Materials and Procedure. An aqueous solution of tetrabutylammonium fluoride was prepared by neutralization of an aqueous solution of tetrabutylammonium hydroxide with hydrofluoric acid. The hydroxide solution was prepared by reacting tetrabutylammonium iodide, which was prepared and purified by the same procedure as in earlier papers,[4,5] with freshly prepared silver hydroxide in water, followed by filtration of the silver iodide precipitate. An aqueous solution of tetrabutylammonium propionate was prepared by reacting the tetrabutylammonium iodide with silver propionate in water, followed by filtration of the silver iodide precipitate. The silver

propionate was prepared by reacting sodium propionate with silver nitrate in water, followed by repeated washing with water to remove sodium nitrate. The concentration of the mother solutions of the tetrabutylammonium salts was determined by titration with tetraphenylborate aqueous solution standardized by pure tetrabutylammonium iodide. Radioactive methyl and ethyl alcohols were purchased from The Japan Radioisotope Association. Sample solutions were prepared by dissolving a known amount (0.2—1.0 g) of the sample containing 0.1—0.3 μCi in 4—5 cm^3 of scintillator, Insta-gel (Packard Instrument Co., Inc.). The radioactivity was measured using the TRI-CARB 460C Automatic Liquid Scintillation System (Packard Instrument Co., Inc.).

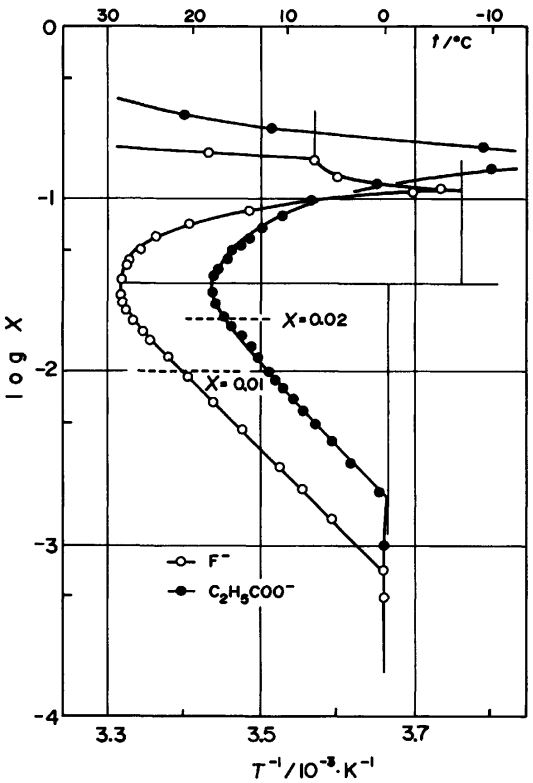

Fig. 1. The solid-liquid phase diagrams for the binary systems of $(n\text{-}C_4H_9)_4NF+H_2O$(○) and $(n\text{-}C_4H_9)_4NOOCC_2H_5+H_2O$(●). The mole fraction ($X$) which is kept constant throughout this study is shown for each salt.

Determination of the Experimental Conditions. In Fig. 1, the solid-liquid phase diagrams for the binary systems of $(n\text{-}C_4H_9)_4NF\text{-}H_2O$[7] and of $(n\text{-}C_4H_9)_4NOOCC_2H_5\text{-}H_2O$[4] are shown, in which the ordinate represents the logarithm of the concentration expressed by the mole fraction (X) of each salt and abscissa represents the reciprocal of the absolute temperature. These phase diagrams clearly indicate the formation of hydrates for both salts. The congruent composition of the hydrate is around X=0.032 for both hydrates and the congruent melting point is 28.3 °C[7] for the fluoride hydrate and 18.0 °C[4] for the propionate hydrate, respectively. As is obvious from this figure, the experimental temperature range is inevitably limited between the eutectic point (around 0 °C for both hydrates) and the congruent melting point of the hydrate, and is highly dependent upon the concentration of each tetrabutylammonium salt. Therefore, the concentration of the tetrabutylammonium salt, which is kept constant throughout this experiment, is determined to be X=0.01 for the systems containing the $(n\text{-}C_4H_9)_4NF$ and X=0.02 for those containing the $(n\text{-}C_4H_9)_4NOOCC_2H_5$, respectively. This situation is also depicted in Fig. 1.

In Fig. 2 the melting points of the two hydrates are plotted against the concentration of the alcohol added. These data were obtained by the usual ampoule method used in

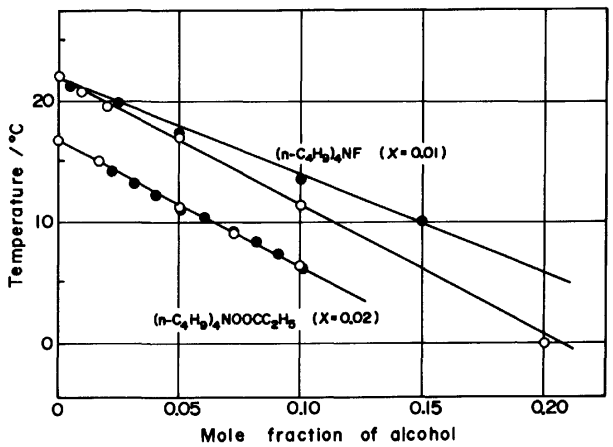

Fig. 2. The effect of added alcohols on the melting points of the clathrate-like hydrates of $(n\text{-}C_4H_9)_4NF$ and of $(n\text{-}C_4H_9)_4NOOCC_2H_5$. The mole fraction of each salt is kept constant at the value given in parenthesis. ○: CH_3OH; ●: C_2H_5OH.

Table 1. List of the Experimental Conditions

No.	Tetrabutylammonium salt	Alcohol	X_{TBA}	X_{alc}	Experimental temperature/°C
1	$(n\text{-}C_4H_9)_4NF$	CH_3OH	0.01	0.01	15.0
2	$(n\text{-}C_4H_9)_4NF$	CH_3OH	0.01	0.10	5.0
3	$(n\text{-}C_4H_9)_4NF$	C_2H_5OH	0.01	0.01	17.5
4	$(n\text{-}C_4H_9)_4NF$	C_2H_5OH	0.01	0.10	9.5
5	$(n\text{-}C_4H_9)_4NOOCC_2H_5$	CH_3OH	0.02	0.02	12.0
6	$(n\text{-}C_4H_9)_4NOOCC_2H_5$	CH_3OH	0.02	0.10	3.1
7	$(n\text{-}C_4H_9)_4NOOCC_2H_5$	C_2H_5OH	0.02	0.02	12.5
8	$(n\text{-}C_4H_9)_4NOOCC_2H_5$	C_2H_5OH	0.02	0.10	3.2

previous papers.[4,5,7] The concentration of the tetrabutylammonium salts are kept constant as mentioned above. This figure indicates that the melting point of each hydrate is lowered almost linearly with increasing concentration of the alcohol. At temperatures above each line only a single liquid phase is present and at temperatures several degrees below the line the mixture apparently looks like a single solid phase in which the coexisting liquid phase is absorbed in the interstice between the hydrate crystal. Therefore, the experimental temperature at which both liquid and solid phases are present in nearly equal proportion is limited to a temperature of a few degrees below each line.

From these standpoints all the experimental conditions are determined. They are summarized in Table 1. The X_{TBA} and X_{alc} represent the mole fraction of tetrabutylammonium salt and of alcohol added, respectively.

Results and Discussion

(1) Estimation of the Amount of the Liquid Phase Adhering to the Solid Phase. Prior to the main experiment, the weight fraction, P, of the liquid phase adhering to the wet solid phase must be estimated. The process for estimating the P is divided into the following processes: (1) a ternary mixture (about 5 cm^3) containing a given amount of tetrabutylammonium salt, of nonradioactive alcohol, and of water was cooled down to about −20 °C in order to deposit a solid phase, then a large portion of the solid was dissolved by gradual warming to a temperature about one degree above the experimental temperature; (2) a well-formed crystalline phase is slowly developed by cooling again to the experimental temperature listed in Table 1; (3) a small amount of radioactive alcohol (0.1—0.3 μCi) is added into the solid-liquid mixture which is kept at the experimental temperature and well mixed with the liquid phase by shaking; and (4) the liquid phase is separated from the solid phase by decantation, followed by suction through a long thin syringe needle. The radioactivity per unit weight is then measured for the liquid phase and for the solid phase, respectively.

If we represent the radioactivity (dpm) and the weight (g) of the sample by r and m, and the liquid phase by a suffix 1 and the wet solid phase by s, P can be calculated by the following equation:

$$P = \frac{r_s/m_s}{r_l/m_l}, \quad (1)$$

since the amount of the liquid phase contained in the m_s g wet solid is equal to the quantity $(m_l/r_l)r_s$. In this procedure, it is assumed that radioactive alcohol is not present in the solid phase since additional solid phase deposition owing to the addition of alcohol is impossible: i.e., the addition of alcohol never causes the rise in the melting point as shown in Fig. 2 and the temperature is always kept constant. The P values of all the systems determined by this procedure are summarized in Table 2. The number of the system is the same as that listed in Table 1. These values are averages of 5—10 measurements and the limits of error attached to each value simply represent the deviation from the mean value from experiment to experiment. In general, a long and well-shaped, parallelepiped crystal was formed in the systems 1 to 4, especially in the systems containing ethyl alcohol, leading to small values of P. However, in the systems containing $(n\text{-}C_4H_9)_4NOOCC_2H_5$ (systems 5—8), many thin and wedge-shaped crystals were developed almost simultaneously over the whole part of the solution, resulting in relatively large and less accurate values of P.

Table 2. Summary of P Values for All the Systems Examined

System[a)]	P	System[a)]	P
1	0.097±0.006	5	0.09±0.04
2	0.097±0.005	6	0.29±0.06
3	0.017±0.010	7	0.24±0.03
4	0.040±0.009	8	0.12±0.03

a) The number of the system stands for the same one listed in Table 1.

(2) Enclathration of Alcohols within the Clathrate-Like Hydrates of Tetrabutylammonium Fluoride and of Tetrabutylammonium Propionate. Through the measurements of radioactivity of ^{14}C-labeled alcohols, the amount of either methyl or ethyl alcohol included in the hydrate solid which is formed in ternary mixtures of tetrabutylammonium fluoride (or propionate)–radioactive methyl (or ethyl) alcohol–water has been determined. The solid phase was carefully developed by the same procedure as the processes (1) and (2) described in the preceding section.

Since water networks which have the possibility to enclathrate alcohol molecules are vacant pentagonal dodecahedra, the molar ratio of the tetrabutylammonium salt to water in the hydrate solid remains unchanged, i.e., 1:30, irrespective of the presence of alcohol within the hydrate solid. Therefore, the molecular formula of the solid phase may be expressed as (Tetrabutylammonium salt)$(Alcohol)_x30H_2O$. The maximal value of x is equal to 2 according to the crystal structure examination by Jeffrey et al.[3] Thus, the following relation can be obtained with respect to the amount of alcohol existing in the solid phase:

$$\frac{M_{alc}x}{M_{TBA}+M_{alc}x+30M_{H_2O}} = \frac{w_s-Pw_l}{1-P}, \quad (2)$$

in which M_{TBA}, M_{alc}, and M_{H_2O} are the molecular weights of tetrabutylammonium salt, alcohol, and water, and w_s and w_l, are the weight fractions of the alcohol in the wet solid phase and in the liquid phase, respectively. These two weight fractions were

Table 3. The x Values Determined for All the Systems Examined

System[a)]	x	System[a)]	x
1	0.12±0.03	5	0.03±0.03
2	0.71±0.10	6	0.21±0.25
3	0.10±0.01	7	0.12±0.05
4	0.75±0.10	8	0.79±0.10

a) The number of systems is the same as listed in Table 1.

determined by the radioactivity measurements for both phases separated from each other by the same procedure as the process (4) in the previous section. From Eq. 2 we can get the following relation:

$$x = \frac{w_s - Pw_l}{1 - P - (w_s - Pw_l)} \cdot A, \quad (3)$$

where A is a constant calculated from the molecular weight of each component in ternary mixtures: A is equal to 25.03 for systems 1 and 2; 17.41 for systems 3 and 4; 26.72 for systems 5 and 6; and 18.58 for systems 7 and 8.

The values of x determined for all the systems are summarized in Table 3. These values are averages of 5—10 measurements. The limit of error attached to each x is estimated by taking into consideration the uncertainty of the P values (Table 2) and the error arising from the radioactivity measurements. In system 6 the deviation from the mean value is exceptionally large because of the difficulty to obtain a well-formed crystal in this system as partly exemplified by large P value for this system (Table 2).

From these results the following conclusions can be drawn:

(1) In the systems containing tetrabutylammonium fluoride (systems 1—4), both methyl and ethyl alcohols are intercalated within the hydrate solid.

(2) In the systems 1—4, the amounts of alcohol intercalated increase with increasing concentration of alcohol in the initial solutions, showing a feature characteristic of a nonstoichiometric inclusion compound. The increment of x is 5.9 times for methyl alcohol and 7.5 times for ethyl alcohol for the 10 times increment of the mole fraction of each alcohol, i.e., from X=0.01 to 0.10.

(3) For the systems 5 and 6, taking into account the relatively small values of x and the deviations from the mean values, it may be concluded that methyl alcohol is not intercalated within the tetrabutylammonium propionate hydrate.

(4) On the other hand, the values of x for the systems 7 and 8 clearly indicate that ethyl alcohol is intercalated within the tetrabutylammonium propionate hydrate. The values of x for the systems 7 and 8 are similar to those of the systems 3 and 4, respectively.

As mentioned in the introduction section, in the structure of the tetrabutylammonium fluoride hydrate[3] there exists a vacant space which is made of five pentagonal dodecahedra face-sharing with each other. However, this space must be appreciably deformed by the arrangement of other large polyhedra like tetrakaidecahedra and pentakaidecahedra which accommodate butyl groups of a tetrabutylammonium cation. The experimental above listed facts may be explained if we assume the presence of at least two types of pentagonal dodecahedra, i.e., geometrically highly deformed pentagonal dodecahedra which exist near the tetrabutylammonium cation (denoted by S-type hereafter) and geometrically less deformed ones which exist somewhat apart from the tetrabutylammonium cation (denoted by L-type hereafter).

Taking into account the fact that free diameter of a nondeformed pentagonal dodecahedron is about 5.2 Å[8] and the molecular diameter of methyl alcohol is about 5.2 Å and that of ethyl alcohol is about 6.3 Å, it will be reasonable to assume that methyl alcohol is enclathrated in the S-type pentagonal dodecahedra and ethyl alcohol in the L-type ones. This assumption means that the free diameter of the L-type pentagonal dodecahedron is elongated enough to accommodate an ethyl alcohol molecule. These assumptions lead to a conclusion compatible with the experimental facts: (1) since in the $(n\text{-}C_4H_9)_4NF$ hydrate the S-type pentagonal dodecahedron is vacant, it can enclathrate methyl alcohol; (2) however, the S-type pentagonal dodecahedron in the $(n\text{-}C_4H_9)_4NOOCC_2H_5$ hydrate must accommodate the C_2H_5 group of the $C_2H_5COO^-$ ion, it can enclathrate methyl alcohol no longer; and (3) since the L-type pentagonal dodecahedra are considered to be in a similar situation in both hydrates, their ability to enclathrate ethyl alcohol is expected to be similar in both hydrates.

The present work was supported by a Grant-in-Aid for Scientific Research No. 60470006 from the Ministry of Education, Science and Culture.

References

1) H. Nakayama and M. Hashimoto, *Bull. Chem. Soc. Jpn.*, **53**, 2427 (1980).

2) H. Matsui and H. Nakayama, *Bull. Chem. Soc. Jpn.*, **57**, 2663 (1984).

3) R. K. McMullan, M. Bonamico, and G. A. Jeffrey, *J. Chem. Phys.*, **39**, 3295 (1963).

4) H. Nakayama and S. Torigata, *Bull. Chem. Soc. Jpn.*, **57**, 171 (1984).

5) H. Nakayama and H. Usui, *J. Inclusion Phenomena*, **2**, 249 (1984).

6) Yu. A. Dyadin, L. S. Aladko, L. A. Gaponenko, and T. M. Polyanskaya, *Izv. Sib. Otd. Akad. Nauk SSSR, Ser. Khim. Nauk*, **1981** (9), 19.

7) H. Nakayama, *Bull. Chem. Soc. Jpn.*, **56**, 877 (1983).

8) D. W. Davidson, "Water," ed by F. Franks, Plenum Press, New York (1973), Vol. 2, Chap. 3.

Homogeneous Isomerization of 1-Butene Catalyzed by $[MX_2(PR_3)_2]$-$NaBH_4$ Systems (M=Co, Ni, X=Halides, SCN, $PR_3=PPh_nEt_{3-n}$)— Acceleration by Phosphine Addition and Stereoselectivity

Hiroyoshi KANAI,* Shigeyoshi SAKAKI,† and Takenobu SAKATANI††
Department of Hydrocarbon Chemistry, Faculty of Engineering, Kyoto University, Sakyo-ku, Kyoto 606
(Received October 2, 1986)

The stoichiometric or a little excess amount of $NaBH_4$ was treated with $[MX_2(PR_3)_2]$ (M=Co, Ni, X= halides, SCN, $PR_3=PPh_nEt_{3-n}$) in THF-1,2-dimethoxyethane to form monohydride species which were active for isomerization of 1-butene. The reaction was accelerated by excess PPh_3 in $[CoX_2(PPh_3)_2]$-$NaBH_4$ systems. Other catalytic systems have optimum ratios of excess phosphine to metal for getting maximum activities. Thiocyanate-metal complexes are the most active in each Co- and Ni-catalyst system. Cis-selectivity depends on the cone angle of PR_3, the size of anion ligands, and the congested structure of complexes.

Double bond migration of linear terminal olefins is homogeneously catalyzed by many transition metal catalysts.[1] Cocatalysts are frequently required: hydrogen,[2] acids,[3] and oxygenated compounds[4] have been used for heavy transition metal complexes to give metal hydrides. Alkylaluminum, Grignard reagents, and alkali metal alkyls and hydrides are effective cocatalysts for complexes of the first row transition metal complexes.[5]

We have found the isomerization of 1-butene catalyzed by $[MX_2(PR_3)_2]$ (M=Co, Ni, X=halogen, SCN, NO_3, CN, $PR_3=PPh_nEt_{3-n}$) with sodium tetrahydroborate as a cocatalyst. One of characteristic features in these systems is that *cis*-2-butene is preferentially formed to the trans-isomer. Another is that the more PPh_3 is added, the more the rates of isomerization increase in the cobalt system. Since rates and stereoselectivity are dependent on halogen ligands, active species are cobalt or nickel hydrides containing Co-X or Ni-X bonding.

Experimental

Materials. The 1-butene which was purchased from Takachiho Chemicals had a purity of 99.8%. Tetrahydrofuran (THF) and 1,2-dimethoxyethane (glyme) were refluxed over sodium and distilled before use. Cobalt and nickel halides were obtained from Nakarai Chemicals and used without purification. PPh_3 was recrystallized from methanol. Phosphines containing ethyl group were prepared by standard Grignard synthesis. $[CoX_2(PR_3)_2]$ (X=halides, SCN, $PR_3=PPh_nEt_{3-n}$, n=0—3) were prepared from cobalt halides and PR_3 in ethanol or acetone by the methods described in the literatures.[6] $[NiX_2(PR_3)_2]$ (X=halides, SCN, NO_3, CN) were similarly prepared from NiX_2 and phosphines in 1-butanol or ethanol according to the literatures.[7] Elemental analytical data of complexes agree with those of calculated values.

Procedure and Analysis. Three ml of THF solution of a cobalt or a nickel complex (0.1 or 0.15 mmol) and 2 ml of glyme solution of $NaBH_4$ (0.025—0.1 mmol) were placed in each 10-ml ampule connected with each other. 1-Butene (4.2 mmol) was added to the ampules which were degassed and chilled in liquid nitrogen. After they were sealed and stored at 0 °C, two solutions were mixed and allowed to stand at 0 °C for a given interval. The reaction was stopped by freezing the solution in liguid nitrogen and the reaction mixture was distilled rapidly in vacuo. The distillate was analyzed by a Shimadzu-6A gas chromatograph on a column packed with 30% dimethylsulfolane on Celite 545 (5.6 m) at r.t. The concentration of $NaBH_4$ in glyme was determined by the titration with 1/100 N HCl using Methyl Red as an indicator.

Results

Formation of Metal Hydrides and Their Catalysis. Anhydrous cobalt chloride dissolved in THF was reacted with $NaBH_4$ at 0 °C to yield black precipitates. They had very little activity for isomerization of 1-butene. The presence of hydrogen caused isomerization but less rapidly compared to hydrogenation.[8]

Cobalt halide complexes containing phosphine ligands such as $[CoCl_2(PPh_3)_2]$, were found to react with $NaBH_4$ to give green homogeneous solution, which effectively catalyzed isomerization of 1-butene. The rate of isomerization gradually decreased due to the decomposition of active species where cobalt metal began to be deposited. The decomposition was prevented by adding excess phosphine. A hydrogenated product, butane, was formed at the beginning of the rection, but the amount did not increase with the elapse of time. The ratios of *cis*-2-butene to the trans-isomer (abbreviated as c/t) remain constant until 1-butene has almost been consumed. Scrambling of 2-butenes was much slower compared to double-bond migration.

Effects of the Concentration of $NaBH_4$ on the Isomerization of 1-Butene Catalyzed by $[CoX_2(PPh_3)_2]$ (X=Halides, SCN). Sodium tetrahydroborate is nec-

† Present address: Department of Synthetic Chemistry, Faculty of Engineering, Kumamoto University, Kurokami, Kumamoto 860.

†† Present address: Lion Corporation, 13-12, 7-Chome, Hirai, Edogawa-ku, Tokyo 132.

essary for the formation of metal hydrides as active species. The effects of the ratio of $NaBH_4$ to cobalt complexes on the isomerization are shown in Fig. 1. In the case of $[CoCl_2(PPh_3)_2]$, the apparent rate, which is expressed as the conversion of 1-butene, increases proportionally with the increase of $NaBH_4$. The reaction at $H^-/Co=4$ proceeded in suspension from the beginning. The initial state of the reaction mixture was homogeneous at $H^-/Co \leqq 2$, and metal deposited at the end of the reaction at $H^-/Co \geqq 1$. The c/t ratio was almost independent of H^-/Co ratios. The rates reach maxima at nearly stoichiometric concentration of $NaBH_4$ to produce monohydride in cases of $[CoX_2(PPh_3)_2]$ (X=Br, I, SCN). The c/t ratios remain constant when H^-/Co is less than 2, but decrease at $H^-/Co>2$.

The amounts of butane produced are nearly proportional to the concentration of $NaBH_4$ for any complexes. They decrease in the order Cl>Br>I>SCN at the same ratio of $NaBH_4$ to the cobalt complex.

Similar effect of the $NaBH_4$ concentration was observed for $[CoX_2(PPh_nEt_{3-n})_2]$ (n=0—2) and $[NiX_2(PPh_nEt_{3-n})_2]$ (n=0—3) whereas H^-/M values giving maximum rates shift to somewhat higher ones than stoichiometry.

Effect of Addition of Excess Phosphine. The reaction mixture of Co-PPh_3 complexes at $H^-/Co \leqq 2$ was kept homogeneous for several hours after which metallic precipitates began to be formed. The addition of excess PPh_3 kept homogeneity throughout the reaction and accelerated the isomerization (Fig. 1). The low values of c/t in Fig. 1 (the dotted lines) indicate the completion of double-bond migration of 1-butene followed by the scrambling of 2-butenes. The dependence of the rate on H^-/Co is the same with and without excess PPh_3.

Rate Constants and Stereoselectivity in the Isomerization of 1-Butene Catalyzed by Co- and Ni-Phosphine Complexes. The isomerization was first order in 1-butene and the rates were proportional to the metal concentrations. The second-order rate constants, k', are expressed as follows:

$$\frac{-d[1\text{-}C_4H_8]}{dt} = k[1\text{-}C_4H_8] \quad (1)$$

$$k=k'[M] \quad (2)$$

where [M] stands for the concentration of metal complexes.

Cobalt catalysts, on the whole, are more active than nickel ones for the same ligands (Table 1, Fig. 2). $[Co(SCN)_2(PPh_3)_2]$-$NaBH_4$ system is by far the most

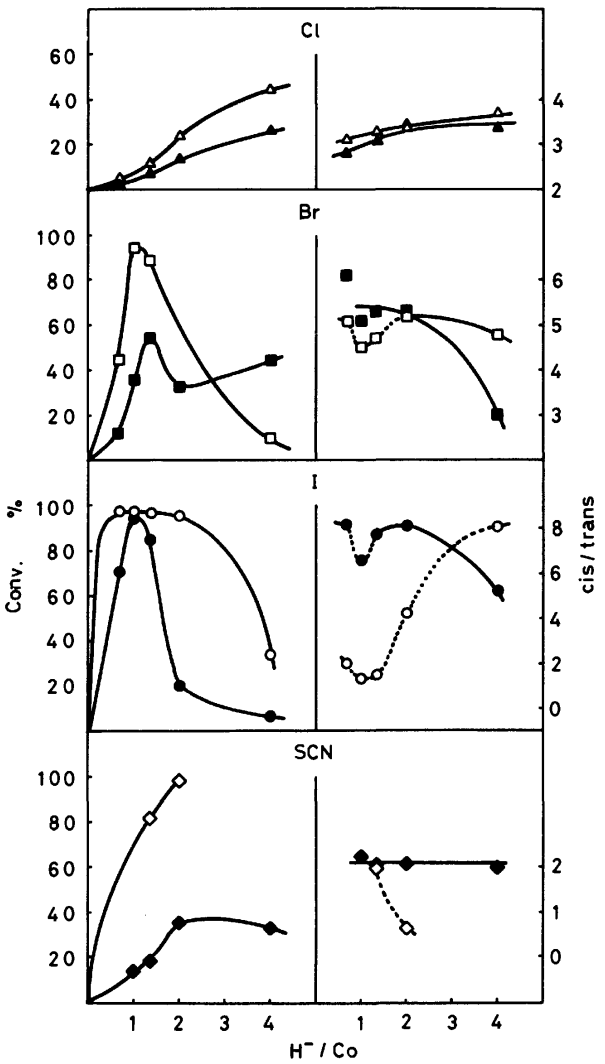

Fig. 1. The apparent rates and cis-selectivity of the isomerization of 1-butene by $[CoX_2(PPh_3)_2]$-$NaBH_4$ depend on the concentration of $NaBH_4$. [Co]=3×10^{-2} mol dm^{-3} (X=halogen), 8×10^{-3} mol dm^{-3} (X=SCN), [1-C_4H_8]=0.83 mol dm^{-3}. ▲■●◆: Without free PPh_3; △□○◇: free PPh_3/Co=2 (X=Cl, Br, SCN), 1.2 (X=I).

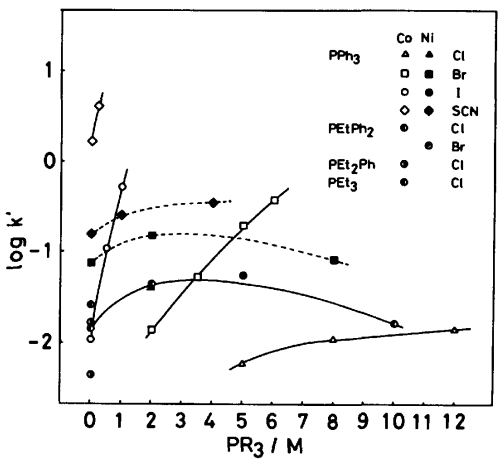

Fig. 2. Rate constants for the isomerization of 1-butene by $[MX_2(PR_3)_2]$-$NaBH_4$ systems as a function of the PR_3/M ratio.

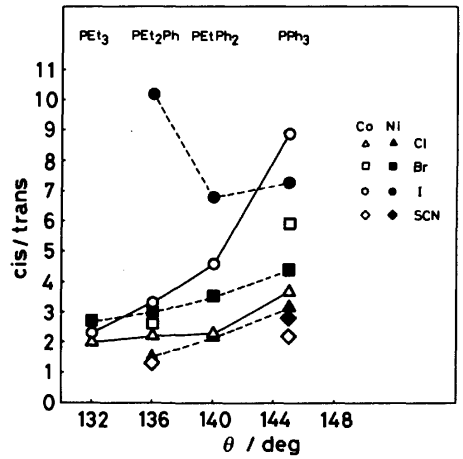

Fig. 3. Cis-selectivity depends on the cone angle of PR_3.

active among them, where a very small amount of excess PPh_3 increases the rate. The same tendency is observed for $[CoI_2(PPh_3)_2]$ system. A large excess of PPh_3 never retards the ismerization for all Co-PPh_3 complexes. However, a small excess of PPh_3 increases the rate, but a large excess retards the isomerization for Ni-PPh_3 complexes. The rates decrease in the order SCN>I>Br>Cl for cobalt catalysts, and SCN>Br>I>Cl>NO_3 for nickel catalysts. The substituents of ethyl group in PR_3 lower the rates and much more in nickel catalyst systems.

The c/t ratios which give a measure for stereoselectivity are dependent on both halogen and PR_3 ligands (Table 2, Fig. 3). The c/t ratio decreases in the order I>Br>Cl>SCN for Co-PPh_3 catalysts, and

Table 1. Rate Constants in the Isomerization of 1-Butene Catalyzed by $[MX_2(PR_3)_2]$-$NaBH_4$ Systems[1)]

M-PR_3	k' [2)]/10^{-2} dm^3 mol^{-1} s^{-1}				
	Cl	Br	I	SCN	NO_3
Co-PPh_3	0.59[d] (5)	1.4[b] (2)	1.1[b]	170[d]	
	1.4[d] (12)	38[b] (6)	52[b] (1)	420[d] (0.2)	
-PPh_2Et	1.4[b]				
	4.4[b] (2)				
	1.7[b] (10)				
-$PPhEt_2$	1.2[b]				
	1.7[d]				
-PEt_3	0.45[d]				
Ni-PPh_3	4.3[c] (2)	7.3[c]	2.9[c] (2)	16[d]	0.027[d]
		15[c] (2)	5.6[c] (5)	26[d] (1)	0.035[d] (2)
		8.2[c] (8)		36[d] (4)	
-PPh_2Et	0.49[c]	1.9[c]	0.98[b]		
	0.64[d]		0.76[d]		
-$PPhEt_2$	0.030[c]	0.054[c]	0.15[a]		
			0.29[b]		
-PEt_3		0.011[c]			

1) H^-/M=[a] 0.64, [b] 1.0, [c] 1.3, [d] 2.0. 2) The number in parentheses is the mole ratio of excess PR_3 to metal.

Table 2. Stereoselectivity in the Isomerization of 1-Butene Catalyzed by $[MX_2(PR_3)_2]$-$NaBH_4$ Systems

PR_3	c/t[a)] ($(c/t)_x/(c/t)_{Cl}$)[b)]					
	Cl	Br	I	SCN	NO_3	CN
Co-catalysts						
PPh_3	3.7	5.9 (1.6)	8.9 (2.4)	2.2 (0.59)		
PPh_2Et	2.3		4.6 (2.0)			
$PPhEt_2$	2.2	2.6 (1.2)	3.3 (1.5)	1.3 (0.59)		
PEt_3	2.0		2.3 (1.2)			
Ni-catalysts						
PPh_3	3.2	4.4 (1.4)	7.3 (2.3)	2.8 (0.88)	3.4 (1.1)	2.0 (0.62)
PPh_2Et	2.2	3.5 (1.4)	6.8 (3.1)			
$PPhEt_2$	1.5	3.0 (2.0)	10.5 (7.0)			
PEt_3		2.7				

a) *cis*-2-C_4H_8/*trans*-2-C_4H_8. b) The number in parentheses is the ratio of c/t of a catalytic system to that of the chloro-catalyst system in M-PR_3 catalyst series.

I>Br>Cl>NO_3>SCN>CN for Ni-PPh_3 catalysts. Cis-selectivity increases with cone angle of PR_3 (Fig. 3). An exception is observed with $[NiI_2(PPhEt_2)_2]$-$NaBH_4$ system where the less stoichiometric ratio of H^-/Ni gives high cis-selectivity. The increase of H^-/Ni decreases the c/t ratio from 10.5 at H^-/Ni=0.6 to 3.3 at H^-/Ni=1. The effect of the change from Cl to Br and I on the cis-selectivity becomes less pronounced with the substituents of ethyl group of PR_3 for cobalt catalysts, but is magnified for nickel catalysts (numbers in parentheses in Table 2).

Discussion

Active Species. The stoichiometric amount of $NaBH_4$ to form cobalt monohydride species gives maximum rates for the isomerization of 1-butene catalyzed by $[CoX_2(PPh_3)_2]$-$NaBH_4$ systems (X=Br, I) (Fig. 1). Active species should be metal hydrides containing halogen ligands since cis-selectivity of 2-butene is dependent on halogen ligands.

$$[MX_2(PR_3)_2] + NaBH_4 \longrightarrow [MHX(PR_3)_2] \quad (3)$$
$$M = Co, Ni,\ X = \text{halogen, SCN},\ PR_3 = PPh_nEt_{3-n}$$

Metal hydrides are stabilized by phosphines which act as σ-donors and π-acceptors.[9] More basic phosphines strengthen M-H bonds[10] to give less active catalysts. The coordination number of PR_3 is mostly two, but exceptionally three (vide post).

The isomerization has occurred through a metal-hydride addition and elimination mechanism. A small amount of butane was formed in the beginning of reactions. The amount of butane decreases in the order, Cl(33)>Br(22)>I(22)>SCN(10) for $[CoX_2(PPh_3)_2]$, PPh_3(33)>PPh_2Et(16)>$PPhEt_2$(6)>PEt_3(8) for $[CoCl_2(PR_3)_2]$ and does not change regularly with anion or PR_3 ligands (17—33) for $[NiX_2(PR_3)_2]$ (the number in parentheses is the percentage of H^- (from $NaBH_4$) consumed into butane). No increase of butane during kinetic runs shows that butane was produced via Eq. 4 rather than Eq. 5.

$$M\text{-}R + H^-(\text{from } NaBH_4) \longrightarrow M(+M\text{-}H) + RH \quad (4)$$
$$M\text{-}R + M\text{-}H \longrightarrow 2M + RH \quad (5)$$

Rate Enhancement and Retardation by Excess PR_3. Phosphines are very convenient and efficient ligands for many homogeneous catalytic reactions.[11] The disadvantages are susceptibility of orthometallation[12] and the inhibition of reactions by excess phosphines.[13,14] Some reactions which need drastic conditions such as high temperatures contain excess phosphines to maintain catalytic species irrespective of lowering of rates.[14] Many catalytic reactions by transition metal phosphine complexes are retarded by a small amount of phosphines.[14,15] Here are presented two cases where (1) the more PR_3 is added, the more the reaction is accelerated, and (2) an optimum addition of excess PR_3 gives a maximum rate as is often observed.

Acceleration of reactions by excess phosphines has been rarely observed.[16] Cobalt(II) hydrides are too unstable to be isolated and identified due to thermal unstability and lability.[17] $[CoX_2(PPh_3)_2]$ are originally tetrahedral.[6] The stoichiometric amount of $NaBH_4$ reacts with $[CoX_2(PPh_3)_2]$ to give monohydrido-substituted complexes.[18] Since hydride is a strong σ-donor but halides are weak ones,[19] monohydridocobalt complexes may change their structure into square planar one.[20] The active species should be bis(triphenylphosphine)cobalt complexes which holds the same stereoselectivity with and without free PPh_3. Excess PPh_3 can stabilize unstable cobalt hydrides which are easily decomposed by dissociation of PPh_3,[6a,b] and prevent coupling of alkyl- and hydrido-metal complexes (Eq. 5). Accelerating effect per unit PPh_3 addition decreases in the order SCN>I>Br>Cl parallel to their soft character.[21]

Large excess of $NaBH_4$ gives $[CoH_3(PPh_3)_3]$ in Ar,[22] $[CoH(N_2)(PPh_3)_3]$ in N_2,[23] and $[Co(BH_4)(PPh_3)_2]$ and $[Co(BH_4)(PPh_3)_3]$.[17] These are assigned to be tri- and monovalent. $[CoX(PPh_3)_3]$ forms on standing of $[CoHX(PPh_3)_2]$ with PPh_3 in THF. A less bulky phosphine such as PMe_3 coordinates to Co(II) to give a five-coordinate complex, $[CoMe_2(PMe_3)_3]$.[24] The reason why the third molecule of PPh_3 does not coordinate to halogenohydridocobalt(II) complexes is not obvious, but steric bulkiness of ligands may prevent further coordination.[25] In fact, excess of less bulky phosphine, PPh_2Et, hinders the isomerization catalyzed by cobalt chloride system.

A small amount of PPh_3 accelerates but large excess inhibits the reaction in $[NiX_2(PPh_3)_2]$-$NaBH_4$ systems. The c/t ratio of nickel iodide system drops at H^-/Ni>1.3 due to the partial dissociation of PPh_3. The addition of 2 mol of PPh_3 maintains the c/t ratio of 7.3. However, large excess inhibits the reaction with the coordination site for 1-butene blocked by PPh_3.[26] Less reactivity of nickel systems may come from the strength of coordinated 1-butene onto the metal.[27] More basic phosphines retard the reaction and the tendency is pronounced for nickel catalyst systems. This is caused by the stability of hydrido and alkyl metal complexes as intermediates. Many σ-alkylnickel(II) complexes including PPh_3 were isolated and characterized,[28] but only a few alkylcobalt complexes with basic phosphines were identified.[20]

Cobalt catalysts are more active than nickel ones for the complexes with the same ligands. On the contray, $[(\eta^6\text{-toluene})Ni(C_6F_5)_2]$ is a very active catalyst for 1-butene isomerization, but the analogous cobalt complex is not.[29] The electronic state of metals reflects the strength of metal-ligand bonds[30] leading to different reactivity. It is interesting that a metal

Table 3. Comparison of Stereoselectivity between Co- and Ni-Catalytic Systems

PR_3	$(c/t)_{Co}/(c/t)_{Ni}$				
	Cl	Br	I	SCN	
PPh_3	1.2	1.3	1.2	0.78	↑ π-acceptor
PPh_2Et	1.0		0.68		
$PPhEt_2$	1.5	0.87	0.32		↓ σ-donor
PEt_3		0.78			
		soft →			

complex is active but another is not where they are isostructural. It is very hard to expect which metal complex is active or not.

Stereoselectivity. Bulky phosphines and large-sized anions lead high cis-selectivity in the cobalt catalyst systems similar to $[NiX(PPh_3)_3]$.[15] Such tendency is not necessarily observed in the nickel catalyst systems. Nickel iodide complex with less bulky $PPhEt_2$ in the range of $H^-/Ni \leqq 0.6$ gives the highest cis-selectivity among Ni-catalyst systems. This is due to congested $[NiHI(PR_3)_3]$[26,31] which is formed from $[NiHI(PR_3)_2]$ and dissociated PR_3. A similar congested complex, $[CoH(N_2)(PPh_3)_3]$, gives high cis-selectivity (c/t=14) in the isomerization of 1-pentene.[32]

The atomic radius of cobalt is almost the same as that of nickel. The dependency of cis-selectivity on the metal (Table 3) is not due to the metal size. The strong σ-donor (the weak π-acceptor) character of phosphines and the soft character of anions lead the ratios, $(c/t)_{Co}/(c/t)_{Ni}$, less than unity. The electronic factor of these ligands may control stereoselectivity similar to the isomerization of 1-pentene with $[PdX_2(RCN)_2]$.[33]

Some nickel(I) complexes might be formed analogously to cobalt complexes.[34] Nickel(I) complexes effectively catalyze isomerization of olefins,[15] though cobalt(I) complexes do not. The c/t ratios in the isomerization of 1-butene catalyzed by $[NiX(PPh_3)_3]$ are 3.0, 3.7, and 8.1 for X=Cl, Br, I, respectively. The cis-selectivity is somewhat diffecrent from that by $[NiX_2(PPh_3)_2]$-$NaBH_4$ systems suggesting that Ni(I) species are rarely responsible for the reaction.

References

1) C. W. Bird, "Transition Metal Intermediates in Organic Synthesis," Logos Press, London (1967), pp. 69—87; G. W. Parshall, "Homogeneous Catalysis," Wiley-Interscience, New York (1980), pp. 27—36; A. Nakamura and M. Tsutsui. "Principles and Applications of Homogeneous Catalysis", John Wiley and Sons, New York (1980), pp. 123—125; S. G. Davies, "Organotransition Metal Chemistry, Application to Organic Synthesis," Pergamon Press, Oxford (1982), pp. 266—303.

2) G. C. Bond and M. Hellier, *J, Catal.*, **7**, 217 (1967); I. Yasumori and K. Hirabayashi, *Trans. Faraday Soc.*, **67**, 3283 (1971).

3) R. Cramer and R. V. Lindsey, Jr., *J. Am. Chem. Soc.*, **88**, 3534 (1966); C. A. Tolman, *ibid.*, **94**, 2972 (1972).

4) J. F. Harrod and A. J. Chalk, *J. Am. Chem. Soc.*, **86**, 1776 (1964); T. A. Manuel, *J. Org. Chem.*, **27**, 3941 (1962).

5) P. W. Jolly and G. Wilke, "The Organic Chemistry of Nickel," Vol. II, Academic Press, New York, (1975), pp. 54—66; M. Akita, H. Yasuda, K. Nagasuna, and A. Nakamura *Bull. Chem. Soc. Jpn.*, **56**, 554 (1983).

6) a) F. A. Cotton, O. D. Faut, D. M. L. Goodgame, and R. H. Holm, *J. Am. Chem. Soc.*, **83**, 1780 (1961); b) F. A. Cotton, D. M. L. Goodgame, M. Goodgame, and A. Sacco, *ibid.*, **83**, 4157 (1961); c) K. A. Jensen, *Z. Anorg. Allg. Chem.*, **229**, 265 (1936).

7) L. M. Venanzi, *J. Chem. Soc.*, **1958**, 719; G. N. Schrauzer and P. Glockner, *Chem. Ber.*, **97**, 2451 (1964); R. G. Hayter and F. S. Humiec, *Inorg. Chem.*, **4**, 1701 (1965).

8) The reaction was carried out with 0.20 mmol of $CoCl_2$, 0.20 mmol of $NaBH_4$ and 4.17 mmol of 1-butene in 3 ml of THF and 2 ml of glyme in an H_2 atmosphere at 0 °C for 24 h. V.p.c. analysis gave 67.4% of 1-butene, 15.3% of butane, 10.9% of *trans*-2-butene and 6.4% of *cis*-2-butene.

9) M. L. H. Green and D. J. Jones, *Adv. Inorg. Chem. Radiochem.*, **7**, 115 (1965).

10) G. L. Geoffroy and J. R. Lehman, *Adv. Inorg. Chem. Radiochem.*, **20**, 189 (1977).

11) "Catalytic Aspects of Metal Phosphine Complexes," ed by E. C. Alyea and D. W. Meek, ACS. Washington, D. C., 1982; "Honogeneous Catalysis with Metal Phosphine Complexes," ed by L. H. Pignolet, Plenum Press, New York (1983).

12) G. Parshall, *Acc. Chem. Res.*, **3**, 139 (1970); **8**, 113 (1975); M. I. Bruce, *Angew. Chem., Int., Ed. Engl.*, **16**, 73 (1977).

13) B. R. James, "Homogeneous Hydrogenation," John Wiley & Sons, New York (1973).

14) E. R. Tucci, *Ind. Eng. Chem., Prod. Res. Dev.*, **9**, 516 (1970).

15) H. Kanai, K. Kushi, K. Sakanoue, and N. Kishimoto, *Bull. Chem. Soc. Jpn.*, **53**, 2711 (1980).

16) J. X. McDermott, J. F. White, and G. M. Whitesides, *J. Am. Chem. Soc.*, **98**, 6521 (1976).

17) a) H. D. Kaesz and R. B. Saillant, *Chem. Rev.*, **72**, 231 (1972); b) R. D. W. Kemmitt and D. R. Russell, "Comprehensive Organometallic Chemistry," Pergamon Press, Oxford, 1982, Vol. 5, p. 1.

18) D. G. Holah, A. N. Hughes, B. C. Hui, and C. T. Kan, *Can. J. Chem.*, **56**, 814 (1978); R. C. Wade, D. G. Holah, A. N. Hughes, and B. C. Hui, *Catal. Rev. Sci. Eng.*, **14**, 211 (1976).

19) F. R. Hartley, *Chem. Soc. Rev.*, **2**, 163 (1973) G. Butler, J. Chatt, G. J. Leigh, and C. J. Pickett, *J. Chem. Soc., Dalton Trans.*, **1979**, 113; J. Chatt, C. T. Kan, G. J. Leigh, C. J. Pickett, and D. R. Stanley, *ibid.*, **1980**, 2032.

20) Ref. 17 b), p. 74.

21) U. Belluco, L. Cattalini, F. Basolo, R. G. Pearson, and A. Turco, *J. Am. Chem. Soc.*, **87**, 241 (1965); R. G. Pearson, H. Sobel, and J. Songstad, *ibid.*, **90**, 319 (1968).

22) A. Sacco and M. Rossi, *J. Chem. Soc., Chem. Commun.*, **1967**, 316; *Inorg. Chim. Acta*, **2**, 127 (1968).

23) A. Yamamoto, S. Kitazume, L. S. Pu, and S. Ikeda, *J. Am. Chem. Soc.*, **93**, 371 (1971); E. Balogh-Hergovich, G. Speier, and L. Marko, *J. Organomet. Chem.*, **66**, 303 (1974).
24) H. F. Klein and H. H. Karsh, *Chem. Ber.*, **109**, 1453 (1976).
25) B. E. Mann and A. Musco, *J. Chem. Soc., Dalton Trans.*, **1975**, 1673 and references cited therein.
26) A. N. Nesmeyanov, L. S. Isaeva, and L. N. Lorens, *J. Organomet. Chem.*, **129**, 421 (1977).
27) M. Herberhold, "Metal π-Complexes," Elsevier Pub., Amsterdam, (1972), Vol. II, pp. 95—101, 125—132; Ref. 17 b), pp. 177—192; C. A. Tolman, *J. Am. Chem. Soc.*, **96**, 278 (1974).
28) P. W. Jolly, "Comprehensive Organometallic Chemistry," ed by G, Wilkinson F. G. A. Stone, and E. W. Abel, Pergamon Press, Oxford (1982) Vol. 6, p. 37.
29) H. Kanai, S. B. Choe, and K. J. Klabunde, *J. Am. Chem. Soc.*, **108**, 2019 (1986).
30) L. J. Radonovich, K. J. Klabunde, C. B. Behrens, D. P. McCollor, and B. B. Anderson, *Inorg. Chem.*, **19**, 1221 (1980).
31) A. N. Nesmeyanov, L. S. Isaeva, L. N. Lorens, and V. S. Kolesov, *Dokl. Chem.*, **223**, 477 (1975).
32) F. Pennella, *J. Organomet. Chem.*, **78**, C10 (1974).
33) S. Sakaki, H. Kanai, and K. Tarama, *Can. J. Chem.*, **52**, 2857 (1974).
34) D. G. Holah, A. N. Hughes, B. C. Hui, and C. T. Kan, *Can. J. Chem.*, **56**, 2552 (1978).

 © 1987 The Chemical Society of Japan Bull. Chem. Soc. Jpn., 60, 1595—1605 (1987)

Raman Spectra and Electronic Structure of Alkaline Metal Doped Polyacetylene and β-Carotene

Jiro TANAKA,* Yasuyoshi SAITO, Masaaki SHIMIZU, Chizuko TANAKA, and Masashi TANAKA†
Department of Chemistry, Faculty of Science, Nagoya University, Chikusa-ku, Nagoya 464
†College of General Education, Nagoya University, Chikusa-ku, Nagoya 464
(Received October 8, 1986)

Raman spectra of alkaline metal doped polyacetylene were studied at various levels of doping for $(CHM_y)_x$, and $(CDM_y)_x$, M=Na and K, with y=0—0.18. Several steps in the doping process can be recognized in changes of the Raman spectra; the initial Raman lines remain for y=0—0.06 but change completely into a new pattern at y=0.13. Raman and ESR spectra of alkaline metal doped β-carotene were measured as a model study of the alkaline metal doping of polyacetylene. The correlation of these spectra together with the ab initio SCF MO calculation on model compounds show that a heavily alkaline metal doped polyacetylene chain does not have a uniform bond length structure but is composed of a charged soliton structure connected by a uniform chain. The new Raman bands were assigned based on this structure, implying that a bond alternation still exists in the metallic state of alkaline doped polyacetylene.

Raman spectra of neat and doped polyacetylene (PA) provide characterizing insight regarding the molecular structure of the polymer.[1] The change in the Raman spectra upon doping the polymer has been extensively investigated; however, only a relatively few studies have appeared which discuss the quantitative aspect of alkaline metal doping of PA.[2,3] Recently, Heeger et al.[4,5] discussed the structural change from a spinless soliton lattice to a metallic polaron lattice in alkaline metal doping of PA by an ESR measurement. In this paper we present Raman spectral evidence of a structural change occurring at a definite level of Na and K doping of $(CH)_x$ and $(CD)_x$. The Raman and ESR spectra of Na-doped β-carotene were measured; here, the structure of the anion radical is discussed in terms of an analysis of the hyperfine structure and chemical information. The structure of alkaline metal doped PA is considered from an ab initio SCF MO calculation of the model compound[6] and a close similarity of the Raman spectra between the Na doped PA and Na doped β-carotene. The present study gives information regarding the structural aspect of a heavily doped PA lattice and the nature of the structural change occurring in the doping of PA.

Experimental

Materials. Thin films of PA were synthesized by Shirakawa's method[7] on the inner surface of a quartz cell for UV, visible, near IR and Raman spectral measurements. Doping was carried out by the use of naphthalene anions in a dried THF solution. The film was immersed into the solution under a completely sealed condition and washed with THF for five to ten times until the solution became colorless. β-Carotene was recrystallized from benzene and stored under a nitrogen atmosphere.

Spectrometers. Visible and near IR spectra were measured by a Hitachi model 330 spectrophotometer (40000—4000 cm^{-1}). In situ doping and combined visible, near IR and Raman spectral measurements were carried out using a JEOL Model JRS 400T spectrometer with Ar-ion (Spectra Physics 164-05) and He-Ne lasers (Spectra Physics 125A) and a Varian Model 2300 spectrophotometer at the Instrument Center of Institute for Molecular Science (IMS). ESR spectra were obtained by a Varian E112 at X-band in IMS. IR spectra were measured with a Hitachi 230-50 spectrophotometer.

Analysis. The dopant content was analyzed by a flame analysis using an Evans Model 100 flame photometer. A radiation chemical analysis was performed with some films by Dr. Tohru Kishi of National Police Science Institute.

Conductivity. All conductivity measurements were carried out by a four-probe technique, and the mechanical pressed contacts were applied between the film and the Pt leads. The measurement was carried out down to 80 K in cold N_2 gas.

Results and Discussion

(1) Doping and Electronic Spectra. The visible and near IR spectra of PA are largely dependent on the concentration of the dopant in PA.[8-10] In order to estimate the doping level of the polymer, the visible and near IR absorption of Na-doped PA were measured at several concentrations of the dopant. The spectra were taken on different films of approximately the same thickness; the absorbance was recorded by normalizing the absorption peak of *cis*-PA at 18500 cm^{-1} to unity. The change in the spectra upon doping in the near IR region was recorded with reference to the peak intensity of an undoped *cis*-rich film. The dopant content was analyzed on each thin film; the thickness of the film was estimated before doping by the absorption intensity[11] and the total amount of PA was determined from the area and the thickness of the film. Then, the composition was determined on each film. The optical densities of the doped film were found to change with the dopant concentration.[10] It appears that the 6000 cm^{-1} band increases almost linearly, while the 18500 cm^{-1} band

also decreases linearly with the dopant concentration. A change in the spectra might be recognized as being due to a transition from the undoped *cis*-$(CH)_x$ to the doped state of PA. A doped film has a characteristic electronic absorption band at about the 6000 cm^{-1} region.[8] Another broad peak was recognized around the 38000 cm^{-1} region, which may indicate that the electronic structure of the polyene chain is completely changed. By the use of a linear relation[10] between the dopant concentration and the absorption intensities, the dopant level was estimated for each doped film in the following measurements. The ratio of the optical densities in the near IR region to the maximum in the visible region before the doping was used to estimate the dopant concentration at each stage of doping.

The change in the electronic spectra after compensation of the dopant by H_2O in the air is shown in Fig. 1. The spectrum of the cis-rich film before Na doping is shown by curve 0 and curve 1 is that of a heavily doped film. The vacuum system was leaked to 0.1 Torr (1 Torr=133.322 Pa) and the spectral change was recorded. The intensity of the 6000 cm^{-1} peak decreased and the 16000 cm^{-1} band increased by a reaction of the Na doped film with H_2O. After three hours the intensity at 6000 cm^{-1} almost disappeared and a new peak of the trans form was found at 16000 cm^{-1}; the cis-form band was not found. The result indicated that the cis-trans isomerization occurred completely by Na doping and that the trans film was obtained by a reaction of Na with H_2O. A side reaction, such as bond cleavage, was not involved since the spectral curve 7 (Fig. 1) was coincident with that of native trans film.

The origin of the 6000 cm^{-1} band is not unique; at the initial stage of doping, the so-called mid gap absorption was found in this region.[8] However, a heavily doped film may show broad absorption due to free carriers, as was observed in the case of an I_2 doped PA film.[12] A distinction between the two origins is not easy; however, the predominance of the mid gap band in the initial stage and the free carrier in the final stage was confirmed by reflectivity measurements as well.[9]

(2) Near IR and Raman Spectra of Doped *trans*-$(CH)_x$. Measurements of near IR absorption and Raman spectra of doped PA films were carried out systematically with in situ doping and monitoring of

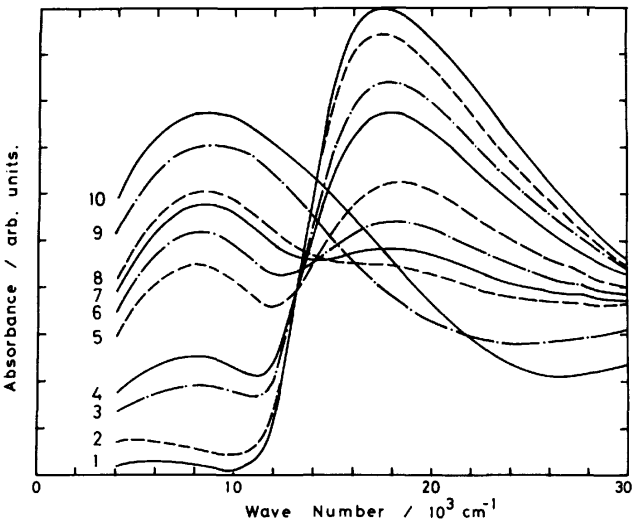

Fig. 2. Absorption spectra of the same thin *trans*-PA film doped with Na. The numbers of the curves correspond to the doping level y in $(CHNa_y)_x$; (1) y=0, (2) y=0.015, (3) y=0.036, (4) y=0.047, (5) y=0.085, (6) y=0.095, (7) y=0.108, (8) y=0.114, (9) y=0.133, and (101) y=0.146.

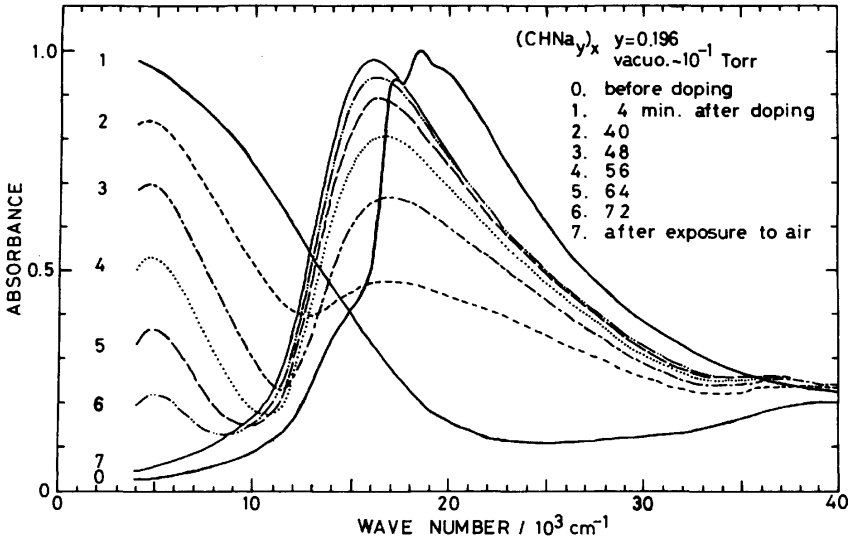

Fig. 1. Absorption spectral change of Na doped as grown $(CH)_x$ film after exposing to the keak of air. (0) undoped film, (1) doped film, after 4 min, (2) 40 min, (3) 48 min, (4) 56 min, (5) 64 min, (6) 72 min, (7) 3 h. exposing to the air.

the dopant level. Figure 2 illustrates changes in the near IR spectra of *trans*-$(CH)_x$ film upon Na doping at each stage; cruve 1 is for undoped *trans*-PA and 10 is for heavily doped film. Two isosbestic points were found in the series of spectra; the first one appears at 13200 cm^{-1} in the initial stage (y=0—0.05; y refers to atomic composition in $(CHNa_y)_x$) and the second one was observed at 14000 cm^{-1} in the intermediate stage (y=0.08—0.11). The same PA film was used for all measurements. These isosbestic points could be clearly found for initially isomerized trans-film; if we use a cis-rich film, the cis-trans isomerization process is involved which shows another spectral change. The appearance of two distinct isosbestic points may imply that the doping proceeds through several steps, and that it is consistent with electrochemical doping results,[13] where several reduction potentials were observed for the doping process of y=0—0.18.

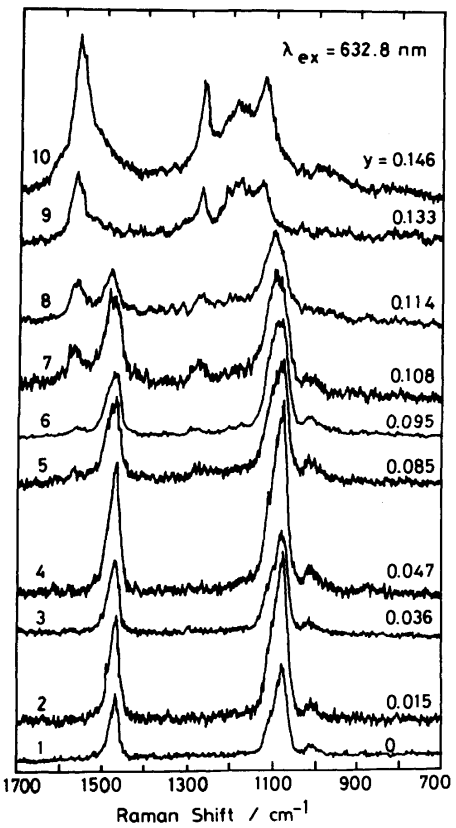

Fig. 3. Raman spectra of thin *trans*-$(CH)_x$ film doped with Na; the composition is shown by the value of y in $(CHNa_y)_x$.

The Raman spectra measured at 632.8 nm (15803 cm^{-1}) excitation are shown in Fig. 3, where the excitation wavelength is selected so as to obtain optimum efficiencies to both the undoped and doped part of PA. The undoped part showed an absorption peak at 18500 cm^{-1}. On the other hand, the doped part displayed an absorption peak at 6000 cm^{-1}, only a post resonance condition is realized by 15803 cm^{-1} excitation. In spite of this, the excitation at 632.8 nm is the best means to find any structural change during the doping process by the Raman spectra. This is because short-wavelength excitation shows little efficiency to the Raman bands of the doped part of PA.

Figure 3 shows that the characteristic Raman bands of *trans*-PA at 1470 and 1080 cm^{-1} did not change at all during the initial stage of doping (curves 1—4). In contrast with this, the characteristic absorption band in the near IR region increased linearly with the dopant; therefore, it is suggested that the skeletal conformation of PA is not significantly changed from the initial structure during the first stage of doping except for the local region where Na is coordinated. The structure of the metal coordinated chain is found by a theoretical calculation[6] (Fig. 4); this particular structure may be called a charged soliton structure in the following discussion. For a light doping level, charged soliton structures are formed in pairs, since no spin susceptibility has been found and such a structure has been called bipolaron.[8,14] The singlet state is obtained by putting two charged soliton structures at distant positions of the conjugated chain with an inversion symmetry; such a chain may give Raman spectra that are almost the same as that of undoped PA.

In the spectra of an intermediate stage of doping (Fig. 3, curves 5—8), new Raman lines appear at 1560, 1275 cm^{-1} etc.; however, a reminiscence of the initial lines suggests that the lightly doped bipolaron structure coexists with the new structure at this stage ($0.08<y<0.11$). The intensities of the new and initial

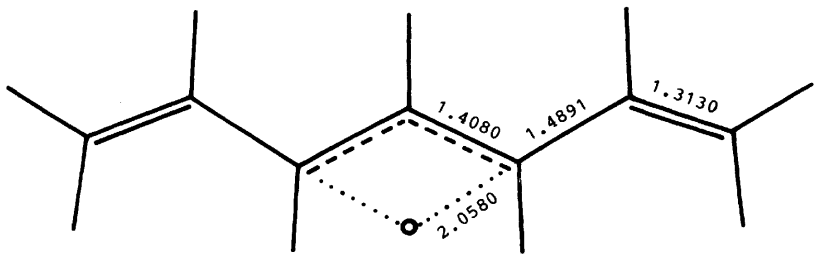

Fig. 4. A model of charged soliton structure, C_7H_9LI, estimated by ab initio SCF MO calculation.

bands are almost equal at y=0.114; the spectra changed completely to a new form above y=0.133. The new structure shows strong peaks at 1570, 1275, 1180, and 1125 cm^{-1} and weak ones at 1040 and 900 cm^{-1}. The transition to the new form may be completed at y≈0.13; the critical point to the new form may be at y=0.12—0.13.

The changes in the visible, near IR and Raman spectra with K doping were almost the same as that of Na doping. The Raman spectrum of a heavily K-doped $(CH)_x$ film showed a peak at 1560 cm^{-1}, about 10 cm^{-1} lower compared to the Na doped film. This result indicates that the 1560 cm^{-1} band is closely connected with the charged soliton structure, since the position is affected by the kind of coordinated metal atom.

(3) Doping and Spectral Changes of *trans*-$(CD)_x$. Changes in the visible and near IR spectra of Na doped *trans*-$(CD)_x$ were measured (Fig. 5). The 18500 cm^{-1} band decreased and the 6000 cm^{-1} band increased as the doping proceeded. Isosbestic points were found at 12500 and 14000 cm^{-1}, as detected in $(CH)_x$ film. The dopant level in $(CD)_x$ was similarly estimated as for $(CH)_x$ film using a calibration curve.[10] The change in the Raman spectra with increasing dopant concentration is illustrated in Fig. 6. The critical point of the Raman-spectral change is much clearer for $(CD)_x$ than $(CH)_x$; the Raman band did not change for y=0—0.09 (curves 1—4) and the transition state appeared at y=0.113 and then changed drastically at y=0.13. The transition from the initial state to the new form occurred rather suddenly and the critical concentration was almost same as $(CH)_x$ at y=0.12.

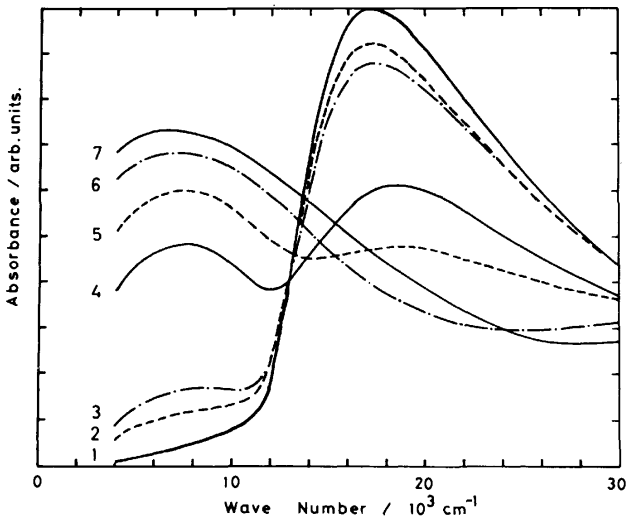

Fig. 5. Absorption spectra of *trans*-$(CD)_x$ film doped with Na. The numbers of absorpiton curves correspond to the content of Na in $(CDNa_y)_x$; (1) y=0, (2) y=0.023, (3) y=0.031, (4) y=0.090, (5) y=0.113, (6) y=0.129, and (7) y=0.140.

The Raman bands of a heavily K-doped $(CD)_x$ film were found at 1500 and 900 cm^{-1}, which were 20 cm^{-1} lower and 10 cm^{-1} higher than the bands of $(CDNa_y)_x$. This result is consistent with the previous argument that these bands are associated with the metal coordinated charged soliton region.

(4) Change of Electronic and Raman Spectra in Na Doping of as Grown $(CH)_x$ and $(CD)_x$ Films. An as-grown $(CH)_x$ film by Shirakawa's method is obtained as a cis-rich form but the isomerization to the trans form occurs to some extent at ambient temperature. The Na doping of a cis-rich film accelerates isomerization to the trans form. The Raman spectra may show the process of a cis-trans isomerization and a transformation to the new form. The change in the visible and near IR spectra of a cis-rich film were measured during Na doping; apparent isosbestic points were found at 14300 cm^{-1} for y=0—0.05 and at 14800 cm^{-1} for y=0.08—0.13. The Raman spectra of the doped cis-rich film were measured and the characteristic cis peaks disappeared almost completely at y=0.10; a new peak appeared at y=0.13 and a transition to the new form occurred at y=0.15 and completed at y=0.17. The critical concentration for this transition was relatively higher than the case starting from a pure trans film.

The changes in the Raman spectra of an as-grown $(CD)_x$ film by Na doping were also measured with the

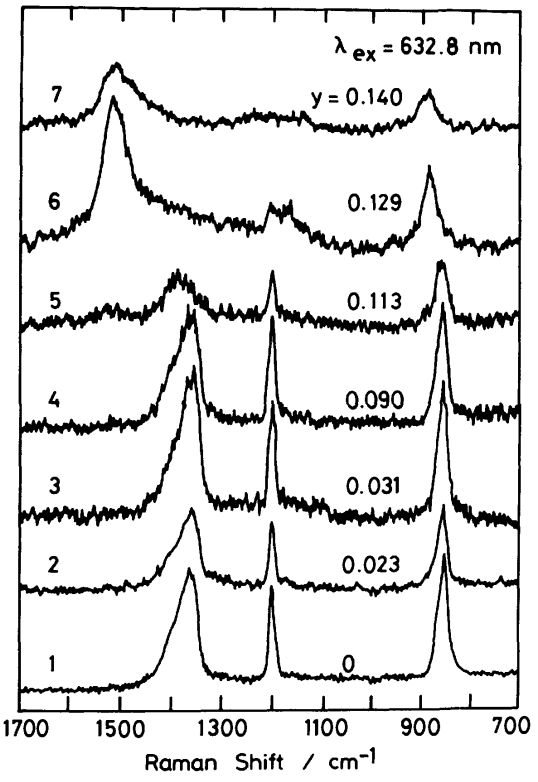

Fig. 6. Raman spectra of *trans*-$(CD)_x$ film doped with Na. The content of Na is shown by y value in the figure.

same film at various stages of doping from $y=0$ to $y=0.18$. The cis-trans isomerization was completed at $y=0.11$ and the new lines were found at $y=0.14$; the transition to the new form was complete at $y=0.18$.

(5) Dispersion of Raman Lines by Changing Excitation Wavelength. The dispersion of the Raman spectra upon changing the excitation wavelength has been found for a *trans*-PA film[1,15-17]; however, it has been explained by an inhomogenous distribution of the chain length of the polymer.[1] Dispersion effects were also found for Na-doped ($y=0.11$ and 0.13) and K-doped ($y=0.15$) *trans*-$(CH)_x$ film. The presence of two forms at $y=0.11$ and 0.13 was clearly indicated by changing the excitation wavelength. The film with $y=0.11$ showed only initial PA lines upon 488.0 and 514.5 nm excitations since the content of the new form was too small. The film with $y=0.13$ showed a new band by 632.8 nm excitation and the initial band which was at 1520 cm^{-1} (514.5 nm) and 1525 cm^{-1} (488.0 nm excitation), considerably higher than the initial PA band. The completely transformed film with $y=0.15$ showed no initial lines, even upon short wavelength excitation. A slight dispersion of the 1555 cm^{-1} line was found at 1585 cm^{-1} (514.5 nm) and 1590 cm^{-1} (488.0 nm).

The dispersion effect was also measured for the film with $y=0.13$ of *trans*-$(CDNa_y)_x$ and $y=0.18$ of initially cis film. Upon short wavelength excitation of $y=0.13$ film, the 1450 cm^{-1} band of a relatively short conjugated double bond was found to be rather strong; however, under 632.8 nm excitation the same film exhibited only Raman lines of the new form. In contrast, the heaviest doped film showed only the new lines under excitation at any wavelength, implying that the PA chain was completely trans formed into the new form. The Raman lines showed a dispersion effect upon changing the excitation wavelength: 1555 cm^{-1} (457.9 nm), 1541 cm^{-1} (514.5 nm), and 1515 cm^{-1} (632.8 nm), respectively.

The dispersion relation upon changing the excitation wavelength for $y=0.11$ as-grown film was almost the same as that of the undoped trans film. However, those for the $y=0.17$ as-grown film showed almost a new form; but a small fraction of the trans form was observed under 457.9 nm excitation. The completely transformed as-grown $(CDNa_y)_x$ film ($y=0.18$) showed a small dispersion effect upon changing the excitation wavelength.

(6) DC Conductivity Measurement of Na Doped as Grown $(CH)_x$. The room-temperature d.c. conductivity of a Na doped as-grown PA film was measured as a function of y. The conductivity increased rapidly from $y=0$ to 0.03 and saturated at about $y=0.10$. The maximum conductivity was 72 S cm^{-1} at 295 K for a film with $y=0.18$ The temperature dependence of the conductivity was measured and plotted for $1/T$ (Fig.

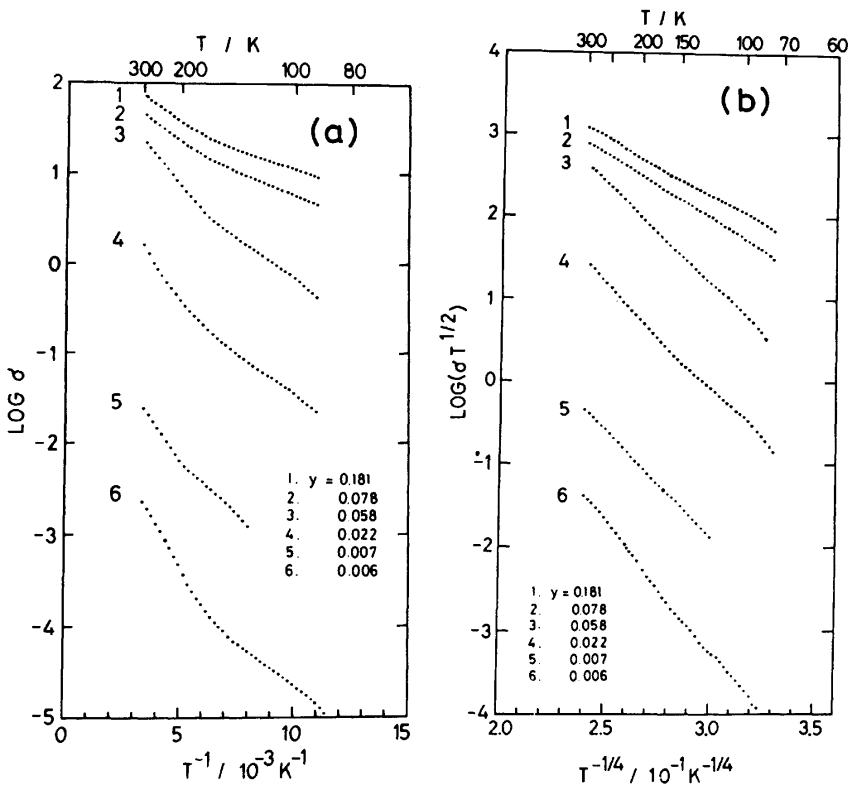

Fig. 7. Temperature dependence of conductivity of Na doped $(CH)_x$; (a) log σ plot for $1/T$, (b) log σ $T^{1/2}$ plot for $T^{-1/4}$; the doping levels are shown in the figure.

7(a)). Also, the activation energies were estimated from the initial slopes; the values were about 0.1 eV for lightly doped films and 0.03 eV for $y=0.18$. A plot of log $(\sigma T^{1/2})$ against $T^{-1/4}$ gave a straight line (Fig. 7(b)). Mott's variable range hopping model[18] could be applied for an analysis of the conduction mechanism. The parameters by this analysis are shown in Table 1, where $T_0=16\,\alpha^3/k_B N(E_F)$ and α^{-1} is the decay length of a localized state. These values are comparable to the values reported for I_2 and $FeCl_3$ doped $(CH)_x$.[19,20]

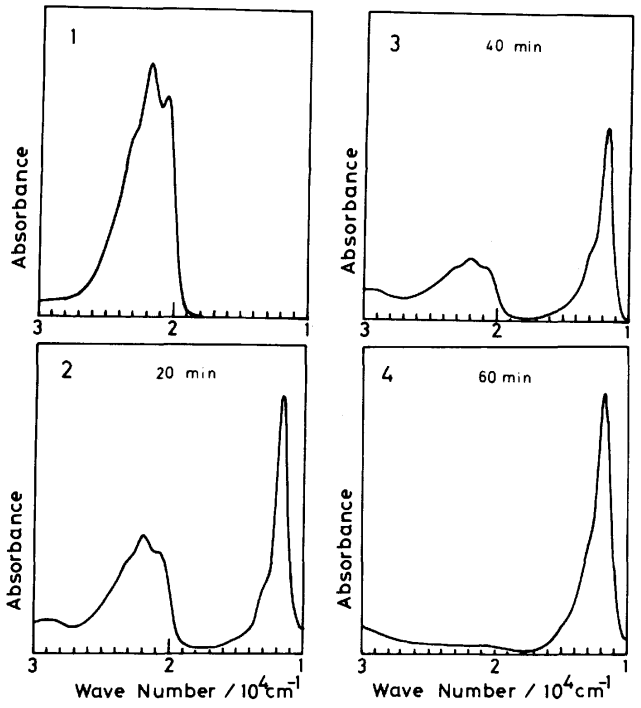

Fig. 8. Absorption spectral changes of β-carotene with Na doping. (1) undoped β-carotene, (2) 20 min, (3) 40 min, (4) 60 min, after doping. (Absorbances are given in arbitrary unit).

(7) Electronic, ESR and Raman Spectra of Na Doped β-Carotene. The characteristic absorption spectra of β-carotene in the visible region was changed upon Na doping (Fig. 8). As the doping proceeded the absorption band around 20000 cm^{-1} decreased and

Table 1. Parameters for Mott's Variable Range Hopping Model

y	σ(300 °K)/S·cm^{-1}	$T_0/10^6$ K°	A/10^7 S·cm^{-1}·K$^{1/2}$
0.181	72	1.2	0.34
0.076	44	1.5	0.38
0.056	22	12	62
0.022	1.7	15	7.5
0.010	0.045	40	20
0.006	0.002	46	2.0

The conductivity σ is given by a formula $\sigma(T)=AT^{-1/2}\exp(-(T_0/T)^{1/4})$, and $A=0.39(N(E_F)/\alpha k_B)^{1/2}\nu_0 e^2$ where ν_0 is optical phonon frequency.

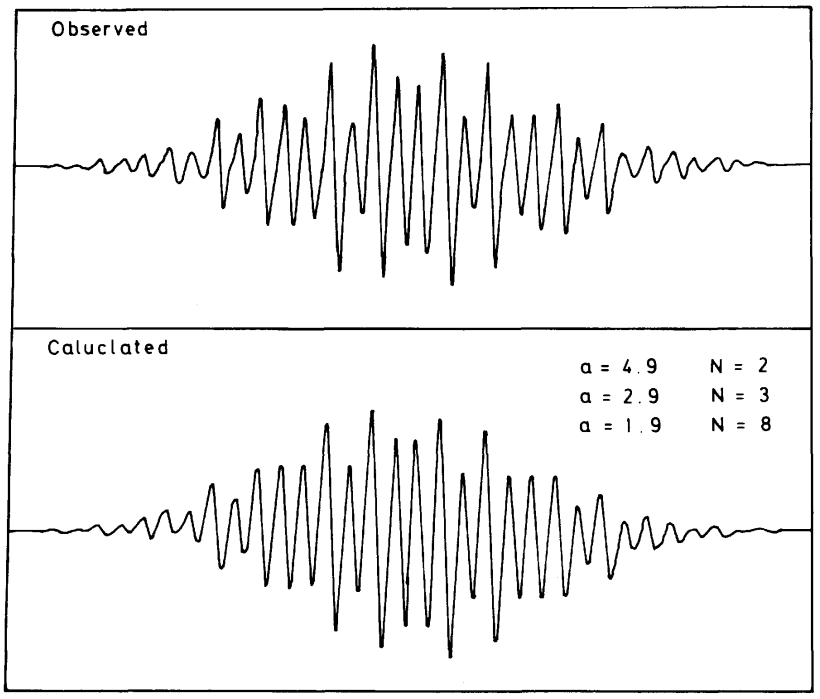

Fig. 9. ESR spectra of Na doped β-carotene in THF solution. Upper curve is the observed ESR spectra by low resolution and the lower one is simulated ESR spectra.

new bands were found at around 12000 cm^{-1} as well as another broad one at a higher energy region. The tail of the higher energy band was found around 30000 cm^{-1}. The ESR spectra of Na-doped β-carotene in a THF solution at low and high resolution were measured (Fig. 9(a)) and the low-resolution spectra were simulated (Fig. 9(b)) by the following coupling parameters: two protons with a_H=4.9 Gauss, three protons with a_H=2.9 Gauss and eight protons with a_H=1.9 Gauss. The agreement between the calculated and the observed spectra are quite satisfactory. In these simulations, the ESR hyperfine structures could be explained by assuming the coupling of an unpaired electron with thirteen hydrogen atoms; this result is important when considering the structure of Na-doped β-carotene.

In order to determine the structure of doped β-carotene, the reaction product of β-carotene with Na was decomposed with H_2O; also, a mass spectral analysis was performed on the product. It showed that eight hydrogen atoms reacted and that the positions of the coordinated alkaline atoms were guessed (Fig. 10(a)) since the mass spectra indicated a fragmentation of the hydrogenerated compound at these positions. This part of the experiment was carried out by Mr. H. Ozeki under the guidance of Dr. M. Kitamura of Prof. Noyori's laboratory. The electrochemical reduction potentials of β-carotene in the THF solution also indicated that the reaction took place to the level of a four-electron reduction.[21] Then, the structure of the radical, which was found in THF solution, is considered as shown in Fig. 10 (b); the localization of the unpaired electron over the chain of nine carbon atoms can be naturally understood by this structure.

The Raman spectra of Na doped β-carotene in a THF solution were significantly changed by the wavelength of excitation (Fig. 11). This result implies that the solution includes both forms shown in Fig. 10 (a) and (b) and that a doped molecule has several chromophoric groups. The Raman spectrum at 457.9 nm excitation was compared with that of the

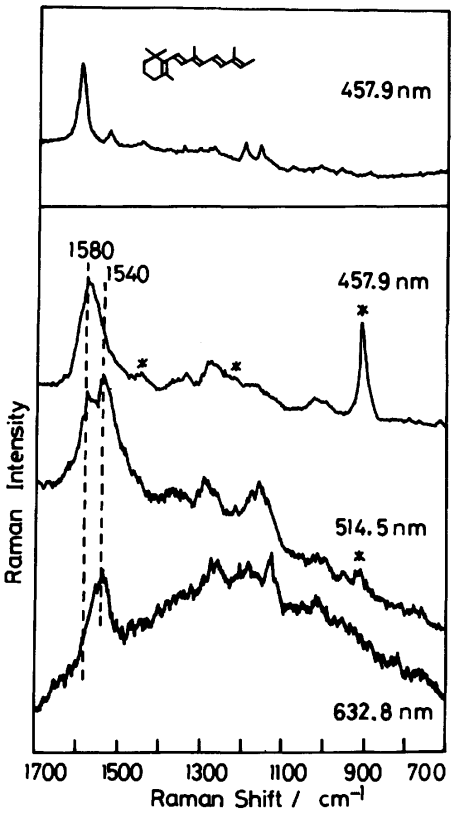

Fig. 11. Raman spectra of Na doped β-carotene and axerophten. The top curve is that of axerophten and the upper one is that of Na doped β-carotene, which are excited by 457.9 nm. The middle curve and the bottom one are Raman spectra of Na doped β-carotene excited by 514.5 and 632.8 nm, respectively.

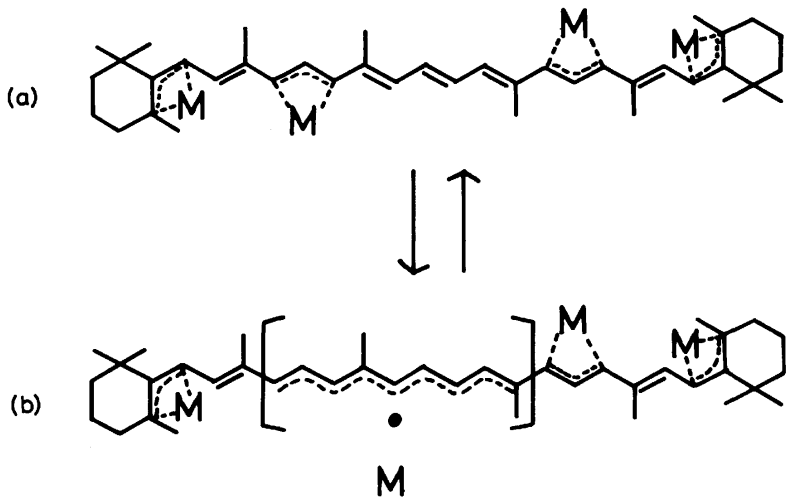

Fig. 10. Equilibrium structures of alkaline metal doped β-carotene.

model compound, axerophten[22], which was kindly prepared by Prof. K. Yamada and Mr. H. Kigoshi of this Department (Fig. 11). The similarity between the two spectra strongly suggests that the doped β-carotene has a partial structure of a short conjugated chain. Regarding SO_2 doping of β-carotene, Harada et al.[1] proposed that the molecule has a shortened double bond system, which is consistent with the present result. By considering these experimental results, the molecular structure of Na-doped β-carotene could be guessed by a formula (a) (Fig. 10).

(8) Structure of Alkaline Metal Doped Polyacetylene. Although a PA film comprises many fibrils and a lightly doped film is never homogeneous, alkaline metal doping proceeds through several stages, implying that a definite conformation exists for each doping step. From the present result and electrochemical studies,[13] three stages are conceivable for the doping process. When the dopant concentration is dilute ($y<0.06$), the doped PA chain can have a charged soliton structure (Fig. 12(a)) in which a bipolaron with about twenty carbon atoms between metal atoms can be formed at first. At a higher dopant level, the PA chain has one Na atom for about six carbon atoms ($y=0.16$) and the chain has unpaired electrons. (Fig. 12(b)) In the intermediate regime ($y=0.06$—0.12) both forms can coexist.

The result of an ab initio SCF MO calculation on the model compound, dilitiopolyenes,[6] is useful for determining the structures of a bipolaron and a heavily doped PA chain. The structure of the singlet state of dilithiopolyene represents a model of the bipolaron structure (Fig. 12 (a)). The triplet state has a unique structure in which a charged soliton structure and a chain without bond alternation are sequentially connected (Fig. 12(b)). Such a structural characteristic was already envisaged in the proposed model of β-carotene anion radical, in which the radical chain is conjugated with a charged soliton structure.

A structural feature of the charged soliton calculated by ab initio SCF MO is represented in Fig. 4; one Li atom coordinates to the end two carbon atoms in a three-carbon chain, the bond alternation being lost in the central coordination region which has an intermediate bond length with weak adjacent bonds. Then, the next adjoining bonds are strong (bond lengths are long and short). The planarity of the conjugated chain including the CH bond is lost ; the effect of coordination is rather limited within the region shown in Fig. 4. The coordinated Li atom forms a domain wall separating the conjugated chain into regions of different phases. Such a characteristic structure of a charged soliton is always found in both the singlet and triplet states of dilithiopolyene and the doublet state of lithiopolyene. In the singlet state such structures are connected by the normal conjugated double bond with an inversion symmetry in the center of the chain and the conjugation between the soliton structure is extended for long range (Fig. 12(a)). This reduces the Raman frequencies to the value of the extended long chain. In the triplet state the charged soliton structures are connected by a uniform bond length chain and the conjugation between the double-bond units are lost (Fig. 12(b)). This difference in conjugation mode is the origin of a drastic change in the Raman spectra from the initial to the final doped level and in magnetic properties during doping. In the intermediate stage of doping, both structural characteristics can coexist, rather than another structure being involved. This is because the Raman spectra exhibit only the mixed bands of the initial and the final structures (Figs. 3 and 6).

(9) Assignment of Vibrational Bands. The neat *trans*-PA has an alternating double bond structure; the double and single bond lengths are estimated as 1.36

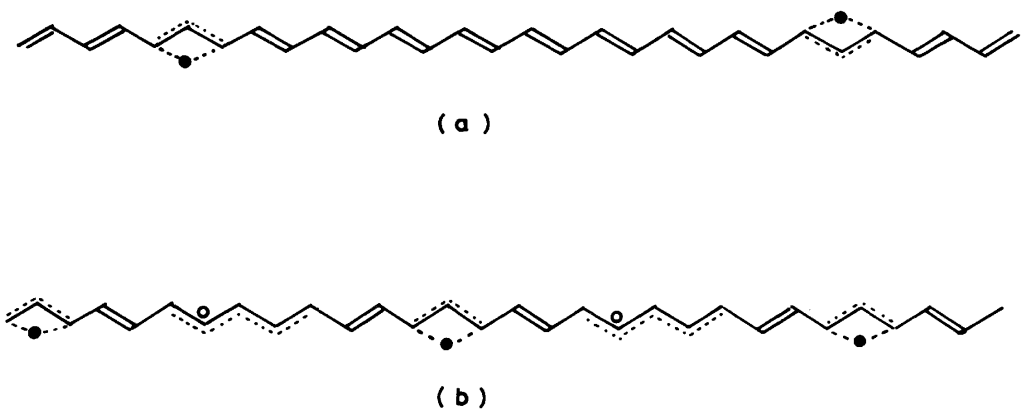

Fig. 12. Proposed model structures of (a) the lightly doped chain (charged soliton pair (bipolaron)) and (b) the heavily doped *trans*-PA chain. The filled circle (●) represents the coordinated alkaline metal ion, and the open circle (○) implies the coordinated alkaline metal atom.

and 1.44 A, respectively.[23] A normal coordinate analysis on Raman bands of *trans*-PA was recently presented by Takeuchi et al.;[24] the 1470 cm^{-1} band and 1079 cm^{-1} band of $(CH)_x$ were assigned to the coupled modes of the -(C=C)- stretching and the C-H in plane bending and the weak band at 1295 cm^{-1} was assigned to the stretching of the -(C-C)- single bond.

In the lightly doped *trans*-PA chain, a pair of soliton structures (bipolaron) were formed (Fig. 12(a)); this particular structure may have characteristic IR and Raman bands. In the IR spectra of Na-doped PA reported by Francois et al.[25] an intense band was observed at 1410 cm^{-1}, weak bands at 1250 cm^{-1}, and broad strong bands below 1100 cm^{-1}. In the IR spectra of Li-doped PA measured by us (Fig. 13), strong peaks were found at 1420 cm^{-1}, a weak one at 1250—1280 cm^{-1}, another weak one at 1160 cm^{-1}, and fairly strong bands below 1060 cm^{-1} at 1060, 950, 830, and 650 cm^{-1}. These band characteristics are common to the n- and p-doped PA;[8] therefore, they may be regarded as the charged soliton characteristic band.

The IR absorption bands associated with the charged soliton are not a simple atomic vibration in the usual sense; this is because the atomic vibration is strongly coupled with the charge flow along the chain and the intensities are extraordinaly large compared to usual infrared absorption of the polymer. In the theoretical treatment of the IR absorption of charged soliton by Horovitz[26], Wada and Terai et al,[27] and Mele and Hicks[28] several in-plane vibrational modes were considered to couple with electron. We suppose that the CH bending and several C-C stretching vibrations around the metal coordinated center are coupled. The prominent IR band at 1400 cm^{-1} is assigned to the C-H in plane bending of the charged soliton structure, because it is largely shifted by deuteration[29,30] and the peak position is dependent on the metal species. The weak 1250—1280 cm^{-1} IR band may be the coupled mode of several C-C stretchings around the charged soliton and the strong band around 1050 cm^{-1} region may be another coupled mode of C-C stretchings.

The Raman spectra of the lightly or medium doped $(CH)_x$ and $(CD)_x$ did not show any characteristic band of the charged soliton. This is because the electronic absorption band of the charged soliton lies in the near IR region and the resonance condition is not satisfied even under 632.8 nm excitation. Also, the short double bonds in the charged soliton structure are coujugated with the chain of a double-bond system in the bipolaron structure; it may give the vibrational mode of the long chain. In the heavily doped regime, the charged soliton structure is rather isolated (Fig. 12(b)) and the Raman bands of the charged soliton may be found at 1570 and 1125 cm^{-1} in addition to the 1270 and 1180 cm^{-1} bands.

Zannoni and Zerbi[31] discussed the vibrational modes of doped PA from a symmetry consideration regarding defect structure and a selection rule. They argued that a C_{2v} local symmetry of the charged soliton is rather unlikely compared to the centro-symmetrical defect structure of C_{2h} symmetry. In our analysis, the charged soliton structures might have appeared in pairs by forming a bipolaron during the

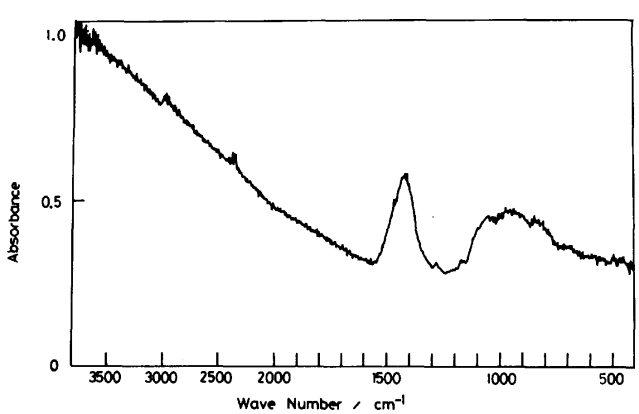

Fig. 13. Infrared spectrum of Li doped thin $(CH)_x$ film.

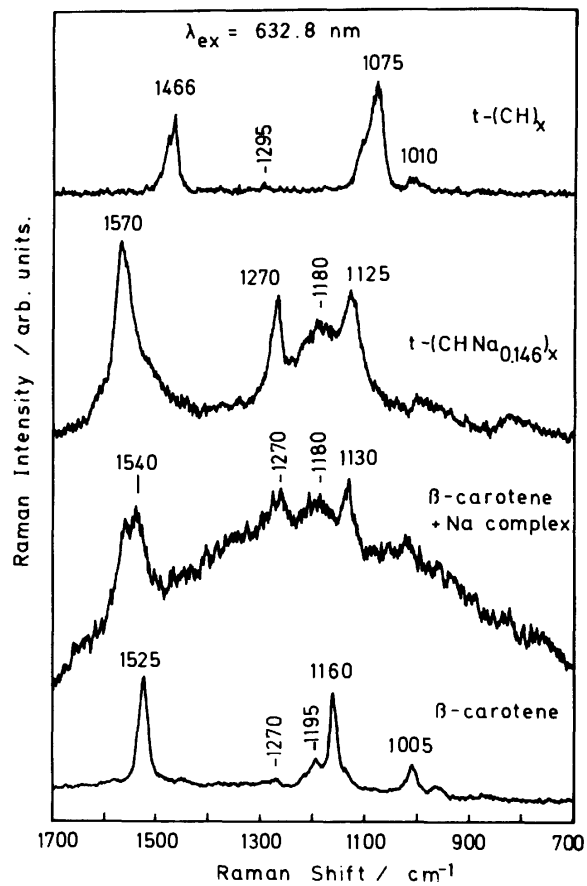

Fig. 14. Comparison of Raman spectra of *trans*-$(CH)_x$, the Na doped film and doped and undoped β-carotene.

early stage of doping; therefore, a center of symmetry is expected in the middle of the conjugated chain and the mutual exclusion of IR and Raman bands may be reasonably understood.

The Raman spectra of a heavily doped $(CH)_x$ film showed a drastically different behavior: -(C=C)- double bond stretching appeared at a higher frequency (1570 cm^{-1}) and CH bending also shifted to the higher side (1125 cm^{-1}). Also, strong Raman bands could be observed at 1270 and 1180 cm^{-1}; the former may be associated with -(C-C-C)- stretching in the center of the charged soliton structure and the broad 1180 cm^{-1} band may be the stretching of the -(C-C-C)- bond in the uniform bond chain. Both bands could be weakly observed in the IR spectra of Li doped PA (Fig. 13). This result is consistent with the selection rule, since an inversion symmetry is lost in the triplet chain model shown in Fig. 12(b) and a local symmetry of C_{2v} may be valid. The observed high-frequency shift can be reasonably explained by the model structure of triplet dilithiopolyene (Fig. 12(b)), where the short double bonds are connected with a uniform chain. In this conformation the cojugation with another double-bond system is interrupted. Takeuchi et al.[24] discussed the relationship between the $-(C=C)_n-$ stretching frequency and the number of double bond units n in a neutral trans-polyene chain. Following their calculation, the observed Raman band at 1540 cm^{-1} in heavily doped PA corresponds reasonably to the ethylenic double bond (Fig. 12(b)).

The similarity of Raman spectra for heavily Na doped *trans*-PA and Na doped β-carotene excited by 632.8 nm is very remarkable when compared it in the same chart (Fig. 14). Skeletal vibrations of -(C=C)- bonds and CH bending modes were found at almost the same position in both spectra; also, the positions of new -(C-C-C)- modes were also the same. Such a close agreement might be explained only when similar backbone structures are involved. The structures of Na doped β-carotene shown in Fig. 11 have an isolated butadiene or ethylene-type skeletons and the uniform radical type chain, and these characteristics are also apparent in the model structure of Fig. 12(b). Following the calculation of Takeuchi et al.[24] the 1580 cm^{-1} band in doped β-carotene might be related to the butadiene or hexatriene skeletons. The observed band positions by 457.9 and 632.8 nm excitation may correspond to butadiene and ethylene type bonds; the observed values are in good agreement with their calculation.

The Raman and IR spectra of Na, K, and Li doped PA at various levels of doping showed that a characteristic structural change from the charged soliton lattice to the new structure occurred in the heavily doped regime. The new structure comprised both charged soliton and the uniform chain units. The structural transformation observed by Raman spectra is in accordance with electrochemical results[13] and ESR experiments.[4,5]

A transition to the new structure started at about $y \approx 0.08$, and was completed at about $y \approx 0.13$ level in $(CH)_x$; this is in partial agreement with ESR results.[4,5] It occurred rather sharply at $y=0.11$ in $(CD)_x$. A simple model of a one-dimensional metal of uniform bond was not substantiated in the present analysis since the Raman spectra of a heavily doped film showed a pattern of isolated short double bonds. In the Raman spectra of the polymethine cyanine dye[32] studied in this laboratory, the skeletal stretching mode of the uniform -(C-C-C)- bond was found at the 1300 cm^{-1} region; this may correspond to the 1280 cm^{-1} band in heavily doped PA. A theory of a polaron metal was presented by Kivelson and Heeger,[33] however, a structural view regarding the polaron lattice was not clearly described. The present structure may afford a model of the regular polaron lattice which was considered in their treatment.

The most important consequence of the present result is that the heavily doped chain is composed of a twill unit comprising a charged soliton structure and a uniform chain unit in an alternating sequential way. Further investigation concerning other aspects of the structure may be required in order to clarify details of the physicochemical properties of doped PA.

All Raman measurements were carried out at the Instrument Center of the Institute for Molecular Science. A part of this study was a joint research program at IMS. We are grateful to the Director General Professor Saburo Nagakura and Professor Iwao Yamazaki for the joint program. A part of this work was supported by a grant in aid of the Ministry of Education (No. 61103003) for organic thin films for information conversion. We also thank Professors Ryoji Noyori and Kiyoyuki Yamada and Dr. Masato Kitamura, Messrs. Hideo Kigoshi and Hiroyuki Ozeki for their help during the experiment and to Dr. Tohru Kishi of the Institute of National Police Science for the radiation chemical analysis.

References

1) I. Harada, Y. Furukawa, M. Tasumi, H. Shirakawa, and S. Ikeda, *J. Chem. Phys.*, **73**, 4746 (1980); Y. Furukawa, I. Harada, M. Tasumi, H. Shirakawa, and S. Ikeda, *Chem. Lett.*, **1981** 1489.

2) E. Faulques, F. Rachdi, S. Lefrant, and P. Bernier, *Synth. Metals*, **9**, 53 (1984).

3) H. Eckhardt, L. W. Shacklette, J. S. Szobota, and R. H. Baughman, *Mol. Cryst. Liq. Cryst.*, **117**, 401 (1985).

4) J. Chen, T.-C. Chung, F. Moraes, and A. J. Heeger, *Solid State Commun.*, **53**, 757 (1985).

5) T. C.-Chung, F. Moraes, J. D. Flood, and A. J. Heeger, *Phys. Rev. B*, **29**, 2341 (1984).

6) C. Tanaka, J. Tanaka, and K. Hirao, to be published.
7) H. Shirakawa and S. Ikeda, *Polym. J.*, **2**, 231 (1971).
8) J. Tanaka and M. Tanaka, "Handbook of Conducting Polymers," ed by T. A. Skotheim, Marcel Dekker, New York (1986) Vol. 2, p. 1269.
9) J. Tanaka, K. Kamiya, M. Shimizu, and M. Tanaka, *Synth. Metals*, **13**, 177 (1986).
10) J. Tanaka, M. Tanaka, H. Fujimoto, K. Kamiya, Y. Saito, and T. Kishi, *Mol. Cryst. Liq. Cryst.*, **117**, 259 (1985).
11) H. Fujimoto, K. Kamiya, J. Tanaka, and M. Tanaka, *Synth. Metals*, **10**, 367 (1985).
12) H. Fujimoto, J. Tanaka, M. Tanaka and T. Kishi, *Synth. Metals*, **16**, 133 (1986).
13) L. W. Shacklette and J. E. Toth, *Phys. Rev. B*, **32**, 5892 (1985).
14) J. L. Bredas, *Mol. Cryst. Liq. Cryst.*, **118**, 49 (1985); J. L. Bredas and G. B. Street, *Acc. Chem. Res.*, **18**, 309 (1985). Bredas did not used a terminology of bipolaron for a pair of charged soliton in PA because of degenerate ground state of undoped PA. However, if we coordinate the dopant rather strongly to the chain, the degeneracy might be lost and the chain with a pair of charged soliton may be called as a bipolaron.
15) H. Kuzmany, *Phys. Stat. Sol. (b)*, **97**, 521 (1980).
16) D. B. Fitchen, *Mol. Cryst. Liq. Cryst.*, **83**, 95 (1982).
17) R. Tubino, *Mol. Cryst. Liq. Cryst.*, **117**, 319 (1985).
18) N. F. Mott and E. A. Davis, "Electronic Processes in Non-Crystalline Materials," (Clarendon, Oxford) (1979).
19) A. J. Epstein, H. Rommelmann, R. Bigelow, H. W. Gibson, D. M. Hoffmann, and D. B. Tanner, *Phys. Rev. Lett.*, **50**, 1866 (1983).
20) M. Przybylski, B. R. Bulka, I. Kulszewics, and A. Pron, *Solid State Commun.*, **48**, 893 (1983).
21) V. G. Mairanovsky, A. A. Engovatov, N. T. Ioffe, and G. I. Samokhvalov, *J. Electroanl. Chem.*, **66**, 123 (1975); S. M. Park, *J. Electroche. Soc.*, **125**, 216 (1978).
22) P. Karrer and J. Benz, *Helv. Chim. Acta*, **31**, 1048 (1948).
23) J. P. Pouget, P. Robin, R. Comes, H. W. Gibson, A. J. Epstein, and D. Billaud, *Physica*, **127B**,158 (1984).
24) H. Takeuchi, Y. Furukawa, I. Harada, and H. Shirakawa, *J. Chem. Phys.*, **84**, 2882 (1986).
25) B. Francois, M. Bernard, and J. J. Andre, *J. Chem. Phys.*, **75**, 4142 (1981).
26) B. Horovitz, *Solid State Commun.*, **41**, 729 (1982).
27) A. Terai, H. Ito, Y. Ono, and Y. Wada, *J. Phys. Soc. Jpn.*, **54**, 196 (1985); A. Terai, Y. Ono, and Y. Wada, *J. Phys. Soc. Jpn.*, **55**, 2889 (1986).
28) E. J. Mele and J. C. Hicks, *Phys. Rev., B*, **32**, 2703 (1985).
29) H. Fujimoto, M. Tanaka, and J. Tanaka, *Bull. Chem. Soc. Jpn.*, **56**, 671 (1983).
30) H. Takeuchi, Y. Furukawa, I. Harada, and H. Shirakawa, *J. Chem. Phys.*, **80**, 2925 (1984).
31) G. Zannoni and G. Zerbi, *J. Mol. Struct.*, **100**, 505 (1983).
32) M. Sano, M. Shimizu, and J. Tanaka, to be published.
33) S. Kivelson and A. J. Heeger, *Phys. Rev. Lett.*, **55**, 308 (1985).

 © 1987 The Chemical Society of Japan Bull. Chem. Soc. Jpn., 60, 1607—1611 (1987)

Epitaxial Growth and Its Growth Mechanism in Physical Vapor Deposited Films of Alkyl Octadecanoates

Michiko TAKAMOTO, Seiji OGIHARA, Kiyoshi YASE,* and Masakazu OKADA
Faculty of Applied Biological Science, Hiroshima University,
2-17 Midori-cho, Fukuyama, Hiroshima 720
(Received October 28, 1986)

Esters of octadecanoic acid and three primary alcohols such as methanol, ethanol, and propanol were deposited on substrates of potassium chloride (KCl), mica and amorphous carbon film under vacuum. The surface morphology of their films was observed by transmission electron microscope. They grew epitaxially to form the rectangular crystals with lateral molecular orientations on KCl substrate. On the other hand, ester molecules tend to arrange normal to the surface of mica and amorphous carbon film and construct the molecular layers like to Langmuir-Blodgett films. The crystal axis relationship between esters and KCl(001) surface was followed; c-axis$_{ester}$ is parallel to $\langle 110\rangle_{KCl}$ direction and $\langle 110\rangle_{ester}$ direction inclines with an angle of about ±16° corresponding to $\langle 110\rangle_{KCl}$. These molecules had resemble crystal structures with trans configuration in the ester moiety. The optimum temperatures of substrates in the former epitaxial growth exist and the temperature decreases in proportion to the chain length of alcohol group with the discrepancy of about 10 to 30 °C.

Organic thin-solid-film was studied for the new devices for electronic, magnetic and optical thin films[1]. The thin-solid-films of octadecanoic acid (stearic acid; $C_{17}H_{35}$ COOH) have been used as the lubricated films,[2] photo-resist and insulators.[3] The preparing of such organic films was carried out by the Langmuir-Blodgett (LB) methods, which were used the air–water interface.[4] Their films, however, had only molecular arrangements normal to the surface and the molecular packing in the first monolayer was not perfect from the results of transmission electron microscopic observation.[5] On the other hand, physical-vapor-deposition (PVD) method could give the alternative molecular orientations.[6] The molecules in the films laid along or stood normal to the surface. The crystal morphology on the substrate had the own habits and molecular orientations in the crystal could be identified by the granularity of the germanium decoration.[6] If the deposition conditions of PVD were controlled, the alternativity in the molecular orientations revealed. Therefore, uniform and well-defined crystal films could be obtained. Furthermore, the lengths of linear chain molecules such as fatty acids of hexadecanoic (palmitic), octadecanoic (stearic), eicosanoic (arachidic) and docosanoic (behenic) acids became clear to relate with the molecular orientations in given deposition conditions of PVD.[7] The longer molecules gave the tendency of normal orientations at same deposition condition than shorter ones.

Fatty acids such as octadecanoic acid form esters with primary alcohols. T. Malkin[8] firstly studied the crystal structures of them by powder X-ray diffractometry. Then single crystal X-ray analysis was carried out for methyl octadecanoate (18-1) by S. Aleby and E. von Sydow[9] and for ethyl octadecanoate (18-2) by S. Aleby[10,11] and A. McL. Mathieson and H. K. Welsh.[12] These crystals belong to monoclinic. The cell dimensions of 18-1[9] are a=5.61, b=7.33, c=106.6 Å, β=116.78° with space group of $A2/a$. Those of 18-2, however, are a=5.59, b=7.40, c=57.1 Å, β=118° with Aa[10] and a=5.59, b=7.40, c=55.0 Å, β=113.5° with Ia[11]. The difference between two cell parameters of 18-2 exists in the configuration of ester group (C_1–O_1–C_{01}–C_{02}). The former has trans configuration, while the latter has cis form as same as that of 18-1 (C_1–O_1–C_{01}). The molecules in the crystal arrange to construct the layer normal to the c-axis. From these cell dimensions the angle of c-axis with $\langle 110\rangle$ direction in the crystal is 105.9° for 18-1 and 106.4° and 103.9° for 18-2, respectively. The crystal structure of 18-3, however, was not revealed yet.

The ester molecules were not good at forming the LB films in order that their ester groups had low hydrophilic properties.[13] The PVD of methyl triacontanoate (30-1; $C_{29}H_{59}COOCH_3$) was carried out by Y. Ueda.[14] He evaporated it on KCl in vacuo. The crystal structure and the growth mechanism were studied by using electron microscope and electron diffraction. The film was composed of V-shape crystals. The 30-1 molecules grew epitaxially with the defined axial relations. The c-axis which is alkyl chain direction of molecule had the angles of ±16° with $\langle 110\rangle$ direction on KCl (001) plane.

This paper describes the preparing of well-defined thin solid films of three esters of fatty acids such as methyl octadecanoate (18-1; $C_{17}H_{35}COOCH_3$), ethyl octadecanoate (18-2; $C_{17}H_{35}COOC_2H_5$) and propyl octadecanoate (18-3; $C_{17}H_{35}COOC_3H_7$) and the film morphology of them.

Experimental

Methyl octadecanoate (18-1), ethyl octadecanoate (18-2), and propyl octadecanoate (18-3) were provided from Sigma Co. Ltd. with the purity of about 99%. These materials have melting points (mp) at the inversely proportional to the alkyl chain lengths of ester groups, as shown in Fig. 1.

The sample was set in the vacuum system and deposited

on three substrates. These substrates were three types; air-cleaved KCl and mica, amorphous carbon film (amorphous film) forming on mica before. The vacuum was kept at 6.7×10^{-4} Pa (5×10^{-6} Torr). After the substrates were baked at the temperature of greater than 100 °C for 1 h, the substrates were cooled down to 30 °C or less temperatures by using a cold trap and then the sample was evaporated. The temperature dependence of substrate with molecular orientations was found from the thin crystal morphology.

As the sample has low mp, it is difficult to evaporate in vacuo. So that the indirectional heating system was performed. The heater of tungsten wire and the sample holder of quartz plate were separated to differ from each other at the distances corresponding with specimen. When the temperature around the heater was kept at 500 to 800 °C, the specimen melted to sublimate.

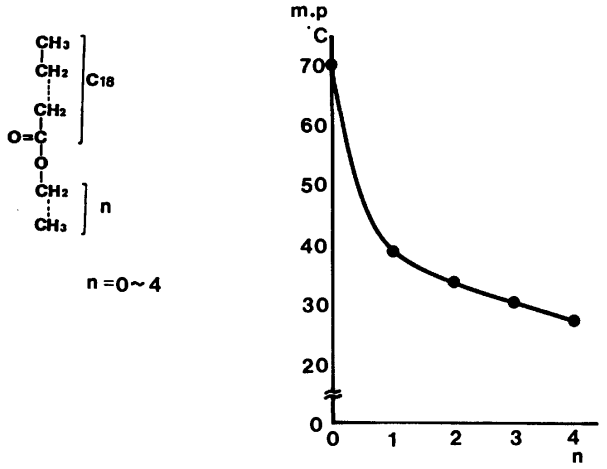

Fig. 1. Molecular shape and its melting point of alkyl octadecanoates (18-*n*; *n*=0, 1, 2, 3, and 4).

After the specimen was deposited on the substrates with the thickness of about 10 nm, germanium and carbon were successively evaporated in same vacuum system. The deposited germanium is surface decoration of organic crystals. When the surface was methyl-end like to (001) plane of octadecanoic acid, germanium grew discrete grains with star-like shapes. While, on the other plane it revealed the continuous layers. So that germanium decoration becomes indirect method for the determination of molecular orientation in thin-solid-films[6].

The three layers of sample, germanium and carbon were stripped off from the substrates on the surface of distilled water. Electron microscope used here was Hitachi HU-11DS with the accelerating voltage of 75 kV. The direct magnification was 5000 and 16000.

Results and Discussion

The typical electron micrographs are represented in Fig. 2(a), (b), and (c). These are thin-solid-films of 18-2 formed at substrate temperature of 10 °C on KCl, 0 °C on mica and −10 °C on amorphous film, respectively. On KCl, 18-2 molecules laid on the substrate surface. The molecular orientation was determined by the appearance of germanium decoration. The axis relation between thin crystal and substrate surface was decided by the shadowing direction of germanium along ⟨110⟩ direction of KCl (001) surface. Molecules formed the rectangular crystals and revealed the epitaxy. The bisectional direction of twinned crystals

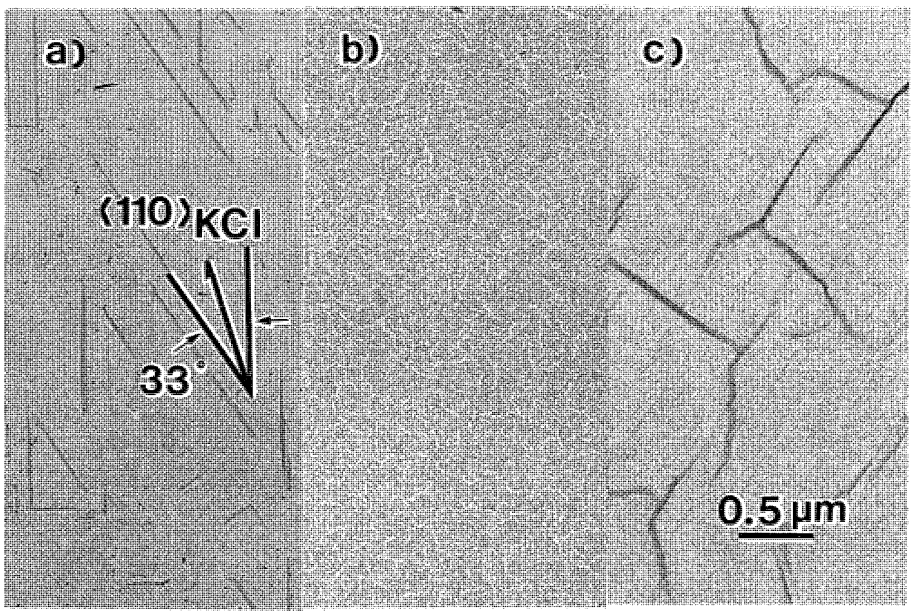

Fig. 2. Electron micrographs of deposited ethyl octadecanoate (18-2) on KCl at sustrate temperature of 10 °C (a), on mica at 0 °C (b) and on amorphous carbon film at −10 °C (c). On KCl (001) surface, 18-2 molecules grew epitaxially along two directions. Each direction indinate an angle of ±16.5° corresponding to KCl ⟨110⟩ direction.

was ⟨110⟩ direction of KCl (001) plane. The longitudinal direction of rectangular crystals crosses with an angle of 33°(±16.5°). This value can be led by the angle relationship between c-axis and ⟨110⟩ direction which is 106.4° (90°+16.4°). The fact shows that deposited films take the cell dimensions of reference [10] and the ester group of 18-2 would have trans configuration. The latitudinal direction is corresponding to c-axis. This result coincides with that for 30-1 by Ueda.[14] On the other hand, the regions covered with granular germanium on mica revealed, as shown in Fig. 2(b). Molecules in the film stood normal to the substrate surface and had no crystal habit. The same result was obtained in the deposition film formed on amorphous carbon film, as shown in Fig. 2(c).

The temperature dependency of substrate with molecular orientations was carried out at −20, −10, 0, and 10 °C for 18-1 and 18-2; from −60 to 10 °C with a step of 10 °C for 18-3 on KCl, mica and amorphous

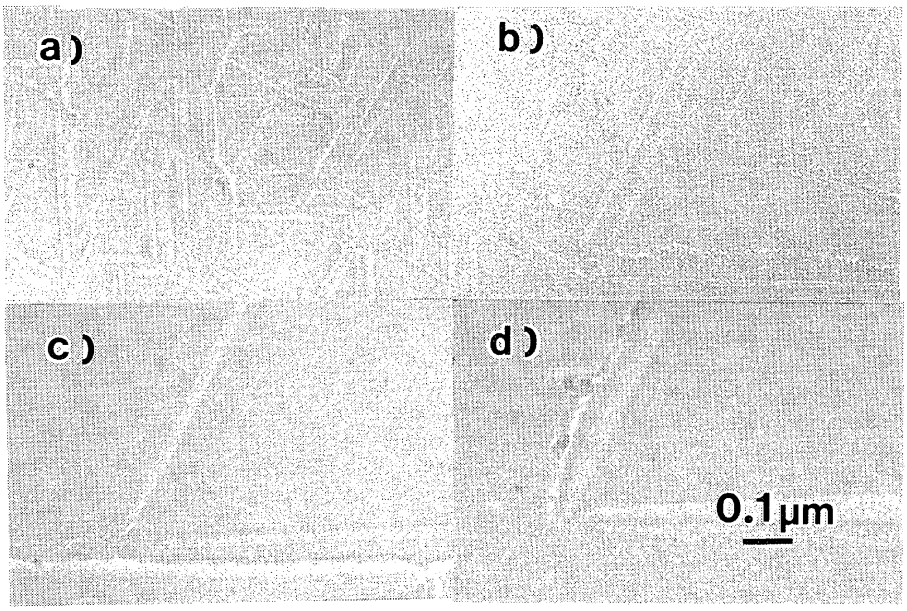

Fig. 3. Thin films of methyl octadecanoate (18-1) formed on KCl at −20 °C (a), −10 °C (b), 0 °C (c), and 10 °C (d).

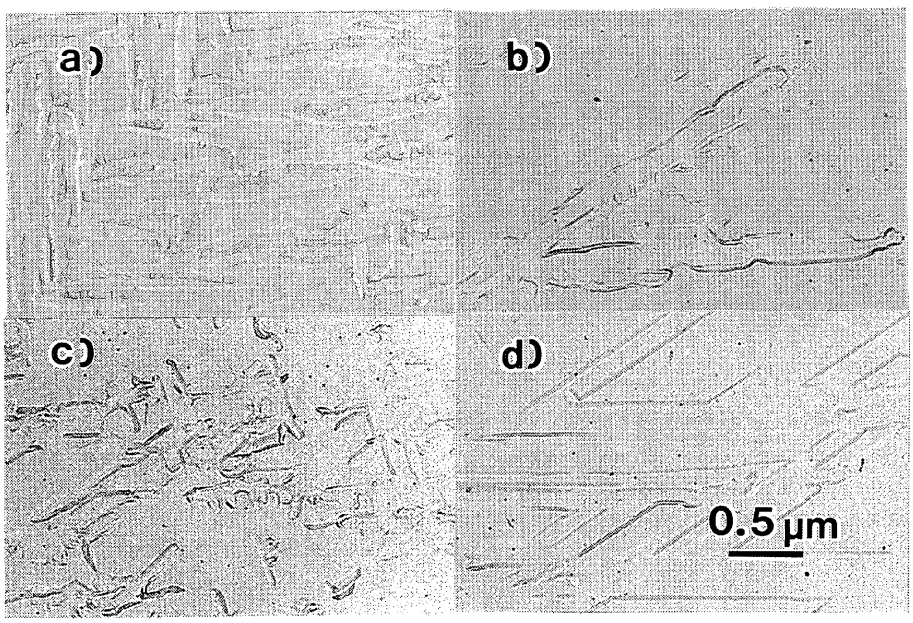

Fig. 4. Thin films of ethyl octadecanoate (18-2) formed on KCl at −20 °C (a), −10 °C (b), 0 °C (c), and 10 °C (d).

carbon film. These results only on KCl substrate are shown in Figs. 3, 4, and 5 for 18-1, 18-2, and 18-3, respectively.

There were the discrepancies of crystal morphology at each substrate temperature on KCl. On the other hand, molecules grew normal to the substrate surface on mica and amorphous carbon film without differency of substrates and substrate temperatures. When the substrate temperature of KCl increases, the thin crystals with parallel molecular orientations to the substrate surface grow greater and reveal more epitaxially. There are the optimum temperatures of substrates for epitaxial growth; 0 °C for 18-1, −10 °C for 18-2 and −40 °C for 18-3, as shown in Fig. 6. The cross angles of rectangular crystals were 58° for 18-1, 33° for 18-2 and 33° for 18-3, in which an angle of 58° is a supplement of 32°. The results represent as followed; three crystals were monoclinic, the angle

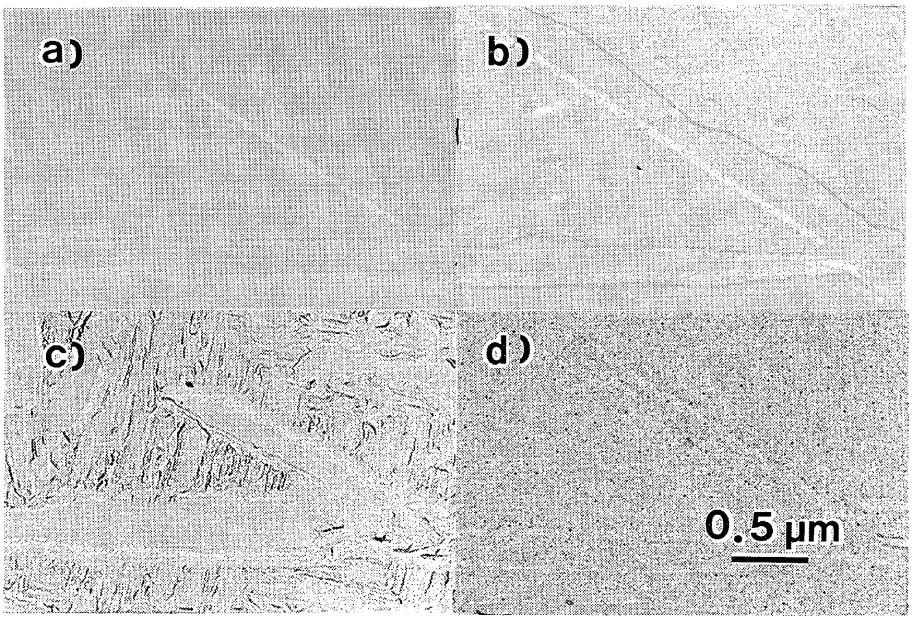

Fig. 5. Thin films of propyl octadecanoate (18-3) formed on KCl at −50 °C (a), −40 °C (b), −10 °C (c), and 0 °C (d).

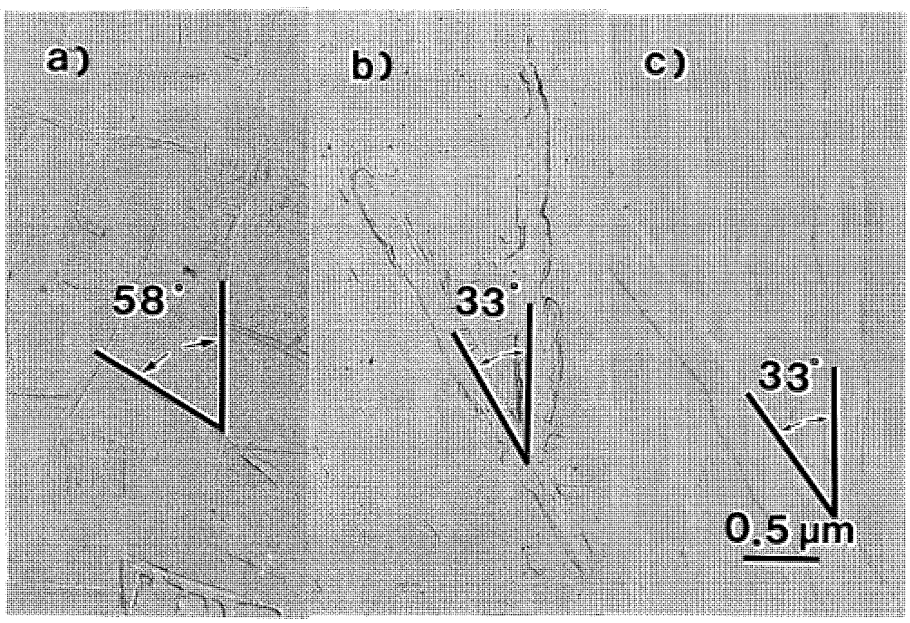

Fig. 6. Crystal morphology at optimum temperature of substrate on KCl. (a) 18-1 at 0 °C, (b) 18-2 at −10 °C, and (c) 18-3 at −40 °C. The angles between rectangular crystals were 58° for 18-1 (a), 33° for 18-2 (b), and 33° for 18-3 (c).

Ts (°C) \ n	1	2	3
10	L	L	L
0	L	L	L
-10	L/N	L	L
-20	L/N	L	L
-30			L
-40			L
-50			L/N
-60			L/N

Fig. 7. Dominant growth hillocks of alkyl octadecanoates at several temperatures of KCl substrate. The symbol of L or N represents the lateral and the normal orientations, respectively.

between the rectangular crystals could be led from the relation between c-axis with ⟨110⟩ direction, these esters had resemble cell shapes and one of crystal parameters for 18-3 which had not determined by other methods was an angle of 106°. Above the optimun temperature of substrate, molecules stood normal to the substrate as same as on mica or amorphous film.

The formation mechanism of thin-solid-films will be explained as followed. The alkyl chain of molecules tends to lay along the substrate surface with the good contact on cations or anions of KCl ⟨110⟩ direction, as described above. If the substrate temperature increased, molecules get the surface migration energy and crystallization energy from the substrate to let the crystal more epitaxial and larger. When the excess energy was supplied, molecules could not contact the substrate surface to stand normal to the surface. The normal crystal has the ability of surface migration and self-aggregation more than lateral one. The tendency revealed the thin crystals on mica and amorphous film. The surface of them had no tetragonal symmetry. The interaction between molecules and substrate surface was lower than ionic crystal surface of KCl. The long chain molecules did not lay on the surface but tended to stand normal to the substrate.

The morphology of deposited thin films on KCl was summarized in Fig. 7. The "L" and "N" are represented the dominant crystals of the film surface with lateral and normal orientations of molecules, respectively. The temperature effect is inversely proportional to the alkyl chain length. The facts are coincided with the resemble study,[7] which was performed on several fatty acids with different chain length.

References

1) F. L. Carter, "Molecular Electronic Devices," Marcel Dekker Inc., N.Y. (1982).
2) K. Nakamura, K. Momono, H. Kawamura, Y. Ota, A. Itoh, and C. Hayashi, *IEEE trans. Magnetics*, **MAG-20**, 833 (1984).
3) P. S. Vincett and G. G. Roberts, *Thin Solid Films*, **68**, 135 (1980).
4) K. B. Blodgett, *J. Am. Chem. Soc.*, **57**, 1007 (1935); K. B. Blodgett and I. Langmuir, *Phys. Rev.*, **51**, 964 (1937).
5) H. E. Ries, Jr., et al., Proc. Int. Congr. Surf. Act., 2nd, 1, 75 (1957); *J. Colloid Sci.*, **16**, 361 (1961).
6) K. Inaoka, F. Matsuzaki, K. Sato, and M. Okada, *Ohyo Butsuri*, **52**, 712 (1983) in Japanese; F. Matsuzaki, K. Inaoka, M. Okada, and K. Sato, *J. Cryst. Growth*, **21**, 201 (1985).
7) T. Inoue, K. Yase, K. Inaoka, and M. Okada, *J. Cryst. Growth.* in press.
8) T. Malkin, *J. Am. Chem. Soc.*, **52**, 3739 (1930); *J. Chem. Soc.*, **133**, 2796 (1931); *Trans. Faraday Soc.*, **29**, 977 (1933).
9) S. Aleby and E. von Sydow, *Acta Crystallogr.*, **13**, 487 (1960).
10) S. Aleby, *Acta Crystallogr.*, **15**, 1248 (1962).
11) S. Aleby, *Acta Chem. Scand.*, **22**, 811 (1968).
12) A. McL. Mathieson and H. K. Welsh, *Acta Crystallogr.*, **18**, 953 (1965).
13) E. Stenhagen, *Trans. Faraday Soc.*, **34**, 1328 (1938).
14) Y. Ueda, *Bull. Chem. Soc. Jpn.*, **59**, 3775 (1986).

 © 1987 The Chemical Society of Japan Bull. Chem. Soc. Jpn., 60, 1613—1615 (1987)

Additivity Law for the Activity of a Counter Ion in Ion-Exchange Resin

Hideo KIMIZUKA,* Hirohiko WAKI, Akira MATSUBARA, and Yōichi ARIMOTO
Department of Chemistry, Faculty of Science, Kyushu University,
Hakozaki, Higashi-ku, Fukuoka 812
(Received November 8, 1986)

The ion-exchange resin–electrolyte solution equilibria were studied on the basis of thermodynamics. The experimental results showed that the external salt activity divided by the co-ion concentration in the ion-exchange resins was linear against the co-ion concentration in the resin. The equilibria were consistently explained by a partition coefficient of salt distribution with the additivity law for the counter ions in the ion-exchange resin. A thermodynamic expression for the ion-exchange reaction was also discussed.

It is of importance to elucidate the behavior of ions in the ion-exchange resin in order to understand the ion transport through the charged membrane and the ion-exchange reaction.

Teorell[1] and Meyer and Sievers[2] explained the membrane potential across a charged membrane by applying the Donnan relation[3] to the membrane surface-electrolyte solution equilibria. Later, the ion concentration in the Donnan relation was replaced by the ionic activity.[4] However, the problem of the change in the activity coefficients of the ions in the ion-exchange resin with the external electrolyte solution has remained unsolved.[5]

On the other hand, it is well-known that the counter-ion activity in a polyelectrolyte solution with an added electrolyte obeys the additivity law;[6] that is, the total activity of counter ions is best expressed as a sum of the independent contributions of counter-ion activities from the polyelectrolyte and the added salt.

Toyoshima et al.[7] treated the membrane properties on the assumption of the additivity law for counter ions in the membrane, disregarding the partition factor. Unfortunately, however, they did not verify the additivity law experimentally.

Since the ion-exchange resin may be regarded as a polyelectrolyte, it is possible to elucidate the salt partition between an ion-exchange resin and an external electrolyte solution on the basis of thermodynamics by taking the additivity law into account.

This paper will describe the theory and the experimental evidence.

Theory

The thermodynamic treatment of the ion-exchange resin-single electrolyte solution equilibria leads to:

$$\bar{a}_{\pm}/a_{\pm} = K \tag{1}$$

and:

$$-RT\ln K = \bar{\mu}^{0}_{\pm} - \mu^{0}_{\pm} + \pi\bar{V}_{\pm} \tag{2}$$

where the overbars refer to the membrane phase; $a_{\pm}$ denotes the mean electrolyte activity; K, the partition coefficient; R, the gas constant; T, the absolute temperature; $\mu^{0}_{\pm}$, the standard chemical potential; π, the swelling pressure, and $\bar{V}_{\pm}$, the mean partial molar volumes of electrolytes, which are assumed identical in both the resin and external-solution phases.

By applying the additivity law[6] to the counter ion α in the membrane with a fixed charge concentration of $\bar{X}$, the activity of the counter ion, $\bar{a}_{\alpha}$, is expressed by;

$$\bar{a}_{\alpha} = (\bar{\gamma}_{f}|Z_{f}|\bar{X} + \bar{\gamma}_{\alpha}|Z_{\beta}|\bar{C}_{\beta})/|Z_{\alpha}| \tag{3}$$

where $\bar{\gamma}_{f}$ denotes the activity coefficirent of ion α referred to the fixed charge; Z_{f}, the valency of the fixed site; $\bar{\gamma}_{\alpha}$, the activity coefficient of the ion α referred to the Donnan salt present in the interstitial space; Z_{β}, the valency of the co-ion; $\bar{C}_{\beta}$, the co-ion concentration, and Z_{α}, the valency of the ion α. The activity of the co-ion β, $\bar{a}_{\beta}$, is given by a usual expression;

$$\bar{a}_{\beta} = \bar{\gamma}_{\beta}\bar{C}_{\beta} \tag{4}$$

where $\bar{\gamma}_{\beta}$ denotes the activity coefficient of the co-ion. By combining Eq. 1 with Eqs. 3 and 4, we obtain;

$$(a_{\pm})^{(\nu_{\alpha}+\nu_{\beta})}/(\bar{C}_{\beta})^{\nu_{\beta}} = (\bar{\gamma}_{\pm}/K)^{(\nu_{\alpha}+\nu_{\beta})}[(\bar{\gamma}_{f}|Z_{f}|\bar{X}/\bar{\gamma}_{\alpha} + |Z_{\beta}|\bar{C}_{\beta})/|Z_{\alpha}|]^{\nu_{\alpha}} \tag{5}$$

where ν_{α} and ν_{β} are the stoichiometric coefficints of the counter ion and the co-ion respectively and $\bar{\gamma}_{\pm}$, the mean activity coefficient of the Donnan salt.

For the system composed of a symmetric electrolyte and a resin having ion-exchange sites with $|Z_{f}|=1$, Eq. 5 is reduced to:

$$(a_{\pm})^{2}/\bar{C}_{\beta} = (\bar{\gamma}_{\pm}/K)^{2}(\bar{\gamma}_{f}\bar{X}/|Z_{\alpha}|\bar{\gamma}_{\alpha} + \bar{C}_{\beta}) \tag{6}$$

Thus, for a symmetric electrolyte, $(a_{\pm})^{2}/\bar{C}_{\beta}$ is linear against $\bar{C}_{\beta}$, providing that $\bar{\gamma}_{\pm}/K$ and $\bar{\gamma}_{f}/\bar{\gamma}_{\alpha}$ are constant.

Experimental

Materials. The anion-exchange membrane used in the present study was a styrene–divinylbenzene copolymer with a quarternary ammonio group developed by the Asahi Chemical Co., Ltd., and coded as CA-1, 0.2 t. The ion-exchange capacity was 1.70 meq. (g dry membrane)$^{-1}$; the water content, 0.37 g H_2O (g dry membrane)$^{-1}$, and the thickness, 0.225 mm. This membrane was prepared without

any other supporting polymer and was of a homogeneous distribution of functional groups within the membrane. The cation-exchange resins were commercial ones, coded as Dowex 50W−X2, −X8, and −X12, whose water contents were 0.75, 0.59, and 0.53 g H_2O (g dry resin)$^{-1}$ respectively and whose ion-exchange capacities were 1.8, 3.2, and 3.8 meq. (g dry resin)$^{-1}$ respectively. The degrees of cross linkage and the water contents of these cation-exchange resins are also different from each other. Pure inorganic salts and twice-distilled water were used for preparing the salt solutions. The concentrations of the electrolyte solutions varied from 0.5 to 3 mol dm^{-3}.

Procedure of Experiments. A membrane of 2×2 cm^2 preconditioned with a test solution was dipped into a 100-ml test solution for 5 days. After equilibration, the solution which had adhered to the membrane was removed by the filter paper; then the Donnan salt was extracted 5 times with 10 ml of distilled water, each extraction being carried out for 1 day. All the extracts were then gathered, and the concentration was determined by measuring the electric conductance of the solution. The Donnan-salt concentration was calculated from the concentration of the extract and the geometry of the membrane determined after equilibration with the test solution. The procedure for determining the ion concentrations in the cation-exchange resin has been described elsewhere.[8] The experiments were carried out at 25±1 °C.

Results and Discussion

The experimental results are shown in Figs. 1 and 2 where the activity data of the external electrolyte solutions were taken from the text book.[9] It is shown in these figures that $(a_\pm)^2/\bar{C}_\beta$ is linear against $\bar{C}_\beta$. This indicates that $\bar{\gamma}_\pm/K$ and $\bar{\gamma}_f/\bar{\gamma}_\alpha$ may be regarded as constants. These values, as estimated from Figs. 1 and 2, are cited in Table 1, together with the ratio of $\bar{\gamma}_f/\bar{\gamma}_\alpha$ to $K/\bar{\gamma}_\pm$, $(\bar{\gamma}_f/K)(\bar{\gamma}_\beta/\bar{\gamma}_\alpha)^{1/2}$.

Table 1 shows that the values of $K/\bar{\gamma}_\pm$ and $\bar{\gamma}_f/\bar{\gamma}_\alpha$ are smaller than unity except for those of $MgSO_4$, while their ratios are of the same order of magnitude. This table also indicates that co-ions in the anion-exchange membrane, Na^+ and K^+, exert different effects on the thermodynamic parameters and that the variation in the cation-exchange resin gives rise to a change in the thermodynamic parameters.

Since $\bar{\gamma}_\pm$ and $\bar{\gamma}_\alpha$ may be regarded as less than unity, both K and $\bar{\gamma}_f$ values for all electrolytes may be deduced to be less than unity. The small values of $\bar{\gamma}_f$ for the uni-univalent electrolyte, a measure of the counter-ion condensation caused by an array of charged sites as a polyelectrolyte, may also be considered to indicate a strong trapping of counter ions by charged sites. The low K values may be ascribed to the co-ion repulsion by charged sites in addition to the exclusion effect due to the resin matrix with a hydrophobic nature. The anomalous values of $K/\bar{\gamma}_\pm$ and $\bar{\gamma}_f/\bar{\gamma}_\alpha$ for $MgSO_4$ may be due to a stronger interaction of magnesium ions with sulfate ions than with charged sites as deduced from the extremely low activity coefficient of $MgSO_4$ in an aqueous solution, an order of 10^{-2}. In fact, the ratio of $\bar{\gamma}_f/\bar{\gamma}_\alpha$ to $K/\bar{\gamma}_\pm$ for $MgSO_4$ was comparable to those for the other

Table 1. Thermodynamic Parameters in the Ion-Exchange Resin-Electrolyte Solution Equilibria

Ion-exchange resin	Electrolyte	$K/\bar{\gamma}_\pm$	$\bar{\gamma}_f/\bar{\gamma}_\alpha$	$(\bar{\gamma}_f/K)(\bar{\gamma}_\beta/\bar{\gamma}_\alpha)^{1/2}$
CA-1 0.2 t	NaCl	0.316	0.015	0.047
	KCl	0.895	0.056	0.063
	$MgSO_4$	6.76	2.15	0.318
Dowex 50W-X12	NaCl	0.121	0.038	0.314
50W-X8	NaCl	0.250	0.074	0.296
50W-X2	NaCl	0.543	0.230	0.424

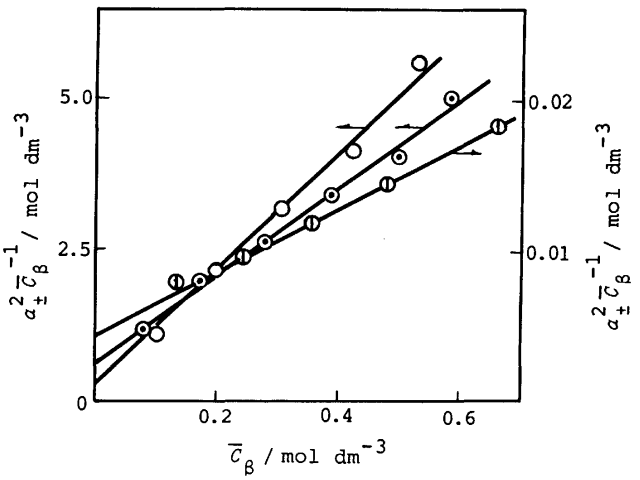

Fig. 1. $a_\pm^2\bar{C}_\beta^{-1}$ vs. $\bar{C}_\beta$ plot for the anion-exchange membrane-electrolyte solution equilibria.
Membrane CA-1 0.2 t; Electrolyte, ○:NaCl, ●:KCl. ⊕:$MgSO_4$

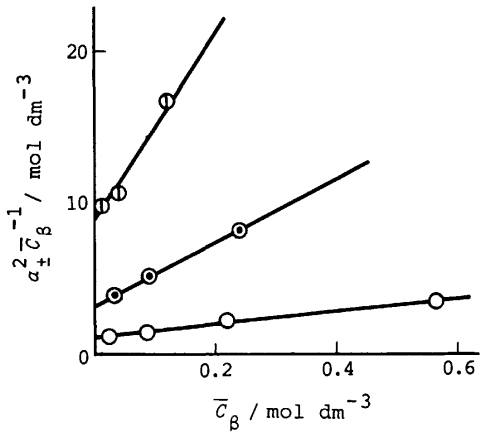

Fig. 2. $a_\pm^2\bar{C}_\beta^{-1}$ vs. $\bar{C}_\beta$ plot for the cation-exchange resin-sodium chloride solution equilibria.
Cation-exchange resin, ○: Dowex 50 W-X2, ●: Dowex 50 W-X8, ⊕: Dowex 50 W-X12.

electrolytes as is shown in Table 1. This may indicate that the interactions of Mg^{2+} and $MgSO_4$ with the ion-exchange resin are not anomalous. Assuming $\bar{\gamma}_\alpha=\bar{\gamma}_\beta=\bar{\gamma}_\pm$, the ratio is reduced to $\bar{\gamma}_f/K$, which expresses the ratio of the counter ion-charged site interaction to the electrolyte-resin interaction.

So far, the difference in the standard chemical potential of an ion between the resin and the external solution has been ignored in thermodynamic treatments of the equilibria.[5] This may, in general, not be valid, since the resin-electrolyte solution equilibria are heterogeneous.

It is likely that $\bar{\gamma}_\pm$ as well as $\bar{\gamma}_\alpha$ varies with the concentration of Donnan salt. Thus, the constant values of $K/\bar{\gamma}_\pm$ and $\bar{\gamma}_f/\bar{\gamma}_\alpha$ observed in the present study may be regarded as apparent ones. A constant value of $K/\bar{\gamma}_\pm$ will be realized if the swelling pressure term is cancelled by $\bar{\gamma}_\pm$. On the other hand, a constant value of $\bar{\gamma}_f/\bar{\gamma}_\alpha$ can not thus be explained, since $\bar{\gamma}_f$ is regarded constant in terms of the additivity law.[6] The apparent constancy of $\bar{\gamma}_f/\bar{\gamma}_\alpha$ is probably related to the fact that the total counter ion concentration did not change so remarkably as the concentration of Donnan salt.

For the ion-exchange reaction:

$$M^+ + NR \rightleftharpoons N^+ + MR$$

where R is the ion-exchange site, we obtain, from Eqs. 1 and 2:

$$\bar{a}_M a_N/\bar{a}_N a_M = K_N^M \quad (7)$$

The equilibrium constant, K_M^N, is given by:

$$-RT \ln K_N^M = (\bar{\mu}_M^\circ-\mu_M^\circ) - (\bar{\mu}_N^\circ-\mu_N^\circ) + \pi(\bar{V}_M-\bar{V}_N) \quad (8)$$

where the subscripts M and N refer to the M and N ions respectively. Since the difference in the ionic molar volume is small, the contribution of the swelling pressure term may be ignored unless the swelling pressure is extremely high.

It is well-known that the selectivity coefficinet for an ion-exchange reaction varies with the composition of the ions involved in the reaction.[5] This indicates the changes in the activity coefficients of ions with the composition. Even in this case, the additivity law may also provide a way of elucidating the behavior of counter ions in the ion-exchange reaction. A more detailed study will be required to establish thermodynamic treatments concerning the ion-exchange resin-electrolyte solution equilibria.

References

1) T. Teorell, *Proc. Natl. Acad. Sci., U. S.*, **21**, 152 (1935).
2) K. H. Meyer and J. F. Sievers, *Helv. Chim. Acta*, **19**, 645, 665, 987 (1936).
3) F. G. Donnan, *Chem. Rev.*, **1**, 73 (1924).
4) G. J. Hills, P. W. M. Jacobs, and N. Lakshminarayanaiah, *Proc. Roy. Soc.*, **A262**, 246 (1961).
5) Y. Marcus and A. S. Kertes, "Ion Exchange and Solvent Extraction of Metal Complexes," Wiley-Interscience (1969).
6) R. A. Mock and C. A. Marshall, *J. Polymer Sci.*, **13**, 163 (1954).
7) Y. Toyoshima, Y. Kobatake, and H. Fujita, *Trans. Farday Soc.*, **63**, 2814 (1967).
8) H. Waki and G. Kura, *Z. Anal. Chem.*, **320**, 268 (1985).
9) R. A. Robinson and R. H. Stokes, "Electrolyte Solutions," London, Butterworths (1970).

 © 1987 The Chemical Society of Japan Bull. Chem. Soc. Jpn., 60, 1617—1623 (1987)

ESR and Mass Spectrometric Studies of Methanol Combustion. II. Correlation between Labile and Stable Chemical Species in Methanol-Oxygen-Argon Flame at Low Pressure

Masayuki TANIGUCHI, Toshiharu YOSHIOKA,† and Hiroshi YOSHIDA*
Faculty of Engineering, Hokkaido University, Kita-ku, Sapporo 060
(Received November 11, 1986)

In order to experimentally elucidate the chemical reactions of methanol combustion, the concentration profiles of ten chemical species were determined in stoichiometric CH_3OH-O_2-Ar flat flame at low pressure, 1.11×10^4 Pa. The concentrations of three labile intermediates (H, O, and OH) as well as that of stable O_2 molecules, were measured by means of the probe-sampling-ESR method. The concentrations of six stable species (CH_3OH, CH_2O, CO, CO_2, H_2, and H_2O) were measured using a quadrupole mass spectrometer. The rates of the net chemical formation (or decay) of these species were determined by subtracting the effect of diffusion from their observed concentration profiles, and were examined on the basis of the reaction mechanisms previously proposed for methanol combustion. The experimental results were found to be consistent with the oxidation pathway $CH_3OH\rightarrow CH_2OH\rightarrow CH_2O\rightarrow CHO\rightarrow CO\rightarrow CO_2$. The results also showed that the reaction $CH_2OH+O_2\rightarrow CH_2O+HO_2$ is an important pathway for O_2 consumption.

In order to elucidate complex combustion reactions in flames, it is indispensable to determine the concentration profiles of as many chemical species, both labile and stable, as possible in the flames. However, it is a difficult task to determine the concentration profiles, especially, of the labile intermediates in high temperature flames. We have been using the probe-sampling-electron spin resonance (ESR) technique to detect the labile intermediates (H, O, and OH; the principal carriers of chain reactions of combustion), in free-burning methane and methanol flames.[1,2] Recently, we carried out a combined ESR-mass spectrometric study in order to examine the concentration profiles of nine (labile and stable) chemical species in free-burning methanol-air flames at atmospheric pressure (in the previous study of this series).[3] The study was extended in our work to the CH_3OH-O_2-Ar flames at a low pressure; this allowed us to control more strictly the physical conditions of combustion and to change more freely the equivalence ratio of the premixed gas.

The reaction mechanism of methanol combustion has theoretically been studied over ten years;[4-7] several numerical models concerning combustion reactions, including more than twenty species, have been proposed.[6-8] However, most of the experimental data so far reported[4,5,9-11] have only partially shown chemical features of the combustion, and have not been sufficiently comprehensive for a comparison with theoretical predictions and to substantiate the proposed models. Akrich et al. first determined the concentration profiles of stable chemical species in methanol-air flames at low pressures by means of the gas chromatographic method.[9] Pauwels et al.[10] later studied the concentration profiles of H, O, and OH by means of the ESR method under the same flame conditions as those in the above gas chromatographic study; these gave general support to the numerical model proposed by Westbrook and Dryer.[6] Very recently, Vandooren and Van Tiggelen,[11] and Andersson et al.[4] performed mass spectrometric studies and obtained a comprehensive set of the profiles of stable species and labile intermediates in methanol flames at low pressures. Based on these results, Dove and Warnatz[7] developed a simplified model of methanol combustion. The present ESR-mass spectrometric study complements these previous studies and serves as an experimental basis for obtaining a further insight into chemical reactions during methanol combustion.

Experimental

The burner and sampling system used in the present study is schematically shown in Fig. 1. The burner comprised two concentric stainless-steel tubes: The inner tube was attached with a porous stainless-steel disk (27-mm diameter) at the end which acted as the burner mouth, and the outer tube (58-mm diameter) enclosed the flame at a low pressure and supported a quartz sampling probe. The sampling probe was pretreated with an aqueous HF solution and cleaned with aqueous NaOH and HNO_3 solutions in order to reduce the surface destruction of labile intermediates.[2,10] Sampling of burning gas was made at several positions on the center axis of the flame by sliding the inner tube with respect to the outer one. The burner was cooled by circulating water.

Oxygen, and argon of purity higher than 99.9% were supplied from cylinders through regulated rotermeters. Methanol of reagent grade was continuously injected into preheated gas flow with a microfeeder. The flames of premixed gas, CH_3OH-O_2-Ar, were stabilized in the burner at a low pressure (1.11×10^4 Pa); this was controlled by adjusting the pumping rate.

The ESR and mass spectrometric measurements of burning gas were made with an X-band ESR spectrometer

† Present address: Nihon Furnace Kogyo, Ltd., Tsurumi-ku, Yokohama 230.

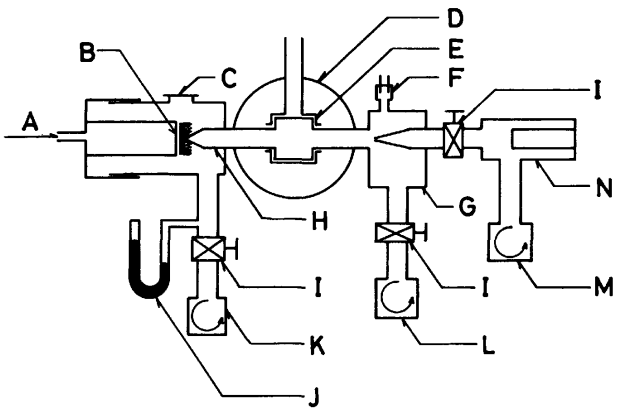

Fig. 1. Schematic drawing of the burner and the sampling system. A) Inlet of premixed gases, B) porous stainless-steel plate, C) viewing window, D) magnet, E) ESR spectrometer, F) vacuum gauge, G) condenser, H) sampling probe, I) vacuum valve, J) Hg manometer, K) primary pumping system (rotary pump), L) secondary pumping system (rotary pump and mechanical booster pump), M) tertiary pumping system (rotary pump and diffusion pump), and N) quadrupole mass spectrometer.

and a quadrupole mass spectrometer (as previously described).[3] About one-tenth of the burning gas was continuously sampled through a tiny hole (about 0.1 mm in diameter) at the tip of the sampling probe; it was subjected to ESR measurements at 13.3 Pa and mass spectroscopic measurements at a total pressure of 10^{-3} Pa. The residence time of the sampled gas in the sampling probe before reaching the ESR cavity was estimated to be about 2 ms. The flame temperature was measured with a SiO_2-coated Pt/Pt-Rh thermocouple.

Analysis of Data

From the apparent local concentration obtained by ESR or mass spectrometric measurements of the i-th species at each position in the flame, the mass flux was calculated as

$$G_i = \frac{X_i M_i}{\bar{M}}\left(1+\frac{V_i}{v}\right), \tag{1}$$

where $\bar{M}$ is the average molecular weight, v the velocity of the flame gas, and X_i, M_i, and V_i the mole fraction, the molecular weight, and the diffusion velocity of the i-th species in the flame gas. By taking the z-axis along the gas flow, the diffusion velocity was calculated as

$$V_i = -\frac{D_{ij}}{X_i}\cdot\frac{dX_i}{dz}, \tag{2}$$

using the binary diffusion coefficients D_{ij} given by

$$D_{ij} = \frac{1.66\times10^{-3}(1/M_i+1/M_j)^{1/2}T^{1.67}}{P\sigma_{ij}^2(\varepsilon_{ij}/\kappa)^{0.17}} \tag{3}$$

as well as the Lennard-Jones potential parameters (σ_{ij} and ε_{ij}/κ) derived by Westenberg and Fristrom,[12] and Warnatz.[13] In actual calculations, argon was always taken as the j-th species.

The net reaction rate was then calculated as

$$K_i = \frac{\rho v}{M_i}\cdot\frac{dG_i}{dz}, \tag{4}$$

where ρ is the density of the flame gas. This quantity gives the rate of net formation (or consumption) at a particular position in the flame solely due to chemical reactions involving the i-th species, i.e., the net formation rate derived by subtracting the effect of diffusion from the concentration profile observed by ESR or mass spectrometric measurements.

Results and Discussion

Concentration Profiles. ESR spectra due to H, O, OH, and O_2 were observed in the present CH_3OH-O_2-Ar flame. The spectral features were essentially the same as those previously observed for methane-air and methanol-air flames.[1-3] The intensity of the spectra of H and O was calibrated with reference to the spectrum of O_2 with a known concentration in order to determine their absolute concentrations in the ESR cavity; while the spectral intensity of OH was calibrated with reference to the NO spectrum.[14,15] A correction for the first-order destruction of H and O on the wall of the sampling probe before reaching the ESR cavity was made by changing the residence time in the sampling probe, as described previously.[3]

A correction for the destruction of OH during sampling was rather difficult, since it did not follow a simple first-order process and was thought to be largely due to unknown reactions occurring at or close to the hole of the sampling probe.[3] The correction factor was, therefore, determined from the observed ESR intensities of H, O, OH, and O_2 in the post flame region and the assumed partial equilibrium of the reaction,

$$H + O_2 \longrightarrow O+OH, \tag{R1}$$

by using the equilibrium constant, $K=300\cdot T^{-0.372}\exp(-8565/T)$ reported previously.[16]

Stable intermediates (H_2, CH_2O, and CO) were detected together with the fuel CH_3OH and the final products (CO_2 and H_2O) by the mass spectrometric method. The concentrations of the stable species were determined from the observed intensities of their mass patterns with reference to those of the mixtures of known compositions. No correction was made for the reactions in the sampling probe for these stable species.

Figure 2 shows the concentration profiles (all in the mole fraction unit) of stable and unstable species in the flame of stoichiometric composition (CH_3OH: 11.7%, O_2: 17.7%, Ar: 70.6%) with the cold gas velocity

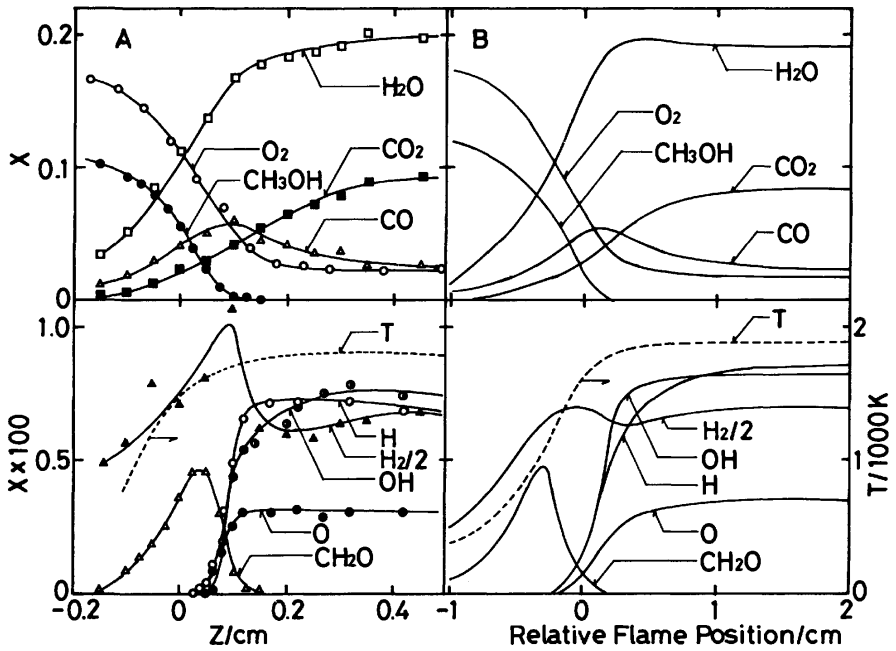

Fig. 2. The profiles of mole fractions (X) of labile and stable species and temperature (A) experimentally observed in stoichiometric methanol-oxygen-argon flame at 1.11×10^4 Pa, and (B) calculated in stoichiometric methanol-air flame at 1.01×10^4 Pa by Westbrook and Dryer (Ref. 6). The scale of abscissa is different between the observed and calculated profiles.

of 41.6 cm s^{-1} (mass flow rate of 6.36×10^{-3} g $cm^{-2}s^{-1}$). The origin of the z-axis corresponds to the beginning of the luminous zone of the flame. The observed profiles resemble those for the low-pressure methanol-air flames of the equivalence ratio (ϕ, $([fuel]/[O_2])_{actual}/([fuel]/[O_2])_{stoichiometric}$) of 1.0 observed by Andersson et al. by means of the mass spectrometric method.[4] There is a slight difference from the previous data regarding the absolute values at the concentration maximum of the profiles. This is probably due to a difference in the flame temperature. The general trend of the present concentration profiles is also very similar to that of low-pressure methanol-air flames of $\phi=1.08$.[9,10]

Westbrook and Dryer[6] have reported on the concentration profiles of chemical species in the stoichiometric methanol-air flame at 1.01×10^4 Pa which have been calculated on the basis of the numerical model of the methanol combustion including 26 species and 84 reactions. The concentration profiles observed in the present study agree with the calculated profiles (as demonstrated in Fig. 2), except that the transient change in the observed concentrations is generally steeper than that expected from model calculations. The same agreement between the observed and calculated profiles has been found for methanol-air flames at atmospheric pressure in the previous study of this series.[3] Thus, it is concluded that the numerical model proposed by Westbrook and Dryer[7] reproduces fairly well the effect of the pressure on the chemical reactions of methanol combustion. A similar conclusion has also been obtained from previous mass spectrometric studies.[4,5]

Formation and Consumption Rates of Chemical Species. In order to examine the chemical aspects of the flame more carefully, the net reaction rate, K, of each species was derived from the concentration profile and Eq. 4, and is shown in Fig. 3. The positive K value indicates net formation, while the negative value indicates net consumption.

The consumption rates of CH_3OH and O_2 and the formation rates of H_2O, H_2, and CO show maxima at almost the same positions. In contrast, the formation rate of CO_2 shows a very broad maximum at the downstream region. It is slowly formed in an extended region of the flame.

For all the labile intermediates (H, O, and OH), the K value first grows in the negative side and then changes to the positive. The features of local K values of the labile intermediates in flame indicates that the labile intermediates are supplied by backward diffusion to the upstream, preheated region, where they are effectively consumed by reactions with CH_3OH.

Reaction Mechanism. The comprehensive reaction mechanism for methanol combustion was first developed by Westbrook and Dryer[6] and was later modified.[5,8] The calculated concentration profiles for one-dimensional flames based on this reaction

mechanism have generally agreed with experimental results.[3,4,9,10] An agreement can also be seen in the present experimental results (already shown in Fig. 2).

Recently, however, Dove and Warnatz proposed a different reaction mechanism, which is simpler (14 species and 40 reactions) than the previous one and explicitly regards the pathway of methanol oxidation to be $CH_3OH \rightarrow CH_2OH \rightarrow CH_2O \rightarrow CHO \rightarrow CO \rightarrow CO_2$.[7] They have argued that the new model predicts well the experimentally observed burning velocity. The formation (or consumption) rates determined in the present experimental study will be examined with reference to the reaction mechanism proposed by Dove and Warnatz. According to the proposed mechanism,[7] CH_3OH reacts mainly with the labile intermediates (H, O, and OH) as follows:

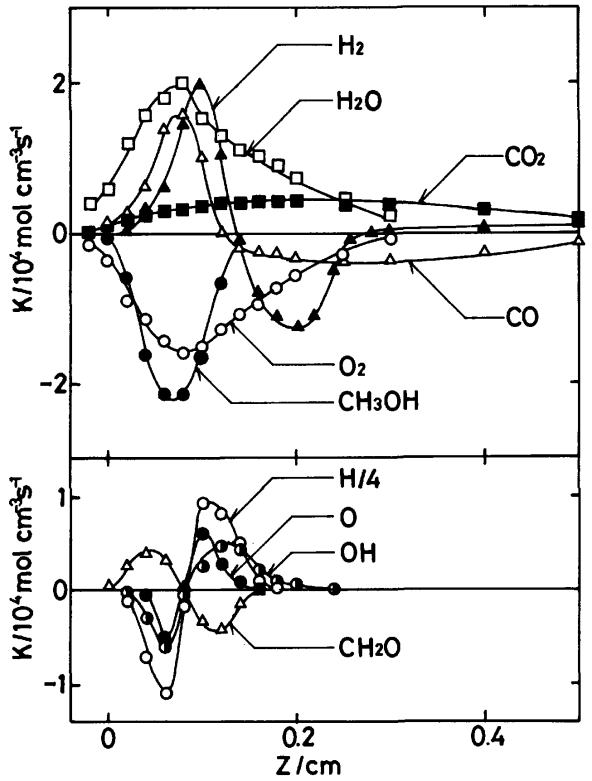

Fig. 3. Net formation (or consumption) rates of labile and stable species in the stoichiometric methanol-oxygen-argon flame at 1.11×10^4 Pa, directly derived from the observed concentration profiles in Fig. 2.

$$CH_3OH + OH \longrightarrow CH_2OH + H_2O, \quad (R2)$$
$$CH_3OH + H \longrightarrow CH_2OH + H_2, \quad (R3)$$

and

$$CH_3OH + O \longrightarrow CH_2OH + OH. \quad (R4)$$

The reactions of CH_2O, CHO, and CO are

$$CH_2O + H \longrightarrow CHO + H_2, \quad (R5)$$
$$CH_2O + O \longrightarrow CHO + OH, \quad (R6)$$
$$CH_2O + OH \longrightarrow CHO + H_2O, \quad (R7)$$
$$CHO + M \longrightarrow CO + H + M, \quad (R8)$$
$$CHO + H \longrightarrow CO + H_2, \quad (R9)$$
$$CHO + OH \longrightarrow CO + H_2O, \quad (R10)$$

and

$$CHO + O_2 \longrightarrow CO + HO_2. \quad (R11)$$

CO_2 is then formed mainly by the reaction,

$$CO + OH \longrightarrow CO_2 + H. \quad (R12)$$

Though CH_3OH can be oxidized also by HO_2 as

$$CH_3OH + HO_2 \longrightarrow CH_2OH + H_2O_2 \quad (R13)$$

and

$$CH_2O + HO_2 \longrightarrow CHO + H_2O_2, \quad (R14)$$

Table 1. Elementary Reactions of Methanol Combustion and Their Rate Parameters Used in the Discussion of the Present Experimental Results

Reaction		A	n	T_0
$H + O_2 \longrightarrow O + OH$	(R1)	2.4×10^{16}	−0.91	8310
$CH_3OH + OH \longrightarrow CH_2OH + H_2O$	(R2)	1.0×10^{13}	0	850
$CH_3OH + H \longrightarrow CH_2OH + H_2$	(R3)	4.0×10^{13}	0	3070
$CH_3OH + O \longrightarrow CH_2OH + OH$	(R4)	1.0×10^{13}	0	2370
$CH_2O + H \longrightarrow CHO + H_2$	(R5)	2.5×10^{13}	0	2010
$CH_2O + O \longrightarrow CHO + OH$	(R6)	3.5×10^{13}	0	1770
$CH_2O + OH \longrightarrow CHO + H_2O$	(R7)	3.0×10^{13}	0	600
$CO + OH \longrightarrow CO_2 + H$	(R12)	4.6×10^{6}	1.5	−370
$CO_2 + H \longrightarrow CO + OH$	(−R12)	1.6×10^{14}	0	13200
$CH_2OH + O_2 \longrightarrow CH_2O + HO_2$	(R16)	1.0×10^{13}	0	3620
$CH_2OH + M \longrightarrow CH_2O + H + M$	(R17)	1.0×10^{14}	0	12600
$CH_2OH + H \longrightarrow CH_2O + H_2$	(R18)	2.0×10^{13}	0	0

The reactions were taken from the reaction mechanism proposed by Dove and Warnatz (Ref. 7). The rate parameters are those in the expression of the reaction rate constant $k = AT^n \exp(-T_0/T)$ in cm^3 mol^{-1} s^{-1} unit.

these oxidation paths are unimportant compared with reactions R2—4 and R5—7 under the present high-temperature conditions. The rate constants of some of these reactions[7] are cited in Table 1.

The above oxidation pathway gives the formation (or consumption) rates, K, as a function of the concentrations of reacting species as following:

$$K(CH_3OH) = -\{k_{R2}[OH]+k_{R3}[H]+k_{R4}[O]\}[CH_3OH] \quad (5)$$

and

$$K(CO_2) = k_{R12}[CO][OH] - k_{-R12}[CO_2][H]. \quad (6)$$

Assuming a quasi-stationary state for CHO,

$$K(CO) + K(CO_2) = \{k_{R5}[H]+k_{R6}[O]+k_{R7}[OH]\}[CH_2O] \quad (7)$$

is also obtained. The K values can be calculated from the observed concentration profiles of the reacting species and the rate constants cited in Table 1. On the other hand, the K values have been directly observed experimentally as shown in Fig. 3 (strictly speaking, directly derived from the concentration profile of the species itself). A comparison between the observed and calculated K's will verify the relevance of the reaction mechanism on which the calculation has been made.

The calculated K is compared with the observed K for the consumption of CH_3OH (Fig. 4). Both K values agree fairly well, except that the calculated K is lower in the very upstream region. The disagreement in the upstream region is attributable to a perturbation due to the inserted sampling probe: The sampling of burning gas acts as a sink for the labile intermediates, and violates their concentration profiles determined by the balance of chemical reactions and diffusion. This effect becomes important when sampling is made at positions close to the burner mouth, since a backward diffusion of the labile intermediates (only source of the labile intermediates existing at the sampling position) is seriously hindered by the sampling probe. Such a perturbation due to the sampling probe has been experimentally shown by observing the OH concentration in the preheated zone of a propane-oxygen flame by mass spectrometric (with sampling) and UV spectroscopic (without sampling) methods.[17]

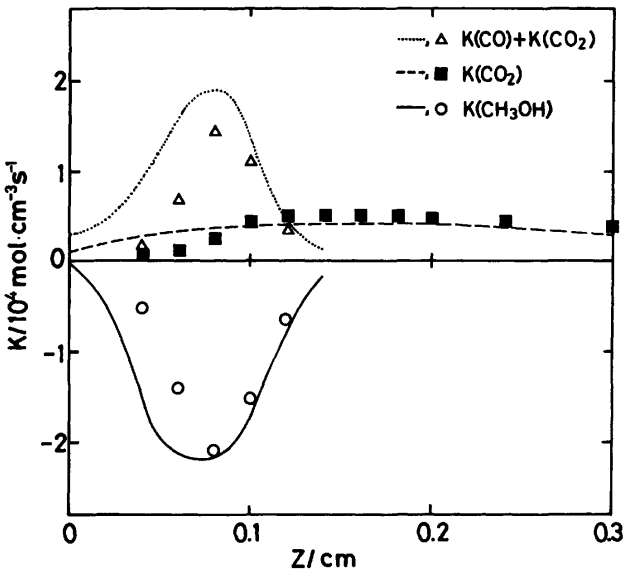

Fig. 4. Comparison between the observed (lines) and the calculated (plots) net formation (or consumption) rates of CH_3OH, CO_2, and sum of CO and CO_2. The lines showing the observed rates were taken from Fig. 3. The plots were obtained by calculating rates based on the rate constants in Table 1 and the concentration profiles of reacting species in Fig. 2. See text also for detail.

Figure 4 shows an agreement between the observation and calculation, also for $K(CO_2)$ and $K(CO)+K(CO_2)$ in the region $z>0.1$ cm, where the concentrations of the labile intermediates reach a plateau value and the perturbation due to the sampling probe is expected to be insignificant. Because the CH_2O consumption appears to balance the formation of CO and CO_2, CHO is very probably short-lived and is converted quickly to CO. Although CH_2O can react with O_2 as

$$CH_2O + O_2 \longrightarrow CHO + HO_2, \quad (R15)$$

numerical examinations based on the observed concentration profiles and the reported rate constants show that the rate of reaction R15 is much smaller than the rates of the reactions of CH_2O with H, O, and OH (reactions R5—7) throughout the flame.

The general agreement between the observed and calculated K values indicates a consistency between the observed concentration profiles of labile and stable chemical species in the flame, and gives experimental support to the simpler mechanism of methanol oxidation.

According to the Dove and Warnatz's mechanism,[7] the consumption of O_2 is mostly due to the following reactions:

$$H + O_2 \longrightarrow O + OH \quad (R1)$$

and

$$CH_2OH + O_2 \longrightarrow CH_2O + HO_2. \quad (R16)$$

The rate of O_2 consumption is, therefore, given as

$$-K(O_2) = \{k_{R1}[H] + k_{R16}[CH_2OH]\}[O_2] - k_{-R1}[O][OH]. \quad (8)$$

However, the consumption rate cannot be calculated in a straight-forwatd manner from the observed concentration profiles, since no experimental data is available for the CH_2OH concentration. If one

assumes that the decay of CH_2OH is exclusively due to its oxidation into CH_2O by

$$CH_2OH + O_2 \longrightarrow CH_2O + HO_2, \quad (R16)$$

$$CH_2OH + M \longrightarrow CH_2O + H + M, \quad (R17)$$

and

$$CH_2OH + H \longrightarrow CH_2O + H_2, \quad (R18)$$

reactions of CH_2OH will determine the sum of the formation rates:

$$K(CH_2O) + K(CO) + K(CO_2) = \{k_{R16}[O_2] + k_{R17}[M] + k_{R18}[H]\}[CH_2OH]. \quad (9)$$

Substituting $[CH_2OH]$ of equation 9 into equation 8,

$$-K(O_2) = k_{R1}[H][O_2] - k_{-R1}[O][OH] + k_{R16}[O_2]\frac{K(CH_2O)+K(CO)+K(CO_2)}{k_{R16}[O_2]+k_{R17}[M]+k_{R18}[H]}. \quad (10)$$

Thus, the O_2 consumption rate can be calculated from the observed $K(CH_2O)$, $K(CO)$, $K(CO_2)$, $[O_2]$, [M], and [H] and from the rate constants cited in Table 1 (the rate constant k_{-R1} can be obtained from the k_{R1} value and the equilibrium constant for reaction R1).

The calculated $-K(O_2)$, by using the rate constants in Table 1, is shown in Fig. 5 (curve B). Thus, calculated $-K(O_2)$ differs from the $-K(O_2)$ determined directly from the observed concentration profile of O_2 (curve A), especially in the downstream region. The agreement between the calculated and observed $-K(O_2)$ is much improved in the downstream region (curve C in Fig. 5), if one uses the rate constant, $k_{R1}=1.2\times10^{17}T^{-0.91}\exp(-8310/T)$, recently recommended by Warnatz.[18] This is five times as large as the previous rate constant (cited in Table 1) at the present flame temperature.

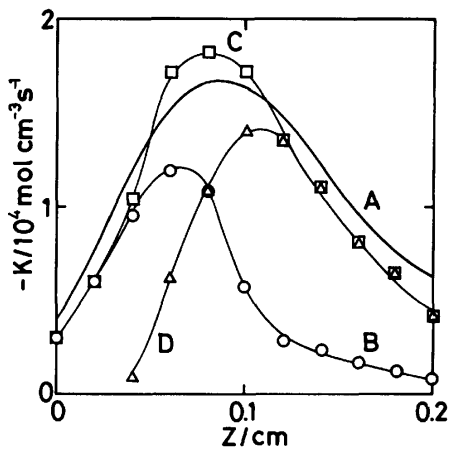

Fig. 5. Comparison of the consumption rates of O_2 obtained in different ways. (A): The observed rate taken from Fig. 3. (B): The rate calculated based on equation 10 and by using the rate constants in Table 1. (C): The rate calculated by using the newly-recommended rate constant for reaction R1. (D): The rate calculated with the newly-recommended rate constant and by excluding reaction R16. See also the text for detail.

$K(O_2)$ calculated with the new K_{R1} and neglecting reaction R16 is also shown in Fig. 5 (curve D). It is evident that reaction R16 is an important process for O_2 consumption in the upstream region of the flame. The observed $-K(O_2)$ appears to agree well with the calculation including reaction R16 rather than the calculation excluding it. We do not, however, dare to stress this agreement in the upstream region, since there is some ambiguities related to perturbation due to the inserted sampling probe in this region (as mentioned before).

Concluding Remarks. Together with seven stable species, three labile intermediates were observed in the CH_3OH-Ar-O_2 stoichiomeric flame at a low pressure by the combined ESR-mass spectrometric method. Their concentration profiles and the local distribution of their net formation (or consumption) rates in the flame were examined to elucidate the chemical reactions of methanol combustion.

The experimental results agree with the concentration profiles predicted by numerical calculations based on the model for methanol combustion consisting of very many elementary reactions previously reported by Westbrook and Dryer.[6] However, the results are also shown to be consistent even with the simplified model for the methanol combustion recently proposed by Dove and Warnatz.[7] As far as the authors are aware, the present study provides some of the most comprehensive experimental data on the distribution of the chemical species in a methanol flame. There is still no need to make the reaction mechanism complex in order to interpret the present experimental results. This does not necessarily means that the reaction mechanism of methanol combustion is really simple. Further progress in combustion chemical experiments is desirable for unambiguous comparisons with the proposed models and to totally elucidate the chemical aspect of combustion.

References

1) S. Noda, M. Miura, and H. Yoshida, *J. Phys. Chem.*, **84**, 3143 (1980).

2) S. Noda, H. Demise, O. Claesson, and H. Yoshida, *J. Phys. Chem.*, **88**, 2552 (1984).

3) M. Taniguchi and H. Yoshida, *Bull. Chem. Soc. Jpn.*, **60**, 1249 (1987), the preceding paper of this series).

4) L. L. Andersson, B. Christenson, A. Höglund, J. O. Olsson, and L. G. Rosengren, *Prog. Astronaut. Aeronaut.*, **95**, 164 (1984).

5) J. O. Olsson, L. S. Karlsson, and L. L. Andersson, *J. Phys. Chem.*, **90**, 1458 (1986).

6) C. K. Westbrook and F. L. Dryer, *Combust. Flame*, **37**, 171 (1980).
7) J. E. Dove and J. Warnatz, *Ber. Bunsenges. Phys. Chem.*, **87**, 1040 (1983).
8) C. K. Westbrook, F. L. Dryer, and K. P. Schug, *Symp. (Int.) Combust. [Proc.]*, **19**, 153 (1982).
9) R. Akrich, C. Vovelle, and R. Delbourgo, *Combust. Flame*, **32**, 171 (1978).
10) J.-F. Pauwels, M. Carlier, and L.-R. Sochet *J. Phys. Chem.*, **86**, 4330 (1982).
11) J. Vandooren and P. J. Van Tiggelen, *Symp. (Int.) Combust. [Proc.]*, **18**, 473 (1981).
12) A. A. Westenberg and R. M. Fristrom, "Flame Structure," McGraw Hill, New York (1965), p. 276.
13) J. Warnatz, *Symp. (Int.) Combust. [Proc.]*, **18**, 369 (1981).
14) A. A. Westenberg and N. de Haas, *J. Chem. Phys.*, **40**, 3087 (1964).
15) A. A. Westenberg, *J. Chem. Phys.*, **43**, 1544 (1965).
16) G. Dixon-Lewis and D. J. Williams, "Comprehensive Chemical Kinetics," ed by C. H. Bamford and C. F. H. Tipper, Elsevier, Amsterdam (1977), Vol. 17, p. 91.
17) J. M. Revet, D. Puechberty, and M. J. Cottereau, *Combust. Flame*, **33**, 5 (1978).
18) J. Warnatz, "Combustion Chemistry," ed by W. C. Gardiner, Jr., Springer, New York (1984), Chap. 5.

 © 1987 The Chemical Society of Japan Bull. Chem. Soc. Jpn., 60, 1625—1629 (1987)

^{129}I Mössbauer Spectroscopic Study of 2:3 Molecular Complexes of Triphenylphosphine Sulfide-Iodine and Acridine-Iodine

Hiroshi SAKAI* and Yutaka MAEDA
Research Reactor Institute, Kyoto University,
Kumatori-cho, Sennan-gun, Osaka 590-04
(Received November 12, 1986)

The ^{129}I Mössbauer effect has been applied to investigate 2:3 molecular complexes of triphenylphosphine sulfide–iodine and acridine–iodine. The Mössbauer spectra indicate the presence of three unequivalent iodine sites (I_A, I_B, and I_C), as expected from the crystallographic data of these complexes. The iodine atom (I_A) coordinating to the sulfur or nitrogen atom of each donor molecule is more positively charged than that of the 1:1 molecular complex containing the same donor atom. This result can be interpreted in terms of the covalency of the S···I_A or N···I_A bond. The degrees of charge transfer in the 2:3 complexes are close to those in the 1:1 complexes, and the transferred charges are mainly localized on the terminal iodine atoms (I_B). The iodine molecule (I_C) cross-linked to two I_B atoms has a slightly negative charge, consistent with the bond distance of the molecule. The iodine moieties of these complexes are very similar to the structure of I_8^{2-} in Cs_2I_8.

The iodine molecule is known to be a typical electron acceptor and to form molecular or charge-transfer complexes with various electron-donor molecules such as amines, ethers, and thioethers. Many of these complexes usually have a 1:1 stoichiometry in the solid phase, consisting of a linear orientation of the iodine molecule with the donor atom. However, triphenylphosphine sulfide (TPPS)[1] and acridine (AC)[2] form 2:3 molecular complexes with the iodine molecule in the solid state, although these donors form 1:1 complexes with iodine monobromide. The crystallographic data of the triphenylphosphine sulfide–iodine (2TPPS–3I_2) complex suggest that two iodine molecules are bonded to each sulfur atom of two TPPS molecules, resulting in a nearly linear S···I_A–I_B arrangement; another iodine molecule is cross-linked to two terminal iodine atoms (I_B) with a Z-shaped structure (Fig. 1).[3] The six iodine atoms of the complex lie in one plane. The intermolecular S···I_A bond distance (2.69 Å) is considerably shorter than the sum of the respective van der Waals radii, whereas the intramolecular I_A–I_B bond disance (2.86 Å) is longer than that of the free iodine molecule. The corresponding bond distances for the usual 1,4-dithiane-iodine complex having a similar S···I_A–I_B configuration have been reported as 2.867 Å for the S···I_A bond and 2.787 Å for the I_A–I_B bond.[4] This comparison of the bond distances for both complexes suggests that the charge-transfer interaction of the unusual 2:3 iodine complex is stronger than that of usual 1:1 iodine complex containing the same donor atom.

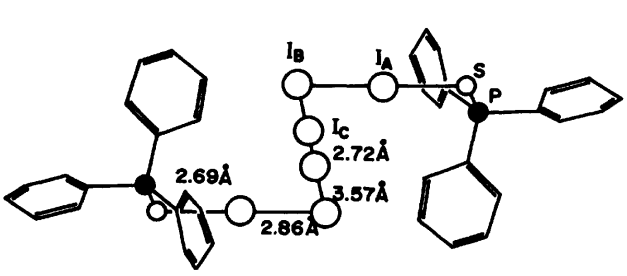

Fig. 1. The structure of the 2TPPS–3I_2 complex (taken from Ref. 3).

Recently, Uchida[5] has revealed the crystal structure of the acridine–iodine (2AC–3I_2) complex, in which the configuration of the iodine atoms is very similar to that of 2TPPS-3I_2. This 2:3 complex is apparently not the ionic compound formulated as $[(AC)_2I]^+I_5^-$, predicted from the low-frequency vibrational spectra.[2] Ichiba et al.[6] previously measured the ^{129}I Mössbauer spectrum of the acridine–iodine complex at 85 K. The analysis of the spectrum with two unequivalent iodine atoms (1:1 type complex) did not give a completely satisfactory result, suggesting the existence of three unequivalent iodine atoms in the complex.

It is of interest to estimate the charge densities on the iodine atoms in the unusual 2:3 iodine complexes of TPPS and AC, in comparison with those in the usual 1:1 iodine complexs of thioethers and amines. The Mössbauer spectroscopy of ^{129}I is favorable for this purpose, since the charge density and the charge distribution on the iodine atom can be directly derived from the such Mössbauer parameters as the quadrupole coupling constant (e^2Qq) and its sign, the asymmetry parameter (η), and the isomer shift (δ). In the present work, the ^{129}I Mössbauer spectra of the 2TPPS–3I_2 and 2AC–3I_2 complexes were measured and the electronic structure on each iodine atom could be determined. The nature of the charge-transfer bond for these 2:3 complexes is discussed in comparison with that for 1:1 complexes of thioether–iodine and amine–iodine.

Experimental

The complexes were prepared on a small scale using radioactive ^{129}I (99% enriched) obtained from the New

England Nuclear Co. as Na ^{129}I in a Na_2SO_3 solution. Molecular iodine, prepared by H_2O_2 oxidation of an acidified solution of NaI, was extracted with carbon tetrachloride or chloroform. Each iodine solution was thoroughly washed with water and passed through a Teflon filter to eliminate any slight amount of water. The 2TPPS-$3I_2$ complex was prepared by adding a solution of a stoichiometric amount of TPPS in carbon tetrachloride to the iodine solution of the same solvent. A purple-red crystalline product was collected by filtration and air-dried. The mole ratio was determined for a complex prepared with nonradioactive (natural) iodine by elemental analysis. Found: C, 31.7; H, 2.5; I, 56.7%. Calcuild for $2(C_6H_5)_3PS$-$3I_2$: C, 32.0, H, 2.2; I, 56.4%. A brown crystalline complex of 2AC-$3I_2$ was prepared in chloroform using a procedure similar to that for the 2TPPS-$3I_2$ complex. The iodine content was determined to be 67.4% by means of iodometry. Calcuild for $2(C_{13}H_9N)$-$3I_2$: I, 68.0%. The thicknesses of the absorber samples, mounted in Teflon sample holders, were in the range of 20 to 30 mg ^{129}I cm^{-2}.

The $^{66}Zn^{129}Te$ Mössbauer source was prepared by irradiation of 150 mg ^{66}Zn ^{128}Te compound at a thermal neutron fluence rate of 2×10^{13} n cm^{-2} s^{-1} for 1 h in the Kyoto University Reactor (KUR). The source, about 10 mCi in radioactivity initially, was immediately used for the measurement since the half life of ^{129}Te is very short (70 min). The Mössbauer measurement was carried out in the transmission geometry by cooling the source and the absorber to 16 K with a closed-cycle helium refrigerator. For the 2AC-$3I_2$ complex the spectra were measured at 78 K in addition to 16 K in order to make a comparison with the previous spectrum.[6] The Mössbauer spectrometer was calibrated using an iron foil spectrum.

Results and Discussion

The Mössbauer spectra of the 2TPPS-$3I_2$ and 2AC-$3I_2$ complexes are shown in Figs. 2 and 3. The top (a)

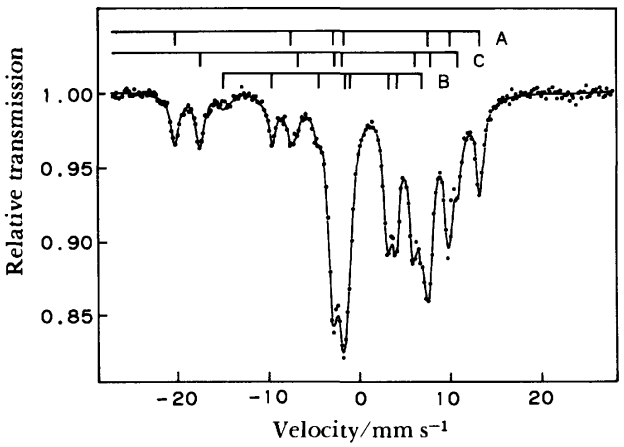

Fig. 2. ^{129}I Mössbauer spectrum of the 2TPPS-$3I_2$ complex at 16 K.

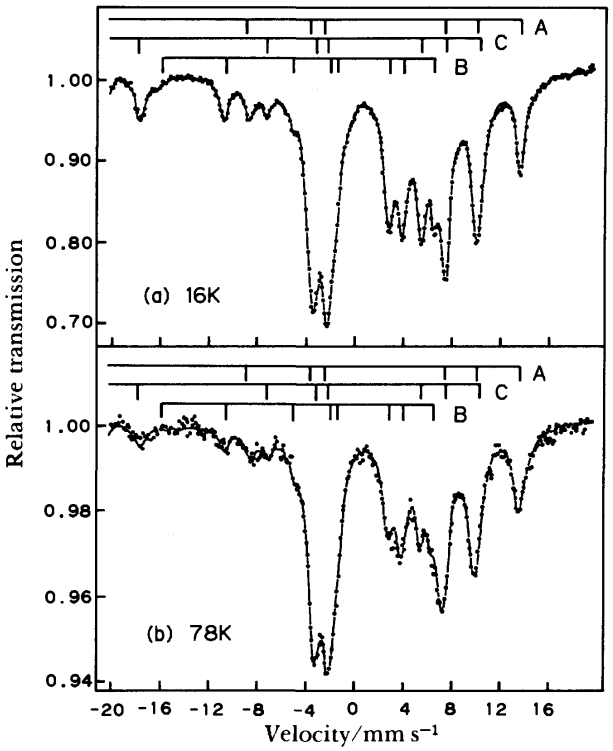

Fig. 3. ^{129}I Mössbauer spectra of the 2AC-$3I_2$ complex at (a) 16 K and (b) 78 K.

Table 1. ^{129}I Mössbauer Parameters for the 2:3 Molecular Complexes of 2TPPS-$3I_2$ and 2AC-$3I_2$ and the 1:1 Molecular Complexes of 1,4-Dithiane-$2I_2$ and Pyridine-I_2

		$\frac{e^2Qq}{\text{MHz}}$ [a]	η	$\frac{\delta}{\text{mm s}^{-1}}$ [b]	U_p [c]	h_p [d]	Ref.
2TPPS-$3I_2$ (16 K)	I_A	−2618±20	0.0	1.47±0.04	1.14	1.34	
	I_B	−1221±20	0.20±0.05	0.38±0.04	0.53	0.61	
	I_C	−2219±20	0.0	0.88±0.04	0.97	0.95	
2AC-$3I_2$ (16 K)	I_A	−2937±20	0.0	1.58±0.04	1.28	1.41	
	I_B	−1326±20	0.17±0.05	0.38±0.04	0.58	0.61	
	I_C	−2276±20	0.0	0.96±0.04	0.99	1.00	
Dithiane-$2I_2$ (16 K)	I_A	−2526±13	0.0	1.47±0.04	1.10	1.34	(7)
	I_B	−1553±13	0.06	0.50±0.04	0.68	0.69	
Pyridine-I_2 in CS_2 (16 K)	I_A	−2631±20	0.10	1.82±0.04	1.15	1.57	(8)
	I_B	−1439±20	0.0	0.39±0.04	0.63	0.62	

a) The e^2Qq values are converted to the ^{127}I nucleus. b) The δ values are relative to the ZnTe source. c) $U_p = -e^2Qq_{obsd}/e^2Qq_{atom}$, $e^2Qq_{atom} = 2292.7$ MHz. d) $\delta = 1.5h_p - 0.54$ (mm s^{-1}).

and bottom (b) spectra of 2AC–3I_2 in Fig. 3 were measured at 16 and 78 K, respectively. These spectra comprise three kinds of quadrupole octets (A, B, and C), as is expected from the crystal structures of 2TPPS–3I_2[3] and 2AC–3I_2[5]. The spectra were fitted with Lorentzian curves of an equal linewidth by a least-squares method using a triple set of the Mössbauer parameters, e^2Qq, η, and δ. The solid curves and the stick diagrams in the figures indicate the best-fitted superimposed Lorentzian curves and the peak positions, respectively. The Mössbauer parameters obtained are summarized in Table 1, together with the results for the usual 1:1 complexes of 1,4-dithiane-iodine[7] and pyridine–iodine.[8] The values of e^2Qq were converted to those for the ^{127}I nucleus.

The Mössbauer spectra of the 2TPPS–3I_2 and 2AC–3I_2 complexes, showing the existence of three unequivalent iodine atoms (I_A, I_B, and I_C), are similar to each other. This observation is in accord with the results of structural analyses for these complexes, in which the iodine groups have a similar configuration. It is established for usual 1:1 molecular complexes that the iodine atom coordinating to the donor atom indicates larger values of e^2Qq and δ than the terminal iodine atom. Therefore, it is appropriate to assign the iodine with the largest quadrupole splting (A) to the iodine atom (I_A) coordinating to the sulfur or nitrogen atom of each donor molecule, whereas the iodine with the smallest quadrupole splitting (B) should be assigned to the terminal iodine atom (I_B). The intermediate quadrupole splitting (C) corresponds to the iodine molecule (I_C) cross-linked to the two terminal iodine atoms, since the values of e^2Qq and δ are close to those for the solid iodine.[9] The Mössbauer spectrum of 2AC–3I_2 at 78 K is very similar to that previously measured at 85 K by Ichiba et al.[6] It was found from the comparison with the spectrum at 16 K that the absorption peaks corresponding to the intermediate quadrupole splitting (C) decrease more rapidly at 78 K than the other absorption peaks. This result implies that the iodine molecule cross-linked to two I_B atoms has a lower Debye temperature than the other iodine atoms.

The values of e^2Qq, η, and δ are closely related to the charge distribution and the charge density localized on the iodine atom as follows:[10,11]

$$U_p = -e^2Qq_{obsd}/e^2Qq_{atom} = -N_z + (N_x+N_y)/2, \quad (1)$$

$$\eta = 3(N_x-N_y)/2U_p, \quad (2)$$

$$\delta = -9.2h_s + 1.5h_p - 0.54, \quad \text{(mm/s, for ZnTe source)}, \quad (3)$$

and

$$h_p = 6-(N_x+N_y+N_z). \quad (4)$$

Here, U_p is the number of unbalanced p-electrons and e^2Qq_{atom}, the atomic iodine quadrupole coupling constant, is equal to 2292.7 MHz for ^{127}I. N_x,N_y, and N_z are the populations of 5p-electrons in the x, y, and z orbitals, respectively. The sign of e^2Qq, obtained directly from the unsymmetrical Mössbauer spectrum, shows whether the main bond of the iodine atom is σ-bonding (z-direction) or π-bonding (x or y direction). The e^2Qq values for all iodine atoms of the present molecular complexes are negative in sign, suggesting that the bonding of each iodine atom is predominantly of the σ-type. The asymmetry parameter (η), the deviation of the electric field from the cylindrical symmetry, is attributed to an additonal π-bonding or an intermolecular bonding in the x or y direction. The large η values for the terminal iodine atoms (I_B) in these complexes are due to the weak intermolecular $I_B\cdots I_C$ bonds, since the bond distances are 3.57 Å and 3.51 Å for 2TPPS–3I_2[3] and 2AC–3I_2[5], respectively (shorter than the sum of the van der Waals radius (4.30 Å)). The isomer shift (δ) is directly related to the s-electron density at the nucleus $|\psi_s(0)|^2$. Since the 5s-electron density is shielded by outer 5p-electrons, the δ value is also dependent on the 5p-electron density. This effect is expressed quantitatively as Eq. 3 by using Slater's shielding coefficients, where h_s and h_p are the numbers of 5s- and 5p-electrons removed from the $5s^25p^6$ (I^-) configuration, respectively. When the bonding of iodine is formed by only $5p_\sigma$-electrons, one expects the relationship $U_p=h_p=1\pm i$ to be valid, where i is the ionic character. If $5p_\pi$-electrons take part in bond formation (π-bonding), in addition to $5p_\sigma$-electrons, the relationship $U_p<h_p$ and non-zero η value are generally observed. On the other hand, the contribution of 5s-electrons (sp hybridization) leads to the relationship that $U_p>h_p$ because of the decrease in the s-electron density at the nucleus. The U_p and h_p values obtained for each iodine atom are presented in Table 1 (assuming that there is no contribution of 5s-electrons to the bonding of iodine).

It can be seen for the I_A atom coordinating to the S or N atom of each donor molecule that the h_p value is larger than the U_p value. The same tendency was found in the I_A atoms of the usual 1:1 complexes, such as thioether–iodine[7] and amine–iodine.[6,8] This relation has generally been explained in terms of the presence of double or intermolecular bonding in the x or y direction. However, it is quite difficult for the I_A atom to consider the presence of the double bond or the intermolecular bond from the crystallographic data of 2TPPS–3I_2[3] or 2AC–3I_2.[5] Furthermore, the η value was observed to be zero for the I_A atom in each complex. This phenomenon has been successfully interpreted in terms of the slight contribution of core $4d_\sigma$-electrons (dp hybridization) to the charge-transfer bond formation, in addition to the delocalized three-center four-electron bonding.[7,8] The promotion energy of the $4d_\sigma$-electron is probably compensated for

by the stabilization of the charge-transfer bond formation. The contribution of the $4d_\sigma$ hybridization remarkably increases the δ value but hardly increases the e^2Qq value. Therefore, the net charge density is close to that obtained from the e^2Qq value. Consequently, the charge densities localized on the I_A atoms of the 2TPPS-$3I_2$ and 2AC-$3I_2$ complexes were evaluated to be approximately +0.12 e and +0.27 e, respectively, by using Eqs. 4 and 5 in Ref. 8. The same calculations lead to charge densities of +0.07 e and +0.11 e for the I_A atoms in dithiane-iodine[7] and pyridine-iodine[8], respectively.

On the other hand, the relationship $U_p<h_p$ and the non-zero η value for the terminal I_B atom are attributable to the additional intermolecular $I_B\cdots I_C$ bond as previously described. Both I_B atoms of the present complexes were estimated to be negatively charged by about 0.39 e from the h_p values (close to the charge densities on the I_B atoms of the 1 : 1 complexes). From the η values for the I_B atoms, very little charge (ca. 0.06 e for 2TPPS-$3I_2$ and ca. 0.04 e for 2AC-$3I_2$) was found to be transferred to the iodine molecule (I_C) cross-linked to the two I_B atoms along the weak $I_B\cdots I_C$ bond. The charge transfer leads to an increase in the charge densities on the I_C atoms of these complexes. The U_p and h_p values for the I_C atoms are in agreement with each other, indicating that the bonding is mainly due to $5p_\sigma$-electrons. The charge densities localized on the I_C atoms are estimated to be −0.04 e and −0.01 e for the 2TPPS-$3I_2$ and 2AC-$3I_2$ complexes, respectively (from the mean values of U_p and h_p). The charge densities obtained for the I_C atoms agree with those transferred from the I_B atoms within the experimental error. Therefore, the slightly negative charge densities on the I_C atoms are apparently due to the charge transfer from the I_B atoms. This result is consistent with the increase in the bond distance (2.73 Å) between the I_C atoms, compared with the gaseous iodine molecule (2.67 Å), since the transferred charges occupy the antibonding molecular orbital (σ_u^*) of the iodine molecule. The charge densities obtained for the I_A, I_B, and I_C atoms of the investigated complexes from the Mössbauer parameters are presented in Fig. 4, together with those for the 1,4-dithiane-iodine[7] and pyridine-iodine[8] complexes.

As shown in Fig. 4, the I_A atoms in the unusual 2:3 molecular complexes are more positively charged than those in the usual 1 : 1 complexes containing the same donor atoms. This result can be qualitatively interpreted on the basis of the strength of a covalent bond between the donor and the I_A atoms. The positive charge on the donor atom, arising from the charge transfer to the iodine molecule, is delocalized on the I_A atom by back donating along the covalent $S\cdots I_A$ or $N\cdots I_A$ bond. The degree of the back donation increases with an increase in the covalency of the intermolecular bond. It is clear from a comparison of the bond distances that the covalency of the $S\cdots I_A$ bond is stronger in the 2TPPS-$3I_2$ complex than in the 1,4-dithiane-$2I_2$ complex. Therefore, it is concluded that the positive charge density on the I_A atom is dependent on the covalency of the intermolecular

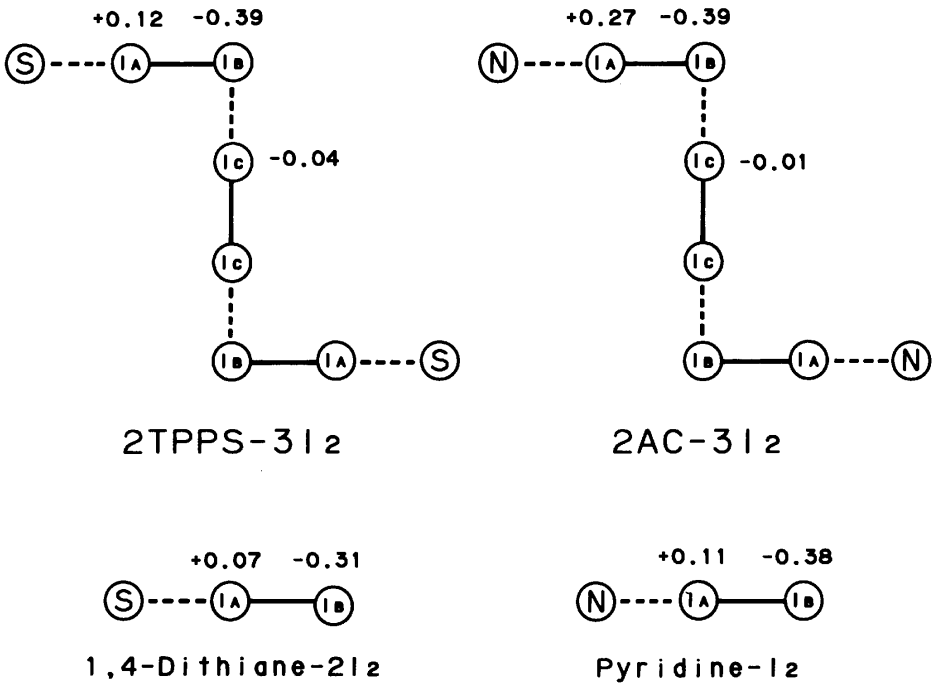

Fig. 4. Charge densities localized on the iodine atoms for the 2TPPS-$3I_2$, 2AC-$3I_2$, 1,4-dithiane-$2I_2$, and pyridine-I_2 complexes.

bond between the donor and the iodine molecules, but not on the degree of the charge transfer from the donor molecule to the iodine molecule. The I_A atoms in the amine complexes are also found to be more positively charged than those in the sulfur-containing donor complexes. As pointed out in our previous paper,[7] this fact is because the amine cations (N^+), produced by a charge transfer, have a larger electron affinity than the sulfur cations (S^+) in the sulfur-containing donor molecules and, therefore, attract more electrons from the I_A atom than do S^+. The charge densities localized on the I_B atoms in the 2:3 complexes are close to those in the 1:1 complexes, suggesting that the degree of the charge transfer is comparable to each other.

The linear S···I_A–I_B or N···I_A–I_B bond can be essentially described in terms of a delocalized three-center four-electron bonding in the electronic ground state, and resembles the linear triiodide anion (I_3^-) very closely in chemical bonding. The similarity seems to explain the formation of the unusual 2:3 complex: the I_3^- anions combine with the I_2 molecules to form polyiodides such as a pentaiodide anion (I_5^-), a heptaiodide anion (I_7^-), and an octaiodide dianion (I_8^{2-}). The structure of the iodine moieties in the 2TPPS-3I_2 and 2AC-3I_2 complexes is very similar to that of Cs_2I_8, in which the iodine atoms consist of two I_3^- units and one I_2 unit with a flat Z-shaped structure.[12] Furthermore, the distances of the intra- and intermolecular bonds in the iodine moiety are close to each other.

The authors wish to thank Prof. Takenobu Higashimura (Research Reactor Institute, Kyoto University) for his useful discussion and encouragement. The authors are also grateful to Prof. Tokiko Uchida (Faculty of Science and Technology, Science University of Tokyo) for her suggestions and advice concerning unpublished crystallographic data of the 2AC-3I_2 complex.

References

1) R. A. Zingaro and E. A. Meyers, *Inorg. Chem.*, **1**, 771 (1962).

2) G. A. Bowmaker and R. J. Knappstein, *Aust. J. Chem.*, **31**, 2131 (1978).

3) W. W. Schweikert and E. A. Meyers, *J. Phys. Chem.*, **72**, 1561 (1968).

4) G. Y. Chao and J. D. McCullough, *Acta Crystallogr.*, **13**, 727 (1960).

5) T. Uchida, private communication. According to her, the iodine moiety of the 2AC-3I_2 complex is confirmed as follows:

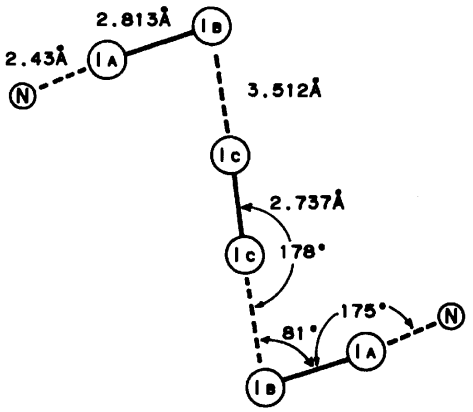

6) S. Ichiba, H. Sakai, H. Negita, and Y. Maeda, *J. Chem. Phys.*, **54**, 1627 (1971).

7) H. Sakai, T. Matsuyama, and Y. Maeda, *Bull. Chem. Soc. Jpn.*, **59**, 981 (1986).

8) H. Sakai, Y. Maeda, S. Ichiba, and H. Negita, *J. Chem. Phys.*, **72**, 6192 (1980).

9) M. Pasternak, A. Simopoulos, and Y. Hazony, *Phys. Rev.*, **140**, 1892 (1965).

10) H. DeWaard, "Mössbauer Effect Data Index 1973," ed by J. G. Stevens and V. E. Stevens, IFI/Plenum Press, New York (1974), P. 447.

11) S. L. Ruby and G. K. Shenoy, "Mössbauer Isomer Shifts," ed by G. K. Shenoy and F. E. Wagner, North-Holland, Amsterdam (1978), Chap. 9b.

12) E. E. Havinga, K. H. Boswijk, and E. H. Wiebenga, *Acta Crystallogr.* **7**, 487 (1954).

Deuterium Nuclear Magnetic Resonance of Oriented DNA Fibers

Heisaburo SHINDO,* Yukio HIYAMA,† Siddhartha ROY,†† Jack S. COHEN,†† and Dennis A. TORCHIA†
Tokyo College of Pharmacy, Hachioji, Tokyo 192-03
†Bone Research Branch, National Institute of Dental Research, NIH, Bethesda, MD 20892, U.S.A
††Clinical Pharmacology Branch, National Cancer Institute, NIH, Bethesda, MD 20892, U.S.A.
(Received December 1, 1986)

Solid-state ^{2}H NMR spectra were measured as a function of relative humidity for nonoriented DNA films and oriented DNA fibers deuterated at C8 carbons of the purine bases. The line-shape analyses of the quadrupole echo spectra from oriented DNA fibers demonstrated that the purine base planes of the A form of DNA were tilted by about 70° relative to the helix axis, and that base planes of the B form varied significantly, although they were, on average, perpendicular to the helix axis. These results were generally consistent with the X-ray fiber diffraction studies and the single crystal structures of oligonucleotides. Analyses of ^{2}H relaxation times, T_1 and T_2, showed at 79% RH that the orientation of the base planes fluctuated about an axis normal to the helix axis with a correlation time, $\tau_c=3.6\times10^{-8}$ s and amplitude of 8.5°. The correlation time of the base plane fluctuation was 1.5×10^{-8} s and the amplitude was 13.5° at 92% RH. In addition, at 92% RH, but not at 79% RH, the base planes reoriented slowly, $\tau_c \approx 10^{-6}$ s, about the helix axis, through an rms angle of ca. 30°.

We have recently reported ^{31}P nuclear magnetic resonance (NMR) studies of the structure and dynamics of DNA in the fibers as a function of relative humidity.[1,2] The results were in general agreement with the structure inferred from the X-ray diffraction studies of the fibers at relatively low humidities, but differed from the X-ray results, in some respects, at high humidities. The most interesting conclusion derived from the NMR studies is the finding of heterogeneity in the structure and dynamics in the backbone of the B form of DNA at high relative humidities. It seems likely that local heterogeneity in dynamics and structure also occurs in base domains as well.

However, some lines of evidence indicate that the base domains are less mobile than the DNA backbone in the fiber;[3] in crystals,[4] and in solution.[5,6] Since ^{31}P NMR only provides information about the phosphodiester groups of DNA, a question arises as to whether the conclusions derived from ^{31}P NMR studies correctly represent the nature of the base domains as well. It is therefore important to examine the base domains of DNA using the same conditions as employed in ^{31}P NMR studies. ^{2}H NMR is the most suitable probe if nonexchangeable protons of the bases of DNA are selectively substituted by deuterium nuclei. DiVerdi and Opella[3] and later Bendel et al.[7] have reported the solid state ^{2}H NMR studies of DNA with the deuterium-labeled purine bases at C8 position. The former group has attributed the different behavior of ^{2}H and ^{31}P NMR line-shapes, observed when humidity or temperature was changed, to differences in flexibility in the backbone and base domains in hydrated DNA. We have pointed out, however, that differences in the ^{2}H and ^{31}P NMR time scales must be taken into account in the line-shape analysis, and we also suggested that more clear-cut conclusions could be obtained if oriented DNA samples were used for NMR measurements.[2] Recently Vold et al.[8] reported a ^{2}H NMR study of oriented Na- and Li-DNA samples at relatively low humidities.

In the present study, we prepared highly oriented Na-DNA fibers by the traditional method, rather than the wet-spinning technique[9] employed by Vold et al.[8] that produces a block of oriented sample. Humidity control is easier for the fibers than for the DNA block because of the size of sample. We report measurements of ^{2}H NMR spectra and relaxation times of two typical forms of DNA, i.e., the A and B forms of oriented DNA fibers with deuterated purine bases, and discuss the structure and dynamics of DNA fibers. We also show that ^{2}H and ^{31}P NMR results are consistent and discuss the relative merits of ^{2}H and ^{31}P NMR spectroscopy for studying DNA.

Experimental

Deuterium Labeled Nucleosides and DNA. Lyophilized salmon sperm DNA was purchased from P. L. Biochemicals and purine nucleosides were from Sigma Chemical company U.S.A. Nucleosides were dissolved in D_2O, heated at 90 °C for 6 h, dried in vacuo. They were redissolved in H_2O and dried, and this procedure was repeated several times to remove the residual D_2O. The degree of deuteration at C8 position was checked by ^{1}H NMR. Deuterium exchange of C8 position of purine bases of DNA was carried out following the method of tritium exchange of DNA by Doppler-Bernardi and Felsenfeld.[10] Lyophilized DNA was dissolved overnight into D_2O (10 mM††† Tris-HCl, 1 mM EDTA, pH 7.5) and then the solution was mixed with 4.0 M NaCl and 10 mM Tris in D_2O to a final concentration of 2.0 M NaCl and 10 mM Tris (pH 7.5). The solution was held at 83 °C in a thermostat for 10 h and then cooled in an ice bath. Two volumes of cold ethanol were added, yielding a fibrous precipitate. The precipitate was dried in the atmosphere and redissolved in H_2O, 10 mM Tris, at 4 °C overnight. The solution was exaustively dialyzed against H_2O, 10 mM NaCl, for 2 d.

††† 1 M=1 mol dm^{-3}

DNA Films and Fibers. The solution of DNA (1—2% w/v) prepared above was centrifuged at 50000 rpm for 16 h, yielding viscous pellets. The viscous pellets were dried on a plastic sheet in the atmosphere to make films, and many pieces of films were collected for NMR measurements. To make an oriented fiber a drop of the pellet was placed between the ends of tooth picks and left to dry in the atmosphere. Optically homogeneous fibers of 3—5 mm length and 0.1—0.3 mm diameter were usually obtained. The fibers gave excellent X-ray fiber diffraction images of the A type of DNA at 79% RH.

NMR Measurements. About 40 fibers were aligned in parallel on a sample holder and held overnight for equilibration in the atmosphere of a given humidity. The DNA films prepared above were also equilibrated at an appropriate humidity before NMR measurements. Relative humidity was controlled by saturated solutions of various salts.[11] The sample holder was inserted into a sample tube (6 mm o.d.), capped tightly and mounted on a goniometer. ^{2}H NMR spectra were obtained at 38.45 MHz with a quadrupole echo pulse sequence, 90°-τ-90°-τ-FID, on a home-built spectrometer with a NIC-1280 computer (for details, see Sarkar et al.[12]). Some ^{2}H NMR spectra were observed at 76.77 MHz on a NIC-500 spectrometer (Nicolet Inc.). The 90° pulse was 2.5 μs at 38.45 MHz and 3.0 μs at 76.77 MHz. A time interval of 50 μs was used between the two pulses of the echo sequence, unless otherwise stated, to eliminate the base line distortion caused by probe ringing after the pulse.

Relaxation times T_1 and T_2 were measured by a progressive saturation method with variable repetition time, and a quadrupole echo with variable pulse interval, respectively. All measurements were performed at 22 °C.

Analysis of ^{2}H NMR Spectra

In the case of the ^{2}H nucleus the solid-state NMR spectrum is dominated by the electric quadrupole interaction whose coupling constant for ^{2}H in C-^{2}H bonds e^2qQ/h=180 kHz can lead to spectra up to 250 kHz wide. As a result, the quadrupole echo spectrum may be distorted depending on the ^{2}H relaxation time and the instrumental performance. A general rewiew of ^{2}H NMR spectroscopy[13] has appeared recently and spectral distortions have been analyzed in detail, taking into account the effect of relaxation (Spiess and Sillescu[14]) and finite pulse power (Bloom et al.[15]).

Analysis of the ^{2}H NMR spectrum from an axially oriented specimen is straightforward. By the analogy with the analysis of the ^{31}P NMR from oriented DNA fibers,[1,16] the frequencies of the observed quadrupolar split lines, $\nu^{obsd}(\phi,\alpha)$, are give by

$$\nu^{obsd}(\phi,\alpha) = \pm\sqrt{\frac{3}{2}}\frac{eQ}{2\hbar}\rho_{20}^{lab}$$

$$\rho_{20}^{lab}(\phi,\alpha) = \sum_{m,n,p=-2}^{2} D_{p0}^{(2)}(0,\phi,0)D_{np}^{(2)}(\psi,\theta,0)D_{nm}^{(2)}(\alpha,\beta,\gamma)\rho_{2n} \quad (1)$$

for ^{2}H with I=1. Here $D_{nm}^{(2)}(\alpha,\beta,\gamma)$ is the Wigner rotation matrix of the second rank, ρ_{2n} is the irreducible EFG tensor in the principal axis system[17] and the Euler angle notations are given in Figs. 1A and B. The principal axis system of the tensor is defined by Euler angles α, β, and γ with respect to the molecular fixed axis system (a, b, c). The fiber axis system is taken to be identical to the goniometer axis system (Fig. 1B). The goniometer angle ϕ between the fiber axis and the magnetic field direction can be varied. The spectrum in which ϕ=0° corresponds to the spectrum of the fibers oriented parallel to the magnetic field, and the spectrum at ϕ=90° is that of fibers oriented perpendicular to the field. The angle θ is the angle made by the molecular fixed axis, c, and the fiber axis. As described previously,[1] the spectrum at a given ϕ can be calculated by the superposition of the spectral lines with appropriate weights over all the possible angles for α, β, γ, θ, and ψ. Gaussian distributions were also assumed for β and θ with standard deviations, $\langle\Delta\beta\rangle$ and $\langle\Delta\theta\rangle$, respectively.

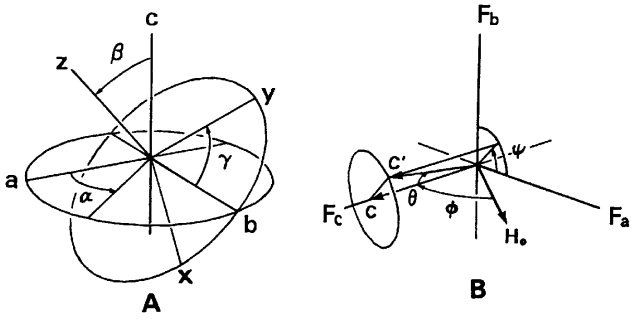

Fig. 1. Coordinate systems. (A) System (a, b, c) represents the molecular fixed system and axis c coincides with the helix axis of DNA. The principal axis system (x, y, z) of the quadrupolar coupling tensor is described by Euler angles α, β, and γ with respect to the molecular axis system as a reference frame. (B) Vector c lies along the fiber axis and vector c′ represents the helix axis of misaligned DNA which makes an angle θ with respect to the fiber axis. H_0 is the magnetlc fieid and ϕ is the goniometer angle.

Results

The degree of deuteration at the C8 positions of guanosine and adenosine was estimated to be about 70 and 75%, respectively, from the signal intensity in the ^{1}H NMR spectrum of each molecule in $CDCl_3$. According to the tritium-exchange reaction[10] of DNA in D_2O solution at 83 °C for 10 h, 30% of the total number of guanosine and adenosine residues, about 20% of the adenosine and 40% of the guanosine residues, were assumed to be deuterated. No appreciable degradation was expected under our experimental conditions.

^{2}H Powder Pattern Spectra. The spectra from polycrystalline guanosine and adenosine exhibited a typical static powder pattern with a quadrupolar splitting of 126±2 kHz as shown in Fig. 2. The long relaxation time T_1 of these samples at 22 °C, 30±10 s, indicated that the molecules were virtually immobile. It is interesting to note that the sugar ring of deoxyguanosine is found to be mobile.[18] The best visual fit with the observed spectrum of adenosine, shown in the bottom of Fig. 2, yielded values of principal frequencies of the quadrupolar coupling tensor, ν_1, ν_2, and ν_3, of −72±1, −63±1, and 135±3 kHz, respectively. The resulting nuclear quadrupole coupling constant and asymmetry parameter were 180±3 kHz and 0.06—0.07(±0.01), respectively. On the other hand, the parameter η of guanosine was a little larger than that of adenosine but it was in the above error range. The non-zero asymmetry parameter observed for the C8-^{2}H bonds in guanosine and adenosine is not surprising because a value of η=0.07—0.08 have been reported for the C2-^{2}H bonds in imidazole and benzimidazole at 77 K by Hiyama et al.[19]

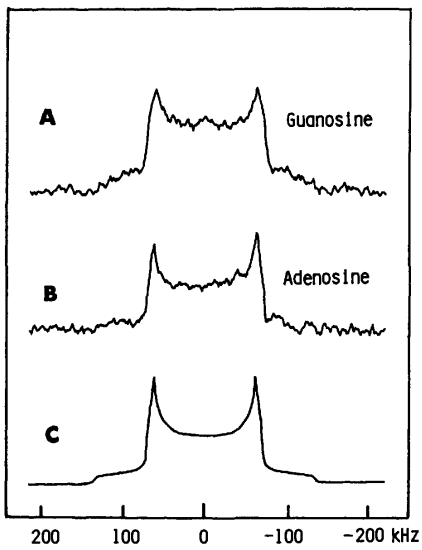

Fig. 2. Quadrupole echo ^{2}H NMR spectra (38.5 MHz) of polycrystalline guanosine (A), adenosine (B), and simulated powder pattern (C) at 22 °C. Measurement conditions: Spectral window 1 MHz; data points 4096 with zero filling; pulse width 2.2 μs; pulse interval 50 μs; delay time 40 s; exponential line broadening 2 kHz; scan number 1600. The simulated spectrum (C) was calculated using line broadening of 2 kHz and the principal values, 132, −64, and −70 kHz for ν_3, ν_2, and ν_1, respectively.

Figure 3 shows the ^{2}H powder patterns of DNA films, labeled at C8 position of guanosine and adenosine, at 79 and 92% RH. Note that a spike at the center of each spectrum arises from the natural abundance of deuterium water in the sample. At each relative humidity, two spectra were obtained by the quadrupole echo method with different pulse intervals (the time between $\pi/2$ pulses). The top spectrum was obtained with a 50 μs pulse interval and the bottom was with a 100 μs interval.

The reduction of signal intensity observed at 79% RH with the larger interval is a consequence of the finite T_2 value (200 μs) of the sample. The anisotropy in T_2 is evidently quite small, since the line-shapes observed using both pulse intervals are virtually identical to those of guanosine and adenosine (Fig. 2). The quadrupolar splitting (123±2 kHz) is slightly smaller than that observed for adenosine (126±1 kHz). The large splitting observed in the DNA sample shows that the amplitudes of molecular motions are small, and the small intensity losses (due to finite T_2) show that the amplitudes of motion on the time scale of ω_Q^{-1} (10^{-4}—10^{-6} s) are insignificant.

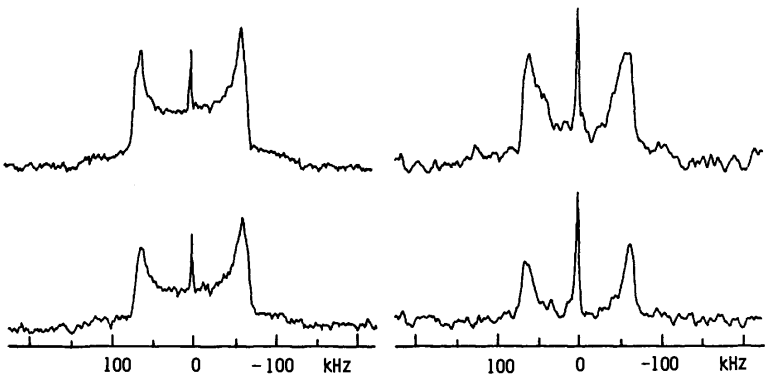

Fig. 3. Quadrupole echo spectra (38.5 MHz) of ^{2}H NMR of nonoriented DNA films at 79% RH (left) and 92% RH (right). Top and bottom spectra were taken with different pulse intervals, 50 and 100 μs, which may be used for examining the anisotropy effect of the relaxation time T_2. The measurement conditions were almost the same for all the samples as in Fig. 2, with delay time 0.6 s and scan number 32000.

Although the line-shape and T_2 data at 79% RH are similar to those observed in the model compounds, the measured T_1 is much smaller in DNA than in the model bases (Table 1). This implies that a small amplitude motion is taking place on the time scale of ω_0^{-1} (10^{-7}—10^{-10} s) in the 79% RH sample.

We can obtain an estimate of the amplitude of this motion by comparing the observed quadrupole splitting in DNA with the splitting observed in the model compounds. $2|\nu_1|$ and $2|\nu_2|$ (the quadrupole splittings) in DNA were smaller by 5.0 (±1) and 4.0 (±1) kHz, respectively, than in the model compounds. Because the reduction in splittings is much less than $2|\nu_1|-2|\nu_2|$ for either guanosine or adenosine, 16 kHz, there is little likelihood of the principal axis interchange between the nucleoside and DNA. Therefore, we make the reasonable assumption that the orientation of the nonaveraged ^{2}H EFG tensor is the same in the nucleoside and in the DNA molecule.

Table 1. Relaxation Times T_1 and T_2 of ^{2}H NMR at 38.5 MHz of Unoriented DNA Films and Oriented DNA Fibers at 22 °C

Relative Humidity/%	T_1/ms[a]		T_2/μs[a]	
	DNA Film	Fiber[b]	DNA Film	Fiber[b]
75	177±20	—	164±15	—
79	167±13 (480±80)[c]	158±25	183±20	—
87	75±9	—	134±14	—
92	30±6 (71±14)[c]	25±7	96±9	100±20
98	16±3	—	101±8	—

a) Relaxation times measured for the perpendicular component of the tensor in the powder pattern spectrum of DNA films. b) Relaxation times measured for the parallel spectrum of DNA fibers. c) T_1 values measured at 76.8 MHz.

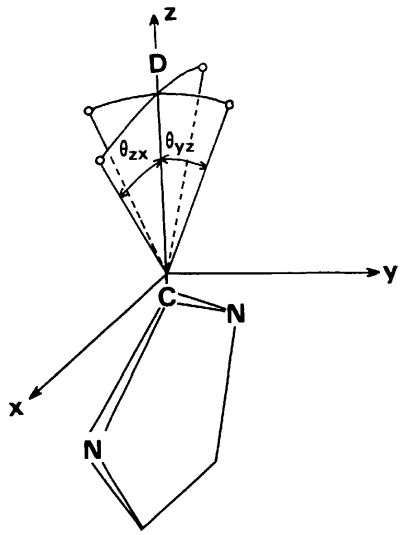

Fig. 4. Principal axis system (x, y, z) of the EFG tensor relative to the atomic coordinates of a purine base, and two sets of two jump sites for the C8-^{2}H bond whose fluctuation amplitude are represented by θ_{zx} and θ_{yz}.

The reduced splittings were analyzed using the four-site jump model illustrated in Fig. 4. If the jump rate is much larger than ω_Q, the motionally averaged principal frequencies, $\bar{\nu}_1$ and $\bar{\nu}_2$, are related to the motional amplitudes, θ_{zx} and θ_{yz}, by following equations

$$\bar{\nu}_1 = \frac{1}{2}(\nu_1+\nu_1\cos^2\theta_{zx}+\nu_3\sin^2\theta_{zx}), \quad (2)$$

$$\bar{\nu}_2 = \frac{1}{2}(\nu_2+\nu_2\cos^2\theta_{yz}+\nu_3\sin^2\theta_{yz}). \quad (3)$$

Using these equations together with two sets of the observed values of ν_i and $\bar{\nu}_i$ (i=1, 2), θ_{yz} and θ_{zx} were calculated to be 8.1° and 8.9°, respectively. Since these angles are nearly equal, the motion does not appear to have a preferential axis.

As mentioned earlier, the spin-lattice relaxation time, T_1 at 79% RH, 167 ms, is substantially shorter than that found in the nucleosides. The possible minimum T_1 resulting from dipole-dipole interactions with the nearest neighbor protons is about 10 s. Therefore, T_1 is determined by quadrupolar relaxation.

Since in the line-shape we assumed that the rotation about a single axis is not likely at 79% RH, we analyse the measured T_1 values at 38.5 and 76.8 MHz using the diffusion-in-a-cone model. In this model we assume that the C–^{2}H bond diffuses uniformly over the surface of a cone having semiangle θ_0. In this case the rms fluctuation in θ is $\sqrt{\theta_0^2/2}$, and θ_{rms} is taken to be the average of θ_{zx} and θ_{yz}, 8.5°, calculated from the line-shape analysis. Using the general formalism of Torchia and Szabo[17] together with the condition that $\theta_{rms}^2 \ll 1$, we find that

$$\left\langle \frac{1}{T_1} \right\rangle = (\omega_Q^2/10)\sin^2 2\theta_{rms}[g(\tau,\omega_0) + 4g(\tau,2\omega_0)], \quad (4)$$

where $\langle\cdots\rangle$ indicates the average overall orientations of the field relative to a crystal fixed axis system, and $g(\tau,\omega)$ equals $\tau(1+\omega^2\tau^2)^{-1}$. In writing Eq. 4 we have made the approximation that η equals zero and $\omega_Q/2\pi$ is taken to be the average of $2|\nu_1|$ and $2|\nu_2|$ of the nucleoside. Inserting the measured values of $\langle 1/T_1\rangle$, ω_Q, θ_{rms}, and $\omega_0/2\pi$ (38.5 MHz) into Eq. 4 we obtain two solutions τ_c=2.5×10^{-10} and 3.6×10^{-8} s. Only the larger value is consistent with the observation of a strong frequency dependence of T_1 (Table 1). The ratio of T_1 at 76.8 MHz to T_1 at 38.5 MHz was 2.9±0.5 which was a little smaller than the theoretical value of 4.0.

In contrast with the 79% RH DNA spectra (left, Fig. 3) the 92% RH DNA powder patterns (right, Fig. 3) are distinctly different from the static powder patterns of the model compounds, Fig. 2. Only the perpendicular components of the pattern have significant intensity. This observation suggests that the DNA molecule reorients about the helix axis with a correlation time in the 10^{-4}—10^{-7} s range. Such a motion would cause T_2 to be very short for all orientations of the field relative to the helix axis, except for the field parallel to the rotation (helix) axis.

In order to estimate the rate and amplitude of the axial motion, the observed spectra were simulated using an N-site jump model, in which jumps were restricted to nearest neighbors (Fig. 5). The computer program includes correction for the relaxation effect on the line-shape of quadrupole echo spectrum as reported by Speiss and Sillescu.[14] Six sites are sufficient to approximate rotational diffusion, and limit computational costs. Figure 6 shows spectral shape as a function of maximum rotation amplitude (i.e., 5 ω). Each jump rate, k, shown in the figure legend was estimated so as to give a reasonable fit to the observed spectra (right, Fig. 3). It was found that a maximum rotation amplitude of 150°, i.e., root mean square fluctuation for each jump Φ_{rms}, of at least 30°, was required to simulate the observed 92% RH DNA spectrum. As expected, the jump rate required to fit the spectrum, $(2\pm1)\times10^6$ s^{-1}, was approximately equal to $\omega_Q/2\pi$. Motions on the time scale of ω_Q result in anisotropic T_2 values which cause intensity losses and line-shape distortions in ^{2}H spectra. Although satisfactory spectral simulations were also obtained with values of Φ_{rms} greater than 30°, again with the jump rate approximately equal to ω_Q, these solutions were ruled out by the ^{31}P spectra of 92% RH DNA. These spectra showed that the ^{31}P chemical shift anisotropy, $\sigma_{33}-\sigma_{11}$, observed in the spectra of 92% RH at 24 MHz (Shindo et al.[20]) and 40 MHz (not shown) were only 12% smaller than that in the spectra of the 79% RH DNA. Futhermore, by applying a restricted rotation model with a rectangular potential well to the ^{31}P NMR data of DNA fibers at 92% RH, the average rotation amplitude about the helix axis was estimated to be about 130° (Fujiwara and Shindo[2]). This amplitude is close to the maximum rotation angle of 150° as estimated above. Therefore only the motions of restricted six-site jump model having a root mean square fluctuation less than 35° are consistent with the ^{31}P data.

Although the restricted, slow azimuthal reorientation of the DNA molecule accounts for the line-shape observed at 92% RH, this motion does not explain

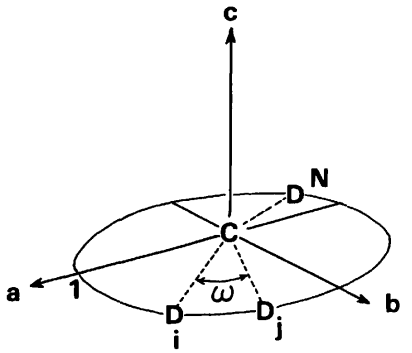

Fig. 5. N site jump model for rotational motion about the helix axis. Jumping is allowed only between nearest neighbors with jump rate k and jumping matrix $R_{i,i+1}=k$. For free jump, site N+1 equals site 1, allowing $R_{1N}=R_{N1}=k$. For restricted jump, $R_{1N}=R_{N1}=0$.

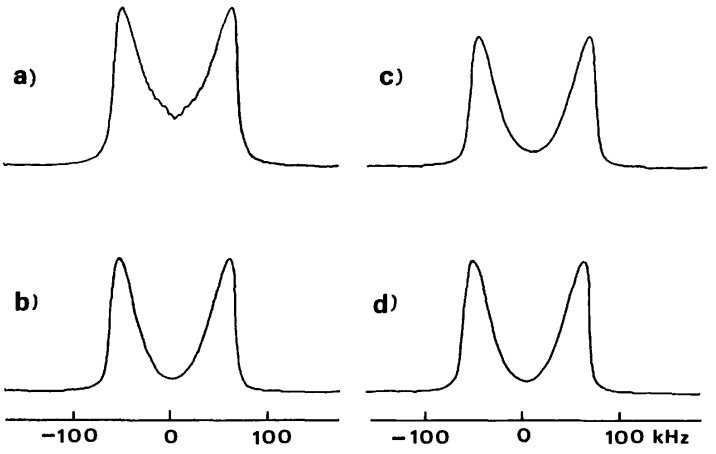

Fig. 6. Calculated ^{2}H NMR powder patterns based on the six-site jump model, (a) $5\omega=100°$, $k=2.5\times10^6$ rad s^{-1}, (b) $5\omega=150°$, $k=3\times10^6$ rad s^{-1}, (c) $5\omega=200°$, 1.5×10^6 rad s^{-1}, (d) $5\omega=250°$, $k=10^6$ rad s^{-1}. Angle ω represents the azimuthal angle between nearest neighbor sites as in Fig. 5.

either the small average T_1 value, Table 1, measured at 92% RH or the 5 kHz reduction in $2|\nu_1|$ observed when RH is increased from 79 to 92%. The rotational motion is too slow, i.e., the correlation time is too far from the T_1 minimum, to account for the small T_1 value, and the motion about the helix axis does not affect the value of $2|\nu_1|$ regardless of time scale. The reduction of $2|\nu_1|$ with increasing RH can be explained by assuming that the amplitude of the C-^{2}H bond fluctuation in the cone, θ_{rms}, increases from 8.5 to 13.5° upon increasing RH from 79 to 92%. Using this value in Eq. 5 together with the measured values of $\langle 1/T_1 \rangle$, ω_0, and ω_Q, we calculate $\tau_c = 1.5 \times 10^{-8}$ s, ca. one-half as large as found at 79% RH.

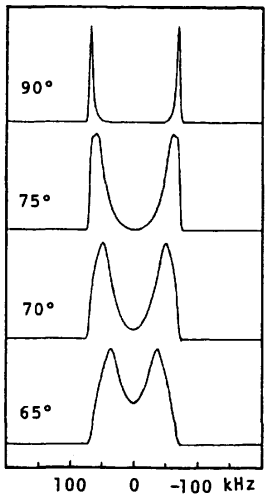

Fig. 7. Effect of Euler angle, β, and the distribution of $\langle \Delta\beta \rangle$ and $\langle \Delta\theta \rangle$ on the spectrum of DNA fibers oriented parallel to the magnetic field direction. A series of spectra show the dependence of spectral pattern on Euler angle β with fixed parameters, $\langle \Delta\beta \rangle = 3°$, $\gamma = 0°$, $\langle \Delta\theta \rangle = 8°$

^{2}H Spectra of Oriented DNA Fibers. Before presenting the experimental spectra of axially aligned DNA fibers we first present theoretical spectra which demonstrate how Euler angle β and standard deviations of β and θ affect the line-shape. The standard deviations $\langle \Delta\theta \rangle$ and $\langle \Delta\beta \rangle$ represent the imperfect alignment of molecules along the fiber axis and heterogeneity of the local structure, respectively. In calculating the theoretical spectra, the orientation of the ^{2}H EFG tensor was assumed to be as shown in Fig. 4, and effects of molecular motion on the line-shape were included with use of motionally averaged principal frequencies.

Figure 7 shows a series of the theoretical spectra calculated for DNA fibers oriented parallel to the magnetic field. The spectra in Fig. 7 demonstrate how the line-shape changes as a function of Euler angle β. The values of the other parameters were goniometer angle $\phi = 0°$, standard deviations $\langle \Delta\beta \rangle = 3°$ and $\langle \Delta\theta \rangle = 8°$, $\gamma = 0°$ and line-width=2 kHz. As expected, the dependence of the peak separation on β is weak around ca. 90°, and becomes stronger as β decreases. It is important to note that at $\phi = 90°$ the spectrum (top, Fig. 7) is hardly affected by either $\langle \Delta\beta \rangle$ or $\langle \Delta\theta \rangle$.

We now turn to an analysis of the experimental spectra. Figure 8 shows the observed and simulated spectra for the fibers at 79% RH oriented parallel, at 45°, and perpendicular to the magnetic field. The fibers at this humidity gave a typical A form of DNA as judged from the X-ray fiber diffraction patterns. Simulated spectra, which reproduced the observed spectra, were calculated using the parameters, $\beta = 70°$, $\langle \Delta\beta \rangle = 3°$, $\gamma = 0°$, and $\langle \Delta\theta \rangle = 8°$. Simulated spectra include 10% of the B form in the A form of DNA,

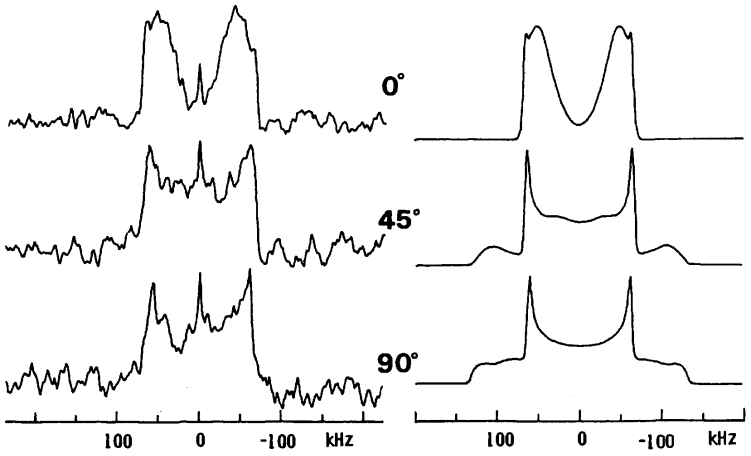

Fig. 8. Quadrupole echo spectra (left) of ^{2}H NMR (38.5 MHz) of oriented DNA fibers at 79% RH at different orientations of fiber axis to the magnetic field as indicated, and simulated spectra (right). Measurement conditions are the same as in Fig. 2, except for pulse width 2.5 μs, delay time 0.3 s, line broadening 2 kHz, scan number 120000—160000.

which gives small peaks at the edges of both sides in the parallel spectrum. The signal components beyond ca. 100 kHz from the carrier were attenuated, because of the finite pulse power of the instrument ($\pi/2$ pulse with 2.5 μs) and were not detectable above the noise level. The standard deviation in θ, $\langle\Delta\theta\rangle=8°$, was estimated from the ^{31}P NMR of the same sample (data not shown), and was close to the value of 10° reported previously (Shindo et al.[1]). The value obtained for β, 70°, has an experimental error of less than three degrees, because the peak separation is very sensitive to the value of β, where β is in the range 65°—75°, Fig. 7. The narrow distribution of β is consistent with the fact that the A form of DNA has a very narrow conformational distribution,[1,16] i.e., the structure is independent of the base composition and sequence.

Although we were able to simulate the 79% RH fiber spectra using the static quadrupole coupling obtained for the model compounds, the splittings in the calculated fiber spectra were always larger than the measured splitting. The best simulations of those measured DNA fiber spectra at 79% RH were obtained using a quadrupole splitting that was 4 kHz smaller than that measured in the model compounds. This result confirms the conclusion, obtained from the analysis of the spectra of DNA films, that a small amplitude motion $\theta_{rms}=8.5°$ takes place in DNA at 79% RH. Further support for this conclusion is provided by the small T_1 value observed in the fiber sample, Table 1, which agreed (within experimental error) with the measurement of T_1 at the perpendicular component in the spectrum of DNA films at 79% RH. Finally we note that because the small amplitude motion takes place on a rapid time scale, $\omega_Q\tau_c\ll1$, T_2 is large for all orientations relative to the external magnetic field H_0. For this reason, the same relative intensity was observed in the spectra of all three orientations shown in Fig. 8.

Figure 9 shows the observed and simulated spectra of the fibers at 92% RH oriented parallel, at 45°, and perpendicular to the magnetic field. All the spectra were measured under the same conditions and were recorded in the absolute intensity mode. The simulated spectra are normalized to have a constant spectral area. The fibers gave an X-ray pattern of the B form of DNA, and therefore we used the X-ray structure of the B form of DNA (Arnott et al.[21]), together with the results of ^{31}P NMR (Shindo et al.[1]) to set initial parameters for simulating the spectra in Fig. 9: The base plane was nearly normal to the helix axis, i.e., $\beta=90°$ and $\gamma=0°$ with standard deviations $\langle\Delta\beta\rangle=10°$ and $\langle\Delta\theta\rangle=8°$. The peak separation measured for the parallel spectrum was 132±2 kHz, corresponding to the peaks at ±66 kHz. The value of 66 kHz is closer to the principal value $|\nu_1|$ than $|\nu_2|$. Considering that the base plane is nearly perpendicular to the helix axis, the axis of ν_1 must be approximately parallel to the helical axis, i.e., $\beta=90°$ and $\gamma=0°$ or 180°. In agreement with the results obtained at 79% RH the best simulation of the observed splittings at 92% RH was obtained by assuming principal values of the EFG tensor were reduced from their static values by small amplitude motion, $\theta_{rms}=13.5°$. The T_1 value observed for the oriented fibers (parallel orientation) is listed in Table 1 where it is seen that the T_1 values measued for the fibers and films at 92% RH are in agreement within experimental error. This result confirms that a small amplitude motion occurs in the fibers. The parallel spectrum is quite sharp (natural line-width ca. 6 kHz)

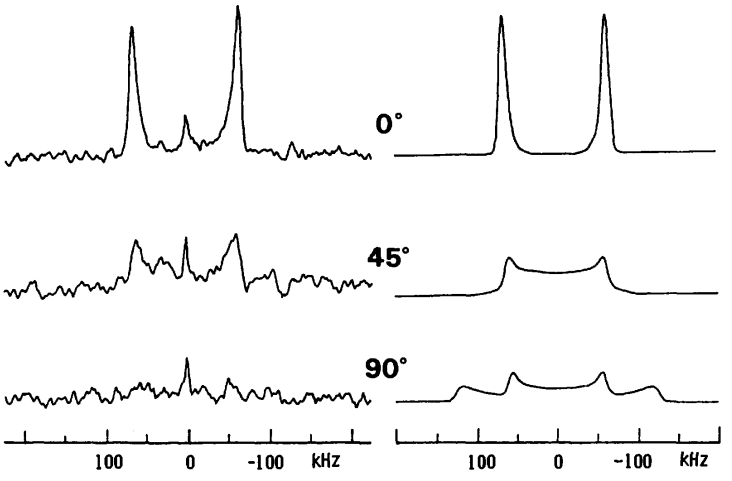

Fig. 9. Quadrupole echo spectra (left) of the ^2H NMR of oriented DNA fibers at 92% RH and at different orientations of the fiber axis, and simulated spectra (right). All the spectra were obtained under the same conditions as in Fig. 6, with delay time 0.3 s and scan number 112000.

in spite of the presence of fairly wide distributions of β and θ. This observation is caused for the fact that the peak positions are very insensitive to changes in β and θ when $\beta=90°$, as mentioned above (Fig. 7). In contrast with the results obtained at 79% RH, large intensity losses were observed when the sample was oriented at 45 and 90° with respect to the field, Fig. 9. In fact, at 90° orientation, the signal intensity was not above the noise level, and at 45°, the signal was observed in the neighborhood of the perpendicular components of the spectrum ($\nu\approx\pm65$ kHz). These observations are explained by the slow reorientation of the DNA about the fiber axis (rms fluctuation 30°, $\tau_c\approx10^{-6}$ s) discussed in conjunction with the analysis of the line-shape of the DNA films at 92% RH. This motion will make the ^{2}H T_2 value very short for all orientations of the fiber axis relative to the field, except for the parallel orientation only where the axis of motion (the fiber axis) is parallel to the field. Therefore spectral intensity at this orientation (where $\nu\approx\pm65$ kHz) only remains unattenuated in the quadrupole echo experiment.

The spectra of oriented DNA fibers at 98% RH (not shown) were similar to those observed at 92% RH. However, the T_1 measured at 98% RH, Table 1, was about one-half as large as measured at 92% RH. Since the splitting observed in the parallel spectra at 92 and 98% RH was the same, the value of θ_{rms} was the same at these RH. Therefore the samller T_1 value observed at 98% RH was due to a shorter correlation time, i.e., $\tau_c=6\times10^{-9}$ s.

Discussion

Powder Pattern Spectra of Purine Bases. According to recent communication from Vold and coworkers,[22] they observed two types of deuterons in polycrystalline guanosine deuterated at the C8 position and they attributed this to two different conformations of guanosine in the unit cell. As shown in Fig. 2, however, the powder pattern of guanosine is rather normal, although the peak is a little broad compared with that of adenosine. The difference between the spectra of Tsang et al.[22] and ours is probably accounted for by the different cystal forms of guanosine. For many other purine bases, including those of 5′-AMP and 5′-GMP, the static quadrupolar coupling constant, $e^2qQ/h=179\pm2$ kHz and asymmetry factor $\eta=0.06$—0.07 (±0.01), appeared to be characteristic of the 8-position in all the purine derivatives. These parameters are in good agreement with those determined by us.

Structure of the Base Domain. Previously reported ^{31}P NMR studies of DNA fibers,[1,5,20,23] have shown that the backbone conformation of the B form of DNA is very heterogeneous, i.e., Euler angles β and γ (structural parameters of the phosphodiester) had a wide distribution of values with standard deviation 5—15° at 92% RH, whereas the backbone of the A form had nearly a single conformation. As for the base domain, according to the structural models inferred from X-ray fiber diffraction studies,[21] the base planes of the A form of DNA tilt by ca. 70° and roll by several degrees with respect to the axis normal to the helix axis, while the base planes of the B form of DNA are almost perpendicular to the helix axis. Assuming that the C8–H bond axis of the purine bases lies on the bisector of the angle made by the base atoms, N7–C8–N9, Euler angles β and γ were calculated using the atomic coordinates of the DNA structure. Because of the small asymmetry factor, $\eta=0.06$, the ^{2}H spectrum was only slightly affected by changes in γ. The angle made by the C8–H bond axis and the helix axis was calculated to be 67.8° (or 112.2°) and 96.1° (or 83.9°) for the A and B forms of DNA, respectively. The values in the parenthesis represent the angles for the antiparallel chain in the duplex. (Both chains give the same spectrum because of the diad symmetry of the DNA model.) On the other hand, the observed value was 70° (at most 73°) and 90°±10 for the A and B forms, respectively. The observed and calculated values agreed with each other within the experimental error. This was also the case for Fuller's B-DNA model[24] as seen in Table 2. Levitt's model[25] gave a value (73.2°) close to the averaged value (75.2°) for the 10 independent purine bases of the single crystal structure[26] of r(GCG)d(AATTCGC). The values of β calculated for two oligonucleotides in the A family of DNA are within the range from 70 to 80°, and their averaged values are slightly higher than the observed value. Several possible reasons for this discrepancy are as follows, 1) the principal axis z of the quadrupolar tensor is not exactly along the C8–^{2}H bond, 2) the C8–^{2}H bond does not lie on the bisector of the atoms, N7–C8–N9, and 3) the average structures of DNA in the fiber and oligonucleotides are not identical. As for the first item, although the orientation of the z

Table 2. Euler Angles β and γ Calculated from the Atomic Coordinates of DNA Models and the Single Crystal Structures of Oligonucleotides[a]

A Form DNA		B Form DNA		Ref./Sample
β	γ	β	γ	
67.8	4.9	96.2	0.1	21/Fiber
73.2±0.2	12.1	97±6	15.5±0.8	25/Fiber
—	—	90.4	4.8	34/Fiber
68.9	0.6	—	—	24/Fiber
75.9±5	5.2±4.3	—	—	35/Octamer
75.2±2.8	8.5±3.5	—	—	36/Decamer
108.1±2.6	174.9±4.4	—	—	
—	—	97±15	18±12	4, 32/
—	—	84±15	163±12	Dodecamer

a) See the data of oligomers in the text.

principal axis is not known for the purine ring, all of the single crystal ^{2}H NMR studies[27-30] have shown that the major principal axis of the ^{2}H bonds is along the C–H bond axis within a couple of degrees. As for the second item, the neutron diffraction study[31] of 1-methylthymine:9-methyladenine crystal has shown that the C8 proton is not on the bisector of the atoms, N7–C8–N9, although the purine base is planar. That is, the C8–H bond axis inclines by about 1.7° from the bisector towards atom N9. Using this result, the Euler angle β was recalculated for the decamer, r(GCG)d-(AATTCGC), and its averaged value changed by only 0.1°. With regard to item three, it is often difficult to determine the helix axis of small oligonucleotides such as those mentioned above. Furthermore, the helix axis often bends, probably due to molecular packing forces.[4] We believe that this factor is the major reason for the discrepancy between the value of β calculated for oligonucleotides and that observed for the fibers.

It is interesting to note the conformational variation in the base planes in the single crystals of oligonucleotides, such as a decamer in the A family of crystalline form of DNA,[26] and two dodecamers, d(CGCGAATTCGCG) and d(CGCGAATTBr5CGCG) in the B family of the crystalline form of DNA.[32] The β values of the decamer are in a very narrow range of a few degrees (±3°), whereas those of the dodecamers are significantly varied over the range of ±15° from the average value. These results indicate that the bases of the A form of DNA are restricted to nearly a single conformation, while those of the B form of DNA have a wide distribution of conformations. The results derived from line-shape analysis of the quadrupole spectra of the A and B DNA fibers are consistent with the above mentioned.

In conclusion, the ^{2}H NMR spectra of DNA fibers studied here demonstrated that the orientations of the bases in the A form of DNA were constant within a few degrees in Euler angle β, whereas value of β in the B form of DNA varied over a range of ±10°. These results are consistent with the distribution of the Euler angles β and γ, calculated on the basis of the structure of oligonucleotides (see Table 2), and they are also consistent with structural features of DNA deduced from ^{31}P NMR studies. It should be noted that the structural information that can be obtained from the spectra of the C8–^{2}H label is limited. Accurate values of γ are not attainable because η is very small, and the values of β and $\langle\Delta\beta\rangle$ have large uncertainties (±7°) in the case of B-DNA because β is ca. 90°, a value in the range where the line-shape and peak splitting are least sensitive to changes in β. More comprehensive and accurate information would be obtained by using synthetic DNA molecules ^{2}H labeled at another position.[18]

Dynamics of the Base Domain. As described earlier in this paper, the relatively small ^{2}H T_1 values observed at 75—79% RH, Table 1, are a consequence of rapid ($\tau_c=3.8\times10^{-8}$ s) motions of the C8–^{2}H bond axis. The line-shape and T_1 data are both well fit using a model in which the orientation of C8–^{2}H bond axis fluctuates in a cone (normal to the helix axis) throughout a rms angle of 8.5°. The reductions in T_1 value and peak splitting observed at higher relative humidity (92% RH) can be accounted for by a large fluctuation of the C8–^{2}H bond axis, rms angle of 13.5°, and smaller correlation time, $\tau_c=1.5\times10^{-8}$ s. It is interesting to note that the amplitude of the base fluctuation, 13.5°, estimated here for Na-DNA at 92 and 98% RH is almost identical to the value 10—13° estimated for Li-DNA at 66% RH by Vold et al.[8] These results suggest that the fluctuation amplitude of the base in the B form of DNA has only a weak humidity dependence over the range from 66 to 98% RH, although its correlation time has an appreciable dependence. The rapid, small amplitude fluctuation of the C8–^{2}H bond axis explains the humidity dependence of quadrupole splittings and T_1, but it does not fully explain the frequency dependence of T_2. Brandes et al.[33] therefore, suggested that a distribution of correlation times must be taken into account for this frequency dependence. We demonstrated that the large distortions and intensity losses in the quadrupole echo spectra of the oriented and unoriented DNA at 92% RH are explained by a slower ($\tau\approx10^{-6}$ s), larger root mean square amplitude (ca. 30°), reorientational motion of the C8–^{2}H bond axis about the helix axis. The six-site model employed here leads to a conclusion consistent with the rotational diffusion about the helix axis as discussed in the ^{31}P NMR study of DNA fibers.[1]

In the course of the present study, we learned that Dr. R. R. Vold in UC San Diego was studying oriented DNA samples by solid-state ^{2}H NMR. We greatly appreciate her kindness for sending us preprints in advance of publication. We thank Robert G. Griffin of MIT for the computer program to calculate spectra of the six-site jump model, and also thank Dr. L. Lerner of NIH for her reading of this manuscript and valuable discussions.

References

1) H. Shindo, T. Fujiwara, H. Akutsu, U. Matsumoto, and Y. Kyogoku, *Biochemistry*, **24**, 887 (1985).

2) T. Fujiwara and H. Shindo, *Biochemistry*, **24**, 892 (1985).

3) J. A. DiVerdi and S. J. Opella, *J. Mol. Biol.*, **149**, 307 (1981).

4) R. Wing, H. Drew, T. Takano, C. Broka, S. Tanaka, K. Itakura, and R. E. Dickerson, *Nature (London)*, **287**, 755 (1980).

5) H. Shindo, "Magnetic Resonance in Biology," ed by

J. S. Cohen, Wiley, New York (1983), Vol. 2, pp. 95—129.
6) T. L. James, "Phosphorus-31 NMR," ed by D. Gorenstein, Academic Press, New York (1984), pp. 340—398.
7) P. Bendel, J. Murphy-Boesch, and T. L. James, *Biochim. Biophys. Acta*, **759**, 205 (1983).
8) R. R. Vold, R. Brandes, P. Tsang, D. R. Kearns, and R. L. Vold, *J. Am. Chem. Soc.*, **108**, 302 (1986).
9) A. Rupprecht, *Acta Chem. Scand.*, **20**, 494 (1966).
10) F. Doppler-Bernardi and G. Felsenfeld, *Biopolymers*, **8**, 733 (1969).
11) F. E. M. O'Brien, *J. Sci. Instru.*, **25**, 73 (1948).
12) S. K. Sarkar, C. E. Sullivan, and D. A. Torchia, *J. Biol. Chem.*, **258**, 7962 (1983).
13) J. H. Davis, *Biochim. Biophys. Acta.*, **737**, 117 (1983).
14) H. W. Spiess and H. J. Sillescu, *J. Magn. Reson.*, **42**, 281 (1981).
15) M. Bloom, J. H. Davis, and M. I. Valic, *Can. J. Phys.*, **58**, 1510 (1980).
16) B. T. Nall, W. P. Rothwell, J. S. Waugh, and A. Rupprecht, *Biochemistry*, **20**, 1881 (1981).
17) D. A. Torchia and A. Szabo, *J. Magn. Reson.*, **49**, 107 (1982).
18) S. Roy, Y. Hiyama, D. A. Torchia, and J. S. Cohen, *J. Am. Chem. Soc.*, **108**, 1675 (1986).
19) Y. Hiyama, E. A. Keiter, and T. L. Brown, *J. Magn. Reson.*, in press.
20) H. Shindo, J. B. Wooten, B. H. Pheiffer, and S. B. Zimmerman, *Biochemistry*, **19**, 518 (1980).
21) S. Arnott, P. Campbell-Smith, and R. Chandrasekaran, "CRC Handbook of Biochemistry," ed by G. D. Fasman, CRC Press, Cleaveland (1976), Vol. 2, pp. 411—422.
22) P. Tsang, R. R. Vold, and R. L. Vold, to be published.
23) H. Shindo, T. Fujiwara, H. Akutsu, U. Matsumoto, and M. Shimidzu, *J. Mol. Biol.*, **174**, 221 (1984).
24) W. Fuller, M. H. F. Wilkins, H. R. Wilson, and L. D. Hamilton, *J. Mol. Biol.*, **12**, 60 (1965).
25) M. Levitt, *Proc. Natl. Acad. Sci. U.S.A.*, **75**, 640 (1978).
26) A. H.-J. Wang, S. Fujii, J. H. Van Boom, G. A. Vander-Marcel, S. A. A. Van Boeckel, and A. Rich, *Nature (London)*, **299**, 601 (1983).
27) A. M. Achlama and Y. Zum, *J. Mag. Reson.*, **36**, 249 (1979).
28) G. J. Adriaenssens and J. L. Bjorkstam, *J. Chem. Phys.*, **56**, 1223 (1972).
29) G. Soda and T. Chiba, *J. Phys. Soc. Jpn.*, **26**, 249 (1969).
30) T. L. Brown, L. G. Butler, D. Y. Curtin, Y. Hiyama, I. C. Paul, and R. B. Wilson, *J. Am. Chem. Soc.*, **104**, 1172 (1982).
31) M. N. Frey, T. E. Koetzle, M. S. Lehmann, and C. W. Hamilton, *J. Chem. Phys.*, **59**, 915 (1973).
32) A. V. Fratini, M. I. Kapka, H. R. Drew, and R. E. Dickerson, *J. Biol. Chem.*, **257**, 14686 (1982).
33) R. Brandes, R. R. Vold, R. L. Vold, and D. R. Kearns, *Biochemistry*, **25**, 7744 (1986).
34) R. Langridge, D. A. Marvin, W. E. Seeds, H. R. Wilson, C. W. Hooper, M. H. Wilkins, and L. D. Hamilton, *J. Mol. Biol.*, **2**, 38 (1960).
35) A. H.-J. Wang, S. Fujii, J. H. Van Boom, and A. Rich, *Proc. Natl. Acad. Sci. U.S.A.*, **79**, 3968 (1982).

 © 1987 The Chemical Society of Japan Bull. Chem. Soc. Jpn., 60, 1641—1643 (1987)

The Reaction of $N(2^4S_{3/2})$ with Hydrogen Halides and Deuterium Iodide

Hironobu UMEMOTO,* Teruo UCHIDA, Shigeru TSUNASHIMA, and Shin SATO†
Department of Applied Physics, Tokyo Institute of Technology,
Ookayama, Meguro-ku, Tokyo 152
†Research Laboratory for Nuclear Reactors, Tokyo Institute of Technology,
Ookayama, Meguro-ku, Tokyo 152
(Received December 4, 1986)

The bimolecular rate constants for the reactions of ground state atomic nitrogen with hydrogen halides and deuterium iodide were measured by employing a pulse radiolysis-resonance absorption technique. As for the reactions of hydrogen iodide and deuterium iodide, the temperature dependence was also measured; it was found that the rate constants were well expressed by the following Arrhenius expressions: $k(N+HI)=(3.6\pm0.6)\times10^5 \exp[-(1530\pm50)/T]$; $k(N+DI)=(1.0\pm0.4)\times10^5 \exp[-(1460\pm130)/T]$, in units of $m^3 mol^{-1} s^{-1}$. The preexponential factors for these reactions are much smaller than the semiempirically calculated ones. These small preexponential factors suggest that these reactions proceed non-adiabatically. The rate constants for hydrogen bromide and hydrogen chloride were found to be very small.

Recently, we have reported the Arrhenius parameters for the reactions of ground-state atomic nitrogen with halogen molecules.[1] The preexponential factors for these reactions were found to be much smaller than those for the analogous reactions of atomic hydrogen and oxygen or those predicted by the semiempirical calculations. It was also found that the preexponential factor increases with the increase in the molecular weight. In order to explain these experimental results, we proposed that the potential barrier for the adiabatic route on the quartet surface is very high and that the major route of the reaction is a non-adiabatic one via a doublet surface. If this hypothesis is true, the preexponential factors for the $N(^4S)+HI$ and DI reactions should also be small, although the production of NH (or ND) and I is spin-allowed and exothermic. In order to check this hypothesis, we have performed experiments with HI and DI. As for the reaction of $N(^4S)+HBr$, Milton and Dunford have reported the bimolecular rate constant to be 2×10^4 $m^3 mol^{-1} s^{-1}$ at 313 K.[2] They considered that the formation of NH and Br is almost thermoneutral, but recent measurement of the heat of the formation of NH suggests that the reaction is 55 kJ mol^{-1} endothermic,[3] and the rate constant they obtained seems to be too large. Although the formation of NH and Cl is unquestionably endothermic in the reaction of $N(^4S)+HCl$, it is not certain if the production of NCl and H is also endothermic, since the NCl bond energy is not known precisely.[4] In the present work, we have measured the rate constants for the reactions of $N(^4S)$ with hydrogen halides and deuterium iodide at various temperatures.

Experimental

The experimental apparatus and the procedures were the same as those reported in a previous paper.[1]

The HI and DI were synthesized from H_2 or D_2 (both Takachiho Kako) and I_2 (Koso Chemical Co.) in the presence of platinized asbestos and were used after repeated trap-to-trap distillations. In order to estimate the isotopic purity of DI, it was photolyzed by the light from a high-pressure mercury lamp; the ratio of D_2 to HD was measured mass-spectrometrically. Since the absorption coefficient of HI is a little larger than that for DI,[5] the HI content must have been overestimated. The initial content of HI was 7%; it increased gradually during the storage, until it was 13% when the experiments were over. Then, all the data for DI were corrected by assuming that it contained 10% of HI. The HBr was separated from its aqueous solution (Wako Pure Chemical Industries) and used after repeated trap-to-trap distillations. The HCl was the product of the Takachiho Kako Co. and was used without further purification.

Results

The decay rate of $N(^4S)$ increased linearly with the increase in the pressure of HI or DI; it also increased with the temperature of the system, while it was independent of the total pressure at a given pressure of HI. On the other hand, in the cases of HBr and HCl, the decay rate did not show any marked dependence on the partial pressures of these gases. In other words, the rate constants for the reactions of $N(^4S)$ with HBr and HCl are too small to be measured by the present technique. From the least-squares slopes of the linear relationships between the decay rates and the pressures of HI and DI, the bimolecular rate constants can be determined. As has been discussed in the previous paper, the apparent rate constants determined from these slopes are considered to be twice the rate constants for the reactions of $N(^4S)$ with HI and DI.[1] This is because one of the products of the reaction, NH or ND, is considered to react with $N(^4S)$ once again very rapidly. The rate constant for the reaction of N and NH (ND) should be of the same order as those for the N+OH, N+CN, and $N+NH_2$ reactions.[6] It should be noted that the formation of NI and H (D) is highly endothermic. Table 1 summarizes the rate

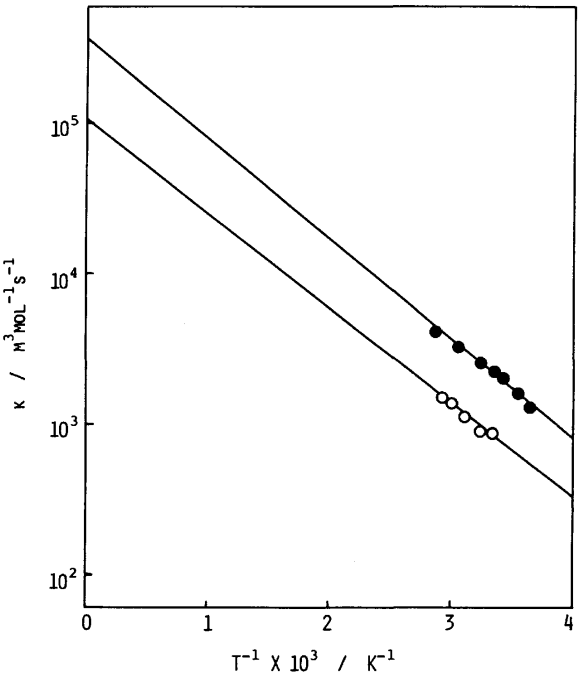

Fig. 1. Arrhenius plots for the reactions of N+HI(●) and N+DI(○).

Table 1. Rate Constants for the Reactions of N(^{4}S) with Hydrogen and Deuterium Halides

Reactant	T/K	$k \times 10^{-3}$/m^3 mol^{-1} s^{-1}
HI	348	4.18±0.39
	327	3.30±0.45
	308	2.54±0.07
	298	2.23±0.11
	292	2.04±0.15
	282	1.61±0.13
	274	1.31±0.07
DI	341	1.46±0.10
	333	1.35±0.08
	322	1.09±0.08
	309	0.87±0.08
	299	0.86±0.09
HBr	376	<0.8
HCl	377	<0.6

constants determined in this way at various temperatures. The rate constants for HI and DI are well expressed by the Arrhenius expressions. This is shown in Fig. 1, while the Arrhenius parameters are listed in Table 2.

The semiempirical LEPS and BEBO calculations were performed to evaluate the preexponential factors for the reactions of N(^{4}S) with HI and DI. The procedure for the LEPS calculation was the same as that described in the previous paper.[1] The Sato parameter was adjusted to give the activation energy experimentally obtained for the N+HI reaction. As

Table 2. Experimental and Semiempirically Calculated Arrhenius Parameters for the Reactions of N(^{4}S) with HI and DI

Reactant	E_a/kJ mol^{-1}	$A \times 10^{-5}$/m^3 mol^{-1} s^{-1}			
	exp[a]	exp[a]	LEPS[b]	BEBO[c]	BEBO[d]
HI	12.7±0.4	3.6±0.6	680	120	140
DI	12.1±1.1	1.0±0.4	680	110	130

a) Experimental value; b) Sato parameter=0.053; c) C_1=4.13, C_2=0.28; d) C_1=3, C_2=0.303.

Table 3. Arrhenius Parameters Calculated by the BEBO Method

Reaction	C_1	C_2	E_a/kJ mol^{-1}	$A \times 10^{-5}$/m^3 mol^{-1} s^{-1}
N+HI	3	0.28	8.4	230
	4.13	0.28	12.7	120
	3	0.303	12.7	140
N+DI	3	0.28	8.5	210
	4.13	0.28	13.1	110
	3	0.303	13.9	130

for the BEBO calculation, in the previous work the factor of the anti-Morse function, C_1, according to the notation by Singleton and Cvetanović,[7] was parametrized and adjusted to give the experimental activation energy. In the present work, not only this factor, but also the Pauling constant, C_2, were parametrized. A similar procedure has been employed by Brown and Smith in the calculation of the rate constant for the O+DCl and DBr reactions.[8] When C_1 was adjusted, C_2 was fixed at 0.28, the recommended value by Gilliom, while, when C_2 was adjusted, C_1 was fixed at 3 considering that atomic nitrogen is a quartet. The rest of the calculational procedure was the same as that reported previously.[1] The results are shown in Tables 2 and 3. The calculations for the N+DI reaction were performed by using the same parameters as those for the N+HI reaction.

Discussion

As has been discussed in the previous paper, the reactions of N(^{4}S) with halogen molecules are considered to proceed non-adiabatically via doublet surfaces.[1] In the present cases, the experimentally obtained preexponential factors for the N+HI and DI reactions were also found to be much smaller than those for the analogous reactions of H and O atoms[7,9] or than the results of the semiempirical LEPS and BEBO calculations, as is shown in Table 2. In general, the agreement between the experimentally obtained Arrhenius parameters and the semiempirically calculated ones is not very good, even in the simple systems, such as H+HX and O+HX, where

HX stands for hydrogen halides.[7,8,10,11] Three-dimensional trajectory calculations are necessary for a quantitative discussion.[12] However, the present disagreement between the experimental and the calculated preexponential factors is outstanding. This discrepancy suggests that these reactions involve transitions between potential surfaces of different multiplicities. Correlation diagrams similar to that presented in the previous paper for the N+halogens systems may also be drawn in the present cases.[1] The preexponential factor for the N+HI reaction was found to be around one-third of that for the $N+I_2$ reaction. This is also consistent with the above consideration that the reactions are not adiabatic, because in the $N+I_2$ system, a stronger spin-orbit coupling is expected and the spin-conservation rule is considered to hold less rigorously. The isotope effect observed in the preexponential factors for HI and DI may be attributed to the difference in the probabilities of crossing from a quartet surface to a doublet surface, since the semiempirical calculations predict no large isotope effect.

The extremely slow reaction rates for HBr and HCl are consistent with the thermodynamical predictions. The formation of NH and halogen atoms from these molecules is endothermic. The production of NCl and H from N(⁴S) and HCl may also be endothermic. The rate constant reported by Milton and Dunford for the N+HBr reaction seems to be erroneous.[2] Their method, a diffusion-flame technique, is too indirect for quantitative measurements. Moreover, their reported value for the $N+C_2H_4$ reaction has not been confirmed in a recent work.[13]

From the present results, together with those of our recent work,[1,13] it can be concluded that N(⁴S) atoms are very inert to stable molecules with even-numbered electrons. This inertness can be attributed to the conservation of the spin-angular momentum. In most practical systems at moderate temperatures, such as discharge-flow systems, the decay of N(⁴S) is governed by the reactions with the molecules with odd-numbered electrons, such as free radicals. In the absence of such active species, the only decay process is the termolecular or heterogeneous recombination reaction between atomic species.

References

1) H. Umemoto, T. Uchida, S. Nakagawa, S. Tsunashima, and S. Sato, *Bull. Chem. Soc. Jpn.*, **59**, 3755 (1986).
2) E. R. V. Milton and H. B. Dunford, *J. Chem. Phys.*, **34**, 51 (1961).
3) N. Washida, G. Inoue, M. Suzuki, and O. Kajimoto, *Chem. Phys. Lett.*, **114**, 274 (1985).
4) R. C. Weast, ed., "CRC Handbook of Chemistry and Physics," CRC Press, 61st ed., Florida (1980/81), p. F-224.
5) J. R. Bates, J. O. Halford, and L. C. Anderson, *J. Chem. Phys.*, **3**, 415 (1935).
6) M. J. Howard and I. W. Smith, *J. Chem. Soc., Faraday Trans. 2*, **77**, 997 (1981); A. R. Whyte and L. F. Phillips, *Chem. Phys. Lett.*, **98**, 590 (1983); A. R. Whyte and L. F. Phillips, *ibid.*, **102**, 451 (1983).
7) D. L. Singleton and R. J. Cvetanović, *Can. J. Chem.*, **56**, 2934 (1978).
8) R. D. H. Brown and I. W. M. Smith, *Int. J. Chem. Kinet.*, **10**, 1 (1978).
9) D. L. Baulch, J. Duxbury, S. J. Grant, and D. C. Montague, *J. Phys. Chem. Ref. Data*, **10**, Suppl. 1 (1981).
10) R. D. H. Brown and I. W. M. Smith, *Int. J. Chem. Kinet.*, **7**, 301 (1975).
11) T. Bérces and J. Dombi, *Int. J. Chem. Kinet.*, **12**, 183 (1980).
12) M. Broida, M. Tamir, and A. Persky, *Chem. Phys.*, **110**, 83 (1986).
13) H. Umemoto, S. Nakagawa, S. Tsunashima, and S. Sato, *Bull. Chem. Soc. Jpn.*, **59**, 1449 (1986).

 © 1987 The Chemical Society of Japan Bull. Chem. Soc. Jpn., 60, 1645—1648 (1987)

Conductance Matrix of Amphoteric Ion-Exchange Membrane in Three Ion System

Akira YAMAUCHI,* Hitoshi SHINOHARA, Makoto SHINODA, Masashi DATE, Yutaka HIRATA, and Hideo KIMIZUKA
Department of Chemistry, Faculty of Science, Kyushu University 33, Hakozaki, Higashi-ku, Fukuoka 812
(Received December 8, 1986)

A conductance matrix describing the ion-transport phenomena in the membrane-three ion system has been determined. It was indicated there that six independent experiments were required in order to determine six independent elements of the conductance matrix. The NaCl-$CaCl_2$-amphoteric membrane system was chosen as the three ion system, and three kinds of fluxes, two kinds of transport numbers, and the membrane conductance were measured. Nine elements were experimentally determined on the assumption of Onsager's reciprocal relation. The results showed that the order of elements in conductance matrix was $g_{CaCa}>g_{ClCl}>g_{NaNa}>g_{CaCl}>g_{NaCl}>g_{CaNa}$. In addition, it was pointed out that the interactions among ions can never be ignored when the ion-transport phenomena across membrane are studied.

The transport phenomena of ions through an ion-exchange membrane have been still important subject in spite of many reported papers with respect to the transport properties. The subject appears in processes concentrating the saline water or obtaining the pure water from the saline water.[1] Probably the practical process would be a complicated one because of involving a number of ions. On the other hand, it is also interesting to understand the transport properties of ions through the membrane physicochemically. Generally, according to nonequilibrium thermodynamics, the fluxes transported across the membrane in the electrolyte solution–ion-exchange membrane system can be expressed by a linear combination of the forces generated in the system such as concentration gradient, potential difference and etc. In the previous studies, we have investigated the relationships among the fluxes and the forces in the system consisting of only a single electrolyte.[2-5] If the number of ions in the system increase, the relationships among the fluxes and the forces would become more complex. However, the thermodynamic examination concerning multi-ionic system simulating the realistic subject should be done. We have therefore chosen to study the three ion system which consisted of the mixed electrolytes having common anion, as representing a typical and simple example of multi-ionic system. Moreover, in order to observe simultaneously the detectable ion fluxes due to both cation and anion, use of the ion-exchange membrane having cation- and anion-exchange sites may be preferable from experimental standpoint. Thus, an amphoteric ion-exchange membrane was employed instead of homogeneous ion-exchange membrane.

The purpose of the present study is to clarify the correlation among behaviors of three ions within membrane.

Theory

We consider three ion system which consists of the amphoteric ion-exchange membrane and the mixed electrolyte solution having the common anion. According to the nonequilibrium thermodynamics,[3-5] the relationship between the current densities, i's and the transmembrane potential, V can be given as the following equation,

$$\begin{pmatrix} i_1 \\ i_2 \\ i_3 \end{pmatrix} = - \begin{pmatrix} g_{11} & g_{12} & g_{13} \\ g_{21} & g_{22} & g_{23} \\ g_{31} & g_{32} & g_{33} \end{pmatrix} \begin{pmatrix} V-V_1 \\ V-V_2 \\ V-V_3 \end{pmatrix}, \quad (1)$$

where subscripts 1—3 refer to the ionic species in the system, V_1—V_3 denote the pseudoequilibrium potentials due to each ionic species, and g_{11}—g_{33}, nine elements of the conductance matrix. In the present system, we assume that Onsager's reciprocal relations are well held among the elements, i.e.,

$$g_{ij} = g_{ji}. \quad (2)$$

With help of Eq. 2, the numbers of elements to be determined are reduced to six from nine. At this point, introducing the contribution due to water, the elements to be determined increase to ten even using Eq. 2. Fortunately, it was pointed out in the previous papers[3-5] that the effect of water on the conductance matrix was negligible when the interaction between ions mainly contribute to the transport phenomena. Therefore, six independent experiments are needed to understand the ion transport phenomena in this system.

The conductance for ions, g_1—g_3 and the membrane conductance, G_m are given as[3]

$$g_k = g_{k1} + g_{k2} + g_{k3} \quad (k=1, 2, 3), \quad (3)$$

$$G_m = g_1 + g_2 + g_3, \quad (4)$$

where subscript k refers to ionic species.

Taking account of Eqs. 3 and 4, one can obtain the alternative expression of Eq. 1 as follows,

$$\begin{pmatrix} i_1 \\ i_2 \\ I \end{pmatrix} = - \begin{pmatrix} g_{11} & g_{12} & g_1 \\ g_{21} & g_{22} & g_2 \\ g_1 & g_2 & G_m \end{pmatrix} \begin{pmatrix} V_3-V_1 \\ V_3-V_2 \\ V-V_3 \end{pmatrix}. \quad (5)$$

On the other hand, when the supplied current is absent, the membrane current, I and the membrane potential, V_0 are written by

$$I = i_1 + i_2 + i_3, \quad (6)$$

$$V_0 = t_1V_1 + t_2V_2 + t_3V_3, \quad (7)$$

$$t_k = g_k/G_m \quad (k=1, 2, 3), \quad (8)$$

$$t_1 + t_2 + t_3 = 1, \quad (9)$$

where the subscript o refers to the absence of the supplied membrane current and t_k's are the transport numbers.

Considering the ionic currents in the presence and absence of the membrane currents, we have from Eq. 1,

$$i_k - i_k^0 = g_k(V-V_0) \quad (k=1, 2, 3), \quad (10)$$

where i_k^0 denotes the ionic current at zero membrane current.

When I=0, we obtain from Eq. 5,

$$i_1^0 = - G_{11}^0(V_3-V_1) - G_{12}^0(V_3-V_2),$$
$$i_2^0 = - G_{21}^0(V_3-V_1) - G_{22}^0(V_3-V_2), \quad (11)$$

where

$$G_{11}^0 = g_{11} - G_m t_1^2,$$
$$G_{12}^0 = G_{21}^0 = g_{12} - G_m t_1 t_2, \quad (12)$$
$$G_{22}^0 = g_{22} - G_m t_2^2.$$

If the measurements of i_1^0 and i_2^0 are performed under the condition, either (V_3-V_1) or (V_3-V_2) is zero, Eq. 11 reduces to

$$i_1^0 = - G_{12}^0(V_3-V_2),$$
$$i_2^0 = - G_{22}^0(V_3-V_2), \quad (13)$$

or

$$i_1^0 = - G_{11}^0(V_3-V_1),$$
$$i_2^0 = - G_{21}^0(V_3-V_1), \quad (14)$$

respectively, Equations 13 and 14 serve to determine G_{11}^0, G_{12}^0, and G_{22}^0.

Combining Eq. 12 with Eqs. 3, 4 and 9, we obtain

$$g_{11} = G_{11}^0 + G_m t_1^2, \; g_{13} = G_m t_1(1-t_1-t_2) - G_{11}^0 - G_{12}^0,$$
$$g_{12} = G_{12}^0 + G_m t_1 t_2, \; g_{23} = G_m t_2(1-t_1-t_2) - G_{12}^0 - G_{22}^0, \quad (15)$$
$$g_{22} = G_{22}^0 + G_m t_2^2, \; g_{33} = G_m(1-t_1-t_2)^2 + G_{11}^0 + G_{22}^0 + 2G_{12}^0.$$

Eq. 15 indicates that all the elements of conductance matrix can be determined when G_{11}^0, G_{12}^0, G_{22}^0, G_m, t_1, and t_2 are experimentally measured.

Experimental

In this study, Na, Ca, and Cl ions were chosen as three ions and six independent experiments were performed in order to determine the six independent conductance elements for the system consisting of membrane and mixed electrolyte solutions having the same concentrations of electrolytes in phases I and II.

Materials. An amphoteric ion-exchange membrane used in this work was supplied by Tokuyama Soda Co. Ltd.,[6,7] and the characteristics of the membrane and the conditioning before use were already described elsewhere.[8-10]

Procedure of Experiments. As outlined in theoretical section, six independent experiments such as the membrane conductance, G_m transport numbers, t_1 and t_2 and the ion fluxes, i_1^0 vs. V_3-V_1 and i_1^0 vs. V_3-V_2 under the condition of $V_3-V_1=0$ and i_2^0 vs. V_3-V_1 under the condition of $V_3-V_2=0$ were measured, respectively. Of these, the procedure of the experiments for G_m, t_1, and t_2 were the same as those described in the preceding papers.[8-10] As to ion fluxes, the concentration change of Na and Ca in mixed electrolyte solutions in chambers I and II across the membrane were measured against a lapse of time by an atomic absorption spectroscopy (Hitachi Co. Ltd., Model 180-50). All the experiments were carried out at 25 °C, and the electrolyte solutions in both chambers were sufficiently stirred by magnetic stirrer throughout the experiment.

Preparation of Mixed Electrolyte Solutions. On the preparation of mixed electrolyte solution, two kinds of electrolytes were suitably mixed so as to eliminate either of two driving forces in Eq. 11. That is, as NaCl and $CaCl_2$ are used in the present system and the subscripts 1, 2, and 3 correspond to Na, Ca, and Cl ion, respectively, the driving forces, V_3-V_1 and V_3-V_2 are written as

$$V_{Cl} - V_{Na} = \frac{RT}{F} \ln \frac{a_{Cl}^{II} a_{Na}^{II}}{a_{Cl}^{I} a_{Na}^{I}}, \quad (16)$$

$$V_{Cl} - V_{Ca} = \frac{RT}{F} \ln \frac{a_{Cl}^{II} (a_{Ca}^{II})^{1/2}}{a_{Cl}^{I} (a_{Ca}^{I})^{1/2}}, \quad (17)$$

where a denotes activity and the superscripts I and II refer to phases I and II, respectively. The prepared electrolyte solutions were summarized in Table 1(a), in which the concentrations of mixed electrolytes in phase II was kept constant while those in phase I were changed so as to make the values of Eq. 16 always zero. Table 1 (b) also shows the prepared electrolyte solutions in which the values of Eq. 17 are zero. For the membrane conductance and transport

Table 1. Concentration of Prepared Electrolyte Solutions

(a)

	NaCl / mol dm^{-3}	$CaCl_2$ / mol dm^{-3}
II	2.00×10^{-2}	1.50×10^{-2}
I-1	3.00×10^{-2}	0.05×10^{-2}
I-2	2.50×10^{-2}	0.60×10^{-2}
I-3	1.70×10^{-2}	2.20×10^{-2}
I-4	1.50×10^{-2}	3.00×10^{-2}

(b)

	NaCl / mol dm^{-3}	$CaCl_2$ / mol dm^{-3}
II	2.00×10^{-2}	1.50×10^{-2}
I-5	3.50×10^{-2}	1.10×10^{-2}
I-6	2.50×10^{-2}	1.40×10^{-2}
I-7	1.00×10^{-2}	1.75×10^{-2}
I-8	0.50×10^{-2}	2.00×10^{-2}

number measurements, the mixed electrolyte solutions of identical composition and concentration were placed in chambers I and II across membrane. The single ion activities in Table 1 were calculated according to Debye-Hückel equation for activity coefficient.[11]

Results and Discussion

The concentration changes of ions in phases I and II in the absence of applied current were examined as a function of time for all the systems in Tables 1(a) and (b), which have the concentration difference of ions between phases I and II. Figure 1 shows a typical example about the system made of first two columns in Table 1(a) in which moles of Ca ions transported across membrane were plotted against times. It can be recognized that Ca ion concentration in phase I increase and that of phase II decrease with a lapse of time, and the concentration changes are linear against time within experimental error. This fact suggests that the transport of Ca ion is in a steady state. The mean absolute values of concentration changes in phases I and II were plotted against time in Figs. 2(a), 2(b), and 2(c). Figures 2(a) and 2(b) indicate Δn_{Na} vs. time plot and Δn_{Ca} vs. time plot under the condition, $V_{Cl}-V_{Na}=0$. The ion flux, J_i^0 was evaluated from the slopes in Fig . 2 as follows,

$$J_i^0 = \frac{\Delta n_i}{tS}, \tag{18}$$

where t and S denote time interval in second and the membrane area in cm^2, respectively. Taking account of the electricity on the ion fluxes, one can obtain the

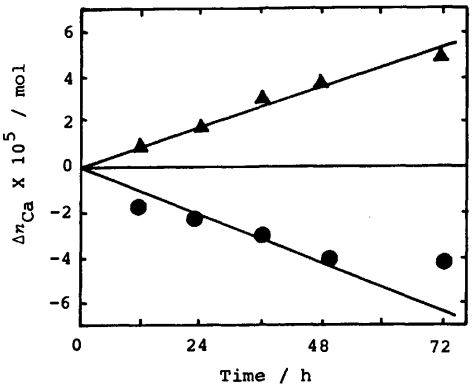

Fig. 1. A typical example of Ca concentration change across membrane against time.
System: NaCl, 3.00×10^{-2} mol dm^{-3}, $CaCl_2$, 0.05×10^{-2} mol dm^{-3} in phase I, ▲; NaCl, 2.00×10^{-2} mol dm^{-3}, $CaCl_2$, 1.50×10^{-2} mol dm^{-3} in phase II, ●.

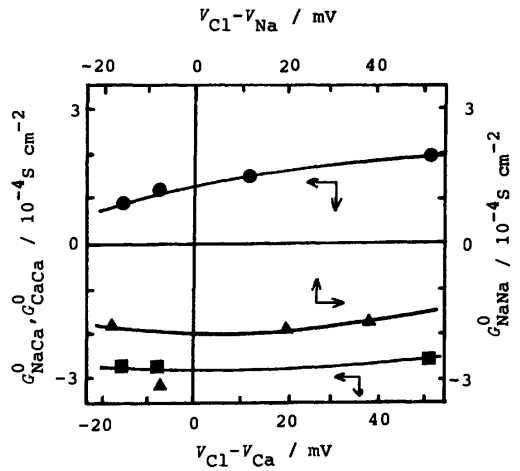

Fig. 3. Relation of G^0_{NaNa}, G^0_{NaCa}, and G^0_{CaCa} vs. $V_{Cl}-V_{Na}$ or $V_{Cl}-V_{Ca}$. ▲: G^0_{NaNa}, ●: G^0_{NaCa}, ■: G^0_{CaCa}.

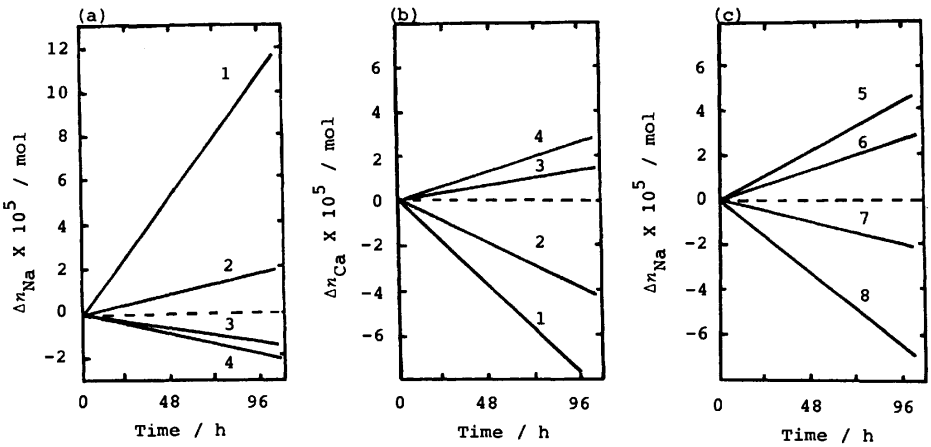

Fig. 2.(a). Na concentration change, Δn_{Na} against time under the condition that $V_{Cl}-V_{Na}=0$. The numbers in figure are those of phase I in Table 1(a).

(b). Δn_{Ca} against time under the condition that $V_{Cl}-V_{Na}=0$. The numbers are the same as in (a).

(c). Δn_{Na} against time under the condition that $V_{Cl}-V_{Ca}=0$. The numbers correspond to those of phase I in Table 1(b).

Table 2. Values of Membrane Conductance and Transport Numbers Together with Values of Conductance Elements

G_m (1.27×10^{-3})	g_{NaNa} (2.45×10^{-4})	g_{CaCa} (5.84×10^{-4})
t_{Na} (0.22)	g_{NaCa} (0.09×10^{-4})	g_{CaCl} (0.29×10^{-4})
t_{Ca} (0.49)	g_{NaCl} (0.25×10^{-4})	g_{ClCl} (3.14×10^{-4})

All the units are S cm^{-2} except the transport number, t.

ion current density, $i_i^0=z_iFJ_i^0$ in the absence of the supplied currents. The obtained i_1^0's were divided by $V_{Cl}-V_{Na}$ or $V_{Cl}-V_{Ca}$ and plotted against $V_{Cl}-V_{Na}$ or $V_{Cl}-V_{Ca}$ in Fig. 3. According to Eq. 12, the quantities in Fig. 3 contain important informations concerning the elements in conductance matrix given by Eqs. 1 or 5. As mentioned in experimental section, the membrane conductance and transport numbers were obtained under the experimental conditions that ionic concentration difference between the mixed electrolyte solutions in phases I and II are all zero. This corresponds to the case in which $V_{Cl}-V_{Na}$ or $V_{Cl}-V_{Ca}$ in Fig. 3 is extrapolated to zero. The values of G^0_{NaNa}, G^0_{NaCa} and G^0_{CaCa}, at $V_{Cl}-V_{Na}=V_{Cl}-V_{Ca}=0$ were estimated from Fig. 3 by interpolation.

On the other hand, the electrodialysis[8] and the membrane resistance were measured to obtain the transport numbers, t_{Na} and t_{Ca} and the membrane conductance, G_m for the membrane-electrolyte solution system in which the electrolyte solutions in phases I and II are identical. The results are shown in Table 2 together with the values of conductance elements estimated according to Eq. 15.

It can be seen in Table 2 that $g_{CaCa}>g_{ClCl}>g_{NaNa}>g_{CaCl}>g_{NaCl}>g_{CaNa}$. It is impressive that the tendency is partly in accord with $g_{CaCa}\simeq g_{ClCl}>-g_{CaCl}$ in the other amphoteric membrane system[3] in contrast to the result in the cation-exchange membrane, $g_{CaCa}>g_{CaCl}>g_{ClCl}$ in the previous paper.[12] As to the first three elements, the order in the present work also corresponds to that of the transport numbers in Table 2 ($t_{Cl}=1-t_{Na}-t_{Ca}=0.29$). This means that the g factors partly reflect the ionic composition within membrane. As seen in comparison with t in a single electrolyte system that $t_{Na}=0.90$ and $t_{Cl}=0.10$ in NaCl system and $t_{Ca}=0.62$ and $t_{Cl}=0.38$ in $CaCl_2$ system, respectively, the situation in mixed electrolyte system is largely different from the single electrolyte system, however. The reason for the inversion of g_{NaNa} and g_{ClCl} in mixed system is not clear in the present, but a possible explanation is that Cl ion within membrane may be relatively concentrated. That is, for the sake of high selectivity of Ca ion over Na ion to the sites in the case of mixed solutions,[8] Na ion may be excluded from the membrane. On the contrary, Cl ion may sufficiently be retained around the anion-exchange sites. The smaller value of g_{NaNa} compared with g_{ClCl} may be attributed to the different behaviors in mixed electrolyte.

The remained three elements, which express the interactions between the different ionic species, can not be ignored. The small but finite values mean that the respective ion fluxes are subject to the coupled forces and the coupling plays an important role in ion-transport phenomena.

Thus, it may be concluded that the transport phenomena can not be predicted by a simple combination of the single electrolyte systems, but the interaction among ions should be taken into account.

The present work was partially supported by Grant-in-Aid for Scientific Research No. 58470007 from the Ministry of Education, Science and Culture.

References

1) M. E. Mattson and M. Lew, *Desalination*, **41**, 1 (1982).
2) H. Kimizuka and K. Kaibara, *J. Colloid Interface Sci.*, **52**, 516 (1975).
3) H. Kimizuka, Y. Nagata, and K. Kaibara, *Bull. Chem. Soc. Jpn.*, **56**, 2371 (1983).
4) Y. Nagata, K. Kohara, W. K. Yang, A. Yamauchi, and H. Kimizuka, *Bull. Chem. Soc. Jpn.*, **59**, 2689 (1986).
5) H. Kimizuka, Y. Nagata, and W. K. Yang, "Membrane and Membrane Process," ed by E. Drioli and M. Nakagaki (1986), p. 85.
6) Y. Mizutani, R. Yamane, H. Ihara, and H. Motomura, *Bull. Chem. Soc. Jpn.*, **36**, 3651 (1963).
7) R. Yamane, T. Izuo, and Y. Mizutani, *Denki Kagaku*, **33**, 589 (1965).
8) M. Shinoda, Y. Hirata, A. Yamauchi, and H. Kimizuka, *Mem. Fac. Sci., Kyushu Univ., Ser. C*, **15**, 195 (1986).
9) Y. Hirata, M. Date. Y. Yamamoto, A. Yamauchi, and H. Kimizuka, this Journal, in press.
10) A. Yamauchi, Y. Okazaki, R. Kurosaki, Y. Hirata, and H. Kimizuka, *J. Memb. Sci.*, in press.
11) R. A. Robinson and R. H. Stoks, "Electrolyte Solutions," Butterworths (London) (1959).
12) H. Kimizuka, K. Kaibara, E. Kumamoto, and M. Shirōzu, *J. Memb. Sci.*, **4**, 81 (1978).

Synthesis and Properties of 5,10,15,20-Tetrakis(3,5-di-*t*-butyl-2-nitrophenyl)porphyrin: Conformational Stabilities of the Respective Atropisomers and Oxygenation Capabilities of the Iron(III) and Manganese(III) Complexes

T. Ken Miyamoto,* Shigeru Takagi, Tai Hasegawa, Seizi Tsuzuki, Eitaro Takahashi, Kojiro Okude, Itsuki Banno, and Yukiyoshi Sasaki
Department of Chemistry, Faculty of Science, The University of Tokyo, Hongo, Bunkyo-ku, Tokyo 113
(Received July 11, 1986)

The synthesis and properties of new, bulky atropisomeric porphyrins are described. Four atropisomers of 5,10,15,20-tetrakis(3,5-di-*t*-butyl-2-nitrophenyl)porphyrins has been easily separated and purified by column chromatography. The isomers all have different thermal stabilities toward atropisomerization. Below 60 °C, however, they have rather high conformational stabilities, and an iron(III) or manganese(III) ion has been incorporated into each isomer, with a retention of the ligand conformation. By the use of these metal complexes, the catalytic oxygenation reactions, i.e., the epoxidation of olefins (styrene, α-methylstyrene, cyclohexene, and cyclooctene) and the hydroxylation of alkanes (cyclohexane and heptane), have been done in the presence of hypochlorite or iodosylbenzene as an oxidant. Products analyses by GLC show that these new complexes effectively catalyze the oxygenations in higher yields or in more selective ways, than the corresponding TPP complexes.

The cytochrome P-450 family of monooxygenase enzymes have increasingly attracted the attention of chemists because of the versatility of its catalyses, i.e., aliphatic hydroxylation, alkene epoxidation, and heteroatom dealkylation.[1] Most of all, an inestimable blessing to inorganic chemists is the fact that iron(II—IV) porphyrin IX serves as an active center throughout enzymatic reactions.[2]

So far many efforts have been made to exploit P-450 models which include the metalloporphyrin–iodosylbenzene,[3–6] the metalloporphyrin–hypochlorite,[7–9] or the metalloporphyrin–O_2-reducing reagent system.[10,11] In these model systems, a variety of protected porphyrins have been used as catalysts. As far as atropisomeric porphyrins are concerned, however, limited numbers of the isomers have been employed, and they are not in extensive use at present.[12] This is surprising in view of the possible unsymmetrical steric protection afforded on both faces of the porphyrin plane by the use of atropisomerism. One factor in explaining this insufficient use is the lack of easily prepared atropisomeric porphyrin that either have a high conformational stability to heating or show no serious deterioration during catalysis. Two types of new atropisomers, i.e., 5,10,15,20-tetrakis(2-methoxy-1-naphthyl)porphyrin (**2**)[13] and 5,10,15,20-tetrakis(2-cyanophenyl)porphyrin (**3**),[14] have been reported. Although the four possible isomers of **2** were cleanly isolated, the instabilities of the 2-methoxy-1-naphthyl groups toward such oxidants as iodosylbenzene or hypochlorite hamper the practical use of their metal complexes as catalysts. Inversely, metal complexes of **3** may not be decomposed by the oxidant, but the separation conditions to the respective atropisomers are very severe. Thus, it is of great interest to develop new synthetic entries into atropisomeric porphyrin chemistry that either have new types of polar bulky groups around the porphyrin plane or lead to recoverable, reusable catalysts for P-450 models.

Recently, we described the synthesis of 5,10,15,20-tetrakis(3,5-di-*t*-butyl-2-nitrophenyl)porphyrin (**1**) and the separation of the four possible isomers (Fig. 2).[15] Each isomer has a relatively high conformational stability to prolonged heating, and the conversion into the iron complex (**1**-FeX) was done with a retention of the ligand conformation. The thermally stable *hydroxy iron(III) complexes* (**1**-FeOH) were also isolated by the treatment of the corresponding halo iron(III) species (**1**-FeBr or **1**-FeCl) with aqueous sodium hydroxide or with basic alumina. The stability of these complexes was explained as a steric

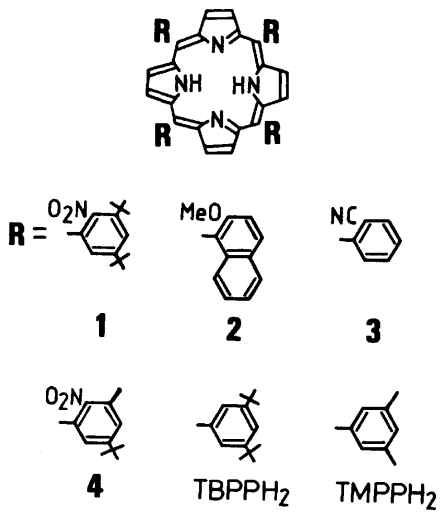

Fig. 1. The porphyrins **1**, **2**,[13] **3**,[14] **4**,[15] $TBPPH_2$,[24] and $TMPPH_2$.[24]

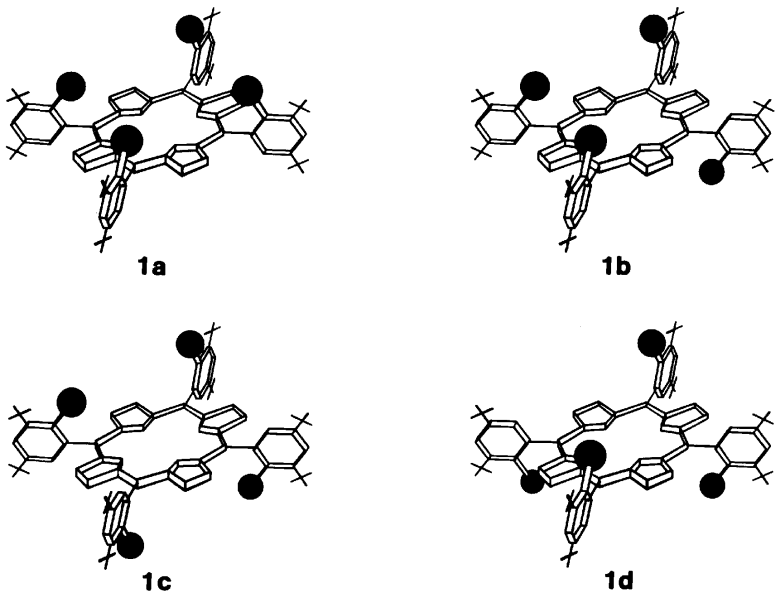

Fig. 2. The four atropisomers of porphyrin **1**: **1a**($\alpha\alpha\alpha\alpha$); **1b**($\alpha\alpha\alpha\beta$); **1c**($\alpha\alpha\beta\beta$); **1d**($\alpha\beta\alpha\beta$).[15]

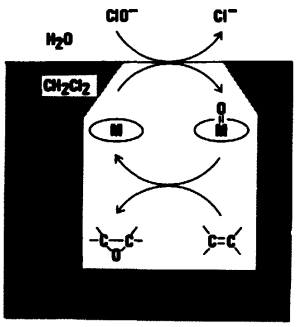

Fig. 3. Olefin epoxidation reaction using hypochlorite.

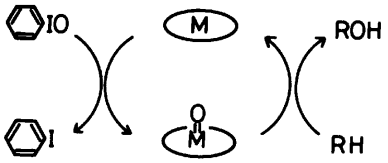

Fig. 4. Alkane hydroxylation reaction using iodosylbenzene.

effect attributable due to *t*-butyl and/or nitro groups.

Herein we wish to report details of the syntheses of **1** and their manganese(III) and iron(III) complexes (**1**-MnX or **1**-FeX) and of GLC analyses of the oxygenation products of the styrene, α-methylstyrene, cyclohexene, cyclooctene, cyclohexane, or heptane catalyzed by these complexes in the presence of hypochlorite or iodosylbenzene (Fig. 3 or 4). A preliminary account of the synthetic and spectral work has appeared.[15-17]

Experimental

The synthetic procedure to **1** is shown in Scheme 1.[15]

3,5-Di-*t*-butyl-2-nitrobenzaldehyde. In a 2 dm^3, three-necked, round-bottomed flask, powder of 3,5-di-*t*-butylbenzaldehyde (214 g, 0.98 mol) was dissolved, with mechanical stirring, in 0.9 dm^3 of sulfuric acid. After the mixture had then cooled to 5 °C, 88 cm^3 of nitric acid (Sp. Gr. about 1.38) was added, drop by drop, at such a rate that the temperature did not rise above 10 °C. After the addition was complete, the mixture was stirred for a further 30 minutes and then poured into 6 dm^3 of water containing chipped ice. The solid product was separated by filtration with a G3 sintered glass filter and washed with three 1-dm^3 portions of water. The solid thus obtained was dissolved in the minimum ammount of the 1:9 chloroform–hexane (about 600 cm^3). The solution was then submitted to 3.5×40 cm of 70—230 mesh Merck alumina 90, and the product was eluted from the column with 1:9 chloroform–hexane. The solution was evaporated to dryness, and the residue was purified by vacuum distillation (bp 150—155 °C/1.3 Pa) to give 214 g (83% based on 3,5-di-*t*-butylbenzaldehyde; mp 90—91 °C) as yellow crystals. Found: C, 68.54; H, 8.07; N, 5.37. Calcd for $C_{15}H_{21}NO_3$: C, 68.41; H, 8.04; N, 5.32. ^{1}H NMR ($CDCl_3$) δ=1.3 (9H, s, 3-*t*-butyl H), 1.4 (9H, s, 5-*t*-butyl H), 7.7 (2H, m, phenyl H), 9.7 (1H, s, CHO). Mass spectrum, *m/z* 263.3.

5,10,15,20-Tetrakis(3,5-di-*t*-butyl-2-nitrophenyl)porphyrin (1). The porphyrin was prepared by a modification of the method of Sorrell's.[18] Two hundred and eighty grams of 3,5-di-*t*-butyl-2-nitrobenzaldehyde were dissolved in 1.3 dm^3 of glacial acetic acid in a 3-dm^3, three-necked, round-bottomed flask fitted with Allihn condensers and a dropping funnel. The solution was heated and stirred with a magnetic bar. To the boiling solution, 74.5 g of pyrrole (1.1 mol) was added, drop by drop. The resulting black mixture was allowed to reflux for 60 min and then left to stand over-night. The purple brown crystals thus precipitated were filtered by suction and washed with

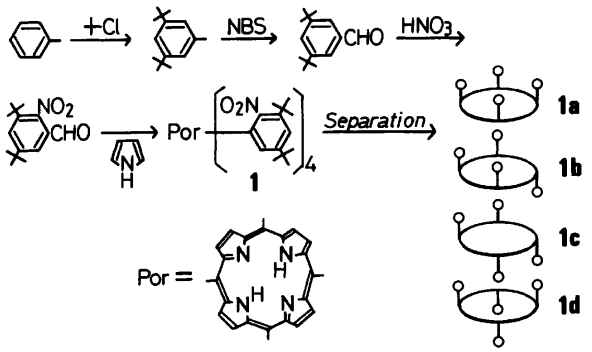

Scheme 1. The synthetic procedure to porphyrin **1**.

methyl alcohol (ca. 500 cm³). Yield: 36.0 g (11%). **1** is very easily soluble in chloroform; very soluble in benzene or toluene; soluble in hexane, dioxane, *N*,*N*-dimethylformamide, or carbon tetrachloride, and sparingly soluble in methyl or ethyl alcohol. **1**: Found: C, 73.28; H, 7.46; N, 8.88. Calcd for $C_{76}H_{90}N_8O_8$: C, 73.40; H, 7.29; N, 9.01. UV-vis. ($CHCl_3$) λ/nm at 25 °C (ε/M^{-1} cm^{-1}),[19] 421 (3.5×10^5), 474 (3.1×10^3), 512 (2.2×10^4), 542 (3.1×10^3), 586 (6.9×10^3), 640 (5.6×10^2). The nitro groups show characteristic infrared absorptions: 760, 840, 1530 cm^{-1}. **1** is a mixture of four atropisomers. TLC on silica (toluene) show four spots; R_f values: **1a**, 0.28; **1b**, 0.65; **1c**, 0.74; **1d**, 0.88.

Separation of Four Isomers. The most polar isomer, the **1a** isomer, could be separated from the other three isomers by means of a skillful column-chromatographic technique. Before the isomer separation, the preferential isomerization was carried out by the utilization of adsorption.[20,21] Ten grams of the porphyrin **1** were dissolved in 2 dm³ of toluene. The solution was then refluxed under Ar, and a 30-g portion of Merck alumina 90 was added nine times every three hours. After refluxing for 30 h, the solution was cooled to the ambient temperature. The isomerized product was then extracted from the alumina with a 1:1 chloroform–acetone mixed solvent. The solvent was removed by the use of a rotary evaporator, and the residue was redissolved in a minimum amount of chloroform (about 300 cm³). The chloroform solution was poured onto a 5.5×60 cm column of Merck alumina 90 prepared as a slurry in chloroform. After all the material had been loaded, chloroform (about 2 dm³) was passed through the column until the eluate became very pale. The **1a** isomer was then removed by the use of a 1:1 chloroform–acetone mixture, and the solvent was removed at a temperature lower than 40 °C. Five grams of the crude **1a** isomer obtained as has been described above was dissolved in 100 cm³ of chloroform and again loaded onto a 3×60 cm column of Merck alumina 90 prepared as a slurry in chloroform. After the loading, the column was eluted with chloroform, and the eluate of the second brown band was collected. The solution was subsequently taken to dryness at room temperature. The residue was redissolved in 300 cm³ of toluene. After it had then been placed in a 3×40 cm column of silicagel (Wako gel C-200) prepared as a slurry in toluene, toluene (about 2 dm³) was passed through the column. The desired pure **1a** isomer was then removed by elution. The solution was concentrated to 40 cm³ at the ambient temperature. The resulting purple brown crystals were filtered, washed with methyl alcohol, and dried in vacuo. Percentage yield: ca. 15%.

The other three isomers were separated in the usual way. Ten grams of **1**, the **1a** isomer of which had been removed in the above procedure, were dissolved in a minimum amount of toluene (about 600 cm³). After the sample had then been placed in a 5.5×60 cm column of alumina (Woelm N-Super 1) prepared as a slurry in toluene, the column was eluted with toluene. The separation was followed by the TLC analysis of the eluate. The fractions of the three bands were separately collected and condensed for crystallization using a rotary evaporator at room temperature. The purple brown crystals were filtered, washed with methyl alcohol, and dried in vacuo. Yields: **1b**, 5.7 g, **1d**, 1.2 g. The **1c** isomer still contained a minor amount of the **1d** isomer at this stage of the separation. Several subsequent recrystallizations from toluene gave 0.9 g of the desired pure **1c** isomer.[22]

Measurement of Atropisomerism. The change in the isomer distribution was measured by the method of the literature[14] with the following modification. A 0.4-g portion of the porphyrin was dissolved in 300 cm³ of toluene or chloroform. Under Ar, the solution was refluxed in a oil bath or photoirradiated with a high pressure mercury lamp (400 W, Riko. UVL-400HA) at the ambient temperature. A few cm³ of the solution was sampled with a pipet at appropriate intervals and spotted on a 20×20 cm TLC plate (Merck silica gel 60). The four isomers were separated with toluene on the TLC plate. The quantity was measured by spectrometry after the extraction of each isomer from the TLC plate with chloroform. The relative abundance of the isomers was photometrically determined using the Soret-band.

Iron Insertion. A 0.4-g portion (0.32 mmol) of **1** was dissolved in a 100-cm³ portion of a mixed solvent of 1:3 chloroform–acetic acid, after which the solution was purged with Ar to remove the O_2. Then, anhydrous $FeBr_2$ (0.34 g, 1.6 mmol), anhydrous sodium acetate (0.4 g, 4.9 mmol), and 2,6-lutidine (0.18 cm³) were added to this solution of **1**. The resulting solution was stirred for 5 h at 50 °C. When **1a** was used, the solution was stirred for 1 h at 50 °C. After a 100-cm³ portion of water was added to the resulting solution, the organic layer was separated and subsequently washed, first with water and then with a dilute sodium hydroxide solution. The crude iron complex of **1** was purified by silica-gel chromatography. The chloroform solution of the product was placed in a silica-gel column (Wako gel C-200) prepared as a slurry in chloroform. Afrer loading, the column was eluted with chloroform. The remaining porphyrin free base was first eluted, and then the desired iron complex of **1** was eluted. The second eluate was collected and then stirred together with 47% hydrobromic acid. The red-brown solution turned dark brown during stirring. After the organic layer had been separated, the solvent was removed by means of a evaporator. The iron complex **1**–FeBr was recrystallized from a benzene–heptane mixed solvent, and the resulting dark blue-purple crystals were dried in vacuo. Percentage yields: **1a**–FeBr, 64%; **1b**–FeBr, 59%; **1c**–FeBr, 65%; **1d**–FeBr, 74%. Found: C, 66.06; H, 6.57; N, 7.99; Br, 5.99. Calcd for $C_{76}H_{88}N_8O_8FeBr$: C, 66.28; H, 6.41; N, 8.14; Br, 5.80. UV-vis. (toluene) λ/nm: 360, 392, 422, 512, 588, 650.

In order to estimate the relative ease of iron insertion in

relation to atropisomeric porphyrins, controlled metal-insertion experiments were carried out. In a typical experiment,[21] a porphyrin free base (0.08 mmol), 2,6-lutidine (0.4 mmol), and anhydrous $FeBr_2$ (0.4 mmol) were dissolved in 20 cm^3 of THF, and the reaction was carried out under Ar for 3 h at 30 °C. The products were separated by the use of a silica-gel column (Wako gel C-200) prepared as a slurry in chloroform. The silica-gel column was eluted by chloroform, and the second band was collected. The second eluate was stirred with 47% of hydrobromic acid. After the solvent had been removed, a bromo iron(III) complex was dried in vacuo and weighed. The insertion ratios were calculated relative to the total amount of porphyrin ligands.

Manganese Insertion. The porphyrin **1** (1.0 g), $MnBr_2 \cdot 4H_2O$ (1.0 g), anhydrous CH_3COONa (0.5 g), and pyridine (10 cm^3) were dissolved in 300 cm^3 of a mixed solvent of 1:3 chloroform–acetic acid under oxygen-free conditions. The resulting solution was stirred for 5 h at 50 °C. When the porphyrin **1a** was used, the manganese insertion was carried out for 5 h at room temperature. The solution was then brought to dryness, and the residue was redissolved in a minimum amount of chloroform. The chloroform solution was poured into the alumina column (Merck alumina 90) prepared as a slurry in chloroform. After loading, the column was eluted by chloroform. The porphyrin free base was eluted, and the desired manganese complex was adsorbed on alumina. Chloroform was passed through the column until the eluate was very pale. Then, a 2:1 chloroform–methanol mixed solvent was added, the desired manganese complex of **1** was removed. The eluate was stirred with 20% hydrobromic acid. After the solvent had been removed by the use of a rotary evaporator, the manganese porphyrin was recrystallized from dichloromethane–hexane; the dark green crystals thus obtained were dried in vacuo. Percentage yields: **1a**–MnBr, 40%; **1c**–MnBr, 18%; **1d**–MnBr, 20%. Found: C, 65.19; H, 6.23; N, 7.97; Br, 5.89. Calcd for $C_{76}H_{88}N_8O_8MnBr \cdot H_2O$: C, 65.46; H, 6.51; N, 8.04; Br, 5.73. UV-vis. (toluene) λ/nm: 376, 490, 588.

Measurement of the Stabilities of the Hydroxy Iron(III) Complexes. The hydroxy iron(III) porphyrins **1a—d**–FeOH were prepared from the corresponding bromo iron(III) complexes. The bromo iron(III) porphyrins **1a—d**–FeBr were treated with aqueous sodium hydroxide. The products (the hydroxy iron complex and the μ-oxo dimer) were purified by the use of an alumina column (Merck alumina 90), using toluene as an eluate, and were identified by spectroscopic methods. The thermal stabilities of the hydroxy iron(III) complexes were measured as follows. Chloroform solutions of **1a—d**–FeOH were refluxed for 8 h, and then the resulting material was analyzed by means of UV-vis. and ^1H NMR spectroscopy.[23] Other porphyrins, $TBPPH_2$ and $TMPPH_2$,[24] were used for comparison.

Oxygenation Reaction. In controlled experiments using iodosylbenzene as an oxidant, the reaction conditions were as follows. In a typical experiment of olefin epoxidation, **1**–FeBr or **1**–MnBr (0.010 mmol) and olefin (1.7 mmol) were dissolved in 5 cm^3 of dichloromethane. Iodosylbenzene (0.3 mmol) was added to this solution, and the resulting mixture was stirred for 3 h in an ice bath. All these operations were carried out under Ar. In the experiments on the hydroxylation of alkane,[25] **1**–FeBr (0.002 mmol), cyclohexane (2 mmol), and iodosylbenzene (0.060 mmol) were employed. The reaction was continued for 3 h at 15—17 °C. In both olefin epoxidation and alkane hydroxylation, the products were analyzed by means of GLC.

When hypochlorite was used as an oxidant, the reaction rates and the yields were also measured for comparison with those of the authentic catalyst, MnTPPBr.[4] All kinetic experiments in the metalloporphyrin–hypochlorite system were controlled, as will be described below.[17] The complex, **1**–FeBr or **1**–MnBr (0.0082 mmol), olefin (7.8 mmol, styrene, α-methylstyrene, cyclohexene, or cyclooctene), the internal standard reagent (*p*-dichlorobenzene or 1,3,5-trichlorobenzene), and the phase-transfer reagent (benzyldimethyltetradecylammonium chloride) were dissolved in 20 cm^3 of dichloromethane. When manganese complexes were used, 1-triphenylmethylimidazole (0.46 mmol) was added to the solution as the N-base ligand. Then, 15 cm^3 of the sodium hypochlorite solution (8.7 mmol) was layered over the organic phase. The epoxidation reaction was initiated by vigorous stirring, and the reaction temperature was maintained at 22 °C during olefin epoxidation. The products were periodically monitored by means of GLC.

Results

In contrast with 5,10,15,20-tetrakis(2-nitrophenyl)-porphyrin, which has hardly shown solubility to any organic solvent,[18] the pophyrin **1** is soluble in common organic solvents. Their iron and manganese complexes of **1** are also well soluble in organic solvents, such as chloroform, benzene, toluene, acetone, alcohol, and *N,N*-dimethylformamide. All the isomers of **1** show identical electronic absorption spectra, but their proton NMR patterns are substantially different from each other (See Table 1).

Atropisomerization. The results of atropisomerization are listed in Table 2. Each isomer is rather stable in refluxing chloroform (61 °C), but is gradually converted to other isomers in refluxing toluene (111 °C). Strong UV irradiation with a mercury lamp for 11 h gives no appreciable amount of other isomers. The time-dependency of the distribution of the isomer which was isomerized from the **1a** isomer to others in refluxing toluene or chloroform is shown in Fig. 5 or 6. The change in the isomer distribution in refluxing toluene has not been observed over 60 h refluxing. The results of this experiment are listed in Table 3.

The Stabilities of Hydroxy Iron(III) Complexes. The treatment of the bromo iron(III) complex of $TMPPH_2$ with sodium hydroxide quantitatively gave the μ-oxo dimer, while that of $TBPPH_2$ afforded a mixture of the hydroxy and μ-oxo compounds, the two species was separated by alumina column chromatography (relative weight of products; hydroxy/μ-oxo=5:1), as is shown in Scheme 2 and Table 4.

The purified hydroxy complex of $TBPPH_2$ was stable in organic solvents at room temperature (ca. 23 °C) for at least 6 d. At higher temperatures, however, the hydroxy complex of $TBPPH_2$ was

Table 1. Proton NMR Data of **1a**—**d**[a)]

Assignment[b)]	**1a**	**1b**	**1c**	**1d**
Internal pyrrole H	−2.97 (s, 2H)	−2.98 (s, 2H)	−2.98 (s, 2H)	−2.99 (s. 2H)
5-*t*-Butyl H	1.45 (s, 36H)	1.43 (s, 9H)	1.47 (s, 36H)	1.52 (s, 36H)
		1.48 (s, 18H)		
		1.52 (s, 9H)		
3-*t*-Butyl H	1.60 (s, 36H)	1.55 (s, 9H)	1.60 (s, 36H)	1.57 (s, 36H)
		1.58 (s, 18H)		
		1.62 (s, 9H)		
Ortho phenyl H	7.93 (d, 4H, J=2.1)	7.81 (m, 1H)	7.97 (d, 4H, J=0.5)	8.23 (d, 4H, J=1.8)
		8.06 (m, 2H)		
		8.17 (m, 1H)		
Para phenyl H	7.99 (d, 4H, J=2.1)	7.99 (m, 4H)	7.99 (d, 4H, J=0.5)	7.99 (d, 4H, J=1.8)
β-Pyrrole H	8.69 (s, 8H)	8.64 (s, 2H)	8.64 (s, 4H)	8.65 (s, 8H)
		8.66 (s, 2H)	8.68 (s, 4H)	
		8.68 (s, 2H)		
		8.69 (s, 2H)		

a) Chemical shifts in ppm relative to TMS, coupling constants J in Hz: solvent $CDCl_3$. b) The assignment of observed proton NMR signals is ably assisted by the use of the nuclear Overhauser method.

Table 2. Thermal and Photo-Induced Atropisomerization

Starting isomer	Solvent	Temp °C	Time h	Conversion ratio[a)] %
1a	Toluene	111	11	90
	Chloroform	61	5	5
	Toluene (hν)[b)]	18	11	5
1b	Toluene	111	11	30
1c	Toluene	111	11	40
	Chloroform	61	5	5
1d	Toluene	111	11	20
	Chloroform	61	11	0
	Toluene (hν)[b)]	18	11	0

a) Original isomer is converted to others. Total percentage represents amount of other isomers converted. b) Photoirradiation with high-pressure mercury lamp (400W, Riko, UVL-400HA).

Table 3. Isomer Distribution of Atropisomerization in Toluene Refluxing

Reflux time h	**1a** %	**1b** %	**1c** %	**1d** %
0	0.4	54.5	33.5	11.6
60	1.5	35.3	17.8	45.4
120	1.6	33.8	17.2	47.5

gradually converted to the μ-oxo dimer. After 8 h heating in toluene (60 °C), the hydroxy complex of $TBPPH_2$ was completely turned into the μ-oxo dimer.

The treatment of bromo iron(III) complexes of **1a**—**d** quantitatively converted them into hydroxy iron(III) complexes. These four hydroxy iron complexes are stable at 60 °C for at least 8 h.

Oxygenation Reaction. The yields of oxygenation reaction using iodosylbenzene are listed in Table 5.

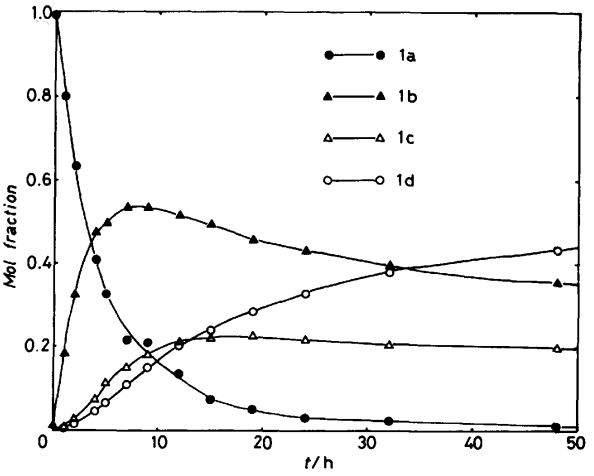

Fig. 5. Time course of isomerization reaction starting from **1a** in refluxing toluene (111 °C).

All the percentage yields are based on the iodosylbenzene consumed. These results show that manganese and iron complexes of the porphyrin **1** are efficient catalyst for both epoxidation and hydroxylation in iodosylbenzene systems.

For obtaining a further understanding of the catalytic activity of **1**–FeBr and **1**–MnBr, we developed olefin epoxidation in hypochlorite systems.

In the estimation of the oxygenation capabilities of the porphyrin catalyst, the oxygenation reaction with hypochlorite was continued until the porphyrins were decomposed by bleaching. The yields in these experiments are represented as "maximum yield in turnovers" in Table 6.[26)]

The kinetic results (the reaction rates and the yields) of controlled experiments in hypochlorite systems are listed in Table 7. The reaction rates are represented by

turnovers/sec, while the yields are represented by turnover numbers. The kinetic results of the epoxidation of olefin using MnTPPBr are also listed in Table 7.

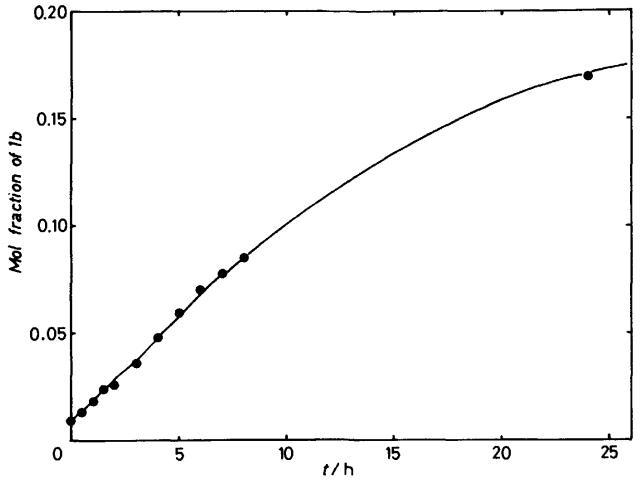

Fig. 6. Time course of isomerization reaction from **1a** to **1b** in refluxing chloroform (61 °C). Other isomers, **1c** and **1d**, were not detected in this experiment.

The epoxides are the main product in all the olefin oxygenation reactions except for the measurements of the "maximum yield in turnovers" using FeTPPCl. When MnTPPBr is used for a control experiment of styrene oxygenation, a notable amount of phenylacetaldehyde (15%) and a small amount of benzaldehyde are also detected. By the use of all the

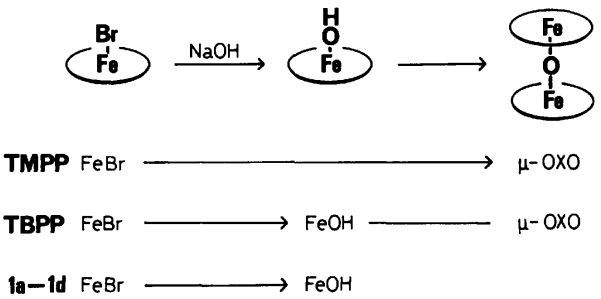

Scheme 2. Interconversion from bromo iron(III) complexes to corresponding hydroxy iron(III) complexes or μ-oxo dimers.

Table 4. Spectroscopic Data of Hydroxy Iron Complexes and μ-Oxo Dimers[a]

Compounds	UV-Vis. (λ/nm)						^{1}H NMR (δ/nm), in benzene-d_6			
							β-pyrrole H	ortho H	t-butyl H[b]	para H
TBPPFe(OH)	336	418	576	617		(Toluene)	81.2		1.8 2.0	
TBPPFe μ-oxo	321	411	576	616	648	(Toluene)	13.9		1.3 1.7	
TMPPFe μ-oxo		410	572	612	648	(Toluene)	13.8	7.2	2.3 2.6	
1a-FeOH	342	419	579			($CHCl_3$)	78.4		1.6 1.9	8.5
1b-FeOH	338	417	579			($CHCl_3$)	82.3		1.7	8.4
1c-FeOH	340	418	576			($CHCl_3$)	79.9		1.7	8.3
1d-FeOH		418	575			($CHCl_3$)	79.5 82.5		1.7	8.1

a) The hydroxy iron complexes and μ-oxo dimers were identified in a way similar to that of Ref. 23. b) In the case of TMPPFe μ-oxo, the chemical shifts of methyl H are listed.

Table 5. Oxygenation Reactions Using Iodosylbenzene

Yield[a] %	Fe salt					Mn salt		
	1a	**1b**	**1c**	**1d**	TPP	**1a**	**1d**	TPP
Cyclohexene								
Cyclohexene oxide	90	89	88	73	44	92	69	31
2-Cyclohexen-1-one	4	4	3	6	7	3	5	12
2-Cyclohexen-1-ol	6	7	9	14	26	5	21	12
Total	100	100	100	93	77	100	95	55
Cyclohexane								
Cyclohexanol	36	27	26	26	Trace	nd[b]	nd	nd
Cyclohexanone	5	6	5	9	Trace	nd	nd	nd
Total	41	33	31	35	Trace	nd	nd	nd
Heptane								
Total[c]	18	18	25	19	0.7	14	7	9

a) The yields are based on the iodosylbenzene consumed. b) Not determined. c) The products are mixtures of the seven oxygenated species.

Table 6. The Maximum Yields in Turnovers[26]

Porphyrin	Styrene	α-Methylstyrene
MnTPPBr	5000	2900
1a-MnBr	23000	95000
1c-MnBr	7300	31000
1d-MnBr	21000	15000
FeTPPCl	300	400
1a-FeBr	4800	2400
1c-FeBr	1600	3500
1d-FeBr	4300	1800

Table 7. The Reaction Rates and Yields. Reaction Rate (yield)

Porphyrin	Styrene	α-Methyl-styrene	Cyclo-hexene	Cyclo-octene
MnTPPBr[a]	3.7(690)	1.6(820)	0.037(50)	0.14(120)
1a-MnBr[a]	2.3(730)	2.6(900)	0.014(310)	0.12(250)
1c-MnBr[a]	0.1(640)	1.2(850)	nd[b]	nd
1d-MnBr[a]	1.2(620)	0.7(840)	0.007(190)	0.05(60)
1a-FeBr	1.3(620)	2.3(790)	0.33 (210)	0.57(290)
1c-FeBr	4.6(860)	3.7(870)	0.48 (570)	0.37(760)
1d-FeBr	1.8(490)	2.5(850)	0.40 (600)	1.1 (850)

a) A 1-triphenylmethylimidazole was added to the solution. b) Not determined.

manganese and iron complexes of **1**, with the exception of **1a**-MnBr, however, the phenylacetaldehyde is not detected during controlled styrene epoxidation.

Discussion

Atropisomerization. The atropisomerization of various ortho-substituted tetraphenylporphyrins has been the subject of several recent studies.[13,14,27,28] For example, when the methanol solution of the $\alpha\alpha\alpha\beta$ isomer of 5,10,15,20-tetrakis(2-hydroxyphenyl)porphyrin was allowed to stand for an hour at 23 °C, the other three isomers began to reappear.[27] On the contrary, each isomer of **1a—d** is stable in refluxing chloroform (61 °C, See Fig. 6 and Table 3). When toluene solution is refluxed for 11 h (111 °C), each isomer of **1a—d** is gradually converted to other isomers. In this experiment, the total conversion ratio from the **1a** isomer is the largest, while that from **1d** is the smallest, among the four isomers (see Table 2). The conversion ratio from **1a** achieves ca. 50% after 3 h refluxing in toluene (111 °C). Hatano et al. investigated the gradual transition of one isomer to the other isomers using 5,10,15-20-tatrakis(2-cyanophenyl)porphyrin **3** at 40—60 °C.[14a] The $\alpha\alpha\alpha\alpha$ isomer of the porphyrin **3** decreased to 50% when the chloroform solution was allowed to stand for 1.5 h at 50 °C[14a] These results clearly show that the porphyrin **1** has a higher conformational stability than 5,10,15,20-tetrakis(2-hydroxyphenyl)porphyrin or the porphyrin **3**.

As a further comparative study, an analogous porphyrin, 5,10,15,20-tetrakis(5-*t*-butyl-3-methyl-2-nitrophenyl)porphyrin **4** (See Fig. 1 and 7), has been prepared by a method similar to that shown in Scheme 1,[15] and its $\alpha\beta\alpha\beta$ isomer has been separated (Fig. 7). Heating in chloroform (61 °C) or photoirradiation in a toluene solution for 11 h results in an easy isomerization of the $\alpha\beta\alpha\beta$ isomer of **4**, with the conversion percentages of 50 and 20 respectively. In the case of the **1d** isomer, the conversion percentage is negligible upon heating in chloroform for 11 h or upon photoirradiation (see Table 2). Although both **1** and **4** are ortho-substituted by nitro groups, the conformational stability of **1** is considerably higher than that of **4**. The conformational stability toward the atropisomerization of the ortho-substituted tetraphenylporphyrins depend on the rotational barrier around the phenyl-porphyrin single bond—in other words, the activation energy to the atropisomerization. The four isomers of **1** apparently have higher activation energies than those of **4**. Judging from the CPK model of the porphyrin **1**, the plane of the nitro group is forced to be almost perpendicular to the phenyl ring by the steric bulk of neighboring *t*-butyl moiety. This steric interaction of *t*-butyl is what is called "the buttressing effect." In contrast, the CPK model of the porphyrin **4** suggests that the steric interaction between the nitro group and the neighboring methyl group is small. Therefore, the nitro group may be supposed to be conjugated with the phenyl ring π system. The planar structure of the

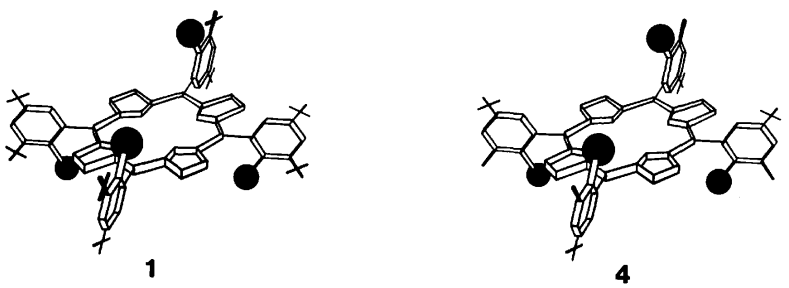

1 **4**

Fig. 7. The porphyrins **1** and **4**.

nitrophenyl group in **4** may cause easy isomerization. The high conformational stability of the porphyrin **1** is given by the strong buttressing effect of the adjacent *t*-butyl group, i.e., by the absence of the conjugation of the nitro group with the phenyl π system.

It has been reported that the four isomers of 5,10,15,20-tetrakis-(2-hydroxyphenyl)porphyrin,[27] 5,-10,15,20-tetrakis(4-*t*-butyl-2-aminophenyl)porphyrin,[21] 5,10,15,20-tetrakis(2-aminophenyl)porphyrin,[14b] and "picket fence" porphyrin[14b] have been equilibrated in a statistical abundance ($\alpha\alpha\alpha\alpha:\alpha\alpha\alpha\beta:\alpha\alpha\beta\beta:\alpha\beta\alpha\beta$= 12.5:50:25:12.5). The isomer distribution of **1a—d** in the equilibrium state ($\alpha\alpha\alpha\alpha:\alpha\alpha\alpha\beta:\alpha\alpha\beta\beta:\alpha\beta\alpha\beta$=1.6: 33.8:17.2:47.5), however, is quite different from that of the statistical abundance. In the equilibrium state, **1d** is the dominant isomer. The amount of the **1a** isomer is much smaller, while the corresponding ratio of **1d** is considerably larger than that of the statistical abundance. In kinetic studies of isomerization, the $\alpha\alpha\alpha\beta$ isomer has been the key compound for the analyses of atropisomerization. Hence, the relative ratios are represented by the amounts of **1a**, **1c**, and **1d** in relation to that of **1b**; the results are listed in Table 8. For the sake of comparison, the relative ratios ($\alpha\alpha\alpha\alpha/\alpha\alpha\alpha\beta$, $\alpha\alpha\beta\beta/\alpha\alpha\alpha\beta$, $\alpha\beta\alpha\beta/\alpha\alpha\alpha\beta$) of the porphyrin **3** and the statistical abundance are also listed in Table 8. These results clearly show that the relative ratios toward **1b** ($\alpha\alpha\alpha\beta$) of the porphyrin **1** or **3** are rather different from those of the statistical abundance and that **1** and **3** porphyrins have similar tendencies. These findings on the isomer distribution in the porphyrin **1** indicate that the thermal stability of the porphyrin **1d** is higher than that of **1b**, while that of **1a** is lower than that of **1b**. In the course of the isomerization, the **1a** isomer is immediately changed into the other three isomers. After 3 h refluxing in toluene (111 °C), the conversion ratio from **1a** is achieved at ca. 50%. The relative ratio of **1d** has been constantly growing during refluxing (see Fig. 5). These results of the time-course experiment also show that the thermal stability of **1d** is higher than those of the other isomers, while that of **1a** is extremely low among the four isomers. The variation in the stabilities of **1a—d** is explained by an electrostatic repulsive model. In the porphyrin **1a—d**, the interactions between the two nitro groups projecting from the diagonal phenyl rings are supposed to be negligible. On the contrary, the two nitro groups projecting to the same side of the porphyrin plane from the adjacent phenyl rings may have large repulsive interactions. The **1a**, **1b**, **1c**, and **1d** isomers have four, two two, and no pairs of such large repulsive interactions respectively. Because of these repulsive interactions, the **1a** isomer has the lowest conformational stability. On the other hand, the **1d** isomer has the highest conformational stability because of the absence of the repulsion between nitro groups.

As has been mentioned above, ortho-substitution by nitro groups with the *t*-butyl moiety at the adjacent position seems to have a great influence on the comformational stability or on the isomer distribution of atropisomerization. At any rate, the extremely high conformational stability toward the isomerization of the porphyrin **1** pushed us to further investigations of the relationship between the shape of the porphyrin and its capability as oxygenation catalyst.

Iron Insertion and Stabilities of Hydroxy Iron(III) Complexes. The insertion ratio of each isomer of **1** in controlled experiments is listed in Table 9. In controlled experiments at 30 °C, the yield of **1a** is rather higher than that of the other three isomers. Therefore, the metal incorporation of **1a** need not maintain a high temperature for a long time. Although the yields of the other three isomers **1b—d** are very low at 30 °C, the metal insertion of these isomers can be carried out at high temperatures. After all, each isomer of the porphyrin **1a—d** is converted to the corresponding iron(III) complex, with a retention of the ligand conformation.

In recent years, several research groups have reported the formation of stable hydroxy iron(III) complexes by the use of such protected porphyrins as 5,10,15,20-tetrakis(2,4,6-trimethoxyphenyl)porphyrin or 5,10,15,20-tetramesitylporphyrin.[23,27,31] Iron(III) complexes of our protected porphyrins **1a—d** have also formed stable hydroxy iron(III) complexes. By contrast, simple unprotected porphyrins, e.g., 5,10,15,20-tetraphenylporphyrin or 2,3,7,8,12,13,17,18-octaethylporphyrin, from the hydroxy iron species in

Table 8. Relative Ratios in the Equilibrium State

Porphyrin	$\frac{\alpha\alpha\alpha\alpha}{\alpha\alpha\alpha\beta}$	$\frac{\alpha\alpha\beta\beta}{\alpha\alpha\alpha\beta}$	$\frac{\alpha\beta\alpha\beta}{\alpha\alpha\alpha\beta}$
1	0.05	0.51	1.41
3	0.06	0.69	1.11
Statistical abundance	0.25	0.50	0.25

Table 9. The Metal-Insertion Ratios in Controlled Experiments

Porphyrin	Ratio[a] / %
1a	60
1b	Trace
1c	Trace
1d	Trace
$TMPPH_2$	80
$TBPPH_2$	60

a) The ratios are based on the porphyrin free base used.

solution; however, these are serious difficulties with the isolation of the species as stable compounds.[32]

The thermal stability of the hydroxy iron(III) complex against transformation into the μ-oxo dimer is supposed to be influenced by the protection of the porphyrin plane. Our results show that the steric bulk of $TBPPH_2$ is just enough for the stabilization of the hydroxy iron(III) species at room temperature, while that of $TMPPH_2$ is insufficient. Furthermore it is certain that ortho substituted nitro groups of **1a—d**, which give rise to great restrictions on the rotation about porphyrin-phenyl single bonds, afford additional thermal stability to the hydroxy iron(III) complexes of **1a—d**.

Oxygenation Reaction. In cyclohexene epoxidation by iodosylbenzene, **1**-FeBr, and **1**-MnBr, but not **1d**-FeBr and **1d**-MnBr, completely consumed the iodosylbenzene (see Table 5). The **1**-FeBr complex sufficiently catalyzed the hydroxylation of alkanes in comparison with FeTPPCl, which generated only a trace amount of the oxygenation products (see Table 5). Groves et al. investigated the influence of the ortho-position substitution of phenyl groups using FeTPPCl and FeTTPCl (TTP=5,10,15,20-tetrakis(2-tolyl)porphyrin)iodosylbenzene system.[33,34] In cyclohexene epoxidation, the total yield and the selectivity for epoxide production of the FeTTPCl catalyst (cyclohexene oxide 67%; 2-cyclohexen-1-ol 15%) were slightly higher than those of the FeTPPCl catalyst (cyclohexene oxide 55%, 2-cyclohexen-1-ol 15%).[33] In the experiment on cyclohexane hydroxylation, the total yields of the FeTTPCl system (cyclohexanol 22%, cyclohexanone 2.4%) were considerably higher than those of the FeTPPCl system (cyclohexanol 7.6%, cyclohexanone 0.5%).[34] These results show that ortho-substitution by the methyl group give rise to high yields in both epoxidation and hydroxylation reactions. The selectivity for epoxide production in cyclohexene oxygenation was also enhanced in the FeTTPCl system. In our **1**-FeBr system, these tendencies are extremely remarkable (see Table 9). Our results indicate that the ortho-substitution of the phenyl moiety by the nitro group is effective and better than the ortho-substitution by the methyl group. Although the yields based on the porphyrin catalyst in these experiments are very small (within 30 turnovers), these results clearly show that the iron and manganese complexes of **1** have quite high catalytic activities compared with FeTPP or MnTPP in metalloporphyrin-iodosylbenzene systems.

The hypochlorite is a cheap, convenient oxygen source for olefin-epoxidation reactions; hence, the manganese porphyrin-hypochlorite systems have been well established for olefin-epoxidation reactions.[7-9] We recently reported a successful olefin epoxidation in iron porphyrin-hypochlorite systems.[17] In order to gain a better understanding of catalysis by our protected metalloporphyrin **1**, the maximum yields in turnovers, the reaction retes, and the yields of the olefin-epoxidation reactions were measured by the use of hypochlorite as an oxidant. The maximum yields in tunovers of manganese complexes of **1a—d** are considerably larger than those of MnTPP, while those of the iron complexes **1**-FeBr are comparable to those of MnTPP (see Table 6). In styrene are α-methylstyrene epoxidation, the reaction rates and the yields of **1**-FeBr or **1**-MnBr are almost the same as those of MnTPP (see Table 7). In cyclohexene and cyclooctene epoxidation, however, the reaction rates and the yields by the use of **1**-FeBr are higher than those of MnTPP and the respective manganese complexes of **1a** and **1d**. These results clearly show that the manganese and iron complexes of the protected porphyrin **1** are useful catalysts for the epoxidation using hypochlorine. In all cases of styrene epoxidation catalyzed by **1**-FeBr or **1**-MnBr except for that catalyzed by **1a**-MnBr, a phenylacetaldehyde is not produced. Thus, the catalytic system of the protected porphyrin **1** has a high selectivity for the epoxide production in styrene oxygenation reactions.

The reaction rates are slightly different among the three isomers (see Table 7). When manganese complexes are used for olefin epoxidation, the orders of the reaction rates in controlled measurements are **1a**>**1d**>**1c** (in styrene epoxidation), **1a**>**1c**>**1d** (in α-methylstyrene epoxidation), and **1a**>**1d** (in cyclohexene and cyclooctene epoxidation). In each reaction, the reaction rates of the **1a** isomer (**1a**-MnBr) are the highest among the isomers. As for the controlled experiments using iron complexes, the orders of the reaction rates are **1c**>**1d**>**1a** (in styrene, α-methylstyrene, and cyclohexene epoxidation) and **1d**>**1a**>**1c** (in cyclooctene epoxidation). When manganese complexes are used, the reaction rates of **1a** are always higher than those of **1d**. When iron complexes are used, however, the reaction rates of **1a** are always lower than those of **1d**. These results indicate that the shape of the porphyrin catalyst might influence the reaction rates in olefin epoxidation, and that the mechanism of olefin epoxidation may be different between manganese and iron complexes.

These kinetic results can be explained by our speculative mechanisms as follows. The isomer **1d** is symmetrical and has two topological identical faces ("half-crowded sites" in Fig. 8). On the contrary, the steric environments of the upper and lower sides of the isomer **1a** are quite different. The porphyrin **1a** has a steric bulk on one side of the porphyrin plane formed by four nitro groups ("crowded site" in Fig. 8), yet leaves the other side comparatively unemcumbered ("open site" in Fig. 8). In the MnBr or FeBr complexes of **1a**, Br is expected to ligate on the "open site" (see Scheme 3-(1)).[35] Employing a N-base such

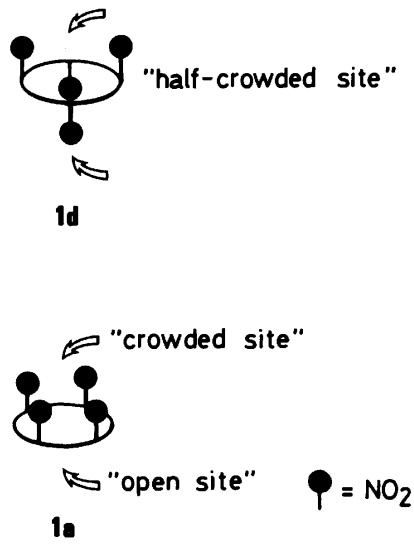

Fig. 8. The reaction site of **1a** and **1d**.

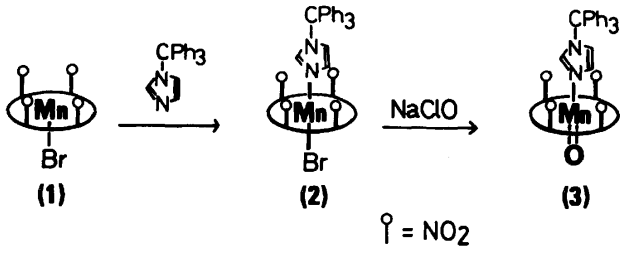

Scheme 3. The speculative oxygenation mechanism of **1a**-MnBr system.

as 1-triphenylmethylimidazole with **1a**-MnBr probably allows the coordination of the N-base on the "crowded site" (see Scheme 3-(2)). The high-valent manganese oxo complex which is illustrated in Scheme 3-(3) may be produced by hypochlorite, and it seems that the oxygenation reaction is carried out on the "open site" in **1a**-MnBr with the N-base system. The oxygenation reaction of **1d**-MnBr and the N-base, however, is done on the "half-crowded site." The analysis of products in styrene oxygenation provides similar information about the reaction site of **1a**-MnBr with the N-base. The ratios of the products in styrene oxygenation are shown in Table 10. In the experiments using **1c**-MnBr and **1d**-MnBr, which oxygenated the olefin on the "half-crowded site," a phenylacetaldehyde cannot be detected. A notable amount of phenylacetaldehyde was, however, produced in the MnTPPBr (15%), MnTBPPBr (11%), and **1a**-MnBr (11%) systems. These results indicated that the reaction site of **1a**-MnBr with the N-base may be the "open site," which is a steric environment similar to that of the reaction site of MnTBPPBr with the N-base. The electronic factors do not influence the rates of oxygenation. In fact, the manganese complexes of **1a**—**d** have similar electronic structures, judging from their identical UV-vis spectra. The reaction rates of the oxygenation reaction using **1**-MnBr and the N-base are only influenced by the steric environments of the reaction site. The epoxidation reaction on an "oprn site" seems to be more reactive than the reaction on a "crowded site" or on a "half-crowded site." Therefore, the reaction rates of **1a**-MnBr with N-base are always higher than those of **1d**-MnBr with the N-base.

When iron complexes of **1a** are used in the absence of the N-base,[36] the reaction mechanism of epoxidation is different from that of the manganese complex of **1a**. In the **1a**-MnBr and N-base system, the axial ligand Br is ligated on the same side ("open site") in the resting state because the "crowded site" is occupied by the N-base. On the contrary, the axial ligand displacement by X (Br^- or other anion in a water solution) may occur on both sides of the porphyrin plane during the oxygenation-reaction cycles in the **1a**-FeBr system.[37] Because of the easy dissociation and scrumbling of the axial ligand, the oxygenation reaction of **1a**-FeBr may take place on both an "open site" and a "crowded site," the average reaction rate of **1a**-FeBr is deduced comparison with the case in which the oxygenation is performed only on an "open site." Accordingly, the reaction rates of **1a**-FeBr are lower than those of **1d**-FeBr whose reaction site is "half-crowded site."

When iron complexes of **1** are used in styrene oxygenation, no phenylacetaldehyde could be detected in any isomer system (see Table 10). In the absence of the N-base, styrene oxygenation catalyzed by **1a**-MnBr or MnTBPPBr afforded no phenylacetaldehyde. These results indicated that phenylacetaldehyde production is affected not only by the reaction site ("open site" or "crowded site"),[38] but also by the N-base. Taking all these findings together, we proposed the speculative mechanism shown in Scheme 3.

At the present stage, we cannot explain completely

Table 10. The Ratios of Products in the Styrene Oxygenation

Catalyst	Styrene oxide	Phenyl-acetaldehyde	Benzal-dehyde
MnTPPBr+N-base[a]	84	15	1
MnTBPPBr+N-base	87	11	2
1a-MnBr+N-base	88	11	1
1c-MnBr+N-base	96	0	4
1d-MnBr+N-base	99	0	1
MnTBPPBr	95	0	5
1a-MnBr	100	0	0
1a-FeBr	99	0	1
1c-FeBr	99	0	1
1d-FeBr	97	0	3

a) N-base = 1-triphenylmethylimidazole.

the relationship between the reaction rates of oxygenation and the shape of the porphyrin catalysts. Spectroscopic measurements were not useful for the specification of the chemical species in each step; further efforts to get kinetic information still continue in our laboratory. However, it has been proved that our protected porphyrins, **1**–FeBr and **1**–MnBr, show sufficient catalytic activity against olefin epoxidation and alkane hydroxylation.

This work was supported in part by a Grant-in-Aid for Scientific Research (No. 61470041) from the Ministry of Education, Science and Culture.

References

1) P. G. Wislocki, G. W. Miwa, and A. Y. H. Hu, "Enzymatic Basis of Detoxication," ed by W. B. Jokoby, Academic Press, New York (1980), Vol. 1, p. 136.

2) R. E. White and M. J. Coon, *Am. Rev. Biochem.*, **49**, 315 (1980).

3) J. T. Groves, T. E. Nemo, and R. S. Meyers, *J. Am. Chem. Soc.*, **101**, 1032 (1979).

4) J. P. Collman, T. Kodadek, S. A. Raybuck, J. I. Brauman, and L. M. Papazian, *J. Am. Chem. Soc.*, **107**, 5537 (1985).

5) T. G. Traylor, J. C. Marsters, Jr., T. Nakano, and B. F. Dunlap, *J. Am. Chem. Soc.*, **107**, 4343 (1985).

6) C. K. Chang and F. Ebina, *J. Chem. Soc., Chem. Commun.*, **1981**, 778.

7) E. Guilmet and B. Meunier, *Nouv. J. Chim.*, **6**, 511 (1982).

8) J. P. Collamn, J. I. Brauman, B. Meunier, T. Hayashi, T. Kodadek, and S. A. Raybuck, *J. Am. Chem. Soc.*, **107**, 2000 (1985).

9) S. Takagi, T. K. Miyamoto, and Y. Sasaki, *Bull. Chem. Soc. Jpn.*, **59**, 2371 (1986).

10) I. Tabushi and N. Koga, *J. Am. Chem. Soc.*, **101**, 6456 (1979).

11) T. Santa, N. Miyata, and M. Hirobe, *Chem. Pharm. Bull.*, **32**, 1252 (1984).

12) J. T. Groves and R. S. Meyers, *J. Am. Chem. Soc*, **105**, 5791 (1983).

13) J. P. Collman, R. R. Gagne, T. R. Halbert, J. C. Marchon, and C. A. Reed, *J. Am. Chem. Soc.*, **95**, 7868 (1973).

14) a) K. Hatano, K. Anzai, T. Kubo, and S. Tamai, *Bull. Chem. Soc. Jpn.*, **54**, 3518 (1981); b) K. Hatano, K. Anzai, A. Nishino, and K. Fujii, *Bull. Chem. Soc. Jpn.*, **58**, 3653 (1985).

15) T. K. Miyamoto, T. Hasegawa, S. Takagi, and Y. Sasaki, *Chem. Lett.*, **1983**, 1181.

16) T. K. Miyamoto, S. Tsuzuki, T. Hasegawa, and Y. Sasaki, *Chem. Lett.*, **1983**, 1587.

17) S. Takagi, E. Takahashi, T. K. Miyamoto, and Y. Sasaki, *Chem. Lett.*, **1986**, 1275.

18) T. N. Sorrell, *Inorg. Synth.*, **20**, 161 (1980).

19) M=mol dm^{-3}.

20) a) J. Lindsey, *J. Org. Chem.*, **45**, 5215 (1980); b) C. M. Elliott, *Anal. Chem.*, **52**, 666 (1980).

21) S. Takagi, T. K. Miyamoto, and Y. Sasaki, *Bull. Chem. Soc. Jpn.*, **58**, 447 (1985).

22) The solubility of the $\alpha\alpha\beta\beta$ isomer against the toluene is rather lower than that of the $\alpha\beta\alpha\beta$ isomer.

23) R. J. Chang, L. L. Grazynski, and A. L. Balch, *Inorg. Chem.*, **21**, 2412 (1982).

24) $TBPPH_2$=5,10,15,20-tetrakis(3,5-di-*t*-butylphenyl)porphyrin; $TMPPH_2$=5,10,15,20-tetrakis(3,5-dimethylphenyl)-porphyrin. The porphyrin free bases, $TBPPH_2$ and $TMPPH_2$, were prepared by the condensation of the corresponding substituted benzaldehyde with pyrrole.

25) In heptane epoxidation, the experiment was carried out as follows: The porphyrin (0.010 mmol) and the heptane (6.8 mmol) were dissolved in 4 cm^3 of CH_2Cl_2. Then, 0.30 mmol of iodosylbenzene was added, and the reaction was performed for 3 h in an ice bath.

26) In a typical experiment, **1a**–MnBr (0.0019 mmol), 1-triphenylmethylimidazole (0.19 mmol), a phase-transfer reagent, and an internal standard reagent (*p*-dichlorobenzene) were dissolved in 40 cm^3 of CH_2Cl_2. Then, 30 cm^3 of α-methylstyrene (230 mmol) and 160 cm^3 of the sodium hypochlorite solution (280 mmol) were added. The resulting two-phase mixture was stirred for 1 d at room temperature. The products (α-methylstyrene oxide and 2-phenylpropionaldehyde) were analyzed by GLC. The total yield of the products, based on the porphyrin catalyst, is represented as the "maximum yield in turnovers."

27) L. K. Gottwald and E. F. Ullman, *Tetrahedron Lett.*, **36**, 3071 (1969).

28)F. A. Walker and G. L. Avery, *Tetrahedron Lett.*, **52**, 4949 (1971).

29) J. T. Groves, R. C. Haushalter, M. Nakamura, T. E. Nemo, and B. J. Evans, *J. Am. Chem. Soc.*, **103**, 2884 (1981).

30) M. J. Gunter, L. N. Manger, and K. S. Murray, *J. Chem. Soc., Chem. Commun.*, **1981**, 799.

31) J. M. Cense and R. M. Lequan, *Tetrahedron Lett.*, **39**, 3725 (1979).

32) a) D. Lexa, M. Momenteau, J. M. Saveant, and F. Xu, *Inorg. Chem.*, **24**, 122 (1985), and the references cited therein. b) L. Fielding, G. R. Eaton, and S. S. Eaton, *Inorg. Chem.*, **24**, 2309 (1985). They reported mechanism of the conversion of iron(III) tetratolylporphyrin hydroxide to the corresponding μ-oxo dimer.

33) J. T. Groves and T. E. Nemo, *J. Am. Chem. Soc.*, **105**, 5786 (1983).

34) J. T. Groves and T. E. Nemo, *J. Am. Chem. Soc.*, **105**, 6243 (1983).

35) M. Sabat and J. A. Ibers, *J. Am. Chem. Soc.*, **104**, 3715 (1982).

36) Employing a N-base with iron complexes of **1** allowed bis-ligated complexes to form. Thus, the oxygenation reaction using **1**–FeBr and N-base was quite slow.

37) M. J. Gunter, G. M. McLaughlin, K. J. Bery, K. S. Murray, M. Irving, and P. E. Clark, *Inorg. Chem.*, **23**, 283 (1984).

38) J. P. Collman, T. Kodadek, and J. I. Brauman, *J. Am. Chem. Soc.*, **108**, 2588 (1986).

The Catalytic Electroreduction of Oxygen in an Aqueous Solution on Glassy Carbon Electrodes Covalently Modified with [5,10,15,20-Tetrakis(4-carboxyphenyl)porphinato]iron(III)

Fumihiro ARIFUKU,* Keizo IWATANI, Kikujiro UJIMOTO, and Hirondo KURIHARA
Department of Chemistry, Faculty of Science, Fukuoka University,
Nanakuma, Jonan-ku, Fukuoka 814-01
(Received April 16, 1986)

The catalytic electroreduction of an oxygen molecule on a glassy carbon electrode covalently modified with [5,10,15,20-tetrakis(4-carboxyphenyl)porphinato]iron(III) (abbreviated as GC-O-Fe(III)TCPP) was investigated in an aqueous solution. The reduction of oxygen on the GC-O-Fe(III)TCPP electrode occurs at a more anodic potential than on the glassy carbon electrode adsorbing Fe(III)TCPP. This anodic shift of the oxygen reduction potential may be closely related to the number of bonds between a metalloporphyrin molecule and the electrode material. The oxygen molecule is reduced via the one-step reduction accompanying four-electron and four-proton transfer at pH 7—11 and via two successive reductions accompanying two-electron transfer and subsequently two-electron and four-proton transfer at pH>11.5. At pH<6, the number of transferred electron could not be reproducibly determined because of the cleavage of several ester linkages.

A number of studies of the application of transition metal complexes with such macrocyclic compounds as porphyrins and phthalocyanines to the electrocatalytic reduction of molecular oxygen have been reported.[1,2] Recently, Kobayashi and Osa reported a study of the catalytic electroreduction of molecular oxygen using 5,10,15,20-tetrakis(4-carboxyphenyl)porphinato iron in aqueous solutions.[3] In their study, molecular oxygen was reduced on either a polished solid electrode in a metalloporphyrin complex solution or a metalloporphyrin-adsorbed electrode in a supporting electrolyte solution. They suggested the mechanism of the catalytic reduction to be an electrochemical (EC) catalytic regeneration.

We have been interested in preparing covalently modified electrodes with iron porphyrin complexes and studying the electrochemical behavior of the modified electrodes.[4] Although solid electrodes have previously been modified by fixing porphyrins through amide[5-9] or ester[4,10] linkage, the reduction of oxygen using these modified electrodes has been rarely studied.[11]

In the present paper, we will report on an electrochemical study of catalytic oxygen reduction on glassy carbon electrodes covalently modified with [5,10,15,20-tetrakis(4-carboxyphenyl)porphinato]iron(III) (represented by Fe(III)TCPP) and will report our finding that the oxygen reduction proceeds with an EC mechanism which changes with the pH-range.

Experimental

Materials. The Fe(III)TCPP was prepared by the metal insertion of 5,10,15,20-tetrakis(4-carboxyphenyl)porphine (Porphyrin Products Inc.) with $FeCl_2$.[12] The purification of Fe(III)TCPP was carried out several times by adding an HCl solution to the crude Fe(III)TCPP alkaline solution until the pH became ca. 5. The precipitated product was dried over phosphorus pentoxide at a reduced pressure for 20 h and identified by means of elemental analysis. Found: C, 65.88; H, 3.46; N, 6.55%. Calcd for Fe(III)TCPP(H_2O)-(OH): C, 65.54; H, 3.55; N, 6.37%.

The water-soluble carbodiimide hydrochloride (WSCD·HCl, 1-ethyl-3-(3-dimethylaminopropyl)carbodiimide hydrochloride) used for dehydration was obtained from the Peptide Institute, Inc. (Osaka). All the other chemicals of a guaranteed reagent grade (Wako Pure Chemical Industries) were used without further purification.

Modification of Glassy Carbon Electrodes. A glassy carbon rod (GC-30, 5.4 mmϕ, Tokai Carbon, Ltd.) was inserted into a Teflon tube to give an exposed disc of area of ca. 0.23 cm^2; this rod then served as a working electrode. The mechanical and chemical treatments in the preparation procedure of each modified electrode are shown in Scheme 1. The numbers, (1) to (6), in Scheme 1 represent the following treatment steps, (1) *Mechanical polishing*: The exposed disc surface of the GC-30 electrode was polished with abrasive paper, followed by suspensions of alumina powders (Marumoto, Ltd.) of decreasing size, down to 0.06 μm, until a mirror-like finish was obtained. (2) *Oxidation*: The polished electrodes were immersed in a 0.4 mol dm^{-3}

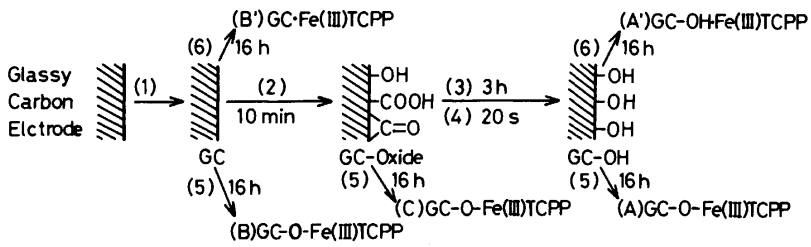

Scheme 1. Modification procedures of GC electrode.

$Na_2Cr_2O_7$ acidic (H_2SO_4) solution and then refluxed at ca. 100 °C. (3) *Reduction*: The oxidized electrodes were immersed in a refluxed 0.1 mol dm^{-3} $LiAlH_4$ diethyl ether solution. (4) *Cleaning*: The $Al(OH)_3$ precipitated on the surface during the (3) treatment was removed by ultrasonic cleaning in a 0.05 mol dm^{-3} H_2SO_4 solution. (5) *Dehydration condensation*: Fe(III)TCPP was linked to the electrode surface covered with a hydroxyl group by dehydration condensation in dichloromethane saturated with Fe(III)TCPP and WSCD·HCl. (6) *Adsorption*: Fe(III)TCPP was adsorbed on the electrodes by immersing the elerctrodes for 16 h in dichloromethane saturated with Fe(III)TCPP.

Each time of treatment is also presented in Scheme 1. The electrodes prepared are identified by abbreviations, such as GC-OH or (A)GC-O-Fe(III)TCPP.

Electrochemical Measurements. The cyclic voltammetric measurement was performed using a Nikko Keisoku NPGFZ-2501-A potentiogalvanostat. For rotating disc voltammetry, a Nikko Keisoku DPGS-1 potentiogalvanostat, an NPS-2 potential sweeper, an RRDE-1 rotator, and an SC-5 speed controller were also used.

In the oxygen-free experiment, the solutions were deaerated by passing nitrogen gas through them for 20 min prior to the electrochemical measurement and by then keeping them blanketed during the measurement, though the reduction experiments of oxygen were carried out in air-saturated solutions. The potentials were referred to a saturated calomel electrode (SCE).

The buffer solutions, which also served as supporting electrolytes, were prepared from acetate, phosphate, borate, and carbonate. The adjustment of the pH was done using H_2SO_4 and/or NaOH, and the ionic strength was adjusted at 0.1 mol dm^{-3} with Na_2SO_4. The pH values were measured with a Toa-5B pH meter. All the measurements were performed at 25 °C.

Results and Discussion

The cyclic voltammetric current-potential (I-E) curves obtained on the (A)GC-O-Fe(III)TCPP and (B)GC-O-Fe(III)TCPP electrodes in oxygen-free electrolytic solutions at pH 7 are shown in Fig. 1. The hatched area for each curve corresponds to the charges consumed during the reduction of modified Fe(III)-TCPP to Fe(II)TCPP. The close potentials of the cathodic and anodic peaks indicate that the corresponding redox process is a surface one.[13,14] The peak current values were so small that we can not examine the dependence of the peak current on the potential sweep rate. In spite of the large difference in residual currents observed on the (A) and (B) electrodes, the same amount of attached Fe(III)TCPP was determined by integrating the cathodic peak current of the wave. The details of these results will be discussed below (see Table 1).

Figure 2 shows the reduction waves of oxygen

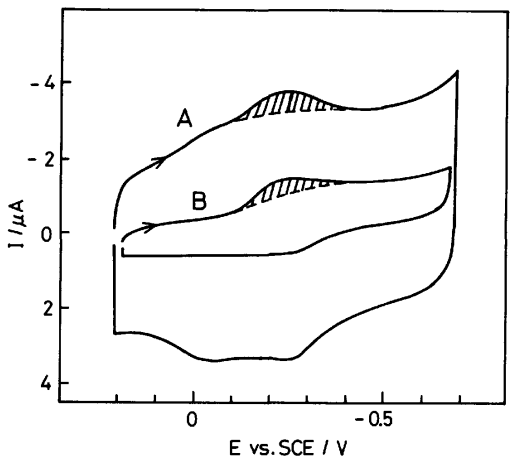

Fig. 1. Cyclic voltammetric I-E curves on the Fe(III)TCPP modified electrodes (A) and (B) obtained in pH 7 solutions in the absence of O_2. Scan rate=0.05 V s^{-1}.

Table 1. The Peak Potential of Oxygen Reduction and the Surface Concentration of Fe(III)TCPP Attached to the Electrodes

Electrode	E_p/V	10^6[Quantity of electricity]/C	10^{11}[Surface concentration]/mol cm^{-2}
A	−0.207	1.30	5.9
B	−0.286	1.60	7.2
C	−0.270	0.60	2.7
A′	−0.300	—	—
B′	−0.350	—	—

Scan rate: 0.05 V s^{-1}.

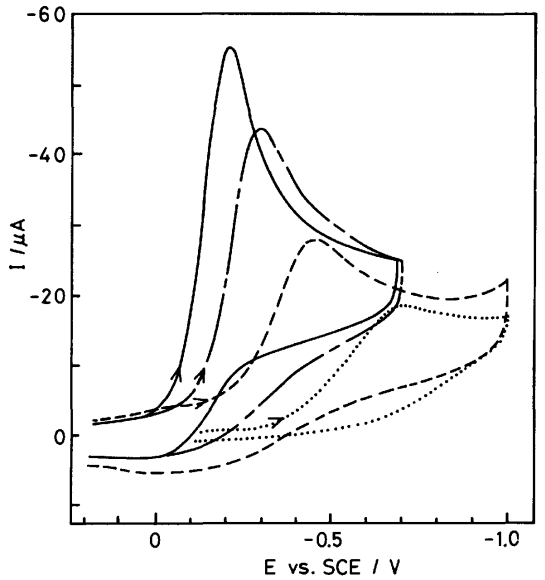

Fig. 2. Cyclic voltammograms for the reduction of O_2 on a glassy carbon and the chemically modified glassy carbon electrodes in the air saturated electrolyte solutions of pH 7. —— (A)GC-O-Fe(III)TCPP, —·— (A′)GC-OH·Fe(III)TCPP, ------ GC-OH, and ····· GC. Scan rates: 0.05 V s^{-1}.

observed on the four kinds of electrodes in air-saturated electrolytic solutions at pH 7. The anodic shift of the peak potential attributable to the Fe(III)TCPP modification is considerably greater on the (A)GC-O-Fe(III)TCPP electrode than on the (A')GC-OH·Fe(III)TCPP-adsorbed electrode (see also Fig. 3).

The peak potentials of oxygen reduction in aqueous solutions of pH 7 and the quantities of Fe(III)TCPP molecules on the modified electrodes (A, B, and C), obtained from the quantity of the charge in the reduction of Fe(III)TCPP, are listed in Table 1, together with the values on the Fe(III)TCPP-adsorbed electrodes. In order to exclude the reduction current attributable to the residual oxygen in the solution, the peak potentials were measured after consecutive scans, in which no variation in the current had been observed. The amounts of Fe(III)TCPP covalently attached to the (A) and (B) electrodes were almost the same, while the amount attached on the (C) electrode was about a half of that value. On the lst scan in the cyclic voltammogram, the (C) electrode gave almost the same area of the reduction peak as those of the (A) and (B) electrodes. In the case of the (C) electrode, however, the consecutive scans caused an abrupt decrease in the area of the reduction peak with a slight decrease in the residual current. This observation suggests that the Fe(III)TCPP attached on the GC-Oxide partially peeled off during the consecutive potential scans.

The amounts of the hydroxyl group on the (A) and (B) electrodes, which was calculated from the quantity of the charge in the reduction of the 3,5-dinitrobenzoyl chloride covalently attached to the OH group of the GC and GC-OH electrodes,[4,15,16] were 1.9×10^{14} and 0.53×10^{14} molecules respectively. In spite of the large difference (ca. 4 times) in the amount of hydroxyl group on the surfaces, the amount of Fe(III)TCPP on the (A) electrode was nearly equal to that on the (B) electrode. This indicates that a large portion of the hydroxyl groups introduced on the (A) electrode is covered with the attached large molecule of Fe(III)-TCPP and is not utilized effectively for the modification. This interpretation is supported by the fact that the redox peak couple at −0.05 V, probably attributable to groups introduced by the oxidation, observed on the (A) electrode was not noticeable on the (B) electrode, as is shown in Fig. 1.[4]

Table 1 shows that the reduction of oxygen on the covalently attached (A)GC-O-Fe(III)TCPP electrode occurs at the most anodic potential among the series of Fe(III)TCPP modified GC electrodes: The peak potential of oxygen reduction on the (A) electrode shifted ca. 80, 90, and 140 mV toward the positive direction compared to those on the (B), (A'), and (B') electrodes respectively.

Figure 3 shows the peak potential of oxygen reduction on the (A)GC-O-Fe(III)TCPP electrode as a function of the condensation time with WSCD·HCl. The complete potential shift, ca. 100 mV, is obtained within 10 min of the condensation. Because of the previously mentioned existence of the excess hydroxyl group on the (A)GC-O-Fe(III)TCPP electrode, all the four carboxyl groups of Fe(III)TCPP may link with the electrode. A preliminary experiment on the modified GC electrode with hemin, which has two carboxyl groups, showed an anodic potential shift of ca. 30—40 mV for oxygen reduction. A similar anodic shift upon the oxygen reduction was reported by Kobayashi et at.[11] on the electrode modified with the metalloporphyrin through amide linkages. Consequently, it can be speculated that this anodic shift of

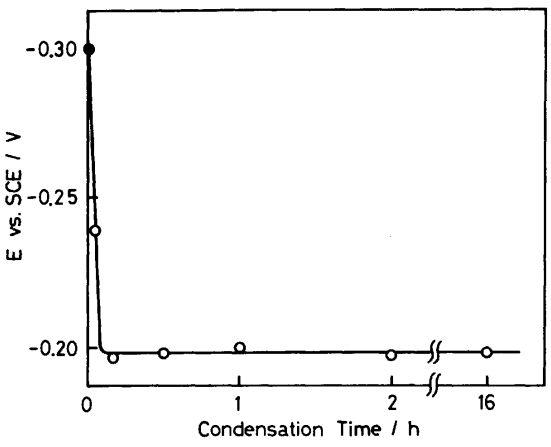

Fig. 3. Plots of the peak potential of oxygen reduction vs. condensation time. ○: (A)GC-O-Fe(III)TCPP, ●: (A')GC-OH·Fe(III)TCPP.

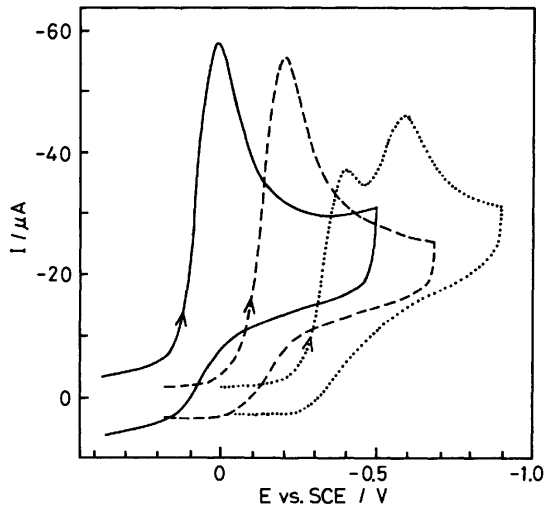

Fig. 4. Cyclic voltammograms for oxygen reduction on the (A)GC-O-Fe(III)TCPP electrode in the air saturated electrolyte solution of pH 1.3 (——), 7.0 (-----), and 12.4 (·····).

the oxygen-reduction potential on the covalently modified electrodes is closely related to the number of bonds between a metalloporphyrin and an electrode material. The more cathodic potential of oxygen reduction on the (B) electrode compared to that on the (A) electrode is probably attributable to the smaller number of covalent bonds per metalloporphyrin molecule on the electrode.

Figure 4 shows some typical cyclic voltammograms obtained on the (A)GC-O-Fe(III)TCPP electrode in air-saturated aqueous solutions of various pHs. The peak potential of oxygen reduction is shifted cathodically with an increase in the pH of the solution. In a high-pH solution, a discrete and successive two-step reduction was observed. The dependence of the peak potential on the pH of the solutions is represented in Fig. 5. Three different potential shifts per unit of pH were observed according as the pH range was pH<5, pH 6—11, or pH>11. The peak-potential shifts with slopes of ca. −55 mV/pH at pH 6—11; that is, the reduction of the oxygen molecule is accompanied by the addition of one electron per one-proton addtition. At pH>11, two successive reduction waves are observed. They shift with slopes of 0 mV/pH and ca. −110 mV/pH; that is, one oxygen molecule is reduced by the electron addition followed by a one-electron addition per two-proton addition. At pH<5, on the other hand, the slope of the peak potential shift is reduced with a decrease in the pH.

In Fig. 5, the dashed line represents the data for oxygen reduction on the GC-20 electrode in Fe(III)-TCPP aqueous solutions, while the open triangle is the peak potential on the Fe(III)TCPP-adsorbed GC-20 electrode in the porphyrin-free solution, as reported by Kobayashi and Osa.[3] Though the peak potential on the adsorbed electrode is almost the same as on the naked electrode in the porphyrin solution, the oxygen reduction potential on our covalently modified electrode shifts anodically by ca. 175 mV in the range of pH 6—11.

In order to estimate the number of transferred electrons in the oxygen reduction, current-potential curves were obtained using an (A)GC-O-Fe(III)TCPP rotating electrode. Figure 6 shows some typical current-potential curves obtained in air-saturated solutions at the pHs corresponding to the ranges in Fig. 5. Because of the lower stability of the modified electrodes at low pHs, the current increased slowly with an increase in the potential, and the reproducibility of the values of limiting current was poor. This behavior suggests the presence of complicating electrode processes, including the cleavage of some ester linkages and the release of Fe(III)TCPP molecules from the surface. Except for the acidic solution, the Levich plots (the limiting current vs. (the rotating rate)$^{1/2}$)[8] showed good straight lines through the point of origin. The number of transferred electrons in the oxygen reduction was calculated by the use of the Levich equation from the limiting current at each rotation rate (250, 500, 750, 1000, and 1250 rpm). In the calculation, the following values were used for the variables in the equation: 2.1×10^{-5} cm^2 s^{-1} and 2.4×10^{-4} mol dm^{-3} [1] for the diffusion coefficient and the concentration of oxygen in air-saturated solutions respectively, 8.9×10^{-3} cm^2 s^{-1} for the kinetic viscosity of aqueous solutins, and 0.23 cm^2 for the surface area of modified electrodes.

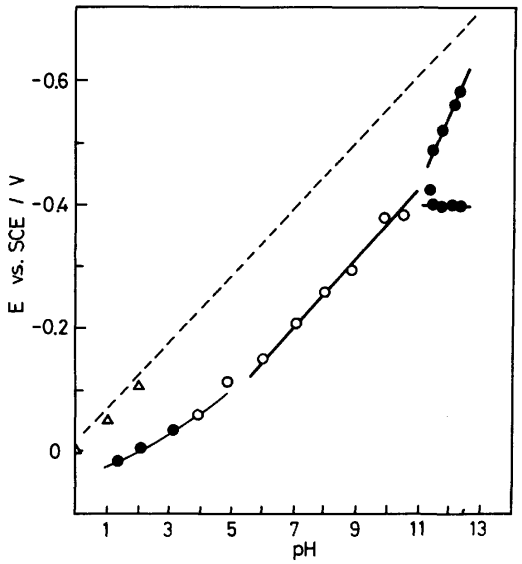

Fig. 5. The peak potentials of oxygen reduction on the (A)GC-O-Fe(III)TCPP electrodes as a function of the pH. ○: in buffered solutions, ●: in non-buffered solutions, △ and dashed line: replotted from Ref. 3.

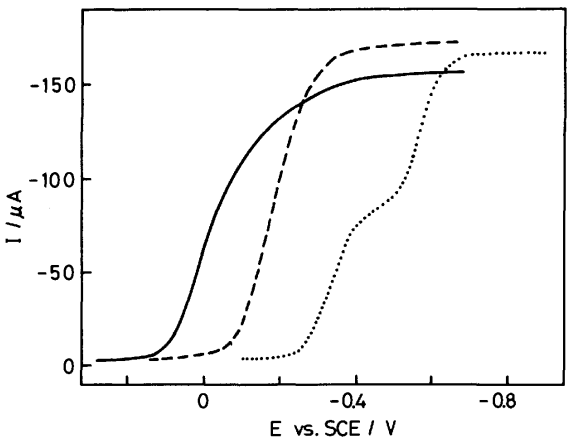

Fig. 6. Current-potential curves of the reduction of oxygen at the rotating disc modified (A) Electrodes. The electrode was rotated at 500 rpm. The potential was scanned at 50 mV s^{-1}. —— pH 3.1, ----- pH 7.1, ·····pH 12.0

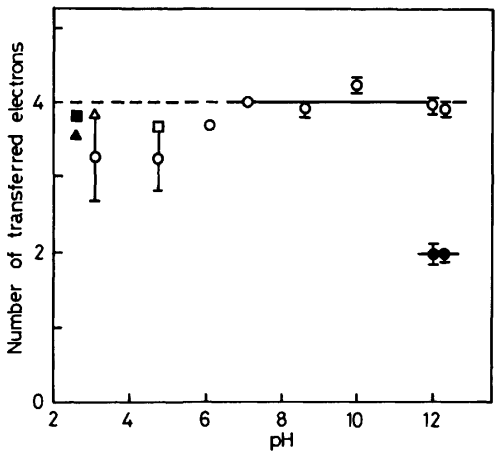

Fig. 7. Number of transferred electrons for the oxygen reduction at the rotating disc modified (A) electrodes as a function of the pH. ○: average overall number of transferred electrons. ●: average number of transferred electrons at the first wave at pH>11.5. Rotation rate (rpm): △250, ▲500, □1000, and ■1250.

Figure 7 shows the relationship between the number of transferred electrons measured on the (A) GC-O-Fe(III)TCPP rotating electrode and the pH of the solutions. At pH>11.5, the solid circle and the open circle indicate the number of transferred electrons in the lst reduction wave and in the overall reduction respectively. Figure 7 indicates that the oxygen molecule is reduced via a one-step reaction with four-electron transfer at pH 7—11 and via two successive reactions, each with a two-electron transfer, at pH>11.5.

The numbers of transferred electrons and protons in the oxygen reduction suggest that the reduction of the oxygen molecules in the solutions on the (A)GC-O-Fe(III)TCPP electrode proceeds via the following EC catalytic regeneration mechanisms. At pH 7—11, the linked Fe(III)TCPP molecules are reduced to Fe(II)-TCPP by Eq. 1 (E step) and reproduced by Eq. 2 (C step), reducing an oxygen molecule to H_2O:

$$\text{Fe(III)TCPP} + e^- \longrightarrow \text{Fe(II)TCPP} \quad (1)$$

$$4\text{Fe(II)TCPP} + O_2 + 4H^+ \longrightarrow 4\text{Fe(III)TCPP} + 2H_2O \quad (2)$$

At pH>11.5, however, the Fe(II)TCPP molecules, which are produced by Eq. 1 (E step), reduce an oxygen molecule to the O_2^{2-} ion by Eq. 3 (C step) at the first peak potential; then they reduce O_2^{2-} by Eq. 4 (C step) at the more cathodic potential:

$$2\text{Fe(II)TCPP} + O_2 \longrightarrow 2\text{Fe(III)TCPP} + O_2^{2-} \quad (3)$$

$$2\text{Fe(II)TCPP} + O_2^{2-} + 2H_2O \longrightarrow 2\text{Fe(III)TCPP} + 4OH^- \quad (4)$$

In the solution at pH<6, there was some scatter in the limiting current of oxygen reduction. However, the largest number of transferred electron determined was nearly equal to four. Therefore, the reduction of oxygen in the solution at pH<6 probably proceed via essentially the same mechanism as that observed in the solution at pH 7—11.

Though the transient formation of an intermediate such as hydrogen peroxide during the reduction of oxygen could be considered, we did not detect the formation of any intermediates by the use of the RDE apparatus.

The authors are grateful to Dr. Kentaro Okuma, Fukuoka University, for the elemental analysis of Fe(III)TCPP and for his helpful suggestions. The present work was partially supported by a Grant-in-Aid for Scientific Research (No. 61740358) from the Ministry of Education, Science and Culture, and a grant from the Central Research Institute of Fukuoka University.

References

1) P. A. Forshey, T. Kuwana, N. Kobayashi, and T. Osa, *Am. Chem. Soc. Advan. Chem.*, **201**, 601 (1982), and the references cited therein.

2) P. A. Forshey and T. Kuwana, *Inorg. Chem.*, **22**, 699 (1983), and the references cited therein.

3) N. Kobayashi and T. Osa, *J. Electroanal. Chem.*, **157**, 269 (1983).

4) F. Arifuku, K. Ujimoto, and H. Kurihara, *Fukuoka Univ. Sci. Rep.*, **13**, 121 (1983).

5) J. C. Lennox and R. W. Murray, *J. Electroanal. Chem.*, **78**, 395 (1977).

6) J. C. Lennox and R. W. Murray, *J. Am. Chem. Soc.*, **100**, 3710 (1978).

7) R. D. Rocklin and R. W. Murray, *J. Electroanal. Chem.*, **100**, 271 (1979).

8) C. P. Jester, R. D. Rocklin, and R. W. Murray, *J. Electrochem. Soc.*, **127**, 1979 (1980).

9) N. Kobayashi, M. Fujihira, T. Osa, and S. Dong, *Chem. Lett.*, **1982**, 575.

10) M. Fujihira, T. Kubota, and T. Osa, *J. Electroanal. Chem.*, **119**, 379, (1981).

11) N. Kobayashi, T. Matsue, M. Fujihira, and T. Osa, *J. Electroanal. Chem.*, **103**, 427 (1979).

12) J. D. Stong and C. R. Hartzell, *Bioinorg. Chem.*, **5**, 219 (1976).

13) E. Laviron, *Bull. Soc. Chim. Fr.*, **1967**, 3717.

14) H. A. Laitinen, C. A. Vincent, and T. J. Bednarski, *J. Electrochem. Soc.*, **115**, 1024 (1968).

15) H. P. Boehm, E. Diehl, W. Eeck, and R. Sappok, *Angew. Chem., Int. Ed. Engl.*, **3**, 669 (1964).

16) R.Vasquez, T. Masujima, H. Yoshida, and H. Imai, *Rev. Polarogr.*, **27** 56 (1981).

Electrochemical and Spectroelectrochemical Speciation of [5-phenyl-10,15,20-tris(4-sulfonatophenyl)porphinato]iron in Aqueous Solution

Fumihiro ARIFUKU,* Rika NISHINO, Kikujiro UJIMOTO, and Hirondo KURIHARA
Department of Chemistry, Faculty of Science, Fukuoka University,
Nanakuma, Jonan-ku, Fukuoka 814-01
(Received August 30, 1986)

The equilibria among the species of [5-phenyl-10,15,20-tris(4-sulfonatophenyl)porphinato]iron (Fe-$TPPS_3$) ion in aqueous solution and the redox reactions of the central metal were investigated by electrochemical and spectro-electrochemical methods. In the range of pH 3—12.5, the species formed by the reduction of Fe(III)-$TPPS_3$ in solution was identified as the monomeric Fe(II)-$TPPS_3$, while Fe(III)-$TPPS_3$ exists in both monomeric and dimeric species in equilibrium. The monomeric Fe(III)-$TPPS_3$ was demetallated at pH below 3 in the course of reduction of the Fe(III)-$TPPS_3$ solution. The μ-oxo-dimer of Fe(III)-$TPPS_3$ in highly basic solution was reversibly reduced to Fe(II)-$TPPS_3$ and subsequently the monomeric Fe(I)-$TPPS_3$. The formation of the stacking-type dimer of Fe(III)-$TPPS_3$, significantly depending on the concentration of Fe(III)-$TPPS_3$, was presumed to have a pH below 6.

Metalloporphyrin complexes are well-known to play important roles in various biological systems.[1,2] These complexes are essential for the carriers and storage of oxygen and as enzymatic cofactors. Recently, noteworthy reports on an electrocatalytic reduction of molecular oxygen by metalloporphyrins, together with metallophthalocyanines, have been reported.[3,4]

Some of these functions of metalloporphyrins must depend on the addition or replacement of axial ligands of the central metals.[5] In order to elucidate the specificity of such macrocyclic compounds, it is important to clarify their solute species and redox properties. Therefore, we have been interested in studying the properties of some water-soluble iron-porphyrin complexes.[6-8]

The characteristics of a monomer and a μ-oxo-dimer of [tetrakis(*p*-sulfonatophenyl)porphinato]iron-(III) (abbreviated as Fe(III)-$TPPS_4$) in aqueous solution was investigated in detail.[9,10] We found, by spectrophotometric and magnetochemical methods, that the solute species in a 1.00×10^{-5} mol dm^{-3} [5-phenyl-10,15,20-tris(4-sulfonatophenyl)porphinato]iron-(III) (abbreviated as Fe(III)-$TPPS_3$) solution were similar to that in a Fe(III)-$TPPS_4$ solution.[11] However, the solute species of the reduced form has not been established. The purpose of the present study is to determine the redox characteristics of Fe(III)-$TPPS_3$ in aqueous solution on the glassy carbon electrode and to identify the solute species of the reduced complex using electrochemical and spectro-electrochemical methods.

Experimental

Materials and Sample Solutions. Fe(III)-$TPPS_3$ was prepared by metal insertion of tetraphenylporphinetrisulfonic acid (Dojindo Laboratories, abbreviated as $TPPS_3$) with $FeSO_4\cdot7H_2O$ according to the method of Fleischer et al.[9] All other chemicals of guaranteed reagent grade (Wako Pure Chemical Industries) were used without further purification. The pH of the sample solution was adjusted with a sulfuric acid and/or sodium hydroxide solution. The ionic strength was adjusted to 0.1 mol dm^{-3} with a sodium sulfate solution except for solutions of pH below 1 or above 13. Where buffered solutions were required, the following buffers were used: acetate buffer at pH 4—6, phosphate-borate buffer at pH 6—9, and carbonate buffer at pH 9—11. Measurements of the pH were made on a Toa HM-5B pH meter.

Spectrophotometric, Electrochemical, and Spectroelectrochemical Measurements. A Hitachi 228A spectrophotometer was used for the spectrophotometric investigation.

The cyclic voltammograms of Fe(III)-$TPPS_3$ in solutions of various pH were obtained by means of Dual Potentiogalvanostat DPGS-1, Potential Sweeper NPS-2 (Nikko Keisoku) and X-Y recorder WX4403 (Watanabe, Inc.) equipped with a conventional three-electrode system. A glassy carbon rod (GC-30, Tokai Carbon) plugged into a Teflon tube was used as the working electrode. The carbon surface exposed to a solution was a circle 0.196 cm^2 in area. The exposed disc surface of a GC-30 electrode was polished with an abrasive paper followed with suspensions of alumina powders (Marumoto, Inc.) of decreasing size, down to 0.06 μm in diameter, until a mirror-like finish was obtained. To completely remove the alumina particles adhering on the polished electrode surfaces,[12,13] the electrodes were thoroughly washed by ultrasonication for 20 s in 0.05 mol dm^{-3} sulfuric acid.[14]

The spectroelectrochemical experiments were achieved with an optically transparent thin-layer electrode (OTTLE)[6,15] constructed with a gold minigrid (500 wires per inch, Backbee Mears) which was sandwiched between two microslide glasses. The distance between the two plates was controlled with Teflon spacers (Delectrix DF-1200). While the Soret and Q band spectra of Fe(III)-$TPPS_3$ and its reduced-form complexes were measured with a Hitachi 228A spectrophotometer, the potential at the gold minigrid as the working electrode was controlled by a Potentiostat NPOT-2501 (Nikko Keisoku).

Prior to both the electrochemical and spectro-electrochemical measurements, the sample solution was deoxygenated by bubbling nitrogen gas through the solution for about 20 min, and the measurements were carried out under

an atmosphere of nitrogen. A saturated calomel electrode (SCE) was employed as a reference electrode. All the measurements were performed at 25 °C.

Results and Discussion

Electrochemistry. Figures 1 and 2 illustrate typical cyclic voltammograms of 5.00×10^{-4} mol dm^{-3} Fe(III)-$TPPS_3$ aqueous solutions at different pH values. The dashed line in Fig. 1 shows the 1st cyclic voltammetric curve observed in Fe(III)-$TPPS_3$ solution of pH 2.04. The catalytic reduction of oxygen, which was not removed from the solution, via the reduction of Fe(III)-$TPPS_3$ was observed at ca. −0.1 V. In addition to this reduction peak, two redox peak couples were clearly observed at the more cathodic potential. The solid line in Fig. 1 shows the stationary cyclic voltammogram (9th cycle) and indicates that the reduction wave at ca. −0.1 V virtually disappeared and the two redox peak couples remained. This disappearance of the 1st current peak must be attributed to a demetallation of Fe(III)-$TPPS_3$ in addition to a consumption of oxygen in an electrical double layer. The 1st current peak at ca. −0.1 V corresponds to the peaks at ca. −0.1 V in Fig. 3 and at ca. −0.07 V in Fig. 4. The redox couple at ca. −0.3 V was observed only in solutions of pH<6 (cf. Fig. 4); the peak current of this redox couple decreased with a decrease in the concentration of the porphyrin complex and the peak couple was then no longer detectable in the solution of 1.00×10^{-5} mol dm^{-3} Fe(III)-$TPPS_3$.

Figure 2 shows the stationary cyclic voltammograms observed in the Fe(III)-$TPPS_3$ solution at pH 7.16 and 12.81. At these pH, the 1st peak attributable to the reduction of Fe(III)-$TPPS_3$ remained intact even after multicycles. The value of

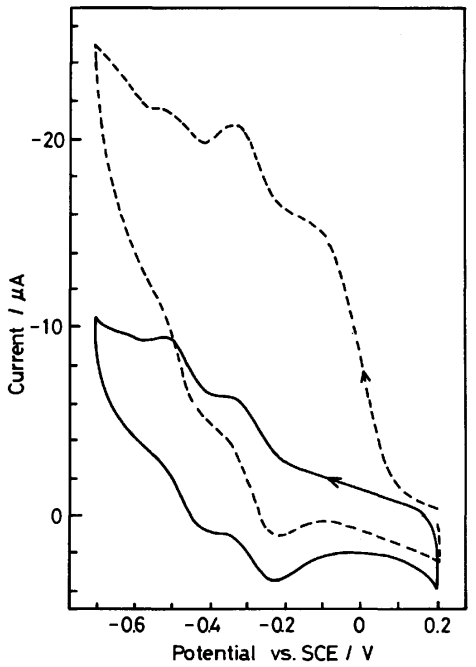

Fig. 1. Cyclic voltammograms of 5.00×10^{-4} mol dm^{-3} Fe(III)-$TPPS_3$ aqueous solution (pH 2.04). ------: 1st cycle, ——: 9th cycle. Scan rate: 0.05 V s^{-1}.

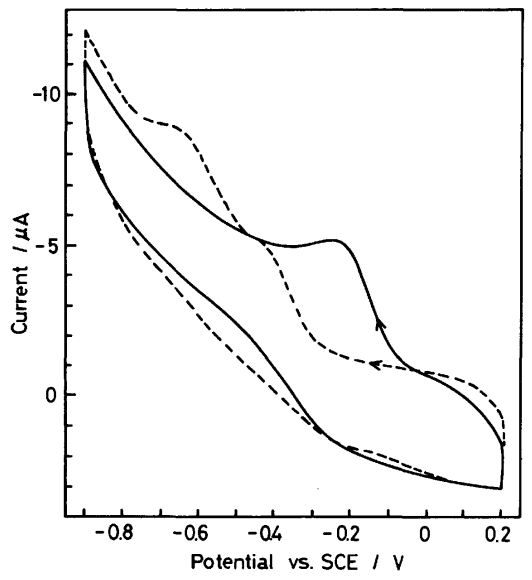

Fig. 2. Cyclic voltammograms of 5.00×10^{-4} mol dm^{-3} Fe(III)-$TPPS_3$ aqueous solutions. ——: pH 7.16, ------: pH 12.81. Scan rate: 0.05 V s^{-1}.

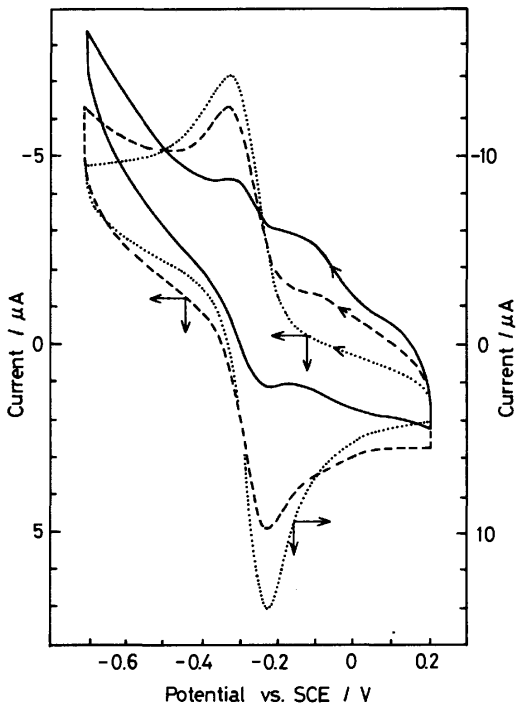

Fig. 3. Cyclic voltammograms of Fe(III)-$TPPS_3$ aqueous solutions (pH 4.21). ——: 1.00×10^{-4} mol dm^{-3}, ------: 3.00×10^{-4} mol dm^{-3}, ·····: 9.00×10^{-4} mol dm^{-3}. Scan rate: 0.05 V s^{-1}.

the reduction current of Fe(III)-TPPS$_3$ at pH 7.16 is almost the same as that of each of two reduction peaks at pH 12.81, respectively. That is to say, the total quantity of electron transfered to Fe(III)-TPPS$_3$ in the two-step reduction at pH 12.81 is twice that at pH 7.16 in the potential range from −0.2 to −0.9 V.

Figure 3 shows the stationary cyclic voltammograms obtained in the Fe(III)-TPPS$_3$ solutions of three different concentrations at pH 4.21, where a well defined redox peak couple appeared around −0.3 V. The reduction wave at ca. −0.1 V, which was observed clearly in 1.00×10^{-4} mol dm^{-3} Fe(III)-TPPS$_3$ solution, diminished with increase in the concentration of Fe(III)-TPPS$_3$ and was scarcely observed in the solution of 9.00×10^{-4} mol dm^{-3}. On the other hand, the reversible redox peak couple around −0.3 V became sharp and well-behaved with increasing concentration of Fe(III)-TPPS$_3$. This phenomenon suggests that a certain species, transformed from Fe(III)-TPPS$_3$ monomer, accumulated in the electrical double layer. However, no significant difference in near-UV and visible absorption spectra obtained in 1.00×10^{-5} and 1.00×10^{-3} mol dm^{-3} Fe(III)-TPPS$_3$ solutions was observed. Furthermore, the excellent linearity between the absorbance at the Soret band peak and the concentration of the solutions at pH 3.9 was obtained over a wide range of concentration.[11]

Figure 4 shows the plot of the reduction peak potential $(E_p)_R$ of the lst cyclic voltammograms obtained in 1.00×10^{-3} mol dm^{-3} Fe(III)-TPPS$_3$ against pH of the solutions. The potential of the lst reduction peak at pH<6 was measured by observing the catalytic peak of dissolved oxygen. The peak potential of the lst and 2nd reduction peaks in the low pH range were −0.07 V (pH<4) and −0.32 V (pH<5), respectively, and no potential shift was observed except for the point at pH 0.6. The 2nd reduction peak was observed at pH<6 and was shifted by ca. −60 mV/pH in the pH range of 5—6. The peak potential ca. −0.5 V of the 3rd reduction peak at low pH is approximately in agreement with that of metal-free TPPS$_3$. The $(E_p)_R$ of the lst reduction peak shifted by ca. −60 mV/pH in the pH range 4—11. At pH>11, a pH-independent reduction peak was observed at −0.47 V followed by a pH-dependent reduction peak by ca. −60 mV/pH.

Spectroelectrochemistry. Figures 5—7 show the typical absorption spectra of the reduced sample solutions, which are prepared by reducing 1.00×10^{-4} mol dm^{-3} Fe(III)-TPPS$_3$ solutions potentiostatically

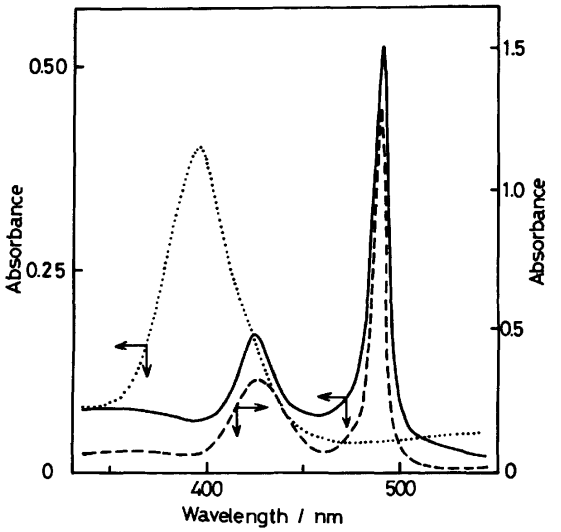

Fig. 5. Soret band spectra of Fe(III)-TPPS$_3$ and its reduced form in aqueous solutions at pH 1.54. ——: 1.00×10^{-3} mol dm^{-3} reduced Fe(III)-TPPS$_3$ at −0.5 V for 3.5 h in OTTLE, ·····: 1.00×10^{-5} mol dm^{-3} Fe(III)-TPPS$_3$ in quartz cell, ------: 1.00×10^{-4} mol dm^{-3} TPPS$_3$ in OTTLE cell.

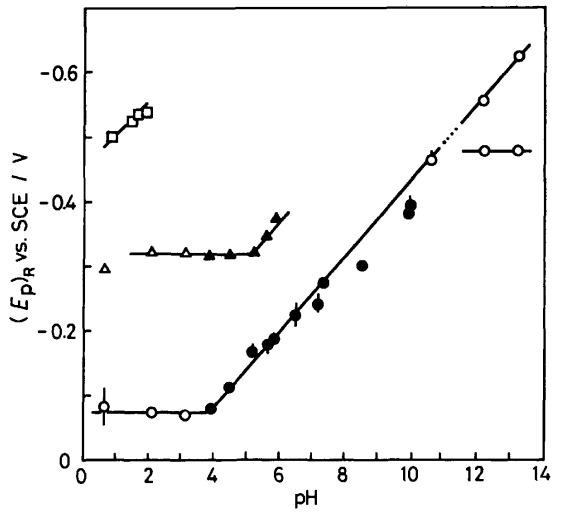

Fig. 4. Plot of $(E_p)_R$ vs. pH for 1.00×10^{-3} mol dm^{-3} Fe(III)-TPPS$_3$ solution. ○, △, □: in nonbuffered solution. ●, ▲: in buffered solution. $(E_p)_R$: see text.

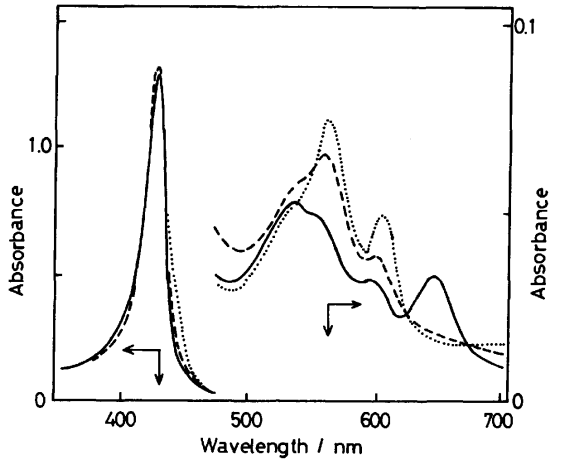

Fig. 6. Absorption spectra of 2.00×10^{-4} mol dm^{-3} Fe(II)-TPPS$_3$ solution. ——: pH 3.05, ------: pH 7.24, ·····: pH 12.00.

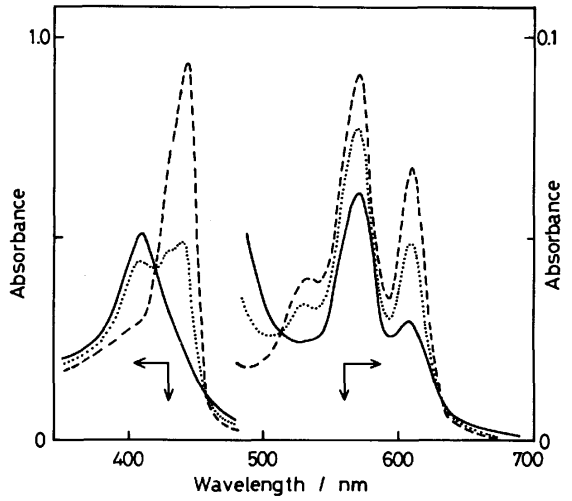

Fig. 7. Absorption spectra of 2.00×10^{-4} mol dm^{-3} Fe(III)-TPPS$_3$ solution during reduction at constant potential of −0.8 V at pH 12.72. Reduction time: ——0 min, ·····10 min, ------40 min.

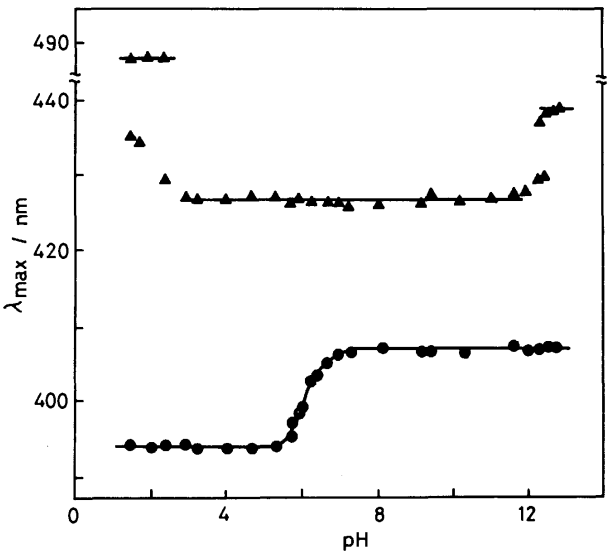

Fig. 8. Wavelength of Soret-band maxima (λ_{max}) vs. pH of 2.00×10^{-4} mol dm^{-3} Fe(III)-TPPS$_3$ solution before (●) and after (▲) the reduction on OTTLE.

in the OTTLE cell at various pH. At pH 1.54 (Fig. 5), the Soret band shifted from 394 to 488 nm, leaving a weak absorption band at 424 nm in the course of the reduction of Fe(III)-TPPS$_3$. The Soret band at 488 nm was also observed in the solutions containing metal-free TPPS$_3$ in contact with an Au-minigrid electrode. Therefore, the appearance of the Soret band at 488 nm suggests the occurrence of a demetallation[16] from the reduced species of Fe(III)-TPPS$_3$ in highly acidic solution of pH<2.5. This phenomena is supported also by the electrochemical results described in the preceding section.

The Soret band and visible absorption spectra in the pH range of 3—12 are represented in Fig. 6. The Soret band shifted from 394 (pH<5.5) or 406 nm (pH>7) to 427 nm by the reduction of Fe(III)-TPPS$_3$ (see Fig. 8 also). The visible absorption of the reduced species changes from a four-band toward a two-band spectrum with an increase of pH. Such a change in the visible absorption spectrum suggests that the unsymmetric structure of the complex species changes with pH toward the more symmetric one in highly basic solutions.

Figure 7 shows the change of the absorption spectrum in the course of reduction at pH>12.5. The Soret band shifted from 406 to 439 nm via 427 nm transiently at pH>12.5. The change in the shape of the visible spectra suggests that a symmetric structure of Fe(III)-TPPS$_3$ with a six-coordination was transformed to an unsymmetric structure of the reduced species with five-coordination. When the reduction potential was put off, the reduced species of Fe(III)-TPPS$_3$ in the solution of pH>3 was rapidly reoxidized to give the initial Fe(III)-species without degradation of the porphyrin ring system.

The relationship between the pH of the sample solution and the wavelength of the Soret band maximum of Fe(III)-TPPS$_3$ or its reduced species is summarized in Fig. 8. No change in the structure of the reduced species was observed at 4<pH<11, while the structure of the Fe(III)-species transformed clearly at around pH 7.

Electrochemical Characteristic and Speciation of Fe(III)-TPPS$_3$ and Its Reduced Fe-TPPS$_3$. The solute species of Fe(III)-TPPS$_3$ and its reduced form in the aqueous solution at the concentration of 1.00×10^{-5} mol dm^{-3} are assigned to those in Scheme 1 from the results of the spectrophotometric experiment[11] and the electrochemical and spectro-electrochemical experiments presented above. Scheme 1 also presents the numbers of protons and electrons transferred in each redox reaction, which were observed from the data in Fings. 2 and 4.

The results of the spectro-electrochemical experiment indicate the reduced complex in aqueous solutions to be a single ionic species over the pH range of 3—12.5. The pattern of the visible absorption spectrum in Fig. 6 together with the numbers of proton and electron added to the Fe(III)-TPPS$_3$ suggest that the species is in the low symmetric structure similar to the five-coordinated Fe(III)-TPPS$_3$(H_2O). In the solution of pH<3, the release of iron ion easily occur in the course of reduction of Fe(III)-TPPS$_3$ because of the enlargement of the electron cloud of the central ion. In the solution of pH>12.5, the data in Fig. 4 suggest that the μ-oxo-dimer of Fe(III)-TPPS$_3$ is first reduced to that of Fe(II)-TPPS$_3$ by the two-electron transfer per dimer, and then the second reduction rapidly follows to give

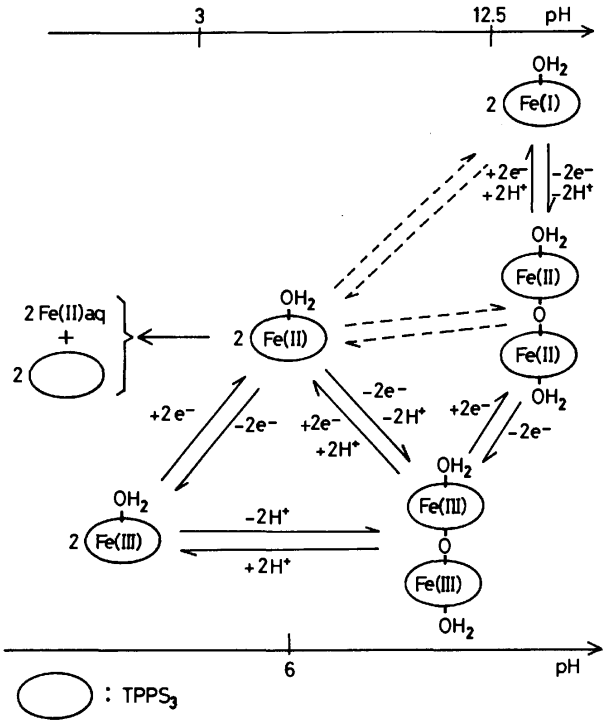

Scheme 1.

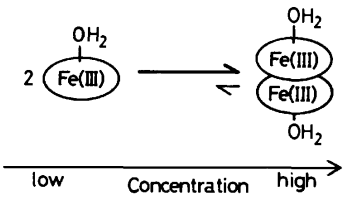

Scheme 2.

Table 1. pH Values of the Inflection Point on the Spectroscopic pH Titration Curves of Fe(III)-TPPS$_3$ Aqueous Solutions

Concentration	Monitoring Wavelength	Inflection Point
mol dm^{-3}	nm	pH
5.60×10^{-6}	394	6.7
8.20×10^{-5}	529	6.3
1.00×10^{-3}	394	5.6
1.00×10^{-3}	529	5.6

two Fe(I)-TPPS$_3$ monomers by the two-proton and two-electron transfer per dimer. The iron(I) monomer is suggested to be a species of low symmetry, such as Fe(I)-TPPS$_3$ (H_2O), by the shape of visible spectrum in Fig. 7 (dashed line).

In accordance with the inference from Fig. 3, it may be presumed that the Fe(III)-TPPS$_3$(H_2O) monomer, in the acidic and relatively concentrated solution (more than 10^{-4} mol dm^{-3}), could make a stacking-type dimer, as suggested for the metal-free TPPS$_4$.[17] The stacking -type dimer, as is shown in Scheme 2, is made up possibly of the two five-coordinated porphyrin complexes, which have an unoccupied axial site and stack each other with the dispersion force such as van der Waals force. The formation of the stacking-type dimer is supported by the data of the pH titration in Table 1. If the stacking-type dimer is formed, the π-electron energy level of the dimer is lowered comparing to the monomer and hence the donation of electron from the axial ligand to the central Fe^{3+} will be increased. The lowering the electron density of the axial ligand will facilitate the deprotonation from the axial ligand of the complex; consequently, the formation of μ-oxo-dimer occur more easily from the two stacking-type dimers compared to the formation from two monomeric species. That is to say, the pH value of the inflection point of the spectrophotometric pH titration curves decreases with the increase in the amount of stacking-type dimer in the solution, as is shown in Table 1.

No difference in near-UV and visible absorption spectra between the monomer and the stacking-type dimer was observed because of the limitation of the resolution of the spectrophotometer used, since the magnitude of the dispersion force corresponded to the order of 10^2 cm^{-1}.

The authors wish to thank Misses Yukari Yonemura and Setsuko Nakamura for their technical collaboration and Professor Hiroko Shimada, Fukuoka University, for her valuable comments.

References

1) K. M. Smith, "Porphyrins and Metalloporphyrins," Elsevier Sci. Pub. Co., Amsterdam (1975).

2) "Iron Porphyrins," ed by A. B. P. Lever and H. B. Gray, Addison-Wesley, MA (1983).

3) P. A. Forshey, T. Kuwana, N. Kobayashi, and T. Osa, *A. C. S. Advan. Chem.*, **201**, 601 (1982) and references cited therein.

4) P. A. Forshey and T. Kuwana, *Inorg. Chem.*, **22**, 699 (1983) and references cited therein.

5) R. F. Pasternack and G. R. Parr, *Inorg. Chem.*, **15**, 3087 (1976).

6) H. Kurihara, F. Arifuku, I. Ando, M. Saita, R. Nishino, and K. Ujimoto, *Bull. Chem. Soc. Jpn.*, **55**, 3515 (1982).

7) F. Arifuku, K. Ujimoto, and H. Kurihara, *Fukuoka Univ. Sci. Reports*, **15**, 27 (1985).

8) F. Arifuku, K. Ujimoto, and H. Kurihara, *Bull. Chem. Soc. Jpn.*, **59**, 149 (1986).

9) E. B. Fleischer, J. M. Palmer, T. S. Srivastava, and A. Chatterjee, *J. Am. Chem. Soc.*, **93**, 3162 (1971).

10) A. A. El-Awady, P. C. Wilkins, and R. G. Wilkins, *Inorg. Chem.*, **24**, 2053 (1985).

11) F. Arifuku, R. Nishino, K. Ujimoto, and H. Kurihara,

Fukuoka Univ. Sci. Reports, **16**, 65 (1986).
12) J. Zak and T. Kuwana, *J. Am. Chem. Soc.*, **104**, 5514 (1982).
13) B. Kazee, D. E. Weisshaar, and T. Kuwana, *Anal. Chem.*, **57**, 2736 (1985).
14) A. Bettelheim, R. Parash, and D. Ozar, *J. Electrochem. Soc.*, **129**, 2247 (1982).
15) R. W. Murray, W. R. Heineman, and G. W. O'Dom, *Anal. Chem.*, **39**, 1666 (1967).
16) O. Ikeda, K. Okabayashi, N. Yoshida, and H. Tamura, *J. Electroanal. Chem.*, **191**, 157 (1985).
17) R. F. Pasternack, P. R. Huber, P. Boyd, G. Engasser, L. Francesconi, E. Gibbs, P. Fasella, G. C. Venturo, and L. deC. Hinds, *J. Am. Chem. Soc.*, **94**, 4511 (1972).

Mössbauer and ESR Spectroscopic Studies on the Mixed-Valence States of 1′,1‴-Dialkyl- and 1′,1‴-Bis(methylbenzyl)biferrocenium Triiodides in Crystalline and Dispersed State

Satoru NAKASHIMA, Yuichi MASUDA, Izumi MOTOYAMA,† and Hirotoshi SANO*
Department of Chemistry, Faculty of Science, Tokyo Metropolitan University, Fukasawa, Setagaya-ku, Tokyo 158
†Department of Chemistry, Faculty of Engineering, Kanagawa University, Rokkakubashi, Kanagawa-ku, Yokohama 221
(Received October 24, 1986)

Iron atoms in the two different crystal forms of 1′,1‴-dibutylbiferrocenium triiodide showed different temperature-depending mixed-valence states; i.e., an averaged-valence state at higher temperatures and a trapped-valence state at lower temperatures in one crystal form but only a trapped-valence state from 78 K to room temperature in the other crystal form. The temperature-depending mixed-valence states were observed in 1′,1‴-diisobutylbiferrocenium triiodide, whereas only a trapped-valence state was found in 1′,1‴-dipentylbiferrocenium triiodide. Both the 1′,1‴-dibutyl- and 1′,1‴-diisobutylbiferrocenium triiodide showed Mössbauer spectra that were different from those of their crystalline states in a dispersed state. A good correlation of the anisotropy of *g*-values with the mixed-valence states was observed in the ESR spectra for a series of 1′,1‴-dialkyl- and 1′,1‴-bis(methylbenzyl)biferrocenium triiodides. The difference in the ESR parameters between these compounds in the crystalline state was reduced in the dispersed state.

It has been known that biferrocene derivatives are easily mono-oxidized to give mixed-valence cations. Those mixed-valence biferrocene compounds can be classified into two types of valence states of iron atoms; a trapped-valence type and an averaged-valence type, by means of Mössbauer spectroscopy.[1] Different states of iron atoms corresponding to ferrocene-like bivalent and ferricenium-like tervalent iron atoms are found in the former, while only an equivalent state of iron atoms is found over the Mössbauer time scale (ca. 10^{-7} s) in the latter.

In studies of bridged biferrocene derivatives it was concluded that the presence of conjugated π-systems between the two ferrocene moieties was necessary to have an interaction between the two metal atoms in well-separated mixed-valence compounds.[2-4] Recently, it has been found that an introduction of a substituent to biferrocenium cations influences the mixed-valence states; e.g., a monocationic salt of 1′,1‴-dichlorobiferrocene[5] shows a trapped-valence state from 4.2 K to room temperature, while monocationic salts of 1′,1‴-diiodo-[6] and 1′,1‴-dibromobiferrocene[5] show an averaged-valence state over the Mössbauer time scale in the same temperature range. Studies by XANES and XPS show that the electron-transfer rate between the two iron atoms in dibromo derivative is lower than ca. 10^{16} s^{-1}.[7] A trapped-valene state of iron atoms in 1′,1‴-diethyl- and 1′,1‴-dipropylbiferrocenium triiodide are known to change into an averaged-valence state at high temperatures.[8]

Similar temperature dependences of the valence state were recently reported for the triiodide salts of monocationic 1′,1‴-dibutyl-,[9] 1′,1‴-dibenzyl-,[9] 1′,1‴-bis(*o*-methylbenzyl)-,[10] and 1′,1‴-bis(*p*-methylbenzyl)-biferrocene.[10] It has been found that a trapped-valence state and an averaged-valence state coexist in 1′,1‴-dibutyl-,[9] 1′,1‴-dibenzyl-,[9] and 1′,1‴-bis(*p*-methylbenzyl)biferrocenium triiodide.[10] In these studies, it has been suggested that the environment surrounding each cation in the solid state should determine the mixed-valence state. The studies on the effects of counter anions were carried out to elucidate the mechanism of the intramolecular electron transfer.[11-15]

It has been suggested that the anisotropy of the *g*-value, $\Delta g = g_{\parallel} - g_{\perp}$, has a close connection with those mixed-valence states obtained from Mössbauer spectra in the studies of mixed-valence biferrocene derivatives.[16] In the present study, the mixed-valence states of 1′,1‴-diisobutyl- and 1′,1‴-dipentylbiferrocenium triiodide and two crystal forms of the 1′,1‴-dibutyl derivative were investigated in a crystalline state and in a state dispersed in poly(methyl methacrylate) by using Mössbauer spectroscopy. The mixed-valence states for a series of 1′,1‴- dialkyl- and 1′,1‴-bis(methylbenzyl)biferrocenium triiodides are also investigated in a crystalline and in a dispersed state by using ESR spectroscopy.

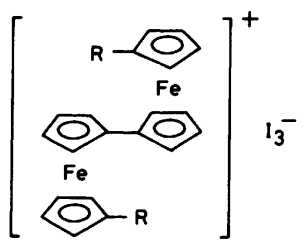

Fig. 1. 1′,1‴-Disubstituted biferrocenium triiodides used in the present studies (R=ethyl, propyl, butyl, isobutyl, pentyl, benzyl, *o*-methylbenzyl, *m*-methylbenzyl, and *p*-methylbenzyl).

Experimental

Materials. 1′,1‴-Dialkyl- and 1′,1‴-bis(methylbenzyl)-biferrocenes were prepared by the Ullmann coupling of 1-bromo-1′-alkylferrocenes and 1-bromo-1′-(methylbenzyl)ferrocenes at 100—110 °C for 18 h, respectively. The products were identified by using ^{1}H NMR and elemental analysis. Data of the elemental analysis and melting points for the new compounds, 1′,1‴-diisobutyl- and 1′,1‴-dipentylbiferrocene, are shown below, respectively: Found: C, 68.69; H, 7.66%. Calcd for $C_{28}H_{34}Fe_2$: C, 69.73; H, 7.11%. mp: 62 °C. Found: C, 69.67; H, 8.27%. Calcd for $C_{30}H_{38}Fe_2$: C, 70.61; H, 7.51%. mp: 36 °C.

The triiodide salts were prepared by a partial oxidation of the corresponding 1′,1‴-dialkyl- and 1′,1‴-bis(methylbenzyl)biferrocenes in benzene with a stoichiometric amount of I_2. The products were recrystallized from CH_2Cl_2 and identified by using elemental analysis. Data of the elemental analysis for the new mixed-valence compounds, 1′,1‴-diisobutyl- and 1′,1‴-dipentylbiferrocenium triiodide, are shown below, respectively: Found: C, 36.86; H, 4.31%. Calcd for $C_{28}H_{34}Fe_2I_3$: C, 38.97; H, 3.97%. Found: C, 40.56; H, 4.99%. Calcd for $C_{30}H_{38}Fe_2I_3$: C, 40.44; H, 4.30%.

1′,1‴-Dibutylbiferrocenium triiodide recrystallized from CH_2Cl_2 gave two kinds of crystal forms. One is needle-like crystals (crystals A), and the other is plate-like crystals (crystals B). Data of elemental analysis for these two crystal forms are shown below. Found for crystals A: C, 39.31; H, 4.14%. Found for crystals B: C, 39.20; H, 4.20%. Calcd for $C_{28}H_{34}Fe_2I_3$: C, 38.97; H, 3.97%.

The samples dispersed in polymer were obtained by evaporating a CH_2Cl_2 solution of poly(methyl methacrylate) containing 1—4% of each triiodide salt.

Mössbauer Spectroscopic Measurements. A ^{57}Co(Rh) source moving in a constant-acceleration mode was used for Mössbauer spectroscopic measurements. Mössbauer spectra were obtained by using an ELSCINT Mössbauer spectrometer and a proportional counter. Isomer shifts were referred to metallic iron foil. Mössbauer parameters were obtained by least-squares fitting to Lorentzian peaks.

ESR Measurements. X-band ESR spectra for powdered crystalline samples and dispersed samples were determined at 78 K using a JEOL JES-PE-3X ESR spectrometer.

Results and Discussion

Mössbauer Spectra. The biferrocene derivatives used in the present studies are shown in Fig. 1. Mössbauer spectrum for crystals obtained by the diffusion of hexane into a CH_2Cl_2 solution of 1′,1‴-dibutylbiferrocenium triiodide at room temperature shows only a single doublet which corresponds to a valence state averaged over ferrocene-like bivalent and ferricenium-like tervalent state. On the other hand,

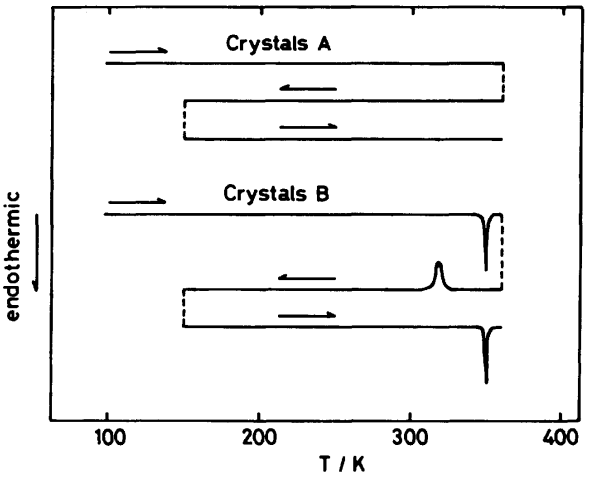

Fig. 3. Differential scanning calorimetric curves for two crystal forms of 1′,1‴-dibutylbiferrocenium triiodide at scanning rate, 5 K min^{-1}.

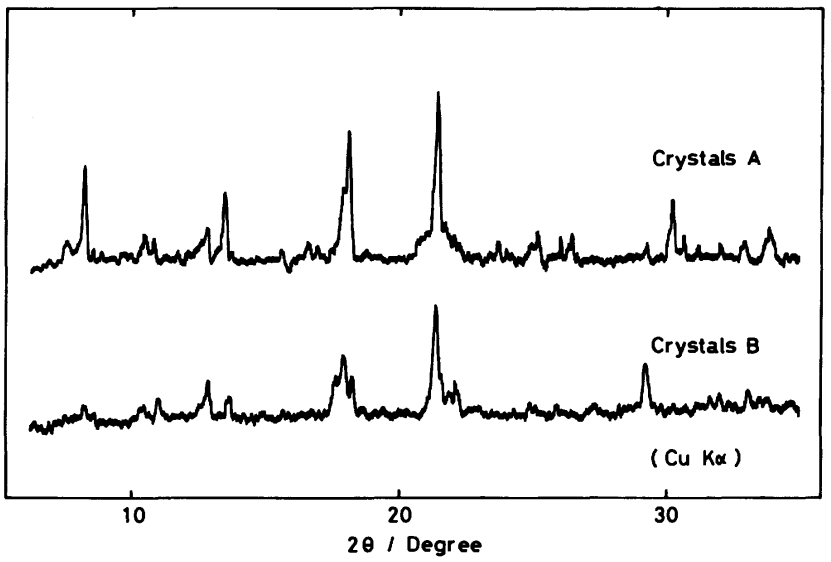

Fig. 2. X-Ray powder patterns for two crystal forms of 1′,1‴-dibutylbiferrocenium triiodide at room temperature.

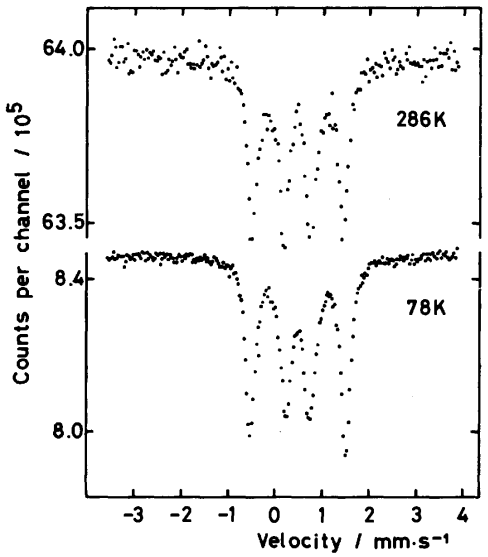

Fig. 4. Mössbauer spectra for crystals A of 1′,1‴-dibutylbiferrocenium triiodide at 78 and 286 K.

the microcrystals obtained by adding a benzene solution of I_2 to a benzene solution of 1′,1‴-dibutylbiferrocene give three doublets in the Mössbauer spectrum, which consist of two doublets corresponding to ferrocene-like bivalent and ferricenium-like tervalent iron atoms and of one doublet of a valence state averaged over the two valence states.[9]

Crystals A and crystals B of 1′,1‴-dibutylbiferrocenium triiodide give different X-ray powder patterns (Fig. 2) and different DSC (differential scanning calorimetry) curves (Fig. 3). An endothermic peak can be observed at 349 K in crystals B under a heating rate of 5 K min^{-1} but not observed in crystals A under the same heating rate. These results suggest that both crystals A and B have crystal structures different from each other.

The Mössbauer spectra in the two crystal forms are shown in Figs. 4 and 5. The Mössbauer spectroscopic data are summarized in Table 1. In crystals A, the spectra at 78 and 286 K consist of an inner- and an outer-doublet with a nearly 1:1 ratio in the areal intensity; these are ascribable to a ferricenium-like tervalent and ferrocene-like bivalent iron, respectively.

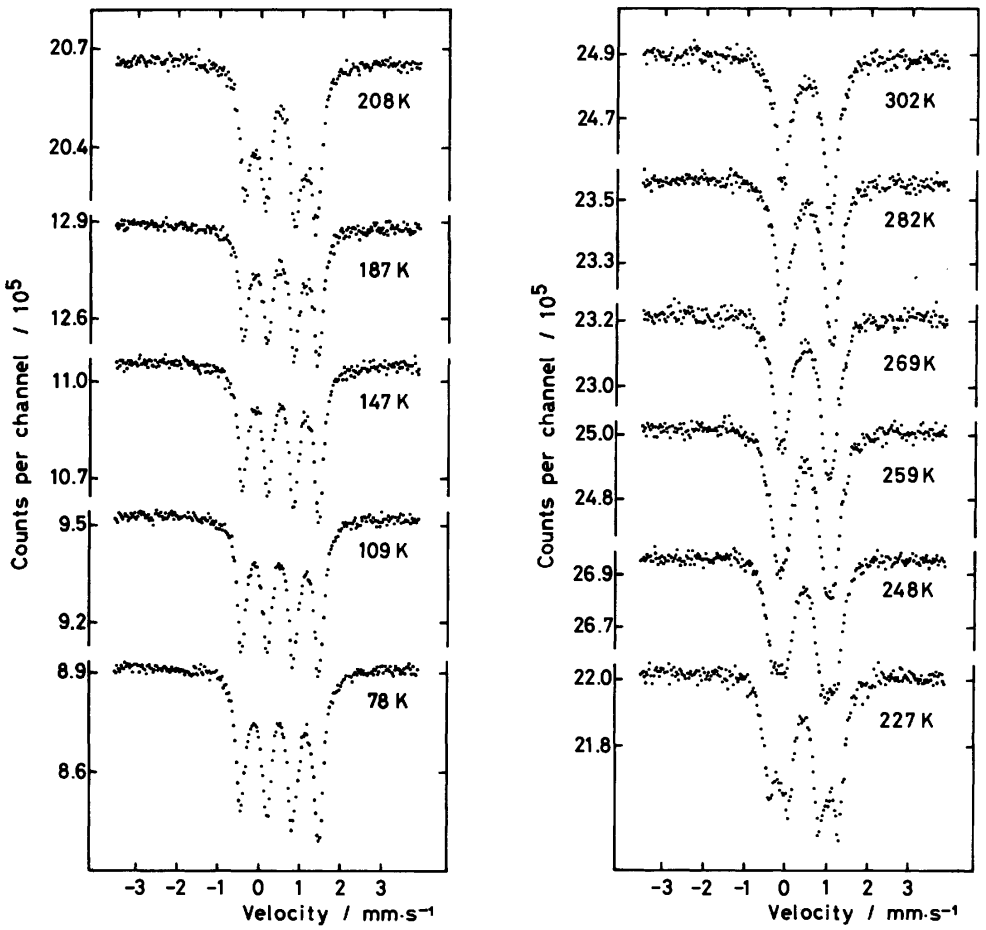

Fig. 5. Mössbauer spectra for crystals B of 1′,1‴-dibutylbiferrocenium triiodide from 78 K to room temperature.

It is clearly concluded that crystals A are of the trapped-valence type from 78 K to room temperature. On the contrary, the spectra of crystals B consist of one doublet ascribed to a state averaged over ferrocene-like and ferricenium-like states near room temperature, but of two doublets below ca. 250 K; i.e., crystals B show temperature-dependent mixed-valence states. The results indicate that the electron-transfer rate between the two iron atoms is dependent on the crystal structure.

The quadrupole splitting, ΔE_q, for the outer doublet ascribed to ferrocene-like iron atoms found in crystals B is a little smaller than that found in crystals A, while the ΔE_q value of the inner-doublet corresponding to ferricenium-like iron atoms is a little larger in crystals B than in crystals A (both at 78 K). This suggests that the interaction between Fe(II) and Fe(III) in crystals B is a little stronger than that in crystals A (even at 78 K).

Figures 6 and 7 show the Mössbauer spectra of 1′,1‴-diisobutyl- and 1′,1‴-dipentylbiferrocenium triiodide. The Mössbauer spectroscopic data are summarized in Table 2. A spectral change from two doublets (trapped-valence state) to one doublet (averaged-valence state) with increased temperatures is observed in 1′,1‴-diisobutylbiferrocenium triiodide, as in the case of crystals B of 1′,1‴-dibutylbiferrocenium triiodide. However, the transition tem-

Table 1. Mössbauer Parameters for 1′,1‴-Dibutylbiferrocenium Triiodide

Species	Temperature/K	$\delta^{a)}$/mm s^{-1}	ΔE_q/mm s^{-1}
Crystals A	286	0.44	1.88
		0.44	0.56
	78	0.50	2.03
		0.50	0.51
Crystals B	302	0.43	1.18
	282	0.44	1.19
	269	0.45	1.18
	259	0.45	1.20
	248	0.46	1.51
		0.46	0.91
	227	0.47	1.65
		0.46	0.80
	208	0.47	1.73
		0.47	0.75
	187	0.48	1.81
		0.48	0.66
	147	0.50	1.86
		0.50	0.64
	109	0.51	1.89
		0.51	0.64
	78	0.52	1.90
		0.52	0.64

a) Isomer-shift data are reported with respect to metallic iron foil.

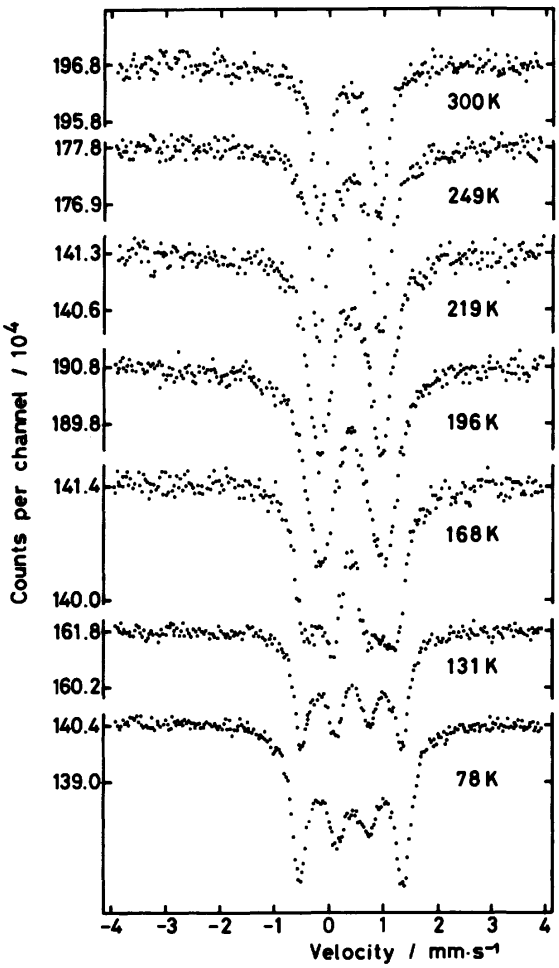

Fig. 6. Mössbauer spectra of 1′,1‴-diisobutylbiferrocenium triiodide from 78 K to room temperature.

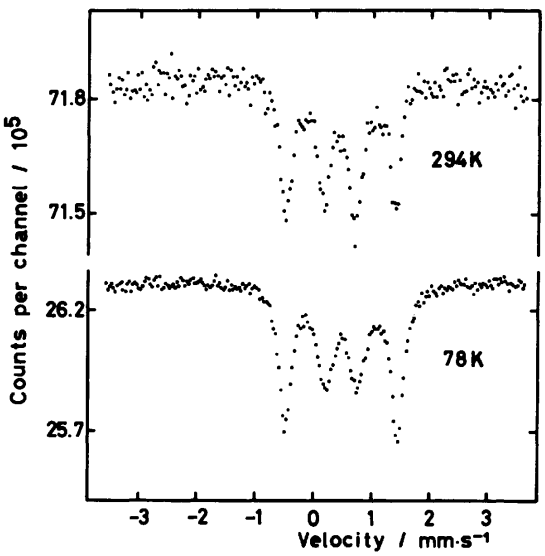

Fig. 7. Mössbauer spectra of 1′,1‴-dipentylbiferrocenium triiodide at 78 and 294 K.

perature, where the valence state changes from a trapped- to an averaged-valence state, is found to be lower in the isobutyl derivative than in crystals B of the butyl derivative. On the other hand, the Mössbauer spectra of the pentyl derivative show only a trapped-valence state from 78 K to room temperature.

It has already been reported that 1′,1‴-dibutylbiferrocenium cations take a trans conformation with respect to a planar fulvalene ligand in structual studies of their needle form triiodide salt (crystals A).[9,17] There are two structural features that also indicate that the structure of the cation is unsymmetric; the carbon-atom framework of one of the butyl groups lies essentially parallel to the Cp ring to which the butyl group is attached; whereas a part of the carbon-atom framework of the other butyl group is folded perpendicular to the Cp ring, and the I_3^- ion has an unsymmetric structure being disposed unequally to the two iron atoms in the cation, putting more negative charge on one terminal iodine atom than the other terminal iodine atom. It is interesting to note that the more negative iodine atom is situated closer to the Fe(III) atom than the other iron atom, Fe(II). It may be concluded that the conformation of the butyl substituents influences the positioning of the I_3^- ion.

Table 2. Mössbauer Parameters for 1′,1‴-Diisobutyl- and 1′,1‴-Dipentylbiferrocenium Triiodide

Compound	Temperature/K	$\delta^{a)}$/mm s^{-1}	ΔE_q/mm s^{-1}
1′,1‴-Diisobutyl-	300	0.45	1.09
biferrocenium	249	0.48	1.13
triiodide	219	0.48	1.14
	196	0.50	1.16
	168	0.50	1.59
		0.51	0.71
	131	0.51	1.82
		0.52	0.64
	78	0.53	1.91
		0.54	0.59
1′,1‴-Dipentyl-	294	0.45	1.88
biferrocenium		0.44	0.54
triiodide	78	0.50	1.94
		0.49	0.55

a) Isomer-shift data are reported with respect to metallic iron foil.

Figure 8 shows the Mössbauer spectra of 1′,1‴-dibutylbiferrocenium triiodide dispersed in poly(methyl methacrylate). The Mössbauer spectroscopic data are summarized in Table 3. The Mössbauer spectra in the dispersed state show two doublets; i. e., a definite trapped-valence state below 196 K and an insufficiently averaged state at 300 K. The collapse of the two doublets of the Mössbauer spectra begins at a higher temperature in the dispersed state than in crystals B, while that is not observed in the temperature range from 78 K to room temperature in crystals A. The Mössbauer spectra and those parameters of 1′,1‴-diisobutylbiferrocenium triiodide dispersed in poly(methyl methacrylate) are shown in Fig. 9 and in Table 3, respectively. Two doublets are found in the Mössbauer spectra for the dispersed state in the temperature range of 78—302 K, whereas an averaged-valence state is observed above ca. 210 K in the crystalline state.

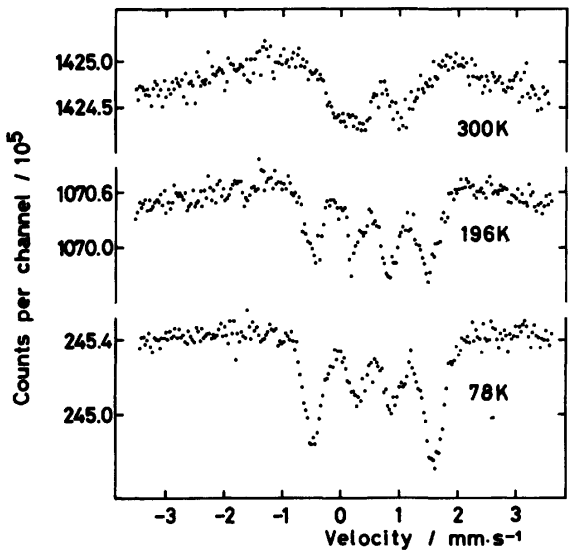

Fig. 8. Mössbauer spectra of 1′,1‴-dibutylbiferrocenium triiodide dispersed in poly(methyl methacrylate) from 78 K to room temperature. See footnote b) in Table 3.

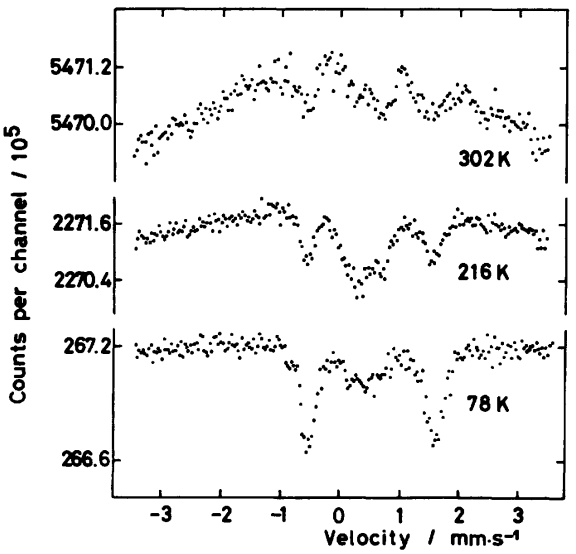

Fig. 9. Mössbauer spectra of 1′,1‴-dibutylbiferrocenium triiodide dispersed in poly(methyl methacrylate) from 78 K to room temperature.

Table 3. Mössbauer Parameters for 1′,1‴-Dibutyl- and 1′,1‴-Diisobutylbiferrocenium Triiodide Dispersed in Poly(methyl methacrylate)

Compound	Temperature / K	δ[a] / mm s^{-1}	ΔE_q / mm s^{-1}
1′,1‴-Dibutylbiferrocenium triiodide dispersed in poly(methyl methacrylate)[b]	300	0.49	1.04
	196	0.50	1.94
		0.51	0.61
	78	0.54	2.06
		0.55	0.60
1′,1‴-Diisobutylbiferrocenium triiodide dispersed in poly(methyl methacrylate)	302	0.47	2.08
		0.44	0.45
	216	0.50	2.13
		0.43	0.41
	78	0.53	2.15
		0.44	0.36

a) Isomer-shift data are reported with respect to metallic iron foil. b) The mixture of the crystals A and B was used for the Mössbauer spectroscopic measurement in the dispersed system, because the observed ESR parameters were close to each other in the crystals A and B dispersed in poly(methyl methacrylate).

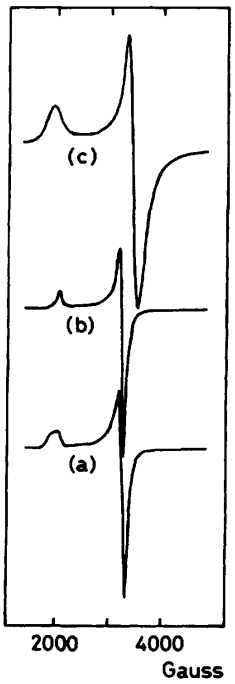

Fig. 10. ESR spectra for (a) crystals A, (b) crystals B, and (c) dispersed state of 1′,1‴-dibutylbiferrocenium triiodide at 78 K.

The difference in the valence state between the dispersed and the crystalline state is also reflected on the quadrupole splittings, ΔE_q, of the 1′,1‴-dibutyl and 1′,1‴-diisobutyl derivatives. For example, the values of ΔE_q for the outer and inner doublet for 1′,1‴-diisobutylbiferrocenium triiodide in the dispersed state are a little larger and smaller than those crystalline state, respectively. This suggests that the interaction between Fe(II) and Fe(III) atoms in dispersed state is a little weaker than that in crystalline state in 1′,1‴-diisobutylbiferrocenium triiodide even at 78 K and that the trapped-valence state remains at higher temperatures in the dispersed state. The same relationship between the valence state and the ΔE_q value is also observed in the dispersed and crystalline (A and B) states in the dibutyl derivative. The results of the valence state reflected on the quadrupole splittings in the dispersed and the crystalline state also indicate that the interaction between the triiodide anions and the biferrocenium monocations plays an important role in the intramolecular electron exchange between the two iron atoms.

ESR Spectra. It has been known that g-tensor anisotropy has a close connection with the mixed-valence states of biferrocene derivatives observed by the method of Mössbauer spectroscopy.[16] Figure 10 shows the ESR spectra of 1′,1‴-dibutylbiferrocenium triiodide (crystals A, crystals B, and a dispersed sample) at 78 K. The $g_{\parallel}$ and $g_{\perp}$ values were found in crystals B to be 3.00 and 1.91, respectively. These g-values are in a good agreement with those previously reported ($g_{\parallel}$=2.98 and $g_{\perp}$=1.92 at 4.2 K);[11] they were obtained by diffusing hexane into a CH_2Cl_2 solution of the triiodide salt. As mentioned above, the Mössbauer spectra of the present crystals B and the crystals obtained by the diffusion method satisfactorily coincide with each other from 78 K to room temperature. These two kinds of crystals obtained by the different methods are considered to have the same crystal structure. The spectral features of the ESR for crystals A are different from those for crystals B. The difference is remarkable in the signal corresponding to $g_{\parallel}$ component; i.e., the sharp signal ($g_{\parallel}$=3.00) was observed for crystals B, while the signal corresponding to $g_{\parallel}$ was observed as a superposition of two kinds of $g_{\parallel}$ values ($g_{\parallel}$=3.04 and 3.26) in crystals A. These differences in the ESR spectra between crystals A and B are in accordance with the results of the Mössbauer spectra.

An intermediate $g_{\parallel}$ value (3.17) in the crystals (3.26 and 3.04) is observed for butyl derivative dispersed in poly(methyl methacrylate).

The ESR parameters of the other dialkylbiferrocenium derivatives in crystalline and dispersed states at 78 K are also shown in Fig. 11 and in Table 4. ESR parameters for 1′,1‴-diethylbiferrocenium triiodide observed in the present experiment ($g_{\parallel}$=3.13 and $g_{\perp}$=2.00 and 1.88) are consistent with those previously reported ($g_{\parallel}$=3.02 and $g_{\perp}$=2.01 and 1.89 at 3.3 K).[11] As discussed above, the Mössbauer spectra of 1′,1‴-diethyl-, 1′,1‴-dipropyl-, 1′,1‴dibutyl-(crystals B), and 1′,1‴-diisobutylbiferrocenium triiodide show an av-

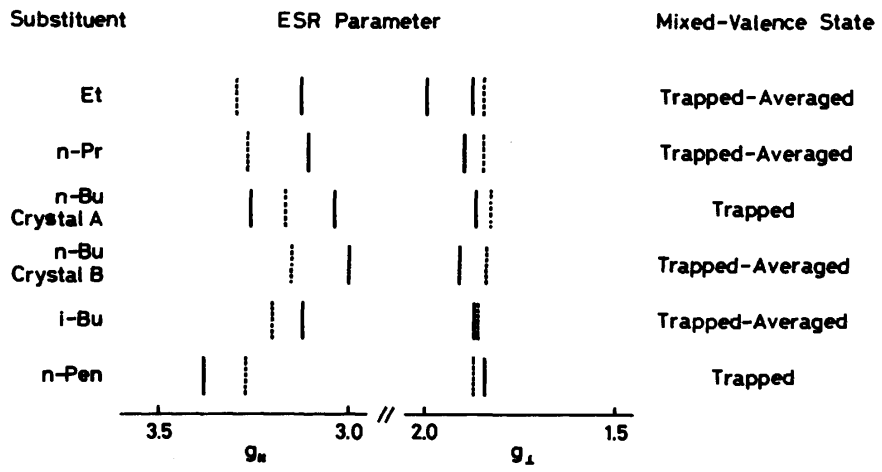

Fig. 11. Summary of ESR parameters in crystalline state (——) and dispersed state (------) at 78 K with those mixed-valence states in crystalline state for 1′,1‴-dialkylbiferrocenium triiodides. "Trapped-Averaged" shows a trapped-valence state at low temperatures and an averaged-valence state near room temperature. "Trapped" shows only the trapped-valence state from low temperature to room temperature.

Table 4. ESR Parameters for 1′,1‴-Dialkylbiferrocenium Triiodide at 78 K

Substituent	State	$g_{\parallel}$	$g_{\perp}$	$\Delta g^{a)}$
Ethyl-	Crystalline	3.13	2.00	1.19
			1.88	
	Glassy	3.30	1.85	1.45
Propyl-	Crystalline	3.11	1.90	1.21
	Glassy	3.27	1.85	1.42
Butyl-	Crystalline	3.26	1.87	1.39
(Crystals A)		3.04		1.17
	Glassy[b)]	3.17	1.83	1.34
Butyl-	Crystalline	3.00	1.91	1.09
(Crystals B)	Glassy[c)]	3.15	1.84	1.31
Isobutyl-	Crystalline	3.12	1.87	1.25
	Glassy	3.20	1.86	1.34
Pentyl-	Crystalline	3.38	1.84	1.54
	Glassy	3.27	1.87	1.40

a) This is the g-tensor anisotropy defined as $\Delta g = g_{\parallel} - g_{\perp}$. When a rhombic signal is seen, an average of two $g_{\perp}$ values is used for $g_{\perp}$. b) Crystals A were dispersed in poly(methyl methacrylate). c) Crystals B were dispersed in poly(methyl methacrylate).

eraged-valence state near room temperature; they change into those for a trapped-valence state with decreasing temperature while only trapped-valence states are observed for 1′,1‴-dibutyl- (crystals A) and 1′,1‴-dipentylbiferrocenium triiodide from 78 K to room temperature. For the above two groups (classified based on the difference of the temperature dependence of the valence states), the Δg value for each group shows a characteristic feature; i.e., the Δg values (Δg=1.09—1.25) for the former group, whose valence state changes from 78 K to room temperature, are smaller than those (Δg=1.39—1.54) for the latter group, whose valence state shows only a trapped-valence state.

As mentioned in the Introduction, 1′,1‴-dibenzyl-, 1′,1‴-bis(*o*-methylbenzyl)- and 1′,1‴-bis(*p*-methylbenzyl)biferrocenium triiodide show temperature-dependences of the mixed-valence state similar to those observed in 1′,1‴-dipropylbiferrocenium triiodide. On the other hand, 1′,1‴-bis(*m*-methylbenzyl)biferrocenium triiodide shows a trapped-valence state from low temperature to room temperature.

Figure 12 and Table 5 summarize the results of ESR spectra for the compounds in crystalline and dispersed states. ESR parameters for 1′,1‴-dibenzylbiferrocenium triiodide observed in the present experiment ($g_{\parallel}$=3.33 and $g_{\perp}$=1.81) are consistent with those previously reported ($g_{\parallel}$=3.42 and $_{\perp}$=1.80 at 4.2 K).[11] In 1′,1‴-bis(methylbenzyl)biferrocenium triiodides, the Δg values also show a characteristic feature; i.e., Δg=1.33—1.52 for the samples whose valence state changes from 78 K to room temperature. The Δg values are much smaller than the value (Δg=2.13) for the sample which shows only a trapped-valence state.

These results indicate that the decrease in the Δg values has a relationship with the nature of the electron exchange between the bivalent and tervalent iron atoms in the biferrocenium derivatives. This consideration is reasonable for explaining the appreciably small Δg values of the 1′,1‴-diiodo- and 1′,1‴-dibromobiferrocenium triiodide whose Mössbauer spectra show an averaged-valence state (only one

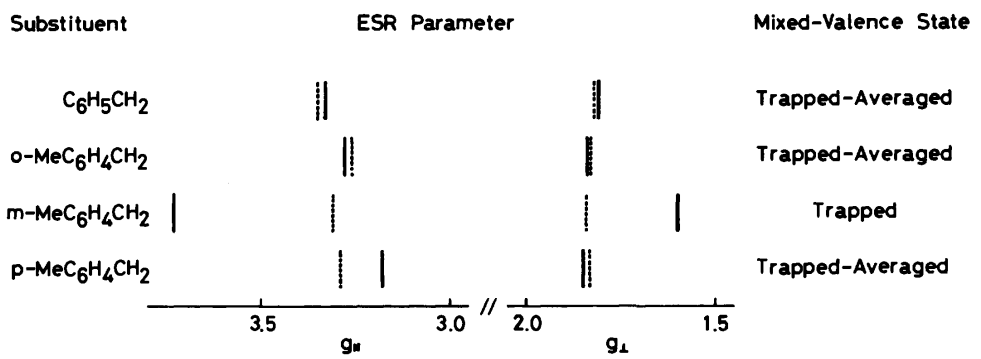

Fig. 12 Summary of ESR parameters in crystalline state (——) and dispersed state (------) at 78 K with those mixed-valence states in crystalline state for 1′,1‴-bis(methylbenzyl)biferrocenium triiodides. "Trapped-Averaged" shows a trapped-valence state at low temperatures and an averaged-valence state near room temperature. "Trapped" shows only the trapped-valence state from low temperature to room temperature.

Table 5. ESR Parameters for 1′,1‴-Bis(methylbenzyl)-biferrocenium Triiodide at 78 K

Substituent	State	$g_{\parallel}$	$g_{\perp}$	$\Delta g^{a)}$
Benzyl-	Crystalline	3.33	1.81	1.52
	Glassy	3.35	1.82	1.53
o-Methylbenzyl-	Crystalline	3.28	1.84	1.44
	Glassy	3.26	1.83	1.43
m-Methylbenzyl-	Crystalline	3.73	1.60	2.13
	Glassy	3.31	1.84	1.47
p-Methylbenzyl-	Crystalline	3.18	1.85	1.33
	Glassy	3.29	1.83	1.46

a) This is the g-tensor anisotropy defined as $\Delta g = g_{\parallel} - g_{\perp}$.

doublet), even at 4.2 K.[11]

The difference of the ESR parameters ($g_{\parallel}$, $g_{\perp}$, and Δg) among the various kinds of 1′,1‴-dialkyl and 1′,1‴-bis(methylbenzyl) derivatives in their crystalline state is reduced in the dispersed state. These differences in the ESR parameters between the crystalline and dispersed state also correspond to the differences in the valence state between both the states observed in the Mössbauer spectra for the derivatives (see the previous section). The difference in ESR parameters in crystalline samples should be attributed not only to intramolecular effects of the alkyl or methylbenzyl substituent but also to intermolecular effects. The results obtained in the present studies indicate that the packing effect of the biferrocenium cations and their counter anions influences the electronic structures and the intramolecular electron transfer rates between the two iron atoms.

References

1) "Mixed-Valence Compounds," ed by D. B. Brown, D. Reidel Publishing Company, Dordrecht (1980).
2) I. Motoyama, M. Watanabe, and H. Sano, *Chem. Lett.*, **1978**, 513.
3) M. Watanabe, S. Iijima, I. Motoyama, and H. Sano, *J. Phys. (Paris), Colloq.*, **C2**, 392 (1979).
4) S. Iijima, I. Motoyama, and H. Sano, *Bull. Chem. Soc. Jpn.*, **53**, 3130 (1980).
5) I. Motoyama, K. Suto, M. Katada, and H. Sano, *Chem. Lett.*, **1983**, 1215.
6) W. H. Morrison, Jr. and D. N. Hendrickson, *Inorg. Chem.*, **14**, 2331 (1975).
7) K. Iwai, M. Iwai, K. Suto, S. Nakashima, I. Motoyama, H. Sano, I. Ikemoto, N. Kosugi, and H. Kuroda, *Bull. Chem. Soc. Jpn.*, **59**, 2675 (1986).
8) S. Iijima, R. Saida, I. Motoyama, and H. Sano, *Bull. Chem. Soc. Jpn.*, **54**, 1375 (1981).
9) T.-Y. Dong, D. N. Hendrickson, K. Iwai, M. J. Cohn, S. J. Geib, A. L. Rheingold, H. Sano, I. Motoyama, and S. Nakashima, *J. Am. Chem. Soc.*, **107**, 7996 (1985).
10) S. Nakashima, M. Katada, I. Motoyama, and H. Sano, *Bull. Chem. Soc. Jpn.*, **59**, 2923 (1986).
11) T.-Y. Dong, D. N. Hendrickson, C. G. Pierpont, and M. F. Moore, *J. Am. Chem. Soc.*, **108**, 963 (1986).
12) M. J. Cohn, T.-Y. Dong, D. N. Hendrickson, S. J. Geib, A. L. Rheingold, *J. Chem. Soc., Chem. Commun.*, **1985**, 1095.
13) T.-Y. Dong, T. Kambara, and D. N. Hendrickson, *J. Am. Chem. Soc.*, **108**, 4423 (1986).
14) T.-Y. Dong, T. Kambara, and D. N. Hendrickson, *J. Am. Chem. Soc.*, **108**, 5857 (1986).
15) M. Katada, S. Nakashima, Y. Uchida, I. Motoyama, H. Sano, H. Sakai, and Y. Maeda, *J. Radioanal. Nucl. Chem., Lett.*, **104**, 349 (1986).
16) J. A. Kramer and D. N. Hendrickson, *Inorg. Chem.*, **19**, 3330 (1980).
17) K. Sato, S. Nakashima, M. Watanabe, I. Motoyama, and H. Sano, *Nippon Kagaku Kaishi*, **1985**, 580.

 © 1987 The Chemical Society of Japan Bull. Chem. Soc. Jpn., 60, 1681—1689 (1987)

Crystal and Molecular Structures of $[Cu_2(taec)X](ClO_4)_3 \cdot nH_2O$ (taec= *N,N',N'',N'''*-Tetrakis(2-aminoethyl)-1,4,8,11-tetraazacyclotetradecane; X=I, F, NO_2, and CH_3COO; n=0, 1, or 2). Effect of Incorporation of an Anion X on the Structure of the Complex Cation

Masahiro MIKURIYA,*,†† Sigeo KIDA,* and Ichiro MURASE†
Coordination Chemistry Laboratories, Institute for Molecular Science, Myodaiji, Okazaki 444
†Laboratory of Chemistry, College of General Education, Kyushu University 01, Ropponmatsu, Chuo-ku, Fukuoka 810
(Received November 11, 1986)

The crystal structures of four binuclear copper(II) complexes of *N,N',N'',N'''*-tetrakis(2-aminoethyl)-1,4,8,11-tetraazacyclotetradecane (taec), $[Cu_2(taec)I](ClO_4)_3$ (**1**), $[Cu_2(taec)F](ClO_4)_3 \cdot H_2O$ (**2**), $[Cu_2(taec)(NO_2)](ClO_4)_3$ (**3**), and $[Cu_2(taec)(CH_3COO)](ClO_4)_3 \cdot 2H_2O$ (**4**), were determined by single-crystal X-ray analysis. In all the complexes, each copper is coordinated by two ring- and two pendant-nitrogen atoms. All the complexes except for **4** adopt similar structures, where I^-, F^-, or NO_2^- is incorporated into the "cavity" of $[Cu_2(taec)]^{4+}$ as a bridging group. The structure of **4** is different from those of **1**, **2**, and **3**. In **4**, one of the oxygen atoms of acetate ion coordinates to one of the copper ions at the apical site and the other oxygen occupies an in-plane coordination site of the other copper ion. The structural effect of incorporation of an anion, X, into $[Cu_2(taec)]^{4+}$ was discussed on the basis of the crystal structures.

Recently we have prepared an octadentate ligand, *N,N',N'',N'''*-tetrakis(2-aminoethyl)-1,4,8,11-tetraazacyclotetradecane (abbreviated as taec) and its metal complexes.[1-5] So far, all the complexes isolated are 2:1 (metal:taec) binuclear complexes where each metal ion is coordinated by two cyclam-ring nitrogens and two pendant amino nitrogens. Two types of binuclear structures are known for these complexes. One is the chair form (Fig. 1(A)) where the cyclam ring adopts the trans III form [6] as found for $[M_2(taec)](ClO_4)_4$ (M=Cu, Ni).[1,2] The other is the boat form (Fig. 1(B)) where the cyclam ring adopts the trans I form,[6] as found for $[Cu_2(taec)X](ClO_4)_3$ (X=Br, N_3, NCO).[2,5] In the latter case, the two coordination planes face to each other forming a space or cavity in the molecule to accommodate an anion which bridges the two copper ions. Owing to this property, we obtained a series of $[Cu_2(taec)X](ClO_4)_3$ complexes (X=F, Br, I, N_3, NCO, NO_2, CH_3COO) as single crystals.[3] Further ligation of X^- to $[Cu_2(taec)]^{4+}$ was investigated by potentiometric and spectrophotometric methods.[3,7] The stabilities of halogeno-copper linkage in aqueous solution are greatly enhanced compared to those of ordinary halogeno copper complexes. Such a high stability should be ascribed not only to the binding to both copper ions but rather to the incorporation of X^- into the "cavity" of $[Cu_2(taec)]^{4+}$. It is expected that the size and shape of the anion, X^-, may affect the structure of $[Cu_2(taec)]^{4+}$, i.e., the size of the "cavity" and the coordination mode of taec. Therefore, we have carried out the X-ray structure analyses of the title complexes and compared their structures with the previous data of the bromo, azido, and cyanato complexes in order to examine the relationship between the anion, X, and the structure of taec in the $[Cu_2(taec)X](ClO_4)_3$ complexes.

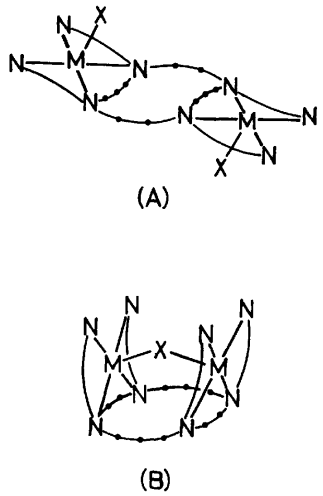

Fig. 1 Coordination modes of taec.

Experimental

The preparative methods for all the complexes were reported in the preceding paper.[3]

A Rigaku AFC-5 automated four-circle diffractometer was used for all measurements at 21±1 °C. Crystal data and details of the data collection are given in Table. 1. Lattice constants were determined by least-squares refinement based on 40 reflections with $20<2\theta<30°$. The intensity data were corrected for Lorentz-polarization effects, but not for absorption. The structures were solved by the direct methods. Refinements were carried out by the block-diagonal least-squares methods. In the course of the refinement it became apparent that the carbon atom, C(3), is

†† Present address: School of Science, Kwansei Gakuin University, Uegahara, Nishinomiya 662.

Table 1. Crystal Data and Data Collection Details[a)]

Complex	$[Cu_2(taec)I](ClO_4)_3$	$[Cu_2(taec)F](ClO_4)_3\cdot H_2O$	$[Cu_2(taec)(NO_2)](ClO_4)_2$	$[Cu_2(taec)(CH_3COO)](ClO_4)_3\cdot 2H_2O$
Formula	$C_{18}H_{44}Cl_3Cu_2IN_8O_{12}$	$C_{18}H_{46}Cl_3Cu_2FN_8O_{13}$	$C_{18}H_{44}Cl_3Cu_2N_9O_{14}$	$C_{20}H_{51}Cl_3Cu_2N_8O_{16}$
F.W.	924.95	835.06	844.05	893.12
Crystal system	Orthorhombic	Orthorhombic	Orthorhombic	Monoclinic
Space group	$Pca2_1$	$Pmn2_1$	$Pmn2_1$	$P2_1/n$
a/Å	15.612(8)	8.925(6)	8.928(4)	13.138(6)
b/Å	14.511(9)	8.124(5)	7.886(2)	28.695(13)
c/Å	14.633(4)	21.560(6)	22.074(5)	9.452(2)
β/°				93.73(3)
V/Å^3	3315.0(27)	1563.2(15)	1554.1(8)	3555.8(23)
Z	4	2	2	4
D_c/gcm^{-3}	1.85	1.77	1.80	1.67
D_m/gcm^{-3}	1.80	1.71	1.78	1.66
$F(000)$	1864	864	872	1856
μ(Mo $K\alpha$)/cm^{-1}	25.16	16.99	17.08	15.02
Crystal dimensions (mm)	0.17×0.32×0.44	0.30×0.36×0.45	0.26×0.35×0.45	0.13×0.25×0.30
2θ range/°	2.5—64.0	1.5—66.0	1.5—68.0	1.0—50.0
Total no. of observed reflections	6354	3368	3611	6714
No. of unique reflections with $\|F_o\|>3\sigma(\|F_o\|)$	3059	2493	2588	3817
Final no. of variables	390	281	299	443
Final residuals				
R	0.078	0.056	0.061	0.070
R'	0.097	0.068	0.072	0.076
Largest peak in final diff Fourier (e/Å^3)	1.20	0.93	0.88	0.71

a) Common data: graphite-monochromated Mo $K\alpha$ radiation (λ=0.71073 Å), scan type θ—2θ, scan speed 3° min^{-1}, scan width $(1.4+0.5\tan\theta)$°.

Table 2. Fractional Positional Parameters(×10^4) and Thermal Parameters of Non-Hydrogen Atoms with Their Estimated Standard Deviations in Parentheses[a)]

Atom	x	y	z	B_{eq} or B_{iso}/Å^2
(1) $[Cu_2(taec)I](ClO_4)_3$				
I	4935(1)	3667(1)	1853(2)	5.3
Cu(1)	5665(1)	1817(1)	1785(2)	3.3
Cu(2)	3923(2)	4099(2)	247(2)	3.6
Cl(1)	7135(3)	-293(4)	3545(4)	4.0
Cl(2)	2468(4)	6288(4)	3776(4)	5.0
Cl(3)	4872(4)	7370(4)	952(6)	6.5
O(1)	6497(11)	-84(15)	4187(11)	7.6
O(2)	7837(10)	-716(11)	4014(12)	6.1
O(3)	6793(14)	-847(14)	2877(15)	8.9
O(4)	7424(12)	517(11)	3154(13)	7.6
O(5)	2818(13)	6209(16)	4676(14)	9.5
O(6)	1627(15)	6252(21)	3819(22)	14.3
O(7)	2599(16)	7327(13)	3581(16)	11.2
O(8)	2822(18)	5901(26)	3294(22)	16.6
O(9)	4995(19)	6610(23)	1309(24)	14.7(10)*
O(10)[a)]	4383(28)	8047(29)	1788(41)	10.0(11)*
O(11)[a)]	5538(29)	7871(31)	1503(31)	9.9(13)*

Table 2. (Continued)

Atom	*x*	*y*	*z*	B_{eq} or B_{iso}/Å^2
O(12)[a]	4407(33)	8272(36)	646(36)	11.3(14)*
O(13)[a]	5577(38)	8054(42)	731(41)	13.7(18)*
O(14)[a]	5287(22)	7236(25)	20(27)	7.2(9)*
O(15)[a]	4272(31)	7517(34)	393(38)	11.2(14)*
N(1)	4622(9)	915(10)	1932(11)	3.4
N(2)	5932(9)	1130(10)	583(11)	3.4
N(3)	4178(13)	3410(14)	-968(11)	5.7
N(4)	2856(10)	3232(11)	358(12)	4.3
N(5)	5695(13)	1778(13)	3218(12)	5.3
N(6)	6885(12)	2231(12)	1694(18)	7.1
N(7)	4794(15)	5031(18)	-120(14)	7.4
N(8)	3215(14)	5066(14)	1016(12)	5.9
C(1)	4772(13)	191(12)	1222(15)	3.9
C(2)	5675(14)	194(14)	895(14)	4.5
C(3)	5494(17)	1304(16)	-298(15)	5.3
C(4)	5378(15)	2318(15)	-478(14)	4.6
C(5)	4494(17)	2474(14)	-1039(14)	5.3
C(6)	3236(20)	3296(20)	-1256(19)	8.4
C(7)	2741(15)	2784(17)	-566(17)	5.9
C(8)	2838(15)	2476(15)	1090(17)	5.6
C(9)	3592(12)	1799(14)	944(14)	3.7
C(10)	3737(11)	1277(13)	1841(17)	3.9
C(11)	4716(15)	515(14)	2837(13)	4.4
C(12)	4886(16)	1165(18)	3510(17)	6.3
C(13)	6845(15)	1138(16)	425(22)	6.4
C(14)	7251(22)	1388(29)	1090(28)	12.8
C(15)	4627(19)	4061(20)	-1509(18)	6.9
C(16)	5173(18)	4686(25)	-953(22)	10.4
C(17)	2155(16)	3913(17)	589(21)	6.6
C(18)	2410(18)	4534(20)	1300(22)	8.1
(2) $[Cu_2(taec)F](ClO_4)_3 \cdot H_2O$				
Cu(1)[a]	0	6402(1)	3151(1)	1.9
Cu(2)[a]	0	6401(1)	5112(1)	1.9
Cl(1)[a]	0	8913(3)	6973(1)	3.4
Cl(2)[a]	0	8907(3)	1290(1)	2.7
Cl(3)[a]	0	10722(3)	-863(3)	3.6
F[a]	0	7002(5)	4162(5)	3.1
O(1)[a]	0	10036(10)	6436(4)	4.4
O(2)[a]	0	7347(12)	6707(6)	10.4
O(3)	1288(7)	9126(10)	7355(4)	6.8
O(4)[a]	0	10030(12)	1752(5)	7.5
O(5)[a]	0	7206(10)	1524(4)	6.9
O(6)	1306(8)	9134(9)	939(4)	7.3
O(7)[a]	0	9140(18)	-739(12)	20.7
O(8)[a]	547(22)	10909(32)	-1418(7)	15.0
O(9)[a]	549(19)	11672(25)	-368(12)	14.1
O(10)[a]	1474(16)	10609(30)	-639(11)	13.1
OW[a]	657(13)	10102(10)	4187(12)	7.1
N(1)	1611(5)	4548(7)	3038(2)	2.5
N(2)	1544(6)	4577(6)	5264(2)	2.4

Table 2. (Continued)

Atom	x	y	z	B_{eq} or B_{iso}/Å^2
N(3)	1679(7)	7901(8)	2893(3)	3.6
N(4)	1650(6)	7973(6)	5389(3)	2.9
C(1)	879(8)	3596(8)	2563(3)	3.2
C(2)	2250(10)	3749(11)	3566(4)	5.2
C(3A)[a]	1639(11)	3619(12)	4146(12)	2.6
C(3B)[a]	2600(12)	4542(13)	4178(11)	2.5
C(4)	2433(9)	3808(12)	4734(3)	4.7
C(5)	627(7)	3072(8)	5494(3)	3.1
C(6)	2977(8)	5474(9)	2770(4)	3.5
C(7)	2671(10)	7018(12)	2504(6)	6.3
C(8)	2411(7)	5160(10)	5794(3)	3.3
C(9)	2908(10)	6902(11)	5697(5)	5.2
(3) $[Cu_2(taec)(NO_2)](ClO_4)_3$				
Cu(1)[a]	0	6476(1)	3386(1)	1.8
Cu(2)[a]	0	6502(1)	5407(1)	1.9
Cl(1)[a]	0	8867(3)	7234(1)	2.6
Cl(2)[a]	0	8860(3)	1573(1)	2.2
Cl(3)[a]	0	10719(2)	-596(3)	2.7
O(1)[a]	0	10023(12)	6765(5)	6.0
O(2)[a]	0	7167(10)	7030(4)	5.1
O(3)	1338(8)	9079(9)	7580(4)	6.3
O(4)[a]	0	10137(10)	2055(4)	4.4
O(5)[a]	0	7196(10)	1881(4)	6.2
O(6)	-1236(9)	9040(9)	1207(5)	7.2
O(7)[a]	0	9017(14)	-675(12)	13.0
O(8)[a]	669(19)	11284(23)	-74(6)	8.9
O(9)[a]	566(18)	11652(29)	-1099(12)	12.6
O(10)[a]	1554(16)	10951(23)	-665(11)	7.8
O(11)[a]	0	7455(6)	4420(7)	2.7
O(12A)[b]	0	9938(16)	4044(6)	3.9
O(12B)[b]	0	9895(22)	4698(9)	4.5
N(1)	1600(7)	4590(6)	3304(2)	2.3
N(2)	1577(6)	4536(6)	5497(3)	2.1
N(3)	1719(6)	7979(6)	3128(3)	2.3
N(4)	1642(7)	8066(7)	5701(3)	2.8
N(5)[a]	0	9062(9)	4298(6)	3.8
C(1)	688(8)	3069(8)	3075(4)	3.0
C(2)	2123(9)	3407(8)	3835(3)	2.7
C(3A)[a]	1603(12)	3838(12)	4393(12)	2.4
C(3B)[a]	2546(13)	4444(13)	4386(12)	2.3
C(4)	2482(8)	4215(9)	4971(3)	3.1
C(5)	862(9)	3521(9)	5960(3)	3.1
C(6)	3024(8)	5331(9)	3054(3)	2.9
C(7)	2844(11)	6930(13)	2800(5)	5.2
C(8)	2426(8)	5256(9)	6026(3)	2.9
C(9)	2806(10)	7014(9)	6007(6)	5.1
(4) $[Cu_2(taec)(CH_3COO)](ClO_4)_3 \cdot 2H_2O$				
Cu(1)	9464(1)	1243(1)	7867(1)	2.5
Cu(2)	5900(1)	942(1)	7808(1)	2.7

Table 2. (Continued)

Atom	*x*	*y*	*z*	B_{eq} or B_{iso}/Å^2
Cl(1)	7477(2)	2461(1)	2739(3)	3.8
Cl(2)	7466(2)	-1490(1)	7573(3)	4.7
Cl(3)	1822(2)	-282(1)	7960(3)	4.2
O(1)	8110(5)	783(2)	7954(7)	3.7
O(2)	6703(4)	369(2)	7480(7)	3.3
O(3)	7282(6)	2800(3)	1651(9)	6.4
O(4)	8459(6)	2267(3)	2657(8)	6.5
O(5)	7392(7)	2679(4)	4068(9)	8.0
O(6)	6741(7)	2104(3)	2583(10)	7.3
O(7)	6513(7)	-1674(4)	7762(11)	9.1
O(8)	7459(8)	-1253(5)	6298(11)	11.5
O(9)	8189(8)	-1843(4)	7642(13)	10.3
O(10)	7736(11)	-1166(4)	8684(13)	13.0
O(11)	1886(12)	-150(4)	6594(10)	13.7
O(12)	2110(6)	-751(3)	8222(9)	6.6
O(13)	822(8)	-236(4)	8308(18)	16.0
O(14)	2408(11)	19(4)	8815(13)	13.3
OW(1)	2651(6)	-3737(3)	6600(10)	7.1
OW(2)	5900(7)	-420(4)	8823(11)	8.3
N(1)	9363(5)	1483(3)	5802(7)	3.0
N(2)	9178(5)	1929(3)	8437(8)	2.7
N(3)	5490(6)	1609(3)	8213(8)	3.2
N(4)	5668(6)	1111(3)	5670(8)	3.4
N(5)	10496(6)	780(3)	7215(9)	4.0
N(6)	9829(6)	1133(3)	9946(8)	3.9
N(7)	5911(6)	840(3)	9922(8)	3.2
N(8)	4381(6)	553(3)	7382(9)	4.6
C(1)	9381(7)	2003(4)	5871(10)	3.8
C(2)	9775(7)	2170(3)	7344(10)	3.3
C(3)	8147(7)	2150(4)	8417(11)	3.7
C(4)	7331(6)	1845(3)	9004(10)	2.8
C(5)	6286(7)	1984(3)	8285(12)	3.8
C(6)	4721(7)	1713(4)	6999(12)	4.1
C(7)	5156(7)	1566(5)	5573(11)	4.8
C(8)	6618(7)	1106(4)	4852(10)	4.0
C(9)	7441(7)	1433(4)	5459(10)	3.0
C(10)	8468(7)	1299(4)	4896(9)	3.9
C(11)	10344(7)	1309(4)	5241(10)	4.1
C(12)	10523(8)	811(4)	5660(12)	4.8
C(13)	9728(8)	1979(4)	9864(11)	4.3
C(14)	9538(8)	1550(4)	10735(10)	4.0
C(15)	4973(8)	1565(4)	9580(11)	4.3
C(16)	5616(7)	1278(3)	10621(10)	3.3
C(17)	4985(8)	737(4)	5048(11)	4.3
C(18)	4036(8)	652(5)	5899(12)	5.5
C(19)	7678(7)	411(3)	7619(10)	3.1
C(20)	8283(8)	-23(4)	7375(14)	5.0

a) Atoms refined with occupancy factors of 0.5. b) Atoms refined with occupancy factors of 0.25. c) Starred values are for atoms refined isotropically. Anisotropically refined atoms are given in the form of the isotropic equivalent thermal parameter defined as $4/3[a^2B_{11}+b^2B_{22}+c^2B_{33}+ab(\cos\gamma)B_{12}+ac(\cos\beta)B_{13}+bc(\cos\alpha)B_{23}]$.

Table 3. Selected Interatomic Distances (l/Å) and Angles (ϕ/°) with Their Estimated Standard Deviations in Parentheses

(1) $[Cu_2(taec)I](ClO_4)_3$			
Cu(1)-Cu(2)	4.841(3)	Cu(1)-N(6)	2.001(19)
Cu(1)-I	2.919(3)	Cu(2)-N(3)	2.078(17)
Cu(2)-I	2.901(3)	Cu(2)-N(4)	2.095(16)
Cu(1)-N(1)	2.101(14)	Cu(2)-N(7)	1.992(25)
Cu(1)-N(2)	2.064(16)	Cu(2)-N(8)	2.111(20)
Cu(1)-N(5)	2.098(18)		
Cu(1)-I-Cu(2)	112.6(1)	N(3)-Cu(2)-N(4)	86.0(7)
N(1)-Cu(1)-N(2)	86.7(6)	N(3)-Cu(2)-N(7)	88.0(8)
N(1)-Cu(1)-N(5)	84.1(7)	N(4)-Cu(2)-N(8)	86.6(7)
N(2)-Cu(1)-N(6)	84.1(8)	N(7)-Cu(2)-N(8)	92.9(9)
N(5)-Cu(1)-N(6)	93.1(10)	I-Cu(2)-N(3)	119.0(5)
I-Cu(1)-N(1)	105.4(4)	I-Cu(2)-N(4)	103.9(5)
I-Cu(1)-N(2)	123.5(4)	I-Cu(2)-N(7)	89.6(6)
I-Cu(1)-N(5)	89.9(5)	I-Cu(2)-N(8)	89.8(5)
I-Cu(1)-N(6)	95.6(5)		
(2) $[Cu_2(taec)F](ClO_4)_3 \cdot H_2O$[a]			
Cu(1)-Cu(2)	4.229(2)	Cu(1)-N(3)	2.009(6)
Cu(1)-F	2.234(10)	Cu(2)-N(2)	2.050(5)
Cu(2)-F	2.106(10)	Cu(2)-N(4)	2.039(6)
Cu(1)-N(1)	2.097(5)		
Cu(1)-F-Cu(2)	154.0(2)	N(2)-Cu(2)-N(2)^i	84.5(2)
N(1)-Cu(1)-N(1)^i	86.6(2)	N(2)-Cu(2)-N(4)	85.4(2)
N(1)-Cu(1)-N(3)	83.8(2)	N(4)-Cu(2)-N(4)^i	92.5(2)
N(3)-Cu(1)-N(3)^i	96.5(3)	F-Cu(2)-N(2)	108.9(2)
F-Cu(1)-N(1)	105.7(2)	F-Cu(2)-N(4)	98.1(2)
F-Cu(1)-N(3)	97.9(2)		
(3) $[Cu_2(taec)(NO_2)](ClO_4)_3$[a]			
Cu(1)-Cu(2)	4.462(2)	Cu(2)-N(2)	2.104(5)
Cu(1)-O(11)	2.411(15)	Cu(2)-N(4)	2.022(6)
Cu(2)-O(11)	2.304(15)	N(5)-O(11)	1.296(10)
Cu(1)-N(1)	2.070(6)	N(5)-O(12A)	0.889(17)
Cu(1)-N(3)	2.021(5)	N(5)-O(12B)	1.102(22)
Cu(1)-O(11)-Cu(2)	142.3(2)	N(2)-Cu(2)-N(2)^i	84.0(2)
Cu(1)-O(11)-N(5)	96.6(10)	N(2)-Cu(2)-N(4)	86.2(2)
Cu(2)-O(11)-N(5)	121.1(10)	N(4)-Cu(2)-N(4)^i	92.9(2)
N(1)-Cu(1)-N(1)^i	87.3(2)	O(11)-Cu(2)-N(2)	109.2(2)
N(1)-Cu(1)-N(3)	82.7(2)	O(11)-Cu(2)-N(4)	96.0(2)
N(3)-Cu(1)-N(3)^i	98.9(2)	O(11)-N(5)-O(12A)	153.1(17)
O(11)-Cu(1)-N(1)	108.2(2)	O(11)-N(5)-O(12B)	114.6(15)
O(11)-Cu(1)-N(3)	94.5(2)	O(12A)-N(5)-O(12B)	92.4(14)
(4) $[Cu_2(taec)(CH_3COO)](ClO_4)_3 \cdot 2H_2O$			
Cu(1)-Cu(2)	4.758(2)	Cu(2)-N(3)	2.031(8)
Cu(1)-N(1)	2.066(7)	Cu(2)-N(4)	2.081(8)
Cu(1)-N(2)	2.083(8)	Cu(2)-N(7)	2.018(8)
Cu(1)-N(5)	2.023(9)	Cu(2)-N(8)	2.301(9)
Cu(1)-N(6)	2.017(8)	C(19)-O(1)	1.240(11)
Cu(1)-O(1)	2.222(6)	C(19)-O(2)	1.284(11)

Table 3. (Continued)

Cu(2)-O(2)	1.990(6)	C(19)-C(20)	1.502(14)
N(1)-Cu(1)-N(2)	85.8(3)	O(2)-Cu(2)-N(7)	93.7(3)
N(1)-Cu(1)-N(5)	86.2(3)	N(8)-Cu(2)-O(2)	91.9(3)
N(2)-Cu(1)-N(6)	86.0(3)	N(8)-Cu(2)-N(3)	104.7(3)
N(5)-Cu(1)-N(6)	94.2(4)	N(8)-Cu(2)-N(4)	82.6(3)
O(1)-Cu(1)-N(1)	103.3(3)	N(8)-Cu(2)-N(7)	93.0(3)
O(1)-Cu(1)-N(2)	113.2(3)	Cu(1)-O(1)-C(19)	148.9(6)
O(1)-Cu(1)-N(5)	100.1(3)	Cu(2)-O(2)-C(19)	116.2(6)
O(1)-Cu(1)-N(6)	90.7(3)	O(1)-C(19)-O(2)	122.9(9)
N(3)-Cu(2)-N(4)	86.6(3)	O(1)-C(19)-C(20)	120.9(9)
N(3)-Cu(2)-N(7)	86.3(3)	O(2)-C(19)-C(20)	116.1(8)
O(2)-Cu(2)-N(4)	94.9(3)		

a) Superscript i refers to the equivalent position $(-x, y, z)$.

subjected to disorder in $[Cu_2(taec)X](ClO_4)_3$ (X=F and NO_2). The carbon atom was divided into two positions with an occupancy factor 0.5 on the basis of a difference Fourier map. Hydrogen atoms were inserted in their calculated positions and fixed at their positions. The final discrepancy factors, $R=\Sigma||F_o|-|F_c||/\Sigma|F_o|$ and $R'=[\Sigma w(|F_o|-|F_c|)^2/\Sigma w|F_o|^2]^{1/2}$, are listed in Table 1. The weighting scheme, $w=[\sigma_{count}^2+(0.015|F_o|)^2]^{-1}$, was employed.

The atomic scattering factors for all the atoms and the anomalous dispersion corrections, $\Delta f'$ and $\Delta f''$, for all the non-hydrogen atoms were taken from Ref. 8. All the calculations were carried out on the HITAC M-680 H computer at the Computer Center of the Institute for Molecular Science using a local version of the MULTAN 78,[9] UNICS-III,[10] and ORTEP[11] programs. Atomic coordinates and thermal parameters of non-hydrogen atoms are listed in Table 2. The anisotropic thermal parameters of non-hydrogen atoms, the atomic coordinates and thermal parameters of hydrogen atoms, and the F_o—F_c tables have been deposited as a Document No. 8737 at the Office of the Editor.

Description of the Structures

$[Cu_2(taec)I](ClO_4)_3$. The crystal and molecular structure of $[Cu_2(taec)I](ClO_4)_3$ is similar to that of $[Cu_2(taec)Br](ClO_4)_3$[2]; they are isomorphous. A perspective drawing of the complex cation, $[Cu_2(taec)I]^{3+}$, and the numbering system are illustrated in Fig. 2. The cyclam ring assumes the trans I form. The taec ligand forms two 5-5-5 fused chelate ring systems with two copper ions. The coordination geometry of each copper ion is an elongated square pyramid. The basal plane is formed by two nitrogens of the cyclam ring and two pendant amino nitrogens. The deviations of the basal atoms from the mean plane are within ±0.15 Å, and Cu(1) and Cu(2) are displaced by 0.48 and 0.38 Å, respectively, from the mean planes toward the iodide ion. The iodide ion coordinates to both copper ions at the apical positions with Cu–I distances of 2.919(3) and 2.901(3) Å in the "cavity" of

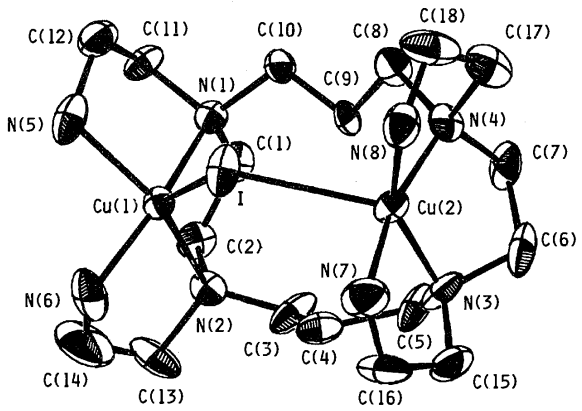

Fig. 2. ORTEP diagram of $[Cu_2(taec)I](ClO_4)_3$.

$[Cu_2(taec)]^{4+}$. The sixth coordination is not feasible because the other axial site of the copper ion is blocked by the CH_2 chains of taec. The pendant amino groups form hydrogen bonds with the iodide ion i.e., I···N(5) 3.593(19), I···N(6) 3.696(19), I···N(7) 3.507(22), I···N(8) 3.582(21) Å. These hydrogen bonds may contribute to the stabilization of the Cu–I bonds. The perchlorate ions are hydrogen-bonded to the pendant amino groups, e.g., O(4)···N(5) 3.262(27) Å.

$[Cu_2(taec)F](ClO_4)_3 \cdot H_2O$. A perspective drawing of the complex cation of $[Cu_2(taec)F](ClO_4)_3 \cdot H_2O$ is shown in Fig. 3. The complex cation has a mirror plane containing Cu(1), Cu(2), and F as required from the crystallographic symmetry. The coordination mode of taec is similar to that of $[Cu_2(taec)I](ClO_4)_3$. The coordination geometry of each copper ion is an elongated square pyramid. The basal planes are perfectly planar as required from the symmetry (the mirror plane) of the complex cation and the copper ions, Cu(1) and Cu(2), are displaced by 0.41 and 0.47 Å, respectively, from the planes toward the fluoride ion. The fluoride ion bridges the two copper

ions at the apical positions with Cu–F distances of 2.234(10) and 2.106(10) Å. The Cu(1)–Cu(2) separation (4.229(2) Å) is the shortest and the Cu(1)–F–Cu(2) angle (154.0 (2)°) is the largest among the $[Cu_2(taec)X](ClO_4)_3$ complexes. The oxygen atom of the water molecule, OW, (whose occupancy factor is 0.5) is located in a vicinity of the "cavity" of $[Cu_2(taec)]^{4+}$ forming a hydrogen bond with the fluoride ion (F···OW 2.587(10) Å).[12] The pendant amino groups form hydrogen bonds to the fluoride ion and perchlorate ions, e.g., F···N(3) 3.203(11), F···N(4) 3.129(11). O(2)···N(4) 3.240(13) Å.

$[Cu_2(taec)(NO_2)](ClO_4)_3$. The crystals of $[Cu_2(taec)(NO_2)](ClO_4)_3$ and $[Cu_2(taec)F](ClO_4)_3 \cdot H_2O$ are isomorphous. The complex cation, $[Cu_2(taec)(NO_2)]^{3+}$, has a mirror plane containing Cu(1), Cu(2), O(11), N(5), O(12A), and O(12B) (Fig. 4). The nitrite ion bridges the two copper ions with one of its oxygen atoms. The other oxygen atom of the nitrite ion is disordered in the ratio 1:1 (O(12A):O(12B)). Such disorder is a common feature of crystal structure of nitrito complexes.[13]

$[Cu_2(taec)(CH_3COO)](ClO_4)_3 \cdot 2H_2O$. A perspective drawing of the complex cation, $[Cu_2(taec)(CH_3COO)]^{3+}$, is illustrated in Fig. 5. The two copper ions are bridged by the acetate ion. There is, however, a significant difference between the coordination geometries about the two copper ions. As found in other $[Cu_2(taec)X](ClO_4)_3$ complexes, the coordination geometry of Cu(1) is a distorted square pyramid with two nitrogens of the cyclam ring and two nitrogens of the pendant amino groups in the basal plane and an oxygen atom of the acetate ion, O(1), in the apical position. The geometry of Cu(2) is also described as a square-pyramid, but in this case the apical position is occupied by the pendant amino nitrogen, N(8), and the basal plane is formed by one of the bridging-acetate oxygens, O(2), the pendant-amino nitrogen, N(7), and two nitrogens of the cyclam ring, N(3) and N(4). Thus, the coordination mode of taec is different from those of other $[Cu_2(taec)X](ClO_4)_3$ complexes (X=F, Br, I, N_3, NCO, NO_2). The Cu(1)–Cu(2) distance is 4.758(2) Å shorter than that of $[Cu_2(taec)I](ClO_4)_3$. One of two water molecules is hydrogen-bonded to the bridging acetate oxygen atom, O(2), and a pendant amino nitrogen, i.e., O(2)···OW(2) 2.831 (12), N(7)···OW(2) $(1-x, -y, 2-z)$ 2.983(12) Å. Another water molecule is hydrogen-bonded to the perchlorate oxygen, O(10), and the pendant-amino nitrogen, N(5), i.e., O(10)···OW(1) $(1/2+x, 1/2-y, 1/2+z)$ 2.780(15), N(5)···OW(1) $(1/2-x, 1/2+y, 3/2-z)$ 2.959 (12) Å.

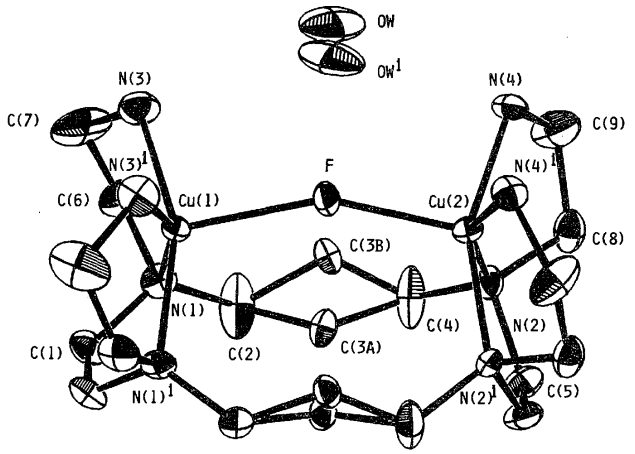

Fig. 3. ORTEP diagram of $[Cu_2(taec)F](ClO_4)_3 \cdot H_2O$.

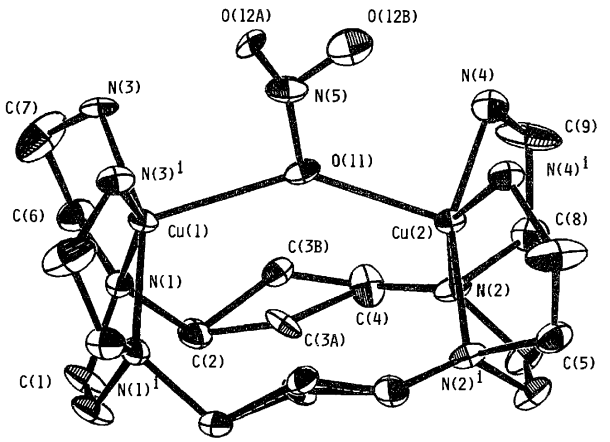

Fig. 4. ORTEP diagram of $[Cu_2(taec)(NO_2)](ClO_4)_3$.

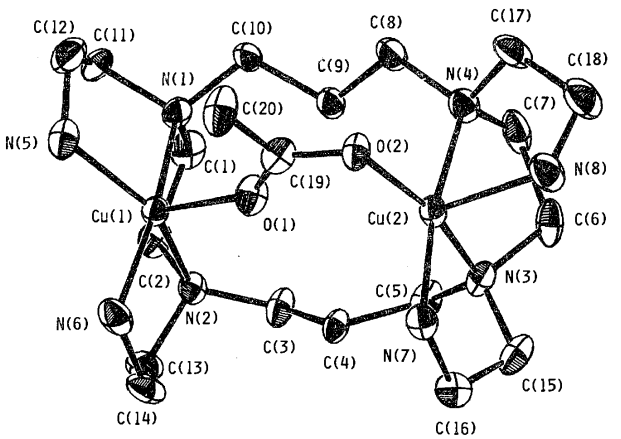

Fig. 5. ORTEP diagram of $[Cu_2(taec)(CH_3COO)](ClO_4)_3 \cdot 2H_2O$.

Discussion

The structures of all the present complexes except for $[Cu_2(taec)(CH_3COO)](ClO_4)_3 \cdot 2H_2O$ are essentially the same as those of previously reported $[Cu_2(taec)X](ClO_4)_3$ (X=Br, N_3, NCO),[2,5] where the coordination

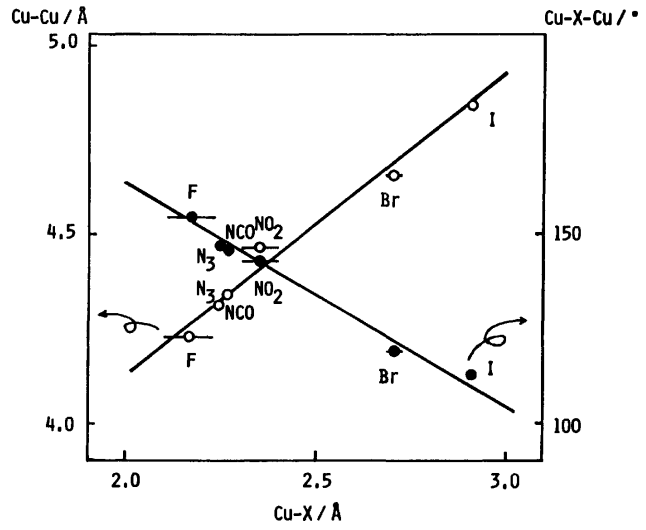

Fig. 6. Correlations of Cu-Cu distance (O) and Cu-X-Cu angle (●) with Cu-X distance.

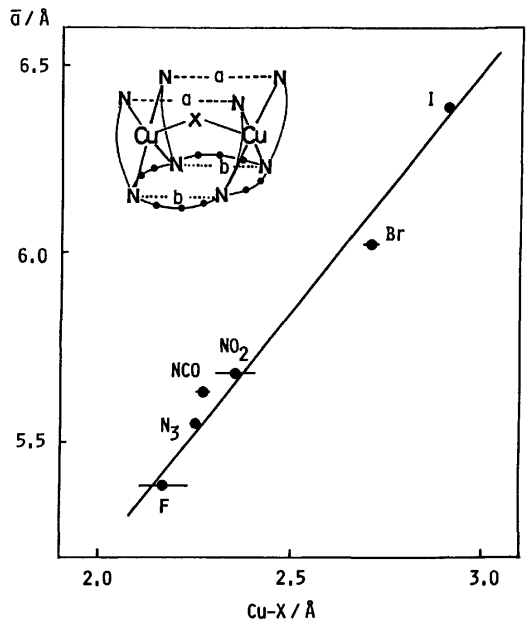

Fig. 7. Correlation between Cu-X and average value of a in $[Cu_2(taec)X](ClO_4)_3$. Parameters a and b represent the N-N distances indicated by ------ and ·····, respectively.

mode of taec is the boat form as shown in Fig. 1(B), and an anion, X, is incorporated into the "cavity" of $[Cu_2(taec)]^{4+}$. Coordination geometry of each copper ion can be described as an elongated square-pyramid. The in-plane Cu-N distances are in the range of 1.988—2.111 Å. The displacement of the copper ion from the basal plane is in the range of 0.38—0.48 Å. The Cu-X and Cu-Cu distances increase and the Cu-X-Cu angle decreases in the increasing order of bridging atom size, $F<N_3<NCO<NO_2<Br<I$ (Fig. 6). The decrease of the Cu-X-Cu angle implies that the anion is pushed out in some degree from the center of the complex cation. It is interesting to see the "cavity" size as a function of the size of X^-. The size may be expressed by two parameters a and b defined in Fig. 7. The a value increases from 5.382 Å to 6.393 Å with increasing the size of bridging atom of X or Cu-X distance, whereas b varies little (4.800—4.912 Å). In other words, the $[Cu_2(taec)]^{4+}$ slightly varies its configuration to accommodate the anion though the expansion of the "cavity" size is limited so that the larger anion tends to be somewhat pushed out from the center of the complex cation as already stated. However, in the case of $X=CH_3COO$, the acetate ion can not take a bridging mode similar to that of NO_2^- in $[Cu_2(taec)(NO_2)](ClO_4)_3$ because of steric hindrance between its methyl group and the pendant amino groups. Thus, one of the pendant amino group (N(8)) is pushed out from the equatorial coordination position of the copper ion and located at the axial position. Instead, the equatorial coordination position is occupied by another oxygen of the acetate ion.

References

1) I. Murase, M. Mikuriya, H. Sonoda, and S. Kida, *J. Chem. Soc., Chem. Commun.*, **1984**, 692.

2) I. Murase, M. Mikuriya, H. Sonoda, Y. Fukuda, and S. Kida, *J. Chem. Soc., Dalton Trans.*, **1986**, 953.

3) S. Kida, I. Murase, C. Harada, L. Daizeng, and M. Mikuriya, *Bull. Chem. Soc. Jpn.*, **59**, 2595 (1986).

4) M. Mikuriya, S. Kida, and I. Murase, *J. Chem. Soc., Dalton Trans.*, in press.

5) M. Mikuriya, S. Kida., and I. Murase, *Bull. Chem. Soc. Jpn.*, **60**, 1355 (1987).

6) B. Bosnich, C. K. Poon, and M. L. Tobe, *Inorg. Chem.*, **4**, 1102 (1965).

7) A. Evers, R. D. Hancock, and I. Murase, *Inorg. Chem.*, **25**, 2160 (1986).

8) "International Tables for X-Ray Crystallography," Kynoch Press, Birmingham (1974), Vol. 4.

9) P. Main, S. E. Hull, L. Lessinger, G. Germain, J. P. Declercq, and M. M. Woolfson, *MULTAN* 78, A System of Computer Programs for the Automatic Solution of Crystal Structures from X-Ray Diffraction Data, University of York (1978).

10) T. Sakurai and K. Kobayashi, *Rikagaku Kenkyusho Hokoku*, **55**, 69 (1979).

11) C. K. Johnson, *Report No. ORNL* 3794, Oak Ridge National Laboratory, Oak Ridge, Tenessee (1965).

12) J. Emsley, N. M. Reza, H. M. Dawes, and M. B. Hursthouse, *J. Chem. Soc., Dalton Trans.*, **1986**, 313.

13) M. A. Hitchman and G. L. Rowbottom, *Coord. Chem. Rev.*, **42**, 55 (1982).

 © 1987 The Chemical Society of Japan Bull. Chem. Soc. Jpn., 60, 1691—1698 (1987)

Calorimetric and Spectrophotometric Studies of Bromo Complexes of Copper(II) in *N,N*-Dimethylformamide

Shin-ichi ISHIGURO,* Kazuhiko OZUTSUMI, László NAGY,† and Hitoshi OHTAKI††
Coordination Chemistry Laboratories, Institute for Molecular Science, Myodaiji, Okazaki 444
††Department of Electronic Chemistry, Tokyo Institute of Technology at Nagatsuta, Nagatsuta, Midori-ku, Yokohama 227
(Received November 17, 1986)

Complexation of copper(II) with Br^- ions has been studied by calorimetry and spectrophotometry in *N,N*-dimethylformamide (DMF) containing 0.16 mol dm^{-3} $(C_2H_5)_4NClO_4$, 1 mol dm^{-3} $LiClO_4$, and 1 mol dm^{-3} NH_4ClO_4 as constant ionic media at 25 °C. Calorimetric titration curves obtained in each solution were well explained in terms of formation of $[CuBr_n]^{(2-n)+}$ (n=1—4) and their formation constants, enthalpies and entropies were determined. Electronic spectra of individual copper(II) bromo complexes were also determined in the $(C_2H_5)_4NClO_4$, $LiClO_4$, and NH_4ClO_4 DMF solutions over the range 260—500 nm, the spectra of each complex being kept practically unchanged in these solutions. The complexation of copper(II) with Br^- ions is considerably weaker in the $LiClO_4$ solution than in the $(C_2H_5)_4NClO_4$ one and is even more weakened in the NH_4ClO_4 solution due to the formation of LiBr and NH_4Br ion pairs in the relevant solutions. The variation of the stepwise enthalpy and entropy values suggests that the coordination structure around copper(II) ion changes from octahedral to tetrahedral at the formation of $[CuBr_3]^-$. The result for the complexation between copper(II) and bromide ions thus obtained was compared with that for the complexation between the metal and chloride ions.

Complexation of copper(II) with chloride ions has so far been studied in aqueous and nonaqueous solutions, and the formation constants and enthalpies of the mononuclear $[CuCl_n]^{(2-n)+}$ (n=1—4) complexes have been determined.[1-6]

On the other hand, as to the copper(II) bromo complexes, the formation constants and enthalpies have been obtained only for the mono- and dibromocopper(II) complexes,[7] although the formation of $[CuBr_4]^{2-}$ was indicated by spectrophotometry in some aprotic solvents.[8-12] The $[CuBr_4]^{2-}$ complex has the flattened tetrahedral D_{2d} structure in the $Cs_2[CuBr_4]$ crystal.[13] By judging from similar electronic spectra of $[CuBr_4]^{2-}$ in solution and in the $Cs_2[CuBr_4]$ crystal,[14-15] the flattened tetrahedral D_{2d} structure of $[CuBr_4]^{2-}$ is also expected in solution, as well as in the case of $[CuCl_4]^{2-}$.[16] In fact, the tetrahedral $[CuBr_4]^{2-}$ complex was revealed in water by the X-ray diffraction method.[17] Although the structure of the tetrahalogenocuprate(II) complex is thus well established both in crystal and in solution, the knowledge of the structure of the mono-, di-, and trihalogeno complexes of copper(II) ion in solution is limited because these complexes have hardly been isolatd as single crystals. We recently elucidated by the X-ray diffraction method that the mono- and trichloro complexes have the distorted octahedral $[CuCl(dmf)_5]^+$ and the distorted tetrahedral $[CuCl_3(dmf)]^-$ structures, respectively, in *N, N*-dimethylformamide (DMF).[18] The formation of the distorted octahedral $[CuBr(H_2O)_5]^+$ complex has been also indicated.[17] Barnes and Hume[10] suggested the formation of the five-coordinate $[CuBr_3(solvent)_2]^-$ complex having a distorted trigonal-bipyramidal structure from measurements of electronic spectra in various aprotic solvents.

In order to throw more light on the formation and the structure of copper(II) bromo complexes in solution, we investigated the complexation between copper(II) and bromide ions in DMF containing 0.16 mol dm^{-3} $(C_2H_5)_4NClO_4$, 1 mol dm^{-3} $LiClO_4$, and 1 mol dm^{-3} NH_4ClO_4 as constant ionic media at 25 °C by using similar calorimetric and spectrophotometric procedures to those employed previously for the copper(II) chloride system in some aprotic solvents.[1,2]

Experimental

Reagent. All chemicals used were of reagent grade. *Lithium bromide* was once recrystallized from methanol. *Ammonium perchlorate, tetraethylammonium bromide,* and *ammonium bromide* were used without further purification. LiBr and $(C_2H_5)_4NBr$ were dried at 150 and 100 °C, respectively, in vacuum and NH_4ClO_4 and NH_4Br at 150 °C under an atmospheric pressure.

Other chemicals were prepared or purified as described elsewhere.[1]

Measurements. Calorimetric and spectrophotometric measurements were carried out in a room thermostated at (25±0.2) °C. Test solutions contained 0.16 mol dm^{-3} $(C_2H_5)_4NClO_4$, 1 mol dm^{-3} $LiClO_4$ or 1 mol dm^{-3} NH_4ClO_4 as a constant ionic medium.

Calorimetric titrations were performed using a Dewar vessel in a water-bath thermostated at (25±0.007) °C. 100 cm^3 of a $Cu(ClO_4)_2$ DMF solution containing 0.16 mol dm^{-3} $(C_2H_5)_4NClO_4$, 1 mol dm^{-3} $LiClO_4$, or 1 mol dm^{-3} NH_4ClO_4 was placed in a Dewar vessel which was filled with dry nitrogen gas and isolated from moisture with a P_2O_5 drying-tube, and then it was titrated with the relevant titrant solution of 0.16 mol dm^{-3} $(C_2H_5)_4NBr$, 1 mol dm^{-3} LiBr, or 1 mol dm^{-3} NH_4Br. The concentration of metal

† Present address: Department of Inorganic and Analytical Chemistry, A. József University, Szeged, Hungary.

ions in the initial test solution was varied over the range 5—20 mmol dm^{-3} in the $(C_2H_5)_4NClO_4$ DMF solution and 20—50 mmol dm^{-3} in the $LiClO_4$ and NH_4ClO_4 DMF solutions. Heats of complexation observed at each titration point were ranged 1—7 J in the $(C_2H_5)_4NClO_4$ and NH_4ClO_4 solutions and 1—12 J in the $LiClO_4$ solution with a certainty ±0.05 J and were corrected for heats of dilution of the titrant. Heats of dilution were measured in advance by separate experiments. All of the measurements were carried out by using a fully automatic on-line system for calorimetry developed in our laboratory.[19] Details of the data treatment have been described elsewhere.[1]

Electronic spectra were measured with a HITACHI 340 spectrophotometer (HITACHI) equipped with a PC-9801 computer (NEC) which recorded data every 2 nm over the wavelength range 260—500 nm. A flow cell with a light-path length of 0.5 cm was connected with a titration vessel through Teflon and glass tubes. 20 cm^3 of a $Cu(ClO_4)_2$ solution was placed in a vessel under a dry nitrogen atmosphere and then titrated with the relevant titrant solution.

Results and Discussion

Calorimetric Results. Calorimetric titration curves for complexation between copper(II) and bromide ions obtained in 0.16 mol dm^{-3} $(C_2H_5)_4NClO_4$, 1 mol dm^{-3} $LiClO_4$, and 1 mol dm^{-3} NH_4ClO_4 DMF solutions are depicted in Figs. 1, 2, and 3, respectively. In each figure, enthalpies $\Delta H^\circ = -q/(\delta v C_{X,tit})$ were plotted against C_X/C_M, where q, δv, C_X, and C_M stand for the heat evolved, the volume of an aliquot of the titrant added and the total concentrations of bromide

Table 1. The Least-Squares Refinement of Overall Formation Constants, $\log(\beta_n/\text{mol}^{-n}\,\text{dm}^{3n})$, and Enthalpies, $\Delta H^\circ_{\beta n}/\text{kJ mol}^{-1}$, of $[CuBr_n]^{(2-n)+}$ Using Calorimetric Data in *N*,*N*-Dimethylformamide Containing 0.16 mol dm^{-3} $(C_2H_5)_4NClO_4$ at 25 °C

	(1, 3)	(1, 2, 3)	(1, 3, 4)	(1-4)
$\log\beta_1$	3.17 (0.13)	3.08 (0.14)	3.30 (0.10)	3.48 (0.08)
$\log\beta_2$	—	5.43 (0.13)	—	5.54 (0.13)
$\log\beta_3$	9.67 (0.13)	7.78 (0.12)	8.26 (0.12)	8.50 (0.09)
$\log\beta_4$	—	—	8.97 (0.38)	9.77 (0.16)
$\Delta H^\circ_{\beta 1}$	20.9 (0.5)	21.5 (0.8)	20.4 (0.3)	19.6 (0.2)
$\Delta H^\circ_{\beta 2}$	—	33.4 (0.8)	—	38.1 (1.5)
$\Delta H^\circ_{\beta 3}$	61.5 (0.4)	65.2 (0.5)	55.8 (0.5)	56.2 (0.5)
$\Delta H^\circ_{\beta 4}$	—	—	96.3 (22)	72.7 (2)
U[a]	3.2	1.48	0.983	0.291
R[b]	0.0522	0.0345	0.0289	0.0158

Values in parentheses refer to standard deviations. The sets (1, 4) and (1-5) gave larger U values. The number of calorimetric data points is 96. a) Error-square sum. b) The Hamilton R-factor.

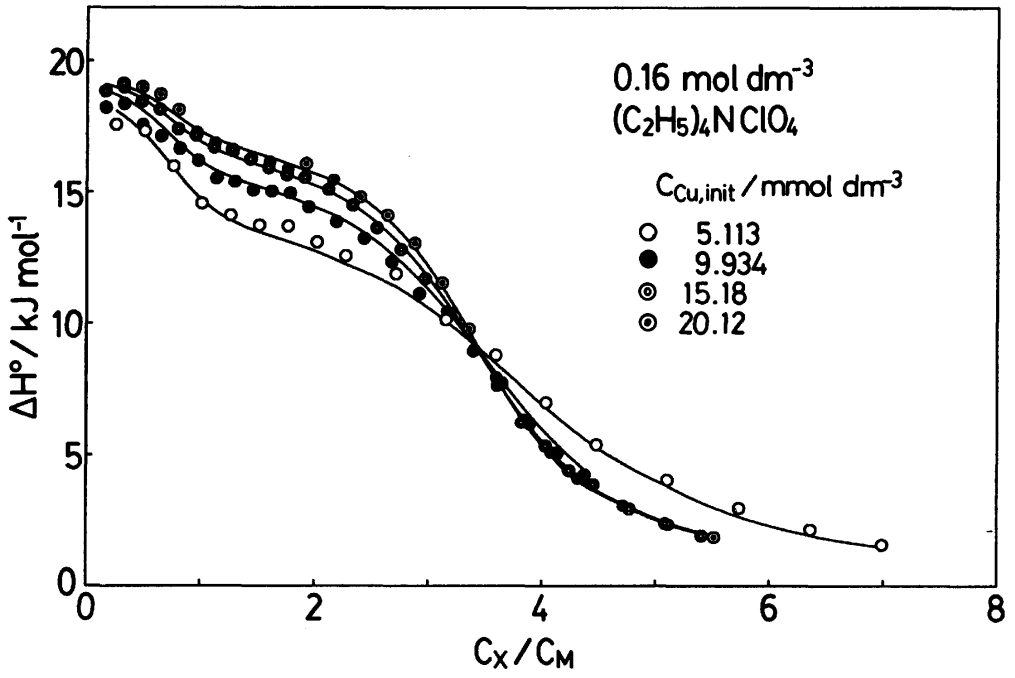

Fig. 1. Calorimetric titration curves of copper(II) bromide DMF solutions containing 0.16 mol dm^{-3} $(C_2H_5)_4NClO_4$ at 25 °C. Concentrations of copper(II) ions, $C_{Cu,init}$/mmol dm^{-3}, in initial test solutions are given in the figure. The solid lines show the curves calculated by using the constants of the set (1—4) by calorimetry in Table 2.

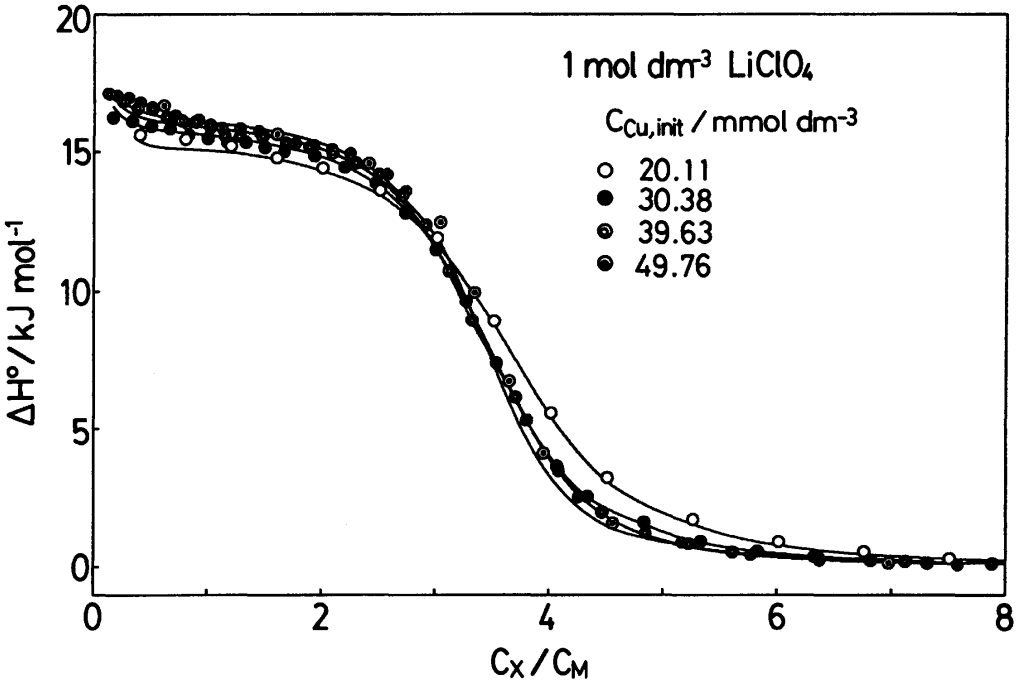

Fig. 2. Calorimetric titration curves of copper(II) bromide DMF solutions containing 1 mol dm^{-3} $LiClO_4$ at 25 °C. Concentrations of copper(II) ions, $C_{Cu,init}$/mmol dm^{-3}, in initial test solutions are given in the figure. The solid lines show the curves calculated by using the constants of the set (1—4) by calorimetry in Table 2.

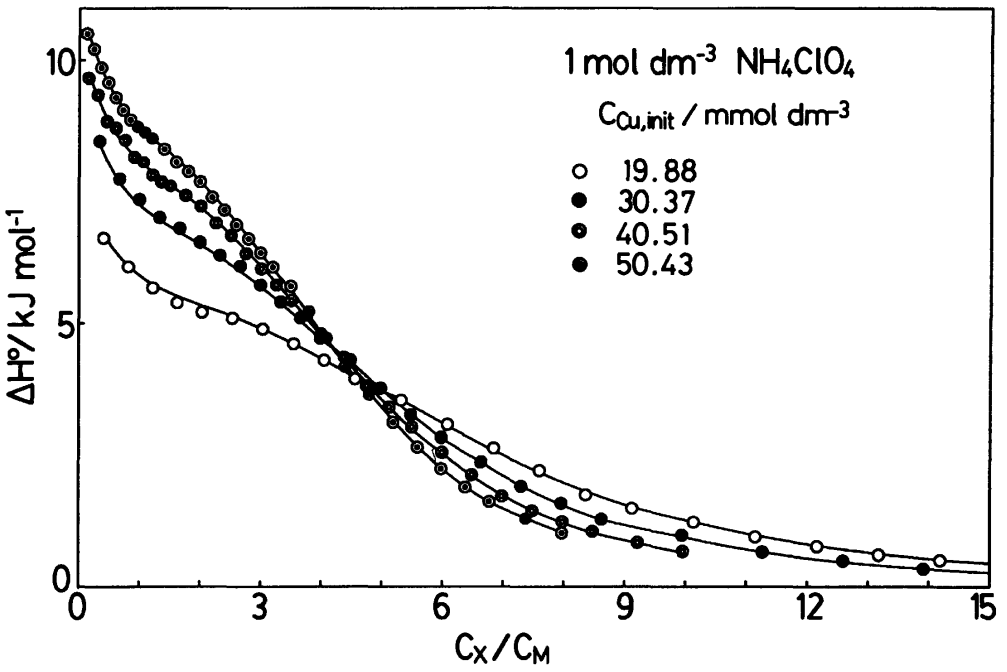

Fig. 3. Calorimetric titration curves of copper(II) bromide DMF solutions containing 1 mol dm^{-3} NH_4ClO_4 at 25 °C. Concentrations of copper(II) ions, $C_{Cu,init}$/mmol dm^{-3}, in initial test solutions are given in the figure. The solid lines show the curves calculated by using the constants of the set (1—4) by calorimetry in Table 2.

and copper(II) ions in solution, respectively, at each titration point, and $C_{X,tit}$ denotes the concentration of bromide ion in the titrant solution.

The calorimetric data obtained in each solution were analyzed by assuming the formation of plausible copper(II) bromo complexes and by simultaneously optimizing their formation constants and enthalpies by the least-squares method, the typical results obtained in the $(C_2H_5)_4NClO_4$ DMF solution being listed in Table 1. As seen in Table 1, among various sets examined the set (1—4) assuming the formation of $[CuBr_n]^{(2-n)+}$ (n=1—4) shows the minimal error-square sum U. The calorimetric data obtained in the $LiClO_4$ and NH_4ClO_4 DMF solutions were also

Table 2. Final Results of the Least-Squares Refinement of Overall Formation Constants, $\log(\beta_n/\text{mol}^{-n}\,\text{dm}^{3n})$, and Enthalpies, $\Delta H^\circ_{\beta n}$/kJ mol^{-1}, of $[CuBr_n]^{(2-n)+}$ in *N,N*-Dimethylformamide at 25 °C

	0.16 mol dm^{-3} $(C_2H_5)_4NClO_4$	1 mol dm^{-3} $LiClO_4$	1 mol dm^{-3} NH_4ClO_4
$\log\beta_1$	3.48 (0.08)	2.29 (0.10)	1.58 (0.02)
$\log\beta_2$	5.54 (0.13)	4.53 (0.06)	2.57 (0.04)
$\log\beta_3$	8.50 (0.09)	7.03 (0.07)	4.00 (0.02)
$\log\beta_4$	9.77 (0.16)	8.22 (0.10)	4.29 (0.08)
$\Delta H^\circ_{\beta 1}$	19.6 (0.2)	20.1 (0.8)	16.5 (0.4)
$\Delta H^\circ_{\beta 2}$	38.1 (1.5)	30.0 (0.4)	27.3 (1.3)
$\Delta H^\circ_{\beta 3}$	56.2 (0.5)	53.5 (0.2)	43.5 (0.7)
$\Delta H^\circ_{\beta 4}$	72.7 (2)	54.4 (0.1)	42.5 (0.8)
U[a]	0.219	1.60	0.292
R[b]	0.0158	0.0146	0.0096
N[c]	96	119	121

Values in parentheses refer to standard deviations. a) Error-square sum. b) The Hamilton R-factor. c) The number of data points.

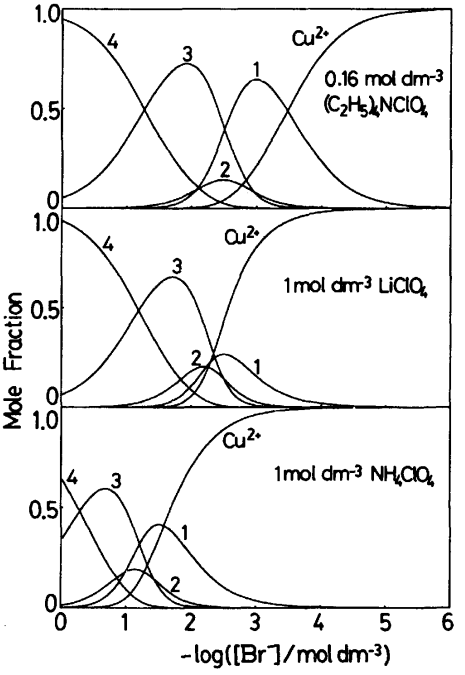

Fig. 4. Distribution of the copper(II) bromo complexes in 0.16 mol dm^{-3} $(C_2H_5)_4NClO_4$, 1 mol dm^{-3} $LiClO_4$, and 1 mol dm^{-3} NH_4ClO_4 DMF solutions. The numbers represent n within $[CuBr_n]^{(2-n)+}$.

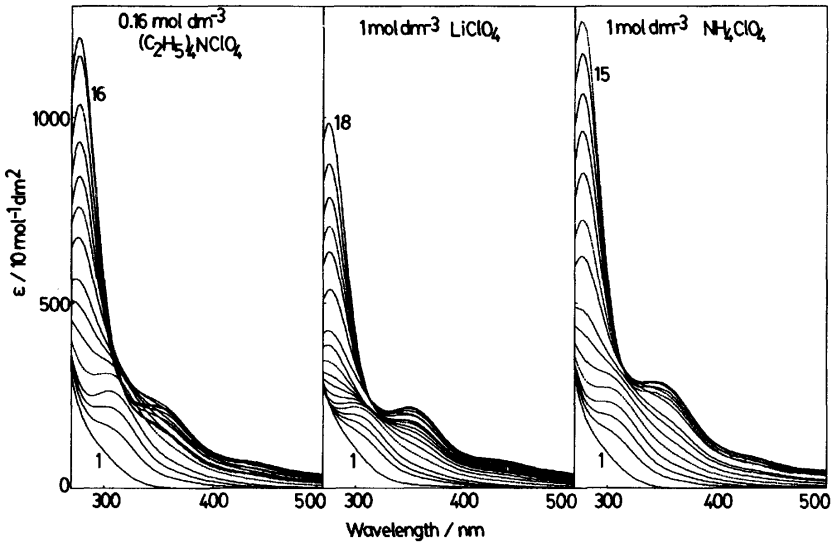

Fig. 5. Electronic spectra of copper(II) bromide DMF solutions in the range 260—500 nm. Intensities are normalized with the unit concentration of the metal ion in solution. Electronic spectra were obtained at various C_X/C_M, the value being varied from 0 (the solution No. 1) to 413 (No. 16), 318 (No. 18) and 2051 (No. 15) in the $(C_2H_5)_4NClO_4$, $LiClO_4$ and NH_4ClO_4 DMF solutions, respectively.

satisfactorily explained by the set (1—4). The overall formation constants and enthalpies of the $[CuBr_n]^{(2-n)+}$ (n=1—4) complexes thus obtained in the DMF solutions are summarized in Table 2. As seen in Figs. 1—3 the solid lines, the titration curves calculated using the constants in Table 2, well reproduce the experimental points over the whole range of C_X/C_M examined in each solution, and thus we conclude the formation of a series of four mononuclear copper(II) bromo complexes in all the solutions examined.

The complexation is weaker in the $LiClO_4$ solution than in the $(C_2H_5)_4NClO_4$ one and is even more weakened in the NH_4ClO_4 solution, as seen in the distribution of the copper(II) bromo complexes in Fig. 4. It is noted that the formation of $[CuBr_2]$ is strongly suppressed in any DMF solution examined. It is also noted that the formation of $[CuBr]^+$ is extensive in the $(C_2H_5)_4NClO_4$ DMF solution but is strongly suppressed in the $LiClO_4$ and NH_4ClO_4 DMF solutions.

Spectrophotometric Results. Electronic spectra of copper(II) bromide DMF solutions in the 0.16 mol dm^{-3} $(C_2H_5)_4NClO_4$, 1 mol dm^{-3} $LiClO_4$, and 1 mol dm^{-3} NH_4ClO_4 DMF solutions are depicted in Fig. 5 over the wavelength range 260—500 nm, absorbance being normalized with the metal concentration in solution. Absorption bands observed are not simply assignable to each coppar(II) bromo complex, because absorbance monotonously increases with increasing concentration of bromide ion in the solutions over the wavelength range measured. Since each measured spectrum should be represented as the sum of electronic spectra of individual copper(II) bromo complexes by taking into account the distribution of species in solution, absorbance data obtained at selected 28 wavelengths in the range 260—500 nm were analyzed by assuming the formation of a series of mononuclear copper(II) bromo complexes, and their formation constants and molar extinction coefficients of each complex at relevant wavelengths were optimized by the least-squares method. The formation constants thus obtained are summarized in Table 3, the values, as a whole, being in satisfactory agreement with those calorimetrically determined.

In the $LiClO_4$ DMF solution, the variation in the measured electronic spectra with C_X/C_M is well explained in terms of the formation of $[CuBr_n]^{(2-n)+}$ (n=1—4). On the other hand, in the $(C_2H_5)_4NClO_4$ and NH_4ClO_4 DMF solutions the corresponding

Table 3. Final Results of the Least-Squares Refinement of Overall Formation Constants, $\log(\beta_n/\text{mol}^{-n}\,\text{dm}^{3n})$ of $[CuBr_n]^{(2-n)+}$ using Spectrophotometric Data in *N,N*-Dimethylformamide at 25 °C

	0.16 mol dm^{-3} $(C_2H_5)_4NClO_4$ (1, 3, 4)	1 mol dm^{-3} $LiClO_4$ (1—4)	1 mol dm^{-3} NH_4ClO_4 (1, 3, 4)
$\log\beta_1$	3.12(0.06)	2.48(0.36)	1.83(0.05)
$\log\beta_2$	—	4.61(0.47)	—
$\log\beta_3$	8.72(0.08)	7.04(0.29)	4.44(0.09)
$\log\beta_4$	10.59(0.11)	8.54(0.82)	5.18(0.16)
$U^{a)}$	0.264	0.913	0.494
$R^{b)}$	0.0248	0.0465	0.0330
$N^{c)}$	1876	1932	1876

Values in parentheses refer to standard deviations. a) Error-square sum. b) The Hamilton R-factor. c) The number of data points.

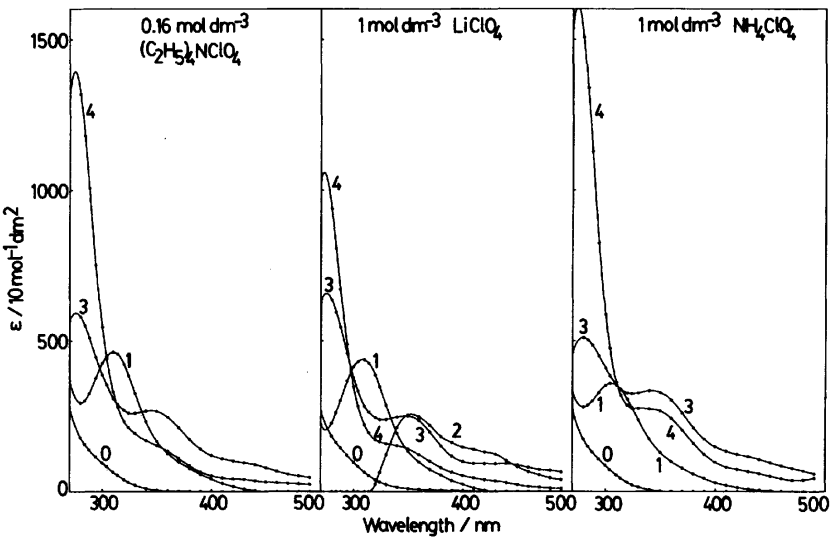

Fig. 6. Electronic spectra of individual copper(II) bromo complexes in the range 260—500 nm obtained in 0.16 mol dm^{-3} $(C_2H_5)_4NClO_4$, 1 mol dm^{-3} $LiClO_4$, and 1 mol dm^{-3} NH_4ClO_4 DMF solutions. The numbers represent n within $[CuBr_n]^{(2-n)+}$.

spectral changes can be explained even without taking the formation of $[CuBr_2]$ into account. The degree of the formation of $[CuBr_2]$ might be too small to extract its characteristic electronic spectrum from the measured spectra in the DMF solutions.

The electronic spectra of individual copper(II) bromo complexes are shown in Fig. 6. In the $LiClO_4$ DMF solution, the electronic spectrum of $[CuBr]^+$ shows a single peak at 310 nm, and the spectrum of $[CuBr_2]$ shows a peak at 350 nm and a weak absorption at ca. 430 nm, over the range measured. On the other hand, the $[CuBr_3]^-$ complex has two peaks at 275 and 350 nm and a weak absorption at ca. 450 nm. It is noted that the absorption band of the $[CuBr_2]$ complex overlaps that of $[CuBr_3]^-$, and thus it is difficult to extract the individual spectrum of the former complex at the coexistence of the $[CuBr_2]$ and $[CuBr_3]^-$ complexes in solution. The $[CuBr_4]^{2-}$ complex shows a peak at 275 nm and a broad peak at ca. 350 nm. The peak positions thus determined for each copper(II) bromo complex are in accordance with those of the ligand to metal charge transfer bands reported by Howard and Keeton.[11] Similar electronic spectra were obtained for each $[CuBr_n]^{(2-n)+}$ (n=1,3, or 4) complex in the $(C_2H_5)_4NClO_4$, $LiClO_4$, and NH_4ClO_4 DMF solutions as seen in Fig. 6, so that the coordination structure of each $[CuBr_n]^{(2-n)+}$ (n=1, 3, or 4) complex may be essentially the same in these ionic medium solutions.

Ion-Pair Formation of Bromide Ions. As noted in a preceding section, the complexation of copper(II) with bromide ions is considerably weaker in the 1 mol dm^{-3} $LiClO_4$ solution than in the 0.16 mol dm^{-3} $(C_2H_5)_4NClO_4$ one, and is even more weakened in the 1 mol dm^{-3} NH_4ClO_4 solution. A similar trend has been observed for the comlexation of copper(II) with chloride ions in the 0.2 mol dm^{-3} $(C_2H_5)_4NClO_4$ and 1 mol dm^{-3} $LiClO_4$ DMF solutions.[1] The ion-pair formation of chloride ion with medium cations

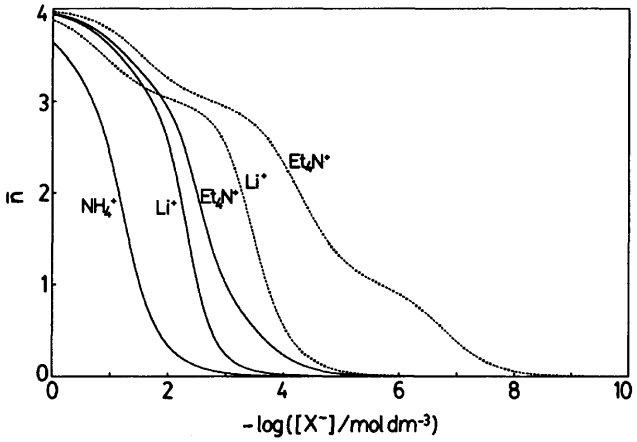

Fig. 7. Formation functions $\bar{n}$ of the copper(II) bromide (the solid lines) and copper(II) chloride (the dotted lines) systems in *N,N*-dimethylformamide containing $(C_2H_5)_4NClO_4$ (Et_4N^+), $LiClO_4$ (Li^+), and NH_4ClO_4 (NH_4^+) at 25 °C.

Table 4. Thermodynamic Quantities, $\log(K_n/\text{mol}^{-1}\,\text{dm}^3)$, ΔG_n°/kJ mol^{-1}, ΔH_n°/kJ mol^{-1}, and ΔS_n°/J K^{-1} mol^{-1}, for the Stepwise Formation of $[CuX_n]^{(2-n)+}$ in *N,N*-Dimethylformamide at 25 °C

	0.16 mol dm^{-3} $(C_2H_5)_4NClO_4$ X=Br	1 mol dm^{-3} $LiClO_4$ X=Br	1 mol dm^{-3} NH_4ClO_4 X=Br	0.2 mol dm^{-3} $(C_2H_5)_4NClO_4$[a] X=Cl
$\log K_1$	3.48	2.29	1.58	6.79
$\log K_2$	2.06	2.24	0.99	4.54
$\log K_3$	2.96	2.50	1.43	4.00
$\log K_4$	1.27	1.19	0.29	1.52
ΔG_1°	−19.9	−13.1	−9.0	−38.8
ΔG_2°	−11.8	−12.8	−5.7	−25.9
ΔG_3°	−16.9	−14.3	−8.2	−22.8
ΔG_4°	−7.3	−6.8	−1.6	−8.7
ΔH_1°	19.6	20.1	16.5	10.3
ΔH_2°	18.5	9.9	10.8	9.7
ΔH_3°	18.1	23.6	16.1	7.3
ΔH_4°	16.5	0.8	−1.0	−8.1
ΔS_1°	132	111	86	165
ΔS_2°	101	76	55	120
ΔS_3°	117	127	82	101
ΔS_4°	80	26	2	2
$\Delta G_{\beta_4}^\circ$[b]	−55.8	−46.9	−24.5	−96.2
$\Delta H_{\beta_4}^\circ$[b]	72.7	54.4	42.5	19.2
$\Delta S_{\beta_4}^\circ$[b]	431	340	225	387

a) Ref. 1. b) For the overall formation of $[CuBr_4]^{2-}$.

is practically negligible in a 0.1—0.2 mol dm^{-3} $(C_2H_5)_4NClO_4$ DMF solution, and thus the weaker complexation between copper(II) and chloride ions in the $LiClO_4$ solution than that in the $(C_2H_5)_4NClO_4$ one is ascribed to the formation of LiCl ion pairs in the former solution.[1] It is expected that the ion-pair formation of bromide ion with medium cations is also negligible in the $(C_2H_5)_4NClO_4$ DMF solution but is appreciably enhanced in the $LiClO_4$ and NH_4ClO_4 solutions. Therefore, the formation of LiBr and NH_4Br ion pairs may be responsible for the weaker complexation of copper(II) with Br^- ions in the $LiClO_4$ and NH_4ClO_4 DMF solutions, respectively. It is noted that, since the complexation between copper(II) and bromide ions in the NH_4ClO_4 solution is weaker than that in the $LiClO_4$ solution, the ion-pair formation of bromide ion should occur more extensively in the former solution than in the latter.

In Fig. 7, the formation functions $\bar{n}$ calculated for the copper(II) chloride and bromide systems in the $LiClO_4$ solution are compared with those in the $(C_2H_5)_4NClO_4$ solution, the shift is larger for the chloride system than for the bromide one, the result suggesting that the LiCl ion pairs are more extensively formed than the LiBr ones in DMF. This is reasonable because hard Li^+ ion prefers hard and small Cl^- to Br^- ion.

As seen in Table 4, the $\Delta H^\circ_{\beta 4}$ and $\Delta S^\circ_{\beta 4}$ values for the overall formation of the $[CuBr_4]^{2-}$ complex in the $LiClO_4$ solution are smaller than those in the $(C_2H_5)_4NClO_4$ one, the values in the NH_4ClO_4 solution being even smaller than those in the $LiClO_4$ one. The result suggests that both enthalpy and entropy values associated with the formation of LiBr and NH_4Br ion pairs are positive. Since the formation of ion pairs may be accompanied by an extensive desolvation of both cation and anion, a positive enthalpy entropy change may be ascribed to the rupture of the M^+–dmf (M^+=Li^+ and NH_4^+) and Br^-–dmf bonds and a positive entropy change to the liberation of DMF molecules from the coordination shells of M^+ and Br^- ions. The entropy increase of the ion-pair formation may be especially large in DMF because DMF molecules are randomly distributed in the bulk,[20] and thus the increased entropy due to the liberation of DMF molecules coordinating to the ions may not be compensated with the entropy decrease due to the intermolecular interactions in the bulk solution. A similar result has also been observed for the complexation of cadmium(II) with bromide ions in dimethyl sulfoxide containing various ionic media.[21]

Stepwise Thermodynamic Quantities. Stepwise formation constants, Gibbs energies, enthalpies and entropies of formation of the $[CuBr_n]^{(2-n)+}$ (n=1—4) complexes in the 0.16 mol dm^{-3} $(C_2H_5)_4NClO_4$, 1 mol dm^{-3} $LiClO_4$, and 1 mol dm^{-3} NH_4ClO_4 DMF solutions are summarized in Table 4, together with those of the $[CuCl_n]^{(2-n)+}$ (n=1—4) complexes in the 0.2 mol dm^{-3} $(C_2H_5)_4NClO_4$ DMF solution.[1]

Copper(II) ion is coordinated with six DMF molecules and the $[Cu(dmf)_6]^{2+}$ solvate species has the distorted octahedral structure in DMF[18] as well as in water.[22] On the other hand, the flattened tetrahedral $[CuBr_4]^{2-}$ complex is formed in a solution of a high concentration of Br^- ion in DMF. Thus, the coordination structure around copper(II) ion changes from the six- to four-coordinate in the course of the complexation with bromide ions. In any ionic medium examined, a relatively large and positive stepwise entropy value is observed at the third step, indicating an extensive liberation of DMF molecules from the primary solvation shell of the metal ion. It is thus suggested that the coordination structure about copper(II) ion changes at the third consecutive step and the $[CuBr_3(dmf)]^-$ complex with the tetrahedral structure is yielded. Relatively large endothermicities are also observed at the third step in the 1 mol dm^{-3} $LiClO_4$ and NH_4ClO_4 DMF solutions, and the result may be reasonably explained in terms of the breaking of more than two metal-solvent bonds accompanying the structure change from the five- or six-coordinate $[CuBr_2]$ complex to the four-coordinate $[CuBr_3]^-$ complex at this step.

In 0.1—0.2 mol dm^{-3} $(C_2H_5)_4NClO_4$ DMF solutions where the fomation of $(C_2H_5)_4NX$ (X^-=Cl^- or Br^-) ion pairs is practically negligible, the formation constants of the copper(II) bromo complexes are significantly smaller than those of the copper(II) chloro complexes,[1] due mainly to more positive ΔH°_n values for the bromide system than those for the chloride one. The result evidently indicates the weaker Cu–Br bond than the Cu–Cl bond as expected from the larger size of Br^- ion.[23]

The present work has been financially supported by the Grant-in-Aid for Special Project Research No. 61134043 from the Ministry of Education, Science and Culture.

References

1) S. Ishiguro, B. G. Jeliazkova, and H. Ohtaki, *Bull. Chem. Soc. Jpn.*, **58**, 1143 (1985); **58**, 1749 (1985): **59**, 1073 (1986).

2) S. Ishiguro, H. Suzuki, B. G. Jeliazkova, and H. Ohtaki, *Bull. Chem. Soc. Jpn.*, **59**, 2407 (1986).

3) M. A. Khan and M. J. Schwing-Weill, *Inorg. Chem.*, **15**, 2202 (1976).

4) M. Elleb, J. Meullemeestre, M. J. Schwing-Weill, and F. Vierling, *Inorg. Chem.*, **19**, 2699 (1980); **21**, 1477 (1982).

5) S. E. Manahan and R. T. Iwamoto, *Inorg. Chem.*, **4**, 409 (1965).

6) T. E. Suarez, R. T. Iwamoto, and J. Kleinberg, *Inorg. Chim. Acta*, **7**, 292 (1973).

7) S. Ahrland, P. Bläuenstein, B. Tagesson, and D. Tuhtar, *Acta Chem. Scand., Ser. A*, **34**, 265 (1980).
8) W. Schneider and A. V. Zelewsky, *Helv. Chim. Acta*, **46**, 1848 (1963).
9) C. Furlani and G. Morpurgo, *Theoret. Chim. Acta*, **1**, 102 (1963).
10) J. C. Barnes and D. N. Hume, *Inorg. Chem.*, **2**, 444 (1963).
11) R. A. Howard and D. P. Keeton, *Spectrochim. Acta*, **22**, 1211 (1966).
12) G. H. Faye, *Can. J. Chem.*, **44**, 1643 (1966).
13) B. Morosin and E. C. Lingafelter, *Acta Crystallogr.*, **13**, 807 (1960).
14) B. Morosin and K. Lawson, *J. Mol. Spectrosc.*, **12**, 98 (1964).
15) P. S. Braterman, *Inorg. Chem.*, **2**, 448 (1963).
16) D. W. Smith, *Coord. Chem. Rev.*, **21**, 93 (1976).
17) M. Ichihashi, H. Wakita, T. Mibuchi, and I. Masuda, *Bull. Chem. Soc. Jpn.*, **55**, 3160 (1982).
18) K. Ozutsumi, S. Ishiguro, and H. Ohtaki, to be published.
19) S. Ishiguro, K. Yamamoto, and H. Ohtaki, *Anal. Sci.*, **1**, 263 (1985).
20) H. Ohtaki, S. Itoh, T. Yamaguchi, S. Ishiguro, and B. M. Rode, *Bull. Chem. Soc. Jpn.*, **56**, 3406 (1983).
21) S. Ahrland and I. Persson, *Acta Chem. Scand., Ser. A*, **35**, 185 (1981).
22) H. Ohtaki, T. Yamaguchi, and M. Maeda, *Bull. Chem. Soc. Jpn.*, **49**, 701 (1976).
23) S. Ahrland, *Pure Appl. Chem.*, **51**, 2019 (1979).

Preparation and Stereochemistry of Cobalt(III) Complexes Containing 3,6-Diphenyl-3,6-diphosphaoctane-1,8-diamine or (2*S*,9*S*)-4,7-Diphenyl-4,7-diphosphadecane-2,9-diamine, $NH_2CHRCH_2P(C_6H_5)CH_2CH_2P(C_6H_5)$-$CH_2CHRNH_2$ (R=H, CH_3)

Masamichi Atoh, Hirofumi Sugiura, Yoji Seki, Kazuo Kashiwabara, and Junnosuke Fujita*
Department of Chemistry, Faculty of Science, Nagoya University, Chikusa-ku, Nagoya 464
(Received November 20, 1986)

Nine new cobalt(III) complexes containing 3,6-diphenyl-3,6-diphosphaoctane-1,8-diamine (NPPN), *trans*-[$CoCl_2$(*rac*(*P*)-NPPN)]$^+$, *cis*α-[Co(L)(*rac*(*P*)-NPPN)]$^{n+}$ (L=en, *n*=3; L=acac, *n*=2) and *Δ*- and *Λ*-*cis*α-[Co(L′)(*rac*(*P*)-NPPN)]$^{n+}$ (L′=*R*-pn, *n*=3; L′=*S*-ala or *S*-pro, *n*=2), and five new cobalt(III) complexes containing (2*S*,9*S*)-4,7-diphenyl-4,7-diphosphadecane-2,9-diamine (*SS*(*C*)-NPPN), *Δ*- and *Λ*-*cis*α-[Co(L)(*rac*(*P*),*SS*(*C*)-NPPN)]$^{n+}$ (L=en, *n*=3; *L*=acac, *n*=2) and *Δ*-*cis*β-[Co(acac)(*meso*(*P*),*SS*(*C*)-NPPN)]$^{2+}$, were prepared, where en, *R*-pn, acac, *S*-ala and *S*-pro denote ethylenediamine, (*R*)-1,2-propanediamine, 2,4-pentanedionate, (*S*)-alaninate and (*S*)-prolinate ions, respectively. Stereochemistries of the complexes and the chiral phosphorus donor atoms were studied on the basis of the absorption, ^{1}H and ^{13}C NMR, and CD spectra. The *rac*(*P*)-NPPN and *rac*(*P*),*SS*(*C*)-NPPN ligands formed selectively either the trans or cisα isomer, while no stable complex was obtained with the meso(P) isomers of NPPN and *SS*(*C*)-NPPN except *cis*β-[Co(acac)(*meso*(*P*),*SS*(*C*)-NPPN)]$^{2+}$ which slowly decomposes in water.

Studies on stereochemistry of optically active octahedral metal complexes containing chiral phosphorus or arsenic donor atoms have little been reported,[1–5] except a systematic study on cobalt(III) complexes containing a quadridentate arsine ligand $(CH_3)_2As(CH_2)_3As(C_6H_5)(CH_2)_3As(C_6H_5)(CH_2)_3As(CH_3)_2$ reported by Bosnich and his co-workers.[6] Since a chiral phosphorus or arsenic atom is stable to racemization,[7] a multidentate ligand containing such chiral donor atoms is expected to exhibit different stereoselectivity in complex formation from that of the corresponding amine ligand which has been studied extensively.[8]

In this paper, we report the preparation and stereochemistry of two quadridentate ligands having two chiral phosphorus donor atoms, $NH_2CH_2CH_2P(C_6H_5)CH_2CH_2P(C_6H_5)CH_2CH_2NH_2$ (NPPN) and (2*S*,9*S*)-$NH_2CH(CH_3)CH_2P(C_6H_5)CH_2CH_2P(C_6H_5)CH_2CH(CH_3)NH_2$ (*SS*(*C*)-NPPN), and their cobalt(III) complexes.

Experimental

The phosphine ligands were prepared and handled under an atmosphere of nitrogen until they formed cobalt(III) complexes. All solvents for the preparation were made oxygen-free by bubbling nitrogen for 20 min immediately before use. Absorption, circular dichroism (CD), and ^{1}H and ^{13}C NMR spectra were recorded on a Hitachi 323 spectrophotometer, a JASCO J-40CS spectropolarimeter, and Jeol PMX-60, FX-100 and GX-400 spectrometers, respectively.

Preparation of Ligands. 3,6-Diphenyl-3,6-diphosphaoctane-1,8-diamine (NPPN). Method 1. This method is a modified one of Issleib and Oehme.[9] To (2-aminoethyl)-phenylphoshine[9] (4.95 g) in dry tetrahydrofuran (THF) (500 cm^3) was added dropwise a 15% hexane solution (14 g) of butyllithium over a period of 1 h with stirring. After further stirring for 1 h, 1,2-dichloroethane (1.6 g) was added dropwise, the solution was refluxed for 3 h, and then cooled. Water (2 cm^3) was added dropwise, the solvent THF was evaporated, and to the residue water (200 cm^3) and then diethyl ether (200 cm^3) were added with stirring. The ethereal layer was separated, dried over $MgSO_4$ (ca. 5 g) overnight, filtered, and evaporated to give an oily product. It was heated at ca. 100 °C under highly reduced pressure (<ca. 135 pa) to remove by-products and starting materials since the NPPN ligand is not distillable under ordinary conditions. Yield: ca. 60%. The crude product was used for preparing cobalt(III) complexes without further purification.

Method 2. A 15% hexane solution (30 g) of butyllithium was added dropwise to a dry THF solution (200 cm^3) of 1,2-bis(phenylphosphino)ethane[10] (7.34 g) over a period of 2 h with stirring. Stirring was continued for 3 h. Aziridine (3.7 g) was added dropwise at 40 °C, and the solution was refluxed for 10 h. After cooling water (1.5 cm^3) was added, and the soluiton was dried over $MgSO_4$ (ca. 10 g) overnight, filtered and evaporated to yield an oily product. It was treated by the same way as described in Method 1. Yield: ca. 60%.

(2*S*,9*S*)-4,7-Diphenyl-4,7-diphosphadecane-2,9-diamine (*SS*-(*C*)-NPPN). This ligand was prepared by the same method as Method 2 for NPPN, using (*S*)-2-methylaziridine[11] instead of aziridine. Yield: 50—60%.

Preparation of Cobalt(III) Complexes. *trans*-[$CoCl_2$(*rac*-(*P*)-NPPN)]$ClO_4 \cdot H_2O$. A methanol solution (30 cm^3) of NPPN (2.89 g, 8.02 mmol) was added dropwise to [CoCl-$(NH_3)_5]Cl_2$[12] (2.21 g) in a mixture (700 cm^3) of methanol and water (1 : 1) with stirring. After the color of the solution had been changed from violet to green (15 min), concd HCl (5 cm^3) was added and the solution was stirred for 15 min. The solvent methanol was removed under reduced pressure, and the unreacted NPPN ligand and by-products were extracted with diethyl ether (100 cm^3×2). The aqueous solution was concentrated to a small volume under reduced

pressure to yield a green precipitate (*trans*-[$CoCl_2$ (*rac*(*P*)-NPPN)]Cl). The precipitate was recrystallized from water by adding $NaClO_4 \cdot H_2O$. Yield: 1.5 g (32%). Found: C, 37.17; H, 5.27; N, 4.63%. Calcd for $C_{18}H_{28}N_2Cl_3CoO_5P_2$: C, 37.30; H, 4.78; N, 4.83%. Perchlorate salts of cobalt(III)-phosphine complexes are potentially explosive, and should be handled carefully.

***cis*α-[Co(en)(*rac*(*P*)-NPPN)]$(ClO_4)_3 \cdot 0.5H_2O$.** A methanol solution (100 cm^3) containing *trans*-[$CoCl_2$(*rac*(*P*)-NPPN)]Cl (300 mg, 0.578 mmol) and en (100 mg, 1.66 mmol) was stirred overnight. The resulting yellow solution was diluted with water (1 dm^3) and applied on a column (ϕ3 cm×60 cm) of SP-Sephadex C-25. The adsorbed product was eluted with 0.15 mol dm^{-3} Na_2SO_4. The yellow eluate (major product) was collected, diluted with water, and applied again on a column (ϕ1 cm×10 cm) of SP-Sephadex C-25. The adsorbed yellow product was eluted with 0.5 mol dm^{-3} $NaClO_4$, and the eluate was concentrated slowly in a desiccator, yielding yellow crystals. Yield: 350 mg (89%). Found: C, 31.69; H, 4.65; N, 7.33%. Calcd for $C_{20}H_{35}N_4CoCl_3O_{12.5}P_2$: C, 31.66; H, 4.65; N, 7.38%.

***cis*α-[Co(acac)(*rac*(*P*)-NPPN)]$(ClO_4)_2$.** The complex was prepared by the same method as for the en complex, using lithium 2,4-pentanedionate (Li(acac)) instead of en. Yield: 65%. Found: C, 39.90; H, 4.86; N, 3.83%. Calcd for $C_{23}H_{33}N_2CoCl_2O_{10}P_2$: C, 40.08; H, 4.83; N, 4.06%.

***Δ-cis*α-[Co(*R*-pn)(*RR*(*P*)-NPPN)]$(ClO_4)_3 \cdot 2H_2O$ and *Λ-cis*α-[Co(*R*-pn)(*SS*(*P*)-NPPN)]$(ClO_4)_3 \cdot 1.5H_2O$.** The complexes were prepared by the same method as that for the en complex, using (*R*)-1,2-propanediamine (*R*-pn) instead of en. By elution with 0.15 mol dm^{-3} Na_2SO_4 two large yellow bands (F1 (faster) and F2 (slower)) were eluted. From each band the complex was isolated by a method similar to that for the en complex. Yields, F1(Δ-*cis*α): 23% and F2 (Λ-*cis*α): 22%. Found for F1: C, 31.50; H, 4.94; N, 6.99%. Calcd for $C_{21}H_{40}N_4CoCl_3O_{14}P_2$:C, 31.54; H, 5.04; N, 7.01%. Found for F2: C, 31.69; H, 4.62; N, 7.01%. Calcd for $C_{21}H_{39}N_4CoCl_3O_{13.5}P_2$: C, 31.90; H, 4.67; N, 7.08%.

***Δ-cis*α-[Co(*S*-ala)(*RR*(*P*)-NPPN)]$(ClO_4)_2 \cdot 2.5H_2O$ and *Λ-cis*α-[Co(*S*-ala)(*SS*(*P*)-NPPN)]$(ClO_4)_2 \cdot 2H_2O$.** The complexes were prepared by a method similar to that for the *R*-pn complex, using sodium (*S*)-alaninate instead of *R*-pn. Yields, F1(Δ-*cis*α): 17% and F2(Λ-*cis*α): 19%. Found for F1: C, 34.65; H, 4.60; N, 5.75%. Calcd for $C_{21}H_{37}N_3CoCl_2O_{12.5}P_2$: C, 34.87; H, 5.16; N, 5.81%. Found for F2: C, 35.01; H, 4.66; N, 5.82%. Calcd for $C_{21}H_{36}N_3CoCl_2O_{12}P_2$: C, 35.31; H, 5.08; N, 5.88%.

***Δ-cis*α-[Co(*S*-pro)(*RR*(*P*)-NPPN)]$(ClO_4)_2 \cdot 0.5H_2O$ and *Λ-cis*α-[Co(*S*-pro)(*SS*(*P*)-NPPN)]$(ClO_4)_2 \cdot 0.5H_2O$.** The complexes were prepared by the same method as for the *S*-ala complexes, using sodium (*S*)-prolinate. Yields, F1 (Δ-*cis*α): 14% and F2 (Λ-*cis*α) : 10%. Found for F1: C, 38.76; H, 4.80; N, 5.78%. Calcd for $C_{23}H_{35}N_3CoCl_2O_{10.5}P_2$: C, 38.73; H, 4.95; N, 5.89%. Found for F2: C, 38.82; H, 4.99; N, 5.90%. Calcd for $C_{23}H_{35}N_3CoCl_2O_{10.5}P_2$: C, 38.73; H, 4.95; N, 5.89%.

***Δ-cis*α-[Co(en)(*RR*(*P*),*SS*(*C*)-NPPN)]$(ClO_4)_3 \cdot 0.5H_2O$ and *Λ-cis*α-[Co(en)(*SS*(*P*),*SS*(*C*)-NPPN)]$Cl_2 \cdot ClO_4 \cdot 0.5H_2O$.** To [Co(en)$_3$]$(ClO_4)_3$[13] (1 g) in a mixture (100 cm^3) of water and methanol (5:3) were added a methanol solution (100 cm^3) of *SS*(*C*)-NPPN (700 mg, 1.94 mmol) and active charcoal (ca. 50 mg). The mixture was stirred overnight, filtered, diluted with water (3 dm^3) added concd HNO_3 (2 cm^3), and applied on a column (ϕ3 cm×60 cm) of SP-Sephadex C-25. By elution with 0.3 mol dm^{-3} Na_2[Sb_2(*d*-tartrate)$_2$], the column gave two large yellow bands (F1 (faster) and F2 (slower)) with a large orange-yellow ([Co(en)$_3$]$^{3+}$) and a few small bands. Each eluate of F1 and F2 was diluted ten times with water, poured again on a column (ϕ2 cm×15 cm) of SP-Sephadex C-25, and the complex was eluted with 2 mol dm^{-3} NaCl. The eluate was concentrated to a small volume under reduced pressure. On addition of excess $NaClO_4 \cdot H_2O$ the concentrate gave crystals of the complex. Yields, F1 (Δ-*cis*α): 80 mg (5%) and F2 (Λ-*cis*α): 200 mg (15%). Found for F1: C, 33.71; H, 4.77; N, 6.61%. Calcd for $C_{22}H_{39}N_4CoCl_3O_{12.5}P_2$: C, 33.58, H, 5.00; N, 7.12%. Found for F2: C, 39.13; H, 6.29; N, 8.16%. Calcd for $C_{22}H_{41}N_4CoCl_3O_{5.5}P_2$: C, 39.04; H, 6.11; N, 8.28%.

***Δ-cis*α-[Co(acac)(*RR*(*P*),*SS*(*C*)-NPPN)]$(ClO_4)_2 \cdot H_2O$, *Λ-cis*α-[Co(acac)(*SS*(P),*SS*(*C*)-NPPN)]$(ClO_4)_2$, and *Δ-cis*β-[Co(acac)(*RS*(P),*SS*(*C*)-NPPN)][$B(C_6H_5)_4$]$_2 \cdot 3H_2O$.** To [Co(acac)$_3$][14] (400 mg, 1.12 mmol) in methanol (200 cm^3) were added a methanol solution (50 cm^3) of *SS*(*C*)-NPPN (550 mg, 1.53 mmol) and active charcoal (ca. 50 mg). The mixture was stirred overnight, filtered, diluted with water (3 dm^3) added concd HNO_3 (2 cm^3), and applied on a column (ϕ3 cm×150 cm) of SP-Sephadex C-25. The adsorbed product was eluted with 0.15 mol dm^{-3} Na_2[Sb_2(*d*-tartrate)$_2$], yielding three large bands (orange F1 (fast), orange F2 (middle), and orange-red F3 (slow)). Each eluate of F1, F2, and F3 was diluted ten times with water acidified with HCl (pH ca. 3.0), and applied again on a column (ϕ2 cm×15 cm) of SP-Sephadex C-25. The adsorbed complex was eluted with 1 mol dm^{-3} Na_2SO_4. Either eluate obtained from F1 and F2 was evaporated to dryness under reduced pressure, and the complex was extracted with methanol. The extract gave orange crystals on addition of excess $NaClO_4 \cdot H_2O$. The complex contained in eluate F3 was isolated by adding sodium tetraphenylborate and purified by column (ϕ2.5 cm×60 cm) chromatography using Toyopearl TSK-GEL and methanol. Yields, F1 (Δ-*cis*α): 95 mg (9%), F2 (Λ-*cis*α): 70 mg (6%) and F3 (Δ-*cis*β): 195 mg (11%). Found for F1 : C, 40.51; H, 5.09; N, 4.07%. Calcd for $C_{25}H_{39}N_2CoCl_2O_{11}P_2$: C, 40.83; H, 5.35; N, 3.81%. Found for F2: C, 41.53; H, 5.29; N, 4.36%. Calcd for $C_{25}H_{37}N_2CoCl_2O_{10}P_2$: C, 41.86; H, 5.20; N, 3.91%. Found for F3: C, 72.15; H, 6.65; N, 2.28%. Calcd for $C_{73}H_{83}N_2B_2CoO_5P_2$: C, 72.41; H, 6.91; N, 2.31%. Complex F3 decomposes slowly in neutral water, so that it should be treated always in slightly acidic conditions.

Derivation of the en Complexes of *SS*(*C*)-NPPN from the acac Complexes. To isomer F1 (10 mg) of the acac complex in a small amount of methanol was added concd HCl (2 cm^3) and the solution was allowed to stand overnight, the color changing gradually from orange to red. The red solution was diluted ten times with water and applied on a column (ϕ1 cm×15 cm) of SP-Sephadex C-25. The adsorbed red complex was eluted with 0.3 mol dm^{-3} HCl. To the red eluate was added a methanol solution of excess en, the color being changed instantly from red to yellow. The yellow eluate was diluted ten times with water and applied on a column (ϕ1 cm×15 cm) of SP-Sephadex C-25. The adsorbed yellow complex was eluted with 0.4 mol dm^{-3} NaCl. The absorption and CD spectra of the yellow eluate coincide with those of isomer F1 of the en complex prepared from

$[Co(en)_3]^{3+}$ and *SS(C)*-NPPN. By the same method, isomer F2 of the en complex was derived from isomer F2 of the acac complex. However, any en complex of *SS(C)*-NPPN could not be obtained from isomer F3 of the acac complex. A methanol solution of F3 turned red by adding concd HCl, but the product gradually decomposed to Co(II) species on addition of excess en.

Optical Resolution of the NPPN Complexes. Partial resolutions of *cisα*-[Co(en)(*rac(P)*-NPPN)]$^{3+}$ and *cisα*-[Co(acac)(*rac(P)*-NPPN)]$^{2+}$ were achieved by an SP-Sephadex C-25 column-chromatographic method using a column (ϕ3 cm×120 cm), and 0.2 mol dm^{-3} and 0.1 mol dm^{-3} $Na_2[Sb_2(d\text{-tartrate})_2]$ as an eluent, respectively. In each resolution the first and last several fractions of the band showed a constant $\Delta\varepsilon/\varepsilon$ value. The fractions with a constant $\Delta\varepsilon/\varepsilon$ value were collected, diluted five times with water and applied on a column (ϕ1 cm×10 cm) of SP-Sephadex C-25. The column was washed with water and the complex was eluted with 0.3 mol dm^{-3} NaCl. The effluent was used for CD measurements, and the concentration of the complex was determined by reference to the ε values of the racemate.

Results and Discussion

NPPN Complexes. We have prepared the NPPN ligand from $(C_6H_5)HPCH_2CH_2PH(C_6H_5)$ and aziridine (Method 2) and also from $NH_2CH_2CH_2PH(C_6H_5)$ and $ClCH_2CH_2Cl$ by Method 1 which is a modified method of Issleib and Oehme.[9] Both methods gave similar yields. The ligand could not be purified by vacuum distillation because it had a high boiling point and decomposed at a high temperature.[9] Thus, the crude product was used without purification for preparing the cobalt(III) complexes.

By reaction of NPPN with $[CoCl(NH_3)_5]Cl_2$, only one isomer of $[CoCl_2(NPPN)]^+$ was isolated, no dichloro complex being formed by oxidizing $[Co(NPPN)]^{2+}$ with Cl_2[15] or O_2.[16] The absorption spectrum of $[CoCl_2(NPPN)]^+$ is similar in pattern to that of *trans(Cl,Cl)*, *cis(P,P)*-$[CoCl_2(ebpp)_2]^+$ (ebpp= $NH_2CH_2CH_2P(C_4H_9)(C_6H_5)$) whose structure has been determined by X-ray analysis (Fig. 1).[2] Although the NPPN complex exhibits strong Co–Cl and Co–P charge-transfer bands[2,15,17] at fairly lower energies, the spectrum indicates that the complex has a trans(Cl,Cl) configuration. For *trans(Cl,Cl)*-$[CoCl_2(NPPN)]^+$, there are two possible diastereomers arising from the combination of chiral phosphorus atoms of the ligand; racemic(RR,SS) and meso(RS)[18] (Fig. 2). The isolated *trans(Cl,Cl)*-$[CoCl_2(NPPN)]^+$ complex can be assigned to have the racemic NPPN ligand, since the complex affords only *cisα*-$[Co(L)(NPPN)]^{n+}$ (L=en, acac) by reaction with L. The meso NPPN ligand can not coordinate to a metal ion in the cisα form, but only in the cisβ form. The filtrate obtained after *trans(Cl,Cl)*-$[CoCl_2(rac(P)\text{-NPPN})]^+$ had been removed contained another green complex which seemed to be *trans(Cl,Cl)*-$[CoCl_2(meso(P)\text{-NPPN})]^+$. However, the complex was rather unstable and decomposed during the course of isolation to give cobalt(II) species and an oily material. The instability of this complex may be attributable to its strained structure, in which the central five-membered P–Co–P chelate ring is forced

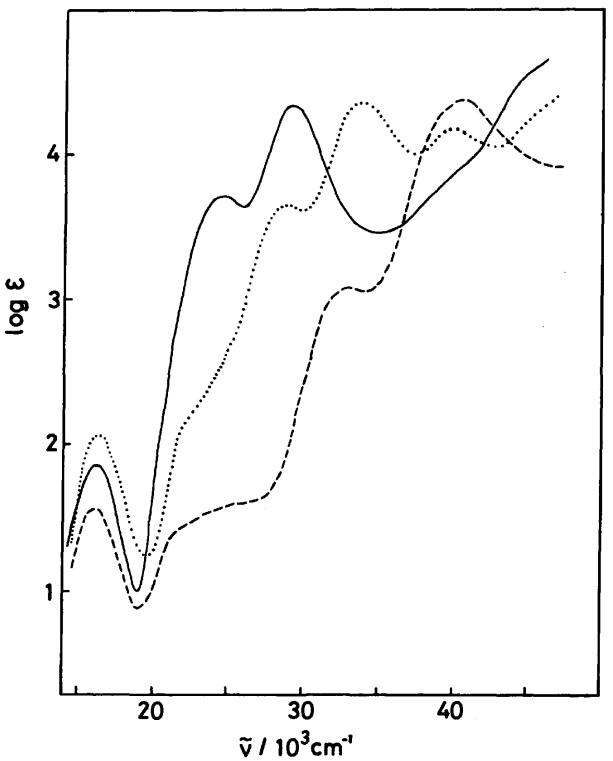

Fig. 1. Absorption spectra of *trans*-$[CoCl_2(rac(P)\text{-NPPN})]^+$ (——), *trans*-$[CoCl_2(en)_2]^+$ (------), and *trans*-$[CoCl_2(ebpp)_2]^+$ (·····).[2]

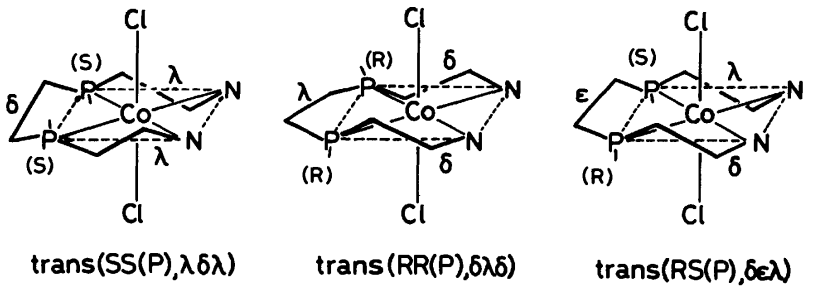

Fig. 2. Three possible isomers of *trans*-$[CoCl_2(NPPN)]^+$.

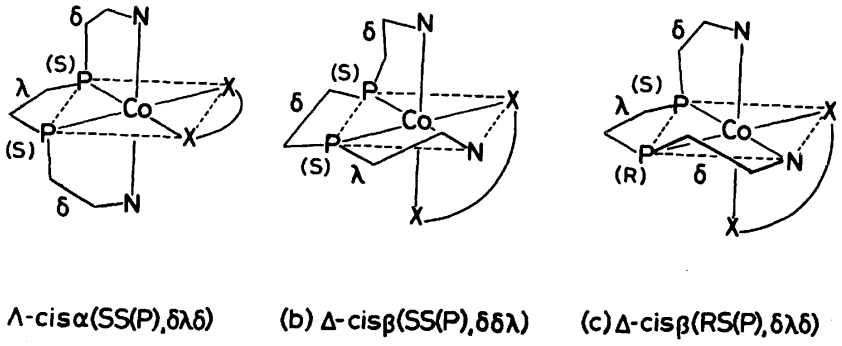

Fig. 3. Three possible isomers of $[Co(L)(NPPN)]^{n+}$.

to take an envelope conformation (Fig. 2), although such an envelope conformation was found in *trans*-$[Co(NH_3)_2(trien)]^{3+}$ (trien=$NH_2CH_2CH_2NHCH_2CH_2NHCH_2CH_2NH_2$).[20] The *trans*(*Cl,Cl*)-$[CoCl_2$ (*rac*(*P*)-NPPN)$]^+$ complex is very stable and does not change in water over several days. Thus only the *rac*(*P*)-NPPN ligand can form stable *trans*(*Cl,Cl*)-$[CoCl_2$-(NPPN)$]^+$.

As stated previously, either reaction of *trans*(*Cl,Cl*)-$[CoCl_2(NPPN)]^+$ with L (L=en, acac) afforded one geometrical isomer of $[Co(L)(NPPN)]^{n+}$. In each reaction product, a very small band (yellow for en and orange for acac) was observed on column chromatography, but they were not characterized because of a very small amount. For [Co(chelate)(NPPN)]$^{n+}$, three geometrical isomers are possible and each isomer has its antipode (Fig. 3). The [Co(chelate)(*meso*(*P*)-NPPN)]$^{n+}$ complex can not form the cisα isomer, since two terminal P–N chelate arms point to the same apical site with respect to the P–Co–P plane. The ^{13}C NMR spectra of the en and acac complexes exhibit eight and ten carbon signals, respectively. Thus these complexes can be assigned to the cisα isomer which has C_2 symmetry. The reason for preferential formation of the cisα isomer in [Co(L)(*rac*(*P*)-NPPN)]$^{n+}$ is not clear at the moment. Molecular models show that the cisβ isomer of the *rac*(*P*)-NPPN complex involves fairly large steric interactions between the phenyl group on the central phosphorus atom of three meridionally coordinated atoms N–P–P and all of three chelate rings formed by NPPN. The instability of the cisβ isomer of the *rac*(*P*)-NPPN complex seems to come from such a steric factor.

The chirality of phosphorus atoms (RR or SS) of *rac*(*P*)-NPPN has a mutual relation with the chirality of [Co(chelate)(*rac*(*P*)-NPPN)]$^{n+}$ (Δ or Λ); *SS*(*P*)-NPPN can form Λ-cisα and Δ-cisβ isomers, while *RR*(*P*)-NPPN Δ-cisα and Λ-cisβ isomers (Fig. 3). Figure 4 shows absorption and circular dichroism spectra of the faster-moving *cis*α-[Co(en)(*rac*(*P*)-NPPN)]$^{3+}$ isomer in column chromatography. The CD spectrum of this isomer is quite similar to that of *Λ-cis*α-[Co(en)(*SS*(*P*),*SS*(*C*)-NPPN)]$^{3+}$ (vide post) whose

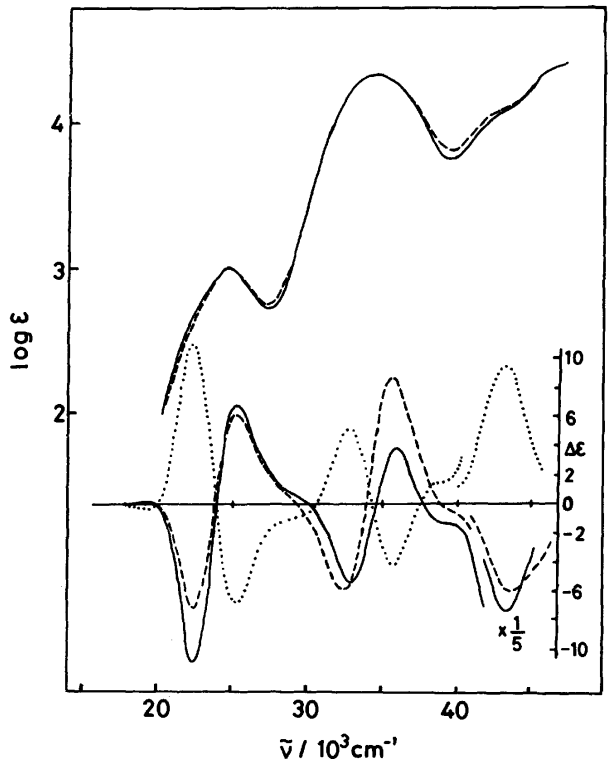

Fig. 4. Absorption and CD spectra of *cis*α-[Co(L)(NPPN)]$^{3+}$: *cis*α-[Co(en)(NPPN)]$^{3+}$ (——) (faster-eluting fractions (see Experimental)), *cis*α-[Co(*R*-pn)(NPPN)]$^{3+}$ (F1) (·····), *cis*α-[Co(*R*-pn)(NPPN)]$^{3+}$ (F2) (------).

absolute configuration has been determined by X-ray analysis.[21] Thus the isomer is assigned to the Λ-cisα isomer and the phosphorus atoms to the S configuration. By reaction of *trans*-$[CoCl_2$(*rac*(*P*)-NPPN)$]^+$ with *R*-pn, two isomers of [Co(*R*-pn)(*rac*(*P*)-NPPN)]$^{3+}$ (F1 and F2) were obtained in similar yields. The isomers were completely separated by SP-Sephadex column chromatography. Both isomers show identical absorption spectrum and the spectrum is nearly the same as that of *cis*α-[Co(en)(*rac*(*P*)-NPPN)]$^{3+}$. The CD spectra of isomers F1 and F2 are also very similar to those of the faster- and slower-

moving isomers of the en complex, *Δ-cisα*-[Co(en)(*RR*(*P*)-NPPN)]$^{3+}$ and *Δ-cisα*-[Co(en)(*SS*(*P*)-NPPN)]$^{3+}$ respectively (Fig. 4). Thus isomers F1 and F2 of the *R*-pn complex can be assigned to *Δ-cisα*-[Co(*R*-pn)(*RR*(*P*)-NPPN)]$^{3+}$ and *Δ-cisα*-[Co(*R*-pn)(*SS*(*P*)-NPPN)]$^{3+}$, respectively. It is noted that the Λ-isomer of these diamine complexes of *rac*(*P*)-NPPN shows a negative main CD band in the first d-d band region. The result is in contrast to the CD pattern for usual chelate complexes of Co(III), although the CD spectra of the present NPPN complexes involve the vicinal effect of chiral phosphorus atoms that can not be evaluated.

Similarly two isomers (F1 and F2) were obtained for each amino acidato complex [Co(L)(*rac*(*P*)-NPPN)]$^{2+}$ (L=*S*-ala, *S*-pro). From comparisons of the absorption and CD spectra with those of the above diamine complexes (Fig. 5), isomer F1 can be assigned to *Δ-cisα*-[Co(L)(*RR*(*P*)-NPPN)]$^{2+}$ and isomer F2 to *Δ-cisα*-[Co(L)(*SS*(*P*)-NPPN)]$^{2+}$. Spectral data for the NPPN complexes are listed in Table 1.

***SS*(*C*)-NPPN Complexes.** The *SS*(*C*)-NPPN ligand was prepared from $(C_6H_5)HPCH_2CH_2PH(C_6H_5)$ and (*S*)-2-methylaziridine by a method similar to Method 2 for NPPN. The *trans*-[$CoCl_2$(*SS*(*C*)-NPPN)]$^+$ complex was yielded from *SS*(*C*)-NPPN and [CoCl$(NH_3)_5$]Cl_2 by the same method as for the NPPN complex, but the yield was very poor. The N-P chelate ring of *SS*(*C*)-NPPN in a complex will be stabilized in a δ-gauche conformation because of the equatorial preference of the methyl group on the (*S*)-carbon atom. Molecular models indicate that when the N-P chelate ring takes a λ-conformation, the methyl group becomes axial and has steric interactions with the phenyl group disposed nearly axially and also with the chloride ion at the apical position of the complex. Of these possible isomers of the *trans*-dichloro complex shown in Fig. 2, only the

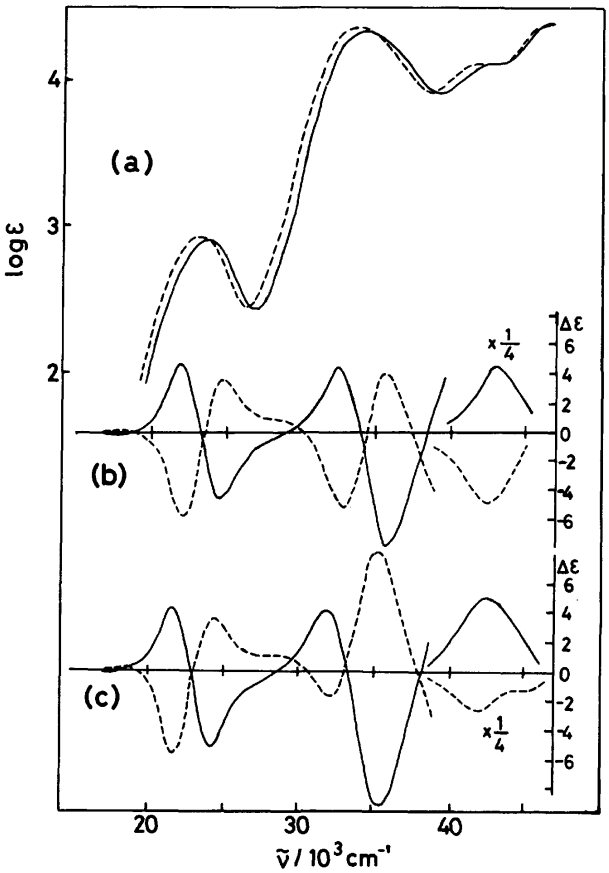

Fig. 5. (a) Absorption spectra of *cisα*-[Co(L)(NPPN)]$^{2+}$ (F2); L=*S*-ala (——), L=*S*-pro (------). (b) CD spectra of *cisα*-[Co(*S*-ala)(NPPN)$^{2+}$; F1 (——), F2 (------). (c) CD spectra of *cisα*-[Co(*S*-pro)(NPPN)]$^{2+}$; F1 (——), F2 (------).

Table 1. Absorption (AB) and CD Spectral Data for [Co(L)(NPPN)]$^{n+}$

L		AB ($\tilde{\nu}$/10^3 cm^{-1} (log ε))	CD ($\tilde{\nu}$/10^3 cm^{-1} (Δε))
Cl_2		16.3(1.82), 24.7(3.67), 29.2(4.29)	
en[a)]		24.7(3.02), 34.4(4.35)	19.6(+0.40), 22.4(−10.63), 25.3(+6.57), 32.9(−5.05), 35.8(+5.42), 43.3(−19.77)
acac[a)]		22.1(2.87), 35.1(4.44)	19.6(+0.32), 23.0(−3.53), 27.0(+1.88), 31.2(−15.29), 35.7(+41.59), 40.3(+31.83)
R-pn	F1	24.6(3.02), 34.2(4.38)	19.6(−0.32), 22.4(+10.97), 25.3(−6.62), 32.9(+5.07), 35.7(−4.16), 43.1(+19.72)
	F2	24.8(3.03), 34.5(4.35)	19.5(+0.20), 22.3(−7.12), 25.3(+6.16), 32.4(−5.89), 35.6(+8.57), 43.5(−11.87)
S-ala	F1	23.8(2.93), 34.1(4.34)	17.5(−0.04), 21.9(+4.68), 24.6(−4.60), 32.5(+4.44), 35.7(−7.62), 42.6(+19.36)
	F2	23.8(4.93), 34.1(4.32)	17.5(+0.05), 22.0(−5.80), 24.8(+3.50), 32.8(−5.24), 35.6(+3.96), 42.4(−18.99)
S-pro	F1	23.3(2.96), 33.6(4.39)	17.2(−0.03), 21.6(+4.35), 24.2(−4.14), 31.9(+4.30), 35.3(−9.27), 42.2(+20.70)
	F2	23.3(2.93), 33.6(4.36)	17.8(+0.05), 22.1(−5.85), 24.3(+3.51), 32.1(−1.72), 35.1(+8.26), 41.7(−10.64)

a) CD data are observed for faster eluting fraction.

trans(RR(P),$\delta\lambda\delta$) isomer[22] has no axial methyl group. The poor yield of *trans*-[$CoCl_2$(*SS*(*C*)-NPPN)]$^+$ will be attributable to such a stereochemical requirement of the complex, neither SS(P)- nor RS(P)-isomer of *SS*(*C*)-NPPN forming the stable *trans*-dichloro complex.

Two isomers (F1 and F2) of [Co(en)(*SS*(*C*)-NPPN)]$^{3+}$ were obtained by the reaction of *SS*(*C*)-NPPN with $[Co(en)_3]^{3+}$. As stated previously, the structure of isomer F2 was determined by X-ray analysis to *Λ-cisα*-[Co(en)(*SS*(*P*),*SS*(*C*)-NPPN)]$^{3+}$ where three chelate rings of *SS*(*C*)-NPPN take $\delta\lambda\delta$ conformations (Fig. 3(a)), and the two methyl groups have an equatorial disposition with respect to the N–P chelate ring. The other isomer F1 can be assigned to Δ-cisα, since the isomer exhibits nine carbon signals in the ^{13}C NMR spectrum, and shows absorption spectrum very similar to that of isomer F2, but the CD spectrum is nearly enantiomeric to that of isomer F2 (Fig. 6). In the Δ-cisα structure, both phosphorus atoms have necessarily the R configuration, and the stable conformation of *RR*(*P*),*SS*(*C*)-NPPN would be λδλ enantiomeric to those of the Λ-cisα isomer (F2). When the P–N chelate ring takes a λ-gauche conformation, the methyl group is disposed axially and approaches very close to one of the methylene groups of the central P–P chelate ring. However, the terminal P–N chelate ring in the cisα configuration is rather flexible and can take other conformation than λ-gauche such as an envelope-type to release the crowding. Such an envelope conformation of a similar P–N chelate ring has been found in *Λ-cisβ*-[Co(acac){(*S*,*S*)-$(CH_3)_2PCH_2$-$CH(CH_3)NHCH_2CH_2NHCH(CH_3)CH_2P(CH_3)_2$}]$^{2+}$.[23] Thus we have assigned isomer F1 to *Λ-cisα*-[Co(en)(*RR*(*P*),*SS*(*C*)-NPPN)]$^{3+}$.

No indication of formation of [Co(en)(*RS*(*P*),*SS*(*C*)-NPPN)]$^{3+}$ was observed in column chromatography. The *RS*(*P*),*SS*(*C*)-NPPN ligand can form only the cisβ isomer as stated previously. However, molecular models indicate that the puckered chelate ring of en has steric interactions with two phenyl groups of *RS*(*P*),*SS*(*C*)-NPPN arranged in the cisβ configuration. Thus the en complex with *RS*(*P*),*SS*(*C*)-NPPN will be unstable by such a steric factor.

The reaction of *SS*(*C*)-NPPN with [Co(acac)$_3$] afforded three isomers of [Co(acac)(*SS*(*C*)-NPPN)]$^{2+}$ (F1, F2, and F3). The ^{13}C NMR spectra suggest the cisα configuration for isomers F1 and F2, and the cisβ configuration for F3. Table 2 lists the NMR data. The assignments were made on the basis of the previous work on analogous complexes.[1,24] The absorption spectra of isomers F1 and F2 are similar, while the CD spectra are nearly enantiomeric to each other (Fig. 7). Isomers F1 and F2 of the acac complex

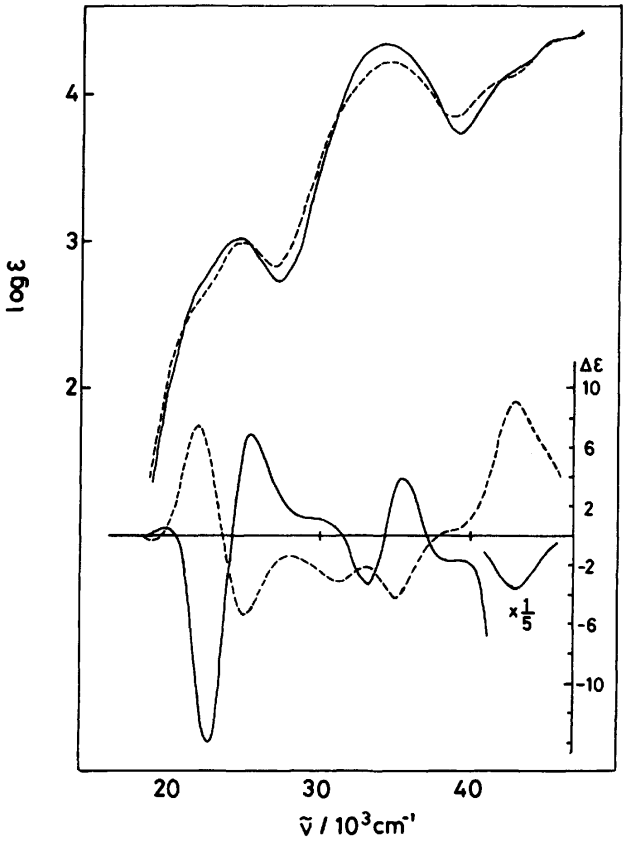

Fig. 6. Absorption and CD spectra of *cisα*-[Co(en)-(*SS*(C)-NPPN)]$^{3+}$; F1 (------), F2 (——).

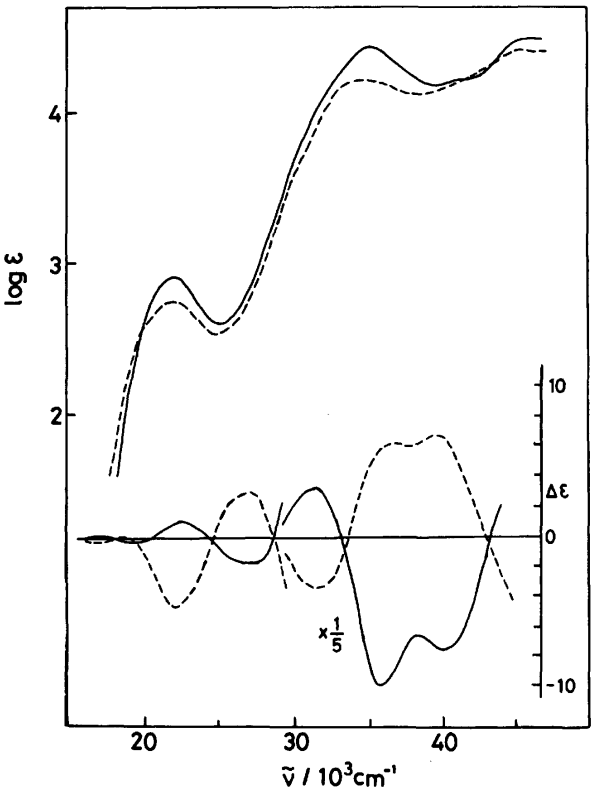

Fig. 7. Absorption and CD spectra of *cisα*-[Co(acac)-(*SS*(*C*)-NPPN)]$^{2+}$; F1 (------), F2 (——).

Table 2. ^{13}C NMR Spectral Data (δ/ppm (J/Hz))

Complexe (Solvent)	acac			en	NPPN or *SS(C)*-NPPN							
	CH_3	CH	CO	$N-CH_2$	PCH_2-(P)	PCH_2-(N)	NCH_2	N-CH	C-CH_3	P-C_1	*o*-	*m*-	*p*-
[Co(acac)(*rac*-NPPN)]$^{2+}$(D_2O)	28.16 s	98.91 s	191.44 s	—	22.96 d (40)	32.62 d (27)	43.20 s	—	—	124.47 t (48)	132.95 s	130.45 s	134.19 s
[Co(en)(*rac*-NPPN)]$^{3+}$(D_2O)	—	—	—	45.59 s	24.61 t (39)	30.94 t (26)	44.02 s	—	—	126.64 t (45)	131.87 t (11)	131.67 t (10)	135.16 s
[Co(acac)(*SS(C)*-NPPN)]$^{2+}$ F1 (D_2O)	28.27 t (5)	99.42 s	—[a]	—	21.54 t (39)	36.65 t (26)	—	50.49 s	20.81 t (15)	125.15 t (15)	133.10 t (7)	130.42 t (11)	134.12 s
[Co(acac)(*SS(C)*-NPPN)]$^{2+}$ F2 (D_2O)	28.51 s	99.08 s	—[a]	—	23.54 t (40)	39.43 t (24)	—	53.78 s	22.08 t (15)	123.94 q (48)	133.20 t (7)	130.61 t (11)	134.17 s
[Co(acac)(*SS(C)*-NPPN)]$^{2+}$ F3 (D_2O)	26.47 s	99.93 s	189.98 s	—	25.64dd (33.5)	35.02 d (29)	—	50.14 s	23.17 d (13)	121.9 d (49)	131.84 d (7)	130.11 d (11)	132.70 s
	27.27 d (4)		191.05 s		31.4dd (33.8)	38.46 d (26)		54.24 s	23.38 d (16)	124.1 d (46)	133.60 d (9)	130.40 d (11)	133.78 s
[Co(en)(*SS(C)*-NPPN)]$^{3+}$ F1 (CD_3CN)	—	—	—	45.56 s	22.23 t (40)	34.33bs	—	53.53 s	21.59 s	124.42 t (44)	—	131.71 b —	134.97 s
[Co(en)(*SS(C)*-NPPN)]$^{3+}$ F2 (D_2O)	—	—	—	45.86 s	25.18 t (38)	37.48 t (27)	—	54.30 s	21.82 s	123.59 t (46)	131.87 s	131.53 s	134.94 s

a) Not obsd. Internal reference: dioxane.

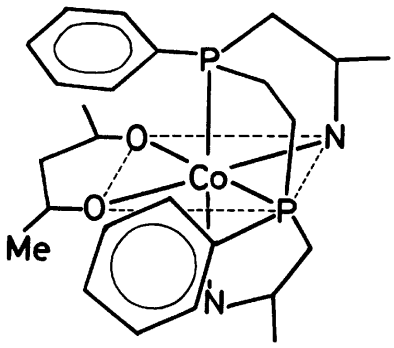

Δ-cisß(RS(P))

Fig. 8. A schematic structure of *Δ-cisβ*-[Co(acac)-(*RS(P),SS(C)*-NPPN)]$^{2+}$ (F3).

afford isomers F1 (Δ-*cisα*) and F2 (Λ-*cisα*) of the en complex, respectively (see Experimental). Thus isomer F1 of the acac complex is assigned to *Δ-cisα*-[Co(acac)(*RR(P),SS(C)*-NPPN)]$^{2+}$ and isomer F2 to *Λ-cisα*-[Co(acac)(*SS(P),SS(C)*-NPPN)]$^{2+}$.

Isomer F3 of the acac complex, which was suggested to be the cis*β* isomer from the ^{13}C NMR spectrum, does not afford any en complex by reaction with en (see Experimental). The result suggests that isomer F3 is the complex containig *RS(P),SS(C)*-NPPN, since the en complex of *RS(P),SS(C)*-NPPN was not formed by the reaction of *SS(C)*-NPPN with $[Co(en)_3]^{3+}$ as described above. A schematic structure of *cisβ*-[Co(acac)(*RS(P),SS(C)*-NPPN)]$^{2+}$ is given in Fig. 8. The assignment of this structure for isomer F3 is supported by the ^1H NMR spectrum. The isomer shows the methine proton signal of acac at a higher field (δ=5.17) than those of isomers F1 (δ=5.93) and F2 (δ=5.80), and also exhibits one of the two methyl proton signals of acac at a remarkably higher field (1.23 and 2.15 ppm) than those of isomers F1 (δ=2.23) and F2 (δ=2.21). The high field shifts of the methine and methyl proton signals of isomer F3 are attributable to the shielding effect of the phenyl groups approached very closely to those protons, as seen in Fig. 8. Such a high field shift of methyl signal is not expected for *cisβ*-[Co(acac)(*RR(P),SS(C)*- or *SS(P),SS(C)*-NPPN)]$^{2+}$ complex. For *cisβ*-[Co(acac)(*RS(P),SS(C)*-NPPN)]$^{2+}$, the Δ isomer will be much more stable than the Λ isomer, since two methyl groups of *RS(P),SS(C)*-NPPN are equatorial in the former, while axial in the latter (Fig. 8). The CD spectrum of isomer F3 suggests a Δ configuration. The isomer shows a similar CD pattern to that of isomer F1 (Δ-cis*α*) in the first d–d band region; both isomers give a negative and a positive CD band from the lower energy side in this region (Figs. 7 and 9). Thus isomer F3 can be assigned to *Δ-cisβ*-[Co(acac)

Table 3. Absorption (AB) and CD Spectral Data for *SS(C)*-NPPN Complexes

Complexe	AB ($\bar{\nu}/10^3$ cm^{-1} (log ε))	CD ($\bar{\nu}/10^3$ cm^{-1} ($\Delta\varepsilon$))
Δ-cisα-[Co(acac)(*SS(C)*-NPPN)]$^{2+}$	22.0(2.78), 34.5(4.28), 45.5(4.51)	16.8(−0.07), 18.7(+0.03), 22.1(−4.74), 26.9(+3.03), 31.9(−5.05), 37.0(+8.60), 39.9(+9.50)
Λ-cisα-[Co(acac)(*SS(C)*-NPPN)]$^{2+}$	22.0(2.96), 35.0(4.52), 45.5(4.56)	16.8(+0.04), 19.3(−0.13), 23.0(+1.34), 27.5(−1.61), 31.5(+3.40), 36.0(−10.0), 40.4(−7.57)
Δ-cisβ-[Co(acac)(*SS(C)*-NPPN)]$^{2+}$	19.9(2.7),[a] 22.7(3.08), 37.2(4.32)	20.0(−5.90), 24.0(+3.69), 29.3(+13.9), 33.0(−5.40), 36.0(+2.16), 38.2(−6.84), 43.5(+3.68)
Δ-cisα-[Co(en)(*SS(C)*-NPPN)]$^{3+}$	24.6(3.06), 34.5(4.31)	19.0(−0.18), 21.9(+7.53), 25.0(−5.54), 31.5(−4.30), 35.0(−6.04), 43.0(12.7)
Λ-cisα-[Co(en)(*SS(C)*-NPPN)]$^{3+}$	24.5(3.02), 34.5(4.33)	19.8(+0.45), 22.5(−14.0), 25.4(+6.78), 33.2(−3.34), 35.5(+3.97), 43.0(−17.8)

a) Shoulder absorption.

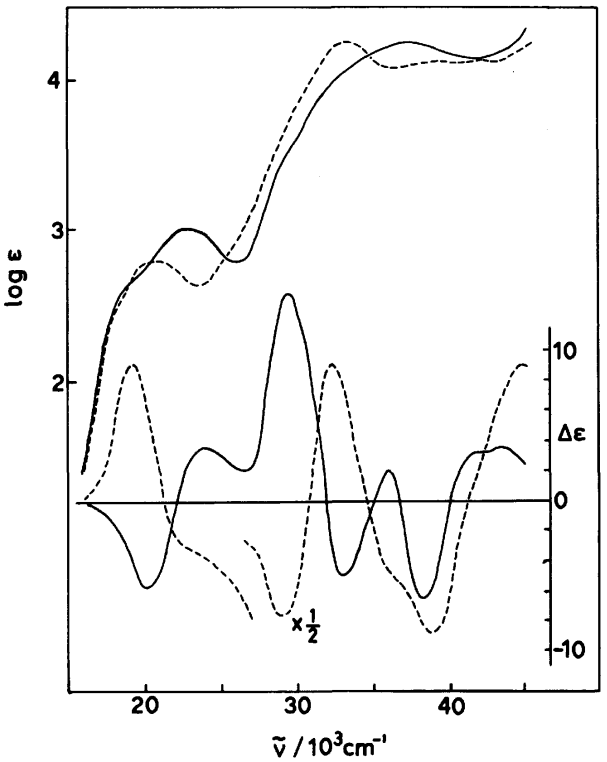

Fig. 9. Absorption and CD spectra of *Δ-cisβ*-[Co(acac)(*RS(P)*,*SS(C)*-NPPN)]$^{2+}$ (F3) (——) and *Λ-cisβ*-[Co(acac){*SR(P)*,*SS(C)*-$(CH_3)(C_6H_5)PCH_2CH(CH_3)NHCH_2CH_2NHCH(CH_3)CH_2P(CH_3)(C_6H_5)$}]$^{2+}$ (------).[4]

(*RS(P)*,*SS(C)*-NPPN)]$^{2+}$. As stated above, this structure is very crowded and will involve steric interactions between the acac ligand and the phenyl groups of *RS(P)*,*SS(C)*-NPPN. In fact, the isomer in aqueous solution changes slowly from orange to red in color, although the red complex could not be isolated.

The first d–d band of isomer F3 (cisβ) splits into two components (Fig. 9), while those of isomers F1 and F2 (cisα) do not (Fig. 7). If it is assumed that the ligand field strengths of donor atoms are P>N>O, a large band-splitting is expected for the cisβ isomer than for

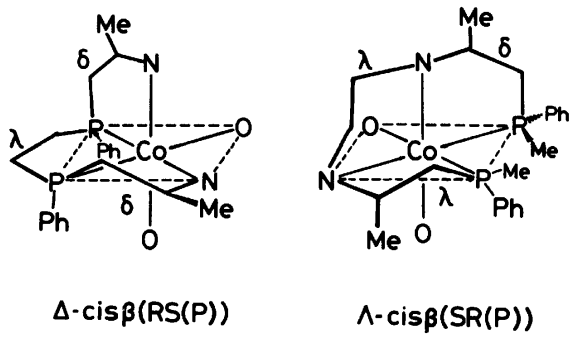

Fig. 10. Molecular models of *Δ-cisβ*-[Co(acac)(*RS(P)*,*SS(C)*-NPPN)]$^{2+}$ (F3) and *Λ-cisβ*-[Co(acac){*SR(P)*,*SS(C)*-$(CH_3)(C_6H_5)PCH_2CH(CH_3)NHCH_2CH_2NHCH(CH_3)CH_2P(CH_3)(C_6H_5)$}]$^{2+}$.

the cisα isomer from Yamatera's rule.[25] Figure 9 compares the CD spectrum of isomer F3 with that of *Λ-cisβ*-[Co(acac){*RS(P)*,*SS(C)*-$(CH_3)(C_6H_5)PCH_2CH(CH_3)NHCH_2CH_2NHCH(CH_3)CH_2P(CH_3)(C_6H_5)$}]$^{2+}$,[4] which has a chelate ring between the two N atoms in place of the P–P chelate ring in isomer F3. Both complexes have the same geometrical arrangement for the coordinating donor atoms, cis(P,P)cis(N,N)cis(O,O), but are antipodal to each other with respect to the arrangement of donor atoms and of chelate rings as seen in Fig. 10. These two complexes show CD spectra nearly enantiomeric to each other except those in the higher energy region.

The absorption and CD spectral data of the *SS(C)*-NPPN complexes are listed in Table 3.

The authors wish to thank the Ministry of Education for Scientific Research Grant-in-Aid No. 60470046 and 61430013.

References

1) K. Kashiwabara, I. Kinoshita, T. Ito, and J. Fujita, *Bull. Chem. Soc. Jpn.*, **54**, 725 (1981).

2) I. Kinoshita, Y. Yokota, K. Matsumoto, S. Ooi, K. Kashiwabara, and J. Fujita, *Bull. Chem. Soc. Jpn.*, **56**, 1067 (1983).

3) M. Takata, K. Kashiwabara, H. Ito, T. Ito, and J. Fujita, *Bull. Chem. Soc. Jpn.*, **58**, 2247 (1985).

4) M. Atoh, K. Kashiwabara, and J. Fujita, *Bull. Chem. Soc. Jpn.*, **59**, 1001 (1986).

5) S. C. Grocott and S. B. Wild, *Inorg. Chem.*, **21**, 3526 (1982); S. C. Grocott and S. B. Wild, *Inorg. Chem.*, **21**, 3535 (1982).

6) a) B. Bosnich, W. G. Jackson, and S. B. Wild, *J. Am. Chem. Soc.*, **95**, 8269 (1973); b) B. Bosnich, W. G. Jackson, and S. B. Wild, *Inorg. Chem.*, **13**, 1121 (1974); c) W. G. Jackson and B. Bosnich, *Inorg. Chem.*, **22**, 2864 (1983).

7) L. Horner and H. Winkler, *Tetrahedron Lett.*, **1964**, 461; H. D. Munro and L. Horner, *Tetrahedron*, **26**, 4621 (1970); G. H. Senkler and K. Mislow, *J. Am. Chem. Soc.*, **94**, 291 (1972).

8) "Chemistry of Octahedral Complexes," Kagaku Sosetu No. 13, 1976.

9) K. Issleib and H. Oehme, *Chem. Ber.*, **100**, 2685 (1967).

10) K. Issleib and H. Weichmann, *Chem. Ber.*, **101**, 2197 (1968).

11) Y. Minoura, M. Takebayashi, and C. C. Price, *J. Am. Chem. Soc.*, **81**, 4689 (1959).

12) *Inorg. Synth.*, Vol. IX, p. 160.

13) *Inorg. Synth.*, Vol. II, p. 221.

14) *Inorg. Synth.*, Vol. V, p. 188.

15) M. Atoh, I. Kinoshita, K. Kashiwabara and J. Fujita, *Bull. Chem. Soc. Jpn.*, **55**, 3179 (1982).

16) T. Ohishi, K. Kashiwabara, and J. Fujita, *Bull. Chem. Soc. Jpn.*, **60**, 575 (1987).

17) M. Atoh, K. Kashiwabara, and J. Fujita, *Bull. Chem. Soc. Jpn.*, **58**, 2793 (1985).

18) The notation of the absolute configurations, R and S, for the chiral phosphorus atoms of a free ligand is reversed upon coordination to the cobalt(III) ion, according to the sequence rule proposed by Cahn et al.[19] In this paper, we use the same notation for the coordinating phosphine ligand as that when it is free.

19) R. S. Cahn, C. K. Ingold, and V. Prelog, *Angew. Chem., Int. Ed. Engl.*, **5**, 385 (1966).

20) S. Utsuno, Y. Sakai, Y. Yoshikawa, and H. Yamatera, *J. Am. Chem. Soc.*, **102**, 6903 (1980).

21) M. Atoh, K. Kashiwabara, and J. Fujita, to be published.

22) In this paper, the absolute configuration of asymmetric phosphorus atoms in an *SS(C)*-NPPN ligand is designated by neglecting two methyl groups on asymmetric carbon atoms to compare with that of an NPPN ligand, otherwise the opposite designation is applied for the same geometry of both *SS(C)*-NPPN and NPPN ligands, and we use the same notation for a coordinating *SS(C)*-NPPN as that when it is free like the case of an NPPN ligand.

23) M. Atoh, K. Kashiwabara, and J. Fujita, *Bull. Chem. Soc. Jpn.*, **58**, 3492 (1985).

24) T. Ohishi, K. Kashiwabara, and J. Fujita, *Bull. Chem. Soc. Jpn.*, **56**, 1553 (1983); M. Atoh, K. Kashiwabara, and J. Fujita, *Bull. Chem. Soc. Jpn.*, **58**, 2793 (1985).

25) H. Yamatera, *Bull. Chem. Soc. Jpn.*, **31**, 95 (1958).

Preparation and Characterization of Cobalt(III) Complexes with L-Cysteinate and S-Methyl-L-Cysteinate. Crystal Structure of (L-Cysteinato)(diethylenetriamine)cobalt(III) Perchlorate

Ken-ichi OKAMOTO,* Hideki UMEHARA, Masayo NOMOTO, Hisahiko EINAGA,† and Jinsai HIDAKA

Department of Chemistry, University of Tsukuba, Sakura, Ibaraki 305
†Institute of Materials Science, University of Tsukuba, Sakura, Ibaraki 305

(Received December 6, 1986)

Of three possible isomers for the (L-cysteinato)(diethylenetriamine)cobalt(III) complex, [Co(L-cys)(dien)]$^+$, two isomers are selectively prepared. Of the two isomers, the crystal structure of the dominantly formed isomer has been determined by the X-ray diffraction method. The greenish brown needle crystal was orthorhombic, space group $P2_12_12_1$, a=16.589(4), b=20.510(9), c=12.479(4) Å, and Z=4. The structure has been refined to R=0.068 on 5913 observed reflections. There are three crystallographically independent complex cations in an asymmetric unit. All the complex cations have trans(N_iS) configuration and the L-cysteinate coordinates facially to the cobalt atoms as terdentate-N,O,S ligand. The isomers of the (*S*-methyl-L-cysteinato)(diethylenetriamine)cobalt(III) complex were derived from [Co(L-cys)(dien)]$^+$ by the reaction with dimethyl sulfate. The electronic absorption, CD, and ^{1}H and ^{13}C NMR spectral behaviors for these complexes are discussed in relation to their geometrical configurations.

Cobalt(III) complexes with the thiolato or thioether type terdentate-N,O,S ligand such as *S*-methyl-L-cysteinate (L-smc), L-penicillaminate (L-pen), and *S*-methyl-L-penicillaminate (L-smp) have been investigated for the stereochemical and spectrochemical interests.[1-10] However, L-cysteinate (L-cys) usually coordinates to cobalt(III) as a bidentate-N,S ligand[11-16] or tends to form the stable *S*-bridged complexes.[17] So we attempted to prepare the (diethylenetriamine)-cobalt(III) complex with L-cysteinate functioning as a terdentate-N,O,S, [Co(L-cys)(dien)]$^+$, and the result is able to compare with the stereochemistry of the corresponding L-penicillaminato complex.[5,7]

In the present paper, the (diethylenetriamine)cobalt(III) complex with L-cysteinate, which could not be prepared by a procedure similar to that used for [Co(L-pen)(dien)]$^+$,[5,7] was successfully obtained for the first time. Two isomers were selectively formed and the crystal structure of the dominantly formed isomer, [Co(L-cys)(dien)]$_3$(ClO_4)$_3$·0.82H_2O, was determined by X-ray diffraction method. The *S*-methyl-L-cysteinato complex, [Co(L-smc)(dien)]$^{2+}$, was prepared by the reaction of [Co(L-cys)(dien)]$^+$ with dimethyl sulfate. The absorption, CD, and ^{1}H and ^{13}C NMR spectra, and the stereochemical properties of [Co(L-cys or L-smc)(dien)]$^{+\text{ or }2+}$ are discussed in comparison with those of the corresponding [Co(L-pen or L-smp)-(dien)]$^{+\text{ or }2+}$ complexes.[5,7]

Experimental

1) Preparation of Complexes. a) [Co(L-cys)(dien)]ClO_4. To a deoxygenated solution containing 4.8 g of $CoCl_2$·6H_2O in 25 cm^3 of water were successively added with stirring a deoxygenated solution containing 2.1 g of diethylenetriamine in 25 cm^3 of water and 2.4 g of L-cystine powder. The mixture was continuously stirred under nitrogen atmosphere at room temperature for 1 h. The greenish brown solution was filtered and the filtrate was poured onto a column of SP-Sephadex C-25 (Na^+ form, 5 cm×45 cm). After the column had been swept with water, the adsorbed band was eluted with a 0.15 mol dm^{-3} aqueous solution of $NaClO_4$. Only a greenish brown band (E-1) was eluted and the eluate was immediately concentrated to a small volume with a rotary evaporator below 25 °C. To the solution was added a small amount of ethanol and then the solution was kept in a refrigerator overnight. A small amount of crystals (A-1) appeared and was collected by filtration. The filtrate was concentrated and kept in a refrigerator again. The greenish brown crystals (A-2) which appeared were collected by filtration. When the A-1 isomer was recrystallized from as little water as possible by adding ethanol, the crystals contained a mixture of the A-1 and A-2 isomers as evidenced from the ^{1}H and ^{13}C NMR spectral measurements. This suggests that the A-1 isomer isomerized to the A-2 one. The A-2 isomer was obtained as pure crystals, collected by filtration, washed with ethanol, and dried in a desiccator. A piece of the crystals of the A-2 isomer was used for the X-ray crystal analysis. The A-1 and A-2 isomers could not be separated using a column chromatographic method because these isomers, especially A-1 isomer, were unstable in the column. Yield for A-2: 39%. Found for A-2: C, 21.94; H, 4.84; N, 14.61%. Calcd for [Co(L-cys)(dien)]ClO_4·0.27H_2O=$C_7H_{18}N_4O_6ClSCo$·0.27H_2O: C, 21.81; H, 4.85; N, 14.53%.

b) [Co(L-smc)(dien)](ClO_4)$_2$. Method 1. To a solution containing 0.3 g of the A-2 isomer, [Co(L-cys)(dien)]-ClO_4·0.27H_2O, in 12 cm^3 of water was added 6 cm^3 of dimethyl sulfate. When the mixture was allowed to stand in a refrigerator overnight, it was separated into two layers. The upper red layer was taken out and poured onto a column of QAE-Sephadex A-25 (ClO_4^- form, 2.5 cm×20 cm) in order to obtain the perchlorate salt. The eluate was concentrated to a small volume with a rotary evaporator and to this was added a small amount of ethanol. After the solution was kept in a refrigerator overnight, the needle

crystals which appeared were collected by filtration, washed with ethanol, and dried in a desiccator. Found: C, 19.38; H, 4.26; N, 11.32%. Calcd for $[Co(L\text{-}smc)(dien)](ClO_4)_2 = C_8H_{21}N_4O_{10}Cl_2SCo$: C, 19.40; H, 4.27; N, 11.32%.

Method 2. The eluate containing $[Co(L\text{-}cys)(dien)]^+$ (E-1) eluted from the SP-Sephadex column in Ia) was methylated by a similar procedure to that used in Method 1. The upper red layer was poured onto a column of Dowex 50W-X8 (200—400 mesh, Na^+ form, 4.5 cm×40 cm). After the column had been swept with water, the adsorbed band was eluted with a 0.5 mol dm^{-3} aqueous solution of NaCl. Two red bands, B-1 and B-2, were eluted in this order. The eluate B-2 showed the identical absorption and CD spectra with the isomer obtained in Method 1. The formation ratio of the isomers, B-1 and B-2, was about 1:3. Then the eluate B-1 was concentrated to a small volume with a rotary evaporator below 25 °C and the deposited NaCl was filtered off. The filtrate was passed through a column of Sephadex G-10 (3 cm×53 cm) in order to eliminate NaCl. The eluate was concentrated to a small volume and poured onto a column of QAE-Sephadex A-25 (ClO_4^- form, 2.5 cm×20 cm). The eluate converted to the perchlorate salt was concentrated to a small volume and to this was added a small amount of ethanol. The solution was kept in a refrigerator for several days. The crystals which appeared were collected by filtration, washed with ethanol, and dried in a desiccator. Found for B-1: C, 19.10; H, 4.43; N, 11.13%. Calcd for $[Co(L\text{-}smc)(dien)](ClO_4)_2 \cdot 0.5H_2O$: C, 19.06; H, 4.40; N, 11.11%.

2) General Data. The electronic absorption spectra were recorded on JASCO UVIDEC-1 and UVIDEC-610 spectrophotometers and the CD spectra on a JASCO J-20 spectropolarimeter. All measurements were carried out in aqueous solution at room temperature. The ^1H and ^{13}C NMR spectra were recorded in deuterium oxide on a JEOL JNM-FX-100 or -FX-90Q NMR spectrometer at the probe temperature. Sodium 2,2-dimethyl-2-silapentane-5-sulfonate was used as an internal reference. The X-ray analysis calculations were carried out on a FACOM M-382 computer at the University of Tsukuba.

3) X-Ray Data Collection. Unit cell parameters and intensity data for the single crystal (A-2) (ca. 0.18×0.20×0.80 mm^3) were measured on a Rigaku-denki four-circle diffractometer (AFC-5) with graphite-monochromatized Mo $K\alpha$ radiation. The unit cell parameters were determined by a least-squares refinement based on 25 reflections.

Table 1. Positional and Thermal Parameters (with e.s.d.'s)

Atom	X	Y	Z	B_{eq}/Å² a)	Atom	X	Y	Z	B_{eq}/Å² a)
CoA	0.44060(8)	0.15381(5)	0.59189(9)	2.00	CoD	0.93161(7)	0.02003(5)	0.38664(9)	1.87
SA	0.5615(2)	0.1777(1)	0.6667(2)	2.74	SD	1.0550(2)	0.0170(1)	0.3073(2)	2.54
OA1	0.4764(4)	0.0652(3)	0.5746(5)	2.76	OD1	0.9465(4)	0.1107(3)	0.4150(5)	2.42
OA2	0.5909(4)	0.0165(3)	0.5239(6)	3.94	OD2	1.0383(4)	0.1766(3)	0.4887(5)	3.39
NA1	0.4940(5)	0.1661(4)	0.4527(6)	3.23	ND1	0.9905(5)	0.0101(3)	0.5221(6)	2.39
NA2	0.3968(5)	0.1331(4)	0.7325(6)	2.88	ND2	0.8765(4)	0.0417(4)	0.2526(7)	2.82
NA3	0.3308(5)	0.1305(4)	0.5349(7)	2.73	ND3	0.8238(5)	0.0219(4)	0.4561(6)	2.59
NA4	0.4012(5)	0.2435(4)	0.5957(7)	3.19	ND4	0.9148(4)	−0.0723(3)	0.3664(7)	2.71
CA1	0.5445(6)	0.0629(4)	0.5254(7)	2.66	CD1	1.0114(6)	0.1226(5)	0.4725(7)	2.70
CA2	0.5672(6)	0.1264(4)	0.4668(7)	2.77	CD2	1.0528(5)	0.0618(4)	0.5137(7)	2.54
CA3	0.6208(6)	0.1648(5)	0.5439(8)	3.26	CD3	1.1128(6)	0.0382(5)	0.4268(8)	2.79
CA4	0.3078(7)	0.1161(6)	0.7281(10)	4.48	CD4	0.7859(6)	0.0370(6)	0.2651(9)	3.71
CA5	0.2927(6)	0.0875(6)	0.6167(10)	4.14	CD5	0.7670(6)	0.0548(6)	0.3814(9)	3.94
CA6	0.2814(7)	0.1924(5)	0.5166(11)	4.85	CD6	0.8017(7)	−0.0453(5)	0.4871(9)	3.86
CA7	0.3381(8)	0.2486(6)	0.5130(12)	5.56	CD7	0.8327(6)	−0.0930(5)	0.4033(10)	4.04
CoB	0.02560(7)	0.18535(6)	0.07290(9)	1.97	C1E	0.6520(2)	0.2175(2)	0.2174(2)	4.35
SB	−0.1015(1)	0.1914(1)	0.1365(2)	2.92	C1F	0.3508(2)	0.0597(2)	0.2557(2)	4.12
OB1	0.0312(4)	0.2790(3)	0.0753(5)	2.80	C1G	0.3582(3)	0.3719(3)	0.2735(3)	7.84
OB2	−0.0384(5)	0.3643(3)	0.0188(6)	3.98	OE1	0.6785(8)	0.1973(6)	0.1198(11)	9.87b)
NB1	−0.0208(5)	0.2010(3)	−0.0691(6)	2.65	OE2	0.6504(8)	0.2880(7)	0.2051(11)	10.56b)
NB2	0.0666(4)	0.1786(4)	0.2189(5)	2.23	OE3	0.7040(6)	0.2011(5)	0.3043(8)	6.71b)
NB3	0.1420(5)	0.1799(4)	0.0283(6)	3.07	OE4	0.5727(7)	0.2021(6)	0.2326(9)	8.68b)
NB4	0.0254(5)	0.0910(3)	0.0540(7)	3.10	OF1	0.3180(7)	0.0580(6)	0.1536(9)	8.69b)
CB1	−0.0237(6)	0.3055(4)	0.0185(7)	2.64	OF2	0.3608(8)	0.1298(7)	0.2734(11)	10.44b)
CB2	−0.0748(6)	0.2585(4)	−0.0496(7)	2.90	OF3	0.4231(11)	0.0352(8)	0.2651(14)	14.23b)
CB3	−0.1447(6)	0.2356(5)	0.0215(8)	3.37	OF4	0.2982(7)	0.0379(6)	0.3386(9)	8.33b)
CB4	0.1547(7)	0.1710(5)	0.2204(8)	3.71	OG1	0.3627(6)	0.3967(5)	0.1690(7)	6.05b)
CB5	0.1896(6)	0.2032(5)	0.1205(9)	3.49	OG2	0.3040(9)	0.3986(7)	0.3445(11)	11.05b)
CB6	0.1630(6)	0.1111(5)	−0.0048(9)	3.88	OG3	0.3152(19)	0.3068(16)	0.2678(25)	28.58b)
CB7	0.0855(7)	0.0745(5)	−0.0326(9)	4.06	OG4	0.4330(10)	0.3547(7)	0.3131(12)	12.49b)
					OW	0.5934(15)	0.0120(12)	0.2227(18)	16.74b)

a) $B_{eq} = 8\pi^2(U_{12}+U_{22}+U_{33})/3$. b) Isotropic temperature factor.

Systematic absences led to the space group $P2_12_12_1$. Crystal Data: $C_{21}H_{55.64}N_{12}O_{18.82}Cl_3S_3Co_3$, $M.W.$=1156.84, orthorhombic, space group $P2_12_12_1$, a=16.589(4), b=20.510(9), c=12.479(4) Å, V=4246(3) Å^3, D_x=1.810 g cm^{-3}, D_m=1.79 g cm^{-3} (by the flotation), Z=12, and μ(Mo Kα)=1.623 mm^{-1}.

The intensity data were collected by the ω-2θ scan technique up to 2θ=60° with scan rate of 3° min^{-1}. The intensity data were converted to the F_o data in the usual manner. Absorption corrections were not applied. A total of 5913 independent reflections with $|F_o|>3\sigma(|F_o|)$ of the measured 6881 reflections were considered as 'observed' and used for the structure analysis.

4) Determination of the Crystal Structure. The positions of three cobalt atoms and the coordinated sulfur, oxygen, and nitrogen atoms were determined by the direct method (program MULTAN[18]) was used). The difference-Fourier maps based on these atomic positions revealed the other nonhydrogen atoms. The structure was refined by a full-matrix least-squares refinement using the positional parameters, the anisotropic thermal parameters of the nonhydrogen atoms of the complex ions, and the isotropic thermal parameters of the oxygen atoms in the perchlorate ions and the water molecule (program RFINE[19]) was used). The occupancy for the oxygen atom of the water molecule was also refined and converged to 0.82(3), since the analytical result of the water molecule indicates the small value. The neutral atomic scattering factors for all the nonhydrogen atoms were taken from the literatures.[20,21]) The final residual values were R=0.068 and R_w=0.076, respectively. The configuration was determined on the basis of the known configuration of L-cysteinate.[22]) The final positional parameters are listed in Table 1. A list of structure factors (Table A) and anisotropic thermal parameters (Table B) are kept at the Chemical Society of Japan as Document No. 8738.

Results and Discussion

Description of the Structure. A perspective drawing of the typical complex cation (CoA species) is shown in Fig. 1, together with the numbering scheme.

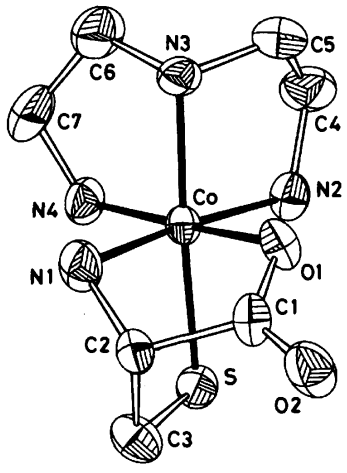

Fig. 1. A. perspective drawing of *trans*(N_iS)-[Co(L-cys)(dien)]$^+$ (CoA species) with the numbering scheme of atoms.

The packing mode is illustrated in Fig. 2. There are three crystallographically independent complex cations in an asymmetric unit, though their shapes and sizes remarkably resemble one another. The cobalt atom was octahedrally surrounded by the oxygen, sulfur, and four nitrogen atoms. The L-cysteinate and diethylenetriamine coordinate facially to the cobalt atom as terdentate ligands. The sulfur atom of the L-cys occupies the trans position to the imino nitrogen atom of the dien. Accordingly, all of these complex cations are determined to take a trans(N_iS) configuration (Figs. 1 and 2).[23])

The bond lengths and angles in the three crystallographically independent complex cations are similar to those for the cobalt(III) complexes with diethylenetriamine and/or sulfur-containing amino carboxylates (Table 2).[1-3,5]) The average Co–N3 distance bonded trans to the sulfur atom is 2.005(8) Å and the average cis Co–N distance is 1.952(8) Å. A difference between the trans and cis Co–N distances, 0.053 Å, indicates the trans effect due to the coordinated sulfur atom, as in the case of the cobalt(III) complexes with the thiolato ligands such as L-penicillaminate[5]) and 2-aminoethanethiolate.[24]) Especially, the CoA and CoB complex cations exhibit the large trans effect, 2.013 Å.

The conformations of the L-cys in the three complex

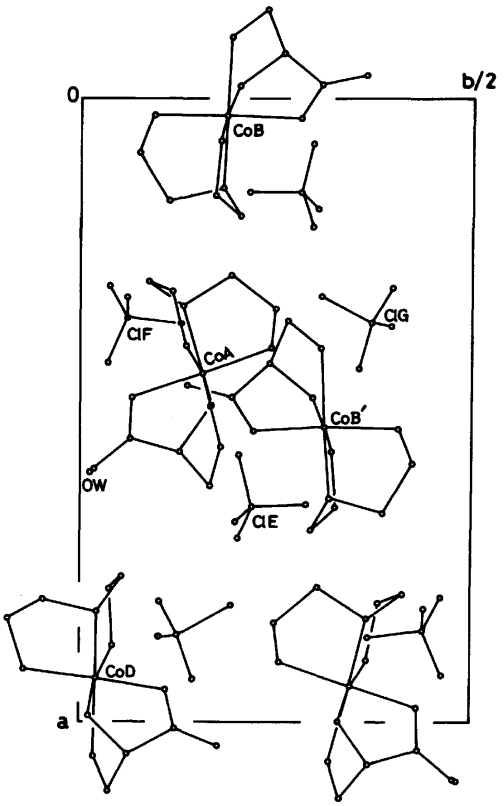

Fig. 2. A partial projection of the crystal packing viewed along the c axis.

Table 2. Interatomic Distances and Bond Angles (with e.s.d.'s) for *trans*(N_iS)-[Co(L-cys)(dien)]$ClO_4 \cdot 0.27H_2O$

(a) Bond distances (l/Å)

	A	B	D		A	B	D
Co-S	2.266(3)	2.256(3)	2.274(3)	N1-C2	1.472(12)	1.501(12)	1.485(11)
Co-O1	1.925(6)	1.922(6)	1.910(6)	N2-C4	1.517(14)	1.470(13)	1.515(12)
Co-N1	1.966(8)	1.959(7)	1.963(8)	N3-C5	1.489(14)	1.475(13)	1.487(13)
Co-N2	1.946(8)	1.950(7)	1.957(8)	N3-C6	1.527(14)	1.511(14)	1.477(13)
Co-N3	2.013(8)	2.013(8)	1.988(8)	N4-C7	1.474(16)	1.508(14)	1.499(12)
Co-N4	1.952(8)	1.949(7)	1.930(7)	C1-C2	1.542(13)	1.540(13)	1.513(13)
S-C3	1.841(10)	1.843(10)	1.825(10)	C2-C3	1.527(14)	1.534(14)	1.550(13)
O1-C1	1.287(11)	1.275(11)	1.318(11)	C4-C5	1.530(18)	1.525(15)	1.529(16)
O2-C1	1.224(12)	1.230(11)	1.209(12)	C6-C7	1.489(17)	1.529(15)	1.522(16)

(b) Bond angles (ϕ/°)

	A	B	D		A	B	D
S-Co-O1	88.7(2)	89.1(2)	89.5(2)	Co-N1-C2	101.3(6)	102.5(5)	102.2(5)
S-Co-N1	86.4(2)	86.7(2)	85.7(2)	Co-N2-C4	112.4(6)	111.5(6)	111.2(6)
S-Co-N2	90.4(3)	90.0(2)	93.1(2)	Co-N3-C5	106.4(6)	106.2(6)	107.8(6)
S-Co-N3	176.2(2)	175.5(2)	179.5(2)	Co-N3-C6	109.9(6)	110.4(6)	108.7(6)
S-Co-N4	94.7(2)	95.5(3)	92.7(2)	C5-N3-C6	111.6(8)	113.1(8)	115.5(8)
O1-Co-N1	83.3(3)	82.5(3)	83.0(3)	Co-N4-C7	106.7(7)	108.0(6)	111.7(6)
O1-Co-N2	90.6(3)	92.3(3)	89.9(3)	O1-C1-O2	126.0(8)	124.0(8)	124.1(9)
O1-Co-N3	90.9(3)	90.8(3)	91.0(3)	O1-C1-C2	114.2(8)	115.6(7)	113.7(8)
O1-Co-N4	174.7(3)	173.4(3)	176.8(3)	O2-C1-C2	119.8(9)	120.4(8)	122.1(9)
N1-Co-N2	173.1(3)	173.9(3)	172.7(3)	N1-C2-C1	108.8(8)	104.6(7)	107.3(7)
N1-Co-N3	97.2(3)	97.8(3)	94.3(3)	N1-C2-C3	105.7(7)	107.7(7)	105.8(7)
N1-Co-N4	93.0(3)	93.0(3)	94.8(3)	C1-C2-C3	106.3(7)	106.8(7)	108.1(7)
N2-Co-N3	85.9(3)	85.4(3)	87.0(3)	S1-C3-C2	106.7(7)	107.9(6)	108.0(6)
N2-Co-N4	93.4(3)	92.5(3)	92.4(3)	N2-C4-C5	106.2(9)	108.7(8)	106.6(8)
N3-Co-N4	85.9(3)	85.0(4)	86.9(3)	N3-C5-C4	109.0(9)	107.1(8)	110.9(8)
Co-S-C3	95.7(3)	96.7(3)	96.3(3)	N3-C6-C7	108.0(9)	109.1(8)	109.6(9)
Co-O1-C1	111.0(5)	112.6(5)	112.8(5)	N4-C7-C6	111.8(11)	106.5(8)	109.6(8)

cations resemble one another and the average displacements of the relevant atoms from the Co-O1-N1 or Co-S-N1 plane are somewhat different from those of *trans*(N_iN)-[Co(L-pen)(dien)]$^+$ (Cl and C2 for the L-cys (L-pen) complex, 0.599(0.371) and 0.942(0.838) Å, λ form; C2 and C3, 1.101(1.154) and 0.590(0.780) Å, δ form).[5] The conformation of the dien in the CoD complex cation are quite similar to those in *trans*(N_iN)-[Co(L-pen)(dien)]$^+$ (the displacement of the CoD-ND2-ND3 or CoD-ND3-ND4 plane: CD4 and CD5 for the L-cys (L-pen) complex, −0.237(−0.239) and 0.366(0.362) Å, δ form; CD6 and CD7, 0.437(0.431) and −0.093(−0.097) Å, λ form). On the contrary, the conformations of the dien in the CoA and CoB complex cations are significantly different from those of the CoD and L-pen ones; namely, both of the diamine chelate rings in the former take an asymmetric skew with λ form (the average displacement of the Co-N2-N3 or Co-N3-N4 plane: C4 and C5, −0.070 and 0.568 Å; C6 and C7, 0.130 and 0.681 Å).

Preparation and Characterization. Three geometrical isomers, trans(N_iN), trans(N_iS), and trans-(N_iO),[23] are possible for [Co(L-cys)(dien)]$^+$, as in the case of [Co(L-pen)(dien)]$^+$.[5,7] The L-cys complex was prepared for the first time by the reaction of cobalt(II) chloride with L-cystine under a nitrogen atmosphere. In this preparative reaction, two isomers, A-1 and A-2 (trans(N_iS) based on the X-ray crystal structure analysis) were selectively formed. The absorption and CD spectra of the A-1 isomer, which were shown by the arbitrary scale in Fig. 3, exhibit quite similar spectral patterns to those of *trans*(N_iN)-[Co(L-pen)(dien)]$^+$ whose structure was determined by the X-ray crystal structure analysis.[7] Therefore, the A-1 isomer can be assigned to the trans(N_iN) configuration.

The absorption, CD, and ^1H and ^{13}C NMR spectra of *trans*(N_iN)-[Co(L-cys)(dien)]$^+$ (A-1) changes with time and these spectral behaviors suggest that the trans(N_iN) isomer isomerizes to the trans(N_iS) one, though *trans*(N_iN)-[Co(L-pen)(dien)]$^+$ did not isomerize in an aqueous solution.[5,7] *trans*(N_iS)-[Co(L-cys)(dien)]$^+$ (A-2) did not isomerize in an aqueous solution and gave only one isomer of [Co(L-smc)(dien)]$^{2+}$ by the reaction with dimethyl sulfate. This fact suggests that the methylation for the A-2 isomer proceeded with retention of the trans(N_iS)

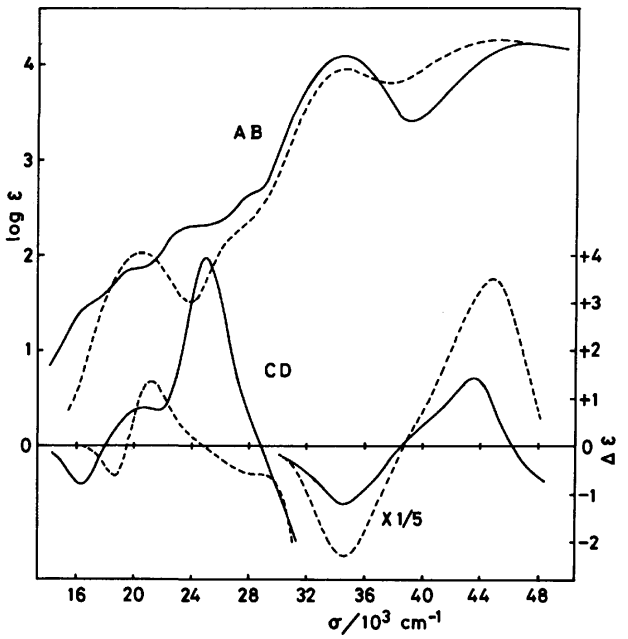

Fig. 3. Absorption and CD spectra of *trans*(N_iN)-[Co(L-cys or L-smc)(dien)]$^{+ \text{ or } 2+}$: L-cys (—) and L-smc (------).

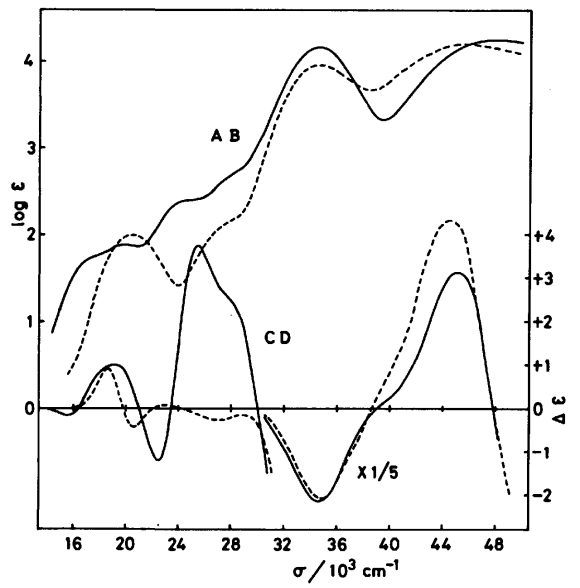

Fig. 4. Absorption and CD spectra of *trans*(N_iS)-[Co(L-cys or L-smc)(dien)]$^{+ \text{ or } 2+}$: L-cys (——) and L-smc (------).

configuration, as in the case of [Co(L-pen)(dien)]$^+$.[7] When the reaction mixture containing [Co(L-cys)(dien)]$^+$ reacted with dimethyl sulfate, two isomers, B-1 and B-2, of [Co(L-smc)(dien)]$^{2+}$ were obtained after the column chromatographic separation. The B-2 isomer showed the identical absorption and CD spectra with *trans*(N_iS)-[Co(L-smc)(dien)]$^{2+}$ (Fig. 4 and Table 3) and the B-1 isomer exhibits quite similar absorption and CD spectra to *trans*(N_iN)-[Co(L-smp)(dien)]$^{2+}$ (Fig. 3 and Table 3), in which the L-smp has a similar framework to the L-smc. This fact seems to indicate that the B-1 isomer has the trans(N_iN) configuration. The formation ratio of the trans(N_iN) and trans(N_iS) isomers was about 1:3 and the two isomers were stable in an aqueous solution. The trans(N_iO) isomer could not be detected. The difference in formation seems to depend on the nitrogen donor atoms, imino and terminal amino nitrogens, in the dien occupying the trans position of the sulfur one in the L-cys.

Table 3. Absorption and CD Spectral Data of [Co(L-cys)(dien)]$^+$ and [Co(L-smc)(dien)]$^{2+}$

Complex	Absorption maxima $\sigma/10^3$ cm^{-1} (log ε/mol^{-1} dm^3 cm^{-1})	CD extrema $\sigma/10^3$ cm^{-1} ($\Delta\varepsilon$/mol^{-1} dm^3 cm^{-1})
trans(N_1N)-[Co(L-cys)-(dien)]$^+$	14.39 (—— sh)	16.31 (−)
	20.00 (—— sh)	20.64 (+)
	24.39 (—— sh)	24.94 (+)
	28.09 (—— sh)	34.48 (−)
	34.48 (——)	43.48 (+)
	47.17 (——)	
trans(N_1S)-[Co(L-cys)-(dien)]$^+$	17.51 (1.74 sh)	15.46 (−0.16)
	19.88 (1.88)	19.12 (+1.01)
	24.69 (2.40 sh)	22.42 (−1.19)
	28.09 (2.71 sh)	25.41 (+3.78)
	34.60 (4.16)	27.70 (+2.59 sh)
	48.08 (4.24)	34.48 (−10.76)
		45.05 (+15.68)
trans(N_1N)-[Co(L-smc)-(dien)]$^{2+}$	20.49 (2.02)	18.62 (−0.61)
	27.03 (2.21 sh)	21.19 (+1.35)
	34.58 (3.95)	28.74 (−0.58 sh)
	45.05 (4.26)	34.48 (−11.50)
		44.84 (+17.59)
trans(N_1S)-[Co(L-smc)-(dien)]$^{2+}$	20.41 (1.99)	18.62 (+0.91)
	27.47 (2.12 sh)	20.62 (−0.43)
	34.60 (3.97)	22.88 (+0.09)
	45.66 (4.21)	26.88 (−0.26)
		34.72 (−10.53)
		44.44 (+21.78)

sh denotes a shoulder.

In the former paper,[7] we assigned the trans(N_iS) and trans(N_iO) configurations for [Co(L-pen)(dien)]$^+$ and [Co(L-smp)(dien)]$^{2+}$ on the basis of the CD spectral patterns of the (diethylenetriamine)cobalt(III) complexes with iminodiacetate, *N*-(carboxylatomethyl)-L-alaninate, and D- or L-aspartate. However, the present assignment for *trans*(N_iS)-[Co(L-cys)(dien)]$^+$ based on the X-ray crystal analysis and the spectral behaviors of the isomers of the derivative, [Co(L-smc)(dien)]$^{2+}$ (Fig. 4), point out that the assignments in the former paper should be reversed.[7]

The ^{1}H NMR spectrum of *trans*(N_iS)-[Co(L-smc)(dien)]$^{2+}$ exhibits two resonance lines at σ=2.18 and 2.35 (intensity ratio; 9.3:1) in the *S*-methyl protons

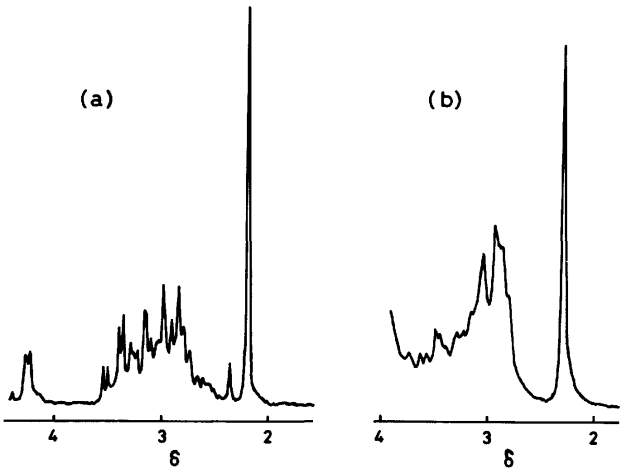

Fig. 5. ^{1}H NMR spectra of $[Co(L\text{-}smc)(dien)]^{2+}$: (a) trans($N_iS$) and (b) trans($N_iN$).

region (Fig. 5). The corresponding resonance lines were also observed for the ^{13}C NMR spectrum at σ=19.8 and 21.8, respectively. For the asymmetric sulfur donor atom, R or S, in the trans(N_iS) isomer, the interligand interaction, which exists between an *S*-methyl group and the amino group of the dien, of the S configuration can be expected to be weaker than that of the R one. The *S*-methyl protons of the S configuration in the trans(N_iS) isomer lies above the carboxyl group, while there is no such steric relation for the *S*-methyl group of the R configuration. Taking account of the model inspections mentioned above and the up field shift due to the methyl group lying above the carboxyl group,[25,26] it is suggested that the major species (2.18 ppm) in the *trans*(N_iS)-$[Co(L\text{-}smc)(dien)]^{2+}$ has the S configuration and the minor one (2.35 ppm) has the R configuration. On the other hand, *trans*(N_iN)-$[Co(L\text{-}smc)(dien)]^{2+}$ exhibits only one resonance line at 2.29 ppm (for ^{1}H NMR) or at 20.69 ppm (for ^{13}C NMR) in the *S*-methyl region (Fig. 5). The model inspection concerning the interligand interaction between the *S*-methyl group and an ethylenediamine moiety in the dien also suggests that the coordinated sulfur atom has only S configuration. These results are in line with the fact that *trans*(N_iN)- and *trans*(N_iS)-$[Co(L\text{-}smp)(dien)]^{2+}$, which exhibit only resonance line in the *S*-methyl protons region, take the S configuration.[7]

The authors wish to express their thanks to Miss Mikako Adachi and Mrs. Yoko Koizumi for their aids in the experiment.

References

1) P. de Meester and D. J. Hodgson, *J. Chem. Soc., Dalton Trans.*, **1976**, 618.
2) P. de Meester and D. J. Hodgson, *J. Am. Chem. Soc.*, **99**, 101 (1977).
3) H. M. Helis, P. de Meester, and D. J. Hodgson, *J. Am. Chem. Soc.*, **99**, 3309 (1977).
4) T. Isago, K. Igi, and J. Hidaka, *Bull. Chem. Soc. Jpn.*, **52**, 407 (1979).
5) K. Okamoto, K. Wakayama, H. Einaga, M. Ohmasa, and J. Hidaka, *Bull. Chem. Soc. Jpn.*, **55**, 3473 (1982).
6) K. Okamoto, K. Wakayama, H. Einaga, S. Yamada, and J. Hidaka, *Bull. Chem. Soc. Jpn.*, **56**, 165 (1983).
7) K. Wakayama, K. Okamoto, H. Einaga, and J. Hidaka, *Bull. Chem. Soc. Jpn.*, **56**, 1995 (1983).
8) T. Konno, K. Okamoto, and J. Hidaka, *Bull. Chem. Soc. Jpn.*, **56**, 2631 (1983).
9) M. Kanesaka, K. Okamoto, M. Nomoto, and J. Hidaka, *Bull. Chem. Soc. Jpn.*, **57**, 3111 (1984).
10) H. Umehara, T. Isago, K. Okamoto, and J. Hidaka, *Bull. Chem. Soc. Jpn.*, **58**, 3623 (1985).
11) V. M. Kothari and D. H. Busch, *Inorg. Chem.*, **8**, 2276 (1968).
12) a) R. D. Gillard and R. Maskill, *Chem. Commun.*, **1968**, 160; b) L. S. Dollimore and R. D. Gillard, *J. Chem. Soc., Dalton Trans.*, **1973**, 933.
13) C. P. Sloan and J. H. Krueger, *Inorg. Chem.*, **14**, 1481 (1975).
14) D. L. Herting, G. P. Sloan, A. W. Cabral, and J. H. Krueger, *Inorg. Chem.*, **17**, 1649 (1978).
15) W. G. Jackson and A. M. Sargeson, *Inorg. Chem.*, **17**, 2165 (1978).
16) H. C. Freeman, C. J. Moore, W. G. Jackson, and A. M. Sargeson, *Inorg. Chem.*, **17**, 3513 (1978).
17) T. Konno, K. Okamoto, and J. Hidaka, *Chem. Lett.*, **1985**, 1017.
18) G. Germain, P. Main, and M. M. Woolfson, *Acta Crystallogr., Sect. A*, **27**, 368 (1971).
19) L. W. Finger, RFINE-2, Geophysical Lab. Carnegie Institute, Washington, D. C., 1972.
20) "International Tables for X-Ray Crystallography," Kynoch Press, Birmingham (1974). Vol. IV.
21) D. T. Cromer and J. B. Mann, *Acta Crystallogr., Sect. A*, **24**, 321 (1968).
22) J. P. Greenstein and M. Wintz, "Chemistry of the Amino Acids," John Wiley & Sons (1961), Vol. 3, Chap. 24.
23) In this paper, N_i denotes the imino nitrogen atom in the dien, and N, S, and O denote the donor atoms in the L-cys: three possible isomers are designated to trans(N_iN), trans(N_iS), and trans(N_iO).
24) a) B. A. Lange, K. Libson, E. Deutsch, and R. C. Elder, *Inorg. Chem.*, **15**, 2985 (1976); b) R. C. Elder, M. J. Heeg, M. D. Payne, M. Trkula, and E. Deutsch, *Inorg. Chem.*, **17**, 431 (1978).
25) L. R. Froebe, S. Yamada, J. Hidaka, and B. E. Douglas, *J. Coord. Chem.*, **1**, 183 (1971).
26) M. Okabayashi, K. Okamoto, H. Einaga, and J. Hidaka, *Bull. Chem. Soc. Jpn.*, **56**, 157 (1983).

Regio- and Stereoselectivity of the Intramolecular C-H Insertion by Cyclopropylidenes Bearing a Remote Oxido Substituent

Toshiro HARADA, Yasunari YAMAURA, and Akira OKU*
Department of Chemistry, Kyoto Institute of Technology, Matsugasaki, Sakyo-ku, Kyoto 606
(Received August 14, 1986)

(ω-Oxidoalkyl)cyclopropylidenes generated from (2,2-dibromo-1-methylcyclopropyl)-CH_2-X-$(CH_2)_n$-OH (X=CH_2 or O, n=1, 2) by the reaction with methyllithium underwent a regioselective intramolecular insertion into the C-H bond at the δ position to the carbenic carbon. The activation effect of the oxido substituent on the reactivity of C-H bonds is discussed on the basis of (1) the ratio of the insertion products to the rearrangement product allenyl alcohol, and (2) the endo stereoselectivity of the present insertion reactions.

The intramolecular C-H insertion by carbenes has been utilized as a powerful tool for the construction of highly strained molecules or cage structures which would be otherwise difficult to synthesize.[1] However, due to the lack of regioselectivity, the utilization of carbenic insertion reactions in organic synthesis has been limited only to the cases where the molecular geometry puts a potential insertion site close to the carbenic centers.[2] One of the most promising approaches to the regio-controlled intramolecular insertion in a less stereo-defined system is to activate a specific C-H bond by an adjacent heteroatom, such as oxygen, nitrogen, and sulfur.[3] Recently, we disclosed a novel oxyanionic substituent effect that facilitates the intermolecular insertion by carbenes into the α C-H bond of alkoxides.[4-8] We also showed in the study of ω-oxidoalkyl(phenylthio)carbenes that a regio-controlled intramolecular insertion is made possible by the utilization of the oxyanionic effect.[9,10]

Baird reported a number of substituent effects of oxygen-containing groups on the intramolecular cyclopropylidene insertion reaction.[11] He observed that the treatment of dibromocyclopropane (**1**) with methyllithium gave the regioselective insertion product **2** to the almost complete exclusion of the expected allene derivative 4-ethoxy-3-methyl-1,2-butadiene (Eq. 1).[12] Paquette and Taylor noted,

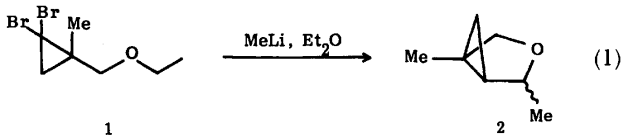

1 2 (1)

however, that alkoxyl substituents in the norcaranylidene system can either activate or deactivate the adjoining C-H bond toward carbene insertion and that the reactvity depends on the site of the alkoxyl group.[13] In contrast to a number of studies on the effect of neutral oxygen-containing substituents in intramolecular insertion reactions,[3] little is known on the effect of oxyanion. Skattebøl reported an activation effect of oxyanion in his study of the cyclopropylidene bearing an oxido substituent at the β position to the carbenic carbon.[14] The similar effect was also noted recently by Baird et al.[15] In order to investigate the effect of oxido substituents located at more remote positions, we examined the reaction of dibromocyclopropyl alcohols (**6**, **7**, and **8**) with methyllithium.[16]

Results

Preparations of Dibromocyclopropyl Alcohols. Dibromocyclopropyl alcohols (**6**, **7**, and **8**) were prepared by the reaction of the tetrahydropyranyl ethers (**3**, **4**, and **5**) of the corresponding alkenols with dibromocarbene generated under the phase-transfer conditions (Eq. 2). We also attempted a direct cyclopropanation of 2-(2-methyl-2-propenyloxy)ethanol under similar reaction conditions, but the desired dibromocyclopropyl alcohol **7** was obtained only in 7% yield.

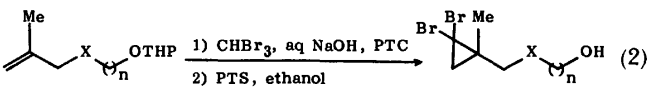

(2)

3; n = 1, X = CH_2
4; n = 2, X = O
5; n = 2, X = CH_2

6; n = 1, X = CH_2
7; n = 2, X = O
8; n = 2, X = CH_2

Reaction of Dibromocyclopropyl Alcohols with Methyllithium. The reaction of dibromocyclopropyl alcohol **6** was carried out in ether utilizing 2.0 equiv of methyllithium to give the insertion products (two stereoisomers *endo*-**9** and *exo*-**9**) together with allenyl alcohol **10**[16] in 49% total yield (*endo*-**9**:*exo*-**9**:**10**=44:6:50)(Eq. 3). In order to evaluate the effect of oxido substitution relatively to the effect of alkoxyl substitution, we also performed the reaction of the

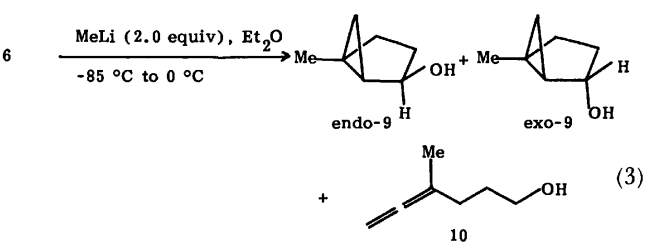

(3)

tetrahydropyranyl ether of alcohol **6** under similar reaction conditions. *endo*-**9**, *exo*-**9**, and **10** were obtained in the ratio of 22:18:60 (73% total yield) after the treatment of the reaction mixture with pyridinium *p*-toluenesulfonate (PTS) in ethanol.

In the previous study of ω-oxidoalkyl(phenylthio)-carbenes,[9] we showed that the five- and six-membered ring formation can be achieved by the substitution of an oxido group at the δ and ε position to the carbenic carbon, respectively. We examined the possibility of six-membered ring formation in the reaction of dibromocyclopropyl alcohols **7** and **8** (Eqs. 4 and 5). The reaction of **7** with methyllithium (2.0 equiv) gave exclusively the endo isomer of δ insertion product *endo*-**11** in 54% yield without forming the allene alcohol. On the other hand, the reaction of **8** with methyllithium followed by quenching the reaction mixture with benzoyl chloride gave the endo and exo isomers of insertion product **12** with a low endo selectivity together with the rearrangement product allenyl benzoate **13** (*endo*-**12**:*exo*-**12**:**13**=24:11:65; 59% total yield). Owing to the difficulty in separating the product alcohols, they were isolated and analyzed as benzoate esters in this reaction. In both reactions, the intramolecular insertion proceeded exclusively at the δ position to the carbenic carbon, and six-membered ring formation was not observed.

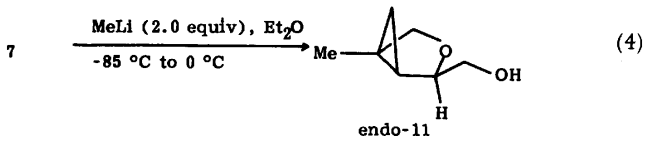

(4)

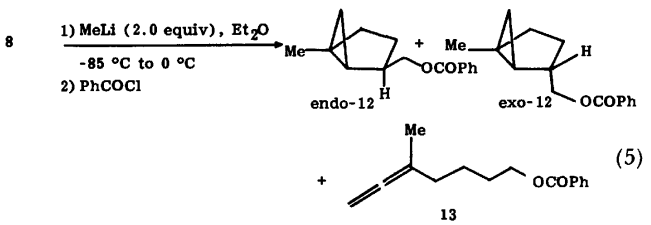

(5)

Determination of the Structure of Insertion Products. The ^{1}H NMR spectrum of the insertion product obtained in the reaction of **7** (Eq. 4) is consistent with either primary alcohol *endo*-**11** (δ insertion product) or secondary alcohol **14** (ε insertion product). The structure, however, was established unambiguously to be *endo*-5-methyl-3-oxabicyclo-[3.1.0]hexane-2-methanol (*endo*-**11**) by the ^{1}H NMR analysis of acetyl derivative **15**: The number of

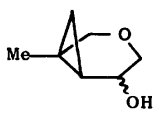

14

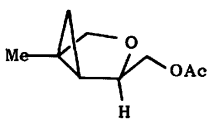

15

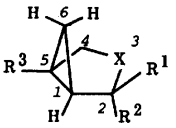

Fig. 1.

Table 1. ^{1}H NMR Coupling Constants between Protons Attached to C(1) and C(2) of Bicyclo[3.1.0]hex-2-yl Derivatives

Compound	endo-Isomer J_{12}/Hz	exo-Isomer J_{12}/Hz
9	4.2	<1
11	2.8	—
12	4.6	<1
16	3.0	<1

proton(s) whose chemical shift was shifted by acetylation to a lower field (δ 3.95 and 4.2) than the corresponding protons of *endo*-**11** was two.

^{1}H NMR spectrum of the major insertion product *endo*-**9** obtained in the reaction of dibromocyclopropyl alcohol **6** was identical with that reported previously.[17] In other cases endo and exo stereochemistry of the insertion products was determined by the comparison of ^{1}H NMR vicinal coupling constants between protons attached to C(1) and C(2) (Fig. 1); J_{12} values for endo isomers range from 2.8 to 4.6 Hz whereas those for the exo isomers are very small (<1 Hz).[17] In Table 1, these coupling constants are summarized together with those reported for the endo and exo isomers of 3-oxabicyclo[3.1.0]hexane-2-methanol (**16**).[18]

Discussion

In a previous study, we clarified that the mechanism of the intermolecular insertion by norcaranylidene into the α C–H bond of alkoxides is different from the concerted insertion which takes place at the C–H bond adjoining to an alkoxyl group,[8] and we proposed the hydride abstraction-recombination mechanism in the reaction of carbenes with alkoxides.[7,8,10] As shown in Scheme 1, if the intramolecular hydride abstraction by the cyclopropylidene proceeds, the intramolecular recombination step becomes unfavorable due to the anti configuration between the generated cyclopropanide anion and the carbonyl-containing side chain: the anion may be consumed by intermolecular reactions. Since the inversion of cyclopropanide anion under the present reaction conditions is unlikely,[19] we conclude that the intramolecular insertion proceeds via a concerted mechanism.

In the reactions of both dibromocyclopropyl

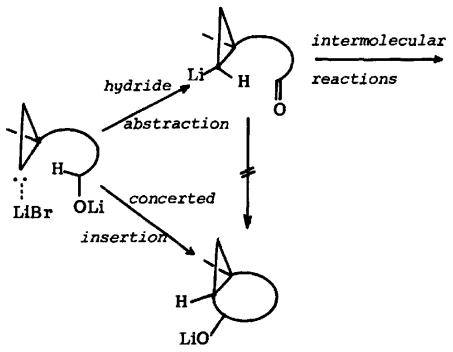

Scheme 1.

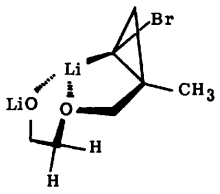

Fig. 2.

alcohol **6** and its tetrahydropyranyl ether with methyllithium, similar ratios of the insertion products to the rearrangement product were observed (Eq. 3). Since the rate of rearrangement to form allenes will not be affected by the oxido group or alkoxyl group located three carbons apart from the cyclopropane ring,[20] these results suggest that the activations by the oxyanion substituent and alkoxyl group are similar in magnitude in the intramolecular insertion by cyclopropylidenes.

It has been known that cyclopropylidenes bearing simple alkyl substituents preferentially undergo the rearrangement to allenes, and when the intramolecular insertion competes with the rearrangement, the insertion generally takes place at the C-H bond β to the carbenoid carbon.[21] Contrastingly, in the present study, the formation of a considerable amount of δ insertion product **12** in the reaction of **8** (Eq. 5) suggests the presence of an activation effect of the adjacent vicinal oxido group which surpasses the other reactions.[22]

It is well-documented in the literature that the cyclopropylidene lithium carbenoids bearing an oxygen-containing substituent at an appropriate position are stabilized by the intramolecular coordination of the oxygen atom with lithium.[23] It has been suggested that the coordination which holds the δ C-H bond in a closer proximity to the carbenic carbon is responsible, at least partly, for the observed efficient insertion of dibromocyclopropyl ether **1** (Eq. 1). As shown in the present study, the reaction of **7** with methyllithium (Eq. 4) which proceeds through the carbenoid intermediate possessing the additional oxido group at the ε position also proceeded efficiently to give *endo*-**11** without forming the allene alcohol. The exclusive formation of the endo isomer can be rationalized by the coordination of two oxygen atoms with lithium on the carbenoid carbon as depicted in Fig. 2. Moreover, the endo selectivity observed in the reaction of dibromocyclopropyl alcohol **6** with methyllithium (product ratio; *endo*-**9**: *exo*-**9**=44:6, Eq. 3) can also be rationalized in terms of the participation of a similar folded conformation of the intermediate carbenoid.

Experimental

Infrared spectra were measured on a JASCO IRA-1 grating spectrophotometer, ^{1}H NMR spectra were recorded on a Varian XL-200 (200 MHz) or a Varian T-60A (60 MHz) spectrometer. Mass spectra were measured on a Hitachi M-80 or a Shimazu QP-1000 mass spectrometer. Silica gel (Wakogel C-300) was used as an adsorbent in flash chromatography. GLC analyses were performed utilizing a capillary column (OV-101, 25 m). Analytically pure products were obtained by preparative GLC (5% OV-17 on Chromosorb W, 0.3×200 cm). Ether and dichloromethane were dried over sodium benzophenone ketyl and CaH_2, respectively, and distilled prior to use. An ethereal solution of methyllithium complexed with lithium bromide (ca. 1.4 mol dm^{-3}) was purchased from Aldrich Chemical Co., and used after titration.

2-(4-Methyl-4-pentenyloxy)tetrahydropyran (3). To a stirred suspension of $LiAlH_4$ (30 mmol) in ether (100 ml) was slowly added ethyl 4-methyl-4-pentenoate (1.66 g, 11.7 mmol) at 0 °C, and the mixture was stirred overnight at a room temperature. Ather the addition of 10% aq HCl followed by the extraction with ethyl acetate, the organic layer was washed with aq $NaHCO_3$, dried over sodium sulfate, and concentrated in vacuo to give the crude alcohol. This was dissolved in CH_2Cl_2 (50 ml), and then 3,4-dihydro-2*H*-pyran (2.52 g, 30.0 mmol) and pyridinium *p*-toluenesulfonate (50 mg) were added at a room temperature. After stirring for 14 h, the reaction mixture was concentrated in vacuo, and the residue was purified by flash chromatography (2% ethyl acetate/petroleum ether) to give 1.82 g (9.91 mmol, 85% yield) of **3**: An oil, IR (neat) 1660, 1150, 1130, 1040, and 890 cm^{-1}.

2-[2-(2-Methyl-2-propenyloxy)ethoxy]tetrahydropyran (4). To a stirred solution of 6.6 g of KOH in ethylene glycol (28 ml) was added 9.76 ml (100 mmol) of 3-chloro-2-methylpropene and the mixture was heated at 100 °C for 7 h. After the addition of water followed by the extraction with ether, the organic layer was dried over sodium sulfate and concentrated in vacuo. The crude material was purified by flash chromatography (30% ethyl acetate/petroleum ether) to give 3.96 g (34 mmol, 34% yield) of 2-(2-methyl-2-propenyloxy)ethanol; an oil, ^{1}H NMR (60 MHz, $CDCl_3$) δ=1.77 (3H, br s, CH_3), 2.57 (1H, br s, OH), 3.53 (2H, m, -C$\underset{\downarrow}{H}_2$O-), 3.73 (2H, m, -$CH_2$O-), 3.97 (2H, br s, =C-$CH_2$-O), and 4.97 (2H, m, CH_2=).

2-(2-Methyl-2-propenyloxy)ethanol (1.00 g 8.61 mmol) was treated with 3,4-dihydro-2*H*-pyran (1.80 g, 21.5 mmol) and

pyridinium *p*-toluenesulfonate (10 mg) in CH_2Cl_2 as described above. A purification by flash chromatography (5% ethyl acetate/petroleum ether) gave **4**: an oil; ^1H NMR (60 MHz, $CDCl_3$) δ=1.2—2.0 (9H, m), 3.4—3.9 (6H, m), 4.65 (1H, m, -OCHO-), and 4.97 (2H, m, CH_2=).

2-(5-Methyl-5-hexenyloxy)tetrahydropyran (5). To the Grignard reagent prepared by the reaction of 2-(4-chlorobutyloxy)tetrahydropyran (10.4 mmol) and Mg (18 mmol) in THF (10 ml) was slowly added a THF solution (10 ml) of acetaldehyde (440 mg, 10 mmol) at 0 °C, and the mixture was stirred at the same temperature for 1 h. After the addition of aq NH_4Cl followed by the extraction with ethyl acetate, the organic layer was washed with aq $NaHCO_3$, dried over sodium sulfate, and concentrated in vacuo to give the crude alcohol, which was dissolved in 5 ml of CH_2Cl_2. To a stirred suspension of pyridinium chlorochromate (3.23 g, 15 mmol) and sodium acetate (205 mg, 2.5 mmol) in CH_2Cl_2 (20 ml) was added the above solution, and the mixture was stirred at a room temperature for 3 h. After the dilution with ether (200 ml) followed by filtration through a short silica-gel column, the reaction mixture was concentrated to give 1.64 g of the crude ketone, which was used without further purification in the next reaction. To a suspension of methyltriphenylphosphonium bromide (3.93 g, 11.0 mmol) in THF (60 ml) was added *t*-BuOK (1.12 g, 10.0 mmol) at a room temperature. After stirring for 1 h, a THF (2 ml) solution of the crude ketone was added to the resulting orange suspension, and the mixture was stirred for 1 h. After the addition of brine followed by the extraction with ether, the organic layer was dried over sodium sulfate and concentrated in vacuo. The crude material was purified by flash chromatography (5% ethyl acetate/petroleum ether) to give 947 mg (4.78 mmol, 46%) of **5**: an oil; ^1H NMR (60 MHz, $CDCl_3$) δ=0.8—2.4 (15H, m), 3.1—4.2 (4H, m), and 4.59 (1H, m, -OCHO-); IR (neat) 1660, 1130, 1085, 1040, and 890 cm^{-1}.

General Procedure for the Preparation of Dibromocyclopropyl Alcohols 6, 7, and 8. A mixture of a THP ether (**3**, **4**, or **5**)(2 mmol), bromoform (2.5 mmol), benzyltriethylammonium chloride (20 mg), and 2 ml of 50% aq NaOH was stirred vigorously at a room temperature for 2 d. After the addition of water followed by extraction with CH_2Cl_2, the organic layer was washed with brine, dried over sodium sulfate, and concentrated in vacuo. The resulting mixture was dissolved in 25 ml of ethanol containing 20 mg of pyridinium *p*-toluenesulfonate, and the solution was heated at 60 °C for several hours. After removing ethanol in vacuo at a room temperature, the residue was subjected to flash chromatography (10—20% ethyl acetate/petroleum ether) to give the dibromocyclopropyl alcohol (**6**, **7**, or **8**).

3-(2,2-Dibromo-1-methylcyclopropyl)-1-propanol (6): An oil; ^1H NMR (60 MHz, $CDCl_3$) δ=1.40 (3H, s, CH_3), 1.55 (3H, m), 1.80 (4H, m), and 3.70 (2H, m, CH_2-OH); IR (neat) 3360, 1060, and 695 cm^{-1}.

2-[(2,2-Dibromo-1-methylcyclopropyl)methoxy]ethanol (7): An oil; ^1H NMR (60 MHz, $CDCl_3$) δ=1.50 (3H, s, CH_3), 1.6 (2H, m), 2.13 (1H, br s, OH), and 3.4—3.9 (6H, m); IR (neat) 3400, 1130, 1070, and 695 cm^{-1}.

4-(2,2-Dibromo-1-methylcyclopropyl)-1-butanol (8): An oil; ^1H NMR (60 MHz, $CDCl_3$) δ=1.37 (3H, s, CH), 1.43 (2H, m), 1.6 (6H, m), 2.25 (1H, m, OH), and 3.65 (2H, m, CH_2OH); IR (neat) 1660, 1130, 1085, 1040, and 890 cm^{-1}.

General Procedure for the Intramolecular Reaction of Dibromocyclopropyl Alcohols 6, 7, and 8. To a solution of a dibromocyclopropyl alcohol (**6**, **7**, or **8**)(1.0 mmol) in dry ether (5 ml) was slowly added methyllithium (ether solution, 2.0 mmol) at −85 °C under a nitrogen atmophere. The reaction mixture was gradually warmed up to 0 °C over a period of 5 h, and quenched by the addition of water. After the extraction with ether, the organic layer was dried over sodium sulfate, and concentrated in vacuo. After a capillary GLC analysis, the residual oil was subjected to flash chromatography (ethyl acetate/petroleum ether) to give a mixture of intramolecular insertion products and the allenyl alcohol. Analytically pure products were obtained after purification by preparative GLC. In the reaction of **8**, the reaction mixture was quenched by addition of benzoyl chloride (1.2 mmol) at 0 °C, and then stirred further for 14 h at a room temperature. By the similar workup procedure, a mixture of the benzoate ester of the insertion product *endo*-**12** and *exo*-**12**, and allenyl alcohol **13** was obtained.

***endo*-5-Methylbicyclo[3.1.0]hexan-2-ol (*endo*-9):**[17] An oil; ^1H NMR (200 MHz, $CDCl_3$) δ=0.25 (1H, dd, J=5.0 and 7.9 Hz, exo C(6)-H), 0.71 (1H, br dd, J=4.2 and 5.0 Hz, endo C(6)-H), 1.07 (1H, ddt, J=11.2, 12.8, and 8.2 Hz, exo C(3)-H), 1.14 (3H, s, CH_3), 1.20 (1H, ddd, J=3.7,. 4.2, and 7.9 Hz, C(1)-H), 1.48 (1H, br s, OH), 1.56 (1H, ddt, J=0.8, 8.0, and 11.2 Hz, exo C(4)-H), 1.73 (1H, dd, J=8.3 and 12.2 Hz, endo C(4)-H), 1.89 (1H, dt, J=12.8 and 8 Hz, endo C(3)-H), and 4.53 (1H, J=3.7 and 8.2 Hz, exo C(2)-H); MS *m/z* (%) 112 (M^+, 6.9), 111 (4.9), 97 (69), 94 (31), 84 (16), and 70 (100); Found: *m/z* 112.0886, Calcd for $C_7H_{12}O$: 112.0889.

***exo*-5-Methylbicyclo[3.1.0]hexan-2-ol (*exo*-9):** An oil; ^1H NMR (200 MHz, $CDCl_3$) δ=0.21 (1H, dd, J=4.0 and 5.2 Hz, endo C(6)-H), 0.33 (1H, dd, J=5.2 and 8.4 Hz, exo C(6)-H), 1.05 (1H, dd, J=4.0 and 8.4 Hz, C(1)-H), 1.26 (3H, s, CH_3), 1.27—1.85 (5H, m), and 4.16 (1H, d, J=4.4 Hz, endo C(2)-H); MS *m/z* (%) 112 (M^+, 12), 97 (76), 94 (4.2), and 70 (100); Found: *m/z* 112.0892, Calcd for $C_7H_{12}O$: 112.0889.

4-Methyl-4,5-hexadien-1-ol (10):[16] An oil; ^1H NMR (200 MHz, $CDCl_3$) δ=1.50 (1H, br s, OH), 1.65—1.80 (5H, m, including t (3H, J=3.2 Hz, CH_3) at 1.68), 2.00 (2H, m, $-CH_2-C$=), 3.68 (2H, t, J=6.4 Hz, CH_2OH), and 4.61 (2H, m, CH_2=); MS *m/z* (%) 112 (M^+, 0.2), 97 (4.6), 94 (4.2), 84 (73), 81 (9.0), and 68 (100).

***endo*-5-Methyl-3-oxabicyclo[3.1.0]hex-2-ylmethanol (*endo*-11):** An oil; ^1H NMR (200 MHz, $CDCl_3$) δ=0.38 (1H, ddd, J=0.8, 4.8, and 7.4 Hz, exo C(6)-H), 0.64 (1H, dd, J=4.2 and 4.8 Hz, endo C(6)-H), 1.16 (1H, ddd, J=2.8, 4.2, and 7.4 Hz, C(1)-H), 1.24 (3H, s, CH_3), 1.56 (1H, br s, OH), 3.7 (3H, m), 3.76 (1H, d, J=8.0 Hz, C(4)-H), and 4.10 (1H, ddd, J=2.8, 4.2, and 7.6 Hz, exo C(2)-H).

***endo*-(5-Methylbicyclo[3.1.0]hex-2-yl)methyl Benzoate (*endo*-12):** An oil; ^1H NMR (200 MHz, $CDCl_3$) δ=0.17 (1H, ddd, J=0.8, 5.1, and 7.6 Hz, exo C(6)-H), 0.46 (1H, dd, J=3.4 and 5.1 Hz, endo C(6)-H), 1.05 (1H, ddd J=3.4, 3.7, and 7.6 Hz, C(1)-H), 1.5—1.8 (5H, m), 2.62 (1H, m, exo C(2)-H), 4.17 (1H, dd, J=7.8 and 9.8 Hz, CHOCOPh), 4.23 (1H, dd, J=5.7 and 9.8 Hz, CHOCOPh), 7.4—7.6 (3H, m), and 8.02 (2H, m); MS *m/z* (%) 122 (M^+, <1), 108 ($M^+ - PhCO_2H$, 100), and 105 (37). The fragment ion peak due to ($M^+ - PhCO_2H$) was observed at *m/z* 108.0940. Calcd for C_8H_{12}: $M^+ - PhCO_2H$, 108.0965.

***exo*-(5-Methylbicyclo[3.1.0]hex-2-yl)methyl Benzoate (*exo*-12):** An oil; ^{1}H NMR (200 MHz, $CDCl_3$) δ=0.32 (1H, dd, J=4.6 and 7.7 Hz, exo C(6)-H), 0.39 (1H, dd, J=3.4 and 4.6 Hz, endo C(6)-H), 0.95 (1H, dd, J=3.4 and 7.7 Hz, C(1)-H), 1.20 (3H, s, CH_3), 1.4—1.7 (4H, m), 2.36 (1H, q, J=6 Hz, endo C(2)-H), 4.15 (2H, d, J=7.1 Hz, CH_2OCOPh), 7.4—7.6 (3H, m), and 8.02 (2H, m); MS m/z (%) 230 (M^+, 0.5) and 108 (100); Found: m/z 230.1329, Calcd for $C_{15}H_{18}O_2$: 230.1307.

5-Methyl-5,6-heptadienyl Benzoate (13): An oil; ^{1}H NMR (200 MHz, $CDCl_3$) δ=1.4—1.9 (7H, m, including t (3H, J=3.2 Hz, CH_3) at 1.68), 1.99 (2H, m), 4.32 (2H, t, J=7.0 Hz, CH_2OCOPh), 4.58 (2H, m, CH_2=), 7.35—7.6 (3H, m), and 8.02 (2H, m); MS m/z (%) 230 (M^+, <1), 125 (13), 108 (39), 105 (56), and 93 (100); Found: m/z 230.1294, Calcd for $C_{15}H_{18}O_2$: 230.1307.

***endo*-(5-Methyl-3-oxabicyclo[3.1.0]hex-2-yl)methyl Acetate (15).** To a solution of *endo*-**11** (22.4 mg, 0.17 mmol) in acetic anhydride (0.032 ml) and pydridine (0.054 ml) was added 3 mg of 4-(dimethylamino)pyridine at a room temperature. After stirring for 3 h, the reaction mixture was diluted with water and extracted with ether. The organic layer was washed successively with 5% aq HCl and aq $NaHCO_3$, dried over sodium sulfate, and concentrated in vacuo. The residue was purified by preparative GLC to give **15**: an oil; ^{1}H NMR (200 MHz, $CDCl_3$) δ=0.40 (1H, dd, J=4.8 and 7.4 Hz, exo C(6)-H), 0.65 (1H, t, J=6 Hz, endo C(6)-H), 1.22 (1H, m, C(1)-H), 1.24 (3H, s, CH_3), 2.06 (3H, s, CH_3CO_2-), 3.59 (1H, br d, J=8.4 Hz, exo C(4)-H) 3.80 (1H, d, J=8.4 Hz, endo C(4)-H), 3.95 (1H, dd, J=9.2 and 12.7 Hz, AcOC$\underline{H}$-), and 4.2 (2H, m, exo C(2)-H and AcOC$\underline{H}$-).

References

1) W. Kirmse, "Carbene Chemistry," Academic Press, New York (1971), Chap. 4; S. D. Burke and P. A. Grieco, *Org. React.*, **26**, 361 (1971).

2) A highly selective intramolecular 1,5-insertion of α-diazo-β-keto ester catalyzed by Rh(II) acetate has been reported recently; D. F. Taber and K. Raman, *J. Am. Chem. Soc.*, **105**, 5935 (1983).

3) Review; K. G. Taylor, *Tetrahedron*, **38**, 2751 (1982).

4) T. Harada and A. Oku, *J. Am. Chem. Soc.*, **103**, 5965 (1981).

5) T. Harada, E. Akiba, and A. Oku, *J. Am. Chem. Soc.*, **105**, 2711 (1983).

6) T. Harada, Y. Nozaki, and A. Oku, *Tetrahedron Lett.*, **24**, 5665 (1983).

7) T. Harada, Y. Nozaki, Y. Yamaura, and A. Oku, *J. Am. Chem. Soc.*, **107**, 2189 (1985).

8) A. Oku, Y. Yamaura, and T. Harada, *J. Org Chem.*, **51**, 3730 (1986).

9) T. Harada, E. Akiba, K. Tsujimoto, and A. Oku, *Tetrahedron Lett.*, **26**, 4483 (1985).

10) See slso, R. H. Ritter and T. Cohen. *J. Am. Chem. Soc.*, **108**, 3718 (1986).

11) M. S. Baird, *J. Chem. Soc., Chem. Commun.*, **1971**, 1145.

12) "Methoden der Organischen Chemie," ed by E. Müller, Thieme, Stuttgart (1977), Vol. 5/2a, p. 985.

13) L. A. Paquette and G. Zon, *J. Am. Chem. Soc.*, **96**, 203 (1974); L. A. Paquette, G. Zon, and R. T. Taylor, *J. Org. Chem.*, **39**, 2677 (1974).

14) N. O. Nilsen, L. Skattebøl, and L. K. Sydnes, *Acta Chem. Scand., Ser. B*, **36**, 587 (1982).

15) M. S. Baird, S. R. Buxton, and P. Sadler, *J. Chem. Soc., Perkin Trans. 1*, **1984**, 1379.

16) Reaction of dibromocyclopropyl alcohol **6** with methyllithium has been reported to give allenyl alcohol **10**; B. Ragonnett, M. Santelli, and M. Bertrand, *Bull. Soc. Chim. Fr.*, **1973**, 3119.

17) W. G. Dauben, L. Schutte, R. E. Wolf, and E. J. Deviny, *J. Org. Chem.*, **34**, 2512 (1969); G. A. Russell, J. J. McDonnell, P. R. Whittle, R. S. Givens, and R. G. Keske, *J. Am. Chem. Soc.*, **93**, 1452 (1971).

18) H. Leininger, F. Lanzendörfer, and M. Christl, *Chem. Ber.*, **116**, 669 (1983).

19) H. M. Walborsky, F. J. Impasstato, and A. E. Young, *J. Am. Chem. Soc.*, **86**, 328 (1964).

20) M. S. Baird, *J. Chem. Soc., Chem. Commun.*, **1979**, 776.

21) L. Skattebøl, *Tetrahedron Lett.*, **1970**, 2361; W. R. Moore, K. G. Taylor, P. Muller, S. S. Hall, and Z. L. F. Gaibel, *ibid.*, **1970**, 2365; D. W. Brown, M. E. Hendrick, and M. Jones, Jr., *ibid.*, **1973**, 3951.

22) The similar activation effect by vicinal alkoxyl group was reported. See Ref. 13.

23) K. G. Taylor, W. E. Hobbs, and M. Saquet, *J. Org. Chem.*, **36**, 369 (1971); K. G. Taylor, W. E. Hobbs, M. S. Clark, and J. Chaney, *ibid.*, **37**, 2436 (1972); K. G. Taylor and J. Chaney, *J. Am. Chem. Soc.*, **98**, 4158 (1976).

Chemo-Selectivity of Group-VIII Metal Catalysts in Hydrogenation of Nonconjugated Enones

Jun-ichi ISHIYAMA,* Satoshi MAEDA,[1a] Kazuhiro TAKAHASHI,[1b] Yasuhisa SENDA,† and Shin IMAIZUMI

Department of Engineering Science, Faculty of Engineering, Tohoku University, Aoba, Sendai 980
†Department of Chemistry, Faculty of Science, Yamagata University, Koshirakawa-cho, Yamagata 990

(Received August 20, 1986)

The chemo-selectivity of group-VIII metal catalysts has been examined in the hydrogenation of nonconjugated enones at ambient temperature under an atmospheric pressure of hydrogen. A cobalt catalyst gave high yields of unsaturated alcohols from trialkylated olefinic ketones. Osmium showed the highest selectivity among platinum metal catalysts for the reduction of the carbonyl bond in the hydrogenation of trialkylated olefinic ketones. The hydrogenation of mono- and dialkylated olefinic ketone ordinarily proceeded with a preferential saturation of the olefinic function, regardless of the catalyst. The hydrogenation of 4-methylene- and 4-ethylidenecyclohexanone was accompanied by the formation of diethyl acetals over ruthenium, rhodium, and palladium black catalysts in an ethanol solvent. The acetals were not detected in the hydrogenation of the other enones and over the other catalysts. In addition, the chemoselectivity on the hydrogenation of acyclic enones was examined over nickel and cobalt catalysts treated with small amounts of alkali and carbon monoxide. The amount of unsaturated alcohols increased when the catalyst was treated with alkali in the case of di- and trialkylated olefinic ketones, whereas the characteristics of cobalt, which selectively reduces the ketonic function in trialkylated olefinic ketones, were completely missing when cobalt was treated with carbon monoxide.

Selective catalytic hydrogenation of nonconjugated enones to the corresponding saturated ketones is achieved easily;[2] however, a selective reduction to afford unsaturated alcohols is a formidable task. This type of compound is usually prepared from a nonconjugated enone by a non-catalytic route. However, it has also been reported that in some structural features the catalyst may have a marked effect on chemo-selectivity.[3] The ketonic function in hexahydronaphthalenedione system was reduced over Ru-on-carbon in preference to the double bond.[4] France et al. reported the preferential reduction of carbonyls in an octahydronaphthalenedione system over platinum oxide in ethanol and the preferential saturation of the double bonds over Pd-on-carbon.[5] Nishimura et al. have reported that 17-oxo group is extensively reduced in preference to Δ^5 unsaturation over unsupported osmium and ruthenium blacks in the hydrogenation of 3-hydroxyandrost-5-en-17-one (dehydroepiandrosterone).[6]

Those available data are, however, insufficient for applications to the selective reduction of the ketonic or olefinic group in unsaturated ketones; little is known about the consistent study concerning the selectivity of group-VIII metal catalysts in the hydrogenation of nonconjugated enones. Recently, we examined the catalytic hydrogenation of 7-methylenebicyclo[3.3.1]nonan-3-one (**1**) and 7-methylbicyclo[3.3.1]non-6-en-3-one (**2**) over group-VIII metals.[7,8] The olefinic bond was selectively reduced to afford 7-endo-methylbicyclo[3.3.1]nonan-3-one (**2A**) over ruthenium, rhodium, and platinum catalysts, whereas the olefinic one remained intact during the reduction of the ketone to give 6-methylbicyclo[3.3.1]-non-6-en-3-endo-ol (**2B**) exclusively in the hydrogenation of **2** over a cobalt catalyst. Hydrogenation over nickel, osmium, and iridium catalysts gave mixtures of **2A** and **2B**.

Therefore, it seems of interest to more precisely study the differences for chemo-selectivity of group-VIII transition metal catalysts by an examination of the hydrogenation of simple nonconjugated aliphatic enones in comparison with their behavior under the same experimental conditions as that of **1** and **2**. The substrates which were chosen comprised the acyclic (5-hexen-2-one: **3**, 5-methyl-5-hexen-2-one: **4**, (*E*) or (*Z*)-5-hepten-2-one: **5**, 6-methyl-5-hepten-2-one: **6**) and alicyclic (4-methylenecyclohexanone: **7**, 4-ethylidenecyclohexanone: **8**) nonconjugated enones. In addition, the chemo-selectivities of the hydrogenation of **3**, **5**, and **6** were also examined using nickel and cobalt catalysts treated with small amounts of alkali and carbon monoxide.

Results and Discussion

Since the reaction of a substrate with a solvent over metal catalysts occurs because of the reactivity of the carbonyl and hydroxy functions when methanol or ethanol is used as a solvent for ketone hydrogenation,[9] the chemo-selectivity of group-VIII metal catalysts in the hydrogenation of nonconjugated enones was examined in a cyclohexane solvent at ambient temperature and approximately atmospheric pressure. Cobalt and nickel catalysts were prepared from Raney alloys using a W-4 method[10] or by reducing the corresponding metal oxides, and platinum metal catalysts by reducing the corresponding metal oxides or hydroxides.[11] The products are saturated ketone (**A**), unsaturated alcohol (**B**), and

saturated alcohol (**C**).

Although the hydrogenation of all substrates used here showed chemo-selectively the saturated ketones over ruthenium, rhodium, palladium,[12] platinum, and iridium[13] catalysts, osmium catalyst showed different chemo-selectivities from that of other platinum metals. Osmium gave unsaturated alcohols together with saturated ketones and saturated alcohols in the hydrogenation of trialkylated ones (**2**, **6**, and **8**). A nickel catalyst showed a similar chemo-selectivity to osmium. The initial chemo-selectivity for unsaturated alcohols of osmium and nickel catalysts are listed in Table 1. Since hydrogenation products increased linearly until 50% of reaction conversion of the substrates, the values shown in Tables give the initial chemo-selectivity of catalysts at 50% conversion. Cobalt catalysts gave high yields of unsaturated alcohols from trialkylated olefinic ketones, and **2B**, 6-methyl-5-hepten-2-ol (**6B**), and 4-ethylidenecyclohexanol (**8B**) were exclusively produced (Table 2).

Table 1. Initial Selectivity for Unsaturated Alcohol(**B**) of Osmium and Nickel Catalysts[a]

Enone	**B**/(**A**+**B**+**C**)[b]	
	Os[c]	Ni[d]
1, **3**, **4**, **5**, **7**	0	0
2	0.24	(0.26)[e]
6	0.15	0.05
8	0.24	0.45

a) Substrate, 0.5 mmol; solvent(cyclohexane), 5 ml. Enones were hydrogenated at ambient temperature under atomospheric pressure. Values are the ratio when 50% of substrate was consumed. b) **A**=Saturated ketone, **B**=unsaturated alcohol, **C**=saturated alcohol. Selectivity for the formation of unsaturated alcohol to all products. c) A 5 mg of catalyst was used. d) A weighed sample of catalyst (500 mg for Raney Ni under wet conditions; 200 mg as NiO for Ni-black) was used. e) Value in parentheses indicates the product ratio over Ni-black catalyst.

Table 2. Hydrogenation of Enones over Cobalt Catalyst[a]

Enone	Product[b]/mol%		
	A	**B**	**C**
1	(64)[c]	(0)	(4)
2	(0)	(100)	(0)
3	100	0	0
4	50	8	42
5	34	12	54
6	0	100	0
7	56(56)	22(44)	22(0)
8	0(0)	100(100)	t[d] (0)

a) See footnote a in Table 1 except for the weight of catalyst. A weighed sample of catalyst (500 mg for Raney Co under wet conditions; 1000 mg as CoO for Co-black) was used. Values in parentheses indicate the product ratios over Co-black catalyst. b) See footnote b in Table 1. c) 1-Adamantanol (26%) and 1-methyl-2-oxa-adamantane (6%) were also detected. d) Trace.

The hydrogenation of **1** and **2** was examined over a variety of group-VIII transition metals in order to evaluate how an intramolecular orbital interaction operates regarding the selectivity of an addition reaction.[7,8,14] Different selectivities were observed depending on the catalysts used in the hydrogenation of **1** and **2**. A novel reductive cyclization occurred to give 1-adamantanol (**2E**) over cobalt, nickel, rhodium, and palladium catalysis in the hydrogenation of **1**,[7] and to give selectively **2E** over palladium in the hydrogenation of **2**.[8] However, reductive cyclization could not be observed in the hydrogenation of acyclic nonconjugated enones (**5** and **6**). We envisage that the proximity between two π-orbitals is closely associated with the formation of reductive cyclization products.[15]

Figure 1 shows the product ratios of unsaturated alcohols (**2B**, **6B**, **7B**, and **8B**) when 50% of the enones were consumed over cobalt, nickel, and osmium catalysts. The high-selectivity to the unsaturated alcohol formation was observed when a carbonyl moiety was associated with a relative hindered olefinic bond. In the case of trialkylated olefinic ketones (**2**, **6**, and **8**), the unsaturated alcohols (**2B**, **6B**, and **8B**) were exclusively produced over cobalt catalyst; however, the formation of **7B** decreased to 22% yield in the case of dialkylated olefinic ketone (**7**). These results show that the reactivity of the carbonyl moiety over cobalt is a little lower than the dialkyl-substituted olefins but is much higher than the trialkyl-substituted ones in nonconjugated enones. This trend was also observed over nickel and osmium catalysts. The hydrogenation

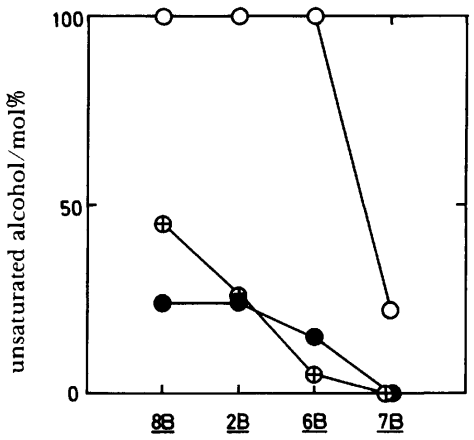

Fig. 1. Product ratios of unsaturated alcohols (**2B**, **6B**, **7B**, **and 8B**) when 50% of substrates were consumed over Co, Ni, and Os catalysts. ○: Co, ⊕: Ni, ●: Os.

of **2**, **6**, and **8** gave 5—45% of **B** over those catalysts, while **7B** was rarely formed in that of **7**. An osmium catalyst showed the highest selectivity for the reduction of the carbonyl bond in platinum metals. Osmium might be expected to be the most suited for reducing the carbonyl function of nonconjugated enones among the platinum metats in this sense.

The selectivity of the reduction of trialkylated olefinic ketones to unsaturated alcohols declined in the series Co≫Ni, Os≫Ir, Ru, Rh, Pd, Pt. This tendency may be attributed to the fact that nickel, osmium, and especially cobalt catalysts have a stronger affinity for the carbonyl moiety than the other catalysts.[16] It is important in organic syntheses that the unsaturated alochol is selectively obtained from trialkylated olefinic ketones during hydrogenation over a cobalt catalyst. The hydrogenation of **2**, **6**, and **8** over cobalt gave those corresponding unsaturated alcohols in 98% yield after absorption of one equivalent of hydrogen. A Raney cobalt catalyst was also remarkably chemoselective in the competitive hydrogenation of a mixture of 6-methyl-2-heptanone (**6A**) and 6-methyl-5-hepten-2-ol (**6B**). The carbonyl moiety of **6A** was completely reduced before the double bond of **6B** was saturated, whereas **6A** and **6B** were converted with a comparable rate over a Raney nickel catalyst (Fig. 2).

Hydrogenations were also carried out in an ethanol solvent. Although the proportion of saturated alcohols decreased according to the catalysts used, the chemo-selectivity of metal catalysts in ethanol showed a similar trend of that in cyclohexane as a whole. Diethyl acetals were rapidly formed in addition to the hydrogenated products by the use of **7** and **8** as nonconjugated enones over ruthenium, rhodium, and palladium catalysts in ethanol. The acetals were a mixture of 4-alkylidenecyclohexanone diethyl acetal (**F**), 4-alkyl-3-cyclohexenone diethyl acetal (**G**), 4-alkylcyclohexanone diethyl acetal (**H**) (Fig. 3). The acetal formation relative to the hydrogenation increased in the order Rh<Ru<Pd. Those were not detected at all during the hydrogenation of the other enones, and were not observed over the other catalysts.

Since **7** and **8**, which have olefinic and carbonyl functions at 1 and 4 positions on a cyclohexane ring, take a rigid and flat chair conformation compared with the other simple nonconjugated enones, it is suggested that the neighborhood of the carbonyl moieties of **7** and **8** is hindered less sterically than that of the other enones. The effect of such steric factors is associated with the formation of diethyl acetals. 4-Ethylidenecyclohexanone diethyl acetal (**8F**) is found to be the most abundant among acetals in the hydrogenation of **8**; it is contemplated that acetal formation occurs faster than a reduction of the olefin. The varying composition of the reaction mixture at the initial stage of the hydrogenation over a Pd catalyst in ethanol is shown in Fig. 4 as an example. Palladium, rhodium, and ruthenium catalysts are the ones which efficiently hydrogenate olefins. It is,

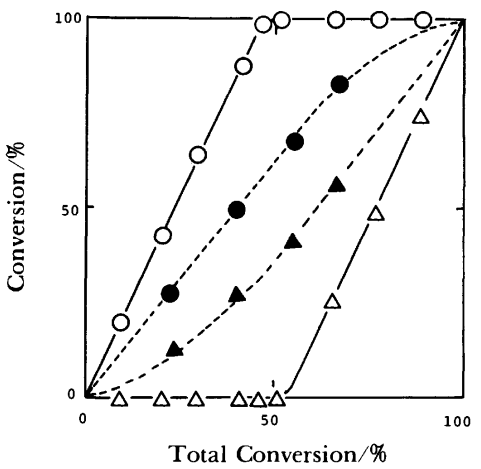

Fig. 2. Conversion of 6-methyl-2-heptanone (**6A**: ○, ●) and 6-methyl-5-hepten-2-ol (**6B**: △, ▲) versus total conversion. Raney Co (○, △: ——), Raney Ni (●, ▲: ------).

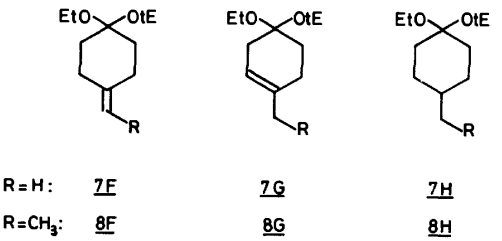

Fig. 3

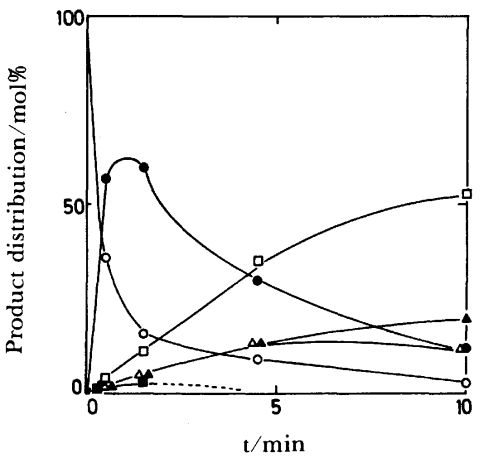

Fig. 4. Product distribution in hydrogenation of 4-ethylidenecyclohexanone (**8**) over Pd catalyst in ethanol. ○: **8**, ▲: 4-ethylcyclohexanone (**8B**), ■: 4-ethyl-3-cyclohexenone (**8D**), ●: 4-ethylidenecyclohexanone diethyl acetal (**8F**), △: 4-ethyl-3-cyclohexenone diethyl acetal (**8G**), □: 4-ethylcyclohexanone diethyl acetal (**8H**).

nevertheless, interesting that the formation of the acetal occurs faster than the hydrogenation of the olefin. Acetal formation is an acid-catalyzed reaction; therefore it may be considered that palladium, rhodium, and ruthenium black catalysts tend to have ionized hydrogens on the surfaces of these metals.[9]

In anticipation of a more preferential reduction of the ketone group of the nonconjugated enones, we also examined the hydrogenation of **5** and **6** over Raney nickel, cobalt, and cobalt black catalysts treated with alkali and carbon monoxide (Table 3). Selectivity to the unsaturated alcohols varied greatly with the additives over cobalt and nickel catalysts. When the catalysts were treated with alkali, the amount of **5B** over Raney cobalt and of **6B** over Raney nickel increased compared with that over the untreated catalysts, respectively. However, the treatment of carbon monoxide for catalysts indicated an opposite and marked effect to that of alkali. The double bond of **6** was selectively reduced to give **6A** over Raney nickel treated with carbon monoxide. When cobalt was treated with carbon monoxide in the hydrogenation of **6**, the characteristics of cobalt, which proceed with the preferential reduction of the ketone group, was completely missing.

Since alkali has a promoting effect on the ketone reduction, the hydrogenation of **3** was examined over Raney cobalt and nickel catalysts which were treated with sodium and potassium hydroxides. However, the chemo-selectivity for **3** was not altered by the treatment of alkali. Gradeff and Formica achieved a preferential reduction of the ketone group in trialkylated olefinic ketones. They have obtained the corresponding unsaturated alcohol using a chromium-promoted Raney nickel catalyst in the presence of a strong inorganic base, triethylamine, and small amounts of water in methanol solvents.[17] The amounts of **5B** and **6B** increased similarly to the results of Gradeff and Formica when the catalysts were treated with alkali (Table 3). The function of alkali in the promotion on the ketone reduction is not always obvious. It may increase the enol content, or change the product-determining step by altering the adsorbability of the substrate.[18]

Table 3. Effect of Modification of Cobalt and Nickel Catalysts in Hydrogenation of Enones **5** and **6**[a]

Enone	Catalyst	Modification (mmol)	Product[b]/mol%		
			A	**B**	**C**
5	Co	——	61	22	17
	Co	NaOH (1)[c]	59	30	11
	Co	KOH (1)	42	42	16
	Ni	——	100	0	0
6	Co	——	(2)[d]	(96)	(2)
	Co	NaOH (0.1)[e]	(0)	(100)	(0)
	Co	CO (0.001)	(100)	(0)	(0)
	Ni	——	61	10	29
	Ni	NaOH (0.1)	34	37	29
	Ni	NaOH (1)	6	88	6
	Ni	NaOH (2)	5	74	21
	Ni	Reflux (CO)[f]	94	2	4

a) Substrate, 0.5 mmol; Raney Ni and Co, 500 mg; Co-black, 1000 mg; Solvent(ethanol), 5 ml. Values are the composition (mol.%) 50% of substrate was consumed. Enones were hydrogenated in ethanol in terms of modification of catalyst. b) See footnote b in Table 1. c) Added ca. 60% solution of NaOH or KOH in water then stirred for 0.5 h at ambient temperature under hydrogen atmosphere. d) Values in parentheses indicate the product ratios over Co-black catalyst. e) Introduced CO, then stirred under the same conditions as alkali. f) Refluxed in ethanol for 2 h under nitrogen atmosphere; when Ni is refluxed in ethanol, CO is adsorbed over catalyst.

Carbon monoxide has no promoting effect on ketone reduction, and the apparent rate of the hydrogenation over a catalyst treated with carbon monoxide decreases compared to an unmodified catalyst. When Raney nickel refluxed in ethanol was used in the hydrogenation of **6**, **6A** increased in a similar manner as a cobalt catalyst treated with carbon monoxide. Ethanol is decomposed to carbon monoxide and methane by refluxing over Raney nickel.[19] It has been known that the amount of the adsorbed hydrogen on nickel pretreated with carbon monoxide is larger than that on an unpoisoned catalyst.[20] Similarly, the adsorption of pyridine on nickel-silica can be promoted if nickel is pretreated with carbon monoxide.[21] Sheets and Hansen considered that if a strong electron withdrawing species like carbon monoxide is already present on the surface of a catalyst, the formation of a coordinated pyridine can be promoted owing to the electron defficiency of the catalyst surface.[22] This suggests that the absorbed state on cobalt and nickel catalysts treated with carbon monoxide is different from that on untreated ones; it may be responsible for the disappearance of the characteristics proceeding with the preferential reduction of the ketone group.

Experimental

All boiling points are uncorrected. ^{1}H and ^{13}C NMR spectra were obtained with either a JEOL JNM-MH100 or a JEOL-JNM-FX100 spectrometer. The frequency was 100 MHz for ^{1}H NMR and 25 MHz for ^{13}C NMR spectra. All IR spectra were obtained with a JASCO A-3 spectrometer as neat samples. Mass spectra were taken at 70 eV on a JEOL JMS-D300 GC/MS spectrometer.

Materials. 5-Hexen-2-one (**3**) and 6-methyl-5-hepten-2-one (**6**) were commercially available: **3** and **6** were obtained from Tokyo Kasei Kogyo and used after distillation: **3**, bp 126 °C/755 mmHg (1 mmHg=133.322 Pa); **6**, bp 73 °C/18 mmHg. The preparation of 5-methyl-5-hexen-2-one (**4**) is described hereinafter. By use of the method of Jones and Sondheimer,[23] 25 g of 2,5-hexanediol, 164 ml of dry

pyridine, 84 g of benzoyl chloride, and 400 ml of dry chloroform gave a 48% yield of 2,5-hexanediol monobenzoate: bp 143—147 °C/1.8 mmHg. The monobenzoate (44.4 g) was oxygenized by pyridinium chlorochromate (PCC) in dichloromethane,[24] affording a 79% yield of 5-benzoyloxy-2-hexanone: bp 130 °C/0.65 mmHg; IR (neat) 1720 (s), 1605 (w), 1590 (w), 1495 (w), 1455 (w), 1320 (m), 1280 (s), 1030 (m), 715 (s). 5-Benzoyloxy-2-methyl-1-hexene was prepared by the Wittig reaction of 5-benzoyloxy-2-hexanone using methylsulfinylmethanide (yield: 70%),[25] a following hydrolysis gave a 50% yield of 5-methyl-5-hexen-2-ol (**4B**). 5-Benzoyloxy-2-methyl-1-hexene: bp 150—155 °C/20 mmHg; IR (neat) 1720 (s), 1650 (w), 1600 (w), 1585 (w), 1450 (m), 1315 (m), 1275 (s), 1115 (m), 1030 (m), 890 (m), 710 (s). **4B**: bp 68—69 °C/20 mmHg; IR (neat) 3350 (s, br), 1650 (m), 1378 (m), 890 (m). A 70% yield of **4** was obtained by the oxidation of **4B** using PCC. **4**: bp 60—62 °C/20 mmHg; IR (neat) 1720 (s), 1660 (m), 1360 (m), 1162 (m), 895 (m); ^{1}H NMR ($CDCl_3$) δ=1.72 (3H, s), 2.15 (3H, s), 2.40 (4H, m), 4.69 (2H, dd); ^{13}C NMR ($CDCl_3$) δ=22.57, 29.77, 31.59, 41.86, 110.17, 144.34, 207.92; MS *m/z* 112 (M^+, 13), 97 (42), 69 (81), 55 (28), 43 (100), 41 (98) 39 (35), 28 (25). Found: C, 74.90; H, 10.81. Calcd for $C_7H_{12}O$: C, 74.95; H, 10.78.

5-Hepten-2-one (**5**) was prepared by the method of Schechter, Green, and LaForge.[26] **5** was a mixture of cis and trans isomers (cis:trans=14:86). **5**: bp 140—150 °C/755 mmHg (yield: 54%); IR (neat) 1720 (s), 1360 (m), 1165 (m), 980 (m); ^{13}C NMR ($CDCl_3$, trans isomer) δ=17.85, 26.89, 29.88, 43.50, 125.81, 129.51, 208.18; MS *m/z* 112 (M^+, 50), 97 (43), 69 (46), 58 (36), 55 (68), 43 (100), 41 (98), 39 (44), 28 (36).

4-Methylenecyclohexanone (**7**) and 4-ethylidenecyclohexanone (**8**) were prepared by a modification of the synthetic method of **4**.[23-25] **7**: bp 65 °C/27 mmHg; IR (neat) 1720 (s), 1650 (w), 1440 (m), 1142 (m), 900 (m), 792 (w); ^{1}H NMR ($CDCl_3$) δ=2.48 (8H, bs), 4.89 (2H, s); ^{13}C NMR ($CDCl_3$) δ=33.14, 41.57, 110.73, 144.34, 210.65; MS *m/z* 110 (M^+, 100), 82 (85), 81 (71), 68 (51), 55 (38), 54 (98), 53 (61), 41 (48), 40 (31), 39 (82), 28 (62). Found: C, 76.53; H, 9.21. Calcd for $C_7H_{10}O$: C, 76.32; H, 9.15. **7B**: bp 78 °C/16 mmHg; IR (neat) 3350 (s. br), 1650 (m), 1070 (m), 895 (m); ^{13}C NMR ($CDCl_3$) δ=31.88, 35.87, 68.98, 107.70, 147.74. **8**: bp 78 °C/20 mmHg; IR (neat) 1720 (s), 1442 (m), 1150 (m), 950 (w), 825 (w), 780 (w), 700 (w); ^{1}H NMR ($CDCl_3$) δ=1.65 (3H, d), 2.43 (8H, bs), 5.41 (1H, q); ^{13}C NMR ($CDCl_3$) δ=13.12, 25.77, 34.14, 40.69, 41.77, 119.36, 134.50, 211.73; MS *m/z* 124 (M^+, 87), 82 (39), 81 (35), 68 (27), 67 (100), 54 (37), 41 (32), 39 (38), 28 (26). Found: C, 77.41; H, 9.74. Calcd for $C_8H_{12}O$: C, 77.37; H, 9.74. **8B**: bp 83—87 °C/14 mmHg: ^{13}C NMR ($CDCl_3$) δ=12.83, 24.57, 33.47, 35.40, 36.40, 69.89, 116.33, 137.70; MS *m/z* 126 (M^+, 7), 108 (50), 93 (79), 79 (100), 67 (38), 41 (32), 39 (26).

Catalysts. Unsupported metal catalysts were prepared by reducing the corresponding metal hydroxides (Ru, Rh, Pd, Ir) or oxides (Pt, Os) with hydrogen in water at atmospheric or elevated pressure using a method which is similar to that described by Nishimura[27] and Tanaka.[11] Care was taken to removal alkaline or acidic impurities with reductions and washings. W-4 Raney Ni and Co were prepared as described earlier.[10] Reduced Ni and Co were prepared by the reduction of NiO and CoO which were obtained from $Ni(NO_3)_2$ and $Co(NO_3)_2$ in hydrogen atmosphere at 350 °C.

Hydrogenation. All hydrogenations were carried out in a 50 ml round glass bottle with a silicone rubber stopper at room temperature (20—25 °C) and approximately atmospheric pressure (1—1.05 atm). A high purity hydrogen gas was used without further purification. In the reaction vessel a weighed sample of catalyst (5 mg for noble metals; 500 mg for Raney Ni and Co under wet conditions; 200 mg as NiO for Ni-black; 1000 mg as CoO for Co-black) was placed along with 5 ml of purified cyclohexane or 99% ethanol, and then the vessel was flushed with hydrogen. The catalyst was stirred magnetically with hydrogen in a solvent for 0.5—1 h; the substrate (0.5 mmol) to be hydrogenated was then added with a microsyringe through a silicone rubber stopper.

Product Analysis. The reaction was followed volumetrically by measuring the hyrogen consumption and also followed gas-chromatographically by analyzing aliquots of the reaction mixture at appropriate time intervals. The reaction mixture was taken into a microsyringe through the silicone rubber stopper during the course of hydrogenation. The gas chromatography was performed on Hitachi F-6 and 164 instruments equipped with a flame ionization detector using nitrogen as the carrier gas. The products were analyzed on a 45 m×0.25 mm Goley column of PEG 400 at 60 °C for **3**, and on a 45 m×0.25 mm Goley column of PEG 4000 at 80—90 °C for **4**, **5**, and **6** or at 120—140 °C for **7** and **8**. The peaks were identified by a comparison of their retention times with those of authentic samples.

References

1) a) Undergraduate Fellow, 1981—1982; b) Undergraduate Fellow, 1982—1983.

2) P. N. Rylander, "Catalytic Hydrogenation over Platinum Metals," Academic Press Inc., New York (1967), p. 271.

3) P. N. Rylander, "Catalytic Hydrogenation in Organic Syntheses," Academic Press Inc., New York (1979), pp. 51, 88.

4) I. A. Kaye and R. S. Mattheus, *J. Org. Chem.*, **29**, 1341 (1964).

5) D. J. France, J. J. Hand, and M. Los, *Tetrahedron*, **25**, 4011 (1969).

6) S. Nishimura, I. Takahashi, M. Shiota, and M. Ishige, *Chem. Lett.*, **1981**, 877.

7)J. -I. Ishiyama, Y. Senda, and S. Imaizumi, *Chem. Lett.*, **1983**, 771.

8) J. -I. Ishiyama, Y. Senda, and S. Imaizumi, *Chem. Lett.*, **1983**, 1243.

9) S. Nishimura, T. Itaya, and M. Shiota, *Chem. Commun.*, **1967**, 422.

10) a) A. A. Pavlic and H. Adkins, *J. Am. Chem. Soc.*, **68**, 1471 (1946); b) H. Adkins and A. A. Pavlic, *J. Am. Chem. Soc.*, **69**, 3039 (1947).

11) K. Tanaka, Y. Takagi, O. Nomura, and I. Kobayashi, *J. Catal.*, **35**, 24 (1974).

12) A 37% of 5-methyl-4-hexen-2-one (**4D**) and a 27% of 4-methyl-3-cyclohexenone (**7D**) were formed besides saturated ketones from **4** and **7** over Pd at the 50% of conversion. **4D** was also present in trace amounts over Ru, Rh, and Pt.

13) A 6% of 6-methyl-2-heptanol (**6C**) was observed over Ir at the 50% of conversion.

14) Y. Senda, J.-I. Ishiyama, and S. Imaizumi, *J. Chem. Soc., Perkin Trans. 2*, **1981**, 90.

15) C. A. Grob and H. Katayama, *Helv. Chim. Acta*, **60**, 1890 (1977).
16) Y. Nitta, T. Imanaka, and S. Teranishi, *Bull. Chem. Soc. Jpn.*, **53**, 3154 (1980).
17) a) P. S. Gradeff and G. Formica, *Tetrahedron Lett.*, **1976**, 4681; b) P. S. Gradeff and G. Formica, U. S. Patent 4041083 (1977).
18) P. N. Rylander, "Catalytic Hydrogenation in Organic Syntheses," Academic Press Inc., New York (1979), p. 84.
19) T. Kubomatsu, S. Kishida, and K. Hotta, *Kagaku To Kogyo (Osaka)*, **40**, 504 (1960).
20) T. A. White and A. F. Benton, *J. Phys. Chem.*, **35**, 84 (1931).
21) B. A. Morrow, J. A. Cody, L. E. Moran, and R. Palepu, *J. Catal.*, **44**, 467 (1976).
22) R. W. Sheets and R. S. Hansen, *J. Phys. Chem.*, **76**, 972 (1972).
23) E. R. H. Jones and F. Sondheimer, *J. Chem. Soc.*, **1949**, 615.
24) E. J. Corey and J. W. Suggs, *Tetrahedron Lett.*, **1975**, 2647.
25) R. Greenwald, M. Chaykovsky, and E. J. Corey, *J. Org. Chem.*, **28**, 1128 (1963).
26) M. S. Schechter, N. Green, and F. B. LaForge, *J. Am. Chem. Soc.*, **71**, 3165 (1949).
27) S. Nischimura, M. Katagiri, T. Watanabe . and M. Uramoto, *Bull. Chem. Soc. Jpn.*, **44**, 166 (1971).

Construction of an Optically Active 7-Oxabicyclo[4.3.0]non-4-en-3-one Skeleton from D-Glucose, and Its Transformation to Some Pseudo-Hexopyranoses

Kin-ichi TADANO,* Yoshihide UENO, Chiyoko FUKABORI, Yukinori HOTTA, and Tetsuo SUAMI*

Department of Applied Chemistry, Faculty of Science and Technology, Keio University, Hiyoshi, Kohoku-ku, Yokohama 223

(Received August 27, 1986)

A versatile chiral compound, (1*R*,6*R*,8*R*,9*R*)-8,9-isopropylidenedioxy-7-oxabicyclo[4.3.0]non-4-en-3-one (**6**), was efficiently synthesized from D-glucose. The synthesis featured an intramolecular aldol cyclization of 3-*C*-acetylmethyl-3-deoxy-1,2-*O*-isopropylidene-α-D-*ribo*-pentodialdo-1,4-furanose, which was readily derivatized from the known Wittig adducts of 1,2:5,6-di-*O*-isopropylidene-α-D-*ribo*-hexofuranos-3-ulose. The utility of this highly functionalized chiral synthon **6** was embodied by conversion to four optically active pseudo-sugars, these are pentaacetyl derivatives of pseudo-α-L-altropyranose, pseudo-β-D-glucopyranose, pseudo-2-amino-2-deoxy-β-L-altropyranose, and pseudo-2-amino-2-deoxy-α-D-glucopyranose (a derivative of pseudo-glucosamine). The transformation of **6** to the pseudo sugars involved 1) a stereospecific epoxidation of the double bond in **6** providing (1*R*,4*S*,5*S*,6*S*,8*R*,9*R*)-4,5-epoxy-8,9-isopropylidenedioxy-7-oxabicyclo[4.3.0]-nonan-3-one (**8**), and 2) an exclusive diaxial ring opening of the β-epoxy alcohols, which were derived from **8**, providing (1*R*,3*R*,4*S*,5*S*,6*S*,8*R*,9*R*)-8,9-isopropylidenedioxy-7-oxabicyclo[4.3.0]nonane-3,4,5-triol (**11**) or (1*R*,3*S*,4*S*,5*R*,6*S*,8*R*,9*R*)-4-azido-8,9-isopropylidenedioxy-7-oxabicyclo[4.3.0]nonane-3,5-diol. Treatment of (1*R*,2*S*,3*S*,4*S*,5*R*)-3,4,5-tris(benzyloxy)-2-hydroxycyclohexanecarbaldehyde, which was derived from **11**, with methanesulfonyl chloride, and successive sodium borohydride reduction provided (3*S*,4*S*,5*R*)-3,4,5-tris(benzyloxy)-1-cyclohexene-1-methanol (**19**). Hydroboration of **19** proceeded from the less hindered side stereoselectively.

1-Hydroxymethyl-2,3,4,5-cyclohexanetetrols, known as "pseudo-sugars," may be regarded as carbocyclic analogues of carbohydrates (mainly, hexopyranoses). They are of current interest in the field of biological chemistry. The pseudo-sugars are found in partial components of antibiotics (validamycins) and enzyme inhibitors (adiposins).[1] In addition to the biological studies, the synthesis of pseudo-sugars is also of current interest. Several approaches directed toward optically active pseudo-sugars synthesis have appeared in the literatures. Ogawa and Suami demonstrated the preparation of the optically active *endo*-7-oxabicyclo[2.2.1]hept-5-ene-2-carboxylic acid, a common intermediate for the synthesis of pseudo-sugars, by optical resolution of the Diels-Alder adduct of furan and acrylic acid.[2] Paulsen and Heiker reported the synthesis of chiral valienamine, a component of validamycin type antibiotics, from quebrachitol (2-*O*-methyl-L-chiroinositol).[3] Paulsen and co-workers also successfully transformed the L-chiroinositol, which was derived from quebrachitol, to pseudo-α-D-galactopyranose and pseudo-β-D-mannopyranose.[4] In connection with the synthesis of prostaglandins employing carbohydrates as chiral starting materials, Ferrier and co-workers extensively pursued chiral cyclopentanoids and cyclohexanoids syntheses. The remarkable strategy developed by their group was the mercury(II)-promoted intramolecular cyclization of the 5,6-unsaturated hexopyranose derivative to the optically active polyhydroxylated cyclohexanone.[5] Applying Ferrier's strategy, Kuzuhara and Sugawara achieved the synthesis of aminocyclitol-containing pseudo-disaccharides by the partial conversion of maltose into cyclohexane derivatives.[6] Recently, Wilcox and co-workers realized an elegant approach towards an optically active carbocycle synthesis. This featured "the radical cyclization" of unsaturated halo sugars.[7] Carbocyclic analogues of D-fructofuranose (pseudo-D-fructofuranose) and D-fructofuranose 6-phosphate were synthesized by this radical cyclization strategy.[8]

In our continuing research on the synthesis of optically active carbocyclic compounds and pseudo-sugars from carbohydrates,[9] we wish to describe herein a novel and utilizable approach directed toward synthesis of pseudo-hexopyranoses.[10] The new approach features an efficient access to the versatile chiral synthon **6** from the readily available **5** by an intramolecular aldol cyclization, and a stereoselective introduction of a triol or an azido diol system on the 2-cyclohexenone moiety of **6** providing the compounds **11** and **22**. From compounds **11** and **22**, four pseudo-hexopyranoses were synthesized in acceptable overall yields.

Results and Discussion

Synthesis of the Chiral Synthon 6 from D-Glucose (Scheme 1). 1,2:5,6-Di-*O*-isopropylidene-α-D-*ribo*-hexofuranos-3-ulose (**1**) was subjected to Wittig olefination with (acetylmethylene)triphenylphosphorane in refluxing benzene according to the literature.[11] This provided an approximately 3 to 1 [(*Z*) to (*E*)] geometrical mixture of the adduct **2** in 96% yield.

Hydrogenation of the mixture **2** in the presence of Raney nickel furnished a diastereomeric mixture of the 3-*C*-(2-hydroxypropyl) derivative. This was directly oxidized with pyridinium chlorochromate (PCC) to provide 3-*C*-acetylmethyl-3-deoxy-1,2:5,6-di-*O*-isopropylidene-α-D-allofuranose (**3**) as crystals in 88% yield. As expected, based on the result of the hydrogenation of the corresponding 3-*C*-methylene derivative,[12] the hydrogenation of **2** proceeded from the β-side to give the α-D-allo derivative **3** exclusively. In the initial stage of the hydrogenation, the presence of **3** was detected in the reaction mixture. However, the compound **3** was rapidly converted to over-hydrogenated products. Selective hydrolysis of the 5,6-*O*-isopropylidene group in **3** with 60% aqueous acetic acid afforded compound **4** in 98% yield. The glycol cleavage of **4** by an aqueous sodium periodate solution gave a 5-aldehyde **5** quantitatively, which was subjected to the next aldol cyclization without purification. The crucial aldol cyclization of **5** to the synthon **6** was examined under the following conditions; 1) with sodium methoxide in methanol; 2) in 1 mol dm^{-3} aqueous NaOH; 3) with triethylamine in refluxing benzene; 4) lithium diisopropylamide (LDA) in THF from −78 to 0 °C; 5) with sodium hydride in refluxing benzene; 6) with BF_3–Et_2O in CH_2Cl_2. None of these reactions gave compound **6** in a practical yield. However, we found finally that 1,8-diazabicyclo[5.4.0]undec-7-ene (DBU) was an effective base for the cyclization. By refluxing **5** in benzene in the presence of 0.05 molar equivalent of DBU for 35 h followed by an acetic anhydride–pyridine treatment of the cyclization products, compound **5** was converted to compound **6** in 45% yield after chromatographic purification on silica gel. For the complete β-elimination of the cyclization products (α,β-enone formation), the acetic anhydride–pyridine treatment was necessary. The β-elimination was presumably proceeded via the β-acetate, which could not be isolated from the reaction mixture. For the Dieckmann cyclization of methyl 3-*C*-(methoxycarbonylmethyl)-1,2-*O*-isopropylidene-3,5,6-trideoxy-α-D-*ribo*-heptofuranuronate (a structurally similar model to the compound **5**), Fraser-Reid and co-workers found potassium *t*-butoxide to be an effective base.[13] We were able to find optimal conditions for the aldol cyclization, but an occurrence of epimerization at C-4 in **5** (an α-position of the aldehyde) under the basic conditions could not be excluded. Accordingly it was necessary to confirm the structure of **6**. Hydrogenation of **6** in the presence of Raney nickel and successive PCC oxidation of a cyclohexanols mixture afforded 7-oxabicyclo[4.3.0]nonan-3-one **7** in 82% yield. In the ^1H NMR spectrum of **7**, a doublet of triplets, which was attributable to H-6, appeared at δ 4.10 with $J_{1,6}=J_{5ax,6}=10.5$ Hz and $J_{5eq,6}=4.5$ Hz. This fact indicated that H-1 and H-6 of **6** (those are H-3 and H-4 of **5**) were in a trans diaxial relationship and no epimerization had occurred under the cyclization conditions. Consequently, the structure of the compound **6** was established.

The Transformation of Compound 6 to Pseudo-α-L-altropyranose Pentaacetate (17) (Scheme 2). Compound **6** possesses the proper functional groups for an introduction of hydroxyl groups (for instance, the carbonyl group or the double bond in the cyclohexenone moiety are convertible to the hydroxyl groups by reduction or oxidation). In addition, a portion of C-1 to C-8 via C-9 is convertible to a hydroxymethyl pseudo-sugar side chain by one-carbon degradation.

Epoxidation of **6** with 35% aqueous hydrogen peroxide in slightly alkaline methanol solution gave a β-epoxy ketone **8** stereospecifically in 96% yield. An α-epoxy ketone **8′** was isoltated in 3% yield. Although the structure of the β-epoxy ketone **8** [(4*S*,5*S*)-configuration] could not be determined unambiguously from the ^1H NMR spectrum, it was confirmed at a later stage. Sodium borohydride reduction of the carbonyl group in **8** gave a 5 to 1 mixture of the epoxy alcohols **9** and **9′**, which were cleanly separated by

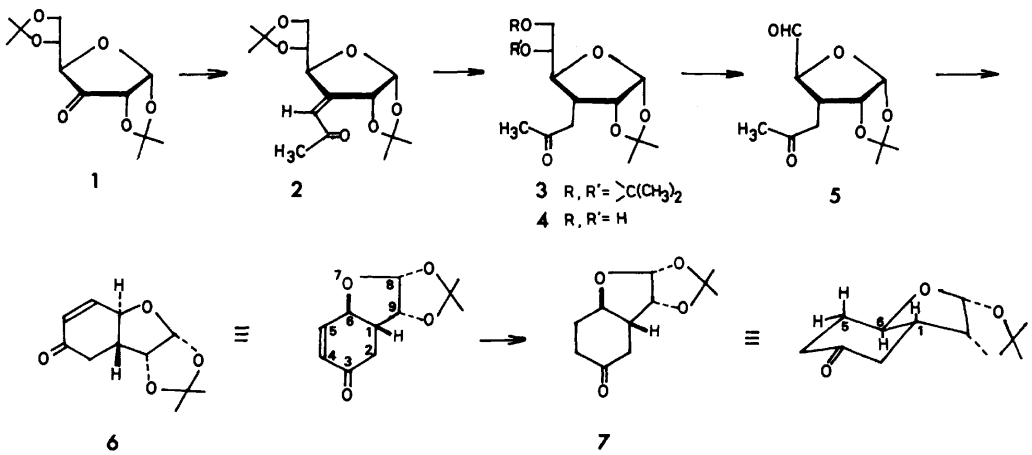

Scheme 1.

silica-gel chromatograpy, in 84% combined yield. The compounds **9** and **9′** were acetylated to afford **10** and **10′**. The ^{1}H NMR spectra of **10** and **10′** revealed a quartet with $J_{2,3}=J_{2',3}=J_{3,4}=4$ Hz for H-3 of **10′** and a triplet with $J_{2,3}=J_{2',3}=8.5$ Hz, $J_{3,4}=0$ Hz for H-3 of **10**. Unfortunately, from these results, we were not able to establish the configurations of the newly introduced acetoxyl groups of **10** and **10′** (therefore hydroxyl groups of **9** and **9′**) unambiguously, since the conformation of the cyclohexane moiety of **10** and **10′** (pseudo-boat form or pseudo-chair form) remained unclear. We tentatively assigned it to a (*S*)-configuration for the major 3-hydroxyl derivative **9** as depicted,[14] and this was confirmed on azidolysis of **9** and **9′** and successive conversion to pseudo-amino sugars (vide infra).

The epoxide-ring opening of **9** and **9′** by solvolysis in refluxing aqueous 2-methoxyethanol in the presence of sodium acetate provided the same triol **11** as a single product in 73 and 81% yield, respectively. Acetylation of **11** afforded the triacetate **12** in 80% yield. In the ^{1}H NMR spectrum of **12**, the protons on carbons bearing acetoxyl groups, (at H-3, 4, and 5), appeared as a quartet at δ 5.00 for H-3 ($J_{2,3}=J_{2',3}=J_{3,4}=3$ Hz) and two triplets at δ 5.12 and 5.37 for H-4 and 5 (or H-5 and 4) ($J_{3,4}=J_{4,5}=J_{5,6}=3$ Hz). This fact supported the view that three acetoxyl groups were in a trans diaxial relationship to one another. Accordingly the structure of **11** [(3*R*,4*S*,5*S*)-configuration] was established. The formation of **11** from **9** is explainable as follows. A neighboring group participation of the α-hydroxyl group in **9** on the

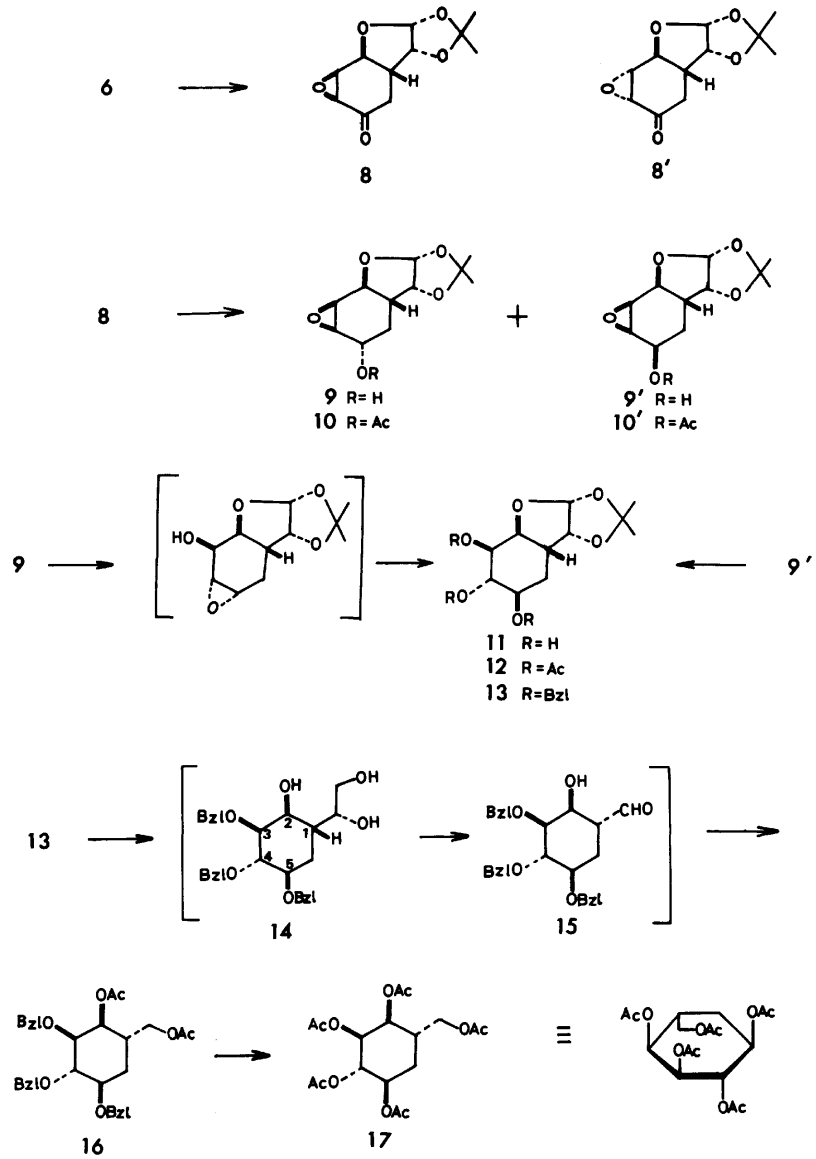

Scheme 2.

occasion of the epoxy-ring opening resulted in the formation of 3,4-α-epoxy-5-β-hydroxyl derivative as an intermediate, which could not be isolated. The intermediate was then attacked by hydroxide anion in a diaxial opening manner providing the compound **11**. The formation of **11** from **9'** was a result of direct diaxial opening of the epoxy ring. Therefore, we could introduce three hydroxyl groups into the cyclohexane moiety of **11** stereospecifically from both compounds **9** and **9'**.

The transformation of compound **11** to pseudo-α-L-altropyranose pentaacetate (**17**) was achieved as follows. Benzylation of **11** furnished a tri-*O*-benzyl derivative **13** in 93% yield. By acid hydrolysis and successive sodium borohydride reduction, the compound **13** was converted to a branched cyclohexane tetrol **14** (a derivative of pseudo-heptopyranose). The glycol cleavage of **14** by periodate gave (1*R*,2*S*,3*S*,4*S*,5*R*)-3,4,5-tris(benzyloxy)-2-hydroxycyclohexanecarbaldehyde (**15**), which was reduced with sodium borohydride, then acetylated providing a fully protected pseudo-α-L-altropyranose **16** in 52% overall yield from **13**. *O*-Debenzylation of **16** with sodium in liquid ammonia and successive acetylation furnished (1*S*,2*S*,3*S*,4*S*,5*R*)-2,3,4,5-tetraacetoxy-1-(acetoxymethyl)cyclohexane, pseudo-α-L-altropyranose pentaacetate (**17**) in 33% yield. The ^{1}H NMR spectrum of **17** was superimposable on that of the known DL-**17**,[15] therefore, the structure of **17** was confirmed.

Synthesis of Pseudo-β-D-glucopyranose Pentaacetate 21 from Compound 15 (Scheme 3). The inversion of the configurations of C-1 and C-2 in compound **17** was next investigated. Treatment of compound **15** with excess methanesulfonyl chloride in pyridine at ambient temperature afforded the α,β-unsaturated aldehyde **18**, which was subjected to the next step without purification. Although we could not detect an intermediate of the reaction, we assumed the β-elimination proceeded via a β-methanesulfonate. Sodium borohydride reduction of compound **18** gave (3*S*,4*S*,5*R*)-3,4,5-tris(benzyloxy)-1-cyclohexene-1-methanol (**19**) in 22% overall yield from **13**. Hydroboration of **19** with borane–THF complex at 0 °C, oxidative work-up with 35% hydrogen peroxide in an alkaline solution, and successive acetylation afforded a pseudo-β-D-glucopyranose derivative **20** accompanied by compound **16**. These were separated on a silica-gel chromatography in 63 and 11% yield, respectively. This result indicates that the hydroboration of **19** proceeded from the α-side preferentially. In this case, a stereocontrolling factor for the attack of borane was probably the configuration of the benzyloxy group at C-3. Consequently, we could establish a methodology for the configurational inversion at the branched carbon. *O*-Debenzylation of compound **20** by hydrogenolysis in the presence of palladium on charcoal and successive acetylation gave the known (**21**), (1*R*,2*R*,3*S*,4*S*,5*R*)-2,3,4,5-tetraacetoxy-1-(acetoxymethyl)cyclohexane, pseudo-β-D-glucopyranose pentaacetate, in 98% yield. The ^{1}H NMR spectrum of **21** was superimposable on that of an authentic sample.[2,16]

Syntheses of Pentaacetyl Derivatives, 29 and 33, of Pseudo-2-amino-2-deoxy-β-L-altropyranose and of Pseudo-2-amino-2-deoxy-α-D-glucopyranose (Scheme 4). Our interest next turned to an access to pseudo-amino sugars from compound **9**. In order to introduce an amino group at an appropriate position in the cyclohexane moiety, azidolysis of **9** was investigated. By refluxing **9** in aqueous 2-methoxyethanol with excess sodium azide in the presence of ammonium chloride, the epoxy ring was cleaved by the azide anion in a diaxial-opening manner providing compound **22** in 84% yield as crystals. No other azido-containing compounds were detected. The structure of **22** was estimated as depicted from the ^{1}H NMR spectrum of the di-*O*-acetyl derivative **23**, in which the H-5 signal revealed at δ 5.38 as a triplet with $J_{4,5}=J_{5,6}=3$ Hz and the H-4 (H–C–N_3) signal revealed at δ 4.02 as a triplet with $J_{3,4}=J_{4,5}=3$ Hz. Azidolysis of the other epoxy alcohol **9'** under the same reaction conditions described above gave another azido containing compound **22'** in 87% yield. The structure of **22'** was determined from the ^{1}H NMR spectrum of the

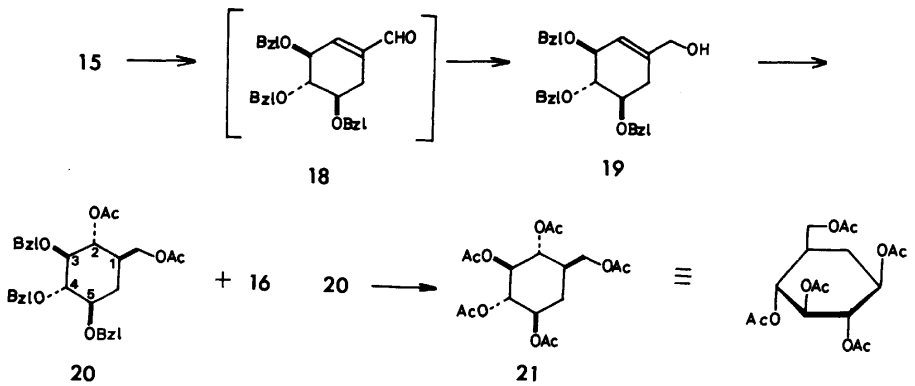

Scheme 3.

di-*O*-acetyl derivative **23′**, in which the H-5 signal appeared at δ 5.32 as a triplet with $J_{4,5}=J_{5,6}=3$ Hz and the H-4 (H–C–N_3) signal appeared at δ 4.09 as a triplet with $J_{3,4}=J_{4,5}=3$ Hz. The structures of **22** and **22′** were confirmed by the ^{1}H NMR spectra (400 MHz) of compounds **24** and **24′**, which were prepared from **22** and **22′** by hydrogenation in the presence of 10% palladium on charcoal and successive acetylation (**24** from **22**, 71%, and **24′** from **22′**, 80%). In the ^{1}H NMR spectrum of **24**, the H-4 signal (H–C–NHAc) appeared at δ 4.47 with $J_{3,4}=J_{4,5}=2.9$ Hz and $J_{NH,4}=7.8$ Hz, which changed to a triplet ($J=2.9$ Hz) on adding D_2O. The H-3 signal appeared at δ 5.20 as a double triplet with $J_{2ax,3}=12.2$ Hz and $J_{2eq,3}=J_{3,4}=2.9$ Hz and H-5 signal appeared at δ 5.59 as a triplet with $J_{4,5}=J_{5,6}=2.9$ Hz. This fact indicated that the acetamido group located at C-4 axially and the acetoxyl groups at C-3 and C-5 were equatorial- and axial-orientation. Therefore, two possibilities that 1) azidolysis of **9** proceeded via a neighboring group participation of the hydroxyl group in the epoxide ring opening, and 2) attack of the azide anion at C-3 in a diaxial opening manner of

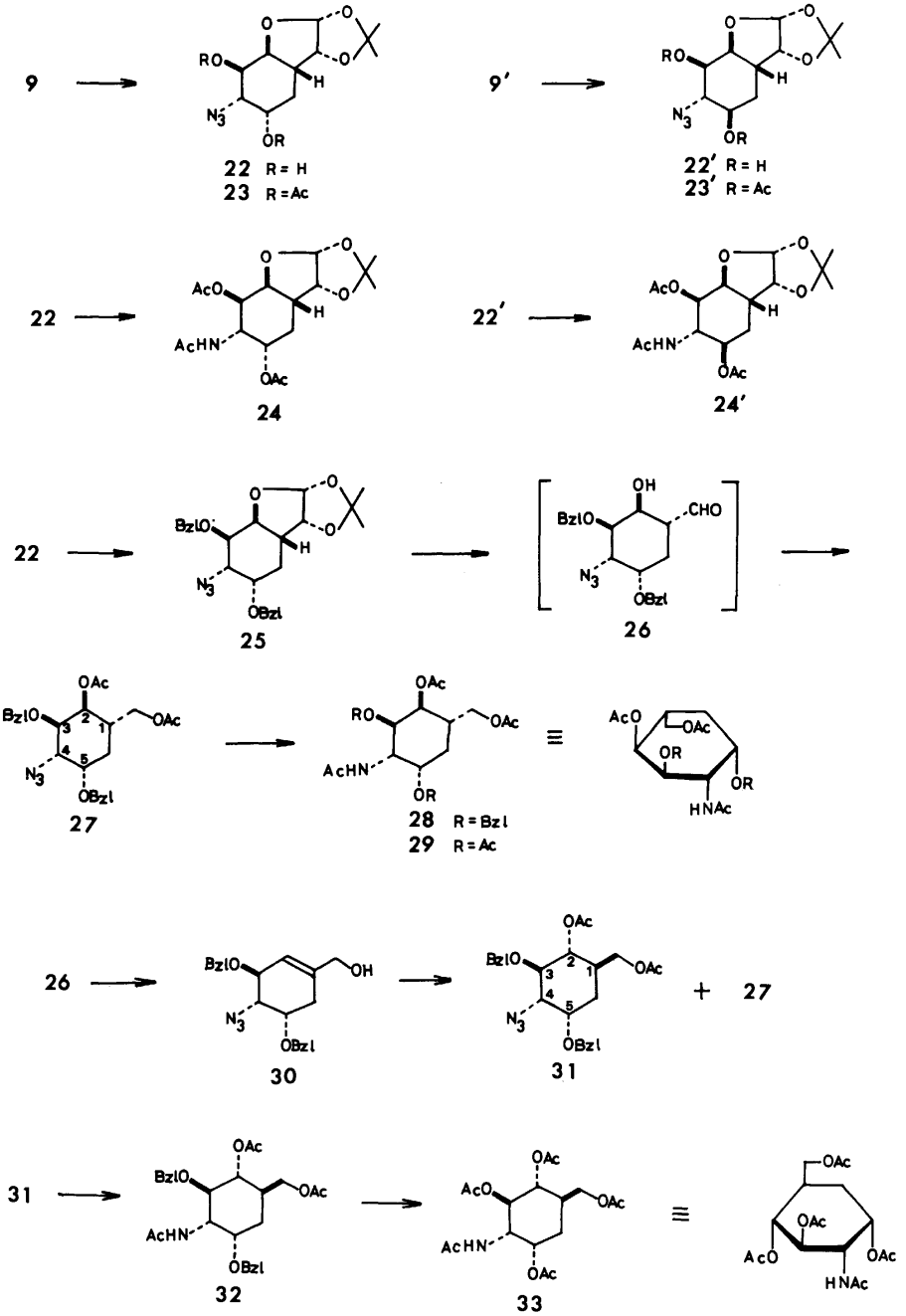

Scheme 4.

the formed 3,4-epoxide were excluded. The azidolysis of **9** proceeded in a diaxial ring opening manner without migration of the epoxide providing **22** exclusively. The ^{1}H NMR spectrum of **24'** was also consistent with the assigned structure. The H-4 signal appeared at δ 4.43 as a broad doublet with $J_{NH,4}$= 8.3 Hz, which changed to a broad singlet (less than 3 Hz for $J_{3,4}$ and $J_{4,5}$). The H-3 appeared at δ 5.00 with less than 3 Hz coupling constants for $J_{2ax,3}$, $J_{2eq,3}$, and $J_{3,4}$. Consequently, compound **22'** was a diaxial ring opening product of **9'**. The compounds **22** and **22'** were considered to be promising precursors for pseudo-2-amino-2-deoxy sugars. The conversion of **22** to two pseudo-amino sugars proceeded as follows. *O*-Benzylation of the compound **22** gave a di-*O*-benzyl derivative **25** in 82% yield. By the reaction sequence described for transformation of **13** to **16**, [1) refluxing in 1 mol dm^{-3} aqueous HCl, 2) sodium borohydride reduction, 3) periodate glycol cleavage, 4) sodium borohydride reduction, and 5) acetylation], the compound **25** was converted to (1*S*,2*S*,3*R*,4*S*,5*S*)-2-acetoxy-1-acetoxymethyl-4-azido-3,5-bis(benzyloxy)cyclohexane (**27**) in 56% overall yield via compound **26**. Hydrogenation of **27** in the presence of Raney nickel and successive acetylation gave an acetamido derivative **28** in 80% yield. *O*-Debenzylation of **28** by hydrogenolysis followed by acetylation afforded pentaacetyl derivative of pseudo-2-amino-2-deoxy-β-L-altropyranose **29** in 96% yield.

Treatment of compound **26**, which was prepared from **25**, with excess methanesulfonyl chloride for formation of an α,β-unsaturated aldehyde and successive diisobutylaluminium hydride reduction afforded (3*S*,4*S*,5*S*)-4-azido-3,5-bis(benzyloxy)-1-cyclohexene-1-methanol (**30**) in 27% yield from **25**. Hydroboration of **30** with borane–THF complex at 0 °C, oxidative work-up with 35% aqueous hydrogen peroxide in an alkaline solution, and successive acetylation provided a pseudo-α-D-glucopyranose derivative **31** and **27** in 21 and 49% yield, respectively. The hydroboration of **30** proceeded from the less hindered side providing **27** as a major product. In this case, the configuration of the 5-*O*-benzyl group was presumably a stereocontrolling factor. Hydrogenation of **31** followed by acetylation afforded compound **32** in 66% yield. *O*-Debenzylation of **32** and successive acetylation provided the pentaacetyl derivative **33** of pseudo-2-amino-2-deoxy-α-D-glucopyranose in 92% yield. Compound **33** is a derivative of pseudo-glucosamine.[17]

Experimental

General. Evaporations were performed under diminished pressure below 40 °C (bath). Melting points were determined with a Mitamura Riken micro mp apparatus and are uncorrected. Specific rotations were measured in a 10 mm cell with a Jasco DIP-4 polarimeter. Column chromatography was performed on Kieselgel 60 (Merck), and thin-layer chromatography (TLC) was performed on a glass plate coated with Kieselgel 60 GF_{254} (Merck) followed by detection by UV light and charring with sulfuric acid. Preparative TLC (PTLC) was performed on a glass plate (20×20 cm) coated with Kieselgel PF_{254} (Merck) and the compounds were extracted with $CHCl_3$. IR spectra were recorded with a Hitachi Model 225 (KBr) or with a Jasco Model A-202 ($CHCl_3$) spectrometer. ^{1}H NMR spectra were recorded with a Varian EM-390 (90 MHz) or with a JEOL JNM-GX FT NMR for compounds **24** and **24'** (400 MHz) spectrometer for solutions in $CDCl_3$ (internal standard Me_4Si). High resolution mass spectra were obtained using a Hitachi Model M-80 spectrometer. Elemental analyses were performed by Messrs. Saburo Nakada and Akio Takahashi of the university to whom our thanks are due.

Dichloromethane and benzene were dried over CaH_2, then distilled. Pyridine was distilled from NaOH. Tetrahydrofuran (THF) was distilled from $LiAlH_4$.

Mixture of (*E*)- and (*Z*)-3-*C*-Acetylmethylene-3-deoxy-1,2:5,6-di-*O*-isopropylidene-α-D-*ribo*-hexofuranose (2). An approximately 3 to 1 [(*Z*) to (*E*)] mixture, **2**, was prepared according to the reported procedure.[11] A mixture of 1,2:5,6-di-*O*-isopropylidene-α-D-*ribo*-hexofuranos-3-ulose (**1**) (8.93 g, 34.6 mmol) and (acetylmethylene)triphenylphosphorane (22.0 g, 69.2 mmol) in benzene (150 ml) was refluxed for 2 h and evaporated. The residue was partitioned between ethyl acetate (500 ml) and water (250 ml). The aqueous layer was extracted with ethyl acetate (500 ml×2). The organic layers were dried (Na_2SO_4) and evaporated. The residue was triturated with petroleum ether (450 ml) at 40 °C and cooled at 5 °C overnight. The precipitated triphenylphosphine oxide was removed by filtration, and the filtrate was evaporated. The residue was chromatographed on silica gel (220 g, ethyl acetate–toluene=1:20). Fractions corresponding to R_f 0.55 to 0.60 (ethanol–toluene=1:10) were evaporated to afford the mixture **2** (9.88 g, 96%) as a colorless syrup.

3-*C*-Acetylmethyl-3-deoxy-1,2:5,6-di-*O*-isopropylidene-α-D-allofuranose (3). A solution of the mixture **2** (9.88 g, 33.1 mmol) in methanol (50 ml) was hydrogenated in the presence of Raney nickel T-4 (ca. 6 g) under atmospheric hydrogen pressure at ambient temperature for 20 h. The catalyst was removed by filtration through a Celite-pad and washed with methanol. The combined filtrate and washing were evaporated to afford a diastereomeric mixture of 3-deoxy-3-*C*-(2-hydroxypropyl)-1,2:5,6-di-*O*-isopropylidene-α-D-allofuranose (TLC R_f 0.24 and 0.29, ethyl acetate–hexane=1:2, 10.3 g) as a colorless syrup. To a solution of the mixture in dichloromethane (150 ml) were added PCC (17.8 g, 82.8 mmol) and molecular sieves (3A, powder, 15.0 g). After stirring at the ambient temperature for 18 h, the mixture was diluted with ether (150 ml), then stirred for 1 h. The mixture was applied to a silica-gel column (200 g), and the column was eluted with ether (3 l). The eluate was evaporated and the residue was chromatographed on silica gel (200 g, ethyl acetate–toluene=1:15). Fractions corresponding to R_f 0.47 (ethyl acetate–toluene=1:2) were evaporated to afford **3** as a colorless syrup which was crystallized gradually upon standing at 5 °C, 8.77 g (88%). Mp 36.5—37 °C; $[\alpha]_D^{20}$ +82.1° (*c* 1.35, $CHCl_3$); IR $\nu_{max}^{CHCl_3}$ 3000, 2950, 2890, 1720, 1455, 1410, 1380, 1250, 1215, 1165, 1100, 1065 cm^{-1};

^{1}H NMR ($CDCl_3$) δ=1.27, 1.30, 1.40, 1.47 (3H×4, each s, 2×C(CH_3)$_2$), 2.17 (3H, s, $COCH_3$), 2.25—2.60 (1H, m, H-3), 2.67—2.93 (2H, m, CH_2COCH_3), 3.40—4.23 (4H, m, H-4,5,6,6'), 4.77 (1H, t, J=4.5 Hz, H-2), 5.75 (1H, d, J=4.5 Hz, H-1). Found: C, 59.77; H 8.02%. Calcd for $C_{15}H_{24}O_6$: C, 59.98; H, 8.05%.

3-*C*-Acetylmethyl-3-deoxy-1,2-*O*-isopropylidene-α-D-allofuranose (4). A solution of **3** (8.26 g, 28.0 mmol) in 60% aqueous acetic acid (120 ml) was stirred at the ambient temperature for 17 h and evaporated. The residue was chromatographed on silica gel (230 g, ethanol-toluene=1:12). Fractions corresponding to R_f 0.11 (ethyl acetate-toluene=1:2) were evaporated to afford **4** (7.00 g, 98%) as crystals, mp 69—69.5 °C; $[\alpha]_D^{24}$ +79.7° (*c* 1.82, $CHCl_3$); IR $\nu_{max}^{CHCl_3}$ 3450, 2980, 2930, 1715, 1405, 1370, 1245, 1215, 1165 cm^{-1}; ^{1}H NMR ($CDCl_3$) δ=1.23, 1.43 (3H×2, each s, C(CH_3)$_2$), 2.13 (3H, s, $COCH_3$), 2.20—2.60 (1H, m, H-3), 2.81 (2H, d, J=6 Hz, CH_2COCH_3), 2.93—3.90 (6H, m, H-4,5,6,6',2×OH), 4.70 (1H, t, J=4.5 Hz, H-2), 5.73 (1H, d, J=4.5 Hz, H-1). Found: C, 55.47; H, 7.52%. Calcd for $C_{12}H_{20}O_6$: C, 55.37; H, 7.75%.

(1*R*,6*R*,8*R*,9*R*)-8,9-Isopropylidenedioxy-7-oxabicyclo[4.3.0]-non-4-en-3-one (6). To a stirred solution of **4** (11.1 g, 42.6 mmol) in methanol (200 ml), an aqueous (50 ml) solution of sodium periodate (10.0 g, 46.9 mmol) was added. After stirring at the ambient temperature for 30 min, the solution was evaporated to ca.50 ml, then diluted with water (300 ml). The aqueous solution was extracted with dichloromethane (500 ml×3). The aqueous layer was saturated with NaCl and extracted with dichloromethane (400 ml×2). The combined organic layers were dried (Na_2SO_4) and evaporated to afford a TLC homogeneous **5** (10.2 g, quantitatively) as a colorless syrup, which was subjected to the next step without purification. **5**: TLC, R_f 0.52, ethanol-toluene=1:5; ^{1}H NMR ($CDCl_3$) δ=1.30, 1.48 (3H×2, each s, C(CH_3)$_2$), 2.17 (3H, s, $COCH_3$), 2.25—2.67 (1H, m, H-3), 2.67—3.00 (2H, m, CH_2COCH_3), 3.33—4.15 (1H, m, H-4), 4.47—4.93 (1H, m, H-2), 5.67—6.03 (1H, m, H-1), 9.67 (1H, d, J=3 Hz, CHO).

A solution of **5** (10.2 g, 42.6 mmol) in benzene (200 ml) containing DBU (0.33 ml, 2.24 mmol) was refluxed for 35 h and evaporated. The residue was dissolved in pyridine (50 ml) and acetic anhydride (50 ml) was added. The mixture was stirred for 19 h and evaporated. The residue was dissolved in water (300 ml) and extracted with dichloromethane (600 ml×3). The extracts were dried (Na_2SO_4) and evaporated. The residue was chromatographed on silica gel (500 g, ethyl acetate-hexane=1:6). Fractions corresponding to R_f 0.50 (ethanol-toluene=1:10) were evaporated to afford **6** (4.01 g, 45%) as crystals, mp 61—62 °C (from hexane); $[\alpha]_D^{17}$ −45.3° (*c* 0.92, $CHCl_3$); IR $\nu_{max}^{CHCl_3}$ 3050, 2980, 2850, 1675, 1600, 1450, 1380, 1335, 1295, 1255, 1210, 1160, 1140 cm^{-1}; ^{1}H NMR ($CDCl_3$) δ=1.35, 1.53 (3H×2, each s, C(CH_3)$_2$), 1.90—2.35 (1H, m, H-1), 2.35—3.00 (2H, m, H-2,2'), 4.47—4.80 (2H, m, H-6,9), 5.73—6.10 (2H, m, H-4,8), 7.28 (1H, d, J=9 Hz, H-5). Found: C, 62.96, H, 6.80%. Calcd for $C_{11}H_{14}O_4$:C, 62.85; H, 6.71%.

(1*R*,6*R*,8*R*,9*R*)-8,9-Isopropylidenedioxy-7-oxabicyclo[4.3.0]-nonan-3-one (7). A solution of **6** (40.0 mg, 0.19 mmol) in ethanol (2 ml) was hydrogenated in the presence of Raney nickel T-4 under hydrogen at atmospheric pressure for 2 h. After removal of the catalyst through a Celite-pad, the filtrate was evaporated to afford a syrupy diastereomeric mixture of (1*R*,6*R*,8*R*,9*R*)-8,9-isopropylidenedioxy-7-oxabicyclo[4.3.0]nonan-3-ol, which was oxidized without purification. To a stirred solution of the mixture in dichloromethane (2 ml) was added PCC (102 mg, 0.48 mmol). After stirring at ambient temperature for 15 h, the mixture was evaporated. The residue was applied to a silica-gel column (3 g), and the column was eluted with ether to afford **7** (33.2 mg, 82%), TLC R_f=0.66 (ethanol-toluene=1:5); mp 98—98.5 °C; $[\alpha]_D^{21.5}$ −33.7° (*c* 1.66, $CHCl_3$); IR $\nu_{max}^{CHCl_3}$ 2980, 2875, 1710, 1450, 1415, 1375, 1325, 1305, 1270, 1245, 1210, 1165, 1150, 1120, 1095 cm^{-1}; ^{1}H NMR ($CDCl_3$) δ=1.35, 1.57 (3H×2, each s, C(CH_3)$_2$), 1.59—2.05 (2H, m, 5,5'), 2.10—2.73 (5H, m, H-1,2,2',4,4'), 4.10 (1H, dt, $J_{1,6}$=$J_{5ax,6}$= 10.5Hz, $J_{5eq,6}$=4.5 Hz, H-6), 4.60 (1H, t, $J_{1,9}$=$J_{8,9}$=4 Hz, H-9), 5.93 (1H, d, $J_{8,9}$=4 Hz, H-8). Found: C, 62.01; H, 7.42%. Calcd for $C_{11}H_{16}O_4$: C, 62.25; H, 7.60%.

(1*R*,4*S*,5*S*,6*S*,8*R*,9*R*)-4,5-Epoxy-8,9-isopropylidenedioxy-7-oxabicyclo[4.3.0]nonan-3-one (8) and the (1*R*,4*R*,5*R*,6*S*,8*R*, 9*R*) stereomer (8'). To a stirred solution of **6** (450 mg, 2.14 mmol) in methanol (3 ml), hydrogen peroxide (35 wt% aqueous solution, 0.56 ml, 6.42 mmol) and an aqueous NaOH solution (1 mol dm^{-3}, 0.07 ml) (pH 9) were added. After stirring at the ambient temperature for 3 h, the mixture was diluted with water (10 ml) and extracted with ethyl acetate (30 ml×5). The extracts were dried (Na_2SO_4) and evaporated. The residue was chromatographed on silica gel (35 g, ethyl acetate-hexane=1:12). Fractions corresponding to R_f 0.62 (ethanol-toluene=1:10) were evaporated to afford **8** (467 mg, 96%) as a colorless syrup, and fractions corresponding to R_f 0.52 were evaporated to afford **8'** (16 mg, 3%) as a colorless syrup. **8**:$[\alpha]_D^{18.5}$ −108.8° (*c* 1.77, $CHCl_3$); IR $\nu_{max}^{CHCl_3}$ 2980, 2940, 2870, 1715, 1450, 1410, 1375, 1320, 1300, 1260, 1210, 1160, 1085 cm^{-1}; ^{1}H NMR ($CDCl_3$) δ=1.32, 1.50 (3H×2, each s, C(CH_3)$_2$), 2.28—2.76 (3H, m, H-1,2,2'), 3.37 (1H, d, J=5 Hz, H-5), 3.90 (1H, d, J=5 Hz, H-4), 4.30 (1H, d, J=10.5 Hz, H-6), 4.57 (1H, t, J=3.5 Hz, H-9), 5.94 (1H, d, J=3.5 Hz, H-8). High-resolution mass spectrum, calcd for $C_{11}H_{15}O_5$: *m/z* 227.0918, found: M+H, 227.0917. **8'**: $[\alpha]_D^{17}$ −11.0° (*c* 0.82, $CHCl_3$); IR $\nu_{max}^{CHCl_3}$ 2990, 2940, 2870, 1715, 1450, 1415, 1375, 1300, 1260, 1240, 1210, 1160, 1115 cm^{-1}; ^{1}H NMR ($CDCl_3$) δ=1.31, 1.52 (3H×2, each s, C(CH_3)$_2$), 1.73—2.18 (1H, m, H-1), 2.42—2.73 (2H, m, H-2,2'), 3.19 (1H, d, J=4 Hz, H-5), 3.79 (1H, d, J=4 Hz, H-4), 4.05 (1H, d, J=10.5 Hz, H-6), 4.57 (1H, t, J=3.5 Hz, H-9), 5.91 (1H, d, J=3.5 Hz, H-8).

(1*R*,3*S*,4*R*,5*S*,6*S*,8*R*,9*R*)- (9) and (1*R*,3*R*,4*R*,5*S*,6*S*,8*R*,9*R*)-(9') 4,5-Epoxy-8,9-isopropylidenedioxy-7-oxabicyclo[4.3.0]nonan-3-ol. The compound **6** (991 mg, 4.72 mmol) was converted to **8** containing a trace of **8'** as described above. The syrupy crude **8** was dissolved in ethanol (10 ml) and sodium borohydride (176 mg, 4.65 mmol) was added. After stirring at 0 °C for 40 min, the mixture was neutralized by addition of 1 mol dm^{-3} HCl, then evaporated. The residue was triturated with chloroform (20 ml) and an insoluble solid was removed by filtration. The filtrate was evaporated and the residue was chromatographed on silica gel (110 g, ethyl acetate-hexane=1:3). Fractions corresponding to R_f 0.29 (ethyl acetate-hexane=1:1) were evaporated to afford **9** (758 mg, 70%) as a colorless syrup, and fractions corresponding to R_f 0.16 were evaporated to afford **9'** (153 mg, 14%) as crystals. **9**: $[\alpha]_D^{27}$ +26.1° (*c* 1.05, $CHCl_3$); IR $\nu_{max}^{CHCl_3}$ 3600, 2990, 2930, 2880, 1450, 1390, 1370, 1300, 1240, 1170,

1130, 1070, 1050 cm^{-1}; ^{1}H NMR ($CDCl_3$) δ=1.36, 1.55 (3H×2, each s, $C(CH_3)_2$), 1.47—2.47 (3H, m, H-1,2,2′), 2.62 (1H, br s, OH), 3.25 (1H, d, $J_{4,5}$=4 Hz, $J_{3,4}$=0 Hz, H-4), 3.67 (1H, d, $J_{4,5}$=4 Hz, $J_{5,6}$=0 Hz, H-5), 4.21 (1H, $J_{1,6}$=10.5 Hz, $J_{5,6}$=0 Hz, H-6), 4.05—4.40 (1H, m, H-3; changed to triplet with $J_{2,3}$=$J_{2',3}$=8 Hz, $J_{3,4}$=0 Hz centered at δ 4.15 by addition of D_2O), 4.57 (1H, t, J=4 Hz, H-9), 5.87 (1H, d, J=4 Hz, H-8). High-resolution mass spectrum, calcd for $C_{11}H_{17}O_5$: m/z 229.1075, found: M+H, 229.1078. **9′**: mp 141—144 °C; $[\alpha]_D^{27}$ +63.2° (c 0.89, $CHCl_3$); IR ν_{max}^{KBr} 3490, 2980, 2930, 2860, 1460, 1440, 1410, 1390, 1380, 1280, 1250, 1210, 1170, 1150, 1130, 1085, 1015 cm^{-1}; ^{1}H NMR ($CDCl_3$) δ=1.30, 1.48 (3H×2, each s, $C(CH_3)_2$), 1.60—2.21 (3H, m, H-1,2,2′), 2.67 (1H, br s, OH), 3.44 (1H, t, $J_{3,4}$=$J_{4,5}$=4 Hz, H-4), 3.72 (1H, d, $J_{4,5}$=4 Hz, $J_{5,6}$=0 Hz, H-5), 4.04 (1H, d, $J_{1,6}$=10 Hz, $J_{5,6}$=0 Hz, H-6), 4.13—4.37 (1H, m, H-3; changed to triplet with J=4 Hz centered at δ 4.24 by addition of D_2O), 4.53 (1H, t, J=4 Hz, H-9), 5.84 (1H, d, J=4 Hz, H-8). Found: C,57.62; H, 7.09%. Calcd for $C_{11}H_{16}O_5$: C, 57.88; H, 7.06%.

(1*R*,3*S*,4*R*,5*S*,6*S*,8*R*,9*R*)-3-Acetoxy-4,5-epoxy-8,9-isopropylidenedioxy-7-oxabicyclo[4.3.0]nonane (10). The compound **9** (33 mg, 0.14 mmol) was acetylated with acetic anhydride (1 ml) and pyridine (1 ml) for 3 h. After removal of the reagents, the residue was chromatographed on silica gel (2 g, ethyl acetate–hexane=1:8) to give **10** (TLC R_f=0.32, ethanol–toluene=1:10) (19 mg, 50%) as a colorless syrup, $[\alpha]_D^{27}$ +50.1° (c0.77, $CHCl_3$); IR $\nu_{max}^{CHCl_3}$ 2980, 2930, 1740, 1455, 1370, 1220, 1165, 1130, 1110, 1055 cm^{-1}; ^{1}H NMR ($CDCl_3$) δ=1.30, 1.50 (3H×2, each s, $C(CH_3)_2$), 1.58—2.58 (3H, m, H-1,2,2′), 2.09 (3H, s, $OCOCH_3$), 3.15 (1H, d, $J_{4,5}$=4 Hz, $J_{3,4}$=0 Hz, H-4) 3.61 (1H, d, $J_{4,5}$=4 Hz, $J_{5,6}$=0 Hz, H-5), 4.15 (1H, d, $J_{1,6}$=10 Hz, $J_{5,6}$=0 Hz, H-6), 4.52 (1H, t, J=4 Hz, H-9), 5.11 (1H, t, $J_{2,3}$=$J_{2',3}$=8.5 Hz, $J_{3,4}$=0 Hz, H-3), 5.83 (1H, d, J=4 Hz, H-8). High-resolution mass spectrum, calcd for $C_{13}H_{19}O_6$: m/z 271.1180, found: M+H, 271.1209.

(1*R*,3*R*,4*R*,5*S*,6*S*,8*R*,9*R*)-3-Acetoxy-4,5-epoxy-8,9-isopropylidenedioxy-7-oxabicyclo[4.3.0]nonane (10′). The compound **9′** (29 mg, 0.13 mmol) was acetylated with acetic anhydride (1 ml) and pyridine (1 ml) for 3 h. After removal of the reagents, the residue was chromatographed on silica gel (2 g, ethyl acetate–hexane=1:8) to give **10′** (R_f=0.32, ethanol–toluene=1:10) (25 mg, 73%), mp 136—138 °C; $[\alpha]_D^{27}$ +84.6° (c 1.04 $CHCl_3$); IR ν_{max}^{KBr} 2990, 1725, 1375, 1320, 1280, 1245, 1210, 1165, 1150, 1125, 1100, 1075, 1050 cm^{-1}; ^{1}H NMR ($CDCl_3$) δ=1.30, 1.50 (3H×2, each s, $C(CH_3)_2$), 1.66—2.32 (3H, m, H-1,2,2′), 2.11 (3H, s, $OCOCH_3$), 3.52 (1H, t, $J_{3,4}$=$J_{4,5}$=4 Hz, H-4), 3.60 (1H, d, $J_{4,5}$=4 Hz, $J_{5,6}$=0 Hz, H-5), 4.06 (1H, d, $J_{1,6}$=10.5 Hz, $J_{5,6}$=0 Hz, H-6), 4.53 (1H, t, J=4 Hz, H-9), 5.25 (1H, q, $J_{2,3}$=$J_{2',3}$=$J_{3,4}$=4 Hz, H-3), 5.83 (1H, d, J=4 Hz, H-8). High-resolution mass spectrum, calcd for $C_{13}H_{19}O_6$: m/z 271.1180, found: M+H, 271.1178.

(1*R*,3*R*,4*S*,5*S*,6*S*,8*R*,9*R*)-8,9-Isopropylidenedioxy-7-oxabicyclo[4.3.0]nonane-3,4,5-triol (11). From **9**. A solution of **9** (153 mg, 0.67 mmol) in a mixture of 2-methoxyethanol and water (10:3, v/v, 7.5 ml) containing sodium acetate (110 mg, 1.34 mmol) was refluxed for 9 h and evaporated. The residue was chromatographed on silica gel (20 g, ethanol–hexane=1:9), and fractions corresponding to R_f 0.26 (ethanol–toluene=1:5) were evaporated to afford **11** (120 mg, 73%), mp 160—162 °C; $[\alpha]_D^{25}$ −6.6° (c 1.00, MeOH); IR ν_{max}^{KBr} 3420, 3250, 2990, 2940, 2910, 1450, 1380, 1370, 1265, 1210, 1170, 1140, 1105, 1075, 1025 cm^{-1}; ^{1}H NMR (CD_3OD) δ=1.32, 1.47 (3H×2, each s, $C(CH_3)_2$), 1.71—2.41 (3H, m, H-1,2,2′), 3.81—4.80 (8H, m, H-3,4,5,6,9, 3×OH), 5.79 (1H, d, J=4 Hz, H-8). Found: C, 49.66; H, 7.51%. Calcd for $C_{11}H_{18}O_6 \cdot H_2O$: C, 49.99; H, 7.63%.

From **9′**. A solution of **9′** (63 mg, 0.67 mmol) in a mixture of 2-methoxyethanol and water (10:3, 4 ml) containing sodium acetate (45 mg) was refluxed for 9 h and evaporated. After chromatographic purification as described above, **11** was obtained (55 mg, 81%).

(1*R*,3*R*,4*S*,5*S*,6*S*,8*R*,9*R*)-3,4,5-Triacetoxy-8,9-isopropylidenedioxy-7-oxabicyclo[4.3.0]nonane (12). A solution of **9** (85 mg, 0.37 mmol) in a mixture of 2-methoxyethanol and water (10:3, 5 ml) containing sodium acetate (61 mg) was refluxed for 8 h and evaporated. The residue was acetylated with acetic anhydride (5 ml) and pyridine (5 ml) for 12 h and evaporated. The residue was partitioned between dichloromethane (40 ml) and water (40 ml). The aqueous layer was extracted with dichloromethane (40 ml×2). The combined organic layers were dried (Na_2SO_4) and evaporated. The residue was chromatographed on silica gel (15 g, ethyl acetate–hexane=1:5), and fractions corresponding to R_f 0.77 (ethanol–toluene=1:5) were evaporated to afford **12** (112 mg, 80%), mp 56—58 °C; $[\alpha]_D^{26}$−7.8° (c 1.26, $CHCl_3$); IR ν_{max}^{KBr} 2985, 2940, 1755, 1745, 1440, 1375, 1250, 1170, 1125, 1115, 1085, 1030 cm^{-1}; ^{1}H NMR ($CDCl_3$) δ=1.32, 1.51 (3H×2, each s, $C(CH_3)_2$), 2.05 (3H, s, $OCOCH_3$), 2.08 (6H, s, 2×$OCOCH_3$), 1.84—2.48 (3H, m, H-1,2,2′), 4.00 (1H, dd, $J_{1,6}$=11 Hz, $J_{5,6}$=3 Hz, H-6), 4.60 (1H, t, J=4 Hz, H-9), 5.00 (1H, q, $J_{2,3}$=$J_{2',3}$=$J_{3,4}$=3 Hz, H-3), 5.12 (1H, t, $J_{4,5}$=$J_{5,6}$=3 Hz, H-5), 5.37 (1H, t, $J_{3,4}$=$J_{4,5}$=3 Hz, H-4), 5.83 (1H, d, J=4 Hz H-8). Found: C, 54.71; H, 6.39%. Calcd for $C_{17}H_{24}O_9$: C, 54.83; H, 6.50%.

(1*R*,3*R*,4*S*,5*S*,6*S*,8*R*,9*R*)-3,4,5-Tris(benzyloxy)-8,9-isopropylidenedioxy-7-oxabicyclo[4.3.0]nonane (13). A stirred suspension of sodium hydride (60% in mineral oil, 431 mg, 10.8 mmol, washed with hexane 10 ml×3 then dried) in dry DMF (5 ml) was added a DMF (10 ml) solution of **11** (442 mg, 1.79 mmol). After stirring for 15 min, benzyl bromide (1.28 ml, 10.8 mmol) was added. The mixture was stirred at ambient temperature for 16 h. The mixture was evaporated and the residue was partitioned between dichloromethane (60 ml) and water (60 ml). The aqueous layer was extracted with dichloromethane (60 ml×2). The organic layers were dried (Na_2SO_4) and evaporated. The residue was chromatographed on silica gel (50 g, ethyl acetate–hexane=1:12), and fractions corresponding to R_f 0.40 (ethyl acetate–hexane=1:5) were evaporated to afford **13** (858 mg, 93%) as a colorless syrup, $[\alpha]_D^{27}$ −0.8° (c 1.22, $CHCl_3$); IR $\nu_{max}^{CHCl_3}$ 3050, 3025, 2995, 2930, 2870, 1600, 1495, 1450, 1380, 1370, 1265, 1240, 1210, 1165, 1120, 1065 cm^{-1}; ^{1}H NMR ($CDCl_3$) δ=1.31, 1.48 (3H×2, each s, $C(CH_3)_2$), 1.79—2.67 (3H, m, H-1,2,2′), 3.69 (1H, q, $J_{2,3}$=$J_{2',3}$=$J_{3,4}$=3 Hz, H-3), 3.84 (1H, t, $J_{3,4}$=$J_{4,5}$=3 Hz or $J_{4,5}$=$J_{5,6}$=3 Hz, H-4 or H-5), 4.08 (1H, dd, $J_{1,6}$=11.5 Hz, $J_{5,6}$=3 Hz, H-6), 4.17 (1H, t, $J_{3,4}$=$J_{4,5}$=3 Hz or $J_{4,5}$=$J_{5,6}$=3 Hz, H-4 or H-5), 4.44—4.69 (6H, m, 3×$OCH_2C_6H_5$), 4.56 (1H, t, J=4 Hz, H-9), 5.84 (1H, d, J=4 Hz, H-8), 7.28 (15H, s, 3×$OCH_2C_6H_5$). High-resolution mass spectrum, calcd for $C_{32}H_{36}O_6$: m/z 516.2509, found: M, 516.2505.

(1*S*,2*S*,3*S*,4*S*,5*R*)-2-Acetoxy-1-acetoxymethyl-3,4,5-tris(benzyloxy)cyclohexane (16). A solution of **13** (648 mg, 1.26 mmol) in a mixture of 80% aqueous acetic acid (20 ml) and

1,4-dioxane (7 ml) was refluxed for 2 h and evaporated. The resulting crude *O*-deisopropylidene derivative (TLC, R_f= 0.41, ethanol-toluene=1:8) was used in the next step directly. To a stirred solution of the residue in methanol (30 ml) was added sodium borohydride (143 mg, 3.78 mmol) at 0 °C. After stirring at the same temperature for 3 h, 35% aqueous hydrogen peroxide (5 ml) was added. After stirring at 0 °C for 1 h, the solution was diluted with saturated aqueous sodium sulfite (25 ml), then acidified (pH 5) with 1 mol dm^{-3} HCl solution. The resulting white precipitate was removed by filtration and washed with ethanol (100 ml). The combined filtrate and washing were evaporated to ca. 20 ml and extracted with dichloromethane (50 ml×5). The extracts were dried (Na_2SO_4) and evaporated. The residue was chromatographed on silica gel (30 g, ethyl acetate-hexane=1:3, 1:2, 1:1, then ethyl acetate-ethanol=1:1). Fractions corresponding to R_f 0.35 (ethanol-toluene=1:8) were evaporated afford (1*R*)-1-[(1*S*,2*S*,3*S*,4*S*,5*R*)-3,4,5-tris-(benzyloxy)-2-hydroxycyclohexyl]-1,2-ethanediol (**14**) (419 mg) as a colorless syrup. To a stirred solution of **14** in methanol (9 ml), an aqueous (1.9 ml) solution of sodium periodate (207 mg, 0.97 mmol) was added. After stirring at the ambient temperature for 1 h, the precipitated solid was removed and the filtrate was evaporated. The residue was dissolved in water (10 ml) and extracted with dichloromethane (10 ml×4). The extracts were dried (Na_2SO_4) and evaporated to afford curde (1*R*,2*S*,3*S*,4*S*,5*R*)-3,4,5-tris(benzyloxy)-2-hydroxycyclohexanecarbaldehyde (**15**) as a colorless syrup, which was reduced directly. To a solution of **15** in ethanol (10 ml), sodium borohydride (73 mg, 1.93 mmol) was added. After stirring at the ambient temperature for 5 h, 35% aqueous hydrogen peroxide (3 ml) was added. After stirring for 1 h, saturated sodium sulfite (15 ml) and 1 mol dm^{-3} HCl (pH 7) were added. The solution was diluted with water (5 ml) and extracted with dichloromethane (100 ml×3, 80 ml×3). The combined extracts were dried (Na_2SO_4) and evaporated. The residue was acetylated with acetic anhydride (3 ml) in pyridine (3 ml) for 5 h. After evaporation of the mixture, the residue was chromatographed on silica gel (20 g, ethyl acetate-hexane=1:10). Fractions corresponding to R_f 0.67 (ethyl acetate-hexane=1:2) were evaporated to afford **16** (350 mg, 52%) as a colorless syrup, $[\alpha]_D^{26}$ −25.7° (*c* 0.74, $CHCl_3$); IR $\nu_{max}^{CHCl_3}$ 3060, 2900, 1735, 1495, 1450, 1365, 1230, 1110, 1085, 1070 cm^{-1}; ^{1}H NMR ($CDCl_3$) δ=1.87 (2H, dd, *J*=5 and 6.5 Hz, H-6,6′), 2.00, 2.06 (3H×2, each s, 2×OCOCH_3), 2.42 (1H, q, *J*=6 Hz, H-1), 3.47—3.82 (3H, m, H-3,4,5), 4.00 (2H, dd, *J*=2.5 and 6.5 Hz, CH_2OAc), 4.59 (4H, s, 2×OCH_2C$_6$H$_5$), 4.72 (2H, s, OCH_2C$_6$H$_5$), 5.28 (1H, dd, *J*=2.5 and 6 Hz, H-2), 7.30 (15H, s, 3×OCH$_2$C$_6$H$_5$). High-resolution mass spectrum, calcd for $C_{32}H_{36}O_7$: *m/z* 532.2466, fornd: M, 532.2459.

(1*S*,2*S*,3*S*,4*S*,5*R*)-2,3,4,5-Tetraacetoxy-1-(acetoxymethyl)-cyclohexane, Pentaacetate of Pseudo-α-L-altropyranose (17). Sodium (180 mg, 7.88 mmol) was added to a liquid ammonia (30 ml) at −78 °C. To the resulting blue solution, a THF (3 ml) solution of **16** (350 mg, 0.66 mmol) was added. After stirring at the same temperature for 25 min, 180 mg of sodium was added. The mixture was stirred for 3 h at −78 °C. Ammonium chloride (200 mg) was added to this, and the mixture was allowed to warm to the ambient temperature. The resulting solid was dried, then acetylated with acetic anhydride (7 ml) in pyridine (7 ml) for 5 h. The mixture was evaporated, and the residue was partitioned between ethyl acetate (50 ml) and water (10 ml). The aqueous layer was extracted with ethyl acetate (50 ml×3). The combined organic layers were dried (Na_2SO_4) and evaporated. The residue was chromatographed on silica gel (12 g, ethyl acetate-hexane=1:4) and fractions corresponding to R_f 0.49 (ethyl acetate-hexane=1:2) were evaporated to afford **17** (85 mg, 33%), mp 84—85 °C, $[\alpha]_D^{26.5}$ −13.7° (*c* 1.36, $CHCl_3$); IR $\nu_{max}^{CHCl_3}$ 2930, 2855, 1740, 1435, 1370, 1220, 1040 cm^{-1}; ^{1}H NMR ($CDCl_3$) δ=1.96 (2H, dd, *J*=5 and 6 Hz, H-6,6′), 2.00, 2.01, 2.04, 2.06, 2.08 (3H×5, each s, 5×OCOCH_3), 2.40 (1H, q, *J*=6 Hz, H-1), 4.15 (2H, d, *J*=6.5 Hz, CH_2OAc), 4.88—5.40 (4H, m, H-2,3,4,5). High-resolution mass spectrum, calcd for $C_{17}H_{25}O_{10}$: *m/z* 389.1446, found: M+H, 389.1463.

(3*S*,4*S*,5*R*)-3,4,5-Tris(benzyloxy)-1-cyclohexene-1-methanol (19). The compound **13** (945 mg, 1.83 mmol) was converted to the crude **15** (326 mg) as described in the preparation of **16**. To a stirred solution of the crude **15** in pyridine (7 ml) was added methanesulfonyl chloride (0.34 ml, 4.40 mmol). After stirring at ambient temperature for 24 h, the mixture was evaporated. The residue was diluted with water (25 ml) and extracted with dichloromethane (40 ml×3). The extracts were dried (Na_2SO_4) and evaporated to give crude α,β-unsaturated aldehyde (**18**) (TLC R_f=0.62, ethyl acetate-hexane=1:2), which was reduced without purification. To a stirred solution of the crude **18** (syrup) in ethanol (7 ml) was added sodium borohydride (51 mg, 1.35 mmol). After stirring at ambient temperature for 3.5 h, the mixture was evaporated. The residue was partitioned between dichloromethane (40 ml) and water (40 ml), and the aqueous layer was extracted with dichloromethane (40 ml×2). The organic layers were dried (Na_2SO_4) and evaporated. The residue was chromatographed on silica gel (30 g, ethyl acetate-hexane=1:10, 1:8, then 1:5). Fractions corresponding to R_f 0.34 (ethyl acetate-hexane=1:2) were evaporated to afford **19** (173 mg, 22% overall yield from **13**) as a colorless syrup, $[\alpha]_D^{26}$ +12.3° (*c* 1.11, $CHCl_3$); IR $\nu_{max}^{CHCl_3}$ 3590, 3000, 2910, 2870, 1590, 1490, 1450, 1360, 1080 cm^{-1}; ^{1}H NMR ($CDCl_3$) δ 1.54—1.80 (1H, m, OH), 1.90—2.64 (2H, m, H-6,6′), 3.63—4.26 (5H, m, H-3,4,5,CH_2OH), 4.50—5.00 (6H, m, 3×OCH_2C$_6$H$_5$), 5.52—5.80 (1H, m, H-2), 7.33 (15H, s, 3×OCH$_2$C$_6$H$_5$). High-resolution mass spectrum, calcd for $C_{28}H_{30}O_4$: *m/z* 430.2142, found: M, 430.2134.

(1*R*,2*R*,3*S*,4*S*,5*R*)-2-Acetoxy-1-acetoxymethyl-3,4,5-tris(benzyloxy)cyclohexane (20) and the (1*S*,2*S*,3*S*,4*S*,5*R*)-Stereoisomer 16. To a stirred solution of **19** (163 mg, 0.38 mmol) in THF (5 ml), borane-THF complex (1 mol dm^{-3} in THF, 1.33 ml, 1.33 mmol) at 0 °C was added under argon atmosphere. After stirring at 0 °C for 20 min, then at ambient temperature for 90 min, 0.20 ml (0.20 mmol) of the reducing reagent was added and stirred for another 1 h. After addition of water (0.8 ml), aqueous NaOH (3 mol dm^{-3}, 1.26 ml) and aqueous hydrogen peroxide (35%, 1.44 ml) were added successively. The mixture was stirred for 3 h, neutralized with 1 mol dm^{-3} HCl, and evaporated. The mixture was diluted with water (30 ml) and extracted with dichloromethane (40 ml×3). The extracts were dried (Na_2SO_4) and evaporated. The residue was acetylated with acetic anhydride (3 ml) in pyridine (3 ml) for 12 h, then evaporated. The residue was chromatographed on silica gel (20 g, ethyl acetate-hexane=1:6). Fractions corresponding

to R_f 0.74 (ethyl acetate-hexane=1:2) were evaporated to afford **16** (17 mg), and fractions corresponding to R_f 0.72 were evaporated to afford **20** (111 mg). In addition, a mixture of **16** and **20** (27 mg) was obtained, from which pure **16** (5 mg) and **20** (17 mg) were separated by repeated PTLC (ethyl acetate-hexane=1:5) [**16** (22 mg, 11%) and **20** (128 mg, 63%)]. **20**: Mp 56—57 °C; $[\alpha]_D^{24}$ +1.9° (*c* 1.03, $CHCl_3$); IR ν_{max}^{KBr} 3080, 2850, 1740, 1490, 1450, 1360, 1240 cm^{-1}; ^1H NMR ($CDCl_3$) δ 1.71—2.26 (3H, m, H-1,6,6'), 1.89, 2.01 (3H×2, each s, 2×$OCOCH_3$), 3.31—3.70 (3H, m, H-3,4,5), 3.86—4.17 (2H, m, CH_2OAc), 4.52—5.19 (7H, m, H-2, 3×$OCH_2C_6H_5$), 7.29, 7.32, 7.37 (15H, each s, 3×$OCH_2C_6H_5$). Found: C, 71.91; H, 6.77%. Calcd for $C_{32}H_{36}O_7$: C, 72.16; H, 6.81%.

(1*R*,2*R*,3*S*,4*S*,5*R*)-2,3,4,5-Tetraacetoxy-1-(acetoxymethyl)cyclohexane, Pentaacetate of Pseudo-β-D-glucopyranose (21). A solution of **20** (80 mg, 0.15 mmol) in methanol (2 ml) was hydrogenolyzed in the presence of 10% palladium on charcoal using a Parr apparatus for 14 h. The catalyst was removed by filtration, washed with methanol, and the filtrate and washing were combined, then evaporated. The residue was acetylated with acetic anhydride (1 ml) in pyridine (1 ml) for 7 h and evaporated. The residue was chromatographed on silica gel (6 g, ethyl acetate-hexane=1:4), and fractions corresponding to R_f 0.58 (ethyl acetate-hexane=1:1) were evaporated to afford **21** (57 mg, 98%), mp 114—116 °C, lit,[2] mp 115—116 °C; $[\alpha]_D^{23}$ +4.4° (*c* 1.23, $CHCl_3$), lit.,[2] $[\alpha]_D^{20}$ +13.8° (*c* 1.0, $CHCl_3$); IR ν_{max}^{KBr} 2860, 1740, 1430, 1370, 1230, 1030 cm^{-1}; ^1H NMR ($CDCl_3$) δ=1.23—2.60 (3H, m, H-1,6,6'), 1.97, 1.99, 2.02, 2.03 (3H, 3H, 6H, 3H, each s, 5×$OCOCH_3$), 3.84—4.26 (2H, m, CH_2OAc), 4.76—5.54 (4H, m, H-2,3,4,5). Found: C, 52.41; H, 6.08%. Calcd for $C_{17}H_{24}O_{10}$: C, 52.57; H, 6.23%.

(1*R*,3*S*,4*S*,5*R*,6*S*,8*R*,9*R*)-4-Azido-8,9-isopropylidenedioxy-7-oxabicyclo[4.3.0]nonane-3,5-diol (22). A solution of **9** (1.24 g, 5.43 mmol) in a mixture of 2-methoxyethanol and water (4:1, v/v, 20 ml) containing sodium azide (1.412 g, 21.7 mmol) and ammonium chloride (581 mg, 10.9 mmol) was refluxed for 4 h, and evaporated. To the residue, ethyl acetate (150 ml) was added and the mixture was stirred for 30 min. Insoluble material was removed by filtration through a Celite-pad, and the filtrate was evaporated to afford a crystalline **22**. Recrystallization from ethyl acetate and hexane gave 1.24 g (84%) of **22**, mp 172—173 °C; TLC R_f 0.18 (ethyl acetate-hexane=1:2); $[\alpha]_D^{27}$ +66.2° (*c* 1.00, MeOH); IR ν_{max}^{KBr} 3460, 3350, 3000, 2910, 2110, 1390, 1380, 1270, 1240, 1210, 1120 cm^{-1}. Found: C, 48.94; H, 6.34; N, 15.23%. Calcd for $C_{11}H_{17}N_3O_5$: C, 48.70; H, 6.32; N, 15.49%.

(1*R*,3*S*,4*S*,5*R*,6*S*,8*R*,9*R*)-3,5-Diacetoxy-4-azido-8,9-isopropylidenedioxy-7-oxabicyclo[4.3.0]nonane (23). The compound **22** (17 mg, 0.06 mmol) was acetylated with acetic anhydride (1 ml) in pyridine (1 ml) for 4 h. After removal of the reagents, the residue was chromatographed on silica gel (2 g, ethyl acetate-hexane=1:6). Fractions corresponding to R_f 0.48 (ethyl acetate-hexane=1:2) were evaporated to afford **23** (21 mg, 96%) as a colorless syrup, $[\alpha]_D^{28}$ +39.6° (*c* 0.89, $CHCl_3$); IR $\nu_{max}^{CHCl_3}$ 2990, 2930, 2110, 1750, 1390, 1380, 1250, 1210, 1130, 1120 cm^{-1}; ^1H NMR ($CDCl_3$) δ=1.31, 1.50 (3H×2, each s, $C(CH_3)_2$), 1.78—2.20 (3H, m, H-1,2,2'), 2.09 (6H, s, 2×$OCOCH_3$), 3.95 (1H, dd, *J*=10.5 and 3 Hz, H-6), 4.02 (1H, t, $J_{3,4}=J_{4,5}$=3 Hz, H-4), 4.54 (1H, t, *J*=4 Hz, H-9), 4.96—5.26 (1H, m, H-3), 5.38 (1H, t, $J_{4,5}=J_{5,6}$=3 Hz, H-5), 5.80 (1H, d, *J*=4 Hz, H-8).

(1R,3*R*,4*S*,5*R*,6*S*,8*R*,9*R*)-4-Azido-8,9-isopropylidenedioxy-7-oxabicyclo[4.3.0]nonane-3,5-diol (22'). A solution of **9'** (220 mg, 0.96 mmol) in a mixture of 2-methoxyethanol and water (4:1, v/v, 5 ml) containing sodium azide (251 mg, 3.86 mmol) and ammonium chloride (103 mg, 1.93 mmol) was refluxed for 6 h, and evaporated. To the residue, ethyl acetate (40 ml) was added and the mixture was stirred for 30 min. Insoluble material was removed by filtration through a Celite-pad, and the filtrate was evaporated to afford crystalline **22'**. Recrystallization from ethyl acetate gave 228 mg (87%) of **22'**, mp 157—159 °C; TLC R_f=0.61 (ethanol-toluene=1:4); $[\alpha]_D^{24}$ −22.0° (*c* 1.00, MeOH); IR ν_{max}^{KBr} 3420, 3260, 2990, 2900, 2110, 1440, 1390, 1380, 1310, 1250, 1220 cm^{-1}.

(1*R*,3*R*,4*S*,5*R*,6*S*,8*R*,9*R*)-3,5-Diacetoxy-4-azido-8,9-isopropylidenedioxy-7-oxabicyclo[4.3.0]nonane (23'). The compound **22'** (22 mg, 0.08 mmol) was acetylated with acetic anhydride (0.5 ml) in pyridine (1 ml) for 10 h. After removal of the reagents, the residue was chromatographed on silica gel (1.5 g, ethyl acetate-hexane=1:6). Fractions corresponding to R_f 0.40 (ethyl acetate-hexane=1:2) were evaporated to afford **23'** (27 mg, 94%) as crystals, mp 95—96 °C; $[\alpha]_D^{22}$ −17.2° (*c* 1.35, $CHCl_3$); IR $\nu_{max}^{CHCl_3}$ 2980, 2960, 2930, 2120, 1740, 1380, 1300, 1250, 1220, 1200 cm^{-1}; ^1H NMR ($CDCl_3$) δ=1.32, 1.51 (3H×2, each s, $C(CH_3)_2$), 1.80—2.44 (3H, m, H-1,2,2'), 2.05, 2.07 (3H×2, each s, 2×$OCOCH_3$), 3.95 (1H, dd, $J_{1,6}$=11.5 Hz and $J_{5,6}$=3 Hz), 4.09 (1H, t, $J_{3,4}=J_{4,5}$=3 Hz, H-4), 4.58 (1H, t, *J*=4 Hz, H-9), 5.04 (1H, q, $J_{2ax,3}=J_{2eq,3}=J_{3,4}$=3 Hz, H-3), 5.32 (1H, t, $J_{4,5}=J_{5,6}$=3 Hz, H-5), 5.81 (1H, d, *J*=4 Hz, H-8).

(1*R*,3*S*,4*S*,5*R*,6*S*,8*R*,9*R*)-4-Acetamido-3,5-diacetoxy-8,9-isopropylidenedioxy-7-oxabicyclo[4.3.0]nonane (24). A solution of **22** (87 mg, 0.32 mmol) in methanol (6 ml) was hydrogenated in the presence of 10% palladium on charcoal (40 mg) under atmospheric hydrogen pressure for 3 h. After removal of the catalyst, the filtrate was evaporated. The residue was acetylated with acetic anhydride (1 ml) in pyridine (3 ml) for 10 h. The solution was evaporated, and the residue was chromatographed on silica gel (3 g, ethanol-toluene=1:30). Fractions corresponding to R_f 0.41 (ethanol-toluene=1:5) were evaporated to afford **24** (84 mg, 71%), mp 110—112 °C; $[\alpha]_D^{24}$ +9.5° (*c* 0.84, $CHCl_3$); IR $\nu_{max}^{CHCl_3}$ 2980, 2930, 1740, 1670, 1490, 1460, 1370, 1300, 1240 cm^{-1}; ^1H NMR (400 MHz, $CDCl_3$) δ 1.33, 1.53 (3H×2, each s, $(CH_3)_2$), 1.68 (1H, q, *J*=12.2 Hz, H-2ax), 2.03, 2.05, 2.09 (3H×3, each s, 2×$OCOCH_3$ and $NCOCH_3$), 1.99—2.18 (2H, m, H-1 and 2eq), 3.83 (1H, dd, $J_{1,6}$=11.2 Hz, $J_{5,6}$=2.9 Hz, H-6), 4.47 (1H, dt, $J_{3,4}=J_{4,5}$=2.9 Hz, $J_{NH,4}$=7.8 Hz, H-4, changed to t with *J*=2.9 Hz by D_2O), 4.58 (1H, t, $J_{1,9}=J_{8,9}$=3.4 Hz, H-9), 5.20 (1H, dt, $J_{2ax,3}$=12.2 Hz, $J_{2eq,3}=J_{3,4}$=2.9 Hz, H-3), 5.43 (1H, d, $J_{NH,3}$=7.8 Hz, NH), 5.59 (1H, t, $J_{4,5}=J_{5,6}$=2.9 Hz, H-5), 5.83 (1H, d, $J_{8,9}$=3.4 Hz, H-8). High-resolution mass spectrum, calcd for $C_{17}H_{25}NO_8$: *m/z* 371.1579, found: M, 371.1595.

(1*R*,3*R*,4*S*,5*R*,6*S*,8*R*,9*R*)-4-Acetamido-3,5-diacetoxy-8,9-isopropylidenedioxy-7-oxabicyclo[4.3.0]nonane (24'). The compound **22'** (100 mg, 0.37 mmol) was converted to **24'** (110 mg, 80%) as described in preparation of **24**. **24'** as a colorless syrup; TLC R_f 0.41 (ethanol-toluene=1:5); $[\alpha]_D^{25}$ −15.1° (*c* 1.32, $CHCl_3$); IR $\nu_{max}^{CHCl_3}$ 2990, 2940, 1740, 1680, 1490,

1440, 1370, 1300, 1240, 1200 cm^{-1}; ^1H NMR (400 MHz, $CDCl_3$) δ=1.34, 1.52 (3H×2, each, s, $(CH_3)_2$), 2.01, 2.07, 2.08 (3H×3, each s, 2×$OCOCH_3$ and $NCOCH_3$), 1.80—2.36 (3H, m, H-1 and H-2ax, 2-eq), 3.79 (1H, dd, $J_{1,6}$=11.2 Hz, $J_{5,6}$=2.9 Hz, H-6), 4.43 (1H, broad d, $J_{NH,4}$=8.3 Hz, changed to broad singlet with less than 3 Hz of $J_{3,4}$, $J_{4,5}$ by D_2O, H-4), 4.60 (1H, t, $J_{1,9}$=$J_{8,9}$=3.9 Hz, H-9), 5.00 (1H, q, $J_{2ax,3}$, $J_{2eq,3}$, $J_{3,4}$ less than 3 Hz, H-3), 5.37 (1H, broad singlet, $J_{4,5}$ less than 3 Hz, $J_{5,6}$=2.9 Hz, H-5), 5.47 (1H, d, $J_{NH,3}$=8.3 Hz, NH), 5.83 (1H, d, $J_{8,9}$=3.9 Hz, H-8). High-resolution mass spectrum, calcd for $C_{17}H_{25}NO_8$: m/z 371.1577, found: M, 371.1558.

(1*R*,3*S*,4*S*,5*R*,6*S*,8*R*,9*R*)-4-Azido-3,5-bis(benzyloxy)-8,9-isopropylidenedioxy-7-oxabicyclo[4.3.0]nonane (25). To a stirred suspension of sodium hydride (60%, 416 mg, 10.4 mmol, washed with hexane, then dried) in DMF (10 ml), a DMF (10 ml) solution of **22** (564 mg, 2.08 mmol) was added. After stirring for 20 min, benzylbromide (1.24 ml, 10.4 mmol) was added to the mixture. The mixture was stirred for 5 h at ambient temperature, then ethanol (10 ml) was added. After evaporation of the mixture, the residue was partitioned between dichloromethane (60 ml) and water (60 ml). The aqueous layer was extracted with dichloromethane (60 ml×2). The organic layers were dried (Na_2SO_4) and evaporated. The residue was chromatographed on silica gel (20 g, ethyl acetate–hexane=1:20), and fractions corresponding to R_f 0.40 (ethyl acetate–hexane=1:6) were evaporated to afford **25** (772 mg, 82%) as a colorless syrup, $[\alpha]_D^{27}$ +48.2° (*c* 1.02, $CHCl_3$); IR $\nu_{max}^{CHCl_3}$ 3000, 2930, 2880, 2110, 1450, 1390, 1380, 1270, 1170, 1140 cm^{-1}; ^1H NMR ($CDCl_3$) δ=1.30, 1.51 (3H×2, each s, $C(CH_3)_2$), 1.66—2.14 (3H, m, H-1,2,2′), 3.80—4.10 (4H, m, H-3,4,5,6), 4.43—4.88 (5H, m, H-9,2×$OCH_2C_6H_5$), 5.81 (1H, d, *J*=4 Hz, H-8), 7.32, 7.34 (10H, each s, 2×$OCH_2C_6H_5$). High-resolution mass spectrum, calcd for $C_{24}H_{26}N_3O_5$: m/z 436.1860, found: M−CH_3, 436.1870.

(1*S*,2*S*,3*R*,4*S*,5*S*)-2-Acetoxy-1-acetoxymethyl-4-azido-3,5-bis(benzyloxy)cyclohexane (27). A solution of **25** (600 mg, 1.33 mmol) in a mixture of 1 mol dm^{-3} HCl (2 ml) and 1,4-dioxane (8 ml) was refluxed for 30 min, neutralized with saturated aqueous $NaHCO_3$, then evaporated. To the residue, ethyl acetate (80 ml) was added and insoluble solids were removed by filtration through a Celite-pad. The filtrate was evaporated to afford crude *O*-deisopropylidene derivative. To a stirred solution of the residue in ethanol (10 ml), sodium borohydride (101 mg, 2.66 mmol) was added. The mixture was stirred at 0 °C for 1 h, diluted with water (2 ml), neutralized with 1 mol dm^{-3} HCl, and evaporated. To the residue, ethyl acetate (80 ml) was added, and insoluble solids were removed by filtration through a Celite-pad. The filtrate was evaporated to afford a foam. The foam was dissolved in methanol (10 ml), and an aqueous (2 ml) solution of sodium periodate (568 mg, 2.66 mmol) was added. The mixture was stirred at the ambient temperature for 1 h and evaporated. To the residue, ethyl acetate (60 ml) was added, and insoluble materials were removed. The filtrate was evaporated to afford crude (1*R*,2*S*,3*R*,4*S*,5*S*)-4-azido-3,5-bis(benzyloxy)-2-hydroxycyclohexanecarbaldehyde (**26**) (TLC R_f 0.70, ethanol–toluene=1:5). To a solution of the crude **26** in ethanol (10 ml), sodium borohydride (101 mg, 2.66 mmol) was added, and the mixture was stirred for 2 h. The mixture was diluted with water (2 ml), neutralized with 1 mol dm^{-3} HCl, and evaporated. To the residue, ethyl acetate (60 ml) was added, and insoluble solids were removed. The filtrate was evaporated. The residue was chromatographed on silica gel (20 g, toluene, then ethanol–toluene=1:5). Fractions corresponding to R_f 0.56 (ethanol–toluene=1:5) were evaporated to afford (1*S*,2*S*,3*R*,4*S*,5*S*)-4-azido-3,5-bis(benzyloxy)-2-hydroxycyclohexanemethanol as a colorless syrup, which was acetylated with acetic anhydride (4 ml) in pyridine (8 ml) for 10 h. The mixture was evaporated, and the residue was chromatographed on silica gel (35 g, ethyl acetate–hexane=1:8). Fractions corresponding to R_f 0.45 (ethyl acetate–hexane=1:3) were evaporated to afford **27** (348 mg, 56% from **25**) as a colorless syrup, $[\alpha]_D^{27}$ −29.1° (*c* 0.70, $CHCl_3$); IR $\nu_{max}^{CHCl_3}$ 2920, 2110, 1730, 1450, 1370, 1320, 1250, 1210 cm^{-1}; ^1H NMR ($CDCl_3$) δ=1.47—2.52 (3H, m, H-1,6,6′), 1.97, 2.02 (3H×2, each s, 2×$OCOCH_3$), 3.78—4.13 (5H, m, H-3,4,5, OH_2OAc), 4.34—4.72 (4H, m, 2×$OCH_2C_6H_5$), 4.92 (1H, dd, *J*=12 and 3 Hz, H-2), 7.30, 7.33 (10H, each s, 2×$OCH_2C_6H_5$).

(1*S*,2*S*,3*R*,4*S*,5*S*)-4-Acetamido-2-acetoxy-1-acetoxymethyl-3,5-bis(benzyloxy)cyclohexane (28). A solution of **27** (198 mg, 0.42 mmol) in ethanol (10 ml) was hydrogenated in the presence of Raney nickel T-4 under hydrogen at atmospheric pressure for 2 h. The catalyst was removed by filtration through a Celite-pad, and the filtrate was evaporated. The residue was acetylated with acetic anhydride (3 ml) in pyridine (6 ml) for 2 h. The mixture was evaporated, and the residue was chromatographed on silica gel (14 g, ethanol–toluene=1:20), and fractions corresponding to R_f 0.35 (ethanol–toluene=1:10) were evaporated to afford **28** (164 mg, 80%) as a colorless syrup, $[\alpha]_D^{24}$ −3.6° (*c* 1.10, $CHCl_3$); IR $\nu_{max}^{CHCl_3}$ 3000, 2930, 2870, 1730, 1670, 1490, 1450, 1370, 1250 cm^{-1}; ^1H NMR ($CDCl_3$) δ=1.44—2.58 (3H, m, H-1,6,6′), 1.91 (3H, s, $NCOCH_3$), 1.97, 2.02 (3H×2, each s, 2×$OCOCH_3$), 3.80—4.26 (4H, m, H-3,5, CH_2OAc), 4.34—4.74 (1H, m, H-4), 4.43, 4.62 (4H, each s, 2×$OCH_2C_6H_5$), 5.06 (1H, dd, *J*=9 and 3 Hz, H-2), 5.69 (1H, d, *J*=7 Hz, NH), 7.30, 7.33 (10H, each s, 2×$OCH_2C_6H_5$). High-resolution mass spectrum, calcd for $C_{27}H_{34}NO_7$: m/z 484.2333, found: M+H, 484.2317.

(1*S*,2*S*,3*R*,4*S*,5*S*)-4-Acetamido-2,3,5-triacetoxy-1-(acetoxymethyl)cyclohexane, Pentaacetate of Pseudo-2-amino-2-deoxy-β-L-altropyranose (29). A solution of **28** (140 mg, 0.29 mmol) in ethanol (10 ml) was hydrogenolyzed in the presence of palladium black in a Parr apparatus for 15 h. The catalyst was removed by filtration through a Celite-pad, and the filtrate was evaporated. The residue was acetylated with acetic anhydride (3 ml) in pyridine (8 ml) for 15 h. The mixture was evaporated, and the residue was chromatographed on silica gel (10 g, ethanol–toluene=1:20). Fractions corresponding to R_f 0.43 (ethanol–toluene=1:4) were evaporated to afford **29** (108 mg, 96%) as a colorless syrup, $[\alpha]_D^{18}$ +37.7° (*c* 0.87, $CHCl_3$); IR $\nu_{max}^{CHCl_3}$ 1760, 1670, 1500, 1370, 1230 cm^{-1}; ^1H NMR ($CDCl_3$) δ=1.57—2.52 (3H, m, H-1,6,6′), 1.94 (3H, s, $NCOCH_3$), 2.06 (12H, s, 4×$OCOCH_3$), 3.98—4.23 (2H, m, CH_2OAc), 4.40—4.70 (1H, m, H-4), 5.10—5.37 (3H, m, H-2,3.5), 5.95 (1H, d, *J*=9 Hz, NH). High-resolution mass spectrum, calcd for $C_{17}H_{25}NO_9$: m/z 387.1528, found: M, 387.1533.

(3*S*,4*S*,5*S*)-4-Azido-3,5-bis(benzyloxy)-1-cyclohexene-1-methanol (30). The compound **25** (802 mg, 1.78 mmol) was converted to the crude **26** as described in preparation of **27**. To the solution of the crude **26** in pyridine (20 ml) was

added methanesulfonyl chloride (0.57 ml, 7.11 mmol). The mixture was stirred at the ambient temperature for 8 h and evaporated. The residue was partitioned between dichloromethane (60 ml) and water (60 ml), and the aqueous layer was extracted with dichloromethane (60 ml×2). The organic layers were dried (Na_2SO_4) and evaporated to afford a brown syrup [main product, R_f 0.63 (ethyl acetate-hexane=1:3)]. To a solution of the syrup in dichloromethane (10 ml) was added diisobutylaluminium hydride (1.5 mol dm^{-3} in toluene, 9.47 ml, 14.2 mmol) at −15 °C. The resulting insoluble materials were removed through a Celite-pad and washed with ethyl acetate. The combined filtrate and washings were evaporated. The residue was chromatographed on silica gel (30 g, ethyl acetate-hexane=1:4), and fractions corresponding to R_f 0.31 (ethyl acetate-hexane=1:2) were evaporated to afford **30** (176 mg, 27% from **25**) as a colorless syrup, $[\alpha]_D^{22}$ +68.1° (*c* 1.39, $CHCl_3$); IR $\nu_{max}^{CHCl_3}$ 2920, 2860, 2110, 1350, 1260 cm^{-1}; ^{1}H NMR ($CDCl_3$) δ=1.57—1.84 (1H, m, OH), 2.20—2.39 (2H, m, H-6,6′), 3.68—4.25 (5H, m, H-3,4,5,C*H*$_2$OH), 4.62 (4H, s, 2×OC*H*$_2$C$_6$H$_5$), 5.66—5.80 (1H, m, H-2), 7.34 (10H, s, 2×OCH$_2$C$_6$*H*$_5$).

(1*R*,2*R*,3*R*,4*S*,5*S*)-2-Acetoxy-1-acetoxymethyl-4-azido-3,5-bis(benzyloxy)cyclohexane (31) and the (1*S*,2*S*,3*R*,4*S*,5*S*)-stereoisomer 27. To a solution of **30** (170 mg, 0.47 mmol) in THF (2 ml) was added borane-THF complex (1.0 mol dm^{-3} in THF, 1.86 ml, 1.86 mmol) at 0 °C under argon atmosphere. The mixture was stirred for 3 h, then hydrogen peroxide (35% aqueous solution, 4 ml) and 3 mol dm^{-3} NaOH (1 ml) were added. After stirring for 6 h, the solution was neutralized with 1 mol dm^{-3} HCl and diluted with water (20 ml). The aqueous solution was extracted with dichloromethane (30 ml×3). The extracts were dried (Na_2SO_4) and evaporated. The residue was acetylated with acetic anhydride (2 ml) in pyridine (4 ml) for 14 h and evaporated. The residue was chromatographed on silica gel (20 g, ethyl acetate-hexane=1:20). Fractions corresponding to R_f 0.61 (ethyl acetate-hexane=1:2) were evaporated to afford **27** (106 mg, 49%), and fractions corresponding to R_f 0.54 were evaporated to afford **31** (46 mg, 21%) as a colorless syrup. **31**: $[\alpha]_D^{18}$ +20.0° (*c* 0.75, $CHCl_3$); IR $\nu_{max}^{CHCl_3}$ 2920, 2100, 1730, 1450, 1360, 1250, 1200 cm^{-1}; ^{1}H NMR ($CDCl_3$) δ=1.16—2.57 (3H, m, H-1,6,6′), 1.92, 2.01 (3H×2, each s, 2×OCOC*H*$_3$), 3.23—3.47 (1H, m, H-5), 3.70—4.23 (4H, m, H-3,4, C*H*$_2$OAc), 4.46—5.30 (4H, m, 2×OC*H*$_2$C$_6$H$_5$), 5.01 (1H, t, *J*=9 Hz, H-2), 7.32, 7.37 (10H, each s, 2×OCH$_2$C$_6$*H*$_5$).

(1*R*,2*R*,3*R*,4*S*,5*S*)-4-Acetamido-2-acetoxy-1-acetoxymethyl-3,5-bis(benzyloxy)cyclohexane (32). A solution of **31** (43 mg, 0.09 mmol) in ethanol (4 ml) was hydrogenated in the presence of Raney nickel T-4 under hydrogen at atmospheric pressure for 1.5 h. After removal of the catalyst, the filtrate was evaporated. The residue was acetylated with acetic anhydride (1 ml) in pyridine (3 ml) for 2 h. The mixture was evaporated, and the residue was chromatographed on silica gel (3 g, ethanol-toluene=1:20). Fractions corresponding to R_f 0.56 (ethanol-toluene=1:6) were evaporated to afford **32** (29 mg, 66%), mp 154—156 °C (recrystallized from ethyl acetate); $[\alpha]_D^{18}$ +65.6° (*c* 0.90, $CHCl_3$); IR ν_{max}^{KBr} 1730, 1640, 1380, 1370, 1280, 1240 cm^{-1}; ^{1}H NMR ($CDCl_3$) δ=1.27—2.57 (3H, m, H-1,6,6′), 1.72 (3H, s, NCOC*H*$_3$), 2.00, 2.04 (3H×2, each s, 2×OCOC*H*$_3$), 3.55—4.74 (9H, m, H-3,4,5, C*H*$_2$OAc, 2×OC*H*$_2$C$_6$H$_5$), 5.08 (1H, dd, *J*=11 and 9 Hz, H-2), 5.46 (1H, d, *J*=8 Hz, NH), 7.30, 7.33 (10H, s, 2×OCH$_2$C$_6$*H*$_5$). High-resolution mass spectrum, calcd for $C_{27}H_{34}NO_7$: *m/z* 484.2333, found: M+H, 484.2345.

(1*R*,2*R*,3*R*,4*S*,5*S*)-4-Acetamido-2,3,5-triacetoxy-1-(acetoxymethyl)cyclohexane, Pentaacetate of Pseudo-2-amino-2-deoxy-α-D-glucopyranose (33). A solution of **32** (22 mg, 0.05 mmol) in ethanol (4 ml) was hydrogenolyzed in the presence of palladium-black in a Parr apparatus for 12 h. The catalyst was removed through a Celite-pad, and the filtrate was evaporated. The residue was acetylated with acetic anhydride (2 ml) in pyridine (4 ml) for 10 h. After evaporation of the mixture, the residue was chromatographed on silica gel (2 g, ethanol-toluene=1:15). Fractions corresponding to R_f 0.43 (ethanol-toluene=1:4) were evaporated to afford **33** (17 mg, 92%) as a colorless syrup, $[\alpha]_D^{23}$ +75.6° (*c* 0.81, $CHCl_3$); IR $\nu_{max}^{CHCl_3}$ 1740, 1670, 1510, 1380, 1370, 1240 cm^{-1}; ^{1}H NMR ($CDCl_3$) δ=1.14—2.66 (3H, m, H-1,6,6′), 1.90 (3H, s, NCOC*H*$_3$) 2.03, 2.05, 2.13 (6H, 3H, 3H, each s, 4×OCOC*H*$_3$), 3.72—4.38 (3H, m, H-4, C*H*$_2$OAc), 4.94—5.34 (3H, m, H-2,3,5), 5.83 (1H, d, *J*=10 Hz, NH). High-resolution mass spectrum, calcd for $C_{17}H_{25}NO_9$: *m/z* 387.1527, found: M, 387.1524.

The authors express their sincere thanks to Professor Seiichiro Ogawa of Keio University for his valuable discussion on the structural identification of the synthesized pseudo-sugars in the present work.

References

1) S. Ogawa, *Yuki Gosei Kagaku Kyokai Shi*, **43**, 26 (1985).
2) S. Ogawa, Y. Iwasawa, and T. Suami, *Chem. Lett.*, **1984**, 355; S. Ogawa, Y. Iwasawa, T. Nose, T. Suami, S. Ohba, M. Ito, and Y. Saito, *J. Chem. Soc., Perkin Trans. 1*, **1985**, 903.
3) H. Paulsen and F. R. Heiker, *Angew. Chem. Int. Ed. Engl.*, **19**, 904 (1980); *idem., Liebigs Ann. Chem.*, **1981**, 2180; *idem., Carbohydr. Res.*, **102**, 83 (1982).
4) H. Paulsen, W. v. Deyn, and W. Roben, *Liebigs Ann. Chem.*, **1984**, 433.
5) R. J. Ferrier and P. Prasit, *Pure Appl. Chem.*, **55**, 565 (1983) and references cited therein.
6) F. Sugawara and H. Kuzuhara, *Agric. Biol. Chem.*, **45**, 301 (1981).
7) C. S. Wilcox and L. M. Thomasco, *J. Org. Chem.*, **50**, 547 (1985).
8) C. S. Wilcox and J. J. Gaudino, *J. Am. Chem. Soc.*, **108**, 3102 (1986).
9) a) T. Suami, K. Tadano, Y. Kameda, and Y. Iimura, *Chem. Lett.*, **1984**, 1919; b) T. Suami, K. Tadano, Y. Ueno, and Y. Iimura, *Chem. Lett.*, **1985**, 37; c) K. Tadano, H. Maeda, M. Hoshino, Y. Iimura, and T. Suami, *Chem. Lett.*, **1986**, 1081; d) K. Tadano and T. Suami, *Yuki Gosei Kagaku Kyokai Shi*, **44**, 633 (1986).
10) A part of the present work was published in a preliminary form, T. Suami, K. Tadano, Y. Ueno, and C. Fukabori, *Chem. Lett.*, **1985**, 1557.
11) J. M. J. Tronchet and B. Gentile, *Carbohydr. Res.*, **44**, 23 (1975).
12) A. Rosenthal and M. Sprinzl, *Can. J. Chem.*, **47**, 3941

(1969).

13) M. Georges, T-F. Tam, and B. Fraser-Reid, *J. Org. Chem.*, **50**, 5747 (1985).

14) In previous papers, we incorrectly assigned the structures of compounds **9** and **9′**. The compounds **96** and **97** in reference 9d) and the compounds **9** (and **10**) and **9′** (and **10′**) in reference 10) should be interchanged.

15) T. Suami, S. Ogawa, T. Ishibashi, and I. Kasahara, *Bull. Chem. Soc. Jpn.*, **49**, 1388 (1976).

16) For DL-**21**: T. Suami, S. Ogawa, K. Nakamoto, and I. Kasahara, *Carbohydr. Res.*, **58**, 240 (1977); S. Ogawa, M. Ara, T. Kondoh, M. Saitoh, R. Masuda, T. Toyokuni, and T. Suami, *Bull. Chem. Soc. Jpn.*, **53**, 1121 (1980).

17) A derivative of pseudo-2-amino-2-deoxy-α-glucopyranose, tetra-*O*-acetyl-(1,2,4/3,5)-5-hydroxymethyl-2-(*p*-toluenesulfonamido)-1,3,4-cyclohexanetriol, was synthesized in a DL-form: S. Ogawa, T. Toyokuni, T. Kondoh, Y. Hattori, S. Iwasaki, M. Suetsugu, and T. Suami, *Bull. Chem. Soc. Jpn.*, **54**, 2739 (1981).

Aryliminodimagnesium Reagents. XI. Two-Electron Oxidation of the Reagent Molecules in the Reaction with Some Oxidizing Agents and with Strongly Push-Pull Substituted α-Benzylideneacetophenones

Masao Ōkubo,* Shunsei Yoshida, Yoshiji Egami, Kōji Matsuo, and Shigeru Nagase†

Department of Chemistry, Faculty of Science and Engineering, Saga University, Honjō-machi, Saga 840
†Department of Chemistry, Faculty of Education, Yokohama National University, Hodogaya-ku, Yokohama 240

(Received September 11, 1986)

The reactions of an aryliminodimagnesium reagent ($ArN(MgBr)_2$) with four oxidizing agents ((i): I_2, OsO_4, $C_6H_5IO_2$, I_2O_5) and four push-pull substituted α-benzylideneacetophenones(ii) were examined. In the reactions with (i), the maximum yield of *sym*-azobenzene was 50%. In the reactions with (ii), in addition to products formed via condensation and the typical radical processes, unexpected products formed via cleavages of C=C and C_β–H bonds were observed. Summarizing these results, a pathway involving the formation of aryl-nitrene-like species via disproportionation of arylaminyl radicals ($Ar\dot{N}MgBr$) has been proposed.

Biaryl is frequently formed as a by-product in the reaction of Grignard reagent(ArMgBr) with a substrate via an electron transfer to the substrate and a subsequent radical dimerization. Similarly, symmetrical(*sym*-) azoarene(ArN=NAr) is formed as a by-product in the reaction of aryliminodimagnesium reagent($ArN(MgBr)_2$, aryl-IDMg), especially with nitrobenzenes[1] and *ortho*-quinones.[2] The formation of *sym*-azoarene is initiated by electron transfer from the reagent, in spite of its weak electron-donating ability(EDA),[3] to produce arylaminyl radical($Ar\dot{N}MgBr$).[4] However, a further removal of electrons is needed for azoarene formation; the pathway has not been studied. The previously reported yield of *sym*-azoarenes, based on the half molar amount of substrate used,[1,2] must be reexamined for elucidating the reaction pathway.

The present authors first studied *sym*-azoarene formation in a reaction of IDMg with four oxidizing agents: iodine(**A**), osmium tetraoxide(**B**), iodylbenzene(**C**), and iodine pentaoxide(**D**). The latter three agents have functional groups($-\overset{+}{X}\!\!\begin{array}{l}/\!/O\\ \backslash O^-\end{array}$: X=Os and I) that are structurally similar to the nitro group(X=N). Agents **A**—**C** proved to be more effective than nitrobenzenes for *sym*-azoarene formation, but the yield never exceeded 50%. On the other hand in the IDMg reaction with some α-benzylideneacetophenones, the formation of an abnormal product via the cleavage of C=C and C_β–H bonds was observed. Summarizing these results, the pathway for the oxidation of IDMg molecules will be discussed.

Results and Discussion

***sym*-Azoarene Formation in IDMg Reactions with Oxidizing Agents.** Oxidants **A**, **C**, and **D** are difficultly soluble in tetrahydrofuran (THF), and reactions with IDMg were carried out by adding a solution of the reagent in THF to the oxidant suspended in the same solvent at room temperature. The resulting mixture was stirred at the same temperature(or at 55 °C) for a certain number of hours. In order to avoid the oxidation of THF, oxidant **B** was dissolved in benzene. Because of the dimeric structure of *sym*-azoarenes, their yields were calculated based on the half molar amount of **A**—**D** used(summarized in Table 1(Runs 1—21)).

In the reaction with **A**(Runs 1—8), the *p*-MeO-substituted reagent is oxidized more easily than *p*-Me- and *p*-Cl-substituted ones(Runs 1, 3, and 6); prolonged heating is also effective for improving the yields (Runs 2 and 7). When two molar equivalents of **A** is used(Runs 4, 5, and 8), the yields given in the table(20 and 25%) correspond to those of 40 and 50%(based on the molar amount of IDMg used). It is thus concluded that the yield does not exceed 50%. The yield was unaffected by the addition of anhydrous $CoCl_2$, which is effective for the formation of biaryl from ArMgBr.[5]

In the reaction of **B** with *p*-$MeOC_6H_4$–IDMg(Runs 9—12), heating the mixture for half an hour is more effective than the use of two molar equivalents of the reagent. Oxidant **B** is more effective than **A** for *sym*-azoarene formation, but the yield does not exceed 50%(again).

In the reaction with **C**(Runs 13—19), the use of two molar equivalents of IDMg and prolonged heating were needed for improving the yields (Runs 17 and 18), but the use of two molar equivalents of the oxidant is not effective(Run 19). The deoxygenation of **C**, affording iodobenzene in yields of 35—70%, was confirmed by GLC analyses, but the yield of *sym*-azoarene did not exceed 50%(again). An attempt to estimate the electron-accepting ability(EAA) of **C** in THF by measuring the reduction potential with cyclic voltammetry[6] was unsuccessful due to the insolubility of **C** in the solvent. The low yield in the reaction with **D**(Runs 20 and 21) is due to its insolubility in THF.

Unusual C=C and C_β–H Cleavage of Some α-Benzylideneacetophenones in IDMg Reactions. The

Table 1. Formation of *sym*-Azoarenes from *p*-RC_6H_4-IDMg in the Reactions with Oxidants **A**—**D**

Run No.	Oxidant[a]	Reagent R	Mol. Ratio [Reag]/[Ox]	Reacn time/h		*sym*-Azoarenes yield/%[b]
				at r.t.	at 55 °C	
1	**A**	Cl	1.0	0	1	24
2	**A**	Cl	1.0	0.5	5	48
3	**A**	Me	1.0	0	1	28
4	**A**	Me	0.5	0.5	1	20
5	**A**	Me	0.5	0.5	5	25
6	**A**	MeO	1.0	0	1	31
7	**A**	MeO	1.0	0	5	42
8	**A**	MeO	0.5	0.5	5	20
9	**B**	MeO	2.0	2.5	0.5	45
10	**B**	MeO	1.0	2.5	0.5	45
11	**B**	MeO	1.0	3.0	0	25
12	**B**	MeO	2.0	2.5	0	29
13	**C**	MeO	1.0	0	1	22
14	**C**	Me	1.0	0	1	28
15	**C**	Me	1.0	1.5	2	23
16	**C**	Me	1.0	0	4	24
17	**C**	Me	2.0	0	3	46
18	**C**	Me	2.0	0	5	45
19	**C**	Me	0.5	0	5	15
20	**D**	Me	1.0	0	2	11
21	**D**	MeO	1.0	0	10	10

a) **A**: I_2, **B**: OsO_4, **C**: $C_6H_5IO_2$, **D**: I_2O_5. b) Yields based on the half molar amount of oxidant used.

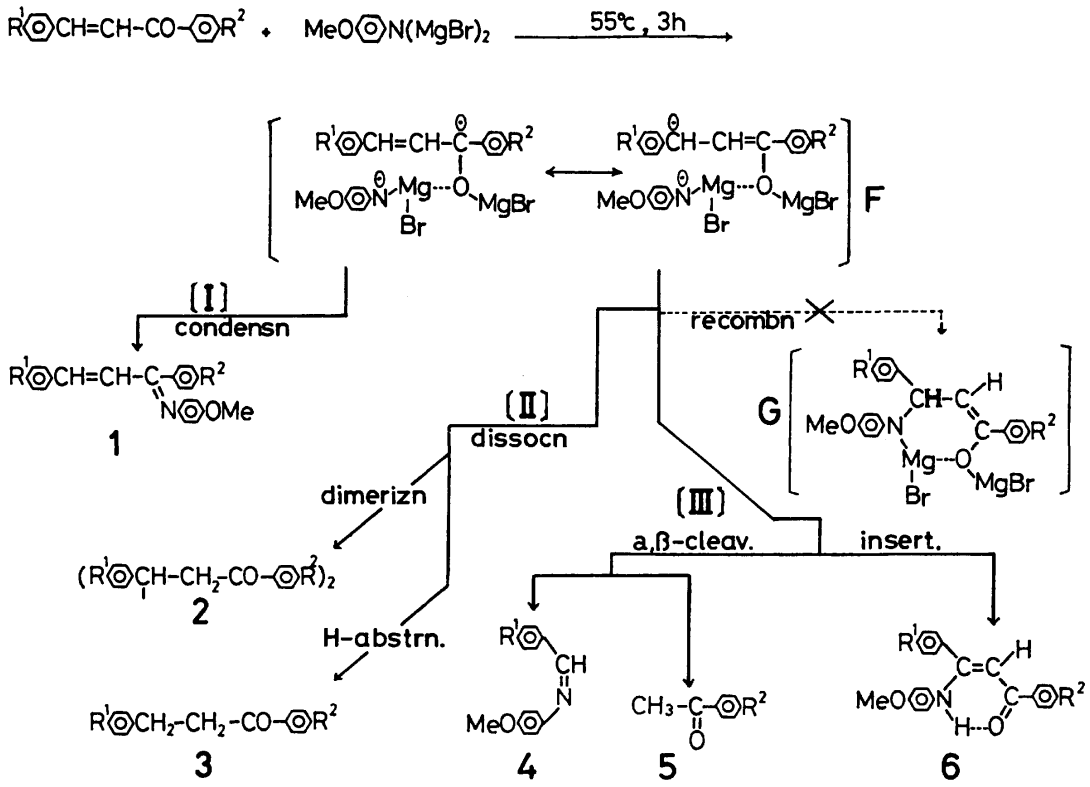

Scheme 1.

IDMg reactions with α-benzylideneacetophenones were independent of those with the oxidants **A**—**C**, and afford no *sym*-azoarene. The results of the reactions with the enones, however, are described in this paper because the formation of some unusual products is explainable(shown below) by a pathway involving two electron oxidation of IDMg molecules. The initial plan was to examine the electronic effect of substituents of the enones on the formation of the 1,4-addition product. This product was obtained in low yield in a preliminary study[2] using an enone having substituents in the weakly pull-push manner, namely, *p*-Cl and *p*-Me substituents on the benzylidene and benzoyl moieties, respectively.

In the present study, enones having substituents in the strongly pull-push(**Ea** and **Ec**) and push-pull(**Eb** and **Ed**) manners were sumbitted to the reaction with 1.2 molar equivalents of *p*-$MeOC_6H_4$-IDMg. The molar ratio of the reagent to enone was the same as that used in the previous study.[2] Six products(**1**—**6**)

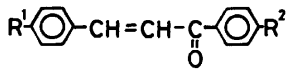

Ea: R^1=Cl, R^2=MeO; **Eb**: R^1=MeO, R^2=Cl;
Ec: R^1=CN, R^2=Me_2N; **Ed**: R^1=Me_2N, R^2=CN.

obtained are shown in Scheme 1 and the yields as well as the amount of recovery are summarized in Table 2. The overall amount of recovery and conversion were sufficiently high with respect to the substrate. In the reaction with **Ea**, *p*-$MeOC_6H_4$-IDMg (oxidation peak potential: 0.941 V[3]) and *p*-MeC_6H_4-IDMg(0.921 V[3]) gave **1**—**6** in almost the same yields.

The relative amounts of recovery(**Ed**>**Eb**>**Ea**>**Ec**) suggest that the σ-complex formation via coordination of an enone carbonyl oxygen to a Mg atom of the reagent governs the reactivity of enone. A similar enhancement of the reactivity by an electron-repelling substituent of the substrate was observed in IDMg reactions with benzophenones.[4] The lowest reactivity of **Ed** may be related to its resonance stabilized structure, indicated by the λ_{max} appearing at much longer wavelnegths (Table 2).

The six products are classified into three types(I—III). Each type of product and its combined yields are given in brackets in the scheme and table. Types-I(**1**) and -II(**2** and **3**) products are those expected from the previous results,[2] the former being formed via condensation and the latter being formed via typical radical pathways: dimerization and hydrogen abstraction. For elucidating the yields of Types-I and -II products, the EAA of enone is an estimate for the rapidness in generating the radical intermediate **F**(Scheme 1). The reduction potentials(redox) of **Ec**(−1.491 V) and **Ed**(−1.527 V) are consistent with the relative reactivities given above and also with the high and low yields of II. The quantumn mechanical calculations were carried out by assuming a planar geometry for estimating the spin density on the carbonyl and β-carbon of anion radicals of **Ec** and **Ed**(Fig. 1). The actual intermediate must be magnesium ketyl(**F**), but not the anion radical; the actual geometry is equivocal. However, the spin density on β-carbon is positive in the case of the

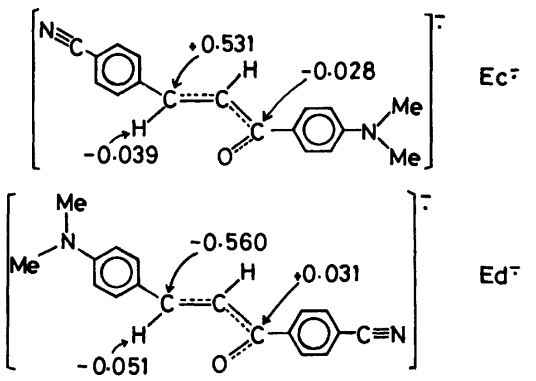

Fig. 1. Spin Density on the Radical Anions of **Ec** and **Ed**.

Table 2. Product Distribution in the Reaction of *p*-MeC_6H_4-IDMg with Pull-Push and Push-Pull α-Benzylideneacetophenones **Ea**, **Eb**, **Ec**, and **Ed**

p-$R^1C_6H_4CH$=$CHCOC_6H_4R^2$-*p*			Product yield/% [Type]/No.						
		λ_{max}/nm	Recovd.	[I]	[II]		[III]		Overall
R^1	R^2			**1**	**2**	**3**	**4**	**5**[a] **6**	
Ea Cl	MeO	318	18	[0] 0	[38] 33	5	9	[24] (10) 15	80
Eb MeO	Cl	340	31	[23] 23	[14] 0	14	3	[29] (2) 26	97
Ec CN	Me_2N	352	2	[9] 9	[48] 48	0	19	[27] (?) 8	86
Ed Me_2N	CN	424	50	[12] 12	[20] 5	15	Trace	[Trace][b] (0) Trace	82

a) The yield of **5** should be the same with that of **4**, and is given in parentheses. The reason for the unsuccessful detection of **5c** is obscure. b) The trace amounts of **4d** and **6d** were identified by ^1H NMR on the basis of the singlets at δ 8.9(-CH=N-) and 13.18(⟩NH···O=C⟨), respectively.

most reactive **Ec**, while it is negative in the case of the least reactive **Ed**. The positive spin density on the β-carbon of **Ec** ketyl, which is effectively generated, is thus responsible for the high yield of II. The yield of **2** is remarkably higher than that of **3** in cases of more reactive **Ea** and **Ec**, while the yields of **3** is slightly higher than that of **2** in cases of the less reactive **Eb** and **Ed**. The relative yield of the dimeric(**2**) and monomeric(**3**) products indicates the relative rapidness in generating **F** from the former and the latter enones, and is explained similarly.

The relative yields of Type-I products(**Eb**>**Ed**>**Ec**>**Ea**) indicate that their formation is favored by the small but positive spin density on the carbonyl carbon of the enone ketyl; the effect, however, is modified by EAA.

Type III products(**4**—**6**) are those formed via an attack of a species generated from IDMg on the β-position of the enone, causing the cleavage of C=C and C_β–H bonds. No evidence for the initially expected attack of the arylaminyl radical on the β-carbon of ketyl leading to 1,4-addition product(**G**, Scheme 1) was obtained. An unusual bond cleavage was observed for the first time in reactions of the enones with Grignard and IDMg reagents;[2] the attacking species will be discussed separately in the following section.

Two-Electron Oxidation of IDMg Molecules. The seemingly poor, but significant, results suggesting the possibility of the formation of an arylnitrene-like species from IDMg molecules were obtained in the following experiments. When reactions of *p*-MeC_6H_4–IDMg with **C** was carried out in the presence of an equimolar amount of bicyclo[2.2.1]hept-2-ene(norbornene), the main product was the *sym*-azoarene and a trace amount of the corresponding 1-azirine was detected. When IDMg derived from 2-aminobiphenyl in THF was electrolyzed using Bu_4NClO_4 as a supporting electrolyte, a trace amount of carbazole was detected. No formation of carbazole was observed in reactions of 2-biphenylyl–IDMg with 2,4,6-Me_3-, 2-Cl-, and 4-Cl-nitrobenzenes.

In contrast to the good yields of 1-azirine and carbazole obtained in photolyses of the corresponding azides[7] and in the thermal deoxygenation of 2-nitrobiphenyl by phosphorus(III) compounds,[8] the results of the above experiments are quite poor. However, the poor yields are reasonable since the arylnitrene-like species is not free from Mg ions and is not effectively trapped by norbornene and/or by the phenyl group (vide infra). The identification of arylnitrene by the electronic absorption spectra[9] was unsuccessful because the reaction mixture was deeply colored.

The most possible pathway for generating arylnitrene-like species from an arylaminyl radical is its disproportionation shown in Scheme 2(i), which is compatible with the maximum yield of *sym*-azoarenes(vide supra). Another pathway involving the dimerization of arylaminyl radicals (Scheme 2(ii)) is suggested from the formation of a product having an *o*-(*N*,*N*′-diarylhydrazino) group in the IDMg reaction with *o*-MeO-nitrobenzene;[11] the latter scheme, however, is incompatible with the maximum yield of *sym*-azoarenes.

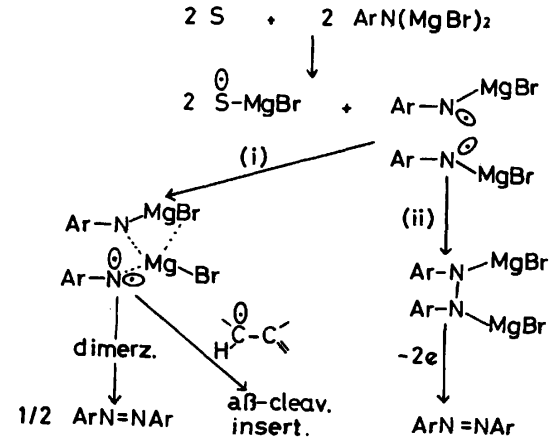

Scheme 2.

In reactions with enones, the correlation of yields of **4** and **6** with those of **2** and **3**, respectively, supports the proposal of a pathway involving the attack of arylnitrene-like species on the β-position of enone ketyl. The poor yields of **4** and **6** in the reaction with **Ed** is consistent with its weak EAA and the lowest reactivity(vide supra). As the enone varies from **Ec** via **Ea** to **Eb**, the yields of **4** and **2** increase while those of **6** and **3** decrease. The yield of **4** is always less than half of that of **2** while the yield of **6** is always higher than that of **3**.

The enone **Ec** having strong EAA generates **F** rapidly, leading to aggregate formation. Inside an aggregate of **F**, a remarkable part of the ketyl dimerizes to afford **2** in high yields, leaving arylaminyl radical behind. The interaction of two arylaminyl radicals leads to generation of an arylnitrene-like species which attacks the ketyl at its β-carbon having positive spin density to give **4**(Scheme 3a). In the case of the less reactive **Eb**, the aggregate of **F** is not greatly accumulated. A part of the ketyl detached from **F** abstracts hydrogen from the solvent, affording the lower yield of **3**. Due to the interaction of **F** with the arylaminyl radicals left behind, an arylnirene-like species is generated; it attacks the ketyl at its β-hydrogen (which has a low spin density) instead of the β-carbon (which has a negative spin density (Scheme 3b)).

The fact that only 36% molar amount of IDMg is available for affording **1**, **4**, and **6** even in the reaction with **Ec** is also compatible with the pathways of Scheme 3. Whether the other ArN-moiety regenerates IDMg or not remains to be determined. The multiplicity of arylnitrene-like species has not yet been determined because of poor direct evidences. However, a triplet state is possible since a cleavage of the C=C bond of α-benzylideneacetophenone in the manner proposed above resembles formally an effective cleavage of the same enone anion radical via an attack of triplet oxygen.[10]

General Discussion. Most probably, *sym*-azoarenes are formed via the dimerization of an arylnitrene-like species,[9] which is generated according to Scheme 2(i). The substrates having strong EAA generate arylaminyl radicals effectively, and are favorable for *sym*-azoarene formation. Another essential factor assisting its formation is the structure of the substrate. An oxidative dimerization leading to *sym*-azoarenes was observed in IDMg reactions with nitrobenzenes,[1] *ortho*-quinones,[2] and the oxidants **B** and **C**, but was not observed in a reaction with 1,4-naphthoquinones, in spite of its strong EAA.[2] The neighboring oxygen atoms of substrates as well as the iodine atoms of **A** assist the arylaminyl radicals in being generated in proximity to each other, effectively leading to *sym*-azoarenes.

α-Benzylideneacetophenones have weaker EAA's than that of nitrobenzenes and quinones, and are less favorable for the rapid generation of an arylaminyl radical. As shown, however, by the formation of **4** and **6** in the reaction of weakly electron-donating IDMg[3] with weakly electron-accepting enones, the aggregation of **F** (vide supra) participates in generating arylnitrene-like species. In the IDMg reaction with benzophenones,[4] only the condensation and typical radical products are formed, probably because the phenyl groups are more resistant than the -CH=CH- group to the attack of arylnitrene-like species. Also, the poor yield of carbazole in the electrolysis of 2-biphenylyl-IDMg is not unexpected.

In accordance with the disproportionation mechanism, the previously reported yields of *sym*-azoarenes calculated based on half molar amount of substrates need not to be revised.

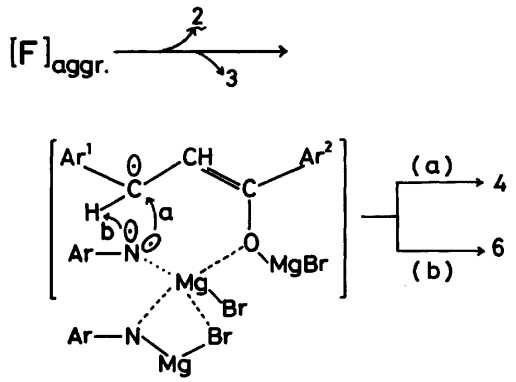

Scheme 3.

Experimental

Melting points are uncorrected.

Materials and Procedures. The oxidizing agents (**A**, **B**, and **D**) were commercially avilable; **C** was prepared from iodobenzene according to a reported method.[12] The enones **Ea—Ed** were prepared according to the usual procedure from the corresponding benzaldehydes and acetophenones. The IDMg reagents in THF were prepared by a reported procedure.[2]

In reactions of IDMg with the oxidants, the reagents(3—5 mmol) in THF(25—40 ml) was added to the suspension of **A—D** in THF or benzene(30 ml). The molar ratio of the reagent to the oxidant and the reaction conditions are given in Table 1. In reactions of IDMg with the enones, the substrates(2.6 mmol) dissolved in THF(20 ml) was added at

Table 3. Melting Points and ^1H NMR Data of Products

No.	Mp θ_m/°C	^1H NMR data/δ
1b	99	7.64—7.84(1H, m), 7.10—7.52(4H, m), 6.42—7.04(7H, m), 3.81(3H, s), 3.79(3H, s).
1c	191	7.39—7.78(6H, m), 6.70—7.12(8H, m), 3.84(3H, s), 3.07(6H, s).
1d	130	7.44—7.90(3H, m), 7.08—7.32(2H, m), 6.86(4H, s), 6.60—6.96(3H, m), 3.82(3H, s), 3.00(6H, s).
2a	oil	6.68 and 7.64(8H, ABq, J=9 Hz), 7.00(8H, s), 3.68(6H, s), 2.82—3.36(6H, m).
2c	196	6.58 and 7.80(8H, ABq, J=10 Hz), 7.20—7.64(8H, m), 3.90—4.10(2H, m), 3.18—3.50 (4H, m), 3.05(12H, s).
2d	oil	7.77 and 8.06(8H, ABq, J=9Hz), 6.48—7.36(8H, m), 3.24—3.96(6H, m), 2.94(6H, m).
3a	oil	7.48—7.72(2H, m), 6.56—7.20(6H, m), 3.78(3H, s), 2.58—3.35(4H, m).
3b	61.5	7.36 and 7.82(4H, ABq, J=9 Hz), 6.72 and 7.06(4H, ABq, J=9 Hz), 3.72(3H, s), 2.92 and 3.06(4H, q, J=8 Hz).
3d	82.5	7.76 and 8.06(4H, ABq, J=8 Hz), 6.70 and 7.16(4H, ABq, J=9 Hz), 2.94—3.38(4H, m), 2.93(6H, s).
6a	114	12.62(1H, s), 7.75—7.88(2H, m), 7.24(4H, s), 6.60—6.94(6H, m), 3.80(3H, s), 3.66 (3H, s).
6b	149	13.04(1H, s), 7.88(2H, d, J=9 Hz), 7.04—7.64(4H, m), 6.56—6.92(6H, m), 5.88(1H, s), 3.90(3H, s), 3.72(3H, s).
6c	176.5	12.69(1H, s), 6.75 and 7.95(4H, ABq, J=8 Hz), 7.50 and 7.64(4H, ABq, J=10 Hz), 6.70(4H, s), 6.02(1H, s), 3.74(3H, s), 3.07(6H, s).
6d	oil	Formation confirmed by 13.18(1H, s) and 6.00(1H, s) signals.

0 °C to a solution of *p*-$MeOC_6H_4$-IDMg (3.1 mmol) in THF(25 ml), and the resulting mixture was stirred at 55 °C for 2 h.

All the reaction mixtures were quenched with aqueous NH_4Cl and the products were isolated by column chromatography on silica gel(Wako Gel C-200 and C-300).

The reaction of IDMg with **C** in the presence of norbornene was carried out as follows: *p*-MeC_6H_4-IDMg(4.0 mmol) in THF(45 ml) was added to the suspension of equimolar amounts of **C** and the hydrocarbon in THF(20 ml), and the resulting mixture was stirred under the same conditions as those of Run 15 (Table 1).

The electrolysis of 2-biphenylyl-IDMg was carried out as follows: In a flask equipped with two Pt-wire electrodes, the reagent(6.0 mmol) in THF(40 ml) containing Bu_4NClO_4 (0.1 M 1 M=21 mol dm^{-3}) was electrolyzed under the conditions of 15.0 V–0.012 A and/or 20.0 V–0.062 A for 8—10 h. Reactions of the same reagent with 2,4,6-Me_3-, 2-Cl-, and 4-Cl-nitrobenzenes were carried out using a molar ratio of 2.5 at 55 °C for 2 h; the reaction mixtures were worked up according to the manner described above.

The reduction potentials(redox) of the enones **Ec** and **Ed** were measured in THF according to the reported method.[6]

The calculation of spin density was carried out within the framework of ab initio spin-unrestricted Hartree-Fock-(UHF) theory, using the STO-3G set[13] and standard geometry.[14]

Products. The results of elemental analyses and ^1H NMR data of the products **1**, **2**, **3**, and **6** are satisfactory. The melting points and ^1H NMR data are summarized in Table 3. Products **4** and **5** were identified by comparing their ^1H NMR spectra with those of commercially available and/or easily prepared authentic samples.

A trace amount of 1-azirine derived from norbornene was detected on the basis of the characteristic doublets appearing at δ 1.5—4.5.[7] A trace amount of carbazole was identified by a comparison with the characteristic doublet appearing at δ 8.2.

The authors are grateful to the Ministery of Education, Science, and Culture for a financial support by a Grant-in-Aid for Scientific Research (No. 60740026). Ab initio calculations were carried out at the Computor Center of the Institute for Molecular Science.

References

1) M. Ōkubo, T. Takahashi, and K. Koga, *Bull. Chem. Soc. Jpn.*, **56**, 199 (1983).

2) M. Ōkubo, M. Yoshida, K. Horinouchi, H. Nishida, and Y. Fukuyama, *Bull. Chem. Soc. Jpn.*, **56**, 1196 (1983).

3) M. Ōkubo, T. Tsutsumi, A. Ichimura, and T. Kitagawa, *Bull. Chem. Soc. Jpn.*, **57**, 2679 (1984).

4) M. Ōkubo , *Bull. Chem. Soc. Jpn.*, **58**, 3108 (1985).

5) M. S. Kharasch and E. K. Fields, *J. Am. Chem. Soc.*, **63**, 2316 (1941)

6) M. Ōkubo, C. Sugimori, M. Tokisada, and T. Tsutsumi, *Bull. Chem. Soc. Jpn.*, **59**, 1644 (1986).

7) R. Huisgen, L. Möbius, G. Müller, H. Stangl, G. Szeimies, and J. M. Vernon, *Chem. Ber.*, **98**, 3992(1965); P. A. S. Smith and J. H. Hall, *J. Am. Chem. Soc.*, **84**, 480 (1962).

8) J. I. G. Cadogan, M. Cameron-Wood, R. K. Mackie, and R. I. G. Searle, *J. Chem. Soc.*, **1965**, 4831.

9) "Nitrenes," ed by W. Lwowski, John Wiley & Sons Inc., New York (1970).

10) I. Rosenthal and A. Frimer, *Tetrahedron Lett.*, **1976**, 2805.

11) M. Ōkubo and Y. Inatomi, Unpublished results.

12) M. W. Formo and J. R. Johnson, *Org. Synth.*, Coll. Vol., **3**, 486 (1955).

13) W. J. Hehre, R. Ditchfield, R. F. Stewart, and J. A. Pople, *J. Chem. Phys.*, **52**, 2769 (1970).

14) J. A. Pople and D. L. Beveridge, "Approximate Moleular Orbital Theory," McGraw-Hill, New York (1970).

 © 1987 The Chemical Society of Japan Bull. Chem. Soc. Jpn., 60, 1747—1752 (1987)

Thermal Rearrangement of 2,5-Bis(allyloxy)tropone, Revisited. Formation of Four Thermolysates under the Claisen Rearrangement Conditions and Structure Revision of the Major Thermolysate

Hitoshi TAKESHITA,* Akira MORI, Yasutomo GOTO,† and Tomohiro NAGAO†
Research Institute of Industrial Science, 86, Kyushu University,
Kasuga-koen, Kasuga, Fukuoka 816
†Graduate School of Engineering Sciences, 39, Kyushu University,
Kasuga-koen, Kasuga, Fukuoka 816
(Received September 12, 1986)

A reinvestigation of the Claisen rearrangement of 2,5-bis(allyloxy)tropone led to the isolation of three diallyl-5-hydroxytropolones along with an intermediary thermolysate, 3-allyl-5-allyloxytropolone. The structure of the formerly identified product was revised from 3,6-diallyl-5-hydroxytropolone to 4,6-diallyl-5-hydroxytropolone. The involvement of no cleavage-recombination process was established by cross-over deuterium labelling experiments. These derivatives were respectively converted to *p*-tropoquinones, one of which was further converted to a cyclohepta[*b*]pyranone derivative by an electrochemical reaction.

The Claisen-type [3,3] sigmatropy of a troponoid derivatives has revealed anomalous features; unsubstituted allyl and propargyl ethers of tropolones gave rearrangement products (**A**) in excellent yields.[1-4] However, allyl groups having a hydrogen-carrying substituent at C-3, e.g., 3-methyl-2-butenyl (prenyl) ethers of tropolones, gave rearrangement products in low yields[2,5] due to a consecutive occurrence of a Woodward-Hoffmann rule-allowed[6] [$_{\pi}6+_{\sigma}2+_{\sigma}2$] process from the proto-Claisen products (**B**).[7] The intramolecular Diels-Alder reaction of Claisen products from 2-allyloxy- and 2-propynyloxy-3,5,7-trimethyltropones constitutes a trapping of unaromatizable protoproducts (**C**).[8] The arylmethoxy- and heteroarylmethoxytropones, which are superficially capable of concerted sigmatropic reactions, yielded homolytic rearrangement products, 3- or/and 5-arylmethyl- and heteroarylmethyltropolones (**D**).[9-11] A sort of degenerated [1,9] sigmatropy[12] was conceived to occur prior to the rearrangement; the heating of two isomeric 2-furylmethyl ethers (**E** and **F**) prepared from hinokitiol (4-isopropyltropolone) gave thermolysates in the same yields.[10] Furthermore, thermolysis in dimethylsulfoxide caused an oxidative fragmentation to carbonyl compounds.[13] These chemical properties of tropolonyl ethers made their thermal reactions very complicated.

A decade ago, we investigated the Claisen rearrangement of 2,5-bis(allyloxy)tropone (**1**) and its various derivatives in order to construct several heterocyclic troponoids, e.g., cycloheptadifurans.[14] From parent **1**, we isolated yellow crystalline thermolysate (**2**) in 39% yield, and assigned it to 3,6-diallyl-5-hydroxytropolone from a mechanistic view point. Although the ^{1}H NMR spectrum of **2** or its acetate (**3**) revealed overlapped signals, indicating the presence of a symmetry element in the molecule, we simply thought that this phenomenon was accidental. During our recent studies regarding the preparation of various *p*-tropoquinone derivatives[15] and their cyclic voltammetry (CV) analysis,[16,17] we have reinvestigated the Claisen rearrangement of **1**, and have found the occurrence of four rearrangement products, suggesting the complicated pathways involved.

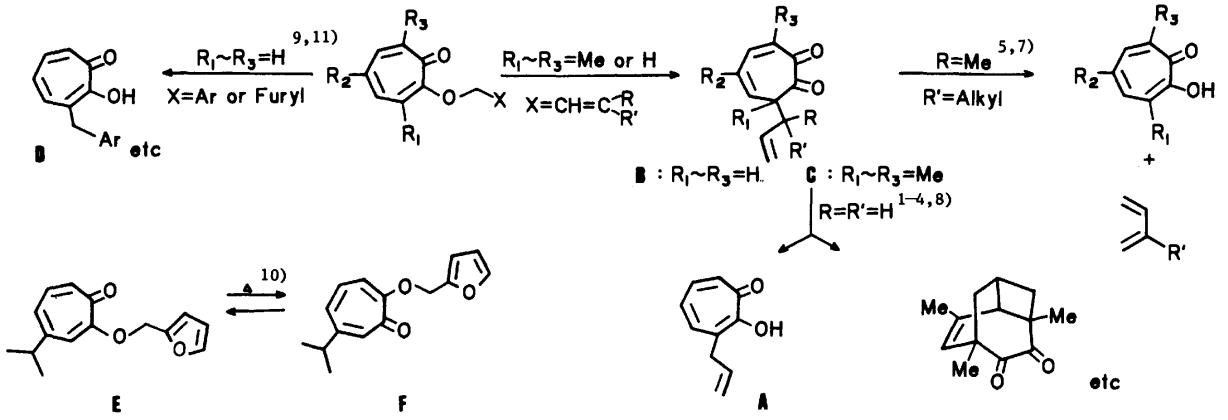

Scheme 1.

In this paper, we describe the structural determination of these thermolysates; this eventually leads to a revision of the structure of former thermolysate, **2**, from 3,6-diallyl-5-hydroxytropolone to 4,6-diallyl-5-hydroxytropolone, and the deuterium-labelling experiments to prove the intramolecular nature of this rearrangement.

Results and Discussion

When **1** was refluxed in xylene for 2 h,[14] four products (**2**, **4**, **5**, and **6**) were formed; however, only three of them (**2**, **4**, and **5**) were detectable on the thin-layer chromatogram (TLC). The major products (**2** and **5**) were isolated by a silica-gel column chromatography and were identical with the previous samples.[14] Repeated silica-gel column chromatography of the intermediary fractions gave another product, **4**. Its ^{13}C and ^{1}H NMR spectra revealed no element of symmetry and no spin-spin coupling between the protons on the seven-membered ring. Consequently, it must be 3,6-diallyl-5-hydroxytropolone; thus, the previously assigned structure of **2** should be revised. These facts suggest that the structure of **2** is either 3,7-diallyl-5-hydroxytropolone (**G**) or 4,6-diallyl-5-hydroxytropolone. To differentiate the point, **2** was converted to two methyl ethers (**7** and **8**) by a treatment with diazomethane. The mixture could be fractionated by silica-gel column chromatography; the ^{1}H NMR spectrum of **8** revealed two aromatic proton signals at different fields (δ=6.59 and 7.15); however, that of **7** showed an overlapped signal for two protons at 7.32. In parallel, the ^{13}C NMR spectrum of **7** showed only eight signals but that of **8** showed fifteen well-resolved lines. If **2** were **G**, **8** should be formulated as 3,7-diallyl-2,5-dimethoxytropone, and its ^{1}H NMR spectrum must exhibit mutually spin-coupled C-4 and C-6 protons (as in the cases of **1**, **10**, and **5**) whose spin-spin coupling constants fall in a range of ca. J=3 Hz.[14] As mentioned, the aromatic proton signals of **8** appeared as two singlet lines. Moreover, the chemical shift of the aromatic protons of **7**, at 7.32, closely resembled the C-3 proton of 4,5-dimethoxytropone. Therefore, **2** must be 4,6-diallyl-5-hydroxytropolone.

From the later fractions of chromatography the third methyl ether (**9**) was isolated, which should be derived from the remaining thermolysate, **6**. Although the isolation of **6** from the thermolysis mixture failed, it was independently prepared in 12% yield together with **4**, in 72% yield, by a further thermolysis of **5**. The samples of methyl ether, **9**, prepared from both sources were mutually identical. The ^{1}H NMR of **6** revealed a pair of AB-signals (J=12 Hz) ascribable to vicinal protons on the seven-membered ring, indicating **6** to be 3,4-diallyl-5-hydroxytropolone and, hence, **9**, 2,3-diallyl-4,7-dimethoxytropone. The undetectability of the isomer, 3,4-diallyl-2,5-dimethoxytropone (**H**) in the methylation product of **6** must be explained in terms of a steric effect.

The product, **5**, was 3-allyl-5-allyloxytropolone. Among the thermolysates, **4** was the expected Claisen rearrangement product, while the major product, **2**, was an abnormal thermolysate, whose formation should involve complicated rearrangement processes.

In order to elucidate the mechanism, we analyzed the isotope distributions of the thermolysates of the deuterio derivatives of **1**, 2,5-bis(allyloxy)tropone-4,6-d_2 (**1**-d_2) and 2,5-bis(allyl-2,3-d_2-oxy)tropone-3,7-d_2 (**1**-d_6). The **1**-d_2 was prepared by a condensation of 3-bromo-1-propene with 5-hydroxytropolone-4,6-d_2 (**11**-4,6-d_2).[18] The **1**-d_6 was prepared by catalytic deuteration with Lindlar's catalyst of 2,5-bis(2-propynyloxy)-tropone-3,7-d_2 (**10**-d_2), prepared by a condensation of 5-hydroxytropolone-3,7-d_2 (**11**-3,7-d_2) with 3-bromo-1-propyne.

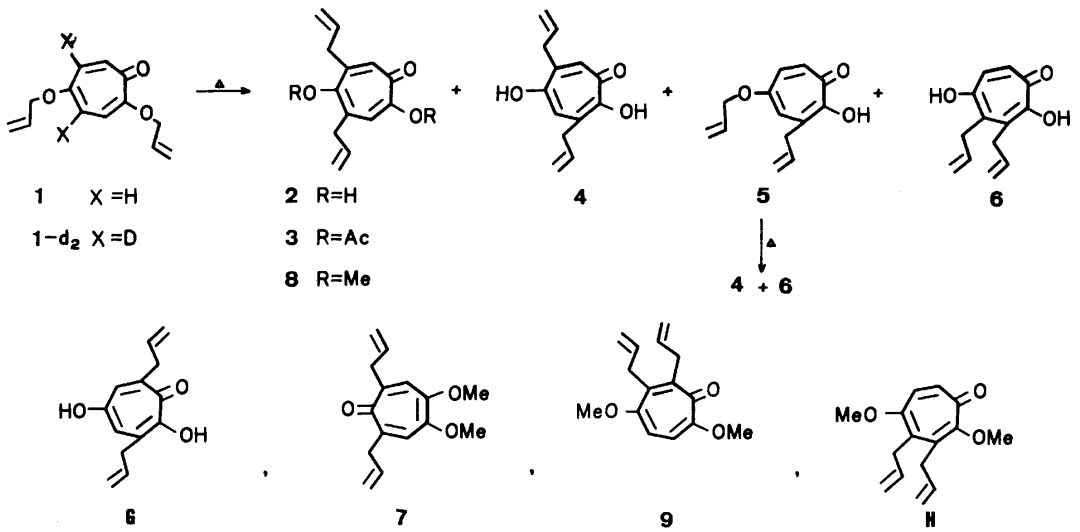

Scheme 2.

The thermolysis of **1**-d_2 determined the location of the allyl groups; the major thermolysate, **2**-*d*, caused a loss of two deuterium atoms, while **4**-*d* retained half of the deuterium atoms and **5**-*d* lost only a fractional amount of deuterium atoms. Table 1 shows a mass-spectral analysis of these thermolysates.

When a 1:2-mixture of **1**-d_6 and **1**-d_0 was heated under similar conditions, again the mass spectrometry of the products isolated after silica-gel column chromatography eliminated the radical dissociation-recombination mechanism; the major product, **2**-*d*, revealed identical deuterium distributions with that of the starting material within the experimental error; i.e., its mass spectrometry deduced to be **2**-d_6 and **2**-d_0 (1:2), and there was no **2**-d_2 or **2**-d_4. Therefore, **2** had been formed by the intramolecular process throughout. Table 2 demonstrates the deuterium distributions of **2**-*d* and other thermolysates to confirm the conclusion. In the cases of **4**-*d* and **5**-*d*, an approximate 1:2:1-distribution of d_4-, d_5-, and d_6-components did not contradict the suggested mechanism, since there were substantial amounts of **1**-d_7 in the starting material. Probably, a partial deuterium exchange of the acidic hydrogen on the sp-carbon might have taken place prior to catalytic deuteration.

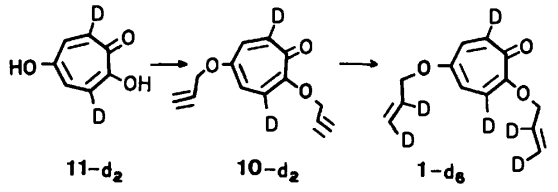

Scheme 3.

Table 1. The Mass-Spectral Determinations of Deuterium Contents of Thermolysates from **1**-d_2

Compound	*m/z* 218(d_0)	219(d_1)	220(d_2)	221(d_3)	222(d_4)
1-d_2	3.2	4.4	53.2	23.2	16.0
2-*d*	55.7	17.6	18.5	8.3	
4-*d*	27.6	50.4	20.7	1.4	
5-*d*	2.0	10.5	49.8	34.5	3.2

Interestingly, the thermolysis of **5** gave only **4** and **6**, whose formation must be straightforward. Hence, **2** might be derived from an undetected intermediary protoproduct (**J**). If it occurred via thermally-allowed concerted processes, either a), two-fold [3,3] sigmatropies, or b), consecutive [3,7] and [3,3] sigmatropies, should be considered, but the deuterium distributions can not distinguish these two routes. In this particular system, the [3,7] process, however, requires a relatively long-distance flight of the allyl group from C-2 oxygen to the C-5 oxygen; in such a case, the [3,7] process should be the rate-determining step of the rearrangement. The absence of the intermediate thermolysates from **J** to **2** may suggest that the possibility is unfavorable.[19]

In addition, the DDQ (2,3-dichloro-5,6-dicyano-*p*-benzoquinone)-oxidation of **4**, similar to that of **2**,[15] afforded 3,6-diallyl-*p*-tropoquinone (**12**) in good yield. The NMR spectra were consistent to the structure assigned in the present study.

Finally, we wish to record the results of an electrolytic reduction of **13**, 4,6-diallyl-*p*-tropoquinone, obtained from the major thermolysate, **2**. As described in the preliminary paper, the CV of several *p*-tropoquinones exhibited an extra oxidation wave after returned at the second oxidation wave.[20] For this extra wave, we assumed the occurrence of a side reaction from the quinones. When **13**, of which the wave was indeed the most pronounced one, was electrolyzed in an *N*,*N*-dimethylformamide (DMF) solution in the presence of a supporting electrolyte, tetrabutylammonium tetrafluoroborate (TBAT) at −0.4 V for 25 h,[21] the formation of a product (**14**) was detected by a TLC analysis. The NMR evidence showed the structure of **14** to be 9-allyl-7-hydroxycyclohepta[*b*]pyran-6(2*H*)-one; particularly, a related model compound, 2-methylfuro[3′,2′:3,4]cyclohepta-[1,2-*b*]pyran-4(8*H*)-one (**K**), identified previously among the Claisen rearrangement products of **10**, provided a closely resembled ^{1}H NMR spectral feature.[14]

Consequently, at least in the case of **13**, the irreversible extra oxidation wave was explainable in terms of the chemical reaction. However, the wave has appeared in the alkyl-*p*-tropoquinones, which should

Table 2. The Deuterium Distributions of the Starting Material and the Thermolysates Obtained from a 1:2-Mixture of **1**-d_6 and **1**-d_0

Compound	*m/z*	218(d_0)	219(d_1)	220(d_2)	221(d_3)	222(d_4)	223(d_5)	224(d_6)	225(d_7)
1-d_6		14.8	4.6	2.1	4.2	8.3	23.1	25.8	17.6[a]
1-(d_6+d_0)		71.1	2.6	1.3	1.4	2.9	8.4	9.6	2.6
2-*d*		68.2	1.9	0.3	1.2	3.9	8.9	13.7	2.0
4-*d*		64.6	2.0	3.4	3.1	7.9	11.7	5.5	1.8
5-*d*		70.6	1.9	1.2	1.8	6.8	12.8	4.0	0.8

a) These figures show that the sample of **1**-d_6 contains nearly equal amount of **1**-d_5, together with some amounts of **1**-d_7.

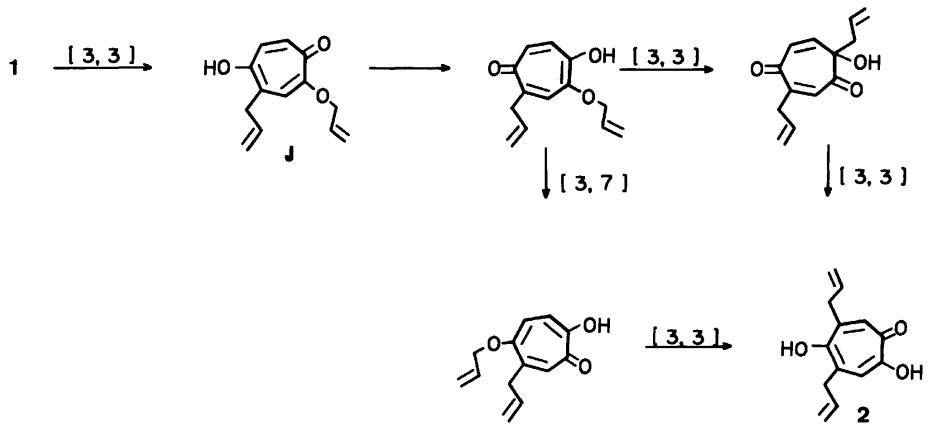

Scheme 4.

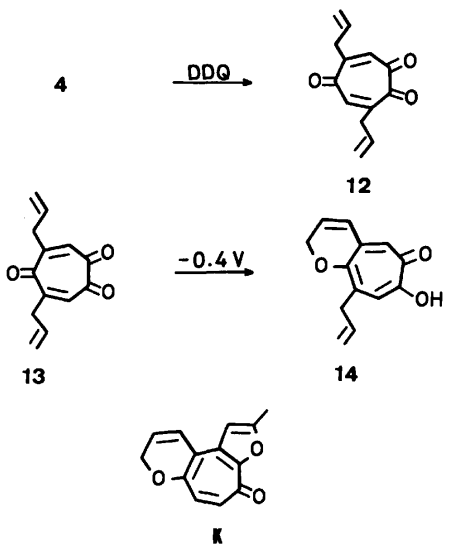

Scheme 5.

not be capable of such a cyclization; thus, more extensive studies are needed.

Experimental

The elemental analyses were carried out by Miss S. Hirashima, of the Research Institute of Industrial Science, Kyushu University. The NMR spectra were measured by a JEOL FX 100 Spectrometer in $CDCl_3$ solution, unless otherwise specified, and the chemical shifts expressed were in δ unit. The mass spectra were measured with a JEOL OISG-2 Spectrometer. The IR spectra were taken as either KBr disks or an inserted liquid film between NaCl plates using a Jasco IR-A 102 Spectrometer.

Preparation of 2,5-Bis(allyloxy)tropone (1). To a mixture of an anhydrous hexamethylphosphoric triamide (HMPA, 100 cm³), **11** (2.0 g), and NaH (55%, 1.3 g), 3-bromo-1-propene (3 cm³) was added under an N_2 atmosphere at 70 °C. After stirring for 4 h, the mixture was acidified with dil HCl and extracted with ether. A silica-gel column chromatography of the extract afforded 5-allyloxytropolone [colorless needles, mp 137—138 °C (lit,[14] 137—138 °C), 485 mg; 19%], and **1** [a colorless oil, 1.65 g; 52%].[14]

Thermal Reaction of 2,5-Bis(allyloxy)tropone (1). Formation of 2, 4, and 5. A xylene solution (50 cm³) of **1** (1.17 g) was refluxed for 5 h under an N_2 atmosphere. The mixture was then heated in vacuo to remove the solvent, and the residue was chromatographed on a silica-gel column to give **5** [colorless needles, mp 72—73 °C (lit,[14] mp 72—73 °C), 316 mg; 27%], **4** [pale yellow crystals, mp 142.5—144.5 °C, 113 mg; 9.7%. Found: C, 71.53; H, 6.48%. Calcd for $C_{13}H_{14}O_3$: C, 71.54; H, 6.47%. ^{1}H NMR δ=3.37 (2H, d, J=5.5 Hz), 3.53 (2H, d, J=5.5 Hz), 4.9—5.3 (4H, m), 5.7—6.2 (2H, m), 7.30 (1H, br s), 7.43 (1H, s), and 8.1 (2H, br s). ^{13}C NMR δ=38.9, 39.2, 117.8, 118.0, 126.7, 128.2, 134.7, 134.9, 136.4, 138.5, 155.1, 164.5, and 167.2. IR ν: 3200—2600, 1395, 1290, 1240, and 925 cm^{-1}. UV λ_{max}^{MeOH}: 246.5 nm (ε=28400), 337.2 (7600), and 390 (11300)], and **2** [colorless needles, mp 126—127 °C (lit, [14] 126—127 °C), 304 mg; 26%].

Acetylation of 2 to 3. A pyridine solution (0.3 cm³) of **2** (15 mg) was treated with Ac_2O (20 mg) at room temperature for 24 h. The mixture was evaporated in vacuo, washed with dil $NaHCO_3$, and chromatographed on a silica-gel column to give **3** [colorless needles, mp 64.5—65.5 °C (lit, [14] 64.5—65.5 °C), 14 mg; 85%. Found: C, 67.41; H, 6.07%. Calcd for $C_{17}H_{18}O_5$: C, 67.54; H, 6.00%. ^{1}H NMR δ=2.28 (6H, s), 3.40 (4H, dd, J=7, 1 Hz), 5.1—5.2 (4H, m), 5.84 (2H, m), and 7.02 (2H, t, J=1 Hz). IR ν: 2980, 1765, and 1635 cm^{-1}].

Methylation of 2. Formation of 7 and 8. A 1:1-mixture of ether and acetone (50 cm³) containing **2** (129 mg) was treated with an excess of ethereal CH_2N_2 at 5—10 °C, and chromatographed on a silica-gel column to give **7** [a colorless oil, 76.4 mg; 53%. Found: M. W., 246.1214. Calcd for $C_{15}H_{18}O_3$: 246.1256. ^{1}H NMR δ=3.46 (4H, dm, J=7 Hz), 3.86 (6H, s), 5.0—5.2 (4H, m), 5.7—6.1 (2H, m), and 7.32 (2H, s). ^{13}C NMR δ=39.9 (2C), 58.9 (2C), 117.5 (2C), 129.5 (2C), 135.9 (2C), 145.8 (2C), 150.5 (2C), and 182.0. IR ν: 3500, 3080, 2990, 2950, 2850, 1735, 1710, 1635, 1560, 1490, 1390, 1255, 1130, 1090, 995, and 915 cm^{-1} UV λ_{max}^{MeOH}: 229 nm (ε=12200), 245 (14300), and 355 (9700)], and **8** [a colorless oil, 56.6 mg; 40%. Found: M. W., 246.1255. ^{1}H NMR δ=3.38 (2H, dm. J=7 Hz), 3.45 (2H, dm, J=7 Hz), 3.64 (3H, s), 3.85 (3H, s), 5.0—5.2 (4H, m), 5.7—6.1 (2H, m), 6.59 (1H, m), and 7.15 (1H, m). ^{13}C NMR δ=38.5, 39.4, 56.1, 61.7, 115.5, 117.7, 117.9, 134.8, 135.6, 136.4, 136.7, 147.6, 155.9, 161.2, and 178.9. IR ν: 3490, 3080, 2980, 2940, 2850, 1590, 1560, 1480, 1390, 1280, 1220, 1170, 1130, 1100, 1010, 990, and 920 cm^{-1}. UV λ_{max}^{MeOH}: 247 nm (ε=24900), 308 (5300, sh), 324 (7100, sh),

351 (7900), and 371 (5300)]. From the intermediary fractions, **9** [a colorless oil, a trace amount. Found: M. W., 246.1308. ^{1}H NMR δ=3.54 (2H, dt, J=6, 1.5 Hz), 3.64 (2H, dt, J=6, 1.5 Hz), 3.76 (3H, d, J=0.5 Hz), 3.81 (3H, d, J=0.5 Hz), 4.8—5.1 (4H, m), 5.7—6.1 (2H, m), 6.26 (1H, dq, J=11, 0.5 Hz), and 6.60 (1H, dq, J=11, 0.5 Hz). IR ν: 3600, 3090, 3000, 2950, 2850, 1600, 1560, 1505, 1460, 1410, 1390, 1240, 1210, 1175, 1125, and 1045 cm^{-1}. UV λ_{max}^{MeOH}: 245 nm (ε=19400), 332 (6900), 362 (7100), and 379 (5400, sh)], were isolated.

Further Thermal Reaction of 5. A xylene solution (4 cm^3) of **5** (70.5 mg) was heated in a sealed tube for 12 h. Silica-gel column chromatography of the mixture afforded **4** [50.8 mg; 72%] and **6** [yellow prisms, mp 172—174 °C, 8.5 mg; 12%. Found: C, 71.66; H, 6.52%. ^{1}H NMR (CD_3OD) δ=3.63 (2H, dt, J=6, 2 Hz), 3.73 (2H, dt, J=6, 2 Hz), 4.95—5.1 (4H, m), 5.75—6.2 (2H, m), 7.08 (1H, d, J=12 Hz), and 7.20 (1H, d, J=12 Hz). ^{13}C NMR (CD_3OD) δ=35.8, 36.3, 116.0 (2C), 123.3, 123.5, 136.5 (2C), 141.0, 141.7, 158.8, 166.0, and 169.7. IR ν: 3080—2330, 1630, 1610, 1520, 1350, and 1260 cm^{-1}. λ_{max}^{MeOH}: 246 nm (ε=25400), 339 (7400), 380 (9000), and 394.5 (9800)].

Methylation of 6. Similarly, **6** (21.4 mg) was methylated with ethereal CH_2N_2 to give **9** [15.3 mg; 63%], which was identical with the sample obtained from the above methylation mixture.

Methylation of 5-Hydroxytropolone. An acetone suspension (7 cm^3) of **11** (20 mg) was treated with ethereal CH_2N_2 (30 cm^3) and kept at 5 °C for 16 h. The resultant homogeneous solution was evaporated in vacuo and chromatographed on an alumina column to give 2,5-dimethoxytropone [17.5 mg; 71%] and 4,5-dimethoxytropone [colorless needles, mp 52—53 °C, 4.2 mg; 17%. Found: C, 65.11; H, 5.98%. Calcd for $C_9H_{10}O_3$: C, 65.05; H, 6.07%. ^{1}H NMR δ=3.91 (6H, s), 6.92 (2H, d, J=12 Hz), and 7.23 (2H, d, J=12Hz). ^{13}C NMR δ=58.6 (2C), 130.8 (2C), 136.3 (2C), 152.3 (2C), and 184.6].

Preparation of 5-Hydroxytropolone-3,7-d_2 (11-3,7-d_2). 2-Methoxytropone-3,5,7-d_3 (1.07 g) was dissolved in a mixed solution (260 cm^3) of MeOH:CS_2:ether (1:9:3) and irradiated by a 400-W tungsten lamp in the presence of tetraphenylporphyrin (42 mg) under the O_2 atmosphere at −30 °C for 10 h. The mixture was then treated with thiourea (5 g) at −5 °C for 4 d to give **11**-3,7-d_2 [665 mg; 62%].

Preparation of 2,5-Bis(2-propynyloxy)tropone-3,7-d_2 (10-d_2). An HMPA solution (5 cm^3) of **11**-3,7-d_2 (100 mg) was treated with NaH (50%, 103 mg) at room temperature, and 3-bromo-1-propyne (270 mg) was added drop by drop at room temperature. After being kept at 60 °C with stirring for 4 h, the mixture was worked up as usual to give **10**-d_2 [36 mg; 24%. ^{1}H NMR δ=2.51 (1H, t, J=2.5 Hz), 2.57 (1H, t, J=2.5 Hz), 4.65[22] (2H, d, J=2.5 Hz), 4.83 (2H. d, J=2.5 Hz), 6.43 (0.86H, br s), and 7.06 (1.14H, br s). m/z, 216:217:218:219=6.9:30.6:60.0:2.5].

Catalytic Deuteration of 10-d_2 with Lindlar's Catalyst to 1-d_6. An AcOEt solution (1.5 cm^3) with quinoline (0.25 cm^3) of **10**-d_2 (47.8 mg) was reduced by Lindlar's catalyst (Pd/$CaCO_3$-Pb, 25 mg) with D_2 gas. After take up of 13.4 cm^3 of D_2 (1.35 mol equiv), the mixture was chromatographed on a silica-gel column to give **1**-d_6 [a colorless oil, 23 mg; 46%. ^{1}H NMR δ=4.44 (2H, br s), 4.59 (2H, br s), 5.25—5.4 (1.82H, m), 6.2—6.4 (0.73H, m), 6.28 (0.24H, d, J=12 Hz), 6.76 (0.24H, d, J=12 Hz), and 6.9—7.2 (1.21H, m). m/z=220:221:222:223:224:225:226:227=14.8:4.6:2.1:4.2:8.3:23.1:25.8:17.0].

Thermal Reaction of 1-4,6-d_2. A xylene solution (6 cm^3) of **1**-4,6-d_2 [93 mg. ^{1}H NMR δ=4.44 (2H, dt, J=5, 1.5 Hz), 4.60 (2H, dt, J=5, 1.5 Hz), 5.2—5.5 (4H, m), 5.8—6.2(2H, m), 6.74 (0.38H, s), and 7.15 (0.38H, s)] was similarly thermolyzed. Silica-gel column chromatographic fractionation gave **5**-d_2 [12.5 mg. ^{1}H NMR (CD_3OD) δ=3.52 (2H,dt, J=6.5, 1.5 Hz), 4.52 (2H, dt, J=5, 1.5 Hz), 5.0—5.5 (4H. m), 5.7—6.2 (2H, m), and 7.26 (0.38H, s)] and **4**-d_1 [11.2 mg. ^{1}H NMR (CD_3OD) δ=3.35—3.65 (4H, m), 4.9—5.3 (4H, m), 5.7—6.2 (2H, m), and 7.35 (0.29H, s)], and **2**-d_0 [20 mg. ^{1}H NMR (CD_3OD) δ=3.35—3.55 (4H, m), 4.9—5.5 (4H, m), 5.7—6.2 (2H, m), and 7.35 (0.68H, s)].

Thermal Reaction of a 1:2-Mixture of 1-d_6 and 1-d_0. A xylene solution (5 cm^3) of 1:2-mixture of **1**-d_6 and **1**-d_0 (69 mg) was similarly refluxed for 3 h. The mixture was fractionated on a silica-gel column to give **2**-d [17.3 mg. ^{1}H NMR (CD_3OD) δ=3.43 (4.3H br d, J=7 Hz), 5.0—5.2 (4.5H, m), 5.7—6.2 (2H, m), and 7.35 (1.9H, s). ^{13}C NMR (CD_3OD) δ=39.6, 116.0, 128.7, 135.5, 141.3, and 156.9 (3C)], **4**-d [10 mg. ^{1}H NMR (CD_3OD) δ=3.35—3.6 (3.8H, m), 5.0—5.2 (5H, m), 5.7—6.2 (2H, m), 7.20 (0.7H, s), and 7.36 (1.3H, s). ^{13}C NMR (CD_3OD) δ=39.7, 40.1, 117.5 (2C), 127.7, 128.8, 136.8, 137.1, 139.4 (2C), 157.5, 166.8, and 167.8], and **5**-d [15.6 mg. ^{1}H NMR (CD_3OD) δ=3.50 (2H, br d, J=7 Hz). 3.82 (2.3H, dt, J=5, 1.5 Hz), 5.0—5.5 (5H, m), 5.7—6.2 (2H, m), 6.94 (1H, dd J=11.5, 3 Hz), and 7.24 (d, J=3 Hz) +7.27 (d, J=11 Hz) for 2.2H. ^{13}C NMR (CD_3OD) δ=39.3, 69.8, 117.7, 118.7, 120.3, 129.8, 132.4, 135.1, 140.4, 157.9, 163.1, and 171.2], respectively.

DDQ-dehydrogenation of 4 to 3,6-Diallyl-*p*-tropoquinone (12). An acetone solution (5 cm^3) of **4** (129 mg) was treated with DDQ (160 mg) at room temperature for 15 h. The mixture was then filtered off to remove the resultant hydroquinone; the filtrate was chromatographed on a silica-gel column to give **12** [a yellow oil, 117 mg; 92%. Found: M. W., 216.0817. Calcd for $C_{13}H_{12}O_3$: 216.0787. ^{1}H NMR δ=3.25 (4H, dm, J=6.5 Hz), 5.0—5.3 (4H, m), 5.68 (2H, ddt, J=16, 10.5, 6.5 Hz), 6.71 (1H, t, J=1 Hz), and 6.78 (1H, t, J=1 Hz). ^{13}C NMR δ=36.4, 37.2, 119.2, 120.0, 132.1, 132.5, 133.0, 138.1, 145.2, 151.2, 188.4, 189.6, and 189.8. IR ν: 1665, 1250, 1235, 995, and 920 cm^{-1}].

Electrolytic Conversion of 13 to 9-Allyl-7-hydroxycyclohepta[*b*]pyran-6(2*H*)-one (14). An anhydrous DMF solution (30 cm^3) of **13** (172.2 mg) was electrolyzed in the presence of TBAT (1 g) at -0.4 V for 25 h. After evaporation of the mixture in vacuo, the residue was chromatographed on a silica-gel column to give **14** [colorless crystats,mp 104—106 °C, 23 mg; 13%. Found: M. W., 216.0786. Calcd for $C_{13}H_{12}O_3$: 216.0787. ^{1}H NMR δ=3.38 (2H, dt, J=6.5, 1.5 Hz), 4.75 (2H, dd, J=3.5, 2 Hz), 5.08 (1H, dq, J=9.5, 1.5 Hz), 5.09 (1H, dq, J=17.5, 1.5 Hz), 5.92 (1H, ddt, J=17.5, 9.5, 6.5 Hz), 6.11 (1H, dt, J=9.5, 3.5 Hz), 6.37 (1H, dt, J=9.5, 2 Hz), 6.96 (1H, s), and 7.24 (1H, s). IR ν: 3450, 3200, 1595, 1582, 1512, 1445, 1230, and 1195 cm^{-1}. UV λ_{max}^{MeOH}: 264 nm (ε=8900, sh), 272 (9700), 284 (6600), 318 (2200), 359 (1800), 407 (2100), and 424 (1900)].

We are grateful to the Ministry of Education, Science, and Culture for a financial assistance through

a Grant-in-Aid for Scientific Research to A. M. (No. 60470025).

References

1) E. Sebe and S. Matsumoto, *Proc. Jpn. Acad.*, **29**, 207 (1953).

2) Y. Kitahara and M. Funamizu, *Bull. Chem. Soc. Jpn.*, **31**, 782 (1958); Y. Kitahara and T. Kato, *ibid.*, **37**, 895 (1964).

3) H. Takeshita, I. Kouno, and K. Miyake, *Kyushu Daigaku Seisan Kagaku Kenkyusho Hokoku*, **66**, 1 (1977); H. Takeshita, K. Tajiri, and I. Kouno, *Heterocycles*, **6**, 1101 (1977).

4) A. Pride, J. Zindely, and H. Schmid, *Helv. Chim. Acta*, **57**, 1598 (1974); R. M. Harrison, J. D. Hobson, and A. W. Midgley, *J. Chem. Soc., Perkin Trans. 1*, **1973**, 1958.

5) H. Takeshita, K. Tajiri, and I. Kouno, *Bull. Chem. Soc. Jpn.*, **52**, 223 (1979).

6) R. B. Woodward and R. Hoffmann, "The Conservation of Orbital Symmetry," Verlag Chemie, GmbH., Weinheim/Bergstr. (1970), p. 114.

7) H. Takeshita, H. Mametsuka, and K. Uchida, Chem. Lett., **1982**, 1061. Even the 2-alkoxy-(or 2-cycloalkoxy)-tropones were thermolyzed via the other concerted process, to alkenes (or cycloalkenes) and tropolones. See H. Takeshita and H. Mametsuka, *J. Chem. Soc., Chem. Commun.*, **1983**, 483; *Can. J. Chem.*, **62**, 2035 (1984).

8) R. M. Harrison, J. D. Hobson, and M. M. Al Holly, *J. Chem. Soc. (C)*, **1971**, 3084.

9) H. Takeshita, H. Mametsuka, A. Chisaka, and N. Matsuo, *Chem. Lett.*, **1981**, 71.

10) H. Takeshita and H. Mametsuka, *Heterocycles*, **22**, 663 (1984).

11) H. Takeshita, H. Mametsuka, and H. Motomura, *J. Heterocyclic Chem.*, **23**, 1211 (1986).

12) H. Takeshita, A. Mori, Y. Watanabe, T. Kusaba, S. Sugiyama, and M. Kodama, in preparation.

13) H. Takeshita, H. Mametsuka, and N. Matsuo, *Bull. Chem. Soc. Jpn.*, **55**, 1137 (1982).

14) H. Takeshita, K. Tajiri, and I. Kouno, *Kyushu Daigaku Seisan Kagaku Kenkyusho Hokoku*, **70**, 65 (1979).

15) A. Mori, Y. Isayama, T. Kusaba, and H. Takeshita, *Kyushu Daigaku Sogo Rikogaku Kenkyuka Hokoku*, **3**, 125 (1981).

16) H. Takeshita, A. Mori, and Y. Goto, *Bull. Chem. Soc. Jpn.*, **59**. 1125 (1986).

17) A. Mori, T. Kusaba Y. Isayama, and H. Takeshita, *Chem. Lett.*, **1986**, 155.

18) The **11**-d_2 was prepared by heating in a sealed tube at 170—180 °C with D_2O (See H. Takeshita, T. Kusaba, and A. Mori, *Chem. Lett.*, **1982**, 701). The product was inevitably contaminated by some amounts of mono-, tri-, and tetradeuterio derivatives. The isotope distributions of **1**-d_2 prepared from this sample can be seen in Table 1.

19) The [3,7] sigmatropy has been proposed in Claisen rearrangement of 3-bromo- and 3-chloro-2-(2-propynyloxy)-tropones to 7-halo-cyclohepta[*b*]furan-8-ones. See R. M. Harrison, J. D. Hobson, and A. W. Midgley, *J. Chem. Soc., Perkin Trans. 1*, **1976**, 2403.

20) The electrolysis was carried out by Hokuto Denko Potentiostat/Galvanostat HA-301.

21) Formation of **14** from **13** constituted another structure proof for **2**.

22) Integrated peak area were calculated from the underlined standard values.

Reaction of Olefins with α-Cyanoacetamide in the Presence of Manganese(III) Acetate

Hidehiko SATO, Hiroshi NISHINO,* and Kazu KUROSAWA
Department of Chemistry, Faculty of Science, Kumamoto University, Kurokami 2-39-1, Kumamoto 860
(Received October 3, 1986)

2-Butenamides and 2-buten-4-olides are formed by the reaction of phenyl or 4-chlorophenyl-substituted olefins with α-cyanoacetamide in the presence of manganese(III) acetate. On the other hand, aryl substituted olefins having electron-donating groups are oxidized under similar reaction conditions to give 1,5-dihydro-2*H*-pyrrol-2-ones and 3-ethenyl-2-pyrrolidones. All these reactions also produce glycols or ketones which are given by the direct oxidation of these olefins with manganese(III) acetate. The question whether an intermediate carbocation in the oxidation process cyclized on an oxygen or a nitrogen atom can be explained by the hard and soft acids and bases (HSAB) concept. A possible mechanism for the formation of 2-butenamides and 2-buten-4-olides is proposed.

Recently, some useful annulation reactions using manganese(III) salts have been reported. Manganese(III) acetate oxidation of alkenes in acetic acid gave γ-lactones,[1] and similar oxidation in the presence of malonic acid or substituted acetic acid yielded spirodi-γ-lactones[2] or α-substituted γ-lactones.[3] On the other hand, alkenes were oxidized with tris(2,4-pentanedionato)manganese(III) to produce dihydrofurans in good yields.[4] One of the authors tried spirodilactamization by the manganese(III) oxidation of malonamide in the presence of alkenes. However, this oxidation did not give spiroannulated products, but α,β-unsaturated γ-lactones and γ-lactams along with other products.[5] This prompted us to investigate the synthesis of γ-lactam analogs, which might be bioactive new compounds or precursors of naturally occurring compounds, by the use of α-cyanoacetamide instead of malonamide. It was found that the reaction gave γ-lactams and γ-lactones together with some other products. We will describe these results and discuss the factors which may govern the mode of the cyclization either on a nitrogen atom or an oxygen atom in the acetamide group.

Results and Discussion

When a mixture of 1,1-diphenylethene (**1a**) and α-cyanoacetamide was oxidized with manganese(III) acetate, products **2a** and **3a** were obtained together with small amounts of **4a**, **5a**, **8a**, **9a**, and benzophenone (**10a**) (Table 1, Entry 1). The ^{1}H NMR spectrum of **2a** showed a singlet due to a vinylic proton at δ 8.51 and the ^{13}C NMR spectrum exhibited three singlets assigned to two carbonyl carbons and a cyano carbon. The IR spectrum of **2a** revealed a characteristic absorption band due to α,β-unsaturated nitrile. These spectral data indicated that the structure of **2a** was 4-acetoxy-2-cyano-4,4-diphenyl-2-butenamide. However, the configuration of the C=C double bond in **2a** could not be determined. The structures of **3a**, **4a**, **5a**, **8a**, and **9a** were determined to be 2-cyano-4,4-diphenyl-2-buten-4-olide, 2-carbamoyl-4,4-diphenyl-2-buten-4-olide, 2-cyano-2-(2,2-diphenylethenyl)-4,4-diphenyl-4-butanolide, 3-cyano-3-(2,2-diphenylethenyl)-5,5-diphenyl-2-pyrrolidone, and 4-acetoxy-2-cyano-4,4-diphenylbutanamide, respectively, on the basis of their spectral data. When a similar reaction was carried out under anhydrous conditions, the carbamoylbutenolide (**4a**) was not formed (Entry

Table 1. Reaction of 1,1-Diphenylethene (**1a**) with α-Cyanoacetamide in the Presence of Manganese(III) Acetate at the Reflux Temperature

Entry	Molar ratio[a]	Time / min	Recovery / %	Product (yield/%)[b]						
				2a	**3a**	**4a**	**5a**	**8a**	**9a**	**10a**
1	1 : 1 : 4	1	3	22	15	2	3	5	3	2
2	1 : 2 : 4	1	5	21	14	2	4	8	5	2
3[c]	1 : 2 : 4	1	3	25	13		4	6	5	3
4	1 : 4 : 4	1	6	20	13	3	4	10	4	2
5	1 : 1 : 6	66		7	13	20	9	10		8
6	1 : 2 : 6	20		14	14	9	7	9		5
7	1 : 6 : 6	1	1	12	12	5		8	2	3

a) **1a** : $CH_2(CN)CONH_2$: manganese(III) acetate. b) The yields are based on the amount of the **1a** used. c) Acetic anhydride (10 equivalents) was added.

3). On the other hand, the oxidation in a molar ratio of **1a**:α-cyanoacetamide:manganese(III) acetate=1:1:6 gave **4a** as the main product and the yield of **2a** decreased, although the reaction time has become longer (Entry 5). It suggests that the **2a** could be hydrolyzed under the reaction conditions to yield **4a**. In fact, the **2a** gave **4a** (27%) on treatment with six molar equivalents of manganese(II) acetate tetrahydrate, $[Mn(OAc)_2]\cdot 4H_2O$, in boiling acetic acid for 2 h. The cyanobutenolide (**3a**) was also hydrolyzed in the presence of manganese(II) acetate tetrahydrates to yield **4a** (21%). However, this route (**3a**→**4a**) would not be important because the **3a** was constantly produced irrespective of the molar ratio.

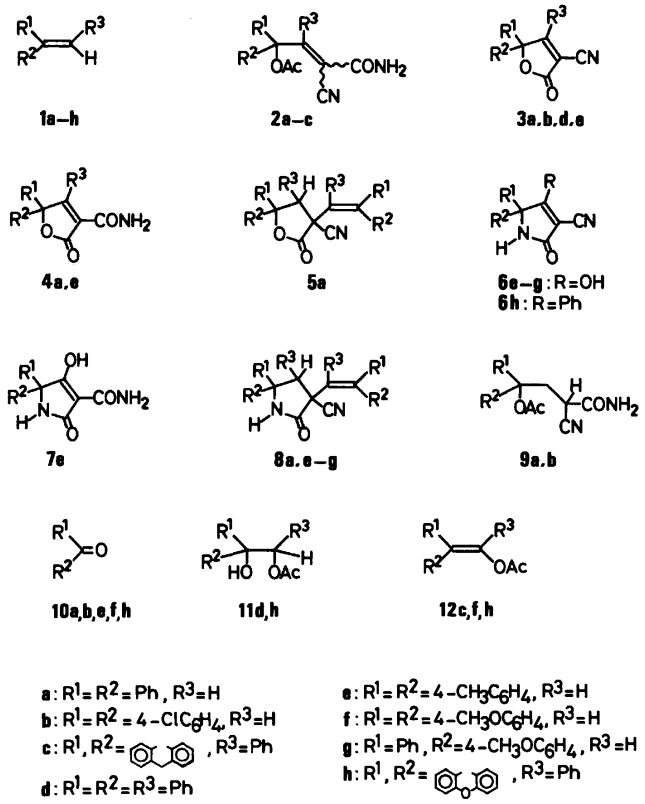

Fig. 1.

The similar oxidations of 1,1-bis(4-chlorophenyl)-ethene (**1b**), 9-benzylidene-9,10-dihydroanthracene (**1c**), and 1,1,2-triphenylethene (**1d**) mainly produced butenamides (**2b** an **2c**) and butenolides (**3b** and **3d**) (Table 2, Entries 2-4).

On the other hand, 1,1-bis(4-methoxyphenyl)ethene (**1f**) was oxidized under similar reaction conditions to yield 3-cyano-4-hydroxy-5,5-bis(4-methoxyphenyl)-1,5-dihydro-2*H*-pyrrol-2-one (**6f**) and 3-cyano-3-[2,2-bis(4-methoxyphenyl)ethenyl]-5,5-bis(4-methoxyphenyl)-2-pyrrolidone (**8f**) along with small amounts of 4,4′-dimethoxybenzophenone (**10f**) and 1-acetoxy-2,2-bis(4-methoxyphenyl)ethene (**12f**) (Table 2, Entry 6).

It has already been discussed that the reaction of aryl-substituted olefins having electron-donating groups with malonamide tends to give such *N*-cyclized products as 1,5-dihydro-2*H*-pyrrol-2-ones.[5] Reactions of 1-(4-methoxyphenyl)-1-phenylethene (**1g**) and 9-benzylidene-9*H*-xanthene (**1h**) with α-cyanoacetamide also yielded 1,5-dihydro-2*H*-pyrrol-2-ones (**6g** and **6h**) and 3-ethenyl-2-pyrrolidone (**8g**). However, the oxidation of **1h** mainly gave 9-xanthenone (**10h**), 9-(α-acetoxybenzyl)-9-xanthenol (**11h**), 9-(α-acetoxybenzylidene)-9*H*-xanthene (**12h**), and α,α-diacetoxytoluene (**14**), which would be formed via an electron-transfer mechanism. This mechanism is well-known in manganese(III) acetate oxidation.[1d,6]

The structure of manganese(III) acetate has been erroneously described in organic chemistry to be a simple acetate, $[Mn(OAc)_3]\cdot 2H_2O$, until a recent date.[5,7,8] However, Fristad et al. explained the radical mechanism for the manganese(III)-mediated γ-lactone annulation by use of the correct structure of manganese(III) acetate: oxygen-centered triangle, $[Mn_3O(OAc)_6(OAc)(HOAc)]\cdot 5H_2O$.[1c,9] In the manganese(III)-α-cyanoacetamide system, a similar mechanism can be considered (Scheme 1), and compound **3** or **6** would be formed via path A. On path A, it was assumed that butanolide(**I**) might be a precursor of **3** and **5**. When 2-cyano-4,4-diphenyl-4-butanolide

Table 2. Reaction of Olefins (**1a—h**) with α-Cyanoacetamide in the Presence of Manganese(III) Acetate at the Reflux Temperature[a,b]

Entry	Substrate	Recovery(%)	Product (yield/%)[c]						
1	**1a**	5	**2a** (21)	**3a** (14)	**4a** (2)	**5a** (4)	**8a** (8)	**9a** (5)	**10a** (2)
2	**1b**	11	**2b** (24)	**3b** (15)	**9b** (7)	**10b** (6)			
3	**1c**	5	**2c** (30)	**12c** (30)	**13** (22)				
4	**1d**	39	**3d** (30)	**10a** (trace)		**11d** (5)			
5	**1e**		**3e** (5)	**4e** (7)	**6e** (3)	**7e** (1)	**8e** (44)	**10e** (3)	
6	**1f**		**6f** (23)	**8f** (33)	**10f** (5)	**12f** (3)			
7	**1g**		**6g** (7)	**8g** (37)					
8	**1h**	1	**6h** (14)	**10h** (26)	**11h** (40)	**12h** (7)	**14** (27)		

a) **1** : $CH_2(CN)CONH_2$: manganese(III) acetate=1 : 2 : 4. b) The reactions were terminated within 1 min. c) The yields are based on the amount of the substrate used.

(**I**, $R^1=R^2=Ph$), which was prepared by an alternative method,[3c,3d,10] was oxidized with manganese(III) acetate, **3a** was not formed, while the oxidation of **I** ($R^1=R^2=Ph$) in the presence of **1a** gave rise to **5a**. Therefore, one can consider another pathway (path B) for the formation of **3** or **6** via 2-cyano-3-butenamide (**III**) as a reaction intermediate. The intermediate **III** was not isolated from the reaction products, probably because **III** was more liable to be oxidized than the parent olefin under the reaction conditions. However, the involvement of **III** is suggested by the fact that 2,2-diphenylethenylmalonate (**15**) was actually isolated together with 2-ethoxycarbonyl-4,4-diphenyl-2-buten-4-olide (**16**) in the manganese(III)-mediated reaction of **1a** with diethyl malonate and that the **15** was subsequently converted to **16** under the reaction conditions (Table 3).

The cyclization of carbocation (**II** or **IV**) depends on whether **II** or **IV** is "hard" or "soft" on the basis of the hard and soft acids and bases (HSAB) concept.[12] That is to say, when the cation is relatively hard (as in the cases of **1a—d**), it cyclizes on an oxygen atom to give butenolide (**3**), while the reaction of **1f—h** yields 1,5-dihydro-2*H*-pyrrol-2-one (**6**) since the carbocation derived from **1f—h** is relatively soft. This tendency is also the case for the reaction with malonamide.[5] Both *O*-cyclized (**3e** and **4e**) and *N*-cyclized products (**6—8e**) were obtained by the reaction of **1e**, indicating that the corresponding carbocation (**IV**) has an intermediate

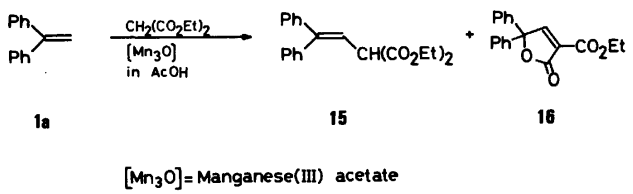

Fig. 2.

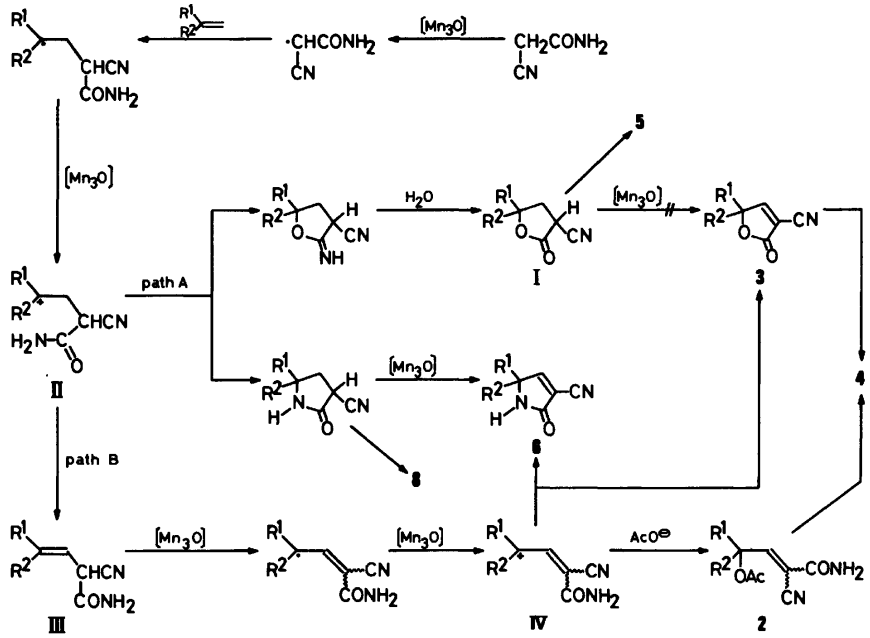

Scheme 1.

Table 3. Reaction of 1,1-Diphenylethene (**1a**) with Diethyl Malonate in the Presence of Manganese(III) Acetate and Oxidation of the Product (**15**)[a]

Entry	Substrate	Molar ratio[b]	Time / min	Recovery / %	Product (yield/%)[c]	
					15	**16**
1	**1a**	1 : 1 : 3	3	28	26	20
2	**1a**	1 : 1 : 4	5	12	26	40
3	**1a**	1 : 1 : 5	6		22	56
4	**1a**	1 : 1 : 6	90			70
5	**15**	1 : 2[d]	5	29		48
6	**15**	1 : 4[d]	210			75

a) The reactions were carried out at the reflux temperature. b) Substrate : $CH_2(CO_2Et)_2$: manganese(III) acetate. c) The yields are based on the amount of the substrate used. d) **15** : manganese(III) acetate.

nature of "hard and soft acids." It seems that the formation of **2** depends on the configuration of **IV**. When the configuration of the cyano group and the $-\overset{+}{C}R^1R^2$ group on **IV** is cis, the **IV** could not cyclize on a nitrogen atom of nitrile, but was probably attacked by an acetate ion to give **2**.

In conclusion, the reaction of olefins with α-cyanoacetamide gave 2-butenamides, 2-buten-4-olides, 1,5-dihydro-2*H*-pyrrol-2-ones, and 3-ethenyl-2-pyrrolidones; these are more complex than the products in the reaction with malonamide.[5] Although the cyano group on α-cyanoacetamide is favorable to the formation of the $\cdot CH(CN)CONH_2$ radical, the cyano group itself is not so reactive in these reactions: the cyclization involving the cyano group did not occur. The reason for the absence of spiroannulation products in the reaction with α-cyanoacetamide or diethyl malonate could be ascribed to the preferential formation of **III** via path B and to the difficulty of the spiroannulation of **5** and **8** involving the cyano group. Moreover, the formation of **3** and **6** could be explained by the HSAB concept.

Experimental

Measurements. Melting points were determined with an Electrothermal apparatus and are uncorrected. The IR spectra were taken on a JASCO A-102 infrared spectrometer. The ^1H and ^{13}C NMR spectra were recorded on a Hitachi Perkin-Elmer R-24 (60 MHz) and a JEOL FX-100 instrument at room temperature. The mass spectra were obtained with a JEOL JMS-DX-300 mass spectrometer using a direct-insertion probe at an ionizing voltage of 70 eV.

Materials. The olefin (**1a—h**) and manganese(III) acetate used were prepared according to methods described in the literature.[5] α-Cyanoacetamide, diethyl malonate, and manganese(II) acetate tetrahydrate were obtained from commercial samples from the Wako Pure Chemical Industries, Ltd.

Reaction of Olefins with α-Cyanoacetamide. The typical procedure for the reaction of olefins with α-cyanoacetamide in the presence of manganese(III) acetate was as follows. To a heated solution of olefin (1 mmol) and α-cyanoacetamide (2 mmol) in acetic acid (25 cm^3), manganese(III) acetate (4 mmol) which was calculated based on the formula weight of $[Mn(OAc)_3 \cdot 2H_2O]$[5] was added. The mixture was heated under reflux until the color of Mn(III) ion changed from brown to transparent. The solvent was removed in vacuo and the residue was triturated with 2 M (1 M=1 mol dm^{-3}) hydrochloric acid (25 cm^3), followed by extraction with chloroform. The products were separated on TLC (Wakogel B-10 or Kieselgel 60G) with chloroform or diethyl ether as the developing solvent. The characteristic data of the new compounds are summarized in Table 4. All spectral data and the melting points of known compounds were identical with those reported in the literatures.

Oxidation Products. 1a: 2a, 3a, 4a,[5] **5a, 8a, 9a,** and **10a.**[5] **1b**: 4-Acetoxy-4,4-bis(4-chlorophenyl)-2-cyano-2-butenamide (**2b**), 4,4-bis(4-chlorophenyl)-2-cyano-2-buten-4-olide (**3b**), 4-acetoxy-4,4-bis(4-chlorophenyl)-2-cyanobutanamide (**9b**), and 4,4'-dichlorobenzophenone (**10b**).[11]

1c: 3-(9-Acetoxy-9,10-dihydro-9-anthryl)-2-cyano-3-phenylpropenamide (**2c**), 9-(α-acetoxybenzylidene)-9,10-dihydroanthracene (**12c**),[5] and 9-acetoxy-9-benzoyl-9,10-dihydroanthracene (**13**).[5]

1d: 2-Cyano-3,4,4-triphenyl-2-buten-4-olide (**3d**), **10a**, 2-acetoxy-1,1,2-triphenylethanol (**11d**).[5]

1e: 2-Cyano-4,4-bis(4-methylphenyl)-2-buten-4-olide (**3e**), 2-carbamoyl-4,4-bis(4-methylphenyl)-2-buten-4-olide (**4e**), 3-cyano-4-hydroxy-5,5-bis(4-methylphenyl)-1,5-dihydro-2*H*-pyrrol-2-one (**6e**), 3-carbamoyl-4-hydroxy-5,5-bis(4-methylphenyl)-1,5-dihydro-2*H*-pyrrol-2-one (**7e**), 3-cyano-3-[2,2-bis(4-methylphenyl)ethenyl]-5,5-bis(4-methylphenyl)-2-pyrrolidone (**8e**), and 4,4'-dimethylbenzophenone (**10e**).[12]

1f: **6f, 8f, 10f,**[13] and **12f.**[14]

1g: 3-Cyano-4-hydroxy-5-(4-methoxyphenyl)-5-phenyl-1,5-dihydro-2*H*-pyrrol-2-one (**6g**) and 3-cyano-3-[2-(4-methoxyphenyl)-2-phenylethenyl]-5-(4-methoxyphenyl)-5-phenyl-2-pyrrolidone (**8g**). The stereochemistry of **6g** and **8g** was not determined.

1h: 4-Cyano-3-phenyl-1,5-dihydrospiro[2*H*-pyrrole-2,9'-xanthen]-5-one (**6h**), **10h,**[15] **11h,**[5] **12h,**[4] and **14.**[16]

Hydrolyses of 2a and 3a. When **2a** (174.0 mg) was treated with manganese(II) acetate tetrahydrate (803.5 mg) in acetic acid (25 cm^3) for 2 h at reflux temperature, **4a** (41.8 mg, 27%) and **2a** (52.0 mg, 30% recovered) were obtained. On the other hand, **3a** (168.9 mg) and manganese(II) acetate tetrahydrate (636.9 mg) were heated under reflux in acetic acid (25 cm^3) for 80 min, giving **4a** (38.0 mg, 21%) and **3a** (90.4 mg, 53% recovered).

Synthesis of 2-Cyano-4,4-diphenyl-4-butanolide (I). A mixture of **1a** (903.5 mg), cyanoacetic acid (3.401 g), and manganese(III) acetate (2.746 g) was heated in acetic acid (50 cm^3) at 70 °C for 15 min according to Fristad method.[3b] On cooling, water (200 cm^3) was added to it and the aqueous solution was extracted with ether. The ethereal extract was washed with aqueous sodium hydrogencarbonate solution and then water. The reaction products were purified on TLC, giving colorless liquid **I** (650.2 mg, 49%). All spectral data were identical with those of the literature.[3b]

Oxidation of 2-Cyano-4,4-diphenyl-4-butanolide (I) with Manganese(III) Acetate. The butanolide **I** (183.6 mg) was oxidized with manganese(III) acetate (373.9 mg) in acetic acid (25 cm^3). The mixture was heated under reflux for 3 min and gave a tarry material, but the butenolide (**3a**) was not detected.

The Reactions of 1,1-Diphenylethene (1a) and 2-Cyano-4,4-diphenyl-4-butanolide (I). A mixture of **1a** (154.5 mg), **I** (223.0 mg), and manganese(III) acetate (457.2 mg) was heated under reflux in acetic acid (25 cm^3) for 1 min. After treatment by the procedure described above, a mixture of **5a** and 3-cyano-1,1,5,5-tetraphenyl-4-penten-1-ol (115.7 mg, 31% yield as **5a**) was obtained and **1a** was recovered (29%).

3-Cyano-1,1,5,5-tetraphenyl-4-penten-1-ol: Colorless prisms (from light petroleum), mp 105.0—105.5 °C; IR ($CHCl_3$) 2236 (CN) and 3200—3600 (OH); ^1H NMR ($CDCl_3$) δ=2.28 (1H, s, OH), 2.6—2.9 (2H, m, CH_2), 3.2—3.7 (1H, m, >CH–), 5.92 (1H, d, J=9.6 Hz, =CH–), and 6.7—7.6 (20H, m, 4×Ph). Found: C, 86.44; H, 6.00; N, 3.32%. Calcd for $C_{30}H_{25}ON$: C, 86.71; H, 6.06; N, 3.37%.

Reaction of 1,1-Diphenylethene (1a) with Diethyl Malonate in the Presence of Manganese(III) Acetate. To a heated solution of **1a** (1 mmol), diethyl malonate (1 mmol), and

Table 4. Characteristic Data of the New Compounds

Compd	Mp θ_m/°C	IR[a] cm^{-1}	^{1}H and ^{13}C NMR[b] δ	MS *m/z* (rel int)	Analysis Formula	Analysis Found(Calcd)
2a	169.7—170.3 (benzene)	1226(C-O-C) 1623(C=C) 1701(C=O) 1748(C=O) 2220(CN) 3100—3600(NH_2)	2.21(3H, s, OAc), 6.17(2H, br. s, NH_2), 7.1—7.5(10H, m, 2×Ph), 8.51(1H, s, =CH-); 21.1(q, CH_3), 84.0(s, C-O), 106.0 (s, =C<), 115.0(s, CN), 127.0(d, Arom. C), 128.5(d, Arom. C), 128.6(d, Arom. C), 140.6(s, Arom. C), 158.0(d, =CH-), 161.0(s, $CONH_2$), 168.7(s, O-CO-)	320(M^+, 5) 278(12) 261(32) 217(75) 173(100) 105(70) 77(40) 43(100)	$C_{19}H_{16}O_3N_2$	*m/z* 320.1142 (M, 320.1161)
2b	187.6—188.1 (CCl_4)	1216(C-O-C) 1623(C=C) 1702(C=O) 1753(C=O) 2220(CN) 3100—3600(NH_2)	2.21(3H, s, OAc), 6.31(2H, br. s, NH_2), 7.23(8H, s, Arom. H), 8.38(1H, s, =CH-)		$C_{19}H_{14}O_3N_2Cl_2$	C 58.56(58.63) H 3.60(3.63) N 7.16(7.20)
2c	112.8—113.7 (benzene/hexane)	1225(C-O-C) 1683(C=O) 1744(C=O) 2200(CN) 3100—3500(NH_2)	2.11(3H, s, OAc), 3.42(2H, s, CH_2), 4.9(1H, br. s, NH_2), 6.02 (1H, br. s, NH_2), 6.3—6.8(2H, m, Arom. H), 6.8—7.7(10H, m, Arom. H), 7.9—8.2(1H, m, Arom. H)	408(M^+, 17) 348(26) 275(100) 232(16)	$C_{26}H_{20}O_3N_2$	*m/z* 408.1477 (M, 408.1474)
3a	140.5—141.5 (methanol)	1627(C=C) 1786(C=O) 2240(CN)	7.1—7.6(10H, m, 2×Ph), 8.50(1H, s, =CH-)	261(M^+, 10) 184(2) 105(100) 77(17)	$C_{17}H_{11}O_2N$	C 78.13(78.15) H 4.16(4.24) N 5.26(5.36)
3b	110.0—110.4 (benzene/hexane)	1629(C=C) 1789(C=O) 2244(CN)	7.0—7.5(8H, m, Arom. H) 8.49(1H, s, =CH-)		$C_{17}H_9O_2NCl_2$	C 61.88(61.84) H 2.78(2.75) N 4·21(4.24)
3d	187.0—188.0 (methanol)	1770(C=O) 2236(CN)	7.1—7.6(15H, m, 3×Ph)		$C_{23}H_{15}O_2N$	C 81.98(81.88) H 4.65(4.48) N 4.30(4.15)
3e	93.8—94.6 (diethyl ether/light petroleum)	1627(C=C) 1785(C=O) 2244(CN)	2.28(6H, s, 2×CH_3), 6.99(8H, s, Arom. H), 8.39(1H, s, =CH-)	289(M^+, 17) 119(100) 91(14)	$C_{19}H_{15}O_2N$	*m/z* 289.1079 (M, 289, 1103)

Table 4. (Continued 1)

Compd	Mp θ_m/°C	IR[a] cm^{-1}	^{1}H and ^{13}C NMR[b] δ	MS m/z (rel int)	Analysis Formula	Found(Calcd)
4e	184.2—184.7 (methanol)	1644 (C=C) 1685 (C=O) 1754 (C=O) 3300—3600 (NH_2)	2.31(6H, s, 2×CH_3), 6.50(1H, br. s, NH_2), 7.17(8H, s, Arom. H), 7.69(1H, br. s, NH_2), 8.70(1H, s, =CH-)		$C_{19}H_{17}O_3N$	C 74.26(74.25) H 5.75(5.58) N 4.66(4.56)
5a	104.5—105.5 (methanol)	1788 (C=O) 2232 (CN)	2.88(1H, d, J=13.8 Hz, CH_2), 3.00 (1H, d, J=13.8 Hz, CH_2), 6.15(1H, s, -CH=), 6.8—7.6(20H, m, 4×Ph)	441 (M^+, 3) 397 (69) 306 (100) 217 (59) 167 (76) 105 (41) 77 (38)	$C_{31}H_{23}O_2N$	m/z 441.1734 (M, 441.1729) C 84.36(84.33) H 5.21(5.25) N 3.10(3.17)
6e	273.7—274.7 (chloroform)	1648 (C=O) 2224 (CN)	2.29(6H, s, 2×CH_3), 3.43(1H, br. s, OH), 7.17(8H, s, Arom. H), 9.45(1H, br. s, NH)		$C_{19}H_{16}O_2N_2$	C 75.17(74.98) H 5.29(5.30) N 9.29(9.21)
6f	185.7—186.2 (chloroform)	1606 (C=C) 1651 (C=O) 2212 (CN) 3100—3500 (NH and OH)	3.72(6H, s, 2×OCH_3), 6.7—7.3(8H, m, Arom. H), 9.50(2H, br. s, NH and OH)		$C_{19}H_{16}O_4N_2$	C 67.57(67.85) H 4.76(4.80) N 8.19(8.33)
6g	210.0—211.0 (chloroform)	1647 (C=O) 2244 (CN) 3000—3600 (NH and OH)	3.71(3H, s, OCH_3), 6.8—7.5(9H, m, Arom. H), 9.54(2H, br. s, NH and OH)		$C_{18}H_{14}O_3N_2$	C 70.41(70.58) H 4.57(4.61) N 9.04(9.15)
6h	over 300 (methanol)	1690 (C=O) 2228 (CN) 3000—3500 (NH)	6.9—7.7(13H, m, Arom. H), 10.11(1H, br. s, NH)	350 (M^+, 100) 321 (15) 222 (66) 195 (70)	$C_{23}H_{14}O_2N_2$	C 78.70(78.84) H 4.05(4.03) N 7.95(8.00)
7e	213.4—214.4 (benzene)	1618 (C=C) 1654 (C=O) 3200—3600 (NH_2 and OH)	2.30(6H, s, 2×CH_3), 5.35(1H, br. s, OH), 6.63(1H, br. s, NH_2), 6.9—7.4(8H, m, Arom. H), 7.54(1H, br. s, NH_2), 8.28(1H, br. s, NH)	322 (M^+, 68) 279 (51) 262 (19) 193 (100) 179 (84)	$C_{19}H_{18}O_3N_2$	m/z 322.1312 (M, 322.1317)
8a	103.5—104.5 (benzene/hexane)	1716 (C=O) 2232 (CN) 3100—3500 (NH)	2.85(1H, d, J=13.8 Hz, CH_2), 2.95(1H, d, J=13.8 Hz, CH_2), 6.23(1H, s, =CH-), 6.9—7.5 (20H, m, 4×Ph), 8.23(1H, br. s, NH)	440 (M^+, 7) 397 (98) 306 (100) 217 (53) 167 (76)	$C_{31}H_{24}ON_2$	m/z 440.1874 (M, 440.1889)

Table 4. (Continued 2)

Compd	Mp θ_m/°C	IR[a] cm^{-1}	^{1}H and ^{13}C NMR[b] δ	MS *m/z* (rel int)	Analysis Formula	Found(Calcd)
8e	121.0—122.0 (benzene)	1715(C=O) 2232(CN) 3200—3500(NH)	2.25(3H, s, CH_3), 2.27(6H, s, 2× CH_3), 2.38(3H, s, CH_3), 2.87(2H, br. s, CH_2), 6.11(1H, s, =CH-), 6.8—7.3(16H, m, Arom, H), 8.72 (1H, br. s, NH)		$C_{35}H_{32}ON_2$	C 84.35(84.64) H 6.45(6.50) N 5.59(5.64)
8f	162.8—163.8 (benzene/hexane)	1720(C=O) 2232(CN) 3200—3500(NH)	2.83(1H, d, J=13.2 Hz, CH_2), 2.97(1H, d, J=13.2 Hz, CH_2), 3.69(3H, s, OCH_3), 3.70(3H, s, OCH_3), 3.75(3H, s, OCH_3), 3.84 (3H, s, OCH_3), 6.11(1H, s, =CH-), 6.6—7.5(16H, m, Arom. H), 8.93 (1H, br. s, NH)	560(M+, 62) 517(100) 396(86) 277(80) 227(63) 121(34)	$C_{35}H_{32}O_5N_2$	*m/z* 560.2388 (M, 560.2311)
8g	224.1—225.1 (benzene)	1716(C=O) 2228(CN) 3100—3500(NH)	2.82(2H, br. s, CH_2), 3.71(3H, s, OCH_3), 3.74(3H, s, OCH_3), 6.15(1H, s, =CH-), 6.6—7.6 (18H, m, Arom. H), 8.27(1H, br. s, NH)		$C_{33}H_{28}O_3N_2$	C 79.26(79.18) H 5.61(5.64) N 5.58(5.60)
9a	84.1—85.1 (benzene)	1227(C-O-C) 1702(C=O) 1740(C=O) 2240(CN) 3100—3600(NH_2)	2.17(3H, s, OAc), 2.8—4.0(3H, m, CH_2 -CH<), 5.90(1H, br. s, NH_2), 6.14(1H, br. s, NH_2), 7.1—7.5(10H, m, 2×Ph)	322(M+, 40) 262(14) 239(91) 220(41) 195(100) 183(83) 165(27) 105(62)	$C_{19}H_{18}O_3N_2$	*m/z* 322.1311 (M, 322.1317)
9b	169.7—170.1 (benzene/hexane)	1209(C-O-C) 1705(C=O) 1745(C=O) 2244(CN) 3100—3600(NH_2)	2.16(3H, s, OAc), 2.8—3.9(3H, m, CH_2-CH<), 6.25(2H, br. s, NH_2), 7.1—7.4(8H, m, Arom. H)		$C_{19}H_{16}O_3N_2Cl_2$	C 58.45(58.33) H 4.21(4.12) N 7.00(7.16)

a) All compounds were measured in $CHCl_3$ except for **6g** and **6h** (KBr disk). b) Compounds (**6e—g**) were dissolved in DMSO-d_6, others were dissolved in $CDCl_3$.

acetic acid (25 cm^3), manganese(III) acetate (3—6 mmol) was added. When the color of the solution turned from brown to transparent, the reaction was stopped and then the solvent was removed in vacuo. After a work-up, **15** and **16** were obtained.

Diethyl (2,2-Diphenylethenyl)malonate (15): Colorless liquid; IR ($CHCl_3$) 1726 (C=O); ^1H NMR (CCl_4) δ=1.25 (6H, t, J=7.2 Hz, 2×CH_3), 4.00 (1H, d, J=9.6 Hz, >CH-), 4.14 (4H, q, J=7.2 Hz, 2×CH_2), 6.21 (1H, d, J=9.6 Hz, =CH-), and 7.0-7.5 (10H, m, 2×Ph); MS *m/z* (rel intensity), 338 (M^+, 14), 266 (13), 191 (100), 165 (19), and 115 (24).

2-Ethoxycarbonyl-4,4-diphenyl-2-buten-4-olide (16): Colorless needles (from ethanol), mp 108—109 °C (lit,[3e] mp 107.9—109.4 °C).

Oxidation of Diethyl (2,2-Diphenylethenyl)malonate (15) with Manganese(III) Acetate. A mixture of **15** (0.5 mmol) and manganese(III) acetate (1 mmol) was heated under reflux in acetic acid (25 cm^3) and worked-up using the method described above, providing **16** in the yields shown in Table 3.

The authors wish to thank Dr. Teruyosi Marunaka of the Taiho Pharmaceutical Co., Ltd., Tokushima, for his kind arrangement for the measurements of the mass and ^{13}C NMR spectra. Thanks are also due to Associate Professor Akira Mori of the Research Institute of Industrial Science, Kyushu University, and Dr. Hiromichi Matsuura of the Wakunaga Pharmaceutical Co., Ltd., Hiroshima, for their arrangement for the measurements of the mass spectra. The present work was supported by a Grant-in-Aid for Encouragement of Young Scientists No. 60740282 from the Ministry of Education, Science and Culture (1985).

References

1) a) J. B. Bush, Jr. and H. Finkbeiner, *J. Am. Chem. Soc.*, **90**, 5903 (1968); b) E. I. Heiba, R. M. Dessau, and W. J. Koehl, Jr., *ibid.*, **90**, 5905 (1968); c) W. E. Fristad and J. R. Peterson, *J. Org. Chem.*, **50**, 10 (1985); d) J. A. Norman, C. B. Thomas, and M. J. Burrow, *J. Chem. Soc., Perkin Trans. 1*, **1985**, 1087.

2) a) N. Ito, H. Nishino, and K. Kurosawa, *Bull. Chem. Soc. Jpn.*, **56**, 3527 (1983); b) W. E. Fristad and S. S. Hershberger, *J. Org. Chem.*, **50**, 1026 (1985).

3) a) E. J. Corey and M. Kang, *J. Am. Chem. Soc.*, **106**, 5384 (1984); b) W. E. Fristad, J. R. Peterson, and A. B. Ernst, *J. Org. Chem.*, **50**, 3143 (1985); c) A. B. Ernst and W. E. Fristad, *Tetrahedron Lett.*, **26**, 3761 (1985); d) E. J. Corey and A. W. Gross, *Tetrahedron Lett.*, **26**, 4291 (1985); e) N. Fujimoto, H. Nishino, and K. Kurosawa, *Bull. Chem. Soc. Jpn.*, **59**, 3161 (1986).

4) a) H. Nishino, *Bull. Chem. Soc. Jpn.*, **58**, 1922 (1985); b) E. I. Heiba and R. M. Dessau, *J. Org. Chem.*, **39**, 3456 (1974).

5) H. Nishino, *Bull. Chem. Soc. Jpn.*, **58**, 217 (1985).

6) a) P. J. Andrulis, Jr., M. J. S. Dewar, R. Dietz, and R. L. Hunt, *J. Am. Chem. Soc.*, **88**, 5473 (1966); b) T. Aratani and M. J. S. Dewar, *ibid.*, **88**, 5479 (1966); c) P. J. Andrulis, Jr. and M. J. S. Dewar, *ibid.*, **88**, 5483 (1966); d) S. A. Zonis and Y. I. Kornilova, *Zhur. Obshchei Khim.*, **20**, 1252 (1950); *Chem. Abstr.*, **45**, 10196e (1951); e) S. A. Zonis and A. G. Pesina, *J. Gen. Chem., USSR*, **20**, 1223 (1950); *Chem. Abstr.*, **46**, 3496i (1952).

7) B. B. Snider, R. Mohan, and S. A. Kates, *J. Org. Chem.*, **50**, 3659 (1985).

8) F. A. Cotton and G. Wilkinson, "Advanced Inorganic Chemistry," 4th ed, John Wiley & Sons, Inc., New York (1980), pp. 736—744.

9) L. W. Hessel and C. Romers, *Recl. Trav. Chim. Pays-Bas*, **88**, 545 (1969).

10) E. I. Heiba, R. M. Dessau, and P. G. Rodewald, *J. Am. Chem. Soc.*, **96**, 7977 (1974).

11) G. I. Nikishin, M. G. Vinogradov, and T. M. Fedorova, *J. Chem. Soc., Chem. Commun.*, **1973**, 693.

12) T. Ho, "Hard and Soft Acids and Bases Principle in Organic Chemistry," Academic Press. Inc., New York (1977).

13) O. G. Backeberg and J. L. C. Marais, *J. Chem. Soc.*, **1945**, 803.

14) W. T. Nauta, M. J. Ernsting, and A. C. Faber, *Recl. Trav. Chim. Pays-Bas*, **60**, 915 (1941).

15) M. Bösler, *Ber.*, **14**, 328 (1881).

16) B. Danieli, F. Ronchetti, and G. Russo, *Chem. Ind. (London)*, **1973**, 1067.

Asymmetric Synthesis of (+)-Phosphinothricin and Related Compounds by the Michael Addition of Glycine Schiff Bases to Vinyl Compounds

Nobuto MINOWA,* Masao HIRAYAMA, and Shunzo FUKATSU
Central Research Laboratories, Meiji Seika Kaisha Ltd., Morooka, Kohoku-ku, Yokohama 222
(Received October 3, 1986)

(*S*)-(+)-Phosphinothricin was prepared in good optical yield by the Michael addition of chiral glycine Schiff base derived from (*S*)-2-hydroxy-3-pinanone to vinyl phosphorus compound. (*R*)-(−)-Phosphinothricin, an enantiomeric isomer, can also be prepared from the same chiral glycine Schiff base by choosing suitable reaction temperature.

The stereochemistry of an amino carbon is a biologically important factor in naturally occurring phosphorus analogues of glutamic acid, such as phosphinothricin ((*S*)-(+)-(**1**)),[1] its alanylalanine derivative **2**,[1] and (+)-2-amino-4-phosphonobutyric acid ((*S*)-(+)-(**3**)),[2] which have been paid a special attention for their herbicidal[3] and antiviral activities.

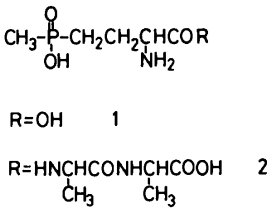

Scheme 1.

Although several methods for the racemic synthesis were already known[4], there have been reported a few example for the asymmetric synthesis.[5] In our preliminary communications,[4g,5] we reported a practical synthesis of (±)-**1** and an effective asymmetric synthesis of (*S*)-(+)-**1**, (*S*)-(+)-**3**, and their enantiomers by the Michael addition of glycine Schiff base to vinyl phosphorus compounds. In the latter, the S- and R-configuration were induced from two glycine Schiff bases bearing different chiral auxiliaries derived from (*S*)-2-hydroxy-3-pinanone ((−)-(**9**)) and its (**R**)-isomer (+)-**9**, respectively. In the course of our study on the asymmetric Michael addition, it has been found that the stereochemistry of the Michael adducts is reversed depending on reaction temperature to yield the *S*-enantiomer at −78 °C and *R*-enantiomer at an elevated temperature. Thus, both enantiomers can be easily prepared from a single chiral glycine Schiff base (−)-**10** by choosing suitable reaction temperature. In this paper, we would like to report the features of the Michael addition of glycine Schiff bases to several kinds of vinyl compounds in detail.

Results and Dicussion

Our basic strategy for the synthesis of glutamic acid analogues involves the Michael addition of glycine Schiff base to appropriate vinyl compounds; The retrosynthetic analysis of **1** is illustrated in Scheme 2.

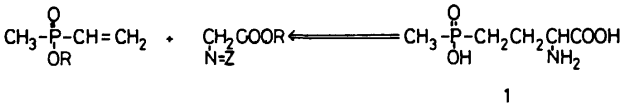

Scheme 2.

Racemic Synthesis of Phosphinothricin 1. Racemic (±)-**1** was synthesized according to the procedures shown in Scheme 3. Methyl vinylmethylphosphinate (**4a**), a Michael acceptor, was conveniently prepared by the following two methods: Trimethyl phosphite (**5**) was converted to methylphosphonochloridate **6** by the Arbusov rearrangement followed by chlorination. Coupling of a vinyl group with phosphorus atom was

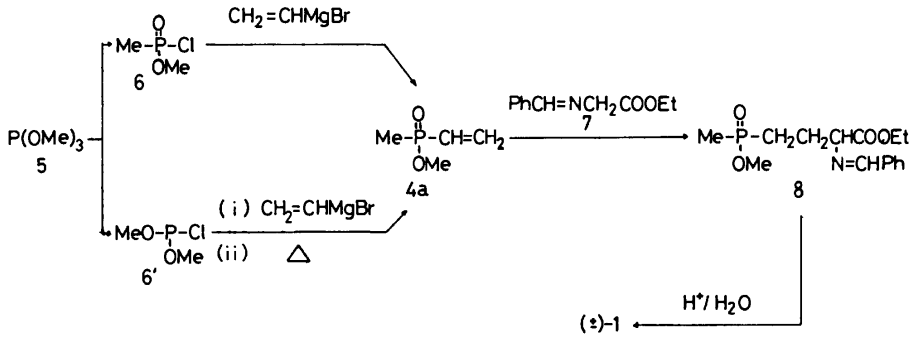

Scheme 3.

accomplished by the addition of vinylmagnesium bromide to **6** in tetrahydrofuran (THF) to give the desired phosphinate **4a** in 61% yield. As a vinyl group could be directly introduced into various phosphonochoridate, this procedure provides a general and facile method for the preparation of vinylalkylphosphinates. According to an alternative method, phosphorochloridite **6'**, prepared by treating **5** with phosphorous trichloride, was subjected to alkylative coupling with vinylmagnesium bromide in THF and the resulting vinylphosphonite was heated to afford **4a**. The α-amino acid part could be successfully introduced into the vinyl group of **4a** by utilizing Schiff base **7** of glycine ethyl ester as a Michael donor. Treatment of the Schiff base with **4a** in the presence of 0.2 equiv of base afforded the adduct **8**, which was successively refluxed with 6M-hydrochloric acid (1 M=1 mol dm^{-3}) for 24 h to give racemic phosphinothricin (±)-**1** as shown in Table 1 after purification (Dowex 50×2). Although the use of either sodium ethoxide or potassium hydroxide in ethanol gave the (±)-**1** in good yield, the latter base was preferable in practice because the reaction is carried out at room temperature (Entries 1—4). The use of the other bases, DBN and Triton B, could not improve the yield of (±)-**1**. (Entries 6, 7).

Asymmetric Synthesis of (*S*)-(+)-1 and (*R*)-(−)-1. A successful Michael addition of the achiral glycine Schiff base **7** suggested that the desired S-configuration of **1** would be prepared by a similar procedure utilizing a chiral Schiff base **7**. Attempted experiment to perform the asymmetric addition of **7** to **4a** in the presence of a chiral base, quinine, was unsuccessful, while the addition of a chiral Schiff base to **4a** provided optically active adduct **1**. Although a number of asymmetric reactions with chiral acceptors has been known,[6] there have been reported a few examples of using chiral Michael donors.[7]

The asymmetric Michael addition was shown in Scheme 4. Chiral Schiff bases (−)-**10** and (+)-**10** having chiral auxiliaries were readily prepared by the condensation of glycine ethyl ester with (*S*)-2-hydroxy-3-pinanone (−)-(**9**) and its (R)-isomer (+)-(**9**) obtained by oxidation of natural (+)-α-pinene and (−)-α-pinene, respectively.[8] The results of the Michael addition of these chiral Schiff base to

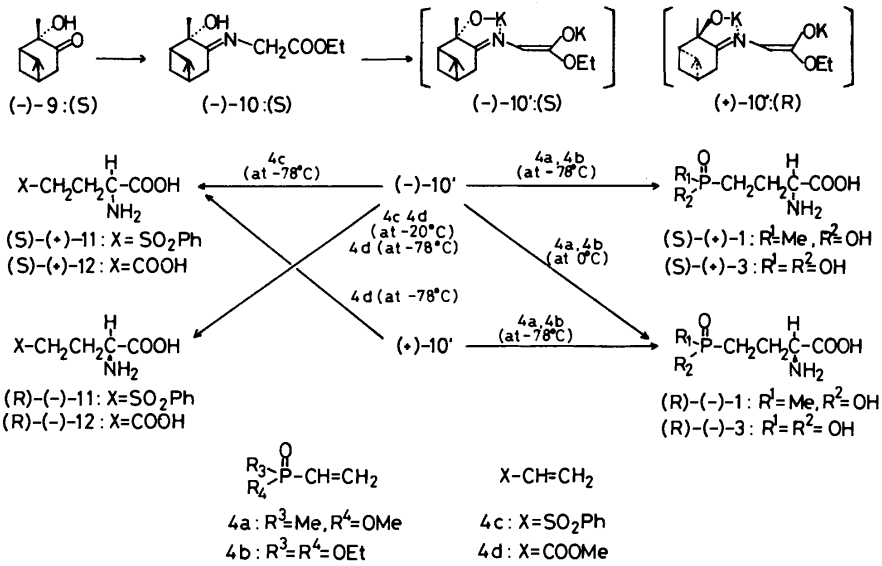

Scheme 4.

Table 1. The Michael Addition of **7** to **4a**

Entry	Base	Ratio[a]	Solvent	Temperature/°C (Time/h)	Yield/% (±)-**1**
1	EtONa	1 : 1.5 : 0.25	EtOH	−10 (5)	64
2	EtONa	1 : 1 : 0.25	EtOH	−10 (4)	50
3	EtONa	1 : 1 : 0.25	EtOH	5 (7)	36
4	KOH	1 : 1.5 : 0.2	EtOH	r.t. (2)	65
5	KOH	1 : 1.5 : 0.2	PhH	r.t. (4)	30
6	DBN	1 : 1.5 : 0.2	$PhCH_3$	r.t. (6)	11
7	Triton B	1 : 1.5 : 0.2	EtOH	r.t. (2)	26

a) Molar ratio of **4a** : **7** : base.

vinylphosphinate **4a** investigated under various conditions at −78 °C are summarized in Table 2. (Entries 1—10) Metalation of the chiral Schiff base (−)-**10** with two equivalents of potassium *t*-butoxide (*t*-BuOK) in THF followed by conjugate addition of the dianion **10′** to an equimolar amount of vinylphosphinate **4a** at −78 °C gave the Michael adduct, which was further converted into the desired phosphinothricin (S)-(+)-**1** with 79% optical purity in 66% yield (Entry 1). The results of the effects of concentration and molar ratio of the reactants, reverse addition of the reactants, and solvent are summarized in Entries 2—9. Particularly, reverse addition of the reactants reduced enantiomeric excess extremely from 79 to 2%. In addition, similar treatment after metalation of (−)-**10** with other base, sodium hydride or lithium diisopropylamide, gave no desired product. Judging from extreme decrease of the optical purities shown in the effects of the reverse addition and change of the molar ratio, a proceeding metalation of (−)-**10** with *t*-BuOK seemed to be important for this asymmetric synthesis. Similar asymmetric addition of the other glycine Schiff base (+)-**10** to **4a** gave unnatural phosphinothricin (*R*)-(−)-(**1**) with 73% optical purity in a similar yield as (*S*)-(+)-**1**. (Entry 10).

The stereoselectivity is not influenced by the kind of the solvents, such as toluene, Et_2O, and THF. (Entries 1, 8, and 9) However, addition of hexamethylphosphoric triamide (HMPA) or dicyclohexano-18-

Table 2. The Asymmetric Michael Addition of (−)-**10** and (+)-**10** to Vinyl Compounds **4a**, **4b**, **4c**, and **4d** in the Presence of *t*-BuOK

Entry	Michael		Condition				Amino acid			
	Acceptor	Donor	Ratio[a]	Additive	Solvent (Concn)[b]	Temperature °C	Compd No.	Total yield/%	$[\alpha]_D^{25}$ deg	Optical purity/% (Confign.)
1	**4a**	(−)-**10**	1 : 1 : 2		THF (16)	−78	**1**	66	+13.4[c]	79[d] (S)
2	**4a**	(−)-**10**	1 : 1 : 2		THF (4)	−78	**1**	63	+8.2[c]	48[d] (S)
3	**4a**	(−)-**10**	1 : 1 : 2		THF (8)	−78	**1**	49	+10.6[c]	62[d] (S)
4	**4a**	(−)-**10**	1 : 1 : 2		THF (79)	−78	**1**	45	+6.0[c]	35[d] (S)
5	**4a**	(−)-**10**	1 : 2 : 2		THF (16)	−78	**1**	59	+12.7[c]	75[d] (S)
6	**4a**	(−)-**10**	2 : 1 : 2		THF (16)	−78	**1**	39	+5.6[c]	33[d] (S)
7	**4a**	(−)-**10**[e]	1 : 1 : 2		THF (16)	−78	**1**	62	+0.3[c]	2[d] (S)
8	**4a**	(−)-**10**	1 : 1 : 2		Et_2O (16)	−78	**1**	65	+13.3[c]	78[d] (S)
9	**4a**	(−)-**10**	1 : 1 : 2		$PhCH_3$ (16)	−78	**1**	56	+10.1[c]	59[d] (S)
10	**4a**	(+)-**10**	1 : 1 : 2		THF (16)	−78	**1**	64	−12.4[c]	73[d] (R)
11	**4b**	(−)-**10**	1 : 1 : 2		THF (16)	−78	**1**	68	+14.6[f]	50[g] (S)
12	**4b**	(+)-**10**	1 : 1 : 2		THF (16)	−78	**3**	65	−13.0[f]	45[g] (R)
13	**4d**	(−)-**10**	1 : 1 : 2		THF (16)	−78	**12**	57	−17.7[f]	56[h] (R)
14	**4d**	(+)-**10**	1 : 1 : 2		THF (16)	−78	**12**	55	+14.9[f]	47[h] (S)
15	**4a**	(−)-**10**	1 : 1 : 2		THF (16)	−60	**1**	49	−4.8[c]	28[d] (R)
16	**4a**	(−)-**10**	1 : 1 : 2		THF (16)	−50	**1**	46	−6.8[c]	40[d] (R)
17	**4a**	(−)-**10**	1 : 1 : 2		THF (16)	−35	**1**	66	−8.0[c]	47[d] (R)
18	**4a**	(−)-**10**	1 : 1 : 2		THF (16)	−20	**1**	43	−11.5[c]	68[d] (R)
19	**4a**	(−)-**10**	1 : 1 : 2		THF (16)	−10	**1**	31	−8.6[c]	51[d] (R)
20	**4a**	(−)-**10**	1 : 1 : 2		THF (16)	0	**1**	24	−11.7[c]	69[d] (R)
21	**4a**	(−)-**10**	1 : 1 : 2		THF (16)	10	**1**	23	−11.8[c]	69[d] (R)
22	**4a**	(−)-**10**	1 : 1 : 2		THF (16)	20	**1**	15	−10.0[c]	59[d] (R)
23	**4a**	(−)-**10**	1 : 1 : 2		THF (16)	−78→0	**1**	57	−6.2[c]	43[d] (R)
24	**4a**	(−)-**10**	1 : 1 : 2	HMPA[i]	THF (16)	−78	**1**	42	+7.6[c]	45[d] (S)
25	**4a**	(−)-**10**	1 : 1 : 2	8-crown[i]	THF (16)	−78	**1**	51	+6.8[c]	40[d] (S)
26	**4b**	(−)-**10**	1 : 1 : 2		THF (16)	−60	**3**	41	−3.57[f]	12[g] (R)
27	**4b**	(−)-**10**	1 : 1 : 2		THF (16)	−40	**3**	30	−20.7[f]	71[g] (R)
28	**4b**	(−)-**10**	1 : 1 : 2		THF (16)	−20	**3**	44	−20.9[f]	72[g] (R)
29	**4b**	(−)-**10**	1 : 1 : 2		THF (16)	0	**3**	35	−19.6[f]	68[g] (R)
30	**4d**	(−)-**10**	1 : 1 : 2		THF (16)	−20	**12**	39	−21.6[f]	69[h] (R)
31	**4c**	(−)-**10**	1 : 1 : 2		THF (16)	−78	**11**	45	+7.23[f]	
32	**4c**	(−)-**10**	1 : 1 : 2		THF (16)	−20	**11**	22	−25.1[f]	

a) Molar ratio of **4** : **10** : base. b) Molar concentration/%. c) *c* 1.0 in H_2O. d) Based on $[\alpha]_D^{25}$ +17° (*c* 1.0, H_2O) in Ref. 14. e) Reverse addition ((−)-**10** was added to **4a**). f) *c* 1.0 in 6M HCl. g) Based on $[\alpha]_D$ +29° (6M HCl) in Ref. 2. h) Based on $[\alpha]_D$ +31.4° of (+)-glutamic acid. i) Five equivalents of the additive was used.

crown-6 (18-crown-6) which has strong ability to solvate cations,[9] at −78 °C, reduced optical purity of the product (Entries 24 and 25). It is assumed that the chelate structure existed in transition state plays an important role in controlling the stereochemistry and a strong coordination of solvent depressed stereoselectivity by interfering the chelation.[10]

Thus, the metalation of (−)-**10** with base resulted in the formation of five-membered rigid chelate structure and next phosphorus oxygen of vinyl phosphorus compound would coordinate to the potassium cation of potassium alkoxide. Consequently, the Michael addition would take place preferentially from the botton face as shown in **14**.

The Asymmetric Michael Addition of 10 to Other Vinyl Compounds. Similar additioin of **10** at −78 °C to three vinyl acceptors, diethyl vinylphosphonate (**4b**), phenyl vinyl sulfone (**4c**), and methyl acrylate (**4d**), was further investigated as shown in Scheme 4. Asymmetric addition of (−)-**10** and (+)-**10** to **4b** smoothly proceeded in a similar way to afford biologically interesting phosphonic acid (*S*)-(+)-**3**,[2] and its isomer (*R*)-(−)-**3** in good optical yields, respectively (Entries 11 and 12). Although addition of (−)-**10** to **4c** also took place smoothly, the data of the optical rotation and high-performance liquid chromatography (HPLC) analysis suggested that the expected chiral sulfone (+)-**11** had less enantiomeric excess than those of phosphorus compound (*S*)-(+)-**1** and (*S*)-(+)-**3** (Entry 31). Interestingly, addition of (−)-**10** and (+)-**10** to **4d** gave (−)-glutamic acid (*S*)-(−)-**12** and and its isomer (*R*)-(+)-**12** in fairly good yields, respectively (Entries 13 and 14). That is, the result of these reactions at −78 °C indicated that the stereochemical course of the addition of (−)-**10** and (+)-**10** to methyl acrylate **4d** was the same as that of alkylation and opposite to that of addition to vinyl phosphorus compounds **4a** and **4b**. However, study of the effect of reaction temperature in these reaction revealed another information about the stereochemistry as described in the following.

Effect of Reaction Temperature. It was found that the reaction temperature is strongly influential on the diastereoface selectivity of the addition as summarized in Table 2 (Entries 15—32). For example, addition product **1** prepared from (−)-**10** with **4a** at 0 °C had negative optical rotation (Entry 20). When the reaction temperature is elevated from −78 up to 20 °C, increase of enantiomeric excess of (*R*)-(−)-**1** was observed. Furthermore, treatment of (−)-**10** with **4a** at −78 °C for 1 h and then at 0 °C for 0.5 h before quenching also afforded (*R*)-(−)-**1** (Entry 23), which was assumed to be produced by isomerization of (*S*)-(+)-**1** formed at −78 °C. These results suggested that (*R*)-(−)-**1** obtained from (−)-**10** with **4a** at 0 °C appeared to be a thermodynamic product.[11] It is assumed that, at low temperature, the reaction

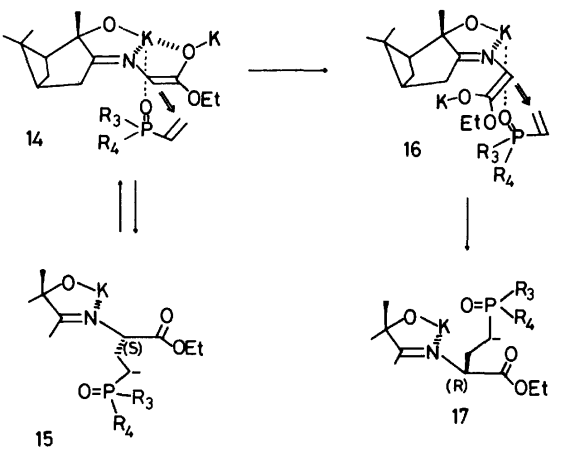

Scheme 5.

proceeds via a double chelated intermediate and the addition takes place from the α face to produce **15** as shown in **14**, **15**, whereas at elevated temperature, the potassium enolate adopts the cisoid conformation shown as the increased molecular mobility leads to the potassium-oxygen interaction being broken. The addition then occurs from the α face as for **14** to produce, this time, **17** as shown in **16**, **17**.

Almost the same results were observed in addition of (−)-**10** to phosphonate **4b** (Entries 11 and 26—29). In the reaction of phenyl vinyl sulfone **4c**, similar change of the stereochemistry was observed by changing reaction temperature from −78 to −20 °C (Entries 31 and 32). Although the change of the configuration was not observed in the reaction of (−)-**10** with **4d**, enantiomeric excess of addition product (*R*)-(−)-**12** at elevated temperature was increased compared with that at −78 °C (Entries 13 and 30). Therefore, in this Michael addition of (−)-**10** to four vinyl acceptors, increase of the product with R-configuration was observed by an elevation of the reaction temperature. From these results, it is assumed that the geometry of the imine and potassium enolate in **10'** at the reaction temperature play an important role in this asymmetric Michael addition. Addition of intermediate **14** or **16** to the acceptor always takes place from the face opposite to the β-methyl in pinanone, resulting in **15** or **17**, respectively.

As the addition products of (−)-**10** to **4a** and **4b** were obtained in good optical yields either −78 or 0 °C, this asymmetric Michael addition was useful for preparation of S- and R-enantiomers of **1** and **3** from (−)-**10** and vinyl phosphorus compounds by just changing reaction temperature.

The herbicidal activity of synthesized (*S*)-(+)-**1** was nearly equal to natural (*S*)-(+)-**1** in foliage treatment. However, synthesized (*R*)-(−)-**1**, unnatural form, had almost no herbicidal activity.

Experimental

The IR spectra were recorded on a JASCO IR-G spectrometer and mass spectra on a JEOL-OISG spectrometer. The ^1H and ^{13}C NMR spectra were taken on a Varian FT-80A spectrometer using TMS or DSS as an internal standared.

Methyl Methylphosphonochloridate (6): The chloride **6** was prepared from trimethyl phosphite and phosphorus pentachloride according to the procedure in Ref. 12; bp 59—61 °C (11 mmHg) (1 mmHg=133.322 Pa) (lit,[12] 64 °C (15 mmHg)).

Dimethyl Phosphorochloridite (6'): The chloride 6' was prepared from trimethyl phosphite and phosphorus trichloride by the procedure in Ref. 13; bp 40 °C (40 mmHg).

Methyl Methylvinylphosphinate (4a): Method A: A solution of 1.00 M vinylmagnesium bromide in THF (18.7 ml, 18.7 mmol) was added dropwise to a solution of methyl methylphosphonochloridate (2.00 g, 15.6 mmol) in THF (5 ml) under argon at −20 °C, and the mixture was stirred at the same temperature for 1 h, 2M ammonium chloride (10 ml) was added to the reaction mixture. The solution was extracted with chloroform (15 ml×3) and dried over magnesium sulfate. The solvent was removed in vacuo, and the residue was distilled to give **4a** (1.14 g, 61%) as a colorless oil; bp 74—76 °C (14 mmHg); IR (neat) 1610 (C=C), 1300 (P=O), 1210 (P=O), and 1030 (P-O-CH_3) cm^{-1}; ^1H NMR ($CDCl_3$) δ=1.51 (3H, d, J=15 Hz), 3.65 (3H, d, J=11 Hz), 5.80—6.50 (3H, m).

Method (B); To a stirred solution of the chloride **6'** (2.00 g, 15.6 mmol) in THF (10 ml) was added 1.00 M vinylmagnesium bromide (1.72 ml, 1.72 mmol) in THF dropwise with cooling to maintain the reaction temperature at −10 °C. The mixture was stirred for 3 h at 0 to 25 °C. After distillation (bp 40—45 °C (30 mmHg)), the colorless oil was heated at 60 °C for 9 h. The solution was distilled to give **4a** (1.42 g, 76%) as a colorless oil; bp, IR, and NMR data were identical with those of **4a** in Method (A).

(±)-Phosphinothricin (±)-(1): Entry 4 in Table 1; To a stirred solution of the Schiff base **7** (1.19 g, 6.24 mmol) and 95% KOH (47 mg, 0.838 mmol) in EtOH (5 ml) was added a solution of vinylphosphinate **4a** (500 mg, 4.16 mmol) in EtOH (5 ml) at room temperature. After the reaction mixture was stirred for 2 h at room temperature, the solvent was removed. To the residue was added 6M HCl (20 ml) and the solution was refluxed for 24 h. After concentration of the resulting solution followed by washing with benzene, the residue was dissolved in EtOH-H_2O (1:1, 12 ml) and a large excess amount of propylene oxide was added. The resulting solution was concentrated and purified by ion-exchange resin (Dowex 50×2). Elution with water and subsequent removal of water gave (±)-**1** as a colorless crystals (490 mg, 69%); mp 211—213 °C (lit, [14] (mp 214 °C); ^1H NMR (D_2O) δ=1.45 (3H, d, J=14 Hz), 1.5—2.6 (4H, m), 4.04 (1H, t, J=6 Hz); ^{13}C NMR (D_2O) δ=14.81 (d, J=92.8), 23.96 (d, J=2.4 Hz), 26.58 (d, J=92.2 Hz), 54.43 (d, J=16.2 Hz), 172.9 (s).

Entry 1 in Table 1; to a stirred solution of sodium (19.2 mg, 0.833 mmol) in EtOH (5 ml) was added a solution of the Schiff base **7** (956 mg, 5.00 mmol) in EtOH (1 ml) at −10°C, followed by addition of a vinylphosphinate **4a** (400 mg, 3.33 mmol) in EtOH (1 ml) at −10 °C. After the same workup and purification, (±)-**1** was obtained as a colorless crystals, (387 mg, 64%); mp 212—214 °C.

(−)- and (+)-2-Hydroxy-3-pinanone (−)-9 and (+)-(9): The ketol (−)-**9** was prepared from (1*R*,5*R*)-(+)-α-pinene ($[\alpha]_D^{22}$ +47.1° (neat)) by the procedure in Ref. 8; bp 115—117 °C (15 mmHg) (lit,[8] 118—119 °C (15 mmHg); $[\alpha]_D^{25}$ −37.0° (*c* 2.60, $CHCl_3$) (lit,[8] $[\alpha]_D^{25}$ −38.9° (*c* 2.64, $CHCl_3$)); IR (neat) 3450 (OH) and 1720 (C=O) cm^{-1}; NMR ($CDCl_3$) δ=0.89 (3H, s), 1.37 (3H, s), 1.38 (3H, s), 1.6—2.6 (6H, m); the optical purity of the ketol (−)-**9** may be estimated to be at least 92.5%.

According to the same procedure, (+)-**9** was prepared from (1*S*,5*S*)-(+)-α-pinene ($[\alpha]_D^{22}$ −42.0° (neat)); $[\alpha]_D^{25}$ +33.0° (*c* 2.60, $CHCl_3$).

The Chiral Schiff Base (−)-(10) and (+)-(10): A solution of glycine ethyl ester hydrochloride (2.99 g, 21.4 mmol), the ketol (−)-**9** (3.00 g, 17.8 mmol), and triethylamine (2.17 g, 21.4 mmol) in benzene (50 ml) containing boron trifluoride etherate (0.1 g) was refluxed for 6 h using a Dean-Stark apparatus under nitrogen. After filtration followed by evaporation, the reasidue was distilled to give (−)-**10** (3.52 g, 78%) as a slight yellow oil; bp 106—108 °C (0.3 mmHg); $[\alpha]_D^{25}$ −7.6° (*c* 3.00, $CHCl_3$); IR (neat) 3250 (OH), 1760 (COOEt), and 1660 (C=N) cm^{-1}; NMR ($CDCl_3$) δ=0.88 (3H, s), 1.29 (3H, t, J=7 Hz), 1.34 (3H, s), 1.52 (3H, s), 1.6—2.6 (6H, m), 2.60 (1H, s), 4.15 (2H, s), 4.20 (2H, q, J=7 Hz); FD MS *m/z* 254 (M+1). According to the same procedure, (+)-**10** was prepared from (+)-**9**; $[\alpha]_D^{25}$ +6.8° (*c* 3.00, $CHCl_3$).

General Procedure for Reaction of the Chiral Schiff Base (10) with Michael Acceptors:. To a stirred solution of potassium *t*-butoxide (1.58 mmol) in THF (3 ml) was added a solution of the chiral Schiff base **10** (0.789 mmol) in THF (1 ml) at −78°C, followed by addition of a solution of vinyl compound (0.789 mmol) in THF (1 ml) at −78 °C under argon. After stirred for 1 h at −78 °C, 1M HCl (3 ml) was added to the resulting yellow solution and the solvent was removed. To the residue was added 6M HCl (4 ml) and the solution was refluxed for 24 h. After concentration of the resulting solution followed by washing with benzene, the residue was dissolved in EtOH-H_2O (4 ml) and a large excess amount of propylene oxide was added. The resulting solution was concentrated and purified by ion-exchange resin (Dowex 50×2). Elution with water and subsequent removal of water gave the amino acid.

(−)-and (+)-Phosphinothricin (−)- and (+)-(1): Entry 1 in Table 2; (S)-(+)-**1** was obtained from vinylphosphinate **4a** as a colorless crystals according to the general procedure; mp 214—216 °C (decomp); ^1H NMR (D_2O) δ=1.45 (3H, d, J=14 Hz), 1.5—2.6 (4H, m), 4.04 (1H, t, J=6 Hz); FD MS *m/z* 182 (M+1).

Entry 23 in Table 2; After the addition reaction according to the general procedure, the reaction mixture was stirred for 1 h at −78 °C and then warmed at 0 °C for 0.5 h.

Entries 24 and 25 in Table 2; To a stirred solution of *t*-BuOK (1.58 mmol) and additive (3.95 mmol) in THF (4 ml) was added a solution of the chiral Schiff base (−)-**10** (0.789 mmol) in THF (1 ml) at −78 °C, followed by addition of a solution of vinylphosphinate **4a** (0.789 mmol) in THF (1 ml) at −78 °C under argon. The reaction mixture was stirred for 1 h at −78 °C.

Entry 18 in Table 2; to a stirred solution of *t*-BuOK

(1.58 mmol) in THF (3 ml) was added a solution of the chiral Schiff base (−)-**10** (0.789 mmol) in THF (1 ml) at −20 °C, followed by addition of a solution of vinylphosphinate **4a** (0.789 mmol) in THF (1 ml) at −20 °C under argon. The reaction mixure was stirred for 1 h at −20 °C.

Recovery of the Ketol (−)-(9): After the reaction according to the general procedure, the workup and purification was carried out as follows. To the reaction mixture was added satd. aq NH_4Cl (3 ml) and the solution was extracted with ethyl acetate (8 ml×2). After the extract was washed with satd. aq NaCl, the solvent was removed in vacuo. The residue was added 1 M aq HCl (2 ml) and the solution was heated at 45 °C for 24 h. The reaction mixture was extracted with benzene (2 ml×2). After the solvent was removed in vacuo, the residue was purified by column chromatography (silica gel, benzene) to give (−)-**9** (95 mg, 72%) as a colorless oil; $[\alpha]_D^{25}$ −34.7° (*c* 2.50, $CHCl_3$).

2-Amino-4-phosphonobutyric acid (3): Entry 28 in Table 2; (R)-(−)-**3** was obtained from the chiral Schiff base (−)-**10** and vinylphosphonate **4b** as colorless crystals according to the procedure in Entry 18 as described above; FD MS *m/z* 184 (M+1); mp 226 °C (decomp); NMR (D_2O) δ=1.5—2.6 (4H, m), 4.03 (1H, t, *J*= 6Hz).

2-Amino-4-phenylsulfonylbutyric Acid (11): Entry 32 in Table 2; (R)-(−)-**11** was obtained from the chiral Schiff base (−)-**10** and phenyl sulfone **4c** as a colorless crystals according to the procedure in Entry 18 as described above; FD MS *m/z* 244 (M+1); mp 216 °C (decomp); ^1H NMR (D_2O) δ=2.1—2.6 (2H, m), 3.5—3.8 (2H, m), 3.92 (1H, t, *J*=6Hz), 7.7—8.2 (5H, m). For elemental analysis, methyl 2-acethylamino-4-phenylsulfonylbutyrate was derived from **11**. Found: C, 51.87; H, 5.95; N, 4.72; S, 10.61%. Calcd for $C_{13}H_{17}NO_5S$: C, 52.16; H, 5.72; N, 4.68; S, 10.71%.

Glutamic Acid (12): Entry 30 in Table 2; (R)-(−)-**12** was obtained from the chiral Schiff base (−)-**10** and methyl acrylate **4c** as colorless crystals according to the procedure in Entry 18 as described above; FD MS *m/z* 148 (M+1); mp 198 °C (decomp).

We are grateful to Professor Teruaki Mukaiyama, The University of Tokyo, and Professor Kikumasa Sato, Yokohama National University, and Mr. Masao Takada, Nippon Chemical Industrial Co., for their valuable advice throughout this work.

References

1) E. Bayel, K. H. Gugel, K. Hagele, H. Hagenmaier, S. Jessipow, W. A. Konich, and H. Zahner, *Helv. Chim. Acta*, **55**, 224 (1972); Y. Kondo, T. Shomura, Y. Ogawa, T. Turuoka, H. Watanabe, K. Totsukawa, T. Suzuki, C. Moriyama, J. Yoshida, S. Inouye, and T. Niida, *Sci. Reports of Meiji Seika Kaisha*, **1973**, 34.

2) S. G. Cull-Candy, J. F. Donnellan, R. W. James, and G. G. Lunt, *Nature*, **1976**, 408; J. F. Koerner and C. W. Cotman, *Brain Research*, **216**, 192 (1981).

3) K. Tachibana, T. Watanabe, Y. Suzuki, and Y. Sekizawa, *Sci. Reports of Meiji Seika Kaisha*, **1980**, 27; K. Weissermel, H. J. Kleiner, M. Finke, and U. H. Felcht, *Angew. Chem., Int. Ed. Engl.*, **20**, 223 (1981).

4) a) Y. Ogawa, H. Yoshida, S. Inoue, and T. Niida, *Sci. Reports of Meiji Seika Kaisha*, **1973**, 49; b) H. Gross and Th. Grouk, *J. Prakt. Chem.*, **318**, 157 (1976); c) E. Gruszecka, P. Mastalerz, and M. Soroka, *Rocz. Chem.*, **49**, 2127 (1975); d) C. Wasielewski and K. Artczak, *Synthesis*, **1981**, 540; e) K. Weissermel, H. J. Kleiner, M. Finke, and U. H. Felcht, *Angew. Chem., Int. Ed. Engl.*, **20**, 223 (1981). f) A. Suzuki, T. Tsuruoka, K. Mizutani, and S. Inoue, *Sci., Reports of Meiji Seika Kaisha*, **1981**, 33; g) N. Minowa, S. Fukatsu, T. Niida, M. Takada, and K. Sato, *Tetrahedron Lett.*, **24**, 2391 (1983).

5) N. Minowa, M. Hirayama, and S. Fukatsu, *Tetrahedron Lett.*, **25**, 1147 (1984).

6) A. I. Meyers and C. E. Whitten, *J. Am. Chem. Soc.*, **97**, 6266 (1975); S. Hashimoto, S. Yamada, and K. Koga, *Chem. Pharm. Bull.*, **27**, 771 (1979); S. Hashimoto, N. Komeshima, S. Yamada, and K, Koga, *ibid.*, **27**, 2437 (1979); T. Mukaiyama, T. Takeda, and M. Osaki, *Chem. Lett.*, **1977**, 1165; T. Mukaiyama and N. Iwasawa, *ibid.*, **1981**, 913; G. Tsuchihashi, S. Mitamura, S. Inoue, and K. Ogura, *Tetrahedron Lett.*, **1973**, 323; G. Posner, J. P. Mallamo, K. Miura, and M. Hulce, *Pure Appl. Chem.*, **53**, 2307 (1981);

7) T. Mukaiyama, Y. Hirako. and T. Takeda, *Chem. Lett.*, **1978**, 461; T. Takeda, T. Hoshiko, and T. Mukaiyama, *ibid.*, **1981**, 797; K. Yamamoto, M. Iijima, and Y. Ojimura, *Tetrahedron Lett.*, **23**, 3711 (1982); H. Malmberg, M. Nilsson, and C. Ullenius, *ibid.*, **23**, 3823 (1982).

8) S. Yamada, T. Oguri, and T. Shioiri, *J. Chem. Soc., Chem. Commum.*, **1976**, 136; T. Oguri, N. Kawai, T. Shioiri, and S. Yamada, *Chem. Pharm. Bull.*, **26**, 803 (1978); J. A. Bajgrowicz, B. Cossec, Ch. Pigiere, R, Jacquier, and Ph. Viallefont, *Tetrahedron Lett.*, **24**, 3721 (1983).

9) HMPA: R. E. Ireland, R. H. Mueller, and A. K. Willard, *J. Am. Chem. Soc.*, **98**, 2868 (1976). Crown ether: G. W. Gokel, H. M. Gerdes, and N. W. Rebert, *Tetrahedron Lett.*, **1976**, 653; T. Mukaiyama, Y. Hirako, and T. Takeda, *Chem. Lett.*, **1978**, 461; T. Takeda, T. Hoshiko, and T. Mukaiyama, *ibid.*, **1981**, 797.

10) K. Tomioka, K. Ando, Y. Takemasa, and K. Koga, *J. Am. Chem. Soc.*, **106**, 2718 (1984); K. Tomioka, K. Ando, Y. Takemasa, and K. Koga, *Tetrahedron Lett.*, **25**, 5677 (1984).

11) S. Shenri and J. K. Stille, *Tetrahedron Lett.*, **23**, 627 (1982).

12) T. M. Balthazor and R. A. Flores, *J. Org, Chem.*, **45**, 529 (1980).

13) H. G. Cook, J. D.Ilett, B. C. Saunder, G. J. Stacey, H. G. Watson, I. G. E. Wilding, and S. J. Woodcock, *J. Chem. Soc.*, **1949**, 2921.

14) Y. Ogawa, T, Tsuruoka, S. Inouye, and T. Niida, *Sci. Reports of Meiji Seika Kaisha*, **1973**, 42.

Convenient Methods for the Preparation of Vinylic and Allylic Sulfones from Alkenes, Haloalkanes, and Aldehydes. Stereochemistry of the Conversion of Vinylic Sulfones to the Corresponding Allylic Sulfones

Katsuhiko INOMATA,* Shin-ichi SASAOKA, Toshifumi KOBAYASHI, Yuhji TANAKA, Susumu IGARASHI, Takashi OHTANI, Hideki KINOSHITA, and Hiroshi KOTAKE
Department of Chemistry, Faculty of Science, Kanazawa University, Kanazawa 920
(Received October 11, 1986)

1- or 2-*p*-Tolylsulfonyl(=tosyl)-1-alkenes, vinylic sulfones, were regioselectively prepared from 1-alkenes via iodosulfonization or sulfonylmercuration and also from 1-haloalkanes by the homologation or unhomologation methods. The vinylic sulfones thus prepared were further converted to the corresponding allylic sulfones under basic conditions. The stereochemistry of this conversion was discussed. One-carbon homologated allylic sulfones were directly obtained from aldehydes in good yields by the reaction with diethyl phenylsulfonylmethylphosphonate and 1,8-diazabicyclo[5.4.0]undec-7-ene (DBU) under mild conditions.

The useful synthetic procedure using vinylic and allylic sulfones as synthons have been recently developed. The importance of vinylic sulfones in synthesis is now well-established.[1-4] Allylic sulfones have been proven to be particularly useful synthetic intermediates,[1] because of the ability of the sulfonyl group to generate an adjacent carbanion[5] and to act as a leaving group in substitution reactions[6] and elimination reactions.[7]

In connection with our continued interest to extend the synthetic utility of sulfones,[8a-e] we have so far investigated the syntheses[9a-c] and reactions[10a-e] of allylic sulfones. Some of them were successfully employed for the synthesis of naturally occurring substances such as recifeiolide,[10b] squalene[10c] and coenzyme Q_{10}.[10e] We herein report facile methods for the preparation of vinylic sulfones from alkenes[11] and haloalkanes and their conversion to the corresponding allylic sulfones under mild basic conditions. On the basis of these facts, a direct preparation of one-carbon homologated allylic sulfones from aldehydes was also achieved.

Results and Discussion

Preparation of Vinylic and Allylic Sulfones from Alkenes. Recently Kao Liu and his coworkers reported a convenient synthesis of various β-iodo sulfones,[12] which involves additions of alkane- and arenesulfonyl iodide to alkenes under the catalytic action of copper(II) chloride in aprotic solvents. Though they and others[13] established from the various evidences that tosyl iodide adds homolytically to alkenes, we thought it was possible to prepare β-iodo sulfones in an ionic fashion from iodine and sulfinate just like iodolactonization. Therefore, we tried the iodosulfonization and the subsequent elimination of hydrogen iodide with a base to yield the corresponding vinylic sulfones (**3**). It was consequently found that the iodosulfonization proceeds readily in methanol or in a two-phase system using ethyl acetate and water. The latter is favorable to avoid the formation of methyl *p*-toluenesulfinate as a by-product when an alkene is sparingly soluble in methanol (See the cases of **1d** in Table 1). The subsequent elimination was accomplished by the treatment with triethylamine in dry acetonitrile at room temperature for 15 min. The results are summarized in Table 1.

We could not exclude the possibility of the initial formation of tosyl iodide as an intermediate in the above iodosulfonization, since the reaction was retarded in the dark as in the case of the reaction of tosyl iodide with alkenes (the yield of **3a** was 75% in the reaction carried out in the dark under similar conditions).[9b] However, it was found that the addition of sodium iodide and sodium *p*-toluenesulfinate was effective to improve the yields of the addition products even for the reaction of tosyl iodide carried out in methanol.[14] These results seem to suggest that the reaction proceeds through the competitive two pathways, ionic one through the iodonium intermediate **4** and radical one for tosyl iodide produced in situ. The advantage of the present method for the preparation of vinylic sulfones from alkenes is obvious, namely it does not require the preparation of unstable tosyl iodide and the use of metal catalyst such as copper(II) chloride.

The results in Table 1 show that the iodosulfonization proceeds regiospecifically. This is considered as follows: If the reaction proceeds in an ionic fashion, *p*-toluenesulfinate ion attacks a less hindered carbon atom of the iodonium intermediate **4**, and if in a radical fashion, the more stable radical intermediate **5** is preferentially formed as shown in Scheme 1.

In contrast to the iodosulfonization, it was found that sulfonyl group is introduced on the C-2 position in sulfonylmercuration of 1-alkenes using mercury(II) chloride and sodium *p*-toluenesulfinate. The treatment of the addition product of sulfonylmercuration

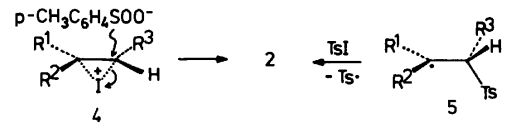

Scheme 1.

with a base afforded exclusively 2-tosyl-1-alkenes (**7a—e**) as shown in Table 2.

This fact seems to suggest that Hg(II) ion of the intermediate **8** does not exist on the central position of olefinic bond, being different from the ionic

Table 1. Preparation of Vinylic Sulfones from Alkenes via Iodosulfonization

Alkene (**1a—j**) —(A) p-$CH_3C_6H_4SOONa \cdot 4H_2O/I_2$→ [Adduct] (**2a—j**) —(B) Et_3N in CH_3CN→ Vinylic Sulfone (**3a—j**)

1a—k	Alkenes	Molar Ratio of 1/TsNa·$4H_2O$/I_2	Condition (A), (B)	Product 3a—j	Yield/% (E/Z)
1a	$C_6H_5CH=CH_2$	1/1.5/1 in MeOH	(A) r.t., 15 min (B) r.t., 15 min	$C_6H_5CH=CHTs$	89 (100/0)
1b	$CH_3(CH_2)_2CH=CH_2$	1.5/1.5/1 in MeOH	(A) r.t., 1 d (B) r.t., 15 min	$CH_3(CH_2)_2CH=CHTs$	94 (78/22)
1c	$CH_3(CH_2)_3CH=CH_2$	1.5/1.5/1 in MeOH	(A) r.t., 1 d (B) r.t., 15 min	$CH_3(CH_2)_3CH=CHTs$	90 (78/22)
1d	$CH_3(CH_2)_7CH=CH_2$	1/1.5/1 in MeOH	(A)[a] r.t., 1 d (B) r.t., 15 min	$CH_3(CH_2)_7CH=CHTs$	77 (83/17)
1e	$(CH_3)_2C=CH_2$	ca. 10/1.5/1 in MeOH	(A) −70 °C/r.t., 3 h (B) r.t., 15 min	$(CH_3)_2C=CHTs$	quant.
1f	$(CH_3)_2C=CHCH_3$	1.5/1.5/1 in MeOH	(A) r.t., 16 h (B) r.t., 17 h	$(CH_3)_2C=C(Ts)CH_3$	80[b]
1g		1/1.5/1 in MeOH	(A) r.t., 3 d (B)[c] r.t., 15 min		76
1d	$CH_3(CH_2)_7CH=CH_2$	1/1.5/1 in EtOAc/H_2O	(A) r.t., 1 d (B) r.t., 15 min	$CH_3(CH_2)_7CH=CHTs$	96 (78/22)
1h	$(CH_3)_2CHCH=CHCH_3$	1/1.5/1 in EtOAc/H_2O	(A) r.t., 2 h (B)[c] r.t., 15 min	$(CH_3)_2CHCH=C(Ts)CH_3$	83 (76/24)
1i		1/1.5/1 in EtOAc/H_2O	(A) r.t., 2 h (B)[c] r.t., 15 min	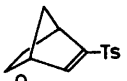	91
1j	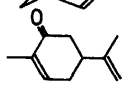	1/1.5/1 in EtOAc/H_2O	(A) r.t., 2 h (B) r.t., 15 min	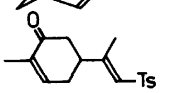	quant. (100/0)

a) MeOH/CH_2Cl_2 (4/1) was used as solvent. b) $CH_2=C(CH_3)CH(Ts)CH_3$ was obtained as a by-product in 6% yield. c) DBU was used instead of Et_3N.

Table 2. Preparation of Vinylic Sulfones from Alkenes via Sulfonylmercuration

RCH=CH_2 (**1a—e**) —p-$CH_3C_6H_4SOONa \cdot 4H_2O/HgCl_2$, in MeOH/$CH_2Cl_2$, (A)→ [RCH(Ts)$CH_2$HgCl] (**6a—e**) —DBU, in THF, (B)→ RC(Ts)=CH_2 (**7a—e**)

Alkene 1a—e	R	Molar Ratio of 1/TsNa·$4H_2O$/$HgCl_2$	Condition (A), (B)	Yield/% 7a—e
1a	C_6H_5	1/1/1	(A) r.t., 1 d (B) DBU (1.2 equiv) r.t., 10 min	61
1b	$CH_3(CH_2)_2$	1.5/1/1	(A) 0 °C, 3 d (B) DBU (1.2 equiv) r.t., 8 h	67[a]
1c	$CH_3(CH_2)_3$	1/1.5/1.2	(A) 0 °C, 3 d (B) DBU (1.7 equiv) r.t., 6 h	72
1d	$CH_3(CH_2)_7$	1/2/2	(A) r.t., 6 h (B) DBU (2.2 equiv) r.t., 12 h	77
1e	$C_6H_5(CH_2)_2$	1/2/2	(A) r.t., 18 h (B) DBU (2.2 equiv) r.t., 16 h	83

a) Based on $HgCl_2$.

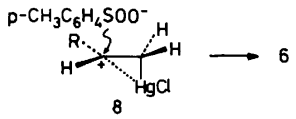

Scheme 2.

intermediate **4** of the iodosulfonization mentioned above, but lies on the less hindered carbon atom. Therefore, the tosylate ion attacks the C-2 position as shown in Scheme 2.

O'Connor and Lyness have reported that the equilibrium between 1-methylsulfonyl-1-hexene (**9**) and 1-methylsulfonyl-2-hexene (**10**) under basic conditions (*t*-BuOK in *t*-BuOH at room temperature) almost completely shifts to **10**.[15] We therefore tried the conversion of **3b—d** to the corresponding allylic sulfones (**11b—d**) with DBU as a base in acetonitrile as shown in Scheme 3. In each case, the proton rearrangement products (**11b—d**) were obtained in excellent yields.

On the other hand, it was found that the 2-tosyl-1-alkenes (**7b—d**), prepared above from 1-alkenes via sulfonylmercuration, were also converted to the corresponding allylic sulfones (**11b—d**) by the treatment with *p*-toluenesulfinic acid and DBU in refluxing dioxane (Table 3). This reaction appears to proceed through the addition of *p*-toluenesulfinate anion to give **12**, elimination (**12** to **3**) reaction of *p*-toluenesulfinic acid and the subsequent isomerization as shown in the scheme of Table 3. The intermediate **12** was actually isolated by decreasing the amount of DBU from 4 to 1.5 equiv.

Consequently, the present reactions provide a convenient method for the preparation of allylic sulfones from alkenes via vinylic sulfones.

Table 3. Conversion of 2-Tosyl-1-alkenes to Allylic Sulfones

$$R'CH_2C(Ts)=CH_2 \xrightarrow[\text{dioxane, reflux}]{p\text{-}CH_3C_6H_4SOOH\cdot xH_2O/DBU} [R'CH_2CH(Ts)CH_2Ts] \xrightarrow[-p\text{-}CH_3C_6H_4SOOH]{} [\mathbf{3b—d}] \xrightarrow{DBU} R'CH=CHCH_2Ts$$

7b—d **12b—d** **11b—d**

Substrates **7b—d**	R′	Reaction time[a] h	Yield of **11b—d**/% (E/Z)
7b	CH_3CH_2	5	95 (81/19)
7c	$CH_3(CH_2)_2$	4.5	94 (81/19)
7d	$CH_3(CH_2)_6$	4	94 (79/21)

a) ca. 2 equiv of p-$CH_3C_6H_4SOOH\cdot xH_2O$ ($x<1$) and 4 equiv of DBU were used.

Preparation of Vinylic and Allylic Sulfones from 1-Haloalkanes. In the previous papers,[9c,10d] we have reported the convenient methods for the preparation of two- or three-carbons homologated allylic sulfones from 1-haloalkanes using 2-(1-pyrrolidinyl)ethyl sulfone[9c] or allyl *p*-tolyl sulfone[10d] as a starting material, respectively. We herein report facile and new methods for the preparation of two- or one-carbon(s) homologated and unhomologated vinylic and allylic sulfones from 1-haloalkanes.

It was previously found that the anions of β-keto sulfones react with formaldehyde to give the corresponding vinylic sulfones via deacylation.[8b] The application of this reaction enabled the preparation of two-carbons homologated vinylic (**15**) and allylic (**16**) sulfones starting from 1-haloalkanes as shown in Scheme 4.

$$R'CH_2CH=CHTs \xrightarrow[\text{in } CH_3CN,\ \text{r.t., overnight}]{\text{DBU (2 equiv)}} R'CH=CHCH_2Ts$$

3b, R′=CH_3CH_2, E/Z=78/22 — **11b**, 91%, E/Z=84/16
3c, R′=$CH_3(CH_2)_2$, E/Z=78/22 — **11c**, 89%, E/Z=52/48
3d, R′=$CH_3(CH_2)_6$, E/Z=83/17 — **11d**, 97%, E/Z=65/35

Scheme 3. Conversion of 1-tosyl-1-alkenes to allylic sulfones.

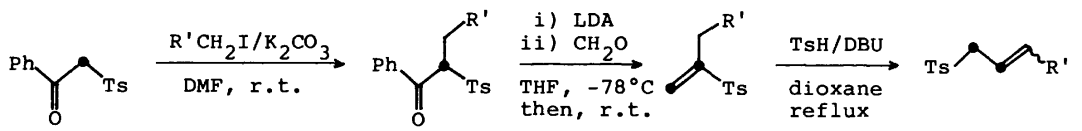

13

14a, R′=CH_3, 79% — **15a**, 95% — **16a**, 95%, E/Z=72/28
14b, R′=CH_2CH_3, 74% — **15b**, 93% — **16b**, 95%, E/Z=81/19
14c, R′=$(CH_2)_4CH_3$, 64% — **15c**, 93% — **16c**, 100%, E/Z=79/21

Scheme 4. Preparation of two-carbons homologated vinylic and allylic sulfones from 1-haloalkanes.

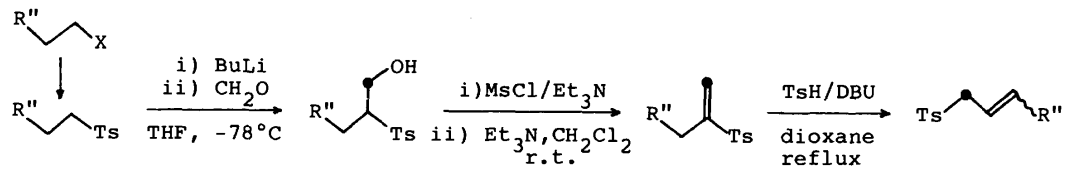

17a, R″=$(CH_2)_5CH_3$ **18a**, 68% **19a**, 93% **20a**, 96%, E/Z=80/20
17b, R″=$(CH_2)_7CH_3$ **18b**, 66% **19b**, 88% **20b**, 100%, E/Z=78/22
17c, R″=$(CH_2)_8CH_3$ **18c**, 62% **19c**, 95% **20c**, 97%, E/Z=77/23

Scheme 5. Preparation of one-carbon homologated vinylic and allylic sulfones from 1-haloalkanes.

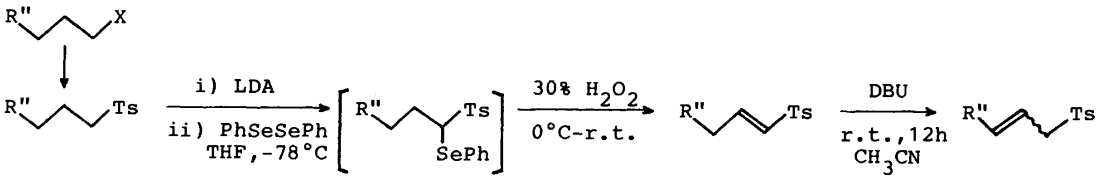

21a, R″=CH_3 **22a—d** **23a**, 86% (E) **24a**, 97%, E/Z=19/81
21b, R″=$(CH_2)_4CH_3$ **23b**, 95% (E) **24b**, 96%, E/Z=31/69
21c, R″=$(CH_2)_6CH_3$ **23c**, 91% (E) **24c**, 97%, E/Z=31/69
21d, R″=$(CH_2)_7CH_3$ **23d**, 87% (E) **24d**, 97%, E/Z=30/70

Scheme 6. Preparation of unhomologated vinylic and allylic sulfones from 1-haloalkanes.

The synthesis of one-carbon homologated vinylic (**19**) and allylic (**20**) sulfones from 1-haloalkanes was accomplished according to Scheme 5. Haloalkanes were initially transformed to the corresponding *p*-tolyl sulfones (**17**) by a general method using sodium *p*-toluenesulfinate.[8e]

Unhomologated vinylic (**23**) and allylic (**24**) sulfones were prepared from 1-haloalkanes in a similar manner used in the preparation of 1-cyano-1-alkenes[16] according to Scheme 6.

In contrast to the case of cyanoalkane,[16] this reaction was found to afford only (E)-isomer of **23** from the observation of its 400 MHz ^{1}H NMR spectrum. This may be due to the bulkiness of tosyl group, namely cis-elimination of benzeneselenenic acid might proceed preferentially via the conformation illustrated in the structure **26** in which the unfavorable steric interaction between alkyl and tosyl groups, represented in the structure **25**, does not exist.

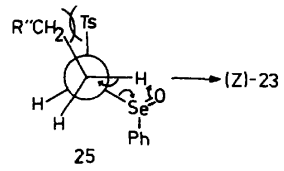

25

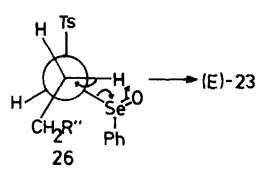

26

The final transformation of (*E*)-vinylic sulfones (**23**) to the corresponding allylic sulfones (**24**) was performed with DBU in acetonitrile at room temperature. It is noteworthy that Z-isomers of **24** were predominantly formed in contrast to the results of similar reaction using E/Z-mixture of vinylic sulfones (**3b—d** to **11b—d** in Scheme 3).

Table 4. Conversion of (*E*)-Vinylic Sulfone (**23d**) to Allylic Sulfone (**24d**) Using DBU as a Base under Various Conditions[a]

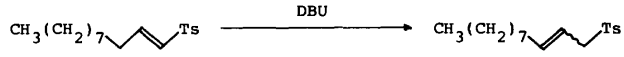

23d **24d**

Entry No.	Condition	Product ratio[b] **23d** : **24d** (E/Z)
1	CH_3CN, r.t., 12 h	3 : 97 (30/70)
2	DMF, r.t., 12 h	5 : 95 (27/73)
3	THF, r.t., 12 h	29 : 71 (18/82)
4	CH_2Cl_2, r.t., 12 h	36 : 64 (22/78)
5	Dioxane, r.t., 12 h	54 : 46 (21/79)
6	Benzene, r.t., 12 h	68 : 32 (10/90)
7	$CHCl_3$, r.t., 12 h	94 : 6 (20/80)
8	CH_3CN, −20 °C, 48 h	77 : 23 (3/97)
9	CH_3CN, 0 °C, 30 h	4 : 96 (22/78)
10	THF, 0 °C, 48 h	28 : 72 (19/81)
11	CH_3CN, reflux, 1.5 h	2 : 98 (78/22)
12	Dioxane, reflux, 1.5 h	4 : 96 (66/34)

a) 2 equiv of DBU (0.26 mmol) was used toward **23d** (0.13 mmol) in each solvent (1 ml). b) Determined by 400 MHz ^{1}H NMR spectra.

Stereochemistry of the Conversion of Vinylic Sulfones to the Corresponding Allylic Sulfones. In order to rationalize the above peculiar phenomenon, the conversion of (*E*)-vinylic sulfone (**23d**) to the corresponding allylic sulfone (**24d**) was investigated using DBU as a base under various conditions as shown in Table 4. The polar solvent such as

acetonitrile (Entry 1) or *N,N*-dimethylformamide (DMF, Entry 2) seemed to be preferable to the less polar ones (Entries 3—7) for the conversion. It is noteworthy that (Z)-isomer of **24d** was preferentially formed at room temperature or at lower temperature in any solvent examined (Entries 1—10), while (E)-isomer was predominant in the reaction carried out at higher temperature (Entries 11 and 12). These results suggest that (Z)-isomer of **24d** is the kinetically-controlled product and the more stable (E)-isomer is the thermodynamically-controlled one.

The results of the similar reaction of **23d** with *t*-BuOK in *t*-BuOH made this point clearer, though the selectivity was not so high as that in the case of DBU. (Z)-Isomer of **24d** was initially formed predominantly and it gradually changed to the (E)-isomer (Table 5).

Table 5. Conversion of (*E*)-Vinylic Sulfone (**23d**) to Allylic Sulfone (**24d**) with *t*-BuOK[a)]

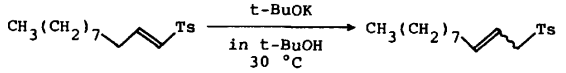

23d **24d**

Reaction time/h	Product ratio[b)]	
	23d :	**24d** (E/Z)
0.5	5	95 (41/59)
1	5	95 (51/49)
2	3	97 (63/37)
4	2	98 (75/25)
15	<1	>99 (86/14)

a) 2 equiv of *t*-BuOK (0.26 mmol) was used toward **23d** (0.13 mmol) in *t*-BuOH (6 ml). b) Determined by 400 MHz ^{1}H NMR spectra.

The question arised from the above experimental results is why (*E*)-**23** afford predominantly (*Z*)-**24** as a kinetically-controlled product. During the preparation of this manuscript, Block and his coworkers reported independently the similar results for the vinylogous Ramberg-Bäcklund reactions as shown in the following.[17)]

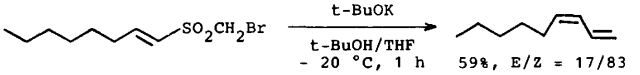

They attributed the stereoselectivity of the reaction to a stabilizing, attractive interaction between the developing negative charge at the α-position and the CH_2 group at the δ-position (a "*syn effect*"[18)]) favoring transition state **27** over **30** for deprotonation (Scheme 7).

Namely, these experimental results including ours suggest that the acidity of the protons at γ-position of vinylic sulfones varies remarkably in each conformation. We would like to propose to call such acidity of a proton chracteristic to each conformation "*Conformational Acidity.*" However, it should be noted that the anionic intermediate **31** is more stable than its (Z)-isomer **28** as can be seen in the above results, while it could not be observed in the Ramberg-Bäcklund reactions since the subsequent desulfonylation proceeded readily at low temperature.

On the other hand, (*Z*)-vinylic sulfone (**33**) and α-alkylated vinylic sulfones (**34a—c**) gave exclusively the corresponding (*E*)-allylic sulfones (**24d** and **35a—c**), respectively, as shown in Scheme 8 and Table 6. It may be due to the steric congestion which precludes

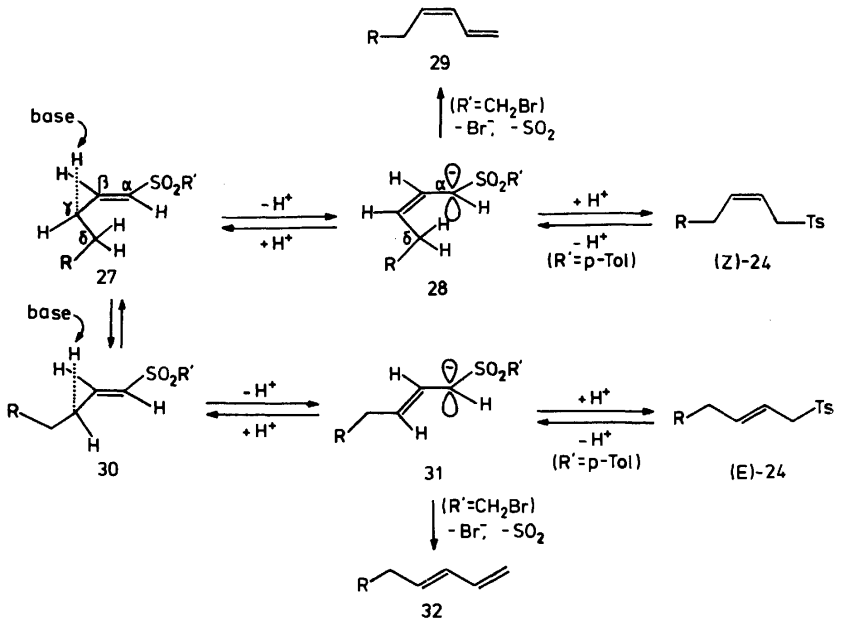

Scheme 7. A probable course of the conversion of (*E*)-vinylic sulfones (**23**=**27**, **30**) to the corresponding allylic sulfones (**24**).

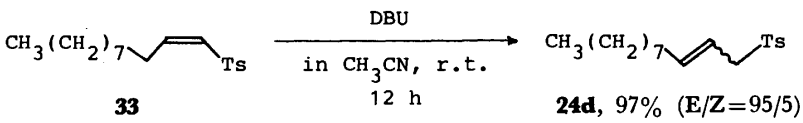

33 **24d**, 97% (E/Z=95/5)

Scheme 8. Conversion of (*Z*)-vinylic sulfone (**33**) to allylic sulfone (**24d**) with DBU.

Table 6. Conversion of α-Alkylated Vinylic Sulfones to Allylic Sulfones

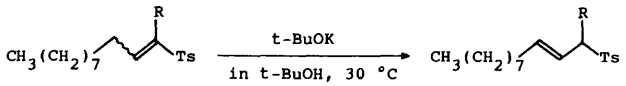

34a—c **35a—c**

Substrate R (E/Z)	Time h	Product ratio[a] 34 : 35	Substrate R (E/Z)	Time h	Product ratio[a] 34 : 35
34a, CH_3 (100/0)	1	58 : 42	**34a**, CH_3 (0/100)	1	32[b] : 68
	3	27 : 73		3	13 : 87
	10	23 : 77		10	14 : 86
	24	22 : 78		24	16 : 84
34b, $CH_3(CH_2)_2$ (100/0)	1	64 : 36	**34b**, $CH_3(CH_2)_2$ (0/100)	1	9[b] : 91
	3	32 : 68		3	10 : 90
	10	13 : 87		10	11 : 89
	24	11 : 89		24	11 : 89
34c, CH_3CH_2 (45/55)	1	24[c] : 76			
	3	12 : 88			
	10	10 : 90			
	24	9 : 91			

a) Determined by 400 MHz ^{1}H NMR spectra. Products consisted of only (*E*)-isomers (**34**, **35**) except the case noted in b). b) (*Z*)-isomer. c) (*E*)-isomer.

Table 7. Direct Preparation of Allylic Sulfones from Aldehydes

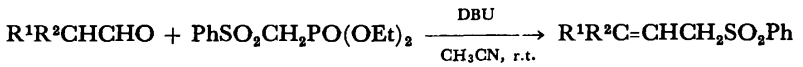

36a—e **37** **38a—e**

36a—e	Aldehyde R[1]	R[2]	Time h	Yield/% (E/Z) 38a—e
36a	$C_6H_5CH_2$	H	4.5	79 (37/63)
36a	$C_6H_5CH_2$	H	67.5	72 (86/14)
36b	$CH_3(CH_2)_6$	H	18	73 (40/60)
36c	$CH_3(CH_2)_7$	H	10.5	87 (46/54)
36d	$(CH_3)_2C=CH(CH_2)_2CH(CH_3)$	H	19.5	81 (50/50)
36e	CH_3	CH_3	12	88

the possibility of a stabilizing syn interaction between the α- and δ-position as being pointed out by Block et al.[17]

It is noteworthy that the Z-ratio of **24a** (R″=CH_3) is higher in the conversion of **23a** (R″=CH_3) than other cases (**23b—d** to **24b—d**) in Scheme 6. This may suggest that the syn interaction between the α- and δ-position is more effective when R″ is methyl group. Further, the reverse conversion of **24a** to **23a** may be retarded by the stabilization of the allylic structure owing to the hyperconjugation of methyl group with the double bond,[19] therefore, the initially formed (Z)-isomer may be retained better when R″ is methyl group than other cases.

Preparation of Allylic Sulfones from Aldehydes. The direct preparation of allylic sulfones from aldehyde was next investigated.

Posner and Brunelle reported the conversion of carbonyl substrates to vinylic sulfones using sulfonylmethylphosphonate carbanions.[20] They gen-

erated the carbanions with butyllithium in THF at −78 °C. On the other hand, we have established above the conversion of the vinylic sulfones to the corresponding allylic sulfones using DBU as a base catalyst. Therefore, the direct preparation of allylic sulfones from aldehydes seemed to be possible if the carbanion of sulfonylmethylphosphonate was generated with DBU itself. Actually, this reaction proceeded well with diethyl phenylsulfonylmethylphosphonate (**37**) and 2 or 3 equiv of DBU in acetonitrile at room temperature as shown in Table 7. The predominant formation of (*Z*)-allylic sulfones (**38a—e**) was observed when the reaction was quenched within a relatively short time (See the cases of **38a**). These results agree with the discussion on the stereochemistry described above since it is known that the present Horner-Wittig type reaction initially affords (*E*)-vinylic sulfones.[20] Similar reaction with ketones afforded neither vinylic sulfones nor allylic sulfones, but a small amount of reduced product, methyl phenyl sulfone, was obtained (3—4%) along with recovery of sulfonylmethylphosphonate (60—70%).

Attempts to prepare the allylic sulfones from aldehydes by Peterson olefination using phenyl trimethylsilylmethyl sulfone and DBU were unsuccessful.[21] Desilylated sulfone was obtained as a main product.

Experimental

All the melting points were determined with a micro melting apparatus (Yanagimoto-Seisakusho) and were uncorrected. The ^{1}H NMR and IR spectra were recorded on JEOL JNM-GX 400 (400 MHz) FT-NMR spectrometer and JASCO IRA-1 diffraction grating infrared spectrometer, respectively. The chemical shifts of NMR are reported in the δ scale relative to TMS as an internal standard.

Materials. All the solvents were distilled and stored over a drying agent. Thin-layer chromatography (TLC) was performed on Merck's silica gel 60 PF_{254} (Art. 7749).

Preparation of 1-Tosyl-2-phenylethene (3a) via Iodosulfonization in methanol. To a mixed solution of styrene (**1a**, 104 mg, 1 mmol) and sodium *p*-toluenesulfinate tetrahydrate (375 mg, 1.5 mmol) in methanol (2 ml) was added iodine (254 mg, 1.0 mmol) at room temperature with stirring. A lot of yellowish solid[22] precipitated immediately. The solvent was replaced by ethyl acetate after stirring for 15 min, and the solution was successively washed with water, aqueous $NaHCO_3$ containing a small amount of $NaHSO_3$, and brine, and dried over Na_2SO_4. The residue obtained by evaporation of the solvent was treated with Et_3N (202 mg, 2 mmol) in dry acetonitrile (2 ml) at room temperature for 15 min. The residue after removal of solvent was taken up in ethyl acetate and successively washed with 1 mol dm^{-3} HCl, aqueous $NaHCO_3$, and brine, and dried over Na_2SO_4. The solvent was evaporated in vacuo and the resulting residue was subjected to preparative TLC (solvent; hexane–AcOEt=5:2, v/v) to afford 229 mg of **3a** (89% yield) as a solid. Mp 120—121 °C (from ethanol, lit,[12] 120—121 °C). IR (KBr) 3032, 1602, 1586, 1442, 1296, 1134, 1076, 964, 800, 738 cm^{-1}; ^{1}H NMR ($CDCl_3$) δ=2.43 (s, 3H), 6.85 (d, 1H, *J*=15 Hz), 7.30—7.52 (m, 7H), 7.65 (d, 1H, *J*=15 Hz), 7.83 (d, 2H, *J*=8 Hz). Found: C, 69.80; H, 5.35%. Calcd for $C_{15}H_{14}O_2S$: C, 69.74; H, 5.46%.

Other vinylic sulfones (**3b—g**) were prepared in a similar manner.

3b: An oil; MS *m/z* 224 (M^+, 71%), 139 (100), 91, 41; IR (neat) 3016, 2908, 2848, 1606, 1580, 1436, 1302, 1130, 1072, 954, 798 cm^{-1}; ^{1}H NMR ($CDCl_3$) δ=0.92 (t, 3H of E and Z, *J*=7.5 Hz), 1.41—1.55 (m, 2H of E and Z), 2.16—2.24 (m, 2H of E), 2.43 (s, 3H of E and Z), 2.60—2.68 (m, 2H of Z), 6.19—6.35 (m, 2H of Z, 1H of E), 6.95 (dt, 1H of E, *J*=7, 15 Hz), 7.33 (d, 2H of E and Z, *J*=8 Hz), 7.76 (d, 2H of E, *J*=8 Hz), 7.80 (d, 2H of Z, *J*=8 Hz); E/Z=78/22.

3c: An oil; MS *m/z* 238 (M^+, 23%), 139 (100), 91, 41; IR (neat) 3024, 2908, 2842, 1606, 1582, 1440, 1304, 1136, 1076, 962, 800 cm^{-1}; ^{1}H NMR ($CDCl_3$) δ=0.89 (t, 3H of E and Z, *J*=7 Hz), 1.27—1.48 (m, 4H of E and Z), 2.19—2.26 (m, 2H of E), 2.43 (s, 3H of E and Z), 2.61—2.68 (m, 2H of Z), 6.18—6.35 (m, 2H of Z, 1H of E), 6.95 (dt, 1H of E, *J*=7, 15 Hz), 7.32 (d, 2H of E and Z, *J*=8 Hz), 7.75 (d, 2H of E, *J*=8 Hz), 7.79 (d, 2H of Z, *J*=8 Hz); E/Z=78/22.

3d: An oil; MS *m/z* 294 (M^+, 13%), 209, 157 (100), 139, 138, 96, 55; IR (neat) 3032, 2916, 2840, 1608, 1582, 1454, 1312, 1139, 1076, 960, 801 cm^{-1}; ^{1}H NMR ($CDCl_3$) δ=0.84—0.92 (m, 3H of E and Z), 1.25 (m, 12H of E and Z), 1.35—1.50 (m, 2H of E and Z), 2.17—2.26 (m, 2H of E), 2.43 (s, 3H of E and Z), 2.61—2.67 (m, 2H of Z), 6.18—6.35 (m, 2H of Z, 1H of E), 6.95 (dt, 1H of E, *J*=7, 15 Hz), 7.32 (d, 2H of E and Z, *J*=8 Hz), 7.75 (d, 2H of E, *J*=8 Hz), 7.79 (d, 2H of Z, *J*=8 Hz); E/Z=83/17.

3e: Mp 62—63 °C (from cyclohexane); IR (KBr) 3020, 1614, 1584, 1430, 1276, 1132, 1076, 800 cm^{-1}; ^{1}H NMR ($CDCl_3$) δ=1.87 (d, 3H, *J*=1 Hz), 2.14 (d, 3H, *J*=1 Hz), 2.43 (s, 3H), 6.17 (m, 1H, *J*=1 Hz), 7.33 (d, 2H, *J*=8 Hz), 7.78 (d, 2H, *J*=8 Hz). Found: C, 62.75; H, 6.72%. Calcd for $C_{11}H_{14}O_2S$: C, 62.83; H, 6.71%.

3f: Mp 65 °C (from cyclohxane, lit,[12] 66—67 °C); IR (KBr) 1610, 1582, 1428, 1286, 1136, 1062, 794 cm^{-1}; ^{1}H NMR ($CDCl_3$) δ=1.86 (s, 3H), 1.99 (s, 3H), 2.21 (s, 3H), 2.43 (s, 3H), 7.31 (d, 2H, *J*=8 Hz), 7.74 (d, 2H, *J*=8 Hz).

3g: Mp 81—82 °C (from ethanol, lit,[12] 81—82 °C); IR (KBr) 3018, 2906, 2842, 1624, 1580, 1434, 1270, 1128, 1082, 802 cm^{-1}; ^{1}H NMR ($CDCl_3$) δ=1.52—1.69 (m, 4H), 2.12—2.21 (m, 2H), 2.21—2.30 (m, 2H), 2.43 (s, 3H), 7.01—7.06 (m, 1H), 7.32 (d, 2H, *J*=8 Hz), 7.73 (d, 2H, *J*=8 Hz).

Preparation of 1-Tosyl-1-decene (3d) via Iodosulfonization in Ethyl Acetate and Water. To a heterogeneous mixture of *p*-$CH_3C_6H_4SOONa \cdot 4H_2O$ (375 mg, 1.5 mmol) in water (1 ml) and ethyl acetate (2 ml) were added 1-decene (**1d**, 140 mg, 1 mmol) and iodine (254 mg, 1 mmol) at room temperature with stirring. The dark brown color of the mixture diminished gradually. After stirring for 24 h, 20 ml of ethyl acetate was added. The organic phase was separated and washed successively with aqueous $NaHCO_3$ containing a small amount of $NaHSO_3$ and brine, and dried over Na_2SO_4. The residue obtained by evaporation of the solvent was treated with Et_3N to give **3d**, in a similar manner described for **3a**. Spectral data of **3d** is given above.

Other vinylic sulfones (**3h—j**) were prepared in a similar way.

3h: (E)- and (Z)-isomers were separated on preparative

TLC (solvent; hexane–AcOEt–Et_2O=10:1:1, v/v) and characterized based on the known deshielding of alkyl groups syn to the sulfonyl group in vinylic sulfones.[23] (*E*)-**3h**: Yield 63%. Mp 71—72 °C (from ethanol); IR (KBr) 2940, 2844, 1626, 1580, 1454, 1298, 1128, 1079, 804 cm^{-1}; ^1H NMR ($CDCl_3$) δ=1.05 (d, 6H, J=7 Hz), 1.82 (s, 3H), 2.43 (s, 3H), 2.49—2.61 (m, 1H), 6.70 (d, 1H, J=10 Hz), 7.32 (d, 2H, J=8 Hz), 7.72 (d, 2H, J=8 Hz). Found: C, 65.30; H, 7.76%. Calcd for $C_{13}H_{18}O_2S$: C, 65.51; H, 7.61%. (*Z*)-**3h**: Yield 20%. An oil; MS *m/z* 238 (M^+, 52%), 140, 139, 83, 82, 67 (100), 55; IR (neat) 2948, 2852, 1626, 1586, 1456, 1278, 1134, 1081, 804 cm^{-1}; ^1H NMR ($CDCl_3$) δ=0.98 (d, 6H, J=7 Hz), 1.94 (s, 3H), 2.44 (s, 3H), 3.61—3.74 (m, 1H), 5.74 (d, 1H, J=11 Hz), 7.33 (d, 2H, J=8 Hz), 7.76 (d, 2H, J=8 Hz).

3i: Mp 89—90 °C (from ethanol); IR (KBr) 3028, 2932, 2852, 1581, 1564, 1434, 1278, 1134, 1081, 806 cm^{-1}; ^1H NMR ($CDCl_3$) δ=0.94—1.02 (m, 1H), 1.07—1.15 (m, 1H), 1.21—1.28 (m, 1H), 1.49—1.56 (m, 1H), 1.62—1.71 (m, 1H), 1.71—1.83 (m, 1H), 2.44 (s, 3H), 3.05—3.12 (m, 1H), 3.12—3.17 (m, 1H), 6.90 (d, 1H, J=3 Hz), 7.32 (d, 2H, J=8 Hz), 7.77 (d, 2H, J=8 Hz). Found: C, 67.60; H, 6.56%. Calcd for $C_{14}H_{16}O_2S$: C, 67.71; H, 6.49%.

3j: An oil; MS *m/z* 304 (M^+, 18%), 165, 149 (100), 148, 133, 123, 108, 107 (100), 105, 91, 82 (100), 54; IR (neat) 3012, 2912, 1658, 1612, 1584, 1438, 1290, 1136, 1078, 806 cm^{-1}; ^1H NMR ($CDCl_3$) δ=1.77 (s, 3H), 2.16 (s, 3H), 2.33—2.56 (m, 4H), 2.45 (s, 3H), 2.69—2.81 (m, 1H), 6.21 (s, 1H), 6.68—6.76 (m, 1H), 7.35 (d, 2H, J=8 Hz), 7.78 (d, 2H, J=8 Hz).

Preparation of 1-Phenyl-1-tosylethene (7a) via Sulfonylmercuration. To a solution of styrene (**1a**, 104 mg, 1 mmol) in methanol (1.5 ml) and dichloromethane (0.7 ml) were added $HgCl_2$ (272 mg, 1 mmol) and sodium *p*-toluenesulfinate tetrahydrate (250 mg, 1 mmol) at room temperatute. After stirring for 1 d, the reaction mixture was diluted with ethyl acetate (ca. 15 ml) and the insoluble substances were filtered off through a Celite bed. The residue obtained by evaporation of solvent was treated with DBU (0.18 ml, 1.2 mmol) in dry THF (4 ml) at room temperature for 10 min. After replacing the solvent by ethyl acetate, the solution was successively washed with water and brine, and dried over Na_2SO_4, followed by evaporation of the solvent. The residue was subjected to preparative TLC (solvent; hexane–ethyl acetate=8:1, v/v) to afford 157 mg of **7a** (61% yield) as a colorless oil. MS *m/z* 258 (M^+, 13%), 139, 103 (100), 77; IR (neat) 3040, 2902, 1583, 1302, 1138, 1058, 800 cm^{-1}; ^1H NMR ($CDCl_3$) δ=2.36 (s, 3H), 5.92 (s, 1H), 6.60 (s, 1H), 7.16—7.37 (m, 7H), 7.56 (d, 2H, J=8 Hz).

Other 2-tosyl-1-alkene were prepared in a similar manner.

7b: An oil, MS *m/z* 224 (M^+, 61%), 157 (100), 139, 119, 92, 91 (100), 69, 68, 65, 41; IR (neat) 2946, 1582, 1439, 1300, 1161, 1128, 1073, 802 cm^{-1}; ^1H NMR ($CDCl_3$) δ=0.86 (t, 3H, J=7 Hz), 1.42—1.55 (m, 2H), 2.20 (t, 2H, J=8 Hz), 2.44 (s, 3H), 5.69 (s, 1H), 6.34 (s, 1H), 7.33 (d, 2H, J=8 Hz), 7.76 (d, 2H, J=8 Hz).

7c: An oil, MS *m/z* 238 (M^+, 100%), 197, 157 (100), 139 (100), 133 (100), 92 (100), 91 (100), 67, 55 (100), 41; IR (neat) 2951, 2863, 1587, 1448, 1305, 1130, 1075, 804 cm^{-1}, ^1H NMR ($CDCl_3$) δ=0.84 (t, 3H, J=7 Hz), 1.21—1.33 (m, 2H), 1.38—1.49 (m, 2H), 2.22 (t, 2H, J=7.5 Hz), 2.44 (s, 3H), 5.69 (s, 1H), 6.33 (s, 1H), 7.33 (d, 2H, J=8.5 Hz), 7.75 (d, 2H, J=8 Hz).

7d: An oil, MS *m/z* 294 (M^+, 1%), 197, 157 (100), 139, 138, 92, 55, 41; IR (neat) 2918, 2847, 1586, 1458, 1305, 1160, 1133, 1075, 803 cm^{-1}; ^1H NMR ($CDCl_3$) δ=0.86 (t, 3H, J=7 Hz), 1.12—1.33 (m, 10H), 1.38—1.50 (m, 2H), 2.22 (t, 2H, J=8 Hz), 2.44 (s, 3H), 5.69 (s, 1H), 6.33 (s, 1H), 7.32 (d, 2H, J=8.5 Hz), 7.75 (d, 2H, J=8 Hz).

7e: An oil, Ms *m/z* 286 (M^+, 78%), 181, 131 (100), 130 (100), 129 (100), 115, 92, 91 (100), 65; IR (neat) 3006, 2900, 1582, 1300, 1137, 1072, 802 cm^{-1}; ^1H NMR δ=2.44 (s, 3H), 2.54 (dd, 2H, J=7, 8 Hz), 2.77 (dd, 2H, J=7, 8 Hz), 5.65 (s, 1H), 6.35 (s, 1H), 7.03—7.39 (m, 7H), 7.75 (d, 2H, J=8 Hz).

Conversion of 1-Tosyl-1-pentene (3b) to 1-Tosyl-2-pentene (11b). To a solution of **3b** (138 mg, 0.62 mmol) in acetonitrile (2 ml) was added DBU (184 µl, 1.23 mmol) at room temperature. After being allowed to stand overnight, the solvent was replaced by ethyl acetate. The resulting solution was successively washed with 1 mol dm^{-3} HCl, aqueous $NaHCO_3$ and brine, followed by being dried over Na_2SO_4. The residue obtained by evaporation of the solvent was subjected to preparative TLC (solvent; hexane–ethyl acetate–ether=10:1:1, v/v) to afford 127 mg of **11b** as an oil. 400 MHz ^1H NMR spectrum showed that it was a mixture of (E)- and (Z)-isomers (E/Z=84/16) of **11b** contaminated with a small amount of **3b** (ca. 1%). Yield 91% (unseparable **3b** was reduced in the calculation of the yield). MS *m/z* 224 (M^+, 1%), 157, 69 (100), 68, 41; IR (neat) 3012, 2952, 1584, 1440, 1294, 1132, 1076, 958, 802 cm^{-1}; ^1H NMR ($CDCl_3$) δ=0.76 (t, 3H of Z, J=8 Hz), 0.91 (t, 3H of E, J=7.5 Hz), 1.73—1.83 (m, 2H of Z), 1.97—2.07 (m, 2H of E), 2.45 (s, 3H of E and Z), 3.72 (d, 2H of E, J=7 Hz), 3.83 (d, 2H of Z, J=8 Hz), 5.32—5.45 (m, 1H of E and Z), 5.55 (dt, 1H of E, J=7, 15 Hz), 5.71 (dt, 1H of Z, J=8, 11 Hz), 7.33 (d, 2H of E and Z, J=8 Hz), 7.73 (d, 2H of E, J=8 Hz), 7.76 (d, 2H of Z, J=8 Hz); E/Z=84/16.

3c and **3d** were also converted to **11c** and **11d**, respectively, in a similar manner.

11c: An oil; MS *m/z* 238 (M^+, 4%), 157 (100), 139, 92 (100), 91 (100), 83, 82 (100), 67 (100), 65, 55, 41 (100); IR (neat) 3012, 2944, 2912, 2852, 1584, 1444, 1306, 1134, 1076, 959, 802 cm^{-1}; ^1H NMR ($CDCl_3$) δ=0.75 (t, 3H of Z, J=7 Hz), 0.82 (t, 3H of E, J=7 Hz), 1.10—1.21 (m, 2H of Z), 1.25—1.36 (m, 2H of E), 1.69—1.77 (m, 2H of Z), 1.94—2.02 (m, 2H of E), 2.44 (s, 3H of E and Z), 3.72 (d, 2H of E, J=7 Hz), 3.83 (d, 2H of Z, J=8 Hz), 5.34—5.45 (m, 1H of E and Z), 5.51 (dt, 1H of E, J=7, 15 Hz), 5.71 (dt, 1H of Z, J=8, 11 Hz), 7.33 (d, 2H of E and Z, J=8 Hz), 7.73 (d, 2H of E, J=8 Hz), 7.76 (d, 2H of Z, J=8 Hz); E/Z=52/48. Recovery of **3c**: 2%.

11d: An oil, MS *m/z* 294 (M^+, 0.1%), 209, 157, 138, 97, 83 (100), 69, 55; IR (neat) 3012, 2908, 2836, 1584, 1448, 1310, 1132, 1078, 958, 804 cm^{-1}; ^1H NMR ($CDCl_3$) δ=0.82—0.93 (m, 3H of E and Z), 1.05—1.34 (m, 10H of E and Z), 1.69—1.78 (m, 2H of Z), 1.94—2.03 (m, 2H of E), 2.44 (s, 3H of E and Z), 3.72 (d, 2H of E, J=7 Hz), 3.83 (d, 2H of Z, J=8 Hz), 5.34—5.44 (m, 1H of E and Z), 5.51 (dt, 1H of E, J=7, 15 Hz), 5.71 (dt, 1H of Z, J=8, 11 Hz), 7.33 (d, 2H of E and Z, J=8 Hz), 7.72 (d, 2H of E, J=8 Hz), 7.75 (d, 2H of Z, J=8.5 Hz); E/Z=65/35. Recovery of **3d**: 3%.

Conversion of 2-Tosyl-1-pentene (7b) to 1-Tosyl-2-pentene (11b). To a solution of **7b** (84 mg, 0.38 mmol) in dioxane (2.5 ml) were added *p*-toluenesulfinic acid hydrate (*p*-$CH_3C_6H_4SOOH \cdot xH_2O$, 133 mg, ca. 0.76 mmol) and DBU (230 µl, 1.52 mmol) at room temperature. After refluxing for 5 h, the solvent was replaced by ethyl acetate.

The solution was successively washed with 1 mol dm^{-3} HCl, aqueous $NaHCO_3$, and brine, followed by being dried over Na_2SO_4. The residue obtained by evaporation of the solvent was subjected to preparative TLC (solvent; hexane–ethyl acetate=8:1, v/v) to afford **11b** as an oil. It was found to be a mixture of (E)- and (Z)-isomers (E/Z=81/19) from its ^1H NMR spectrum. Physical data of **11b—d** are given above.

Alkylation of 2-Tosyl-1-phenylethanone (13). A solution of **13** (685 mg, 2.5 mmol, mp 109—110 °C (from ethanol), prepared by the reaction of 2-bromo-1-phenylethanone and p-$CH_3C_6H_4SOONa \cdot 4H_2O$ in refluxing ethanol according to a general method[8c]) in DMF (8 ml) was added into a flask containing finely powdered dry K_2CO_3 (518 mg, 3.75 mmol) under nitrogen. After stirring for 1 h at room temperature, a solution of iodoethane (468 mg, 3.0 mmol) in DMF (2 ml) was added dropwise. The reaction mixture was quenched, after stirring for 9 h, by the addition of a buffer solution (pH 7) followed by evaporation of the solvent under reduced pressure. The residue was taken up in ethyl acetate and the resulting solution was washed with brine twice and dried over Na_2SO_4. The residue obtained by evaporation of the solvent was subjected to preparative TLC (solvent; hexane–ethyl acetate=5:1) to afford 119 mg of 2-tosyl-1-phenyl-1-butanone (**14a**, 79% yield) as a solid. Mp 72.0—72.5 °C (from hexane–ethanol); IR (KBr) 3048, 2970, 1668, 1585, 1440, 1344, 1310, 1296, 1284, 1262, 1139, 1078, 970, 805, 746, 680 cm^{-1}; ^1H NMR ($CDCl_3$) δ=0.88 (t, 3H, J=7.5 Hz), 1.98—2.22 (m, 2H), 2.43 (s, 3H), 4.99 (dd, 1H, J=4, 11 Hz), 7.31 (d, 2H, J=8 Hz), 7.48 (dd, 2H, J=7, 8 Hz), 7.60 (t, 1H, J=7 Hz), 7.64 (d, 2H, J=8 Hz), 7.97 (d, 2H, J=8 Hz). Found: C, 67.23; H, 6.15%. Calcd for $C_{17}H_{18}O_3S$: C, 67.52; H, 6.00%.

In a similar manner, **14b** and **14c** were prepared.

14b: Mp 89—90 °C (from hexane/ethanol); IR (KBr) 3048, 2950, 1665, 1585, 1440, 1340, 1310, 1290, 1245, 1140, 1075, 950, 804, 742, 675 cm^{-1}; ^1H NMR ($CDCl_3$) δ=0.87 (t, 3H, J=7.5 Hz), 1.26 (m, 2H), 1.96—2.13 (m, 2H), 2.44 (s, 3H), 5.07 (dd, 1H, J=4, 11 Hz), 7.31 (d, 2H, J=8 Hz), 7.48 (dd, 2H, J=7, 8 Hz), 7.60 (t, 1H, J=7 Hz), 7.64 (d, 2H, J=8 Hz), 7.98 (d, 2H, J=8 Hz). Found: C, 68.24; H, 6.39%. Calcd for $C_{18}H_{20}SO_3$: C, 68.33; H, 6.37%.

14c: Mp 78.5—79.5 °C (from hexane/ethanol); IR (KBr) 3044, 2952, 2920, 1665, 1584, 1438, 1336, 1302, 1295, 1138, 1074, 940, 800, 742, 678 cm^{-1}; ^1H NMR ($CDCl_3$) δ=0.81 (t, 3H, J=7 Hz), 1.08—1.31 (m, 8H), 1.96—2.14 (m, 2H), 2.43 (s, 3H), 5.05 (dd, 1H, J=4, 11 Hz), 7.31 (d, 2H, J=8 Hz), 7.48 (dd, 2H, J=7, 8 Hz), 7.61 (t, 1H, J=7 Hz), 7.64 (d, 2H, J=8 Hz), 7.96 (d, 2H, J=8 Hz). Found: C, 70.37; H, 7.43%. Calcd for $C_{21}H_{26}O_3S$: C, 70.36; H, 7.31%.

Synthesis of 2-Tosyl-1-butene (15a) via Deacylation. To a solution of lithium diisopropylamide (LDA, 0.74 mmol, prepared from diisopropylamine (80 mg, 0.79 mmol) and n-BuLi (hexane solution, 0.74 mmol) at −30 °C) in THF (3 ml) was added dropwise a solution of **14a** (211 mg, 0.7 mmol) in THF (7 ml) at −78 °C under nitrogen. After stirring for 30 min at −78 °C, a THF solution of excess amount of formaldehyde was added. The reaction mixture was gradually warmed up to room temperature and stirred overnight. After treatment with a buffer solution (pH 7), the insoluble substance was filtered off through a Celite bed, and the solvent was replaced by ethyl acetate. The resulting solution was washed with brine and dried over Na_2SO_4. The residue obtained by evaporation of the solvent was subjected to preparative TLC (solvent; hexane–ethyl acetate=5:1, v/v) to afford 139 mg of **15a** (95% yield) as a colorless solid. Mp 26—28 °C (crude); MS m/z 210 (M^+, 26%), 139 (100), 92, 55; IR (KBr) 2970, 1582, 1295, 1170, 1128, 1073, 942, 865, 800, 722 cm^{-1}; ^1H NMR ($CDCl_3$) δ=1.07 (t, 3H, J=7 Hz), 2.27 (dq, 2H, J=2, 7 Hz), 2.44 (s, 3H), 5.70 (t, 1H, J=2 Hz), 6.34 (s, 1H), 7.33 (d, 2H, J=8 Hz), 7.75 (d, 2H, J=8 Hz).

In a similar manner, **15b** and **15c** were prepared.

15b: An oil; MS m/z 224 (M^+, 61%), 157 (100), 139, 119, 92, 91 (100), 69, 68, 65, 41; IR (neat) 2956, 1584, 1442, 1302, 1162, 1130, 1080, 940, 802, 726, 701 cm^{-1}; ^1H NMR ($CDCl_3$) δ=0.87 (t, 3H, J=7 Hz), 1.49 (m, 2H), 2.20 (m, 2H), 2.44 (s, 3H), 5.69 (t, 1H, J=2 Hz), 6.34 (s, 1H), 7.34 (d, 2H, J=8 Hz), 7.76 (d, 2H, J=8 Hz).

15c: An oil; MS m/z 266 (M^+, 10%), 197, 157 (100), 139 (100), 92 (100), 69, 55, 41; IR (neat) 2915, 2842, 1584, 1458, 1302, 1160, 1133, 1073, 940, 802, 727 cm^{-1}; ^1H NMR ($CDCl_3$) δ=0.84 (t, 3H, J=7 Hz), 1.14—1.30 (m, 6H), 1.38—1.48 (m, 2H), 2.21 (m, 2H), 2.44 (s, 3H), 5.69 (t, 1H, J=1.5 Hz), 6.34 (s, 1H), 7.33 (d, 2H, J=8 Hz), 7.75 (d, 2H, J=8 Hz).

The conversion of **15a—c** to **16a—c** was carried out in a similar manner described for the conversion of **7b** to **11b**.

16a: An oil; MS m/z 210 (M^+, 22%), 156 (100), 140, 92, 91 (100), 65, 55; IR (neat) 3025, 2920, 1585, 1315, 1135, 1080, 960, 810, 718 cm^{-1}; ^1H NMR ($CDCl_3$) δ=1.37 (dd, 3H of Z, J=2, 7 Hz), 1.68 (dd, 3H of E, J=1, 6 Hz), 2.45 (s, 3H of E and Z), 3.71 (d, 2H of E, J=7 Hz), 3.83 (d, 2H of Z, J=8 Hz), 5.37—5.48 (m, 1H of E and Z), 5.57 (dq, 1H of E, J=6.5, 15 Hz), 5.82 (dq, 1H of Z, J=7, 11 Hz), 7.34 (d, 2H of E and Z, J=8 Hz), 7.73 (d, 2H of E, J=8 Hz), 7.76 (d, 2H of Z, J=8 Hz); E/Z=72/28.

16b: An oil; MS m/z 224 (M^+, 1%), 157, 69 (100), 68, 41; IR (neat) 3020, 2947, 1583, 1305, 1134, 1078, 958, 802, 722 cm^{-1}; ^1H NMR ($CDCl_3$) δ=0.76 (t, 3H of Z, J=7.5 Hz), 0.91 (t, 3H of E, J=8 Hz), 1.78 (m, 2H of Z), 2.01 (m, 2H of E), 2.44 (s, 3H of E and Z), 3.72 (d, 2H of E, J=7.5 Hz), 3.82 (d, 2H of Z, J=8 Hz), 5.32—5.45 (m, 1H of E and Z), 5.55 (dt, 1H of E, J=7, 15 Hz), 5.71 (dt, 1H of Z, J=8, 11 Hz), 7.33 (d, 2H of E and Z, J=8 Hz), 7.73 (d, 2H of E, J=8 Hz), 7.76 (d, 2H of Z, J=8 Hz); E/Z=81/19.

16c: An oil; MS m/z 266 (M^+, 0.2%), 157, 110, 69 (100), 55, 41; IR (neat) 2915, 2842, 1587, 1458, 1310, 1135, 1080, 962, 804, 725 cm^{-1}; ^1H NMR ($CDCl_3$) δ=0.84 (t, 3H of Z, J=7 Hz), 0.87 (t, 3H of E, J=7 Hz), 1.05—1.40 (m, 6H of E and Z), 1.67—1.79 (m, 2H of Z), 1.92—2.07 (m, 2H of E), 2.44 (s, 3H of E and Z), 3.72 (d, 2H of E, J=7.5 Hz), 3.83 (d, 2H of Z, J=8 Hz), 5.33—5.44 (m, 1H of E and Z), 5.50 (dt, 1H of E, J=7, 15 Hz), 5.71 (dt, 1H of Z, J=8, 11 Hz), 7.33 (d, 2H of E and Z, J=8 Hz), 7.73 (d, 2H of E, J=8 Hz), 7.75 (d, 2H of Z, J=8 Hz); E/Z=79/21.

Preparation of 2-Tosyl-1-nonanol (18a). p-Tolyl octyl sulfone (**17a**, 134 mg, 0.50 mmol) was lithiated by the reaction with n-BuLi (hexane solution, 0.55 mmol) in THF (5 ml) at −78 °C for 1 h under nitrogen, followed by the addition of a THF solution of excess amount of formaldehyde at −78 °C. After a few minute, the mixture was quenched with a phosphate buffer solution (pH 7) and the insoluble substance was filtered off through a Celite bed. The residue after removal of the solvent was taken up in ethyl acetate. The organic layer was washed with brine and dried over Na_2SO_4. The residue obtained by evaporation of

the solvent was subjected to preparative TLC (solvent; benzene–ethyl acetate=20:1, v/v) to afford 102 mg of **18a** (68% yield) as an oil. MS *m/z* 299 (M^+ +1, 1%), 280, 157, 92 (100), 83 (100), 69 (100), 55; IR (neat) 3530, 2915, 2847, 1588, 1460, 1294, 1138, 1078, 805 cm^{-1}; ^1H NMR ($CDCl_3$) δ=0.85 (t, 3H, *J*=7 Hz), 1.11—1.49 (m, 10H), 1.49—1.64 (m, 1H), 1.68—1.79 (m, 1H), 2.47 (s, 3H), 2.98 (dd, 1H of OH, *J*=6, 7 Hz), 3.01—3.09 (m, 1H), 3.83—3.95 (m, 2H), 7.38 (d, 2H, *J*=8 Hz), 7.78 (d, 2H, *J*=8 Hz).

18b and **18c** were prepared in a similar manner.

18b: An oil; Ms *m/z* 326 (M^+, 0.4%), 308, 157, 97, 92 (100), 83, 69, 55; IR (neat) 3515, 2958, 2842, 1588, 1458, 1294, 1136, 1078, 805 cm^{-1}; ^1H NMR ($CDCl_3$) δ=0.87 (t, 3H, *J*=7 Hz), 1.08—1.48 (m, 14H), 1.48—1.62 (m, 1H), 1.68—1.79 (m, 1H), 2.47 (s, 3H), 2.99 (dd, 1H of OH, *J*=6, 7 Hz), 3.01—3.09 (m, 1H), 3.85—3.96 (m, 2H), 7.38 (d, 2H, *J*=8 Hz), 7.78 (d, 2H, *J*=8 Hz).

18c: Mp 49.5—50.5 °C (from hexane); MS *m/z* 340 (M^+, 1%), 322, 185, 157 (100), 111, 97, 92, 83, 69, 55; IR (KBr) 3524, 2905, 2840, 1584, 1455, 1270, 1130, 1075, 805 cm^{-1}; ^1H NMR ($CDCl_3$) δ=0.88 (t, 3H, *J*=7 Hz), 1.09—1.48 (m, 16H), 1.48—1.62 (m, 1H), 1.66—1.79 (m, 1H), 2.47 (s, 3H), 2.98 (t, 1H of OH, *J*=7 Hz), 3.00—3.09 (m, 1H), 3.83—3.95 (m, 2H), 7.38 (d, 2H, *J*=8.5 Hz), 7.78 (d, 2H, *J*=8.5 Hz). Found: C, 66.95; H, 9.74%. Calcd for $C_{19}H_{32}O_3S$: C, 67.02; H, 9.47%.

Preparation of 2-Tosyl-1-nonene (19a). To a solution of **18a** (64 mg, 0.215 mmol) and mesyl chloride (30 mg, 0.26 mmol) in dichloromethane (1 ml) was added triethylamine (36 µl, 0.26 mmol) at room temperature. After stirring for 30 min, the reaction mixture was cooled to 0 °C and additional 60 µl (0.43 mmol) of triethylamine was added, followed by stirring for 1.5 d. The solution diluted with ethyl acetate was successively washed with 1 mol dm^{-3} aqueous $NaHCO_3$, and brine, and dried over Na_2SO_4. The residue obtained by evaporation of the solvent was subjected to preparative TLC (solvent; benzene–ethyl acetate=30:1, v/v) to afford 56 mg of **19a** (93% yield) as a colorless oil. MS *m/z* 280 (M^+, 1%), 197, 157 (100), 139, 92, 69, 55, 41; IR (neat) 2920, 2850, 1588, 1308, 1162, 1077, 805 cm^{-1}; ^1H NMR ($CDCl_3$) δ=0.85 (t, 3H, *J*=7 Hz), 1.13—1.31 (m, 8H), 1.38—1.49 (m, 2H), 2.22 (t, 2H, *J*=8 Hz), 2.44 (s, 3H), 5.69 (s, 1H), 6.34 (s, 1H), 7.33 (d, 2H, *J*=8 Hz), 7.75 (d, 2H, *J*=8 Hz).

In a similar manner, **19b** and **19c** were prepared.

19b: An oil; MS *m/z* 308 (M^+, 1%), 197, 157 (100), 152, 139, 92, 55; IR (neat) 2920, 2850, 1588, 1458, 1308, 1160, 1133, 1076, 805 cm^{-1}; ^1H NMR ($CDCl_3$) δ=0.87 (t, 3H, *J*=7 Hz), 1.11—1.36 (m, 12H), 1.36—1.50 (m, 2H), 2.22 (t, 3H, *J*=8 Hz), 2.44 (s, 3H), 5.69 (s, 1H), 6.33 (s, 1H), 7.33 (d, 2H, *J*=8 Hz), 7.75 (d, 2H, *J*=8 Hz).

19c: An oil; MS *m/z* 322 (M^+, 1%), 197, 166, 157 (100), 139, 92, 55; IR (neat) 2922, 2849, 1590, 1460, 1310, 1162, 1134, 1078, 805 cm^{-1}; ^1H NMR ($CDCl_3$) δ=0.88 (t, 3H, *J*=7 Hz), 1.07—1.34 (m, 14H), 1.34—1.49 (m, 2H), 2.21 (t, 2H, *J*=8 Hz), 2.44 (s, 3H), 5.69 (s, 1H), 6.33 (s, 1H), 7.33 (d, 2H, *J*=8 Hz), 7.75 (d, 2H, *J*=8 Hz).

The conversion of **19a—c** to **20a—c** was carried out in a similar manner described for the conversion of **7b** to **11b**.

20a: An oil; MS *m/z* 280 (M^+, 0.2%), 157 (100), 124 (100), 83 (100), 69 (100), 55 (100), 41; IR (neat) 2918, 2845, 1588, 1458, 1314, 1138, 1082, 960, 805 cm^{-1}; ^1H NMR ($CDCl_3$) δ=0.86 (t, 3H of Z, *J*=7 Hz), 0.88 (t, 3H of E, *J*=7 Hz), 0.98—1.36 (m, 8H of E and Z), 1.73 (m, 2H of Z), 1.99 (m, 2H of E), 2.44 (s, 3H of E and Z), 3.72 (d, 2H of E, *J*=7 Hz), 3.83 (d, 2H of Z, *J*=8 Hz), 5.33—5.44 (m, 1H of E and Z), 5.51 (dt, 1H of E, *J*=7, 15 Hz), 5.71 (dt, 1H of Z, *J*=7.5, 11 Hz), 7.33 (d, 2H of E and Z, *J*=8 Hz), 7.73 (d, 2H of E, *J*=8 Hz), 7.76 (d, 2H of Z, *J*=8 Hz); E/Z=80/20.

20b: An oil; MS *m/z* 308 (M^+, 0.2%), 209, 157 (100), 152, 97, 83, 69, 55; IR (neat) 2915, 2840, 1587, 1442, 1312, 1135, 1080, 960, 805 cm^{-1}; ^1H NMR ($CDCl_3$) δ=0.88 (t, 3H of Z, *J*=7 Hz), 0.89 (t, 3H of E, *J*=7 Hz), 1.02—1.48 (m, 12H of E and Z), 1.73 (m, 2H of Z), 1.98 (m, 2H of E), 2.44 (s, 3H of E and Z), 3.72 (d, 2H of E, *J*=7 Hz), 3.83 (d, 2H of Z, *J*=8 Hz), 5.35—5.44 (m, 1H of E and Z), 5.51 (dt, 1H of E, *J*=7, 15.5 Hz), 5.71 (dt, 1H of Z, *J*=7.5, 11 Hz), 7.33 (d, 2H of E and Z, *J*=8 Hz), 7.73 (d, 2H of E, *J*=8 Hz), 7.76 (d, 2H of Z, *J*=8 Hz); E/Z=78/22.

20c: An oil; MS *m/z* 322 (M^+, 0.5%), 166 (100), 157 (100), 111, 97 (100), 83 (100), 69 (100), 55, 43; IR (neat) 2917, 2840, 1590, 1458, 1316, 1138, 1080, 962, 805 cm^{-1}; ^1H NMR ($CDCl_3$) δ=0.88 (t, 3H of E and Z, *J*=7 Hz), 1.00—1.54 (m, 14H of E and Z), 1.72 (m, 2H of Z), 1.98 (m, 2H of E), 2.44 (s, 3H of E and Z), 3.72 (d, 2H of E, *J*=7 Hz), 3.83 (d, 2H of Z, *J*=8 Hz), 5.33—5.44 (m, 1H of E and Z), 5.51 (dt, 1H of E, *J*=7, 15 Hz), 5.70 (dt, 1H of Z, *J*=7.5, 11 Hz), 7.33 (d, 2H of E and Z, *J*=8 Hz), 7.72 (d, 2H of E, *J*=8 Hz), 7.75 (d, 2H of Z, *J*=8 Hz); E/Z=77/23.

Preparation of (*E*)-1-Tosyl-1-butene (23a). To a solution of LDA (2 mmol, prepared from diisopropylamine (280 µl, 2 mmol) and *n*-BuLi (hexane solution, 2 mmol) at −30 °C) in THF (7.5 ml) was added dropwise a THF (1.5 ml) solution of butyl *p*-tolyl sulfone (**21a**, 212 mg, 1 mmol) at −78 °C under nitrogen. After stirring for 1 h at −78 °C, a solution of diphenyl diselenide (343 mg, 1.1 mmol) in THF (1 ml) was added at −78 °C. The mixture was gradually warmed up to room temperature and stirred overnight. After quenching with a phosphate buffer solution (pH 7), the THF was evaporated. The product was extracted from the aqueous phase with ethyl acetate several times and the combined organic extracts were successively washed with aqueous $NaHCO_3$ and brine, and dried over Na_2SO_4. The solution was condensed into ca. 6 ml followed by the addition of 3 ml of THF. To the resulting homogeneous solution was added 30% of hydrogen peroxide (0.43 ml, 5 mmol) at 0 °C. After stirring for 1 h at 0 °C and for 2 h at room temperature, the mixture was treated with aqueous $NaHCO_3$ and the product was extracted with ethyl acetate, followed by being dried over Na_2SO_4. The residue obtained by evaporation of the solvent was subjected to preparative TLC (solvent; benzene–ethyl acetate=50:1, v/v) to afford 181 mg of **23a** (86% yield) as a colorless oil; MS *m/z* 210 (M^+, 29%), 139 (100), 92, 91, 51; IR (neat) 3040, 2960, 1612, 1586, 1448, 1310, 1139, 1079, 958, 808 cm^{-1}; ^1H NMR ($CDCl_3$) δ=1.07 (t, 3H, *J*=7.5 Hz), 2.22—2.32 (m, 2H), 2.44 (s, 3H), 6.29 (d, 1H, *J*=15 Hz), 7.01 (dt, 1H, *J*=6, 15 Hz), 7.33 (d, 2H, *J*=8.5 Hz), 7.76 (d, 2H, *J*=8.5 Hz).

In a similar manner, **23b—d** were prepared.

23b: An oil; MS *m/z* 266 (M^+, 7%), 183, 157 (100), 139 (100), 111, 110 (100), 92, 91, 81 (100), 69 (100), 55, 43, 41; IR (neat) 3036, 2920, 2849, 1588, 1458, 1318, 1140, 1082, 958, 802 cm^{-1}; ^1H NMR ($CDCl_3$) δ=0.86 (t, 3H, *J*=7 Hz), 1.18—1.37 (m, 6H), 1.37—1.51 (m, 2H), 2.17—2.26 (m, 2H), 2.43 (s, 3H), 6.29 (d, 1H, 15 Hz), 6.95 (dt, 1H, *J*=7, 15 Hz), 7.32 (d, 2H, *J*=8 Hz), 7.75 (d, 2H, *J*=8 Hz).

23c: An oil; MS *m/z* 294 (M^+, 23%), 209, 183, 157 (100), 139 (100), 138 (100), 96 (100), 83 (100), 82, 55, 43, 41; IR (neat) 3042, 2918, 2851, 1588, 1460, 1315, 1140, 1080, 962, 802 cm^{-1}; ^1H NMR ($CDCl_3$) δ=0.87 (t, 3H, J=7 Hz), 1.16—1.37 (m, 10H), 1.37—1.61 (m, 2H), 2.17—2.26 (m, 2H), 2.43 (s, 3H), 6.29 (d, 2H, J=15 Hz), 6.95 (dt, 1H, J=7, 15 Hz), 7.32 (d, 2H, J=8 Hz), 7.75 (d, 2H, J=8 Hz).

23d: Mp 44 °C (from hexane); MS *m/z* 308 (M^+, 13%), 209, 157 (100), 152, 139, 96, 92, 82, 68, 55, 43; IR (KBr) 3034, 2918, 1582, 1458, 1280, 1132, 1075, 962, 797 cm^{-1}; ^1H NMR ($CDCl_3$) δ=0.88 (t, 3H, J=7 Hz), 1.24 (broad s, 12H), 1.36—1.51 (m, 2H), 2.15—2.26 (m, 2H), 2.43 (s, 3H), 6.29 (d, 2H, J=15 Hz), 6.95 (dt, 1H, J=7, 15 Hz), 7.32 (d, 2H, J=8 Hz), 7.75 (d, 2H, J=8 Hz). Found: C, 69.90; H, 9.39%. Calcd for $C_{18}H_{28}O_2S$: C, 70.08; H, 9.15%.

The conversion of **23a—d** to **24a—d** was achieved in a similar manner described for **3b** to **11b**. Their physical data were already shown above, namely, those of **24a** were similar to those of **16a**, **24b** to **16c**, **24c** to **11d**, and **24d** to **20b** except only the ratios of E/Z on their ^1H NMR spectra, respectively.

Conversion of (*E*)-1-Tosyl-1-undecene (23d) to 1-Tosyl-2-undecene (24d) with *t*-BuOK. To a solution of *t*-BuOK (29 mg, 0.26 mmol) in *t*-BuOH (4 ml) was added a solution of (*E*)-**23d** (40 mg, 0.13 mmol) in *t*-BuOH (2 ml) at 30 °C with stirring. One-milliliter aliquots were quenched each time shown in Table 5 with 1 mol dm^{-3} HCl followed by the addition of ethyl acetate. The organic phase was separated and washed successively with aqueous $NaHCO_3$ and brine, and dried over Na_2SO_4. The residue obtained by evaporation of the solvent was dissolved in $CDCl_3$ and the resulting solution was passed through a small and short alumina column to dry and to remove insoluble substances. The ratios of products shown in Table 5 were determined by 400 MHz ^1H NMR spectra of the $CDCl_3$ solution thus obtained.

α-Alkylated vinylic sulfones (**34a—c**) were prepared according to the procedure described in the previous paper.[9c] In order to yield the pure (E)- and (Z)-isomers of **34a** and **34b**, their precursors, the 1-alkyl-2-(1-pyrrolidinyl)-alkyl *p*-tolyl sulfones, were separated into each diastereoisomer with preparative TLC prior to Cope elimination reaction. Physical data of **34a—c** are given below. (E)- and (Z)-isomers were characterized based on the known deshielding of alkyl group syn to the sulfonyl group in vinylic sulfones.[23] It was further confirmed by the measurement of NOE for each isomer.

(*E*)-**34a**: An oil; MS *m/z* 322 (M^+, 11%), 197, 166 (100), 157, 139, 69, 55; IR (neat) 2920, 2850, 1640, 1590, 1490, 1460, 1295, 1135, 1070, 805, 707 cm^{-1}; ^1H NMR ($CDCl_3$) δ=0.88 (t, 3H, J=7 Hz), 1.20—1.37 (m, 12H), 1.43—1.54 (m, 2H), 1.81 (s, 3H), 2.14—2.20 (m, 2H), 2.43 (s, 3H), 6.87 (t, 1H, J=7.5 Hz), 7.31 (d, 2H, J=8 Hz), 7.73 (d, 2H, J=8 Hz).

(*Z*)-**34a**: An oil; MS *m/z* 322 (M^+, 25%), 223, 197, 166, 157 (100), 139, 69, 68, 55; IR (neat) 2920, 2850, 1634, 1590, 1490, 1460, 1310, 1135, 1075, 805, 702 cm^{-1}; ^1H NMR ($CDCl_3$) δ=0.89 (t, 3H, J=7 Hz), 1.16—1.44 (m, 14H), 1.96 (s, 3H), 2.44 (s, 3H), 2.60—2.70 (m, 2H), 5.97 (t, 1H, J 7.5 Hz), 7.32 (d, 2H, J=8 Hz), 7.76 (d, 2H, J=8 Hz).

(*E*)-**34b**: An oil; MS *m/z* 350 (M^+, 12%), 194, 157 (100), 139, 119, 83, 69, 55; IR (neat) 2950, 2910, 2840, 1627, 1587, 1450, 1305, 1127, 1078, 803, 710 cm^{-1}; ^1H NMR ($CDCl_3$) δ=0.81—0.96 (m, 6H), 1.17—1.43 (m, 14H), 1.43—1.55 (m, 2H), 2.14—2.24 (m, 4H), 2.43 (s, 3H), 6.88 (t, 1H, J=7 Hz), 7.31 (d, 2H, J=8 Hz), 7.73 (d, 2H, J=8 Hz).

(*Z*)-**34b**: An oil; MS *m/z* 350 (M^+, 44%), 251, 157 (100), 139, 96, 82, 69, 67, 55; IR (neat) 2950, 2910, 2840, 1620, 1587, 1450, 1305, 1130, 1075, 803, 703 cm^{-1}; ^1H NMR ($CDCl_3$) δ=0.85—0.97 (m, 6H), 1.15—1.41 (m, 14H), 1.45—1.58 (m, 2H), 2.27 (t, 2H, J=7.5 Hz), 2.43 (s, 3H), 2.57—2.66 (m, 2H), 5.96 (t, 1H, J=7.5 Hz), 7.31 (d, 2H, J=8 Hz), 7.76 (d, 2H, J=8 Hz).

34c (mixture of E- and Z-forms): An oil; MS *m/z* 336 (M^+, 35%), 237, 211, 180, 157 (100), 139, 82, 69, 55; IR (neat) 2910, 2840, 1625, 1587, 1480, 1450, 1303, 1125, 1075, 803, 701 cm^{-1}; ^1H NMR ($CDCl_3$) δ=0.84—0.96 (m, 6H of E and 3H of Z), 1.05—1.13 (t, 3H of Z, J=7 Hz), 1.16—1.41 (m, 14H of Z and 12H of E), 1.42—1.58 (m, 2H of E), 2.15—2.30 (m, 4H of E), 2.30—2.38 (m, 2H of Z), 2.43 (s, 3H of E and Z), 2.57—2.67 (m, 2H of Z), 5.95 (t, 1H of Z, J=7 Hz), 6.86 (t, 1H of E, J=7.5 Hz), 7.30—7.35 (m, 2H of E and Z), 7.72—7.79 (m, 2H of E and Z).

(*E*)-**34c**: An oil; MS *m/z* 336 (M^+, 9%), 211, 180, 157, 139, 97, 83, 69 (100), 57, 55; IR (neat) 2910, 2840, 1625, 1587, 1480, 1455, 1367, 1307, 1145, 1075, 802, 703 cm^{-1}; ^1H NMR ($CDCl_3$) δ=0.84—0.98 (m, 6H), 1.20—1.37 (m, 12H), 1.42—1.58 (m, 2H), 2.15—2.30 (m, 4H), 2.43 (s, 3H), 6.86 (t, 1H, J=7.5 Hz), 7.31 (d, 2H, J=8 Hz), 7.73 (d, 2H, J=8 Hz).

The conversion of **34a—c** to the corresponding allylic sulfones (**35a—c**) was carried out with *t*-BuOK in *t*-BuOH in a similar manner described for the conversion of **23d** to **24d**. Physical data of **35a—c** were shown below.

(*E*)-**35a**: An oil; CIMS *m/z* 323 (M^+ +1, 12%), 199, 197, 167 (100), 158, 157 (100), 111, 97 (100), 83, 69; IR (neat) 2920, 2850, 1650, 1590, 1450, 1310, 1140, 1085, 965, 807, 710 cm^{-1}; ^1H NMR ($CDCl_3$) δ=0.89 (t, 3H, J=7 Hz), 1.14—1.36 (m, 12H), 1.41 (d, 3H, J=7 Hz), 1.97 (q, 2H, J=7 Hz), 2.44 (s, 3H), 3.62 (quintet, 1H, J=7 Hz), 5.36 (dd, 1H, J=7, 15.5 Hz), 5.45 (dt, 1H, J=6.5, 15.5 Hz), 7.31 (d, 2H, J=8 Hz), 7.70 (d, 2H, J=8 Hz).

(*E*)-**35b**: An oil; MS *m/z* 350 (M^+, 0.1%), 195, 125, 111, 97, 83 (100), 69, 57, 55; IR (neat) 2920, 2850, 1905, 1760, 1650, 1590, 1460, 1310, 1140, 1081, 965, 807 cm^{-1}; ^1H NMR ($CDCl_3$) δ=0.85—0.96 (m, 6H), 1.13—1.36 (m, 13H), 1.36—1.53 (m, 1H), 1.55—1.70 (m, 1H), 1.96 (q, 2H, J=7 Hz), 2.00—2.10 (m, 1H), 2.44 (s, 3H), 3.38—3.47 (m, 1H), 5.17 (dd, 1H, J=9, 15.5 Hz), 5.39 (dt, 1H, J=7, 15.5 Hz), 7.30 (d, 2H, J=8 Hz), 7.69 (d, 2H, J=8 Hz).

(*E*)-**35c**: An oil; CIMS *m/z* 337 (M^+ +1, 20%), 199, 197, 181 (100), 158, 157 (100), 125, 111, 97, 83, 69; IR (neat) 2920, 2840, 1720, 1590, 1450, 1308, 1140, 1080, 960, 805 cm^{-1}; ^1H NMR ($CDCl_3$) δ=0.88 (t, 3H, J=7 Hz), 0.93 (t, 3H, J=7 Hz), 1.14—1.37 (m, 12H), 1.56—1.72 (m, 1H), 1.97 (q, 2H, J=7 Hz), 2.10—2.21 (m, 1H), 2.44 (s, 3H), 3.30—3.38 (m, 1H), 5.18 (dd, 1H, J=9, 15.5 Hz), 5.42 (dt, 1H, J=7, 15.5 Hz), 7.30 (d, 2H, J=8 Hz), 7.69 (d, 2H, J=8 Hz).

Preparation of 4-Phenylsulfonyl-2-methyl-2-butene (38e) from 2-Methylpropanal (36e). To a mixed solution of diethyl phenylsulfonylmethylphosphonate (**37**, 74 mg, 0.25 mmol) and DBU (114 mg, 0.75 mmol) in acetonitrile (1.5 ml) was added 22 mg of **36e** (0.3 mmol) at room temperature with stirring. After 12 h, the reaction mixture was quenched with a phosphate buffer solution (pH 7), followed by replacing the solvent by ethyl acetate. The resulting solution was washed with brine twice and dried over

$MgSO_4$. The residue obtained by evaporation of the solvent was subjected to preparative TLC (solvent; hexane–ethyl acetate=5:1, v/v) to afford 46 mg of **38e** (88% yield) as an oil; MS *m/z* 210 (M^+, 2%), 69 (100), 41; IR (neat) 3048, 2960, 2904, 1578, 1440, 1300, 1144, 1080, 894, 774, 730, 680 cm^{-1}; ^1H NMR ($CDCl_3$) δ=1.31 (s, 3H), 1.71 (s, 3H), 3.79 (d, 2H, J=8 Hz), 5.19 (m, 1H), 7.49—7.59 (m, 2H), 7.61—7.68 (m, 1H), 7.81—7.93 (m, 2H).

In a similar manner, **38a—d** were prepared. Their physical data are given below.

38a: An oil (contaminated with a small amount of vinylic sulfone (ca. 8%), which was reduced in the calculation of the yield of **38a**); CIMS *m/z* 272 (M^+, 100%), 142, 130 (100), 129, 91, 52; IR (neat) 3048, 3012, 2912, 1590, 1486, 1442, 1300, 1142, 1080, 965, 720, 692 cm^{-1}; ^1H NMR ($CDCl_3$) δ=3.13 (d, 2H of Z, J=7 Hz), 3.32 (d, 2H of E J=7 Hz), 3.77 (dd, 2H of E, J=0.5, 7 Hz), 3.95 (d, 2H of Z, J=8 Hz), 5.42—5.60 (m, 1H of E and Z), 5.65 (dt, 1H of E, J=7, 15 Hz), 5.90 (dt, 1H of Z, J=7, 11 Hz), 6.93 (d, 2H of Z, J=7 Hz), 7.00 (d, 2H of E, J=7 Hz), 7.08—7.33 (m, 3H of E and Z), 7.42—7.71 (m, 3H of E and Z), 7.77—7.98 (m, 2H of E and Z).

38b: An oil; CIMS *m/z* 282 (M^+ +2, 77%), 281 (M^+ +1, 100), 183, 143 (100), 139, 138, 83, 53; IR (neat) 3052, 3012, 2920, 2844, 1580, 1440, 1314, 1140, 1080, 962, 720, 680 cm^{-1}; ^1H NMR ($CDCl_3$) δ=0.87 (t, 3H of Z, J=7 Hz), 0.88 (t, 3H of E, J=7 Hz), 0.96—1.36 (m, 10H of E and Z), 1.72 (m, 2H of Z), 1.99 (m, 2H of E), 3.74 (d, 2H of E, J=7 Hz), 3.85 (d, 2H of Z, J=8 Hz), 5.33—5.46 (m, 1H of E and Z), 5.50 (dt, 1H of E, J=7, 15 Hz), 5.71 (dt, 1H of Z, J=7, 11 Hz), 7.49—7.60 (m, 2H of E and Z), 7.60—7.69 (m, 2H of E and Z), 7.80—7.94 (m, 2H of E and Z).

38c: An oil; CIMS *m/z* 295 (M^+ +1, 56%), 183, 153 (100), 143 (100), 97, 83, 69, 53; IR (neat) 3048, 2912, 2840, 1576, 1438, 1310, 1138, 1080, 960, 720, 680 cm^{-1}; ^1H NMR ($CDCl_3$) δ=0.88 (t, 3H of Z, J=7 Hz), 0.89 (t, 3H of E, J=7 Hz), 0.98—1.36 (m, 12H of E and Z), 1.72 (m, 2H of Z), 1.98 (m, 2H of E), 3.74 (d, 2H of E, J=7 Hz), 3.85 (d, 2H of Z, J=8 Hz), 5.34—5.46 (m, 1H of E and Z), 5.50 (dt, 1H of E, J=7, 15 Hz), 5.72 (dt, 1H of Z, J=7, 11 Hz), 7.49—7.59 (m, 2H of E and Z), 7.60—7.69 (m, 1H of E and Z), 7.80—7.95 (m, 2H of E and Z).

(***E***)-**38d**: An oil; CIMS *m/z* 293 (M^+ +1, 62%), 183, 152, 151 (100), 143, 109, 95, 81, 69, 51; IR (neat) 3052, 2952, 2900, 1578, 1440, 1312, 1140, 1080, 962, 730, 680 cm^{-1}; ^1H NMR ($CDCl_3$) δ=0.87 (d, 3H, J=7 Hz), 1.19 (m, 2H), 1.56 (s, 3H), 1.67 (s, 3H), 1.82 (q, 2H, J=7.5 Hz), 2.09 (m, 1H), 3.69—3.82 (m, 2H), 5.01 (m, 1H), 5.30—5.42 (m, 2H, J of olefinic protons=15.5 Hz), 7.50—7.58 (m, 2H), 7.60—7.67 (m, 1H), 7.81—7.92 (m, 2H).

(***Z***)-**38d**: An oil (contaminated with a small amount of vinylic sulfone (ca. 5%), which was reduced in the calculation of the yield of **38d**); CIMS *m/z* 293 (M^+ +1, 100%), 152 (100), 151 (100), 150 (100), 149, 143 (100), 135, 109 (100), 107, 95, 83, 82 (100), 81, 69, 67, 53, 51; IR (neat) 3052, 2952, 2912, 1580, 1440, 1312, 1140, 1080, 886, 722, 680 cm^{-1}; ^1H NMR ($CDCl_3$) δ=0.66 (d, 3H, J=7 Hz), 0.98—1.11 (m, 1H), 1.13—1.27 (m, 1H), 1.54 (s, 3H), 1.66 (d, 3H, J=1 Hz), 1.73 (q, 2H, J=7.5 Hz), 2.02—2.16 (m, 1H), 3.71—3.82 (m, 1H), 3.85—3.95 (m, 1H), 4.95 (m, 1H), 5.31—5.41 (m, 1H), 5.47 (dd, 1H, J=10, 11 Hz), 7.48—7.58 (m, 2H), 7.58—7.69 (m, 1H), 7.82—7.96 (m, 2H).

Authors express their sincere thanks to Professor Shigeyuki Aono and Dr. Kiyoshi Nishikawa of this Institute for their helpful discussions.

References

1) P. D. Magnus, *Tetrahedron*, **33**, 2019 (1977).
2) T. Durst, "Comprehensive Organic Chemistry," ed by D. H. R. Barton and W. D. Ollis, Pergamon, Oxford (1979), Vol. 3, p. 197.
3) J.-L. Fabre, M. Julia, and J.-N. Verpeaux, *Tetrahedron Lett.*, **23**, 2469 (1982).
4) J. Sumner, M. Julia, M. Launay, and J.-P. Stacino, *Tetrahedron Lett.*, **23**, 3265 (1982).
5) B. M. Trost and N. R. Schmuff, *J. Am. Chem. Soc.*, **107**, 396 (1985) and references cited therein.
6) B. M. Trost and M. R. Ghadiri, *J. Am. Chem. Soc.*, **106**, 7260 (1984) and references cited therein.
7) T. Mandai, T. Yanagi, K. Araki, Y. Morisaki, M. Kawada, and J. Otera, *J. Am. Chem. Soc.*, **106**, 3670 (1984) and references cited therein.
8) a) H. Kotake, K. Inomata, Y. Murata, H. Kinoshita, and M. Katsuragawa, *Chem. Lett.*, **1976**, 1073; b) H. Kotake, K. Inomata, and M. Sumita, *ibid.*, **1978**, 717; c) K. Inomata, H. Kinoshita, H. Takemoto, Y. Murata, and H. Kotake, *Bull. Chem. Soc. Jpn.*, **51**, 3341 (1978); d) K. Inomata, Y. Nakayama, M. Tsutsumi, and H. Kotake, *Heterocycles*, **12**, 1467 (1979) references cited therein; e) H. Kotake, K. Inomata, H. Kinoshita, Y. Sakamoto, and Y. Kaneto, *Bull. Chem. Soc. Jpn.*, **53**, 3027 (1980).
9) a) K. Inomata, T. Yamamoto, and H. Kotake, *Chem. Lett.*, **1981**, 1357; b) K. Inomata, T. Kobayashi, S. Sasaoka, H. Kinoshita, and H. Kotake, *ibid.*, **1986**, 289; c) K. Inomata, Y. Tanaka, S. Sasaoka, H. Kinoshita, and H. Kotake, *ibid.*, **1986**, 341.
10) a) H. Kotake, T. Yamamoto, and H. Kinoshita, *Chem. Lett.*, **1982**, 1331; b) A. Ahmed, H. Taniguchi, H. Fukuda, H. Kinoshita, K. Inomata, and H. Kotake, *Bull. Chem. Soc. Jpn.*, **57**, 781 (1984); c) M. Mohri, H. Kinoshita, K. Inomata, and H. Kotake, *Chem. Lett.*, **1985**, 451; d) K. Inomata, Y. Murata, H. Kato, Y. Tsukahara, H. Kinoshita, and H. Kotake, *ibid.*, **1985**, 931; e) M. Mohri, H. Kinoshita, K. Inomata, H. Kotake, H. Takagaki, and K. Yamazaki, *ibid.*, **1986**, 1177.
11) A part of this work has appeared as a preliminary form in Ref. 9b.
12) L. Kao Liu, Y. Chi, and H.-Y. Jen, *J. Org. Chem.*, **45**, 406 (1980).
13) C. M. da Silva Correa and W. A. Waters, *J. Chem. Soc., (C)*, **1968**, 1874.
14) The reaction of tosyl iodide and styrene (**1a**) or 1-pentene (**1b**) in methanol was examined with or without additives under the similar conditions as ones in Table 1. The yields of **3a** and **3b** varied with the additives as follows: Additives (equiv), yields (%) of **3a** and **3b**; none, 40 and 8; NaI (1), 57 and 25; *p*-$CH_3C_6H_4SOONa \cdot 4H_2O$ (0.5), 67 and 35; NaI (1) +*p*-$CH_3C_6H_4SOONa \cdot 4H_2O$ (0.5), 95 and 76. Tosyl iodide was more readily soluble in methanol in the presence of NaI.
15) D. E. O'Connor and W. I. Lyness, *J. Am. Chem. Soc.*, **86**, 3840 (1964).
16) D. N. Brattesani and C. H. Heathcock, *Tetrahedron Lett.*, **1974**, 2279.

17) E. Block, M. Aslam, V. Eswarakrishnan, K. Gebreyes, J. Hutchinson, R. Iyer, J.-A. Laffitte, and A. Wall, *J. Am. Chem. Soc.*, **108**, 4568 (1986).

18) a) D. Cremer, *J. Am. Chem. Soc.*, **101**, 7199 (1979); b) E. Block, R. E. Penn, A. A. Bazzi, D. Cremer, *Tetrahedron Lett.*, **22**, 29 (1981); c) K. N. Houk, R. W. Strozier, N. G. Rondan, R. R. Fraser, and N. Chuaqui-Offermanns, *J. Am. Chem. Soc.*, **102**, 1426 (1980) and references cited therein.

19) I. Fleming, "Frontier Orbitals and Organic Chemical Reactions," John Wiley & Sons, Chichester, New York, Brisbane, Toronto (1978), p. 80.

20) G. H. Posner and D. J. Brunelle, *J. Org. Chem.*, **37**, 3547 (1972).

21) D. Craig, S. V. Ley, N. S. Simpkins, G. H. Whitham, and M. J. Prior, *J. Chem. Soc., Perkin Trans. 1*, **1985**, 1949.

22) This compound was $C_6H_5CHICH_2Ts$. Mp 139—140 °C (from benzene/chloroform=2/1, lit,[12] 138—139 °C).

23) a) C. Y. Meyers and I. Sataty, *Tetrahedron Lett.*, **1972**, 4323; b) W. E. Truce and M. J. Lusch, *J. Org. Chem.*, **43**, 2252 (1978); c) M. Mikolajczyk, S. Grzejszczak, and A. Zatorski, *J. Org. Chem.*, **40**, 1979 (1975).

 © 1987 The Chemical Society of Japan Bull. Chem. Soc. Jpn., 60, 1781—1788 (1987)

$CH_3\cdots O$ Hydrogen Bond. Implications of Its Presence from the Substituent Effects on the Populations of Rotamers in 4-Substituted 9-Ethyl-1-methoxytriptycenes and 9-(Substituted Phenoxymethyl)-1,4-dimethyltriptycenes[1)]

Yoshio TAMURA, Gaku YAMAMOTO, and Michinori ŌKI*
Department of Chemistry, Faculty of Science, The University of Tokyo,
Bunkyo-ku, Tokyo 113
(Received October 13, 1986)

In the series of 4-substituted 9-ethyl-1-methoxytriptycenes, the populations of the *sc* conformer increase as the electron-density on the 1-methoxy-oxygen decreases. This trend was interpreted on the basis of steric repulsion which should increase as the electron density on the oxygen atom becomes high. In contrast, in the series of 9-(substituted phenoxymethyl)-1,4-dimethyltriptycenes, the high electron density on the aryloxy-oxygen favors the *sc* form. The stabilization of the *sc* form relative to the *ap* in the high electron density compounds in the latter series is attributed to the presence of $CH_3\cdots O$ hydrogen bond, since other factors like Coulombic interactions, van der Waals repulsions, and van der Waals attractions could be excluded from being the main factor for the stabilization.

Hydrogen bond is a very important phenomenon both in chemistry and in biology.[2)] Those which involve the OH and NH groups as hydrogen donors are well-documented. However, the hydrogen bond which involves the CH group as a hydrogen donor, though theoretically possible, is controversial at best, except some strong hydrogen donors like hydrogen cyanide, acetylene, and chloroform.[3)] It is a common practice to assume the presence of a hydrogen bond when two groups concerned are placed within the sum of their van der Waals radii in crystals.[4)] Nishio and Hirota have discussed the presence of this kind of interactions from the unusual populations of rotamers but their work is lacking convincing evidence.[5)] Allerhand and Schleyer investigated the presence of hydrogen bond involving the methyl group without success.[6)] As judged from the acidity of methyl groups, the electron-accepting ability of the methyl should be the lowest among the CH groups. And this makes it difficult to detect the hydrogen bond involving the methyl group as a hydrogen donor.

Molecular interactions are generally observable when one of various factors predominates. The factors may be charge-transfer interactions, Coulombic interactions both repulsive and attractive, van der Waals repulsions, and van der Waals attractions (dispersion forces).[3)] Since the charge trasfer interactions involving the methyl group are weak, the attractive forces due to charge transfer may well be cancelled by the strong van der Waals repulsive forces. This is cosidered to be the situation where we do not usually observe hydrogen bond in which the methyl group acts as a hydrogen donor.

1,9-Disubstituted triptycenes comprise a very interesting group of compounds because the substituents are placed well within the sum of the van der Waals radii, as judged from the molecular structures in crystals.[7–9)] That means that the 9-substituent cannot avoid the very strong van der Waals repulsions irrespective of their rotational positions including the otherwise stable staggered positions. In addition, this geometry will enhance the overlap of the atomic orbitals concerned. The fact that this laboratory was able to report the presence of weak molecular interactions such as charge-transfer interactions between n-electrons and π^*-systems of benzene rings,[10)] n-electrons and σ^*-systems of acyloxymethyl groups,[11)] and n-electrons and π^*-systems of various carbonyl moieties[5)] by taking advantage of the 1,9-disubstituted triptycenes owes to these particular steric situations.

We have suggested in some of the previous papers from this laboratory that there have been some phenomena that might be explained by the presence of $CH_3\cdots O$ hydrogen bond. Although the thickness of the π-system is considered to be much smaller than the van der Waals radius of a methyl group, both 9-allyl- (**1**) and 9-ethyl-1,4-dimethoxytriptycene (**2**) show the $\pm sc/ap$ value of ca. 0.7.[12–13)] Similarly, 1,4-dimethoxy-9-(1-methyl-2-propenyl)triptycene (**3**) shows *sc/ap* value of 0.72.[14)] Apparently the methyl group is smaller than the π-system in this case. Although it is possible to argue that these unusual population ratios of rotational isomers are caused by an unexpected instability of the conformation in which the vinyl group takes the *ap* position or the electronic repulsion between the π-system and the methoxy-oxygen is very strong, we cannot overlook a possibility that there are attractive interactions such as $CH_3\cdots O$ hydrogen bond.

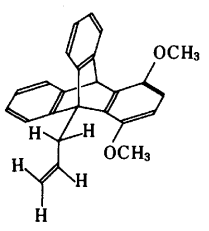

1

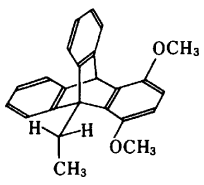

2

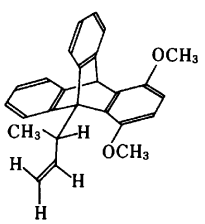

3

1-Substituted 9-(1-methoxyethyl)triptycenes (**4**) are another case that shows anomalous population ratios of rotamers. The *ap* rotamer becomes more favored than the statistical value of 2.0 when the 1-substituent is a methoxyl group whereas other substituents such as chloro, bromo, and methyl all disfavor the *ap* form to a large extent.[15] The results may be interpreted on one hand that the small bulkiness of the methoxyl group favors the *ap* form but on the other it is possible to assume that the $CH_3\cdots O$ hydrogen bond favors the *ap* form especially because all other substituents give small *sc*/*ap* values of 0.3—0.4. This large jump in populations might imply an attractive force in the *ap* form of the 1-methoxy compound.

In order to get further insight into the nature of the abnormal population ratios of these compounds, we have investigated the substituent effects in the population ratios, by introducing a substituent to the para position of the methoxyl group in 9-ethyl-1-methoxytriptycene (**10**) and to the para position (and in one case 3,4-positions) of the phenyl group in 9-(phenoxymethyl)-1,4-dimethyltriptycene (**16**). To the first approximation, it was expected that the lowering of the electron density on the oxygen atom should decrease the stability due to the charge-transfer interactions. The latter compounds behaved as expected, whereas the former did not. The results, however, support the presence of $CH_3\cdots O$ hydrogen bond, as will be discussed in this paper.

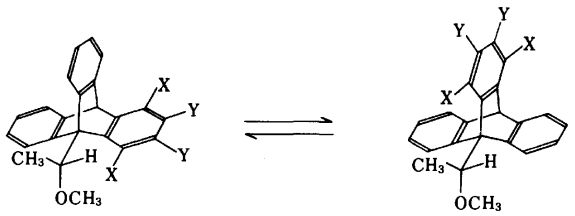

(only *R* configuration shown)

4 (X=OCH_3, Cl, Br, CH_3; Y= H, Cl, Br, H)

Synthesis and Determination of Populations

The synthetic routes for 4-substituted 9-ethyl-1-methoxytriptycenes and 9-(aryloxymethyl)-1,4-dimethyltriptycenes are shown in Schemes 1 and 2, respectively. 9-Ethyl-1,4-dimethoxytriptycene (**2**) had been prepared by treating 9-ethylanthracene with dimethoxybenzyne generated in situ by treating 2-chloro-1,4-dimethoxybenzene with phenylsodium.[12] However, the present method gave much better results including the yield and the ease of purification of the product. 9-Ethylanthracene (**5**) was heated with *p*-benzoquinone to produce the Diels–Alder adduct **6** which was then alternatively treated with aqueous sodium hydroxide and dimethyl sulfate to afford **2**. 4-Methoxy-9-anthrone (**7**) was ethylated with aqueous potassium hydroxide and ethyl iodide and the product **8** was converted to 9-ethyl-1-methoxyanthracene (**9**) by treatment with sodium tetrahydroborate and then with phosphorus pentaoxide. Treatment of the anthracene with benzyne generated from anthranilic acid afforded 9-ethyl-1-methoxytriptycene (**10**). Nitration of the triptycene (**10**) with nitronium tetrafluoroborate afforded a mixture of 2-nitro (**12**) and 4-nitro (**11**) de-

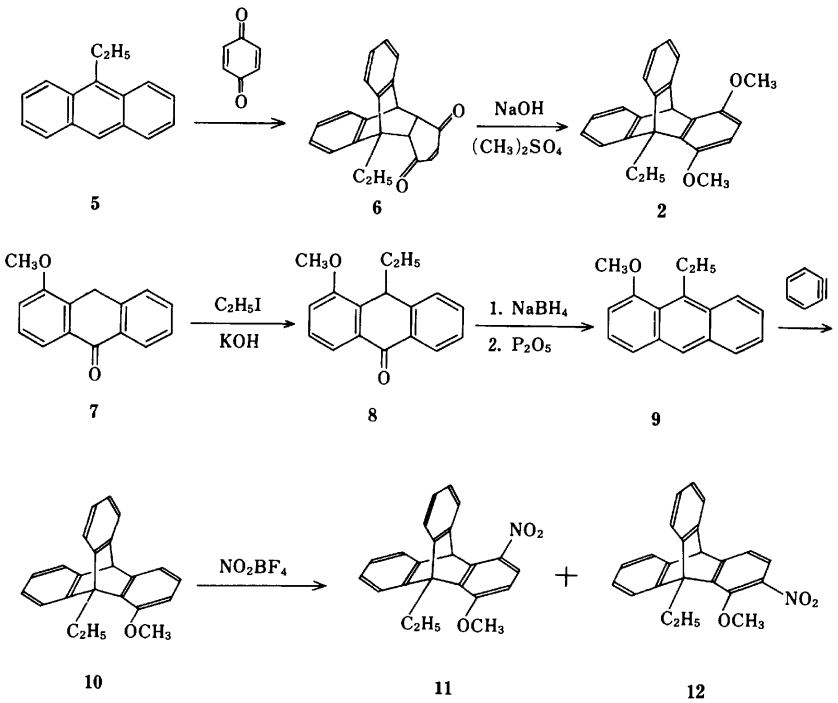

Scheme 1. Synthetic routes to 4-substituted 9-ethyl-1-methoxytriptycenes.

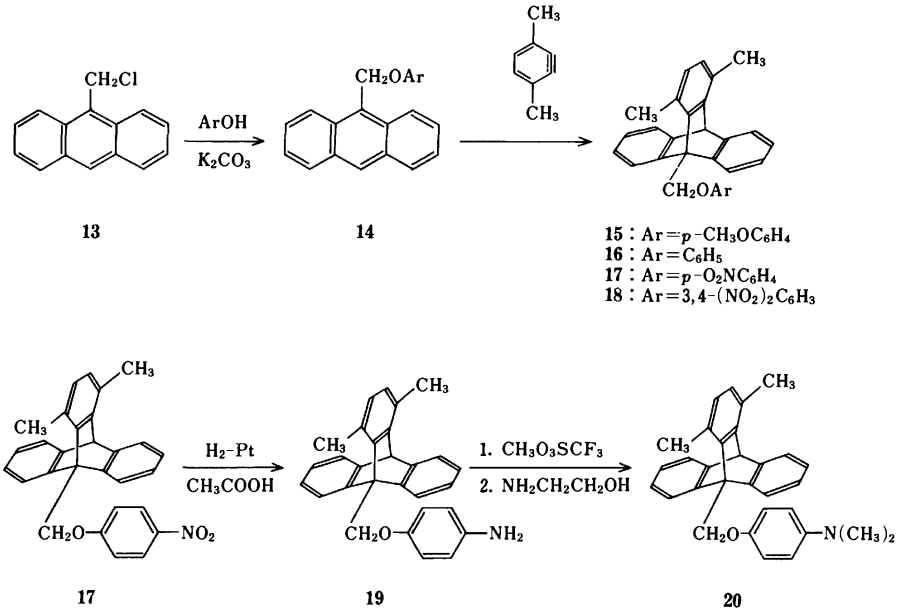

Scheme 2. Synthetic routes to 9-(aryloxymethyl)-1,4-dimethyltriptycenes.

rivatives which could be separated easily by chromatography. The structure of the 4-nitro compound was established by taking advantage of the chemical shift of 9-H in ^1H NMR spectroscopy. Whereas the 4-nitro compound (**11**) exhibits a large low-field shift of the 9-H signal, the 2-nitro compound **12** gives it at a normal range of 9-H signals of triptycenes.

9-(Aryloxymethyl)-1,4-dimethyltriptycenes (**15—18**) were preparad by treating 9-(aryloxymethyl)anthracene (**14**), which was synthesized by treatment of 9-(chloromethyl)anthracene (**13**) with substituted phenols in the presence of potassium carbonate, with 3,6-dimethylbenzyne which was generated from 3,6-dimethylanthranilic acid. 9-(Phenoxymethyl)anthracene had been prepared by treating 9-anthryldiazomethane with phenol,[16] but the present method gives much better results than the reported. 9-[4-(Dimethylamino)phenoxymethyl]-1,4-dimethyltriptycene (**20**) was prepared by reduction of 1,4-dimethyl-9-(4-nitrophenoxymethyl)triptycene (**17**), which was synthesized as above, to afford the amino compound (**19**). The amine (**19**) was then methylated to the corresponding quaternary ammonium salt with methyl triflate and then demethylated with 2-aminoethanol.

Population ratios of the rotational isomers were determined by integration of ^1H NMR spectra at 400 MHz obtained at low temperatures. Assignment of the rotamers was straightforward, because, as is seen in Scheme 3, the *ap* form should exhibit enanthiotopic methylene signal, a singlet, and the $\pm sc$ form diastereotopic, an AB quartet. In practice, however, the separation of the methylene signals was not always perfect to cause errors in integration. In those cases, methyl signals were used for the estimation of populations after completion of assignments by consulting the intensity with the methylene proton signals.

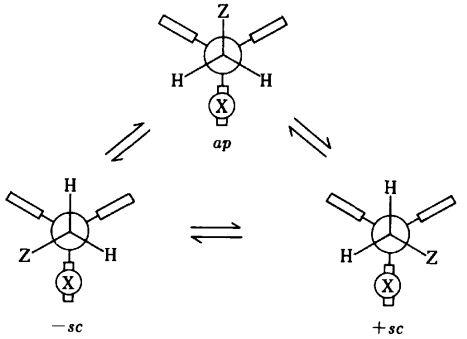

Scheme 3. Rotational circuit of 1,9-disubstituted triptycenes, where the 9-substituent is ZCH_2.

Results and Discussion

4-Substituted 9-Ethyl-1-methoxytriptycenes (2, 10, and 11). The population ratios obtained at ca. −40 °C with these compounds are shown in Table 1 and thermodynamic parameters for the $ap \rightleftarrows \pm sc$ processes in Table 2, where the populations of the $\pm sc$ form were divided by 2 in comparing the *ap* and the *sc* to accommodate the fact that the latter contains two degenerate positions.

The data in Table 1 are rather striking. Clearly the population of the *sc* form increases as the 4-substituent becomes more electron-withdrawing. Namely, the low electron-density on the 1-methoxy-oxygen favors the *sc* form. The changes in enthalpy and entropy were examined to find the possible cause for this phenomenon, but, as are shown in Table 2, rather small *r* values preclude any clear-cut conclusion

Table 1. Populations and Population Ratios of Rotamers of 4-Substituted 9-Ethyl-1-methoxytriptycenes at ca. −40 °C in $CDCl_3$

4-Substituent	σ Value of 4-Substituent	±sc/%	sc/ap[a]	Temp/°C
CH_3O	−0.268	37.7±0.7	0.302	−39.4
H	0.000	40.5±0.7	0.340	−39.4
NO_2	0.778	41.7±0.6	0.358	−39.5

a) The population of the *sc* form is taken as a half of the observed.

Table 2. Thermodynamic Parameters for the $ap \rightleftarrows \pm sc$ Processes in 4-Substituted 9-Ethyl-1-methoxytriptycenes

4-Substituent	$\Delta H°$/kcal mol^{-1} [a]	$\Delta S°$/e.u.[b]	r[c]
CH_3O	0.13±0.05	−1.8±0.2	0.998
H	0.43±0.09	−0.3±0.4	0.994
NO_2	0.18±0.44	−1.3±1.8	0.931

a) 1 cal=4.184 J. b) 1 e.u.=4.184 J mol^{-1} K^{-1}. c) Correlation coefficient in the statistical treatment.

from the data. At least, however, the results imply that there are no abrupt abnormalities associated with the change in the 4-substituent. We may discuss the results in Table 1 by taking advantage of the factors which affect the populations of rotamers.

It is unlikely that the polarity of a molecule examined here changes according to the rotameric positions taken by the substituent, because the ethyl group is the only one which rotates: The methoxyl group(s) is expected to take a coplanar position with the benzene ring[17] with the methyl group away from the 9- or 10-carbon because of the steric effect. We may neglect that Coulombic interactions comprise a main factor which controls the populations of rotamers, because rotation of the ethyl group does not cause appreciable change in dipole–dipole interactions. Charge-transfer interactions between the methyl and the methoxy-oxygen cannot be the main factor either, because if it were the case, the *sc* form should be favored when the electron density on the methoxyl group is high. Dispersion forces are known to be proportional to polarizability and to ionization potential:[18] Whereas the former increases when the electron density of the methoxy-oxygen is high, the latter decreases under the circumstance. Thus dispersion forces should not play an important role here (vide infra).

Then the important factor seems to be the van der Waals repulsion. As the electron density on the 1-methoxy-oxygen becomes high, the effective bulkiness of the group increases, thus increasing the steric repulsion between the groups concerned. It is concluded that the repulsive forces rather than attractive forces are decisive in this case.

The opposite trend seen in the populations in 4-substituted 9-ethyl-1-methoxytriptycenes to that expected for the charge-transfer interactions between the methyl group of the 9-ethyl and the oxygen atom of the 1-methoxyl group prompted us to investigate another series of compounds. The idea was that the acidity of the methyl group in an ethyl may be too low to show significant interactions with the oxygen atom. Since the pK_a value of ethane is known to be much higher than toluene,[19] changing the methyl group from that in an ethyl to that in a toluene derivative should give better chances to observe the presence of the CH_3...O hydrogen bond. Thus we shifted to 9-(substituted phenoxymethyl)-1,4-dimethyltriptycenes.

Table 3. Populations and Population Ratios of Rotamers of 9-(Substituted Phenoxymethyl)-1,4-dimethyltriptycenes in $CDCl_3$ at ca. −50 °C

Substituent	σ Value of Substituent	±sc/%	sc/ap[a]	Temp/°C
4-$(CH_3)_2N$	−0.600	36.6±0.1	0.289	−49.7
4-CH_3O	−0.268	32.6±1.0	0.242	−49.6
H	0.000	30.9±0.8	0.224	−49.4
4-NO_2	0.778	27.6±1.4	0.191	−49.6
3,4-$(NO_2)_2$	1.385[b]	24.8±1.3	0.165	−49.2

a) The population of the *sc* forms was divided by 2. b) The sigma value obtained from the dissociation constant of 3,4-dinitrobenzoic acid.[20]

Table 4. Thermodynamic Parameters for the $ap \rightleftarrows \pm sc$ Processes in 9-(Substituted Phenoxymethyl)-1,4-dimethyltriptycenes

Substituent	$\Delta H°$/kcal mol^{-1}	$\Delta S°$/e.u.	r[a]
4-$(CH_3)_2N$	0.58±0.11	−0.2±0.4	0.996
4-CH_3O	0.51±0.08	−0.6±0.3	0.997
H	0.73±0.23	0.3±0.9	0.989
4-NO_2	1.19±0.06	1.7±0.3	0.999

a) Correlation coefficient in the statistical treatment.

9-(Substituted Phenoxymethyl)-1,4-dimethyltriptycenes (15—18 and 20). The data of populations and the thermodynamic parameters for the process $ap \rightleftarrows sc$ are given in Tables 3 and 4, respectively.

The data in Table 3 clearly show that the populations of the *sc* form increase as the electron density on the aryloxy-oxygen increases. The Hammett plot (Fig. 1) gives a fairly good linearity, the *r* factor being 0.983. The ρ value is −0.114, which is very small if we compare the value with normal reactions that take place at the α-position of the aryl group.[21] Close examination of the straight line reveals that the line does not pass the point for the unsubstituted compound and the plots form a concave curve. This together with the small ρ value will mean that the observed populations base on a delicate balance of attraction and repulsion, because if attractive force is enhanced by virtue of the high electron-density, the

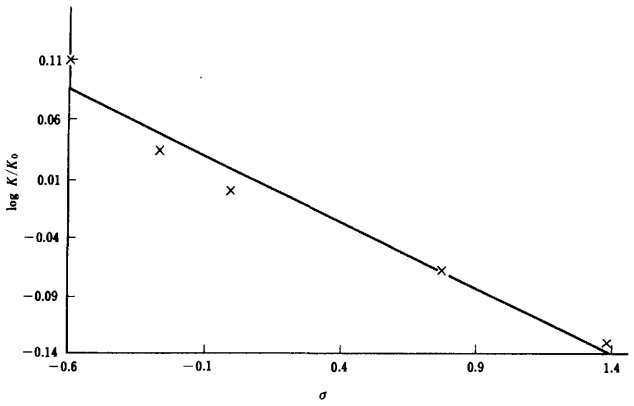

Fig. 1. The Hammett plot for the equilibrium constants of rotamers of 9-(aryloxymethyl)-1,4-dimethyltriptycenes.

same factor simultaneorsly enhances the repulsive forces.

The plot of log K vs. $1/T$ in this case affords better r factors than the case of 4-substituted 9-ethyl-1-methoxytriptycenes and shows the trend that the *sc* forms are more stabilized relative to the *ap* form as the electron-density on the aryloxy-oxygen becomes high. The data are again in conformity with the presence of attractive interactions between the 1-methyl group and the aryloxy-oxygen atom.

The above discussion all favors the presence of charge-transfer type interactions that stabilize the *sc* conformations. However, it may be better to confirm that we can reject possibilities that might favor the same conformation other than charge transfer. Steric repulsion may be excluded from the possibility, because, if it were the case, the *sc* forms in the compounds with an electron-rich oxygen should be disfavored because the high electron-density means the bulky oxygen atom. Coulombic interactions cannot be the main factor which controls the populations, because the only polar part of the molecule is the aryloxy group, that should not give much different electric interactions in different rotameric positions due to the fact that the other parts of the molecules are all hydrocarbons.

High electron density should enhance the polarizability of the oxygen atom and should lower the ionization potential. Since absolute values of these two factors are unknown, it is hard to exclude dispersion forces from the possibility of being a main factor which favors the *sc* conformation. However, since dispersion forces are inversely proportional to the sixth power of the distance concerned, enhanced dispersion forces must be more effective in the *sc* form than the *ap*. This should stabilize the *sc* form even in the 4-substituted 9-ethyl-1-methoxytriptycene series when the electron density of the methoxy-oxygen is high. Since the observed trend is just the opposite to the expectation from the dispersion forces in the said series, we conclude that the dispersion forces cannot be the main factor which controls the populations of the rotamers in the triptycenes. The results imply that, at least in triptycene series, when we compare the population ratios in a series of compounds, the effect of the dispersion forces may be disregarded from the main factor.

From the above results and discussion, we claim that we have observed the presence of CH_3···O hydrogen bond in the series of 9-(substituted phenoxymethyl)-1,4-dimethyltriptycenes. 1,9-Disubstituted triptycenes will continue to be a very convenient system in which we can find very weak molecular interactions that are impossible to find due to severe repulsions in other systems.

Experimental

^{1}H NMR Measurements. ^{1}H NMR spectra were recorded with a Varian EM390 instrument which operated at 90 MHz or with a JEOL GX400 which operated at 400 MHz. The data described in this experimental section are those obtained at 90 MHz at room temperature unless otherwise mentioned.

The assignment of the peaks observed at low temperature were performed by taking advantage of the population ratios and the coalescence phenomena. We assumed that the chemical shift differences for the 4-methoxy or 4-methyl protons should be smaller than those for the 1-methoxy or 1-methyl protons due to the anisotropy effect of the 9-substituent in the *sc* form. Since temperature variation measurements were not done for compounds **18** and **20**, the assignments of the methyl protons in them are tentative especially for the *sc* form.

Determination of Populations of the Rotamers. The ^{1}H NMR spectra at low temperatures were obtained with the use of the 400 MHz NMR machine. The indicated temperatures were calibrated by a thermocouple. The NMR data at low temperatures are summarized in Tables 5 and 6. For the determination of populations, the integrated intensities were obtained by cutting the chart papers and weighing the paper several times. The peaks for the integration were selected so that the best separation of the signals was observed. Signals used for the determination were those due to methyl protons for compounds **15**—**18** and **20** and methylene protons for compounds **2**, **10**, and **11**. The equilibrium data at various temperatures are given in Tables 7 and 8.

9-Ethyl-1,4-dimethoxytriptycene (2). A solution of 0.61 g (3.0 mmol) of 9-ethylanthracene (**5**)[22] and 1.60 g (14.8 mmol) of *p*-benzoquinone in 10 mL of acetonitrile was refluxed for 1 h. After cooling, the adduct **6**, which precipitated, was collected by filtration and washed with ether to remove unreacted *p*-benzoquinone. The residue was dissolved in 20 mL of dioxane and was treated alternatively with a solution of sodium hydroxide (3.00 g) in 30 mL of water and 15 mL of dimethyl sulfate under a nitrogen atmosphere. The reaction mixture was poured into 300 mL of water and the precipitate was collected. The product was purified by recrystallization from dichloromethane–hexane, the yield being 0.71 g (70%). Mp 193.5—195.5 °C (lit,[12] 179—181 °C).

Table 5. ^{1}H NMR Data (δ) of 4-Substituted 9-Ethyl-1-methoxytriptycenes in $CDCl_3$ at ca. −39.4 °C at 400 MHz

Substituent	Form	CH_2(Et)	CH_3(Et)	1-CH_3O	Others
CH_3O	*ap*	3.42 (J=6.4 Hz)	1.50 (J=6.4 Hz)	3.76	3.70 (4-CH_3O)
	sc	2.82, 3.40 (J=14.4, 6.5 Hz)	1.63 (J=6.5 Hz)	3.82	3.74 (4-CH_3O)
H	*ap*	3.45 (J=7.1 Hz)	1.50 (J=7.1 Hz)	3.73	
	sc	2.85, 3.44 (J=14.4, 6.5 Hz)	1.64 (J=6.5 Hz)	3.77	
NO_2	*ap*	3.46 (J=7.5 Hz)	1.51 (J=7.5 Hz)	3.83	
	sc	2.88, 3.48 (J=14.7, 6.8 Hz)	1.59 (J=6.8 Hz)	3.88	

Table 6. ^{1}H NMR Data (δ) of 9-(Substituted Phenoxymethyl)-1,4-dimethyltriptycenes in $CDCl_3$ at ca. −49.6 °C at 400 MHz

Substituent	Form	9-CH_2	Aromatic-2,3	1-CH_3	4-CH_3
4-$(CH_3)_2N$[a]	*ap*	5.72	6.66, 6.74 (J=7.7 Hz)	2.67	2.51
	sc	5.35, 5.68 (J=9.7 Hz)	6.72, 6.81 (J=8.0 Hz)	2.53	2.52
4-CH_3O	*ap*	5.72	6.66, 6.75 (J=7.8 Hz)	2.67	2.51
	sc	5.35, 5.69 (J=10.4 Hz)	6.72, 6.81 (J=8.1 Hz)	2.54	2.50
H[b]	*ap*	5.77	6.66, 6.75 (J=7.6 Hz)	2.68	2.51
	sc	5.40, 5.74 (J=9.8 Hz)	6.72, 6.81 (J=8.1 Hz)	2.54	2.48
4-NO_2	*ap*	5.88	6.69, 6.78 (J=7.6 Hz)	2.69	2.52
	sc	5.53, 5.86 (10.3 Hz)	6.73, 6.83 (J=7.8 Hz)	2.41	2.56
3,4-$(NO_2)_2$[a]	*ap*	5.92	6.69, 6.78 (J=7.6 Hz)	2.41	2.56
	sc	5.57, 5.91 (J=10.2 Hz)	6.73, 6.85 (J=8.0 Hz)	2.39	2.56

a) Assignment uncertain for the 1- and 4-methyls. They may be reversed. b) At −39.6 °C.

Table 7. Temperature Dependence of the Equilibrium Constants of the Rotamers in 4-Substituted 9-Ethyl-1-methoxytriptycenes in $CDCl_3$

Substituent	*sc*/*ap* (Temp/°C)[a]		
CH_3O	0.302 (−39.4)	0.307 (−29.4)	0.310 (−19.4)
H	0.340 (−39.4)	0.357 (−29.4)	0.373 (−14.5)
	0.378 (−9.5)		
NO_2	0.358 (−39.5)	0.360 (−29.5)	0.369 (−19.5)

a) The observed population of the *sc* form was divided by 2 to compensate the degenerate positions of the *sc* form.

Table 8. Temperature Dependence of the Equilibrium Constants of the Rotamers in 9-(4-Substituted Phenoxymethyl)-1,4-dimethyltriptycenes in $CDCl_3$

Substituent	*sc*/*ap* (Temp/°C)[a]		
$(CH_3)_2N$	0.262 (−39.5)	0.276 (−29.4)	0.292 (−19.5)
	0.301 (−9.7)		
CH_3O	0.242 (−49.6)	0.265 (−29.7)	0.274 (−19.7)
	0.294 (−4.8)		
H	0.218 (−49.4)	0.243 (−39.6)	0.267 (−19.7)
	0.283 (−4.7)		
NO_2	0.164 (−49.6)	0.182 (−39.6)	0.203 (−29.7)
	0.245 (−9.8)		

a) The observed population of the *sc* form was divided by 2 to compensate the degeneracy of the + and −*sc* forms.

Found: C, 84.34; H, 6.18%. Calcd for $C_{24}H_{22}O_2$: C, 84.18; H, 6.48%. ^1H NMR ($CDCl_3$) δ=1.54 (3H, t, J=6.6 Hz), 2.8—3.5 (2H, br), 3.67 (3H, s), 3.76 (3H, s), 5.81 (1H, s), 6.45 (2H, s), 6.8—7.6 (8H, m).

10-Ethyl-4-methoxy-9-anthrone (8). To a solution of 5.00 g (22.3 mmol) of 4-methoxy-9-anthrone (**7**)[23] and 34 g (0.22 mol) of methyl iodide in 130 mL of methanol, was added a solution of 1.34 g (24 mmol) of potassium hydroxide in 30 mL of methanol in 2.5 h. After stirring for 15 h, the mixture was poured into water and extracted with dichloromethane. The extract was dried over magnesium sulfate and the solvent was evaporated. The residue was chromatographed on silica gel (hexane–dichloromethane eluent) to give 0.61 g (11%) of 10-ethoxy-1-methoxyanthracene and then 3.11 g (55%) of 10-ethyl-4-methoxy-9-anthrone (**8**). ^1H NMR ($CDCl_3$) δ=0.40 (3H, t, J=9.0 Hz), 2.0 (2H, m), 3.93 (3H, s), 4.57 (1H, t, J=6.0 Hz), 7.0—8.4 (8H, m). This compound was directly used for the synthesis of 9-ethyl-1-methoxyanthracene (**9**).

The following ^1H NMR data ($CDCl_3$, δ) were recorded for 10-ethoxy-1-methoxyanthracene: 1.59 (3H, t, J=6.0 Hz), 4.03 (3H, s), 4.21 (2H, q, J=6.0 Hz), 6.67 (1H, d, J=6.0 Hz), 7.1—8.4 (6H, m), 8.61 (1H, s).

9-Ethyl-1-methoxyanthracene (9). To a refluxing solution of 2.55 g (10.1 mmol) of 10-ethyl-4-methoxyanthrone (**8**) in 100 mL of ethanol, was added a solution of 3.82 g (101 mmol) of sodium tetrahydroborate in 100 mL of 10% aqueous ethanol in 1 h. After heating for further 1 h, ethanol was removed by distillation and the mixture was poured into water. The mixture was extracted with dichloromethane and the extract was dried over magnesium sulfate. The solvent was evaporated and the residue was taken up in 250 mL of carbon tetrachloride. The solution was refluxed with 50 g of phosphorus pentaoxide for 2 h. After cooling the supernatant liquid was decanted and evaporated to give 2.29 g (96%) of almost pure 9-ethyl-1-methoxyanthracene (**9**). ^1H NMR ($CDCl_3$) δ=1.49 (3H, t, J=7.5Hz), 3.86 (2H, q, J=7.5 Hz), 4.02 (3H, s), 6.75 (1H, d, J=7.8 Hz), 7.2—8.8 (6H, m), 8.26 (1H, s). This compound was directly used for the synthesis of 9-ethyl-1-methoxytriptycene (**10**).

9-Ethyl-1-methoxytriptycene (10). To a boiling solution of 2.29 g (9.7 mmol) of 9-ethyl-1-methoxyanthracene (**9**) in 40 mL of dichloromethane, were added a solution of 2.04 g (15.0 mmol) of anthranilic acid in 40 mL of acetone and 2.60 g (22.2 mmol) of isopentyl nitrite in 40 mL of dichloromethane, from two funnels, in 3 h. After refluxing for further 30 min, the solvent was removed by distillation and the residue was submitted to chromatography on silica gel (hexane–dichloromethane eluent). The pure compound was obtained in 2.37 g (78%) yield after recrystallization from dichloromethane–hexane, mp 185—186 °C. Found: C, 88.30; H, 6.18%. Calcd for $C_{23}H_{20}O$: C, 88.42; H, 6.45%. ^1H NMR ($CDCl_3$) δ=1.54 (3H, t, J=6.3 Hz), 2.9—3.5 (2H, m), 3.66 (3H, s), 5.22 (1H, s), 6.48 (1H, dd, J=2.2, 7.8 Hz), 6.7—7.7 (10H, m).

Nitration of 9-Ethyl-1-methoxytriptycene (10). To a solution of 1.90 g (6.1 mmol) of **10** in 30 mL of acetonitrile, was added 7.33 g (5.5 mmol) of saturated solution (ca. 10%) of nitronium tetrafluoroborate in acetonitrile at −30 °C. The completion of the nitration was checked by TLC, and a few drops of the saturated solution of nitronium tetrafluoroborate were added if unreacted materials were detected. The mixture was poured into 500 mL of water and the precipitate was collected by filtration. After drying, the product was submitted to chromatography on silica gel (hexane–dichloromethane eluent). The desired 4-nitro compound **11** was eluted first, the yield being 0.32 g (15%). After recrystallization from dichloromethane–hexane, the pure sample melted at 260—261 °C. Found: C, 77.25; H, 5.23; N, 3.89%. Calcd for $C_{23}H_{19}NO_3$: C, 77.29; H, 5.36; N, 3.92%. ^1H NMR ($CDCl_3$) δ=1.55 (3H, t, J=5.7 Hz), 3.0—3.6 (2H, br), 3.81 (3H, s), 6.52 (1H, s), 6.54 and 7.62 (2H, ABq, J=10.2 Hz), 6.8—7.2 (8H, m).

The 2-nitro compound **12** was obtained in 0.11 g (5%) yield. Recrystallization from tetrahydrofuran–hexane afforded the pure sample, mp 235—236.5 °C. Found C, 77.38; H, 5.29; N, 3.83%. Calcd for $C_{23}H_{19}NO_3$: C, 77.29; H, 5.36; N, 3.92%. ^1H NMR ($CDCl_3$) δ=1.55 (3H, t, J=6 Hz), 3.30 (2H, q, J=6 Hz), 3.74 (3H, s), 5.33 (1H, s), 6.8—7.7 (10H, m).

9-(Aryloxymethyl)anthracenes (14). The following is a typical procedure for the syntheses of a series of compounds. Phenols were available from commercial sources, except for 3,4-dinitrophenol which was prepared according to the published procedure.[24]

A mixture of 415.7 mg (1.834 mmol) of 9-(chloromethyl)-anthracene (**13**),[25] 228.6 mg (2.429 mmol) of phenol, and 0.37 g (2.7 mmol) of potassium carbonate and 30 mL of acetone were refluxed for 48 h. After cooling, the precipitate was removed by filtration and the filtrate was poured into water. The mixture was extracted with dichloromethane and the extract was washed with aqueous sodium hydroxide. 9-(Phenoxymethyl)anthracene was obtained almost quantitatively.

These compounds were used directly for the syntheses of the corresponding triptycenes.

The following ^1H NMR data ($CDCl_3$, δ) were recorded (only aryl groups given for compounds **14**). Phenyl: 5.97 (2H, s), 6.8—8.5 (13H, m), 8.53 (1H, s). *p*-Methoxyphenyl: 3.77 (3H, s), 5.87 (2H, s), 6.86 and 7.04 (2H, ABq, J=9 Hz), 7.3—8.4 (8H, m), 8.48 (1H, s). *p*-Nitrophenyl: 6.05 (2H, s), 7.1—8.5 (12H, m), 8.54 (1H, s). 3,4-Dinitrophenyl: 6.11 (2H, s), 7.3—8.4 (11H, m), 8.60 (1H, s).

9-(Aryloxymethyl)-1,4-dimethyltriptycenes (15—18). The following is the typical procedure for the syntheses of the triptycenes. The results and analytical data are given in Table 9.

To a refluxing solution of 0.30 g (1.0 mmol) of 9-[(4-methoxyphenoxy)methyl]anthracene in 20 mL of dichloromethane, were added 0.66 g (4.0 mmol) of 3,6-dimethylanthranilic acid[26] in 40 mL of acetone and 1.14 g (9.7 mmol) of isopentyl nitrite in 40 mL of dichloromethane, from separate funnels, in 2 h. The whole was heated for further 30 min and the solvents were removed by distillation. The residue was submitted to chromatography on alumina (hexane–dichloromethane eluent). The product was recrystallized from tetrahydrofuran–hexane.

The following ^1H NMR data ($CDCl_3$, δ) were recorded except for the 3,4-dinitro compound, which was too sparingly soluble (only aryl groups given for compounds **15—17**). Phenyl: 2.57 (3H, s), 2.50 (3H, s), 5.66 (1H, s), 5.2—5.9 (2H, br), 6.64 and 6.72 (2H, ABq, J=7.8 Hz), 6.8—7.8 (12H, m). *p*-Methoxyphenyl: 2.57 (3H, s), 2.50 (3H, s),

Table 9. Yields, Melting Points, and Analytical Data of 9-(Aryloxymethyl)-1,4-dimethyltriptycenes

Compd	Yield	Mp θ_m/°C	Found			Calcd		
			C	H	N	C	H	N
15	60	216—217	86.13	6.16	—	86.09	6.26	—
16	61	176—176.5	89.84	6.15	—	89.65	6.23	—
17	67	319—321	80.27	5.22	3.27	80.35	5.35	3.23
18	42	319	72.54	4.52	5.73	72.79	4.64	5.86

3.82 (3H, s), 5.63 (1H, s), 5.3—6.0 (2H, br), 6.63 and 6.72 (2H, ABq, J=7.8 Hz), 6.8—7.8 (12H, m). *p*-Nitrophenyl: 2.55 (3H, s), 2.51 (3H, s), 5.89 (1H, s), 5.4—6.1 (2H, br), 6.64 and 6.74 (2H, ABq, J=8.0 Hz), 6.9—7.7 (10H, m), 8.35 (2H, d, J=9.0 Hz).

1,4-Dimethyl-9-[4-(dimethylamino)phenoxymethyl]triptycene (20). A solution of 97.0 mg (0.224 mmol) of 9-(4-nitrophenoxymethyl)-1,4-dimethyltriptycene (**17**) in 20 mL of acetic acid was shaken under a hydrogen atmosphere in the presence of 19.5 mg of platinum oxide for 19 h. The catalyst was removed by filtration and the filtrate was diluted with water. The mixture was neutralized with sodium hydrogencarbonate and extracted with dichloromethane. Evaporation of the solvent gave the almost pure amino compound **19**. ^{1}H NMR ($CDCl_3$) δ=2.55 (3H, s), 2.48 (3H, s), 3.89 (2H, br), 5.60 (1H, s), 5.6 (2H, br), 6.4—7.6 (14H, m).

To a solution of the amine (89 mg or 0.22 mmol) in 15 mL of dichloromethane, was added 73.4 mg (0.447 mmol) of methyl triflate in 5 mL of dichloromethane at room temperature under a nitrogen atmosphere, until the spot due to the starting amine was not detected in TLC. Water was added and the pH of the aqueous layer was adjusted to 7.0. The organic layer afforded a product which was practically insoluble in chloroform. The product was heated with 67 mg of 2-aminoethanol at 200 °C for 5 min and then poured into water. The precipitate was collected and recrystallized from tetrahydrofuran–hexane, mp 242—244 °C. The yield was 0.05 g (50%). Found: C, 86.23; H, 6.80; N, 2.97%. Calcd for $C_{31}H_{29}NO$: C, 86.27; H, 6.77; N, 3.25%. ^{1}H NMR ($CDCl_3$) δ=2.50 (3H, s), 2.57 (3H, s), 2.94 (6H, s), 5.63 (1H, s), 5.3—5.9 (2H, br), 6.63 and 6.72 (2H, ABq, J=8.4 Hz), 6.8—7.8 (12H, m).

The 400 MHz ^{1}H NMR spectra at low temperatures were measured at Institute for Molecular Science. We wish to thank Dr. Shigeru Murata of the Institute for technical assistance in the measurement.

References

1) A preliminary note has been published: Y. Tamura, G. Yamamoto, and M. Ōki, *Chem. Lett.*, **1986**, 1619.
2) G. C. Pimentel and A. L. McCllelan, "The Hydrogen Bond," W. H. Freeman, San Francisco (1960).
3) R. D. Green, "Hydrogen Bonding by C-H Groups," John-Wiley, New York (1974).
4) R. Taylor and O. Kennard, *J. Am. Chem. Soc.*, **104**, 5063 (1982); J. A. R. P. Sarma and G. R. Desiraju, *Acc. Chem. Res.*, **19**, 222 (1986).
5) S. Zushi, Y. Kodama, K. Nishihata, K. Umezawa, M. Nishio, J. Uzawa, and M. Hirota, *Bull. Chem. Soc. Jpn.*, **53**, 3631 (1980).
6) A. Allerhand and P. von R. Schleyer, *J. Am. Chem. Soc.*, **85**, 1715 (1963).
7) M. Mikami, T. Toriumi, K. Konno, and Y. Saito, *Acta Crystallogr, Sect. B*, **31**, 2474 (1975).
8) M. Ōki, G. Izumi, G. Yamamoto, and N. Nakamura, *Bull. Chem. Soc. Jpn.*, **55**, 159 (1982).
9) N. Nogami, M. Ōki, S. Sato, and Y. Saito, *Bull. Chem. Soc. Jpn.*, **55**, 3580 (1982).
10) F. Suzuki and M. Ōki, *Bull. Chem. Soc. Jpn.*, **48**, 596 (1975); M. Kono, H. Kihara, N. Nakamura, F. Suzuki, and M. Ōki, *ibid.*, **52**, 1682 (1979).
11) G. Izumi, G. Yamamoto, and M. Ōki, *Bull. Chem. Soc. Jpn.*, **54**, 3064 (1981).
12) H. Nakanishi and O. Yamamoto, *Bull. Chem. Soc. Jpn.*, **51**, 1777 (1978).
13) G. Izumi, S. Hatakeyama, G. Yamamoto, and M. Ōki, *Bull. Chem. Soc. Jpn.*, **54**, 258 (1981).
14) H. Kikuchi, S. Hatakeyama, G. Yamamoto, and M. Ōki, *Bull. Chem. Soc. Jpn.*, **54**, 3832 (1981).
15) Y. Tanaka, G. Yamamoto, and M. Ōki, *Bull. Chem. Soc. Jpn.*, **56**, 3023, 3028 (1983).
16) T. Nakaya, T. Tomomoto, and M. Imoto, *Bull. Chem. Soc. Jpn.*, **40**, 691 (1967).
17) G. M. Anderson III, P. M. Kollman, L. N. Domelsmith, and K. N. Houk, *J. Am. Chem. Soc.*, **101**, 2344 (1979).
18) T. Kihara, "Bunshikanryoku (Intermolecular Forces)," Iwanami, Tokyo (1976), pp. 34—51.
19) R. E. Dessy, W. Kitching, T. Psarras, R. Salinger, A. Chen, and T. Chivers, *J. Am. Chem. Soc.*, **88**, 460 (1966).
20) J. F. Dippy, B. P. Hawkins, and B. V. Smith, *J. Chem. Soc.*, **1964**, 154.
21) H. H. Jaffé, *Chem. Rev.*, **53**, 191 (1953); P. R. Wells, *ibid.*, **63**, 171 (1963).
22) R. LaLonde and R. Calas, *Bull. Soc. Chim. Fr.*, **1959**, 766.
23) G. Yamamoto and M. Ōki, *Bull. Chem. Soc. Jpn.*, **54**, 473 (1981).
24) N. V. Sidgwick and W. M. Aldous, *J. Chem. Soc.*, **1921**, 1001.
25) F. H. C. Stewart, *Aust. J. Chem.*, **13**, 478 (1960).
26) S. Gronowitz and G. Hansen, *Ark. Kemi*, **27**, 145 (1967).

Synthesis and Properties of Chiral Macrobicyclic and Macrotricyclic Cryptands Containing the *trans*-Tetrahydrofuran-2,5-diylbis(methylene) Subunit as the Chiral Center

Koichiro NAEMURA,* Yuji KANDA, Hiroshi IWASAKA, and Hiroaki CHIKAMATSU
Department of Chemistry, Faculty of Engineering Science, Osaka University, Toyonaka, Osaka 560
(Received October 23, 1986)

The macrobicyclic and macrotricyclic cryptands containing the *trans*-tetrahydrofuran-2,5-diylbis(methylene) molecular framework as the chiral subunit were prepared in optically active forms. The enantiomer recognition property of the macrotricyclic tetracarboxamide (+)-**6** in transport of enantiomeric molecules was examined, and the cation-binding abilities of the macrotricyclic and macrobicyclic amines **7**, **10**, and **13** were also investigated.

Azamacropolycyclic polyethers (cryptands), as well as crown ethers, are of interest in host-guest chemistry. Various kinds of optically active crown ethers have been prepared and their chiral recognition behaviors have been extensively studied.[1] On the other hand, little synthesis of optically active cryptand have been reported, and chiral recognition property of the compound has been scarcely investigated.

Chiral macrotricyclic cryptands yield complexes by using a macrocyclic subunit as anchor site for binding a substrate. With primary ammonium salts, the NH_3^+-group binds directly to the macrocycle, and with alkali salts of organic anions, a cascade process is involved with first binding of the alkali cation followed by electrostatic pairing with the molecular anion. When the substrates are chiral, enantiomer recognition is expected to occur in both cases.[2]

In our preceding papers,[3,4] we have reported the preparations and the enantiomer recognition properties of optically active crown ethers and open-chain polyethers which contained the *trans*-tetrahydrofuran-2,5-diylbis(methylene) subunit as the chiral center. Our continuing interest in chiral crown ethers and analogous compounds prompted us to prepare chiral macrotricyclic cryptand incorporating the *trans*-tetrahydrofuran-2,5-diylbis(methylene) subunit, and we present here our results on the syntheses and some properties of the chiral macrotricyclic and macrobicyclic cryptands.

Results and Discussion

One of our target compounds is the chiral cylindrical macrotricyclic cryptand containing two chiral centers, and Lehn and coworkers[2] have reported the synthesis of the cylindrical macrotricyclic tetracarboxamide by condensation of two molecules of the acid dichloride with two macrocyclic amine molecules.

The synthetic strategy was to introduce the chiral centers by condensation of optically active acid dichloride with achiral macrocyclic amine. We previously reported the synthesis and the determination of absolute configuration of enantiomerically pure *trans*-tetrahydrofuran-2,5-dicarboxylic acid (**1**),[3] from which the chiral acid dichloride **3** was prepared. Treatment of (−)-(2*S*,5*S*)-**1**, $[\alpha]_D$ −5.4° (MeOH), with thionyl chloride gave the acid dichloride **3**, which was condensed with 1,7-diaza-12-crown-4 (**4**) in benzene in the presence of triethylamine under high dilution conditions.[5] Chromatography of the resulting mixture on alumina followed by recrystallization from benzene–hexane provided the desired macrotricyclic tetracarboxamide **6**, mp 240 °C (decomp), $[\alpha]_D$ +14.9° ($CHCl_3$), (26% yield) together with the macrobicyclic dicarboxamide **5**, mp 275 °C (decomp), $[\alpha]_D$ +41.0° ($CHCl_3$), (11% yield). The structures of these amides were proved by their mass spectra as well as elemental analyses and ^1H NMR spectra. The predominant formation of the macrotricyclic dimer **6** in condensation of **3** with **4** is rationalized by assuming that *trans*-tetrahydrofuran-2,5-dicarboxylic acid (**1**) contains diglycolic acid moiety.[2]

The reduction of (+)-**6** to the macrotricyclic tetramine **7** was carried out with lithium aluminium hydride in dry tetrahydrofuran (THF), and chromatography of the product on alumina afforded a 51% yield of **7**, $[\alpha]_D$ +32.5° ($CHCl_3$), as a colorless oil.

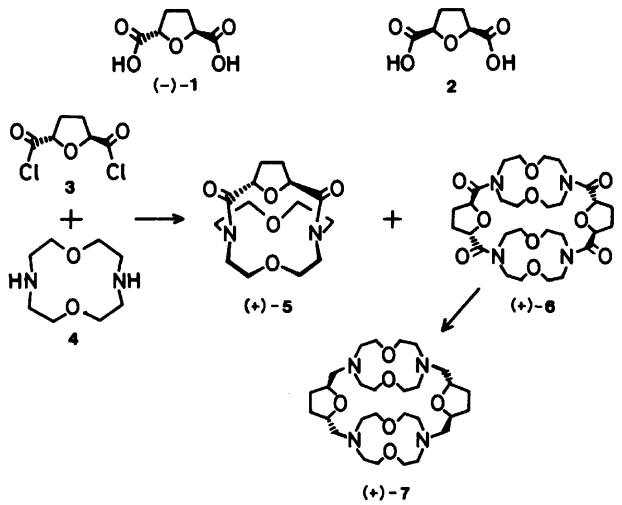

Next, we attempted to prepare the macrotricyclic cryptand, possessing the larger cavities than those of

(+)-**6**, by condensation of two molecules of **3** with two 1,10-diaza-18-crown-6 (**8**) molecules. Condensation of **3** with **8** in benzene was carried out by the same procedure described for the preparation of **6**. The product was chromatographed on alumina to give a 46% yield of the macrobicyclic dicarboxamide **9**, mp 203—205 °C, $[\alpha]_D$ +27.8° ($CHCl_3$), whose structure was also confirmed by the mass spectrum, and the cylindrical macrotricycle corresponding to **6** was not obtained. The dicarboxamide (+)-**9** was converted to the macrobicyclic diamine **10** by diborane reduction.[5] Refluxing of (+)-**9** with a freshly prepared diborane in dry THF gave the borane–amine adduct, which was hydrolyzed with 6M-hydrochloric acid (1 M=1 mol dm^{-3}) to afford the macrobicyclic diamine **10**, mp 190—192 °C, $[\alpha]_D$ +61.7° ($CHCl_3$), in 75% yield after recrystallization from hexane.

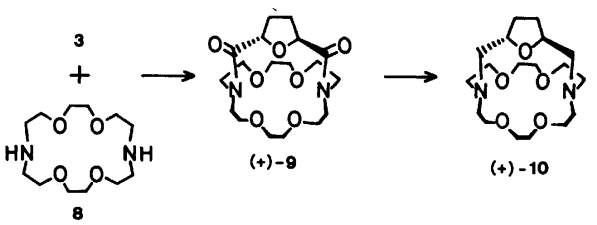

Finally, we prepared the macrobicyclic diamine incorporating achiral *cis*-tetrahydrofuran-2,5-diylbis-(methylene) residue. The acid dichloride **11** was obtained from *cis*-tetrahydrofuran-2,5-dicarboxylic acid (**2**) with thionyl chloride. Condensation of **11** with **8** under high dilution conditions followed by alumina column chromatography and recrystallization provided a 32% yield of **12**, mp 173—174 °C, and the cylindrical macrotricycle was not detected. Diborane reduction of **12** followed by hydrolysis with 6M-hydrochloric acid gave the achiral macrobicyclic diamine **13**, mp 208—209 °C, in 22% yield after recrystallization from hexane.

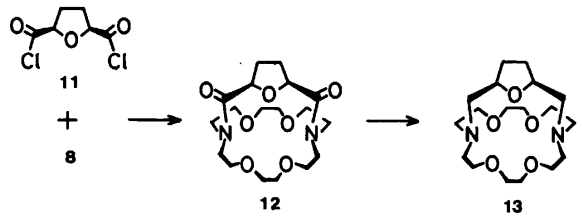

Chiral recognition property of the macrotricyclic tetracarboxamide (+)-**6** in transport of racemic primary ammonium cations; (±)-1,2-diphenylethylamine, (±)-2-aminotetralin and methyl (±)-phenylglycinate hydrochloride was examined and the results are given in Table 1.

The cryptand **6** has a higher enantiomer selectivity towards these guest molecules rather than 18-crown-6 and dibenzo-18-crown-6 derivatives incorporating the *trans*-tetrahydrofuran chiral center.[4] The cylindrical macrotricyclic cryptand (+)-**6** with D_2 symmetry contains two lateral and one central cavities.[6] Each lateral cavity possesses two chiral groups attached to nitrogen, and a large central cavity defined by the two macrocycles and the two bridges linking them incorporates two chiral subunits in the ring system. Both the lateral and the central cavities may bind NH_3^+-group, but in the complex formed by the binding of the substrate to the central cavity, the bound substrate may interact appreciably with the chiral center and therefore be subject to chiral discrimination.

Next, we studied extraction experiment for testing the chiral discrimination ability of the macrotricyclic amine **7** towards chiral molecular anion. Aqueous solution of potassium (±)-mandelate was extracted with a solution of (+)-**7** in $CDCl_3$. But, ^1H NMR spectrum of the organic layer obtained showed no signal due to the substrate. It appears that the molecular cavity of **7** is too small for inclusion of mandelate anion.

The macrobicyclic diamine **10** and **13** are analogues of cryptand 221[5] and possess the ethano bridge between C20 and C22 of the cryptand 221 molecular framework. We next turned our attention to the comparison of the cation-binding abilities of the macropolycyclic amines **7**, **10**, and **13** with that of

Table 2. Extraction of Alkali Metal Picrates

	Extractability/%				
	Li^+	Na^+	K^+	Rb^+	Cs^+
7	30	29	25	22	30
10	80	72	71	79	72
13	78	71	70	78	80
Cryptand 221	78	74	74	80	54

Table 1. Differential Transport of Enantiomeric Molecules through Bulk Liquid Membrane Containing (+)-**6**

Guest	Time / h	Transported / %	Configuration of dominantry transported enantiomer	Optical purity / %
(±)-1,2-Diphenylethylamine	3	10.1	S	46
(±)-2-Aminotetralin	5	10.3	R	25
Methyl (±)-phenylglycinate	12	11.0	R	16

Table 3. Transport Properties of Macrobicyclic Diamines

Host	Transport rate $\times 10^6$/mol h^{-1}				
	Li^+	Na^+	K^+	Rb^+	Cs^+
10	0.65	0.11	1.5	0.55	0.14
13	0.85	0.12	1.7	0.60	0.15

cryptand 221. The abilities were assessed by solvent extraction of aqueous solution of alkaline metal picrate with a chloroform solution containing cryptand. The results are summarized in Table 2.

As can be seen from Table 2, the alteration in the configuration of tetrahydrofuran moiety scarcely results in the variation in the cation-binding abilities of cryptands **10** and **13**. The striking difference between the cryptands **10** and **13** and the parent cryptand 221 is seen in their extractabilities for Cs^+ ion among alkali metal ions. The differences in extractabilities of three cryptands for the other alkali metal cations cannot be regarded as significant.

We also examined cation transport properties of **10** and **13** by using a chloroform liquid membrane system, and Table 3 lists the results.

Although potassium ion transport was most rapid in both cases, cryptands **10** and **13** hardly mediated transport of guest cations.

Experimental

Infrared spectral data were taken on a Hitachi 260-10 spectrophotometer, and ^{1}H NMR spectra were obtained from a JNM-MH-100 and a JNM-C-60. Chemical shifts are reported in parts per million (δ) down field from tetramethylsilane. Optical rotations were measured with a JASCO DIP-140 automatic polarimeter. Electronic spectral data were measured with a Hitachi 220A spectrophotometer and circular dichroism data were collected with a JASCO J-40 spectropolarimeter. Mass spectra were taken with a Hitachi RMS-4 spectrometer. Elemental analyses were determined on a Yanagimoto CHN-Corder, Type II. All melting and boiling points are uncorrected.

(2*S*,5*S*)-Tetrahydrofuran-2,5-dicarbonyl Dichloride (3). A mixture of (−)-(2*S*,5*S*)-tetrahydrofuran-2,5-dicarboxylic acid (**1**), $[\alpha]_D$ −5.4° (MeOH),[3] (1.50 g, 8.43 mmol) and thionyl chloride (10.5 g, 88.1 mmol) was stirred for 48 h at room temperature. The excess of thionyl chloride was evaporated under reduced pressure to give 1.60 g of **3**, which was used for the next reaction without further purification.

(+)-(3*S*,6*S*)-3,6-Epoxy-11,16-dioxa-1,8-diazabicyclo[6.5.5]-octadecane-2,7-dione (5) and (+)-(3*S*,6*S*,16*S*,19*S*)-3,6:16,19-Diepoxy-11,24,29,34-tetraoxa-1,8,10,21-tetraazatricyclo[20.5.5.5^{8,14}]-hexatriacontane-2,7,15,20-tetrone (6). The acid dichloride (**3**) (1.97 g, 10.0 mmol) and a mixture of 1,7-diaza-12-crown-4 (**4**)[5] (1.65 g, 9.48 mmol) and triethylamine (2.69 g, 26.6 mmol), each dissolved in 200 mL of dry benzene, were dripped over a period of 10.5 h from separate addition funnels into 400 mL of rapidly stirred dry benzene at room temperature. After the mixture was stirred for an additional 30 min, a precipitate was filtered off and the benzene was evaporated in vacuo. The residue was chromatographed on alumina. Fractions eluted with $CHCl_3$ gave 1.01 g of **5** (11% yield), which was recrystallized from benzene–hexane: mp 275 °C (decomp); $[\alpha]_D^{23}$ +41.0° (*c* 0.666, $CHCl_3$); IR (KBr) 1640, 1120, 1060 cm^{-1}; MS *m/z* 298 (M^+). Fractions eluted with $CHCl_3$–MeOH (95:5 v:v) afforded 2.35 g of **6** (26% yield), which was recrystallized from benzene–hexane: mp 240°C (decomp); $[\alpha]_D^{23}$ +14.9° (*c* 0.603, $CHCl_3$); IR (KBr) 1640, 1140, 1080, 1070 cm^{-1}; ^{1}H NMR ($CDCl_3$) δ=2.0—2.3 (8H, m, $-(CH_2)_2-$), 3.0—4.0 (32H, m, $-NCH_2CH_2O-$), 4.93 (4H, br s, CH); MS *m/z* 596 (M^+).

(+)-**5**: Found: C, 56.43; H, 7.34; N, 9.52%. Calcd for $C_{14}H_{22}O_5N_2$: C, 56.36; H, 7.34; N, 9.39%.

(+)-**6**: Found: C, 56.16; H, 7.30; N, 9.35%. Calcd for $C_{28}H_{44}O_{10}N_4$: C, 56.36; H, 7.34; N, 9.39%.

(+)-(3*S*,6*S*,16*S*,19*S*)-3,6:16,19-Diepoxy-11,24,29,34-tetraoxa-1,8,10,21-tetraazatricyclo[20.5.5.5^{8,14}]hexatriacontane (7). A solid $LiAlH_4$ (200 mg, 4.20 mmol) was added by portions to a solution of (+)-**6** (500 mg, 0.900 mmol) in 75 mL of dry THF at room temperature and then the mixture was refluxed for 16 h. To the chilled reaction mixture was slowly added 10% aqueous NaOH solution and a deposited solid was filtered off. The solvent was evaporated in vacuo and the residue was dissolved in 20 mL of $CHCl_3$. The organic solution was washed with water, dried over Na_2SO_4, and concentrated in vacuo. The residue was chromatographed on alumina, and fractions eluted with $CHCl_3$–MeOH (95:5 v:v) gave 230 mg of **7** (51% yield) as a colorless oil: $[\alpha]_D^{23}$ +32.5° (*c* 0.560, $CHCl_3$); ^{1}H NMR ($CDCl_3$) δ=1.4—2.2 (8H, m, $-(CH_2)_2-$), 2.6—2.9 (24H, m, $-NCH_2-$), 3.5 (16H, t, *J*=5 Hz, $-OCH_2-$), 3.9—4.2 (4H, m, CH). Found: C, 61.95; H, 9.50; N, 10.33%. Calcd for $C_{28}H_{52}O_6N_4$: C, 62.19; H, 9.69; N, 10.36%.

(+)-(20*S*,23*S*)-20,23-Epoxy-4,7,13,16-tetraoxa-1,10-diazabicyclo[8.8.6]tetracosane-19,24-dione (9). Condensation of **3** (2.39 g, 1.21 mmol) with 1,10-diaza-18-crown-6 (**8**);[5] (3.10 g, 11.2 mmol) was carried out by the same procedure described for the preparation of **5** and **6**. The product was chromatographed on alumina and fractions eluted with $CHCl_3$ gave 2.48 g of **9** (46% yield), which was recrystallized from benzene–hexane: Mp 203—205 °C; $[\alpha]_D^{22}$ +27.8° (*c* 0.410, $CHCl_3$); IR (KBr) 1660, 1110, 1060 cm^{-1}; MS *m/z* 386 (M^+). Found: C, 55.63; H, 7.89; N, 7.19%. Calcd for $C_{18}H_{30}O_7N_2$: C, 55.94; H, 7.83; N, 7.25%.

(+)-(20*S*,23*S*)-20,23-Epoxy-4,7,13,16-tetraoxa-1,10-diazabicyclo[8.8.6]tetracosane (10). To a solution of (+)-**9** (1.46 g, 3.00 mmol) in dry THF (20 mL) was added a freshly prepared solution of diborane (18 mmol) in 27 mL of dry THF at room temperature, and then the mixture was refluxed for 18 h. After cooling to room temperature, 3 mL of water was added to the mixture and the mixture was stirred for 1 h at room temperature. After the mixture was concentrated in vacuo, 70 mL of $CHCl_3$ was added to the residue and a deposited inorganic solid was filtered off. The solvent was evaporated in vacuo, and 50 mL of ether and 5 mL of 6M-HCl were added to the residue. After the mixture was stirred for 1 h at room temperature, the acidic aqueous layer was separated and the organic layer was extracted with water. The combined aqueous solutions were made alkaline with 25% aqueous NaOH solution and extracted with $CHCl_3$. The extract was dried over Na_2SO_4

and concentrated to give a solid, which was recrystallized from benzene–hexane to afford 785 mg of **10** (57% yield): Mp 190—192 °C; $[\alpha]_D^{23}$ +61.7° (*c* 0.505, $CHCl_3$); ^1H NMR ($CDCl_3$) δ=1.1—2.0 (4H, m, $-(CH_2)_2-$), 2.4—3.0 (12H, m, $-NCH_2-$), 3.1—3.8 (16H, m, $-OCH_2-$), 4.0—4.3 (2H, m, CH). Found: C, 60.15; H, 9.57; N, 7.80%. Calcd for $C_{18}H_{34}O_5N_2$: C, 60.30; H, 9.56; N, 7.82%.

***cis*-Tetrahydrofuran-2,5-dicarbonyl Dichloride (11).** By the same procedure described for the preparation of **3**, *cis*-tetrahydrofuran-2,5-dicarbonyl dichloride (**11**) (3.60 g) was prepared from *cis*-tetrahydrofuran-2,5-dicarboxylic acid (**2**)[7] (3.30 g, 0.0205 mol) and thionyl chloride (21.0 g, 0.176 mol). Without further purification, the product was used in the next reaction.

(20*S*,23*R*)-20,23-Epoxy-4,7,13,16-tetraoxa-1,10-diazabicyco-[8.8.6]tetracosane-19,24-dione (12). In the same manner described for the preparation of **5** and **6**, the acid dichloride **11** (1.20 g, 6.09 mmol) was condensed with 1,10-diaza-18-crown-6 (**8**) (1.55 g, 5.92 mmol), and the product was chromatographed on alumina. Fractions eluted with $CHCl_3$ provided 810 mg, of **12** (32% yield), which was recrystallized from benzene–hexane: Mp 173—174 °C; IR (KBr) 1650, 1120 cm^{-1}; ^1H NMR ($CDCl_3$) δ=1.7—2.2 (2H, m, $-(CH_2)_2-$), 2.3—3.2 (6H, m, $-(CH_2)_2-$ and $-NCH_2-$), 3.5—4.4 (20H, m, $-NCH_2-$ and $-OCH_2-$); MS *m/z* 386 (M^+). Found: C, 55.80; H, 7.86; N, 7.11%. Calcd for $C_{18}H_{30}O_7N_2$: C, 55.94; H, 7.83; N, 7.25%.

(20*S*,23*R*)-20,23-Epoxy-4,7,13,16-tetraoxa-1,10-diazabicyclo-[8.8.6]tetracosane (13). Treatment of **12** (650 mg, 1.68 mmol) with a solution of diborane (8.04 mmol) in dry THF followed by hydrolysis with 6M-HCl was carried out by the same procedure described for the preparation of **10**. The same workup described for **10** gave a solid which was recrystallized from hexane to provide 130 mg of **13** (22% yield): Mp 208—209 °C. Found: C, 60.18; H, 9.53; N, 7.80%. Calcd for $C_{18}H_{34}O_5N_2$: C, 60.30; H, 9.56; N, 7.82%.

Enantiomer Differential Transport. Enantiomer differential transport was carried out in a conventional apparatus which consisted of an outer cylindrical glass vessel (24.5 mm inner diameter) and a central glass tube (15.5 mm inner diameter). The 0.005 M $CHCl_3$ solution of the host separated the inner aqueous phase (0.1 M HCl) and the outer aqueous phase (0.08 M HCl) which contained $LiPF_6$ (0.4 M) and the racemic guest (0.04 M). The $CHCl_3$ layer was stirred at a constant speed (60 rpm) at 25±1 °C.

Cation Transport. The same apparatus described above was used. The $CHCl_3$ (5 mL) layer contained the cryptand (2.4×10^{-4} M) and the outer aqueous layer (5 mL) contained the metal picrate (2.4×10^{-4} M). The $CHCl_3$ layer was stirred at 25±1 °C.

Extraction Procedure. The aqueous solution (5 mL) of the metal picrate (2.4×10^{-4} M) and the $CHCl_3$ solution (5 mL) containing the host (2.4×10^{-4} M) were placed in a screw cap glass tube (30 mL) and the tube was shaken for 30 min at room temperature. Extraction of the picrate was followed by monitoring the absorbance at 357 nm of the aqueous phase.

References

1) G. W. Gokel and S. H. Koreniowski, "Macrocyclic Polyether Syntheses" Springer-Verlag, Berlin, Heiderberg, and New York (1982).

2) J. Cheney and J. M. Lehn, *J. Chem. Soc., Chem. Commun.*, **1972**, 487; J. Cheney, J. M. Lehn, J. P. Sauvage, and M. E. Stubbs, *ibid.*, **1972**, 1100; B. Dietrich, J. M. Lehn, and J. Simon, *Angew. Chem. Int. Ed. Engl.*, **13**, 406 (1974); J. M. Lehn, J. Simon, and A. Moradpour, *Helv. Chim. Acta*, **61**, 2407 (1978).

3) M. Nakazaki, K. Naemura, M. Makimura, A. Matsuda, T. Kawano, and Y. Ohta, *J. Org. Chem.*, **47**, 2429 (1982).

4) K. Naemura, I. Ebashi, and A. Matsuda, *Bull. Chem. Soc. Jpn.*, **58**, 3057 (1985); K. Naemura, I. Ebashi, A. Matsuda, and H. Chikamatsu, *J. Chem. Soc., Chem. Commun.*, **1986**, 666.

5) B. Dietrich, J. M. Lehn, J. P. Sauvage, and J. Blazat, *Tetrahedron*, **29**, 1629 (1973); B. Dietrich, J. M. Lehn, and J. P. Sauvage, *ibid.*, **29**, 1647 (1973).

6) J. M. Lehn and J. Simon, *Helv. Chim. Acta*, **60**, 141 (1977).

7) B. Lean, *J. Chem. Soc.*, **1900**, 103.

A New Synthesis of Cyclic Ureas, Cyclic Urethanes, and a Quinazolinedione.[1] Selenium-Assisted Carbonylation of Aromatic Amines with Carbon Monoxide

Tohru YOSHIDA, Nobuaki KAMBE, Shinji MURAI, and Noboru SONODA*
Department of Applied Chemistry, Faculty of Engineering, Osaka University, Suita, Osaka 565
(Received November 4, 1986)

Five-, six-, and seven-membered cyclic ureas were synthesized in excellent yields from various aromatic diamines by reaction with carbon monoxide and a stoichiometric or excess amount of selenium in the presence of *N*-methylpyrrolidine. The carbonylation also proceeded using a catalytic amount of selenium in the presence of an oxidizing agent such as oxygen or dimethyl sulfoxide producing selectively the five- and six-membered cyclic ureas. In the case of 2-(2-aminoethyl)aniline under the catalytic conditions, intra- and intermolecular carbonylation competed resulting in the formation of a mixture of the seven-membered cyclic urea, 1,3,4,5-tetrahydro-2*H*-1,3-benzodiazepin-2-one and the acyclic urea, 1,3-bis[2-(2-aminophenyl)ethyl]-urea. The distribution ratio of these two products varied depending on the reaction conditions, but selective formation of the cyclic urea was attained only when a stoichiometric or excess amount of selenium was used. In addition to the above diamino compounds, 2-carbamoylaniline, 2-amino-3-pyridinol, and 2-(hydroxymethyl)-aniline also underwent similar carbonylation to give 2,4(1*H*,3*H*)-quinazolinedione, oxazolo[4,5-*b*]pyridin-2-(3*H*)-one, and 1,4-dihydro-2*H*-3,1-benzoxazin-2-one, respectively.

Many cyclic urea derivatives have been used as important precursors to pigments,[2] resins,[3] and bioactive compounds.[4] These cyclic ureas can be synthesized by intramolecular amination of in situ formed isocyanates via Hoffman, Curtius, or Lossen rearrangement,[5] or carbonylation of diamines using carbonylating reagents such as phosgene, ethyl chloroformate,[6] 1,1′-carbonyldiimidazole,[6] and 1,1′-[carbonylbis(oxy)]bis-2,5-pyrrolidinedione.[7]

In addition to these stoichiometric reactions, the catalytic *N*-carbonylation of diamines with carbon monoxide is an alternative approach to the synthesis of cyclic urea derivatives.[8] Although a number of studies on catalytic carbonylation of monoamines with carbon monoxide have been reported using a variety of transition metal complexes as the catalysts, these reaction often gave mixtures of urea, formamide, and oxamide.[9–15] The selectivity depends largely on the ligands as well as the metal used.[11] However, there are only two reports of the catalytic carbonylation of diamines: One uses $Mn_2(CO)_{10}$[16a] and the other $Ni(CO)_4$[16b]; selective formation of cyclic ureas has not been achieved using these two reaction systems.

Continuing an ongoing project on selenium-assisted carbonylation, we have established a convenient method for the synthesis of symmetrical ureas using a variety of amines which are reacted with carbon monoxide and oxygen in the presence of a catalytic amount of selenium under mild conditions.[17]

This catalytic reaction has been postulated[17a,b] to proceed via selenolcarbamate ammonium salt **1**[18] which undergoes aminolysis by the nucleophilic attack of a second amine molecule at the carbonyl carbon of **1** to form urea derivatives **2** in the presence of oxygen (Scheme 1). The intermediacy of the

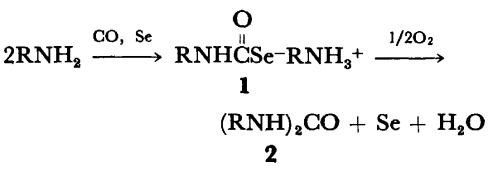

Scheme 1.

selenolcarbamate **1** is strongly supported by the facts that the selenolcarbamate derived from piperidine was isolated[17a] and that the selenolcarbamate from diethylamine was trapped by alkyl halides to give alkyl selenolcarbamates.[17b]

We have expected that application of this reaction system to diamino compounds may provide a simple and convenient method for the synthesis of cyclic ureas **4**. In this paper, we will present full details of a study aimed at the selective formation of cyclic ureas from aromatic diamines by carbonylation with carbon monoxide using selenium (Scheme 2).[1]

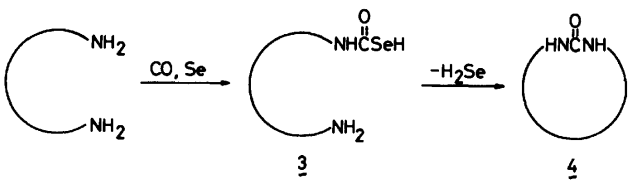

Scheme 2.

Results and Discussion

Carbonylation of Aromatic Diamines with Carbon Monoxide Using Stoichiometric Amount of Selenium. We have shown that aliphatic amines react with carbon monoxide at room temperature in the presence of stoichiometric amount of selenium leading to the

selenolcarbamate **1**.[17a,b] Oxidation of **1** with oxygen afforded corresponding ureas in good yields.[17a] Alternatively, aromatic amines such as anilines were less reactive, and the reaction of aromatic amines required a tertiary amine as the base and higher reaction temperature.[17c]

A solution of *o*-phenylenediamine (**5**) was allowed to react at 100 °C with 31 kg cm^{-2} of carbon monoxide and a stoichiometric amount of selenium in the presence of *N*-methylpyrrolidine (NMP) in THF. The uptake of carbon monoxide ceased within 20 h. After the reaction was complete, the remaining carbon monoxide was purged and the mixture was stirred for 1 h under air to oxidize the resulting hydrogen selenide (see Scheme 2). The following workup gave an 89% yield of the cyclic urea **17**. Unreacted starting

Table 1. Intramolecular Carbonylation of Aromatic Amines with Carbon Monoxide

Entry	Substrate		Product		Yield/% (Conditions)[a]	
					Excess	Catalytic
1	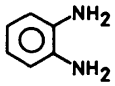	**5**	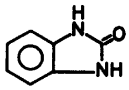	**17**	99(A)	99(E) 98(I)
2	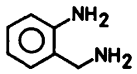	**6a**	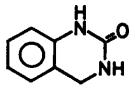	**18a**	86(A)	92(F)
3	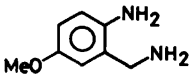	**6b**	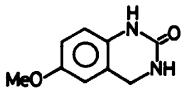	**18b**	92(A)	—
4	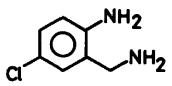	**6c**	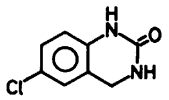	**18c**	86(A)	—
5	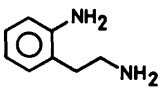	**7**	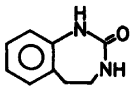	**19**	81(A)	b)
6	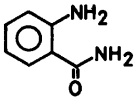	**8**	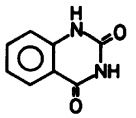	**20**	21(B)	20(G) 23(J)
7	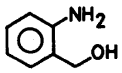	**9**	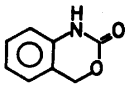	**21**	—	85(F)
8	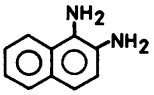	**10**	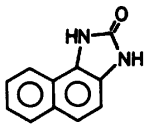	**22**	98(A)	96(E) 97(I)
9	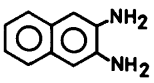	**11**	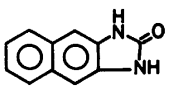	**23**	98(A)	97(E)
10	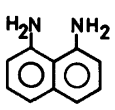	**12**	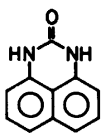	**24**	97(A)	96(E) 95(I)
11	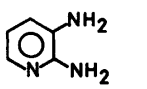	**13**	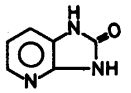	**25**	98(C)	97(G)
12	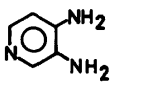	**14**	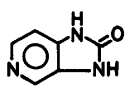	**26**	96(C)	98(G)

Table 1. (Continued)

Entry	Substrate		Product		Yield/% (Conditions)[a]	
					Excess	Catalytic
13	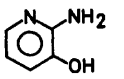	**15**	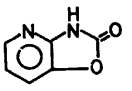	**27**	75(D)	71(H) 74(I)
14	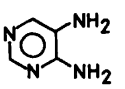	**16**	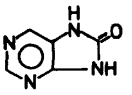	**28**	87(D)	89(H) 83(I)

a) Conditions: (A) Substrate (2.5 mmol), selenium (7.5 mmol), *N*-methylpyrrolidine (0.79 mL, 7.5 mmol), THF (10 mL), carbon monoxide (31 kg cm^{-2}), 100 °C, 20 h. (B) Substrate (2.5 mmol), selenium (7.5 mmol), *N*-methylpyrrolidine (0.79 mL, 7.5 mmol), DMF (10 mL), carbon monoxide (31 kg cm^{-2}), 100 °C, 20 h. (C) Substrate (5 mmol), selenium (15 mmol), THF (10 mL), carbon monoxide (31 kg cm^{-2}), 100 °C, 20 h. (D) Substrate (5 mmol), selenium (15 mmol), DMSO (1 mL), carbon monoxide (31 kg cm^{-2}), 100 °C, 20 h. (E) Substrate (2.5 mmol), selenium (0.125 mmol), *N*-methylpyrrolidine (0.79 mL, 7.5 mmol), THF (10 mL), carbon monoxide (29 kg cm^{-2}), oxygen (2 kg cm^{-2}), 100 °C, 20 h. (F) Substrate (2.5 mmol), selenium (0.125 mmol), *N*-methylpyrrolidine (0.79 mL, 7.5 mmol), THF (10 mL), under atmospheric pressure of a gas mixture of carbon monoxide (0.94 kg cm^{-2}) and oxygen (0.06 kg cm^{-2}), 15 °C, 10 h. (G) Substrate (2.5 mmol), selenium (0.125 mmol), THF (10 mL), carbon monoxide (29 kg cm^{-2}), oxygen (2 kg cm^{-2}), 100 °C, 20 h. (H) Substrate (2.5 mmol), selenium (0.125 mmol), DMSO (1 mL), carbon monoxide (29 kg cm^{-2}), oxygen (2 kg cm^{-2}), 100 °C, 20 h. (I) Substrate (2.5 mmol), selenium (0.125 mmol), *N*-methylpyrrolidine (0.79 mL, 7.5 mmol), THF (10 mL), DMSO (250 mg), carbon monoxide (31 kg cm^{-2}), 100 °C, 20 h. (J) Substrate (2.5 mmol), selenium (0.125 mmol), DMSO (2 mL), carbon monoxide (31 kg cm^{-2}), 100 °C, 20 h. b) See Table 2.

diamine was recoverd. When the reaction was carried out at 25 °C, only the starting material was recovered. In the absence of NMP, **5** gave **17** in 67% yield under similar conditions. This carbonylation was accelerated by using excess amounts of selenium. For example, when three-fold excess of selenium was used, **17** was obtained in 99% yield. Table 1 summarizes the results obtained when the reaction was carried out at 100 °C with 31 kg cm^{-2} of carbon monoxide and three-fold excess of selenium (conditions A-D in Table 1).

Other aniline derivatives having an aminoalkyl substituent in the ortho position **6a—c** and **7** underwent similar carbonylation to yield the corresponding cyclic ureas **18a—c** and **19** in good yields.

It should be noted that the carbamoyl nitrogen could be carbonylated under similar conditions as demonstrated by the reaction of 2-carbamoylaniline **8** in DMF (Entry 6 in Table 1). In this reaction, unreacted starting material was recovered. In THF, **8** did not react, probably due to the low solubility of **8** in THF.

The present carbonylation reaction is postulated to proceed via a selenolcarbamate intermediate formed by the reaction of the diamines with carbon monoxide and selenium (Scheme 3). The aliphatic amino group is more reactive than the aromatic one and may react faster with carbon monoxide in the presence of selenium, so that 2-(aminomethyl)aniline (**6a**) is preferentially converted to selenolcarbamate **29**.[19] In case of 2-carbamoylaniline **8**, the selenolcarbamate is formed at the site of the aromatic amino group, because of the low reactivity of the carbamoyl

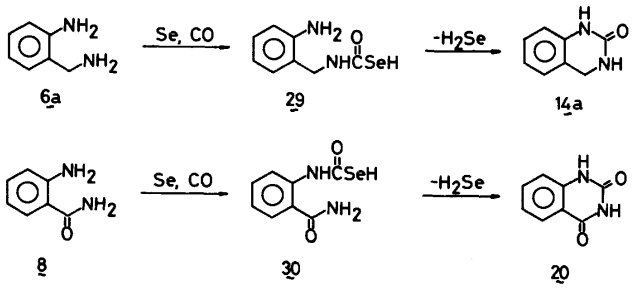

Scheme 3.

nitrogen.

The intermediates **29** and **30** then undergo aminolysis by the intramolecular nucleophilic attack of the remaining NH_2 group to give the corresponding cyclic ureas **14a** and **20**, respectively, together with the formation of hydrogen selenide.

Naphthalene-, pyridine-, and pyrimidinediamines were also examined. The reaction of 1,2-, 2,3-, and 1,8-naphthalenediamine **10—12** under similar conditions gave rise to cyclic ureas **22—24**, respectively in good yields. Pyridine- and pyrimidinediamines **13**, **14**, and **16** which have the tertiary amino moiety in the aromatic ring underwent similar carbonylation even in the absence of NMP to give the corresponding cyclic ureas **25**, **26**, and **28** in good yields. In case of 2-amino-3-pyridinol **15**, the carbonylation reaction also proceeded without NMP to afford the corresponding cyclic urethane **27** in 87% yield.

Selenium-Catalyzed Carbonylation with Carbon Monoxide Using Oxidizing Agents. In addition to

the stoichiometric reaction described above, a similar carbonylation using a catalytic amount of selenium in the presence of an oxidizing agent was developed.[17a,c]

Reaction of *o*-phenylenediamine (**5**) was carried out at 100 °C using 0.05 equiv of selenium with 3 equiv of NMP under a gas mixture of carbon monoxide (29 kg cm^{-2}) and oxygen (2 kg cm^{-2}). After a similar workup as previously mentioned, the cyclic urea **17** was obtained in 99% yield. At room temperature **5** gave **17** in 77% yield.[20]

Other aromatic diamines **10**—**12** underwent intramolecular carbonylation catalytically in a similar manner to afford the corresponding cyclic compounds in good yields (Table 1). As described in the stoichiometric reactions, a tertiary amine was not required in the catalytic carbonylation of **13**—**16**. 2-Carbamoylaniline **8** and 2-amino-3-pyridinol **15** also afforded 2,4(1*H*,3*H*)-quinazolinedione **20** (20%) and **27** (71%).

This selenium-catalyzed carbonylation also proceeded using dimethyl sulfoxide[21] as the oxidizing agent instead of oxygen. Formation of dimethyl sulfide was confirmed by capillary gas chromatography and ^{1}H NMR.

Scheme 4 shows a plausible reaction path for this catalytic carbonylation under these reaction conditions.[22]

The catalytic carbonylation was found to proceed under much milder conditions in comparison with those of stoichiometric reactions.[20] For example, at room temperature under atmospheric pressure of a mixture of carbon monoxide and oxygen, 2-(aminomethyl)aniline **6a** and 2-(hydroxymethyl)aniline **9** were converted to the corresponding cyclic urea **18a** and urethane **21** in good yields, respectively, although the reaction using a stoichiometric amount of selenium in the absence of oxygen at room temperature resulted in the recovery of the starting materials. Under the catalytic conditions at room temperature in the presence of oxygen, 2-(2-aminoethyl)aniline (**7**) gave acyclic urea **33** (95%) together with a trace amount of cyclic urea **19** (<1%). In the stoichiometric reaction **19** was the sole product.

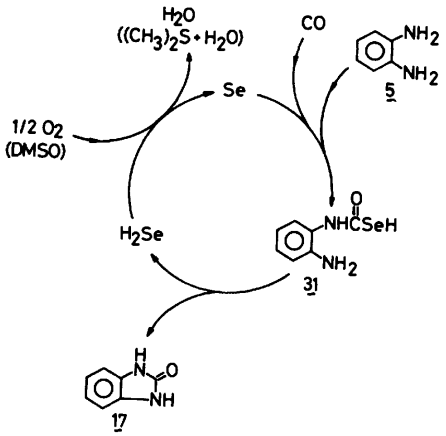

Scheme 4.

Selectivity between Intra- and Intermolecular Reactions of Selenium-Catalyzed Carbonylation of 2-(2-Aminoethyl)aniline (7). As mentioned above, intra- and intermolecular carbonylations competed in case of 2-(2-aminoethyl)aniline (**7**). Then we examined the effects of temperature, concentration, carbon monoxide and oxygen pressure, and amount of selenium used on the selectivity. The representative results were summarized in Table 2.

The cyclic urea **19** was preferentially formed under more dilute conditions (compare Entries 1, 6, and 7) and at higher temperatures (compare Entries 1, 2, and 3). The acyclic urea **33** was obtained selectively when the reaction was carried out at room temperature (Entries 3 and 4). Selective formation of cyclic urea **19** was attained only when a stoichiometric or excess amount of selenium was used (Entry 5).

These results are interpreted as follows. The aliphatic amino group of **7** is more nucleophilic than the aromatic amino group and reacts faster with selenium and carbon monoxide to form selenolcarbamate **32**. Therefore when a stoichiometric or excess amount of selenium is used, all of the aliphatic amino groups are converted rapidly to selenolcarbamate moieties which undergo intramolecular cyclization by the attack of the aromatic amino group.

On the other hand, in the catalytic reaction, there remains most of the starting material possessing the aliphatic amino group which can attack the carbamoyl carbon of **32** intermolecularly to form acyclic urea **33**. Thus, both intra- and intermolecular reactions take place competitively (Scheme 5).

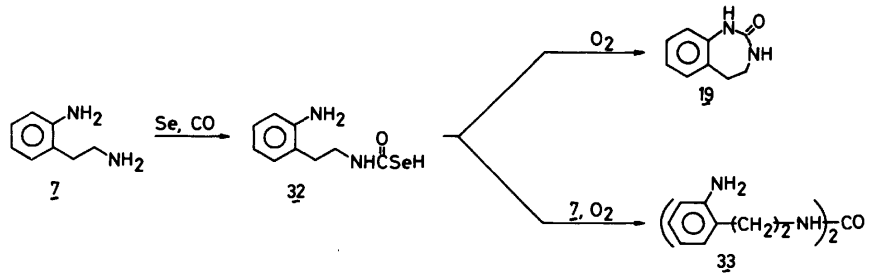

Scheme 5.

Table 2. Selenium-Assisted Carbonylation with Carbon Monoxide

Entry	7	CO	O_2	Se	Temp	THF	Yield/%	
	mmol	kg cm^{-2}		mmol	°C	mL	**19**	**33**
1	2.5	29	2	0.125	100	10	61	29
2	2.5	29	2	0.125	65	10	49	45
3	2.5	29	2	0.125	15	10	<1	96
4	2.5	0.8	0.2	0.125	15	10	<1	95
5	2.5	29	2	2.5	100	10	85	<1
6	2.5	29	2	0.125	100	0.3	24	64
7	0.5	29	2	0.025	100	20	79	12

NMP (0.79 mL, 7.5 mmol)

Experimental

Apparatus. Melting points were determined on a Yanagimoto HP-S2 and were uncorrected. ^{1}H NMR spectra were recorded on a Hitachi R-24B or a JEOL JNM-PS-100 with Me_4Si as an internal standard. ^{13}C NMR spectra were obtained on a JEOL FX-60s with Me_4Si as an internal standard. Infrared spectra were obtained on a Shimadzu IR-400. Mass spectra were recorded on a Hitachi Model RMU-6E. Gas chromatography were carried out on a Shimadzu GC-8A using a 0.2 mm×25 m fused silica capillary column CBP1-M25-025. Elemental analyses were performed on a Yanagimoto CHN-Corder MT-2.

Materials. THF was freshly distilled from sodium-benzophenone prior to use. DMF and DMSO were distilled from CaH_2. Metallic selenium (99.9%) and carbon monoxide (99.9%) were purchased from Nakarai Chemicals, Ltd. and Seitetsu Chem., Co., respectively. *N*-Methylpyrrolidine (NMP) was distilled from CaH_2. 2-(Aminomethyl)-aniline **6a**[23] and its derivatives **6b** and **6c**, and 2-(2-aminoethyl)aniline **7**[24] were prepared from nitriles following the procedures reported. All other starting materials were purchased from commercial sources and purified by distillation or recrystallization.

Carbonylation of *o*-Substituted Aromatic Diamines with Carbon Monoxide Using a Stoichiometric or Excess Amount of Selenium.

Formation of 2*H*-benzimidazol-2(3*H*)-one 17 as a Typical Experiment. *o*-Phenylenediamine (**5**) (270 mg, 2.5 mmol), selenium (592 mg, 7.5 mmol), NMP (0.79 mL, 7.5 mmol), and THF (10 mL) were placed in a 50 mL stainless-steel autoclave under a nitrogen atmosphere. Carbon monoxide (31 kg cm^{-2}) was introduced to the system, and the reaction vessel was heated to 100 °C with stirring. After 20 h, the apparatus was cooled to room temperature, and the remaining carbon monoxide was evacuated and the resulting mixture was stirred in the air for 1 h to oxidize resulting hydrogen selenide. The reaction mixture was extracted into THF (50 mL) by a Soxhlet extractor and the extract was evaporated in vacuo. The crude solid was recrystallized from THF–hexane to give 331 mg (99%) of **17**: Mp 299—300 °C (lit,[25] mp 300 °C); ^{1}H NMR (DMSO-d_6) δ=10.58 (br s, 2H), 7.02 (s, 4H); IR (KBr) 3025, 1715, 1020, 868, 714 cm^{-1}; MS *m/z* 134 (M$^+$). When a stoichiometric amount of selenium was used, **17** was obtained in 89% (295 mg) yield by a similar procedure.

Reactions under the same conditions and similar workup as described above gave cyclic ureas **18a—c**, **19**, and **21—23**.

3,4-Dihydro-2(1*H*)-quinazolinone (18a): 86%; mp 241—242 °C; ^{1}H NMR (DMDO-d_6) δ=9.08 (br s, 1H), 7.50—6.80 (m, 5H), 4.40 (s, 2H); IR (KBr) 3240, 1720, 1264, 740 cm^{-1}; MS *m/z* 148 (M$^+$). Found: C, 64.60; H, 5.20; N, 18.95. Calcd for $C_8H_8N_2O$: C, 64.85; H, 5.44; N, 18.92.

6-Methoxy-3,4-dihydro-2(1*H*)-quinazolinone (18b): 92%; mp 230—231 °C; ^{1}H NMR (DMSO-d_6) δ=8.81 (br s, 1H), 6.81 (s, 3H) 6.66 (br s, 1H), 4.32 (s, 2H), 3.71 (s, 3H); IR (KBr) 2970, 1660, 1031, 763 cm^{-1}; MS *m/z* 178 (M$^+$). Found: C, 60.28; H, 5.55; N, 15.60. Calcd for $C_9H_{10}N_2O_2$: C, 60.66; H, 5.66; N, 15.72.

6-Chloro-3,4-dihydro-2(1*H*)-quinazolinone (18c): 86%; mp 285—286 °C; ^{1}H NMR (DMSO-d_6) δ=9.38 (br s, 1H), 7.45—6.80 (m, 4H), 4.43 (s, 2H); IR (KBr) 3200, 1678, 1191, 802, 757 cm^{-1}; MS: *m/z* 182 (M$^+$). Found: C, 52.55; H, 3.77; N, 15.40. Calcd for $C_8H_7N_4ClO$: C, 52.62; H, 3.86; N, 15.34.

1,3,4,5-Tetrahydro-2*H*-1,3-benzodiazepin-2-one (19): 81%: mp 170.5—171 °C (lit,[26] mp 169—171 °C); ^{1}H NMR (DMSO-d_6) δ=8.90 (br s, 1H), 7.22—6.55 (m, 5H), 3.21 (m, 2H), 2.85 (m, 2H); IR (KBr) 3225, 1685, 1241, 750 cm^{-1}; MS *m/z* 162 (M$^+$).

2,4(1*H*,3*H*)-Quinazolinedione (20). A similar treatment of 2-carbamoylaniline (**8**) (340 mg, 2.5 mmol) with selenium (593 mg, 7.5 mmol), NMP (0.79 mL, 7.5 mmol) in DMF (10 mL) under a pressure of carbon monoxide (31 kg cm^{-2}), followed by a similar workup as described for the preparation of **17** afforded 85 mg (21%) of **20**: Mp >300 °C; ^{1}H NMR (DMSO-d_6) δ=11.50 (br s, 1H), 11.20 (br s, 1H), 8.07—6.59 (m, 4H); IR (KBr) 3200, 1704, 1141, 758, 683 cm^{-1}; MS *m/z* 162 (M$^+$). **20** showed the spectral data in complete accordance with those of the authentic sample (Aldrich).

1*H*-Naphth[1,2-*d*]imidazol-2(3*H*)-one (22): 98%; mp 347—347.5 °C; ^{1}H NMR (DMSO-d_6) δ=11.55 (br s, 1H), 10.75 (br s, 1H), 7.88—7.45 (m, 6H); IR (KBr) 3020, 1705, 787, 728 cm^{-1}; MS: *m/z* 184 (M$^+$). Found: C, 71.34; H, 4.41; N, 15.04. Calcd for $C_{11}H_8N_2O$: C, 71.73; H, 4.38; N, 15.21.

1*H*-Naphth[2,3-*d*]imidazol-2(3*H*)-one (23): 98%; mp >340 °C; ^{1}H NMR (DMSO-d_6) δ=10.65 (br s, 2H), 7.95—7.00 (m, 4H), 7.29 (s, 2H); IR (KBr) 3012, 1751, 825, 760, 700 cm^{-1}; MS *m/z* 184 (M$^+$). **23** showed the spectral data in complete accordance with the authentic sample.[27]

1*H*-Perimidin-2(3*H*)-one (24): 97%; mp >310 °C. ^{1}H NMR (DMSO-d_6) δ=10.11 (br s, 2H), 7.41—6.98 (m, 4H),

6.64—6.46 (m, 2H); IR (KBr) 3200, 1714, 813, 758 cm^{-1}; MS *m/z* 184 (M^+). **24** showed the spectral data in complete accordance with the authentic sample.[4b]

1*H*-Imidazo[4,5-*b*]pyridin-2(3*H*)-one (25). Treatment of 2,3-pyridinediamine (**13**) (546 mg, 5 mmol) with selenium (1.184 g, 15 mmol), in THF (10 mL) under pressure of carbon monoxide (31 kg cm^{-2}) at 100 °C for 20 h, followed by a similar workup as described for the preparation of **17** gave 660 mg (98%) of **21**: Mp 272—273 °C (lit,[28] mp 270—273 °C); ^1H NMR (DMSO-d_6) δ=10.99 (br s, 1H), 10.49 (br s, 1H), 6.74 (d, *J*=4.0 Hz, 1H), 7.56 (dd, *J*=4.0, 7.0 Hz, 1H), 7.06 (d, *J*=7.0 Hz, 1H); IR (KBr): 3000, 1685, 1459, 1107, 862, 714 cm^{-1}; MS: *m/z* 135(M^+).

1*H*-Imidazo[4,5-*c*]pyridin-2(3*H*)-one (26). Reaction of 3,4-pyridinediamine (14) (546 mg, 5 mmol) under the same conditions followed by a similar workup as described for the preparation of **25**, gave 648 mg (96%) of **26**: Mp 312—313 °C (lit,[29] mp 315 °C); ^1H NMR (DMSO-d_6) δ=11.57—10.09 (br, 2H), 8.33 (s, 1H), 8.32 (d, *J*=7.0 Hz, 1H), 7.20 (d, *J*=7.0 Hz, 1H); IR (KBr) 3000, 1710, 1227, 998, 905, 760, 697 cm^{-1}; MS *m/z* 135 (M^+).

Oxazolo[4,5-*b*]pyridin-2(3*H*)-one (27). 2-Amino-3-pyridinol (**15**) (550 mg, 5 mmol), selenium (1.184 g, 15 mmol), and DMSO (1 mL) was reacted under a pressure of carbon monoxide (31 kg cm^{-2}) at 100 °C for 20 h. The carbon monoxide and resulting dimethyl sulfide was evacuated through aqueous calcium hypochlorite solution. A similar workup as described for the preparation of **17** gave 517 mg (75%) of **27**: Mp 211—212 °C (lit,[29] 211—212 °C) ^1H NMR (DMSO-d_6) δ=10.31 (br s, 1H), 8.08 (d, *J*=5.0 Hz, 1H), 7.62 (d, *J*=7.0 Hz, 1H), 7.12 (dd, *J*=5.0, 7.0 Hz); IR (KBr) 3000, 2700, 1772, 1221, 791, 703 cm^{-1}; MS *m/z* 136 (M^+).

7*H*-Purin-8(9*H*)-one (28). Reaction of 4,5-pyrimidinediamine (**16**) (555 mg, 5 mmol) under the same conditions as described for the preparation of **27**, followed by a similar workup gave 682 mg (87%) of **28**: Mp >330 °C (lit,[30] 305—307 °C); ^1H NMR (DMSO) δ=11.76 (br s, 1H) 10.98 (br s, 1H), 8.54 (s, 1H), 8.04 (s, 1H); IR (KBr): 3050, 1730, 1459, 1107, 989, 714 cm^{-1}; MS *m/z* 136 (M^+). **28** showed the spectral data in complete accordance with the authentic sample.[30]

Carbonylation with Carbon Monoxide Using a Catalytic Amount of Selenium in the Presence of Oxygen. A typical experimental procedure is as follows. In a 50 mL stainless-steel autoclave, were placed *o*-phenylenediamine **5** (270 mg, 2.5 mmol), selenium (10 mg, 0.125 mmol), NMP (0.79 mL, 2.5 mmol), and THF (10 mL) under nitrogen atmosphere. The autoclave was charged with oxygen (2 kg cm^{-2}), and carbon monoxide (29 kg cm^{-2}) to the total pressure of 31 kg cm^{-2}. The reaction mixture was stirred at 100 °C for 20 h, and then cooled to room temperature. After evacuation of the remaining gas, the product was extracted into THF (50 mL) with a Soxhlet extractor. The solvent was evaporated in vacuo, and the residue was recrystallized from THF-hexane to give 328 mg (99%) of **17**.

The reactions of 2-carbamoylaniline (**8**), and 1,2-, 2,3-, 1,8-naphthalenediamine (**9—11**), were performed in a similar manner as exemplified by *o*-phenylenediamine (**5**).

Under similar conditions 1,2- and 3,4-pyridinediamine (**13**) and (**14**) (273 mg, 2.5 mmol) reacted with selenium (10 mg, 0.125 mmol), carbon monoxide (31 kg cm^{-2}), and oxygen (2 kg cm^{-2}) in the absence of NMP and gave **25** (98%, 327 mg) and **26** (96%, 324 mg), respectively. Similar reactions of 2-amino-3-pyridinol (**15**) (275 mg, 2.5 mmol), and 4,5-pyrimidinediamine (**16**) (278 mg, 2.5 mmol) in DMSO (1 mL) gave (**27**) (71%, 261 mg) and **28** (89%, 306 mg), respectively.

Catalytic Carbonylation under Atmospheric Pressure. A typical experimental procedure is as follows. In a three-necked 100 mL flask, were placed 2-(aminomethyl)aniline (**6a**) (305 mg, 2.5 mmol), selenium (10 mg, 0.125 mmol), NMP (0.79 mL, 7.5 mmol), and THF (10 mL) and carbon monoxide (4.5 mL min^{-1}) was bubbled into the reaction mixture at room temperature with stirring. All of metallic selenium reacted and a colorless homogeneous solution was obtained within 1 h. Oxygen (0.3 mL min^{-1}) was bubbled into the mixture, and after 3 h, the feed of carbon monoxide was stopped. The addition of oxygen was increased to 20 mL min^{-1}, and was continued for another 2 h. At this time, all of the selenium used was deposited. The product was extracted into THF (50 mL) with a Soxhlet extractor. The extract was evaporated in vacuo, and the residual solid was recrystallized from THF-hexane to give 315 mg (92%) of **18a**.

1,4-Dihydro-(2*H*)-3,1-benzoxazin-2-one (21). 2-(Hydroxymethyl)aniline(**9**) (307 mg. 2.5 mmol) was reacted under the same conditions as descrived above. A similar workup afforded 316 mg (85%) of **21**: Mp 118.5—119 °C (lit,[31] 118—120 °C); ^1H NMR ($CDCl_3$) δ=9.07 (br s, 1H), 7.67—6.43 (m, 4H), 5.40 (s, 2H); IR (KBr) 2980, 1701, 1446, 730 cm^{-1}; MS *m/z* 149 (M^+).

1,3-Bis[2-(2-aminophenyl)ethyl]urea (33). In a three-necked 50 mL flask, were placed 2-(2-aminoethyl)aniline (**7**) (340 mg, 2.5 mmol) selenium (10 mg, 0.125 mmol), NMP (0.79 mL, 7.5 mmol), and THF (5 mL). Carbon monoxide was bubbled (5 mL min^{-1}) into the reaction mixture at room temperature for 1 h. Oxygen was bubbled at a rate of 0.3 mL min^{-1} through the system for 3 h. The flow of carbon monoxide was then stopped, and the resulting mixture was stirred for another 1 h under oxygen. The selenium was filtered off and the solvent was evaporated in vacuo, and the residue was recrystallized from THF-pentane to afford 365 mg (95%) of **33**: Mp 103—104 °C; ^1H NMR ($CDCl_3$) δ=7.25—6.27 (m, 8H), 4.64 (br s, 2H), 3.39 (br s, 4H), 3.31 (t, *J*=7.6 Hz, 4H), 2.66 (t, *J*=7.6 Hz, 4H); ^{13}C NMR (DMSO-d_6) δ=162.74, 130.37, 127.57, 127.36, 123.38, 116.82, 115.31, 40.55, 40.12; IR (KBr) 3330, 2930, 1630, 1562, 1270, 1043, 752 cm^{-1}; MS *m/z* 298 (M^+). Found: C, 75.92; H, 7.53; N, 10.43. Calcd for $C_{17}H_{24}N_4O$: C, 76.09; H, 7.51; N, 10.44.

Catalytic Carbonylation with Carbon Monoxide Using a Catalytic Amount of Selenium in the Presence of Dimethyl Sulfoxide. In a 50 mL stainless-steel autoclave, were placed *o*-phenylenediamine (**5**) (270 mg, 2.5 mmol), selenium (10 mg, 0.125 mmol), DMSO (250 mg, 3.2 mmol), NMP (0.79 mL, 7.5 mmol), and THF (10 mL). The autoclave was charged with carbon monoxide (31 kg cm^{-2}) and the reaction was carried out at 100 °C for 20 h. The remaining carbon monoxide was purged, and the resulting mixture was analyzed by capillary gas chromatography, and the yield of dimethyl sulfide was found to be 85% (2.1 mmol) using octane as the internal standard. A similar workup gave **17** in 98% yield (328 mg).

In a similar manner, **8, 10, 12, 15,** and **16** were converted to **20, 22, 24, 27,** and **28**, respectively, in 23—98% yields.

This work was supported in part by a Grant-in-Aid for Scientific Research from the Ministry of Education, Science and Culture.

References

1) A portion of this study has been reported; T. Yoshida, N. Kambe, S. Murai, and N. Sonoda, *Tetrahedron Lett.*, **27**, 3037 (1986).

2) J. A. Dodd and R. L. Robert, U. S. Patent 4343655 A; *Chem. Abstr.*, **97**, 164847k (1982).

3) P. W. Sherwood, *J. Coat. Technol.*, **54**, 61 (1982).

4) a) E. J. Lien and W. D. Kumler, *J. Med. Chem.*, **11**, 214 (1968); b) M. H. Hussain and E. J. Lien, *ibid.*, **14**, 138 (1971); c) P. S. Liu, V. E. Marquetz, J. S. Driscoll, and R. W. Fuller, *ibid.*, **24**, 662 (1981); d) C.-d. Li, S. L. Mella, and A. C. Sartorelli, *ibid.*, **24**, 1089 (1981); e) H. A. Bate, N. Condulis, and N. L. Srein, *J. Org. Chem.*, **51**, 2228 (1986).

5) F. M. Hershenson, L. Bauer, and K. F. King, *J. Org. Chem.*, **33**, 2543 (1968).

6) A. M. Felix and R. I. Fryer, *J. Heterocyclic Chem.*, **5**, 291 (1968).

7) K. Takeda and H. Ogura, *Synth. Commun.*, **12**, 213 (1982).

8) For reductive *N*-carbonylation reactions, see; Y. Tsuji, R.-Takeuchi and Y. Waranabe, *J. Organomet. Chem.*, **290**, 249 (1985); P. Braunstein, J. Kervennal, and J.-L. Richert, *Angew. Chem., Int. Ed. Engl.*, **24**, 768 (1985).

9) For instance, manganese,[10] rhodium,[11] and iron[12] give a mixture of the corresponding urea and formamide, palladium[13] gives both of these compounds and oxamide, silver[14] gives a mixture of ureas and oxamides, and rhenium, ruthenium, cobalt, nickel, and copper give formamide as a sole product.[15] For reviews see, a) R. J. Angelici, *Acc. Chem. Res.*, **5**, 335 (1972). b) J. Falbe, "New Syntheses with Carbon Monoxide," Springer-Verlag, Berlin (1980), p. 291.

10) F. Calderazzo, *Inorg. Chem.*, **4**, 293 (1965).

11) D. Durand and C. Lassau, *Tetrahedron Lett.*, **1969**, 2329.

12) W. Reppe, *Libigs Ann. Chem.*, **582**, 1 (1953).

13) J. Tsuji and N. Iwamoto, *J. Chem. Soc., Chem. Commun.*, **1966**, 380.

14) T. Tsuda, Y. Isegawa, and T. Saegusa, *J. Org. Chem.*, **37**, 2670 (1972).

15) C. W. Bird, *Chem. Rev.*, **62**, 283 (1962).

16) a) B. D. Dombek and R. J. Angelici, *J. Organomet. Chem.*, **134**, 203 (1977); b) W. E. Martin and M. F. Farona, *ibid.*, **206**, 393 (1981).

17) a) N. Sonoda, T. Yasuhara, K. Kondo, T. Ikeda, and S. Tsutsumi, *J. Am. Chem. Soc.*, **93**, 6344 (1971); b) K. Kondo, M. Takarada, S. Murai, and N. Sonoda, *Synthesis*, **1979**, 597; c) N, Sonoda, G. Yamamoto, K. Kondo, and S. Murai, *Tetrahedron Lett.*, **1975**, 1969; d) K. Kondo, N. Sonoda, K. Yoshida, M. Koishi, and S. Tsutsumi, *Chem. Lett.*, **1972**, 373; e) K. Kondo, N. Sonoda, K. Yoshida, M, Koishi, and S. Tsutsumi, *Chem. Lett.*, **1972**, 401; f) K. Kondo, N. Sonoda, and S. Tsutsumi, *J. Chem. Soc., Chem. Commun.*, **1972**, 307; g) K. Kondo, K. Murata, N. Miyoshi, S. Murai, and N. Sonoda, *Synthesis*, **1979**, 735; h) K. Kondo, S. Yokoyama, N. Miyoshi, S. Murai, and N. Sonoda, *Angew. Chem. Int. Ed. Engl.*, **18**, 692 (1979).

18) The intermediate, selenolcarbamic acid **1** may exist as the ammonium salt in the actual reaction mixture (Scheme 1). However, in the following Schemes 2—6, it will be shown in the free state for simplification.

19) In case of the carbonylation of 2-(aminomethyl)-aniline (**6a**), theoretical amount of carbon monoxide was absorbed at room temperature. Unfortunately, an attempt for the trapping of the corresponding selenolcarbamate with butyl iodide under nitrogen failed resulting in the formation of a mixture of cyclic urea **14a** and *N*-alkylated compounds of **14a**.

20) The fact that the intramolecular carbonylation of *o*-phenylendiamine (**5**) proceeded even at room temperature under catalytic conditions indicates that an alternative path may exist in the presence of oxygen. One of the possible paths is the intramolecular aminolysis of the corresponding diselenide which is formed in situ by the oxidation of the selenolcarbamate **31** with oxygen.[17c] An attempt for the isolation of the diselenide failed. In the absence of an oxidizing reagent (i.e., in the stoichiometric reaction), the cyclization via aminolysis of **31** may occur only at elevated temperatures to give **17** and hydrogen selenide (Scheme 4).

21) The use of dimethyl sulfoxide as an oxidizing agent rather than that of oxygen is recommended, because the limit of inflammablility of carbon monoxide in oxygen has large extent ranging from 15.5 to 93.9%. See, R. C. Wheast, "CRC Handbook of Chemistry and Physics," CRC Press, Inc. Boca Raton, Florida (1985), p. D-124.

22) For the oxidation of thiol with dimethyl sulfoxide, see, R. Tanikaga, K. Tanaka, and A. Kaji, *J. Chem. Soc., Chem. Commun.*, **1978**, 865.

23) N. Kornblum and D. C. Iffland, *J. Am. Chem. Soc.*, **71** 2137 (1949).

24) B. A. Burdick, P. A. Benkovic, and S. J. Benkovic, *J. Am. Chem. Soc.*, **99**, 5716 (1977).

25) A. W. Scott and B. L. Wood, *J. Org. Chem.*, **7**, 508 (1942).

26) T. Jen, P. Bender, H. V. Hoeven, B. Dienel, and B. Dienel, *J. Med. Chem.*, **16**, 407 (1973).

27) M. S. Cauhan and R. G. Cooke, *Aust. J. Chem.*, **23**, 2133 (1970).

28) D. Harrison and A. C. B. Smith, *J. Chem. Soc.*, **1959**, 3157.

29) M. Debeljak-Suster, B. Stanovnik, M. Tisler, and Z. Zrimsek, *J. Org. Chem.*, **43**, 393 (1978).

30) A. Albert and D. J. Brown, *J. Chem. Soc.*, **1954**, 2060. 2060.

31) D. Aelony and W. J. Mckillop, *J. Med. Chem.*, **9**, 923 (1972).

Redox-Photosensitized Reactions. XIV.[1] Photochemistry of 4-Alkylated NADH Models, 1-Benzyl-4-(1-hydroxyalkyl)-1,4-dihydronicotinamides

Osamu Ishitani, Shozo Yanagida, Setsuo Takamuku, and Cyongjin Pac*
Department of Chemical Process Engineering, Faculty of Engineering, Osaka University, Suita, Osaka 565
(Received November 4, 1986)

There were investigated photochemical behaviors of 4-alkylated 1-benzyl-1,4-dihydronicotinamides (**1a—c**) having $R^1R^2C(OH)$ as the substituent (a: R^1=Ph and R^2=H; b: R^1=Ph and R^2=CF_3; c: R^1=*p*-NC-C_6H_4 and R^2=H). The direct photolysis of **1a—c** gave R^1R^2CO and the dimers of the dihydronicotinamide (BNA) fragment along with a minor amount of $[C_6H_5CH(OH)]_2$, being thus interpreted in terms of the homolysis between the $R^1R^2(OH)$ and BNA moieties. In the $[Ru(bpy)_3]^{2+}$-photosensitized reactions, it is suggested that **1a—c**$^{+\cdot}$ was generated as a key intermediate by electron transfer to excited $[Ru(bpy)_3]^{2+}$, undergoing a bond cleavage to give R^1R^2CO and the BNA· dimers. In the case of **1c**, however, $R^1R^2CH(OH)$ was formed, being attributed to a product from **1c**$^{-\cdot}$ that is formed by electron transfer from $[Ru(bpy)_3]^+$ to **1c**.

In previous papers,[2,3] we reported that the photosensitized reactions of 1-benzyl-1,4-dihydronicotinamide (BNAH), a typical NADH model, with either olefins or aromatic carbonyl compounds by $[Ru(bpy)_3]^{2+}$ (bpy=2,2′-bipyridine) yielded 1:1 adducts, new classes of 4-alkylated 1,4-dihydronicotinamides. These findings prompted us to investigate chemical behaviors of these adducts, since chemistry of 4-substituted 1,4-dihydronicotinamides has been of synthetic and biological significance.[4—7] We have found that the adducts with carbonyl compounds **1a—c** reveal interesting behaviors in either the direct photolysis or the photosensitization by $[Ru(bpy)_3]^{2+}$.

Experimental

Materials. The preparation and purification of BNAH[8] and $[Ru(bpy)_3Cl_2]\cdot 6H_2O$[9] were carried out according to the literature methods. The 4-alkylated dihydronicotinamides, **1a—c**, were obtained as 1:1 mixtures of the diastereoisomers by the $[Ru(bpy)_3]^{2+}$-photosensitized reactions of BNAH with benzaldehyde, 1,1,1-trifluoroacetophenone, and *p*-cyanobenzaldehyde as previously reported.[1,3] The diastereoisomers were separated by either repeated column chromatography on basic alumina or HPLC.[1] However, we confirmed that the photochemical behaviors of the isolated diastereoisomers are essentially identical with those of 1:1 mixtures. Therefore, we used 1:1-diastereoisomeric mixtures of **1a—c** in the present investigation. The other materials were obtained from Nakarai Chemicals and used after distillation and/or recrystallization.

Analytical Methods. The formation of **2**, **6c**, and 1,2-diphenyl-1,2-ethanediol was followed by GLC, whereas both the disappearance of **1a—c** and the formation of **3—5** were analyzed by HPLC. GLC was carried out on a Shimadzu GC-7A dual column instrument with flame-ionization detectors, and HPLC analysis were done on a Chemicosorb 7-ODS-H column using a Toyosoda CCPD dual pump coupled with a Yanaco M-315 spectromonitor working at 355 nm. A Hitachi 850 spectrofluorometer was used for luminescence-quenching experiments; deaerated solutions of the ruthenium complex (0.25 mM†) were photoexcited at 550 nm and intensities of the luminescence were monitored at 610 nm. Polarographic measurements were carried out for N_2-saturated water-free methanolic solutions containing **2a—c** (1 mM) and $NaClO_4$ (0.1 M) as the supporting electrolyte using an $Ag/AgNO_3$ reference electrode, a dropping mercury working electrode, and a Yanagimoto P-1100 potentiostat.

Direct Photolysis. A 3 cm^3-methanolic solution containing **1a—c** (50 mM) was bubbled with a gentle stream of Ar for 15 min and then irradiated with a high-pressure mercury lamp using a uranil glass filter (>330 nm) under cooling with water. The progress of the photoreactions was followed by GLC and HPLC.

Photosensitized Reactions by $[Ru(bpy)_3]^{2+}$. A 3 cm^3-methanolic solution containing **1a—c** (50 mM) and $[Ru(bpy)_3]^{2+}$ (1 mM) was bubbled with Ar for 15 min and then irradiated with a tungsten-halogen lamp using a solution filter of potassium chromate (20 g dm^{-3}), sodium nitrate (200 g dm^{-3}), and sodium hydroxide (6.7 g dm^{-3})(>470 nm)[2] under cooling with water. The progress of the reactions was followed by GLC and HPLC.

Results and Discussion

Direct Photolysis. Irradiation of a methanolic solution of **1a—c** (50 mM) at >330 nm mainly gave a carbonyl compound (**2a—c**) and the three isomeric dimers of 1-benzyl-3-carbamoyldihydro-4-pyridinyl radical, i.e. the 4,4′-bonded dimer (**3**), 4,6′-bonded dimer (**4**), and the diastereoisomer of **4** (**5**), as shown in Scheme 1. The dimers were isolated and identified by direct comparison with authentic samples,[10] while the other isomers could not be detected. In the case of **1a**, 1,2-diphenyl-1,2-ethanediol was formed in a 12% yield by GLC. Although the diol formation from **1b,c** can be presumed to occur, GLC and HPLC methods could not be used for the analysis.[11] In any case, moreover, we could not detect the alcohols, $R^1R^2CH(OH)$, nor the positional isomers of **1a—c** by extensive GLC and HPLC analyses. Table 1 summarizes yields of **2—5**.

These observations strongly suggest that the photoexcitation of **1a—c** results in a selective homolytic fission to generate a pair of $R^1R^2\dot{C}(OH)$ and the dihydropyridinyl radical (BNA·). The radical

† 1 M=1 mol dm^{-3}.

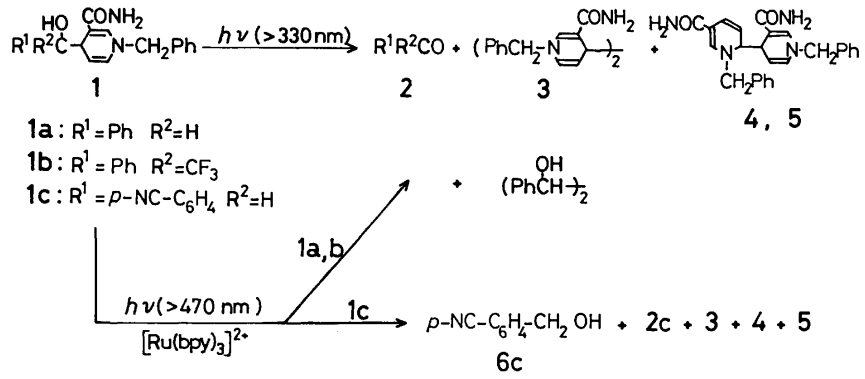

Scheme 1.

Table 1. Direct Photolysis of **1a**—**c**[a]

	1		Time	Convn.	Yield/%[b]			
	R^1	R^2	h	%	**2**	**3**	**4**	**5**
a	Ph	H[c]	4	47	49	37	26	17
b	Ph	CF_3	12	25	52	80	7	4
c	*p*-NCC_6H_4	H	10	35	57	43	26	20

a) For 3-cm³ methanolic solutions containing **1a**—**c** (0.05 M) irradiated at >330 nm. b) Based on **1a**—**c** consumed. c) 1,2-Diphenyl-1,2-ethanediol was formed in a 12% yield.

pair might diffuse apart out of a solvent cage in competition with the radical coupling regenerating **1a**—**c**. The free BNA· exclusively dimerizes to give **3**, **4**, and **5** in a kinetic controlled ratio. The predominant formation of **3** in the photolysis of **1b** appears to arise from a consequence of a secondary photoreaction, since irradiation of either **4** or **5** leads to the selective isomerization to **3** though the reverse photoisomerization does not occur.[12] On the other hand, the $R^1R^2\dot{C}(OH)$ are perhaps oxidized to **2a**—**c** by impurities and/or by unreclaimed reactions in competition with the dimerization. We attempted to detect other possible products arising from the $R^1R^2\dot{C}(OH)$ fragment, since yields of **2a**—**c** are lower than the combined yields of **3**—**5** in each case. However, we could not detect other definite products than those mentioned here. A possible mechanism is shown in Eqs. 1—6.

$$R^1R^2C(OH)\text{-BNA} \overset{h\nu}{\rightleftharpoons} \overline{R^1R^2\dot{C}(OH)\ \ BNA\cdot} \quad (1)$$

$$\overline{R^1R^2\dot{C}(OH)\ \ BNA\cdot} \longrightarrow R^1R^2\dot{C}(OH) + BNA\cdot \quad (2)$$

$$R^1R^2\dot{C}(OH) \xrightarrow[-H\cdot]{} R^1R^2C{=}O \quad (3)$$

$$2R^1R^2\dot{C}(OH) \longrightarrow R^1R^2C(OH)C(OH)R^1R^2 \quad (4)$$

$$R^1R^2\dot{C}(OH) \longrightarrow \text{Others} \quad (5)$$

$$2BNA\cdot \longrightarrow \mathbf{3} + \mathbf{4} + \mathbf{5} \quad (6)$$

It is of interest to note that the radical pair can be regarded as a mechanistic equivalent to a key intermediate that is involved in an ECE mechanism[13] proposed for the reduction of carbonyl compounds by BNAH in the dark as shown in Eqs. 7 and 8. According to this mechanism, BNA· could donate an electron to $Ph\dot{C}(OH)CF_3$ and *p*-$NCC_6H_4\dot{C}H(OH)$ since the reductions of trifluoroacetophenone and *p*-cyanobenzaldehyde by BNAH do occur in the dark to give the corresponding alcohols. However, the photolysis of either **1b** or **1c** did not afford the corresponding alcohols, thus indicating that BNA· is incapable of undergoing one-electron reduction of $R^1R^2\dot{C}(OH)$.[1,14]

Furthermore, the lack of the BNAH formation in the photolysis of **1a**—**c** suggests that transfer of a hydrogen-atom equivalent from $R^1R^2\dot{C}(OH)$ to BNA·, the reverse pathway of Eq. 7, is very unlikely to occur.

$$R^1R^2C{=}O + BNAH \rightleftharpoons$$

$$\overline{R^1R^2CO^{-}\cdot\ \ BNAH^{+}\cdot} \rightleftharpoons \overline{R^1R^2\dot{C}(OH)\ \ BNA\cdot} \quad (7)$$

$$\overline{R^1R^2\dot{C}(OH)\ \ BNA\cdot} \rightleftharpoons \overline{R^1R^2\bar{C}(OH)\ \ BNA^{+}} \xrightarrow{H^{+}} R^1R^2CH(OH) + BNA^{+} \quad (8)$$

Photosensitization by $[Ru(bpy)_3]^{2+}$. The photosensitized reactions of **1a**—**c** were carried out by the irradiation at >470 nm in order to achieve the selective photoexcitation of $[Ru(bpy)_3]^{2+}$. In the cases of **1a,b**, the results are similar to those of the direct photolysis with some differences in product ratios. The major products are again **2a,b**, and the BNA· dimers without the formation of BNAH and $R^1R^2CH(OH)$, and 1,2-diphenyl-1,2-ethanediol was also formed in a 13% yield in the case of **1a**.[11] Prominently, the photosensitized reaction of **1c** yielded *p*-cyanobenzyl alcohol (**6c**) in a 50% yield along with **2c** and the BNA· dimers, showing a sharp contrast to the lack of the alcohol formation in the direct photolysis. In this case, moreover, it is notable that the combined yield of **3**—**5** is significantly lower than that of **2c** and **6c** though BNAH is not formed, an observation contrary

Table 2. $[Ru(bpy)_3]^{2+}$-Photosensitized Reactions[a]

	1		Time	Convn.	Yield/%[b]				
	R^1	R^2	h	%	2	3	4	5	6
a	Ph	H[c]	8	67	67	56	30	10	0
b	Ph	CF_3	16	10	30	50	20	12	Trace
c	*p*-NCC_6H_4	H	10	20	40	10	22	29	50

a) For 3-cm³ methanolic solutions containing **1a—c** (0.05 M) and $[Ru(bpy)_3Cl_2]\cdot 6H_2O$ (1 mM) irradiated at >470 nm. b) Based on **1a—c** consumed. c) 1,2-Diphenyl-1,2-ethanediol and hydrogen were detected in 13 and 2% yields respectively.

Table 3. Rate Constants for Quenching of $[Ru(bpy)_3]^{2+}$ Luminescence[a]

Quencher	$k_q\tau/M^{-1}$	k_q[b]$/M^{-1}\,s^{-1}$
1a	57	7.1×10^7
1b	17	2.1×10^7
1c	15	1.9×10^7
BNAH	120	1.5×10^8
DMT[c]	840	1.1×10^9
3	1700	2.1×10^9

a) Obtained from linear Stern-Volmer plots of the luminescence quenching for deaerated methanolic solutions. b) Calculated from the $k_q\tau$ values using $\tau=800$ ns at 20 °C in methanol.[2] c) *N,N*-Dimethyl-*p*-toluidine.

to those of the other cases. The results are summarized in Table 2 and in Scheme 1.

The luminescence of $[Ru(bpy)_3]^{2+}$ was quenched by **1a—c** at rate constants, which are significantly smaller than the quenching rate constant of BNAH and which decrease with increasing inductive effects of R^1 and/or R^2 as shown in Table 3. It is therefore reasonable to assume that electron transfer from **1a—c** to $[Ru(bpy)_3]^{2+}$ in the metal-to-ligand charge-transfer excited state occurs to initiate the photosensitized reactions (Eq. 9). Electron-withdrawing inductive effects of the aromatic rings and the trifluoromethyl group should weaken the electron-donating power of the dihydronicotinamide moiety of **1a—c** compared with BNAH.

$$\mathbf{1a—c} + [Ru(bpy)_3]^{2+} \overset{h\nu}{\rightleftharpoons} \mathbf{1a—c}^{+\cdot} + [Ru(bpy)_3]^{+} \quad (9)$$

The follow-up reaction of $\mathbf{1a—c}^{+\cdot}$ has two choices; one is the bond cleavage to yield **2a—c**, H^+, and BNA· (Eq. 10) and the other involves the formation of $R^1R^2\dot{C}(OH)$ and BNA^+ (Eq. 11). Although there is no unequivocal evidence supporting either or both of the two pathways, comparisons of reduction potentials between **2a—c** and BNA^+ in methanol might imply that Eq. 10 is thermodynamically more favorable than Eq. 11. The polarographic reduction waves of **2a** and **2c** in methanol appear at −1.86 and −1.52 V vs. Ag/Ag^+, respectively, which are more negative than the reduction wave of BNA^+ (−1.445 V).[1,15] Reduction waves of aromatic carbonyl compounds in the presence of a proton donor usually occur as the consequences arising from the formation of $R^1R^2\dot{C}$-(OH) by sequential electron-proton transfer to R^1R^2CO.[16] Therefore electron transfer from $R^1R^2\dot{C}$-(OH) to BNA^+ should be exothermic to yield **2a—c** and BNA· (Eq. 12).

$$\mathbf{1a—c}^{+\cdot} \longrightarrow R^1R^2CO + H^+ + BNA\cdot \quad (10)$$

$$\mathbf{1a—c}^{+\cdot} \longrightarrow R^1R^2\dot{C}(OH) + BNA^+ \quad (11)$$

$$R^1R^2\dot{C}(OH) + BNA^+ \xrightarrow[(\Delta G<0)]{} R^1R^2CO + H^+ + BNA\cdot \quad (12)$$

However, the formation of 1,2-diphenyl-1,2-ethanediol implies the intervention of $Ph\dot{C}H(OH)$. This can be easily interpreted by assuming the occurrence of electron transfer from $[Ru(bpy)_3]^+$ to **2a** (Eq. 13), which has already been discussed previously.[3] This might be a major origin for lower yields of **2a,b** compared with the BNA· dimers, provided that $\mathbf{2a,b}^{-\cdot}$ and $R^1R^2\dot{C}(OH)$ afford unreclaimed products even in part.

$$[Ru(bpy)_3]^+ + \mathbf{2a—c} \rightleftharpoons [Ru(bpy)_3]^{2+} + \mathbf{2a—c}^{-\cdot} \quad (13)$$

$$\mathbf{2a—c}^{-\cdot} + H^+ \longrightarrow R^1R^2\dot{C}(OH) \quad (14)$$

$$2R^1R^2\dot{C}(OH) \longrightarrow R^1R^2CH(OH)CH(OH)R^1R^2 \quad (15)$$

$$\mathbf{2a—c}\cdot \text{ and } R^1R^2\dot{C}(OH) \longrightarrow \text{Others} \quad (15')$$

The formation of **6c** is of particular interest with regard to the electron-transfer mechanism. In order to obtain further mechanistic insights, we carried out the $[Ru(bpy)_3]^{2+}$-photosensitized reactions of **1a—c** in the presence of BNAH or *N,N*-dimethyl-*p*-toluidine (DMT) in an equimolar amount, a concentration at which excited $[Ru(bpy)_3]^{2+}$ is exclusively quenched by BNAH or DMT (Table 3) via electron transfer (Eq. 16). Interestingly, the photosensitized reaction of **1c** in the presence of either BNAH or DMT selectively gave **6c** at a rate 3.7 or 2 times each more efficient than that in its absence, while **2c** was not formed at all. Furthermore, we could not detect BNAH in the photoreaction with DMT but **3**, **4**, and **5** though yields were not determined. In contrast, the photosensitized

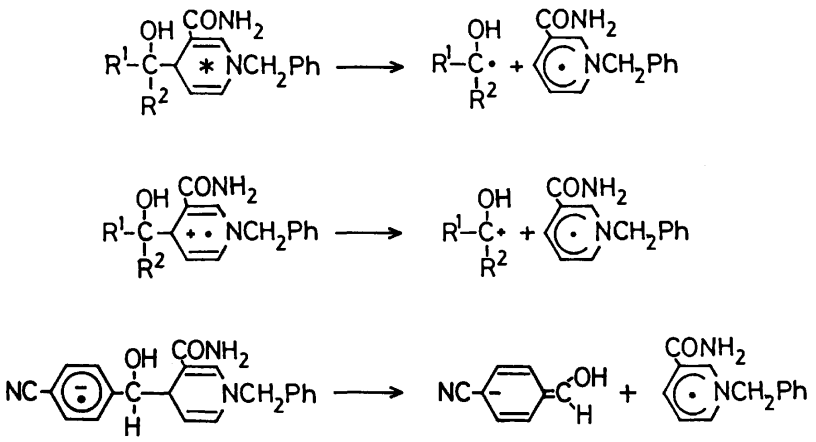

Scheme 2.

reactions of **1a,b** in the presence of BNAH or DMT did not give the corresponding alcohols at all.

$$[Ru(bpy)_3]^{2+} + D \overset{h\nu}{\rightleftharpoons} [Ru(bpy)_3]^{+} + D^{+\cdot} \quad (16)$$
(D=BNAH or DMT)

$$[Ru(bpy)_3]^{+} + \mathbf{1c} \longrightarrow [Ru(bpy)_3]^{2+} + \mathbf{1c}^{-\cdot} \quad (17)$$

$$[Ru(bpy)_3]^{+} + \mathbf{1a,b} \dashrightarrow [Ru(bpy)_3]^{2+} + \mathbf{1a,b}^{-\cdot} \quad (18)$$

$$\mathbf{1c}^{-\cdot} + H^{+} \begin{cases} \longrightarrow p\text{-NC-C}_6\text{H}_4\text{-CH}_2\text{OH} + \text{BNA}\cdot & (19) \\ \dashrightarrow p\text{-NC-C}_6\text{H}_4\text{-}\dot{\text{C}}\text{H(OH)} + \text{BNAH} & (20) \end{cases}$$

On the basis of these observations, the formation of **6c** can be interpreted in terms of Eqs. 16, 17, and 19. A key pathway is the electron transfer from $[Ru(bpy)_3]^{+}$ to **1c**, in which the cyanophenyl group should be essential because of the electron-accepting nature. Since **3** is a much more efficient quencher of excited $[Ru(bpy)_3]^{2+}$ than either **1c** or BNAH (Table 3), it is expected that the BNA· dimers formed can also act as D in Eq. 16, being thus consumed during the photosensitized reaction of **1c**. This would be a reason for the lower yield of the BNA· dimers compared with the combined yield of **2c** and **6c** as shown in Table 2. On the other hand, $[Ru(bpy)_3]^{+}$ appears to be incapable of donating an electron to **1a,b** since the phenyl group has no extra electron-withdrawing substituent. The anion radical ($\mathbf{1c}^{-\cdot}$) thus formed undergoes a bond cleavage to give **6c** and BNA· in the presence of a proton donor. On the other hand, little participation of Eq. 20 can be expected, since both **2c** and BNAH were not formed in the photoreaction in the presence of DMT.

Summary

The present investigation exemplifies chemical bahaviors of photoexcited **1a—c**, the cation radicals, and the anion radical of **1c** as shown in Scheme 2. In the direct photolysis, the photoexcitation should be localized on the BNA moiety since it absorbs the incident light at >330 nm. This leads to the homolysis between the $R^1R^2\dot{C}(OH)$ and BNA moieties, while intramolecular electron transfer from the excited BNA chromophore to the R^1 group does perhaps not occur. Likewise, the positive charge of $\mathbf{1a—c}^{+\cdot}$ should be localized on the BNA chromophore, being apparently the driving force for the bond cleavage between $R^1R^2C(OH)$ and BNA. This is reminescent of the very acidic nature of $BNAH^{+\cdot}$.[17] On the other hand, the negative charge of $\mathbf{1c}^{-\cdot}$ should be localized on the *p*-cyanophenyl group, thus leading to the formation of *p*-cyanobenzyl alcohol. In any case, BNA· is commonly formed.

This work was partly supported by Grant-in-Aid for Special Project Research (No. 61123001) from the Ministry of Education, Science and Culture.

References

1) Part XIII: O. Ishitani, S. Yanagida, S. Takamuku, and C. Pac, *J. Org. Chem.*, in press.

2) C. Pac, Y. Miyauchi, O. Ishitani, M. Ihama, M. Yasuda, and H. Sakurai, *J. Org. Chem.*, **49**, 26 (1984).

3) O. Ishitani, C. Pac, and H. Sakurai, *J. Org. Chem.*, **48**, 2941 (1983).

4) For a review, see: D. M. Staut and A. I. Meyers, *Chem. Rev.*, **82**, 223 (1982).

5) A. Ohno, J. Nakai, K. Nakamura, T. Goto, and S. Oka, *Bull. Chem. Soc. Jpn.*, **54**, 3482 (1981).

6) S. H. Mashraqui and D. M. Kellogg, *J. Am. Chem. Soc.*, **105**, 7792 (1983).

7) A. I. Meyers and T. Oppenlaender, *J. Am. Chem. Soc.*, **108**, 1989 (1986).

8) D. Mauzarall and F. M. Westheimer, *J. Am. Chem. Soc.*, **77**, 2261 (1955).

9) J. A. Broomhead and C. G. Yaung, *Inorg. Synth.*, **22**, 127 (1983).

10) Y. Ohnishi and M. Kitami, *Bull. Chem. Soc. Jpn.*, **52**, 2674 (1979).

11) The diols, $[p\text{-NC-C}_6\text{H}_4\text{CH(OH)}]_2$ and $[\text{PhC(OH)-CF}_3]_2$, which had been independently prepared, revealed no peak on GLC, whereas HPLC peaks of the diols were inseparably overlapped with many other peaks.

12) O. Ishitani and C. Pac, unpublished results.

13) J. J. Steffens and D. M. Chipman, *J. Am. Chem. Soc.*, **93**, 6694 (1971).

14) In a previous paper,[3] we reported that the $Ru(bpy)_3^{2+}$-photosensitized reactions of BNAH with **2b** and **2c** give the corresponding alcohols (**6c** and **6d**) as minor products. Although these observations would indicate the occurence of electron transfer from BNA· to $R_1R_2\dot{C}OH$, close analyses of the reactions[1] demonstrate that **6c** is not a primary product but a secondary one, perhaps from the $Ru(bpy)_3^{2+}$-photosensitized reduction of **1c** by BNAH as described in the present paper; see Eqs 16, 17, and 19. Furthermore, it was confirmed that the formation of **6b** is not photochemical but thermally arises from the reduction of **2b** by BNAH in the dark.

15) In polarography, **2b** shows no significant reduction wave in methanol because of the formation of the hemiacetal.[1]

16) D. H. Evans, "Encyclopedia of Electrochemistry of the Elements," ed by A. J. Bard, and H. Lund, Marcel Dekker Inc., New York (1978) Vol. XII, pp. 1—259.

17) F. M. Maltens and J. W. Verhoven, *Rec. Trav. Chim. Pays-Bas*, **100**, 228 (1981).

Oxidation of 2,4-Alkadienoic Esters with Selenium Dioxide. A New Synthesis of Furans and Selenophenes

Sadao Tsuboi, Shigetoshi Mimura, Shin-ichiro Ono, Kenji Watanabe, and Akira Takeda*
Department of Synthetic Chemistry, School of Engineering, Okayama University, Tsushima, Okayama 700
(Received November 4, 1986)

Direct oxidation of 2,4-alkadienoic esters with selenium dioxide gave 5-alkyl-2-furancarboxylic esters along with 5-alkyl-2-selenophenecarboxylic esters. Ethyl 5-methylfurancarboxylate was converted to 5-hydroxymethyl-2-furancarbaldehyde, a component of honey, via ethyl 5-bromomethyl-2-furancarboxylate (**5**) in good yield. The compound **5** was converted to (5-ethoxycarbonyl-2-furyl)methyl dimethyldithiocarbamate possessing fungicidal activity. Reaction of triphenylphosphonium salt of **5** with nonanal gave ethyl 5-(1-decenyl)-2-furancarboxylate (E/Z=88:12) in 86% yield. Ethyl 5-methyl-2-selenophenecarboxylate was also converted to ethyl 5-(1-decenyl)-2-selenophenecarboxylate (E/Z=7:3) in 30% total yield.

Selenium dioxide is a conventional and useful reagent for the oxidation of olefins to α,β-unsaturated ketones and allylic alcohols.[1] As our continuing interest in the chemistry of 2,4-alkadienoic esters **1**,[2] we carried out the oxidation of **1** with selenium dioxide.[3] Here we describe a novel synthesis of furans **2** and selenophenes **3** via the oxidation of **1** with selenium dioxide, as summarized below.

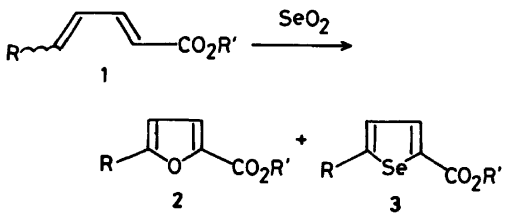

Oxidation of α,β-unsaturated carboxylic acids with SeO_2 gave a γ-acetoxy derivative[4] and an α,β-unsaturated γ-butyrolactone derivative.[5] However, oxidation of conjugated dienoic esters with SeO_2 is little known. Only the oxidation of methyl 3-(2,6,6-trimethyl-2-cyclohexenyl)-1-methyl-2-propenylideneacetate with SeO_2 in ethanol to give the corresponding 1- and 4-hydroxy-cyclohexenyl derivatives is reported.[6] Recently we reported a convenient synthesis of (2*E*,4*Z*)-alkadienoic esters.[2a,b] For its application to the syntheses of natural products, we oxidized some 2,4-alkadienoic esters **1** with SeO_2.

Oxidation of commercially available methyl (2*E*,4*E*)-2,4-hexadienoate (sorbate) (**1a**) with SeO_2 gave unexpectedly a mixture of methyl 5-methyl-2-furancarboxylate (**2a**) (56%) and methyl 5-methyl-2-selenophenecarboxylate (**3a**) (29%). Any trace amount of 6-hydroxy- or 6-oxosorbates which were expected to be produced could not be detected. To generalize the present synthesis, various kinds of 2,4-alkadienoic esters were oxidized with SeO_2 and the results are summarized in Table 1. Methyl (2*E*,4*Z*)-hexadienoate (**1b**) was also oxidized with SeO_2, giving an 1:1

Table 1. Oxidation of **1** with SeO_2

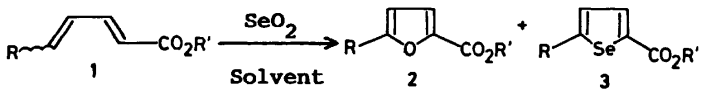

Run	1[a]			SeO_2 (equiv)	Solvent	Reaction Time	Yield/%[b] of Products			
							2		3	
	No.	R	R′			h	No.	Yield	No.	Yield
(1)	**1a**	CH_3	CH_3	1.1	Benzene	5	**2a**	56	**3a**	29
(2)	**1b**	CH_3	CH_3	1.1	Benzene	0.5	**2a**	46	**3a**	48
(3)	**1c**	CH_3	C_2H_5	1.5	Bromobenzene	2	**2b**	37	**3b**	5
(4)	**1d**	n-C_3H_7	CH_3	1.0	Xylene	6	**2c**	57	**3c**	29
(5)	**1e**	n-C_3H_7	C_2H_5	1.5	Xylene	2	**2d**	58	**3d**	15
(6)	**1e**	n-C_3H_7	C_2H_5	2.2	DME	6.5	**2d**	22[c]	**3d**	9[c]
(7)	**1f**	$(CH_3)_2CH$	C_2H_5	1.1	Xylene	1.5	**2e**	45	**3e**	2
(8)	**1g**	n-C_5H_{11}	C_2H_5	3.0	Xylene	26	**2f**	17[c]	**3f**	6[c]

a) Geometries of **1a** and **1c** are (2*E*,4*E*), and those of others are (2*E*,4*Z*). b) Unless otherwise indicated, determined by ^1H NMR analysis after removal of polymerized products by short-path distillation or short column chromatography. c) Isolated yield.

mixture of **2a** and **3a** in good yields. Although the oxidation of ethyl (2*E*,4*Z*)-octadienoate (**1d**) with SeO_2 afforded furan **2c** (57%) and selenophene **3c** (29%), the yield in that of alkadienoates bearing a longer chain such as **1g** decreased.

Oxidations of **1a** with SeO_2 under various reaction conditions were conducted to optimize the yields, and the results were tabulated in Tables 2 and 3. Oxidation with 1—2 equiv of SeO_2 gave the best result. Most of the reaction gave the furan **2a** as a major product. However, the reaction in acetic acid afforded an 1:1 mixture of **2a** and **3a**.

Table 2. Oxidation of **1a** with a Various Amount of SeO_2[a]

Run	SeO_2 (equiv)	Yield/%[b] of Product	
		2a	**3a**
1	0.5	3[c]	0
2	1	60	20
3	2	52	30
4	5	13[d]	3[d]

a) Conducted in benzene at the reflux temperature for 6.5 h. b) Calculated by GLC analysis after purification by flash column chromatography. c) Starting material (**1a**) was recovered. d) Resinous materials were produced.

Table 3. Oxidation of **1a** with SeO_2 in Various Solvents[a]

Solvents	Reaction Time/h	Yield/%[b] of Products	
		2a	**3a**
Xylene	2.5	62	15
Toluene	4	56	8
Dioxane	4	50	25
Ethanol	1	66	2.4
Acetic Acid	4	32	32

a) SeO_2 (1.1 equiv) was used. b) Calculated by ^1H NMR analysis of a reaction mixture.

Structural determination was carried out on the basis of IR, NMR, and elemental analysis which were tabulated in Tables 4 and 5. IR spectra of furancarboxylates **2** showed characteristic absorptions at 1520, 1536, and 1600 cm^{-1}. On the other hand, IR spectra of selenophenecarboxylates **3** exhibited signals due to a selenophene ring at 1550, 1616, and 1640 cm^{-1}. Proton NMR spectra of **2a** showed two singlets at δ 2.36 and 3.78 and two doublets (J=3.2 Hz) at δ 6.00 and 6.92. Signals due to ring protons of selenophene **3** appeared at ca. δ 6.8 and 7.7 as two doublets (J= 3.7 Hz). Mass spectrum of **3a** showed characteristic signals of a selenium compound at m/z 204, 202, and 200.

To examine the synthetic utility of the product obtained by the present method, some chemical conversions of **2b** and **3b** were conducted representatively. Many natural products possessing 2,5-disubstituted furan rings have been reported.[7] The present synthesis will be useful for these compounds. For example, **2b** was successfully converted to 5-hydroxymethyl-2-furancarbaldehyde (**4**), a component of honey.[7a] The synthetic sequence are shown in Scheme 1. Furan **2b** was brominated with NBS to give ethyl 5-bromomethyl-2-furancarboxylate (**5**) in 85% yield which was subsequently hydrolyzed with aqueous $AgNO_3$ to ethyl 5-hydroxymethyl-2-furancarboxylate (**6**). After the alcohol **6** was converted to tetrahydropyranyl (THP) ether **7**, reduction of the latter with $LiAlH_4$ followed by oxidation with MnO_2 gave aldehyde **9** in good yield. Deprotection of THP

Table 4. Spectral Data of **2**

Compd	IR/cm^{-1}	^1H NMR (δ, CCl_4)
2a[a]	1730, 1600, 1520, 1536	2.35(s, 3H), 3.77(s, 3H), 6.0(d, 3H, J=4 Hz), 6.90(d, 1H, J=4 Hz)
2b[a]	1720, 1600, 1539, 1521, 1020, 760	1.32(t, 3H, J=7 Hz), 2.35(s, 3H), 4.23(q, 2H, J=7 Hz), 6.02(d, 1H, J=3.2 Hz), 6.92(d, 1H, J=3.2 Hz)
2c[b]	1720, 1596, 1530, 1519, 1018, 756	0.98(t, 3H, J=7 Hz), 1.38—2.05(m, 2H), 2.66(t, 2H, J=7 Hz), 3.77 (s, 3H), 6.02(d, 1H, J=3.2 Hz), 6.92(d, 1H, J=3.2 Hz)
2d[b]	1720, 1600, 1535, 1520, 1018, 760	1.00(t, 3H, J=7 Hz), 1.35(t, 3H, J=7 Hz), 1.3—2.1(m, 2H), 2.65 (t, 2H, J=7 Hz), 4.28(q, 2H, J=7 Hz), 6.0(d, 1H, J=3.2 Hz), 6.92 (d, 1H, J=3.2 Hz)
2e[b]	1720, 1601, 1535, 1520, 1300, 1140	1.34(d, 6H, J=6.5 Hz), 1.37(t, 3H, J=6.5 Hz), 1.9—2.5(m, 1H), 4.25(q, 2H, J=6.5 Hz), 5.96(d, 1H, J=3.2 Hz), 6.90(d, 1H, J= 3.2 Hz)
2f[c]	1720, 1595, 1520, 1300, 1015, 760	0.93(t, 3H, J=6 Hz), 1.36(t, 3H, J=6.5 Hz), 1.2—2.1(m, 6H), 2.67 (t, 2H, J=7 Hz), 4.26(q, 2H, J=6.5 Hz), 6.00(d, 1H, J=3.2 Hz), 6.90(d, 1H, J=3.2 Hz)

a) Known compound; see Ref. 13. b) The corresponding acid is known; see Ref. 14. c) The corresponding methyl ester is known; see Ref. 15.

Table 5. Spectral and Analytical Data of **3**

Compd	IR/cm^{-1}	^{1}H NMR (δ, CCl_4)	Formula	Found (Required) C	H
3a[a]	1705, 1555, 1280, 1260, 1080, 740	2.58(s, 3H), 3.78(s, 3H), 6.83(d, 1H, J=3.7 Hz), 7.69(d, 1H, J=3.7 Hz)			
3b[a]	1720, 1560, 1280, 1265, 1080, 760	1.32(t, 3H, J=7 Hz), 2.55(s, 3H), 4.22(q, 2H, J=7 Hz), 6.81(d, 1H, J=3.7 Hz), 7.63 (d, 1H, J=3.7 Hz)			
3c	1710, 1550, 1275, 1260, 1082, 740	1.00(t, 3H, J=7 Hz), 1.3—2.0(m, 2H), 2.83(t, 2H, J=7 Hz), 3.77(s, 3H), 6.86(d, 1H, J=3.7 Hz), 7.74(d, 1H, J=3.7 Hz)	$C_9H_{12}O_2Se$	46.83 (46.77	5.45 5.23)
3d	1705, 1550, 1260, 1470, 1080, 740	1.00(t, 3H, J=6.5 Hz), 1.32(t, 3H, J=7 Hz), 1.4—2.1(m, 2H), 2.82(t, 2H, J=7 Hz), 3.63(s, 3H), 4.20(q, 2H, J=7 Hz), 6.82(d, 1H, J=3.7 Hz), 7.66(d, 1H, J=3.7 Hz)	$C_{10}H_{14}O_2Se$	49.03 (48.99	5.96 5.75)
3f	1705, 1550, 1270, 1270, 1080, 740	0.90(br t, 3H, J=6.5 Hz), 1.32(t, 3H, J=7 Hz), 1.1—2.0(m, 6H), 2.80(t, 2H, J=6 Hz), 4.20(q, 2H, J=6.5 Hz), 6.82(d, 1H, J=3.7 Hz), 7.65(d, 1H, J=3.7 Hz)	$C_{12}H_{18}O_2Se$	52.58 (52.75	6.79 6.64)

a) Known compound although spectral data are not reported; see Ref. 11.

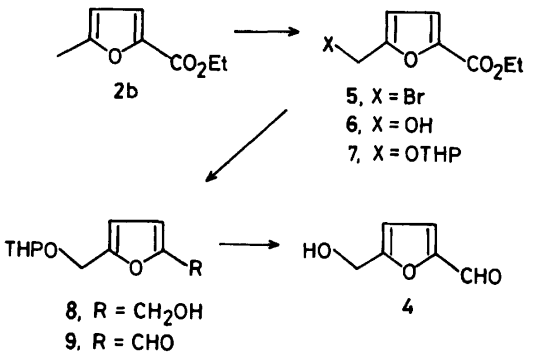

Scheme 1.

ether **9** with pyridinium *p*-toluenesufonate (PPTS) provided **4**[7a] in 21% yield from **7**. Pianka[8] has reported (5-ethoxycarbonyl-2-furyl)methyl dimethyldithiocarbamate (**10**) showed fungicidal activity. We prepared **10** in 65% yield by the reaction of **5** with sodium dimethyldithiocarbamate.

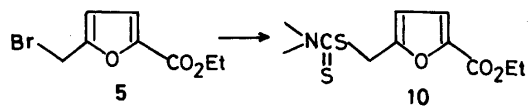

Furthermore, the bromide **5** was treated with triphenylphosphine to afford phosphonium salt **11**. The Wittig reaction of **11** with nonanal in the presence of butyllithium gave ethyl 5-(1-decenyl)-2-furancarboxylate (**12**) in 86% yield with the geometry of E/Z (88:12). Similarly, selenophenecarboxylate **3b** was also brominated with NBS to give bromide **13** in 71% yield. Reaction of **13** with triphenylphosphine

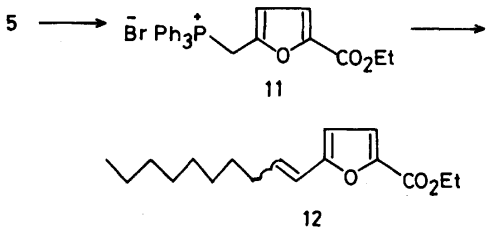

yielded triphenyl phosphonium salt **14**. Reaction of **14** with nonanal in the presence of butyllithium gave ethyl 5-(1-decenyl)-2-selenophenecarboxylate (**15**) in 85% yield with the geometry of E/Z (7:3).

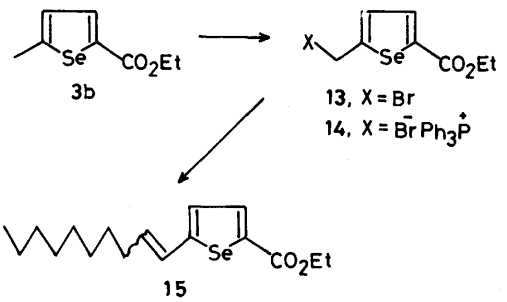

On the other hand, similar treatment of 3,5-alkadienoates such as methyl (3*E*,5*E*)-3,5-octadienoate (**16**) and methyl (3*E*,5*E*)-3,5-decadienoate (**17**) with

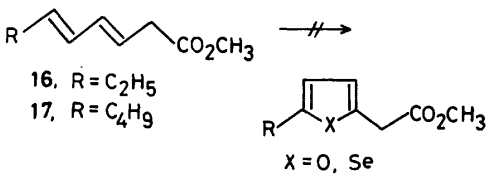

SeO_2 resulted in the recovery of the starting material. This fact shows that conjugated system between a diene and an ester group is required for the formation of furan and selenophene rings.

Although the accurate mechanism of the present reaction can not be clarified, the formation of **2** and **3** can be explained by the assumption of an intermediate **18** which is similar to the adduct of butadiene derivatives with SeO_2.[9] Thermal decomposition of **18** will give **2** along with selenium and water, and the reduction of **18** with selenium will give **3** and selenium(II) dihydroxide.

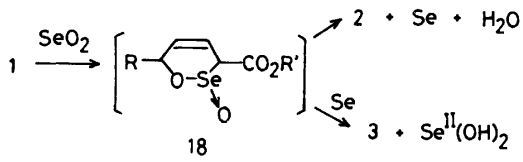

To our knowledge, syntheses of furans via the oxidation of alkadienes are quite few. Parthasarathy and Hort[10] reported the oxidative dehydrogenation of butadiene in the presence of silver ion to yield furan. But their methods required drastic conditions (258 °C[10a], 483 °C[10b]) and special techniques to control the reaction (4 second reaction[10a]). In particular, no reference was found on the use of selenium dioxide for furan synthesis from 2,4-alkadienoates **1**. The present method provides straightforwardly furans and selenophenes under comparatively mild conditions, and the simplicity makes it considerably attractive. Noteworthy is that this procedure for the synthesis of 5-methyl-2-selenophenecarboxylate is simpler than the previously reported one.[11]

Experimental

The melting and boiling points are uncorrected. Infrared (IR) spectra were obtained with a JASCO Model A-102 infrared spectrophotometer. ^1H NMR spectra (60 MHz) were recorded with a JEOL JNM-PMX60SI apparatus. ^1H NMR (100 MHz) and ^{13}C NMR spectra (25 MHz) were obtained with a JEOL JNM-FX100 apparatus using $CDCl_3$ as a solvent. All chemical shifts are reported in δ units downfield from internal Me_4Si, and J values are given in herz. Mass spectra were obtained with an ESCO EMD-05B apparatus. Column chromatography was accomplished using 100—200 mesh Wakogel C-200. Analytical determinations by GLC were performed on a Hitachi Model 163 gas chromatograph fitted with 10% Silicone SE-30 on Chromosorb W column (3 mm o.d.×1 m). Preparative GLC was performed on a Yanagimoto Model G-80 gas chromatogaph fitted with 10% Apiezone Grease L on Chromosorb W column (3 mm o.d.×1 m). High-performance liquid chromatography (HPLC) was obtained with a Yanagimoto liquid chromatograph L-2000.

All solvents and reagents were reagent grade, and solvents were dried according to the literature procedures.[12] Methyl sorbate and ethyl sorbate were distilled prior to use. Methyl (or ethyl) (2*E*,4*Z*)-2,4-alkadienoates (**1b** and **1d—g**) were prepared by the procedure reported previously.[2a,b]

Oxidation of 1 with SeO_2. The reaction was carried out under nitrogen at the reflux temperature of the solvent as shown in Table 1 until the starting material was consumed. The crude product was purified by column chromatography or preparative TLC. Spectral data and elemental analyses of **2**[13-15] and **3** are shown in Tables **4** and **5**. Representative procedures are detailed below.

Methyl 5-Methy-2-furancarboxylate (2a) and Methyl 5-Methyl-2-selenophenecarboxylate (3a). A mixture of **1a** (2 g, 15.9 mmol), SeO_2 (1.94 g, 17.5 mmol), and benzene (1 ml) was heated under reflux for 5 h with stirring. After filtration, the solvent was removed in vacuo. The residual oil was chromatographed on SiO_2 (hexane–ethyl acetate, 20:1) to give 2.18 g of a mixture of **2a**[13] (56% yield) and **3a** (29% yield) as an oil; **2a**/**3a** =57:43 by ^1H NMR analysis. Preparative TLC (SiO_2, hexane–ethyl acetate (4:1)) gave analytical samples, **2a** (R_f=0.52) and **3a** (R_f=0.61). Spectral and analytical data were shown in Tables 4 and 5.

Ethyl 5-Propyl-2-furancarboxylate (2d) and Ethyl 5-Propyl-2-selenophenecarboxylate (3d). A mixture of **1e** (0.10 g, 0.60 mmol), SeO_2 (0.1 g, 0.9 mmol), and xylene (0.5 ml) was heated under reflux for 2 h. The mixture was filtered off, and the solvent was removed in vacuo to give a brown oil. Flash column chromatography [SiO_2, hexane–ethyl acetate (4:1)] gave 85.3 mg of a mixture of **2d** (58%) and **3d** (15%) as an oil; **2d**/**3d**=74/26 by ^1H NMR analysis. Medium pressure liquid chromatography [SiO_2, hexane–ethyl acetate (4:1)] gave pure **2d** and **3d**: TLC analysis (SiO_2, hexane–ethyl acetate=4:1), **2d** (R_f=0.55) and **3d** (R_f=0.60).

Ethyl 5-Pentyl-2-furancarboxylate (2f) and Ethyl 5-Pentyl-2-selenophenecarboxylate (3f). A mixture of **1g** (1.0 g, 5.1 mmol), SeO_2 (0.85 g, 7.6 mmol), and xylene (10 ml) was heated under reflux for 20 h. After being mixed with celite, the mixture was filtered and the filtrate was concentrated in vacuo. The crude products were purified by column chromatography [SiO_2, hexane–ethyl acetate (30:1—0:1)] to give 0.179 g (17%) of **2f** and 43 mg (6.0%) of **3f**. Spectral and analytical data are shown in Tables 4 and 5.

Ethyl 5-Bromomethyl-2-furancarboxylate (5).[16] A mixture of **2b** (1.2 g, 7.8 mmol), NBS (1.52 g, 8.6 mmol), carbon tetrachloride (12 ml), and benzoyl peroxide (50 mg) was heated at the reflux temperature for 2 h. After filtration, the filtrate was concentrated to give 1.9 g of crude **5** which was distilled with a bulb-to-bulb distillation apparatus to afford 1.70 g (94%) of **5**:[16] Bp 120—140 °C (bath temp)/2 Torr (1 Torr=133.322 Pa); IR (neat)1720, 1590, 1535, 1520, 1300, 1221, 1145, 1020, 760 cm^{-}; ^1H NMR data were consistent with those reported.[16]

Ethyl 5-Hydroxymethyl-2-furancarboxylate (6).[17] To a mixture of **5** (0.15 g, 0.65 mmol), acetone (2.5 ml), and water (2.5 ml) was added $AgNO_3$ (0.267 g, 1.7 mmol). The mixture was stirred for 6 h at 22 °C, and then organic materials were extracted with ether. The combined extracts were washed with water, dried over $MgSO_4$ and concentrated. The crude product (111 mg) was purified by preparative TLC [SiO_2, hexane–ethyl acetate (2:1)] to give 33 mg (30%) of **6**:[17] R_f=0.13; IR (neat) 3500, 1730, 1600, 1550, 1540, 1320, 1225, 1160, 1038, 780 cm^{-1}; ^1H NMR (CCl_4) δ=1.35 (t, 3H, $CO_2CH_2C\underline{H}_3$), 3.50 (br s, 1H, OH), 4.25 (q, 2H, J=7 Hz, $CO_2C\underline{H}_2CH_3$), 4.55 (s, 2H, $C\underline{H}_2OH$), 6.30 (d, 1H, J=3.2 Hz,

=CHCH=CCO$_2$Et), 7.00 (d, 1H, J=3.2 Hz, CH=CCO$_2$Et).

Ethyl 5-Hydroxymethyl-2-furancarboxylate THP Ether (7). To a solution of **6** (64 mg, 0.38 mmol) and 3,4-dihydro-2*H*-pyran (34 mg, 0.4 mmol) in 0.2 ml of ether was added a catalytic amount of *p*-toluenesulfonic acid. The mixture was stirred for 90 min at room temperature, and then neutralized with NaHCO$_3$. After the mixture was filtered, washed with ether, and the filtrate was concentrated to give 74 mg (84%) of **7**: IR (neat) 1730, 1600, 1535, 1520, 1300, 1205, 1130, 1020 cm^{-1}; ^{1}H NMR (CCl_4) δ=1.37 (t, 3H, J=7 Hz $CO_2CH_2CH_3$), 1.65 (br s, 6H, $3CH_3$), 3.55 (m, 2H, OCH_2), 4.28 (q, 2H, J=7 Hz, $CO_2CH_2CH_3$), 4.53 (d, 2H, J=3.5 Hz, THPOCH$_2$), 4.68 (m, 1H, >CHO), 6.33 (d, 2H, J=3.2 Hz, CHCH=C-CO$_2$Et), 7.00 (d, 2H, J=3.2 Hz, CH=C-CO$_2$Et).

2,5-Bis(hydroxymethyl)furan MonoTHP Ether (8). To a mixture of $LiAlH_4$ (11.4 mg, 0.30 mmol) and dry ether (2 ml) was added at −40 °C a solution of **7** (73 mg, 0.29 mmol) in 0.5 ml of dry ether. The mixture was stirred for 1 h at −40 °C. The mixture was worked up as shown in **6**, giving 52.8 mg (93%) of **8**: IR (neat) 3450, 1560, 1260, 1120, 1020, 800 cm^{-1}; ^{1}H NMR (CCl_4) δ=1.0—2.0 (m, 6H, $3CH_2$), 3.0 (br s, 1H, OH), 3.5 (m, 2H, OCH_2CH_2), 4.38 (s, 2H, OCH_2), 4.45 (s, 2H, OCH_2C=), 4.61 (s, 1H, OCHO), 6.10 (s, 2H, 2CH=).

5-Hydroxymethyl-2-furancarbaldehyde THP Ether (9). To a mixture of activated MnO_2 (226 mg, 2.6 mmol), petroleum ether (2 ml), and diethyl ether (1 ml) was added a solution of **8** (50 mg, 0.26 mmol) in 1 ml of ether at room temperature. The mixture was stirred for 7d at room temperature and the organic materials were extracted with ether. The combined extract was washed with water, dried over $MgSO_4$. Removal of the solvent gave 70 mg of crude **9**: IR (neat) 1680, 1660, 1530, 1260, 1155, 1020, 965, 900, 815 cm^{-1}; ^{1}H NMR (CCl_4) δ=1.6 (br s, 6H, $3CH_2$), 3.55 (m, 2H, CH_2O), 4.56 (d, 2H, J=3.5 Hz, OCH_2C=), 4.65 (m, 1H, OCHO), 6.41 (d, 2H, J=3.2 Hz, =CHCH=C-CHO), 7.10 (d, 2H, J=3.2 Hz, CH=C-CHO), 9.64 (s, 1H, CHO). Crude **9** was used for the next step without further purification.

5-Hydroxymethyl-2-furancarbaldehyde (4).[7a] To a solution of pyridinium *p*-toluenesulfonate[18] (6.6 mg, 0.03 mmol) in ethanol (1 ml) was added 70 mg (0.33 mmol) of crude **9**, and the mixture was stirred for 12 h at 55 °C. After removing the solvent, the residual oil (57 mg) was purified by preparative TLC [SiO_2, hexane-ethyl acetate (2:1)] to give 10 mg (21% yield from **6**) of **4**:[7a] IR (neat) 3440, 1680, 1530, 1195, 1020, 810, 780 cm^{-1}; ^{1}H NMR (CCl_4) δ=1.66 (br s, 1H, OH), 4.77 (s, 2H, CH_2OH), 6.55 (d, 1H, J=3.2 Hz, CHCH=CCHO), 7.25 (d, 1H, J=3.2 Hz), 9.60 (s, 1H, CHO).

(5-Ethoxycarbonyl-2-furyl)methyl Dimethyldithiocarbamate (10).[8] To a solution of sodium dimethyldithiocarbamate (170 mg, 1.2 mmol) in methanol (2 ml) was added **5** (200 mg, 1.08 mol) at 0 °C with stirring. The mixture was stirred for 20 h at room temperature, and then poured into water. The organic materials were extracted with water, and dried over $MgSO_4$. Removal of the solvent gave 250 mg of crude **10**, which was purified by preparative TLC [SiO_2, hexane-ethyl acetate (4:1)] to yield 192 mg (65%) of **10**:[8] R_f=0.23; IR (neat) 1720, 1595, 1520, 1380, 1300, 1150, 1020, 980, 760 cm^{-1}; ^{1}H NMR (CCl_4) δ=1.35 (t, 3H, J=7 Hz, $CO_2CH_2CH_3$), 3.43 (s, 6H, $N(CH_3)_2$), 4.26 (q, 2H, J=7 Hz, $CO_2CH_2CH_3$), 4.58 (s, 2H, SCH_2), 6.39 (d, 1H, J=3.2 Hz, =CHCH=C-CO$_2$Et), 6.96 (d, 1H, J=3.2 Hz, CH=CO$_2$Et).

(5-Ethoxycarbonyl-2-furylmethyl)triphenylphosphonium Bromide (11). A mixture of triphenylphosphine (310 mg, 1.18 mmol), **5** (200 mg, 1.08 mmol), and benzene (2 ml) was stirred for 25 h at room temperature, and then filtered, washed with benzene, and dried in vacuo, giving 370 mg (74%) of **11**: Mp 194.5—195 °C; IR (KBr) 3450, 2900—2800, 1710, 1590, 1530, 1340, 1240, 1140, 760 cm^{-1}.

Ethyl 5-(1-Decenyl-2-furancarboxylate (12). To a solution of **11** (120 mg, 0.242 mmol) in dry THF (2 ml) was added dropwise 1.5 M† *n*-BuLi (0.162 ml, 0.242 mmol) at 0 °C with stirring under an atmosphere of nitrogen. After 30 min, nonanal (35 mg, 0.242 mmol) was added dropwise over 10 min, and the mixture was stirred for 30 min at 0 °C and for 4 h at room temperature. After being poured into ice water, the mixture was neutralized with dil HCl. The organic materials were extracted with ether, and the ethereal layer was washed with water, dried over $MgSO_4$, and concentrated. The residual oil (180 mg) was chromatographed on SiO_2 (hexane–ethyl acetate=40:1—0:1) to give 58 mg (86%) of **12**: IR (neat) 1730, 1650, 1580, 1500, 1380, 1300, 1200, 1010, 960, 760 cm^{-1}; ^{1}H NMR (CCl_4) δ=0.7—1.6 (m, 18H, $CH_3(CH_2)_6$ and $CO_2CH_2CH_3$), 2.20 (m, 2H, CH_2CH=CH), 4.28 (q, 2H, J=7 Hz, $CO_2CH_2CH_3$), 6.12 (d, 1H, J=3.2 Hz, CHCH=C-CO$_2$Et), 6.97 (d, 1H, J=3.2 Hz, CH=C-CO$_2$Et). Found: C, 73.43; H, 9.56%. Calcd for $C_{17}H_{26}O_3$: C, 73.35; H, 9.41%. HPLC analysis [column, Unisil Q (10.7 mm o.d.×250 mm); eluent, hexane–ethyl acetate (20:1), 2.0 ml min^{-1}] showed two peaks at R_t17.6 and 20.2 min in an intensity ratio of 12:88. Each component was separated by preparative HPLC. The first fraction gave 5 mg of (*Z*)-**12**: IR (neat) 1730, 1720, 1640, 1502, 1300, 1020, 760 cm^{1}; ^{1}H NMR (CCl_4) δ=0.86 (t, 3H, J=5.5 Hz, CH_3), 1.28 (br s, 14H, $(CH_2)_7$), 1.32 (t, 3H, J=7 Hz, $CO_2CH_2CH_3$), 2.45 (m, 2H, CH_2CH=CH), 4.22 (q, 2H, J=7 Hz, $CO_2CH_2CH_3$), 5.61 (td, 1H, J=6.3 and 11.0 Hz, CH_2CH=CH), 6.12 (d, 1H, J=11.0 Hz, CH=CH-furyl) 6.14 (d, 1H, J=3 Hz, CH=C-CO$_2$Et), 6.98 (d, 1H, J=3 Hz, =CH=C-CO$_2$Et), 6.98 (d, 1H, J=3 Hz, =CH-CH=C-CO$_2$Et). The second fraction gave 35 mg of (*E*)-**12**: IR (neat) 1730, 1720, 1660, 1580, 1505, 1300, 1022, 1110, 968, 770 cm^{-1}; ^{1}H NMR (CCl_4) δ=0.89 (t, 3H, J=5 Hz, CH_3), 1.30 (br s, 14H, $(CH_2)_7$), 1.32 (t, 3H, J=6Hz, $CO_2CH_2CH_3$), 2.15 (m 2H, CH_2CH=CH), 4.22 (q, 2H, J=8 Hz, $CO_2CH_2CH_3$), 6.03 (d, 1H, J=15 Hz, CH=C-CO$_2$Et), 6.42 (dt, 1H, J=5 and 15 Hz, CH_2CH=CH-), 6.08 (d, 1H, J=3 Hz, =CH-CH=C-CO$_2$Et), 6.93 (d, 1H, J=3 Hz, CH=C-CO$_2$Et).

Ethyl 5-Bromomethyl-2-selenophenecarboxylate (13). A mixed solution of **3b** (300 mg, 1.4 mmol), NBS (274 mg, 1.5 mmol), a catalytic amount of benzoyl peroxide and CCl_4 (3 ml) was heated under reflux for 10 h. The mixture was cooled and the precipitates were filtered off. Concentration of the filtrate gave 510 mg of crude products, which were purified by preparative TLC [SiO_2, hexane–ethyl acetate (4:1)] giving 90 mg of **3b** (R_f=0.59) and 290 mg (71%) of **13**: R_f=0.53; IR (neat) 1710, 1550, 1470, 1330, 1220, 1100, 1030, 1000, 750 cm^{-1}; ^{1}H NMR (CCl_4) δ=1.35 (t, 3H, J=7 Hz, $CO_2CH_2CH_3$), 4.27 (q, 2H, J=7 Hz, $CO_2CH_2CH_3$), 4.67 (s, 2H, CH_2Br), 7.18 (d, 1H, J=3.7 Hz, =CHCH=C-CO$_2$Et), 7.74 (d, 1H, J=3.7 Hz, CH=C-CO$_2$Et). Found: C, 32.55; H, 3.18%. Calcd for $C_8H_9BrO_2Se$: C, 32.46; H, 3.06%.

† 1 M=1 mol dm^{-3}.

(5-Ethoxycarbonyl-2-selenophenylmethyl)triphenylphosphonium Bromide (14). A mixture of **13** (200 mg, 0.86 mmol), triphenylphosphine (247 mg, 0.95 mmol), and benzene (2 ml) was heated at the reflux temperature for 20 h. The mixture was cooled and then filtered to afford 230 mg (50%) of **14** as white crystals: Mp 211—213 °C; IR (KBr) 1710, 1695, 1585, 1545, 1460, 1270, 1115, 1080, 745, 725 cm^{-1}.

Ethyl 5-(1-Decenyl)-2-selenophenecarboxylate (15). To a solution of **14** (190 mg, 0.34 mmol) in THF (2 ml), 1.5 M *n*-BuLi in hexane (0.20 ml, 0.34 mmol) was added at 0 °C. After 30 min nonanal (48 mg, 0.34 mmol) was added dropwise over 10 min, and the mixture was stirred for 30 min at 0 °C and for 6 h at room temperature and then worked up as shown in **12**, giving 180 mg of an oil. Preparative TLC [SiO_2, hexane–ethyl acetate(4:1)] gave 98 mg (85%) of **15**: R_f=0.62; E/Z=7:3; IR (neat) 1710, 1530, 1360, 1270, 1080, 945, 740 cm^{-1}; ^1H NMR (CCl_4) δ=0.7—0.8 (m, 18 Hz, $(CH_2)_6CH_3$ and $CO_2CH_2CH_3$), 2.20 (m, 2H, CH_2CH=CH), 4.24 (q, 2H, J=7 Hz, $CO_2CH_2CH_3$); 5.60 (dt, 0.3H, J=10 and 7Hz, CH_2CH=CH), 5.95 (dt, 0.7H, J=7 and 15 Hz, CH_2CH=CH), 6.42 (d, 0.7H, J=15 Hz, CH_2CH=CH), 6.48(d, 0.3H, J=10 Hz, CH_2CH=CH), 6.86 (d, 0.7 H, J=3.5 Hz CHCH=CCO_2Et), 6.98 (d, 0.3H, J=3.5 Hz, CHCH=C-CO_2), 7.68 (d, 0.7 H, J=3.5 Hz, CH=C-CO_2Et), 7.75 (d, 0.3H, J=3.5 Hz, CH=C-CO_2Me). Found: C, 59.61; H, 7.69%. Calcd for $C_{17}H_{26}O_2Se$: C, 59.82; H, 7.68%.

Treatment of Methyl (3*E*, 5*E*)-3,5-Octadienoate (16) with SeO_2. A mixture of **16** (49 mg, 0.32 mmol), SeO_2 (71 mg, 0.64 mmol), and xylene (2 ml) was heated under reflux for 3 h with stirring. After column chromatography [SiO_2, hexane–ethyl acetate(10:1)], the starting material **16** (30 mg) was recovered.

Treatment of Methyl (3*E*,5*E*)-3,5-Decadienoate (17) with SeO_2. A mixture of **17** (84 mg, 0.46 mmol), SeO_2 (102 mg, 0.92 mmol), and benzene (3 ml) was heated under reflux for 12 h with stirring. Column chromatography [SiO_2, hexane–ethyl acetate(10:1)] gave 52mg of the starting material **17**.

We thank Mr. Eiichiro Amano in our laboratory for elemental analyses.

References

1) For examples, see reviews: a) G. R. Waitkins and C. W. Clark, *Chem. Rev.*, **36**, 235 (1945); b) N. Rabjohn, *Org. React.*, **5**, 331 (1949); c) R. A. Jerussi, "Selective Oxidations with Selenium Dioxide", John Wiley, New York (1970), p. 301; d) N. Sonoda, *Yuki Gosei Kagaku Kyokai Shi*, **30**, 728 (1972); e) N. Rabjohn, *Org. React.*, **24**, 261 (1976).

2) a) S. Tsuboi, T. Masuda, H. Makino, and A. Takeda, *Tetrahedron Lett.*, **23**, 209 (1982); b) S.Tsuboi, T. Masuda, and A. Takeda, *J. Org. Chem.*, **47**, 4478 (1982); c) S. Tsuboi, T. Masuda, and A. Takeda, *Chem. Lett.*, **1983**, 1829; d) S. Tsuboi, Y. Nooda, and A. Takeda, *J. Org. Chem.*, **49**, 1204 (1984); e) S. Tsuboi, A. Kuroda, T. Masuda, and A. Takeda, *Chem. Lett.*, **1984**, 1541.

3) Preliminary communication: S. Tsuboi, K. Watanabe, S. Mimura, and A. Takeda, *Tetrahedron Lett.*, **27**, 2643 (1986).

4) J. Colonge and M. Reymermier, *Bull. Soc. Chim. Fr.*, **1956**, 195.

5) N. Danieli, Y. Mazur, and F. Sondheimer, *Tetrahedron*, **23**, 509 (1967).

6) T. Oritani and K. Yamashita, *Agr. Biol. Chem.*, **38**, 801 (1974).

7) a) W. N. Haworth and W. G. M. Jones, *J. Chem. Soc.*, **1944**, 667; b) J. A. Elix and M. V. Sargent, *J. Chem. Soc.*, **1968**, 595; c) H. Okajima, K. Ishii, and H. Watanabe, *Chem. Pharm. Bull.*, **32**, 3281 (1984).

8) M. Pianka, J. D. Edwards, and C. B. F. Smith, *J. Sci. Food Agr.*, **17**, 407 (1966); *Chem. Abstr.*, **66**, 2169d (1967).

9) a) W. L. Mock and J. H. McCausland, *Tetrahedron Lett.*, **1968**, 391; b) H. J. Backer and J. Strating, *Rec. Trav. Chim.*, **53**, 1113 (1934).

10) a) R. Parthasarathy and E. V. Hort, U. S. Patent 4280959 (1981); *Chem. Abstr.*, **95**, 168975g (1981); b) R. Parthasarathy and E. V. Hort, U. S. Patent 4320031 (1982); *Chem. Abstr.*, **96**, 217686v (1982).

11) Yu. K. Yurev, N. K. Sadovaya, and A. B. Ibragimova, *Zh. Obshchei Khim.*, **29**, 3647 (1959); *Chem. Abstr.*, **54**, 19644e (1960).

12) J. A. Riddick and W. B. Bunger, "Organic Solvents," 3rd ed, Wiley-Interscience (A Division of John Wiley & Sons, Inc.), New York (1970), Chap. 5.

13) J.-P. Morizur, Y. Pascal, and F. Vernier, *Bull. Soc. Chim. Fr.* **1966**, 2296.

14) H. Matsue, *Bull. Chem. Soc. Jpn.*, **48**, 491 (1975).

15) H. Gilman and N. O. Calloway, *J. Am. Chem. Soc.*, **55**, 4197 (1933).

16) a) A. Jurasek, J. Kovac, and R. Belko, *Collect. Czech. Chem. Commun.*, **45**, 746 (1980). b) W. B. Smith, *J. Phys. Chem.*, **67**, 2841 (1963).

17) L. A. Solonenko and V. G. Kulnevich, *Tr. Krasnodar. Politekhn In-t*, **1979**, 39; *Chem. Abstr.*, **94**, 65405w (1981).

18) M. Miyashita, A. Yoshikoshi, and P. A. Grieco, *J. Org. Chem.*, **42**, 3772 (1977).

 © 1987 The Chemical Society of Japan Bull. Chem. Soc. Jpn., 60, 1813—1817 (1987)

Chemo- and Regioselective Reduction of Epoxides with Sodium Borohydride in Mixed Solvent Containing Methanol

Atsuhiro Ookawa, Hiroshi Hiratsuka, and Kenso Soai*
Department of Applied Chemistry, Faculty of Science, Science University of Tokyo, Shinjuku, Tokyo 162
(Received November 5, 1986)

Mono- and *gem*-disubstituted epoxides were reduced to more substituted alcohols in good to high yields (73—100%) and in high regioselectivities (89—100:11—0) by sodium borohydride in a mixed solvent of *t*-butyl alcohol-methanol or 1,2-dimethoxyethane-methanol. The reaction of disubstituted epoxide depends on the steric hindrance and the position of the substituents. Trisubstituted epoxides were not reduced by the present reducing system. The reactivity order of epoxides by the present reducing system was mono->2,2-di->2,3-di-≫trisubstituted epoxides. The chemoselectivity of the present reducing system is excellent. Thus, epoxides were selectively reduced in the presence of such reducible groups as carbamoyl, carboxyl, nitro, cyano, and bromo.

Epoxides are important synthetic intermediates,[1a] and their transformation reactions have been the subject of increasing interest in recent years.[1b] Among the many types of reactions involving epoxides, the reduction to alcohols by metal hydrides is one of the most fundamental reactions.[1b,2] Several kinds of metal hydrides[3] such as lithium aluminum hydride ($LiAlH_4$), lithium 9,9-dibutyl-9-borabicyclo[3.3.1]-nonane,[3f] lithium triethylhydroborate ($LiBHEt_3$)[4] and aluminum hydride are known to reduce epoxides.[3a-c] However, because of the poor chemoselectivities of most of these reducing agents, a selective reduction of epoxides can not usually be achieved in the presence of such reducible functional groups as carbamoyl, carboxyl, cyano, or halo. Regioselectivity and synthetic yield of lithium borohydride ($LiBH_4$) reduction of epoxides are low to moderate.[5]

Sodium borohydride ($NaBH_4$) is a mild chemoselective reducing reagent for ketones and aldehydes. It is generally accepted, however, that the reduction rate of epoxides with $NaBH_4$ is very slow.[3a-c] Exceptional epoxides, which are reported to be reduced with $NaBH_4$, contain neighboring functional groups which may in some way take part in the reduction.[6] To the best of our knowledge, no systematic study has been reported on the selective reduction of epoxides with $NaBH_4$.

We have studied chemoselective[7,8] and diastereoselective[9,10] reductions using $NaBH_4$ in a mixed solvent containing MeOH as one component, and chemoselective[11] and asymmetric[12] reductions using $LiBH_4$. In this paper, we describe a chemo- and regioselective reduction of epoxides with $NaBH_4$ in a mixed solvent containing MeOH.

Results and Discussion

We examined the effect of a solvent in the reduction of 2-phenyloxirane (**1a**) with $NaBH_4$. The reaction was carried out as follows. To a refluxing mixture of $NaBH_4$, **1a** and solvent, MeOH was added dropwise over a period of 1 h. Then, the reflux was continued for an additional 1 h. As shown in Table 1, the reaction in *t*-BuOH afforded 2-phenylethanol (**2a**) and 1-phenylethanol (**3a**) in 97% total yield with high regioselectivity (**2a**:**3a**=89:11). On the other hand, when a reduction was carried out in each single solvent (MeOH or *t*-BuOH), the yields of alcohols (**2a** and **3a**) dropped considerably to 33% (Table 1, Entries 1 and 2). Thus, the presence of a small amount of MeOH (about 5 molar equivalent to $NaBH_4$) in *t*-

Table 1. Effect of the Solvent for the Reduction of 2-Phenyloxirane with $NaBH_4$

Entry	Solvent	Yield/%	Ratio[a] **2a** : **2b**
1	MeOH	33	c)
2	*t*-BuOH	33	87 : 13
3	*t*-BuOH-MeOH[d]	97	89 : 11
4	DME[b]-MeOH[d]	82	83 : 17
5	THF-MeOH[d]	44	96 : 4
6	Hexane-MeOH[d]	28	65 : 35
7	Benzene-MeOH[d]	10	67 : 33

a) Determined by ^1H NMR. b) 1,2-Dimethoxyethane. c) Not determined. d) Molar ratio, 2-phenyloxirane : $NaBH_4$: MeOH = 1 : 2.5 : 12.

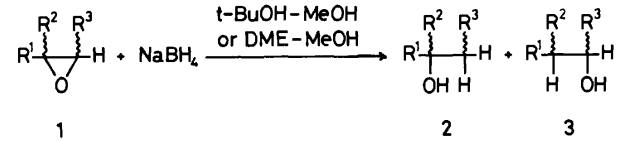

1 2 3

a; R^1=Ph, R^2=H, R^3=H
b; R^1=n-C_6H_{13}, R^2=H, R^3=H
c; R^1=Ph, R^2=CH_3, R^3=H
d; R^1=H, R^2, R^3=-$(CH_2)_4$-
e; R^1=Ph, R^2=H, R^3=Ph (cis)
f; R^1=Ph R^2=H, R^3=Ph (trans)
g; R^1=Ph, R^2=H, R^2=H, R^3=CH_3
h; R^1=CH_3, R^2, R^3=-$(CH_2)_4$-
i; R^1=Ph, R^2=CH_3, R^3=CH_3

BuOH was apparently effective to increase the chemical yields of **2a** and **3a**. 1,2-Dimethoxyethane (DME) was also a suitable co-solvent with MeOH for the reduction of **1a**. Reactions in such hydrocarbon solvents as benzene and hexane were very sluggish and showed low regioselectivities (Table 1, Entries 6 and 7).[13]

For one molar amount of monosubstituted oxirane, 2.5 molar amounts of $NaBH_4$ was sufficient to perform the reaction (Table 2, Entries 1—3). As to the amount of MeOH, about five molar amounts of MeOH to $NaBH_4$ were suitable for the reduction (Table 2, Entries 5—7). Thus, the optimum molar ratio was as follows: epoxide: $NaBH_4$: MeOH=1:2.5:12. Under the above conditions (in *t*-BuOH, molar ratio 1: $NaBH_4$: MeOH=1:2.5:12), aromatic and aliphatic monosubstituted epoxides (**1a** and **1b**) were reduced to the corresponding alcohols in 96—97% yields (Table 2, Entries 1 and 8). The reduction of 2-methyl-2-phenyloxirane (**1c**) proceeded with high regioselectivity; 2-phenyl-1-propanol (**2c**) was obtained as the sole product in 73% yield (Table 2, Entry 9). The reaction with 2,3-disubstituted oxirane was slower than that with 2,2-disubstituted one. A long reaction time was required for the reduction of cyclohexene oxide (**1d**) (Table 2, Entry 10).

One of the characteristic features of the present reducing system is chemoselectivity. Chemoselective or competitive reductions of **1a** in the presence of other functional groups such as carbamoyl, carboxyl, nitro or cyano are shown in Table 3. **1a** was reduced in good to high yields while other functional groups were not reduced (Table 3, Entries 1—3). The reduction of 2-(4-bromophenyl)oxirane proceeded to

Table 2. Reduction of Various Types of Epoxides with $NaBH_4$ in a Mixed Solvent

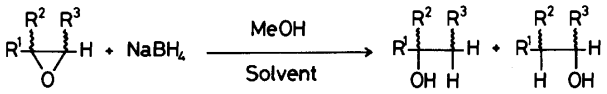

1 2 3

Entry	1 R¹	R²	R³	Molar Ratio 1 : $NaBH_4$: MeOH	Solvent	Time/h	Yield/%[a] 2+3	Ratio[b] 2 : 3
1	Ph	H	H (**1a**)	1 : 2.5 : 12	*t*-BuOH	2.0	97	89 : 11
2		**1a**		1 : 1.5 : 7	*t*-BuOH	2.0	71	
3		**1a**		1 : 0.5 : 2.5	*t*-BuOH	2.0	49	
4		**1a**		1 : 2.5 : 20	*t*-BuOH	2.0	88	89 : 11
5		**1a**		1 : 2.5 : 6	THF	2.0	22	95 : 5
6		**1a**		1 : 2.5 : 12	THF	2.0	44	96 : 4
7		**1a**		1 : 2.5 : 20	THF	2.0	26	95 : 5
8	*n*-C_6H_{13}	H	H (**1b**)	1 : 2.5 : 12	*t*-BuOH	2.0	96	97 : 3[c]
9	Ph	CH_3	H (**1c**)	1 : 5.0 : 25	*t*-BuOH	2.0	73	100 : 0
10	H	$-(CH_2)_4-$	(**1d**)	1 : 5.0 : 25	*t*-BuOH	9.5	72	
11	Ph	H	Ph(cis, **1e**)	1 : 5.0 : 25	*t*-BuOH	2.0	12	
12	Ph	H	CH_3 (**1g**)[d]	1 : 5.0 : 25	*t*-BuOH	4.0	36 (63)[e]	68 : 32
13	CH_3	$-(CH_2)_4-$	(**1h**)	1 : 5.0 : 25	THF	2.0	0	
14	Ph	CH_3	CH_3 (**1i**)	1 : 5.0 : 25	*t*-BuOH	2.0	9	

a) The values in parentheses were the yields of recovered **1**. b) Unless otherwise noted, the ratio was determined by ^1H NMR. c) Determined by GLC analysis. d) The ratio of cis/trans was 32/68. e) The ratio of cis/trans of recovered **1g** was 35/65.

Table 3. Chemoselective or Competitive Reduction of Epoxide by $NaBH_4$-MeOH-*t*-BuOH System

1a + **4** $\xrightarrow[t\text{-BuOH-MeOH}]{NaBH_4}$ **2** + **3** + **4**(Recovery)

Entry[a]	1	4	Yield/% 2+3	Ratio[b] 2 : 3	Recovery/% 4
1[a]	**1a**	$PhCONHCH_2CO_2H$	71	88 : 12[c]	84
2[a]	**1a**	$PhNO_2$	91	89 : 11[c]	83
3[a]	**1a**	PhCN	90	88 : 12[c]	77
4[b]	2-(4-Bromophenyl)oxirane		100	91 : 9[d]	—

a) Molar ratio **1a** : **4** : $NaBH_4$=1 : 1 : 2.5—2.8. b) Molar ratio **1** : $NaBH_4$=1 : 2.5. c) Determined by GLC. d) Determined by ^1H NMR.

Table 4. Comparison of Regioselectivities in the Reduction of Epoxides

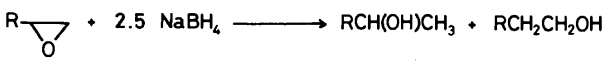

Entry	R	Reducing system	Yield/% 2+3	Ratio 2 : 3
1	Ph(**1a**)	$NaBH_4$-*t*-BuOH	33	87 : 13
2	Ph(**1a**)	$NaBH_4$-MeOH-*t*-BuOH	97	89 : 11
3[a]	Ph(**1a**)	$LiBH_4$-Et_2O	66	56 : 44
4[a]	Ph(**1a**)	$LiBH_4$-MeOH-Et_2O	99	65 : 35
5	Ph(**1a**)	KBH_4-MeOH-*t*-BuOH	18	100 : 0
6	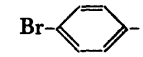	$NaBH_4$-MeOH-*t*-BuOH	100	91 : 9
7[b]	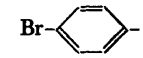	$LiBH_4$-Et_2O	66	84 : 16
8	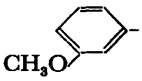	$NaBH_4$-MeOH-*t*-BuOH	100	95 : 5
9[b]	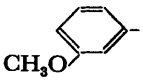	$LiBH_4$-Et_2O	63	77 : 23
10	*n*-C_6H_{13}-(**1b**)	$NaBH_4$-MeOH-*t*-BuOH	96	97 : 3

a) Data from Ref. 11. b) Data from Ref. 5.

afford 2-(4-bromophenyl)ethanols in 100% yield (Table 3, Entry 4).

Another feature is high regioselectivity. Results are summarized in Table 4. Both aromatic and aliphatic epoxides were reduced with high regioselectivities (89—97:11—3) by $NaBH_4$-*t*-BuOH-MeOH (Table 4, Entries 2, 6, 8, and 10). The regioselectivities of $NaBH_4$ were higher than those of $LiBH_4$ (Entries 3, 4, 7, and 9). The regioselectivity was excellent in the reduction of **1a** with potassium borohydride (KBH_4)-MeOH-*t*-BuOH, although the chemical yield was low. The addition of MeOH caused an increace in the chemical yield and regioselectivity (Entries 1—4).

Though many reports have appeared regarding reductions of epoxide to alcohol, most of them (for example, $LiAlH_4$,[14] $LiBEt_3H$,[15] $LiAlH_4$-$AlCl_3$,[14]) reduce epoxides exceedingly rapidly, regardless of the structure of epoxide. In the competitive reduction of **1a** and *trans*-2,3-diphenyloxirane (**1f**) by a $NaBH_4$-*t*-BuOH-MeOH reducing system, **1a** was selectively reduced to **2a** and **3a** in 96% total yield, while **1f** was in 100% recovered. Thus, the present method can differentiate the structure of epoxides.

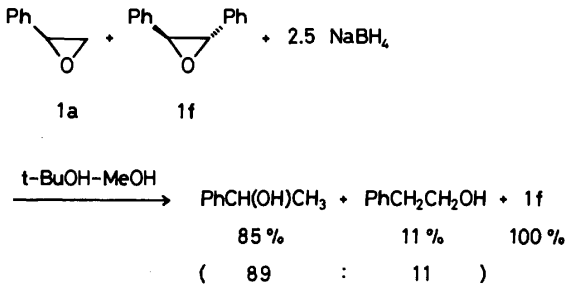

Furthermore, a competitive reduction between disubstituted epoxides was also performed. 2-Methyl-2-phenyloxirane (**1c**) was selectively reduced to 2-phenyl-2-propanol in 97% yield, while *trans*-2,3-disubstituted (**1f**) was quantitatively recovered.

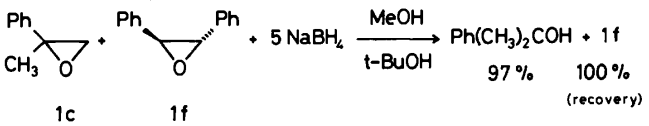

Conclusion

The reduction of epoxides with $NaBH_4$ in a mixed solvent containing MeOH is of practical utility. The unique characteristic features of the present reducing system are exemplified by the regioselective and chemoselective reductions of epoxide in the presence of carbamoyl, carboxyl, nitro, cyano, bromo, and methoxyl groups and/or a structure selective reduction of the terminal epoxide in the presence of an internal one. A small amount of MeOH caused an increase in the reducing ability of $NaBH_4$ and the use of $NaBH_4$ in a *t*-BuOH-MeOH mixed solvent enabled the above-mentioned unique selective reduction.

Experimental

Melting and boiling points were uncorrected. IR spectra were recorded with a Hitachi 260-10 spectrophotometer. ^1H NMR spectra (60 MHz) were recorded using either a JEOL JNM-PMX-60 NMR spectrometer or a JEOL-PMX 60 SI NMR spectrometer. GLC analyses were carried out with a Shimadzu Gas Chromatograph (either model GC-4A

or model GC-4C). All of the reactions were run under an argon atmosphere. Organic extracts were dried over anhydrous sodium sulfate.

Materials Methanol and ethanol were stored, respectively, over 3A and 4A molecular sieves. *t*-Butyl alcohol (Kanto), sodium borohyride (Nakarai), potassium borohydride (Nakarai), and lithium borohydride (Wako) were used without further purification. 2-Phenyloxirane, *trans*-2,3-diphenyloxirane, α-methylstyrene and cyclohexene oxide were purchased from Aldrich. 2-Methyl-3-phenyloxirane was prepared by the method of Eliel et al.[14] Bp 49 °C/1.5 mmHg (lit,[14] 62 °C/2.3 mmHg)(1 mmHg=133.322 Pa). 2-(4-bromophenyl)oxirane and 2-(3-methoxyphenyl)-oxirane were prepared from the corresponding phenacyl bromide according to a procedure from the literature.[4] Other epoxides were synthesized by an oxidation of the corresponding olefin with *m*-chloroperbenzoic acid.[16] *trans*-2,3-Diphenyloxirane: Mp 68.2—70.0 °C (lit,[17] 65—67 °C). *cis*-2,3-Diphenyloxirane: Mp 38.2—39.O °C (lit,[18] 37—38 °C). 1-Methylcyclohexene oxide: Bp 58.0—58.4 °C/20 mmHg (lit,[18] 136—137 °C). 2-Methyl-3-phenyl-oxirane: Bp 115 °C/39 mmHg (bath temp). This oxirane was identified by ^{1}H NMR, compared to those of an authentic sample;[19] the ratio of cis/trans was determined by a GLC analysis.

Reduction of 2-Phenyloxirane (1a): To a refluxing mixture of $NaBH_4$ (0.095 g, 2.5 mmol) and **1a** (0.120 g, 1.0 mmol) in *t*-BuOH (4.0 ml), MeOH (0.5 ml) was added over a period of 1 h. After the reflux was continued for an additional 1 h, water and satd. aq. ammonium chloride were added to quench the reaction. Most of the solvent was evaporated under reduced pressure at an ambient temperature, and the residue was extracted with ether. An ethereal extract was dried, evaporated on a rotary evaporator and the residual oil was purified on silica gel TLC (dichloromethane–MeOH (10:1) as a developing solvent). A mixture of 1- and 2-phenylethanol was obtained in 93% yield (0.114 g).

Reduction of 2-Methyl-3-phenyloxirane (1g): Methanol (1.08 ml) was added dropwise to a refluxing mixture of 2-methyl-3-phenyloxirane (0.1465 g, 1.08 mmol), sodium borohydride (0.205 g, 5.42 mmol) and *t*-BuOH (6 ml) over a period of 1.5 h and the reflux was continued for additional 2.5 h. After cooling the mixture to room temperature, water, satd. aq ammonium chloride and ether were added. An organic layer was separated and an aq layer was extracted with dichloromethane. The combined organic layer was dried and evaporated. The residue was purified on silica-gel TLC (chloroform as developing solvent) to afford 1- and 2-phenylpropanols (**2g** and **3g**, 0.053 g, 36%). The recovery of **1g** was 63%. A GLC analysis showed that the ratio of alcohol (**2g**:**3g**) was 68:32. Analytical conditions were as follows; Shimadzu Gas chromatograph GC-4C model, OV-1 50 m capillary column, column temperature 120 °C, retention time, *trans*-**1g** (17.0 min), *cis*-**1g** (15.9 min); SE-30 25 m capillary column, column temp 95 °C, retention time, **2g** (7.1 min), **3g** (7.8 min).

Selective Reduction of 2-Phenyloxirane (1a) in the Presence of Nitrobenzene: Methanol (0.5 ml) was added dropwise to a mixture of **1a** (0.120 g, 1 mmol), nitrobenzene (0.123 g, 1 mmol), sodium borohydride (0.095 g, 2.5 mmol), and *t*-BuOH (4 ml) over a period of 1 h. The mixture was refluxed for an additional 1 h, cooled to room temperature, followed by the addition of water and MeOH. After evaporating most of the MeOH under reduced pressure, the mixture was extracted with dichloromethane. The extract was then dried and evaporated in vacuo. The residue was purified on silica-gel TLC (dichloromethane as developing solvent) to afford 1-phenyl- and 2-phenylethanol (0.111 g, 91% yield) and nitrobenzene (0.102 g, 83% recovery). A GLC analysis showed that the ratio of **2a** and **3a** was 89:11.

Structural Selective Reduction of 2-Phenyloxirane (1a) in the Presence of *trans*-2,3-Diphenyloxirane (1f): To a refluxing mixture of **1a** (0.118 g, 0.98 mmol), **1f** (0.193 g, 0.98 mmol), sodium borohydride (0.093 g, 2.46 mmol) and *t*-BuOH (6 ml), MeOH (0.5 ml) was added dropwise over a period of 1 h and the mixture was refluxed for additional 1 h. After quenching the reaction by the addition of water and satd. aq. ammonium chloride, the mixture was extracted with dichloromethane. The extract was dried and evaporated under reduced pressure. Purification on silica-gel TLC (benzene–chloroform=3:1 as developing solvent) afforded a mixture of **2a** and **3a** (0.115 g, 96% yield). ^{1}H NMR analyses of the mixture showed that the ratio of **2a** to **3a** was 89:11.

The present work was partially supported by a Grant from The Foundation "Hattori-Hokokai."

References

1) a) S. Masamune, C. U. Kim, K. E. Wilson, G. O. Spessard, P. E. Georghiou, and G. S. Bates, *J. Am. Chem. Soc.*, **97**, 3512 (1975); E. J. Corey, E. J. Trybulski, L. S. Melvin, Jr., K. C. Nicolaou, J. A. Secrist, R. Lett, P. W. Sheldrake, J. R. Falck, D. J. Brunelle, M. F. Haslanger, S. Kim, and S. Yoo, *ibid.*, **100**, 4618 (1978); E. J. Corey, S. Kim, S. Yoo, K. C. Nicolaou, L. S. Melvin, Jr., D. J. Brunelle, J. R. Falck, E. J. Trybulski, R. Lett, and P. W. Sheldrake, *ibid.*, **100**, 4620 (1978); P. A. Grieco, M. Nishizawa, T. Oguri, S. D. Burke, and N. Marinovic, *ibid.*, **99**, 5773 (1977); A. S. Kende and Y. G. Tsay, *J. Chem. Soc., Chem. Commun.*, **1977**, 140; Y. Kishi, *Aldrichimica Acta*, **13**, 23 (1980); b) For a review, J. G. Smith, *Synthesis*, **1984**, 629.

2) a) H. B. Henbest and R. A. L. Wilson, *J. Chem. Soc.*, **1956**, 3289; Y. L. Fu and M. Bobek, *J. Org. Chem.*, **45**, 3836 (1980).

3) a) A. Hajós, "Complex Hydrides," Elsevier Scientific Publishing Co., Budapest, (1979); b) E. R. H. Walker, *Chem. Soc. Rev.*, **5**, 23 (1976); c) H. C. Brown and S. Krishnamurthy, *Tetrahedron*, **35**, 567 (1979); d) J. Maleh and M. Cerry, *Synthesis*, **1972**, 217; e) J. M. Ross, D. S. Tarbell, W. E. Lovett, and A. D. Cross, *J. Am. Chem. Soc.*, **78**, 4675 (1956); S. Corsano and G. Piancatelli, *J. Chem. Soc., Chem. Commun.*, **1971**, 1106; f) Y. Yamamoto, H. Toi, A. Sonoda, and S.-L. Murahashi, *J. Chem. Soc., Chem. Commun.*, **1976**, 672.

4) H. C. Brown, S. Narasimhan and V. Somayaji, *J. Org. Chem.*, **48**, 3091 (1983).

5) R. Fuchs and C. A. V. Werf, *J. Am. Chem. Soc.*, **76**, 1631 (1945); R. Fuchs, *ibid.*, **78**, 5612 (1956).

6) M. Bharucha, H. Jaeger, K. Meyer, T. Reichstein and O. Schindler, *Helv. Chim. Acta*, **42**, 1395 (1959); H. H. Baer and C. B. Hadumelu, *Can. J. Chem.*, **56**, 1177 (1978).

7) a) K. Soai, H. Oyamada, and A. Ookawa, *Synth.*

Commun., **12**, 463 (1982); b) K. Soai, H. Oyamada, M. Takase, and A. Ookawa, *Bull. Chem. Soc. Jpn.*, **57**, 1948 (1984); c) K. Soai, and H. Oyamada, *Synthesis*, **1984**, 605; d) K. Soai, H. Oyamada, and M. Takase, *Bull. Chem. Soc. Jpn.*, **57**, 2327 (1984); e) A. Ookawa, S. Yokoyama, and K. Soai, *Synth. Commun.*, **16**, 819 (1986).

8) Preliminary communication. K. Soai, A. Ookawa, H. Oyamada, and M. Takase, *Heterocycles*, **19**, 1371 (1982).

9) K. Soai, K. Komiya, Y. Shigematsu, H. Hasegawa, and A. Ookawa, *J. Chem. Soc., Chem. Commun.*, **1982**, 1282; K. Soai, H. Hasegawa, *J. Chem. Soc., Perkin Trans. 1*, **1985**, 769.

10) K. Soai and K. Ohi, *Bull. Chem. Soc. Jpn.*, **58**, 1601 (1985).

11) K. Soai, A. Ookawa and H. Hayashi, *J. Chem. Soc., Chem. Commun.*, **1983**, 668; K. Soai and A. Ookawa, *J. Org. Chem.*, **51**, 4000 (1986).

12) K. Soai, T. Yamanoi, and H. Oyamada, *Chem. Lett.*, **1984**, 251; K. Soai, H. Oyamada, and T. Yamanoi, *J. Chem. Soc., Chem. Commun.*, **1984**, 413; K. Soai, T. Yamanoi, H. Hikima, and H. Oyamada, *ibid.*, **1985**, 138; K. Soai, T. Yamanoi, and H. Hikima, *J. Organomet. Chem.*, **290**, C23 (1985); K. Soai, S. Niwa, T. Yamanoi, and H. Hikima, *J. Chem. Soc., Chem. Commun.*, **1986**, 1018.

13) The same tendency was observed in the reduction of **1a** with lithium aluminum hydride. T. K. Jones and J. H. J. Prect, *Chem. Ind. (London)*, **1971**, 995.

14) E. L. Eliel and M. N. Rerick, *J. Am. Chem. Soc.*, **82**, 1362 (1960).

15) H. C. Brown, S. C. Kim and S. Krishnamurthy, *J. Org. Chem.*, **45**, 1 (1980). For a kinetic study, see Ref. 4.

16) L. F. Fieser and M. Fieser, "Reagents for Organic Synthesis," John Wiley & Sons, Inc., New York (1967), p. 135.

17) D. J. Reif and H. O. House, "Organic Synthesis," Coll, Vol. IV, p. 860 (1963).

18) J. R. L. Smith and P. R. Sleath, *J. Chem. Soc., Perkin Trans. 2*, **1982**, 1009.

19) M. Imuta and H. Ziffer, *J. Org. Chem.*, **44**, 1351 (1979).

Photoresponsive Crown Ethers. 19. Photocontrol of Reversible Association-Dissociation Phenomena in "Tail(Ammonium)-Biting" Crown Ethers

Seiji SHINKAI,* Tohru YOSHIDA, Kiminori MIYAZAKI, and Osamu MANABE
Department of Industrial Chemistry, Faculty of Engineering, Nagasaki University, Nagasaki 852
(Received November 7, 1986)

The aggregation properties of photoresponsive crown ethers (**1**) having a crown ring and an ammonioalkyl (H_3N^+-$(CH_2)_n$-, n=4, 6, 10) group attached to the two sides of an azobenzene have been evaluated through the measurements of average molecular weights and electric conductance. Osmometric determination of average molecular weights established that all trans-isomers (*trans*-**1** (n=4, 6, 10)) form the pseudo-cyclic dimers due to intermolecular crown-ammonium complexation. Photoisomerized *cis*-**1** (n=6) and *cis*-**1** (n=10), which have been designed so that intramolecular "biting" of the ammonio group to the crown can occur upon photoisomerization, existed as the discrete monomers. On the other hand, *cis*-**1** (n=4), which cannot form the intramolecular "tail-biting" complex because of the short tetramethylene spacer, existed as the pseudo-cyclic dimer. This difference was well reflected by electric conductance: in **1** (n=6) and **1** (n=10), the conductance increased synchronously with trans-to-cis photoisomerization and decreased with cis-to-trans photoisomerization. Such a photoresponsive conductance change was scarcely detected for **1** (n=4). Furthermore, the additives which enforce dissociation of the dimeric species to the monomeric species suppressed the magnitude of the photoinduced conductance change. This is a novel example that the light energy is transmitted to the conductance change.

The development of photofunctional systems which change their chemical and physical properties in response to photoirradiation is currently a focal interest in the fields of biomimetic chemistry.[1] The photofunctional systems reported so far are related to the photocontrol of ion permeability,[2-6] solution pH,[7,8] membrane potentials,[9-12] polymer conformations,[13-16] binding to host molecules,[17-20] etc. In these intriguing fields, the purpose of our investigation has been to control the functions of a crown ether family by an on-off light switch, which would eventually lead to the photocontrol of ion-extraction and membrane transport.[1] Recently, we reported novel photoresponsive crown ethers (**1**) having a crown ether ring and an ammonioalkyl [-$(CH_2)_nNH_3^+$] group attached to the two sides of an azobenzene.[21] These photoresponsive crown ethers have been designed so that intramolecular "biting" of the crown to the tail(ammonium) group can only occur upon photoisomerization of the azobenzene segments to the cis-configuration (Scheme 1: Ts^-, *p*-toluenesulfonate). We found that this "tail-biting" really occurs in *cis*-**1** (n=6) and *cis*-**1** (n=10) but in *cis*-**1** (n=4) the tetramethylene spacer is too short to allow intramolecular "tail-biting".[21]

Through this study we noticed that *trans*-**1** might not be monomeric but form polymeric aggregates or pseudo-cyclic oligomers due to intermolecular crown$\cdots$ NH_3^+ complexation.[21] This idea arised from the fact that K^+ ion is transported across a liquid membrane against its concentration gradient from a basic aqueous phase to an acidic aqueous phase even in the dark although the transport efficiency is much improved by UV light irradiation.[21] This suggests that K^+ ion is released to the acidic aqueous phase because of the competitive binding with the ammonio group in *trans*-**1**.[22,23] Since the intramolecular crown-NH_3^+ complexation is sterically impossible in *trans*-**1**, this phenomenon can be rationalized only by the intermolecular crown-NH_3^+ complexation. If this is the case, UV light irradiation which mediates trans-to-cis isomerization of the azo segment and thus facilitates intramolecular "tail-biting" should enforce the dissociation of the intermolecular complex to the intramolecular one. To obtain an insight into the photoresponsive change in the aggregation properties of **1**, we assessed the effect of photoirradiation on the electric conductance and the average molecular weight. As a working hypothesis, we considered two possible aggregation modes, polymeric aggregates and pseudo-cyclic (e.g., dimeric) oligomers (Scheme 2). **2** and **3** were used as reference compounds.

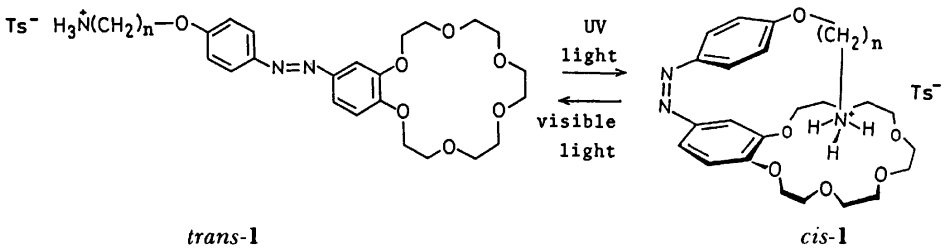

trans-**1** *cis*-**1**

Scheme 1.

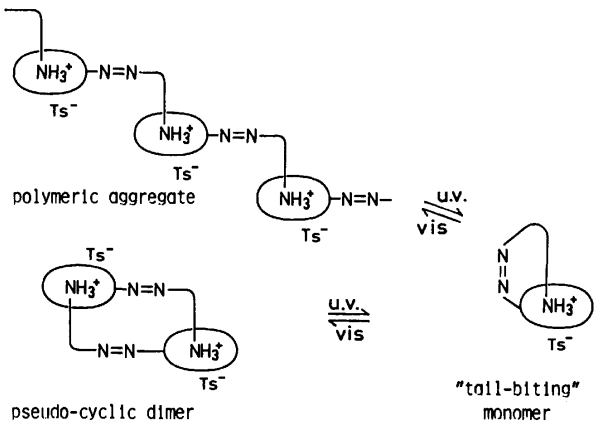

Scheme 2.

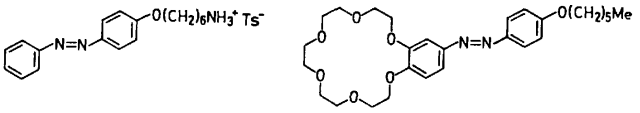

2 3

Experimental

Materials. Preparations of 4′-[*p*-(4-aminobutoxy)phenylazo]benzo-18-crown-6, 4′-[*p*-(6-aminohexyloxy)phenylazo]-benzo-18-crown-6, and 4′-[*p*-(10-aminodecyloxy)phenylazo]-benzo-18-crown-6 were described previously.[21] Treatment of these amines with an equimolar amount of *p*-toluenesulfonic acid gave *trans*-**1** (n=4), *trans*-**1** (n=6), and *trans*-**1** (n=10), respectively, in quantitative yields.

4-(6-Aminohexyloxy)azobenzene. 4-Hydroxyazobenzene (5.38 g; 27.1 mmol) and *N*-(6-bromohexyl)phthalimide (8.18 g; 26.4 mmol) was heated at 100 °C in 150 ml of dimethyl sulfoxide in the presence of K_2CO_3 (1.92 g; 13.9 mmol). After 11 h, the reaction mixture was poured into excess water. The aqueous solution was extracted with chloroform, the chloroform solution being dried over Na_2SO_4. After filtration, the solution was evaporated in vacuo to dryness. The residue was washed with aqueous NaOH solution to remove unreacted 4-hydroxyazobenzene. Recrystallization of the orange powder from acetonitrile gave *N*-[6-[*p*-(phenylazo)phenoxy]hexyl]phthalimide: Mp 113—114 °C, yield 39%. IR (KBr) ν_{c-o-c} 1260 cm^{-1}; $\nu_{c=o}$ 1700 and 1770 cm^{-1}. Found: C, 73.64; H, 5.83; N, 9.92%. Calcd for $C_{26}H_{25}N_3O_3$: C, 73.05; H, 5.89; N, 9.38%.

Treatment of *N*-[6-[*p*-(phenylazo)phenoxyl]hexyl]phthalimide with hydrazine hydrate in ethanol gave 4-(6-aminohexyloxy)azobenzene. The method was described previously.[21] Mp 108—109 °C, yield 100%. It was very difficult to obtain good elemental analysis data because this compound readily absorbed CO_2 to form the carbonate. A similar behavior was observed previously for the free amines of **1**.[21] Found: C, 70.69; H, 7.66; N, 13.80%. Calcd for $C_{18}H_{23}N_3O \cdot 0.5H_2CO_3$: C, 70.87; H, 7.64; N, 13.65%. Treatment of 4-(6-aminohexyloxy)azobenzene with an equimolar amount of *p*-toluenesulfonic acid gave **2** in quantitative yield.

4′-(*p*-Hexyloxyphenylazo)benzo-18-crown-6 (3). Sodium salt of 4′-(*p*-hydroxyphenylazo)benzo-18-crown-6[21] (0.30 g; 0.66 mmol) and 1-bromohexane (0.88 g; 3.3 mmol) was heated at 100 °C in 50 ml of dimethyl sulfoxide in the presence of K_2CO_3 (0.2 g). The progress of the reaction was monitored by a TLC method (silica gel, chloroform–methanol (10:1 v/v)). After 5 h, the reaction mixture was poured into excess water. The aqueous solution was extracted with chloroform. After evaporating the chloroform solution to dryness, the residue was recrystallized from chloroform–ligroine; mp 115—117 °C, yield 50%. IR (KBr) ν_{c-o-c} 1120 and 1250 cm^{-1}; $\nu_{N=N}$ 1500 cm^{-1}. Found: C, 65.11; H, 7.92; N, 5.09%. Calcd for $C_{28}H_{40}N_2O_7$: C, 65.10; H, 7.80; N, 5.42%.

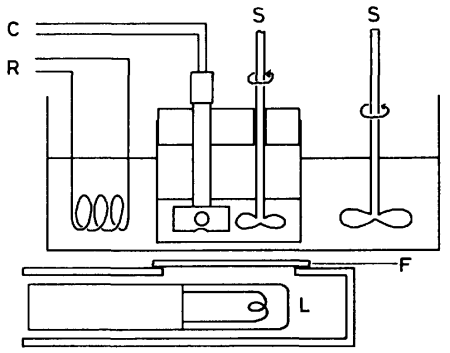

Fig. 1. Apparatus for measurements of the photo-induced conductance change. L: High-pressure Hg lamp, F: colored glass filter, S: stirrer, C: conductance electrode, R+ thermo-regulator.

Table 1. Average Aggregation Numbers (N_{av}) of *trans*-**1** and *cis*-**1**[a]

Crown ether	Concentration / g dm^{-3}	cis%[b]	N_{av}
trans-**1**(n=4)	0.370	—	2.3±0.3
cis-**1**(n=4)	0.370	76→53	2.3±0.2
trans-**1**(n=6)	0.380	—	2.3±0.2
cis-**1**(n=6)	0.380	85→80	1.1±0.1
trans-**1**(n=10)	0.410	—	1.9±0.1
cis-**1**(n=10)	0.410	72→50	1.2±0.1

a) 50 °C, 1-butanol. b) The values indicate the cis% before and after the measurement of vapor pressure.

Photoisomerization and Measurements of Electric Conductance. Trans-cis isomerization was carried out at 30 °C by using a 100W high-pressure Hg lamp with a colored glass filter: Toshiba UV-D35 ($330<\lambda<380$ nm) for UV light and Toshiba Y-46 ($\lambda>460$ nm) for visible light.

Conductance measurements were carried out at 30 °C by using an apparatus illustrated in Fig. 1. The containers for a thermostatted water-bath and a sample solution were made of transparent Pyrex glass. The sample solution was photoirradiated from the bottom of the water bath by a Hg lamp through a colored glass filter. In order to avoid the heat effect of the Hg lamp on electric conductance, both the water-bath and the sample solution were stirred effeciently.

Measurements of Average Molecular Weights. The average molecular weights (MW_{av}) of *trans*-**1** and *cis*-**1** were

determined by vapor pressure osmometry[24-26] (1-butanol at 50 °C). The apparatus (Corona, Type 117) was first calibrated by compound **2** and then used for the measurement of *trans*-**1**. On the other hand, the measurement of *cis*-**1** is more complicated: The 1-butanol solution of *trans*-**1** was irradiated by UV light and the cis% at the photostationary state was determined spectrophotometrically. This solution was immediately set up in the apparatus. After the measurement of MW_{av} (about 15 min), the cis% was determined again spectrophotometrically. The results are summarized in Table 1.

Results and Discussion

Osmometric Determination of MW_{av}. It is well-established that 18-crown-6 and its analogs can form stable complexes with ammonium cations, the stability being comparable with that of the K^+ complexes.[27-30] Thus, they are frequently employed as receptors to fix the ammonium moiety in guest molecules. The detailed studies have been reported by Sutherland, Lehn, and others.[27-34] For example, bis(crown ethers) and polymethylene-α,ω-diammonio cations can form pseudo-cyclic 1:1 complexes when the distance between the two crown systems is close to the distance between the two ammonium cations.[31-34] On the other hand, intermolecular, polymeric complexes result when the two crown systems are not located suitably to form pseudo-cyclic 1:1 complexes.[31,34]

It is sterically impossible for *trans*-**1** to form the intramolecular complex between the ammonium tail and the crown ring. Therefore, it should form either polymeric aggregates or pseudo-cyclic oligomers. In *cis*-**1**, on the other hand, examination of Corey-Pauling-Koltun models suggests that introduction of a proper spacer between the ammonium tail and the crown ring allows the intramolecular complexation and that the hexamethylene group optimizes the interaction. This means that *cis*-**1** (n=6) has the potential capability to form the intramolecular "tail-biting" complex.

The average aggregation numbers ($N_{av}=MW_{av}/MW$ of monomer) were calculated from MW_{av} determined by vapor pressure osmometry (Table 1). As the cis% at the photostationary state cannot be enhanced up to 100%, the N_{av} values for *cis*-**1** imply the cis-rich mixtures. It is clearly seen from Table 1 that all trans-forms give $N_{av}=2.0\pm0.3$. This suggests that they favorably form the pseudo-cyclic "dimers" but not the polymeric aggregates. It is not yet clear why the pseudo-cyclic dimers are more energetically-favorable than the polymeric aggregates. In the polymeric aggregates (Scheme 2) the terminal ammonium cation always remains uncomplexed. In contrast, the uncomplexed cation no longer exists in the cyclic forms. The polymeric aggregates may not be formed in the solution state because of this disadvantage.

When the trans-forms were photoisomerized to the corresponding cis-forms, the N_{av} values for **1** (n=6) and **1** (n=10) decreased very close to unity, 1.1±0.1. The finding supports that the cis-forms of **1** (n=6) and **1** (n=10) exist mainly as "monomers" in solution. In other words, the intramolecular "tail-biting" really occurs and the pseudo-cyclic dimers are dissociated into the discrete monomers. This is reasonably explained by the cis-configuration of the azo segment which facilitates the intramolecular "tail-biting" sterically. In contrast, the N_{av} for **1** (n=4) was scarcely affected by photoirradiation. The difference is readily ascribed to the incapability of *cis*-**1** (n=4) to bite at the intramolecular ammonium tail. One can conclude, therefore, that in **1** (n=4) not only the trans-form but also the cis-form should form the pseudo-cyclic dimers in solution.

Photoresponsive Conductance Change. Electric conductance is defined as a function of mobility of charged particles in solution. Therefore, it should reflect the photoinduced change in the molecular size. First, we examined the photoirradiation effect on **1** (n=6) in 1-butanol which was used for the determination of MW_{av} (Fig. 2). Very interestingly, the conductance (Λ=7.59 ohm^{-1} cm^2 mol^{-1} for *trans*-**1** (n=6)) increased on UV light irradiation ($330<\lambda$ 380 nm) and finally saturated at Λ=8.59 ohm^{-1} cm^2 mol^{-1} (cis 80%). On visible light irradiation (λ >460 nm) it decreased gradually and finaly reached the Λ value for *trans*- **1** (n=6). This process could be repeated several times by alternate irradiation of UV and visible light. We found, however, that the absolute Λ values in 1-butanol were affected sensitively by a small amount of concomitant water. On the other hand, the reproducible Λ values can be obtained when the concentration of 1-butanol was reduced by mixing with aprotic solvents. We thus employed a mixed solvent of *o*-dichlorobenzene-1-butanol=(9:1 v/v) for detailed examinations.

Figure 3 shows the effect of photoirradiation on cis% and conductance. Two curves were obtained by

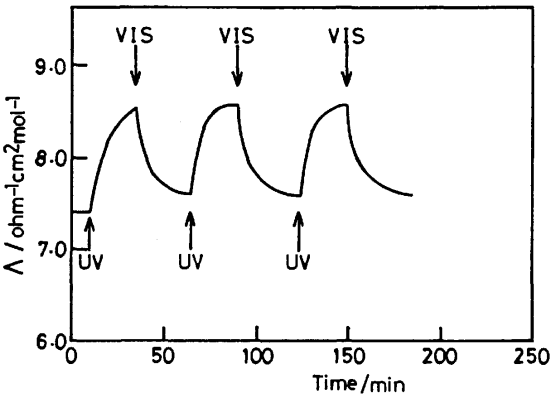

Fig. 2. Photoresponsive conductance change for **1**(n=6) in 1-butanol. [**1**(n=6)]=5.40×10^{-4} mol dm^{-3}.

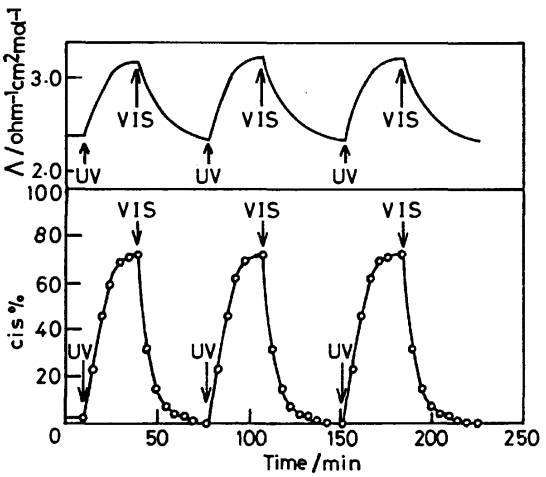

Fig. 3. Photoresponsive conductance change and cis% change for **1**(n=6) in o-dichlorobenzene-1-butanol=9:1 (v/v). [**1**(n=6)]=5.40×10^{-4} mol dm^{-3} for both conductance and cis% determination.

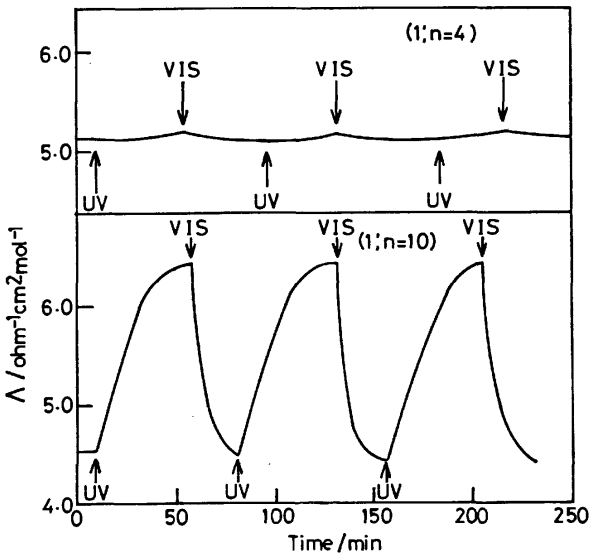

Fig. 4. Photoresponsive conductance change for **1**(n=4) and **1**(n=10) in o-dichlorobenzene-1-butanol=9:1 (v/v). [**1**(n=4)]=5.57×10^{-4} mol dm^{-3}, [**1**(n=10)=5.39×10^{-4} mol dm^{-3}.

using the same apparatus (Fig. 1) and the same conditions (see caption to Fig. 3). It is seen from Fig. 3 that two curves show excellent coincidence. Similar photoresponsiveness of both cis% and conductance was also observed for **1** (n=10) (Fig. 4: cis% is not illustrated here). The magnitude of the conductance change ($\Delta\Lambda$=2.00 ohm^{-1} cm^2 mol^{-1}) was somewhat greater than that for **1** (n=6) (0.85 ohm^{-1} cm^2 mol^{-1}). When visible light was not irradiated, the thermal cis-to-trans isomerization took place slowly. The first-order rate constants (k) determined at 30 °C by following the appearance of the absorption maxima of *trans*-(**1**) (364—368 nm)[21] were 2.39×10^{-5} s^{-1} for **1** (n=6) and 8.90×10^{-5} s^{-1} for **1** (n=10). The k values in the dark could be also determined by following the slow decrease in the conductance; k=2.30×10^{-5} s^{-1} for **1** (n=6) and 8.65×10^{-5} s^{-1} for **1** (n=10). Several lines of excellent coincidence between the spectroscopic data and the conductance data support that the conductance change is caused by the photoinduced trans-cis isomerization. In other words, the monomeric cis-forms have the Λ value higher than the dimeric trans-forms and two aggregation modes can be rever-

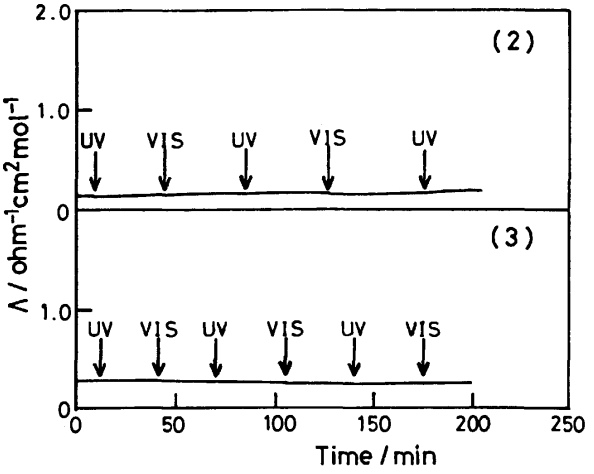

Fig. 5. Photoresponsive conductance change for **2** and **3** in o-dichlorobenzene-1-butanol=9:1 (v/v). [**2**]=5.45×10^{-4} mol dm^{-3}, [**3**]=5.36×10^{-4} mol dm^{-3}.

Table 2. Influence of Photoirradiation on Electric Conductance of **1**[a]

Conductance / ohm^{-1} cm^2 mol^{-1}	Additive (concd mmol dm^{-3})	**1**(n=4)	**1**(n=6)	**1**(n=10)
Λ_{dark}[b]	—	5.08	2.34	4.43
Λ_{light}[c]	—	5.16	3.19	6.43
$\Delta\Lambda$[d]	—	0.08	0.85	2.00
$\Delta\Lambda$[d]	18-Crown-6 (5.00)	—	0.11	—
$\Delta\Lambda$[d]	$C_{12}H_{25}OSO_3^-K^+$ (0.56)	—	0.26	—
$\Delta\Lambda$[d]	$CH_3NH_3^+Ts^-$ (21.3)	—	0.48	—

a) 30 °C, o-dichlorobenzene-1-butanol=9:1 (v/v). b) Electric conductance in the dark. c) Maximum electric conductance under UV light irradiation. cis% at the maximum conductance: 58% for **1**(n=4), 72% for **1**(n=6), and 78% for **1**(n=10). d) $\Delta\Lambda=\Lambda_{light}-\Lambda_{dark}$.

sibly interconverted by photoirradiation. The finding would be rationalized in terms of the difference in the mobility between the monomeric species and the dimeric species.

In contrast, the conductance change was scarcely detected for **1** (n=4) which could not form the "tail-biting" monomeric complex. Reference compounds, **2** and **3**, which have neither a crown ring nor an ammonium tail, showed no conductance change although the trans-cis photoisomerization really occurred in the conductance cell (maximum cis% under UV light irradiation, 51% for **2** and 58% for **3**: Fig. 5). As a summary of the foregoing results (Table 2), one can draw a conclusion that the photoinduced conductance change is observed only for the "tail-biting" crown ethers which can realize reversible interconversion between the monomeric form and the pseudo-cyclic, dimeric form.

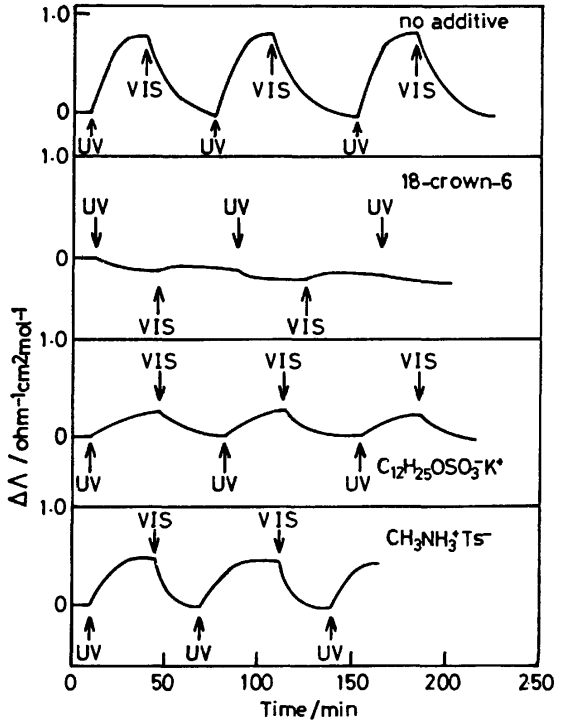

Fig. 6. Effect of additives on the photoresponsive conductance change for [**1**(n=6)] (5.40×10^{-4} mol dm^{-3}) in o-dichlorobenzene-1-butanol=9:1 (v/v). [18-Crown-6]=5.00×10^{-3} mol dm^{-3},[$C_{12}H_{25}OSO_3^-K^+$]=5.60×10^{-4} mol dm^{-3}, [$CH_3NH_3^+Ts^-$]=2.13×10^{-2} mol dm^{-3}.

Effects of Additives. In solvent extraction with **1** (n=6), we found that *trans*-**1** (n=6) can extract K^+ into the organic phase while *cis*-**1** (n=6) has almost no metal affinity.[21] On the other hand, the present study has established that both *trans*- and *cis*-**1** (n=6) form the complexes with the ammonio groups. The difference in the K^+ affinity should be related to the stability of the ammonium complexes: That is, the intermolecular ammonium cation in *trans*-**1** (n=6) can be replaced competitively by K^+, whereas the intramolecular ammonium-crown complex in *cis*-**1** (n=6) is so stable that the ammonium cation binds to the crown cavity in preference to K^+. This suggests that the added K^+ ion would selectively dissociate the dimeric aggregates of *trans*-**1** (n=6).

Figure 6 indicates the influence of K^+ and $CH_3NH_3^+$ on the photoresponsive wave of **1** (n=6). Separately, we confirmed that the cis% is scarcely affected by the addition of these ions. It is clearly seen from Fig. 6 that the photoresponsive wave for **1** (n=6) becomes significantly smaller in the presence of potassium dodecyl sulfate and methylammonium p-toluenesulfonate (Table 2). The finding suggests that these cations can dissociate the pseudo-cyclic dimers into the monomers through competitive binding to the crown cavity (Scheme 3).

Similar suppression of the conductance change can be induced by the additive which selectively interacts with the ammonio group. For instance, addition of 18-crown-6 effectively suppressed the photoinduced conductance change (Fig. 6). Conceivably, added 18-crown-6 competes with the crown ring in **1** for the ammonio group. As a result, the pseudo-cyclic dimers would be dissociated into the monomers.

Conclusions

The present study demonstrated that the conductance of the solution containing **1** (n=6) and **1** (n=10) changes reversibly in response to photoirradiation. The novel phenomenon is ascribed, on the basis of several lines of experimental evidence, to photo-induced association-dissociation phenomena in the "tail(ammonium)-biting" crown ethers. Since the conductance change is sensitively affected by added K^+, ammonium ions, etc., the concept may be applicable more generally to interdisciplinary fields between photochemistry and electrochemistry including sensors, membrane systems, etc.

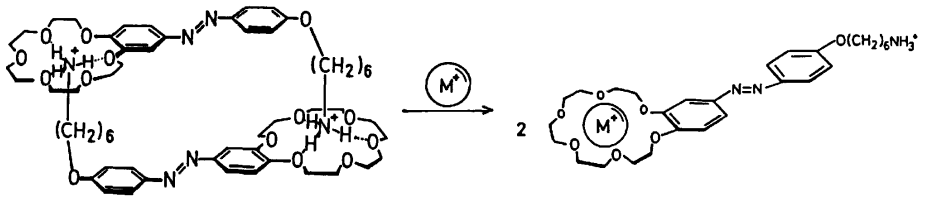

Scheme 3.

We are indebted to Professor Kazuo Kondo (Kyushu University) for measuring the molecular weights. This work was supported by the Grant-in-Aid from the Ministry of Education, Science and Culture.

References

1) For comprehensive reviews see S. Shinkai and O. Manabe, *Top. Curr. Chem.*, **121**, 67 (1984); A. Ueno and T. Osa, *Yuki Gosei Kagaku Kyokai Shi*, **38**, 207 (1980).
2) M. Montal, *Biochim. Biophys. Acta*, **559**, 231 (1979).
3) D. F. O'Briene, *Photochem. Photobiol.*, **29**, 679 (1979).
4) A. Kumano, O. Niwa, T. Kajiyama, M. Takayanagi, K. Kano, and S. Shinkai, *Chem. Lett.*, **1983**, 1327.
5) T. Shimidzu and M. Yoshikawa, *Polym. J.*, **15**, 631 (1983).
6) T. Kinoshita, M. Sato, A. Takizawa, and Y. Tsujita, *J. Chem. Soc., Chem. Commun.*, **1984**, 929.
7) M. Irie, *J. Am. Chem. Soc.*, **105**, 2078 (1983).
8) N. Negishi, K. Tsunemitsu, K. Ishihara, I. Shinohara, T. Okano, K. Katooka, T. Akaike, and Y. Sakurai, *Kobunshi Ronbunshu*, **37**, 287 (1980).
9) S. Kato, M. Aizawa, and S. Suzuki, *J. Membr. Sci.*, **2**, 39 (1977).
10) J. R. Duchek and J. S. Huebner, *Biophys. J.*, **27**, 317 (1979).
11) J. Anzai, H. Sasaki, A. Ueno, and T. Osa., *J. Chem. Soc., Perkin Trans. 2*, **1985**, 903; *Chem. Lett.*, **1985**, 1443.
12) K. Honda, H. Komizu, and M. Kawasaki, *J. Chem. Soc., Chem. Commun.*, **1982**, 253.
13) A. Ueno, K. Takahashi, J. Anzai, and T. Osa, *J. Am. Chem. Soc.*, **103**., 6410 (1981).
14) O. Pieroni, J. L. Houben, A. Fissi, P. Costantino, and F. Ciardelli, *J. Am. Chem. Soc.*, **102**, 5913 (1980).
15) M. Irie, "Molecular Models of Photoresponsiveness," ed by G. Montanagnoli and B. F. Erlanger, Plenum, New York (1983), p. 291.
16) For a comprehensive review see G. Smets, *Adv. Polym. Sci.*, **50**, 17 (1983).
17) H. Bouas-Laurent, A. Castellan, and J.-P. Desvergne, *Pure Appl. Chem.*, **52**, 2633 (1980).
18) A. Ueno, H. Yoshimura, R. Saka, and T. Osa, *J. Am. Chem. Soc.*, **101**, 2779 (1979).
19) S. Shinkai, T. Nakaji, Y. Nishida, T. Ogawa, and O. Manabe, *J. Am. Chem. Soc.*, **102**, 5860 (1980).
20) S. Shinkai, T. Nakaji, T. Ogawa, K. Shigematsu, and O. Manabe, *J. Am. Chem. Soc.*, **103**, 111 (1981).
21) S. Shinkai, M. Ishihara, K. Ueda, and O. Manabe, *J. Chem. Soc., Perkin Trans. 2*, **1985**, 511; *J. Inclusion Phenom.*, **2**, 111 (1984).
22) H. Tsukube, *J. Membr. Sci.*, **14**, 155 (1983).
23) Y. Nakatsuji, H. Kobayashi, and M. Okahara, *J. Chem. Soc., Chem. Commun.*, **1983**, 800.
24) F. Y. Lo, B. M. Escott, E. J. Fendler, E. T. Adams, Jr., R. D. Larsen, and P. W. Smith, *J. Phys. Chem.*, **79**, 2609 (1975).
25) U. Herrmann and Z. A. Schelly, *J. Am. Chem. Soc.*, **101**, 2665 (1979).
26) K. Tamura and Z. A. Schelly, *J. Am. Chem. Soc.*, **103**, 1013 (1981).
27) D. J. Cram, *Acc. Chem. Res.*, **11**, 8 (1978).
28) J.-M. Lehn, *Acc. Chem. Res.*, **11**, 49 (1978).
29) E. Weber and F. Vögtle, *Top. Curr. Chem.*, **98**, 1 (1981).
30) G. W. Gokel and S. H. Korzeniowski, "Macrocyclic Polyether Syntheses," Springer-Verlag, Berlin (1982).
31) M. R. Johnson, I. O. Sutherland, and R. F. Newton, *J. Chem. Soc., Chem. Commun.*, **1979**, 306; *J. Chem. Soc., Perkin Trans. 2*, **1980**, 586.
32) J.-P. Kintzinger, F. Kotzyba-Hibert, J.-M. Lehn, A. Pagelot, and K. Saigo, *J. Chem. Soc., Chem. Commun.*, **1981**, 833.
33) A. H. Alberts, R. Annunziata, and J.-M. Lehn, *J. Am. Chem. Soc.*, **99**, 8502 (1977).
34) R. Mageswaran, S. Mageswaran, and I. O. Sutherland, *J. Chem. Soc., Chem. Commun.*, **1979**, 722.

 © 1987 The Chemical Society of Japan Bull. Chem. Soc. Jpn., 60, 1825—1829 (1987)

Syntheses of 3-Deoxy-3-*C*-methyl-3-nitro-D- and L-glucosides and Their Denitrohydrogenation with Tributyltin Hydride

Sinichi OTANI* and Shiro HASHIMOTO
Department of Chemistry, College of Liberal Arts and Sciences, Kyoto University, Yoshida, Sakyo-ku, Kyoto 606
(Received November 11, 1986)

Cyclization, with nitroethane in the presence of sodium methoxide, of the dialdehyde produced by periodate oxidation of methyl β-D-glucopyranoside and acetylation led to methyl 2,4,6-tri-*O*-acetyl-3-*C*-methyl-3-nitro-β-D- and -α-L-glucopyranoside (**1**, 12% and **2**, 8.8%). In the case of methyl α-D-glucopyranoside, products **3** (8.6%) and **4** (8.0%) were antipodes of **1** and **2**, respectively. Denitrohydrogenation of **1** or **3** with tributyltin hydride in toluene led to 3-deoxy-3-*C*-methyl-β-D-pyranosides (gluco, **5**, 61% and allo, **6**, 22%) or L-pyranosides (gluco, **9**, 65% and allo, **10**, 19%), respectively. This sequence of the reaction was a novel method for the syntheses of 3-deoxy-3-*C*-methyl-L-glucose and -L-allose. Denitrohydrogenation of **2** or **4** led to a mixture of 3-deoxy-3-*C*-methyl-α-L-pyranosides (allo, **7**, 39% and gluco, **8**, 41%) or mixture of 3-deoxy-3-*C*-methyl-α-D-pyranosides (allo, **11**, 38% and gluco, **12**, 41%), respectively. Methyl 2-*O*-acetyl-4,6-*O*-benzylidene-3-deoxy-3-nitro-β-D-glucopyranoside was denitrohydrogenated to the corresponding 3-deoxy sugar (**14**) in 68% yield.

Deoxy sugars are important constituents of some natural products, especially of antibiotics. The deoxy sugars may be prepared by the reduction of oxiranes with lithium aluminium hydride.[1] The most direct methods for preparing monodeoxy sugars are by homolytic replacement of a good leaving group modified from a hydroxyl group. Thiocarbonates,[2] *O*-alkyl thiobenzoates,[3] *O*-alkyl *S*-methyl dithiocarbonates,[3] [alkoxy(thiocarbonyl)]imidazolides,[3,4] dimethyl thiocarbamates,[5] trifluoromethanesulfonates[6] and thionocarbonates[7] were deoxygenated.

3-Deoxy-3-*C*-methylhexopyranosides were synthesized from 2,3-anhydro sugars and methyllithium[8] or methylmagnesium chloride,[9,10] from 3-oxo sugars by Wittig reaction and the following reduction,[11] from 3-deoxy-3-nitro-3-*C*-methyl sugar by electrochemical reduction,[12] and from 3-*O*-acetyl-3-*C*-methyl sugar by photoreduction.[13]

An efficient method became available for replacing the nitro group of secondary or tertiary nitro compounds by hydrogen using tributyltin hydride in refluxing benzene or toluene in the presence of azobisisobutyronitrile.[14—16] The reaction proceeds via free radical chain mechanism. The reduction was selective without affecting other functional groups such as chloro, cyano, alkoxycarbonyl, carbonyl, sulfinyl, sulfonyl, and carbon–carbon double bond.

Cyclization, with nitroethane or nitromethane in the presence of sodium methoxide, of the dialdehyde produced by periodate cleavage of methyl α- or β-D-glucopyranoside, led to 3-deoxy-3-nitro sugars.[17—20] In this paper the authors wish to report the synthesis of 3-deoxy-3-*C*-methyl-3-nitro-D- and -L-glucopyranosides and their denitrohydrogenation with tributyltin hydride.

Results and Discussion

Preparation of Nitro Sugars. Baer obtained crystalline mixture of methyl 3-deoxy-3-*C*-methyl-3-nitrohexopyranosides in 18—20% yield[17] from the dialdehyde, prepared by periodate oxidation of methyl α-D-glucopyranoside, and nitroethane in methanol in the presence of sodium methoxide. Catalytic hydrogenation of the product afforded two stereoisomeric amino glycosides, which were separated, acetylated, and hydrolysed to a pair of enantiomers of reducing amino sugars. The acetylated products were reported to be β-L-gluco (or allo) and α-D-gluco (or allo) derivatives. When a sequence of the above reaction was performed from methyl β-D-glucopyranoside, a set of nitrogeneous glycosides were obtained as the antipodes of the products from methyl α-D-glucopyranoside, having α-L-gluco (or allo) and β-D-gluco (or allo) configurations.[17]

The author acetylated crystalline cyclized products from the dialdehyde, prepared by periodate cleavage of methyl β-D-glucopyranoside, and nitroethane. The acetylated products were separated with a column of silica gel (benzene–ethyl acatate 4:1) to crystals **1** (12%) and a sirup **2** (8.8%) which were both levorotatory.

In ^{1}H NMR spectrum of **1** in $CDCl_3$, H-1, H-2, and H-4 appeared as doublets with $J_{1,2}$=7.9 Hz and $J_{4,5}$=10.1 Hz, indicating that these hydrogens were axial. Irradiation of the C–CH_3 induced nuclear Overhauser effect (NOE) to H-1 and H-5. Therefore, the C–CH_3 was axial. ^{13}C NMR spectrum showed C-1 at δ 100.5 and O–CH_3 at δ 57.0, indicating the presence of equatorial OCH_3.[21] Taking into account that **1** was levorotatory, **1** was methyl 2,4,6-tri-*O*-acetyl-3-deoxy-3-*C*-methyl-3-nitro-β-D-glucopyranoside.

^{1}H NMR spectrum of **2** in $CDCl_3$ showed C–CH_3 at δ 1.89. Irradiation of the C–CH_3 induced NOE to H-5 but not to H-1. Thus the C–CH_3 and O–CH_3 were axial and H-1 was equatorial. The doublet signal due to H-1 and H-2 with small splitting ($J_{1,2}$=4.3 Hz) in ^{1}H NMR and C-1 at δ 96.5 and OCH_3 at 56.0 ppm in ^{13}C NMR indicated the presence of axial OCH_3. $J_{4,5}$

(10.2 Hz) proved the diaxial H-4 and H-5 arrangement. Considering that **2** was levorotatory and that Baer obtained a pair of enantiomers of reducing amino sugars by catalytic hydrogenation,[17] **2** was methyl 2,4,6-tri-*O*-acetyl-3-deoxy-3-*C*-methyl-3-nitro-α-L-glucopyranoside.

When the above reaction sequence was performed with the dialdehyde from methyl α-D-glucopyranoside, acetylated products, crystals **3**, (8.6%) and a sirup **4**, (8.0%), were both dextrorotatory. NMR spectra of these products coincided with those of the products from methyl β-D-glucopyranoside. Therefore, **3** and **4** were methyl 2,4,6-tri-*O*-acetyl-3-deoxy-3-*C*-methyl-3-nitro-β-L-glucopyranoside and -α-D-glucopyranoside, antipodes of **1** and **2**, respectively.

All the products, **1**—**4**, had the nitro and the vicinal hydroxyl groups in equatorial orientation. In **2** and **3**, the epimerization was observed at C-1 and C-5, evidently owing to base-catalyzed epimerization of the starting dialdehydes.[20]

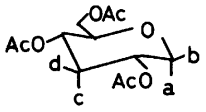

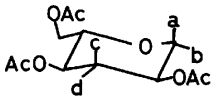

	a	b	c	d		a	b	c	d
1	H	OMe	Me	NO_2	2	OMe	H	Me	NO_2
4	OMe	H	Me	NO_2	3	H	OMe	Me	NO_2
5	H	OMe	H	Me	7	OMe	H	Me	H
6	H	OMe	Me	H	8	OMe	H	H	Me
11	OMe	H	Me	H	9	H	OMe	H	Me
12	OMe	H	H	Me	10	H	OMe	Me	H

Denitrohydrogenation. The nitro group of tertiary or secondary nitro compounds is replaced by hydrogen with tributyltin hydride. Refluxing a mixture of a nitro compound, tributyltin hydride and azobisisobutyronitrile (AIBN) in benzene or toluene for 1—2 h in a stream of nitrogen gave the denitrohydrogenated product in good yield.[14]

$$RNO_2 + n\text{-}Bu_3SnH \longrightarrow RH + n\text{-}Bu_3SnONO$$

A mixture of **1**, tributyltin hydride and AIBN in toluene was boiled under reflux for 1.5 h in a stream of nitrogen. The solution was evaporated and chromatographed on a column of silica gel (benzene–ethyl acetate 4:1) to give levorotatory products, **5** (61%) and **6** (22%).

^{1}H NMR spectrum of **5** showed the presence of C–CH_3 (δ 0.92, doublet) and diaxial H-1 and H-2 ($J_{1,2}$=7.8 Hz). Signals of C-1 (δ 103.0) and OCH_3 (δ 56.6) in ^{13}C NMR supported the presence of equatorial OCH_3 and axial H-1. Signal of H-3 (sextet, $J_{2,3}$=$J_{3,4}$=10.6 Hz, $J_{3,Me}$=6.4 Hz) showed that H-3 and H-4 were axial. Consequently, **5** was methyl 2,4,6-tri-*O*-acetyl-3-deoxy-3-*C*-methyl-β-D-glucopyranoside.

^{13}C NMR spectrum of **6** showed axial C–CH_3 at δ 9.2, differing from equatorial C–CH_3 at δ 13.2 in **5**. Signal of H-3 (sextet, $J_{2,3}$=$J_{3,4}$=4.7 Hz, $J_{3,Me}$=7.2 Hz) showed that H-3 and C–CH_3 were equatorial and axial, respectively. $J_{1,2}$ (5.8 Hz) and $J_{4,5}$ (6.8 Hz) were rather small for diaxial protons. But C-1 at δ 99.2 and OMe at δ 56.5 in ^{13}C NMR supported the presence of axial H-1. Therefore, **6** was proved to be methyl 2,4,6-tri-*O*-acetyl-3-deoxy-3-*C*-methyl-β-D-allopyranoside. These results showed that the predominant product had an equatorial methyl in denitrohydrogenation.

Denitrohydrogenation of **3**, antipode of **1**, gave methyl 2,4,6-tri-*O*-acetyl-3-deoxy-3-*C*-methyl-β-L-glucopyranoside (**9**, 65%) and -allopyranoside (**10**, 19%). This reaction was proved to be a novel method for the syntheses of 3-deoxy-3-*C*-methyl-L-glucose and -L-allose.

Products of denitrohydrogenation of **2** were a levorotatory mixture of C-3 epimers with 51:49 ratio on the basis of the methyl peak of methoxyl group in ^{1}H NMR. Coupling constants of H-3, $J_{2,3}$ and $J_{3,4}$, were both 5.5 Hz for a minor product (**7**, 39%) and both 10.4 Hz for a major product **8** (41%). These showed that **7** and **8** had axial and equatorial C–CH_3, respectively. Consequently, **7** and **8** were methyl 2,4,6-tri-*O*-acetyl-3-deoxy-3-*C*-methyl-α-L-allopyranoside and -glucopyranoside, respectively. We could not find an appropriate developer for the separation of the mixture on TLC and on a column of silica gel. Similarly, denitrohydrogenation of **4**, antipode of **2**, gave a mixture of methyl 2,4,6-tri-*O*-acetyl-3-deoxy-3-*C*-methyl-α-D-allopyranoside (**11**, 38%) and -glucopyranoside (**12**, 41%) with the ratio of 48:52.

The stereochemistry of denitrohydrogenation was explained as follows. For the β-glycosides, intermediate C-3 radical was preferentialy attacked from axial direction by tributyltin hydride to form a product with equatorial methyl, for equatorial attack was sterically hindered with axial H-2 and H-4. For the α-glycosides, axial attack was considerably hindered with axial methoxyl group at C-1. Therefore, axial and equatorial attack occurred with the same difficulty.

The secondary nitro sugar, methyl 2-*O*-acetyl-4,6-*O*-benzylidene-3-deoxy-3-nitro-β-D-glucopyranoside (**13**), synthesized by cyclization of the dialdehyde from methyl β-D-glucopyranoside with nitromethane,[19] was denitrohydrogenated with tributyltin hydride to give methyl 2-*O*-acetyl-4,6-*O*-benzylidene-3-deoxy-β-D-glucopyranoside (**14**) in 68% yield. Secondary nitro compounds were generally denitrohydrogenated in lower yield than tertiary nitro compounds.[14]

Experimental

Melting points were measured in capillary tubes with a Yamato melting-point apparatus MP-21 and are uncorrected. Column chromatography was performed on

Wakogel C-200 (100—200 mesh). ^{1}H NMR spectra were recorded with a JEOL JNM-GX-400 spectrometer (400 MHz) and ^{13}C NMR spectra with a JEOL FX-90Q spectrometer (22.5 MHz) using tetramethylsilane as an internal standard in deuteriochloroform unless otherwise stated. Chemical shifts and coupling constants were recorded in δ and Hz units. TLC was performed on precoated HPTLC plates, silica gel 60 (E. Merck). Optical rotations were determined with a Jasco DIP-140 digital polarimeter.

Methyl 2,4,6-Tri-*O*-acetyl-3-deoxy-3-*C*-methyl-3-nitro-β-D-glucopyranoside (1) and -α-L-glucopyranoside (2). Methyl β-D-glucopyranoside (38.8 g) was oxidized with sodium periodate (85.6 g) to the sirupy colorless dialdehyde, which was treated with nitroethane in the presence of sodium methoxide in methanol to the crystalline product (12.3 g) according to Baer.[17] The crystalline product (10 g) in pyridine (180 ml) was acetylated with acetic anhydride (50 ml) overnight at room temperature. The reaction mixture was poured into water and extracted with chloroform. The extract was evaporated and treated with ethanol to crystals (**1**, 6.7 g). The mother liquor was evaporated and passed through a column of silica gel (60×5 cm, hexane–ethyl acetate 1:1). The additional crystalline **1**, (2.1 g) and a sirup **2**, (6.4 g) were obtained.

1: 8.8 g (12% yield from methyl β-D-glucopyranoside): Mp 124—125 °C; $[\alpha]_D^{22}$ −25.5° (*c* 1, chloroform); ^{1}H NMR δ=5.71 (H-4, 1H, d, $J_{4,5}$=10.1), 5.67 (H-2, 1H, d, $J_{1,2}$=7.9), 4.44 (H-1, 1H, d), 4.27 (H-6R, 1H, q, $J_{5,6R}$=4.6, $J_{6,6}$=12.4), 4.15 (H-6S, 1H, q, $J_{5,6S}$=2.8), 3.75 (H-5, 1H, octet), 3.51 (OMe, 3H, s) and 1.78 (CMe, 3H, s). NOE of H-1 (+12%) and H-5 (+12%) were measured by irradiation at δ 1.78. ^{13}C NMR δ=170.6, 168.2, 168.1 (C=OMe), 100.5 (C-1), 91.1 (C-3), 71.5, 71.4, 69.6 (C-2,4,5), 62.2 (C-6), 57.0 (OMe), 20.7, 20.5, 20.3 (CO<u>Me</u>), and 12.0 (C<u>Me</u>).

Found: C, 46.17; H, 5.82; N, 3.89%. Calcd for $C_{14}H_{21}NO_{10}$: C, 46.28; H, 5.83; N, 3.86%.

2: 6.4 g (8.8% yield from methyl β-D-glucopyranoside), $[\alpha]_D^{22}$ −96.7° (*c* 1, chloroform); ^{1}H NMR δ=5.63 (H-2, 1H, d, $J_{1,2}$=4.3), 5.58 (H-4, 1H, d, $J_{4,5}$=10.2), 5.11 (H-1, d), 4.31 (H-6S, 1H, q, $J_{5,6S}$=4.5, $J_{6,6}$=12.3), 4.11 (H-6R, 1H, q, $J_{5,6R}$=2.4), 3.94 (H-5, 1H, octet), 3.41 (OMe, 3H, s), and 1.89 (CMe, 3H, s). NOE of H-5 (+12%) was measured by irradiation at δ 1.89. ^{13}C NMR δ=170.5, 169.1, 168.3 (C=OMe), 96.5 (C-1), 91.2 (C-3), 71.2, 69.4, 66.2 (C-2,4,5), 61.8 (C-6), 56.0 (OMe), 20.6, 20.4, 20.2 (CO<u>Me</u>), and 13.1 (C<u>Me</u>).

Found: C, 46.28; H, 5.83; N, 3.61%. Calcd for $C_{14}H_{21}NO_{10}$: C, 46.28; H, 5.83; N, 3.86%.

Methyl 2,4,6-Tri-*O*-acetyl-3-deoxy-3-*C*-methyl-3-nitro-β-L-glucopyranoside (3) and -α-D-glucopyranoside (4). Methyl α-D-glucopyranoside (38.8 g) was oxidized with sodium periodate (85.6 g), and treated with nitroethane to crystals (7.9 g, 17% yield).[17] The crystalline product (5.9 g) was acetylated in a similar manner as the preceded procedure. Crystals (**3**, 4.7 g, 8.6% from methyl α-D-glucoside) and a sirup (**4**, 4.2 g, 8.0% from methyl α-D-glucoside) were obtained.

3: Mp 124—125 °C; $[\alpha]_D^{18}$ +29.0° (*c* 1, chloroform); ^{13}C NMR δ= 170.4, 168.1, 167.8 (C=OMe, each s), 100.8 (C-1, d), 91.3 (C-3, s), 71.9, 71.8, 70.1 (C-2,4,5, each d), 62.6 (C-6, t), 56.6 (OMe, q), 20.6, 20.3, 20.2 (CO<u>Me</u>, q), and 12.2 (C<u>Me</u>, q).

Found: C, 46.21; H, 5.81; N, 3.74%. Calcd for $C_{14}H_{21}NO_{10}$: C, 46.28; H, 5.83; N, 3.86%.

4: $[\alpha]_D^{22}$ +102° (*c* 1, chloroform); ^{13}C NMR δ=170.2, 168.9, 168.1 (C=OMe, each s), 96.8 (C-1, d), 91.5 (C-3, s), 71.6, 70.0, 66.6 (C-2,4,5, each d), 62.2 (C-6, t), 55.9 (OMe, q), 20.4, 20.2, 20.0 (CO<u>Me</u>, each q), and 13.2 (C<u>Me</u>, q).

Found: C, 45.98; H, 5.79; N, 3.86%. Calcd for $C_{14}H_{21}NO_{10}$: C, 46.28; H, 5.83; N, 3.86%.

Denitrohydrogenation of 1. A mixture of **1** (1.0 g, 2.7 mmol), tributyltin hydride (3 ml, 11 mmol), and AIBN solution (120 mg in 10 ml of toluene) in toluene (100 ml) was boiled under reflux.[14] A half an hour later, AIBN solution (60 mg in 5 ml of toluene) was added. Boiling under reflux for an hour, the solution was evaporated and chromatographed on a column of silica gel (60×3 cm, benzene–ethyl acetate 4:1). Methyl 2,4,6-tri-*O*-acetyl-3-deoxy-3-*C*-methyl-β-D-glucopyranoside (**5**, 0.52 g, 61%) and -allopyranoside (**6**, 0.19 g, 22%) were crystallized from ethanol and from hexane, respectively.

5: Mp 85 °C; $[\alpha]_D^{22}$ −39.7° (*c* 1, chloroform); ^{1}H NMR δ=4.79 (H-4, 1H, t, $J_{3,4}$=$J_{4,5}$=10.2), 4.70 (H-2, 1H, q, $J_{1,2}$=7.8, $J_{2,3}$=10.8), 4.34 (H-1, 1H, d), 4.23 (H-6R, 1H, q, $J_{5,6R}$=4.9, $J_{6,6}$=12.2), 4.10 (H-6S, 1H, q, $J_{5,6S}$=2.4), 3.63 (H-5, 1H, octet), 3.48 (OMe, 3H, s), 2.10, 2.09, 2.08 (3×COMe, 3×3H, each s), 1.91 (H-3, 1H, octet, $J_{3,Me}$=6.4), and 0.92 (CMe, 3H, d). ^{13}C NMR δ=170.7, 169.8 (overlapped) (C=OMe, each s), 103.0 (C-1, d), 74.6, 72.9, 70.4 (C-2,4,5, each d), 62.6 (C-6, t), 56.6 (OMe, q), 39.8 (C-3, d), 20.8, 20.7 (overlapped) (CO<u>Me</u>, q), and 13.6 (C<u>Me</u>, q).

Found: C, 52.60; H, 7.10%. Calcd for $C_{14}H_{22}O_8$: C, 52.82; H, 6.97%.

6: Mp 55 °C; $[\alpha]_D^{19}$ −35.5° (*c* 0.5, chloroform); ^{1}H NMR δ=4.94 (H-4, 1H, q, $J_{3,4}$=4.7, $J_{4,5}$=6.8), 4.82 (H-2, 1H, q, $J_{1,2}$=5.8, $J_{2,3}$=4.7), 4.60 (H-1, 1H, d), 4.25 (H-6, 2H, d, $J_{5,6}$=4.9), 3.98 (H-5, 1H, sextet), 3.45 (OMe, 3H, s), 2.66 (H-3, 1H, sextet, $J_{3,Me}$=7.2), 2.11, 2.090, 2.086 (3×COMe, 3×3H, each s), and 0.99 (CMe, 3H, d); ^{13}C NMR δ=170.7, 169.8, 169.7 (C=OMe, each s), 99.2 (C-1, d), 63.4 (C-5, t), 56.5 (OMe, q), 30.7 (C-3, d), 20.83, 20.75 (overlapped) (CO<u>Me</u>), and 9.2 (C<u>Me</u>, q).

Found: C, 52.71; H, 7.08%. Calcd for $C_{14}H_{22}O_8$: C, 52.82; H, 6.97%.

Denitrohydrogenation of 2. Compound **2** (1.0 g) was denitrohydrogenated in a similar manner as **1**. NMR spectra of the sirupy product (0.70 g, 80% yield) showed that it was a mixture of two components, methyl-2,4,6-tri-*O*-acetyl-3-deoxy-3-*C*-methyl-α-L-allopyranoside (**7**) and -glucopyranoside (**8**). According to the methyl peak of methoxyl group, components ratio **7**/**8** was 49/51. Separation of the components was unsuccessful on TLC and on a column of silica gel. $[\alpha]_D^{20}$ −114° (*c* 0.5, chloroform).

Found: C, 53.03; H, 7.20%. Calcd for $C_{14}H_{22}O_8$: C, 52.82; H, 6.97%.

7: ^{1}H NMR δ=4.94 (H-2, 1H, q, $J_{1,2}$=3.7, $J_{2,3}$=5.5), 4.94 (H-4, 1H, q, $J_{3,4}$=5.5, $J_{4,5}$=11.2), 4.65 (H-1, 1H, d), 4.29 (H-6R, 1H, q, $J_{5,6R}$=5.0, $J_{6,6}$=12.1), 4.17 (H-6S, 1H, q, $J_{5,6S}$=2.4), 4.07 (H-5, 1H, octet), 3.40 (OMe, 3H, s), 2.69 (H-3, 1H, q, $J_{3,Me}$=7.3), 2.12, 2.09, 2.08 (3×COMe, 3×3H, each s), and 1.12 (CMe, 3H, d). ^{13}C NMR δ=97.9 (C-1, d), 69.6, 68.4, 63.7 (C-2,4,5, each d), 62.6 (C-6, t), 55.5 (OMe, q), 33.3 (C-3, d), 20.9, 20.7 (overlapped) (CO<u>Me</u>, each q), and 8.51 (C<u>Me</u>, q). Signals of carbonyl carbons were appeared at 170.7, 170.3,

169.8, and 169.3, of which assignment to **7** or **8** was not determined.

8: ^{1}H NMR δ=4.83 (H-2, 1H, q, $J_{1,2}$=3.7, $J_{2,3}$=10.5), 4.78 (H-4, 1H, t, $J_{3,4}$=$J_{4,5}$=10.4), 4.62 (H-1, 1H, d), 4.22 (H-6R, 1H, q, $J_{5,6R}$=4.9, $J_{6,6}$=12.2), 4.05 (H-6S, 1H, q, $J_{5,6S}$=2.4), 3.88 (H-5, 1H, octet), 3.42 (OMe, 3H, s), 2.27 (H-3, 1H, sextet, $J_{3,Me}$=6.4), 2.12, 2.09, 2.07 (3×COMe, 3×3H, each s), and 0.92 (CMe, 3H, d); ^{13}C NMR δ=96.1 (C-1, d), 73.1, 70.5, 68.1 (C-2,4,5, each d), 62.9 (C-6, t), 55.2 (OMe, q), 34.9 (C-3, d), 20.9, 20.7 (overlapped) (COMe, each q), and 13.4 (CMe, q). Concerning signals of carbonyl carbons, see the data of **7**.

Denitrohydrogenation of 3. Compound **3** (1.0 g) was denitrohydrogenated in a similar manner as **1**. Methyl 2,4,6-tri-*O*-acetyl-3-deoxy-3-*C*-methyl-β-L-glucopyranoside (**9**, 0.57 g, 65%) and -allopyranoside (**10**, 0.17 g, 19%) were obtained.

9: Mp 85 °C; $[\alpha]_D^{20}$ +40.5° (*c* 1, chloroform); ^{13}C NMR δ=170.5, 169.7, 169.6 (COMe, each s), 103.2 (C-1, d), 75.0, 73.4, 71.1 (C-2,4,5, each d), 63.0 (C-6, t), 56.2 (OMe, q), 40.1 (C-3, d), 20.6 (overlapped) (COMe, q), and 13.7 (CMe, q).

Found: C, 52.83; H, 7.06%. Calcd for $C_{14}H_{22}O_8$: C, 52.82; H, 6.97%.

10: Mp 56 °C; $[\alpha]_D^{20}$ +36.5° (*c* 1, chloroform); ^{1}H NMR: 4.94 (H-4, 1H, q, $J_{3,4}$=4.7, $J_{4,5}$=6.7), 4.82 (H-2, 1H, q, $J_{1,2}$=5.8, $J_{2,3}$=4.7), 4.60 (H-1, 1H, d), 4.25 (H-6, 2H, d, $J_{5,6}$=5.2), 3.98 (H-5, 1H, sextet), 3.48 (OMe, 3H, s), 2.66 (H-3, 1H, sextet, $J_{3,Me}$=7.1), 2.11 2.089, 2.085 (3×COMe, 3×3H, each s), and 0.99 (CMe, 3H, d).

Found: C, 52.54; H, 7.02%. Calcd for $C_{14}H_{22}O_8$: C, 52.82; H, 6.97%.

Denitrohydrogenation of 4. Compound **4** (1.0 g) was denitrohydrogenated in a similar manner as **1**. A mixture of methyl 2,4,6-tri-*O*-acetyl-3-deoxy-3-*C*-methyl-α-D-allopyranoside (**11**) and -glucopyranoside (**12**) (0.71 g, 79% yield) was obtained. $[\alpha]_D^{20}$ +116° (*c* 0.5, chloroform).

Found: C, 53.06; H, 7.02%. Calcd for $C_{14}H_{22}O_8$: C, 52.82; H, 6.97%.

According to the methyl peak of methoxyl group, products ratio **11**/**12** was 48/52.

11: ^{1}H NMR δ=4.93 (H-2, 1H, q, $J_{1,2}$=3.8, $J_{2,3}$=5.5), 4.93 (H-4, 1H, q, $J_{3,4}$=5.6, $J_{4,5}$=11.0), 4.65 (H-1, 1H, d), 4.29 (H-6R, 1H, q, $J_{5,6R}$=5.2, $J_{6,6}$=12.2), 4.17 (H-6S, 1H, q, $J_{5,6S}$=2.4), 4.06 (H-5, 1H, octet), 3.40 (OMe, 3H, s), 2.68 (H-3, 1H, q), 2.13, 2.11, 2.08 (3×COMe, 3×3H, each s), and 1.12 (CMe, 3H, d).

12: ^{1}H NMR δ=4.82 (H-2, 1H, q, $J_{1,2}$=3.7, $J_{2,3}$=10.4), 4.77 (H-4, 1H, t, $J_{3,4}$=$J_{4,5}$=10.4), 4.62 (H-1, 1H, d), 4.21 (H-6R, 1H, q, $J_{5,6R}$=5.0, $J_{6,6}$=12.2), 4.05 (H-6S, 1H, q, $J_{5,6S}$=2.4), 3.88 (H-5, 1H, octet), 3.42 (OMe, 3H, s), 2.27 (H-3, 1H, sextet), 2.12, 2.09, 2.07 (3×COMe, 3×3H, each s), and 0.92 (CMe, 3H, d).

Denitrohydrogenation of Methyl 2-*O*-Acetyl-4,6-*O*-benzylidene-3-deoxy-3-nitro-β-D-glucopyranoside (13). Compound **13**[19] (1.0 g, 2.8 mmol) was denitrohydrogenated in a similar manner as **1**. Methy 2-*O*-acetyl-4,6-*O*-benzylidene-3-deoxy-β-D-glucopyranoside (**14**, 0.60 g, 68% yield) were obtained as crystals after the evaporation of the developer. Mp 147—148 °C; $[\alpha]_D^{22}$ −89.2° (*c* 1, chloroform). ^{1}H NMR δ=5.51 (C_6H_5CH, 1H, s), 4.81 (H-2, 1H, octet, $J_{1,2}$=7.6, $J_{2,3e}$=4.9, $J_{2,3a}$=11.6), 4.43 (H-1, 1H, d), 4.33 (H-6e, 1H, q, $J_{5,6e}$=4.9, $J_{6,6}$=10.4), 3.76 (H-6a, 1H, t, $J_{5,6a}$=10.4), 3.62 (H-5, 1H, octet, $J_{4,5}$=9.3), 3.45 (H-4, 1H, multiplet), 2.51 (H-3e, 1H, sextet, $J_{3,3}$=11.6, $J_{3e,4}$=4.9) and 1.73 (H-3a, 1H, q, $J_{3a,4}$=11.6).

Found: C, 62.06; H, 6.60%. Calcd for $C_{16}H_{26}O_6$: C, 62.32; H, 6.54%.

The authors wish to express their thanks to Dr. Noboru Ono, Faculty of Science in Kyoto University, for his helpful suggestions. The authors also would like to thank Professor Jun-ichi Hayami and Mr. Ryuichi Imamura for obtaining ^{13}C and ^{1}H NMR spectra. This work was supported (in part) by Grant-in-Aid for Scientific Research No. 56430008 from the Ministry of Education, Science and Culture.

References

1) D. A. Prins, *J. Am. Chem. Soc.*, **70**, 3955 (1948).
2) D. H. R. Barton and R. Subramanian, *J. Chem. Soc., Perkin Trans. 1*, **1977**, 1718.
3) D. H. R. Barton and S. W. McCombie, *J. Chem. Soc., Perkin Trans. 1*, **1975**, 1574.
4) J. R. Rasmussen, C. J. Slinger, R. J. Kordish, and D. D. Newman-Evans, *J. Org. Chem.*, **46**, 4843 (1981).
5) R. H. Bell, D. Horton, D. H. Williams, and E. W-Mihaly, *Carbohydr. Res.*, **58**, 109 (1977); R. H. Bell, D. Horton, and D. H. Williams, *J. Chem, Soc., Chem, Commun.*, **1968**, 323.
6) T. Tsuchiya, F. Nakamura, and S. Umezawa, *Tetrahedron Lett.*, **1979**, 2805.
7) M. E. Haque, T. Kikuchi, K. Kanemitsu, and Y. Tsuda, *Chem. Pharm. Bull.*, **34**, 430 (1986).
8) A. A. J. Feast, and W. G. Overend, and N. R. Williams, *J. Chem. Soc.*, **1965**, 7378; M. Sharma and K. K. Brown, *Can. J. Chem.*, **46**, 758 (1968).
9) T. D. Inch and G. J. Lewis, *Carbohydr. Res.*, **15**, 1 (1970).
10) J-R. Pougny and P. Sinay, *J. Chem. Res. (S)*, **1982**, 1.
11) A. Rosenthal and M. Sprinzl, *Can. J. Chem.*, **47**, 3941 (1969).
12) A. K. Ganguly, P. Kabsasakalian, J. Morton, O. Sarre, A. Westcott, S. Kalliney, P. Mangiaracina, and A. Papaphilippou, *J. Chem. Soc., Chem. Commun.*, **1980**, 56.
13) R. Bonjouklian and B. Ganem, *Carbohydr. Res.*, **76**, 245 (1979).
14) N. Ono, H. Miyake, R. Tamura, and A. Kaji, *Tetrahedron Lett.*, **22**, 1705 (1981); N. Ono and A. Kaji, *Synthesis*, **1986**, 693.
15) D. D. Tanner, E. V. Blackburn, and D. D. Diaz, *J. Am. Chem. Soc.*, **103**, 1557 (1981).
16) F. Baumberger and A. Vasella, *Helv. Chim. Acta*, **66**, 2210 (1983).
17) H. H. Baer and G. V. Rao, *Chem. Ind. (London)*, **1965**, 137; *Justus Liebigs Ann. Chem.*, **686**, 210 (1965).
18) H. H. Baer and H. O. L. Fischer, *Proc. Natl. Acad. Sci. U.S.A.*, **44**, 991 (1958); *J. Am. Chem. Soc.*, **82**, 3709 (1960); H. H. Baer, *Chem. Ber.*, **93**, 2865 (1960); *J. Am. Chem. Soc.*, **83**, 1882 (1961); **84**, 83 (1962); G. Baschang, *Justus Liebigs Ann. Chem.*, **663**, 167 (1963); H. H. Baer and F. Kienzle, *Can. J. Chem.*, **41**, 1606 (1963); F. W. Lichtenthaler, *Angew. Chem., Int. Ed. Engl.*, **3**, 211 (1964); H. H. Baer and F. Kienzle, *Can. J. Chem.*, **43**, 3047 (1965); H. H. Baer, F. Kienzle, and T. Neilson, *ibid.*, **43**, 1829 (1965); H. H. Baer and F. Kienzle,

ibid., **45**, 983 (1967); M. L. Wolfrom, U. G. Nayak, and T. Radford, *Proc. Natl. Acad. Sci. U.S.A.*, **58**, 1848 (1967); H. H. Baer, *Advan. Carbohydr. Chem. Biochem.*, **24**, 67 (1969); H. H. Baer and W. Rank, *Can. J. Chem.*, **50**, 1216 (1972).

19) H. H. Baer, *Methods Carbohydr. Chem.*, **6**, 245, 302 (1972).

20) M. M. Abuaan, J. S. Brimacombe, and J. N. Low, *J. Chem. Soc., Perkin Trans. 1*, **1980**, 995.

21) K. Bock and C. Pedersen, *J. Chem. Soc., Perkin Trans. 2*, **1974**, 293.

Fluoride Ion-Induced Horner-Emmons Reaction of α-Silylalkylphosphonic Derivatives with Carbonyl Compounds

Takayuki KAWASHIMA,* Takafumi ISHII, and Naoki INAMOTO*
Department of Chemistry, Faculty of Science, The University of Tokyo,
Hongo, Bunkyo-ku, Tokyo 113
(Received November 12, 1986)

Dimethyl α-trimethylsilylbenzylphosphonate was allowed to react with carbonyl compounds in the presence of fluoride ion to give the corresponding olefins in fairly good yields. Use of CsF in tetrahydrofuran gave the best result. On the other hand, dimethyl trimethylsilylmethylphosphonate was allowed to react similarly with benzophenone to afford 1,1-diphenylethylene, dimethyl methylphosphonate, and dimethyl 2,2-diphenylethenylphosphonate. A similar result was obtained by using *O,O*-diethyl trimethylsilylmethylphosphonothioate. But, reaction of trimethylsilylmethylphosphonic bis(diethylamide) afforded only the protodesilylation product.

Since Si–F bond energy is high,[1] fluoride-induced desilylation has been utilized as a powerful tool for the generation of stabilized carbanions under neutral and relatively mild conditions.[2] The first application to the Wittig reaction was demonstrated by Vedejs and Martinez during the investigation on the generation and reaction of a carbanion stabilized by positively charged nitrogen, sulfur, or phosphorus.[3] Recently, this desilylation of α-silylalkylphosphonium salts has been studied in detail and shown to be a useful method for trisubstituted olefins by Bestmann and Bomhard.[4] If this fluoride ion-induced desilylation can be applied to α-silylalkylphosphonates, it is possible to undergo to Horner–Emmons reaction under neutral and mild conditions. A few of the results have already been described in a previous report.[5] In this paper we wish to report the detailed results.

Results and Discussion

Preparation of α-Trimethylsilylalkylphosphonic Derivatives 1. Dimethyl α-trimethylsilylbenzylphosphonate (**1a**) was prepared in 92% yield by α-lithiation of dimethyl benzylphosphonate (**2a**) and subsequent silylation with chlorotrimethylsilane.

$$X_2P(O)CH_2R \xrightarrow[2)\ Me_3SiCl]{1)\ BuLi} X_2P(O)CHRSiMe_3$$

2 **1**

a: R=Ph, X=OMe; b: R=H, X=OMe;
c: R=H, X=NEt_2

Dimethyl trimethylsilylmethylphosphonate (**1b**) was obtained similarly in 27% yield. The formation of dimethyl α,α-bis(trimethylsilyl)methylphosphonate could not be inhibited since the reaction was carried out under conditions where the quencher existed in more excess than the reactant (See Experimental). Very efficient distillation with a spinning band was necessary for removal of the by-product. According to the literature,[6] **1b** can be prepared by the Arbuzov reaction of trimethyl phosphite with trimethylsilylmethyl halide. Trimethylsilylmethylphosphonic bis(diethylamide) (**1c**) was also prepared in 43% yield by the same method as described above. *O,O*-Diethyl trimethylsilylmethylphosphonothioate (**1d**) was given in 74% yield by reaction of chlorodiethoxyphosphine with trimethylsilylmethylmagnesium chloride, followed by sulfurization.

$$(EtO)_2PCl + Me_3SiCH_2MgCl \longrightarrow \xrightarrow{S_8} (EtO)_2P(S)CH_2SiMe_3$$

1d

Reaction of 1a with Benzaldehyde in the Presence of Various Fluoride Ion Sources. Dimethyl α-trimethylsilylbenzylphosphonate (**1a**) was allowed to react with benzaldehyde in tetrahydrofuran (THF) in the presence of various fluoride ion sources to give stilbene (**3a**) and a protodesilylation product, dimethyl benzylphosphonate (**2a**). The reaction proceeds as shown in the following scheme. The results are summarized in Table 1.

$$Me_3SiCHPhP(O)(OMe)_2 \xrightarrow[-Me_3SiF]{F^-}$$

1a

$$^-CHPhP(O)(OMe)_2 \xrightarrow{H^+} PhCH_2P(O)(OMe)_2$$

2a

$$\downarrow PhCHO$$

$$PhCH{=}CHPh + (MeO)_2P(O)O^-$$

3a

When cesium fluoride dried freshly by a heat gun under vacuum was used, the best result was obtained. Use of acetonitrile as a solvent gave a similar result, but in toluene the reaction became very slow. Potassium fluoride was less effective even in the presence of 18-crown-6. On the other hand, ammonium fluorides could undergo desilylation efficiently even at room temperature, however, the

Table 1. Reaction of **1a** with Benzaldehyde in the Presence of Various Fluoride Ion Sources

Fluoride	Reaction condition			Stilbene	
	Solvent	Temp	Time	Yield[a]/%	E/Z[b]
CsF[c]	THF	RT	overnight		
		Reflux	40 min	32	100/0
CsF[d]	THF	RT	2.5 h		
		Reflux	overnight	36	100/0
CsF[e]	THF	50 °C	overnight		
		Reflux	2 h	64	100/0
CsF[f]	THF	Reflux	6 h	52	100/0
CsF[g]	THF	Reflux	1 d	85	100/0
CsF[g]	CH_3CN	50 °C	overnight	64	100/0
CsF[g]	Toluene	75 °C	1 d		
		90 °C	12 h	60	100/0
CsF[g]	DME	RT	6 h		
		Reflux	2.5 h	51	100/0
KF[h]-18-crown-6	THF	Reflux	1 d	9.5	100/0
Freeze dry KF[i]	THF	Reflux	2 d	40	100/0
Freeze dry KF[i]	CH_3CN	Reflux	2 d	57	100/0
TBAF[j]	THF	RT	2.5 h	65	90/10
TBAF[k]	THF	RT	3.5 h	26	90/10
TMAF[l]	THF	RT	1.5 h	30	90/10

a) Isolated yields based on **1a**. b) By ^{1}H NMR analysis. c) Heated at 120 °C under vacuum. d) Dried by heating at 115 °C over P_2O_5 under vacuum. e) Dried by benzene azeotrope. f) Dried with molecular sieves 4A. g) Heated with a heat gun under vacuum. h) Heated at 120 °C over P_2O_5 under vacuum. i) Heated at 180 °C under vacuum. j) Commercially available one. k) Half mol equivalent of TBAF was used with molecular sieves 4A. l) Heated at 110 °C under vacuum.

yield of **3a** was rather poor. It seems to be due to the difficulty in drying because of its thermal instability and/or the existence of acidic hydrogens easily abstractable by the resulting carbanion. Considering that the yield of **3a** was less than 60% in spite of drying of tetrabutylammonium fluoride (TBAF) by various procedures such as absorption of water with molecular sieves 4A, removal of water as the benzene azeotrope and so on, the latter reason seems more likely.

It is interesting to point out that when metal fluorides were used only (*E*)-**3a** was obtained, while use of ammonium fluorides afforded a mixture of (*E*)- and (*Z*)-**3a** in a ratio of 90:10. In general the Horner–Emmons reaction using the phosphonates with substituents stabilizing carbanion at the α-position gives selectively thermodynamically more stable (*E*)-olefins through a reversible addition of the carbanion to the carbonyl compound at the first step of the reaction.[7] Therefore, it can reasonably be explained as follows: Ammonium cation makes counter anion more naked so that the second step of the reaction, cycloelimination of the phosphate ion, proceeds more readily to give kinetically (*Z*)-stilbene. Such an acceleration of the second step has been alternatively achieved by stabilizing a pentavalent intermediate by use of five-membered phosphonates[8] or electronegative group such as 2,2,2-trifluoroethyl.[9]

The following labeling experiment indicates that **1a** can not act as a proton source for the formation of **2a**, and that the resulting carbanion seems to be protonated by water which still remained in the system: A similar reaction using dimethyl α-deuterio-α-trimethylsilylbenzylphosphonate (**1a**-*d*) gave stilbene-*d* and dimethyl α-deuteriobenzylphosphonate (**2a**-*d*). No evidence was obtained for the formation of dimethyl α,α-dideuteriobenzylphosphonate. It can be concluded that the carbanion generated by desilylation does not abstract the α-proton of **1a**. Therefore, if water could be removed completely, the yield of the olefin is expected to increase.

The reaction can be followed by ^{31}P NMR spectroscopy. As the signal at δ_P 31.4 due to **1a** decreased gradually, the peak at δ_P 28.5 assignable to protodesilylation product **2a** appeared in a low intensity, but no peak of the phosphate ion could be observed around δ_P 0 except for use of TBAF, because of low solubility of metal phosphate.

Reactions of 1a with Other Carbonyl Compounds in the Presence of CsF. A mixture of **1a** and carbonyl compounds was refluxed overnight in THF in the presence of CsF to give the corresponding olefins in moderate yields. The results are shown in Table 2.

It is noteworthy that 1,2-diphenylpropene (**3c**) was obtained by reaction of **1a** with acetophenone in 67% yield, whereas the reaction using the lithio derivative caused mainly deprotonation of acetophenone and gave **3c** only in 8% yield, suggesting that the carbanion generated by the present desilylation is less basic than the lithio derivative. However, in the case of reactions with more easily enolizable carbonyl compounds such as cyclohexanone and isobutyraldehyde, the corresponding olefins were obtained in quite low yields. The latter result shows the limitation of the present reaction.

Determination of geometry of olefins was done by comparing their ^{1}H NMR spectra with those reported in the literature.[10,11] In the case of 3-methyl-1-phenyl-1-butene (**3e**) the upper field doublet due to the isopropyl group was assigned to Z-isomer based on shielding effect of benzene ring. This assignment is also supported by the fact that, on irradiating the minor peak due to the methine proton of the isopropyl group, the upper doublet became singlet and double doublet at δ 5.44 changed to a doublet with J=11.5 Hz, a typical vicinal coupling constant between the *Z*-protons. Considering that the Z-isomer formed predominantly in the case of **3c**, while the E-

Table 2. Reaction of **1a** with Other Carbonyl Compounds in the Presence of CsF in Refluxing THF

Carbonyl compound / mmol	**1a** mmol	CsF[a] mmol	Time	Olefin **3**	Yield[b] %	E/Z[c]
$Ph_2C{=}O$ 4.00	1.90	2.70	5 h	b : $PhCH{=}CPh_2$	79	
PhCOMe 4.21	1.80	5.20	Overnight	c : PhCH=CMePh	67	1/3
=O 4.83	2.50	3.65	5 h	d : PhCH=	35	
i-PrCHO 6.06	2.06	3.62	5.5 h	e : PhCH=CH-Pr^i	35	70/30
PhCH=CHCHO 5.80	2.48	4.94	Overnight	f : PhCH=CH-CH=CHPh[d]	67	

a) Heated with a heat gun under vacumm. b) Isolated yields based on **1a**. c) By ^1H NMR analysis. d) Only E,E-isomer was obtained.

isomer predominated over the Z-isomer in the case of **3e**, what determines stereochemistry of the olefin remains unclear.

Reaction of Dimethyl Trimethylsilylmethylphosphonate (1b) with Benzophenone in the Presence of CsF. A mixture of **1b**, benzophenone, and CsF in THF was refluxed for 1 d to afford 1,1-diphenylethylene (**3g**), dimethyl 2,2-diphenylethenylphosphonate (**4a**), and dimethyl methylphosphonate (**2b**) in 20, 30, and 50% yields, respectively. The following two mechanisms can be considered for the formation of **4a**: (i) Elimination of CsOH from the adduct **6** of the α-phosphinyl carbanion with benzophenone (Path a) and (ii) the Peterson reaction of α-trimethylsilyl-α-phosphinylmethylide anion (**7**) with benzophenone (Path b).[12]

$$(MeO)_2P(O)CH_2^-\ Cs^+ \xrightarrow{Ph_2C=O} (MeO)_2P(O)CH_2CPh_2O^-\ Cs^+ \quad \mathbf{6}$$

$$\xrightarrow[-CsOH]{} (MeO)_2P(O)CH{=}CPh_2 \quad \mathbf{4a} \qquad \text{(Path a)}$$

$$\mathbf{5} + \mathbf{1b} \longrightarrow \mathbf{2b} + Cs^+\ {}^-CH(SiMe_3)P(O)(OMe)_2 \quad \mathbf{7}$$

$$\xrightarrow{Ph_2C=O} (MeO)_2P(O)CH(SiMe_3)CPh_2O^-\ Cs^+ \quad \mathbf{8}$$

$$\xrightarrow[-Me_3SiOCs]{} (MeO)_2P(O)CH{=}CPh_2 \quad \mathbf{4a} \qquad \text{(Path b)}$$

In order to decide which mechanism is operative, an attempt to generate the intermediate β-oxido phosphonate (**6**) alternatively was done. Namely, dimethyl 2,2-diphenyl-2-(trimethylsiloxy)ethylphosphonate (**9**) was treated with CsF to afford 1,1-diphenylethylene (**3g**) in high yield and no 2,2-diphenylethenylphosphonate (**4**), indicating that path a can be ruled out. Therefore, the resulting carbanion **5** by desilylation may abstract a proton from **1b** in competition with an attack on a carbonyl compound to give α-silylalkylphosphonate carbanion (**7**) which undergoes the Peterson reaction with benzophenone to afford **3g**.

$$(MeO)_2P(O)CH_2CPh_2OSiMe_3 \xrightarrow[THF,\ reflux]{CsF} CH_2{=}CPh_2$$
$$\mathbf{9} \qquad\qquad \mathbf{3g}$$

It has been reported by Ando and Sekiguchi that dimethyl α-trimethylsilylalkylphosphonates such as **1b** are heated at 250 °C to give alkylidenedimethoxy(trimethylsiloxy)phosphoranes (**10**) through 1,3-silyl shift from carbon to oxygen atom, which undergo the Wittig-type olefination with carbonyl compounds.[13]

$$(MeO)_2P(O)CHRSiMe_3 \xrightarrow[O]{250\,^\circ C} (MeO)_2(Me_3SiO)P{=}CHR \quad \mathbf{10}$$

$$\xrightarrow{Ph_2C=O} RCH{=}CPh_2 + (MeO)_2P(O)OSiMe_3$$

From the fact that the thermal reaction of **1b** with benzophenone affords **3g** in good yield and no Peterson reaction product,[13] it can reasonably be concluded that methylenephosphorane (**10**), which was proposed as an intermediate in the above reaction, is less basic than the carbanion **7** formed by an attack of fluoride ion on **1b**.

Reaction using other trimethylsilylmethylphosphonic derivatives, trimethylsilylphosphonic bis(diethylamide) (**1c**) and *O,O*-diethyl trimethylsilylmethylphosphonothioate (**1d**), failed to raise the yield of the methylene derivative. Use of **1c** caused mainly protodesilylation because strong hygroscopic property of **1c** made it difficult to remove water. Use of **1d** gave a result similar to that for **1b**, and the yield of the olefin was also quite poor, in marked contrast to the fact that reaction of dimethyl lithiomethylphosphonothioate with carbonyl compounds gives the corresponding methylene derivatives in good yields.[14] Two phase reaction in the presence of phase-transfer catalyst does not work in this system, either.

Experimental

All melting points and boiling points are not corrected. ^{1}H NMR spectra were measured with a Varian EM-390 (90 MHz), a Hitachi R-24B (60 MHz), and a JEOL FX-90Q (90 MHz) spectrometers using tetramethylsilane (TMS) as internal standard. ^{13}C NMR spectra were taken with a JEOL FX-90Q (22.53 MHz) specrometer using TMS as internal standard. ^{31}P NMR spectra were recorded with a JEOL FX-90Q (36.28 MHz) spectrometer using 85% H_3PO_4 as external standard. Mass spectra were measured at 70 eV with a JEOL 300-D mass spectrometer.

Preparation of α-Trimethylsilylalkylphosphonic Derivatives 1. Dimethyl α-Trimethylsilylbenzylphosphonate (1a). Dimethyl benzylphosphonate (**2a**) was prepared as described previously.[15] To a solution of **2a** (18.3 g, 91.7 mmol) in THF (300 ml), distilled over benzophenone ketyl, was added butyllithium (commercially available, 1.5 M (1 M=1 mol dm^{-3}) solution in hexane, 101 mmol) at −78 °C under argon. After 5 min chlorotrimethylsilane (16.3 g, 150 mmol) was added to the reaction mixture. The solution was allowed to warm to room temperature. After neutralization with aq $NaHCO_3$ THF was removed under reduced pressure, then the residue was treated with water and dichloromethane. Organic layers were collected and aq solution was extracted four times with dichloromethane. All extracts were combined, dried over anhydrous $MgSO_4$, and then the solvent was evaporated to give a colorless oil which was distilled under vacuum to afford 22.9 g (92%) of **1a**. Bp 90—92 °C/0.05 Torr (1 Torr=133.322 Pa). ^{1}H NMR ($CDCl_3$) δ=0.11 (9H, s, Si(C$\underline{H}_3$)$_3$), 2.71 (1H, d, J=24.6 Hz, P-C$\underline{H}$-Si), 3.59 (3H, J=10.7 Hz, P(OC$\underline{H}_3$)(OCH′$_3$)), 3.66 (3H, d, J=11.0 Hz, P(OCH$_3$)(OC$\underline{H}$′$_3$)), and 7.2 (5H, br s, Ph). ^{13}C NMR ($CDCl_3$) δ_C=−1.35 (d, $^3J_{C,P}$=2.4 Hz, Si(C$\underline{H}_3$)$_3$), 36.84 (d, $^1J_{C,P}$=125.7 Hz, P-C$\underline{H}_2$Si), 51.78 (d, $^2J_{C,P}$=6.7 Hz, P(OC$\underline{H}_3$)(OC′H$_3$)), 52.98 (d, $^2J_{C,P}$=7.3 Hz, P(OCH$_3$)-(OC$\underline{H}$′$_3$)), 125.76 (d, $^5J_{C,P}$=2.4 Hz, para-C), 128.46 (d, $^3J_{C,P}$=1.8 Hz, ortho-C), 129.53 (d, $^4J_{C,P}$=8.5 Hz, meta-C), and 135.08 (d, $^2J_{C,P}$=7.3 Hz, ipso-C). ^{31}P NMR ($CDCl_3$) δ_P=31.4. MS m/z (rel intensity) 272 (M^+; 49), 257 (43), 167 (33), 151 (96), and 105 (100). Found: C, 53.04; H, 7.80%. Calcd for $C_{12}H_{21}O_3PSi$: C, 52.92; H, 7.77%.

Dimethyl α-Deuterio-α-trimethylsilylbenzylphosphonate (1a-*d*). To a solution of **1a** (2.1 g, 7.7 mmol) in 50 ml of THF was added n-BuLi (9.2 mmol) at −78 °C. After 5 min a solution of D_2O (0.55 g, 27.7 mmol) in THF (10 ml) was added to the reaction mixture. The reaction mixture was allowed to warm to room temperature, neutralized with aq NH_4Cl, and extracted with dichloromethane. After removal of the solvent the residue was distilled under vacuum with Kugelrohr to give 1.79 g (85%) of **1a**-*d*. Bp 100 °C/0.01 Torr. ^{1}H NMR ($CDCl_3$) δ=0.114 (9H, s, Si(C$\underline{H}_3$)$_3$), 3.55 (3H, d, $^3J_{H,P}$=10.8 Hz, P(OC$\underline{H}_3$)(OCH′$_3$)), 3.66 (3H, $^3J_{H,P}$= 11.0 Hz, P(OCH$_3$)(OC$\underline{H}$′$_3$)), and 7.24 (5H, br s, C$_6\underline{H}_5$). ^{31}P NMR ($CDCl_3$) δ_P=31.4. High resolution mass spectrum (HRMS) m/z Found: 273.1064. Calcd for $C_{12}H_{20}DO_3PSi$: 273.1061. D contents was estimated to be 98 and 87% by ^{1}H NMR and mass spectroscopies, respectively.

Dimethyl Trimethylsilylmethylphosphonate (1b). To a solution of dimethyl methylphosphonate (**2b**) (20.0 g, 160 mmol) in THF (200 ml) was added n-BuLi (176 mmol) at −78 °C. After 5 min chlorotrimethylsilane (34.7 g, 320 mmol) was added dropwise to the solution, the cooling bath was taken off. After aq $NaHCO_3$ was added, THF was evaporated, and the residue was extracted with dichloromethane. Organic layer was dried over anhydrous $MgSO_4$, then the solvent was evaporated to give 32.4 g of an equimolar mixture of **1b**, **2b**, and dimethyl α,α-bis(trimethylsilyl)methylphosphonate. Fractional distillation with a spinning band gave 8.42 g (27%) of **1b**. **1b**; bp 100 °C/12 Torr (lit,[6] 111—114 °C/21.5 Torr). ^{1}H NMR ($CDCl_3$) δ=0.1 (9H, s, Si(C$\underline{H}_3$)$_3$), 1.1 (2H, d, J=20 Hz, P-C$\underline{H}_2$), and 3.7 (6H, d, J=13 Hz, P(OC$\underline{H}_3$)$_2$). ^{13}C NMR ($CDCl_3$) δ_C=−0.42 (d, $^3J_{C,P}$=4.3 Hz, Si(C$\underline{H}_3$)$_3$), 13.65 (d, $^1J_{C,P}$=128.2 Hz, P-C$\underline{H}_2$), and 51.83 (d, $^2J_{C,P}$=6.7 Hz, (OC$\underline{H}_3$)$_2$). ^{31}P NMR ($CDCl_3$) δ_P=35.6.

Trimethylsilylmethylphosphonic bis(diethylamide) (1c). Methylphosphonic bis(diethylamide) (**2c**) was prepared by the Arbuzov reaction of ethoxybis(diethylamino)phosphine with iodomethane in 85.5% yield. Bp 120 °C/0.9 Torr. (lit,[16] bp 166 °C/33 Torr). To a solution of methylphosphonic bis(diethylamide) (0.4 ml, 1.88 mmol) in THF (10 ml) was added butyllithium (1.2 equiv) at −78 °C, and the mixture was allowed to warm to 0 °C. To a cooled solution of chlorotrimethylsilane (1.5 equiv) was added by means of a syringe the solution of α-lithio derivative of methylphosphonic bis(diethylamide) at −40 °C for 30 min. After stirring was continued overnight aq NH_4Cl was added, the organic layer was extracted with dichloromethane, dried over anhydrous $MgSO_4$. The solvent was evaporated to give colorless oil, which was distilled with Kugelrohr to give **1c** as a colorless oil in 43% yield. Bp 70 °C/0.03 Torr. ^{1}H NMR ($CDCl_3$) δ=0.16 (9H, s, Si(C$\underline{H}_3$)$_3$), 1.08 (12H, t, J=7.0 Hz, (N(CH$_2$C$\underline{H}_3$)$_2$)$_2$), 1.15 (2H, d, J=17.2 Hz, P-C$\underline{H}_2$), and 2.70—3.35 (8H, m, (N(C$\underline{H}_2$CH$_3$)$_2$)$_2$). ^{13}C NMR ($CDCl_3$) δ_C =0.36 (d, $^3J_{C,P}$=4.3 Hz, Si(C$\underline{H}_3$)$_3$), 14.44 (d, $^3J_{C,P}$=2.2 Hz, N(CH$_2$C$\underline{H}_3$)$_2$), 15.72 (d, $^1J_{C,P}$=106.4 Hz, P-C$\underline{H}_2$), and 39.05 (d, $^2J_{C,P}$=4.4 Hz, N(C$\underline{H}_2$CH$_3$)$_2$). ^{31}P NMR ($CDCl_3$) δ_P=35.41. HRMS m/z Found: 278.1952. Calcd for $C_{12}H_{31}N_2PSi$: 278.1942.

***O,O*-Diethyl Trimethylsilylmethylphosphonothioate (1d).** Diethoxychlorophosphine was prepared as described in a previous paper[16] in 40% yield, which was contaminated with about less than 8% of ethoxydichlorophosphine. Ten ml of trimethylsilylmethylmagnesium chloride solution, prepared from chloromethyltrimethylsilane (4.39 g, 35.8 mmol) and Mg (0.933 g, 38.4 mmol) in ether (27 ml), was added to a solution of diethoxychlorophosphine (1.64 g, 10.47 mmol) in ether (20 ml) with stirring at −78 °C under argon atmosphere, then dry excess amount of sulfur (0.4 g) was added by portions to the solution. The reaction mixture was allowed to warm to room temperature, the reaction was quenched by adding aq NH_4Cl. The organic layer was extracted with dichloromethane, dried over anhydrous $MgSO_4$. The solvent was removed under reduced pressure, and the residue was distilled fractionally under vaccum to give 1.869 g (74%) of **1d** as a colorless oil. Bp 115 °C/7 Torr. ^{1}H NMR ($CDCl_3$) δ=0.17 (9H, s, Si(C$\underline{H}_3$)$_3$), 1.29 (6H, t, J=7.1 Hz, (OCH$_2$C$\underline{H}_3$)$_2$), 1.53 (2H, d, J=20.0 Hz, P-C$\underline{H}_2$), and 3.75—4.42 (4H, m, (OC$\underline{H}_2$CH$_3$)$_2$). ^{13}C NMR ($CDCl_3$) δ_C=−0.12 (d, $^3J_{C,P}$=3.9 Hz, Si(C$\underline{H}_3$)$_3$), 16.19 (d, $^3J_{C,P}$=7.3 Hz, P(OCH$_2$C$\underline{H}_3$)$_2$), 25.47 (d, $^1J_{C,P}$=100.1 Hz, P-C$\underline{H}_2$), and 61.97 (d, $^2J_{C,P}$=6.8 Hz, P(OC$\underline{H}_2$CH$_3$)$_2$). ^{31}P NMR ($CDCl_3$) δ_P=97.80. HRMS: m/z Found: 240.0768. Calcd for

$C_8H_{21}O_2PSSi$: 240.0768.

Preparation of Dimethyl 2,2-Diphenyl-2-(trimethylsiloxy)-ethylphosphonate (9). To a solution of dimethyl methylphosphonate (**1b**) (1.74 g, 14 mmol) in THF (50 ml) was added dropwise *n*-BuLi (15.4 mmol) at −78 °C. After 5 min a solution of benzophenone (2.80 g, 15.4 mmol) in THF (5 ml) was added to the solution, and the reaction mixture was allowed to warm gradually to room temperature. After cooling the reaction mixture at −78 °C again was added chlorotrimethylsilane (2.28 g, 21 mmol) by means of a syringe. The reaction mixture was allowed to warm to room temperature and it was neutralized with aq $NaHCO_3$. After removal of the solvent the residue was treated with water, and extracted with dichloromethane. The extracts were dried over anhydrous $MgSO_4$ and the solvent was removed under reduced pressure to give crude **4**, which was recrystallized from hexane to afford 4.97 g (97%) of pure **9**. **9**: Mp 86—88 °C (hexane). ^1H NMR ($CDCl_3$) δ=−0.04 (9H, s, $Si(C\underline{H}_3)_3$), 3.05 (2H, d, J=19.6 Hz, $PC\underline{H}_2$), 3.42 (6H, d, J=11.0 Hz, $P(OC\underline{H}_3)_2$), and 7.1—7.3 (10H, m, 2×Ph). ^{31}P NMR ($CDCl_3$) δ_P=29.0. MS (70 eV) m/z (rel intensity) 378 (M^+; 2), 363 (59), 301 (33), and 255 (100). HRMS (70 eV) m/z Found: 378.1413. Calcd for $C_{19}H_{27}O_4PSi$: 378.1414. Found: C, 60.02; H, 7.07%. Calcd for $C_{19}H_{27}O_4PSi$: C, 60.30; H, 7.19%.

Reaction of 1a with Benzaldehyde in the Presence of CsF. 1) In a 30 ml two-necked flask was placed CsF (0.354 g, 2.33 mmol), dried at 120 °C under vacuum for 2 h. Into the flask were added benzaldehyde (0.24 ml, 2.37 mmol) and THF (10 ml) under argon atmosphere, and a solution of **1a** (0.708 g, 2.60 mmol) in THF (10 ml) was added to the mixture cooled at −19 °C. The reaction mixture was stirred at room temperature overnight, and refluxed for 40 min. Thin-layer chromatography (SiO_2, CCl_4) showed the existence of unreacted benzaldehyde and (*E*)-stilbene (**3a**). After evaporating the solvent the residue was treated with water and dichloromethane, and the organic layer was dried over anhydrous $MgSO_4$. The solvent was removed under reduced pressure to give 0.477 g of an oil, which was subjected to dry column chromatography (DCC)(SiO_2, CCl_4) to afford 0.13 g (32%) of (*E*)-**3a**. Identification of this compound was done by comparing its ^1H NMR spectrum with that previously reported[10] and R_f value with that of authentic sample.

2) A mixture of CsF (0.349 g, 2.3 mmol), which was dried overnight at 115 °C over phosphorus pentaoxide under vacuum, benzaldehyde (0.35 ml, 3.46 mmol), and **1a** (0.476 g, 1.75 mmol) in THF (20 ml) was stirred at room temperature for 2.5 h, and refluxed overnight. The work-up as described above gave a mixture of **2a**, unreacted benzaldehyde, and (*E*)-**3a**, which was subjected to DCC (SiO_2, CCl_4) to give 0.113 g (36%) of (*E*)-**3a** and 0.23 g (66%) of crude **2a**.

3) In a 30 ml two-necked flask were placed CsF (0.410 g, 2.70 mmol) and dry benzene (15 ml), and water was removed as an azeotrope with benzene. Into the flask were added THF (20 ml), benzaldehyde (0.210 g, 1.98 mmol), and **1a** (0.204 g, 0.75 mmol), the mixture was stirred overnight at 50 °C and refluxed for 2 h. The usual work-up gave 0.087 g (64%) of (*E*)-**3a**.

4) A mixture of CsF (0.340 g, 2.24 mmol) and molecular sieves 4A (1 g) was refluxed for 1 h in THF (20 ml). After cooling was added benzaldehyde (0.29 ml, 2.87 mmol) and **1a** (0.463 g, 1.70 mmol) to the suspension, and the reaction mixture was refluxed for 6 h. The usual work-up afforded (*E*)-**3a** in 52% yield.

5) In a 30 ml flask was placed CsF (0.347 g, 2.29 mmol) and dried by heating with a 400 W heat-gun under vacuum. After adding THF (20 ml), benzaldehyde (0.51 ml, 5.05 mmol), and **1a** (0.558 g, 2.05 mmol) the mixture was refluxed for 1 d, and was treated as described above. DCC (SiO_2, CCl_4) of the residue gave 0.311 g (85%) of (*E*)-**3a**.

6) CsF dried as described in 5) was used, the reaction was carried out in acetonitrile at 50 °C overnight, in toluene at 75 °C for 1 d plus at 90 °C for 12 h, and in 1,2-dimethoxyethane at room temperature for 6 h plus at reflux for 2.5 h to afford (*E*)-**3a** in 64, 60, and 51% yields after usual work-up, respectively.

Reaction of Dimethyl α-Deuterio-α-trimethylsilylbenzylphosphonate (1a-*d*) with Benzaldehyde in the Presence of CsF. Dimethyl α-deuterio-α-trimethylsilylbenzylphosphonate (**1a**-*d*) (0.625 g, 2.29 mmol) was allowed to react with benzaldehyde (0.740 g, 6.97 mmol) in the presence of CsF (0.896 g, 5.90 mmol) in THF (8 ml) as described above to give (*E*)-**3a**-*d* (0.29 g, 70%) and dimethyl α-deuteriobenzylphosphonate (**2a**-*d*) (0.15 g, 33%). (*E*)-**3a**-*d*: ^1H NMR ($CDCl_3$) δ=7.09 (1H, br s, -CD=C$\underline{H}$-) and 7.18—7.62 (10H, m, aromatic). HRMS m/z Found: 181.1007. Calcd for $C_{14}H_{11}D$: 181.1002. D contents was estimated to be 95% by the ^1H NMR spectrum. **2a**-*d*: ^1H NMR ($CDCl_3$) δ=3.16 (1H, br d, $^2J_{H,P}$=21.5 Hz, P-C$\underline{D}$H), 3.65 (6H, d, $^3J_{H,P}$=10.7 Hz, $P(OC\underline{H}_3)_2$), and 7.29 (5H, br s, aromatic). HRMS m/z Found: 201.0665. Calcd for $C_9H_{12}DO_3P$: 201.0665. D contents was estimated to be 95 and 86% by ^1H NMR and mass spectroscopies, respectively.

Reaction of 1a with Benzaldehyde in the Presence of Other Fluorides. 1) In a 30 ml two-necked flask was weighted potassium fluoride (0.14 g, 2.41 mmol), and it was dried at 120 °C over phosphorus pentaoxide under vacuum overnight. Drying was continued at 200 °C for additional 5 h. Into the flask were added benzaldehyde (0.41 ml, 4.06 mmol), THF (20 ml), and **1a** (0.409 g, 1.50 mmol), and the mixture was refluxed for 1 d. As the ^{31}P NMR showed that **1a** still remained in a significant amount, a trace of 18-crown-6 was added to the reaction mixture. After stirring at room temperature for 1 d the usual work-up gave 0.034 g (9.5%) of (*E*)-**3a**.

2) Freeze dry KF (0.67 g, 11.5 mmol), which was prepared according to the literature,[18] was dried at 180 °C under vacuum for 1 h in a 50 ml two-necked flask, and THF (40 ml), benzaldehyde (1.04 ml, 10.3 mmol), and **1a** (2.124 g, 7.80 mmol) were added into the flask, and then the mixture was refluxed for 2 d. (*E*)-Stilbene (**3a**) and crude **2a** were obtained in 40 and 69% yields after the usual work-up, respectively.

3) Reaction of **1a** (1.69 g, 6.20 mmol) with benzaldehyde (1.24 ml, 12.2 mmol) in the presence of freeze dry KF (0.71 g, 12.2 mmol) in refluxing acetonitrile (40 ml) afforded 0.58 g (57%) of (*E*)-**3a**.

4) To a solution of **1a** (0.43 g, 1.59 mmol) and benzaldehyde (0.32 ml, 3.18 mmol) in THF (18 ml) was added dropwise commercially available tetrabutylammonium fluoride (TBAF)(1 M THF solution, 1.91 ml) at room temperature. Stirring was continued for 2.5 h. In the ^{31}P NMR spectrum of the reaction mixture two peaks were

observed at δ_P=27.7 and 0.87 in almost same ratio, which can be assignable to the signals due to **2a** and tetrabutylammonium dimethyl phosphate, respectively. The usual work-up afforded a mixture of (*E*)- and (*Z*)-**3a** (0.168 g, 65%) and crude **2a** (0.128 g, 44%). The ratio of (*E*)- to (*Z*)-stilbene was determined to be 90:10 by ^{1}H NMR spectroscopy.[10]

5) A mixture of benzaldehyde (0.41 ml, 4.06 mmol), TBAF (1 ml, 1 mmol), and molecular sieves 4A (1 g) in THF (5 ml) was stirred overnight at room temperature. To the suspension was added a solution of **1a** (0.54 g, 1.98 mmol) in THF (15 ml), and the mixture was stirred for 3.5 h at room temperature. The usual work-up afforded (*E*)- and (*Z*)-**3a** (0.085 g, 26%) in the same ratio and crude **2a** (0.30 g, 80%).

6) A mixture of benzaldehyde (0.41 ml, 4.06 mmol), tetramethylammonium fluoride (TMAF) (0.372 g, 4.00 mmol), and **1a** (0.368 g, 1.35 mmol) in THF (15 ml) was stirred for 1.5 h at room temperature. The usual work-up gave (*E*)- and (*Z*)-**3a** in 30% yield. The ratio of (*E*)- and (*Z*)-**3a** was 90:10.

Reaction of Dimethyl α-Trimethylsilylbenzylphosphonate (1a) with Other Carbonyl Compounds in the Presence of CsF. Benzophenone. Cesium fluoride (0.410 g, 2.70 mmol) was dried in a 30 ml two-necked flask as described above, and a solution of dry benzophenone (0.729 g, 4.00 mmol) in THF (18 ml) and **1a** (0.518 g, 1.90 mmol) were added into the flask, and then the mixture was refluxed for 5 h and stirred at 50 °C overnight. The usual work-up gave a mixture (0.870 g) of 1,1,2-triphenylethylene (**3b**), **2a**, and unreacted benzophenone, which was subjected to DCC (SiO_2, CCl_4) to afford **3b** (0.385 g, 79%) as a viscous oil. ^{1}H NMR ($CDCl_3$) δ=6.87 (1H, s, C=C<u>H</u>Ph), 6.97 (5H, s, Ph), and 7.06—7.40 (10H, m, 2×Ph).

Acetophenone. In a 30 ml two-necked flask was weighted CsF (0.790 g, 5.20 mmol), dried as described above. After subsequent addition of acetophenone (0.49 ml, 4.21 mmol), THF (20 ml), and **1a** (0.490 g, 1.80 mmol), the mixture was refluxed overnight. The usual DCC (SiO_2, CCl_4) afforded a mixture of (*E*)- and (*Z*)-1,2-diphenylpropenes (**3c**) (0.234 g, 67%) as a colorless oil. (*E*)-**3c**: ^{1}H NMR ($CDCl_3$) δ=2.19 (3H, d, J=1.5 Hz, =CC<u>H</u>$_3$), 6.46 (1H, q, J=1.5 Hz, =C<u>H</u>Ph), and 6.90—7.62 (10H, m, Ph). (*Z*)-**3c**: ^{1}H NMR ($CDCl_3$) δ=2.26 (3H, d, J=1.2 Hz, =CC<u>H</u>$_3$), 6.83 (1H, q, J=1.2 Hz, =C<u>H</u>Ph), and 6.90—7.62 (10H, m, Ph). The ratio of (*E*)- and (*Z*)-**3c** was determined to be 1:3 from the integral ratio between the doublet at δ 2.26 due to E-isomer and the doublet at δ 2.19 due to Z-isomer.[11]

Cyclohexanone. In a 30 ml two necked flask was placed CsF (0.544 g, 3.65 mmol), and dried. Into the flask were added cyclohexanone (0.50 ml, 4.83 mmol), THF (20 ml), and **1a** (0.681 g, 2.50 mmol), and the mixture was refluxed for 5 h, and then it was stirred at 50 °C overnight. The residue obtained after the usual work-up was submitted to DCC (SiO_2, CCl_4) to give 0.146 g (35%) of benzylidenecyclohexane (**3d**). ^{1}H NMR ($CDCl_3$) δ=1.37—1.87 (6H, m, -CH_2-(C<u>H</u>$_2$)$_3$-CH_2-), 2.01—2.47 (4H, m, -C<u>H</u>$_2$-(CH_2)$_3$-C<u>H</u>$_2$-), 6.10 (1H, br s, =C<u>H</u>Ph), and 6.90—7.40 (5H, m, Ph).

Isobutyraldehyde. Cesium fluoride (0.55 g, 3.62 mmol) was dried, mixed with isobutyraldehyde (0.55 ml, 6.06 mmol), THF (30 ml), and **1a** (0.561 g, 2.06 mmol) and the mixture was refluxed for 5.5 h. The reaction mixture was treated as described above to give 0.535 g of an oil which was subjected to DCC (SiO_2, CCl_4) to afford a mixture of (*E*)- and (*Z*)-3-methyl-1-phenyl-1-butenes (**3e**) (0.10 g, 35%). (*E*)-**3e**: ^{1}H NMR ($CDCl_3$) δ=1.07 (6H, d, J=6.6 Hz, CH(C<u>H</u>$_3$)$_2$), 2.18—2.67 (1H, m, C<u>H</u>(CH_3)$_2$), 6.12 (1H, dd, J=5.4, 16 Hz, =C<u>H</u>CH(CH_3)$_2$), 6.36 (1H, d, J=16 Hz, =C<u>H</u>Ph), 6.9—7.6 (5H, m, Ph). (*Z*)-**3e**: ^{1}H NMR ($CDCl_3$) δ=1.02 (6H, d, J=6.6 Hz, CH(C<u>H</u>$_3$)$_2$), 2.67—3.14 (1H, m, C<u>H</u>(CH_3)$_2$), 5.44 (1H, dd, J=10.0, 11.5 Hz, =C<u>H</u>CH(CH_3)$_2$), 6.29 (1H, d, J=11.5 Hz, =C<u>H</u>Ph), and 6.9—7.6 (5H, m, Ph). The ratio of (*E*)- and (*Z*)-**3e** was determined to be 70:30 from the integral ratio of the doublet at δ 1.07 due to E-isomer to the doublet at δ 1.02 due to Z-isomer.

Cinnamaldehyde. A mixture of **1a** (0.675 g, 2.48 mmol), cinnamaldehyde (0.73 ml, 5.80 mmol), and CsF (0.75 g, 4.94 mmol) in THF (25 ml) was refluxed overnight. After removal of the solvent the residue was treated with water and extracted several times with dichloromethane. The extracts were combined, dried over anhydrous $MgSO_4$, and then the solvent was evaporated. The residue was subjected to DCC (SiO_2, CCl_4) to afford (*E*,*E*)-1,4-diphenyl-1,3-butadiene (**3f**) (0.326 g, 67%). Mp 151—152 °C (EtOH) (lit,[19] 152—153 °C).

Reaction of Trimethylsilylmethylphosphonic Derivatives (1b—d) with Benzophenone in the Presence of CsF. Dimethyl Trimethylsilymethylphosphonate (1b). A mixture of CsF (0.744 g, 4.90 mmol), dried as described above, benzophenone (1.35 g, 7.40 mmol), **1b** (0.420 g, 2.14 mmol), and THF (20 ml) was refluxed for 1 d with stirring. The usual work-up afforded 1,1-diphenylethylene (**3g**), dimethyl 2,2-diphenylethenylphosphonate (**4a**), and dimethyl methylphosphonate (**2b**) in 20, 30, and 50% yields, respectively. **4a**: ^{1}H NMR ($CDCl_3$) δ=3.49 (6H, d, J=11 Hz, P(OC<u>H</u>$_3$)$_2$), 6.18 (1H, d, J=15 Hz, =C<u>H</u>), and 7.3—7.5 (10H, m, 2×Ph). ^{31}P NMR ($CDCl_3$) δ_P=19.32. HRMS: *m/z* Found: 288.0913. Calcd for $C_{16}H_{17}O_3P$: 288.0914.

Trimethylsilylmethylphosphonic Bis(diethylamide) (1c). A mixture of CsF (0.559 g, 3.68 mmol), benzophenone (0.399 g, 2.19 mmol), and **1c** (0.381 g, 1.37 mmol) in THF (20 ml) was refluxed overnight to give methylphosphonic bis(diethylamide) (**2c**) almost quantitatively after usual work-up.

***O,O*-Diethyl Trimethylsilylmethylphosphonothioate (1d).** A mixture of CsF (0.577 g, 3.80 mmol), benzophenone (0.292 g, 1.60 mmol), and **1d** (0.250 g, 1.05 mmol) in THF (20 ml) was refluxed overnight. The usual work-up afforded **3g**, *O,O*-diethyl 2,2-diphenylethenylphosphonothioate (**4b**), and *O,O*-diethyl methylphosphonothioate (**2d**) in 30, 25, and 42% yields, respectively, from analysis of ^{1}H NMR and ^{31}P NMR spectra of the mixture. **4b**: Bp 175 °C/0.05 Torr. ^{1}H NMR ($CDCl_3$) δ=1.08 (6H, t, J=7.1 Hz, C<u>H</u>$_3$), 3.51—4.19 (4H, m, OC<u>H</u>$_2$), 6.36 (1H, d, J=20.3 Hz, =C<u>H</u>), 7.25 (5H, br s, Ph), and 7.35 (5H, br s, Ph). ^{31}P NMR ($CDCl_3$) δ_P=80.16. HRMS: *m/z* Found: 332.1008. Calcd for $C_{18}H_{21}O_2PS$: 332.1000.

Reaction of Dimethyl 2,2-Diphenyl-2-(trimethylsiloxy)-ethylphosphonate (9) with CsF. A mixture of CsF (0.749 g, 4.93 mmol) and **9** (0.867 g, 2.29 mmol) in THF (20 ml) was refluxed for 3 d. The usual work-up gave 1,1-diphenylethylene (0.351 g) in 85% yield.

Reaction of Dimethyl α-Lithiobenzylphosphonate with Acetophenone. To a solution of dimethyl benzylphosphonate (**2a**) (0.544 g, 2.72 mmol) in THF (20 ml) was added *n*-BuLi (2.0 ml, 1.64 M) at −78 °C. After 5 min a

solution of acetophenone (0.63 ml, 2.0 equiv) in THF (5 ml) was added to the solution at the same temperature and the reaction mixture was allowed to warm to room temperature, and then was stirred for 1 d. The usual work-up gave 0.856 g of crude mixture, which was chromatographed on silica gel (DCC, CCl_4) to give 0.043 g (8.1%) of **3c**.

The authors wish to express their thanks to Miss Toshiko Seki and Mrs. Kimiyo Saeki, who made the elemental analyses. They also thank to Shinetsu Kagaku Co. for a gift of chlorotrimethylsilane. The present work was partially supported by a Grant-in-Aid for Scientific Research No. 61540365 from the Ministry of Education, Science and Culture.

References

1) L. H. Sommer, "Stereochemistry, Mechanism, and Silicon," McGraw Hill, New York (1965), p. 25.

2) Silyl enol ethers: a) I. Kuwajima and E. Nakamura, *J. Am. Chem. Soc.*, **97**, 3259 (1975); b) W. A. Kleschick, C. T. Buss, and C. H. Heathcock, *ibid.*, **99**, 247 (1977); c) R. Noyori, K. Yokoyama, J. Sakata, I. Kuwajima, E. Nakamura, and M. Shimizu, *ibid.*, **99**, 1265 (1977); d) I. Kuwajima, E. Nakamura, and M. Shimizu, *ibid.*, **104**, 1025 (1982); allylsilanes: e) A. Hosomi, A. Shirahata, and H. Sakurai, *Tetrahedron Lett.*, **1978**, 3043; propargylsilanes: f) J. Pornet, *ibid.*, **22**, 455 (1981); 2-silyl-1,3-dithianes: g) N. H. Andersen, D. A. McCrae, D. B. Grotjahn, S. Y. Gabhe, L. J. Theodore, R. M. Ippolito, and T. K. Sarkar, *Tetrahedron*, **37**, 4069 (1981).

3) E. Vedejs and G. R. Martinez, *J. Am. Chem. Soc.*, **101**, 6452 (1979).

4) H. J. Bestmann and A. Bomhard, *Angew. Chem., Int. Ed. Engl.*, **21**, 545 (1982).

5) T. Kawashima, T. Ishii, and N. Inamoto, *Tetrahedron Lett.*, **24**, 739 (1983).

6) A. E. Canavan and C. Eaborn, *J. Chem. Soc.*, **1962**, 592.

7) B. J. Walker, "Organophosphorus Reagents in Organic Synthesis," ed by J. I. G. Cadogan, Academic Press, London-New York-Toronto-Sydney-San Francisco (1979), Chap. 3.

8) a) E. Breuer and D. M. Bannet, *Tetrahedron Lett.*, **1977**, 1141; b) R. O. Larsen and G. Aksnes, *Phosphorus and Sulfur*, **16**, 339 (1983).

9) W. C. Still and C. Gennari, *Tetrahedron Lett.*, **24**, 4405 (1983).

10) C. J. Pouchert and J. R. Campbell, "The Aldrich Library of NMR Spectra," Aldrich Chemical Company, Inc., Milwaukee, Wisconsin (1974), Vol. 4, 19B, 19C.

11) A. F. Casey, A. Parulkar, and P. Pocha, *Tetrahedron*, **24**, 3031 (1968).

12) F. A. Carey and A. S. Court, *J. Org. Chem.*, **37**, 939 (1972).

13) A. Sekiguchi and W. Ando, *Chem. Lett.*, **1978**, 1385.

14) E. J. Corey and G. T. Kwiatkowski, *J. Am. Chem. Soc.*, **88**, 5654 (1966).

15) K. D. Berlin, C. Hildebrand, A. South, D. M. Hellwege, M. Peterson, E. A. Pier, and J. G. Verkade, *Tetrahedron*, **20**, 323 (1954).

16) G. M. Kosolapoff and L. B. Payne, *J. Org. Chem.*, **21**, 413 (1956).

17) H. G. Cook, J. D. Ilett, B. C. Saunders, G. J. Stacey, H. G. Watson, I. G. E. Wilding, and S. J. Woodcock, *J. Chem. Soc.*, **1949**, 2921.

18) N. Ishikawa, T. Kitazume, and M. Nakabayashi, *Chem. Lett.*, **1980**, 1089.

19) J. H. Pinckard, B. Wille, and L. Zechmeister, *J. Am. Chem. Soc.*, **70**, 1938 (1948).

α,β-Epoxy Sulfoxides as Useful Intermediates in Organic Synthesis. X.[1] An Improved Synthesis of α,β-Unsaturated Carbonyl Compounds from Carbonyl Compounds with Carbon Homologation through α,β-Epoxy Sulfoxides

Tsuyoshi SATOH, Masayuki ITOH, Teruhiko OHARA, and Koji YAMAKAWA*
Faculty of Pharmaceutical Sciences, Science University of Tokyo,
Ichigaya-funagawara-machi, Shinjuku-ku, Tokyo 162
(Received November 17, 1986)

Treatment of the α,β-epoxy sulfoxides derived from **ketones** and chloromethyl phenyl sulfoxide or 1-chloroalkyl phenyl sulfoxides with lithium perchlorate in the presence of tributylphosphine oxide in toluene at 110 °C for about 1—3 h gave α,β-unsaturated aldehydes or α,β-unsaturated ketones in high yields. In contrast to these results, the α,β-epoxy sulfoxides derived from **aldehydes** did not give the desired α,β-unsaturated ketones. In this case, a sequential treatment of the α,β-epoxy sulfoxides with benzenethiolate and *m*-chloroperbenzoic acid afforded α-phenylsulfinylated ketones, which were heated in toluene at 110 °C to give the desired enones in good overall yields. The oxidation of the α,β-unsaturated aldehydes obtained by this method gave α,β-unsaturated carboxylic acids in high yields. These procedures afforded a new method for the synthesis of α,β-unsaturated carbonyl compounds, including α,β-unsaturated esters, from carbonyl compounds with carbon homologation.

The statement made by Roberts and Caserio[2] ("the chemistry of carbonyl compounds is virtually the backborn of synthetic organic chemistry") clearly indicates that carbonyl compounds, including α,β-unsaturated types, are of most importance in synthetic organic chemistry. Especially, α,β-unsaturated carbonyl compounds are quite useful in various synthetic reactions such as the Diels–Alder reaction[3] and Michael-type reactions.[4] Almost an uncountable numbers of methods for the preparation of carbonyl compounds have already been reported; however, as a consequence of the usefulness of carbonyl compounds, the exploration of a new procedure for their syntheses from readily available precursors is always welcome.

Recently, we reported[5] a new and useful method for the syntheses of various kinds of carbonyl compounds by the homologation of carbonyl compounds through α,β-epoxy sulfoxides (**3**). In the course of our studies on new synthetic method from carbonyl compounds **1** through α,β-epoxy sulfoxides (**3**)[6] we report here on a new and simple procedure for the synthesis of α,β-unsaturated ketones and α,β-unsaturated aldehydes from carbonyl compounds **1** with carbon homologation. These procedure are shown in Scheme 1.

Results and Discussion

A Synthesis of α,β-Unsaturated Ketones and α,β-Unsaturated Aldehydes from Ketones through α,β-Epoxy Sulfoxides. Before our first publication in 1984[7] only two kinds of synthetic methods through α,β-epoxy sulfoxides had been reported: One was a thermal reaction resulting in α,β-unsaturated carbonyl compounds,[8] and the other was a rearrangement of sulfinyl group with Lewis acids, such as $BF_3 \cdot Et_2O$, giving α-sulfinylated ketones.[9] These reactions, themselves, are quite interesting; unfortunately, the yields were not satisfactory for the

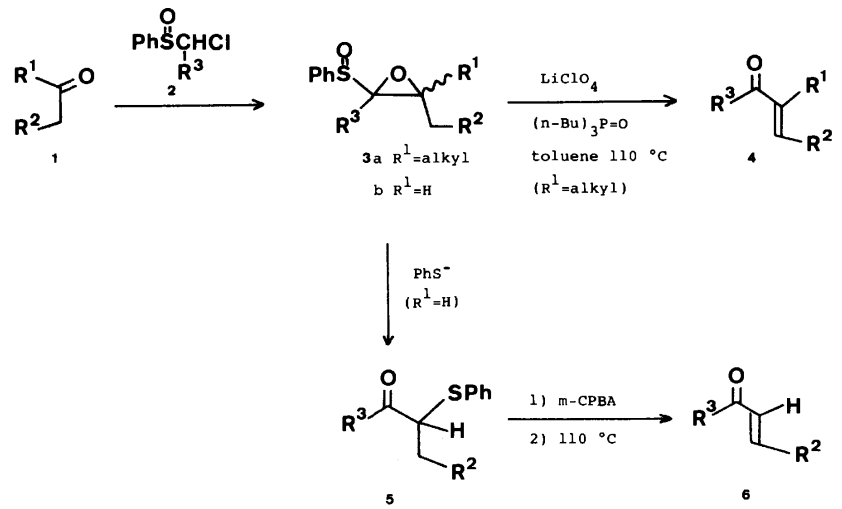

Scheme 1.

practical use in synthetic organic reactions. In fact, in our reexamination, upon heating in xylene at 140 °C for 3 h, the α,β-epoxy sulfoxide (**7**) gave a brown mixture in which the desired enone **8** was obtained in only 46% yield. On the other hand, a treatment of **7** with $BF_3 \cdot Et_2O$ in CH_2Cl_2 at room temperature for 4 h gave only a complex mixture.

We thought that a treatment of α,β-epoxy sulfoxides **3** with a weak Lewis acid under heating resulted in a sulfinyl group rearrangement followed by a thermal elimination of the rearranged sulfinyl group to afford the desired α,β-unsaturated carbonyl compounds under relatively mild conditions. First of all, we started to find the appropriate weak Lewis acid under heating (a temperature around refluxing benzene) by using the α,β-epoxy sulfoxide **7** as a substrate (Table 1). As shown in Table 1, aluminum, titanium, and magnesium alkoxides were not effective for this reaction; finally, lithium perchlorate in the presence of one equivalent of tributylphosphine oxide[10] was found to be quite effective for the desired reaction. This reaction was rather sluggish in refluxing benzene but in toluene at 110 °C the reaction took place quite smoothly and cleanly to afford the desired enone **8** in 74% yield. These conditions were used throughout this study.

The results of the preparation of α,β-unsaturated carbonyl compounds from ketones via α,β-epoxy sulfoxides upon a treatment with lithium perchlorate in toluene at 110 °C (the temperature of the oil bath used) are summarized in Table 2. The remarkable characteristics of the presented procedure are as follows: a) The yields are uniformly quite good except the result in Entry 8; b) the conditions were neutral, and the temperature of the reaction was much lower than that previously reported,[8] and the reaction time was less than 3 h; c) the reaction mixture was quite clean except the result in Entry 8; d) in Entry 8, though some by-products were observed, because of the mildness of the conditions, no double-bond migration giving conjugated divinyl ketone occured; e) usually, but not always, the reactions giving α,β-unsaturated aldehydes tended to proceed faster than those giving α,β-unsaturated ketones (Entries 10—14).

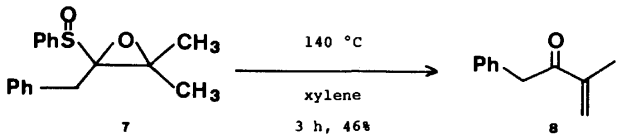

Scheme 2.

A Synthesis of α,β-Unsaturated Ketones from Aldehydes through α,β-Epoxy Sulfoxides. In contrast to the good results mentioned above a treatment of the α,β-epoxy sulfoxides **3b**, derived from aldehydes and **2**, with lithium perchlorate under the same conditions used above, did not give any good results. The reaction was very sluggish and prolonged heating resulted in a complex mixture. The reason for this results may be interpreted as being a stability problem involving a secondary carbocation[10] of the inter-

Table 1. Treatment of **7** with Weak Lewis Acid under Heating

Lewis Acid	Temp °C	Time	Enone **8**[a] %
$Al(OPr^i)_3$	83[b]	8 h	20
$Ti(OPr^i)_4$	80[c]	6 d	—
$Mg(OMe)_2$	80[c]	3 d	—
$LiClO_4 \cdot 3H_2O$[d]	80[c]	1 d	54
$LiClO_4 \cdot 3H_2O$[d]	110[e]	2 h	74

a) Isolated purified yield after silica-gel column chromatography. b) The reaction was carried out in refluxing 2-propanol. c) The reaction was carried out in refluxing benzene. d) With tributylphosphine oxide. e) The reaction was carried out in toluene. The temperature of the oil bath used.

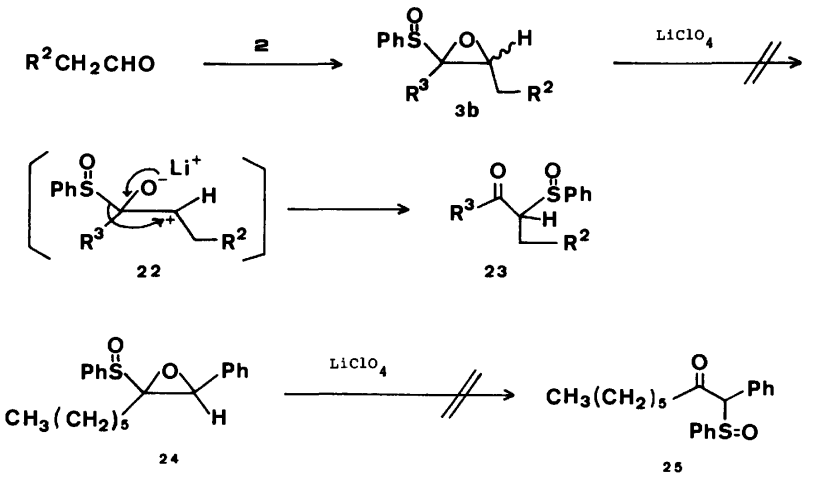

Scheme 3.

Table 2. Preparation of α,β-Unsaturated Carbonyl Compounds from Ketones through α,β-Epoxy Sulfoxides

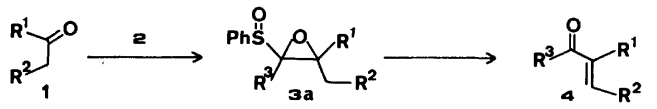

Entry	Ketone **1**	R^3 in **2**	Time	α,β-Unsaturated carbonyl compound	Yield[a] %
1	CH_3COCH_3	$PhCH_2$	2 h	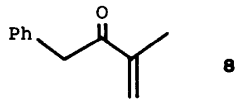 **8**	74
2	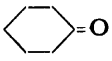	$PhCH_2$	2.5 h	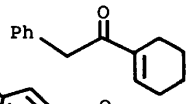 **9**	98
3	—	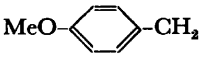	2.5 h	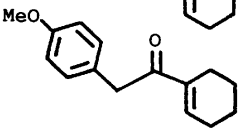 **10**	87
4	—	$CH_3(CH_2)_5$	2 h	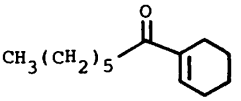 **11**	89
5	—		50 min	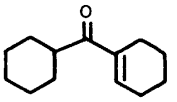 **12**	83
6	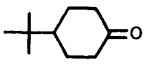	CH_3	3 h	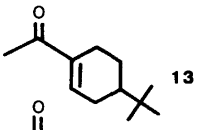 **13**	91
7	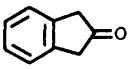	CH_3	2.5 h	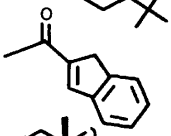 **14**	90
8	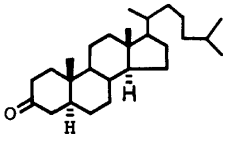	CH_2=CH-CH_2	2 h	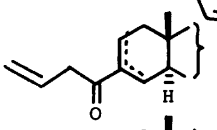 **15**	64
9	—	CH_3	50 min	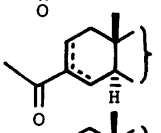 **16**	95
10	—	H	40 min	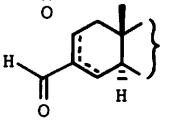 **17**	83
11		H	30 min	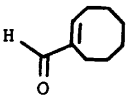 **18**[8a]	97
12	$[CH_3(CH_2)_3]_2CO$	H	1 h	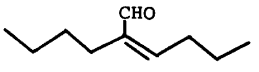 **19**	85
13	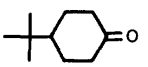	H	50 min	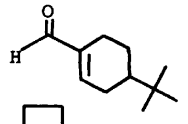 **20**	98
14	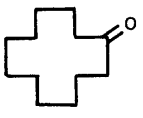	H	2 h	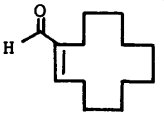 **21**[11]	88

a) Isolated purified yield after silica-gel column chromatography.

mediate (**22**). In the case of the α,β-epoxy sulfoxides derived from ketones, the cationic intermediate was tertiary, which may proceed to a rearrangement followed by a thermal elimination to afford α,β-unsaturated carbonyl compounds **4**. It is noteworthy that the α,β-epoxy sulfoxide having a phenyl group at the β position **24**, in which the carbocationic intermediate is thought to be stabilized by a phenyl ring, still did not give the rearranged product **25**.

This difficulty regarding the preparation of enones from α,β-epoxy sulfoxides could be overcome by taking another route (shown in Scheme 1). As already reported by us,[5b] the treatment of **3b** with benzenethiolate gave α-phenylthio ketones (**5**) in excellent yields. The sequential oxidation of **5** and the elimination of the resultant sulfoxide[12] must give the desired enone **6**.

Three example are listed in Table 3. Though two more steps were required, compared to the method described above, the overall yields from α,β-epoxy sulfoxides were equally good.

Here, we should like to describe the interesting characteristic of the presented procedure. As shown in Scheme 4, the famous aldol reaction affords α,β-unsaturated carbonyl compounds from carbonyl compounds with a carbon-chain elongation at the α-position of the carbonyl group. In contrast to this, the presented procedure gives α,β-unsaturated carbonyl compounds with a carbon-chain elongation from the carbonyl carbon itself.

An Application of This Method to a Synthesis of α,β-Unsaturated Esters from Ketones by One-Carbon Homologation. α,β-Unsaturated esters have received considerable attention for a long time in synthetic

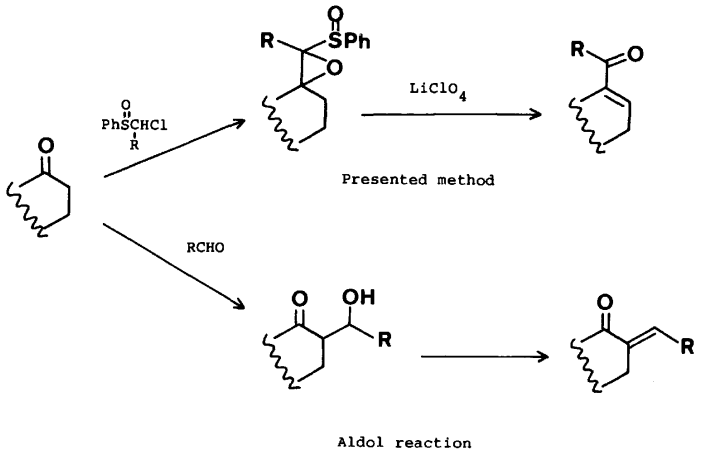

Scheme 4.

Table 3. Preparation of α,β-Unsaturated Ketones from Aldehydes through α,β-Epoxy Sulfoxides

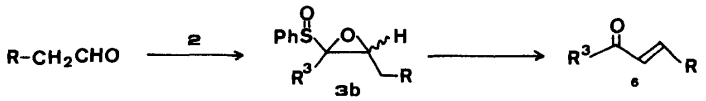

Entry	Aldehyde	R^3 in **2**	α,β-Unsaturated ketone	Yield[a] %
1	$CH_3(CH_2)_8CHO$	$PhCH_2$	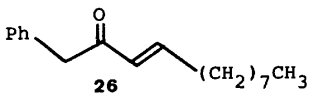 **26**	77
2	$PhCH_2CH_2CHO$	CH_3	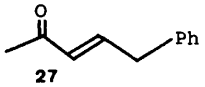 **27**	77
3	$CH_3(CH_2)_4CHO$		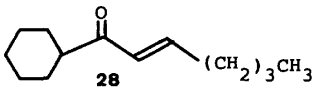 **28**	88

a) Three steps overall yield from the α,β-epoxy sulfoxide. The product was purified by silica-gel column chromatography.

organic chemistry. The Michael-type conjugate addition of various kinds of nucleophiles, especially carbon nucleophiles, to α,β-unsaturated esters is one of the most useful tools for constructing a carbon framework.[13] Recently, a diastereo- and/or enantioselective Michael addition of some enolates to α,β-unsaturated esters was also reported.[14] Several methods for the synthesis of saturated esters from ketones by one-carbon homologation have been reported;[15] however, very few methods for the synthesis of α,β-unsaturated ones from ketones by one-carbon homologation have been published.[16]

With the new method described above in hand, it was anticipated that the desired α,β-unsaturated ester, such as **31**, could be derived from α,β-unsaturated aldehyde **20** or α,β-unsaturated methyl ketone **13** by two types of oxidations: the oxidation of aldehydes to carboxylic acids[17] or the haloform-type oxidation of methyl ketone **13** to carboxylic acid.[18]

Several method for the oxidation of enals to α,β-unsaturated carboxylic acids have been reported;[17] we used the most recent method reported by Dalcanale and Montanari[17c] with a slight modification. The enal **20** was oxidized with sodium chlorite–hydrogen peroxide in *t*-butyl alcohol followed by methylation with diazomethane to afford the desired α,β-unsaturated ester **31** in 89% yield. Parallel to this reaction, several haloform-type oxidations[18] of the methyl ketone **13** were carried out, but it was found that the reaction were quite sluggish and gave only complex mixtures. Table 4 shows the results of the preparation of α,β-unsaturated esters from various kinds of ketones through the α,β-unsaturated aldehydes.

Beacuse of its overall simplicity and high overall yields, we believe that the presented procedure will prove valuable in the preparation of synthetically useful α,β-unsaturated carbonyl compounds.

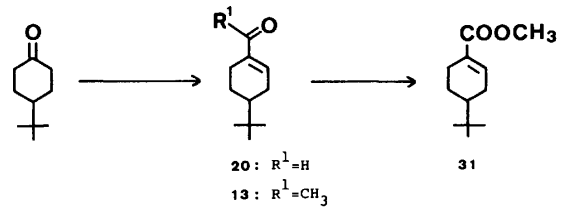

Scheme 5.

Experimental

All melting points are uncorrected. Infrared (IR) spectra were measured directly on a NaCl plate or in KBr disks with a Hitachi 215 spectrometer. ^{1}H Nuclear magnetic resonance (NMR) spectra were measured in a $CDCl_3$ solution with a JOEL FX-100 spectrometer using Me_4Si as an internal standard. Ultraviolet (UV) spectra were measued in an EtOH solution with a Hitachi 200 spectrometer. Electron-impact mass spectra (MS) were obtained on a Hitachi M-80 double-focusing spectrometer at 70 eV by direct insertion. Silica-gel BW-127 ZH (Fuji-Devison) containing 2% fluoresence reagent 254 and quartz column were used for column chromatography and the products having UV absorption were detected by UV irradiation.

Table 4. Preparation of α,β-Unsaturated Esters from Ketones through α,β-Epoxy Sulfoxides and α,β-Unsaturated Aldehydes

Entry	Ketone	α,β-Unsaturated aldehyde/%[a]	α,β-Unsaturated ester	Yield[b] %
1	$CH_3(CH_2)_5\overset{O}{\overset{\|}{C}}(CH_2)_5CH_3$	**29** (91)	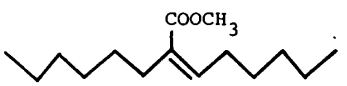 **30**	95
2	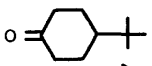	**20**	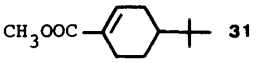 **31**	89
3	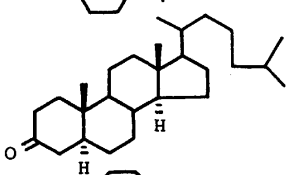	**17**	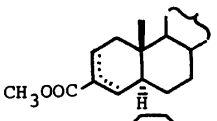 **32**	92
4	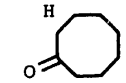	**18**	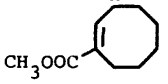 **33**	96
5	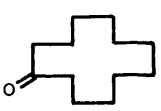	**21**	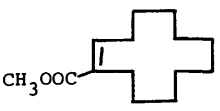 **34**	82

a) The isolated yields of the treatment of the α,β-epoxy sulfoxides with lithium perchlorate. b) Isolated purified yields.

α,β-Epoxy Sulfoxides. All α,β-epoxy sulfoxides, except the ones cited below, used in this study were prepared from carbonyl compounds and **2** (R^3=H or alkyl) through chlorohydrins nearly quantitative yields, which were reported previously.[5] α,β-Epoxy sulfoxides in Table 2; Entry 6: Colorless oil; IR (Neat) 1090, 1055 (SO) cm^{-1}; ^1H NMR δ=0.91 (9H, s), 1.30 (3H, s), 7.4—7.7 (5H, m); MS *m/z* (%) 307 ($[M+H]^+$, 0.7), 181 ($[M-PhSO]^+$, 64), 43 (100). Entry 7: Colorless prisms; mp 155—157 °C (AcOEt-hexane); IR (KBr) 1055 (SO) cm^{-1}; ^1H NMR δ=1.37 (3H, s), 2.97, 3.35, 3.47, 3.97 (each 1H, d, *J*=18 Hz), 7.21 (4H, bs), 7.40—7.75 (5H, m); Found: C, 71.74; H, 5.68; S, 11.43%. Calcd for $C_{17}H_{16}O_2S$: C, 71.80; H, 5.67; S, 11.25%. Entry 9: Colorless needles; mp 164—165 °C (hexane-MeOH); IR (KBr) 1055 (SO) cm^{-1}; ^1H NMR δ=0.66 (3H, s), 0.87 (6H, d, *J*=7 Hz), 0.98 (3H, d, *J*=7 Hz), 1.01 (3H, s), 1.28 (3H, s), 7.36—7.72 (5H, m); Found: C, 78.09; H, 10.25; S, 6.12%. Calcd for $C_{35}H_{54}O_2S$: C, 78.01; H, 10.10; S, 5.95%. Entry 11: Colorless oil; IR (neat) 1085, 1.40 (SO) cm^{-1}; ^1H NMR δ=1.32—2.24 (14H, m), 3.68 (1H, s), 7.4—7.7 (5H, m). Entry 12: Colorless oil: IR (neat) 1055 (SO) cm^{-1}; ^1H NMR δ=3.60 (1H, s), 7.3—7.8 (5H, m). Entry 13: Colorless crystals; mp 91—93 °C (recrystallized from EtOH); IR (KBr) 1050 (SO) cm^{-1}; ^1H NMR δ=0.91 (9H, s), 3.65 (1H, d, *J*=1 Hz), 7.40—7.70 (5H, m); MS *m/z* (%): 292 (M^+, 0.2), 167 ($[M-PhSO]^+$, 26), 126 (83), 57 (100); Found: C, 69.77; H, 8.39; S, 10.97%. Calcd for $C_{17}H_{24}O_2S$: C, 69.82; H, 8.27; S, 10.96%. Entry 14: Colorless needles; mp 97—98 °C (recrystallized from benzene-hexane); IR (KBr): 1085, 1045, 1040 (SO) cm^{-1}; ^1H NMR δ=1.10—2.32 (22H, m), 3.62 (1H, d, *J*=1 Hz), 7.38—7.76 (5H, m); MS *m/z* (%): 195 ($[M-PhSO]^+$, 26), 126 (100); Found: C, 71.40; H, 9.04; S, 10.14%. Calcd for $C_{19}H_{28}O_2S$: C, 71.21; H, 8.81; S, 10.00%. α,β-Epoxy sulfoxides in Table 3; Entry 1: Colorless oil; IR (neat) 1090, 1055 (SO) cm^{-1}; ^1H NMR δ=0.98 (3H, bt, *J*=6 Hz), 3.00, 3.05 (each 1H, d, *J*=16 Hz, benzyl-H), 3.70 (1H, t, *J*=6 Hz), 7.00—7.24, 7.36—7.64 (each 5H, m). Entry 2: Colorless oil; IR (neat) 1085, 1045 (SO) cm^{-1}; ^1H NMR δ=1.23 (3H, s), 3.61 (1H, t, *J*=7 Hz), 7.04—7.32, 7.38—7.70 (each 5H, m). α,β-Epoxy sulfoxide in Table 4; Entry 1: Coloress oil; IR (neat) 1055 (SO) cm^{-1}; ^1H NMR δ=3.65 (1H, s), 7.40—7.72 (5H, m); MS *m/z* (%): 211 ($[M-PhSO]^+$, 30), 126 (100).

3-Methyl-1-phenyl-3-buten-2-one (8). A solution of **7** (69 mg; 0.24 mmol) in xylene (3 ml) was heated at reflux for 3 h under N_2 atmosphere. The mixture was diluted with benzene and washed with sat. aq NH_4Cl. The solvent was evaporated and the residue was purified by silica-gel column chromatography (hexane:AcOEt=40:1) to give 18 mg (46%) of **8** as a pale yellow oil. IR (neat) 1670 (CO) cm^{-1}; ^1H NMR δ=1.87 (3H, m), 3.98 (2H, s), 5.79 (1H, m), 6.04 (1H, m), 7.0—7.4 (5H, m); UV λ_{max} 218 nm; MS *m/z* (%) 160 (M^+, 38), 91 ($[M-C_4H_5O]^+$, 59), 69 ($[M-PhCH_2]^+$, 100).

Treatment of 7 with Aluminum Isoproposide. Aluminum isopropoxide (161 mg; 0.79 mmol) was dissolved in 2 ml of isopropyl alcohol; to this was added a solution of **7** (120 mg; 0.42 mmol) in 1 ml of isopropyl alcohol and the reaction mixture was stirred and refluxed for 8 h. The reaction mixture was diluted with AcOEt and washed with sat. qa NH_4Cl. After the usual workup, the product was purified by silica-gel column chromatography to give 14 mg (20%) of **8** as a pale yellow oil.

General Procedure for the Preparation of α,β-Unsaturated Ketones and α,β-Unsaturated Aldehydes from α,β-Epoxy Sulfoxides. A typical procedure is described for a synthesis of 1-(1-cyclohexenyl)-2-phenylethanone (**9**). To a solution of $LiClO_4 \cdot 3H_2O$ (32 mg; 0.2 mmol) and $(n\text{-}Bu)_3PO$ (43.6 mg; 0.2 mmol) in 3 ml of toluene was added a solution of 2'-benzyl-2'-(phenylsulfinyl)spiro[cyclohexane-1,1'-oxirane][5a] (65 mg; 0.2 mmol) in 1 ml of toluene. The mixture was stirred and heated at 110 °C (the temperature of the oil bath used) under a N_2 atmosphere until all the α,β-epoxy sulfoxide was consumed (2.5 h). The solution was cooled to room temperature and diluted with benzene. The whole mixture was washed once with sat. aq NH_4Cl and dried over Na_2SO_4. The solvent was evaporated under reduced pressure and the reside was purified by silica-gel column chromatography (hexane:AcOEt=20:1) to give 39 mg (98%) of **9** as a colorless oil. IR (neat) 1685 (CO), 1640 (C=C) cm^{-1}; ^1H NMR δ=1.60 (4H, m), 2.23 (4H, m), 3.92 (2H, s), 6.98 (1H, m), 7.0—7.3 (5H, m); UV λ_{max} 233.5 nm; MS *m/z* (%): 200 (M^+, 4), 186 ($[M-CH_2]^+$, 5), 109 ($[M-PhCH_2]^+$, 100).

1-(1-Cyclohexenyl)-2-(4-methoxyphenyl)ethanone (10). Colorless needles (AcOEt-hexane); mp 106—108 °C; IR (KBr): 1675 (CO), 1645, 1625 (C=C) cm^{-1}; ^1H NMR δ=1.60 (4H, m), 2.22 (4H, m), 3.76 (3H, s), 3.86 (2H, s), 6.98 (1H, m, vinyl-H), 6.7—7.2 (4H, m); UV λ_{max} 228.5 nm; Found: C, 78.44; H, 7.99%. Calcd for $C_{15}H_{18}O_2$: C, 78.23; H, 7.88%.

1-(1-Cyclohexenyl)-1-heptanone (11). Colorless oil; IR (neat) 1675 (CO), 1645 (C=C) cm^{-1}; ^1H NMR δ=0.88 (3H, bt, *J*=7 Hz), 2.04—2.36 (4H, m), 2.60 (2H, t, *J*=8 Hz), 6.85 (1H, m, vinyl-H); UV λ_{max} 234 nm; MS *m/z* (%) 194 (M^+, 20), 124 ($[M-C_5H_{10}]^+$, 72), 109 ($[M-C_6H_{13}]^+$, 100); Found: *m/z* 194.1672. Calcd for $C_{13}H_{22}O$: M, 194.1669.

Cyclohexyl 1-Cyclohexenyl Ketone (12). Colorless oil; IR (neat) 1660 (CO), 1635 (C=C) cm^{-1}; ^1H NMR δ=6.83 (1H, m, vinyl-H), UV λ_{max} 234.5 nm; MS *m/z* (%) 192 (M^+, 21), 163 ($[M-C_2H_5]^+$, 3), 109 ($[M-C_6H_{11}]^+$, 100); Found: *m/z* 192.1524. Calcd for $C_{13}H_{20}O$: M, 192.1513.

1-Acetyl-1-(4-*t*-butyl)cyclohexene (13). Colorless oil; IR (neat) 1675 (CO), 1655 (C=C) cm^{-1}; ^1H NMR δ=0.89 (9H, s), 2.27 (3H, s), 6.86 (1H, m); UV λ_{max} 233.5 nm; MS *m/z* (%) 180 (M^+, 70), 165 ($[M-CH_3]^+$, 21), 123 ($[M-C_4H_9]^+$, 61), 43 (100).

2-Acetyl-1*H*-indene (14). Colorless crystals (Et_2O-hexane); mp 56—58 °C; IR (KBr) 1660 (CO) cm^{-1}; ^1H NMR δ=2.48 (3H, s), 3.64 2H, d, *J*=2 Hz), 7.20—7.62 (5H, m); UV λ_{max} 233, 239.5, 301 nm; MS *m/z* (%) 158 (M^+, 100), 143 ($[M-CH_3]^+$, 37), 115 ($[M-CH_3CO]^+$, 86).

3-(1-Oxo-3-butenyl)cholestene ($\Delta^{2,3}$-, $\Delta^{3,4}$-mixture) (15). Colorless oil; IR (neat) 1680 (CO), 1640 (C=C) cm^{-1}; ^1H NMR δ=3.43 (2H, m, CH_2=CH-C<u>H_2</u>CO-), 5.03 (1H, m, C<u>H_2</u>=CH-), 5.17 (1H, m, C<u>H_2</u>=CH-), 5.75—6.16 (1H, m, CH_2=C<u>H</u>-), 6.58 (bs, vinyl-H of 4-position), 6.75 (m, vinyl-H of 2-position); From these protones, the ratio of $\Delta^{2,3}$:$\Delta^{3,4}$ could be determined to be 5:6; UV λ_{max} 240 nm; MS *m/z* (%) 438 (M^+, 78), 397 ($[M-C_3H_5]^+$, 100); Found: *m/z* 438.3869. Calcd for $C_{31}H_{50}O$: M, 438.3859.

3-Acetylcholestene ($\Delta^{2,3}$-,$\Delta^{3,4}$-mixture) (16). Colorless solid; IR (neat) 1675 (CO), 1645 (C=C) cm^{-1}; ^1H NMR δ=2.27, 2.29 (each s, CH_3CO), 6,56 (bs, vinyl-H of 4-position); From these protones the ratio of $\Delta^{2,3}$:$\Delta^{3,4}$ could

be determined to be 4:5; UV λ_{max} 238 nm; MS *m/z* (%) 412 (M^+, 100), 397 ($[M-CH_3]^+$, 10), 369 ($[M-CH_3CO]^+$, 7); Found: *m/z* 412.3685. Calcd for $C_{29}H_{48}O$: M, 412.3702.

3-Formylcholestene ($\Delta^{2,3}$-, $\Delta^{3,4}$-mixture) (17). A mixture of $\Delta^{2,3}$- and $\Delta^{3,4}$-enal in a ratio of 2:5. Colorless solid; IR (KBr) 1680 (CO), 1655 (C=C) cm^{-1}; ^1H NMR δ=6.48 (bs, vinyl-H), 6.66 (m, vinyl-H), 9.36, 9.38 (each s, CHO); UV λ_{max} 233.5 nm; MS *m/z* (%) 398 (M^+, 100), 383 ($[M-CH_3]^+$, 13), 315 ($[M-C_5H_7O]^+$, 25); Found: *m/z* 398.3553. Calcd for $C_{28}H_{46}O$: M, 398.3546.

5-Formyl-4-nonene (19). Colorless oil; IR (neat) 2730 (CHO), 1700 (CO), 1650 (C=C) cm^{-1}; ^1H NMR δ=2.00—2.48 (4H, m), 6.41 (1H, t, *J*=7 Hz, vinyl-H), 9.32 (1H, s, CHO); UV λ_{max} 229.5 nm; MS *m/z* (%) 154 (M^+, 73), 139 ($[M-CH_3]^+$, 12), 125 ($[M-C_2H_5]^+$, 26), 111 ($[M-C_3H_7]^+$, 100).

4-*t*-Bultyl-1-cyclohexene-1-carbaldehyde (20). Colorless oil; IR (neat) 1690 (CO), 1650 (C=C) cm^{-1}; ^1H NMR δ=0.91 (9H, s), 6.78 (1H, m), 9.37 (1H, s); UV λ_{max} 231.5 nm; MS *m/z* (%) 166 (M^+, 18), 123 (21), 110 (71), 57 (100).

General Procedure for the Preparation of α,β-Unsaturated Ketones from the α,β-Epoxy Sulfoxides Derived from Aldehydes. A typical procedure is described for the synthesis of 1-phenyl-3-dodecen-2-one (**26**). To a solution of $NaBH_4$ (946 mg; 2.5 mmol) in 4 ml of EtOH was added diphenyl disulfide (273 mg; 1.25 mmol); the whole mixture was stirred and refluxed under a N_2 atmosphere for 30 min. The mixture was cooled to room temperature and to this was added 100 mg (0.26 mmol) of 2,3-epoxy-1-phenylsulfinyldodecane (the α,β-epoxy sulfoxide in Table 3, Entry 1); the reaction mixture was stirred at room temperature for 30 min. The reaction was quenched by adding sat. aq NH_4Cl and the EtOH was evaporated under vacuum and the residue was extracted with benzene-ether. The combined organic layer was washed once with sat. aq NH_4Cl, dried and concentrated. The residue was separated by silica-gel column chromatography to afford 98 mg (100%) of 1-phenyl-3-phenylthio-2-dodecanone as a colorless oil. IR (neat) 1705 (CO) cm^{-1}; ^1H NMR δ=0.88 (3H, bt, *J*=7 Hz), 3.67 (1H, t, *J*=7 Hz), 3.83, 3.84 (each 1H, d, *J*=16 Hz), 7.0—7.4 (10H, m). This α-phenylthio ketone (98 mg; 0.26 mmol) was dissolved in 4 ml of CH_2Cl_2 and the solution was cooled to −50 °C. To this was added *m*-CPBA (0.29 mmol) and after being stirred for 10 min, 10% aq NaOH (10 ml) was added. The whole mixture was extracted with CH_2Cl_2 and after the usual workup, the product was purified by silica-gel column chromatography to afford 99.6 mg (99%) of 1-phenyl-3-phenylsulfinyl-2-dodecanone as a colorless oil. IR (neat) 1705 (CO), 1045 (SO) cm^{-1}. This sulfoxide (57.7 mg; 0.15 mmol) was dissolved in 3 ml of toluene and the solution was refluxed under N_2 atmosphere for 15 min. The solvent was evaporated under reduced pressure and the residue was purified by silica-gel column chromatography to afford 30 mg (78%) of the desired enone **26** as a colorless oil. IR (neat) 1690, 1670 (CO), 1630 (C=C) cm^{-1}; ^1H NMR δ=0.88 (3H, bt, *J*=6 Hz), 2.00—2.32 (2H, m), 3.79 (2H, s), 6.09 (1H, dt, *J*=16, 1.5 Hz, vinyl-H), 6.88 (1H, dt, *J*=16, 7 Hz, vinyl-H), 7.04—7.40 (5H, m); UV λ_{max} 226.5 nm; MS *m/z* (%) 258 (M^+, 6), 188 ($[M-C_5H_{10}]^+$, 6), 167 ($[M-PhCH_2]^+$, 100); Found: *m/z* 258.1971. Calcd for $C_{18}H_{26}O$: M, 258.1981.

5-Phenyl-3-penten-2-one (27). α-Phenylthio ketone: Colorless oil; IR (neat) 1705 (CO) cm^{-1}; ^1H NMR δ=1.8—2.2 (2H, m), 2.24 (3H, s), 2.75 (2H, t, *J*=7 Hz), 3.55 (1H, t, *J*=7 Hz), 7.0—7.4 (10H, m); MS *m/z* (%) 270 (M^+, 24), 227 ($[M-CH_3CO]^+$, 4), 166 ($[M-C_8H_8]^+$, 42), 117 ($[M-C_8H_9OS]^+$, 100); Found: *m/z* 270.1090. Calcd for $C_{17}H_{18}OS$: M, 270.1077. α-Phenylsulfinylated ketone: Colorless oil; IR (neat) 1710 (CO), 1085, 1050 (SO) cm^{-1}. The enone **27**: Colorless oil; IR (neat) 1670 (CO), 1625 (C=C) cm^{-1}; ^1H NMR δ=2.23 (3H, s), 3.53 (2H, dd, *J*=7, 1.5 Hz), 6.03 (1H, dt, *J*=16, 1.5 Hz), 6.88 (1H, dt, *J*=16, 7 Hz), 7.0—7.4 (5H, m); UV λ_{max} 219 nm; MS *m/z* (%) 161 ($[M+H]^+$, 97), 126 (28), 117 ($[M-CH_3CO]^+$, 28), 91 ($[M-C_4H_5O]^+$, 100).

1-Cyclohexyl-2-hepten-1-one (28). α-Phenylthio ketone; see Ref. 5b. α-Phenylsulfinylated ketone: Colorless oil; IR (neat) 1700 (CO), 1085, 1050 (SO) cm^{-1}. The enone **28**: Colorless oil; IR (neat) 1695, 1670 (CO), 1635 (C=C) cm^{-1}; ^1H NMR δ=0.91 (3H, bt, *J*=6.5 Hz), 2.00—2.32 (2H, m), 2.54 (1H, m), 6.10 (1H, dt, *J*=15.5, 1.5 Hz), 6.82 (1H, dt, *J*=15.5, 7 Hz); UV λ_{max} 228.5 nm; MS *m/z* (%): 194 (M^+, 3), 137 ($[M-C_4H_9]^+$, 69), 111 ($[M-C_6H_{11}]^+$, 100); Found: *m/z* 194.1673. Calcd for $C_{13}H_{22}O$: M, 194.1670.

(*Z*)-7-Formyl-6-tridecene (29). Colorless oil; IR (neat) 1695 (CO), 1645 (C=C) cm^{-1}; ^1H NMR δ=0.90 (6H, m), 2.00—2.46 (4H, m), 6.40, (1H, t, *J*=7.5 Hz); UV λ_{max} 231.5 nm; MS *m/z* (%): 210 (M^+, 37), 167 (25), 155 (41), 141 (51), 113 (96), 43 (100).

General Procedure for the Preparation of α,β-Unsaturated Esters from α,β-Unsaturated Aldehydes. A typical procedure is described for the synthesis of 4-*t*-butyl-1-(methoxycarbonyl)cyclohexene (**31**). A solution of $NaClO_2$ (85%; 48 mg; 0.45 mmol) in 0.42 ml of H_2O was added dropwise over a period of 2 h to a stirred solution of **20** (49 mg; 0.3 mmol) in *t*-BuOH (0.5 ml), 10 mg of Na_2HPO_4 in 0.12 ml of H_2O and 35 μl of H_2O_2 (35%). The reaction mixture was vigorously stirred at room temperature for 20 h. The reaction was quenched by adding 6 mg of Na_2SO_3; the mixture was acidified with 10% HCl to pH 2 and the whole was extracted with ether. The combined ether layer was dried over Na_2SO_4 and the ether was evaporated. The residue, without further purification, was treated with slight excess CH_2N_2 in ether. The product was purified by silica-gel column chromatography with a mixture of hexane and AcOEt (50:1) as an eluent to give **31** (51 mg; 88%) as a colorless oil; IR (neat) 1720 (CO), 1655 (C=C), 1265 (COC) cm^{-1}; ^1H NMR δ=0.88 (9H, s), 3.70 (3H, s), 6.94 (1H, m); UV λ_{max} 220 nm; MS *m/z* (%) 196 (M^+, 31), 181 ($[M-CH_3]^+$, 6), 153 (19), 140 ($[M-C_4H_8]^+$, 100); Found: *m/z* 196.1455. Calcd for $C_{12}H_{20}O_2$: M, 196.1461.

(*Z*)-7-Methoxycarbonyl-6-tridecene (30). Colorless oil; IR (neat) 1715 (CO), 1640 (C=C), 1275, 1250 (COC) cm^{-1}; ^1H NMR δ=0.89 (6H, m), 2.0—2.4 (4H, m), 3.71 (3H, s), 6.69 (1H, t, *J*=7.5 HZ); UV λ_{max} 218 nm; MS *m/z* (%) 240 (M^+, 34), 209 ($[M-OCH_3]^+$, 9), 197 ($[M-C_3H_7]^+$, 13), 169 ($[M-C_5H_{11}]^+$, 100); Found: *m/z* 240.2092. Calcd for $C_{15}H_{28}O_2$: M, 240.2088.

The Ester 32. A mixture of $\Delta^{2,3}$- and $\Delta^{3,4}$-ester in a ratio of 2:5. Colorless solid; IR (KBr) 1715 (CO), 1675 (C=C), 1265, 1255, 1245 (COC); ^1H NMR δ=3.72 (3H, s), 6.68 (bs, vinyl-H), 6.08 (m, vinyl-H); UV λ_{max} 224 nm; MS *m/z* (%) 428 (M^+, 100), 413 ($[M-CH_3]^+$, 19), 315 (34); Found: *m/z* 428.3641. Calcd for $C_{29}H_{48}O_2$: M, 428.3651.

1-(Methoxycarbonyl)cyclooctene (33). Colorless oil; IR

(neat) 1730, 1720 (CO), 1650 (C=C), 1290, 1215 (COC); ^{1}H NMR δ=3.71 (3H, s), 6.95 (1H, t, J=8.5 Hz); UV λ_{max} 223 nm; MS m/z (%) 168 (M^+, 73), 153 ([M−CH_3]$^+$, 13), 137 (35), 109 (100).

1-(Methoxycarbonyl)cyclododecene (34). Colorless oil; IR (neat) 1720 (CO), 1645 (C=C), 1285, 1220 (COC) cm^{-1}; ^{1}H NMR δ=2.04—2.45 (4H, m), 3.72 (3H, s), 6.72 (1H, t, J=8 Hz); UV λ_{max} 220 nm; MS m/z (%) 224 (M^+, 75), 193 (23), 153 (27), 95 (75), 81 (100).

The authors are grateful to Dr. Sei-ichi Saito, Tanabe Seiyaku Co., Ltd., for elemental analysis and Miss Noriko Sawabe and Mrs. Noriko Yamatani of this laboratory for NMR and MS measurements.

References

1) Part IX: T. Satoh, T. Kumagawa, A. Sugimoto, and K. Yamakawa, *Bull. Chem. Soc. Jpn.*, **60**, 301 (1987).

2) J. D. Roberts and M. C. Caserio, "Basic Principles of Organic Chemistry," W. A. Benjamin, Inc. (1964), p. 426.

3) M. C. Kloetzel, *Org. React.*, **4**, 1 (1948); H. L. Holmes, *ibid.*, **4**, 60 (1948); L. W. Butz and A. W. Rytina, *ibid.*, **5**, 136 (1949). J. Sauer, *Angew. Chem., Int. Ed. Engl.*, **5**, 211 (1966), **6**, 16 (1967); G. Desimoni and G. Tacconi, *Chem. Rev.*, **75**, 651 (1975); G. Brieger and J. N. Bennett., *ibid.*, **80**, 63 (1980); M. Petrizilka, *Synthesis*, **1981**, 753, A. G. Fallis, *Can. J. Chem.*, **62**, 183 (1984); E. Ciganek, *Org. React.*, **32**, 1 (1984).

4) E. D. Bergmann, D. Ginsburg, and R. Pappo, *Org. React.*, **10**, 179 (1959); G. Posner, *ibid.*, **19**, 1 (1972); W. Carruthers, *Chem. Ind.*, **1973**, 931; M. E. Jung, *Tetrahedron*, **32**, 3 (1976); O. W. Lever, Jr., *ibid.*, **32**, 1943 (1976); R. E. Gawley, *Synthesis*, **1976**, 777.

5) a) T. Satoh, Y. Kaneko, T. Izawa, K. Sakata, and K. Yamakawa, *Bull. Chem. Soc. Jpn.*, **58**, 1983 (1985); b) T. Satoh, T. Kumagawa, and K. Yamakawa, *ibid.*, **58**, 2849 (1985); c) T. Satoh, Y. Kaneko, K. Sakata, and K. Yamakawa, *ibid.*, **59**, 457 (1986); d) T. Satoh, S. motohashi, and K. Yamakawa, *ibid.*, **59**, 946 (1986); e) T. Satoh, T. Kumagawa, and K. Yamakawa, *Tetrahedron Lett.*, **27**, 2471 (1986); f) T. Satoh, S. Motohashi, and K. Yamakawa, *ibid.*, **27**, 2889 (1986).

6) T. Satoh, Y. Kaneko, and K. Yamakawa, *Bull. Chem. Soc. Jpn.*, **59**, 2463 (1986) and references cited therin.

7) T. Satoh, Y. Kaneko, T. Kumagawa, T. Izawa, K. Sakata, and K. Yamakawa, *Chem. Lett.*, **1984**, 1957.

8) V. Reutrakul and W. Kanghae, *Tetrahedron Lett.*, **1977**, 1377; D. F. Taber and B. P. Gunn, *J. Org. Chem.*, **44**, 450 (1979).

9) T. Durst and K. C. Tin, *Tetrahedron Lett.*, **1970**, 2369; D. F. Tavares, R. E. Estep, and M. Blezard, *ibid.*, **1970**, 2373.

10) B. Rickborn and E. M. Gerkin *J. Am. Chem. Soc.*, **90**, 4193 (1968).

11) D. R. Williams and K. Nishitani, *Tetrahedron Lett.*, **21**, 4417 (1980).

12) B. M. Trost and T. N. Salzmann, *J. Am. Chem. Soc.*, **95**, 6840 (1973); B. M. Trost, T. N. Salzmann, and K. Hiroi, *ibid.*, **98**, 4887 (1976); B. M. Trost and G. S. Massiot, *ibid.*, **99**, 4405 (1977); B. M. Trost, *Chem. Rev.*, **78**, 363 (1978).

13) Y. Yamamoto and K. Maruyama, *J. Am. Chem. Soc.*, **100**, 3240 (1978); Y. Yamamoto, S. Yamamoto, H. Yatagai, Y. Ishihara, and K. Maruyama, *J. Org. Chem.*, **47**, 119 (1982). (1982).

14) M. Yamaguchi, K. Hasebe, S. Tanaka, and T. Minami, *Tetrahedron Lett.*, **27**, 959 (1986); D. Enders, K. Papadopoulos, and B. E. M. Rendenbach, *ibid.*, **27**, 3491 (1986).

15) S. E. Dinizo, R. W. Freerksen, W. E. Pabst, and D. S. Watt., *J. Am. Chem. Soc.*, **99**, 182 (1977); S. F. Martin, *Synthesis*, **1979**, 633; K. Takahashi, K. Shibasaki, K. Ogura, and H, Iida, *J. Org. Chem.*, **48**, 3566 (1983).

16) G. Gousseau, P. LePerchec, and J. M. Conia, *Synthesis*, **1978**, 67.

17) a) E. J. Corey and N. W. Gilman, *J. Am. Chem. Soc.*, **90**, 5616 (1968); b) H. W. Pinnick, *Tetrahedron.*, **37**, 2091 (1981); c) E. Dalcanale and F. Montanari, *J. Org. Chem.*, **51**, 567 (1986).

18) K. E. Harding, K. S. Clement, J. C. Gilbert, and B. Wiechman, *J. Org. Chem.*, **49**, 2049 (1984); M. J. Taschner and A. Shahripour, *J. Am. Chem. Soc.*, **107**, 5570 (1985).

Photoinduced Substitution Reaction Initiated by Electron-Transfer. Photochemical Reaction of 2,3-Dichloro-1,4-naphthoquinone with Thiophenes

Kazuhiro MARUYAMA* and Hitoshi TAMIAKI
Department of Chemistry, Faculty of Science, Kyoto University, Kyoto 606
(Received November 18, 1986)

Photochemical reaction of 2,3-dichloro-1,4-naphthoquinone (**1**) with thiophenes **2** afforded 2-chloro-3-(2-thienyl)-1,4-naphthoquinones. The reaction might be initiated by the photoelectron transfer from **2** to **1**, resulting in the formation of combined products via recombination of the formed ion radicals $\mathbf{1}^{\cdot-}$ and $\mathbf{2}^{\cdot+}$ by accompanying elimination of chloro and hydro radicals. In the photoreaction, reactivity of **2** was estimated from the observed oxidation potentials of **2** and the calculated electron densities in $\mathbf{2}^{\cdot+}$.

Photoinduced reactions initiated by electron transfer are one of the recent topics. The reactions are attractive from the viewpoints of synthesis and mechanism in organic and bio-reactions.[1] We have already reported several photosubstitution reactions induced by photoelectron transfer; photochemical reactions of 2-halo-1,4-naphthoquinones with olefins[2] and olefin analogues[3] (Scheme 1). In this paper, we report the photoreaction of 2,3-dichloro-1,4-naphthoquinone (**1**) with thiophenes **2** to afford 2-chloro-3-(2-thienyl)-1,4-naphthoquinones **3** which are of interest as precursors of alkylated quinones,[4] and then discuss the reaction pathway.

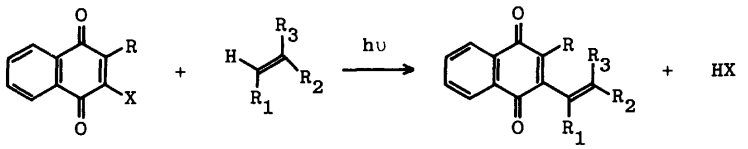

X = Cl, Br.

R_1 = H, R_2,R_3 = Alkyl, Aryl, *O*-Alkyl, *O*-Silyl;
R_1,R_2 = -O-CH=CH-, R_3 = H;
R_1,R_2 = -NH-CH=CH-, R_3 = H.

Scheme 1. Substitution reaction of quinones with olefins initiated by photoelectron transfer.

Table 1. Photochemical Reaction of **1** with **2**

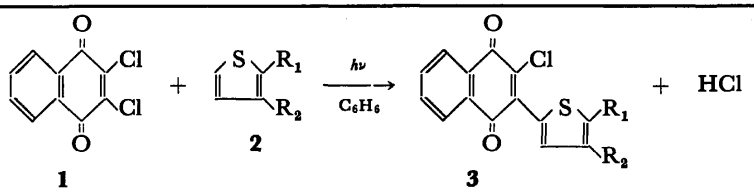

1 **2** **3**

R_1	R_2		E_{pa}[a]/V	I_p[b]/eV	v_{rel}[c]		Yield[d]/%
I	H	(**2a**)	1.42	8.55	0.82	(**3a**)	78
Br	H	(**2b**)	1.48	8.66	1.24	(**3b**)	70
Cl	H	(**2c**)	1.50	8.70	1.51	(**3c**)	65
H	H	(**2d**)	1.54	8.80	1	(**3d**)	57
H	I	(**2e**)	1.55	—	0.11	(**3e**)	17
H	Br	(**2f**)	1.60	8.90	0.07	(**3f**)	5
H	Cl	(**2g**)	1.64	—	0.02	(**3g**)	2
CO_2H	H	(**2h**)	<1.77	—	0		0
COMe	H	(**2i**)	1.79	—	0		0
CO_2Et	H	(**2j**)	≈1.84	—	0		0
CHO	H	(**2k**)	1.85	—	0		0

a) Anodic peak potential of **2**, error was within ±0.02 V, vs. ferrocene/ferrocenium ([**2**] = 10^{-3} mol dm^{-3}, [*n*-Bu_4NClO_4] = 0.1 mol dm^{-3}, in CH_2Cl_2, 100 mV s^{-1}, 24 °C). b) Adiabatic first ionization potential of **2**, data of Ref. 8. c) v_{rel} was the value of the initial rate in the formation of **3** relative to that in the formation of **3d** ([**1**] = 10^{-4} mol dm^{-3}, [**2**] = 10^{-3} mol dm^{-3}, in benzene, upon irradiation with light of 313 nm). d) All yields were based on consumed **1**, see Experimental part.

Results and Discussion

Photochemical reaction of quinone **1** with thiophenes **2** generally gave thienylquinones **3** (Table 1). Thiophenes **2a—g** successfully afforded **3a—g**, but the photoreaction of **2h—k** resulted in vain.[5] To explain reactivities of **2**, we tried to measure the oxidation potentials $E_{1/2}$ of **2**. All the thiophenes (**2**) were electrooxidized irreversibly,[6] and their anodic peak potentials E_{pa} are listed in Table 1. The order of their E_{pa} is supposed to be equal to that of their $E_{1/2}$ because the E_{pa} is nearly linear with the ionization potential I_P; $E_{pa}=0.501\ I_P-2.68$ (correlation coefficient =99.8%).[7] As shown in Table 1, thiophenes **2a—g** whose E_{pa} were smaller than 1.7 V reacted with **1** to give **3a—g**, and **2h—k** whose E_{pa} were greater than 1.7 V did not react. In the cases of 3-halothiophenes **2e—g**, the increase in their E_{pa} suppressed their reactivities v_{rel}, the value of the initial rate in the formation of **3** relative to that in the formation of **3d**. When **2d** was added to a benzene solution of **1**, a new absorption band (λ_{max}=422 nm, the formation constant K=0.08 dm^3 mol^{-1} at 22 °C[9]) appeared. In the ground state, thiophene **2d** formed apparently the charge-transfer (CT) complex with **1** absorbing light of wavelengths above 500 nm. Selective irradiation of the CT band (514.5 nm-irradiation, see Experimental part) led to the formation of **3d**. In the initial stage of the reaction, therefore, photoelectron transfer could occur from **2a—g** to **1**.

In order to understand the high regioselectivity in the reactions affording **3a—g** as well as less reactivity of 3-halothiophenes **2e—g**, we calculated the electron densities q in the cation radials of **2** ($\mathbf{2}^{\cdot+}$) formed by the photoelectron transfer process by using Hückel molecular orbital (HMO) method (Table 2). In the cases of **2a—d**, the substitution reaction occurred at the lowest q position. This position is the electron-poorest in $\mathbf{2}^{\cdot+}$, which must be attacked by the anion radical of **1** ($\mathbf{1}^{\cdot-}$) more easily than any other position. On the other hand, in the cases of 3-substituted thiophenes **2e—g**, the lowest q position is crowded with iodo, bromo, and chloro atoms on its neighbouring carbon atom. Such a situation could make attacking by the fairly bulky $\mathbf{1}^{\cdot-}$ difficult, so the substitution occurred at the second lowest q position sterically less hindered. The q values of C-5 atom in the cation radicals of 3-halothiophenes **2e—g** are over

Table 2. Calculated Electron Density q of $\mathbf{2}^{\cdot+}$ [a]

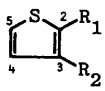

$\mathbf{2}^{\cdot+}$

R_1	R_2		C-2	C-3	C-4	C-5
I	H	($\mathbf{2a}^{\cdot+}$)	(0.764)	0.877	1.012	0.646
Br	H	($\mathbf{2b}^{\cdot+}$)	(0.764)	0.874	1.014	0.641
Cl	H	($\mathbf{2c}^{\cdot+}$)	(0.742)	0.884	1.003	0.637
H	H	($\mathbf{2d}^{\cdot+}$)	0.623	0.932	0.932	0.623
H	I	($\mathbf{2e}^{\cdot+}$)	0.586	(0.955)	0.983	0.712
H	Br	($\mathbf{2f}^{\cdot+}$)	0.583	(0.950)	0.991	0.711
H	Cl	($\mathbf{2g}^{\cdot+}$)	0.586	(0.950)	0.978	0.698

a) HMO calculation (ω-technique), see Ref. 10. Parenthesis indicates the position which possesses no hydrogen.

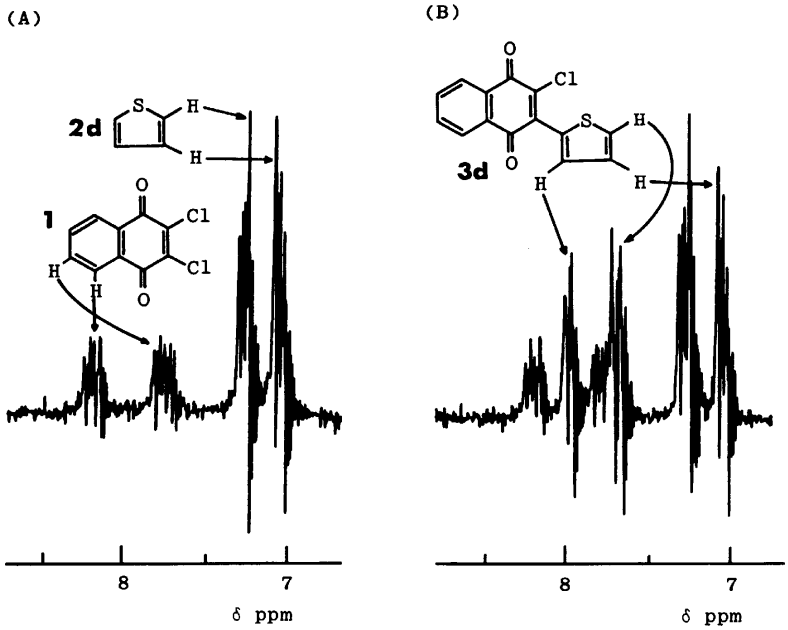

Fig. 1. ^{1}H NMR spectra observed in a CCl_4 solution of **1** and **2d**. (A) In the dark, (B) during irradiation.

0.69 and greater than those of highly reactive thiophenes **2a—d**. So the relatively high q values of C-5 atom in $\mathbf{2e}^{\ddagger}$, $\mathbf{2f}^{\ddagger}$, and $\mathbf{2g}^{\ddagger}$ might suppress their reactivities. Thus, the experimental results could be clearly explained by simple HMO calculation.

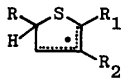

4·

As shown in Fig. 1, in all the cases in which **3** were obtained except for **3a** and **3g**, photo-^{1}H CIDNP signals were observed at the protons in the thienyl moiety of **3**. The polarized patterns indicated that at least the structure of **4·** might exist in the course of the reaction and that all the radical pairs were in the triplet multiplicity.[11]

Under the conditions (see footnote a) in Table 1), the CT state in the ground state was much less than 1% (about 0.08% in **2d**) and the absorption at 313 nm was mainly due to quinone **1**. Upon irradiation with light of 313 nm, the local excitation of **1** was dominant and the CT excitation was negligible. Considering the fact that **1** photoreacted with various olefins via the triplet quenching mechanism,[12] the initially formed singlet excited state of **1** might immediately intersystem-cross to the triplet excited state, where it was quenched by **2** in the ground state to give the ion radical pair $^3(\mathbf{1}^{\cdot-}\cdots\mathbf{2}^{\ddagger})$. Above results lead us to the reaction mechanism in Scheme 2.

Experimental

Apparatus. All melting points were measured with a Yanagimoto micro melting point apparatus and were uncorrected. Ultraviolet and visible spectra were measured with a Shimadzu UV-200 spectrometer. Infrared spectra were measured with a JASCO IRA-1 spectrometer. Normal ^{1}H and ^{13}C NMR spectra were recorded on a JEOL JNM-FX400 instrument; chemical shifts (δ) are expressed in parts per million relative to tetramethylsilane. Mass spectra were measured with a JEOL JMS-DX-300 spectrometer. HPLC analyses were carried out with a Waters liquid chromatograph equipped with a LiChrosorb RP-18 column. The elemental analyses were performed at the Microanalysis Center of Kyoto University.

Materials. Reagent-grade solvents were simply distilled and used except otherwise noted. Quinone **1**, thiophenes **2b—d**, **2f**, and **2h—k** were commercially available and used after distillation. Thiohenes **2a**,[13] **2e**,[14] and **2g**[15] were synthesized according to the procedure in the literature.

Preparation of 2-Chloro-3-(2-thienyl)-1,4-naphthoquinones 3. General Procedure: A benzene solution (700 ml) of **1** (0.7 mmol) and 10 equiv of **2** (7 mmol) was irradiated with a high-pressure mercury arc lamp (300 W) through an aqueous $CuSO_4$ solution filter under argon atmosphere at room temperature. After irradiation for a suitable time (1 h for **3a—d** and **3g**, 3 h for **3e**, and 12 h for **3f**), the starting quinone **1**, thiophene **2**, and the photosubstituted product **3** were isolated by using flash column chromatography on silica gel with hexane and ether as eluents. Recrystallization from dichloromethane and hexane gave a pure sample. All yields were based on consumed **1**.

2-Chloro-3-(5-iodo-2-thienyl)-1,4-naphthoquinone (3a): 78% yield; red needles; mp 151.5—152 °C; UV ($CHCl_3$) 466 nm (ε 5450); IR (KBr) 1660 cm^{-1} (C=O); ^{1}H NMR ($CDCl_3$) δ=7.37 (1H, d, J=4 Hz, 4-H), 7.74 (1H, d, J=4 Hz, 3-H), 7.77—7.81 (2H, m), and 8.16—8.20 (2H, m); MS (70 eV) m/z (rel intensity) 400, 402 (M^+; 100, 34), 365 (M^+ −Cl; 45), 337 (M^+ −Cl−CO; 21), 273 and 275 (M^+ −I; 37, 18); Found: C, 41.76; H, 1.48; Cl, 8.87; I, 31.76%; M^+, 399.8822 and 401.8796. Calcd for $C_{14}H_6ClIO_2S$: C, 41.97; H, 1.51; Cl, 8.85; I, 31.68%; M, 399.8824 and 401.8794.

2-(5-Bromo-2-thienyl)-3-chloro-1,4-naphthoquinone (3b): 70% yield; red plates; mp 153—153.5 °C; UV ($CHCl_3$) 460 nm

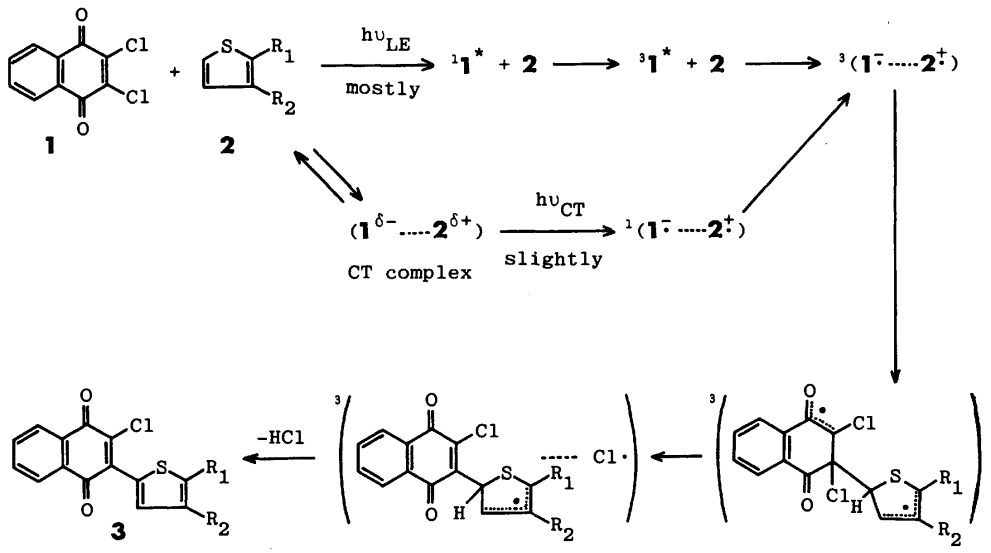

Scheme 2. Proposed mechanism for photoreaction of **1** with **2** on 313 nm-irradiation. $h\upsilon_{LE}$: The local excitation of **1**, $h\upsilon_{CT}$: The excitation of the CT complex.

(ε 4500); IR (KBr) 1665 cm^{-1} (C=O); ^{1}H NMR ($CDCl_3$) δ=7.17 (1H, d, J=4 Hz, 4-H), 7.75—7.80 (2H, m), 7.86 (1H, d, J=4 Hz, 3-H), and 8.12—8.20 (2H, m); MS (70 eV) m/z (rel intensity) 352, 354, 356 (M^+; 75, 100, 31), 317, 319 (M^+ −Cl; 47, 50), 289, 291 (M^+ −Cl−CO; 22, 22), 273, and 275 (M^+ −Br; 71, 29); Found: C, 47.51; H, 1.64; Br, 22.46; Cl, 9.97; S, 9.23%; M^+, 351.8960, 353.8936, and 355.8914. Calcd for $C_{14}H_6BrClO_2S$: C, 47.55; H, 1.71; Br, 22.60; Cl, 10.03; S, 9.07%; M, 351.8961, 353.8931, 353.8941, and 355.8912.

2-Chloro-3-(5-chloro-2-thienyl)-1,4-naphthoquinone (3c): 65% yield; red needles; mp 141—141.5 °C; UV ($CHCl_3$) 426 (sh, ε 4500), 445 (sh, 5000), and 463 nm (5100); IR (KBr) 1660 cm^{-1} (C=O); ^{1}H NMR ($CDCl_3$) δ=7.05 (1H, d, J=4 Hz, 4-H), 7.77—7.82 (2H, m), 7.94 (1H, d, J=4 Hz, 3-H), and 8.16—8.20 (2H, m); MS (70 eV) m/z (rel intensity) 308, 310, 312 (M^+; 76, 61, 12), 273, 275 (M^+ −Cl; 100, 36), 245, and 247 (M^+ −Cl−CO; 36, 12); Found: C, 54.15; H, 1.79; Cl, 22.95; S, 10.46%; M^+, 307.9465, 309.9433, and 311.9403. Calcd for $C_{14}H_6Cl_2O_2S$: C, 54.39; H, 1.96; Cl, 22.93; S, 10.37%; M, 307.9466, 309.9436, and 311.9406.

2-Chloro-3-(2-thienyl)-1,4-naphthoquinone (3d): 57% yield; red prisms; mp 95 °C; UV ($CHCl_3$) 275 (ε 23000), 320 (50000), and 441 nm (4400); IR (KBr) 1670 cm^{-1} (C=O); ^{1}H NMR ($CDCl_3$) δ=7.22 (1H, dd, J=4 and 5 Hz, 4-H), 7.73 (1H, dd, J=1 and 5 Hz, 5-H), 7.75—7.79 (2H, m), 7.95 (1H, dd, J=1 and 4 Hz, 3-H), and 8.13—8.18 (2H, m); ^{13}C NMR ($CDCl_3$) δ=181.86 (s), 177.62 (s), 139.68 (s), 138.10 (s), 134.11 (d, C-3), 134.07 (d), 134.02 (d), 132.28 (d, C-5), 131.44 (s), 131.12 (s), 130.91 (s), 127.30 (d), 126.87 (d), and 126.57 (d, C-4); MS (70 eV) m/z (rel intensity) 276, 274 (M^+; 87, 37), 239 (M^+ −Cl; 100), and 211 (M^+ −Cl−CO; 30); Found: C, 60.96; H, 2.43; Cl, 12.78; S, 11.64%; M^+, 273.9856 and 275.9826. Calcd for $C_{14}H_7ClO_2S$: C, 61.21; H, 2.57; Cl, 12.90; S, 11.67%; M, 273.9855 and 275.9826.

2-Chloro-3-(4-iodo-2-thienyl)-1,4-naphthoquinone (3e): 17% yield; red needles; mp 141—143 °C; UV ($CHCl_3$) 444 nm (ε 4060); IR (KBr) 1670 cm^{-1} (C=O); ^{1}H NMR ($CDCl_3$) δ=7.77 (1H, d, J=1 Hz, 5-H), 7.78—7.82 (2H, m), 7.92 (1H, d, J=1 Hz, 3-H), and 8.16—8.22 (2H, m); MS (70 eV) m/z (rel intensity) 400, 402 (M^+; 100, 30), 365 (M^+ −Cl; 58), 337 (M^+ −Cl−CO; 25), 273, and 275 (M^+ −I; 12, 5); Found: m/z 399.8823 and 401.8791. Calcd for $C_{14}H_6ClIO_2S$: M, 399.8824 and 401.8794.

2-(4-Bromo-2-thienyl)-3-chloro-1,4-naphthoquinone (3f): 5% yield; orange needles; mp 125—127 °C; UV ($CHCl_3$) 433 nm (ε 3960); IR (KBr) 1670 cm^{-1} (C=O); ^{1}H NMR ($CDCl_3$) δ=7.61 (1H, d, J=1 Hz, 5-H), 7.78—7.82 (2H, m), 7.88 (1H, d, J=1 Hz, 3-H), and 8.16—8.21 (2H, m); MS (70 eV) m/z (rel intensity) 352, 354, 356 (M^+; 73, 100, 30), 317, 319 (M^+ −Cl; 69, 70), 289, 291 (M^+ −Cl−CO; 26, 27), 273, and 275 (M^+−Br; 12, 5); Found: m/z 351.8961, 353.8934, and 355.8916. Calcd for $C_{14}H_6BrClO_2S$: M, 351.8961, 353.8931, 353.8941, and 355.8912.

2-Chloro-3-(4-chloro-2-thienyl)-1,4-naphthoquinone (3g): 2% yield; red needles; mp 143—144 °C; UV ($CHCl_3$) 434 nm (ε 5730); IR (KBr) 1670 cm^{-1} (C=O); ^{1}H NMR ($CDCl_3$) δ=7.51 (1H, d, J=1.5 Hz, 5-H), 7.78—7.83 (2H, m), 7.84 (1H, d, J=1.5 Hz, 3-H), and 8.17—8.21 (2H, m); MS (70 eV) m/z (rel intensity) 308, 310, 312 (M^+; 75, 58, 11), 273, 275 (M^+ −Cl; 100, 35), 245, and 247 (M^+ −Cl−CO; 45, 16); Found: m/z 307.9465, 309.9438, and 311.9412. Calcd for $C_{14}H_6Cl_2O_2S$: M, 307.9466, 309.9436, and 311.9406.

Measurement of v_{rel}. A benzene solution (1 ml) of **1** (0.1 μmol) and **2** (1 μmol) was irradiated with light of 313 nm and sampled at an appropriate interval. The molar quantity of **3** was determined by measuring the area of HPL chromatogram (H_2O-MeOH=1/9) and plotted versus time. The initial rate in the formation of **3** was determined from a slope of the straight line. The value of v_{rel} was obtained by dividing each rate by the rate in the formation of **3d**.

Measurement of E_{pa} of Thiophenes 2. Electrochemical measurement was performed with PAR Model 174 polarographic analyzer, a standard H-cell, glassy carbon (working electrode), and a platinum wire (counter electrode). The solution was 10^{-3} mol dm^{-3} in **2**, in a 0.1 mol dm^{-3} tetrabutylammonium perchlorate-dried dichloromethane solution. All the cyclic voltammograms were recorded at 24 °C under single sweep conditions (scan rate; 100 mV s^{-1}). Anodic peak potentials were corrected vs. ferrocene/ ferrocenium. The peak potentials were measured with an error of ±0.02 V. It was necessary to repeat polishing of the electrode during the experiment, because thiophene polymers and others[6] were frequently adsorbed on the electrode surface.

Examination of CT Excitation. When thiophene **2d** was added to a benzene solution of quinone **1**, color of the solution was turned from pale yellow to pale orange, owing to the formation of the CT complex of **1** with **2d**. In a benzene solution, **1** had no absorption at wavelengths above 500 nm, but the CT complexes had the absorption in the region. For selective irradiation of the CT complex, NEC GLS 3300 Argon ion laser (514.5 nm, 1 W) was used. After irradiating a benzene solution of **1** and **2d** for a few minutes, **3d** was detected by thin-layer chromatography.

Observation of ^{1}H CIDNP Signals. Suitable amounts of **1** and **2** were dissolved in CCl_4, $CDCl_3$, or C_6D_6. The sample was irradiated in a Pyrex glass NMR sample tube with a high-pressure mercury arc projector lamp at room temperature and the ^{1}H NMR signals were recorded before, during, and after irradiation by a JEOL JNM-PS-100 instrument.

We thank Dr. Atsushi Terahara and Mr. Kohji Ichimori, Dr. Satoshi Okazaki and Mr. Kouichi Nozaki, and Mr. Ken Hosoya, Kyoto University, for their help on calculation, measurement of E_{pa}, and HPLC analyses.

References

1) "Photochemical, Photoelectrochemical and Photobiological Processes," ed by D. O. Hall and W. Palz, D. Reidel, Dordrecht, Holland (1982); G. J. Kavarnos and N. J. Turro, *Chem. Rev.*, **86**, 401 (1986).

2) K. Maruyama and T. Otsuki, *Chem. Lett.*, **1975**, 87; K. Maruyama, T. Otsuki, and K. Mitsui, *Bull. Chem. Soc. Jpn.*, **49**, 3361 (1976); *J. Org. Chem.*, **45**, 1424 (1980); K. Maruyama, T. Otsuki, K. Mitsui, and M. Tojo, *J. Heterocycl. Chem.*, **17**, 695 (1980); K. Maruyama, S. Tai, M. Tojo, and T. Otsuki, *Heterocycles*, **16**, 1963 (1981); K. Maruyama, T. Otsuki, and S. Tai, *J. Org. Chem.*, **50**, 52 (1985); K. Maruyama, S. Tai, and H. Imahori, *Bull. Chem. Soc. Jpn.*, **59**, 1777 (1986).

3) K. Maruyama and T. Otsuki, *Bull. Chem. Soc. Jpn.*, **50**, 3429 (1977); K. Maruyama, T. Otsuki, and H. Tamiaki,

ibid., **58**, 3049 (1985).

4) Preliminary report; K. Maruyama and T. Otsuki, *Chem. Lett.*, **1977**, 851.

5) In dioxane, carbon tetrachloride, dichloromethane, ethanol, methanol, and acetonitrile, the same behavior was observed as in benzene.

6) R. J. Waltman and J. Bargon, *Can. J. Chem.*, **64**, 76 (1986).

7) W. C. Neikam, G. R. Dimeler, and M. M. Desmond, *J. Electrochem. Soc.*, **111**, 1190 (1964).

8) J. W. Robinson, "Handbook of Spectroscopy," CRC press (1974), Vol. 1, pp. 257—511.

9) The *K* value was determined by UV technique; H. A. Benesi and J. H. Hildebrand, *J. Am. Chem. Soc.*, **71**, 2703 (1949).

10) A. Streitwieser, Jr., "Molecular Orbital Theory for Organic Chemists," John Wiley & Sons, New York (1961).

11) R. Kaptein, *J. Chem. Soc., Chem. Commun.*, **1971**, 732; N. J. Turro, "Modern Molecular Photochemistry," Benjamin/Cummings, Menlo Park, CA (1978), pp. 275—288.

12) K. Maruyama and H. Imahori, 52nd National Meeting of the Chemical Society of Japan, Kyoto, April 1986, Abstr., No. 3L16.

13) J. M. Barker, R. R. Huddleston, and M. L. Wood, *Synth. Commun.*, **5**, 59 (1975).

14) S. Gronowitz and V. Vilks, *Ark. Kemi*, **21**, 191 (1963).

15) S. Conde, C. Corral, R. Madronero, and A. S. Alvarez-Insúa, *Synthesis*, **1976**, 412.

Stereoselective Synthesis of (*E*)- or (*Z*)-α-Alkylidene-γ-butyrolactone from γ-Butyrolactone and Bis[ethoxy(thiocarbonyl)] Disulfide and Mechanistic Studies of the Effect of Metal Complexes on the Stereoselection

Syuichi MATSUI
Department of Industrial Chemistry, Fukui Technical College, Geshi, Sabae, Fukui 916
(Received November 25, 1986)

Treatment of γ-butyrolactone with bis[ethoxy(thiocarbonyl)] disulfide in the presence of 2.2 equiv of lithium diisopropylamide (LDA) produced lithium enolate of *O*-ethyl *S*-(tetrahydro-2-oxo-3-furanyl) dithiocarbonate, which reacted with an aldehyde to afford exclusively (*E*)-α-alkylidene-γ-butyrolactone. Interestingly, when the reaction was quenched below −20 °C or when it was carried out in the presence of metal complex such as zinc chloride, copper(I) iodide, or tributyltin chloride, (*Z*)-α-alkylidene-γ-butyrolactone was obtained as the major product. The stereoselectivity of this reaction was sensitive to the reaction temperature and the metal cation employed.

Much attention has been focused on the stereocontrolled synthesis of α-alkylidene-γ-butyrolactones (3-alkylidenedihydro-2(3*H*)-furanone) since these compounds serve as useful intermediates in organic synthesis[1] and constitute the biologically active natural products.[2] In particularly, the general stereoselective synthesis of (*Z*)-α-alkylidene-γ-butyrolactones has been attractive since these compounds can serve as important intermediate in the synthesis of obtusilactone isolated from *Lindela obtusiloba*[3] as cytotoxic natural product. Although several methods have been reported for the direct introduction of an alkylidene group to α position of a γ-butyrolactone.[2,4] there has been no general method for the stereoselective introduction. Recently, the stereoselective synthesis of (*E*)-α-alkylidene-γ-butyrolactones using the monoanion of *O*-ethyl *S*-(tetrahydro-2-oxo-3-furanyl) thiocarbonate, or the dianion of α-mercapto-γ-butyrolactone has been reported by Tanaka et al.[5a] (*E*)- or (*Z*)-α-Alkylidene-γ-butyrolactones can also be synthesized with high stereoselectivity, starting with easily available γ-butyrolactone and bis[methoxy-(thiocarbonyl)] disulfide.[5b] The observation that the presence of metal complex such as zinc chloride, copper(I) iodide, or tributyltin chloride causes a dramatic alternation in the stereoselectivity of the reaction is very interesting.

In this paper the mechanistic aspects of these reaction and the effect of metal complexes on the stereoselection are described in greater detail.

Results and Discussion

One Pot Synthesis of α-Alkylidene-γ-butyrolactones (2) from γ-Butyrolactone. Treatment of γ-butyrolactone with bis[methoxy(thiocarbonyl)] disulfide in the presence of 2.2 equiv of lithium amide at −78 °C in THF gave the lithium enolate **1** which reacted with heptanal to give exclusively (*E*)-α-heptylidene-γ-butyrolactone (**2a**). Among the various lithium amides examined, lithium diisopropylamide (LDA) is the most efficient base for converting γ-butyrolactone into the enolate **1** as shown in Table 1.

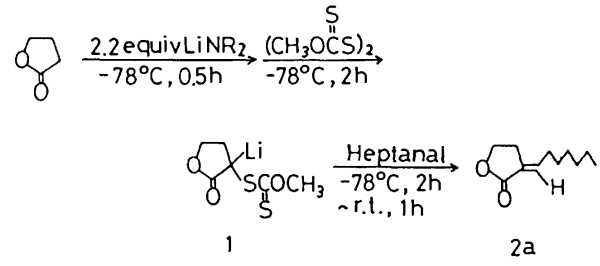

1 2a

Generality of this new methodology is apparent from the results summarized in Table 2. In all cases examined, (E)-isomers were obtained exclusively. The E/Z ratio of product **2** was determined in same manner as reported previously.[5a] For example, the ^{1}H NMR spectrum of **2a** shows the vinyl proton β to the carbonyl at δ 6.58 for (E)-isomer and at δ 6.06 for (Z)-isomer, respectively.[6] Integration showed a **96:4** mixture of (*E*)-**2a** and (*Z*)-**2a**, being identical with the ratio obtained by GLC analysis (E/Z=95/5). (Z)-Isomer could be readily separated from (E)-isomer, which eluted more slowly than (Z)-isomer.

Table 1. Effect of Lithium Amide in the Reaction of γ-Butyrolactone with Heptanal

Lithium amide	Yield[a] of **2a** %	E/Z[b]
$(i\text{-Pr})_2$NLi	65	96/4
i-PrN(Li)-cyclohexyl	54	87/13
$(Me_3Si)_2$NLi	38	92/8
N(Li)-cyclohexyl	49	83/17
$(cyclohexyl)_2$NLi	31	93/7

a) Isolated yields. b) Determined by ^{1}H NMR and GLPC analyses of the isolated product.

Table 2. Stereoselective Synthesis of (*E*)-α-Alkylidene-γ-butyrolactones (**2**) from γ-Butyrolactone and Carbonyl Compounds

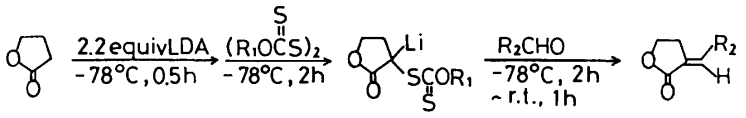

2

$R_1OCSSCOR_1$ (S, S) R_1	Carbonyl compound	Product **2**	Yield[a] %	E/Z[b]
CH_3	Heptanal	(**2a**)	65	96/4
CH_3	Benzaldehyde	(**2b**)	52	100/0
CH_3	Pentanal	(**2c**)	58	96/4
CH_3	Propanal	(**2d**)	37	96/4
CH_3	Butanal	(**2e**)	57	96/4
CH_3	Cyclohexanecarbaldehyde	(**2f**)	65	89/11[c]
C_2H_5	Heptanal	**2a**	71	95/5[d]
C_2H_5	Heptanal	**2a**	60	93/7[c]
C_2H_5	Benzaldehyde	**2b**	59	100/0[c]
$(CH_3)_2CH$	Heptanal	**2a**	58	100/0[c]
$(CH_3)_2CH$	Butanal	**2e**	54	90/10[c]

a) Isolated yields. b) Determined by ^1H NMR and GLPC analyses of the isolated product. c) Triethyl phosphite was added before adding carbonyl compound as a desulfurization agent. d) Ethyl bromide was added before adding carbonyl compound.

In contrast, when the reaction was carried out in the presence of metal complex such as anhydrous zinc chloride, copper(I) iodide, or tributyltin chloride, (*Z*)-α-alkylidene-γ-butyrolactone was obtained as the major product as shown in Table 3. For example, the reaction of the lithium enolate **1** with heptanal in the presence of 1.5 equiv of zinc chloride afforded predominantly (*Z*)-α-heptylidene-γ-butyrolactone in 68% (E/Z=17/83) isolated yield.

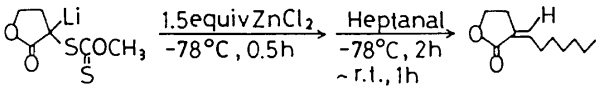

1 2a

As can be seen from the data listed in Tables 2 and 3, the alternation of substituent R of disulfide ROCSSCOR gave little significant improvement in the yield and the stereoselectivity of **2**. The effect of solvent on the yield and E/Z ratio of **2a** has been examined in the reaction of **1** with heptanal in the presence of 1.5 equiv of copper(I) iodide. The results (Table 4) indicate that among the solvents examined, tetrahydrofuran is the most efficient solvent for converting γ-butyrolactone into **2a** and the stereoselectivity of (*Z*)-**2a** is correlative with the solubility of metal complex in solvent.

One Pot Synthesis of α-Alkylidene-γ-valerolactone (4) from γ-Valerolactone. (*E*)- or (*Z*)-α-Alkylidene-γ-valerolactones (**4**) were also synthesized with high stereoselectivity according to the following route.

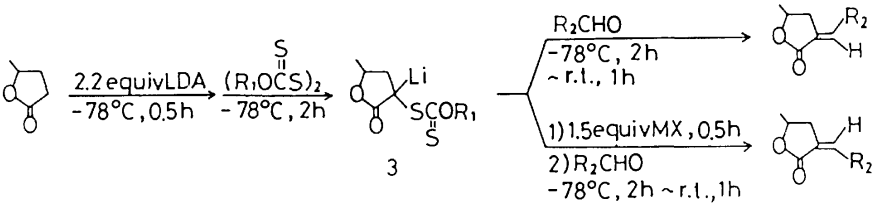

3 4

Table 3. Stereoselective Synthesis of (*Z*)-α-Alkylidene-γ-butyrolactones (**2**) from γ-Butyrolactone and Carbonyl Compounds in the Presence of Metal Complex (MX)

$R_1OCSSCOR_1$ (S, S; R_1)	Carbonyl compound	MX	Product **2**	Yield[a] %	E/Z[b]
CH_3	Heptanal	$ZnCl_2$	**2a**	68	17/83
CH_3	Heptanal	$ZnCl_2$	**2a**	67	15/85[c]
CH_3	Heptanal	$(n\text{-Bu})_3SnCl$	**2a**	68	19/81
CH_3	Heptanal	CuI	**2a**	70	25/75[d]
CH_3	Heptanal	CuI	**2a**	67	19/81[e]
CH_3	Pentanal	$ZnCl_2$	**2c**	65	11/89
CH_3	Butanal	$ZnCl_2$	**2e**	58	9/91
C_2H_5	Heptanal	$ZnCl_2$	**2a**	67	15/85[c]
C_2H_5	Heptanal	$MgCl_2$	**2a**	66	92/8
C_2H_5	Heptanal	$HgCl_2$	**2a**	52	37/63[d]
C_2H_5	Heptanal	$ZnCl_2$	**2a**	68	11/89
C_2H_5	Heptanal	$(i\text{-Pro})_3TiCl$	**2a**	38	45/55[d]
$(CH_3)_2CH$	Heptanal	$ZnCl_2$	**2a**	67	23/77
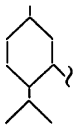	Heptanal	$ZnCl_2$	**2a**	59	28/72
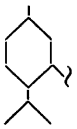	Heptanal	$ZnCl_2$	**2a**	68	9/91[e]

a) Isolated yields. b) Determined by ^1H NMR and GLPC analyses of the isolated product. c) Metal complex was added before treating with disulfide. d) Triethyl phosphite was added before adding carbonyl compound as a desulfurization agent. e) 100 ml of THF was used for the reaction of 20 mmol of γ-butyrolactone with aldehyde.

Table 4. Effect of Solvent on the Yields and E/Z Ratios of **2a**

Solvent	Yield[a] of **2a** %	E/Z[b]
THF	69	16/84[c]
THF	61	33/67[d]
DEE	0	—
DME	47	20/80[c]
THF-HMPA[e]	35	15/85[c]

a) Isolated yields. b) Determined by ^1H NMR and GLPC. c) 60 ml of solvent was used for the reaction of 20 mmol of γ-butyrolactone with heptanal. d) 40 ml of solvent was used for the reaction of 20 mmol of γ-butyrolactone with heptanal. e) A mixture of THF and HMPA (8 : 1, v/v) was used as a solvent.

The results were summarized in Table 5. Thus, the observations presented here represent a new and general method for the stereoselective introduction of alkylidene functionality on the α-position of γ-butyrolactone or γ-valerolactone by one pot procedure. These procedures are synthetically significant in respect of utilizing easily available γ-butyrolactone or γ-valerolactone as the starting material.

The Reaction of Lithium Enolate of *O*-Ethyl *S*-(tetrahydro-2-oxo-3-furanyl) Dithiocarbonate (5a) and Thiocarbonate (5b) with Carbonyl Compounds. When γ-butyrolactone was treated with bis[ethoxy(thiocarbonyl)] disulfide in the presence of 2.2 equiv of LDA at −78 °C for 2 h and followed by quenching with saturated aqueous ammonium chloride solution, *O*-ethyl *S*-(tetrahydro-2-oxo-3-furanyl) dithiocarbonate (**5a**) was obtained in 72% isolated yield.

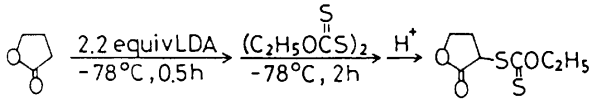

5a

On the other hand, when the reaction was carried out in the presence of 1.1 equiv of LDA, lactone **6** was obtained in the place of **5a** as the major product in 41% (82% based on disulfide) isolated yield and γ-butyrolactone (37%) was recovered. The formation of **6** appears to involve a deprotonation of **5a**, followed by an attack toward disulfide.[7]

Table 5. Stereoselective Synthesis of α-Alkylidene-γ-valerolactones (**4**) from γ-Valerolactone and Carbonyl Compounds

$R_1OCSSCOR_1$ (S S) R_1	Carbonyl compound	MX	Product **4**	Yield[a] %	E/Z[b]
CH_3	Heptanal	—	(**4a**)	58	91/9
CH_3	Hexanal	—	(**4b**)	65	89/11[c]
CH_3	2-Methylbutanal	—	(**4c**)	64	89/11
CH_3	Pentanal	—	(**4d**)	62	94/6
CH_3	2-Methylpropanal	—	(**4e**)	60	94/6
C_2H_5	Hexanal	—	**4b**	57	96/4
CH_3	Hexanal	$(n\text{-Bu})_3SnCl$	**4b**	92	9/91[c]
CH_3	Pentanal	$ZnCl_2$	**4d**	76	16/84
CH_3	2-Methylbutanal	$ZnCl_2$	**4c**	54	12/88
CH_3	2-Methylpropanal	$ZnCl_2$	**4e**	62	11/89
C_2H_5	Heptanal	CuI	**4a**	68	21/79
C_2H_5	Butanal	$ZnCl_2$	(**4f**)	70	27/73

a) Isolated yields. b) Determined by ^1H NMR and GLPC analyses of the isolated product. c) Triethyl phosphite was added before adding carbonyl compound as a desulfurization agent.

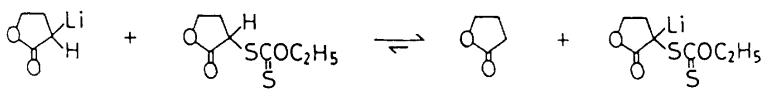

5a

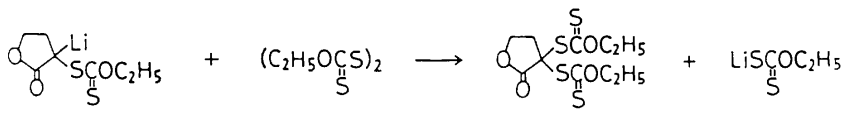

6

Above observation suggests that the reaction of lithium enolate of γ-butyrolactone with aldehydes in the presence of bis[ethoxy(thiocarbonyl)] disulfide to give α-alkylidene-γ-butyrolactone (**2**) proceeds via *O*-ethyl *S*-(tetrahydro-2-oxo-3-furanyl) dithiocarbonate (**5a**) as intermediate. In this paper the author has examined the effect of the starting material **5a** or **5b**, the reaction temperature and time, and metal complex (MX) added on the yields and E/Z ratios of **2** produced in the following reactions, and studied the mechanistic aspects of these reactions.

The geometrical compositions of **2** obtained under various conditions are summarized in Table 6. When the reaction of lithium enolate **7** with aldehyde was carried out in the presence of metal complex (MX) such as $ZnCl_2$, CuI, or $(n\text{-Bu})_3SnCl$, (*Z*)-**2** was obtained as major product, whereas these reactions in the absence of metal cations other than Li^+ gave exclusively (*E*)-**2**. However, $MgBr_2$ was less effective. An increase in the proportion of (*Z*)-product using

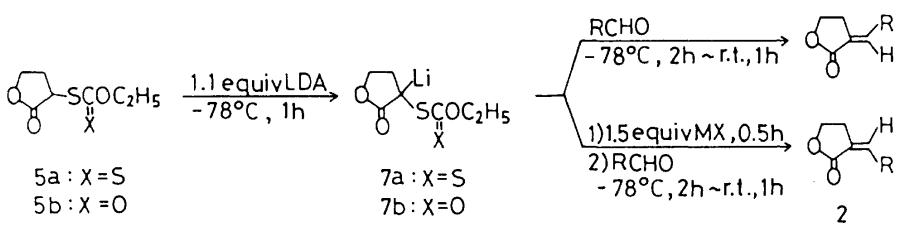

5a : X=S
5b : X=O

7a : X=S
7b : X=O

2

Table 6. Stereoselective Synthesis of α-Alkylidene-γ-Butyrolactones (**2**) from *O*-Ethyl *S*-(Tetrahydro-2-oxo-3-furanyl)dithiocarbonate (**5a**) or Thiocarbonate (**5b**) and Carbonyl Compounds

Starting material	Carbonyl compound	MX	Product **2**	Yield[a] %	E/Z[b]
5a	Heptanal	—	**2a**	63	95/5
5a	Heptanal	—	**2a**	87	97/3[c]
5a	Hexanal	—	**2g**	58	92/8
5a	Benzaldehyde	—	**2b**	60	94/6
5a	Benzaldehyde	CuI	**2b**	90	15/85[c]
5a	Heptanal	CuI	**2a**	76	28/72
5a	Heptanal	$ZnCl_2$	**2a**	56	18/82
5a	Heptanal	$ZnCl_2$	**2a**	94	23/77[c]
5a	Heptanal	$(n\text{-Bu})_3SnCl$	**2a**	60	20/80
5a	Heptanal	$MgBr_2$	**2a**	64	45/55
5a	Hexanal	$ZnCl_2$	**2g**	64	20/80
5a	Hexanal	$ZnCl_2$	**2g**	70	28/72[d]
5b	Heptanal	—	**2a**	48	100/0
5b	Heptanal	$ZnCl_2$	**2a**	46	50/50
5b	Heptanal	$ZnCl_2$	**2a**	63	47/53[e]
5b	Heptanal	$(i\text{-PrO})_2TiCl_2$	**2a**	67	45/55[d,e]
5b	Hexanal	$(EtO)_3Al$	**2g**	85	67/33[e]
5b	Pentanal	$MgBr_2$	**2c**	89	37/63[d,e]

a) Isolated yields. b) Determined by ^1H NMR and GLPC analyses of the isolated product. c) Carbonyl compound was instantly added after **5a** was treated with 1.1 equiv of LDA for 1 min. d) Triethyl phosphite was added before adding carbonyl compound as a desulfurization agent. e) *n*-BuLi was used as a base and THF-HMPA (v/v, 16/1) was used as a co-solvent.

metal complex, but to a lesser extent than for **5a**, was also observed for the reaction of **5b** with aldehyde. Therefore, the common mechanism is taken into cosideration for the reactions of **5a** and **5b** with aldehyde to afford **2**.

In order to examine the stability of lithium enolate **7a**, **5a** was treated with 1.1 equiv of LDA in THF at −78 °C for 1 h, and then quenched with saturated aqueous ammonium chloride solution. Upon work-up, lactone **8** was isolated in 18% yield in addition to 68% recovery of **5a**. The transformation of **7a** to **8** appears to involve the formation of a thiirane by intramolecular cyclization, followed by expulsion of sulfur.

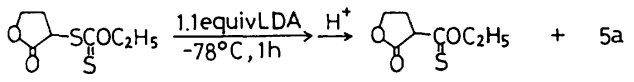

5a 8

As is apparent from Table 6, when the treating time of **5a** with 1.1 equiv of LDA was shortened to 1 min from 1 h, the yield of **2a** was enhanced to 87% from 63% in the reaction of **5a** with heptanal. The result suggests that the self-rearrangement of lithium enolate **7a** takes place competitively.

The Generation of Aldol Adducts 9. As shown in Table 7, when the reactions of **7a** with aldehydes were carried out at −78 °C for 2 h and then quenched with dilute hydrochloric acid, aldol adduct **9** (X=S) were isolated in good yields but **2** was not detected.

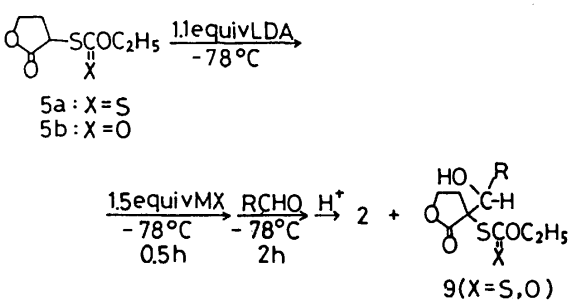

On the other hand, in the reactiion of **7b** with butanal, **2e** was isolated in 23—28% yields but the aldol adduct (X=O) was little isolated. These results may be attributed to the difference in the amount of polarization between thiocarbonyl (C=S) and carbonyl group (C=O) of **9**, that is, in the reaction of **7a** with aldehydes, the small amount of polarization of thiocarbonyl group may reduce the rearrangement of the adduct **10** to **11** (described later).

The aldol adduct **9** should consist of a mixture of diastereomers (erythro and threo isomers).

The stereoselectivity of the resulting α-alkylidene-γ-butyrolactone (**2**) may be closely correlated with the stereo-structure of the aldol adduct **9** from which it is formed. The aldol adduct **9** was separated into the

e-9(erythro) t-9(threo)

Table 7. Aldol Condensations of **5** with Carbonyl Compounds at −78 °C

Starting material	Carbonyl compound	MX	**2** %	E/Z[a]	**9** %	erythro/threo[b]	**5** %
5a	Propanal	—	0	—	70	52/48	19
5a	Propanal	$ZnCl_2$	0	—	84	54/46	11
5a	Butanal	—	0	—	65	53/47	21
5a	Butanal	$ZnCl_2$	0	—	84	55/45	9
5b	Butanal	—	28	58/42	Trace	—	42
5b	Butanal	$ZnCl_2$	23	52/48	Trace	—	45
5a	Heptanal	—	0	—	67	55/45	26
5a	Heptanal	$ZnCl_2$	0	—	74	58/42	19

a) Determined by ^1H NMR and GLPC analyses of the isolated product. b) Determined by ^1H NMR and MPLC (LiChroprep Si60 column, 2:1 hexane-ethyl acetate eluent, Flow rate 1 ml min^{-1}).

Table 8. Effects of Reaction Temperature and Time After Adding Carbonyl Compound on the Yields and Stereoselectivities of **2** and **9**

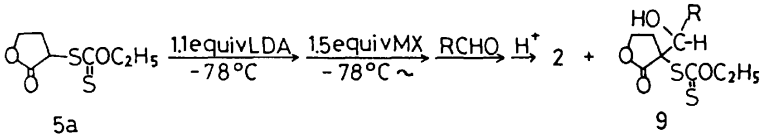

5a 9

Carbonyl compound	MX	Reaction conditions	**2** %	E/Z[a]	**9** %	erythro/threo[b]	**5a** %
Butanal	—	−78 °C, 1 min	0	—	57	48/52	28
Butanal	—	−78 °C, 15 min	0	—	70	49/51	19
Butanal	—	−78 °C, 2 h	0	—	65	53/47	21
Butanal	—	−78 °C, 6.5 h	0	—	77	56/44	7
Heptanal	—	−78 °C, 2 h	0	—	67	55/45	26
Heptanal	—	−78 °C, 2 h——50 °C,[c] 1 h	26	28/72	58	67/33	10
Heptanal	—	−78 °C, 2 h——40 °C,[c] 1 h	51	37/63	36	62/38	4
Heptanal	—	−78 °C, 2 h——20 °C,[c] 1 h	71	41/59	19	66/34	0
Heptanal	—	−78 °C, 2 h—0 °C,[c] 1 h	83	91/9	0	—	0
Heptanal	—	−78 °C, 2 h—r.t.,[c] 1 h	87	97/3	0	—	0
Heptanal	—	−78 °C, 2 h 25 °C,[d] 4 min	70	56/44	0	—	0
Heptanal	$ZnCl_2$	−78 °C, 2 h	0	—	74	58/42	19
Heptanal	$ZnCl_2$	−78 °C. 2 h——40 °C,[c] 1 h	23	10/90	61	55/45	7
Heptanal	$ZnCl_2$	−78 °C, 2 h—r.t.,[c] 1 h	94	23/77	0	—	0

a) Determined by ^1H NMR and GLPC analyses of the isolated product. b) Determined by ^1H NMR and MPLC (LiChroprep Si60 column, hexane-ethyl acetate eluent, Flow rate 1 ml min^{-1}). c) The reaction temperature was gradually raised to room temperature from −78 °C by removing cooling bath. d) The reaction temperature was immediately raised by dipping the reaction mixture in water bath maintained at 25 °C.

faster-eluting diastereomer and the slower-eluting diastereomer by column chromatography on silica gel with 3:1 hexane-ethyl acetate as eluent. The ^1H NMR spectrum of **9a** derived from heptanal shows the hydroxymethine proton at δ 3.70 for the faster-eluting isomer and at δ 4.04 for the slower-eluting isomer. The slightly major isomer resulting from the aldol condensation was in all instances the slower-eluting diastereomer which was assigned erythro form (**e-9**), whereas the slightly minor and mobile isomer was assigned threo form (**t-9**).[8] The stereochemical compositions (**e-9**/**t-9**) of the aldol adducts obtained from various aldehydes were determined by ^1H NMR and/or MPLC (medium-pressure liquid chromatography) system, and summarized in Table 7. These results show that the metal enolate of **5a** condensed with aldehydes to exhibit consistently low diastereoselectivity, regardless of the metal cation employed.

Effects of Reaction Temperature and Time. Effects of reaction temperature and time after adding aldehyde on the yields and stereoselectivities of **2** and **9** were next examined. These results under the various conditions were summarized in Table 8. When the reaction of **5a** with heptanal was carried out at −78 °C for 2 h and at −50 °C for 1 h, 58% of aldol adduct **9a** was isolated in addition to 26% of **2a**. Interestingly, the geometry selectivity of **2a** was Z-selective (E/Z=28/72) in spite of absence of metal cation other than Li^+. With only the lithium cation present, as the reaction temperature before quenching was raised gradually to 0 °C or above the yields and E-selectivity of **2a** increased. On the other hand, in the

presence of $ZnCl_2$ Z-selectivity of **2a** was observed even if the reaction temperature before quenching was raised gradually to room temperature. Next, in the reaction of **7a** with butanal at −78 °C, the effect of reaction time on the yields and the erythro/threo ratios of aldol adducts **9e** was examined but it was little observed. It is reasonable to consider that the aldol-type reacition of **7a** with an aldehyde is so rapid that the equilibrium described later is reached almost instantly.

The satisfactory yield of the aldol adduct **9** was obtained only at low temperature (−78 to −20 °C).

The Retro-Aldolization of 9. The results listed in Tables 7 and 8 predict the retro-aldolization of **9** to the lithium enolate **7a** and aldehyde, since the diastereomer ratios of aldol adducts **9** do not correspond to the E/Z ratios of the final product **2**. When the purified adduct **9a** (erythro/threo=45/55) was lithiated with 1.1 equiv of LDA at −78 °C, and followed by warming to room temperature, α-alkylidene-γ-butyrolactone (**2a**) was obtained in 73% (E/Z=94/6) isolated yield.

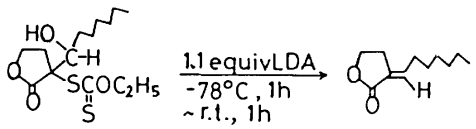

9a 2a

erythro/threo=45/55 73%(E/Z=94/6)

The same reaction for the adduct **9e** afforded (*E*)-**2e** with high stereoselectivity, regardless of the stereochemistry of **9e**.

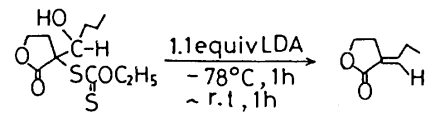

9e 2e

erythro/threo = 20/80 → 63%(E/Z=97/3)

=73/27 → 71%(E/Z=100/0)

On the other hand, when the same reaction for the nearly erythro **9a** (erythro/threo=91/9) was carried out in the presence of $ZnCl_2$, (*Z*)-**2a** was obtained as the major product (E/Z=27/73) in 78% isolated yield.

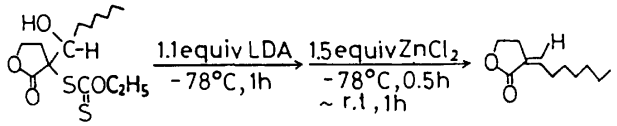

9a 2a

erythro/threo=91/9 78%

(E/Z=27/73)

Furthermore, in the reaction of **7a** with heptanal, even when $ZnCl_2$ was added after treating with heptanal at −78 °C for 2 h, (*Z*)-**2a** was obtained as major product as well as the results listed in Table 6.

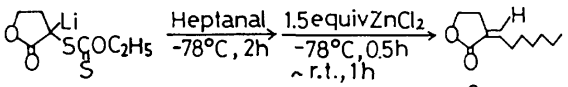

7a 2a

65%

(E/Z=22/78)

From these results, it is reasonable to consider that **10** is in equilibrium with **7a** as follows, and that the effect of the metal complex employed is exhibited in the conversion of the aldol adduct **10** to the final product **2**.

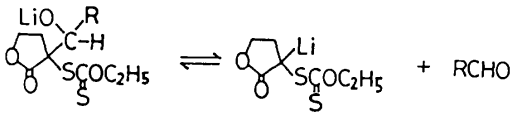

10 7a

Mechanistic Aspects. As reported previously,[5a,9] it is reasonable to assume that the mechanism of this reaction involves aldol condensation of **7** with carbonyl compound, rearrangement of an adduct **10** to **11**, subsequent conversion of **11** to thiirane species **12**, and elimination of sulfur to give α-alkylidene-γ-butyrolactone (**2**) (Scheme 1). The equilibrium between (*E*)-**2** and (*Z*)-**2** was not observed even after allowding to stand at room temperature for several days. The elimination of sulfur from **12** to give **2** is explained by a stereospecific mechanism.[10] Furthermore, it is reasonable to consider that **e-11** is not in equilibrium with **t-11**, since, in both conformations, the intramolecular rearrangement of $\underset{\underset{X}{\|}}{COC_2H_5}$ group is already occured. Thus, the aldol adduct **e-10** (erythro) and **t-10** (threo) should convert to (*E*)- and (*Z*)-**2** stereospecifically, respectively. It is considered that the geometry of final product **2** is dependent on whether the aldol condensation proceeds via erythro or threo isomer as intermediate. However, as is apparent from Tables 7 and 8, the aldol-type reactions of **7** with aldehydes at low temperature have exhibited low diastereoselectivity regardless of metal cation employed. That is, the diastereomer ratio of aldol adduct **9** does not correspond to the geometry of **2**. It is documented that, in the kinetically controlled aldol-type reaction, the appearance of stereoselection is attributed to the form of the transition state.[8g,11] It is generally believed that, when an aldol-type reaction is carried out at relatively low temperature in ethereal solvent, even lithium enolate is satisfactory to stabilize the metal chelate.[8g,12] Recently, acyclic transition states have been also proposed to account for the erythro-selective aldol reaction with enol silyl ethers and acetals,[13] zirconium enolates,[14] and crotyltrialkyltins.[15] Furthermore, Heathcock et al. have reported that the reactions of lithium enolate of dioxolanones

with aldehydes occur through the conventional Zimmerman–Traxler transition state[16] with the hydrogen of the aldehyde RCHO, rather than the R group, over the face of the dioxolanone ring.[17] The transition state models **A, B, C,** and **D** were proposed for the reactions of **7** with aldehydes (Scheme 2).

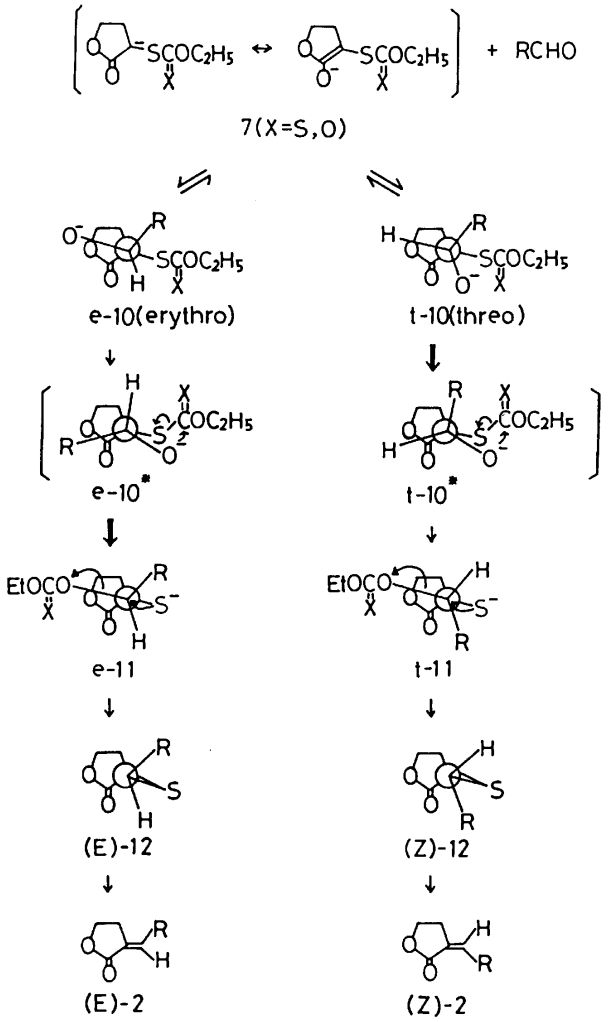

Scheme 1.

It is reasonable to consider that , among four possible transition state models (Scheme 2), **A** leading to erythro isomer and **D** leading to threo isomer, in both which the lactone carbonyl group and R group of aldehyde RCHO are anti-oriented, must be favored for the steric reason. Thus, the aldol condensations of **7** with aldehydes under the kinetically controlled reaction conditions occur through the transition states **A** and **D**, giving consistently almost 1:1 mixture of diastereomers of **9**. In these reactions, the effect of metal complex added was little observed for the stereoselection of **9**. The results listed in Table 8 show that, even in the absence of metal cation other than Li^+, when the reaction of **7** with aldehyde was carried out below −20 °C (*Z*)-**2** was obtained as major product, while (*E*)-**2** was exclusively obtained when the reaction was quenched after warming to 0 °C or above. On the contrary, in the presence of metal cation such as Zn^{2+} or Cu^+, Z-selectivity of **2** was observed even when the reaction was quenched after warming to room temperature. The observations presented here can be rationalized by considering that a retro-aldolization of **10** to the starting materials is in competition with the rearrangement of **10** to **11**, that is, the reaction of **7** with aldehyde proceeds via erythro or threo isomer to give **2** is the thermodynamically controlled process, and that the erythro isomer **e-10** become energetically more favorable than the threo isomer **t-10** as the reaction temperature is raised. Since it seems that the cyclic transition state **D** can not be controlled by lithium coordination as the reaction temperature is raised to room temperature.[8g,12] In addition, in two possible stereoisomeric precursors (**e-**

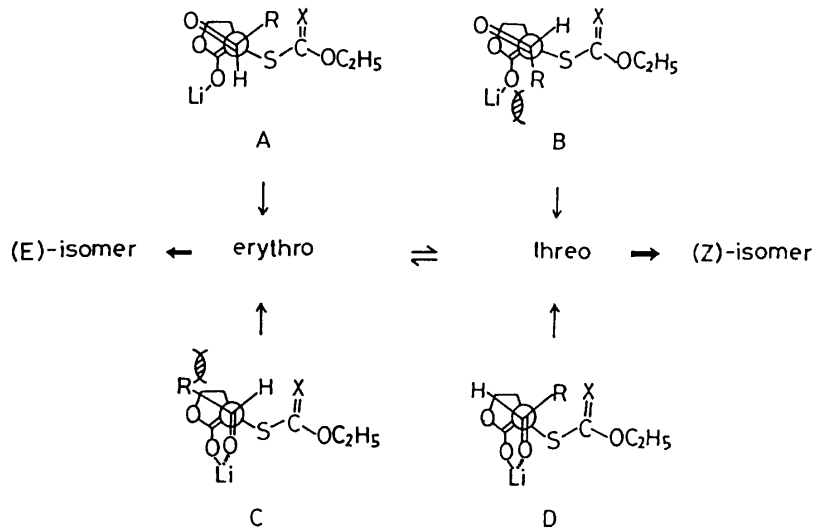

Scheme 2.

11 and **t-11**) leading to **2** as shown in Scheme 1, if the conformer, in which the $OCOC_2H_5$ and S^- groups are

anti-periplanar, is favorable one for the subsequent intramolecular attack of S^- group and elimination of the $OCOC_2H_5$ species, the orientation of R group is

thus represented as **e-11** and **t-11**, respectively. The rearrangement reaction of **e-10** to **e-11** would proceed more smoothly than that of **t-10** to **t-11**, since the steric interaction between a bulky R group and a lactone carbonyl is minimized in **e-11**. On the other hand, the stereoisomer **t-11**, in which the alkyl and carbonyl group are gauche, would exhibit severe interactions. Thus, (*E*)-**2** predominates. However, if a metal complex such as $ZnCl_2$ or CuI is added, the reaction of **7** with aldehyde proceeds via threo isomer **t-10** to give (*Z*)-**2** as major product. Since the threo isomer **t-10**, which seems to exist as structure with the six-membered ring containing coordination to metal cation of an alcoholate anion and a lactone carbonyl oxygen, can become energetically more favorable than the more charged-separated erythro isomer **e-10**. Furthermore, the difference in rotational energy between the conformational conversion of **e-10** to **e-10*** and that of **t-10** to **t-10*** (Scheme 1) is proposed to account for the threo-selective reaction at low temperature (−78 to −20 °C) to give (*Z*)-**2**. That is, the rotation about C–C bond formed by the aldol-type reaction must occur, since the both conformations **e-10*** and **t-10***, in which an alcoholate anion and $SCOC_2H_5$ group are cis or gauche, are favorable for

the subsequent intramolecular attack of O^- group toward $SCOC_2H_5$ group. The conformational

conversion of **t-10** to **t-10*** must be energetically more favorable than that of **e-10** to **e-10*** for the steric interaction between a lactone carbonyl and an alcoholate anion coordinated to a metal cation or a bulky R group.

It is concluded that the stereoselectivity of α-alkylidene-γ-butyrolactone (**2**) results from the aldol-type reaction of **7** with aldehyde which takes a different course as functions of the metal cation employed and the reaction temperature. That is, in the presence of only Li^+, this reaction occurs through erythro adduct **e-10** leading to (*E*)-**2**, whereas the reaction occurs predominantly through threo adduct **t-10** leading to (*Z*)-**2** when it was quenched below −20 °C or when it was carried out in the presence of metal cation such as Zn^{2+}, Cu^+, or Sn^{4+}. Furthermore, the effect of the metal complex employed and the reaction temperature on the stereoselectivity of **2** is exhibited in the rearrangement reaction of aldol adduct **10** to **11**.

Experimental

General. All reactions were performed under a nitrogen atmosphere. The glassware was dried by flaming in a nitrogen stream. Tetrahydrofuran (THF) was dried by distillation from calcium hydride and by subsequent distillation from lithium aluminum hydride under a nitrogen atmosphere. Diisopropylamine were distilled from calcium hydride and stored over molecular sieves. Butyllithium was titrated by the Kofron's method[18] before use. γ-Butyrolactone, γ-valerolactone, triethyl phosphite, and carbonyl compounds were purified by distillation under a nitrogen atmosphere. Zinc chloride was successively fused under reduced pressure and then cooled under nitrogen. Copper(I) iodide and magnesium bromide was prepared by the reported procedure.[8g,19] Magnesium chloride and tributyltin chloride were obtained commercially. Diisopropoxytitanium dichloride and triisopropoxytitanium chloride were prepared from titanium tetrachloride and tetraisopropyl titanate by the Dijkgraaf's method.[20] *O*-Ethyl *S*-(tetrahydro-2-oxo-3-furanyl) dithiocarbonate (**5a**) and thiocarbonate (**5b**) were prepared by the reported procedure.[5a] Melting points were determined with a Yamato Kagaku melting point apparatus and are uncorrected. Boiling points were determined during distillation and are uncorrected. Infrared spectra were determined on a Hitachi Model 260-30 spectrophotometer. Nuclear magnetic resonance spectra were determined on a JEOLCO MH-100 spectrometer. Chemical shifts are given in δ units, part per million relative to tetramethylsilane as an internal standard. Carbon tetrachloride (CCl_4), chloroform-*d* ($CDCl_3$) and benzene-d_6 (C_6D_6) were used as solvent. Gas chromatograms were obtained using a Varian Aerograph Model 920 instrument with a 0.15 cm×120 cm glass column (20% Silicone DC-550 on Celite 545). Silica gel (Wakogel) of the size 100—300 mesh was used for column chromatography. Medium-pressure liquid chromatography (MPLC) was performed on a unit constructed from various commercial components.

Preparation of Disulfides. Bis[methoxy(thiocarbonyl)], bis[ethoxy(thiocarbonyl)], and bis[isopropoxy(thiocarbonyl)] disulfides were prepared by the reported procedure.[21]

Preparation of Bis[menthyl(thiocarbonyl)] Disulfide. To a solution of 6.26 g (40 mmol) of *l*-methol in 50 ml of THF was added dropwise 40 mmol of butyllithium at 0 °C. After stirring for 1 h, 3.2 ml (50 mmol) of carbon disulfide was added dropwise and the reaction mixture was stirred for 1 h. 5.06 g (20 mmol) of iodide in 40 ml of THF was then added dropwise and the reaction mixture was stirred for 1 h. To this was added 10 ml of saturated aqueous ammonium chloride solution and the mixture was extracted four times with ether. The ether extracts were washed with dilute aqueous sodium thiosulfate solution and saturated aqueous sodium chloride solution, dried on anhydrous sodium sulfate, and concentrated under reduced pressure. The recrystallization from ethanol gave 1.31 g (71%) of bis[menthyl(thiocarbonyl)] disulfide: Mp 94.0—95.0 °C; ^1H NMR (CCl_4) δ=5.20—5.48 (m, 2H, 2CHO), 2.04—2.25 (m, 2H, 2CH), 0.72—2.04 (m, 34H, 4CH, $6CH_2$, and $6CH_3$). IR (KBr pellet) 2950, 1050, 630 cm^{-1}. Found: C, 56.94; H, 8.31%. Calcd for $C_{22}H_{38}O_2S_4$: C, 57.10; H, 8.28%.

Reaction of Lithium Enolate of γ-Butyrolactone with Carbonyl Compounds. General Procedure: Lithium diisopropylamide (LDA) (44 mmol) was prepared as usual in 60 ml of THF at −78 °C. After 10 min, a solution of 1.72 g (20 mmol) of γ-butyrolactone in 5 ml of THF was added over a period of 3 min. After stirring for 1 h at −78 °C, a solution of 22 mmol of disulfide in 6 ml of THF was added over a period of 10 min and the reaction mixture was stirred for 2 h at −78 °C. To this was added dropwise a solution of 22 mmol of carbonyl compound in 6 ml of THF over a period of 10 min and the reaction mixture was stirred for 2 h at −78 °C. Usually, the reaction mixture was then warmed gradually to room temperature from −78 °C by removing the cooling bath and it was stirred for 1 h before quenching with saturated aqueous ammonium chloride solution (10 ml). It was then poured into dilute hydrochloric acid and extracted with ether (50 ml×4). The extracts were washed with saturated aqueous sodium chloride solution, dried on anhydrous sodium sulfate, and concentrated under reduced pressure. Product isolation and purification by silica-gel chromatography gave (*E*)-α-alkylidene-γ-butyrolactone as main product.

Reaction of Lithium Enolate of γ-Butyrolactone with Carbonyl Compounds Using Metal Complexes. The preparation of α-heptylidene-γ-butyrolactone (**2a**) using zinc chloride is given here as a typical experiment. To a solution of lithium enolate in THF produced by treatment of γ-butyrolactone with bis[methoxy(thiocarbonyl)] disulfide in the presence of 2.2 equiv of LDA was added a solution of 4.10 g (30 mmol) of zinc chloride in 30 ml of THF. After 30 min, a solution of 2.20 g (22 mmol) of heptanal in 3 ml of THF was added dropwise. After stirring at −78 °C for 2 h, the reaction mixture was warmed gradually to room temperature from −78 °C and it was stirred for 1 h before quenching with saturated aqueous ammonium chloride solution (10 ml). The usual work-up and the purification by silica-gel chromatography (hexane-benzene) gave 2.48 g (68%) of **2a**.

Physical Properties of α-Alkylidene-γ-butyrolactones. The analytical samples were obtained by silica-gel chromatography. The (E)- and (Z)-isomers of **2a** were separated by silica-gel chromatography using hexane-benzene as eluent, and were identified by comparison of ^{1}H NMR and IR spectra with corresponding data reported previously.[5]

(*Z*)-α-Heptylidene-γ-butyrolactone (2a): ^{1}H NMR (CCl_4) δ=6.06 (m, 1H, CH=C), 4.18 (t, *J*=7 Hz, 2H, CH_2O), 2.46—2.92 (m, 4H, $2CH_2$), 1.02—1.50 (m, 8H, $4CH_2$), 0.88 (m, 3H, CH_3). IR (neat) 1758 (COO), 1675 (C=C) cm^{-1}. Found: C, 72.76; H, 9.92%. Calcd for $C_{11}H_{18}O_2$: C, 72.49; H, 9.95%.

(*Z*)-α-Pentylidene-γ-butyrolactone (2c): ^{1}H NMR (CCl_4) δ=6.00 (m, 1H, CH=C), 4.13 (t, *J*=7 Hz, 2H, CH_2O), 2.44—2.90 (m, 4H, $2CH_2$), 1.00—1.60 (m, 4H, $2CH_2$), 0.88 (m, 3H, CH_3). IR (neat); 1750 (COO), 1670 (C=C) cm^{-1}. Found: C, 69.71; H, 9.22%. Calcd for $C_9H_{14}O_2$: C, 70.10; H, 9.15%.

(*Z*)-α-Butylidene-γ-butyrolactone (2e): ^{1}H NMR (CCl_4) δ=6.12 (m, 1H, CH=C), 4.20 (t, *J*=7 Hz, 2H, CH_2O), 2.88 (m, 2H, CH_2), 2.64 (m, 2H, CH_2), 1.20—1.70 (m, 2H, CH_2), 0.94 (m, 3H, CH_3). IR (neat) 1750 (COO), 1670 (CH=C) cm^{-1}. Found: C, 68.43; H, 8.68%. Calcd for $C_8H_{12}O_2$: C, 68.55; H, 8.63%.

Reaction of Lithium Enolate of γ-Valerolactone with Carbonyl Compounds. The same procedure as above was employed, except using γ-valerolactone instead of γ-butyrolactone.

α-Heptylidene-γ-valerolactone (4a): (E)-Isomer: ^{1}H NMR (CCl_4) δ=6.46 (m, 1H, CH=C), 4.48 (m, 1H, CH-O-), 1.90—3.10 (m, 4H, $2CH_2$), 1.10—1.60 (m, 11H, CH_3 and $4CH_2$), 0.88 (m, 3H, CH_3). IR (neat) 1750 (COO), 1680 (CH=C) cm^{-1}. (Z)-Isomer: ^{1}H NMR (CCl_3) δ=6.02 (m, 1H, CH=C), 4.48 (m, 1H, CH-O-), 2.22—3.10 (m, 4H, $2CH_2$), 1.10—1.62 (m, 11H, CH_3 and $4CH_2$), 0.88 (m, 3H, CH_3). IR (neat) 1750 (COO), 1680 (CH=C) cm^{-1}. Found: C, 73.17; H, 10.40%. Calcd for $C_{12}H_{20}O_2$: C, 73.43; H, 10.27%.

α-Hexylidene-γ-valerolactone (4b): (E)-Isomer: ^{1}H NMR (CCl_4) δ=6.44 (m, 1H, CH=C), 4.50 (m, 1H, CH-O-), 1.98—3.06 (m, 4H, $2CH_2$), 1.00—1.56 (m, 9H, CH_3 and $3CH_2$), 0.88 (m, 3H, CH_3). IR (neat) 1750 (COO), 1670 (CH=C) cm^{-1}. Found: C, 72.40; H, 10.11%. Calcd for $C_{11}H_{18}O_2$: C, 72.49; H, 9.95%. (Z)-isomer: ^{1}H NMR (CCl_4) δ=5.94 (m, 1H, CH=C), 4.40 (m, 1H, CH-O-), 2.10—3.00 (m, 4H, $2CH_2$), 1.08—1.60 (m, 9H, CH_3 and $3CH_2$), 0.88 (m, 3H, CH_3). IR (neat) 1750 (COO), 1680 (CH=C) cm^{-1}.

α-(2-Methylbutylidene)-γ-valerolactone (4c): (E)-Isomer: ^{1}H NMR (CCl_4) δ=6.22 (dt, *J*=9.9, 2.7 Hz, 1H, CH=C), 4.52 (m, 1H, CH-O-), 2.00—3.20 (m, 3H, CH_2 and CH), 1.38 (d, *J*=7 Hz, 3H, CH_3), 1.05 (d, *J*=7 Hz, 3H, CH_3), 0.88 (m, 5H, CH_2 and CH_3). IR (neat); 1750 (COO), 1680 (CH=C) cm^{-1}. (Z)-Isomer: ^{1}H NMR (CCl_4) δ=5.72 (dt, *J*=9.8, 2.2 Hz, 1H, CH=C), 4.42 (m, 1H, CH-O-), 3.48 (m, 1H, CH), 2.20—3.20 (m, 2H, CH_2), 1.36 (d, *J*=7 Hz, 3H, CH_3), 0.97 (d, *J*=7 Hz, 3H, CH_3), 0.85 (m, 5H, CH_2 and CH_3). Found: C, 71.15; H, 9.70%. Calcd for $C_{10}H_{16}O_2$: C, 71.39; H, 9.59%. IR (neat); 1750 (COO), 1670 (CH=C) cm^{-1}.

α-Pentylidene-γ-valerolactone (4d): (E)-Isomer: ^{1}H NMR (CCl_4) δ=6.50 (m, 1H, CH=C), 4.52 (m, 1H, CH-O-), 2.00—3.20 (m, 4H, $2CH_2$), 1.10—1.70 (m, 7H, CH_3 and $2CH_2$), 0.80—1.10 (m, 3H, CH_3). IR (neat) 1750 (COO), 1680 (CH=C) cm^{-1}. Found: C, 71.66; H, 9.70%. Calcd for $C_{10}H_{16}O_2$: C, 71.39; H, 9.59%. (Z)-Isomer: ^{1}H NMR (CCl_4) δ=6.04 (m, 1H, CH=C), 4.48 (m, 1H, CH-O-), 2.20—3.20 (m, 4H, $2CH_2$), 1.20—1.60 (m, 7H, CH_3 and $2CH_2$), 0.90 (m, 3H, CH_3).

α-(2-Methylpropylidene)-γ-valerolactone (4e): (E)-Isomer: ^{1}H NMR (CCl_4) δ=6.20 (dt, *J*=9.3, 2.6 Hz, 1H, CH=C), 4.44 (m, 1H, CH-O-), 2.20—3.20 (m, 3H, CH_2 and CH), 1.35 (d, *J*=7 Hz, 3H, CH_3), 1.05 (d, *J*=7 Hz, 6H, $2CH_3$). IR (neat) 1750 (COO), 1680 (CH=C) cm^{-1}. Found: C, 70.03; H, 9.38%. Calcd for $C_9H_{14}O_2$: C, 70.10; H, 9.15%. (Z)-Isomer: ^{1}H NMR (CCl_4) δ=5.74 (dt, *J*=9.6, 2.1 Hz, 1H, CH=C), 4.42 (m, 1H, CH-O-), 3.66 (m, 1H, CH), 2.20—3.10 (m, 2H, CH_2), 1.34 (d, *J*=6 Hz, 3H, CH_3), 0.98 (d, *J*=7 Hz, 6H, $2CH_3$). IR (neat) 1750 (COO), 1670 (CH=C) cm^{-1}.

α-Butylidene-γ-valerolactone (4f): (E)-Isomer: ^{1}H NMR (CCl_4) δ=6.36 (m, 1H, CH=C), 4.42 (m, 1H, CH-O-), 1.96—3.00 (m, 4H, $2CH_2$), 1.28—1.60 (m, 5H, CH_2 and CH_3), 0.92 (t, *J*=7 Hz, 3H, CH_3). (Z)-Isomer: ^{1}H NMR (CCl_4) δ=5.96 (m, 1H, CH=C), 4.44 (m, 1H, CH-O-), 2.24—3.04 (m, 4H, $2CH_2$), 1.20—1.56 (m, 5H, CH_3 and CH_2), 0.90 (t, *J*=7 Hz, 3H, CH_3). IR (neat) 1750 (COO), 1680 (CH=C) cm^{-1}. Found: C, 69.95; H, 9.17%. Calcd for $C_9H_{14}O_2$: C, 70.10; H, 9.15%.

Reaction of γ-Butyrolactone with Bis[ethoxy(thiocarbonyl)] Disulfide. To a solution of lithium diisoprop-

ylamide (LDA) (44 mmol) in 60 ml of THF was added a solution of 1.72 g (20 mmol) of γ-butyrolactone in 5 ml of THF at −78 °C. After stirring for 1 h, a solution of 5.32 g (22 mmol) of bis[ethoxy(thiocarbonyl)] disulfide in 5 ml of THF was added and the reaction mixture was stirred at −78 °C for 2 h. The cooling bath was removed and the reaction mixture was quenched with 10 ml of saturated aqueous ammonium chloride solution. The usual work-up and the purification by silica-gel chromatography (benzene) gave 2.97 g (72%) of **5a**. The product was identified by comparison of the ^{1}H NMR spectrum and retention time of GLC with the correponding data from independently synthesized material described above.

On the other hand, the reaction of 20 mmol of γ-butyrolactone treated by 22 mmol of LDA with 22 mmol of bis[ethoxy(thiocarbonyl)] disulfide gave 2.67 g (41%) of **6**: Mp 130.5—131.5 °C. ^{1}H NMR ($CDCl_3$) δ=4.72 (q, *J*=7 Hz, 4H, $2CH_2O$), 4.58 (t, *J*=7 Hz, 2H, CH_2O), 3.21 (t, *J*=7 Hz, 2H, CH_2O), 1.50 (t, *J*=7 Hz, 6H, $2CH_3$). IR (KBr pellet) 2990, 1780 (COO), 1035 cm^{-1}. Found: C, 36.49; H, 3.98%. Calcd for $C_{10}H_{14}O_4S_4$: C, 36.79; H, 4.32%.

Reaction of Lithium Enolate of 5a or 5b with Carbonyl Compounds. The preparation of α-heptylidene-γ-butyrolactone from **5a** and heptanal is given here as a typical experiment. To a solution of lithium diisopropylamide (LDA) (22 mmol) in 60 ml of THF was added 4.13 g (20 mmol) of *O*-ethyl *S*-(tetrahydro-2-oxo-3-furanyl) dithiocarbonate (**5a**) at −78 °C. After 30 min, a solution of 2.51 g (22 mmol) of heptanal in 3 ml of THF was added over 2 min. After stirring at −78 °C for 2 h, the reaction mixture was warmed gradually to room temperature from −78 °C and it was stirred for 1 h before quenching with saturated aqueous ammonium chloride solution (10 ml). The usual work-up and the purification by silica-gel chromatography (benzene) gave 2.22 g (61%) of **2a**.

The procedure using butyllithium instead of LDA as base and THF-HMPA (v/v, 16/1) instead of THF as solvent was also employed for the reaction of lithium enolate of **5b** with carbonyl compounds.

(*Z*)-α-Benzylidene-γ-butyrolactone (2b): Mp 90.5—91.5 °C. ^{1}H NMR ($CDCl_3$) δ=7.50 (m, 2H, aromatic), 7.04 (m, 3H, aromatic), 6.70 (m, 1H, CH=C), 4.20 (t, *J*=7 Hz, 2H, CH_2O), 3.00 (m, 2H, CH_2). IR (KBr pellet); 1740 (COO), 1650 (CH=C) cm^{-1}. Found: C, 75.67; H, 5.88%. Calcd for $C_{11}H_{10}O_2$: C, 75.84; H, 5.79%.

(*Z*)-α-Hexylidene-γ-butyrolactone (2g): ^{1}H NMR (CCl_4) δ=6.22 (m, 1H, CH=C), 4.30 (t, *J*=7 Hz, 2H, CH_2O), 2.60—3.00 (m, 4H, $2CH_2$), 1.00—1.58 (m, 6H, $3CH_2$), 0.92 (m, 3H, CH_3). IR (neat) 1758 (COO), 1675 (CH=C) cm^{-1}. Found: C, 71.20; H, 9.65%. Calcd for $C_{10}H_{16}O_2$: C, 71.39; H, 9.59%.

Decomposition of Lithium Enolate 7a. The lithium enolate **7a** was prepared as usual from 4.13 g (20 mmol) of **5a** and 22 mmol of LDA in 60 ml of THF. After stirring at −78 °C for 1 h, the reaction mixture was quenched by adding 10 ml of saturated aqueous ammonium chloride solution. The usual work-up and the product isolation gave 2.81 g (68%) of **5a** and 0.63 g (18%) of α-[ethoxy(thiocarbonyl)]-γ-butyrolactone (**8**): ^{1}H NMR (CCl_4) δ=4.56 (q, *J*=7 Hz, 2H, CH_2O), 4.30 (m, 2H, CH_2O), 3.84 (t, *J*=7 Hz, 1H, CH), 2.72 (m, 2H, CH_2O), 1.44 (t, *J*=7 Hz, 3H, CH_3). Found: C, 47.88; H, 5.91%. Calcd for $C_7H_{10}O_3S$: C, 48.26; H, 5.79%.

Therefore, in the subsequent experiments carbonyl compound was instantly added after treating of **5a** with 1.1 equiv of LDA.

General Procedure for the Preparation of Aldol Adducts 9. To a solution of LDA (22 mmol) in 60 ml of THF was added 4.13 g (20 mmol) of **5a** at −78 °C. When the addition was complete, a solution of 22 mmol of carbonyl compound in 5 ml of THF was added and the reaction mixture was stirred at −78 °C for 2 h. The cooling bath was removed and the reaction mixture was poured into dilute hydrochloric acid, and extracted with ether (50×3 ml). The combined organic layer was washed twice with saturated aqueous sodium chloride solution, dried on anhydrous sodium sulfate, and concentrated under reduced pressure. The chromatography on silica gel (hexane-ethyl acetate 3:1) gave a purified but unseparated diastereomers **9** in high yields. The diastereomers were separated by MPLC system using hexane-ethyl acetate 3:1 as eluent, and the diastereomer ratios were determined.

α-(1-Hydroxyheptyl)-α-[ethoxy(thiocarbonyl)thio]-γ-butyrolactone (9a): Chromatography (hexane-ethyl acetate 3:1) afforded in 67% yield a 45:55 mixture of the faster eluting (assigned threo) and slower eluting (assigned erythro) isomers. The faster eluting diastereomer was obtained as a viscous oil: ^{1}H NMR ($CDCl_3$) δ=4.46 (q, *J*=7 Hz, 2H, CH_2O), 4.20 (m, 2H, CH_2O), 3.70 (bt, 1H, CH), 3.40 (bs, 1H, OH), 2.60 (m, 2H, CH_2), 1.08—1.60 (m, 13H, $5CH_2$ and CH_3), 0.70—0.88 (m, 3H, CH_3). IR (neat) 3402 (OH), 1740 (COO) cm^{-1}.

The slower eluting diastereomer was obtained as crystals: Mp 81.5—82.5 °C. ^{1}H NMR ($CDCl_3$) δ=4.64 (q, *J*=7 Hz, 2H, CH_2O), 4.36 (t, *J*=7 Hz, 2H, CH_2O), 4.04 (m, 1H, CH), 3.68 (bs, 1H, OH), 2.08—2.84 (m, 2H, CH_2O), 1.08—1.60 (m, 13H, $5CH_2$ and CH_3), 0.64—0.84 (m, 3H, CH_3). IR (KBr pellet) 3400 (OH), 1736 (COO) cm^{-1}. Found: C, 52.14; H, 7.17%. Calcd for $C_{14}H_{24}O_4S_2$: C, 52.47; H, 7.55%.

α-(1-Hydroxypropyl)-α-[ethoxy(thiocarbonyl)thio]-γ-butyrolactone (9d): Chromatography (hexane-ethyl acetate 2:1) afforded in 70% yield a 48:52 mixture of the faster eluting (assigned threo) and slower eluting (assigned erythro) isomers. The faster eluting diastereomer was obtained as a viscous oil: ^{1}H NMR ($CDCl_3$) δ=4.58 (q, *J*=7 Hz, 2H, CH_2O), 4.32 (t, *J*=7 Hz, 2H, CH_2O), 4.02 (m, 1H, CH), 3.44 (bs, 1H, OH), 2.12—2.96 (m, 2H, CH_2), 1.06—1.80 (m, 5H, CH_3 and CH_2), 1.02 (t, *J*=7 Hz, 3H, CH_3). IR (neat) 3500 (OH), 1770 (COO) cm^{-1}.

The slower-eluting diastereomer was obtained as a viscous oil: ^{1}H NMR ($CDCl_3$) δ=4.71 (q, *J*=7 Hz, 2H, CH_2O), 4.46 (t, *J*=7 Hz, 2H, CH_2O), 3.74—3.94 (m, 1H, CH), 3.89 (s, 1H, OH), 2.50—3.00 (m, 2H, CH_2), 1.20—1.80 (m, 5H, CH_2 and CH_3), 1.04 (t, *J*=7 Hz, 3H, CH_3). IR (neat) 3480 (OH), 1760 (COO) cm^{-1}. Found: C, 45.20; H, 5.98%. Calcd for $C_{10}H_{16}O_4S_2$: C, 45.43; H, 6.10%.

α-(1-Hydroxybutyl)-α-[ethoxy(thiocarbonyl)thio]-γ-butyrolactone (9e): Chromatography (hexane-ethyl acetate 3:1) afforded in 84% yield a 47:53 mixture of the faster eluting (assigned threo) and slower eluting (assigned erythro) isomers. The faster elutiong diastereomer was obtained as a viscous oil: ^{1}H NMR ($CDCl_3$) δ=4.72 (q, *J*=7 Hz, 2H, CH_2O), 4.44 (t, *J*=7 Hz, 2H, CH_2O), 4.16 (m, 1H, CH), 3.54 (bs, 1H, OH), 2.24—2.96 (m, 2H, CH_2), 1.08—1.64 (m, 7H, $2CH_2$ and CH_3), 0.64—1.08 (m, 3H,

CH_3). IR (neat) 3480 (OH), 1770 (COO) cm^{-1}.

The slower-eluting diastereomer was obtained as a viscous oil: ^1H NMR ($CDCl_3$) δ=4.74 (q, J=7 Hz, 2H, CH_2O), 4.46 (t, J=7 Hz, 2H, CH_2O), 3.78—4.24 (m, 2H, CH and OH), 2.30—3.00 (m, 2H, CH_2), 1.08—1.90 (m, 7H, $2CH_2$ and CH_3), 0.80—1.08 (m,3H, CH_3). IR (neat) 3480 (OH), 1760 (COO) cm^{-1}. Found: C, 47.41; H, 6.70%. Calcd for $C_{11}H_{18}O_4S_2$: C, 47.46; H, 6.52%.

Preparation of α-Heptylidene-γ-butyrolactone (2a) from α-(1-Hydroxyheptyl)-α-[ethoxy(thiocarbonyl)thio]-γ-butyrolactone (9a): Into a solution of 8.10 mmol of LDA in 15 ml of THF, 2.36 g (7.36 mmol) of **9a** in 6 ml of THF was added at −78 °C. After stirring at −78 °C for 1 h and then at room temperature for 2 h, the usual work-up and chromatographic isolation afforded 0.98 g (73%) of **2a**, which was identical by spectroscopic comparison with an authentic sample.

α-Butylidene-γ-butyrolactone (2e): The similar reactions utilizing 2.13 g (7.65 mmol) and 1.61 g (5.80 mmol) of **9e** gave 0.68 g (63%) and 0.58 g (71%) of **2e**, respectively.

Preparation of 2a from 9a Using $ZnCl_2$. Into a solution of 7.21 mmol of LDA in 15 ml of THF, 2.10 g (6.55 mmol) of **9a** in 6 ml of THF was added at −78 °C. After stirring at −78 °C for 1 h, 1.34 g (9.83 mmol) of zinc chloride in 9 ml of THF was added. After stirring at −78 °C for 30 min and then at room temperature for 2 h, the usual work-up and chromatographic isolation afforded 0.93 g (78%) of **2a**.

The author would like to thank Drs. Aritsune Kaji and Kazuhiko Tanaka, Department of Chemistry, Faculty of Science, Kyoto University, for their helpful discussion during this work.

References

1) a) O. E. Edwards and P.-T. Ho, *Can. J. Chem.*, **55**, 371 (1977); b) Y. S. Rao, *Chem. Rev.*, **76**, 625 (1976); c) T. G. Back, O. E. Edwards, and G. A. MacAlpine, *Tetrahedron. Lett.*, **1977**, 2651; d) T. R. Hoye and A. J. Caruso, *Tetrahedron Lett.*, **1978**, 4611.

2) a) P. A. Grieco, *Synthesis*, **1975**, 67; b) R. B. Grammil, C. A. Wilson, and T. A. Bryson, *Synth. Commun.*, **5**, 245 (1975); c) S. S. Newaz, *Aldrichica Acta*, **10**, 64 (1977); d) R. A. Amos and J. A. Katzenellenbogen, *J. Org. Chem.*, **43**, 560 (1978); e) J. L. Herrmann, M. H. Berger, and R. H. Schlessinger, *J. Am. Chem. Soc.*, **101**, 1544 (1979); f) P. A. Grieco, M. Nishizawa, T. Oguri, S. D. Burke, and N. Marinovic, *J. Am. Chem. Soc.*, **99**, 5773 (1977); g) S. Danishefsky, T. Kitahara, P. F. Schuda, and S. J. Etheredge, *J. Am. Chem. Soc.*, **98**, 3028 (1976); h) S. Danishefsky, P. F. Schuda, T. Kitahara, and S. J. Etheredge, *J. Am. Chem. Soc.*, **99**, 6066 (1977); i) G. R. Kieczykowsky and R. H. Schlessinger, *J. Am. Chem. Soc.*, **100**, 1938 (1978); J) Y. Ohfune, P. A. Grieco, C.-L. J. Wang, and G. Majetich, *J. Am. Chem. Soc.*, **100**, 5946 (1978).

3) a) M. Niwa, M. Iguchi, and S. Yamamura, *Tetrahedron Lett.*, **1975**, 1539; b) M. Niwa, M. Iguchi, and S. Yamamura, *Chem. Lett.*, **1975**, 655; c) M. Niwa, M. Iguchi, and S. Yamamura, *Tetrahedron Lett.*, **1975**, 4395.

4) a) G. M. Ksander, J. E. McMurry, and M. Johnson, *J. Org. Chem.*, **42**, 1180 (1977); b) P. A. Grieco, C.-L. J. Wang, and S. D. Burke, *J. Chem. Soc., Chem. Commun.*, **1975**, 537; c) T. Minami, I. Nishi, and T. Agawa, *J. Org. Chem.*, **39**, 3236 (1974); d) J. L. Roberts, P. S. Borromeo, and C. D. Poulten, *Tetrahedron Lett.*, **1977**, 1621; e) H. Zimmer and J. Rothe, *J. Org. Chem.*, **24**, 28 (1959); f) P. A. Grieco and C. S. Pogonowsky, *J. Org. Chem.*, **39**, 1958 (1974); g) K. Yamamoto, Y. Tomo, and S. Suzuki, *Tetrahedron Lett.*, **21**, 2861 (1980).

5) a) K. Tanaka, H. Uneme, N. Yamagishi, R. Tanikaga, and A. Kaji, *Bull. Chem. Soc., Jpn.*, **53**, 2910 (1980); b) K. Tanaka, N. Tamura, and A. Kaji, *Chem. Lett.*, **1980**, 595.

6) G. A. Howie, P. E. Manni, and J. M. Cassady, *J. Med. Chem.*, **17**, 840 (1974).

7) G. H. Posner and G. L. Loomis, *J. Chem. Soc., Chem. Commun.*, **1972**, 892.

8) a) B. J. Hunt and W. Rigby, *Chem. Ind. (London)*, **1967**, 1868; b) T. Nakata and T. Oishi, *Tetrahedron Lett.*, **21**, 1640 (1980); c) M. Hirama and S. Masamune, *Tetrahedron Lett.*, **1979**, 2225; d) S. Masamune, S. Mori, D. E. Vanhorn, and D. W. Brooks, *Tetrahedron Lett.*, **1979**, 1665; e) D. E. Vanhorn and S. Masamune, *Tetrahedron Lett.*, **1979**, 2229; f) M. Hirama, D. S. Garvey, L. D.-L. Lu, and S. Masamune, *Tetrahedron Lett.*, **1979**, 3937; g) H. O. House, D. S. Grumrine, A. Y. Teranishi, and H. D. Olmstead, *J. Am. Chem. Soc.*, **95**, 3310 (1973); h) F. A. Carey and M. E. Kuehne, *J. Org. Chem.*, **47**, 3811 (1982); i) D. Seebach and V. Prelog, *Angew. Chem., Int. Ed. Engl.*, **21**, 654 (1982); j) C. H. Heathcock, C. T. Buse, W. A. Kleischick, M. C. Pirrung, J. E. Sohn, and J. Lampe, *J. Org. Chem.*, **45**, 1066 (1960).

9) S. Matsui, *Bull. Chem. Soc. Jpn.*, **57**, 426 (1984).

10) a) M. Sander, *Chem. Rev.*, **66**, 297 (1966); b) N. P. Neureiter, and F. G. Bordwell, *J. Am. Chem. Soc.*, **81**, 578 (1959); c) D. B. Denny and M. J. Boskin, *J. Am. Chem. Soc.*, **82**, 4736 (1960).

11) a) D. A. Evans, E. Vogel, and J. V. Nelson, *J. Am. Chem. Soc.*, **101**, 6120 (1979); b) W. A. Kiebshick, C. T. Buse, and C. H. Heathcock, *J. Am. Chem. Soc.*, **99**, 247 (1977); c) C. T. Buse and C. H. Heathcock, *J. Am. Chem. Soc.*, **99**, 8109 (1977); d) C. H. Heathcock and C. T. White, *J. Am. Chem. Soc.*, **101**, 7076 (1979); e) C. H. Heathcock, M. C. Pirrung, C. T. Buse, J. P. Hagen, S. D. Young, and J. E. Sohn, *J. Am. Chem. Soc.*, **101**, 7077 (1979).

12) a) C. R. Hauser and W. H. Puterbaugh, *J. Am. Chem. Soc.*, **75**, 1068 (1953); b) E. M. Kaiser and C. R. Hauser, *J. Am. Chem. Soc.*, **89**, 4566 (1967); c) M. W. Rathke, *J. Am. Chem. Soc.*, **92**, 3222 (1970); d) E. M. Kaiser, D. M. von Schriltz, and C. R. Hauser, *J. Org. Chem.*, **32**, 2610 (1967); **33**, 4275 (1969); e) J. E. Dubois and M. Dubois, *Bull. Soc. Chim. Fr.*, **1969**, 3553, 3120; f) J. E. Dubois and J. F. Fort, *Tetrahedron*, **28**, 1653, 1665 (1972); g) J. E. Dubois and P. Fellmann, *C. R. Acad. Sci., Ser. C*, **274**, 1307 (1972).

13) S. Murata, M. Suzuki, and R. Noyori, *J. Am. Chem. Soc.*, **102**, 3248 (1980).

14) a) Y. Yamamoto and K. Maruyama, *Tetrahedron Lett.*, **21**, 4607 (1980); b) D. A. Evans and L. R. McGee, *Tetrahedron Lett.*, **21**, 3975 (1980).

15) Y. Yamamoto, H. Yatagai, Y. Naruta, and K. Maruyama, *J. Am. Chem. Soc.*, **102**, 7107 (1980).

16) a) H. Zimmerman and M. Traxler, *J. Am. Chem. Soc.*, **79**, 1920 (1975); b) P. Fellmann and J. E. Dubois, *Tetrahedron Lett.*, **1978**, 34, 1349.

17) C. H. Heathcock, M. C. Pirrung, S. D. Young, J. P. Hagen, E. T. Jarvi, U. Badertscher, H. P. Märki, and S. H. Montgomery, *J. Am. Chem. Soc.*, **106**, 8161 (1984).
18) W. G. Kofron and L. M. Baclawski, *J. Org. Chem.*, **43**, 373 (1978).
19) a) G. H. Posner and J. J. Sterling, *J. Am. Chem. Soc.*, **95**, 3076 (1973); b) G. H. Posner, C. E. Whitten, and J. J. Sterling, *J. Am. Chem. Soc.*, **95**, 7788 (1973).
20) C. Dijkgraaf and J. P. G. Rousseau, *Spectrochim. Acta.*, **24**, 1213 (1967).
21) G. Fuchs, *Ark. Kemi.*, **26**, 111 (1966); *Chem. Abstr.*, **66**, 28363 (1967).

Preparation of New Nitrogen-Bridged Heterocycles. 15.[1] Synthesis and Reaction of 1,9a-Dihydropyrido[2,1-*c*][1,4]thiazines

Akikazu KAKEHI,* Suketaka ITO, Shingo YONEZU, Katsunori MARUTA, Kazuhiro YUITO, Morio SHIOHARA, and Kyoko ADACHI
Department of Industrial Chemistry, Faculty of Engineering, Shinshu University, Wakasato, Nagano 380
(Received November 29, 1986)

Alkaline treatment of 1-[2-(substituted methylthio)vinyl]pyridinium bromides, readily obtainable from the *S*-alkylation of pyridinium 1-(thiocarbonyl)methylides with various alkyl bromides such as bromoacetonitrile, ethyl bromoacetate, and some phenacyl bromides, gave smoothly 1,9a-dihydropyrido[2,1-*c*][1,4]thiazine derivatives as almost isomeric mixtures. These dihydropyridothiazines are very unstable and decomposed rapidly at ordinary temperature, but by treating them with a dehydrogenating agent such as lead tetraacetate (LTA) or 2,3-dichloro-5,6-dicyano-*p*-benzoquinone (DDQ) at 0 °C the desulfurized and the rearranged aromatic indolizine derivatives were formed in moderate to good yields.

A compound having a planar cyclic $4n\pi$ system is very intriguing molecule because various interesting reactions to avoid the high energic state caused by its resonance destabilization can be expected. Our recent reports[1,2] showed that neutral pyrido[1,2-*d*][1,3,4]thiadiazines bearing a planar 12π system are 1,3,4-thiadiazinyl anion congeners[3] and undergo smoothly the desulfurization or the rearrangement to give the aromatized pyrazolo[1,5-*a*]pyridine derivatives in good yields. On the other hand, the extension of this reaction to its 1-deaza analogue gave only 1,9a-dihydropyrido[2,1-*c*][1,4]thiazine derivatives and did not afford the initially expected indolizine derivatives except a few examples.[4] All our attempts to obtain the corresponding aromatic indolizines from these primary bicyclo adducts in the presence or absence of various dehydrogenating agents at ordinary temperature were unsuccessful, but we found that the treatment of them with LTA and DDQ at the limited temperature (0 °C) afforded the expected indolizines in moderate to good yields. In this paper we wish to report convenient syntheses of 1,9a-dihydropyrido[2,1-*c*][1,4]thiazines and their dehydrogenative transformations to the desulfurized and the rearranged indolizine derivatives.

Results and Discussion

Preparations of 1,9a-Dihydropyrido[2,1-*c*][1,4]thiazines. The treatment of 1-[1-cyano-2-methylthio-2-(substituted methylthio)vinyl]pyridinium bromides **10**—**23**, obtainable quantitatively from the *S*-alkylations of the corresponding pyridinium (thiocarbonyl)-methylides **1** and **2** with bromoacetonitrile (**3**), ethyl bromoacetate (**4**), phenacyl bromide (**5**), *p*-chlorophenacyl bromide (**6**), *p*-bromophenacyl bromide (**7**), *p*-methylphenacyl bromide (**8**), and *p*-phenylphenacyl bromide (**9**), with 1,8-diazabicyclo[5.4.0]undec-7-ene (DBU) in chloroform at 0 °C for 10 min afforded unstable yellow products **24**—**37** in 43—84% yields, respectively. Similar reactions of 1-[1-[1-(ethoxycarbonyl) and 1-benzoyl]-2-methylthio-2-(substituted methylthio)vinyl]pyridinium bromides **42**—**53** with DBU gave the corresponding compounds **54**—**65** in 39—89% yields and those of pyridinium bromides **68**—**78** possessing a methyl group at the 2-position yielded compounds **79**—**89** in 49—97% yields (Schemes 1 and 2). All products except **62**—**65**, **82**, **84**, and **86** were isomeric mixtures, and their isolatons other than **24a** were unsuccessful because of their thermal instability. These isomeric ratios (see Schemes 1 and 2) determined by their proton NMR (^{1}H NMR) spectra suggest the following inclinations for the substituent effect in these cyclization reactions: 1) In the adducts **24a,b**—**37a,b**, **54a,b**—**65a,b**, and **79a,b**—**89a,b** having 9a-hydrogen, the formations of the trans isomers (type b) increase with the increase of the steric hindrance of the substituent (R_2) derived from the alkylating agents **3**—**9**. 2) In the adducts **79c,d**—**89c,d** bearing a 9a-methyl group, the cis isomer (type c) is always predominant or exclusive. 3) The 2-methyl group of salts **68**—**78** does not cause large steric hinderance toward the cyclization at the 2-position. 4) When the group (R) is an ethoxycarbonyl and the substituent (R_2) is a bulky aroyl group, their cyclization reactions afford sole products **62b**—**65b**, **84b**, and **86b**, respectively.

The structures of compounds **24**—**37**, **54**—**65**, and **79**—**89**, were determined by their analytical and spectral inspections and by the mechanistic consideration of their transformations to indolizine derivatives. Adducts **24**, **25**, **28**—**37**, **54**—**56**, **59**, **61**—**65**, **79**, **80**, **83**—**86**, and **88** gave the satisfactory elemental analyses, though almost adducts of them were isomeric mixtures, and more evidently their ^{1}H NMR spectra (Table 1) supported our proposed 1,9a-dihydropyrido[2,1-*c*][1,4]-thiazine structure. For example, the spectrum of compound **24** indicated the proton signals due to the major isomer at δ 2.50 (3H, s, MeS), 4.02 (1H, d, J= 2.0 Hz, 1-H), 4.60 (1H, m, 9a-H), 4.99 (1H, br t, J=7.0 and 6.0 Hz, 7-H), 5.41 (1H, br q, J=10.0 and 4.0 Hz, 9-H), 6.21 (1H, br q, J=10.0 and 6.0 Hz, 8-H), and 6.72 (1H, br d, J=7.0 Hz, 6-H), together with weak proton

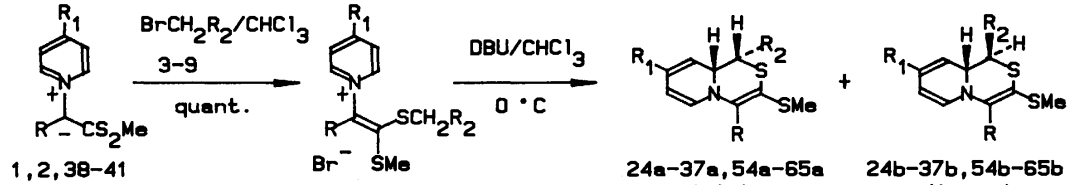

	R_1	R
1	H	CN
2	Me	CN
38	H	COOEt
39	Me	COOEt
40	H	Bz
41	Me	Bz

	R_2
3	CN
4	COOEt
5	Bz
6	*p*-ClBz
7	*p*-BrBz
8	*p*-MeBz
9	*p*-PhBz

Prod.	Salt	R_1	R_2	R	a/b
24a,b	10	H	CN	CN	8/1
25a,b	11	Me	CN	CN	5/1
26a,b	12	H	COOEt	CN	10/7
27a,b	13	Me	COOEt	CN	5/1
28a,b	14	H	Bz	CN	7/10
29a,b	15	Me	Bz	CN	2/3
30a,b	16	H	*p*-ClBz	CN	5/6
31a,b	17	Me	*p*-ClBz	CN	4/5
32a,b	18	H	*p*-BrBz	CN	2/3
33a,b	19	Me	*p*-BrBz	CN	3/4
34a,b	20	H	*p*-MeBz	CN	2/3
35a,b	21	Me	*p*-MeBz	CN	4/7
36a,b	22	H	*p*-PhBz	CN	2/3

Prod.	Salt	R_1	R_2	R	a/b
37a,b	23	Me	*p*-PhBz	CN	8/13
54a,b	42	H	CN	COOEt	2/1
55a,b	43	Me	CN	COOEt	2/1
56a,b	44	H	CN	Bz	6/1
57a,b	45	Me	CN	Bz	5/1
58a,b	46	H	COOEt	COOEt	5/9
59a,b	47	Me	COOEt	COOEt	2/3
60a,b	48	H	COOEt	Bz	5/2
61a,b	49	Me	COOEt	Bz	5/2
62b	50	H	Bz	COOEt	0/1
63b	51	Me	Bz	COOEt	0/1
64b	52	H	*p*-ClBz	COOEt	0/1
65b	53	Me	*p*-ClBz	COOEt	0/1

Scheme 1.

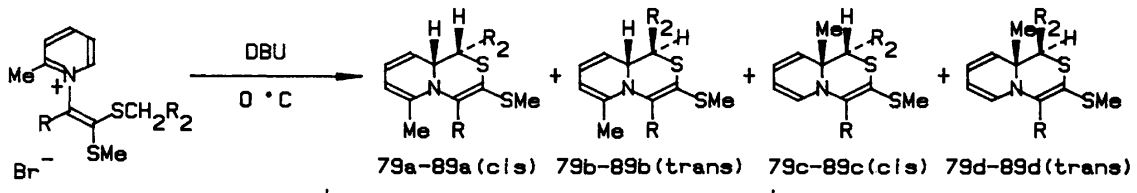

Products	Salt	R_2	R	a/b/c/d
79a,b,c,d	68	CN	CN	9/3/7/4
80a,b,c,d	69	CN	COOEt	4/5/2/1
81a,b,c	70	COOEt	CN	6/5/6/0
82b	71	COOEt	COOEt	0/1/0/0

Prod.	Salt	R_2	R	a/b/c/d
83b,c	72	Bz	CN	0/7/2/0
84b	73	Bz	COOEt	0/1/0/0
85b,c	74	*p*-ClBz	CN	0/3/1/0
86b	75	*p*-ClBz	COOEt	0/1/0/0
87b,c	76	*p*-BrBz	CN	0/5/1/0
88b,c	77	*p*-MeBz	CN	0/3/1/0
89b,c	78	*p*-PhBz	CN	0/4/1/0

	R
66	CN
67	COOEt

Scheme 2.

signals of the minor one appeared at δ 4.03 (1H, d, J=8.0 Hz, 1-H), 4.41 (1H, br q, J=8.0 and 4.0 Hz, 9a-H), and 6.45 (1H, br d, J=7.0 Hz, 6-H). The chemical shifts (δ 4.02—6.72) and the signal patterns of these skeletal protons indicated distinctly the presence of a nonaromatic 1,2-dihydropyridine moiety in **24**, and the presence of the two kinds of the 1-H signals coupled with 2.0 or 8.0 Hz showed that **24** was a cis and trans mixture at the 1- and 9a-positions. From the consideration of Karplus relationship between the coupling constant and the dihedral angle using Dreiding models, we concluded that the major isomer (its dihedral angle is about 60°) is *cis* (**24a**) and the other (its dihedral angle is about 180°) is *trans* (**24b**). The ^{1}H NMR spectrum of **79** obtained from the alkaline treatment of 2-methylpyridinium salt **68** exhibited four methyl proton singlets at δ 1.43, 1.54, 2.08, and 2.25, and a pair of the 6-proton signals at δ 6.54 (br d, J=7.0 Hz) and 6.82 (br d, J=7.0 Hz), together with two methylthio singlets (δ 2.50 and 2.57) and many undistinguishable multiplets in the range of δ 4.0—6.5. From these spectral data we also concluded that

Table 1. ^{1}H NMR Data of Pyrido[2,1-*c*][1,4]thiazines

Compd[a)]	C-1	C-6	C-7	C-8	C-9	C-9a	SMe	R_2	R
24a	4.02 d	6.72 br d	4.99 br t	6.21 br q	5.41 br q	4.60 m	2.50 s	—	—
24b	4.03 d	6.45 br d	b)	b)	b)	4.41 br q	b)	—	—
25a	4.00 d	6.70 d	4.90 dd	1.85 s	5.29 br s	4.56 m	2.52 s	—	—
25b	3.96 d	6.42 d	b)	b)	5.49 br s	b)	b)	—	—
26a	3.90 d	6.62 br d	4.85 br t	6.02 br q	5.38 br q	4.61 m	2.50 s	1.24 t 4.18 q	—
26b	4.00 d	6.48 br d	4.98 br t	b)	b)	b)	2.51 s	1.32 t 4.29 q	—
27a	3.84 d	6.59 d	4.73 dd	1.74 s	5.08 br s	4.50 m	2.48 s	1.21 t 4.15 q	—
27b	b)	6.42 d	b)	b)	b)	b)	b)	1.33 t 4.15 q	—
28a	4.98 d	6.72 br d	c)	5.80 br q	4.4—5.2 m		2.50 s	7.4—8.2 m	—
28b	5.08 d	6.54 br d	c)	5.90 br q	5.38 br q	c)	2.50 s	7.4—8.2 m	—
29a	b)	6.64 d	d)	1.42 s	4.3—5.2 m		2.50 s	7.4—8.2 m	—
29b	4.99 d	6.50 d	d)	1.65 s	4.3—5.2 m		2.50 s	7.4—8.1 m	—
30a	4.91 d	6.68 br d	c)	5.78 br q	b)	c)	2.50 s	7.3—8.2 m	—
30b	5.00 d	6.53 br d	c)	5.91 br q	5.33 br q	c)	2.50 s	7.3—8.2 m	—
31a	b)	6.62 d	e)	1.47 s	4.3—5.3 m		2.55 s	7.3—8.1 m	—
31b	4.96 d	6.49 d	e)	1.64 s	4.3—5.3 m		2.55 s	7.3—8.1 m	—
32a	c)	6.70 br d	c)	5.79 br q	b)	c)	2.49 s	7.5—8.2 m	—
32b	c)	6.55 br d	c)	5.94 br q	5.35 br q	c)	2.49 s	7.5—8.2 m	—
33a	b)	6.65 d	e)	1.45 s	4.3—5.3 m		2.50 s	7.5—8.1 m	—
33b	4.97 d	6.52 d	e)	1.63 s	4.3—5.3 m		2.50 s	7.5—8.1 m	—
34a	4.98 d	6.73 br d	b)	5.78 br q	b)	4.88 m	2.48 s	7.2—8.1 m 2.44 s	—
34b	5.07 d	6.56 br d	4.77 br t	5.93 br q	5.37 br q	4.59 br q	2.48 s	7.2—8.1 m 2.44 s	—
35a	b)	6.66 d	d)	1.41 s	4.3—5.2 m		2.48 s	7.2—8.1 m 2.44 s	—
35b	4.99 d	6.51 d	d)	1.60 s	4.3—5.2 m		2.48 s	7.2—8.1 m 2.44 s	—
36a	5.02 d	6.75 br d	b)	5.80 br q	b)	b)	2.49 s	7.4—8.3 m	—
36b	5.12 d	6.57 br d	4.88 br t	5.96 br q	5.40 br q	4.61 br q	2.49 s	7.4—8.3 m	—
37a	b)	6.69 d	e)	1.41 s	4.3—5.3 m		2.49 s	7.3—8.3 m	—
37b	5.07 d	6.55 d	e)	1.61 s	4.3—5.3 m		2.49 s	7.3—8.3 m	—
54a	3.90 d	6.10 br d	4.88 br t	6.10 br q	5.46 br q	f)	2.40 s	—	1.38 t 4.40 q
54b	f)	b)	5.05 br t	b)	b)	b)	2.45 s	—	1.33 t f)
55a	3.85 d	6.10 d	4.77 dd	1.82 s	5.13 br s	f)	2.40 s	—	1.38 t 4.37 q
55b	f)	5.97 d	4.92 dd	1.84 s	5.44 br s	f)	2.45 s	—	1.34 t f)

Table 1. (Continued)

Compd[a)]	C-1	C-6	C-7	C-8	C-9	C-9a	SMe	R_2	R
56a	3.97 d	6.02 br d	4.73 bt t	6.05 br q	5.40 br q	4.88 m	2.07 s	—	7.3—8.3 m
56b	4.16 d	b)	b)	b)	b)	b)	2.25 s	—	7.3—8.3 m
57a	3.98 d	6.05 d	4.64 dd	1.78 s	5.16 br s	4.84 m	2.08 s	—	7.3—8.3 m
57b	4.14 d	5.91 d	b)	b) s	b)	b)	2.28 s	—	7.3—8.3 m
58a	3.78 d	b) br t	4.70 br t	b)	b)	b)	2.36 s	g)	g)
58b	f)	6.01 br d	4.90 br t	5.98 br q	5.35 br q	f)	2.41 s	g)	g)
59a	3.74 d	6.00 d	4.61 dd	1.73 s	5.11 br s	f)	2.39 s	g)	g)
59b	f)	6.00 d	4.80 dd	1.73 s	5.11 br s	f)	2.44 s	g)	g)
60a	3.85 d	5.90 br d	4.57 br t	5.90 br q	5.35 br q	4.81 m	2.08 s	7.3—8.3 m	1.29 t 4.23 q
60b	b)	b)	b)	b)	b)	b)	2.27 s	7.3—8.3 m	1.32 t 4.27 q
61a	3.84 d	5.88 d	4.48 dd	1.69 s	5.13 br s	4.72 m	2.07 s	7.3—8.3 m	1.28 t 4.23 q
61b	b)	b)	b)	b)	b)	b)	2.27 s	7.3—8.3 m	1.34 t 4.29 q
62b	5.23 d	6.12 br d	4.92 br t	5.95 br q	5.40 br q	f)	2.42 s	7.3—8.3 m	1.38 t 4.36 q
63b	5.12 d	6.05 br d	4.81 br d	1.59 s	5.05 br s	f) m	2.40 s	7.3—8.3 m	1.34 t 4.33 q
64b	5.15 d	6.11 br d	4.91 br t	5.93 br q	5.34 br q	4.40 m	2.40 s	7.3—8.2 m	1.36 t 4.33 q
65b	5.05 d	5.99 br d	4.85 br d	1.60 s	4.99 br s	4.30 m	2.41 s	7.3—8.1 m	1.36 t 4.34 q
79a	4.00 d	2.25 s	———	4.8—6.5 m	———		h)	—	—
79b	b)	2.08 s	b)	b)	b)	b)	h)	—	—
79c	3.63 s	6.82 br d	b)	b)	b)	1.43 s	h)	—	—
79d	b)	6.54 br d	b)	b)	b)	1.54 s	h)	—	—
80a	3.97 d	1.90 s	4.92 br d	6.25 q	5.39 br q	f)	2.50 s	—	1.36 t 4.32 q
80b	f)	1.77 s	i)	i)	i)	f)	2.53 s	—	g)
80c	3.59 s	i)	i)	i)	i)	1.43 s	2.39 s	—	g)
80d	f)	b)	b)	b)	b)	1.54 s	2.44 s	—	g)
81a	3.90 d	2.12 s	i)	i)	i)	f)	2.57 s	g)	—
81b	f)	2.07 s	b)	b)	b)	f)	2.57 s	g)	—
81c	3.46 s	6.75 br d	b)	b)	b)	1.40 s	2.45 s	g)	—
82b	f)	1.73 s	4.88 br d	6.00 q	5.28 br q	3.86 q	2.46 s	g)	g)
83b	5.21 d	2.13 s	4.99 br d	5.92 q	5.35 br q	4.18 q	2.54 s	7.3—8.2 m	—
83c	4.52 s	6.86 br d	b)	b)	b)	1.53 s	2.38 s	7.3—8.2 m	—
84b	5.38 d	1.81 s	4.92 br d	5.97 q	5.31 br q	f)	2.40 s	7.3—8.2 m	1.33 t 4.31 q

Table 1. (Continued)

Compd[a)]	C-1	C-6	C-7	C-8	C-9	C-9a	SMe	R_2		R	
85b	5.12 d	2.11 s	5.00 br d	5.93 q	5.33 br q	4.13 q	2.54 s	7.3—8.1 m		—	
85c	4.46 s	6.87 br d	b)	b)	b)	1.53 s	2.38 s	7.3—8.1 m		—	
86b	5.28 d	1.80 s	4.92 br d	5.95 q	5.23 br q	f)	2.47 s	7.3—8.1 m		1.33 t	4.30 q
87b	5.15 d	2.12 s	4.99 br d	5.95 q	5.33 br q	4.16 q	2.52 s	7.4—8.1 m		—	
87c	4.46 s	6.87 br d	b)	b)	b)	1.53 s	2.37 s	7.4—8.1 m		—	
88b	5.17 d	2.11 s	4.97 br d	5.90 q	5.33 br q	4.16 q	2.50 s	7.1—8.1 m	2.43 s	—	
88c	4.47 s	6.85 br d	b)	b)	b)	1.51 s	2.36 s	7.1—8.1 m	2.43 s	—	
89b	5.24 d	2.13 s	4.99 br d	5.94 q	5.38 br q	4.20 q	2.51 s	7.3—8.3 m		—	
89c	4.55 s	6.90 br d	b)	b)	b)	1.53 s	2.37 s	7.3—8.3 m		—	

a) The coupling constants are as follows: $J_{1,9a}$=2.0(cis) or 8.0(trans), $J_{6,7}$=7.0, $J_{7,8}$=6.0, $J_{8,9}$=10.0, $J_{9,9a}$=4.0, $J_{7,9}$=2.0, J_{Et}=7.0 Hz. b) Overlapped with the signals of the major isomer. c) Overlapped with the signals at δ 4.4—5.2. d) Overlapped with the signals at δ 4.3—5.2. e) Overlapped with the signals at δ 4.3—5.3. f) Overlapped with the signals at δ 3.9—4.7. g) Overlapped with each others at δ 1.0—1.6 and 4.0—4.7. h) 2.57 or 2.50 (s). i) Overlapped with each others at δ 3.7—6.5.

compound **79** consisted of both cis and trans mixtures of 6-methyl and 9a-methyl derivatives and both cyclization to 2- and 6-positions on the pyridine ring took place. In the same way the distinction between the cis isomer and the trans one in the 9a-methyl derivatives **79c,d**—**89c,d** were carried out by the comparisons of the chemical shifts (δ 6.75—6.90 for the cis isomers **79c**, **81c**, **83c**, **85c**, and **87c**—**89c**, and δ 6.54 for the trans isomer **79d**) of each 6-proton with those (δ 6.59—6.73 for the cis isomers **24a**—**37a** and δ 6.42—6.57 for the trans isomers **24b**—**37b**) of the 9a-H derivatives. These chemical shifts and the signal patterns were very similar to those of 4,4a-dihydropyrido[1,2-*d*][1,3,4]-thiadiazine derivatives synthesized earlier by us.[2b] Furthermore, the transformations of these compounds **24**—**37**, **54**—**65**, and **79**—**89** to the corresponding indolizine derivatives using a dehydrogenating agent supported strongly our proposed structures (See below).

Transformations to Indolizine Derivatives. Because of the thermal instability, the transformations from these dihydropyridothiazines to the corresponding indolizines did not take place except in compounds **26**, **27**, and **58**, and their treatment with an oxidizing or a dehydrogenating agent at a temperature over 0 °C resulted always in polymeric tars. Among many reagents examined for purpose of this transformation, we found that LTA and DDQ gave satisfactory results only when they were used at 0 °C. The reactions of dihydropyridothiazines **24**—**27** and **54**—**61** bearing a cyano or an ethoxycarbonyl group at the 1-position with LTA in tetrahydrofuran (THF) or with DDQ in chloroform in an ice bath afforded the desulfurized indolizines **90**—**101**, and those of compounds **28**—**37** and **62**—**65** having an aroyl group at that position with the same reagents gave the rearranged indolizines **102**—**115** in considerable yields. On the other hand, the reactions of dihydropyridothiazines **79**—**89**, synthesized from 2-methylpyridinium bromides **68**—**78**, with LTA or DDQ gave always only 5-methylindolizine derivatives **116**—**126** which were convertible from 9a-H adducts (types a and b), and did not afford any significant product which might be derived from 9a-methyl compounds (types c and d). The reaction of 1,4-dicyano adduct **79** with LTA, however, gave only 6-acetoxy-1,3-dicyano-5-methyl-2-methylthioindolizine **127** in very low yield (3%) instead of the expected 1,3-dicyano-5-methyl-2-methylthioindolizine **116**, while that of **79** with DDQ yielded normal product **116**. These results are summarized in Schemes 3 and 4. These dehydrogenating agents, LTA and DDQ, were effective to the same extent unless the substituents R and/or R_2 were an ethoxycarbonyl group, but, when the group(s) was so, the latter reagent was superior in the yield and the easy separation to the former.

The same indolizine derivatives could be also synthesized by adding directly DDQ to 1,9a-dihydropyridothiazines generated in situ from the alkaline treatment of the corresponding pyridinium salts (See Scheme 3). It was found that this method has high synthetic value because it can be carried out without the isolation of unstable dihydropyridothiazines.

In above reactions, the desulfurized indolizines **90**—

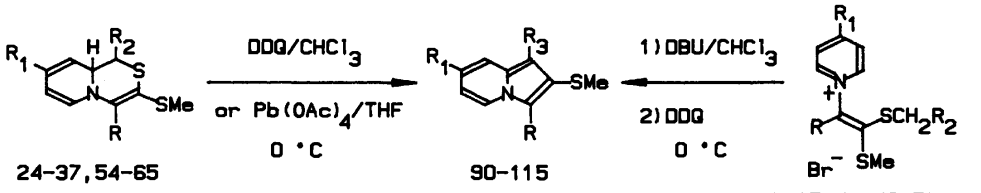

Prod.	React.	R_1	R_3	R
90	24	H	CN	CN
91	25	Me	CN	CN
92	26	H	COOEt	CN
93	27	Me	COOEt	CN
94	54	H	CN	COOEt
95	55	Me	CN	COOEt
96	56	H	CN	Bz
97	57	Me	CN	Bz
98	58	H	COOEt	COOEt
99	59	Me	COOEt	COOEt
100	60	H	COOEt	Bz
101	61	Me	COOEt	Bz
102	28	H	BzS	CN
103	29	Me	BzS	CN
104	30	H	*p*-ClBzS	CN
105	31	Me	*p*-ClBzS	CN
106	32	H	*p*-BrBzS	CN
107	33	Me	*p*-BrBzS	CN
108	34	H	*p*-MeBzS	CN
109	35	Me	*p*-MeBzS	CN
110	36	H	*p*-PhBzS	CN
111	37	Me	*p*-PhBzS	CN
112	62	H	BzS	COOEt
113	63	Me	BzS	COOEt
114	64	H	*p*-ClBzS	COOEt
115	65	Me	*p*-ClBzS	COOEt

Scheme 3.

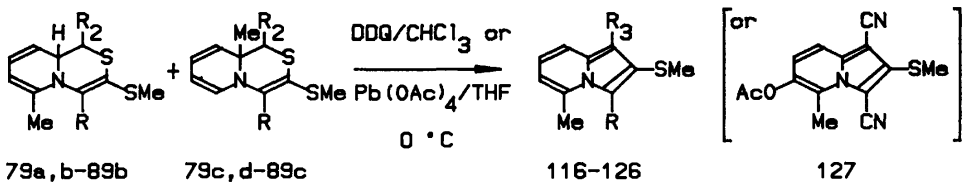

Prod.	React.	R_3	R
116	79	CN	CN
117	80	CN	COOEt
118	81	COOEt	CN
119	82	COOEt	COOEt
120	83	BzS	CN
121	84	BzS	COOEt
122	85	*p*-ClBzS	CN
123	86	*p*-ClBzS	COOEt
124	87	*p*-BrBzS	CN
125	88	*p*-MeBzS	CN
126	89	*p*-PhBzS	CN

Scheme 4.

101 and **116—119** were always formed when R_2 was a cyano or an ethoxycarbonyl group, and the rearranged indolizines **102—115** and **120—126** were obtained whenever R_2 was an aroyl group. These substituent effects are all the same as those observed in the formations from 4,4a-dihydropyrido[1,2-*d*][1,3,4]thiadiazines to the desulfurized and rearranged pyrazolo-[1,5-*a*]pyridines.[1,2]

The structures of these indolizines **90—127** were determined mainly by their spectral and elementary analyses and in part by the comparison with authentic samples **94** (mp 142—143°C, Lit,[5] mp 139°C) and **96** (mp 143—144 °C, Lit,[5] mp 138—139 °C). In particular, the chemical shifts and signal patterns due to the skeletal protons in their ^{1}H NMR spectra (Table 2) were grossly similar to those of known indolizine derivatives prepared by us[6] and by other investigators.[5,7] The mass spectra of compounds **90**, **92**, **102**, **104**, **106**, **108**, and **110** gave molecular ion peaks at *m/z* 213, 260, 324, 360, 404, 338, and 401, respectively. On the other hand, the structure of unusual 6-acetoxyindolizine **127** was decided on the basis of the presences of a AB type signal coupled with 9.0 Hz (vicinal coupling) at δ 7.18 and 7.63 and of an acetoxy methyl signal at δ 2.41

Table 2. ^{1}H NMR Data of Indolizines in $CDCl_3$

Compd[a)]	C-5	C-6	C-7	C-8	SMe	R_2	R
90	8.36 br d	7.10 dt	7.45 br t	7.77 br d	2.77 s	—	—
91	8.24 d	6.97 dd	2.49 s	7.51 br s	2.76 s	—	
92	8.29 br d	6.98 dt	7.37 br t	8.25 br d	2.81 s	1.44 t 4.42 q	—
93	8.19 d	6.83 dd	2.44 s	8.03 br s	2.79 s	1.43 t 4.41 q	—
94	9.59 br d	7.04 dt	7.41 br t	7.77 br d	2.89 s	—	1.47 t 4.50 q
95	9.42 d	6.83 dd	2.47 s	7.48 br s	2.86 s	—	1.46 t 4.46 q
96	9.48 br d	7.04 dt	b)	b)	2.52 s	—	7.3—8.0 m
97	9.32 d	6.84 dd	2.48 s	b)	2.50 s	—	7.3—8.9 m
98	9.47 br d	6.90 dt	7.29 br t	8.28 br d	2.53 s	1.47 t c)	1.47 t c)
99	9.40 d	6.79 dd	2.43 s	8.09 br s	2.54 s	1.48 t d)	1.48 t d)
100	9.25 br d	6.95 dt	b)	8.40 br d	2.28 s	1.47 t 4.49 q	7.3—8.3 m
101	9.23 d	6.84 dd	2.49 s	8.20 br d	2.26 s	1.48 t 4.50 q	7.3—8.0 m
102	8.36 br d	6.95 dt	b)	b)	2.63 s	7.2—8.3 m	—
103	b)	6.79 dd	2.37 s	7.26 br s	2.61 s	7.4—8.3 m	—
104	8.33 br d	6.95 dt	7.21 br t	b)	2.63 s	7.4—8.2 m	—
105	8.16 d	6.74 dd	2.36 s	7.20 br s	2.59 s	7.3—8.2 m	—
106	8.32 br d	6.94 dt	7.21 br t	7.51 br d	2.62 s	7.5—8.2 m	—
107	8.21 d	6.80 dd	2.39 s	7.26 br s	2.62 s	7.2—8.2 m	—
108	8.33 br d	6.92 dt	b)	b)	2.61 s	7.1—8.2 m 2.43 s	—
109	8.18 d	6.77 dd	2.36 s	b)	2.59 s	7.2—8.2 m 2.43 s	—
110	8.34 br d	6.95 dt	7.22 br t	b)	2.64 s	7.3—8.4 m	—
111	b)	6.79 dd	2.39 s	7.30 br s	2.63 s	7.4—8.4 m	—
112	9.55 br d	6.88 dt	7.15 br t	b)	2.50 s	7.3—8.3 m	1.48 t 4.49 q
113	9.48 d	6.74 dd	2.36 s	7.30 br s	2.48 s	7.4—8.3 m	1.47 t 4.48 q
114	9.54 br d	6.88 dt	7.14 br t	7.51 br d	2.48 s	7.4—8.1 m	1.47 t 4.49 q
115	9.42 d	6.73 dd	2.36 s	7.24 br s	2.48 s	7.3—8.3 m	1.46 t 4.48 q
116	3.03 s	6.82 br d	7.34 q	7.66 br d	2.76 s	—	—
117	2.57 s	6.78 br d	7.28 q	7.63 br d	2.70 s	—	1.44 t 4.48 q
118	3.04 s	6.73 br d	7.30 q	8.32 br d	2.72 s	1.45 t 4.47 q	—
119	2.57 s	6.67 br d	7.15 q	8.28 br d	2.50 s	1.44 t e)	1.44 t e)
120	3.04 s	6.70 br d	7.18 q	b)	2.57 s	7.3—8.3 m	—

Table 2. (Continued)

Compd[a)]	C-5	C-6	C-7	C-8	SMe	R_2		R	
121	2.60 s	6.71 br d	7.11 q	b)	2.46 s	7.3—8.4 m		1.47 t	4.51 q
122	3.03 s	6.72 br d	7.16 q	b)	2.56 s	7.3—8.3 m		—	
123	2.58 s	6.67 br d	7.07 q	b)	2.43 s	7.3—8.3 m		1.45 t	4.49 q
124	3.03 s	6.69 br s	7.12 q	7.44 br d	2.55 s	7.6—8.2 m		—	
125	3.02 s	6.68 br d	7.12 q	b)	2.57 s	7.2—8.2 m	2.46 s	—	
126	3.03 s	6.68 br d	7.13 q	b)	2.58 s	7.3—8.4 m		—	
127	2.90 s	2.41 s	7.18 d	7.63 d	2.77 s	—		—	

a) The coupling constants are as follows: $J_{5,6}=J_{6,7}=7.0$, $J_{7,8}=9.0$, $J_{6,8}=2.0$, and $J_{Et}=7.0$ Hz. b) Overlapped with the phenyl proton signals. c) 4.48 or 4.44 (q). d) 4.48 or 4.49 (q). e) 4.47 or 4.49 (q).

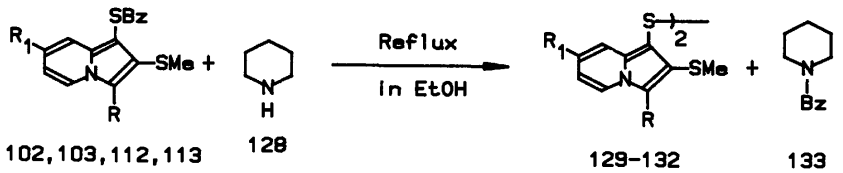

102,103,112,113 128 129-132 133

Prod.	React.	R_1	R
129	102	H	CN
130	103	Me	CN
131	112	H	COOEt
132	113	Me	COOEt

Scheme 5.

(s) and by the comparison of the chemical shifts of the pyridine protons in the ^{1}H NMR spectrum.

In order to obtain further evidences for the rearranged indolizine structure, the aminolysis of compounds **102**, **103**, **112**, and **113** with piperidine **128** were carried out in ethanol at the reflux temperature, and the corresponding disulfides **129—132** were obtained in good yields together with *N*-benzoylpiperidine **133** (Scheme 5). The structures of disulfides **129—132** were also determined by their IR and ^{1}H NMR spectral inspections in which the absence of the benzoyl group was clearly exhibited.

Reaction Mechanisms. Possible mechanisms for the reactions of pyridinium sals **10—23**, **42—53**, and **68—78** to desulfurized indolizines **90—101** and **116—119**, and rearranged indolizines **102—115** and **120—126** and of the rearranged indolizines to disulfides **129—132** are summarized in Scheme 6. This mechanisms are formally the same as those proposed to the reactions of a 1,3,4-thiadiazinyl anion by Schmidt et al.[3] and of a pyrido[1,2-*d*][1,3,4]thiadiazine by us.[1,2] In contrast with our previos works[1,2] for its aza-analogue, 1,9a-dihydropyrido[2,1-*c*][1,4]thiazine intermediates could be separated actually and the effect of dehydrogenating agents in the conversion from them to aromatic indolizines derivatives was confirmed distinctly. On the other hand, the lowness of the stereoselectivity and the regioselectivity in the 1,6-cyclizations of the zwitterionic species **134** to 1,9a-dihydropyrido[2,1-*c*][1,4]thiazines **24—37**, **54—65**, and **79—89** may be largely owing to the one plane and one anionic pyramidal approach (see Fig. 1) which undergoes less steric hindrance than the two plane approach as seen in normal cycloaddition reactions. The increase of the formation ratios of the trans isomers to cis isomers with the increase of the bulkiness of the group R_2 in the 9a-H adducts **24—37**, **54—65**, and **79a,b—89a,b** can be explained reasonably by considering the sterically less hindered conformation (**B**) in the transition state, and the predominance of the cis isomers in 9a-methyl adducts **79c,d—89c,d** can be understand similarly by thinking the larger steric hindrance of the 2-methyl group than that of the flat pyridine ring. Furthermore, the fact that the

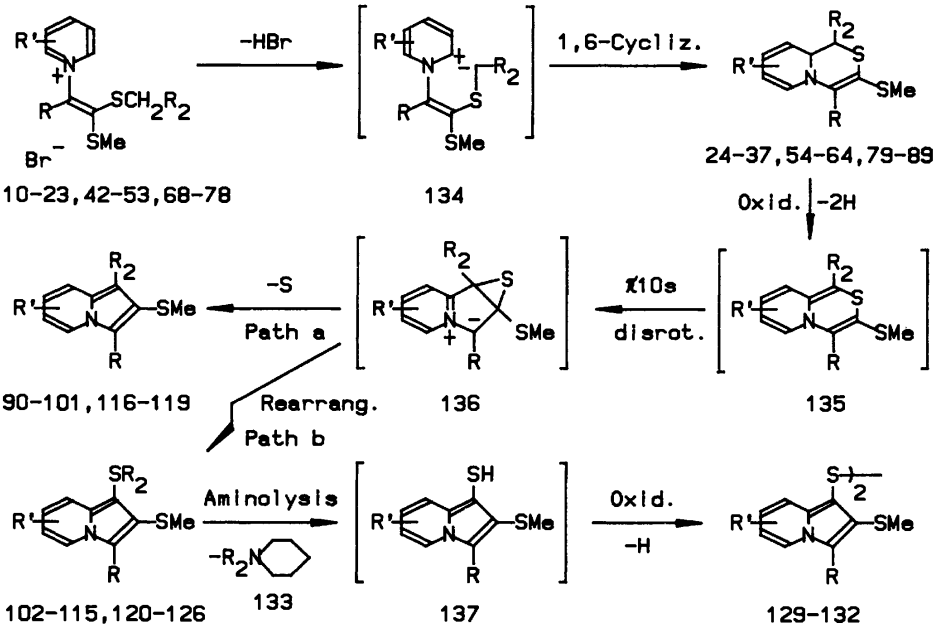

Scheme 6.

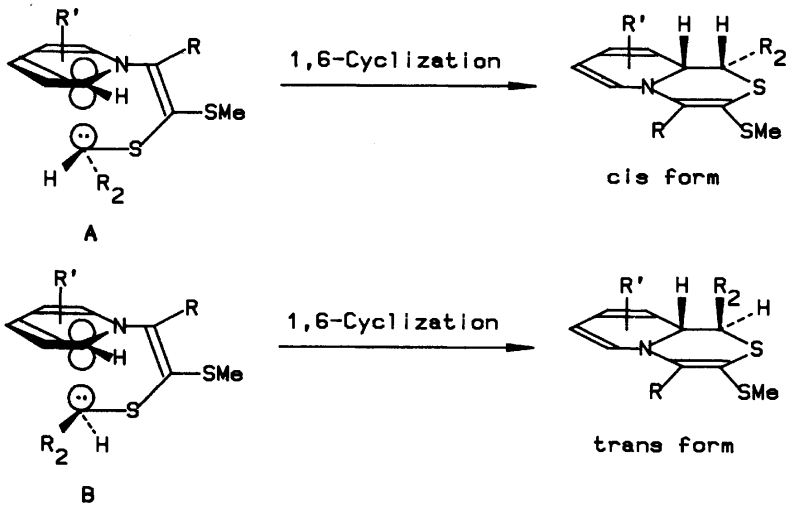

Fig. 1.

effect of the substituent R_2 in these reactions was all the same that as in the transformations of pyridothiadiazines to pyrazolo[1,5-*a*]pyridines suggests strongly a mechanistic similarity between these two reactions.

On the other hand, the mechanism for the formation of 6-acetoxyindolizine **127** is uncertain, but it may involve an attack of the acetoxyl radical generated from LTA onto the electron-rich sp^2 carbon in the pyridothiazine or indolizine intermediate.

Our reactions described here have a theoretical and practical values because only the desulfurizaion has been reported in the reaction of a 1,4-thiazinyl anion system[8] and the *S*-containing indolizine has been scarcely synthesized.[5,9]

Experimental

Melting points were measured with a Yanagimoto micro-melting point apparatus and are uncorrected. Microanalyses were carried out on a Perkin-Elmer 240 Elemental analyzer. The ^1H NMR spectra were determined with a Varian EM360A spectrometer in deuteriochloroform with tetramethylsilane as an internal standard. The chemical shifts are expressed in δ values. The IR spectra were taken with a Hitachi 260-10 Infrared spectrophotometer, and the mass specta with a JEOL LMS-01SG-2 mass spectrometer attached with a JEC-6 spectrocomputer.

Preparations of Pyridinium 1-(Thiocarbonyl)methylides. These pyridinium 1-(thiocarbonyl)methylides **1**, **2**, **38**—**41**, **66**, and **67** were synthesized from the alkaline treatment of

Table 3. Some Data of 1,9a-Dihydropyrido[2,1-*c*][1,4]thiazines

Compd No.	Salt(S.M[a])	Yield %	Mp θ_m/°C	IR[KBr] (cm^{-1})		Formula	Calcd%(Found%) C	H	N
24a, b	**10(1, 3)**	47	131—133[b]	2230	2210	$C_{11}H_9N_3S_2$	53.41 (53.21	3.67 3.63	16.99 17.23)
25a, b	**11(2, 3)**	56	c)	2230	2212	$C_{12}H_{11}N_3S_2$	55.15 (55.06	4.24 4.19	16.08 15.84)
26a, b	**12(1, 4)**	72	c)	2212	1728[d]	Unstable[e,f]			
27a, b	**13(2, 4)**	74	c)	2213	1722[d]	Unstable[e,g]			
28a, b	**14(1, 5)**	55	c)	2208	1677	$C_{17}H_{14}N_2OS_2$	62.55 (62.78	4.32 4.27	8.58 8.40)
29a, b	**15(2, 5)**	84	c)	2208	1664	$C_{18}H_{16}N_2OS_2$	63.50 (63.37	4.74 4.67	8.23 8.33)
30a, b	**16(1, 6)**	44	c)	2205	1687	$C_{17}H_{13}ClN_2OS_2$	56.58 (56.46	3.63 3.51	7.76 8.00)
31a, b	**17(2, 6)**	62	c)	2205	1678	$C_{18}H_{15}ClN_2OS_2$	57.67 (57.54	4.03 3.88	7.47 7.37)
32a, b	**18(1, 7)**	43	c)	2206	1670	$C_{17}H_{13}BrN_2OS_2$	50.37 (50.44	3.23 3.09	6.91 6.97)
33a, b	**19(2, 7)**	57	c)	2210	1679	$C_{18}H_{15}BrN_2OS_2$	51.55 (51.59	3.61 3.53	6.68 6.73)
34a, b	**20(1, 8)**	54	c)	2205	1670	$C_{18}H_{16}N_2OS_2$	63.50 (63.79	4.74 4.59	8.23 8.09)
35a, b	**21(2, 8)**	67	c)	2199	1663	$C_{19}H_{18}N_2OS_2$	64.38 (64.36	5.12 4.97	7.90 8.08)
36a, b	**22(1, 9)**	57	c)	2215	1670	$C_{23}H_{18}N_2OS_2$	68.63 (68.68	4.51 4.35	6.96 7.07)
37a, b	**23(2, 9)**	63	c)	2219	1668	$C_{24}H_{20}N_2OS_2$	69.20 (69.46	4.84 4.89	6.73 6.52)
54a, b	**42(38, 3)**	78	c)	2235	1710	$C_{13}H_{14}N_2O_2S_2$	53.04 (53.01	4.79 4.55	9.52 9.79)
55a, b	**43(39, 3)**	50	c)	2240	1717	$C_{14}H_{16}N_2O_2S_2$	54.52 (54.34	5.23 5.27	9.08 9.24)
56a, b	**44(40, 3)**	89	88—88[c]	2232	1669	$C_{17}H_{14}N_2OS_2$	62.55 (62.55	4.32 4.30	8.58 8.60)
57a, b	**45(41, 3)**	82	c)	2230	1666[d]	Unstable[e]			
58a, b	**46(38, 4)**	50	c)	1720[d]		Unstable[e]			
59a, b	**47(39, 4)**	90	c)	1710		$C_{16}H_{21}NO_4S_2$	54.06 (53.95	5.95 5.87	3.94 3.84)
60a, b	**48(40, 4)**	82	c)	1731	1666[d]	Unstable[e]			
61a, b	**49(41, 4)**	72	c)	1716	1658	$C_{20}H_{21}NO_3S_2$	61.99 (61.83	5.46 5.42	3.61 3.82)
62b	**50(38, 5)**	80	94	1715	1675	$C_{19}H_{19}NO_3S_2$	61.10 (61.10	5.13 5.31	3.75 3.72)
63b	**51(39, 5)**	75	96—97	1670	1650	$C_{20}H_{21}NO_3S_2$	61.99 (61.98	5.46 5.37	3.61 3.71)
64b	**52(38, 6)**	63	92—94	1674		$C_{19}H_{18}ClNO_3S_2$	55.94 (55.86	4.45 4.59	3.43 3.36)
65b	**53(39, 6)**	39	106—108	1676	1640	$C_{20}H_{20}ClNO_3S_2$	56.93 (56.79	4.78 4.69	3.32 3.32)
79a, b, c, d	**68(66, 3)**	67	c)	2232	2203	$C_{12}H_{11}N_3S_2$	55.15 (55.05	4.24 4.21	16.08 16.20)
80a, b, c, d	**69(67, 3)**	91	c)	2235	1723	$C_{14}H_{16}N_2O_2S_2$	54.52 (54.50	5.23 5.14	9.08 9.19)
81a, b, c	**70(66, 4)**	77	c)	2205	1732[d]	Unstable[e]			
82b	**71(67, 4)**	89	Oil	1720	1687[d]	Unstable[e]			
83b, c	**72(66, 5)**	94	c)	2204		$C_{18}H_{16}N_2OS_2$	63.50 (63.64	4.74 4.84	8.23 7.99)
84b	**73(67, 5)**	58	91—92	1670		$C_{20}H_{21}NO_3S_2$	61.99 (61.96	5.46 5.22	3.61 3.88)
85b, c	**74(66, 6)**	97	c)	2207	1688	$C_{18}H_{15}ClN_2OS_2$	57.67 (57.58	4.03 3.99	7.47 7.60)
86b	**75(67, 6)**	49	99—100	1676		$C_{20}H_{20}ClNO_3S_2$	56.93 (56.64	4.78 4.70	3.32 3.52)

Table 3. (Continued)

Compd No.	Salt(S.M[a])	Yield %	Mp θ_m/°C	IR[KBr] (cm^{-1})		Formula	Calcd% (Found%) C	H	N
87b, c	**76 (66, 7)**	74	c)	2210	1668[d]	Unstable[e]			
88b, c	**77 (66, 8)**	76	c)	2199	1662	$C_{19}H_{18}N_2OS_2$	64.38 (64.51	5.12 5.08	7.90 7.92)
89b, c	**78 (66, 9)**	77	c)	2210	1674[d]	Unstable[e]			

a) Starting materials. b) Cis isomer. c) Mixture. d) Neat. e) The preparation of pure sample for its analysis was unsuccessful because of its instability. f) This compound decomposed smoothly to indolizine **92** on standing in a freezer (76%). g) This compound decomposed smoothly to indolizine **93** on standing in a freezer (66%).

Table 4. Some Data of Indolizines

Compd No.	React	Method(%) A	B	C	Mp θ_m/°C	IR[KBr] (cm^{-1})		Formula	Calcd% (Found%) C	H	N
90	**24**	41		27	140—141	2201		$C_{11}H_7N_3S+1/2H_2O$	59.94 (59.46	3.63 3.72	18.96 18.80)
91	**25**	56		47	173—175	2201		$C_{12}H_9N_3S$	63.41 (63.64	3.99 3.96	18.49 18.29)
92	**26**	42		43	152—154	2201	1678	$C_{13}H_{12}N_2O_2S$	59.98 (60.14	4.65 4.75	10.76 10.50)
93	**27**	57		55	130—132	2201	1680	$C_{14}H_{14}N_2O_2S$	61.29 (61.58	5.14 5.17	10.21 9.90)
94	**54**	33		65	142—143	2194	1669	Known Compound[a]			
95	**55**	63		51	168—169	2202	1671	$C_{14}H_{14}N_2O_2S$	61.29 (61.40	5.14 5.18	10.21 10.06)
96	**56**	31	62		143—144	2212	1608	Known Compound[b]			
97	**57**	59	60		176—178	2203	1606	$C_{18}H_{14}N_2OS$	70.56 (70.46	4.61 4.32	9.14 9.20)
98	**58**	23			58	1680	1660	$C_{15}H_{17}NO_4S$	58.62 (58.46	5.58 5.42	4.56 4.48)
99	**59**	13			55	1680	1660	$C_{16}H_{19}NO_4S$	59.79 (59.83	5.96 5.37	4.36 4.41)
100	**60**	62	53		126—128	1691		$C_{19}H_{17}NO_3S$	67.24 (67.13	5.05 5.02	4.13 4.22)
101	**61**	56	45		84—85	1670		$C_{20}H_{19}NO_3S$	67.97 (67.92	5.42 5.49	3.96 3.95)
102	**28**	50	81	57	134	2196	1672	$C_{17}H_{12}N_2OS_2$	62.94 (62.68	3.73 3.68	8.63 8.52)
103	**29**	49	63	44	158—159	2196	1673	$C_{18}H_{14}N_2OS_2$	63.88 (63.69	4.17 4.12	8.28 8.58)
104	**30**	58	94		139	2190	1670	$C_{17}H_{11}ClN_2OS_2$	56.90 (56.80	3.09 3.07	7.81 7.64)
105	**31**	64	79		171—172	2192	1671	$C_{18}H_{13}ClN_2OS_2$	57.98 (57.93	3.51 3.53	7.51 7.53)
106	**32**	54	83		141—142	2206	1679	$C_{17}H_{11}BrN_2OS_2$	50.63 (50.46	2.75 2.58	6.95 6.69)
107	**33**	59	80		179	2189	1672	$C_{18}H_{13}BrN_2OS_2$	51.80 (51.54	3.14 2.89	6.71 6.45)
108	**34**	59	61		140	2192	1668	$C_{18}H_{14}N_2OS_2$	63.88 (63.73	4.17 4.12	8.28 8.48)
109	**35**	59	56		208—209	2204	1670	$C_{19}H_{16}N_2OS_2$	64.74 (64.74	4.58 4.45	7.95 8.08)
110	**36**	57	93		174	2199	1676	$C_{23}H_{16}N_2OS_2$	68.97 (68.98	4.03 3.95	6.99 7.13)
111	**37**	47	77		120—121	2185	1674	$C_{24}H_{18}N_2OS_2$	69.54 (69.31	4.38 4.21	6.76 6.76)
112	**62**	22	68	53	89—90	1670		$C_{19}H_{17}NO_3S_2$	61.43 (61.21	4.61 4.59	3.77 3.66)
113	**63**	37	53	51	105—106	1670		$C_{20}H_{19}NO_3S_2$	62.31 (62.38	4.97 4.91	3.63 3.58)

Table 4. (Continued)

Compd No.	React	Method(%) A	B	C	Mp θ_m/°C	IR^{KBr} (cm^{-1})		Formula	Calcd% (Found%) C	H	N
114	**64**	25	76		93	1667		$C_{19}H_{16}ClNO_3S_2$	56.22 (56.27	3.97 3.88	3.45 3.49)
115	**65**	10	51		137—140	1679	1670	$C_{20}H_{18}ClNO_3S_2$	57.20 (57.22	4.32 4.31	3.34 3.44)
116	**79**	0	39		147—148	2202		$C_{12}H_9N_3S$	63.41 (63.75	3.99 3.92	18.49 18.22)
117	**80**	c)	56		59	2205	1705	$C_{14}H_{14}N_2O_2S$	61.29 (61.37	5.14 5.13	10.21 10.14)
118	**81**	46			138—139	2206	1681	$C_{14}H_{14}N_2O_2S$	61.29 (61.40	5.14 5.26	10.21 9.98)
119	**82**	18	53		Oil	1695[d]		$C_{16}H_{19}NO_4S$	59.79 (59.70	5.96 5.99	4.36 4.42)
120	**83**	32	41		149	2195	1662	$C_{18}H_{14}N_2OS_2$	63.88 (64.12	4.17 4.15	8.28 7.98)
121	**84**	20	24		75—76	1690	1667	$C_{20}H_{19}NO_3S_2$	62.31 (62.03	4.97 4.92	3.63 3.86)
122	**85**	21	33		93—95	2200	1665	$C_{18}H_{13}ClN_2OS_2$	57.98 (57.83	3.51 3.51	7.51 7.47)
123	**86**	25	26		113—114	1710	1670	$C_{20}H_{18}ClNO_3S_2$	57.20 (57.05	4.32 4.37	3.34 3.56)
124	**87**	c)	31		125—127	2200	1670	$C_{18}H_{13}BrN_2OS_2$	51.80 (51.86	3.14 3.13	6.71 6.53)
125	**88**	24	40		154—156	2190	1664	$C_{19}H_{16}N_2OS_2$	64.74 (64.61	4.58 4.50	7.95 8.10)
126	**89**	18	42		187—190	2198	1668	$C_{24}H_{18}N_2OS_2$	69.54 (69.28	4.38 4.30	6.76 6.47)
127	**79**	3			205—207	2218	2195[e]	$C_{14}H_{11}N_3O_2S$	58.93 (58.67	3.89 3.89	14.73 14.45)

a) Mp 139 °C, see Ref. 5. b) Mp 138—139 °C, see Ref. 5. c) Trace. d) Neat.

the corresponding pyridinium chlorides, carbon disulfide, and dimethyl sulfate according to the procedure described in the literature.[10] Some properties of new compounds **2** and **66** are as follows: **2**, 76%, yellow needles, mp 180—181 °C (from EtOH-$CHCl_3$), IR (KBr) 2165 (CN) and 1399 cm^{-1}. Found: C, 54.27; H, 4.52; N, 12.65%. Calcd for $C_{10}H_{10}N_2S_2$: C, 54.02; H, 4.53; N, 12.60%. **66**, 68%, yellow prisms, mp 145—146 °C (from EtOH-$CHCl_3$), IR (KBr) 2160 (CN) and 1385 cm^{-1}. Found: C, 53.96; H, 4.54; N,12.65. Calcd for $C_{10}H_{10}N_2S_2$: C, 54.02; H, 4.53; N, 12.60.

Preparations of Pyridinium Bromides. General Method. These pyridinium salts **10—23**, **42—53**, and **68—78** (2 mmol) were prepared in quantitatively yields from the reactions of the corresponding pyridinium methylides **1**, **2**, **38—41**, **66**, and **67** (2 mmol) with small excess of alkyl bromides **3—9** (2.4 mmol) in chloroform at room temperature for 1—10 d. After the evaporation of the solvent followed by the removal of an unaltered alkylating agent by washing them three times with 30 ml portions of ether, they were used immediately to the next reactions without further purification.

Preparations of 1,9a-Dihydropyrido[2,1-*c*][1,4]thiazines. General Method. To a chloroform solution (20 ml) of pyridinium bromide (2 mmol) DBU (0.380 g, 2.5 mmol) was added dropwise under stirring in an ice bath. The resulting dark red solution was kept for further 10 min at the temperature, and then concentrated immediately at reduced pressure at below 40 °C. The residue was quickly separated by short pass column chromatography (alumina, 1.7 cm diameter×7 cm long) using chloroform as an eluent. The chloroform layer was concentrated at reduced pressure without heating. The same column separation was repeated further two times. Recrystallizations of the resulting 1,9a-dihydropyrido[2,1-*c*][1,4]thiazines from chloroform-hexane in a freezer afforded pure samples.

The preparations of pure samples of compounds **26**, **27**, **57**, **58**, **81**, **82**, and **89** for analyses and the separations of the cis and trans mixtures were unsuccessful because of their thermal instability, but pure **24a** was isolated by the repeated recrystallization. Compounds **26**, **27**, and **58** were decomposed in a freezer to give the aromatized indolizines **92**, **93**, and **98** in 76, 66, and 15% yields, respectively.

Some data of these products are listed in Tables 1 and 3.

Preparations of Indolizines. General Method A. To a tetrahydrofuran solution (30 ml) of dihydropyridothiazine (1 mmol) LTA (0.443 g, 1 mmol) was added under stirring in an ice bath and the solution was stirred for further 6 h at the temperature. The resulting solution was filtered to remove insoluble substances and the filtrate was concentrated at reduced pressure. The residue was separated by column chromatography (alumina) using ether and then chloroform as eluents. The combined chloroform layer was concentrated and the recrystallization of the residue from chloroform-hexane gave the corresponding indolizine derivatives.

General Method B. DDQ (0.227 g, 1 mmol) as a dehydrogenating agent and chloroform as a solvent were

employed here instead of LTA and tetrahydrofuran in Method A. The same work-ups yielded the corresponding indolizines.

General Method C. To a chloroform solution (30 ml) of pyridinium bromide (2 mmol) DBU (0.380 g, 2.5 mmol) was added dropwise under stirring in an ice bath and the resulting dark red solution was stirred for further 10 min at the temperature. An equimolar amount of DDQ was added to the reaction mixture and the resulting solution was stirred for 6 h in an ice bath. The same work-ups described in Method A gave indolizine derivatives.

The treatment of dihydropyridothiazines with LTA or DDQ at over 0°C gave always polymeric tars, and those at below 0 °C required more prolonged reaction time (a week to a month). When LTA was used as a dehydrogenating agent in the preparations of indolizines **92—95**, **98—101**, **117—119**, **121**, and **123** possessing an ethoxycarbonyl groups, the isolations of their indolizines from the reaction mixtures were considerably troublesome due to the formation of polymeric tars with similar solubility.

These data were summarized in Tables 2 and 4.

Preparations of Disulfides. General Method. An ethanolic solution (30 ml) of 1-benzoylthioindolizine (1 mmol) and piperidine **128** (0.50 g, 5.9 mmol) was heated under reflux for 6 h, the resulting solution was cooled overnight in a freezer, the separated crystals were collected by filtration, and the recrystallization from ethanol afforded the corresponding disulfide. The concentration of the filtrate, followed by its column separation (alumina) gave 1-benzoylpiperidine **133** in very good yields (88—96%). The structure of compound **133** was determined by comparison with the authentic sample.[11]

Some data of these disulfides are as follows: **129**, 90%, yellow prisms, mp 190—193 °C, IR (KBr) 2199 cm^{-1} (CN), ^1H NMR ($CDCl_3$) δ=2.62 (6H, s, 2×SMe), 6.6—7.1 (6H, m, 6, 7, 8, 6′, 7′, and 8′-H), and 8.11 (2H, br d, J=7.0 Hz, 5 and 5′-H). Found: C, 54.54; H, 3.19; N, 13.03%. Calcd for $C_{20}H_{14}N_4S_4$: C, 54.77; H, 3.22; N, 12.77%. **130**, 90%, yellow needles, mp 206—207 °C, IR (KBr) 2190 cm^{-1} (CN), ^1H NMR, ($CDCl_3$) δ=2.24 (6H, s, 2×Me), 2.66 (6H, s, 2×SMe), 6.5—6.9 (4H, m, 6, 8, 6′, and 8′-H), and 7.99 (2H, d, J=7.0 Hz, 5 and 5′-H). Found: C, 56.54; H, 3.86; N, 12.28%. Calcd for $C_{22}H_{18}N_4S_4$: C, 56.62; H, 3.89; N, 12.01%. **131**, 73%, yellow needles, mp 120—121 °C, IR (KBr) 1681 cm^{-1} (CO), ^1H NMR ($CDCl_3$) δ=1.46 (6H, t, J=7.0 Hz, 2×$\underline{CH_3}CH_2O$), 2.59 (6H, s, 2×SMe), 4.47 (4H, q, J=7.0Hz, 2×$CH_3\underline{CH_2}O$), 6.5—7.1 (6H, m, 6, 7, 8, 6′, 7′, and 8′-H), and 9.31 (2H, m, 5 and 5′-H). Found: C, 54.10; H, 4.53; N, 5.43%. Calcd for $C_{24}H_{24}N_2O_4S_4$: C, 54.11; H, 4.54; N, 5.26%. **132**, 86%, yellow prisms, mp 141 °C, IR (KBr) 1664 cm^{-1} (CO), ^1H NMR ($CDCl_3$) δ=1.45 (6H, t, J=7.0 Hz, 2×$\underline{CH_3}CH_2O$), 2.01 (6H, s, 2×Me), 2.64 (6H, s, 2×SMe), 4.47 (4H, q, J=7.0 Hz, 2×$CH_3\underline{CH_2}O$), 6.47 (2H, br d, J=7.0 Hz, 6 and 6′-H), 6.51 (2H, br s, 8 and 8′-H), and 9.20 (2H, d, J=7.0 Hz, 5 and 5′-H). Found: C, 55.67; H, 4.92; N, 4.80%. Calcd for $C_{26}H_{28}N_2O_4S_4$: C, 55.69; H, 5.03; N, 5.00%.

References

1) For part 14 of this series, see A. Kakehi, S. Ito, K. Nagata, M. Kinoshita, and N. Kakinuma, *Chem. Pharm. Bull.*, **35**, 156 (1987).

2) a) A. Kakehi, S. Ito, M. Ito, and T. Yotsuya, *Heterocycles*, **22**, 2237 (1984); b) A. Kakehi, S. Ito, M. Ito, T. Yotsuya, and K. Nagata, *Bull. Chem. Soc. Jpn.*, **58**, 1432 (1985).

3) a) R. R. Schmidt, *Angew. Chem. Int. Ed. Engl.*, **14**, 581 (1975); b) R. R. Schmidt and H. Huth, *Tetrahedron Lett.*, **1975**, 33

4) A. Kakehi, S. Ito, S. Yonezu, K. Maruta, and K. Yuito, *Heterocycles*, **23**, 33 (1985).

5) a) C. Maseda, M. Sone, Y. Tominaga, R. Natsuki, Y. Matsuda, and G. Kobayashi, *Yakugaku Zasshi*, **94**, 839 (1974); b) Y. Tominaga, H. Fujito, K. Mizuyama, Y. Matsuda, and G. Kobayashi, *Chem. Pharm. Bull.*, **25**, 1519 (1977).

6) a) A. Kakehi and S. Ito, *Bull. Chem. Soc. Jpn.*, **47**, 938 (1974); b) A. Kakehi, S. Ito, T. Maeda, R. Takeda, M. Nishimura, M. Tamashima, and T. Yamaguchi, *J. Org. Chem.*, **43**, 4837 (1978); c) S. Kakehi, S. Ito, B. Wada, K. Watanabe, K. Nishimura, and A. Kumagai, *Bull. Chem. Soc. Jpn.*, **55**, 3590 (1982).

7) a) Y. Tamura, Y. Sumida, and M. Ikeda, *J. Chem. Soc., Perkin Trans. 1*, **1973**, 2089; b) H. Pauls and F. Krohnke, *Chem. Ber.*, **110**, 1294 (1977); c) E. K. Pohjara, *J. Heterocyclic Chem.*, **15**, 955 (1978); d) J. Alvarez-Builla, M. G. Quintanilla, C. Abril, and M. T. Gandasegui, *J. Chem. Research (S)*, **1984**, 202.

8) L. F. Lee and R. K. Howe, *J. Org. Chem.*, **49**, 4780 (1984).

9) a) S. McKenzie and D. H. Reid, *J. Chem. Soc. C*, **1970**, 145; b) E. E. Glover, K. D. Vaughan, and D. C. Bishop, *J. Chem. Soc., Perkin Trans. 1*, **1973**, 2595.

10) Y. Tominaga, Y. Miyake, H. Fujito, Y. Matsuda, and G. Kobayashi, *Yakugaku Zasshi*, **97**, 927 (1977)

11) C. Schotten, *Chem. Ber.*, **17**, 2544 (1884).

 © 1987 The Chemical Society of Japan Bull. Chem. Soc. Jpn., 60, 1881—1886 (1987)

In-beam EIMS and Molecular SIMS of Quaternary Ammonium Chlorides of Benzylamine Derivatives

Yasuo SHIDA,* Kazuo TSUJIMOTO,† Takashi IKEDA,† and Mamoru OHASHI*,†
Tokyo College of Pharmacy, Horinouchi 1432-1, Hachioji, Tokyo 192-03
†Department of Materials Science, The University of Electro-Communications, Chofu, Tokyo 182
(Received December 1, 1986)

The in-beam EIMS and SIMS of three quaternary ammonium chlorides of benzylamine derivatives have been examined, and their fragmentation processes have been clarified by means of the B/E costant and B^2/E constant linked scanning techniques. The B/E constant linked scan of the benzyltrimethylammonium ion (m/z 150) in the in-beam EIMS indicated a fragment ion at m/z 126 as a daughter ion. A substitution reaction between the m/z 150 ion and a chlorine atom in the first field free region is proposed. The characteristics of SIMS of those compounds were demonstrated in comparison with those of EIMS and the fragmentation processes of the salts upon Xe^+ bombardment were established based on the linked scanning techniques.

In order to test the suitability of the unified model for soft ionization proposed by Vestal[1] we have examined the matrix effects on the in-beam Electron Ionization Mass Spectrometry (EIMS) of quaternary ammonium salts.[2] During the course of this investigation we tried to clarify the fragmentation processes of those quaternary ammonium salts upon electron ionization (in-beam EI) and upon Xe^+ bombardment [molecular Secondary Ion Mass Spectrometry (SIMS)] on the basis of the B/E constant and the B^2/E constant linked scanning mass spectra. We found that the linked scans indicated the unusual behavior of the benzyltrimethylammonium ion in the in-beam EIMS. This article deals with the fragmentation processes of three quaternary ammonium salts of benzylamine derivatives upon electron impact and upon Xe^+ ion bombardment.

Experimental

The in-beam EIMS were taken with a Hitachi RMU-6 and a Hitachi M-80 spectrometers. The in-beam EIMS were obtaind with an electron energy of 70 eV (80 μA) and at a source temperature of 200 °C. Samples were introduced into the in-beam system with probe heating at 300 °C. The molecular SIMS were performed with a double focusing Hitachi M-80B spectrometer. Xenon was used as the primary ion source and was accelerated to 8 kV. In these studies the samples dissolved in glycerol matrix were applied to the stainless steel target for the molecular SIMS. The B/E constant and the B^2/E constant linked scanning techniques were applied to each spectrum.

Benzyltrimethylammonium chloride (**1**), benzyltriethylammonium chloride (**2**) and benzyldimethylphenylammonium chloride (**3**) were purchased from Tokyo Kasei Co. and used without further purification.

Results and Discussion

1. In-beam EIMS. Figure 1a shows the in-beam EIMS of **1**. The intact quaternary ammonium ion is observed at m/z 150 (C^+), and the fragment ions at m/z 135 (C^+–Me), 126 ($PhCH_2Cl^+$), 91 ($C_7H_7^+$) and 58 ($CH_2{=}NMe_2$) are also abundant. The fragment ion at m/z 126 must contain chlorine atom because of the relative abundance of the isotope peak at m/z 128, and must correspond to the molecular ion of benzyl chloride. This ion seems to come from a thermal SN-2 type reaction under the in-beam conditions producing benzyl chloride molecules followed by electron ionization. In order to confirm the origins of the ion at m/z 126 as well as the other fragment ions, we examined the B/E constant linked scan of the C^+ at m/z 150. Figure 2a represents its spectrum. As expected, the ions at m/z 135, 134, 91, and 58 are shown to be derived from C^+ in accorded with the general fragmentation of quaternary ammonium salts in the in-beam EI.[3-5]

Surprisingly, this linked scan also indicates that the ion at m/z 126 is a daughter ion of C^+. The same technique showed that the m/z 126 ion is the parent ion of the m/z 91 ion, consistant with the structure of benzyl chloride. To ascertain the origin of the m/z 126 ion, we examined the B^2/E constant linked scan and found abroad weak peak around m/z 135 as the parent ion. Figure 3a shows the linked scanning spectrum. However, the B/E constant linked scan of m/z 135 ion did not show any peaks at m/z 126, but strong praks at m/z 91 and 58 as shown in Fig. 3b. If the ion at m/z 135 is the parent ion of m/z 126 ion, the fragmentation processes involving a charge exchange mechanism as shown in Scheme 1 may account for this unusual

$$\underset{(m/z\ 150)}{PhCH_2\text{-}N^+Me_3} \longrightarrow \underset{(m/z\ 135)}{PhCH_2\text{-}N^{+\cdot}Me_2} \xrightarrow{PhCH_2Cl} \underset{(m/z\ 126)}{PhCH_2Cl^{+\cdot}} + PhCH_2NMe_2$$

Scheme 1.

transition. However, it is hard to rationalize that collision between the *m/z* 135 ion and benzyl chloride transfers not only an electron but also the kinetic energy to each other.

The second possibility is a collision between the C^+ and a chlorine atom in the first field free region in accordance with the result of the *B/E* constant linked scan. Scheme 2 shows an example of the reaction. Since, under the in-beam conditions, large amounts of neutral species are vaporized in the ion source,[1] many

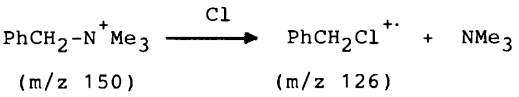

Scheme 2.

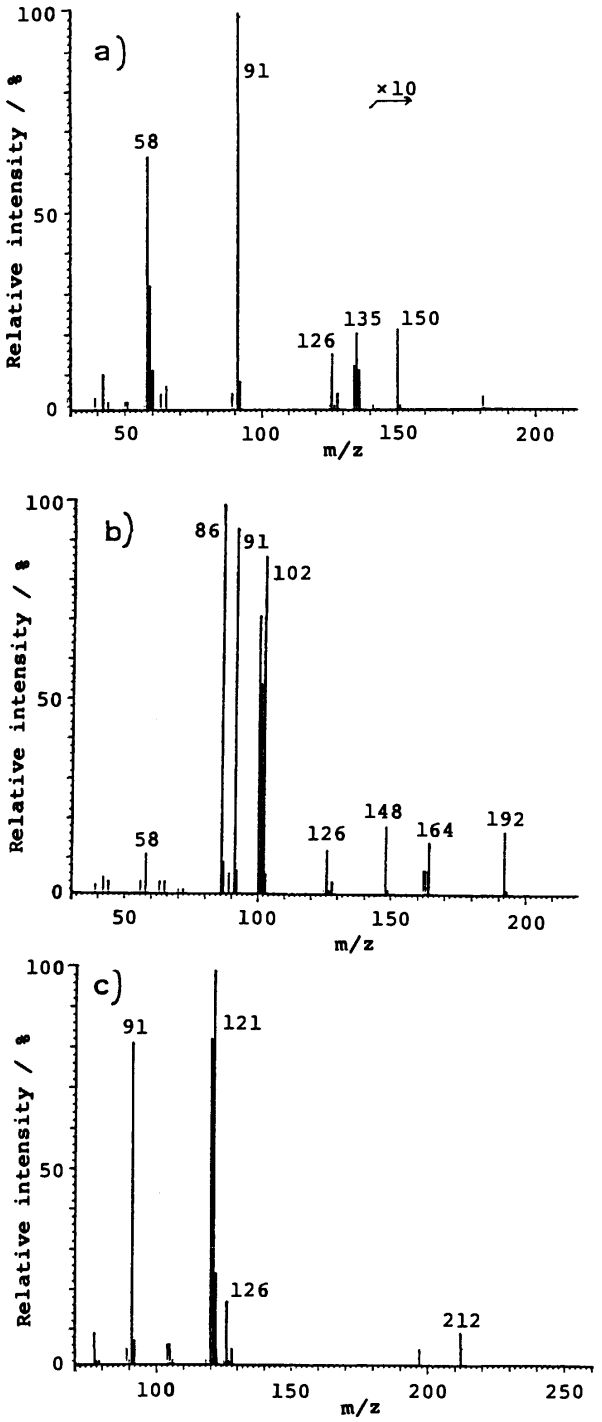

Fig. 1. In-beam EIMS of three quaternary ammonium chlorides of benzylamine derivatives.
a): **1**, b): **2**, c): **3**.

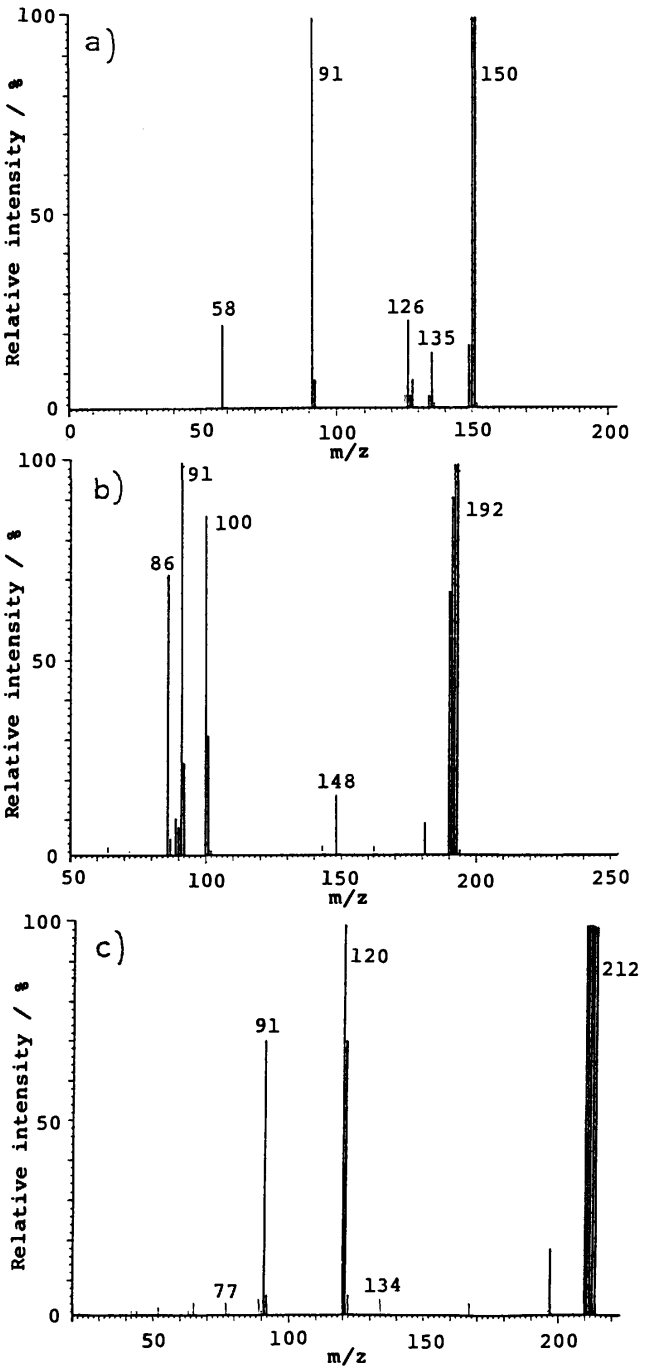

Fig. 2. B/E constant linked scanning spectra of C^+ in the in-beam EIMS.
a): **1**, *m/z* 150, b): **2**, *m/z* 192, c): **3**, *m/z* 212.

ion-molecular reactions are also expected to happen in the first field free region. At this stage, the processes shown in Scheme 2 are reasonably conceivable. The third possibility is the so-called "artifact peak" discussed by Beynon et al.[6] Suppose that there are a parent ion m_1, a daughter ion m_2, and another ion m_3 formed in the source and fully accelerated, which then decomposes to give an ion m_4. The only necessary condition for the detection of m_4 in the B/E constant linked scanning spectra is as follows;

$$m_3=m_2^2/m_1,\ m_4=m_2m_3/m_1.$$

In our case, $m_1=150$ and $m_2=126$. Then substituting these values for the equations, we obtained $m_3=106$, $m_4=89$. However, we found no peak corresponding to those ions. Thus the possibility of the artifact peak is excluded. The fragmentation processes of the in-beam EIMS of **1** are summarized in Scheme 3.

The in-beam EIMS of **2** and **3** are shown in Figs. 1b and 1c, respectively. The B/E constant linked scanning spectra of each C^+ at m/z 192 or 212 are shown in Figs. 2b and 2c, respectively. Figures 2b and 2c also show the presence of benzyl chloride ion at m/z 126 and 128, but the linked scanning spectra do not. Thus we conclude that the unusual behavior of **1** in the B/E constant linked scan is not general, but very specific. The fragmentation processes of **2** and **3** upon in-beam EI are summarized in Scheme 4 and 5, respectively.

2. SIMS. Figures 4a—c show the glycerol assisted SIMS os **1, 2,** and **3**, respectively. The major fragment ions from the quaternary ammonium ion (C^+) are similar to those of the in-beam EIMS. Several major differences between the SIMS and the in-beam EIMS are also noticed: i.e., (1) the cluster ions of $(R_4N^+)_2Cl$ are observed in the SIMS but not in the in-beam EIMS, (2) the ions at m/z 126 and 128 due to the benzyl chloride molecular ion observed in the in-beam EIMS are absent in the SIMS, (3) the fragment ions having not only even electrons but also odd electrons are often observed in the in-beam EIMS but the ions carrying only even electrons are observed in the SIMS. For instance, in the SIMS spectrum of **2** (Fig. 4b), the peaks at m/z 163, 102, and 101 observed in the in-beam EIMS are absent, but the peaks at m/z 192, 162, 148, 100, 91, and 86 are commonly observed in both spectra. Similarly, in the case of **3**, the peaks at m/z 212, 121,

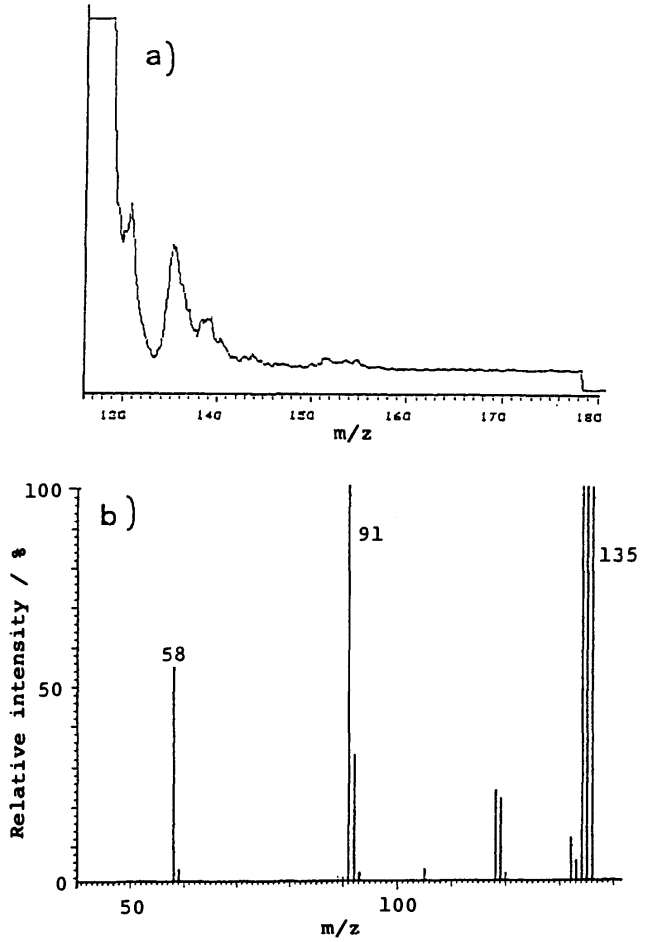

Fig. 3. a) B^2/E constant linked scanning spectrum of m/z 126 ion, and b) B/E constant linked scannining spectrum of m/z 135 ion of the in-beam EI spectrum of **1**.

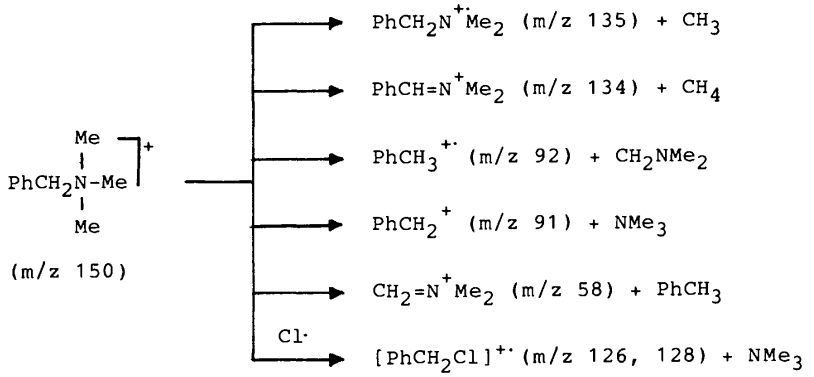

Scheme 3.

and 91 are common in both spectra, but strong peak at *m/z* 120 observed in the in-beam EIMS is absent in the SIMS.

The *B/E* constant and B^2/E constant linked scanning spectra of major peaks of **1** are shown in Figs. 5 and 6, respectively. On the basis of these spectra, the fragment processes of **1** are summarized as shown in Scheme 6: i.e., the cluster ion at *m/z* 335 forms only a C^+ ion at *m/z* 150, which decomposes to yield ions at *m/z* 134, 91, and 58 and the ion at *m/z* 134 also produces the *m/z* 91 ion.

Similarly, the fragmentation processes of **2** and **3** in the SIMS are also summarized in Scheme 7 and 8, respectively.

In conclusion we have clarified the characteristics of the in-beam EIMS and the SIMS of three quaternary

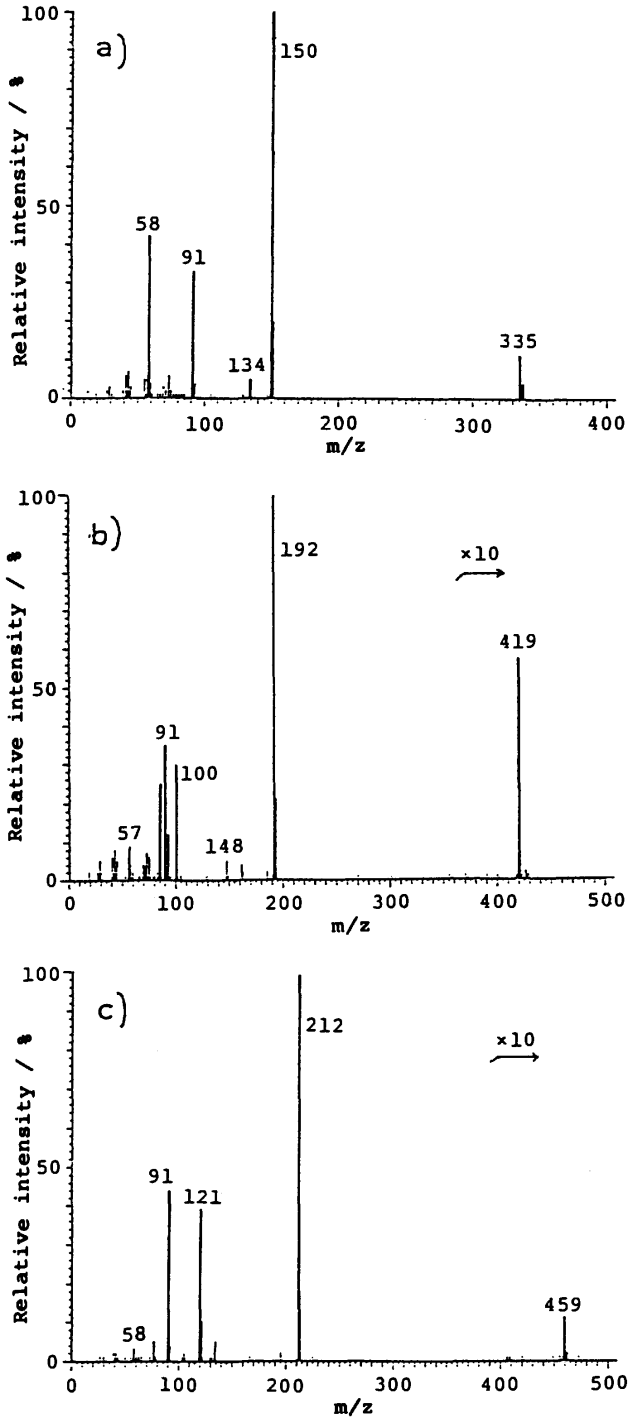

Fig. 4. Molecular SIMS (glycerol assisted) of a) **1**, b) **2**, and c) **3**.

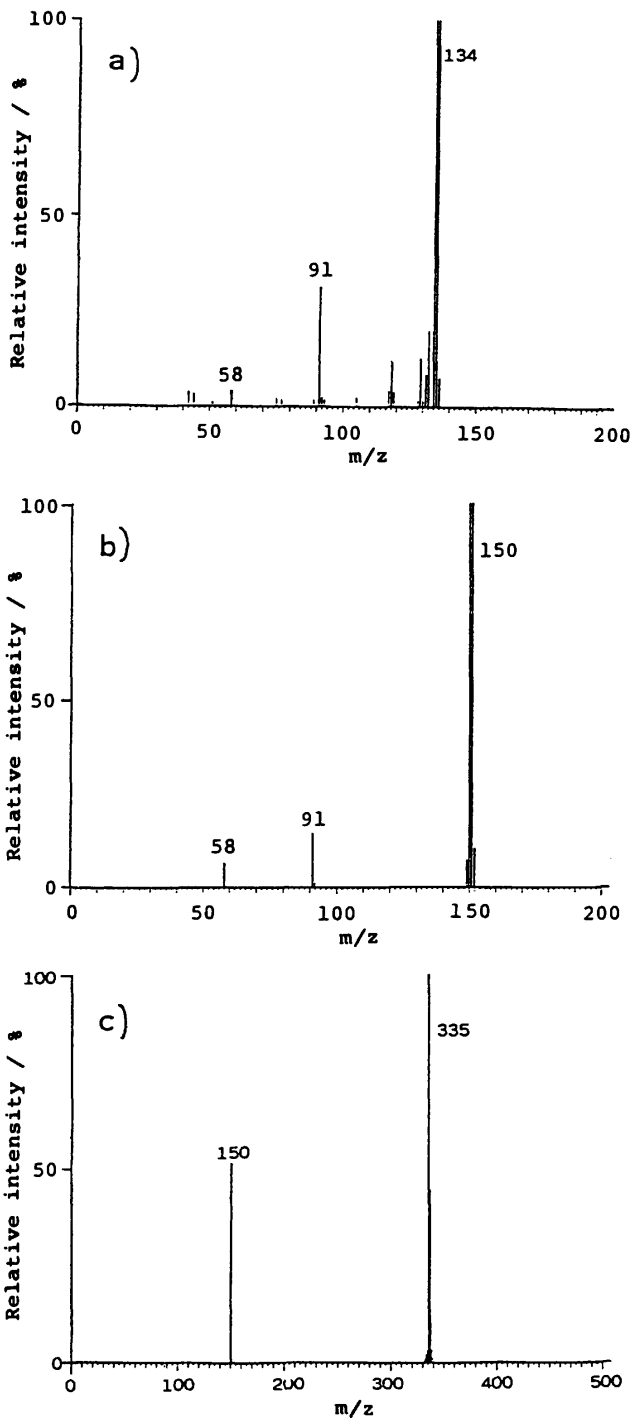

Fig. 5. *B/E* constant linked scanning spectra of C^+ in the SIMS: a) *m/z* 134; b) *m/z* 150; c) *m/z* 335.

ammonium chlorides of benzylamine derivatives, and indicated the unusual behavior of benzyltrimethylammonium chloride in the *B/E* constant linked scanning spectra. Care must be taken for the interpretation of the *B/E* constant linked scanning spectra, considering the possibilities of the ion-molecular reactions in the first field free region in the in-beam EIMS.

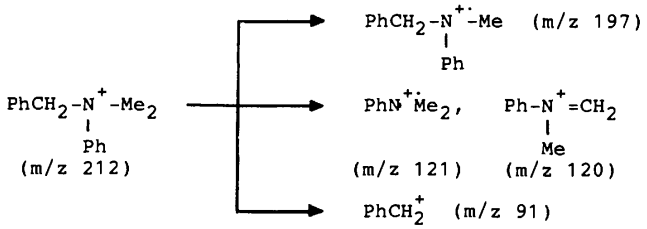

Scheme 5.

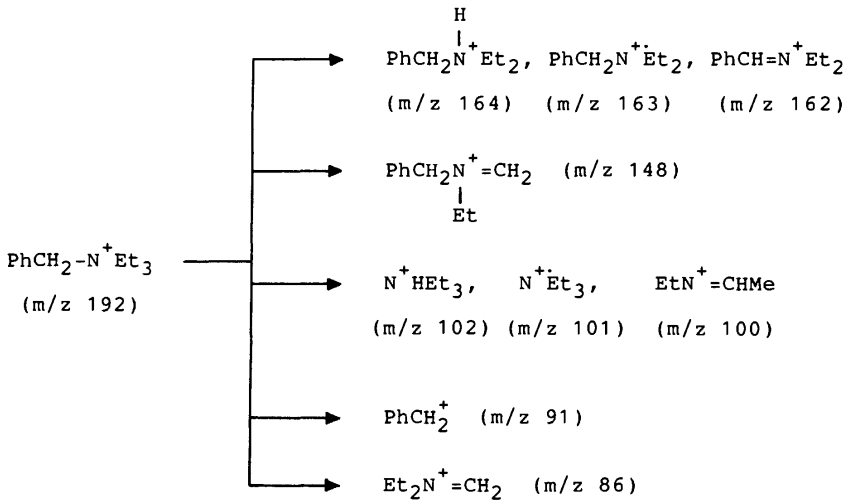

Scheme 4.

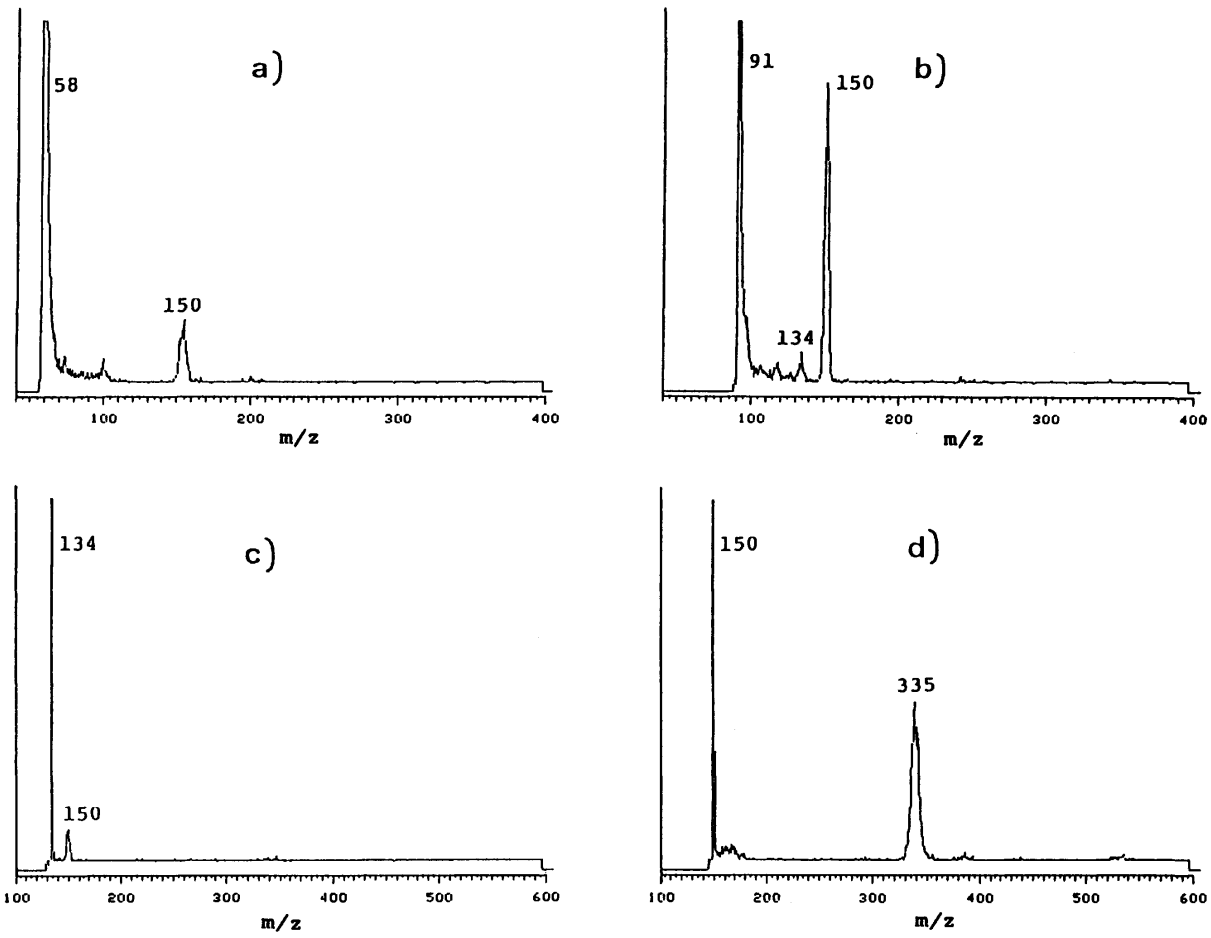

Fig. 6. B^2/E constant linked scanning spectra of a) *m/z* 58, b) *m/z* 91, c) *m/z* 134, and d) *m/z* 150 in the SIMS of **1**.

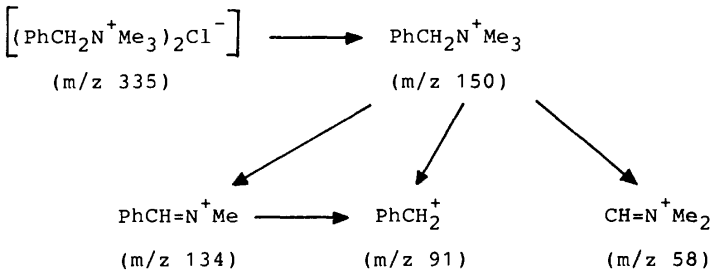

Scheme 6.

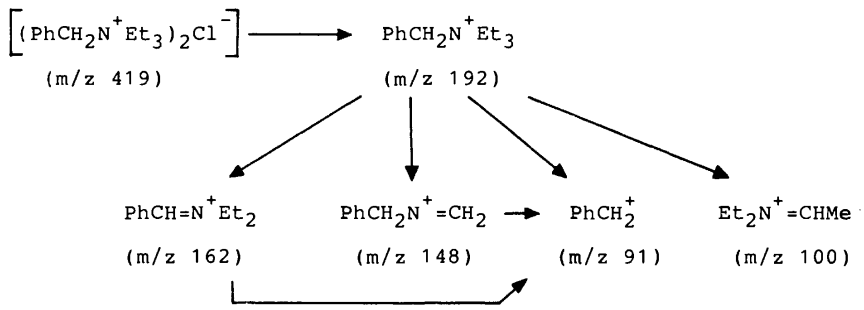

Scheme 7.

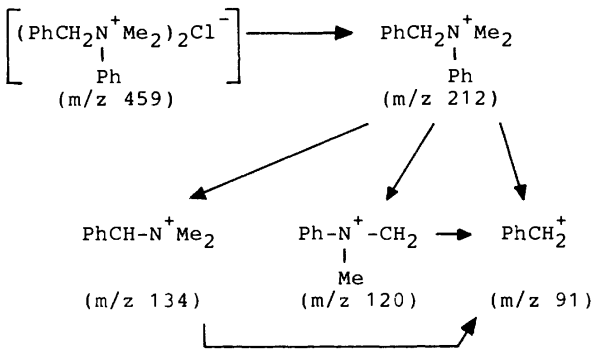

Scheme 8.

This work was supported by the Grant-in-Aid for Scientific Research No. 60430007 from the Ministry of Education, Science and Culture.

References

1) M. L. Vestal, *Mass Spectrom. Rev.*, **2**, 447 (1983).
2) M. Ohashi, M. Iijima, and K. Tsujimoto, *Shitsuryo-bunseki*, **34**, 287 (1986).
3) M. Ohashi, R. P. Barron, and W. P. Benson, *J. Am. Chem. Soc.*, **103**, 3943 (1981).
4) M. Ohashi, *Shitsuryobunseki*, **32**, 463R (1984).
5) H. J. Veith, *Mass Spectrom. Rev.*, **2**, 419 (1983).
6) R. P. Morgan, C. J. Porter, and J. H. Beynon, *Org. Mass Spectrom.*, **12**, 735 (1977).

Metal Ion-Catalyzed Reduction of Substituted Nitrosobenzenes by 1-Benzyl-3,5-bis(1-pyrrolidinylcarbonyl)-1,4-dihydropyridine in Acetonitrile

Hiroshi AWANO, Kazuo TAKEMOTO, Hirohisa OHYA, Minaki TOMIO, Seizo TAMAGAKI, and Waichiro TAGAKI*
Department of Applied Chemistry, Faculty of Engineering, Osaka City University, Sugimoto 3, Sumiyoshi-ku, Osaka 558
(Received December 1, 1986)

Metal ion catalyzed reduction of substituted nitrosobenzenes by 1-benzyl-3,5-bis(1-pyrrolidinylcarbonyl)-1,4-dihydropyridine (BPDH) in acetonitrile has been studied for seven bivalent metal ions. The reduction of *N*-methylacridinium salt (MA) has also been examined. In the former cases, it was found that the metal ions catalyze the reduction by forming a 1:1 complex with BPDH according to a Michaelis-Menten type saturation kinetics which allowed to derive the association constants, K_M, for the complexation and the second-order rate constants, k_2, for the reduction. A linear relationship was found between log k_2 and the ionization potentials of metal ions with a positive slope. A linear Hammett relationship was also observed between log k_2 and the Hammett σ constants with a positive ρ value for three metal ions. These results suggest that a bivalent metal ion is sandwiched between the BPDH and the substrate and acts as a Lewis acid to stabilize the incipient *N*-oxide anion of the substrate which is formed by hydride transfer in the transition state. In the cases of MA, all metal ions inhibited the reduction. Repulsion between the positive charges of the metal ion-BPDH complex and the substrate salt appears to be prevailing.

The role of zinc ion at the active site of alcohol dehydrogenase has attracted much attention in recent years.[1] Recent crystallographic and the related studies[2-5] have disclosed the following features for the structure of reactive ternary complex at the active site of the enzyme: (a) A zinc ion sits at the bottom of a hydrophobic pocket, (b) the oxygen atom of substrate is directly coordinated to the zinc ion, and (c) there is no direct contact between the zinc ion and the coenzyme. These features strongly suggest that the zinc ion performs as an electrophile to polarize the carbonyl group or to ionize the hydroxyl group of substrate.

In the model studies, it has also been observed that a bivalent metal ion such as Mg^{2+} or Zn^{2+} ion accelerates the rate of reduction of some carbonyl substrates,[6-22] and it has been considered that a metal ion may also polarize the substrate carbonyl group as a Lewis acid as in enzymic systems.[6-8,12,15] However, the role of a bivalent metal ion in model systems so far studied seems to be somewhat different from the one suggested for the above enzymic systems on the following grounds.[13-22] Namely, it has been demonstrated that a bivalent metal ion such as Mg^{2+} or Zn^{2+} ion forms a complex with the 1,4-dihydronicotinamide moiety of the reductants.[14-22] It has also been indicated that Mg^{2+} ion does not show any measurable complexation with such a substrate as ethyl benzoylformate, in spite of the rate acceleration.[16]

We have also been interested in the activation of model systems of NADH coenzyme by acids and metal ions. In our previous paper, we reported the carboxylic acid-catalyzed reduction of substituted nitrosobenzenes by BPDH in acetonitrile.[23,24] We proposed a mechanism that a carboxylic acid acts as a general acid by protonating the oxygen atom of nitroso group of the substrate in the transition state. The acid-catalyzed rate was faster for a substrate having a more electron-donating substituent. As a natural extension, we have now studied the metal ion-catalyzed reduction of substituted nitrosobenzenes (NB) by BPDH in acetonitrile (Eq. 1). We will describe in this paper that bivalent metal ion catalysis is much more efficient than carboxylic acid one and the rate is faster for a substrate having a more electron-withdrawing substituent, in contrast to the case of the above acid-catalysis.

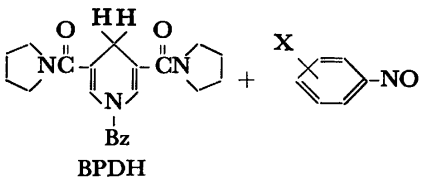

BPDH (1)

Results

Products, Kinetic Analysis, and Metal Ion Catalysis. The reduction was carried out in anhydrous acetonitrile under nitrogen atmosphere. The substrate nitrosobenzenes were confirmed to be reduced to hydroxylamines quantitatively by HPLC analysis as described before.[23,24] The rates of reduction were followed spectrophotometrically by observing the decrease of absorbance at 355 nm due to the disappearence of BPDH. The rate of reduction was slow in the absence of metal ion. In the presence of a metal ion, the pseudo-first-order rate constant, k_{obsd} increased with increasing concentration of the metal ion according to a manner to obey a Michaelis-Men-

ten type saturation kinetics, as shown in Fig. 1. Here the metal ions were used as the perchlorates with water of crystallization. The results suggest the complexation of the metal ion with either BPDH or a nitrosobenzene, or both before the rate-limiting step. As for the substrate, it was observed that the rates (k_{obsd}) were first-order with respect to the concentration of the nitrosobenzene, as shown in Fig. 2. Therefore, the complexation between the substrate nitrosobenzene and the metal ion prior to the reduction seems to be unimportant.

It was confirmed spectrophotometrically that the complexation occurs between Zn^{2+} ion and BPDH. As shown in Fig. 3a, the absorption maximum of BPDH at 355 nm in the absence of metal ion shifts to a shorter wavelength of 320 nm in the presence of Zn^{2+} ion. The plots of absorbance change as a function of the Zn^{2+} ion concentration gave a saturation curve of Fig. 3b which indicates a complexation and fits nicely with the curve for Zn^{2+} ion in Fig. 1. Thus, it is likely that the rate acceleration by Zn^{2+} ion is due to the

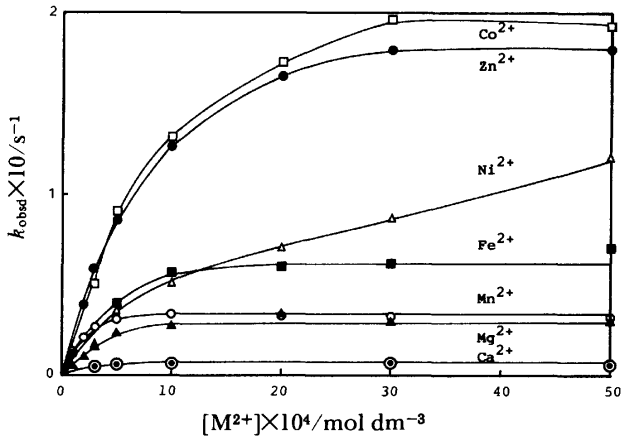

Fig. 1. Pseudo-first-order rate constants for the reduction of nitrosobenzene plotted as a function of the concentration of bivalent metal ions: In acetonitrile at 25 °C; ◎: Ca^{2+}, ▲: Mg^{2+}, ○: Mn^{2+}, ■: Fe^{2+}, △: Ni^{2+}, ●: Zn^{2+}, □: Co_q^{+}. [BPDH]=1×10^{-4} mol dm^{-3}, [C_6H_5NO]=1×10^{-3} mol dm^{-3}.

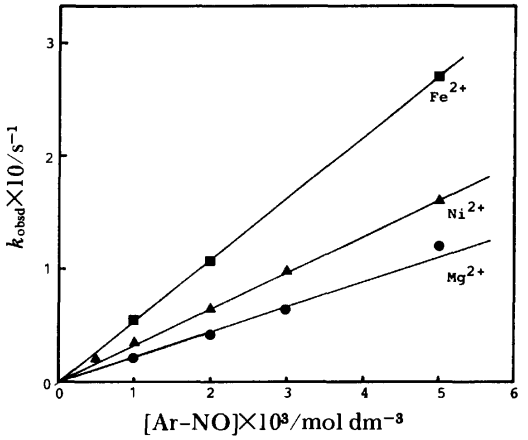

Fig. 2. Plots of pseudo-first-order rate constants as a function of substrate concentration: In acetonitrile, 25 °C; ■: Fe^{2+}, ▲: Ni^{2+}, ●: Mg^{2+}.

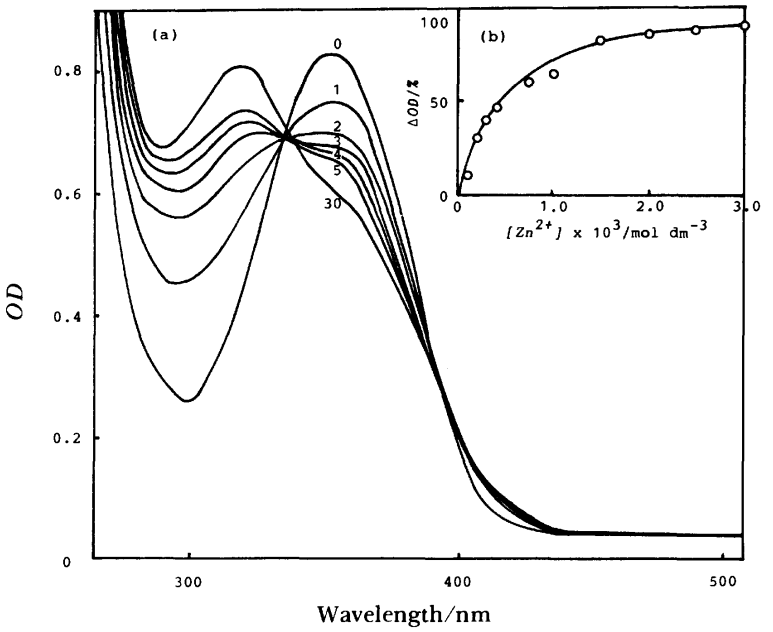

Fig. 3. Spectral changes of BPDH induced by added zinc ion: In acetonitrile, 25 °C; [BPDH]=1×10^{-4} mol dm^{-3}; (a) observed UV spectra. The numbers indicate the concentration of zinc ion [(Zn^{2+}]×10^4). The shift was saturated above 3×10^{-3} mol dm^{-3}; (b) saturation curve of absorbance change, %.

complexation of BPDH with the Zn^{2+} ion. A similar correlation between the rate acceleration and the spectral change was also confirmed for the other metal ions. Furthermore, the rate of reduction was observed to be inhibited in the presence of water and this rate inhibition was perfectly parallel to the loss of complexation as shown in Fig. 4.

The saturation curves in Fig. 1 can be described by assuming a reaction scheme shown in Scheme 1 in which BPDH (DH) and a metal ion (M^{2+}) form a 1:1 complex ($DH \cdot M^{2+}$) with an association constant, K_M, and the complex reacts with the substrate (ArNO) with a second-order rate constants, k_2, to give the products, D^+ and $ArNHO^-$. Uncatalyzed rate (k_2') must also be taken into account, although its contribution to the total rate was negligible. The scheme leads to a rate equation shown by Eq. 1, and under the conditions of $[M]_T \gg [DH \cdot M]$, Eqs. 2 and 3 can be derived by an approximation, where $[DH]_T$ and $[M]_T$ are the total concentration BPDH and metal ion, respectively, and $[ArNO]_0$ is the initial concentration of substrate which is used in a large excess and taken to be constant under a pseudo-first-order conditions. Experimentally, the k_2 and K_M values were obtained as usual from the reciprocal plots of Eq. 4. The results are shown in Table 1.

$$\text{Rate} = k_{obsd}[DH]_T = k_2'[ArNO]_0[DH]_T + k_2[ArNO]_0[DH \cdot M^{2+}] \quad (1)$$

$$[DH \cdot M^{2+}] = \frac{K_M[M]_T[DH]_T}{1+K_M[M]_T} \quad ; \quad [M]_T \gg [DH \cdot M^{2+}] \quad (2)$$

$$k_{obsd} = k_0 + \frac{k_2K_M[ArNO]_0[M]_T}{1+K_M[M]_T} \quad ; \quad k_0 = k_2'[ArNO]_0 \quad (3)$$

$$\frac{1}{(k_{obsd}-k_0)} = \frac{1}{k_2[ArNO]_0} + \frac{1}{k_2K_M[ArNO]_0} \cdot \frac{1}{[M]_T} \quad (4)$$

$$DH + M^{2+} \overset{K_M}{\rightleftharpoons} DH \cdot M^{2+} \xrightarrow{k_2[ArNO]_0} D^+ + Ar\text{-}NHO^- + M^{2+}$$

$$DH + ArNO \xrightarrow{k_2'} D^+ + ArNHO^-$$

Scheme 1.

The k_2 and K_M values as the Functions of Ionization Potentials of Metal Ions. In Table 1 are shown the ionization potentials (I_P) of metal ions[25] in addition to the above k_2 and K_M values. It can be seen that there is a good linear relationship between I_P and $\log k_2$ values, as shown in Fig. 5. It indicates that a metal ion having a higher I_P is more active. In Fig. 6 is also shown a correlation between I_P and $\log K_M$ values. Although the correlation is not so good as in the case

Table 1. Second-Order Rate Constants and Association Constants for the Metal Ion-Catalyzed Reduction of Nitrosobenzene by BPDH in Acetonitrile (25 °C)[a]

M^{2+}	I_P / eV	k_2 / $s^{-1}\,mol^{-1}\,dm^3$	K_M / $mol^{-1}\,dm^3$
Ni^{2+}	18.17	261	245
Zn^{2+}	17.96	180	1865
Co^{2+}	17.06	195	1060
Fe^{2+}	16.18	70.9	2523
Mn^{2+}	15.64	32.2	6932
Mg^{2+}	15.04	30.8	2899
Ca^{2+}	11.87	7.2	10430

a) $[BPDH] = 1 \times 10^{-4}$ mol dm^{-3}, $[C_6H_5NO] = 1 \times 10^{-3}$ mol dm^{-3}.

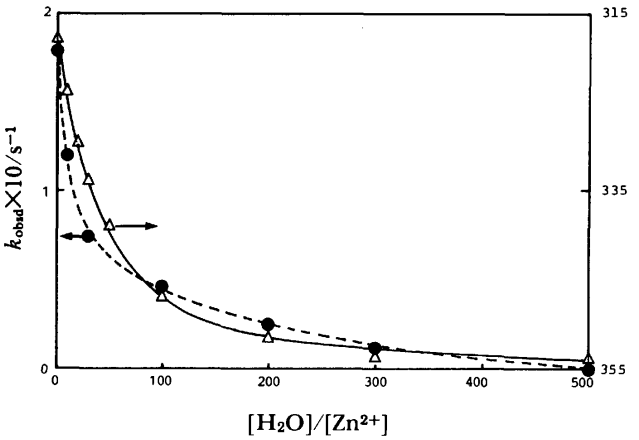

Fig. 4. Effect of H_2O on the shift of absorption maximum of BPDH (△) from 355 nm and the reduction rate constants of nitrosobenzene (●) in the presence of zinc ion: In acetonitrile, 25 °C; [BPDH]=1×10^{-4} mol dm^{-3}, $[C_6H_5NO] = 1 \times 10^{-3}$ mol dm^{-3}, $[Zn^{2+}] = 3 \times 10^{-3}$ mol dm^{-3}.

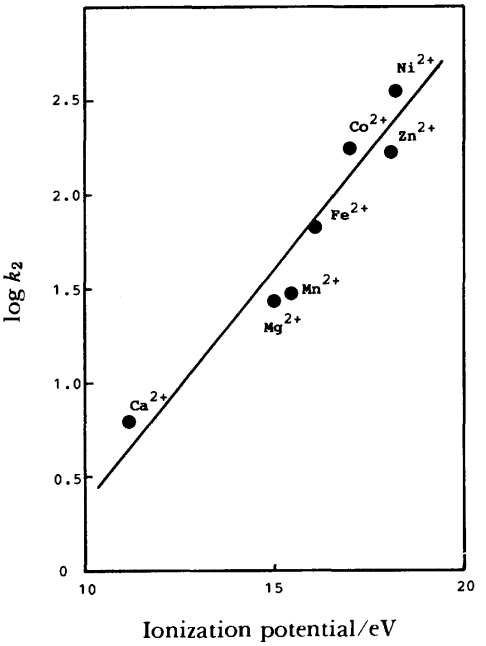

Fig. 5. Correlation between I_P and $\log k_2$.

of Fig. 5, there is a clear tendency that a metal ion having a lower I_P forms a stronger complex with the dihydropyridine (BPDH). The Table 1 also indicates that, at a high metal ion concentration, i.e., $K_M[M]_T \gg 1$, the observed reactivity (k_{obsd}) is governed by k_2 value (see Eq. 3) which is in the order of $Ni^{2+}>Co^{2+}>Zn^{2+}>Fe^{2+}>Mn^{2+}>Mg^{2+}>Ca^{2+}$, but at a low metal ion concentration, i.e., $K_M[M]_T \ll 1$, the reactivity is governed by k_2K_M which is in the order of $Zn^{2+}>Mn^{2+}>Co^{2+}>Fe^{2+}>Mg^{2+}>Ca^{2+}>Ni^{2+}$. It may be interesting that biologically important Zn^{2+} ion is the most active at a low metal ion concentration.

The Effects of Substrate-Substituents on the Rates. Figure 1 indicates that the rates of reaction (k_{obsd}) become saturated with the use of 3×10^{-3} M† of metal ion in the presence of 1×10^{-4} M of BPDH and 1×10^{-3} M of NB (X=H) for all the metal ions except for Ni^{2+} ion. For the other substituted NB's (X=*p*-CH_3 to *m*-CF_3), the rate saturation was also observed at the metal ion concentration of 3×10^{-3} M except for Ni^{2+} ion. Therefore, these saturated rates can be used as the substitutes of k_2 values (see Eq. 3) to examine the Hammett relationships. The results are shown in Table 2 and Fig. 7. A good linear relationship can be seen for each of the five metal ions. The ρ values

Table 2. Saturation Rate Constants for the Reduction of Nitrosobenzenes by BPDH in the Presence of Metal Ions in Acetonitrile (25 °C)[a]

	k_2[b] / s^{-1} mol^{-1} dm^3				
	Co^{2+}	Zn^{2+}	Ni^{2+},[c]	Mn^{2+}	Mg^{2+}
p-Me	154	133	59.4	23.4	22.1
m-Me	182	154	74.7	28.0	26.3
H	202	174	87.2	32.3	30.7
p-Cl	307	275	136	62.2	63.1
m-Cl	397	358	183	92.0	96.6
m-CF_3	437	382	—	102	101

a) [BPDH] = 1×10^{-4} mol dm^{-3}, [ArNO] = 1×10^{-3} mol dm^{-3}, [metal ion] = 1×10^{-3} mol dm^{-3}. b) $k_2=k_{obsd}$/[ArNO]. c) These values are not the saturated rate constants.

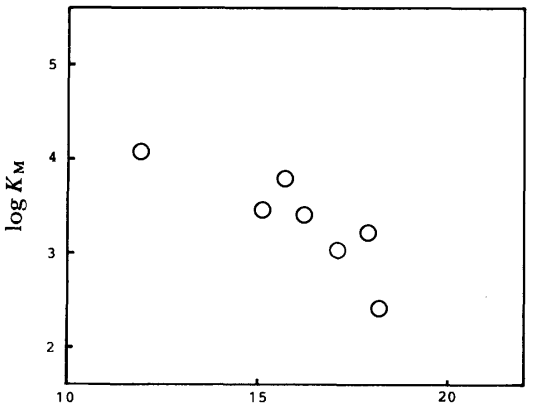

Fig. 6 Correlation between I_P and log K_M.

† 1 M=1 mol dm^{-3}.

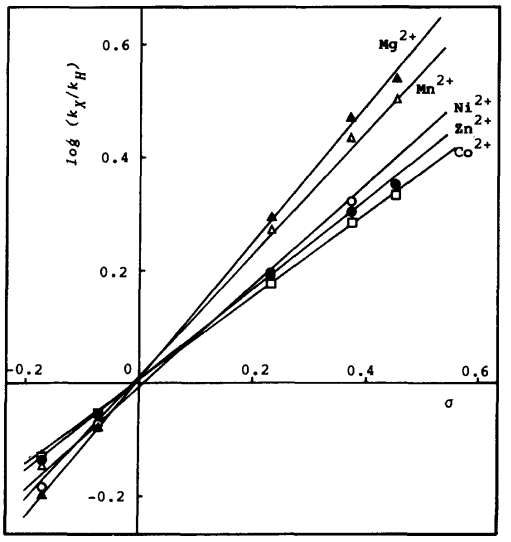

Fig. 7. Hammett substituent effect on the rates of metal ion-catalyzed reduction of nitrosobenzenes by BPDH: In acetonitrile, 25 °C; [BPDH]=1×10^{-4} mol dm^{-3}, [ArNO]=1×10^{-3} mol dm^{-3}, [metal ion]=3×10^{-3} mol dm^{-3}.

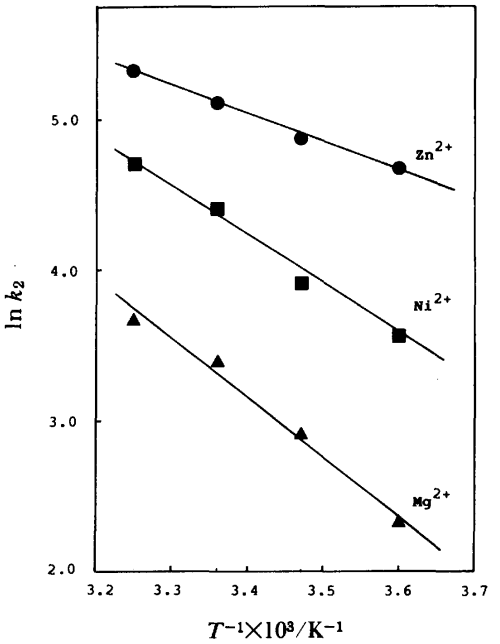

Fig. 8. Arrhenius plots for the metal ion-catalyzed reduction of nitrosobenzene by BPDH: In acetonitrile, 25 °C; [BPDH]=1×10^{-4} mol dm^{-3}, [C_6H_5-NO]=1×10^{-3} mol dm^{-3}, [metal ion]=3×10^{-3} mol dm^{-3}.

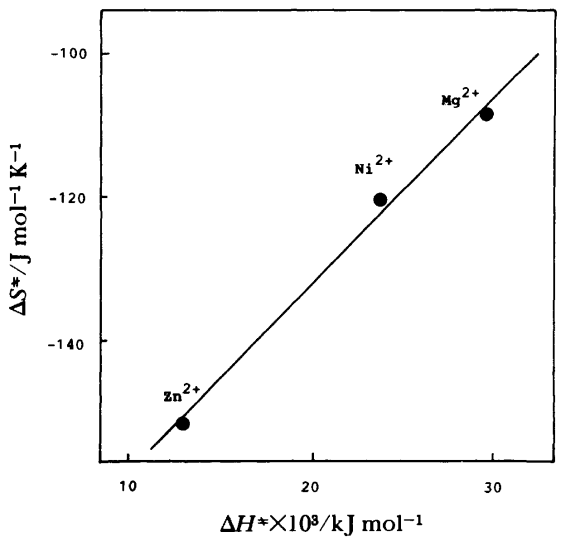

Fig. 9. Isokinetic relationship between ΔH^* and ΔS^* for three metal ions.

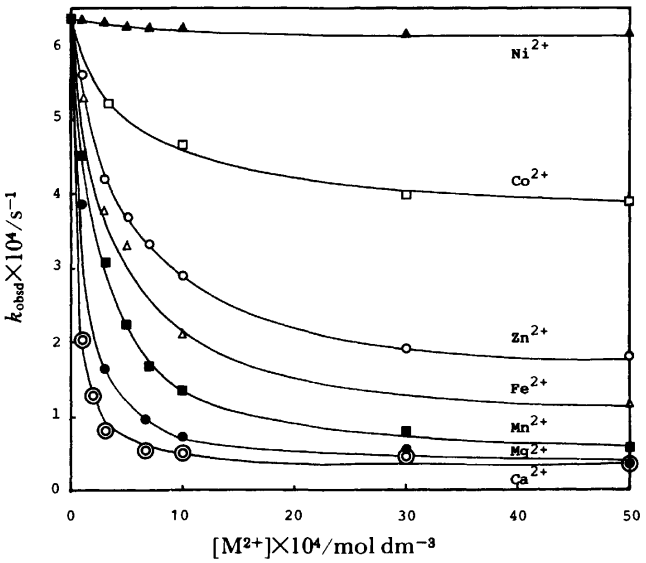

Fig. 10. Pseudo-first-order rate constants for the reduction of *N*-methylacridinium salt plotted as the function of the concentration of various metal ions: in acetonitrile, 25 °C; [BPDH]=1×10^{-4} mol dm^{-3}, [MA]=1×10^{-4} mol dm^{-3}.

Table 3. Temperature Effect on the Second-Order Rate Constants for the Reduction of Nitrosobenzene by BPDH in the Presence of Metal Ions in Acetonitrile[a)]

	k_2 / s^{-1} mol^{-1} dm^3		
T	Zn^{2+}	Ni^{2+}	Mg^{2+}
5 °C	108	36.5	10.1
15 °C	131	51.1	18.5
25 °C	171	83.4	30.0
35 °C	206	109	39.7
ΔH^* / kJ mol^{-1}	13.0	23.9	30.0
ΔS^* / J K^{-1} mol^{-1}	152	121	109
$T\Delta S^*$ / kJ mol^{-1}	45.2	36.0	32.4

a) [BPDH] = 1 × 10^{-4} mol dm^{-3}, [C_6H_5NO] = 1 × 10^{-3} mol dm^{-3}, [metal ion] = 3 × 10^{-3} mol dm^{-3}.

obtained from the slopes of the straight lines are 0.76, 0.81, 0.89, 1.12, and 1.23 for Co^{2+}, Zn^{2+}, Ni^{2+}, Mn^{2+}, and Mg^{2+} ion, respectively. The ρ value for Ni^{2+} ion may be somewhat larger than that expected for the saturated rates. At any rate, these ρ values are all positive, indicating that the rate-determining k_2 step is assisted by an electron-withdrawing substituent on the substrate NB. It is also noticed that the ρ value is smaller for a more active metal ion.

Temperature Effects. The temperature effects on the above saturation rates were examined for three metal ions as shown in Table 3 and in Figs. 8 and 9. It may be seen that the weight of ΔH^* term to the total rate is relatively small as compared to the ΔS^* term, especially in the case of Zn^{2+} ion. A linear isokinetic relationship in Fig. 9 may indicate the mechanism of catalysis to be the same for these three metal ions.

Metal Ion Inhibition in the Reduction of *N*-Methylacridinium Cation (MA). As shown in Fig. 10, the reduction of MA ion by BPDH was found to be inhibited by all metal ions. The order of inhibition is $Ni^{2+}<Co^{2+}<Zn^{2+}<Fe^{2+}<Mn^{2+}<Mg^{2+}<Ca^{2+}$ and almost the same as in the order of the association constants between BPDH and metal ions shown in Table 1. It may be suggested that the inhibition is due to a charge repulsion between the positive charge of substrate salt and metal ion-BPDH complex.

Discussion

It has been established in the model studies of NADH coenzyme that the metal ions such as Zn^{2+} and Mg^{2+} enhance the rates of reduction of some carbonyl substrates.[6-22)] However, much remain to be clarified for the mechanism of metal ion catalysis. As mentioned in the introductory part, it has been proposed that a metal ion may polarize the substrate carbonyl group as a Lewis acid to facilitate the reduction.[6-8,12,15)] However, confusing facts for this idea are the spectral evidence for the complexation between a metal ion and the dihydropyridine moiety, but not between a metal ion and the substrate carbonyl group. Namely, the electronic absorption at around 350 nm due to the π-π^* transition of the dihydropyridine moiety undergoes a red shift on complexation with a metal ion.[9,14-16,18,19)] Two explanations were proposed for the modes of complexation. Ohno et al.

proposed a sandwich type complexation for the transition state of reduction in which Mg^{2+} ion is located between the dihydropyridine and the substrate based on the electronic and infrared spectra.[13,16,17] Gase et al., however, explained differently based on the ^{13}C NMR spectra that Mg^{2+} ion coordinates to the amide oxygen of 1-benzyl-1,4-dihydronicotinamide.[20] Hughes et al. also considered the complexation on the amide moiety based on the electronic[9] and ^{1}H and ^{13}C NMR[14] spectra.

The present BPDH was also found to show a strong complexation with a bivalent metal ion in dry acetonitrile as manifested from the changes of absorption spectra at around 355 nm (Fig. 3) and from the saturation kinetics (Fig. 1). Here it should be noticed that the spectral change was a blue shift of 355 nm absorption, in contrast to a red shift mentioned above. There may be two conceivable types of complexation which result in different spectral changes as illustrated in Fig. 11. One is the complexation on the amide-oxygen (a) which would result in a red shift because of the metal ion stabilization of an excited state. The other is the complexation on the dihydropyridine ring involving an enamine π-system (b) which would result in a blue shift because of the metal ion destabilization of an excited state.[21,22] The observed blue shift seems to conform to the latter possibility.

As shown in Table 1 and Fig. 6, there is a tendency that a metal ion having a lower I_P forms a stronger complex with BPDH. As for the transition metal ions, it can also be shown that the magnitude of $\log K_M$ increases linearly with increasing ionic radius of metal ion in the order of $Ni^{2+}<Co^{2+}<Zn^{2+}<Fe^{2+}<Mn^{2+}$. This order is contrary to that of commonly observed Irving-Williams series.[26] This order is also difficult to correlate with the softness parameters σ_p of Pearson and Mawby[27] and σ_A of Ahrland[28] proposed for these metal ions. On the other hand, the rates of exchange of hydrated water molecule of aqua complexes of metal ions are known to be in the order of $Ni^{2+}<Co^{2+}<Fe^{2+}<Mn^{2+}$,[29] similarly as in the above order. For further discussions, however, it is necessary to know the ligand-exchange equilibrium between the hydrated water and BPDH since in this study the hydrated metal ions were used.

It is well-known that the pK_a's of aqua complexes of metal ions are linearly correlated with the ionization potentials (I_P) of metal ions.[30] Namely, the acidity of hydrated water becomes stronger on a metal ion of higher I_P. Thus, a linear correlation between the k_2 and the I_P values in Fig. 5 strongly suggests that the k_2 step is facilitated by the stabilization of the incipient *N*-oxide anion formed as the proceeding of hydride transfer in the transition state. The postulated mechanism is illustrated in Fig. 12. The figure also indicates a concerted process in which the exchange of ligand on the metal ion occurs from the dihydropyridine to the anion of product hydroxylamine. In this mechanism, it is important to know whether a metal ion does polarize the substrate N=O double bond before the hydride transfer or not, which might be answerd by looking at the Hammett substituent effect. In Fig. 7, the Hammett ρ values were observed to be in a range 0.76—1.23 which indicates the k_2 step to be facilitated by an electron-withdrawing substituent of the substrate. On the other hand, we reported previously that the ρ values for uncatalyzed and the carboxylic acid-catalyzed rates are 1.35 and −0.93, respectively.[24] The present ρ values are thus very close to that of uncatalyzed rates, suggesting that, in the present metal ion-catalyzed reduction, the substrate NO bond is not perturbed much by metal ion before the hydride transfer. It should be noticed that a negative ρ value (−0.93) for the carboxylic acid-catalysis indicates the importance of protonation of NO group in the transition state. Thus, the metal ion catalysis is found to be quite different from the carboxylic acid catalysis in anhydrous acetonitrile.

A sandwich structure in Fig. 12 proposed for the ternary complex in the transition state appears to be similar to that proposed by Ohno et al. for the

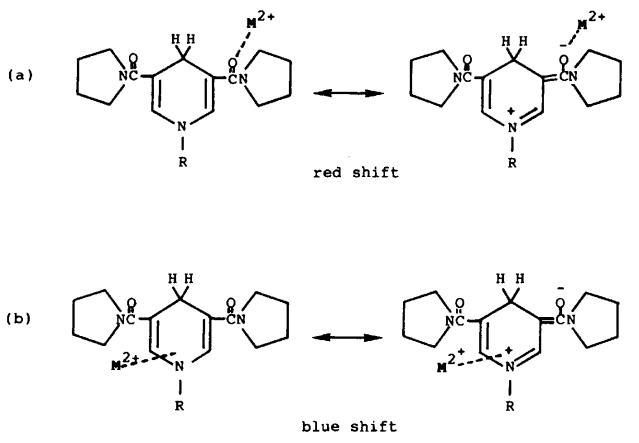

Fig. 11. Schematic illustration to explain a red shift (a) and blue shift (b) of electronic absorption at around 355 nm of BPDH on complexation with a metal ion.

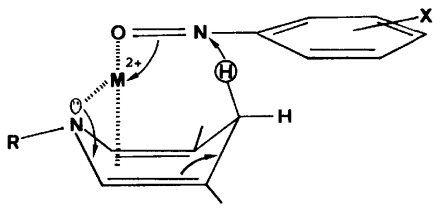

Fig. 12. Schematic illustration of the transition state for an M^{2+} ion-catalyzed reduction of substituted nitrosobenzene.

reduction of carbonyl substrate.[13,16,17] Important difference is that in the latter model electron movement occurs from the dihydropyridine to the substrate through the metal ion, in a reversed way as considered in the former case.

In Fig. 12, it is assumed that the hydrogen to be transferred is the pseudo axial one in the 4-position in the boat conformation of 1,4-dihydropyridine moiety. This assumption is based on a recent proposal that the axial hydrogen is more reactive than the equatorial one.[31] Finally, it must be mentioned that a metal coordination on the amide group may also explain most of the present results except the blue shift of electronic absorption on complexation.

In conclusion, the function of a metal ion seems to be dual in the present system: (a) to form a ternary complex, and (b) to facilitate the hydride transfer by stabilizing the incipient product anion. The two functions seem to be compensating to each other so that a metal ion such as Zn^{2+} ion having a proper balance in the two functions becomes the most active under certain conditions.

Experimental

Materials. Anhydrous acetonitrile was prepared by distilling over phosphorus pentoxide. Substituted nitrosobenzenes were prepared by the reduction of the corresponding commercially available nitrobenzenes with zinc powder as reported previously.[24] Metal ions were used as the perchlorates which were commercially available as special grade reagents.

1-Benzyl-3,5-bis(1-pyrrolidinylcarbonyl)-1,4-dihydropyridine (BPDH) was prepared according to a previous method, mp. 46 °C.[24]

Product analysis was performed for unsubstituted nitrosobenzene (X=H) by HPLC method as described before.[24]

Kinetics. The procedures were essentially the same as those reported previously.[24] In a 1 cm quartz UV cell stoppered with a rubber septum cover was placed a 3 mL acetonitrile solution of BPDH and the solution was well bubbled with acetonitrile saturated pure nitrogen gas through inserted needles. Stock solutions of nitrosobenzene and metal ion in acetonitrile were treated similarly. Then the quartz cell was mounted on a water-jacketed UV cell holder and nitrosobenzene and a metal ion stock solutions in water bath were kept at 25 °C for 15 min. The reaction was started by adding 10 μL each of the solution of nitrosobenzene and the metal ion in this order to the quartz cell by a Hamilton microsyringe. The rates of reduction were followed by monitoring the decrease of absorbance of BPDH at 355 nm. In most cases the reaction was carried out under pseudo-first-order conditions by using 10 molar excess of nitrosobenzene over BPDH.

References

1) A. Ferst, "Enzyme Structure and Mechanism," 2nd ed., W. H. Freeman and Co., New York (1985), pp. 390—404.

2) C.-I. Brändén, H. Jornvall, H. Eklund, and B. Furugren, "The Enzymes," ed by P. D. Boyer, Academic Press, New York (1975), 3rd. ed., Vol. 11, p. 103.

3) H. Eklund, B. V. Plapp, J.-P. Samama, and C.-I. Brändén, *J. Biol. Chem.*, **257**, 14349 (1982).

4) E. Cedergren-Zeppe Zauer, J.-P. Samama, and H. Eklund, *Biochemistry*, **21**, 4895 (1982).

5) J. Kvassman, A. Larsson, and G. Pettersson, *Eur. J. Biochem.*, **114**, 555 (1981).

6) D. J. Creighton and D. S. Sigman, *J. Am. Chem. Soc.*, **93**, 6314 (1971).

7) D. J. Creighton, J. Hajdu, and D. S. Sigman, *J. Am. Chem. Soc.*, **98**, 4619 (1976).

8) M. Shirai, Y. Chishima, and M. Tanaka, *Bull. Chem. Soc. Jpn.*, **48**, 1079 (1975).

9) M. Hughes and R. H. Prince, *J. Inorg. Nucl. Chem.*, **40**, 703 (1978).

10) K. Watanabe, R. Kawaguchi, and H. Kato, *Chem. Lett.*, **1978**, 255.

11) Y. Ohnishi, M. Kagami, and A. Ohno, *Tetrahedron Lett.*, **1975**, 2437.

12) J. B. Steevens and U. K. Pandit, *Tetrahedron*, **39**, 1395 (1983).

13) A. Ohno and S. Ushida, "Mechanistic Model of Asymmetric Reductions," in Lecture Notes in Bioorganic Chemistry, No. 1, Springer-Verlag, Heidelberg (1986), pp. 1—105.

14) M. Hughes, R. H. Prince, and P. Wyeth, *J. Inorg. Nucl. Chem.*, **40**, 713 (1978).

15) M. Hughes and R. H. Prince, *J. Inorg. Nucl. Chem.*, **40**, 719 (1978).

16) A. Ohno, T. Kimura, H. Yamamoto, S. G. Kim, S. Oka, and Y. Ohnishi, *Bull. Chem. Soc. Jpn.*, **50**, 1535 (1977).

17) A. Ohno, H. Yamamoto, T. Okamoto, S. Oka, and Y. Ohnishi, *Bull. Chem. Soc. Jpn.*, **50**, 2385 (1977).

18) A. Ohno, H. Kobayashi, T. Goto, and S. Oka, *Bull. Chem. Soc. Jpn.*, **57**, 1279 (1984).

19) A. Ohno, J. H. Lee, T. Yasuma, and S. Oka, *Tetrahedron Lett.*, **25**, 1995 (1984).

20) R. A. Gase, G. Boxhoorn, and U. K. Pandit, *Tetrahedron Lett.*, **1976**, 2889.

21) S. Fukuzumi, Y. Kondo, and T. Tanaka, *Chem. Lett.*, **1983**, 485.

22) S. Fukuzumi, N. Nishizawa, and T. Tanaka, *Chem. Lett.*, **1983**, 1755.

23) H. Awano, T. Hirabayashi, and W. Tagaki, *Tetrahedron Lett.*, **25**, 2005 (1984).

24) H. Awano and W. Tagaki, *Bull. Chem. Soc. Jpn.*, **59**, 3117 (1986).

25) "Lange's Handbook of Chemistry," ed by J. A. Dean., McGraw-Hill, New York (1985), 13th ed.

26) H. Irving and R. J. P. Williams, *J. Chem. Soc.*, **1953**, 3192.

27) P. G. Pearson and R. J. Mawby, "Halogen Chemistry," ed by V. Gutmann, Academic Press, New York (1967), Vol. 3, p. 55.

28) S. Ahrland, *Structure and Bonding*, **5**, 118 (1968).

29) M. Eigen, *Pure Appl. Chem.*, **6**, 105 (1963).

30) J. Bailor Ed., "Comprehensive Inorganic Chemistry," Pergamon, Oxford (1972), Vol. 4, p. 611.

31) K. P. Nambiar, D. M. Stauffer, P. A. Kolodziej, and S. A. Benner, *J. Am. Chem. Soc.*, **105**, 5886 (1983).

32) S. A. Benner, K. P. Nambiar, and G. K. Chambers, *J. Am. Chem. Soc.*, **107**, 5513 (1985).

Optically Active Polyamides Having (−)-Anti Head-to-Head Coumarin Dimer Component. 2. Chiroptical Property in the Film State

Yun CHEN, Kazuhiko SAIGO,* Noriyuki YONEZAWA, and Masaki HASEGAWA
Department of Synthetic Chemistry, Faculty of Engineering, The University of Tokyo, Bunkyo-ku, Tokyo 113
(Received December 6, 1986)

The chiroptical property of optically active polyamides (**3a—i**), derived from (−)-anti head-to-head coumarin dimer (**1**), was investigated by comparing their UV and circular dichroism (CD) spectra with those of the corresponding model diamides (**8a—i**) in the film state. The result suggests that the polyamides (**3a—c,g**) derived from acyclic aliphatic diamines, exist in a random conformation due to the flexibility of the diamine components. The polyamides (**3d,h**), consisting of piperazine, are assumed to be in a rod-like conformation, resulting from their rigid and fixed main chains. The polyamides (**3e,f,i**), prepared from aromatic diamines, show reversed and split Cotton effects at 270—300 nm in comparison with those of model diamides. This phenomenon is interpreted by the formation of an ordered conformation of macromolecular asymmetry.

Recently, we have synthesized a series of optically active polyamides by the ring-opening polyaddition reaction of (—)-anti head-to-head coumarin dimer with diamines,[1,2] and have shown that these polyamides exist in a random or ordered conformation in solution depending on the medium and/or on the structure of diamine components.[1,2] For example, the polyamide, consisting of (—)-anti head-to-head coumarin dimer and 1,4-phenylenediamine components, exists in a random coil in *N,N*-dimethylacetamide solution, while in basic media it exists in an ordered conformation due to the electronic repulsion of the phenolate anions formed by the base. It is well-known that CD spectral study is very effective to investigate the chiroptical property of polypeptides in the film-state.[3,4] These observation and fact prompted us to disclose the conformations of the optically active polyamides in the film state, since it is considered to be possible that these polyamides form an ordered conformaion even in film state depending on the rigidity of the diamine component.

In this paper, we wish to report the chiroptical property of the optically active polyamides, derived from (—)-anti head-to-head coumarin dimer, in the film state on the basis of the comparison of their UV and CD spectra with those of the corresponding model diamides.

Results and Discussion

Synthesis of Optically Active Polyamides and Model Diamides. Optically active polyamides **3a—f** were synthesized by the ring-opening polyaddition reaction of (−)-anti head-to-head coumarin dimer **1** as described in detail in the literature.[2]

Optically active *O*-methylated polyamides **3g—i** were prepared by the interfacial polycondensation reaction of bis(acid chloride) **6** with diamines using benzyltriethylammonium chloride as a phase-transfer catalyst. The starting material **6** could be obtained from **1** by three steps as shown in the following Scheme 2.

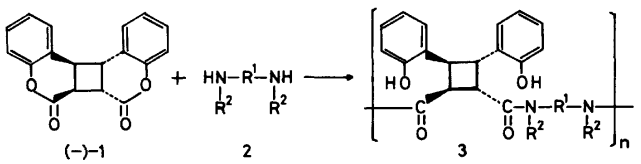

Scheme 1.

The notations for the optically active polyamides are as follows:

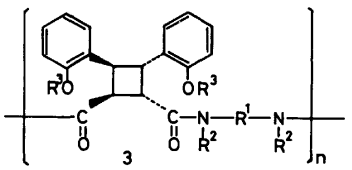

Polyamide	R^1	R^2	R^3	η_{inh}
3a	$-(CH_2)_6-$	H	H	0.88
3b	$-(CH_2)_6-$	CH_3	H	0.35
3c	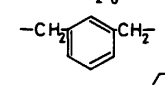	H	H	0.63
3d	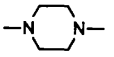		H	0.51
3e		H	H	0.36
3f	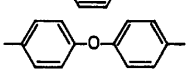	H	H	0.31
3g	$-(CH_2)_6-$	H	CH_3	1.01
3h	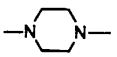		CH_3	1.00
3i	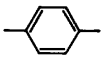	H	CH_3	0.50

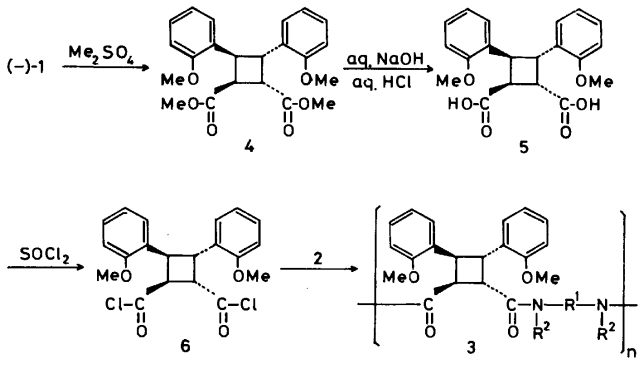

Scheme 2.

Similar to the ring-opening polyaddition reaction, the interfacial polycondensation also gave high-molecular-weight polyamides (η_{inh}=0.50—1.01 dl g^{-1}). These *O*-methylated polyamides showed no solubility in common organic solvents, but could dissolve in *m*-cresol, *N,N*-dimethylacetamide (DMAc), dimethyl sulfoxide (DMSO), *N*-methyl-2-pyrrolidone (NMP), and acetic acid very slowly.

Model diamides **8a—f** were synthesized by ring-opening addition reaction as reported in the literature.[2] In order to study the influence of the extension of resonance on UV and CD spectra, model diamides **8e′, f′** were synthesized in a similar manner.

O-Methylated model diamides **8g—i** were synthesized by interfacial condensation without the phase-transfer catalyst.

The notations for the model diamides are as follows:

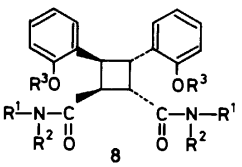

Diamide	R^1	R^2	R^3
8a	$-(CH_2)_5CH_3$	H	H
8b	$-(CH_2)_5CH_3$	CH_3	H
8c	$-CH_2-C_6H_4-CH_3$	H	H
8d			H
8e		H	H
8e′	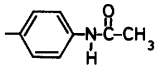	H	H
8f	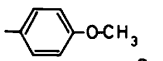	H	H
8f′	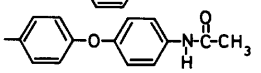	H	H
8g	$-(CH_2)_5CH_3$	H	CH_3
8h			CH_3
8i		H	CH_3

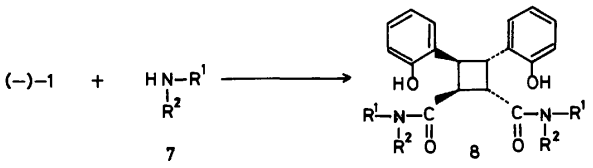

Scheme 3.

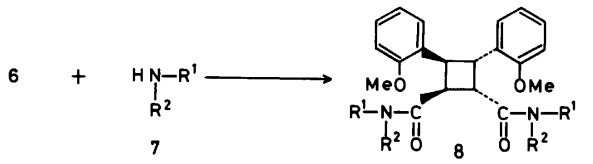

Scheme 4.

Chiroptical Property in the Film State. Polyamide **3** was cast on the outside surface of a quartz cell and dried to give a clear and homogeneous thin film. In the case of model diamide **8**, a clear and homogeneous thin deposit could also be obtained with the exception of **8b**. The cast sample was found to be isotropic on the basis of the fact that UV and CD spectra, obtained by rotating the sample around the axis of the incident beam, were identical to each other.

It is known that the chiroptical property of synthetic polyamides can be investigated by comparing their CD spectra with those of the corresponding model diamides.[5] In general, the random conformation of the polymer results in weaker Cotton effect at about the same wavelength than that of the corresponding model diamide. In this study, we compared mainly the Cotton effects of the amide carbonyl and aromatic chromophores in polyamide **3** with those of model diamide **8**, respectively.

As listed in Table 1, model diamides **8a, c, d, g, h**, derived from aliphatic amines, show maximum absorption(s) at about 275 nm in their UV spectra, which apparently corresponds to the π-π^* transition of hydroxyphenyl group. In CD spectra, all of the model diamides show *negative* Cotton effects at about 235 and 275 nm. The former negative CD band may be assigned to a component of the split π-π^* transition due to an exciton coupling of amide carbonyl chromophore,[6] although a short-wavelength component of this split cannot be observed because of the limit of measurement. Moreover, the latter can be assigned to the π-π^* transition of the aromatic[2] chromophore.

In the case of model diamides **8e, f, i** derived from aromatic amines, their molar extinction coefficients are much larger than those of the model diamides derived from aliphatic amines. Negative CD bands of the amide carbonyl and aromatic chromophores in **8**, **f**, **i** appear at about 240 and 280 cm, respectively, namely, the CD bands red-shifted about 5 nm in

Table 1. Optical Properties of Model Diamides in the Film State

Diamide	UV spectra		CD spectra	
	ε	λ_{max}	$\Delta\varepsilon$	λ_{max}
8a	4780	273.2	−2.60	270.8
	4500	280.0	−7.92	236.0
8c	5150	275.0	−3.50	275.0
	4700	281.0	−9.02	235.0
8d	3820	280.0	−3.42	277.0
			−4.36	236.5
8g	3880	273.1	−1.93	270.0
	3780	280.0	−1.59	230.0
8h	4318	276.0	−3.79	274.0
			−11.14	235.5
8e	21700	249.0	−7.95	279.0
			−13.63	241.0
8e'	39000	272.0	−6.00	282.5
			−7.80	238.5
8f	24900	257.5	−10.33	279.0
			−19.25	238.5
8f'	59300	262.0	−7.25	282.5
			−9.08	241.0
8i	19700	251.3	−11.00	279.0
			−10.82	243.0

comparison with those of the aliphatic counterparts. These phenomena would be attributable to the resonance effect of the amide carbonyl chromophore with the aromatic amine residue and to the effect of the aromatic amine residue as an aromatic chromophore. Moreover, **8e'** and **8f'**, synthesized to clarify the influence of the extension of the resonance on CD spectra in the film state, show also only a little decrease and shift in CD bands, although they show an enhanced molar extinction coefficient in UV spectra.

From these facts, it is clear that the negative CD bands of model diamide **8** result simply from the chiral carbons of cyclobutane ring and that the extension of the resonance in the aromatic amine residue results only in a little decrease and shift of the CD bands.

The UV and CD spectra of polyamide **3a** and model diamide **8a** in the dry film state are shown in Fig. 1. The negative CD bands of **3a** at 230—240 and 260—280 nm are, as mentioned for model diamides, assigned to a component of the split π-π^* transition of the amide carbonyl chromophore and to the π-π^* transition of the hydroxyphenyl chromophore, respectively. Comparing the bands with those of **8a**, the former band shows enhanced intensity with a blue shift although the latter exhibits weaker intensity.

Similar enhanced intensity and blue shift of the CD band of polyamide at 230—240 nm in comparison with that of the corresponding model diamide were also

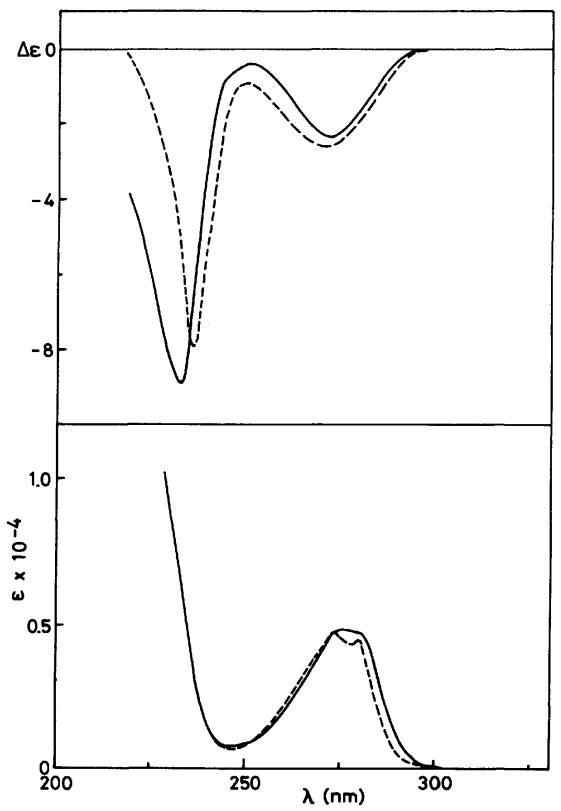

Fig. 1. CD and UV spectra of polyamde **3a** (——) and model diamide **8a** (------) in the film state.

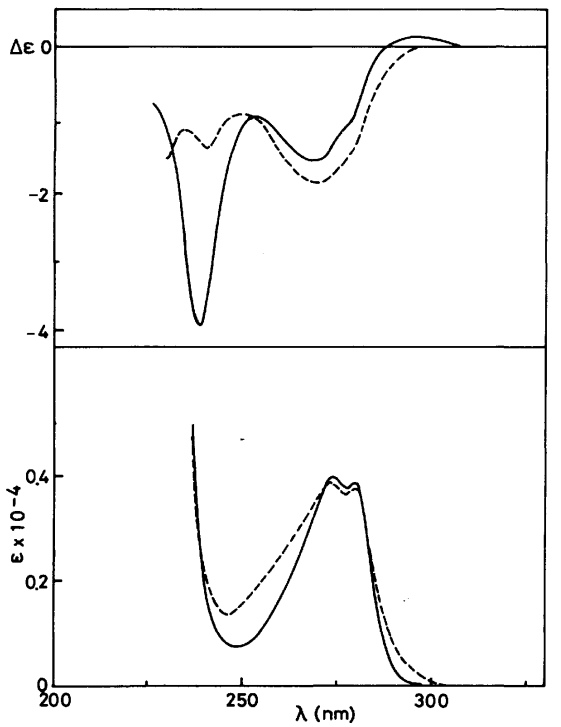

Fig. 2. CD and UV spectra of polyamide **3g** (——) and model diamide **8g** (------) in the film state.

observed for **3g**. Namely, *O*-methylated polyamide **3g** shows stronger CD band at ca. 240 nm than that of model diamide **8g**, while the band at 270 nm is weaker than that of **8g** as shown in Fig. 2.

Similarity in the CD shape between **3a** and **8a**, and between **3g** and **8g**, suggests that they possess similar conformational preference, resulting from the asymmetric cyclobutane ring. But the enhancement of the band at 230—240 nm indicates that **3a** and **3g** aggregate by the interaction between the amide groups, respectively, although **3a** and **3g** exist essentially in a random conformation.

In the case of polyamide **3c**, both negative CD bands are weaker in intensity than those of model diamide **8c** (Fig. 3). This is a typical phenomenon for a completely random conformation.[5] Then, **3c** would exist in a random conformation in the film state.

The preparation of the thin film of **8b** was not successful since it precipitated out and became opaque on drying. Then, the chiroptical study of polyamide **3b** could not be conducted by comparing directly the CD spectrum of **3b** with that of **8b**. But the CD spectrum is very similar to that of **3c**, indicating that **3b** exists in a random conformation in the film state. The random conformation would result from the flexibility of the diamine component and the lack of amide hydrogen.

Considering the structural difference between **3a**, **3b**, and **3g**, it would be concluded that the amide hydrogen plays an important role for macromolecular aggregation but the phenolic hydroxyl does not. The lack of aggregation in polyamide **3c** would be attributed to the steric crowd near by the amide group.

The CD bands of polyamides **3d** and **3h** at the wavelength shorter than 250 nm degenerate significantly in comparison with those of **8d** and **8h**, respectively, as shown in Figs. 4 and 5. The much smaller mean residue rotation and molecular circular dichroism of **3h** in DMAc than those of **8h**, similar to that observed between **3d** and **8d**,[1,2] indicate the existence of a rigid conformation of **3h** in DMAc. The Corey-Pauling-Koltun space-filling molecular models of **3d** and **3h** show that the diacid component is in a very tight conformation and that neither polymer main chain nor hydroxyphenyl (or methoxyphenyl) group in the side chain can rotate. On the basis of these observations, it seems possible to say that polyamides **3d** and **3h**, derived from piperazine, have a fixed rod-like conformation in the film state as well as in solution.

The film-state UV and CD spectra of polyamide **3e** and model diamides **8e**, **e'** are shown in Fig. 6. Model diamide **8e** shows normal negative CD bands at 235—245 and 270—285 nm, which can be assigned to a component of the split π-π^* transition of the amide carbonyl chromophore and the π-π^* transition of the

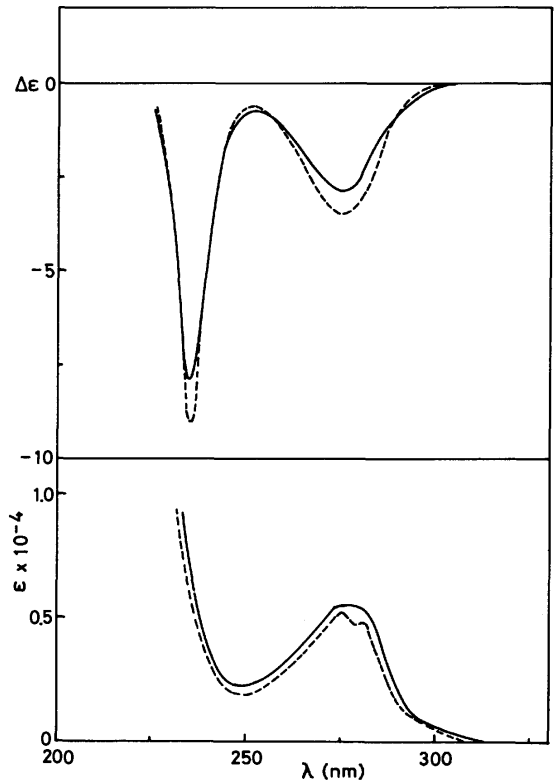

Fig. 3. CD and UV spectra of polyamide **3c** (——) and model diamide **8c** (------) in the film state.

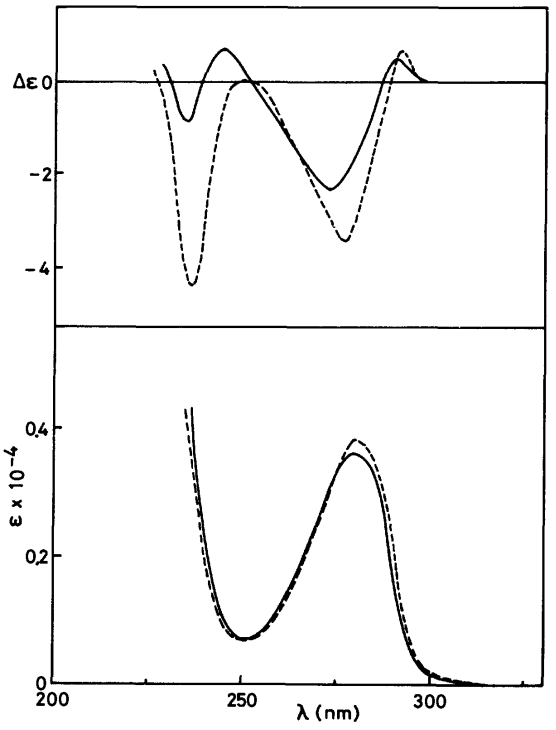

Fig. 4. CD and UV spectra of polyamide **3d** (——) and model diamide **8d** (------) in the film state.

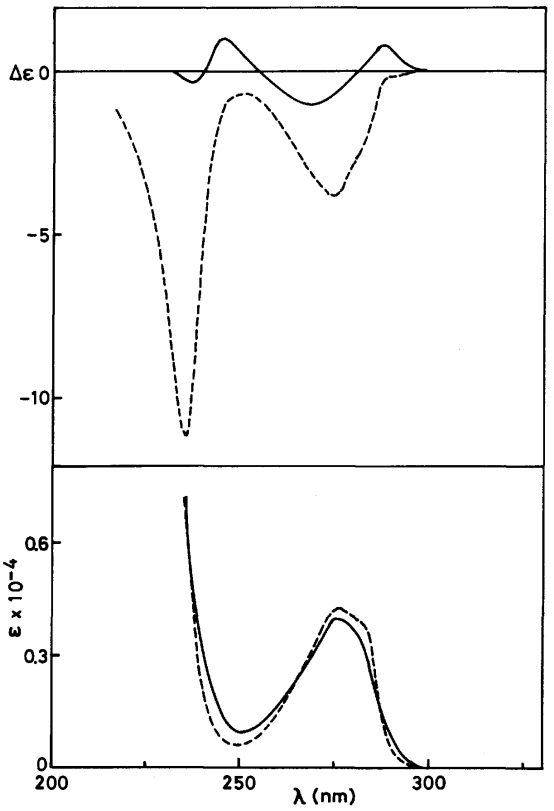

Fig. 5. CD and UV spectra of polyamide **3h** (——) and model diamide **8h** (------) in the film state.

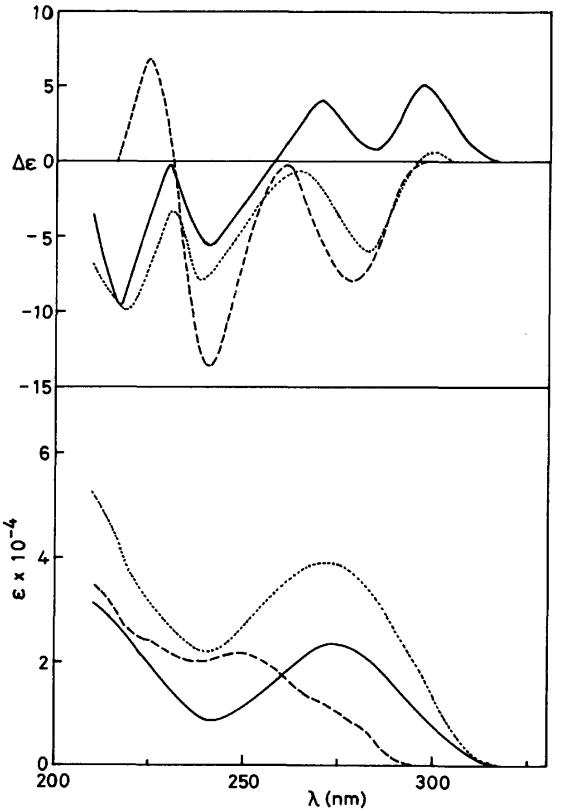

Fig. 6. CD and UV spectra of polyamide **3e** (——) and model diamide **8e** (------), **8e′** (·····) in the film state.

aromatic chromophore, respectively. The red shift and increased intensity of the UV absorption of **8e′** in comparison with that of **8e** would be attributed to the extension of its mesomeric region. But, this extension in **8e′** results only in a little decrease and shift of the CD bands at 235—245 and 270—285 nm. However, in the CD spectrum of **3e**, two *positive* CD bands appear at 265—275 and 290—302 nm in contrast to the *negative* bands of **8e** and **8e′** at 270—285 nm. These two positive CD bands would be attributed to the π–π^* transitions of 2-hydroxyphenyl group in the side chain and 1,4-phenylenediamine residue in the main chain. Then, the drastic difference is considered to result from a second ordered conformation, for which the aromatic residues in the main and side chains probably play an important role. Similar CD spectral change was observed for **3e** in DMAc on addition of 1,8-diazabicyclo[5.4.0]undec-7-ene (DBU). The CD spectrum of **3e** in the film state is quite similar to that of **3e** in DMAc when DBU/hydroxyphenyl in the side chain is 2.[2] But, it is not so developed as observed in 0.2 M (1 M=1 mol dm^{-3}) NaOH, in which **3e** exists in a fully developed ordered conformaion.[2] This means that in the dry film state **3e** exists in an ordered conformation of macromolecular asymmetry though it is incomplete.

As shown in Fig. 7, *O*-methylated polyamide **3i**

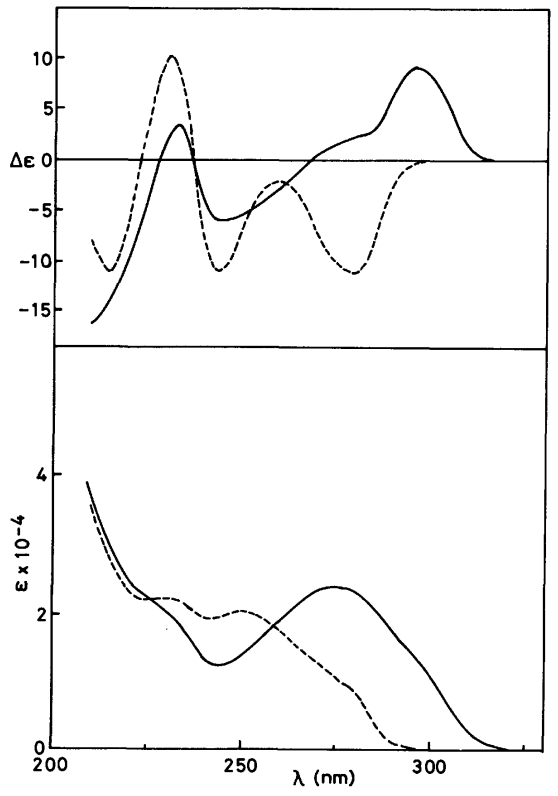

Fig. 7. CD and UV spectra of polyamide **3i** (——) and model diamide **8i** (------) in the film state.

shows CD bands similar to that of **3e**, i.e. the *positive* band at 290—300 nm with shoulder at 270—285 nm. This means that **3i** forms an ordered conformation similar to that of **3e** in spite of its lack of phenolic hydroxyl group in the side chain.

From these results, it is considered that the ordered conformation of **3e** and **3i** in the film state would be attributed to the hydrogen bonding of amide residue, which renders the polymer main chain taking a macromolecular asymmetry to release the strain.[7,8] To ascertain the contribution of the amide hydrogen to the ordered conformation, the preparation of the polyamide, consising of **1** and *N,N'*-dimethyl-1,4-phenylenediamine, was tried. But, the reaction gave only low-molecular-weight polyamide. Then, the contribution could not be demonstrated directly.

As shown in Fig. 8, the CD bands of **3f** at 255—300 nm tends to appear in *positive* region in contrast to those of negative bands of **8f** and **8f'**. This means that **3f** is also in an ordered conformation of macromolecular asymmetry, although this ordered conformation is less developed than that of **3e** due to the flexibility of the diphenyl ether linkage.

On the basis of these CD spectral studies, the following chiroptical property in the dry film state is concluded for polyamide **3**: Polyamides **3a**—c and **3g**, derived from acyclic aliphatic diamines, exist essentially in a random conformation due to the flexibility of the diamine components, but **3a** and **3g** show an aggregation phenomenon, for which the amide hydrogen is important. Polyamides **3d** and **3h**, derived from piperazine, have a fixed rod-like conformation due to their very rigid and tight main chain. Polyamides **3e**, **3f**, and **3i** exist in an ordered conformation of macromolecular asymmetry though it is incomplete. In the formation of the ordered conformation, the structure of the diamine component and the amide hydrogen play an important role. At present, these ordered conformations of **3e**, **3f**, and **3i** cannot be specified, but they possess the possibility to form a sheet and/or helical conformation in the dry film state. The chiroptical property of the polyamides in the film state is summarized in Table 2 with that in solution.[2]

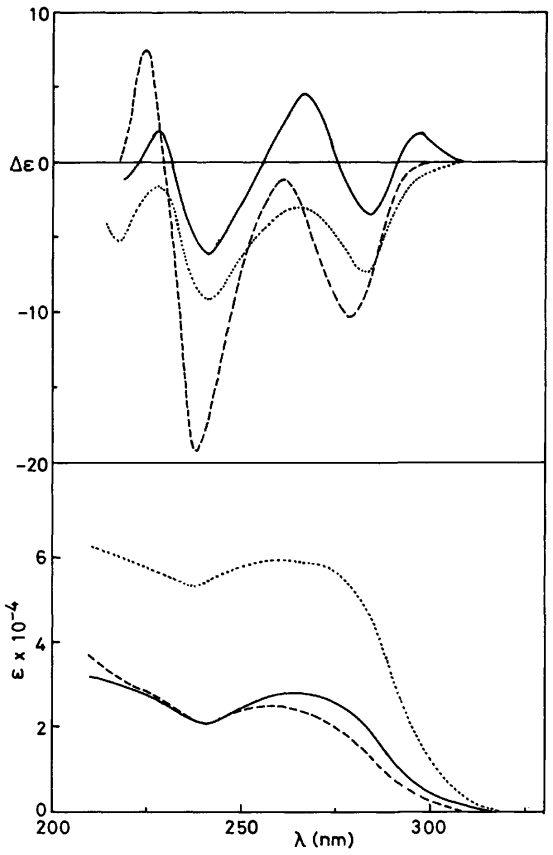

Fig. 8. CD and UV spectra of polyamide **3f** (——) and model diamide **8f** (------), **8f'** (·····) in the film state.

Table 2. Conformation of Polyamides **3a**—**i** in the Film State with that in Solution

Polyamide	In solution		Film state
	DMAc	Basic media	
3a	random	random	aggregation
3b	random	—[a]	random
3c	random	random	random
3g	random[b]	—[a]	aggregation
3d	ordered (rigid)	ordered (rigid)	ordered (rigid)
3h	ordered[b] (rigid)	—[a]	ordered (rigid)
3e	random	ordered	ordered
3f	random	ordered	ordered
3i	ordered[b]	—[a]	ordered

a) Insoluble. b) The chiroptical property of *O*-methylated polyamides in DMAc was investigated in this work.

Experimental

Measurement. Melting points were determined on a Laboratory Devices Mel-Temp and are uncorrected. The IR spectra were obtained on a Jasco IR-810 spectrophotometer. ^{1}H NMR spectra were recorded with a Hitachi R-40 (90 MHz) spectrometer. The optical rotations were measured with a Jasco DIP-360 digital polarimeter at 20 °C in a 1.0 dm cell. The inherent viscosities of the polyamides were measured at 30 °C with an Ostwald viscometer at the concentration of 0.30 g dl^{-1}. The circular dichroism and UV spectra were measured on a Jasco J-500 spectropolarimeter and on a Shimadzu UV-260 spectrophotometer, respectively, at room temperature.

Materials. (−)-Anti head-to-head coumarin dimer (**1**) was obtained from the racemate by the diasteriomeric resolution method as reported in the previous paper.[9] Before use, **1** was recrystallized from benzene and dried at 60 °C in vacuo (ca. 2 mmHg) for 24 h: $[\alpha]_D$ −9.0° (*c* 1.00, benzene), almost 100% enantiomeric excess on the basis of

HPLC analysis of its diamide derivative with *S*-(−)-1-phenylethylamine.[10]

3,4-Bis(2-methoxyphenyl)-1,2-cyclobutanedicarbonyl Dichloride (6). To a solution of **1** (7.31 g, 25.0 mmol) in acetone/2.0 M NaOH (73 ml/150 ml) was added dropwise dimethyl sulfate (99.21 g, 786 mmol) in a period of one hour at room temperature. After stirring for 4 h at the temperature, acetone was evaporated, and the mixture was extracted with carbon tetrachloride (150 ml×3). The evaporation of the solvent to dryness gave an oily product. The purification of the crude product by silica-gel chromatography (eluent: hexane/ethyl acetate=60/40 (v/v)), followed by recrystallization from hexane/acetone, gave 6.00 g (63%) of dimethyl 3,4-bis(2-methoxyphenyl)-1,2-cyclobutanedicarboxylate (**4**): Mp 85.5—86.5 °C; $[\alpha]_D$ −169.8° (*c* 0.5, chloroform); IR (KBr) 1720, 1240, 1020, and 759 cm^{-1}; ^1H NMR ($CDCl_3$) δ=3.25 (6H, s), 3.77 (8H, s with shoulder), 4.75 (2H, pseudo d, *J*=8.0 Hz), and 6.5—7.2 (8H, m).

Found: C, 68.93; H, 6.40%. Calcd for $C_{22}H_{24}O_6$: C, 68,74; H, 6.29%.

Diester **4** (4.61 g, 12.0 mmol) was hydrolyzed in a solution of 1.0 M NaOH/MeOH (50 ml/25 ml) at 50 °C for 5 h, and then the solution was acidified with 1.0 M HCl after evaporation of methanol. The precipitates appeared were collected by filtration and recrystallized from water/ethanol to give 3.65 g (85%) of 3,4-bis(2-methoxyphenyl)-1,2-cyclobutanedicarboxylic acid (**5**): Mp 268.0—269.5 °C: $[\alpha]_D$ −121.2° (*c* 0.5, MeOH); IR (KBr) 2600, 1700, 1246, 1030, and 757 cm^{-1}; ^1H NMR (Me_2SO-d_6) δ=3.5 (2H, pseudo d, *J*=8.0 Hz), 4.6 (1H, pseudo d, *J*=8.0 Hz), 3.75 (6H, s), 6.4—7.2 (8H, m), and 11.75 (2H, s).

Found: C, 67.37; H, 5.65%. Calcd for $C_{20}H_{20}O_6$: C, 67.41; H, 5.66%.

Dicarboxylic acid **5** (3.65 g, 10.2 mmol) was refluxed in a mixture of thionyl chloride/benzene (75 ml/90 ml) for 2 h until the solution became clear. After evaporation of thionyl chloride and benzene, the residue was recrystallized from hexane to give 3.70 g (92%) of 3,4-bis(2-methoxyphenyl)-1,2-cyclobutanedicarbonyl dichloride (**6**): ^1H NMR ($CDCl_3$) δ=3.78 (6H, s), 4.2—4.7 (4H, m), and 6.5—7.3 (8H, m). Bis(acid chloride) **6** was immediately used in the interfacial synthesis of polyamides and model diamides without further purification

General Procedure for Synthesis of Polyamides 3. The synthesis of optically active polyamides **3a—f** by ring-opening polyaddition reaction has been described in the previous paper.[2]

O-Methylated polyamides **3g—i** were synthesized by the interfacial polycondensation reaction of **6** with the corresponding diamines as follows: To a solution of diamine (2.78 mmol) in 12 ml of 1.0 M NaOH was added 0.63 g of benzyltriethylammonium chloride (2.78 mmol) as a phase-transfer catalyst. Then, a chloroform solution (11 ml) of **6** (1.09 g, 2.78 mmol) was added to the aqueous solution at once under vigorous stirring at room temperature. The precipitates appeared were collected by filtration, washed successively with methanol and hot water, and dried in vacuo at 80 °C for 48 h.

Polyamide 3g: Yield 84%; η_{inh}=1.01 dl g^{-1} (*m*-cresol); $[\alpha]_D$ −70.3° (*c* 0.3, *m*-cresol); IR (KBr) 3500—3300, 3000—2800, 1645, 1525, 1247, 1024, and 755 cm^{-1}.

Found: C, 68.47; H, 6.97; N, 5.85%. Calcd for $(C_{26}H_{32}N_2O_4 \cdot H_2O)_n$:C, 68.70; H, 7.54; N, 6.16%.

Polyamide 3h: Yield 86%; η_{inh}=1.00 dl g^{-1} (DMAc); $[\alpha]_D$ −40.7° (*c* 0.3, DMAc); IR (KBr) 3600—3300, 3100—2800, 1630, 1243, 1028, and 755 cm^{-1}.

Found: C, 67.25; H, 6.25; N, 6.36%. Calcd for $(C_{24}H_{26}N_2O_4 \cdot H_2O)_n$: C, 67.90; H, 6.65; N, 6.60%.

Polyamide 3i: Yield 99%; η_{inh}=0.50 dl g^{-1} (DMAc); $[\alpha]_D$ +5.7° (*c* 0.3, DMAc); IR (KBr) 3600—3200, 3100—2800, 1668, 1545, 1245, 1026, and 755 cm^{-1}.

Found: C, 69.82; H,5.24; N, 6.07%. Calcd for $(C_{26}H_{24}N_2O_4 \cdot H_2O)_n$: C, 69.94; H, 5.87; N, 6.27%.

General Procedure for the Synthesis of Model Diamides 8. The synthesis of optically actically active diamides (**8a—f**) by ring-opening addition reaction has been reported in the previous paper.[2] Model diamides **8e′**, **8f′** were also synthesized by this method.

The general procedure for the synthesis of *O*-methylated model diamides **8g—i** by interfacial condensation reaction is described as follows: To a solution of amine (4.00 mmol) in 2.0 ml of 1.0 M NaOH was added dropwise a chloroform solution (2.0 ml) of **6** (0.16 g, 0.40 mmol) in a period of 5 min under vigorous stirring at room temperature. After stirring for additional 10 min, chloroform was evaporated, and the remaining solid mass was collected by filtration. The recrystallization gave the corresponding 3,4-bis(2-methoxyphenyl)-1,2-cyclobutanedicarboxamide (**8g—i**).

***N,N′*-Bis(4-acetylaminophenyl)-3,4-bis(2-hydroxyphenyl)-1,2-cyclobutanedicarboxamide (8e′)**: Light brown prism (EtOH-H_2O); yield 79%; mp 198 °C (decomp); $[\alpha]_D$ −131.4° (*c* 0.3, DMAc), −109.9° (*c* 0.3, 0.37 M NaOH); IR (KBr) 3600—2800, 1660, 1610, 1255, 1020, 940, 840, and 760 cm^{-1}; ^1H NMR (Me_2SO-d_6) δ=1.90 (6H, s), 3.81 (2H, pseudo d, *J*=8.0 Hz), 4.73 (2H, pseudo d, *J*=8.0 Hz), 6.4—7.5 (16H, m), 9.2—9.5 (4H, 2 peaks), and 9.61 (2H, s).

Found: C, 66.92; H, 5.40; N, 9.07%. Calcd for $C_{34}H_{32}N_4O_6 \cdot H_2O$: C, 66.87; H, 5.61; N, 9.18%.

***N,N′*-Bis[4-(4-acetylaminophenoxy)phenyl]-3,4-bis(2-hydroxyphenyl)-1,2-cyclobutanedicarboxamide (8f′)**: Light yellow needle (dioxane-EtOH); yield 48%; mp 184.0—185.5°C; $[\alpha]_D$ −69.6° (*c* 0.3, DMAc); IR (KBr) 3600—3000, 1660, 1610, 1220, 1020, 830, and 755 cm^{-1}: ^1H NMR (Me_2SO-d_6) δ=2.00 (6H, s), 3.87 (2H, pseudo d, *J*=8.0 Hz), 4.80 (2H, pseudo d, *J*=8.0 Hz), 7.3—8.6 (24H, m), 9.43 (4H, s), and 9.80 (2H, s).

Found: C, 69.63; H, 5.29; H,7.30%. Calcd for $C_{46}H_{40}N_4O_8 \cdot H_2O$: C, 69.51; H, 5.33; N, 7.05%.

***N,N′*-Dihexyl-3,4-bis(2-methoxyphenyl)-1,2-cyclobutanedicarboxamide (8g)**: Colorless prism (EtOH-H_2O); yield 66%; mp 131.5—132.0 °C; $[\alpha]_D$ −81.0 ° (*c* 0.3, *m*-cresol); IR (KBr) 3330, 3000—2800, 1645, 1250, 1030, and 750 cm^{-1}; ^1H NMR (Me_2SO-d_6) δ=0.5—1.4 (22H, m), 3.42 (2H, pseudo d, *J*=8.0 Hz), 3.75 (6H, s), 4.57 (2H, pseudo d, *J*=8.0 Hz), and 6.3—7.3 (8H, m).

Found: C, 73.26; H, 8.84; N, 5.06%. Calcd for $C_{32}H_{46}N_2O_4$: C, 73.53; H, 8.87; N, 5.36%.

***N,N′*-[3,4-Bis(2-methoxyphenyl)-1,2-cyclobutanedicarbonyl] bis[piperidine] (8h)**: Colorless prism (EtOH-H_2O); yield 80%; mp 212.5—214.0 °C; $[\alpha]_D$ −83.0 ° (*c* 0.3, DMAc); IR (KBr) 3450, 3100—2800, 1622, 1245, 1030, and 760 cm^{-1}; ^1H NMR ($CDCl_3$) δ=0.4—1.5 (12H, m), 2.6—3.4 (8H, m), 3.7 (6H, s), 4.17 (2H, pseudo d, *J*=8.0 Hz), 4.86 (2H, pseudo d, *J*=8.0 Hz), and 6.5—7.3 (8H, m).

Found: C, 73.17; H, 7.72; N, 5.42%. Calcd for $C_{30}H_{38}N_2O_4$: C, 73.44; H, 7.81; N, 5.71%.

3,4-Bis(2-methoxyphenyl)-1,2-cyclobutanedianilide (8i): Colorless needle (benzene–hexane); yield 73%; mp 221.0—222.0 °C; $[\alpha]_D$ −32.7° (*c* 0.3, DMAc); IR (KBr) 3400, 3100—2800, 1675, 1600, 1245, 1022, and 755 cm^{-1}: ^1H NMR (Me_2SO-d_6) δ=3.73 (8H, s with shoulder), 4.67 (2H, pseudo d, J=8.0 Hz), 6.2—7.5 (18H, m), and 9.37 (2H, s).

Found: C, 75.75; H, 5.90; N, 5.39%. Calcd for $C_{32}H_{30}N_2O_4$: C, 75.87; H, 5.97; N, 5.53%.

Preparation of Thin Films for Chiroptical Study. The thin films of the polyamides and model diamides were prepared by casting their solution (ca. 30 mg ml^{-1} DMAc) on the outside surface of a quartz cell (10×45×10 mm). The coated films were dried at ambient air and then in vacuo for 24 h at room temperature. The obtained thin films were at the concentration of ca. 10^{-4} repeating-unit mmol (or mmol) cm^{-2}. All CD spectra were given in $\Delta\varepsilon$, molecular circular dichroism, with cm^2/repeating-unit-mmol (or mmol) unit, which was calculated by the following equation:

$$\Delta\varepsilon = [\theta]/3300 \text{ and } \theta = 0.1 \times [\theta] \times m/MW$$

where MW is the repeating-unit molecular weight (or molecular weight) of the polyamide (or the model diamide); m is the sample weight per unit area (g cm^{-2}); θ is the measured ellipticity (deg); and $[\theta]$ is the molecular ellipticity (deg·$cm^2$$dmol^{-1}$).

Thin film were also cast on the outside surface of a cylindrical quartz cell [10×20 (o.d.) mm], and each CD measurement was repeated four times by rotating the sample cell by 45, 90, and 120 degrees from the first position around the axis of the incident light beam to give almost identical spectra.

References

1) N. Yonezawa, T. Kanoe, K. Saigo, Y. Chen, K. Tachibana, and M. Hasegawa, *J. Polym. Sci., Polym. Lett. Ed.*, **23**, 617 (1985).

2) K. Saigo, Y. Chen, N. Yonezawa, T. Kanoe, K. Tachibana, and M. Hasegawa, *Macromolecules*, **19**, 1552 (1986).

3) G. D. Fasman, H. Hoving, and S. N. Timasheff, *Biochemistry*, **9**, 3316 (1970).

4) N. Ito and T. Takagi, *Biochem. Biophys. Acta.*, **221**, 430 (1970).

5) C. G. Overberger and D. W. Wang, *J. Polym. Sci., Polym. Chem. Ed.*, **22**, 1153 (1984), and the references cited therein.

6) C. G. Overberger and Y. Shimokawa, *Macromolecules*, **4**, 718 (1971); C. G. Overberger and T. Nishiyama, *J. Polym. Sci., Polym. Chem. Ed.*, **19**, 331 (1981).

7) F. Ciardelli, E. Chiellini, C. Carlini, O. Pieroni, P. Salvadori, and R. Menicagli, *J. Polym. Sci., Polym. Symp.*, **62**, 143 (1978).

8) F. Ciardelli, M. Alietto, C. Carlini, E. Chiellini, and R. Solaro, *Pure Appl. Chem.*, **54**, 521 (1982).

9) K. Saigo, N. Yonezawa, K. Sekimoto, M. Hasegawa, K. Ueno, and H. Nakanishi, *Bull. Chem. Soc. Jpn.*, **58**, 1000 (1985).

10) K. Saigo, K. Sekimoto, N. Yonezawa, F. Ishii, and M. Hasegawa, *Bull. Chem. Soc. Jpn.*, **58**, 1006 (1985).

Stereoelectronic Control in the Hydrolysis of RNA by Imidazole

Kazunari TAIRA*
Department of Chemistry, The Pennsylvania State University,
University Park, PA 16802, U.S.A.
(Received June 23, 1986)

The cleavage of poly(uridylic acid) by imidazole buffer was studied recently by Breslow and Labelle, and a bell-shaped profile was observed for the rate vs. buffer protonation state. The reaction, however, was kinetically first-order in buffer (R. Breslow and M. Labelle, *J. Am. Chem. Soc.*, **108**, 2655 (1986)). The sequential base-acid mechanism proposed by those authors is in agreement with the expectation based on the stereoelectronic effects. In addition, the alternative sequential acid-base mechanism, which could not be excluded on the basis of their kinetic data, may be excluded based on the stereoelectronic considerations.

The hydrolysis of RNA and simpler model compounds has been the subject of much investigation.[1-9] In the hydrolysis of both RNA[1,9] and a simpler phosphate diester, such as methyl 2-hydroxyethyl hydrogenphosphate,[5,6] the mechanistic sequence involves two steps: The formation of a five-membered cyclic phosphate via an intramolecular nucleophilic attack by the vicinal hydroxyl group with concomitant exocyclic cleavage, followed by the hydrolysis of the cyclic diester intermediate. The formation of a 2′,3′-cyclic diester suggests why RNA, which functions as a carrier of genetic information and thus has a high turnover rate, is capable of undergoing rapid degradation. On the other hand, DNA, which serves to store genetic information and from which the requisite 2′-hydroxyl group is absent, is resistant to hydrolysis.

The rate of hydrolysis of five-membered ring cyclic phosphate such as methyl ethylene phosphate (MEP) and ethylene hydrogenphosphate (EP) is 10^6 to 10^8 times faster than that of their acyclic analogues, trimethyl phosphate and dimethyl hydrogenphosphate, respectively. Westheimer and coworkers proposed that this rate acceleration was due to the energy released in going from a strained five-membered cyclic ester to a "strain-free" cyclic phosphorane transition state.[3] However, as pointed out by Gerlt et al.,[10] the amount of ring strain is insufficient to explain the total lowering of activation energy of the five-membered cyclic phosphates. Therefore, Gorenstein et al.[11-14] proposed, based upon molecular orbital calculations on the basic hydrolysis of model phosphate diesters, that a significant fraction of this difference in reactivity between five-membered cyclic phosphates and their acyclic counterparts comes from orbital stereoelectronic effects in the trigonal bipyramid transition state. Gorenstein and coworkers have provided

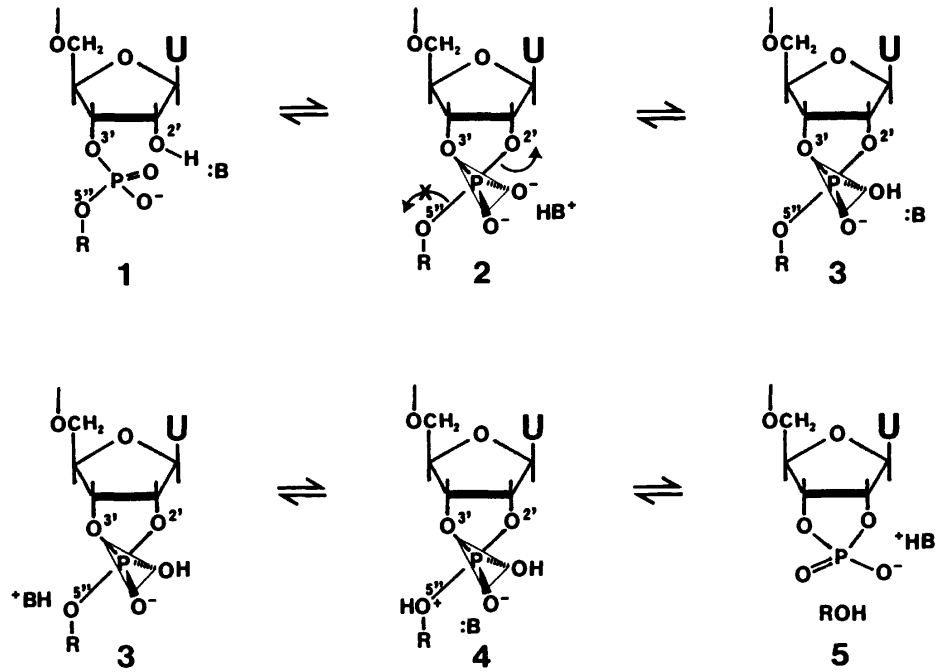

Fig. 1 Breslow and Labelle's mechanism for the hydrolysis of RNA by imidazole.[9] The equatorial positions are indicated by triangle planes.

* Present address: Fermentation Research Institute, Agency of Industrial Science & Technology, Yatabe-machi, Tsukuba Science City, Ibaraki 305.

theoretical justification[11-19] as well as experimental support[20-28] for these stereoelectronic effects.

Breslow and Labelle[9] recently investigated the hydrolysis of poly(uridylic acid) (poly-U) by imidazole buffers and proposed the sequential general base-acid catalysis mechanism, as shown in Fig. 1. In the first step, nucleophilic attack is catalyzed when the imidazole (:B) removes a proton from the 2′-hydroxyl group of **1**. The resulting more nucleophilic oxygen adds to phosphorus, and the temporarily formed imidazolium ion ($^+$BH) puts a proton back onto one of the equatorial phosphorus oxygens of **2** to generate intermediate **3**. In the reversal of this reaction, the same sequence runs backwards: The endocyclic cleavage of the phosphorane intermediate, **3**, occurs by deprotonation of **3** and eventual protonation of the leaving 2′-oxygen. However, in the forward direction, exocyclic cleavage takes place with the loss of 5′-oxygen of the next nucleotide by a process preferentially catalyzed by imidazolium ion ($^+$BH), but not by imidazole (:B). In the case of the imidazolium ion catalysis, a proton is added presumably to the leaving group first followed by proton removal from the phosphorus oxygen so that the final product monoanion, **5**, is formed.[9]

As Breslow and Labelle pointed out,[9] their mechanism is quite curious: The endocyclic cleavage of **3** (backward reaction) is catalyzed by a base (:B), however, the exocyclic cleavage of **3** (forward reaction) is catalyzed by an acid ($^+$HB). Furthermore, due to the well-known kinetic ambiguity, the alternative sequential acid-base mechanism, in which the formation of intermediate **3** is catalyzed by imidazolium ion ($^+$HB) and its forward decomposition is catalyzed by imidazole (:B), cannot be cxcluded on the basis of their kinetic data.

In this paper, we suggest that the mechanism proposed by Breslow and Labelle could be rationalized by the stereoelectronic effect. This explanation not only supports their mechanism, in which an imidazole catalyzes the endocyclic cleavage and an imidazolium ion catalyzes the exocyclic cleavage, but also uniquely excludes the alternative sequential general acid-base mechanism.

Discussion

Stereoelectronic Effects in the Hydrolysis of MEP. The role of orbital orientation in organic and enzymatic reactions has been of considerable interest over the last decade.[11-41] Deslongchamps and coworkers[29] in studying tetracovalent carbon species have demonstrated selective cleavage of bonds which are *trans*-antiperiplanar (app) to lone pairs on directly bonded oxygen and nitrogens. Molecular orbital calculations have provided theoretical justification for these stereoelectronic effects in tetracovalent carbon and phosphorus species and pentacovalent phosphoranes.[11-19,33-38] For example, in the cyclic transition state/intermediate, **8**, which corresponds to Breslow's intermediate, **2**, (the ribose ring portion is omitted) the two lone pairs on the equatorial ring oxygen are oriented partially antiperiplanar (app) to the axial ring ester bond, which corresponds to the phosphorus-(2′-oxygen) bond in **2**.

Thus, the stereoelectronic theory suggests that this app lone pair can significantly facilitate the endocyclic P—O ester bond cleavage. As Deslongchamps argues that a cleavage is stereoelectronically controlled when and only when **two** heteroatoms possess lone pair orbitals app to the departing bond,[29] the exocyclic cleavage (P–OR bond cleavage) can also be stereoelectronically assisted by the lone-pair orbitals on the **two** equatorial anionic oxygens (orbitals not shown in **8**). However, the endocyclic cleavage is still favored over the exocyclic cleavage because the endocyclic breakage is assisted by **all three** equatorial oxygen lone pairs, especially those on the equatorial ring-oxygen. Note that the equatorial ring oxygen lone-pairs (orbitals are shown in Scheme 1) of **8** are app **only** to the apical endocyclic ester bond and **not** to the exocyclic bond. Indeed, as Gorenstein argued earlier, in the five-membered-ring cyclic esters the ring constrained the lone pairs in a stereoelectronically favorable orientation while

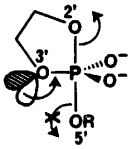

8

Scheme 1.

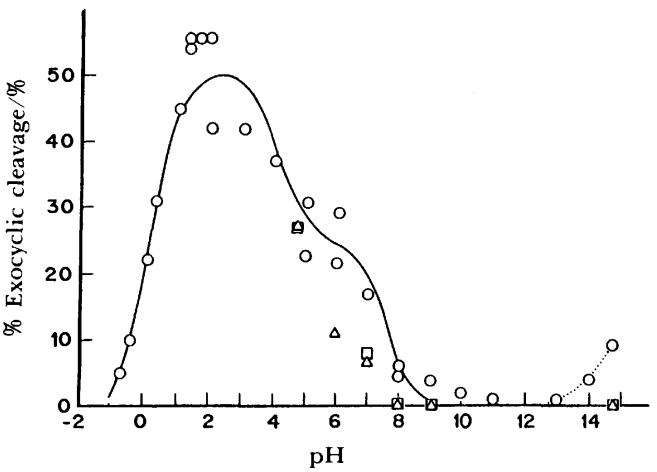

Fig. 2 Percentage exocyclic cleavage of methyl ehylene phosphate (○,△) and ethyl ethylene phosphate (□) vs. pH. Data from Kluger et al.[4] (○) and our own work (△, MEP; □, EEP).[6]

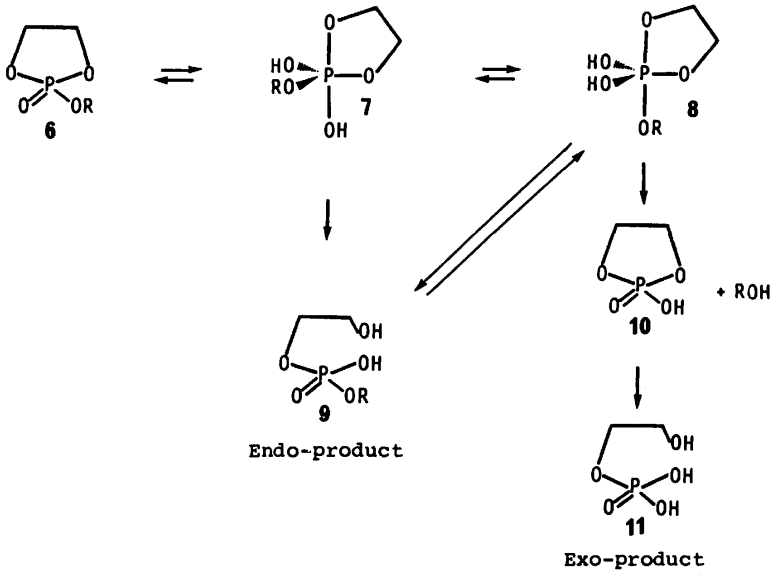

Fig. 3 Reaction paths for the formation of endocyclic and exocyclic cleavage products.

in the acyclic transition state, proper app lone pair overlap would require "freezing" of one or more rotational degrees of freedom about the ester bonds. It is thus significant that a considerable portion of the rate difference between cyclic and acyclic reactions is driven entropically.

However, a major difficulty with the stereoelectronic effect explanation for a portion of the rate acceleration was the observation of significant exocyclic cleavage (Fig. 2) in the hydrolysis of methyl ethylene phosphate (MEP) (Fig. 3).[3,4] As shown in Figures 2 and 3, hydrolysis of **6** (MEP) yielded not only the endocyclic cleavage product **9** but also as much as 1—50% of the exocyclic cleavage product **11**, formed by rapid hydrolysis of the initially formed ethylene hydrogenphosphate (EP), **10**. While the exocyclic cleavage in acid could be reconciled with the "reverse anomeric effect"[30] (see below), the 9 and 15% exocyclic cleavage in 5 and 10 M† alkali, respectively, was at odds with the stereoelectronic effect: Recall that the lone pairs on the ring oxygen are app only to the endocyclic bond (**8** in Scheme 1).

We carried out the hydrolysis of ethyl ethylene phosphate (EEP)[5] as well as MEP[24] at **low** concentration of ester in 5 M NaOH and analyzed the reaction products by phosphorus NMR instead of the earlier proton NMR and GC methodology.[4] We found that, compared with Kluger et al.'s earlier results,[4] there was much less (0±3% vs. the reported 9%) exocyclic cleavage product produced in the hydrolysis of MEP in 5 M NaOH. These results were consistent with the prediction of the stereoelectronic effect. However, recently Kluger and Thatcher[7,8] rechecked Kluger et al.'s earlier results[4] by proton NMR (and to a lesser extent by phosphorus NMR), employing **much higher** concentration of the starting ester. By monitoring the appearance of the methanol peak, they found that at strong alkaline conditions the fraction of "methanol" (which they equate with the exocyclic cleavage product) in fact appeared to increase to as much as 24% exocyclic cleavage in saturated NaOH (18.5 M) and 9.2% in 5.6 M NaOH.

However, Gorenstein et al. now report[41] that, in contrast to the claims of Kluger and Thatcher,[7,8] the increase in exocyclic cleavage product with increasing strong base is shown to arise from an artifactual sidereaction in the base-catalyzed hydrolysis of MEP. The initial product of endocyclic cleavage, methyl 2-hydroxyethyl hydrogenphosphate **9**, reacts with a second molecule of MEP **6**, when the reaction is carried out at **high** concentration of MEP, to yield a reactive "triester dimer" which subsequently releases methanol to yield a relatively stable "diester dimer": note that Kluger and Thatcher equate the amount of "methanol" with the exocyclic cleavage product. Although a small amount of exocyclic cleavage product is observed in strong alkali (<0.5%±1.5% for EEP and 2—4%±1.5% for MEP), these results are still completely consistent with arguments regarding stereoelectronic control in these reactions.[41]

In conclusion, a base-catalyzed hydrolysis of five-membered-ring cyclic phosphates, such as EEP and MEP, preferencially undergoes endocyclic cleavage. It is important to notice that, in Fig. 1, the endocyclic cleavage of **3** (backward reaction) occurs by a prior deprotonation of an equatorial oxygen (base catalysis).

† 1 M=1 mol dm^{-3}.

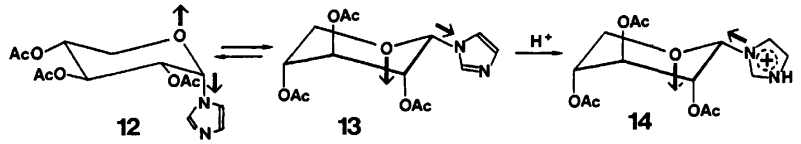

Scheme 2.

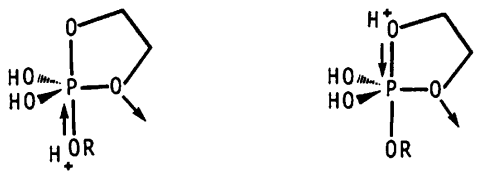

Scheme 3.

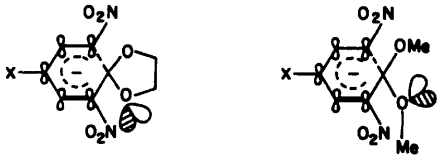

Scheme 5.

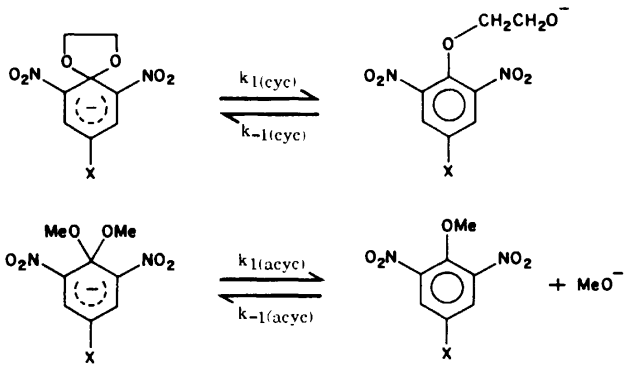

Scheme 4.

The Reverse Anomeric Effect. Electron-withdrawing substituents show a powerful preference for the axial position in 2-substituted tetrahydropyrans (ground state stereoelectronic effect or anomeric effect). However, groups such as *N*-alkylpyridinium appear to show a preference for the equatorial position, and there is evidence to suggest that this preference is stronger than the usual steric preferences found in cyclohexanes.[30] This reversed equatorial preference by protonated or positively charged substituents, which are even stronger electron-withdrawing groups, is called "the reverse anomeric effact." Although, to date, the origin of the reverse anomeric effect is not well understood, dipole moment interaction appears to operate, since the preference of imidazole for the equatorial position (**13**) in the equilibrium (**12**⇄**13**) of Scheme 2 is greater in more polar solvent and, when sufficient trifluoroacetic acid is added to the solvent ($CDCl_3$), only the isomer **14** with the imidazolium group equatorial exists.[30]

In the acid-catalyzed hydrolysis of MEP, the above-mentioned dipole moment arguments suggest that protonation on the exocyclic ester oxygen is favored over the endocyclic oxygen. This would thus favor exocyclic cleavage in acidic media (Scheme 3).

In strong acid, protonation of both exo- and endo-oxygens may be possible, in which case the mode of cleavage is again governed by the stereoelectronic effect (see Fig. 2).

In related systems, Bernasconi and Howard[42] thoroughly investigated the breakdown of spiro cyclic and acyclic Meisenheimer complexes derived from 1-(2-hydroxyethoxy)-2,6-dinitro-4-X-benzenes and 2,6-dinitro-4-X-anisoles, respectively, where X was Cl, CF_3, NO_2, or SO_2CF_3.

They concluded that the difference in intrinsic reactivity between the two families was quite large ($\Delta\Delta G^{\ddagger}=\Delta G^{\ddagger}[k_{1(acyc)}]-\Delta G^{\ddagger}[k_{1(cyc)}]=3.80$ to 5.34 kcal mol^{-1} (1 cal=4.184 J)) and this difference increased as the X substituent became more electron-withdrawing. The most likely cause for the difference in reactivity is of stereoelectronic origin. As described in the above-mentioned endocyclic cleavage of **8**, the orientation of the lone-pair orbitals on oxygen in the spiro cyclic complexes is such as to lead to n–σ^* overlap (app orientation) in the transition state. On the other hand, in the acyclic (1,1-dimethoxy-) complexes the orientation of the lone-pair orbitals does not lead to such overlap unless the complex first undergoes an unfavorable conformational change (Scheme 5).

The fact that $\Delta\Delta G^{\ddagger}$ increases with the electron-withdrawing strength of the X substituent supports this interpretation because the n–σ^* overlap leading to a transfer of electron density from the nonreacting oxygen into the antibonding orbital of the scissile bond becomes more important when a transfer of electron density from the benzene ring (p–σ^* type interaction) is less available because of an electron-withdrawing X group.

More importantly, the study of Bernasconi and Howard[42] further indicates that the difference in intrinsic reactivity is smaller for the acid-catalyzed compared to the noncatalyzed pathway, and this difference diminishes with increasing acidity of the catalyst. For the specific acid-catalyzed pathway the reactivity difference between the two families nearly disappears ($\Delta\Delta G^{\ddagger}$ spans a range ca. 0.09 to 0.2 kcal mol^{-1}). This means that in acidic media one does not observe much of a stereoelectronic effect. This indicates that for the acid-catalyzed lower activation-energy pathway a further lowering of the activation energy by the stereoelectronic effect becomes less important, compared to the noncatalyzed pathway. The breakdown behavior of these Meisenheimer complexes is very similar to that of the hydrolysis of EEP, MEP, and as well as RNA by imidazole: Under basic conditions the cyclic C(P)-O bond breaks (endocyclic cleavage) much faster than the acyclic C(P)-O bond (exocyclic cleavage), however, the exocyclic bond cleavage $k_{1(acyc)}$ starts to compete with the endocyclic bond cleavage $k_{1(cyc)}$ upon an increase in acidity of the medium, as shown by the percentage of exocyclic cleavage in Fig. 2.

Favored Protonation on 5′ Oxygen. If we use the above-mentioned dipole moment analysis in the protonation of the Meisenheimer complexes, it can easily be shown (Scheme 6) that protonation of the acyclic complexes is favored. This interpretation is consistent with Bernasconi and Howard's observation[42] of less negative ρ values and smaller Bronsted α values in the cyclic Meisenheimer complexes, indicating that less positive charge (H^+) has been transferred to the cyclic system than to the acyclic counterpart from the catalyst in the transition state.

The favorable protonation of the acyclic complexes is also consistent with the Hammond Postulate. In case of the breakdown of the cyclic complexes, one might expect an early transition state due to the intrinsically high reactivity of these compounds.[43] Because of the early transition state, the pK_{app} of the departing oxygen for the cyclic complexes would be low, and hence would not be subject to appreciable protonation. The acyclic complexes, on the other hand, would be less reactive than the cyclic counterparts, and in turn would have their transition states further along the reaction coordinate. Because of this later position on the reaction coordinate, one might expect the pK_{app} of the oxygens of the acyclic complexes to be higher than that of the cyclic counterparts and in turn more susceptible to transition state protonation. These predictions would lead to more positive ρ values and larger Bronsted α values in the acyclic families.

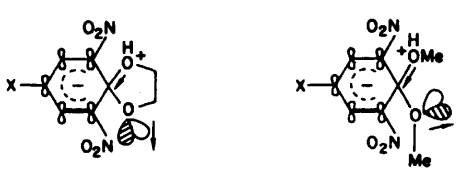

Scheme 6.

Similar argument would support our earlier analysis in that the exocyclic 5′ oxygen, in **3** (Fig. 1) or **8** (Scheme 1), is more susceptible to transition state protonation. In case of the exocyclic cleavage of the strain-free[3] intermediates, **3**, or **8**, one might expect a later transition state due to an increase in ring strain in the transition state in forming the five-membered cyclic diesters, **5** or **10**. The endocyclic cleavage, on the other hand, would not experience any increase in ring stain and therefore would have an earlier transition state, resulting in a less favorable protonation for the endocyclic 2′ oxygen.

Hydrolysis of RNA by Imidazole. The elegant work by Breslow and Labelle[9] has given us insight into a sequential catalytic mechanism for the hydrolysis of RNA by imidazole buffer. As they pointed out, their preferred mechanism (Fig. 1) is quite curious since, for the cleavage of the phosphorus-(2′-oxygen) bond (endocyclic cleavage) in **3**, the basic form of imidazole is utilized, whereas for the cleavage of the phosphorus-(5″-oxygen) bond (exocyclic cleavage) the conjugate acid form of imidazole acts as a catalyst. They pose the question: "*Why is it that loss of the C-5″ oxygen from intermediate* **3** *occurs by a prior protonation of the leaving group oxygen, while loss of the C-2′ oxygen from* **3** *occurs by a prior deprotonation of an oxygen on the phosphorus? If in the alternative slower path the loss of the 5″ oxygen can also occur with imidazole catalysis, and thus with a prior deprotonation, why is it that the prior protonation mechanism is not the best for the loss of C-2′ oxygen? It is hard to see a good reason for this mechanistic distinction* ...."

However, taken together with the observation, in the hydrolysis of MEP, that an endocyclic cleavage is preferred in basic media due to the stereoelectronic effect and an exocyclic cleavage becomes competitive in acidic media because protonation is more favorable on the exocyclic oxygen (the reverse anomeric effect), a similar analysis to the hydrolysis of RNA provides a capability for uniquely supporting the mechanism of Breslow and Labelle. The deprotonation of **3** by imidazole leads to **2**, which is equivalent to **8** in Scheme 1, resulting in stereoelectronically favorable P-(2′-O) bond cleavage. For the forward reaction, protonation is preferred on the exocyclic 5″-oxygen, leading to the loss of 5″ oxygen of the next nucleotide. Apparently, this analysis disfavors the kinetically equivalent alternative mechanism, a sequential general acid-base catalysis, since protonation is never favored on an endocyclic 2′-

oxygen and at the same time the stereoelectronic effect disfavors an exocyclic cleavage.

This mechanism may indeed be significant for the action of Ribonuclease.[9] At the active site of Ribonuclease, the basic imidazole of the enzyme (His-12) acts to remove the proton from the attacking 2′-hydroxyl group which then adds to phosphorus from the opposite side of the leaving 5″-OR group, leading to the in-line mechanism[44-46] intermediate, **2**. In order to shift the equilibrium toward the exocyclic cleavage, via the monoanion intermediate, **3**, the temporarily formed imidazolium ion (His-12) transfers its proton to one of the equatorial oxygens (the equatorial positions are indicated by a triangle plane in Fig. 1). Recall that without this proton transfer, the dianion intermediate, **2**, stereoelectronically favors the decomposition to the starting diester, **1**. The imidazolium ion of the enzyme (His-119) then acts to put a proton on the leaving 5″-oxygen atom, and indeed this is the preferred protonation site, as discussed in terms of the reverse anomeric effect as well as the Hammond Postulate.

It is important to realize that all the reaction steps discussed in the previous paragraph are also the chemically favored lower energy pathways (i.e., in-line over adjacent, endo- over exo-cleavage of the basic form of the intermediate, and 5′- over 2′-protonation). For the first transesterification step, the more electron-withdrawing 2′-oxygen and 5′-OR groups occupy the apical positions, as required by the preference rule,[3] leading to the in-line mechanism. The first stereochemical study of an enzymatic P–O bond cleavage was that of Usher, Eckstein, and their associates on pancreatic ribonuclease A.[44,45] They showed that each of the two P–O bond cleavage steps catalyzed by this enzyme proceeded with inversion of configuration at phosphorus (in-line mechanism). Presently, over thirty stereochemical studies of enzymatic substitution at phosphorus have been carried out.[46] There is as yet no indication of an adjacent mechanism which involves pseudorotatory rearrangements in pentavalent intermediates of enzymatic substitutions at phosphorus. All reactions studied to date are stereospecific, and the available data strongly supports the hypothesis that each enzymatic substitution at phosphorus proceeds by an in-line mechanism with inversion of configuration at phosphorus. Together with the probable involvement of the stereoelectronic and reverse anomeric effects in the action of Ribonuclease, this enzyme appears to take advantage of any energy lowering effects at each reaction steps (in-line over adjacent, endo-over exo-cleavage, 5′- over 2′-protonation, etc.), in accord with the "evolutionary perfection."[47]

In conclusion, as can be seen in Fig. 2, the mode of cleavage of MEP and EEP is pH-dependent: The exo- and endocyclic cleavages are preferred in acidic and basic media, respectively. Similarly, the exo- and endocyclic cleavages of the RNA intermediate, **3**, are catalyzed by the acidic and basic forms of imidazole, respectively. These observations are consistent with the arguments regarding the stereoelectronic effect and the reverse anomeric effect.

There is no way for the author to express his great appreciation to Prof. David G. Gorenstein then at University of Illinois/Chicago and presently at Purdue University and Prof. William L. Mock at University of Illinois/Chicago for their wonderful hospitality and guidance during the author's stay at UIC. Influence by these professors has greatly enhanced the author's interest in the role of orbital interactions in reaction mechanisms. The author wishes to express his appreciation for the support and understanding, in addition to an excellent tutelage, of Prof. Stephen J. Benkovic and Patricia Benkovic at Pennsylvania State University. This article is dedicated to the author's outstanding teachers: Professors S. J. Benkovic at Penn State, D. G. Gorenstein at Purdue, W. L. Mock at Univ. of Illinois, T. Koizumi at Toyama Medical and Pharmaceutical University, J. Sunamoto at Nagasaki University, E. Tsukamoto, A. Hamano, H. Nagasue at Sasebo Technical College, R. Tanaka at Kyushu University, and K. Furukawa at Fermentation Research Institute, Tsukuba. Lastly, the very helpful discussion and comments of the author's colleague, Dr. Robert J. Miller, are much appreciated.

References

1) D. Lipkin, P. T. Talbert, and M. Cohn, *J. Am. Chem. Soc.*, **76**, 2871 (1954).
2) D. M. Brown and N. K. Hamer, *J. Chem. Soc.* **1960**, 406.
3) F. H. Westheimer, *Acc. Chem. Res.*, **1**, 70 (1968).
4) R. Kluger, F. Covitz, E. Dennis, L. D. Williams, and F. H. Westheimer, *J. Am. Chem. Soc.*, **91**, 6066 (1969).
5) D. G. Gorenstein and K. Taira, *J. Am. Chem. Soc.*, **104**, 6130 (1982).
6) K. Taira, T. Fanni, and D. G. Gorenstein, *J. Org. Chem.*, **49**, 4531 (1984).
7) R. Kluger and G. R. Thatcher, *J. Am. Chem. Soc.*, **107**, 6006 (1985).
8) R. Kluger and G. R. Thatcher, *J. Org. Chem.*, **51**, 207 (1986).
9) R. Breslow and M. Labelle, *J. Am. Chem. Soc.*, **108**, 2655 (1986).
10) J. A. Gerlt, F. H. Westheimer, and J. M. Sturtevant, *J. Biol. Chem.*, **250**, 5059 (1975).
11) D. G. Gorenstein, J. B. Findlay, B. A. Luxon, and D. Kar, *J. Am. Chem. Soc.*, **99**, 3473 (1977).
12) D. G. Gorenstein, B. A. Luxon, J. B. Findlay, and R. Momii, *J. Am. Chem. Soc.*, **99**, 4170 (1977).
13) D. G. Gorenstein, B. A. Luxon, and J. B. Findlay, *J. Am. Chem. Soc.*, **99**, 8048 (1977).

14) D. G. Gorenstein, B. A. Luxon, and J. B. Findlay, *J. Am. Chem. Soc.*, **101**, 5869 (1979).
15) D. G. Gorenstein, B. A. Luxon, and E. M. Goldfield, *J. Am. Chem. Soc.*, **102**, 1757 (1980).
16) D. G. Gorenstein and K. Taira, *Biophys. J.*, **46**, 749 (1984).
17) K. Taira and D. G. Gorenstein, *J. Am. Chem. Soc.*, **106**, 7825 (1984).
18) A. Chang, K. Taira, S. Urano, and D. G. Gorenstein, submitted for publication.
19) K. Taira and D. G. Gorenstein, submitted for publication.
20) D. G. Gorenstein and R. Rowell, *J. Am. Chem. Soc.*, **101**, 4925 (1979).
21) D. G. Gorenstein, R. Rowell, and J. B. Findlay, *J. Am. Chem. Soc.*, **102**, 5077 (1980).
22) D. G. Gorenstein, R. Rowell, and K. Taira, "Phosphorus Chemistry," ACS Symposium No. 171, Washington D. C. (1981), p. 69.
23) R. Rowell and D. G. Gorenstein, *J. Am. Chem. Soc.*, **103**, 5894 (1981).
24) K. Taira, T. Fanni, and D. G. Gorenstein, *J. Am. Chem. Soc.*, **106**, 1521 (1984).
25) K. Taira and D. G. Gorenstein, *Tetrahedron*, **40**, 3215 (1984).
26) K. Taira, W. L. Mock, and D. G. Gorenstein, *J. Am. Chem. Soc.*, **106**, 7831 (1984).
27) J-C. Yang and D. G. Gorenstein, *Tetrahedron Lett.*, **25**, 4627 (1984).
28) K. Taira, K. Lai, and D. G. Gorenstein, *Tetrahedron*, **42**, 229 (1986).
29) P. Deslongchamps, "Stereoelectronic Effects in Organic Chemistry," Pergamon Press, Oxford (1983).
30) A. J. Kirby, "The Anomeric Effect and Related Stereoelectronic Effect at Oxygen," Springer-Verlag, Berlin (1983).
31) D. R. Storm and D. E. Koshland Jr., *J. Am. Chem. Soc.*, **94**, 5815 (1972).
32) W. L. Mock, *Bioorg. Chem.*, **4**, 270 (1975).
33) J. M. Lehn and G. Wipff, *J. Chem. Soc., Chem. Commun.*, **1975**, 800.
34) J. M. Lehn and G. Wipff, *J. Am. Chem. Soc.*, **96**, 4048 (1974).
35) J. M. Lehn and G. Wipff, *J. Am. Chem. Soc.*, **98**, 7498 (1976).
36) J. M. Lehn and G. Wipff, *Helv. Chim. Acta*, **61**, 1274 (1978).
37) J. M. Lehn and G. Wipff, *J. Am. Chem. Soc.*, **102**, 1347 (1980).
38) L. Radom, W. L. Hehre, and J. A. Pople, *J. Am. Chem. Soc.*, **94**, 2371 (1972).
39) S. A. Bizzozero and H. Dutler, *Bioorg. Chem.*, **10**, 46 (1981).
40) H. Dugas and C. Penney, "Bioorganic Chemistry. A Chemical Approach to Enzyme Action," Springer-Verlag, New York (1981).
41) D. G. Gorenstein, A. Chang, and J-C. Yang, Tetrahedron, in press (1987).
42) C. F. Bernasconi and K. A. Howard, *J. Am. Chem. Soc.*, **105**, 4690 (1983).
43) W. P. Jencks, "Catalysis in Chemistry and Enzymology," McGraw-Hill, New York (1969).
44) D. A. Usher, E. S. Erenrich, and F. Eckstein, *Proc. Natl. Acad. Sci. U.S.A.*, **69**, 115 (1972).
45) D. A. Usher and D. I. Richardson, Jr., *Nature*, **228**, 663 (1970).
46) P. A. Frey, *Tetrahedron*, **38**, 1541 (1982).
47) W. J. Albery and J. R. Knowles, *Biochemistry*, **15**, 5631 (1976).

Activation of Glassy Carbon Electrodes by Polishing with Ceramics Particles

Makoto AIHARA* and Masahiro KOMATSU†
Faculty of Home Life Science, Fukuoka Women's University,
Kasumigaoka, Higashi-ku, Fukuoka 813
†Government Industrial Research Institute, Kyushu, Tosu 841
(Received December 5, 1986)

Synopsis. Glassy carbon electrode polished with ceramics particles (TiB_2, SiC, and TiC) showed higher oxidation rate of ascorbic acid. The activation seems to depend on hardness of glassy carbon and ceramics particles and to be influenced by fresh edges formed on glassy carbon surface.

Glassy carbon electrode (GCE) has been used for voltammetry and amperometry. Renewal of glassy carbon (GC) is usually perfomed by polishing GC surface with an abrasive such as α-alumina. It was recently shown that an oxide (α-Al_2O_3, CeO_2, ZrO_2, etc.) dispersed on GC surface enhances the rate of electrochemical reaction of ascorbic acid and other compounds.[1-3] A model has been proposed to explain the enhancement. A porous thin layer of carbon embracing metal oxide particles adheres to the surface of base GC.[1-3] The current is enhanced due to additional current from an electroactive species in the porous layer. These studies are, however, limited to the experiments on metal oxides.

In this paper, activity of three types of glassy carbon electrode polished with ceramics particles (titanium boride (TiB_2), silicone carbide (SiC), and titanium carbide (TiC)) was investigated for oxidation of ascorbic acid by cyclic voltammetry.

Experimental

L-Ascorbic acid (Wako Pure Chem. Co.) was used without further purification. α-Al_2O_3 was obtained from Buehler Co. (Chicago), TiB_2 (particle size: 2 μm, hardness: 3200—3400 kg mm^{-2}) from Hermann C. Starck Co., SiC (particle size: 2 μm, hardness: 2700 kg mm^{-2}) from Fujimi Kenmazai Kogyo Co., and TiC (particle size: 2 μm, hardness: unknown[4]) from Japan New Metals Co. The supporting electrolyte was 0.1 M (1 M=1 mol dm^{-3}) phosphate buffer at pH 2.0. Twice distilled water was used throughout the experiments. Other chemicals used are of reagent grade.

Three types of GC (GC-10, GC-20, and GC-30, Tokai Carbon Co.) with a geometric area of 0.071 cm^2 were used. Each GC was polished succesively with α-Al_2O_3 of 1.0, 0.3, and 0.05 μm in diameter as a slurry with water, until a mirrorlike surface was obtained. After polishing, the electrode was washed with water for 15 min in an ultrasonic field. The each electrode was repolished with an aqueous slurry of an abrasive (TiB_2, SiC, or TiC) for 30 s on a polishing pad (Yanaco) under pressure and rinsed with water. The electrode was electrochemically examined immediately. GCE was deactivated by a polishing cloth.[5]

A Yanaco model VMA-010 cyclic voltammetric analyzer was employed for cyclic voltammetric measurements. The reference and counter electrodes were Ag/AgCl (Yanaco, MR-P3) and a Pt wire, respectively. The differential capacitance of GCE was evaluated from a.c. measurements with a Fuso phase sensitive amplifier.

Electrodes activated by polishing with the abrasives were immersed into a solution of 1×10^{-3} M ascorbic acid in 0.1 M phosphate buffer solution at pH 2.0 and cyclic voltammograms were recorded to examine the activity of GCE at a scan rate of 100 mV s^{-1}.

Table 1. Electrochemical Data for Ascorbic Acid Oxidation

GC	Abrasive	Size μm	E_{pa} V. vs. Ag/AgCl	$E_{pa/2}$ V. vs. Ag/AgCl	i_{pa}^*/i_{pd}
GC-10	TiC	2	0.257	0.190	0.90
	SiC	2	0.233	0.166	1.21
	TiB_2	2	0.216	0.159	1.40
	α-Al_2O_3	0.05	0.209	0.171	1.27
		0.3	0.205	0.160	1.40
		1.0	0.205	0.163	1.52
GC-20	TiC	2	0.185	0.155	1.87
	SiC	2	0.175	0.141	2.44
	TiB_2	2	0.171	0.139	2.50
	α-Al_2O_3	0.05	0.190	0.158	1.72
		0.3	0.176	0.144	2.07
		1.0	0.169	0.135	3.13
GC-30	TiC	2	0.181	0.155	2.02
	SiC	2	0.171	0.139	3.22
	TiB_2	2	0.171	0.139	3.80
	α-Al_2O_3	0.05	0.181	0.151	1.89
		0.3	0.179	0.141	2.43
		1.0	0.170	0.139	3.58

* i_{pa} is peak current value measured at about 10 s after polishing.

Results and Discussion

By preliminary experiments using GCE activated with α-Al_2O_3 (1.0, 0.3, and 0.05 μm in diameter) it was revealed that the enhancement of oxidation of ascorbic acid depends on the particle size of α-Al_2O_3 as shown in Table 1. In this study, GCE surface was activated by polishing it with ceramic particles(TiB_2, SiC, and TiC) with a same particle size of 2 μm.

Typical cyclic voltammograms of ascorbic acid solution in phosphate buffer are shown in Fig. 1. No cathodic wave was observed for deactivated and activated GCE. A broad oxidation wave was obtained at the deactivated GCE. The avarage of 20 peak potential (E_{pd}) values at deactivated GCE was 0.476 V vs. Ag/AgCl. Peak current (i_{pa}) was enhanced and peak potential (E_{pa}) shifted to a less positive potential by polishing GCE with seramics particles. Similar voltammetric behavior was observed at GCE activated with each of the ceramics. The results for oxidation of ascorbic acid are summarized in Table 1, indicating that the activation of ascorbic acid occurs at GCE activated with the ceramics particles. The presence of metal oxide particles dispersed on GC surface will not necessary for activation of ascorbic acid. The order of activation is TiB_2>SiC>TiC at the same type of GCE. TiB_2 is assumed to have the highest hardness in three abrasives examined. The results indicate that the activation depends on the hardness of ceramics particles at a constant particle size.

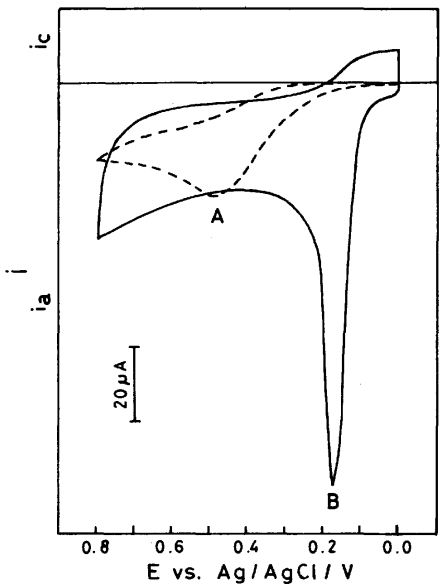

Fig. 1. Cyclic voltammograms of 1×10^{-3} M ascorbic acid at pH 2.0 at GC-30 GCE. Scan rate 0.1 V s^{-1}. (A): Deactivated by final polishing on a polishing cloth. (B): Activated by polishing with TiB_2.

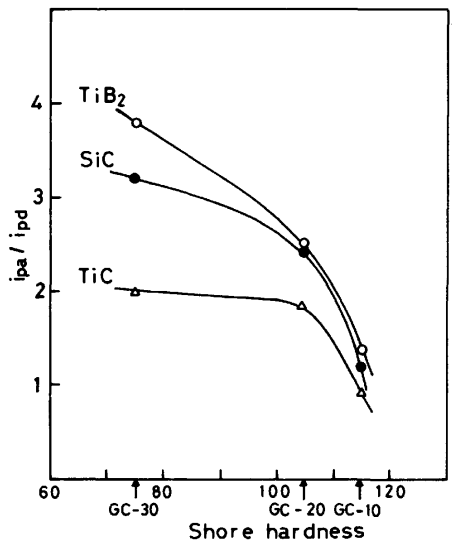

Fig. 2. Plots of the ratio of i_{pa} to i_{pd} versus the average Shore hardness of GC.

Figure 2 shows the relationship between the ratio of peak current at activated GCE(i_{pa}) to peak current at deactivated GCE (i_{pd}) and the average Shore hardness of GC. The order of oxidation activation for three types of GCE is GC-30>GC-20>GC-10. GC-30 GCE which has the lowest hardness shows the most enhanced oxidation of ascorbic acid. These results suggest that active edges are formed on carbon surface of GCE(GC-30) polished with TiB_2.

On the other hand, the differential capacitance at peak potential for deactivated GCE(GC-30) in ascorbic acid solution was 62 μF cm^{-2}. The values for GCE(GC-30) polished with TiB_2, SiC, and TiC were 570, 554, and 463 μF cm^{-2}, respectively. These values are seven to nine times greater than that for deactivated GCE and similar to that for edge orientation of pyrolytic graphite.[6] It is likely that ascorbic acid is adsorbed on fresh carbon edges. The activation of ascorbic acid oxidation will be ascribed to fresh carbon edges formed on GCE surface.

The authors wish to thank Dr. Minoru Nakamizo of Government Industrial Research Institute, Kyushu for valuable discussion. We also would like to thank Professor Eiichi Sekido and Assistant Professor Yoshitaka Masuda of Kobe University for double layer experiments. One of the authors(M. A.) was supported by a grant from Fukuoka Prefecture.

References

1) J. Zak and T. Kuwana, *J. Am. Chem. Soc.*, **104**, 5514 (1982).

2) J. Zak and T. Kuwana, *J. Electroanal. Chem.*, **150**, 645 (1983).

3) S. Dong and T. Kuwana, *J. Electrochem. Soc.*, **131**, 813 (1984).

4) The hardness of TiC is assumed to be slightly lower than that of SiC. "Handbook of Chemistry and Physics," ed by R. C. Weast, CRC Press, Cleveland (1977), p. F-24.

5) D. H. Karweik, I-F Hu, S. Weng, and T. Kuwana, in "Catalyst Characterization Science," ed by M. L. Deviney and J. L. Gland, ACS Symposium series No. 288, Amer. Chem. Soc, Washington, D. C., (1985) Chap. 48, 582.

6) J. P. Randin, "Enccyclopedia of Electrochemistry of The Elements," ed by A. J. Bard, Marcel Dekker, New York (1976), Vol. 7, pp. 12—41.

The Magnetic Properties of the Ammonium Chloride Adducts of Copper(II) Fluoroacetate and Copper(II) Bromoacetate

Shuji EMORI,* Nobuhide MORISHITA, and Yoneichiro MUTO
Department of Chemistry, Faculty of Science and Egineering, Saga University, Honjo-machi, Saga 840
(Received November 11, 1986)

Synopsis. Compounds of formula $Cu(XCH_2COO)_2 \cdot nACl$ (A=NH_4, CH_3NH_3, $(CH_3)_2NH_2$, $(CH_3)_4N$ and X=F, Br) have been prepared, and characterized by magnetic susceptibility and IR spectroscopy measurements. Factors affecting the magnetic moments of copper(II) salts of monosubstituted alkanoic acids are discussed.

Most copper(II) carboxylates have the familiar bridged copper(II) acetate monohydrate structure,[1,2] and their magnetic properties have been studied extensively to elucidate the factors which determine the magnitude of spin-exchange coupling between copper(II) ions.

According to the Edwards equation with 'hard' base and 'borderline' acid,[3] their stability constants depend primarily to the basicities of the carboxylato ligands. Therefore it seems likely that their magnetic properties relate to the acidities of their parent acids. Actually, in some series of dinuclear copper(II) carboxylates,[4-9] the magnetic moment tends to increase as the pK_a value of the parent acid decreases. This empirical relationship has been explained in terms of the inductive effect of the carboxylato substituents, and is supported by molecular orbital analyses.[10,11]

However, there exist a few exceptions; e.g., the room temperature-magnetic moments of copper(II) haloacetate hydrates[4] vary from 1.32 BM for fluoroacetate to 1.43, 1.54, and 1.49 BM for chloro-, bromo-, and iodoacetates, whereas the pK_a values of the parent acids are 2.66, 2.86, 2.90, and 3.17, respectively. Since the magnitude of the spin-exchange coupling in these hydrates may be affected by other factors, such as the intermolecular hydrogen bonds between the water molecules in the axial positions and the oxygen atoms of the carboxylato groups,[1,2] it is preferable to accumulate the magnetic data and to examine the general tendency for the compounds with the same axial ligands. We have prepared various ammonium chloride adducts of copper(II) fluoroacetate and copper(II) bromoacetate, and compared their magnetic data with those of other dinuclear copper(II) salts of monosubstituted alkanoic acids with chloride ions in the axial positions.

Compounds with a stoichiometry of $Cu(XCH_2COO)_2 \cdot nACl$, where X=F or Br and A=$NH_4$, CH_3NH_3, $(CH_3)_2NH_2$, or $(CH_3)_4N$, were prepared by a previously described method for the corresponding chloroacetates.[8] These compounds were obtained as green crystals.

The effective magnetic moments of these compounds (Table 1) were evaluated from the room-temperature magnetic susceptibilities, corrected for the diamagnetic contribution of the constituent atoms using Pascal constants[12] with a value of $N\alpha=60\times10^{-6}$ emu mol^{-1} (1 emu=$4\pi\times10^{-6}$ m^3).

For the methylammonium chloride adducts of copper(II) fluoroacetate and copper(II) bromoacetate, the temperature dependence of their magnetic susceptibilities was measured in the temperature range of 80—300 K to confirm their dinuclear structures. The results agreed well with the Bleaney-Bowers equation,[13] using the following parameters: $g=2.17$ and $2J=-359$ cm^{-1} for the fluoroacetate and $g=2.19$ and $2J=-300$ cm^{-1} for the bromoacetate, respectively. The IR spectra of the solid compounds show the characteristic bands in the ranges 1450—1460 and 1625—1660 cm^{-1} connected with symmetric and unsymmetric COO stretching vibrations of the carboxyl groups.[14]

Table 1. Analytical Data and Effective Magnetic Moments at 20 °C

Compound	Found (Calcd)/%					μ_{eff}/BM
	Cu	Cl	C	H	N	
$Cu(BrCH_2COO)_2 \cdot 3/2NH_4Cl$	15.07 (15.14)	12.33 (12.67)	11.45 (11.45)	2.46 (2.40)	5.01 (5.01)	1.40
$Cu(BrCH_2COO)_2 \cdot CH_3NH_3Cl$	15.80 (15.62)	8.85 (8.71)	14.84 (14.76)	2.53 (2.48)	3.26 (3.44)	1.41
$Cu(BrCH_2COO)_2 \cdot (CH_3)_2NH_2Cl$	15.02 (15.10)	8.33 (8.42)	17.09 (17.12)	2.81 (2.87)	3.09 (3.33)	1.43
$Cu(FCH_2COO)_2 \cdot 2NH_4Cl$	19.59 (19.58)	21.77 (21.84)	14.77 (14.80)	3.67 (3.73)	8.44 (8.63)	1.29
$Cu(FCH_2COO)_2 \cdot CH_3NH_3Cl$	21.59 (22.29)	12.34 (12.42)	20.77 (21.06)	3.65 (3.53)	4.95 (4.91)	1.27
$Cu(FCH_2COO)_2 \cdot (CH_3)_2NH_2Cl$	20.90 (21.24)	12.42 (11.85)	23.88 (24.09)	3.96 (4.04)	4.59 (4.68)	1.26
$Cu(FCH_2COO)_2 \cdot (CH_3)_4NCl$	19.88 (19.42)	10.81 (10.83)	29.09 (29.37)	4.92 (4.93)	4.18 (4.28)	1.28

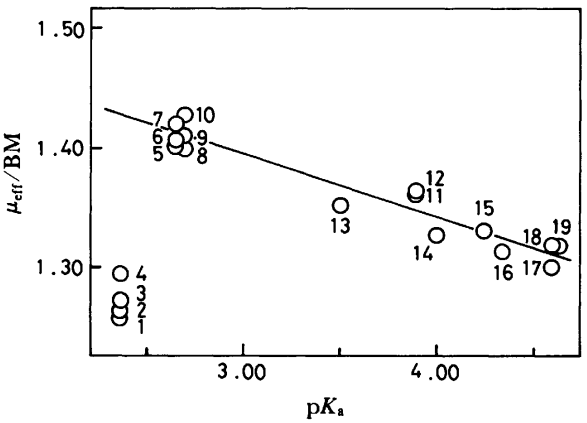

Fig. 1. The magnetic monent at 20 °C plotted against the pK_a value of the parent carboxylic acid for the copper(II) salts of monosubstituted alkanoic acids with chloride ions in the axial positions; the fluoroacetates (**1**—**4**), the chloroacetates (**5**—**7**),[8] the bromoacetates (**8**—**10**), the 3-chloropropionates (**11**, **12**),[15] the ω-ammonioalkanoates (**13**—**16**),[9] the butyrates (**17**, **18**),[15] and the propionate (**19**).[15]

The magnetic and IR spectral data indicate that the present compounds have the bridged dinuclear structure similar to copper(II) acetate monohydrate.[1,2]

In order to examine the correlation between the room-temperature magnetic moment of dinuclear copper(II) carboxyate and the pK_a value of its parent acid, the data for the present compounds, together with those of other dinuclear copper(II) salts of monosubstituted alkanoic acids with chloride ions in the axial positions, are plotted in Fig. 1. The magnetic moments of the chloroacetates[8] were corrected for the difference of room temperature by use of the Bleaney-Bowers equation[13] with g=2.15. As can be seen from Fig. 1, the magnetic moments of the fluoroacetates are much smaller than those expected from the pK_a value of fluoroacetic acid. However, except for fluoroacetates, there is a linear relation between these magnetic moments and the pK_a values of the parent acids in the range of those measurements. The best line has a slope of −0.052 BM and the intercept of 1.31$_8$ BM at pK_a=4.56 (the pK_a value of acetic acid). The variation of single-triplet separation values (e.g.,$-2J$=278, 300, and 320 cm^{-1} for the dimethylammonium chloride adduct of copper(II) chloroacetate,[8] the methylammonium chloride adduct of copper(II) bromoacetate, and the copper(II) chloride compound with 4-aminobutyric acid,[9] respectively) is consistent with this general trend, and agrees well with the molecular orbital analyses.[10,11]

It is still unclear why the magnetic data for the fluoroacetates deviate from the general trend. Porter and Doedens have pointed out that there is an apparent relationship between the singlet-triplet separation values and the group polarizabilities of the carboxlato substituents.[16] However the ordering for the above-mentioned $-2J$ values is contrary to the proposal that lower $-2J$ values are associated with increasing group polarizabilities. From the study of ^{19}F NMR in the series of fluorochloromethanes,[17] it is known that the fluorine nuclei are shielded in the opposite manner from that predicted by electronegativity considerations. In order to explain these anomalous chemical shifts, Gutowsky and Hoffman have suggested the use of higher energy orbitals in the hybridized orbitals of atoms attached to fluorine atoms.[18] This idea may explain the small magnetic moment observed for the present fluoroacetates, because the higher energy orbitals interact more strongly with the electronic system of neighboring carboxylato group, through which spin-exchange coupling between copper(II) ions operates. However, the elucidation of cause and mechanism depends upon future multilateral studies.

References

1) J. N. van Niekerk and F. R. L. Schoening, *Acta Crystallogr.*, **6**, 227 (1953).
2) G. M. Brown and R. Chidambaram, *Acta Crystallogr.*, **B29**, 2393 (1973).
3) J. O. Edwards and R. G. Pearson, *J. Am. Chem. Soc.*, **84**, 16 (1961).
4) M. Melnik, *Coord. Chem. Rev.*, **36**, 1 (1981).
5) R. W. Jotham, S. F. A. Kettle, and J. A. Marks, *J. Chem. Soc., Dalton Trans.*, **1972**, 428.
6) D. Hibdon and J. H. Nelson, *Inorg. Chim. Acta*, **7**, 629 (1973).
7) Y. Muto, T. Tokii, K. Chijiwa, and M. Kato, *Bull. Chem. Soc. Jpn.*, **57**, 1008 (1984).
8) S. Emori, N. Haramaki, and Y. Muto, *Bull. Chem. Soc. Jpn.*, **58**, 761 (1985).
9) S. Emori, T. Noguchi, and Y. Muto, *Bull. Chem. Soc. Jpn.*, **58**, 2733 (1985).
10) P. J. Hay, J. C. Thibeaul, and R. Hoffmann, *J. Am. Chem. Soc.*, **97** 4884 (1975).
11) P. de Loth, P. Cassoux, J. P. Daudey, and J. P. Malriew, *J. Am. Chem. Soc.*, **103**, 4007 (1981).
12) G. Foex, "Constants Sélectionées, Diamagnétisme et Paramagnétisme," Masson, Paris (1957).
13) J. Lewis, Y. C. Lin, L. K. Royston, and R. C. Thomson, *J. Chem. Soc.*, **1965**, 428.
14) S. Yamada, H. R. Nakamura, and R. Tsuchida, *Bull. Chem. Soc. Jpn.*, **31**, 303 (1958).
15) S. Emori and Y. Muto, unpublished data. The magnetic moments of $Cu(ClCH_2CH_2COO)_2 \cdot CH_3NH_3Cl$, $Cu(ClCH_2CH_2COO)_2 \cdot C_4H_9NH_3Cl$, $Cu(CH_3CH_2CH_2COO)_2 \cdot 2(CH_3)_2NH_2Cl$, $Cu(CH_3CH_2CH_2COO)_2 \cdot CH_3NH_3Cl \cdot H_2O$, and $Cu(CH_3CH_2COO)_2 \cdot (CH_3)_2NH_2Cl \cdot H_2O$ are 1.38, 1.37, 1.30, 1.32, 1.32 BM, respectively, at 20 °C.
16) L. C. Porter and R. J. Doedens, *Inorg. Chem.*, **23**, 997 (1984).
17) L. H. Meyer and H. S. Gutowsky, *J. Phys. Chem.*, **57**, 481 (1953).
18) H. S. Gutowsky and C. J. Hoffman, *J. Chem. Phys.*, **19**, 1259 (1951).

Structure of Protonated Products of Potassium 1-(Dimethylamino)naphthylide

Akira Oku* and Yukio Homoto
Department of Chemistry, Kyoto Institute of Technology, Matsugasaki, Sakyo-ku, Kyoto 606
(Received December 8, 1986)

Synopsis. Potassium 1-(dimethylamino)naphthylide (K^+DMAN^-) was protonated by aqueous THF and the structures of protonated products (overall yield of three isomeric products was almost quantitative) were analyzed by ^1H NMR and their 2D-NOE correlation. Products were 1-(dimethylamino)-5,8-dihydronaphthalene (major product, 88%), 7,8-dihydro- (9%), and 5,6-dihydro-isomer (3%). Deducing from the structures, the protonation pathway as well as the spin distribution in K^+DMAN^- is discussed.

Potassium 1-(dimethylamino)naphthylide radical anion (abbreviated as K^+DMAN^-) has recently been appearing in literatures as a useful reductant instead of parent naphthylide[1,2] because of the ease with which DMAN and its derivatives can be removed from the reaction mixture by the workup with aqueous acid, and which enables easy product analysis as well as the accomplishment of synthetic purposes. Although $DMAN^-$ can be used in diverse ways,[3-6] it seemed strange to us that the structure of the most common workup products from $DMAN^-$, i.e., dihydro-DMAN (abbreviated as DMAN-H_2), has not yet been elucidated. Since $DMAN^-$ is an unsymmetrically substituted naphthalene radical anion, the structural analysis of its protonated products will also afford information for the spin distribution in this radical anion. We report here the structural elucidation of protonated products of $DMAN^-$.

When a THF solution of K^+DMAN^-, prepared from potassium metal and DMAN in THF under a nitrogen atmosphere (60% of the initially charged DMAN was active), was treated at −70 °C with aqueous THF, a mixture of isomeric 1-(dimethylamino)dihydronaphthalenes (DMAN-H_2) was obtained besides DMAN. The most likely protonation mechanism is:[7]

$$[DMAN^-] + H_2O \longrightarrow [DMAN\text{-}H_1]^\cdot + OH^- \quad (1)$$

$$[DMAN\text{-}H_1]^\cdot + [DMAN^-] \longrightarrow [DMAN\text{-}H_1]^- + DMAN \quad (2)$$

$$[DMAN\text{-}H_1]^- + H_2O \longrightarrow DMAN\text{-}H_2 + OH^- \quad (3)$$

$$2[K^+DMAN^-] + 2H_2O \longrightarrow 2DMAN + 2KOH + H_2. \quad (4)$$

According to Eqs. 1—3, one mol each of DMAN and DMAN-H_2 should be produced from two moles of $DMAN^-$. In fact, the protonation mixture was analyzed by VPC to be consisting of DMAN (retention time, t_r=23.74 min) and three other products **1** (t_r=22.87 min), **2** and **3** (t_r=21.27 min) in the ratio DMAN/**1**/**2**/**3**=67/29/3/1.[8] Taking into account that the titrated concentration of active K^+DMAN^- before protonation was 60% based on the initially charged DMAN, the calculated (theoretical) product distribution based upon this correction should be DMAN/DMAN-H_2=70/30,[9] which agrees well with the observed distribution DMAN/(**1**+**2**+**3**)=67/33. Consequently, it is concluded that active K^+DMAN^- was transformed almost quantitatively into dihydronaphthalenes **1**, **2**, and **3** (corrected yields: **1**=88%, **2**=9%, **3**=3%). The participation of a reduction process (Eq. 4)[10] which may partially account for the production of DMAN is thus negligible.

Product **1** and a mixture of **2** and **3** were separated and purified by column as well as by VPC. The mass spectral analysis of both **1** and the mixture of **2** and **3** showed M^+ (m/z)=173 which agrees with DMAN-H_2. The ^1H NMR spectra of these products showed the same proton ratio of *N*-methyl/Ar-H/(aliphatic+olefinic)=6/3/6, indicating that the protonation took place mainly on the unsubstituted ring. Three structures which agree with the above observations are shown below.

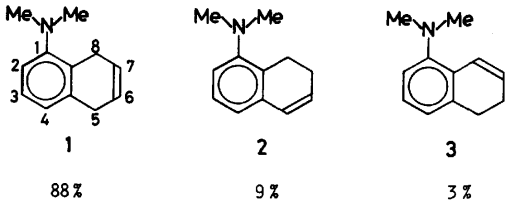

1 88% **2** 9% **3** 3%

The structure of the major product was determined to be **1** by its ^1H NMR spectrum: Two sets of methylene protons with roughly the same chemical shift are appearing at δ 3.26 as doublets, and two olefinic protons at δ 5.93 as a doublet.

Structural determination of **2** and **3** was somewhat complicated because their separation was possible only by the use of a capillary column (OV-101 30 m, ΔR_f=0.03, isomer ratio=3/1) and their ^1H NMR spectra are almost identical: *N*-Methyl protons are appearing as two singlets at δ 2.61 and 2.65 (ratio 1:3), and β-methylene protons between 2.16—2.33, benzylic α-methylene protons at δ 2.68 (partially overlapping *N*-methyls), β-olefinic methines at δ 6.0, α-olefinic methines at δ 7.0 (overlapping aromatic protons, identified by the irradiation at δ 6.06).

To determine which isomer predominates in the mixture of **2** and **3**, a two-dimensional Nuclear Overhauser Effect (2D-NOE) correlation diagram was taken.[11] The expected NOE between *N*-methyl (δ 2.65) and α-methylene protons (δ 2.68) of **2** was indecipherable due to the mutual overlapping of their signals. However, an appreciable correlation between *N*-methyl (δ 2.65) and β-methylene protons (δ 2.20) was observed. By a molecular model analysis it is shown that protons of *N*-methyls and 7-methylene group of **2** stay within the interproton distance of 2.4—2.6 Å, whereas those of *N*-methyls and 6-

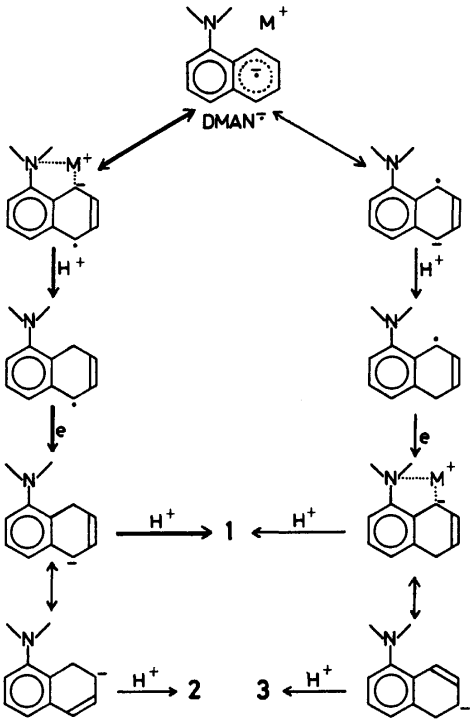

Scheme 1.

methylene group of **3** stay more apart. This observation supports at least the presence of isomer **2**. In addition, the anticipated strong correlation between methyls (δ 2.61) and 8-methine proton (δ 7.0) of **3** appeared only weakly. Although 2D-NOE measurements are generally considered not so reliable for quantitative analysis, yet the above results reasonably lead us to conclude that isomer **2** predominates over the other isomer **3** (isomer ratio **2**/**3**=3 by VPC).

Structures and the product distribution both provide information for solving the major channel of the protonation mechanism (Scheme 1). First of all, the protonation takes place exclusively on the unsubstituted ring of $DMAN^-$. This may be due to the spin distribution which is greatly shifted toward the unsubstituted half of the molecule. Second, the peri-position spatially adjacent to the dimethylamino group in $DMAN^-$ is predominantly protonated. This selectivity can be explained in terms of both the stability of benzylic carbanion intermediates and the coordination effect between the alkali metal cation and the nitrogen atom.

Experimental

General. 1-(Dimethylamino)naphthalene (DMAN) was commercially available and was purified by distillation before use. ^1H NMR spectra and homonuclear NOE correlated 2D-NMR were taken on Varian XL 200 spectrometer equipped with a 2D-NOE program. Mass spectra were taken on Hitachi M-80A spectrometer. For the VPC analysis Shimazu GC-9A was used.

Preparation and Determination of K^+DMAN^-. A THF solution of K^+DMAN^- was prepared under a nitrogen atmosphere by mixing 2.0 g (0.05 gram atom) of potassium metal and 8.6 g (0.05 mol) of DMAN in 100 mL of THF at 0 °C. The concentration of active radical anion was determined to be 0.30 dm^{-3} according to the titration method reported previously.[12]

Reaction and Workup Procedures. The radical anion solution prepared above was cooled to 0 °C, to which was slowly added dropwise a 5:1 mixture (20 cm^3) of THF and water. The reaction mixture was warmed up to 20 °C and was extracted with diethyl ether. After drying over anhydrous Na_2SO_4 and concentrating the ethereal solution, the product mixture was analyzed by VPC (packed column Apiezon Grease-L 2 m; fused silica capillary column OV-101 0.5 mm×30 m). Results are described in the main text.

^1H NMR Spectra of 1-(Dimethylamino)-5,8-dihydronaphthalene (5,8-Dihydro-DMAN, 1). δ=2.67 (6H, s, 2Me); 3.26 (4H, d, CH_2, $J(5,6)=J(8,7)=1.0$ Hz); 5.93 (2H, bs, -CH=, $J(6,5)=J(7,8)=1.0$ Hz); 6.85 (1H, dd, ArH(4), $J(4,3)=7.6$, $J(4,2)=1.0$ Hz); 6.95 (1H, dd, ArH(2), $J(2,3)=7.6$, $J(2,4)=1.0$ Hz); 7.14 (1H, t, ArH(3), $J(3,2)=J(3,4)=7.6$ Hz). Mass spectrum M^+ (m/z)=173. Anal. Calcd for $C_{12}H_{15}N$: C, 83.19; H, 8.73; N, 8.08%. Found: C, 83.03; H, 8.98; N, 7.87%.

^1H NMR Spectra of a Mixture of 7,8-Dihydro-DMAN (2) and 5,6-Dihydro-DMAN (3). δ=2.20 (2H, m, 7-CH_2 of **2** and 6-CH_2 of **3**, $J(7,8)=8.0$ Hz); 2.61 (s, Me's of **3**) and 2.65 (s, Me's of **2**), total integration of 2.61 plus 2.65 is equivalent to 6H; 2.68 (2H, bt, 8-CH_2 of **2** and 5-CH_2 of **3**, $J(8,7)$ of **2**=$J(5,6)$ of **3**=8.0 Hz); 6.00 (1H, dt, 6-CH= of **2** and 7-CH= of **3**, $J(6,7)$ of **2**=$J(7,6)$ of **3**=4.4 Hz, $J(6,5)$ of **2**=$J(7,8)$ of **3**=10.0 Hz); 6.74 (1H, d, 5-CH= of **2**, $J(5,6)$ of **2**=10.0 Hz); 6.73 (1H, d, ArH(4) of **2** and **3**, $J(4,3)$ of **2** and **3**=7.6 Hz); 6.81 (1H, d, ArH(2) of **2** and **3**, $J(2,3)=7.6$ Hz); 7.00 (1H, t, ArH(3) of **2** and **3**, $J(3,4)=J(3,2)=7.6$ Hz); 8-CH= of **3** may be hidden near 7.0. Mass spectrum M^+ (m/z)=173. Anal. Found: C, 83.07; H, 9.05; N, 7.78%.

Authors are grateful for the support of this research to the Grant-in-Aid for Environmental Science from the Ministry of Education and Culture (No. 61035037).

References

1) Reviews on naphthalene radical anion: a) B. J. McClelland, *Chem. Rev.*, **64**, 301 (1964); b) N. J. Holy, *Chem. Rev.*, **74**, 243 (1974).

2) For examples, a) A. Oku, H. Tsuji, N. Yoshiura and M. Yoshida, *J. Am. Chem. Soc.*, **103**, 1244 (1981); b) A. Oku and K. Yagi, *ibid.*, **96**, 1966 (1974).

3) S. Bank and M. Platz, *Tetrahedron Lett.*, **1973**, 2097.

4) T. Cohen and J. P. Sherbine, *J. Am. Chem. Soc.*, **106**, 3245 (1984).

5) A. Oku and N. Yoshiura, *J. Org. Chem.*, **48**, 617 (1983).

6) C. G. Screttas and M. M. Screttas, *J. Org. Chem.*, **43**, 1046 (1978).

7) J. F. Garst, *Acc. Chem. Res.*, **4**, 400 (1971).

8) No more volatile component was detected in the mixture and the total weight of products did not decrease appreciably after a column chromatography.

9) The ratio corresponds to [(100-60)+1/2(60)]/[1/2(60)].

10) G. R. Stevenson, J. Valentin, C. Meverden, L. Echegoyen, and R. Maldonado, *J. Am. Chem. Soc.*, **100**, 353 (1978).

11) Varian XL-200 NMR spectrometer equipped with a 2D-NOE program was used. A supplementary material for the NOE correlated 2D-^1H NMR spectra of the mixture (**2**+**3**) is available.

12) A. Oku, K. Harada, T. Yagi, and Y. Shirahase, *J. Am. Chem. Soc.*, **105**, 4400 (1983).

Chemical Studies on the Lichen. I. The Structure of Isolecanoric Acid, a New *ortho*-Depside Isolated from *Parmelia tinctorum* Despr.

Atsushi SAKURAI* and Yohko GOTO
Department of Chemistry, Faculty of Science, Shizuoka University, Ohya, Shizuoka 422
(Received December 15, 1986)

Synopsis. A new *ortho*-depside, isolecanoric acid was isolated from *Parmelia tinctorum* Despr. and 2-(2,4-dihydroxy-6-methylbenzoyloxy)-4-hydroxy-6-methylbenzoic acid was assigned to this substance from studies on the hydrolysis products and from analyses of the ^1H and ^{13}C NMR spectra. This substance is the first *ortho*-depside isolated from the genus Lichen.

Lichens produce many unusual secondary metabolites ("lichen substance") hardly found in other plants.[1] The major phenolic substances, among them are divided into classes of *meta*-depside, *para*-depside, depsidone, etc, but *ortho*-depside has not been isolated. From a lichen, *Parmelia tinctorum* Despr. (Umenoki-goke in Japanese) *para*-depsides, atranolin and lecanoric acid have been isolated.[2]

In our studies on the constituents of *Parmelicaeae* we found the presence of a new depside in *P. tinctorum* Despr. besides them and named it isolecanoric acid (**1**). In this paper we wish to report the isolation and structure of **1**.

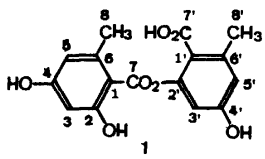

1

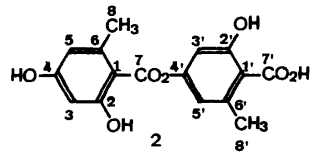

2 8'

The lichen which occurred on stone walls was collected and extracted with acetone followed by reextraction with methanol. The later extract was subjected to chromatography on a column of Sephadex LH-20 eluting with methanol. The last effluent gave **1** as colorless powder, mp >300 °C (colored at 220 °C) in 0.03% yield from wet plant. Compound **1** is optically inactive and from its elemental analyses was suggested the formula $C_{16}H_{14}O_7$. The UV spectrum of **1** in ethanol shows the absorption maxima at 211, 269, and 303 nm, which was similar to that of lecanoric acid (**2**) in the spectral pattern.[2]

The ^1H NMR spectrum of **1** in a mixture of $CDCl_3$ and CD_3OD shows the small difference in the chemical shifts as compared with that of **2**.[3] And the spectrum of **1** shows the signals ascribed to two aromatic methyl protons at δ 2.56 (3H, s) and 2.62 (3H, s), and to the protons attached to two 1,2,3,5-tetrasubstituted benzene rings at δ 6.22 (1H, d, J=2 Hz) and 6.30 (1H, d, J=2 Hz), and 6.48 (1H, d, J=2.1 Hz) and 6.54 (1H, d, J=2.1 Hz).

Treatment of **1** with diazomethane in methanol gave a tetramethyl derivative of **1** as colorless needles, mp 154—155 °C [MS (20 eV): M^+ 374], and its ^1H NMR spectrum in $CDCl_3$ shows the signals ascribed to three methoxyl groups and to one

Table 1. Carbon-13 NMR Chemical Shifts of **1**, **2**, **3**, and **4** in DMSO-d_6

Compound	1	2	3	4
1	107.6	107.7	107.0	—
2	160.7[a]	160.7[a]	161.2[a]	—
3	100.6	100.6	100.4	—
4	161.4[a]	161.4[a]	161.5[a]	—
5	110.1	110.2	110.3	—
6	140.3	140.0	141.1	—
7	167.6	167.4	170.3	—
8	21.7	21.3	22.2	—
1′	116.3	116.0	—	105.0
2′	151.1	159.3	—	161.8
3′	107.1	107.5	—	100.6
4′	165.6	152.6	—	164.5
5′	112.5	114.9	—	110.9
6′	142.2	140.7	—	142.9
7′	171.8	170.9	—	173.3
8′	23.0	21.7[b]	—	23.5
CH_3	—	—	51.6	—

In parts per million downfield from tetramethylsilane. Values bearing the same superscript may be interchanged.

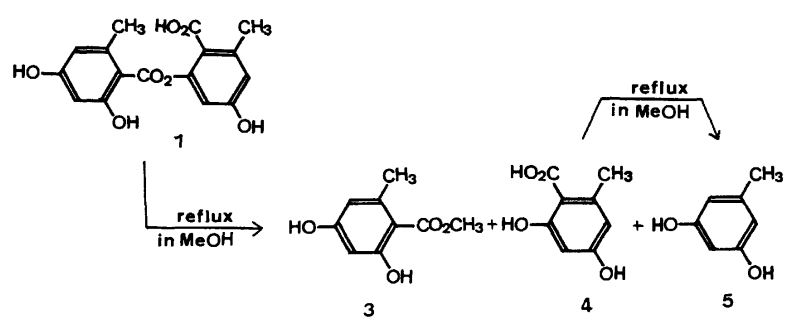

Scheme 1.

methoxycarbonyl group at δ 3.82 (6H, s), 3.86 (3H, s), and 3.90 (3H, s).

After having been refluxed in methanol followed by separation with a column of Sephadex LH-20 in the same manner as described above, compound **1** gave methyl orsellinate (**3**) and orsellinic acid (**4**) in a molar ratio of ca. 1:1 and a trace amount of orcinol (**5**).[4] Since **4** gives **5** by further treatment with boiled methanol, compound **5** should be formed by decarboxylation of **4** after methanolysis of **1**.

In the ^{13}C NMR spectra of **1**, **2**, **3**, and **4** in DMSO-d_6 as shown in Table 1, the signals ascribed to the carbons at the left hand of **1** (C-1—C-8) show the good agreement with those of **2**, whereas the signals at the right hand (C-1′—C-8′) show a little difference between **1** and **2**. The 2′-carbon bearing a benzoyloxy group in **1** appears at a field higher by 10.7 ppm than that of **4**, and 1′-, 3′-, and 5′-carbons in **1** (*ortho*- and *para*-potitions to C-2′) appear at fields lower by 11.3, 6.5, and 1.6 ppm respectively than those of **4**. The 4′-carbon in **2** appears at a field higher by 11.9 ppm than that of **4**, and 1′-, 3′-, and 5′-carbons in **2** appear at fields lower by 11.0, 6.9, and 4.0 ppm respectively than those of **4**. These results indicate that the ester bond in **1** should be linked at the 2′-position.

These ^1H NMR and ^{13}C NMR spectral data and all experimental results described above support the structure of isolecanoric acid (**1**) to be 2-(2,4-dihydroxy-6-methylbenzoyloxy)-4-hydroxy-6-methylbenzoic acid.

Compound **1** is the first *ortho*-depside isolated from the genus Lichen. Moreover we found the presence of **1** in *P. clavurifera* Räs. (Matsuge-goke in Japanese)[5] as a minor constituents with **2**.

Experimental

All melting points are uncorrected. The ^1H NMR spectra were measured with a Varian EM-390 90 MHz NMR spectrometer. The ^{13}C NMR spectra were measured with a JEOL JNM-PFT-60 NMR spectrometer at 15.04 MHz. Chemical shifts were expressed by δ value (ppm) from tetramethylsilane as internal standard. The IR spectra were measured with a Hitachi EPI-G3 spectrophotometer and the UV spectra were measured with a JASCO UVIDEC-510 spectrophotometer.

Isolation of Isolecanoric Acid (1). The lichen (300 g) which occurred on stone walls was collected and extracted with acetone (1500 cm^3) followed by reextraction with methanol (1500 cm^3) at room temperature for a week. The later extract was condensed to a syrup under reduced pressure and the syrup was subjected to chromatography on a column of Sephadex LH-20 (3.5×120 cm) eluting with methanol. The last effluent gave **1** as colorless powder after recrystallization from methanol: Mp >300 °C (colored at 220 °C); yield, 90 mg (0.03% from wet plant); UV (EtOH) 211 (log ε 4.56), 269 (4.21), and 303 nm (3.99); ^1H NMR (CD_3OD–$CDCl_3$) δ=2.56 (3H, s, Ar–CH_3), 2.62 (3H, s, Ar–CH_3), 6.22 (1H, d, J=2 Hz, Ar–H), 6.30 (1H, d, J=2 Hz, Ar–H), 6.48 (1H, d, J=2.1 Hz, Ar–H), and 6.54 (1H, d, J=2.1 Hz, Ar–H); ^{13}C NMR (DMSO-d_6) δ=21.7 (q), 23.0 (q), 107.6 (s), 110.1 (d), 112.5 (d), 116.3 (s), 140.3 (s), 142.2 (s), 151.1 (s), 160.7 (s), 161.4 (s), 165.6 (s), 167.6 (s), and 171.8 (s). Found: C, 58.93; H, 4.78%. Calcd for $C_{16}H_{14}O_7 \cdot 0.5H_2O$: C, 58.72; H, 4.63%.

Treatment of **1** (10 mg) in methanol (10 cm^3) with an ether solution containing diazomethane followed by chromatography through silica gel with hexane–ethyl acetate (4:1) afforded a tetramethyl derivative of **1** as colorless needles after recrystallization from acetone–hexane: Mp 154—155 °C; yield, 4 mg; MS (20 eV): M^+ 374; ^1H NMR ($CDCl_3$) δ=2.30 (3H, s, Ar–CH_3), 2.42 (3H, s, Ar–CH_3), 3.82 (6H, s, OCH_3), 3.86 (3H, s, OCH_3), 3.90 (3H, s, OCH_3), 6.37 (2H, s, Ar–H), and 6.67 (2H, brs, Ar–H). Found: m/z 374.1374. Calcd for $C_{20}H_{22}O_7$: M, 374.1365.

Methanolysis of 1. Compound **1** (44 mg) was dissolved in methanol (50 cm^3) and the solution was refluxed for 20 h. The mixture was concentrated and was subjected to chromatography on a column of Sephadex LH-20 in the same manner as described above, and afforded methyl orsellinate (**3**) (23 mg; mp 142—144 °C), orsellinic acid (**4**) (22 mg; mp 180—183 °C), and orcinol (**5**) (*ca.* 2 mg; mp 104—106 °C). Further treatment of **4** with boiled methanol gave **5**. These substances **3**, **4**, and **5** were proved to be identical with authentic samples which were prepared by methanolysis of lecanoric acid (**2**) in the same manner.

The present work was partially supported by a Grant-in-Aid for Science Research No. 59540341 from the Ministry of Education, Science and Culture.

References

1) Y. Asahina and S. Shibata, "Chemistry of Lichen Substances," Kawaide Shobo, Tokyo (1949), Part 1, Chap. 2; C. F. Culberson, "Chemical and Botanical Guide to Lichen Products," University of N. Carolina Press, Chapel Hill (1969), Chap. II.

2) Y. Asahina, *Yakugaku Zasshi*, **47**, 533 (1926); G. B. Ahmann and A. Mathey, *Bryologist*, **70**, 93 (1967).

3) **2**: ^1H NMR ($CDCl_3$–CD_3OD) δ=2.57 (6H, s, Ar–CH_3), 6.21 (1H, d, J=3 Hz, Ar–H), 6.28 (1H, d, J=3 Hz, Ar–H), 6.60 (1H, d, J=3 Hz, Ar–H), and 6.67 (1H, d, J=3 Hz, Ar–H).

4) Y. Asahina and M. Yanagita, *Ber.*, **66**, 36 (1933); Y. Asahina and H. Akagi, *ibid*, **68**, 1130 (1935); G. Koller and J. Hamburg, *Monatsh*, **65**, 373 (1935).

5) From this lichen only salazinic acid was identified by means of microcrystal test. See, C. F. Culberson, "Chemical and Botanical Guide to Lichen Products," University of N. Carolina Press, Chapel Hill (1969), p. 413 and the references cited therein.

A Facile Preparation of Flavones Using Nonaqueous Cation-Exchange Resin

Yukio HOSHINO* and Noboru TAKENO†
Department of Natural Science, Muroran Institute of Technology, Mizumoto-cho, Muroran 050
†Department of Industrial Chemistry, Muroran Institute of Technology, Mizumoto-cho, Muroran 050
(Received December 12, 1986)

Synopsis. Flavone was prepared from 1-(2-hydroxyphenyl)-3-phenyl-1,3-propanedione by using nonaqueous cation-exchange resin in a nearly quantitative yield. Of several reaction media, isopropyl alcohol gave the best result. Eight substituted flavones were also synthesized from the corresponding diketones in satisfactory yields.

Organic syntheses using ion-exchange resins have long been known, which are exemplified by esterification of acids and alcohols,[1] addition of acids to olefins,[2] Knoevenagel condensation,[3] and von Pechmann reaction.[4] Recently, the utilization of ion-exchange resins is in rapid progress. The use of the resin as catalyst has the following advantages: (1) Products can be stripped of catalyst resin simply by filtering reaction mixtures; (2) the resin can be recovered simply by filtration; (3) it is possible to minimize side reactions. But, hitherto, only few examples using ion-exchange resin have been known in the field of flavonoid synthesis. On the other hand, Baker-Venkataraman's method[5] is one of the best known procedures of a number of synthetic methods for flavones. In this method flavone (**2a**) is usually prepared by intramolecular dehydration, followed by cyclization, of 1-(2-hydroxyphenyl)-3-phenyl-1,3-propanedione (**1a**) with sulfuric acid in glacial acetic acid; **1a** is obtained from *o*-(benzoyloxy)acetophenone by the Baker-Venkataraman transformation.

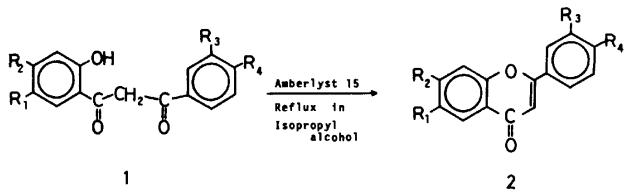

1 2

Now we attempted this cyclization by using a nonaqueous cation-exchange resin, Amberlyst 15, instead of sulfuric acid, and succeeded in obtaining satisfactory results. In this work, flavones (**2**) were also obtained in high yields by very simple procedures and under comparatively mild conditions. When a mixture of **1a** and a resin in a solvent was heated at the reflux temperature for several hours, a crude product was obtained almost quantitatively simply by filtering off the resin.

Reactions were carried out in benzene, chloroform, acetonitrile, or isopropyl alcohol. The results obtained are summarized in Table 1. We avoided using glacial acetic acid as the reaction medium, because its boiling point is close to the limiting temperature for the use of Amberlyst 15 (120 °C). The reactions were monitored by means of TLC analyses, and were taken as finished when the spot of starting material disappeared or when no change was observed in spots of substrate and product for more than three hours. In the case of chloroform, the reaction did not finish even after 27 h.

Amberlyst 15 is a macroreticular (MR) sulfonic acid type cation-exchange resin and has a huge network structure. When this kind of resin is used as an organic reaction catalyst, the key point is the rate of diffusion of substrate into the network of resin. The best yield of **2a** in the case of isopropyl alcohol may be due to the facility of the diffusion of substrate into the resin. Furthermore, it is remarkable that solvents having a comparatively high dielectric constant give high yields of **2a**. In those solvents the exchange groups in the resin might get more activated than in low dielectric solvents.

The total capacity of Amberlyst 15 is 4.6—5.0 meq/g-R, and accordingly one gram of resin is formally equivalent to ca. 5 mmol of substrate. But it is considered that in this reaction the resin acts as a catalyst for the substrate. This was confirmed by the following experimental result: When a recovered resin was used again for the same reaction without any regenerating treatment, **2a** reappeared and its yield did not extremely decrease (crude 90% and pure 75%; 3 h), although degradation of the resin was observed to

Table 1. Yields of Flavone (**2a**) and Reaction Times in Four Solvents[a]

Solvent[b]	Reaction Time / h	Yield[c] / %
Benzene	14	65[d]
Chloroform	>27	79[d]
Acetonitrile	6	83
Isopropyl alcohol	4	90

a) Substrate: 3.0 g (12.5 mmol); resin: 3.0 g (15.0 meq). b) 80 ml. c) Isolated yield. d) Isolated by column chromatography.

Table 2. Influence of Reaction Composion on the Yield of Flavone (**2a**) in Isopropyl Alcohol[a]

Composion (**1a** : Resin)	Reaction Time / h	Isolated Yield / %
1 : 0.33	14.5	90
1 : 1.20	4	90[b]
1 : 1.43	4	91
1 : 2.64	3	92
1 : 5.0	3	90

a) Solvent: 30 ml. b) From the value in Table 1.

Table 3. Reaction Times and Yields of Mono- or Disubstituted Flavones (**2b—i**) in Isopropyl Alcohol in the Presence of Amberlyst 15

Product No.	R_1	R_2	R_3	R_4	Reaction Time h	Isolated Yield %
2b	H	OCH_3	H	H	8.5	80
2c	H	H	H	OCH_3	2.5	78
2d	H	H	OCH_3	H	8	85
2e	H	OCH_3	OCH_3	H	19	83
2f	H	H	H	Cl	9	80
2g	H	H	Br	H	19.5	67
2h	CH_3	H	H	H	5	90
2i	H	CH_3	H	H	6	83

some extent.

In search for the optimum reaction conditions, reactions were repeated in isopropyl alcohol with several compositions of **1a** and resin. The results are shown in Table 2. Although there is not a great difference in the yield caused by changing the reaction composition, it can be concluded from the viewpoint of reaction time and economy that nearly equivalent composition of substrate and resin is optimum.

Eight mono- or disubstituted flavones (**2b—i**) were also prepared from the corresponding diketones (**1b—i**) by the same procedure. The results obtained are summerized in Table 3. Syntheses of a few 2′-substituted derivatives were also attempted in vain. This may be due to the steric hindrance by the introduction of the 2′-substituent close to the reaction center. From the results in Table 3, this method may be regarded as a general synthetic procedure for the flavones except the above-mentioned examples.

Thus we believe that this reaction allows a facile preparation of flavones, although the behavior of the substrate and product molecules in the network structure of the resin is not clear at present.

Experimental

All melting points were uncorrected. ^{1}H NMR spectra were obtained with a Hitachi R-22 (90 MHz) spectrometer by using tetramethylsilane as an internal standard. Physical data of isolated flavones agreed with those of independently synthesized authentic samples, which have already been reported.[6]

Materials. Solvents were of commercially available grade and were purified by ordinary procedures before use. Amberlyst 15 (Rohm and Haas Co., Ltd., U. S. A.) was employed without any treatment. Diketones were prepared according to known procedures,[5] and were identified on the basis of values in literatures[7] except for the following derivatives.

1-(2-Hydroxyphenyl)-3-(3-methoxyphenyl)-1,3-propanedione (1d): Mp 85.0—86.0 °C; ^{1}H NMR (CCl_4) δ=3.82 (3H, s, 3-OCH_3), 6.76 (2H, s, -CH_2-), 6.79—7.72 (8H, m, Aromatic), and 11.77 (1H, s, 2-OH). Found: C, 71.05; H, 5.10%. Calcd for $C_{16}H_{14}O_4$: C, 71.10; H, 5.22%.

1-(2-Hydroxy-4-methoxyphenyl)-3-(3-methoxyphenyl)-1,3-propanedione (1e): Mp 102.0—103.0 °C; ^{1}H NMR (CCl_4) δ=3.78 (3H, s, 4-OCH_3), 3.80 (3H, s, 3-OCH_3), 6.56 (2H, s, -CH_2-), 6.27—7.59 (7H, m, Aromatic), and 12.22 (1H, s, 2-OH). Found: C, 67.95; H, 5.30%. Calcd for $C_{17}H_{16}O_5$: C, 67.99; H, 5.37%.

1-(2-Hydroxyphenyl)-3-(3-bromophenyl)-1,3-propanedione (1g): Mp 115.0—116.0 °C; ^{1}H NMR (CCl_4) δ=6.71 (2H, s, -CH_2-), 6.81—8.00 (8H, m, Aromatic), and 11.71 (1H, s, 2-OH). Found: C, 56.48; H, 3.50; Br, 25.01%. Calcd for $C_{15}H_{11}O_3Br$: C, 56.45; H, 3.47; Br, 25.04%.

1-(2-Hydroxy-5-methylphenyl)-3-phenyl-1,3-propanedione (1h): Mp 88.0—91.0 °C; ^{1}H NMR ($CDCl_3$) δ=2.32 (3H, s, 5-CH_3), 6.79 (2H, s, -CH_2-), 6.83—7.98 (8H, m, Aromatic), and 11.86 (1H, s, 2-OH). Found: C, 75.54, H, 5.61%. Calcd for $C_{16}H_{14}O_3$: C, 75.58; H, 5.55%.

1-(2-Hydroxy-4-methylphenyl)-3-phenyl-1,3-propandione (1i): Mp 83.0—84.5 °C; ^{1}H NMR (CCl_4) δ=2.30 (3H, s, 4-CH_3), 6.68 (2H, s, -CH_2-), 6.51—7.89 (8H, m, Aromatic), and 11.82 (1H, s, 2-OH). Found: C, 75.60; H, 5.50%. Calcd for $C_{16}H_{14}O_3$: C, 75.58; H, 5.55%.

General Procedure. In a 50 ml conical flask equipped with a reflux condenser, a mixture of diketone (3.0 g, 12.5 mmol) and resin (3.0 g, 15.0 meq) was placed. Then isopropyl alcohol (30 ml) was added and the flask was heated on a hot plate for several hours under reflux with magnetic stirring. During the reaction, trace amounts of the reaction solution were withdrawn at hourly intervals with a glass capillary and subjected to TLC analyses. When the reaction was taken as finished, the flask was cooled to room temperature and had 20 ml chloroform added. Then the resin was filtered off and washed with a small amount of chloroform. The solvent of filtrate was removed by using an evaporator and the residue was dried overnight in a desicator under reduced pressure. Then the pure product was obtained by recrystallization from hexane or ligroine and benzene.

References

1) D. Saletan and R. White, *Chem. Eng. Prog.*, **4**, 59 (1952).
2) Rohm and Haas Co., *Amber-hi-lite*, No. 27 (1972).
3) M. J. Astle and W. C. Gergel, *J. Org. Chem.*, **21**, 493 (1956).
4) Rohm and Hass Co., *Amberlyst 15, Tech. Notes* (1962).
5) W. Baker, *J. Chem. Soc.*, **1933**, 1381; H. S. Mahal and K. Venkataraman, *Curr. Sci.*, **4**, 214 (1933).
6) Y. Hoshino, S. Takeda, M. Hamada, and N. Takeno, *Nippon Kagaku Kaishi*, **1982**, 1564; N. Takeno, T. Fukushima, S. Takeda, and K. Kishimoto, *Bull. Chem. Soc. Jpn.*, **58**, 1599 (1985).
7) R. Mozingo and H. Adkins, *J. Am. Chem. Soc.*, **60**, 669 (1938); H. Schmid and K. Banholzer, *Helv. Chem. Acta*, **37**, 1706 (1954); L. Reichel and H.-G. Henning, *Justus Liebigs Ann. Chem.*, **621**, 72 (1959); W. Baker, J. B. Harborn, and W. D. Ollis, *J. Chem. Soc.*, **1952**, 1294.

^{1}H and ^{19}F NMR Spectra of Some Fluorocyclobutane Derivatives

Kensuke TAKAHASHI,* Hiroshi KIMOTO,† and Hiroshige MURAMATSU†
Department of Applied Chemistry, Nagoya Institute of Technology, Gokiso-cho, Showa-ku, Nagoya 466
†Government Industrial Research Institute, Nagoya, Hiratemachi, Kita-ku, Nagoya 462
(Received October 2, 1986)

Synopsis. ^{1}H and ^{19}F NMR spectra were observed at 60.00 and 56.46 MHz, respectively, for ten 1,1,2,2-tetrahalo-1,2,2a,7a-tetrahydro-7*H*-cyclobut[*a*]inden-7-ones. NMR parameters, thus obtained, are discussed in connection with molecular structures and properties. The structures were partly confirmed by NOE measurements. The signs of all coupling constants observed for six compounds were determined by a selective decoupling technique (except for one with a small magnitude). A deshielding effect of the carbonyl group to a particular ^{19}F atom has also been obtained; it is useful for a structural determination.

Although many fluorocyclobutanes have been synthesized by the thermal cycloaddition of fluoroolefines, only a few NMR spectral parameters of cyclobutanes have been reported.[1] Recently, we obtained several title compounds by the photocycloaddition of indene to chlorofluoroethylenes as a part of studies on the syntheses of fluorine-containing fused polycyclic compounds.[2] During these studies, ^{1}H and ^{19}F NMR spectral data were found to be potentially useful in determining the structures of the compounds. Therefore, we wish to report on some NMR data in this article in order to contribute to the structural determination of similar compounds. This article makes clear that the configuration between fluorine and proton can be ascertained by NOE measurements. The signs of several fluorine-proton and fluorine-fluorine coupling constants were also determined relative to the vicinal proton-proton coupling constants.

Experimental

All ^{1}H and ^{19}F NMR spectra were recorded on a Hitachi R-20B spectrometer at a probe temperature (31.5 °C). ^{19}F and ^{1}H selective decoupling and tickling experiments were performed with the aid of a R-201SD decoupler, a R-209PA power amplifier, and a MG-514C synthesizer(Anritsu Electric Co., Ltd).

Chemical shifts were measured at 60 and 56.46 MHz for ^{1}H and ^{19}F nuclei, respectively; accuracies were within 0.2 Hz for ^{1}H and 0.4 Hz for ^{19}F measurements. All iterative calculations of the spectral analyses were carried out with a Hitachi-8450 computer system using a modification of LAOCN3 program.[3]

Samples of the title cyclobutane derivatives were synthesized from chlorofluoroethylenes and indene and the preparative methods were published.[2] The samples were dissolved in CCl_4 or $CDCl_3$ with small amounts of TMS and C_6F_6 served as internal references for ^{1}H and ^{19}F spectra, respectively. All sample solutions were degassed by the freeze-pump-thaw technique and sealed in 5-mm NMR sample tubes under vacuum.

Results and Discussion

The compounds studied are shown in Table 1;

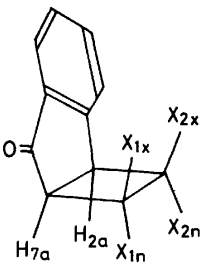

X= F or Cl

Scheme 1.

Table 1. ^{1}H and ^{19}F Chemical Shifts of Fluorocyclobutanes in Carbon Tetrachloride

Compound No.	Conc. wt%	Chemical Shift/ppm					
		H_{2a}	H_{7a}	F_{1x}	F_{1n}	F_{2x}	F_{2n}
1	5.7	4.43	3.94	62.48	Cl	Cl	Cl
2	7.5	4.40	3.95	Cl	74.93	Cl	Cl
3	7.5	4.30	3.94	63.35	70.35	Cl	Cl
4	2.6	4.32	3.88	55.85	Cl	62.78	Cl
5	ca. 10	a	a	Cl	51.8	Cl	55.0
6	3.8	4.40	3.75	Cl	68.35	60.95	Cl
7	5.0	4.43	3.77	46.40	Cl	Cl	49.24
8	4.1	4.30	3.76	51.00	67.43	44.92	Cl
9	10.1[b]	4.25	3.90	59.65	55.80	Cl	45.07
10	7.1[c]	4.29	3.67	48.1	52.8	50.1	47.9

a) Uncertain because **5** could not be isolated. b) The sample contains **8** in the amount of 40%. c) In $CDCl_3$ solution.

Scheme 1 shows the numberings of positions (x=exo and n=endo). The NMR spectral parameters obtained from iterative refinements are shown in Tables 1 and 2. The parameters for compound **5** could not be obtained since the sample was impure.

^{1}H and ^{19}F Chemical Shifts. As shown in Table 1, the ^{1}H chemical shifts fall in a narrow range. The H_{2a} chemical shifts are always larger than those of H_{7a}. ^{19}F chemical shifts show a range of variations. The ranges of the chemical shifts for H_{2a}, H_{7a}, F_{1x}, F_{1n}, F_{2x}, and F_{2n} are about 0.18, 0.28, 16.95, 23.1, 17.9, and 9.9 ppm, respectively. The range is larger for H_{7a} than for H_{2a}; among fluorine nuclei, the F_{1n} shows the largest variation and the F_{2n} shows the smallest. The introduction of a chlorine atom instead of a fluorine atom caused a shielding effect for the fluorine chemical shift. This tendency is contrary to the strong inductive effect of fluorine, and is interpreted by the magnetic anisotropy effect of the chlorine atom.

When a carbonyl group was introduced to the 7-position of a precursor hydrocarbon, a large effect was observed on the ^{19}F chemical shifts of F_{1x}. The effect on the chemical shift of F_{1x} amounts to about 10 ppm while that of F_{1n} is smaller than 2.5 ppm in magnitude. This deshielding of F_{1x} is ascribed to a magnetic anisotropy effect of the 7-positioned carbonyl group; it seems to be useful for assigning of the F_{1x} signal. The observed chemical-shift displacements of F_{1x} and F_{1n} are given in Table 3. The values for F_{1x} are about 9.5 ppm. However, those for the F_{1n} are separated into two groups: one group falls at about 0.5 ppm and the other is at about −2.5 ppm. Compounds **2** and **6**, which belong to the latter group, have a trans-dichloro configuration. These chlorine atoms seem to contribute to the displacement.

Spin-Spin Coupling Constants. The coupling constants obtained from the spectral analyses of the compounds studied (except for **5** and **10**) are given in Table 2. Among the values, the relative signs of the coupling constants were determined by using selective decoupling and tickling techniques (except for the values for **8** and **9**). Typical decoupled spectra of **1** are given in Fig. 1 as examples. The upfield doublet of H_{2a} was decoupled when the upfield doublet of F_{1x} was irradiated as shown in Fig. 1C. The result shows that the $^3J_{2a7a}$ and the $^3J_{7a1x}$ of **1** have the same sign. The sign of $^4J_{2a1x}$ of **7** could not be determined because of its small magnitude. From the values given in Table 2, the signs of $^2J_{FF}$, $^3J_{HF}$, and $^4J_{HF}$ are positive, while those of $^3J_{FF}$ are negative. The values of fluorine-proton and fluorine-fluorine coupling constants vary largely in magnitude, while the vicinal proton coupling constants are almost constant. Therefore, care should be taken for the use of the coupling constants in order to determine the structures of the samples. For example, $^3J_{2a2x}$ of **4** and **6** and the $^3J_{2a2n}$ of **7** and **9** vary largely in magnitude.

NOE Enhancement. NOE observations can give valuable informations for structural determination.[4] The results of the present investigation are shown in Table 4. The signals of the H_{7a} of **2** and **6** increase in intensity by about 15% when the F_{1n} resonance is irradiated; for H_{2a}, irradiation of the F_{2n} resonance is effective. The results are consistent both with the structures determined from other chemical and physical properties and with the relative positions of the atoms shown in Scheme 1.

Table 2. Coupling Constants of Fluorocyclobutanes in Hz[a]

Compound	**1**	**2**	**3**	**4**	**6**	**7**	**8**	**9**
$^3J_{2a7a}$	+7.1	+7.3	+7.2	+7.4	+7.3	+7.1	7.4	7.5
$^4J_{2a1x}$	+0.8	—	+2.7	+0.3	—	(−)0.1	2.0	2.5
$^4J_{2a1n}$	—	+4.0	+5.6	—	+4.1	—	5.7	6.2
$^3J_{2a2x}$	—	—	—	+15.9	+2.9	—	2.1	—
$^3J_{2a2n}$	—	—	—	—	—	+2.8	—	17.2
$^3J_{7a1x}$	+10.6	—	+8.1	+8.8	—	+8.6	6.9	7.0
$^3J_{7a1n}$	—	+15.1	+10.1	—	+15.5	—	10.9	13.0
$^4J_{7a2x}$	—	—	—	+2.7	+1.3	—	0.5	—
$^4J_{7a2n}$	—	—	—	—	—	+0.6	—	3.9
$^2J_{1x1n}$	—	—	+188.0	—	—	—	200.7	202.9
$^3J_{1x2x}$	—	—	—	−8.8	—	—	10.0	—
$^3J_{1x2n}$	—	—	—	—	—	−8.5	—	1.4
$^3J_{1n2x}$	—	—	—	—	−1.2	—	4.8	—
$^3J_{1n2n}$	—	—	—	—	—	—	—	5.1

a) The signs of the coupling constants were determined relative to the $^3J_{2a7a}$ which is assumed to be positive.

Table 3. Fluorine Chemical-Shift Change for Introduction of a Carbonyl Group at the 7-Position of the Precursors Studied

Compound	**1**	**2**	**3**	**4**	**5**	**6**	**7**	**8**	**9**	**10**
F_{1x}	9.5	—	10.0	9.3	—	—	9.0	10.1	10.0	10.0
F_{1n}	—	−2.4	0.3	—	0.0	−2.5	—	0.4	0.8	0.2

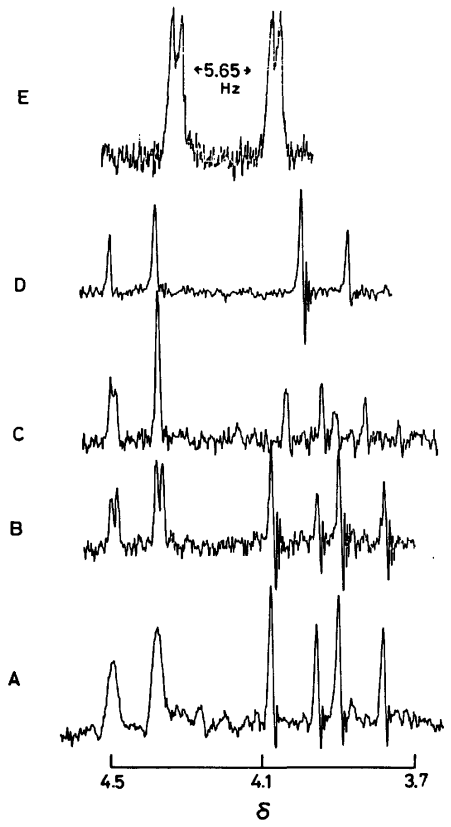

Fig. 1. ^{1}H and ^{19}F NMR spectra of the cyclobutane ring of **1** in CCl_4 at 60 and 56.46 MHz and 31.5 °C: (A) A normal ^{1}H spectrum, (B) an aromatic-proton decoupled ^{1}H spectrum, (C) a weak fluorine and aromatic-proton decoupled ^{1}H spectrum, (D) a strong fluorine and aromatic-proton decoupled ^{1}H spectrum, and (E) a ^{19}F spectrum.

Table 4. Proton-Fluorine Nuclear Overhauser Effects

Compound No.	^{19}F irradiated	% Enhancement observed[a]	
		H_{2a}	H_{7a}
1	1_x	2	4
2	1_n	0	14
4	1_x	2	−1
	2_x	3	2
6	1_n	0	13
	2_x	3	4
7	1_x	3	3
	2_n	10	1
8	2_x	2	−1
9[b]	2_n	5	

a) The area of the absorption was determined with an error of ±2%. b) The experiment was made in a mixture containing 40% of **8**. The enhancement of the H_{2a} and H_{7a} signals could not be obtained separately by overlapping of the signals. However, the result is significant.

References

1) W. D. Phillips, *J. Chem. Phys.*, **25**, 949 (1956); J. B. Lambert and J. D. Roberts, *J. Am. Chem. Soc.*, **87**, 3884, 3891 (1965); R. R. Ernst, *Mol. Phys.*, **16**, 241 (1969); R. K. Harris and V. J. Robinson, *J. Magn. Reson.*, **1**, 362 (1969); V. J. Gazzard and R. K. Harris, *Org. Magn. Reson.*, **6**, 404 (1974).

2) H. Kimoto, K. Takahashi, and H. Muramatsu, *Bull. Chem. Soc. Jpn.*, **53**, 764 (1980).

3) A. A. Bothner-By and S. M. Castellano, "Computer Programs for Chemistry," ed by D. F. DeTar and W. A. Benjamin, New York (1968), Vol. 1, p. 10.

4) J. H. Noggle and R. E. Schirmer, "The Nuclear Overhauser Effect," Academic Press, New York (1971).

Crystal Structure of Trichloroacetamide and Inequivalent Reorientations of CCl_3 Groups in the Crystal

Masao HASHIMOTO,* Kensaku HAMADA,† and Koichi MANO††
Department of Chemistry, Faculty of Science, Kobe University, Rokkodaicho, Nadaku, Kobe 657
†Graduate School of Science, Kobe University, Rokkodaicho, Nadaku, Kobe 657
††Research Institute for Atomic Energy, Osaka City University, Sugimotocho, Sumiyoshiku, Osaka 556
(Received December 8, 1986)

Synopsis. The crystal structure of trichloroacetamide has been determined by the single crystal X-ray diffraction method. Intermolecular contacts have been found to be responsible for the inequivalent reorientations of the CCl_3 groups of two crystallographically-independent molecules in the crystal.

It is well-known that CCl_3 groups in organic compounds undergo reorientations around the C_3 axis in crystalline state.[1] For several trichloromethyl derivatives, the magnitudes of the potential barrier height hindering the reorientation (V_0) have been determined by means of pulsed ^{35}Cl NQR method.[2-6] Chlorine NQR studies on trichloroacetamide (TCAA) indicated that the asymmetric unit of the crystal contains two independent CCl_3 groups with relatively different V_0 values (20.1 and 46.8 kJ mol^{-1}).[6,7] The origin of this difference has been unknown. Besides, our preliminary thermal analysis by a differential scanning calorimeter (DSC) showed that TCAA has a peculiar phase transition. Because of these reasons we decided to carry out the crystal structure analysis of TCAA.

Experimental

Recrystallizations of commercial trichloroacetamide (Nakarai Chemicals, LTD.) from diethyl ether gave colorless plate crystals (mp 415 K by DSC). A crystal with approximate dimensions of 0.5×0.4×0.3 mm^3 was used for the X-ray measurements. The unit cell parameters and intensities were measured on a Rigaku AFC-5 automatic four circle diffractometer with graphite-monochromatized Mo-K_α radiation. 1562 reflections within the range $2\theta<55°$ were collected by the ω-2θ scan technique. The ω scan width, scan rate and back ground counting time at both ends of a scan were $\omega=(1.4+0.35\tan\theta)°$, 8° min^{-1}, and 5.0 s, respectively. Lorentz and polarizetion corrections were made. Independent 1340 reflections with $|F_o|>3\sigma(F_o)$ were used in structure analysis. The structure was solved by the direct method (MULTAN 78)[8] and refined by the block-diagonal least-squares method (HBLS-V) with anisotropic temperature factors.[9] The function minimized was $\Sigma w(|F_o|-|F_c|)^2$. All the hydrogen atoms were found in the difference Fourier map and included in the refinement with isotropic temperature factors. The final R value was 0.058 (R_w=0.068). The weighting scheme adopted at the final stage was w=1.0 for $|F_o|\leq10.0$ and $w=[1.0+0.096(|F_o|-10.0)]^{-1}$ for $|F_o|>10.0$. Atomic scattering factors were taken from International Tables for X-Ray Crystallography.[10] The computations were carried out on an ACOS-1000 computer at Kobe University. Final atomic parameters are listed in Table 1.[11]

Crystal data: $C_2H_2Cl_3NO$, M=162.4, monoclinic, $P2_1$, a=10.415(2), b=5.785(1), c=10.182(2) Å, β=107.61° (2), Z=4, D_c=1.845 Mg m^{-3}, D_m=1.82 Mg^{-3}, μ=1.5 mm^{-1}, F(000)=320.

Results and Discussion

In accordance with the prediction of the NQR work,[7] the asymmetric unit of the crystal of TCAA contains two independent molecules (designated as Molecule A and B) shown in Fig. 1 (ORTEP-drawings).[12] The bond lengths, bond angles, and dihedral angles are listed in Table 2. The values of bond lengths and angles are comparable with those found in several amides.[13-17]

An ORTEP drawing of the crystal structure is shown in Fig. 2. A pair of N-H···O hydrogen bonds of lengths 2.982 and 3.019 Å couples Molecule A and B to form a dimer. Interestingly, the two molecules are related by a local two-fold axis. Each molecule of a dimer is also connected by other kinds of hydrogen bonds of lengths 2.915 and 2.957 Å to its nearest neighbors in the c direction. This results in a two-dimensional system of hydrogen bonds similar to those found in tetradecanamide and decanamide.[16,17]

Table 1. Final Atomic Coordinates (×10^4, H×10^3) with e. s. d.'s in Parentheses, and Equivalent Isotropic Thermal Parameters (Å^2)

	x	y	z	B_{eq}
Molecule A				
Cl(1)	9099(2)	492(4)	4132(2)	4.56(5)
Cl(2)	7538(2)	3985(4)	2342(2)	4.13(6)
Cl(3)	7462(2)	3642(4)	5122(2)	4.05(6)
C(1)	7576(6)	2056(12)	3670(6)	2.7(1)
C(2)	6447(6)	221(13)	3187(6)	2.8(2)
N	5925(6)	−649(12)	4120(5)	3.3(2)
O	6139(5)	−401(10)	1976(4)	3.6(1)
H(1)	608(9)	4(20)	494(9)	4.8(25)[a]
H(2)	518(7)	−183(16)	383(7)	2.2(16)[a]
Molecule B				
Cl(1)	2759(2)	764(5)	1200(4)	9.45(14)
Cl(2)	1283(3)	3814(8)	2388(3)	7.31(12)
Cl(3)	1251(2)	4410(6)	−379(2)	7.57(9)
C(1)	2240(6)	3617(13)	1270(6)	2.8(2)
C(2)	3545(5)	5112(11)	1795(6)	2.5(2)
N	4068(5)	5873(12)	850(5)	3.3(2)
O	4014(5)	5472(11)	3029(4)	3.8(1)
H(1)	367(9)	568(22)	−15(9)	4.4(23)[a]
H(2)	484(7)	660(17)	117(7)	2.5(18)[a]

a) Isotropic temperature factors.

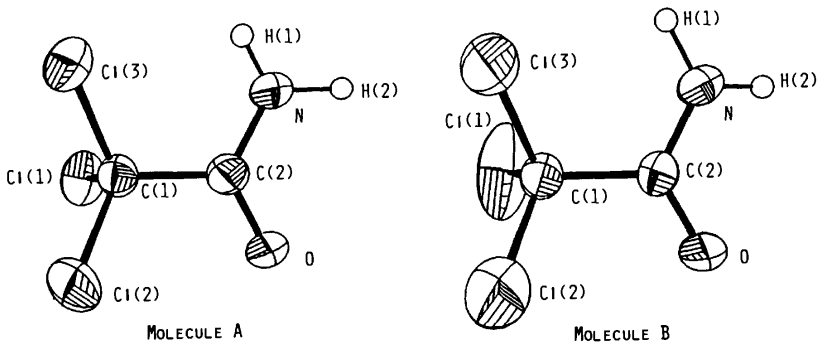

Fig. 1. ORTEP drawings of molecular structures with the numbering scheme. Non-hydogen atoms are expressed as thermal ellipsoids with 50% probability level and hydrogen atoms as spheres of radius 0.1 Å.

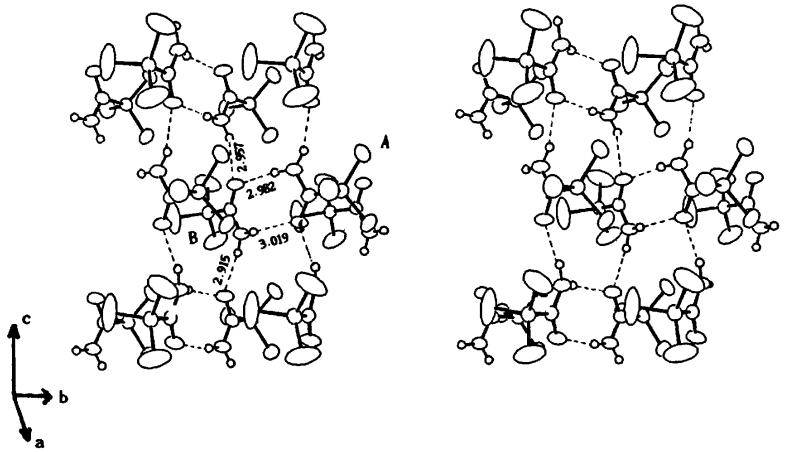

Fig. 2. An ORTEP drawing of the crystal structure of trichloroacetamide viewed along the normal to the bc plane. A: Molecule A; B: Molecule B.

Table 2. Bond Lengths, Bond Angles, and Dihedral Angles of Molecule A and B

	Molecule A	Molecule B
	l/Å	
C(1)-Cl(1)	1.762(8)	1.745(9)
C(1)-Cl(2)	1.745(7)	1.729(9)
C(1)-Cl(3)	1.775(7)	1.745(8)
C(1)-C(2)	1.550(10)	1.563(10)
C(2)-N	1.328(10)	1.316(10)
C(2)-O	1.230(9)	1.220(9)
	ϕ/deg	
Cl(1)-C(1)-Cl(2)	110.1(4)	109.7(4)
Cl(1)-C(1)-Cl(3)	109.0(4)	108.0(4)
Cl(2)-C(1)-Cl(3)	108.9(4)	109.0(4)
Cl(1)-C(1)-C(2)	105.6(5)	106.8(5)
Cl(2)-C(1)-C(2)	110.8(5)	110.7(5)
Cl(3)-C(1)-C(2)	112.5(5)	112.5(5)
C(1)-C(2)-O	117.5(6)	118.8(6)
C(1)-C(2)-N	117.9(6)	116.4(6)
N-C(2)-O	124.5(7)	124.8(7)
	χ/deg	
Cl(1)-C-C-N	91.2(7)	87.1(7)
Cl(2)-C-C-N	−149.6(6)	−153.6(6)
Cl(3)-C-C-N	−27.5(8)	−31.3(8)
Cl(1)-C-C-O	−85.6(7)	−92.2(7)
Cl(2)-C-C-O	33.6(8)	27.2(8)
Cl(3)-C-C-O	155.7(6)	149.5(6)

The gross feature of the solid is determined by van der Waals contacts of chlorine atoms in CCl_3 groups on both sides of the layer.

The crystal and molecular structures of TCAA suggest that the observed difference in V_0 is attributable to intermolecular contacts between CCl_3 groups and their neighboring atoms. Then, by rotating the group around its C_3 axis, we calculated the atom-atom potential energy (U) as a function of rotation angle (ϕ) on the basis of the following function[18]

$$U = \Sigma\varepsilon_i(2.90\times 10^5 \exp(-12.50/P_i) - 2.25P_i^6)$$

where P_i stands for the sum of van der Waals radii (Σr_i^*) divided by the distance (r_i) between interacting centers. The values of van der Waals radii and ε_i were taken from Ref. 19.

The results of the calculations shown in Fig. 3 indicate that the intermolecular Cl···Cl interactions dominate to determine the magnitude of the potential, and that the value of $V_0=U_{max}-U_{min}$ of Molecule A is considerably larger than that of Molecule B. These findings are consistent with the result of the NQR study. However, for both Molecule A and B, the calculated V_0 values are twice as high as the observed ones. Unfortunately, the discussion on the magnitude of V_0 will be artificial, because it depends strongly on the choice of van der Waals radius of chlorine atom.

As seen in Table 1, the magnitudes of the tem-

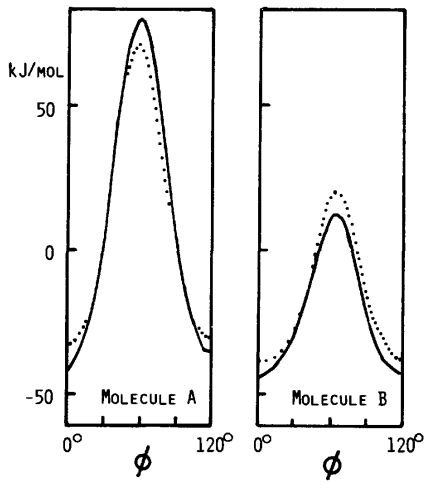

Fig. 3. Calculated atom-atom potential curves of CCl_3 groups in trichloroacetamide crystal as a function of rotation angle (ϕ), where the orientation with ϕ=0 corresponds to the structure determined by the present X-ray work. ——: Including interactions with all atoms within 4.1 Å (twice of the van der Waals radius of chlorine atom); ·····: including interactions only with chlorine atoms within 4.1 Å.

perature factor (B_{eq}) for Cl atoms in Molecule B are considerably larger than those in Molecule A. Moreover, the thermal ellipsoids of Cl atoms of Molecule B indicate the ease of the reorientation of the CCl_3 group around the C_3 axis (see Fig. 2). Thus, the CCl_3 group with the higher V_0 value may be assigned to Molecule A, although a complete assignment should be done by the Zeeman NQR study on a single crystal.

References

1) M. Buyle-Bodin, *Ann. Phys. (Paris)*, **10**, 533 (1955).
2) I. V. Izmest'ev and V. S. Grechishkin, *Zh. Strukt. Khim.*, **11**, 927 (1970).
3) M. E. Ainbinder, B. F. Amirhanov, I. V. Izmest'ev, A. N. Osipenko, and G. B. Soifer, *Sov. Physics-Solid State*, **13**, 344 (1971).
4) T. Kiichi, N. Nakamura, and H. Chihara, *J. Magn. Reson.*, **6**, 516 (1972).
5) H. Chihara and N. Nakamura, *Bull. Chem. Soc. Jpn.*, **45**, 3530 (1972).
6) I. V. Izmest'ev and G. B. Soifer, *Opt. Spektrosk.*, **30**, 479 (1971).
7) H. C. Allen, Jr., *J. Am. Chem. Soc.*, **74**, 6074 (1952).
8) P. Main, S. E. Hull, L. Lessinger, G. Germain, J-P, Declercq, and M. M. Woolfson, "A System of Computer Program for the Automatic Solution of Crystal Structures from X-ray Diffraction Data, *MULTAN* 78," University of York.
9) T. Ashida, "The Universal Crystallographic Computing Systems-Osaka, *HBLS*-V," The Computation Center, Osaka University (1979), p. 53.
10) "International Tables for X-Ray Crystallography," Vol. IV, Kynoch Press, Birmingham (1974).
11) Tables of anisotropic temperature factors and observed and calculated structure factors are kept at Chemical Society of Japan, Document No. 8741.
12) C. K. Johnson, "*ORTEP*-II: A FORTRAN Thermal Ellipsoid Plot Program for Crystal Structure Illustratins, ORNL-5138," March, 1976, Oak Ridge National Laboratory.
13) F. Senti and D. Harker, *J. Am. Chem. Soc.*, **62**, 2008 (1940).
14) W. C. Hamilton, *Acta Crystallogr.*, **18**, 866 (1965).
15) P. J. Dejace, *Acta Crystallogr.*, **8**, 851 (1955).
16) J. D. Turner and E. C. Lingafelter, *Acta Crystallogr.*, **8**, 551 (1955).
17) J. Brathovde and E. C. Lingafelter, *Acta Crystallogr.*, **11**, 729 (1958).
18) N. L. Allinger, *J. Am. Chem. Soc.*, **99**, 8127 (1977).
19) N. L. Allinger and Y. H. Yuh, *QCPE*, **395**, 41 (1980).

Crystal Structure of Bis(2,2′-bipyridine)copper(I) Perchlorate

Megumu MUNAKATA,* Susumu KITAGAWA, Akio ASAHARA, and Hideki MASUDA†
Department of Chemistry, Faculty of Science and Technology, Kinki University, Kowakae, Higashi-Osaka 577
†Faculty of Pharmaceutical Sciences, Kyoto University, Shimoadachi-cho, Sakyo-ku, Kyoto 606
(Received May 20, 1986)

Synopsis. The crystal structure of the title complex was determined by X-ray diffraction: Orthorhombic, space group $C222_1$, a=20.553(2) Å, b=11.210(1) Å, c=8.980(2) Å, and Z=4. The structure was solved by the direct method and was refined anisotropically by the full-matrix least-squares method: R was 0.062 for 1206 observed reflections. The $[Cu(bpy)_2]^+$ cation has a pseudo-tetrahedral arrangement (average Cu–N=2.021 Å). The interligand dihedral angle in $[Cu(bpy)_2]^+$, 75.2°, differs significantly from that previously reported $[Cu(1,10\text{-phenanthroline})_2]ClO_4$ (49.9°).

2,2′-Bipyridine(bpy) and 1,10-phenanthroline (phen) are bidentate ligands, whose π acceptor capability significantly contributes to the stabilization of their low valent metal complexes.[1,2] Regarding their complexation, it is interesting to compare these ligands with 2,9-dimethyl-1,10-phenanthroline (dmp) and 6,6′-dimethyl-2,2′-bipyridine (dmbp). Four-coordinate copper(I) cations tend to favor a regular tetrahedral arrangement[3] due to its d^{10} configuration. The interligand dihedral angles, between the mean planes defined by the metal ion and each set of bidentate nitrogen atoms, were 80.2° and 85.7° for $[Cu(dmp)_2]^+$,[4,5] and 80.7° for $[Cu(dmbp)_2]^+$,[6] indicating a pseudo-tetrahedral geometry. Recently, two interesting structures, $[Cu(phen)_2]ClO_4$ and $[Cu(phen)_2][CuBr_2]$, have been reported,[7] whose interligand dihedral angles were 49.9° and 76.8°, respectively. Although both structures have the same $[Cu(phen)_2]^+$ unit, these two angles are quite different. In the case of the $[Cu(bpy)_2]^+$ cation, the question arose as to how large is the interligand dihedral angle. In order to answer this question, an X-ray structural determination of $[Cu(bpy)_2]ClO_4$ was carried out.

Experimental

Preparations. $[Cu(bpy)_2]ClO_4$ was synthesized in the following way.[8] Under a nitrogen atmosphere, an 8-ml methanol solution of bpy(80 mM) (1 M=1 mol dm^{-3}) was added to tetrakis(acetonitrile)copper(I) perchlorate (40 mM) and stirred at 298 K. Brown prism-like crystals suitable for diffraction studies were grown from this solution in a sealed tube at 273 K.

Crystal Data. $C_{20}N_4H_{16}Cu$, ClO_4, $F.W.$ 475.35, orthorhombic, space group $C222_1$ (No. 20, systematic absences, hkl: $h+k=2n+1$ and $00l$: $l=2n+1$), a=20.553(2), b=11.210 (1), c=8.980(2) Å, D_c=1.526 g cm^{-3} for Z=4.

A crystal with approximate dimensions of 0.15×0.15×0.20 mm^3 was mounted on a Rigaku AFC-6B four-circle diffractometer with graphite-monochromatized Cu $K\alpha$ radiation ($\bar{\lambda}$=1.54178 Å). The intensity data were collected at 296 K in the θ–2θ scan mode with a 1.2° scan width, $2\theta_{max}$ of 120° ($-22\leq h\leq 22$, $0\leq k\leq 12$, $0\leq l\leq 10$), and scan rate of 4° min^{-1}. They were converted to $|F_o|$ data in the usual manner. An absorption correction was not applied (μ=2.98 mm^{-1}). Of the 1834 measured reflections, 1206 were observed ($|F_o|>3\sigma(F_o)$), where $\sigma(F_o)$ is the standard deviation estimated by countig statistics.

Structure Solution and Refinement. The structure was solved by a direct method (*MULTAN* 78),[9] and refined by full-matrix least-squares calculations with anisotropic thermal parameters, including isotropic H atoms located on a difference Fourier synthesis. The final R and R_w values were 0.062 and 0.060, respectively. The atomic parameters of non-hydrogen atoms are given in Table 1.#

The atomic scattering factors[10] and anomalous dispersion[11] terms for all atoms were obtained from International Tables for X-Ray Crystallography, Vol. IV. All computation were performed on a FACOM M-382 computer at the Data Processing Center, Kyoto University using the program system KPPXRAY.[12]

Results and Discussion

The view of the cation in Fig. 1 shows that the central copper atom, with a pseudo-tetrahedral geometry, is coordinated to two bpy molecules via the pyridine nitrogens. Selected bond lengths and angles are also given in Fig. 1. A perchlorate anion does not coordi-

Table 1. Atomic Coordinates of Non-hydrogen Atoms, with Estimated Standard Deviations in Parentheses and Equivalent Isotropic Temperature Factors

Atom	x	y	z	B_{eq}[a)]/Å^2
Cu	0.0	0.0918(3)	0.2500	7.41
Cl	0.1316(2)	0.5000	0.5000	8.15
C1	0.1350(5)	0.0656(10)	0.1952(11)	4.71
C2	0.1973(6)	0.0236(13)	0.2090(15)	7.10
C3	0.2120(7)	−0.0769(14)	0.2964(15)	8.88
C4	0.1622(7)	−0.1280(13)	0.3778(15)	7.92
C5	0.1031(7)	−0.0841(12)	0.3561(14)	7.43
C6	0.1161(5)	0.1675(10)	0.1077(12)	5.07
C7	0.1573(6)	0.2311(12)	0.0156(21)	7.27
C8	0.1339(8)	0.3262(13)	−0.0696(15)	8.82
C9	0.0692(7)	0.3526(11)	−0.0689(15)	6.75
C10	0.0310(6)	0.2867(11)	0.0233(18)	6.95
N1	0.0876(4)	0.0116(9)	0.2690(13)	6.44
N2	0.0505(5)	0.1956(9)	0.1068(12)	6.10
O1	0.1704(6)	0.4022(12)	0.4947(26)	17.43
O2	0.0887(7)	0.5158(23)	0.3957(18)	22.18

a) Equivalent isotropic temperature factor defined by Hamilton.[20]

Tables of thermal parameters of non-hydrogen atoms, fractional coordinates of hydrogen atoms, and the observed and calculated structure factors are being kept at the Chemical Society of Japan, Document No. 8734.

nate to the copper because the closest Cu···O contact is 5.26 Å. The bpy ligand is planar within 0.04 Å, with the twisting about the Cl-C6 bond (dihedral angle is 2.2°). The Cu-N lengths are slightly shorter than that of $[Cu(dmbp)_2]BF_4$,[6] indicating that the steric interaction between copper atom and methyl group is unexpectedly little. On the other hand, a steric effect of the methyl group has been found in $[Cu(phen)_2]^+$ and $[Cu(dmp)_2]^+$, and the Cu-N length for the former is clearly shorter than that for the latter (Table 2). The interligand dihedral angle, α, of the present complex is of particular interest. The angle 75.2° is slightly smaller (by 5.7°) than that in $[Cu(dmbp)_2]^+$, and an apparent difference between two complexes is not appreciated; this indicates that there are no marked substituent effects. Table 2 shows that α of $[Cu(phen)_2]NO_3$ differs by 27° from that of $[Cu(phen)_2][CuBr_2]$.

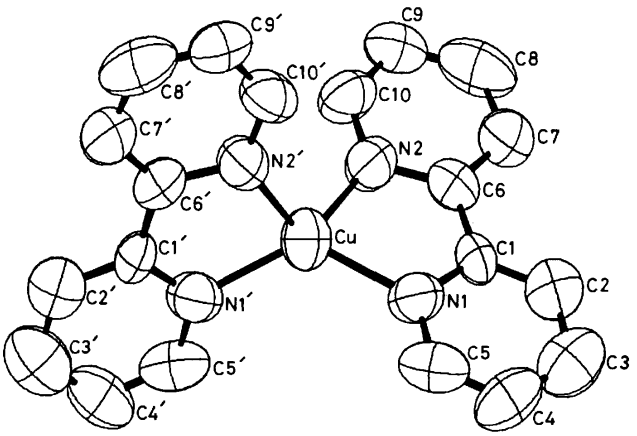

Fig. 1. View of the $[Cu(bpy)_2]^+$ cation. Thermal ellipsoids are drawn at 50% probability level: Hydrogen atoms are omitted. The labeling scheme used for the atom in the molecule is also shown. The primed atom notes the atom translated by two-fold axis. Selected bond lengths (Å) and angles (deg.) are as follows: Cu-N1=2.020(9); Cu-N2=2.021 (11); Cl-C6=1.440(15); Cl-N1=1.325(14); C6-N2= 1.385(15); N1-Cu-N1′=127.1(4); N1-Cu-N2′=131.3 (4); N1-Cu-N2=81.5(4); N2-Cu-N2′=109.7(4); C6-Cl-N1=115.9(9); Cl-C6-N2=116.5(9); Cu-N1-Cl= 114.2(8); Cu-N1-C5=127.3(8); Cu-N2-C6=111.4(8); Cu-N2-C10=130.3(9).

The small angle for the former is not necessarily due to a counter anion because of no coordination of the anion; the angle is associated with the intermolecular interaction from a crystal packing, rather than the intramolecular interaction inherent in copper(I). The α of 49.9° is close to that of a copper(II) complex, $[Cu(bpy)_2]^{2+}$.[14] In the copper(II) complex, the small angle α is reasonable since the copper(II) cation prefers a near square-planar structure to a tetrahedral one.[15] According to Table 2, α for the methyl complex, $[Cu(dmbp)_2]^+$, is about 81°, larger by ca. 6° than that for methyl group-free complexes. On the other hand, it is surprising to find that α for $[Cu(tmbp)_2]^+$ is smaller than that for the present complex in spite of the dmbp analog.[16] These facts suggest that α for tetrahedral copper(I) complexes with the bidentate ligand *in the solid state* depends on the crystal packing dominating over the steric effect of methyl groups. The effect of the methyl group should be considered, especially in the case of a square-planar arrangement, rather than a tetrahedral arrangement. The near neighboring methyl groups probably play an important role in inhibiting the deformation toward a square-planar geometry. This role is advantageous for copper(I) complexes. In fact, dmp favors a copper(I) ion rather than a copper(II) ion: the stability con-

Table 2. Comparison of Average Bond Parameters in Some $[Cu(biL)_2]X_n$ Type Complexes

biL	Oxidation Number of Copper (n)[a]	X	Bond Length (Å) Cu-N[b]	Angles (deg.)		Reference	Redox Potential $E_{1/2}$ (V. vs. NHE)
				N-Cu-N[b]	Dihedral[c]		
2,2′-Bipyridine (bpy)	+1 (1)	ClO_4^-	2.021 (11)	81.5 (4)	75.2	Present work	0.12[d], 0.254[e]
6,6′-Dimethyl-2,2′-bipyridine (dmbp)	+1 (1)	BF_4^-	2.034 (1)	81.9 (1)	80.7	(6)	0.574[e]
4,4′,6,6′-Tetramethyl-2,2′-bipyridine (tmbp)	+1 (1)	ClO_4^-	2.057 (10)	80.6 (4)	68	(14)	
1,10-Phenanthroline (phen)	+1 (1)	ClO_4^-	2.049 (9)	81.4 (3)	49.9	(7)	0.174[d]
1,10-Phenanthroline (phen)	+1 (1)	$CuBr_2^-$	2.039 (8)	82.2 (3)	76.8	(7)	
2,9-Dimethyl-1,10-phenanthroline (dmp)	+1 (1)	NO_3^-	2.071 (8)	82.7 (3)	80.2	(4)	0.603[f]
2,9-Dimethyl-1,10-phenanthroline (dmp)	+1 (1)	NO_3^- [g]	2.063	83.4	85.7	(5)	
2,2′-Bipyridine (bpy)	+2 (2)	PF_6^-	1.985 (11)	83.0 (7)	44.6	(14)	

a) Number of counter ions. b) Bond lengths and intraligand N-Cu-N angle. Two values are averaged. c) An interligand dihedral angle. d) Ref. 1. e) Present work. Obtained from cyclic voltammograms of acetone solution at 25 °C. f) Ref. 18. g) Dihydrate.

stant $10^{19.1}$ of $[Cu(dmp)_2]^+$ is very much larger than that, $10^{11.7}$, of $[Cu(dmp)_2]^{2+}$.[17] This is also well-illustrated in terms of the redox properties of the copper complexes of dmp and dmbp since both $[Cu(dmp)_2]^+$ and $[Cu(dmbp)_2]^+$ have higher redox potentials of copper than the corresponding complexes without methyl substituents (Table 2).[1,18,19] These facts indicate that the steric interaction of the methyl groups in the 2 and 9 positions of phen and in the 6 and 6′ positions of bpy favor the tetrahedral geometry of the copper(I) complex *in solution* since there is no effect owing to closed packing, forcing the copper(II) complex to avoid a square planar geometry.

References

1) B. R. James and R. J. P. Williams, *J. Chem. Soc.*, **1961**, 2007.

2) R. J. P. Williams, *J. Chem. Soc.*, **1955**, 137.

3) I. Csoeregh, P. Kierkegaard, and R. Norrestam, *Acta Crystallogr. Sect. B*, **31**, 314 (1975); A. H. Lewin and R. J. Michl, *J. Chem. Soc., Chem. Commun.*, **1971**, 1400; W. Clegg, S. R. Acott, and C. D. Garner, *Acta Crystallogr. Sect. C*, **40**, 768 (1984); C. L. Raston, B. Walter, and A. H. White, *Aust. J. Chem.*, **32**, 2751 (1979); J. Garaj, *Inorg. Chem.*, **8**, 304 (1969); K. Nilsson and A. Oskasson, *Acta Chem. Scand.*, **A36**, 605 (1982).

4) R. Haemaelaeinen, M. Ahlgren, U. Turpeinen, and T. Raikas, *Cryst. Struct. Commun.*, **8**, 75 (1979).

5) R. Haemaelaeinen, U. Turpeinen, M. Ahlgren and T. Raikas, *Finn. Chem. Lett.*, **1978**, 199.

6) P. J. Burke, D. R. McMillin, and W. R. Robinson, *Inorg. Chem.*, **19**, 1211 (1980).

7) P. C. Healy, L. M. Engelhardt, V. A. Patrick, and A. H. White, *J. Chem. Soc., Dalton Trans.*, **1985**, 2541.

8) S. Kitagawa and M. Munakata, *Inorg. Chem.*, **20**, 2261 (1981).

9) P. Main, S. E. Hull, L. Lessinger, G. Germain, J.-P. Declercq, and M. M. Woolfson, 1978. "*MULTAN* 78. A System of Computer Programms for the Automatic Solution of Crystal Structures from X-Ray Diffraction Data," Univ. of York, England and Louvain, Belgium.

10) International Tables for X-Ray Crystallography: Kynoch Press, Birmingham, 1974, Vol. IV, Table 2. 2B.

11) Ref. 10. Table 2. 31.

12) T. Taga, T. Higashi, and H. Iizuka, "*KPPXRAY*. Kyoto Program Package for X-ray Crystal Structure Analysis" Kyoto University, Japan (1985).

13) The electron-density distribution of the oxygen atoms of the ClO_4^- ion was much diffuse with the shortening of the Cl–O bond lengths (1.30—1.36 Å), but the configuration of the ClO_4^- ion was evidently indicative of tetrahedral type. The large distribution will be interpreted as static disorder rather than thermal motion. This indicates rather weak interaction between $[Cu(bpy)]_2^+$ cation and ClO_4^- anion.

14) J. Foley, S. Tyagi, and B. J. Hatheway, *J. Chem. Soc., Dalton Trans.*, **1984**, 1.

15) G. Brubaker, J. N. Brown, M. K. Yoo, R. A. Kinsey, T. M. Kutchan, and E. A. Mottel, *Inorg. Chem.*, **18**, 299 (1979).

16) P. J. Burke, K. Henrick, and D. R. McMillin, *Inorg. Chem.*, **21**, 1881 (1982).

17) R. M. Smith and A. E. Martell, "Critical Stability Constants: Amines " Vol. 2, Plenum Press, New York, 1975.

18) S. Kitagawa, M. Munakata, and H. Higashie, *Inorg. Chim. Acta*, **59**, 219 (1982).

19) M. A. Augastin and J. K. Yandell, *Inorg. Chem.*, **18**, 577 (1979).

20) W. C. Hamilton, *Acta Crystallogr.*, **12**, 609 (1959).

Inductively Coupled Plasma Atomic Emission Spectrometric Determination of Copper by Suction-Flow On-Line Liquid-Liquid Extraction of Its Macrocyclic Dioxotetramine Chelate

Takahiro KUMAMARU,* Yoko NITTA, Hiroshi MATSUO, and Eiichi KIMURA†
Department of Chemistry, Faculty of Science, Hiroshima University,
Higashisenda-machi, Naka-ku, Hiroshima 730
†Department of Medicinal Chemistry, Hiroshima University School of Medicine,
Kasumi, Minami-ku, Hiroshima 734
(Received December 8, 1986)

Synopsis. The flow manifold described permits suction-flow liquid-liquid extraction of copper(II) in a discrete aqueous sample as its macrocyclic dioxotetramine (6-hexadecyl-1,4,8,11-tetraazacyclotetradecane-5,7-dione, HDC) chelate into chloroform. The organic extract is successively fed into the inductively coupled plasma by a peristaltic pump. The detection limit is 1.5 ng cm^{-3} copper(II) and the relative standard deviation is 2.2% (n=10) for 100 ng cm^{-3} copper(II).

The chemical properties of macrocyclic polyamines have received much attention in recent years.[1] However their applications to chemical analysis have been limited.[2] Kimura et al.[3] recently synthesized HDC and found that it selectively encloses copper(II) with simultaneous deprotonation of two amides as a neutral 1 : 1 complex in alkaline pH and is potentially useful for the separation of copper(II) by solvent extraction.

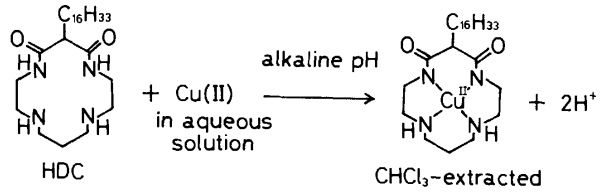

This paper demonstrates an analytical application of HDC as a chelating agent for copper(II) to an on-line liquid-liquid extraction for the inductively coupled plasma atomic emission spectrometry (ICPAES) of copper. The limiting factors for the extraction and the ICPAES were investigated to obtain the maximum sensitivity of copper, and the technique was applied to the analysis of some biological samples.

Experimental

Apparatus and Reagents. A Kyoto Koken Model UOP-1S ICP atomic emission spectrometer was used. The flow system comprised a Teflon suction cup,[4] a 6-channel variable-speed peristaltic pump (Tokyo Rikakikai Model MP-3), T-joints, a segmentor, a Teflon extraction coil (1 mm i.d., 2 m long) and a phase separator (4 mm i.d., 40 mm horizontal long, 60 mm vertical long). The phase separator was made up of a T-piece glass fitting into which a Teflon fiber string was inserted at one of the bends.[5] As for the pump tubing, Acidflex (Technicon Corp.) for chloroform and Tygon (Norton Co.) for aqueous solutions were used. The inner diameters of the tubing for sample, HDC, buffer, and chloroform were 2.4, 1.6, 1.6, and 1.6 mm, respectively. The other parts of the flow system were made of 1-mm i.d. Teflon tubing. The assembly is shown in Fig. 1.

HDC was prepared by refluxing dimethyl hexadecylmalonate and 3,7-diazanonane-1,9-diamine in methanol (25% yield, mp 113°C from methanol-benzene).[3] A solution of the chelating agent [5.0×10^{-4} M (1 M=1 mol dm^{-3})] was prepared by dissolving HDC in dilute hydrochloric acid and diluting with water. A 1000 μg cm^{-3} copper(II) standard stock solution was prepared by dissolving 0.500 g of copper metal (99.999%) in dilute hydrochloric acid diluting to 500 cm^3 with water. Solutions of suitable concentrations were prepared by dilution. A 1000 μg cm^{-3} nickel(II) solution was prepared by dissolving 0.500 g of nickel metal

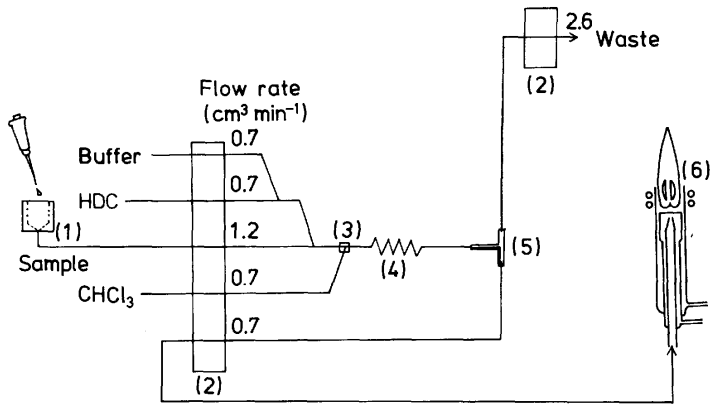

Fig. 1. Flow diagram for extraction of copper(II) with HDC into chloroform.
(1) Teflon suction cup, (2) peristaltic pump, (3) segmentor, (4) extraction coil, (5) phase separator, (6) ICP.

(99.999%) in dilute hydrochloric acid and diluting to 500 cm^3 with water. A borate buffer solution (1 M, pH 9) was prepared by mixing boric acid and sodium hydroxide. Chloroform was used without further purification.

Recommended Procedure for Copper Determination. A sample solution ([Cu(II)]$\lesssim$500 ng cm^{-3}) in which nickel(II) had been added in the concentration of 30 μg cm^{-3}, usually 2 cm^3, was added to the suction cup from a Pipetman P-5000 (Gilson International). As shown in Fig. 1, the sample was sucked into the mixture of the HDC and the buffer solutions, and with chloroform in the segmentor. The segmented solution was carried into the extraction coil and the phase separator. The organic extract was introduced by the peristaltic pump into the nebulizer of the ICP spectrometer. The transient Cu I 324.754-nm emission signal at an observation height of 13 mm above load coil was recorded on a strip-chart recorder, and the peak height was measured. The optimum argon gas flow rates for the ICP were 12 dm^3 min^{-1} of plasma gas, 1.0 dm^3 min^{-1} of auxiliary gas and 0.325 dm^3 min^{-1} of nebulizer gas.

Results and Discussion

The effect of pH on the extraction was investigated, keeping the other variables in the recommended procedure constant. The HDC-copper(II) complex was confirmed to be quantitatively extracted into chloroform in the pH 8—14; a pH 9 borate buffer solution (1 M) was used throughout. Under the conditions, the pH of the sample solution had to be above ca. 0.8 to obtain a maximum and constant intensity.

It is interesting to note that the extraction rate of copper(II) was much accelerated by addition of nickel(II). When a 1-mm i.d. and 2-m long Teflon extraction coil was used and nickel(II) was absent in the aqueous phase, the recovery of copper(II) was no more than about 50%. However, in the presence of nickel(II) of more than 60-fold amounts of copper(II), the extraction of copper(II) was confirmed to be complete even with the same length of the extraction coil. The behavior of nickel(II) is not understood as yet and awaits further investigation.

The volume of sample taken in the suction cup was varied by using the volume-adjustable pipet. Figure 2 shows some typical signals obtained with different volumes of a 100 ng cm^{-3} copper(II) solution at a time constant for the electronic circuit of 10 s. Variation of the time constant had no appreciable effect on the sensitivity provided that it was in the range 3—10 s. However, the signal became noisy at the smaller time constant. The best reproducibility was obtained at 10 s. The peak height was proportional to the volume added up to about 3 cm^3 and thereafter was constant. A 2-cm^3 sample plug showed ca. 80% of the plateau intensity. This volume seems to be a good compromise between high sensitivity and the practical requirements of high sampling rate and low reagent consumption.

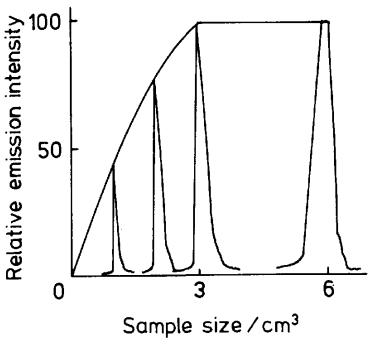

Fig. 2. Recorder tracings obtained with various sample volumes. Copper(II): 100 ng cm^{-3}.

Table 1. Determination of Copper in Human Organs[a)]

Sample	Copper found/μg g^{-1}	
	Present method	GF-AAS[b)]
Liver 3374	9.3±0.2	9.7±0.2
Liver 3355	4.8±0.1	4.7±0.1
Liver 3308	4.2±0.2	4.5±0.2
Pancreas 3355	1.2±0.0	1.3±0.1
Kidney 3354	4.0±0.1	3.8±0.3

a) Wet base. b) Mean±av. dev., 2 results.

Under the recommended procedure, a linear calibration graph was obtained for up to 500 ng cm^{-3} copper(II). The detection limit (S/N=3) was 1.5 ng cm^{-3} copper. The detection limit is about 11-fold better than that obtained by direct aspiration of the aqueous solution. The improvement is attributed not only to the preconcentration of copper by extraction, but also to the enhancement effect of chloroform.[6] The relative standard deviation for 10 replicate measurements was 2.2% for 100 ng cm^{-3} copper(II) and the sample throughput was 25 h^{-1}.

The interferences of large amounts of alkali and alkaline earth metal salts could be avoided by the extraction. Most other metal ions such as cobalt(II), nickel(II), zinc(II), cadmium(II), tin(II), antimony(III), mercury(II), lead(II), and bismuth(III) did not interfere with the determination of copper when present in 200-fold amounts of 100 ng cm^{-3} copper(II). Interferences were encountered only with aluminum(III), chromium(III), and ion(III); the maximum permissible amounts within 10% error of these species were 91-, 45-, and 32-fold, respectively. The interferences may arise from metal hydrolysis during the extraction process of copper(II) under the alkaline condition.

The reliability of the present method was examined by comparing the analytical results of some human organ samples with those obtained by the graphite-furnace atomic absorption spectrometry (GF-AAS) combined with dithizone-carbon tetrachloride batch-extraction.[7] The samples were prepared by digesting in Teflon beakers with nitric acid and perchloric acid on a hot plate. As Table 1 shows, the data are in good agreement with each other.

The authors wish to express their thanks to Professor Mitsuo Kiboku of Kinki University and Dr. Koji Kirimoto of Kure National Hospital for providing the human organ samples.

References

1) E. Kimura, *Yuki Gosei Kagaku Kyokai Shi*, **44**, 871 (1986).
2) A. Jyo and M. Takagi, *Bunseki*, **1985**, 185.
3) E. Kimura, C. A. Dalimunte, A. Yamashita, and R. Machida, *J. Chem. Soc., Chem. Commun.*, **1985**, 1041.
4) M. Ikeda, F. Nakata, H. Matsuo, and T. Kumamaru, *Bunseki Kagaku*, **33**, 416 (1984).
5) B. Karlberg and S. Thelander, *Anal. Chim. Acta*, **98**, 1 (1978).
6) T. Kumamaru, M. Matsuo, and Y. Yamamoto, Presented at the 1984 International Chemical Congress of Pacific Basin Societies, Honolulu, December 1984, Abst. No. 01I05.
7) Y. Yamamoto, T. Kumamaru, T. Kamada, T. Tanaka, and M. Kawabe, *Nippon Kagaku Kaishi*, **1975**, 836.

Synthesis, Properties, and Crystal and Molecular Structure of Diaquatetrakis(thiocyanato)cobalt(II)mercury(II)-2-pyrrolidone (1/2), $[CoHg(SCN)_4(H_2O)_2]\cdot 2C_4H_7NO$

Hisashi KINOSHITA* and Akira OUCHI†
Department of Chemistry, Faculty of Liberal Arts, Shizuoka University, Ohya, Shizuoka 422
†Department of Chemistry, College of Arts and Sciences, The University of Tokyo, Komaba, Meguro-ku, Tokyo 153
(Received September 3, 1986)

Synopsis. The title inclusion compound, which has a new-type "double decker" host skeleton, has been obtained, and its crystal and molecular structure has been determined by the X-ray diffraction technique using its single crystal. 2-Pyrrolidone molecules are not directly coordinated to any metal atoms, but are hydrogen-bonded with coordinated water-oxygen atoms in the two-dimensional polymer planes of $[CoHg(SCN)_4(H_2O)_2]_n$. In the complex polymer, each pair of adjacent Hg(4S(SCN) four-coordinated in a tetrahedral geometry) and Co(4N(SCN), 2O(water, trans) six-coordinated in an octahedral geometry) atoms are bridged with a thiocyanate (SCN) ion. Such two types of networks are spread approximately parallel to the (010) plane at 1/4 and 3/4 heights, and the included Lewis base molecule layers are also doubled. Compared with the previously reported single-layer host skeleton of $[CoHg(SCN)_4(H_2O)_2]\cdot 2L$ (L=Lewis base), the present one is short in its inter-complex layer distance, in spite of the analogous size of the included molecule. The crystallographic data are: orthorhombic, space group $P2_1nb$, a=12.004(4), b=15.330(5), c=11.985(4) Å, and Z=4. The final R value was 0.054.

Previously, the present authors[1,2] have reported about the crystal structures of some adducts of tetrakis(thiocyanato) cobalt(II)mercury(II), $CoHg(SCN)_4$ (**1**), with the general formula of $CoHg(SCN)_4(H_2O)_2\cdot 2L$ (L=*N*,*N*-dimethylacetamide (dma), (**2**)[1] or *N*-methyl-2-pyrrolidone (mpd) (**3**).[2] These complexes were found to be a new type of inclusion compound in which the Lewis bases were not coordinated to any metal atoms directly, but were kept between the two-dimensional polymeric planar networks only by the hydrogen bondings. The cage structure of **2** and **3** are almost the same.

In this line of research, the title complex was obtained. From the preliminary test, its crystal system and the unit cell size were found to be different from those of **2** and **3**. Expecting to find a new type of structure of the inclusion compound, we have investigated the crystal and molecular structures of this complex by means of the X-ray diffraction method, using its single-crystal.

Experimental

Synthesis of Diaquatetrakis(thiocyanato)cobalt(II)mercury(II)-2-pyrrolidone(1/2), $CoHg(SCN)_4(H_2O)_2\cdot 2pd$ (4). The crystalline powder of **1** (1.0 g, 2.0 mmol) was dissolved into 2-pyrrolidone (pd) (10 cm³), and 20 cm³ of water was added to the solution. The mixture was left standing for several days; thereby the red-brown crystals of **4** were deposited. They were filtered off and dried over silica gel. Yield: 0.8 g, 57%. Anal. Found: Co, 8.22; C, 20.75; H, 2.76; N, 12.33%. Calcd for $CoHgC_{12}H_{18}N_6O_4S_4$: Co, 8.44; C, 20.65; H, 2.60; N, 12.04%.

X-Ray Structure Analysis. A crystal of **4** with the dimensions of 0.3×0.3×0.12 mm³ was used for the intensity measurement. Crystallographic data: $CoHgC_{12}H_{18}N_6O_4S_4$ $F.W.$=698.10, orthorhombic, with the space group of $P2_1nb$, a=12.004(4), b=15.330(5), c=11.985(4) Å, U=2205.5(11) Å³, Z=4, D_m=2.07(3) Mg m⁻³, D_x=2.07 Mg m⁻³, μ(Mo $K\alpha$)=8.28 mm⁻¹. Reflections within a range of $3°<2\theta<60°$ were collected on a Rigaku AFC-6A automated four-circle X-ray diffractometer, with graphite-monochromated Mo $K\alpha$ radiation, the ω-2θ scan technique was employed (scan speed, 4° min⁻¹ in θ; scan width, 1.12+0.5tanθ°). Of the 3564 independent reflections measured, 1841 $|F_o|>3\sigma(|F_o|)$ reflections were used for the structure determination. The intensities were corrected for the Lorentz and polarization factors as well as for the absorption. The last correction was made using a numerical Gaussian integration.[3] The structure was solved by the heavy atom method. The final R value obtained by applying the anisotropic temperature parameters was 0.054.[4] As the R value for the structure with an inversed chirality was 0.059, the value was not adopted.

All the calculations were carried out on a HITAC M-680H computer apparatus at the Computer Center of the University of Tokyo, using the local version of the UNICS program system.[5] The atomic scattering factors were taken from Ref. 6.

Other Measurements. The infrared absorption spectra were obtained by means of a Hitachi EPI-G3 grating infrared spectrophotometer using mineral oil and hexachloro-1,3-butadiene mull. The magnetic moment of the solid sample was measured at 20 °C using a Gouy balance.

Results and Discussion

The selected bond-lengths and bond angles, and also some interatomic distances, are shown in Table 1.[7] A perspective drawing of the complex around a cobalt atom, together with the hydrogen bondings between the neighboring cobalt atoms along the b-axis, is shown in Fig. 1. The projection of the structure along the b-axis is shown in Fig. 2.

Each mercury atom is coordinated tetrahedrally to four SCN sulfur atoms. The cobalt atom is six-coordinated and is in an octahedral geometry, where four SCN nitrogen atoms are ligated equatorially, and two water oxygen atoms, axially, approximately from the b-axis directions. The bond lengths of Hg–S, Co–O, and Co–N (on the average, 2.536, 2.089, and 2.12 Å respectively) are not much different from the respective sums of Shannon's ionic radii: Hg–S, 2.80; Co–O, 2.00; and Co–N, 2.11 Å.[8] Both of the bond angles, Co–N–C (169° on the average) and N–C–S (177° on the average) deviate a little from 180°.

As is shown in Fig. 1, both kinds of pd molecules

Table 1. Selected Bond Lengths and Bond Angles, with Estimated Standard Deviations in Parentheses

Bond length	l/Å	Bond length	l/Å	Bond length	l/Å
Hg-S(1^{i})	2.551(7)	Co-N(1)	2.138(16)	S(1)-C(1)	1.64(2)
Hg-S(2^{ii})	2.514(7)	Co-N(2)	2.08(2)	S(2)-C(2)	1.66(2)
Hg-S(3)	2.548(7)	Co-N(3)	2.11(2)	S(3)-C(3)	1.62(2)
Hg-S(4^{iii})	2.529(7)	Co-N(4)	2.149(18)	S(4)-C(4)	1.66(3)
Co-O(W1)	2.085(11)	O(W1)···O(11)	2.71(2)	C(1)-N(1)	1.15(3)
Co-O(W2)	2.093(11)	O(W1)···O(21)	2.72(2)	C(2)-N(2)	1.16(3)
C(11)-O(11)	1.22(3)	O(W2^{iv})···O(21)	2.64(2)	C(3)-N(3)	1.13(3)
C(21)-O(21)	1.26(3)	O(W2^{iv})···O(21)	2.68(2)	C(4)-N(4)	1.11(3)
Boud angle	ϕ/°	**Bond angle**	ϕ/°	**Bond angle**	ϕ/°
S(1^{i})-Hg-S(2^{ii})	101.9(2)	N(1)-Co-N(2)	92.7(8)	N(1)-Co-O(W1)	88.0(5)
S(1^{i})-Hg-S(3)	121.3(2)	N(1)-Co-N(3)	175.0(7)	N(1)-Co-O(W2)	87.7(5)
S(2^{ii})-Hg-S(3)	104.8(2)	N(2)-Co-N(3)	89.7(8)	N(2)-Co-O(W1)	93.8(7)
S(3)-Hg-S(4^{iii})	102.5(2)	N(1)-Co-N(4)	87.6(7)	O(W1)-Co-O(W2)	175.7(5)
Hg-S(1^{i})-C(1^{i})	99.2(8)	Co-N(1)-C(1)	167.6(16)	S(1)-C(1)-N(1)	176.8(19)
Hg-S(2^{ii})-C(2^{ii})	97.3(9)	Co-N(2)-C(2)	172(2)	S(2)-C(2)-N(2)	174(2)
Co-O(W1)···O(11)	136.0(10)	O(11)···O(W1)···O(21)	91.7(6)	O(W1)···O(11)···O(W2^{iv})	87.7(8)
Co-O(W1)···O(21)	126.9(10)	O(11)···O(W2^{iv})···O(21)	94.0(6)	O(W1)···O(21)···O(W2^{iv})	86.6(7)

Key to the symmetry operations: i, $-1+x, y, z$; ii, $-0.5+x$, $0.5-y$, $-0.5+z$; iii, $-0.5+x$, $0.5-y$, $0.5+z$; iv, x, $0.5+y$, $0.5-z$; v, x, $-0.5+y$, $0.5-z$.

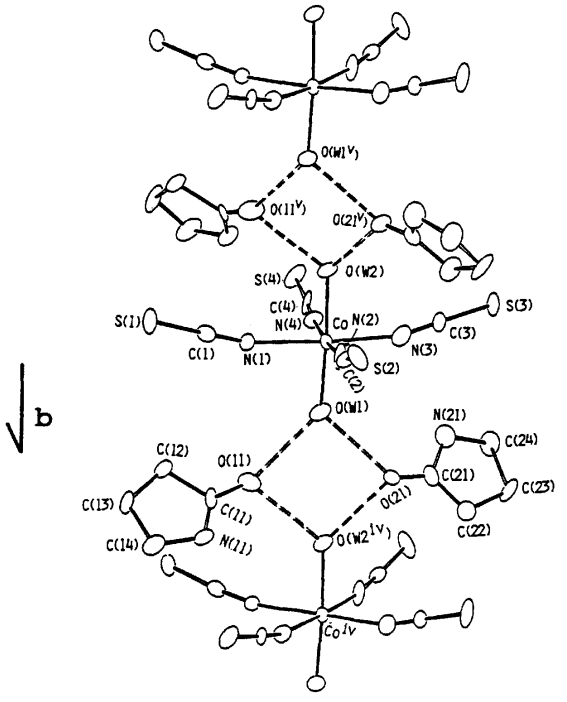

Fig. 1. The perspective drawing of the complex around a cobalt atom and the included Lewis bases.

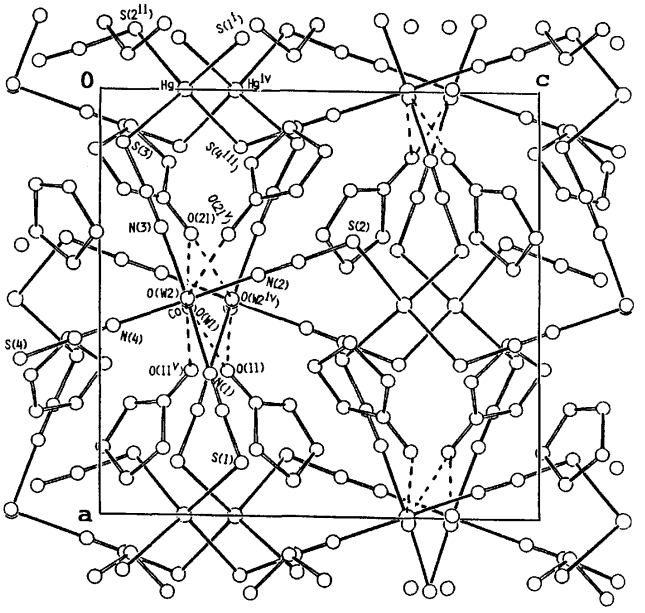

Fig. 2. The projection of the unit cell of the complex to the (010) plane.

are linked by hydrogen-bondings to the water oxygen atoms, which are ligated to the cobalt atoms. As is shown in Fig. 2, two mercury(II), two cobalt(II), and four SCN ions make a sixteen-membered ring which organizes the unit of the two-dimensional network of the polymeric complex and which is about the same as those of **2** and **3**.

The 1/4 of the ac face of the unit cell of **4** is 35.97 Å^2, while those of **2** and **3** (1/4 of the ab face) are 36.75 and 36.17 Å^2 respectively. Therefore, the areas of this sixteen-membered rings (exactly, the projections to the average plane) are approximately the same.

However, the crystal structures **2** or **3**, and **4** are very different with each other. In the cases of **2** and **3**, the network of the complex as well as the base molecule layer spread parallel to the ab-plane, and the separation of the plane corresponds with the c-axis length: 7.985 Å in **2** and 8.097 Å in **3** respectively. On the other hand, there are two such networks in the **4**

Table 2. Infrared Absorption Data of **1**, mpd, **3**, pd, and **4** (in σ/cm^{-1})

1[1]	mpd[9]	**3**	pd[9]	**4**	Tentative Assignment
		3360 (s)		3290 (s)	ν(O-H)
			3240 (w)	3400 (w)	ν(N-H)
	2895 (m)	2950 (m)	2940 (m)	2980 (m)	ν(C-H)
2150 (s)		2140 (s)		2140 (s)	ν(CN)
		1650 (m)		1655 (m)	δ(HOH)
	1682 (s)	1640 (s)	1687 (s)	1640 (s)	ν(CO)
720 (s)		730 (m)		720 (m)	ν(CS)
470 (s)		460 (s)		470 (m)	δ(SCN)
447 (s)		440 (s)		445 (m)	δ(SCN)

1, $CoHg(SCN)_4$; **3**, $CoHg(SCN)_4(H_2O)_2 \cdot 2mpd$; **4**, $CoHg(SCN)_4(H_2O)_2 \cdot 2pd$.

complex, approximately 1/4 and 3/4 in height respectively, parallel to the (0 1 0) plane. Therefore, the separation of the network plane is a half of the b-axis length, 7.665 Å, which is much shorter than those of **2** and **3**. On both network layers, the respective metal atomic positions deviated only a little, approximately in the c-axis direction, from each other. However, the positions of the pd molecules in the two intervals are very different. Each pd molecule exists in a interval space where the top and bottom walls are concave, while the space between the convexed walls is vacant. Thus, the filled and empty intervals are laid alternately, perpendicular to the plane. This is probably the main cause of the shorter inter-layer distance of this complex.

If we define the cage volumes of this type of inclusion compound by the unit-cell volume divided by the number of the included base molecule, they are 292 and 296 $Å^3$ in the cases of **2** and **3** respectively. On the other hand, the volume of the **4** complex is $2205.5/8=276$ $Å^3$, which is smaller than the former two, showing the more compact packing in this complex.

Some infrared spectral data are shown in Table 2. When the wavenumbers of the peaks of **4** are compared with those of the free-ligand molecules,[9] its ν(C=O) peak is found to be red-shifted by 40—50 cm^{-1}. Such a red shift has also been observed in the spectra of **3** as well as **2**,[1] and it is considered to be due to the strong hydrogen bonds between the Lewis-base molecule and the ligating water molecules. The hydrogen bondings are manifested by the ν(O-H) at high frequencies, too.[10] The ν(N-H) of **4** is shifted from 3240 (free pd) to 3400 cm^{-1} as a result of the release from mutual hydrogen bondings in the free ligand molecules.[11] The wavenumbers of the bands caused by the SCN ions of **1**, **2**,[1] **3**, and **4** are not very different from one another.

The magnetic moment of **4** is about 5.05 BM at 20 °C, about the same as that of **3**, 4.98 BM (1 BM=$9.274078(36)\times10^{-24}$ JT^{-1}). These are typical values for the cobalt(II) ion in the octahedral geometry.

References

1) H. Kinoshita, M. Shimoi, A. Ouchi, and S. Sato, *Bull. Chem. Soc. Jpn.*, **58**, 2782 (1985).

2) H. Kinoshita, M. Shimoi, and A. Ouchi, *Bull. Chem. Soc. Jpn.*, **59**, 1253 (1986).

3) W. R. Busing and H. A. Levy, *Acta Crystallogr.*, **10**, 180 (1957).

4) $R=\sum||F_o|-|F_c||/\sum|F_o|$

5) "The Universal Crystallographic Computation Program-System (UNICS)," ed by T. Sakurai, Crystallographic Society of Japan, Tokyo (1967).

6) "International Tables for X-ray Crystallography," Kynoch Press, Birmingham (1974), Vol. IV, pp. 72, 150.

7) The final atomic positional and thermal parameters, and the final F_o-F_c table, are deposited as Document No. 8730 at the Office of the Editor of *Bull. Chem. Soc. Jpn.*

8) R. D. Shannon, *Acta Crystallogr., Sect. A*, **32**, 751 (1976). Shannon's Ionic Radii: Hg (Val=2+, CN=4) 0.96, Co (Val=2+, CN=6) 0.65, O (Val=2−, CN=2) 1.35, N (Val=3−, CN=4) 1.46, S (Val=2−, CN=6) 1.84 Å.

9) K. Kurosaki, *Nippon Kagaku Zasshi*, **82**, 1691 (1961).

10) K. Nakamoto, "Infrared and Raman Spectra of Inorganic and Coordination Compounds," 3rd ed., Wiley Interscience, N. Y. (1978), p. 119.

11) L. T. Bellamy, "The Infrared Spectra of Complex Molecules," 2nd ed., Methuen, London (1958), p. 245.

The Relationships between the Formation Constants of 2,2′-Bipyridine Metal(II) Complexes and the Donor Numbers of Solvents

Yuriko Abe* and Goro Wada†
Graduate Division of Human Culture and Faculty of Science,† Nara Women's University, Nara 630
(Received September 29, 1986)

Synopsis. The complex formation constants of cobalt(II) or zinc(II) with 2,2′-bipyridine (bpy) were determined spectrophotometrically in various solvents. The values of $\log K_1$, $\log K_2$, and $\log K_3$ for the Co(II) complexes obtained were 4.06±0.06, 3.09±0.04, and 1.15±0.02 respectively in dimethyl sulfoxide, while those of $\log K_1$ for the Zn(II)–bpy complexes were 6.27±0.10, 4.14±0.01, 4.71±0.03, and 3.44±0.12 in trimethyl phosphate, *N,N*-dimethylformamide, *N,N*-dimethylacetamide, and dimethyl sulfoxide respectively. It was found that the linear relationships hold between logarithms of the formation constants of the bpy complexes and the donor numbers of the solvents when both the solvated metal ions and the bpy complexes are octahedral in the solvents.

In recent years, studies of the solvent effects on the chemical reactions have been extensively reported.[1-3] However, there are few quantitative equilibrium data to account for the solvent effects for the first transition metal complexes.[1,4,5]

In this study, we determined spectrophotometrically the complex formation constants of cobalt(II) or zinc(II) with 2,2′-bipyridine (bpy) in dimethyl sulfoxide (DMSO), trimethyl phosphate (TMP), *N,N*-dimethylformamide (DMF), and *N,N*-dimethylacetamide (DMA) for the purpose of clarifying the solvent effects on the chemical equilibria. The linear relationship between the logarithms of the complex formation constants and the donor numbers of the solvents will be discussed on the basis of the experimental data.

Experimental

Materials and Preparations. DMSO and DMF of a guaranteed reagent grade were purified as has been described elsewhere.[6,7] TMP and DMA were distilled under a reduced pressure of nitrogen, after having been dried with 5A molecular sieves. 2,2′-Bipyridine was recrystallized from a hexane solution. Solvated complexes of the metal ions $[M(s)_6](ClO_4)_2$ (M=Co(II) or Zn(II), and s=dmso, dmf, or dma) were synthesized by methods similar to those of $[M(hmpa)_4](ClO_4)_2$:[8] hydrated metal perchlorate was treated with a large excess of 2,2-dimethoxypropane for one hour with stirring. At the end of the dehydration period, a slight excess of the solvent was added. After several minutes, a large excess of anhydrous ether was added, and then the precipitate was filtered. They were dried in a vaccum desiccator. Solvated Zn(II) perchlorate in TMP was prepared as follows: hydrated Zn(II) perchlorate was dissolved in TMP, where 5A molecular sieves were present for the purpose of dehydration. After standing overnight, 5A molecular sieves were removed from the solution. Portions of stock solutions of these metal perchlorates were taken to analyze the metal ion concentrations by the spectrophotometric methods already reported.[9] The bpy complex solutions were prepared by mixing aliquots of the stock solutions of metal perchlorates with those of the bpy solution. The ionic strength was kept at I=0.06 M (mol dm^{-3}) with sodium perchlorate.

Apparatus. The absorptivities of complex solutions were measured by using a Shimadzu Spectrophotometer, Model UV-200S, with a thermostated cell compartment. The temperature was kept at 25±0.1 °C.

Results and Discussion

The value of the first formation constant, $K_1=[[M(bpy)]^{2+}]/[M^{2+}][bpy]$, for the Co(II)–bpy complex in DMSO, and those for the Zn(II)–bpy complexes in DMSO, DMF, DMA, and TMP were obtained by the use of Job's curves.[10,11] The value of the second formation constant, $K_2=[[M(bpy)_2]^{2+}]/[[M(bpy)]^{2+}][bpy]$, and that of the third formation constant, $K_3=[[M(bpy)_3]^{2+}]/[[M(bpy)_2]^{2+}][bpy]$, for the Co(II)–bpy complex in DMSO were obtained by the linear relationship method.[10,11] The results are summarized in Table 1, together with the results in hexamethylphosphoric triamide (HMPA) and those for the Mn(II)–bpy complex previously reported.[11-13] The $\log K$ values decrease roughly in accordance with the increase in the donor number (D) of the solvents, except for the K_1 and K_2 values for the Co(II)–bpy complexes and for the K_1 value for the Mn(II)–bpy complex in HMPA, as shown in Table 1.

It is accepted that, in solvents such as water, methanol, DMSO, and DMF, the solvated ions of first transition metals are mostly octahedral.[14-16] On the other hand, we have already reported that, in HMPA, they prefer the tetrahedral configurations to the octahedral ones since the HMPA molecule is very bulky as compared with the molecules of the other solvents.[9,11] Therefore in all the solvents used here other than in HMPA, $[M(s)_6]^{2+}$ (M(II)=Mn(II), Co(II), or Zn(II), s=solvent) is octahedral.[14-16] Their bpy complexes are probably be octahedral also, for the bpy ligand gives a stronger ligand field than the solvents. Nevertheless, $[Zn(hmpa)_6]^{2+}$, $[Zn(hmpa)_4(bpy)]^{2+}$, and $[Co(hmpa)_2(bpy)_2]^{2+}$ in HMPA are octahedral, in contrast with the tetrahedral configurations of $[M(hmpa)_4]^{2+}$ and $[M(hmpa)_2(bpy)]^{2+}$ (M(II)=Mn(II) or Co(II)).[9,11] Therefore, when the octahedral–octahedral equilibria are established in the solvents, the linear relationship can be said to hold roughly between $\log K$ vs. D as shown in Table 1. The deviation from the linearity in HMPA may be due to the establishment of a tetrahedral–tetrahedral or tetrahedral–octahedral equilibrium, in consequence of the steric hindrance caused by the bulkiness of the HMPA molecule in the coordination sphere.[11]

When bpy coordinates to a metal ion, the metal ion liberates two solvent molecules from the coordination sphere. Therefore, the true formation constant should

Table 1. Formation Constants of the Complexes of Mn(II), Co(II), and Zn(II) with bpy in Various Solvents at 25 °C and $I=0.06$ mol dm^{-3}

M^{2+}	Ligand	log K[a]	Solvent (Donor Number)						
			H_2O[12] (18)	CH_3OH[13] (19)	TMP (23)	DMF (26.6)	DMA (27.8)	DMSO (29.8)	HMPA[11] (38.8)
		log K_1	5.65					4.06	5.84[b]
Co^{2+}	bpy	log K_2	5.60					3.09	3.58[c]
		log K_3	4.80					1.15	−0.4
Zn^{2+}	bpy	log K_1	5.20		6.27	4.14	4.71	3.44	1.77
Mn^{2+}	bpy	log K_1	2.62	2.7				2.5	3.10[b]

a) log K in octahedral-octahedral equilibrium except for b) and c). b) log K_1 in tetrahedral-tetrahedral equilibrium. c) log K_2 in tetrahedral-octahedral equilibrium.

be $K_{x+1}[s]^2$ rather than $K_{x+1}=[[M(bpy)_{x+1}]^{2+}]/[[M(bpy)_x]^{2+}][bpy]$ (x=0, 1, or 2) in an octahedral-octahedral equilibrium, where [s] is the molar concentration of the solvent. Since the [s] values are not equal to each other for various solvents, the plots of log $K_{x+1}[s]^2$ *vs.* D are probably more reasonable than those of log K_{x+1}. Figure 1 shows the plots of log $K_{x+1}[s]^2$ *vs.* D. The linearity for the K_1 of the Zn(II)-bpy complex corresponding to the octahedral-octahedral equilibria in all solvents is improved from that in Table 1.

When octahedral-octahedral equilibria hold in various solvents, the following linear equation is given:

$$\log K[s]^2 = \alpha D + \text{const.} \quad (1)$$

where α is the slope of the straight line. Moreover, the following equation holds in the solvents:

$$-RT \ln K[s]^2 = \Delta H - T\Delta S \quad (2)$$

It is considered that the ΔS values of the equilibria in various solvents are roughly equal, because one bpy molecule is taken in, and two solvent molecules are liberated in each reaction. Thus, the changes in the K values upon changing solvents are due mainly to the changes in the ΔH values upon changing solvents, which depend upon the properties of the solvent; the bond strength between the metal ion and the solvent in the coordination sphere increases with the increase in the basicities of the solvents. The donor number is a measure of the basicity of the solvent, being equal to the heat of the reaction between $SbCl_5$ and the solvent in 1,2-dichloroethane.[2] All the solvents used in the present study coordinate with the oxygen atom to the first transition metal ion, with no back donation in the coordination. Thus, it is considered that Eq. 1 might hold for the metal ion in various solvents in octahedral-octahedral equilibria.

It has been reported that, in the cases of halide (X^-), the stabilities of $[Co(X)_4]^{2-}$ are affected by both the donor number and the acceptor number of the solvents.[2] However, since bpy is electrically neutral and the solvation to bpy occurs more weakly than that to the Cl^- ion, the acceptor number is not important here.

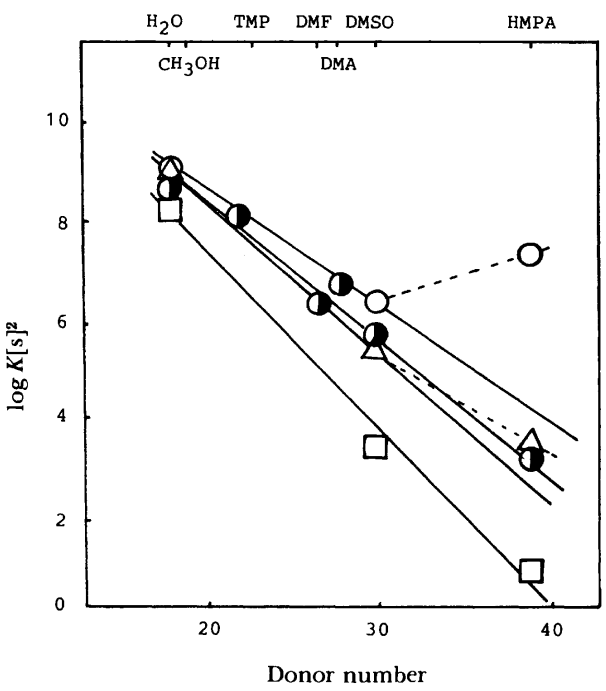

Fig. 1. Linear relations of log $K[s]^2$ vs. donor numbers in various solvents. For Co(II)-bpy complexes, (○): log $K_1[s]^2$, (△): log $K_2[s]^2$, (□): log $K_3[s]^2$. In HMPA, the value of log K_2 is plotted since the tetrahedral-octahedral equilibrium holds at the second step. For Zn(II)-bpy complexes, (◑): log $K_1[s]^2$.

In conclusion, log $K[s]^2$ is linear with respect to the donor number only when the solvation to the ligand is weak and the octahedral-octahedral equilibria hold in the solvents, as is shown in Fig. 1.

References

1) E. S. Amis, "Solvent Effects on Reaction Rates and Mechanisms," Academic Press, New York (1966).
2) V. Gutmann, "The Donor and Acceptor Approach to Molecular Interactions," Plenum Press, New York (1978).
3) M. Senoo and T. Arai, "Solvent Effects on Organic Reactions," Sangyotosho, Tokyo (1965).
4) V. Gutmann, A. Weisz, and W. Kerber, *Monatsh.*

Chem., **100**, 2096 (1969).
5) A. Miezis, *Acta. Chem. Scand., A.*, **28**, 407 (1974).
6) Y. Unno and G. Wada, *Bull. Chem. Soc. Jpn.*, **46**, 1188 (1973).
7) G. Wada, Y. Sahira, K. Ohsaki, and F. Shinoda, *Bull. Chem. Soc. Jpn.*, **47**, 851 (1974).
8) J. T. Donoghue and R. S. Drago, *Inorg. Chem.*, **1**, 866 (1962).
9) Y. Abe and G. Wada, *Bull. Chem. Soc. Jpn.*, **53**, 3547 (1980).
10) G. Wada, *Bull. Chem. Soc. Jpn.*, **41**, 882 (1968).
11) Y. Abe and G. Wada, *Bull. Chem. Soc. Jpn.*, **54**, 3334 (1981).
12) L. G. Sillén and A. E. Martell, "Stability Constants Supplements No. 1 Special Publication 25," ed by The Chemical Society, Alden Press, Oxford (1971).
13) D. P. Douglas, "Stability Constants of Metal-Ion Complexes Part 8. Organic Ligands," Pergamon Press, New York (1979).
14) A. B. P. Lever, "Inorganic Electronic Spectroscopy," Elsevier Publishing Company, Amsterdam (1968), Chap. 9.
15) H. B. Silber, D. Simon, and F. Gaizer, *Inorg. Chem.*, **23**, 2844 (1984).
16) W. Libuś, B. Chachulski, W. Grzybkowski, M. Pilarczyk, and D. Puchalska, *J. Solution Chem.*, **10**, 631 (1981).

Preparation and Structure of {Bis(3-aminopropyl)amine}(*r*-1, *c*-3, *c*-5-cyclohexanetriamine)cobalt(III) Complex

Minoru Ishii,* Michiko Umehara, and Masayoshi Nakahara
Department of Chemistry, College of Science, Rikkyo (St. Paul's) University, Nishiikebukuro 3, Toshima-ku, Tokyo 171
(Received August 8, 1986)

Synopsis. {Bis(3-aminopropyl)amine}(*r*-1,*c*-3,*c*-5-cyclohexanetriamine)cobalt(III) complex was prepared and the crystal structure of its iodide has been analyzed by X-ray diffraction. The complex cation has a facial configuration and an exo-type of N(secondary)-H bond orientation in bis(3-aminopropyl)amine. There is only a little distortion in the octahedron of this complex cation.

Although the complexes of five-membered rings of diethylenetriamine (dien) ligand have been extensively studied, reports on those of six-membered ring bis(aminopropyl)amine (dpt) are relatively few.

In a previous paper, the authors described the preparation of *mer*-$[Co(dpt)_2]^{3+}$ complex and the resolution to their optical isomers.[1] We also reported the structure of a bis-type complex of *r*-1,*c*-3,*c*-5-cyclohexanetriamine (chta), which takes a facial position and forms six-membered rings.[2]

The title complex, which is the mixed complex of chta and dpt, has necessary a facial geometry and exo and endo isomers in dpt as shown in Fig. 1.

In this paper, the authors will report the preparation of {bis(3-aminopropyl)amine}(*r*-1,*c*-3,*c*-5-cyclohexanetriamine)cobalt(III) complex, $[Co(chta)(dpt)]^{3+}$, and the crystal structure of its iodide.

Experimental

Preparation. To 80 mg of finely ground $[CoCl_3(chta)]$,[3] 5 ml of dpt solution (45 mg dpt/ml ethanol) was added, and the solution was stirred for 5 h on a water bath. The reddish-orange solution was diluted with a small amount of water and filtered to remove unreacted materials. The filtrate was poured into a column (ϕ 40 mm, h 300 mm) containing SP-Sephadex C-25 resin of Na^+ form. After the column was washed with 1 dm^3 water, elution was carried out with 1.0 mol dm^{-3} hydrochloric acid. A faster red layer and a slower reddish-orange layer descended. The reddish-orange fraction was concentrated to a small volume by an evaporator at 35 °C. With addition of ethanol to this solution, orange powders were obtained. Yield 21 mg (18%). Found: C, 32.50; H, 7.49; N, 18.87%. Calcd for $CoCl_{12}N_6H_{32}Cl_3 \cdot H_2O$: C, 32.48; H, 7.72; N, 18.94%. Absorption maxima of ligand field bands and their extinction coefficients are as follows: ,20300 cm^{-1} (log ε=1.90), 28300 cm^{-1} (log ε=1.94). The crystal for X-ray analysis was grown from an aqueous solution, after the chloride was converted into iodide with an I^- form anion-exchange resin.

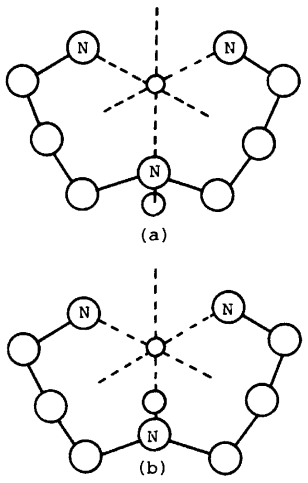

Fig. 1. Coordination mode of bis(3-aminopropyl)-amine. (a) exo (b) endo.

Crystal Structure Determination. The crystal data are as follows: $[Co(chta)(dpt)]I_3 \cdot H_2O$, $CoC_{12}N_6H_{32}I_3 \cdot H_2O$, $F.W.$= 818.09, monoclinic, space group $P2/a$,[4] a=23.424(7), b=12.079(3), c=9.761(3) Å, β=123.93(11)°, V=2291.6(1) Å^3, D_x=2.03 Mg m^{-3}, D_m=2.05 Mg m^{-3}, Z=4. A polyhedral crystal of approximately spherical shape with the radius of 0.5 mm was used for the X-ray intensity measurement. The intensity was measured on a Rigaku AFC-5 four-circle diffractometer (Keio University) with graphite-monochromated Mo $K\alpha_1$ radiation (λ=0.7093 Å) up to 2θ of 55°. The θ-2θ scan technique was employed. Independent 4482 reflections with $|F_o|>3\sigma(|F_o|)$ were used for structure determination. Corrections were made for the Lorentz and polarization factors, but no correction for absorption and extinction was applied. The structure was analyzed by the Patterson method by means of UNICS.[5] The calculation was carried out on a UNIVAC 1100 computer at Rikkyo University Computer Center. Scattering factors were taken from International Tables for X-ray Crystallography.[6] The refinement was carried out using the block-diagonal least-squares program HBLS IV based on $\Sigma w(|F_o|-k|F_c|)^2$, w=1, with anisotropic thermal parameters for nonhydrogen atoms and isotropic ones for hydrogen atoms. Fifteen among thirty-two hydrogen atoms (except those of the water molecule) were found from different synthesis. The remaining seventeen hydrogen atoms were located at sites calculated by assuming a tetrahedral geometry around C and N and fixed bond lengths. The atomic and thermal parameters of the complex are given in Table 1.[7] The R and R_2 values were 4.09 and 4.60%, respectively. A perspective drawing of the complex cation is shown in Fig. 2.

Results and Discussion

The chta and dpt ligands coordinate with six nitrogen atoms from above and below cobalt atom to form an octahedral complex. Each ligand spreads across a face of the octahedron, that is, it coordinates in facial positions as expected. In the dpt chelate, N-(secondary)-H (N(5)-H) bond orientation has apparently an exo-type (Fig. 1-(a)). In the chta chelate, triplet six-membered chelate rings have stable chair-

Table 1. Final Atomic Coordinates ($\times 10^5$ for I and Co, $\times 10^4$ for N, C, and O), with Estimated Standard Deviations in Parentheses, and Their Equivalent Isotropic Thermal Parameters

Atom	x	y	z	B_{eq}/Å^2 a)
I(1)	45741(3)	15598(5)	62913(7)	3.1_0
I(2)	39326(3)	47072(4)	16768(6)	2.6_6
I(3)	18670(3)	45524(5)	20682(6)	3.1_2
Co	10394(4)	23261(7)	46387(10)	1.3_3
N(1)	2033(3)	1947(5)	5877(7)	2.1_1
N(2)	1107(3)	2438(5)	6755(7)	1.2_3
N(3)	1276(3)	3913(4)	4805(7)	1.8_8
N(4)	31(3)	2693(5)	3436(7)	2.3_1
N(5)	954(3)	2199(5)	2473(7)	2.0_1
N(6)	792(3)	723(5)	4538(7)	2.0_0
C(1)	2530(4)	2602(6)	7424(9)	2.4_7
C(2)	2358(4)	2452(7)	8686(9)	2.9_1
C(3)	1695(4)	3026(6)	8175(8)	2.5_9
C(4)	1672(4)	4229(6)	7708(9)	2.9_1
C(5)	1851(4)	4368(6)	6451(9)	2.5_6
C(6)	2522(4)	3806(6)	6973(9)	2.6_7
C(7)	−321(4)	3501(7)	2059(11)	3.3_7
C(8)	−2(4)	3583(7)	1066(10)	3.2_4
C(9)	266(4)	2480(8)	931(9)	3.4_8
C(10)	1216(4)	1158(6)	2174(10)	2.7_2
C(11)	856(4)	135(6)	2209(10)	2.9_3
C(12)	1056(4)	−138(6)	3913(10)	2.7_7
O(1)	2806(4)	2229(7)	4371(11)	5.6_5

a) $B_{eq}=4/3(B_{11}a^2+B_{22}b^2+B_{33}c^2+B_{13}ac\cdot\cos\beta)$

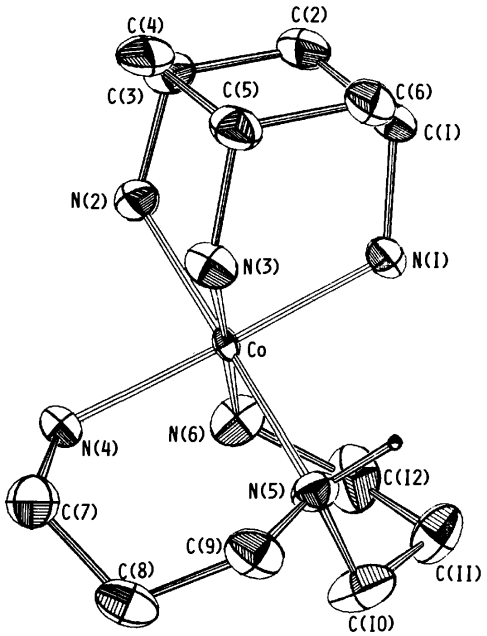

Fig. 2. Perspective drawing of the $[Co(chta)(dpt)]^{3+}$ cation.

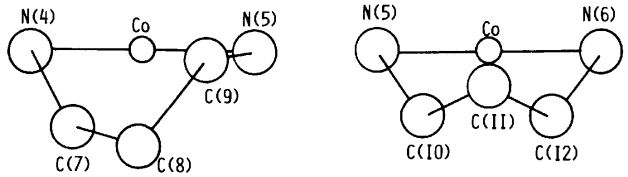

Fig. 3. Conformation of dpt chelate rings.

Table 2. Bond Distances (l/Å) in the Chelate Rings with Their Standard Deviations in Parentheses

Co-N(1)	1.910(5)	C(1)-C(2)	1.494(15)
Co-N(2)	1.989(7)	C(2)-C(3)	1.456(12)
Co-N(3)	1.972(5)	C(3)-C(4)	1.515(11)
Co-N(4)	1.933(6)	C(4)-C(5)	1.499(15)
Co-N(5)	2.020(7)	C(5)-C(6)	1.462(12)
Co-N(6)	2.002(6)	C(6)-C(1)	1.517(11)
		C(7)-C(8)	1.496(17)
N(1)-C(1)	1.459(8)	C(8)-C(9)	1.512(13)
N(2)-C(3)	1.495(8)	C(10)-C(11)	1.488(12)
N(3)-C(5)	1.483(11)	C(11)-C(12)	1.498(14)
N(4)-C(7)	1.474(8)		
N(5)-C(9)	1.485(11)		
N(5)-C(10)	1.497(11)		
N(6)-C(12)	1.487(12)		

Table 3. Bond Angles (ϕ/°) in the Chelate Rings with Their Standard Deviations in Parentheses

N(1)-Co-N(2)	89.8(3)	Co-N(1)-C(1)	118.2(6)
N(1)-Co-N(3)	89.6(2)	Co-N(2)-C(3)	119.9(6)
N(2)-Co-N(3)	89.6(3)	Co-N(3)-C(5)	118.9(4)
		Co-N(4)-C(7)	123.4(6)
N(4)-Co-N(5)	90.5(3)	Co-N(5)-C(10)	117.1(6)
N(4)-Co-N(6)	88.4(3)	Co-N(6)-C(12)	121.0(6)
N(5)-Co-N(6)	91.0(3)		
		C(6)-C(1)-C(2)	112.8(8)
N(1)-Co-N(5)	91.0(3)	C(1)-C(2)-C(3)	111.7(6)
N(1)-Co-N(6)	90.9(2)	C(2)-C(3)-C(4)	113.4(8)
N(1)-Co-N(4)	178.4(3)	C(3)-C(4)-C(5)	111.8(8)
N(2)-Co-N(4)	88.8(3)	C(4)-C(5)-C(6)	112.5(6)
N(2)-Co-N(6)	88.3(3)	C(5)-C(6)-C(1)	111.7(8)
N(2)-Co-N(5)	179.0(3)		
N(3)-Co-N(4)	91.1(3)	N(1)-C(1)-C(2)	110.2(7)
N(3)-Co-N(5)	91.1(3)	N(1)-C(1)-C(6)	109.5(6)
N(3)-Co-N(6)	177.8(3)	N(2)-C(3)-C(2)	109.7(7)
		N(2)-C(3)-C(4)	108.7(5)
		N(3)-C(5)-C(4)	109.7(7)
		N(3)-C(5)-C(6)	109.7(7)
		N(4)-C(7)-C(8)	113.4(7)
		C(7)-C(8)-C(9)	112.0(8)
		C(8)-C(9)-N(5)	112.1(6)
		C(9)-N(5)-C(10)	108.7(6)
		N(5)-C(10)-C(11)	112.9(9)
		C(10)-C(11)-C(12)	112.0(6)
		C(11)-C(12)-N(6)	110.8(6)

conformation. In contrast to this, the double fused six-membered dpt chelate rings take chair and skew-boat conformations (Fig. 3) which are the same as that observed in *s-fac*-[Co(dien)(dpt)](S_2O_6)(ClO_4)·H_2O.[8] There is a little difference in the Co–N distances between chta and dpt chelates in the $[Co(chta)(dpt)]^{3+}$ complex, but these values agree with the results obtained for the complex having six-membered chelate rings[9] (Table 2). The N–Co–N angles in the chelate rings are close to 90° (Table 3), distinct from other complexes containing facial type dpt (for example, in *s-fac*-$[Co(dien)(dpt)]^{3+}$,[8] 96.2°, 87.9°, and 92.5°, in *u-fac*-$[Co(dien)(dpt)]^{3+}$,[10] 96.6°, 88.7°, and 90.5°, and in $[Co_2(OH)_3(dpt)_2]^{3+}$,[11] 95.5°, 98.4°, and 93.1°) and comparable to those of chta complex (in $[Co(chta)_2]^{3+}$,[2] 90.1°, 90.0°, and 89.9°). The trans N–Co–N angles are slightly smaller than 180° and the non-chelate N–Co–N angles are slightly larger or smaller than 90°. These facts indicate that six nitrogen atoms form a slightly distorted octahedron around cobalt atom; the axis perpendicular to facial plane of octahedron elongates. In the complexes containing dpt, *s-fac*-,[8] *mer*-,[12] *u-fac*-$[Co(dien)(dpt)]^{3+}$,[10] and *mer*-$[Co(dpt)_2]^{3+}$,[13] there exists a considerable deviation from 90° in their N–Co–N angles of six-membered chelate rings. However, in the title complex, $[Co(chta)(dpt)]^{3+}$, the octahedral configuration is retained. It is known that chta ligands in $[Co(chta)_2]^{3+}$ [2] form a robust octahedron with cobalt atom. It seems that the particular structure of the title dpt complex is due to combination of dpt with chta and that distortion is fairly reduced by soft conformation of six-membered dpt chelate rings to retain octahedra of CoN_6 chromophores.

References

1) S. Yamada, M. Umehara, M. Ishii, and M. Nakahara, *Nippon Kagaku Kaishi*, **1983**, 1733.
2) M. Ishii, M. Umehara, T. Nomura, and M. Nakahara, *Chem. Lett.*, **1983**, 541.
3) M. Umehara, M. Ishii, I. Muramatsu, and M. Nakahara, *Nippon Kagaku Kaishi*, **1980**, 675.
4) Standard space group is No.13, *P2/c*.
5) T. Sakurai, UNICS, the Universal Crystallographic Computing System, The Crystallographic Society of Japan (1967).
6) "International Tables for X-Ray Crystallography," Kynoch Press, Birmingham (1974), Vol. IV, pp. 72, 73, 78, 86.
7) The observed and calculated structure factors, anisotropic thermal parameters for non-hydrogen atoms, and atomic parameters for hydrogen atoms are deposited at the Chemical Society of Japan (Document No. 8733).
8) T. W. Hambley and G. H. Searle, *Acta Crystallogr., Sect. C*, **40**, 383 (1984).
9) S. Sato and Y. Saito, *Acta Crystallogr., Sect. B*, **34**, 420 (1978); R. Nagao, F. Marumo, and Y. Saito, *Acta Crystallogr., Sect. B*, **29**, 2438 (1973).
10) G. H. Hambley and G. H. Searle, *Aust. J. Chem.*, **37**, 249 (1984).
11) G. H. Searle and T. W. Hambley, *Aust. J. Chem.*, **35**, 1975 (1982).
12) G. H. Searle and T. W. Hambley, *Aust. J. Chem.*, **35**, 2399 (1982).
13) T. W. Hambley, G. H. Searle, and M. R. Snow, *Aust. J. Chem.*, **35**, 1285 (1982).

The Molecular Structure of (+)$_{589}$-β_2-(3-Methyl-2-iminobutanoato) ((2*S*,10*S*)-4,8-diazaundecane-2,10-diamine)cobalt(III) Perchlorate: α-Imino Acidato Complex

Motowo YAMAGUCHI,* Takamichi YAMAGISHI, and Mitsuhiko HIDA
Department of Industrial Chemistry, Faculty of Engineering, Tokyo Metropolitan University, Fukasawa, Setagaya-ku, Tokyo 158
(Received December 25, 1986)

Synopsis. The crystal structure of (+)$_{589}$-β_2-(3-methyl-2-iminobutanoato)((2*S*,10*S*)-4,8-diazaundecane-2,10-diamine)cobalt(III) perchlorate has been determined by the single-crystal X-ray diffraction method. The complex ion adopts *Λ*-β_2 configuration, and it has the Co–N(imine) bond length of 1.90 Å, which is shorter than the Co–N(amine) bond lengths. The chelate ring of the 2-imino carboxylato is planar.

α-Imino acids (2-imino carboxylic acids) chelated to a metal ion are stable in an aqueous solution, while free α-imino acids are subject to be hydrolyzed. The syntheses and properties of cobalt(III) complexes of α-imino acids have been reported.[1–3] It reacts with nucleophile on its α-carbon, while it reacts with electrophile on its β-carbon and imino nitrogen. These facts make this ligand a useful building block for the synthesis of α-amino acid derivatives.

Recently, we obtained α-imino acidato Co(III) complexes by the dehydrogenation of the corresponding α-amino acidato complexes: The reaction of the [Co(α-amino acidato)(tetraamine)]$(ClO_4)_2$ complex with potassium permanganate gave a dehydrogenated product [Co(α-imino acidato)(tetraamine)]-$(ClO_4)_2$.[2] Asymmetric addition of a nucleophile to the imino carbon atom of α-imino acidate ligand can be expected, when optically active tetraamine ligand is employed. Since the tetraamine ligand seems to have a significant influence on the stereoselectivity, the structure of the complex is important, but the structure of the simple α-imino acidato complex has not yet been determined, as far as we know.[4] In this paper, we wish to report the X-ray structure determination of the molecular structure of (+)$_{598}$-β_2-[Co(oval)(2,10-Me_2-2,3,2-tet)]$(ClO_4)_2$.[5]

Experimental

(+)$_{598}$-β_2-[Co(oval)(2,10-Me_2-2,3,2-tet)]$(ClO_4)_2$ was prepared in a manner similar to that described previously.[3] Red crystals were obtained by crystallization from an aqueous solution. Found: C, 30.03; H, 5.78; N, 12.23%. Calcd for $C_{14}H_{32}Cl_2CoN_5O_{10}$: C, 30.01; H, 5.76; N, 12.50%.

The crystal used in the data collection was a red needle with the approximate dimentions of 0.1×0.05×0.05 mm^3. The diffraction data were measured on a Rigakudenki AFC-5R diffractometer using Mo *Kα* radiation monochromated by graphite (*λ* 0.7107 Å). Within the range of $2\theta<60°$, 1729 independent reflections with $|F_o| \geqq 2.5\sigma(F_o)$ were obtained. The intensities were corrected for Lorentz and polarization effects.

Crystal data for $C_{14}H_{32}Cl_2CoN_5O_{10}$: *F.W.*=560.3; Orthorhombic; $P2_12_12_1$; a=14.743(4), b=15.165(3), c=10.568(2) Å; V=2362.7(10) Å^3; Z=4; D_m=1.565 g cm^{-3}; D_x=1.575 g cm^{-3}; μ=10.07 cm^{-1}.

The structure was solved by the heavy-atom method and refined by a full-matrix least-squares method with anisotropic temperature factors for non-H atoms (for hydrogen atoms isotropically). The final discrepancy factors were $R=\Sigma||F_o|-|F_c||/\Sigma|F_o|=0.062$ and $R_w=[\Sigma w(|F_o|-|F_c|)^2/\Sigma w|F_o|^2]^{1/2}=0.060$ with a weighting scheme, $1/w=a|F_o|^2+b|F_o|+c$, were a, b, and c were calculated automatically. The absolute configuration of the whole complex ion was determined by the known absolute configuration of the asymmetric carbon atoms. All the hydrogen atoms except those of the terminal methyl groups of the isopropyl group were located and refined. The atomic scattering factors and the corrections for anomalous dispersion of Co, Cl, O, N, and C were taken from the literature.[6] Final positional and thermal parameters for non-hydrogen atoms are listed in Table 1.[7]

All the calculations were carried out on a HITAC M200H computer at the Computer Center of the Institute for Molecular Science and a HITAC M280H computer at the Computer Center of the University of Tokyo with Universal Program System UNICS-III.[8]

Results and Discussion

The observed structure of the complex ion (+)$_{589}$-[Co(oval)(2,10-Me_2-2,3,2-tet)]$^{2+}$ is shown in Fig. 1. The

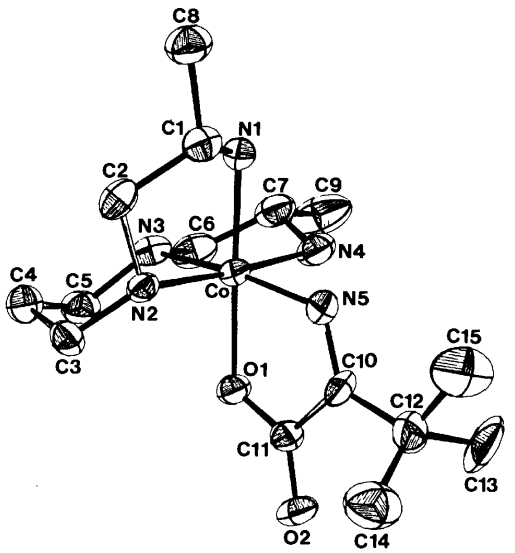

Fig. 1. An ORTEP[9] drawing of the complex cation *Λ*-β_2-[Co(oval)(2,10-Me_2-2,3,2-tet)]$^{2+}$. Ellipsoids enclose 30% probability. Hydrogen atoms are omitted for clarity.

Table 1. Fractional Positional Parameters ($\times 10^4$) and Thermal Parameters of Non-Hydrogen Atoms with Their Estimated Standard Deviations in Parentheses

Atom	x	y	z	B_{eq}/Å^2
Co	213(1)	3365(1)	3102(2)	3.6
Cl(1)	2907(2)	1166(2)	3062(4)	4.9
Cl(2)	2086(4)	3885(3)	6475(6)	8.8
N(1)	382(7)	4522(6)	3830(10)	4.6
N(2)	−1106(6)	3600(5)	3279(9)	3.6
N(3)	208(8)	3796(6)	1345(9)	4.4
N(4)	1541(7)	3228(7)	2852(12)	5.3
N(5)	262(8)	2799(6)	4710(9)	4.5
O(1)	−5(6)	2184(4)	2519(7)	4.0
O(2)	−131(6)	799(4)	3226(9)	5.1
C(1)	−436(9)	4779(8)	4522(12)	4.7
C(2)	−1232(9)	4537(8)	3674(13)	4.5
C(3)	−1703(7)	3348(9)	2223(12)	4.5
C(4)	−1456(12)	3759(10)	1000(13)	6.2
C(5)	−514(10)	3472(9)	491(13)	5.1
C(6)	1089(11)	3578(9)	765(15)	5.7
C(7)	1831(9)	3707(8)	1713(16)	5.6
C(8)	−431(11)	5748(9)	4966(14)	6.2
C(9)	2754(12)	3428(11)	1191(22)	9.8
C(10)	135(10)	1955(7)	4705(13)	5.2
C(11)	−19(7)	1594(7)	3399(11)	4.1
C(12)	149(11)	1377(9)	5884(15)	6.7
C(13)	1038(18)	930(18)	5938(35)	10.1
C(14)	−737(20)	890(18)	6020(28)	9.6
C(15)	383(36)	1848(22)	7037(26)	14.4
O(C11)1	2209(8)	1379(7)	2253(14)	10.0
O(C11)2	2952(8)	288(6)	3373(15)	10.0
O(C11)3	3046(14)	1726(10)	4053(13)	12.9
O(C11)4	3685(14)	1367(15)	2424(20)	17.6
O(C12)1	2308(14)	3104(11)	6008(21)	15.7
O(C12)2	2597(11)	4157(9)	7495(14)	11.7
O(C12)3	1189(12)	3875(15)	6773(20)	15.8
O(C12)4	2109(13)	4462(10)	5477(19)	15.4

Table 2. Selected Bond Distances (l/Å) with Their Estimated Standard Deviations in Parentheses

Co-N(1)	1.933(10)	C(5)-N(3)	1.48(2)
Co-N(2)	1.986(10)	N(3)-C(6)	1.47(2)
Co-N(3)	1.969(10)	C(6)-C(7)	1.50(2)
Co-N(4)	1.985(11)	C(7)-C(9)	1.53(2)
Co-N(5)	1.905(10)	C(7)-N(4)	1.47(2)
Co-O(1)	1.922(7)	N(5)-C(10)	1.29(1)
		C(10)-C(11)	1.50(2)
N(1)-C(1)	1.46(2)	C(10)-C(12)	1.52(2)
C(1)-C(2)	1.52(2)	C(12)-C(13)	1.48(3)
C(1)-C(8)	1.54(2)	C(12)-C(14)	1.51(3)
C(2)-N(2)	1.49(1)	C(12)-C(15)	1.45(3)
N(2)-C(3)	1.47(2)	C(11)-O(1)	1.29(1)
C(3)-C(4)	1.48(2)	C(11)-O(2)	1.23(1)
C(4)-C(5)	1.55(2)		

tetraamine ligand and the α-imino acidato are coordinated to a cobalt ion in the cis-β_2 geometry.[10] The absolute configuration of the complex ion deduced from the known absolute configuration of the asymmetric carbon atoms of the tetraamine ligand is Λ. The geomtry around metal ion showed no change during the oxidation reaction. The electronic and circular dichroism (CD) spectra are shown in Fig. 2. The CD spectrum in a neutral solution showed a positive Cotton effect corresponding to the first absorption band, which is consistent with the absolute configuration. The solution showed characteristic

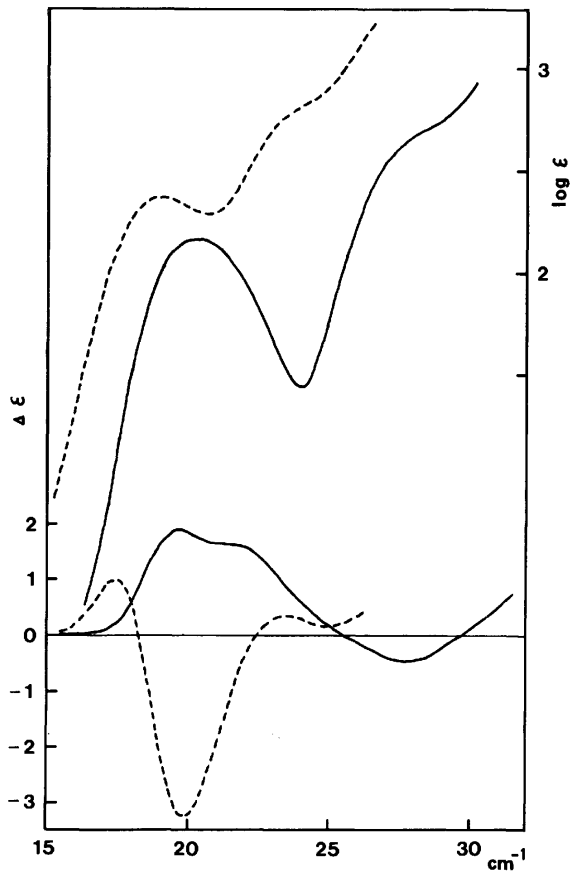

Fig. 2. Electronic absorption and circular dichroism spectra of Λ-β_2-[Co(oval)(2,10-Me_2-2,3,2-tet)]$(ClO_4)_2$: (a) in H_2O(——); (b) in N/10 NaOH (---).

Table 3. Selected Bond Angles (ϕ/°) with Their Estimated Standard Deviations

N(1)-Co-N(2)	85.7(4)	C(10)-C(11)-O(1)	114.0(9)
N(2)-Co-N(3)	91.5(4)	N(5)-C(10)-C(12)	124.4(12)
N(3)-Co-N(4)	85.0(5)	C(11)-C(10)-C(12)	122.9(10)
N(5)-Co-O(1)	82.7(4)	C(10)-C(11)-O(2)	120.9(10)
		O(1)-C(11)-O(2)	125.1(11)
Co-N(5)-C(10)	115.9(9)	C(10)-C(12)-C(13)	107.9(18)
Co-O(1)-C(11)	114.7(7)	C(10)-C(12)-C(14)	110.3(16)
N(5)-C(10)-C(11)	112.7(11)	C(10)-C(12)-C(15)	114.0(16)

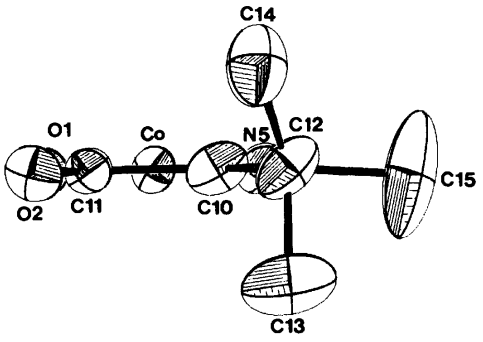

Fig. 3. An ORTEP[9] drawing of the α-imino acidato ligand. Ellipsoids enclose 30% probability.

changes of the electronic and CD spectra on basification because of the dissociation of the imino proton.[3]

Selected bond lengths and bond angles are given in Table 2 and 3, respectively. The bond length between the imino nitrogen atom and cobalt atom, Co–N(5) is 1.90(1) Å, which is shorter than the average of other Co–N bond lengths (1.97 Å). This value is similar to the Co–N(imine) bond lengths of the α-imino acidato Co(III) complex reported previously.[4] The bond angle N(5)–Co–O(1) (82.7(4)°) is smaller than that of α-amino acidato chelate ring, and, therefore, is more strained. The bond length C(10)–N(5) (1.29(1) Å) is consistent with that expected for a C=N bond.[4]

The chelate ring of the α-imino acidate moiety is planar as expected (Fig. 3). The deviations from the least-squares plane through the five atoms are within 0.0030 Å.[11]

The isopropyl group appeared to be a *t*-butyl group, due to disordering in the crystal. Its conformation was gauche to the carboxylato group.

The authors are grateful to Prof. Sadao Yoshikawa of the University of Tokyo for helpful discussion, and to Drs. Takehiko Mori and Tamotsu Inabe of the Institute for Molecular Science for kindly collecting the diffracting data. This work was partly supported by a Grant-in-Aid for Scientific Research No. 60750810 from the Ministry of Education, Science and Culture.

References

1) J. M. Harrowfield and A. M. Sargeson, *J. Am. Chem. Soc.*, **96**, 2634 (1974); J. M. Harrowfield and A. M. Sargeson, *J. Am. Chem. Soc.*, **101**, 1514 (1979) and references cited therein.

2) E. K. Chang, J. M. Harrowfield, W. G. Jackson, A. M. Sargeson, and J. Springborg, *J. Am. Chem. Soc.*, **107**, 2015 (1985).

3) M. Yamaguchi, M. Saburi, and S. Yoshikawa, *J. Am. Chem. Soc.*, **106**, 8293 (1984).

4) X-Ray structure determination of the N-substituted 2-imino carboxylato Co(III) complex has been reported: G. B. Robertson and P. O. Whimp, *Aust. J. Chem.*, **28**, 2129 (1975).

5) Abbreviations used: oval=3-Methyl-2-iminobutanoato; 2,10-Me_2-2,3,2-tet=(2*S*,10*S*)-4,8-diazaundecane-2,10-diamine.

6) D. T. Cromer, *Acta Crystallogr.*, **18**, 17 (1965); D. T. Cromer and D. Liberman, *J. Chem. Phys.*, **53**, 1891 (1970).

7) The tables of the anisotropic temperature factors for nonhydrogen atoms, the atomic parameters for the hydrogen atoms, and the F_o–F_c table are kept at the Chemical Society of Japan (Document No. 8739).

8) T. Sakurai and K. Kobayashi, *Rep. Inst. Phys. Chem. Res.*, **55**, 69 (1979).

9) C. K. Johnson, *ORTEP*, Report ORNL-3794, Oak Ridge National Laboratory, Oak Ridge, TN, USA, 1965.

10) β_2 refers to the unsymmetrical topology of the tetraamine ligand with the oxygen atom of α-imino acidato trans to the apical nitrogen: A. M. Sargeson and G. H. Searle, *Inorg. Chem.*, **6**, 787 (1967).

11) The equation of the least-squares plane through the chelate ring of the α-imino acidato is 0.9841X−0.1395Y−0.1100Z+0.7619=0, and the deviations from the plane are as follows: Co, −0.011; N(5), 0.0026; O(1), −0.0002; C(10), −0.0030; C(11), 0.0018 Å.

Favorskii-Type Rearrangement of α,α'-Dihalo Ketones Induced by Enolates of (Diethoxyphosphinyl)acetic Esters and Its Application to the Synthesis of α,α'-Divinyl Ketones

Takashi SAKAI,* Eiichiro AMANO, Kazuyoshi MIYATA, Masanori UTAKA, and Akira TAKEDA
Department of Synthetic Chemistry, School of Engineering, Okayama University, Tsushima, Okayama 700
(Received October 16, 1986)

Synopsis. A Favorskii-type rearrangement of 1,3-dihalo-3-methyl-2-butanone with enolate of ethyl (diethoxyphosphinyl)acetate or *t*-butyl (diethoxyphosphinyl)acetate gave ethyl 2-(diethoxyphosphinyl)-5-methyl-3-oxo-4-hexenoate (**3a**) or its *t*-butyl ester (**3b**). Compound **3b** was applied to the preparation of (*E*)-5-methyl-1-(*p*-tolyl)-1,4-hexadien-3-one and diethyl (4-methyl-2-oxo-3-pentenyl)phosphonate, which are the important intermediates for natural product syntheses.

Recently, we have made considerable efforts[1a-d] to extend the base of the Favorskii rearrangement[2] to carbanions such as enolates of malonic ester and (phenylsulfonyl)acetic ester. In a preceding paper,[1d] we reported that sodium enolates of β-keto esters reacted with 1,3-dihalo-3-methyl-2-butanone to give dihydro-4-pyrone derivatives via the Favorskii-type rearrangement. In this paper, we elucidate that the reaction is adaptable to enolates of (diethoxyphosphinyl)acetic esters, giving α-(diethoxyphosphinyl) β-keto esters (**3a,b**) in good yields. Products having a phosphinyl-functionality were utilized for the preparation of α,α'-divinyl ketones.

A reaction of 1,3-dichloro-3-methyl-2-butanone (**1a**) with sodium enolate of ethyl (diethoxyphosphinyl)-acetate (**2a**) in THF at room temperature gave ethyl 2-(diethoxyphosphinyl)-5-methyl-3-oxo-4-hexenoate (**3a**) in 42% yield (Scheme 1). The yield was improved up to 79% by using 3-bromo-1-chloro-3-methyl-2-butanone (**1b**). The *t*-butyl ester **3b** was similarly obtained in 36% yield from **1a** or in 81% yield from **1b**. The reaction can be explained in parallel with that described previously.[1d]

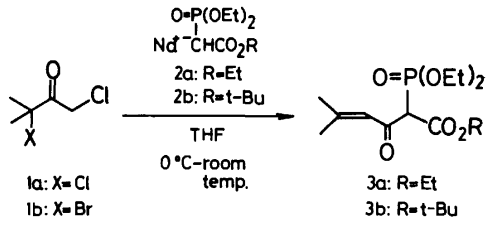

Scheme 1.

Attempts to apply the above reaction to 3-bromo-3-methyl-2-butanone (**4**) and 3,4-dibromo-4-methyl-2-pentanone (**6**) resulted in giving **5** (43% yield) and **8** (41% yield), respectively (Scheme 2). The formation of **8** suggests to us that the enolate **2a** may attack C-3 methylene carbon, instead of the carbonyl carbon, of the cyclopropanone intermediate **7**, which is produced under the basic conditions in a manner similar to the conventional Favorskii rearrangement.[2] It is interesting that the mode of the ring cleavage[3] of **7** is in marked contrast to that of the Favorskii rearrangement although a further investigation is required to confirm the mechanism.

The Horner–Wadmorth–Emmons reaction of sodium

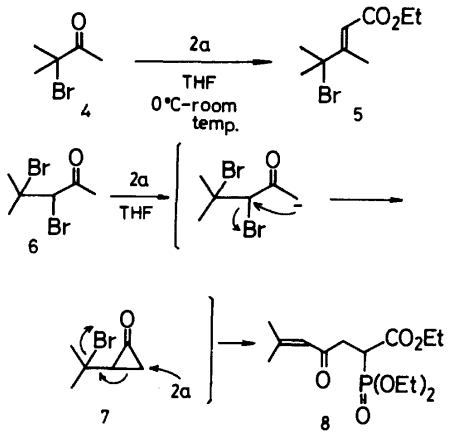

Scheme 2.

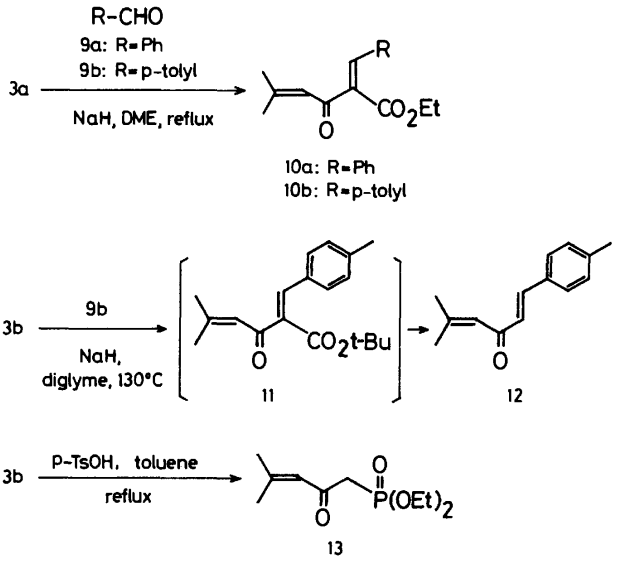

Scheme 3.

enolate derived from **3a** with benzaldehyde (**9a**) was carried out in refluxing 1,2-dimethoxyethane (DME), giving α-benzylidenation product **10a** in 31% yield[4] (Scheme 3). A similar reaction with *p*-tolualdehyde (**9b**) gave **10b** in only 17% yield.[4] On the other hand, sodium enolate derived from **3b** was allowed to react with aldehyde **9b** at an elevated temperature (130 °C) in diglyme to give (*E*)-5-methyl-1-(*p*-tolyl)-1,4-hexadien-3-one (**12**) in 47% yield. In this case, deesterification of **11** may have occurred thermally[5] in the course of the reaction. Furthermore, the treatment of **3b** with a catalytic amount of *p*-toluenesulfonic acid in refluxing toluene gave (4-methyl-2-oxo-3-pentenyl)-phosphonate (**13**) in 78% yield. Compounds **12** and **13** are the important intermediates for the syntheses of *ar*-turmerone[1d,6] and related sesquiterpenes.[7]

Experimental

IR spectra were taken on a JASCO Model A-102 spectrometer. ^{1}H NMR spectra (60 MHz) were measured with a JEOL Model JNM-60 SI spectrometer by using Me_4Si as an internal standard. Preparative TLC was carried out on silica gel (Kieselgel 60 PF_{254}, Merck A. G. Darmstadt).

Materials: 1,3-Dichloro-3-methyl-2-butanone (**1a**)[8] was prepared by chlorination of 3-methyl-2-butanone with 2.4 equiv of sulfuryl chloride. 3-Bromo-3-methyl-2-butanone (**4**)[9] was prepared by bromination of the starting ketone with *N*-bromosuccinimide. 3-Bromo-1-chloro-3-methyl-2-butanone (**1b**)[10] was obtained by chlorination of **4** with sulfuryl chloride. (Diethoxyphosphinyl)acetates **2a**[11] and **2b**[12] were prepared by the reported procedures.

Ethyl 2-(Diethoxyphosphinyl)-5-methyl-3-oxo-4-hexenoate (3a). To a suspension of NaH (48 mg, 2 mmol) in THF (6 ml) was added a solution of ethyl (diethoxyphosphinyl)-acetate (448 mg, 2 mmol) in THF (2 ml); stirring was continued at room temperature for 2 h. To this was added **1b** (199 mg, 1 mmol) with stirring during an additional 48 h at room temperature. The mixture was poured into water and acidified with 10% HCl. The organic layer was extracted with ether, washed with aqueous $NaHCO_3$ and brine, dried ($MgSO_4$), and concentrated. The residue was purified by preparative TLC on silica gel (hexane–acetone, 3:1) to give 242 mg (79%) of **3a**: IR (neat) 1740, 1693, 1620, and 1555 cm^{-1}; ^{1}H NMR (CCl_4) δ=1.32 (9H, t, *J*=7 Hz), 1.96 (3H, d, *J*=1.5 Hz), 2.14 (3H, d, *J*=1.2 Hz), 3.74—4.36 (6.77H, m), 6.32 (0.77H, m), 6.79 (0.23H, m), 14.65 (0.23H, br s, enol OH). Found: C, 50.87; H, 7.64%. Calcd for $C_{13}H_{23}O_6P$: C, 50.98; H, 7.57%.

A similar reaction of **1a** with **2a** gave **3a** in 42% yield.

***t*-Butyl 2-(Diethoxyphosphinyl)-5-methyl-3-oxo-4-hexenoate (3b).** A similar reaction of **1a** and **1b** with sodium enolate of *t*-butyl (diethoxyphosphinyl)acetate (**2b**) gave **3b** in 36% and 81% yields, respectively. **3b**: IR (neat) 1730, 1690, 1620, and 1555 cm^{-1}; ^{1}H NMR (CCl_4) δ=1.31 (6H, t, *J*=7 Hz), 1.45 (9H, s), 1.93 (3H, br s), 2.09 (3H, br s), 3.67—4.36 (4.8H, m), 6.30 (0.2H, m), 6.73 (0.8H, m), 13.90 (0.2H, br s, enol OH). Found: C, 53.97; H. 8.06%. Calcd for $C_{15}H_{27}O_6P$: C, 53.89; H, 8.18%.

Ethyl (*E*)-4-Bromo-3,4-dimethyl-2-pentenoate (5):[13] 43% yield after purification by column chromatography (hexane–ether, 30:1); IR (neat) 1725 and 1640 cm^{-1}, ^{1}H NMR (CCl_4) δ=1.28 (3H, t, *J*=7 Hz), 1.93 (6H, s), 2.36 (3H, s), 4.11 (2H, q, *J*=7 Hz), 5.85 (1H, m).

Ethyl 2-(Diethoxyphosphinyl)-6-methyl-4-oxo-5-heptenoate (8). To a mixture of mesityl oxide (98.1 mg, 1.0 mmol), $NaHCO_3$ (35 mg, 0.42 mmol), and ether (1 ml), was added bromine (159 mg, 1.0 mmol) dropwise; the mixture was stirred for 2 h. The resulting ether solution of 3,4-dibromo-4-methyl-2-pentanone (**6**)[14] was slowly introduced to a suspension of **2a** which was prepared from ethyl (diethoxyphosphinyl)acetate (448 mg, 2.0 mmol) and NaH (48 mg, 2 mmol) in THF (2 ml) in a manner similar to that described above. After being stirred for 21 h at room temperature, the usual work up of the mixture gave 128 mg (41%) of **8** after purification by preparative TLC (hexane–acetone, 4:1; twice development, R_f=0.16—0.26). **8**: IR (neat) 1740, 1695, and 1625 cm^{-1}; ^{1}H NMR (CCl_4) δ=1.28, 1.30, 1.32 (each with 3H, t, *J*=7 Hz), 1.88 (3H, br s), 2.10 (3H, br s), 2.7—3.7 (3H, m), 4.13 (6H, q, *J*=7 Hz), 6.02 (1H, m). Found: C, 52.43; H, 7.93%. Calcd for $C_{14}H_{25}O_6P$: C, 52.50; H, 7.87%.

Ethyl 2-Benzylidene-5-methyl-3-oxo-4-hexenoate (10a). To a suspension of NaH (72 mg, 3 mmol) in DME (3 ml) was added a solution of ester **3a** (918 mg, 3 mmol) and benzaldehyde (**9a**) (501 mg, 3.6 mmol) in DME (4 ml). The mixture was stirred for 1 h at room temperature and then for an additional 3 h under reflux. It was poured into water and acidified with 10% HCl. The organic layer was extracted with ether, washed with brine, dried ($MgSO_4$), and concentrated. The residual oil was purified by preparative TLC (hexane–acetone, 3:1) to give 240 mg (31%) of **10a**: IR (neat) 1720, 1705, 1672, and 1618 cm^{-1}; ^{1}H NMR (CCl_4) δ=1.30 (3H, t, *J*=7 Hz), 1.84 (2.2H, br s), 1.95 (0.8H, br s), 2.17 (3H, br s), 4.20 (2H, q, *J*=7 Hz), 5.92 (0.7H, m), 6.20 (0.3H, m), 7.26 (5H, m), 7.40 (0.3H, s), 7.47 (0.7H, s). Found: C, 74.46; H, 6.94%. Calcd for $C_{16}H_{18}O_3$: C, 74.40; H, 7.02%.

Ethyl 5-Methyl-3-oxo-2-(*p*-tolylmethylene)-4-hexenoate (10b). A similar reaction of **3a** with *p*-tolualdehyde (**9b**) gave **10b** (17%): IR (neat) 1719, 1670, and 1610 cm^{-1}; ^{1}H NMR ($CDCl_3$) δ=1.27 (3H, t, *J*=7 Hz), 1.83 (1.7H, s), 1.94 (1.3H, s), 2.18 (3H, br s), 2.33 (3H, s), 4.21 (1.1H, q, *J*=7 Hz), 4.28 (0.9H, q, *J*=7 Hz), 6.02 (0.56H, m), 6.27 (0.44H, m), 6.9—7.4 (4H, m), 7.43 (0.44H, s), 7.51 (0.56H, s). Found: C, 75.16; H, 7.34%. Calcd for $C_{17}H_{20}O_3$: C, 74.97; H, 7.40%.

(*E*)-5-Methyl-1-(*p*-tolyl)-1,4-hexadien-3-one (12). A similar reaction of enolate of **3b** with **9b** was carried out in diglyme at 130 °C for 16 h. The crude product was purified by preparative TLC (hexane–acetone, 3:1) to afford **12** (47%), whose ^{1}H NMR spectral data were identical with those reported.[6]

Diethyl (4-Methyl-2-oxo-3-pentenyl)phosphonate (13). A mixture of **3b** (131 mg, 0.39 mmol), *p*-toluensulfonic acid (40 mg, 0.23 mmol), and toluene (3 ml) was stirred for 3.5 h under reflux. The cooled mixture was washed with aqueous $NaHCO_3$ and water. The organic layer was separated and the aqueous layer was extracted with ether. The combined organic layer was dried ($MgSO_4$) and then concentrated. Distillation of the crude product [bp 100—105 °C (0.3 mm Hg) (1 mmHg=133.322 Pa)] gave **13** (89 mg, 78%): IR (neat) 1680, 1620, and 1255 cm^{-1}; ^{1}H NMR (CCl_4) δ=1.33 (6H, t, *J*=7 Hz), 1.93 (3H, br s), 2.13 (3H, br s), 2.88 (2H, d, *J*=22 Hz), 3.97 and 4.11 (each with 2H, q, *J*=7 Hz), 6.20 (1H, m). Found: C, 59.25; H, 9.53%. Calcd for $C_{10}H_{19}O_2P$: C, 59.39; H, 9.47%. These spectral data are consistent with those of the corresponding dimethyl ester.[6a]

References

1) a) T. Sakai, E. Amano, A. Kawabata, and A. Takeda, *J. Org. Chem.*, **45**, 43 (1980); b) T. Sakai, T. Katayama, and A. Takeda, *J. Org. Chem.*, **46**, 2924 (1981); c) T. Sakai, H. Tabata, and A. Takeda, *J. Org. Chem.*, **48**, 4618 (1983); d) T. Sakai, K. Miyata, M. Ishikawa, and A. Takeda, *Tetrahedron*

Lett., **26**, 4727 (1985).

2) A. S. Kende, "Organic Reactions," John Wiley & Sons, New York (1960), Vol. 11, Chap. 4.

3) Synthesis of α,β-unsaturated aldehyde by the hydrolysis of 1-methoxy-(1-mesyloxyalkyl)cyclopropane through a similar type of the ring-cleavage: E. J. Corey and P. Ulrich, *Tetrahedron Lett.*, **1975**, 3685.

4) Products other than **10a,b** were obtained as a complex mixture. Their purification and structural identification were unsuccessful. The starting esters **3a,b** were not recovered.

5) Formation of radical species in the pyrolysis of β-keto esters was reported: M. B. S. Kirkiacharian, *C. R. Acad. Sci. Ser. C.*, **269**, 721 (1969).

6) a) Preparation of **13** by the reaction of 3-methyl-2-pentenoyl chloride with lithium (dimethoxyphosphinyl)-methanide and its application to the synthesis of **12**: J. Motoyoshiya, M. Miyajima, K. Hirakawa, and T. Kakurai, *J. Org. Chem.*, **50**, 1326 (1985); b) Preparation of **12** by the reaction of **9b** with lithium enolate of mesityl oxide and subsequent dehydration: O. S. Park, Y. Grillasca, G. A. Garcia, and L. A. Maldonado, *Synth. Commun.*, **7**, 345 (1977), and references cited in these literatures.

7) L. A. Paquette, W. E. Fristad, D. S. Dime, and T. R. Bailey, *J. Org. Chem.*, **45**, 3017 (1980).

8) N. Schamp, N. De. Kimpe, and W. Coppens, *Tetrahedron*, **31**, 2081 (1975).

9) J. W. Thorpe and J. Warkentin, *Can. J. Chem.*, **51**, 927 (1973).

10) A. A. Petrov, *J. Gen. Chem.*, **15**, 931 (1945).

11) H. Takahashi, K. Fujiwara, and M. Ohta, *Bull. Chem. Soc. Jpn.*, **35**, 1498 (1962).

12) G. F. Griffiths, G. W. Kenner, S. W. McCombie, K. M. Smith, and N. J. Sutton, *Tetrahedron*, **32**, 275 (1976).

13) C. E. Moppett and J. K. Sutherland, *J. Chem. Soc.*, **1968**, 3040.

14) a) H. Rupe and S. Kessler, *Chem. Ber.*, **42**, 4715 (1909); b) K. S. Ayyar, R. C. Cookson, and D. A. Kagi, *J. Chem. Soc., Perkin Trans. 1*, **1975**, 1727.

Preparation of Isoxazolines by Thermolysis of Ethyl 2-Nitroalkanoates in the Presence of Dipolarophiles

Tomio SHIMIZU,* Yoshiyuki HAYASHI, Hiroshi SHIBAFUCHI, and Kazuhiro TERAMURA
Department of Color Chemistry and Technology, Faculty of Engineering and Design, Kyoto Institute of Technology, Matsugasaki, Sakyo-ku, Kyoto 606
(Received November 28, 1986)

Synopsis. 3-Alkyl-2-isoxazolines and 3-alkylisoxazole were prepared by thermolysis of ethyl 2-nitroalkanoates at about 230 °C in the presence of dipolarophiles.

1,3-Dipolar cycloaddition reactions using nitrile oxides are one of versatile methods for the preparation of five-membered heterocycles. A variety of preparative methods for nitrile oxides are known so far.[1-12] Recently, we reported[10,11] the thermolysis of nitromalonates (**1**) and the mono anilides (**2**) at 160—170 °C to give nitrile oxides effectively, which could be trapped by a variey of dipolarophiles as cycloadducts

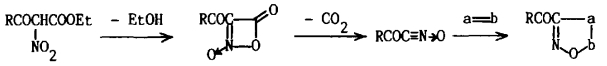

1 : R = OEt
2 : R = NHAr

in high yields. Although ethyl 2-nitrobutanoate (**3**) remained unchanged under similar reaction conditions,[11] a thermolysis of **3** under more vigorous thermal conditions in the presence of dipolarophiles did give cycloadducts. For example, a mixture of **3** and 1-dodecene in an appropriate solvent was heated to reflux for several hours under nitrogen and the following work-up of the reaction mixture gave a desired cycloadduct, 5-decyl-3-ethyl-2-isoxazoline (**4a**), in yields shown in Table 1. It was found from the

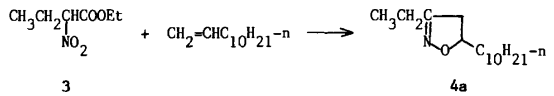

3 4a

Table that the yield of **4a** was not so varied from the employment of an excess of the dipolarophile and was effectively affected by the reaction temperature. Though a considerable amount of both substrates was recovered from the reaction mixture of Runs 1—4 and 6—8, none of **3** could be recovered from the reaction mixture of Run 5 in which formation of a considerable amount of tarry material was observed. Although the optimum reaction conditions were not yet attained, the best yield (48%) of the cycloadduct (**4a**) obtained is comparable with that by Mukaiyama method.[5]

Table 2. Yields and Melting Points of the Cycloadducts (**4**, **6**, **8**, and **9**)[a]

Adduct	R^2	R^3	Yield / %	Mp(θ_m/°C) (Bp(θ_b/°C)/mmHg)
4a	H	$C_{10}H_{21}$-*n*	48	(130—135/0.3)
4b	H	C_8H_{17}-*n*	43	(110—115/0.2)
4c	H	$C_{12}H_{25}$-*n*	37	33—34[b]
4d	H	$C_{14}H_{29}$-*n*	21	41—43
4e	$-(CH_2)_{10}-$		20	(128—135/0.2)
4f	H	$CH_2C_6H_4OCH_3$-*p*	34	(166—170/0.4)
4g	H	$CH_2OC_6H_4NO_2$-*p*	10	83—85[b]
4h	$COOCH_3$	$COOCH_3$	10	(110—115/0.3)[b]
4i	Ph	Ph	25	(140—145/0.5)
4j	CH_3	$C_6H_4OCH_3$-*p*	24	(144—149/0.4)
6a	H	$C_{10}H_{21}$-*n*	12	(130—136/0.6)
6b	H	C_8H_{17}-*n*	5	(110—115/0.5)
6c	H	$C_{12}H_{25}$-*n*	28	(145—151/0.4)
6e	$-(CH_2)_{10}-$		8	(137—140/0.4)
6f	H	$CH_2C_6H_4OCH_3$-*p*	15	(158—165/0.4)
8a	H	$C_{10}H_{21}$-*n*	33	(160—167/0.4)
8b	H	C_8H_{17}-*n*	30	(110—115/0.6)
8c	H	$C_{12}H_{25}$-*n*	39	34—36
8e	$-(CH_2)_{10}-$		20	(165—173/0.4)
8f	H	$CH_2C_6H_4OCH_3$-*p*	33	(160—165/0.4)
9	H	C_8H_{17}-*n*	14	(83—91/0.2)

a) Satisfactory microanalyses are obtained (C, H, N: ±0.25%). b) Lit, mp; **4c**: 35—36 °C,[7] **4g**: 83—85 °C,[7] **4h**: 83 °C/0.3 mmHg.[12] [1 mmHg=133.322 Pa].

Table 1. The Reaction of **3** with 1-Dodecene

Run No.	Molar ratio of **3**: 1-dodecene	Solvent	Reaction temperature[a]	Reaction time	Yield of **4a**[b]	Recovery of **3**
1	1 : 1	Mesitylene	164 °C	6 h	0%	>90%
2	1 : 1	Decalin	190 °C	6 h	trace	>90%
3	1 : 1	Tridecane	234 °C	3 h	31%	50%
4	1 : 1	Tridecane	234 °C	6 h	48%	40%
5	1 : 1	Tridecane	234 °C	12 h	40%	0%
6	1 : 1	Tetradecane	254 °C	4.5 h	42%	38%
7	1 : 2	None	213 °C	3 h	25%	57%
8	1 : 2	None	213 °C	6 h	42%	45%

a) The boiling point of the solvent is shown except for the cases of Runs 7 and 8, in which that of 1-dodecene is shown. b) Yields were calculated on the basis of **3** used.

The results of the reaction of **3** with some dipolarophiles under similar conditions such as Run 4 in Table 1 were summarized in Table 2 along with those obtained by the reactions using ethyl 2-nitropropanoate (**5**) or ethyl 2-nitropentanoate (**7**) instead of **3**. In cases using **5**, yields of the desired cycloadducts (**6**) were generally lower than those from **3** or **7**. This results may be ascribed to the nature of the boiling point (195 °C) of **5**, lower than those (>230 °C) of **3** and **7**.

Table 3. ^{1}H NMR Spectral Data of the Cycloadducts (**4**, **6**, **8**, and **9**)

Adduct	^{1}H NMR, ppm (in $CDCl_3$)
4a	0.9 (t, 3H, J=7), 1.15 (t, 3H, J=7), 1.1—1.8 (m, 18H), 2.35(q, 2H, J=7), 2.45(dd, 1H, J= 8, 16), 3.0(dd, 1H, J=10, 16), 4.1—4.7(m, 1H).
4b	0.85(t, 3H, J=7), 1.15(t, 3H, J=7), 1.0—1.7 (m, 14H), 2.33(q, 2H, J=7), 2.45(dd, 1H, J= 8, 16), 3.0(dd, 1H, J=10, 16), 4.1—4.7(m, 1H).
4d	0.9 (t, 3H, J=7), 1.16 (t, 3H, J=7), 1.0—1.8 (m, 26H), 2.35(q, 2H, J=7), 2.45(dd, 1H, J= 8, 16), 3.0(dd, 1H, J=10, 16), 4.1—4.7(m, 1H).
4e	1.17 (t, 3H, J=7), 1.1—1.8 (m, 20H), 2.3 (q, 2H, J=7), 2.6—3.2(m, 1H), 4.2—4.7(m, 1H).
4f	1.1(t, 3H, J=7), 2.3(q, 2H, J=7), 2.5—3.2(m, 4H), 3.8(s, 3H), 4.5—5.0(m, 1H), 6.83(d, 2H, J=9), 7.17(d, 2H, J=7).
4i	1.05 (t, 3H, J=7), 1.9—2.45 (m, 2H), 4.17 (d, 1H, J=7), 5.4(d, 1H, J=7), 7.3(brs, 10H).
4j	1.05(t, 3H, J=7), 1.25(d, 3H, J=7), 1.9—2.6 (m, 2H), 2.7—3.4(m, 1H), 3.8(s, 3H), 4.95(d, 1H, J=9), 7.0(d, 2H, J=9), 7.3(d, 2H, J=9).
6a	0.9(t, 3H, J=7), 1.0—1.7(m, 18H), 1.95(s, 3H), 2.47(dd, 1H, J=8, 16), 2.95(dd, 1H, J=10, 16), 4.0—4.7(m, 1H).
6b	0.9(t, 3H, J=7), 1.0—1.7(m, 14H), 1.95(s, 3H), 2.47(dd, 1H, J=8, 16), 2.95(dd, 1H, J=10, 16), 4.0—4.7(m, 1H).
6c	0.9(t, 3H, J=7), 1.0—1.7(m, 22H), 1.97(s, 3H), 2.45(dd, 1H, J=8, 16), 3.0(dd, 1H, J=10, 16), 4.1—4.7(m, 1H).
6e	1.0—1.8(m, 20H), 1.95(s, 3H), 2.6—3.1(m, 1H), 4.2—4.7(m, 1H).
6f	1.93(s, 3H), 2.3—3.2(m, 4H), 3.77(s, 3H), 4.4—5.0 (m, 1H), 6.8(d, 2H, J=9), 7.15 (d, 2H, J=9).
8a	0.9 (t, 3H, J=7), 0.97 (t, 3H, J=7), 1.1—1.9 (m, 20H), 2.3(t, 2H, J=7), 2.47 (dd, 1H, J= 8, 16), 2.97(dd, 1H, J=10, 16), 4.1—4.7(m, 1H).
8b	0.9 (t, 3H, J=7), 0.96 (t, 3H, J=7), 1.1—1.9 (m, 16H), 2.3(t, 2H, J=7), 2.47 (dd, 1H, J= 8, 16), 2.97(dd, 1H, J=10, 16), 4.1—4.7(m, 1H).
8c	0.9 (t, 3H, J=7), 0.96 (t, 3H, J=7), 1.1—1.9 (m, 24H), 2.3(t, 2H, J=7), 2.47 (dd, 1H, J= 8, 16), 2.97(dd, 1H, J=10, 16), 4.1—4.7(m, 1H).
8e	0.9(t, 3H, J=7), 1.0—1.9(m, 22H), 2.25(t, 2H, J=7), 2.6—3.1(m, 1H), 4.2—4.7(m, 1H).
8f	0.9 (t, 3H, J=7), 1.5 (hexet, 2H, J=7), 2.3(t, 2H, J=7), 2.5—3.2 (m, 4H), 3.77(s, 3H), 4.5—5.0(m, 1H), 6.8(d, 2H, J=9), 7.15(d, 2H, J=9).
9	0.9(t, 3H, J=7), 1.0—1.5(m, 15H), 2.6(q, 2H, J=7), 2.67(t, 2H, J=7), 5.8(s, 1H).

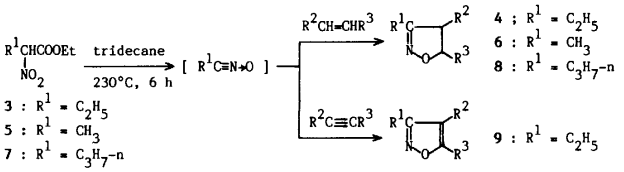

The structure of the cycloadducts (**4**, **6**, **8**, and **9**) were assigned on the basis of elemental, MS, NMR, and IR spectral analyses (see Table 3). The assignment of the structure (**4c**, **4g**, and **4h**) was further supported by comparison of the physical properties with those of authentic specimens prepared according to literatures.[7,12] The structure of **9** was supported by the evidence that the physical properties of **9** agreed with those of the specimen prepared by dehydrogenation of **4b** with *N*-bromosuccinimide.[13]

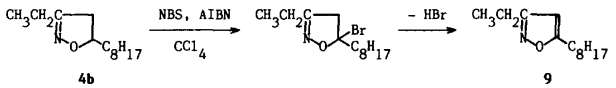

Gradual evolution of carbon dioxide and ethanol was observed in the course of the reactions. From these evidences, one of the probable mechanism of the formation of the isoxazolines and isoxazole may be explained on the basis of the formation of nitrile oxide intermediate from the decomposition of ethyl 2-nitroalkanoates though we failed to isolate 3,4-dialkylfurazan 2-oxides, a dimer of the nitrile oxide, from the decomposition of those in the absence of dipolarophiles. This results may be explained as follows: a reverse reaction of the furazan 2-oxides to nitrile oxide has been known to be possible under the reaction temperature,[14] and consequently, the nitrile oxide is consumed by irreversible reactions such as the rearrangement to isocyanates or the reaction with ethanol giving ethyl hydroximic acid which, then,

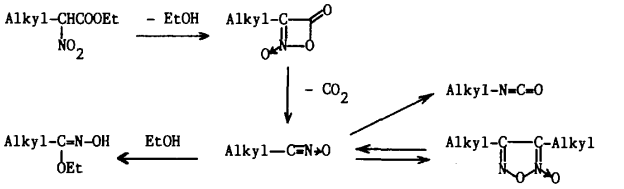

undergo further transformations such as decomposition, polymerization, and reaction with ethanol and/or the staring material to give complex tarry materials under the conditions, though we failed to isolate any compound that supports this mechanism from the tarry mixture. The lower yields of the cycloadducts (**4**, **6**, **8**, and **9**) from **3**, **5**, or **7** than those from **1** or **2** can be ascribed to the result of the difficulty of thermolysis of **3**, **5**, and **7** into nitrile oxides. In other words, the introduction of electron-withdrawing group such as carbalkoxy and carbamoyl groups at α-position of ethyl nitroacetate promotes the tautomerization to the corresponding aci-nitro isomers and,

consequently, intramolecular condensation and the following decarboxylation giving nitrile oxides are accelerated.

Experimental

Measurements. Melting and boiling points are all uncorrected. ^{1}H NMR spectra were recorded on Varian T-60A instrument with TMS as an internal standard; chemical shifts are given in δ-units and coupling constants (J) are in herz units: s=singlet; d=doublet; t=triplet; m=multiplet; brs=broad singlet.

Materials. Ethyl 2-nitroalkanoates (**3, 5,** and **7**) were prepared according to the method described in literature.[15] The other chemicals were of commercial origin and were used without further purification.

Reaction of Ethyl 2-Nitroalkanoates with Dipolarophiles; General Procedure: A mixture of ethyl 2-nitrobutanoate (**3**) (1.61 g, 10 mmol), 1-dodecene (1.68 g, 10 mmol), and tridecane (3.0 g) is heated to reflux over free flame for 6 h under nitrogen. After distillation of the unreacted substrates and the solvent from the reaction mixture by water aspirator, the residue was further distilled *in vacuo* to give analytically pure 5-decyl-3-ethyl-2-isoxazoline (**4a**) in 48% yield.

References

1) C. Grundmann and P. Grünanger, "The Nitrile Oxides," Springer Verlag, New York (1971), pp. 31—61.
2) P. Caramella and P. Grünanger, "1,3-Dipolar Cycloaddition Chemistry," ed by A. Padwa, John-Wiley & Sons, New York (1984), Vol. 1, Chap. 3, pp. 293—295.
3) R. Sustmann, R. Huisgen, and H. Huber, *Chem. Ber.*, **100**, 1802 (1967).
4) L. Gajesler, R. M. Paton, J. H. Hall, and D. J. Harper, *J. Polym. Sci., Polym. Lett. Ed.*, **18**, 635 (1980).
5) T. Mukaiyama and T. Hoshino, *J. Am. Chem. Soc.*, **82**, 5339 (1960).
6) T. Shimizu, Y. Hayashi, and K. Teramura, *Bull. Chem. Soc. Jpn.*, **57**, 2531 (1984).
7) T. Shimizu, Y. Hayashi, H. Shibafuchi, and K. Teramura, *Bull. Chem. Soc. Jpn.*, **59**, 2827 (1986).
8) R. A. Whitney and E. S. Nicholas, *Tetrahedron Lett.*, **22**, 3371 (1981).
9) T. Shimizu, Y. Hayashi, T. Taniguchi, and K. Teramura, *Tetrahedron*, **41**, 727 (1985).
10) T. Shimizu, Y. Hayashi, and K. Teramura, *Bull. Chem. Soc. Jpn.*, **58**, 2519 (1985).
11) T. Shimizu, Y. Hayashi, T. Ito, and K. Teramura, *Synthesis*, **1986**, 488.
12) K. Harada, E. Kaji, and S. Zen, *Chem. Pharm. Bull.*, **28**, 3296 (1980).
13) G. Bianchi and P. Grünanger, *Tetrahedron*, **21**, 817 (1965).
14) J. A. Chapman, J. Crosby, C. A. Cummings, R. A. C. Rennie, and R. M. Paton, *J. Chem. Soc., Chem. Commun.*, **1976**, 240.
15) K. Kornblum, R. K. Blackwood, and J. W. Powers, *J. Am. Chem. Soc.*, **79**, 2507 (1957).

Reductive Dimerization of Allyl and Benzyl Halides in Pb/*n*-Bu_4NBr-DMF and $PbBr_2$/Al-DMF Systems

Hideo Tanaka, Shiro Yamashita, and Sigeru Torii*
Department of Industrial Chemistry, School of Engineering, Okayama University, Okayama 700
(Received December 1, 1986)

Synopsis. Reductive dimerization of allyl and benzyl halides has been performed by treatment with Pb/*n*-Bu_4NBr and catalytic $PbBr_2$/Al in *N*,*N*-dimethylformamide.

Reductive coupling of organic halides is of importance for making carbon–carbon linkage in organic synthesis. Various metals, e.g., Cu,[1] Te,[2] Mo,[3] Fe,[4,5] Zn,[6] V,[7] Sm,[8] Co,[9] and Ni,[10,11] have been utilized for the reductive dimerization of allyl and benzyl halides. The combination of metal halides, e.g., $TiCl_3$,[12] VCl_3,[13] $CrCl_3$,[14] and WCl_6,[15] with $LiAlH_4$ has also proved to be useful. However, many of these reagents require scrupulous attention and/or hazardous conditions to use. Meanwhile, lead is still untouched for this purpose, presumably due to the lack of suitable reaction media for the generation of organolead reagents.[16] Recently, we have reported an effective lead-promoted "Barbier-type" reaction, wherein the combination of lead with tetrabutylammonium bromide (*n*-Bu_4NBr) in *N*,*N*-dimethylformamide (DMF) is quite effective for the generation of the intermediary active lead species for the allylation of carbonyl compounds.[17] Furthermore, we have found a new lead(0)-recycling system for the allylation of carbonyl compounds, which has been successfully performed with a combination of catalytic $PbBr_2$ and Al.[18]

In the lead-promoted allylation of carbonyl compounds, especially less reactive carbonyl compounds, an excess amount of allyl bromide was required to complete the reaction.[17] Notably, when allyl bromide was treated with lead in DMF prior to treatment with carbonyl compounds, any appreciable amount of the allylation products was not obtained. These facts suggest that the reductive dimerization of allyl bromide takes place competitively and, in turn, enable us to investigate allyl–allyl coupling in the Pb/*n*-Bu_4NBr–DMF and $PbBr_2$/Al–DMF systems. Herewith, we describe that both the unique combinations of Pb/*n*-Bu_4NBr and $PbBr_2$/Al are effective for the reductive dimerization of a variety of allyl and benzyl halides at ambient temperature.

Reductive Dimerization in a Pb/*n*-Bu_4NBr System (Method A). The reductive dimerization of a variety of allyl and benzyl halides in a Pb/Bu_4NBr system took place to give the corresponding coupling products (Table 1). Thus, into a stirred mixture of cinnamyl bromide (**1a**, X=Br), *n*-Bu_4NBr, and trimethylsilyl chloride (Me_3SiCl) in DMF was immersed a Pb plate. The reaction was continued at ambient temperature until most of **1a** was consumed (Entry 1). After taking out the Pb plate (loosing ca. 0.5 equiv. Pb), usual workup of the mixture afforded the corresponding dimers **2a** (73%). The addition of Me_3SiCl was indispensable for initiation of the reaction. However, when the Pb plate was treated with aqueous 5% HCl and air-dried immediately before use, the reaction took place similarly without addition of Me_3SiCl (yield; 72%), suggesting that the addition of Me_3SiCl and/or HCl liberated in situ would effect the activation of Pb plate surface. The effect of *n*-Bu_4NBr was remarkable; in the absence of *n*-Bu_4NBr, the reductive dimerization of allyl halides scarcely occurred except for **1a** (X=Br) (Entries 1 and 4 in Table 1). When *n*-Bu_4NBr was replaced with other salts, the yield of coupling products of cinnamyl chloride (**1a**, X=Cl) decreased in the order: *n*-Bu_4NBr(63%)>NaBr(50%)>$C_6H_5CH_2N(CH_3)_3Br$(none). Although the role of *n*-Bu_4NBr in the reductive dimerization is still unclear, it is likely that *n*-Bu_4NBr effects the generation of an active organolead reagent, e.g., *n*-Bu_4NPb·[19] and (*n*-Bu_4N)($PbBr_2$($CH_2CH{=}CH_2$)).[20] The effect of solvent is also remarkable since the yield of coupling products of **1a** (X=Br) varies significantly

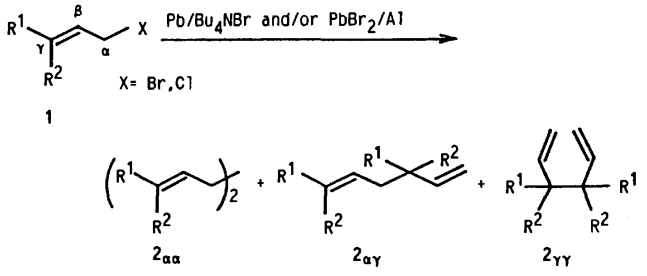

Scheme 1.

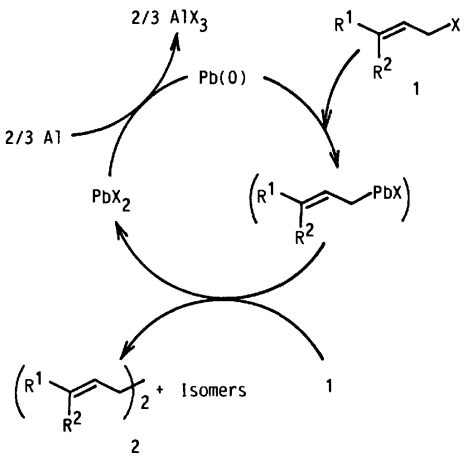

Scheme 2.

Table 1. Reductive Dimerization of Allyl and Benzyl Halides[a)]

Entry	Halide	Method[b)]	Time[c)] / h	Product	Yield[d)] / %
1	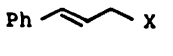 1a (X= Br)	A	14	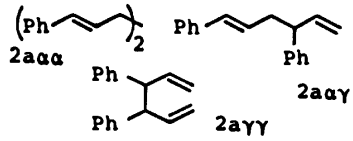 2aαα, 2aαγ, 2aγγ	73[e)] (83)
2	1a (X= Br)	B_1	24	2a	90[e)]
3	1a (X= Br)	B_2	14	2a	85[e)]
4	1a (X= Cl)	A	14	2a	63[e)] (-)
5	1a (X= Cl)	B_1	2[f)]	2a	54[e)]
6	1a (X= Cl)	B_2	15	2a	72[e)]
7	1a (X= Cl)	B_3	19	2a	74[e)]
8	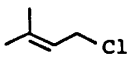 1b	A	24	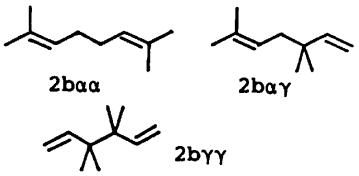 2bαα, 2bαγ, 2bγγ	60[g)]
9	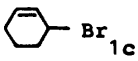 1c	A	3	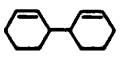 2c	100[h)]
10	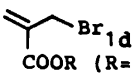 1d COOR (R= Me)	A	4	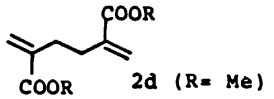 2d (R= Me)	60
11	1d (R= Me)	B_1	10	2d (R= Me)	62
12	1d (R= Et)	B_1	15	2d (R= Et)	71
13	$PhCH_2Br$ 3	A	4[f)]	$PhCH_2CH_2Ph$ 4	50
14	3	B_1	24	4	37
15	Ph_2CHBr 5	B_1	30	$Ph_2CHCHPh_2$ 6	67

a) Carried out at ambient temperature. b) A: With Pb/*n*-Bu_4NBr/Me_3SiCl in DMF; B_1: With $PbBr_2$/Al in DMF; B_2: with $PbBr_2$/Al in THF; B_3: with $PbBr_2$/Al in THF-H_2O (1:1). c) Unless otherwise noted, the reaction was continued until most of halides (1 mmol) were consumed. d) Isolated yields; numbers in parentheses showing the yields of coupling products obtained in the absence of *n*-Bu_4NBr. e) **2aαα/2aαγ/2aγγ** ratio of ca. 2:2:1 (^1H NMR and/or GLPC). f) Carried out at 60—65 °C. g) **2bαα/2bαγ/2bγγ** ratio of 77:20:3 (^1H NMR and/or GLPC). h) meso/dl ratio of 1:1 (GLPC).

depending on the choice of the solvent: DMF(73%)> MeCN(27%)>CH_2Cl_2(trace)>THF(none), MeOH(none).

The coupling products **2a** and **2b** were mixtures of three regio-isomers (**2aαα/2aαγ/2aγγ** ratio: ca. 2/2/1 (Entries 1—7); **2bαα/2bαγ/2bγγ** ratio: ca. 77/20/3 (Entry 8)).[21)] The product **2c** was a mixture of the corresponding meso and dl isomers in a ratio of 1:1 (Entry 9). The yield of the reductive dimerization of benzyl bromide (**3**) was not satisfactory (yield, 9%), but was improved to some extent (up to 50% yield) when the reaction was carried out at higher temperature (60—65 °C, Entry 13).

Reductive Dimerization in a $PbBr_2$/Al System (Method B). Furthermore, we found that the reductive dimerization of allyl and benzyl halides was successfully performed with the combination of $PbBr_2$ (7 mol%) and Al foils (1 equiv.) in DMF. The representative results are summarized in Table 1 (Method B_{1-3}). The reductive dimerization of **1a** (X=Br, Cl) in the $PbBr_2$/Al-DMF system took place smoothly (Entries 2 and 5). The satisfactory results were also obtained when the reaction was operated in THF (Entries 3 and 6) and THF-H_2O (1:1) (Entry 7). In a similar manner, the reaction of α-(bromomethyl)-acrylic esters **1d** (R=Me, Et), **3**, and bromodiphenylmethane (**5**) afforded the corresponding coupling products (Entries 11, 12, 14, and 15) respectively.

Although the details on the mechanism of the

$PbBr_2$/Al-promoted reductive dimerization have not been clarified yet, this system seems to involve the regeneration of Pb(0) by the reduction of $PbBr_2$ with Al (Scheme 2). The Pb(0) generated in this way would effect the reductive dimerization of the halides, since in the absence of $PbBr_2$ no appreciable coupling products were obtained. Further applications of the $PbBr_2$/Al system are in progress and will be reported in due course.

Experimental

IR spectra were taken on a JASCO IRA-1 grating spectrometer. ^1H NMR spectra were obtained on a Hitachi R-24 (60 MHz) and/or JEOL FX-100 (100 MHz), and ^{13}C NMR spectra on a JEOL FX-100 (25.05 MHz) spectrometer. Chemical shifts are expressed in parts per million downfield from Me_4Si used as internal standard. Analytical gas chromatography was carried out on a Yanaco GCG-550T using a column packed with Silicone SE-30 (10%) on Chamelite CK.

Materials. Cinnamyl halides (**1a**) (X=Br, Cl), 1-chloro-3-methyl-2-butene (**1b**), 3-bromocyclohexene (**1c**), benzyl bromide (**3**), and bromodiphenylmethane (**5**) were purchased from Tokyo Kasei Kogyo Co., LTD. and used as received. Methyl and ethyl α-(bromomethyl)acrylates (**1d**) (R=Me, Et) were prepared according to the method described in the literature.[22]

General Procedure of the Reductive Dimerization. A typical reaction procedure is as follows.

Method A: Into a stirred mixture of cinnamyl bromide (**1a**, X=Br) (1 mmol), *n*-Bu_4NBr (1 mmol), and Me_3SiCl (0.2 ml) in DMF (6 ml) was immersed a Pb plate (>99.9%; 1.5×2.0 cm^2, 0.5 mm thick) and the stirring was continued at ambient temperature until most of **1a** was consumed (14 h). After taking out the Pb plate (loosing ca. 0.5 mmol of Pb), the mixture was quenched with aqueous 5% HCl and extracted with AcOEt (6 ml×5). The extracts were washed with aqueous $NaHCO_3$ (6 ml) and brine (6 ml×4), dried (Na_2SO_4), and concentrated. The residue was chromatographed (SiO_2, hexane–AcOEt (3:1)) to give a mixture of the corresponding dimers **2a** (73%), whose GLPC analysis showed the presence of three regio-isomers **2a**$\alpha\alpha$, **2a**$\alpha\gamma$, and **2a**$\gamma\gamma$ in a ratio of 39:43:18. Identification of the products was performed by comparison of its IR, ^1H NMR, and/or ^{13}C NMR spectra with reported ones.[2]

Method B: Into a mixture of $PbBr_2$ powders (0.07 mmol) and finely cut Al foils (1 mmol) in DMF (5 ml) was added cinnamyl bromide (**1a**, X=Br) (1 mmol) and the mixture was stirred at ambient temperature until most of **1a** was consumed (24 h). The unreacted Al foils were separated and the reaction mixture was worked up in a similar manner to that described above. The corresponding dimers **2a** were obtained in 90% yield. GLPC analysis of the products showed the presence of three regio-isomers **2a**$\alpha\alpha$, **2a**$\alpha\gamma$, and **2a**$\gamma\gamma$ in a ratio of 40:41:19 (Method B_1). In a similar manner, the reductive dimerization of cinnamyl chloride (**1a**, X=Cl) (1 mmol) with $PbBr_2$ (0.07 mmol)/Al (1 mmol) in THF (Method B_2) and THF–H_2O (1:1) (Method B_3) afforded the dimers **2a** in 72 and 74% yields, respectively. GLPC analysis of these products showed the presence of three regio-isomers (the ratio of 41:40:19 and 35:43:22).

The present work was partially supported by a Grant-in-Aid for Scientific Research No. 61225018 from the Ministry of Education, Science and Culture.

References

1) Y. Kitagawa, K. Oshima, H. Yamamoto, and H. Nozaki, *Tetrahedron Lett.*, **1975**, 1859.
2) D. L. J. Clive, P. C. Anderson, N. Moss, and A. Singh, *J. Org. Chem.*, **47**, 1641 (1982).
3) H. Alper and D. D. Roches, *J. Org. Chem.*, **41**, 806 (1976).
4) G. M. Shakhnazaryan, L. A. Saakyan, R. S. Avoyan, and Sh. L. Shakhbatyan, *Arm. Khim. Zh.*, **36**, 504 (1983); *Chem. Abstr.*, **100**, 34090c (1984).
5) S. Nakanishi, T. Oda, T. Ueda, and Y. Otsuji, *Chem. Lett.*, **1978**, 1309.
6) V. F. Cherstkov, S. R. Sterlin, L. S. German, and I. L. Knunyants, *Izv. Akad. Nauk SSSR, Ser. Khim.*, **1984**, 2152; *Chem. Abstr.*, **102**, 78303v (1985).
7) T. A. Cooper, *J. Am. Chem. Soc.*, **95**, 4158 (1973).
8) P. Girard, J. L. Namy, and H. B. Kagan, *J. Am. Chem. Soc.*, **102**, 2693 (1980).
9) Y. Yamada and D. Momose, *Chem. Lett.*, **1981**, 1277.
10) S. Inaba, H. Matsumoto, and R. D. Rieke, *Tetrahedron Lett.*, **23**, 4215 (1982).
11) S. Inaba, H. Matsumoto, and R. D. Rieke, *J. Org. Chem.*, **49**, 2093 (1984).
12) G. A. Olah and G. K. S. Prakash, *Synthesis*, **1976**, 607.
13) T.-L. Ho and G. A. Olah, *Synthesis*, **1977**, 170.
14) Y. Okude, T. Hiyama, and H. Nozaki, *Tetrahedron Lett.*, **1977**, 3829.
15) Y. Fujiwara, R. Ishikawa, and S. Teranishi, *Bull. Chem. Soc. Jpn.*, **51**, 589 (1978); and references cited therein.
16) P. G. Harrison, "Comprehensive Organometallic Chemistry," ed by G. Wilkinson, Pergamon Press (1982), Vol. 2, p. 629; V. G. K. Das and C. K. Chu, "The Chemistry of the Metal-Carbon Bond," ed by F. R. Hartrey and S. Patai, John Wiley & Sons Ltd. (1985), Vol. 3, p. 1.
17) H. Tanaka, S. Yamashita, T. Hamatani, Y. Ikemoto, and S. Torii, *Chem. Lett.*, **1986**, 1611.
18) H. Tanaka, S. Yamashita, T. Hamatani, Y. Ikemoto, and S. Torii, to be published.
19) E. Kariv-Miller, P. B. Lawin, and Z. Vajtner, *J. Electroanal. Chem. Interfacial Electrochem.*, **195**, 435 (1985); *Chem. Abstr.*, **104**, 12224e (1986).
20) H. Tanaka, T. Hamatani, S. Yamashita, and S. Torii, *Chem. Lett.*, **1986**, 1461.
21) It has been reported that upon the reductive dimerization of **1a** and **1b**, the ratio of **2**$\alpha\alpha$/**2**$\alpha\gamma$/**2**$\gamma\gamma$ varies depending on the choice of the metal promoter: Te^{2-} ($\alpha\alpha/\alpha\gamma/\gamma\gamma$=38/49/13 for **2a**);[2] SmI_2 (67/26/7 for **2a**, 58/34/8 for **2b**);[8] $CrCl_3$–$LiAlH_4$ (72/22/6 for **2b**).[14]
22) K. Ramarajan, K. Ramalingam, D. J. O'Donnell, and K. D. Berlin, *Org. Synth.*, **61**, 56 (1983). Methyl ester was prepared from α-(bromomethyl)acrylic acid and methanol.

Useful Synthetic Routes to Pure *exo*-5-Vinyl-2-norbornene and *endo*-5-Vinyl-2-norbornene

Yoshiharu INOUE
Research Institute for Production Development,
15, Shimogamo Morimoto-cho, Sakyo-ku, Kyoto 606
(Received November 20, 1986)

Synopsis. Hydroboration of 5-vinyl-2-norbornene (**1**) with 9-BBN mainly affords 5-(2-hydroxyethyl)-2-norbornene (**2**). The iodo ether cyclization of **2** can convert only *endo*-5-(2-hydroxyethyl)-2-norbornene (**2b**) to iodo ether **10**, followed by reductive elimination and subsequent dehydration to furnish *endo*-5-vinyl-2-norbornene (**1b**) which has not been isolated in pure form. Meanwhile, unreacted *exo*-5-(2-hydroxyethyl)-2-norbornene (**2a**) produces *exo*-5-vinyl-2-norbornene (**1a**) via dehydration.

5-Vinyl-2-norbornene (**1**), the principal product from the Diels–Alder reaction between cyclopentadiene and butadiene consists of *exo*-5-vinyl-2-norbornene (**1a**) and *endo*-5-vinyl-2-norbornene (**1b**).[1] Although a successful separation of these two isomers was accomplished by preparative gas chromatography,[1] the procedure encounters the difficulty in obtaining the isomers in pure form and in large quantities. As an alternative approach to the isolation of **1a**, of considerable utility is the thermal isomerization[2] in which **1b** was transformed into 4,7,3a,7a-tetrahydro-1*H*-indene whereas **1a** remained unchanged, allowing it to be isolated. It is difficult, however, to prevent the **1a** thus obtained from being contaminated by unreacted **1b**. Except these processes above mentioned, to the best of our knowledge no one appears to have reported on the stereoselective synthesis or isolation of **1a** and **1b**.

We now wish to report herein a convenient method for the isolation of **1a** and **1b** as well as the investigation of their chemical behavior.

Results and Discussion

One of the most facile methods to separate **1a** and **1b** from **1**, the mixture of **1a** and **1b**, is outlined in Scheme 1.

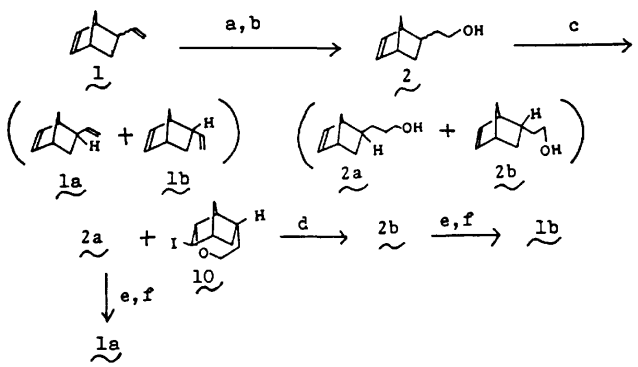

Scheme 1.

Reagents: a, 9-BBN, THF; b, H_2O_2, NaOH; c, I_2, KI, $NaHCO_3$, dioxane, H_2O; d, Zn, CH_3CO_2H; e TsCl, pyridine; f, pyridine, 100 °C.

Hydroboration of **1** with 9-borabicyclo[3.3.1]nonane (9-BBN), followed by oxidation with alkaline hydrogen peroxide, resulted in the formation of **2** in 70.7% yield, together with a 5.8% yield of a mixture of 6-vinyl-2-norbornanol (**3**) and 5-vinyl-2-norbornanol (**4**) and a 4.3% yield of a mixture of 6-(2-hydroxyethyl)-2-norbornanol (**5**) and 5-(2-hydroxyethyl)-2-norbornanol (**6**).

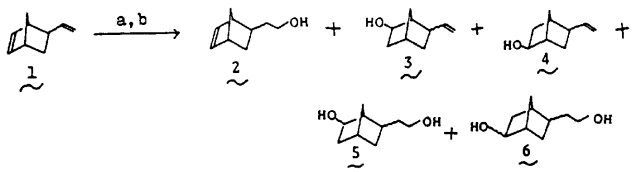

Reagents: a, 9-BBN, THF; b, H_2O_2, NaOH

Although this reaction could be achieved using B_2H_6 in THF, the selectivity of the hydroboration toward the vinyl group was decreased, resulting in the product ratio of **2**, the mixture of **3** and **4**, and the mixture of **5** and **6** being ca. 29:6:11. In this case, it was expected that the endo-isomer **7** of the initially formed [2-(5-norbornen-2-yl)ethyl]borane might undergo an intramolecular hydroboration[3] to give no *endo*-2-hydroxyethyl isomer **2b** as illustrated below, but in fact, evidence that this is not the case was presented by the experimental results on the formation of the iodo ether **10** from **2**, which will be described later.

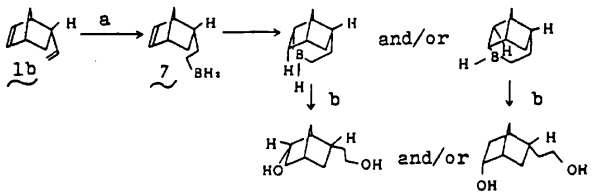

Reagents: a, B_2H_6, THF; b, H_2O_2, NaOH.

Further purification of **2** can be accomplished by utilizing the readily isolable intermediates, 2-(5-norbornen-2-yl)ethyl 3,5-dinitrobenzoate (**8**) and 2-(5-norbornen-2-yl)ethyl tetrahydro-2-pyranyl ether (**9**), which are, in turn, converted to **2**.

Turning here to Scheme 1, treatment of a solution of **2** in dioxane with iodine and KI in 0.5 M $NaHCO_3$ solution (1 M=1 mol dm^{-3}) led to the iodo ether cyclization of **2b** to form the iodo ether **10** in 42.1% yield, while **2a** remained unreacted. Separation of both products was readily achieved by a fractional distillation or recrystallization.

In considering possible modes of the iodo ether cyclization, examination of molecular models suggested that the seven-membered ring cyclization should be prohibited on steric grounds.[4]

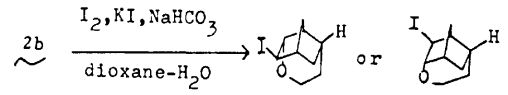

favored

An attempt to follow the Kropp's procedure[5] where **2** was treated with I_2 and $N(C_2H_5)_3$ in methanol at a reflux temperature for 2 d failed to complete the iodo ether cyclization, providing 18% yield (based on **2b**) of **10** along with the unreacted starting material **2a** containing **2b**.

It was now ready to convert the iodo ether **10** to **2b** via a reductive elimination. Treatment of **10** with zinc in acetic acid furnished **2b** in 75.7% yield. Although the procedure for this reaction is similar to that applied to the reductive elimination of the iodo lactone[6] and the β-halo ether,[7] the observation that the β-halo ether compound in this system could be successfully effected by this treatment is noteworthy.

With these two stereoisomers **2a** and **2b** available, the dehydration step was now examined utilizing the conventional manners.[8] Both alcohols were converted individually to **1a** and **1b** in 26.8 and 28.3% yield, respectively, by treatment with tosyl chloride in pyridine, followed by elimination with pyridine at 100 °C. These two stereoisomers **1a** and **1b** thus obtained have a refractive index of n_D^{20} 1.4791 (lit,[2a] n_D^{20} 1.4794) and n_D^{20} 1.4806, respectively.

Experimental

Melting and boiling points are uncorrected. GC analysis was carried out on a Hitachi Model 163 gas chromatograph fitted with a FID detector, using a 5 mm×2 m stainless-steel column packed with 10% Silicone-30 on Chromosorb W. ^{1}H NMR spectra were recorded with a Hitachi Model R-24B, using $Si(CH_3)_4$ as an internal reference. IR spectra were obtained with a Hitachi Model 160-10 infrared spectrophotometer. Elemental analysis was performed by the Laboratory for Organic Elemental Microanalysis, Faculty of Pharmaceutical Science, Kyoto University.

Materials. 5-Vinyl-2-norbornene, obtained from Nippon Petrochemical Corp., was vacuum distilled before use. The 5-vinyl-2-norbornene employed, on the basis of ^{1}H NMR spectroscopy, consisted of *exo*- and *endo*-5-vinyl-2-norbornene in a ratio 2:3.[1]

5-(2-Hydroxyethyl)-2-norbornene (2). Method A. To a stirred solution of 5-vinyl-2-norbornene (**1**, 24.0 g, 0.200 mol) in dry THF (20 mL) at ambient temperature under a nitrogen stream was added dropwise 9-BBN (0.50 M THF solution, 400 mL) over about 1 h. The mixture was stirred at 25 °C for 2 h, and to this mixture was added dropwise water (5 mL), aq NaOH (3 M, 67 mL), then 30% aq H_2O_2 (67 mL). After being stirred at 40 °C for 2 h, the mixture was extracted three times with ether (150 mL). The ether layer was dried over $MgSO_4$ and concentrated in vacuo. The residue was distilled under reduced pressure to give a mixture of **3** and **4** (1.6 g, 5.8%) as the first fraction [64 °C/0.5 mmHg (1 mmHg=133.322 Pa) (lit,[9] 60—61 °C/0.35 mmHg)], **2** (19.5 g, 70.7%) as the second fraction (70 °C/0.5 mmHg), and then a mixture of **5** and **6** (1.3 g, 4.2%) as the third fraction (130—135 °C/1.5 mmHg). The spectroscopic data of the second and third fractions were as follows:

Alcohol **2**: IR (neat film) cm^{-1} 3350, 3080, 2930, 2870, 1640; ^{1}H NMR ($CDCl_3$) δ=6.20—5.80 (m, 2H), 3.60 (t, 2H), 2.80 (m, 2H), 2.40 (s, 1H), 2.60—1.10 (m, 7H). Found: C, 78.31; H, 10.19; O, 11.50%. Calcd for $C_9H_{14}O$: C, 78.26; H, 10.14; O, 11.60%.

A Mixture of **5** and **6**: IR (neat film) cm^{-1} 3345, 2935, 2870, 1100; ^{1}H NMR ($CDCl_3$) δ=4.75—4.50 (s, 1H), 4.35—3.75 (m, 1H), 3.60—3.20 (m, 1H), 2.45—0.80 (m, 13H). Found: C, 69.18; H, 10.35; O, 20.47%. Calcd for $C_9H_{16}O_2$: C, 69.23; H, 10.26; O, 20.51%.

Method B. To an ice-cooled, stirred solution of **1** (48.0 g, 0.400 mol) in dry THF (250 mL) was added $NaBH_4$ (4.2 g, 0.110 mol) and then added dropwise $BF_3 \cdot O(C_2H_5)_2$ (18.1 mL, 20.8 g, 0.147 mol). After being stirred at room temperature for 3 h, the reaction was quenched by adding water (32.5 mL), and then to the mixture was added aq NaOH (3 M, 44.0 mL) and 30% aq H_2O_2 (44.0 mL). After being allowed to stir at 40 °C for an additional 3 h, the reaction mixture was cooled to room temperature and then extracted three times with ether (200 mL). The organic extracts were washed with water and dried over $MgSO_4$. After removal of the solvent, the residue was distilled under reduced pressure to give a mixture of **3** and **4** (3.2 g, 5.8%), **2** (15.9 g, 28.8%), and a mixture of **5** and **6** (6.8 g, 10.9%).

Purification of 2. Via 3,5-Dinitrobenzoate 8. To an ice-cooled solution of **2** (5.0 g, 0.036 mol) in pyridine (20 mL) was added 3,5-dinitrobenzoyl chloride (7.5 g, 0.033 mol) with stirring. The reaction mixture was heated over a steam bath for 5 min and poured, with vigorous stirring, into water (50 mL). The precipitate was collected, washed with 5% aq Na_2CO_3 (25 mL), and recrystallized from a mixture of ethanol and water to give **8** (8.6 g, 78.5%): mp 68—69 °C; IR (nujol) cm^{-1} 3090, 2930, 2875, 1720, 1665, 1200; ^{1}H NMR ($CDCl_3$) δ=9.20 (s, 3H), 6.35—5.90 (m, 2H), 4.70—4.35 (t, 2H), 2.85 (broad s, 2H), 2.45—1.25 (m, 7H). Found: C, 57.92; H, 4.82; N, 8.32; O, 28.94%. Calcd for $C_{16}H_{16}O_6N_2$: C, 57.83; H, 4.85; N, 8.43; O, 28.89%.

The ester **8** (5.0 g, 0.015 mol) was added to a mixture of methanol (10 mL) and 20% aq NaOH (3.5 mL), and the mixture was refluxed for 1 h. After removal of methanol, the residue was extracted with ether–benzene (100 mL). The extract was washed with water, dried over $MgSO_4$, and concentrated in vacuo, and subsequent distillation afforded **2** (1.8 g, 87.0%) whose purity was determined to be more than 99.9% by GC analysis.

Via Tetrahydro-2-pyranyl Ether 9. A solution of **2** (10.0 g, 0.072 mol), 3,4-dihydro-2*H*-pyran (4.8 g, 0.057 mol), and *p*-toluenesulfonic acid (0.5 g) in ether (100 mL) was stirred at room temperature for 3 h and treated with 10% aq Na_2CO_3 (10 mL). The ethereal layer was washed with water, dried over $MgSO_4$, and concentrated in vacuo. The residue was distilled (102—104 °C/2.0 mmHg) to yield **9** (8.5 g, 67.2%): IR (neat film) cm^{-1} 3050, 2930, 2870, 1660; ^{1}H NMR (CCl_4) δ=6.25—5.80 (m, 2H), 3.95—3.85 (t, 1H), 3.60—3.45 (m, 4H), 2.60—1.10 (m, 15H). Found: C, 75.48; H, 9.88; O, 14.64%. Calcd for $C_{14}H_{22}O_2$: C, 75.63; H, 9.97; O, 14.40%.

A solution of the ether **9** (6.0 g, 0.027 mol), methanol (10 mL), and 2% aq HCl (3 mL) was refluxed for 3 h, and then this solution was treated with 5% aq $NaHCO_3$ (10 mL). After removal of methanol, the residual oil was extracted three times with ether–benzene (50 mL). The extracts were washed with water, dried over $MgSO_4$, and concentrated in vacuo. Distillation yielded **2** of more than 99.5% purity (2.8 g, 75.1%).

***exo*-7-Iodooctahydro-4,6-methanocyclopenta[*b*]pyran (10).** To a solution of **2** (16.2 g, 0.117 mol) in dioxane (30 mL), with stirring at room temperature, was added aq $NaHCO_3$ (0.5 M, 720 mL) and an aqueous solution (360 mL) of iodine (70.0 g, 0.276 mol) and potassium iodide (120.0 g, 0.723 mol). After being stirred at room temperature for 1 h, the mixture was extracted three times with ether–benzene (200 mL). The extracts were washed with sat. aq Na_2SO_3, water, and dried over $MgSO_4$. After removal of the solvent, the residue was distilled under reduced pressure to yield **2a** (4.4 g, 27.3%) as the first fraction (66 °C/0.2 mmHg) and then **10** (13.0 g, 42.1%) as the second fraction (100—103 °C/1.0 mmHg). The ester formed on treatment of **2a** with 3,5-dinitrobenzoyl chloride in pyridine had the mp of 72—74 °C.

The physical properties of **10** were as follows: IR (neat film) cm^{-1} 2925, 2870, 1470; ^1H NMR (CCl_4) δ=4.75—4.60 (broad s, 1H), 4.15—4.05 (t, 1H), 3.70—3.40 (m, 2H), 2.60—1.20 (m, 9H). Found: C, 41.06; H, 4.98%. Calcd for $C_9H_{13}OI$: C, 40.91; H, 4.92%.

Reaction of 2 with Iodine and Triethylamine in Methanol. A solution of **2** (10.0 g, 0.072 mol), iodine (17.9 g, 0.070 mol), and triethylamine (9.9 g, 0.098 mol) in methanol (55 mL) was refluxed for 2 d. After removal of the solvent, the reaction mixture was treated with water (35 mL), extracted twice with ether (50 mL). The extracts were washed with sat. aq Na_2SO_3, water, dried over $MgSO_4$, and concentrated in vacuo. Distillation gave **10** (2.3 g, 12.1%) and recovered **2** (6.0 g).

***endo*-5-(2-Hydroxyethyl)-2-norbornene (2b).** To an ice-cooled solution of **10** (12.0 g, 0.045 mol) in acetic acid (60 mL) was added slowly, with stirring, zinc dust (11.8 g, 0.183 mol), keeping the reaction temperature below 30 °C. Following the addition, the mixture was stirred at room temperature for 5 h, and then filtered. The resulting precipitate was washed with a 1:2 mixture of acetic acid and water (50 mL). The combined filtrates were concentrated in vacuo to remove the acetic acid. The residue was extracted with ether–benzene (200 mL), and then the extract was washed with water, dried over $MgSO_4$, and concentrated in vacuo. The residual oil was distilled (62 °C/0.6 mmHg) to furnish **2b** (4.7 g, 75.7%). The ester formed on treatment of **2b** with 3,5-dinitrobenzoyl chloride in pyridine had the mp of 77 °C.

***exo*-5-Vinyl-2-norbornene (1a) and *endo*-5-Vinyl-2-norbornene (1b).** To an ice-cooled, stirred solution of **2a** (15.0 g, 0.109 mol) in pyridine (80 mL) was added in several portions of *p*-toluenesulfonyl chloride (22.8 g, 0.120 mol). After being stirred at room temperature overnight, the mixture was treated with water (5 mL), and the pyridine was evaporated in vacuo. The residue was treated with water (50 mL) and extracted with ether–benzene (200 mL). The organic extract was washed with water, dried over $MgSO_4$, and concentrated under reduced pressure to give 2-(5-norbornen-*exo*-2-yl)ethyl *p*-toluenesulfonate (15.5 g, 48.7%) as an oil which was used in the next step without further purification: IR (neat film) cm^{-1} 3090, 2925, 2875, 1660, 1640, 1180; ^1H NMR ($CDCl_3$) δ=7.80—7.50 (m, 4H), 6.30—5.95 (m, 2H), 4.10—3.90 (t, 2H), 2.80 (broad s, 2H), 2.60 (s, 3H), 2.35—1.35 (m, 7H).

A solution of the above oil (15.5 g, 0.053 mol) in pyridine (50 mL) was refluxed for 12 h. Upon cooling to room temperature the mixture was poured into ice-water (50 mL) and extracted three times with pentane (100 mL), and the combined organic extracts were washed with water, dried over $MgSO_4$, and concentrated in vacuo. The residue was distilled [55—62 °C/25 mmHg (lit,[2a] 66.5 °C/66 mmHg)] to furnish **1a** (3.5 g, 55.0%): ^1H NMR (CCl_4) δ=6.05—6.00 (m, 2H), 5.95—5.70 (m, 1H), 5.30—4.85 (m, 2H), 2.85 (broad s, 1H), 2.70 (broad s, 1H), 2.25—1.95 (m, 2H), 1.45—1.35 (m, 3H); n_D^{20} 1.4791.

In place of **2a**, **2b** was treated in the identical manner described above to produce 2-(5-norbornen-*endo*-2-yl)ethyl *p*-toluenesulfonate (17.5 g, 55.0%) and **1b** (3.7 g, 51.4%), respectively. The physical properties of **1b** were as follows: bp 51—55 °C/20 mmHg; ^1H NMR (CCl_4) δ=6.05—5.95 (m, 2H), 5.80—5.40 (m, 1H), 5.10—4.70 (m, 2H), 2.95—2.65 (m, 3H), 2.10—1.80 (m, 1H), 1.50—1.30 (m, 2H), 1.00—0.80 (m, 1H); n_D^{20} 1.4806.

The author expresses his sincere thanks to Professor Teijiro Yonezawa of Kyoto University for helpful discussions. Special appreciation is due Nippon Petrochemical Corp. for parts of the synthetic work.

References

1) T. Maeda, M. Muranaka, S. Hamanaka, and M. Ogawa, *Nippon Kagaku Kaishi*, **1974**, 1587.

2) a) A. A. Bobyleva, N. A. Belikova, A. N. Kalinichenko, A. T. Baryshnikov, N. F. Dubitskaya, T. I. Pekhk, E. T. Lippmaa, and A. F. Plate, *Zh. Org. Khim.*, **16**, 1645 (1980); b) G. Just, U. Linder, W. Pritzkow, and M. Roellig, *J. Prakt. Chem.*, **317**, 979 (1975).

3) H. C. Brown and E. Negishi, *J. Am. Chem. Soc.*, **89**, 5477 (1967).

4) H. O. House, R. G. Carlson, and H. Babad, *J. Org. Chem.*, **28**, 3359 (1963).

5) P. J. Kropp, P. R. Worsham, R. I. Davidson, and T. H. Jones, *J. Am. Chem. Soc.*, **104**, 3972 (1982).

6) B. M. Trost and P. G. McDougal, *J. Org. Chem.*, **49**, 458 (1984).

7) a) C. G. Schmitt and C. E. Boord, *J. Am. Chem. Soc.*, **54**, 751 (1932); b) D. C. Rowlands, K. W. Greenlee, J. M. Derfer, and C. E. Boord, *J. Org. Chem.*, **17**, 807 (1952).

8) a) J. P. Kutney and F. Bylsma, *J. Am. Chem. Soc.*, **92**, 6090 (1970); b) W. Reusch and D. W. Frey, *Tetrahedron Lett.*, **1967**, 5193; c) J. Schmutz and F. Künzle, *Helv. Chim. Acta*, **53**, 89 (1970); d) A. A. Bobyleva, A. N. Kalinichenko, N. A. Belikova, S. I. Korol'kov, N. F. Dubitskaya, and A. F. Platé, *Zh. Org. Khim.*, **10**, 1885 (1974).

9) E. A. Rick and S. W. Tinsley, U. S. Patent 3459775 (1969).

Pressure Effect in Syngas Conversion to Ethylene Glycol. A Behavior of Rhodium-Tributylphosphine-*N*-Methylpyrrolidone System under 1000 atm

Kazuhisa MURATA,* Akio MATSUDA, Takashi MASUDA, Eiichi WATANABE,† and Keisuke WADA†
National Chemical Laboratory for Industry, Yatabe, Tsukuba, Ibaraki 305
†Research Center, Mitsubishi Chemical Industries Limited,
1000 Kamoshida-chou, Midori-ku, Yokohama 227
(Received September 27, 1986)

Synopsis. In syngas ($CO+H_2$) conversion to ethylene glycol (EG), rhodium catalyst modified by tributylphosphine (P^nBu_3) was found to be ca. 20 times more active under 1000 atm at 210 °C than under 500 atm. This unusual pressure effect was discussed on the basis of IR spectral data.

A pressure effect has been observed in syngas conversion to ethylene glycol (EG), where *N*-methylpyrrolidone (NMP) solution of rhodium compound was used as catalyst system.[1] Also, rhodium systems modified by phosphine have been found to be more effective than Rh alone under the syngas pressure below 500 atm.[2] We have reported the effectiveness of the addition of some phosphines for the glycol synthesis using Co–Ru mixed system in toluene or dioxane solvent under 1000 atm.[3] These findings led us to examine briefly the behavior of Rh–phosphine–NMP catalyst system under 1000 atm, in comparison with that under 500 atm.

Results and Discussion

NMP was employed as solvent, since it is one of the solvents suitable for Rh-catalyzed syngas conversion.[1] The reaction was carried out at 210 °C. The equimolar addition of some phosphines raised the catalytic activity. The effectiveness of phosphines when employed under the conditions of 1000 atm was in the order. $PCy_3(15.5)>P^iPr_3(14.6)>Cy_2PCH_2CH_2PCy_2(8.8)$[4]$>P^nBu_3(8.2)>$none$(5.8)>OPPh_3(4.4)>Me_2OPCH_2CH_2POMe_2(3.9)>P^nBu_3(2.7)>P^tBu_3(2.1)>P^sBu_3(1.8)>PPh_3(0)=P(OPh)_3(0)=P(O^nBu)_3(0)=P(O^iPr)_3(0)=PPh_2Me(0)=Ph_2PCH_2CH_2PPh_2(0)$. (Numerical values refer to turnover frequencies of ethylene glycol (N_{EG} (mol (Rh mol)$^{-1}$ h^{-1}). Here Cy denotes cyclohexyl, Pr propyl, Bu butyl, Ph phenyl, and Me methyl; the superscripts *i*, *n*, and *t* are for iso-, normal, tertiary, respectively.)

The effect of P/Rh ratio on the activity is illustrated

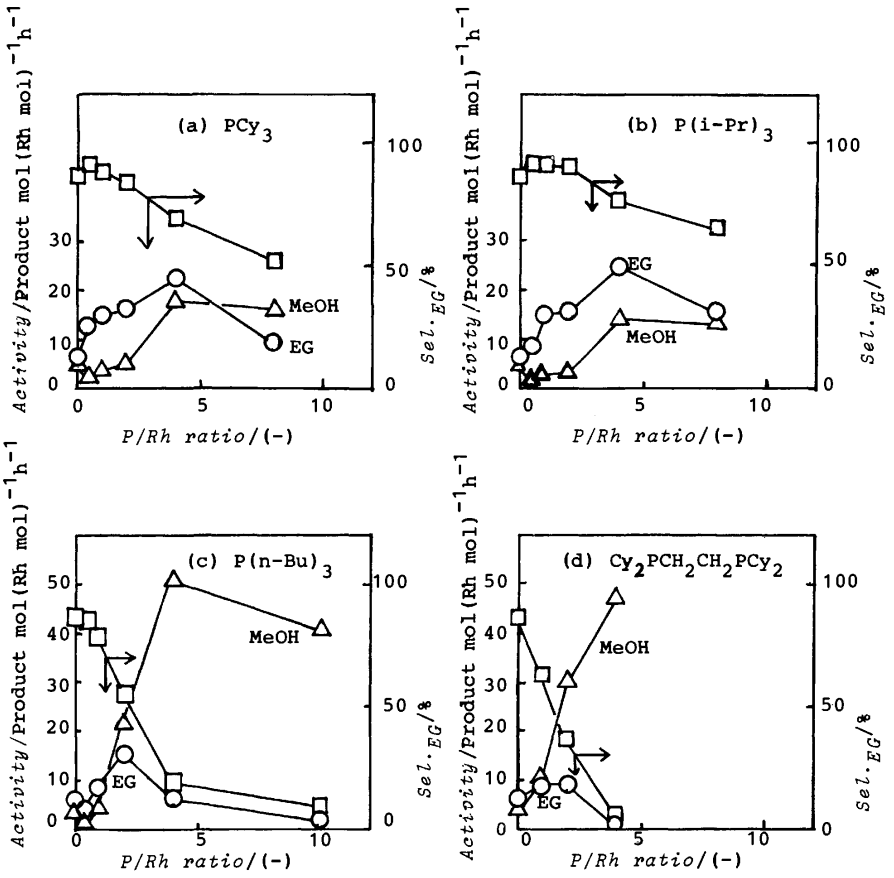

Fig. 1. Effect of P/Rh atomic ratio on catalytic activity and selectivity($Sel._{EG}$). Conditions: $Rh_4(CO)_{12}$ 0.05 mmol, NMP 20 ml, 210 °C, 3 h, 1000 atm(CO/H_2=1).

in Fig. 1. In the cases of PCy_3 and P^iPr_3, the maximum activity was achieved at P/Rh ratio of 4,[2b] whereas, in the cases of P^nBu_3[2b] and $Cy_2PCH_2CH_2PCy_2$, the optimum ratio was found to be 2. However, the methanol formation was remarkably accelerated by these catalyst systems including P^nBu_3 or $Cy_2PCH_2CH_2PCy_2$ at the P/Rh ratio above 2 and, consequently, the selectivity to the glycol decreased (Fig. 1c, d).

The activity depends on the total pressure (Fig. 2). The rate of glycol formation for the catalyst systems containing PCy_3 or P^iPr_3 under 1000 atm was 3—4 times higher than that under 500 atm. These trends were similar to that of Rh alone (▽). However, the rate for Rh-P^nBu_3 system under 1000 atm was ca. 20 times higher than that under 500 atm (Fig. 2, ○).

In order to explain this unusual improvement of the activity in Rh-P^nBu_3 system, IR spectra of catalyst solution were measured at ambient temperature under 20 atm (CO/H_2=1). The catalyst solution pretreated at 210 °C under 1000 atm exhibited IR absorption at 1952 cm^{-1}, characteristic of a dimeric rhodium such as $[Rh(CO)_3(P^nBu_3)]_2$, **A**,[2b,5] and at 1895 cm^{-1}, assigned to $[Rh(CO)_4]^-$, **B**,[2b,6] with weak shoulder bands near 2000 cm^{-1}. These spectral patterns were analogous to those[7] of Rh-PCy_3 system after the reaction under 500 atm as well as under 1000 atm. On the other hand, the solution of Rh-P^nBu_3, pretreated under 500 atm, showed weak IR absorptions of both **A** and **B** and additional broad bands at 2050—1940 cm^{-1} with 1849 cm^{-1} band, characteristic of rhodium clusters.[8] Thus, in the case of Rh-P^nBu_3 under 1000 atm conditions, two rhodium species, **A** and **B**, which seem to be responsible for the catalysis,[1b,2b] are predominantly formed at a P/Rh ratio of 2,[9] whereas cluster species, the activity of which are low,[8a] predominates under 500 atm (Scheme 1).[2,8] In conclusion, the unusual pressure effect is considered to be due to the increase in the concentration of more active Rh species than clusters: This result supports the possibility of non-cluster Rh complex as active species, as suggested previously.[1b,2]

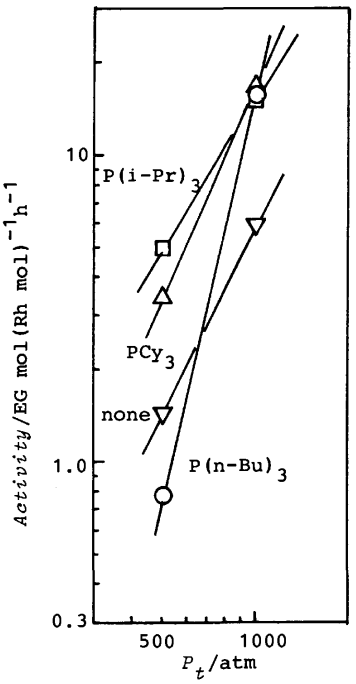

Fig. 2. Effect of total pressue. Conditions: $Rh_4(CO)_{12}$ 0.05 mmol, NMP 20 ml, phosphine 0.4 mmol, 210° C, 3 h.

Experimental

Materials. NMP and phosphines were obtained commercially and used with no further purification. $Rh_4(CO)_{12}$ was purchased from Nippon Engelhard Co.

Reaction Procedure. A catalyst solution containing $Rh_4(CO)_{12}$ (0.05 mmol) and phosphine in NMP solvent (20 ml) was placed in a Hastelloy C-autoclave (100 ml), which was subsequently charged with syngas (CO/H_2=1, 650 atm at room temp). After the reaction at 210 °C for 3 h under 1000 atm, the reaction vessel was cooled to room temperature and the solution was analyzed by GLC. The high pressure IR spectra were recorded on a JEOL A302-type spectrometer.

Product selectivity is defined by

$$\text{Sel.}_{EG} = \frac{2EG \times 100}{MeOH + MF + 2(EG + EtOH)}$$

This work is a part of "C_1 Chemistry Project," a National Research and Development Program of Agency of Industrial Science and Technology, Ministry of International Trade and Industry (M.I.T.I.), Japan.

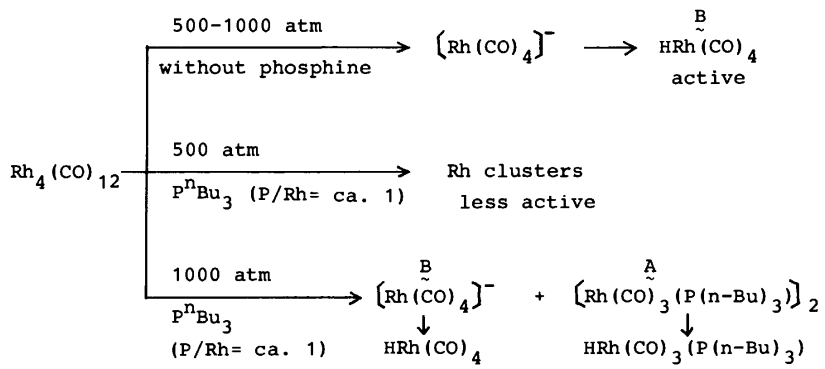

Scheme 1.

References

1) W. Keim, M. Berger, and J. Schulupp, *J. Catal.*, **61**, 359 (1980); T. Masuda, K. Murata, and A. Matsuda, *Bull. Chem. Soc. Jpn.*, **59**, 1287 (1986); E. Watanabe, K. Murayama, Y. Hara, Y. Kobayashi, K. Wada, and T. Onoda, *J. Chem. Soc., Chem. Commun.*, **1986**, 227.

2) a) E. Watanabe, Y. Hara, K. Wada, and T. Onoda, *Chem. Lett.*, **1986**, 285; b) E. Watanabe, Y. Hara, T. Matsuzaki, K. Wada, and T. Onoda, *Shokubai*, **28**, 154 (1986); c) Y. Tomotake, T. Matsuzaki, K. Murayama, E. Watanabe, K. Wada, and T. Onoda, *J. Organomet. Chem.*, in press; d) H. Tanaka, Y. Hara, E. Watanabe, K. Wada, and T. Onoda, *J. Organomet. Chem.*, **312**, C71 (1986); e) M. Tamura, M. Ishino, T. Deguchi, and S. Nakamura, *ibid.*, **312**, C75 (1986).

3) K. Murata, A. Matsuda, T. Masuda, M. Ishino, and M. Tamura, *Bull. Chem. Soc. Jpn.*, **60**, 438 (1987).

4) For the first time, the effectiveness of diphosphine was demonstrated for the Rh-catalyzed syngas conversion; for $MePCH_2CH_2PMe_2$ and $^tBu_2P(CH_2)_5P^tBu_2$, the reactions were found to be inhibited under 500 atm of syngas. H. Murakami, E. Watanabe, K. Wada, and T. Onoda, unpublished results.

5) B. L. Booth, M. J. Else, R. Fields, and R. N. Hazeldine, *J. Organomet. Chem.*, **27**, 119 (1971).

6) The catalyst solution of Rh–NMP system without phosphine showed the only IR band at 1895 cm^{-1}. P. Chini and S. Martinengo, *Inorg. Chim. Acta*, **3**, 21 (1969).

7) These exhibited the IR absorption at 1950(m) and 1895(m) cm^{-1}.

8) The formation of $[Rh_9P(CO)_{21}]^{2-}$ and $[Rh_6(CO)_{15}]^{2-}$ is likely.[2] a) J. L. Vidal and W. E. Walker, *Inorg. Chem.*, **19**, 896 (1980); b) J. L. Vidal, W. E. Walker, R. L. Pruett, and R. C. Shoening, *ibid.*, **18**, 129 (1979); c) S. Martinengo, A. Fumagalli, P. Chini, V. G. Albano, and G. Ciani, *J. Organomet. Chem.*, **116**, 333 (1976).

$[Rh_9P(CO)_{21}]^{2-}$: ν(CO) 2010(s), 1840 cm^{-1}
$[Rh_6(CO)_{15}]^{2-}$: ν(CO) 2050, 1990, 1984(s), 1960, 1790, 1767 cm^{-1}.

9) Under the 1000 atm-conditions, where non-cluster species are predominantly present, the dependence of reactivity on the P^nBu_3/Rh atomic ratio (Fig. 1c) could be explained by the equilibria (a), as is the case for Rh–P^iPr_3 system under 500 atm.[2]

$$HRh(CO)_4 \overset{L,\,-CO}{\rightleftharpoons} HRh(CO)_3L \overset{L,\,-CO}{\rightleftharpoons} HRh(CO)_2L_2 \overset{L,\,-CO}{\rightleftharpoons} HRh(CO)L_3 \overset{L,\,-CO}{\rightleftharpoons} HRhL_4 \qquad (a)$$

Studies on the Lattice Dynamics in Ferrocene Derivatives by Means of Recoil-Free Fraction and Thermal Shift in Mössbauer Spectra

Kumiko IWAI,* Motomi KATADA, Izumi MOTOYAMA,† and Hirotoshi SANO
Department of Chemistry, Faculty of Science, Tokyo Metropolitan University, Fukasawa, Setagaya-ku, Tokyo 158
(Received October 4, 1986)

Lattice dynamics in ferrocene derivatives, mono- and disubstituted acetyl-, carboxy-, and ethylferrocenes, tetrachloro(1,1′-diacetylferrocenato-*O*,*O*′)tin(IV) and tetrachlorobis(acetylferrocenato-*O*)tin(IV) have been studied by determining the temperature dependence of the recoil-free fraction and the thermal shift in the Mössbauer spectra. It was found that the lattice vibrations in acetyl- and carboxyferrocenes and adducts could be satisfactorily explained by assuming a harmonic oscillation model, while those of ethyl-substituted ferrocenes could not be interpreted by assuming harmonic vibrations.

Ferrocene derivatives are of great interest to the authors, since they exhibit various kinds of mesophase transitions associated with intermolecular interactions.[1-4] In order to investigate the effect of substituent groups on the lattice dynamics, such ferrocene derivatives as mono- and disubstituted acetyl-, carboxy-, and ethyl-ferrocene have been synthesized and the lattice dynamical nature of these compounds investigated in the solid state by comparing their Mössbauer spectra with the crystal structures and thermal data.

Lattice dynamics in more complicated systems, tetrachloro(1,1′-diacetylferrocenato-*O*,*O*′)tin(IV) and tetrachlorobis(acetylferrocenato-*O*)tin(IV), were also studied by Mössbauer spectroscopy. The temperature dependence of the recoil-free fraction and the thermal shift were determined for each of two the Mössbauer nuclides, ^{57}Fe and ^{119}Sn, included in the adducts, in order to investigate the total vibration of molecules.

Experimental

Preparation of Mono- and Disubstituted Ferrocenes. Mono- and disubstituted ferrocenes were prepared by following the method described in Ref. 5. The purification was carried out by repeated sublimations and recrystallizations. The purities were confirmed by checking the melting point and by elemental analyses. No impurity was detected in infrared(IR), NMR, and Mössbauer spectra.

Preparation of Adducts. Tetrachloro(1,1′-diacetylferrocenato-*O*,*O*′)tin(IV) and tetrachlorobis(acetylferrocenato-*O*)tin(IV) were prepared by modifying the method described in Ref. 6. Since the adducts are very sensitive to air, the samples for IR and Mössbauer measurements were mounted under nitrogen in a glove box. The IR spectra agreed with those of the literature.[6] However, the data of elemental analyses are not in good agreement with the calculated values, since the partial decomposition of adducts seems to occur upon exposure to air.

Mössbauer Spectra. Mössbauer spectra were measured using an Austin Science Associate Mössbauer spectrometer. A velocity calibration was carried out based on the spectra of metallic iron at room temperature. By fitting the resonance line-shape to a Lorentzian function, the Mössbauer parameters could be extracted. Low-temperature measurements were carried out by using a CA thermocouple embedded in a copper sample holder in a cryostat. The precision of this measurement was approximately ±1°.

Structure Determination and Refinement for Ferrocenecarboxylic Acid. A yellow-needle single crystal suitable for an X-ray study was obtained by slowly evaporating a methanol solution. The crystal size employed for data collection was approximately 0.05 m×0.15 mm×0.35 mm. Intensity data were collected on a four-circle diffractometer using an ω-2θ scan technique. A total of 2356 reflections were measured with Mo$K\alpha$ radiation ($2\theta<55°$); of these, 1252 were considered to have a significant intensity ($|F_o|>3\sigma|F_o|$). The intensities of the four standard reflections remained almost constant during data collection.

Crystal data for ferrocenecarboxylic acid are tabulated in Table 1. The positions of carbon and iron atoms were deduced from sharpened Patterson maps and all of the hydrogen atoms were deduced from difference syntheses. The block-least-squares program HBLS-4[7] was employed using anisotropic thermal parameters for non-hydrogen atoms and isotropic thermal parameters for hydrogen atoms. The atomic scattering factors were taken from the International Tables for X-ray Crystallograpy (1974).[8] Unit weights were adopted for all reflections. The R value reduced to 0.040 and final atomic parameters are given in Table 2. The complete F_o-F_c data have been deposited as Document No. 8736 at the

Table 1. Summary of Crystallographic Data for Ferrocenecarboxylic Acid at 24°C

Molecular formula	$C_{11}H_{10}O_2Fe$
Molecular weight	M.W. 235.0
Crystal system	Monoclinic
Space group	$P2_1/c$
a	5.8183(5) Å[a]
b	12.8535(11) Å
c	13.2064(13) Å
β	108.734(8)°
V	935.32(14) Å^3
D_c	1.67 g cm^{-3}
Z	4
R	4.0%

a) 1 Å=10^{-8} cm.

†Present address: Department of Chemistry, Faculty of Engineering, Kanagawa University, Rokkakubashi, Yokohama, Kanagawa 221.

Table 2. Positional Parameters ($\times 10^4$; for H$\times 10^3$)

	X	Y	X	$U_{eq}\times 10^2$(Å^2)		X	Y	X	$U_{eq}\times 10^2$(Å^2)
Fe	3066(1)	1807(1)	1791(1)	31(1)	O(1)	−94(8)	4392(3)	1084(4)	65(2)
C(1)	−129(10)	1047(5)	1184(6)	61(3)	O(2)	2921(8)	4341(3)	377(4)	65(2)
C(2)	1651(12)	363(5)	1770(5)	55(2)	H(1)	−159(10)	127(4)	121(4)	59(17)
C(3)	3495(10)	339(4)	1297(4)	46(2)	H(2)	166(12)	−6(5)	242(5)	89(23)
C(4)	2870(11)	1014(4)	429(4)	47(2)	H(3)	497(12)	4(6)	155(5)	95(24)
C(5)	633(11)	1468(5)	353(5)	57(2)	H(4)	384(10)	113(5)	−2(5)	72(20)
C(6)	2597(9)	2953(4)	2770(4)	38(2)	H(5)	−18(12)	196(5)	−11(5)	80(21)
C(7)	4422(11)	2264(5)	3354(4)	47(2)	H(6)	108(8)	313(4)	291(4)	36(13)
C(8)	6283(10)	2244(5)	2878(4)	49(2)	H(7)	442(9)	179(4)	391(4)	50(15)
C(9)	5664(9)	2914(4)	2003(4)	42(2)	H(8)	766(9)	180(4)	313(4)	44(14)
C(10)	3358(10)	3371(4)	1921(4)	38(2)	H(9)	661(10)	309(5)	154(4)	67(18)
C(11)	1929(11)	4070(4)	1097(5)	45(2)	H(10)	194(12)	479(6)	−18(5)	95(24)

Office of the Editor of the Bulletin of the Chemical Society of Japan.

Results and Discussion

First, suitable model compounds having similar molecular weights and volumes but different intermolecular interactions caused by the substituent groups (mono- and disubstituted acetyl-, carboxy-, and ethylferrocenes) were synthesized and the temperature dependence of Mössbauer spectra was measured in order to elucidate the relationship between the recoil-free fraction or the thermal shift and the lattice vibration in these ferrocene derivatives.

The recoil-free fraction, f, can be estimated from the areal intensity of Mössbauer spectrum and is expressed by the mean-square amplitude of a Mössbauer atom, $<U^2>$:

$$f = \exp[-4\pi^2<U^2>/\lambda_\gamma^2] \quad (1)$$

where λ_γ is the wavelength of a Mössbauer γ-ray. It is difficult to obtain an absolute recoil-free fraction by using the areal intensity method, because of the absence of a suitable standard sample. Therefore, the mean-square amplitude was estimated by a high-temperature-approximation method.[2] At a temperature sufficiently high to assume $T \gg \Theta_D/2$ (where Θ_D is the Debye characteristic temperature), it is known that the mean-square amplitude is proportional to the absolute temperature. The values of the mean-square amplitude are estimated from the slope of the linear relationship.

Figure 1 shows the temperature dependence of the mean-square amplitude estimated from the areal intensities of the Mössbauer spectra for iron atoms in acetyl- and carboxyferrocenes. The mean-square amplitude is considered to be proportional to the absolute temperature nearly up to room temperature, indicating that the molecules are in harmonic vibration. The values of the mean-square amplitude at room temperature determined by applying the high-temperature approximation from 78 K to room temperature are 2.6×10^{-2}, 2.8×10^{-2}, 3.0×10^{-2}, and 4.5×10^{-2} Å^2 for ferrocenecarboxylic acid, 1,1′-diacetylferrocene, acetylferrocene, and 1,1′-ferrocenedicarboxylic acid, respectively, while those determined based on the isotropic thermal factors in X-ray diffraction study are 3.1×10^{-2}, 2.8×10^{-2},[10] 3.2×10^{-2},[3] and 4.0×10^{-2} Å^2,[11] respectively. Both values for the same compound are in fairly good agreement with each other. The value of the mean-square amplitude of ferrocenecarboxylic acid is slightly less than those of acetylferrocenes, while the value of 1,1′-ferrocenedicarboxylic acid was estimated to be about 1.5-times larger than those of other compounds.

Figure 2 shows the crystal structure of ferrocenecarboxylic acid determined by X-ray diffraction. The C-C distances in the cyclopentadienyl rings are 1.289—1.426 Å; the Fe-C distances are 2.019—2.045 Å. These results are in good agreement with acetylferrocene[3] and 1,1′-diacetylferrocene,[10] as well as molecules that exhibit an eclipsed conformation. The C(11), O(1), and O(2) atoms lie approximately on the plane of the aromatic rings, because of a existence of a

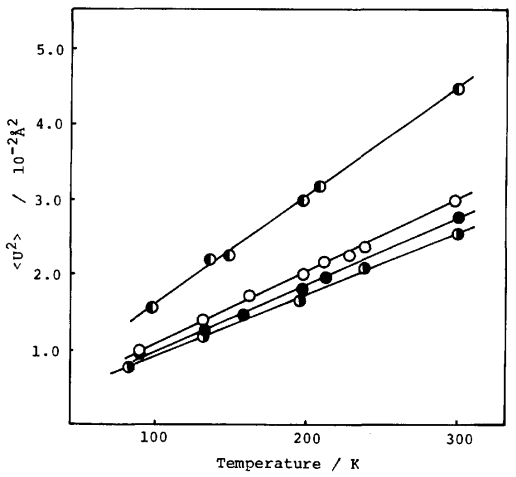

Fig. 1. The temperature dependence of mean-square amplitude for acetylferrocene (○), 1,1′-diacetylferrocene (●), ferrocenecarboxylic acid (◑), and 1,1′-ferrocenedicarboxylic acid (◐).

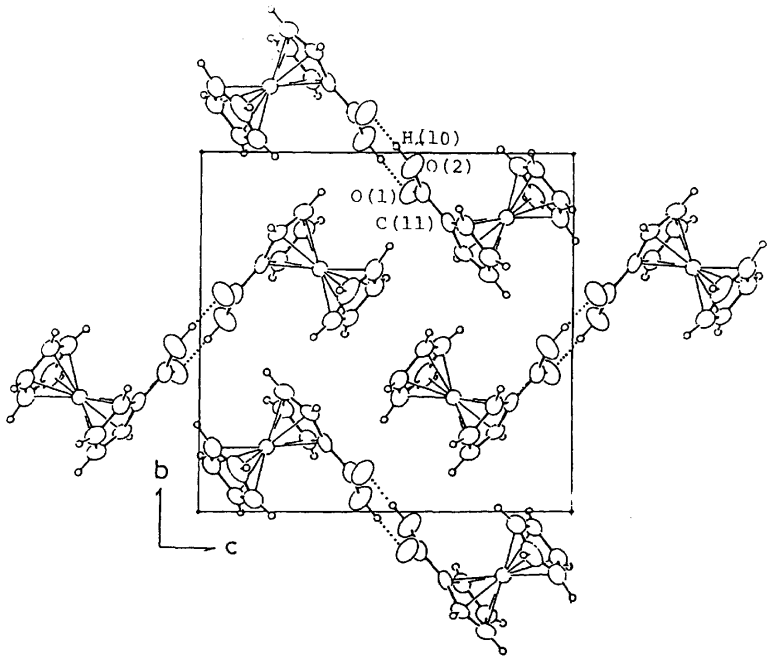

Fig. 2. Projection of the crystal structure of ferrocenecarboxylic acid along the a axis at room temperature. The hydrogen bonding O(1)···H(10) is indicated by broken lines.

complete conjugation between the carboxyl group and cyclopentadienyl rings. Two molecules of ferrocenecarboxylic acid have an intermolecular hydrogen bonding as shown in Fig. 2. The hydrogen-bonding distance between O(1) and H(10) is 1.69 Å and that between O(1) and O(2) is 2.65 Å. The H(10) is covalently bonded to the O(2) on one side of the carboxyl group. Molecules of ferrocenecarboxylic acid seem to be rigid in the crystal state owing to a significant interaction of hydrogen bonding between carboxyl groups.

On the other hand, the values of the mean-square amplitude of iron atom in 1,1′-ferrocenedicarboxylic acid are about 1.5-times larger than those found in other ferrocene derivatives. It was found by means of X-ray diffraction measurements that two 1,1′-ferrocenedicarboxylic acid molecules form a dimer through two intermolecular hydrogen bonds.[11] The present sample was determined to be a monoclinic form by Weissenberg photographs. The intermolecular hydrogen bonds seem to be so strong that the dimer molecules of 1,1′-ferrocenedicarboxylic acid behave like one molecular unit in regard to the molecular motion.

An attempt to interpret the molecular motion for 1,1′-ferrocenedicarboxylic acid was made by applying a rigid-body model. The center of gravity for this compound associated with the molecular motion is assumed to be located at the center of a dimer. Since iron atoms are far apart from the center of gravity in a dimer and its moment of inertia for librational vibration seems to be large, the large values of the mean-square amplitude for iron atoms could be explained by assuming both translational and librational motion. For the other compounds, it is roughly assumed that all the iron atoms sit at the center of mass of the molecules and, thus, the mean-square amplitudes of iron atoms have been estimated to be much smaller than that of 1,1′-ferrocenedicarboxylic acid.

As can be seen in Fig. 3, the temperature dependence of the mean-square amplitude for mono- and 1,1′-diethylferrocene derivates from a single straight line, which shows anomaly at about 150 K. There seems to

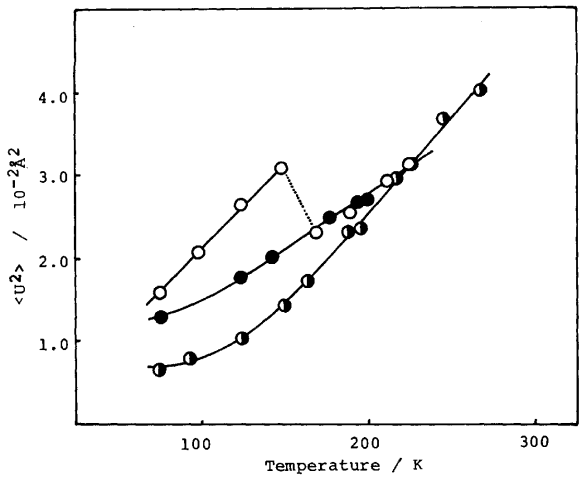

Fig. 3. The temperature dependence of mean-square amplitude in ethylferrocene (◑) and in 1,1′-diethylferrocene (○) and (●), in which open circles were obtained by heating the samples where were first cooled down to liquid nitrogen temperature; closed circles were obtained on cooling 1,1′-diethylferrocene heated up to 224 K in the heating experiment.

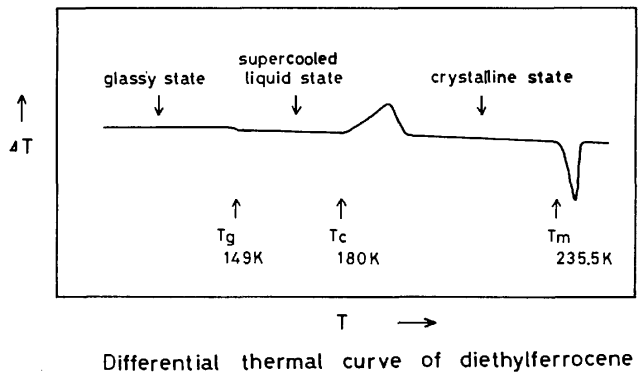

Fig. 4. Differential thermal curve of 1,1′-diethylferrocene at scanning rate of 2.2 deg min^{-1}, Tg: Transition temperature from glass to supercooled liquid state (glass transition temperature); Tc: Transition temperature from supercooled liquid to crystal state (crystallizing temperature); Tm: Melting point.

exist an anharmonicity of the intermolecular vibration in the low-temperature region owing to a loosely packed crystal structure caused by the flexibility of the ethyl groups. This observation suggests that the thermal vibration in acetyl- and carboxy-substituted ferrocenes differs considerably from that in the ethyl-substituted ones.

1,1′-Diethylferrocene was found to have a glassy state through a thermal analysis (Fig. 4).[2] The Differential Thermal Analysis (DTA) data of 1,1′-diethylferrocene reveal that this compound in a glassy state turns into a supercooled liquid state at 149 K, the glass transition temperature, T_g. After heating beyond T_g, crystallization takes place at 180 K, the crystallizing temperature, T_C, followed by melting at 235.5 K. Although the apparent T_g and T_c depend upon the scanning rate of the temperature, nearly constant values of T_g and T_c are obtained with good reproducibility at various slow scanning rates (<2 deg min^{-1}).

In Fig. 3, the open circles indicate the data obtained while heating a sample which was first cooled down to liquid-nitrogen temperature. The closed circles indicate the data obtained while cooling 1,1′-diethylferrocene (heated to 224 K during the heating experiment). The drastic anomaly observed in the recoil-free fraction at 150—170 K during the heating process could be attributed to a transition from the glass to the crystal state via a supercooled liquid state (based on the DTA data shown in Fig. 4). The apparent crystallizing temperature is a little lower than 180 K for a lower scanning speed than 2.2 deg min^{-1}. Since a measurement of the Mössbauer spectra requires about 24 h at a constant temperature, values of the mean-square amplitude between 80 and 149 K are attributed to the thermal motion of molecules in a glass state. The values above 169 K (corresponding to the T_c (180 K) in DTA) may reflect the thermal motion in a crystal state. The larger value of the mean-square amplitude found near 149 K indicates that the molecules in a glass state are much more mobile compared to the molecules near 200 K in a crystal state. Since it is impossible to change from a crystal state to a glass state during cooling, the data of the mean-square amplitude obtained in the recooled process from 224 to 80 K are ascribed to the values for the crystal state. It has been clearly observed that the mean-square amplitude of 1,1′-diethylferrocene in the crystal state differs from that in the glassy state at the same temperature. The value of the mean-square amplitude obtained for 1,1′-diethylferrocene in the crystal state near the melting point is similar in magnitude to that found at the glass transition point.

Lattice dynamics in tetrachlorobis(acetylferrocenato-*O*)tin(IV) and tetrachloro(1,1′-diacetylferrocenato-*O*,*O*′)tin(IV) have been observed by Mössbauer spectroscopy in order to investigate the total vibration of molecules.

These adducts were synthesized by Pavlik et al. in 1968 and were suggested to have a molecular structure in which oxygen atoms of acetyl groups are coordinated to tin atoms. The isomer shift and quadrupole splitting values of iron atoms in the Mössbauer spectra at nitrogen temperature for the sample mounted under nitrogen are 0.51 and 2.17 mm s^{-1} for tetrachlorobis(acetylferrocenato-*O*)tin(IV) and 0.49 and 1.98 mm s^{-1} for tetrachloro(1,1′-diacetylferrocenato-*O*,*O*′)tin(IV), respectively. The values of quadrupole splitting are smaller than other ferrocene derivatives because of the electron-attracting effect of the acetyl group coordinating to the tin atom. The isomer shift values of tin atoms in the Mössbauer spectra at nitrogen temperature are 0.46 mm s^{-1} for tetrachlorobis(acetylferrocenato-*O*′)tin(IV) and 0.39 mm s^{-1} for tetrachloro(1,1′-diacetylferrocenato-*O*,*O*′)tin(IV), respectively, which are smaller than those, 1,45—1.55 mm s^{-1}, of starting materials, $SnCl_4$. These adducts are found to have an octahedral structure which consists of an sp^3d^2 orbital since the s-electron density around tin atoms in these adducts is lower than that of $SnCl_4$. Mössbauer spectroscopic data support the results offered by Pavlik et al.

Figure 5 shows the temperature dependence of the mean-square amplitude obtained for these adducts. The values of the mean-square amplitude of iron atoms were found to be larger than those of tin atoms. The reason may be that iron atoms require not only a translational motion of the center of gravity but also a librational motion around the center of gravity, since iron atoms are located far from the center of gravity and possess a large moment of inertia for librational motion around the center of gravity. Although the crystal structures of these adducts cannot be determined because of instability in air and the difficulty of preparing a single crystal, the results obtained from the temperature dependence of the mean-square amplitude indicate that the mean-square amplitude of iron and tin atoms are apparently proportional to the

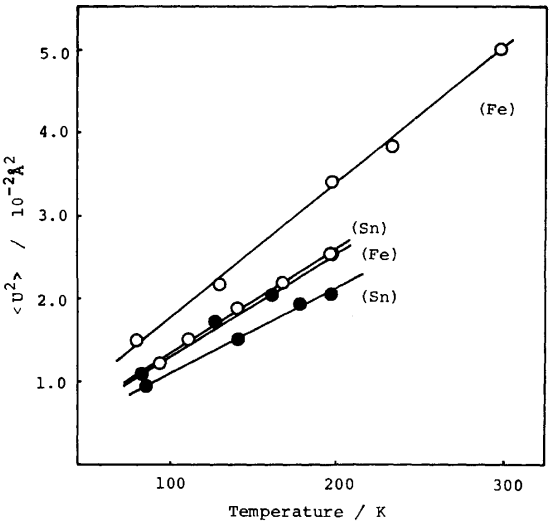

Fig. 5. The temperature dependence of mean-square amplitude determined for each of two Mössbauer nuclei, iron and tin atoms, included in the respective adducts, in which open circles were obtained for tetrachlorobis(acetylferrocenato-*O*)tin(IV); closed circles were obtained for tetrachloro(1,1′-diacetylferrocenato-*O*,*O*′)tin(IV).

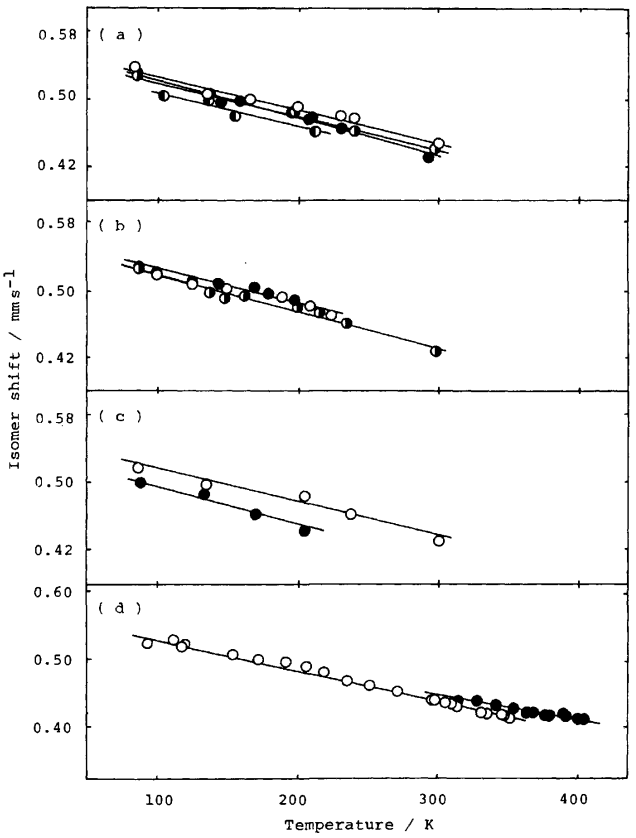

Fig. 6. The temperature dependence of thermal shift for (a) acetylferrocene (○), 1,1′-diacetylferrocene (●), ferrocenecarboxylic acid (◑), and 1,1′-ferrocenedicarboxylic acid (◐), (b) ethylferrocene (◑) and 1,1′-diethylferrocene (○) and (●), in which open circles were obtained in the crystal state; closed circles were obtained in the glassy state, (c) tetrachlorobis(acetylferrocenato-*O*)tin(IV) (○) and tetrachloro(1,1′-diacetylferrocenato-*O*,*O*′)tin(IV) (●), (d) formylferrocene (○) and 1,1′,2,2′-tetrachloroferrocene (●).

absolute temperature in the temperature range studied and that the molecular vibration for these adducts can be explained by assuming the harmonic vibration and the rigid-body model.

The thermal shift, so-called 2nd-order Dopplar Shift, extracted from the Mössbauer spectra also gives significant information about the lattice dynamics in the solid state. The thermal shift originates from the mass defects of the Mössbauer nuclei associated with a γ-ray transition. When the high-temperature approximation of the Debye model is applied, the thermal shift, ΔE, can be expressed as,

$$\Delta E = 3kTE_\gamma/2c^2M, \quad (2)$$

where E_γ is the energy of the Mössbauer γ-ray and M is the effective vibrational mass. It was known that the Mössbauer spectra shift position by both thermal and isomer shifts. Since the former depends on the temperature, the temperature dependence of center shifts in Mössbauer spectra can provide information concerning the magnitude of the thermal shift.

Figure 6 shows the temperature dependence of the center shifts. It was found that all the values are proportional to the absolute temperature and that their slopes are constant in spite of the different molecular structure. When the thermal shifts was interpreted by applying the Debye model (as shown in Eq. 2) the effective vibrational mass was estimated to be ca. 100 for all the studied samples. This fact indicates that the thermal shift dose not depend on the intermolecular interaction and that the iron atom and some atoms in its neighbourhood are involved as a unit in the molecular vibration.

It is interesting to note that the values of the thermal shifts obtained in the crystal phase and the glassy phase for 1,1′-diethylferrocene are approximately equal (Fig. 6(b)) in spite of the drastic difference in the mean-square amplitude between the crystal and glassy phases. The results were also observed in other ferrocene derivatives having a mesophase. The authors have reported that the mean-square amplitudes of formylferrocene and 1,1′,2,2′-tetrachloroferrocene drastically change at the plastic crystal phase transition points, 296.5 and 391 K, respectively.[4] In the case of the formylferrocene, the value of the mean-square amplitude in the plastic phase is about 4-times larger than those in the crystal phase. However, as shown in Fig. 6(d), the thermal shift of formylferrocene shows no significant change in the range from 78 to 343 K. For formyl- and 1,1′,2,2′-tetrachloroferrocene, the effective masses were estimated to be ca. 100, similar to the values obtained in the present work.

It is concluded that acetyl- and carboxyferrocene and

adducts exhibit harmonic thermal vibrations in the range of whole temperature but that ethyl-substituted ferrocenes do not exhibit harmonic thermal vibration at low temperatures. The values of the mean-square amplitude of iron atoms significantly depend upon the position of the iron atom in the compound associated with the moment of inertia in molecular motion. The magnitude of the mean-square amplitude is affected by the molecular arrangement in the solid state, such as the crystal and the glassy states. On the other hand, the thermal shift dose not depend on the intermolecular interaction for ferrocene derivatives studied and the values of vibrational mass estimated from Debye model remain in a constant value. It was found that the thermal shift depends on the bonding state between the Mössbauer atoms and the atoms around the Mössbauer atom.

The authors are indebted to Prof. Michiko Konno at Ochanomizu University for her kind help regarding the use of the X-ray diffractometer at the Institute for Solid State Physics, The University of Tokyo and for discussions concerning the results.

References

1) F. L. Hedberg and H. Rosenberg, *J. Therm. Anal.*, **6**, 571 (1974); J. Malthete and J. Billard, *Mol. Cryst. Liq. Cryst.*, **34**, 117 (1976); M. F. Daniel, A. J. Leadbetter, R. E. Meads, and W. G. Parker, *J. Chem. Soc., Faraday Trans. 2*, **1978**, 456.

2) K. Sato, M. Katada, and H. Sano, *Chem. Lett.*, **1980**, 217.

3) K. Sato, M. Katada, H. Sano, and M. Konno, *Bull. Chem. Soc. Jpn.*, **57**, 2361 (1984).

4) K. Sato, M. Konno, snd H. Sano, *Chem. Lett.*, **1984**, 17; K. Sato, M. Iwai, H. Sano, and M. Konno, *Bull. Chem. Soc. Jpn.*, **57**, 634 (1984).

5) M. Rosenblum and R. B. Woodward, *J. Org. Chem.*, **80**, 5443 (1958); K. L. Rinehart, Jr. K. L. Motz, and S. Moon, *J. Org. Chem.*, **79**, 2749 (1957); R. B. Woodward, M. Rosenblum, and M. C. Whiting, *J. Org. Chem.*, **74**, 3458 (1952); R. A. Benkeser and J. L. Bach, *J. Org. Chem.*, **86**, 890 (1964).

6) I. Pavlik, J. Klikorka, and K. Handlir, *Z. Chem.*, **8**, Jg. 10, 390 (1968).

7) T. Ashida (1976) UNICS. The Universal Crystallographic Computing System, The Crystallographic Society of Japan.

8) "International Tables for X-Ray Crystallography." Kynoch Press, Birmingham (1974), Vol. IV.

9) H. Sano, Mössbauer Spectroscopy The Chemical Applications, Kodansha Ltd., 1972.

10) G. J. Palenik, *Inorg. Chem.*, **9**, 2424 (1974).

11) F. Takusagawa and T. F. Koetzle, *Acta. Cryst.*, **B35**, 2888 (1979); G. J. Palenik, *Inorg. Chem.*, **8**, 2744 (1969).

 © 1987 The Chemical Society of Japan Bull. Chem. Soc. Jpn., 60, 1967—1973 (1987)

Fluorescence Behavior and Energy Transfer of Cyanine Dyes Bound to Bilayer Membranes of Double-Chain Ammonium Amphiphiles[1)]

Naotoshi NAKASHIMA, Reiko ANDO, and Toyoki KUNITAKE*
Department of Organic Synthesis, Faculty of Engineering, Kyushu University, Fukuoka 812
(Received November 1, 1986)

Negatively-charged cyanine dyes are bound specifically to aqueous bilayer membranes of double-chain ammonium amphiphiles, as reflected in their absorption spectra. The quantum yield of the fluorescence emission of a trimethine-thiacyanine dye is remarkably enhanced (up to 0.64) when the dye is bound to crystalline bilayer membranes of certain double-chain ammonium amphiphiles. The fluorescence intensity diminished drastically with the liquid crystalline bilayers. Efficient energy transfer is noted from an oxacyanine to the thiacyanine dye in the crystalline membrane matrix. The efficiency decreases by the membrane phase transition to the liquid crystalline state. These results are discussed in terms of specific dye binding and concentration of dyes at the membrane surface.

It has been shown by us and others that a large variety of synthetic amphiphiles produce bilayer aggregates spontaneously.[2-4)] Double-chain ammonium amphiphiles belong to a representative class of the bilayer-forming compounds. These synthetic bilayers possess the two-dimensional organization which is unique as sites for controlling aggregation and orientation of chromophores.

Chromophores can be introduced into bilayers as part of component molecules and as noncovalently adsorbed guest molecules. In the former case, unique spectral and related characteristics such as extraordinary enhancement of circular dichroism, large shifts in absorption spectra, and efficient energy transfer are observed for bilayers containing benzene,[5)] biphenyl,[6)] naphthalene,[7)] anthracene,[8)] azobenzene,[5,9-11)] carbazole,[12,13)] and viologen units[14,15)] as chromophores. The latter cases include membrane-bound dyes (Methyl Orange,[16)] cyanines and merocyanines,[17,18)] and phenylenediamine[19)]) of which spectra reflect specific modes of aggregation and orientation.

As an extention of these studies, we discuss in this paper the fluorescence behavior and the energy transfer of cyanine dyes bound to ammonium bilayer membranes. Cyanine dyes have attracted wide attention because of their characteristic photochemical and photophysical properties: as sensitizers in the photographic process,[20)] as spectroscopic probes for the physical state of the biological membrane,[21)] liposomes,[22,23)] and monolayers.[24,25)] The photophysical aspects of these dyes in highly organized bilayer assemblies pose an exciting topic, since it is known that specific aggregation and orientation of chlorophyll and carotenoid molecules play crucial roles in the efficient energy transfer in the biological photosynthetic machine.

The molecular structures of amphiphiles and dyes employed in this study are given in Scheme 1. We have reported preliminary results on the fluorescence characteristics of cyanine dye **5** bound to bilayer membranes of $2C_{12}$-L-Glu-ph$C_n N^+$, (**1**, n=2 and 4) and $2C_{16}N^+2C_1$ (**4**).[18)] Amphiphiles **2** and **3** possess molecular structures closely related to **1**. The difference is in the connector portion which connects the double chain portion and the phenyl group. The glutamic acid unit is used as connector in **1**, while **2** and **3** contain aspartic acid and diethanolamine, respectively, as connector. These small structural differences lead to different binding modes of thiacyanine dye **5**. Oxacyanine dye **6** was employed to study the efficiency of energy transfer to **5** at the membrane surface.

Experimental

Materials. Preparation of amphiphile **1** (n=4) was described before,[5)] and **1** (n=2 and 10), **2**, and **3** were obtained by similar procedures. The synthesis of the whole series will be discussed separately. The preparation of $2C_{16}N^+2C_1$ was given.[26)] Cyanine dyes **5** (NK 2012) and **6** (NK 1952) were purchased from Nippon Kanko Shikiso and used without further purification.

Measurement. Amphiphiles **1**—**4** suspended in distilled water were sonicated for 3 min (Branson Cell Disruptor 185, sonic power 40 W). The transparent dispersions obtained were incubated in ice water for 30 min. The dispersions were brought to given temperatures, aqueous dyes were added, and the mixtures were kept for 20 min. The 20-min aging at temperatures of the spectral measurement was required in order to secure reproducible spectra. This aging time may correspond to equilibration of dye molecules at the membrane surface. Absorption and emission spectra were measured with Hitachi 220 spectrophotometer and Hitachi 650-10S or 650-60 spectrofluorimeter, respectively. The 650-60 instrument possesses the correction function. The emission measurement was conducted under the aerated conditions, since no spectral difference was observed between the air saturated and N_2 saturated conditions. The excitation wavelength was set at the isosbestic point when the absorption spectrum showed temperature dependence. The quantum yield of emission of Rhodamin B (Wako Pure Chemical, recrystallized twice from ethanol, absorption maximum 542 nm, emission maximum 570 nm (corrected)) was assumed to be 0.5[27)] and used as the reference.

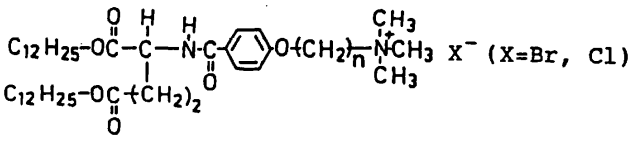

1, $2C_{12}$-L-Glu-ph-C_nN^+ (n=2, 4, 10)

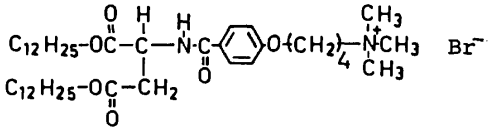

2, $2C_{12}$-L-Asp-ph-C_4N^+

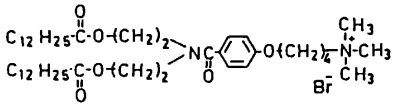

3, $2C_{12}$-Dea-ph-C_4N^+

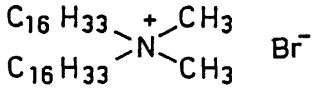

4, $2C_{16}N^+2C_1$

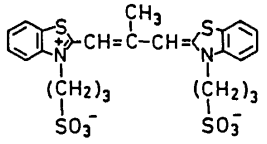

5, thiacyanine dye

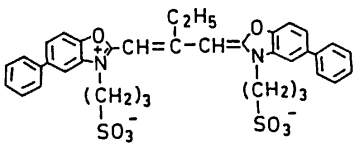

6, oxacyanine dye

Scheme 1.

Results and Discussion

Absorption and Fluorescence Spectra. Figure 1 displays temperature dependences of absorption and emission spectra of cyanine dye **5** bound to the bilayer matrix of $2C_{12}$-L-Glu-phC_4N^+ (**1**, n=4, X=Cl) at a molar ratio of 1/4000 (dye/bilayer). Both spectra show remarkable variations at a narrow temperature range of 27 to 29 °C. The spectral changes are small at lower temperatures (below 27 °C) and at higher temperatures (above 30 °C). The crystal-to-liquid crystal phase-transition temperature (T_c) of this bilayer is located at 31 °C (peak top temperature),[5] and the spectral variation is undoubtedly associated with the phase transition.

Similar results are found for other bilayers. The relative emission intensity (I_F) in different bilayers is plotted against temperature in Fig. 2. The dye concentration is very small (1/4000) relative to those of bilayers, and I_F is not affected by the dye concentration at this molar ratio (see below). Drastic I_F decreases are seen for the $2C_{12}$-L-Glu-phC_nN^+ (**1**) bilayers with different spacer lengths (n=2, 4, and 10) near the respective phase-transition temperatures: T_c=27 °C for n=2

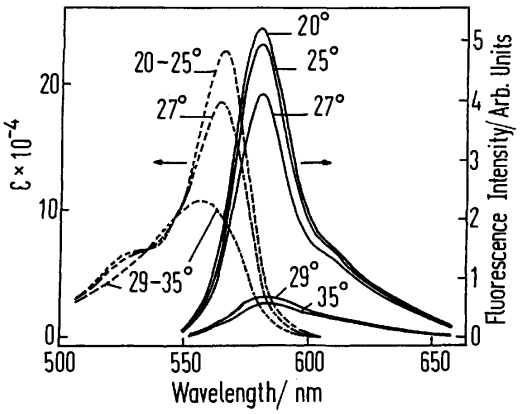

Fig. 1. Absorption (dotted line) and fluorescence (solid line, excitation at 545 nm) spectra of cyanine dye **5** (NK 2012) bound to the aqueous bilayer of $2C_{12}$-L-Glu-ph-C_4N^+ (**1**, n=4, X=Cl). [**5**]= 5.0×10^{-7} M.

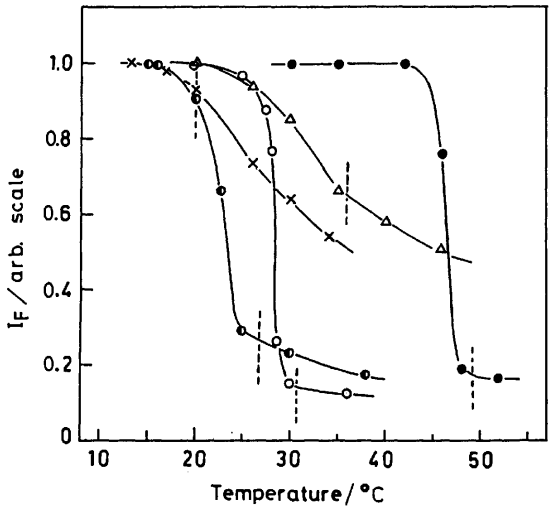

Fig. 2. Plots of I_F (arb. scale) of cyanine dye **5** against temperatures. [bilayer]=2.0×10^{-3} M, [**5**]=5.0×10^{-7} M. —◐—: $2C_{12}$-L-Glu-phC_2N^+ (**1**, n=2), —○—: $2C_{12}$-L-Glu-phC_4N^+ (**1**, n=4), —●—: $2C_{12}$-L-Glu-ph$C_{10}N^+$ (**1**, n=10), —△—: $2C_{12}$-L-Asp-phC_4N^+ (**2**), —×—: $2C_{12}$-Dea-phC_4N^+ (**3**). The emission intensity at 15 °C is taken as unity for the respective bilayer system. The dotted lines indicate the respective phase transition temperatures (peak top).

and 49 °C for n=10. The dependence on T_c is less drastic for bilayers **2** (T_c=36 °C) and **3** (T_c=20 °C). The temperature effect was also not remarkable for the bilayer of $2C_{16}N^+2C_1$ (**4**) (data not shown). These different sensitivities clearly indicate that the mode of dye binding is strongly affected by the chemical structure of the bilayer component. In particular, the structures of $2C_{12}$-L-Glu-phC_4N^+ (**1**, n=4) and $2C_{12}$-L-Asp-phC_4N^+ (**2**) are different only by one CH_2 unit in the connector portion (glutamate vs. aspartate).

Klausner and Wolf[28] incorporated a series of long-chain (C_{10} to C_{22}) cyanine dyes into lecithin vesicles and examined their fluorescence characteristics. However, the variation of I_F with the phase transition was very small.

Table 1. Quantum Yield for Cyanine Dye **5** in Various Media

Media	Φ_F		P	
	20 °C	35 °C	20 °C	35 °C
1 (n=2) (X=Br)	0.40	—	0.47	0.45
1 (n=4) (X=Cl)[a]	0.64	0.08	0.47	0.45
1 (n=6) (X=Br)	0.60	—	0.47	—
1 (n=10)(X=Br)	0.64	—	0.46	—
2	0.25	—	0.45	—
3	0.064	—	0.46	—
4	0.063	0.047	0.43	0.42
CTAC	0.035	0.019	0.39	0.39
Water	ca. 0.0025	ca. 0.0018	0.40	0.40
Methanol	ca. 0.0024	ca. 0.0017	0.39	0.38
Glycerol	0.24	—	0.47	—

a) Φ_F is almost the same when Cl is replaced by Br.

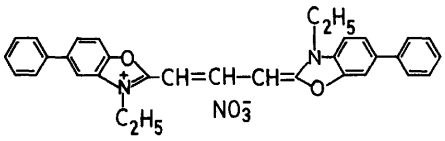

7

Scheme 2.

Onuki et al.[29] recognized that the fluorescence intensity of double-chain cyanine dyes was modified by the phase transition of matrix liposomes, though a single-chain cyanine dye did not show such an effect.

The fluorescence quantum yields (Φ_F) of thiacyanine dye **5** in various media are summarized in Table 1. Φ_F is small in water and in methanol (ca. 0.0025), and is enhanced by a factor of 15 in the hexadecyltrimethylammonium chloride (CTAC) micelle. A similar Φ_F enhancement was reported by Grätzel and coworkers.[30] They found that the fluorescence intensity of cyanine dye **7** is enhanced 5 times in the sodium dodecyl sulfate micelle and 8 times in the cadmium lauryl sulfate micelle relative to that in methanol.

Greater Φ_F enhancements are observed in the bilayer system at $T<T_c$. Φ_F values in bilayers of $2C_{12}$-L-Glu-phC_nN^+ are ca. 20 times greater than that in the CTAC micelle and ca. 250 times greater than those in water and alcohol. Large changes in Φ_F among bilayers are noteworthy. In spite of the structural similarity, $2C_{12}$-L-Glu-phC_4N^+ and $2C_{12}$-L-Asp-phC_4N^+ give a 10 fold difference. These data are again indicative of the specific nature of the binding mode. In fact, Φ_F is drastically diminished by the gel-to-liquid crystal phase transition of the matrix bilayer. The binding specificity appears lost in the liquid crystalline bilayer.

The Φ_F enhancement may be explained in terms of suppression of the nonradiative decay due to "rigidization" of the dye specifically bound to the membrane surface. The specific binding would constrain the conformation of the dye in such ways that large absorption shifts and fluorescence enhancements result.

The influence of the dye concentration on the spectral characteristics was subsequently examined. Cyanine dye **5** bound to the rigid $2C_{12}$-L-Glu-phC_4N^+ bilayer gives an absorption maximum at 565 nm and an emission maximum at 580 nm at a molar ratio of 1/4000 (see Fig. 1). When the molar ratio is raised to 1/20, these maxima undergo red shifts by ca. 10 nm each: λ_{max} 574 nm (absorption) and 590 nm (emission). Figure 3 demonstrates the effect of the relative dye concentration on the fluorescence intensity at 20 °C (below the phase transition) and at 35 °C (above the phase transition). The absolute emission intensity is much smaller at 35 °C as shown in Fig. 2. The dye concentration is fixed at 5.0×10^{-6} M (1 M=1 mol dm^{-3}), while the bilayer concentration is varied. The relative emission intensity is constant at molar ratios of 1/1000 and below. The intensity is lessened at higher ratios, prob-

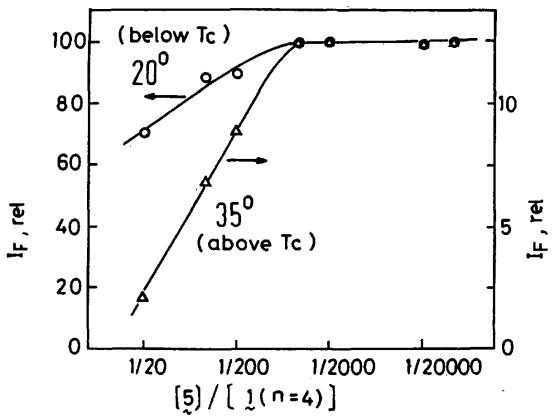

Fig. 3. Influence of the dye/bilayer molar ratio on the fluorescence intensity. [5]=5.0×10⁻⁶ M (constant). Bilayer, $2C_{12}$-L-Glu-phC_4N^+.

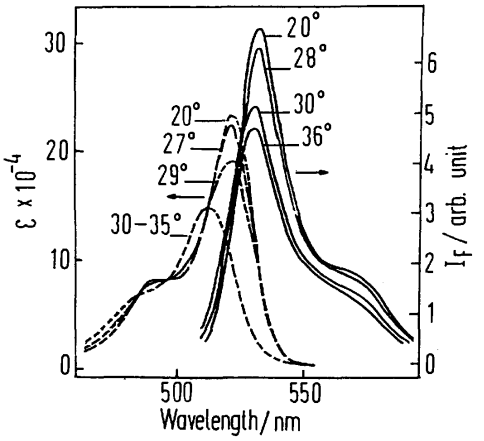

Fig. 4. Absorption (dotted line) and fluorescence (solid line, excitation at 500 nm) spectra of cyanine dye **6** bound to the aqueous bilayer of $2C_{12}$-L-Glu-phC_4N^+. [bilayer]=4.0×10⁻³ M, [dye]=1.0×10⁻⁶ M.

ably due to concentration quenching. The decrease is much larger in the crystalline bilayer, the intensity becoming ca. one third at the ratio of 1/20. This appears to be related to the enhanced energy transfer in the crystalline bilayer to be discussed later.

The emission intensity decreases drastically at T_c at the whole molar ratio range. The position of the descending line moves to higher temperatures with increasing dye concentrations. This is ascribed to the T_c rise of the dye-bound bilayer, as confirmed by the DSC measurement.[30] Similar trends were observed for absorption spectra and induced circular dichroism of this system.

The sharp emission with a small Stokes shift and the red shift in the absorption spectrum strongly suggest the formation of the J-like aggregates[20] for cyanine dye **5** concentrated in the bilayer matrix of $2C_{12}$-L-Glu-phC_nN^+. We have shown separately that many other cyanine and merocyanine dyes form the J-like aggregates in this bilayer matrix.[31] The latter dye aggregates similarly give rise to enhanced fluorescence emission.

On the other hand, a blue shift is observed in the absorption spectrum (λ_{max} 498 nm), when dye **5** is bound to the bilayer of $2C_{12}$-L-Asp-phC_4N^+. The fluorescence emission is barely recognized in this system. These spectral data are indicative of the formation of the H-aggregates.[20] It is interesting that the mode of the dye binding — orientation and aggregation — is quite different between bilayers with a minor structural variation (glutamate vs. aspartate). The bilayer physical state also plays a crucial role. The J-aggregates act as better photosensitizers. Therefore, it is expected that the migration and transfer of the excitation energy among bilayer-bound dyes are similarly affected by the variation of the binding mode.

Fluorescence Quenching and Energy Transfer. The energy transfer from an oxacyanine dye to a thiacyanine dye in the multilayer system was pioneered by Kuhn and Möbius.[24] We similarly employed an oxacyanine dye (**6**, NK 1952) as an energy donor in this study. Figure 4 snows absorption and emission spectra of **6** in the bilayer matrix of $2C_{12}$-L-Glu-phC_4N^+. The absorption maximum is located at 531 nm at 20 °C. As the temperature is raised, the maximum shifts to shorter wavelengths (511 nm at 30 °C) and the intensity decreases. The change is most drastic at 27 to 30 °C and is negligible at 30 to 35 °C. The phase transition of the bilayer is responsible for the spectral change, as also observed for bilayer-bound **5** (see Fig. 1). The emission maximum is located at 530 nm, and the intensity decreases with temperature. A comparison of Figs. 1 and 4 indicates that the emission spectrum of **6** overlap with the absorption range of **5**. Therefore, the Förster-type energy transfer from the oxacyanine to the thiacyanine is anticipated.

Figure 5 compares emission spectra of membrane-bound oxacyanine **6** alone and in the presence of equimolar (1.0×10⁻⁶ M) thiacyanine **5**. The emission of oxacyanine **6** (excitation at 500 nm) decreases in the presence of thiacyanine **5** and the emission from the latter is enhanced. This clearly indicates the energy transfer from **6** to **5**. The transfer efficiency is largest at 20—25 °C, and decreases with increasing temperatures, as can be estimated by the relative emission intensity at 530 nm and at 584 nm.

The decrease in the oxacyanine emission becomes pronounced with increasing concentrations of the thiacyanine acceptor. The quenching process can be represented by the Stern-Volmer relation

$$I_F^\circ/I_F - 1 = K_{sv}[A] \quad (1)$$

where I_F° and I_F are emission intensities of a donor dye in the absence and presence of acceptor dye A, respectively. K_{sv} is the Stern-Volmer quenching constant.

Figure 6 gives Stern-Volmer plots in the bilayer and micelle systems. The quenching process obeys Eq. 1.

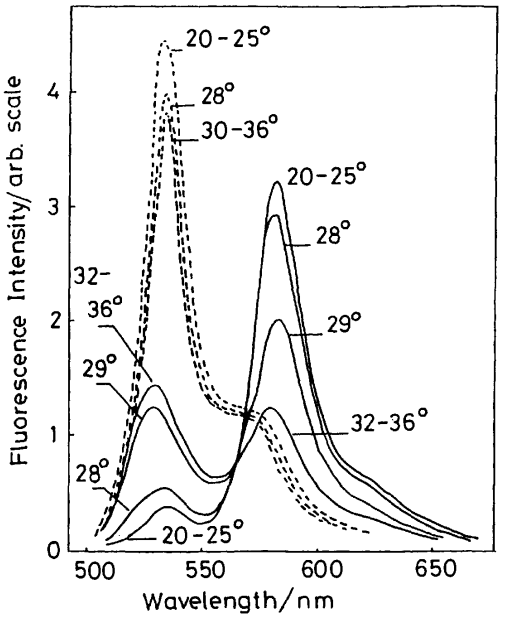

Fig. 5. Temperature dependence of fluorescence spectra of cyanine dyes (**5** or **6**) bound to the aqueous bilayer of $2C_{12}$-L-Glu-phC_4N^+. [bilayer]=1.0×10^{-3} M. Excitation at 500 nm. ----: Fluorescence spectra of **6** (1.0×10^{-6} M) alone. ——: Fluorescence spectra of **6** (1.0×10^{-6} M) plus **5** (1.0×10^{-6} M).

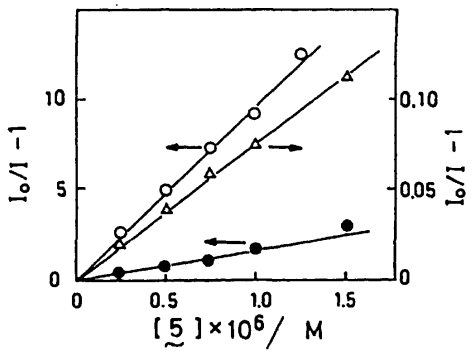

Fig. 6. Stern-Volmer plots for the emission quenching of cyanine dye **6** in the presence of dye **5**. [**6**]=1.0×10^{-6} M (constant). —○—: **1** (n=4), 1.0×10^{-3} M. —●—: **1** (n=4), 4.0×10^{-3} M. —△—: CTAB, 4.0×10^{-3} M.

The slopes in Fig. 6 give $K_{sv}=1.6\times10^6$ M^{-1} for the bilayer ($2C_{12}$-L-Glu-phC_4N^+) concentration of 4.0×10^{-3} M. The K_{sv} value is enhanced to 9.5×10^6 when the bilayer concentration is lowered to 1.0×10^{-3} M. In the CTAB micelle (4.0×10^{-3} M), $K_{sv}=7.5\times10^4$ M^{-1}, a value only 1/20 of the corresponding bilayer system. Thus the bilayer membrane provides a vehicle for energy transfer superior to the globular micelle. Concentration and specific binding of donor and acceptor dyes at the rigid bilayer surface must be responsible for the enhanced energy transfer.

Factors Affecting Fluorescence Quenching. It is apparent from Fig. 5 that the fluorescence quenching is strongly temperature-dependent. Figure 7 shows the

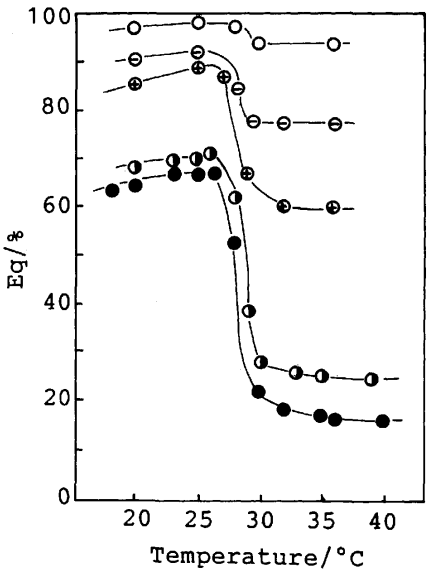

Fig. 7. Quenching efficiency (E_q) vs. temperature in the presence of the $2C_{12}$-L-Glu-phC_4N^+ bilayer. [**5**]=[**6**]=1.0×10^{-6} M. The bilayer concentration is as follows; —○—, 1.0×10^{-4} M; —⊖—, 5.0×10^{-4} M; —⊕—, 1.0×10^{-3} M; —◑—, 2.0×10^{-3} M; —●—, 4.0×10^{-3} M.

temperature dependence of the quenching efficiency

$$E_q = (1-I_F/I_F^\circ)\times 100\ (\%) \qquad (2)$$

at different concentrations of the $2C_{12}$-L-Glu-phC_4N^+ bilayer. E_q is reduced slightly at ca. 30 °C in the presence of 1×10^{-4} M of the bilayer, but remains almost unchanged at higher and lower temperature ranges. The reduction at 25—30 °C becomes drastic with increasing bilayer concentrations. In accordance with the spectral change in Fig. 5, the quenching is more efficient in the rigid bilayer matrix. The fluorescence quenching is well above 90% at all temperatures at the bilayer concentration of 1×10^{-4} M. A sonicated sample of $2C_{12}$-L-Glu-phC_4N^+ in water contains lamellar dispersions of which molecular weight cannot be less than ten millions.[31] We cannot at the moment distinguish the inter- and intra-aggregate processes. A crude estimate indicates that an average distance of the donor and acceptor dyes that are randomly distributed at the bilayer surface is 30—40 Å (the cross section of the bilayer component is 50—60 Å^2). The energy transfer via the Förster mechanism would proceed efficiently at this distance.

Reduction of the quenching efficiency with increasing bilayer concentrations is pronounced in the liquid crystalline region. For the crystalline bilayer, however, E_q is only reduced from 97 to 63% by the concentration change from 1×10^{-4} to 4×10^{-3} M. This reduction is too small to be accounted for by the concentration effect alone. It appears that E_q in the crystalline bilayer matrix remain high either due to the nonrandom distribution of dye molecules or due to the enhanced transfer rate. Absorption spectra of the dyes

bound to these bilayers display characteristic variations, implying that the modes (orientaion and aggregation) of dye binding are specific. This binding specificity may be responsible for these small concentration effects. The larger E_q reduction in the liquid crystalline bilayer matrix can be accounted for solely by the dilution effect.

The other bilayer matrices were similarly used for the quenching experiment, and the results are summarized in Fig. 8. The abrupt reduction in E_q is observed commonly for the bilayers of $2C_{12}$-L-Glu-phC_nN$^+$ (n=2, 4, and 10) at temperatures slightly below T_c (peak top temperature). However, the extent of the reduction is quite different. The difference is produced by an especially small quenching efficiency observed in the crystalline $2C_{12}$-L-Glu-phC_2N$^+$ bilayer. The binding mode in this bilayer appears not different from those in other bilayers of longer spacers, as the absorption spectrum of the bound cyanine is not sensitive to the spacer length. There could be changes in the mode of dye distribution that are not reflected in the absorption spectrum.

There are common trends in the T_c effect between the specificity of absorption spectra and the reduction of E_q. The $2C_{16}N^+2C_1$ bilayer which cannot bind dye molecules in specific manners,[31] gives almost constant E_q's at temperatures above and below T_c (28 °C). The fluid micelle of CTAB similarly gives temperature-independent E_q values. The smaller E_q value for CTAB (ca. 11%) relative to that of $2C_{16}N^+2C_1$ (ca. 21%) may reflect the smaller size of the CTAB micelle. E_q values in the fluid micelle and in the liquid crystalline bilayers are in the range of 10—20%. These data, together with the data shown in Fig. 7, unmistakably endorse the thesis that the specific nature of the dye binding enhance the efficiency of energy transfer.

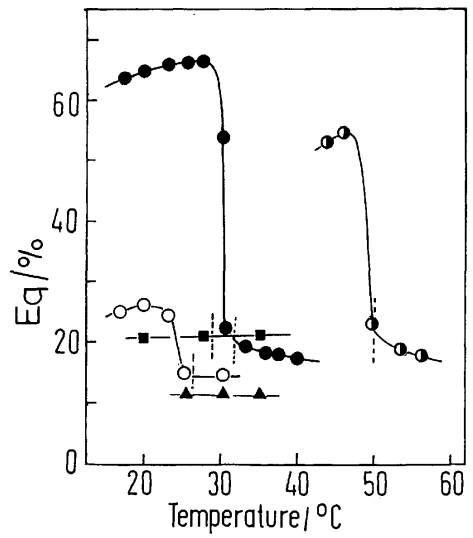

Fig. 8. Quenching efficiency (E_q) vs. temperatures in bilayers and micelles. [**5**]=[**6**]=1.0×10^{-6} M, [amphiphile]=4.0×10^{-3} M. —○—: $2C_{12}$-L-Glu-phC_2N$^+$. —●—: $2C_{12}$-L-Glu-phC_4N$^+$. —◑—: $2C_{12}$-L-Glu-phC_{10}N$^+$. —■—: $2C_{16}N^+2C_1$. —△—: CTAB. The dotted lines indicate the phase transition temperature (peak top) of the respective bilayer.

Conclusion

The present study leads to the following conclusions.

(1) The emission characteristics of anionic cyanine dyes bound to cationic bilayer membranes are strongly affected by the chemical structure and the physical state of the matrix membrane. The fluorescence emission is remarkably enhanced in crystalline bilayers of double-chain glutamate derivatives, and is characteristic of the J-like aggregate when the dye concentration is high. These unique spectral properties are related to binding of dyes to the specific space created at the membrane surface.

(2) Dye molecules concentrated at bilayer surfaces give rise to efficient energy transfer. The efficiency is affected by the nature of the matrix bilayer. The observed data imply that the energy flow in the bilayer can be regulated by appropriate disposition of dye molecules.

It is demonstrated that bilayer membranes provide superior media for organizing chromophores in specific manners.

References

1) Contribution No. 839 from Department of Organic Synthesis.

2) For our recent article; T. Kunitake, N. Kimizuka, N. Higashi, and N. Nakashima, *J. Am. Chem. Soc.*, **106**, 1978 (1984).

3) J. H. Fendler, "Membrane Mimetic Chemistry," Wiley-Interscience Pub., New York (1982).

4) J. H. Fuhrhop and J. Mathieu, *Angew. Chem., Int. Ed. Engl.*, **23**, 100 (1984).

5) T. Kunitake, N. Nakashima, M. Shimomura, Y. Okahata, K. Kano, and T. Ogawa, *J. Am. Chem. Soc.*, **102**, 6642 (1980).

6) T. Kunitake, N. Nakashima, and T. Morimitsu, *Chem. Lett.*, **1980**, 1347.

7) N. Nakashima, N. Kimizuka, and T. Kunitake, *Chem. Lett.*, **1985**, 1817.

8) M. Shimomura, H. Hashimoto, and T. Kunitake, *Chem. Lett.*, **1982**, 1285.

9) M. Shimomura, R. Ando, and T. Kuntiake, *Ber. Bunsenges. Phys. Chem.*, **87**, 1134 (1983).

10) N. Nakashima, K. Morimitsu, and T. Kunitake, *Bull. Chem. Soc. Jpn.*, **57**, 3253 (1984).

11) T. Kunitake, *Colloid and Surfaces*, **19**, 225 (1986).

12) T. Kunitake, M. Shimomura, Y. Hashiguchi, and T. Kawanaka, *J. Chem. Soc., Chem. Commun.*, **1985**, 833.

13) N. Takeyama, S. Sakaguchi, Y. Hashiguchi, M. Shimomura, T. Kunitake, and T. Matsuo, *Chem. Lett.*, **1985**, 1735.

14) E. Baumgartner and J. H. Fuhrhop, *Angew, Chem., Int. Ed. Engl.*, **19**, 550 (1980).

15) T. Nagamura, K. Tanaka, N. Takeyama, and T. Matsuo, *Ber. Bunsenges. Phys. Chem.*, **87**, 1129 (1983).

16) N. Nakashima, H. Fukushima, and T. Kunitake, *Chem. Lett.*, **1981**, 1555.
17) N. Nakashima, R. Ando, H. Fukushima, and T. Kunitake, *J. Chem. Soc., Chem. Commun.*, **1982**, 707.
18) N. Nakashima and T. Kunitake, *J. Am. Chem. Soc.*, **104**, 4261 (1982).
19) J. H. Fuhrhop and D. Fritsch, *J. Am. Chem. Soc.*, **106**, 4287 (1984).
20) e.g., A. H. Herz, *Adv. Colloid Interface Sci.*, **8**, 237 (1977).
21) A. S. Waggoner and A. Grinvald, *Ann. N. Y. Acad. Sci.*, **303**, 217 (1977).
22) K. Kurihara, Y. Toyoshima, and M. Sukigara, *J. Phys. Chem.*, **81**, 1833 (1977).
23) T, Handa, C. Ichibashi, I. Yamamoto, and M. Nakagaki, *Bull. Chem. Soc. Jpn.*, **56**, 2548 (1983).
24) H. Kuhn, D. Möbius, and H. Bücher, "Techniques of Chemistry," ed by A. Weissberger and B. W. Rossiter, Wiley (1972), Vol. 1. Part IIIB, p. 577.
25) D. Möbius, *Acc. Chem. Res.*, **14**, 63 (1981).
26) Y. Okahata, R. Ando, and T. Kunitake, *Ber. Bunsenges. Phys. Chem.*, **85**, 789 (1981).
27) T. Karsten and K. Kobs, *J. Phys. Chem.*, **84**, 1871 (1980).
28) R. D. Klausner and D. E. Wolf. *Biochem.*, **19**, 6199 (1980).
29) K. Onuki, K. Kurihara, Y. Toyoshima, and M. Sukigara, *Bull. Chem. Soc. Jpn.*, **53**, 1914 (1980).
30) R. Humphrey-Baker, M. Grätzel, and R. Steiger, *J. Am. Chem. Soc.*, **102**, 847 (1980).
31) N. Nakashima, T. Kunitake, et al. manuscript in preparation.

 © 1987 The Chemical Society of Japan Bull. Chem. Soc. Jpn., 60, 1975—1980 (1987)

Kinetic Study of Liquid-Phase Esterification with Sulfonic Acid Cation-Exchange Resin of the Macroreticular Type. II.[1] Solvent Effects on Resin Catalysis

Shoichi SHIMIZU* and Choichiro HIRAI
Department of Industrial Chemistry, College of Industrial Technology, Nihon University, Izumi-cho, Narashino, Chiba 275
(Received November 28, 1986)

The rates of the esterification of octanoic acid with 1-butanol catalyzed by macroreticular sulfonated ion-exchange resin in the presence of various organic solvents and water were measured by the use of a batch reactor. The solvent effects on the rate were investigated by applying the heterogeneous-pseudohomogeneous reaction mechanism. From these results, it was found that the effects can be quantitatively estimated by means of the magnitude of the equilibrium constants, $K_{sol}^{(S)}$, for the solvent-separated ion-pair formations, which are due to the interaction of the sulfo groups in the resin with the solvents. The correlations of the $K_{sol}^{(S)}$ value with the physical properties, μ and ε; the solvatochromic parameters, π^*,α, and β, and Gutmann's parameters, AN_E and DN_B, have been examined by using linear regression analysis methods. The results of the correlations in which the protic solvents have been excluded suggest that the positions of the equilibria of solvent-separated ion-pair formations depend mainly on the electron-donor property of the solvents; that is to say, the solvents with a strong donor property diminish the number of un-ionized sulfo groups which act as catalytic species for the heterogeneous reaction.

The advantages cited most frequently for the use of ion-exchange resins as catalysts are the elimination of the necessity for product isolation by distillation or extraction procedures and their possible re-utilization. Therefore, experimental studies of the use of resin have been carried out on almost all the reactions homogeneously catalyzed by acids or bases.[2] Little, however, is known concerning the solvent effects on resin catalysis.

Tartarelli et al.[3] studied the kinetics of the esterification of benzoic acid with 1-butanol catalyzed by sulfonic acid resin of the standard type and sulfuric acid in the presence of heptane, benzene, and toluene as solvents; they reported that, taking into account the distribution of the components between the external solution and the micropore liquid in the resin, the solvent effects on the reaction rate can be explained on the basis of a mechanism involving the reaction between a positive ion and a dipolar molecule. The kinetics of ethyl acetate reesterification with methanol and 1-propanol catalyzed by a sulfonated ion-exchanger MS-25 in 1,4-dioxane and cyclohexane were likewise investigated by Setinek and Rodriguez,[4] who noted that cyclohexane behaved as an inert solvent, while 1,4-dioxane interacted with the catalyst. Recently, Regen et al.[5] pointed out that, from a qualitative point of view, the nature of the organic solvent used for polymer-based triphase catalysts may influence the observed activity of the catalysts in the following ways: (1) it can be important in determining the absorption equilibria for the reactants on the polymer; (2) when a gelular resin is used, it can control the extent of swelling, which in turn will determine the number of active sites available for catalysis, and (3) it may be important in establishing the nature of the microenvironment at the active site.

On the other hand, Gates and his coworkers have published a series of fundamentally important papers.[6-8] These papers have shown that an excess of water or alcohol can shift the catalytic species from the more active undissociated sulfonic acid to the less active solvated proton; this finding was also substantiated by our preceding work.[1] The shift of catalytically active species reveals an important relationship between the solvent system and the nature of the catalytic species.[9]

In this work, in order to clarify the solvent effects on the resin catalysis from such a point of view, we have measured the kinetics of the esterification of octanoic acid with 1-butanol catalyzed by macroreticular sulfonic acid resin (Amberlyst 15) in the presence of various organic solvents and water.

Experimental

Catalyst Preparation and Reagents. The catalyst was a macroporous sulfonated copolymer of styrene and divinylbenzene, Amberlyst 15 (Rohm and Haas Company). The hydrogen-form resin, 0.59—0.84 mm particles, was pretreated as usual[1] and then stored in a desiccator in sealed vials over silica gel. The ion-exchange capacity was 5.05 meq g^{-1} of dry resin, and the water content was 6.87 wt%.

The octanoic acid (reagent-grade for the automatic analysis of amino acids from Wako Pure Chemical Industries, Ltd.) was used without further purification. The 1-butanol was purified by drying over potassium carbonate and distillation.

Solvents. All the chemicals were of a guaranteed reagent grade. The octane and toluene were distilled and then dried over magnesium sulfate. The anisole was washed with a 0.5 mol dm^{-3} aqueous solution of sodium hydroxide and twice with distilled water, dried over calcium chloride, and then distilled. The dibutyl ether was purified by distillation and passing it through a column of activated alumina. The 2-butanol was purified in the same manner as 1-butanol. The 1,4-dioxane was refluxed over sodium and then dis-

tilled. The dimethyl sulfoxide was dried over calcium chloride and distilled under reduced pressure.

Reaction-Rate Measurement. The apparatus was the same as that described in Part I.[1] The esterification was measured at 80±0.05 °C, and the reaction medium was agitated at 250 rpm. In all experiments, the total volume of the reaction mixture, consisting of octanoic acid, 1-butanol (or with water in the runs so denoted in Fig. 2), and a solvent, was kept constant at 30 ml. The initial concentration of octanoic acid and the amount of resin were also held constant at 0.150 mol dm^{-3} and 1.25 g respectively. The initial ratio of the volume of 1-butanol to that of solvent was changed in every run for the kinetic analysis. After the start of a reaction, 40.0-μl samples were removed by using a microsyringe at appropriate time intervals and then transferred to individual capped microtubes containing a mixture of hexadecane as an internal standard and the solvent used in each run. For gas-chromatographic (GC) analysis, samples of about 1—2 μl were taken from these microtubes. The reaction rates were determined from the analyses of butyl octanoate. The instrument used to carry out the GC analyses and the operating conditions were described in detail in an earlier paper.[10]

The ester-concentration increments from 0.0200 to 0.0400 mol dm^{-3}, divided by the time required for the reaction progress, were set equal to the reaction rates for each solution composition at a conversion of 20 % and were adopted as the kinetic data, since a short induction period rarely appeared and since an initial reaction rate could not be employed.

Results and Discussion

Effects of Various Organic Solvents and Water on the Rate. The influences of various organic solvents upon the reaction rate are shown in Fig. 1. When 2-butanol was used as a solvent, *s*-butyl octanoate was formed as a by-product. However, the rate of the by-product reaction was negligibly small compared to that of the reaction of octanoic acid with 1-butanol under the present reaction conditions. In other cases, no side reaction occurred. As can be seen from Fig. 1, dimethyl sulfoxide most strongly interacted with the catalyst and inhibited the reaction, while octane did so most weakly or not at all; octane is, therefore, regarded as an inert solvent.[11] Water also inhibited the reaction, as is shown in Fig. 2.

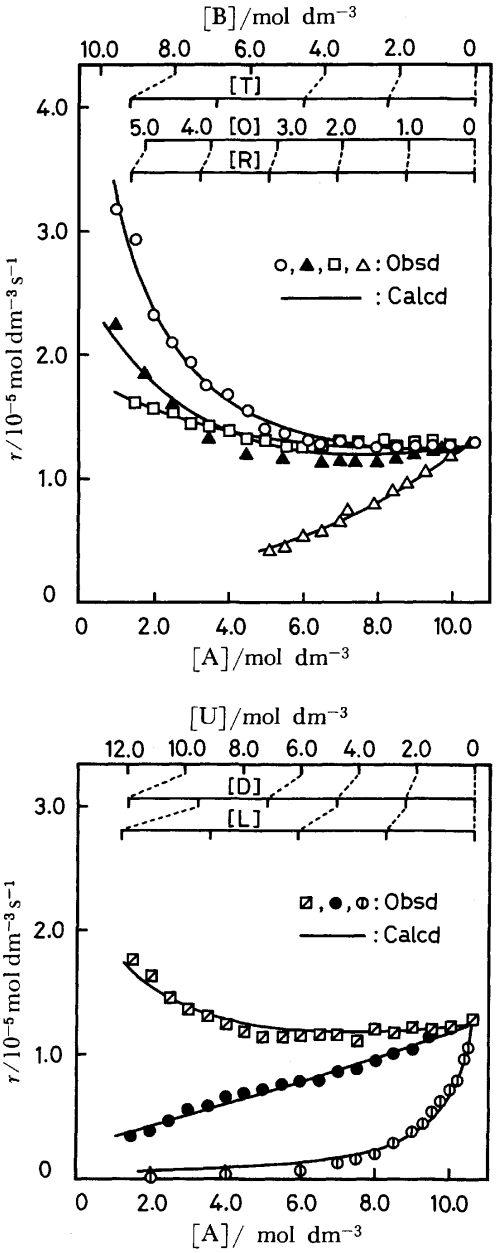

Fig. 1. Solvent effects on reaction rate (r).
[F]=0.120 mol dm^{-3}, [E],[W]=0.030 mol dm^{-3}.
○; Octane (O), ▲; toluene (T), □; dibutyl ether (R), △; 2-butanol (B), ⊠; anisole (L), ●; 1,4-dioxane (D), ⊕; dimethyl sulfoxide (U).

Evaluation of Solvent Effects in the Dielectric Approach. The swelling of an unsulfonated styrene-divinylbenzene copolymer of the macroreticular type was scarcely even observed in either polar or nonpolar organic solvents, whereas the sulfonated ion-exchange resin, Amberlyst 15, was slightly swollen only in polar solvents.[12] This swelling was considered to be due to the interaction between solvents and sulfo groups in the resin.[12] In practice, even when a polar reactant or a solvent such as 2-methyl-2-propanol[13] or 1,4-dioxane[4] was used, no sulfo groups located within the gelular microspheres in about 20% crosslinked resins took part in the catalytic reaction. Therefore, it is considered that only the sulfo groups residing on the surface of the microspheres are available for a catalytic reaction, that the number of the available sulfo groups varies hardly at all with the polarity of the reaction medium, and that it is not necessary to take into account the distribution of the reactants between an external solution and micropore liquid in the microspheres, which conforms to Helfferich's standpoint.[14]

On the assumption that a reaction between a neutral dipolar molecule and a positive ion is the rate-controlling step, Tartarelli et al.[3] interpreted the solvent effects on the rate of esterification with sulfonic acid resin in the dielectric approach. According to this treatment, the kinetic data presented in Figs. 1 and 2

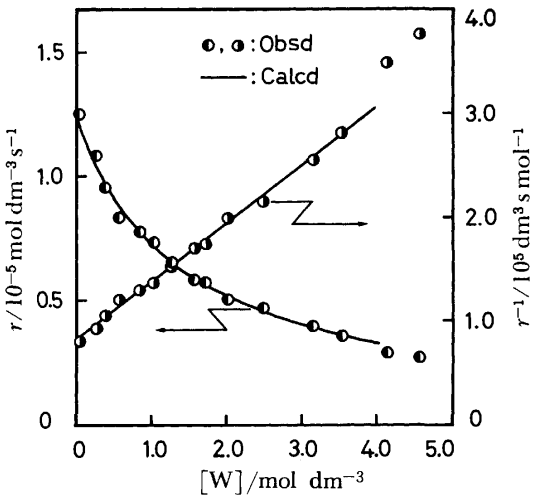

Fig. 2. Effect of water on reaction rate (r). [F]=0.120 mol dm^{-3}, [A]=9.7 mol dm^{-3}, [E]=0.030 mol dm^{-3}, solvent; octane.

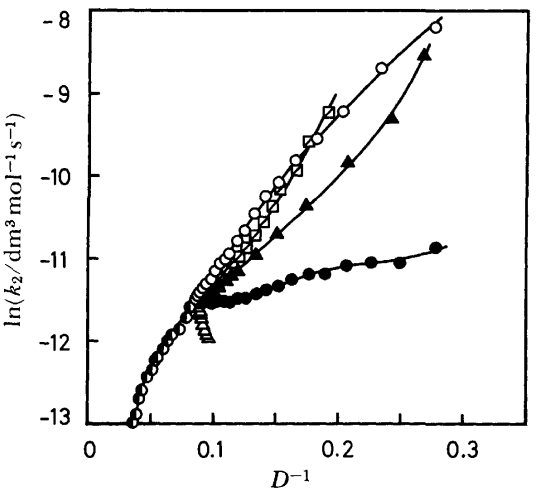

Fig. 3. Dependence of dielectric constant of reaction medium (D) on reaction rate constant ($k_2=r[F]^{-1}[A]^{-1}$). ○; Octane, ▲; toluene, △; 2-butanol, ☒; anisole, ●; 1,4-dioxane, ◐; water.

should give a straight line in the plot of ln k_2 vs. $1/D$ with a positive slope. As is shown in Fig. 3, however, curves and a line with a negative slope were obtained. These results indicate that the dielectric approach is inadequate to interpret the solvent effects on the resin catalysis.

Application of Heterogeneous-Pseudohomogeneous Reaction Mechanism[1] and Estimation of Solvent Effects by Means of Kinetic Analysis. In the preceding paper,[1] it was reported that water and 1-butanol solvate the matrix-bound sulfo groups, and that the esterification system consists of a heterogeneous reaction catalyzed by matrix-bound sulfo groups which are not ionized and a pseudo-homogeneous reaction by protons solvated with alcohol. Rate Equation 1, values calculated from which were in fair agreement with the observed ones, was presented.

$$r=\frac{\{k_{het}[F]+k_{phom}^{(A)}K_{phom}^{(A)}K_{sol}^{(A)}[F][A]^{\alpha+1}\}[Cat]M}{1+K_{sol}^{(A)}[A]^{\alpha}+K_{sol}^{(W)}[W]^{\beta}} \quad (1)$$

In the present case, it is necessary to take into account the interaction of an additional solvent with the catalyst, that is, with sulfo groups in the resin. Assuming that appropriate polar solvents also behave as solvating agents (Eq. 2), and then that the protons solvated with the solvents become catalytic agents (Eqs. 3 and 4), the reaction rate is expressed by Eq. 5.

$$\gamma X+Ⓟ\text{—}SO_3H \overset{K_{sol}^{(X)}}{\rightleftarrows} Ⓟ\text{—}SO_3^-/\gamma X/H^+ \quad (2)$$

$$F+Ⓟ\text{—}SO_3^-/\gamma X/H^+ \overset{K_{phom}^{(X)}}{\rightleftarrows} Ⓟ\text{—}SO_3^-/\gamma X+HF^+ \quad (3)$$

$$A+HF^++Ⓟ\text{—}SO_3^-/\gamma X \xrightarrow{k_{phom}^{(X)}} E+W+Ⓟ\text{—}SO_3^-/\gamma X/H^+ \quad (4)$$

$$r=\frac{\{k_{het}[F]+k_{phom}^{(A)}K_{phom}^{(A)}K_{sol}^{(A)}[F][A]^{\alpha+1}+k_{phom}^{(X)}K_{phom}^{(X)}K_{sol}^{(X)}[F][A][X]^{\gamma}\}[Cat]M}{1+K_{sol}^{(A)}[A]^{\alpha}+K_{sol}^{(W)}[W]^{\beta}+K_{sol}^{(X)}[X]^{\gamma}} \quad (5)$$

The application of Eq. 5 based on the heterogeneous-pseudohomogeneous reaction mechanism makes it possible to estimate the solvent effects on the resin catalysis in a quantitative way, provided that Eq. 5 gives good representations of the observed data plotted in Figs. 1 and 2. Hence, octane was chosen as the reference solvent, for it does not interact with the sulfo groups, that is to say, $K_{sol}^{(O)}=0$ dm^3 mol^{-1}, and the optimum values of α, β, k_{het} [Cat], $k_{phom}^{(A)}K_{phom}^{(A)}$ [Cat], $K_{sol}^{(A)}$, and $K_{sol}^{(W)}$ were determined from the results observed with octane according to the procedure previously described.[1] Next, in order to determine the values of $k_{phom}^{(X)}K_{phom}^{(X)}$ [Cat] and $K_{sol}^{(X)}$ for each solvent for integral values of the γ exponent ranging from one to three, the sum of the squares of the deviations of the predicted rates from the observed rates has been calculated with a computer. By substituting the values of these parameters, which are listed in Table 1, into Eq. 5, the most precise representation of the data for each solvent is given. When the calculated values are compared to the data in Figs. 1 and 2, the agreement between the observed and calculated values is satisfactory. These results give support to this approach for the quantitative estimation of the solvent effects on the resin catalysis.

Correlations with Physical Properties and Empirical Parameters of Solvents. The least-squares analyses were carried out for the equilibrium constants for solvent-separated ion-pair formation, $K_{sol}^{(S)}$, vs. the molecular dipole moment, μ, and the dielectric constant, ε. Equation 6 is the least-squares fit for $K_{sol}^{(S)}$ vs. μ with seven solvents, and Eq. 7, for $K_{sol}^{(S)}$ vs. ε with nine solvents.

$$K_{sol}^{(S)}=2.66\mu-1.19, \qquad R=0.838 \quad (6)$$

$$K_{sol}^{(S)}=0.103\varepsilon+0.461, \qquad R=0.814 \quad (7)$$

Table 1. Optimum Values of γ, $K_{sol}^{(S)}$, and $k_{phom}^{(S)}K_{phom}^{(S)}$[Cat], and Empirical Parameters of Solvents

No.	Solvent	γ (α, β)	$K_{sol}^{(S)}$ / dm^3 mol^{-1}	$k_{phom}^{(S)}K_{phom}^{(S)}$[Cat] / 10^{-6} dm^3 mol^{-1} s^{-1} g^{-1}	AN_E[a,b]	DN_B[a,c]	π^*[d]	α[d]	β[d]
1	Octane (O)	—	0	—	—	—	(−0.08[f])	(0.00[f])	(0.00[f])
2	Toluene (T)	1	0.133	0.00	3.3	3.9	0.54	0.00	0.11
3	Anisole (L)	1	0.205	0.00	7.6	7.9	0.73	0.00	0.22
4	Dibutyl ether (R)	1	0.384	9.36	2.6	18.1	0.24	0.00	0.46
5	1-Butanol[e] (A)	1	0.823	4.23	24.4	24.0	0.47	0.79	0.88[g]
6	1,4-Dioxane (D)	1	2.08	4.86	6.0	18.0	0.55	0.00	0.37
7	2-Butanol[e] (B)	2	2.59[h]	4.86	—	—	—	—	—
8	Water[e] (W)	1	6.07	0.00	41.0	17.0	1.09	1.17	0.18[g]
9	Dimethyl sulfoxide (U)	1	9.88	0.00	17.6	30.1	1.00	0.00	0.76

a) Values taken from Ref. 22. b) AN_E values are calculated from the E_T values using $AN_E=-40.52+1.29E_T$. c) DN_B values are calculated from the B^* or B values using $DN_B=-6.36+0.19B^*$. d) Values taken from Ref. 19. e) Highly-structured protic solvents. f) Values of hexane and heptane. g) Data are relatively less certain. h) dm^6 mol^{-2}.

These correlation coefficients for Eqs. 6 and 7 are not statistically acceptable. This result is consistent with the information[15] that the extent of ionization is governed by the ability of a solvent to heterolyze covalent bonds and not by its dipolar characteristics, such as the dipole moment or the dielectric constant.

Recently, an empirical solvent scale based on the solvatochromic comparison method[16] and an equation based on the linear solvation energy relationship,[17-19] which expresses the role of the contributions of individual types of solvent-solute interactions, have been proposed by Kamlet, Taft, and their coworkers.[20] In general form, this solvatochromic equation is given by

$$XYZ = XYZ_0 + s\pi^* + a\alpha + b\beta, \quad (8)$$

where XYZ is the measured quantity (a free energy or heat of transfer between solvents, the logarithm of a reaction rate or an equilibrium constant, etc.) in the given solvent, and where XYZ_0 is the same quantity obtained for a reference solvent. The π^* scale is an index of solvent dipolarity/polarizability (SPP). The α scale of hydrogen-bond donor (HBD) acidities describes the ability of the solvent to donate a proton. Similarly, the β scale of hydrogen-bond acceptor (HBA) basicities expresses the solvent's ability to accept a proton (donate an electron pair). The s, a, and b terms in Eq. 8 are measures of the responses of XYZ to changing SPP, HBD acidity and HBA basicity; they are called the solvatochromic coefficients.

For the seven solvents whose solvatochromic parameters are known, the multiple-parameter least-squares correlation of ln $K_{sol}^{(S)}$ with the π^*, α, and β values leads to

$$\ln K_{sol}^{(S)} = -3.72 + 3.88\pi^* + 0.26\alpha + 2.57\beta, \quad R=0.827. \quad (9)$$

If the data for 1-butanol and water, which are highly-structured protic solvents, are excluded, a correlation equation with an acceptable correlation coefficient,

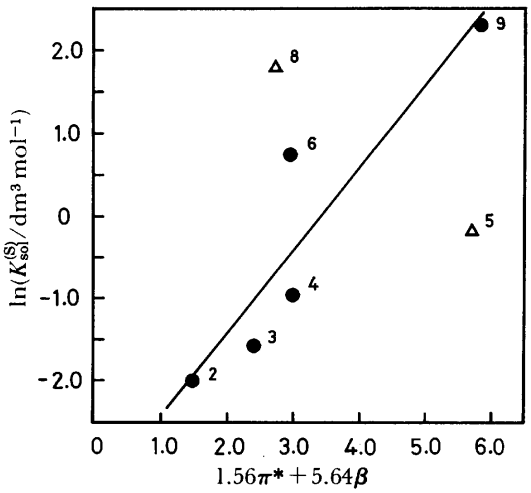

Fig. 4. Relationship between equilibrium constants ($K_{sol}^{(S)}$) and solvatochromic parameters (π^* and β). △; Highly-structured protic solvents.

represented by the regression line in Fig. 4, is given by

$$\ln K_{sol}^{(S)} = -3.43 + 1.56\pi^* + 5.64\beta, \quad R=0.917. \quad (10)$$

It is considered that, since the data points representing 1-butanol and water, which can also act as stronger hydrogen-bond donors, are not displaced from the regression line in the same direction in Fig. 4, there is no contribution of solvent HBD acidities to the $K_{sol}^{(S)}$. Furthermore, because the π^*, α, and β parameters are roughly normalized to cover the range from near 0.0 to near 1.0,[19] the b/s (5.64/1.56) ratio obtained from Eq. 10 may indicate that the positions of the equilibria of solvent-separated ion-pair formations depend largely on the solvent HBA basicities.

In contrast to the solvatochromic parameter scales of Kamlet and Taft, Gutmann and his coworkers[15,21] have proposed a "donor-acceptor" approach to describe the total solvent effects in terms of the electron-donor and electron-acceptor properties of the solvent.

As quantitative measures of these solvent properties, two empirical parameter scales, termed "donor number" (*DN*) and "acceptor number" (*AN*), have been introduced. The *DN* was defined as the negative ΔH° value for the interaction between the reference acid, $SbCl_5$, and a basic solvent in a highly dilute 1,2-dichloroethane solution. The *AN* was derived from the infinite-dilution ^{31}P NMR solvent shifts (relative to hexane) of triethylphosphine oxide in the bulk solvents.

The plot of $\ln K_{sol}^{(S)}$ vs. DN_B[22] values is shown in Fig. 5. If the points for the highly-structured protic solvents are excluded, the correlation with DN_B leads to

$$\ln K_{sol}^{(S)} = -2.857 + 0.163DN_B, \quad R = 0.934. \tag{11}$$

With the allowance of a partial dependence on AN_E also, the multiple linear regression equation becomes

$$\ln K_{sol}^{(S)} = -2.918 + 0.082AN_E + 0.129DN_B, \quad R = 0.953. \tag{12}$$

The $\ln K_{sol}^{(S)}$ values are plotted against the values of $0.082AN_E+0.129DN_B$ in Fig. 6. By a consideration of the small difference in the magnitude of the correlation coefficient between the two linear regression analyses, it is found that $K_{sol}^{(S)}$ is sensitive mainly to the donor ability of solvents. A comparison of Eqs. 11 and 12 with Eq. 10 shows that the correlations with Gutmann's parameters are somewhat better than those with the solvatochromic parameters. However, since no normalization of the AN_E and DN_B parameters has been carried out, the relative contributions of the individual solvent properties can not be discussed by a direct comparison of the coefficient value of AN_E with that of DN_B.

Taft et al.[18] have examined the relationships between Gutmann's *AN* and *DN* and the solvatochromic parameters, π^*, α, and β; they have reported that *AN* correlates well with a linear combination of π^* and α, and that *DN* is linear with β when the result for pyridine is excluded. Therefore, it seems that the signification of the correlation (Eq. 12) with Gutmann's parameters is essentially the same as that (Eq. 10) with the solvatochromic parameters. These significations are in harmony with Gutmann's description[23] that the formation of solvent-separated ion pairs is primarily influenced by the coordinating properties of the solvent.

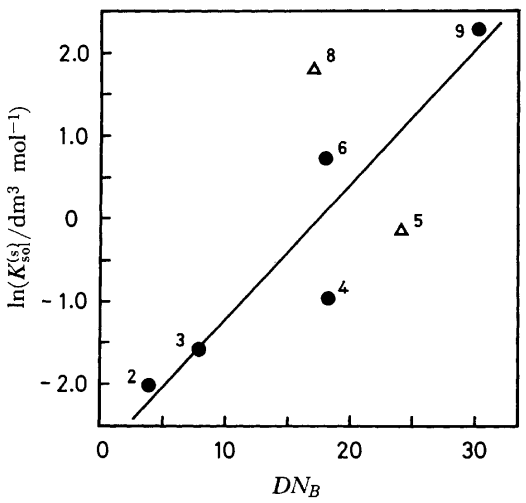

Fig. 5. Relationship between equilibrium constants ($K_{sol}^{(S)}$) and solvent donor numbers (DN_B). △; Highly-structured protic solvents.

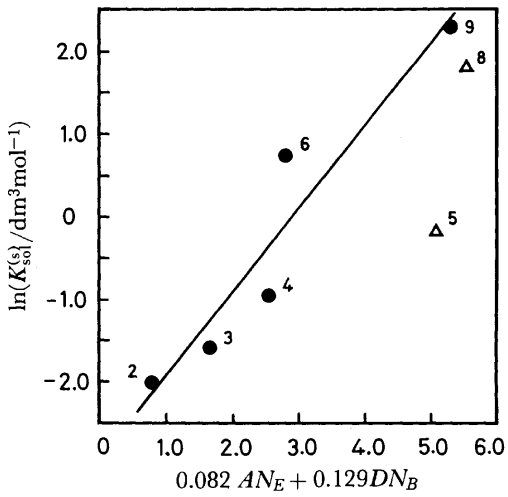

Fig. 6. Relationship between equilibrium constants ($K_{sol}^{(S)}$) and solvent acceptor and donor numbers (AN_E and DN_B). △; Highly-structured protic solvents.

As is shown in Table 1, the protons produced by the interaction of the sulfo groups with anisole and toluene, whose $K_{sol}^{(S)}$ values are relatively small, have no catalytic activity as those with water and dimethyl sulfoxide: $k_{phom}^{(S)} K_{phom}^{(S)}[Cat]=0\ dm^3\ mol^{-1}\ s^{-1}\ g^{-1}$. This result may indicate that, when the resins are immersed in anisole and toluene, some of the sulfo groups residing on the surface of the microspheres exist as contact ion pairs (or intimate ion pairs),[24] in which cations and anions are considered to be in immediate contact with each other, rather than as solvent-separated ion pairs.

In conclusion, if the solvents with a strong electron-donor property are employed as diluents in the esterification with the macroreticular sulfonic acid resin, this donor property diminishes the number of unionized sulfo groups which act as catalytic species for the heterogeneous reaction and, consequently, a decrease in the total catalytic activity is observed. Hence, it can be presumed that the extent of the selectivity of the resin catalyst related to the alkyl chain length of normal fatty acids, which was reported in an earlier paper,[10] also decreases.

The authors are grateful to Mr. Shigeru Itoh and Miss Sawako Onoda for their experimental assistance. The present work was partially supported by a Grant-in-Aid from Nihon University.

Notation

A 1-Butanol
F Octanoic acid
W Water
E Butyl octanoate
O Octane
T Toluene
L Anisole
R Dibutyl ether
D 1,4-Dioxane
B 2-Butanol
U Dimethyl sulfoxide
X Additional solvent (O,T,L,R,D,B, or U)
k_2 Specific rate constant, calculated by assuming that the esterification was second-order, $dm^3\ mol^{-1}\ s^{-1}$
D Dielectric constant of the reaction medium
r Reaction rate, $mol\ dm^{-3}\ s^{-1}$
[Cat] Number of sulfo groups participating in the reaction per g of the resin catalyst, mol of sulfo groups g^{-1}
M Amount of the resin catalyst, g
Ⓟ—SO_3H Matrix-bound sulfo group which is not ionized
Ⓟ—$SO_3^-/\gamma X/H^+$ Solvent-separated ion pair
α, β, γ Number of molecules participating in solvation
k_{het} Specific rate constant for the heterogeneous chemisorption reaction of fatty acid, s^{-1} (mol of -SO_3H groups participating in the reaction)$^{-1}$
$K_{sol}^{(A)}, K_{sol}^{(W)}, K_{sol}^{(X)}$ Equilibrium constants for solvent-separated ion-pair formations, $dm^3\ mol^{-1}$ (except $K_{sol}^{(B)}/dm^6\ mol^{-2}$)
$k_{phom}^{(A)}, k_{phom}^{(X)}$ Specific rate constants for the pseudo-homogeneous reactions of the protonated fatty acid with alcohol, $dm^3\ mol^{-1}\ s^{-1}$ (mol of -SO_3H groups)$^{-1}$
$K_{phom}^{(A)}, K_{phom}^{(X)}$ Equilibrium constants for the protonations of fatty acid, dimensionless

References

1) Part I: S. Shimizu and C. Hirai, *Bull. Chem. Soc. Jpn.*, **59**, 7 (1986).

2) See, for example, D. C. Sherrington, "Polymer-supported Reactions in Organic Synthesis," ed by P. Hodge and D. C. Sherrington, John Wiley & Sons, New York (1980), Chap. 3; N. K. Mathur, C. K. Narang, and R. E. Williams, "Polymers as Aids in Organic Chemistry," Academic Press, New York (1980), Chap. 13, pp. 199—205; Y. Ogiwara and K. Arai, "Kobunshi-Shokubai no Kougyouka," ed by T. Higaki, CMC, Tokyo (1981), Chap. 4; K. Itagaki and T. Itoh, "Ion-Kokan-Jushi · Maku no Saishin-Ohyou-Gijutsu," ed by T. Higaki, CMC, Tokyo (1982), Chap. 4, and the references cited therein.

3) R. Tartarelli, F. Piladi, G. Stoppato, and A. Lucchesi, *Chim. Ind. (Milan)*, **53**, 150 (1971).

4) O. Rodriguez and K. Setinek, *J. Catal.*, **39**, 449 (1975); K. Setinek and O. Rodriguez, *Vses. Konf. Mekhan. Katal. Reak., Moskva* (1974).

5) S. L. Regen, J. C. K. Heh, and J. McLick, *J. Org. Chem.*, **44**, 1961 (1979).

6) B. C. Gates and W. Rodriguez, *J. Catal.*, **31**, 27 (1973).

7) R. Thornton and B. C. Gates, *J. Catal.*, **34**, 275 (1974).

8) R. B. Wesley and B. C. Gates, *J. Catal.*, **34**, 288 (1974).

9) A. R. Pitochelli, "Ion Exchange Catalysis and Matrix Effects," Rohm & Haas, Philadelphia (1980), p. 12.

10) S. Shimizu, K. Ishii, and C. Hirai, *Yukagaku*, **30**, 771 (1981).

11) In Part I, toluene was regarded as an inert solvent. In practice, however, there is a slightly appreciable interaction between the toluene and the catalyst.

12) S. Kamata and M. Gohara, *Nippon Kagaku Kaishi*, **1977**, 532.

13) H. W. Heath, Jr., and B. C. Gates, *AIChE J.*, **18**, 321 (1972).

14) F. Helfferich, *J. Am. Chem. Soc.*, **76**, 5567 (1954).

15) V. Gutmann, "The Donor-Acceptor Approach to Molecular Interactions," Plenum Press, New York (1978), p. 157.

16) M. J. Kamlet and R. W. Taft, *J. Am. Chem. Soc.*, **98**, 377 (1976); R. W. Taft and M. J. Kamlet, *ibid.*, **98**, 2886 (1976); T. Yokoyama, R. W. Taft, and M. J. Kamlet, *ibid.*, **98**, 3233 (1976); M. J. Kamlet, E. G. Kayser, M. E. Jones, J. L. Abboud, J. W. Eastes, and R. W. Taft, *J. Phys. Chem.*, **82**, 2477 (1978); R. R. Minesinger, M. E. Jones, R. W. Taft, and M. J. Kamlet, *J. Org. Chem.*, **42**, 1929 (1977); M. J. Kamlet, J. L. Abboud, and R. W. Taft, *J. Am. Chem. Soc.*, **99**, 6027 (1977); M. E. Jones, R. W. Taft, and M. J. Kamlet, *ibid.*, **99**, 8452 (1977).

17) M. J. Kamlet and R. W. Taft, *J. Chem. Soc., Perkin Trans. 2*, **1979**, 337; M. J. Kamlet, M. E. Jones, R. W. Taft, and J.-L. Abboud, *ibid.*, **1979**, 342; M. J. Kamlet and R. W. Taft, *ibid.*, **1979**, 349; R. W. Taft and M. J. Kamlet, *ibid.*, **1979**, 1723; M. J. Kamlet, A. Solomonovici, and R. W. Taft, *J. Am. Chem. Soc.*, **101**, 3734 (1979); M. J. Kamlet, T. N. Hall, J. Boykin, and R. W. Taft, *J. Org. Chem.*, **44**, 2599 (1979).

18) R. W. Taft, N. J. Pienta, M. J. Kamlet, and E. M. Arnett, *J. Org. Chem.*, **46**, 661 (1981).

19) M. J. Kamlet, J.-L. M. Abboud, M. H. Abraham, and R. W. Taft, *J. Org. Chem.*, **48**, 2877 (1983).

20) The printing type of the solvatochromic parameters π^*, α, and β is bold to distinguish them from the solvation numbers α, β, and γ.

21) V. Gutmann and E. Wychera, *Inorg. Nucl. Chem. Lett.*, **2**, 257 (1966); V. Gutmann, *Angew. Chem., Int. Ed. Engl.*, **9**, 843 (1970); V. Gutmann and R. Schmid, *Coord. Chem. Rev.*, **12**, 263 (1974); V. Gutmann, *ibid.*, **15**, 207 (1975).

22) To enlarge the *AN* and *DN* scales, Schmid and Sapunov have, in addition, introduced AN_E and DN_B values: R. Schmid and V. N. Sapunov, "Non-Formal Kinetics," Verlag Chemie, Weinheim (1982), p. 140.

23) Ref. 15, p. 151.

24) S. Winstein, E. Clippinger, A. H. Fainberg, and G. C. Robinson, *J. Am. Chem. Soc.*, **76**, 2597 (1954).

1,4-Dihydropyrrolo[3,2-*b*]pyrrole: The Electronic Structure Elucidated by Photoelectron Spectroscopy

Shoji TANAKA, Tsutomu KUMAGAI, Toshio MUKAI,* and Tsunetoshi KOBAYASHI*,†
Department of Chemistry, Faculty of Science, Tohoku University, Aramaki, Sendai 980
†The Institute of Physical and Chemical Research, Wako, Saitama 351-01
(Received December 2, 1986)

The electronic structures of 1,4-dihydropyrrolo[3,2-*b*]pyrrole and some of its alkyl derivatives were studied by means of He(I) photoelectron spectroscopy combined with the MNDO calculation and a first-order perturbation theoretical method. The first five bands of the parent pyrrolopyrrole are assigned, from the top, to the $\pi_5(a_u)$, $\pi_4(a_u)$, $\pi_3(b_g)$, $\pi_2(b_g)$, and $\sigma(a_g)$ bands respectively. The MO model, which explains well the spectral data, indicates that the nitrogen lone-pair electrons are mainly delocalized in the π_4, π_2, and π_1 orbitals. The ionization potentials of the HOMO levels of these compounds, which are characterized by the large p_z contributions from the α-carbons, are the lowest among the hitherto known π-electron-excessive heteroaromatic compounds. 1,4-Dihydropyrrolo[3,2-*b*]pyrrole is concluded to be the system with the most efficient π-electron-donating ability among 10π-electron systems.

The purpose of this work is to elucidate the electronic character of 1,4-dihydropyrrolo[3,2-*b*]pyrrole in comparison with pyrrole and indole. Dihydropyrrolopyrroles are fundamentally important heteroaromatic compounds. These heterocycles are expected to be new candidates for conducting polymers and are also of interest from the standpoint of pharmacology.[1] Their electronic structures, however, have not been explored in detail. Although the photoelectron spectrum of the parent [2,3-*b*] isomer has been measured and analyzed by Gleiter et al.,[2] recent MNDO and ab initio MO calculations suggest that the proposed assignments of the first and the second bands are questionable.[1] Here, the He(I) photoelectron (PE) spectra of 1,4-dihydropyrrolo[3,2-*b*]pyrroles **1a—d** are reported and compared with the results of semiempirical MO calculations. In addition, the shifts of the bands induced by the alkyl substitutions are analyzed by a first-order perturbation method. This approach gives information on the assignments of ionizations and on the validity of the MO models used.

Experimental

Materials. The pyrrolopyrroles **1a** and **1c** were synthesized as has been reported formerly.[3] Their 1,4-dimethyl derivatives **1b** and **1d** were obtained by the reduction of the corresponding 1,4-bis(methoxycarbonyl) derivatives[3] with lithium aluminium hydride-aluminium chloride (3 : 1) in ether.

Measurements. The vapor phase He(I) photoelectron spectra of **1a—d** were measured with the PE spectrometer described in Ref. 4. Xe gas was used as the internal standard for the calibration of the energy scale.

Results and Discussion

The He(I) photoelectron spectra of the pyrrolopyrroles **1a—d** are shown in Fig. 1. The vertical ionization potentials and the results of MO calculations for the parent compound **1a** using the HMO[5] and MNDO[6] methods are listed in Table 1.

According to the empirically parameterized method

Table 1. Comparison of the Observed Vertical Ionization Potentials of **1a** with the Orbital Energies Calculated by the HMO and MNDO Methods

Band	I_v/eV	$-\varepsilon^{HMO}$/eV	$-\varepsilon^{MNDO}$/eV
[1]	7.27	7.51 $\pi_5(a_u)$	7.85 $\pi_5(a_u)$
[2]	8.00	8.20 $\pi_4(a_u)$	8.36 $\pi_4(a_u)$
[3]	9.42	9.65 $\pi_3(b_g)$	9.82 $\pi_3(b_g)$
[4]	11.42	11.59 $\pi_2(b_g)$	12.44 $\sigma(a_g)$
[5]	12.10	—	12.66 $\pi_2(b_g)$

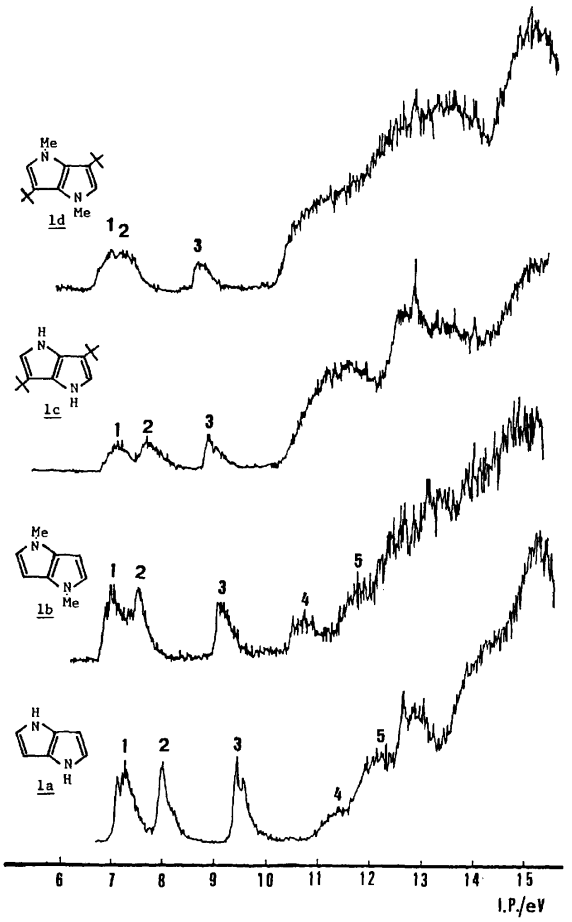

Fig. 1. Vapor phase He(I) photoelectron spectra of 1,4-dihydropyrrolo[3,2-*b*]pyrroles **1a—d**.

Table 2. Comparison of the Observed Vertical Ionization Potentials (I_v) of **1b—d** with Those Calculated by the Perturbation Methods

Compound		I_v/eV				
	Band	[1]	[2]	[3]	[4]	[5]
	Obsd	6.95	7.48	9.00	10.67	11.68
1b	Calcd[a]	6.94	7.43	9.16	10.57	—
		$\pi_5(a_u)$	$\pi_4(a_u)$	$\pi_3(b_g)$	$\pi_2(b_g)$	
	Obsd	6.92	7.49	8.68	—	—
1c	Calcd[a]	6.66	7.43	8.53	—	—
		$\pi_5(a_u)$	$\pi_4(a_u)$	$\pi_3(b_g)$		
	Obsd	6.76	6.98	8.42	—	—
1d	Calcd[b]	6.59	6.92	8.42	—	—
		$\pi_5(a_u)$	$\pi_4(a_u)$	$\pi_3(b_g)$		

a) Calculated by the perturbation method. The reference standard compound is **1a**; $I_v^{calcd}=I_v^{obsd}$ (**1a**)$+\Delta I_v^{calcd}$.
b) Calculated by the perturbation method. The reference standard compound is **1c**; $I_v^{calcd}=I_v^{obsd}$ (**1c**)$+\Delta I_v^{calcd}$.

based on the first order perturbation theory, the vertical ionization potential changes (ΔI_v) of π bands induced by alkyl substitutions can be estimated by using the following formula:[7]

$$-\Delta I_{v,j}=a(\sum_{\alpha} C_{\alpha j}^2+m\sum_{\beta} C_{\beta j}^2)+b$$

where j denotes the j-th MO corresponding to the certain PE spectral band in question, $C_{\alpha j}$ is the AO coefficient of the atom α in the j-th MO at which a certain substitution is introduced, and $C_{\beta j}$ is the AO coefficient of the atom β just adjacent to the atom α. The a, b, and m are the empirical parameters for a certain substitution. The parameter m is a kind of damping factor and is put equal to 1/3, as in Ref. 7. The parameters a and b are reevaluated by the least-squares method using the ionization energy data of hydrocarbons and the AO coefficients obtained by the MNDO method.[8] The ionization potentials estimated by this method and the corresponding experimental values are summarized in Table 2.

For the first three bands of the parent compound **1a**, the orbital energies calculated by the HMO and the MNDO methods correlate reasonably well with the observed ionization potentials. Therefore, these bands are assigned, from the top, to the ionization from the π orbitals, $\pi_5(a_u)$, $\pi_4(a_u)$, and $\pi_3(b_g)$ respectively. In the cases of **1a** and **1b**, the 4th and the 5th bands are rather well resolved. The HMO calculation predicts that the ionization potentials for the $\pi_2(b_g)$ and the $\pi_1(a_u)$ orbitals of **1a** are 11.59 and 13.58 eV respectively. The former is close to the observed value of the 4th band, while the latter is much higher than that of the 5th band. From these results, the 4th and the 5th bands may be ascribed to the ionizations from the $\pi_2(b_g)$ orbital and the σ orbital respectively. On the other hand, our MNDO calculation and the ab initio calculation reported by Verbist et al.[1] predict that the 4th and the 5th bands should correspond to the ionizations from the $\sigma(a_g)$ and $\pi_2(b_g)$ orbitals respectively. It is difficult to assign these bands only on the basis of the MO calculations, but additional information can be obtained from a consideration of the substituent effects on the ionization potentials.

As is shown in Table 2, the perturbation method reproduces reasonably well the observed changes for the first three bands of the alkyl-substituted derivative **1b**. This finding supports both the above assignments of the first three bands of **1a** and the applicability of this method in the assignments of the spectra of the pyrrolopyrroles. In the PE spectrum of **1b**, shifts of 0.75 and 0.42 eV were observed for the 4th and 5th bands relative to those of **1a** respectively. The shift of the $\pi_2(b_g)$ band of the parent compound **1a** by *N,N'*-dimethylation is estimated to be 0.85 eV. (This value is very close to the energy difference between the 4th band of **1a** and that of the 1,4-dimethyl derivative **1b**, 0.75 eV.) Therefore, the 4th bands of these compounds are ascribed to the ionizations from their $\pi_2(b_g)$ orbitals. As a result, the 4th and the 5th bands of the pyrrolopyrroles (**1a** and **1b**) are assigned to the $\pi_2(b_g)$ and the $\sigma(a_g)$ orbitals, and their first three bands, to the $\pi_5(a_u)$, $\pi_4(a_u)$, and $\pi_3(b_g)$ orbitals from the top, respectively. In the case of compounds **1c** and **1d** also, the first three bands are unambiguously ascribed from the top to the ionizations from the $\pi_5(a_u)$, $\pi_4(a_u)$, and $\pi_3(b_g)$ orbitals respectively, based on the perturbation theoretical calculations. Furthermore, the reasonable correspondence between the observed band shifts and those calculated by the perturbation method supports the validity of the delocalized MO pictures for these compounds given by the MO calculations. Figure 2 shows the AO coefficients of the occupied π orbitals in **1a** with the HOMO levels of pyrrole [$\pi_3(a_2)$] and indole [$\pi_5(a'')$].

The above MO model indicates that the nitrogen lone-pair electrons of **1a** are mainly delocalized in the π_4, π_2, and π_1 orbitals. The HOMO level of the pyrrolopyrrole is characterized by large p_z contributions from the α-carbon atoms. This is similar with the nature of the pyrrole HOMO level and is in contrast with that of the indole HOMO level, which has large p_z contributions from the β-carbon atom. Consistent with these results, we have found that some electrophilic substitution reactions, which are known to occur at the β-position of indoles, take place selectively at the α-position of the pyrrolopyrroles.[9] The ionization potential of the HOMO level of the parent pyrrolopyrrole **1a** (7.27 eV) is lower than those of pyrrole (8.21 eV)[10] and indole (7.91 eV).[11] In the case of indole, the oxidation potential and basicity are almost the same as those of pyrrole, although the ionization potential is appreciably lower. In contrast with this, the oxidation potential of **1a** (0.51 V vs. SCE) is much lower than those of pyrrole (1.2 V) and indole (1.2 V).[3]

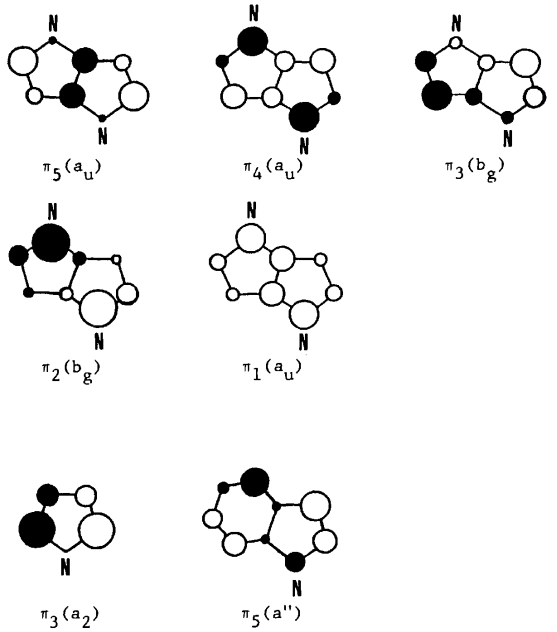

Fig. 2. Schematic representation of the occupied π molecular orbitals of 1,4-dihydropyrrolo[3,2-*b*]pyrrole, pyrrole, and indole given by the MNDO calculations.

The basicity (the pK_a value of the conjugate acid) of the pyrrolopyrrole **1c**, a stable derivative in acidic media, is +3.6; this value is much higher than those of pyrrole (−3.8)[12] and indole (−3.6).[13] In addition, it should be noted that the first ionization potential of **1a** is lower than those of the previously reported π-electron-excessive heterocycles; furan[5] (8.90 eV), thiophene[14] (8.90 eV), 1,6-dihydropyrrolo[2,3-*b*]pyrrole[2] (7.46 eV), thieno[2,3-*b*]pyrrole[2] (7.97 eV), thieno[3,2-*b*]pyrrole[2] (7.70 eV), thieno[2,3-*b*]thiophene[14] (8.32 eV), and thieno[3,2-*b*]thiophene[14] (8.10 eV). In conclusion, all the experimental results are consistent with the description of 1,4-dihydropyrrolo[3,2-*b*]pyrrole as a 10π-heteroaromatic compound possessing a more efficient π-electron-donating ability compared to the previously known π-electron-excessive heteroaromatic compounds.

References

1) R. Lazzaroni, J. P. Boutique, J. Riga, J. J. Verbist, J. G. Fripiat, and J. Delhalle, *J. Chem. Soc., Perkin Trans. 2*, **1985**, 97; H. Hemetsberger and D. Knittel, *Monatsh. Chem.*, **103**, 194 (1972); H. Prinzbach, *Chimia*, **33**, 332 (1979).

2) This parent [2,3-*b*] isomer was synthesized in 1975, but its properties have not been explored except for some spectral data. K. N. Java, S. Soth, M. Farnier, and C. Paulmier, *C. R. Acad. Sci., Ser. C*, **281**, 793 (1975); R. Gleiter, M. Kobayashi, J. Spanget-Larsen, S. Gronowitz, A. Konar, and M. Farnier, *J. Org. Chem.*, **42**, 2230 (1977).

3) T. Kumagai, S. Tanaka, and T. Mukai, *Tetrahedron Lett.*, **25**, 5669 (1984); K. Satake, T. Kumagai, and T. Mukai, *Chem. Lett.*, **1984**, 2033.

4) T. Kobayashi, K. Yokota, and S. Nagakura, *J. Electron Spectrosc. Relat. Phenom.*, **3**, 449 (1973); T. Kobayashi, T. Kubota, and K. Ezumi, *J. Am. Chem. Soc.*, **105**, 2172 (1983).

5) J. H. D. Eland, *Int. J. Mass Spectrom. Ion Phys.*, **2**, 471 (1969).

6) M. J. S. Dewar and W. Thiel, *J. Am. Chem. Soc.*, **99**, 4899 (1977).

7) T. Kobayashi, T. Kubota, K. Ezumi, and C. Utsunomiya, *Bull. Chem. Soc. Jpn.*, **55**, 3915 (1982); T. Kobayashi, T. Arai, H. Sakuragi, K. Tokumaru, and C. Utsunomiya, *Bull. Chem. Soc. Jpn.*, **54**, 1658 (1981), and the references cited therein.

8) The parameters *a* and *b* for methyl substitution were evaluated on the basis of the ionization energy data of the ethylene, butadiene, benzene, and naphthalene derivatives as reported in Ref. 7. The values are as follows: a=1.019±0.024 eV, b=0.043±0.016 eV. The standard deviation of $\Delta I_{v,j}$ is 0.036 eV. We applied these parameters for the assignments of the π bands of pyrrolopyrroles in this paper. These parameters are able to reproduce the shifts of the bands of pyrroles and indoles induced by *N*-methylations with a standard deviation of 0.044 eV. The parameters (a=1.316± 0.076 eV and b=0.042±0.069 eV) for *t*-butyl substitution were also estimated based on the data for ethylene, propene, and benzene derivatives. The standard deviation of $\Delta I_{v,j}$ is 0.087 eV. We did not estimate the band shift of the σ orbital by the perturbation method because of the complicated treatment. The photoelectron spectral datum of the parent [2,3-*b*] isomer has been published in 1977; at that time, the first and the second bands were assigned to the a_2 and the b_1 orbitals respectively.[2] Recent ab initio calculations, however, have called the proposed assignments into question.[1] Additional research using a perturbation method will be needed for the exact assignment.

9) T. Mukai, S. Tanaka, T. Hirano, and T. Kumagai, 52nd Annual Meeting of the Chemical Society of Japan, Kyoto, April, 1986, Abstr., No. 1R40.

10) P. J. Derrick, L. Åsbrink, O. Edqvist, B.-Ö. Jonsson, and E. Lindholm, *Int. J. Mass Spectrom. Ion Phys.*, **6**, 191 (1971).

11) H. Güsten, L. Klasinc, J. V. Knop, and N. Trinajstić, *Excited States Biol. Mol. Proc. Int. Conf.*, **1974**, 45.

12) Y. Chiang and E. B. Whipple, *J. Am. Chem. Soc.*, **85**, 2763 (1963).

13) R. L. Hinman and J. Lang, *J. Am. Chem. Soc.*, **86**, 3796 (1964).

14) P. A. Clark, R. Gleiter, and E. Heilbronner, *Tetrahedron*, **29**, 3085 (1973).

 © 1987 The Chemical Society of Japan Bull. Chem. Soc. Jpn., 60, 1985—1992 (1987)

Atropisomerism of Zinc Tetrakis(*o*-cyanophenyl)porphyrins. The Crystal Structure of the $\alpha\beta\alpha\beta$-Isomer and the Atropisomerization Rates

Keiichiro HATANO,* Kyoko KAWASAKI, Sonono MUNAKATA, and Yoichi IITAKA†
Department of Pharmaceutical Sciences, Nagoya City University, Mizuho-ku, Nagoya 467
†Faculty of Pharmaceutical Sciences, The University of Tokyo, Bunkyo-ku, Tokyo 113
(Received December 3, 1986)

The structure of one of the four atropisomers of tetrakis(*o*-cyanophenyl)porphyrin has been determined as the zinc complex by X-ray crystallographic methods. The five-coordinate zinc porphyrin with pyridine as the axial ligand also has a pyridine solvate in the crystal lattice. The conformation of the *o*-cyanophenyl rings is $\alpha\beta\alpha\beta$ as predicted previously. The two nitrogen atoms of the CN groups on the same side of the coordinated pyridine have close *intramolecular* contacts to pyridine at the van der Waals distance. However, the structural parameters, bond distances and angles of this molecule do not indicate distinct steric effects of the CN groups. Thermal atropisomerization among the four zinc porphyrin atropisomers occurs in solution. The quantitative composition of the atropisomers at equilibrium and the rates of the isomerization reaction have been determined with aliquots separated by TLC. A nonstatistical equilibrium distribution of the atropisomers suggests some mutual interactions among the CN groups. The slower isomerization rates of the zinc complexes compared to those of the free base have been discussed in connection with the molecular structure.

The synthetic model study has been one of the most powerful approaches in probing the relationship between function and structure of the prosthetic heme group in multifunctional hemoproteins. The fundamental functions of hemes such as ligand binding and electronic state changes of the central iron are controlled by various factors including the electronic and steric effects of substituents of the porphyrin periphery. In recent years, the subtle control of the electronic properties of hemes has been investigated by means of a wide and systematic variation of the porphyrin peripheral substitution.[1-3] Steric control of the functions of hemes and metalloporphyrins is an interesting subject in the model studies considering the role of proteins. A typical steric control of oxygen binding to heme models has been accomplished notably as the "picket fence" porphyrin in which the role of the bulky pivaloylamino substituents on the one side of the porphyrin plane is attributed to the appropriate pocket for dioxygen binding and the hindrance for dimer formation.[4] However, there have been few studies to evaluate the steric effects quantitatively using a systematic variation of substituents and so on.[4d,5-7] We have been interested in the four atropisomers of *o*-substituted tetraarylporphyrin since there is a possibility in designing three dimensional models using the steric effect of the substituents under the isoelectronic conditions to control the functions of metalloporphyrin molecules. On this line, we have reported some properties of the tetrakis (*o*-substitutedphenyl)porphyrin atropisomers, i.e., electronic spectra, redox potential and metal incorporation rates, rotational rate of phenyl rings, and axial coordination reactions of bases.[7,8] The molecular structure determination of porphyrin atropisomers is expected to offer essential information as to the steric effects and the stereochemical environment around the porphyrin.

On the other hand, there is some ambiguity in the assignment of the conformation of $\alpha\beta\alpha\beta$- and $\alpha\alpha\beta\beta$-isomers of 5,10,15,20-tetrakis(*o*-cyanophenyl)porphyrin(ToCNPP[9]) free bases because of small difference in TLC separation and nonstatistical equilibrium population of these isomers.[8a] The present X-ray crystal structure determination originally aimed to establish the conformation of the $\alpha\beta\alpha\beta$-form and, subsequently, all conformations of the four atropisomers of ToCNPP. However, the ToCNPP free bases are thermally unstable and isomerize under the ambient recrystallization conditions. The coordination of metal ions to the porphyrin has been predicted to retard the rotational isomerization rate of the substituted phenyl rings.[10] Thus, the metallation of the porphyrin is expected to make it possible to isolate a pure isomer. At the same time, we are interested in the effect of the coordination of metal ions on the isomerization rate, its relationship to the structure of porphyrin, and the effect of axial ligands of the metal ion on the atropisomerization. Herein we report the X-ray structural analysis of the $\alpha\beta\alpha\beta$-isomer of ZnToCNPP and the atropisomerization rates among the isomers.

Experimental

Synthesis and Isolation of Atropisomers of ZnToCNPP. All reagents and solvents were reagent grade and used without further purification. ToCNPP was prepared as described.[8a] Metallation of ToCNPP was performed by refluxing zinc acetate and a mixture of the four atropisomers in DMF. The completion of the reaction was checked by UV-visible spectra recorded on a Shimadzu 200-S spectrophotometer. The products were precipitated by pouring an excess of water into the reaction mixture and were collected by filtration. The metallated porphyrins, ZnToCNPP, were separated by TLC (Merck; eluting solvent, 5:95 ether-

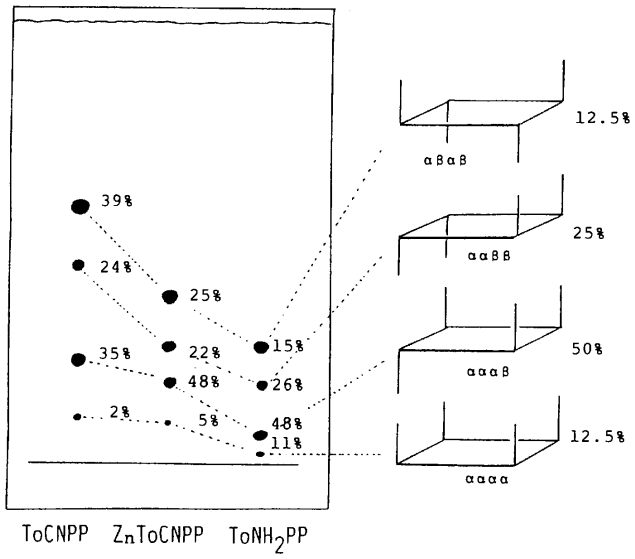

Fig. 1. The separation of atropisomers by thin layer chromatography and the distribution percentage of the isomers at the equilibrium. On the right the schematic representation of the assignment of four atropisomers and the statistical distribution are shown.

$CHCl_3$). The resolution of the four atropisomers is shown in Fig. 1 along with those of the corresponding ToCNPP and $ToNH_2PP$. The isolation of the respective atropisomers was accomplished by column chromatography on silica gel eluted with 98:2 chloroform-ether. The fractions of each isomer were evaporated to dryness immediately after elution from the column to avoid atropisomerization. The purity of each isomer was found to be more than 85%, satisfactory for the following kinetic experiments. Only the $\alpha\beta\alpha\beta$-isomer was purified further by recrystallization from chloroform-methanol, yielding purple crystals. Anal. Calcd for Zn(ToCNPP) $CHCl_3$, $C_{49}H_{25}N_8Cl_3Zn$: C, 65.57; H, 2.81; N, 12.48%. Found: C, 65.58; H, 2.51; N, 12.52%.

Crystal Structure Determination. Single crystals suitable for X-ray diffraction were obtained by vapor diffusion of pentane into a pyridine solution of the $\alpha\beta\alpha\beta$-isomer of ZnToCNPP. Crystals of $\alpha\beta\alpha\beta$-ZnToCNPP(Py)·Py were examined on a Philips PW-1100 automated diffractometer. This established a four-molecule monoclinic unit cell with *Cc* or *C2/c* as the possible space group. Least-squares refinement of the setting angles of 25 reflections gave the cell constants reported in Table 1. Table 1 also reports other details of crystal data and intensity collection. Intensity data were reduced to the structure factors without absorption corrections.

The choice of *C2/c* as the space group requires that the molecule possess a two-fold axis passing through Zn in porphyrin plane or an inversion center on Zn. However, the probable zinc locations calculated from the Patterson map lead to featureless difference Fourier maps and the Patterson map itself was incompatible with a crystallographic two-fold axis passing through the center of the tetragonal porphyrin molecule.[11] Thus, the *Cc* space group was chosen and all subsequent developments of the structure analysis of the complex were consistent with this choice.

A series of difference Fourier syntheses, phased initially by the zinc atom, revealed all non-hydrogen atoms of the porphyrin framework and a coordinated pyridine. After several cycles of refinement using these atoms, a difference Fourier map revealed six atomic positions of a solvate pyridine and several hydrogen positions of the porphyrin skeleton. The solvated pyridine was refined by assuming it as benzene i.e., six carbon atoms. All hydrogen atoms of the porphyrin and coordinated pyridine were idealized with C-H=0.95 Å and assigned isotropic temperature factors one unit higher than the associated atom. Refinement was then carried to convergence with anisotropic temperature factors for all non-hydrogen atoms using the block-diagonal least-squares and two-block 'full matrix' least-squares method.[11] At covergence, the final R and R_w values were 0.053 and 0.051, respectively. Calculations for the opposite enantiomorph gave R=0.059 and R_w=0.061. The coordinates of the first choice are reported. A final difference Fourier synthesis was featureless (<0.48 e/Å^3). A listing of observed and calculated structure factors is available as supplementary material (Table S1[12]). Tables 2 and S2[12] list final atomic coordinates with isotropic equivalent temperature factors and the associated anisotropic temperature factors, respectively.

Table 1. Summary of Crystal Data and Intensity-Collection Parameters for ZnToCNPP(Py)·Py

Formula	$ZnC_{58}H_{34}N_{10}$
F.W., amu	936.4
Crystal dimensions	0.3×0.3×0.7 mm^3
Space group	*Cc*
Temperature	293 K
a, Å	18.805(2)
b, Å	16.647(4)
c, Å	16.724(2)
β, °	115.49(12)
V, Å^3	4725.6
Z	4
Calcd density	1.316 g cm^{-3}
Obsd density	1.314 g cm^{-3}
2 theta range	6—54°
Criterion for observation	$F_o>2\sigma(F_o)$
Unique obsd data	3898
R	0.053
R_w	0.051
Data/Parameters	6.3

Atropisomerization. A toluene or 1,1,2-trichloroethane solution of each isolated isomer (ca. 5 mg/20 ml) in a flask was placed in a heated oil bath. Aliquots sampled by a glass capillary were spotted at intervals on TLC and developed with 95:5 $CHCl_3$-ether. The separated isomers were extracted two times with $CHCl_3$ and diluted to a constant volume in a cuvette. The quantity of the four isomers was analyzed by the spectrometric absorption area in the 390—450 nm region and was normalized to a molecular ratio of four atropisomers. The rates of isomerization were determined by a combination of the Runge-Kutta simulation and least-squares curve-fitting techniques.[8]

Results and Discussion

Molecular Structure of $\alpha\beta\alpha\beta$-Zn(ToCNPP)(Py). The structure of the ZnToCNPP(Py) molecule is shown in two different orientations in Figs. 2 and 3,

Table 2. The Fractional Coordinates and Isotropic Equivalent Temperature Factors

Atom	x	y	z	B_{eq}	Atom	x	y	z	B_{eq}
Zn	1/2	0.3632(0)	1/4	4.3	C5	0.3461(4)	0.5763(5)	0.5059(5)	7.8
NP1	0.6120(3)	0.3597(3)	0.3644(3)	4.8	C6	0.3848(4)	0.5418(5)	0.4617(5)	6.8
N1	0.4689(2)	0.4824(3)	0.2530(3)	4.3	C7	0.3905(3)	0.1059(4)	0.2978(4)	5.1
N2	0.4172(3)	0.3314(3)	0.2949(3)	4.6	C8	0.4441(4)	0.0549(3)	0.3624(4)	5.1
N3	0.4951(3)	0.2464(3)	0.2054(3)	4.9	C9	0.4207(4)	−0.0186(4)	0.3838(5)	6.8
N4	0.5466(3)	0.3979(3)	0.1619(3)	4.6	C10	0.3425(5)	−0.0402(4)	0.3389(6)	8.5
CP1	0.6576(4)	0.2959(4)	0.3839(5)	7.4	C11	0.2887(4)	0.0107(5)	0.2779(5)	7.3
CP2	0.7347(5)	0.2976(5)	0.4484(7)	9.2	C12	0.3131(4)	0.0817(4)	0.2569(5)	6.0
CP3	0.7636(4)	0.3635(5)	0.4949(6)	8.5	C13	0.5677(3)	0.6217(3)	0.1536(4)	5.0
CP4	0.7175(4)	0.4337(5)	0.4753(5)	7.4	C14	0.5393(4)	0.6476(4)	0.0661(5)	6.1
CP5	0.6434(4)	0.4290(4)	0.4091(4)	5.9	C15	0.5652(4)	0.7207(4)	0.0447(5)	7.1
CA1	0.4952(3)	0.5472(3)	0.2232(4)	4.4	C16	0.6198(4)	0.7678(4)	0.1116(5)	7.6
CA2	0.4251(3)	0.5117(3)	0.2940(4)	5.0	C17	0.6467(4)	0.7451(4)	0.1984(5)	6.7
CA3	0.3839(3)	0.3816(3)	0.3337(4)	4.6	C18	0.6217(4)	0.6724(4)	0.2208(4)	5.2
CA4	0.3975(3)	0.2541(3)	0.3084(4)	4.6	C19	0.6100(4)	0.2192(4)	0.0694(5)	6.6
CA5	0.5332(3)	0.2174(3)	0.1583(4)	5.7	C20	0.5668(4)	0.2013(4)	−0.0172(5)	7.3
CA6	0.4629(3)	0.1805(3)	0.2287(4)	4.6	C21	0.6030(6)	0.1584(5)	−0.0654(6)	10.5
CA7	0.5645(3)	0.4737(3)	0.1472(4)	4.3	C22	0.6818(6)	0.1337(5)	−0.0176(8)	12.6
CA8	0.5770(3)	0.3476(3)	0.1203(4)	4.9	C23	0.7230(5)	0.1505(6)	0.0680(7)	10.8
CB1	0.4646(4)	0.6196(3)	0.2442(5)	6.2	C24	0.6889(5)	0.1942(5)	0.1133(6)	9.5
CB2	0.4213(4)	0.5993(4)	0.2872(5)	5.8	CN1	0.2179(4)	0.4889(4)	0.2506(5)	6.6
CB3	0.3448(4)	0.3338(4)	0.3756(4)	5.8	NC1	0.1791(4)	0.4666(5)	0.1773(5)	10.1
CB4	0.3538(3)	0.2572(4)	0.3604(4)	5.3	CN2	0.5238(4)	0.0802(4)	0.4083(5)	5.7
CB5	0.5256(4)	0.1303(4)	0.1516(4)	6.0	NC2	0.5868(3)	0.1004(4)	0.4462(4)	7.5
CB6	0.4808(4)	0.1091(3)	0.1934(4)	5.5	CN3	0.6519(4)	0.6492(4)	0.3107(5)	6.0
CB7	0.6083(4)	0.4718(4)	0.0953(4)	5.9	NC3	0.6783(4)	0.6313(4)	0.3839(4)	8.3
CB8	0.6142(4)	0.3934(4)	0.0760(4)	5.8	CN4	0.4858(5)	0.2221(4)	−0.0608(5)	7.2
CM1	0.3872(3)	0.4648(3)	0.3338(4)	4.7	NC4	0.4196(4)	0.2359(4)	−0.0935(5)	8.6
CM2	0.4179(3)	0.1842(3)	0.2767(4)	4.5	NP2	−0.0383(5)	0.3485(6)	0.2219(6)	9.1
CM3	0.5421(3)	0.5441(3)	0.1765(4)	4.6	CP6	−0.0050(6)	0.3861(6)	0.1729(7)	11.0
CM4	0.5724(4)	0.2631(4)	0.1202(4)	5.6	CP7	−0.0405(6)	0.4081(6)	0.0909(6)	10.6
C1	0.3441(3)	0.5099(3)	0.3772(4)	5.2	CP8	−0.1207(6)	0.3993(6)	0.0436(7)	11.5
C2	0.2622(3)	0.5184(3)	0.3357(4)	5.0	CP9	−0.1593(6)	0.3564(7)	0.0879(9)	13.6
C3	0.2237(4)	0.5549(4)	0.3816(5)	6.6	CP10	−0.1171(6)	0.3368(7)	0.1788(8)	13.3
C4	0.2657(4)	0.5807(5)	0.4672(6)	8.7					

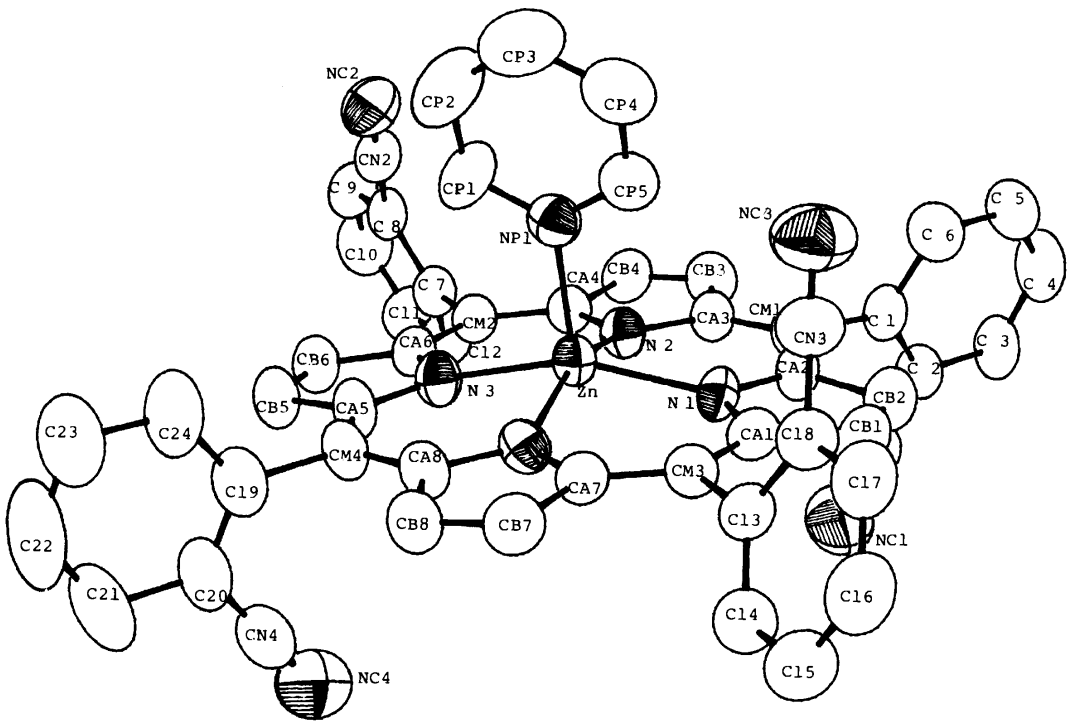

Fig. 2. Computer-drawn model of the ZnToCNPP(Py) molecule. The labeling scheme for the atoms is given. Zinc and nitrogen atoms are shown by the octant shading ellipsoids. Ellipsoids are contoured to enclose 50% of the electron density.

Table 3. Average Values of Bond Distances and Angles of the Porphyrin Skeleton in ZnToCNPP(Py)·Py

		Bond Distance/Å			
$Zn-N_{por}$	2.076(12)	$N_{por}-Ca$	1.369(11)	Ca-Cb	1.444(13)
Cb-Cb	1.347(14)	Ca-Cm	1.398(8)		
		Bond Angle/deg.			
$Zn-N_{por}-Ca$		126.2(5)	$N_{por}-Ca-Cb$		109.5(4)
$Ca-N_{por}-Ca$		106.8(4)	$N_{por}-Ca-Cm$		125.4(4)
Ca-Cm-Ca		125.9(4)	Ca-Cb-Cb		107.1(9)

Ca, Cb, and Cm denote atoms of pyrrole-α, pyrrole-β, and methine(5,10,15,20-) positions of porphyrin skeleton, respectively.

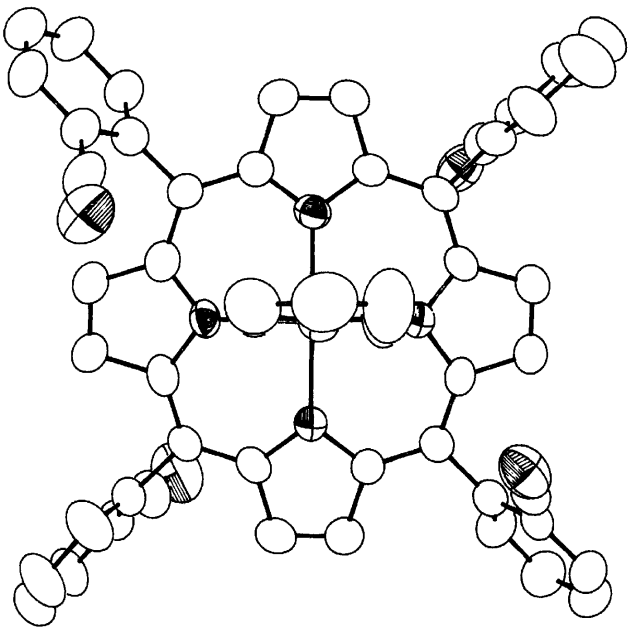

Fig. 3. Perspective view of the ZnToCNPP(Py) molecule looking down the nomal of the porphyrin plane, showing the relative orientation of coordinating pyridine and geometry of the CN groups.

which demonstrate the most significant feature of the molecule: The arrangement of the CN groups and nonbonded intramolecular contacts between the CN group and the coordinated pyridine. Figure 2 also gives the labels assigned to each non-hydrogen atom. The structure is in agreement with the conformation ($\alpha\beta\alpha\beta$) of the atropisomer identified previously by chemical properties and chromatographic separation, i.e., the atropisomer eluting most rapidly on silica gel and consequently being least polar.

Average values for the chemically equivalent bond lengths and angles of the porphinato core are given in Table 3. The numbers in parentheses are the standard deviations calculated from the differences between the average of the equivalent bonds and the individual values (Table S3[12]).[13]

The coordination state of the present zinc porphyrin is five-coordinate with a pyridine molecule in the fifth axial position. The coordination sphere around Zn is apparently normal. The average $Zn-N_{por}$ bond length of 2.076 (12) Å and the displacement (0.37 Å) of the zinc ion out of the mean plane of the four porphinato N atoms are in general accord with those observed in the five-coordinate zinc porphyrins as shown in Table 4. The $Zn-N_{py}$ bond length of 2.151 (4) Å does not display any elongation due to a steric effect between the pyridine and the two CN substituents projecting toward pyridine. Indeed the bond length is significantly shorter (by 0.049 Å) than the 2.200 (3) Å value reported for Zn(OEP)(Py)[14] which has no hindering substituents on the porphyrin periphery. This indicates that the CN substituents on the ortho position in the $\alpha\beta\alpha\beta$ phenyl conformation have little steric effect on the coordinated pyridine molecule, or, even if there is any, the effect is not necessarily hindering or repulsive.

The dihedral angle between the axial pyridine plane and the plane containing three nitrogen atoms, those of pyridine and two opposite pyrroles of the porphyrin core, is small at 8.8°. The actual ligand orientation

Table 4. Comparison of the Stereochemical Parameters of the Coordination Group for Five-Coordinate Zinc Porphyrins

Zn Porphyrin	Distance/Å			ϕ/°	Ref.
	$Zn-N_{por}$	$Zn-N_{Py}$	Zn-Ct		
$ZnTPP(H_2O)$	2.05	2.20*	0.19	—	(15)
ZnTPyP(Py)	2.073(3)	2.143(4)	0.33	23	(16)
ZnOEP(Py)	2.067(3)	2.200(3)	0.31	4	(14)
Zn(TPP side arm Py)	2.059(7)	2.147(7)	0.37	5.8	(17)
ZnToCNPP	2.076(12)	2.151(4)	0.37	8.9	This work

* $Zn-O_{water}$ distance.

would appear to have ϕ[18] closer to a completely eclipsed conformation (i.e. ϕ=0°); the apparent value of 8.8° results in part from the pyridine plane not being precisely perpendicular to the 24-atom porphinato plane, the angle is 77.0°. As reported in Table 4, the ligand orientation of five-coordinate zinc porphyrins have, in general, small values. This means that sterically unfavoring contacts between α-hydrogen of pyridine and porphinato pyrrole nitrogen result if no other constraint controls the orientation. Although the constraint of the side arm has been explained to lead to an exceptionally small ϕ value of Zn(TPP side arm Py),[17] the present structure indicates no distinct evidence that the orientation of the ligand is controlled by the CN substituents. The closest contact of N_{CN} to non-hydrogen atoms of the coordinated pyridine is 3.49 Å (NC2-CP2), which is a normal van der Waals contact. Even if there would be a closer contact, it can be circumvented by the small rotation about the aryl-porphine bond. There is a considerable room for the rotation since the dihedral angles between cyanophenyl rings and the mean porphyrin plane are 73.3° and 64.7° on the pyridine side and 77.9° and 87.8° on the other side.

Recently, Scheidt et al. suggest that the electronic spin-state is one of the important factors correlating with ligand orientation in some iron(III) porphyrin cases.[19] The zinc ion has a d^{10} electronic configuration and all five 3d orbitals are occupied by spin-paired electrons, hence, the drastic changes in the electronic states or spin states depending implicitly on the change of axial ligands, bond lengths, or ligand orientation are *not* expected for zinc porphyrins. Consequently, the small orientation angle observed in all of the pyridine-ligated zinc porphyrins reported so far should be explained by an intrinsic electronic nature of zinc(II) ion. A possible explanation comes from consideration of the overlap of the occupied d_{zx} or d_{yz} orbital over pπ* at the N_{Py} atom, namely dπ-pπ* backdonation, because the d_{zx} or d_{yz} has a common nodal plane with pπ* at ϕ=0°.

The structural similarity of six- and five-coordinate porphyrin complexes of zinc(II) and high-spin iron(II) has been pointed out by Schauer et al.[20] The similarity includes the bond distances between the metal ion and porphinato nitrogen atoms and the axial N_{base}-metal bond length. The structural similarity can also extend to five-coordinate high-spin iron(III) complexes since a novel structure of five-coordinate [Fe(OEP)(2Mim)]ClO_4 molecule has been determined recently.[21] The structural parameters, 2.038(6) Å for average Fe-N_{por}, 2.068(4) Å for Fe-N_{2Mim}, and 0.35 Å for displacement of Fe(III) out of plane, are comparable to those of five-coordinate zinc porphyrins in Table 4. Here, a small orientational angle (ϕ=3.0—7.3°) of the 2-methylimidazole ligand can be particularly emphasized as part of the similarity. This suggests that the occupation of electrons in all of the five 3d orbitals has an essential and common effect on the coordination structure in porphyrin complexes of these two metal ions.

The structure of four peripheral cyanophenyl groups shows no abnormal feature in the bond distances and angles irrespective of whether the CN substituents are on the same side as the coordinated pyridine or not. The CN group is coplanar to each phenyl ring within 0.07 Å from the mean plane. Figure 4 shows the average bond parameters for the four chemically equivalent types with the standard deviations in parentheses. The average C-C_{CN} bond length is 1.411(13) Å, similar to the C-C bonds of the phenyl ring. Thus, the bond has a conjugated double bond character. The C≡N distance ranges from 1.128(8) Å to 1.184(9) Å and the average is 1.151(24) Å. These bond values agree well with those of benzonitrile or cyanomethanide ion disregarding whether the molecule or ion is free or coordinated to a metal.[22,23]

The nonbonded intramolecular N_{CN}-N_{CN} atomic distances are measured to be 9.15 Å at a level 3.2 Å above the porphyrin plane on the pyridine side and 8.56 Å at a level 3.4 Å below the plane on the other side. These distances correspond to a diameter of the cavity defined by the CN substituents. The diameter is comparable with the interior size of some inclusion compounds, e.g., ca. 8.5 Å for cyclohexaamyloses or ca. 8.6 Å for cyclophanes.[24,25] We have noted previously that the free base atropisomers (ToCNPP) populate in a nonstatistical equilibrium ratio (cf. Fig. 1) because of the mutual nonbonded interaction of the CN substituents on the same side of the porphyrin plane. A similar nonstatistical distribution is also observed in ZnToCNPP. The rather large diameter of the cavity requires the idea of the nonbonded tran-

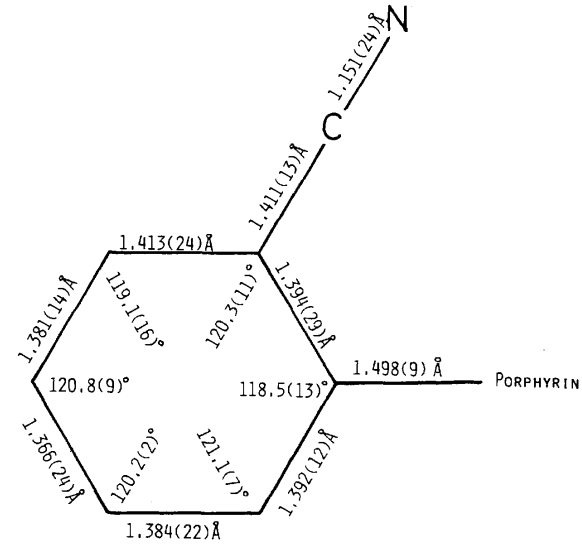

Fig. 4. A formal diagram of the average structure of four cyanophenyl rings of the molecule. Average values of bond distances and angles are displayed with the standard deviations[13] of the least significant digits in parentheses.

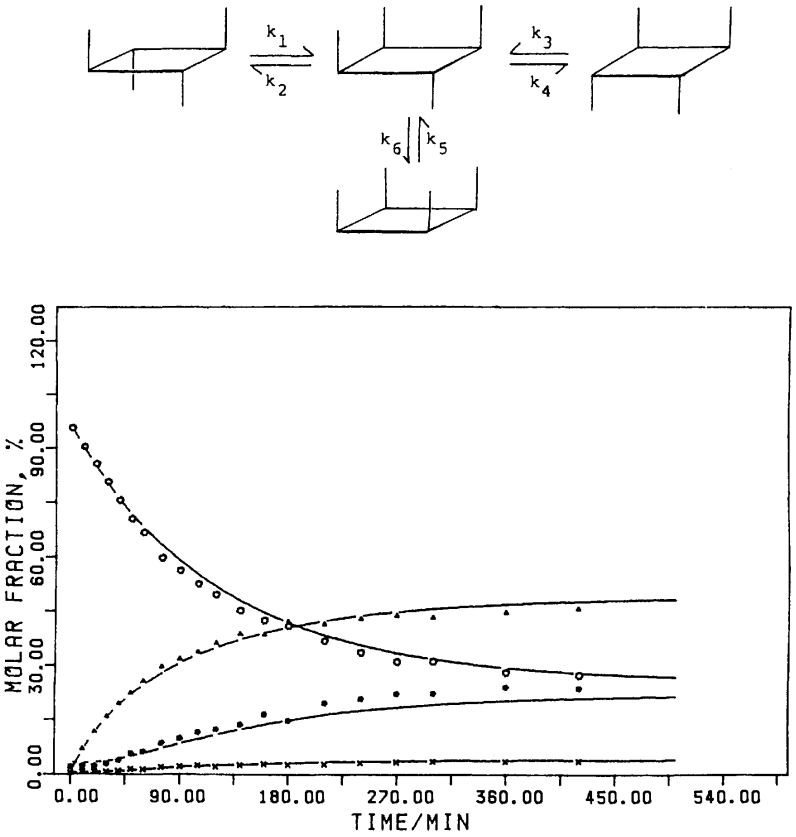

Fig. 5. The reaction scheme of the atropisomerization and a time course diagram of the reactions initiating from $\alpha\beta\alpha\beta$-isomer of ZnToCNPP at 96 °C, (○) $\alpha\beta\alpha\beta$; (●) $\alpha\alpha\beta\beta$; (▲) $\alpha\alpha\alpha\beta$; (×) $\alpha\alpha\alpha\alpha$. The solid lines in the diagram were computed by the Runge-Kutta method from the rate constants in Table 5.

sannular interaction to be not necessarily direct but maybe indirect through axial ligands or solvents in the vicinity of the cavity.

The maximum displacement from the 24-atom mean porphyrin plane is as small as 0.16 Å of the CB2 atom, namely, the porphyrin skeleton is fairly planar for ZnToCNPP. Although there seems to be no clear-cut general interpretation as to whether the porphyrin takes planar or "ruffled" skeleton depending on the metal ions and so on, the zinc coordination has a trend in favor of the planar structure. The planar structure of the porphyrin core may correlate with the inflexibility of the core for the deformation required in the transition state of the atropisomerization reaction as discussed below.

Atropisomerization of ZnToCNPP. Figure 5 depicts schematic isomerization reactions among the atropisomers along with the definition of rate constants and a typical result of kinetic experiments. The relative ratio of the amount of four atropisomers equilibrating at 96 °C for 2 d was as follows: $\alpha\alpha\alpha\alpha$,5 (2); $\alpha\alpha\beta\beta$, 48 (4); $\alpha\alpha\beta\beta$, 22 (4); $\alpha\beta\alpha\beta$, 25 (3). The ratio was found to be independent of temperatures in the range of 75° to 105 °C within the experimental deviations in parentheses. The individual reaction rates were investigated in several independent runs at 65, 75, 85, 96, and 105 °C. The observed average rate constants are listed in Table 5. Considering the constant population of the isomers in the equilibrium at any temperature in our experiments, we analyzed the rates by obtaining first the average Arrhenius activation energy (E_a) and then individual preexponential terms for six rate constants using the least-squares method. This treatment demands a constant ratio in the six rate constants at any temperature. The ratio is $1:0.51:2.9:1.3:5.3:0.46$ for $k_1:k_2:k_3:k_4:k_5:k_6$. The thermodynamic parameters could be obtained by the use of relation-

Table 5. Observed Rate Constants for Atropisomerization Reactions of Tetrakis(*o*-cyanophenyl)-porphinatozinc(II)

Temperature	Observed Rate Constant ($\times 10^5$)/s^{-1}					
°C	k_1	k_2	k_3	k_4	k_5	k_6
65	0.50	0.27	1.42	0.75	2.65	0.22
75	1.15	0.58	3.85	1.65	6.35	0.64
85	3.35	1.60	9.20	4.15	16.5	1.60
96	10.5	5.5	26.5	11.5	53.5	4.5
105	21.0	11.0	65.0	30.0	115.0	8.5

Table 6. Comparative Activation Parameters for the Atropiosomerization Rate (k_1)

Porphyrin	Temperature	ΔH^*	ΔS^*	ΔG^*[a)]	Ref.
	°C	(kJ mol^{-1})	(JK^{-1} mol^{-1})	(kJ mol^{-1})	
ZnToCNPP	85	97.6	−59.5	118.9	This work
	65	97.6	−59.9	117.7	This work
ToCNPP	60	85.8	−68.2	108.4	(8a)
ToNH_2PP	65	91.3	−61.5	112.2	(8b)

a) Extrapolated values.

ships, $\Delta H^*=E_a-RT$ and $\Delta G^*=\Delta H^*-T\Delta S^*$, and the Eyring equation, $k=(k_BT/h)\exp(-\Delta G^*/k_BT)$. The values for the one representative reaction (k_1) are shown in Table 6. The kinetic data processed as above were consistent with all of the observed rate constants within the experimental errors. The activation parameters calculated similarly for the same reaction (k_1) of ToCNPP[8a)] and ToNH_2PP[8b)] are also shown in Table 6 for comparison.

The slower rates of ZnToCNPP relative to those of ToCNPP are remarkable. The ΔG^* value of 118.9 kJ mol^{-1} at 85 °C is high and comparable to the 113.1 kJ mol^{-1} value at 81 °C reported for the bulky hexadecyl derivative of ToNH_2PP.[26)] The phenyl ring rotation in *o*-substituted tetraarylporphyrins is thought to require the severe deformation of the porphyrin skeleton. The slow rates of the Zn complex suggest that the zinc ion coordination (perhaps metal ion coordination in general) brings a reinforcement of the skeletal tension against the required deformation. The higher free energy of activation of ZnToCNPP, consequently the slower rate, compared to that of ToCNPP at 60 or 65 °C also reflect the reinforcement as the part of the stabilization energy of the porphyrin acquired by the incorporation of the zinc ion. The reinforcement effect seems to correlate with the enthalpy term of the free energy of activation because of the identical entropy values obtained from the reactions of ZnToCNPP and ToCNPP (Table 6). This is contrasting with the entropy control of activation observed in a series of the free base porphyrins with bulky *o*-substituents.[8b)]

The retardation factor of the isomerization reaction induced by the coordination of zinc reaches about 20 at 60 °C and the factor is appreciably larger than the apparent value of 12.5 calculated from the data for the ToOHPP-Cu system.[10)] The difference in the retardation factor may come from the difference in the porphyrin core expansion by the two metal ions. In this connection, the bond length between the metal and the porphyrin nitrogen can be cited as 1.981 Å for CuTPP[27)] and 2.036 Å for ZnTPP:[28)] both metalloporphyrins are four-coordinate; CuTPP is ruffled whereas ZnTPP is planar.[29)] Thus, the coordination of zinc ion is thought to bring forth not simply the reinforcement against deformation but also to some extent as expansion effect on the porphyrin skeleton. The expansion of porphyrin core should weaken the transannular interaction among *o*-substituents on the same side of the porphyrin plane. This may be a possible explanation for why the equilibrium distribution of atropisomers of ZnToCNPP becomes closer to the statistical ratio than that of metal-free ToCNPP. We have speculated that the nonbonded distance between two adjacent nitrogen atoms of CN group is responsible for the nonstatistical isomer distribution.[8a)] However, the transannular interaction occur not always through the directly measured *intramolecular* distance since short *intermolecular* contacts such as van der Waals distance are frequently observed in the solid state. In solution, the intramolecular transannular interaction must be affected by the solvent molecule therein, especially the coordinating impurities in the case of metalloporphyrin. The present five-coordinate ZnToCNPP structure demonstrate a possibility of some interaction through the coordinated pyridine by the shortest contact of 3.49 Å with the CN substituent as mentioned above. The addition of pyridine as an effector into the reaction solution did not give distinct changes in the equilibrium distribution of isomers. A drastic change was observed in the presence of some other particular molecules such as 2Mim[9)] in the reaction mixture. The observed distribution in the presence of 2Mim is as follows: $\alpha\alpha\alpha\alpha$, 15(3); $\alpha\alpha\alpha\beta$, 52(5); $\alpha\alpha\beta\beta$, 19(4); $\alpha\beta\alpha\beta$, 14(3). This is almost the statistical ratio. Although the details of the mechanism and effect of 2Mim or other ligands on the atropisomerization is forthcoming, the effect must be due to the interaction through 2Mim coordinated to ZnToCNPP. This is a novel control of the rotational isomerization by the steric effect of the axial ligand. By this axial ligand effect, the distribution ratio is controlled in the favor of the $\alpha\alpha\alpha\alpha$-form.

We thank the Ministry of Education, Science, and Culture of Japan for support of the part of this work under a Grant-in-Aid for Scientific Research (#60571024). We acknowledge the discussions on the crystal structure of ZnToCNPP(Py)·Py with Professor W. R. Scheidt.

References

1) D. K. Geiger and W. R. Scheidt, *Inorg. Chem.*, **23**, 1970 (1984).

2) F. A. Walker, M.-W. Lo, and M. T. Ree, *J. Am. Chem. Soc.*, **98**, 5552 (1976).

3) V. L. Balke, F. A. Walker, and J. T. West, *J. Am. Chem. Soc.*, **107**, 1226 (1985).

4) a) J. P. Collman, R. R. Gagne, C. A. Reed, T. R. Halbert, G. Lang, and W. T. Robinson, *J. Am. Chem. Soc.*, **97**, 1427 (1975); b) G. B. Jameson, G. A. Rodley, W. T. Robinson, R. R. Gagne, C. A. Reed, and J. P. Collman, *Inorg. Chem.*, **17**, 850 (1978); c) G. B. Jameson, F. S. Molinaro, J. A. Ibers, J. P. Collman, J. I. Brauman, E. Rose, and K. S. Suslick, *J. Am. Chem. Soc.*, **102**, 3224 (1980); d) J. P. Collman, J. I. Brauman, B. L. Iverson, J. L. Sessler, R. M. Morris, and Q. H. Gibson, *J. Am. Chem. Soc.*, **105**, 3052 (1983).

5) D. Lexa, M. Momenteau, P. Rentien, G. Rytz, J.-M. Saveant, and F. Xu, *J. Am. Chem. Soc.*, **106**, 4755 (1984).

6) K. M. More, G. R. Eaton, and S. S. Eaton, *Inorg. Chem.*, **24**, 3698 (1985).

7) a) K. Anzai and K. Hatano, *Chem. Pharm. Bull.*, **32**, 1273 (1984); b) *Idem, ibid.*, **32**, 2067 (1984); c) K. Anzai, T. Hosokawa, and K. Hatano, *ibid.*, **34**, 1865 (1986).

8) a) K. Hatano, K. Anzai, T. Kubo, and S. Tamai, *Bull. Chem. Soc. Jpn.*, **56**, 422 (1983); b) K. Hatano, K. Anzai, A. Nishino, and K. Fujii, *ibid.*, **58**, 3653 (1985).

9) Abbreviations: DMF, *N,N*-dimethylformamide; ToCNPP, 5,10,15,20-tetrakis(*o*-cyanophenyl)porphyrin dianion; ToNH_2PP, 5,10,15,20-tetrakis(*o*-aminophenyl)-porphyrin dianion; ToOHPP, 5,10,15,20-tetrakis(*o*-hydroxyphenyl)porphyrin dianion; TPyP, tetra-4-pyridylporphyrin dianion; TPP side arm Py, 5-[2-[2-(3-pyridyl)ethylcarbonylamino]phenyl]-10,15,20-triphenylporphyrin dianion; OEP, octaethylporphyrin dianion; TPP, tetraphenylporphyrin dianion; Py, pyridine; 2Mim, 2-methylimidazole; N_{por}, porphinato nitrogen atom. N_X, a nitrogen atom belonging to X (X generally denotes a molecule or a group of atoms.).

10) L. K. Gottwald and E. F. Ullman, *Tetrahedron Lett.*, **1969**, 3071.

11) The programs used in this study included local versions and modifications of Sakurai's KFR-5, Okaya and Ashida's XNBLS and FMLS, and Johnson's ORTEP2.

12) Table Sl(listings of the observed and calculated structure amplitudes (×10, 13 pages)), Table S2 (anisotropic temperature factors), and Table S3 (individual bond distances and angles) are deposited as Document No. 8732 at the office of this Bulletin.

13) We use two kinds of estimated standard deviations (esd) in this report. The esd's of the individual positional, thermal, and bond parameters come from the least-squares treatment, i.e., the statistics of F_o and F_c. The other derives from the average statistical treatment of several *chemically equivalent* parameters.

14) D. L. Cullen and E. F. Meyer, Jr., *Acta Crystallogr., Sect B*, **32**, (1976).

15) M. D. Glick, G. H. Cohen, and J. L. Hoard, *J. Am. Chem. Soc.*, **89**, 1996 (1967).

16) D. M. Collins and J. L. Hoard, *J. Am. Chem. Soc.*, **92**, 3761 (1970).

17) M. A. Bobrik and F. A. Walker, *Inorg. Chem.*, **19**, 3383 (1980).

18) a) D. M. Collins, R. Countryman, and J. L. Hoard, *J. Am. Chem. Soc.*, **94**, 2066 (1972); b) J. L. Hoard, in "Porphyrins and Metallopophyrins," ed by K. M. Smith, Elsevier, Amsterdam (1975), pp. 317—380.

19) a) W. R. Scheidt, D. K. Geiger, R. G. Hayes, and G. Lang, *J. Am. Chem. Soc.*, **105**, 2625 (1983); b) D. K. Geiger, V. Chunplang, and W. R. Scheidt, *Inorg. Chem.*, **24**, 4736 (1985).

20) C. K. Schauer, O. P. Anderson, S. S. Eaton, and G. R. Eaton, *Inorg. Chem.*, **24**, 4082 (1985).

21) W. R. Scheidt, D. K. Geiger, Y. J. Lee, C. A. Reed, and G. Lang, *J. Am. Chem. Soc.*, **107**, 5693 (1985).

22) a) P. G. Fauvet, M. Massaux, and R. Chevalier, *Acta Crystallogr., Sect B*, **34**, 1376 (1978); b) I. W. Bassi, C. Benedicenti, M. Calcaterra, and G. Rucci, *J. Organomet. Chem.*, **117**, 285 (1976).

23) D. A. Summerville, I. A. Cohen, K. Hatano, and W. R. Scheidt, *Inorg. Chem.*, **17**, 2906 (1978), and the references cited therein.

24) a) A. Hybl, R. E. Rundle, and D. E. Williams, *J. Am. Chem. Soc.*, **87**, 2779 (1965); b) K. Harata, *Bull. Chem. Soc. Jpn.*, **48**, 2409 (1975).

25) a) K. Odashima, A. Itai, Y. Iitaka, and K. Koga, *J. Am. Chem. Soc.*, **102**, 2504 (1980); b) I. Tabushi, K. Yamanaka, H. Nonoguchi, K. Hirotsu, and T. Higuchi, *J. Am. Chem. Soc.*, **106**, 2621 (1984).

26) F. A. Freitag, J. A. Mercer-Smith, and D. G. Whitten, *J. Am. Chem. Soc.*, **103**, 1226 (1981).

27) E. B. Fleisher, C. K. Miller, and L. E. Webb, *J. Am. Chem. Soc.*, **86**, 2342 (1964).

28) W. R. Scheidt, M. E. Kastner, and K. Hatano, *Inorg. Chem.*, **17**, 706 (1978).

29) W. R. Scheidt, in "The Porphyrins," ed by D. Dolphin, Academic Press, New York (1978), Vol. III, pp. 463—511.

The Molecular Structure of Tricarbonyl(triple-layered [2.2]-paracyclophane)chromium at −95°C(Monoclinic Form) and −160°C (Triclinic Form)†

Hitoshi OIKE,†† Yasushi KAI,* Kunio MIKI, Nobuo TANAKA,††† and Nobutami KASAI*
Department of Applied Chemistry, Faculty of Engineering, Osaka University, Suita, Osaka 565
(Received December 5, 1986)

The tricarbonylchromium complex of triple-layered [2.2]paracyclophane shows a reversible phase transition in the solid state from the monoclinic to the triclinic form at a temperature between −100 and −110 °C. The monoclinic form crystallizes in the space group $P2_1/c$, with a=15.095(6), b=9.950(3), c=15.641(5) Å, β=103.46(3)° (−95 °C), and Z=4: The triclinic form belongs to the space group $P\bar{1}$, with a=15.037(5) Å, b=9.913(2), c=15.662(5) Å, α=89.41(3), β=104.51(3), γ=89.39(4)° (−160 °C), and Z=4. In the triclinic crystal, two molecules are crystallographically independent. The crystal structures were solved by the direct method and then refined by the block-diagonal least-squares procedure to the R indices of 0.067 for 3530 (monoclinic form) and 0.079 for 6776 (triclinic form) observed reflections. No essential difference is found between the structures of the monoclinic-form molecule and the two triclinic-form molecules. The interlayer distance between the upper-layer benzene ring coordinated to the $Cr(CO)_3$ group and the middle-layer benzene ring is unusually shorter than the corresponding distance between the middle- and lower-layer benzene rings. No bond alternation is found in the upper-layer benzene ring, unlike as in the tricarbonyl(benzene)chromium complex and the (tricarbonyl)chromium complex of double-layered [2.2]paracyclophane. The phase transition of the crystal can be explained by a slight change in the molecular packing.

In a series of structural studies of layered cyclophanes, the X-ray structure determination of the (tricarbonyl)chromium complex of double-layered [2.2]-paracyclophane (TCPC).[1] has been carried out. The molecular structure of TCPC showed an unusual shortening of the distance between two benzene rings compared with the corresponding distances in other double-layered [2.2]paracyclophanes, [2.2]paracyclophane (PC),[2] 4,7,13,16-tetramethyl[2.2]paracyclophane (TMPC),[3] and 4,7-dimethyl[2.2]paracyclophane (DMPC).[3] Stimulated by this interesting feature of the [2.2]paracyclophane structure, we then determined the molecular structure of the (tricarbonyl)chromium complex of triple-layered [2.2]paracyclophane (TC3PC) by means of X-ray diffraction. A low-temperature experiment on the TC3PC revealed a reversible phase transition between the monoclinic and triclinic forms. The molecular structures determined are compared with that of 12-bromo(triple-layered [2.2]paracyclophane) (BR3PC),[4] which is the only example of a triple-layered [2.2]paracyclophane whose structure has been determined by the X-ray diffraction method.

Experimental

All the X-ray measurements were undertaken on a Rigaku automated, four-circle diffractometer with graphite-monochromatized Mo$K\alpha$ radiation. A Rigaku low-temperature apparatus was attached to the diffractometer, and the low temperature was attained by the gas-flow method of liquid nitrogen. During the process of cooling the crystal down to −160 °C from room temperature, an interesting phase transition has been found. At a temperature between −100 and −110 °C, the split and complexity of the diffraction profile of the monitor reflections were observed. At temperature below −110 °C, the profile of the same diffraction became sharp and simple again. These changes were observed reversibly. The process of the phase transition was confirmed by the oscillation photographs which were taken on the four-circle diffractometer by the use of a special film-cassette and ω-oscillation mechanism. It was revealed that the crystal belongs to the monoclinic system at −80 °C and to the triclinic system at −130 °C. The X-ray diffraction data have been collected at −95 °C for the monoclinic form and at −160 °C for the triclinic form with the same crystal. The crystal data are listed in Table 1. The triclinic form has two crystallographically independent molecules per unit cell.

The integrated intensities were measured by the θ-2θ scan technique at a 2θ scan rate of 4° min^{-1} in the range of $\Delta 2\theta=(2.0+0.7\tan\theta)°$. The backgrounds were counted for 5 s before and after the scan of each peak. Totals of 3530 and 6776 observed reflections [$|F_o|>3\sigma(F_o)$] were collected up to 2θ=54 and 50° for the monoclinic and triclinic forms respectively. The intensity data were corrected for the usual Lorentz and polarization effects, but not for the absorption [μ(Mo$K\alpha$)=5.5 and 5.6 cm^{-1} for monoclinic and triclinic crystals].

Structure Solution and Refinement

The crystal structures of the monoclinic and triclinic forms of TC3PC were solved by the direct method (*MULTAN* 78)[5] and were refined by the block-diagonal least-squares procedure (*HBLS* V),[6] with anisotropic temperature factors for nonhydrogen atoms and isotropic temperature factors for hydrogen atoms. The final R indices are 0.067 and 0.079 (R_W=0.083 and 0.135) for 3530 and 6776 observed reflections of the monoclinic and triclinic forms respectively. The weighting scheme used was $w=\{\sigma^2(F_o)+a|F_o|+b|F_o|^2\}^{-1}$. The weighting parameters

† Structural Chemistry of Layered Cyclophane. XI.
†† Present address: Oike Industry Corporation, Shimogyo-ku, Kyoto 615.
††† Present address: Institute for Protein Research, Osaka University, Suita, Osaka 565.

Table 1. Crystal Data of Tricarbonyl(triple-layered [2.2]paracyclophane)chromium

Formula	$C_{29}H_{26}O_3Cr$	
Formula Weight	474.5	
$F(000)$	992	
Temperature/°C	−95	−160
System	Monoclinic	Triclinic
Space Group	$P2_1/c$	$P\bar{1}$
a/Å	15.095(6)	15.037(5)
b/Å	9.950(3)	9.913(2)
c/Å	15.641(5)	15.662(5)
α/°		89.41(3)
β/°	103.46(3)	104.51(3)
γ/°		89.39(4)
V/Å^3	2284.8(13)	2259.8(12)
Z	4	4
D_c/g cm^{-3}	1.379	1.394
D_m/g cm^{-3}	1.37 (room temp)	
μ(Mo $K\alpha$)/cm^{-1}	5.54	5.60

Table 2. Final Atomic Parameters for Nonhydrogen Atoms together with the Estimated Standard Deviations in Parentheses

Monoclinic Form (at −95°C):

Atom	x	y	z	B_{eq}/Å^2[7]
Cr	0.79662(5)	0.23301(7)	0.83800(4)	1.83
O(1)	0.8871(3)	0.2405(4)	1.0301(3)	4.4
O(2)	0.6440(3)	0.0540(5)	0.8607(3)	4.6
O(3)	0.8996(3)	-0.0192(4)	0.8222(3)	3.7
C(1)	0.5768(4)	0.4531(5)	0.6031(4)	3.2
C(2)	0.5906(4)	0.3374(6)	0.6747(4)	4.4
C(3)	0.6870(4)	0.3395(5)	0.7298(3)	2.9
C(4)	0.7080(3)	0.4114(5)	0.8099(3)	2.6
C(5)	0.7964(3)	0.4529(4)	0.8454(3)	2.3
C(6)	0.8667(3)	0.4279(4)	0.8008(3)	2.0
C(7)	0.8480(4)	0.3353(4)	0.7311(3)	2.3
C(8)	0.7600(4)	0.2900(5)	0.6964(3)	2.7
C(9)	0.9482(3)	0.5188(5)	0.8142(4)	2.8
C(10)	0.9229(3)	0.6557(5)	0.7616(3)	2.6
C(11)	0.8293(3)	0.6520(4)	0.6996(3)	2.1
C(12)	0.8136(3)	0.5944(5)	0.6145(3)	2.2
C(13)	0.7292(4)	0.5352(5)	0.5830(3)	2.5
C(14)	0.6551(3)	0.5532(5)	0.6221(3)	2.3
C(15)	0.6638(3)	0.6570(5)	0.6846(3)	2.5
C(16)	0.7522(3)	0.6938(5)	0.7273(3)	2.3
C(17)	0.5832(4)	0.7392(5)	0.6991(4)	3.3
C(18)	0.5487(4)	0.8456(6)	0.6238(4)	3.9
C(19)	0.6211(4)	0.8760(5)	0.5735(4)	2.9
C(20)	0.7004(4)	0.9458(5)	0.6127(4)	3.0
C(21)	0.7810(4)	0.9233(5)	0.5869(3)	2.9
C(22)	0.7838(4)	0.8316(5)	0.5188(3)	2.9
C(23)	0.7007(4)	0.7878(5)	0.4686(3)	3.4
C(24)	0.6214(4)	0.8091(6)	0.4954(4)	3.4
C(25)	0.8732(4)	0.7621(6)	0.5174(4)	3.6
C(26)	0.8778(4)	0.6135(5)	0.5537(3)	3.2
C(27)	0.8510(4)	0.2355(5)	0.9561(3)	2.8
C(28)	0.7030(4)	0.1244(6)	0.8539(3)	3.1
C(29)	0.8605(3)	0.0797(5)	0.8277(3)	2.5

Table 2. (Continued 1)

Triclinic Form (at −160°C):
Molecule 1

Atom	x	y	z	B_{eq}/Å^2
Cr	0.78752(6)	0.23825(9)	0.83997(6)	1.12
O(1)	0.8889(4)	0.2405(5)	1.0315(3)	2.4
O(2)	0.8871(4)	-0.0164(5)	0.8160(4)	2.4
O(3)	0.6351(4)	0.0616(6)	0.8654(4)	3.0
C(1)	0.9138(4)	0.6508(6)	0.7512(4)	1.6
C(2)	0.9426(4)	0.5134(7)	0.8028(5)	1.9
C(3)	0.8577(4)	0.4268(6)	0.7971(4)	1.2
C(4)	0.8293(5)	0.3357(6)	0.7282(4)	1.8
C(5)	0.7362(5)	0.3000(6)	0.6984(4)	1.9
C(6)	0.6712(5)	0.3555(6)	0.7389(4)	1.7
C(7)	0.7014(4)	0.4253(6)	0.8190(4)	1.5
C(8)	0.7955(4)	0.4577(6)	0.8487(4)	1.4
C(9)	0.5710(5)	0.3629(8)	0.6910(5)	2.5
C(10)	0.5575(4)	0.4657(7)	0.6103(4)	1.8
C(11)	0.6364(4)	0.5648(7)	0.6218(4)	1.6
C(12)	0.6508(4)	0.6685(6)	0.6841(4)	1.6
C(13)	0.7421(4)	0.7006(6)	0.7228(4)	1.4
C(14)	0.8161(4)	0.6524(6)	0.6918(4)	1.3
C(15)	0.7938(4)	0.5971(6)	0.6073(4)	1.5
C(16)	0.7063(4)	0.5399(6)	0.5788(4)	1.6
C(17)	0.8542(5)	0.6128(7)	0.5426(4)	2.0
C(18)	0.8525(5)	0.7641(7)	0.5088(5)	2.2
C(19)	0.7663(5)	0.8399(7)	0.5148(4)	1.9
C(20)	0.6793(5)	0.8027(6)	0.4656(4)	1.9
C(21)	0.6016(5)	0.8307(7)	0.4960(4)	2.0
C(22)	0.6082(5)	0.8956(7)	0.5757(4)	1.9
C(23)	0.6914(5)	0.9582(7)	0.6141(5)	2.0
C(24)	0.7703(5)	0.9306(6)	0.5844(4)	1.7
C(25)	0.5389(5)	0.8668(8)	0.6296(5)	2.4
C(26)	0.5742(5)	0.7517(7)	0.7030(4)	2.0
C(27)	0.8487(5)	0.2371(6)	0.9580(4)	1.7
C(28)	0.8495(4)	0.0820(6)	0.8252(4)	1.5
C(29)	0.6947(4)	0.1333(6)	0.8578(4)	1.7

Table 2. (Continued 2)

Molecule 2

Atom	x	y	z	B_{eq}/Å^2
Cr	0.19516(6)	0.72992(9)	0.66257(6)	1.03
O(1)	0.1166(5)	0.7408(5)	0.4653(3)	3.4
O(2)	0.0833(4)	0.4826(5)	0.6658(4)	2.7
O(3)	0.3482(4)	0.5395(6)	0.6519(4)	3.1
C(1)	0.0655(4)	1.1573(6)	0.7306(4)	1.7
C(2)	0.0403(4)	1.0195(7)	0.6792(4)	1.8
C(3)	0.1233(4)	0.9266(6)	0.6962(4)	1.4
C(4)	0.1405(4)	0.8317(6)	0.7656(4)	1.4
C(5)	0.2300(5)	0.7857(7)	0.8050(4)	1.8
C(6)	0.3040(4)	0.8340(6)	0.7743(4)	1.7
C(7)	0.2848(4)	0.9061(6)	0.6938(4)	1.7
C(8)	0.1958(4)	0.9506(6)	0.6549(4)	1.4
C(9)	0.4003(5)	0.8274(8)	0.8342(5)	2.8
C(10)	0.4122(4)	0.9481(7)	0.9016(4)	2.0
C(11)	0.3333(4)	1.0491(6)	0.8796(4)	1.5
C(12)	0.3258(4)	1.1537(6)	0.8174(4)	1.6
C(13)	0.2374(4)	1.1934(6)	0.7714(4)	1.4
C(14)	0.1582(4)	1.1517(6)	0.7965(4)	1.4
C(15)	0.1732(4)	1.0924(6)	0.8818(4)	1.5
C(16)	0.2576(4)	1.0326(6)	0.9154(4)	1.5
C(17)	0.1069(4)	1.1127(7)	0.9397(4)	1.8
C(18)	0.1129(5)	1.2578(7)	0.9788(4)	2.0
C(19)	0.2042(5)	1.3261(7)	0.9794(4)	1.8
C(20)	0.2863(5)	1.2747(7)	1.0339(4)	2.1
C(21)	0.3687(5)	1.2949(7)	1.0106(4)	2.2
C(22)	0.3721(5)	1.3643(7)	0.9342(4)	2.0
C(23)	0.2933(5)	1.4399(7)	0.8904(5)	2.1
C(24)	0.2095(4)	1.4209(7)	0.9141(4)	1.9
C(25)	0.4450(5)	1.3328(7)	0.8862(5)	2.3
C(26)	0.4074(4)	1.2339(7)	0.8063(5)	1.9
C(27)	0.1478(5)	0.7359(7)	0.5418(5)	2.2
C(28)	0.1260(4)	0.5793(6)	0.6669(4)	1.5
C(29)	0.2888(4)	0.6142(7)	0.6537(4)	1.8

used at the final stage of the refinement were: a=0.0767 and b=0.0005 for the monoclinic form and a=0.2271 and b=0.0032 for the triclinic form. The final atomic parameters of both forms are listed in Table 2.††††

The atomic scattering factors for the Cr, O, and C atoms were taken from the International Tables for X-Ray Crystallography, Vol. IV,[8] and those for H atom, from Stewart, Davidson, and Simpson.[9] Calculations were done on an ACOS 900 computer (Computation Center) and, at the final stage, on an ACOS 850 computer, (Crystallographic Research Center, Institute for Protein Research), Osaka University.

††††Tables of the anisotropic temperature factors, the coordinates of the hydrogen atoms, and the observed and calculated structure factors are kept at the Chemical Society of Japan, Document No. 8735.

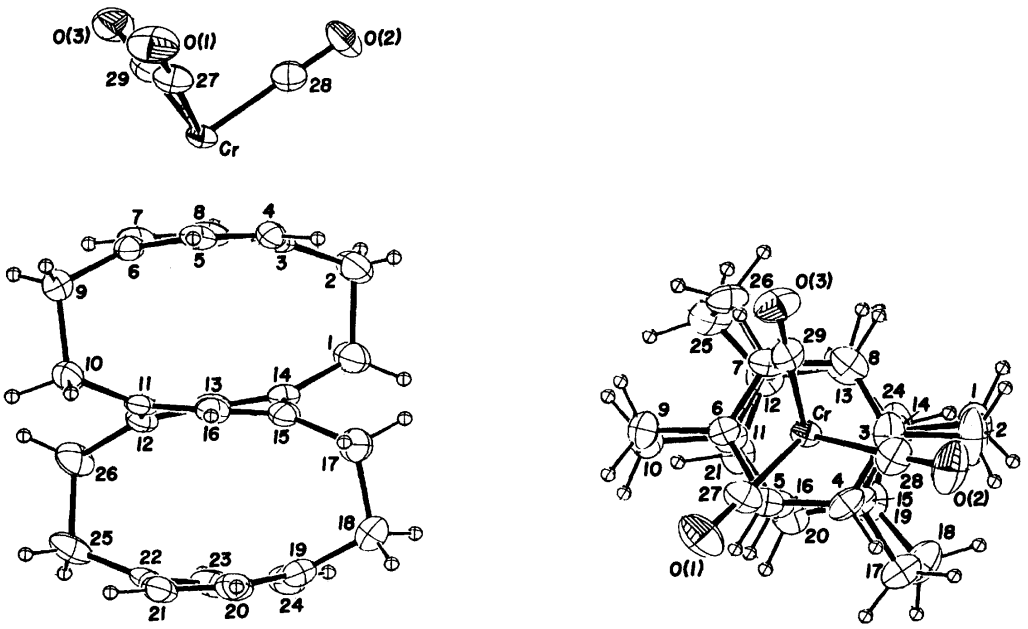

Fig. 1. A perspective view[10] of the molecule, together with the numbering scheme of the nonhydrogen atoms. Nonhydrogen atoms are drawn as thermal ellipsoids with 30% probability level, and the hydrogen atoms as spheres with B=1.0Å^2. a) Projected down from the C(16) to C(13) atoms in the middle layer benzene ring, b) projected onto the base plane of the upper layer benzene.

Table 3. Interatomic Bond Distances and Angles in Tricarbonyl(triple-layered [2.2]paracyclophane)-chromium, together, with the Estimated Standard Deviations in Parentheses

Bond distance/Å

	Monoclinic form (−95 °C)	Triclinic form (−160 °C)	
		Molecule 1	Molecule 2
Cr -C(27)	1.839(5)	1.847(6)	1.846(7)
Cr -C(28)	1.841(5)	1.846(6)	1.839(6)
Cr -C(29)	1.832(4)	1.824(6)	1.839(6)
O(1) -C(27)	1.159(7)	1.159(8)	1.172(9)
O(2) -C(28)	1.158(6)	1.151(7)	1.157(7)
O(3) -C(29)	1.160(6)	1.179(8)	1.161(8)
C(1) -C(2)	1.586(8)	1.576(9)	1.593(9)
C(1) -C(14)	1.521(6)	1.529(8)	1.513(8)
C(2) -C(3)	1.509(7)	1.531(8)	1.511(8)
C(3) -C(4)	1.413(6)	1.399(8)	1.403(8)
C(3) -C(8)	1.415(7)	1.415(8)	1.420(8)
C(4) -C(5)	1.385(6)	1.410(9)	1.401(8)
C(5) -C(6)	1.421(6)	1.402(9)	1.405(9)
C(6) -C(7)	1.405(6)	1.413(8)	1.406(8)
C(6) -C(9)	1.502(6)	1.506(10)	1.516(9)
C(7) -C(8)	1.388(7)	1.415(8)	1.389(8)
C(9) -C(10)	1.591(7)	1.587(9)	1.585(10)
C(10)-C(11)	1.516(6)	1.525(8)	1.514(9)
C(11)-C(12)	1.417(6)	1.406(8)	1.400(8)
C(11)-C(16)	1.397(6)	1.404(8)	1.400(8)
C(12)-C(13)	1.386(6)	1.397(8)	1.394(8)
C(12)-C(26)	1.520(7)	1.499(9)	1.514(9)
C(13)-C(14)	1.405(6)	1.403(8)	1.409(8)
C(14)-C(15)	1.408(6)	1.400(8)	1.418(8)
C(15)-C(16)	1.395(6)	1.407(8)	1.373(8)
C(15)-C(17)	1.525(7)	1.529(9)	1.519(9)
C(17)-C(18)	1.580(8)	1.583(9)	1.563(9)
C(18)-C(19)	1.518(7)	1.514(9)	1.536(9)
C(19)-C(20)	1.396(7)	1.397(9)	1.399(9)
C(19)-C(24)	1.393(7)	1.411(9)	1.400(9)
C(20)-C(21)	1.387(7)	1.395(9)	1.394(9)
C(21)-C(22)	1.411(7)	1.393(9)	1.386(9)
C(22)-C(23)	1.387(7)	1.400(9)	1.414(9)
C(22)-C(25)	1.520(7)	1.523(9)	1.509(9)
C(23)-C(24)	1.374(7)	1.403(9)	1.414(9)
C(25)-C(26)	1.579(8)	1.600(10)	1.590(9)

Table 3. (Continued)

Bond distance/Å			
Cr -C(3)	2.329(5)	2.330(5)	2.347(6)
Cr -C(4)	2.205(5)	2.219(6)	2.232(6)
Cr -C(5)	2.191(5)	2.234(7)	2.236(6)
Cr -C(6)	2.347(4)	2.335(6)	2.333(6)
Cr -C(7)	2.245(5)	2.223(6)	2.201(6)
Cr -C(8)	2.228(5)	2.183(6)	2.190(6)
Bond angle/°			
C(27)-Cr -C(28)	92.8(3)	89.6(3)	88.6(3)
C(27)-Cr -C(29)	88.8(3)	93.5(3)	92.3(3)
C(28)-Cr -C(29)	87.7(3)	88.1(3)	87.1(3)
Cr -C(27)-O(1)	177.7(5)	177.5(6)	179.0(7)
Cr -C(28)-O(2)	177.4(5)	179.0(6)	176.7(6)
Cr -C(29)-O(3)	178.3(4)	176.5(6)	177.0(6)
C(2) -C(1) -C(14)	111.7(4)	113.9(5)	112.9(5)
C(1) -C(2) -C(3)	110.1(4)	109.9(5)	110.4(5)
C(2) -C(3) -C(4)	120.1(5)	120.5(6)	121.1(6)
C(2) -C(3) -C(8)	121.0(5)	120.4(5)	120.8(5)
C(4) -C(3) -C(8)	118.1(5)	117.6(6)	116.9(6)
C(3) -C(4) -C(5)	120.2(5)	121.0(6)	121.1(6)
C(4) -C(5) -C(6)	120.8(4)	119.6(6)	119.8(6)
C(5) -C(6) -C(7)	117.2(4)	119.4(6)	118.5(6)
C(5) -C(6) -C(9)	120.5(4)	120.8(6)	119.6(6)
C(7) -C(6) -C(9)	120.9(4)	119.0(6)	121.2(6)
C(6) -C(9) -C(10)	110.7(4)	109.2(6)	108.9(6)
C(9) -C(10)-C(11)	112.7(4)	112.3(6)	113.1(6)
C(10)-C(11)-C(16)	121.0(4)	118.9(6)	120.0(6)
C(12)-C(11)-C(16)	116.2(4)	117.2(6)	115.8(6)
C(11)-C(12)-C(13)	116.4(4)	116.4(6)	117.1(6)
C(11)-C(12)-C(26)	123.0(4)	123.2(6)	122.9(5)
C(13)-C(12)-C(26)	119.8(4)	120.2(6)	119.6(6)
C(12)-C(13)-C(14)	123.4(5)	123.2(6)	122.6(6)
C(1) -C(14)-C(13)	119.5(4)	120.8(5)	120.2(6)
C(1) -C(14)-C(15)	124.0(4)	123.0(6)	123.5(6)
C(14)-C(15)-C(16)	116.7(4)	116.9(6)	116.3(6)
C(14)-C(15)-C(17)	123.3(4)	122.9(6)	122.5(6)
C(16)-C(15)-C(17)	119.7(4)	119.7(6)	120.5(6)
C(11)-C(16)-C(15)	123.2(5)	121.9(6)	124.2(6)
C(15)-C(17)-C(18)	112.6(5)	110.8(6)	111.9(6)
C(17)-C(18)-C(19)	111.6(5)	112.4(6)	112.5(6)
C(18)-C(19)-C(20)	121.3(5)	121.8(6)	119.8(6)
C(18)-C(19)-C(24)	120.6(5)	119.5(6)	120.6(6)
C(20)-C(19)-C(24)	116.4(5)	117.3(6)	118.3(6)
C(19)-C(20)-C(21)	120.9(5)	120.4(6)	119.6(6)
C(20)-C(21)-C(22)	120.4(5)	121.4(6)	121.8(6)
C(21)-C(22)-C(23)	116.7(5)	117.1(6)	117.6(6)
C(21)-C(22)-C(25)	119.2(5)	120.2(6)	121.3(6)
C(23)-C(22)-C(25)	122.5(5)	120.7(6)	119.2(6)
C(22)-C(23)-C(24)	121.1(5)	120.7(6)	119.6(6)
C(19)-C(24)-C(23)	121.5(5)	120.2(6)	120.2(6)
C(22)-C(25)-C(26)	112.7(5)	112.4(6)	111.1(6)
C(12)-C(26)-C(25)	111.2(5)	111.9(6)	112.6(6)

Results and Discussion

Molecular Structure. A perspective view (*ORTEP* drawing[10]) of the TC3PC molecule of the monoclinic form is shown in Fig. 1, along with the numbering scheme of the atoms. The interatomic bond distances and angles in the monoclinic-form and triclinic-form molecules are given in Table 3. Other important structural parameters of the cyclophane skeleton in the three TC3PC molecules are compared in Table 4 with those of BR3PC and TCPC. No essential difference is found between the structures of the one monoclinic-form molecule and the two triclinic-form molecules. Therefore, the discussion hereafter will be done on the molecular structure of the monoclinic form unless otherwise stated.

Some remarkable features of the triple-layered [2.2]paracyclophane moiety are observed. Both the upper- and lower-layer benzene rings take the boat form. This fact is commonly observed for the outermost benzene rings of multiple-layered [2.2]paracyclophanes. The upper-layer benzene ring in the present complex is less deformed from the plane than that of the lower layer benzene ($p+q<p'+q'$ in Table 4). On the other hand, the second layer benzene ring is twisted along the line passing through the C(13) and C(16) atoms, which are not linked by $-CH_2-CH_2-$ bridges; the twist angle is 13.4°, which is equal to that [13.4°] in tetramethyl quadruple-layered [2.2]paracyclophane.[11]

Table 4. Mean Molecular Structures of TC3PC and Related Compounds

	TC3PC			BR3PC[4]	TCPC[1]
	Monoclinic form (−95°C)	Triclinic form (−160°C)			
		Molecule 1	Molecule 2		
Upper-layer benzene ring					
p/°	11.0	11.3	11.4	12.1	12.2
q/°	10.3	10.5	9.7	11.4	8.9
s/°	117.7	118.5	117.7	117.2	118.3
-CH_2-CH_2- bridge between upper- and middle-layer benzene rings					
g/Å	1.506	1.519	1.514	1.513	1.510
h/Å	1.589	1.582	1.589	1.580	1.595
j/Å	1.519	1.527	1.514	1.515	
r/°	110.4	109.6	109.7	112.4	110.9
t/°	112.2	113.1	113.0	112.0	112.8
ϕ/°	11.5	17.4	10.4	15.1	3.8
Middle-layer benzene ring					
δ/°	13.4	13.6	13.5	13.6	
-CH_2-CH_2- bridge between middle- and lower-layer benzene rings					
g'/Å	1.519	1.519	1.523		1.519
h'/Å	1.580	1.592	1.577		
j'/Å	1.523	1.514	1.517		
r'/°	112.2	112.4	111.8		
t'/°	111.9	111.4	112.3		
ϕ'/°	21.9	21.4	21.7		
Lower-layer benzene ring					
p'/°	11.8	11.8	11.9		11.4
q'/°	12.5	12.8	9.5		11.2
s'/°	116.6	117.2	118.0		116.9
Interring distances between upper and middle (d_1) and between middle and lower benzenes (d_2)					
d_1/Å	2.979	3.004	2.989	3.046	
d_2/Å	3.057	3.053	3.049	3.046	

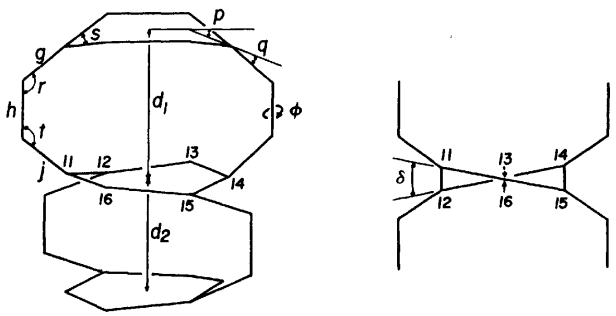

The C-C distances of the -CH_2-CH_2- bridges are 1.591(7) and 1.586(8) Å (from the upper layer to the middle) and 1.579(8) and 1.580(8) Å (from the middle layer to the lower), values which are comparable to those of TCPC [1.591(7) and 1.599(8) Å] and much longer than the usual C-C single bond. The torsional angles around the -CH_2-CH_2- bond between the upper and middle layers [13.2 and 9.7°] are much smaller than those between the middle and lower layers [20.1 and 23.6°]. As may be seen in Fig. 1(b), the three benzene rings are not in the eclipsed position; they are mutually rotated slightly in a helical way, similar to those in BR3PC and inner triple-layered paracyclophanequinone.[12]

The $Cr(CO)_3$ group in tricarbonyl(benzene)chromium (TCB)[13] takes the staggered configuration to the benzene ring because of the crystallographic mirror symmetry of the molecule, each of the three Cr-C≡O branches projected is perpendicular to the C-C bond of the benzene ring. The C-C bond distances in the benzene ring show a bond alternation. The $Cr(CO)_3$ in TCPC shows a slight deviation from the staggered position. The mean angular deviation (θ_{av}) of a Cr-C≡O branch from the staggered configuration is 3.6° in TCPC, while the remainder of the bond alternation can be seen in the upper-layer benzene ring. In the present complex, the relative positions of the $Cr(CO)_3$ group projected onto the upper-layer benzene

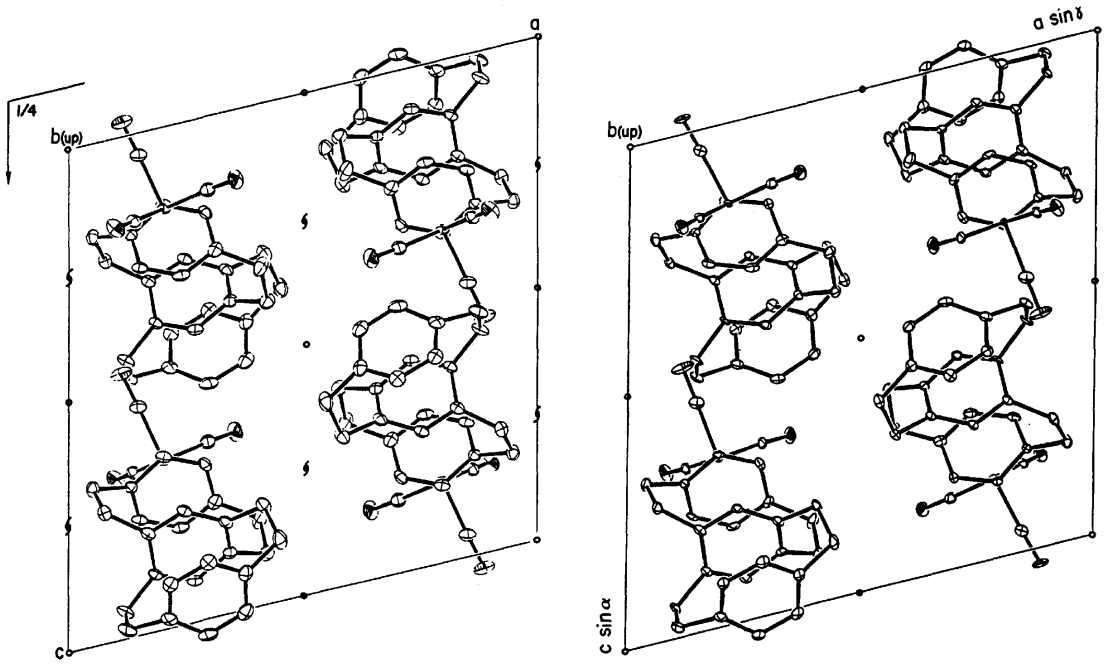

Fig. 2. Crystal structure projected along the b axis.[10] a) Monoclinic form, b) Triclinic form.

ring in the monoclinic- (θ_{av}: 15.6°) and triclinic-form (θ_{av}: 18.9 and 18.4°) molecules are in between the staggered and eclipsed configurations. No bond alternation is observed in the upper-layer benzene rings in these complexes.

The interlayer distances from the base planes of the boat-shaped upper- and lower-layer benzene rings to the least-squares plane of middle-layer twisted benzene are compared with those in BR3PC in Table 4. In TC3PC, the d_1 distance between the upper- and middle-layer benzene rings is significantly shorter than the d_2 distance between the middle- and lower-layer benzenes. The d_2 distances are essentially equal to that in BR3PC. The shortening of the d_1 compared with d_2 results from the strong electron-withdrawing effect of the $Cr(CO)_3$ group coordinated to the upper-layer benzene. However, the electronic effect of the $Cr(CO)_3$ group may not account for the shortening of d_2. The shortening of the interlayer distance by the coordination of the $Cr(CO)_3$ group to the benzene has also been found in the crystal structure of TCPC.

Crystal Structure. The packing of the molecules in the monoclinic- and triclinic-form crystals are shown in Fig. 2. The corresponding space group of the crystal changed from $P2_1/c$ to $P\bar{1}$ upon cooling. A slight difference is observed between the crystals of the two forms in their unit-cell dimensions (0.38% in a, 0.37% in b, and 0.13% in c; Table 1). Intermolecular contacts shorter than 3.5 Å were found between an oxygen atom of the $Cr(CO)_3$ moiety and a carbon atom of the upper-layer benzene ring or that of a $-CH_2-CH_2-$ bridge; in a monoclinic crystal: C(7)(x, y, z)···O(1)(x, 0.5−y, −0.5+z)=3.416(6) Å, in a triclinic crystal: C(1^{ii})(x, y, z)···O(2^{ii})(x, 1+y, z)=3.404(8) Å, C(4^{i})(x, y, z)···O(1^{ii})-($1-x$, $1-y$, $1-z$)=3.420(9) Å, and C(2^{i})(x, y, z)···O(2^{ii})($1+x$, y, z)=3.383(8) Å, where the superscripts i and ii show the two independent molecules.

The authors wish to express their deep thanks to Professor Soichi Misumi and his coworkers of the Institute of Scientific and Industrial Research, Osaka University, for supplying the crystals and for their helpful discussions.

References

1) Y. Kai, N. Yasuoka, and N. Kasai, *Acta Crystallogr., Sect. B*, **34**, 2840 (1978).

2) H. Hope, J. Bernstein, and K. N. Trueblood, *Acta Crystallogr., Sect. B*, **28**, 1733 (1972).

3) Y. Kai, H. Goto, N. Yasuoka, and N. Kasai, *Acta Crystallogr., Sect. A*, **34**, S292 (1978).

4) Y. Koizumi, T. Toyoda, K. Miki, N. Kasai, and S. Misumi, *Bull. Chem. Soc. Jpn.*, **59**, 239 (1986).

5) P. Main, S. E. Hull, L. Lessinger, G. Germain, J.-P. Declercq, and M. M. Woolfson, *MULTAN* 78, "A System of Computer Programs for the Automatic Solution of Crystal Structures from X-Ray Diffraction Data," Univ. of York, England, 1978.

6) T. Ashida, *HBLS* V, "The Universal Crystallographic Computing System-Osaka," The Computation Center, Osaka Univ., 1973, pp. 55—61.

7) W. C. Hamilton, *Acta Crystallogr.*, **12**, 609 (1959).

8) International Tables for X-Ray Crystallography, Vol. IV, Kynoch Press, Birmingham (1974), p. 71.

9) R. F. Stewart, E. R. Davidson, and W. T. Simpson, *J. Chem. Phys.*, **42**, 3175 (1965).

10) C. K. Johnson, *ORTEP* II, Report ORNL-5138, Oak Ridge National Laboratory, Tennessee (1976).

11) H. Mizuno, K. Nishiguchi, T. Toyoda, T. Otsubo, S. Misumi, and N. Morimoto, *Acta Crystallogr., Sect. B*, **33**, 329 (1977).
12) T. Toyoda, H. Tatemitsu, Y. Sakata, N. Kasai, and S. Misumi, *Bull. Chem. Soc. Jpn.*, **59**, 3994 (1986).
13) B. Ree and P. Coppens, *Acta Crystallogr., Sect. B*, **29**, 2515 (1973).

Stabilization of Platinum-Loaded CdS Photocatalyst by Addition of EDTA

Michio MATSUMURA,* Hideyuki OHNISHI, Koji HANAFUSA, and Hiroshi TSUBOMURA
Laboratory for Chemical Conversion of Solar Energy and Department of Chemistry, Faculty of Engineering Science, Osaka University, Toyonaka, Osaka 560
(Received December 6, 1986)

The photocatalytic activity of platinum-loaded CdS powder in sulfite solutions declined by illumination over 200 h, and became half the initial activity at 600 h. By addition of small amount (2 mM) of ethylenediaminetetraacetic acid (EDTA) to the solution, however, the photocatalyst was guarded from deterioration. The effect of EDTA is to prevent the platinum part of photocatalyst from the impurity metal deposition by forming stable metal-EDTA complexes in the solution. The reactivities of sulfite ions, EDTA, and metal-EDTA complexes on illuminated CdS are examined electrochemically by use of CdS-sinter electrodes.

A variety of photocatalytic reactions are induced by semiconductor particles. Hydrogen and many organic compounds are produced from aqueous solutions of organic materials, such as alcohols, aromatic hydrocarbons, etc., over the illuminated semiconductor particles loaded with noble metals.[1,2] Hydrogen production occurs also from aqueous solutions of inorganic materials, such as sulfide ions.[3,4] Efficient hydrogen production from aqueous solutions of sulfite was reported by use of noblel metal loaded CdS powder,[5-8] the sulfite ions being oxidized to sulfate and dithionate ions. This photocatalytic reaction is interesting from the viewpoint of industrial waste disposal.

The platinum-loaded CdS photocatalyst used for the hydrogen production from sulfite solutions was stable for 65 h in our previous experiment.[5] Ciba-Geigy group reported that the photocatalyst was deactivated after 6 d.[7] In this paper, the durability of the photocatalyst and its stabilization by addition of EDTA to the solution is reported.

Experimental

Photocatalytic Reaction. CdS powder of 99.999% purity purchased from Furuuchi Chemical Co., Inc. was used after heat treatment at 700 °C for 2 h under a nitrogen stream. The particle size after the heat treatment was ca. 2 μm. For the platinum loading, the CdS powder was shaken with platinum powder (Japan-Engelhard) in a glass vessel for 1 h. Aqueous solutions were prepared by use of deionized water having resistivities higher than 3.3 MΩ cm. The pH was adjusted at 8.4 by addition of boric acid (0.3 M, 1 M=1 mol dm^{-3}) and sodium hydroxide. All chemicals used were of reagent grade.

In a 100-ml glass flask, 0.5 g photocatalyst was suspended in a 50 ml sodium sulfite solution. The suspension was illuminated with a 500-W high-pressure mercury lamp, after it was deaerated by bubbling with high purity nitrogen gas for 15 min. The evolved hydrogen gas was introduced into a measuring cylinder.

Electrochemical Measurements. The CdS sintered disks for use as electrodes were prepared from CdS powder by use of a hot press under pressure of 1×10^7 Pa at 750 °C for 6 h in a nitrogen atmosphere. Electrochemical measurements were performed in a three-electrode cell with a sintered CdS electrode, a platinum counterelectrode, and an Ag/AgCl reference electrode under potentiostatic and galvanostatic conditions. A tungsten-halogen lamp was used as the light source for the photoelectrochemical measurements.

Results

The photocatalytic hydrogen evolution from sulfite solutions proceeded in our experimental conditions at the initial rate of ca. 2.7×10^{-3} mol h^{-1}. It declined to nearly zero after 50 h as shown in Fig. 1, as the sulfite ions were consumed, and the pH shifted to ca. 13. The decline of the hydrogen evolution rate was also due to the shift of pH, because the hydrogen evolution is inefficient in alkaline solutions.[5] The rate of hydrogen evolution recovered to the initial value by renewing the solution as shown by an arrow in Fig. 1.

The long-term stability of the photocatalyst was tested, renewing the solution at every 45 h. The rate of hydrogen evolution measured at 4 h after each of the renewal of the solution is shown by a solid line in Fig. 2. The rate of hydrogen evolution began to decline at ca. 200 h, and dropped to half the initial value at 600 h. However, the activity of the photocatalyst after illumination for 650 h recovered to 95% of the initial value by washing it in 0.4 M HCl for 30 min.

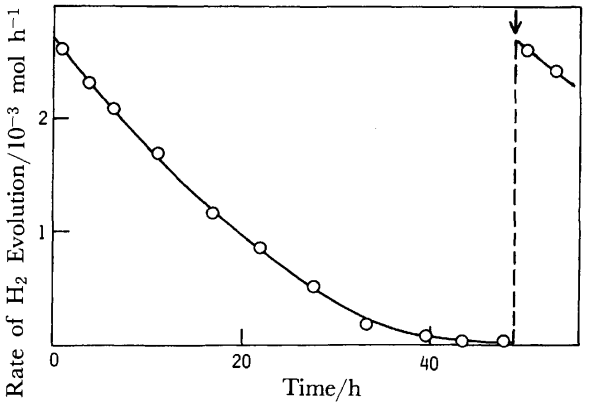

Fig. 1. Time-course of the rate of hydrogen evolution for the solution of 1 M sodium sulfite buffered at pH 8.4; the solution was renewed at the arrow.

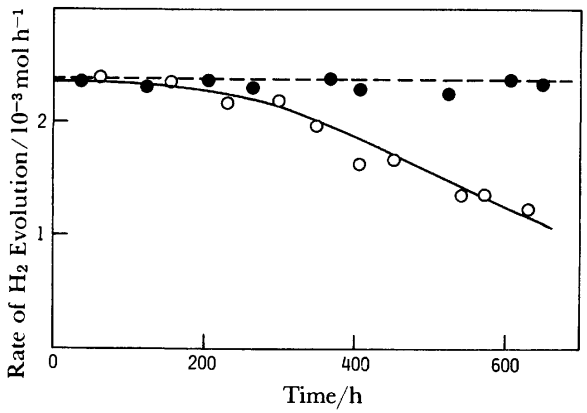

Fig. 2. Time-course of the rate of hydrogen evolution for the solutions of 1 M sodium sulfite buffered at pH 8.4 without EDTA, solid line, and with 5 mM EDTA, broken line.

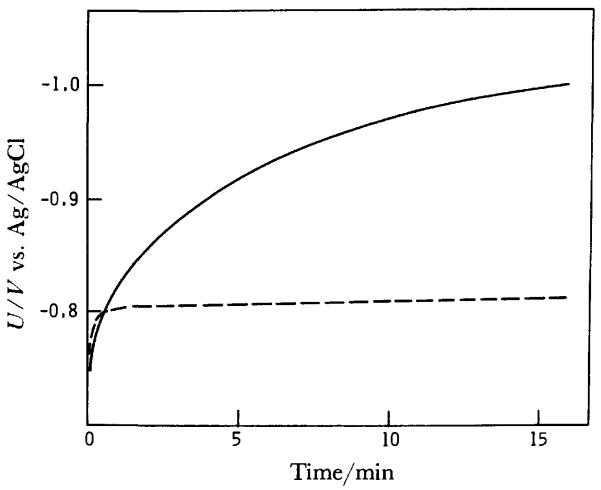

Fig. 3. Time-course of the potential of a platinum electrode observed under galvanostatic conditions at the current density of $-0.5\,mA\,cm^{-2}$ in the solutions of 0.5 M sodium sulfite buffered at pH 8.4 without EDTA, solid line, and with 5 mM EDTA, broken line.

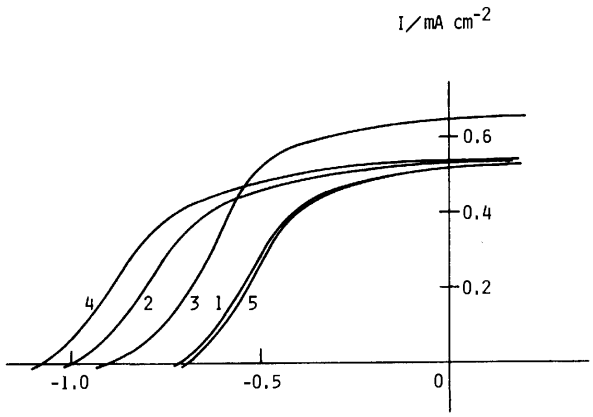

Fig. 4. *I-U* curve of a CdS sinter electrode measured under illumination with a tungsten-halogen lamp in 0.5 M sodium sulfate (curve 1), and those obtained by the addition of 0.1 sodium sulfite (curve 2), 0.1 M EDTA (curve 3), 0.1 M sodium sulfite and 0.1 M EDTA (curve 4), and 0.1 M cadmium chloride and 0.1 M EDTA (curve 5); the pH of the solutions is adjusted to 8.4.

When a small amount of ethylenediaminetetraacetic acid (EDTA, 5 mM) was added to the sulfite solution, the photocatalyst showed no decay of the activity even after illumination over 650 h, as shown by a broken line in Fig. 2. The amounts of hydrogen evolved during 650 h illumination from the solutions with and without EDTA were 13.6 and 10.7 l, respectively. Platinum-loaded CdS powder has been reported to photocatalyze hydrogen evolution from the aqueous solution of EDTA.[9] However, the rate of hydrogen evolution was negligibly small from the solution of 5 mM EDTA without sulfite. Therefore, the oxidation of EDTA at the illuminated CdS surface is excluded from the reasons of the stabilization of the photocatalyst and the increase of the amount of evolved hydrogen. By addition of 2 mM EDTA to the sulfite solution, practically the same stability of the photocatalyst was obtained as the case of 5 mM EDTA. The lower limit of the concentration of EDTA needed to stabilize the photocatalyst has not been determined.

In order to clarify the reason for the enhancement of the durability of the photocatalyst by the addition of EDTA and the deactivation of the photocatalyst in the absence of EDTA, we measured the potential of a hydrogen-evolving platinum electrode under galvanostatic conditions in 1 M sodium sulfite with and without EDTA. In the solution without EDTA, the potential of the platinum electrode shifted to negative rapidly as shown by a solid line in Fig. 3. This suggests that the catalytic activity of the platinum electrode for the hydrogen evolution decays with time. The shift of the potential of the platinum electrode was retarded drastically by addition of EDTA as shown by a broken line.

In Fig. 4 are shown the *I-U* curves of the illuminated CdS electrode in various solutions. The photocurrent in a sodium sulfate solution (curve 1) is caused by the dissolution of the CdS electrode. By addition of sulfite ions (curve 2) or EDTA (curve 3), the photocurrents now start at -1.0 and -0.91 V, respectively, which are caused by the oxidation of these species by the photogenerated positive holes in CdS. The higher reactivity of sulfite ions than that of EDTA is suggested by comparing curves 2 and 3. The increase of the saturated photocurrent density by the addition of EDTA (curve 3) is attributed to the "current doubling effect"[10] arising from the oxidation of EDTA. The disappearance of the "current doubling effect" in the presence of both EDTA and sulfite ions (curve 4) suggests that the sulfite ions are solely oxidized on the illuminated CdS electrode due to their higher reactivity than that of EDTA. The negative shift of the onset

potential of the photocurrent by the addition of EDTA to the sulfite solution (compare curves 2 and 4) is probably due to the shift of the flat band potential of the CdS electrode caused by the chemisorption of EDTA on the surface of CdS.[11] In the solution containing both EDTA and heavy metal ions, such as cadmium ions, at the same concentrations (0.1 M), the *I-U* curve nearly coincided with that measured in sodium sulfate solution (curves 1 and 5). This suggests that the heavy metal ions present in the solution are complexed with EDTA and that the complexes have very low reactivities with the positive holes photogenerated in CdS.

Discussion

The properties of the platinum-loaded CdS photocatalyst are well explained by assuming that each photocatalyst particle works as a photoelectrochemical cell having a CdS electrode and a platinum electrode.[12] Then, the deposition of metals on the platinum from impurity metal ions existing in the solution is likely to occur electrochemically in competition with the hydrogen evolution. Therefore, the deactivation of the photocatalyst by illumination in the absence of EDTA is attributable to the deposition of impurity metals on a platinum part of the photocatalyst. The recovery of the photocatalytic activity by the washing treatment of the deactivated photocatalyst in hydrochloric acid suggests the removal of metals deposited on platinum.

The metal ions which deteriorate the activity of the photocatalyst are supposed to come from water, sodium sulfite, or the photocatalyst itself. The shift of the potential of the hydrogen-evolving platinum electrode under galvanostatic conditions was accelerated by addition of CdS powder to the solution. This suggests that not only the impurities in the solution but also impurities, probably cadmium ion, from the surface of CdS powder also deactivate the photocatalyst.

It is plausible to conclude that EDTA forms stable complexes with metal ions, prevents them from depositing on the platinum, and raises the durability of the photocatalyst. The electrochemical activity of EDTA itself with positive holes photogenerated in CdS is lowered by the formation of metal complexes as shown by curve 5 in Fig. 4. This gives a good reason why the effect of EDTA is sustained for the solutions containing EDTA at low concentrations. The low reactivity of the metal-EDTA complexes is presumably due to the stabilization of the lone-electron pair of nitrogen atoms in EDTA by formation of coordination bonds with the metal ions.

On the basis of these properties of EDTA and metal-EDTA complexes, it is expected that the stability of many photocatalysts other than platinized CdS, e.g., TiO_2, ZnO, etc., and also the hydrogen-evolving electrodes of photoelectrochemical cells can be improved by addition of small amounts of EDTA or other chelating agents to the solutions. The present results for the effect of EDTA on the platinum-loaded CdS photocatalyst are, aside from aforementioned practical significances, interesting from the viewpoint of the elucidation of the working mechanism of the photocatalysts.

References

1) T. Sakata and T. Kawai, "Energy Resources through Photochemistry and Catalysis," ed by M. Grätzel, Academic Press, New York (1983), Chap. 10.

2) M. A. Fox, *Acc. Chem. Res.*, **16**, 314 (1983).

3) E. Borgarello, K. Kalyanasundaram, M. Grätzel, and E. Pelizzetti, *Helv. Chim. Acta*, **65**, 243 (1982).

4) D. H. M. W. Thewissen, A. H. A. Tinnemans, M. Eeuwhorst-Reinten, K. Timmer, and A. Mackor, *Nouv. J. Chim.*, **7**, 191 (1983).

5) M. Matsumura, Y. Saho, and H. Tsubomura, *J. Phys. Chem.*, **87**, 3807 (1983).

6) M. Matsumura, S. Furukawa, Y. Saho, and H. Tsubomura, *J. Phys. Chem.*, **89**, 1327 (1985).

7) N. Bühler, K. Meier, and J.-F. Reber, *J. Phys. Chem.*, **88**, 3261 (1984).

8) J.-F. Reber and M. Rusek, *J. Phys. Chem.*, **90**, 824 (1986).

9) J. R. Darwent, *J. Chem. Soc., Faraday Trans. 2*, **77**, 1703 (1981).

10) S. R. Morrison, "Electrochemisty at Semiconductor and Oxidized Metal Electrodes," Plenum Press, New York (1981), Chap. 6.

11) The flat band potential of a CdS electrode determined by Mott-Schottky plots was shift ca. 0.2 V to negative by addition of EDTA; the details will be reported.

12) M. Matsumura, M. Hiramoto, T. Iehara, and H. Tsubomura, *J. Phys. Chem.*, **88**, 248 (1984).

 © 1987 The Chemical Society of Japan Bull. Chem. Soc. Jpn., 60, 2005—2010 (1987)

Characteristic Polynomial Expression and Integral Expression for Imaginary Bond-Bond Polarizability. Rules for London Susceptibility and for Ring Current

Noriyuki MIZOGUCHI
Department of Physics, Meiji College of Pharmacy, Nozawa, Setagaya-ku, Tokyo 154
(Received December 12, 1986)

The McWeeny theory for calculating magnetic properties of conjugated hydrocarbons is studied from a graph-theoretical point of view. Imaginary bond-bond polarizability is expressed in terms of characteristic polynomial. The expression clarifies the dependence of imaginary bond-bond polarizability on the structure. It is shown that the expression enables one easily to derive the equations for the quantity proved in two previous papers. The characteristic polynomial expression for imaginary bond-bond polarizability is rewritten in Coulson's integral form. The rules for London susceptibility and for ring current are proved from the integral expression.

The application of the graph theory[1] in the Hückel molecular orbital (HMO) theory enabled one mathematically to prove statements valid for a large class of unsaturated conjugated systems which clarify that there are close relationships between the chemical properties of a conjugated hydrocarbon and the topologies.[2] One of the most significant achievements is the proof of the Hückel rule, which states that cyclic conjugation of the π-electron system causes drastically different effects on the thermodynamic stability, depending on the size of the circuit.[3]

The HMO method with London's approximations[4] for calculating magnetic properties of conjugated hydrocarbons was established in differents forms by Pople[5] and by McWeeny.[6] Pople calculated ring currents from a knowledge of the field-dependent secular determinant (characteristic polynomial) while McWeeny used the usual perturbation method and expressed the magnetic susceptibility due to π-electrons (London susceptibility) in terms of imaginary bond-bond polarizability.

Although Pople did not give an explicit expression for London susceptibility (and ring current), some time ago Aihara[7] was able to express London susceptibility in terms of a characteristic polynomial and showed that the London susceptibility of a polycyclic conjugated molecule can be given as a sum of the circuit susceptibilities over all the circuits found in the system. By using Coulson's integral method[8] the present author proved a rule for London susceptibility valid for any alternant polycyclic conjugated system which states that the sign of the circuit susceptibility for a circuit in the system is determined by the number of carbon atoms in the circuit.[9] This rule has very similar aspects to Hückel rule for thermodynamical stability.[10]

The McWeeny method has been widely applied to conjugated systems by a large number of authors.[11] However the properties of imaginary bond-bond polarizability had not been studied. Recently the present author clarified the dependence of imaginary bond-bond polarizability on the mode of branching[12] and the role of "acyclic" bond in the magnetic properties of conjugated molecules.[13] Although the McWeeny theory has also been pointed out to have some topological aspects associated with a spanning tree,[6,14] the close relationship between London susceptibility and the circuit found in the Pople-Aihara theory is not known in the McWeeny theory.

The purpose of this paper is to clarify the dependence of magnetic properties on the circuit in the McWeeny method.[15] In the first part of the present paper 1) imaginary bond-bond polarizability will be expressed in terms of a characteristic polynomial and 2) it will be shown that the characterist polynomial expression for imaginary bond-bond polarizability enables one to derive easily the equations proved in two previous papers. In the second part 3) imaginary bond-bond polarizability will be represented in Coulson's integral form and the rules for London susceptibility and for ring current will be proved.

Characteristic Polynomial Expression for Imaginary Bond-Bond Polarizability

In McWeeny's perturbation approach, the partial London susceptibility for the J-th MO, χ_J, of a polycyclic conjugated system is given by[6]

$$\chi_J = 2\beta(e/\hbar c)^2\Big(\sum_{(rs)} P_{J,rs}S_{rs}^2 + \sum_{(rs)}\sum_{(tu)} \beta\pi_{J,(rs)(tu)}S_{rs}S_{tu}\Big), \quad (1)$$

where β is the field-free resonance integral, which is assumed to be equal for all the bonds in the molecule; e, $\hbar$, and c are the usual fundamental constants with these symbols; S_{rs} is the signed area of the triangle formed by an arbitrary origin and bond r-s; the sum $\sum_{(rs)}$ runs over all the bonds in the molecule; $P_{J,rs}$ is the partial Coulson bond order for the J-th MO;[8] $\bar{\pi}_{J,(rs)(tu)}$ is the partial imaginary bond-bond polarizability given by[6]

$$\bar{\pi}_{J,(rs)(tu)} = \sum_{K(\neq J)} \frac{(C_{rJ}C_{sK} - C_{sJ}C_{rK})(C_{tK}C_{uJ} - C_{uK}C_{tJ})}{(X_J - X_K)\beta}, \quad (2)$$

where X_J and C_{rJ} are the J-th eigenvalue (in units of β) and the eigenvector of the field-free Hückel Hamiltonian matrix, respectively.

In the later discussions attention should be paid to the order of the suffices in $\bar{\pi}_{J,(rs)(tu)}$ since

$$\bar{\pi}_{J,(rs)(tu)} = -\bar{\pi}_{J,(rs)(tu)} = -\bar{\pi}_{J,(rs)(tu)}. \tag{3}$$

The sign of χ_J is not dependent on the order of the suffices in the right-hand side of Eq. 1 because of Eq. 3 and $S_{sr}=-S_{rs}$.

Following Aihara,[7] in Pople's approach,[5] the London susceptibility of a polycyclic conjugated system is expressed in terms of a characteristic polynomial as follows:

$$\chi_J = \sum_j 2\beta(e/\hbar c)^2(P(G\ominus C_j; X_J)/P'(G; X_J))S(C_j)^2$$
$$= \sum_j \chi_J(C_j). \tag{4}$$

In Eq. 4 G is the graph representing the system; the sum runs over all the circuits found in G; $G\ominus C_j$ is a subgraph of G obtained by deleting circuit C_j and all the bonds incident to C_j from G; $P(G;X)$ and $P(G\ominus C_j;X)$ are the field-free characteristic polynomials of G and of $G\ominus C_j$, respectively; $P'(G;X)$ is the first derivative of $P(G;X)$ with respect to X; $S(C_j)$ is the area of C_j; $\chi_J(C_j)$ denotes the contribution of a circuit C_j to the London susceptibility of the system (circuit susceptibility).

For example, the London susceptibility of naphthalene is given by a sum of the circuit susceptibilities over three circuits C_1, C_2, and C_3 shown in Fig. 1. The circuit C_3 is produced by the fusion of two rings (fundamental circuits) R_1 and R_2 (see Fig. 1).

Equation 4 shows that the factor determining the magnetic properties of a polycylcic conjugated system is not the rings but the circuits. In other words, it shows that every circuit in the system acts as a driving force for the induction of ring current. The number of the modes of cyclic conjugation of the π-electrons is the number of the circuits found in the system. This aspect resembles Randić's "conjugated circuit" based on classical valence bond method.[16]

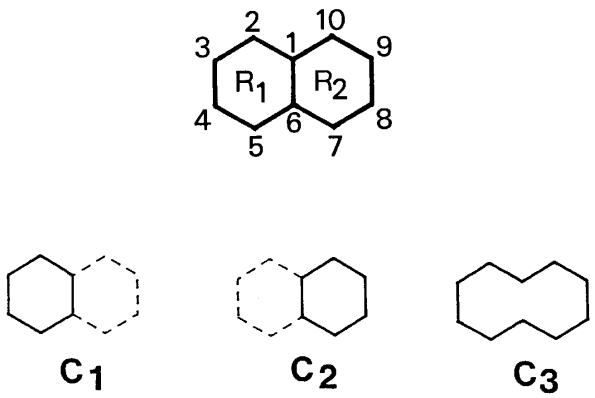

Fig. 1. Two rings and three circuits in naphthalene.

The expression for London susceptibility in McWeeny's theory, namely Eq. 1, is based on the concept "bond" while that in the Pople-Aihara theory, namely Eq. 4, is based on the concept "circuit." Since the two equations are obtained with the same approximations (London's approximations), they are equivalent mathematically.[17] Therefore comparison of the two equations will enable us to express imaginary bond-bond polarizability in terms of a characteristic polynomial. Before doing so, however it is necessary to express the London susceptibility in terms of the ring area $S(R_j)$ because the two equations are expressed in terms of the different area terms, that is, Eq. 1 is expressed in terms of triangle area S_{rs} while Eq. 4 is expressed in terms of the circuit area $S(C_j)$. Fortunately we have a unitary transformation devised by McWeeny,[6,14] which enables one to rewrite Eq. 1 in a form suitable for our purpose.

Due to McWeeny's unitary transformation we can obtain the transformed Hamiltonian matrix in which the elements for "circuit-completing" bonds for a chosen spanning tree[18] depend on an applied magnetic field but the other elements are independent of the field. From the transformed Hamiltonian matrix for a chosen spanning tree T we obtain in stead of Eq. 1 the following equation:

$$\chi_J = 2\beta(e/\hbar c)^2\Big(\sum_j (P_{J,(b_j)} + \beta\bar{\pi}_{J,(b_j)(b_j)})S(C_j)^2$$
$$+ 2\sum_j \sum_{k(>j)} (-1)^{\zeta}\beta\bar{\pi}_{J,(b_j)(b_j)}S(C_j)S(C_k)\Big). \tag{5}$$

In Eq. 5 C_j denotes a circuit completed by inserting a "circuit-completing" bond b_j for T; the sum is over all the "circuit-completing" bonds for T; ζ is a topological quantity defined as

$\zeta=0$ if the direction of the bond b_j in the circuit C_j is identical with that of the bond b_k in the circuit C_k,
$\zeta=1$ otherwise. (6)

It should be noted that the circuits appearing in Eq. 5 are only the circuits completed by inserting the "circuit-completing" bonds for a chosen spanning tree although all the circuits of the original graph appears in Eq. 4. The number of the "circuit-completing" bonds for a spanning tree for a polycyclic conjugated system equals the number of the rings (fundamental circuits) of the system. After representing the circuit area $S(C_j)$ in Eqs. 4 and 5 in terms of the ring area $S(R_j)$ and by equating the coefficients of $S(R_j)^2$ or $S(R_j)S(R_k)$ in the two equations, we can obtain the following equations:

$$P_{J,rs} + \beta\bar{\pi}_{J,(rs)(rs)} = \sum_j^{rs\,\epsilon\,C_j} (P(G\ominus C_j; X_J)/P'(G; X_J)), \tag{7}$$

and

$$\beta\bar{\pi}_{J,(rs)(tu)} = \sum_j^{rs,\,tu\,\epsilon\,Cj} (-1)^{\eta}(P(G\ominus C_j; X_J)/P'(G; X_J)), \tag{8}$$

In Eq. 7 the sum $\sum_{j}^{rs\epsilon C_j}$ runs over all the circuits which pass through the bond r-s. In Eq. 8 the sum $\sum_{j}^{rs,tu\epsilon C_j}$ runs over all the circuits which pass through the two bonds r-s and t-u and

$\eta=0$ if the directions of $r\rightarrow s$ and $t\rightarrow u$ are same in the circuit C_j

$\eta=1$ if they are different.

Further, by substituting the following equation[19]

$$P_{J,rs}=(P(G\ominus e_{rs};X_J)+\sum_{j}^{rs\,\epsilon\,C_j}P(G\ominus C_j;X_J))/P'(G;X_J), \quad (9)$$

into Eq. 7 we find that

$$\beta\bar{\pi}_{J,(rs)(rs)}=-P(G\ominus e_{rs};X_J)/P'(G;X_J), \quad (10)$$

where $G\ominus e_{rs}$ is a subgraph of G obtained by deleting bond (edge) r-s and all the bonds incident to e_{rs} from G. Figure 2 shows a subgraph $G\ominus e_{23}$ for bond 2-3 of naphthalene.

Let us take naphthalene as an example in order to illustrate the above procedure. Figure 3 shows a spanning tree for naphthalene, $T1$. The "circuit-completing" bonds for $T1$ are bonds 2-3 and 6-1. Insertion of bond 6-1 into $T1$ completes circuit C_2 (ring R_2) and that of bond 2-3 completes circuit C_3 which contains two rings R_1 and R_2 (see Fig. 1). If the spanning tree $T1$ is chosen, then in McWeey's method χ_J of naphthalene is given by (see Eq. 5):

$$\begin{aligned}\chi_J=2\beta(e/\hbar c)^2\{&(P_{J,23}+\beta\bar{\pi}_{J,(23)(23)})(S(R_1)+S(R_2))^2\\&-2\beta\bar{\pi}_{J,(23)(61)}(S(R_1)+S(R_2))S(R_2)\\&+(P_{J,61}+\beta\bar{\pi}_{J,(61)(61)})S(R_2)^2\},\end{aligned} \quad (11)$$

where the negative sign before the second term is due to the fact that the direction of $2\rightarrow 3$ is anticlockwise in circuit C_3 but the direction of $6\rightarrow 1$ is clockwise in circuit C_2 (see Figs. 1 and 3).

In Pople's method χ_J of naphthalene is expressed as a sum of the partial circuit susceptibilities for three circuits, C_1, C_2, and C_3:

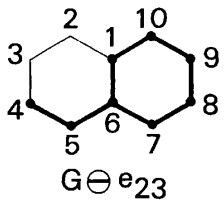

Fig. 2. Subgraph $G\ominus e_{23}$ of naphthalene.

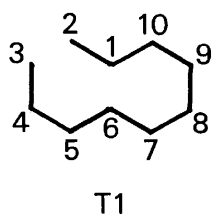

Fig. 3. Spanning tree, $T1$, for naphthalene.

$$\chi_J=\chi_J(C_1)+\chi_J(C_2)+\chi_J(C_3). \quad (12)$$

The explicit expressions for $\chi_J(C_1)$, $\chi_J(C_2)$, and $\chi_J(C_3)$ will be obvious. For example, from Eq. 4 $\chi_J(C_3)$ is

$$\chi_J(C_3)=2\beta(e/\hbar c)^2(P(G\ominus C_3;X_J)/P'(G;X_J))\,(S(R_1)+S(R_2))^2. \quad (13)$$

By equating the coefficients of $S(R_j)S(R_k)$ in Eqs. 11 and 12 we obtain the following equations:

$$P_{J,23}+\beta\bar{\pi}_{J,(23)(23)}=(P(G\ominus C_1;X_J)+P(G\ominus C_3;X_J))/P'(G;X_J), \quad (14)$$

$$\beta\bar{\pi}_{J,(23)(61)}=P(G\ominus C_1;X_J)/P'(G;X_J), \quad (15)$$

$$P_{J,61}+\beta\bar{\pi}_{J,(61)(61)}=(P(G\ominus C_1;X_J)+P(G\ominus C_2;X_J))/P'(G;X_J). \quad (16)$$

It can be ascertained that the equations obtained for $T1$, namely Eqs. 14—16, are the examples of Eqs. 7 and 8. Even if the other spanning tree is chosen, we can ascertain the validity of Eqs. 7, 8, and 10.

The Eqs. 7, 8, and 10 are the desired equations. Equation 7 shows that the quantity $P_{J,rs}+\beta\bar{\pi}_{J,(rs)(rs)}$ for bond r-s is expressed as a sum of the characteristic polynomials of the subgraphs $G\ominus C_j$ over all the circuits passing through bond r-s. Equation 8 shows that the partial imaginary mutual bond-bond polarizability for two bonds r-s and t-u, $\beta\bar{\pi}_{J,(rs)(tu)}$, is expressed as a sum of the characteristic polynomials of the subgraphs $G\ominus C_j$ over all the circuits passing through the two bonds r-s and t-u. Equation 10 shows that the partial imaginary self bond-bond polarizability for bond r-s is expressed in terms of the characteristic polynomial of the subgraph $G\ominus e_{rs}$.

Although the imaginary bond-bond polarizability represents the imaginary part of the change of Coulson's bond order due to an applied magnetic field, we can find from Eqs. 7 and 8 a similarity between the two quantities $P_{J,rs}+\beta\bar{\pi}_{J,(rs)(rs)}$ and $\beta\bar{\pi}_{J,(rs)(tu)}$ that the two quantities are expressed in terms of the same type of characteristic polynomial such as $P(G\ominus C;X)$.[13] Further it is seen from Eqs. 8 and 10 that the imaginary mutual bond-bond polarizability and the imaginary self bond-bond polarizability are different quantities because the former is associated with the subgraph $G\ominus C_j$ but the latter is associated with the subgraph $G\ominus e_{rs}$.

From Eqs. 7, 8, and 10 we can clarify the dependence of imaginary bond-bond polarizability on the topologies (circuit and connectivity). Let us first consider the properties related to the circuit. Equation 7 shows that the quantity $P_{J,rs}+\beta\bar{\pi}_{J,(rs)(rs)}$ for the bond r-s consists of the contributions of all the circuits passing through the bond r-s, and Eq. 8 shows that the partial imaginary mutual bond-bond polarizability $\beta\bar{\pi}_{J,(rs)(tu)}$ for bonds r-s and t-u consists of the contributions of all the circuits passing through the two bonds r-s and t-u. Although, as seen from Eq. 1, two quantities $P_{J,rs}+\beta\bar{\pi}_{J,(rs)(rs)}$ and $\beta\bar{\pi}_{J,(rs)(tu)}$ represent the contribution of a

bond to London susceptibility, it is interesting that the two quantities themselves show the circuit dependence mentioned above.

In a previous paper[13] we classified bonds into "acyclic" and "cyclic" and pointed out the importance of this classification in the study of magnetic properties of conjugated molecules. We proved that for an "acyclic" bond r-s,

$$P_{J,rs}+\beta\bar{\pi}_{J,(rs)(rs)}=0, \tag{17}$$

and

$$\bar{\pi}_{J,(rs)(vw)}=0, \tag{18}$$

where v-w is an arbitrary bond but not equal to r-s. The set of Eqs. 17 and 18 shows that an "acyclic" bond makes no contribution to London susceptibility and to ring current. Since an "acyclic" bond, by definition, has no circuits passing through it,[13] from Eqs. 7 and 8 we can easily obtain Eqs. 17 and 18.

The branching in a graph is one of the important factors determining the physical and chemical properties of unsaturated hydrocarbons.[2] Figure 4 shows two modes of branching in the graph representing a conjugated molecule. Since the difference in the modes of branching appears in the difference of the circuits passing through the bonds, Eqs. 7 and 8 give the imformation on the dependence of imaginary bond-bond polarizability on branching.

Let C be a circuit which passes through bond r-s in G1 shown in Fig. 4. Then the circuit C necessarily passes through bond s-t in G1 also and the directions of $r\rightarrow s$ and of $s\rightarrow t$ are the same in the circuit C. Therefore we obtain from Eqs. 7 and 8

$$\beta\bar{\pi}_{J,(vw)(rs)}=\beta\bar{\pi}_{J,(vw)(st)}, \tag{19}$$

$$P_{J,rs}+\beta\bar{\pi}_{J,(rs)(rs)}=P_{J,rs}+\beta\bar{\pi}_{J,(st)(st)}, \tag{20}$$

$$P_{J,rs}+\beta\bar{\pi}_{J,(rs)(rs)}=\beta\bar{\pi}_{J,(rs)(st)}, \tag{21}$$

where v-w is an arbitrary bond except the bonds in G1. In a similar way, it follows from Eqs. 7 and 8 that for vertices r', s', t', and u' in subgraph G2 shown in Fig. 4

$$\beta\bar{\pi}_{J,(vw)(r's')}=\beta\bar{\pi}_{J,(vw)(s't')}+\beta\bar{\pi}_{J,(vw)(s'u')}, \tag{22}$$

$$P_{J,r's'}+\beta\bar{\pi}_{J,(r's')(r's')}=\beta\bar{\pi}_{J,(r's')(s't')}+\beta\bar{\pi}_{J,(r's')(s'u')}, \tag{23}$$

where v-w is an arbitrary bond except the bonds in G2. The above five equations show the dependence of imaginary bond-bond polarizability on the mode of branching. Although Eqs. 19—23 were proved in a previous paper,[12] as seen above, Eqs. 7 and 8 provide an easier way to derive Eqs. 19—23 than that used in Ref. 12.

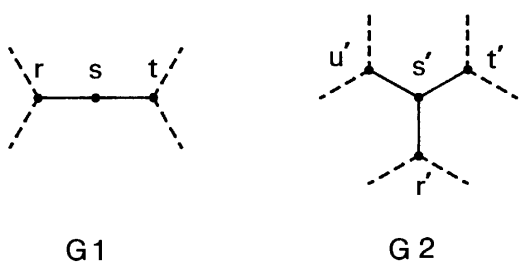

Fig. 4. Subgraphs G1 and G2.

Integral Expressions for Imaginary Bond-Bond Polarizability. Rules for London Susceptibility and for Ring Current

Coulson's integral representation technique[8] has been shown to be very powerful in the study of the dependence of the HMO π-electron indices on the structure of the conjugated molecule.[2] The characteristic polynomial expression for imaginary bond-bond polarizability obtained above is the first step for obtaining the integral expression for the quantity.

It follows from Eqs. 7, 8, and 10 that

$$P_{rs}+\beta\bar{\pi}_{(rs)(rs)}=\sum_J g_J \sum_j^{rs\in C_j}(P(G\ominus C_j;X_J)/P'(G;X_J)), \tag{24}$$

$$\beta\bar{\pi}_{(rs)(tu)}=\sum_J g_J \sum_j^{rs,tu\in C_j}(-1)^{\eta}(P(G\ominus C_j;X_J)/P'(G;X_J)), \tag{25}$$

and

$$\beta\bar{\pi}_{(rs)(rs)}=-\sum_J g_J P(G\ominus e_{rs};X_J)/P'(G;X_J), \tag{26}$$

where g_J is the occupation number of the J-th MO. According to the same procedure as in Ref. 9, for closed shell molecules Eqs. 24—26 can be written in the integral form as follows:

$$P_{rs}+\beta\bar{\pi}_{(rs)(rs)}=(-1/\pi)\sum_j^{rs\in C_j}\int_{-\infty}^{\infty}(P(G\ominus C_j;iy)/P(G;iy))dy, \tag{27}$$

$$\beta\bar{\pi}_{(rs)(tu)}=(-1/\pi)\sum_j^{rs,tu\in C_j}(-1)^{\eta}\int_{-\infty}^{\infty}(P(G\ominus C_j;iy)/P(G;iy))dy, \tag{28}$$

and

$$\beta\bar{\pi}_{(rs)(rs)}=(1/\pi)\int_{-\infty}^{\infty}(P(G\ominus e_{rs};iy)/P(G;iy))dy. \tag{29}$$

With the quantity $F(C)$ defined as[9]

$$F(G,C)=\int_{-\infty}^{\infty}(P(G\ominus C;iy)/P(G;iy))dy, \tag{30}$$

Eqs. 27 and 28 are written as follows:

$$P_{rs}+\beta\bar{\pi}_{(rs)(rs)}=(-1/\pi)\sum_j^{rs\in C_j}F(G,C_j), \tag{31}$$

and

$$\beta\bar{\pi}_{(rs)(tu)}=(-1/\pi)\sum_j^{rs,tu\in C_j}(-1)^{\eta}F(G,C_j). \tag{32}$$

It was shown that if the system G is alternant, the sign of $F(G,C)$ is determined only by the size of the circuit, $N(C)$:[9]

$$F(G,C)\begin{cases}<0 & \text{if } N(C)=4n+2\\ >0 & \text{if } N(C)=4n.\end{cases} \tag{33}$$

This equation means that the contribution of a $(4n+2)$-membered circuit is diamagnetic and that of a

$(4n)$-membered circuit is paramagnetic.

In a similar fashion it can be shown from Eq. 29 that the sign of the imaginary self bond-bond polarizability is always positive

$$\bar{\pi}_{(rs)(rs)} > 0, \tag{34}$$

where we used the fact that β is negative. This result was already obtained in another manner.[12]

If we remember that bond current for bond r-s (ring current) is expressed in terms of imaginary bond-bond polarizability as follows:[20]

$$Q(rs) = (P_{rs} + \beta\bar{\pi}_{(rs)(rs)})\, S_{rs} + \sum_{(tu)} \beta\bar{\pi}_{(rs)(tu)}\, S_{tu}, \tag{35}$$

it is seen from Eqs. 31 and 32 that the driving forces for the bond current for bond r-s are the presence of the circuits which contain the bond r-s. In other words, cyclic conjugation is the basis for the induction of bond current.

From Eqs. 31—33 we can obtain the rule for imaginary bond-bond polarizability which states that

(1) $P_{rs}+\beta\bar{\pi}_{(rs)(rs)}$ is expressed as a sum of the contributions over all the circuits passing through bond r-s and the sign of the contribution of a circuit is determined only by the size of the circuit as shown in Eq. 33.

(2) $\beta\bar{\pi}_{(rs)(tu)}$ is expressed as a sum of the contributions over all the circuits passing through two bonds r-s and t-u, and the sign of the contribution of a circuit is determined only by the size of the circuit as shown in Eq. 33.

From this rule we can predict the sign of the imaginary bond-bond polarizability by counting the size of the circuit only. For example, it is seen for naphthalene that

$$P_{23} + \beta\bar{\pi}_{(23)(23)} > 0,$$

$$\beta\bar{\pi}_{(23)(61)} > 0,$$

because the circuits passing through 2-3 are C_1 and C_3, the circuit passing through 2-3 and 6-1 is C_1, $N(C_1)=6$ and $N(C_3)=10$. Similarly we can predict that the signs of $P_{rs}+\beta\bar{\pi}_{(rs)(rs)}$ and $\beta\bar{\pi}_{(rs)(tu)}$ for any bond in a catacondensed benzenoid hydrocarbon are positive (diamagnetic) because all the circuits found in a catacondensed benzenoid hydrocarbon are $(4n+2)$-membered circuits.

Since London susceptibility and bond current are expressed in terms of $P_{rs}+\beta\bar{\pi}_{(rs)(rs)}$ and $\beta\bar{\pi}_{(rs)(tu)}$ (see Eqs. 1 and 35), we can obtain the rules for London susceptibility and for bond current. For example, we can predict for a catacondensed benzenoid hydrocarbon that the London susceptibility and the bond current for any bond are diamagnetic because all the contributions of the circuits in the system to $P_{rs}+\beta\bar{\pi}_{(rs)(rs)}$ and $\beta\bar{\pi}_{(rs)(tu)}$ are diamagnetic. This is in agreement with experimental results.[21]

Concluding Remarks

By using the equality of the expressions for London susceptibility in two different methods (McWeeny and Pople-Aihara), imaginary bond-bond polarizability was expressed in terms of characteristic polynomial (see Eqs. 7, 8, and 10). It was shown that the characteristic polynomial expressions for imaginary bond-bond polarizability reveal the dependence of the quantity on the structures such as circuit and branching and that the equations proved in previous papers[12,13] can easily be derived from these expressions. The integral expressions for imaginary bond-bond polarizability (see Eqs. 27—29) were obtained from Eqs. 7, 8, and 10. It was shown that Eqs. 27—29 give a rule for imaginary bond-bond polarizability (and for London susceptibility and for ring current) of any alternant conjugated systems.

Equations 7, 8, and 10 hold only for nondegenerate molecular orbitals because Eqs. 4 and 5 do not hold for degenerate molecular orbitals. However, Eqs. 27—29 are valid for neutral alternant conjugated systems even with degenerate orbitals provided that they have filled bonding and empty antibonding molecular orbitals.[9]

In the present paper we neglect the effect of bond alternation. Since [$4n$]-annulene without bond alternation has nonbonding molecular orbitals, the rule proved in this paper cannot be applied to the system. However it has been reported that [$4n$]-annulene with bond alternation which has no nonbonding orbitals bears a paramagnetic ring current.[22] Further we can find the numerical results by Aihara for biphenylene, cycloocta[*def*]biphenylene and dicycloocta[1,2,3,4-*def*:1′,2′,3′,4′-*jkl*]biphenylene with bond alternation, which show that circuit susceptibilities for the $(4n+2)$-membered circuits in these systems are diamagnetic and those for the $(4n)$-membered circuits are paramagnetic.[23] Accordingly it seems that the introduction of bond alternation changes the magnitude of a circuit susceptibility but does not change its sign.

References

1) F. Harary, "Graph Theory," Addison-Wesley, Reading (1969); H. Sachs, *Publ. Math.*, **11**, 119 (1964).

2) A. Graovac, I. Gutman, and N. Trinajstić, "Topological Approach to the Chemistry of Conjugated Molecules," Springer-Verlag, Berlin (1977); N. Trinajstić, "Chemical Graph Theory," CRC Press, Inc., Boca Raton, Florida (1983).

3) H. Hosoya, K. Hosoi, and I. Gutman, *Theoret. Chim. Acta.*, **38**, 37 (1975).

4) F. London, *J. Phys. Radium*, **8**, 397 (1937).

5) J. A. Pople, *Mol. Phys.*, **1**, 175 (1958).

6) R. McWeeny, *Mol. Phys.*,**1**, 311 (1958); L. Salem, "The Molecular-Orbital Theory of Conjugated Systems," W. A. Benjamin, New York (1966), Chap. 4; J. D. Memory, "Quantum Theory of Magnetic Resonance Parameters," McGraw-Hill, New York (1968). Chap. 6.

7) J. Aihara, *J. Am. Chem. Soc.*, **101**, 558 (1979); **101**, 5913 (1979).

8) C. A. Coulson and H. C. Longuet-Higgins, *Proc. R. Soc. London, Ser. A.*, **191**, 39 (1947).

9) N. Mizoguchi, *Chem. Phys. Lett.*, **106**, 451 (1984).
10) I. Gutman, *Chem. Phys. Lett.*, **117**, 614 (1985).
11) C. W. Haigh and R. B. Mallion, "Progress in NMR Spectroscopy," ed by J. W. Emsley, J. Feeney and L. H. Sutctliffe, Pergamon, Oxford (1980), Vol. 13, p. 303 and references therein.
12) N. Mizoguchi, *Bull. Chem. Soc. Jpn.*, **56**, 1588 (1983).
13) N. Mizoguchi, *Bull. Chem. Soc. Jpn.*, **58**, 540 (1985).
14) J. Gayoso and A. Boucekkine, *C. R. Acad. Sci. Paris, Ser. C*, **272**, 184 (1971); R. B. Mallion, *Proc. R. Soc. London, Ser. A.*, **341**, 429 (1975).
15) Attention should be paid to the recent results of Lazzeretti and Zanasi for $C_3H_3^+$ and benzene which show that local electron circulations also provide a relevant contribution to the in-plane component of the magnetic susceptibility. See P. Lazzeretti and R. Zanasi, *Chem. Phys. Lett.*, **80**, 553 (1981); *J. Chem. Phys.*, **75**, 5019 (1981).
16) M. Randić, *Pure Appl. Chem.*, **55**, 347 (1983) and references therein; J. Gayoso, *C. R. Acad. Sci. Ser. C*, **228**, 327 (1979); J. A. N. F. Gomes, *Theor. Chim. Acta*, **59**, 333 (1981); S. Kuwajima, *J. Am. Chem. Soc.*, **106**, 6496 (1984).
17) J. Aihara, *Bull. Chem. Soc. Jpn.*, **58**, 1045 (1985).
18) A tree which connects all the vertices (carbon atoms) of the graph representing a polycyclic conjugated system is called a spanning tree. The edge (bond) which must be added to a spanning tree in order to re-form the original graph is called the "circuit-completing" bond.
19) H. Hosoya and K. Hosoi, *J. Chem. Phys.*, **64**, 1065 (1976).
20) R. B. Mallion, *Mol. Phys.*, **25**, 1415 (1973).
21) H. J. Dauben, Jr., J. D. Wilson, and J. L. Laity, *J. Am. Chem. Soc.*, **91**, 1991 (1969).
22) J. A. Pople and K. G. Untch, *J. Am. Chem. Soc.*, **88**, 4811 (1966); T. Nakajima and S. Kohda, *Bull. Chem. Soc. Jpn.*, **39**, 804 (1966).
23) J. Aihara, *J. Am. Chem. Soc.*, **107**, 298 (1985).

 © 1987 The Chemical Society of Japan Bull. Chem. Soc. Jpn., 60, 2011—2017 (1987)

The Effect of the Chain Length and the End-Groups on the Epitaxial Growth of Long-Chain Molecules

Yasukiyo UEDA
Department of Industrial Chemistry, Faculty of Engineering, Kobe University, Rokko, Nada, Kobe 657
(Received December 17, 1986)

Five paraffins (C_{30}—C_{44}) and three linear compounds with polar end-groups,such as hydroxyl, methyl-ester, and carboxyl groups, were deposited on the cleavage surface of an alkali halide crystal in vacuo. Paraffin films deposited on the substrate took the same crystal structure and molecular orientation, independent of the number of carbon atoms in the chain. In the case of derivatives, the morphology and orientation of the crystals, however, differed with the end-groups. The (110) planes of paraffins, alcohol,and methyl-ester crystals were oriented parallel to the substrate (001) plane, and their *c*-axes were parallel to the [110] direction of the substrate crystal. On the other hand, the (001) plane of the acid crystal lay parallel to the substrate surface, so that the *c*-axis of the crystal was oblique to the substrate surface. The epitaxial growth of linear molecules with different end-groups was explained by the difference in the interaction between the end-groups and the substrate.

In recent years, attempts have been made to prepare many organic compounds in the form of an ultrathin film and study the relation between the physical properties and molecular arrangements in the films. The main methods of preparing oriented thin films are the Langmiur-Blodgett method and the physical vapor deposition (PVD) method. The former has been widely applied to amphiphilic linear molecules. The orientation of their films, however, is a single-molecular arrangement normal to the substrate and it was reported, on the basis of microscopic observation, that the uniformity of the molecular packing was incomplete even in the first monolayer.[1] On the other hand, the PVD method has been applied to planar and linear molecules and could give an alternative molecular orientation, depending on the evaporation conditions.[2-10] In the case of linear molecules such as paraffin,[11] they took two orientations on the cleavage surface of alkali halide. The films deposited on the substrate kept at room temperature were found to be composed of raft-like crystallites. The (110) plane of these crystals was oriented parallel to the substrate (001) plane, while their fiber axes were parallel to the [110] direction of the substrate crystal. On the other hand, the films deposited on the substrate kept at temperatures near or above their melting points were composed of discrete, disk-like crystals, and their fiber axes were perpendicular to the substrate.

The linear polar molecules such as methyl triacontanoate also took two similar orientations.[12] The crystal morphology, however, was different from that of paraffin, although methyl triacontanoate molecules were oriented parallel to the substrate surface. It seems that the epitaxial growth of linear molecules from the vapor phase depends on the kind of end-group as well as on their crystal structures. It is well-known that paraffins have many polymorphic forms. Their polymorphs depend on even and odd number of carbon atoms,[13,14] as well as the crystallization conditions. It seemed that it would be interesting to investigate the effects of end-groups and the number of carbon atoms on the morphology and orientation of linear molecular crystals.

In this paper, paraffins containing an even or odd number of carbon atoms and their derivatives with different polar end-groups, such as hydroxyl, methyl-ester, and carboxyl groups, were evaporated on alkali halide crystals. The epitaxial growth and growth mechanisms of these linear molecules were then studied by using an electron micrograph and by electron-diffraction.

Experimental

The materials used were five paraffins ($C_{30}H_{62}$, $C_{35}H_{72}$, $C_{36}H_{74}$, $C_{40}H_{82}$, and $C_{44}H_{90}$) and three linear polar compounds containing 30 carbons($C_{30}H_{61}OH$, $C_{29}H_{59}COOCH_3$, and $C_{29}H_{59}COOH$). These materials, obtained from the Tokyo Chemical Industry Co., Ltd., were of a purity higher than 99%. These samples were sublimated from a quartz crucible heated with a tungusten coil onto the clean surface of an alkali halide in a vacuum of 1.33×10^{-3} Pa. Single crystals of alkali halide, NaCl and KCl, were cleaved in air and mounted on a metal block equipped with an electric heater as well as a thermocouple for the temperature measurement of the substrate crystal. After being heated to a higher temperature, the substrate was kept at a temperature between 20 and 100 °C. About 5 mg of each material was deposited vertically onto the substrate surface, which faced downwards on a horizontal plane separated from the crucible by about 10 cm. The rate of sublimation was about 1.5 nm min^{-1}. The temperature of the evaporation source was kept in the range from 180 to 200 °C. The thickness of the deposited films was estimated to be in the range from 80 to 100 nm by using a quartz crystal microbalance. The specimens used for electron microscopy were prepared by the dissolution of the substrate in water after they had been reinforced with evaporated carbon film. The orientation of the deposited crystal relative to the substrate crystal was determined by chromium shadowcasting along the [100] direction of the substrate crystal. Thallium(I) chloride, prepared by evaporation, was used as the standard calibration material for spacing measurements.

Results and Discussion

Crystal morphology and molecular orientation have a close relation to the surface treatment, mainly

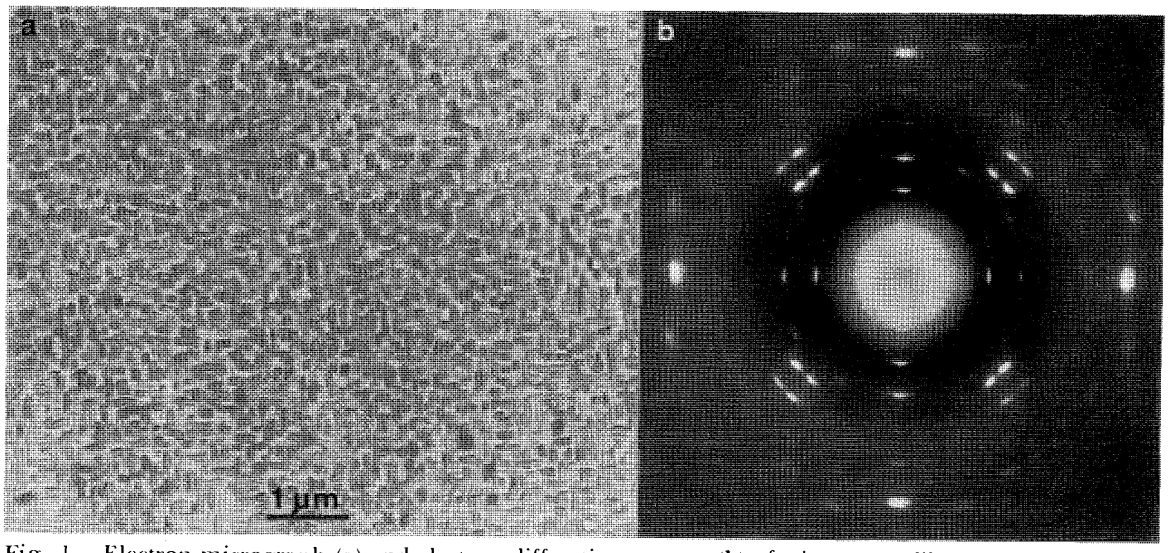

Fig. 1. Electron micrograph (a) and electron-diffraction pattern (b) of triacontane film vacuum-deposited on the (001) plane of KCl kept at 20 °C after being preheated at 150 °C.

depending on the bake-out procedure. When these compounds were evaporated onto a cleavage surface of alkali halide without any heat-treatment, the films were composed of granules with various orientations. The triacontane film vacuum-condensed on the substrate which had been heated at 150 °C for 1 h in advance and then kept at 20 °C was composed of small rod-like crystals crossing each other orthogonally, as is shown in Fig. 1(a). The needle axis of the deposited crystals was parallel to the substrate [110] direction. Corresponding to such a configuration of the film, the diffraction pattern shown in Fig. 1(b) also had an orthogonal appearance. This pattern is a superposition of two identical fiber diagrams rotated at 90° to each other. The crystals vacuum-condensed on the KCl and NaCl surfaces had the same morphology and showed identical diffraction patterns.

Crystals of such linear molecules as paraffin and its derivatives generally have a lamellar structure. They are composed of stacked layers which consist of chain molecules lying with their axes parallel to each other. In order to generalize the similarity detected among the crystal structures of chain molecules, Vand has introduced the concept of a subcell which is determined by the position of the methylene groups.[15] The most widely encountered type of subcell is an orthorhombic one occupied by two C_2H_4 groups. The diffraction pattern shown in Fig. 1(b) is composed of reflections situated at the reciprocal lattice points hkl_s of the sublattice and a series of $00l$ reflections in the small-angle region; the suffix s indicates the subcell lattice. A triacontane crystal has an orthorhombic subcell with dimensions of a_s=0.733, b_s=0.492, and c_s=0.2546 nm.[16] On the basis of the dimensions, the reflection spots in Fig. 1(b) were indexed as is shown in Fig. 2, in which the open circles represent the basic single-crystal pattern. The total pattern is overlapped by rotating the pattern at 90°. This pattern

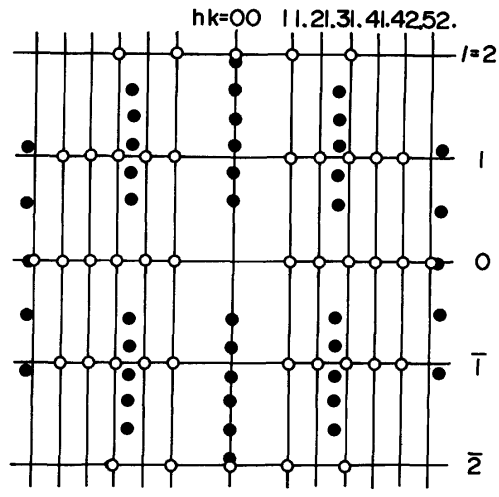

Fig. 2. The interpretation of the diffraction pattern shown in Fig. 1(b). The open circles represent the basic single crystal pattern.

is similar to the pattern obtained from hexatriacontane film grown epitaxially. From the same consideration as that applied to the orientation of the hexatriacontane crystal, the (110) plane of the triacontane crystal is found also to be oriented parallel to the substrate (001) plane, while its c-axis lies parallel to the [110] direction of the substrate crystal. The crystals of the other paraffins vacuum-condensed on alkali halide surfaces had the same morphology and showed the diffraction pattern of the identical subcell independent of the carbon atoms. This suggests that all the paraffin crystals used are composed of the same subcell and take the same orientation when they grow epitaxially on alkali halide. In addition to the reflection spots of the identical subcell, a series of reflections was found on the equator in the small-angle region. Figure 3 shows the series of $00l$ reflections corresponding to the long-spacings from each paraffin crystal. In the case of molecules with an odd number of carbon atoms, the

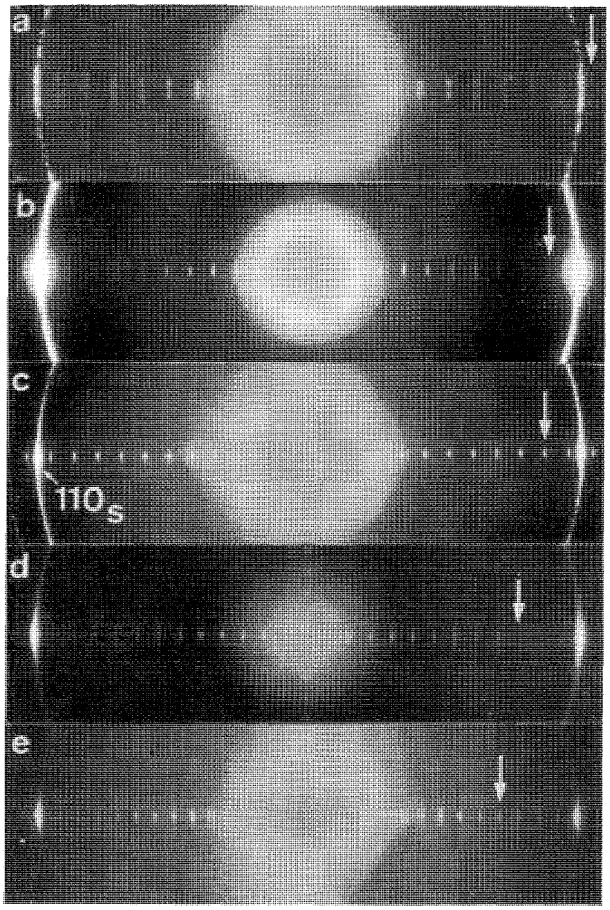

Fig. 3. Electron-diffraction patterns of the long-spacings of (a) $C_{30}H_{62}$, (b) $C_{35}H_{72}$, (c) $C_{36}H_{74}$, (d) $C_{40}H_{82}$, and (e) $C_{44}H_{90}$. Arrow indicates the tenth reflection spot.

long-spacings indicate the thickness of two molecules because of the crystal symmetry. Considering the extinction law for the crystal symmetry, l is integer for the molecules with an even number of carbon atoms, while it is even for the molecules with an odd number of carbon atoms. It is noted that the reflections can be clearly observed over the tenth order. Consequently, it seems that the crystallinities of the evaporated paraffin films are very high. These $00l$ reflections demonstrate the lamellar structure of paraffin crystals directly. The individual long-spacings obtained from the $00l$ reflections are given in Table 1. In the crystal of the orthorhombic form, the chain is perpendicular to the basal plane and the length of one zig-zag of a chain is estimated to be 0.2546 nm. The long-spacings may be expressed by an equation of this type;

$$d\,(\mathrm{nm}) = 0.1273 \times m + 0.183$$

m is the number of carbon atoms.[14] The long-spacings calculated from the equation are given in Table 1. The observed values from C_{30} to C_{44} coincide with the calculated values within the error of measurement. Figure 4 shows the high-resolution electron micrograph of hexatriacontane film. A periodicity of 4.77 nm corresponding to the molecular length is

Table 1. Long-Spacings of Paraffins

Sample	Observed Value/nm	Calculated Value/nm
$C_{30}H_{62}$	3.993	4.002
$C_{35}H_{72}$	4.634	4.639
$C_{36}H_{74}$	4.769	4.766
$C_{40}H_{82}$	5.305	5.275
$C_{44}H_{90}$	5.829	5.784

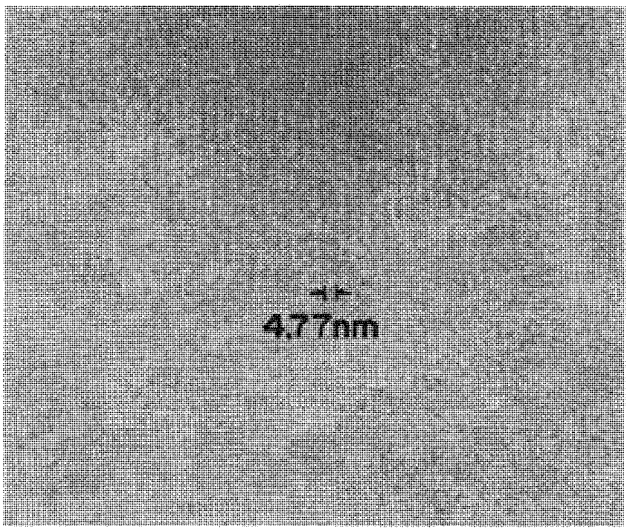

Fig. 4. The 001 lattice image of $C_{36}H_{74}$ crystal.

observed, although the paraffin crystal is very sensitive to the radiation damage by an electron beam. This finding indicates directly that hexatriacontane molecules lie parallel to the substrate surface.

The 1-triacontanol film vacuum-deposited on the substrate kept at 20 °C was composed of rod-like crystals crossing each other orthogonally, as is shown in Fig. 5(a). The electron-diffraction pattern from the film shows a pattern similar to that of triacontane film. It is well-known that linear alcohols, like other linear molecules, exhibit polymorphism.[17,18] The alcohols have a hexagonal high-temperature form (α) which is stable just below the melting point. The alcohols with an even number of carbon atoms possess two low-temperature forms; the one form is orthorhombic (β), with its chains normal to the (001) plane, while the other is monoclinic (γ), with chains inclined to the plane. In all forms, the long-spacings indicate the thickness of two molecules. The experimental formulae for the long-spacings of the three forms were classified as follows,

$$l_\alpha = 0.252n + 0.45$$
$$l_\beta = 0.252n + 0.55$$
$$l_\gamma = 0.215n + 0.32$$

n is the number of carbon atoms.[17]

The long-spacing obtained from the $00l$ reflections shown in Fig. 5(c) was 8.10 nm. This value coincided with the spacing calculated by the formula for the β form. The subcell dimensions of the β form are a_s=0.733, b_s=0.504, and c_s=0.252 nm.[17] Con-

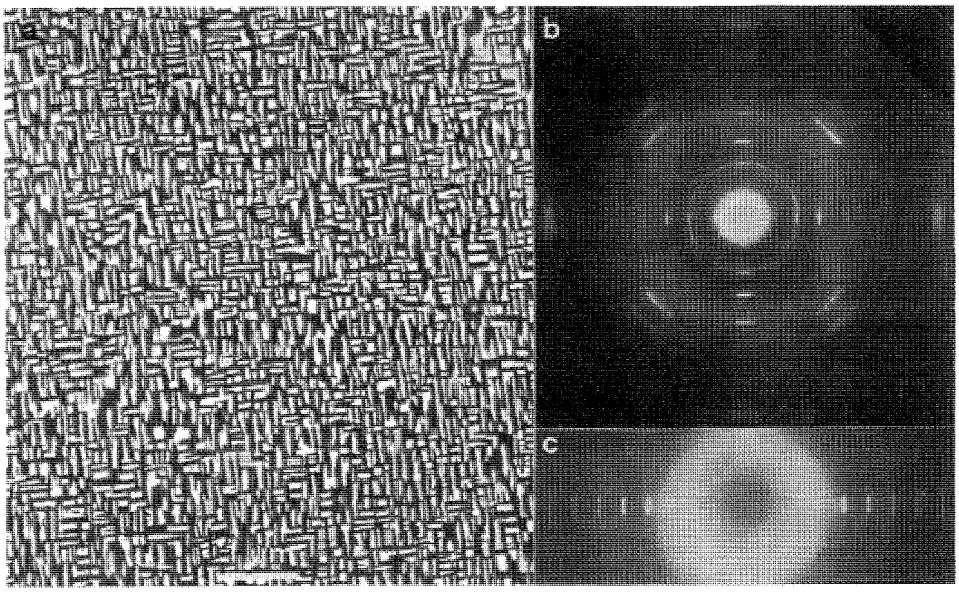

Fig. 5. Electron micrograph (a), electron-diffraction pattern (b), and the long-spacings (c) of 1-triacontanol film.

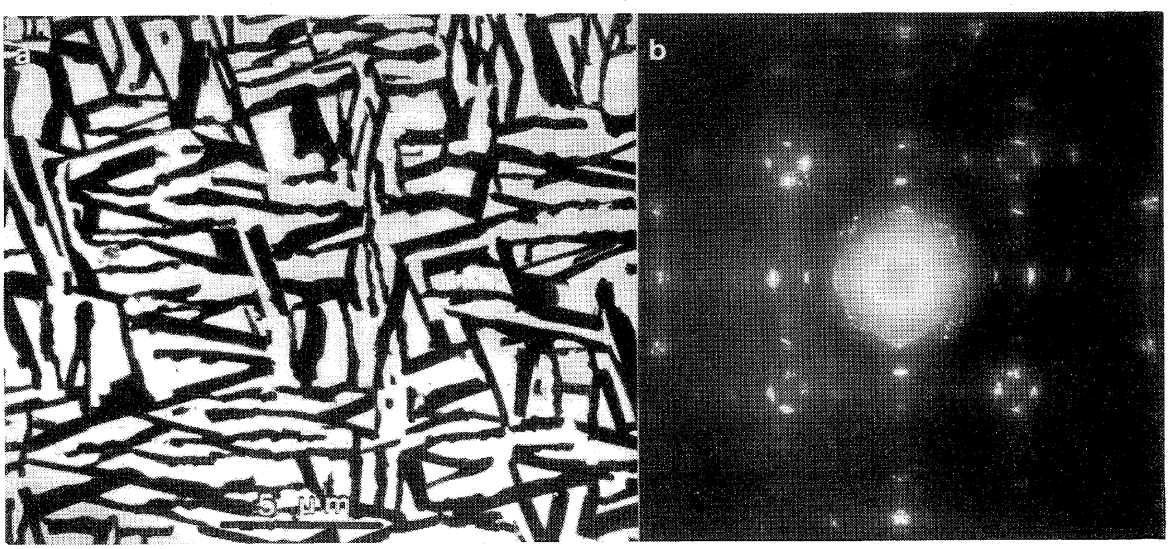

Fig. 6. Electron micrograph (a) and electron-diffraction pattern (b) of methyl triacontanoate film.

sequently, the crystal form of 1-triacontanol deposited on the substrate was assumed to be of the orthorhombic form, with dimensions of $a_s(=a)=0.733$, $b_s(=b)=0.504$, $c_s=0.252$, and $c=8.10$ nm. On the basis of these subcell dimensions, the reflection spots in Fig. 5(b) were indexed so as to be similar to the diffraction pattern of the triacontane film shown in the previous section. Therefore, it seems that the epitaxial overgrowth of 1-triacontanol molecules vacuumcondensed on the substrate is similar to that of triacontane molecules.

Figure 6(a) shows the electron micrograph of the methyl triacontanoate film deposited on the substrate kept at 30 °C. The film was composed of V-shaped crystals growing along two directions crossing at 32°, and the [110] direction of the substrate crystal corresponded to the bisectional direction of the V-shaped crystals. These crystals intersected at right angles to each other. Figure 6(b) shows the electron-diffraction pattern from the film. As has been described in a previous paper,[12] the (110) planes of the two crystals related by mirror symmetry, whose mirror plane corresponds to the (110) plan of KCl, are oriented parallel to the substrate surface. Their c-axes are parallel to the [110] direction of the substrate KCl.

The crystal morphologies differed with the end-groups when the linear molecules grew epitaxially on KCl. The epitaxial overgrowth of paraffins and 1-triacontanol crystals on the surface of KCl is represented schematically in Figs. 7(a) and (b). The (110) planes are oriented parallel to the substrate surface. The c-axes are parallel to the [110] direction of KCl. Figures 7(c) and (d) show the schematic representation of the relative orientation and the epitaxial over-

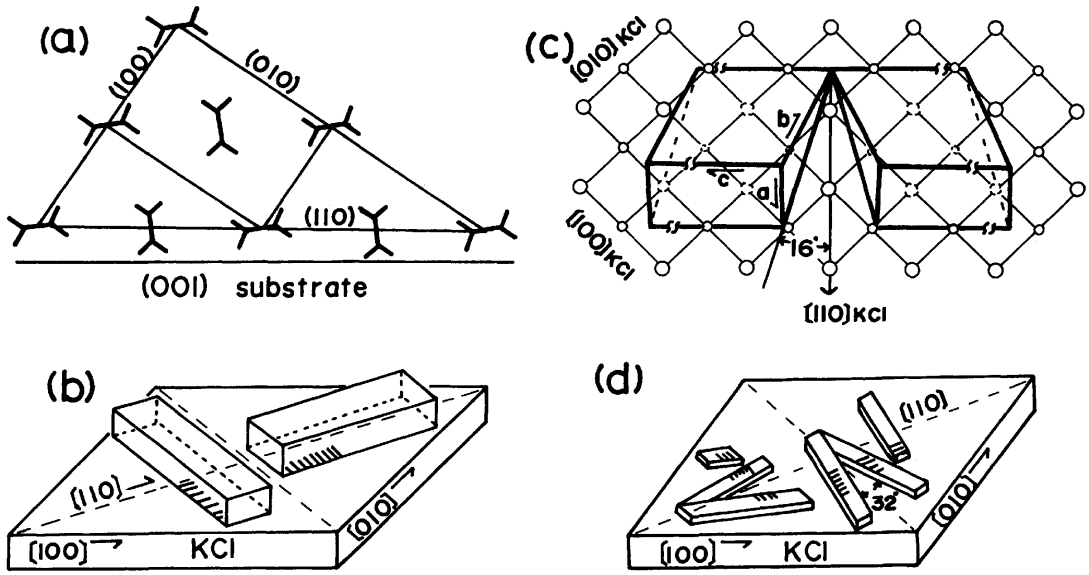

Fig. 7. (a): The relation between paraffin and alcohol molecules and the substrate surface. (b): Orientation of the deposited paraffin and alcohol crystals on the substrate surface. The chain molecules are shown in the crystals. (c): Schematic diagram of the relative orientation of methyl ester crystals and KCl (001) surface. (d): Orientation of the deposited methyl triacontanoate crystals on the substrate surface.

growth of the methyl triacontanoate crystals on the KCl (001) surface. The [110] direction of the methyl triacontanoate crystals crosses the [110] direction of the substrate crystal at 16°. The morphology of the deposited methyl triacontanoate is V-shaped, and these V-shaped crystals grow epitaxially, crossing each other orthogonally, corresponding to the C_{4v} symmetry of the substrate crystal.

The triacontanoic acid film deposited on the substrate at 20 °C was composed of randomly-oriented rod-like crystals and lamellar crystals filling in the space among the former, as is shown in Fig. 8(a). The high-resolution electron-diffraction pattern from the film showed the arc reflection spots on the ring pattern, as is shown in Fig. 8(b). This pattern was similar to the pattern obtained from hexatriacontane film, in which the crystal c-axis was oriented perpendicular to the substrate.[11] However, not all spots were indexed to the series of $hk0$ reflections. When the film was tilted about 40° around the a-axis of the crystal, the pseudo-hexagonal net-pattern appeared, as is shown in Fig. 8(c). The normal-chain carboxylic acids are known to possess several crystalline modifications. The crystals of even-numbered acids have three forms which are called the A-, B-, and C-form respectively, in order of the decrease in long-spacings.[19] The chain molecules in the B-and C-forms tilt to the basal (001) plane at angles of 62.76° and 51.54° respectively; these angles correspond to the β angle in respective monoclinic form. The B- and C-forms have the same subcell dimensions; a_s=0.740 nm and b_s=0.496 nm,[20,21] and the long-spacing of the C-form triacontanoic acid crystal is 6.52 nm.[22] The crystal parameters of the C-form triacontanoic acid crystal are a=0.936, b=0.496, c=6.52 nm, and β=128.4°. The net pattern in Fig. 8(c) was indexed with $hk0$ reflection series of the C-form. Therefore, the triacontanoic acid crystal deposited on the substrate is the C-form, and its c-axis tilts at an angle about 50° to the basal plane. Consequently, the (001) plane of the triacontanoic acid crystal is

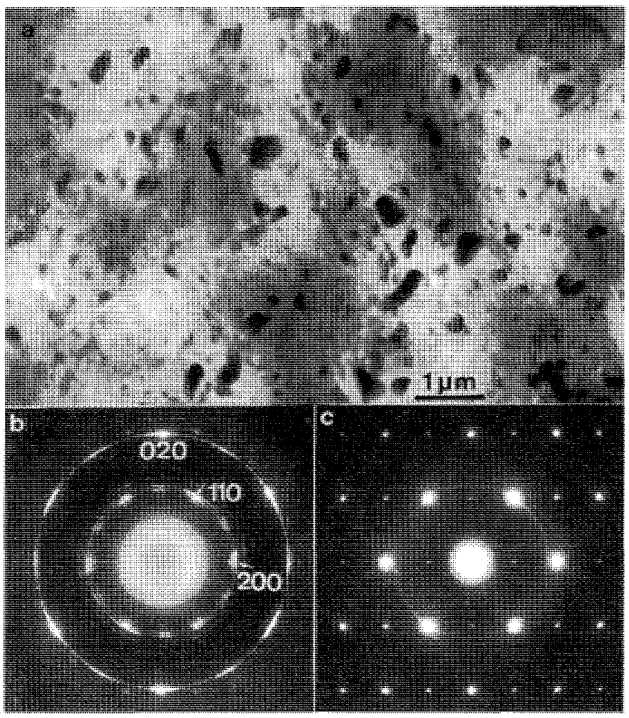

Fig. 8. Electron micrograph (a) and electron-diffraction patterns (b) (c) of triacontanoic acid film. Electron-diffraction pattern (c) was obtained from the film tilted about 40° around the a-axis of the crystal.

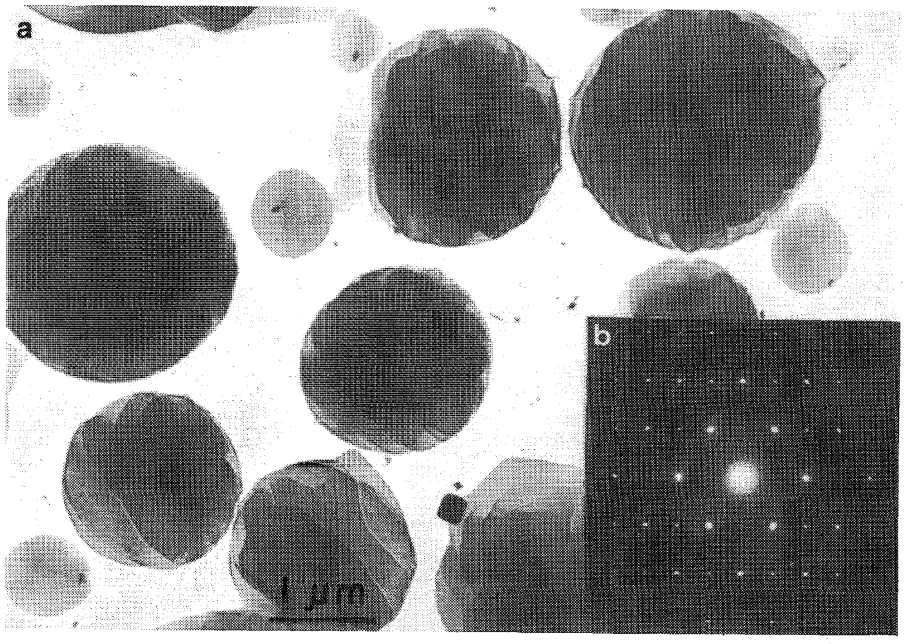

Fig. 9. Electron micrograph (a) and electron-diffraction pattern (b) of triacontane film deposited on the substrate kept at 100°C.

oriented parallel to the substrate (001) plane; as a result of such an orientation, the *c*-axis tilts at an angle of 51.54° to the substrate.

When the substrate was kept at a temperature higher than the melting point of each linear molecule, each sample vacuum-condensed on the surface formed discrete, disk-like crystals which were composed of overlapping lamellae, as is shown in Fig. 9(a). The electron-diffraction patterns from these crystals shows a single net-pattern of higher-order reflections of 100_s and 010_s, as is shown in Fig. 9(b); this indicates that the *c*-axes of the crystals are perpendicular to the substrate surface. Therefore, when linear molecules are evaporated on a substrate which is kept at a temperature above their melting points, the liquid deposit condenses in droplets due to the surface energy. On cooling, the deposited molecule probably crystallizes independently of the molecule-substrate interaction and forms the disk-like crystals composed of lamellae.

Paraffins, 1-triacontanol, and methyl triacontanoate crystals took their *c*-axes parallel to the substrate surface. On the other hand, the triacontanoic acid crystals took their *c*-axes perpendicularly to the substrate surface. It seems that the epitaxial overgrowth of long-chain molecules is dependent on the interaction between the end-groups and the substrate. Mauritz et al. pointed out that the non-polar aliphatic long-chain was oriented parallel to the alkali halide surface to minimize the total energy of molecular interaction and that the dispersion-repulsive force was most sensitive to orientation and was greater in magnitude than the electrostatic forces.[23] On the contrary, the polar end-groups probably have a tendency to come in contact with ionic species by means of dipole-dipole interaction. If the dipole-dipole interaction is strong and the interaction between the deposited molecule and the substrate is rather weak, the molecule comes into close contact with the ionic species on the substrate by the end group; the resultant orientation of the crystals is a standing *c*-axis one in order to maintain their molecular configuration. The adsorption strength of long-chain molecules with polar end-groups on metal increases in the following sequence: ester<alcohol <acid.[24] This order on metal may be applied on such ionic substrates as KCl. The more strongly the polar end-groups interact with the substrate, the more the tendency turned the standing *c*-axis orientation increases. It seems that the standing *c*-axis orientation of the triacontanoic acid crystal is caused by the strong interaction between the end-group and the substrate. If long-chain acid molecules have more carbon atoms than that of triacontanoic acid, it is probable that the influence of the polar end-group decreases and its *c*-axis becomes parallel to the substrate.

The author wishes to express his thanks to Professor Michio Ashida for his helpful discussions. Thanks are also due to Mr. Hideaki Yajima and Mr. Hisao Yanagi for their kind assistance.

References

1) R. D. Neuman, S. Fereshtehkhou, and F. Ovalle, *J. Colloid and Interface Sci.*, **101**, 309 (1984).
2) N. Uyeda, M. Ashida, and E. Suito, *J. Appl. Phys.*, **36**, 1453 (1964).
3) M. Ashida, N. Uyeda, and E. Suito, *Bull. Chem. Soc. Jpn.*, **39**, 2610 (1966).
4) M. Ashida, *Bull. Chem. Soc. Jpn.*, **39**, 2625 (1966); *ibid.*, **39**, 2632 (1966).
5) M. Ashida, A. Hamada, and T. Watanabe, *Bull.*

Chem. Soc. Jpn., **45**, 2312 (1972).
6) Y. Murata, T. Kobayashi, N.Uyeda, and E. Suito, *J. Crystal Growth*, **26**, 187 (1974).
7) T. Kobayashi, Y. Fujiyoshi, and N. Uyeda, *Acta Crystallogr. Sect. A*, **38**, 356 (1982).
8) Y. Hattori, M. Ashida, and T. Watanabe, *Nippon Kagaku Kaishi*, **1975**, 496.
9) M. Ashida, Y. Ueda, and T. Watanabe, *J. Polym. Sci., Polym. Phys. Ed.*, **16**, 179 (1978).
10) M. Ashida, Y. Ueda, and H. Yanagi, *Bull. Chem. Soc. Jpn.*, **59**, 1437 (1986)
11) Y. Ueda and M. Ashida, *J. Electron Microscopy*, **29**, 38 (1980).
12) Y. Ueda, *Bull. Chem. Soc. Jpn.*,**59**, 3775 (1986).
13) M. O. Stanley, *J. Phys. Chem.*, **63**, 248 (1959).
14) G. Strobl, B. Ewen, E. W. Fischer, and W. Piesczek,*J. Chem. Phys.*, **61**, 5257 (1974).
15) V. Vand, *Acta Crystallogr.*, **4**, 465 (1951).
16) A. Muller, *Proc. R. Soc. London, Ser. A.* **138**, 514 (1932).
17) K. Tanaka, T. Seto, and T. Hayashida, *Bull. Inst. Chem. Res. Kyoto Univ.*, **35**, 123 (1958).
18) K. Tanaka, T. Seto, A. Watanabe, and T. Hayashida, *Bull. Inst. Chem. Res. Kyoto Univ.*, **37**, 281 (1959).
19) F. Francis, S. H. Piper, and T. Malkin, *Proc. R. Soc. London, Ser. A.* **128**, 214 (1930).
20) V. Malta, G. Gelotto, R. Zanetti, and A. F. Martelli, *J. Chem. Soc. B*, **1971**, 548.
21) M. Goto and E. Asada, *Bull. Chem. Soc. Jpn.*, **51**, 2456 (1978).
22) F. Francis, F. J. E. Collins, and S. H. Piper, *Proc. R. Soc. London, Ser. A*, **158**, 691 (1937).
23) K. A. Mauritz, E. Baer, and A. J. Hopfinger, *J. Polym. Sci. Polym. Phys. Ed.*, **11**, 2185 (1973).
24) S. G. Daniel, *Trans. Faraday Soc.*, **47**, 1345 (1951).

The Reaction of Dibutyl Disulfide with Hydrogen Atom

Jie TANG,* Tohru KAMO, Muneyoshi YAMADA, Yozo OHSHIMA,† and Akira AMANO
Department of Applied Chemistry, Faculty of Engineering, Tohoku University, Aoba, Aramaki, Sendai 980
†Department of Fuel Chemistry, Faculty of Mining, Akita University, Gakuen-cho, Tegata, Akita 010
(Received December 25, 1986)

The title reaction was investigated at room temperature and under pressures ranging from 133 to 2660 Pa. 1-Butanethiol, butane, and 1-butene were the main products. In the reaction with deuterium atom, dibutyl disulfide and 1-butanethiol were not deuterated, while butane was monodeuterated. The following mechanism was proposed to account for the product composition and its pressure dependency as well as the deuterium labeling of the products. $C_4H_9SSC_4H_9+D\cdot \rightarrow n\text{-}C_4H_9SD + n\text{-}C_4H_9S\cdot$, $n\text{-}C_4H_9S\cdot + D\cdot \rightarrow n\text{-}C_4H_9SD^*$, $n\text{-}C_4H_9SD^*+M \rightarrow n\text{-}C_4H_9SD$, $n\text{-}C_4H_9SD^* \rightarrow \Delta'\text{-}C_4H_8+HDS$, $n\text{-}C_4H_9SD^* \rightarrow n\text{-}C_4H_9\cdot + DS\cdot$, $n\text{-}C_4H_9\cdot + D\cdot \rightarrow n\text{-}C_4H_9D$, $n\text{-}C_4H_9\cdot + D\cdot \rightarrow \Delta'\text{-}C_4H_8+HD$.

In our continuing effort to work out the mechanism of the reactions between thiols with H atom,[1-3] involvement of chemically activated thiols and metastable intermediate containing trivalent sulfur has been pointed out as its characteristic feature. The overall reaction is the hydrodesulfurization of thiols, which is initiated by

$$RSH + H\cdot \rightarrow RS\cdot + H_2 \quad (1)$$

and

$$RSH + H\cdot \rightarrow R\cdot + H_2S \quad (2)$$

taking place simultaneously. Thiyl radical, produced in reaction (1), subsequently forms chemically activated thiol, RSH*, which in turn becomes a source of the unique hydrodesulfurization. Reaction (2), a novel metathesis characteristic to the reactions of sulfur containing compounds with H atom, is considered to take place via the formation of metastable intermediate, $RSH_2\cdot$. Product composition of the overall reaction is governed by the relative importance between reactions (1) and (2).

In the present work, the study is extended to the reactions of disulfide with H and D atoms. Dibutyl disulfide is chosen as the substrate. The present experimental results can thus be compared conveniently with those of 1-butanethiol already accumulated in our laboratory.[1] As a result of the present study, mechanistic interpretation of reaction pathway turns out to be much less equivocal with this particular substrate, since it does not directly produce R· as in reaction (2).

Experimental

A conventional discharge flow apparatus was adopted. Details were described elsewhere.[1] Dibutyl disulfide and H_2 (or D_2), both diluted with excess He, were introduced into a Pyrex reactor tube of 400 mm in length and 27 mm in inside diameter. Flow rates of dibutyl disulfide, H_2 (or D_2), and He were 0.001 ml(NTP) s^{-1}, 0.01 ml(NTP) s^{-1}, and 0.72—14.4 ml(NTP) s^{-1} respectively. H atom (or D atom) was generated by passing H_2 (or D_2) through a microwave discharge cavity placed at the upstream side of the reactor. The reactor surface was coated with boric acid to prevent H atom (or D atom) from recombination.

The reaction was carried out at room temperature and under pressures ranging from 133 to 2660 Pa. Reacting gas mixture was intermittently withdrawn through a nozzle and was isolated into a side arm chilled by liquid N_2. The isolated sample was then analyzed by GC and GC-MS, using VZ-10 column (2 m, 328 K) for hydrocarbons and polyethylene glycol column (1 m, 363 K) for organosulfur compounds.

Commercially available purest grade dibutyl disulfide was purified by trap-to-trap distillation, and the fraction of better than 99% purity was used. Cylindered gases of H_2, D_2, and He were dried by passing through a train of liquid N_2 traps.

Results

1-Butanethiol, butane, and 1-butene were the main products of the reaction with H atom. Small amounts of *cis*-2-butene, *trans*-2-butene, and fragmental products such as propane, propylene, ethane, and ethylene were also formed. No sulfide was detected in the product. Based on the mass balance, methane, if any, was formed only in a limited amount.

Product composition vs. conversion relations observed with the three major products under 133, 530, and 2660 Pa are shown in Figs. 1, 2, and 3, respectively. Although 1-butanethiol was by far the most important, all the three major components were clearly the

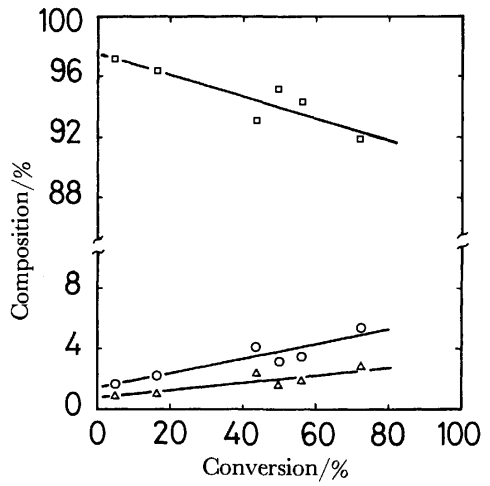

Fig. 1. Composition vs. conversion relation under 133 Pa. □: 1-Butanethiol, ○: butane, △: 1-butene.

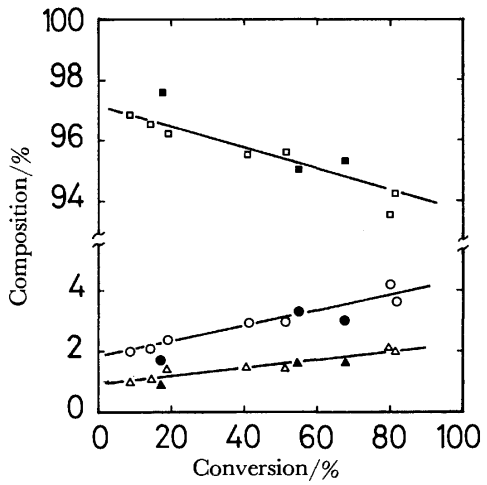

Fig. 2. Composition vs. conversion relation under 530 Pa. □: 1-Butanethiol, ○: butane, △: 1-butene. Filled symbols indicate the reaction with D atom.

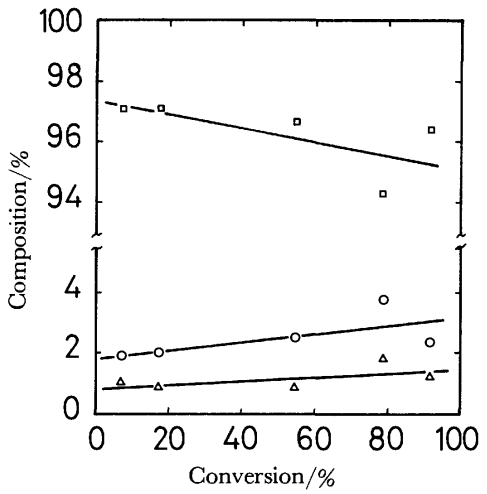

Fig. 3. Composition vs. conversion relation under 2660 Pa. □: 1-Butanethiol, ○: butane, △: 1-butene.

initial products. And, up to 90% conversion, these three together accounted practically for all the substrate consumed. As can be seen with filled symbols in Fig. 2, the product composition remained unchanged when D atom was used instead of H atom. The decreasing trend in 1-butanethiol compensated the increasing trend in butane and 1-butene. Thus, the reaction can be described by the following stoichiometry:

$$(C_4H_9S)_2 + H \rightarrow (2-a-b)\ C_4H_9SH + a\ C_4H_{10} + b\ C_4H_8$$

where a and b are stoichiometric coefficients. Irrespective of the pressure used, the ratio a/b of about 0.5 was deduced from the figures. The ratio $(a+b)/(2-a-b)$, however, decreased as the pressure increased. The latter ratios were 0.08 at 133 Pa, 0.05 at 530 Pa, and 0.03 at 2660 Pa.

Practically no isotopic mixing was observed with dibutyl disulfide left unreacted. Deuterium distributions observed with butane and 1-butene are listed in Table 1 for a few different conversions. Approximately one D atom was introduced into each butane molecule produced. Both 1-butene[D_0] and 1-butene-[D_1] were formed, and the latter became progressively important as conversion increased.

Table 1. Relative Abundance of Deuterium Labeled Products

Conversion/%	Butane			1-Butene		
	D_0	D_1	D_2	D_0	D_1	D_2
16.8	9	100	1	100	27	1
46.6	2	100		100	71	1
68.1		100		100	116	
89.1	3	100	2	100	103	2

The conventional GC-MS analysis showed no D-labeled 1-butanethiol. But, with a quadrapole mass spectrometer connected directly to the reactor tube, 1-butanethiol[D_1] was found to be an exclusive constituent. It may therefore be concluded that 1-butanethiol was monodeuterated in the course of the reaction, and that the result as observed with GC-MS was due to the retro H-D exchange between residual water in the ionization chamber and mercapto-D of 1-butanethiol[D_1].

Discussion

Heat of Formation of the Species in Relevance with the Present System. The values of the heat of formation of the species involved in the present study are estimated using a conventional additivity rule,[4] and are listed in Table 2. Error limits of the listed values are ±1.0 kcal mol^{-1} (1 kcal$_{th}$=4.184 kJ) for stable molecules, and ±2.0 kcal mol^{-1} for radicals. The reliability level of the additivity rule used here may be seen by comparing the tabulated data with literature values of $\Delta H^0_f(C_4H_9SH)$=−21.06 kcal mol^{-1},[5] and $\Delta H^0_f(C_4H_9SSC_4H_9)$=−37.63 kcal mol^{-1}.[6]

Initial Step. In analogy with the reactions of thiols and sulfides with H atom, and based on the fact that fragmentation of alkyl group was only trivial, the initial act of H atom is presumably its addition to one of the S atoms of the substrate molecule. Therefore, the following reactions are plausible.

$$C_4H_9SSC_4H_9 + D\cdot \rightarrow n\text{-}C_4H_9SD + C_4H_9S\cdot \quad (3)$$

$$C_4H_9SSC_4H_9 + D\cdot \rightarrow n\text{-}C_4H_9SSD + C_4H_9\cdot \quad (4)$$

For the sake of clarity, we hereafter write D standing for both hydrogen and deuterium atoms. Based on the

Table 2. Standard Heat of Formation of the Related Species[a)]

Species	ΔH^0_f / kcal mol^{-1}
n-C_4H_9SH	−21.1
n-C_4H_9SSH	−16.8
$C_4H_9SSC_4H_9$	−37.3
n-$C_4H_9\cdot$	15.8
n-$C_4H_9S\cdot$	17.8

a) Ref. 4.

values listed in Table 2, reactions (3) and (4) are exothermic by 18.1 and 15.8 kcal mol^{-1}, respectively. Therefore, reaction (3) is thermochemically more favorable.

We may also reject reaction (4) as a reaction of importance on the ground of the following argument. If reaction (4) takes place significantly, butyl radical should subsequently form butane and butenes through the intermolecular H transfer or else should form sulfide through the following reaction:

$$C_4H_9\cdot + C_4H_9SSC_4H_9 \rightarrow C_4H_9SC_4H_9 + C_4H_9S\cdot. \quad (5)$$

The results observed, however, turned out to be contrary to the above presumption. As will be described later, small amount of hydrocarbons observed in the product can be simply accounted for by the secondary reactions of $C_4H_9S\cdot$ produced in reaction (3). And, dibutyl sulfide, expected product of reaction (5), was not detected in the product.

The initiation quite analogous to reaction (3) was also suggested in the reactions of dimethyl and diethyl disulfides with H atom.[7] The reaction is considered to take place via the intermediary formation of the novel adduct $C_4H_9SS(H)C_4H_9$.[2] However, to date, no mention has been made on the structure and stability of such adduct. Recently, it was proposed that S-S bond in RSS(R)SR$\cdot$, formed in the reaction between RS$\cdot$ and RSSR, was weakened by at least one quarter of a normal S-S *sigma*-bond.[8]

Secondary Reactions. In their study on the reactions of dimethyl and diethyl disulfides with H atom, Strausz et al. reported the formation of a considerable amount of polymers.[7] The formation of polymers in the above instance, being due to the low concentration of H atom used in their work, made it difficult for them to elucidate the fate of thiyl radical produced by reaction (3). In the present work, H atom concentration was maintained at the level not less than the concentration of the substrate. Consequently, practically no polymer was formed, and the amount of 1-butanethiol in the product accounted for more than 90% of dibutyl disulfide consumed over the wide conversion range. This indicates that reaction (3) is followed by

$$C_4H_9S\cdot + D\cdot \rightarrow n\text{-}C_4H_9SD^* \quad (6)$$

and

$$n\text{-}C_4H_9SD^* + M \rightarrow n\text{-}C_4H_9SD, \quad (7)$$

and that dibutyl disulfide is considerably more reactive than 1-butanethiol in the reaction with H atom. The latter statement is in accord with some existing rate data listed in Table 3. Further reactions of 1-butanethiol may therefore be ignored in formulating a group of secondary reactions. It should be noted here that the asterisk denotes chemically activated species and M the bath molecule.

Conceivable reactions of the chemically activated 1-butanethiol, other than reaction (7), are

$$n\text{-}C_4H_9SD^* \rightarrow \Delta'\text{-}C_4H_8 + HDS \quad (8)$$

and

$$n\text{-}C_4H_9SD^* \rightarrow n\text{-}C_4H_9\cdot + DS\cdot. \quad (9)$$

Reactions subsequent to reaction (9) are the following:

$$n\text{-}C_4H_9\cdot + D\cdot \rightarrow n\text{-}C_4H_9D \quad (10)$$

and

$$n\text{-}C_4H_9\cdot + D\cdot \rightarrow \Delta'\text{-}C_4H_8 + HD. \quad (11)$$

According to the scheme, consisting of reactions (7)—(11), [hydrocarbon]/[1-butanethiol] ratio should decrease as pressure increases. This is quite in accord with the result mentioned earlier that the ratio $(a+b)/(2-a-b)$ decreased from 0.08 at 133 Pa to 0.03 at 2660 Pa. One D atom is introduced into butane through reaction (10), while no channel exists to produce D-labeled 1-butene. During a later stage, however, D-labeled 1-butene may be formed through the sequence comprising D-addition and H-abstraction. These are also quite in accord with the present result.

It should be noted that the sequence of elementary reactions, from reaction (6) through reaction (11), is identical with the one proposed for the reaction of 1-butanethiol with H atom, and was, therefore, thoroughly discussed already.[1,3]

1-Butene/Butane Ratio. According to the proposed mechanism, the following formula can be obtained to relate the ratio of 1-butene to butane.

$$[\text{1-butene}]/[\text{butane}] = k_8/k_9 + k_{11}/k_{10}(1 + k_8/k_9).$$

The ratio [1-butene]/[butane] was observed to be 0.5 in the present study. The ratio k_{11}/k_{10}=0.05 was estimated in the reactions of ethyl radical with H atom[10] and propyl radical with methyl radical.[11] Based on

Table 3. Rate Constant and Activation Energy of the Reaction of Sulfur Compounds with H Atom

Compound	Rate constant	Activation energy	Reference
	l mol^{-1} s^{-1}	kcal mol^{-1}	
Dimethyl disulfide	4.80×10^9	0.1	7
Diethyl disulfide	2.74×10^9	1.7	7
Dimethyl sulfide	2.10×10^8	2.6	9
Diethyl sulfide	0.80×10^8	3.8	9
Thiolane	2.92×10^8	2.0	3
Methanethiol	7.80×10^8	1.7[a], 2.6[b]	2
1-Butanethiol	1.01×10^8	2.2[a], 3.2[b]	1

a) Assigned for reaction (1). b) Assigned for reaction (2).

these values, the value of 0.43 can be deduced for the ratio k_8/k_9. On the other hand, k_8/k_9=0.18 was reported in the very low pressure pyrolysis of 1-butanethiol.[12] There is, therefore, a considerable difference between the chemically activated 1-butanethiol and the thermo-energized 1-butanethiol in their H-addition and H-abstraction rate ratios.

References

1) O. Horie, J. Nishino, and A. Amano, *Int. J. Chem. Kinet.*, **10**, 1043 (1978); T. Kamo, J. Tang, M. Yamada, and A. Amano, *Nippon Kagaku Kaishi*, in press.

2) K. Hashimoto and M. Yamada, *Nippon Kagaku Kaishi*, **1983**, 678; A. Amano, M. Yamada, K. Hashimoto, and K. Sugiura, *ibid.*, **1983**, 385.

3) O. Horie, K. Onuki, and A. Amano, *J. Phys. Chem.*, **81**, 1706 (1977).

4) S. W. Benson, "Thermochemical Kinetics," 2nd ed, John Wiley & Sons, New York (1976); S. W. Benson, *Chem. Rev.*, **78**, 23 (1978).

5) D. W. Scott and J. M. McCullough, U. S. Bureau of Mines Bulletin 595, U. S. Government Printing Office, Washington, D. C., 1961.

6) S. W. Benson, F. R. Cruickshank, D. M. Golden, G. R. Haugen, H. E. O'Neal, A. S. Rodgers, R. Shaw, and R. Walsh, *Chem. Rev.*, **1968**, 279.

7) M. M. Ekwenchi, A. Jodhan, and O. P. Strausz, *Int. J. Chem. Kinet.*, **12**, 431 (1980); M. M. Ekwenchi, I. Safarik, and O. P. Strausz, *ibid.*, **13**, 799 (1981).

8) M. Bonifacic and K-D. Asmus, *J. Phys. Chem.*, **88**, 6286 (1984).

9) T. Yokota and O. P. Strausz, *J. Phys. Chem.*, **83**, 3196 (1979); M. M. Ekwenchi, I. Safarik, and O. P. Strausz, *Can. J. Chem.*, **59**, 3226 (1981).

10) J. O. Terry and J. H. Futrell, *Can. J. Chem.*, **45**, 2327 (1967).

11) J. W. Kraus and J. G. Calvert, *J. Am. Chem. Soc.*, **79**, 5921 (1957).

12) M. Yamada, Y. Takahashi, T. Kamo, Y. Ohshima, and A. Amano, *Nippon Kagaku Kaishi*, **1985**, 1560; M. Yamada, T. Kamo, J. Tang, Y. Ohshima, and A. Amano, *ibid.*, **1985**, 2283.

Microenvironmental Effects of Water-Soluble Polymers on the Chemiluminescence of Luminol and Its Analogs

Hajime KARATANI
Laboratory of Analytical Chemistry, Faculty of Textile Science, Kyoto Institute of Technology, Matsugasaki, Sakyo-ku, Kyoto 606
(Received July 31, 1986)

The effects of water-soluble polymers(WSPs), such as bovine serum albumin(BSA) and polyethylenimine-(PEI), on chemiluminescence(CL) in an aqueous solution have been studied. The CL emission, particularly in the initial stage of the CL reaction, was strongly enhanced by increasing the concentrations of these WSPs. This was attributed to the acceleration of the chemical reactions prior to the formation of the light-emitting species. BSA was also peculiar in that it could enhance CL under neutral pH conditions. It was suggested that these WSPs offered hydrophobic and basic microenvironments well suited to the CL reaction.

The microenvironment of an aqueous solution has a substantial effect on the chemi- and the bioluminescence.[1-4] In particular, the microenvironmental effects of surfactants, such as hexadecyltrimethylammonium bromide(CTAB), polyoxyethylene sorbitan monostearate(Tween 60), polyoxyethylene(10)octylphenyl ether(Triton X-100), polyoxyethylene(23)-dodecanol(Brij-35), and sodium dodecyl sulfate(SDS), to enhance the CL emission of lucigenin(*N,N'*-dimethyl-9,9'-biacridinium dinitrate) and of luminol(5-amino-2,3-dihydro-1,4-phthalazinedione) are interesting from the standpoint of analytical chemistry.[5-8]

CL-enhancement effects can arise from several factors: (1) The rate of the reaction leading to the formation of the light-emitter, (2) the CL excitation efficiency, (3) the fluorescence quantum yield of the emitter, and (4) some combination of these factors.[6]

To date, only a few reports have dealt with the relationship between the CL-emission intensity in the presence of surfactants and the above-mentioned factors.[1,4,6] In the CL of cypridina luciferin, two factors, (1) and (3), have a substantial effects on the enhancement of its CL emission,[1] while the (2) factor is significant in the CL of MAD(9-methylene-10-dodecylacridane).[4] Two factors, (1) and (2), contribute to an increase in the CL-emission intensity of lucigenin.[6]

Such WSPs as BSA and PEI show a strong binding affinity to small aromatic anions.[9,10] These are expected to influence the CL reaction significantly. However, the effects of the WSPs on the CL emission have not yet been studied. In this paper, the effects of BSA and PEI(Mw: 70,000) on the CL emission centering around luminol were studied and were evaluated from the analytical standpoint. The other compounds used in this study were isoluminol(6-amino-2,3-dihydro-1,4-phthalazinedione) and *N*-(4-aminobutyl)-isoluminol derivatives (ABI derivatives: 6-[*N*-(4-aminobutyl)alkylamino]-2,3-dihydro-1,4-phthalazinedione) (Fig. 1).

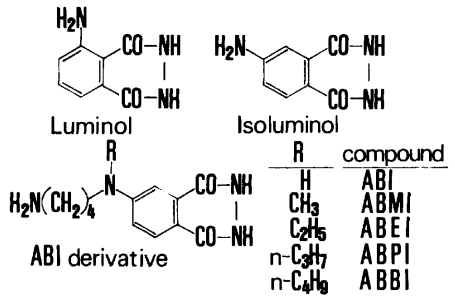

Fig. 1. Chemical structures of luminol and its analogs.

Results

The CL reaction in this study was initiated with a hydrogen peroxide(H_2O_2)-potassium peroxodisulfate($K_2S_2O_8$) co-oxidation system in 0.1 mol dm^{-3} aqueous sodium carbonate (Na_2CO_3, pH 11.4). The following scheme, Scheme 1, is proposed as the CL reaction mechanism of luminol(pK_a=6 and 13).[14,15] The CL reaction of the other compounds also seems to follow Scheme 1. The reaction is of the first order in the CL

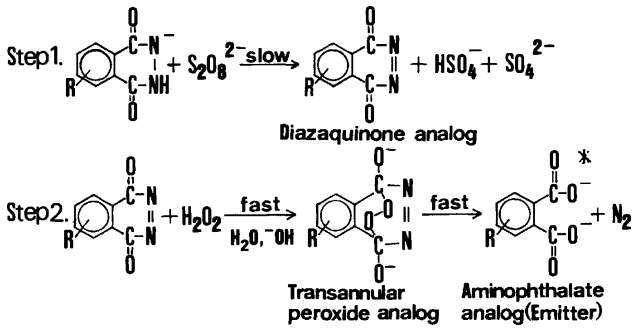

Scheme 1.

compound and in peroxodisulfate($S_2O_8^{2-}$), but is of zero order in H_2O_2 and at hydroxide(OH^-) concentration under the conditions of this experiment.[14]

The CL quantum yield(ϕ_{CL}) based on the starting luminols is the product of several variables:[15]

$$\phi_{CL} = \phi_r \cdot \phi_{es} \cdot \phi_{fl}, \quad (1)$$

where ϕ_r is the fraction of molecules following the correct chemical reaction path, ϕ_{es} is the fraction of those product molecules that are formed in the excited emitter, i.e., the CL excitation efficiency, and ϕ_{fl} is the fluorescence quantum yield of the emitter. In this study, the ϕ_{fl} values were determined on the basis of the

Table 1. Quantum Yields of Luminol and Its Analogs[a)]

Compound[b)]	$\phi_r \cdot \phi_{es}$[c)]	ϕ_{fl}	ϕ_{CL}
Luminol	0.059	0.16	0.0094[d)]
Isoluminol	0.048	0.034	0.0017[e)]
ABI	0.12	0.040	0.0049
ABMI	0.29	0.053	0.016
ABEI	0.19	0.044	0.0083
ABPI	0.16	0.038	0.0059
ABBI	0.070	0.039	0.0027

a) Oxidation system: H_2O_2–$K_2S_2O_8$. b) [Compound]= 1.6×10^{-5} mol dm^{-3} in 0.1 mol dm^{-3} Na_2CO_3. c) The product, $\phi_r \cdot \phi_{es}$, was calculated according to Eq. 1 from the experimentally determined ϕ_{fl} and ϕ_{CL} values. ϕ_r is usually assumed to be approximately unity. Ref. 15. d) Reported value=0.006—0.009. Ref. 14, 20. e) Reported value=0.0012 (it was measured in 0.1 mol dm^{-3} K_2CO_3 with H_2O_2 and hemin.). Ref. 16.

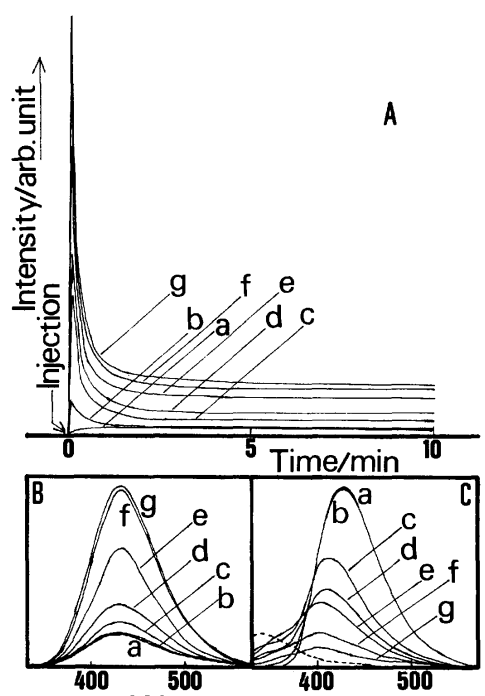

Fig. 2. Time course of luminol chemiluminescence (A), chemiluminescence spectra at 10—12.5 min after the initiation of the reaction (B), and fluorescence spectra of the total reaction mixture at 48 h after the initiation of the reaction (C) with and without BSA. [Luminol]=8.0×10^{-5} mol dm^{-3} in 0.1 mol dm^{-3} Na_2CO_3. [H_2O_2]=0.1 mol dm^{-3}. [$K_2S_2O_8$]=2.5×10^{-4} mol dm^{-3}. [BSA]/wt%: a=0, b=0.020, c=0.40, d=0.60, e=1.2, f=2.4, g=4.0. Excitation: 306 nm. Broken line in (C): Fluorescence spectrum of 1.0 wt% of BSA in 0.1 mol dm^{-3} Na_2CO_3 (pH 11.4).

total reaction mixture at the end of the CL reaction(48 h after CL initiation). The values of these variables are summarized in Table 1.

Figure 2 shows the effects of BSA on the CL of luminol. In the presence of BSA, the CL emission reached its maximum intensity at about 10 s after the initiation of the reaction and thereafter rapidly to a constant level. The CL emission intensities in both the initial stage and in the plateau region increased with the increase in the BSA concentration. The CL-spectrum maximum from 10 to 12.5 min after the initiation of the reaction was affected little by the addition of BSA, whereas the fluorescence-spectrum maximum of the total reaction mixture at the end of the reaction, 48 h after the initiation of the reaction, shifted considerably to shorter wave lengths and its intensity was lower than that obtained for the total reaction mixture in the absence of BSA. The inherent fluorescence of BSA in the total reaction mixture also

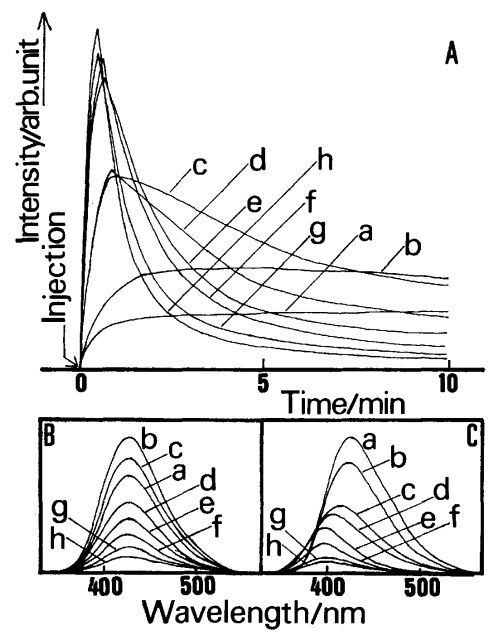

Fig. 3. Time course of luminol chemiluminescence (A), chemiluminescence spectra at 10—12.5 min after the initiation of the reaction (B) and fluorescence spectra of the total reaction mixture at 48 h after the initiation of the reaction (C) with and without BSA. [Luminol]=8.0×10^{-5} mol dm^{-3} in 0.1 mol dm^{-3} Na_2CO_3. [H_2O_2]=0.10 mol dm^{-3}. [$K_2S_2O_8$]=2.5×10^{-4} mol dm^{-3}. [PEI]/wt%: a=0, b=0.010, c=0.050, d=0.10, e=0.25, f=0.50, g=1.0, h=2.0. Excitation: 306 nm.

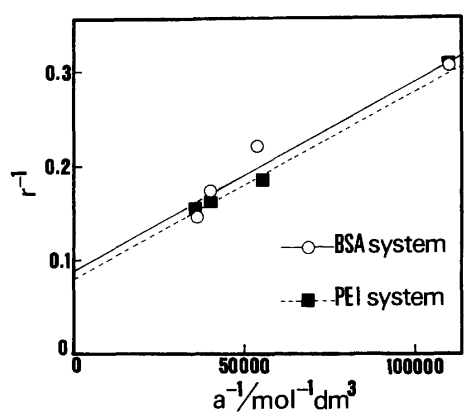

Fig. 4. Reciprocal of average mole ratio of bound luminol monoanions to WSP ($1/r$) vs. reciprocal of equilibrium concentration of luminol monoanions ($1/a$). Solvent: 0.1 mol dm^{-3} Na_2CO_3. [WSP]=0.10 wt%. [Luminol]=1.0×10^{-5}—3.0×10^{-5} mol dm^{-3}.

become weaker than in the 0.1 mol dm^{-3} Na_2CO_3 solution.

PEI also influenced the CL emission, particularly in the initial stage, as is shown in Fig. 3. In this case, much more time was required for the attainment of the CL-emission peak than in the BSA system. By analogy to the BSA, the fluorescence spectrum shifted to a shorter wavelength, and its intensity decreased, with the increase in the PEI concentration. In this case, PEI was non-fluorescent, unlike BSA.

The binding constant(K, mol^{-1} dm^3) between the luminol monoanions and the WSPs and the maximum possible number of bound luminol monoanions per WSP molecule(n) were determined using the equilibrium dialysis method following Eq. 2, as suggested by Klotz et al.:[9]

$$1/r = 1/n + 1/n \cdot K \cdot a, \quad (2)$$

where r is the moles of luminol monoanions bound to the total moles of WSP and where a is the molar concentration of free luminol monoanions at equilibrium. The measurements were made in 0.1 mol dm^{-3} aqueous Na_2CO_3. Both K and n can be calculated from a linear plot of $1/r$ vs. $1/a$. Figure 4 shows the results of the analysis of the relationship between the luminol monoanions and the WSPs. In this system containing 0.1 wt% of BSA, the K and n values were 4.41×10^4 mol^{-1} dm^3 and 11 respectively, while they were 3.72×10^4 mol^{-1} dm^3 and 12 respectively in the presence of 0.1 wt% of PEI(Mw: 70000).

Figure 5 indicates the relationship between the initial CL-emission intensity(CL intensity, I; at 10 s after the initiation of the reaction) and the concentration of WSP. The ratio of the CL intensity in the presence of WSP to that in the absence of WSP was plotted as a function of the WSP concentration.

Figure 6 indicates the effects of various surfactants on the CL emission. As is shown in Fig. 6, the surfactants did not affect the initial CL emission nearly as much as the WSPs. In addition, unlike the system containing the WSPs, the shifts of the fluorescence-spectrum maximum were not observed.

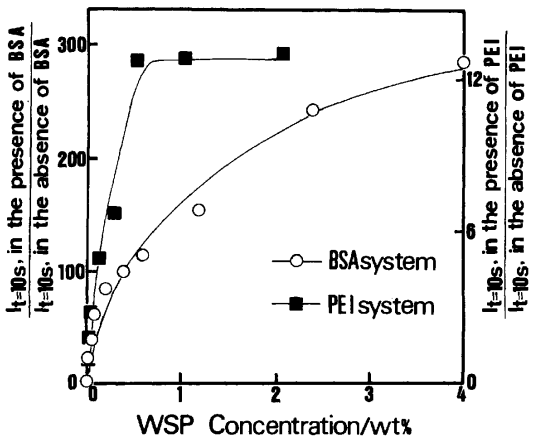

Fig. 5. Effects of BSA and PEI on the initial chemiluminescence intensity($I_{t=10s}$). [Luminol]= 8.0×10^{-5} mol dm^{-3} in 0.1 mol dm^{-3} Na_2CO_3. [H_2O_2]=0.10 mol dm^{-3}. [$K_2S_2O_8$]=2.5×10^{-4} mol dm^{-3}. [BSA]=0.10 wt%. [PEI]=0.10 wt%.

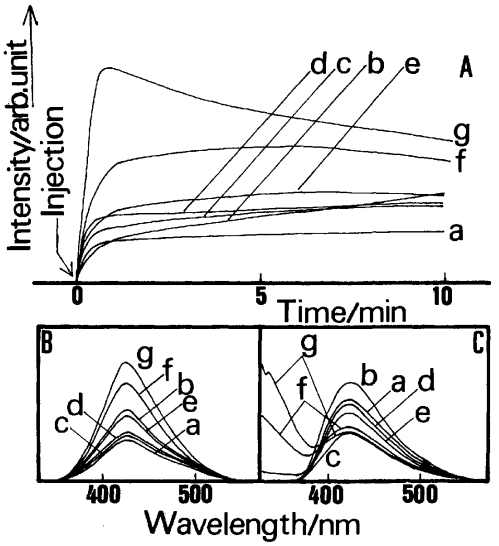

Fig. 6. Time course of luminol chemiluminescence (A), chemiluminescence spectra at 10—12.5 min after the initiation of the reaction (B) and fluorescence spectra of the total reaction mixture at 48 h after the initiation of the reaction (C) with and without surfactants. [Luminol]=8.0×10^{-5} mol dm^{-3} in 0.1 mol dm^{-3} Na_2CO_3. [H_2O_2]=0.10 mol dm^{-3}. [$K_2S_2O_8$]=2.5×10^{-4} mol dm^{-3}. [Surfactant]/mol dm^{-3}: a; surfactant free, b; [CTAB]=1.8×10^{-3}, c; [SDS]=1.6×10^{-2}, d; [Brij 35]=2.0×10^{-4}, e; [Triton X-100]=8.0×10^{-4}, f; [Triton X-100]=8.0×10^{-3}, g; [Triton X-100]=2.0×10^{-2}. a—e: cmc×2, f: cmc×20, g: cmc×50. These cmc values are in water (Refs. 6, 8).

Table 2. Effect of BSA on ϕ_{fl} and on CL Intensity(I). $\phi_{fl,BSA\text{-free}}$, $\phi_{fl,BSA}$, and Initial I Ratio

Compound[a]	$\phi_{fl,BSA\text{-free}}$	$\phi_{fl,BSA}$[b]	$I_{BSA}/I_{BSA\text{-free}}$[c]
Luminol	0.16	0.17	66.7
Isoluminol	0.034	0.030	40.3
ABI	0.040	0.050	5.3
ABMI	0.053	0.045	10.3
ABEI	0.044	0.043	9.7
ABPI	0.038	0.043	4.5
ABBI	0.039	0.040	5.5

a) [Compound]=1.6×10^{-5} mol dm^{-3} in 0.1 mol dm^{-3} Na_2CO_3. b) [BSA]=0.10 wt%. c) I in the presence of BSA to I in the absence of BSA at 10 s after the initiation of the reaction.

The effects of BSA on various CL reactions were also examined. Table 2 shows the ϕ_{fl} values with and without BSA and the initial I ratio(I in the presence of BSA to I in the absence of BSA) at 10 s after the initiation of the reaction. As has been referred to earlier, the ϕ_{fl} values were determined based on the total reaction mixture at the end of the CL reaction(48 h after CL initiation). The concentration of BSA was 0.10 wt%. In such a fairly dilute system, BSA had only a small influence on the fluorescence of the total reaction mixture.

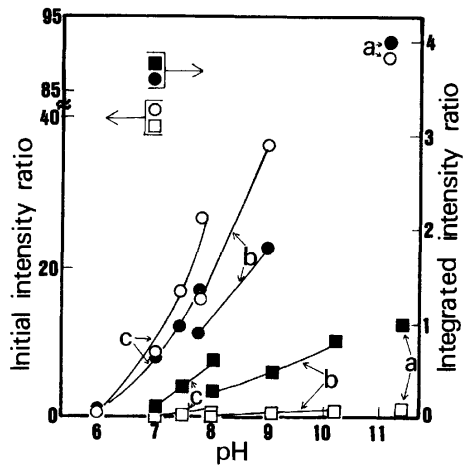

Fig. 7. Comparison of the chemiluminescence-emission intensity of luminol under various pH conditions with and without BSA. [Luminol]=8.0×10^{-5} mol dm^{-3}. [H_2O_2]=0.10 mol dm^{-3}. [$K_2S_2O_8$]=2.5×10^{-4} mol dm^{-3}. [BSA]=0.50 wt%. a: Prepared with 0.1 mol dm^{-3} Na_2CO_3, b: prepared with 0.05 mol dm^{-3} borate/NaOH buffer solution, c: prepared with 0.1 mol dm^{-3} phosphate buffer solution. ○, ●: With BSA. □, ■: Without BSA. The intensity ratios were calculated on the basis of the initial intensity (t=10 s) or the integrated intensity (during 10 min after the initiation of the reaction) measured in 0.1 mol dm^{-3} Na_2CO_3 without BSA.

Figure 7 shows the CL-emission intensities measured under various pH conditions in the presence of BSA.

Discussion

Time Course of CL Emission. The effects of BSA and PEI on the time course will be described briefly, since it is important to evaluate the features of the time course of CL emission if we are to use CL for analytical chemistry.

In the presence of BSA (Fig. 2A), the time required to reach the CL-emission peak is nearly constant and is independent of the BSA concentration, irrespective of the peak intensity. In the decay part in Fig. 2A, there are at least two decay components, one of them decays rapidly, while the other one lasts more than 10 min.

On the other hand, in the presence of PEI (Fig. 3A), the time required to reach the CL-emission peak depends on the PEI concentration and becomes shorter, approaching an almost constant value, as the PEI concentration increases. The decay feature with no prolonged emission is also different from that in the presence of BSA.

It is difficult to elucidate the time course in detail, since the interaction between these WSPs and the dissolved chemical species may well be very intricate. However, the effects of these WSPs, especially BSA, on enhancing the initial CL emission seem to have a great practical value from the analytical standpoint.

Enhancement of CL Emission. The most remarkable feature of the absorption spectra of luminol and its analogs in the 0.1 mol dm^{-3} Na_2CO_3 solution containing BSA or PEI was that the absorption peak near 230 nm becomes small and shifts to the longer wavelength side by 5—10 nm. This suggests that the monoanions of these CL compounds are bound to the hydrophobic region of BSA or PEI, like other aromatic anions.[9-13] In this connection, it was worth noting that most of the acidic groups in BSA are dissociated in the 0.1 mol dm^{-3} Na_2CO_3 solution. A similar thing is true with the ammonium protons on PEI(pK_a≈6). Therefore, BSA and PEI under the present reaction conditions are likely to afford basic binding sites(for binding acidic CL compounds) in addition to their inherent hydrophobic sites within the polymer matrix. The binding affinities of the luminol monoanions to both BSA and PEI seem similar, for there is no marked difference in the K values or n values determined in the two WSP systems.

As is shown in Figs. 2A and 3A, the microenvironments offered by BSA or PEI mentioned above caused remarkable CL-enhancing effects in the initial stage of the CL reaction. Such effects were remarkable, especially in the presence of BSA, as is shown in Fig. 5. The difference in the effects of WSPs on the initial CL emission seems to depend significantly on their basic properties rather than on their hydrophobic properties. This seems to be supported by the fact that no strong initial CL emission is observed in the presence of surfactants without basic groups in their micelles (Fig. 6A).

It should also be emphasized that the CL-enhancing effects were even observed in a very dilute WSP. Such was not the case with surfactants. They usually did not show any CL-enhancing effects below their critical micelle concentrations(cmcs).[5,6]

As is listed in Table 2, the initial I ratios in various CL reactions increased in the presence of BSA. The introduction of the electron-donating substituent to the amino group of isoluminol results in the higher ϕ_{es}.[15] This was also observed in the CL of ABI derivatives, as is summarized in Table 1. This is because the electron-donating property of the aminobutylalkyl substituents of the ABI derivatives is advantageous for the intramolecular chemically initiated electron-exchange luminescence(CIEEL) mechanism.[17,18] In the BSA molecule, various basic groups carrying lone-pair electrons seem to be able to interact with the protons of the amino and hydrazide groups of luminol, as is generally observed in the interaction between enzymes and substrates.[19] In other words, BSA in a basic solution is considered to be able to give an advantageous reaction field to the intramolecular CIEEL mechanism, particularly in the CL of luminol or isoluminol. However, in this study it is difficult to relate the microenvironmental effects to ϕ_{es} directly.

On the other hand, the effects of the WSPs on ϕ_{fl} are rather detrimental to the enhancement of the CL emission, as is shown in Figs. 2C and 3C. This was also

observed in the presence of a surfactant (Fig. 6C). The fluorescence intensity of 3-aminophthalate dianions (8.0×10^{-5} mol dm^{-3}) in 0.1 mol dm^{-3} Na_2CO_3 solutions containing various concentrations of BSA or PEI also decreased compared with that in the absence of BSA or PEI. However, the shifts in the fluorescence spectra shown in Figs. 2C and 3C were in conflict with the fact that there was no difference in the fluorescence-spectra maxima of 3-aminophthalate dianions in the system both with and without BSA or PEI (the shift was also not observed at 48 h after the preparation of the test solution). The shifts shown in Figs. 2C and 3C are thus at present difficult to explain.

Effects of WSP from the Analytical Standpoint. For the application of CL to clinical and biochemical analysis, it is important to obtain a strong CL emission, even under neutral pH conditions.[20] As is well known, the CL-emission intensity of luminol is much weaker under neutral conditions than under strongly alkaline conditions.[21] Thus, BSA was studied under neutral or weakly alkaline conditions in order to enhance the CL emission. As is shown in Fig. 7, the microenvironments of BSA were highly effective in producing a sufficient CL emission, even under neutral pH conditions. This indicates that BSA can be very useful enhancer of CL emission for analytical application. As is shown in Table 2, the effects of BSA on the CL emission of ABI derivatives are smaller than those of BSA in the CL emission of luminol, but BSA seems to be of practical value as a CL-enhancer with ABI derivatives also.

Experimental

Instruments. The UV and visible absorption spectra were measured by using a JASCO-610C spectrophotometer. The fluorescence and CL spectra were recorded with a Shimadzu RF-540 spectrofluorometer. In recording the CL spectra, the window of the excitation-light source was shut. In the measurements of the time course of the CL emission, the CL emission was received by a EMI 9893A/100 photomultiplier, and then the output photocurrent was amplified by a home-made preamplifier and recorded by a Matsushita VP-6431B recorder. The operational amplifier used in the I-V converter part of the preamplifier was an AD515KH apparatus. The guard ring was placed around the input terminals, and they were put on stand-off terminals made of Teflon for perfect insulation. In the measurements of the monochromatic-light-emission intensity, a Jovan-Yvon H-20 monochromator was set between the photomultiplier and a black box equipped with the CL reaction cell(inner-volume: 5 cm^3). The temperature in the black box was controlled using a thermistor. All the measurements were done at 25 °C. Mass-spectral analysis was performed by means of a Hitachi M-80B mass spectrometer.

Reagents. The BSA(F-V)(Mw: 70,000, Nakarai) was used as received. The PEI(Mw: 70,000, Wako) was dialysed against cellophane membrane for 3 days in distilled water, and then the solvent was evaporated to give a highly viscous liquid. The CTAB, SDS, Triton X-100, and Brij-35 were all purchased from Wako and used as received. The luminol (Wako), isoluminol(Tokyo Kasei), and 3-aminophthalate (Kanto Kagaku) were used after recrystallization from 0.6 mol dm^{-3} HCl. The ABI, ABMI, ABEI, ABPI, and ABBI were synthesized by a modification of the method of Schroeder et al. for ABEI.[22] The melting-point data are uncorrected values. These compounds were synthesized according to Scheme 2.

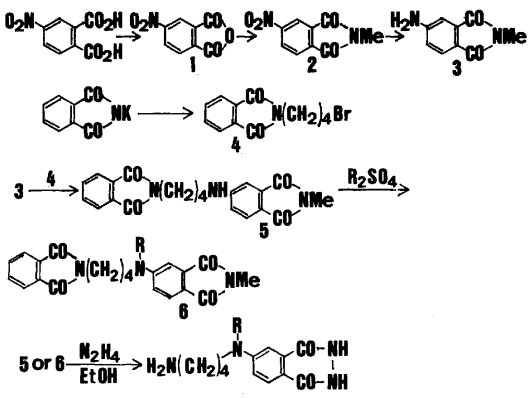

Scheme 2.

4-Amino-*N*-methylphthalimide (3). A modification of the method of Nicolet et al. was used for the syntheses of 4-nitrophthalic anhydride (**1**).[23] Compound **2** was synthesized as has been described in the literature.[22] Concentrated HCl (303 cm^3) and 48 cm^3 of water was added, drop by drop and successively, to a mixture of 50 g (0.24 mol) of **2** and 215 g (0.95 mol) of $SnCl_2\cdot2H_2O$, and then the reaction mixture was vigorously stirred for 1 h at 85 °C, resulting in a pale yellow solution. This solution was allowed to stand at room temperature over night. The product was precipitated as a white powder. Filtration and thorough washing with much water gave **3** as a yellow powder. This powder was dried at 120 °C for several hours; mp 246—248 °C.

***N*-(4-Bromobutyl)phthalimide (4).** This compound was synthesized according to the procedure in the literature.[24]

***N*-Methyl-4-*N*[4-(*N*-phthalimide)butyl]aminophthalimide (5).** This compound was likewise synthesized as has been described in the literature.[22]

The *N*-alkylation of **5** was performed by a reaction with dialkyl sulfate by reference to the literature.[22] To synthesize ABMI, a mixture of 7.5 g (0.02 mol) of **5** and 25 cm^3 (0.15 mol) of dimethylsulfate was stirred for 60 min at 140 °C under anhydrous conditions. After it had cooled to room temperature, the mixture was poured into 500 cm^3 of ice water to deposit a dark green-colored viscous fluid. This product was recrystallized from 50% H_2O-acetic acid several times to give yellow green crystals. Next, a mixture of 5 g (0.012 mol) of **6**, 14 cm^3 of anhydrous hydrazine, and 50 cm^3 of absolute ethanol was stirred for 4 h at 85 °C. Then the reaction mixture was cooled to room temperature. In the next step, after the excess hydrazine and ethanol had been removed by vaccum distillation, ABMI including the by-product was deposited as a faintly gray-colored solid. After filtration, it was mixed with 100 cm^3 of 3 mol dm^{-3} HCl to dissolve the ABMI. An insoluble by-product was removed by filtration. The filtrate was adjusted at pH 7—9 with 5 mol dm^{-3} potassium hydroxide, and soon ABMI precipitated as white crystals. They were recrystallized from 50% H_2O-*N*,*N*-dimethylformamide. Other ABI derivatives were

synthesized similarly.

Mass-Spectral Data. ABI; MS (70 eV) m/z (rel intensity) 248 (M^+; 45), 231 (15), 204 (48), 190 (100), and 177 (37); Found: m/z 248.1272. Calcd for $C_{12}H_{16}O_2N_4$: M, 248.2738. ABMI; MS (70 eV) m/z (rel intensity) 262 (M^+; 28), 218 (7), 204 (100), and 191 (11); Found: m/z 262.1415. Calcd for $C_{13}H_{18}O_2N_4$: M, 262.3007. ABEI; MS (70 eV) m/z (rel intensity) 276 (M^+; 26), 232 (5), 218 (100), 204 (8), and 190 (28); Found: m/z 276.1587. Calcd for $C_{14}H_{20}O_2N_4$: M, 276.3276. ABPI; MS (70 eV) m/z (rel intensity) 290 (M^+; 4), 248 (58), 204 (43), 190 (100), and 177 (21); Found: m/z 290.1739. Calcd for $C_{15}H_{22}O_2N_4$: M, 290.3545. ABBI; MS (70 eV) m/z (rel intensity) 304 (M^+; 34), 246 (68), 204 (34), 190 (50), and 72 (100); Found: m/z 304.1898. Calcd for $C_{16}H_{24}O_2N_4$: M, 304.3814.

The other reagents used in this study were of a reagent grade.

Determination of ϕ_{fl} and ϕ_{CL}. The fluorescence and CL spectra were corrected according to the method in the literature.[25] The correction of the intensity of the excitation light was made on the basis of the excitation spectrum of Rohdamine B (3 g dm^{-3} in ethylene glycol). The ϕ_{fl} was determined relative to the quantum yield of quinine sulfate.[25] The unknown ϕ_{fl} was given by the following equation:

$$\phi_{fl,sample}=\frac{A_{standard}\cdot N^2_{sample}\cdot I_{sample}}{A_{sample}\cdot N^2_{standard}\cdot I_{standard}}\cdot\phi_{fl,standard}, \quad (3)$$

where A, I, and N are, respectively, the absorbance, the fluorescence intensity (I=the area under the fluorescence spectrum), and the refractive index of the solution. $\phi_{fl,standard}$ is 0.55 at 25 °C. ϕ_{CL} was determined relative to the ϕ_{CL} of luminol in dimethyl sulfoxide. The unknown ϕ_{CL} was given by:[26]

$$\phi_{CL,sample}=\frac{q_{\lambda max,sample}\cdot A_{standard}\cdot f_{\lambda max,standard}}{q_{\lambda max,standard}\cdot A_{sample}\cdot f_{\lambda max,sample}}\cdot\phi_{CL,standard}, \quad (4)$$

where $q_{\lambda max}$ is the time integral of the measured phototube current at the peak wavelength of the CL spectrum, and where A is the number of the molecules reacted in the CL reaction. The fractional CL emission at λ_{max}, $f_{\lambda max}$, is calculated by integrating the area under the portion of the curve at the CL-spectrum maximum bound by the exact wavelength-band pass and by dividing it by the total area under the CL spectrum. $\phi_{CL,standard}$ is 0.0125 at 25 °C.[27]

Initiation of the CL Reaction. The CL reaction was initiated with a H_2O_2–$K_2S_2O_8$ co-oxidation system. The H_2O_2 and the $K_2S_2O_8$ were mixed just before use and then immediately injected into the CL reaction cell using a microsyringe while being stirred by the use of a magnetic stirrer for 30 s. The time required to make the solution homogeneous was within about 3 s in all CL reaction systems. In this study, a mixture of 40 μdm^3 of 35% H_2O_2 and 20 μdm^3 of 0.05 mol dm^{-3} aqueous $K_2S_2O_8$ was injected against 4 cm^3 of the solution of the CL compound in 0.1 mol dm^{-3} aqueous Na_2CO_3 (pH 11.4) (or in an appropriate pH-buffer solution). The concentrations of H_2O_2 and $K_2S_2O_8$ in the CL reaction mixtures were 0.10 and 2.5×10^{-4} mol dm^{-3} respectively.

Determination of pK_a. The pK_a values of the protonated PEI were determined by the titration of 0.46 wt% aqueous PEI (pH 10.2) with 0.05 mol dm^{-3} hydrochloric acid.

Determination of K and n. Both the K and n values were determined by reference to the literature.[9,28] The pretreatment of dialysis bags (Union Carbide, Cellophane Tubing-Seamless 30/32 inch for dialysis) was done according to the usual method.[29] The dialysis bags were filled with 20 cm^3 of the test solution, which contained 0.1 mol dm^{-3} Na_2CO_3, 0.1 wt% WSP, and various known concentrations of luminol (1.0×10^{-5}—3.0×10^{-5} mol dm^{-3}). The solution in the outside compartment (in which the dialysis bags were immersed) was the same as the test solution in volume, in Na_2CO_3 concentration, and in luminol concentration, but it contained no WSP. Three days were allowed for equilibration at 25 °C. The solution in the outside compartment was then analyzed by absorption spectrophotometry. In all systems, corrections were applied to take into account the absorption due to the WSP and due to the leachable material from the dialysis bag. The interaction between luminol and the dialysis bag was found to be negligible in the concentration range of luminol studied.

The author is grateful to Mr. Nobuaki Ohnishi, Faculty of Engineering and Design, Kyoto Institute of Technology, for the mass-spectral measurements.

References

1) T. Goto and H. Fukatsu, *Tetrahedron Lett.*, **1969**, 4299.

2) J. W. Hastings, Q. H. Gibson, J. Friendland, and J. Spudich, "Bioluminescence in Progress," ed by F. H. Johnson and Y. Haneda, Princeton University Press (1966), pp. 151—186.

3) J. W. Hastings, T. O. Baldwin, and M. Z. Nicoli, *Methods Enzymol.*, **51**, 135 (1978).

4) S. Shinkai, Y. Ishikawa, O. Manabe, and T. Kunitake, *Chem. Lett.*, **1981**, 1523.

5) L. L. Klopf and T. A. Nieman, *Anal. Chem.*, **51**, 1539 (1984).

6) W. L. Hinze, T. E. Riehl, H. N. Singh, and Y. Baba, *Anal. Chem.*, **56**, 2180 (1984).

7) M. Yamada, S. Kamiyama, and S. Suzuki, *Chem. Lett.*, **1985**, 1597.

8) T. Komatsu, M. Ohira, M. Yamada, and S. Suzuki, *Bull. Chem. Soc. Jpn.*, **59**, 1849 (1986).

9) I. M. Klotz, F. M. Walker, and R. B. Pivan, *J. Am. Chem. Soc.*, **68**, 1486 (1946).

10) J. J. Fischer and O. Jardetzky, *J. Am. Chem. Soc.*, **87**, 3237 (1965).

11) J. A. Reynolds, S. Herbert, and J. Steinhardt, *Biochemistry*, **7**, 1357 (1968).

12) T. Takagishi and I. M. Klotz, *Biochemistry*, **11**, 483 (1972).

13) T. W. Johnson and I. M. Klotz, *Biopolymers*, **13**, 791 (1974).

14) M. M. Rauhut, A. M. Semsel, and B. G. Roberts, *J. Org. Chem.*, **31**, 2431 (1966).

15) E. H. White and D. F. Roswell, "Clinical and Biochemical Analysis. 16, Chemi- and Bioluminescence," ed by J. G. Burr, Marcel Dekker, New York (1985), Chap.4, pp. 215—244.

16) K. B. Brundrett, D. F. Roswell, and E. H. White, *J. Am. Chem. Soc.*, **94**, 7536 (1972).

17) G. B. Schuster, *Acc. Chem. Res.*, **12**, 366 (1979).

18) T. Goto, "Kagaku Sōsetsu No. 33," Gakkai Shuppan

Center, Tokyo (1982), Chap. 13, pp. 229—240.
19) A. Nomura and Y. Mizuno, *Kagaku No Ryoiki*, **26**, 333 (1972).
20) M. L. Grayeski, "Clinical and Biochemical Analysis. 16, Chemi- and Bioluminescence," ed by J. G. Burr, Marcel Dekker, New York (1985), Chap. 12, pp. 469—493.
21) J. Lee and H. H. Seliger, *Photochem. Photobiol.*, **15**, 227 (1972).
22) H. R. Schroeder, R. C. Boguslaski, R. J. Carrico, and R. T. Buckler, *Methods Enzymol.*, **51**, 424 (1978).
23) B. H. Nicolet and J. A. Bender, *Org. Synth.* **1941**, **I**. 410.
24) R. H. Mizzoni, M. A. Hennessey, and C. R. Scholz, *J. Am. Chem. Soc.*, **76**, 2414 (1954).
25) W. H. Melhuish, *J. Phys. Chem.*, **64**, 762 (1960).
26) H. H. Seliger, *Methods Enzymol.*, **51**, 560 (1978).
27) J. Lee and H. H. Seliger, *Photochem. Photobiol.*, **4**, 1015 (1965).
28) P. Molyneux and H. P. Frank, *J. Am. Chem. Soc.*, **83**, 3169 (1961).
29) T. Tobita, "Shin-jikken Kagaku Kōza, Kihon Sōsa 1, II," ed by T. Tachibana, Maruzen, Tokyo (1975), Chap. 4, pp. 498—500.

The Determination of a Small Amount of a Biological Constituent by the Use of Chemiluminescence. XI. The Determination of Protein Using a 1,10-Phenanthroline-Hydrogen Peroxide-Osmium(VIII) System

Tadashi HARA* and Kazuhiko TSUKAGOSHI
Department of Chemical Engineering, Faculty of Engineering, Doshisha University, Karasuma Imadegawa, Kamigyo-ku, Kyoto 602
(Received November 12, 1986)

Osmium(VIII) was found by the authors to show extremely sensitive catalytic activity for the 1,10-phenanthroline-hydrogen peroxide chemiluminescence system. By optimizing the measurement conditions, 3.2×10^{-11}—1.3×10^{-8} mol dm^{-3} osmium(VIII) could be determined by chemiluminescence flow-injection analysis with a detection limit of 0.4 pg. The method for the determination of protein was established; it was based on the lowering of the catalytic activity of osmium(VIII) attributable to the complex formation between osmium(VIII) and protein. Similar calibration curves were obtained for bovine serum albumin, human serum albumin, and human serum γ-globulin under the optimum conditions for the determination of protein. According to the method, 5.0×10^{-6}—1.0×10^{-3} g dm^{-3} protein could be determined with a detection limit of about 250 pg and with a coefficient of variation of 2.9% (n=10) for a 1.0×10^{-4} g dm^{-3} protein solution.

Various sensitive methods for the determination of protein have been reported previously by the present authors;[1-4] in those methods, use is made of chemiluminescence(CL) flow-injection analysis for a small amount of a metal ion or a metal complex. The method is based on the lowering of the catalytic activity of a metal ion by the complex formation between a metal ion and protein. Though protein was determined by the present authors by the use of the luminol-hydrogen peroxide(H_2O_2)-osmium(VIII) oxide (Os(VIII)) CL system, neither the stability of the CL intensity nor the detection limit of protein was satisfactory.[1]

As a method for the determination of protein using the 1,10-phenanthroline(phen)-H_2O_2-ruthenium(III) system was reported in one of the previous papers,[4] the catalytic activities of iridium(III), osmium(VIII), palladium(II), platinum(IV), and rhodium(III) for the phen-H_2O_2 CL system have been investigated in the present study. Os(VIII) has been found to be very sensitive. By optimizing the measurement conditions, a micro amount of Os(VIII) could be determined by CL flow-injection analysis. The present method for the determination of Os(VIII) is 5—60 times as sensitive as the methods using a lucigenin or luminol CL system.[5-7] Here, this sensitive method for the determination of Os(VIII) was combined with the complex formation between Os(VIII) and protein to established a sensitive method for the determination of protein using CL flow-injection analysis. According to the present method, a micro amount of protein can be rapidly determined with a stable CL intensity.

The present method is 4×10^2—1×10^6 times as sensitive as the non-labeling colorimetric or fluorometric method[8] for the determination of protein and is the most sensitive method among those reported by the present authors[1-4] for the determination of protein using CL flow-injection analysis.

Experimental

All the reagents were of a commercially available special grade. Ion-exchanged water was distilled before use. A 1.2×10^{-4} mol dm^{-3} phen solution contained 5.0×10^{-3} mol dm^{-3} ethylhexadecyldimethylammonium bromide(EHDAB), 1.0×10^{-1} mol dm^{-3} sodium hydroxide(NaOH), and 1.0×10^{-9} mol dm^{-3} tetraethylenepentamine(TEPA). A 5.0 wt% H_2O_2 solution was prepared by diluting 30 wt% H_2O_2 with water. A 1.3×10^{-3} mol dm^{-3} Os(VIII) catalyst solution was prepared as a stock solution by diluting a 4% osmium(VIII) oxide aqueous solution (2 ml) (Nakarai Chemical, Ltd.) with water; it was then further diluted to the desired concentration with a buffer solution (pH 10.2) consisting of 1.0×10^{-1} mol dm^{-3} boric acid and 1.0×10^{-1} mol dm^{-3} potassium hydroxide. Bovine serum albumin(BSA) and human serum albumin (HSA) from Nakarai Chemical, Ltd., human serum γ-globulin(HγG) from the Sigma Chemical Company, and control serum(Q-PAC-Chemistry Control Serum I) from Hyland were prepared by diluting them with the above-mentioned buffer solution.

The experiment was carried out using the same apparatus as in a previous paper.[9] A phen-H_2O_2 solution and the above-mentioned buffer solution as a carrier were mixed at the point X of the apparatus. The optimum distance from the point X to a photometric flow cell and the optimum flow rates were decided by experimentation. A definite volume of Os(VIII) catalyst solution was added to a sample solution containing protein, and the resulting solution was heated for a definite period for the complexation reaction of Os(VIII) with protein. After the solution has then cooled to room temperature, an aliquot of the solution (50 mm^3) was injected into the line of a buffer solution as a carrier and the CL intensity-time profile was measured at the flow cell.

Results and Discussion

Cl Flow-Injection Analysis for a Micro Amount of Os(VIII). As the method for the determination of protein using a phen-H_2O_2-ruthenium(III) system was reported in the previous paper, the catalytic activities of iridium(III), osmium(VIII), palladium(II), pla-

tinum(IV), and rhodium(III) for the phen-H_2O_2 CL system were investigated in the present study; Os(VIII) was found to be very sensitive. Then, the effects of the flow rates, the tube length, and the reagent concentration on the CL intensity of a Os(VIII) catalyst solution were examined in the following way, and the conditions for the determination of a micro amount of Os(VIII) were established.

The CL intensity of a 6.3×10^{-9} mol dm^{-3} Os(VIII) catalyst solution was measured by the use of 10-, 100-, 200-, and 300-cm portions of tubing, which corresponded to the distance between the point X and a photometric flow cell. The maximum CL intensity was observed by the use of a 200-cm tube. Both the flow rate of a phen solution and that of a H_2O_2 solution were chosen at the same time as follows: 0.5, 0.8, 1.0, 1.3, 1.5, and 1.7 ml min^{-1}, and the CL intensity of a 6.3×10^{-9} mol dm^{-3} Os(VIII) catalyst solution (volume injected, 50 mm^3) was measured. The CL intensity increased with the increase in the flow rate, but was accompanied by an increasing noise. The flow rate of a carrier buffer solution was always set at 2.3 ml min^{-1}, the maximum capacity of the pump, so as to deal with as many samples as possible within a definite time. On the basis of the experimental results, the optimum conditions were established as follows: tube length, 200 cm; flow rates of a phen, a H_2O_2, and a buffer solution, 1.3, 1.3, and 2.3 ml min^{-1} respectively.

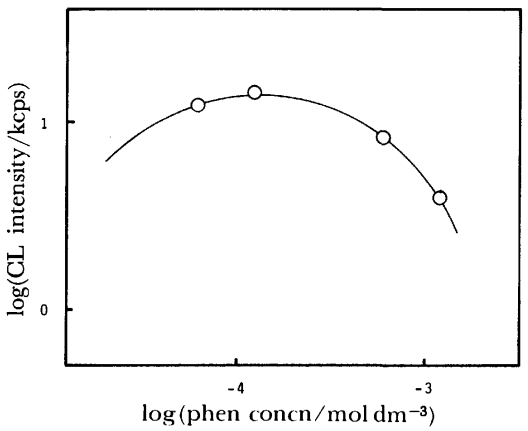

Fig. 1. Effect of phen concn on CL intensity. Conditions: 5.0×10^{-3} mol dm^{-3} EHDAB, 1.0×10^{-1} mol dm^{-3} NaOH, 1.0×10^{-9} mol dm^{-3} TEPA, 7.5 wt% H_2O_2, and 1.3×10^{-8} mol dm^{-3} Os(VIII).

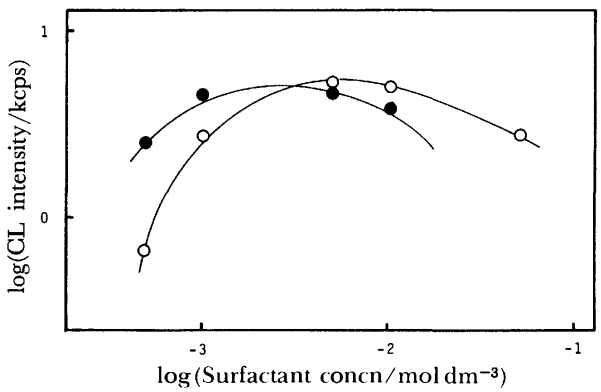

Fig. 2. Effect of surfactants on CL intensity. ○: EHDAB and ●: TOAC. Conditions: 1.2×10^{-4} mol dm^{-3} phen, 1.0×10^{-1} mol dm^{-3} NaOH, 1.0×10^{-9} mol dm^{-3} TEPA, 5.0 wt% H_2O_2, and 6.3×10^{-9} mol dm^{-3} Os(VIII).

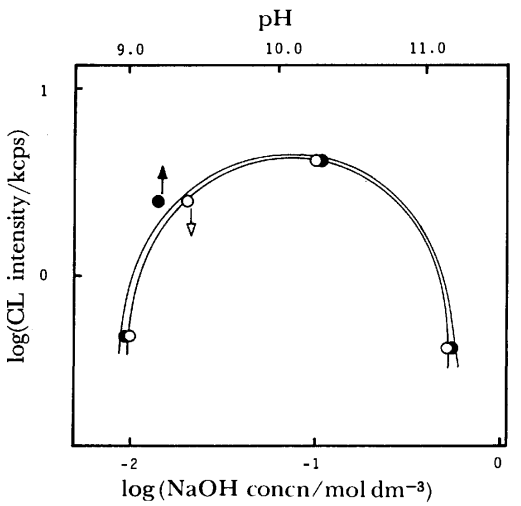

Fig. 3. Effect of NaOH concn or pH[1] on CL intensity. ○: CL intensity against NaOH concn and ●: CL intensity against pH. Conditions: 1.2×10^{-4} mol dm^{-3} phen, 5.0×10^{-3} mol dm^{-3} EHDAB, 1.0×10^{-3} mol dm^{-3} TEPA, 5.0 wt% H_2O_2, and 6.3×10^{-9} mol dm^{-3} Os(VIII). 1) The pH value refers to the value of a solution just before CL intensity is measured.

The effect of the phen, surfactant, and NaOH concentration in the phen solution on the peak CL intensity are shown in Figs. 1—3 under the optimum flow rates, as has been described above. Trimethyloctadecylammonium chloride(TOAC) and EHDAB were examined as cationic surfactants, for they had been known to show a high, enhanced action for a phen-H_2O_2-copper(II) system.[10] As can be seen from Figs. 1—3, 1.2×10^{-4} mol dm^{-3} phen, 5.0×10^{-3} mol dm^{-3} EHDAB, and 1.0×10^{-1} mol dm^{-3} NaOH were chosen as the optimum concentrations. A phen solution also contained 1.0×10^{-9} mol dm^{-3} TEPA as a masking reagent for a small amount of the metal ion. The effect of the H_2O_2 concentration on the CL intensity is shown in Fig. 4. The CL intensity increased with the increase in the concentration of H_2O_2, but was accompanied by an increasing noise. From these results, 5.0 w% H_2O_2 was chosen as the optimum concentration.

The relationship between the CL intensity and the Os(VIII) catalyst concentration was obtained under the above-mentioned conditions and is shown in Fig. 5. According to the present method, a micro amount of Os(VIII) could be determined over a range of concentration of 3.2×10^{-11}—1.3×10^{-8} mol dm^{-3}, with the detection limit of 0.4 pg at the rate of about 40 samples per hour. The coefficient of variation was 2.2% for 10 analyses of a 6.3×10^{-9} mol dm^{-3} Os(VIII) catalyst solu-

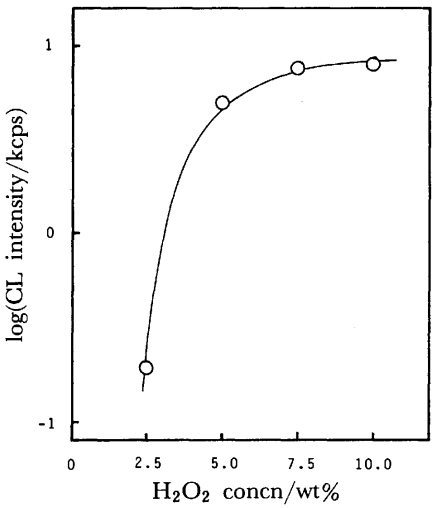

Fig. 4. Effect of H_2O_2 concn on CL intensity. Conditions: 1.2×10^{-4} mol dm^{-3} phen, 5.0×10^{-3} mol dm^{-3} EHDAB, 1.0×10^{-1} mol dm^{-3} NaOH, 1.0×10^{-9} mol dm^{-3} TEPA, and 6.3×10^{-9} mol dm^{-3} Os(VIII).

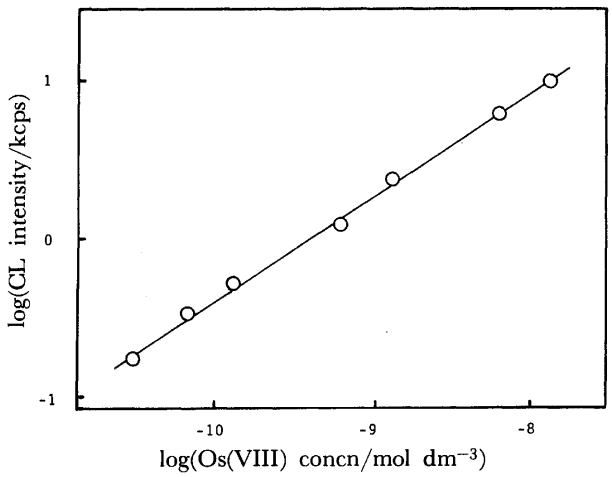

Fig. 5. Relationship between CL intensity and Os(VIII) concn. Conditions: 1.2×10^{-4} mol dm^{-3} phen, 5.0×10^{-3} mol dm^{-3} EHDAB, 1.0×10^{-1} mol dm^{-3} NaOH, 1.0×10^{-9} mol dm^{-3} TEPA, and 5.0 wt% H_2O_2.

Table 1. Detection Limit of Elements of the Platinum Group

Sample	Detection limit/mol dm^{-3}
OsO_4(VIII)	3.2×10^{-11}
$RuCl_3$(III) $3H_2O$	1.0×10^{-7}[4]
$PdCl_2$(II)	1.1×10^{-6}
$IrCl_3$(III) $1.5H_2O$	5.0×10^{-6}
$RhCl_3$(III) $3H_2O$	1.0×10^{-5}
H_2PtCl_6(IV)	1.0×10^{-4}

tion. The present method for the determination of Os(VIII) was 5—60 times as sensitive as the methods using the lucigenin or luminol CL system. By the present CL flow-injection analysis, iridium(III), palladium(II), platinum(IV), and rhodium(II) were determined with the detection limits of 5.0×10^{-6}, 1.1×10^{-6}, 1.0×10^{-4}, and 1.0×10^{-5} mol dm^{-3} respectively (Table 1).

Determination of Protein. Though protein was formerly determined by the authors by the use of the luminol-H_2O_2-Os(VIII) system, both the stability of the CL intensity and the detection limit of protein were not satisfactory. Here, a sensitive method for the determination was carried out by the use of a CL flow-injection technique using a phen-H_2O_2-Os(VIII) system.

Since protein was determined after the reaction between Os(VIII) and protein, the reaction time, the reaction temperature, and the Os(VIII) concentration required for the determination of protein were investigated in advance. Figure 6 shows the relationship between the relative CL intensity and the reaction time at 20, 60, and 95 °C. The relative CL intensity is represented as the value against the CL intensity of a BSA-free sample solution at the reaction time of 0, for

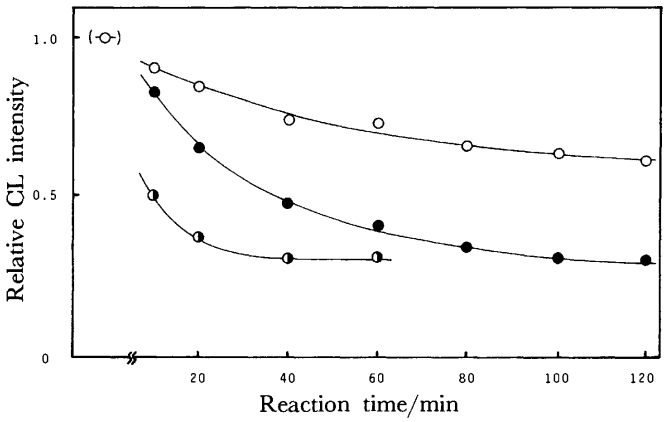

Fig. 6. Relationship between CL intensity and reaction time. ○: 20, ●: 60, ◑: 95 °C, and (—○—): BSA free. Conditions: 5.0×10^{-4} g dm^{-3} BSA and 6.3×10^{-9} mol dm^{-3} Os(VIII).

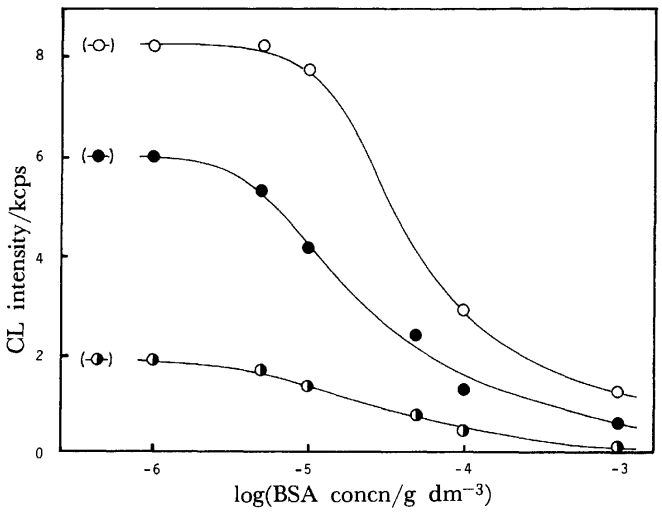

Fig. 7. Effect of Os(VIII) concn on the calibration curve of BSA. ○: 1.3×10^{-8} mol dm^{-3}-, ●: 6.3×10^{-9} mol dm^{-3}-, ◑: 3.2×10^{-9} mol dm^{-3} Os(VIII), and (—○—): BSA free.

Table 2. Lowering of CL Intensity in the Presence of 1.0×10^{-4} g dm^{-3} BSA

System	Lowering of CL intensity	Relative lowering CL intensity[a)]
phen-H_2O_2-Cu(II)	0.05	1
phen-H_2O_2-Ru(III)	0.14	2.8
phen-H_2O_2-Os(VIII)	0.75	15

a) Based on the value of the lowering of the CL intensity for the phen-H_2O_2-Cu(II) system.

the CL intensity of the BSA-free sample solution did not change upon heat treatment up to 60 min at 95 °C or up to 120 min at 20 and 60 °C. On the basis of the results pertaining to the decrease in the CL intensity and the reaction time, the CL intensity of a sample solution containing protein was examined after it had been treated for 45 min at 95 °C in the following experiments. Figure 7 shows the calibration curve of BSA obtained by the use of 3.2×10^{-9}, 6.3×10^{-9}, and 1.3×10^{-8} mol dm^{-3} portions of the Os(VIII) catalyst. The detection limit of the protein concentration and the decrease in the CL intensity for a definite amount of protein suggested that a 6.3×10^{-9} mol dm^{-3} Os(VIII) catalyst solution should be used in the present study.

The calibration curves for BSA, HSA, and HγG were obtained under the conditions specified above (Fig. 8). They could be used for the determination of protein in the concentration range of 5.0×10^{-6}—1.0×10^{-3} g dm^{-3} with a detection limit of about 250 pg. The coefficient of variation was 2.9% for 10 analyses of a 1.0×10^{-4} g dm^{-3} protein solution by the present method. The lowering of the CL activity of an Os(VIII) catalyst solution in the presence of protein seemed to be due to the formation of an Os(VIII)-polypeptide linkage, as in the previous paper.

Table 2 shows the lowering of the CL intensity by the use of copper(II), ruthenium(II), or osmium(VIII) as a catalyst for the phen-H_2O_2 CL system in the presence of 1.0×10^{-4} g dm^{-3} BSA. The values for the lowering of the CL intensity were obtained by subtracting the relative CL intensity for a sample solution in the

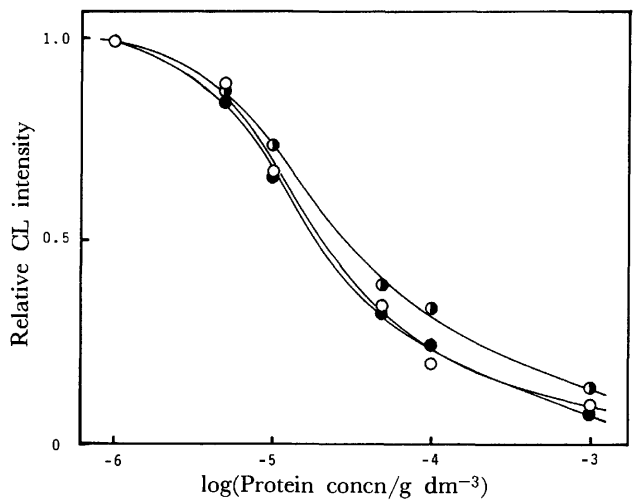

Fig. 8. Calibration curves of various proteins. ○: BSA, ●: HSA, and ◑: HγG. Conditions: 6.3×10^{-9} mol dm^{-3} Os(VIII).

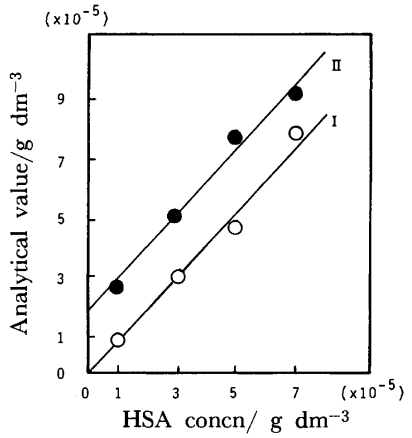

Fig. 9. Relationship between HSA concn and the observed protein concn. ○: HSA alone and ●: HSA+control serum. Conditions: 2.2×10^{-5} g dm^{-3} control serum and 6.3×10^{-9} mol dm^{-3} Os(VIII).

presence of 1.0×10^{-4} g dm^{-3} BSA from the relative CL intensity (=1.00) for a sample solution in the absence of BSA. As can be seen from these values, the present method using the Os(VIII) catalyst for a phen-H_2O_2 CL system was 5—15 times as sensitive as those using ruthenium(III) or copper(II). The present method was 4×10^2—1×10^6 times as sensitive as the non-labeling colorimetric or fluorometric method for the determination of protein and was the most sensitive method among those reported by the present authors for the determination of protein using CL flow-injection analysis.

Application to Serum Analysis. A human serum sample was measured after having been diluted because the present method was too sensitive to estimate protein in an original human serum sample and these was the possibility of interference with the coexisting constituents in human serum. Various amounts of HSA were estimated in either the presence or absence of a definite amount of control serum (diluted to a volume of 2×10^6 times with a buffer solution), and the relationship between the HSA concentration and the analytical value was obtained by the use of the calibration curve of HSA shown in Fig. 8. All the analytical values of the ordinate in Fig. 9 are represented as the amount of HSA. The difference between the straight lines, I and II, in the analytical value was approximately equal to the amount of protein in the added control serum, which was determined to be 2.2×10^{-5} g dm^{-3} by the use of the biuret method. This means that the present method was applicable to the determination of protein in a serum sample, without

any interference from coexisting constituents, when a sample solution was diluted to 2×10^6 times with a buffer solution and the resulting solution was then measured.

The authors wish to thank Mr. Masakatsu Imaki (Horiba, Ltd.) for providing the apparatus necessary for the present study.

References

1) T. Hara, M. Toriyama, and K. Tsukagoshi, *Bull. Chem. Soc. Jpn.*, **56**, 1382 (1983).
2) T. Hara, M. Toriyama, and K. Tsukagoshi, *Bull. Chem. Soc. Jpn.*, **57**, 289 (1984).
3) T. Hara, M. Toriyama, K. Kitamura, and M. Imaki, *Bull. Chem. Soc. Jpn.*, **58**, 2135 (1985).
4) T. Hara, K. Tsukagoshi, and M. Imaki, *Bull. Chem. Soc. Jpn.*, **60**, 1537 (1987).
5) Lukovskaya. N. M. and Teletskaya A. V., *Ukr. Khim. Zh.*, **40**, 1311 (1974).
6) L. A. Montano and J. D. Ingle, *Anal. Chem.*, **51**, 919 (1979).
7) K. Tsukagoshi, M. Toriyama, and T. Hara, *Sci. Eng. Rev. Doshisha Univ.*, **23**, 119 (1982).
8) K. Sugawara and M. Soejima, "Seibutsu Kagaku Jikken-hō 7 Tanpakushitsu No Teiryo-hō," Japan Scientific Societies Press, Tokyo (1981).
9) T. Hara, K. Tsukagoshi, A. Arai, and T. Iharada, *Bull. Chem. Soc. Jpn.*, **59**, 3681 (1986).
10) M. Yamada and S. Suzuki, *Anal. Lett.*, **17**, 251 (1984).

Preparation of Some Lanthanoid Picrates and the Behavior of Their Water of Hydration[1)]

Kazuharu NAKAGAWA,* Kayoko AMITA,† Hifumi MIZUNO,†† Yoshihisa INOUE,*,††† and Tadao HAKUSHI††††
Leather Research Institute of Hyogo Prefecture, 3 Higashigawara, Nozato, Himeji, Hyogo 670
†Industrial Research Institute of Hyogo Prefecture, Yukihira-cho, Suma, Kobe 654
††Ako Kasei Co., 329 Sakoshi, Ako, Hyogo 678-01
†††Basic Research Laboratory, Himeji Institute of Technology, 2167 Shosha, Himeji, Hyogo 671-22
††††Department of Applied Chemistry, Himeji Institute of Technology, 2167 Shosha, Himeji, Hyogo 671-22
(Received November 22, 1986)

Lanthanoid(III) picrates (Ln=La, Ce, Pr, Nd, Sm, Eu, Gd, Dy, and Yb) were prepared from picric acid and the corresponding lanthanoid carbonates in good yields. Combustion analyses, ICP emission analyses, and UV spectrophotometry have shown that the light lanthanoid picrates, i.e. Ln=La-Gd, are all undecahydrates, while the heavy ones, Dy and Yb, are octahydrates. An examination by TG-DTA has revealed that these hydrates, being fairly stable in air at ambient temperature, are quite labile to give partially or completely dehydrated samples upon drying under vacuum, in a desiccator, and/or at elevated temperatures just above 30 °C.

Picrates have long been used in industry as initiating explosives and fuel additives.[2)] They have also been used in analyses, especially in the solvent extraction technique owing to the highly lipophilic nature of the picrate ion. Recently, the cation-binding abilities of neutral ligands like crown ethers have been conveniently evaluated by the extractability of aqueous metal picrates.[3)] For this purpose, alkali (Na-Cs),[4)] alkaline earth (Mg-Ba),[3,5)] and some heavy metal (Ag, Tl) picrates[3,6)] were synthesized and isolated. On the other hand, lanthanoid picrates have only been prepared in situ in solvent extraction experiments with some crown ethers;[7)] no practical method for preparing lanthanoid picrates has been published and their characterization has not been fully described. In this paper, we wish to report on a method for preparing some lanthanoid picrates and the characterization of their crystals.

Results and Discussion

Synthesis. The reaction of picric acid with metal hydroxide is a common route to obtain metal picrates, as in the case of alkali metal picrates.[4)] Since lanthanoid hydroxides are not commercially available and some heavy metal picrates have been prepared from the metal oxides,[3,6)] we first tried lanthanoid oxide. The reaction of picric acid with La oxide was carried out in hot water, but only the starting materials were recovered from the mixture.

Lanthanoid carbonates were then tried and gave satisfactory results regarding the preparation of La, Ce, Pr, Nd, Sm, Eu, Gd, Dy, and Yb picrates. The reaction conditions were optimized in order to obtain the recommended procedure shown in the Experimental section. First examined were the effects of the molar ratio of picric acid to lanthanoid carbonate upon the product yield and purity. With Ce carbonate taken as an example, the picric acid/carbonate ratio (n) was changed from 1 to 9. Although no precipitation was obtained upon cooling when n=1, a yellow precipitate was formed at $n>3$. The yield generally increased with increasing n. However, as shown by spectrophotometric examination of dichloromethane extracts of the crystalline products, the use of excess picric acid, i.e. $n>6$, led to a significant contamination of the resulting picrate with picric acid, even after repeated recrystallizations from water. Therefore, $n<6$ should be used in order to obtain a pure sample free from picric acid in high yield.

The fresh lanthanoid picrate recrystallized from water gradually lost its weight (by ca. 10—18%) upon air-drying for 3—5 d at room temperature; after that period, practically no weight change (>1%) was observed during the next 85 d. The samples used in subsequent experiments were, therefore, air-dried for more than one week and stored in stoppered vials in the dark.

The lanthanoid picrates prepared as above were analyzed by means of an inductively coupled plasma (ICP) atomic emission analysis as well as by a combustion analysis. As shown in Table 1, the results from both analyses are in good agreement with the values calculated for the undecahydrates of light lanthanoid picrates (Ln=La-Gd) and for octahydrates of heavy ones (Dy, Yb). The UV spectra of their aqueous solutions also support this conclusion. As shown in Table 1, all picrates show almost identical molar extinction coefficients around 42000 $M^{-1}cm^{-1}$,§ indicating that they contain the same numbers of water of hydration as determined by the elemental analyses.

The fact that the light and heavy lanthanoid picrates contain different numbers of water of hydration may be related to the well-documented "*gadolinium break*" observed for thermodynamic data of the lanthanoid series in aqueous solution, where a plot of such data as a function of ionic radius often exhibits a break somewhere in the middle of the lanthanoid series. This break is considered to reflect a discontinuous variation in the hydration structures of the lanthanoid ions.[8)]

§1 M=1 mol dm^{-3}.

Table 1. Elemental Analyses and Some Properties of Lanthanoid Picrate Hydrates ($Ln(Pic)_3 \cdot xH_2O$)

Compound	Mol wt	Yield/%	Content/%[a]				Dp/°C[b]	Ep/°C[c]	$\varepsilon_{max}/M^{-1}cm^{-1}$[d]
			Ln	H	C	N			
$La(Pic)_3 \cdot 11H_2O$	1021.40	56	12.9 (13.6)	2.57 (2.76)	21.21 (21.17)	12.22 (12.34)	292	340	42100
$Ce(Pic)_3 \cdot 11H_2O$	1022.61	86	13.6 (13.7)	2.54 (2.76)	20.98 (21.14)	12.35 (12.33)	270	316	42200
$Pr(Pic)_3 \cdot 11H_2O$	1023.40	76	13.6 (13.8)	2.76 (2.76)	21.44 (21.13)	12.19 (12.32)	284	337	41600
$Nd(Pic)_3 \cdot 11H_2O$	1026.73	56	14.0 (14.1)	2.35 (2.75)	20.85 (21.06)	12.15 (12.28)	288	344	42100
$Sm(Pic)_3 \cdot 11H_2O$	1032.84	65	14.8 (14.6)	2.65 (2.73)	20.68 (20.93)	11.90 (12.21)	286	342	42100
$Eu(Pic)_3 \cdot 11H_2O$	1034.45	45	15.5 (14.7)	2.50 (2.73)	20.60 (20.90)	11.83 (12.19)	292	342	40900
$Gd(Pic)_3 \cdot 11H_2O$	1039.74	33	15.2 (15.1)	2.42 (2.71)	20.49 (20.79)	11.89 (12.12)	288	346	42100
$Dy(Pic)_3 \cdot 8H_2O$	990.95	69	16.5 (16.4)	2.13 (2.24)	21.73 (21.82)	12.71 (12.72)	285	350	42700
$Yb(Pic)_3 \cdot 8H_2O$	1001.49	42	17.4 (17.3)	2.13 (2.21)	21.59 (21.59)	12.51 (12.59)	260	348	43000

a) Determined by ICP for Ln and by combustion analysis for H, C, and N; calculated values (%) are shown in the parentheses. b) Decomposition point determined by DTA. c) Explosion point determined by DTA. d) Molar absorption coefficient at the absorption maximum (354 nm) in water.

Studies on the apparent molal volume and X-ray diffraction data of aqueous rare earth salt solutions suggest that the coordination number in the first solvation shell of a lanthanoid ion shifts from nine to eight between neodymium and terbium.[8f,g] The present change in the number of the water of hydration lies in the same line, although the coordination number in the crystalline state is not necessarily identical to that in an aqueous solution.

The Behavior of the Water of Hydration. Interestingly, the water in lanthanoid picrate hydrates was shown to be quite labile. Although the light lanthanoid picrates, La–Gd, do not change in weight (within ±1%) in open air, they gradually lose weight to reach ca. 85 % of the original weights when stored over SiO_2 in a desiccator for 3 d or more. Thus, SiO_2 removes 8—9 out of 11 water molecules, leaving a tri- or dihydrate. Vacuum-drying over P_2O_5 resulted in complete dehydration, as indicated by a 17—19% loss of the original weight which corresponds to a loss of 11 water molecules from each picrate of a light lanthanoid.

In order to further investigate the behavior of the water of hydration, samples of La picrate at different drying stages were subjected to thermal analyses. The thermogravimetry-differential thermal analysis (TG-DTA) curves obtained are shown in Fig. 1. For the air-dried sample (curves A), the first endothermic peak in the DTA curve starts just above room temperature (30 °C) and reaches a maximum at 50 °C. This causes a considerable loss of weight (cf. the TG curve A). The second weak endothermic peak appears near 90 °C with a smaller loss of weight. The weight loss at each peak roughly coincides with that observed upon drying over SiO_2 and P_2O_5 in vacuo, respectively. Further heating gives an exothermic peak at 292 °C, i.e. the

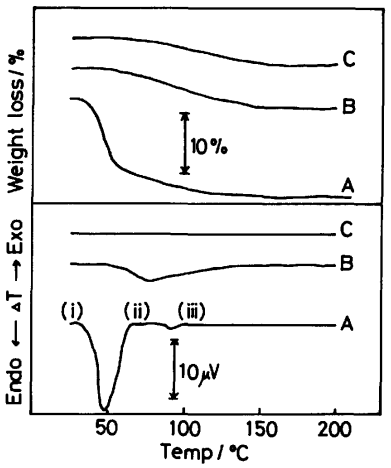

Fig. 1. TG-DTA curves for air-dried (A), SiO_2-dried (B), and P_2O_5-in vacuo dried (C) samples of La picrate; see Experimental for detailed conditions of measurement.

decomposition point of La picrate, and finally results in an explosion at 340 °C.[§§]

With the SiO_2-dried sample (curves B), only a broad peak around 75 °C appears in DTA curve B with a small decrease in the TG curve. The sample vacuum-dried over P_2O_5 did not show any evident peak in DTA curve C; TG curve C declined slightly, but this could be ascribed to the loss of a small amount of water reabsorbed before the DTA measurement since the vacuum-dried sample was highly hygroscopic.

Air-dried samples of Ce, Pr, and Nd picrate hydrates

[§§]Caution should be exercised in handling metal picrates, since they are shock- and heat-sensitive. Although most lanthanoid picrates did not explode below 300 °C, heating of sodium picrate at >250 °C resulted in an explosion which destroyed the thermocouple of the DTA apparatus.

also gave analogous TG-DTA curves with the first large endothermic peak at ca. 50 °C and a subsequent small peak at ca. 90 °C; Sm, Eu, and Gd picrates gave an additional endothermic peak around 140 °C. Dy and Yb picrate octahydrates exhibited similar TG-DTA curves with two endothermic peaks around 55 and 85 °C; however, the peak intensities were inverted. These observations support the idea that lanthanoid picrate hydrates possess at least two kinds of water; one is loosely bound and is released easily by mild drying over SiO_2 or by heating just above room temperature. The other is tightly bound and is removed by vacuum-drying over P_2O_5 or by heating up to 90—140 °C. This behavior of the water of hydration in lanthanoid picrates is in sharp contrast with that of alkali or alkaline earth picrate hydrates which do not lose water at such low temperatures as 30—50 °C. It has been reported that most mono- and divalent metal picrates show the first endothermic peak well above 100 °C,[9] which would correspond to the second peak in the lanthanoid picrate case.

The structural change of an air-dried La picrate caused by dehydration can be visualized by X-ray diffraction patterns. As can be seen in Fig. 2, the diffraction pattern of the air-dried sample (stage i in Fig. 1), indicates the presence of a well-defined crystal structure, while the sample obtained by rapid cooling just after the first endothermic peak (stage ii) yielded a more complicated diffraction pattern (which still maintained the original peaks at the same angles). This indicates that a certain phase change takes place between stages i and ii. Further heating up to 110 °C, i.e. to the end of the second endothermic peak (stage iii), leads to the disappearance of all sharp diffraction peaks (top trace in Fig. 2), indicating that the original crystal structure is totally broken by a complete loss of water. The samples dried over SiO_2 or P_2O_5 in vacuo also show no sharp X-ray diffraction patterns at all; these samples are all highly hygroscopic but do not regenerate the original undecahydrate upon standing in a moderately humid atmosphere at room temperature. Also observed was an apparent change in color of the crystalline lanthanoid picrates from yellow to deep orange or to red upon heating up to ca. 120 °C or upon drying in vacuo, which may again be accounted for in terms of the drastic structural change.

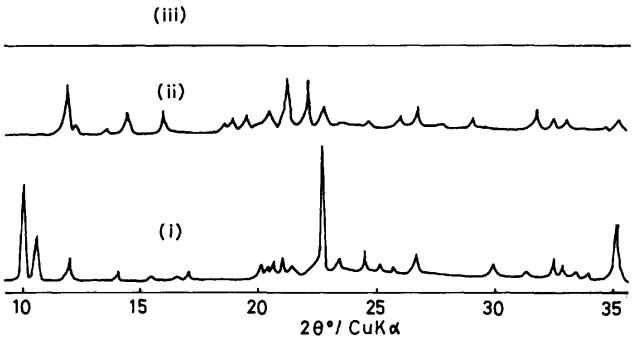

Fig. 2. X-Ray diffraction patterns of La picrate at different stages (i—iii) of the thermal analysis as shown in Fig. 1.

It may be summarized as follows: 1) the lanthanoid(III) picrates (Ln=La-Gd, Dy, Yb) are prepared in good yield by the reaction of picric acid with the corresponding carbonate in hot water, 2) the picrates prepared are undecahydrates for the light lanthanoids La-Gd and octahydrates for the heavy lanthanoids Dy and Yb, and 3) the water of hydration can be removed easily when stored over a desiccant under atmospheric or reduced pressure, to give partially or completely dehydrated samples, which suffer a phase change and turn highly hygroscopic. It is therefore recommended that the lanthanoid picrates recrystallized from water should merely be air-dried and be used as hydrates without further drying. The present method should be applicable to the synthesis of the rest of lanthanoid picrates, which are inferred to be octa- or undecahydrates.

Experimental

Materials. Commercially available picric acid and lanthanoid carbonates and oxides (G.R. or E.P. grade) were used without further purification. Deionized water was used throughout the study.

Instruments. It was first attempted to measure the melting and decomposition points in a capillary tube with a Yanaco hot-stage micro melting point apparatus. However, the obtained mps were the same (around 65 °C) for some light lanthanoid picrates, for which the release of the water of hydration must be responsible. Measurements on an open glass plate are also difficult due to an apparent carbonization of a sample above 230 °C. Decomposition and explosion points (dp and ep) were therefore determined from the extrapolated onsets of the exothermic peaks of DTA curves; these peaks accompanied a moderate and an extreme loss of weight in the TG curve, respectively.

TG-DTA curves were recorded on a Rigaku differential thermal balance model 8076 equipped with a platinel thermocouple; sample size: 5 mg picrate + 5 mg baked α-alumina; air-flow: 75 ml min^{-1} for air-dried samples and no flow for the samples dried over desiccants; scanning speed: 5 or 10 °C min^{-1}. Electronic spectra were obtained on a Shimadzu UV-365 spectrophotometer. Infrared spectra were recorded on a Jasco IR-810 instrument. X-Ray diffraction patterns were recorded on a Rigaku X-ray diffraction equipment. ICP analyses were performed on a Shimadzu GVM100P inductively coupled plasma atomic emission spectrometer. The ICP instrument was calibrated for each metal with standard solutions prepared by dissolving lanthanoid oxides which were baked at 900 °C for 2 h in hydrochloric acid or, in Ce oxide case, in a 1 : 1 mixture of sulfuric acid and concentrated hydrogen peroxide.

Synthesis. Lanthanum Picrate Undecahydrate. To picric acid (3.4 g, 15 mmol) dissolved in hot water (100 ml) was added portionwise La carbonate (trihydrate; 1.3 g, 2.5 mmol) with stirring on a water bath at 80—90 °C. The stirring was continued for an additional 10 min at that temperature. The hot mixture was filtrated and then cooled with ice. The crude La picrate, obtained as a yellow precipitate, was recrystallized three times from water and air-dried at room temper-

ature for more than one week. Yellow crystals; yield 2.8 g (56%); dp 292 °C; ep 340 °C. No further significant change of weight (>1%) was observed for at least 85 d.

Undecahydrates of the Light Lanthanoids (Ce-Gd) and Octahydrates of the Heavy Lanthanoids (Dy, Yb). These were prepared from picric acid and the corresponding carbonate as above, typically using 15 mmol of the former and 2.5 mmol of the latter. They are all yellow crystals; their yields and decomposition and explosion points are given in Table 1.

In order to check the contamination of unreacted picric acid, the crystalline lanthanoid picrates obtained above were extracted with dichloromethane. A spectral examination of the dichloromethane extracts did not show any absorbance greater than 0.01 at wavelengths >290 nm; therefore, the samples were free from picric acid. Aqueous solutions of La-Gd, Dy, and Yb picrates all showed absorption maxima at an identical wavelength of 354 nm with very close absorption coefficients (Table 1). The coefficients around 42000 $M^{-1}cm^{-1}$ are reasonable in view of those for alkali metal picrates (14400—14800 $M^{-1}cm^{-1}$) and for alkaline earth metal picrates (29100—31000 $M^{-1}cm^{-1}$).

The IR spectra of light lanthanoid picrate undecahydrates (La-Gd) are all superimposable with respect to the frequencies and relative intensities of their peaks: ν(KBr) 3400 (br), 3090, 1635, 1615, 1565, 1560, 1500, 1485, 1440, 1370, 1335, 1280, 1270, 1240, 1165, 1080, 940, 905, 795, 745, 710, 705, 545, 520 cm^{-1}. The heavy lanthanoid picrate octahydrates (Dy, Yb) also exhibit quite analogous spectra but evidently weaker absorption at 3400 cm^{-1}; ytterbium picrate possesses a broadened 3400 cm^{-1} band and two additional weak absorptions at 1425 and 1405 cm^{-1}. These spectra are essentially identical as that of sodium picrate monohydrate[4] or calcium picrate pentahydrate[3,5] except for the intensity of the O-H stretching band around 3400 cm^{-1}.

This work was supported in part by a grant from the Hyogo Foundation for the Promotion of Science and Technology, which is gratefully acknowledged.

References

1) Part of this work has been presented at the 4th Symposium on Rare Earths, Kyoto, March 1986, Abstr., p. 162.

2) For recent examples, see: M. T. Scholtz, U.S. Patent 132119 (1981); R. W. Simmons, Ger. Patent 2759055 (1979).

3) Y. Takeda, *Topics Curr. Chem.*, **121**, 1 (1984); Y. Inoue, M. Ouchi, and T. Hakushi, *Bull. Chem. Soc. Jpn*, **58**, 525 (1985); and earlier references cited therein.

4) T. Maeda, K. Kimura, and T. Shono, *Bull. Chem. Soc. Jpn.*, **55**, 3506 (1982); K. Kimura, T. Maeda, and T. Shono, *Talanta*, **26**, 945 (1979).

5) T. Maeda, K. Kimura, and T. Shono, *Fresenius Z. Anal. Chem.*, **313**, 407 (1982).

6) T. Maeda, K. Kimura, and T. Shono, *Fresenius Z. Anal. Chem.*, **298**, 363 (1979).

7) I. J. Borowitz, W. Lin, T. Wun, R. Bittman, L. Weiss, V. Diakiw, and G. B. Borowitz, *Tetrahedron*, **33**, 1697 (1977); W. Wenji, C. Bozhong, J. Zhong-kao, and W. Ailing, *J. Radioanal. Chem.*, **76**, 49 (1983); K. Yuan and N. Jiazan, *He Huaxue Yu Fangshe Huaxue*, **5**, 146 (1983); V. V. Yakshin, A. T. Fedorova, A. V. Val'kov, and B. N. Laskorin, *Dokl. Akad. Nauk. SSSR.*, **277**, 1417 (1984); Y. Fukuhara, K. Hirose, M. Masuda, and Y. Hasegawa, 3rd. Symp. Rare Earths, Tokyo, March 1985, Abstr., p. 64.

8) a) F. H. Spedding and G. Atkinson, "The Structure of Electrolytic Solutions," ed by W. J. Hamer, Wiley, New York, NY (1959), Chapter 22; b) I. Grenthe, *Acta Chem. Scand.*, **18**, 293 (1964); c) P. L. E. de la Praudiere and L. A. K. Staveley, *J. Inorg. Nucl. Chem.*, **26**, 1713 (1964); d) G. R. Choppin and A. J. Graffeo, *Inorg. Chem.*, **4**, 1254 (1965); e) S. L. Bertha and G. R. Choppin, *ibid.*, **8**, 613 (1969); f) F. H. Spedding and M. J. Pikal, *J. Phys. Chem.*, **70**, 2430 (1966); g) F. H. Spedding, P. F. Cullen, and A. Habenschuss, *ibid.*, **78**, 1106 (1974).

9) K. Vladimir and L. Pavel, *Chem. Prum.*, **32**, 43 (1982).

The Wetting of an Alumina Substrate by Liquid Silver

Masumi USHIO* and Yoshihiro SUMIYOSHI
Department of Applied Chemistry, Faculty of Engineering, Gunma University, Tenjin-cho, Kiryu 376
(Received December 5, 1986)

The wetting of the Al_2O_3 substrate by liquid silver was investigated by means of the sessile-drop technique in an atmosphere of argon. An empirical relation was established between the contact angle and the temperature or surface tension of the liquid drop by the use of the diameter and the height of the sessile drop. The contact angle was constant as the time increased while it decreased linearly with the increase in the temperature. The variation in the contact angle with the temperature is correlated with the surface tension of the sessile drop. The critical surface tension (γ_c) of Al_2O_3 is 361 dyn cm^{-1}, while the surface tension of liquid silver at 0 K is 790 dyn cm^{-1}.

As for all the properties of the engineering materials, the phenomenon of liquid wetting on a solid surface is an especially important problem, among the many engineering problems on the surface, in the sense that interaction between a solid and a liquid is involved. This phenomenon is also important as a fundamental factor in the related fields of electronics, printing, dyeing and metallurgy, composite materials, adhesion, etc. This wetting phenomenon may be broadly classified into three types of wetting: adhesion, diffusion, and dipping.

Metal-alumina substrates are very attractive as engineering materials. The properties of such substrates are, however, greatly influenced by the nature of the metal-alumina interface. Thus, it is essential to understand metal-alumina interactions in substrate materials.

In the present paper, the wettability of a sintered alumina subetrate, its surface polished and smooth, by liquid silver is investigated by means of the sessile-drop technique in an atmosphere of argon.

Experimental

High-purity silver (99.99%, Ishifuku Co.) was cut into a desk. The disk was 4 mm in diameter and 3 mm thick. The sintered alumina (99.5%, Kyocera Co.) used as the substrate had dimensions of 20×20×3 mm^3, and its surface had been polished to a mirrorlike finish.

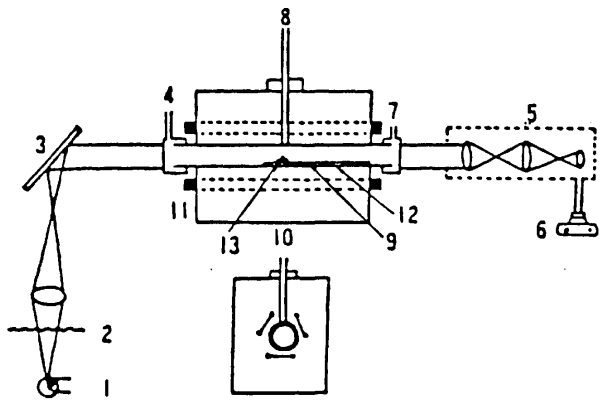

Fig. 1. Experimental apparatus for measuring the wettability. 1: Mercury lamp, 2: Green filter, 3: Reflecting mirror, 4: Argon gas inlet, 5: Microscope, 6: Camera, 7: Argon gas outlet, 8: Pt/Pt13%Rh thermocouple, 9: Porcelain plate, 10: Electric furnace, 11: SiC heater element, 12: Porcelain pipe, 13: Test sample.

An outline of the sessile-drop apparatus used to measure the contact angle is shown in Fig. 1. The temperature of a drop was measured by means of a Pt—Pt. 13% Rh thermocouple, which was located near the drop. The furnace was operated in an atmosphere of argon. The flow rate was about 0.9 L min^{-1}. The silver disk and the substrate were cleaned with acetone and then dried in a vacuum. The silver disk was placed in the furnace on an alumina substrate. The sessile drop was allowed to rest on the substrate at 980 °C for 30 min. The value of the contact angle after 30 min was assumed to be the equilibrium contact angle. The shadow of the sessile drop was then photographed from the back by using light shed by a mercury lamp. The contact angle of the drop was bilaterally measured, and its mean value was taken as the measured value.

In the case of the constant temperature, the contact angle was measured at 5-minute intervals for 60 min. On the other hand, at different temperatures from 960 to 1000 °C the contact angle of a drop was also measured at intervals of 5 °C. From these many photographs taken at 5-minute intervals for 60 min and at intervals of 5 °C, the diameters and the heights of the sessile drops were measured. These dimensions were used to calculate the surface tension of liquid silver and the critical surface tension for spreading (γ_c) for the Ag/Al_2O_3 system.

The human error was found to be about ±1 °C by measuring the contact angle from ten photographs. The temperature deviation was ±2 °C. The silver/alumina interface regions were exemined with an optical microscope and a scanning electron microscope.

Results

In the case of a constant temperature of 980 °C, the photographs used in measuring the contact angles of the drops are shown in Fig 2, while the measured values of the contact angles are shown in Table 1 and Fig. 3. These experimental results shown that a constant angle of a liquid silver sessile drop resting on an alumina substrate was about 90 °C, although there were some differences in the wettability depending on the test pieces of the alumina substances. Each straight line in Fig. 3 represents the results of two independent runs.

In the case of different temperatures from 960 to

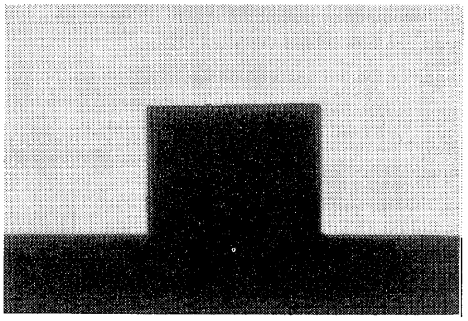

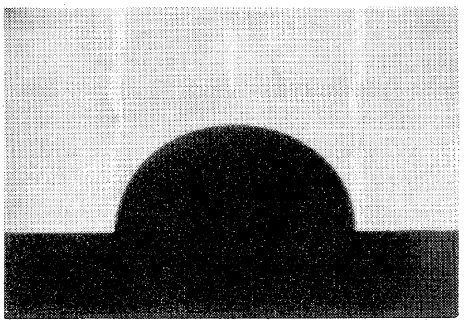

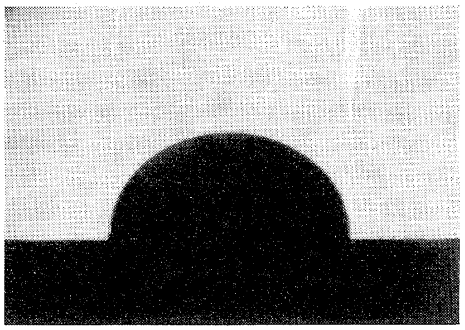

Fig. 2. Sessile drops of liquid silver on alumina at 980 °C for Run No. (S-1). A) T=0 min (Ag metal disk), B) T=30 min, C) T=60 min.

Table 1. Experimental Results of the Contact Angles of Liquid Silver Sessile Drops for Each Substrate at 980 °C

Run No. / t / min	S-1 θ_1 / °	S-1 θ_2 / °	S-2 θ_1 / °	S-2 θ_2 / °	$\theta_{ave.}$ / °
5	90.5	91.8	90.0	89.0	90.3
10	91.0	90.8	89.0	89.0	90.0
15	91.0	90.0	89.0	89.0	89.8
20	90.8	91.3	89.0	89.0	90.0
25	90.8	91.8	89.5	88.0	90.0
30	90.5	90.8	89.5	88.5	89.8
35	90.3	91.8	89.0	89.5	90.2
40	90.0	90.0	89.0	89.0	89.6
45	90.5	90.5	90.0	88.0	89.8
50	90.5	89.8	89.0	88.5	89.5
55	90.5	90.8	89.5	89.0	90.0
60	90.0	90.5	89.5	90.0	90.0
Ave.	90.5	90.8	89.3	88.9	89.9

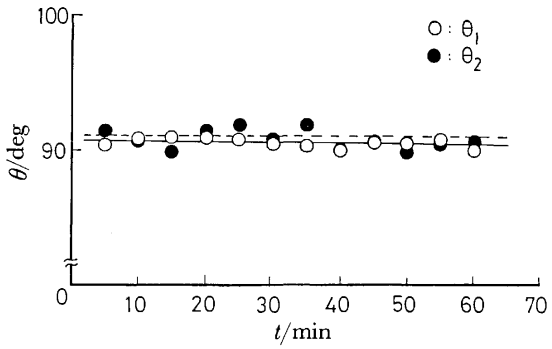

Fig. 3. Change in contact angle with time for a system Ag/Al_2O_3 of Run No. (S-1).

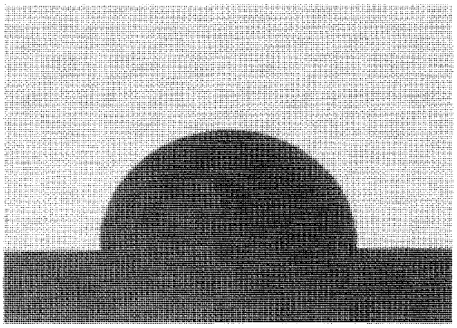

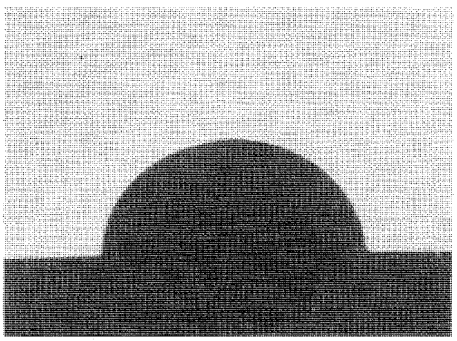

Fig. 4. Sessile drop of liquid silver on alumina for Run No. (S-3). A) At 970 °C, B) at 1000 °C.

1000 °C, with the contact angle measured at intervals of 5 °C, the photographs used in measuring the contact angle of a liquid silver sessile drop resting on an alumina substrate are shown in Fig. 4. The effect of the temperature on the contact angle is shown in Table 2 and Fig. 5. Each straight line in Fig. 5 also represents the results of two independent runs.

Table 2 shows that the degree of the variation in the θ_1 and θ_2 values for runs of (S-3) and (S-4) was different, but the contact angles of a liquid silver on the alumina substrate decrease linearly with an increase in the temperature. That is, a liquid silver is liable to wet an alumina substrate.

The condition of the surface of an alumina substrate was investigated before and after the thermal treatment. Before, it was smooth and flat, but after the thermal treatment, it was revealed that the flatness of

Table 2. Experimental Results of the Effects of Different Temperatures on the Contact Angles of Liquid Silver for Each Substrate at Intervals of 5 °C

Run No. / t / °C	S-3 θ_1 °	S-3 θ_2 °	S-4 θ_1 °	S-4 θ_2 °	$\theta_{ave.}$ °
960	97.3	98.9	98.1	97.8	98.0
965	96.8	98.4	96.2	96.8	97.1
970	95.2	96.7	93.8	93.3	94.8
975	93.8	95.9	92.2	93.9	94.0
980	93.1	94.5	90.1	92.8	92.6
985	93.3	94.3	88.7	91.3	91.9
990	91.6	91.8	86.8	89.8	90.0
995	89.9	90.4	85.2	88.5	88.5
1000	89.0	89.7	83.2	87.8	87.4

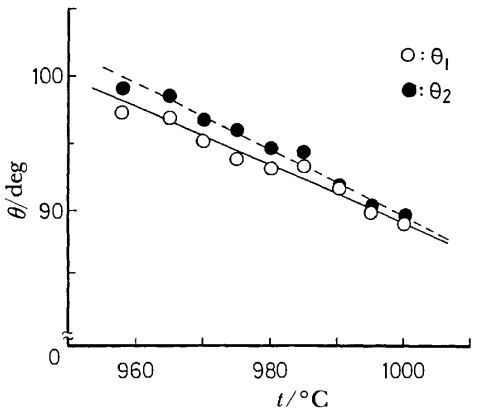

Fig. 5. Change in contact angle with temperature for a system Ag/Al_2O_3 for Run No. (S-3).

the surface had been destroyed. If the surface of an alumina substrate was magnified and then examined, alumina particles were observed on the surface and this surface became rough.

Discussion

As for runs of (S-1) and (S-2), the effect of the time on the contact angle of a liquid silver sessile drop resting on the alumina substrates was investigated at a constant temperature of 980 °C. Each straight line in Fig. 3 can be fitted by means of this equation:

Run (S-1)

$$\theta_1 = -0.0121x + 91.0$$

$$\theta_2 = -0.0030x + 91.4$$

Run (S-2)

$$\theta_1 = 0.0014x + 91.4$$

$$\theta_2 = 0.0045x + 88.7$$

where x is the time in minutes and where θ is the contact angle.

The slopes of these equations were within the range of the absolute value: | 0.0014—0.00121 |. These values were very small. Therefore, it can be assumed, considering the accuracy of the temperature control, the human errors of the measurements, etc., that the contact angle of a liquid silver on an alumina substrate was scarcely changed at a constant temperature of 980 °C. That is, it is not too much to say that the contact angle does not change within the present experimental range if the temperature is kept constant.

The effect of the temperature on the constant angle of a liquid silver on an alumina substrate was also investigated for the runs of (S-3) and (S-4). The values of the slopes of all the straight lines are negative, as is obvious from Fig. 5. The figure indicates that the contact angle decreases linearly with an increase in the temperature and that a liquid silver is apt to wet an alumina substrate better. The reason for this may be considered to be that the contact angle becomes small as the forces between molecules of silver decrease with an increase in the temperature and that the surface tension of silver therefore decreases.

The amount of scattering in the measured values of the contact angle (θ_1 and θ_2) is shown in Tables 1 and 2. It may be assummed, considering the human errors of measurement of ±2 °C, etc., that its scattering is due to other causes. That is, if the sintered alumina is used as a substrate, the effect of the binder agents, the difficulty of producing homogeneous finished goods, the effect of the atmosphere, etc. must be considered.

The alumina substrate was chemically inert to liquid silver in the temperature range investigated, judging from the optical-microscopy and scanning-electron-microscope studies. However, from the surface observation after the thermal treatment shown in Fig. 6, the surface of an alumina substrate became fairly rough. If the surface was worn by the thermal treatment and the atmosphere, the rough surface may be fairly much influenced by the contact angle of the liquid silver. It is necessary to increase the reproducibility in order to produce homogeneous finished goods, to clean the surface of the alumina substrate, to standarize the roughness of the work surface, to decrease the temperature fluctuation, etc.

The values of the surface tension of liquid silver have been variously reported.

The values of the surface tension were 800 dyn cm^{-1} (1 dyn=10^{-5} N) at 970 °C in air,[1] 893 dyn cm^{-1} at

Table 3. Critical Surface Tension (γ_c) and Surface Tension at 0 K (γ°_{LV}) for the Ag/Al_2O_3, AlN, and TiC Systems

Liquid metal	γ_c (dyn cm^{-1}) for ceramic		γ°_{LV} (dyn cm^{-1}) for liquid silver
Ag	Al_2O_3	361	790
	AlN	873[4]	1474[4]
	TiC	783[4]	1474[4]

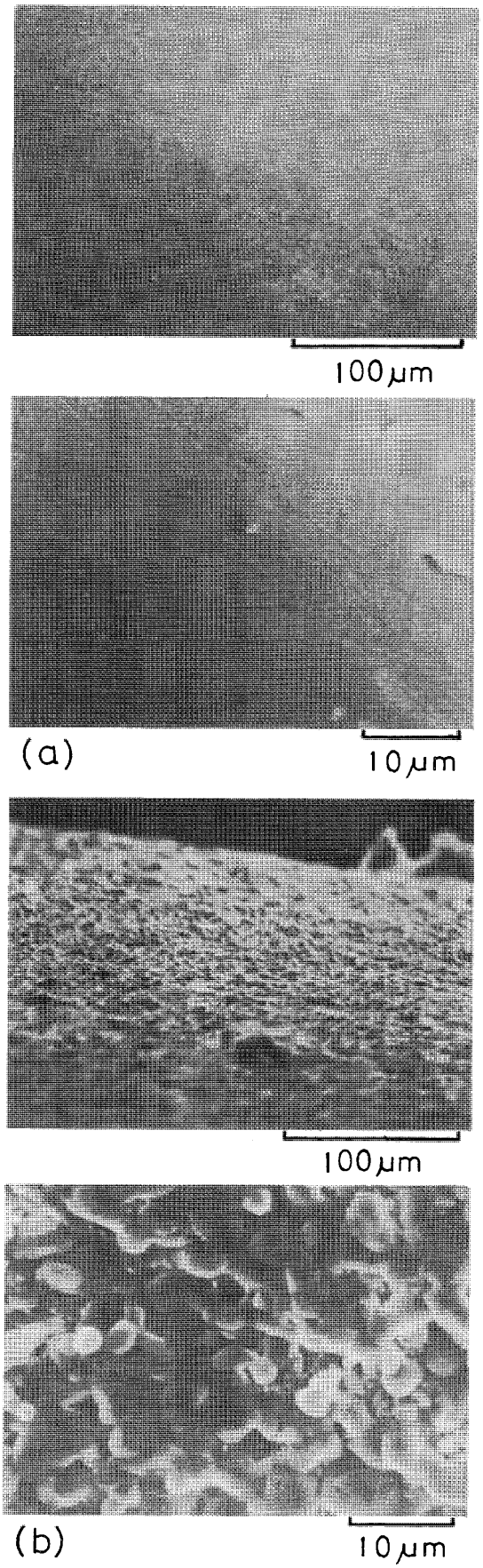

Fig. 6. Photographs of the surfaces of alumina before and after treatment for Run No. (S-3). (a) Before heat treatment, (b) after heat treatment.

1000 °C, and 849 dyn cm^{-1} at 1250 °C.[2] According to Semenchenko's publication,[3] the values of the surface tension of liquid silver are 940 dyn cm^{-1} as calculated by the Zadumkin formula, 991 dyn cm^{-1} as calculated by the Samoilovich formula, and 904 dyn cm^{-1} as calculated by the Kunin formula. On the other hand, Rhee reported that the surface tension of liquid silver followed the following equation: γ_{LV}(Ag)(dyn cm^{-1})=1092−0.14 T (°C).[4] Therefore, the surface tension at 961 °C (melting point) could be estimated to be 957 dyn cm^{-1} by the use of this equation. The values reported by Flint[5] vary from about 785 to 980 dyn cm^{-1}. Krause et al.[6] obtained the values of 930 dyn cm^{-1} at 980.8 °C and 923 dyn cm^{-1} at 1000 °C. According to Kingery,[7] the surface tension of liquid silver is 920 dyn cm^{-1} at 1000 °C in vacuo or in an atmosphere of inert gas. The surface tension of 1140 dyn cm^{-1} at 1180 K (907 °C) has also been reported.[8]

The liquid-solid interface energy, γ_{LS}, is 126 dyn cm^{-1} for silver.[9] It has also been reported that, for metal, γ_{LS}=(0.12±0.03) T_m, where T_m is the melting point (K).[10] From this equation, we can now estimate it to be from 111 to 185 dyn cm^{-1}, while Southin et al. and Zellenmoyer reported that γ_{LS}=130 dyn cm^{-1} on the average.[11]

The temperature coefficient of the surface tension of liquid silver was reported by Rhee[4] to be −0.14 dyn cm^{-1} °C, while Krause et al.[6] reported the very near value of −0.15 dyn cm^{-1} °C. On the other hand, Pawlek et al. reported a somewhat smaller value of −0.11 dyn cm^{-1} °C.[12] We should, therefore, pay special attention to controlling the temperature when high accuracy is required.

By using the present experimental results of the total height, the drop height above the maximum diameter, the maximum diameter, and the θ-value of the sessile drop that is, 0.322, 0.295, 0.499 cm and 98° (at 980 °C) respectively, and 0.311, 0.254, 0.523 cm and 89° (at 1000 °C) respectively, the surface tension of liquid silver was calculated. The calculated values of the surface tension of liquid silver were from 390 to 420 dyn cm^{-1}, as predicted by Tartar et al.'s formula,[13] 380 to 550 dyn cm^{-1} as predicted by the Porter formula,[14] and 610 dyn cm^{-1} as predicted by the Dorsey formula[15] and other formulas.[3] It was found that the values calculated by using their formulas were about 15 to 25% smaller than the values in the literature cited above.

We also attempted to calculate the critical surface tension and the surface tension at 0 K for the Ag/Al_2O_3 system and therefore adopted the values obtained by using the Dorsey formula.[15] The critical surface tension and the surface tension at 0 K were discussed by Rhee.[4]

The work of the adhesion of a liquid-solid interface can be generally defined by this equation:

$$S_{LS}=(\gamma_{LV}+\gamma_{SV})-\gamma_{LS}$$

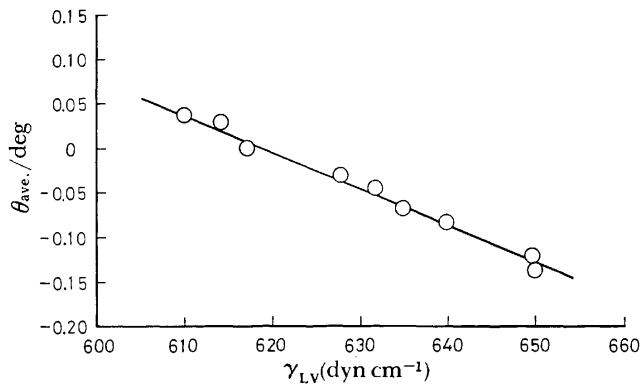

Fig. 7. Cosine of contact angle vs. surface tension of liquid silver for system Ag/Al_2O_3.

where γ_{LV}, γ_{SV}, and γ_{LS} represent the interfacial energies between the phases actually present in the Ag/Al_2O_3 system at the time of measurement. Substituting Young's equation, $\gamma_{SV}-\gamma_{LS}=\gamma_{LV}\cos\theta$, where θ is the contact angle, into the above equation gives:

$$S_{LS}=\gamma_{LV}(1+\cos\theta).$$

Since S_{LS} and $\cos\theta$ are linear functions of the temperature in the Ag/Al_2O_3 system, S_{LS} and $(\gamma_{SV}-\gamma_{LS})$ in Young's equation will vary parabolically with the temperature. If complete wetting occurs, that is, if $\cos\theta=+1$, and $\gamma_{LV}=\gamma_c$, then:

$$S_{LS}=2\gamma_{LV}=2\gamma_c=S_{LL}$$

where γ_c is the critical surface tension. The work of the adhesion of the liquid become equal to the work of cohesion. That is, the layer of vapor adsorbed on the solid surface behaves as does the liquid itself. Therefore, the critical surface tension for spreading is the surface tension of the solid with adsorbed vapor which has attained a liquidlike behavior.

As has been described above, the cosine of the contact angle increases linearly with an incresse in the temperature in the Ag/Al_2O_3 system. The variation in the cosine of the contact angle with a decrease in the surface tension of liquid silver is shown in Fig. 7 for the Ag/Al_2O_3 system. The extrapolation of the straight line to $\cos\theta=+1$ produces the critical surface tension for spreading (γ_c) for the Ag/Al_2O_3 system, with the surface tension of liquid silver at 0 K. For a liquid silver, γ_c for Al_2O_3 is always smaller than that for aluminium nitride (783 dyn cm^{-1}) and for TiC (873 dyn cm^{-1} [14]). When we obtain the values of the critical surface tension, etc., the silver vapor near the melting point may be nearly ignored and thought not to absorb on the Al_2O_3 substrate.

The writers wish to thank Mr. Hiromichi Watanuki for his assistance in the experimental work.

References

1) Landolt-Börnstein, "Physikalisch-Chemische Tabellen," **1**, 198 (1923); "International Critical Tables," McGraw-Hill Book Co., New York, **1**, 103 (1926); *ibid.*, **4**, 435 (1928); I. Lauermann, *Z. Phys. Chem.*, **216**, 42 (1928).

2) "International Critical Tables," **4**, 436 (1928).

3) V. K. Semenchenko, "Surface Phenomena in Metals and Alloys," Pergamon Press, New York (1962), p. 236; V. K. Semenchenko and L. P. Shikhobalova, *J. Phys. Chem. (USSR).*, **21**, 613,707 (1947).

4) S. K. Rhee, *J. Am. Ceram. Soc.*, **53**, 639 (1970).

5) O. Flint, *J. Nucl. Mater.*, **16**, 233 (1965).

6) W. Krause and F. Sauerwald, *Z. Anorg. Chem.*, **181**, 353 (1928).

7) W. D. Kingery, "Property Measurement at High Temperatures," John Wiley & Sons (1959), p. 368.

8) J. M. Blakey and P. S. Maiya, "Surface snd Interfaces," Syracuse University Press (1967), p. 325.

9) J. C. Brice, "The Growth of Crystals from Liquid," North-Holland, London (1973), p. 92.

10) J. C. Brice, "The Growth of Crystals from Liquid," North-Holland, London (1973), p. 93.

11) R. J. Southin and G. A. Chadwick, *Sci. Prog.*, **57**, 353 (1969); A. C. Zelllenmoyer, "Nucleation," Dekker, New York (1969), p. 341.

12) F. Pawlek, W. Thielsch, and W. Wuth, *Metall.*, **15**, 1076 (1961).

13) G. Quinche, *Ann. Physik.*, **105**, 1 (1858); H. V. Tartar, V. Siverts, and R. E. Reitmeier, *J. Am. Chem. Soc.*, **62**, 2375 (1940); G. C. Long, *ibid.* **63**, 84 (1941).

14) A. W. Porter, *Phil. Mag.*, **15**, 163 (1933); R. S. Bradley, *J. Phys. Chem.*, **33**, 232 (1934).

15) N. E. Dorsey, *J. Wash. Acad. Sci.*, **18**, 606 (1928).

 © 1987 The Chemical Society of Japan Bull. Chem. Soc. Jpn., 60, 2047—2052 (1987)

Prediction of Dissociation Constants of Ammonium Ion in Artificial Seawaters and in Concentrated Sodium Chloride Solutions

Masunobu MAEDA,* Masato HAYASHI, Shoichiro IKEDA, Yoshiaki KINJO,† and Kaname ITO
Department of Applied Chemistry, Nagoya Institute of Technology, Showa-ku, Nagoya 466
†Chemical Laboratory, College of Education, University of the Ryukyus, Okinawa 903-01
(Received December 11, 1986)

The dissociation constants of ammonium ion were determined at 25 °C by potentiometry with glass and ammonium-ion-selective electrodes in artificial seawaters at various salinities (25—45‰) and in concentrated sodium chloride aqueous solutions (0.72—3.2 mol kg^{-1}). The activity coefficients of ammonia in sodium chloride solutions of the same ionic strengths as those of the artificial seawaters and in the concentrated sodium chloride solutions, which were used for the theoretical estimation of the dissociation constants, were measured by a transpiration method. The dissociation constants were theoretically evaluated in terms of the ionic interaction model developed by Pitzer and co-workers, and compared with the experimental ones. The predicted dissociation constants showed a good agreement with the observed ones.

The majority of the values of thermodynamic properties such as free energy and enthalpy changes for ionic equilibria have been determined in solution containing an inert salt at a high and constant concentration.[1-3] The high electrolyte concentration is employed mainly in order to decrease the variation of the activity coefficients of the reacting species. The natural consequence is that the values of these thermodynamic properties are strongly influenced by the type and concentration of the electrolyte. Thus, the theoretical evaluation of these properties in a specified solution, or the recalculation from one ionic medium to another, is of theoretical as well as practical interest. From a theoretical point of view, the problem is reduced to estimating the effect of the ionic medium on the activity coefficients of the species participating in the ionic equilibria. The estimation of the activity coefficients of the relevant ionic species in concentrated single and mixed electrolyte solutions has been made by using various specific ion interaction theories.[4,5] Various important improvements to these theories have been made in recent years by Pitzer and coworkers.[6,7] The main point in the treatment is the consideration of short-range interactions between the species in solution through two second virial coefficient factors, $\beta^{(0)}$ and $\beta^{(1)}$, which can be a function of ionic strength. The equations derived, with various values of the β parameters along with the values of higher order electrostatic terms, give excellent fits to the experimental results up to the substantially high concentration level.

In previous works[8,9] the dissociation constant of ammonium ion, K_a,

$$NH_4^+ = H^+ + NH_3;\ K_a = [H^+][NH_3]/[NH_4^+]$$

was evaluated in $LiNO_3$, $NaNO_3$, $LiClO_4$, and $NaClO_4$ media with different concentrations (0.5—5 mol dm^{-3}) in terms of both the Brønsted-Guggenheim-Scatchard (BGS)[4,5] and the Pitzer ionic interaction models.[6,7] The predicted and observed values agreed fairly well, although in the lithium salt systems at higher concentration levels the deviations between the estimated and observed values exceeded by far the experimental uncertainties. As far as the sodium salt solutions were concerned, it was found that the values evaluated according to the Pitzer approach were in closer agreement with the observed ones than the values from the BGS approach. The Pitzer ionic interaction theory was successfully applied also to the evaluation of enthalpy changes for dissociation of ammonium ion in LiCl, NaCl, $LiNO_3$, $NaNO_3$, $LiClO_4$, and $NaClO_4$ media with different concentrations (0.5—5 mol dm^{-3}).[10]

In the present work the pK_a values for ammonium ion in artificial seawaters at salinites of 25, 30, 35, 40, and 45‰, the values at 35 and 45‰ being already reported by Khoo et al.,[11] and in the sodium chloride solutions of 0.72—3.2 mol kg^{-1} were determined at 25 °C by potentiometry with glass and ammonium-ion-selective electrodes. The activity coefficients of ammonia (γ_{NH_3}) in sodium chloride solutions at the same ionic strengths as those of the artificial seawaters and in the concentrated sodium chloride solutions were measured by a transpiration method. Since the γ_{NH_3} values in the seawaters could not be measured due to the precipitation of $Mg(OH)_2$ caused by the addition of ammonia, the experimental values for the sodium chloride solutions at the same ionic strengths must be employed. The observed pK_a values were compared with those calculated with the measured γ_{NH_3} values and the activity coefficients of H^+ and NH_4^+ evaluated in terms of the model developed by Pitzer and coworkers.

Whitfield[12,13] estimated the pK_a values for ammonium ion in artificial seawaters and sodium chloride solutions (0.5—3 mol dm^{-3}) according to a few different ionic interation approaches, and compared them with the values reported previously. It does not seem clear whether the agreement is satisfactory especially in the sodium chloride solutions, because of the divergence of the experimental values. In his calculations the γ_{NH_3} values used for the seawaters and concentrated sodium chloride solutions were just read from a straight line drawn through the reference point at

infinite dilution (ionic strength I=0, γ_{NH_3}=1) and the γ_{NH_3} values measured at 0.5, 1.0, and 1.5 mol dm^{-3} NaCl by Abegg and Riesenfeld[14] or a straight line drawn between the reference point at infinite dilution and the mean of the experimental values reported previously in electrolyte solutions at an ionic strength of 0.7 mol dm^{-3}.[14-16]

Experimental

Reagents. Sodium chloride of primary analytical standard quality was dried at 360 °C in an electric furnace and used without further purification. Reagent-grade ammonium chloride was recrystallized twice from water. A stock solution of ammonium chloride was analyzed gravimetrically for Cl^- as AgCl. Other salts and ammonia, of reagent quality, were used without further purification. Artificial seawaters were prepared according to Khoo et al.[11] The molal compositions of the artificial seawaters at five different salinities are shown in Table 1. The ionic strengths were calculated in the usual way with neglect of ion pairing.

Potentiometric Titration Procedures. The dissociation of ammonium ion was monitored by measuring the equilibrium hydrogen-ion and ammonium-ion concentrations with a glass electrode and an ammonium-ion-selective electrode, respectively. The emf's were measured for the cell of the type

$$\text{GE, } NH_4^+\text{-ISE} \mid \text{test solution} \parallel \text{ref}$$

where GE and NH_4^+-ISE denote a glass electrode and an ammonium-ion-selective electrode, respectively, and ref the reference half-cell, e.g., in the artificial seawater of 35‰ salinity.

$$\parallel \text{35‰ artificial seawater} \parallel \text{0.72 mol kg}^{-1}\text{ NaCl, satd. AgCl} \mid \text{AgCl-Ag}$$

From the emf's the equilibrium hydrogen-ion and ammonium-ion concentrations were calculated according to the equations

$$E^H = E_0^H + 59.16 \log[H^+] + E_j, \quad (1)$$

$$E^{NH_4} = E_0^{NH_4} + 59.16 \log[NH_4^+] + E_j, \quad (2)$$

where E_0's are constants, which were determined in situ in solution of known hydrogen-ion and ammonium-ion concentrations. E_j is a liquid junction potential arising between the test solution and the salt bridge. The E_j values, which were mainly caused by H^+ and OH^- ions, were negligibly small over the $-\log[H^+]$ range from 3 to 10 in all the solutions examined. The potentiometric titrations were performed by coulometric generation of OH^- ions.

A glass electrode of Beckman No.39314 and an ammonium-ion-selective liquid membrane electrode purchased from Denki Kagaku Keiki (DKK) were used in combination with a silver-silver chloride reference electrode prepared as recommended by Brown.[17] The emf's were measured (up to 0.1 mV) with pH meters(DKK, Ion-Meter model IOC-10). The titration cell was of the type designed by Tsukuda et al.[18] It was kept in a paraffin oil-thermostat maintained at 25.00±0.02 °C in a room thermostated at 25±1 °C. The hydroxide ions were generated by means of a coulometer (Metrohm, Coulostat E524) using the analogous cell assembly to that described by Biedermann and Ciavatta.[19] To avoid losses of ammonia the titration cell was kept tightly closed. Stirring was performed with a magnetic rod.

Table 1. Molal Compositions of Artificial Seawaters at Five Salinities

Component and ionic strength I	Salinity/‰				
	25.24	30.20	35.11	40.00	44.84
NaCl	0.3041	0.3657	0.4274	0.4893	0.5514
$MgCl_2$	0.03933	0.04730	0.05527	0.06328	0.07131
Na_2SO_4	0.02086	0.02507	0.02931	0.03356	0.03780
$CaCl_2$	0.00768	0.00924	0.01079	0.01236	0.01392
KCl	0.00754	0.00907	0.01060	0.01213	0.01368
I	0.5153	0.6196	0.7241	0.8290	0.9636

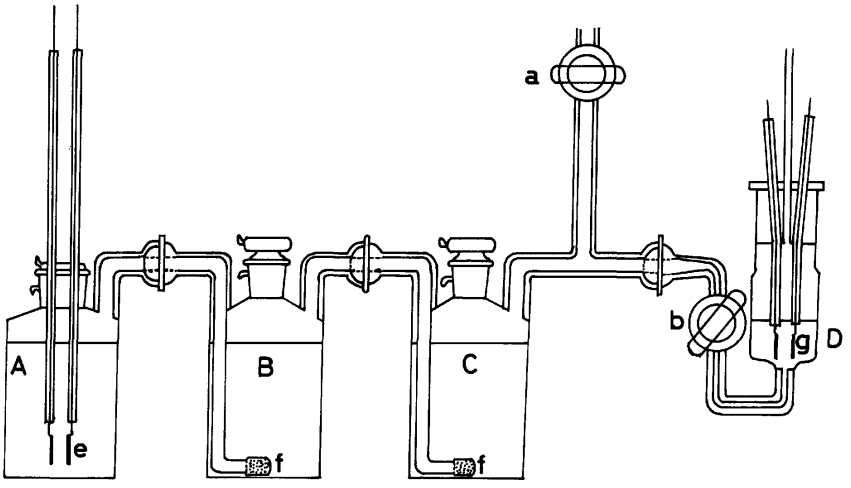

Fig. 1. Apparatus for measurement of ammonia activity. e: Platinum plates, f: sintered glass, g: platinum plates coated with platinum black.

Measurement of Activity Coefficient of Ammonia. The transpiration experiments were performed with a glass apparatus essentially similar to that used by Gaus.[20] It is schematically shown in Fig. 1. Vessel *A* was filled with a 0.5 mol dm^{-3} NaOH solution, and in vessels *B* and *C* were charged 0.4 mol dm^{-3} NH_3 solutions containing NaCl at a desired ionic strength. 10 ml of a 0.01 mol dm^{-3} HCl solution were introduced in conductivity cell *D*. The whole apparatus was immersed in a water thermostat kept at 25.00±0.01 °C. First, the detonating gas was generated in vessel *A* with stopcock *a* open and stopcock *b* closed until the empty spaces in the vessels and the tubes were saturated with the NH_3 gas. And then, in a condition of stopcock *a* being closed and stopcock *b* being open, the electrolysis of the detonating gas was carried out in small steps so that the NH_3 gas transpired by the "purging" gas was absorbed in the HCl solution in cell *D*, while the conductivity of the HCl solution being measured in each step. The electrolysis was carried out by means of a coulometer (Metrohm, Coulostat E524), and the conductivity measurement with an A. C. bridge (Delica, model DlS). The concentration of the NH_3 solution in vessel *C* before and after the experiment was measured by acid-base titrations to ascertain the invariance of the NH_3 concentration during the experiment.

Results and Discussion

Dissociation Constant of Ammonium Ion. The dissociation constants of ammonium ion were determined by the usual graphical and least-squares methods.[21] The ion products of H_2O in the artificial seawaters were taken from Culberson and Pytkowicz.[22] The pK_a values in the seawaters and in the sodium chloride solutions are tabulated in Table 2, together with those previously reported. The pK_a values obtained with a glass electrode and an ammonium-ion-selective electrode are in fairly good agreement with each other, although the uncertainties of the pK_a values determined with data from the ammonium-ion-selective electrode potentiometry are very large. The pK_a values increase with rising salinity and sodium chloride concentration. The pK_a value at 0.725 mol kg^{-1} NaCl is larger than the value in the 35‰ artificial seawater with the same formal ionic strength. The pK_a values at salinities of 35 and 45‰ are consistent with those reported by Khoo et al.[11]

Activity Coefficient of Ammonia. The experimental plots of the conductivities κ against the quantities of electricity passed (for generation of the detonating gas) Q in salt-free and 3.2 mol kg^{-1} NaCl solutions are illustrated in Fig. 2. The amount of electricity passed Q_e for the transpiration of NH_3 needed to neutralize 10 ml of a 0.01 mol dm^{-3} HCl solution was calculated from the point of the slope change. The activity coefficients of ammonia γ_{NH_3} in the sodium chloride solutions with different concentrations were determined by the use of Q_e values and ammonia concentrations C_{NH_3} (in molal units) according to Eq. 3 on the assumption that the γ_{NH_3} value in a salt-free solution be unity.

$$\gamma_{NH_3}=(Q_e^0/Q_e)\times(C_{NH_3}^0/C_{NH_3}) \quad (3)$$

where the superscript 0 is for a salt-free solution. The values of C_{NH_3} and $C_{NH_3}^0$ were adjusted practically equal to each other. The γ_{NH_3} values determined in the sodium chloride solutions of different ionic strengths are given in Table 3. It is seen that the γ_{NH_3} values increase with increasing sodium chloride concentration.

The γ_{NH_3} values in the artificial seawaters could not be determined due to the precipitation of $Mg(OH)_2$ caused by the addition of NH_3. Thus, the adequacy of the employment of the γ_{NH_3} value in the sodium chloride solution for the seawater at the same ionic strength was examined with reference to the artificial seawater at 35‰ salinity. It was suggested in the previous paper[8] that the activity coefficient of ammonia is strongly influenced by the extent of polarization of water molecules coordinated to cations. Accordingly, the Mg^{2+} ions in the artificial seawater of 35‰ salinity were replaced by the Li^+ ions which have the analogous surface charge density to that of the Mg^{2+} ions, with the ionic strength being kept at 0.725 mol kg^{-1}. The γ_{NH_3} value measured in the "artificial seawater" containing Li^+ ions was found to be 1.021, which is smaller than the value (1.057) in the 0.725 mol kg^{-1}

Table 2. Comparison between Observed and Estimated Dissociation Constants of Ammonium Ion in Artificial Seawaters and Sodium Chloride Solutions at 25 °C (pK_a values in molal units)
The Numbers in Parentheses are the Uncertainties of the Last Decimal Place

Solution	Salinity/‰ and ionic strength/mol kg^{-1}	Obsd					Est
		Present work		Khoo et al.[11]	Fouad[26]	Whitfield[12]	
		GE	NH_4^+-ISE				
Artificial seawater	25.24	9.30(1)	9.29(3)				9.316
	30.26	9.33(1)	9.34(3)				9.329
	35.11	9.35(1)	9.33(3)	9.354[a]			9.343
	40.00	9.38(1)	9.37(3)				9.357
	44.84	9.39(1)	9.40(3)	9.374[b]			9.371
NaCl solution	0.725	9.41(1)	9.44(3)				9.372
	1.022	9.44(1)	9.45(3)		9.56	9.51	9.417
	2.087	9.60(2)			9.71	9.66	9.578
	3.202	9.77(2)			9.89	9.80	9.739

a) At 35.00‰. b) At 44.55‰.

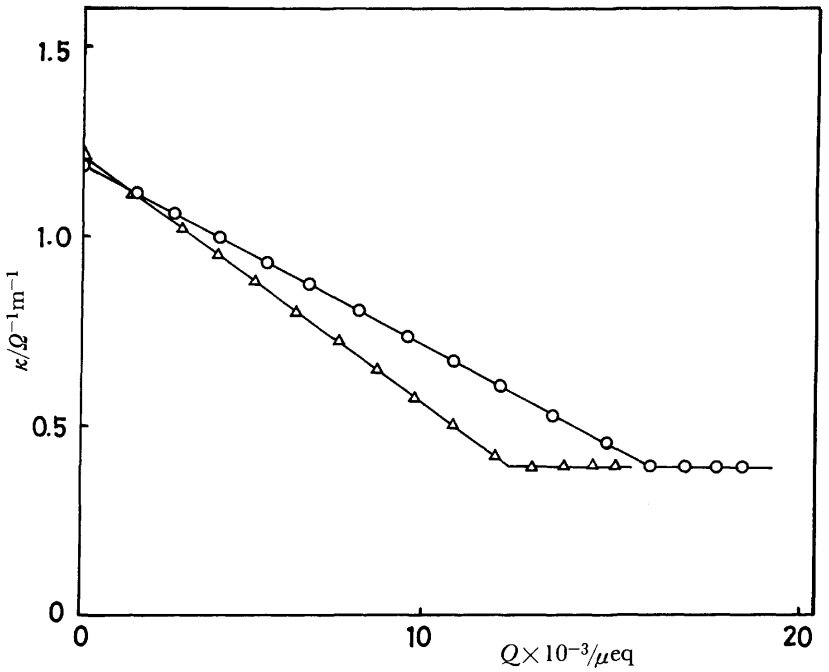

Fig. 2. Plot of conductivity κ against quantity of electricity Q. ○: Salt-free solution, △: 3.202 mol kg^{-1} NaCl solution.

Table 3. Activity Coefficients of Ammonia γ_{NH_3} at 25 °C in Sodium Chloride Solutions with Different Ionic Strengths (in molal units)

Ionic strength/mol kg^{-1}	γ_{NH_3}
0.516	1.040
0.621	1.048
0.725	1.057
0.829	1.066
0.966	1.077
1.022	1.076
2.087	1.158
3.202	1.228

NaCl solution at the same ionic strength as that of the seawater at 35‰. If this is true in the real artificial seawater of 35‰ salinity, the theoretical pK_a value is lowered by 0.025 units compared with the value calculated by use of the γ_{NH_3} value (1.057) in the 0.725 mol kg^{-1} NaCl solution. However, since the concentration of the Li^+ ions in the "artificial seawater" is 2.5 times larger than that of the Mg^{2+} ions in the artificial seawater at 35‰, the adoption of 1.021 as the γ_{NH_3} value in the 35‰ artificial seawater would lead to an underestimation of the theoretical pK_a value. In conclusion, it may be said that the use of the γ_{NH_3} values obtained in the NaCl solutions at the same ionic strengths as those of the artificial seawaters is unlikely to introduce an error of more than 0.02 units into the calculation of the pK_a values in the artificial seawaters.

Prediction of p*K*a Values. The relation between the dissociation constant of ammonium ion, $K_a(I)$, and the activity coefficients of the relevant species in solution of ionic strength I is represented by Eq.4.

$$pK_a(I) = pK_a(0) + (\ln \gamma_{H^+} + \ln \gamma_{NH_3} - \ln \gamma_{NH_4^+})/2.303 \quad (4)$$

where pK_a(0) denotes the dissociation constant in a salt-free solution. The pK_a(0) value =9.245 reported by Bates and Pinching[23] was accepted in the present calculations. As is evident from Eq. 4, since the pK_a(0) value is available and the γ_{NH_3} values have been measured in the preceeding section, the present problem is reduced to the estimation of the γ values of H^+ and NH_4^+ ions in the solution at ionic strength I. For these calculations the Pitzer ionic interaction approach[6,7] was employed. The trace activity coefficients of the ionic components of unit charge, H^+ and NH_4^+, in the solution containing cations c's and anions a's of ionic strength I can be determined from Pitzer's equations which can be expressed in the ionic form.[24]

$$\ln \gamma_{M^+} = f^\gamma + \sum_c \sum_a m_c m_a B'_{ca} + \sum_{c<c'} \sum m_c m_{c'} \theta'_{cc'} + \sum_{a<a'} \sum m_a m_{a'} \theta'_{aa'} + \sum_a m_a (2B_{Ma} + ZC_{Ma}) + \sum_c m_c (2\theta_{Mc} + \sum_a m_a \psi_{Mca}) + \sum_{a<a'} \sum m_a m_{a'} \psi_{aa'M} + \sum_c \sum_a m_c m_a C_{ca} \quad (5)$$

where M^+ denotes H^+ and NH_4^+, and m the concentration (in molal units) of the ion represented by the subscript,

$$f^\gamma = -A_\phi [I^{1/2}/(1+1.2\,I^{1/2}) + (2/1.2)\ln(1+1.2\,I^{1/2})] \quad (6)$$

with A_ϕ=0.392 at 25 °C,

$$B_{Ma} = \beta_{Ma}^{(0)} + (\beta_{Ma}^{(1)}/2I)[1-\exp(-2\,I^{1/2})(1+2\,I^{1/2})] \quad (7)$$

$$B'_{ca} = (\beta_{ca}^{(1)}/2\,I^2)[-1+\exp(-2\,I^{1/2})(1+2\,I^{1/2}+2\,I)] \quad (8a)$$

Table 4. Single Electrolyte Parameters in Pitzer's Equations at 25 °C

Cation	Anion	$\beta^{(0)}$	$\beta^{(1)}$	$\beta^{(2)}$	C^{ϕ}
H	Cl	0.1775	0.2945		0.00080
H	SO_4	0.0027	0		0.0416
NH_4	Cl	0.0522	0.1918		−0.00301
NH_4	SO_4	0.0409	0.659		−0.00116
Na	Cl	0.07650	0.2664		0.00127
Na	SO_4	0.01958	1.1130		0.00497
K	Cl	0.04835	0.2122		−0.00084
K	SO_4	0.04995	0.7793		0
Mg	Cl	0.35235	1.6815		0.00519
Mg	SO_4	0.22100	3.3430	−37.25	0.025
Ca	Cl	0.31590	1.6140		−0.00034
Ca	SO_4	0.20000	2.650	−57.70	0

$$B'_{ca} = (\beta_{ca}^{(1)}/I^2)(2/1.96)[-1+\exp(-1.4I^{1/2})(1+1.4I^{1/2}+0.98I)] + (\beta_{ca}^{(2)}/I^2)(1/72)[-1+\exp(-12I^{1/2})\times(1+12I^{1/2}+72I)] \quad (8b)$$

$$Z = \sum_i m_i|z_i| \quad (9)$$

z_i being the charge of ion i,

$$C_{ca} = C_{ca}^{\phi}/2|z_c z_a|^{1/2}. \quad (10)$$

Equation 8a is for 1-1 and 1-2 electrolytes and Eq. 8b for higher valence types such as 2-2 electrolytes. The θ and θ' terms are related to like charge interactions, and the ψ term accounts for triplet ion interactions.

The values of $\beta^{(0)}$, $\beta^{(1)}$, $\beta^{(2)}$, and C^{ϕ} used in the calculations[7] are listed in Table 4. The calculations were made without the higher order terms θ, θ', and ψ, the contributions of which are usually small,[25] because their values for all the ions are not available. A comparison between the measured pK_a values and ones estimated using Pitzer's equations is shown in Table 2. It is seen that the values observed and those predicted in the present work are in good agreement each other in almost all the solutions. The pK_a values in the sodium chloride solutions measured in the present work are in closest agreement with the theoretically estimated values.

In view of the previous[8-10]and present results, it may be said that the ionic interaction model developed by Pitzer and coworkers is adequately applied to estimate free energy and enthalpy changes both in concentrated single electrolyte solutions and in mixed electrolyte solutions as complex as seawaters. However, the large discrepancies between the observed and estimated pK_a values occurred at higher ionic strengths in the lithium salts solutions.[8,9] This may be ascribed to the fact that the higher order terms θ, θ' and ψ for binary mixtures NH_4A-LiA with a common anion A(A=NO_3 or ClO_4), the contributions of which might unexpectedly be too large to be neglected, were omitted in the calculations because of their unavailableness. Thus, it may be necessary to measure the higher order terms in order to predict the values of the thermodynamic properties more accurately. With the intention to make clear this point, isopiestic measurements of NH_4A-LiA(A=NO_3 or ClO_4) are in progress.

The work was supported in part by a Grant-in-Aid for Scientific Research No. 61540444 from the Ministry of Education, Science and Culture.

References

1) L. G. Sillén and A. E. Martell, "Stability Constants," The Chemical Society, London (1964) and "Stability Constants," Supplement No. 1, The Chemical Society, London (1970).
2) D. D. Perrin, "Stability Constants of Metal-Ion Complexes," Part B, Pergamon Press, Oxford (1979).
3) E. Högfeldt, "Stability Constants of Metal-Ion Complexes," Part A, Pergamon Press, Oxford (1982).
4) K. S. Pitzer and L. Brewer, "Thermodynamics" (Revision of Lewis and Randall), McGraw-Hill Press, New York (1961), Chap. 23.
5) E. A. Guggenheim, "Application of Statistical Mechanics," Clarendon Press, Oxford (1966).
6) K. S. Pitzer, *J. Phys. Chem.*, **77**, 268 (1973).
7) K. S. Pitzer, "Activity Coefficients in Electrolyte Solutions," Vol. 1, ed by R. M. Pytkowicz, CRC Press, Boca Raton, Florida (1979), p. 157.
8) M. Maeda, G. Nakagawa, and G. Biedermann, *J. Phys. Chem.*, **87**, 121 (1983).
9) M. Maeda, *J. Electrochem. Soc. Jpn (Denki Kagaku)*, **55**, 61 (1987).
10) M. Maeda, *J. Phys. Chem.*, **90**, 1134 (1986).
11) K. H. Khoo, C. H. Culberson, and R. G. Bates, *J. Solution Chem.*, **6**, 281 (1977).
12) M. Whitfield, *J. Mar. Biol. Assoc. U. K.*, **54**, 565 (1974).
13) M. Whitfield, *J. Mar. Biol. Assoc. U. K.*, **58**, 781 (1978).
14) R. Abegg and H. Riesenfeld, *Z. Phys. Chem.*, **40**, 84 (1902).
15) H. M. Dawson and J. McRea, *J. Chem. Soc.*, **79**, 493 (1901).
16) H. E. Matthews and C. W. Davies, *J. Chem. Soc.*, **1933**, 1435.
17) A. S. Brown, *J. Am. Chem. Soc.*, **56**, 646 (1934).
18) H. Tsukuda, T. Kawai, M. Maeda, and H. Ohtaki, *Bull. Chem. Soc. Jpn.*, **48**, 691 (1975).
19) G. Biedermann and L. Ciavatta, *Arkiv Kemi*, **22**, 253 (1964).

20) W. Gaus, *Z. Anorg. Allg. Chem.*, **25**, 236 (1900).
21) M. Maeda, R. Arnek, and G. Biedermann, *J. Inorg. Nucl. Chem.*, **41**, 343 (1979).
22) C. H. Culberson and R. M. Pytkowicz, *Mar. Chem.*, **1**, 309 (1973).
23) R. G. Bates and G. D. Pinching, *J. Res. Natl. Bur. Stand.*, **42**, 419 (1949).
24) C. E. Harvie and J. H. Weare, *Geochim. Cosmochim. Acta*, **44**, 981 (1980).
25) K. S. Pitzer and J. J. Kim, *J. Am. Chem. Soc.*, **96**, 5701 (1974).
26) M. G. Fuoad, *Motatshefte für Chemie und verwandte Teile anderer Wissenschaften*, **86**, 141 (1955).

Calorimetric and Spectrophotometric Studies of Ternary Copper(II) Complexes with Bromide Ions and 2,2′-Bipyridyl in *N,N*-Dimethylformamide

Shin-ichi Ishiguro,* László Nagy,§ and Hitoshi Ohtaki†
Coordination Chemistry Laboratories, Institute for Molecular Science, Myodaiji, Okazaki 444
†Department of Electronic Chemistry, Tokyo Institute of Technology at Nagatsuta, Nagatsuta, Midori-ku, Yokohama 227
(Received December 18, 1986)

Mixed ligand complexation of copper(II) with bromide ions and 2,2′-bipyridyl (bpy) has been calorimetrically studied in *N,N*-dimethylformamide (DMF) containing 0.16 mol dm^{-3} $(C_2H_5)_4NClO_4$ at 25 °C. Complexation of the metal ion with 2,2′-bipyridyl has been also studied in the same solution. The calorimetric titration curves obtained were satisfactorily explained in terms of formation of the mononuclear $[CuBr_p(bpy)_q]^{(2-p)+}$ (denoted as (1*pq*)) complexes such as (101), (102), (103), (111), (121), and (112), and their formation constants and enthalpies were determined. The mixed ligand (111), (112), and (121) complexes are quite stable and yielded to a large extent in the DMF solution. Electronic spectra of these complexes have been measured in DMF over the range 400—1500 nm. The thermodynamic quantities of formation and electronic spectra of the complexes thus obtained are discussed in connection with the coordination structure of the complexes in DMF. The formation of the five-coordinate $[Cu(bpy)_2(dmf)]^{2+}$ and $[CuBr(bpy)_2]^+$ complexes is suggested in the DMF solution as well as in crystal.

Complexation of bivalent transition metal ions with nitrogen-coordinating bidentate ligands such as 1,10-phenanthroline (phen) and 2,2′-bipyridyl (bpy) has so far been studied in water.[1] Mixed ligand complexes involving these ligands and a variety of amino acids (or peptides) have also been intensively studied from the biochemical point of view.[2]

As to mixed ligand complexes of copper(II) involving 2,2′-bipyridyl, Barclay et al.[3] reported the five-coordinate trigonal-bipyramidal $[CuI(bpy)_2]^+$ complex in crystal. A similar coordination structure has also been revealed for the $[CuX(bpy)_2]^+$ (X^-=Cl^-, Br^- and I^-) complex with varying counter anions.[4-8] The trigonal-bipyramidal $[Cu(bpy)_2(H_2O)]^{2+}$ complex has been observed in crystal,[9] as well as the corresponding $[Cu(phen)_2(H_2O)]^{2+}$ complex.[10-12] Besides, Faye[13] suggested from measurements of electronic spectra that both bis(1,10-phenanthroline)copper(II) and monochlorobis(1,10-phenanthroline)copper(II) complexes have the triginal-bipyramidal structure in acetone and nitromethane solutions.

Although the knowledge of the structure and electronic spectra of the five-coordinate copper(II) complexes has been so far accumulated, the thermodynamic behavior of these complexes in solution has not been well elucidated yet.

In the present work, we calorimetrically investigated the formation of ternary copper(II) complexes with bromide ions and 2,2′-bipyridyl in *N,N*-dimethylformamide containing 0.16 mol dm^{-3} $(C_2H_5)_4NClO_4$ at 25 °C. The formation of binary copper(II) complexes with 2,2′-bipyridyl has been also explored in the same ionic medium solution. The complexation of copper(II) with bromide ions has already been examined in the $(C_2H_5)_4NClO_4$ DMF solution.[14] In order to elucidate the coordination structure of the ternary copper(II) complexes in DMF, electronic spectra were measured over the range 400—1500 nm in DMF solutions in which one of the ternary complexes was predominantly formed. Electronic spectra of the 2,2′-bipyridyl complexes of copper(II) have also been measured in DMF. The thermodynamic quantities of formation and electronic spectra of the $[Cu(bpy)_n]^{2+}$ and $[CuCl_p(bpy)_q]^{(2-p)+}$ complexes thus determined will be discussed in connection with the coordination structure of the complexes in DMF.

Experimental

Reagent. All chemicals used were of reagent grade. 2,2′-*Bipyridyl* was used without further purification and dried in vacuum over P_2O_5 in a desiccator. Other chemicals were prepared or purified as described elsewhere.[14,15]

Measurements. Calorimetric measurements were carried out in a room thermostated at (25.0±0.2) °C, a Dewar vessel for calorimetric titrations being immersed in a water bath controlled at (25±0.007) °C. All test solutions contained 0.16 mol dm^{-3} $(C_2H_5)_4NClO_4$ as a constant ionic medium. 100 cm^3 of a DMF solution containing copper(II) perchlorate or copper(II) bromide with varying molar ratios of bromide to the metal ions was placed in a Dewar vessel which was filled with dry nitrogen gas and isolated from moisture with a P_2O_5 drying-tube, and then it was titrated with 0.1 mol dm^{-3} 2,2′-bipyridyl DMF solution. Heats of complexation observed at each titration point were ranged 1—5 J with certainty ±0.05 J and were corrected for heats of dilution of the titrant, although the correction was very small. Heats of dilution were determined in advance by separate experiments by titrating a 0.16 mol dm^{-3} $(C_2H_5)_4NClO_4$ DMF solution with the 2,2′-bipyridyl solution. All of the measurements were carried out by using a fully automatic on-line system for calorimetry developed in our laboratory.[16,17]

Calorimetric data were treated with the least-squares method by taking into account the mass-balance equations for the metal and bromide ions and 2,2′-bipyridyl in solution, and the formation constants and enthalpies of assumed complexes were simultaneously optimized. The least-

§Present address: Department of Inorganic and Analytical Chemistry, A. József University, Szeged, Hungary.

squares program having been used for the binary systems in previous works[14-16] was extended for the ternary system in this work.

Electronic spectra were measured using a Cary 2300 spectrophotometer (Varian) over the range 400—1500 nm.

Results and Discussion

Calorimetric titration curves for the complexation of copper(II) ion with 2,2′-bipyridyl are depicted in Fig. 1. The corresponding curves in the ternary system are depicted in Fig. 2. In both figures, enthalpies $\Delta H^\circ = -q/(\delta v C_{L,tit})$ were plotted against C_L/C_M, where q, δv, C_L, and C_M stand for the heat evolved, the volume of an aliquot of the titrant added and the concentrations of 2,2′-bipyridyl and copper(II) ion in solution, respectively, at each titration point, and $C_{L,tit}$ denotes the concentration of 2,2′-bipyridyl in the titrant soluton.

In Fig. 1 the ΔH° values are negative and kept practically constant in the range $C_L/C_M<1$, indicating a formation of $[Cu(bpy)]^{2+}$ complex. The ΔH° values drastically change at $C_L/C_M=1$ and are slightly dependent on the concentration of the metal ion over the range $C_L/C_M=1$—4, rather weak $[Cu(bpy)_2]^{2+}$ and $[Cu(bpy)_3]^{2+}$ complexes being expected to be formed in the range. As expected, the calorimetric data were well explained in terms of the formation of $[Cu(bpy)_n]^{2+}$ (n=1—3), and their formation constants and enthalpies were optimized by the least-squares method. The overall formation constants and enthalpies of formation of the complexes thus obtained are summarized in Table 1. As seen in Fig. 1, the solid lines, the titration curves calculated by using the constants in Table 1, satisfactorily reproduce the experimental points over the whole range of C_L/C_M examined.

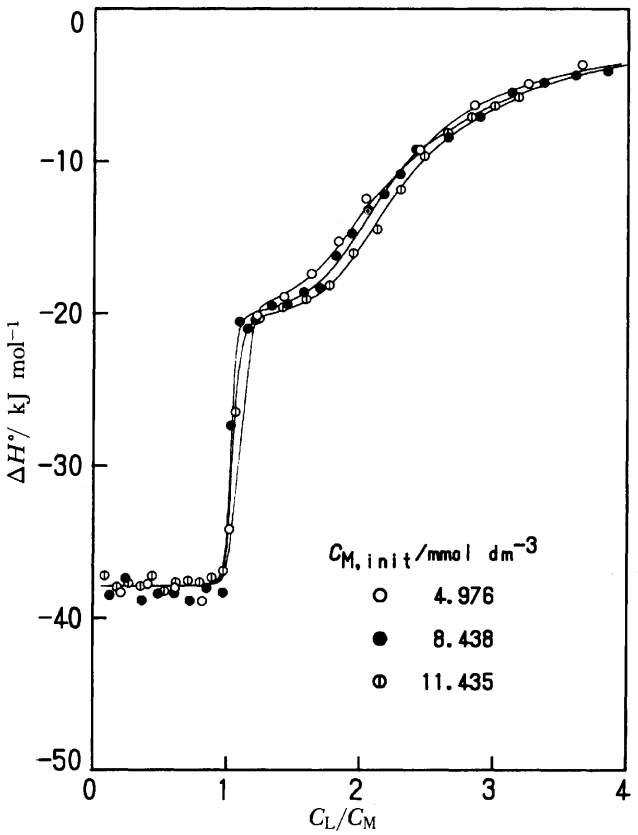

Fig. 1. Calorimetric titration curves of copper(II) 2,2′-bipyridyl DMF solutions containing 0.16 mol dm^{-3} $(C_2H_5)_4NClO_4$ at 25°C. Concentrations of copper(II) ions, $C_{M,init}$/mmol dm^{-3}, in the initial test solutions are given in the figure. The solid lines show the curves calculated by using the constants in Table 1.

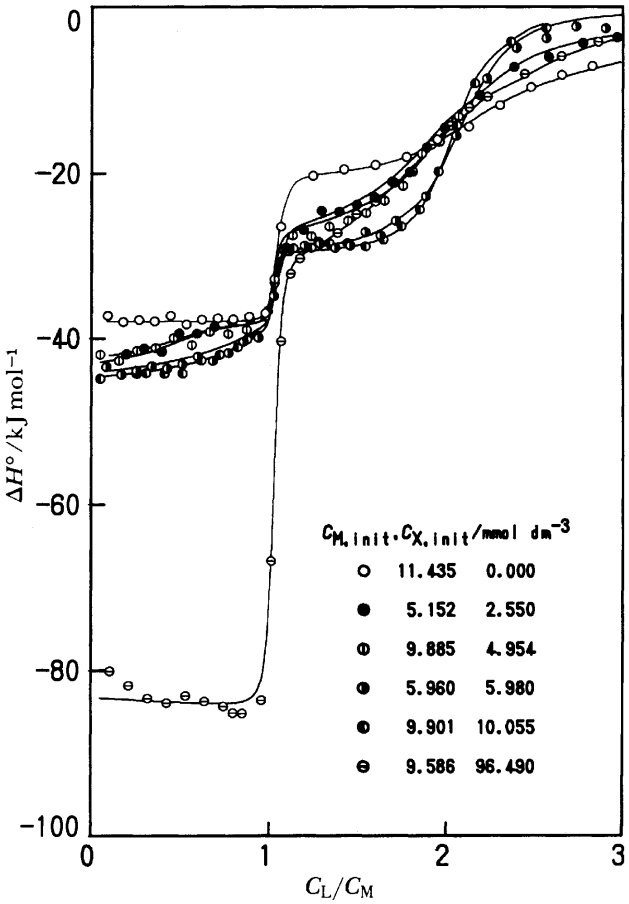

Fig. 2. Calorimetric titration curves in the ternary system obtained by titrating copper(II) bromide DMF solutions with a 2,2′-bipyridyl DMF solution, each containing 0.16 mol dm^{-3} $(C_2H_5)_4NClO_4$ at 25°C. Concentrations of copper(II) and bromide ions, $C_{M,init}$ and $C_{X,init}$/mmol dm^{-3}, in initial test solutions are given in the figure. The solid lines show the curves calculated by using the constants in Table 1.

In Fig. 2 the calorimetric titration curves are strongly dependent on the molar ratio of bromide to copper(II) ions in the solution. The curves calculated by using the only known formation constants and enthalpies of $[CuBr_n]^{(2-n)+}$ (n=1—4)[14] and those of $[Cu(bpy)_n]^{2+}$ (n=1—3) determined above hardly reproduce the experimental points, and thus the formation of ternary $[CuBr_p(bpy)_q]^{(2-p)+}$ (denoted as ($1pq$)) complexes must be considered. Ternary ($1pq$) complexes with $p+2q\leq 6$ may be plausibly formed by taking into

Table 1. The Least-Squares Refinement of Overall Formation Constants, $\log(\beta_{1pq}/\mathrm{mol}^{-(p+q)}\mathrm{dm}^{3(p+q)})$, and Enthalpies, $\Delta H^\circ_{\beta 1pq}/\mathrm{kJ\,mol}^{-1}$, of $[CuBr_p(bpy)_q]^{(2-p)+}$ (bpy=2,2′-bipyridyl) in *N,N*-Dimethylformamide Containing 0.16 mol dm^{-3} $(C_2H_5)_4NClO_4$ at 25 °C

	$[Cu(bpy)_q]^{2+}$	$[CuBr_p(bpy)_q]^{(2-p)+}$
$\log\beta_{101}$	7.04(0.41)	7.20(0.33)
$\log\beta_{102}$	10.55(0.45)	10.74(0.35)
$\log\beta_{103}$	12.34(0.48)	12.56(0.37)
$\log\beta_{111}$	—	11.90(0.26)
$\log\beta_{121}$	—	14.12(0.22)
$\log\beta_{112}$	—	15.87(0.23)
$\Delta H^\circ_{\beta 101}$	−37.9(0.3)	−37.9(0.3)
$\Delta H^\circ_{\beta 102}$	−58.7(0.8)	−58.7(0.6)
$\Delta H^\circ_{\beta 103}$	−86.2(3.9)	−85.7(3.7)
$\Delta H^\circ_{\beta 111}$	—	−24.0(0.5)
$\Delta H^\circ_{\beta 121}$	—	−18.7(0.7)
$\Delta H^\circ_{\beta 112}$	—	−54.5(0.7)
U[a]	0.178	0.520
R[b]	0.0197	0.0210
N[c]	84	220

Values in parentheses refer to three standard deviations. The formation constants and enthalpies of formation of $[CuBr_n]^{(2-n)+}$ (n=1—4)[14] were fixed in the course of the least-squares analysis. a) Error-square sum. b) The Hamilton R-factor. c) The number of data points.

account the six-coordinate about the metal ion, together with the mono- and bidentate coordinations of bromide ion and 2,2′-bipyridyl, respectively. The possible compositions of the ternary complexes are thus (111), (121), (131), (141), (112), and (122). However, the formation of the (131), (141), and (122) complexes were eliminated in the course of the least-squares analysis. The formation constants and enthalpies of these ternary complexes were finally optimized together with those of the binary $[Cu(bpy)_n]^{2+}$ (n=1—3) complexes by using the whole set of data shown in Figs. 1 and 2, the results being also listed in Table 1. The Hamilton R-factor was 2.10% and the thermodynamic quantities of each complex was obtained with relatively small standard deviations. As seen in Fig. 2, the solid lines calculated by using the constants in Table 1 and those for the $[CuBr_n]^{(2-n)+}$ (n=1—4) previously determined,[14] satisfactorily reproduce the experimental points. The $\log\beta_{10q}$ (q=1—3) values thus obtained in the mixed ligand ternary system were in satisfactorily good agreement with those in the binary system without bromide ions.

In Fig. 3 the distribution of species is shown as the function of $-\log([bpy]/\mathrm{mol\,dm}^{-3})$ in solution with varying $R(=C_X/C_M)$ values, which is calculated by using the formation constants of the ternary copper(II) complexes with 2,2′-bipyridyl and bromide ions, together with those of relevant binary copper(II) complexes. It is indicated from the figure that the (111) and (112) complexes are predominantly formed in solution containing equimolar amounts of copper(II)

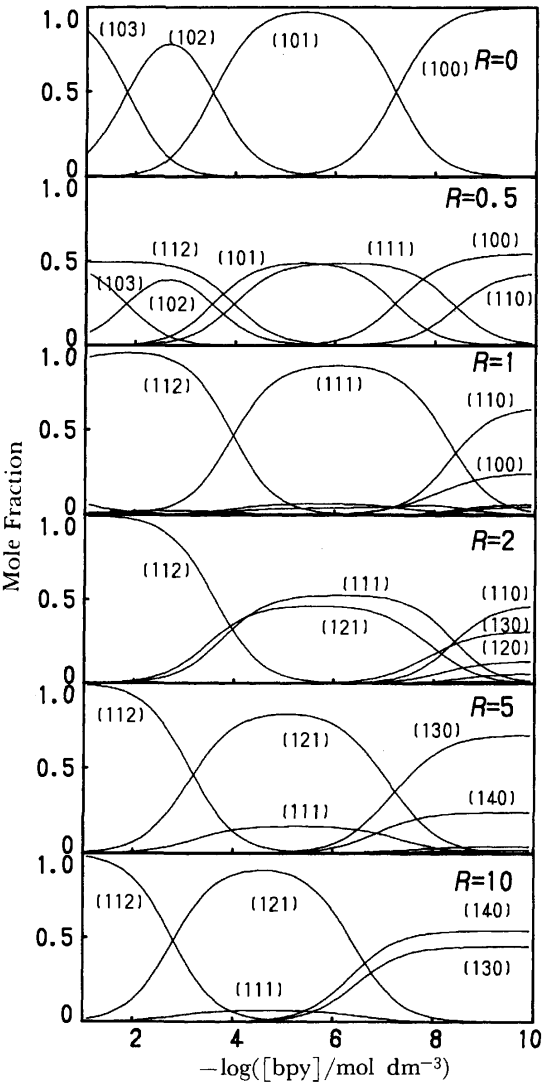

Fig. 3. Distribution of the $[CuBr_p(bpy)_q]^{(2-p)+}$ (denoted as (lpq)) complexes as the function of $-\log([bpy]/\mathrm{mol\,dm}^{-3})$ in DMF containing 0.16 mol dm^{-3} $(C_2H_5)_4NClO_4$ at 25 °C. The R value stands for the molar ratio of bromide to copper(II) ions in solution.

and bromide ions (R=1). With increasing R, the formation of the ternary copper(II) complexes is suppressed for the (111) complex but is enhanced for the (121) one. The (112) complex is formed in all the solutions. In Fig. 4 the distribution of species is represented as the function of $-\log([Br^-]/\mathrm{mol\,dm}^{-3})$ in solution with varying R' $(=C_L/C_M)$ ratios of 2,2′-bipyridyl to copper(II) ion, for comparison.

The distribution of species in Figs. 3 and 4 indicates that each of the (101), (102), (103), (111), (112), and (121) complexes is yielded as a main species in a DMF solution with a suitable composition of the ligands to copper(II) ion. Electronic spectra of DMF solutions in which each of the $[Cu(bpy)_n]^{2+}$ (n=0—3) complex is predominantly formed are depicted in Fig. 5. As well, electronic spectra of the $[CuBr(bpy)]^+$, $[CuBr(bpy)_2]^+$ and $[CuBr_2(bpy)]$ complexes are shown in Fig. 6.

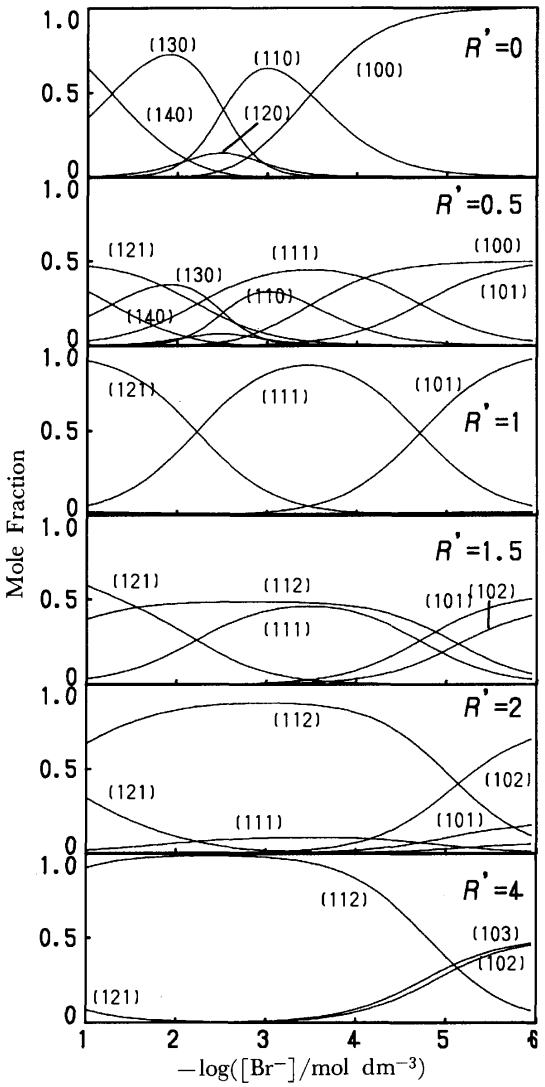

Fig. 4. Distribution of the $[CuBr_p(bpy)_q]^{(2-p)+}$ (denoted as (l*pq*)) complexes as the function of $-\log([Br^-]/\text{mol dm}^{-3})$ in DMF containing 0.16 mol dm^{-3} $(C_2H_5)_4NClO_4$ at 25°C. The *R'* value stands for the molar ratio of 2,2'-bipyridyl to copper(II) ion in solution.

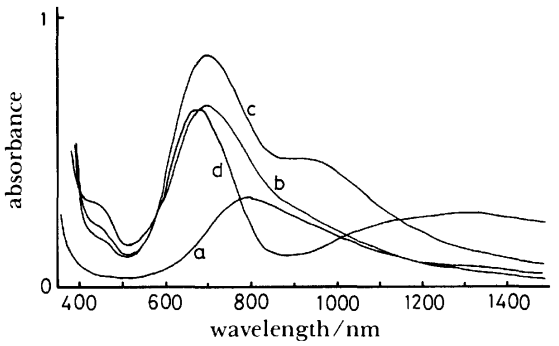

Fig. 5. Electronic spectra of various copper(II) 2,2'-bipyridyl DMF solutions. Concentrations of metal ions and ligands, C_M and C_L/mmol dm^{-3}: 9.69, 0.0 (spectrum a for $[Cu(dmf)_6]^{2+}$); 10.17, 11.60 (b for $[Cu(bpy)]^{2+}$); 9.92, 21.2 (c for $[Cu(bpy)_2]^{2+}$); 10.67, 100. (d for $[Cu(bpy)_3]^{2+}$).

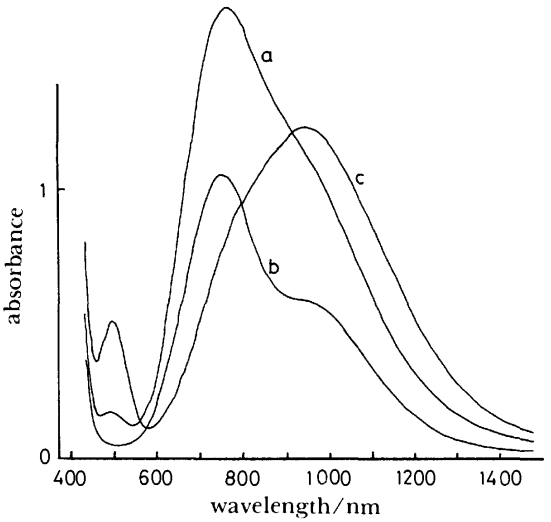

Fig. 6. Electronic spectra of the ternary copper(II) complexes with bromide ions and 2,2'-bipyridyl in DMF. Concentrations of metal and bromide ions and 2,2'-bipyridyl, C_M, C_X and C_L/mmol dm^{-3}: 10.15, 11.01, 9.97 (spectrum a for $[CuBr(bpy)]^+$); 9.87, 10.47, 20.35 (b for $[CuBr(bpy)_2]^+$); 4.00, 16.0, 4.25 (c for $[CuBr_2(bpy)]$).

These electronic spectra observed in the wavelength range 400—1500 nm may be ascribed to the d-d transition bands of copper(II) ion within the complexes.

Binary (2,2'-Bipyridyl)copper(II) Complexes. In DMF, copper(II) ion is present as $[Cu(dmf)_6]^{2+}$ with the distorted octahedral structure according to X-ray diffraction measurements.[19] The DMF molecules coordinating to copper(II) ion are stepwise replaced with 2,2'-bipyridyl molecules and the $[Cu(bpy)_3]^{2+}$ complex is finally formed in the solution. The $[Cu(bpy)_3]^{2+}$ complex may have the distorted octahedral structure in DMF because its electronic spectrum in DMF is very similar to that in crystals,[20] and the distorted octahedral $[Cu(bpy)_3]^{2+}$ complex has been revealed in the $[Cu(bpy)_3](ClO_4)_2$ crystal.[21] Similarly, the mono(2,2'-bipyridyl) complex may have the distorted octahedral structure as represented by $[Cu(bpy)(dmf)_4]^{2+}$ with two DMF molecules at the equatorial position and the others at the axial position, because its electronic spectrum shows a similar single peak to that of the $[Cu(dmf)_6]^{2+}$ complex, although the peak position of the former complex is shifted to shorter wavelength by ca. 100 nm than that of the latter.

The bis(2,2'-bipyridyl)copper(II) complex exhibits two absorption bands at ca. 690 and 950 nm in DMF as well as in water,[22] suggesting a similar coordination structure of the complex in both solutions. It is noted that the electronic spectrum of the bis(2,2'-bipyridyl) complex in solution is also very similar to that (with peaks at 708 and 930 nm) arising from the five-coordinate $[Cu(bpy)_2(H_2O)]^{2+}$ moiety in the $[Cu(bpy)_2(H_2O)]S_5O_6$ crystal.[9] Therefore, the five-coordinate $[Cu(bpy)_2(dmf)]^{2+}$ complex is plausibly formed in

Table 2. Thermodynamic Quantities, $\log(K_n/\text{mol}^{-1}\,\text{dm}^3)$, $\Delta G_n^\circ/\text{kJ mol}^{-1}$, $\Delta H_n^\circ/\text{kJ mol}^{-1}$, and $\Delta S_n^\circ/\text{J K}^{-1}\,\text{mol}^{-1}$, for the Stepwise Formation of the 2,2′-Bipyridyl and Ethylenediamine Complexes of Copper(II)

	2,2′-Bipyridyl DMF[a]	2,2′-Bipyridyl Water[b]	Ethylenediamine Water[c]
$\log K_1$	7.20	7.81	11.38
$\log K_2$	3.54	4.64	9.97
$\log K_3$	1.82	4.17	
ΔG_1°	−41.1	−44.6	−65.0
ΔG_2°	−20.2	−26.5	−56.9
ΔG_3°	−10.4	−23.8	
ΔH_1°	−37.9	−49.7	−67.7
ΔH_2°	−20.8	−22.6	−71.0
ΔH_3°	−27.0	−27.7	
ΔS_1°	11	−17	−9
ΔS_2°	−2	13	−47
ΔS_3°	−56	−13	

a) This work in *N*,*N*-dimethylformamide containing 0.16 mol dm^{-3} $(C_2H_5)_4NClO_4$. b) Ref. 1, in 0.1 mol dm^{-3} $NaClO_4$ aqueous solution. c) Ref. 18, in 3 mol dm^{-3} $LiClO_4$ aqueous solution.

DMF.

The thermodynamic quantities of stepwise formation of $[Cu(bpy)_n]^{2+}$ (n=1—3) in DMF are summarized in Table 2, together with those of $[Cu(bpy)_n]^{2+}$ (n=1—3)[1] and $[Cu(en)_n]^{2+}$ (n=1 and 2)[18] in water. The ΔH_1° value for the formation of the $[Cu(bpy)]^{2+}$ complex is large and negative and the corresponding ΔS_1° value is slightly positive in DMF. It is noted that the ΔH_2° value is significantly less negative than the ΔH_1° value in the copper(II)-2,2′-bipyridyl system both in DMF and in water. On the other hand, the ΔH_2° value is even more negative than the ΔH_1° value in the copper(II)-ethylenediamine system in water. According to X-ray diffraction measurements,[23] the bis(ethylenediamine) complex has the distorted octahedral (or practically the square planar) $[Cu(en)_2(H_2O)_{ax}(H_2O)_{ax}]^{2+}$ structure with extremely elongated two axial water molecules in water. Therefore, the significant difference observed for the ΔH_2° values in the 2,2′-bipyridyl and ethylenediamine systems may be ascribable to the difference in the coordination structure of the bis(2,2′-bipyridyl) and bis(ethylenediamine) complexes of copper(II). It is also noted that the ΔH_3° and ΔS_3° values are more negative than the corresponding ΔH_2° and ΔS_2° values in the copper(II)-2,2′-bipyridyl system. Considering the five-coordinate $[Cu(bpy)_2(dmf)]^{2+}$ complex as discussed in a preceding section, we expect that the more negative ΔH_3° and ΔS_3° values than the corresponding ΔH_2° and ΔS_2° ones may be explained in terms of the liberation of only one DMF molecule within the five-coordinate $[Cu(bpy)_2(dmf)]^{2+}$ complex followed by the formation of the six-coordinate $[Cu(bpy)_3]^{2+}$ complex.

Table 3. Thermodynamic Quantities, $\Delta G^\circ/\text{kJ mol}^{-1}$, $\Delta H^\circ/\text{kJ mol}^{-1}$, and $\Delta G^\circ/\text{J K}^{-1}\,\text{mol}^{-1}$, of Stepwise Formation of $[CuBr_p(bpy)_q]^{(2-p)+}$ (bpy=2,2′-bipyridyl), Together with Those of Stepwise Formation of $[CuBr_n]^{(2-p)+}$ (n=1—4) in *N*,*N*-Dimethylformamide at 25 °C

Reaction	ΔG°	ΔH°	ΔS°
$[CuBr(bpy)]^+ + bpy = [CuBr(bpy)_2]^+$	−22.7	−30.5	−26
$[Cu(bpy)_2]^{2+} + Br^- = [CuBr(bpy)_2]^+$	−29.3	4.2	112
$[CuBr]^+ + bpy = [CuBr(bpy)]^+$	−48.1	−43.6	15
$[Cu(bpy)]^{2+} + Br^- = [CuBr(bpy)]^+$	−26.8	13.9	137
$[CuBr_2] + bpy = [CuBr_2(bpy)]$	−49.0	−56.7	−26
$[CuBr(bpy)]^+ + Br^- = [CuBr_2(bpy)]$	−12.7	5.3	64
$Cu^{2+} + Br^- = [CuBr]^+$[a]	−19.9	19.6	132
$[CuBr]^+ + Br^- = [CuBr_2]$[a]	−11.8	18.5	101
$[CuBr_2] + Br^- = [CuBr_3]^-$[a]	−16.9	18.1	117
$[CuBr_3]^- + Br^- = [CuBr_4]^{2-}$[a]	−7.3	16.5	80

a) Ref. 14, in 0.16 mol dm^{-3} $(C_2H_5)_4NClO_4$ DMF solution.

Ternary (2,2′-Bipyridyl)bromocopper(II) Complexes. The thermodynamic quantities of stepwise formation of ternary copper(II) complexes with bromide ions and 2,2′-bipyridyl, together with those of binary copper(II) bromo complexes, in DMF are summerized in Table 3.

As seen in Table 3, the coordination of a bromide ion to the $[Cu(bpy)_2]^{2+}$ complex is endothermic with a large and positive entropy change. Such a result can not be expected from a simple addition of bromide ion to the $[Cu(bpy)_2(dmf)]^{2+}$ complex to form a six-coordinate $[CuBr(bpy)_2(dmf)]^+$ complex. We thus expect the rupture of a Cu-dmf bond within $[Cu(bpy)_2(dmf)]^{2+}$ followed by the formation of the five-coordinate $[CuBr(bpy)_2]^+$ complex without any DMF molecule coordinating to the central metal ion, as having already been found in crystal.[7,8] The conclusion may be supported by the electronic spectra of the bis(2,2′-bipyridyl)monobromocopper(II) complex in DMF because it exhibits peaks at ca. 750 and 950 nm, and a similar spectrum with peaks at 755 and 955 nm has been observed for the five-coordinate $[CuCl(bpy)_2]^{2+}$ moiety within the $[CuCl(bpy)_2]_2S_5O_6\cdot 6H_2O$ crystal.[9] The monobromocopper(II) complex may exist as $[CuBr(dmf)_5]^+$ in DMF, as well as $[CuCl(dmf)_5]^+$.[19] DMF molecules coordinating to the $[CuBr(dmf)_5]^+$ complex are replaced with 2,2′-bipyridyl molecules and the five-coordinate $[CuBr(bpy)_2]^+$ complex may be finally formed in DNF. As seen in Table 3, in the course of the successive reactions of $[CuBr]^+$ with 2,2′-bipyridyl molecules in DMF, the formation of the $[CuBr(bpy)]^+$ complex exhibits a positive ΔS° value and the subsequent formation of $[CuBr(bpy)_2]^+$ a negative ΔS° one. Since a relatively large ΔS° value may be associated with the change from the six- to five-coordinate structure in the course of a complexation reaction, the coordination structure may be changed at the formation of the $[CuBr(bpy)]^+$ complex. As seen in Fig. 6, the electronic spectrum of the $[CuBr(bpy)]^+$ complex shows a

Table 4. Thermodynamic Quantities, $\log K$, $\Delta G°$/kJ mol^{-1}, $\Delta H°$/kJ mol^{-1}, and $\Delta S°$/J K^{-1} mol^{-1}, of Reaction, $[CuBr_p]^{(2-p)+}+[Cu(bpy)_q]^{2+}=[CuBr_p(bpy)_q]^{(2-p)+}+Cu^{2+}$ (bpy=2,2′-bipyridyl), in *N*,*N*-dimethylformamide at 25°C

Complex formed	$\log K$	$\Delta G°$	$\Delta H°$	$\Delta S°$
$[CuBr(bpy)]^+$	1.23	−7.0	−5.7	4
$[CuBr(bpy)_2]^+$	1.65	−9.4	−15.4	−20
$[CuBr_2(bpy)]$	1.38	−7.9	−18.9	−37

peak at 750 nm and a shoulder at ca. 950 nm, these bands being also observed in the spectrum of the five-coordinate $[CuBr(bpy)_2]^+$ complex. Therefore, we expect the formation of the five-coordinate $[CuBr(bpy)(dmf)_2]^+$ complex in DMF.

The electronic spectrum of the mono(2,2′-bipyridyl)-dibromocopper(II) complex exhibits a peak at 950 nm and a shoulder at ca. 750 nm, these peak positions being similar to that observed for the $[CuBr(bpy)_2]^+$ and $[CuBr(bpy)]^+$ complexes, while the relative intensity of the 950 nm band to the 750 nm one is significantly strong in the $[CuBr_2(bpy)]$ complex. It seems thus difficult to conclude whether the $[CuBr_2(bpy)]$ complex has the four- or five-coordinate structure in DMF.

The thermodynamic quantities of formation of the ternary $[CuBr(bpy)]^+$, $[CuBr(bpy)_2]^+$, and $[CuBr_2(bpy)]$ complexes according to the reaction, $[CuBr_p]^{(2-p)+}+[Cu(bpy)_q]^{2+}=[CuBr_p(bpy)_q]^{(2-p)+}+Cu^{2+}$, are summarized in Table 4. The $\Delta G°$ values are all appreciably negative, indicating the favorable formation of each ternary complex with respect to the relevant binary bromo and 2,2′-bipyridyl complexes of copper(II) ion in DMF. It should be noted that the corresponding $\Delta H°$ values are significantly large and negative.

The formation reactions of the $[CuBr(bpy)]^+$ and $[CuBr(bpy)_2]^+$ complexes may be represented as $[CuBr(dmf)_5]^+ + [Cu(bpy)(dmf)_4]^{2+} = [CuBr(bpy)(dmf)_2]^+ + [Cu(dmf)_6]^{2+} + dmf$ and $[CuBr(dmf)_5]^+ + [Cu(bpy)_2(dmf)]^{2+} = [CuBr(bpy)_2]^+ + [Cu(dmf)_6]^{2+}$, respectively, by taking into account the coordination of DMF molecules within the relevant complex species. We note that one DMF molecule may be liberated at the formation of the $[CuBr(bpy)]^+$ complex but no DMF molecule at the formation of $[CuBr(bpy)_2]^+$. In Table 4 the $\Delta H°$ and $\Delta S°$ values for the formation of $[CuBr(bpy)]^+$ are appreciably less negative than those for the formation of $[CyBr(bpy)_2]$, the result might be thus ascribed to the rupture of the metal-dmf bond at the formation of the former complex.

The present work has been financially supported by the Grant-in-Aid for Special Project Research No. 61134043 from the Ministry of Education, Science and Culture.

References

1) W. A. E. McBryde, "A Critical Review of Equilibrium Data for Proton- and Metal Complexes of 1,10-Phenanthroline, 2,2′-Bipyridyl and Related Compounds," IUPAC Chemical Data Series No. **17**, Pergamon Press (1978).
2) H. Sigel and R. B. Martin, *Chem. Rev.*, **82**, 385 (1982).
3) G. A. Barclay, B. F. Hoskins, and C. H. L. Kennard, *J. Chem. Soc.*, **1963**, 5691.
4) W. D. Harrison, B. J. Hathaway, and D. Kennedy, *Acta Crystallogr., Sect. B*, **35**, 2301 (1979).
5) F. S. Stephens and P. A. Tucker, *J. Chem. Soc., Dalton Trans.*, **1973**, 2293.
6) J. Keiser, G. Brauner, F. A. Schröder, I. F. Taylor, and S. E. Rasmussen, *J. Chem. Soc., Dalton Trans.*, **1974**, 1490.
7) B. J. Hathaway and A. Murphy, *Acta Crystallogr., Sect. B*, **36**, 295 (1980).
8) M. A. Khan and D. G. Tuck, *Acta Crystallogr., Sect. B*, **37**, 1409 (1981).
9) W. D. Harrison and B. J. Hathaway, *Acta Crystallogr., Sect. B*, **35**, 2910 (1979).
10) H. Nakai and Y. Deguchi, *Bull. Chem. Soc. Jpn.*, **48**, 2557 (1975).
11) H. Nakai and Y. Noda, *Bull. Chem. Soc. Jpn.*, **51**, 1386 (1978).
12) A. Bencini and D. Gatteschi, *Inorg. Chem.*, **16**, 1994 (1977).
13) G. H. Faye, *Can. J. Chem.*, **44**, 2165 (1966).
14) S. Ishiguro, K. Ozutsumi, L. Nagy, and H. Ohtaki, *Bull. Chem. Soc. Jpn.*, **60**, 1691 (1987).
15) S. Ishiguro, B. G. Jeliazkova, and H. Ohtaki, *Bull. Chem. Soc. Jpn.*, **58**, 1143 (1985).
16) S. Ishiguro, K. Yamamoto, and H. Ohtaki, *Anal. Sci.*, **1**, 263 (1985).
17) S. Ishiguro and H. Ohtaki, *J. Coord. Chem., Sect. B*, **15**, 237 (1987).
18) S. Ishiguro, Y. Oka, and H. Ohtaki, *Bull. Chem. Soc. Jpn.*, **57**, 391 (1984).
19) K. Ozutsumi, S. Ishiguro, and H. Ohtaki, to be published.
20) R. A. Palmer and T. S. Piper, *Inorg. Chem.*, **5**, 864 (1966).
21) O. P. Anderson, *J. Chem. Soc., Dalton Trans.*, **1972**, 2597.
22) C. K. Jørgensen, *Acta Chem. Scand.*, **9**, 1362 (1955); "Inorganic Complexes," Academic Press London and New York (1963).
23) T. Fujita and H. Ohtaki, *Bull. Chem. Soc. Jpn.*, **56**, 3274 (1983).

Association of Benzene and Alkylbenzenes with Cyclodextrins in Aqueous Medium

Isao SANEMASA* and Youko AKAMINE
Department of Chemistry, Faculty of Science, Kumamoto University, Kurokami 2-39-1, Kumamoto 860
(Received December 23, 1986)

Formation constants of the following aromatic hydrocarbons with α-,β-, and γ-cyclodextrin(CyD) were determined in aqueous medium at 25 °C in the presence of excess CyD: benzene, toluene, ethylbenzene, propylbenzene, isopropylbenzene, (*o*-, *m*-, and *p*-)xylene, and (1,2,3-, 1,2,4-, and 1,3,5-)trimethylbenzene. The technique used to study association between host(CyD) and guest (hydrocarbon) is based on the facts that the guest molecules can be driven out to gaseous phase by introducing an inert gas at a constant flow rate into the aqueous solution and that the volatilization rate of guest decreases with increasing association with the host in the aqueous solution. The 1:1 and 2:1 (host:guest) formation constants were evaluated. As a measure of hydrophobicity of guest molecules, the free energy change of dehydration derived from Henry's law constant was used. Based on hydrophobicity and a host-guest spatial-fitting model, the formation constants have been discussed.

α-, β-, and γ-Cyclodextrins(CyD) are cyclic oligosaccharides consisting of six, seven, and eight D-glucopyranose units linked by α(1—4) bonds with a central cavity. The cavity is thought to be hydrophobic and a wide variety of inorganic and organic compounds is held if they suitably fit in the space, making CyD act as a host. Aromatic hydrocarbons, which are generally hydrophobic, have been extensively studied, but most of the hydrocarbons so far examined have hydrophilic substituent groups in order to increase solubility. There have been two reports concerning the benzene-CyD association system,[1,2] and there appears no data on alkylbenzene-CyD system. The scarcity of examination of these substances may be partially attributed to low aqueous solubility of these nonelectrolytes and partially to their high volatility; both reasons make it difficult to estimate accurately the amount of CyD-associated species formed in the aqueous medium.

In our preveous papers,[3,4] a method was presented which estimates 1:1 association constants between volatile and nonvolatile solutes in aqueous medium. The method is based on volatility of nonelectrolyte solute in aqueous solution. Volatile molecules are driven out to gaseous phase by introducing an inert gas at a constant flow rate into the aqueous solution. The volatilization rate was measured with and without addition of nonvolatile solute which associates with the volatile solute and decreased with the degree of association between the solutes. The method is simple, versatile, and applicable to such systems where (a) one of the solutes is volatile, (b) the concentration of nonvolatile solute is sufficiently high in comparison with that of volatile solute, and (c) the rate of association is rapid compared with the volatilization rate.

The method seems to be particularly suitable for studying association where solutes such as benzene and alkylbenzenes are concerned, because these solutes are highly volatile and scarecely soluble in water. The present study was undertaken to demonstrate the volatilization method and to interpret formation constants by a host-guest spatial-fitting model and hydrophobicity of guest molecule. A series of alkylbenzene have been chosen for this purpose: straight-chain series and some isomers (propylbenzenes, xylenes, and trimethylbenzenes).

Experimental

Materials and Preparation of Sample Solutions. Distilled deionized water was used throughout the experiments. Aromatic hydrocarbons used for guest are of analytical reagent grade (the purity is listed in Table 1). Cyclodextrins (α-, β-, and γ-CyD) used for host were of guaranteed grade from Nakarai Chemicals Co. Both guest and host reagents were used without further purification. An aqueous solution of each guest was prepared using a technique previously described.[5] The solute vapor in equilibrium with the liquid solute was introduced into water at 25 °C and circulated in a closed system. An aqueous solution saturated with guest liquid hydrocarbon can be prepared within 5 min by this technique. A portion of the saturated guest solution was transferred into a separatory funnel and the concentration of guest was determined by solvent extraction with chloroform, and another portion was transferred into a 2.5φ×25 cm cylindrical glass tube. A suitable amount of CyD, which had been dried over phosphorus pentaoxide under vacuum, was weighed and dissolved into the guest solution. The solution

Table 1. Experimental Conditions

Guest substance	Purity	λ[a]	N_2 flow rate
	%	nm	$cm^3 min^{-1}$
Benzene	99.5	254.4	15.8
Toluene	99.0	261.4	18.0
Ethylbenzene	98	261.0	20.0
o-Xylene	96	263.0	20.2
m-Xylene	98	264.0	20.9
p-Xylene	99	267.2	20.9
Propylbenzene	97.0	260.6	19.9
Isopropylbenzene	98.0	259.6	22.2
1,2,3-Trimethylbenzene	97	262.0	30.0
1,2,4-Trimethylbenzene	98	267.4	29.0
1,3,5-Trimethylbenzene	97.0	264.8	28.0

a) The wavelength for determining the concentration of guest molecules after $CHCl_3$ extraction.

was then diluted to 100 cm^3 with water. Ranges of concentration of guest and host are given in Table 3.

Amberlite XAD-2 resin (Rohm and Hass) as an adsorbent of guest vapor was ground in an agate mortar, a 150—200 mesh portion was collected and washed with ethanol by decantation until the supernatant became clear.

Apparatus and Procedures. The cylindrical glass tube containing guest and host at each desired concentration was immersed in a bath thermostated at 25.0±0.1 °C. A gas-inlet-type adaptor was mounted on the tube and N_2 was blown in the solution through Teflon tube of 1 mm i.d. at a constant flow rate controlled by a Stec Type Sec 400 mass-flow controller in the range of 15.8 to 30.0 $cm^3 min^{-1}$ (Table 1) depending on the volatility of guest and its association with host in aqueous solution. The N_2 flow rate was kept same irrespective of the presence of host. The N_2 leaving the sample solution was passed through a 0.5ϕ×12 cm glass column filled with XAD-2 resin beads of 8 cm in length. The exit and the bed top of column was plugged and covered with glass wool. After a fixed time, N_2 stream was interrupted, the XAD column was replaced by a fresh one and N_2 flow was resumed. This operation was repeated at regular time intervals. The guest hydrocarbon adsorbed on the resin was completely eluted out with $CHCl_3$ of 3 or 4 cm^3. The amount of hydrocarbon expelled from the sample solution during a fixed time, ΔQ, i.e., the amount of guest collected on a single XAD column, was determined by UV spectroscopy at the optimum wavelength for each guest hydrocarbon (Table 1) with reference to a calibration curve prepared for each guest-$CHCl_3$ solution. The XAD column can be used repeatedly by washing with $CHCl_3$ and drying in hot air.

Results

Derivation of Equation Estimating 1:1 and 2:1 (Host:Guest) Formation Constants. As for the CyD-benzene systems, the possible host : guest stoichiometric ratios are 1 : 1, 2 : 1, and 1 : 2.[2] The last one is, however, excluded under the present experimental condition that host molecules are always excess over guest molecules. Then, the reactions that should be taken into account are:

$$\mathrm{CyD}+\phi \rightleftharpoons \mathrm{CyD}\cdot\phi, (K_1) \quad (1)$$

$$\mathrm{CyD}\cdot\phi+\mathrm{CyD} \rightleftharpoons \mathrm{CyD_2}\cdot\phi, (K_2), \quad (2)$$

$$\phi\,(\mathrm{aq}) \rightarrow \phi\,(\mathrm{gas}), (k), \quad (3)$$

where ϕ refers to a hydrocarbon molecule, K_1 and K_2 are the corresponding stepwise formation constants, and k is the rate constant for transfer of guest molecules from aqueous to gaseous phase.

The guest molecules expelled into the gaseous phase are collected successively by the adsorbent, and the total amount, Q_ϕ, which is the summation of ΔQ_ϕ, is measured as a function of aeration time, t. Here, we assume that the releasing of guest molecules at a constant N_2 flow rate is of first-order with respect to the concentration of free species in the solution as follows:

$$dQ_\phi V^{-1}/dt = k[\phi], \quad (4)$$

where V is the volume of the aqueous solution. The mass-balance equations are:

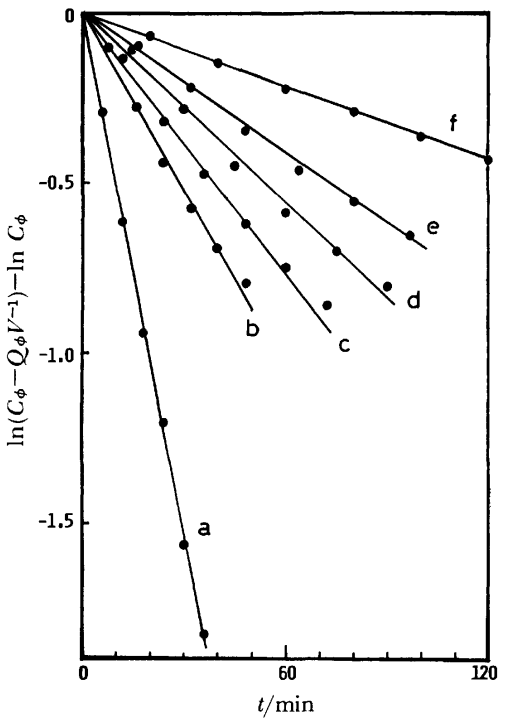

Fig. 1. Propylbenzene-α-CyD system. The plots of $\ln(C_\phi - Q_\phi V^{-1}) - \ln C_\phi$ vs. t in the absence and presence of cyclodextrin. N_2 gas flow rate 19.9 $cm^3 min^{-1}$; $C_{CyD}/10^{-3}$ M; (a) 0, (b) 2.52, (c) 5.04, (d) 7.56, (e) 10.1, (f) 20.2; $C_\phi/10^{-4}$ M: (a) 4.46, (b) 2.42, (c) 2.61, (d) 3.91, (e) 3.91, (f) 3.63.

Table 2. The Rate Constant for Transfer of Propylbenzene from Aqueous to Gaseous Phase with and without α-, β-, and γ-Cyclodextrin

k or k'[a]	C_ϕ[b]	Total concentration of α-CyD	β-CyD	γ-CyD
$10^{-2} min^{-1}$	10^{-4} M	10^{-3} M	10^{-3} M	10^{-3} M
5.40	4.44			
5.14	4.46			
5.30	3.35			
5.16	3.14			
5.26	3.14			
1.72	2.42	2.52		
1.28	2.61	5.04		
0.932	3.91	7.56		
0.694	3.91	10.1		
0.361	3.63	20.2		
3.04	1.04		1.42	
2.53	1.04		2.13	
2.01	2.08		2.85	
1.09	1.97		4.19	
4.51	2.04			4.78
3.27	2.08			7.97
2.94	2.08			15.9

a) $k' = k/(1+K_1C_{CyD}+K_1K_2C_{CyD}^2)$, where C_{CyD} is the total concentration of cyclodextrin. b) The initial concentration of propylbenzene.

$$C_{CyD} = [\mathrm{CyD}] + [\mathrm{CyD}\cdot\phi] + 2[\mathrm{CyD_2}\cdot\phi], \quad (5)$$

$$C_\phi = [\phi] + [\mathrm{CyD}\cdot\phi] + [\mathrm{CyD_2}\cdot\phi] + Q_\phi V^{-1}$$
$$= [\phi] + K_1[\mathrm{CyD}][\phi] + K_1K_2[\mathrm{CyD}][\phi] + Q_\phi V^{-1}, \quad (6)$$

where C_{CyD} and C_ϕ denote the total concentration of CyD and the total concentration of guest, respectively. Substituting Eq. 6 by Eq. 4 we obtain

$$dQ_\phi V^{-1}/dt = k(C_\phi - Q_\phi V^{-1})/(1+K_1[CyD]+K_1K_2[CyD]^2), \quad (7)$$

which becomes, on integration and with $Q_\phi=0$ at $t=0$,

$$\ln(C_\phi - Q_\phi V^{-1}) = -kt/(1+K_1[CyD]+K_1K_2[CyD]^2) + \ln C_\phi = -k't + \ln C_\phi, \quad (8)$$

where

$$k' = k/(1+K_1[CyD]+K_1K_2[CyD]^2). \quad (9)$$

Plots of $\{\ln (C_\phi - Q_\phi V^{-1}) - \ln C_\phi\}$ vs. t will give a straight line with a slope which corresponds to $-k'$ in the presence of CyD or to $-k$ in the absence of CyD. Under the condition that the total concentration of CyD is sufficiently higher than that of the associated complexes formed, that is, $C_{CyD} \gg [CyD\cdot\phi]+[CyD_2\cdot\phi]$, [CyD] in Eq. 9 is equal to C_{CyD}. Rearrangement of Eq. 9 gives the equation:

$$1/k' = K_1K_2C_{CyD}^2/k + K_1C_{CyD}/k + 1/k, \quad (10)$$

from which we can estimate K_1 and K_2 by plotting $1/k'$ against C_{CyD}.

Preliminary experiments show that the rate constant k is a function of gas flow rate and that the constant k' is proportional to k at a constant CyD concentration. We assume from the latter observation that the reaction (3) is the rate-determining step.

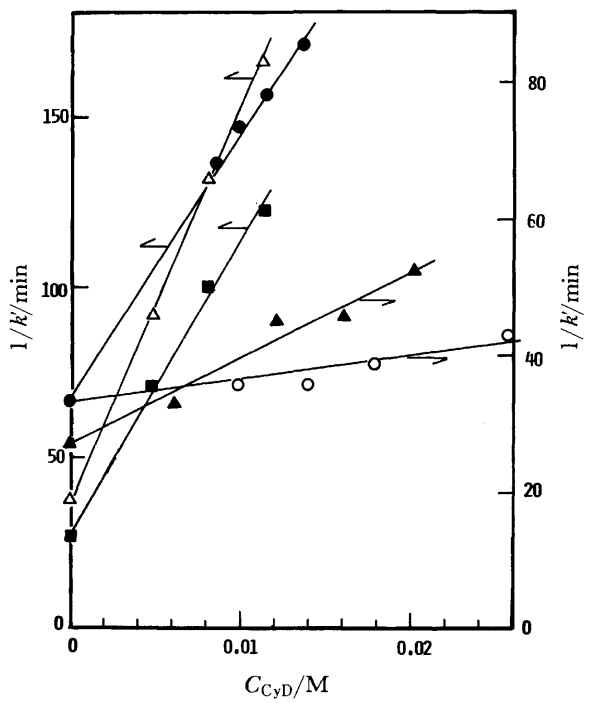

Fig. 2. The plots of $1/k'$ vs. C_{CyD}. Examples of straight line. Benzene-β-CyD(●), benzene-γ-CyD (○), 1,2,4-trimethylbenzene-α-CyD(▲), o-xylene-β-CyD(△), ethylbenzene-β-CyD(■).

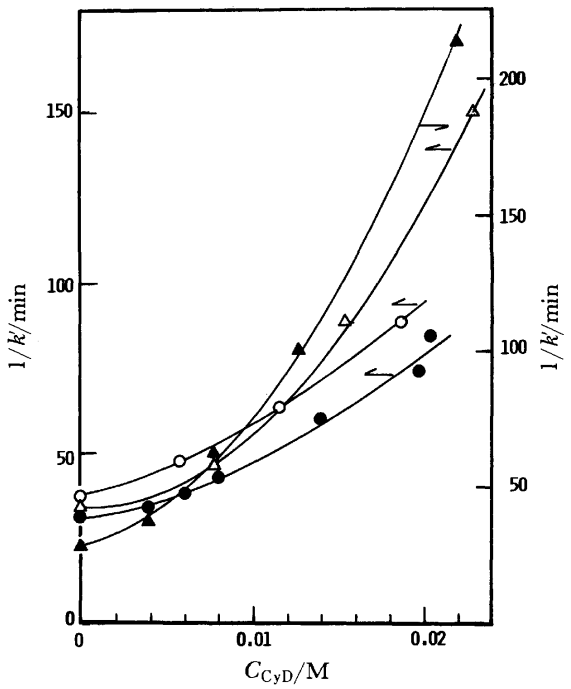

Fig. 3. The plots of $1/k'$ vs. C_{CyD}. Examples of parabolic curve. Benzene-α-CyD(●), o-xylene-γ-CyD(○), p-xylene-α-CyD(▲), 1,2,3-trimethylbenzene-α-CyD(△).

Estimation of K_1 and K_2. Plots according to Eq. 8 for propylbenzene-α-CyD system are shown in Fig. 1. The plots give straight lines up to ca. 70% release of the guest hydrocarbon from the solution. This linearity verifies the validity of the assumption that the volatilization of guest molecules follows a first-order reaction at a constant gas flow rate. The slopes of resulting straight lines, k and k', were evaluated using the least-squares method; the results for propylbenzene are shown in Table 2. Figures 2 and 3 show some typical results plotted by a curve-fitting method with the aid of Eq. 10. The $1/k'$ vs. C_{CyD} plots appear to be linear (Fig. 2) or parabolic (Fig. 3) depending on the host-guest combination. All the data were first treated by quadratic equations and when coefficients of the C_{CyD}^2 term were slightly negative, the plots were taken to be linear. The K_1 (and K_2) values thus determined are summarized in Table 3.

Discussion

Comparison of Results with Those in the Literature. In a previous paper,[4] which concerns with 1 : 1 associations of molecular iodine with α-, β-, and γ-CyD, we reported that the method making use of the difference in I_2 volatility rate with and without CyD provides formation constants in reasonable agreement with the literature values and that the method can be used to study association with a small formation constant in the order of 10. The present work is based on the same technique. In order to discuss whether we

Table 3. Concentration Ranges of Host and Guest and the Formation Constants, K_1 (1:1) and K_2 (2:1) of (Host:Guest) Complexes at 25.0 °C

	Concentration		Formation constant	
	C_ϕ [a]	C_{CyD} [b]	K_1	K_2 [c]
	10^{-4} M	10^{-3} M	M^{-1}	M^{-1}
Benzene				
α-CyD	6.20—17.5	10.5 —51.0	17±2	17±3
β-CyD	7.17—10.4	8.54—13.7	(1.2±0.1)×10²	—
γ-CyD	6.78—10.4	9.93—25.8	12±2	—
Toluene				
α-CyD	3.99—5.14	6.07—60.7	33±3	11±5
β-CyD	4.83—5.11	7.30—10.5	(1.4±0.1)×10²	—
γ-CyD	4.72—5.31	5.83—19.4	20±1	—
Ethylbenzene				
α-CyD	3.23—3.79	7.95—23.8	(1.1±0.1)×10²	21±9
β-CyD	3.13—3.76	4.87—11.3	(3.3±0.1)×10²	—
γ-CyD	3.25—3.76	5.83—19.4	36±6	—
o-Xylene				
α-CyD	2.86—3.50	7.57—22.7	22±8	—
β-CyD	3.03—3.38	4.87—11.4	(3.0±0.1)×10²	—
γ-CyD	3.13—3.44	5.80—18.7	34±1	61±2
m-Xylene				
α-CyD	3.41—3.59	7.94—23.8	40±1	37±5
β-CyD	2.29—3.59	4.82—11.2	(1.6±0.1)×10²	—
γ-CyD	3.37—3.59	12.2 —20.3	27±2	—
p-Xylene				
α-CyD	2.28—2.83	3.90—22.0	72±7	(1.4±0.4)×10²
β-CyD	2.79—2.90	4.87—11.4	(2.4±0.1)×10²	13±3
γ-CyD	2.78—2.81	5.93—19.5	7.9±0.1	32±1
Propylbenzene				
α-CyD	2.42—4.46	2.52—20.2	(5.9±0.1)×10²	6.6±2.5
β-CyD	1.04—4.46	1.42—4.19	46±9	(4.3±0.9)×10³
γ-CyD	2.04—4.46	4.78—15.9	52±14	—
Isopropylbenzene				
α-CyD	2.21—2.47	7.83—22.5	72±11	—
β-CyD	1.76—2.46	2.61—7.80	(1.2±0.1)×10³	—
γ-CyD	2.21—2.51	4.59—15.3	94 [d]	—
1,2,3-Trimethylbenzene				
α-CyD	2.50—2.76	7.63—23.0	13±1	(4.7±0.2)×10²
β-CyD	2.19—2.76	2.98—7.45	(1.8±0.1)×10²	74 [d]
γ-CyD	1.65—2.76	3.94—13.1	(2.9±0.1)×10²	—
1,2,4-Trimethylbenzene				
α-CyD	1.59—2.32	6.05—20.2	46±5	—
β-CyD	1.65—2.32	2.92—8.69	(8.7±0.5)×10²	—
γ-CyD	1.98—2.31	3.91—13.0	53±3	15 [d]
1,3,5-Trimethylbenzene				
α-CyD	1.94—2.12	5.05—20.2	61±5	—
β-CyD	1.60—1.94	3.05—6.87	60±4	—
γ-CyD	1.83—1.94	3.44—13.7	24±4	—

a) The initial concentration of guest substance. b) The total concentration of cyclodextrin. c) The dash-sign indicates that K_2 was not evaluated, because $1/k'$ vs. C_{CyD} plots by Eq. 10 gave nearly straight line only. d) The mean of two determinations.

can apply the method in the cases of aromatic hydrocarbons as guest molecules, the estimated formation constants are to be compared with those in the literature. Of the guest substances studied in this work, however, the literature data are only available for benzene. Then, we applied the method to naphthalene-β-CyD to find the formation constant K_1 to be 680 M^{-1} (M=mol dm^{-3}) at 25 °C.[6] Our estimation was in reasonable agreement with the literature value of 630 M^{-1} at 25 °C.[7]

Hoshino et al. measured fluorescence enhancement of benzene by forming inclusion complex with β-CyD, and reported K_1 for benzene-β-CyD at 28 °C to be 196 M^{-1}.[1] Tucker and Christian measured vapor pressure of benzene with and without CyD in aqueous solutions at various temperatures.[2] Their K values at 25 °C are as follows; for α-CyD K_1=31.6 M^{-1}, K_1K_2= 325 M^{-2}, for β-CyD K_1=169 M^{-1}, and for γ-CyD K_1= 9.1 M^{-1}.

The present result for benzene-β-CyD (K_1=120 M^{-1})

is smaller than each literature value. Compared with Tucker-Christian's results for benzene-α-CyD, the present K_1 (17 M^{-1}) seems considerably small. Since their K_1K_2 product (325 M^{-1}) is in reasonable agreement with our corresponding value (289 M^{-2}), our K_2 is larger than their K_2. Because of lack of data available in the literature, it is difficult at present to judge which is more reliable and to know if the agreement observed for benzene-γ-CyD is meaningful.

The vapor pressure method employed by Tucker and Christian makes use of the fact that the volatility of substrate is depressed by forming inclusion complexes with CyD and it resembles our method in this respect: the former may be called "static" and the latter "dynamic" technique. Their method seems, however, to be only applicable to a high volatile guest like benzene, because it is the total vapor pressure that can be measured. Accurate measurement of vapor pressure for low volatile solute is difficult due to the vapor pressure of water. Our present technique seems advantageous in this respect. The present method, however, accompanies large deviation of formation constants. This may arise from uncertainty in determining the amount of released guest. The overall error in Q_ϕ becomes large due to the accumulation of error in ΔQ_ϕ. Moreover, it should be noted that the present method cannot be applied for determining formation constants of guest-rich complexes. This is an unavoidable disadvantage. Tucker and Christian succeeded in determining the 1 : 2 (host : guest) formation constant for benzene-α-CyD.

Henry's Law Constant as a Measure of Hydrophobicity of Guest. Hydrogen bonding, van der Waals forces, and hydrophobic interaction are generally accepted to be the binding forces between CyD and guest molecules. The first one is excluded in the present case because the guests used have no ability to form hydrogen-bond with CyDs. It is considered that the host-guest spatial fitting plays a dominant part in van der Waals forces. On the other hand, it is generally difficult to evaluate the contribution of hydrophobic interaction. Some physico-chemical parameters such as aqueous solubility and partition coefficient of 1-octanol-water or chloroform-water systems have been used as a measure of hydrophobicity: Their logarithmic values plotted against log K gave fairly good linear relationships for some guest substances.[8,9]

Tabushi et al. have calculated the free-energy change caused by hydrophobic interaction of three model guests including benzene.[10] Their theory is reasonably based on the idea that the hydrophobic interaction arises from dehydration process, that is, a guest molecule is transferred from a hydrated state to an ideal gas state leaving behind a cavity (water cluster) which is collapsed and redistributed. A suitable parameter for describing hydrophobicity of nonelectrolyte guests like those employed in this work is Henry's law constant, K_H, a measure of free-energy

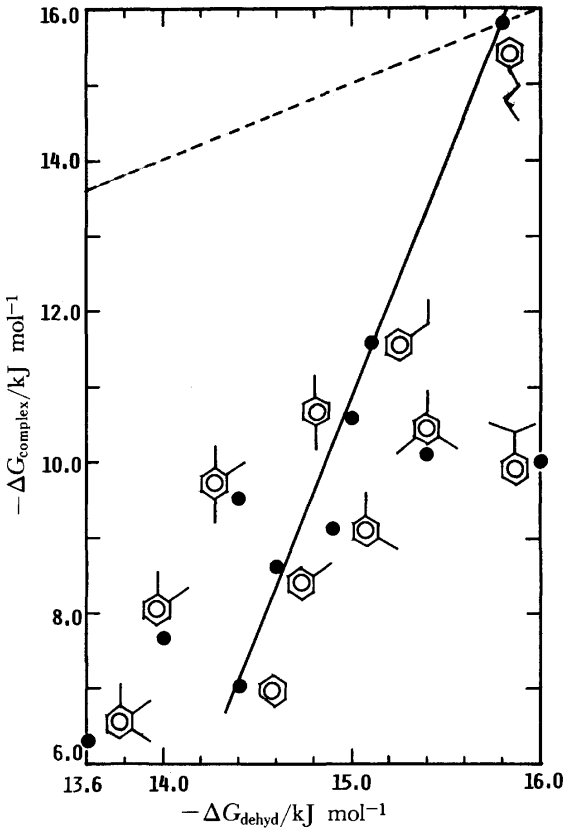

Fig. 4. The plots of $-\Delta G_{complex}$ vs. $-\Delta G_{dehyd}$. α-Cyclodextrin. The dotted lines in Figs. 4—6 indicate $-\Delta G_{complex}=-\Delta G_{dehyd}$.

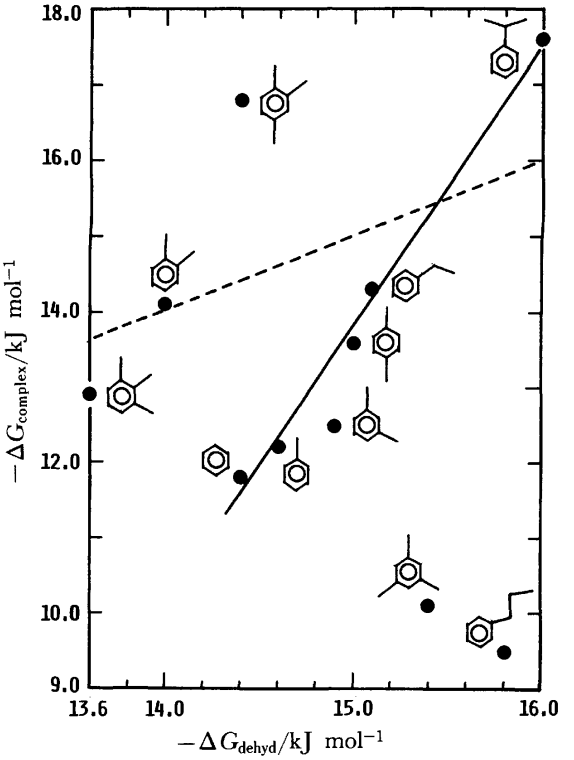

Fig. 5. The plots of $-\Delta G_{complex}$ vs. $-\Delta G_{dehyd}$. β-Cyclodextrin.

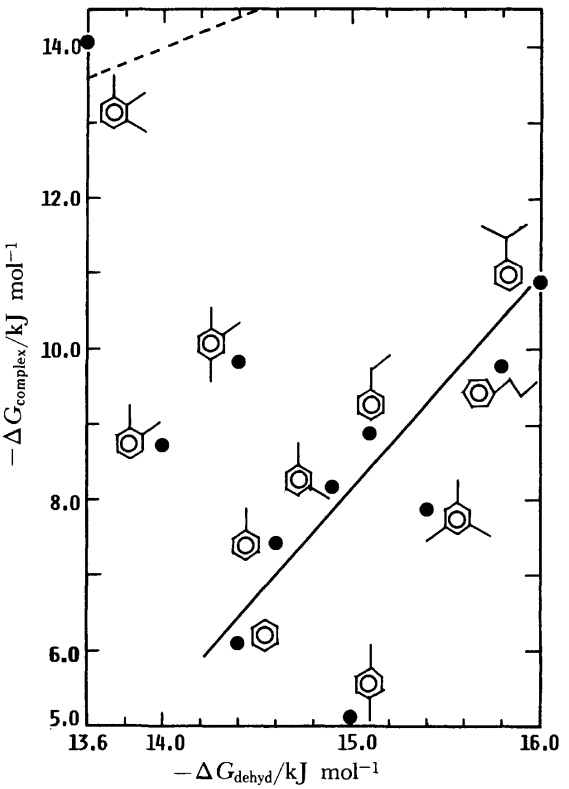

Fig. 6. The plots of $-\Delta G_{complex}$ vs. $-\Delta G_{dehyd}$. γ-Cyclodextrin.

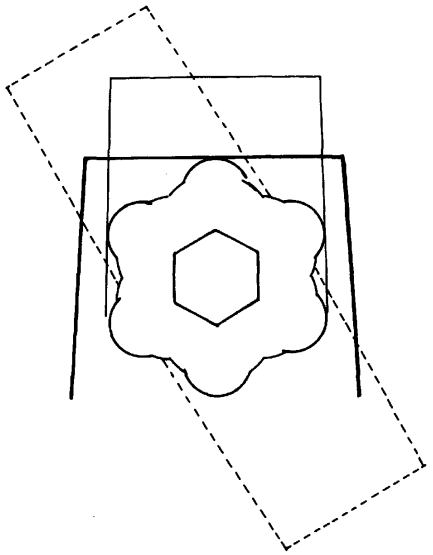

Fig. 7. Benzene-CyD inclusion model. α-, β-, and γ-cyclodextrin cavities in Figs. 7—9 are drawn by dotted, thin solid, and thick solid lines, respectively.

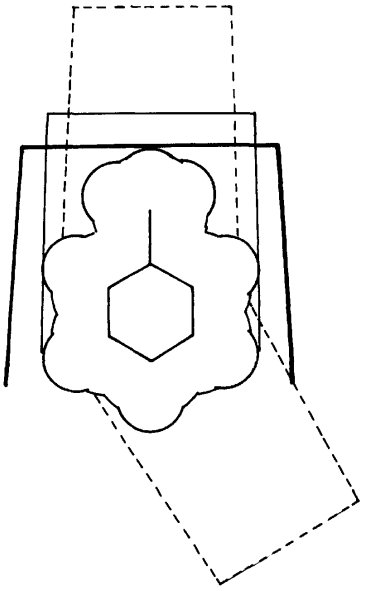

Fig. 8. Toluene-CyD inclusion model.

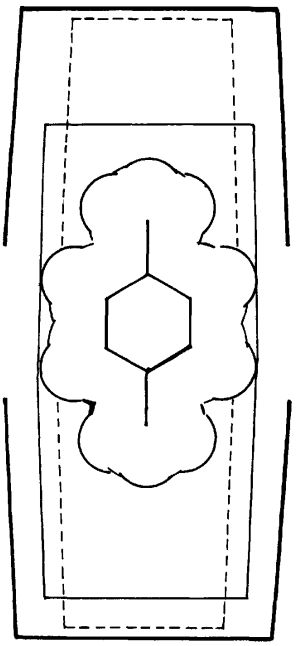

Fig. 9. *p*-Xylene-CyD inclusion model.

necessary to bring a nonelectrolyte from aqueous medium to vapor phase. The free-energy change associated with dehydration of a guest, ΔG_{dehyd}, can be evaluated by $\Delta G_{dehyd}=-RT \ln K_H$. The ΔG_{dehyd} values for all the guests examined were already reported in a previous paper.[5] The free-energy change in the 1 : 1 complex formation, $\Delta G_{complex}$ ($=-RT \ln K_1$) is plotted against ΔG_{dehyd} in Figs. 4 to 6; a dotted line indicates $\Delta G_{dehyd}=\Delta G_{complex}$.

Figures 4—6 show that most of the guests have considerably smaller $-\Delta G_{complex}$ than $-\Delta G_{dehyd}$ for three CyDs, especially for α- and γ-CyD. If we postulate that a guest molecule is fully embraced in the cavity of a given CyD and that the environment for the guest is just like a gaseous phase, $-\Delta G_{dehyd}$ for the nonelectrolyte will contribute in full to the $-\Delta G_{complex}$. Such circumstances are, however, hardly realized. Therefore, $-\Delta G_{dehyd}$ from K_H can be taken as an upper limit of the hydrophobic contribution.

Interpretation of Formation Constants. We try to interpret the magnitude of K_1 and K_2 determined for each host-guest combination by an inclusion (or asso-

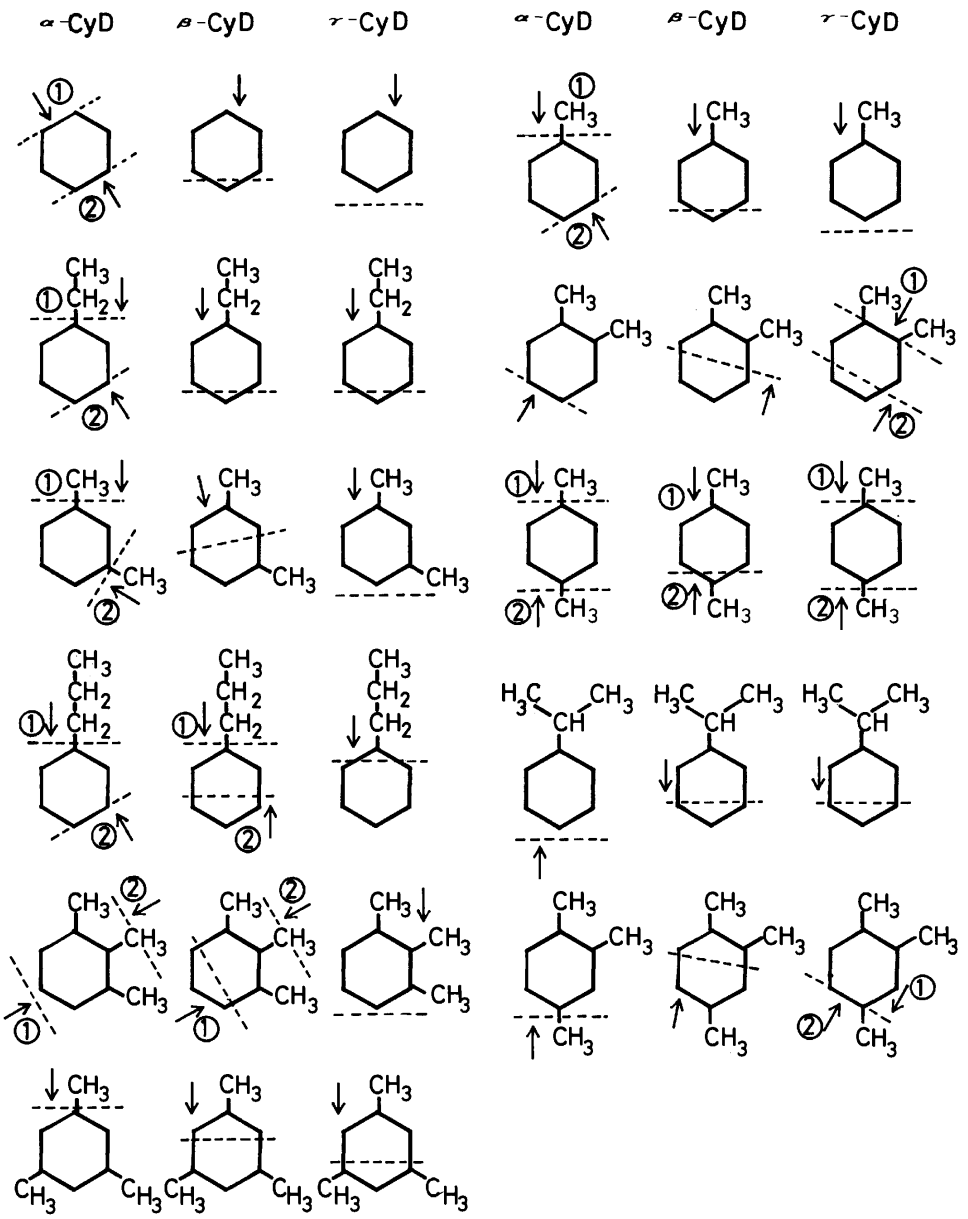

Fig. 10. Host-guest inclusion model. The direction from which the host includes the guest and the extent to which the guest penetrates the host are indicated by an arrow and a dotted line, respectively. The numbers, 1 and 2, in the circle refer to the binding sites corresponding to K_1 and K_2, respectively.

ciation) model and by taking into account the hydrophobicity of guest molecule. The following data in Å unit (1 Å=0.1 nm) are used for guests; bond length: 1.04 for C-C, 1.08 for C-H in benzene ring, 1.54 for C-C, 1.08 for C-H in alkyl group, van der Waals radius:[11] 1.0 for H, 1.7 for C. Concerned with CyDs, the following data in Å reported in the literature are used; the inner diameter of cavity:[12] 4.7—5.2 for α-CyD, 6.0—6.4 for β-CyD, 7.5—8.3 for γ-CyD (the smaller value is for the primary hydroxyl group side and the larger is for the secondary hydroxyl group side), the cavity depth:[13] 6.7 for α-CyD, ≈7 for β- and γ-CyD.

Typical inclusion models are depicted for benzene, toluene, and *p*-xylene in Figs. 7—9, and their simplified models are illustrated in Fig. 10. These models were made on the following assumptions. (A) A guest enters into CyD through wider secondary hydroxyl side. (B) Alkyl group is included in CyD cavity preferentially to benzene ring if the cavity entrance radius admits. This assumption is based on the fact that aliphatic series are more hydrophobic than aromatic hydrocarbons.[14] (C) When two hosts share a single guest and K_2 is larger or nearly equal to K_1, the cross-section of secondary hydroxyl group sides of two CyDs are situated in parallel to each other in a suitable distance to form hydrogen bond,[15] and when K_2 is smaller than K_1, the distance between two CyDs is too

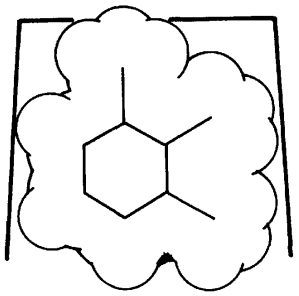

Fig. 11. 1,2,3-Trimethylbenzene-γ-CyD inclusion model.

short or too far to form hydrogen bonding or the axis along the cavity is not coincident with each CyD. (D) Guests come into contact with the wall of host as to increase contact area or to be included by host as deeply as possible. (E) The cavity size of β-CyD is a little small to include two adjacent methyl groups together. (F) The cavity size of γ-CyD is a little small to include adjacent three or alternate two methyl groups together.

For benzene and three straight-chain alkylbenzenes, $-\Delta G_{complex}$ increases almost linearly with $-\Delta G_{dehyd}$ for α-CyD (Fig. 4). The linear relationship is not so good for γ-CyD, but isopropylbenzene-γ-CyD showed a line in Fig. 6. For α-CyD, propylbenzene is far from the straight line as shown in Fig. 5, though the isomer falls on the line. These observations can be explained in terms of the host-guest spatial fitting. α-CyD accepts *n*-propyl group within the cavity, but is incapable of including bulky isopropyl group. Isopropyl group, on the other hand, can be accepted within cavities of β- and γ-CyD, which are large enough to accept the *n*-propyl group, but they are so shallow that only a part of benzene ring of propylbenzene is included; γ-CyD seems to exert less critical effect on isomeric propyl groups than does β-CyD because of its sufficiently large cavity size.

Among three trimethylbenzenes, 1,3,5-isomer exhibits an extremely low K_1 for β-CyD, while 1,2,3-isomer exhibits a large K_1 for γ-CyD. These observations can also be explained by the steric viewpoint. Two bulky methyl groups in 1,3,5-isomer hinder this guest from entering deeply into the cavity of β-CyD; *m*-xylene enters more deeply into β-CyD due to the lack of another methyl group in meta-position. For γ-CyD this steric hindrance of 1,3,5-isomer seems to operate to a less extent. The inclusion model illustrated in Fig. 11 may account for the extremely high *K* value observed for 1,2,3-isomer-γ-CyD; a large van der Waals stabilization works in this case.

The host-guest spatial fitting and the hydrophobicity of guest will be a useful guide to understand formation constants. There are, however, some host-guest combinations difficult to be interpreted. In view of hydrophobicity, *o*-xylene, 1,2,4- and 1,2,3-trimethylbenzene seem to exhibit large K_1 for three CyDs. For γ-CyD, favorable fitting may be responsible as mentioned above, but it is difficult to explain for α- and β-CyD on the same basis. β-CyD as well as α-CyD cannot include two adjacent methyl groups together, then both hosts will come into contact with these guests preferentially on the opposite site of methyl groups. Of the host-guest combinations studied in this work, two are most difficult to interpret. For α-CyD, *m*-xylene complex gave K_1 and K_2, whereas only K_1 was observed for 1,3,5-trimethylbenzene. For γ-CyD, K_1 of *p*-xylene was extraordinarily small.

Spatial fitting will contribute to van der Waals stabilization and hydrophobicity to driving force of complexation, but they don't give satisfactory explanation of the measured formation constants. Other possible energy factors, as Tabushi et al. have pointed out in their theoretical considerations,[10] and motional freedom of host, guest, and water molecules should be taken into account.

References

1) M. Hoshino, M. Imamura, K. Ikehara, and T. Hama, *J. Phys. Chem.*, **85**, 1820 (1981).
2) E. E. Tucker and S. D. Christian, *J. Am. Chem. Soc.*, **106**, 1942 (1984).
3) I. Sanemasa, Y. Nishimoto, A. Tanaka, and T. Deguchi, *Bull. Chem. Soc. Jpn.*, **59**, 1459 (1986).
4) I. Sanemasa, Y. Nishimoto, A. Tanaka, and T. Deguchi, *Bull. Chem. Soc. Jpn.*, **59**, 2269 (1986).
5) I. Sanemasa, M. Araki, T. Deguchi, and H. Nagai, *Bull. Chem. Soc. Jpn.*, **55**, 1054 (1982).
6) To be published.
7) S. Hamai, *Bull. Chem. Soc. Jpn.*, **55**, 2721 (1982).
8) K. A. Connors and D. D. Pendergast, *J. Am. Chem. Soc.*, **106**, 7607 (1984).
9) K. Uekama, M. Otagiri, Y. Kanie, S. Tanaka, and K. Ikeda, *Chem. Pharm. Bull.*, **23**, 1421 (1975).
10) I. Tabushi, Y. Kiyosuke, T. Sugimoto, and K. Yamamura, *J. Am. Chem. Soc.*, **100**, 916 (1978).
11) A. Bondi, *J. Phys. Chem.*, **68**, 441 (1964).
12) W. Saenger, *Angew. Chem., Int. Ed. Engl.*, **19**, 344 (1980).
13) M. L. Bender and M. Komiyama, "Cyclodextrin Chemistry," Springer-Verlag, New York (1978).
14) G. Némethy and H. A. Scheraga. *J. Chem. Phys.*, **36**, 3401 (1962).
15) W. C. Cromwell, K. Byström, and M. R. Eftink, *J. Phys. Chem.*, **89**, 326 (1985).

 © 1987 The Chemical Society of Japan Bull. Chem. Soc. Jpn., 60, 2067—2071 (1987)

Topological Ligand Design. III. Parent Ligand Graphs, Simple Cage Graphs, and Donor-Atomic Graphs for the Octahedral Coordination

Susumu TAKAMOTO* and Chikako ENKAKU
Department of Chemistry, Faculty of Science, Gakushuin University, Mejiro, Toshima-ku, Tokyo 171
(Received December 23, 1986)

Various computer processes to determine all parent ligand graphs, simple cage graphs, and donor-atomic graphs for the octahedral coordination are described in order to design new sexidentate ligands. A complex ligand graph is represented by a numeral comprising of 12 figures, each of which indicates the code of a unit graph of six kinds placed on 12 edges of an octahedron. Then, 1055 parent ligand graphs, excluding chiral isomers, are selected from 6^{12} permutations of the complex ligand graphs. A simple cage graph is produced by fusing a pair of adjacent lines around every point of an octahedral graph; 102 kinds of simple cage graphs, excluding chiral isomers, have been obtained. Another more practical method for ligand design has been proposed by starting from 62 donor-atomic graphs.

Recently, the enumeration and classification of various complicated compounds have been enormously developed by the use of a graph theory and computer processing. However, such applications involving ligand design remain very few.

A ligand molecule can be considered to be a set of donor atoms joined by some carbon chains capable of forming a medium-sized chelate ring. A graph-theoretical path corresponding to such a carbon chain is called a "chelate path". One of the authors has already published a designing method for ligands using a simple ligand graph, which is defined as a set of m points and n lines representing m donor-atoms and n chelate-paths, respectively. Then, all the simple ligand graphs with $m \leqq 8$ were systematically derived and clearly documented by a numeral code of eight figures.[1]

However, a simple ligand graph cannot distinguish a ligand structure which has chelate paths branched at their carbon atoms. Thus, some modifications have been applied to the ligand graphs in order to represent all the structures of general chelating ligands.[2] Also, a complex ligand graph has been preferably adopted, which is a set of main points and sub-points connected by lines (where main points, sub-points, and lines correspond to donor atoms, carbon atoms forming chelate ring, and chemical bonds among these atoms, respectively). When a metal chelate ring is limited to five or six members, including a metal ion, each chelate path consists of two or three sub-points and three or four lines. Since no more than three chelate rings can branch at a donor atom or at a carbon atom, the maximum degree of a main point and a sub-point is three (the degree of a point is the number of lines incident on it).

Complex ligand graphs can faithfully express their original ligand structures, but they are so complicated that their systematic derivation and complete enumeration are quite difficult. In order to design all the chelate ligands for a given coordination structure, a "parent ligand graph" was defined.[2] This is a complex ligand graph to which no more sub-points nor lines can be added, i.e., highest density graphs in such coordination. Several kinds of parent ligand graphs may exist for a certain coordination structure. Then, all the other complex ligand graphs can be derived by neglecting some sub-points or by removing some lines from these parent ligand graphs.

Hence, finding all of the parent ligand graphs is a step in designing complex ligand graphs. Although the parent ligand graphs for the square planar and the tetrahedral coordinations have already been published,[2] it is difficult to obtain parent graphs for octahedral coordination by similar procedures, since four edges are incident on each vertex of an octahedron, whereas the degree of a main point cannot exceed three. Thus, the degree of each main point has to be reduced by a partial fusing of some adjacent graphs. Besides, an increasing number of donor atoms causes a much accelerated increase in the number of parent ligand graphs. But whatever difficulty may arise, designing sexidentate ligands should be achieved, since the octahedral coordination is one of the most popular and important structures in complex chemistry.

Methods

(1) Parent Ligand Graphs. Unit Graphs: In order to determine all of the parent ligand graphs for octahedral coordination, "unit graphs" of six kinds are defined. These unit graphs with direction and their own codes are shown in Fig. 1. Unconnected unit graph (0), and any unit graphs containing less than five-membered ring are omitted hereafter.

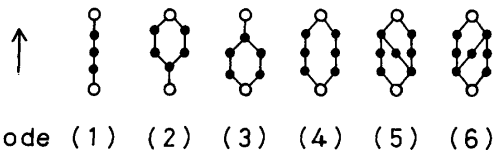

Fig. 1. Unit graphs for the parent ligand graph.

Since these unit graphs are introduced for composing the parent ligand graphs, each chelate path in these unit graphs contains three sub-points. Unit graphs (2) and (3) have directions opposite to each other. Unit graphs (5) and (6) cause an antipode relation when placed on a solid surface. The order of the unit graphs in chelate-path density is (5), (6)>(4), (3), (2)>(1).

Then, a "composite graph" is assembled by placing one of above unit graphs on every line of a donor-atomic graph with common main point each other. (A donor-atomic graph is a set of main points and lines, each of which connects a pair of main points having at least one chelate path.[2]) Next a complex ligand graph is generated when these unit graphs in a composite graph are partially fused around every vertex. As a simplified example using a terdentate ligand, a derivation of these graphs is shown in Fig. 2.

When an octahedral graph is adopted as a starting donor-atomic graph, all the complex ligand graphs derived from it have a complete cage structure, where every pair of adjacent main points is connected; they must include all the parent ligand graphs of the octahedral coordination.

In this case the fusing manner of unit graphs is uniquely definable so that the ligand molecules may have its most strainless cage structure; hence, these complex ligand graphs have one-to-one correspondence with their composite graphs. Then, the design of the complex ligand graphs may be substituted for assembling of the composite graphs.

A parent ligand graph should have the highest density as to the chelate paths; that is, it should be assembled from unit graphs of higher order as possible. Although unit graphs (5) and (6) have the highest order as to the chelate paths (both of them are parent ligand graphs of the bidentate ligand), when four such unit graphs are incident on a vertex of an octahedron, the degree of the central main point exceeds three even if they are effectively fused. Therefore, some unit graphs of the lower order are still necessary as the constituents of the parent ligand graph.

Fusing Restrictions: There are some restrictions in partially fusing the unit graphs arround a main point, subjected to the limitation of the degree of main points and sub-points, and to the steric requirements which may be confirmed by use of molecular models.

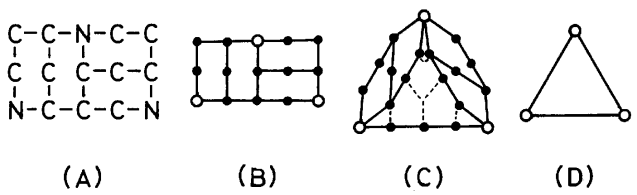

Fig. 2. Graph representations of a ligand. (A) Ligand, (B) complex ligand graph, (C) composite graph (Dotted lines indicate fusing sites.), (D) donor-atomic graph.

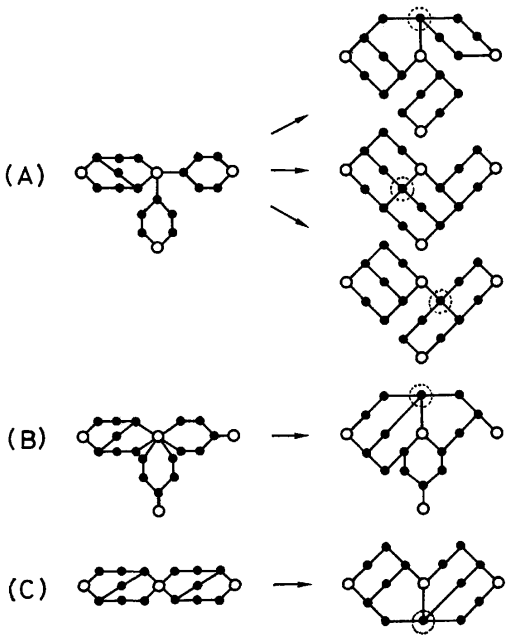

Fig. 3. Examples of impossible fusions. (A) (2)(2)(6), (B) (3)(3)(5), (C) trans (5)(5) (each dotted circle indicates over degree of a vertex.).

The following fusions of unit graphs arround a main point (a vertex on an octahedron) are impossible, and some examples are shown in Fig. 3.

(i) Two unit graphs (5) and (5), or (6) and (6) in trans position.

(ii) Two unit graphs (5) and (6), or (6) and (5) in cis position.

(iii) Following arrangements of three unit graphs in clockwise order: (6)(6)(4), (6)(6)(3), (6)(4)(4), (6)(4)(3), (6)(3)(4), (6)(3)(3), (4)(5)(5), (3)(5)(5), (4)(4)(5), (4)(3)(5), (3)(4)(5), (3)(3)(5), (6)(4)(5), (6)(3)(5), (5)(2)(6), (2)(6)(6), (2)(6)(4), (2)(6)(3), (5)(5)(2), (4)(5)(2), and (3)(5)(2).

(iv) Four unit graphs (2).

(v) Four unit graphs other than (1) or (2).

We should thus determine all the composite graphs in which any arrangement of unit graphs does not offend against above fusing restrictions.

Canonical Name: If unit graphs of six kinds are simply placed on 12 edges of an octahedron, there exist 6^{12} (=2,176,782,848) permutations, including some duplications in each structure. Hence, it is necessary to define a "canonical name" which is the unique expression of a composite ligand graph (and also of a complex ligand graph) corresponding to a structure in one to one.

Labeling of Vertices and Edges of an Octahedron: Six vertices on an octahedron are labeled along one of the Hamiltonian paths, and twelve directed edges are labeled along one of Eulerian trails (like a picture drawn with a single stroke) in the graph theory as shown in Fig. 4. Hereafter, these labels of vertices and directed edges are represented by①,②,③, ····,⑥, and

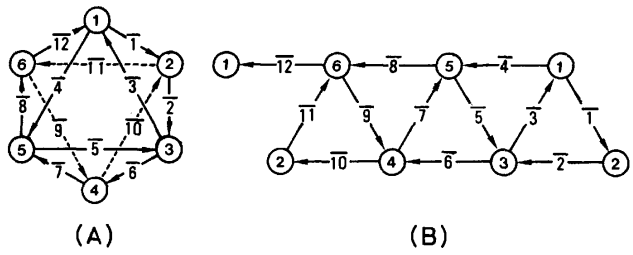

Fig. 4. Labeling of vertices and edges on an octahedron. (A) Perspective view, (B) developed diagram.

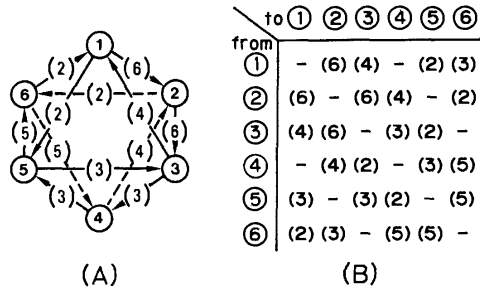

Fig. 5. An example of the composite graph. (A) Octahedral structure composing of 12 unit graphs, (B) its connection matrix.

$\overline{1}, \overline{2}, \overline{3}, \cdots, \overline{12}$ respectively, as well as (1), (2), (3), ····, (6) indicate codes of unit graphs.

Then a composite graph, as well as its complex ligand graph can be described by a numeral of 12 figures, each of which represents the code of a unit graph placed on every edge and lined up in the above-defined order. However, there exist 24 (=6×4) line-up ways of 12 edges in each octahedral structure, since such an Eulerian trail may start from any one of six vertices, and may take any one of four initial directions. The canonical name is defined as the maximum numerical in these 24 numerical names, thus the duplication of the same structure can be avoided.

For example, a composite graph for which the structure is shown in Fig. 5 can be expressed by 24 ways of numerical name given in Table 1. Then, their maximum numeral is 664 233 355 422, which becomes the canonical name of this graph.

The computer selects the possible arrangements of unit graphs from 6^{12} permutations under the abovementioned fusing restrictions, and finds their canonical names.

Parent Ligand Graph: If a complex ligand graph becomes a parent ligand graph, it must contain neither a unit graph (2), (3), nor (4) on any edge which can be replaced with another unit graph of higher order (5) or (6) subjecting to the fusing restrictions; similarly, it must contain no unit graph (1) replaceable with (2), (3), (4), (5), or (6). The computer examines all such rearrangements of unit graphs in each structure, and if every replacement causes offense against the fusing

Table 1. 24 Expressions of a Composite Graph in Fig. 5

Start	Name	Start	Name
①→②	664 233 355 422	④→⑤	333 464 622 255
①→③	423 352 534 266	④→③	264 536 353 422
①→⑤	252 625 463 334	④→②	425 352 234 663
①→⑥	336 464 222 553	④→⑥	552 223 466 334
②→③	646 222 553 334	⑤→⑥	522 346 634 253
②→①	633 455 222 346	⑤→①	342 226 453 635
②→⑥	254 633 342 526	⑤→③	333 554 226 642
②→④	425 642 335 253	⑤→④	255 333 646 422
③→④	333 425 262 546	⑥→①	225 533 346 462
③→⑤	234 663 345 522	⑥→⑤	525 342 664 233
③→①	466 342 535 223	⑥→④	542 266 423 335
③→②	642 225 533 364	⑥→②	363 534 222 645

restrictions, then the original structure can become a parent ligand graph. For example, in a structure named 664 214 553 222, if the unit graph (3) (the nineth figure) is replaced with (5), the resulting structure named 664 214 555 222 is allowed for the fusing around every vertex, then that the original structure is not a parent ligand graph. Also, the computer showed that no other unit graph in the latter structure can be replaced with any unit graph of higher order without breaking fusing restrictions; thus, the latter graph 664 214 555 222 is proved to be a parent ligand graph.

Chiral Isomers: In oreder to search the chiral-isomer couples in the parent ligand graphs, the mirror-image graphs of a given graph should be generated. Since an octahedron is reflected by a mirror (as shown in Fig. 6(A)), the correspondences of each vertex and edge between original and mirror-image graphs would be obvious.

Vertices ①, ②, ③, ④, ⑤, and ⑥, are converted into ①, ⑥, ⑤, ④, ③, and ②, respectively; also edges $\overline{1}$, $\overline{2}$, $\overline{3}$, $\overline{4}$, $\overline{5}$, $\overline{6}$, $\overline{7}$, $\overline{8}$, $\overline{9}$, $\overline{10}$, $\overline{11}$, and $\overline{12}$ are converted into $\overline{12}$, $\overline{8}$, $\overline{4}$ $\overline{3}$, $\overline{5}$, $\overline{7}$, $\overline{6}$, $\overline{2}$, $\overline{10}$, $\overline{9}$, $\overline{11}$, and $\overline{1}$, respectively, by a mirror-image transformation. As this transformation inverts also the chirality and direction of the unit graph, the unit graphs (5) and (6), as well as (2) and (3) should be converted each other.

For example, in Fig. 6(B), the graph 664 233 355 422 is transformed into its mirror-image graph 363 422 254 635; however, this representation is not its canonical name. Then the computer produces 24 kinds of numeral espressions for this structure, and finds the maximum numeral in them. Thus, 663 334 545 222 is obtained as the canonical name of the chiral isomer for the original graph.

If the canonical name of the mirror image is identical with that of the original graph, e.g. the graph named 643 541 624 522, it has no chiral isomer; in other words, its structure is achiral.

(2) Simple Cage Graph. A simple cage graph is a

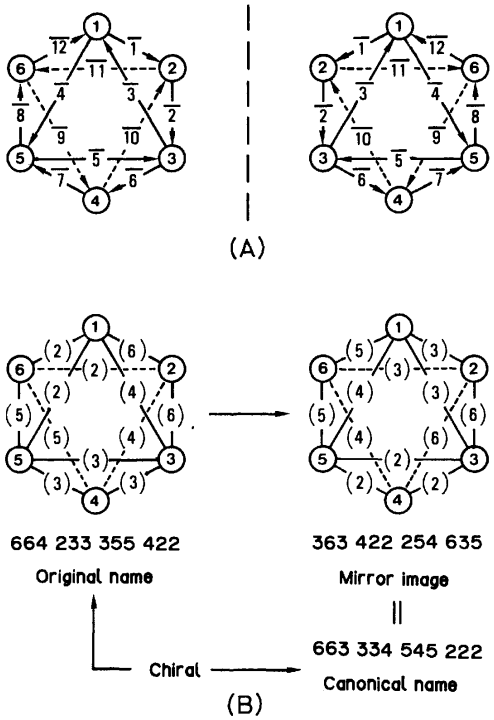

Fig. 6. An example of chiral couples. (A) Mirror reflection, (B) mirror-image transformation.

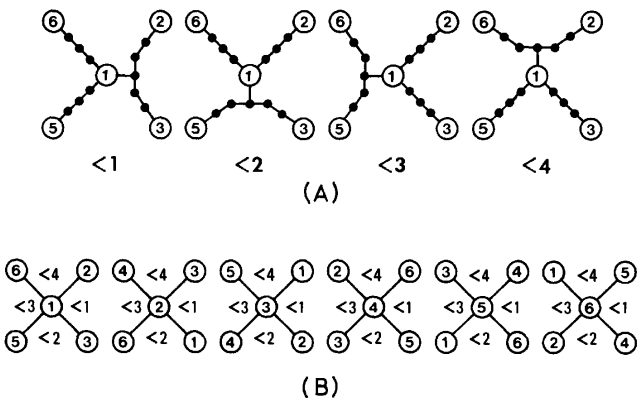

Fig. 7. Labeling of the fusing sites in the simple cage graph. (A) Four sites of fusing around the vertex 1, (B) fusing sites around each vertex.

complex ligand graph where every pair of adjacent main points is joined by only one chelate path. Accordingly, both its donor-atomic graph and its composite graph are an octahedron. Since the degree of every vertex on an octahedron is four, one adjacent pair of unit graphs (1) around every vertex must be partially fused so that the degree of each main point may become three. As there are four adjacent pairs of four edges at each of six vertices, the permutations of fusing ways come to 4^6=4096 kinds including symmetrical duplications.

Labeling of the sites, where each adjacent pair of unit graphs (1) is partially fused around every vertex, are defined as Fig. 7.

Then, a simple cage graph is expressed by a numeral consisting of six figures, each of which represents the label of fusing site around each of six vertices which are lined up in the previous order. Also, in this case 24 expressions are possible in a given structure; thus, a canonical name may be defined as the minimum numeral in these expressions. An example is shown in Fig. 8. The chiral isomers are found by the same method in the parent ligand graphs.

(3) Direct Designing of Complex Ligand Graphs. Simpler complex ligand graphs may be produced directly from some donor-atomic graphs not having complete-cage structure through neither the parent ligand graph nor the simple cage graph. When unit graphs in Fig. 9 are placed on every line of a certain donor-atomic graph in Fig. 10, a composite graph is directly generated.

Directed or chiral isomers of unit graphs are neglected in Fig. 9 for symplifying. Geometrical (or configurational) isomers of donor-atomic graphs are also omitted in Fig. 10. Then several complex ligand graphs are designed by proper fusing around main points under similar restrictions. In this case fusing is not alwalys necessary unless the degree of a main point exceeds three; thus, one-to-one correspondence is lost between a composite graph and its complex ligand graph.

These donor-atomic graphs in Fig. 10 are partial graphs of an octahedral graph, and can be systematically derived from it by removing some lines. Then each of them consists of six points and n lines ($5 \leqq n < 12$), and maximum degree of its points is four. Naturally, a pair of points in trans position of an octahedron is never connected.

The above calcurations are performed by use of a HP9831A Desktop Computer (Hewlett & Packard Co.) and a PC9801F2 Personal Computer (Nippon Electric Co.).

Results and Discussion

It was already discussed[2] that the complex ligand

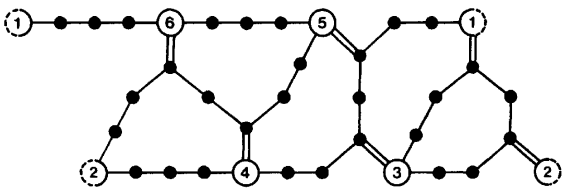

Fig. 8. An example of the simple cage graph.

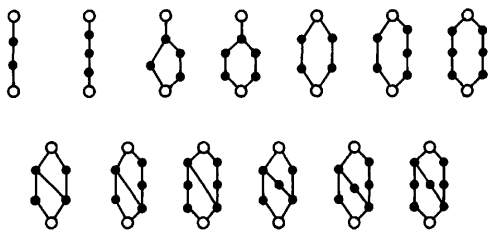

Fig. 9. General unit graphs.

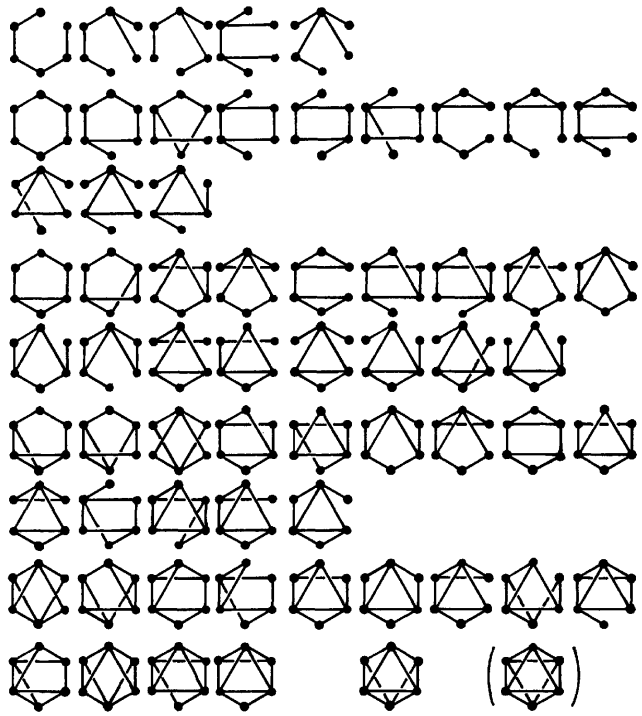

Fig. 10. Donor-atomic graphs for the octahedral coordination.

graph is the best mean for the expression of a ligand structure. The complex graph which has main points and sub-points would be very useful especially in designing of hetero-atomic compounds. The complex ligand graph can be "uniquely" decomposed into several unit graphs, and reversely assembled from them. These procedures may be also available in complicated chemical designs. In this case "uniquely" is important, because any complicated graph should have definable components as if a chemical compound consists of definite atoms. The concept of "fusing" is extensively applicable not only to the graph but also to other geometrical figures in various designings, e.g. a naphthalene frame is formed by fusing of two benzene rings.

Simple numerical expressions of molecular structures are necessary for computer processing. Since an arrangement of six kinds of unit graphs can fully express intricate ligand structures, including optical isomers, the above procedures can be extended to determine the parent ligand graphs for any other coordinations.

Computer calculations show that as many as 1055 kinds of parent ligand graphs for the octahedral coordination may exist even if chiral isomers are excluded, whereas the number of parent ligand graphs for the tetrahedral structure is only nine. They would be too many and too complicate for the application to ligand design. Although more severe restriction to the local fusing of unit graphs around a main point would be difficult, some sifting out may be possible with the totally steric hindrance as to the whole structure of a graph. Neverthless, a drastic reduction of their number would be hopeless, even upon applying such modifications. Moreover, the ligands which will be synthesized in near future will not have such complicated networks as the parent ligand graphs.

The simple cage graphs are the least complete cage-graph, where every pair of adjacent main points is connected, and they are much simpler and much fewer than the parent ligand graphs for the octahedral coordination. Computer calculations have proved that 90 chiral couples and 12 achiral graphs exist in these simple cage graphs. Therefore, they may be preferably adopted as the new starting points of the ligand design instead of parent ligand graphs, and many complex ligand graphs can be introduced by adding or omitting some sub-points and/or lines on them. Especially, this method would be well suited for designing ligands with cage or nearly cage structures.

Method (3) is most useful and most hopeful for the practical designing of ligands. When one or more donor-atomic graphs are selected from Fig. 10 for a certain purpose, some series of related structures can be systematically derived by diverse combinations of unit graphs. Since almost known ligands have topologically simple structure, various new ligands of quite different from old ones would be easily created. As the geometrical structure of a ligand largely effects on the properties and the reactions of the metal chelates, such design would extensively contribute to the development of the coordination chemistry. The applications of these ligand graphs to the designing of new ligands have already been discussed in previous papers.[1-3]

The donor-atomic graph is regarded as a back-bone of a ligand, then all ligands can be classified by their donor-atomic graphs. As this graph is one of the most simplified expression of a ligand, it is available for an easy determination of several geometrical (or configurational) isomers of a metal chelate with a complicated ligand. The donor-atomic graph resembles the simple ligand graph[1] in the graph shape. The only difference is that the degree of each point in the simple ligand graph cannot exceed three. Therefore, the donor-atomic graphs completely include the simple ligand graphs. Although the configurational isomers of donor-atomic graphs are omitted here, most of them were shown as those of the simple ligand graphs in a previous paper.[1]

References

1) S. Takamoto, *Bull. Chem. Soc. Jpn.*, **52**, 2477 (1979).
2) S. Takamoto, *Bull. Chem. Soc. Jpn.*, **53**, 595 (1980).
3) S. Takamoto, *Talanta*, **32**, 757 (1985).

 © 1987 The Chemical Society of Japan Bull. Chem. Soc. Jpn., 60, 2073—2077 (1987)

Stereoselective Synthesis of Anomers of 5-Substituted 2′-Deoxyuridines

Hajime Aoyama
Research Laboratories, Toyama Chemical Co., Ltd., Shimookui, Toyama 930
(Received July 17, 1986)

The substitution reaction of 5-substituted 2,4-bis(trimethylsilyloxy)pyrimidines with 3,5-bis(*O*-*p*-chlorobenzoyl)-2-deoxy-α-D-ribofuranosyl chloride was investigated. In the presence of *p*-nitrophenol, β anomers were formed stereoselectively, whereas the addition of organic bases brought forth stereoselective formation of α anomers. Stereoselectivity of the reaction depends on the substituents at 5-position of disilylpyrimidines, additives, and the concentration of each reagent. The α and β anomers of 5-substituted 2′-deoxy-uridines were synthesized through the deacylation of α and β anomers of 5-substituted 3′,5′-di-*O*-(*p*-chlorobenzoyl)-2′-deoxyuridines.

It is well-known that 5-substituted 2′-deoxy-β-uridines (**6a—f**) have useful physiological activity for antitumor[1,2] and anti-viral[3-5] drugs. Usually, only β anomers show the physiological activity. Many investigations have been carried out to synthesize β anomers under different conditions by the Hilbert-Johnson reaction, such as reactions of sugar halide with mercury salt of uracils,[6-8] 2,4-dimethoxypyrimidines,[9-14] silylpyrimidines by fusion,[15,16] and silylpyrimidines in the presence of $SnCl_4$.[17] But up to date, no general and efficient methods have been reported for the stereoselective synthesis of 2′-deoxyuridines.

We reported recently that the reaction of 5-fluoro-2,4-bis(trimethylsilyloxy)pyrimidine (**1c**) with 3,5-bis(*O*-*p*-chlorobenzoyl)-2-deoxy-α-D-ribofuranosyl chloride (**2**) in the presence of Brönsted acids selectively gives 3′,5′-di-*O*-(*p*-chlorobenzoyl)-5-fluoro-2′-deoxy-β-uridine (**4c**).[18] Further studies on stereoselectivity of the reaction of **1c** with **2** suggested that the addition of a base such as pyridine changed the stereoselectivity of the reaction from β- to α-selectivity in proportional degrees to the concentration of the base.

This paper describes the stereoselective synthetic method of both the α and β anomers of 5-substituted 2′-deoxyuridines (**5a—f** and **6a—f**) based on the following observation. 1) In the presence of *p*-nitrophenol, **1a—f** reacts with **2** to give β anomers stereoselectively in high yields. 2) Combined use of *p*-nitrophenol and pyridine as catalyst changes β-stereoselective reaction of **1c** with **2** to an α-stereoselective reaction. 3) In the presence of other organic bases or their salts, reaction of **1c** with **2** also gives an α anomer (**3c**) stereoselectively. 4) Similarly to the reactin of **1c**, 5-substituted 2,4-bis(trimetylsilyloxy)-pyrimidines reacts with **2** in the presence of pyridine to give α anomers in high yields.

Results

Identification of Anomers of 2′-Deoxyuridine Derivatives. Rapid identification of the anomers of 2′-deoxyuridine derivatives in the reaction mixture was carried out by mean of ^{1}H NMR spectroscopy and chromatography. The properties of 5-substituted 3′,5′-di-*O*-(*p*-chlorobenzoyl)-2′-deoxyuridines are summarized in Table 1. The anomeric protons of all β anomers **4a—f** were observed as triplet at δ 6.15—6.40, whereas those of α anomers **3a—f** were multiplet.

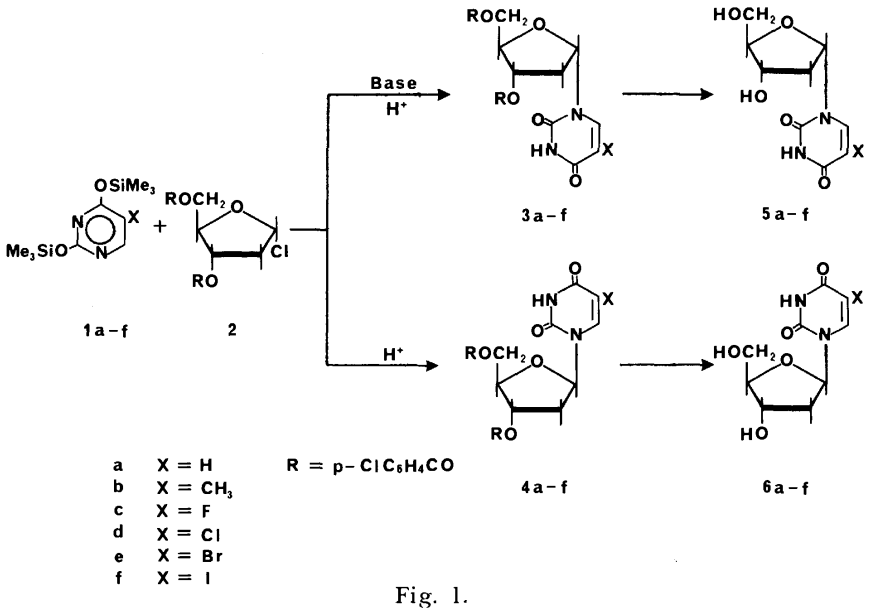

Fig. 1.

Table 1. 5-Substituted 3′,5′-Di-*O*-(*p*-chlorobenzoyl)-2′-deoxyuridines

Compound No.	Substituent and Anomer	Mp θ_m/°C	TLC R_f Value	HPLC Retention time/min	$[\alpha]_D^{20}$ (C2, dioxane) (°)	IR (KBr) $\nu_{C=O}$/cm^{-1}	^{1}H NMR[a] δ(ppm) Anomeric H
3a	H, α	190.5—191	0.29	9.25	−46.2	1720, 1690, 1670	6.17—6.37m
4a	H, β	212 —213	0.25	11.47	−14.7	1718, 1685	6.25 t, *J*=8 Hz
3b	CH_3, α	179 —180	0.34	11.45	−23.7	1725, 1685	6.18—6.42m
4b	CH_3, β	197.5—198.5	0.38	14.02	−30.7	1715, 1675	6.33 t, *J*=8 Hz
3c	F, α	176 —177	0.41	11.89	−67.4	1725, 1690, 1670	6.15—6.41m
4c	F, β	198 —199	0.45	14.59	− 4.7	1710, 1700, 1665	6.25 t, *J*=7 Hz
3d	Cl, α	184 —185	0.48	13.65	− 1.2	1725, 1690	6.11—6.35m
4d	Cl, β	189.5—190	0.59	16.39	−28.4	1710, 1692	6.37 t, *J*=8 Hz
3e	Br, α	168 —170	0.49	14.38	+22.5	1720, 1690	6.14—6.34m
4e	Br, β	188 —189	0.61	17.18	−35.4	1715, 1680	6.30 t, *J*=8 Hz
3f	I, α	182 —183	0.50	15.43	+56.1	1715, 1665	6.24—6.36m
4f	I, β	187 —188	0.64	18.33	−50.3	1712, 1675, 1650	6.18 t, *J*=8 Hz

a) DMSO-d_6.

Table 2. 5-Substituted 2′-Deoxyuridines

Compound No.	Substituent and Anomer	Mp θ_m/°C	TLC R_f Value	$[\alpha]_D^{20}$ (C2, N-NaOH) (°)	IR (KBr) $\nu_{C=O}$/cm^{-1}	^{1}H NMR[a] δ(ppm) H_6	^{1}H NMR[a] δ(ppm) Anomeric H
5a	H, α	oil	0.25	− 4.2	1700, 1690	7.72 d, *J*=8Hz	6.09 dd, *J*=5 and 6Hz
6a	H, β	164 —165	0.27	+50.4	1690, 1660	7.60 d, *J*=8Hz	6.24 t, *J*=Hz
5b	CH_3, α	187.5—188	0.32	+19.3	1682	7.60s	6.15 dd, *J*=5 and 6Hz
6b	CH_3, β	192 —193	0.34	+30.8	1700, 1655	7.43s	6.28 t, *J*=6.5Hz
5c	F, α	177 —178	0.39	−13.7	1722, 1690	7.80 d, *J*=7Hz	6.09m
6c	F, β	150 —151	0.44	+55.1	1710, 1685	7.70 d, *J*=7Hz	6.18 t, *J*=7Hz
5d	Cl, α	194 —196	0.44	+ 4.6	1695, 1680(sh)	7.93s	6.11 dd, *J*=3.5 and 7Hz
6d	Cl, β	177 —178	0.50	+49.4	1730, 1672	7.86s	6.15 t, *J*=7Hz
5e	Br, α	197 —199	0.47	+11.2	1682	8.04s	6.05 dd, *J*=3.5 and 7Hz
6e	Br, β	186 —187	0.52	+39.4	1710, 1685	7.99s	6.24 t, *J*=8Hz
5f	I, α	188.5—189.5	0.51	+21.5	1685	8.09s	6.03 dd, *J*=4 and 7Hz
6f	I, β	187 —188	0.55	+27.4	1700, 1672	8.08s	6.16 t, *J*=7Hz

a) N-NaOD.

Thin-layer chromatograph using a precoated silica-gel plate (Art 5715, $60F_{254}$) and a mixted solvent of hexane, benzene, and ethyl acetate (1 : 1 : 2) as well as HPLC were successfully used for separating α and β anomers (**3a—f** and **4a—f**).

The properties of 5-substituted 2′-deoxyuridines are shown in Table 2. ^{1}H NMR spectra of the anomeric protons show triplet about δ 6.03—6.28 for all β anomers, and double doublet or multiplet for α anomers. ^{1}H NMR spectra of H_6 of pyrimidine ring show doublet or singlet peaks and those of β anomers appear at higher magnetic fields in comparison with those of α anomers. The α and β anomers (**5a—f and 6a—f**) were identified by thin-layer chromatogrph using a precoated silica-gel plate (HPTLC, Art 5628, $60F_{254}$) with a mixed solvent of ethyl acetate, formic acid, and water (65 : 5 : 5).

Reaction of 1a—f with 2 in the Presence of *p*-Nitrophenol. Pyrimidine derivatives **1a—f** reacted with **2** in the presence of *p*-nitrophenol to give β anomers **4a—f** in high yields. Among Brönsted acids used, *p*-nitrophenol gave β anomer most efficiently in the reaction of **1c** with **2**.[18] The results are shown in Table 3. The β-stereoselectivity was affected by a substituent in 5-position of silylpyrimidine; electron-releasing substituents seem to give more β anomer.

Table 3. β-Selective Synthesis of 5-Substituted 3′,5′-Di-*O*-(*p*-chlorobenzoyl)-2′-deoxy-β-uridines

Run	Substituent group	Yield/%[a] α Anomer	Yield/%[a] β Anomer
1	H	2.5	96.5
2	CH_3	trace	96
3	F	4.5	92
4	Cl	4.5	92
5	Br	10	85
6	I	9	87

a) Yields refer to isolated products.

Reaction of 1c with 2 in the Presence of Base and *p*-Nitrophenol. During investigation of the reaction of **1c** with **2** it was happened that β anomer **4c** is not formed, but formed α anomer **3c** when **1c** and/or **2** containing a trace of trietylamine hydrochloride[20] and/or pyridine were used. This result made the author to examine the effect of base on the stereoselectivity.

First, the effect of concentration of pyridine on the

stereoselectivity was investigated. The results are shown in Fig. 2. In the presence of a trace of pyridine, β-stereoselective reaction changed to α-stereoselective reaction in proportion to the concentration of pyridine.

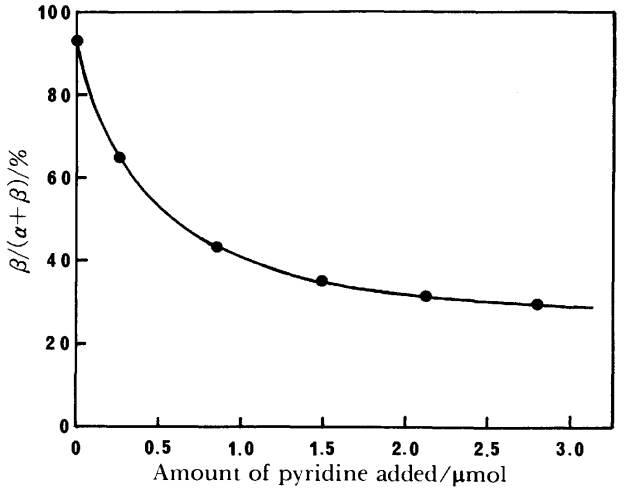

Fig. 2. The effect of the concentration of pyridine on the stereoselectivity of the reaction **1c** with **2**. Reaction conditions; **1c**: 0.197 g (0.768 mmol), **2**: 0.300 g (0.698 mmol), *p*-nitrophenol: 0.034 g (0.244 mmol), chloroform: 2.1 cm³, reaction temp: 25 °C, reaction time: 12 h.

Table 4. Effect of Additives on the Formation of **3c**[a)]

Run	Additive	Amount[b)]	Yield/%[c)]
1	Pyridine	0.1	77.8
2	α-Picoline	0.1	76.5
3	β-Picoline	0.1	78.1
4	2,6-Lutidine	0.1	62.3
5	Triethylamine	0.1	73.4
6	Triethylamine Hydrochloride	0.35	77.5
7	*N*,*N*-Dimethylformamide	0.1	39.7
8	Acetamide	0.1	50.9

a) Reaction conditions; **1c**: 1.1 mmol, **2**: 1.0 mmol, *p*-nitrophenol: 0.35 mmol, chloroform: 3.0 cm³, reaction temp: 25 °C, reaction time: 12 h. b) Based on 2. c) Yield is measured by HPLC.

Table 5. α-Selective Synthesis of 5-Substituted 3′,5′-Di-*O*-(*p*-chlorobenzoyl)-2′-deoxy-α-uridines

Run	Substituent group	Yield/%[a)]	
		α Anomer	β Anomer
1	H	74.8	21.1
2	CH_3	67.4	32.5
3	F	79.3	14.6
4	Cl	77.3	10.4
5	Br	77.0	21.0
6	I	81.5	15.4

a) Yields refer to isolated products.

Second, the effect of additives such as organic bases or triethylamine hydrochloride in the reaction of **1c** with **2** on the stereoselectivity was investigated. The results are shown in Table 4. Pyridine showed higher α-stereo-selectivity than lutidine. This seems to be due to steric hindrance of methyl radicals of 2,6-lutidine to sugar halide. On the other hand, triethylamine hydrochloride showed considerable α-stereoselectivity, but *N*,*N*-dimethylformamide and acetamide showed no stereoselectivity.

α-Stereoselective Synthesis. The effect of substituents at 5-position of silylpyrimidine on α-stereoselective reactions of **1a—f** with **2** was investigated and α anomers **3a—f** were synthesized. In the presence of pyridine, **1a—f** reacted with **2** α-stereoselectively to give **3a—f** in high yields. The results are shown in Table 5.

The α-stereoselectivity was affected by the substituents at 5-position of silylpyrimidine and halogen substituents showed higher selectivity than methyl group. It is, therefore, considered that electron-attracting substituents cause higher α-stereoselectivity than electron-releasing substituents.

Deprotection by the treatment of ammonia-methanol solution to **3a—f** or **4a—f** smoothly gave **5a—f** or **6a—f**, respectively, in high yields.

Discussion

On the substitution reactions of **1a—f** with **2**, it became apparent that the stereoselectivity varies with

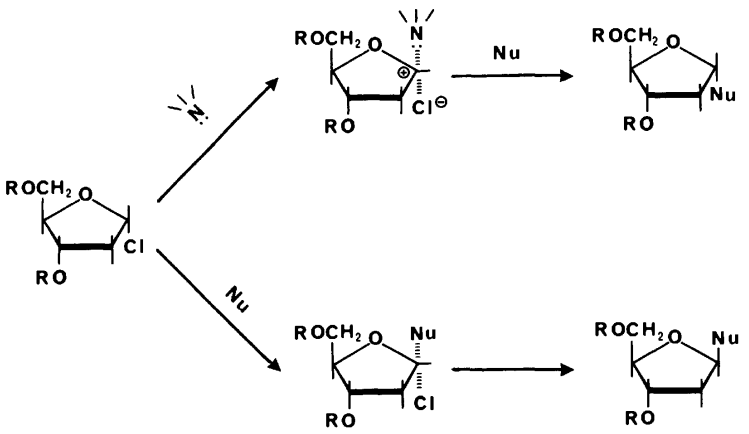

Fig. 3.

the substituent group of 5-position of silylpyrimidine, the additives, and concentration of additives.

It is improbable that both the α and β nucleosides are stereoselectively formed in the substituting reaction, by the Hilbert-Johnson reaction through nucleophilic attack of a sugar cation on aromatic pyrimidine ring.[13] In the preceding work,[18] it was proposed that β-stereoselective reaction occurs between silylpyrimidine as nucleophilic reagent and the β-face of sugar halide which is pure α anomer, in the presence of Brönsted acid.

On the other hand, the presence of organic base or its salt turned β-stereoselective substitution reaction into α-stereoselective reaction.

α-Stereoselectivity. The α-stereoselective reaction mechanism can be depicted in Fig. 3. While nucleophilic reagent attacks the β-face of sugar halide, a base attacks the nucleophilic reagent competitively. If the base has higher active in nucleophilicity than the nucleophilic reagent, the base coordinates with the β-face of sugar halide predominantly. Then the nucleophilic reagent cannot attack the β-face of sugar halide but attacks the α-face to produce an α-nucleoside. Thus, nucleophilicity of reagent seems to contribute to the stereoselectivity in substitution reaction.

Experimental

Apparatus. All the melting points measured were not corrected. IR spectra were recorded by a Hitachi 260—30 infrared spectrophotometer using KBr disk method. ^{1}H NMR spectra were obtained by a Hitachi Perkin-Elmer P-24 (60 MHz) using TMS as the internal standard. The specific rotation was measured by a JASCO DIP-181 digital polarimeter. The spectrophotometric measurement of TLC spots was done on a Shimadzu High-Speed TLC Scanner CS-920. High-performance liquid chromatography was experimented by a Shimadzu LC-3A equipped with a Shimadzu variable length spectrophotometric detector SPD-2A and a Shimadzu Chromatopac C-RIA.

Analysis by Thin-Layer Chromatography. The anomeric ratio of nucleoside was monitored during the reaction by thin-layer chromatography. Anomers were separated on the plates precoated with silica-gel $60F_{254}$ (Merck, Art 5715) with a mixed solvent of hexane, benzene, and ethyl acetate (1 : 1 : 2). R_f values of anomers **3a—f** and **4a—f**, are shown in Table 1. Measurements were run according to the preceding work[18] by using of high-speed TLC scanner.

Anomers **5a—f** and **6a—f**, were separated the plates precoated with silica-gel $60F_{254}$ (HPTLC, Merck, Art 5628) a mixed solvent of ethyl acetate, formic acid, and water (65 : 5 : 5). R_f values of the anomers are shown in Table 2.

Analysis by High-Performance Liquid Chromatography. A column (25 cm×4 mm i.d.) was packed with RP-18 chemically bonded silica-gel (LiChrosorb, 10 μm, Merck). The mobil phase was a 45 : 55 mixture of 0.03 mol dm^{-3} ammonium dihydrogenphosphate solution and acetonitrile, which was made to 1 cm^3 min^{-1} and 25 °C. The retention time values of each compound of **3a—f** and **4a—f** are shown in Table 1.

Materials. Chloroform were refluxed for 2 h over P_2O_5 and distilled. Uracil, thymine, and 5-fluorouracil purchased were used without further purification. 5-Chlorouracil, 5-bromouracil, and 5-iodouracil were prepared by the reaction of uracil with the corresponding *N*-halosuccinimide[19] in acetic acid. 3,5-Bis(*O*-*p*-chlorobenzoyl)-2-deoxy-α-D-ribofuranosyl chloride (**2**) was prepared as described in the preceding report.[18]

Table 6. Boiling Point of 5-Substituted 2,4-Bis-(trimethylsilyloxy)pyrimidines

Compound		Bp/θ_b/°C/mmHg†
No.	Substituent group	
1a	H	113—114/16
1b	CH_3	124—131/16
1c	F	110—111/15
1d	Cl	130—131/16
1e	Br	138—139/16
1f	I	124—132/4

5-Substituted 2,4-Bis(trimethylsilyloxy)pyrimidines (1a—f). These compounds were all prepared in an analogous manner.[18] A mixture of appropriate uracil (1 mol), hexamethyldisilazane (260 cm^3, 1.25 mol), and trimethylsilyl chloride (1 cm^3, 7.8 mmol) was refluxed in dry atomosphere. Ammonia gas vigorously evolved. The excess of hexamethyldisilazane was removed after 2 h of the reaction under 50 mmHg† and finally 12 mmHg at 90 °C. The residue was distilled in vacuo to give **1a—f**. The boiling point values are shown in Table 6.

Synthesis of β Anomers (4a—f). To a mixture of **1a—f** (17.9 mmol), *p*-nitrophenol (0.8 g, 5.77 mmol) in dry chloroform (49 cm^3), was added **2** (7 g, 16.3 mmol) and stirred for 12 h at 30 °C. The reaction mixture was then evaporated under a reduced pressure to give crystalline residue, which was recrystallized from acetic acid to give β anomers. From mother liquor, anomers were isolated by fractional crystallization. Results are shown in Table 3.

Effect of Pyridine on the Reaction of 1c with 2. To a mixture of **1c** (0.197 g, 0.768 mmol), *p*-nitrophenol (0.034 g, 0.244 mmol), and pyridine in chloroform (2.1 cm^3), was added **2** (0.300 g, 0.698 mmol) and stirred for 12 h at 25 °C. The ratio of each anomer was analyzed by TLC scanner. The result is shown in Fig. 2.

Effect of Additives on the Formation of 3c. To a mixture of **1c** (0.302 g, 1.1 mmol), *p*-nitrophenol (0.049 g, 0.35 mmol), and additives in chloroform (3.0 cm^3), was added **2** (0.430 g, 1.0 mmol) and stirred for 12 h at 25 °C. The ratio of each anomer was analyzed by HPLC. The results are shown in Table 4.

Synthesis of α Anomers (3a—f). To a mixture of **1a—f** (17.9 mmol), *p*-nitrophenol (0.8 g, 5.77 mmol), and pyridine (0.4 g, 5.05 mmol) in dry chloroform (49 cm^3), was added **2** (7 g, 16.3 mmol) and stirred for 12 h at 30. The reaction mixture was then evaporated under a reduced pressure to give an oily residue, which was subjected to crystallization with ethanol to give α anomers. The anomers were isolated from mother solutions by fractional crystallization. The results are shown in Table 5.

5-Substituted 2′-Deoxyuridines (5a—f, 6a—f). To a saturated ammonia-methanol solution (20 cm^3), was added 1 g of each anomer **3a—f** and **4a—f**, and stirred for 16 h at 30 °C. The reaction mixture was then treated similarly to the

† 1 mmHg=133.3 Pa.

manner as described in preceding report.[18] The 2′-deoxyuridine derivatives were isolated in 90—99% yield, of which physical properties are shown in Table 2.

References

1) C. Heidelberger, L. Griesbach, O. Cruz, R. J. Schnitzer, and E. Grunberg, *Proc. Soc. Exp. Biol. Med.*, **97**, 470 (1958).
2) J. H. Burchenal, E. A. D. Holmberg, J. J. Fox, S. C. Hemphill, and J. A. Reppert, *Cancer Res.*, **19**, 497 (1959).
3) F. Weygand, A. Wacker, and H. Dellweg, *Z. Naturforsch., Teil B*, **7**, 19 (1952).
4) R. E. Belts and D. Visser, *J. Am. Chem. Soc.*, **77**, 736 (1955).
5) D. W. Visser, D. M. Frisch, and B. Huang, *Biochem. Pharmacol.*, **5**, 157 (1960).
6) M. Hoffer, R. Duschinsky, J. J. Fox, and N. Yung, *J. Am. Chem. Soc.*, **81**, 4112 (1959).
7) M. Hoffer, *Ber.*, **93**, 2777 (1960).
8) M. Prystaš and F. Šorm, *Collect. Czech. Chem. Commun.*, **29**, 121 (1964).
9) M. Prystaš, J. Farkaš, and F. Šorm, *Collect. Czech. Chem. Commun.*, **28**, 3140 (1963).
10) M. Prystaš and F. Šorm, *Collect. Czech. Chem. Commun.*, **29**, 131 (1964).
11) M. Prystaš and F. Šorm, *Collect. Czech. Chem. Commun.*, **29**, 143 (1964).
12) M. Prystaš and F. Šorm, *Collect. Czech. Chem. Commun.*, **30**, 2960 (1965).
13) M. Prystaš, J. Farkaš, and F. Šorm, *Collect. Czech. Chem. Commun.*, **30**, 3124 (1965).
14) M. Prystas, and F. Šorm, *Collect. Czech. Chem. Commun.*, **30**, 1900 (1965).
15) T. J. Bardos, M. P. Kotick, and C. Szantay, *Tetrahedron Lett.*, **16**, 1759 (1969).
16) M. P. Kotick, C. Szantay, and T. J. Bardos, *J. Org. Chem.*, **34**, 3806 (1969).
17) U. Niedballa and H. Vorbrüggen, *J. Org. Chem.*, **39**, 3654 (1974).
18) H. Aoyama, Y. Kusayanagi, M. Yotsuji, I. Kitayama, T. Yamaguchi, and T. Kodama, *Nippon Kagaku Zasshi*, in press.
19) T. Nishiwaki, *Tetrahedron*, **22**, 2401 (1966).
20) T. Nishimura, B. Shimizu, and I. Iwai, *Chem. Pharm. Bull.*, **11**, 1470 (1963).

Synthesis on 1,4-Diaminocyclitol Antibiotics. IV. Synthesis of 7′-Phenylfortimicin A and 7′-Phenyl-6′-epifortimicin A

Kazuaki KANAI, Seiichiro OGAWA,* and Tetsuo SUAMI†
Department of Applied Chemistry, Faculty of Science and Technology, Keio University, Hiyoshi, Yokohama 223
(Received September 18, 1986)

7′-Phenylfortimicin A and 7′-phenyl-6′-epifortimicin A have been synthesized by condensation of newly prepared 1-*O*-acetyl-2,6-bis(2,4-dinitrophenylamino)-2,3,4,6,7-pentadeoxy-7-phenyl-L-*lyxo*-heptopyranose and -D-*ribo*-heptopyranose, respectively, with 2,5-di-*O*-benzoyl-1,4-bis[*N*-(methoxycarbonyl)]fortamine B, followed by deprotection.

In the preceding paper,[1] the chemical synthesis of 7′-propylfortimicin A and its antibacterial assay were reported. In continuation of our study on modification of the diamino sugar moiety of antibiotic fortimicins,[1,2] replacement of the 6′-methyl group with benzyl group would be of interest because of anticipated enhancement both in its lipohilic nature and in the steric congestion. We now describe the synthesis and biological activities of 7′-phenylfortimicin A and 7′-phenyl-6′-epifortimicin A.

Results and Discussion

1-*O*-Acetyl-2,6-bis(2,4-dinitrophenylamino)-2,3,4,6,7-pentadeoxy-7-phenyl-L-*lyxo*-heptopyranose (**7**) and -D-*ribo*-heptopyranose (**8**) have been first prepared from methyl 2-acetamido-2,3,4,6-tetradeoxy-6-nitro-α-*erythro*-hexopyranoside (**1**).[1]

The nitro aldol reaction of **1** with benzaldehyde was effected in the presence of methanolic sodium methoxide in methanol for 2 h at 0 °C. The products were acetylated with acetic anhydride and boron trifluoride etherate, and then hydrogenated with sodium borohydride in dimethyl sulfoxide to give an inseparable mixture of methyl 2-acetamido-2,3,4,6,7-pentadeoxy-6-nitro-7-phenyl-β-L-*lyxo*- and -α-D-*ribo*-heptopyranoside (**2**) in 54% yield. The reaction using KF or CsF in acetonitrile instead of sodium methoxide resulted in a poor yield. However, when excess KF was used, **2** was obtained in 38% yield. Catalytic hydrogenation of **2** with Raney nickel in a mixture of ethanol and ethyl acetate, followed by *N*-acetylation with acetic anhydride, gave two compounds (**3**, 47% and **4**, 15%) after chromatography. The value of specific rotation +129° of **4** was more dextrorotatory than +28.2° of **3**. In addition, the ^{13}C NMR spectra of **3** and **4** revealed that C-7 signal of **4** shifted upfield by 1.83 ppm compared to that of **3** (Table 1). These results corresponded to those of the respective 7-propyl derivatives. The stereochemistry at C-6[3] of **3** and **4** has thus been confirmed as depicted in Scheme.

Compound **3** was *N*-deacetylated with sodium hydroxide in refluxing 95% aqueous 2-methoxyethanol and the free base was converted to the bis[*N*-(2,4-dinitrophenyl)] derivative **5** in 81% yield. Hydrolysis of **5** with acetic acid containing 2M†† hydrochloric acid, followed by acetylation, gave the acetate (**7**) in 61% yield.

Table 1. ^{13}C NMR Chemical Shifts[a] of **3** and **4**

	3	**4**
C-1	99.71	99.56
C-2	49.79	49.31
C-3	24.74	25.18
C-4	28.29	28.22
C-5	69.77	71.30
C-6	54.78	55.34
C-7	38.75	36.93
Phenyl	127.27	127.20
Phenyl	129.26	129.24
Phenyl	130.21	130.19
Phenyl	140.07	140.28
OMe	55.75	55.56
$\underline{C}OCH_3$	173.07	172.90
	172.83	172.76
$CO\underline{C}H_3$	22.38	22.45
	22.50	22.53

a) In parts per million downfield from TMS.

Condensation of **7** with 2,5-di-*O*-benzoyl-1,4-bis[*N*-(methoxycarbonyl)]fortamine B (**9**)[4] in 1,2-dichloroethane in the presence of trimethylsilyl trifluoromethanesulfonate under argon gave a single condensate (**10**) in 43% yield. The ^{1}H NMR spectrum of **10** exhibited a doublet (δ 5.38, J=3 Hz) due to H-1′, supporting the conformation of the anomeric proton to be equatorial in the α-D-glycoside. Hydrolysis of **10** in refluxing aqueous 1,4-dioxane with barium hydroxide, followed by treatment with Amberlite IRA-400 (OH^-) resin, gave 7′-phenylfortimicin B (**12**) in 70% yield. Compound **12** was converted into the tris[*N*-(benzyloxycarbonyl)] derivative (**14**) in 54% yield. Treatment of **14** with *N*-[*N*-(benzyloxycarbonyl)glycyloxy]succinimide and triethylamine afforded the tetrakis-[*N*-(benzyloxycarbonyl)] derivative of 7′-phenylfortimicin A (**16**) in 77% yield. Finally, catalytic hydrogenation of **16** in the presence of 10% palladium on

†Present address: Department of Chemistry, Faculty of Science and Technology, Meisei University, Hodokubo, Hino, Tokyo 191.

††1 M=1 mol dm^{-3}.

Table 2. Antimicrobial Activity of **18**, **19**, and Fortimicin A[a)]

Test Organisms	**18**	**19**	FM A
Streptococcus faecalis KY4280	12.5	>100	6.3
Pseudomonas aeruginosa KY4276	25	>100	6.3
Staphylococcus aureus KY4279	0.2	0.39	0.2
Escherichia coli KY4271	3.1	3.1	0.78
Bacillus subtilis KY4273	0.2	3.1	0.1
Shigella sonnei KY4281	3.1	25	1.6
Klebsiella pneumoniae KY4275	0.39	1.6	0.2

a) Minimum inhibitory concentration in μg ml^{-1}.

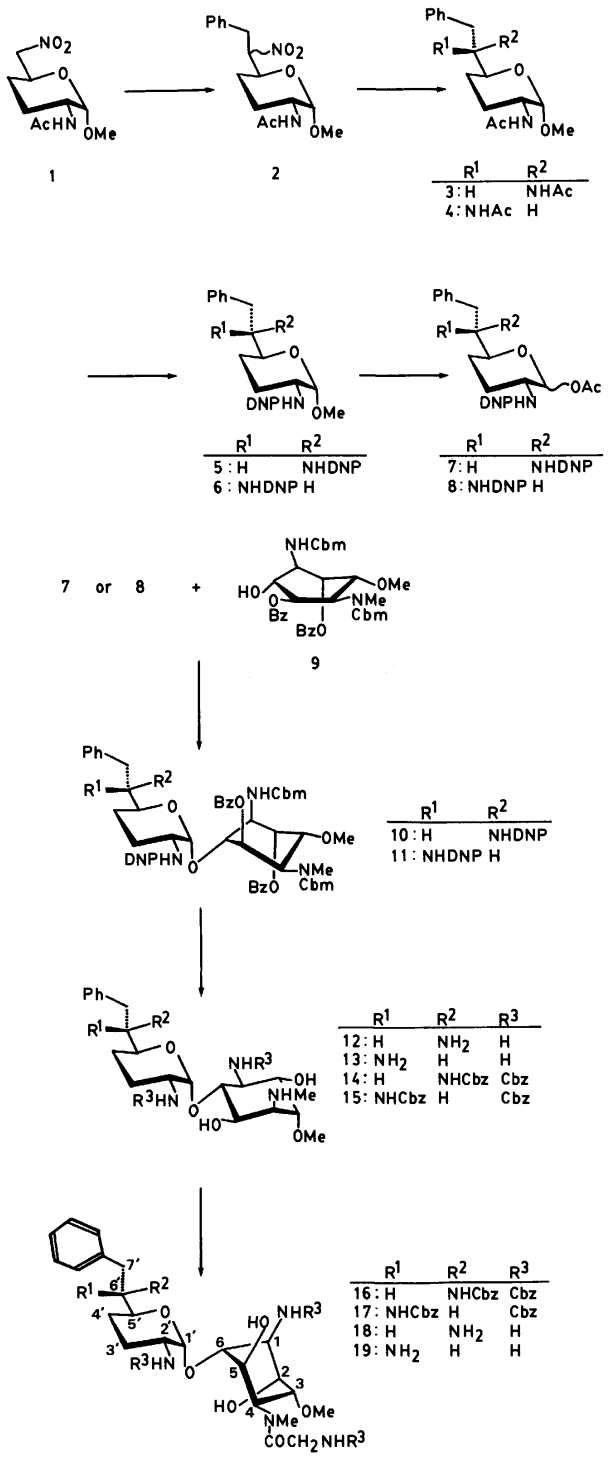

charcoal, followed by treatment with AG1-X2 (SO_4^{2-}) resin, gave 7′-phenylfortimicin A (**18**) as the sulfate.

7′-Phenyl-6′-epifortimicin A (**19**) has been similarly synthesized starting from **4** as described in the preparation of **18** from **3**.

The minimum inhibitory concentrations of **18** and **19** were listed together with those of fortimicin A (Table 2). 7′-Phenylfortimicin A (**18**) exhibited slightly weak activity compared to that of fortimicin A against many micro organisms. However, 7′-phenyl-6′-epifortimicin A (**19**) showed weak activity. Generally, the 6′-epi analogs[5)] of fortimicin A seem to be less active against micro organisms than those of the natural type.

Experimental[6)]

Methyl 2-Acetamido-2,3,4,6,7-pentadeoxy-6-nitro-7-phenyl-β-L-*lyxo*- and -α-D-*ribo*-heptopyranoside (2). To a solution of methyl 2-acetamido-2,3,4,6-tetradeoxy-6-nitro-α-D-*erythro*-hexopyranoside[1)] (**1**) (1.50 g) in methanol (3 ml) were added benzaldehyde (0.70 ml) and 1M sodium methoxide methanolic solution (6.7 ml) under ice cooling, and the mixture was stirred at 0 °C for 2 h. After neutralization with Amberlite IR-120 (H^+) resin, the mixture was concentrated. The residue was dissolved in acetic anhydride (10 ml) and boron trifluoride etherate (1.5 ml) was added to it under ice cooling. After stirring for 1 h, the mixture was poured into ice water (100 ml) and the mixture was extracted with dichloromethane (150 ml). The extract was successively washed with saturated aqueous $NaHCO_3$ (300 ml), brine (100 ml) and water (100 ml), and dried. After concentration, the residue was dissolved in dimethyl sulfoxide (18 ml), and a suspension of $NaBH_4$ (200 mg) in dimethyl sulfoxide (2 ml) was added to it. After stirring for 0.5 h, the mixture was acidified with Amberlite IR-120 (H^+) resin. The mixture was extracted with chloroform (100 ml) and the extract was dried. After concentration, the residue was chromatographed on silica gel with chloroform–methanol (90 : 1) to give **2** (1.13 g, 54%) and recovered **1** (0.60 g): IR (KBr) 1640 (amide), 1545, 1370 (NO_2) cm^{-1}; ^{1}H NMR ($CDCl_3$) δ=1.42—2.10 (4H, m, H-3,4), 1.96 (3H, s, NAc), 3.08 (2H, m, H-7), 3.33 (3H, s, OMe), 4.15 (2H, m, H-2,5), 4.58 (1H, d, *J*=3 Hz, H-1), 4.65 (1H, m, H-6), 5.73 (1H, d, *J*=8 Hz, NH), 7.04—7.42 (5H, m, phenyl).

Found: C, 59.23; H, 6.79; N, 8.46%; *m/z*, 323.1607. Calcd for $C_{16}H_{22}N_2O_5$: C, 59.62; H, 6.88; N, 8.69%; M+1, 323.1605.

Methyl 2,6-Diacetamido-2,3,4,6,7-pentadeoxy-7-phenyl-β-L-*lyxo*- (3) and -α-D-*ribo*-heptopyranoside (4). A solution of **2** (1.10 g) in ethanol (10 ml) and ethyl acetate (10 ml) was hydrogenated in the presence of Raney nickel in an initial hydrogen pressure of 3.4 kg cm^{-2} overnight. After removal of the catalyst, the solution was concentrated. The residue was acetylated with acetic anhydride (5 ml) in methanol (10 ml). The product was purified by chromatography on silica gel with toluene–ethanol (10 : 1) to give **3** (546 mg, 47%) and **4** (170 mg, 15%): Compound **3**; mp 241—242 °C; $[\alpha]_D^{20}$ +28.2° (*c* 0.77, MeOH); ^{1}H NMR (CD_3OD) δ=1.50—1.82 (4H, m, H-3,4), 1.87, 1.94 (each 3H, s, NAc), 2.83 (1H, dd, *J*=8.5, 14 Hz, H-7a), 2.91 (1H, dd, *J*=7, 14 Hz, H-7b), 3.42 (3H, s, OMe), 3.77 (1H, ddd, *J*=2.5, 6, 8.5 Hz, H-5), 3.90 (1H, ddd, *J*=3, 4.5, 11.5 Hz, H-2), 4.18 (1H, ddd, *J*=2.5,

7, 8.5 Hz, H-6), 4.67 (1H, d, J=3 Hz, H-1), 7.24 (5H, m, phenyl).

Found: C, 64.81; H, 7.48; N, 8.21%. Calcd for $C_{18}H_{26}N_2O_4$: C, 64.65; H, 7.84; N, 8.38%.

Compound **4**; mp 266.5—267.5 °C; $[\alpha]_D^{20}$ +129° (c 1.41, MeOH); ^{1}H NMR (CD_3OD) δ=1.60—1.90 (4H, m, H-3,4), 1.79, 1.94 (each 3H, s, NAc), 2.61 (1H, dd, J=11 Hz, 14 Hz, H-7a), 3.15 (1H, dd, J=4, 14 Hz, H-7b), 3.40 (3H, s, OMe), 3.70 (1H, ddd, J=2, 6, 11 Hz, H-5), 3.93 (1H, ddd, J=3, 6, 11 Hz, H-2), 4.07 (1H, ddd, J=4, 6, 11 Hz, H-6), 4.68 (1H, d, J=3 Hz, H-1), 7.24 (5H, m, phenyl).

Found: C, 64.44; H, 7.77; N, 8.14%. Calcd for $C_{18}H_{26}N_2O_4$: C, 64.65; H, 7.84; N, 8.38%.

Methyl 2,6-Bis(2,4-dinitrophenylamino)-2,3,4,6,7-pentadeoxy-7-phenyl-β-L-*lyxo*-heptopyranoside (5). A solution of **3** (435 mg) in 95% aqueous 2-methoxyethanol (20 ml) containing sodium hydroxide (1.6 g) was refluxed for 26 h. An additional amount of sodium hydroxide (1.6 g) was added to it and the reflux was continued for further 21 h. After cooling, the mixture was neutralized with 1M hydrochloric acid and concentrated. The residue was extracted with cold ethanol and the solution was concentrated. The residue was dissolved in methanol (20 ml), and 1-fluoro-2,4-dinitrobenzene (0.50 ml) and triethylamine (2.0 ml) were added to it. After stirring for 20 h, the mixture was extracted with chloroform (30 ml), and the extract was dried and concentrated to give a residue, which was chromatographed on silica gel with toluene-2-butanone (30:1) to give **5** (612 mg, 81%). Recrystallization from acetone-2-propanol gave an analytical sample: mp 109—114 °C; $[\alpha]_D^{20}$ −147° (c 0.95, acetone); IR (KBr) 1620, 1590 (aromatic), 1520, 1330 (NO_2) cm^{-1}; ^{1}H NMR ($CDCl_3$) δ=1.66—2.12 (4H, m, H-3,4), 3.10 (2H, d, J=7 Hz, H-7), 3.63 (3H, s, OMe), 5.00 (1H, d, J=3 Hz, H-1), 6.57, 6.95 (each 1H, d, J=10 Hz, H-6 of DNP), 8.03, 8.21 (each 1H, dd, J=3, 10 Hz, H-5 of DNP), 9.03, 9.09 (each 1H, d, J=3 Hz, H-3 of DNP).

Found: C, 53.36; H, 4.52; N, 14.45%. Calcd for $C_{26}H_{26}N_6O_{10}$: C, 53.61; H, 4.50; N, 14.43%.

1-*O*-Acetyl-2,6-bis(2,4-dinitrophenylamino)-2,3,4,6,7-pentadeoxy-7-phenyl-L-*lyxo*-heptopyranose (7). A solution of **5** (610 mg) in acetic acid (30 ml) containing 2M hydrochloric acid (5 ml) was stirred at 80 °C for 5 h. After cooling, the mixture was concentrated to the half volume and extracted with chloroform (60 ml). The extract was successively washed with saturated aqueous $NaHCO_3$ (20 ml) and water (20 ml), dried, and concentrated. The residue was acetylated with acetic anhydride (5 ml) in pyridine (10 ml). The mixture was concentrated to a residue, which was extracted with chloroform (100 ml) and the extract was successively washed with 1M hydrochloric acid (30 ml), saturated aqueous $NaHCO_3$ (30 ml) and water (30 ml), and dried. After concentration, the residue was chromatographed on silica gel with toluene-2-butanone (30:1) to give **7** (386 mg, 61%): mp 223 °C (decomp); $[\alpha]_D^{23}$ −172° (c 1.18, pyridine); IR (KBr) 1760 (ester), 1620, 1590 (aromatic), 1520, 1340 (NO_2) cm^{-1}; ^{1}H NMR (pyridine-d_5) δ=2.31 (3H, s, OAc), 3.20 (2H, d, J=9 Hz, H-7), 7.47 (5H, m, phenyl), 8.34 (2H, dd, J=3 Hz, 10 Hz, H-5 of DNP).

Found: C, 53.00; H, 4.33; N, 13.90%. Calcd for $C_{27}H_{26}N_6O_{11}$: C, 53.12; H, 4.29; N, 13.77%.

2,5-Di-*O*-benzoyl-2′,6′-bis[*N*-(2,4-dinitrophenyl)]-1,4-bis[*N*-(methoxycarbonyl)]-7′-phenylfortimicin B (10). To a solution of **7** (350 mg) and 2,5-di-*O*-benzoyl-1,4-bis[*N*-(methoxycarbonyl)]fortamine B (**9**)[1] (310 mg) in freshly distilled 1,2-dichloroethane in the presence of powdered molecular sieve 4A (300 mg) was added trimethylsilyl trifluoromethanesulfonate (0.12 ml), and the mixture was stirred for 5.5 h under argon. An insoluble material was filtered and washed with chloroform. The filtrate was successively washed with 5% aqueous $NaHCO_3$ (40 ml) and water (40 ml), dried, and concentrated to give a residue, which was chromatographed on silica gel with toluene-2-butanone (15:1) to give **10** (274 mg, 43%). Recrystallization from acetone-2-propanol gave an analytical sample: mp 147—153 °C; $[\alpha]_D^{27}$ −128° (c 1.08, acetone); ^{1}H NMR ($CDCl_3$) δ=2.84 (3H, s, NMe), 3.06 (2H, m, H-7′), 3.46 (3H, s, OMe), 3.56 (6H, s, Cbm×2), 4.12 (1H, dd, J=4, 9 Hz, H-3), 4.36 (1H, bs, H-6), 5.32 (1H, d, J=10 Hz, NH-1), 5.38 (1H, d, J=3 Hz, H-1′), 5.51 (1H, t, J=5 Hz, H-5), 5.78 (1H, bs, H-2), 6.32 and 6.84 (each 1H, d, J=9 Hz, H-6 of DNP), 7.15 (5H, s, phenyl), 7.40—7.66 (6H, m, benzoyl), 7.86 and 8.08 (3H and 1H, each d, J=8.5 Hz, benzoyl), 8.21 (2H, dd, J=3, 9 Hz, H-5 of DNP×2), 8.61 and 8.86 (each 1H, d, J=9 Hz, NH-2′,6′), 8.99 and 9.10 (each 1H, d, J=3 Hz, H-3 of DNP).

Found: C, 56.27; H, 4.84; N, 10.31%. Calcd for $C_{51}H_{53}N_8O_{19}$: C, 56.62; H, 4.94; N, 10.36%.

7′-Phenylfortimicin B (12). A stirred solution of **10** (206 mg) in dioxane (10 ml) and water (3 ml) in the presence of barium hydroxide octahydrate (3.5 g) was refluxed for 6 h. After cooling, the solid was filtered. Carbon dioxide was introduced to the filtrate and an insoluble material was filtered. After concentration, the residue was treated with Amberlite IRA-400 (OH^-) resin (10 ml) in a mixture of water (5 ml), methanol (10 ml) and acetone (10 ml). After stirring for 18 h, the resin was filtered, and the filtrate was concentrated. The residue was chromatographed on a column of Amberlite CG-50 (NH_4^+) resin (35 ml) with 0—0.15 M aq ammonia with gradient increase in concentration to give **12** (56 mg, 70%): $[\alpha]_D^{23}$ −23.8° (c 1.05, water); ^{1}H NMR (CD_3OD) δ=1.72 (4H, m, H-3′,4′), 2.39 (3H, s, NMe), 3.45 (3H, s, OMe), 7.27 (5H, s, phenyl).

Found: C, 55.79; H, 8.12; N, 12.40%. Calcd for $C_{21}H_{36}N_4O_5 \cdot 2/3H_2CO_3$: C, 55.86; H, 8.08; N, 12.03%.

1,2′,6′-Tris[*N*-(benzyloxycarbonyl)]-7′-phenylfortimicin B (14). To a solution of **12** (51 mg) in methanol (4 ml) was added *N*-(benzyloxycarbonyloxy)succinimide (92 mg) under ice cooling and the mixture was stirred for 1 h at 0 °C, and stirring was continued for 20 h at room temperature. The mixture was extracted with chloroform (60 ml) and the extract was dried. After concentration, the residue was chromatographed on silica gel with chloroform–methanol (50:1) to give **14** as a solid (53 mg, 54%): $[\alpha]_D^{24}$ +3.8° (c 1.98, $CHCl_3$); ^{1}H NMR ($CDCl_3$) δ=1.53 (4H, m, H-3′,4′), 2.30 (3H, bs, NMe), 3.43 (3H, s, OMe), 7.18, 7.28 and 7.31 (20H in total, each s, phenyl×4).

Found: C, 65.46; H, 6.70; N, 6.65%. Calcd for $C_{45}H_{54}N_4O_{11}$: C, 65.37; H, 6.58; N, 6.78%.

1,2′,6′-Tris[*N*-(benzyloxycarbonyl)]-4-[*N*-[*N*-(benzyloxycarbonyl)glycyl]]-7′-phenylfortimicin B (16). To a solution of **14** (44 mg) in dioxane (5 ml) were added *N*-[*N*-(benzyloxycarbonyl)glycyloxy]succinimide (20 mg) and triethylamine (0.01 ml), and the mixture was stirred for 14 h at 50 °C. After addition of 5% aqueous $NaHCO_3$ (10 ml), the mixture was extracted with chloroform (30 ml) and the extract was dried. After concentration, the residue was chromatographed on silica gel with chloroform–methanol

(50:1) to give **16** as a solid (41 mg, 77%): $[\alpha]_D^{24}$ +24.8° (*c* 1.04, $CHCl_3$); ^1H NMR ($CDCl_3$) δ=1.64 (4H, m, H-3′,4′), 2.80 (5H, bs, NMe and H-7′), 3.29 (3H, s, OMe), 7.22, 7.27, 7.30, and 7.34 (25H in total, each s, phenyl×5).

Found: C, 64.71; H, 6.29; N, 6.76%. Calcd for $C_{55}H_{63}N_5O_{14}$: C, 64.89; H, 6.24; N, 6.88%.

7′-Phenylfortimicin A (18). A solution of **16** (28 mg) in methanol (2 ml) was hydrogenated in the presence of 10% palladium on charcoal (30 mg) under hydrogen atmosphere for 3 h. After removal of the catalyst, the filtrate was concentrated. The residue was dissolved in water, and then the solution was passed through a column of AG1-X2 (SO_4^{2-}) resin (2 ml). The eluent was concentrated to give a solid of 7′-phenylfortimicin A (**18**, 14 mg) as the sulfate: $[\alpha]_D^{24}$ +52.5° (*c* 0.48, water); ^1H NMR (D_2O) δ=1.76, 2.10 (4H in total, each m, H-3′,4′), 3.18 (3H, s, NMe), 3.54 (3H, s, OMe), 5.37 (1H, d, *J*=3 Hz, H-1′), 7.48 (5H, m, phenyl).

MS (SIMS) Found: *m/z*, 482. Calcd for $C_{23}H_{40}N_5O_6$: M+1, 482.

Methyl 2,6-Bis(2,4-dinitrophenylamino)-2,3,4,6,7-pentadeoxy-7-phenyl-α-D-*ribo*-heptopyranoside (6). A solution of **4** (392 mg) in 95% aqueous 2-methoxyethanol (18 ml) containing sodium hydroxide (1.93 g) was refluxed for 29 h. After neutralization with 1M hydrochloric acid, the mixture was concentrated and the residue was extracted with cold ethanol. The solution was concentrated to a residue, which was treated with 1-fluoro-2,4-dinitrobenzene (0.73 ml) and triethylamine (2.0 ml) in methanol (10 ml) for 13 h. The product was purified as described for the preparation of **5** to give **6** (410 mg, 60%): mp 102—108 °C; $[\alpha]_D^{20}$ +132° (*c* 1.29, acetone); IR (KBr) 1620, 1590 (aromatic), 1515, 1335 (NO_2) cm^{-1}; ^1H NMR ($CDCl_3$) δ=1.95 (4H, m, H-3,4), 2.72—3.35 (2H, m, H-7), 3.53 (3H, s, OMe), 4.91 (1H, d, *J*=3 Hz, H-1), 6.06, 6.93 (each 1H, d, *J*=10 Hz, H-6 of DNP), 7.20 (5H, s, phenyl), 7.92, 8.20 (each 1H, dd, *J*=3 Hz, 10 Hz, H-5 of DNP), 8.27, 8.89 (each 1H, d, *J*=9 Hz, NH-2,6), 8.97, 9.07 (each 1H, d, *J*=3 Hz, H-3 of DNP).

Found: C, 53.70; H, 4.50; N, 14.39%. Calcd for $C_{26}H_{26}N_6O_{10}$: C, 53.61; H, 4.50; N, 14.43%.

1-*O*-Acetyl-2,6-bis(2,4-dinitrophenylamino)-2,3,4,6,7-pentadeoxy-7-phenyl-D-*ribo*-heptopyranose (8). A solution of **6** (390 mg) in acetic acid (20 ml) containing 2M hydrochloric acid (3.5 ml) was stirred at 80 °C for 6 h. The crude product was acetylated with acetic anhydride (5 ml) in pyridine (10 ml), and the product was purified as described for the preparation of **7** to give **8** (337 mg, 83%): mp 104—108 °C; $[\alpha]_D^{25}$ +52.0° (*c* 1.2, acetone); IR (KBr) 1755 (ester), 1615, 1590 (aromatic), 1515, 1330 (NO_2) cm^{-1}; ^1H NMR ($CDCl_3$) δ=2.19 (3H, s, OAc), 3.05 (2H, m, H-7), 4.12 (3H, m, H-2,5,6), 5.70 (1/5H, d, *J*=9 Hz, H-1), 6.34 (4/5H, d, *J*=3 Hz, H-1), 6.87, 7.08 (each 1H, d, *J*=10 Hz, H-6 of DNP), 7.21 (5H, s, phenyl), 8.06, 8.26 (each 1H, dd, *J*=3 Hz, 10 Hz, H-5 of DNP), 8.54, 8.71 (each 1H, d, *J*=9 Hz, NH-2,6), 8.98, 9.05 (each 1H, d, *J*=3 Hz, H-3 of DNP).

Found: C, 53.28; H, 4.39; N, 13.55%. Calcd for $C_{27}H_{26}N_6O_{11}$: C, 53.12; H, 4.29; N, 13.77%.

2,5-Di-*O*-benzoyl-2′,6′-bis-*N*-(2,4-dinitrophenyl)-1,4-bis-*N*-(methoxycarbonyl)-7′-phenyl-6′-epifortimicin B (11). To a solution of **10** (330 mg) and **9** (290 mg) in freshly distilled 1,2-dichloroethane (8 ml) in the presence of powdered molecular sieve 4A (300 mg) was added trimethylsilyl trifluoromethanesulfonate (0.11 ml) and the mixture was stirred for 2 h. The product was purified as described for the preparation of **10** to give **11** (206 mg, 35%). Recrystallization from acetone-2-propanol gave an analytical sample: mp 144—149 °C; $[\alpha]_D^{25}$ +60.5° (*c* 1.03, acetone); ^1H NMR ($CDCl_3$) δ=2.72 (1H, dd, *J*=10 Hz, 14 Hz, H-7′a), 2.88 (3H, s, NMe), 3.06 (1H, d, *J*=4 Hz, 14 Hz, H-7′b), 3.47 (3H, s, OMe), 3.50, 3.55 (each 3H, s, Cbm), 5.18 (1H, d, *J*=10 Hz, NH-1), 5.27 (1H, d, *J*=3 Hz, H-1′), 5.47 (1H, t, *J*=5 Hz, H-5), 5.73 (1H, bs, H-2), 6.66, 6.80 (each 1H, *J*=9 Hz, H-6 of DNP), 7.16 (5H, m, pheny), 7.38—7.66 (6H, m, benzoyl), 7.88 (3H, m, H-5 of DNP×2 and benzoyl), 8.06, 8.20 (3H in total, each d, *J*=9 Hz, benzoyl), 8.66, 8.83 (each 1H, d, *J*=9 Hz, NH-2′,6′), 8.98 (1H, d, *J*=3 Hz, H-3 of DNP), 9.06 (1H, bs, H-3 of DNP).

Found: C, 56.23; H, 4.84; N, 10.07%. Calcd for $C_{51}H_{53}N_8O_{19}$: C, 56.62; H, 4.94; N, 10.36%.

7′-Phenyl-6′-epifortimicin B (13). A stirred solution of **11** (172 mg) in dioxane (10 ml) and water (3 ml) in the presence of barium hydroxide octahydrate (3.0 g) was refluxed for 21 h. The solid was filtered and carbon dioxide was introduced to the filtrate, and then an insoluble material was filtered. After concentration, the residue was treated with Amberlite IRA-400 (OH^-) resin (10 ml) in a mixture of water (5 ml), methanol (10 ml), and acetone (10 ml) for 43 h. The product was purified as described for the preparation of **12** to give **13** (47 mg, 70%): $[\alpha]_D^{26}$ +42.8° (*c* 0.57, H_2O); ^1H NMR (CD_3OD) δ=1.69 (4H, m, H-3′,4′), 2.42 (3H, s, NMe), 3.45 (3H, s, OMe), 4.98 (1H, d, *J*=3 Hz, H-1′), 7.32 (5H, s, phenyl).

Found: C, 57.12; H, 8.33; N, 12.66%. Calcd for $C_{21}H_{36}N_4O_5 \cdot 1/3H_2CO_3$: C, 57.56; H, 8.30; N, 12.58%.

1,2′,6′-Tris[*N*-(benzyloxycarbonyl)]-7′-phenyl-6′-epifortimicin B (15). To a solution of **13** (37 mg) in methanol (3 ml) was added *N*-(benzyloxycarbonyloxy)succinimide (65 mg) under ice cooling and the mixture was stirred for 1 h at 0 °C, and stirring was continued for 6 h at room temperature. The product was purified as described for the preparation of **14** to give **15** as a solid (39 mg, 56%): $[\alpha]_D^{26}$ +32.3° (*c* 0.36, $CHCl_3$); ^1H NMR ($CDCl_3$) δ=1.58 (4H, m, H-3′,4′), 2.34 (3H, bs, NMe), 3.42 (3H, s, OMe), 7.18, 7.28, and 7.33 (20H in total, each s, phenyl×4).

Found: C, 64.94; H, 6.56; N, 6.29%. Calcd for $C_{45}H_{54}N_4O_{11} \cdot 1/2H_2O$: C, 64.66; H, 6.63; N, 6.70%.

1,2′,6′-Tris[*N*-(benzyloxycarbonyl)]-4-[*N*-[*N*-(benzyloxycarbonyl)glycyl]]-7′-phenyl-6′-epifortimicin B (17). To a solution of **15** (29 mg) in dioxane (3 ml) were added *N*-[*N*-(benzyloxycarbonyl)glycyloxy]succinimide (15 mg) and triethylamine (0.01 ml), and the mixture was stirred for 21 h at 50 °C. The product was purified as described for the preparation of **16** to give **17** as a solid (29 mg, 79%): $[\alpha]_D^{26}$ +60.0° (*c* 0.3, $CHCl_3$); ^1H NMR ($CDCl_3$) δ=1.65 (4H, m, H-3′,4′), 2.70 (3H, bs, NMe), 3.30 (3H, bs, OMe), 7.21, 7.29, 7.35 (25H in total, each s, phenyl×5).

Found: C, 64.49; H, 6.29; N, 6.72%. Calcd for $C_{55}H_{63}N_5O_{14}$: C, 64.89; H, 6.24; N, 6.88%.

7′-Phenyl-6′-epifortimicin A (19). A solution of **17** (26 mg) in methanol (2 ml) was hydrogenated in the presence of 10% palladium on charcoal (30 mg) under hydrogen atmosphere for 3 h. The product was purified as described for the preparation of **18** to give a solid of 7′-phenyl-6′-epifortimicin A (**19**, 11 mg) as the sulfate: $[\alpha]_D^{26}$ +104° (*c* 0.55, water); ^1H NMR (D_2O) δ=1.70, 1.92 (each 2H, m, H-3′,4′), 3.12 (3H, s, NMe), 3.50 (3H, s, OMe), 7.44 (5H, m, phenyl).

MS (SIMS) Found: *m/z*, 482. Calcd for $C_{23}H_{40}N_5O_6$: M+1, 482.

The authors wish to express their thanks to Dr. Hiroshi Sano of Kyowa Hakko Co. for the antibacterial assay. We also would like to thank Mr. Osamu Sakanaka of Meiji Seika Co. for the measurement of mass, ^{13}C and ^{1}H NMR (200 MHz) spectra, and Mr. Akio Takahashi for elemental analyses.

References

1) K. Kanai, J. Nishigaki, S. Ogawa, and T. Suami, *Bull. Chem. Soc. Jpn.*, **60**, 261 (1987).

2) K. Kanai, I. Sakamoto, Y. Miyamoto, S. Ogawa, and T. Suami, *Bull. Chem. Soc. Jpn.*, **60**, 255 (1987).

3) In a manner as described in the preceding paper,[1] the structure of **4** could be assigned on the basis of both ^{13}C NMR (the upfield shift of C-7 of **4** compared to that of **3** due to antiperiplanar arrangement of C-7/C-6/C-5/O-5) and the ^{1}H NMR ($J_{5,6}$=6 Hz) data.

4) Judging from the ^{1}H NMR data, the conformation of **9** is assumed to adopt the skew-boat form[1] and that of the fortamine moiety of **10** or **11** the chair form. However, the conformations of the fortamine moieties of **12**—**19** would not be deduced by analogy with these results.

5) J. Tadanier, R. Hallas, J. R. Martin, and R. S. Stanaszek, *Tetrahedron*, **37**, 1309 (1981).

6) The general procedures used in the present work have been described in the preceding paper.[1]

Correlation of Oxidation and Reduction Potentials of Reactants with Product Distribution in the Reactions of Various Organomagnesium Reagents with Aromatic Carbonyl and Nitro Compounds

Masao Ōkubo,* Toshiki Tsutsumi, and Kōji Matsuo
Department of Chemistry, Faculty of Science and Engineering, Saga University, Honjō-machi, Saga 840
(Received October 2, 1986)

In the electron transfer initiated fifteen reactions of five organomagnesium reagents, a semiquantitative relationship between the product distribution and the electron-donating and -accepting abilities (EDA and EAA) of reactants was obtained. The EDA was estimated by cyclic voltammetry of oxidation peak potentials of reagents and/or by the product distribution in their reactions, the decreasing order of EDA being: ArMgBr > ArSMgBr > ArNHMgBr > ArN(MgBr)$_2$ > ArOMgBr. The EAA of six quinones, eight nitroarenes, eleven aromatic ketones and an imine, and five azoxyarenes were similarly estimated by their reduction potentials (redox) in THF. The values of differences between the oxidation peak and reduction potentials were taken as an estimate of the relative efficiency of electron transfer, and were correlated to the distribution of normal (addition, condensation, replacement, and azoxy-deoxygenation) and abnormal (radical) products. Some exceptional cases were explained by modifying EDA and/or EAA based on the effect of coordination of substrate's oxygen to reagent's Mg atom.

Carbon-carbon bond formation with the use of Grignard addition to carbonyl compounds has been thoroughly investigated. In our laboratory, the methods for the formation of nitrogen-carbon and nitrogen-nitrogen double bonds based on the condensation of aryliminodimagnesium reagents (ArN(MgBr)$_2$, aryl-IDMg) with aromatic carbonyl[1] and nitro[2] compounds have been developed. A qualitative classification of reactions of the two magnesium reagents on the basis of the distribution of normal and abnormal products in terms of the combination of electron-donating and -accepting abilities(EDA and EAA) of reactants was previously proposed.[3] The lower EDA of IDMg than that of ArMgBr suggested from the product distribution[3] was established by comparing their polarographic oxidation peak potentials;[4] the reactions of these reagents with benzophenones were mechanistically distinguished.[5] The product distribution in C-C, C-S, and C-N bond formations with the use of the replacement of bromo and methoxyl groups on the β-position of α,β-enone and α,β-eneimine by ArMgBr(***C***), ArSMgBr(***S***), ArNHMgBr(***NH***), ArN(MgBr)$_2$(***N***), and ArOMgBr(***O***) was correlated to the relative EDA: ***C>S>NH>N>O***.[6] The product distribution in the deoxygenation of azoxyarenes by IDMg was also explained on the basis of relative EAA's estimated by reduction potentials.[7]

These results suggest the general applicability of the EDA-EAA concept independently of reaction manners; a quantitative basis is needed. In this study, the EAA's of aromatic nitro and carbonyl compounds were estimated from their reduction potentials(redox) measured by cyclic voltammetry in THF used as reaction solvent. The values of differences between the oxidation peak and reduction potentials were correlated to the previously given classification,[3] and the EDA-EAA concept was established semiquantitatively. The results will be described in the following.

Results and Discussion

Reduction and Oxidation Potentials of Substrates and Reagents in Tetrahydrofuran. Cyclic voltammetry by polarography was carried out in THF using n-Bu$_4$NClO$_4$ as the supporting electrolyte. The positive and negative limits of the potential window of this system are +1.5 and −2.1V, respectively. The observed reduction potentials (redox) of substrates were normalized by use of bisbiphenylchromiun(I) tetraphenylborate (BCTB) as internal reference,[8] and are summarized in the following. The negative large values indicate weak EAA.

I	Quinones	
1)	2,6-Cl$_2$-1,4-benzoquinone	−0.443V
	2-Br-4-*t*-Bu-1,4-benzoquinone	−0.568V
	2-Me-1,4-benzoquinone	−0.787V
2)	2-Me-1,4-naphthoquinone	−0.935V
	2-MeO-1,4-naphthoquinone	−0.957V
3)	9,10-Anthraquinone	−1.074V
II	Nitroarenes	
1)	4-MeO-nitrobenzene	−1.608V
	4-Me-nitrobenzene	−1.418V
	4-Cl-nitrobenzene	−1.254V
2)	4-Nitrobenzothiazole	−1.314V
	5-Nitrobenzothiazole	−1.299V
	6-Nitrobenzothiazole	−1.220V
	7-Nitrobenzothiazole	−1.142V
3)	Nitroferrocene	−1.693V
III	Carbonyl Compounds and an Imine	
1)	Benzophenone	−1.989V
	Xanthone	Unobservable
	1-Br-9-fluorenone	−1.337V
	N-(1-Br-9-fluorenylidene)-*p*-methylaniline	−1.604V
2)	*p*-R^{1}C$_6$H$_4$CH=CHCOC$_6$H$_4$R^2-*p*	
	R^1 R^2	
	H H	−1.586V
	Cl MeO	−1.590V
	MeO Cl	−1.606V
	CN Me$_2$N	−1.491V

	Me_2N	CN	−1.527V
3)	*p*-MeO, *p*-Me, and *p*-Cl-benzoylferrocenes		Unobservable
4)	*p,p'*-Me_2-benzil		−1.386V

IV Azoxyarenes(Ar^1-N(O)=N-Ar^2)

	Ar^1	Ar^2	
1)	4-MeC_6H_4	4-$MeOC_6H_4$	−1.786V
	C_6H_5	C_6H_5	−1.596V
	C_6H_5	4-ClC_6H_4	−1.423V
2)	4-ClC_4H_4	2-(4-Me)pyridyl	−1.312V
3)	Ferrocenyl	4-ClC_4H_4	−1.640V

In each group of substrates, the electron-repelling substituents give larger negative potentials[9] indicative of a weaker EAA. Taking the effect of a π-electron rich ferrocenyl group into account, the larger negative potentials (weaker EAA's) of nitro- and benzoylferrocenes than those of nitrobenzene and benzophenone, respectively, are reasonable. The potentials of the latter were unobservable since they are located out of the potential window. Also, the potential of xanthone is located out of the window due to the effect of electron-repelling resonance effect of ethereal oxygen atom.

The oxidation peak potentials, including those reported previously,[4] observed in the same solvent system were normalized by the use of ferrocene as an internal reference, and are summarized in the following. The electrode process was irreversible, and no reduction peak was observed. The positive large values are indicative of weak EDA.

C	ArMgBr[4]		
	Ar= 4-$MeOC_6H_4$	4-MeC_6H_4	4-ClC_6H_4
	0.749V	0.819V	0.897V
S	ArSMgBr	Unobservable	
NH	ArNHMgBr[4]		
	Ar= 4-MeC_6H_4	0.883—0.901V	
N	$ArN(MgBr)_2$		

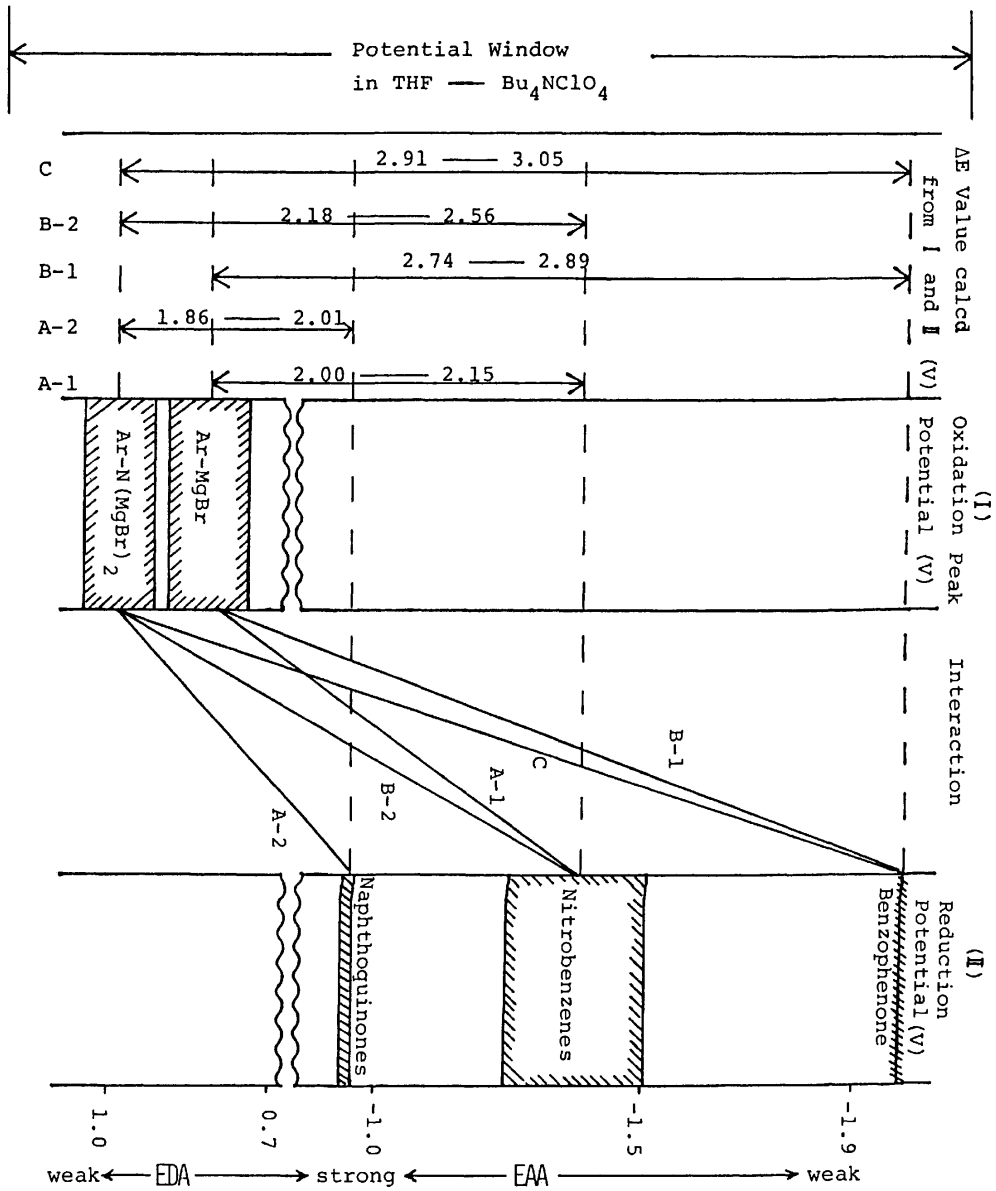

Fig. 1. Correlation of oxidation peak and reduction potentials with classes of reactions of ArMgBr and $ArN(MgBr)_2$.

1)[4]	Ar= 4-$MeOC_6H_4$	4-MeC_6H_4	4-ClC_6H_4
	0.912V	0.941V	1.056V
2)[7]	Ar= 2-(4-Me)pyridyl	1.295V	
NN	Ph(Me)N-N($MgBr)_2$	Undetermined	
O	ArOMgBr	Unobservable	

The lower oxidation peak potential of ***C*** than that of ***N*** was reported previously.[4] In both cases, the electron-repelling substituents gave smaller positive potentials[9] indicating stronger EDA. The large positive potential of 2-pyridyl-IDMg is responsible for its low reactivity observed in condensation with diaryl ketones.[1] The unsuccessful observation of the oxidation peak potential of aryloxyl reagent(***O***) derived from phenol is due to its much larger potential located out of the potential window. The reason for the unsuccessful observation of the oxidation peak potential of ***S*** is equivocal. Probably, the long and weak S-Mg bond will be responsible for the electron transfer followed by an extraordinarily quick dimerization. This is shown not only by the previous result involving a replacement reaction[6] but also by many examples concerning the one-electron oxidation of sulfide anions.[10] The oxidation peak potential of ***S*** is suggested to be located between those of ***C*** and ***NH***,[6] and to have an approximate value of 0.86V. The oxidation peak potential of the IDMg-type reagent ***NN***, which was derived from 1-methyl-1-phenylhydrazine,[1] shifts from ca. 1.0 to 1.9V during the course of repeated measurements: The reason is equivocal.

Correlation of Relative Value of Difference between Oxidation Peak and Reduction Potentials with Product Distribution in Addition, Condensation, Replacement, and Azoxy-Deoxygenation. The relative efficiency of electron transfer in individual reactions depends on the combination of EDA and EAA of reactants. It is thus reasonable that the relative values of differences (ΔE) between oxidation peak and reduction potentials are correlated to the distribution of normal and abnormal (radical) products. Previously, five reactions of ***C*** and ***N*** with some carbonyl and nitro compounds were classified into Classes A, B, and C on the basis of the product distribution.[3] As shown in Fig. 1, the three classes proved to be correlated to the relative ΔE values.

In Table 1, fifteen reactions of ***C***, ***S***, ***NH***, and ***N***, including not only addition and condensation but also replacement and azoxy-deoxygenation, are summarized. The three classes given above are designated. The ΔE values listed in the Table are approximate and were calculated using the oxidation peak potentials of *p*-Me-substituted reagents and mean values of reduction potentials of nitrobenzenes (A-1 and B-2), naphthoquinones (A-2), azoxybenzenes (B-6), and nitrobenzothiazoles (B-9) cited above. The applied reaction conditions are usual and are similar to each other, as reported previously.[1-7,11,13-15]

In Class A reactions, the ΔE values smaller than 2.2 as well as the formation of large amounts of abnormal (radical) products at the expense of normal ones are in accord with the previous characterization, i.e., "hardly controllable reactions due to a vigorous electron transfer."[3] The reduction potential of 1,3-diaryl-3-MeO-2-propen-1-one(β-MeO-α,β-enone) used in A-3 (and also in B-5) reactions[6] could not be determined. The potential was estimated with use of the ΔE values to be −1.3—−1.5 V, comparable to those of nitro-

Table 1. Correlation of Classes of Reactions, Potential Differences, and Distribution of Normal and Abnormal Products

Class of reacn	Reagent	Substrate[a]	Manner of reacn[b]	Approx. ΔE/V[c]	Product Yield/% Normal	Abnormal	Ref.
A-1	***C***	$ArNO_2$	A	2.2	ca. 50	ca. 60	2
A-2	***N***	NQ	C	1.9	10—20	ca. 80	3
A-3	***S***	MeOChl	R	—	5	95	6
A-4	***N***	Azx-Py	D	2.0—2.1	<30	>70	7
B-1	***C***	Ar_2CO	A	2.8	90	5	5
B-2	***N***	$ArNO_2$	C	2.3	85	10—20	2
B-3	***S***	BrFl	R	2.2	80	—	6, 15
B-4	***C***	BrFl-An	R	2.4	65—90	0—25	6, 15
B-5	***N***(***NH***)	MeOChl	R	—	85—92	0	6
B-6	***N***	Azx-Bz	D	2.5	75—90	0—21	7, 11
B-7	***N***	AQ	C	2.0[d]	>70	0	3
B-8	***N***	NBT	C	2.0—2.2	50—60	15—28[d]	13
B-9	***NN***	Xnt	C	—	90	5	3
C-1	***N***	Ar_2CO	C	2.9	60—90	10[d]	1, 5
C-2	***N***	Bzl	C	2.4	50—60	0[d]	3, 14

a) Abbreviations. NQ=1,4-naphthoquinones, MeOChl=β-MeO-chalcone (α-benzylideneacetophenone), Azx-Py=Azoxypyridine, BrFl=1-Br-9-fluorenone, BrFl-An=*N*-(1-Br-9-fluorenylidene)aniline, Azx-Bz=azoxybenzenes, AQ=9,10-anthraquinone, NBT=nitrobenzothiazoles, Xnt=xanthone, Bzl=benzil. b) Abbreviations. A=addition, C=condensation, R=replacement, D=deoxygenation. c) Calculation of approximate ΔE values is given in the text. d) The seemingly exceptional results are discussed in the text.

benzenes. The yields of normal products could be improved using lower temperatures (−20—−40 °C), which suppress the electron transfer (as confirmed by the present authors in A-3 reaction[6] and also by Bartoli in A-1 reaction[12]).

In Class B reactions, the medium ΔE values (2.2—2.8) are responsible for the yields of normal products higher than 65% and those of abnormal ones lower than 28%. The previously given "electron transfer controlled" character of Class B reactions is based on the fact that in B-1 and B-2 reactions the electron-attracting substituents of substrates and electron-repelling ones of reagents accelerate electron transfer leading to the higher concentration of intermediate radicals[3,5] and, consequently to a better yields of normal products. In kinetic terms, the B-1 reaction proceeds via a rapid but incomplete coordination and rate-determining electron transfer.[5] The B-2 reaction proceeds step by step via condensation and subsequent deoxygenation.[2,11] The comparable reduction potentials of nitro- and azoxybenzenes cited above may be responsible for the dependence of the final distribution of products simply on the relative EAA of substrate. The 65—90% yields of replacement products are obtained in B-3, B-4, and B-5 reactions.[6] The ΔE value in the B-5 reaction is estimated to be 2.3—2.5 (vide supra). The effect of EAA on the deoxygenation of azoxybenzenes (B-6) and an azoxypyridine (A-4) was recently reported.[7,11] In condensation reactions B-7 and B-8,[13] good yields of normal products were obtained in spite of the small ΔE values comparable to those of Class A reactions. The precise results concerning product distribution in a B-8 reaction will be reported elsewhere, but the reduction of EDA of *p*-MeC_6H_4-IDMg due to the coordination of thiazolyl group to Mg atom of reagent was confirmed.[13] In the B-9 reaction of ***NN*** with xanthone, the corresponding hydrazone was obtained in good yield.[1] The high yield and the observed manner of fluctuation of oxidation peak potential (vide supra) suggest that the actual potential of ***NN*** is lower than 0.8V (which is responsible for an efficient electron transfer to xanthone having weak EAA).

Even in the C-1 reaction having a ΔE value larger than 2.9 (which seems to be unfavorable for electron transfer), the condensation product was obtained in good yield.[5] In this reaction, the substituent effect of substrate appears in the manner reverse to that of the B-1 reaction (vide supra). The electron-repelling substituents favor the σ-complex formation by the rate-determining coordination of carbonyl oxygen to Mg atom of reagent, the reaction being thus characterized as "coordination controlled" one.[3] The weak EDA and EAA of reactants of C-1 reflect their low HOMO and high LUMO levels, respectively, but the σ-complex formation assists the substrate in lowering its HOMO and LUMO levels and in accepting electrons from the mild reagent.[3] The good yield of the normal product in C-1 is, thus, reasonable. The mechanisms of initial steps of C-1 distinct from those of B-1 were proposed for elucidating the formation of dimeric and monomeric types of abnormal products, respectively.[5]

Table 2. Relative Efficiency of Electron Transfer from ArOMgBr to Quinones Depending on EDA and EAA

ArOMgBr / Quinone	*p*-RC_6H_4OMgBr (R): MeO	Me	Cl
	strong ← (EDA) → weak		
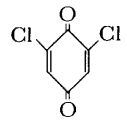	○○○○[a] 0 °C immediate	○○○ 0 °C immediate	○○ 55 °C 10 min
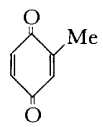	○○○ 0 °C 5 min	○○ 55 °C 20 min	○ 55 °C 40 min
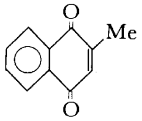	△[b] complex formation	×	×
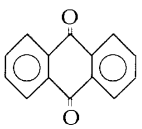	×	×	×

(EAA) ↑ strong, ↓ weak

a) Relative efficiency of electron transfer is indicated by number of circles, and no color change by X.
b) In this case, the mixture turned yellow-brown but no radical species was detected by ESR. The coloration is ascribed to σ-complex formation.[3,5]

Irrespective of the small ΔE value comparable to that of B-2, the reaction of *p*-substituted benzils with IDMg reagent is characterized as C-type because the reaction is accelerated by the *p*-MeO-substituent of substrate.[3] The anomaly in C-2 reaction, however, is understood by a measurement of reduction potential of benzil in the presence of an equimolar amount of anhydrous $MgBr_2$. The potential becomes large at least in ca. 0.2V. The reduction of EAA is ascribable to chelate formation by the coordination of α-dicarbonyl oxygen atoms to Mg atom of the reagent. The actual ΔE value in the C-2 reaction may be larger than 2.5. The precise results of the study of substituent effect will be reported elsewhere.[14]

Undoubtedly, the Grignard addition to carbonyl compounds owes its great success about eighty years ago to the lucky selection of Class B combination of reactants.

Electron Transfer from Aryloxymagnesium Reagents to Quinones. Among the reagents examined, aryloxymagnesium (***O***) is suggested to be the weakest electron donor because it is unable to react with monofunctional carbonyl compounds.[6] Its oxidation peak potential was undetermined in the present measurements (vide supra), but it donates electrons to benzoquinones having strong EAA. When *p*-$MeOC_6H_4O$-MgBr was allowed to react with a sixth molar amount of 2-Br-5-*t*-Bu-1,4-benzoquinone, ca. 80% of the quinone was recovered unchanged but a small amount of quinhydrone was obtained. No replacement product was detected. Also, in the reaction with 2-MeO-5-*t*-Bu-1,4-benzoquinone, the results were similar. The precise results on product distribution will be reported elsewhere.

As shown in Table 2, the relative efficiency of electron transfer in cases of benzoquinones and no electron transfer in cases of naphtho- and anthraquinones are in line with the expectation based on the EDA-EAA concept. By mixing the THF solutions of reactants in 1 : 1 molar ratio, the mixture turned deep blue-green due to the formation of semiquinone and aryloxyl radicals. The time given in the Table indicates the period of time needed for obtaining the highest concentration of radicals under the given temperatures. Taking into account the correlation of potential difference shown in Table 1, the results of Table 2 suggest that *p*-RC_6H_4OMgBr has oxidation peak potential higher than 1.6V.

General Discussion. The characteristics of the three typical classes of reactions under usual conditions are summarized in the following.

Class A: High yields of radical products are formed as the result of a vigorous electron transfer. The small ΔE values indicate the strong EDA and/or EAA.

Class B: Good yields of normal products are formed as the result of efficient electron transfer arising from medium ΔE values. The favorable electronic effect of substituents of reactants appears in the manner raising the oxidation potential and lowering the reduction potential, i.e., strengthening both EDA and EAA.

Class C: As far as the initial formation of the σ-complex is not sterically retarded, good yields of products are formed in spite of the large ΔE values. The σ-complex formation is favored by the electron-repelling substituent of the substrates, and assists them in strengthening their EAA, resulting in a mild electron transfer.

The correlation of product distribution with the ΔE value as the first approximation must originate from the remarkable feature of reactions of magnesium reagents. As established in B-1 and C-1 reactions,[3,5] the rate-determining step is located in one of the common initial processes, i.e., the σ-complex formation and the subsequent electron transfer. Due to the strong affinity of magnesium with oxygen, the modification of EDA and/or EAA based on the second important effect of coordination is reasonable.

The EDA-EAA concept is extended further to additional cases, in which no chemical change takes place and no radical species is detected even though the mixture turns yellow-brown indicating the formation of σ-complex: The combination of *N*-(1-Br-9-fluorenylidene)aniline with ***S***,[6] and those of β-MeO-α,β-enone[6] and anthraquinone with ***O*** (Table 2). The much larger ΔE value is responsible for no transfer of electrons, even after the α-complex formation. Similarly, no color change after mixing the components, indicating no interaction, is ascribed to the very large ΔE value as exemplified by the combination of anthraquinone with ***O*** (Table 2) and/or to the steric inhibition of σ-complex formation.[5]

So far, the reactants were confined to aromatic types; the rather simple types of products obtained assisted us in revealing the governing factor. The combination of magnesium reagents with α-benzylideneacetophenones,[16] β-nitrostyrenes,[17] nitro- and benzoylferrocenes,[18] were also studied. These substrates have carbonyl and nitro groups that are not bound directly to the benzene ring; the types of products as well as the effect of substituents are explainable partly on the basis of the EDA-EAA concept. However, some additional factors have to be taken into account.[16,18] The reactions are, thus, excluded from the present classification and will be reported elsewhere.

Electron transfers in organic reactions, including that of a Grignard reagent, have been studied on the general basis of the Marcus theory.[19] Further quantitative studies are needed. However, the present classification will contribute to studies on the mechanisms and molecular orbital picture of electron transfers (vide supra) in the field of organomagnesium chemistry.[20,21] The simple relationship will also be helpful for the selection of reaction conditions and for the expectation of product yields in the synthetic applica-

tions of magnesium reagents.

Experimental

Materials, Reaction Procedures, and Measurements. Almost all the quinones, nitrobenzenes, and benzophenone were commercially available. Nitrobenzothiazoles, nitroferrocene, 1-bromo-9-fluorenone, α-benzylideneacetophenones, *p,p'*-dimethylbenzil, and azoxyarenes were prepared according to the manner given in the references. Some references will be given in the forthcomig papers. The preparation of magnesium reagents in THF was reported previously.

The reaction of *p*-$MeOC_4H_4OMgBr$ with 2-bromo-4-*t*-butylbenzoquinone was carried out by heating the mixture at 55 °C for 3 h. The products were separated by column chromatography on silica gel.

Cyclic voltammetry of oxidation peak potentials[4] and reduction potentials[7] were reported previously.

The gift of samples of BCTB by Professor Gerhard Gritzner, University of Linz, and Professor Kohsuke Izutsu, Shinshu University, is gratefully acknowledged. The authors also wish to thank Dr. Akio Ichimura and Professor Toyokichi Kitagawa, Osaka City University, for helpful advice on cyclic voltammetry. The authors are grateful also to Ministry of Education, Science, and Culture for a financial support by a Grant-in-Aid for Scientific Research (No. 60470026).

This paper is dedicated to the late Professor Ryozo Goto, Kyoto University.

References

1) M. Ōkubo and S. Ueda, *Bull. Chem. Soc. Jpn.*, **53**, 281 (1980); M. Ōkubo, S. Hayashi, M. Matsunaga, and Y. Uematsu, *ibid.*, **54**, 2337 (1981).

2) M. Ōkubo, T. Takahashi, and K. Koga, *Bull. Chem. Soc. Jpn.*, **56**, 199 (1983).

3) M. Ōkubo, M. Yoshida, K. Horinouchi, H. Nishida, and Y. Fukuyama, *Bull. Chem. Soc. Jpn.*, **56**, 1196 (1983).

4) M. Ōkubo, T. Tsutsumi, A. Ichimura, and T. Kitagawa, *Bull. Chem. Soc. Jpn.*, **57**, 2679 (1984).

5) M. Okubo, *Bull. Chem. Soc. Jpn.*, **58**, 3108 (1985).

6) M. Ōkubo, Y. Nakagawa, M. Yoshida, and H. Yanase, *Bull. Chem. Soc. Jpn.*, **58**, 2707 (1985).

7) M. Ōkubo, C. Sugimori, M. Tokisada, and T. Tsutsumi, *Bull. Chem. Soc. Jpn.*, **59**, 1644 (1986).

8) G. Gritzner and J. Kuta, *Pure Appl. Chem.*, **56**, 461 (1984).

9) P. Zuman, "Substituent Effects in Organic Polarography," Plenum Press, New York (1967).

10) S. Bank and D. A. Noyd, *J. Am. Chem. Soc.*, **95**, 8203 (1973); N. Kornblum, S. C. Carlson, and R. G. Smith, *ibid.*, **101**, 647 (1979); N. Kornblum, J. Widmer, and S. C. Carlson, *ibid.*, **101**, 658 (1979).

11) M. Ōkubo and K. Koga, *Bull. Chem. Soc. Jpn.*, **56**, 203 (1983).

12) G. Bartoli, M. Bosso, R. D. Pozzo, and F. Ciminale, *J. Org. Chem.*, **45**, 5227 (1982); G. Bartoli, *Acc. Chem. Res.*, **17**, 109 (1984).

13) M. Ōkubo, K. Asao, and H. Hyakutake, submitted to this Bulletin.

14) M. Ōkubo, Y. Fukuyama, and M. Satoh, unpublished results.

15) M. Ōkubo and Y. Uematsu, *Bull. Chem. Soc. Jpn.*, **55**, 1121 (1982).

16) M. Ōkubo, Y. Egami, T. Tsutsumi, and S. Nagase, *Bull. Chem. Soc. Jpn.*, **60**, 1741 (1987).

17) M. Ōkubo and K. Inoue, unpublished results.

18) M. Ōkubo and T. Tsutsumi, submitted to this Bulletin.

19) L. Eberson, *Adv. Phys. Org. Chem.*, **18**, 79—185 (1982); T. Holm., *Acta Chem. Scand., B* **37**, 567 (1983).

20) R. G. Pearson, "Symmetry Rules for Chemical Reactions," John Wiley & Sons Inc., New York (1976).

21) S. Nagase and Y. Uchibori, *Tetrahedron Lett.*, **23**, 2585 (1982).

Total Synthesis of 6-Hydroxy-*epi*-PS 5 and 6-Methoxy-*epi*-PS 5

Azuma WATANABE,* Yasuo FUKAGAWA, Tomoyuki ISHIKURA, and Takeo YOSHIOKA
SANRAKU INC., Central Research Laboratories, 9-1 Johnan 4 Chome, Fujisawa, 251
(Received November 13, 1986)

The stabilizing effect of the 6-methoxyl or 6-hydroxyl substituent on dehydropeptidase I sensitivity of PS 5 was examined by a new total synthesis of 6-methoxy-*epi*-PS 5 and 6-hydroxy-*epi*-PS 5 from dimethyl benzyloxycarbonylaminomalonate. The Wittig reaction of α-(*t*-butoxycarbonyl)propylidenetriphenylphosphorane with a pyrrolidine derivative predominantly afforded a *trans*-α,β unsaturated ester, which was epoxidated, *N*-deprotected and cyclized to give a bicyclic carbapenam with a C-6 hydroxyl group. After the 6-hydroxyl group was methylated, the 2-(acetamido)ethylthio side chain was introduced at C-3 of the carbapenam by benzeneselenenylation of the geminal diester, followed by eliminatlon of the seleninyl group. The resulting carbapenam was converted to 6-methoxy-*epi*-PS 5. Furthermore, 6-hydroxy-*epi*-PS 5 was synthesized by the use of tetrahydropyranyl and trimethylsilyl ethers for protection of the 6-hydroxyl group in a process similar to that for synthesis of 6-methoxy-*epi*-PS 5.

Although the carbapenem antibiotic PS 5[1] and related compounds[2] have very broad spectra of potent antimicrobial activity and high resistance to β-lactamase, they are unexpectedly sensitive to renal dehydropeptidase I (DHP-I), resulting in poor therapeutic effects in vivo. In a continued effort to improve the DHP-I stability of PS 5 to a clinically acceptable level, a variety of C-3 side chains have been introduced into PS 5,[3] but no PS 5 derivative with satisfactory DHP-I stability has yet been prepared.

Considered from the observations that the stability of cephalosporins to β-lactamase is improved by introduction of the 7α-methoxyl group[4] and that the stereochemistry of C-6 of carbapenems is not critically important for antimicrobial activity,[5] it is interesting to examine whether the introduction of the 6α-methoxyl or 6α-hydroxyl substituent serves to stabilize carbapenem against DHP-I or not. For this purpose, a new route of total synthesis of carbapenem has been developed using dimethyl benzyloxycarbonylaminomalonate as starting material. This paper describes the stereoselective total synthesis of 6-methoxy-*epi*-PS 5 (**1**) and 6-hydroxy-*epi*-PS 5 (**2**) together with their enzymological and antimicrobial evaluation.

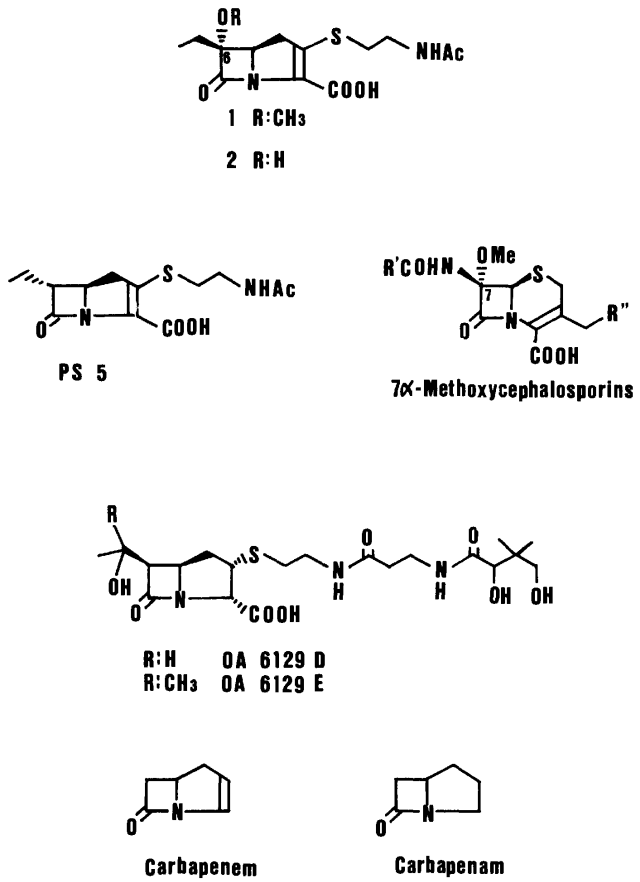

Fig. 1.

Results and Discussion

Carbapenam compounds such as OA 6129D and E[6] are physicochemically very stable and easily convertible to carbapenems. In hitherto known routes of synthesis of carbapenems, the β-lactam ring is formed before the 5-membered pyrrolidine ring is closed, whereas the reverse route has least been reported.[7] Thus it is interesting to develop a new route to synthesize 6-methoxy-*epi*-PS 5 (**1**). This comprises the initial closure of the pyrrolidine ring, the susequent formation of the β-lactam ring and the final conversion of carbapenam to carbapenem, starting from dimethyl (*N*-protected amino)malonate **H** according to the retrosynthetic strategy as shown below (Fig. 2).

The key points to the successful synthesis seem to be in the introduction of a leaving group X at C-2 (derivative **B**), followed by conversion to carbapenem **A**, and in the stereoselective preparation of a *trans*-α,β-unsaturated ester by the Wittig reaction of a pyrrolidine derivative **G** with a stable ylid **F**. If this route of synthesis is operative as described above, an optically active compound **B** will be obtained from D- or L-glutamic acid.[8]

A key intermediate carbapenam **9** for 6-methoxy-*epi*-PS 5 (**1**) was prepared as shown above. The Michael addition of dimethyl benzyloxycarbonylaminomalonate (**3**) (readily preparable from dimethyl malonate)

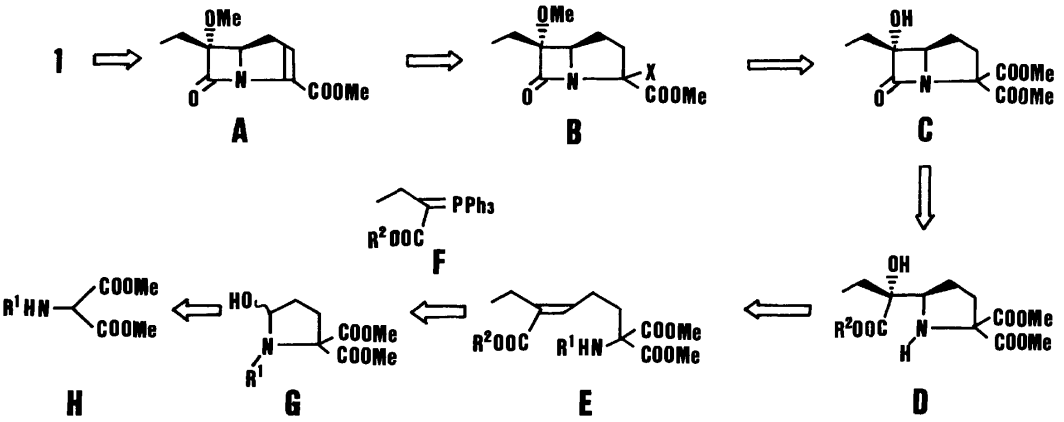

Fig. 2.

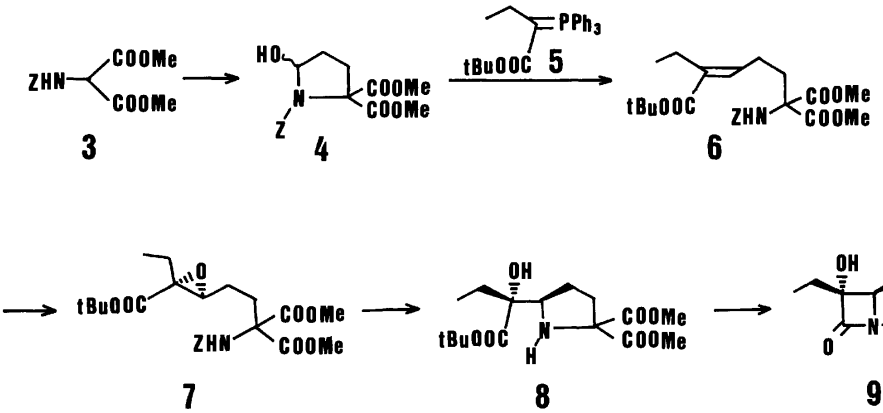

Fig. 3.

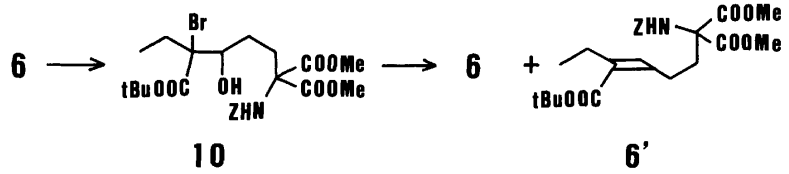

Fig. 4.

with acrylaldehyde in the presence of sodium methoxide catalyst afforded 5-hydroxypyrrolidine **4** in 85% yield. The Wittig reaction of **4** with α-(*t*-butoxycarbonyl)propylidenetriphenylphosphorane (**5**) predominantly provided a *trans*-α,β-unsaturated ester **6** in good yield under reflux in benzene for 16 h. The geometrical isomerism of **6** was examined by transformation to the cis isomer **6'** according to the following scheme (Fig. 4):

The treatment of the unsaturated ester **6** with *N*-bromoacetamide in aqueous acetone gave bromohydrins **10**, which were subjected to reduction with tributyltin hydride, methylsulfonylation with methanesulfonyl chloride and triethylamine, and β-elimination with 1,6-diazabicyclo[5.4.0]undec-7-ene, affording geometrical isomers **6** and **6'**. The cis isomer **6'** was separated by preparative silica-gel thin-layer chromatography (TLC). The NMR spectrometric comparison of these isomers by the chemical shift of the vinyl proton clearly showed that the isomerism of the predominant compound **6** was trans (δ=6.44; δ=5.64 for **6'**).[9] The oxidation of **6** with *m*-chloroperbenzoic acid in dichloromethane at 40 °C for 4 h afforded an epoxide **7** (90% yield). The cleavage of the *N*-benzyloxycarbonyl group from **7** by hydrogenation gave a pyrrolidine derivative **8** in 89% yield. After the *t*-butyl ester group was hydrolyzed in 4 mol dm^{-3} HCl in dioxane, the resulting β-amino acid was cyclized at 60 °C for 4 h with dicyclohexylcarbodiimide in acetonitrile to provide the bicyclic β-lactam **9** in 70% yield.

The methylation of the hydroxyl group of **9** with methyl iodide in the presence of silver oxide in *N*,*N*-dimethylformamide resulted in a methoxycarbapenam **11** (90% yield). The carbapenam **11** was transformed to a carbapenem **14** by selenoxide elimination which was operative under milder conditions than sulfoxide elimination. Benzeneselenenyl derivatives **13a** and **13b** are preparable from the diester **11** by two routes.

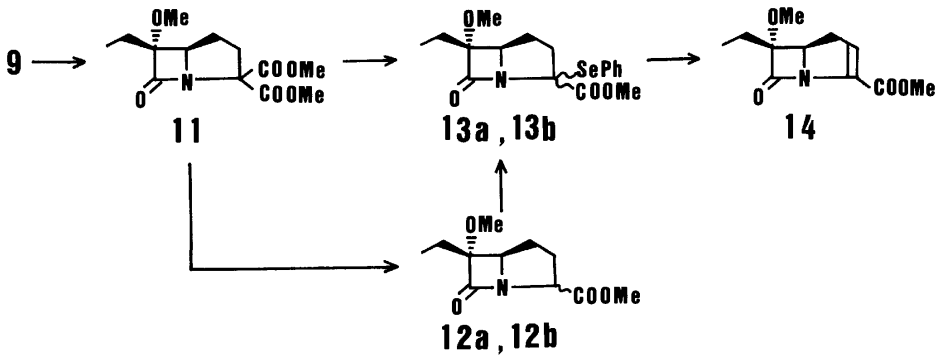

Fig. 5.

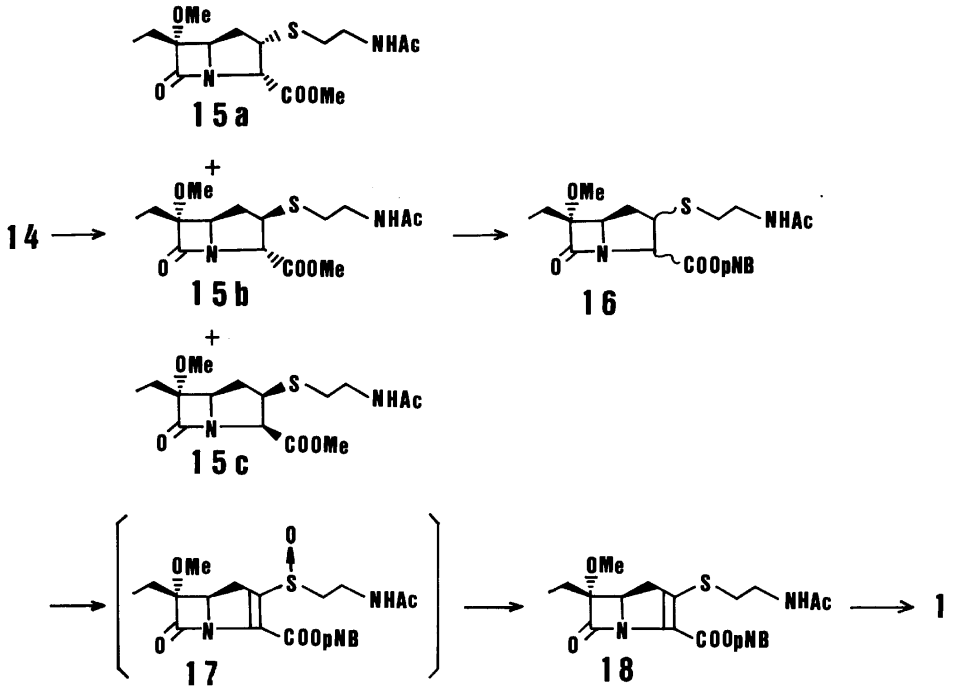

Fig. 6

First, the diester **11** was converted to the benzeneselenenyl compounds **13a** and **13b** via mono(methoxycarbonyl) derivatives **12a** and **12b**. More particularly, the diester **11** was hydrolyzed in 1 mol dm^{-3} NaOH and then heated at 100 °C in pyridine to give a diastereoisomeric mixture of the mono(methoxycarbonyl) derivatives **12a** and **12b** in 52% yield. After treatment with lithium diisopropylamide in tetrahydrofuran, the mixture was allowed to react with benzeneselenenyl chloride, leading to the benzeneselenenyl compounds **13a** and **13b** (a mixture of the two diastereoisomers) in a total yield of 61% from **12a** and **12b**.

Then the direct route of benzeneselenenylation was investigated by replacing sulfur by selenium in the procedure of Asaoka et al.[10] which was used to sulfenylate a geminal diester by demethoxycarbonylation. The reaction of 1 mol of the diester **11** with 1 mol of diphenyl diselenide in the presence of 2 mol of NaI in hexamethylphosphoric triamide at 80 °C for 2 h gave a mixture of **13a** and **13b** in 50% yield together with 31% of the unreacted diester **11**. The treatment of the isomeric mixture of the selenides **13a** and **13b** with *m*-chloroperbenzoic acid at −30 °C, followed by triethylamine addition, produced the carbapenem **14** in 78% yield via selenoxide.

The introduction of a 2-(acetamido)ethylthio side chain at C-3 of the carbapenem **14** in the presence of triethylamine in *N*,*N*-dimethylformamide give a diastereoisomeric mixture of **15a**, **15b**, and **15c** in a good yield of 95%. They were separated from each other by silica-gel column chromatography. ^{1}H NMR analysis indicated that the molar ratio of **15a** (δ=4.72, $J_{2,3}$=8.0 Hz), **15b** (δ=4.33, $J_{2,3}$=6.0 Hz), and **15c** (δ=4.19, $J_{2,3}$=8.0 Hz) was 2 : 5 : 3.[11]

The mixture **15a**, **15b**, and **15c** was hydrolyzed in 0.1 mol dm^{-3} NaOH and subjected to ester exchange with *p*-nitrobenzyl bromide to give a carbapenam *p*-nitrobenzyl ester **16** in 72% yield. The ester **16** was converted to a carbapenem **18** via a sulfoxide **17** in 54% yield by the method of Bateson et al.[12] 6-Methoxy-*epi*-PS 5 (**1**)

(sodium salt) was obtained from the *p*-nitrobenzyl ester (**18**) in 70% yield by hydrogenolytic removal of the *p*-nitrobenzyl group, followed by column chromatographic purification on QAE-Sephadex A-25 and Diaion CHP-20P.

Generally speaking, penicillins and cephalosporins are sensitive to β-lactamase and insensitive to DHP-I, whereas carbapenems are sensitive to DHP-I and insensitive to β-lactamase. The introduction of the 7α-methoxyl or 7α-hydroxyl group to cephalosporins improves the resistance to β-lactamase, but accompanies a reduction in antimicrobial activity. Thus it is interesting to compare the 6-methoxyl and 6-hydroxyl substituents of carbapenems to give useful information on the structure-activity relationship of carbapenems in antimicrobial activity, β-lactamase sensitivity, and DHP-I resistance. For this purpose, 6-hydroxy-*epi*-PS 5 (**2**) was prepared using a similar procedure.

Without protecting the 6-hydroxyl group, the alcohol **9** was converted directly to a benzeneselenenyl derivative **19** in a poor yield, which was then converted to a 6-hydroxycarbapenem **20**, also in a poor yield by oxydation, followed by elimination of the benzeneseleninyl group. For improvement of the reaction yields, the 6-hydroxyl group of **9** was protected with a tetrahydropyranyl (THP) group which survived the subsequent treatment.

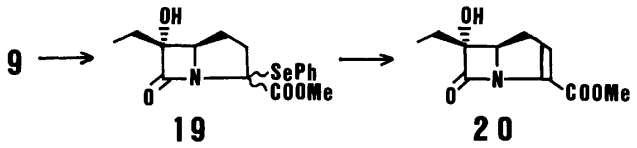

Fig. 7.

The alcohol **9** was treated with 3,4-dihydro-2*H*-pyran in the presence of *p*-toluenesulfonic acid to yield an anomeric *O*-THP derivative mixture **21**, which was led to a carbapenam **25** in four steps in the same manner as described for 6-methoxy-*epi*-PS 5. The carbapenam **25** was convertible to the corresponding carbapenem, but the deprotection of the *O*-THP group without breakdown of the β-lactam ring was unsuccessful. Therefore the *O*-THP group of the carbapenam **25** was removed by treatment with pyridinium *p*-toluenesulfonate (PPTS)[13] in ethanol to provide an alcohol **26**. As no direct conversion to the corresponding carbapenem was successful, the alcohol **26** was reprotected with the trimethylsilyl (TMS) group which was readily deprotectable under mild conditions to give an *O*-TMS carbapenam **27**. The carbapenam **27** was transformed to a carbapenem **28** and the hydrolytic cleavage of the TMS ether **28** in 0.001 mol dm^{-3} HCl-ethanol (1 : 1) at 0 °C for 30 min gave a 6-hydroxycarbapenem **29** in 87% yield. The *p*-nitrobenzyl ester **29** was hydrogenated to yield 6-hydroxy-*epi*-PS 5 (**2**), as described above for 6-methoxy-*epi*-PS 5 (**1**). It is worth noting that the TMS group is useful for protection of hydroxyl groups on the carbapenem system.

Table 1 shows the comparative antimicrobial activities of 6-methoxy-*epi*-PS 5 (**1**), 6-hydroxy-*epi*-PS 5 (**2**), PS 5 and cefazolin. It seems highly probable that the introduction of the methoxyl or hydroxyl group at C-6 of PS 5 results in a significant reduction of the antimicrobial potency, as is reported for 7α-methoxy- and 7α-hydroxycephalosporins.[14] It is interesting to note that the 6-hydroxyl group is more influential than the 6-methoxyl in reduction of the antimicrobial activity.

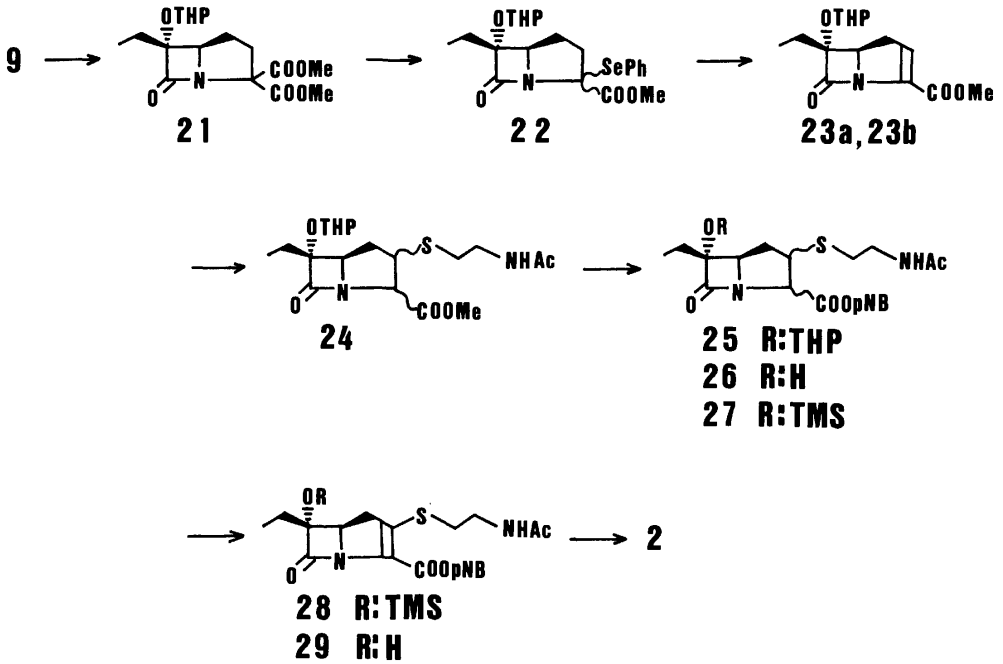

Fig. 8.

Table 1. Comparative Antimicrobial Activities of 6-Methoxy-*epi*-PS 5 (**1**), 6-Hydroxy-*epi*-PS 5 (**2**), PS 5 and Cefazolin (MIC in $\mu g\,ml^{-1}$)

Microorganism	1	2	PS 5	Cefazolin
Bacillus subtilis ATCC 6633	6.25	50	0.10	0.10
Staphylococcus aureus FDA209P	0.78	50	0.024	0.05
Staphylococcus aureus Smith	3.13	25	0.20	0.20
Citrobacter freundii GN346	>50	>50	1.56	>100
Comamonas terrigena IFO12685	0.78	—	0.012	0.10
Enterobacter cloacae 45	>50	>50	3.13	>100
Escherichia coli K-12	25	6.25	1.56	0.78
Proteus vulgaris GN76	>50	>50	12.5	>100
Pseudomonas aeruginosa NCTC10490	>50	>50	25	>100
Salmonella gallinarum ATCC9184	25	25	1.56	1.56
Serratia marcescens IFO3736	>50	>50	6.25	>100
Shigella sonnei EW33	50	>50	3.13	3.13

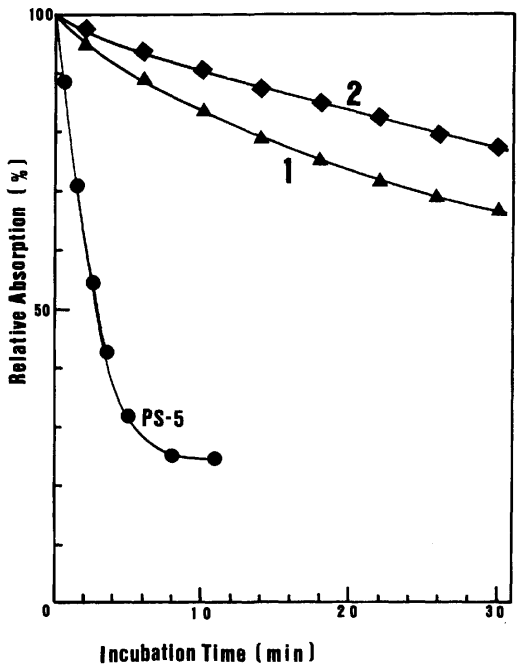

Fig. 9. Comparative DHP-I stabilities.

The comparative DHP-I stabilities of the three carbapenem derivatives are compared in Fig. 9, using the time course curves of hydrolysis by DHP-I on the relative UV absorptions at 300 nm. The DHP-I enzyme used in these assays was a partially purified preparation from hog kidney. The 6-hydroxyl substituent seems more effective than the 6-methoxyl in stabilization of carbapenem against DHP-I.

In conclusion, the introduction of the 6α-methoxyl or 6α-hydroxyl group in carbapenem significantly improves the DHP-I stability as expected, but with drastic reduction in antimicrobial activity.

Experimental

General. All mp's were measured with a YANACO apparatus and are uncorrected. Silica-gel thin-layer chromatography (TLC) and column chromatography were carried out on precoated TLC plates silica gel 60 F-254 (E. Merck) and silica gel 60 (70—230 mesh, E. Merck), respectively. Infrared (IR), ultraviolet (UV), ^{1}H NMR and ^{13}C NMR spectra were recorded with a Hitachi 260-30 infrared spectrophotometer, a Hitachi 200-20 spectrophotometer, a Varian EM-390 (90 MHz) spectrometer and a JEOL FX-100 spectrometer, respectively. Chemical shifts are given in ppm from internal TMS in $CDCl_3$ or TSP [sodium 3-(trimethylsilyl)propionate] in D_2O. Mass spectrometric data were collected on a Hitachi EM-80 spectrometer. Antimicrobial activity and DHP-I stability were measured as previously described.[15]

1-Benzyloxycarbonyl-2,2-bis(methyoxycarbonyl)-5-hydroxypyrrolidine (4). To a solution of 28.1 g (0.10 mol) of dimethyl benzyloxycarbonylaminomalonate **3** in 250 ml of benzene, 0.5 g of sodium methoxide, and 10 ml (0.20 mol) of acrylaldehyde were added and stirred for 1 h at room temperature. The reaction mixture was poured into 100 ml of cold 0.1 mol dm^{-3} HCl and the aqueous layer was separated and extracted twice with 100 ml each of benzene. The organic layer and the benzene washes were combined and rinsed with brine, dried (Na_2SO_4) and concentrated in vacuo to give a liquid. The liquid was chromatographed on a silica-gel column (250 g) using benzene-acetone (7:1) as eluent to provide 28.9 g of **4** as an oil in 85% yield: IR ($CHCl_3$) 1750, 1740, and 1700 cm^{-1}; ^{1}H NMR ($CDCl_3$) δ=1.75—2.25 (2H, m), 2.25—2.85 (2H, m), 3.53 (3H, s), 3.75 (3H, s), 4.02 (1H, s), 5.10 (1H, s), 5.17 (1H, s), 5.67 (1H. br) and 7.30 (5H, s); MS (EI) m/z 319 (M^+-H_2O).

***trans*-2-Benzyloxycarbonylamino-6-(*t*-butoxycarbonyl)-2-methoxycarbonyl-5-octenoic Acid Methyl Ester (6).** A mixture of 1.1 g (3.3 mmol) of 1-benzyloxycarbonyl-2,2-bis-(methoxycarbonyl)-5-hydroxypyrrolidine (**4**) and 1.73 g (4.3 mmol) of α-(*t*-butoxycarbonyl)propylidenetriphenylphosphorane (**5**) in 50 ml of benzene was refluxed for 16 h and concentrated to dryness in vacuo. Purification by silica-gel column (50 g) chromatography with benzene-acetone (10:1) resulted in isolation of 1.20 g of **6** as needles (80% yield) (recrystallized from benzene-hexane): mp 93—94 °C; IR ($CHCl_3$) 1740, 1720, and 1700 cm^{-1}; ^{1}H NMR ($CHCl_3$) δ=0.94 (3H, t, J=7.0 Hz), 1.47 (9H, s). 1.85—2.55 (6H, m), 3.73 (6H, s), 5.08 (2H, s), 6.15 (1H, s), 6.44 (1H, t, J=7.5 Hz), and 7.30 (5H, s).

Found: C, 62.45; H, 7.28; N, 3.01%; M^++1, 464. Calcd for $C_{24}H_{33}NO_8$: C, 62.19; H, 7.18; N, 3.02%; M+1, 464.

6' (isomer of **6**): IR ($CHCl_3$) 1740 and 1715 cm^{-1}; ^1H NMR δ=0.99 (3H, t, J=7.5 Hz), 1.47 (9H, s), 2.18 (2H, q, J=7.5 Hz), 2.2—2.5 (4H, m), 3.77 (6H, s), 5.09 (2H, s), 5.64 (1H, t, J=7.5 Hz), 6.27 (1H, br), and 7.35 (5H, s).

Found: m/z 464.2270. Calcd for $C_{24}H_{34}NO_8$: M+1, 464.2281.

2-Benzyloxycarbonylamino-6-(*t*-butoxycarbonyl)-5,6-epoxy-2-(methoxycarbonyl)octanoic Acid Methyl Ester (7). *m*-Chloroperbenzoic acid (2.80 g, 16.2 mmol) was added to a solution of 3.83 g (8.3 mmol) of *trans*-2-benzyloxycarbonylamino-6-(*t*-butoxycarbonyl)-2-(methoxycarbonyl)-5-octenoic acid methyl ester **6** in 50 ml of dichloromethane, and stirred for 4 h at 40 °C. After quenching with 1.15 ml (8.0 mmol) of triethylamine, the reaction mixture was washed with aqueous saturated $NaHCO_3$ and brine, dried (Na_2SO_4), and concentrated to dryness. The residue was purified by silica-gel column (140 g) chromatography using benzene-ethyl acetate (10 : 1), providing 3.56 g of **7** as needles (recrystallized from benzene-hexane) (90% yield): mp 61—62 °C; IR ($CHCl_3$) 1740 and 1725 cm^{-1}; ^1H NHR $CDCl_3$) δ=1.01 (3H, t, J=7.5 Hz), 1.47 (9H, s), 1.2—2.05 (4H, m), 2.35—2.6 (2H, m), 3.04 (1H, t, J=6.0 Hz), 3.73 (6H, s), 5.08 (2H, s), 6.14 (1H, s) and 7.34 (5H, s).

Found: C, 60.07; H, 6.94; N, 2.94; M^+, 479. Calcd for $C_{24}H_{33}NO_9$: C, 60.11; H, 6.94; N, 2.92; M, 479.

2,2-Bis(methoxycarbonyl)-5-[1-(*t*-butoxycarbonyl)-1-hydroxypropyl]pyrrolidine (8). A suspension of the epoxide **7** (9.24 g, 19.3 mmol) and 10% Pd-charcoal (2.0 g) in 200 ml of dioxane was agitated at room temperature for 5 h at 1 atm under hydrogen, and then filtered. After the dioxane was evaporated off, the residue was chromatographed on silica gel with benzene-ethyl acetate (5 : 1) as eluent. From the eluate 5.90 g of **8** (89% yield) was provided as needles (recrystallized from benzene-hexane): mp 105—105.5 °C; IR ($CHCl_3$) 1735 cm^{-1}; ^1H NMR ($CDCl_3$) δ=0.87 (3H, t, J=7.0 Hz), 1.46 (9H, s), 1.6—2.65 (6H, m), 3.08 (1H, d, J=5.0 Hz), 3.41 (1H, s), 3.53 (1H, m), 3.73 (3H, s), and 3.78 (3H, s); ^{13}C NMR ($CDCl_3$) δ=7.7 (q), 26.1 (t), 27.9 (q), 30.0 (t), 32.9 (t), 52.7 (q), 52.9 (q), 65.2 (d), 71.9 (s), 78.9 (s), 82.3 (s), 170.1 (s), 172.7 (s), and 173.5 (s).

Found: C, 55.73; H, 7.92; N, 4.00; M^++1, 346.1865. Calcd for $C_{16}H_{27}NO_7$: C, 55.64; H, 7.88; N, 4.06; M+1, 346.1864.

2,2-Bis(methoxycarbonyl)-6-ethyl-6-hydroxy-1-azabicyclo-[3.2.0]heptane (9). The *t*-butyl ester **8** (439 mg, 1.3 mmol) in 10 ml of 4 mol dm^{-3} HCl-dioxane was kept for 4 h at room temperature and the solution was concentrated to dryness in vacuo. The residue was subjected to Sephadex LH-20 column chromatography using methanol to give 336 mg of a β-amino acid as an amorphous solid (81% yield): IR (KBr) 1750 cm^{-1}; ^1H NMR (D_2O) δ=0.92 (3H, t, J=7.5 Hz), 1.6—3.0 (6H, m), 3.90 (6H, s), and 4.25 (1H, dd, J=8.0 and 9.5 Hz).

Dicyclohexylcarbodiimide (42 mg, 0.20 mmol) was added to a solution of 59 mg (0.18 mmol) of the β-amino acid in 5 ml of acetonitrile and stirred for 10 min. After 37 μl (0.27 mmol) of triethylamine was dropped into the solution, stirring was continued at 60 °C for 4 h. Concentration under reduced pressure gave a solid, which was taken into 4 ml of ethyl acetate and filtered. The ethyl acetate was removed by evaporation. The residue was applied on a silica-gel column (4 g) and developed with benzene-ethyl acetate (2 : 1), providing 43 mg of a bicyclic β-lactam **9** (88% yield): IR ($CHCl_3$) 1770 and 1740 cm^{-1}; ^1H NMR ($CDCl_3$) δ=1.02 (3H, t, J=7.5 Hz), 1.65—2.2 (6H, m), 2.62 (2H, dd, J=4.5 and 9.0 Hz), 3.64 (1H, s), 3.80 (6H, s), and 3.83 (1H, m); MS (FD) m/z 271 (M^+).

2,2-Bis(methoxycarbonyl)-6-ethyl-6-methyoxy-1-azabicyclo-[3.2.0]heptan-7-one (11). A suspension of 50 mg (0.19 mmol) of the alcohol **9**, 215 mg (0.93 mmol) of silver dioxide and 0.23 ml (3.8 mmol) of methyl iodide in 5 ml of *N,N*-dimethylformamide was heated at 40 °C for 4.5 h and diluted with 20 ml of ethyl acetate. After filtration, the filtrate was evaporated to give an oil, which was purified by silica-gel column chromatography with benzene-ethyl acetate (5 : 1). A colorless oil of a methyl ether **11** (48 mg, 90% yield) was obtained from the eluate: IR ($CHCl_3$) 1765 and 1740 cm^{-1}; ^1H NMR ($CDCl_3$) δ=0.95 (3H, t, J=7.5 Hz), 1.5—2.15 (4H, m), 2.60 (2H, dd, J=7.0 and 9.0 Hz), 3.47 (3H, s), 3.80 (6H, s), and 3.91 (1H, dd, J=7.5 and 8.5 Hz); ^{13}C NMR ($CDCl_3$) δ=6.8 (q), 23.8 (t), 25.5 (t), 39.7 (t), 53.3 (q), 53.4 (q), 68.5 (d), 70.8 (s), 84.6 (s), 167.4 (s), 168.9 (s), and 173.8 (s).

Found: C, 52.88; H, 6.28; N, 5.10; M^+, 285. Calcd for $C_{12}H_{17}NO_6$: C, 53.13; H, 6.32; N, 5.16; M, 285.

6-Ethyl-6-methoxy-2-methoxycarbonyl-1-azabicyclo[3.2.0]-heptan-7-ones (12a and 12b). A solution of 130 mg (0.46 mmol) of the diester **11** in 10 ml of acetone was mixed at 0 °C with 4.6 ml of 0.1 mol dm^{-3} NaOH, and stirred for 1 h. After the acetone was removed by evaporation, the concentrate was diluted with 26 ml of ethyl acetate and then carefully acidified to pH 2 with 0.1 mol dm^{-3} HCl (about 4.7 ml). The organic layer was separated, washed with brine, dried (Na_2SO_4), and concentrated to dryness in vacuo to afford 123 mg of a monocarboxylic acid. The crude monocarboxylic acid was dissolved in 10 ml of pyridine and heated at 100 °C for 7 h. Evaporation of the solvent gave a residue, which was dissolved in 1 ml of dichloromethane and chromatographed on 8 g of silica gel with benzene-ethyl acetate (5 : 1) to provide 45 mg (43% yield) of **12a** and 9 mg (9% yield) of **12b**. From the silica-gel column, 40 mg (31%) of the monocarboxylic acid was recovered with methanol. **12a**: IR ($CHCl_3$) 1750 cm^{-1}; ^1H NMR ($CDCl_3$) δ=0.98 (3H, t, J=7.0 Hz), 1.4—2.35 (6H, m), 3.49 (3H, s), 3.73 (3H, s), 3.97 (1H, t, J=6.5 Hz), and 4.44 (1H, t, J=6.0 Hz); MS (FD) m/z 227 (M^+).

12b: IR ($CHCl_3$) 1755 and 1735 cm^{-1}; ^1H NMR ($CDCl_3$) δ=0.98 (3H, t, J= 7.0 Hz), 1.6—2.0 (4H, m), 2.15—2.5 (2H. m), 3.46 (3H, s), 3.74 (3H, s) and 3.7—4.0 (2H, m); MS (FD) m/z 227 (M^+), 212 (M^+-CH_3).

6-Ethyl-6-methoxy-2-phenylseleno-7-oxo-1-azabicyclo-[3.2.0]heptane-2-carboxylic Acid Methyl Esters (13a and 13b). A solution of 6.6 mmol of butyllithium in 2.83 ml of hexane was added at −30 °C under nitrogen to a solution of 0.94 ml (6.6 mmol) of diisopropylamine in 30 ml of THF and cooled to −70 °C. A solution of 285 mg (1.3 mmol) of an isomeric mixture of **12a** and **12b** was added dropwise to the reaction mixture within 5 min. After the temperature of the solution was raised to −30 °C, 1.27 g (1.3 mmol) of benzeneselenenyl chloride in 3 ml of THF was added to the mixture and stirred for 30 min below −30 °C. Ammonium chloride (0.5 g) was added to the reaction mixture and then poured in 300 ml of ethyl acetate. The ethyl acetate was separated, rinsed with water, dried (Na_2SO_4) and concentrated to dryness in vacuo. The residue was subjected to silica-gel column chromatography with benzene-ethyl acetate (10 : 1) to afford a mixture of **13a** and **13b** (300 mg, 61% total yield), and a portion of the mixture was subjected to preparative silica-gel TLC (benzene-ethyl acetate 5 : 1) to give **13a** and **13b**, respectively.

13a: IR ($CHCl_3$) 1760 and 1735 cm^{-1}; ^1H NMR ($CDCl_3$) δ=0.92 (3H, t. J=7.5 Hz), 1.65—2.0 (4H, m), 2.25—2.75 (2H, m), 3.33 (3H, s), 3.42 (1H, t, J=7.5 Hz), 3.82 (3H, s), 7.3—7.5 (3H, m), and 7.6—7.8 (2H, m); MS (EI) m/z 384, 383, and 382.

13b: IR ($CHCl_3$) 1755 and 1730 cm^{-1}; ^1H NMR ($CDCl_3$) δ=1.00 (3H, t, J=7.5 Hz), 1.65—2.1 (2H, m), 2.4—2.85 (2H, m), 3.49 (3H, s), 3.57 (3H, s), 3.90 (1H, dd, J=6.5 and 10.0 Hz), 7.3—7.45 (3H, m), and 7.6—7.8 (2H, m): MS (EI) m/z 384, 383, 382, and 381.

Direct Derivation of 13a and 13b from 11. A mixture of 242 mg (0.85 mmol) of the methyl ester **11**, 253 mg (1.70 mmol) of sodium iodide and 265 mg (0.85 mmol) of diphenyl diselenide in 2 ml of hexamethylphosphoric triamide was heated at 80 °C for 2 h, poured into 5 ml of ice-water, and extracted 3 times with 10 ml each of benzene. The combined benzene extracts were washed with brine, dried (Na_2SO_4), and concentrated in vacuo, giving an oil. The oil was chromatographed on silica gel using benzene-acetone (10 : 1) to provide 95 mg of **13a** and 55 mg of **13b** (50% total yield) together with 75 mg of the methyl ester **11** (31% yield).

6-Ethyl-6-methoxy-7-oxo-1-azabicyclo[3,2,0]hept-2-ene-2-carboxylic Acid Methyl Ester (14). Into a solution of the isomeric mixture of the selenides **13a** and **13b** (45 mg, 0.12 mmol) in 8 ml of dichloromethane was dropped a solution at −30 °C of 20.3 mg (0.12 mmol) of *m*-chloroperbenzoic acid in 1 ml of dichloromethane and stirred at −30 °C for 15 min. The reaction mixture was quenched with 17 μl (0.16 mmol) of triethylamine and diluted with 50 ml of dichloromethane. The organic layer was separated, washed twice with 25 ml each of aqueous saturated $NaHCO_3$ and once with 25 ml of brine, dried (Na_2SO_4), and concentrated to dryness under reduced pressure. The residue was purified by preparative TLC (benzene-acetone 5 : 1), affording 20 mg of a carbapenem **14** as a colorless oil (76% yield): UV (CH_2Cl_2) 282 nm (ε 5000); IR ($CHCl_3$) 1775 and 1728 cm^{-1}; ^1H NMR ($CDCl_3$) δ=1.02 (3H. *t*, J=7.0 Hz), 1.65—2.05 (2H, m), 2.81 (2H, dd, J=3.0 and 9.8 Hz), 3.53 (3H, s), 3.83 (3H, s), 4.45 (1H, t, J=9.8 Hz), and 6.37 (1H, t, J=3.0 Hz).

3-[2-(Acetamido)ethylthio]-6-ethyl-6-methoxy-7-oxo-1-azabicyclo[3.2.0]heptane-2-carboxylic Acid Methyl Esters (15a—c). Triethylamine (127 μl, 0.92 mmol), and then a solution of 94 mg (0.79 mmol) of *N*-acetylcysteamine in 1 ml of *N*,*N*-dimethylformamide were added at −30 °C to 130 mg (0.61 mmol) of the carbapenem **14** in 12 ml of *N*,*N*-dimethylformamide, warmed to 25 °C, and stirred for 1 h at the same temperature. After the solvent was removed by evaporation under reduced pressure, the residue was purified by Bio-Beads S-X3 (200—400 mesh) column (100 ml) chromatography using benzene and by silica-gel column chromatography with benzene-acetone (2 : 1), giving an isomeric mixture (193 mg, 95% total yield) which was further subjected to silica-gel column chromatography for separation of each isomer (**15a**, **15b**, or **15c**) under delicately controlled development conditions:

15a: IR ($CHCl_3$) 1760 and 1670 cm^{-1}; ^1H NMR ($CDCl_3$) δ=1.06 (3H, t, J=7.0 Hz), 1.3—2.6 (4H. m), 2.00 (3H, s), 2.77 (2H, m), 3.1—3.6 (3H, m), 3.50 (3H, s), 3.79 (3H, s), 4.18 (1H, dd, J=3.0 and 8.0 Hz), 4.72 (1H, d, J=8.0 Hz), and 6.0—6.4 (1H, br); MS (EI) m/z 344 (M^+) and 316.

15b: IR ($CHCl_3$) 1760 and 1670 cm^{-1}; ^1H NMR ($CDCl_3$) δ=0.98 (3H, t, J=7.0 Hz), 1.4—3.2 (6H, m), 2.01 (3H, s), 3.2—3.6 (2H, m), 3.50 (3H, s), 3.6—4.1 (2H, m), 3.81 (3H, s), 4.33 (1H, d, J=6.0 Hz), and 6.0—6.5 (1H, br); MS (EI) m/z 344 (M^+) and 316.

15c: IR ($CHCl_3$) 1760, 1740, and 1670 cm^{-1}; ^1H NMR ($CDCl_3$) δ=0.97 (3H, t, J=7.0 Hz), 1.5—2.4 (4H, m), 2.00 (3H, s), 2.5—3.0 (2H, m), 3.2—3.5 (2H, m), 3.47 (3H, s), 3.6—4.0 (2H, m), 3.80 (3H, s), 4.19 (1H, d, J=8.0 Hz), and 5.9—6.4 (1H, br); MS (EI) m/z 344 (M^+) and 316.

3-[2-(Acetamido)ethylthio]-6-ethyl-6-methoxy-7-oxo-1-azabicyclo[3.2.0]heptane-2-carboxylic Acid *p*-Nitrobenzyl Ester (16). A tenth mol dm^{-3} NaOH (476 μl) was dropped at 0 °C into a solution of 15.8 ml (48 μmol) of the methyl ester isomers **15a—c** in 3 ml of acetone and agitated for 1.5 h. The reaction mixture was mixed at 0 °C with 240 μl of 0.1 mol dm^{-3} HCl and concentrated to dryness by repeated azeotropic evaporation with benzene. The residue was dissolved in 1.5 ml of *N*,*N*-dimethylformamide. *p*-Nitrobenzyl bromide (15.4 mg, 71 μmol) and triethylamine (17 μl, 120 μmol) were added at 0 °C to the solution, and stirred for 12 h at room temperature. The reaction mixture was diluted with 20 ml of ethyl acetate and washed twice with 7 ml each of brine. Drying (Na_2SO_4) and evaporation in vacuo give an oil, which was purified by preparative silica-gel TLC with benzene-acetone (1 : 1) to afford a mixture of *p*-nitrobenzyl esters **16** (15.3 mg, 72% yield): IR ($CHCl_3$) 1760 and 1670 cm^{-1}; ^1H NMR ($CDCl_3$) δ=0.96 (3H, t, J=7.5 Hz), 1.4—3.1 (6H, m), 2.0 (3H, s), 3.2—3.6 (2H, m), 3.50 (3H, s), 3.6—4.1 (2H, m), 4.38 (1H, d, J=6.0 Hz), 5.3 (2H, s), 5.8—6.2 (1H, br), 7.55 (2H, d, J=9.0 Hz), and 8.27 (2H, d, J=9.0 Hz).

Found: m/z 466.1629. Calcd for $C_{21}H_{28}N_3SO_7$: M^++1, 466.1644.

3-[2-(Acetamido)ethylthio]-6-ethyl-6-methoxy-7-oxo-1-azabicyclo[3.2.0]hept-2-ene-2-carboxylic Acid *p*-Nitrobenzyl Ester (18). To a solution of 15 mg (32 μmol) of the carbapenam **16** in 2 ml of dichloromethane was added dropwise at 0 °C first 13 μl (160 μmol) of pyridine containing 0.57 μl (32 μmol) of water, and then 23 mg (81 μmol) of (dichloroiodo)benzene in 0.5 ml of dichloromethane. After stirring for 30 min, 12 μl (81 μmol) of triethylamine was added to the mixture and was stirred for 15 min. further 30 min. The reaction mixture was mixed with 8 μl (33 μmol) of tributyl phosphine at 0 °C and stirred for 15 min. Silica-gel column chromatography using benzene-acetone mixtures of (10 : 1), (5 : 1), (2 : 1), and (1 : 1) gave 8.0 mg (54% yield) of a carbapenem **18**: UV ($CHCl_3$) 271 (ε 10200) and 324 nm (11400); IR ($CHCl_3$) 1772, 1700, and 1675 cm^{-1}; ^1H NMR ($CDCl_3$) δ= 1.03 (3H, t, J=7.5 Hz), 1.7—2.05 (2H, m), 1.98 (3H, s), 2.8—3.55 (6H, m), 3.50 (3H, s), 4.40 (1H, t, J=10.0 Hz), 5.22 (1H, d, J=14.0 Hz), 5.51 (1H, d, J=14.0 Hz), 6.17 (1H, br), 7.67 (2H, d, J=9.0 Hz), and 8.20 (2H, d, J=9.0 Hz).

Found: m/z 463.1401. Calcd for $C_{21}H_{25}N_3SO_7$: M, 463.1410.

3-[2-(Acetamido)ethylthio]-6-ethyl-6-methoxy-7-oxo-1-azabicyclo[3.2.0]hept-2-ene-2-carboxylic Acid Sodium Salt (6-Methoxy-epi-PS 5 Na Salt: 1). A solution of 95 mg (0.20 mmol) of the *p*-nitrobenzyl ester **18** was dissolved in 12 ml of a 2 : 1 mixture of tetrahydrofuran and 0.1 mol dm^{-3} phosphate buffer (pH 7.6) and hydrogenated at room temperature for 3 h at a hydrogen pressure of 4 kg cm^{-2} in the presence of platinum dioxide (100 mg). The filtrate was subjected to column chromatographic purification on QAE-Sephadex A-25 (Pharmacia Fine Chemicals AB, Sweden) and on Diaion CHP-20P (Mitsubishi Chemical Industries Ltd., Japan). Eluate fractions which indicated a UV absorption maximum

at 305.5 nm were combined and lyophilized to provide a white powder of the sodium salt of **1** in 70% yield (50 mg): UV (H_2O) 305.5 nm (ε 8000); IR (KBr) 1752, 1665, and 1608 cm^{-1}; ^1H NMR (D_2O) δ=0.96 (3H, t, J=7.5 Hz), 1.87 (2H, q, J=7.5 Hz), 1.97 (3H, s), 2.7—3.5 (6H, m), 3.50 (3H, s), and 4.43 (1H, t, J=10.0 Hz); ^{13}C NMR (D_2O, Dioxane) δ=7.1 (q), 22.8 (q), 23.9 (t), 31.7 (t), 35.8 (t), 40.4 (t), 54.2 (d), 60.4 (q), 92.6 (s), 128.3 (s), 130.8 (s), 168.5 (s), 175.2 (s), and 177.1 (s).

2,2-Bis(methoxycarbonyl)-6-ethyl-6-tetrahydropyranyloxy-1-azabicyclo[3.2.0]heptan-7-one (21). 3,4-Dihydro-2*H*-pyran (3.87 ml, 43 mmol) and anhydrous *p*-toluenesulfonic acid (0.15 g, 0.85 mmol) were added at 0 °C to a solution of 2.30 g (8.5 mmol) of **9** in 60 ml of ethyl acetate and stirred for 2 h at room temperature. After quenching with 0.18 ml (1.3 mmol) of triethylamine, the reaction solution was diluted with 100 ml of ethyl acetate, washed with aqueous saturated $NaHCO_3$ and brine, and dried (Na_2SO_4). The solvent was eliminated by evaporation and the residue was purified by silica-gel column chromatography with benzene-ethyl acetate mixtures of (20 : 1), (10 : 1), (5 : 1), and (3 : 1) as eluents to afford 2.91 g (97% yield) of an anomeric mixture of **21**: ^1H NMR ($CDCl_3$) δ=0.85—1.2 (3H, m), 1.25—2.25 (10H, m), 2.25—2.75 (2H, m), 3.3—4.4 (3H, m), 3.70 (6H, s), and 4.8—5.25 (1H, m), MS (FD) m/z 356 (M^++1).

6-Ethyl-7-oxo-2-phenylseleno-6-tetrahydropyranyloxy-1-azabicyclo[3.2.0]heptane-2-carboxylic Acid Methyl Ester (22). A solution containing 2.85 g (8.0 mmol) of **21**, 2.53 g (8.0 mmol) of diphenyl diselenide, and 2.41 g (16 mmol) sodium iodide in 15 ml of hexamethylphosphoric triamide was heated at 80 °C for 4 h. As described for **13a** and **13b**, a mixture of the four isomers of **22** (2.22 g, 61% yield) was obtained together with unreacted **21** (0.64 g): IR ($CHCl_3$) 1755 and 1725 cm^{-1}; ^1H NMR ($CDCl_3$) δ=0.80—1.25 (3H, m), 1.3—2.25 (10H, m), 2.25—2.8 (2H, m), 3.3—4.45 (6H, m), 4.8—5.25 (1H, m), 7.2—7.5 (2H, m), and 7.6—7.9 (2H, m).

6-Ethyl-7-oxo-6-tetrahydropyranyloxy-1-azabicyclo[3.2.0]-hept-2-ene-2-carboxylic Acid Methyl Esters (23a and 23b). The treatment described for **14** was repeated with the isomeric mixture **22**, giving a 1 : 1 mixture of two anomers **23a** and **23b** in 80% yield. **23a**: IR ($CHCl_3$) 1780, 1737, and 1618 cm^{-1}; ^1H NMR ($CDCl_3$) δ=1.07 (3H, t, J=7.5 Hz), 1.35—2.05 (8H, m), 2.65—2.95 (2H, m), 3.3—4.2 (2H, m), 3.80 (3H, s), 4.72 (1H, t, J=10.0 Hz), 5.00 (1H, br), and 6.32 (1H, t, J=3.0 Hz); MS (FD) m/z 295 (M^+).

23b: IR ($CHCl_3$) 1780, 1737, and 1618 cm^{-1}; ^1H NMR ($CDCl_3$) δ=1.10 (3H, t, J=7.5 Hz), 1.35—2.1 (8H, m), 2.65—2.9 (2H, m), 3.4—4.2 (2H, m), 3.84 (3H, s), 4.52 (1H, t, J=10.0 Hz), 5.18 (1H, br), and 6.33 (1H, t, J=3.0 Hz); MS (FD) m/z 295 (M^+).

3-[2-(Acetamido)ethylthio]-6-ethyl-7-oxo-6-tetrahydropyranyloxy-1-azabicyclo[3.2.0]heptane-2-carboxylic Acid Methyl Ester (24). Under reaction conditions similar to those described for **15a**, **15b**, and **15c**, 4.4 g (84% yield) of an isomeric mixture of **24** was obtained from 3.7 g of the mixture of **23a** and **23b**: IR ($CHCl_3$) 1758 and 1665 cm^{-1}; ^1H NMR ($CDCl_3$) δ=0.8—1.2 (3H, m), 1.3—2.15 (9H, m), 2.00 (3H, s), 2.15—3.0 (3H, m), 3.0—4.8 (7H, m), 3.77 (3H, m), 4.8—5.25 (1H, m), and 6.20 (1H, br); MS (FD) m/z 415 (M^++1).

3-[2-(Acetamido)ethylthio]-6-ethyl-7-oxo-6-tetrahydropyranyloxy-1-azabicyclo[3.2.0]heptane-2-carboxylic Acid *p*-Nitrobenzyl Ester (25). Treatment of 134 mg (0.32 mmol) of **24** with 0.1 mol dm^{-3} NaOH and *p*-nitrobenzyl bromide gave 131 mg (76% yield) of **25**: IR ($CHCl_3$) 1750 and 1665 cm^{-1}; ^1H NMR ($CDCl_3$) δ=0.85—1.2 (3H, m), 1.3—2.15 (9H, m), 2.15—3.0 (3H, m), 3.2—3.65 (3H, m), 3.65—4.05 (2H, m), 4.15 (1H, t, J=7.0 Hz), 4.33 (1H, d, J=6.0 Hz), 4.8—5.2 (1H, m), 5.35 (2H, s), 6.00 (1H, br), 7.50 (2H, d, J=9.0 Hz), and 8.13 (2H, d, J=9.0 Hz); MS (FD) m/z 536 (M^++1).

3-[2-(Acetamido)ethylthio]-6-ethyl-6-hydroxy-7-oxo-1-azabicyclo[3.2.0]heptane-2-carboxylic Acid *p*-Nitrobenzyl Ester (26). Pyridinium *p*-toluenesulfonic acid (0.71 g, 2.8 mmol) was added to a solution of 6.0 g (11 mmol) of the tetrahydropyranyl ether **25** in 120 ml of ethanol and stirred at 50 °C for 5 h. After dilution with 600 ml of ethyl acetate, the reaction mixture was washed successively with saturated aqueous $NaHCO_3$ and with brine, dried (Na_2SO_4), and evaporated to dryness. The residue was chromatographed on a silica-gel column with benzene-acetone (2 : 1), providing 4.1 g (81% yield) of an alcohol **26**: IR ($CHCl_3$) 1745 and 1665 cm^{-1}; ^1H NMR ($CDCl_3$) δ=0.85—1.2 (3H, m), 1.45—2.0 (3H, m), 1.94 (3H, s), 2.2—2.75 (3H, m), 3.2—3.6 (3H, m), 3.6—4.0 (2H, m), 4.0—4.8 (2H, m), 5.25 (2H, s), 6.22 (1H, br), 7.45 (2H, d, J=9.0 Hz), and 8.12 (2H, d, J=9.0 Hz); MS (FD) m/z 451 (M^+).

3-[2-(Acetamido)ethylthio]-6-ethyl-7-oxo-6-trimethylsilyloxy-1-azabicyclo[3.2.0]heptane-2-carboxylic Acid *p*-Nitrobenzyl Ester (27). The alcohol **26** (2.61 g, 5.8 mmol), triethylamine (16.0 ml, 120 mmol), and trimethylchlorosilane (13.9 ml, 110 mmol) were dissolved in 100 ml of tetrahydrofuran and stirred for 12 h at room temperature. The reaction mixture was diluted with 300 ml of ethyl acetate, washed with brine, dried (Na_2SO_4), and concentrated to give a residue. The residue was purified by silica-gel column chromatography with benzene-acetone (3 : 1) to give 2.22 g of **27** (73% yield): IR ($CHCl_3$) 1755 and 1668 cm^{-1}; ^1H NMR ($CDCl_3$) δ=0.20 (9H, s), 0.8—1.15 (2H, m), 1.3—2.0 (3H, m), 1.96 (3H, s), 2.25—2.9 (3H, m), 3.2—3.55 (2H, m), 3.55—4.0 (2H, m), 4.3—4.75 (1H, m), 5.27 (2H, s), 6.51 (1H, br), 7.48 (2H, d, J=9.0 Hz), and 8.13 (2H, d, J=9.0 Hz); MS (FD) m/z 523 (M^+).

3-[2-(Acetamido)ethylthio]-6-ethyl-7-oxo-6-trimethylsilyloxy-1-azabicyclo[3.2.0]hept-2-ene-2-carboxylic Acid *p*-Nitrobenzyl Ester (28). The treatment of the carbapenam **27** as described for **18** gave a carbapenem **28**: IR ($CHCl_3$) 1770, 1700, and 1678 cm^{-1}; UV ($CHCl_3$) 271 (ε 10700) and 325 nm (12000); ^1H NMR ($CDCl_3$) δ=0.27 (9H, s), 1.07 (3H, t, J=7.5 Hz), 1.78 (2H, q, J=7.5 Hz), 1.99 (3H, s), 2.8—3.7 (6H, m), 4.20 (1H, t, J=10.0 Hz), 5.22 (1H, d, J=14.0 Hz), 5.47 (1H, d, J=14.0 Hz), 6.15 (1H, br), 7.63 (2H, d, J=9.0 Hz), and 8.16 (2H, d, J=9.0 Hz), MS (FD) m/z 521 (M^+).

3-[2-(Acetamido)ethylthio]-6-ethyl-6-hydroxy-7-oxo-1-azabicyclo[3.2.0]hept-2-ene-2-carboxylic Acid *p*-Nitrobenzyl Ester (29). Twenty milliliter of 0.001 mol dm^{-3} HCl was added dropwise at 0 °C to a solution of 46 mg (88 μmol) of the trimethylsilyl ether **28** in 20 ml of ethanol and agitated for 30 min. The solution was mixed with 200 ml of ethyl acetate, washed with cold 5% $NaHCO_3$ and brine, dried (Na_2SO_4), and concentrated to dryness. The residue was chromatographed on silica gel with benzene and acetone (1 : 1) to give 34.5 mg (87% yield) of **29** as plates (recrystallized from benzene): mp 74—75 °C: IR (KBr) 1760 and 1690 cm^{-1}; UV (CH_2Cl_2) 271 (ε 11000) and 325.5 nm (11600); ^1H NMR ($CDCl_3$) δ=1.08 (3H, t, J=7.5 Hz), 1.62 (1H, br), 1.82 (2H, q, J=7.5 Hz), 1.96 (3H, s), 2.7—3.85 (6H, m), 4.23 (1H, t, J=10 Hz), 5.18 (1H, d, J=14.0 Hz), 5.45 (1H, d, J=14.0 Hz), 5.90 (1H, br), 7.60 (2H, d, J=9.0 Hz), and 8.12 (2H, d, J=9.0 Hz).

3-[2-(Acetamido)ethylthio]-6-ethyl-6-hydroxy-7-oxo-1-azabicyclo[3.2.0]hept-2-ene-2-carboxylic Acid Sodium Salt (6-Hydroxy-*epi*-PS 5 Na Salt: 2). Under the same conditions as for **1**, the *p*-nitrobenzyl ester **29** was hydrogenated to give a white powder of **2**: IR (KBr) 1750 and 1600 cm^{-1}; UV (H_2O) 304.5 nm (ε 8900); ^1H NMR (D_2O) δ=1.00 (3H, t, *J*=7.3 Hz), 1.82 (2H, q, *J*=7.3 Hz), 2.00 (3H, s), 2.7—3.5 (6H, m), and 4.22 (1H, t, *J*=9.6 Hz).

The authors are grateful to Professor Yasuji Yamada, Tokyo College of Pharmacy, for his valuable advice throughout this study, and to Mrs. Michiko Sakamoto and Miss Fumito Satoh for the antimicrobial and enzymological evaluations.

References

1) K. Okamura, S. Hirata, Y. Okumura, Y. Fukagawa, Y. Shimauchi, K. Kouno, T. Ishikura, and J. Lein, *J. Antibiot.*, **31**, 480 (1978).

2) N. Shibamoto, A. Koki, M. Nishino, K. Nakamura, K. Kiyoshima, K. Okamura, M. Okabe, R. Okamoto, Y. Fukagawa, Y. Shimauchi, T. Ishikura, and J. Lein, *J. Antibiot.*, **33**, 1128 (1980).

3) K. Yamamoto, T. Yoshioka, Y. Kato, K. Isshiki, M. Nishino, F. Nakamura, Y. Shimauchi, and T. Ishikura, *Tetrahedron Lett.*, **23**, 897 (1982).

4) C. M. Cimarusti, *J. Med. Chem.*, **27**, 247 (1984).

5) Y. Fukagawa, K. Kubo, K. Okamura, and T. Ishikura, "Trends in Antibiotic Research: Genetics, Biosyntheses, Actions & New Substances," ed by H. Umezawa, A. Demain, T. Hata, and C. R. Hutchinson, Japan Antibiot. Research Association, Tokyo (1982), p. 248.

6) T. Yoshioka, A. Watanabe, I. Kojima, Y. Shimauchi, M. Okabe, Y. Fukagawa, and T. Ishikura, *J. Antibiot.*, **37**, 211 (1984).

7) M. Miyashita, N. Chida, and A. Yoshikoshi, *J. Chem. Soc., Chem. Commun.*, **1984**, 195.

8) M. D. Bachi, R. Breiman, and H. Meshulam, *J. Org. Chem.*, **48**, 1439 (1983).

9) T. H. Kinstle and B. Y. Mandanas, *J. Chem. Soc., Chem. Commun.*, **1968**, 1699.

10) M. Asaoka, K. Miyake, and H. Takei, *Bull. Chem. Soc. Jpn.*, **51**, 3008 (1978).

11) J. H. Bateson, R. I. Hickling, P. M. Roberts, T. C. Smale, and R. Southgate, *J. Chem. Soc., Chem. Commun.*, **1980**, 1084.

12) J. H. Bateson, P. M. Roberts, T. C. Smale, and R. Southgate, *J. Chem. Soc., Chem. Commun.*, **1980**, 185.

13) M. Miyashita, A. Yoshikoshi, and P. A. Grieco, *J. Org. Chem.*, **42**, 3772 (1977).

14) J. D. Hood, A. G. Brown, A. L. Elson, M. L. Gilpin, and R. Holmes. "Recent Advances in the Chemistry of Beta-Lactam Antibiotics," ed by A. G. Brown and S. M. Roberts, The Royal Society of Chemistry, Burlington House, London (1985), p. 52.

15) T. Yoshioka, K. Isshiki, F. Nakamura, K. Yamamoto, Y. Shimauchi, M. Sakamoto, N. Shibamoto, Y. Fukagawa, and T. Ishikura. Abstracts of the 24th Interscience Conference on Antimicrobial Agents and Chemotherapy, Washington, D. C., October 1984, Abstr. No. 132.

Studies of a Peptide Antibiotic "Gratisin". II

Makoto TAMAKI,* Michiaki TAKIMOTO, and Ichiro MURAMATSU†
Department of Chemistry, Faculty of Science, Toho University, Miyama, Funabashi-shi, Chiba 274
†Department of Chemistry, College of Science, Rikkyo University, Nishi-ikebukuro, Tokyo 171
(Received November 29, 1986)

In order to investigate the structure-activity relationship of the "gratisin"-related peptide, *cyclo*(-Val-Orn-Leu-D-Phe-Pro-D-Tyr-)$_2$ (GR-I), its two analogs, *cyclo*(-Val-Orn-Leu-D-Ala-Pro-D-Tyr-)$_2$ (**6a**) and *cyclo*(-Val-Orn-Leu-D-Phe-Pro-D-Ala-)$_2$ (**6b**), were synthesized. The CD spectra of these synthetic peptides in an aqueous solution were similar to that of GR-I, indicating that these peptides have similar conformations in an aqueous solution. The activity of **6b** was half that of GR-I, whereas **6a** did not show any antibiotic activity. These results indicated that the phenyl group of the D-Phe residue preceding the Pro residue is essential for exhibiting the activity, while the *p*-hydroxyphenyl group of the D-Tyr residue following the Pro residue is not essential.

A peptide antibiotic, gratisin, which shows activity against *Bacillus subtilis* 720, was isolated from *Bacillus brevis* Y-33 by Silaev et al.[1,2] In order to determine the primary structure of natural gratisin, we have ourselves synthesized several peptides on the basis of the primary structure proposed by Silaev et al. In these synthetic studies,[3] we found that *cyclo*(-Val-Orn-Leu-D-Phe-Pro-D-Tyr-)$_2$ (GR-I)[4] possesses the strongest activity against the gram-positive microorganisms tested and that it shows the same activity as that of gramicidin S-1 (GS)[5] toward *Bacillus subtilis;* we proposed that the amino-acid sequence of GR-I is most probable as that of natural peptide. We also reported that *cyclo*(-Val-Orn-Leu-D-Phe-Pro-D-Phe-)$_2$, in which D-Tyr residues at positions 6 and 6′ of GR-I are replaced with D-Phe residues, shows almost the same activity as does GR-I, indicating that the hydroxyl groups of the D-Tyr residues at positions 6 and 6′ are not necessary for exhibiting antibiotic activity.[3]

In order to investigate further the structure-activity relationship of GR-I, we synthesized two analogs, *cyclo*(-Val-Orn-Leu-D-Ala-Pro-D-Tyr-)$_2$ (**6a**) and *cyclo*(-Val-Orn-Leu-D-Phe-Pro-D-Ala-)$_2$ (**6b**) (Fig. 1), in which D-Phe-Pro-D-Tyr sequences in GR-I are replaced with D-Ala-Pro-D-Tyr and D-Phe-Pro-D-Ala sequences respectively. The roles of the side chains of the D-Phe residues at positions 4 and 4′ and of the D-Tyr residues at positions 6 and 6′ in GR-I for exhibiting the antibiotic activity were elucidated.

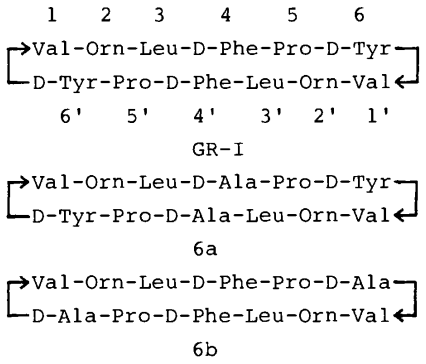

Fig. 1. Primary structures of GR-I and its analogs (**6a** and **6b**).

The routes of the syntheses of these peptides are shown in Fig. 2. In the synthesis of peptide **6a**, the Boc-hexapeptide benzyl ester (**1a**) was synthesized from the Pro benzyl ester by step-by-step elongation using dicyclohexylcarbodiimide (DCC) and 1-hydroxybenzotriazole (HOBt). Then, a part of the **1a** was converted into the corresponding hydrazide (**2a**). The coupling of **2a** with the hexapeptide benzyl ester derived from **1a** was carried out using the azide method; this afforded the Boc-dodecapeptide benzyl ester (**3a**). This ester **3a** was treated with hydrazine hydrate to give the corresponding hydrazide (**4a**), and then the Boc-group of **4a** was removed by the action of trifluoroacetic acid. The dodecapeptide hydrazide trifluoroacetate (**4a′**) thus obtained was changed to the azide by using isopentyl nitrite at −20 °C for 15 min. The azide could be cyclized under a high dilution in pyridine at 0 °C for 3 d. The resulting product was purified by means of silica-gel column chromatography, followed by recrystallization. The cyclododecapeptide (**5a**) was obtained in a 53% yield. The removal of all the masking group of **5a** by hydrogenolysis yielded **6a**. Peptide **6b** was synthesized in a similar manner. In the synthesis of **1b**, 1-ethyl-3-(3-dimethylaminopropyl)carbodiimide hydrochloride (WSCD·HCl) was used as the coupling reagent instead of DCC. The yield of cyclization by the azide method was 67%. The homogeneities of the products were confirmed by means of thin-layer chromatography (TLC), amino-acid analysis, high-performance liquid chromatography (HPLC), and fast-atom-bombardment (FAB) mass spectrum.

The CD spectra of GR-I and its two analogs were measured in aqueous solutions (Fig. 3). Peptide **6a** showed almost the same CD curve as GR-I, although this analog does not contain aromatic side chains at positions 4 and 4′. In the CD spectrum of peptide **6b** we observed a curve similar to that of GR-I, but its trough was shallower than the troughs of GR-I. These results indicated that, in aqueous solutions, these synthetic peptides possess a conformation similar to that of GR-I; they also show that the aromatic side chains of the D-Phe residues at positions 4 and 4′ make only a

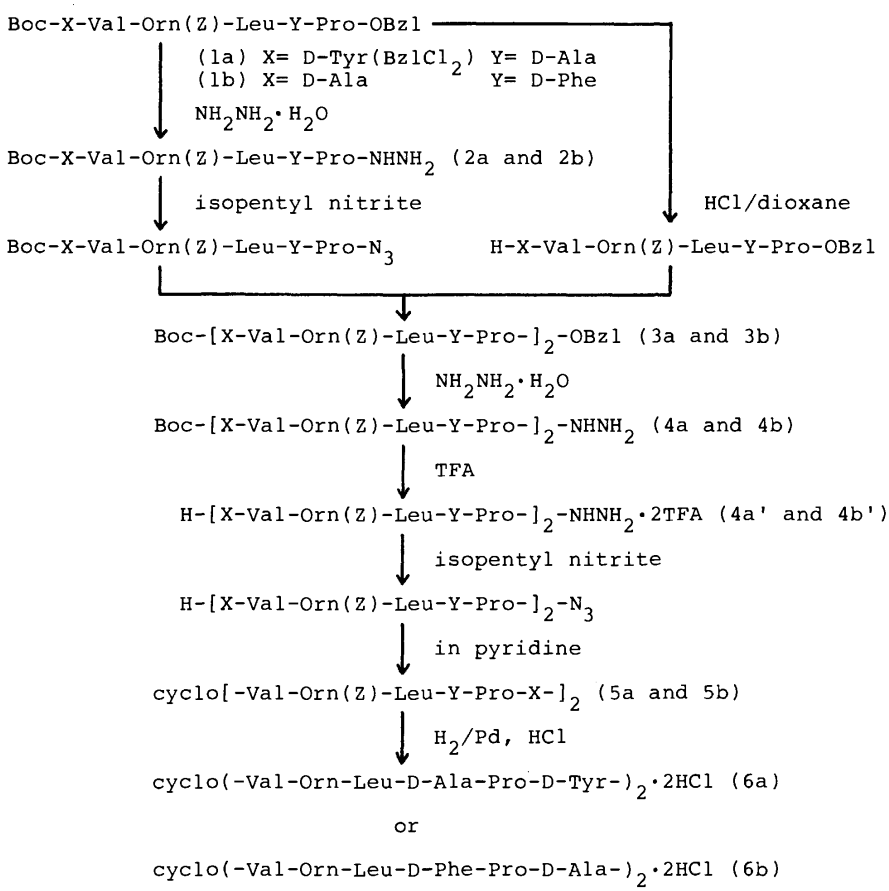

Fig. 2. Synthesis of peptides **6a** and **6b**.

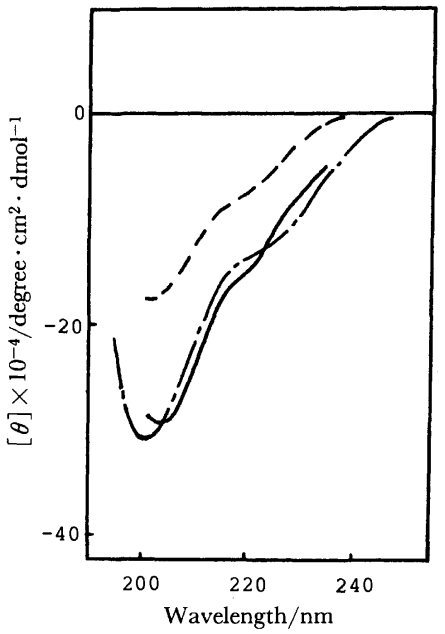

Fig. 3. CD spectra of **6a** ——, **6b**----, GR-I -·-·- in water.

small contribution to the conformation in an aqueous solution.

The antibiotic activity of these synthetic peptides is summarized in Table 1. Peptide **6a**, which has a D-Ala-Pro-D-Tyr sequence, showed no activity against the microorganisms tested, although this peptide possesses almost the same CD curve as GR-I in an aqueous solution. Lee et al.[6] reported that [D-Ala$^{4,4'}$]GS containing D-Ala residues in place of D-Phe residues preceding Pro residues possesses about 1/8 of the activity of the natural GS against *Bacillus subtillis* and *Staphylococcus aureus*, and that its ORD spectrum is similar to that of GS. The difference in activity between **6a** and [D-Ala$^{4,4'}$]GS may result from the difference in their ring sizes, in other words, the difference in the rigidity of their ring conformations. The activity of **6b**, which has a D-Phe-Pro-D-Ala sequence, was half that of GR-I. These results indicated that, in GR-analog peptides, the phenyl group of the D-Phe residue preceding the Pro residue is essential for the activity, while the *p*-hydroxyphenyl group of the D-Tyr residue following the Pro residue is not essential. Further, no relationship between the CD spectra in aqueous solution and the antibiotic activities could be found.

As for the mode of action of gratisin and GS, it is considered that the most significant role for their antibiotic action is played by each ring conformation induced during the binding of their antibiotics to the bacterial cell.[7-9] In the present studies, it is suggested that peptides **6a** and **6b** in aqueous solutions have conformations similar to that of GR-I, but that, when these peptides interact with the bacterial cell, peptide

Table 1. Antibiotic Activity of GR-I and Its Analogs[a)]

Test organism	GR-I	6a	6b
Staph. aureus ATCC 6538 P	6.3	>50	12.5
Strept. pyogenes N.Y. 5	3.1	>50	6.25
Micrococcus flavus ATCC 10240	3.1	>50	6.25
Corynebact. diphtheriae P.W. 8	3.1	>50	3.13
Bac. subtilis ATCC 6633	3.1	>50	6.25
E. coli NIHJ-JC2	>50	>50	>100
Proteus vulgaris OX 19	>50	>50	>100

a) The minimum inhibitory concentration ($\mu g\,ml^{-1}$) was determined by means of an agar-dilution method with 10^6 organisms per milliliter.

6b can take an active conformation similar to that of GR-I, while peptide **6a** can not take the active conformation. This great contrast between the two peptides is caused by the removal of the aromatic ring of the residues at positions 4 and 4'.

Experimental[4)]

All the melting points are uncorrected. The CD spectra were obtained by use of a JASCO spectropolarimeter, model J-500, using a 1-mm quartz cell at room temperature. The CD spectroscopy of GR-I and its two analogs was carried out with an aqueous solution of their dihydrochlorides at the concentration of $1.1—1.5\times10^{-4}$ M (1 M=1 mol dm^{-3}). The molecular weights of these synthetic peptides were determined by FAB mass spectrometry using a JEOL D-300 mass spectrometer. Amino-acid analyses were carried out by means of a Hitachi 835 amino-acid analyzer after the hydrolysis of the peptides in 6 M HCl at 110 °C for 24 h. HPLC was performed by means of an ODS column (ϕ 4.6×250 mm), using MeOH-5% $NaClO_4$ aq (5:1) as the elution solvent. TLC was performed on Merck silica-gel F_{254} plates with the following solvent systems (v/v): R_f^1, $CHCl_3$-MeOH (9:1); R_f^2, $CHCl_3$-MeOH-AcOH (95:5:3); R_f^3, *n*-BuOH-AcOH-H_2O (4:1:1); R_f^4, *n*-BuOH-pyridine-AcOH-H_2O (4:1:1:2).

Boc-D-Tyr(BzlCl$_2$)-Val-Orn(Z)-Leu-D-Ala-Pro-OBzl (1a). DCC (2.06 g, 10 mmol) was added to a solution of Boc-D-Ala (1.90 g, 10 mmol), HOBt (1.49 g, 11 mmol), Pro-OBzl·HCl (2.42 g, 10 mmol), and NMM (1.1 ml, 10 mmol) in $CHCl_3$ (50 ml) at 0 °C. This solution was stirred for 2 h at 0 °C and then overnight at room temperature. After the reaction mixture has then been concentrated in vacuo, AcOEt (20 ml) was added to the residue and insoluble substances were removed by filtration. The filtrate was then diluted with AcOEt (200 ml). The solution was washed successively with 5% citric acid, water, 5% Na_2CO_3 and water, and dried over sodium sulfate. After the removal of the drying reagent, the solvent was evaporated in vacuo. The residue was dissolved in 4 M HCl/dioxane (20 ml) containing anisole (0.2 ml) at 0 °C. After stirring for 30 min at room temperature, the solution was concentrated in vacuo. The residue was dissolved in $CHCl_3$ (50 ml). The solution was washed with 10% Na_2CO_3 and water under cooling with an ice bath. To this solution we then added Boc-Leu (2.40 g, 10 mmol), HOBt (1.49 g, 11 mmol), and DCC (2.06 g, 10 mmol) at 0 °C. The same procedure as has been described above was repeated for this reaction mixture. Further, Boc-Orn(Z), Boc-Val, and Boc-D-Tyr(BzlCl$_2$) were successively coupled by the same method. All the reactions were followed by TLC on a silica-gel plate. The crude, protected hexapeptide obtained from the final reaction mixture was purified by chromatography on a silica-gel column (ϕ 2×50 cm), using a solvent system of $CHCl_3$-MeOH (50:1). The fractions containing the desired product were combined and concentrated. The product was reprecipitated from AcOEt-ether; overall yield, 3.28 g (28% from Pro-OBzl); mp 161—163 °C; $[\alpha]_D^{29}$ −13.2° (*c* 1, DMF); R_f^1 0.63, R_f^2 0.55.

Found: C, 62.20; H, 6.81; N, 8.82%. Calcd for $C_{60}H_{77}O_{12}N_7Cl_2$: C, 62.17; H, 6.69; N, 8.46%.

Boc-D-Ala-Val-Orn(Z)-Leu-D-Phe-Pro-OBzl (1b). This compound was prepared from Pro-OBzl·HCl (1.45 g, 6 mmol) in a manner similar to that described for the preparation of **1a**. In the synthesis of this compound, WSCD·HCl was used instead of DCC as the coupling reagent, and the reaction mixture was washed successively in a $CHCl_3$ solution with 5% citric acid and 5% Na_2CO_3; yield, 3.84 g (64%); mp 188—193 °C; $[\alpha]_D^{29}$ −33.5° (*c* 1, DMF); R_f^1 0.76, R_f^2 0.53.

Found: C, 64.54; H, 7.47; N, 10.05%. Calcd for $C_{53}H_{73}O_{11}N_7$: C, 64.68; H, 7.48; N, 9.96%.

Boc-D-Tyr(BzlCl$_2$)-Val-Orn(Z)-Leu-D-Ala-Pro-NHNH$_2$ (2a). A solution of **1a** (1.17 g, 1 mmol) and hydrazine hydrate (1.5 ml) in DMF (10 ml) was allowed to stand for 2 d at room temperature. The solution was concentrated in vacuo, and then water was added to the residue. The resulting solid product was collected by filtration; yield, 0.96 g (88 %); mp 167—170 °C; $[\alpha]_D^{29}$ −17.6° (*c* 1, DMF); R_f^1 0.49, R_f^2 0.33.

Found: C, 58.44; H, 6.92; N, 11.69%. Calcd for $C_{53}H_{73}O_{11}N_9Cl_2$: C, 58.77; H, 6.79; N, 11.64%.

Boc-D-Ala-Val-Orn(Z)-Leu-D-Phe-Pro-NHNH$_2$ (2b). Compound **1b** (1.81 g, 1.84 mmol) was treated with hydrazine hydrate in the manner described for the preparation of **2a**; yield, 1.20 g (72%); mp 171—173 °C; $[\alpha]_D^{29}$ −34.2° (*c* 1, DMF); R_f^1 0.54, R_f^2 0.49.

Found: C, 60.64; H, 7.74; N, 13.56 %. Calcd for $C_{46}H_{69}O_{10}N_9$: C, 60.84; H, 7.66; N, 13.88%.

Boc-[D-Tyr(BzlCl$_2$)-Val-Orn(Z)-Leu-D-Ala-Pro-]$_2$-OBzl (3a). Compound **1a** (0.95 g, 0.82 mmol) was dissolved in 4 M HCl/dioxane (15 ml) containing anisole (0.5 ml) at 0 °C. After stirring at room temperature for 30 min, the solution was concentrated in vacuo. Ether was added to the residue, and the resulting solid, H-D-Tyr(BzlCl$_2$)-Val-Orn(Z)-Leu-D-Ala-Pro-OBzl·HCl, was collected by filtration. To a solution of **2a** (0.86 g, 0.8 mmol) in DMF (20 ml) we added 4 M HCl/dioxane (0.6 ml, 2.4 mmol) and isopentyl nitrite (0.12 ml, 0.9 mmol) at −40 °C. After stirring at −20 °C for 15 min, the solution was cooled again to −40 °C and neutralized with TEA (0.34 ml, 2.4 mmol). This solution was combined with the chilled solution of H-D-Tyr(BzlCl$_2$)-Val-Orn(Z)-Leu-D-Ala-Pro-OBzl·HCl mentioned above and TEA (0.12 ml, 0.82 mmol) in DMF (12 ml). The mixture was stirred at 0 °C

for 3 d and then concentrated. The residue was dissolved in AcOEt (200 ml), and the solution was washed with 5% citric acid, water, 5% Na_2CO_3, and water, and dried over sodium sulfate. After the solution has been concentrated, the residue was purified by chromatography on a silica-gel column (ϕ 1.8×30 cm), using a solvent system of $CHCl_3$-MeOH (20 : 1), and the fractions containing the desired product were combined and concentrated. Further purification was performed by reprecipitation from $CHCl_3$-ether; yield, 0.90 g (53%); mp 202—205 °C; $[\alpha]_D^{29}$ −9.36° (*c* 1, DMF); R_f^1 0.55, R_f^2 0.77.

Found: C, 61.19; H, 6.81; N, 9.43%. Calcd for $C_{108}H_{138}O_{21}N_{14}Cl_4$: C, 61.47; H, 6.59; N, 9.29%.

Boc-[D-Ala-Val-Orn(Z)-Leu-D-Phe-Pro-]$_2$-OBzl (3b). This compound was prepared from **1b** (1.08 g, 1.1 mmol) and **2b** (1.00 g, 1.1 mmol) in a manner similar to that described for the preparation of **3a**. Purification was performed by silica-gel column chromatography, followed by recrystallization from AcOEt-ether; yield, 1.16 g (60%); mp 213—216 °C; $[\alpha]_D^{29}$ −35.8° (*c* 1, DMF); R_f^1 0.53, R_f^2 0.68.

Found: C, 64.02; H, 7.67; N, 11.13%. Calcd for $C_{94}H_{130}O_{19}N_{14}$: C, 64.14; H, 7.44; N, 11.14%.

Boc-[D-Tyr(BzlCl$_2$)-Val-Orn(Z)-Leu-D-Ala-Pro-]$_2$-NHNH$_2$ (4a). Compound **3a** (0.76 g, 0.36 mmol) was treated with hydrazine hydrate as has been described for the preparation of **2a**; yield, 0.61 g (83%); mp 206—210 °C; $[\alpha]_D^{29}$ −15.8° (*c* 1, DMF); R_f^1 0.51, R_f^2 0.26.

Found: C, 59.34; H, 6.83; N, 10.98%. Calcd for $C_{101}H_{134}O_{20}N_{16}Cl_4$: C, 59.64; H, 6.64; N, 11.02%.

Boc-[D-Ala-Val-Orn(Z)-Leu-D-Phe-Pro-]$_2$-NHNH$_2$ (4b). Compound **3b** (1.00 g, 0.57 mmol) was treated with hydrazine hydrate as has been described for the preparation of **2a**; yield, 0.90 g, (92%); mp 214—218 °C; $[\alpha]_D^{29}$ −36.0° (*c* 1, DMF); R_f^1 0.59, R_f^2 0.49.

Found: C, 61.43; H, 7.61; N, 13.13%. Calcd for $C_{87}H_{126}O_{18}N_{16}\cdot H_2O$: C, 61.39; H, 7.58; N, 13.16%.

***Cyclo*[-Val-Orn(Z)-Leu-D-Ala-Pro-D-Tyr(BzlCl$_2$)-]$_2$ (5a).** Compound **4a** (0.55 g, 0.27 mmol) was dissolved in TFA (10 ml) containing anisole (0.2 ml). The mixture was stirred for 40 min at room temperature and then concentrated in vacuo. The residue was triturated with ether and collected by filtration. To a solution of the trifluoroacetate of the dodecapeptide hydrazide in DMF (5 ml), we then added 4 M HCl/dioxane (0.2 ml) and isopentyl nitrite (0.041 ml, 0.30 mmol) at −40 °C. After stirring at −20 °C for 15 min, the mixture was poured, drop by drop, into pyridine (300 ml) at 0 °C. After stirring for 3 d at 0 °C, the solution was concentrated. The addition of water to the residue afforded a precipitate, which was then filtered and washed with water. Purification was performed by recrystallization from MeOH-ether; yield, 272 mg (53%); mp 270—275 °C (decomp); $[\alpha]_D^{29}$ −9.1° (*c* 0.8, DMF); R_f^1 0.72, R_f^2 0.55.

Found: C, 59.91; H, 6.75; N, 9.59 %. Calcd for $C_{96}H_{122}O_{18}N_{14}Cl_4\cdot 2H_2O$: C, 59.50; H, 6.55; N, 10.12%.

***Cyclo*[-Val-Orn(Z)-Leu-D-Phe-Pro-D-Ala-]$_2$ (5b).** This compound was prepared from **4b** (0.70 g, 0.42 mmol) as has been described for the preparation of **5a**. The purification of this compound was performed by chromatography on a silica-gel column (ϕ 1.8×20 cm), using a solvent system of $CHCl_3$-MeOH (50 : 1), followed by recrystallization from MeOH-ether; yield, 438 mg (67%); mp 271—276 °C (decomp); $[\alpha]_D^{29}$ −86.0° (*c* 0.8, DMF); R_f^1 0.72, R_f^2 0.53.

Found: C, 62.87; H, 7.49; N, 12.01%. Calcd for $C_{82}H_{114}O_{16}N_{14}\cdot 1.5\ H_2O$: C 62.37; H, 7.46; N, 12.41 %.

***Cyclo*(-Val-Orn-Leu-D-Ala-Pro-D-Tyr-)$_2\cdot$2HCl (6a).** Compound **5a** (100 mg, 0.052 mmol) was dissolved in 90% MeOH (20 ml) and dioxane (10 ml), and then 1 M HCl (0.11 ml) was added to the solution. The mixture was hydrogenated in the presence of palladium black for 15 h. After the removal of the catalyst, the filtrate was concentrated in vacuo. The product was purified by gel filtration on a Sephadex LH-20 column (ϕ 1.3×120 cm), using MeOH as the solvent, and by reprecipitation from MeOH-ether; yield, 40 mg (55 %); mp 256—259 °C (decomp); $[\alpha]_D^{29}$ −56.0° (*c* 0.2, EtOH); R_f^3 0.76, R_f^4 0.44. Amino acid ratios: Val, 0.98; Orn, 0.97; Leu, 1.00; Ala, 1.11; Pro, 1.01; Tyr, 0.94. MS (FAB), *m/z* 1316 ($C_{66}H_{102}O_{14}N_{14}$, MH^+).

Found: C, 53.75; H, 7.60; N, 13.27%. Calcd for $C_{66}H_{102}O_{14}N_{14}\cdot 2\ HCl\cdot 5\ H_2O$: C, 53.61; H, 7.77; N, 13.26%.

***Cyclo*(-Val-Orn-Leu-D-Phe-Pro-D-Ala-)$_2\cdot$2HCl (6b).** This compound was prepared from **5b** (200 mg, 0.13 mmol) as has been described for the preparation of **6a**; yield, 164 mg (93%); mp 276—279 °C (decomp) $[\alpha]_D^{29}$ −134.1° (*c* 0.4, EtOH); R_f^3 0.62, R_f^4 0.65. Amino acid ratios: Val, 1.00; Orn, 0.98; Leu, 1.00; Phe, 1.02; Pro, 1.03; Ala, 1.07. MS(FAB), *m/z* 1283 ($C_{66}H_{102}O_{12}N_{14}$, MH^+).

Found: C, 55.12; H, 7.42; N, 13.23%. Calcd for $C_{66}H_{102}O_{12}N_{14}\cdot 2\ HCl\cdot 4.5\ H_2O$: C, 55.14; H, 7.92; N, 13.64%.

Cellulose-Plate Electrophoresis. The electrophoresis of the products was carried out with a cellulose (Avicel) plate and a solvent system of HCOOH-AcOH-MeOH-H_2O (1 : 3 : 6 : 10 v/v, pH 2.2) for 2 h at 500 V /20 cm. Each of the peptides revealed a single spot, the mobility being the same as that of GS.

We are grateful to the staff of the Research Laboratories of the Toyo Jozo Co. for their elemental analyses, microbiological assays, and the measurement of the FAB Mass.

References

1) G. G. Zharikova, S. P. Myaskovskaya, and A. B. Silaev *Vesten. Mosk. Univ., Biol. Pochovoved.*, **27**, 110 (1972).

2) S. P. Myaskovskaya, G. G. Zharikova, and A. B. Silaev, *Vestn. Mosk. Univ., Biol. Pochovoved.*, **28**, 123 (1973).

3) M. Tamaki, *Bull. Chem. Soc. Jpn.*, **57**, 3210 (1984).

4) The amino acid residues with no prefix have the L-configuration. The abbreviations for amino acids and peptides are in accordance with the rules of the IUPAC-IBU Commission of Biological Nomencalture. The abbreviations used are as follows: Boc, *t*-butoxycarbonyl; Z, benzyloxycarbonyl; OBzl, benzyloxy; $BzlCl_2$ 2,6-dichlorobenzyl; TFA, trifluoroacetic acid; TEA, triethylamine; NMM, *N*-methylmorpholine; DMF, *N*,*N*-dimethylformamide; AcOEt, ethyl acetate.

5) S. Nozaki and I. Muramatsu, *J. Anitibiot.*, **37**, 689 (1984).

6) S. Lee, R. Ohkawa, and N. Izumiya, *Bull. Chem. Soc. Jpn.*, **44**, 158 (1971).

7) S. N. Semenov, E. I. Mel'nik, L. G. Snezhkov, A. I. Miroshnikov, and V. T. Ivanov, *Bioorg. Khim.*, **3**, 1055 (1977).

8) A. B. Kaprel'yants, V. V. Nikiforev, A. I. Miroshnikov, L. G. Snezhkova, V. A. Eremin, and D. N. Ostrovskii, *Biokhimiya*, **42**, 329 (1977).

9) M. Tamaki, M. Takimoto, S. Nozaki, and I. Muramasu, *J. Chromatogr.*, **413**, 287 (1987).

The Reactions of Tropone Tosylhydrazone Sodium Salt with Acetylene Derivatives Possessing Electron-Withdrawing Groups: A Novel Method of Synthesis of 1*H*-1,2-Benzodiazepine Derivatives

Katsuhiro SAITO
Department of Chemistry, Nagoya Institute of Technology, Gokiso-cho, Showa-ku, Nagoya 466
(Received December 4, 1986)

Reactions of tropone tosylhydrazone sodium salt with dimethyl and diethyl acetylenedicarboxylate gave dimethyl and diethyl 1*H*-1,2-benzodiazepin-3,4-dicarboxylate, respectively. The same reactions, but using ethyl acetylenecarboxylate and 3-butyn-2-one, afforded ethyl 1*H*-1,2-benzodiazepin-4-carboxylate and 4-acetyl-1*H*-1,2-benzodiazepine, respectively, accompanied by 8-azaheptafulvene derivatives derived from the sodium salt and the acetylene derivatives, and *p*-toluenesulfinic esters formed from *p*-toluenesulfinic acid and the acetylene derivatives. Reactions of the sodium salt with ethyl 2-butynoate gave the corresponding sulfinic ester but afforded no diazepine derivative.

It is known that upon heating or irradiation, tropone tosylhydrazone sodium salt (**1**) generates nitrogen gas, sodium *p*-toluenesulfinate (**2**), and cycloheptatrienylidene (**3**), which is considered to be a singlet nucleophilic carbene[1] and to isomerize to an allene, cycloheptatetraene (**4**).[2] When heated in the presence of silver chromate, **1** affords 2-tosyl-2*H*-indazole (**6**) via a hydrazyl radical intermediate (**5**).[3]

The reactions of **1** with olefins have been well-studied and the following results are known. In reactions with ethylene derivatives **1** gives spiro[2.6]nonatriene derivatives (**7**) via the carbene (**3**),[1] on the other hand, in reactions with suitable dienes, such as anthracene, cyclopentadienone, or isobenzofuran derivatives, **1** affords the Diels-Alder-type addition products **8** via the allene (**4**).[2] However, papers concerning the reaction of **1** with acetylene derivatives are limited to reports concerning the reaction of **1** with phenylacetylene, where [2+2]-type adduct (**9**) and 2-phenylindene (**10**) are formed. The former is afforded via the allene-form (**4**) and the latter via an isomerization of **9**.[2]

As one part of the study on the reactivity of **1**, reactions of **1** with acetylene derivatives possessing electron-withdrawing groups were investigated to form benzo-1,2-diazepine derivatives, heptafulvene derivatives, and esters of *p*-toluenesufinic acid. Here, these results will be discussed.

Results

Tropone tosylhydrazone sodium salt (**1**) was allowed to react with two molar equivalents of dimethyl acetylenedicarboxylate (**11**) at 120 °C for 15 min in anhydrous diglyme. The ether extraction of the reaction mixture followed by silica-gel column chromatographic purification gave benzo-1,2-diazepine derivative (**12**) in a 34.0% yield. The same reaction, but using diethyl acetylenedicarboxylate (**13**), afforded the corresponding benzo-1,2-diazepine derivative (**14**)[4] in a 32.3% yield.

Reactions of **1** with ethyl acetylenecarboxylate (**15**) under analogous conditions as above afforded three products, benzo-1,2-diazepine derivative (**16**), 8-azaheptafulvene derivative (**17**), and ester of *p*-toluenesufinic acid (**18**) in the yields of 51.9, 1.5, and 24.8%, respectively. The same type of reaction of **1** with 3-butyn-2-one (**19**) gave benzo-1,2-diazepine derivative (**20**) and heptafulvene derivative (**21**) in the yields of 5.7 and 6.3%, respectively. The reaction of **1** with ethyl 2-butynoate (**22**) yielded sulfinic ester (**23**) in a 9.1% yield but gave no benzo-1,2-diazepine derivative. Reactions of **1** with diphenylacetylene (**24**) and 1-butyne (**25**) afforded no reaction product except **2** and polymeric resinous material.

The structure of **14** was determined on the basis of

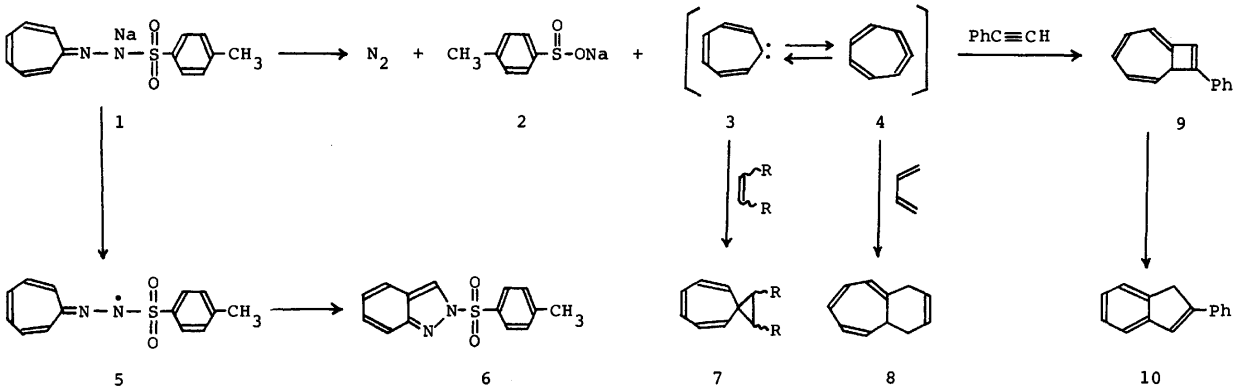

Fig. 1.

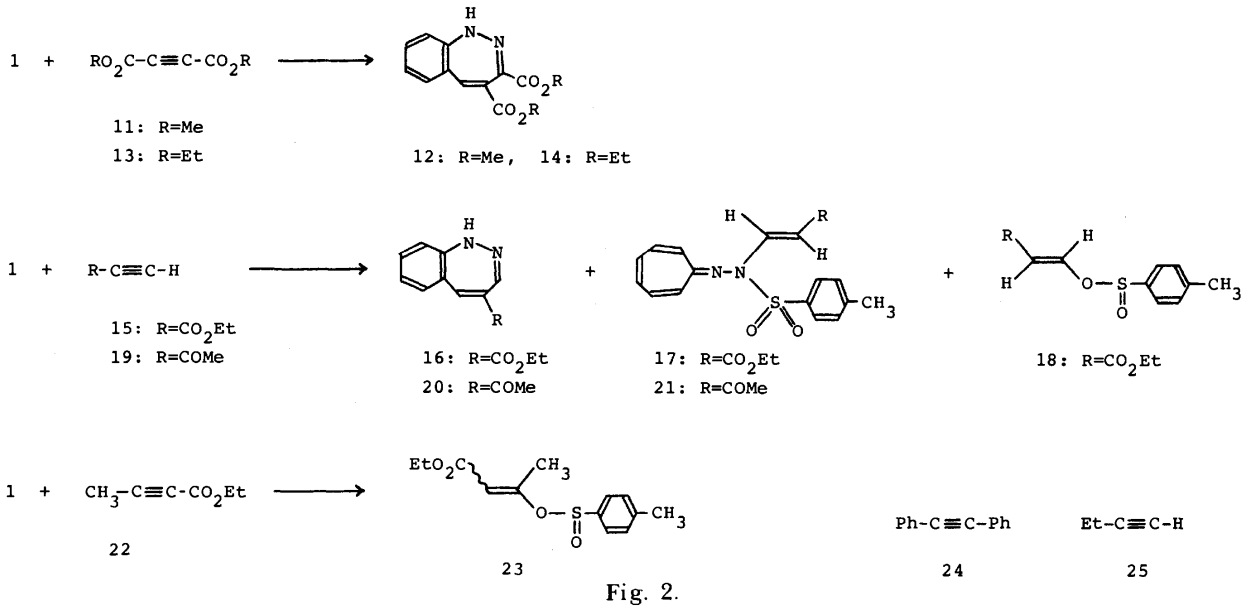

Fig. 2.

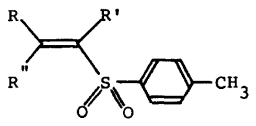

26

Fig. 3.

its spectral properties and was confirmed by a comparison of its melting point and spectral properties with those of the authentic sample.[4] The structures of the another benzo-1,2-diazepines were determined by the resemblance of their spectral properties to those of the analogous benzo-1,2-diazepines containing **14**.[4] The structures of **17** and **21** were determined as follows. The molecular ion peaks in their mass spectra and the elemental analyses show that **17** and **21** are the addition products of tropone tosylhydrazone and the corresponding acetylene derivatives (**15** and **19**), respectively. The multiplet signals corresponding to six protons at around δ 6.5—7.1 in the NMR spectra[5] and the absorption maximum at long wavelength in the UV spectra[6] suggest the existence of the 8-azaheptafulvene moiety in these products. The coupling constants (14 Hz) between the olefinic protons show that the configuration of these two protons is trans-configuration.[7]

The structures of **18** and **23** were determined on the basis of their spectral properties as follows. The coupling constant (15 Hz) between the olefinic protons shows that these two protons in **18** are in trans-configuration each other.[7] The absorption at 1150 cm^{-1} in the IR spectra demonstrates that the SO_2 groups of these products are sulfinyl groups and not sulfonyl groups such as **26**.[8]

Discussion

The formation of benzo-1,2-diazepine derivatives can be explained to be as follows. The thermal decomposition of the sodium salt (**1**) generates diazotropilidene (**27**).[9] The Michael-type addition of the anionic nitrogen atom of **27** to the acetylene derivatives[10] forms an ionic intermediate (**28**),[9e,11] which gives the bicyclic intermediate (**29**) by intramolecular cyclization. The valence tautomerization in the tropylidene moiety of **29** affords the norcaradiene-type intermediate (**30**),[12] which then forms the final products, benzo-1,2-diazepine derivatives via the cleavage of the three-membered ring.

The formation of the 8-azaheptafulvene dereivatives (**17**, **21**) and the sulfinic esters (**18**, **23**) are considered to proceed through Michael-type additions of the anions of tropone tosylhydrazone and *p*-toluenesulfinic acid to the corresponding acetylene derivatives, respectively.

There is an evident difference between reactions of **1** with acetylenes and reactions of **1** with olefins. It was clarified that reactions of **1** with acetylenes possessing electron-withdrawing groups proceed via diazotropilidene but that reactions with olefins proceed via carbene (**3**) or the allene (**4**). For example, the reaction of **1** with dimethyl acetylenedicarboxylate gives the benzo-1,2-diazepine derivative via diazotropilidene (**27**); on the other hand, reactions of **1** with dimethyl fumarate or maleate afford the spiro compounds **7** via the carbene (**3**).[1] No such product as **31** has ever been formed.

These differences in the reactivity can be explained as follows. The primary product of the decomposition of **1** is diazotropylidene (**27**).[9,13] In the case of the existence of acetylenes possessing electron-withdrawing groups, **27** reacts with the acetylenes to form **29** [Path A]. It is known that the nucleophilic reactions of reagents such as amines or imines with acetylene derivatives proceed easily more than do reactions with ethylene derivatives.[10] If there are no suitable acetylenes, **27** further decomposes to the carbene (**3**) or the allene (**4**) [Path B]. Probably, this decomposition of **27** proceeds more quickly than the reaction of **27** with olefins

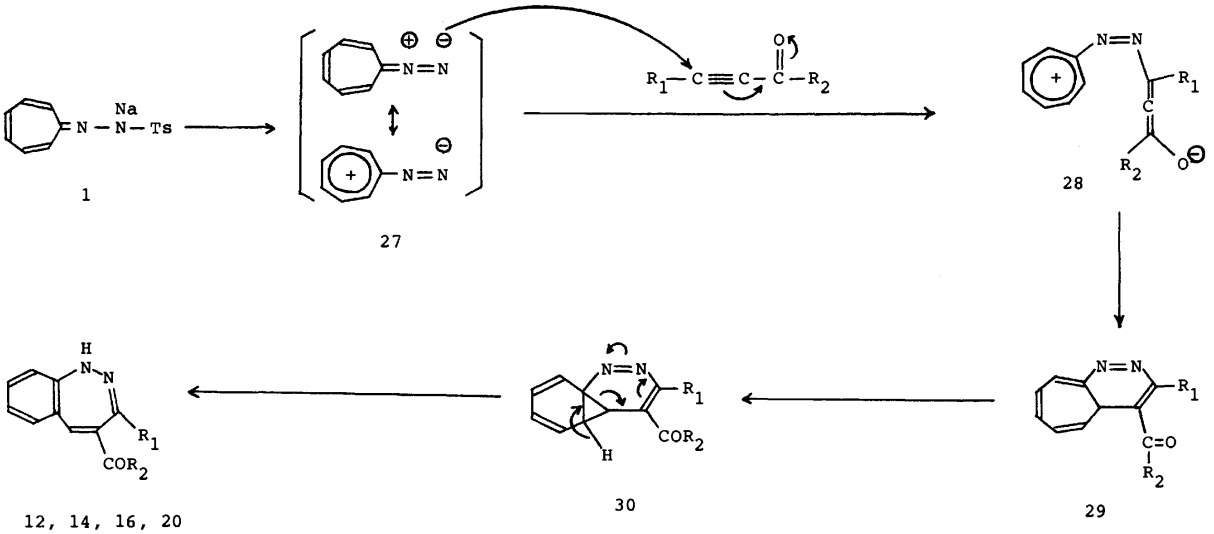

Fig. 4.

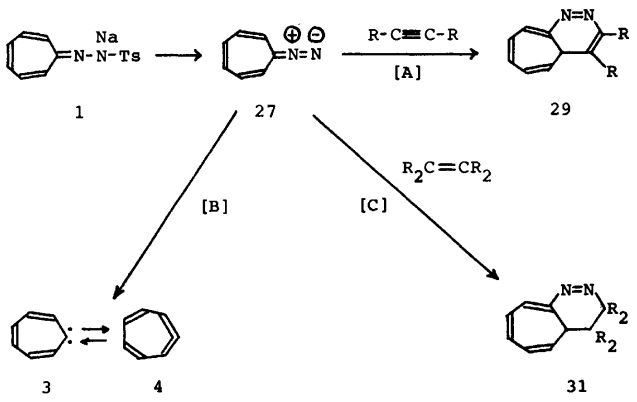

Fig. 5.

to give **31** [Path C].

The fact that reactions of **1** with the acetylene derivatives **22** and **25**, which have electron-donating groups do not afford the benzo-1,2-diazepine derivatives seems to partially support the above considerations. The inactivity of **27** toward diphenylacetylene (**24**) can be attributed to the fact that **24** have no strong electron-withdrawing groups.

Experimental

All melting points were uncorrected. NMR spectra were measured with Varian XL 200 or Hitachi R-20B spectrometers with tetramethylsilane as an internal standard. UV and IR spectra were measured with Hitachi 220A and DS-701G spectrometers, respectively. Mass spectra were measured with Hitachi M-52 or JMS-DX300 spectrometers. Wako gel C 200 and Wako gel B5F were used for column and thin-layer chromatography, respectively. Diglyme was dried over Molecular Sieves 3A 1/16.

Reaction of Tropone Tosylhydrazone Sodium Salt (1) with Dimethyl Acetylenedicarboxylate (11). A mixture of **1** (14.80 g, 50 mmol) and **11** (14.60 g, 100 mmol) in anhydrous diglyme (70 ml) was heated at 120 °C for 15 min. The reaction mixture was poured into water, extracted with ether, washed with water and brine, and dried over anhydrous sodium sulfate. After filtration the solvent was removed on a rotary evaporator to give a mixture of crystals of **12** and an oil. The crystals of **12** (4.010 g) were removed by filtration and the filtrate was column-chromatographed on silica gel to give the crystals of **12** (405 mg) by the use of benzene-ether 8:2. The total yield of **12** was 4.415 g, 34.0%. The crystals were recrystallized from cyclohexane to give pure crystals **12**.

12: Mp 153—154 °C. Found: C, 60.10; H, 4.95; N, 10.85%. Calcd for $C_{13}H_{12}N_2O_4$: C, 59.99; H, 4.95; N, 10.77%. Mass *m/z* (rel intensity) 260 (M^+, 22), 175 (12), 143 (100), 142 (30), 139 (29), 115 (34). IR (KBr) 3350, 3020, 2950, 1730, 1640, 1600 cm^{-1}. UV (EtOH) 204 nm (log ε, 4.21), 257 (4.16), 285 (sh, 4.02). ^1H NMR (CD_3COCD_3) δ=3.70 (3H, s), 3.71 (3H, s), 6.8—7.4 (4H, m), 7.86 (1H, s), 8.10 (1H, broad s).

Reaction of Tropone Tosylhydrazone Sodium Salt (1) with Diethyl Acetylenedicarboxylate (13). A mixture of **1** (5.92 g, 20 mmol) and **13** (17.00 g, 100 mol) in anhydrous diglyme (50 ml) was heated at 120 °C for 15 min. The reaction mixture was treated as usual and chromatographed on silica gel to give crystals of **14** (1.86 g, 32.3%, mp 113—114 °C, lit,[4] 114° C) by the use of benzene-ether 8:2.

14: ^1H NMR (CD_3COCD_3) δ=1.28 (6H, two triplets), 4.15 (4H, two quartets), 6.75 (4H, m), 7.45 (1H, s), 7.80 (1H, broad s).

Reaction of Tropone Tosylhydrazone Sodium Salt (1) with Ethyl Acetylenecarboxylate (15). A mixture of **1** (5.92 g, 20 mmol) and **15** (9.80 g, 100 mmol) in anhydrous diglyme (50 ml) was heated at 120 °C for 15 min and the reaction mixture was treated as usual. The resulted oily material was column-chromatographed on silica gel to give crystals of **18** (1.26 g, 24.8%) by the use of benzene, crystals of **17** (110 mg, 1.5%) by the use of benzene-ether 50:1, and crystals of **16** (3.02 g, 51.9%) by the use of benzene-ether 50:1. The crystals of **16**, **17**, and **18** were recrystallized from cyclohexane to give pure compounds, respectively.

16: Mp 93—94 °C. Found: C, 66.59; H, 5.49; N, 13.09%. Calcd for $C_{12}H_{12}N_2O_2$: C, 66.65; H, 5.59; N, 12.96%. MS *m/z* (rel intensity): 216 (M^+, 63), 171 (14), 144 (18), 143 (100). IR (KBr) 3320, 3020, 2950, 1710, 1630. 1595 cm^{-1}. UV (EtOH): 211 nm (log ε, 4.13), 258 (4.22), 303 (sh, 3.45). ^1H NMR (CD_3COCD_3) δ=1.30 (3H, t), 4.24 (2H, q), 6.7—7.2 (4H, m), 7.32 (1H, d, J=1.5 Hz), 7.68 (1H, broad s), 7.78 (1H, d, J=1.5 Hz).

17: Mp 125—126 °C. Found: C, 61.33; H, 5.32; N, 7.41%.

Calcd for $C_{19}H_{20}N_2O_4S$: C, 61.27; H, 5.41; N, 7.52%. MS *m/z* (rel intensity): 372 (M^+, 2), 327 (3), 217 (100), 190 (3), 189 (5). IR (KBr) 3060, 2970, 1712, 1615, 1360, 1160 cm^{-1}. UV (EtOH): 235 nm (log ε, 4.39), 277 (4.18), 315 (4.05), 346 (sh, 3.95). ^1H NMR ($CDCl_3$) δ=1.25 (3H, t), 2.40 (3H, t), 4.11 (2H, q), 4.93 (1H, d, *J*=14 Hz), 6.5—7.2 (6H, m), 7.24 (2H, d, *J*=8 Hz), 7.74 (2H, d, *J*=8 Hz), 8.08 (1H, d, *J*=14 Hz).

18: Mp 89—90 °C: Found: C, 56.89, H, 5.52%. Calcd for $C_{12}H_{14}O_4S$: C, 56.69; H, 5.55%. MS *m/z* (rel intensity): 254 (M^+, 13), 145 (10), 139 (100), 97 (19). IR (KBr): 3050, 2970, 1720, 1595, 1310, 1240, 1150 cm^{-1}. UV (EtOH): 246 nm (log ε, 3.99). ^1H NMR ($CDCl_3$) δ=1.28 (3H, t), 2.47 (3H, s), 4.26 (2H, q), 6.26 (1H, d, *J*=15 Hz), 7.34 (2H, d, *J*=8 Hz), 7.36 (1H, d, *J*=15 Hz), 7.77 (2H, D, *J*=8 Hz).

Reaction of Tropone Tosylhydrazone Sodium Salt (1) with 3-Butyn-2-one (19). A mixture of **1** (5.92 g, 20 mmol), **19** (6.80 g, 100 mmol) in anhydrous diglyme (50 ml) was heated at 120 °C for 15 min. After the usual workup, the resulted oily material was column-chromatographed on silica gel to give an oily material, which was then thin-layer-chromatographed on silica gel using ether as a developing solvent to give an oil of **20** (210 mg, 5.7%, R_f=0.80) and an oil of **21** (430 mg, 6.3%, R_f=0.55).

20: Found: *m/z* 186.0814. Calcd for $C_{11}H_{10}N_2O$: *m/z* 186.0793. MS *m/z* (rel intensity) 186 (M^+, 100), 171 (18), 144 (58), 116 (25). IR (oil): 3350, 3020, 2960, 1670, 1600, 1465 cm^{-1}. UV (EtOH): 258 nm (log ε, 4.21, 310 (sh, 3.58). ^1H NMR (CD_3COCD_3) δ=2.41 (3H, s), 6.7—7.2 (4H, m), 7.45 (1H, d, *J*=1.5 Hz), 7.60 (1H, bs), 7.73 (1H, d, *J*=1.5 Hz).

21: Found: *m/z* 342.1027. Calcd for $C_{18}H_{18}N_2O_3S$: *m/z* 342.1038. MS *m/z* (rel intensity) 342 (M^+, 2), 230 (100), 215 (90), 187 (83), 135 (69). IR (oil): 3030, 2970, 1680, 1535, 1365, 1160 cm^{-1}. UV (EtOH): 237 nm (log ε, 4.32), 282 (4.15), 331 (sh, 3.80). NMR ($CDCl_3$) δ=2.3 (3H, s), 5.20 (1H, d, *J*=14 Hz), 6.5—7.0 (6H, m), 7.16 (2H, d, *J*=8 Hz), 7.60 (2H, *J*=8 Hz), 7.90 (1H, d, *J*=14 Hz).

Reaction of Tropone Tosylhydrazone Sodium Salt (1) with Ethyl 2-Butynoate (22). A mixture of **1** (5.92 g, 20 mmol) and **22** (4.48 g, 40 mmol) in anhydrous diglyme (30 ml) was heated at 120 °C for 15 min. After the usual treatment the resulted oily material was column-chromatographed on silica gel to give an oily material (1.04 g) by the use of benzene–ether 9:1. The oily material was thin-layer-chromatographed on silica gel using benzene–ether 9:1 as a developing solvent to give an oil of **23** (490 mg, 9.1%, R_f=0.8).

23: Found: *m/z* 268.0794. Calcd for $C_{13}H_{16}O_4S$: *m/z* 268.0770. MS *m/z* (rel intensity) 268 (M^+, 16), 222 (30), 139 (38), 103 (100). IR (oil): 3030, 2970, 1720, 1595, 1320, 1200, 1150 cm^{-1}. UV (EtOH) 247 nm (log ε , 4.07). ^1H NMR ($CDCl_3$) δ=1.23 (3H, t), 2.20 (3H, s), 2.36 (3H, s), 4.12 (2H, q), 6.23 (1H, s), 7.18 (2H, d), 7.58 (2H, d).

The author is indebted to Professor Toshio Mukai of Tohoku University and Professor Takashi Toda of Utsunomiya University for their fruitful suggestions. The present work was partially supported by a Grant-in-Aid for Science Research No. 274152 from the Ministry of Education, Science and Culture.

References

1) W. M. Jones and C. L. Ennis, *J. Am. Chem. Soc.*, **89**, 3069 (1967); T. Mukai, T. Nakazawa, and K. Isobe, *Tetrahedron Lett.*, **1968**, 565; W. M. Jones and C. L. Ennis, *J. Am. Chem. Soc.*, **91**, 6391 (1969); R. C. Joines, A. B. Turner, and W. M. Jones, *ibid.*, **91**, 7754 (1969); J. W. Baron, M. Jones, Jr., *ibid.*, **92**, 4739 (1970); W. D. Crow and M. N. Paddon-Row, *ibid.*, **94**, 4746 (1972); L. W. Christensen, E. E. Waali, and W. M. Jones, *ibid.*, **94**, 2118 (1972); E. E. Waali and W. M. Jones, *ibid.*, **95**, 8114 (1973); *idem*, *J. Org. Chem.*, **38**, 2573 (1973); T. Mitsuhashi and W. M. Jones, *J. Chem. Soc., Chem. Commun.*, **1974**, 103.

2) C. Mayor and W. M. Jones, *Tetrahedron Lett.*, **1977**, 3855; K. Saito, Y. Omura, and T. Mukai, *Chem. Lett.*, **1980**, 349; J. W. Harris and W. M. Jones, *J. Am. Chem. Soc.*, **104**, 7329 (1982); K. Saito, Y. Omura, and T. Mukai, *Bull. Chem. Soc. Jpn.*, **58**, 1663 (1985); K. Saito and H. Ishihara, *ibid.*, **58**, 2664 (1985); R. O. Angus, Jr., M. W. Schmidt, and R. P. Johnson, *J. Am. Chem. Soc.*, **107**, 532 (1985); K. Saito and H. Ishihara, *Bull. Chem. Soc. Jpn.*, **59**, 1095 (1986).

3) K. Saito, T. Toda, and T. Mukai, *Heterocycles*, **3**, 445 (1975); K. Saito, T. Toda, and T. Mukai, *Bull. Chem. Soc. Jpn.*, **57**, 1567 (1984).

4) L. Garanti, A. Scandroglio, and G. Zecchi, *Tetrahedron Lett.*, **1975**, 3349; L. Garanti and G. Zecchi, *J. Chem. Soc., Perkin Trans. 1*, **1977**, 2092.

5) D. J. Bertelli and T. G. Andrews, Jr., *J. Am. Chem. Soc.*, **91**, 5280, 5286 (1969); Y. Kitahara, T. Asao, and M. Oda, "Kagaku Sosetsu," ed by S. Ito, Chemical Society of Japan (1977), pp. 109, 113.

6) T. Nozoe, T. Mukai, and T. Suzuki, *Bull. Chem. Soc. Jpn.*, **36**, 38 (1963); M. Oda and Y. Kitahara, *Chem. Ind.*, **1969**, 920; C. Jutz, *Chem. Ber.*, **97**, 2050 (1964); H. Tsuruta, T. Sugiyama, and T. Mukai, *Chem. Lett.*, **1972**, 185; T. Asao, N. Morita, and Y. Kitahara, *J. Am. Chem. Soc.*, **94**, 3655 (1972); T. Toda, K. Saito, and T. Mukai, *Bull. Chem. Soc. Jpn.*, **52**, 151 (1979).

7) T. Schaefer, *Can. J. Chem.*, **40**, 1 (1962); M. Karplus, *J. Am. Chem. Soc.*, **85**, 2870 (1963); P. Laszlo and P. von R. Schleyer, *Bull. Soc. Chim. Fr.*, **1964**, 87.

8) J. S. Waugh and F. A. Cotton, *J. Phys. Chem.*, **65**, 562 (1961); M. Oki and H. Iwamura, *Bull. Chem. Soc. Jpn.*, **35**, 1428 (1962); J. W. Wilt and W. J. Wagner, *Chem. Ind.*, **1964**, 1389; K. Nakanishi, "Sekigaisen Kyushu Supekutoru," Nankodo, Japan (1967).

9) a) D. M. Kaufman, J. A. Smith, G. G. V. Stouw, and H. Shechter, *J. Am. Chem. Soc.*, **87**, 935 (1965); b) R. M. McDonald and R. A. Krueger, *J. Org. Chem.*, **31**, 488 (1966); c) T. Miyashi, Y. Nishizawa, T. Sugiyama, and T. Mukai, *J. Am. Chem. Soc.*, **99**, 6109 (1977); d) R. M. Willson and J. W. Reckers, *ibid.*, **101**, 4005 (1979); e) A. Padwa and Hao Ku, *Tetrahedron Lett.*, **1979**, 4425; **21**, 1009 (1980).

10) C. W. Kruse and R. F. Kleinschmidt, *J. Am. Chem. Soc.*, **83**, 213, 216 (1961); K. E. Schulte, J. Reisch, and H. Walker, *Chem. Ber.*, **98**, 98 (1965); I. A. Chekulaeva and L. V. Kondrateva, *Usp. Khim.*, **34**, 1583 (1965); K. Bowden and M. J. Price, *J. Chem. Soc., B*, **1970**, 1466; E. K. Raunio and T. G. Frey, *J. Org. Chem.*, **36**, 345 (1971).

11) N. El-Ghandour, O. Henri-Rousseau, and J. Soulier, *Tetrahedron Lett.*, **1972**, 2817; J. Hamelin and R. Carrier, *Bull. Soc. Chim. Fr.*, **1972**, 3511; A. A. Reid, J. T. Sharp, H. R. Sood, and P. B. Thorogood, *J. Chem. Soc., Perkin Trans. 1*, **1973**, 2543; J. T. Sharp, R. H. Findlay, and P. B. Thorogood, *ibid.*, **1975**, 102; J. Dingwall and J. T. Sharp, *J. Chem. Soc., Chem. Commun.*, **1975**, 128; R. Huisgen, H. U.

Reissig, and H. Hulber, *J. Am. Chem. Soc.*, **101**, 3647 (1979).
12) T. Mukai, T. Nakazawa, and K. Okayama, *Tetrahedron Lett.*, **1968**, 1695; T. Toda, M. Nitta, and T. Mukai, *ibid.*, **1969**, 4401; W. R. Hoffmann, *ibid.*, **1970**, 2907; H. Gunther, *ibid.*, **1970**, 5173; R. H. Bradbury, T. L. Gilchrist, and C. W. Rees, *J. Chem. Soc., Chem. Commun.*, **1979**, 528; O. D. Lucchi, F. Filipuzzi, and V. Lucchini, *Tetrahedron Lett.*, **25**, 1407, (1984); G. Bocche and R. Eiben, *ibid.*, **26**, 1289 (1985).
13) I. Moritani, S. I. Murahashi, M. Nishino, Y. Yamamoto, K. Itoh, and N. Mataga, *J. Am. Chem. Soc.*, **89**, 1259 (1967); S. I. Murahashi, I. Moritani, and M. Nishino, *Tetrahedron*, **27**, 5131 (1971).

 © 1987 The Chemical Society of Japan Bull. Chem. Soc. Jpn., 60, 2111—2115 (1987)

Crystal Structure of TTF·BTDA-TCNQ Complex. A New Type of CT Complex with an Inclusion Behavior and a Multi-Dimensional Structure

Takanori SUZUKI, Chizuko KABUTO,† Yoshiro YAMASHITA, and Toshio MUKAI*
Department of Chemistry, Faculty of Science, Tohoku University, Aramaki, Sendai 980
†Instrumental Analysis for Chemistry, Faculty of Science, Tohoku University, Aramaki, Sendai 980
(Received December 5, 1986)

The crystal structure of TTF·BTDA-TCNQ complex was determined by an X-ray diffraction method. The crystals are monoclinic, space group $P2_1/n$ with a=9.660(1), b=7.231(1), c=14.628(2) Å, β=91.31(1)°, and Z=2. The structure was solved by the direct method and refined by the block-diagonal least-squares method to give an R value of 0.040 for non-zero 2620 reflections. The complex is nonionic and the molecules form equally spaced mixed stacks along the b axis. These stacks are connected by strong transverse interactions resulting in a three-dimensional structure. BTDA-TCNQ molecules make cavities by S-N≡C interactions in which TTF molecules are included. This complex is not a simple CT complex with mixed stacks but rather the one with some inclusion behavior.

Recently, we have reported the preparation[1] and crystal structure[2] of bis(1,2,5-thiadiazolo)tetracyanoquinodimethan (BTDA-TCNQ),[3] which forms a two-dimensional "sheet-like network" by strong S-N≡C interactions in crystalline state. Thus, the charge-transfer complex or ion-radical salt of BTDA-TCNQ is proposed to exhibit a high-dimensional structure which could stabilize the metallic state[4] and induce the electrical conductivity along the side-by-side directions. In the course of our examination for the CT complexes of BTDA-TCNQ, the donors with the larger size such as tetrathianaphthacene (TTN) and dimethyldihydrophenazine (DMPH) have been proved to give highly conductive complexes with BTDA-TCNQ.[5,6] On the other hand, the CT complexes with tetrathiafulvalene (TTF) and its analogues exhibit very low electrical conductivities[5,6] though TTF·TCNQ complex is a representative organic metal.[7] We have succeeded in obtaining single crystals of TTF·BTDA-TCNQ.[8] This report describes the structural analysis of the title complex from which the causes of the low conductivity are discussed.

Experimental

TTF·BTDA-TCNQ complex (decomp 247—248 °C) was prepared by a diffusion method in dichloromethane using an H-shaped tube. The molar ratio was determined to be 1 : 1 on the basis of the elemental analysis. Found: C, 41.26; H, 0.58; N, 20.69; S, 36.72%. Calcd for $C_{18}H_4N_8S_6$: C, 41.20; H, 0.77; N, 21.35; S, 36.68%. A platelike crystal with dimensions of 0.15×0.20×0.25 mm was used for the data collection on a Rigaku automated four-circle diffractometer (AFC-5), equipped with a rotating anode (50 kV, 200 mA), using graphite-monochromated MoK_α radiation (λ=0.71069 Å). Crystal data are as follows; a=9.660(1), b=7.231(1), c=14.628(2) Å, β=91.31(1)°, V=1021.5(4) Å^3, $P2_1/n$, Z=2, D_{calcd}=1.71 g cm^{-3}. The ω—2θ scan mode with a scan rate of 4° min^{-1} was employed with the ω scan range (1.0+0.5 tanθ)°. A total of 2915 reflections within 2θ=55° was collected. No absorption correction was applied.

The structure was solved by the direct method using RANTAN81[9] with some modification. The parameters of all the non-hydrogen atoms were refined by the block-diagonal least-squares method with the anisotropic temperature factors. Although the positions of hydrogen atoms were located by a difference Fourier map, the geometrically calculated ones were included in the refinement. The final R value ($R=\sum||F_o|-|F_c||/\sum|F_o|$) is 0.040 for 2620 non-zero reflections. The atomic coordinates are given in Table 1.

The atomic scattering factors from the International Tables for X-ray Crystallography[10] were used. All the computation were carried out by an ACOS 1000 computer at Tohoku University using the applied library program of UNICSIII system.[11]

Results and Discussion

Molecular Structure. Figures 1 and 2 show the thermal ellipsoids of the BTDA-TCNQ and TTF molecule, respectively. Since Z=2 in the space group $P2_1/n$, BTDA-TCNQ and TTF molecules are both restrictly related by a center of symmetry in the unit cell. Each molecule takes an almost planar conformation and the slight deviations of atoms from the

Table 1. Fractional Atomic Coordinates (×10^4) and Equivalent Temperature Factors (Å^2)

Atom	x	y	z	B_{eqv}[a)]
S 1	7057(1)	432(1)	3598(0)	3.1
N 1	7269(2)	870(3)	4676(1)	2.8
N 2	8594(2)	−271(3)	3356(1)	2.8
C 1	8587(2)	456(3)	4889(2)	2.3
C 2	9352(2)	−196(3)	4132(2)	2.3
C 3	9188(2)	722(3)	5806(2)	2.3
C 4	8467(2)	1391(3)	6520(2)	2.4
C 5	7001(2)	1786(3)	6498(2)	3.0
C 6	9067(2)	1764(3)	7411(2)	2.8
N 3	5863(2)	2097(4)	6589(2)	4.7
N 4	9404(2)	2130(4)	8140(2)	3.8
S 2	6862(1)	961(1)	9323(0)	2.9
S 3	6336(1)	−122(1)	11228(0)	2.9
C 7	8231(2)	1122(4)	10118(2)	3.4
C 8	7988(3)	636(4)	10961(2)	3.5
C 9	5667(2)	187(3)	10114(2)	2.4

a) $B_{eqv}=(4/3)\sum_{ij}\beta_{ij}(a_i\cdot a_j)$.

Table 2. Comparison of Bond Lengths (Å) in BTDA-TCNQ

Bond	BTDA-TCNQ^{0} a)	BTDA-TCNQ^{-} b)	TTF complex
a	1.617(6)	1.614(4)	1.616(2)
b	1.330(4)	1.346(6)	1.338(3)
c	1.422(6)	1.443(5)	1.426(3)
d	1.457(6)	1.437(6)	1.462(3)
e	1.356(7)	1.390(6)	1.358(3)
f	1.438(6)	1.429(7)	1.442(3)
g	1.143(5)	1.140(6)	1.136(4)

a) Ref. 2. b) Ref. 20.

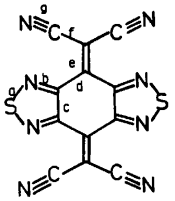

Table 3. Comparison of Bond Lengths (Å) in TTF

Bond	TTF^{0} a)	TTF^{+} b)	BTDA-TCNQ complex
a	1.349(3)	1.404(14)	1.352(3)
b	1.757(2)	1.713(9)	1.750(2)
c	1.730(2)	1.725(11)	1.743(3)
d	1.314(3)	1.306(16)	1.309(4)

a) Ref. 12. b) Ref. 13.

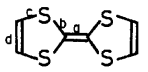

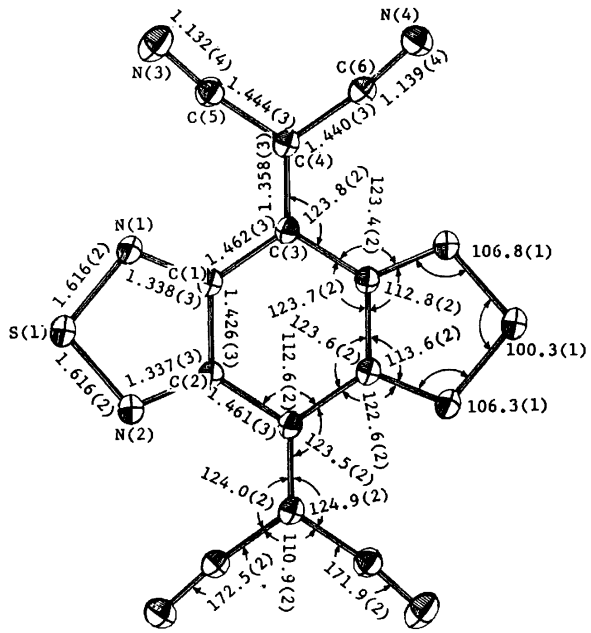

Fig. 1. ORTEP drawing of BTDA-TCNQ molecule with the bond lengths (l/Å) and bond angles (ϕ/°).

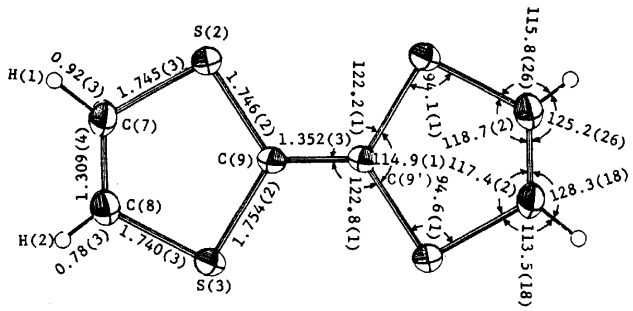

Fig. 2. ORTEP drawing of TTF molecule with the bond lengths (l/Å) and bond angles (ϕ/°).

molecular plane in BTDA-TCNQ indicate the twisting around the *exo*-methylene double bond (5.1°). Tables 2 and 3 show the comparisons of bond lengths of BTDA-TCNQ and TTF in the present complex with those in the neutral molecules or the ion-radical species. It is apparent that the present complex is nonionic as indicated by the degree of charge transfer (Z=0.06) estimated from the bond lengths of C(3)=C(4) (bond e) of BTDA-TCNQ and C(9)=C(9′) (bond a) of TTF.[14]

Crystal Structure and Molecular Packing. Three views of the crystal structure are shown in Figs. 3—5. TTF and BTDA-TCNQ form a mixed stack with the equal space of 3.40 Å. This type of a mixed stacking is often observed in the CT complexes of TCNQ which exhibit low electrical conductivities.[15] The low conductivity of the present complex can be attributed to this mixed stack formation as well as the small degree of the charge transfer from TTF to BTDA-TCNQ. The mixed stack formation is favored when the symmetry of HOMO of the donor is similar to that of LUMO of the acceptor.[15] Thus, molecules tend to overlap in a "ring-double bond type"[16] with a highly symmetrical superimposition so as to maximize the

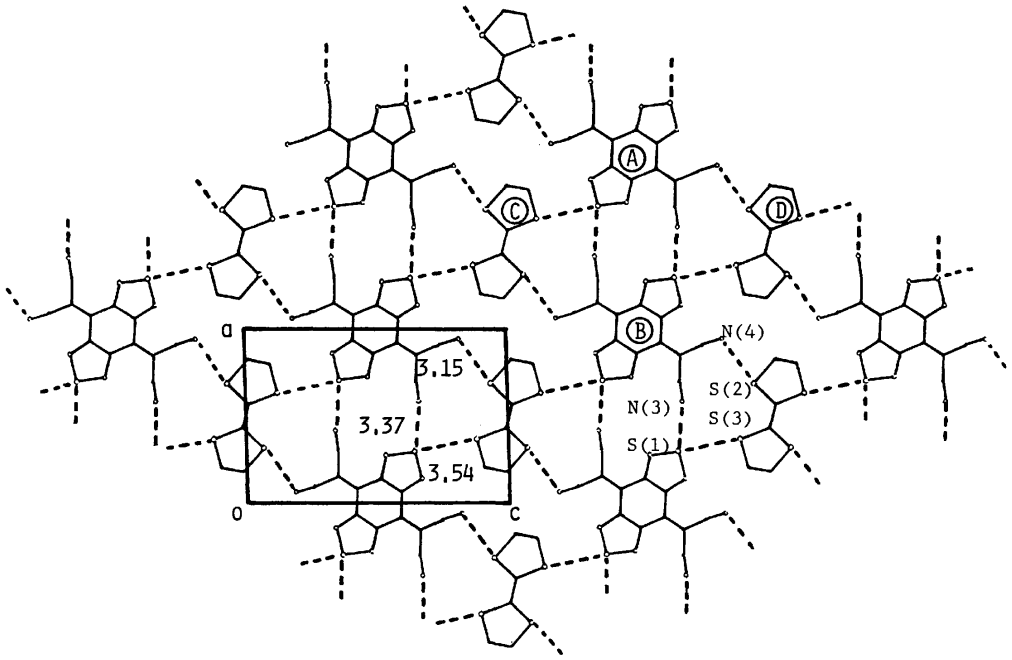

Fig. 3. "Sheet-like network" in the ac plane. S(1)-N(3)≡C(5) (3.37 Å), S(2)-N(4) (3.15 Å) and S(1)-S(3) (3.54 Å) interactions are indicated by broken line. Molecules A-D are related by the following symmetry operations: A (x,y,z and $2-x,-y,1-z$); B ($-1+x,y,z$ and $1-x,-y,1-z$); C ($x,y,-1+z$ and $1-x,-y,1-z$); D (x,y,z and $1-x,-y,2-z$).

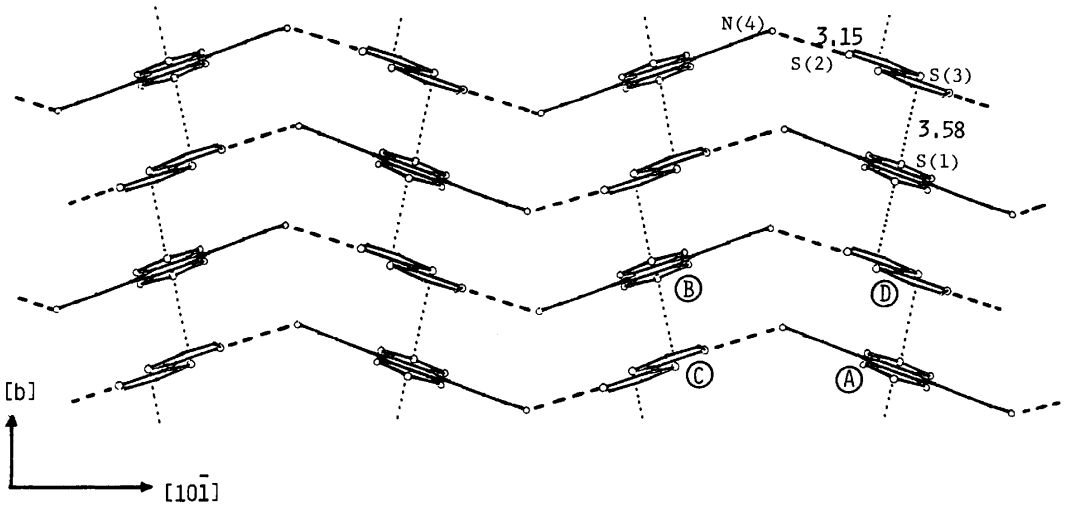

Fig. 4. Corrugation of the "sheet". The drawing of (10$\bar{1}$) plane. S(2)-N(4) (3.15 Å) interactions are indicated by broken line. S(1)-S(3) (3.58 Å) interactions along the b axis are indicated by dotted line. Molecules A—D are related by the following symmetry operations: A (x,y,z and $2-x,-y,1-z$); B ($-0.5+x,0.5-y,0.5+z$ and $1.5-x,0.5+y,1.5-z$); C (x,y,z and $1-x,-y,2-z$); D ($0.5+x,0.5-y,-0.5+z$ and $1.5-x,0.5+y,1.5-z$).

CT interaction in the mixed stacks. As shown in Fig. 6, the molecular overlapping of this complex is not such a type, but BTDA-TCNQ and TTF molecules are tightly connected by S(1)-S(3) (3.58 Å) and N(1)-S(3) (3.47 Å) interactions. These facts indicate that the mixed stacks in the present complex are formed by the direct interactions between heteroatoms rather than the charge-transfer interaction through the π-electron overlapping. Similar mode of overlapping is found in TTF·bis(1,2,5-thiadiazolo)benzoquinone[3] (1 : 1) complex and TTF·(1,2,5-thiadiazolo)naphthoquinone[3] (1 : 2) complex.[17]

The more interesting feature in the crystal is that the mixed stacks are connected by several transverse interactions resulting in the formation of a complicated three-dimensional network as a whole. In the ac plane perpendicular to the stacking b axis, the TTF and BTDA-TCNQ molecules form lines along the a axis and arranged alternately along the c axis. In this ac plane BTDA-TCNQ molecules are connected by weak S(1)-N(3)≡C(5) linkages (3.37 Å; molecules A and B in Fig. 3) and also connected by strong S(1)-S(3) (3.54 Å;

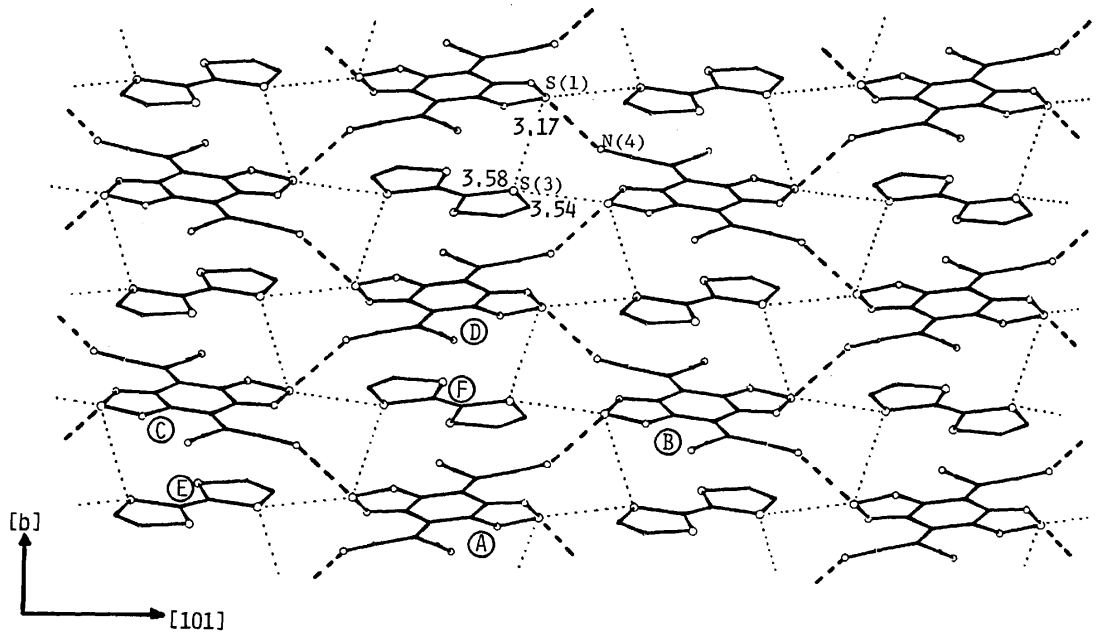

Fig. 5. Cavity formation of BTDA-TCNQ. The drawing of (101) plane. S(1)-N(4)≡C(6) (3.17 Å) interactions are indicated by broken line. S(1)-S(3) interactions along the b axis (3.58 Å) and along [101] direction (3.54 Å) are indicated by dotted line. Molecules A—F are related by the following symmetry operations: A (x,y,z and $2-x,-y,1-z$); B ($0.5+x,0.5-y,0.5+z$ and $2.5-x,0.5+y,1.5-z$); C ($-0.5+x,0.5-y,-0.5+z$ and $1.5-x,0.5+y,0.5-z$); D ($x,1+y,z$ and $2-x,1-y,1-z$); E ($x,y,z-1$ and $1-x,-y,1-z$); F ($0.5+x,0.5-y,-0.5+z$ and $1.5-x,0.5+y,1.5-z$).

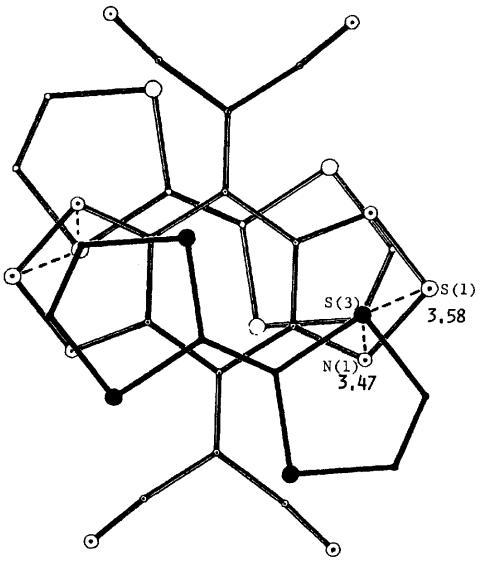

Fig. 6. Molecular overlapping of TTF and BTDA-TCNQ viewed perpendiculer to the molecular plane of BTDA-TCNQ. S(1)-S(3) (3.58 Å) and S(3)-N(1) (3.47 Å) interactions are indicated by broken line.

molecules A and C in Fig. 3) and S(2)-N(4)≡C(6) (3.15 Å; molecules A and D in Fig. 3) interactions along [101] and [10$\bar{1}$] directions with TTF, thus forming a sheet-like network on this plane. Since the molecules incline ca. 20° from the ac plane,[18] this network is not coplanar but somewhat corrugated (Fig. 4). The more important finding is that there exist strong S(1)-N(4)≡C(6) interactions (3.17 Å; molecules A, B, C, and D in Fig. 5) along [111] and [1$\bar{1}$1] directions. As a result, four BTDA-TCNQ molecules are connected to each other which surround a TTF molecule from top, bottom, and two sides. In other words, cavities which include TTF molecules are formed by BTDA-TCNQ molecules. This fact indicates that the present CT complex is more stabilized by the contribution of inclusion behavior. This inclusion behavior is also observed in the BTDA-TCNQ complexes with some aromatic hydrocarbons such as benzene.[19] It is suggested here that the present complex is not a simple CT complex with mixed stacks but rather the one with some inclusion behavior resulted from the multi-dimensional structure.

Conclusion

The crystal structure of TTF·BTDA-TCNQ complex does not exhibit a segregated columnar stack as found in TTF·TCNQ but a mixed stack resulting in the low electrical conductivity. However, the more important finding is the effects of the network formed by the strong interheteroatom interactions. It has been manifested in the anion-radical salts that the two-dimensional network of BTDA-TCNQ can enhance the electrical conductivity.[20] However, it is also true that these interactions can create the cavities leading to a mixed stack formation with the inclusion behavior for some CT complexes. In conclusion, it is suggested that a donor with a larger size and a relatively low oxidation potential which excludes the inclusion behavior observed in the present complex is needed in

order to form a highly conductive CT complex with BTDA-TCNQ.

Tables of anisotropic thermal parameters, coordinates of hydrogen atoms, and observed and calculated structure factors are kept at the Chemical Society of Japan (Document No. 8740).

References

1) Y. Yamashita, T. Suzuki, T. Mukai, and G. Saito, *J. Chem. Soc., Chem. Commun.*, **1985**, 1044.

2) C. Kabuto, T. Suzuki, Y. Yamashita, and T. Mukai, *Chem. Lett.*, **1986**, 1433.

3) Bis(1,2,5-thiadiazolo)tetracyanoquinodimethan; 4*H*,8*H*-4,8-bis(dicyanomethylene)benzo[1,2-*c*: 4,5-*c'*]bis[1,2,5]thiadiazole. Bis(1,2,5-thiadiazolo)benzoquinone; 4*H*,8*H*-benzo-[1,2-*c*: 4,5-*c'*]bis[1,2,5]thiadiazole-4,8-dione. (1,2,5-Thiadiazolo)-naphthoquinone; naphtho[2,3-*c*][1,2,5]thiadiazole-4,9-dione.

4) H. Kobayashi, A. Kobayashi, Y. Sasaki, G. Saito, T. Enoki, and H. Inokuchi, *J. Am. Chem. Soc.*, **105**, 297 (1983).

5) Y. Yamashita, T. Suzuki, G. Saito, and T. Mukai, *Chem. Lett.*, **1985**, 1759.

6) The electrical resistivities (ρ_{RT}/Ω cm) measured on compressed pellet at room temperature are as follows: TTN complex; 0.19. DMPH complex; 0.29. TTF complex; 2.0×10^7.

7) J. Ferraris, D. O. Cowan, V. V. Walatka, Jr., and J. H. Perlstein, *J. Am. Chem. Soc.*, **95**, 948 (1973).

8) Single crystals of highly conductive complexes have not been obtained yet.

9) Y. Jia-xing, *Acta Crystallogr., Sect. A*, **37**, 642 (1981); **39**, 35 (1983).

10) "International Tables for X-Ray Crystallography," Vol. 3, Kynoch Press, Birmingham (1962), p. 202.

11) T. Sakurai and K. Kobayashi, *Rikagaku Kenkyusho Hokoku*, **55**, 69 (1979).

12) W. F. Cooper, N. C. Kenny, J. W. Edmonds, A. Nagel, F. Wudl, and P. Coppens, *J. Chem. Soc., Chem. Commun.*, **1971**, 889.

13) K. Yakushi, S. Nishimura, T. Sugano, H. Kuroda, and I. Ikemoto, *Acta Crystallogr., Sect. B*, **36**, 358 (1980).

14) H. Kobayashi and J. Nakayama, *Bull. Chem. Soc. Jpn.*, **54**, 2408 (1981).

15) J. B. Torrance, J. J. Mayerle, V. Y. Lee, and K. Bechgaard, *J. Am. Chem. Soc.*, **101**, 4747 (1979).

16) C. J. Fritchie, Jr., *Acta Crystallogr.*, **20**, 892 (1966).

17) A. Gieren, V. Lamm, T. Hübner, M. Rabben, R. Neidlein, and D. Droste, *Chem. Ber.*, **117**, 1940 (1984).

18) The dihedral angles between the ac plane and the molecular plane of BTDA-TCNQ and TTF are 20.3° and 19.5°, respectively.

19) The crystal structure of benzene·BTDA-TCNQ (1:2) complex will be soon reported elsewhere by C. Kabuto, T. Suzuki, Y. Yamashita, and T. Mukai.

20) C. Kabuto, T. Suzuki, Y. Yamashita, T. Mukai, and G. Saito, submitted for publication.

Basic Autoxidation of Friedelin[1)]

Tadaaki NISHIHAMA* and Takeyoshi TAKAHASHI†
School of Industrial Chemistry, The Meiji University, Tama-ku, Kawasaki 214
†Department of Chemistry, Faculty of Science, The University of Tokyo, Hongo, Bunkyo-ku, Tokyo 113
(Received December 9, 1986)

Base-catalyzed autoxidation of a triterpene ketone, friedelin, in the presence of potassium *t*-butoxide gave four products, and their structures and formation mechanism were investigated. The common intermediate to these compounds was suggested to be 4-hydroperoxyfriedelan-3-one, not friedelane-2,3-dione. 3-Oxafriedel-1-ene-2-carboxylic acid was a dehydration product of the main product, 2-hydroxy-3-oxafriedelane-2-carboxylic acid.

Autoxidation of ketones with gaseous oxygen in the presence of strong bases is known as a convenient oxidation method for the syntheses of α-diketones from the corresponding α-methylene ketones and many investigations on synthesis of steroidal α-diketones were reported, but the yields were generally not good.[2)] The autoxidation of a triterpene with a 4,4-dimethyl-3-keto structure was examined by Hanna et al. and they reported a formation of the corresponding α-diketone in 68% yield together with a lactol which was derived by the further oxidation of the α-diketone.[3)] Thus it is generally difficult to control the oxidation reaction which often proceeds exceedingly, or aldol condensation may take place concomitantly. The reaction products, therefore, consist of a complex mixture of many compounds, and frequently the isolation of desired product is difficult. Consequently, applicability of this oxidation to organic synthesis is considerably restricted.

In connection with a study on effective degradation of triterpene ketones, friedelin (**1**)** was autoxidized in the presence of potassium *t*-butoxide and a dihydropyrancarboxylic acid (**2a**) was isolated as a ring-cleavage product in ca. 30% yield.[1)] Although this oxidation reaction was found to be not useful for a practical method to degradate the triterpene ketone effectively, examination on the complicated reaction mixture gave a different result from those obtained in steroids and triterpenes with the 4,4-dimethyl-3-keto structure and offered many interesting problems from the structural and mechanistic viewpoints. This paper describes the structures and formation mechanism of autoxidation products of friedelin (**1**) and some α-oxygenated derivatives.

The oxidation reaction of friedelin (**1**) was carried out in *t*-butyl alcohol and benzene using ten-molar excess of potassium *t*-butoxide with bubbling dry oxygen at room temperature. Although the absorption of oxygen usually stopped within 2 h, the reaction was continued for 24 h to be completed. The reaction mixture was acidified with hydrochloric acid and extracted with ether. The extract (A) was concentrated to afford a residue, which, on trituration with petroleum benzine–chloroform, was separated into a soluble fraction (B) and an insoluble materials (C).

The insoluble material (C) was a crude carboxylic acid (**3a**) containing a trace amount of hydrochloric acid, and crystallized from chloroform–petroleum benzine to yield a less polar carboxylic acid (**2a**) in 20% yield, which was shown to be apparently different from **3a** by TLC examination. The insoluble material (C) was esterified with diazomethane. The crude ester (**3b**) was crystallized from the same solvents as above under acid-free conditions to yield a methyl ester (**3b**) in 35% yield, while on crystallization from the acid-containing solvents gave a less polar ester (**2b**) in 30% yield, which was identical with a methyl ester of **2a**. These observations, therefore, suggest that the less polar acid (**2a**) is a secondary reaction product derived from the polar acid (**3a**) by heating with a catalytic amount of acid.

Since the soluble fraction (B) was revealed to be a mixture of carboxylic acids, the whole extract (A) was methylated with diazomethane, separated by chromatography and recrystallized to afford four methyl esters, **3b**, **4b**, **5b**, and **6b** in 50—35, 20—3, 5—6, and 20—10% yields, respectively.

The methyl esters (**2b** and **3b**) gave the molecular formulas, $C_{31}H_{50}O_3$ and $C_{31}H_{52}O_4$, respectively, from elemental analysis and the mass spectra, and the latter showed the presence of a hydroxyl group by the IR spectrum. Therefore, **2b** was a dehydration product of **3b**. The ester (**2b**) showed the presence of α,β-unsaturated ester (IR: 1720 and 1640 cm^{-1}) with an oxygenfunction at α-position (UV: 253 nm). The ^1H NMR spectrum suggested the presence of a methoxycarbonyl (δ 3.8), -C-(C$\underline{H_3}$)-O- (δ 3.92, 1H, q, J=7 Hz), and -C=CH-CH- (δ 2.08 and 6.01, each 1H, d, J=2 Hz). These spectral data lead to the structure, methyl 3-oxafriedel-1-ene-2-carboxylate for **2b**. The structure proposed for **2b** was further confirmed including the configurations at C-4 and C-10 as follows. The oxidation of **2b** with ozone and hydrogen peroxide gave a ring-cleavage product (not isolated), which was subjected to partial reduction with lithium aluminium hydride (LAH), followed by a treatment with hydrochloric acid to afford a γ-lactone (**7**), $C_{28}H_{46}O_2$, IR 1765

**Friedelin (=friedelan-3-one); friedelane is used as a conventional skeletal name instead of D:A-friedooleanane throughout this paper.

cm^{-1}. The same γ-lactone (**7**) was also obtained by the following route from friedelin (**1**). 3a-Oxa-3a-homofriedelan-3-one (**8**)[4] derived from **1** was treated with phenylmagnesium bromide and then with acetic anhydride in acetic acid to give a diphenylethylene derivative (**9**). On oxidation with chromium trioxide, **9** afforded a δ-lactone, 3-oxafriedelan-2-one (**10**)[5], $C_{29}H_{48}O_2$. Then the δ-lactone (**10**) was submitted to a Grignard reaction using phenylmagnesiun bromide to yield 2-phenyl-3-oxafriedel-1-ene (**11**), $C_{35}H_{52}O$. Ozonolysis of **11** followed by a treatment with LAH yielded a γ-lactone (**7**) and a hemiacetal (**12**), $C_{28}H_{48}O_2$, and the latter (**12**) gave the γ-lactone (**7**) on oxidation with chromium trioxide. The dihydropyran derivative (**11**) was submitted to ozonization followed by a treatment with peracetic acid, and the reaction mixture was saponified with alkali. Acid treatment gave a mixture of two γ-lactones (**7** and **13**). One (**7**) of them was identical with that obtained by either route described above in every respect, and the configuration at C-10 was shown to be the same as that of friedelin (**1**). The other (**13**) is a C-10 epimer derived from a partial isomerization at C-10 under alkaline conditions and therefore possesses $C_{(10\beta)}$-H configuration. Since Baeyer-Villiger reaction is known to proceed with retention of the configuration of the chiral center α to the carbonyl group, the configuration at C-4 of the γ-lactone (**7**) is concluded to be the same 4R-configuration as that of friedelin (**1**). Thus the structure of 2a

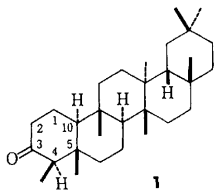

1

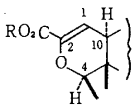

2a R =H
b R =Me

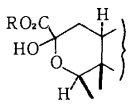

3a R =H
b R =Me

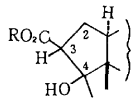

4a R =H
b R =Me

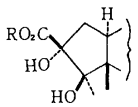

5a R =H
b R =Me

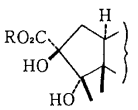

6a R =H
b R =Me

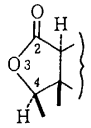

7

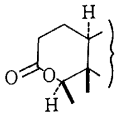

8

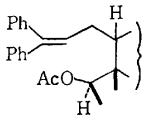

9

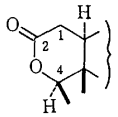

10

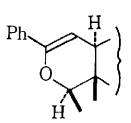

11

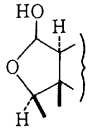

12

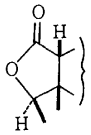

13

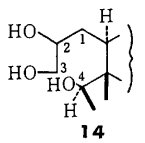

14

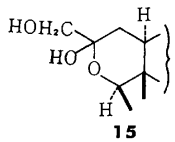

15

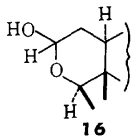

16

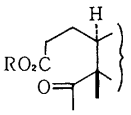

17a R =H
b R =Me

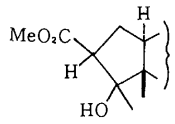

18 (a diastereomer of **4b**)

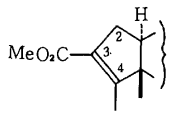

19

was deteremined to be 3-oxa-friedel-1-ene-2-carboxylic acid.

The structure of **3b** was deduced to be methyl 2-hydroxy-3-oxafriedelane-2-carboxylate from the spectral data and a chemical relation with **2b**. The fact that **3b** was easily converted into **2b** with $C_{(4\beta)}$-Me and $C_{(10\alpha)}$-H, implies that these configurations of **3b** are the same as those of **2b**. However, ^{1}H NMR signal due to $C_{(4\alpha)}$-H of **3b** was changed from a quartet into a multiplet on standing the solution, which indicates that **3b** in solution would exist in an equilibrium mixture of a pair of $C_{(2)}$-epimers.

Reduction of **3b** with LAH in THF under reflux gave 3,4-secofriedelane-2,3,4-triol (**14**), $C_{30}H_{54}O_3$, while in ether at room temperature afforded an unstable hemiacetal, 2-hydroxymethyl-3-oxafriedelan-2-ol (**15**) as an amorphous solid. When the hemiacetal (**15**) was warmed in benzene for recrystallization, dimerization occurred to give a dimeric ether, $C_{60}H_{100}O_4$, as a white powder, the structure of which was not further investigated. A treatment of the hemiacetal (**15**) with lead tetraacetate (LTA) gave a hemiacetal (**16**), $C_{29}H_{50}O_2$, which, on oxidation with chromium trioxide, yielded the δ-lactone (**10**). These derivations described above can be explained based on the structure **3b**.

The methyl ester (**4b**) gave the molecular formula, $C_{31}H_{52}O_3$ and showed the presence of a hydroxyl group by IR and -CH-CO- grouping (δ 2.5) by ^{1}H NMR spectrum. The ester (**4b**) did not react with lead tetraacetate nor with acetic anhydride in pyridine. The structure of **4b** was, therefore, inferred to be methyl 4-hydroxy-A(1)-norfriedelane-3-carboxylate and the structure was confirmed synthetically. Methyl 4-oxo-3,4-secofriedelan-3-oate (**17b**)[4] prepared from **1**, was refluxed with potassium *t*-butoxide in toluene and the aldol condensation mixture was esterified with diazomethane. Chromatographic separation of the product afforded a pair of hydroxy esters (**4b** and **18**) and methyl A(1)-norfriedel-3-ene-3-carboxylate (**19**).[4] One of the hydroxy ester, obtained as the major product, was identical with **4b**. The stereochemistry at C-3 and C-4 remains undetermined.

The methyl esters (**5b** and **6b**) gave the same molecular formulas, $C_{31}H_{52}O_4$, and the presence of two

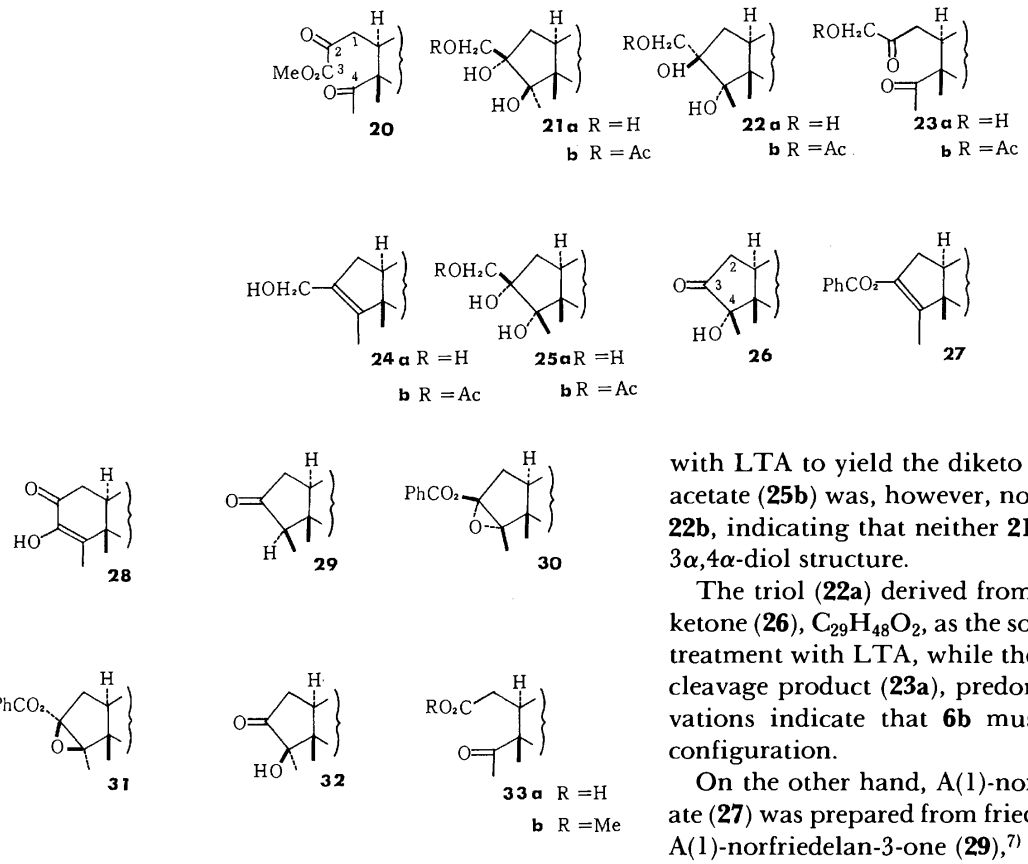

hydroxyl groups was shown from IR and chemical degradation (vide infra). No signal due to any hydrogen atom on a carbon bearing the hydroxyl group was observed in the ^{1}H NMR spectra and both esters resisted acetylation under normal conditions, indicating that two hydroxyl groups were tertiary. On treatment with LTA, **5b** and **6b** gave the same diketo ester, methyl 2,4-dioxo-3,4-secofriedelan-3-oate (**20**), structure of which was supported by the ^{1}H NMR spectrum (δ 2.07, 3H, CH_3CO-; 2.2—3.0, 2H, -CH_2CO-; and 3.80, 3H, -$COOCH_3$). From these observations, methyl 3,4-dihydroxy-A(1)-norfriedelane-3-carboxylate was proposed as a planar structure for **5b** and **6b**. Stereostructures for **5b** and **6b** were determined by following examination.

The methyl esters (**5b** and **6b**) were reduced with LAH to afford triols, **21a** and **22a**, which on acetylation gave monoacetates **21b** and **22b**, respectively. The monoacetates **21b** and **22b** were treated with LTA to afford the same diketo acetate (**23b**), $C_{32}H_{52}O_4$. The structure of **23b** was shown to be 2,4-dioxo-3,4-secofriedelan-3-yl acetate by the ^{1}H NMR spectrum, and was identical with a specimen prepared by the following route. The unsaturated ester (**19**) was subjected to reduction with LAH to afford an unsaturated alcohol (**24a**), which, after acetylation, was treated with osmium tetraoxide. The oxidizing reagent would attack the double bond from the less hindered α-side of the norfriedelene skeleton, giving rise to a *cis*-glycol acetate, 3β-acetoxymethyl-A(1)-norfriedelane-3α,4α-diol (**25b**). The glycol acetate (**25b**) was then treated with LTA to yield the diketo acetate (**23b**). The diol acetate (**25b**) was, however, not identical with **21b** nor **22b**, indicating that neither **21b** nor **22b** possesses the 3α,4α-diol structure.

The triol (**22a**) derived from **6b**, gave a norhydroxy ketone (**26**), $C_{29}H_{48}O_2$, as the sole reaction product on a treatment with LTA, while the triol (**25a**) gave a ring-cleavage product (**23a**), predominantly. These observations indicate that **6b** must possess a trans diol configuration.

On the other hand, A(1)-norfriedel-3-en-3-yl benzoate (**27**) was prepared from friedelane-2,3-dione (**28**) via A(1)-norfriedelan-3-one (**29**),[7] and subjected to epoxidation with peracetic acid. Since the double bond would be attacked by the reagent from the less hindered α-side, it was expected that the α-epoxide (**30**) would be formed as the major product. Therefore, the epoxide mixture (**30** and **31**) was hydrolyzed with potassium hydroxide to afford 4α-hydroxy-A(1)-norfriedelan-3-one (**26**) as the major product and 4β-hydroxy isomer (**32**) as the minor product. Both hydroxy norketones (**26** and **32**) gave the same keto norester (**33**)[4] on a treatment with LTA followed by methylation. The major hydroxy ketone (**26**) was identical with a specimen obtained from triol (**22a**) (vide supra). A support for the assignment of configuration at C-4 was observed on IR measurement. The pseudoequatorial[8] 4β-hydroxyl of **32** was considered to form stronger intramolecular hydrogen bond with carbonyl group than pseudoaxial 4α-hydroxyl of **26**.[9] Actually, absorption bands due to hydroxyl groups of **26** and **32** in dilute carbon tetrachloride solution appeared at 3606 and 3563 cm^{-1} respectively.

Since the hydroxyl group at C-4 of **26** was shown to be located in α-configuration and the relative configuration of $C_{(3)}$-OH and $C_{(4)}$-OH of **22b** is trans, the hydroxyl group at C-3 of **22b** and therefore that of **6b** is concluded to be in β-configuration.

The oxidation of **21a** with LTA was found to give a complicated reaction mixture, from which the hydroxy norketone (**32**) was isolated along with a small amount of the ring-cleavage diketo alcohol (**23a**). Since this observation implies that **21a** possesses a trans 3,4-diol with 4β-hydroxy configuration, the

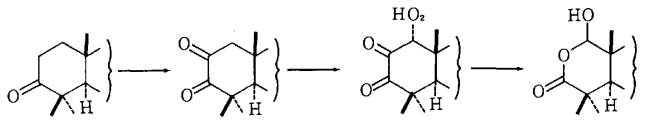

Scheme 1.

hydroxyl group at C-3 should be in α-configuration.

From these observations described above, it is concluded that **5a** and **6a** are formulated as 3α,4β-dihydroxy-A(1)-norfriedelane-3β-carboxylic acid and 3β,4α-dihydroxy-A(1)-norfriedelane-3α-carboxylic acid, respectively.

The basic autoxidation of ketones is known to proceed by an initial formation of α-keto carbanion (enolate anion) and followed by an attack of oxygen to yield α-hydroperoxy ketone. If the α-hydroperoxide is primary or secondary, it usually converts rapidly into the corresponding α-diketone, and then the α-diketone would be submitted to further oxidation. Many examples are reported in steroids and triterpenes with the 4,4-dimethyl-3-keto structure.[2] In the latter case, the primary oxidation product is a 2,3-dione, which is converted into a lactol via 1-hydroperoxy-2,3-dione with elimination of carbon monoxide[3] (Scheme 1). The basic autoxidation of friedelin (**1**) is not the case. The Δ^3-enolate anion being more stable than the Δ^2-enolate anion, attack of oxygen must occur at C-4 to afford a tertiary hydroperoxide (**34**) preferentially. Attack to C-2 yielding friedelane-2,3-dione (**28**) would be the minor process. In fact friedelane-2,3-dione (**28**) and several oxidation products derived from **28** were detected in the autoxidation product of **1** but in very minute quantities, and therefore, it is concluded that the process through 2,3-dione (**28**) would be of no importance.

From product analysis of the autoxidation of friedelin (**1**), it is inferred that the hydroperoxy ketone (**34**) would be submitted to the following reactions;[10] i) an attack of the hydroperoxide anion of **34** to the carbonyl carbon followed by the $C_{(3)}$-$C_{(4)}$ bond fission, ii) the participation with a *t*-butoxide anion followed by the $C_{(3)}$-$C_{(4)}$ bond fission, iii) a reaction with friedelin (**1**) or some unknown process yielding 4α-hydroxyfriedelin (**35**) (Scheme 2). Process i) would produce 4-oxo-3,4-secofriedelan-3-oic acid (**17a**), but the keto acid (**17a**) was not detected in the reaction mixture. Since a separate experiment revealed that the keto acid (**17a**) was fairly stable in the autoxidation conditions and survived for long time, no detection of **17a** would deny the occurrence of process i). Process ii) would at least, partially, be responsible for the formation of 4-hydroxy-A(1)-norfriedelane-3-carboxylic acid (**4a**).

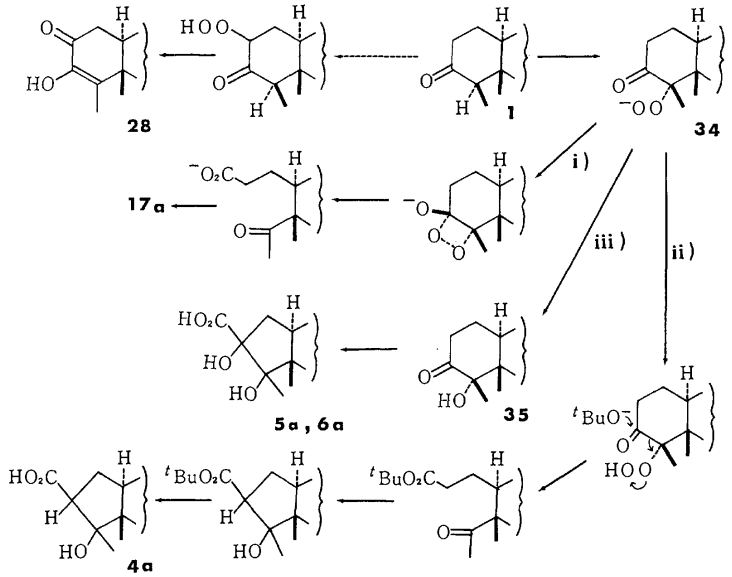

Scheme 2.

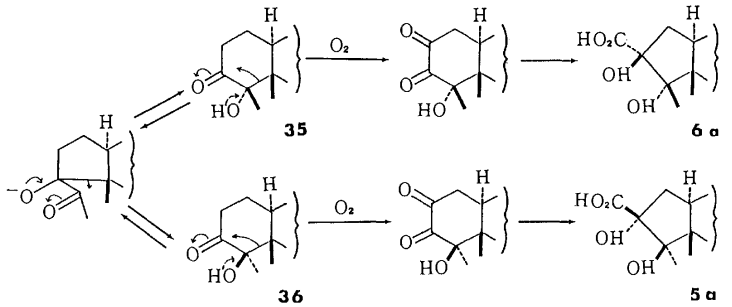

Scheme 3.

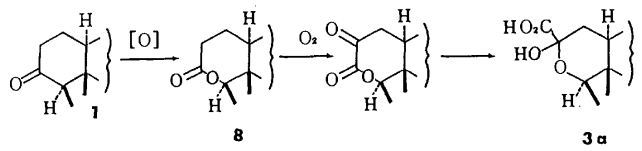

Scheme 4.

Process iii) was revealed to be the main route leading to dihydroxy carboxylic acids (**5a** and **6a**). 4α-Hydroxyfriedelan-3-one (**35**), the important intermediate in the process iii), and its 4β-hydroxy isomer (**36**) were prepared from friedelin (**1**) through an epoxidation of 3-friedelen-3-yl benzoate. The epoxidation gave a mixture of α- and β-epoxides, and the former was the main product from the reasons described for **27**. The 4α-hydroxyfriedelan-3-one (**35**) was subjected to the autoxidation under the same conditions as in the case of **1**. The reaction products, after methylation, were shown to be **5b** and **6b**. The autoxidation of 4β-hydroxy isomer (**36**) gave also **5b** and **6b** after methylation. Therefore, a rapid interconversion between **35** and **36** was suggested prior to the autoxidation and the autoxidation of **35** and **36** is considered to proceed as depicted in Scheme 3.

Since 2-hydroxy-3-oxafriedelane-2-carboxylic acid (**3a**) was not detected in the autoxidation product of **35** nor **36**, these two compounds were not intermediates leading to **3a**. A speculative formation process leading to **3a** was given in Scheme 4, and the investigation on the formation process is now under way.

Experimental

General Procedures. All melting points were uncorrected. Infrared spectra (IR) were taken on Perkin Elmer "Infracord," or Hitachi EPI-G2 spectrometer in Nujol mull. Ultra violet spectra (UV) were measured on a Hitachi EPS-3 spectrometer. ^{1}H NMR spectra were taken using Hitachi R-24 (60 MHz), Varian A-60 (60 MHz), or Varian EM-390 (90 MHz) and mass spectra (MS) were run on a Hitachi RMU-6L or JEOL DX-300 mass spectrometer at 70 eV unless otherwise noted and the relative intensities were indicated in parentheses. High performance liquid chromatography (HPLC) was run on Waters Associates 6000A with μ-PORASIL (silica gel) column and RI detector. Reduction with lithium aluminium hydride (LAH), acetylation with acetic anhydride-pyridine, methylation with diazomethane, and oxidation of glycols with lead tetraacetate (LTA) in acetic acid were done in usual manner unless specially noted.

Materials and Solvents. Friedelin (**1**) was extracted from "cork smoker wash solid"[6] (not available now) or cork powder and purified by column chromatography (alumina, benzene) and by crystallization from ethyl acetate, mp 261 °C. Friedelane-2,3-dione (**28**) was extracted from "cork smoker wash solid" and the crude material was subjected to column chromatography on alumina eluted with benzene-ethyl acetate followed by crystallization from the same solvent, mp 222 °C. Benzene was distilled before use. Dry *t*-butyl alcohol was prepared by distillation from a solution of *t*-butyl alcohol (100 parts) containing sodium *t*-butoxide (1 part). Potassium *t*-butoxide solution was prepared by dissolving potassium (1 g) in dry *t*-butyl alcohol (100 ml).

Autoxidation of Friedelin (1) with Potassium *t*-Butoxide. A solution of friedelin (**1**; 1 g) in dry benzene (100 ml) was placed in a two-necked Erlenmeyer flask equipped with a gas buret. The air inside was transferred by oxygen, and the potassium *t*-butoxide solution (100 ml) was added through a rubber septum cap. The solution, kept at 25 °C, was stirred for 24 h. A rapid absorption of oxygen was observed within first 30 min and the absorption stopped when about 85 ml of oxygen was consumed. Ether and 1 M hydrochloric acid (1 M=1 mol dm^{-3}) were added and the organic layer (A) was washed once with water and concentrated under reduced pressure to afford a residue. The residue was trituated with petroleum benzine and a soluble fraction (B) and an insoluble material (C) were obtained. A part of the insoluble material (C) crystallized from benzine-chloroform to afford 3-oxafriedel-1-ene-2-carboxylic acid (**2a**) in ca. 20% yield, mp 241—245 °C (needles from ether); IR 2360, 2340, 1705, 1640, 1460, 1390, 1285, 1140, 1120, and 1080 cm^{-1}; ^{1}H NMR (90 MHz, $CDCl_3$) δ=2.1 (1H, d, J=2 Hz; $C_{(10)}H$), 3.9 (1H, q, J=5 Hz, -O-C<u>H</u>-CH_3), 6.1 (1H, d, J=2 Hz; $C_{(1)}H$), and 7.5 (1H, br s; COOH); MS m/z (%) 456 (M^+; 11), 441 (7), 426 (37), 411 (11), 382 (27), 341 (53), 205 (100), 135 (55), 123 (62), and 109 (84). The remaining part of C was esterified with diazomethane. Recrystallization from the same solvents gave a methyl ester (**2b**) of **2a** in 30% yield, while recrystallization, after the solvents were free from acid, gave methyl 2-hydroxy-3-oxafriedelane-2-carboxylate (**3b**) in 35% yield. **2b**; Mp 214.5—215 °C; IR 1720 and 1640 cm^{-1}; UV (EtOH) 253 nm (ε 8900); ^{1}H NMR (60 MHz, $CDCl_3$) δ=2.08 (1H, d, J=2 Hz; C=CH-C<u>H</u>), 3.79 (3H, s; $COOCH_3$), 3.92 (1H, q, J=7 Hz; -O-C<u>H</u>-CH_3), and 6.01 (1H, d, J=2 Hz; C=C<u>H</u>-CH); MS m/z 470 (M^+); Found: C, 78.70; H, 10.79%. Calcd for $C_{31}H_{50}O_3$: C, 79.10; H, 10.71%. **3b**; Mp 204.5—205 °C (from petroleum benzine); IR 3670, 1740, and 1640 cm^{-1}; ^{1}H NMR (60 MHz, $CDCl_3$) δ=3.7 (1H, m; -$OC_{(4)}H$) and 3.8 (3H, s; -$COOCH_3$); MS (20 eV) m/z (%) 488 (M^+; 13), 470 (47), 429 (50), 341 (38), 218 (33), and 205 (100); Found: C, 76.04; H, 10.73%. Calcd for $C_{31}H_{52}O_4$: C, 76.18; H, 10.72%.

The extract (A) was treated with diazomethane until a yellow color persisted for 5 min. Removal of the solvent in vacuo and the residue was chromatographed on silica gel. Elution with benzene gave methyl 2-hydroxy-3-oxafriedelane-2-carboxylate (**3b**), methyl 4-hydroxy-A(1)-norfriedelane-3-carboxylate (**4b**), methyl 3α,4β-dihydroxy-A(1)-norfriedelane-3β-carboxylate (**5b**), and methyl 3β,4α-dihydroxy-A(1)-norfriedelane-3α-carboxylate (**6b**) in turn. **4b**; Needles from methanol, mp 224—225 °C; IR 3630 and 1725 cm^{-1}; ^{1}H NMR (60 MHz, $CDCl_3$) δ=2.5 (1H, m; -CH-CO) and 3.9 (3H, s; $COOCH_3$); MS m/z (%) 472 (M^+; 33), 454 (19), 356 (16), 274 (44), 205 (73), and 109 (100); Found: C, 78.88; H, 11.09%. Calcd for $C_{31}H_{52}O_3$: C, 78.76; H, 11.09%. **5b**; Needles from petroleum benzine, mp 205—205.5 °C; IR 3700, 3500, and 1720 cm^{-1}; ^{1}H NMR (60 MHz, $CDCl_3$) δ=3.8 (3H, s; -$COOCH_3$); MS m/z (%) 488 (M^+; 70), 428 (49), 341 (36), 205 (83), and 109 (100); Found: C, 75.59; H, 10.59%. Calcd for $C_{31}H_{52}O_4$: C, 76.18; H, 10.72%. **6b**; Needles from petroleum benzine, mp 240—241 °C; IR 3500 and 1725 cm^{-1}; ^{1}H NMR (60 MHz, $CDCl_3$) δ=3.75 (3H, s; -$COOCH_3$); MS m/z (%) 488 (M^+; 100), 428 (46), 205 (64), 149 (46), 123 (68), and 109 (92); Found: C, 75.94; H, 10.65%. Calcd for $C_{31}H_{52}O_4$: C, 76.18; H, 10.72%.

Oxidation of 2b with Ozone and Hydrogen Peroxide. Ozone was introduced to a solution of **2b** (100 mg) in dichlo-

romethane (50 ml), kept at −78 °C, until the solution developed blue color. A mixture of hydrogen peroxide (30%, 20 ml), acetic acid (20 ml), and sulfuric acid (1 ml) was added and the solution was heated at 100 °C. After 30 min, the solution was cooled to room temperature, neutralized with an aqueous solution of sodium carbonate, and extracted with ether. The ether layer was concentrated and chromatographed (silica gel-benzene). 3-Oxa-A(1)-norfriedelan-2-one (**7**; 53 mg) was obtained, mp 263—264 °C (from ethyl acetate); IR 1780, 1170, 1060, 1015, and 920 cm^{-1}; ^1H NMR (60 MHz, $CDCl_3$) δ=2.1 (1H, s; $C_{(10)}H$) and 4.05 (1H, q, J=7 Hz; $-OC_{(4)}H$); MS m/z (%) 414 (M^+; 23), 399 (14), 290 (70), 262 (84), 247 (26), 221 (20), and 205 (44); Found: C, 81.24; H, 11.32%. Calcd for $C_{28}H_{46}O_2$: C, 81.10; H, 11.18%.

3a-Oxa-3a-homofriedelan-3-one (8). To a solution of friedelin (**1**; 5 g) in chloroform (300 ml) was added 39% peracetic acid (40 ml) and the mixture was stirred overnight at 60 °C. Water was added and the organic layer was washed with water several times, concentrated, and crystallized from ethyl acetate to yield **8** (3.2 g), mp 292—293 °C; IR 1730, 1290, and 1230 cm^{-1}; ^1H NMR (60 MHz, $CDCl_3$) δ=2.5—2.7 (2H, m; $C_{(2)}H_2$-CO-) and 4.23 (1H, q, J=6 Hz; $-OC_{(4)}H$-); MS m/z (%) 442 (M^+; 16), 398 (25), 274 (19), 245 (23), 218 (42), 205 (61), 123 (79), and 109 (100); Found: C, 81.39; H, 11.38%. Calcd for $C_{30}H_{50}O_2$: C, 81.40; H, 11.60%.

Diphenylethylene Acetate (9). 3a-Oxa-3a-homofriedelan-3-one (**8**; 2 g) was treated with 10 molar excess of phenylmagnesium bromide in usual manner and the reaction product was dissolved in benzene, dried over sodium sulfate, and then concentrated. The residue was dissolved in a mixture (1 : 1, 200 ml) of acetic anhydride and acetic acid containing sodium acetate (2 g), and the solution was refluxed overnight. The usual work-up and chromatography (silica gel-petroleum benzine) afforded diphenylethylene acetate (**9**) as an amorphous solid, IR 1725, 1595, 1235, 1040, and 760 cm^{-1}; ^1H NMR (60 MHz, $CDCl_3$) δ=1.95 (3H, s; AcO-), 2.0—2.3 (2H, m; $C_{(1)}H_2$-C=C), 4.77 (1H, q, J=7 Hz; $-OC_{(4)}H$), 5.99 (1H, t, J=7 Hz; -C=$C_{(2)}H$), and 7.3—7.5 (5H, br s; C_6H_5-).

3-Oxafriedelan-2-one (10). Chromium trioxide (1 g) was added to a solution of **9** (1 g) in acetic acid (200 ml) with stirring at room temperature and the solution was stirred for 10 h. After removal of the solvent in vacuo, the residue was shaken with ether and 1% sulfuric acid. The organic layer was concentrated, dissolved in a mixture of dioxane (100 ml) and concd sulfuric acid (1 g). The solution was refluxed for 1 h and then poured into water to yield precipitates, which recrystallized from methanol. 3-Oxafriedelan-2-one (**10**; 300 mg) was obtained, mp 263—264 °C; IR 1735, 1245, 1080, and 1050 cm^{-1}; ^1H NMR (60 MHz, $CDCl_3$) δ=2.0—2.6 (2H, m; CH_2CO-) and 4.05 (1H, q, J=7 Hz); MS m/z (%) 428 (M^+; 9), 304 (28), 276 (23), 205 (74), 203 (20), 123 (74), 107 (69), and 109 (100); Found: C, 81.29; H, 11.35%. Calcd for $C_{29}H_{48}O_2$: C, 81.25; H, 11.29%.

2-Phenyl-3-oxafriedel-1-ene (11). One gram of **10** was added to 3 molar excess of phenylmagnesium bromide solution in ether, and the solution was refluxed for 1 h. After dil hydrochloric acid was added, the ether layer was concentrated to give a residue. The residue was chromatographed (silica gel-petroleum benzine) and crystallized from ethyl acetate to afford 2-phenyl-3-oxa-1-friedelene (**11**; 650 mg) as lustrous platelets, mp 223—225 °C; MS m/z (%) 488 (M^+; 23), 300 (9), 205 (17), and 185 (23).

Ozonolysis of 11 by Reductive Treatment. A solution of 2-phenyl-3-oxa-1-friedelene (**11**; 500 mg) in dichloromethane (200 ml) was cooled in Dry Ice-methanol bath and ozone was bubbled into the solution until the color of the solution changed to blue. A solution of LAH (200 mg) in ether (50 ml) was added and the mixture was allowed to warm up to room temperature. After addition of a small amount of acetone, the mixture was shaken with dil hydrochloric acid. The organic layer was concentrated and chromatographed (silica gel-benzene) to afford 3-oxa-A(1)-norfriedelan-2-one (**7**; 155 mg) and 3-oxa-A(1)-norfriedelan-2-ol (**12**; 75 mg), mp 236—238 °C (from benzene); IR 3200, 1100, 1060, 1010, and 730 cm^{-1}; ^1H NMR (90 MHz, $CDCl_3$) δ=3.55 (1H, q, J=6.5 Hz; $-OC_{(4)}H$) and 3.6—3.7 (2H, m; $C_{(1)}\underline{H}OH$); MS m/z (%) 398 ([M−18]$^+$; 15), 356 (17), 341 (6), 205 (56), 123 (100), and 109 (97); Found: C, 80.70; H, 11.82%. Calcd for $C_{28}H_{48}O_2$: C, 80.71; H, 11.61%. 3-Oxa-A(1)-norfriedelan-2-ol (**12**; 35 mg) in acetic acid (20 ml) was oxidized with chromium trioxide (50 mg) at reflux temperature for 1 h to afford **7** (25 mg).

Ozonolysis of 11 by Alkaline Treatment. Ozonation of **11**(500 mg) in dichloromethane was carried out in the same manner as above and the reaction product was treated with 39% peracetic acid (20 ml). The mixture was heated up to 100 °C in a hood until no peroxide was detected with a potassium iodide-acetic acid solution. After the solvent was removed in vacuo, an excess ethanolic potassium hydroxide solution was added and the alkaline mixture was refluxed for 1 h. The solution was then acidified to pH ca. 1 by addition of dil hydrochloric acid and left for 1 h at 80 °C. The reaction product was extracted with ether and subjected to separation by chromatography (silica gel-benzene) to yield 3-oxa-A(1)-norfriedelan-2-one (**7**; 75 mg) and 10-epi-3-oxa-A(1)-norfriedelan-2-one (**13**; 53 mg), mp 181—181.5 °C (from ethyl acetate); IR 1760, 1140, 1120, and 1055 cm^{-1}; ^1H NMR (60 MHz, $CDCl_3$) δ=3.90 (1H, q, J=7 Hz; $-OC_{(4)}H$), 2.0 (1H, s; $C_{(10)}HCO$-), and 3.0—3.6 (1H, m; $C_{(11)}H$); MS m/z (%) 414 (M^+; 17), 399 (20), 290 (57), 261 (100), 235 (38), and 205 (45); Found: C, 81.03; H, 11.33%. Calcd for $C_{28}H_{46}O_2$: C, 81.10; H, 11.18%.

Reduction of Methyl 2-Hydroxy-3-oxafriedelane-2-carboxylate (3b) with LAH. A solution of **3b** (500 mg) in tetrahydrofuran (THF) (100 ml) was refluxed with excess LAH for 6 h and the usual work-up gave 3,4-secofriedelane-2,3,4-triol (**14**; 280 mg) as needles, mp 203—203.5 °C (from benzene); IR 3400, 3250, 3150, 1095, 1080, and 680 cm^{-1}; ^1H NMR (90 MHz, $CDCl_3$) 3.5—3.8 (4H, m; -OCH-); MS m/z (%) 462 (M^+; trace), 413 (11), 273 (7), 219 (11), 205 (40), and 109 (100); Found: C, 78.06; H, 11.71%. Calcd for $C_{30}H_{54}O_3$: C, 77.86; H, 11.76%.

A solution of **3b** (200 mg) in ether (100 ml) was reduced with LAH (50 mg) at room temperature. After 24 h, the reaction mixture was cooled with an ice bath, and treated with a small amount of acetone and then dil hydrochloric acid. The ether layer was washed with water several times and then concentrated in vacuo to give 2-hydroxymethyl-3-oxafriedelan-2-ol (**15**; ca. 150 mg) as an amorphous solid. The hemiacetal (**15**; 100 mg) was dissolved in benzene (200 ml) and the solvent was evaporated slowly on a water bath. The residue was chromatographed (silica gel-benzene) to give the dimeric ether (73 mg) as white powder, which crystallized from benzene, mp 298—299 °C; IR 1280, 1110, 1090, 1050, 980, 970, and 795 cm^{-1}. ^1H NMR (60 MHz, $CDCl_3$) δ=3.2—4.0 (6H, m; -OCH); MS m/z (%) 888 (M^+; trace), 440 (0.9), 438 (1), 424 (20), 409 (21), 341 (17), 229 (20), 205 (55), 191

(24), 138 (100), 137 (54), 123 (35), and 109 (40); Found: C, 81.20; H, 11.16%. Calcd for $C_{60}H_{100}O_4$: C, 81.39; H, 11.38%.

3-Oxafriedelan-2-ol (16). An ethereal solution of **15** (120 mg) obtained by the reduction of **3b** was added to a solution of LTA (300 mg) in acetic acid (100 ml) and the mixture was stirred for 1 h at room temperature. Ethylene glycol was added and the reaction mixture was worked up as usual to afford 3-oxafriedelan-2-ol (**16**; 83 mg), mp 228—232 °C (from benzene); IR 3400, 1270, 1245, 1105, 1050, 990, 950, and 725 cm^{-1}; MS *m/z* (%) 430 (M^+; trace), 412 (16), 218 (22), 205 (46), 135 (43), 123 (61), 121 (46), and 109 (100); Found: C, 80.67; H, 11.72%. Calcd for $C_{29}H_{50}O_2$: C, 80.87; H, 11.70%. Poor ^1H NMR spectrum was obtained due to the low solubility.

Modified Preparation of 4-Oxa-3,4-secofriedelan-3-oic Acid (17a). A solution of friedel-3-en-3-yl benzoate[6] (3 g) in dichloromethane (300 ml) was cooled in an ice-salt bath and ozone was passed though the solution until the blue color did not fade. A solution of chromium trioxide (3 g) in 90% acetic acid (300 ml) was added, and the mixture was heated at 60 °C for 1 h. Water and ether were added and the ether layer was worked up as usual. The residue crystallized from acetone-water to afford 4-oxo-3,4-secofriedelan-3-oic acid (**17a**; 2.1 g), mp 205—207 °C (needles from ether); IR 3100 (br), 1735, 1670, 1365, 1290, 1240, and 1190 cm^{-1}; ^1H NMR (60 MHz, $CDCl_3$) δ=2.1 (3H, s; Ac), 2.2—2.5 (2H, m; $-CH_2-CO-$), and 7.0—7.6 (1H, br s; -COOH); MS (20 eV) *m/z* (%) 458 (M^+; 18), 415 (14), 219 (41), and 205 (100). Preparation of **17a** by this method is more convenient than by chromic acid-oxidation of **1**.[4] On methylation, **17a** afforded methyl 4-oxo-3,4-secofriedelan-3-oate (**17b**), mp 157—158 °C (silky needles from methanol); IR 1735, 1695, and 1165 cm^{-1}. ^1H NMR (60 MHz $CDCl_3$) δ=2.1 (2H, t, *J*=3 Hz; $-CH_2CO-$), 2.15 (3H, s; CH_3CO-), and 3.65 (3H, s; $-COOCH_3$); MS *m/z* (%) 472 (M^+; 9), 429 (42), 205 (95), 123 (66), 121 (42), 109 (100), and 107 (45).

Aldol Condensation of 17b. To a solution of methyl 4-oxo-3,4-secofriedelan-3-oate (**17b**; 1 g) in toluene (200 ml) was added 200 ml of the potassium *t*-butoxide solution (the same solution as that used for the basic autoxidation) under nitrogen atmosphere and the mixture was refluxed for 24 h. After 2% hydrochloric acid (500 ml) was added, the organic layer was treated with diazomethane. The usual work-up afforded a residue, which was separated by chromatography on silica gel. Elution with benzene yielded methyl 4-hydroxy-A(1)-norfriedelane-3-carboxylate (**4b**; 143 mg), the stereoisomer (**18**; 118 mg) of **4b**, and methyl A(1)-norfriedel-2-ene-3-carboxylate (**19**; 85 mg) successively. **18**; Mp 226—228 °C (from benzene-cyclohexane); IR 3400, 1710, 1230, 1210, 1180, 1150, 1110, 1040, and 900 cm^{-1}; ^1H NMR (90 MHz, $CDCl_3$) δ=2.8—3.1 (1H, m; $-C_{(3)}HCO-$) and 3.7 (3H, s; $COOCH_3$); MS *m/z* (%) 472 (M^+; 16), 356 (11), 273 (26), 218 (39), 205 (76), 137 (59), 123 (84), and 109 (100); Found; C, 78.75; H, 10.96%. Calcd for $C_{31}H_{52}O_3$: C, 78.76; H, 11.09%. **19**; Mp 230—231.5 °C (platelet from methanol); IR 1710, 1630, 1310, 1215, and 1065 cm^{-1}; ^1H NMR (60 MHz, $CDCl_3$) δ=1.95 (3H, br s; $CH_3-C=C-$), 2.1—2.5 (2H, m; $C_{(1)}H_2-C=C$), and 3.70 (3H, s; $-COOCH_3$); MS *m/z* (%) 454 (M^+; 30), 235 (38), 234 (37), 233 (43), 205 (60), 191 (36), 165 (53), 123 (70), and 109 (100).

Oxidation of 5b and 6b with Lead Tetraacetate. An ethereal solution of **5b** (72 mg) was added dropwise to a solution of LTA (200 mg) in acetic acid. The usual work-up and crystallization from methanol aforded methyl 2,4-dioxo-3,4-secofriedelan-3-oate (**20**; 53 mg), mp 134—135 °C; IR 1730, 1695, 1365, 1275, 1265, and 1085 cm^{-1}. ^1H NMR (90 MHz, $CDCl_3$) δ=2.07 (3H, s; Ac), 2.2—3.0 (2H, m; $-C_{(1)}H_2CO-$), and 3.80 (3H, s; $-COOCH_3$); MS *m/z* (%) 486 (M^+; 15), 443 (39), 427 (29), 205 (83), 149 (56), 123 (78), and 109 (100); Found: C, 76.78; H, 10.42%. Calcd for $C_{31}H_{50}O_4$: C, 76.50; H, 10.36%. The same diketo ester (**20**; 32 mg) was obtained from **6b** (55 mg) by the same treatment.

3β-Hydroxymethyl-A(1)-norfriedelane-3α,4β-diol (21a) and Its Monoacetate (21b). Reduction of **5b** with LAH afforded **21a**, mp 260 °C (with decomp) (from petroleum benzine); IR 3430, 1365, and 1275 cm^{-1}; ^1H NMR (90 MHz, $CDCl_3$) δ=3.3—3.9 (2H, m; $-CH_2OH$); MS *m/z* (%) 442 ($[M-18]^+$; 4), 424 (20), 409 (21), 406 (27), 231 (26), 218 (68), 205 (94), 191 (45), 163 (42), 123 (64), and 109 (100); Found: C, 78.06; H, 11.16%. Calcd for $C_{30}H_{52}O_3$: C, 78.20; H, 11.38%. On acetylation, **21a** gave 3β-acetoxymethyl-A(1)-norfriedelane-3α,4β-diol (**21b**), mp 198.5—199 °C (from ether-cyclohexane); IR 3500, 1730, 1285, and 1055 cm^{-1}; ^1H NMR (60 MHz, $CDCl_3$) δ=2.10 (3H, s; AcO-) and 4.20 (2H, s; -OH); MS *m/z* (%) 502 (M^+; 1), 442 (1), 399 (7), 273 (11), 205 (57), and 109 (100); Found: C, 76.36; H, 10.78%. Calcd for $C_{32}H_{54}O_4$: C, 76.44; H, 10.83%.

3α-Hydroxymethyl-A(1)-norfriedelane-3β,4α-diol (22a) and Its Monoacetate (22b). By the same treatment as above, methyl 3β,4α-dihydroxy-A(1)-norfriedelane-3α-carboxylate (**6b**) afforded **22a** and 3α-acetoxymethyl-A(1)-norfriedelane-3β,4α-diol (**22b**). **22a**; Mp 255 °C (with decomp) (from ethyl acetate); IR 3400, 1135, 1070, 1060, 940, 920, and 890 cm^{-1}; ^1H NMR (90 MHz, $CDCl_3$) δ=3.55 and 3.93 (each 1H, d, *J*=12 Hz); MS *m/z* (%) 442 ($[M-18]^+$; 4), 427 (4), 399 (10), 273 (8), 219 (12), 205 (55), 142 (100), 113 (63), and 109 (88); Found: C, 78.15; H, 11.08%. Calcd for $C_{30}H_{52}O_3$: C, 78.20; H, 11.38%. **22b**; Mp 156—157 °C (from ether-cyclohexane); IR 3700, 3460, 1760, 1735, 1270, 1220, and 1045 cm^{-1}; ^1H NMR (60 MHz, $CDCl_3$) δ=2.10 (3H, s; AcO-), 4.13 and 4.36 (each 1H, d, *J*=10 Hz); MS *m/z* (%) 502 (M^+; trace), 442 (2), 427 (3), 409 (3), 399 (7), 381 (2), 371 (3), 341 (5), 273 (8), 205 (54), 123 (68), 121 (61), and 109 (100); Found: C, 76.25; H, 10.84%. Calcd for $C_{32}H_{54}O_4$: C, 76.44; H, 10.83%.

Treatment of 21b and 22b with Lead Tetraacetate. 3β-Acetoxymethyl-A(1)-norfriedelane-3α,4β-diol (**21b**) was treated with LTA to afford 2,4-dioxo-3,4-secofriedelan-3-yl acetate (**23b**), mp 196—197 °C (from petroleum benzine); IR 1760, 1745, 1695, 1230, 1060, and 1040 cm^{-1}; ^1H NMR (60 MHz, $CDCl_3$) δ=2.10 and 2.13 (each 3H, s; AcO- and Ac), 2.2—2.5 (2H, m; $C_{(1)}H_2CO-$), 4.50 and 4.73 (each 1H, d, *J*=18 Hz, $AcOC\underline{H}_2-CO-$); MS *m/z* (%) 500 (M^+; 1), 457 (38), 341 (20), 205 (100), 137 (52), 135 (45), 123 (66), 121 (56), 109 (80), and 107 (47); Found: C, 76.95; H, 10.68%. Calcd for $C_{32}H_{52}O_4$: C, 76.75; H, 10.47%. The same treatment of **22b** with LTA gave the same diketo acetate (**23b**).

3-Acetoxymethyl-A(1)-norfriedel-3-ene (24b). A solution of methyl A(1)-norfriedel-3-ene-3-carboxylate (**19b**) in ether was treated with LAH to give 3-hydroxymethyl-A(1)-norfriedel-3-ene (**24a**), mp 234—236 °C (from benzene); IR 3400 (br), 1640, 995, 720, and 410 cm^{-1}; ^1H NMR (60 MHz, $CDCl_3$) δ=4.10 (2H, s; $=C-CH_2OH$); MS *m/z* (%) 426 (M^+; 5), 411 (84), 205 (95), 137 (100), 123 (98), 121 (89), 119 (87), 109 (67), 107 (93), and 105 (62); Found: C, 84.61; H, 11.84%. Calcd for $C_{30}H_{50}O$; C, 84.44; H, 11.81%. Acetylation of **24a** yielded 3-acetoxymethyl-A(1)-norfriedel-3-ene (**24b**), mp 179—183.5 °C (from methanol); IR 1735, 1665, 1260, and 1030 cm^{-1}; ^1H NMR (60 MHz, $CDCl_3$) δ=2.10 (3H, s; Ac); MS

m/z (%) 468 (M^+; 2), 453 (18), 408 (14), 393 (33), 273 (11), 259 (14), 205 (42), 123 (72), 121 (78), 119 (67), 109 (100), 107 (83), and 105 (53); Found: C, 81.77; H, 11.11%. Calcd for $C_{32}H_{54}O_3$: C, 81.99; H, 11.18%.

3β-Hydroxymethyl-A(1)-norfriedelane-3α,4,α-diol (25a). To a solution of 3-acetoxymethyl-A(1)-norfriedel-3-ene (**24b**; 300 mg) in ether (20 ml) was added osmium tetraoxide (0.3 g) and the solution was allowed to stand for 1 week. After addition of ether and excess LAH, the mixture was refluxed for 30 min and then a small amount of acetone was added. The usual work-up followed by chromatographic separation (silica gel-benzene and ether) gave 3β-hydroxymethyl-A(1)-norfriedelane-3α,4α-diol (**25a**; 185 mg), mp 263—267 °C (with decomp) (from ethyl acetate); IR 3850, 1120, 1060, 1045, 1005, and 940 cm^{-1}. ^1H NMR (90 MHz, $CDCl_3$) δ=3.60 (2H, s; $-CH_2O-$); MS *m/z* (%) 460 (M^+; trace), 442 (10), 417 (68), 343 (21), 273 (23), 219 (30), 205 (100), 191 (34), 142 (55), and 109 (80); Found: C, 78.06; H, 11.21%. Calcd for $C_{30}H_{52}O_3$: C, 78.20; H, 11.38%.

3β-Acetoxymethyl-A(1)-norfriedelane-3α,4α-diol (25b). On acetylation of **25a** afforded the acetate (**25b**), mp 212—214 °C (needles from ether-cyclohexane); IR 3500, 3300, 1750, 1730, 1260, and 1065 cm^{-1}. ^1H NMR (60 MHz, $CDCl_3$) δ=2.10 (3H, s; CH_3COO-) and 4.10 (2H, s; $-CH_2OOC-$); MS *m/z* (%) 460 (M^+; trace), 442 (10), 417 (68), 273 (23), 219 (30), 205 (100), 191 (34), 142 (55), and 109 (80); Found: C, 76.17; H, 10.67%. Calcd for $C_{32}H_{54}O_4$: C, 76.44; H, 10.83%.

4α-Hydroxy-A(1)-norfriedelan-3-one (26) and 4β-Hydroxy-A(1)-norfriedelan-3-one (32). Friedelane-2,3-dione (**28**; 5 g) and potassium hydroxide (5 g) were dissolved in diethylene glycol (400 ml) and the mixture was heated at 200 °C for 10 h under a nitrogen atmosphere. The solution was then poured into 2% hydrochloric acid (1 l) with formation of white precipitates, which were collected on a filter paper and dried. Although the benzilic acid rearrangement product consisted of a mixture of stereoisomers, further purification was not done.

The crude product obtained above, was suspended in acetic acid (300 ml) and LTA was added until no starting material was detected on TLC. Then the reaction mixture was poured into water and extracted with ether. The ether layer was worked up as usual and chromatographed (silica gel-benzene) to give a mixture of A(1)-norfriedelan-3-one (**29**) and its 4-epimer.

The mixture (1 g) of **29** and its 4-epimer was refluxed with benzoyl chloride (30 ml) for 1 h. After cooling, pyridine (10 ml) and then water (10 ml) were added dropwise, and the mixture was allowed to stand until the exothermic reaction ceased. Ether was added and the ethereal solution was washed with dil hydrochloric acid. The organic layer was worked up in usual manner and subjected to chromatography on silica gel. Elution with benzene-petroleum benzine afforded A(1)-norfriedel-3-en-3-yl benzoate (**27**; 0.93 g), mp 206—209 °C (from dichloromethane-cyclohexane); IR 1740, 1685, 1250, 1100, and 710 cm^{-1}; ^1H NMR (60 MHz, $CDCl_3$) δ=7.3—8.3 (5H, m; C_6H_5-); MS *m/z* (%) 516 (M^+; 0.4), 501 (4), 155 (5), 135 (7), 121 (11), 109 (14), 107 (14), and 105 (100); Found: C, 83.41; H, 10.14%. Calcd for $C_{36}H_{52}O_2$: C, 83.66; H, 10.14%.

To a solution of the benzoate (**27**; 1 g) in dichloromethane (300 ml) was added 39% peracetic acid solution (20 ml, a trace amount of sulfuric acid in the solution was neutralized by addition of potassium acetate before use). The reaction mixture was kept in a dark place for a week, and then the remaining peroxide was decomposed with an aqueous solution of potassium iodide and sodium sulfite. The organic layer was washed with sodium carbonate solution and concentrated to yield a residue, which was hydrolyzed with ethanolic potassium hydroxide solution at room temperature for 2 d. After most of ethanol was removed in vacuo, the residue was extracted with benzene and chromatographed on silica gel. Elution was performed with benzene to afford 4α-hydroxy-A(1)-norfriedelan-3-one (**26**; 530 mg) and the 4β-epimer (**32**; 3 mg) in turn. **26**; mp 286 °C (with decomp) (from benzene); IR 3450, 1740, 1090, and 915 cm^{-1}; ν^{OH} (0.001 M carbon tetrachloride solution) 3606 cm^{-1}; ^1H NMR (90 MHz, $CDCl_3$) δ=2.18 (1H, s; -OH); MS *m/z* (%) 428 (M^+; 36), 341 (63), 205 (69), 137 (56), 135 (46), 123 (72), 121 (53), and 109 (100); Found: C, 80.95; H, 11.02%. Calcd for $C_{29}H_{48}O_2$: C, 81.25; H, 11.29%. **32**; Mp 214—216.5 °C (from cyclohexane); IR 3450, 3400, 1755, and 1745 cm^{-1}; ν^{OH} (0.001 M carbon tetrachloride solution) 3563 cm^{-1}; ^1H NMR (90 MHz, $CDCl_3$) δ=2.0 (1H, s; -OH); MS *m/z* 428 (M^+; 38), 341 (50), 205 (78), 137 (46), 123 (75), 121 (54), 109 (100), and 107 (54); Found: *m/z* 428.3624. Calcd for $C_{29}H_{48}O_2$: M, 428.3654.

Methyl 4-Oxo-3,4-seco-A(1)-norfriedelan-3-oate (33b). 4-Oxo-3,4-seco-A(1)-norfriedelan-3-oic acid (**33a**) was prepared from friedelane-2,3-dione (**28**) by the same procedure as that for the preparation of 4-oxo-3,4-secofriedelan-3-oic acid (**17a**) from friedel-3-en-3-yl benzoate (vide supra). **33a**; Mp 215—217 °C (from ethanol); IR 3450, 1740, 1200, 1180, 1150, 1070, 1050, 1010, 990, and 900 cm^{-1}; ^1H NMR (60 MHz, $CDCl_3$) δ=2.20 (3H,s; Ac) and 1.9—2.5 (2H, m; $-C\underline{H}_2-COOH$); MS *m/z* (%) 444 (M^+; 2), 401 (40), 219 (19), 205 (100), 137 (28), 135 (26), 123 (48), 121 (37), and 109 (88). On methylation with diazomethane, **33a** afforded methyl 4-oxo-3,4-seco-A(1)-norfriedelan-3-oate (**33b**), mp 166—167 °C (from ethanol); IR 1740, 1695, 1295, 1170, and 995 cm^{-1}; ^1H NMR (60 MHz, $CDCl_3$) δ=2.20 (3H, s; Ac) and 3.63 (3H, s; $-COOCH_3$); MS *m/z* (%) 458 (M^+; 6), 415 (35), 219 (12), 205 (45), 163 (20), 135 (50), 121 (78), and 109 (100).

4α-Hydroxyfriedelan-3-one (35) and 4β-Hydroxyfriedelan-3-one (36). The preparation procedure of **35** and **36** was almost the same as that of 4α- and 4β-hydroxy-A(1)-norfriedelan-3-ones (**26** and **32**) from friedelane-2,3-dione (**28**). **35**; Mp 269—271 °C (from ethyl acetate); IR 3440, 1710, 1110, and 1070 cm^{-1}; ν^{OH} (0.001 M carbon tetrachloride solution) 3620 cm^{-1}; ^1H NMR (60 MHz, $CDCl_3$) no signals below δ 2.5 were observed. MS *m/z* (%) 442 (M^+; 40), 205 (74), 123 (81), 121 (52), 109 (100), and 107 (56); Found: C, 81.16; H, 11.11%. Calcd for $C_{30}H_{50}O_2$: C, 81.39; H, 11.38%. **36**; Mp 234.5—236 °C (from ethyl acetate); IR 3470, 1720, 1160, and 1125 cm^{-1}; ν^{OH} (0.001M carbon tetrachloride solution) 3520 cm^{-1}; ^1H NMR (60 MHz, $CDCl_3$) δ=2.55 (2H, m; $C_{(2)}H_2CO-$) and 3.9 (1H, s; -OH); MS *m/z* (%) 442 (M^+; 19), 399 (5), 205 (39), 189 (17), 135 (39), 121 (64), and 109 (100).

References

1) T. Nishihama and T. Takahashi, *Bull. Chem. Soc. Jpn.*, **39**, 200 (1966).

2) E. J. Bailey, D. H. R. Barton, J. Elks, and J. F. Templeton, *J. Chem. Soc.*, **1962**, 1578; B. Camerio, B. Patelli, and R. Sciaky, *Tetrahedron Lett.*, **1961**, 554; H. Mori, V. S. Gandhi, and E. Schwenk, *Chem. Pharm. Bull.*, **10**, 842 (1962).

3) R. Hanna and G. Ourisson, *Bull. Soc. Chim. Fr.*, **1961**, 1945.

4) N. L. Drake and J. K. Wolfe, *J. Am. Chem. Soc.*, **61**, 3074 (1939).

5) The Baeyer-Villiger reaction was known to proceed with the retention of the configuration of the chiral carbon α to the carbonyl group; this is exigent of the 4R-configuration for **10**. The other δ-lactone,[4] 4-epi-3-oxafriedelan-2-one (**10′**), obtained by reduction of **33a** with sodium and 1-propanol was not identical with **10**. This leads to the 4S-configuration for **10′**. The alcohol (**10′**) was also obtained by $NaBH_4$ reduction of **33b** in a quantitative yield. The presence of **10** was not detected in the reaction product. **10′**; IR 1720, 1215, 1198, 1175, 1062, 1055, and 977 cm^{-1}; ^1H NMR (60 MHz, $CDCl_3$) δ=2.3—2.5 (2H, m; CH_2CO-) and 4.05 (1H, q, J=7 Hz); MS m/z (%) 428 (M^+; 2.2), 342 (12), 304 (13), 276 (13), 235 (18), 205 (39), and 109 (100).

6) T. Tsuyuki, R. Aoyagi, S. Yamada, and T. Takahashi, *Tetrahedron Lett.*, **1968**, 5263.

7) V. V. Kane and R. Stevenson, *J. Org. Chem.*, **25**, 1394 (1960).

8) F. V. Brutcher, Jr. and W. Bauer, Jr., *J. Am. Chem. Soc.*, **84**, 2236 (1962). Ring D of steroidal 16-one is known to adopt a half chair conformation. The conformational situation of ring A in **26** and **32** is considered to be almost the same as that of the steroidal ring D.

9) M. Oki, H. Iwamura, J. Aihara, and H. Iida, *Bull. Chem. Soc. Jpn.*, **41**, 176 (1968); L. Joris and P. von R. Schleyer, *J. Am. Chem. Soc.*, **90**, 4599 (1968).

10) T. Matsuura, "Sanso-sanka-hanno," Maruzen, Tokyo, (1977), p. 174.

A New Synthesis of 3-Amino-2-alkenoates. Novel Synthetic Route to Amino Sugars *N*-Benzoyl-L-daunosamine and -L-acosamine

Tamejiro HIYAMA,* Kazuhiro KOBAYASHI, and Kiyoharu NISHIDE
Sagami Chemical Research Center, 4-4-1 Nishiohnuma, Sagamihara, Kanagawa 229
(Received December 9, 1986)

Alkanoate esters are found to couple with various nitriles to give (*Z*)-3-amino-2-alkenoates in good yields with the aid of a magnesium amide prepared by the reaction of ethylmagnesium bromide and diisopropylamine. The C-C bond forming reaction was applied to (2*S*,3*S*)-2,3-(cyclohexylidenedioxy)butanenitrile and the resulting adduct was successfully converted into *N*-benzoyl-L-daunosamine in 41% overall yield through a sequence of functional group manipulation; acetylation, hydrogenation, hydrolysis and benzoylation, lactonization and finally reduction. By the similar process, (2*R*,3*S*)-2,3-(cyclohexylidenedioxy)butanenitrile was transformed to *N*-benzoyl-L-acosamine in 25% overall yield.

Carbonyl addition of the enolates of carboxylic acids and their esters is well-documented and widely used for the construction of carbon framework of various target molecules.[1] For this carbonyl addition, a variety of metal enolates are employed which exhibit characteristic reactivity with respect to stereo-selection.[2] Addition of the metal enolates with nitrogen analogs of aldehydes is especially useful for β-lactam synthesis.[3] However, nitriles as the substrates remained unexplored until recently, possibly due to low reactivity of conventional enolates.[4] In fact, when we examined the reaction of *t*-butyl lithioacetate with benzonitrile, we observed that no trace of the expected adduct was produced. The failure of the nitrile addition was ascribed to the incapability of the lithium ion to take a nitrile in its ligand sphere as well as to the instability of the primary adduct. Thus, we searched for higher valent metal counter ions appropriate to the C-C bond formation. Zinc enolates grew promising upon literature survey.[5] We could not, however, achieve the nitrile addition of the Reformatsky reagent in good yields, although Hannick and Kishi later established an improved procedure for the Blaise reaction.[6] After several screening experiments, we found the magnesium enolates of alkanoate esters undergo the desired reaction to afford 3-amino-2-alkenoates efficiently[7] and applied the reaction successfully to the synthesis of amino sugars *N*-benzoyl-L-daunosamine[8] and *N*-benzoyl-L-acosamine.[9] Details of the new transformation are reported herein.

Results and Discussion

Nitrile Addition of Alkanoate Magnesium Enolates. The reaction of *t*-butyl acetate with benzonitrile was first studied. Magnesium amide was prepared by mixing equimolar amounts of ethylmagnesium bromide and a secondary amine[10] such as diisopropylamine, isopropylcyclohexylamine and hexamethyldisilazane. *t*-Butyl acetate was treated with each base at −10 to 0 °C in diethyl ether for 1 h and then with benzonitrile to give, after quenching with aqueous ammonium chloride solution and extractive workup followed by distillation, *t*-butyl 3-amino-3-phenylpropenoate (**2i**) in 53, 49, and 62% yield respectively. The yields were improved when the magnesium amide was prepared by 2 : 1 molar ratio of secondary amine and ethylmagnesium bromide. Diethyl ether was proved to be a superior solvent to tetrahydrofuran (THF). Although the structure of the magnesium amide reagent is unclear at present, a report by Wannagat and Kuckertz is informative.[11] They treated hexamethyldisilazane with a Grignard reagent in diethyl ether and obtained a complex $[(Me_3Si)_2N]_2Mg : MgX_2 : OEt_2$ which upon treatment with more basic solvent dioxane gave $[(Me_3Si)_2N]_2Mg$: (dioxane)$_3$ and MgI_2 : (dioxane)$_2$. Thus, we assumed the reagent generated from a 1 : 1 mixture of EtMgBr and HN(*i*-Pr)$_2$ would be a mixture of $[(i\text{-Pr})_2N]_2Mg$ and $MgBr_2$ solvated by diethyl ether. By use of excess diisopropylamine, the Lewis acid $MgBr_2$ would be preferentially neutralized, and, as the results, the reactivity of the magnesium amide base is enhanced.

$$2\,EtMgBr + 4\,HN(i\text{-}Pr)_2 \longrightarrow Mg[N(i\text{-}Pr)_2]_2 + MgBr_2 \cdot [HN(i\text{-}Pr)_2]_2$$

We employed diisopropylamine for all cases, as it is relatively cheap and volatile enough to be removed readily. At the early stage of our research,[7a] we employed 4 : 2 : 2 molar ratio of diisopropylamine, ethylmagnesium bromide and ester, but later found a 4 : 2 : 1 ratio is better for the reaction, since an excess ester sometimes underwent self-condensation.

The nitrile addition of magnesium ester enolate is applicable to various nitriles (Scheme 1). The mol ratio of the ester enolate to a nitrile was changed from 1 : 1 to large excess depending on the reactivity of the nitrile as summarized in Table 1. Nitriles having rela-

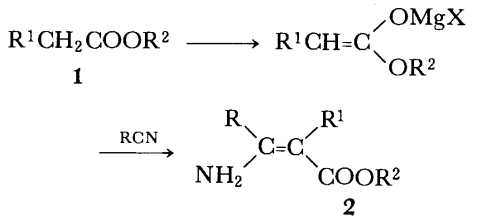

Scheme 1.

Table 1. Nitrile Addition of the Magnesium Enolates of Alkanoate Esters

Run	Nitrile	Alkanoate Ester 1	Reaction Condition	Product (Yield)
1	MeCN (62 mg, 1.5 mmol)	AcOt-Bu (0.35 g, 3 mmol)[a]	0 °C, 3 h	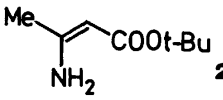 **2a** (0.156 g, 66%)
2	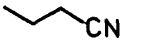 (0.104 g, 1.5 mmol)	AcOt-Bu (0.35 g, 3 mmol)[a]	0 °C, 4 h	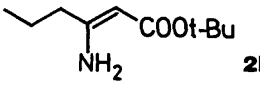 **2b** (0.158 g, 57%)
3	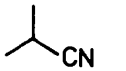 (0.104 g, 1.5 mmol)	AcOt-Bu (0.174 g, 1.5 mmol)[a]	0 °C, 1.5 h	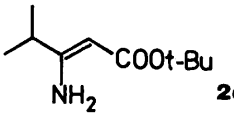 **2c** (0.21 g, 74%)
4	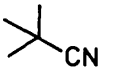 (0.127 g, 1.5 mmol)	AcOt-Bu (0.174 g, 1.5 mmol)[a]	0 °C, 1.5 h	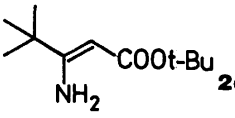 **2d** (0.143 g, 48%)
5	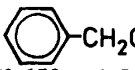 (0.176 g, 1.5 mmol)	AcOt-Bu (0.176 g, 1.5 mmol)[a]	0 °C, 1.5 h	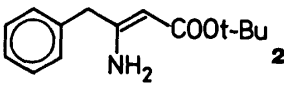 **2e** (94 mg, 27%)
6	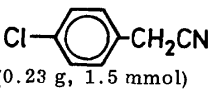 (0.23 g, 1.5 mmol)	AcOt-Bu (0.70 g, 6 mmol)[a]	0 °C, 0.7 h	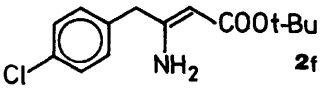 **2f** (0.120 g, 30%)
7	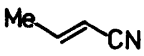 (0.101 g, 1.5 mmol)	AcOt-Bu (0.174 g, 1.5 mmol)[a]	0 °C, 1.5 h	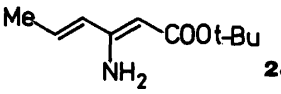 **2g** (49 mg, 18%)
8	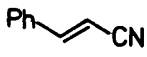 (0.194 g, 1.5 mmol)	AcOt-Bu (0.35 g, 3 mmol)[b]	0 °C, 1.5 h	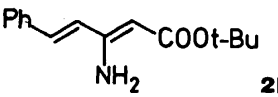 **2h** (0.163 g, 44%)
9	PhCN (0.155 g, 1.5 mmol)	AcOt-Bu (0.134 g, 1.5 mmol)[b]	0 °C, 1 h	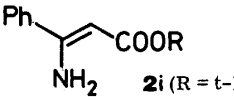 **2i** (R = t-Bu, 0.27 g, 83%)
10	PhCN (0.155 g, 1.5 mmol)	AcOEt (0.26 g, 3 mmol)[b]	-78 °C to 0 °C, 1.5 h	**2j** (R = Et, 0.163 g, 57%)
11	PhCN (0.155 g, 1.5 mmol)	EtCOOt-Bu (0.195 g, 1.5 mmol)[b]	-78 °C, 5 h; then 0 °C	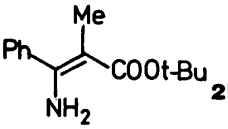 **2k** (0.105 g, 30%)
12	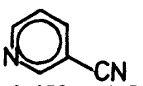 (0.156 g, 1.5 mmol)	AcOt-Bu (0.174 g, 1.5 mmol)[a]	0 °C, 1.5 h	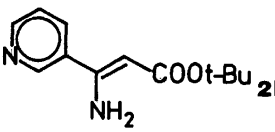 **2l** (0.22 g, 65%)
13	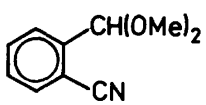 (0.35 g, 2 mmol)	AcOt-Bu (0.91 g, 8 mmol)[a]	0 °C, 5 h	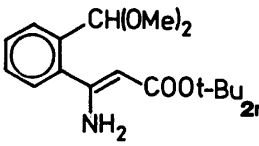 **2m** (0.50 g, 85%)
14	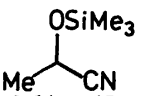 (2.14 g, 15 mmol)	AcOt-Bu (3.48 g, 30 mmol)[b]	0 °C, 3 h	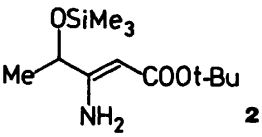 **2n** (2.52 g, 65%)

Table 1. (Continued)

Run	Nitrile	Alkanoate Ester **1**	Reaction Condition	Product (Yield)
15	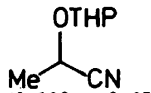 (0.100 g, 0.65 mmol)[c]	AcOt-Bu (87 mg, 0.75 mmol)[b]	0 °C, 1.5 h	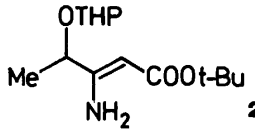 **2o** (0.150 g, 86%)
16	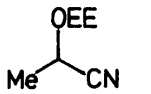 (12.9 g, 90 mmol)[c]	AcOt-Bu (20.9 g, 180 mmol)[b]	0 °C, 3 h	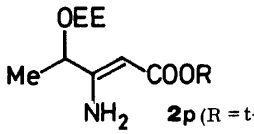 **2p** (R = t-Bu, 18.9 g, 81%)
17	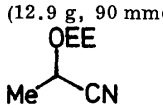 (0.143 g, 1 mmol)[c]	AcOEt (0.35 g, 4 mmol)[b]	-78 °C to 0 °C, 5 h	**2q** (R = Et, 0.122 g, 53%)
18	CCl_3CN (0.29 g, 2 mmol)	AcOt-Bu (0.23 g, 2 mmol)[b]	0 °C, 5 min	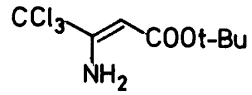 **2r** (0.43 g, 83%)

a) A mol ratio of diisopropylamine:ethylmagnesium bromide:ester was 4:2:2. b) A mol ratio of diisopropylamine:ethylmagnesium bromide:ester was 4:2:1. c) THP is tetrahydropyran-2-yl; EE is 1-ethoxyethyl group.

tively acidic α-hydrogen(s) gave slightly lower yields of adducts (Runs 5 and 6). The yields were not improved even by use of 6 fold mol of the ester enolate. 3-Butenenitrile did not give the desired adduct at all. The nitrile addition was applied particularly effectively to α-alkoxy nitriles or protected cyanohydrins (Runs 14 to 17). Ethyl acetate and *t*-butyl propionate can be employed in place of *t*-butyl acetate, but these required milder conditions: Both generation of magnesium enolate and the reaction with benzonitrile were preferably carried out at −78 °C, and the reaction mixture was allowed to warm up gradually (Runs 10, 11, and 17) to avoid self-condensation of the esters.

The configuration of the products **2** is all assigned as (Z) on the basis of ^{1}H NMR spectra. For example, **2a** and **2c** showed olefinic singlet absorptions at δ 4.42 and 4.47 respectively consistent with the literature values δ 4.49 and 4.56 for the ethyl ester of Z-configuration corresponding to **2a** and **2c** respectively.[12] The Z-preference is ascribed to intramolecular hydrogen bonding between amino and alkoxycarbonyl groups.[12] The geometrical preference was retained after the 3-amino-2-alkenoates were acetylated, though small amounts of (E)-isomers were produced. The resultant 3-acetamido-2-alkenoates are stable to moisture and was readily purified by preparative TLC or column chromatography in contrast to the parent compounds **2**.

As 3-amino-2-alkenoates are versatile synthetic intermediates for heterocycles such as pyridines,[13] pyrimidines, indoles,[14] and isothiazoles,[15] and, in addition, some *N*-aroyl derivatives of 3-amino-2-alkenoic acids exhibit anti-inflammatory activity,[16] various synthetic approaches have appeared.[6,17] The magnesium enolate-nitrile addition reported herein

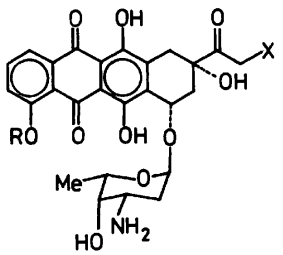

3a R=Me, X=OH adriamycin
3b R=Me, X=H daunomycin
3c R=H, X=H carminomycin

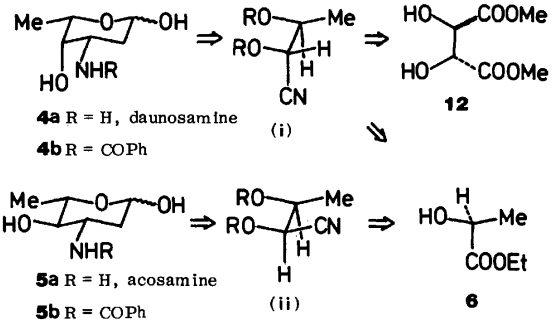

Scheme 2.

can be characterized by simple experimental version coupled with wide applicability. We applied the new synthetic method to the total synthesis of physiologically active amino sugars.

Synthesis of *N*-Benzoyl-L-daunosamine and -L-acosamine. The nitrile-ester enolate coupling reaction is applied to the synthesis of amino sugars such as L-daunosamine (**4a**) and L-acosamine (**5a**). These are sugar moieties of highly potent antitumor antibiotics adriamycin, daunomycin, and carminomycin.[18] Particularly, the cardiotoxicity is lowered remarkably by

changing the sugar part of adriamycin from daunosamine to acosamine.[19] The structural features of these amino sugars led us to retrosynthetic analysis as shown in Scheme 2. Addition of acetic acid ester enolate to the nitrile (i) or (ii) followed by stereoselective reduction of the resulting configurationally fixed C=C bond and appropriate functional group manipulation should afford daunosamine or acosamine derivatives respectively. The requisite nitriles (i) and (ii) may be derived from ethyl (*S*)-(−)-lactate (**6**). Methyl L-tartrate (**12**) can be the precursor of the nitrile (i), as the tartrate possesses the needed C_4 framework, oxygen functional groups and stereochemical arrangements all in a single molecule. Synthetic operations were carried out according to the Schemes 3 and 4.

Ethyl (*S*)-(−)-lactate (**6**) was protected with ethyl vinyl ether, and reduced with lithium aluminium hydride to give (*S*)-2-ethoxyethyl ether of 1,2-propanediol (**7**). Oxidation of **7** with dimethyl sulfoxide (DMSO)[20] gave the aldehyde **8** which was isolated by distillation. Cyanohydrin formation was effected with acetone cyanohydrin and triethylamine catalyst. The resulting cyanohydrin **9** was converted into a cyclohexylidene acetal by acetal exchange reaction with cyclohexanone dimethyl acetal and bis(trimethylsily) sulfate catalyst.[21] The diastereomeric ratio of **10** and **11** was estimated before isolation to be 45 : 55. When the cyanohydrin formation was carried out with Me_3SiCN and Et_2AlCN catalyst, the diastereomeric ratio changed to 73 : 27. These nitriles were readily separated by column chromatography. ^1H NMR study with $Eu(tfc)_3$ showed >95% optical purity of **10** and **11**. Thus, no trace of racemization occurred during the oxidation of **7**, cyanohydrin formation or acetalization leading to **10** and **11**. All attempts to epimerize the C(2) stereocenter with base failed. Either recovery of the starting nitriles (NaOEt) or total decomposition ($LiN(i\text{-}Pr)_2$) was observed in sharp contrast to the facile epimerization of the corresponding aldehydes.[22]

The (2S,3S)-isomer **10** was alternatively prepared according to the Scheme 4. Dimethyl L-tartrate (**12**) was acetalized to **13**[23] which was reduced with lithium aluminium hydride to a diol. Selective monotosylation followed by sodium borohydride reduction of the resulting tosylate gave an alcohol **14**. Oxidation by the Swern's method[20] afforded **15**.[24] Derivatization of **15** to its oxime followed by dehydration gave **10**.

With the required nitriles now at hand, we studied subsequent C_2 homologation. The (2*S*,3*S*)-nitrile **10**

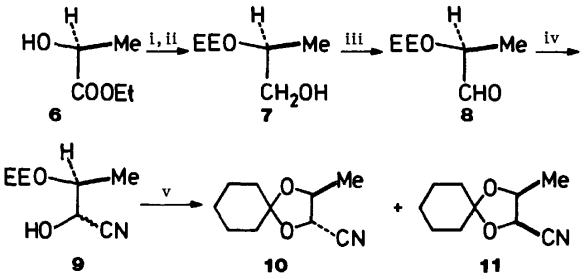

i) CH_2=CHOEt, PyH·OTs, CH_2Cl_2, 0 °C to r.t.
ii) $LiAlH_4$, Et_2O, reflux
iii) DMSO, $(COCl)_2$, Et_3N, CH_2Cl_2, −65 to −70 °C
iv) $Me_2C(OH)CN$, Et_3N, 0 °C
v) $(CH_2)_5C(OMe)_2$, $(Me_3SiO)_2SO_2$, Molecular Sieve 4A, 0 °C to r.t.

Scheme 3.

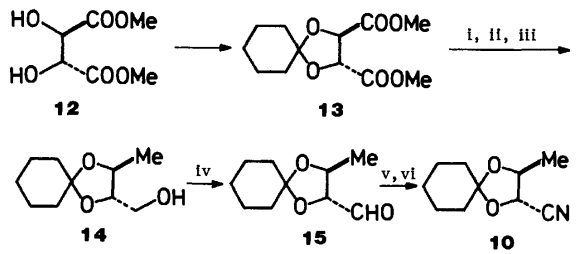

i) $LiAlH_4$, Et_2O, 0 °C to reflux
ii) TsCl, Et_3N, CH_2Cl_2, 0 °C
iii) $NaBH_4$, DMSO
iv) DMSO, $(COCl)_2$, Et_3N, CH_2Cl_2
v) NH_2OH·HCl, Py, 80 °C
vi) CCl_4, Ph_3P, Et_3N, 80 °C

Scheme 4.

With the required nitriles now at hand, we studied subsequent C_2 homologation. The (2*S*,3*S*)-nitrile **10**

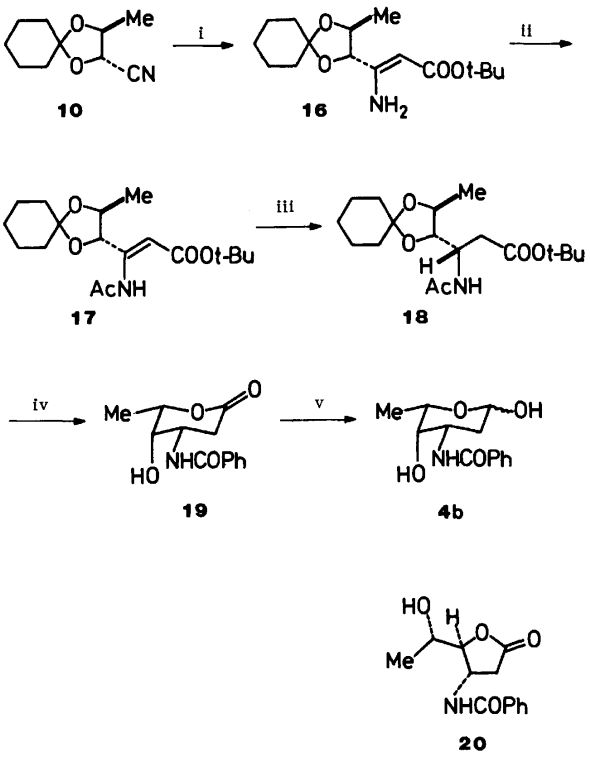

i) CH_2=C(O*t*-Bu)OMgX, Et_2O, 0 °C
ii) Ac_2O, Py, 50 to 60 °C
iii) H_2(55 kg cm^{-2}=5.6×10^6 Pa), PtO_2, AcOEt, 70 °C
iv) 2M (1M=1 mol dm^{-3}) HCl, reflux; PhCOCl, sat aq $NaHOC_3$-acetone (5 : 2), r.t.; 2 M HCl
v) *i*-Bu_2AlH, THF, −60 to −50 °C

Scheme 5.

Table 2. Catalytic Hydrogenation of **17**

Run	Catalyst	Solvent	Temp °C	H_2 kg cm^{-2} [a]	Reaction Time/d	Yield %	**18**:Epimer
1	5% Rh/C	THF	55	60	0.6	90	1:2
2	5% Rh/C	THF-AcOH (40:1)	55	60	2.5	68	2:3
3	5% Pd/Al_2O_3	AcOEt	55	60	0.6	Quant.	1:2
4	PtO_2	AcOEt	55	1	3.5	31	3:2
5	PtO_2	AcOEt	70	55	1	98	5.1:1

a) 1 kg cm^{-2} = 1.01×10^5 Pa.

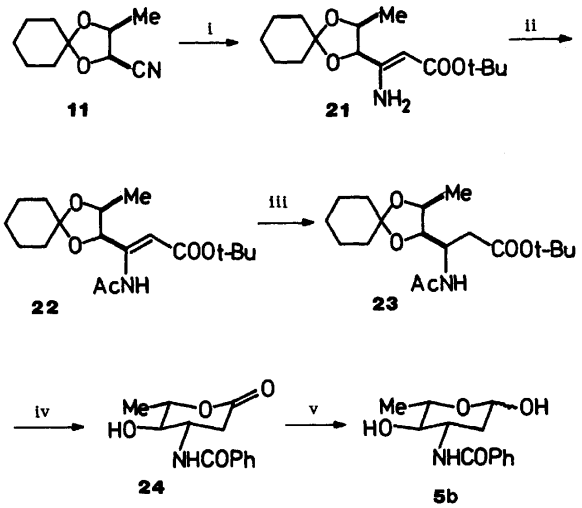

i) CH_2=C(O*t*-Bu)OMgX, Et_2O, 0 °C
ii) Ac_2O, Py, 50 to 60 °C
iii) H_2(70 kg cm^{-2}=7.1×10^6 Pa), Rh/C, THF, 55 °C
iv) 2M HCl, reflux; PhCOCl, sat aq $NaHOC_3$-acetone (5:2), r.t.; 2 M HCl
v) *i*-Bu_2AlH, THF, −60 to −50 °C

Scheme 6.

was revealed to be reactive enough to afford **16** in 99% yield (Scheme 5). Although the C=C bond of 3-amino-2-alkenoates is recorded to be reduced under several conditions,[25] the known conditions were not applicable to **16** possibly due to unrecognized electronic and/or steric reasons. To reduce the electron density of the C=C bond of **16**, we acetylated **16** to **17**. A part of the product isomerized to the (E)-isomer.[26] The acetamide **17** was proved to be acid-stable and was readily purified by chromatography. Catalytic hydrogenation was studied under various conditions. Results are summarized in Table 2. Platinum catalyst produced predominantly the desired product **18**, whereas rhodium and palladium catalysts preferred the formation of the epimer of **18**. Under the conditions of Run 5, **18** was isolated in 82% yield in a pure form. Its epimer was isolated in 16% yield. Treatment of **18** with hydrochloric acid induced hydrolysis of the acetal, ester and amide moieties all in a single operation. Subsequent benzoylation under the Schotten-Baumann conditions followed by lactonization gave a δ-lactone **19**. The lactonization was found to proceed stepwise: Initially a γ-lactone **20** was formed which gradually isomerized to **19**. Reduction of **19** with diisobutylaluminium hydride gave *N*-benzoyl-L-daunosamine.[27,28,31]

For the synthesis of *N*-benzoyl-L-acosamine (**5b**), (2*R*,3*S*)-2,3-(cyclohexylidenedioxy)butanenitrile (**11**) is a requisite starting material. Addition of the magnesium enolate of *t*-butyl acetate to **11** was found relatively sluggish and took place at 0 °C to give **21** in 54% yield after isolation by distillation. Acetylation under the standard conditions gave **22**. Again (E)-isomer of **22** accompanied. Hydrogenation of **22** with rhodium or platinum catalyst was satisfactory in respect to stereochemical outcome. Of these, rhodium on carbon was employed in an autoclave under a hydrogen pressure of 70 kg cm^{-2}. Hereby a single isomer **23** was isolated in 84% yield. It is worthy of note that the stereochemical course of the hydrogenation of C(2)=C(3) is oriented by the configuration of C(5) rather than that of C(4) (compare the reduction of **17** with that of **22**), even though C(4) is situated closer to the reaction site.[32] Hydrolysis of **23** followed by *N*-benzoylation and lactonization afforded **24** which exhibited spectral data fully identical with the reported values.[28a] Diisobutylaluminium hydride reduction gave finally *N*-benzoyl-L-acosamine.[28,29]

Experimental

Distillation of a sample of less than 1 g was carried out by bulb-to-bulb distillation technique with Kugelrohr (Büchi) or Glass Tube Oven GTO 250R (Shibata). Larger amount of sample was distilled by a micro distillation apparatus. Reactions were carried out under an argon atmosphere unless otherwise specified. All mps and bps were uncorrected values. ^{1}H NMR spectra were obtained on a Varian EM 390 or Varian XL-100A spectrometer, chemical shifts being given in ppm units from the tetramethylsilane standard. ^{13}C NMR spectra were recorded on a Bruker AM-400 spectrometer with tetramethylsilane as the internal standard. IR spectra were taken on a JASCO A 202 spectrometer. Specific rotation was measured with a Horiba SEPA-200 or Union PM-201 machine. Low resolution mass spectra were recorded with a Hitachi RMU-6MG machine (70 eV); millimass with a Hitachi M-80A spectrometer. GLC analyses were performed with a Shimadzu GC-7A chromatograph with a FID detector. TLC analyses were performed on com-

mercial glass plates coated with Merck Silica Gel 60 F_{254} in 0.25 mm thick layer. Preparative TLC plates were prepared using Merck Kieselgel 60 PF_{254}. Column chromatography was carried out using silica gel such as Wacogel C-100 (Wako) or Kieselgel 60 (Merck). THF and diethyl ether were distilled before use from sodium-benzophenone. Diisopropylamine, *t*-butyl acetate, and DMSO were distilled over calcium hydride.

***t*-Butyl 3-Amino-2-butenoate (2a). A Typical Procedure for Generation and Nitrile Addition of the Magnesium Enolate of *t*-Butyl Acetate.** Diisopropylamine (0.61 g, 6.0 mmol) was added to an ethereal solution (0.70 M, 4.3 ml) of ethylmagnesium bromide (3.0 mmol) at 0 °C, and the reaction mixture was stirred for 1 h. To the resulting turbid solution was added *t*-butyl acetate (0.35 g, 3.0 mmol) at 0 °C. After 0.5 h acetonitrile (62 mg, 1.5 mmol) was injected with the aid of a microsyringe to the reaction mixture and allowed to react for 3 h at 0 °C. Quenching with aqueous ammonium chloride solution, extraction with diethyl ether, and purification by distillation gave *t*-butyl 3-amino-2-butenoate (**2a**) (0.156 g, 66% yield). Bp 73 °C/0.3 Torr† (lit,[16] 66 °C/0.4 Torr). IR (neat) 3460, 3345, 1650, 1615, 1558 cm^{-1}. ^1H NMR ($CDCl_3$) δ=1.46 (s, 9H), 1.84 (s, 3H), 4.42 (s, 1H), 5.0—6.7 (br, 2H).

The *t*-butyl esters of **2** (Table 1) were prepared by the similar procedure described above, and the physical properties of these are listed below.

***t*-Butyl 3-Amino-2-hexenoate (2b):** Bp 78 °C/0.25 Torr; IR (neat) 3460, 3345, 1655, 1615, 1560 cm^{-1}; ^1H NMR ($CDCl_3$) δ=0.93 (t, 3H), 1.45 (s, 9H), 1.5—1.8 (m, 2H), 2.05 (t, 2H), 4.43 (s, 1H), 5.3—6.6 (br, 2 H). Found: C, 64.89; H, 10.10; N, 7.42%. Calcd for $C_{10}H_{19}NO_2$: C, 64.83; H, 10.34; N, 7.56%.

***t*-Butyl 3-Amino-4-methyl-2-pentenoate (2c):** Bp 95 °C/0.7 Torr; IR (neat) 3460, 3345, 1660, 1615, 1545 cm^{-1}; ^1H NMR ($CDCl_3$) δ=1.14 (d, 6H), 1.47 (s, 9H), 2.1—2.5 (m, 1H), 4.47 (s, 1H), 5.8—6.8 (br, 2H). Found: C, 64.59; H, 10.23; N, 7.40%. Calcd for $C_{10}H_{19}NO_2$: C, 64.83; H, 10.34; N, 7.56%.

***t*-Butyl 3-Amino-4,4-dimethyl-2-pentenoate (2d):** Bp 104 °C/0.4 Torr; mp 75 °C; IR (neat) 3500, 3455, 3345, 1675, 1615, 1540 cm^{-1}; ^1H NMR δ=1.14 (s, 9H), 1.45 (s, 9H), 4.52 (s, 1H), 5.9—7.0 (br, 2H). Found: C, 66.16; H, 10.72; N, 7.01%. Calcd for $C_{11}H_{21}NO_2$: C, 66.29; H, 10.62; N, 7.03%.

***t*-Butyl 3-Amino-4-phenyl-2-butenoate (2e):** Bp 116 °C/0.25 Torr (lit,[30] 120 °C/0.01 Torr); IR (neat) 3460, 3340, 1660, 1615, 1555 cm^{-1}; ^1H NMR ($CDCl_3$) δ=1.46 (s, 9H), 3.70 (s, 2H), 4.53 (s, 1H), 5.5—6.3 (br, 2H), 7.31 (s, 5H).

***t*-Butyl 3-Amino-4-(4-chlorophenyl)-2-butenoate (2f):** Bp 138 °C/0.25 Torr; IR (neat) 3450, 3340, 1660, 1610, 1555 cm^{-1}; ^1H NMR ($CDCl_3$) δ=1.48 (s, 9H), 3.36 (s, 2H), 4.49 (s, 1H), 5.4—6.4 (br, 2H), 7.0—7.5 (m, 4H); MS *m/z* (rel intensity) 269 (M^++2, 1), 267 (M^+, 3), 212 (28), 211 (19), 195 (27), 194 (20), 193 (43), 152 (18), 127 (11), 126 (13), 125 (30), 89 (11), 57 (100). Found: *m/z* 267.1027. Calcd for $C_{14}H_{18}NO_2Cl$: M^+ 267.1030.

***t*-Butyl 3-Amino-2,4-hexadienoate (2g):** Bp 103 °C/0.3 Torr; IR (neat) 3475, 3350, 1670, 1610, 1550 cm^{-1}; ^1H NMR ($CDCl_3$) δ=1.48 (s, 9H), 1.7—2.0 (m, 3H), 4.56 (br s, 1H), 5.1—6.9 (m, 5H); MS *m/z* (rel intensity) 183 (M^+, 11), 127 (100), 126 (14), 112 (77), 110 (41), 109 (13), 82 (14), 81 (17), 80 (11), 68 (31), 67 (30), 66 (11), 57 (28). Found: *m/z* 183.1270. Calcd for $C_{10}H_{17}NO_2$: M^+ 183.1260.

***t*-Butyl 3-Amino-5-phenyl-2,4-pentadienoate (2h):** Viscous oil, R_f=0.70 (hexane-ethyl acetate 3 : 1); IR (neat) 3460, 3340, 1655, 1635, 1605, 1540 cm^{-1}; ^1H NMR ($CDCl_3$) δ=1.48 (s, 9H), 4.76 (s, 1H), 5.9—6.3 (br, 2H), 6.37 (d, 1H), 6.90 (d, 1H), 7.2—7.5 (m, 5H). MS *m/z* (rel intensity) 245 (M^+, 5), 189 (9), 188 (4), 172 (10), 145 (13), 144 (100), 143 (20), 57 (10). Found: *m/z* 245.1417. Calcd for $C_{15}H_{19}NO_2$: M^+ 245.1416.

***t*-Butyl 3-Amino-3-phenyl-2-propenoate (2i):** R_f=0.51 (hexane-ethyl acetate 5 : 1); mp 93 °C; IR (KBr) 3460, 3425, 3345, 1665, 1645, 1615, 1550 cm^{-1}; ^1H NMR ($CDCl_3$) δ=1.49 (s, 9H), 4.86 (s, 1H), 5.8—6.8 (br, 2H), 7.3—7.6 (m, 5H). Found: C, 71.18; H, 7.77; N, 6.38%. Calcd for $C_{13}H_{17}NO_2$: C, 71.21; H, 7.81; N, 6.39%.

***t*-Butyl 3-Amino-3-(3-pyridyl)-2-propenoate (2l):** Bp 144 °C/0.25 Torr; mp 50—50.5 °C; IR (KBr) 3400, 3310, 3275, 3190, 1665, 1595, 1555 cm^{-1}; ^1H NMR ($CDCl_3$) δ=1.51 (s, 9H), 4.86 (s, 1H), 6.0—7.0 (br, 2H), 7.2—7.4 (m, 1H), 7.80 (dt, 1H), 8.62 (dd, 1H), 8.82 (d, 1H). Found: C, 65.46; H, 7.45; N, 12.48%. Calcd for $C_{12}H_{16}N_2O_2$: C, 65.43; H, 7.32; N, 12.72%.

***t*-Butyl 3-Amino-4-trimethylsilyloxy-2-pentenoate (2n):** Bp 72 °C/0.3 Torr; IR (neat) 3400, 3345, 1665, 1615, 1540 1140, 840 cm^{-1}; ^1H NMR (CCl_4) δ=0.18 (s, 9H), 1.38 (d, 3H), 1.48 (s, 9H), 4.25 and 4.30 (q and s, totally 2H), 5.9—7.4 (br, 2H). MS *m/z* (rel intensity) 259 (M^+, 10), 203 (37), 188 (21), 186 (34), 185 (100), 170 (16), 158 (13), 142 (10), 117 (10), 96 (16), 85 (12), 75 (25), 73 (49), 57 (18). Found: C, 55.64; H, 9.82; N, 5.32%. Calcd for $C_{12}H_{25}NO_3Si$: C, 55.56; H, 9.71; N, 5.40%.

***t*-Butyl 3-Amino-4-(tetrahydro-2-pyranyloxy)-2-pentenoate (2o):** Bp 160 °C/0.25 Torr; IR (neat) 3500, 3440, 1665, 1540 cm^{-1}; ^1H NMR ($CDCl_3$) δ=1.2—1.9 (m and s (δ=1.45), totally 18 H), 3.2—4.7 (m, 5H), 5.8—6.6 (br, 2H). Found: C, 62.19; H, 9.16; N, 5.08%. Calcd for $C_{14}H_{25}NO_4$: C, 61.97; H, 9.29; N, 5.16%.

***t*-Butyl 3-Amino-2-methyl-3-phenylpropenoate (2k):** Bp 112 °C/0.3 Torr; ^1H NMR (CCl_4): δ=1.50 (s, 9H), 1.53 (s, 3H), 6.2 (br, 2H), 7.30 (s, 5H); IR (neat) 3460, 3330, 3050, 2970, 2920, 1660, 1610, 1595, 1280, 1130, 1100, 770, 700 cm^{-1}; MS *m/z* (rel intensity) 233 (M^+, 15), 178 (13), 177 (100), 176 (26), 160 (29), 132 (40), 131 (43), 130 (25), 105 (11), 104 (57), 77 (20). Found: *m/z* 233.1427. Calcd for $C_{14}H_{19}NO_2$: M^+ 233.1416.

***t*-Butyl 3-Amino-3-[2-(dimethoxymethyl)phenyl]propenoate (2m):** Bp 159 °C/0.17 Torr; ^1H NMR ($CDCl_3$) δ=1.52 (s, 9H), 3.35 (s, 6H), 4.62 (s, 1H), 5.47 (s, 1H), 7.1—7.5 (m, 2H), 6.0—7.0 (br, 2H), 7.0—7.7 (m, 2H); IR (neat) 3450, 3330, 2960, 2920, 2830, 1660, 1605, 1545, 1360, 1310, 1200, 1140, 1090, 1070, 980, 790, 770, 750 cm^{-1}; MS *m/z* (rel intensity) 293 (M^+, 1), 278 (10), 261 (10), 223 (11), 222 (84), 206 (16), 205 (39), 204 (58), 174 (70), 172 (52), 160 (13), 156 (100), 146 (87), 130 (44), 129 (13), 128 (27), 57 (53). Found: *m/z* 293.1627. Calcd for $C_{16}H_{23}NO_4$: M^+ 293.1627.

***t*-Butyl 3-Amino-4-(1-ethoxyethoxy)-2-pentenoate (2p):** Bp 102 °C/0.37 Torr; ^1H NMR ($CDCl_3$) δ=1.1—1.6 (m+s (δ=1.47), 18H), 3.3—3.7 (m, 2H), 3.9—4.3 (m, 1H), 4.38 and 4.43 (2s, 1H), 4.57 and 4.67 (2q, 1H), 5.6—6.9 (br, 2H); IR (neat) 3500, 3440, 1660, 1615, 1540 cm^{-1}; MS *m/z* (rel intensity) 259 (M^+, 0.5), 187 (16), 171 (5), 170 (2), 158 (11), 131 (3), 115 (60), 114 (46), 113 (16), 97 (10), 96 (20), 85 (14), 73 (100), 57 (24). Found: *m/z* 259.1779. Calcd for $C_{13}H_{25}NO_4$: M^+ 259.1783. Found: C, 60.07; H, 9.99; N, 5.30%. Calcd for $C_{13}H_{25}NO_4$: C, 60.21; H, 9.72; N, 5.40%.

Ethyl 3-Amino-4-(1-ethoxyethoxy)-2-pentenoate (2q): Bp 98 °C/0.5 Torr; ^1H NMR (CCl_4) δ=1.0—1.6 (m, 12H), 3.4—

† 1 Torr=133.322 Pa.

3.9 (m, 2H), 4.0—4.9 (m, 5H), 6.0—7.0 (br, 2H); IR (neat) 3450, 3340, 2970, 2920, 1660, 1620, 1560, 1265, 1150, 1070, 1040 cm^{-1}; MS *m/z* (rel intensity) 231 (M^+, 0.1), 186 (M^+—OEt, 5), 170 (3), 160 (2), 159 (23), 143 (28), 124 (11), 114 (32), 113 (14), 97 (12), 96 (27), 85 (14), 73 (84), 69 (9), 68 (7), 54 (6), 45 (100). Found: *m/z* 231.1460. Calcd for $C_{11}H_{21}NO_4$: M^+ 231.1469.

***t*-Butyl 3-Amino-4,4,4-trichloro-2-butenoate (2r):** Bp 123 °C/0.3 Torr; mp 37—39 °C; ^1H NMR ($CDCl_3$) δ=1.49 (s, 9H), 5.41 (s, 1H), 6.0—7.1 (br, 2H); IR (KBr) 3445, 3330, 2980, 1665, 1625, 1620, 1545, 1365, 1275, 1250, 1140, 820, 775 cm^{-1}; MS *m/z* (rel intensity) 263 (M^++4, 0.7), 262 (M^++2, 2), 259 (M^+, 2), 224 (4), 207 (12), 205 (36), 203 (37), 188 (12), 186 (12), 170 (12), 168 (19), 86 (11), 68 (27), 57 (100). Found: *m/z* 258.9927. Calcd for $C_8H_{12}NO_2Cl_3$: M^+ 258.9907.

Ethyl 3-Amino-3-phenyl-2-propenoate (2j). The magnesium amide was prepared by the addition of diisopropylamine (0.61 g, 6.0 mmol) to an ethereal solution (4.3 ml) of ethylmagnesium bromide (3 mmol) at 0 °C and by stirring the solution of 1 h. To the base solution cooled at −78 °C, ethyl acetate (0.132 g, 1.5 mmol) was added drop by drop and the resulting enolate solution was stirred at −78 °C for 30 min. Benzonitrile (0.155 g, 1.5 mmol) was then added, and the reaction mixture was allowed to warm to 0 °C and stirred for 1.5 h. Workup as before followed by distillation gave **2j** (0.163 g, 57% yield). Bp 112 °C/0.3 Torr (lit,[30] bp 110—112 °C/0.2 Torr).

Acetylation of 2n. A mixture of *t*-butyl 3-amino-4-trimethylsilyloxy-2-pentenoate (**2n**) (1.00 g, 3.9 mmol), acetic anhydride (10 ml) and pyridine (0.53 g, 6.6 mmol) was heated at 80 °C for 9 h. Excess acetic anhydride and pyridine was evaporated under reduced pressure, and the residue was purified by column chromatography (silica gel, hexane-ethyl acetate 3:1) to give *t*-butyl (*Z*)-3-acetamido-4-acetoxy-2-pentenoate (R_f=0.56, 0.68 g, 65% yield). IR (neat) 3230, 1745, 1720, 1660, 1630 cm^{-1}; ^1H NMR (CCl_4) δ=1.42 and 1.46 (d and s, totally 12 H), 2.03 (s, 3H), 2.11 (s, 3H), 4.99 (s, 1H), 6.31 (q, 1H), 12.2 (br, 1H). Found: C, 57.24; H, 7.66; N, 4.84%. Calcd for $C_{13}H_{21}NO_5$: C, 57.55; H, 7.80; N, 5.16%.

The (E) isomer (R_f=0.13, 0.198 g) also was obtained in 19% yield. Mp 104—105.5 °C; IR (KBr) 3350, 1745, 1710 (sh), 1695, 1640 cm^{-1}; ^1H NMR ($CDCl_3$) δ=1.43 and 1.46 (d and s, totally 12H), 2.09 (s, 3H), 2.14 (s, 3H), 6.68 and 6.80 (q and s, 2H), 7.2 (br, 1H).

(*S*)-2-(1-Ethoxyethoxy)-1-propanol (7). A dichloromethane (26 ml) solution of pyridinium *p*-toluenesulfonate (1.53 g, 0.01 mol) was added drop by drop to a mixture of ethyl (*S*)-lactate (11.8 g, 0.10 mol), ethyl vinyl ether (10.8 g, 0.15 mol) and dichloromethane (100 ml), and the mixture was stirred at 0 °C for 50 min and at room temperature for 1 h. The reaction mixture was diluted with diethyl ether (300 ml) and washed twice with brine (50 ml) and then twice with water (50 ml). The organic layer was dried over anhydrous sodium sulfate and concentrated under reduced pressure. Distillation at 77—78 °C/26 Torr gave ethyl (*S*)-*O*-ethoxyethyl lactate (18.4 g, 97% yield). ^1H NMR ($CDCl_3$) δ=1.06—1.50 (m, 12H), 3.33—3.90 (m, 2H), 4.20 (q, *J*=7.5 Hz, 2H), 4.30 (q, *J*=6.0 Hz, 1H), 4.76 (q, *J*=6.0 Hz). IR (neat) 3000, 2950, 1750, 1445, 1390, 1370, 1270, 1200, 1175, 1150, 1090, 1055, 1025, 965 cm^{-1}. MS *m/z* (rel intensity) 189 (M^+ −1, 1), 175 (15), 145 (99), 117 (53), 102 (73), 101 (44), 74 (49), 73 (100), 72 (15), 55 (13), 45 (100). $[\alpha]_D^{24}$ −54.1° (*c* 3.87, $CHCl_3$); $[\alpha]_D^{28}$ −71.7° (*c* 4.18, MeOH). Found: C, 57.05; H, 9.77%. Calcd for $C_9H_{18}O_4$: C, 56.82; H, 9.54%.

The above lactate (14.9 g, 78.3 mmol) dissolved in diethyl ether (100 ml) was added to an ethereal solution (100 ml) of lithium aluminium hydride (4.05 g, 0.100 mol) over 25 min. After the addition was completed, the reaction mixture was heated to reflux for 7 h. Quenching the excess hydride was effected by dropwise addition of aqueous saturated solution of sodium sulfate and successively by the addition of magnesium sulfate. Filtration through a Hyflosupercell pad, concentration, followed by distillation, gave **7** (10.9 g, 94% yield). Bp 77—79 °C/17 Torr; ^1H NMR ($CDCl_3$) δ=1.06—1.38 (m, 9H), 2.62 and 3.20 (dd, *J*=(6.8, 5.3 Hz) and (8.3, 4.1 Hz) respectively, totally 1H, OH), 3.37—3.96 (m, 5H), 4.70 and 4.78 (2q, *J*=5.3 Hz each, totally 1H); IR (neat) 3450, 3000, 2950, 1450, 1380, 1340, 1130, 1105, 1060, 970 cm^{-1}; MS *m/z* (rel intensity) 147 (M^+−1, 1), 133 (2), 117 (5), 103 (15), 73 (92), 59 (43), 45 (100), 43 (12). $[\alpha]_D^{29}$ +42.2° (*c* 5.87, $CHCl_3$). Found: C, 56.91; H, 11.03%. Calcd for $C_7H_{16}O_3$: C, 56.73; H, 10.88%.

(*S*)-2-(1-Ethoxyethoxy)propanal (8). A dichloromethane (40 ml) solution of DMSO (7.9 g, 7.2 ml, 0.101 mol) was added drop by drop over 15 min to a dichloromethane (100 ml) solution of oxalyl dichloride (6.4 g, 4.4 ml, 0.050 mol) at −70 °C. After stirring for 10 min a dichloromethane (50 ml) solution of **7** (5.0 g, 0.034 mol) was added over 15 min, and the resulting mixture was stirred for 30 min at −70 °C before addition (over 15 min) of triethylamine (17.1 g, 23.5 ml, 0.168 mol). The mixture was stirred at −70 °C for 25 min, allowed to warm to 10 °C in 20 min, and then treated with brine (100 ml). The organic layer was separated, washed with brine (50 ml×2), dried over magnesium sulfate and concentrated. Distillation at 53—54 °C/17 Torr gave **8** (3.8 g, 78% yield) as a colorless oil. ^1H NMR ($CDCl_3$) δ=1.06—1.38 (m, 9 H), 3.20 (q, *J*=7.5 Hz, 2H), 3.70—4.27 (m, 1H), 4.71 and 4.81 (2q, *J*=5.3 Hz, totally 1H), 9.59 and 9.64 (2d, *J*=3.0 and 1.5 Hz respectively, totally 1H); IR (neat) 1735 cm^{-1}. $[\alpha]_D^{23}$ −56.9° (*c* 6.31, $CHCl_3$). The aldehyde was immediately used for the next transformation.

(3*S*)-3-(1-Ethoxyethoxy)-2-hydroxybutanenitrile (9). A mixture of **8** (2.2 g, 15 mmol), acetone cyanohydrin (bp 53—55 °C/8 Torr, 1.53 g, 1.64 ml, 18 mmol) and triethylamine (21 μl, 15 mg) was stirred in an ice bath for 1 h. TLC assay revealed the starting material **8** was all consumed. Evaporation of excess acetone cyanohydrin and triethylamine followed by brief column chromatography (Wacogel C-100, hexane-ethyl acetate 3:1 to 1:1) gave **9** (2.6 g, quantitative yield) as a viscous oil. ^1H NMR ($CDCl_3$) δ=1.10—1.40 (m, 9H), 3.36—4.14 (m, 3H), 4.25 and 4.28 (2d, *J*=1.5 and 4.5 Hz, respectively, totally 1H), 4.60—6.00 (m, 1H); IR (neat) 3425, 3000, 2950, 2250, 1450, 1395, 1340, 1130, 1070, 970, 940, 855, 810 cm^{-1}. The cyanohydrin was directly used for the next reaction.

(2*S*,3*S*)-2,3-(Cyclohexylidenedioxy)butanenitrile (10) and (2*R*,3*S*)-2,3-(Cyclohexylidenedioxy)butanenitrile (11). In a 100-ml flask were placed successively activated Molecular Sieve 4A (ca. 5 g), a dichloromethane (20 ml) solution of **9** (2.55 g, 14.7 mmol), a dichloromethane (20 ml) solution of 1,1-dimethoxycyclohexane (2.39 g, 16.5 mmol). The mixture was cooled to 0 °C and a 1 M dichloromethane solution of bis(trimethylsilyl) sulfate (0.45 ml, 0.45 mmol) was added and the resulting mixture was stirred at 0 °C for 10 min and at room temperature for 30 min. The reaction mixture was neutralized with pyridine (0.1 ml), and the insoluble mate-

rial was filtered off. Concentration and purification by column chromatography (Kieselgel 60, hexane-ethyl acetate 10 : 1 to 6 : 1) afforded **10** (0.69 g, R_f=0.67, hexane-ethyl acetate 3 : 1, 28% yield) and **11** (1.05 g, R_f=0.55 (vide supra), 40% yield).

Physical properties of **10** are as follows. Bp 60—61 °C/0.25 Torr; ^{1}H NMR (CCl_4) δ=1.38 (d, J=6.0 Hz, 3H), 1.50—1.80 (m, 10H), 4.02 (d, J=7.5 Hz, 1H), 4.36 (quintet, J=6.0 Hz, 1H); IR (neat) 2950, 2870, 2250, 1450, 1370, 1285, 1160, 1120, 1065, 930, 910 cm^{-1}; MS m/z (rel intensity) 181 (M^+, 9), 152 (11), 138 (100), 55 (29), 41 (15); $[\alpha]_D^{24}$ +15.5° (c 8.84, $CHCl_3$). Found: C, 66.38; H, 8.39; N, 7.57%. Calcd for $C_{10}H_{15}NO_2$: C, 66.27; H, 8.34; N, 7.73%.

Physical properties of **11** are following. Bp 73—75 °C/0.25 Torr; ^{1}H NMR (CCl_4) δ=1.45, (d, J=6.0 Hz, 3H), 1.30—1.80 (m, 10H), 4.21 (quintet, J=6.0 Hz, 1H), 4.58 (d, J=5.3 Hz, 1H); IR (neat) 2950, 2875, 2250, 1450, 1370, 1285, 1240, 1170, 1120, 1080, 920 cm^{-1}. MS m/z (rel intensity) 181 (M^+, 9), 152 (12), 138 (100), 84 (10), 55 (31), 42 (10), 41 (15); $[\alpha]_D^{26}$ +26.4° (c 5.57, $CHCl_3$). Found: C, 66.40; H, 8.44; N, 8.09%. Calcd for $C_{10}H_{15}NO_2$: C, 66.27; H, 8.34; N, 7.73%. The optical purity of **11** was checked by ^{1}H NMR with a chiral shift reagent Eu(tfc)$_3$ (1.2 mol eq) in dry CCl_4 solution. Under these conditions the doublet methine proton of (±)-**11** splitted into base-line resolved two doublets. The sample of **11** prepared as above gave only one doublet at higher field and the other doublet was not detected even after 5 times enlargement. The sample of **10** also was subjected to the chirality check, and similar results were obtained. Thus, the optical purity of **11** as well as **10** was estimated to be more than 95%.

(2*S*,3*S*)-2,3-(Cyclohexylidenedioxy)-1-butanol (14). An ethereal (20 ml) solution of dimethyl (2*R*,3*R*)-2,3-(cyclohexylidenedioxy)butanedioate[23] (5.16 g, 20 mmol) was added to an ethereal (20 ml) solution of lithium aluminium hydride (2.0 g) at 0 °C. After the addition was completed, the reaction mixture was heated to reflux for 1 h, and the excess hydride was quenched by addition of saturated aqueous solution of sodium sulfate under cooling. The reaction mixture was further dried by addition of anhydrous magnesium sulfate under vigorous stirring. Filtration through a pad of Hyflo-supercell followed by concentration gave a crude oil of (2*S*,3*S*)-2,3-(cyclohexylidenedioxy)-1,4-butanediol (2.78 g, 69% yield). Mp 52—54 °C; ^{1}H NMR ($CDCl_3$) δ=1.4—1.8 (m, 10H), 2.90 (t, J=6 Hz, 2H), 3.68—4.03 (m, 6H); IR (KBr) 3400, 2940, 1450, 1160, 1120, 1040 cm^{-1}.

The diol (13.7 mmol) was dissolved in dichloromethane (10 ml) and triethylamine (3 ml, 21.4 mmol). To the solution was added at 0 °C *p*-toluenesulfonyl chloride (2.86 g, 15 mmol) dissolved in dichloromethane (15 ml) drop by drop over a period of 3 h with the aid of a syringe drive. Stirring was continued at 0 °C for 1 h and at room temperature for 1 h. Concentration under reduced pressure, trituration of the resulting solid with diethyl ether, filtration, concentration of the ethereal filtrate, followed by purification by column chromatography (Wacogel C-100, hexane-ethyl acetate 2 : 1), afforded a ditosylate (2.13 g, 30% yield). Further elution with hexane-ethyl acetate (1 : 1) gave a monotosylate (2.13 g, 44% yield, 70% yield based on the consumed diol). Elution with ethyl acetate and methanol afforded a recovered diol (0.96 g). The monotosylate exhibited ^{1}H NMR ($CDCl_3$) δ=1.2—1.7 (m, 10H), 2.10 (s, 1H), 2.43 (s, 3H), 3.5—3.8 (m, 2H), 3.8—4.2 (m, 4H), 7.33 (d, J=8 Hz, 2H), 7.88 (d, J=8 Hz, 2H); IR (neat) 3500, 2940, 1740, 1600, 1360, 1180, 810 cm^{-1}.

The monotosylate (2.05 g, 5.7 mmol) was dissolved in DMSO (5 ml). To this solution was added sodium borohydride (0.68 g, 18 mmol) and the reaction mixture was heated at 80 °C for 2 h. At the initial stage, foaming of the reaction mixture was observed which ceased at the end of the reaction time. The reaction mixture was diluted with dichloromethane and the excess hydride was carefully quenched with brine. Dichloromethane extraction followed by usual work-up and purification by column chromatography (Wacogel C-100, hexane-ethyl acetate 3 : 1, R_f=0.27) gave **14** (0.94 g, 88% yield). ^{1}H NMR (CCl_4) δ=1.23 (d, J=6 Hz, 3H), 1.3—2.0 (m, 10H), 2.25 (br s, 1H), 3.3—3.7 (m, 3H), 3.88 (dq, J=8 and 6 Hz, 1H); IR (neat) 3450, 2940, 1440, 1360, 1160, 1100, 940 cm^{-1}.

(2*R*,3*S*)-2,3-(Cyclohexylidenedioxy)butanal (15). A dichloromethane (1 ml) solution of DMSO (0.34 ml, 4.8 mmol) was added to a dichloromethane (4 ml) solution of oxalyl dichloride (0.195 ml, 2.2 mmol) at −78 °C over a period of ca. 5 min, and the resulting solution was stirred at −78 °C for 10 min before the addition of a dichloromethane (2 ml) solution of **14** (0.375 g, 2.0 mmol) at −78 °C. After 15 min, triethylamine (1.4 ml) was added at −78 °C, and stirring was continued for 10 min. The reaction mixture was then warmed to room temperature, treated with water (ca. 6 ml), and vigorously stirred for 10 min. Separation of the organic layer, extraction of the aqueous layer with dichloromethane, drying the combined dichloromethane extract with anhydrous sodium sulfate, followed by concentration and purification by column chromatography (Wacogel C-100, CH_2Cl_2), afforded **15** (0.32 g, 87% yield). ^{1}H NMR (CCl_4) δ=1.33 (d, J=6.0 Hz, 3H), 1.4—2.0 (m, 10 H), 3.67 (dd, J=7.8 and 2.7 Hz, 1H), 4.00 (dq, J=7.8 and 6.0 Hz, 1H), 9.62 (d, J=2.7 Hz, 1H); IR (neat) 3450, 2940, 1740, 1370, 1100 cm^{-1}.

(2*S*,3*S*)-2,3-(Cyclohexylidenedioxy)butanenitrile (10). A mixture of **15** (0.29 g, 1.58 mmol), hydroxylamine hydrochloride (0.30 g, 4.3 mmol), ethanol (2 ml) and pyridine (2 ml) was heated at 80 °C for 2 h. Concentration followed by short column chromatography (Wacogel C-100, CH_2Cl_2) gave the oxime (0.32 g, quantitative yield) which exhibited ^{1}H NMR ($CDCl_3$) absorptions at δ=1.30 (d) and 1.43 (d) along with absorptions ascribed to aldoxime methine hydrogen at δ=6.80, 7.36, 7.68, and 8.60. Thus, syn-anti isomers as well as their conformational ones seem to coexist.

The oxime (40 mg, 0.20 mmol) dissolved in dichloroethane (1 ml) was heated in the presence of triphenylphosphine (80 mg, 0.30 mmol), triethylamine (42 μl, 0.3 mmol) and carbon tetrachloride (29 μl, 0.3 mmol) at 80 °C for 2 h. The reaction mixture was passed through an 8 cm column of Wacogel C-100 (CH_2Cl_2 elution) to give **10** (30 mg, 83% yield). Bp 150 °C/10 Torr.

***t*-Butyl (4*S*,5*S*,2*Z*)-3-Amino-4,5-(cyclohexylidenedioxy)-2-hexenoate (16).** The magnesium enolate of *t*-butyl acetate (0.42 ml, 3.3 mmol) was prepared as before using ethylmagnesium bromide (2.0 M ethereal solution, 3.3 ml, 6.6 mmol), diethyl ether (9.6 ml), diisopropylamine (1.96 ml, 14 mmol) at 0 °C. To this enolate solution was added an ethereal solution (3.0 ml) of **10** (0.30 g, 1.66 mmol) at 0 °C over a period of 5 min, and the mixture was stirred at 0 °C for 4 h. Workup gave a colorless solid **16** (0.49 g, 99% yield) which was homogeneous by silica gel TLC assay (R_f=0.70 (hexane-ethyl acetate 3 : 1)). Mp 102—103 °C (hexane). ^{1}H NMR ($CDCl_3$) δ=1.35 (d, J=5.3 Hz, 3H), 1.48 (s, 9H), 1.50—1.77 (m, 10H), 3.77—4.10 (m, 2H), 4.43 (s, 1H), 6.40 (br, 2H); IR (KBr) 3510,

3470, 3370, 3350, 2980, 2950, 1670, 1630, 1610, 1555, 1445, 1365, 1285, 1255, 1140, 1110, 1060, 1000, 935, 790 cm^{-1}; MS *m/z* (rel intensity) 297 (M^+, 6), 241 (22), 198 (85), 180 (19), 154 (15), 144 (16), 143 (56), 127 (13), 126 (100), 125 (15), 99 (13), 98 (12), 81 (13), 57 (34), 55 (24), 41 (38); $[\alpha]_D^{26}$ −62.5° (*c* 5.19, $CHCl_3$). Found: C, 64.57; H, 9.04; N, 4.63%. Calcd for $C_{16}H_{27}NO_4$: C, 64.62; H, 9.15; N, 4.71%.

***t*-Butyl (4*S*,5*S*,2*Z*)-3-Acetamido-4,5-(cyclohexylidenedioxy)-2-hexenoate (17).** A mixture of **16** (0.45 g), pyridine (4 ml) and acetic anhydride (4.0 ml) was heated at 50 °C for 6.5 d. Concentration in vacuo followed by preparative TLC (hexane-ethyl acetate 3:1) gave **17** (R_f=0.62, 0.31 g, 59% yield) along with its (E)-isomer (R_f=0.53, 97 mg, 19% yield) both as viscous oil. The compound **17** exhibited ^1H NMR ($CDCl_3$) δ=1.42 (d, *J*=6.0 Hz, 3H), 1.50 (s, 9H), 1.60—1.85 (m, 10H), 2.13 (s, 3H), 3.99 (quintet, *J*=6.0 Hz, 1H), 5.62 (s, 1H), 5.65 (d, *J*=6.0 Hz, 1H), 11.12 (br s, 1H, NH); IR (neat) 3450, 3250, 3000, 2950, 2880, 1720, 1635, 1490, 1450, 1370, 1250, 1150 cm^{-1}. The (E) isomer gave ^1H NMR ($CDCl_3$) δ= 1.37 (d, *J*=6.0 Hz, 3H), 1.47 (s, 9H), 1.60—1.80 (m, 10H), 2.08 (s, 3H), 3.80 (dq, *J*=8.3 and 6.0 Hz, 1H), 5.65 (d, *J*=8.3 Hz, 1H), 6.93 (br s, 1H), 7.87 (br s, 1H, NH).

***t*-Butyl (3*S*,4*S*,5*S*)-3-Acetamido-4,5-(cyclohexylidenedioxy)-hexanoate (18).** In an autoclave were placed **17** (34 mg, 0.1 mmol), ethyl acetate (2 ml) and platinum oxide (34 mg), and the atmosphere was replaced by hydrogen of 55 kg cm^{-2}. The autoclave was agitated at 70 °C for 24 h. Filtration of the catalyst through a Celite pad, concentration, followed by preparative TLC (hexane-ethyl acetate 1:1) afforded **18** (R_f=0.33, 28 mg, 82% yield) as a viscous oil. ^1H NMR ($CDCl_3$) δ=1.27 (d, *J*=6.0 Hz, 3H), 1.47 (s, 9H), 1.50—1.70 (m, 10H), 1.97 (s, 3H), 2.57 (dd, *J*=4.5 and 3.0 Hz, 2H), 3.55 (t, *J*=7.5 Hz, 1H), 3.75—4.10 (m, 1H), 4.15—4.50 (m, 1H), 6.40 (br d, *J*=7.5 Hz, 1H, NH); IR (neat) 3400 (br), 3100 (br), 2950, 1735, 1660, 1550, 1450, 1370, 1160, 1110, 950, 850 cm^{-1}; MS *m/z* (rel intensity) 341 (M^+, 16), 285 (18), 243 (18), 242 (100), 170 (61), 155 (37), 144 (31), 128 (35), 111 (27), 88 (23), 81 (20), 57 (35), 55 (24), 43 (40); $[\alpha]_D^{20}$ −4.8° (*c* 1.47, $CHCl_3$). Found: *m/z* 341.2186. Calcd for $C_{18}H_{31}NO_5$: M^+ 341.2200.

(3*R*)-Isomer (5 mg, 15% yield, R_f=0.60) also was isolated and showed ^1H NMR ($CDCl_3$) δ=1.30 (d, *J*=6.0 Hz, 3H), 1.45 (s, 9H), 1.50—1.70 (m, 10H), 1.97 (s, 3H), 2.50 (d, *J*=6.8 Hz, 2H), 3.40—3.85 (m, 1H), 6.0 (br d, *J*=10.5 Hz, 1H, NH).

(3*S*,4*S*,5*S*)-3-Benzamido-4-hydroxy-5-hexanolide (19). A mixture of the *t*-butyl ester **18** (73 mg, 0.22 mmol) and 2 M hydrochloric acid (3 ml) was heated to reflux for 5 h. Excess acid and volatile material were evaporated, and the residue was dissolved in saturated aqueous sodium hydrogencarbonate solution (7.5 ml) and acetone (2.6 ml). To the resulting solution was added benzoyl chloride (0.2 ml) at 0 °C. The mixture was stirred at room temperature for 2.5 h, then acidified with 2 M hydrochloric acid to pH 1, stirred for 20 min at room temperature and extracted with ethyl acetate. Workup and preparative TLC purification gave the desired lactone **19** (50 mg, 93% yield). Mp 138—140 °C (lit,[28b] 125—127 °C); R_f=0.06 (hexane-ethyl acetate 1:1); IR (Nujol) 3500, 3350, 1745, 1740, 1640, 1530, 1460, 1380, 1035 cm^{-1}; ^1H NMR (DMSO-d_6) δ=1.14 (d, *J*=6.2 Hz, 3 H), 2.54 (AB dd, *J*=18.0 and 4.0 Hz, 1H), 2.94 (AB dd, *J*=18.0 and 9.0 Hz, 1H), 3.91 (m, 1H), 4.30 (t, *J*=3.0 Hz, 1H), 4.63 (m, 1H), 5.10 (d, *J*=5.1 Hz, 1H, OH), 7.40—7.65 (m, 3H), 7.82—8.02 (m, 2H), 8.92 (br d, *J*=7.0 Hz, 1H, NH); ^{13}C NMR (DMSO-d_6) δ=19.3 (C-6), 34.5 (C-2), 48.3 (C-3), 66.5 (C-5), 88.9 (C-4), 127.2, 128.2, 131.3, 133.7 (aromatic), 166.1 (NHCO), 175.7 (lactone C=O); $[\alpha]_D^{20}$ −20.5° (*c* 0.39, ethanol); lit,[28b] $[\alpha]_D^{20}$ −15.8° (*c* 1, ethanol). Found: *m/z* 249.1024. Calcd for $C_{13}H_{15}NO_4$: M^+ 249.1000.

At the early stage of the lactonization, 1,4-lactone (**20**) was produced and isolated. The physical properties of **20** is as follows. R_f=0.13 (hexane-ethyl acetate 1:1); ^1H NMR ($CDCl_3$) δ=1.34 (d, *J*=6.2 Hz, 3H), 2.32 (br, 1H, OH), 2.60 (AB dd, *J*=18.0 and 4.0 Hz, 1H), 3.17 (AB dd, *J*=18.0 and 9.0 Hz, 1H), 4.16 (m, 1H), 4.41 (t, *J*=3.0 Hz, 1H), 4.85 (m, 1H), 6.89 (br d, *J*=7.0 Hz, 1H, NH), 7.45—7.62 (m, 3H), 7.76—7.92 (m, 2H). IR ($CHCl_3$) 3460, 3350, 2950, 1780, 1660, 1515, 1290, 1200, 1180, 1160, 990 cm^{-1}; $[\alpha]_D^{20}$ −10.6° (*c* 0.64, EtOH).

***N*-Benzoyl-L-daunosamine (4b).** A 1 M hexane solution of diisobutylaluminium hydride (0.07 ml, 5 mol equiv) was added to a THF (1.0 ml) solution of **19** (3.4 mg, 0.014 mmol) at −60 °C, and the resulting solution was stirred at −60 to −50 °C for 1.5 h before the addition of a 1:1 mixture (2 ml) of methanol and acetone. Warming up to room temperature, filtration through a Celite pad, concentration and purification by column chromatography (ethyl acetate) gave *N*-benzoyl-L-daunosamine (3.2 mg, 94% yield). Mp 153—155 °C (ether) (lit,[31] 152 °C); $[\alpha]_D^{20}$ −109° (*c* 0.08, EtOH) (lit,[31] −108° (*c* 0.5, EtOH)); ^1H NMR (DMSO-d_6) δ=1.10 and 1.15 (each d, *J*=6 Hz, 3H, Me of α,β-isomers), 1.35—2.16 (m, 2H, C(2)-H_2 of α,β-isomers), 3.14—4.90 (C(3-5)-H of α,β-isomers and C(1)-H of β-isomer, totally 7H), 5.18 (br m, 1H, C(1)-*H* of α-isomer), 6.18 (br d, *J*=3.8 Hz, 1H, OH of α-isomer), 6.50 (br d, *J*=6.3 Hz, 1H, OH of α-isomer), 7.38—7.66 (m, 3H, aromatic), 7.80—8.10 (m, aromatic and NH, 3H); ^{13}C NMR (DMSO-d_6) δ=17.1 (C-6), 30.2 (C-2 of α-isomer), 32.9 (C-2 of β-isomer), 45.6 (C-3 of α-isomer), 49.5 (C-3 of β-isomer), 65.4 C-5 of α-isomer), 66.8 (C-4 of β-isomer), 68.1 (C-4 of α-isomer), 70.8 (C-5 of β-isomer), 90.2 (C-1 of α-isomer), 94.1 (C-1 of β-isomer), 127.2, 128.0, 130.9, 134.6 (aromatic) and 165.5 (CONH), all consistent with the literature values.[28a]

***t*-Butyl (4*R*,5*S*,2*Z*)-3-Amino-4,5-(cyclohexylidenedioxy)-2-hexenoate (21).** The nitrile **11** (1.40 g, 7.7 mmol) in diethyl ether (20 ml) was allowed to react at 0 °C for 3.5 h with the magnesium enolate of *t*-butyl acetate, which was prepared from ethylmagnesium bromide (31 mmol), diisopropylamine (8.7 ml, 62 mmol) and diethyl ether (40 ml) at 0 °C. Workup followed by distillation afforded **21** (1.23 g, 54% yield). Bp 112—113 °C/0.3 Torr; ^1H NMR ($CDCl_3$) δ=1.21 (d, *J*=6.0 Hz, 3H), 1.30—1.90 (m, 10H), 1.48 (s, 9H), 4.30—4.60 (m, 3H), 6.50 (br, 2H, NH_2); IR (neat) 3525, 3350, 1670, 1620, 1050 cm^{-1}; MS *m/z* (rel intensity) 297 (M^+, 8), 241 (28), 199 (14), 198 (93), 197 (28), 180 (30), 154 (26), 144 (20), 143 (72), 127 (14), 126 (100), 125 (29), 99 (24), 98 (15), 81 (19), 69 (14), 57 (44), 55 (33), 41 (41); $[\alpha]_D^{26}$ −7.40° (*c* 3.59, $CHCl_3$). Found: *m/z* 297.1937. Calcd for $C_{16}H_{27}NO_4$: M^+ 297.1938.

***t*-Butyl (4*R*,5*S*,2*Z*)-3-Acetamido-4,5-(cyclohexylidenedioxy)-2-hexenoate (22).** A mixture of **21** (0.143 g, 0.48 mmol), acetic anhydride (1 ml) and pyridine (1 ml) was heated at 50 to 60 °C for 2 d. Concentration followed by preparative TLC (silica gel, hexane-ethyl acetate 3:1) gave **22** (R_f=0.47, 0.125 g, 77% yield) along with its (E) isomer (R_f=0.37, 33 mg, 20% yield) both as viscous oil.

The spectral data of **22** are as follows. ^1H NMR ($CDCl_3$) δ=1.10 (d, *J*=6.0 Hz, 3H), 1.30—1.80 (m, 10H), 1.50 (s, 9H), 2.14 (s, 3H), 4.73 (quintet, *J*=6.0 Hz, 1H), 5.55 (d, *J*=1.0 Hz, 1H), 5.74 (dd, *J*=6.0 and 1.0 Hz, 1H), 11.34 (br, 1H, NH); IR (neat) 3525, 3250, 3000, 2950, 2875, 1720, 1670, 1635, 1490,

1450, 1370, 1320, 1250, 1150, 1115 cm^{-1}; MS *m/z* (rel intensity) 339 (M^+, 2) 283 (21), 241 (14), 240 (28), 185 (74), 168 (32), 167 (21), 151 (13), 150 (100), 143 (21), 142 (21), 141 (27), 126 (20), 125 (48), 124 (13), 123 (35), 99 (10), 98 (11), 97 (11), 81 (14), 69 (13), 57 (33), 55 (33), 43 (58), 41 (40). Found: *m/z* 339.2012. Calcd for $C_{18}H_{29}NO_5$: M^+ 339.2043. $[\alpha]_D^{20}$ −131.7° (*c* 2.26, $CHCl_3$). Spectral data of the (E) isomer of **22** are following. ^1H NMR ($CDCl_3$) δ=1.05 (d, *J*=6.0 Hz, 3H), 1.43 (s, 9H), 1.60—1.80 (m, 10H), 2.03 (s, 3H), 4.63 (quintet, *J*=6.0 Hz, 1H), 5.62 (br d, *J*=7.5 Hz, 1H), 6.77 (br s, 1H), 7.82 (br s, 1H, NH); IR (neat) 3420, 1720, 1700, 1635, 1500, 1370, 1235, 1135, 1110 cm^{-1}.

***t*-Butyl (3*S*,4*R*,5*S*)-3-Acetamido-4,5-(cyclohexylidenedioxy)-hexanoate (23).** In an autoclave were placed **22** (0.57 g, 1.67 mmol), THF (10 ml) and 5% rhodium on carbon (0.64 g) and the atmosphere was replaced by hydrogen of 70 $kg\,cm^{-2}$. The reaction mixture was heated at 55 °C for 24 h. Filtration, concentration and preparative TLC (hexane-ethyl acetate 1 : 1) gave recovered **22** (26 mg, 5%) and the desired product **23** (0.48 g, 84% yield) as a viscous oil. R_f=0.19 (silica-gel TLC, hexane-ethyl acetate 3 : 1), >99.3% pure by GLC assay (Diasolid ZS, 2 m, 180 °C, R_t=10.7 min). ^1H NMR ($CDCl_3$) δ=1.25 (d, *J*=6.0 Hz, 3H), 1.47 (s, 9H), 1.50—1.80 (m, 10H), 1.95 (s, 3H), 2.48 (d, *J*=6.8 Hz, 2H), 4.10—4.50 (m, 3H), 5.93 (br d, *J*=7.5 Hz, 1H, NH); IR (neat) 3450, 3200, 1730, 1660, 1370, 1160, 1120, 1070 cm^{-1}; MS *m/z* (rel intensity) 341 (M^+, 15), 285 (17), 243 (16), 242 (100), 188 (18), 187 (16), 170 (63), 155 (62), 144 (14), 137 (10), 131 (26), 130 (21), 128 (24), 111 (19), 99 (13), 88 (30), 81 (19), 70 (12), 60 (16), 57 (38), 55 (25), 43 (42), 41 (31); $[\alpha]_D^{26}$ +21.2° (*c* 2.04, $CHCl_3$). Found: *m/z* 341.2232. Calcd for $C_{18}H_{31}NO_5$: M^+ 341.2201.

(3*S*,4*R*,5*S*)-3-Benzamido-4-hydroxy-5-hexanolide (24). A mixture of **23** (17 mg, 0.050 mmol) and 2 M hydrochloric acid (1.0 ml) was heated to reflux for 12 h. Concentration in vacuo gave a solid which was treated with saturated sodium hydrogencarbonate (0.5 ml), acetone (0.1 ml) and benzoyl chloride (15 μl) at room temperature for 4 h. Then, the reaction mixture was acidified with 2 M hydrochloric acid to pH 1, diluted with brine (2 ml) and extracted with ethyl acetate (30 ml×3 times). The combined extract was dried over sodium sulfate, concentrated, and the residue was chromatographed to give **24** (9.1 mg, 73% yield). Mp 188 °C (MeOH) (lit,[28b] 190 °C); R_f=0.25 (silica-gel TLC, hexane-ethyl acetate 1 : 2); ^1H NMR (acetone-d_6) δ=1.42 (d, *J*=6.2 Hz, 3H), 2.67 (AB dd, *J*=17.5 and 7.5 Hz, 1H), 3.17 (AB dd, *J*=17.5 and 7.5 Hz, 1H), 3.71 (dt, *J*=8.5 and 4.5 Hz, 1H), 4.33 (dq, *J*=8.5 and 6.0 Hz, 1H), 4.44 (m, 1H), 4.98 (d, *J*=4.5 Hz, 1H, OH), 7.30—7.60 (m, 3H), 7.70 (br m, 1H, NH), 7.85—8.05 (m, 2H); IR (Nujol) 3550—3200, 1735, 1720, 1640 cm^{-1}; MS *m/z* (rel intensity) 249 (M^+, 2), 231 (2), 192 (6), 144 (7), 122 (14), 105 (100), 77 (31), 51 (6). $[\alpha]_D^{20}$ +11.5° (*c* 0.80, EtOH) (lit,[28b] +11.5° (*c* 1.1, EtOH)). Found: *m/z* 249.1035. Calcd for $C_{13}H_{15}NO_4$: M^+ 249.1000.

***N*-Benzoyl-L-acosamine (5b).** A 1.0 M hexane solution (0.11 ml) of diisobutylaluminium hydride (0.11 mmol) was added to a THF (1 ml) solution of **24** (5.4 mg, 0.022 mmol) at −60 °C, and the reaction mixture was stirred at −50 to −60 °C for 1.5 h before quenching with a 1 : 1 mixture (3 ml) of methanol and acetone. Warming to room temperature, filtration through a Celite pad and finally purification by preparative TLC (ethyl acetate) gave *N*-benzoyl-L-acosamine (**5b**) (5.3 mg, 98% yield). R_f=0.38 (silica-gel TLC, AcOEt); mp 218—220 °C (Et_2O); $[\alpha]_D^{20}$ −18.6° (*c* 0.30, EtOH, 3 h); ^1H NMR (DMSO-d_6) for α-isomer: δ=1.15 (C(6)-H), 4.85 (C(4)-OH), 5.12 (C(1)-H), 6.13 (C(1)-OH), 8.10 (NH) and for β-isomer: δ=1.20 (C(6)-H), 4.70 (C(1)-*H*), 4.85 (C(4)-O*H*), 6.49 (C(1)-O*H*), 8.22 (NH). ^{13}C NMR (DMSO-d_6) for α-isomer: δ=18.2 (C-6), 36.9 (C-2), 48.2 (C-3), 67.6 (C-5), 74.1 (C-4), 89.7 (C-1), and for β-isomer: δ=18.2 (C-6), 51.5 (C-3), 72.8 (C-5), 73.5 (C-4), 93.5 (C-1), and 127.2, 127.9, 130.8, 134.9 (aromatic), 166.0 (*C*ONH). These data are fully consistent with the literature values.[28a]

References

1) a) R. L. Shriner, *Org. React.*, **1**, 1 (1942); b) M. W. Rathke, *ibid.*, **22**, 423 (1975); c) T. Mukaiyama, *ibid.*, **28**, 203 (1982); d) J. d'Angelo, *Tetrahedron*, **32**, 2979 (1976); e) L. M. Jackman and B. C. Lange, *ibid.*, **33**, 2737 (1977).

2) a) D. A. Evans, J. V. Nelson, and T. R. Tabler, *Topics in Stereochemistry*, **13**, 1 (1982); b) C. H. Heathcock, "The Aldol Addition Reaction," in Asymmetric Synthesis, **3**, 111 (1984).

3) a) T. Iimori and M. Shibasaki, *Tetrahedron Lett.*, **27**, 2149 (1986); T. Iimori, Y. Ishida, and M. Shibasaki, *ibid.*, **27**, 2153 (1986) and references cited therein; b) T. Chiba and T. Nakai, *ibid.*, **26**, 4647 (1985).

4) Nitriles having an alkoxyl group at C(α) react with α-metallo nitriles: K. Kobayashi and T. Hiyama, *Tetrahedron Lett.*, **24**, 3509 (1983).

5) H. B. Kagan and Y.-H. Suen, *Bull. Soc. Chim. Fr.*, **1966**, 1819; b) J. Cason, K. L. Rinehart, Jr., and S. D. Thornton, Jr., *J. Org. Chem.*, **18**, 1594 (1953).

6) S. M. Hannick and Y. Kishi, *J. Org. Chem.*, **48**, 3833 (1983) and references therein. See also R. B. Silverman, J. Mathew, and B. J. Invergo, *Synth. Commun.*, **15**, 377 (1985).

7) a) T. Hiyama and K. Kobayahsi, *Tetrahedron Lett.*, **23**, 1597 (1982); b) K. Kobayashi and H. Suginome, *Bull. Chem. Soc. Jpn.*, **59**, 2635 (1986).

8) T. Hiyama, K. Nishide, and K. Kobayashi, *Chem. Lett.*, **1984**, 361.

9) T. Hiyama, K. Nishide, and K. Kobayashi, *Tetrahedron Lett.*, **25**, 569 (1984).

10) a) K. Sisido, H. Nozaki, and O. Kurihara, *J. Am. Chem. Soc.*, **74**, 6254 (1952); b) K. Sisido, K. Kumazawa, and H. Nozaki, *ibid.*, **82**, 125 (1960).

11) U. Wannagat and H. Kuckertz, *Angew. Chem., Int. Ed. Engl.*, **2**, 47 (1963).

12) a) T. Kato, H. Yamanaka, and T. Shibata, *Yakugaku Zasshi*, **89**, 1637 (1969); b) D. J. Aberhart and H. -J. Lin, *J. Org. Chem.*, **46**, 3749 (1981); c) T. L. Shieh, C. -T. Lin, A. T. McKenzie, and S. R. Byrn, *ibid.*, **48**, 3103 (1983).

13) a) N. Katagiri, A. Koshihara, S. Atsuumi, and T. Kato, *Chem. Pharm. Bull.*, **31**, 2288 (1983); b) T. Kato, H. Yamanaka, and T. Hozumi, *Yakugaku Zasshi*, **91**, 740 (1971); c) G. Hörlein, B. Kübel, A. Studeneer, and G. Salbeck, *Liebigs Ann. Chem.*, **1979**, 371.

14) K. Grohe and H. Heitzer, *Liebigs Ann. Chem.*, **1973**, 1025.

15) D. Raileanue, M. Palaghita, and C. D. Nenitzescu, *Tetrahedron*, **27**, 5031 (1971).

16) R. T. Buckler, H. E. Hartzler, and B. M. Phillips, *J. Med. Chem.*, **18**, 509 (1975).

17) a) H. G. O. Becker, *J. Prakt. Chem.*, **4**, 294 (1961); b) T. Iwasaki H. Horikawa, K. Matsumoto, and M. Miyoshi, *J. Org. Chem.*, **42**, 2419 (1977); c) F. Risitano, G. Grassi, F.

Foti, F. Caruso, and G. L. Vecchio, *J. Chem. Soc., Perkin Trans. 1*, **1979**, 1522; d) P. H. Lambert, M. Vaultier, and R. Carrie, *J. Org. Chem.*, **50**, 5352 (1985); e) M. Basato, B. Corain, M. Coffer, A. C. Veronese, and G. Zanotti, *J. Chem. Soc., Chem. Commun.*, **1984**, 1593; f) P. G. Baraldi, A. Barco, S. Benetti, F. Moroder, G. P. Pollini, and D. Simoni, *J. Org. Chem.*, **48**, 1297 (1983); g) J.-P. Célérier, E. Deloisy, P. Kapron, G. Lhommet, and P. Maitte, *Synthesis*, **1981**, 130; h) F. Scavo and P. Helquist, *Tetrahedron Lett.*, **26**, 2603 (1985) and references therein; i) J. G. Buchanan, G. Singh, R. H. Wightman, *J. Chem. Soc., Chem. Commun.*, **1984**, 1299; j) J. P. Célérier, M. G. Richand, and G. Lhommet, *Synthesis*, **1983**, 195.

18) F. Arcamone, "Daunomycin and Related Antibiotics," in "Topics in Antibiotic Chemistry," ed by P. G. Sammes, Ellis Horwood Ltd., Chichester (1978) Vol 2; S. Terashima, *Yuki Gosei Kagaku Kyokai Shi*, **40**, 20 (1982).

19) F. Arcamone, S. Penco, A. Vigevani, S. Redaelli, G. Tranchi, A. Di Marco, A. M. Casazza, T. Dasdia, F. Formelli, A. Necco, and S. Coranzo, *J. Med. Chem.*, **18**, 703 (1975).

20) K. Okamura and D. Swern, *Tetrahedron*, **34**, 1651 (1978).

21) Y. Morizawa, I. Mori, T. Hiyama, and H. Nozaki, *Synthesis*, **1981**, 899; Y. Morizawa, T. Hiyama, K. Oshima, and H. Nozaki, *Bull. Chem. Soc. Jpn.*, **57**, 1123 (1984).

22) A. W. M. Lee, V. S. Martin, S. Masamune, K. B. Sharpless, and F. J. Walker, *J. Am. Chem. Soc.*, **104**, 3515 (1982).

23) J. A. Musich and H. Rapoport, *J. Am. Chem. Soc.*, **100**, 4865 (1978).

24) T. Mukaiyama, Y. Goto, and S. Shoda, *Chem. Lett.*, **1983**, 671; T. Sakai, T. Nakamura, K. Fukuda, E. Amano, M. Utaka, and A. Takeda, *Bull. Chem. Soc. Jpn.*, **59**, 3185 (1986).

25) M. Slopianka, A. Gossaur, *Liebigs Ann. Chem.*, **1981**, 2258; J. D. Rozzell, *Tetrahedron Lett.*, **23**, 1767 (1982); M. Furukawa, T. Okawara, Y. Noguchi, and Y. Terawaki, *Chem. Pharm. Bull.*, **27**, 2223 (1979); K. Achiwa and T. Soga, *Tetrahedron Lett.*, **1978**, 1119.

26) Acetylation with Ac_2O and AcONa took place slightly more effectively: 72% yield and the (Z)/(E) ratio was 86 : 14 for racemic material.

27) Daunosamine synthesis: a) F. M. Hauser, S. R. Ellenberger, J. P. Glusker, C. J. Smart, and H. L. Carrell, *J. Org. Chem.*, **51**, 50 (1986); b) M. Hirama, J. Nishizaki, T. Shigemoto, and S. Itô, *J. Chem. Soc., Chem. Commun.*, **1986**, 393; c) A. Warm and P. Vogel, *Tetrahedron Lett.*, **26**, 5127 (1985); d) S. Hanessian and J. Kloss, *ibid.*, **26**, 1261 (1985); e) P. G. Sammes and D. Thetford, *J. Chem. Soc., Chem. Commun.*, **1985**, 352; f) Y. Hamada, A. Kawai, and T. Shioiri, *Tetrahedron Lett.*, **25**, 5409 (1984); g) P. M. Wovkulich and M. R. Uskoković, *Tetrahedron*, **41**, 3455 (1985) and references cited therein; h) I. Pelyvás, A. Hasegawa, and R. L. Whistler, *Carbohydr. Res.*, **146**, 193 (1986).

28) a) G. Fronza, C. Fuganti, and P. Grasselli, *J. Chem. Soc., Perkin Trans. 1*, **1982**, 885; b) *idem, ibid.*, **1980**, 442.

29) a) T. Suami, K. Tadano, A. Suga, and Y. Ueno, *J. Carbohydr. Chem.*, **3**, 429 (1984); b) Ref. 27g and references therein.

30) R. H. Howe, T. A. Gruner, L. G. Carter, and J. E. Franz, *J. Heterocyclic Chem.*, **15**, 1001 (1978).

31) C. Fuganti, P. Grasselli, and G. P. Fantoni, *J. Org. Chem.*, **48**, 909 (1983).

32) Stereoselective reduction of olefins having homoallylic chiral centers by means of homogeneous catalysts: A. G. Schultz and P. J. McCloskey, *J. Org. Chem.*, **50**, 5905 (1985); D. A. Evans, M. M. Morrissey, and R. L. Dow, *Tetrahedron Lett.*, **26**, 6005 (1985).

Synthesis of 4-Amino-2(5*H*)-furanones through Intra- and Intermolecular Nitrile Addition of Ester Enolates. Construction of Carbon Framework of an Antitumor Antibiotic Basidalin

Tamejiro HIYAMA,* Haruhito OISHI, Yukari SUETSUGU (nee KUSANO), Kiyoharu NISHIDE, and Hiroyuki SAIMOTO
Sagami Chemical Research Center, 4-4-1 Nishiohnuma, Sagamihara, Kanagawa 229
(Received December 9, 1986)

Two new routes to 4-amino-2(5*H*)-furanones are disclosed. The one is based on the reaction of a magnesium enolate of *t*-butyl acetate or propionate with *O*-protected cyanohydrins followed by acid-treatment which effects hydrolysis of the ester group, deprotection, olefin isomerization and lactonization all in a single operation. The other is base-induced ringclosure of α-acyloxy nitriles. The two methods are applied to construction of the carbon framework of an antitumor antibiotic basidalin.

Nitrile addition of an ester enolate is proved to be a promising alternative to 3-amino-2-alkenoates[1] which are versatile synthetic intermediates.[2] The addition is particularly facilitated to nitriles having α-alkoxy groups.[3] Though the (Z)-configuration of the produced 3-amino-2-alkenoates predominates due to intramolecular hydrogen bonding, Z to E isomerization takes place readily under various conditions.[2] Thus, protected cyanohydrins, after coupling with an ester enolate, isomerization of C=C bond of the adduct followed by appropriate functional group manipulations, are expected to give rise to 4-amino-2(5*H*)-furanones[4] which are precursors of defoliant, plant growth retardants,[5] and anti-hypertensive agents.[6]

An alternative approach to 4-amino-2(5*H*)-furanones emerges which employes intramolecular nitrile addition of an ester enolate, i.e., cyclization of α-alkanoyloxy nitriles.[7] Reported herein are details of the two synthetic approaches based on the inter- and intramolecular nitrile addition of ester enolates as well as their application to the construction of the carbon framework of an antibiotic basidalin.[8]

Results and Discussion

Synthesis of 4-Amino-2(5*H*)-furanones through Intermolecular Nitrile-Ester Enolate Addition. Cyanohydrins protected by 1-ethoxyethyl (=EE) ether **1** were allowed to react with the magnesium enolate of *t*-butyl acetate or propionate (Scheme 1). The resulting adduct, *t*-butyl 4-(1-ethoxyethoxy)-3-amino-2-alkenoates **2**, were treated with various acids in order to effect hydrolysis of the ester group, deprotection, (Z)→(E) isomerization, and lactonization all in a single operation without the enamine moiety affected.

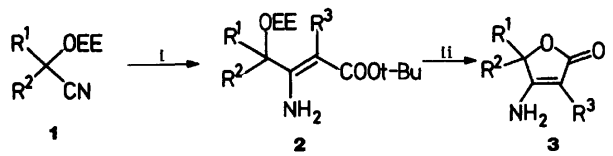

1 2 3

i) $R^3CH{=}C(Ot\text{-}Bu)OMgX$, Et_2O, 0 °C
ii) HX, PhH (or PhMe), 0 °C to r.t.

Scheme 1.

Organic acids like *p*-toluenesulfonic acid and trifluoroacetic acid gave intractable material. The best conditions we found were those which involve treatment of **2** with hydrogen halide gas in anhydrous nonpolar solvents like benzene and toluene, and the desired 4-amino-2(5*H*)-furanones (**3**) precipitated from the reaction medium. Purification by preparative TLC or column chromatography allowed us to isolate pure material. Typical results are summarized in Table 1. As the *N*-acyl derivatives of **2** are stable to acid and some of these derivatives are shown to exhibit biological activity, we prepared *N*-aroyl derivatives **4**, which underwent cyclization to give rise to 4-aroylamino-5-methyl-2(5*H*)-furanones **5**.[4] These results also are summarized in Table 1.

We also intended to prepare the *N*-ureido derivatives (vide infra) of **3** by the acid-catalyzed cyclization of the *N*-ureido derivatives of **2**. Actually, **2a** was converted into the corresponding urea derivative by the reaction

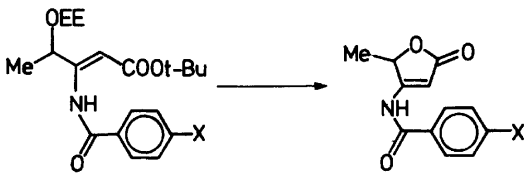

4 **5**

r: X=H, **s**: X=Br, **t**: X=CN, **u**: X=F, **v**: X=NO_2, **w**: X=Me

Table 1. Acid-Catalyzed Cyclization of **2** (or **4**) to **3** (or **5**)

Substrate	HX and Condition	Product	Yield/%
2a	HCl, PhH, r.t.	**3a**	65
2a	HCl, PhMe, 0 °C	**3a**	60
2a	HBr, PhH, 0 to 5 °C	**3a**	72
2b	HBr, PhH, 0 to 5 °C	**3b**	32
2c	HBr, PhH, 0 to 5 °C	**3c**	39
2d	HCl, PhH, 0 to 5 °C	**3d**	34
2e	HCl, PhH, 0 to 5 °C	**3e**	47
4r	HCl, CH_2Cl_2, 0 °C	**5r**	14
4s	HCl, CH_2Cl_2, 0 °C	**5s**	54
4t	HCl, CH_2Cl_2, 0 °C	**5t**	30
4u	HCl, CH_2Cl_2, 0 °C	**5u**	43
4v	HCl, CH_2Cl_2, 0 °C	**5v**	72
4w	HCl, CH_2Cl_2, 0 °C	**5w**	27

Table 2. Base-Promoted Ringclosure of **7**

Substrate	Condition	Product	Yield/%
7a	$LiN(SiMe_3)_2$, THF, −78 °C	**3a**	6
7b	$LiN(SiMe_3)_2$, THF, −78 °C	**3b**	0
7b	$LiN(SiMe_3)_2$-$Ni(acac)_2$,[a] −76 °C	**3b**	28
7d	$LiN(SiMe_3)_2$, THF, −78 °C	**3d**	82
7d	$LiN(i\text{-}Pr)_2$, THF, −78 °C	**3d**	60
7d	$Mg[N(i\text{-}Pr)_2]_2$, THF, −78 to −74 °C	**3d**	24
7e	$LiN(SiMe_3)_2$, THF, −78 °C	**3e**	74
7f	$LiN(SiMe_3)_2$, THF, −78 °C	**3f**	62
7g	$LiN(SiMe_3)_2$, THF, −78 °C	**3g**	63
7h	$LiN(SiMe_3)_2$, THF, −78 °C	**3h**	87
7i	$LiN(SiMe_3)_2$, THF, −78 °C	**3i**	96
7j	$LiN(SiMe_3)_2$, THF, −78 °C	**3j**	95
7k	$LiN(SiMe_3)_2$, THF, −78 °C	**3k**	65
7l	$LiN(SiMe_3)_2$, THF, −78 °C	**3l**	88
7m	$LiN(SiMe_3)_2$, THF, −78 °C	**3m**	16
7n	NaH, THF, reflux	**3n**	28
	Et_3N, THF, r.t.[b]	**3n**	38
7o	NaH, THF, reflux	**3o**	55
7p	NaH, THF, reflux	**3p**	22
7q	NaH, THF, reflux	**3q**	86

a) The reaction was carried out in the presence of 0.2 mol equiv of $Ni(acac)_2$. b) A mixture of 2-hydroxy-2-methylpropanenitrile (1.18 mmol), diketene (1.26 mmol), triethylamine (1.28 mmol) in THF (5 ml) was stirred at room temperature for 6 h.

with *t*-butyl isocyanate (KO*t*-Bu catalyst) in 58% yield. However, the acid-catalyzed transformation of the urea derivative to **6a** turned out futile.

Synthesis of 4-Amino-2(5*H*)-furanones through Intramolecular Nitrile-Ester Enolate Addition. Intramolecular nitrile addition of an ester enolate under ringclosure[9] is an alternative way to **3**. The requisite precursor is an α-acyloxy nitrile **7** which are derived from a cyanohydrin by acylation. In case that the cyanohydrin was commercially unavailable or thermodynamically unfavorable, the parent ketone was transformed to a cyanohydrin trimethylsilyl ether[10] which was subsequently acylated with an acid anhydride and iron(III) chloride catalyst.[11] Intramolecular nitrile addition of ester enolates were studied with **7d** as the model substrate. Ring closure was effected with KO*t*-Bu (0 °C), $Mg[N(i\text{-}Pr)_2]_2$ (−78 to −74 °C), $LiN(i\text{-}Pr)_2$ (−78 °C) or $LiN(SiMe_3)_2$ (−78 °C) all in tetrahydrofuran (THF) to afford **3d** in 4, 24, 60, or 82% yield respectively. In contrast to the intermolecular nitrile addition,[2] lithium amide was more effective than the magnesium amide. Since the use of 2.4 mol equiv of lithium hexamethyldisilazanide gave best yields, these conditions were applied to various kinds of α-acyloxy nitriles **7**, and the results are summarized in Table 2. Ringclosure of nitriles **7n—q** which have more acidic α-CH was preferably carried out with sodium hydride as the base. Desulfurization of **3p** with Raney Nickel is a byway to **3d**. It is apparent that the base-promoted cyclization proceeds highly efficiently, although **7a** and **7b** underwent competitive proton abstraction from C-H α to CN, and the expected product **3a** and **3b** were obtained in low yields. For **3b**, in particular, addition of $Ni(acac)_2$[12] improved the

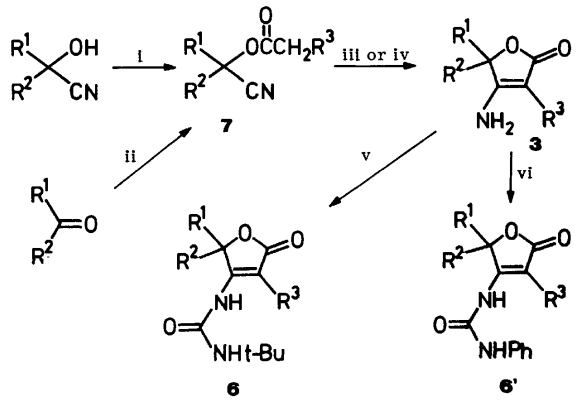

i) $(R^3CH_2CO)_2O$ (or R^3CH_2COCl), Py (or Et_3N)
ii) Me_3SiCN, ZnI_2; $(R^3CH_2CO)_2O$, $FeCl_3$
iii) $LiN(SiMe_3)_2$(2.4 mol), THF, −78 °C
iv) NaH, THF, reflux
v) *t*-BuN=C=O, *t*-BuOK
vi) PhN=C=O, *t*-BuOK

	R^1	R^2	R^3		R^1	R^2	R^3
a	Me	H	H	**j**	6-MeO-2-$C_{10}H_6$	Me	H
b	Et	H	H				
c	Me	H	Me	**k**	Et	Et	H
d	Me	Me	H	**l**	Me	Me	Me
e	$-(CH_2)_5-$		H	**m**	Me	Me	Cl
f	*i*-Pr	Me	H	**n**	Me	Me	COMe
g	*n*-C_9H_{19}	Me	H	**o**	Me	Me	Ph
h	Ph	Me	H	**p**	Me	Me	SPh
i	$PhCH_2$	Me	H	**q**	Me	Me	SOPh

(Substituents for **2**, **3**, **6**, **6'**, and **7**)

Scheme 2.

Table 3. Derivatization of **3** to Ureas **6** and

4-Amino-2(5*H*)-furanone	Isocyanate	Reaction Time	Product	Yield/%
3a	*t*-BuNCO	3 h	**6a**	47
3a	PhNCO	4 h	**6'a**	58
3b	*t*-BuNCO	1 d	**6b**	35
3d	*t*-BuNCO	2 d	**6d**	89
3d	PhNCO	2 d	**6'd**	82
3e	*t*-BuNCO	Overnight	**6e**	82
3f	*t*-BuNCO	2.5 d	**6f**	66
3g	PhNCO	Overnight	**6'g**	50
3h	*t*-BuNCO	3 d	**6h**	80
3h	PhNCO	Overnight	**6'h**	88
3i	*t*-BuNCO	Overnight	**6i**	51
3i	PhNCO	Overnight	**6'i**	62
3j	*t*-BuNCO	Overnight	**6j**	76
3j	PhNCO	Overnight	**6'j**	88
3k	*t*-BuNCO	2.5 d	**6k**	67
3l	*t*-BuNCO	2 d	**6l**	47
3q	*t*-BuNCO	2.5 d	**6q**	80

yields. Anyhow, to these substrates, the intermolecular method is applicable as disclosed before. With various kinds of 4-amino-2(5*H*)-furanones in hand, we derivatized these to the urea **6** or **6'** by the reaction to *t*-butyl isocyanate or phenyl isocyanate with potassium *t*-butoxide catalyst. In addition to the parent 4-amino-2(5*H*)-furanones (**3**), these as well as the *N*-aroyl analogs **5** were subjected to biological screening test. Although any of **5** did not show remarkable pharmacological activity, **6d**, **6'd**, and **3j** exhibited herbicidal activity against broad leaf weeds such as *Amaranthus retroflexus* at the level of 200 g/10 a by foliage application.

Synthetic Approach to Basidalin. With the two methods in hand, we undertook synthesis of basidalin. Basidalin is an antibiotic[8] which has an antibacterial activity and antitumor activity against L1210 mouse leukemia and possesses a 4-amino-2(5*H*)-furanone structure as well as formylmethylene substituent at C(5). We planned two synthetic routes to basidalin: Key intermediates we considered were 4-amino-2(5*H*)-furanones **12** and **17**, which were synthesized according to Schemes 3 and 4.

Cyanation of commercially available 1,1,3,3-tetramethoxypropane with trimethylsilyl cyanide and boron trifluoride etherate catalyst[13] induced substitution of one MeO group with CN to give **8** in 99% yield. The required introduction of acetoxyl group was achieved as follows. Bromination of **8** under radical conditions selectively took place at CN-substituted carbon to afford a labile bromide **9** which was immediately subjected to substitution reaction with silver acetate to give the key compound **10** needed for the intramolecular nitrile addition strategy in 74% overall yield. The success of regioselective radical bromination is ascribed to the stabilization of the intermediary radical species by "capto-dative" substituents CN and MeO.[14] The α-acetoxy nitrile **10** was treated with various bases such as lithium diisopropylamide, magnesium bis(diisopropylamide) and diethylaluminium diisopropylamide in 1.0 to 4.0 mol equiv to afford 4-amino-2(5*H*)-furanone **11** in 2 to 7% yields only. The yield of **11** was improved to 76% by use of 10 mol equiv of $Et_2AlN(i\text{-}Pr)_2$ at -78 to -60 °C for 1.7 h. Hydrolysis of the acetal moiety with a standard reagent trimethylsilyl iodide or boron tribromide turned out to induce total decomposition solely. However, combination of the Lewis acid with an amine base effectively converted **11** into **12**. Best combination was BBr_3 (3 mol) and $HN(SiMe_3)_2$ (3 mol) and thus **12** was obtained in 56% yield.

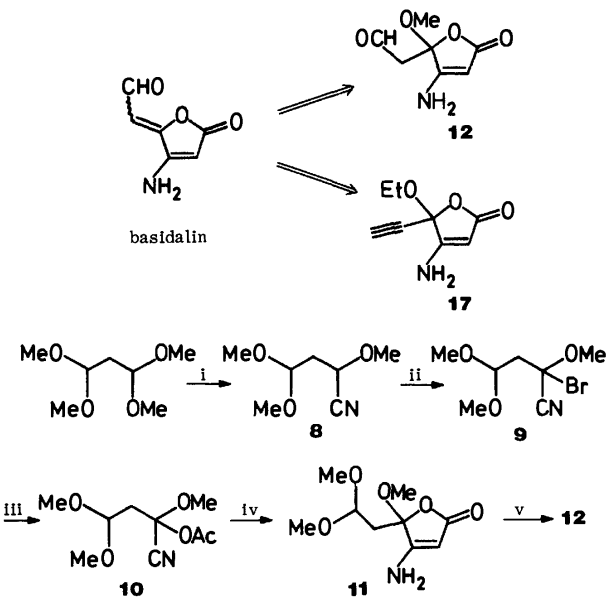

i) Me_3SiCN, $BF_3 \cdot OEt_2$(cat), 99%
ii) NBS, AIBN(cat), 94%
iii) AcOAg, 79%
iv) $Et_2AlN(i\text{-}Pr)_2$(10 equiv), 76%
v) $BBr_3 \cdot HN(SiMe_3)_2$(3 equiv), 56%

Scheme 3.

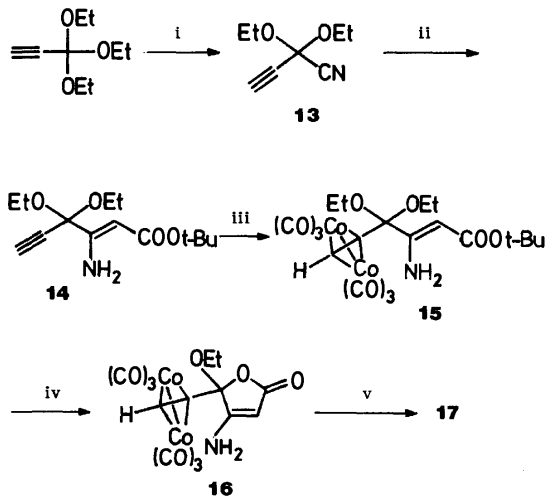

i) Me_3SiCN, $SnCl_2$, 71%
ii) CH_2=C(O*t*-Bu)OMgX, Et_2O, 85%
iii) $Co_2(CO)_8$, pentane, 81%
iv) CF_3COOH, 77%
v) $(NH_4)_2Ce(NO_3)_6$, 83%

Scheme 4.

The final step, elimination of methanol from **12**, grew to be extremely tough. Under various possible basic, acidic, or even neutral conditions, only decomposition resulted possibly via competitive ring opening of the lactone moiety of **12** by elimination and/or loss of the amino group.

We switched to the intermolecular strategy which required a nitrile whose α-carbon is a protected form of ketone carbonyl. For the candidate, we chose **13** which was derived from 3,3,3-triethoxypropyne[15] by a tin(II) chloride-catalyzed cyanation[13] in good yields. Reaction of **13** with *t*-butyl acetate through the magnesium enolate afforded **14** in 85% yield. Direct cyclization of **14** with various kinds of acids[4] failed to give the expected product **17**. However, protection of the C≡C bond of **14** with $Co_2(CO)_8$ followed by treatment with trifluoroacetic acid induced the desired ringformation to afford **16** in 77% yield. Complexation of the acetylene moiety with cobalt rendered us following advantages:[16] (a) Protection of the acetylenic triple bond and (2) stabilization of the cationic species involved in this transformation. Oxidative deprotection under the standard conditions gave **17**. Final transformation to basidalin unfortunately turned out fruitless in spite of numerous experiments including hydrometallation/oxidation.

Although total synthesis was unsuccessful, we could construct the basic carbon framework of basidalin and thus subjected the synthetic intermediates to in vitro test for cell growth inhibition of L1210 and P388. Of these, **15** exhibited IC_{50} (μmol ml^{-1}) 8.5×10^{-3} for L1210 and 3.1×10^{-3} for P388 comparable to the cytotoxicity of prostaglandin A_2 (2.6×10^{-3} and 2.8×10^{-3} for L1210 and P388 respectively).[17]

In conclusion, inter- and intramolecular nitrile-addition of ester enolates is found to be a facile and promising route to a biologically important 4-amino-2(5*H*)-furanone structure. As the structural feature is closely related to tetronic acids,[18] the new synthetic methods will provide us with an additional way to physiologically important tetronic acids and their derivatives.

Experimental

Experimental apparatus and instrumental facilities are the same as those of the preceding paper.[2] Additionally, FT ^{1}H NMR spectra were recorded on a Hitachi R-90H spectrometer. Trimethylsilyl cyanide and hexamethyldisilazane were purchased from Petrach Systems Inc. and distilled before use. *t*-Butyl 3-amino-4-(1-ethoxyethoxy)-2-alkenoates **2a—e** were prepared according to the procedure described in the preceding paper.[2] The yields and spectral properties are as follows. The compounds **2b** and **2d** were oily substance and labile to thin layer, column or gas chromatographic purification. Thus, these were characterized only spectrometrically.

***t*-Butyl 3-Amino-4-(1-ethoxyethoxy)-2-hexenoate (2b):** 65% yield. Bp 100—120 °C (bath temperature)/0.1 Torr.† ^{1}H NMR ($CDCl_3$) δ=0.92 and 0.95 (2t, J=6.5 Hz, 3H), 1.17 and 1.19 (2t, J=6.5 Hz, 3H), 1.30 (d, J=6.0 Hz, 3H), 1.47 (s, 9H), 1.63 (q, J=6.5 Hz, 2H), 3.30—3.78 (m, 2H), 3.84 (q, J=6.0 Hz, 1H), 4.43 and 4.47 (2s, totally 1H), 4.63 and 4.70 (2q, J=6.0 Hz, 1H), 5.5—6.7 (br, 2H). IR (neat) 3500, 3350, 2990, 2940, 1665, 1620, 1555, 1280, 1250, 1080, 1045, 795 cm^{-1}. MS m/z 201 (M^+ $-CH_2$=CHOEt).

***t*-Butyl 3-Amino-4-(1-ethoxyethoxy)-2-methyl-2-pentenoate (2c):** 47% yield. Bp 110—150 °C (bath temperature)/0.2 Torr. ^{1}H NMR ($CDCl_3$) δ=0.90—2.0 (m+2s (δ=1.50 and 1.67), 21 H), 3.25—3.90 (m, 2H), 4.40—4.90 (m, 2H), 6.2—6.8 (br, 2H). IR (neat) 3540, 3360, 3020, 2960, 1670, 1610, 1530, 1460, 1400, 1375, 1275, 1255, 1180, 1125, 1085, 970, 855, 790 cm^{-1}. MS m/z (rel intensity) 273 (M^+, 6), 172 (8), 171 (7), 156 (9), 145 (42), 129 (19), 128 (49), 127 (12), 110 (12), 99 (19), 82 (7), 73 (100), 72 (4), 57 (18), 56 (5), 55 (6), 54 (4), 45 (74). Found: m/z 273.1941. Calcd for $C_{14}H_{27}NO_4$: M^+ 273.1938.

***t*-Butyl 3-Amino-4-(1-ethoxyethoxy)-4-methyl-2-pentenoate (2d):** 79% yield. Bp 70—75 °C (bath temperature)/0.25 Torr. ^{1}H NMR ($CDCl_3$) δ=1.08—1.23 (t, J=13.5 Hz, 3H), 1.27 and 1.33 (2d, J=5.4 Hz, 3H), 1.43 (br s, 6H), 1.48 (s, 9H), 3.37—3.60 (q, J=6.9 Hz, 2H), 4.53 (s, 1H), 4.65—4.83 (q, J=5.4 Hz, 1H), 5.67—7.00 (br, 2H). IR (neat) 3525, 3350, 3000, 2950, 2900, 1670, 1610, 1550, 1390, 1370, 1295, 1150, 1080, 980, 800 cm^{-1}. MS m/z 227 (M^+ $-$EtOH).

***t*-Butyl 3-Amino-3-[1-(1-ethoxyethoxy)cyclohexyl]-2-propenoate (2e):** 79% yield. Bp 120—132 °C (bath temperature)/0.8 Torr. Mp 69—70 °C (hexane-ethyl acetate 3:1). ^{1}H NMR ($CDCl_3$) δ=1.13 (t, J=6 Hz, 3H), 1.30 (d, J=5 Hz, 3H), 1.47 (s, 9H), 1.40—2.20 (m, 10H), 3.47 (q, J=6 Hz, 2H), 4.60 (s, 1H), 4.63 (q, J=5 Hz, 1H), 6.0—7.0 (br, 2H). IR (KBr) 3520, 3350, 3000, 2980, 2950, 2900, 2870, 2850, 1670, 1615, 1550, 1450, 1385, 1365, 1270, 1245, 1150, 1080, 1055, 980, 790, 660 cm^{-1}. Found: C, 65.18; H, 10.14; N, 4.39%. Calcd for $C_{17}H_{31}NO_4$: C, 65.14; H, 9.97; N, 4.47%.

Synthesis of 4-Amino-5-methyl-2(5*H*)-furanone (3a). A Typical Procedure for Hydrogen Halide Induced Formation

†1 Torr=133.322 Pa.

of 4-Amino-2(5*H*)-furanones. Dry hydrogen chloride gas was bubbled into a benzene (100 ml) solution of *t*-butyl 3-amino-4-(1-ethoxyethoxy)-2-pentenoate (**2a**)[2] (100 mg, 0.39 mmol) over a period of 2 h. Colorless material precipitated after 30 min's bubbling. The precipitates were collected and washed twice with benzene. Purification by preparative TLC (silica gel, dichloromethane-methanol 10 : 1, R_f=0.19—0.29) gave colorless solid **3a**[5a,6] (29 mg, 65% yield), mp 151—152 °C (lit,[5a] 150—152 °C). ^{1}H NMR ($CDCl_3$-DMSO-d_6) δ=1.47 (d, J=6 Hz, 3H), 4.56 (s, 1H), 4.76 (q, J=6 Hz, 1H), 6.40—6.70 (br, 2H). IR (KBr) 3450, 3395, 3230, 3000, 1710, 1660, 1580, 1335, 1190, 1050, 950, 905, 785 cm^{-1}. MS *m/z* (rel intensity) 114 (M^++1, 7), 113 (M^+, 66), 98 (64), 70 (100), 43 (22), 42 (33), 41 (56).

Spectral properties of 4-amino-2(5*H*)-furanones prepared by the similar procedures are listed below.

4-Amino-5-ethyl-2(5*H*)-furanone (3b).[5a,b] Mp 143—143.5 °C (lit,[5a] 143—145.5 °C). ^{1}H NMR ($CDCl_3$-DMSO-d_6) δ=0.95 (t, J=6.5 Hz, 3H), 1.4—2.2 (m, 2H), 4.45—4.90 (m+s (δ=4.60), 2H), 6.0—6.6 (br, 2H). IR (neat) 3450, 3240, 2980, 2950, 2900, 1710, 1650, 1580, 1540, 1345, 1190, 1080, 980 910, 780, 720 cm^{-1}.

4-Amino-3,5-dimethyl-2(5*H*)-furanone (3c).[6] Mp 96—98 °C. ^{1}H NMR ($CDCl_3$-DMSO-d_6) δ=1.48 (d, J=6 Hz, 3H), 1.66 (s, 3H), 4.73 (q, J=6 Hz, 1H), 4.83 (br s, 2H). IR (KBr) 3480, 3370, 3250, 3025, 2950, 2900, 1720, 1670, 1620, 1430, 1340, 1122, 1105, 1060, 990, 770, 740 cm^{-1}. Found: C, 56.42; H, 7.20; N, 10.90%. Calcd for $C_6H_9NO_2$: C, 56.68; H, 7.13; N, 11.02%.

4-Amino-5,5-dimethyl-2(5*H*)-furanone (3d). Mp 205—207 °C. ^{1}H NMR ($CDCl_3$-DMSO-d_6) δ=1.48 (s, 6H), 4.48 (s, 1H), 6.4—6.7 (br, 2H). IR (KBr) 3400, 3350 (sh), 3220, 3000, 1720, 1680, 1660, 1615, 1600, 1390, 1375, 1300, 1255, 1200, 1130, 985, 945, 900, 800 cm^{-1}. MS *m/z* (rel intensity) 128 (M^++1, 6), 127 (M^+, 53), 112 (100), 70 (42), 66 (11), 59 (12), 43 (77). Found: C, 56.55; H, 7.14; N, 10.90%. Calcd for $C_6H_9NO_2$: C, 56.68; H, 7.13; N, 11.02%.

3'-Aminospiro[cyclohexane-1,2'(5'*H*)-furan]-5'-one (3e). Mp 194.5—195.5 °C. ^{1}H NMR ($CDCl_3$-DMSO-d_6 1 : 1) δ=1.2—2.0 (m, 10H), 4.48 (s, 1H), 6.4—6.7 (br, 2H). IR (KBr) 3400, 3200, 2950, 2870, 1710, 1660, 1600, 1295, 1210, 1140, 1065, 975, 940, 860, 795 cm^{-1}. MS *m/z* (rel intensity) 168 (M^++1, 5), 167 (M^+, 38), 124 (27), 112 (16), 111 (100), 99 (32), 84 (65), 83 (10), 81 (27), 69 (20), 66 (77), 55 (16). Found: C, 64.56; H, 7.60; N, 8.38%. Calcd for $C_9H_{13}NO_2$: C, 64.65; H, 7.84; N, 8.38%.

Aroylation of 3a. Benzoyl chloride (1.37 g, 9.7 mmol) and 4-dimethylaminopyridine (0.20 g, 1.64 mmol) were added to a pyridine (20 ml) solution of **3a** (1.68 g, 6.5 mmol) at 0 °C, and the reaction mixture was stirred at 0 °C for 30 min and at 50 °C overnight. The pyridine was evaporated in vacuo and the residue was purified by column chromatography (Kieselgel 60) to give an E/Z mixture of *t*-butyl 3-(benzoylamino)-4-(1-ethoxyethoxy)-2-pentenoate (**4r**) (1.03 g, 44% yield) and a compound assigned as *t*-butyl 3-benzoylamino-4-benzoyloxy-2-pentenoate (0.20 g, 10% yield). **4r** (viscous oil, R_f=0.50 (hexane-ethyl acetate 5 : 1)) showed ^{1}H NMR ($CDCl_3$) δ=1.00—1.70 (2t+d+s (δ=1.43), 18H), 3.25—3.70 (m, 2H), 3.90—4.30 (m, 1H), 4.30 (s, 1H), 4.30—4.90 (m, 1H), 7.20—7.70 (m, 3H), 7.90—8.20 (m, 2H), 12.00—12.30 (br, 1H). IR (neat) 3500, 3230, 3080, 2950, 1700, 1660, 1635, 1490, 1370, 1300, 1265, 1250, 1150, 1070, 960, 920, 740, 710 cm^{-1}. Found: C, 66.19; H, 8.22; N, 3.71%. Calcd for $C_{20}H_{29}NO_5$: C, 66.09; H, 8.04; N, 3.85%.

The *N,O*-dibenzoate (R_f 0.40) showed mp 152—153 °C; ^{1}H NMR ($CDCl_3$) δ=1.71 (d, J=7 Hz, 3H), 1.20 (s, 9H), 5.38 (s, 1H), 6.93 (q, J=7 Hz, 1H), 7.33—7.73 (m, 6H), 7.93—8.23 (m, 4H), 11.13—11.43 (br, 1H). Found: C, 70.01; H, 6.38; N, 3.45%. Calcd for $C_{23}H_{25}NO_5$: C, 69.85; H, 6.37; N, 3.54%.

In similar manners and by using the corresponding aroyl chloride, **4s**—w were prepared.

***t*-Butyl 3-(4-Bromobenzoylamino)-4-(1-ethoxyethoxy)-2-pentenoate (4s).** Pale yellow viscous oil, R_f=0.69 (hexane-ethyl acetate 5 : 1). ^{1}H NMR ($CDCl_3$) δ=1.0—1.65 (m+s (δ=1.53), 18H), 3.35—3.90 (m, 2H), 4.73 and 4.79 (2q, 1H), 5.50—5.85 (m+2s (δ=5.32 and 5.42), 2H), 7.55—7.90 (AB q, 4H), 12.4—12.7 (br, 1H). IR (neat) 3230, 3000, 2950, 1700, 1660, 1630, 1595, 1485, 1370, 1305, 1270, 1250, 1155, 1075, 1015, 920, 825, 750, 740 cm^{-1}. Found: C, 54.11; H, 6.35; N, 3.09%. Calcd for $C_{20}H_{28}BrNO_5$: C, 54.30; H, 6.38; N, 3.17%.

***t*-Butyl 3-(4-Cyanobenzoylamino)-4-(1-ethoxyethoxy)-2-pentenoate (4t).** Colorless viscous oil, R_f=0.48 (hexane-ethyl acetate 5 : 1). ^{1}H NMR ($CDCl_3$) δ=1.00—1.60 (m+s (δ=1.53), 18H), 3.35—3.80 (m, 2H), 4.60—4.90 (2q, 1H), 5.55—5.80 (2s(δ=5.57 and 5.70)+q (δ=5.70), 2H), 7.75—8.20 (AB q, 4H), 12.3—12.6 (br 1H). IR (neat) 3500, 3350, 3200, 3100, 3000, 2950, 2230, 1700, 1660, 1630, 1490, 1370, 1300, 1270, 1240, 1150, 1080, 960, 920, 860, 760 cm^{-1}. Found: C, 64.67; H, 7.41; N, 6.93%. Calcd for $C_{21}H_{28}N_2O_5$: C, 64.93; H, 7.27; N, 7.21%.

***t*-Butyl 4-(1-Ethoxyethoxy)-3-(4-fluorobenzoylamino)-2-pentenoate (4u).** Colorless viscous oil, R_f=0.54 (hexane-ethyl acetate 5 : 1). ^{1}H NMR ($CDCl_3$) δ=1.10—1.90 (m+s (δ=1.55), 18H), 3.35—3.90 (m, 2H), 4.65—4.95 (2q, 1H), 5.50—5.90 (2s (δ=5.53 and 5.67)+q (δ=5.75, J=6 Hz), totally 2H), 7.17 (t, J=9.0 Hz, 2H), 8.03 (dd, J=9.0 and 5.0 Hz, 2H), 12.0—12.5 (br, 1H). IR (neat) 3220, 3000, 2950, 1700, 1660, 1635, 1605, 1495, 1250, 1155, 1080, 760, 740 cm^{-1}. Found: C, 63.00; H, 7.33; N, 3.58%. Calcd for $C_{20}H_{28}FNO_5$: C, 62.98; H, 7.40; N, 3.67%.

***t*-Butyl 4-(1-Ethoxyethoxy)-3-(4-nitrobenzoylamino)-2-pentenoate (4v).** Pale yellow viscous oil, R_f=0.57 (hexane-ethyl acetate 5 : 1). ^{1}H NMR ($CDCl_3$) δ=1.05—1.65 (m+s (δ=1.54), 18 H), 3.40—3.80 (m, 2H), 4.60—4.90 (2q, 1H), 5.55—5.80 (2s (δ=5.59 and 5.71) +m, totally 2H), 8.10—8.45 (AB q, 4H), 12.30—12.60 (br, 1H). IR (neat) 3210, 3140, 3000, 2950, 1700, 1660, 1640, 1605, 1535, 1485, 1350, 1300, 1265, 1250, 1155, 1080, 955, 920, 870, 850, 735, 715 cm^{-1}. Found: C, 58.70; H, 6.97; N, 6.73%. Calcd for $C_{20}H_{28}N_2O_7$: C, 58.81; H, 6.91; N, 6.86%.

***t*-Butyl 4-(1-Ethoxyethoxy)-3-(4-methylbenzoylamino)-2-pentenoate (4w).** Colorless viscous oil, R_f=0.48 (hexane-ethyl acetate 5 : 1). ^{1}H NMR ($CDCl_3$) δ=1.00—1.80 (m+s (δ=1.57), 18H), 2.43 (s, 3H), 3.30—3.80 (m, 2H), 4.55—4.90 (2q, 1H), 5.45—5.85 (2s (δ=5.48 and 5.60)+m, totally 2H), 7.10—7.95 (AB q, 4H), 12.1—12.4 (br, 1H). IR (neat) 3250, 3000, 2950, 1700, 1600, 1635, 1560, 1495, 1375, 1305, 1270, 1250, 1160, 1135, 1080, 920, 840, 750, 740 cm^{-1}. Found: C, 66.99; H, 8.37; N, 3.56%. Calcd for $C_{21}H_{31}NO_5$: C, 66.82; H, 8.28; N, 3.71%.

4-Aroylamino-5-methyl-2(5*H*)-furanones. Into a dichloromethane solution of *t*-butyl 3-aroylamino-4-(1-ethoxyethoxy)-2-pentenoate (**4r**—w) (0.27 M††), dry hydrogen chloride gas was bubbled at 0 °C for 3 h, and the reaction mixture was

††1 M=1 mol dm^{-3}.

Table 4. Physical Properties of **5**

Compound	Mp(θ_m/°C) (solvent)	IR/cm^{-1}	^{1}H NMR ($CDCl_3$) (δ)
5r[a]	Colorless needles 176—178 (Hexane–ethanol)	3325, 1730 1715, 1690 1600	1.50 (d, J=5.4 Hz, 3 H), 5.22 (q, J=5.4 Hz, 1 H), 6.15 (s, 1 H), 7.77—8.07 (m, 5 H), 11.2—11.4 (br, 1 H)
5s[b]	Colorless prisms 201—202 (Ethanol)	3345, 1730 1705, 1630 1590	1.57 (d, J=6 Hz, 3 H), 5.22 (q, J=6 Hz, 1 H), 6.22 (s, 1 H), 7.87—7.95 (AB q, 4 H), 10.3—10.5 (br, 1 H)
5t[c]	Colorless needles 203—204.5 (Ethanol)	3320, 3250 2250, 1760 1750 (sh) 1730 (sh) 1720, 1625 (sh)	1.57 (d, J=6 Hz, 3 H), 5.22 (q, J=6 Hz, 1 H), 6.23 (s, 1 H), 7.79—8.18 (AB q, 4 H), 10.9 (br, 1 H)
5u[d]	Colorless needles 206—208 (Ethanol)	3350, 3250 1745, 1730 1705, 1630	1.54 (d, J=6 Hz, 3 H), 5.20 (q, J=6 Hz, 1 H), 6.16 (s, 1 H), 7.26 (t, J=9 Hz, 2 H), 8.06 (dd, J=9 and 5 Hz, 2 H), 10.8 (br, 1 H)
5v[e]	Pale yellow prisms 244—246 (Methanol)	3350, 3250 (sh) 1730, 1710 1630, 1605 1555, 1350 1330	1.54 (d, J=7 Hz, 3 H), 5.22 (q, J=7 Hz, 1 H), 6.20 (s, 1 H), 8.15—8.40 (AB q, 4 H), 11.2 (br, 1 H)
5w[f]	Colorless needles 191—192 (Hexane–ethanol)	3350, 3250 (sh) 3150 (sh) 1745, 1730 1690, 1630	1.59 (d, J=7 Hz, 3 H), 2.43 (s, 3 H), 5.23 (q, J= 7 Hz, 1 H), 6.17 (s, 1 H), 7.20—8.05 (AB q, 4 H), 10.8 (br, 1 H)

a) MS m/z (rel intensity) 218 (M^++1, 12), 217 (M^+, 57), 174 (10), 173 (80), 172 (66), 171 (14), 129 (4), 128 (5), 105 (24), 104 (100), 103 (22), 77 (29), 76 (8), 70 (59), 69 (9), 51 (14), 43 (56). Found: m/z 217.0757. Calcd for $C_{12}H_{11}NO_3$: M^+ 217.0738. b) MS m/z (rel intensity) 297 (M^++2, 11), 295 (M^+, 11), 185 (100), 183 (100), 157 (24), 155 (25), 76 (26), 75 (20), 50 (15). Found: C, 48.63; H, 3.33; N, 4.61; Br, 26.71%. Calcd for $C_{12}H_{10}BrNO_3$: C, 48.67; H, 3.40; N, 4.73; Br, 26.98%. c) MS m/z (rel intensity) 242 (M^+, 7), 214 (10), 131 (9), 130 (100), 103 (4), 102 (39), 76 (6), 75 (9), 68 (7), 51 (6). Found: m/z 242.0709. Calcd for $C_{13}H_{10}N_2O_3$: M^+ 242.0727. d) MS m/z (rel intensity) 235 (M^+, 7), 205 (4), 124 (8), 123 (100), 95 (33), 75 (11), 68 (4). Found: C, 61.40; H, 4.17; N, 5.83%. Calcd for $C_{12}H_{10}FNO_3$: C, 61.28; H, 4.29; N, 5.95%. e) MS m/z (rel intensity) 262 (M^+, 9), 234 (10), 151 (8), 150 (100), 120 (18), 104 (29), 92 (11), 76 (19), 75 (6), 68 (6), 50 (8). Found: C, 54.94; H, 3.80; N, 10.61%. Calcd for $C_{12}H_{10}N_2O_5$: C, 54.96; H, 3.84; N, 10.68%. f) MS m/z (rel intensity) 232 (M^++1, 2), 231 (M^+, 13), 120 (27), 119 (100), 92 (7), 91 (88), 90 (7), 89 (9), 68 (5), 65 (34), 63 (7), 51 (4), 41 (5). Found: m/z 231.0898. Calcd for $C_{13}H_{13}NO_3$: M^+ 231.0895.

allowed to stand for a couple of days. The precipitated crystals were collected and recrystallized from the solvent shown in Table 4. The yields listed in Table 1 are those after recrystallization. Physical properties are summarized in Table 4.

Derivatization of 2a by the reaction with *t*-butyl isocyanate was effected by the procedure described in the derivatization of **3a**, and the resulting urea derivative showed following spectra.

***t*-Butyl 4-(1-Ethoxyethoxy)-3-(*N'*-*t*-butylureido)-2-pentenoate.** Colorless prisms, mp 114—117 °C, R_f=0.56 (hexane–ethyl acetate 5:1). ^{1}H NMR ($CDCl_3$) δ=1.07—1.43 (m, 9H), 1.33 (s, 9H), 1.48 (s, 9H), 3.37—3.67 (m, 2H), 4.50—4.80 (m, 2H), 5.20 and 5.32 (2s, 1H), 5.43—5.65 (2q, 1H), 10.1—10.5 (br, 1H). Found: C, 60.30; H, 9.78; N, 7.54%. Calcd for $C_{18}H_{34}N_2O_5$: C, 60.30; H, 9.56; N, 7.82%.

Acylation of Cyanohydrin. A typical procedure is shown for the synthesis of 2-acetoxy-2-methylpropanenitrile (**7d**). To a dichloromethane (20 ml) solution of commercially available 2-hydroxy-2-methylpropanenitrile (1.70 g, 20 mmol) were added acetic anhydride (4.0 ml) and pyridine (3.2 ml) under cooling with ice, and the reaction mixture was stirred at room temperature for 2 d. The reaction mixture was then washed 3 times with 3% hydrochloric acid and once with brine, dried over magnesium sulfate, and then concentrated. Distillation at 70—75 °C/9 Torr gave **7d** (1.28 g, 50% yield). ^{1}H NMR ($CDCl_3$) δ=1.76 (s, 6H), 2.09 (s, 3H), IR (neat) 2260 (vw), 1760, 1470, 1420, 1390, 1370, 1355, 1275, 1230, 1190, 1140 cm^{-1}.

Similarly, **7e** (36%), **7m** (81%), and **7l** (46%) were prepared. Nitriles **7a** and **7b** were finally purified by preparative GLC.

2-Acetoxypropanenitrile (7a): Bp 70—75 °C/9 Torr. ^{1}H NMR ($CDCl_3$) δ=1.63 (d, J=7.2 Hz, 3H), 2.13 (s, 3H), 5.36 (q, J=7.2 Hz, 1H).

2-Acetoxybutanenitrile (7b): Bp 75—80 °C/22 Torr. ^{1}H NMR ($CDCl_3$) δ=1.10 (t, J=6.6 Hz, 3H), 1.89 (quintet, J=6.6 Hz, 2H), 2.13 (s, 3H), 5.25 (t, J=6.6 Hz, 1H). IR (neat) 3000, 2950, 2900, 2250 (vw), 1750, 1460, 1370, 1220 cm^{-1}.

1-Cyanocyclohexyl Acetate (7e): Bp 120 °C/13 Torr, mp 48.5—49 °C, colorless prisms. ^{1}H NMR ($CDCl_3$) δ=1.15—1.95 (m, 8H), 2.10 (s, 3H), 2.18—2.42 (m, 2H). IR (KBr) 3500,

2950, 2875, 2250, 1750, 1450, 1365, 1260, 1230, 1165, 1060 cm^{-1}.

2-Chloroacetoxy-2-methylpropanenitrile (7m): Bp 70—71 °C/0.5 Torr. ^1H NMR ($CDCl_3$) δ=1.80 (s, 6H), 4.04 (s, 2H). IR (neat) 3025, 2975, 2250 (w), 1770, 1750 (sh), 1470, 1410, 1390, 1370, 1320, 1290, 1230, 1185, 1135 cm^{-1}.

2-Methyl-2-propanoylpropanenitrile (7l): Bp 50 °C/0.5 Torr. ^1H NMR ($CDCl_3$) δ=1.15 (t, J=7.5 Hz, 3H), 1.74 (s, 6H), 2.34 (q, J=7.5 Hz, 2H). IR (neat) 3000, 2950, 2250, 1775, 1470, 1420, 1390, 1370, 1355, 1225, 1190, 1140 cm^{-1}.

Synthesis of α-Acyloxy Nitriles by Silylcyanation of Ketones and Acylation with Iron(III) Chloride Catalyst. Zinc iodide (20 mg, 0.06 mmol) was added to acetophenone (1.21 g, 10 mmol) and trimethylsilyl cyanide (1.5 ml, 11 mmol) dissolved in benzene (10 ml) at 0 °C and the reaction mixture was stirred at room temperature overnight. The reaction mixture was diluted with benzene (30 ml) and washed with brine (50 ml), dried over magnesium sulfate, and concentrated in vacuo to give crude 2-phenyl-2-trimethylsilyloxypropanenitrile which was dissolved in acetic anhydride (5.0 ml), to which solution was added iron(III) chloride (0.10 g) at 0 °C. Stirring was continued for 1 h at 0 °C to room temperature. The color of the reaction mixture turned to green before dilution with dichloromethane (30 ml) and quenching with water (30 ml). The organic layer was separated, washed with brine, dried over magnesium sulfate, and concentrated under reduced pressure. Distillation gave **7h** (1.70 g, 90% yield). Bp 56—58 °C/0.15 Torr. ^1H NMR ($CDCl_3$) δ=2.00 (s, 3H), 2.12 (s, 3H), 7.2—7.9 (m, 5H). IR (neat) 3080, 3050, 3010, 2950, 2250, 1760, 1600, 1495, 1370, 1220, 1140, 1090, 1070, 1010, 950, 760, 695 cm^{-1}.

By this procedure following 2-acyloxy nitriles were prepared. Overall yield from the corresponding ketone or aldehyde is given.

2-Acetoxy-2,3-dimethylbutanenitrile (7f): 65%, bp 70—73 °C/16 Torr. ^1H NMR ($CDCl_3$) δ=1.08 and 1.13 (2d, J=4.5 Hz, 6H), 1.68 (s, 3H), 2.08 (s, 3H), 2.08—2.16 (m, 1H). IR (neat) 3000, 2250 (w), 1755, 1470, 1370, 1235 cm^{-1}.

2-Acetoxy-2-methylundecanenitrile (7g): 82% yield, bp 88—90 °C/0.15 Torr. ^1H NMR ($CDCl_3$) δ=0.82—0.95 (t, 3H), 1.28 (m, 14H), 1.72 (s, 3H), 1.76—2.03 (m, 2H), 2.07 (s, 3H). IR (neat) 2925, 2855, 2230 (vw), 1750, 1710, 1460, 1370, 1230 cm^{-1}.

2-Acetoxy-2-ethylpentanenitrile (7k): 66% yield, bp 95—96 °C/20 Torr. ^1H NMR ($CDCl_3$) δ=1.05 (t, J=6.9 Hz, 6H), 2.04 (q, J=6.9 Hz, 4H), 2.09 (s, 3H). IR (neat) 3000, 2950, 2245 (vw), 1750, 1460, 1370, 1230 cm^{-1}.

2-Acetoxy-2-methyl-3-phenylpropanenitrile (7i): 63% yield, bp 140—150 °C/1 Torr. ^1H NMR ($CDCl_3$) δ=1.40 (s, 3H), 2.13 (s, 3H), 3.23 (AB q, 2H), 7.36 (br s, 5H). IR (neat) 3100, 3060, 2970, 2250 (vw), 1760, 1500, 1455, 1375, 1265, 1230, 1170, 1070, 1020, 760, 700 cm^{-1}.

2-Methyl-2-[(phenylthio)acetoxy]propanenitrile (7p). To a dichloromethane (30 ml) solution of phenylthioacetyl chloride (2.40 g, 12.8 mmol) were added 2-hydroxy-2-methylpropanenitrile (1.00 g, 11.7 mmol) and then triethylamine (1.79 ml, 0.128 mmol) at 0 °C. The reaction mixture was stirred and gradually warmed to room temperature over 3 h, then washed twice with 3% hydrochloric acid (30 ml), then with brine (30 ml) and finally with aq sat. sodium hydrogencarbonate solution (30 ml), dried over magnesium sulfate, and concentrated under reduced pressure. Distillation afforded **7p** (1.20 g, 43% yield). Bp 150—160 °C (bath temperature)/0.7 Torr. ^1H NMR ($CDCl_3$) δ=1.65 (s, 6H), 3.58 (s, 2H), 7.17—7.47 (m, 5H). IR (neat) 3075, 3020, 2950, 2340, 1740, 1585, 1470, 1435, 1390, 1370, 1265, 1225, 1200, 1115, 1025, 975 cm^{-1}. MS m/z (rel intensity) 237 (M^++2, 2), 236 (M^++1, 5), 235 (M^+, 32), 168 (10), 123 (100), 109 (13), 77 (12), 65 (10), 51 (12), 45 (41), 41 (10).

Similarly, **7o** (0.64 g, 32% yield) was prepared from 2-hydroxy-2-methylpropanenitrile (0.85 g, 10 mmol), phenylacetyl chloride (1.80 g, 11.7 mmol) and triethylamine (1.60 ml, 11.5 mmol). Bp 145—150 °C/0.8 Torr. ^1H NMR ($CDCl_3$) δ=1.40 (s, 6H), 3.62 (s, 2H), 7.28 (br s, 5H). IR (neat) 3075, 3050, 3010, 2950, 2250, 1750, 1605, 1500, 1470, 1455, 1390, 1370, 1350, 1255, 1225, 1125, 970, 730, 700 cm^{-1}. MS m/z (rel intensity) 204 (M^++1, 2), 203 (M^+, 14), 119 (4), 92 (9), 91 (100), 68 (5), 65 (10), 41 (9), 39 (7).

2-Methyl-2-[(phenylsulfinyl)acetoxy]propanenitrile (7q). *m*-Chloroperoxybenzoic acid (80—85% purity, 0.19 g) was added to a dichloromethane (5 ml) solution of **7p** (0.20 g, 0.85 mmol), and the reaction mixture was stirred at room temperature overnight before dilution with dichloromethane (20 ml) and treatment with 10% sodium thiosulfate aq solution (20 ml). Extractive workup followed by preparative TLC (hexane-ethyl acetate 1 : 1, R_f=0.25) gave **7q** (0.165 g, 77% yield) as a viscous oil. ^1H NMR ($CDCl_3$) δ=1.65 (s, 3H), 1.71 (s, 3H), 3.81 and 3.71 (AB q, J=13.5 Hz, 2H), 7.45—7.80 (m, 5H). IR (neat) 3500, 3075, 3010, 2950, 2250, 1745, 1475, 1445, 1390, 1370, 1270, 1230, 1200, 1150, 1115, 1090, 1050, 975 cm^{-1}. MS m/z (rel intensity) 253 (M^++2, 1), 252 (M^++1, 3), 251 (M^+, 20), 184 (2), 167 (3), 126 (13), 125 (100), 97 (22), 77 (27), 51 (20), 41 (11).

2-Methyl-2-(3-oxobutanoyloxy)propanenitrile (7n). Diketene (1.0 g, 12 mmol) and pyridine (0.94 g, 12 mmol) were successively added to a dichloromethane (20 ml) solution of 2-hydroxy-2-methylpropanenitrile (0.85 g, 10 mmol) at 0 °C, and the reaction mixture was stirred at room temperature overnight, then poured into 5% hydrochloric acid (30 ml), extracted with dichloromethane. The organic layer was washed with brine, dried over magnesium sulfate and concentrated. Distillation gave **7n** (1.52 g, 90% yield). Bp 155—160 °C/21 Torr. ^1H NMR ($CDCl_3$) δ=1.78 (s, 6H), 2.26 (s, 3H), 3.48 (s, 2H). IR (neat) 3015, 2950, 2250, 1760, 1725, 1630, 1560, 1470, 1410, 1370, 1365, 1320, 1260, 1230, 1135, 1025, 995, 970 cm^{-1}. MS m/z (rel intensity) 168 (M^+−1, 3), 126 (2), 100 (2), 85 (12), 84 (14), 70 (75), 69 (15), 68 (10), 58 (6), 44 (12), 43 (100), 42 (18), 41 (16).

Synthesis of 4-Amino-5,5-dimethyl-2(5*H*)-furanone (3d). A Typical Procedure for the Preparation of 5,5-Disubstituted 4-Amino-2(5*H*)-furanones with $LiN(SiMe_3)_2$. A THF solution of **7d** (0.127 g, 1.0 mmol) was added to $LiN(SiMe_3)_2$ (2.5 mmol in 3 ml of THF) drop by drop at −78 °C under an argon atmosphere. After 2 h, sat. ammonium chloride aq solution (5 ml) was added to the reaction mixture to quench the reaction. The resulting mixture was warmed to room temperature and concentrated under reduced pressure. The residue was extracted with methanol. The methanolic extract was concentrated and the residual oil was purified by preparative TLC (silica gel, dichloromethane-methanol 10 : 1) to give **3d** (0.104 g, 82% yield).

In a similar manner, following amino furanones were prepared. Physical properties of these are listed below.

4-Amino-5-isopropyl-5-methyl-2(5*H*)-furanone (3f). Mp 171—172 °C. ^1H NMR ($CDCl_3$-DMSO-d_6 10 : 1) δ=0.86 and

1.05 (2d, J=6.6 Hz, 6H), 1.42 (s, 3H), 1.93 (heptet, J=6.6 Hz, 1H), 4.54 (s, 1H), 6.23 (br s, 2H). IR (KBr) 3380, 3205, 3000, 1730 (sh), 1700, 1665, 1610, 1590, 1580, 1415, 1290, 1230 cm^{-1}. MS m/z (rel intensity) 156 (M^++1, 2), 155 (M^+, 8), 113 (11), 112 (100), 70 (23), 43 (35), 41 (12). Found: C, 61.90; H, 8.56; N, 8.97%. Calcd for $C_8H_{13}NO_2$: C, 61.91; H, 8.44; N, 9.03%.

4-Amino-5-methyl-5-nonyl-2(5*H*)-furanone (3g). Mp 104—107 °C. ^1H NMR ($CDCl_3$-DMSO-d_6 20:1) δ=0.87 (t, J=6.0 Hz, 3H), 1.0—1.4 (br s, 14H), 1.44 (s, 3H), 1.55—1.90 (m, 2H), 4.65 (s, 1H), 5.58 (br s, 2H). IR (KBr) 3440, 3350, 3225, 2925, 2870, 1735, 1710, 1660, 1585 cm^{-1}. MS m/z (rel intensity) 240 (M^++1, 3), 239 (M^+, 5), 211 (6), 154 (11), 140 (12), 127 (21), 113 (59), 112 (100), 85 (24), 70 (29), 43 (44). Found: m/z 239.1868. Calcd for $C_{14}H_{25}NO_2$: M^+ 239.1883.

4-Amino-5-methyl-5-phenyl-2(5*H*)-furanone (3h). Mp 69—71 °C. ^1H NMR ($CDCl_3$-DMSO-d_6 10:1) δ=1.90 (s, 3H), 4.68 (s, 1H), 6.31 (br s, 2H), 7.3—7.6 (m, 5H). IR (KBr) 3400, 3205, 1700, 1665 (sh), 1585, 1445, 1405, 1290, 1285, 1230, 1075, 965 cm^{-1}. MS m/z (rel intensity) 191 (M^++2, 1), 190 (M^++1, 11), 189 (M^+, 83), 175 (13), 174 (100), 146 (22), 121 (33), 112 (30), 105 (67), 103 (20), 77 (38), 70 (14), 69 (17), 68 (14), 51 (20), 43 (72), 41 (42). Found: C, 66.54; H, 6.24; N, 6.99%. Calcd for $C_{11}H_{11}NO_2 \cdot 0.5\ H_2O$: C,66.65; H, 6.10; N, 7.07%. Found: m/z 189.0776. Calcd for $C_{11}H_{11}NO_2$: M^+ 189.0788.

4-Amino-5-benzyl-5-methyl-2(5*H*)-furanone (3i). Mp 158—161 °C. ^1H NMR ($CDCl_3$-DMSO-d_6 10:1) δ=1.50 (s, 3H), 3.37 (s, 2H), 4.43 (s, 1H), 6.15 (br s, 2H), 7.20 (br s, 5H). IR (KBr) 3420, 3225, 1715, 1700, 1665, 1605, 1590, 1450, 1415, 1300, 1255, 1170, 970 cm^{-1}. MS m/z (rel intensity) 203 (M^+, 6), 112 (100), 91 (7), 84 (33), 70 (15), 66 (40), 43 (19). Found: C, 70.75; H, 6.36; N, 6.76%. Calcd for $C_{12}H_{13}NO_2$: C, 70.92; H, 6.45; N, 6.89%.

4-Amino-5-(6-methoxy-2-naphthyl)-5-methyl-2(5*H*)-furanone (3j). Mp 206—208 °C. ^1H NMR ($CDCl_3$-DMSO-d_6 4:1) δ=1.97 (s, 3H), 3.90 (s, 3H), 4.73 (s, 1H), 6.25 (br s, 2H), 7.0—7.9 (m, 6H). IR (KBr) 3450, 3350, 3240, 1730 (sh), 1725, 1645, 1595, 1440, 1390, 1370, 1270, 1220, 1200, 1165, 1140, 1020, 950 cm^{-1}. MS m/z (rel intensity) 271 (M^++2, 2), 270 (M^++1, 15), 269 (M^+, 79), 255 (18), 254 (100), 226 (10), 201 (10), 185 (40), 157 (18). Found: C, 71.23; H, 5.49; N, 5.13%. Calcd for $C_{16}H_{25}NO_3$: C, 71.36; H, 5.61; N, 5.20%.

4-Amino-5,5-diethyl-2(5*H*)-furanone (3k). Mp 162—164 °C. ^1H NMR ($CDCl_3$-DMSO-d_6 3:1) δ=0.83 (t, J=7 Hz, 6H), 1.54—1.89 (m, 4H), 4.67 (s, 1H), 5.94 (br s, 2H). IR (KBr) 3425, 3375, 3200, 3000, 1715, 1665, 1650, 1605, 1590 cm^{-1}. MS m/z (rel intensity) 156 (M^++1, 1), 155 (M^+, 9), 127 (18), 126 (100), 84 (10), 70 (14), 57 (53), 41 (12). Found: C, 61.81; H, 8.40; N, 8.95%. Calcd for $C_8H_{13}NO_2$: C, 61.91; H, 8.44; N, 9.03%.

4-Amino-3,5,5-trimethyl-2(5*H*)-furanone (3l). Mp 205—208 °C. ^1H NMR ($CDCl_3$-DMSO-d_6 3:1) δ=1.43 (s, 6H), 1.61 (s, 3H), 5.69 (br s, 2H). IR (KBr) 3400, 3230, 3000, 2950, 1710, 1665, 1600, 1475, 1430, 1345, 1215, 1195, 1100, 1000 cm^{-1}. MS m/z (rel intensity) 142 (M^++1, 16), 141 (M^+, 71), 126 (100), 98 (23), 70 (16), 56 (19), 55 (32), 54 (15), 43 (38). Found; m/z 141.0770. Calcd for $C_7H_{11}NO_2$: M^+ 141.0790.

4-Amino-3-chloro-5,5-dimethyl-2(5*H*)-furanone (3m). Mp 170—172 °C. ^1H NMR ($CDCl_3$-DMSO-d_6 1:1) δ=1.48 (s, 6H), 6.88 (br s, 2H). IR (KBr) 3450 (sh), 3375, 3220, 3000, 1720, 1670, 1650, 1600, 1300, 1225, 1140, 1040 cm^{-1}. MS m/z (rel intensity) 164 (M^++3, 3), 163 (M^++2, 18), 162 (M^+1, 8), 161 (M^+, 54), 148 (33), 146 (100), 118 (36), 104 (39), 82 (11), 76 (13), 75 (17), 70 (24), 68 (21), 43 (60). Found: m/z 161.0209. Calcd for $C_6H_8ClNO_2$: M^+ 161.0242.

4-Amino-5,5-dimethyl-3-phenylsulfinyl-2(5*H*)-furanone (3q). A Typical Procedure for the Synthesis of 3 Having Electron-Withdrawing Substituent at C(3). A THF (3 ml) solution of **7q** (50 mg, 0.20 mmol) was added drop by drop to sodium hydride (50% in oil, 20 mg, 0.40 mmol) suspended in THF (30 ml) under reflux, and the reaction mixture was heated to reflux for 2 h until all the starting material was consumed. Excess hydride was carefully quenched with sat. ammonium chloride aq solution and worked up. Isolation by column chromatography (dichloromethane-methanol 10:1) gave **3q** (43 mg, 86% yield). Mp 137—138 °C. ^1H NMR ($CDCl_3$-DMSO-d_6 10:1) δ=1.41 (s, 3H), 1.53 (s, 3H), 6.9—7.3 (br, 2H), 7.33—7.57 (m, 3H), 7.57—7.90 (m, 2H). IR (KBr) 3350, 3200, 3000, 1715, 1665, 1590, 1580 (sh), 1480, 1460, 1410, 1370, 1280, 1225, 1220, 1160, 1080, 1045 (sh), 1025 cm^{-1}. MS m/z (rel intensity) 251 (M^+, 3) 235 (5), 204 (15), 203 (100), 188 (32), 160 (42), 158 (11), 126 (9), 86 (27), 78 (25), 77 (17), 68 (18), 51 (18), 43 (23), 39 (10). Found: C, 57.27; H, 5.11; N, 5.48; S, 12.94%. Calcd for $C_{12}H_{13}NO_3S$: C, 57.35; H, 5.21; N, 5.57; S, 12.76%.

By the similar procedure, **3n**, **3o**, and **3p** were prepared and their physical data are listed below.

3-Acetyl-4-amino-5,5-dimethyl-2(5*H*)-furanone (3n). Mp 188—189 °C. ^1H NMR ($CDCl_3$-DMSO-d_6) δ=1.56 (s, 6H), 2.46 (s, 3H), 8.43 and 8.82 (br 2s, 2H). IR (KBr) 3370, 1710, 1650, 1540, 1360, 1320, 1025 cm^{-1} MS m/z (rel intensity) 169 (M^+, 11), 154 (12), 112 (8), 87 (67), 86 (67), 66 (100), 48 (14), 46 (24), 43 (19). Found: C, 56.77; H, 6.65; N, 8.02%. Calcd for $C_8H_{11}NO_3$: C, 56.80; H, 6.55; N, 8.28%.

4-Amino-5,5-dimethyl-3-phenyl-2(5*H*)-furanone (3o). Mp 148—150 °C (hexane-ethyl acetate). ^1H NMR ($CDCl_3$-DMSO-d_6 1:1) δ=1.57 (s, 6H), 6.40 (br s, 2H), 7.15—7.65 (m, 5H). IR (KBr) 3400, 3330, 3000, 1700, 1640, 1615, 1595, 1500, 1470, 1425, 1370, 1330, 1245, 1200, 1155, 1120, 1010, 970, 920 cm^{-1}. MS m/z (rel intensity) 205 (M^++2, 1), 204 (M^++1, 15), 203 (M^+, 100), 188 (49), 160 (55), 158 (11), 132 (22), 118 (33), 117 (63), 115 (14), 91 (14), 89 (24), 77 (6), 43 (55). Found: C, 70.91; H, 6.49; N, 6.85%. Calcd for $C_{12}H_{13}NO_2$: C, 70.92; H, 6.45; N, 6.89%.

4-Amino-5,5-dimethyl-3-phenylthio-2(5*H*)-furanone (3p). Mp 154.5—156.5 °C. ^1H NMR ($CDCl_3$) δ=1.55 (s, 6H), 6.66 (br s, 2H), 7.00—7.33 (m, 5H). IR (KBr) 3460, 3325, 3270, 3200, 1710, 1640, 1585, 1480, 1410, 1290, 1035, 740 cm^{-1}. MS m/z (rel intensity) 237 (M^++2, 6), 236 (M^++1, 16), 235 (M^+, 100), 220 (8), 192 (7), 176 (5), 151 (10), 150 (28), 149 (12), 142 (43), 141 (12), 123 (10), 121 (24), 114 (22), 113 (15), 110 (6), 109 (8), 105 (11), 86 (14), 77 (16), 68 (15), 65 (10), 51 (19), 45 (11), 43 (65), 42 (12), 39 (15). Found: m/z 235.0646. Calcd for $C_{12}H_{13}NO_2S$: M^+ 235.0665.

Desulfurization of 3p. A mixture of **3p** (15 mg, 0.064 mmol), Raney Nickel (W-2) (0.06 g) and ethanol (3 ml) was heated to reflux for 3 h. Filtration, concentration and purification by preparative TLC (dichloromethane-methanol 10:1) gave **3d** (10 mg, quantitative yield) which showed identical chromatographic and spectrometric data to those of the sample prepared before.

Derivatization of 3d to 6d. A Typical Procedure for the Synthesis of Urea 6 and 6′. To a THF (50 ml) solution of **3d** (1.27 g, 10 mmol) was added *t*-butyl isocyanate (1.50 g, 15 mmol) at room temperature and the mixture was cooled with ice bath. Potassium *t*-butoxide (1.68 g, 15 mmol) was then added, and the whole was warmed to room temperature

and stirred for 2 d. Neutralization with sat. ammonium chloride aq solution, dilution with brine (30 ml), extraction with ethyl acetate (30 ml), drying the organic extract over magnesium sulfate followed by careful evaporation of the organic solvents to ca. 5 ml afforded 4-(*N'*-*t*-butylureido)-5,5-dimethyl-2(5*H*)-furanone (**6d**) as colorless crystals (1.53 g) which were filtered. From the filtrate, another portion (0.5 g) of **6d** was obtained. Total yield was 89%. Mp 247.5—248 °C. ^{1}H NMR ($CDCl_3$–DMSO-d_6 3:1) δ=1.37 (s, 9H), 1.48 (s, 6H), 5.85 (s, 1H), 6.25 (br s, 1H), 8.56 (br s, 1H). IR (KBr) 3390, 3005, 2955, 1745, 1730, 1700, 1625, 1540 (sh), 1450, 1395, 1370, 1320, 1280, 1255, 1200, 1180, 1170, 1005, 975, 950, 820, 775, 740, 710, 700 cm^{-1}. MS *m/z* (rel intensity) 227 (M^++1, 0.6), 226 (M^+, 1), 138 (9), 128 (10), 127 (88), 112 (100), 84 (15), 70 (11), 58 (38), 57 (77), 43 (25), 42 (16), 41 (38), 39 (11), 29 (20). Found: C, 58.30; H, 8.19; N, 12.25%. Calcd for $C_{11}H_{18}N_2O_3$: C, 58.39; H, 8.02; N, 12.38%.

Similarly, other urea derivatives listed in Table 3 were prepared and exhibited following characteristics.

4-(*N'*-*t*-Butylureido)-5-methyl-2(5*H*)-furanone (6a).[5] Mp 197—201 °C (decomp); lit,[5a,b] 204—206 °C (decomp). ^{1}H NMR ($CDCl_3$–DMSO-d_6) δ=1.37 (s, 9H), 1.50 (d, *J*=6 Hz, 3H), 4.98 (q, *J*=6 Hz, 1H), 5.86 (s, 1H), 5.97 (s, 1H), 8.70 (s, 1H). IR (KBr) 3425, 3325, 3175, 3080, 3000, 1710, 1625, 1550, 1510, 1255, 1195, 1170, 1085, 1050, 1005, 950, 905, 815, 700 cm^{-1}. MS *m/z* (rel intensity) 213 (M^++1, 2), 212 (M^+, 2), 181 (2), 173 (9), 155 (2), 154 (3), 140 (2), 139 (1), 115 (3), 114 (13), 113 (100), 112 (6), 101 (6), 98 (44), 84 (10), 70 (42), 58 (61), 57 (100).

5-Methyl-4-(*N'*-phenylureido)-2(5*H*)-furanone (6'a).[6] ^{1}H NMR ($CDCl_3$–DMSO-d_6) δ=1.54 (d, *J*=6 Hz, 3H), 5.02 (q, *J*=6 Hz, 1H), 5.90 (s, 1H), 7.50 (s, 5H), 8.41 (br, 1H), 8.96 (br, 1H). IR (KBr) 3380 (sh), 3350, 3150, 3075, 2990, 1715, 1630, 1605, 1550, 1500, 1440, 1330, 1295, 1230, 1190, 1170, 1095, 1050, 820, 755, 695, 685 cm^{-1} MS *m/z* (rel intensity) 233 (M^++1, 3), 232 (M^+, 14), 213 (2), 212 (10), 204 (4), 188 (2), 149 (2), 139 (2), 124 (4), 121 (1), 120 (16), 119 (100), 113 (35), 98 (29), 93 (100), 91 (31), 77 (24), 70 (35), 63 (9), 64 (20).

4-(*N'*-*t*-Butylureido)-5-ethyl-2(5*H*)-furanone (6b).[6] Mp 140—144 °C (decomp); lit,[5a] 142—144 °C. ^{1}H NMR ($CDCl_3$) δ=0.95 (t, *J*=7 Hz, 3H), 1.37 (s, 9H), 1.5—2.3 (m, 2H), 4.87 (dd, *J*=3 and 6 Hz, 1H), 3.90 (s, 1H), 3.95 (br s, 1H), 8.62 (br s, 1H). IR (neat) 3420, 3300, 3000, 1700, 1620, 1520, 1460, 1350, 1250, 1190, 1160, 1010, 980, 820, 695, 655 cm^{-1}. MS *m/z* (rel intensity) 227 (M^++1, 5), 226 (M^+, 3), 128 (21), 127 (64), 100 (17), 99 (84), 98 (99), 84 (9), 72 (4), 71 (7), 70 (16), 58 (40), 57 (100).

5,5-Dimethyl-4-(*N'*-phenylureido)-2(5*H*)-furanone (6'd). Mp 239—240 °C. ^{1}H NMR ($CDCl_3$–DMSO-d_6 3:1) δ=1.53 (s, 6H), 6.01 (s, 1H), 7.04—7.53 (m, 5H), 8.49 (br s, 1H), 8.85 (br s, 1H). IR (KBr) 3400, 3230, 3160, 3070, 1750 (sh), 1730 (sh), 1705, 1625, 1600, 1565 (sh), 1555 (sh), 1530, 1435, 1330, 1295, 1285, 1215, 1195, 1175, 1115, 1010, 975, 905, 860, 830, 760, 740, 695 cm^{-1}. MS *m/z* (rel intensity) 247 (M^++1, 2), 246 (M^+, 13), 138 (29), 127 (43), 120 (15), 119 (100), 112 (82), 93 (60), 92 (16), 91 (32), 77 (20), 70 (22), 68 (10), 67 (10), 66 (21), 65 (20), 64 (23), 63 (11), 51 (14), 43 (72), 41 (33). Found: C, 63.31; H, 5.82; N, 11.29%. Calcd for $C_{13}H_{14}N_2O_3$: C, 63.40; H, 5.73; N, 11.38%.

3'-(*N'*-*t*-Butylureido)spiro[cyclohexane-1,2'(5'*H*)-furan]-5'-one (6e). Mp 249.5—250 °C. ^{1}H NMR ($CDCl_3$–DMSO-d_6 10:1) δ=1.37 (s, 9H), 1.5—2.1 (m, 10H), 5.92 (s, 1H), 6.14 (br s, 1H), 8.61 (br s, 1H). IR (KBr) 3390, 3350, 2960, 1740, 1720 (sh), 1695, 1625, 1540, 1430, 1395, 1370, 1295, 1280, 1255, 1195, 1135, 1100, 1010, 980, 960, 940, 910, 855, 830, 760, 750, 700 cm^{-1}. MS *m/z* (rel intensity) 266 (M^+, 2), 168 (11), 167 (77), 124 (18), 112 (17), 111 (100), 68 (11), 58 (33), 57 (60), 42 (12), 41 (34), 29 (16). Found: C, 63.15; H, 8.28; N, 10.47%. Calcd for $C_{14}H_{22}N_2O_3$: C, 63.13; H, 8.33; N, 10.52%.

5-(*N'*-*t*-Butylureido)-5-isopropyl-5-methyl-2(5*H*)-furanone (6f). Mp 182—183 °C. ^{1}H NMR ($CDCl_3$–DMSO-d_6 5:1) δ=0.78 and 1.08 (2d, *J*=6.6 Hz, 6H), 1.35 (s, 9H), 1.43 (s, 3H), 1.5—2.0 (m, 1H), 5.90 (s, 1H), 6.13 (br s, 1H), 8.24 (br s, 1H). IR (KBr) 3410, 3300, 3240, 3170, 3070, 3000, 1730, 1710, 1690, 1615, 1550 (sh), 1535, 1455, 1395, 1370, 1365, 1340, 1280, 1255, 1190, 1145, 1110, 1040, 1000, 975, 820, 775, 750, 710 cm^{-1}. MS *m/z* (rel intensity) 255 (M^++1, 0.4), 254 (M^+, 1), 155 (20), 113 (20), 112 (100), 58 (14), 57 (30), 43 (26), 41 (17), 29 (11). Found: C, 61.42; H, 8.52; N, 10.98%. Calcd for $C_{13}H_{22}N_2O_3$; C, 61.39; H, 8.72; N, 11.02%

4-(*N'*-*t*-Butylureido)-5-methyl-5-nonyl-2(5*H*)-furanone (6g). Mp 120—120.5 °C. ^{1}H NMR ($CDCl_3$) δ=0.87 (t, 3H), 1.1—2.1 (m+2s (δ=1.37 and 1.48), totally 28H), 6.00 (s, 1H), 6.12 (br s, 1H), 8.62 (br s, 1H). IR (KBr) 3430, 3320, 3240, 3175, 3080, 2980, 2950, 2875, 1735, 1625, 1555, 1515, 1460, 1395, 1390, 1370, 1340, 1255, 1090, 1050, 1005, 965, 820, 745, 720 cm^{-1}. MS *m/z* (rel intensity) 339 (M^++1, 1), 338 (M^+, 3), 239 (11), 222 (9), 211 (14), 180 (11), 154 (20), 141 (15), 140 (20), 139 (21), 138 (34), 127 (41), 113 (100), 112 (95), 85 (29), 84 (85), 83 (13), 70 (31), 68 (22), 58 (94), 57 (87), 56 (31), 51 (26), 43 (63), 42 (29), 41 (87), 40 (10). Found: C, 67.46; H, 10.04; N, 8.30%. Calcd for $C_{19}H_{34}N_2O_3$: C, 67.42; H, 10.13; N, 8.28%.

5-Methyl-5-nonyl-4-(*N'*-phenylureido)-2(5*H*)-furanone (6'g). Mp 114—115 °C. ^{1}H NMR ($CDCl_3$) δ=0.75—0.90 (m, 3H), 1.22 (br s, 14H), 1.56 (s, 3H), 1.73—1.93 (m, 2H), 6.21 (s, 1H), 7.07—7.53 (m, 5H), 8.27 (br s, 1H), 8.98 (br s, 1H). IR (KBr) 3400, 3320, 3260, 3170, 3080, 2980, 2940, 2880, 1745, 1710 (sh), 1695, 1625, 1605, 1540, 1475, 1440, 1325, 1295, 1225 (sh), 1190, 1135, 1085, 1070, 1055, 1010, 975, 910, 885, 875, 870, 830, 755, 725, 695 cm^{-1}. MS *m/z* (rel inensity) 359 (M^++1, 1), 358 (M^+, 4), 232 (9), 222 (10), 154 (12), 140 (11), 139 (27), 138 (44), 127 (19), 119 (58), 113 (54), 112 (100), 94 (11), 93 (84), 92 (11), 91 (37), 77 (11), 70 (29), 68 (15), 66 (18), 65 (16), 64 (24), 63 (11), 57 (14), 55 (20), 43 (72), 42 (18), 41 (55). Found: C, 70.25; H, 8.39; N, 7.74%. Calcd for $C_{21}H_{30}N_2O_3$: C, 70.36; H, 8.44; N, 7.82%.

4-(*N'*-*t*-Butylureido)-5-methyl-5-phenyl-2(5*H*)-furanone (6h). Mp 207—208 °C. ^{1}H NMR ($CDCl_3$–DMSO-d_6 3:1) δ=1.32 (s, 9H), 1.88 (s, 3H), 6.08 (s, 1H), 6.25 (br s, 1H), 7.40 (s, 5H), 8.23 (br s, 1H). IR (KBr) 3370, 2990, 1740 (sh), 1700, 1620, 1530, 1450, 1390, 1365, 1310, 1280, 1255, 1200, 1100, 1070, 1000, 970, 950, 820, 770, 740, 700 cm^{-1}. MS *m/z* (rel intensity) 289 (M^++1, 1), 288 (M^+, 1) 200 (17), 190 (14), 189 (88), 175 (12), 174 (100), 146 (17), 144 (12), 143 (10), 121 (21), 112 (12), 105 (33), 84 (16), 77 (25), 69 (10), 68 (15), 58 (41), 57 (87), 51 (13), 43 (39). Found: C, 66.78; H, 7.00; N, 9.74%. Calcd for $C_{16}H_{20}N_2O_3$: C, 66.64; H, 6.99; N, 9.72%.

5-Methyl-5-phenyl-4-(*N'*-phenylureido)-2(5*H*)-furanone (6'h). Mp 234—235 °C. ^{1}H NMR ($CDCl_3$–DMSO-d_6 3:1) δ= 1.95 (s, 3H), 6.25 (s, 1H), 7.2—7.6 (m, 10H), 8.56 (br s, 2H). IR (KBr) 3360, 3325, 3175, 3075, 1755, 1730 (sh), 1710, 1640, 1605, 1555, 1545, 1505, 1445, 1385, 1330, 1300, 1280, 1255, 1245, 1215, 1185, 1100, 1085, 1075, 1030, 1010, 995, 970, 935, 920, 905, 890, 860, 820, 780, 755, 705 cm^{-1}. MS *m/z* (rel intensity) 309 (M^++1, 4), 308 (M^+, 25), 215 (10), 200 (59), 189 (58), 175 (11), 174 (92), 172 (17), 146 (20), 121 (25), 120 (14), 119 (100), 112 (20), 105 (82), 103 (15), 93 (76), 92 (17), 91 (50),

78 (11), 77 (67), 70 (11), 69 (12), 68 (16), 67 (13), 66 (28), 65 (25), 64 (31), 63 (18), 52 (12), 51 (40), 50 (17), 41 (68). Found: C, 70.00; H, 5.25; N, 9.07%. Calcd for $C_{18}H_{16}N_2O_3$: C, 70.11; H, 5.23; N, 9.09%.

4-(*N'-t*-Butylureido)-5-benzyl-5-methyl-2(5*H*)-furanone (6i). Mp 241—243 °C. ^{1}H NMR ($CDCl_3$–DMSO-d_6 20:1) δ= 1.35 (s, 9H), 1.46 (s, 3H), 3.01 (AB, 2H), 5.76 (s, 1H), 6.20 (br s, 1 H), 7.21 (br s, 5H), 8.64 (br s, 1H). IR (KBr) 3420, 3310, 3170, 3075, 3000, 2975, 1735, 1710 (sh), 1700, 1625, 1555, 1510, 1460, 1395, 1385, 1370, 1310, 1255, 1190, 1170, 1130, 1090, 1065, 1050, 1005, 965, 885, 820, 765, 745, 725, 700 cm^{-1}. MS *m/z* (rel intensity) 303 (M^++1, 1), 302, (M^+, 5), 211 (15), 155 (13), 112 (100), 91 (29), 58 (17), 57 (32), 43 (21), 41 (16). Found: C, 67.47; H, 7.45; N, 9.20%. Calcd for $C_{17}H_{22}N_2O_3$: C, 67.52; H, 7.33; N, 9.27%.

5-Benzyl-5-methyl-4-(*N'*-phenylureido)-2(5*H*)-furanone (6'i). Mp 206.5 °C. ^{1}H NMR ($CDCl_3$–DMSO-d_6 20:1) δ=1.55 (s, 3H), 3.07 (AB, 2H), 6.00 (s, 1H), 7.10—7.55 (m+s (δ=7.18), 10H), 8.34 (br s, 1H), 8.96 (br s, 1H). IR (KBr) 3380 (sh), 3350, 3300, 3270, 3080, 2930, 1745, 1705, 1640, 1605, 1550, 1500, 1445, 1385, 1325, 1300, 1235, 1210, 1185, 1090, 1005, 980, 870, 815, 780, 750, 700 cm^{-1}. MS *m/z* (rel intensity) 323 (M^++1, 2), 322 (M^+, 9), 231 (40), 138 (12), 119 (18), 112 (100), 93 (26), 92 (14), 91 (86), 77 (13), 70 (22), 66 (12), 65 (23), 64 (10), 51 (10), 43 (55). Found: C, 70.75; H, 5.63; N, 8.66%. Calcd for $C_{19}H_{18}N_2O_3$: C, 70.79; H, 5.63; N, 8.69%.

4-(*N'-t*-Butylureido)-5-(6-methoxy-2-naphthyl)-5-methyl-2(5*H*)-furanone (6j). Mp 234—235 °C ^{1}H NMR ($CDCl_3$–DMSO-d_6 10:1) δ=1.30 (s, 9H), 1.98 (s, 3H), 3.91 (s, 3H), 6.16 (br s, 1H), 6.18 (s, 1H), 7.1—7.9 (m, 6H), 8.18 (br s, 1H). IR (KBr) 3390, 3350, 3020, 2970, 1740, 1710, 1635, 1615, 1550, 1530, 1495, 1460, 1400, 1380, 1370, 1320, 1280, 1260, 1210, 1170, 1130, 1100, 1075, 1040, 1010, 970, 950, 930, 890, 855, 830, 820, 750, 725 cm^{-1}. MS *m/z* (rel intensity) 370 (M^++2, 1), 369 (M^++1, 7), 368 (M^+, 30), 296 (15), 295 (79), 281 (19), 280 (100), 269 (40), 255 (11), 254 (60), 252 (16), 201 (12), 186 (11), 185 (75), 157 (37), 142 (19), 128 (10), 127 (10), 115 (11), 114 (27), 84 (18), 67 (10), 63 (10), 58 (97), 57 (36), 43 (62). Found: C, 68.38; H, 6.77; N, 7.45%. Calcd for $C_{21}H_{24}N_2O_4$: C, 68.46; H, 6.57; N, 7.60%.

5-(6-Methoxy-2-naphthyl)-4-(*N'*-phenylureido)-2(5*H*)-furanone (6'j). Mp 221—222 °C. ^{1}H NMR ($CDCl_3$–DMSO-d_6 10:1) δ=2.02 (s, 3H), 3.90 (s, 3H), 6.30 (s, 1H), 6.9—7.9 (m, 11 H), 8.56 (br s, 2H). IR (KBr) 3350, 3300 (sh), 1745, 1730 (sh), 1705, 1630, 1555, 1540, 1500, 1445, 1395, 1325, 1290, 1270, 1205, 1185, 1090, 1075, 1030, 1005, 970, 960, 920, 885, 855, 845, 820, 755, 750, 695 cm^{-1}. MS *m/z* (rel intensity 388 (M^+, 1), 311 (9), 269 (42), 255 (12), 254 (66), 212 (10), 201 (11), 185 (47), 157 (21), 142 (11), 119 (40), 114 (14), 93 (100), 92 (14), 91 (31), 77 (13), 66 (21), 65 (20), 64 (25), 63 (16), 57 (11), 51 (14), 43 (57). Found: C, 70.98; H, 5.24; N, 7.16%. Calcd for $C_{23}H_{20}N_2O_4$: C, 71.12; H, 5.19; N, 7.21%.

4-(*N'-t*-Butylureido)-3,5,5-trimethyl-2(5*H*)-furanone (6l). Mp 200.5—201 °C. ^{1}H NMR ($CDCl_3$–DMSO-d_6 1:1) δ=1.35 (s, 9H), 1.54 (s, 6H), 1.81 (s, 3H), 6.28 (br s, 1H), 7.85 (br s, 1H). IR (KBr) 3400, 3325, 3210, 3080, 3020, 2960, 1775, 1765, 1720, 1610, 1595, 1500, 1470, 1450, 1410, 1370, 1330, 1295, 1190, 1115, 1085, 890, 865, 845, 780, 740, 710 cm^{-1}. MS *m/z* (rel intensity) 241 (M^++1, 1), 240 (M^+, 2), 142 (9), 141 (100), 126 (80), 123 (10), 98 (23), 84 (10), 58 (28), 57 (74), 55 (12), 43 (20), 42 (12), 41 (33). Found: C, 59.99; H, 8.38; N, 11.43%. Calcd for $C_{12}H_{20}N_2O_3$: C, 59.98; H, 8.39; N, 11.66%.

4-(*N'-t*-Butylureido)-5,5-dimethyl-3-phenyl-2(5*H*)-furanone (6o). Mp 201—201.5 °C. ^{1}H NMR ($CDCl_3$–DMSO-d_6 5:1) δ=1.27 (s, 9H), 1.78 (s, 6H), 6.58 (br s, 1H), 7.23—7.53 (m, 5H), 8.28 (br s, 1H). IR (KBr) 3400, 3230, 3140, 3000, 1745, 1730, 1680, 1645, 1605, 1535, 1515, 1455, 1395, 1370, 1350, 1320, 1290, 1230, 1210, 1195, 1150, 1080, 1035, 1015, 970, 960, 930, 790, 780, 750, 705 cm^{-1}. MS *m/z* (rel intensity) 303 (M^++1, 1), 302 (M^+, 3), 229 (10), 204 (15), 203 (100), 188 (27), 186 (12), 160 (41), 158 (15), 130 (11), 117 (13), 115 (14), 89 (22), 77 (5), 58 (30), 57 (39), 43 (49). Found: C, 67.42; H, 7.40; N, 9.16%. Calcd for $C_{17}H_{22}N_2O_3$: C, 67.52; H, 7.33; H, 9.27%.

4-(*N'-t*-Butylureido)-5,5-dimethyl-3-phenylsulfinyl-2(5*H*)-furanone (6q). Mp 179.5—180 °C. ^{1}H NMR ($CDCl_3$–DMSO-d_6 10:1) δ=1.36 (s, 9H), 1.74 and 1.78 (2s, 6H), 6.19 (br s, 1H), 7.47—7.60 (m, 3H), 7.76-7.93 (m, 2H), 9.95 (br s, 1H). IR (KBr) 3330, 3250, 3120, 3070, 3000, 2950, 1750 (sh), 1725, 1615, 1540, 1480, 1445, 1395, 1365, 1275, 1220, 1155, 1040, 995, 930, 920, 790, 770, 760, 695 cm^{-1}. MS *m/z* (rel intensity) 351 (M^++1, 0.2), 350 (M^+, 0.4), 229 (17), 203 (66), 188 (13), 186 (15), 160 (20), 125 (14), 109 (15), 95 (11), 94 (12), 86 (12), 84 (36), 78 (23), 77 (40), 68 (14), 65 (14), 58 (100), 57 (38), 56 (15), 53 (12), 52 (12), 51 (48), 50 (15), 45 (48), 43 (94). Found: C, 58.29; H, 6.38; N, 7.96; S, 8.96%. Calcd for $C_{17}H_{22}N_2O_4S$: C, 58.27; H, 6.33; N, 7.99; S, 9.15%.

2,4,4-Trimethoxybutanenitrile (8). Boron trifluoride etherate (0.15 ml, 1.2 mmol) was added to a mixture of 1,1,3,3-tetramethoxypropane (1.65 g, 10 mmol) and trimethylsilyl cyanide (1.35 ml, 10 mmol) at 0 °C and the mixture was stirred at 0 °C for 3 h. GLC assay (PEG 20 M, 10%, 3 m, 180 °C) showed a single new peak. Dilution with dichloromethane, treatment with sat. sodium hydrogencarbonate aq solution, extraction with dichloromethane (4 times), drying over magnesium sulfate, followed by concentration gave **8** (1.63 g, 99% yield) as a colorless oil. Bp 70—73 °C/15 Torr. ^{1}H NMR ($CDCl_3$) δ=2.10 (t, *J*=6 Hz, 2H), 3.34 (s, 6H), 3.47 (s, 3H), 4.15 (t, *J*=6 Hz, 1 H), 4.54 (t, *J*=6 Hz, 1H). IR (neat) 3400, 2950, 2850, 2250, 1460, 1390, 1370, 1335, 1190, 1120, 1065, 1020, 980, 920, 900, 800, 605 cm^{-1}. MS *m/z* (rel intensity) 158 (M^+−1, 1), 128 (M^+−OMe, 37), 98 (11), 96 (27), 75 (100), 71 (5), 70 (89), 47 (17), 45 (17). Found: C, 52.52; H, 8.12; N, 8.85%. Calcd for $C_7H_{13}NO_3$: C, 52.81; H, 8.23; N, 8.80%.

2-Acetoxy-2,4,4-trimethoxybutanenitrile (10). A mixture of **8** (0.62 g, 3.9 mmol), *N*-bromosuccinimide (NBS) (0.76 g, 4.3 mmol), azobis(isobutyronitrile) (7 mg, 0.043 mmol) and benzene (15 ml) was heated gradually over 10 min to 90 °C and stirred for 30 min at 90 °C. The reaction mixture was diluted with hexane, and the insoluble material was filtered off through a Celite pad. Concentration gave **9** (0.87 g, 93% yield) as a pale yellow oil which exhibited ^{1}H NMR ($CDCl_3$) δ=2.76 (d, *J*=5.6 Hz, 2H), 3.40 (s, 3H), 3.41 (s, 3H), 3.70 (s, 3H), 4.73 (t, *J*=5.6 Hz, 1H), and IR (neat) 2250 cm^{-1}.

Without purification, this was employed for the next reaction. Silver acetate (0.60 g, 3.6 mmol) was added to an acetonitrile (13 ml) solution of **9** (0.87 g, 3.6 mmol) at 0 °C, and the mixture was stirred at 0 °C for 40 min. Filtration through a Celite pad followed by concentration and distillation gave **10** (0.62 g, 79% yield) as a colorless oil. Bp 110—114 °C/0.65 Torr. ^{1}H NMR ($CDCl_3$) δ=2.12 (s, 3H), 2.53 (d, *J*=6 Hz, 2H), 3.33 (s, 3H), 3.35 (s, 3H), 3.62 (s, 3H), 4.68 (t, *J*=6 Hz, 1H). IR (neat) 3025, 2975, 2860, 2260, 1760, 1735 (sh), 1450, 1375, 1235, 1200, 1120, 1075, 1015, 950, 840 cm^{-1}. MS *m/z* (rel intensity) 186 (M^+−OMe, 2), 142 (3), 126 (38), 117 (4), 112 (7), 103 (4), 100 (6), 85 (5), 75 (99), 70 (9), 58 (5), 47 (12), 43 (100). Found: C, 49.09; H, 6.87; N, 6.28%. Calcd for

$C_9H_{15}NO_5$: C, 49.09; H, 6.96; N, 6.34%.

4-Amino-5-(2,2-dimethoxyethyl)-5-methoxy-2(5*H*)-furanone (11). Lithium diisopropylamide (4.6 mmol in THF (2 ml) and hexane (2.8 ml)) was added to a mixture of diethylaluminium chloride (2.2 M hexane solution, 2.2 ml, 4.7 mmol) and THF (1 ml) at 0 °C, and the resulting solution was stirred for 1 h then cooled to −78 °C. To this base solution was added **10** (0.100 g, 0.46 mmol) dissolved in THF (1.5 ml) over 5 min. After 1.2 h, the starting material was all consumed. Quenching was effected by addition of sat. ammonium chloride aq solution (0.2 ml) at −78 °C. The mixture was warmed to room temperature, dried over magnesium sulfate, charged on the top of a short silica-gel column (Wakogel C-100, 1 cm) and eluted with methanol-dichloromethane (1 : 10). Concentration followed by prepartive TLC (dichloromethane-methanol 10 : 1) gave **12** (68 mg, 68% yield). R_f= 0.48 (CH_2Cl_2-MeOH 10 : 1). Mp 109—111 °C (colorless plates). ^{1}H NMR ($CDCl_3$) δ=2.28 (d, J=5.7 Hz, 2H), 3.23 (s, 3H), 3.32 (s, 3H), 3.37 (s, 3H), 4.63 (t, J=5.5 Hz, 1H), 4.88 (s, 1H), 5.27 (br, 2H). IR (neat) 3370, 3220, 2950, 2850, 1735, 1660, 1610, 1440, 1410, 1390, 1370, 1290, 1210, 1190, 1165, 1115, 1070, 1000, 915, 795, 730 cm^{-1}. MS m/z (rel intensity) 217 (M^+, 2), 185 (28), 155 (22), 154 (23), 128 (63), 100 (49), 75 (100). Found: m/z 217.0968. Calcd for $C_9H_{15}NO_5$: M^+ 217.0950.

4-Amino-5-methoxy-5-(2-oxoethyl)-2(5*H*)-furanone (12). Hexamethyldisilazane (0.29 ml, 1.39 mmol) and then boron tribromide (1.0 M dichloromethane solution, 1.38 ml, 1.38 mmol) were added successively to a dichloromethane (12 ml) solution of **11** (0.100 g, 0.46 mmol) at −23 °C (CCl_4-Dry Ice bath). The mixture was stirred at −23 °C for 2 h and neutralized with sat. sodium hydrogencarbonate aq solution (1 ml) at −23 °C. Concentration under reduced pressure gave a solid material which was charged on TLC plate with the aid of a solvent mixture of dichloromethane-methanol (10 : 1). Development with the same solvent mixture afforded **12** (45 mg, 56% yield). R_f=0.27 (CH_2Cl_2-MeOH 10 : 1). ^{1}H NMR ($CDCl_3$) δ=2.92 (dd, J=1.97 and 5.27 Hz, 2H), 3.21 (s, 3H), 4.87 (s, 1H), 5.28 (br, 2H), 9.67 (t, J=2.0 Hz, 1H). MS m/z (rel intensity) 171 (M^+, 8), 143 (9), 140 (M^+—OMe, 12), 129 (19), 128 (35), 115 (30), 112 (27), 111 (20), 101 (37), 100 (47), 83 (7), 71 (10), 70 (16), 69 (31), 68 (57), 59 (6), 58 (4), 57 (9), 55 (5), 44 (6), 43 (42). Found: m/z 171.0552. Calcd for $C_7H_9NO_4$: M^+ 171.0530.

2,2-Diethoxy-3-butynenitrile (13). Tin(II) chloride (0.162 g, 0.85 mmol) was added to a mixture of 3,3,3-triethoxypropyne (1.72 g, 10 mmol) and trimethylsilyl cyanide (1.50 ml, 11.2 mmol) at 0 °C under a nitrogen atmosphere, and the whole was stirred at room temperature for 30 min before dilution with ether (20 ml). The mixture was washed with brine, dried over magnesium sulfate and concentrated. Distillation gave **13** (1.08 g, 71% yield). Bp 75—80 °C (bath temperature)/5 Torr. ^{1}H NMR ($CDCl_3$) δ=1.30 (t, J=7.5 Hz, 6H), 2.80 (s, 1H), 3.80 (q, J=7.5 Hz, 4H). IR (neat) 3300, 3000, 2960, 2920, 2250, 2140, 1485, 1445, 1400, 1180, 1120, 1105, 1085, 1050, 885, 680 cm^{-1}. MS m/z (rel intensity) 108 (M^+—OEt, 72), 80 (100), 53 (65), 45 (15). Found: C, 62.41; H, 7.29; N, 9.06%. Calcd for $C_8H_{11}NO_2$: C, 62.72; H, 7.24; N, 9.14%.

***t*-Butyl 3-Amino-4,4-diethoxy-2-hexen-5-ynoate (14).** Magnesium amide base was prepared by addition of ethylmagnesium bromide (2.0 M ethereal solution, 10 ml, 20 mmol) to diisopropylamine (5.6 ml, 40 mmol) in ether (15 ml) and aged at 0 °C for 1.5 h. To this base solution *t*-butyl acetate (1.30 ml, 20 mmol) was added drop by drop over 5 min, and the mixture was stirred at 0 °C for 30 min. An ethereal solution (15 ml) of **13** (0.77 g, 5.0 mmol) was added over a period of 5 min, and the reaction mixture was stirred for 30 min. Quenching with sat. ammonium chloride aq solution (20 ml), extraction with ether (30 ml×3), washing the ethereal extract with brine, drying over magnesium sulfate, concentration, followed by distillation, gave **14** (1.14 g, 85% yield) as a pale yellow oil. Bp 115—120 °C (bath temperature)/0.15 Torr. ^{1}H NMR ($CDCl_3$) δ=1.23 (t, J=7.5 Hz, 6H), 1.48 (s, 9H), 2.60 (s, 1H), 3.63 (q, J=7.5 Hz, 4H), 5.05 (s, 1H), 6.45 (br, 2H, NH_2). IR (neat) 3525, 3360, 3300, 3000, 2950, 2910, 2130, 1675, 1625, 1555, 1455, 1395, 1370, 1290, 1255, 1155, 1130, 1100, 1080, 1050, 980, 805, 670 cm^{-1}. MS m/z (rel intensity) 269 (M^+, 3), 225 (19), 224 (23), 196 (15), 170 (11), 169 (100), 168 (27), 140 (43), 127 (34), 53 (26), 51 (16), 44 (19), 43 (17), 41 (37). Found: m/z 269.1616. Calcd for $C_{14}H_{23}NO_4$: M^+ 269.1625.

Hexacarbonyl(*t*-butyl 3-amino-4,4-diethoxy-2-hexen-5-ynoate)dicobalt (15). A pentane (50 ml) solution of **14** (0.84 g, 3.1 mmol) was added to a pentane (20 ml) solution of octacarbonyldicobalt(0) (1.06 g, 3.1 mmol) at 0 °C. The reaction mixture was warmed to room temperature over a period of 1 h, and the solvent was evaporated at ambient temperature by passing nitrogen gas. The residue was purified by column chromatography on silica gel to give **15** (1.33 g, 81% yield) as a red viscous oil. R_f=0.47 (hexane-ethyl acetate 5 : 1). ^{1}H NMR ($CDCl_3$) δ=1.21 (t, J=7.5 Hz, 6H), 1.45 (s, 9H), 3.63 (q, J=7.5 Hz, 4H), 4.88 (s, 1H), 6.13 (s, 1H). IR (neat) 3525, 3350, 3100, 3000, 2950, 2900, 2110, 2070, 2040, 1670, 1620, 1545, 1500, 1455, 1390, 1365, 1285, 1255, 1155, 1120, 1090, 1050, 980, 920, 805, 635, 580, 520, 500, 450 cm^{-1}. MS m/z (rel intensity) 527 (M^+—CO, 2), 499 (3), 471 (4), 443 (3), 415 (6), 387 (6), 359 (2), 343 (3), 331 (4), 225 (4), 224 (3), 169 (29), 149 (26), 140 (28) 122 (40), 59 (100). Found: C, 42.98; H, 4.29; N, 2.47%. Calcd for $C_{20}H_{23}NO_{10}Co_2$: C, 43.28; H, 4.40; N, 2.66%.

Hexacarbonyl(4-amino-5-ethoxy-5-ethynyl-2(5*H*)-furanone)-dicobalt (16). Trifluoroacetic acid (3.0 ml) was added to **15** (0.187 g, 0.34 mmol) at 0 °C and stirred for 30 min at 0 °C before evaporation of the trifluoroacetic acid in vacuo. Preparative TLC of the residue (hexane-ethyl acetate 1 : 1) gave **16** as red viscous oil (0.110 g, 77% yield). R_f=0.44 (hexane-ethyl acetate 1 : 1). ^{1}H NMR ($CDCl_3$) δ=1.20 (t, J=7.5 Hz, 3H), 3.40—3.80 (m, 2H), 4.90 (s, 1H), 5.00 (br, 2H), 6.08 (s, 1H). IR (neat) 3500, 3425 (sh), 3360, 3300 (sh), 3250 (sh), 3220, 3000, 2960, 2920, 2120, 2075, 2040, 1740, 1650, 1610, 1530, 1395, 1280, 1210, 1130, 1035, 985, 925, 800, 750, 630, 610, 520, 500, 450 cm^{-1}. MS m/z (rel intensity) 425 (M^+—CO, 2), 397 (4), 369 (3), 341 (7), 313 (5), 286 (6), 167 (8), 149 (7), 125 (6), 103 (5), 96 (5), 75 (4), 73 (5), 70 (5), 69 (6), 61 (6), 46 (21), 45 (51), 44 (11), 43 (23), 31 (58), 28 (100). Found: C, 37.18; H, 2.03; N, 2.89%. Calcd for $C_{14}H_9O_9Co_2N$: C, 37.10; H, 2.00; N, 3.09%.

4-Amino-5-ethoxy-5-ethynyl-2(5*H*)-furanone (17). Cerium-(IV) ammonium nitrate (0.68 g) was added portionwise to an acetone (5.0 ml) solution of **16** (47 mg, 0.11 mmol) at −78 °C under an argon atmosphere, and the reaction mixture was stirred at −78 °C for 2 h. The solvent was evaporated in vacuo, and the residue was treated with ethyl acetate (30 ml) and water (30 ml). Separation of the organic extract, drying the organic layer over sodium sulfate, concentration, followed by preparative TLC (hexane-ethyl acetate 1 : 1) gave

17 (15 mg, 83% yield). Mp 113—114 °C. R_f=0.30 (hexane-ethyl acetate 1 : 1) gave **17** (15 mg, 83% yield). Mp 113—114 °C, R_f=0.30 (hexane-ethyl acetate 1 : 1). ^{1}H NMR ($CDCl_3$) δ=1.27 (t, J=7.5 Hz, 3 H), 2.73 (s, 1H), 3.65—4.05 (m, 2H), 4.85 (s, 1H), 4.95 (br, 2H, NH_2). IR (KBr) 3420, 3350, 3300, 3275, 3220, 3000, 2925, 2130, 1735, 1660, 1610, 1490, 1410, 1400, 1280, 1210, 1130, 1100, 1040, 980, 920, 890, 790, 700, 610, 590 cm^{-1}. MS m/z (rel intensity) 167 (M^+, 13), 123 (28), 122 (98), 95 (15), 94 (12), 71 (17), 69 (58), 68 (21), 53 (38), 51 (24), 44 (26), 41 (75). Found: m/z 167.0580. Calcd for $C_8H_9NO_3$: M^+ 167.0581.

References

1) a) T. Hiyama and K. Kobayashi, *Tetrahedron Lett.*, **23**, 1597 (1982).; b) S. M. Hannick and Y. Kishi, *J. Org. Chem.*, **48**, 3833 (1983).

2) T. Hiyama, K. Kobayashi, and K. Nishide, preceding article.

3) K. Kobayashi and T. Hiyama, *Tetrahedron Lett.*, **24**, 3509 (1983).

4) K. Kobayashi and H. Suginome, 50th National Meeting of the Chemical Society of Japan, Tokyo, April 1985, Abstr., No. 2O01.

5) a) P. E. Aldrich, Japan Kokai Tokkyo Koho 77-139056 [*Chem. Abstr.*, **88**, 169947s (1978)]; b) B. I. Dittmar and W. A. Price, Jr., Ger. Patent 2516555; Japan Kokai Tokkyo Koho 75-148352 [*Chem. Abstr.*, **84**, 74087q (1976)].

6) P. Gerike, U.S. Patent Re 27894 [*Chem. Abstr.*, **80**, P82435j (1974)].

7) Preliminary report has appeared in T. Hiyama, H. Oishi, and H. Saimoto, *Tetrahedron Lett.*, **26**, 2459 (1985).

8) H. Iinuma, H. Nakamura, H. Naganawa, T. Masuda, S. Takano, T. Takeuchi, H. Umezawa, Y. Iitaka, and A. Obayashi, *J. Antibiot.*, **1983**, 448.

9) Similar base-promoted ringclosure of α-acetoxyalkanoic esters: a) BrMgN(i-Pr)$_2$: L. J. Haynes and A. H. Stanners, *J. Chem. Soc.*, **1956**, 4103; b) LiN(i-Pr)$_2$: R. E. Ireland and W. J. Thompson, *J. Org. Chem.*, **44**, 3041 (1979); c) LiN($SiMe_3$)$_2$: S. Brandänge, L. Flodman, and A. Norberg, *J. Org. Chem.*, **49**, 927 (1984).

10) D. A. Evans, G. L. Carroll, and J. K. Truesdale, *J. Org. Chem.*, **39**, 914 (1974).

11) T. Hiyama, M. Inoue, and K. Saito, *Synthesis*, **1986**, 645.

12) Nickel effect is observed in the reaction of benzoyl cyanide with β-diketones: M. Basato, B. Corain, M. Cofler, A. C. Veronese, and G. Zanotti, *J. Chem. Soc., Chem. Commun.*, **1984**, 1593.

13) K. Utimoto, Y. Wakabayashi, Y. Shishiyama, M. Inoue, and H. Nozaki, *Tetrahedron Lett.*, **22**, 4279 (1981).

14) L. Stella, Z. Janousek, R, Merényi, and H. G. Viehe, *Angew. Chem., Int. Ed. Engl.*, **17**, 691 (1978); H. G. Viehe, R. Merényi, L. Stella, and Z. Janousek, *ibid.*, **18**, 917 (1979).

15) H. Stetter and W. Uerdingen, *Synthesis*, **1973**, 207; H. Saimoto, M. Shinoda, S. Matsubara, K. Oshima, T. Hiyama, and H. Nozaki, *Bull. Chem. Soc. Jpn.*, **56**, 3088 (1983).

16) M. Saha and K. M. Nicholas, *J. Org. Chem.*, **49**, 417 (1984); S. Padmanabhan and K. M. Nicholas, *Tetrahedron Lett.*, **24**, 2239 (1983).

17) The in vitro test was carried out by Ms. Kaoru Yamada of our Institute. We are indebted to her greatly.

18) L. J. Haynes and J. R. Plimmer, *Quart. Rev.*, **1960**, 292; A. S. Wengel, T. Reffstrup, and P. M. Boll, *Tetrahedron*, **35**, 2181 (1979); P. J. Jerrils, P. M. Wovkulich, and A. B. Smith, III, *Tetrahedron Lett.*, **1979**, 4517; J. E. Wrobel and B. Ganem, *J. Org. Chem.*, **48**, 3761 (1983).

 © 1987 The Chemical Society of Japan Bull. Chem. Soc. Jpn., 60, 2151—2161 (1987)

An Enantiospecific Synthesis of the C-21–C-37 Segment of the Aglycon of Amphotericin B†

Mitsuhiro KINOSHITA,* Hitoshi TAKAMI, Masato TANIGUCHI, and Tetsuro TAMAI
Department of Applied Chemistry, Faculty of Science and Technology, Keio University, Hiyoshi, Kohoku-ku, Yokohama 223
(Received December 17, 1986)

3-Deoxy-1,2-*O*-isopropylidene-3-*C*-methyl-α-D-allofuranose was stereoselectively converted into 3,5-dideoxy-4-*O*-(methoxymethyl)-3,5-di-*C*-methyl-6-*O*-pivaloyl-L-talose ethylene dithioacetal (**31**) via 3,5-dideoxy-4-*O*-(methoxymethyl)-3,5-di-*C*-methyl-L-talopyranuro-6,2-lactone ethylene dithioacetal (**24**) in 10 steps (23.6% overall yield). Desulfurization [Raney Ni W-4, 92% yield] of **31** followed by three-step transformation (91% yield) afforded 2,4,6-trideoxy-5-*O*-(diethylisopropylsilyl)-3-*O*-(methoxymethyl)-2,4-di-*C*-methyl-L-altrose, which was olefinated by using methyl (2*E*,4*E*)-6-(dimethoxyphosphinyl)-2,4-hexadienoate twice to give the target compound, all-*trans*-hexaenal **4** (12 steps, 38.6% overall yield from **31**).

Amphotericin B (**1**),[1] produced by *Streptomyces nodosus*, is the only member of the polyene antibiotic group which is widely used for treatment of the "deep seated" systemic fungal infections and the only polyene macrolide whose absolute structure is firmly established by X-ray crystallographic analysis.[2] Though the extremely difficult problem to isolate the free type of aglycon **2** from natural amphotericin B still remains unsolved, many synthetic approaches toward construction of such aglycon molecule have so far been reported.[3] The preparation in a protected

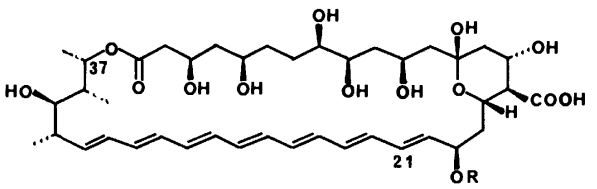

1, R = 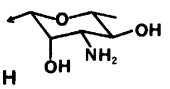

2, R = H

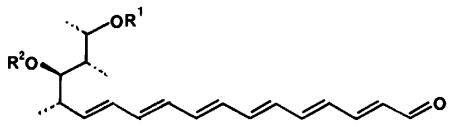

3a R¹ = TES, R² = TBS
3b R¹ = MEM, R² = TBS
3c R¹ = H, R² = TBS
4 R¹ = H, R² = MOM

TBS = *t*-Bu-Si(Me)(Me)-, TES = Et_3Si-, MEM = $MeOCH_2CH_2OCH_2$-
MOM = $MeOCH_2$-

form of **2** (or its C-13 epimer) from naturally derived C-1–C-20 and C-21–C-37 segments has recently been announced by Nicolaou et al.[4] As can be seen in some of these synthetic approaches, the C-21–C-37 segments **3a**,[3l] **3b**,[3m] and **3c**[4] have already been enantiospecifically synthesized from chiral carbon sources other than carbohydrates. In our studies directed toward the total synthesis of amphotericin B (**1**), general plan for synthesis of the free aglycon **2** which was considered to be a synthetic precursor of **1**, required **4** as the C-21–C-37 synthetic segment of **2** (Scheme 1). This strategic segment was expected to be synthesized enantiospecifically from carbohydrate. In this paper, we wish to describe a synthesis of **4** from D-glucose.

The synthetic plan as broadly outlined in Scheme 1 was devised by considering that the key intermediate **B** (whose absolute stereochemistry at C-2, C-3, and C-4 correlates to that at C-17, C-16, and C-15, respectively, of **4**) is obtainable from the known sugar derivative **5**,[5] and the formation of a new chiral center (corresponding to C-14, the last asymmetric carbon atom in **4**) on C-5 of **B** should be possible by asymmetric conversion[6] of **5** into **A** which is a precursor of **B**. The synthetic route to **C** via the lactone **B** from **A** should be indispensable for the regioselective *O*-methoxymethylation toward the C-3 hydroxyl group of C. The successful pursuit of the basic elements of this synthetic plan forms the topic of this report.

The starting diol **5**,[5] which was obtainable in large scale from 1,2:5,6-di-*O*-isopropylidene-α-D-glucofuranose in 41% yield, was acetylated with acetic anhydride and triethylamine in dichloromethane to afford an 85% yield of a ca. 10:1 mixture of the monoacetates **6a** and **6b**, and a 6.4% yield of the diacetate **6c** after chromatographic isolation through a

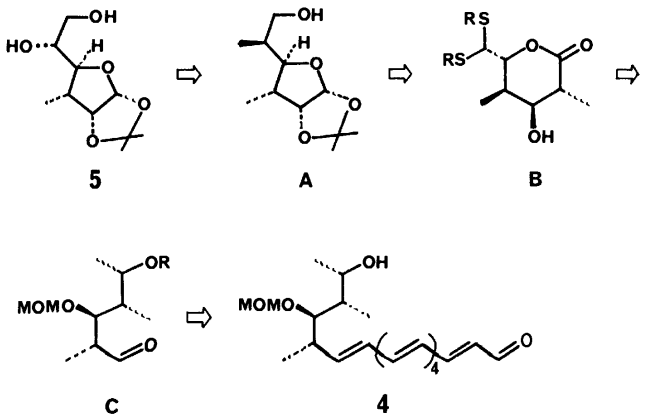

5 **A** **B**

C **4**

Scheme 1.

† A part of this paper was read at the 52nd National Meeting of the Chemical Society of Japan, Kyoto, April 1986, Abstr., No. 4N06.

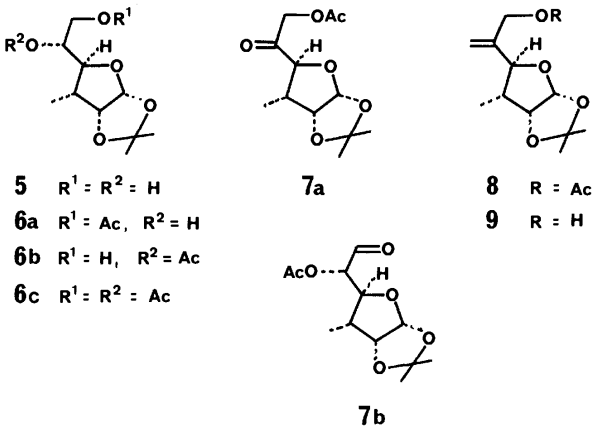

short silica-gel column. Since the preparative separation of the desired acetate **6a** from the minor regioisomer **6b** by column chromatography was impracticable, the mixture was directly oxidized with pyridinium chlorochromate (PCC) and molecular sieves 3A powder[7] to give the chromatographically separable ketone **7a** and the aldehyde **7b** in 87.9 and 8.9% yields, respectively. Wittig methylenation[8] of **7a** with methylenetriphenylphosphorane in ether afforded a 71.5% yield of **8** and 5.4% yield of **9**. Treatment of **8** with methanolic sodium hydroxide provided **9** in 97% yield; the total yield of **9** from **5** amounted to 55.8%. Homogeneous hydrogenation of **9** with 0.2 molar equivalents of tris(triphenylphosphine)chlororhodium (I) in benzene gave a 2.3 : 1 mixture of **10a** and **10b** in 95% yield. Because the preparative separation of **10a**

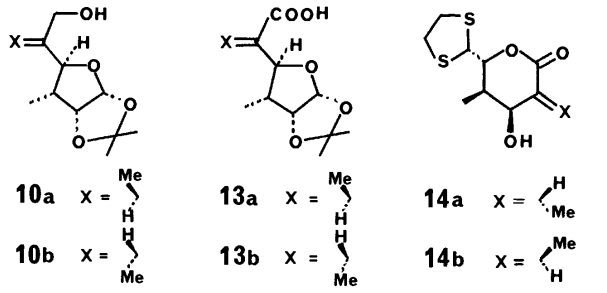

from its epimer **10b** was not practicable in this stage, the separation had to be carried over to the later synthetic step. The isomeric ratio was assumed based on the intensities of the double-doublet signals due to the H-4 protons at δ 3.91 (**10a**) and δ 3.72 (**10b**) in the 250 MHz ^{1}H NMR spectrum of the mixture. The configuration at C-5 of the isolated major isomer **10a** was assigned as (*S*) by the following fashions: (a) The product **10a** was converted into **11** in four steps (Scheme 2). The ^{1}H NMR spectrum of **11** showed

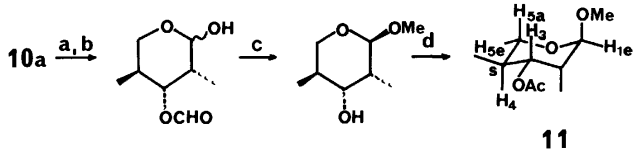

Scheme 2.[a]

a) (a) 1 M HCl, rt, 5 h, 91%; (b) $NaIO_4$, 1 : 1 Me_2CO–H_2O, rt, 1 h, ca. 100%; (c) 0.15 M HCl–MeOH, rt, 1 h, α-anomer (68%); (d) Ac_2O, DMAP, py, rt, 1 h, 97%.

signals in line with the depicted structure with 4(*S*) configuration (see Experimental section). (b) The compound **11** proved to be identical spectroscopically and chromatographically with an authentic sample of **11** which was derived from the known sugar derivative **12**[9] by the sequence of reactions shown in Scheme 3.

The low stereoselectivity (**10a** : **10b**=2.3 : 1) in the hydrogenation of **9** may suggest that the difference in free energy between the possible transition states **I** and **II** (Scheme 4) corresponding to **10a** and **10b** should be very small. This result prompted us to examine the homogeneous hydrogenation of the 1,6-anhydro-derivative **15** whose rigid conformation in the ground state may be similar to that in the transition state **I**. The compound **15** could be obtained by exposure of **9** to 50% aqueous trifluoroacetic acid[6b] in 13% yield. Though direct hydrogenation of **15** could not be accomplished, its silyl ether **16** was smoothly hydrogenated with rhodium catalyst to afford **17** as a sole reduction product, which was identical with a sample of **17** derived from **10a** via **18**. This highly stereoselective hydrogenation process, however, could not be utilized in the asymmetric conversion of **9** into **B**(**14a**), because of the low yield of **15** and of undesired elongation of the synthetic route by this process.

Chromium trioxide oxidation[10] of the mixture of **10a** and **10b** provided in 98.5% yield a mixture of the carboxylic acids **13a** and **13b**, which were quite difficult to separate each other. Dithioacetalization of the mixture with 1,2-ethanedithiol and boron trifluoride etherate afforded the chromatographically separable epimeric lactones **14a** and **14b** in 46.9 and 23.4% yields, respectively. The major lactone **14a** proved to correspond to **10a** by transformation of the isolated **10a** into **14a**.

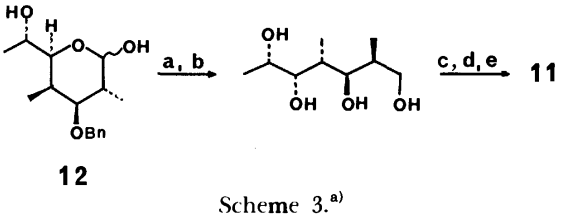

Scheme 3.[a]

a) (a) H_2/Pd, MeOH; (b) $NaBH_4$, H_2O, rt, 1 h; (c) $NaIO_4$, 1 : 1 Me_2CO–H_2O, rt, 0.5 h; (d) 0.15 M HCl–MeOH, rt, 15 min, α:β=10 : 1; (e) Ac_2O, Py, rt.

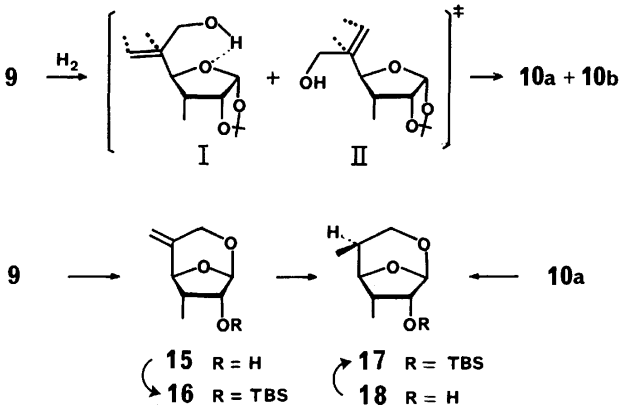

Scheme 4.

Direct desulfurization of the thioacetal group of **14a** with Raney Ni W-4 in methanol yielded only a 20% yield of **19**. Therefore, the first route to **21** via **20** from **14a** was not practicable (Scheme 5). The second route to **21** from **14a** was successful as follows. Reduction of **14a** with diisobutylaluminium hydride (DIBAL) followed by selective *t*-butyldimethylsilylation gave α-**22** (α-anomer) and β-**22** (β-anomer) in 34.8 and 43.5% yields, respectively. Desulfurization of α-**22** and β-**22** with Raney Ni W-4 in methanol afforded smoothly the corresponding α-**23** and β-**23** in 89.8 and 85.1% yields. Methoxymethylation of α-**23** and β-**23** followed by desilylation gave **21** in 96 and 99% yields, respectively. In the third route to **21**, methoxymethylation of **14a** afforded in 98% yield **24** which was treated with DIBAL to give **25** in good yield. However, desulfurization of **25** provided **21** in unsatisfactory yield (44%). The desulfurization reactions of **14a**, **22**, and **25** were carried out with irradiation in the water bath of an ultrasound laboratory cleaner. The TLC inspection of the reaction mixtures showed that, in all cases, no starting material could be detected in the supernatant layer after ultrasonic irradiation for 0.5—1 h, while at that time, only the spot of desulfurized product was observed. The precipitated nickel residue was thoroughly extracted with methanol in twenty times to provide an additional amount of product in almost pure state. The reason the desulfurizations of **14a** and **25** resulted in low yields is now indefinable.

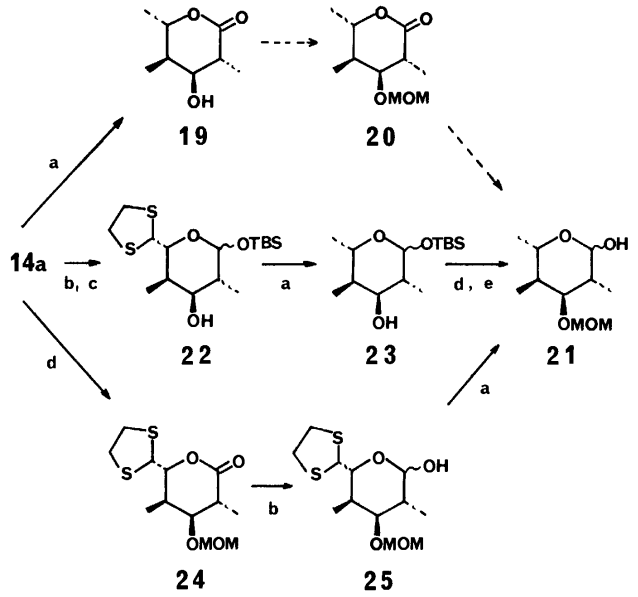

Scheme 5.[a]

a) (a) Raney Ni W-4, MeOH; (b) DIBAL, PhMe, −78°C; (c) TBSCl, imidazole, DMF; (d) MOMCL, *i*-Pr$_2$NEt, DMF; (e) *n*-Bu$_4$NF, THF.

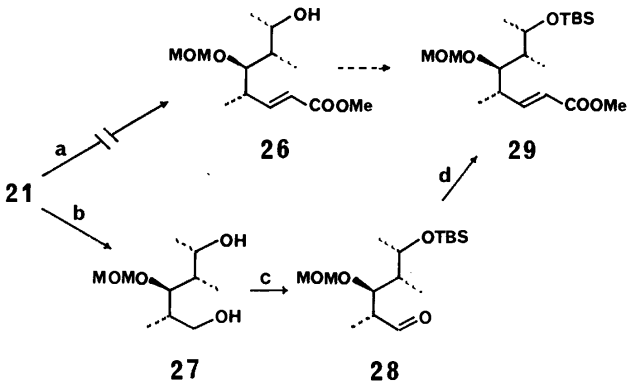

Scheme 6.[a]

a) (a) Ph_3P=CHCOOMe, PhMe, 90°C, 24 h, (b) $NaBH_4$, 2:1 MeOH–H_2O, rt, 0.5 h, ca. 100%; (c) (1) *t*-BuCOCl, py, rt, 20 h, 69%; (2) TBSCl, imidazole, DMF, 35°C, 1 h, 99%; (3) MeLi, ether, rt, 0.5 h, 92%; (4) $(COCl)_2$, CH_2Cl_2, DMSO (−60°C), Et_3N (−25°C), 98%; (d) Ph_3P=CHCOOMe, PhMe, 90°C, 1 h, 90%.

Having thus prepared the hemiacetal **21** which contains entire chiral sequence of **4** in the proper absolute configuration, we turned our attention to the facile transformation of **21** into **4**. The first attempt to convert **21** through direct Wittig olefination into a model intermediate **29** failed, because the condensation of **21** and (methoxycarbonylmethylene)triphenylphosphorane (or trimethyl phosphonoacetate) afforded no desired product **26**. The compound **29**, therefore, had to be prepared from **21** via the diol **27** and the free aldehyde **28** (Scheme 6). The overall yield of **28** from **14a** was 40.9%.

In keeping with these experimental results, the last and more facile synthetic route to **35** (equivalent to **28**) from **24** was pursued (Scheme 7). Lithium aluminium hydride reduction of **24** afforded the alcohol **30** in almost quantitative yield, which was selectively 6-*O*-pivaloylated to give **31** in 96.5% yield. Desulfurization of **31** with Raney Ni W-4 in methanol yielded **32** in 91.6% yield. *O*-Silylation of **32** with diethylisopropylsilyl chloride[11] in the presence of imidazole followed by depivaloylation of the resulting **33** with methyllithium in ether, afforded **34** in almost quantitative yield, which was subjected to Swern oxidation[12] to give the aldehyde **35** in 92% yield. The overall yield of **35** from

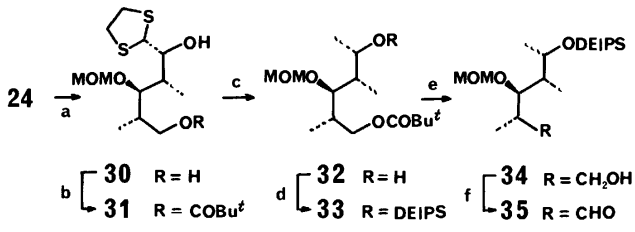

Scheme 7.[a]

a) (a) $LiAlH_4$, THF, rt, 1 h; (b) *t*-BuCOCl, Py, rt, 3 h; (c) Raney Ni W-4, MeOH, 0.5 h; (d) DEIPSCl, imidazole, DMF, rt, 0.5 h; (e) MeLi, ether, rt, 0.5 h; (f) $(COCl)_2$, CH_2Cl_2, DMSO, Et_3N.

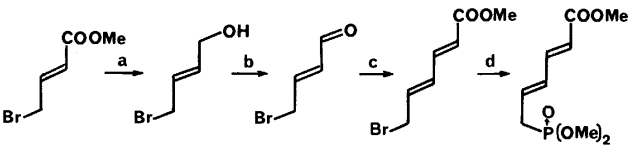

Scheme 8.[a]

a) (a) DIBAL, PhMe, −78°C, 0.5 h, ca. 100%; (b) MnO_2, CH_2Cl_2, rt, 1 h, 88%; (c) Ph_3P=CHCOOMe, PhMe, 90°C, 2 h, 70.5%; (d) $(MeO)_3P$, 120—130°C, 3 h, 88%.

14a was 79.2%.

Having effectively arrived at the key intermediate **35**, the task remained to complete a synthesis of **4** was effective elaboration of **35** to all-*trans*-hexaenal **49**. After many unsuccessful attempts, the effective construction of **49** from **35** was achieved by the repeated Wittig-type olefination procedure using methyl (2*E*,4*E*)-6-(dimethoxyphosphinyl)-2,4-hexadienoate (**40**). The preparation of **3c** by the similar olefination procedure using ethyl (2*E*,4*E*)-6-(diethoxyphosphinyl)-2,4-hexadienoate instead of **40**, have recently been reported by Nicolaou et al.[4] after our work had been completed.

A facile preparation of the reagent **40** starting from methyl 4-bromocrotonate (**36**) was first accomplished as detailed in Scheme 8. Condensation of **35** with the lithio derivative of **40** which was prepared by treatment of **40** with lithium diisopropylamide(LDA) in THF afforded a 1:2 mixture of the (2*E*,4*E*,6*E*)-trienoic ester **41** and its (6*Z*)-isomer **42** in 99.7% yield. The mixture was then isomerized[13] with 0.01 molar equivalent of iodine in dichloromethane to give a ca. 8:1 mixture of **41** and **42** in almost quantitative yield. Reduction of this mixture with DIBAL followed by oxidation of the resulting mixture of the allylic alcohol **43** and its (6*Z*)-isomer **44** with manganese dioxide, afforded after chromatographic isomeric separation, the (2*E*,4*E*,6*E*)-trienal **45** and its (6*Z*)-isomer **46** in 70 and 13% overall yields from **35**, respectively. The olefinic structures of **41**, **42**, **45**, and **46** were confirmed by ^{1}H NMR spectroscopy. It is noteworthy that the iodine-catalyzed isomerization of **46** to **45** is not practicable, because the reaction proceeds with considerable decomposition of both **45** and **46**.

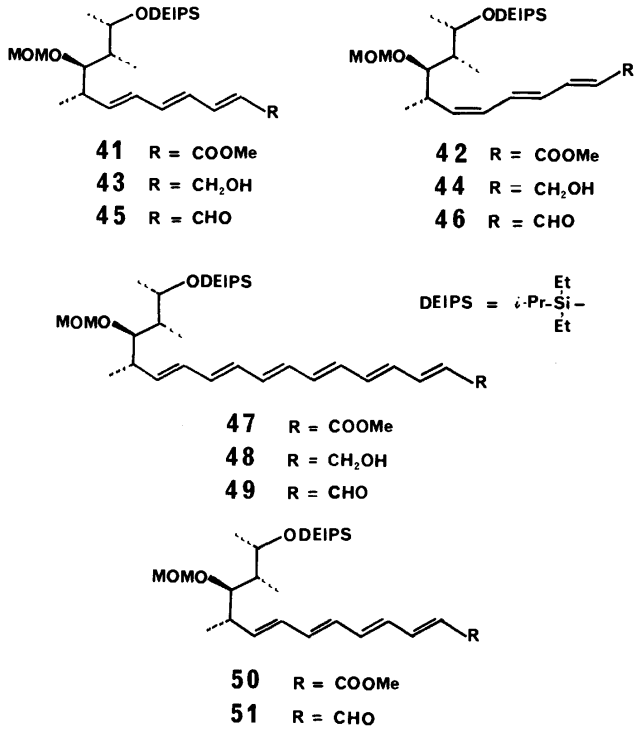

The isolated **45** was again coupled with lithium derivative of **40** to give the pure all-*trans*-hexaenoic ester **47** in 96.2% yield as the only detectable product. DIBAL reduction of **47** followed by manganese dioxide oxidation of the resulting allylic alcohol **48** afforded the all-*trans*-hexaenal **49** in 73.5% overall yield. Finally, exposure of **49** to a 1M[††] solution of tetrabutylammonium fluoride in THF led to **4** in 96.8% yield. The *O*-diethylisopropylsilyl protecting group in **49** could be removed more smoothly than the *O*-*t*-butyldimethylsilyl group. The structures of **49** and **4** were confirmed[14] by their 250 MHz ^{1}H NMR spectra.

Experimental

Melting points were determined on a micro hot-stage Yanaco MP-S3 and were uncorrected. IR spectra were recorded on a Hitachi Perkin-Elmer 225 spectrometer, UV spectra on a JAS·CO UVIDEC-1 spectrometer, and ^{1}H NMR spectra in $CDCl_3$ using TMS as the internal standard on either a Varian EM-390 or a Bruker WM 250 spectrometer. Optical rotations were measured on a JAS·CO DIP-360 photoelectric polarimeter in chloroform. TLC was carried out on Merck TLC plates (60F-254, 0.25 mm). Column chromatography was performed on silica gel, Wakogel C-200 and Merck Kieselgel 60 (230—400 mesh) for "Flash Chromatography." In general, organic solvents were purified and dried by the appropriate procedure, and evaporation and concentration were carried out under reduced pressure below 30 °C, unless otherwise noted.

Acetylation of Diol 5. A mixture of **5**[5] (10.1 g, 46.4 mmol), acetic anhydride (5.30 ml, 55.6 mmol), and triethylamine (7.80 ml, 55.6 mmol) in dichloromethane (101 ml) was stirred at room temperature for 4 h, after which period ethanol (3.30 ml) was added and stirring was continued for 0.5 h. The reaction mixture was then evaporated and the residue was coevaporated with ether to a yellow syrup (18.3 g), which was chromatographed on silica gel (600 g) with 2:1 toluene-ethyl acetate to afford a mixture of **6a** and **6b** (10.2 g, 85%) and **6c** (0.90 g, 6.4%) as syrups. The mixture of **6a** and **6b** was used for the next step without further purification. Pure samples of **6a** (0.27 g) and **6b** (0.02 g) were obtained from a sample of the mixture (0.42 g) by flash chromatography on silica gel (42 g) with 2:3 toluene-ethyl acetate.

6a: R_f=0.36 (1:1 toluene-ethyl acetate); $[\alpha]_D^{27}$ +32° (*c* 1.00); IR($CHCl_3$) 1740 and 1230 cm^{-1}; ^{1}H NMR (90 MHz) δ=1.17 (3H, d, 3-Me, *J*=6.6 Hz), 1.36 and 1.53 (each 3H, each s, CMe_2), 1.7—2.0 (1H, m, H-3), 2.12 (3H, s, OAc), 2.53 (1H, d, OH, *J*=3.9 Hz), 3.8—4.3 (4H, m, H-4,5, 2×H-6), 4.57 (1H, t, H-2, *J*=3.9 Hz), and 5.78 (1H, d, H-1, *J*=3.9 Hz).

Found: C, 55.23; H, 7.71%. Calcd for $C_{12}H_{20}O_6$: C, 55.37; H, 7.74%.

6b: R_f=0.33 (1:1 toluene-ethyl acetate); ^{1}H NMR(90 MHz) δ=1.13 (3H, d, 3-Me, *J*=6.6 Hz), 1.33 and 1.51 (each 3H, each s, CMe_2), 2.12 (3H, s, OAc), 1.8—2.4 (2H, m, H-3, OH), 3.8—4.1 (3H, m, H-4 and 2×H-6), 4.55 (1H, t, H-2, *J*=4.5 Hz), 4.8—5.1 (1H, m, H-5), and 5.79 (1H, d, H-1, *J*=4.5 Hz).

6c: R_f=0.67 (1:1 toluene-ethyl acetate); $[\alpha]_D^{17}$ +53° (*c* 0.99); IR ($CHCl_3$) 1740 and 1230 cm^{-1}; ^{1}H NMR (90 MHz) δ=1.12 (3H, d, 3-Me, *J*=6.0 Hz), 1.31 and 1.50 (each 3H, each s, CMe_2), 1.7—2.0 (1H, m, H-3), 2.03 and 2.08 (each 3H, each s, 2×OAc), 3.91 (1H, dd, H-4, *J*=5.1 and 9.6 Hz), 4.20 (1H,

[††] 1 M=1 mol dm^{-3}.

dd, H-6, J=7.2, 12.0 Hz), 4.43 (1H, dd, H-6′, J=4.2, 12.0 Hz), 4.53 (1H, t, H-2, J=4.2 Hz), 5.1—5.3 (1H, m, H-5), and 5.75 (1H, d, H-1, J=4.2 Hz).

Found: C, 55.36; H, 7.30%. Calcd for $C_{14}H_{22}O_7$: C, 55.62; H, 7.33%.

6-*O*-Acetyl-3-deoxy-1,2-*O*-isopropylidene-3-*C*-methyl-α-D-*ribo*-5-hexulofuranose (7a) and 5-*O*-Acetyl-3-deoxy-1,2-*O*-isopropylidene-3-*C*-methyl-α-D-allodialdo-1,4-furanose (7b). To a stirred mixture of PCC (22.3 g, 0.10 mol), molecular sieves 3A powder (34.5 g), and dichloromethane (86 ml) was added a solution of the mixture of **6a** and **6b** (8.98 g, 34.5 mmol) in dichloromethane (50 ml) at room temperature over a period of 15 min. After being stirred at room temperature for 1 h, the reaction mixture was diluted with ether (140 ml) and filtered through a column filled with silica gel (230 g). Evaporation of the eluates left a syrupy residue (8.90 g) which was chromatographed on silica gel (600 g) with 2:1 toluene-ethyl acetate to afford **7a** (7.83 g, 87.9%) and **7b** (0.75 g, 8.4%).

7a: Colorless plates, mp 72—74 °C (ethyl acetate-hexane); R_f=0.66 (3:2 toluene-ethyl acetate); $[\alpha]_D^{27}$ −40° (c 1.01); IR (KBr) 1760, 1730, and 1240 cm^{-1}; ^{1}H NMR (90 MHz) δ=1.19 (3H, d, 3-Me, J=6.6 Hz), 1.35 and 1.51 (each 3H, each s, CMe_2), 2.16 (3H, s, OAc), 2.0—2.4 (1H, m, H-3), 4.20 (1H, d, H-4, J=10.8 Hz), 4.58 (1H, t, H-2, J=3.3 Hz), 4.77 and 5.07 (2H, ABq, 2×H-6, J=18.0 Hz), and 5.90 (1H, d, H-1, J=3.3 Hz).

Found: C, 55.52; H, 6.91%. Calcd for $C_{12}H_{18}O_6$: C, 55.81; H, 7.02%.

7b: Pale yellow syrup, R_f=0.46 (3:2 toluene-ethyl acetate); ^{1}H NMR (90 MHz) δ=1.11 (3H, d, 3-Me, J=6.9 Hz), 1.33 and 1.54 (each 3H, each s, CMe_2), 2.21 (3H, s, OAc), 1.9—2.5 (1H, m, H-3), 4.14 (1H, dd, H-4, J=3.6, 11.1 Hz), 4.53 (1H, t, H-2, J=4.5 Hz), 5.05 (1H, d-like, H-5), 5.72 (1H, d, H-1, J=4.5 Hz), and 9.53 (0.4H, s-like, CHO).

6-*O*-Acetyl-3,5-dideoxy-1,2-*O*-isopropylidene-3-*C*-methyl-5-*C*-methylene-α-D-*ribo*-hexofuranose (8) and 3,5-Dideoxy-1,2-*O*-isopropylidene-3-*C*-methyl-5-*C*-methylene-α-D-*ribo*-hexofuranose (9). A 4 M solution of methylsulfinylmethanide anion in DMSO (9.87 ml, 39.5 mmol) prepared from sodium hydride and DMSO,[8] was added dropwise to a stirred suspension of methyltriphenylphosphonium bromide (14.1 g, 39.5 mmol) in dry ether (188 ml) under argon at room temperature. The mixture was stirred at room temperature for 10 min and then to the resulting yellow suspension of ylide was added dropwise a solution of **7a** (4.08 g, 15.8 mmol) in dry ether (94 ml). After the mixture had been stirred at room temperature for 0.5 h, the reaction mixture was poured into an ice-water mixture, which was extracted with ether (3×250 ml). The organic layer was washed with saturated aqueous NaCl, dried, and evaporated. The residue (8.71 g) was chromatographed on silica gel (600 g) with 3:1 hexane-ethyl acetate to afford **8** (2.89 g, 71.5%) and **9** (0.22 g, 5.4%).

8: R_f=0.57 (3:2 hexane-ethyl acetate); IR ($CHCl_3$) 3010, 1740, 1210, and 1020 cm^{-1}; $[\alpha]_D^{25}$ +17° (c 0.99); ^{1}H NMR (90 MHz) δ=1.05 (3H, d, 3-Me, J=7.2 Hz), 1.34 and 1.52 (each 3H, each s, CMe_2), 2.07 (3H, s, OAc), 1.8—2.1 (1H, m, H-3), 4.20 (1H, d, H-4, J=10.8 Hz), 4.53 (1H, t, H-2, J=4.2 Hz), 4.60 (2H, s, 2×H-6), 5.2—5.3 (2H, m, =CH_2), and 5.77 (1H, d, H-1, J=4.2 Hz).

Found: C, 60.65; H, 7.63%. Calcd for $C_{13}H_{20}O_5$: C, 60.92; H, 7.87%.

Preparation of 9 from 8. To a solution of **8** (2.71 g, 10.6 mmol) in methanol (32 ml) was added a solution of NaOH (0.64 g) in methanol (16 ml), and stirred at room temperature for 1 h. After being neutralized (pH 7) with CO_2 gas, the reaction mixture was diluted with water (30 ml), and extracted with chloroform (3×30 ml). The organic layers were washed with a saturated aqueous NaCl solution, dried, and evaporated. The residue (2.62 g) was chromatographed on silica gel (150 g) with 3:2 hexane-ethyl acetate to afford **9** (2.20 g, 97%) as a syrup.

9: R_f=0.28 (3:2 hexane-ethyl acetate); $[\alpha]_D^{27}$ +7.5° (c 0.99); IR ($CHCl_3$) 3510, 3010, and 1020 cm^{-1}; ^{1}H NMR (90 MHz) δ=1.04 (3H, d, 3-Me, J=6.6 Hz), 1.35 and 1.54 (each 3H, each s, CMe_2), 1.8—2.3 (2H, m, H-3, OH), 4.1—4.4 (3H, m, H-4, 2×H-6), 4.60 (1H, t, H-2, J=4.2 Hz), 5.16 and 5.27 (each 1H, each s, =CH_2), and 5.84 (1H, d, H-1, J=4.2 Hz).

Found: C, 61.80; H, 8.24%. Calcd for $C_{11}H_{18}O_4$: C, 61.66; H, 8.47%.

3,5-Dideoxy-1,2-*O*-isopropylidene-3,5-di-*C*-methyl-α-L-talofuranose (10a) and D-allo Epimer (10b). A solution of **9** (2.30 g, 10.7 mmol) and tris(triphenylphosphine)chlororhodium(I) (1.99 g, 2.15 mmol) in benzene (115 ml) was stirred under an atmospheric pressure of hydrogen at room temperature for 4 h. The reaction mixture was then evaporated and the residue was passed through Florisil (100—200 mesh, 160 g) with ether to afford a pale yellow syrup after evaporation of the solvent, a mixture of **10a** and **10b** (2.20 g, 95%). This sample was utilized without further purification in the subsequent transformation. Part of this syrup was flash chromatographed on silica gel with 1:1 hexane-ethyl acetate to give pure **10a** and **10b**.

10a: R_f=0.49 (1:1 hexane-ethyl acetate); $[\alpha]_D^{26}$ +45° (c 0.54); ^{1}H NMR (90 MHz) δ=0.90 and 1.04 (each 3H, each d, 3 and 5-Me, J=6.9 and 7.2 Hz), 1.32 and 1.49 (each 3H, each s, CMe_2), 1.7—2.0 (2H, m, H-3, 5), 2.52 (1H, br-s, OH), 3.64 (2H, d, after addition of D_2O, 2×H-6, J=6.0 Hz), 3.91 (1H, dd, H-4, $J_{4,5}$=2.4, $J_{4,3}$=9.9 Hz), 4.51 (1H, t, H-2, $J_{2,1}$=$J_{2,3}$=3.6 Hz), and 5.72 (1H, d, H-1).

Found: C, 60.90; H, 9.17%. Calcd for $C_{11}H_{20}O_4$: C, 61.09; C, 9.32%.

10b: R_f=0.47 (1:1 hexane-ethyl acetate); $[\alpha]_D^{27}$ +12° (c 1.00); ^{1}H NMR (90 MHz) δ=1.06 and 1.10 (each 3H, each d, 3 and 5-Me, J=7.2, 6.9 Hz), 1.33 and 1.51 (each 3H, each s, CMe_2), 1.7—2.1 (2H, m, H-3,5), 2.5—2.7 (1H, m, OH), 3.63 (2H, d, 2×H-6, J=4.8 Hz), 3.72 (1H, dd, H-4, $J_{4,5}$=5.1, $J_{4,3}$=9.9 Hz), 4.54 (1H, t, H-2, $J_{2,1}$=$J_{2,3}$=3.9 Hz), and 5.76 (1H, d, H-1).

Found: C, 61.17; H, 9.15%. Calcd for $C_{11}H_{20}O_4$: C, 61.09; H, 9.32%.

Methyl 3-*O*-Acetyl-2,4-dideoxy-2,4-di-*C*-methyl-α-L-lyxopyranoside (11). (A) From **12**: A solution of **12**[9] (70.8 mg) in methanol (1.4 ml) was stirred with Pd-black under bubbling with H_2 gas at 25 °C for 2.5 h, and the suspension was filtered. The filtrate was evaporated to a colorless syrup (52 mg) of debenzylation product, which was treated with $NaBH_4$ (10 mg) in water (0.52 ml) at room temperature for 1 h. The reaction mixture was neutralized with CO_2 gas and evaporated. The residue was chromatographed on silica gel (5 g) with 3:1 chloroform-methanol to afford the crystalline tetrol (30.5 mg). To a solution of the tetrol (30.5 mg) in acetone (0.61 ml) was added a solution of $NaIO_4$ (32.4 mg) in water (0.72 ml) and the mixture allowed to stand at room temperature for 0.5 h. The mixture was extracted with

chloroform three times and then with ethyl acetate seven times. The combined extracts were dried and evaporated to give crude crystals of 2,4-dideoxy-2,4-di-*C*-methyl-L-lyxose (31 mg). A solution of the crystals (24.7 mg) in a 0.15M methanolic hydrogen chloride (0.49 ml) was allowed to stand at room temperature for 15 min. The reaction mixture was neutralized with saturated aqueous $NaHCO_3$, concentrated, and extracted with ethyl acetate. The dried extracts were evaporated to a syrup which was chromatographed on silica gel (2.7 g) with 8:1 benzene-acetone to afford the major anomer of methyl 2,4-dideoxy-2,4-di-*C*-methyl-L-lyxopyranoside [R_f=0.28 (8:1 benzene-acetone), 10.1 mg] and the minor anomer [R_f=0.37 (8:1 benzene-acetone), 0.9 mg]. The major anomer (9 mg) was acetylated with Ac_2O in dry pyridine and worked up by the usual way to give a crude syrup of **11**, which was chromatographed on silica gel (1 g) with 3:1 hexane-ethyl acetate to afford a pure sample of **11**: Colorless syrup, R_f=0.81 (1:1 hexane-ethyl acetate); $[\alpha]_D^{26}$ −35° (*c* 0.65); ^{1}H NMR (250 MHz) δ=0.85 and 0.97 (each 3H, each d, 2- and 4-Me, J=6.6 and 6.9 Hz), 1.9—2.3 (2H, m, H-2,4), 2.06 (3H, s, OAc), 3.36 (3H, s, OMe), 3.46 (1H, dd, H-5a, $J_{5a,4}$=10.0, $J_{5a,5e}$=11.5 Hz), 3.61 (1H, dd, H-5e, $J_{5e,4}$=5.0 Hz), 4.45 (1H, d, H-1, $J_{1,2}$=2.7 Hz), and 4.95 (1H, dd, H-3, $J_{2,3}$=4.8, $J_{3,4}$=9.0 Hz). (B) From **10a**: A solution of **10a** (166 mg) in 1M hydrochloric acid (1.7 ml) was allowed to stand at room temperature for 5 h. The reaction mixture was neutralized with saturated aqueous $NaHCO_3$, diluted with acetone, and evaporated. The residue was chromatographed on silica gel (17 g) with 5:1 chloroform-methanol to afford 3,5-dideoxy-3,5-di-*C*-methyl-L-idofuranose (123 mg, 91.2%). To a solution of the free sugar (19.2 mg) in acetone (0.38 ml) was added a solution of $NaIO_4$ (35 mg) in water (0.35 ml) and the mixture was stirred at room temperature for 1 h. The reaction mixture was extracted with ethyl acetate (3×2 ml). The extracts were washed with saturated aqueous NaCl, dried, and evaporated to a syrup (21.3 mg). The syrup (19.0 mg) was dissolved in 0.15M methanolic HCl (0.38 ml) and the solution was allowed to stand at room temperature for 1 h. The reaction mixture was neutralized (pH 8) with saturated aqueous $NaHCO_3$ and evaporated. The residue was taken with ethyl acetate (2.0 ml), which was washed with saturated aqueous NaCl, dried, and evaporated to a pale yellow syrup (30 mg). This syrup was chromatographed on silica gel (2.0 g) with 8:1 benzene-acetone to afford two syrupy anomers of methyl 2,4-dideoxy-2,4-di-*C*-methyl-L-lyxopyranoside: Major anomer [R_f=0.28 (8:1 benzene-acetone)], 11.9 mg; minor anomer [R_f=0.37 (8:1 benzene-acetone)], 5.3 mg. The major anomer (8.6 mg) was acetylated with Ac_2O (6.1 µl), DMAP (0.66 mg) in dry pyridine (86 µl) at room temperature for 1 h, and worked-up to afford a syrup which was chromatographed on silica gel (1 g) with 3:1 hexane-ethyl acetate to give a colorless syrup of **11** (10.5 mg); R_f=0.81 (1:1 hexane-ethyl acetate). This sample was identical in all respects with the sample of **11** described in (A).

1,6-Anhydro-3,5-dideoxy-3-*C*-methyl-5-*C*-methylene-β-D-*ribo*-hexofuranose (15). A solution of **9** (24.1 mg) in 50% aqueous trifluoroacetic acid (TFA)(0.24 ml) was kept at room temperature for 50 h and then neutralized with Amberlite IRA-45 resin. The resin was filtered and washed with methanol (3×5.0 ml). The combined filtrates were evaporated and the residue was chromatographed on silica gel (1.8 g) with 1:1 benzene-ethyl acetate to afford **15** (2.2 mg, 13%): mp 219—224 °C; R_f=0.40 (1:1 benzene-ethyl acetate); $[\alpha]_D^{25}$ −84° (*c* 0.39); ^{1}H NMR (90 MHz) δ=1.00 (3H, d, 3-Me, J=6.6 Hz), 1.58 (1H, br-s, OH), 2.5—2.8 (1H, m, H-3), 3.70 (1H, d, H-6, $J_{6,6'}$=9.0 Hz), 4.02 (1H, d, H-4, $J_{4,3}$=4.2 Hz), 4.35 (1H, d, H-6′), 4.90 (1H, d, H-2, $J_{2,3}$=9.3 Hz), 4.91 (1H, s, H-1), and 5.07 and 5.25 (each 1H, each s, $=CH_2$).

2-*O*-*t*-Butyldimethylsilyl Derivative (16). To a stirred solution of **15** (5.0 mg) in DMF (50 µl) was added imidazole (8.7 mg) and TBSCl (14.5 mg) at 0 °C. After being stirred at room temperature for 2 h, the reaction mixture was poured into cold water, which was extracted with ethyl acetate (3×1.0 ml). The extracts were washed with saturated aqueous NaCl, dried, and evaporated to a syrup (24.1 mg), which was chromatographed on silica gel (0.9 g) with 2:1 hexane-ethyl acetate to give colorless needles of **16** (8.3 mg, 95.8%): mp 139—144 °C; R_f=0.56 (20:1 benzene-ethyl acetate); $[\alpha]_D^{26}$ −29° (*c* 0.40); ^{1}H NMR (90 MHz) δ=0.8—1.0 (12H, m, *t*-Bu, 3-Me), 2.4—2.7 (1H, m, H-3), 3.63 (1H, d, H-6, $J_{6,6'}$=9.3 Hz), 3.93 (1H, d, H-4, $J_{4,3}$=3.9 Hz), 4.31 (1H, d, H-6′), 4.73 (1H, s, H-1), 4.84 (1H, d, H-2, $J_{2,3}$=9.6 Hz), and 5.03 and 5.20 (each 1H, each s, $=CH_2$).

1,6-Anhydro-3,5-dideoxy-3,5-di-*C*-methyl-α-L-talofuranose (18) and Its 2-*O*-*t*-Butyldimethylsilyl Derivative (17). A solution of **10a** (33.2 mg) in 75% aqueous TFA (0.33 ml) was kept at room temperature for 1 h. The reaction mixture was poured into saturated aqueous $NaHCO_3$ containing solid $NaHCO_3$. The mixture (pH=8) was saturated with NaCl and extracted with ethyl acetate. The extracts were dried and evaporated to a syrup which was chromatographed on silica gel (1.2 g) with 1:1 benzene-ethyl acetate to afford **18** (18.5 mg, 76.2%) as a colorless syrup; ^{1}H NMR (90 MHz) δ=0.70 (3H, d, 5-Me, J=6.9 Hz), 1.11 (3H, d, 3-Me, J=7.2 Hz), 1.62 (1H, br-s, OH), 2.2—2.5 (2H, m, H-3, 5), 3.25 (1H, dd, H-6, $J_{5,6}$=$J_{6,6'}$=10.8 Hz), 3.81 (1H, dd, H-6′, $J_{5,6'}$=6.3 Hz), 3.8—4.0 (1H, m, H-4), 4.37 (1H, d, H-2, $J_{2,3}$=7.5 Hz), and 5.15 (1H, s, H-1).

By the procedure described for the silylation of **15**, **18** (8.0 mg) obtained above was silylated to give **17** (11.6 mg, 84.4%) as a colorless syrup; R_f=0.47 (20:1 benzene-ethyl acetate); $[\alpha]_D^{27}$ −9.5° (*c* 0.37); ^{1}H NMR (90 MHz) δ=0.68 (3H, d, 5-Me, J=6.6 Hz), 0.91 (9H, s, *t*-Bu), 1.04 (3H, d, 3-Me, J=7.8 Hz), 2.1—2.5 (2H, m, H-3, 5), 3.24 (1H, dd, H-6, $J_{5,6}$=$J_{6,6'}$=11.7 Hz), 3.79 (1H, dd, H-6′, $J_{5,6'}$=6.3 Hz), 3.8—4.0 (1H, m, H-4), 4.35 (1H, d, H-2, $J_{2,3}$=7.2 Hz), and 5.03 (1H, s, H-1).

Homogeneous Hydrogenation of 16. By the procedure described for hydrogenation of **9**, **16** (4.5 mg) was hydrogenated with $(Ph_3P)_3RhCl$ (3.1 mg), to afford **17** (3.2 mg, 70.6%) after silica-gel column chromatography, by which no isomeric product was detected in the reduction product. The product **17** was identical with the sample of **17** derived from **10a** via **18** by TLC and ^{1}H NMR.

3,5-Dideoxy-1,2-*O*-isopropylidene-3,5-di-*C*-methyl-L-talofuranuronic Acid (13a) and D-allo Epimer (13b). Chromium trioxide (5.0 g, 49.9 mmol) was dissolved in a 30:1 mixture of acetic acid and pyridine (155 ml). This chromium oxidation reagent (142 ml, 45.8 mmol) was added to the aforesaid mixture of **10a** and **10b** (1.65 g, 7.63 mmol). After being stirred at room temperature for 15 h, the reaction mixture was poured into cold water (300 ml) which was extracted with chloroform (3×200 ml). The extracts were washed with saturated aqueous NaCl, dried, and evaporated. The residue was co-evaporated with ether repeatedly to a

syrup (2.60 g), which was chromatographed on silica gel (200 g) with 150:5:1 chloroform-methanol-acetic acid to afford a mixture of **13a** and **13b** (1.73 g, 98.5%). Analytical samples of **13a** and **13b** were obtained from pure samples of **10a** and **10b** by the procedure described above.

13a: Colorless syrup, R_f=0.53 (100:10:1 chloroform-methanol-acetic acid) $[\alpha]_D^{31}$ +18° (*c* 0.58); IR ($CHCl_3$) 3080 and 1710 cm^{-1}; ^1H NMR (90 MHz) δ=1.09 and 1.22 (each 3H, each d, 3 and 5-Me, *J*=7.2 and 7.8 Hz), 1.34 and 1.53 (each 3H, each s, CMe_2), 1.7—2.1 (1H, m, H-3), 2.5—2.7 (1H, m, H-5), 4.10 (1H, dd, H-4, *J*=5.4, 10.5 Hz), 4.54 (1H, t, H-2, *J*=3.6 Hz), 5.76 (1H, d, H-1, *J*=3.6 Hz), and 9.67 (1H, br-s, COOH).

Found: C, 57.12; H, 7.77%. Calcd for $C_{11}H_{18}O_5$: C, 57.38; H, 7.88%.

13b: Colorless needles, R_f=0.53 (100:10:1 chloroform-methanol-acetic acid); mp 110—114 °C (ethyl acetate-hexane); $[\alpha]_D^{30}$ +43° (*c* 0.84); IR(KBr) 3200 and 1730 cm^{-1}; ^1H NMR (90 MHz) δ=1.11 and 1.29 (each 3H, each d, 3-and 5-Me, *J*=7.2 and 7.8 Hz), 1.34 and 1.53 (each 3H, each s, CMe_2), 1.9—2.3 (1H, m, H-3), 2.6—2.9 (1H, m, H-5), 4.00 (1H, dd, H-4, *J*=4.5, 9.6 Hz), 4.57 (1H, t, H-2, *J*=3.6 Hz), 5.80 (1H, d, H-1, *J*=3.6 Hz), and 10.2 (1H, br-s, COOH).

Found: C, 57.28; H, 7.69%. Calcd for $C_{11}H_{18}O_5$: C, 57.38; H, 7.88%.

3,5-Dideoxy-3,5-di-*C*-methyl-L-talopyranurono-6,2-lactone Ethylene Dithioacetal (14a) and D-allo Epimer (14b). To an ice-cooled solution of a mixture of **13a** and **13b** (1.96 g, 8.51 mmol) in 1,2-ethaneditiol (19.6 ml) was added boron trifluoride etherate (0.59 ml) and the mixture was stirred at room temperature for 1 h. The reaction mixture was neutralized (pH 7) with 10% aqueous K_2CO_3, and extracted with ethyl acetate (3×50 ml). The extracts were washed with saturated aqueous NaCl, dried, and evaporated. The residue was chromatographed on silica gel (100 g) with 1:1 benzene-ethyl acetate to afford the mixture of **14a** and **14b** (1.52 g, 71.9%). The mixture was separated by flash chromatography on silica gel (200 g) with 3:2 benzene-ethyl acetate to give **14a** (0.87 g, 46.9%) and **14b** (0.49 g, 23.4%).

14a: Colorless plates, mp 113—114 °C (ethyl acetate-hexane); R_f=0.43 (1:1 hexane-ethyl acetate); $[\alpha]_D^{30}$ −42° (*c* 0.51); IR (KBr) 3400, 1700, and 1210 cm^{-1}; ^1H NMR (90 MHz) δ=1.13 and 1.36 (each 3H, each d, 3-and 5-Me, each *J*=6.9 Hz), 1.9—2.3 (1H, m, H-3), 2.72 (1H, dq, H-5, *J*=3.3 and 6.9 Hz), 2.73 (1H, br-s, OH), 3.1—3.7 (4H, m, SCH_2CH_2S), 3.76 (1H, t after addition of D_2O, H-4, *J*=3.0 Hz), 4.51 (1H, dd, H-2, $J_{2,1}$=1.8, $J_{2,3}$=9.0 Hz), and 4.73 (1H, d, H-1).

Found: C, 48.34; H, 6.50%. Calcd for $C_{10}H_{16}O_3S_2$: C, 48.36; H, 6.49%.

14b: Colorless needles, mp 115—119 °C (ethyl acetate-hexane); R_f=0.49 (1:1 hexane-ethyl acetate) $[\alpha]_D^{25}$ −36° (*c* 1.01); IR (KBr) 3460, 1710, and 1200 cm^{-1}; ^1H NMR (90 MHz) δ=1.17 and 1.33 (each 3H, each d, 3- and 5-Me, each *J*=6.9 Hz), 1.8—2.2 (1H, m, H-3), 2.23 (1H, br-s, OH), 2.63 (1H, dq, H-5, *J*=2.4 and 7.2 Hz), 3.0—3.6 (4H, m, SCH_2CH_2S), 3.83 (1H, br-s, H-4), 4.52 (1H, dd, H-2, $J_{2,1}$=1.8, $J_{2,3}$=10.2 Hz), and 4.74 (1H, d, H-1).

Found: C, 48.06; H, 6.40%. Calcd for $C_{10}H_{16}O_3S_2$: C, 48.36; H, 6.49%.

2,4,6-Trideoxy-3-*O*-(methoxymethyl)-2,4-di-*C*-methyl-L-altropyranose (21). To a cooled (−78 °C) solution of **14a** (171 mg, 0.689 mmol) in dry toluene (1.7 ml) was added a 1M solution of DIBAL in toluene (1.38 ml, 1.38 mmol) and stirred at −78 °C for 0.5 h. A 50% aqueous acetic acid solution (0.28 ml) was added to the reaction mixture which was stirred at −78 °C for 5 min and then warmed to room temperature. The mixture was filtered through a Celite and washed with acetone (3×5.0 ml). The organic layer was evaporated to afford a colorless syrup (175 mg). A mixture of this syrup (57.6 mg), TBSCl (52.0 mg), imidazole (31.3 mg), and dry DMF (0.58 ml) was stirred at room temperature for 3 h, and the mixture was poured into cold water, which was extracted with ethyl acetate (3×3.0 ml). The extracts were washed with saturated aqueous NaCl, dried, and evaporated to a syrup, which was chromatographed on silica gel (8.5 g) with 7:1 hexane-ethyl acetate to **α-22** (α-anomer, 29.2 mg), **β-22** (β-anomer, 36.5 mg), and di-*O*-TBS derivative (18.6 mg). A suspension of Raney Ni W-4 (0.3 g) in a solution of **α-22** (44.8 mg) in methanol (1.1 ml) was irradiated in the water bath of an ultrasound laboratory cleaner (65W, 48KHz) for 1 h. The supernatant layer was separated and the precipitate was extracted with methanol (20×0.5 ml). The combined extracts were evaporated to a colorless syrup (48 mg), which was chromatographed on silica gel (2.4 g) with 7:1 hexane-ethyl acetate to afford **α-23** (30.3 mg, 89.8%) as a colorless syrup. By the same way, **β-23** (31.6 mg, 81.1%) was obtained from **β-22** (49.3 mg). A mixture of **α-23** (31.8 mg), methoxymethyl chloride (70.4 μl), *N*,*N*-diisopropylethylamine (242 μl), and DMF (0.32 ml) was stirred at 50 °C for 6 h. The reaction mixture was poured into cold water, which was extracted with ethyl acetate (3×2.0 ml). The extracts were worked up to give a brown syrup, which was chromatographed on silica gel (2.6 g) with 6:1 hexane-ethyl acetate to afford the 3-*O*-methoxymethyl derivative of **α-23** (35.4 mg, 95.8%). By the same way, the corresponding β-anomer (30.1 mg, 98.6%) was obtained from **β-23** (26.3 mg). The combined α- and β-anomeric 3-*O*-methoxymethyl derivatives (65.1 mg) were treated with 2 equivalents of n-Bu_4NF in THF, and worked up to a syrup, which was chromatographed on silica gel (3.3 g) with 1:1 benzene-ethyl acetate to afford **21** (39 mg): Colorless syrup, ^1H NMR (90 MHz) δ=0.8—1.3 (9H, m, 3×Me), 1.5—1.9 (1H, m, H-4), 2.0—2.3 (1H, m, H-2), 3.40 (0.8H, s, β-OMe), 3.44 (2.2H, s, α-OMe), 3.5—3.7 (1H, m, H-3), 3.8—4.0 (0.3H, m, β-OH), 3.8—4.1 (1H, m, H-5), 4.59 and 4.74 (0.7H, ABq, OCH_2O (β), *J*=6.9 Hz), 4.63 and 4.77 (1.3H, ABq, OCH_2O (α), *J*=6.3 Hz), 4.84 (0.7H, d, H-1(α), *J*=9.9 Hz), 5.06 (0.7H, d, α-OH, *J*=9.9 Hz), and 5.1—5.3 (0.3H, m, H-1(β)).

3,5-Dideoxy-4-*O*-(methoxymethyl)-3,5-di-*C*-methyl-L-talopyranurono-6,2-lactone Ethylene Dithioacetal (24). To a solution of **14a** (248 mg, 0.99 mmol) in DMF (2.50 ml) was added *N*,*N*-diisopropylethylamine (0.87 ml, 4.99 mmol) and methoxymethyl chloride (0.30 ml, 3.99 mmol) at 0 °C. After being stirred at 60 °C for 10 h, the reaction mixture was poured into an ice-water mixture, which was extracted with ethyl acetate (3×5 ml). The extracts were washed with saturated aqueous NaCl, dried, and evaporated to a syrup (520 mg), which was chromatographed on silica gel (11 g) with 2:1 benzene-ethyl acetate to afford **24** (271 mg, 98.3%) as a colorless syrup: R_f=0.72 (1:1 benzene-ethyl aceta); $[\alpha]_D^{27}$ −25.9° (*c* 0.99); IR ($CHCl_3$) 1725 and 1030 cm^{-1}; ^1H NMR (90 MHz) δ=1.11 (3H, d, 3-Me, *J*=6.9 Hz), 1.34 (3H, d, 5-Me, *J*=7.5 Hz), 1.9—2.3 (1H, m, H-3), 2.84 (1H, dq, H-5, *J*=3.3, 7.5 Hz), 3.1—3.6 (4H, m, SCH_2CH_2S), 3.35 (3H, s, OMe), 3.59 (1H, t, H-4, *J*=3.3 Hz), 4.43 (1H, dd, H-2, *J*=2.1, 9.3 Hz), and 4.6—4.8 (3H, m, H-1, OCH_2O).

Found: C, 49.03; H, 6.87%. Calcd for $C_{12}H_{20}O_4S_2$: C, 49.29, H, 6.89%.

3,5-Dideoxy-4-*O*-(methoxymethyl)-3,5-di-*C*-methyl-L-talose Ethylene Dithioacetal (30). To a solution of **24** (288 mg, 1.04 mmol) in dry THF (4.30 ml) was added lithium aluminium hydride (790 mg, 2.08 mmol) at 0 °C. After being stirred at room temperature for 1 h, saturated aqueous NaCl was added to the reaction mixture until bubbling was stopped. Then, the mixture was filtered through a Celite and the filter cake was washed with acetone (5×7 ml). The filtrate and washings were evaporated and the residue was chromatographed on silica gel (20 g) with 1 : 1 benzene-ethyl acetate to afford **30** (297 mg, ca. 100%) as a colorless syrup: R_f=0.18 (1 : 1 benzene-ethyl acetate); $[\alpha]_D^{28}$ +34° (*c* 0.93); IR($CHCl_3$) 3460 and 1020 cm^{-1}; ^1H NMR (90 MHz) δ=0.89 and 1.00 (each 3H, each d, 3- and 5-Me, *J*=6.6 and 6.9 Hz), 1.8—2.4 (3H, m, H-3, H-5, OH), 2.8—3.1 (1H, m, OH), 3.2—3.4 (4H, m, SCH_2CH_2S), 3.43 (3H, s, OMe), 3.4—3.7 (3H, m, H-2, 2×H-6), 3.91 (1H, dd, H-4, *J*=3.3, 7.5 Hz), 4.65 and 4.79 (2H, ABq, OCH_2O, *J*=6.6 Hz), and 4.90 (1H, d, H-1, *J*=5.7 Hz).

Found: C, 48.67; H, 8.13%. Calcd for $C_{12}H_{24}O_4S_2$: C, 48.62; H, 8.16%.

6-*O*-Pivalate (31) of 30. To a solution of **30** (184 mg, 0.655 mmol) in dry pyridine (5.50 ml) was added pivaloyl chloride (121 µl, 0.982 mmol) at room temperature. After being stirred at room temperature for 3 h, the reaction mixture was diluted with ethyl acetate (6.0 ml) and washed with saturated aqueous K_2SO_4 (2×5.0 ml), $NaHCO_3$ (2×5.0 ml), and NaCl, dried, and evaporated. The residual syrup (350 mg) was chromatographed on silica gel (8.0 g) with 3 : 1 benzene-ethyl acetate to afford **31** (230 mg, 96.5%) as a colorless syrup: R_f=0.75 (1 : 1 benzene-ethyl acetate); $[\alpha]_D^{28}$ +6.5°, $[\alpha]_{365}$=+17° (*c* 0.99); IR ($CHCl_3$) 3500, 1720, 1280, 1150, and 1020 cm^{-1}; ^1H NMR (90 MHz) δ=0.95 and 0.98 (each 3H, each d, 3- and 5-Me, *J*=6.6 and 7.2 Hz); 1.21 (9H, s, O-Bu^t), 2.0—2.4 (2H, m, H-3, H-5), 3.1—3.4 (4H, m, SCH_2CH_2S), 3.37 (3H, s, OMe), 3.4—3.7 (1H, m, H-2), 3.74 (1H, dd, H-4, *J*=3.0, 6.9 Hz), 3.91 and 3.99 (each 1H, each s, 2×H-6), 4.59 and 4.67 (2H, ABq, OCH_2O, *J*=6.3 Hz), and 4.86 (1H, d, H-1, *J*=6.3 Hz).

Found: C, 53.67; H, 8.48%. Calcd for $C_{17}H_{32}O_5S_2$: C, 53.65; H, 8.48%.

2,4,6-Trideoxy-3-*O*-(methoxymethyl)-2,4-di-*C*-methyl-1-*O*-pivaloyl-L-altritol (32). A flask containing a solution of **31** (480 mg, 1.3 mmol) in methanol (4.80 ml) in the presence of Raney Ni W-4 (3.0 g) was ultrasonificated for 40 min. The organic layer was separated from insoluble matter which was washed with methanol (10×5.0 ml). The combined organic layers were concentrated to a crude syrup of **32** (525 mg) contaminated with a small amount of impurity. The crude syrup was chromatographed on silica gel (30 g) with 2 : 1 benzene-ethyl acetate to afford **32** (350 mg, 91.6%) as a colorless syrup: R_f=0.36 (2 : 1 benzene-ethyl acetate); $[\alpha]_D^{29}$ +11° (*c* 1.01); ^1H NMR (90 MHz) δ=0.83 and 0.96 (each 3H, each d, 2 and 4-Me, *J*=6.9 and 7.2 Hz), 1.17 (3H, d, 3×H-6, *J*=4.8 Hz), 1.23 (9H, s, Bu^t), 1.5—2.2 (2H, m, H-2, H-4), 2.83 (1H, s, OH), 3.43 (3H, s, OMe), 3.4—3.6 (1H, m, H-5), 3.7—4.1 (3H, m, 2×H-1 and H-3), and 4.68 (2H, s, OCH_2O).

Found: C, 62.10; H, 10.15%. Calcd for $C_{15}H_{30}O_5$: C, 62.04; H, 10.41%.

2,4,6-Trideoxy-5-*O*-(diethylisopropylsilyl)-3-*O*-(methoxymethyl)-2,4-di-*C*-methyl-1-*O*-pivaloyl-L-altritol (33). To a solution of **32** (134 mg, 0.462 mmol) in DMF (1.34 ml) were added at 0 °C imidazole (62.9 mg, 0.924 mmol) and diethylisopropylsilyl chloride[11] (129 µl, 0.693 mmol). After being stirred at room temperature for 0.5 h, the reaction mixture was poured into an ice-water mixture, which was extracted with ethyl acetate (3×2.0 ml). The extracts were washed with saturated aqueous NaCl, dried, and evaporated. The residual syrup (326 mg) was chromatographed on silica gel (5.8 g) with 10 : 1 hexane-ethyl acetate to afford **33** (192 mg, 99.1%) as a colorless syrup: R_f=0.69 (5 : 1 hexane-ethyl acetate); $[\alpha]_D^{26}$ +7.1°, $[\alpha]_{365}$+22° (*c* 1.02); IR ($CHCl_3$) 1720, 1290, 1160, and 1030 cm^{-1}; ^1H NMR (90 MHz) δ=0.5—1.2 (26H, m, 2-, 4-, and 5-Me, $SiEt_2Pr^i$), 1.21 (9H, s, Bu^t), 1.5—2.3 (2H, m, H-2, H-4), 3.3—3.5 (4H, m, H-3, -OMe), 3.96 and 4.04 (each 1H, each d, 2×H-1, *J*=1.8, 3.3 Hz), 4.19 (1H, dq, H-5, *J*=3.3 Hz), and 4.61 (2H, s, OCH_2O).

Found: C, 63.00; H, 10.79%. Calcd for $C_{22}H_{46}O_5Si$: C, 63.11; H, 11.07%.

2,4,6-Trideoxy-5-*O*-(diethylisopropylsilyl)-3-*O*-(methoxymethyl)-2,4-di-*C*-methyl-L-altritol (34). To a solution of **33** (213 mg, 0.506 mmol) in ether (2.13 ml) was added at 0 °C 0.5M methyllithium in ether (2.02 ml, 1.01 mmol). After being stirred at room temperature for 10 min, to the reaction mixture was added saturated aqueous NH_4Cl (3.0 ml). The mixture was extracted with ether (3×3.0 ml), and the extracts were washed with saturated aqueous NaCl, dried, and evaporated. The crude syrup (254 mg) was chromatographed on silica gel (8.5 g) with 2 : 1 hexane-ethyl acetate to afford **34** (171 mg, almost quantitative yield) as a colorless syrup: R_f=0.38 (5 : 1 hexane-ethyl acetate); $[\alpha]_D^{30}$ +50° (*c* 1.02); ^1H NMR (90 MHz) δ=0.4—1.2 (26H, m, 2-, 4-, and 5-Me, $SiEt_2Pr^i$), 1.7—2.1 (2H, m, H-2, H-4), 2.7—3.0 (1H, m, OH), 3.44 (3H, s, OMe), 3.4—3.6 (3H, m, 2×H-1 and H-3), 4.11 (1H, dq, H-5, *J*=3.0, 6.3 Hz), and 4.65 (2H, s, OCH_2O).

Found: C, 61.11; H, 11.10%. Calcd for $C_{17}H_{38}O_4Si$: C, 61.03; H, 11.45%.

2,4,6-Trideoxy-5-*O*-(diethylisopropylsilyl)-3-*O*-(methoxymethyl)-2,4-di-*C*-methyl-L-altrose (35). To a solution of oxalyl dichloride (70.1 µl, 0.803 mmol) in dry dichloromethane (374 µl) was added a mixture of dry DMSO (114 µl, 1.61 mmol) and dry dichloromethane (449 µl) at −60 °C. After being stirred at −60 °C for 0.5 h, a solution of **34** (150 mg, 0.446 mmol) in dichloromethane (446 µl) was added, and the mixture was stirred at −60 °C for 1 h. Triethylamine (311 µl, 2.23 mmol) was added to the reaction mixture, which was stirred at −40 °C for 1 h. The mixture was diluted with ether (1.50 ml) and poured into an ice-water mixture, which was extracted with ether (3×2.0 ml). The extracts were washed with saturated aqueous NaCl, dried, and evaporated to give a syrup (143 mg), which was chromatographed on silica gel (7.5 g) with 3 : 1 hexane-ethyl acetate to afford **35** (137 mg, 91.9%) as a colorless syrup: R_f=0.66 (3 : 1 hexane-ethyl acetate); $[\alpha]_D^{26}$ −43° (*c* 0.95); IR ($CHCl_3$) 2966, 1720, and 1030 cm^{-1}: ^1H NMR (90 MHz) δ=0.5—1.3 (26H, m, 2,4, and 5-Me, $SiEt_2Pr^i$), 1.7—2.1 (1H, m, H-4), 2.49 (1H, dq, H-2, *J*=2.1, 6.9 Hz), 3.28 (1H, s, OMe), 3.95 (1H, dd, H-3, *J*=2.1, 9.6 Hz), 4.15 (1H, dq, H-5, *J*=3.6, 6.0 Hz), 4.50 and 4.57 (2H, ABq, OCH_2O, *J*=6.3 Hz), and 9.77 (1H, s, CHO).

Found: C, 61.62; H, 10.65%. Calcd for $C_{17}H_{36}O_4Si$: C, 61.40; H, 10.91%.

Methyl (2*E*,4*E*)-6-(Dimethoxyphosphinyl)-2,4-hexadienoate (40). To a solution of methyl 4-bromocrotonate (**36**) (1.00 g, 5.59 mmol) in toluene (20.0 ml) was added dropwise a 1M solution of DIBAL in hexane (14.0 ml, 14.0 mmol) at

−78 °C. After being stirred at −78 °C for 0.5 h, 50% aqueous acetic acid (1.60 ml, 14.0 mmol) was added and the mixture was warmed to room temperature. The resulting insoluble material was removed by filtration through a Celite, and the filter cake was washed with acetone (5×10 ml). The filtrate and washings were evaporated to give a yellow syrup of allylic alcohol **37** (0.97 g). A mixture of **37** (0.73 g, 4.82 mmol), MnO_2 (12.6 g, 145 mmol), and dichloromethane (36.0 ml) was stirred at room temperature for 1 h. The insoluble material was filtered through a column filled with silica gel (2.0 g) with ethyl acetate. The filtrate was evaporated to give a syrup of crude aldehyde **38** (0.63 g, 88%). To a solution of the crude **38** (72.3 mg) in toluene (1.0 ml) was added (methoxycarbonylmethylene)triphenylphosphorane (206 mg, 0.615 mmol). The mixture was stirred at 90 °C for 2 h, and then evaporated. The residue was chromatographed on silica gel (20 g) with 5 : 1 hexane-ethyl acetate to afford **39** (70 mg, 70.5%) as a pale yellow liquid. A sample of **39** (116 mg, 0.567 mmol) was added dropwise to trimethyl phosphite (62.8 μl, 0 536 mmol) at 120—130 °C. After being stirred at 120—130 °C for 3 h, the reaction mixture was chromatographed on silica gel (7.5 g) with 10 : 1 chloroform-methanol to afford **40** (111 mg, 88%) as a pale yellow syrup: R_f=0.61 (10:1 chloroform-methanol); IR ($CHCl_3$) 3000, 2950, 2850, 1710, 1250, and 1030 cm^{-1}; UV(EtOH) 257 nm (log ε=4.45); ^1H NMR (90 MHz) δ=2.59 and 2.84 (each 1H, each d, 2×H-6, J=6.9 Hz), 3.69 , 3.74, and 3.83 (each 3H, each s, 3×OMe), 5.84 (1H, d, H-2, $J_{2,3}$=15.6 Hz), 6.08 (1H, dd, H-5, $J_{4,5}$=14.4, $J_{5,6}$=6.9 Hz), 6.29 (1H, dd, H-4, $J_{3,4}$=9.9 Hz), and 7.25 (1H, dd, H-3).

Found: C, 46.18; H, 6.38%. Calcd for $C_9H_{15}O_5P$: C, 46.16; H, 6.46%.

Methyl (8*S*,9*R*,10*R*,11*S*)-(2*E*,4*E*,6*E*)-11-[(Diethylisopropylsilyl)oxy]-9-(methoxymethoxy)-8,10-dimethyl-2,4,6-dodecatrienoate (41) and (6*Z*)-Isomer (42). To a stirred solution of *N*,*N*-diisopropylamine (32.1 μl, 0.229 mmol) in dry THF (153 μl) was added a 1.37 M solution of butyllithium in hexane (167 μl, 0.229 mmol) at −60 °C. After being kept at −60 °C for 1 h, to this solution was added a solution of **40** (50.0 mg, 0.191 mmol) in dry THF (0.50 ml). The reaction mixture was stirred at −60 °C for 0.5 h. A solution of **35** (31.7 mg, 0.0953 mmol) in dry THF (0.32 ml) was added at −60 °C and stirring was continued at −60—−40 °C for 1 h. Saturated aqueous NH_4Cl (1.5 ml) was added to the reaction mixture, which was warmed to room temperature and extracted with ethyl acetate (3×1.5 ml). The extracts were washed with saturated aqueous NaCl, dried, and evaporated. The residue (93.7 mg) was chromatographed on silica gel (1.3 g) with 4 : 1 hexane-ethyl acetate to afford a 1 : 2 mixture of **41** and **42** (41.9 mg, 99.7%) as a pale yellow syrup. The R_f-values (200 : 20 : 1 hexane-ethyl acetate-methanol) of **41** and **42** were 0.42 and 0.46, respectively. The mixture (40.0 mg, 0.0908 mmol) was dissolved in a solution of iodine (0.23 mg, 9.08×10^{-4} mmol) in dry dichloromethane (1.20 ml) and the resulting mixture was stirred at room temperature for 8 h without shading the light. Then saturated aqueous $Na_2S_2O_3$ (1.5 ml) was added to the reaction mixture, which was extracted with ethyl acetate (3×2.0 ml). The extracts were washed with saturated aqueous NaCl, dried, and evaporated to give a 8 : 1 mixture of **41** and **42** (40.0 mg, almost quantitative) as a pale yellow syrup. This syrup was used for the next reaction without further purification. A pure sample of **41** was obtained by flash chromatography of the isomerized product: $[\alpha]_D^{26}$ −4.6°, $[\alpha]_{577}$ −5.1°, $[\alpha]_{546}$ −5.2°, $[\alpha]_{435}$ −2.7° (*c* 0.78); IR ($CHCl_3$) 2950, 1700, and 1615 cm^{-2}; UV (EtOH) 304 nm (log ε=4.54); ^1H NMR (250 MHz) δ=0.60 (4H, q, 2×SiC<u>H</u>$_2$CH$_3$, J=8.5 Hz), 0.87 (3H, d, 10-Me, J=7.0 Hz), 1.9—1.1 (13H, m, 2×SiCH$_2$C<u>H</u>$_3$, *i*-Pr), 1.06 (3H, d, 8-Me, J=7.0 Hz), 1.07 (3H, d, 11-Me, J=6.3 Hz), 1.8—2.0 (1H, m, H-10), 2.54 (1H, ddq, H-8, J=3.8, 7.0 Hz), 3.31 (1H, dd, H-9, J=3.8, 8.3 Hz), 3.35 (3H, s, OCH$_2$O<u>Me</u>), 3.74 (3H, s, COOMe), 4.13 (1H, dq, H-11, J=4.0, 6.3 Hz), 4.54 and 4.57 (2H, ABq, OCH$_2$O, J=7.0 Hz), 5.85 (1H, d, H-2, $J_{2,3}$=15.0 Hz), 5.99 (1H, dd, H-7, $J_{7,8}$=7.0, $J_{7,6}$=15.0 Hz), 6.16 (1H, dd, H-6, $J_{6,5}$=10.5 Hz), 6.25 (1H, dd, H-4, $J_{4,3}$=11.5, $J_{4,5}$=15.0 Hz), 6.54 (1H, dd, H-5), and 7.30 (1H, dd, H-3).

Found: C, 65.57; H, 9.89%. Calcd for $C_{24}H_{44}O_5Si$: C, 65.41; H, 10.06%.

(8*S*,9*R*,10*R*,11*S*)-(2*E*,4*E*,6*E*)-11-[(Diethylisopropylsilyl)oxy]-9-(methoxymethoxy)-8,10-dimethyl-2,4,6-dodecatrienal (45) and (6*Z*)-Isomer (46). To a stirred solution of the 8 : 1 mixture of **41** and **42** (40.4 mg) in dry toluene (1.20 ml) was added dropwise a 1 M solution of DIBAL in hexane (229 μl) at −78 °C. After being stirred at −78 °C for 10 min, 50% aqueous acetic acid (262 μl) was added to the mixture, which was warmed to room temperature. The resulting insoluble matter was removed by filtration through a Celite, and the filter cake was washed with acetone (5×3.0 ml). The filtrate and washings were evaporated to give a yellow syrup (40.2 mg), which was chromatographed on silica gel (3.8 g) with 1 : 1 hexane-ethyl acetate to afford a mixture of the allylic alcohol **43** and its isomer **44** (35.4 mg, 93.6%) as a yellow syrup [R_f=0.17 (4 : 1 hexane-ethyl acetate)]. To this syrup (35.4 mg, 0.0858 mmol) was added dichloromethane (1.42 ml) and MnO_2 (423 mg, 4.87 mmol), and the mixture was stirred at room temperature for 0.5 h. The insoluble material was removed by filtration through a column filled with silica gel (0.35 g). The filtrate was evaporated to give an orange syrup (35.1 mg), which was flash-chromatographed on silica gel (7.0 g) with 140 : 20 : 1 hexane-ethyl acetate-methanol to afford **45** (27.5 mg) and **46** (5.1 mg) in 71 and 13% overall yields from **35**, respectively. **45**: Pale yellow syrup, R_f=0.41 (4 : 1 hexane-ethyl acetate); $[\alpha]_D^{25}$ −14.3° (*c* 0.48); IR ($CHCl_3$) 2960, 1725, 1670, and 1610 cm^{-1}; UV (EtOH) 319 nm (log ε=4.75); ^1H NMR (250 MHz) δ=0.61 (4H, q, 2×SiC<u>H</u>$_2$Me, J=7.8 Hz), 0.87 (3H, d, 10-Me, J=7.3 Hz), 0.9—1.1 (13H, m, 2×SiCH$_2$C<u>H</u>$_3$, *i*-Pr), 1.07 (6H, d, 8-and 11-Me, J=7.0 Hz), 1.88 (1H, m, H-10), 2.57 (1H, ddq, H-8, J=3.3, 7.0 Hz), 3.33 (1H, dd, H-9, J=3.3, 8.3 Hz), 3.36 (3H, s, OMe), 4.13 (1H, dq, H-11, J=4.5, 7.0 Hz), 4.54 and 4.58 (2H, ABq, OCH$_2$O, J=7.0 Hz), 6.10 (1H, dd, H-7, $J_{7,8}$=7.0, $J_{7,6}$=15.0 Hz), 6.14 (1H, dd, H-2, $J_{2,1}$=8.3, $J_{2,3}$=15.3 Hz), 6.21 (1H, dd, H-6, $J_{6,5}$=9.8 Hz), 6.37 (1H, dd, H-4, $J_{4,3}$=11.3, $J_{4,5}$=15.0 Hz), 6.66 (1H, dd, H-5), 7.12 (1H, dd, H-3, $J_{3,2}$=15.3 Hz), and 9.56 (1H, d, CHO, J=8.3 Hz).

Found: C, 67.45; H, 10.11%. Calcd for $C_{23}H_{42}O_4Si$: C, 67.27; H, 10.31%.

46: R_f=0.47 (4 : 1 hexane-ethyl acetate), ^1H NMR (250 MHz) δ=2.9—3.1 (1H, m, H-8), 5.77 (1H, dd, H-7, $J_{7,6}$=$J_{7,8}$=10.8 Hz), 6.10 (1H, dd, H-6, $J_{6,5}$=$J_{6,7}$=10.8 Hz), 6.17 (1H, dd, H-2, $J_{2,1}$=7.3, $J_{2,3}$=15.0 Hz), 6.44 (1H, dd, H-4, $J_{4,3}$=10.8, $J_{4,5}$=14.5 Hz), 6.65 (1H, dd, H-5), 7.17 (1H, dd, H-3), and 9.58 (1H, d, CHO).

Methyl (14*S*,15*R*,16*R*,17*S*)-(2*E*,4*E*,6*E*,8*E*,10*E*,12*E*)-17-[(Diethylisopropyl)oxy]-15-(methoxymethoxy)-14,16-dimethyl-2,4,6,8,10,12-octadecahexaenoate (47). To a stirred solution

of LDA in THF prepared from *N,N*-diisopropylamine (15.0 μl, 0.107 mmol) by the procedure described in the preparation of **41** was added a solution of **40** (23.4 mg, 0.0892 mmol) in dry THF (234 μl) at −60 °C and the mixture was stirred at −60 °C for 0.5 h. A solution of **45** (18.3 mg, 0.0446 mmol) in dry THF (183 μl) was added and stirred at −30 °C for 2 h. The reaction mixture was quenched with saturated aqueous NH_4Cl (1.0 ml), and extracted with ethyl acetate (3×1.0 ml). The extracts were washed with saturated aqueous NaCl, dried, and evaporated. The residue (53.3 mg) was chromatographed on silica gel (2.0 g) with 40:1 chloroform–ethyl acetate to afford **47** (21.4 mg, 92.6%) as a yellow plates: R_f=0.45 (5:1 hexane-ethyl acetate); mp 154—157 °C; $[\alpha]_D^{25}$ +2.5°, $[\alpha]_{577}$ +4.1°, $[\alpha]_{546}$ +7.1° (*c* 0.42); IR (KBr) 1710, 1615, 1010 cm^{-1}; UV (EtOH), nm (log ε) 224 (4.07), 282 (4.10), 381 (4.90); ^1H NMR (250 MHz) δ=0.61 (4H, q, 2×SiC$\underline{H_2}$Me, *J*=7.3 Hz), 0.85 (3H, d, 16-Me, *J*=6.8 Hz), 0.9—1.1 (19H, m, 14- and 17-Me, 2×SiCH$_2$$\underline{Me}$, *i*-Pr), 1.8—1.9 (1H, m, H-16), 2.4—2.6 (1H, m, H-14), 3.29 (1H, dd, H-15, *J*=4.0, 8.8 Hz), 3.36 (3H, s, CH$_2$O$\underline{Me}$), 3.74 (3H, s, COOMe), 4.34 (1H, dq, H-17, *J*=4.3, 6.5 Hz), 4.54 and 4.58 (2H, ABq, OCH_2O, *J*=7.5 Hz), 5.83 (1H, dd, H-13, $J_{13,14}$=7.3, $J_{13,12}$=15.0 Hz), 5.88 (1H, d, H-2, $J_{2,3}$=15.3 Hz), 6.0—6.7 (9H, m, H-4,5,6,7,8,9,10,11,12), and 7.32 (1H, dd, H-3, $J_{3,4}$=11.3 Hz).

Found: C, 69.41; H, 9.52%. Calcd for $C_{30}H_{50}O_5Si$: C, 69.45; H, 9.71%.

(14*S*,15*R*,16*R*,17*S*)-(2*E*,4*E*,6*E*,8*E*,10*E*,12*E*)-17-[(Diethylisopropylsilyl)oxy]-15-(methoxymethoxy)-14,16-dimethyl-2,4,6,8,10,12-octadecahexaenal (49). By the procedure described in the preparation of **45** from **41**, above obtained **47** (49.3 mg) was transformed via the allylic alcohol **48** into **49** (33.2 mg, 73.5%).

49: Orange crystals; R_f=0.39 (5:1 hexane-ethyl acetate); mp 146—149 °C; $[\alpha]_D^{28}$ +3.5°, $[\alpha]_{577}$ +4.1°, $[\alpha]_{546}$ +9.4° (*c* 0.34); IR (KBr) 1665, 1600, 1550, 1005 cm^{-1}; UV (EtOH) nm (log ε) 228 (4.18), 288 (4.20), 408 (4.99); ^1H NMR (250 MHz) δ=0.61 (4H, q, 2×SiC$\underline{H_2}$Me, *J*=8.3 Hz), 0.87 (3H, d, I6-Me, *J*=7.0 Hz), 0.9—1.1 (13H, m, 2×SiCH$_2$$\underline{Me}$, *i*-Pr), 1.05 and 1.06 (each 3H, each d, 14- and 17-Me, *J*=6.5 Hz), 1.87 (1H, m, H-16), 2.52 (1H, ddq, H-14, *J*=3.3, 6.8 Hz), 3.30 (1H, dd, H-15, *J*=3.3, 7.8 Hz), 3.36 (3H, s, OMe), 4.15 (1H, dq, H-17, *J*=4.3, 7.0 Hz), 4.54 and 4.58 (2H, ABq, OCH_2O, *J*=7.0 Hz), 5.85 (1H, dd, H-13, $J_{13,14}$=6.8, $J_{13,12}$=15.0 Hz), 6.15 (1H, dd, H-2, $J_{2,1}$=3.4, $J_{2,3}$=15.3 Hz), 6.0—6.8 (9H, m, H-4,5,6,7,8,9,10,11,12), 7.15 (1H, dd, H-3, $J_{3,4}$=11.3 Hz), and 9.57 (1H, d, CHO).

Found: C, 71.24; H, 9.73%. Calcd for $C_{29}H_{48}O_4Si$: C, 71.26; H, 9.90%.

(14*S*,15*R*,16*R*,17*S*)-(2*E*,4*E*,6*E*,8*E*,10*E*,12*E*)-17-Hydroxy-15-(methoxymethoxy)-14,16-dimethyl-2,4,6,8,10,12-octadecahexaenal (4). To a solution of **49** (19.6 mg, 0.04 mmol) in dry THF (0.39 ml) was added a 1 M solution of *n*-Bu_4NF in THF (80.2 μl, 0.08 mmol) at 0 °C. After being stirred at 0 °C for 15 h, the reaction mixture was poured into an ice-water mixture which was extracted with ethyl acetate (3×1.0 ml). The extracts were washed with saturated aqueous NaCl, dried, and evaporated. The residue (23.4 mg) was chromatographed on silica gel (2.2 g) with 2:3 hexane-ethyl acetate to afford **4** (14.0 mg, 96.8%) as orange crystals: R_f=0.15 (7:3 hexane-ethyl acetate); mp 105—114 °C; IR (KBr) 3340, 1670, 1550, and 1010 cm^{-1}; UV (EtOH) nm (log ε) 288 (4.01), 406 (4.73); ^1H NMR (250 MHz) δ=0.88 (3H, d, 16-Me, *J*=7.0 Hz), 1.08 (3H, d, 17-Me, *J*=6.8 Hz), 1.17 (3H, d, 14-Me, *J*=6.3 Hz), 1.76 (1H, q-like, H-16, *J*=7.0 Hz), 2.5—2.7 (1H, m, H-14), 3.3—3.5 (2H, m, H-15, OH), 3.40 (3H, s, OMe), 3.83 (1H, dq, H-17, *J*=6.8 Hz), 4.65 and 4.67 (2H, ABq, OCH_2O, *J*=7.5 Hz), 5.82 (1H, dd, H-13, $J_{13,14}$=7.5, $J_{13,12}$=14.5 Hz), 6.16 (1H, dd, H-2, $J_{2,1}$=8.0, $J_{2,3}$=15.0 Hz), 6.1—6.8 (9H, m, H-4,5,6,7,8,9,10,11,12), 7.14 (1H, dd, H-3, $J_{3,4}$=11.5 Hz), and 9.56 (1H, d, CHO).

Found: C, 73.02; H, 8.65%. Calcd for $C_{22}H_{32}O_4$: C, 73.30; H, 8.95%.

We are grateful to Prof. Sumio Umezawa, Institute of Bioorganic Chemistry, and Prof. Hamao Umezawa, Institute of Microbial Chemistry for their generous support of our program. The present work was partially supported by a Grant-in-Aid for Scientific Research No. 60470091 from the Ministry of Education, Science and Culture. We would like to thank Miss Yoshiko Koyama of the Institute for 250 MHz ^1H NMR spectral analyses, and Mr. Akio Takahashi of Keio University, for elemental analyses.

References

1) J. Vandeputte, J. L. Wachtel, and E. T. Stiller, *Antibiot. Annu.*, **1956**, 587.

2) W. Mechliuski, C. P. Schaffner, P. Ganis, and G. Avitabile, *Tetrahedron Lett.*, **1970**, 3873; P. Ganis, G. Avitabile, W. Mechlinski, and C. P. Schaffner, *J. Am. Chem. Soc.*, **93**, 4560 (1971).

3) a) D. M. Floyed and A. W. Fritz, *Tetrahedron Lett.*, **22**, 2847 (1981); b) D. W. Brooks and R. P. Kellogg, *ibid.*, **23**, 4991 (1982); c) S. Masamune, T. Kaiho, and D. S. Garvey, *J. Am. Chem. Soc.*, **104**, 5521 (1982); d) P. Ma, V. S. Martin, S. Masamune, K. B. Sharpless, and S. M. Viti, *J. Org. Chem.*, **47**, 1378 (1982); e) K. C. Nicolaou and J. Venishi, *J. Chem. Soc., Chem. Commun.*, **1982**, 1292; f) M. Hirama and M. Vie, *Tetrahedron Lett.*, **23**, 5307 (1982); g) B. H. Lipshutz and J. A. Kozlowski, *J. Org. Chem.*, **49**, 1149 (1984); h) S. Masamune, P. Ma, H. Okamoto, J. W. Ellingboe, and Y. Ito, *J. Org. Chem.*, **49**, 2843 (1984); i) D. Liang, H. W. Pauls, and B. Fraser-Reid, *J. Chem. Soc., Chem. Commun.*, **1984**, 1123; j) M. A. Blanchette, W. Choy, J. T. Davis, A. P. Essenfeld, S. Masamune, W. R. Roush, and T. Sakai, *Tetrahedron Lett.*, **25**, 2183 (1984); k) J. M. Williams and G. J. McGarvey, *ibid.*, **26**, 4891 (1985); l) D. Boschell, T. Takemasa, Y. Nishitani, and S. Masamune, *ibid.*, **26**, 5239 (1985); m) G. J. McGarvey, J. M. Williams, R. N. Hiner, Y. Matsubara, and T. Oh, *J. Am. Chem. Soc.*, **108**, 4943 (1986); J. M. Williams and G. J. McGarvey , *Tetrahedron Lett.*, **26**, 4891 (1985).

4) K. C. Nicolaou, T. K. Chakraborty, R. A. Daines, and N. S. Simpkins, *J. Chem. Soc., Chem. Commun.*, **1986**, 413.

5) M. Kinoshita and S. Mariyama, *Bull. Chem. Soc. Jpn.*, **48**, 2081 (1975); A. Rosenthal and M. Spinze, *Can. J. Chem.*, **47**, 3941 (1969).

6) a) H. Redlich and H.-J. Neumann, *Chem. Ber.*, **114**, 2029 (1981); b) M. Kinoshita, N. Ohsawa, and S. Gomi, *Carbohydr. Res.*, **109**, 5 (1982).

7) J. Herscovici and K. Antonakis, *J. Chem. Soc., Chem. Commun.*, **1980**, 561.

8) E. J. Corey and M. Chaykovsky, *J. Am. Chem. Soc.*, **84**, 866 (1962); M. Nakata, Y. Ikeyama, H. Takao, and M. Kinoshita, *Bull. Chem. Soc. Jpn.*, **53**, 3252 (1980).

9) M. Nakata, H. Takao, Y. Ikeyama, T. Sakai, K. Tatsuta, and M. Kinoshita, *Bull. Chem. Soc. Jpn.*, **54**, 1749

(1981).

10) J. C. Sheehan, H. G. Zachan, and W. B. Lawson, *J. Am. Chem. Soc.*, **80**, 3349 (1958).

11) K. Toshima, K. Tatsuta, and M. Kinoshita, *Tetrahedron Lett.*, **27**, 4741 (1986).

12) A. J. Mancuso, S.-L. Huang, and D. Swern, *J. Org. Chem.*, **33**, 2480 (1978).

13) I. Ernest, A. J. Main, and R. Menassé, *Tetrahedron Lett.*, **23**, 167 (1982).

14) Direct ^{1}H NMR spectroscopic confirmation of the (6E)-configuration of **47** and **49** was impossible, because, in their spectra, the signals of the H-6 and 7 protons were found in a complex multiplet due to nine olefinic protons. Therefore, their (6E)-configuration was indirectly confirmed. The reaction of **45** with (methoxycarbonylmethylene)triphenylphosphorane afforded the all-*trans*-tetraenoic ester **50** in 89% yield: ^{1}H NMR (90 MHz) δ=5.88 (1H, d, H-2, $J_{2,3}$=15.6 Hz), 6.0—6.7 (6H, m, H-4,5,6,7,8,9), and 7.37 (1H, d, H-3, $J_{3,4}$=10.8 Hz). The ester **50** was converted , by the procedure described in the preparation of **45**, into the all-*trans*-tetraenal **51** in 43.3% yield: ^{1}H NMR (90 MHz) δ=6.17 (1H, dd, H-2, $J_{2,1}$=8.1, $J_{2,3}$=15.3 Hz), 6.0—6.8 (6H, m, H-4,5,6,7,8,9), 7.16 (1H, dd, H-3, $J_{3,4}$=9.9 Hz), and 9.62 (1H, d, CHO). The reaction of **51** with methyl (2*E*)-4-(dimethoxyphosphinyl)-2-butenoate (THF, LDA, −60 °C, 0.5h) provided in almost quantitative yield the hexaenoic ester **47**, which proved to be identical in all respects with a sample of **47** obtained by the reaction of **45** and **40**.

 © 1987 The Chemical Society of Japan Bull. Chem. Soc. Jpn., 60, 2163—2167 (1987)

Kinetic Studies of Antioxidant Activity of New Tocopherol Model Compounds in Solution

Kazuo MUKAI,* Satoshi YOKOYAMA, Kazuyuki FUKUDA, and Yuichi UEMOTO
Department of Chemistry, Faculty of Science, Ehime University, Matsuyama 790
(Received December 26, 1986)

The second-order rate constants k_s for the reaction of 10 kinds of tocopherol (vitamin E) model compounds with stable phenoxyl radical in ethanol have been measured at 25.0 °C, using a stopped-flow spectrophotometer, as a model reaction of tocopherols with unstable free radicals (ROO·, RO·, and HO·) in biological systems. The absolute k_s values of α-, β-, γ-, and δ-tocopherol models are similar to or slightly smaller than those of the corresponding tocopherols having a long-phytyl-chain. The relative k_s values (α : β : γ : δ=100 : 53 : 50 : 24), that is, relative antioxidant activities, of α-, β-, γ-, and δ-tocopherol models are in good agreement with those (100 : 44 : 47 : 20) of α-, β-, γ-, and δ-tocopherols. The antioxidant activities of tocopherol models having two alkyl substituents, such as methyl, ethyl, isopropyl, and *t*-butyl groups, at ortho positions of OH group are similar to each other, suggesting that the effect of steric hindrance on the reaction rate is small. 5,7-Dimethyltocol model has quite similar rate constants with those of β- and γ-tocopherol models, whereas δ-tocopherol model is only ca. 24% as reactive as α-tocopherol model and tocol model is only ca. 10% as reactive as α-tocopherol model. The result indicates that the rate constants increase as the total electron donating capacity of the alkyl substituents at aromatic ring increases. For the tocopherol models log k_s was found to correlate with $\Sigma\sigma^+$ substituent constants with a ρ^+ value of −1.0.

Vitamin E (α-, β-, γ-, and δ-tocopherols) is known to scavenge peroxyl, alkoxyl, and hydroxyl radicals.[1,2] The above free radical scavenging actions by vitamin E have been ascribed to the initial reaction of the phenolic hydroxyl group with the production of a tocopheroxyl† radical.[3-7] Recently, Burton et al. have reported absolute second-order rate constants, k_1, for the reaction of α-, β-, γ-, and δ-tocopherols with poly(styrylperoxyl) radicals, using the inhibited autoxidation of styrene method (reaction 1).[8-10]

$$\mathrm{ROO\cdot + Toc \xrightarrow{k_1} ROOH + Toc\cdot} \quad (1)$$

They suggested that the relative magnitude of the second-order rate constant, k_1, of α-, β-, γ-, and δ-tocopherols is in agreement with in vivo and in vitro tests of their relative biological activities which yield: α>β>γ>δ-tocopherol.[9]

In a previous work, we have determined spectrophotometrically the rates of reaction of α-, β-, γ-, and δ-tocopherols with stable phenoxyl radical (2,6-di-*t*-butyl-4-(4-methoxyphenyl)phenoxyl (PhO·) (see Fig. 1)) in ethanol solution using stopped-flow technique, as a model reaction of tocopherols with unstable free radicals (ROO·, RO·, and HO·) in biological systems (reaction 2).[11]

$$\mathrm{PhO\cdot + Toc \xrightarrow{k_s} PhOH + Toc\cdot} \quad (2)$$

The second-order rate constants, k_s, obtained are $(5.12\pm0.36)\times10^3$ (α-Toc), $(2.24\pm0.04)\times10^3$ (β-Toc), $(2.42\pm0.16)\times10^3$ (γ-Toc), and $(1.02\pm0.10)\times10^3$ (δ-Toc) $M^{-1}s^{-1}$ in ethanol at 25.0 °C. The relative k_s values (α : β : γ : δ=100 : 44 : 47 : 20) obtained by the stopped-flow technique are in good agreement with the values (100 : 41 : 44 : 14)[10] obtained by the inhibited autoxidation of styrene method, although the absolute k_s values are about 600 times smaller than those for the reaction of tocopherols with poly(styrylperoxyl) radical in chlorobenzene. The results suggest that the relative reactivities, that is, relative antioxidant activities of tocopherols in homogeneous solution do not change depending on the kinds of radicals (phenoxyl and poly(styrylperoxyl) radicals) used, while the absolute

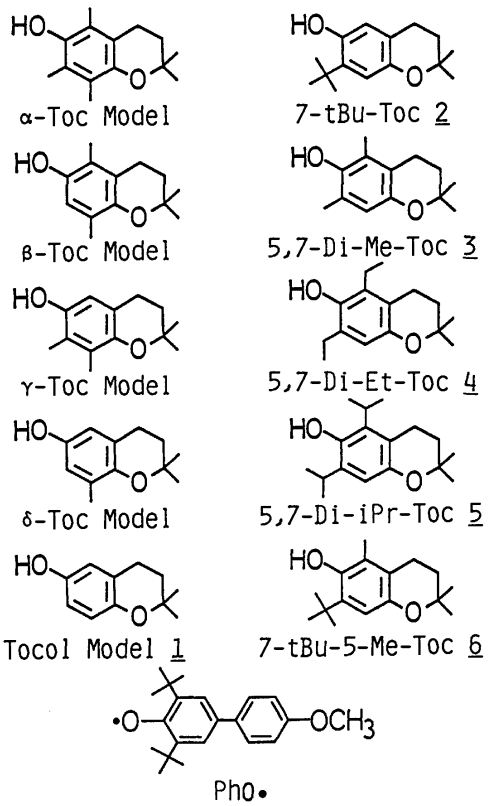

Fig. 1. Molecular structures of tocopherol model compounds and phenoxyl radical (PhO·).

†The phenoxyl radicals generated from tocopherols are named in this paper as widely used tocopheroxyl radicals for convenience rather than tocopheryloxyl radicals that conform to rules of nomenclature.

rates are considerably different from each other. Further, the above results indicate that α-tocopherol having two methyl groups at ortho positions of OH group is about two times as reactive as β- and γ-tocopherols having one methyl group at ortho positions, and, then, δ-tocopherol which has no methyl substituents at ortho positions is only ca. 20% as reactive as α-tocopherol. Antioxidant activities of tocopherols seem to increase in the order of the number of methyl substituents at ortho positions of OH group. These findings suggest that the presence of two methyl groups at ortho positions in tocopherols is of great importance to their antioxidant action.

Therefore, in the present work, in order to get the tocopherol compounds having higher antioxidant activity than α-tocopherol and in order to clear the structure-activity relationship in antioxidant action of tocopherols, we have prepared several tocopherol model compounds which have especially two alkyl substituents, such as methyl, ethyl, isopropyl, and *t*-butyl groups, at ortho positions of OH group (see Fig. 1), and measured the rates of reaction of tocopherol models with phenoxyl radical in ethanol solution, using stopped-flow spectrophotometer.[11]

Experimental

Materials. α-, β-, γ-, δ-Tocopherol models, tocol model (**1**), and 5,7-dimethyl-tocol model (**3**) were prepared according to the method of Nilsson et al.[12] Preparation of 7-*t*-butyl-tocol model (**2**), 5,7-diisopropyl-tocol model (**5**), and 7-*t*-butyl-5-methyl-tocol model (**6**) was reported in a previous paper.[13] 2,6-Diethylhydroquinone (mp 105.0—106.0 °C) were prepared from 2,6-diethylphenol by the standard procedure, as reported for the syntheses of the 2,3-, 2,5-, and 2,6-dimethylhydroquinone.[14]

The 2,6-di-*t*-butyl-4-(4-methoxyphenyl)phenoxyl (PhO·) was prepared according to the method of Müller et al.[15] Radical concentration of phenoxyl radical was obtained from the results of the paramagnetic susceptibility measurements at 20 °C. The value was 100% for phenoxyl, assuming the Curie law.

5,7-Diethyl-Tocol Model (4). 2,6-Diethylhydroquinone (3.7 g, 22 mmol) was dissolved in formic acid (99%) (50 ml) and THF (tetrahydrofuran) (5 ml), and the solution was heated to reflux. A THF (2 ml) solution of 2-methyl-3-buten-2-ol (1.9 g, 22 mmol) was added dropwise slowly during 1 h, and the refluxing was continued for an additional 3 h with stirring. The reaction mixture was poured onto crushed ice (150 g), and extracted with diethyl ether (5×25 ml). Petroleum ether (bp 40—50 °C) (25 ml) was added to the combined diethyl ether extracts and the mixture was washed with water (5×25 ml). After removal of the solvent, the residue was dissolved in methanol (75 ml), 1 ml of concn HCl was added, and the solution refluxed for 20 min to hydrolyze formate of **4** produced. The methanol was then evaporated, and the residue was taken up in diethyl ether (100 ml), washed with $NaHCO_3$ solution and with water, and the solution was dried over anhydrous sodium sulfate. The solvent was evaporated, and the residual oil was extracted three times with hot petroleum ether (bp 50—60 °C) (3×100 ml). After removal of the solvent, a viscous oil remained. The oily residue obtained was chromatographed on 50 g of silica gel with ether-petroleum ether (1 : 5) as the eluting agent. After removal of the solvent, the oily solids remained were recrystallized from petroleum ether (bp 60—70 °C), giving white crystals. Mp 80.0—80.4 °C. (Found: C, 76.63; H, 9.50%. Calcd for $C_{15}H_{22}O_2$: C, 76.88; H, 9.46%). UV spectrum (λ_{max}=294 nm, log ε=3.55 in ethanol). NMR spectrum (δ=1.13 (3H, t, 5- or 7-CH_2CH_3, J=7.3 Hz), 1.21 (3H, t, 5- or 7-CH_2CH_3, J=7.3 Hz), 1.28 (6H, s, 2-CH_3), 1.78 (2H, t, 3-CH_2, J=6.6 Hz), 2.56 (2H, q, 5- or 7-CH_2CH_3, J=7.3 Hz), 2.63 (2H, q, 5- or 7-CH_2CH_3, J=7.3 Hz), 2.67 (2H, t, 4-CH_2, J=6.6 Hz), 4.17 (1H, s, 6-OH), 6.46 (1H, s, 8-H); δ in $CDCl_3$ with TMS as an internal standard).

Measurement of k_s Values by the Stopped-Flow Spectrophotometer. The stopped-flow data were obtained on a UNISOKU stopped-flow spectrophotometer Model RS-450 by mixing equal volumes of ethanol solutions of phenoxyl and tocopherol model. The oxidation reactions were studied under pseudo-first-order conditions, and the observed rate constants, k_{obsd}, were calculated in the usual way using a standard least-squares analysis. All measurements were performed at 25.0±0.5 °C.

Results

The phenoxyl radical (PhO·) is stable in the absence of tocopherol models, and shows absorption peaks at λ_{max}=376 nm (ε=17600 $M^{-1}cm^{-1}$(1 M=1 mol dm^{-3})) and 580 nm (ε=4280 $M^{-1}cm^{-1}$) in ethanol. By adding an ethanol solution of α-tocopherol model (1.00 mM) to an ethanol solution of phenoxyl (0.10 mM) (1 : 1 in volume) at 25.0 °C, the absorption spectrum of the phenoxyl immediately changed to that of α-tocopheroxyl model. The absorption spectrum of α-tocopheroxyl model shows weak absorption peaks at 427 and 405 nm.[16] However, the α-tocopheroxyl model is unstable, and the absorption peaks rapidly disappeared. Similarly, the phenoxyl radical has been reacted with excess tocopherol models, showing rapid decrease of the absorption spectrum, respectively. Therefore, the oxidation rates of tocopherol model compounds by phenoxyl were studied spectrophotometrically using

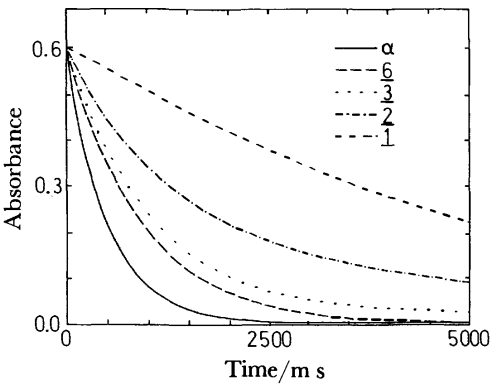

Fig. 2. The decay of phenoxyl radicals for the reaction of phenoxyls with tocopherol model compounds in ethanol at 25.0 °C. $[PhO\cdot]_{t=0}$ 0.05 mM and $[Toc]_{t=0}$ 0.50 mM. At 376 nm.

stopped-flow technique in the presence of excess tocopherol model in ethanol. The details of experiments are reported in a previous paper.[11] The rate was measured by following the decrease in absorbance at 376 and 580 nm of phenoxyl radical. The time dependence of the decrease in absorbance at 376 nm observed when 0.10 mM ethanol solution of phenoxyl is mixed with 1.00 mM ethanol solution of tocopherol models (1 : 1 in volume; final concentration of phenoxyl is 0.05 mM) is shown in Fig. 2. The stopped-flow reactions were performed at 25.0±0.5 °C.

The pseudo-first-order rate constants, k_{obsd}, observed at 376 nm and at 580 nm were linearly dependent on the concentration of tocopherol model, and, thus, the rate law is expressed as

$$-d[PhO\cdot]/dt = k_{obsd}[PhO\cdot] = k_s[Toc][PhO\cdot] \quad (3)$$

where k_s is the second-order rate constant for oxidation of tocopherol model by phenoxyl radical. The values of k_s calculated from k_{obsd} are listed in Table 1. For each tocopherol model, k_s was measured in at least 4 independent experiments. The experimental errors in k_s values was $<\pm 10\%$ in every case.

Discussion

The effect of phytyl side chain of vitamin E on its antioxidant activity has been studied by Fukuzawa et al.[17] and Niki et al.[18] They examined the inhibition effect of the oxidation of unsaturated lipids in homogeneous solution and in liposomes by α-tocopherol and α-tocopherol model. It was concluded that the antioxidative properties of α-tocopherol and α-tocopherol model without the phytyl side chain are quite similar within liposomes as well as in homogeneous solution but that the phytyl side chain enhances the retainment of α-tocopherol in liposomes and suppresses the transfer of α-tocopherol between liposomal membranes. Burton et al. have measured the rate constants k_1 for the reaction of α-tocopherol and α-tocopherol model with poly(styrylperoxyl) radical in homogeneous solution.[9,10,19] In an early report, they suggested that α-tocopherol and α-tocopherol model have similar in vitro antioxidant activity in solution.[9] However, both the absolute rate constants k_1 of α-tocopherol and α-tocopherol model and the relative rate constants ($k_1/k_1(\alpha\text{-Toc})\times 100$) reported by Burton et al. varied from early work to recent work. The values are as follows: i) α-tocopherol: $k_1 = (2.35\pm0.50)\times10^6$ M^{-1} s^{-1} (100) and α-tocopherol model: $(2.14\pm0.81)\times10^6$ (91) (1981);[9] ii) α-tocopherol: $(3.24\pm0.15)\times10^6$ (100) and α-tocopherol model: $(3.77\pm0.19)\times10^6$ (116) (1983);[19] iii) α-tocopherol: $(3.20\pm0.32)\times10^6$ (100) and α-tocopherol model: $(3.80\pm0.38)\times10^6$ (119) (1985).[10]

In the present work, we have measured the rate constants k_s for the reaction of α-, β-, γ-, and δ-tocopherol models with the stable phenoxyl radical in ethanol, using a stopped-flow spectrophotometer. The results listed in Table 1 indicate that α-, β-, γ-, and δ-tocopherol models have reactivities similar to or slightly less than those of corresponding α-, β-, γ-, and δ-tocopherols (see Table 2) in homogeneous solution. Further, the relative k_s values (α : β : γ : δ = 100 : 53 : 50 : 24), that is, relative antioxidant activities, obtained for α-, β-, γ-, and δ-tocopherol models are in good agreement with those (100 : 44 : 47 : 20) for α-, β-, γ-,

Table 1. Second-Order Rate Constants (k_s) and Relative Rate Constants for Oxidation of Tocopherol Models by Phenoxyl Radical in Ethanol at 25.0 °C, and $\Sigma\sigma^+$ Values

Tocopherol Model	$10^{-3}\,k_s$ ($M^{-1}\,s^{-1}$)	$\frac{k_s\text{ (Toc Model)}\times 100}{k_s\text{ (α-Toc Model)}}$	$\Sigma\sigma^+$
α-Toc Model	4.20±0.04	100	−0.688
β-Toc Model	2.24±0.07	53	−0.377
γ-Toc Model	2.10±0.17	50	−0.377
δ-Toc Model	1.00±0.01	24	−0.066
Toc Model **1**	0.41±0.01	10	0.000
Toc Model **2**	1.36±0.13	32	−0.256
Toc Model **3**	2.00±0.01	48	−0.622
Toc Model **4**	1.91±0.01	45	−0.590
Toc Model **5**	2.82±0.02	67	−0.560
Toc Model **6**	2.34±0.15	56	−0.567

Table 2. Second-Order Rate Constants (k_s) and Relative Rate Constants for Oxidation of Tocopherols by Phenoxyl radical in Ethanol at 25.0 °C

Tocopherol	$10^{-3}\,k_s$ ($M^{-1}\,s^{-1}$)	$\frac{k_s\text{ (Toc)}\times 100}{k_s\text{ (α-Toc)}}$	$\frac{k_s\text{ (Toc Model)}}{k_s\text{ (Toc)}}$
α-Toc	5.12±0.36[a]	100	0.82
β-Toc	2.24±0.04	44	1.00
γ-Toc	2.42±0.16	47	0.87
δ-Toc	1.02±0.10	20	0.98

a) See Ref. 11.

and δ-tocopherols having a long-phytyl-chain, respectively.

As described in a previous section, α-tocopherol which has two methyl substituents at ortho positions of OH group showed the highest antioxidant activity among α-, β-, γ-, and δ-tocopherols. Therefore, we have prepared several tocopherol model compounds especially having two alkyl substituents, such as methyl, ethyl, isopropyl, and *t*-butyl groups, and measured the antioxidant activity of tocopherol models in ethanol solution. By comparing the second-order rate constants observed for 5,7-dimethyl-tocol model (**3**) having two methyl groups at ortho position with that of α-tocopherol model, the former is only ca. 48% as reactive as the latter, against to our expectation. On the other hand, as is clear from the results listed in Table 1, the antioxidant activities of tocopherol models (**3**), (**4**), (**5**), and (**6**) having two alkyl substituents at ortho position of OH group are similar to each other, although the 5,7-diisopropyl-tocol model (**5**) shows 12—15% higher antioxidant activity than the other tocopherol models. The result suggests that the effect of steric hindrance on the reaction rate is not remarkable, but small. Further, to our surprise, 5,7-dimethyl-tocol model (**3**) has quite similar rate constants with those of β- and γ-tocopherol models, whereas δ-tocopherol model is only ca. 24% as reactive as α-tocopherol model and tocol model (**1**) is only ca. 10% as reactive as α-tocopherol model. Therefore, the relative rate constants are plotted against to the number of alkyl substituents at aromatic ring in tocopherol models. The results shown in Fig. 3 clearly suggest that the antioxidant activity of tocopherol models depends on the number of alkyl substituents at aromatic ring rather than the position of substitution. This implies that the values of the rate constants for this reaction increase as the total electron donating capacity of the alkyl substituents increases.

Howard and Ingold have measured the rate constants k_4 for the reaction of ortho-alkyl phenols with poly(styrylperoxyl) radicals.[20] They found that the logarithms of rate constants correlate with the sum of the Brown's σ^+ constants[21] for all the substituents on the phenol ($\Sigma\sigma^+$). They also reported that the steric effects due to ortho alkyl substituents are important. However, for the tocopherol models, it was observed that the steric effect on the reaction rate is not remarkable. Therefore, the values of log k_s for tocopherol models have been plotted against $\Sigma\sigma^+$. As shown in Fig. 4, the logarithms of rate constants (k_s) were found to roughly correlate with $\Sigma\sigma^+$ substituent constants. The slope of the best straight line, i.e., the ρ factor, was −1.0.

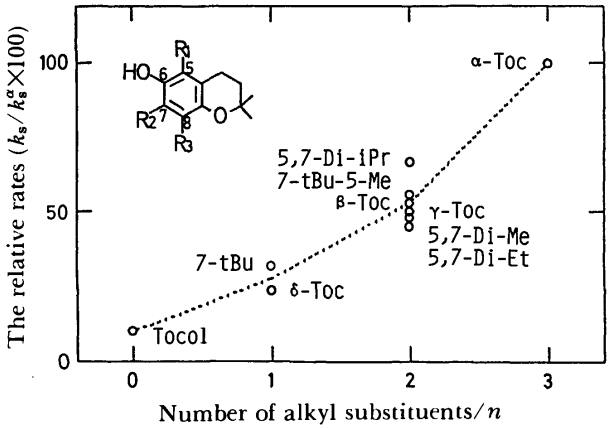

Fig. 3. Plot of the relative rate constant (k_s(Toc Model)/k_s(α-Toc Model)×100) vs. the number of alkyl substituents (n) at aromatic ring in tocopherol model compounds.

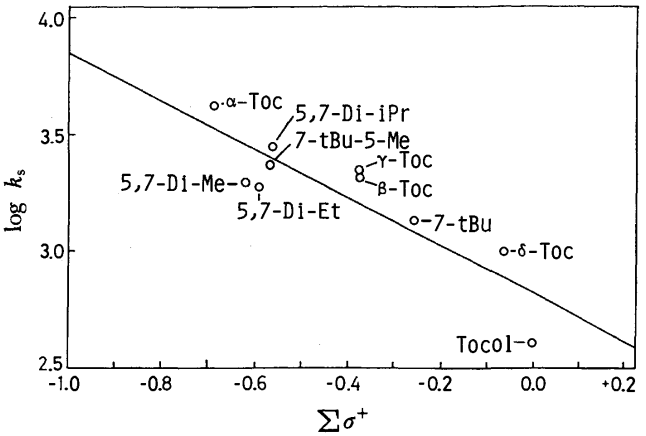

Fig. 4. Plot of log k_s for tocopherol models vs. $\Sigma\sigma^+$. The σ^+ values are from Ref. 21.

Recently, Burton et al. have reported absolute rate constants k_1 for the reaction of α-tocopherol and some related phenols (for example, 4-methoxy-2,3,5,6-tetramethylphenol) with peroxyl radicals (ROO·) (reaction 1).[9,10,19,22] By comparing the k_1 value for α-tocopherol with those found for structurally related phenols that lacked the 6-membered heterocyclic ring, they suggested that the structure of this ring was largely responsible for the high reactivity of α-tocopherol. The relative magnitudes of k_1 values for α-tocopherols and phenols can be correlated with the degree of stabilization of the radical produced by oxidation. Here, stabilization of radical depends on two factors: (i) the extent of orbital overlap between the 2p type lone pair on the para oxygen atom and the aromatic π electron system and (ii) the electron-donating or withdrawing character of the group bonded to the para oxygen atom. Therefore, Burton et al. have prepared new tocopherol model compounds having 5-membered heterocyclic ring, which is generally more planar than 6-membered ring. They found that two tocopherol models having 5-membered ring are 1.7—1.8 times as reactive as α-tocopherol. However, to our regret, all the tocopherol model compounds we have studied in the present work showed smaller reactivity than that of α-tocopherol.

We are very grateful to Professor Kazuhiko Ishizu for his valuable discussions. We also wish to thank Professor Youichi Kitamura for use of stopped-flow spectrophotometer and his helpful discussions.

References

1) P. Schudel, H. Mayer, and O. Isler, "The Vitamins," 2nd ed., ed by W. H. Sebrell, Jr. and R. S. Harris, Academic Press, New York (1972), Vol. 5, pp. 168—218.

2) M. L. Scott, "The Fat-Soluble Vitamins," ed by H. F. Deluca, Plenum Press, New York (1978), pp. 133—210.

3) W. Boguth and H. Niemann, *Biochim. Biophys. Acta*, **248**, 121 (1971).

4) K. Mukai, N. Tsuzuki, K. Ishizu, S. Ouchi, and K. Fukuzawa, *Chem. Phys. Lipids*, **29**, 129 (1981).

5) K. Mukai, N. Tsuzuki, S. Ouchi, and K. Fukuzawa, *Chem. Phys. Lipids*, **30**, 337 (1982).

6) M. Matsuo and S. Matsumoto, *Lipids*, **18**, 81 (1983).

7) J. Tsuchiya, E. Niki, and Y. Kamiya, *Bull. Chem. Soc. Jpn.*, **56**, 229 (1983).

8) G. W. Burton, Y. Le Page, E. J. Gabe, and K. U. Ingold, *J. Am. Chem. Soc.*, **102**, 7791 (1980).

9) G. W. Burton and K. U. Ingold, *J. Am. Chem. Soc.*, **103**, 6472 (1981).

10) G. W. Burton, T. Doba, E. J. Gabe, L. Hughes, F. L. Lee, L. Prasad, and K. U. Ingold, *J. Am. Chem. Soc.*, **107**, 7053 (1985).

11) K. Mukai, Y. Watanabe, Y. Uemoto, and K. Ishizu, *Bull. Chem. Soc. Jpn.*, **59**, 3113 (1986).

12) J. L. G. Nilsson, H. Sievertsson, and H. Selander, *Acta Chem. Scand.*, **22**, 3160 (1968).

13) K. Mukai, K. Takamatsu, and K. Ishizu, *Bull. Chem. Soc. Jpn.*, **57**, 3507 (1984).

14) J. L. G. Nilsson, H. Sievertsson, and H. Selander, *Acta Pharm. Suecica*, **5**, 215 (1968).

15) E. Müller, A. Schick, and K. Scheffler, *Chem. Ber.*, **92**, 474 (1959).

16) K. Mukai, Y. Watanabe, and K. Ishizu, *Bull. Chem. Soc. Jpn.*, **59**, 2899 (1986).

17) K. Fukuzawa, H. Chida, A. Tokumura, and H. Tsukatani, *Arch. Biochem. Biophys.*, **206**, 173 (1981).

18) E. Niki, A. Kawakami, M. Saito, Y. Yamamoto, J. Tsuchiya, and Y. Kamiya, *J. Biol. Chem.*, **260**, 2191 (1985).

19) G. W. Burton, L. Hughes, and K. U. Ingold, *J. Am. Chem. Soc.*, **105**, 5950 (1983).

20) J. A. Howard and K. U. Ingold, *Can. J. Chem.*, **41**, 2800 (1963).

21) H. C. Brown and Y. Okamoto, *J. Am. Chem. Soc.*, **80**, 4979 (1958).

22) T. Doba, G. W. Burton, and K. U. Ingold, *J. Am. Chem. Soc.*, **105**, 6505 (1983).

 © 1987 The Chemical Society of Japan Bull. Chem. Soc. Jpn., 60, 2169—2172 (1987)

Synthesis of 1,2-Di-*O*-alkyl-*sn*-glycero-3-phosphatidylcholine Using 2-Methoxyethoxymethyl and 2-(Trimethylsilyl)ethoxymethyl Protective Groups[1)]

Kiyoshi YAMAUCHI,* Mitsuyoshi HIHARA, and Masayoshi KINOSHITA
Department of Applied Chemistry, Osaka City University, Sumiyoshi-ku, Osaka 558
(Received January 12, 1987)

2-Methoxyethoxymethyl (MEM) and 2-(trimethylsilyl)ethoxymethyl (SEM) groups were used to protect the *sn*-3-OH of optically active glycerols in the synthesis of 1,2-di-*O*-octadecyl-*sn*-glycero-3-phosphatidylcholine. Both MEM and SEM protective groups had advantages of a classical benzyl group by virtue of (i) the facile preparation of 1,2-*O*-isopropylidene-3-*O*-(2-methoxyethoxymethyl)-*sn*-glycerol and its *sn*-3-*O*-SEM analog as starting materials and (ii) the rapid demasking of the MEM and SEM moieties in lipid precursors, especially by means of titanium tetrachloride.

With increasing physicochemical and biological interests in biomembranes, various glycerophospholipids are in great demand now.[2,3)] Of representative glycerophospholipids, 1,2-di-*O*-acyl-*sn*-glycero-3-phosphatidylcholine is prepared conveniently by direct acylation of *sn*-glycero-3-phosphatidylcholine (GPC)[4)] which is derived from egg lecithin.[5)] Another representative glycerophospholipid, 1,2-di-*O*-alkyl-*sn*-glycero-3-phosphatidylcholine, can not be produced from GPC but has been obtained via the multistep synthesis which begins generally with long-chain alkylation of the *sn*-1- and *sn*-2-OH groups of 3-*O*-benzyl-*sn*-glycerol (**1**) followed by demasking of the benzyl group of the resulting 1,2-di-*O*-alkyl-3-*O*-benzyl-*sn*-glycerol by means of catalytic hydrogenolysis and the subsequent attachment of phosphorylcholine unit or the analog to the naked *sn*-3-OH group.[6-8)]

However, one would often encounter difficulty in the hydrogenolysis because of extreme sensitivity of palladium catalyst to poisoning by a trace of contaminants in the substrate or on the appratus used; thus, a large scale preparation being often rendered unpractical. Furthermore, to our experience, the hydrogenolysis tends to become inefficient with increasing alkyl-chain length in the lipid precursors.

In view of these inconveniences of the benzyl group in the glycerolipid synthesis, we attempted to protect the *sn*-3-OH groups of optically active glycerols with 2-methoxyethoxymethyl (MEM) and 2-(trimethylsilyl)-ethoxymethyl (SEM) groups, choosing natural 1,2-di-*O*-octadecyl-*sn*-glycero-3-phosphatidylcholine (**10**) as a synthetic target. The MEM and SEM groups are acid-labile protective groups and have been utilized in the preparation of carbohydrates and nucleic acid-related compounds.[9)]

Results and Discussion

D-Mannitol was transformed into 1,2-*O*-isopropylidene-*sn*-glycerol (**2**) in a routine yield of 65—82% upon modifing a literature procedure.[10,11)] The compound **2** in THF was treated with sodium hydride, and the resulting sodium alkoxide was allowed to react with 2-methoxyethoxymethyl chloride or 2-(trimethylsilyl)ethoxymethyl chloride at ca. 0 °C for 2h. Distillation of the reaction mixtures furnished the corresponding 3-*O*-MEM and 3-*O*-SEM glycerols (**3** and **4**, respectively) in the yields of >80%.

Now, although the *O*-isopropylidene moiety and the *O*-MEM or *O*-SEM moiety of **3** and **4** are acid-labile, a treatment with 0.4 equiv of *p*-toluenesulfonic acid in 90% aqueous methanol at 25 °C for 2—3h cleaved the acetal moiety only to give 3-*O*-[(2-methoxyethoxymethyl)]- and 3-*O*-[2-(trimethylsilyl)-ethoxymethyl]-*sn*-glycerols (**4** and **5**, respectively) in the yields of 90—95% (NMR). Thus, in comparison with an analogous preparation of 3-*O*-benzyl-*sn*-glycerol (**1**) from **2**,[6)] **5**, and **6** were synthesized much readily with the yields comparable with or better than that of **1**.

Next, the sodium salts of **5** and **6** were allowed to react with octadecyl *p*-toluenesulfonate at ca. 190 °C for 0.5 h in the absence of any solvent. The modified procedure for the Williamson ether synthesis took place rapidly to give the corresponding 1,2-di-*O*-octadecylglycerols (**7** and **8**) in the yields of ca. 60%, which were higher than the values (45—47%) obtained in an ordinary procedure-reactions of the sodium alkoxide with octadecyl bromide with reflux in THF for 30h. No cleavage of the MEM and SEM protective groups was observed during the reactions.

Deprotection of the MEM and SEM-ether linkages could be performed by means of diphosphorus tetraiodide, triphenylmethyl tetrafluoroborate and zinc bromide.[9)] But, titanium tetrachloride ($TiCl_4$) was the most effective reagent of converting **7** and **8** into 1,2-di-*O*-octadecyl-*sn*-glycerol (**9**); i.e., an action of 0.6—1 equiv of $TiCl_4$ to a dichloromethane solution of **7** or **8** at ca. 0 °C for 0.5—1 h resulted in a quantitative demasking of the *sn*-3-*O*-ether moiety. No racemization occurred during the demasking reaction as judged from an optical activity of the resulting **9**.

Transformation of **9** into the phospholipid **10** was achieved as usual;[7,12)] i.e., a reaction of **9** with 2-bromoethyl phosphorodichloridate and the subsequent treatment of the reaction mixture with trimethy-

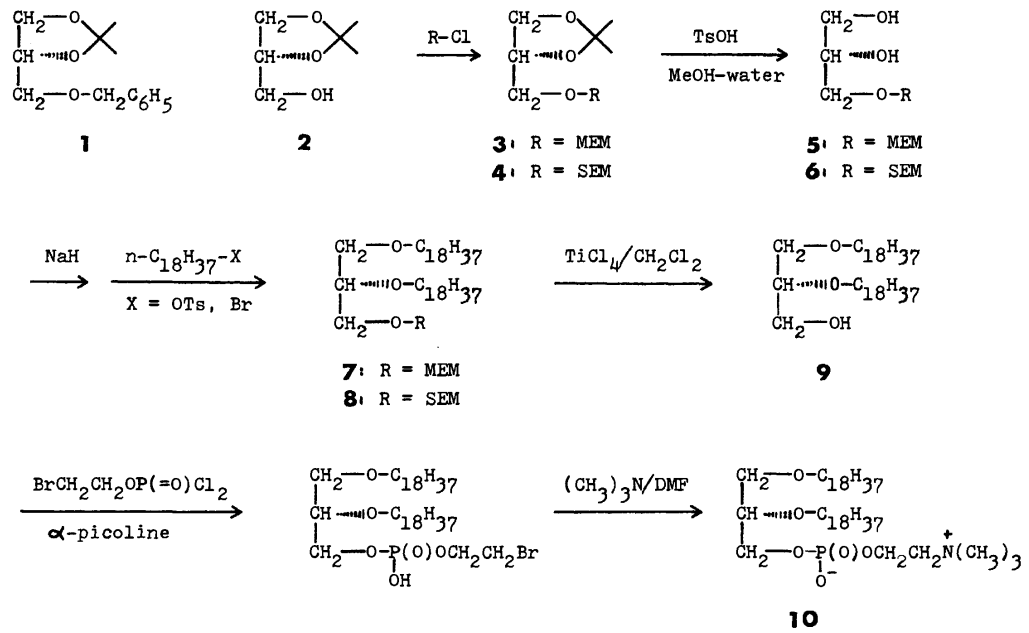

lamine afforded **10** in the yield of 35—51%.

In conclusion, the MEM and SEM groups were very useful to protect the *sn*-3-OH groups of the optically active glycerols (**2**—**8**). The protective groups were superior to the classical benzyl group with regard to (i) the facile preparation of **3** and **4** and (ii) the rapid demasking of the *sn*-3-*O*-MEM and -SEM moieties from **7** and **8**, especially by means of $TiCl_4$. Both MEM and SEM groups were similar in reactivity in the masking and demasking reactions.

Experimental

1,2-*O*-Isopropylidene-*sn*-glycerol (**2**) was derived from D-mannitol as described previously.[11] 2-Methoxyethoxymethyl chloride, 2-(trimethylsilyl)ethoxymethyl chloride, and deprotecting reagents including $TiCl_4$ were used without further purification. Column chromatography was carried out using silica gel (Merck 7734, 70—230 mesh). Mobility (R_f) in thin-layer chromatography was measured on precoated silica-gel sheet (Merck 17345, $60F_{254}$) using the following solvent systems: A, hexane-ethyl acetate (10 : 1 v/v); B, hexane-ethanol (7 : 1 v/v); C, chloroform-methanol-concentrated ammonia (65 : 35 : 5 v/v/v). Compound spots in TLC were visualized under ultraviolet light spraying with 0.0012% aqueous Rhodamine 6G (for compounds having long-chain alkyl groups) and the Dittmer-Lester reagent[13] (for phosphoric acid esters). Mp's were measured using a Yanagimoto hot stage appratus and uncorrected. Optical rotations were recorded by means of a JASCO DIY-360 polarimeter. ^{1}H NMR spectra were measured on a JEOL PS-100 using dilute solution in $CDCl_3$ or $CDCl_3$-methanol-d_4 (2 : 1 v/v) with $SiMe_4$ as an internal standard.

1,2-*O*-Isopropylidene-3-*O*-(2-methoxyethoxymethyl)-*sn*-glycerol (3). Sodium hydride (60% in oil, 1.4 g, 35 mmol) was added to a stirred THF solution (200 ml) of **2** (3.5 g, 26.5 mmol) at room temperature. After 30 min, (2-methoxyethoxy)-methyl chloride (3.6 ml, 31.5 mmol) was added dropwise to the sodium alkoxide solution cooled in an ice-water bath, and the mixture was swirled at ca. 0 °C for 2 h. The solution was then concentrated and the residue was extracted with chloroform (300 ml). The organic layer was filtered and concentrated to afford the liquid, which was distilled under reduced pressure to give **3** as a colorless substance, 4.8 g (82%); bp 92—94 °C/2 mmHg (1 mmHg=133.322 Pa); $[\alpha]_D^{25}$ +11.3° (neat); ^{1}H NMR ($CDCl_3$) δ=1.34 and 1.40 (3H, s, CH_3), 3.38 (3H, s, OCH_3), 3.47—4.16 (8H, complex m, CH_2CHCH_2 and OCH_2CH_2O), 4.28 (1H, m, CH), and 4.76 (2H, s, OCH_2O). Anal. ($C_{10}H_{20}O_5$) C, H.

1,2-*O*-Isopropylidene-3-*O*-[2-(trimethylsilyl)ethoxymethyl]-*sn*-glycerol (4). Using sodium hydride (60% in oil, 1.5 g, 37.5 mmol), **2** (4.1 g, 31 mmol) was converted into the sodium alkoxide, which was then allowed to react with 2-(trimethylsilyl)ethoxymethyl chloride (5.6 ml, 32 mmol) in a manner similar to that mentioned in the preparation of **3**, 6.5 g (80%); bp 118—120 °C/8 mmHg; $[\alpha]_D^{18}$ +10.0° (neat); ^{1}H NMR ($CDCl_3$) δ=0.0 [9H, s, $Si(CH_3)_3$], 0.93 (2H, t, J=16.4 Hz, CH_2Si), 1.30 and 1.37 (3H, s, $C(CH_3)_2$), 3.3—4.3 (7H, complex m, CH_2CHCH_2 and OCH_2CH_2Si), and 4.56 (2H, s, OCH_2O). Anal. ($C_{12}H_{26}O_4Si$) C, H.

3-*O*-(2-Methoxyethoxymethyl)-*sn*-glycerol (5). *p*-Toluenesulfonic acid monohydrate (1.5 g, 7.9 mmol) was added to a methanol-water (10 : 1 v/v) solution (55 ml) of **3** (4.7 g, 21 mmol) at 25 °C. After stirring the mixture at the same temperature for 2 h, the solution was neutralized with powdery sodium hydrogencarbonate. The supernatant was concentrated to give the residue which was extracted with chloroform. Evaporation of the solvent from a dried organic extract on anhydrous sodium sulfate furnished **5** as a colorless liquid, 3.4 g (89%); the ^{1}H NMR and IR spectra were almost identical with those of an authentic sample obtained by distillation, 1.2 g (31%); bp 120—125 °C/1 mmHg; $[\alpha]_D^{26}$ −1.58° (*c* 9.2, methanol); ^{1}H NMR ($CDCl_3$) δ=3.33 (3H, s, OCH_3), 3.1—4.5 (9H, complex m, CH_2CHCH_2 and OCH_2CH_2O), and 4.68 (2H, s, OCH_2O). Anal. ($C_7H_{16}O_5$) C, H.

3-*O*-[2-(Trimethylsilyl)ethoxymethyl]-*sn*-glycerol (6). Compound (**4**, 5.1 g, 19.4 mmol) was processed with *p*-toluenesulfonic acid monohydrate (1.5 g, 7.9 mmol) in 90% aqueous methanol (55 ml) in a manner similar to that men-

tioned in the preparation of **5**. The reaction mixture was neutralized with sodium hydrogencarbonate, concentrated and extracted with chloroform. Evaporation of the solvent from the dried organic extract on anhydrous sodium sulfate gave crude **6** (3.9 g, 91%), which that the IR and ^{1}H NMR spectra almost identical with those of the distilled material, 1.9 g (43%); bp 129—131 °C/3 mmHg; $[\alpha]_D^{24}$ +4.1° (neat); ^{1}H NMR ($CDCl_3$) δ=0.0 [9H, s, $Si(CH_3)_3$], 0.93 (2H, t, J=16.4 Hz, CH_2Si), 3.46—4.21 (7H, complex m, CH_2CHCH_2 and OCH_2CH_2Si), and 4.54 (2H, s, OCH_2O). Anal. ($C_9H_{22}O_4Si$) C, H.

1,2-Di-*O*-octadecyl-3-*O*-(2-methoxyethoxymethyl)-*sn*-glycerol (7). Compound **5**, (1.5 g, 8.3 mmol) in THF (100 ml) was stirred with sodium hydride (60% in oil, 0.7 g, 18 mmol) at room temperature for 30 min. Octadecyl *p*-toluenesulfonate (8.5 g, 20.0 mmol) was added to the alkoxide solution, and the mixture was heated to remove the solvent. The resulting semisolid residue was further heated in an oil bath at 190—200 °C for 30 min. A chloroform solution of the cooled reaction mixture was washed with water and concentrated to provide a residue which was dissolved in ethanol (150 ml) and allowed to stand in a refrigerator of ca. 10 °C overnight. The resulting solid was collected by suction-filtration, then applied to a silica-gel column. Elution with hexane-ethyl acetate (10 : 1 v/v) gave **7**, which was purified by recrystallization from acetone, 3.1 g, (54%). The mother liquior provided another crop of **7** through a similar purification process, 0.8 g (14%); mp 32—33 °C; $[\alpha]_D^{22}$ −2.2° (*c* 2.68, chloroform); R_f=0.54 (solvent B); ^{1}H NMR ($CDCl_3$) δ=0.89 (6H, two t separated by ca. δ 0.002, $2CH_3$), 1.25 [64H, coherent peak, $2(CH_2)_{16}$], ca. 1.53 (4H, m, $2OCH_2$), 3.38 (3H, s, OCH_3), 3.38—3.77 (9H, complex m, CH_2CHCH_2 and OCH_2CH_2O), and 4.73 (2H, s, OCH_2O). Anal. ($C_{43}H_{88}O_5$) C, H.

1,2-Di-*O*-octadecyl-3-*O*-[2-(trimethylsilyl)ethoxymethyl]-*sn*-glycerol (8). In a manner similar to that mentioned above, **8** was prepared from **6** in a yield of 65%. It was also obtained by the next Williamson synthesis. Compound (**6**, 2.4 g, 10.8 mmol) in THF (100 ml) was stirred with sodium hydride (60% in oil, 1.0 g, 25 mmol) at room temperature for 30 min. Octadecyl bromide (9.0 ml, 26.4 mmol) was added to the alkoxide solution, and the mixture was heated with reflux for 30 h. The cooled reaction mixture was concentrated to afford the residue which was then extracted with chloroform. The organic solution was washed with water, dried over anhydrous sodium sulfate, concentrated and applied to a silica-gel column. Elution with hexane-ethyl acetate (10 : 1 v/v) gave crude **8**, which was purified by recrystallization from acetone, 3.6 g (46%); mp 29—30 °C; $[\alpha]_D^{18}$ −1.5° (*c* 5.6, chloroform); R_f=0.54 (solvent A); ^{1}H NMR ($CDCl_3$) δ=0.0 [9H, s, $Si(CH_3)_3$], 0.80—1.07 (8H, complex m, $2CH_3$ and CH_2Si), 3.25—3.79 (9H, complex m, CH_2CHCH_2 and two $OCH_2C_{17}H_{35}$), and 3.64 (2H, t, J=16.4 Hz, CH_2CH_2Si); *m/z* (rel intensity, %) (a JEOL JMS-06 spectrometer at 75 eV at 70 °C ion source temperature) 727 (M^+, 18), and 578 (M^+ −HO-SEM, 7). Found: C, 73.92; H, 13.50%. Calcd for $C_{45}H_{94}O_4Si$: C, 74.31; H, 13.03%.

1,2-Di-*O*-octadecyl-*sn*-glycerol (9). Titanium tetrachloride (0.4 ml, 3.64 mmol) was added to a cooled dichloromethane solution of **7** (0.74 g, 1.1 mmol) in an ice-water bath. After swirling 1 h, the reaction mixture was stirred vigorously with 1 M (1 M=1 mol dm^{-3}) sodium hydrogencarbonate, then extracted with chloroform. The organic solution was washed with water, dried over anhydrous sodium sulfate and concentrated to give **9**, 0.64 g (≈100%) which was purified by a silica-gel column chromatography using a mixture of hexane and ethyl acetate (8 : 1 v/v), 0.39 g (61%); mp 57—58 °C (lit,[6] 53.5—54.5 °C); $[\alpha]_D^{25}$ −7.47° (*c* 1.6, chloroform) (lit,[6] −6.85°); R_f=0.43 (solvent B); the IR and ^{1}H NMR spectra as well as the R_f of the product were identical with those of an authentic sample, which was prepared by hydrogenolysis of 1,2-di-*O*-octadecyl-3-*O*-benzyl-*sn*-glycerol.[11]

Similarly, **8** was demasked into **9** in a yield of 72% after column chromatographic purification. The mp and the ^{1}H NMR spectrum were identical with those of **9** obtained from **7**.

1,2-Di-*O*-octadecyl-*sn*-glycero-3-phosphatidylcholine (10). The literature procedure[6] was slightly modified. A mixture of **9** (0.5 g, 0.83 mmol), 2-bromoethyl phosphorodichloridate (0.31 g, 1.3 mmol) and α-picoline (2 ml) in chloroform (30 ml) was stirred at ca. 40 °C overnight. The reaction mixture was then processed in a manner similar to that reported to give rise crude 2-bromoethyl 1,2-di-*O*-octadecyl-*sn*-glyceryl hydrogenphosphate, which was subsequently heated with 6.25 M DMF solution of trimethylamine (25 ml) at 55 °C overnight. The resulting solution was concentrated to give the residue which in 90% aqueous methanol (30 ml) was stirred vigorously with silver acetate (1.1 g, 6.6 mmol) for 1 h. The resulting precipitate was removed by filtration and the filtrate was concentrated and applied to a silica-gel column. Elution with a mixture of chloroform, methanol and water (65 : 35 : 5 v/v/v) furnished **10** as amorphous solid which was recrystallized from ethyl acetate, 0.26 g (42%); mp 205 (softening)—210 °C (melting) (lit,[8] 201—202 °C); $[\alpha]_D^{25}$ +2.1° [*c* 0.5, chloroform-methanol (2 : 1 v/v)] (lit,[8] +1.3°); R_f=0.30 (solvent C). The IR and ^{1}H NMR spectra as well as the R_f were identical with those of an authentic sample.

References

1) Compounds are named according to the recommendation of the IUPAC-IUB commision on biochemical nomenclature (1967).

2) H. Eibl, *Angew. Chem., Int. Ed. Engl.*, **23**, 257 (1984); D. Papahadjopoulos,"Medical Application of Liposomes," ed by K. Yagi, Japan Scientific Societies Press, Tokyo (1986), p. 1.

3) F. Ramirez, and J. F. Marecek, *Synthesis*, **1985**, 449.

4) R. Radhakrishnan, R. J. Robson, Y. Takagaki, and H. G. Khorana, *Methods in Enzymology*, **72**, 408 (1981).

5) J. S. Chadha, *Chem. Phys. Lipid.*, **4**, 104 (1970).

6) M. Kates, T. H. Chan, and N. Z. Stanacev, *Biochemistry*, **2**, 394 (1963).

7) S. Tsushima, Y. Yoshikawa, S. Tanida, H. Nomura, S. Nojima, and M. Hozumi, *Chem. Pharm. Bull. (Tokyo)*, **30**, 3260 (1982).

8) S. Funahashi, I. Hara, and T. Yamakawa, "Shishitsu (Lipids)," Kyoritsu, Tokyo (1963), part 1, p. 359.

9) T. W. Greene, "Protective Groups in Organic Synthesis," Wiley, New York (1981), p 19; T. Ito, S. Ueda, and H. Takaku, *J. Org. Chem.*, **51**, 931 (1986); H. Saimoto, Y. Kusano, and T. Hiyama, Abstracts, 52nd Meeting of the Japan Chemical Society, April 1986, No. 1O33; other references are cited therein.

10) E. Baer and H. O. L. Fisher, *J. Biol. Chem.*, **128**, 463 (1939).

11) K. Yamauchi, F. Une, S. Tabata, and M. Kinoshita, *J. Chem. Soc., Perkin Trans. 1*, **1986**, 765.
12) M. Ohno, K. Fujita, H. Nakai, S. Kobayashi, K. Inoue, and S. Nojima, *Chem. Pharm. Bull. (Tokyo)*, **33**, 572 (1985).
13) J. C. Dittmer and R. L. Lester, *J. Lipid Res.*, **5**, 126 (1964).

Electrogenerated Acid-Catalyzed Reactions of Acetals, Aldehydes, and Ketones with Organosilicon Compounds, Leading to Aldol Reactions, Allylations, Cyanations, and Hydride Additions

Sigeru Torii,* Tsutomu Inokuchi, Sadahito Takagishi, Hirofumi Horike, Hideki Kuroda, and Kenji Uneyama
Department of Industrial Chemistry, School of Engineering, Okayama University, Okayama 700
(Received January 21, 1987)

Exquisite use of electrogenerated acid (EG acid) in the silicon-mediated acid-catalyzed reactions; e.g., aldol reactions, allylations, cyanations, and hydride additions is described. The aldol reaction of acetals **1** with enol trimethylsilyl ethers **3** and 1,2-bis(trimethylsiloxy)alkenes **4** gives the corresponding adducts **5** and **6**, respectively. The reaction proceeds smoothly with EG acid derived from perchlorate salts such as $LiClO_4$, n-Bu_4NClO_4, and $Mg(ClO_4)_2$ in dichloromethane using platinum electrodes. The amount of electricity required to complete the reaction implies a cationic process which is mediated by the trimethylsilyl moiety. This aldol reaction is further developed with unprotected carbonyl compounds **2** with **3**, giving the trimethylsilyl ethers of the adducts **7**. Further utility of this EG acid as a catalyst for a chain reaction is exemplified by the successful application in the following conversions: (1) The allylation of acetals **1** with allyltrimethylsilane (**8**) to give **9**, (2) the cyanation of acetals **1** and unmasked **2** with trimethylsilyl cyanide (**10**) to give **11**, **12**, and **13**, and (3) the hydride addition of acetals **1** with triethylsilane (**14**) to give **15**.

The reaction of organosilicon compounds[1] bearing a nucleophilic site with an electron-deficient center has demonstrated one of the most efficiently designed examples of acid-catalyzed reactions, in which the silyl moiety serves as a chain carrier.[2] This reaction can be understood as illustrated in Scheme 1.

Thus, acetals and aldehydes **A** are activated by an acid-catalyst to give cationic intermediates **B**. These carbocations $[R^1R^2C\text{-}X]^+$ (X=OR, NR'R", etc.) may be stabilized by buffering with counter ion such as perchlorate ion or triflate ion present in the media. When nucleophilic silicon compounds are added to this media, cation **B** undergoes nucleophilic attack to produce the substituted product C together with a stable methoxysilane **D**. The formation of methoxysilane **D**, therefore, favors the equilibration of this acid-catalyzed reaction to proceed to completion. These silicon-mediated cationic reactions including aldol reaction,[2,3] acetalization,[2,12] allylation,[2] hydride additions,[2] cyanation,[2,4] and others[2,5] have been effected by very oxophilic reagents such as trimethylsilyl triflate (TMSOTf),[2] triphenylmethyl perchlorate ($TrClO_4$),[3,5,6] and other Lewis acids.[4] Unfortunately, these moisture sensitive reagents are cumbersome to use and it is still of considerable interest to develop new effective reagents which can be easily prepared and handled. In the previous paper from our laboratory, we have explored the potential utility of an electrogenerated acid (EG acid)[7] as a catalyst for selective epoxy ring openings,[8] tetrahydropyranylation of alcohols,[9] conversion of nerolidol to bisaborol,[10] biogenetic-type cyclization,[11] and acetalization of carbonyl compounds.[12] These results indicates an oxophilic ability of EG acid to oxygen containing compounds and prompted us to investigate the possibility of EG acid as an alternative to hitherto known catalysts in the above silicon-mediated catalytic reactions. In this paper, we describe an EG acid-assisted activation of acetals as well as unprotected aldehydes and ketones in the presence of organosilicon compounds bearing a nucleophilic site, leading to (1) aldol reactions, (2) allylations, (3) cyanations, and (4) hydride additions.

Results and Discussion

Aldol Reaction of Acetals, Aldehydes, and Ketones with Enol Trimethylsilyl Ethers. The aldol condensation has long been recognized to be one of the most versatile synthetic tools for a carbon-cabon bond formation.[13] The reaction of acetals **1** with enol silyl

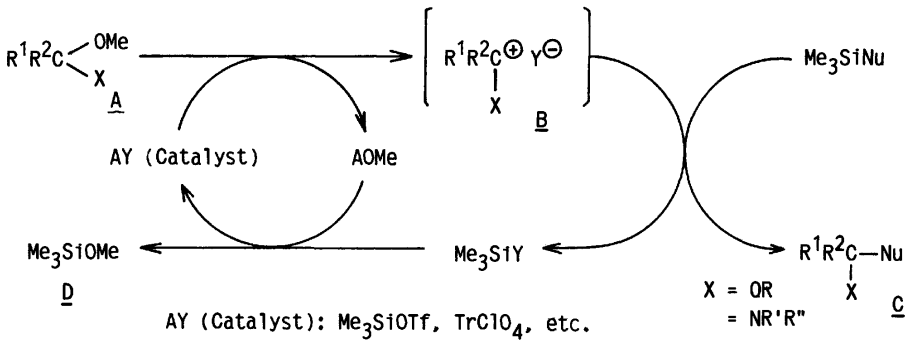

Scheme 1.

ethers **3** is an important method of obtaining the corresponding adducts **5**, selectively.[3,14-16] The electrochemical version of this condensation was attempted using benzaldehyde dimethyl acetal (**1a**) and cyclohexanone enol trimethylsilyl ether (**3a**) as a typical substrate. Thus, the electrolysis was carried out by using platinum foil electrodes in dichloromethane (CH_2Cl_2) containing lithium perchlorate ($LiClO_4$) and/or tetrabutylammonium perchlorate (n-Bu_4NClO_4) for both an electrolyte and a source of the electrogenerated acid (EG acid). During the electrolysis a constant current of 2.67 mA cm^{-2} (applied voltage: 8—10 V) was charged until the starting materials **1a** or **3a** disappeared completely on TLC. After the electrolysis (0.07 F mol^{-1} of electricity based on the starting **3a** as one electron process has been passed), the reaction was quenched with a few drops of triethylamine and the concentrated products, without aqueous working up, were purified by column chromatography on silica gel to give *threo*-**5a** and *erythro*-**5a** in 93% yield as an isolable 14:86 mixture. No polycondensation product, self-condensation product, or α,β-unsaturated enone was formed by this reaction. The stereochemistry of the diastereoisomers **5a** was determined based on the ^{1}H NMR signals due to the methine proton on the methoxylated carbon (spectral data are given in the Experimental).[14b] On the other hand, no aldol reaction was observed for the acetal **1a** with cyclohexanone enol acetate, cyclohexanone enol methyl ether, and cyclohexanone morpholine enamine by treatment with the EG acid.

In order to know the applicability of the present procedure to the large-scale operation, we attempted to perform this reaction in the circulating flow-cell system as illustrated in Fig. 1, in which the electrolyte was circulated at a linear rate of about 15 cm min^{-1}. By using this flow-cell system, we were capable of preparing the aldol **5a** in 82—86% yields by the electrolysis of an appreciably concentrated solution of **1a** and **3a** (0.8—1.3 M in $ClCH_2CH_2Cl$) with SUS-27 electrodes.

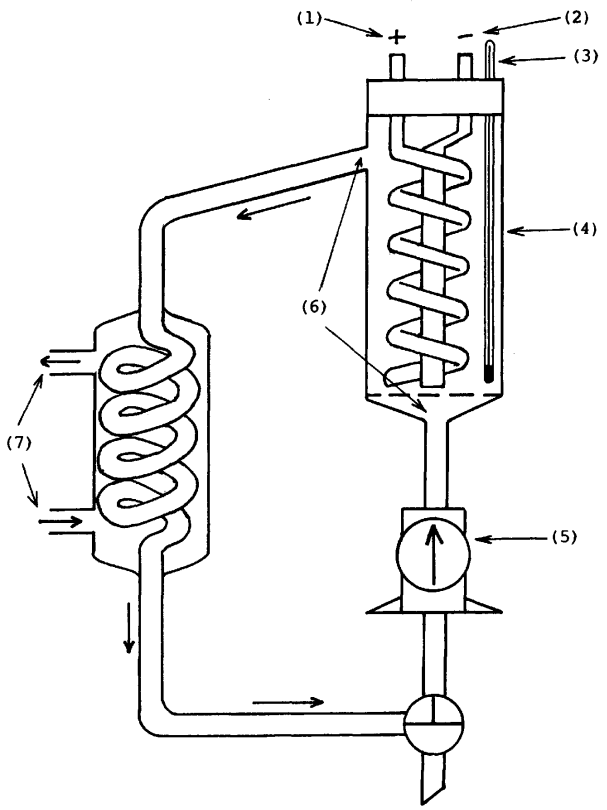

Fig. 1. Schematic drawing of a circulating flow cell for EG acid catalyzed reaction; (1): anode (SUS-27), (2): cathode (SUS-27), (3): thermometer, (4): glass electrolysis cell. (ca. 30 mm diameter and 150 mm height), (5): circulating pump, (6): electrolyte outlet and inlet, (7): heat exchanger by cold ethanol.

The effect of a supporting electrolyte is remarkable in this aldol reaction. The current efficiencies summarized in Table 1 were determined at the time when the necessary amount of electricity for the complete conversion has been passed based on the starting material **3a**. As shown in Entries 5—7, good to excellent conversion yields were obtained with perchlorate salts

Table 1. Effect of Electrolytes and Temperature in the Aldol Reaction of **1a** and **3a** to **5a**[a]

Entry	Electrolyte[b]	Solvent[c]	Temp °C	F mol^{-1}[d]	Yield of **5a**[e]/% (CE)[f]	(erythro/threo)[g]
1	$LiClO_4$-n-Bu_4NClO_4 (1:1)	CH_2Cl_2	20	0.01	75 (7500)	(79/21)
2	$LiClO_4$-n-Bu_4NClO_4 (1:1)	CH_2Cl_2	0	0.02	78 (3900)	(85/15)
3	$LiClO_4$-n-Bu_4NClO_4 (1:1)	CH_2Cl_2	−30—−40	0.04	86 (2150)	(83/17)
4	$LiClO_4$-n-Bu_4NClO_4 (1:1)	CH_2Cl_2	−78	0.07	93 (1329)	(86/14)
5	n-Bu_4NClO_4	CH_2Cl_2	−78	0.07	92 (1314)	(86/14)
6	$LiClO_4$	CH_2Cl_2-THF (10:1)	−78	0.02	84 (4200)	(84/16)
7	$Mg(ClO_4)_2$	CH_2Cl_2-THF (10:1)	−78	0.05	70 (1400)	(81/19)
8	$LiBF_4$	CH_2Cl_2-THF (10:1)	−78	0.30	24 (80)	(75/25)
9	Et_4NOTs	CH_2Cl_2	−78	0.30	—	
10	Et_4NBr	CH_2Cl_2	−78	0.30	—	

a) Carried out by using **1a** (1.2 mmol) and **3a** (1.0 mmol) with Pt electrodes (1.5 cm^2) at a constant current density of 2.67 mA cm^{-2} in an undivided cell. b) 0.1 Mol equivalent of the electrolyte to the substrate **3a** was used. c) 3 Ml was used. d) Electricity consumed (based on **3a** as an one-electron process). e) Based on isolated products. f) Current efficiency on the basis of one electron reaction. g) Determined based on isolated materials.

such as $LiClO_4$, n-Bu_4NClO_4, and $Mg(ClO_4)_2$. A combination of $LiClO_4$ and n-Bu_4NClO_4 (1/1 mixture), employed to get enough electric conductivity through the electrolysis media, gave the best conversion yield of **5a** (Entry 4). Other supporting electrolytes such as lithium tetrafluoroborate, tetraethylammonium tosylate, and tetraethylammonium bromide are less useful for this purpose (Entries 8—10). Halogenated solvents such as dichloromethane and 1,2-dichloroethane are highly effective for the formation of the aldol **5a**, while AcOEt, hexane, and THF are less effective. In order to increase the solubility of $LiClO_4$, $Mg(ClO_4)_2$, and $LiBF_4$ in CH_2Cl_2, THF was added to the solution in approximately 10 vol% (Entries 6—8). As shown in Table 1, Entries 1—4, the yield and erythro/threo selectivity of **5a** increase with lowering the temperature from 20 to −78 °C, although the current efficiency decreases. Meanwhile, feasibility of the present reaction at wide temperature range enables to raise the reactivity of rather less reactive acetals and unmasked carbonyl compounds (Entries 4 and 26 in Table 2). The yield and erythro/threo (e/t) selectivity of **5a** obtained by an EG acid-catalyzed reaction are comparable to the literature data obtained by other reagents such as TMSOTf (−75 °C/10 h, 89% yield, e/t=93 : 7),[2] $TrClO_4$ (−75 °C/0.25 h, 96% yield, e/t=88 : 12),[3a] and $TiCl_4$ (1 equiv) (−75 °C/2 h, 95% yield, e/t=50 : 50).[15a] The erythro selectivity of this reaction can be rationalized in terms of an acyclic extended transition state of Type **A** (Scheme 2), in good accordance with the results obtained with TMSOTf[2] or $TrClO_4$[3a] as a catalyst. This EG acid-catalyzed procedure could be applied to aldol reaction of a variety of acetals **1** and enol silyl ethers **3**, and the results are shown in Table 2, Entries 1—12. Acetals of aromatic aldehydes generally gave reasonable results, whereas acetals of saturated aliphatic aldehydes and ketones provided the corresponding adducts slightly lower yields or lower current efficiencies.

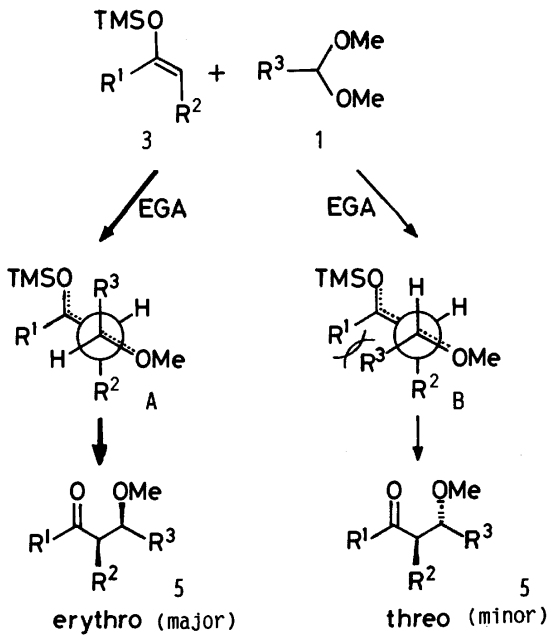

Scheme 2.

Aldols derived from 1,2-bis(trimethylsiloxy)cycloalkenes **4** and acetals **1** are synthetically valuable as precursors of 1,3-cycloalkanediones by rearrangement.[16a] Keto esters can also be prepared from these aldol products by oxidative or reductive ring cleavage.[16] These aldol reactions of **4** with acetals **1** have been carried out by using a stoichiometric amount of Lewis acid such as $TiCl_4$ and $BF_3 \cdot OEt_2$. However, aldol products derived from 1,2-bis(trimethylsiloxy)-cyclobutene **4c** are susceptible to undergo further rearrangement with acid-catalyst such as TMSOTf, TFA, and p-TsOH to give 1,3-cyclopentanediones. We have succeeded in the EG acid-catalyzed aldol reaction of **4** with acetals **1**, giving the corresponding adducts **6**, selectively (Table 2, Entries 13—20). Any by-products due to acid-catalyzed rearrangement have not been observed in the reaction products, except for the free alcohols which is due to partial hydrolysis of the trimethylsiloxy group of **6** (4—6%).

On the other hand, it is noted that the aldol reaction of enol silyl ethers **3** with unmasked ketones and aldehydes **2** is unsuccessful with a catalytic amount of TMSOTf[14a] as an acid-catalyst, while $TrClO_4$ effects this condensation, smoothly.[3] Stimulated by these findings, we attempted the EG acid-catalyzed aldol reaction of aldehydes **2** with enol silyl ethers **3** to compare the stereochemical outcome of the product with that obtained from **1** and **3**. The electrolysis of benzaldehyde **2a** and **3a** in CH_2Cl_2 containing an 1 : 1 mixture of $LiClO_4$ and n-Bu_4NClO_4 produced the desired aldol product **7a** in 85% yield. However, erythro/threo ratio of the product **7a** decreased to 69 : 31 in comparison with the ratio 86 : 14 obtained from the acetal **1a** and **3a**. In this reaction, aldols **7** are isolated as a silyl ether. The aldol reaction with ketones required a higher temperature than that for the reaction with aldehydes. Typical results of electrochemical aldol reaction of unmasked **2** with enol silyl ethers **3** are summarized in Table 2, Entries 21—26.

In order to gain an insight into the behavior of the EG acid in this aldol reaction, an electrolysis procedure different from that above mentioned was examined. Thus, electrolysis of the solution in the absence of **1a** and **3a** by passing about 0.05 F mol^{-1} of electricity was followed by the addition of the substrates **1a** and **3a** at −78 °C (stirring was continued for 10 min) to give the following results. The desired aldol adducts **5a** were obtained in almost identical yields with those obtained in the concurrent electrolysis. However, the electrolysis in the presence of a small amount of bases such as pyridine and triethylamine prevents the condensation, completely. These results along with erythro-selectivity of the adducts suggest the formation of EG acid of Brønsted acid character like as $HClO_4$[7]

Table 2. Aldol Reaction of Enol Silyl Ethers **3** and **4** with Acetals **1**, Aldehydes, and Ketones **2** Catalyzed by Electrogenerated Acid (EG Acid)[a)]

Entry	Acetal or Aldehyde	Enol Silyl Ether	Electricity / F mol^{-1}[b)]	Product[c)] (Yield[d)]/%, erythro/threo[e)])
1	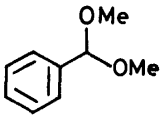 **1a**	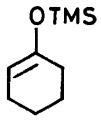 **3a**	0.07	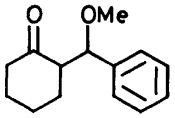 (93, 86:14) **5a**
2	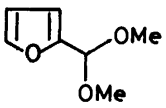 **1b**	**3a**	0.05	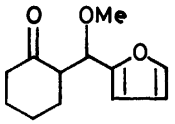 (82, 93: 7) **5b**
3	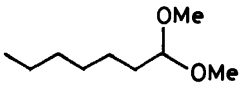 **1c**	**3a**	0.075	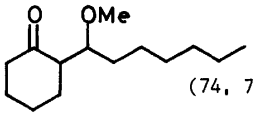 (74, 72:28) **5c**
4	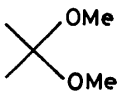 **1d**	**3a**	0.15	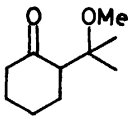 (52) **5d**
5	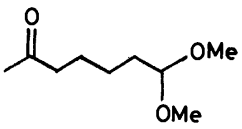	**3a**	0.11	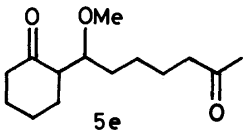 (60, ca, 60:40) **5e**
6	**1a**	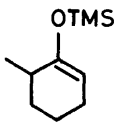 **3b**	0.15	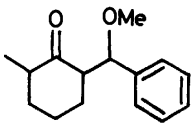 (64, 44:56) **5f**
7	**1a**	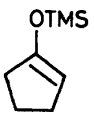 **3c**	0.065	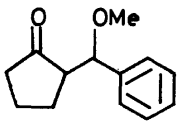 (88, 75:25) **5g**
8	**1c**	**3c**	0.075	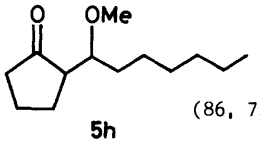 (86, 73:27) **5h**
9	**1a**	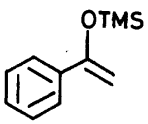 **3d**	0.075	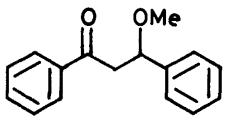 (85) **5i**

Table 2. (Continued)

Entry	Acetal or Aldehyde	Enol Silyl Ether	Electricity / F mol^{-1}[b]	Product[c] (Yield[d]/%, erythro/threo[e])
10	1c	3d	0.18	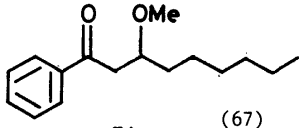 (67) **5j**
11	1d	3d	0.15	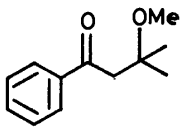 (73) **5k**
12	1a	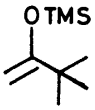 **3e**	0.15	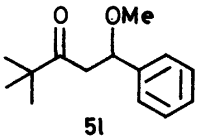 (33) **5l**
13	1a	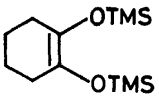 **4a**	0.87	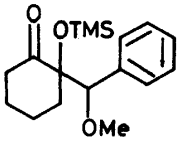 (91) **6a**
14	1b	4a	0.112	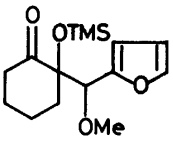 (66) **6b**
15	1c	4a	0.124	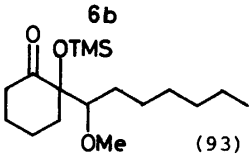 (93) **6c**
16	1a	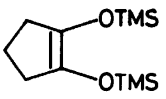 **4b**	0.01	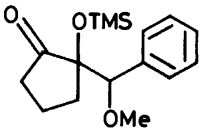 (82) **6d**
17	1c	4b	0.174	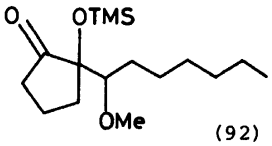 (92) **6e**
18	1d	4b	0.174	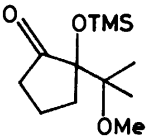 (74) **6f**

Table 2. (Continued)

Entry	Acetal or Aldehyde	Enol Silyl Ether	Electricity / F mol^{-1}[b]	Product[c] (Yield[d]/%, erythro/threo[e])
19	1a	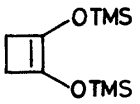 4c	0.087	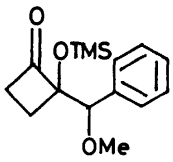 (81) 6g
20	1c	4c	0.137	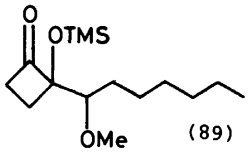 (89) 6h
21	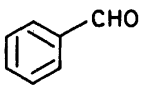 2a	3a	0.124	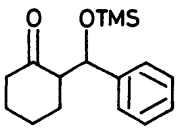 (85, 69:31) 7a
22	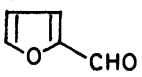 2b	3a	0.124	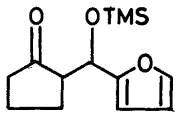 (88, 83:17) 7b
23	2a	3c	0.114	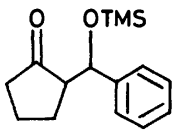 (87, 97: 3) 7c
24	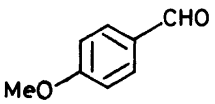 2c	3c	0.075	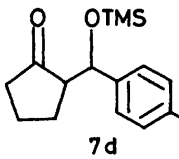 (84, 99: 1) 7d
25	2a	3d	0.150	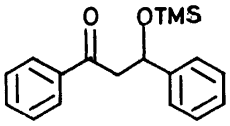 (80) 7e
26	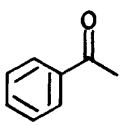 2d	3d	0.224	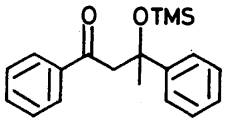 (84) 7f

a) Unless otherwise noted electrolyses were carried out under a constant current of 2.67 mA cm^{-2} with two platinum electrodes (1.5 cm^2) in an undivided cell under argon at −78 to −60 °C (for unmasked aldehyde as well as acetals derived from aldehydes) or at 0 °C (for unmasked ketone as well as acetal derived from ketone). b) Faradays/mole during preparative run. c) Products from **1** and **4** (Entries 13—20) are contaminated with 4—6% of the free alcohol due to the partial hydrolysis of silyl protecting group. d) Based on isolated products in complete conversion of 1.0—1.2 mmol of the substrates. e) Determined either by direct separation of isomers by SiO_2 column chromatography or by ^{1}H NMR spectra.

during the electrolysis in a CH_2Cl_2-$LiClO_4$-*n*-Bu_4NClO_4-(Pt) system. The EG acid could be concentrated at the vicinity of the anode during the electrolysis so that the aldol condensation proceeds even with EG acid generated with a catalytic amount of electricity.

Allylation with Allyltrimethylsilane. Addition of an allyl group to carbonyl compounds using allyltrimethylsilane (**8**) is of value due to the versatility of adducts in organic transformation.[17] The activation of the carbonyl function for this transformation has been effected by a stoichiometric amount of Lewis acid[18] such as $TiCl_4$, $BF_3 \cdot OEt_2$, and $AlCl_3$ and a catalytic amount of TMSOTf.[19] We attempted to use the EG acid as a catalyst for this allylation. Thus, allyltrimethylsilane was reacted with acetals **1** at 0 °C in CH_2Cl_2 with the aid of the EG acid to give the corresponding homoallylic alcohol methyl ethers **9** in high yields. However, the reaction of aldehyde **2** with allyltrimethylsilane was unsuccessful. The reaction of 4-*t*-butylcyclohexanone dimethyl acetal **1k** at 0 °C furnished a mixture of equatorial:axial adducts **9k** in 90:10 ratio (80% yield).[2] Some additional results are given in Table 3.

Table 3. Preparation of Homoallyl Ethers **9** from Allylsilane **8** and Acetals **1**[a]

Entry	Acetal **1**	Electricity / F mol^{-1}[b]	Homoallyl ether **9** (Yield/%)[c]
1	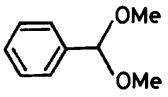 **1a**	0.07	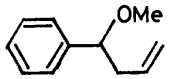 (82) **9a**
2	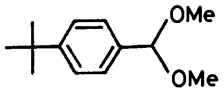 **1f**	0.06	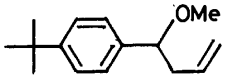 (98) **9f**
3	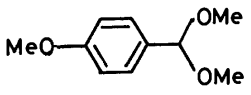 **1g**	0.04	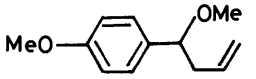 (93) **9g**
4	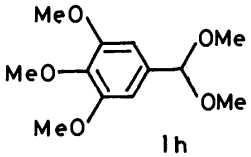 **1h**	0.03	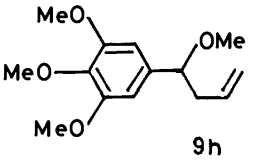 (95) **9h**
5	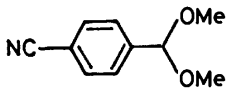 **1i**	0.03	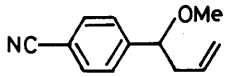 (79) **9i**
6	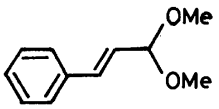 **1j**	0.12	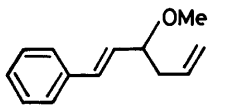 (78) **9j**
7	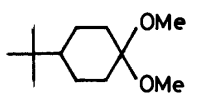 **1k**	0.21	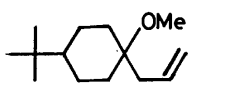 (80) **9k**

a) Unless otherwise noted electrolyses were carried out under a constant current of 2.67 mA cm^{-2} with two platinum electrodes (1.5 cm^2) in an undivided cell under argon at 0 °C. b) Faradays/mole during preparative run. c) Based on isolated products in complete conversion of 1.0—1.2 mmol of the substrates.

Cyanation of Acetals with Trimethylsilyl Cyanide. α-Alkoxyalkanenitriles **11**, a protected form of cyanohydrins, are synthetically useful compounds as precursors of 3-amino-2-alkenenitriles,[20] α-alkoxy ketone[21] and are accepted as synthons of acyl carbanion equivalents.[22] Although the preparation of α-alkoxy nitriles by cyanation of acetals with trimethylsilyl cyanide (**10**) using Lewis acid has been reported,[4,24] a highly convenient procedure is still in demand. We have succeeded in a facile cyanation of dimethyl acetals **1** with trimethylsilyl cyanide (**10**) by using EG acid, giving **11**.

The reaction procedure is similar to that of the aldol reaction. Thus, a mixture of heptanal dimethyl acetal (**1c**) and trimethylsilyl cyanide (**10**) in CH_2Cl_2 containing $LiClO_4$ and Et_4NClO_4 (1 : 1) was electrolyzed with plat-

Table 4. Preparation of Cyanohydrin Methyl Ether **11** from Acetal **1** and Trimethylsilyl Cyanide (**10**)[a]

Entry	Acetal **1**	Electricity[b] / F mol^{-1}	Cyanohydrin Methyl Ether **11** (Yield/%)[c]
1	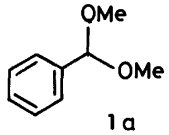 **1a**	0.04	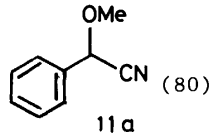 (80) **11a**
2	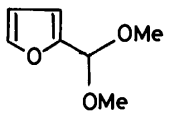 **1b**	0.01	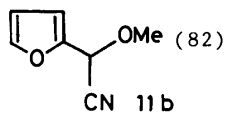 (82) **11b**
3	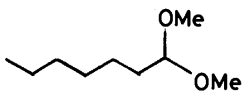 **1c**	0.08	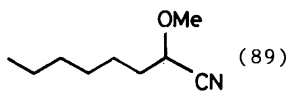 (89) **11c**
4	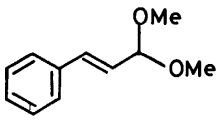 **1j**	0.40	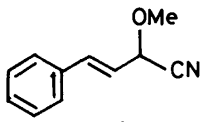 (81) **11j**
5	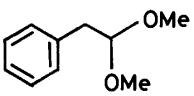 **1l**	0.03	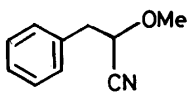 (87) **11l**
6	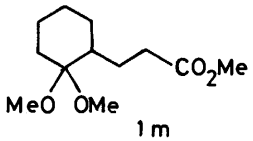 **1m**	0.06	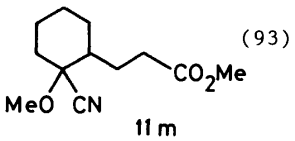 (93) **11m**
7	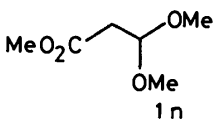 **1n**	0.15	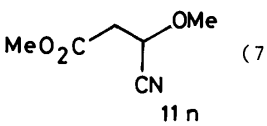 (72) **11n**
8	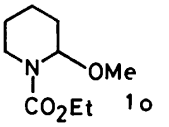 **1o**	0.28	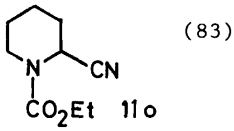 (83) **11o**

a) Unless otherwise noted electrolyses were carried out at an applied voltage of 15 V (current: 12 mA) with two platinum electrodes (1.5 cm^2) in an undivided cell under argon at room temperature. b) Faradays/mole during preparative run. c) Based on isolated products in complete conversion of 1.0—1.2 mmol of the substrates.

inum electrodes at an applied voltage of 15 V (current: 12—13 mA). After electrolysis for 32 min (electricity: 0.077 F mol^{-1} based on acetal **1c** as one electron process) and an additional stirring for 5 min, the reaction was quenched with pyridine (2 drops). Concentration in vacuo followed by either column chromatography (SiO_2, hexane-AcOEt, 50:1) or bulb to bulb distillation gave the cyanide **11c** in 89% yield. Electrolysis with either $LiBF_4$ or Et_4NOTs as a supporting electrolyte resulted only in the recovery of the starting acetal **1c**.

As shown in Table 4, most of the acetals **1** could be smoothly converted into the corresponding cyanohydrin methyl ethers **11** with a catalytic amount of electricity. Cyclic α-methoxy amine **1o** underwent smooth cyanation through the replacement of the methoxyl group to give 2-cyanopiperidine **11o**.

Alternatively, the EG acid-catalyzed cyanation of unprotected aldehydes and ketones with trimethylsilyl cyanide (**10**) was examined. Cyanohydrin derived from ketones were obtained as a form of trimethylsilyl ethers **12**, while adducts of aldehydes were isolated as a cyanohydrins **13** due to the instability of the corresponding silyl ether to moisture. The reaction of α,β-enone **2i** with trimethylsilyl cyanide gave 1,2-adducts **12i**, predominantly (Table 5).

Table 5. Preparation of Cyanohydrin Derivatives from Ketones and Aldehydes **2**[a]

Entry	Ketone or Ardehyde **2**	Electricity[b] / F mol^{-1}	Product, **12**, **13** (Yield/%)[c]
1	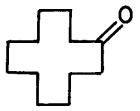 **2e**	0.28	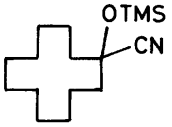 **12e** (95)
2	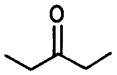 **2f**	0.15	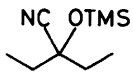 **12f** (93)
3	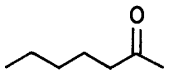 **2g**	0.15	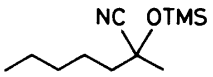 **12g** (97)
4	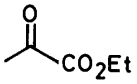 **2h**	0.38	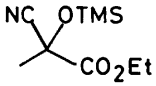 **12h** (82)
5	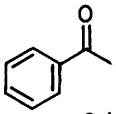 **2d**	0.47	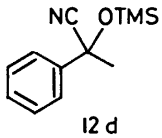 **12d** (88)
6	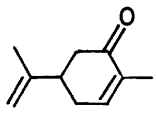 **2i**	0.30	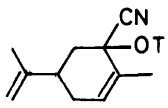 **12i** (88)
7	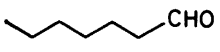 **2j**	0.37	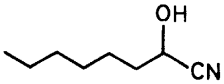 **13j** (82)
8	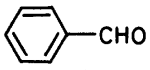 **2a**	0.16	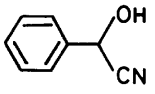 **13a** (88)

Table 5. (Continued)

Entry	Ketone or Ardehyde **2**	Electricity[b] / F mol^{-1}	Product, **12**, **13** (Yield/%)[c]
9	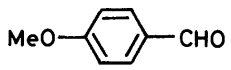 **2c**	0.03	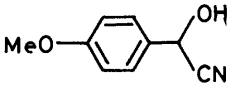 **13c** (97)
10	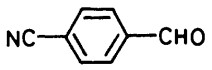 **2k**	0.13	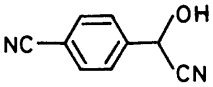 **13k** (66)
11	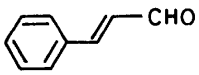 **2l**	0.33	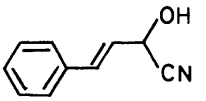 **13l** (91)

a) Unless otherwise noted electrolyses were carried out under a constant current of 20 mA cm^{-2} (for ketones) or 6.67 mA cm^{-2} (for aldehydes) with two platinum electrodes (1.5 cm^2) in an undivided cell under argon at room temperature. b) Faradays/mole during preparative run. c) Based on isolated products in complete conversion of 1.0—1.2 mmol of the substrates.

Table 6. Preparation of Methyl Ether **15** by the Reaction of Acetal **1** and Triethylsilane (**14**)[a]

Entry	Acetal **1**	Electricity[b] / F mol^{-1}	Methyl Ether **15** (Yield/%)[c]
1	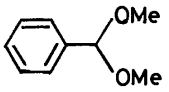 **1a**	0.02	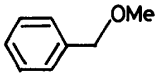 **15a** (88)
2	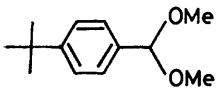 **1f**	0.06	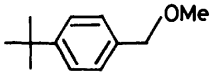 **15f** (87)
3	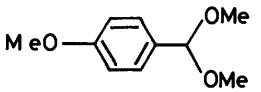 **1g**	0.02	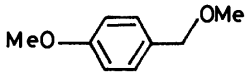 **15g** (95)
4	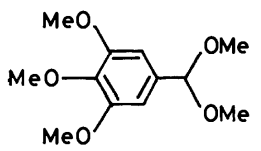 **1h**	0.02	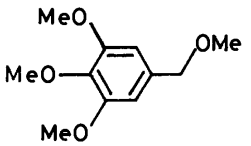 **15h** (95)
5	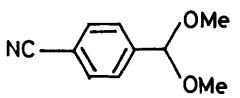 **1i**	0.04	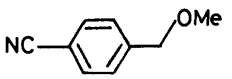 **15i** (74)

a) Unless otherwise noted electrolyses were carried out under a constant current of 2.67 mA cm^{-2} with two platinum electrodes (1.5 cm^2) in an undivided cell under argon at 0°C. b) Faradays/mole during preparative run. c) Based on isolated products in complete conversion of 1.0—1.2 mmol of the substrates.

Hydride Addition to Acetals. Trialkylsilanes have attracted a considerable interest because of their utility as a mild hydrogen doner in modern synthetic reaction.[23] Acetals have been reduced to ethers with this reagent by the aid of TMSOTf.[24] We have also succeeded in this transformation using EG acid as a catalyst. Thus, the electrolysis of acetals **1** in the presence of a slightly excess of triethylsilane (**14**), performed in a similar manner as described for the aldol reaction, resulted in the replacement of methoxyl group with hydrogen to give the corresponding ethers **15** in good yields. Some examples of this reaction are listed in Table 6.

In this paper the EG acid has been shown to be a viable alternative as a catalyst for silicon-mediated cationic reaction in terms of its easy and clean operation, short reaction time, and high current efficiency. By analogy with the reactions catalyzed by TMSOTf[2] and $TrClO_4$,[3,5,6] the present EG acid catalyzed reactions of acetals **a** and Me_3SiNu are rationalized as depicted in Scheme 3. Thus, the EG acid generated from perchlorate salts is strong enough to activate **a** to allow the carbenium ion **b** buffered by perchlorate ion. The cation **b** undergoes smoothly nucleophilic attack of Me_3SiNu to produce the desired **c**. In this step, the intermediacy of trimethylsilyl perchlorate (Me_3SiClO_4) is considered, but the Me_3SiClO_4 is quickly hydrolyzed by methoxide ion to stable methoxytrimethylsilane **d**, allowing to regenerate the EG acid. Although the nature of EG acid was not unveiled completely, its electrophilic character to the oxygen function was demonstrated, resembling with that of conventional catalyst such as TMSOTf and $TrClO_4$ especially in the aldol reactions. As noted above briefly, if EG acid, generated in a CH_2Cl_2-$LiClO_4$-n-Bu_4NClO_4-(Pt) system, has a character of Brønsted acid like $HClO_4$, the results accomplished in this paper are the first example, to our knowledge, that is achieved by the acid not having Lewis acid character. Further study aimed at the extended application of the EG acid for organic transformation is currently under investigation.

Experimental

General. Melting points are uncorrected and boiling points are indicated by an air-bath temperature without correction. IR spectra were recorded with a JASCO IRA-1 grating spectrometer. Unless otherwise noted, ^1H NHR spectra were determined at 60 MHz with either a Hitachi R-24 or a JEOL JNM-PMX 60 and ^{13}CNMR spectra were recorded with a JEOL FX-100 (25.05 MHz) spectrometer. Samples were dissolved in $CDCl_3$ and the chemical shifts are expressed in δ values (ppm) relative to Me_4Si as an internal standard. Satisfactory elemental analyses were obtained for the new compounds: C ±0.29, H ±0.29.

Materials. Enol silyl ethers **3**[25] and 1,2-bis(trimethylsiloxy)-cycloalkenes **4**[26] were prepared by the reported methods. Commercially available allyltrimethylsilane (**8**), trimethlsilyl cyanide (**10**), triethylsilane (**14**) were used as received. $LiClO_4$, n-Bu_4NClO_4, and Et_4NClO_4 purchased from Tokyo Kasei Kogyo (Japan) were used without further purification. Dichloromethane and 1,2-dichloroethane were distilled once over P_2O_5 before use.

Electrolysis Apparatus. A simple cylindrical glass tube (1.5 cm diameter×10.5 cm height) was equipped with a gas inlet tube, stirring bar, and two platinum foil electrodes (1.5 cm^2) placed parallel to each other 3 mm apart. The vessel was immersed in a cooling bath as indicated in the Experimental. The reactions were usually carried out under argon.

Typical Procedure for the Aldol Condensation of Acetal 1 with Enol Trimethylsilyl Ether 3. Into the electrolysis vessel were added $LiClO_4$ (10.6 mg, 0.1 mmol) and n-Bu_4NClO_4 (34.2 mg, 0.1 mmol) and the resulting mixture was dried at about 100 °C under vacuum for 1 h and then purged with argon. To this mixture was added a solution of cyclohexanone enol trimethylsilyl ether (**3a**, 170.3 mg, 1.0 mmol), benzaldehyde dimethyl acetal (**1a**, 182.6 mg, 1.2 mmol) in

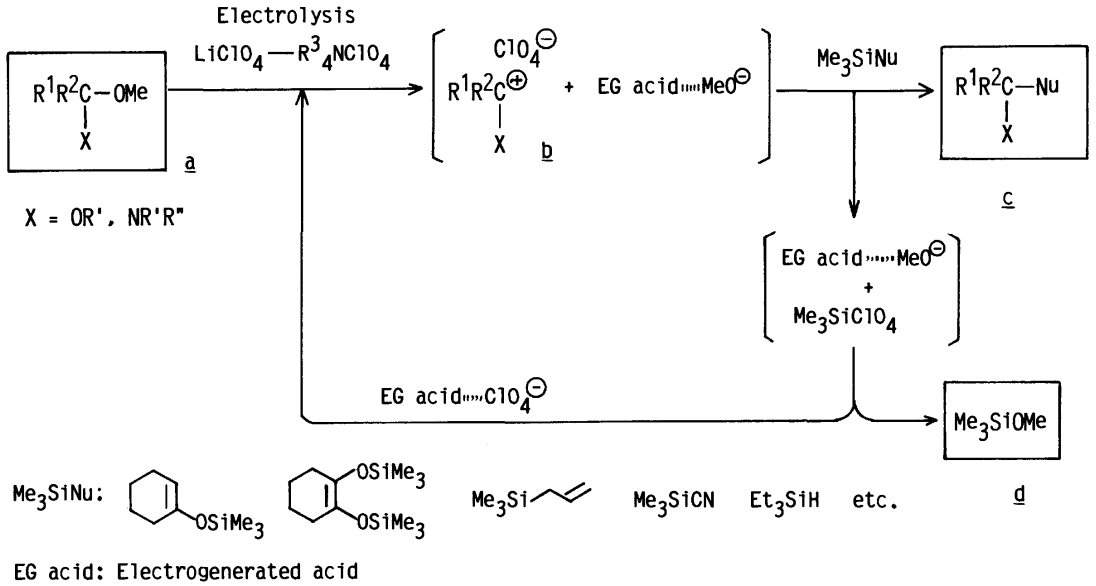

Scheme 3.

CH_2Cl_2 (3 ml). The entire mixture was electrolyzed under a constant current of 2.67 mA cm^{-2} (applied voltage: 8—10 V) at −78 °C. Soon after electric current was communicated, the surface of the cathode was covered with a black deposite (presumably with lithium metal). The progress of reaction was monitored by TLC and the reaction was quenched with Et_3N (3 drops) when the starting **3a** was completely consumed (about 30 min and after 0.07 F mol^{-1} of electricity has been passed). The volatiles were removed on a rotary evaporator and the residue was subjected to purification by column chromatography (SiO_2, hexane-AcOEt 5 : 1) to give 174 mg (80 %) of *erythro*-**5a** (R_f 0.5, Merck Silica Gel 60 F-254, hexane-AcOEt 5 : 1) and 29 mg (13 %) of *threo*-**5a** (R_f 0.3). *erythro*-**5a**:[3a] bp 56—58 °C/0.009 Torr (1 Torr=133.322 Pa); IR (neat) 3040, 3010, 2920, 2840, 2800, 1710 (C=O), 1610 (C=C), 1500, 1450, 1140, 1125 cm^{-1}; ^1H NMR ($CDCl_3$) δ=1.2—2.1 (m, 6, CH_2), 2.27—2.93 (m, 3, CH_2CO, CHCO), 3.27 (s, 3, OCH_3), 4.78 (d, J=5 Hz, 1, CH-O), 7.3 (s, 5, PhH); ^{13}C NMR ($CDCl_3$) δ=24.6 (t), 26.4 (t), 27.0 (t), 42.2 (t), 57.2 (q), 57.4 (d), 80.1 (d), 126.9 (d, 2c), 127.2 (d), 128.2 (d, 2c), 140.9 (s), 210.4 (s). *threo*-**5a**: bp 56—58 °C/0.009 Torr; IR (neat) 3040, 3010, 2920, 2840, 2800, 1710 (C=O), 1610 (C=C), 1500, 1450, 1140, 1125 cm^{-1}; ^1H NMR ($CDCl_3$) δ=1.05—2.20 (m, 6, CH_2), 2.27—2.93 (m, 3, CH_2CO, CHCO), 3.18 (s, 3, OCH_3), 4.55 (d, J=9 Hz, 1, CH-O), 7.25 (s, 5, PhH).

The electrolysis of **1a** and **3a** in 1,2-dichloroethane was carried out in the same manner as that in dichloromethane, giving the adducts in 90% yield.

The procedure for the aldol reaction by using a circulating flow cell system: Into a flow cell as dipicted in Fig. 1 were added consecutively a solution of benzaldehyde dimethyl acetal (**1a**, 4.87 g, 35 mmol), trimethylsiloxycyclohexene (**3a**, 5.1 g, 30 mmol), $LiClO_4$ (0.32 g, 3 mmol), and n-Bu_4NClO_4 (0.34 g, 1 mmol) in THF (2 ml) and 1,2-dichloroethane (60 ml). These stuffs were mixed by circulating at a linear rate of ca. 15 cm min^{-1} by flowing pump. The mixture was then electrolyzed at a current of 15 mA with stainless steels (SUS-27, anode area: 0.5×32 cm^2) as electrodes. During the electrolysis, temperature of the solution was maintained at −20 °C by cooling externally from heat-exchanger. The electrolysis was continued until 0.02 F mol^{-1} of electricity (based on **3a**) has been passed. The mixture was then treated with triethylamine (0.5 ml) and then concentrated. The crude product thus obtained was purified by column chromatography (SiO_2, hexane-AcOEt 10 : 1) to give 5.5 g (84%, erythro/threo 71 : 29) of **5a** (based on **3a**).

Preparation of **6g** from 1,2-Bis(trimethylsiloxy)cyclobutene (**4c**). A similar electrolysis of **1a** (152.2 mg, 1.0 mmol) and **4c** (277 mg, 1.2 mmol) in CH_2Cl_2 (3 ml) in the presence of $LiClO_4$ (10.6 mg, 0.1 mmol) and n-Bu_4NClO_4 (34.2 mg, 0.1 mmol) at −78 °C for 30 min (0.087 F mol^{-1} of electricity being passed) provided **6g** in 81% yield.

Spectral data for the adducts **5—7** listed in the Table 2 are as follows.

***erythro*-2-[(2-Furyl)methoxymethyl]cyclohexanone (5b):** IR (neat) 3100, 2840, 2800, 1710 (C=O), 1500, 1450, 1190, 1120, 1005, 950, 920, 730 cm^{-1}; ^1H NMR ($CDCl_3$) δ=1.40—2.15 (m, 6, CH_2), 2.15—3.00 (m, 3, CH_2CO, CHCO), 3.30 (s, 3, OCH_3), 4.73 (d, J=5 Hz, 1, CH-O), 6.30 (m, 2, CH=C), 7.35 (m, 1, CH=C). Found: C, 69.37; H, 7.63%. Calcd for $C_{12}H_{16}O_3$: C, 69.21; H, 7.74%.

***threo*-5b**: IR (neat) 3100, 2840, 2800, 1710 (C=O), 1500, 1450, 1320, 1230, 1150, 1125, 1117, 1090, 1010, 920, 750 cm^{-1}; ^1H NMR ($CDCl_3$) δ=1.20—2.20 (m, 6, CH_2), 2.30—3.20 (m, 3, CH_2CO, CHCO), 3.25 (s, 3, OCH_3), 4.58 (d, J=9 Hz, 1, CH-O), 6.32 (m, 2, CH=C), 7.40 (m, 1, CH=C).

***erythro*-2-(1-Methoxyheptyl)cyclohexanone (5c):** Bp 51—53 °C/0.013 Torr; IR (neat) 2850, 2800, 1715 (C=O), 1470, 1455, 1380, 1320, 1190, 1150, 1135, 1130, 1105, 1190 cm^{-1}; ^1H NMR ($CDCl_3$) δ=0.89 (m, 3, CH_3), 1.30 (br, 10, CH_2), 1.60—2.15 (m, 6, CH_2), 2.15—2.60 (m, 3, CH_2CO, CHCO), 3.36 (s, 3, OCH_3), 3.55—3.90 (m, 1, CH-O); ^{13}C NMR ($CDCl_3$) δ=14.0 (q), 20.9 (t), 22.6 (t), 22.6 (t), 23.0 (t), 25.9 (t), 29.4 (t), 31.8 (t), 32.7 (t), 39.1 (t), 52.7 (d), 58.3 (q), 79.6 (d), 220.9 (s). Found: C, 74.37; H, 11.33%. Calcd for $C_{14}H_{26}O_2$: C, 74.29; H, 11.58%.

***threo*-5c**: IR (neat) 2810, 1716 (C=O), 1470, 1455, 1380, 1370, 1320, 1135, 1105, 1085, 830 cm^{-1}; ^1H NMR ($CDCl_3$) δ=0.88 (m, 3, CH_3), 1.32 (br, 10, CH_2), 1.55—2.20 (m, 6, CH_2), 2.20—2.90 (m, 3, CH_2CO, CHCO), 3.32 (s, 3, OCH_3), 3.50—3.80 (m, 1, CH=O).

2-(1-Methoxy-1-methylethyl)cyclohexanone (5d):[3a] Bp 53—55 °C/3.5 Torr; IR (neat) 2820, 1715(C=O), 1455, 1385, 1370, 1320, 1150, 1130, 1080, 1035, 995, 915, 900, 850, 840, 740 cm^{-1}; ^1H NMR ($CDCl_3$) δ=1.20, 1.28 (s, 6, CH_3), 1.40—2.76 (m, 9, CH_2, CH_2CO, CHCO), 3.16 (s, 3, OCH_3); ^{13}C NMR ($CDCl_3$) δ=21.2 (q), 23.2 (q), 25.4 (t), 28.5 (t), 29.0 (t), 43.8 (t), 48.3 (q), 58.3 (d), 75.2 (s), 211.6 (s).

2-(1-Methoxy-6-oxoheptyl)cyclohexanone (5e): Bp 76—77 °C/0.005 Torr; IR (neat) 2805, 1710 (C=O), 1450, 1365, 1160, 1120, 1090 cm^{-1}; ^1H NMR ($CDCl_3$) δ=1.30—2.70 (m, 17, CH_2, CH_2CO, CHCO), 2.11 (s, 3, CH_3CO), 3.29, 3.31 (s, 3, OCH_3), 3.60 (m, 1, CH-O).

***erythro*-2-(1-Methoxy-1-phenylmethyl)-6-methylcyclohexanone (5f):** Mp 58—61 °C (from hexane); IR (Nujol) 3040, 3023, 2820, 1705 (C=O), 1602 (C=C), 1580, 1485, 1443, 1355, 1310, 1280, 1215, 1120, 1094, 1020, 995, 956, 917, 862, 760, 700 cm^{-1}; ^1H NMR ($CDCl_3$) δ=0.91, 1.01 (d, J=6 Hz, 3, CH_3), 1.30—2.30 (m, 6, CH_2), 2.35—2.80 (m, 2, CHCO), 3.21 (s, 3, OCH_3), 4.67 (d, J=6 Hz, 1, CH-O), 7.28 (s, 5, PhH). Found: C, 77.34; H, 8.71%. Calcd for $C_{15}H_{20}O_2$: C, 77.55; H, 8.68%.

***threo*-5f**: IR ($CHCl_3$) 3040, 3020, 2822, 1706 (C=O), 1601 (C=C), 1440, 1370, 1238, 1203, 1083, 1000, 860, 760, 697 cm^{-1}; ^1H NMR ($CDCl_3$) δ=1.12, 1.21 (d, J=6 Hz, 3, CH_3), 1.30—2.30 (m, 6, CH_2), 2.50—2.90 (m, 2, CHCO), 3.13 (s, 3, OCH_3), 4.58 (d, J=10 Hz, 1, CH-O), 7.35 (s, 5, PhH).

***erythro*-2-(1-Methoxy-1-phenylmethyl)cyclopentanone (5g):**[3a] Bp 69—71 °C/0.02 Torr; IR (neat) 3080, 3020, 2880, 2805, 1745 (C=O), 1602 (C=C), 1590, 1495, 1450, 1403, 1380, 1370, 1200, 1150, 1140, 1120, 1080, 1030, 950, 875, 844, 782, 740, 700 cm^{-1}; ^1H NMR ($CDCl_3$) δ=1.20—2.40 (m, 7, CH_2, CH_2CO, CHCO), 3.19 (s, 3, OCH_3), 4.70 (d, J=1.5 Hz, 1, CH-O), 7.22 (s, 5, PhH). Found: C, 76.37; H, 8.03%. Calcd for $C_{13}H_{16}O_2$: C, 76.44; H, 7.90%.

***threo*-5g**: IR (neat) 3080, 3055, 3020, 2805, 1740 (C=O), 1602 (C=C), 1590, 1495, 1450, 1405, 1370, 1150, 1100, 960, 740, 700 cm^{-1}; ^1H NMR ($CDCl_3$) δ=1.30—2.40 (m, 6, CH_2, CH_2CO), 2.50—2.90 (m, 1, CHCO), 3.25 (s, 3, OCH_3), 4.63 (d, J=5 Hz, 1, CH-O), 7.25 (s, 5, PhH).

***erythro*-2-(1-Methoxyheptyl)cyclopentanone (5h):** Bp 47—50 °C/0.01 Torr; IR (neat) 2840, 2810, 1740 (C=O), 1460, 1402, 1375, 1260, 1150, 1095 cm^{-1}; ^1H NMR ($CDCl_3$, 100 MHz) δ=0.88 (m, 3, CH_3), 1.29 (br, 10, CH_2), 1.70—2.40 (m, 7, CH_2, CH_2CO, CHCO), 3.22 (s, 3, OCH_3), 3.65 (m, 1, CH-O). Found: C, 73,58; H, 11.24%. Calcd for $C_{13}H_{24}O_2$: C, 73.54; H, 11.39%.

threo-**5h**: IR (neat) 2840, 2810, 1735 (C=O), 1465, 1405, 1264, 1090 cm^{-1}; ^1H NMR ($CDCl_3$, 100 MHz) δ=0.88 (m, 3, CH_3), 1.30 (br, 10, CH_2), 1.70—2.70 (m, 7, CH_2, CH_2CO, CHCO), 3.32 (s, 3, OCH_3), 3.45 (m, 1, CH-O).

3-Methoxy-1,3-diphenyl-1-propanone (5i):[3a] Bp 150—153 °C/3 Torr; IR (neat) 3040, 3020, 2810, 1690 (C=O), 1600 (C=C), 1580, 1490, 1450, 1360, 1265, 1200, 1100, 1055, 1000, 985, 750, 700 cm^{-1}; ^1H NMR ($CDCl_3$) δ=2.81—3.82 (m, 2, CH_2), 3.22 (s, 3, OCH_3), 4.87 (dd, J=8, 4.5 Hz, 1, CH-O), 7.20—7.60 (m, 8, PhH), 7.80—8.10 (m, 2, PhH).

3-Methoxy-1-phenyl-1-nonanone (5j): Bp 83—85 °C/0.015 Torr; IR (neat) 3040, 2840, 2800, 1690 (C=O), 1600 (C=C), 1580, 1460, 1442, 1360, 1100, 1000, 750, 690 cm^{-1}; ^1H NMR ($CDCl_3$) δ=0.88 (m, 3, CH_3), 1.30 (m, 10, CH_2), 2.60—3.50 (m, 2, CH_2CO), 3.31 (s, 3, OCH_3), 3.87 (m, 1, CH-O), 7.20 (m, 5, PhH). Found: C, 77.38; H, 9.74%. Calcd for $C_{16}H_{24}O_2$: C, 77.38; H, 9.74%.

3-Methoxy-3-methyl-1-phenyl-1-butanone (5k): Bp 62—64 °C/0.007 Torr; IR (neat) 3080, 3000, 2840, 1690 (C=O), 1610, 1600 (C=C), 1480, 1460, 1080, 770, 700 cm^{-1}; ^1H NMR ($CDCl_3$) δ=1.31 (s, 6, CH_3), 3.14 (s, 2, CH_2CO), 3.20 (s, 3, OCH_3), 7.30—8.10 (m, 5, PhH); ^{13}C NMR ($CDCl_3$) δ=25.0 (q, 2C), 48.0 (t), 49.3 (q), 74.8 (s), 128.4 (d, 3c), 132.8 (d, 2c), 138.3 (s), 198.9 (s).

5-Methoxy-2,2-dimethyl-5-phenyl-3-pentanone (5l): IR (neat) 3070, 3050, 3020, 2810, 1710 (C=O), 1602 (C=C), 1495, 1480, 1450, 1370, 1105, 1043, 995, 840, 760, 740, 700 cm^{-1}; ^1H NMR ($CDCl_3$) δ=1.07 (s, 9, CH_3), 2.40—3.45 (m, 2, CH_2CO), 3.20 (s, 3, OCH_3), 4.72 (dd, J=8, 5.5 Hz, 1, CH-O), 7.30 (s, 5, PhH); ^{13}C NMR ($CDCl_3$) δ=25.9 (q, 3C), 44.2 (s), 45.4 (t), 56.8 (q), 79.4 (d), 126.6 (d), 127.7 (d, 2c), 128.4 (d, 2c), 141.6 (s), 212.8 (s). Found: C, 76.18; H, 9.09%. Calcd for $C_{14}H_{20}O_2$: C, 76.32; H, 9.15%.

2-(1-Methoxy-1-phenylmethyl)-2-(trimethylsiloxy)cyclohexanone (6a): (Less polar component on SiO_2 column chromatography): Bp 65—66 °C/0.007 Torr; IR (neat) 3080, 3060, 3020, 2820, 1730 (C=O), 1605 (C=C), 1498, 1455, 1340, 1310, 1250, 1180, 1150, 1130, 1100, 1075, 996, 843, 760, 704 cm^{-1}; ^1H NMR ($CDCl_3$) δ=0.04 (s, 9, $OSiMe_3$), 1.20—2.40 (m, 6, CH_2), 2.50—2.80 (m, 2, CH_2CO), 3.29 (s, 3, OCH_3), 4.53 (s, 1, CH-O), 7.39 (s, 5, PhH). Found: C, 66.33; H, 8.43%. Calcd for $C_{17}H_{26}O_3Si$: C, 66.62; H, 8.55%.

(More polar component on SiO_2 column chromatography): IR (neat) 3075, 3040, 3010, 2800, 1720 (C=O), 1600 (C=C), 1485, 1443, 1250, 1180, 1150, 1127, 1110, 1080, 1000, 890, 850, 760, 710 cm^{-1}; ^1H NMR ($CDCl_3$) δ=0.06 (s, 9, $OSiMe_3$), 1.10—2.30 (m, 6, CH_2), 2.40—2.75 (m, 2, CH_2CO), 3.15 (s, 3, OCH_3), 3.68 (s, 1, CH-O), 7.30 (s, 5, PhH).

2-[(2-Furyl)methoxymethyl]-2-(trimethylsiloxy)cyclohexanone (6b): (Less polar component on SiO_2 column chromatography): IR (neat) 3100, 2850, 2805, 1725 (C=O), 1507, 1455, 1250, 1190, 1150, 1130, 1115, 1100, 1015, 912, 845, 790, 760, 738 cm^{-1}; ^1H NMR ($CDCl_3$) δ=0.04 (s, 9, $OSiMe_3$), 1.45—2.20 (m, 6, CH_2), 2.30—2.70 (m, 2, CH_2CO), 3.26 (s, 3, OCH_3), 4.60 (s, 1, CH-O), 6.33 (m, 2, CH=C), 7.36 (m, 1, CH=C). Found: C, 64.42; H, 8.46%. Calcd for $C_{15}H_{24}O_3Si$: C, 64.24; H, 8.63%.

(More polar component on SiO_2 column chromatography): IR (neat) 3100, 2855, 2810, 1730 (C=O), 1505, 1450, 1250, 1180, 1143, 1130, 1100, 1070, 980, 915, 840, 750 cm^{-1}; ^1H NMR ($CDCl_3$) δ=0.12 (s, 9, $OSiMe_3$), 1.40—2.20 (m, 6, CH_2), 2.30—2.80 (m, 2, CH_2CO), 3.20 (s, 3, OCH_3), 4.73 (s, 1, CH-O), 6.37 (m, 2, CH=C), 7.38 (m, 1, CH=C).

2-(1-Methoxyheptyl)-2-(trimethylsiloxy)cyclohexanone (6c): (Less polar component on SiO_2 column chromatography): Bp 64—66 °C/0.008 Torr; IR (neat) 2820, 1720 (C=O), 1470, 1450, 1380, 1250, 1100, 1022, 940, 900, 840, 760 cm^{-1}; ^1H NMR ($CDCl_3$) δ=0.11 (s, 9, $OSiMe_3$), 0.88 (m, 3, CH_3), 1.33 (br, 10, CH_2), 1.60—2.62 (m, 8, CH_2, CH_2CO), 3.42 (s, 3, OCH_3), 3.50 (m, 1, CH-O). Found: C, 65.14; H, 11.02%. Calcd for $C_{17}H_{34}O_3Si$: C, 64.92; H, 10.90%.

(More polar component on SiO_2 column chromatography): IR (neat) 2875, 1720 (C=O), 1460, 1250, 1180, 1140, 1120, 1100, 1070, 1050, 937, 840, 760 cm^{-1}; ^1H NMR ($CDCl_3$) δ=0.11 (s, 9, $OSiMe_3$), 0.88 (m, 3, CH_3), 1.32 (br, 10, CH_2), 1.65—2.66 (m, 8, CH_2, CH_2CO), 3.32 (s, 3, OCH_3), 3.50 (m, 1, CH-O).

2-(1-Methoxy-1-phenylmethyl)-2-(trimethylsiloxy)cyclopentanone (6d): (Less polar component on SiO_2 column chromatography): Bp 57—59 °C/0.008 Torr; IR (neat) 3080, 3055, 3025, 2820, 1750 (C=O), 1602 (C=C), 1590, 1500, 1458, 1404, 1360, 1336, 1250, 1200, 1145, 1100, 1080, 982, 900, 843, 760, 705 cm^{-1}; ^1H NMR ($CDCl_3$) δ=0.03 (s, 9, $OSiMe_3$), 1.30—2.50 (m, 6, CH_2, CH_2CO), 3.18 (s, 3, OCH_3), 4.34 (s, 1, CH-O), 7.33 (s, 5, PhH); ^{13}C NMR ($CDCl_3$) δ=1.93 (q), 17.7 (t), 33.3 (t), 36.4 (t), 57.3 (q), 83.5 (s), 85.9 (d), 127.9 (d, 3c), 128.5 (d, 2c), 136.7 (s), 216.8 (s).

(More polar component on SiO_2 column chromatography): IR (neat) 3075, 3040, 3020, 2810, 1742 (C=O), 1600 (C=C), 1495, 1450, 1400, 1255, 1200, 1150, 1105, 1080, 990, 900, 850, 760, 710 cm^{-1}; ^1H NMR ($CDCl_3$) δ=0.08 (s, 9, $OSiMe_3$), 1.20—2.30 (m, 6, CH_2, CH_2CO), 3.22 (s, 3, OCH_3), 4.36 (s, 1, CH-O), 7.24 (s, 5, PhH).

2-(1-Methoxyheptyl)-2-(trimethylsiloxy)cyclopentanone (6e): Bp 56—58 °C/0.01 Torr; IR (neat) 2820, 1750 (C=O), 1470, 1405, 1250, 1155, 1104, 1080, 962, 900, 844, 760 cm^{-1}; ^1H NMR ($CDCl_3$) δ=0.09 (s, 9, $OSiMe_3$), 0.90 (m, 3, CH_3), 1.30 (br, 10, CH_2), 1.80—2.45 (m, 6, CH_2, CH_2CO), 3.29 (s, 3, OCH_3), 3.33 (m, 1, CH-O). Found: C, 63.67; H, 10.71%. Calcd for $C_{16}H_{32}O_3Si$: C, 63.95; H, 10.73%.

2-(1-Methoxy-1-methylethyl)-2-(trimethylsiloxy)cyclopentanone (6f): Bp 44—46 °C/0.005 Torr; IR (neat) 2830, 1750 (C=O), 1470, 1410, 1380, 1365, 1253, 1160, 1115, 1060, 920, 890, 842, 760 cm^{-1}; ^1H NMR ($CDCl_3$) δ=0.05 (s, 9, $OSiMe_3$), 1.16 (s, 6, CH_3), 1.55—2.70 (m, 6, CH_2, CH_2CO), 3.12 (s, 3, OCH_3); ^{13}C NMR ($CDCl_3$) δ=1.9 (q, 3C), 17.9 (t), 18.7 (q), 19.5 (q), 34.1 (t), 38.5 (t), 49.3 (q), 80.4 (s), 83.3 (s), 219.6 (s). Found: C, 58.76; H, 9.97%. Calcd for $C_{12}H_{24}O_3Si$: C, 58.97; H, 9.90%.

2-(1-Methoxy-1-phenylmethyl)-2-(trimethylsiloxy)cyclobutanone (6g):[19] IR (neat) 3080, 3060, 3020, 2815, 1790 (C=O), 1500, 1460, 1390, 1250, 1220, 1178, 1104, 1070, 1016, 875, 850, 760, 700 cm^{-1}; ^1H NMR ($CDCl_3$) δ=0.04 (s, 9, $OSiMe_3$), 1.52—3.00 (m, 4, CH_2, CH_2CO), 3.28 (s, 3, OCH_3), 4.30 (s, 1, CH-O), 7.37 (s, 5, PhH).

2-(1-Methoxyheptyl)-2-(trimethylsiloxy)cyclobutanone (6h): IR (neat) 2840, 2810, 1780 (C=O), 1460, 1385, 1255, 1174, 1110, 850, 760 cm^{-1}; ^1H NMR ($CDCl_3$) δ=0.12 (s, 9, $OSiMe_3$), 0.88 (m, 3, CH_3), 1.29 (br, 10, CH_2), 1.60—2.95 (m, 4, CH_2, CH_2CO), 3.15 (m, 1, CH-O), 3.30 (s, 3, OCH_3). Found: C, 62.85; H, 10.43%. Calcd for $C_{15}H_{30}O_3Si$: C, 62.88; H, 10.55%.

erythro-**2-[(Trimethylsiloxy)phenylmethyl]cyclohexanone (7a)**:[3b] IR (neat) 3055, 3040, 3020, 2840, 1710 (C=O), 1602 (C=C), 1495, 1450, 1370, 1250, 1130, 1100, 1065, 1010, 905, 840, 700 cm^{-1}; ^1H NMR ($CDCl_3$) δ=−0.05 (s, 9, $OSiMe_3$),

1.07—2.07 (m, 6, CH_2), 2.07—2.67 (m, 3, CH_2CO, CHCO), 5.30 (d, J=4 Hz, 1, CH-O), 7.17 (s, 5, PhH).

***threo*·7a:** IR (neat) 3040, 3020, 2845, 1716 (C=O), 1600 (C=C), 1497, 1450, 1307, 1250, 1205, 1123, 1080, 1060, 1030, 880, 840, 765, 700 cm^{-1}; ^1H NMR ($CDCl_3$) δ=0.01 (s, 9, $OSiMe_3$), 1.00—2.10 (m, 6, CH_2), 2.20—3.00 (m, 3, CH_2CO, CHCO), 5.05 (d, J=8 Hz, 1, CH-O), 7.22 (s, 5, PhH).

***erythro*·2·[(2·Furyl)(trimethylsiloxy)methyl]cyclopentanone (7b):** IR (neat) 2960, 2880, 1745 (C=O), 1250, 1155, 1120, 1050, 1005, 955, 915, 860, 845, 755, 740 cm^{-1}; ^1H NMR ($CDCl_3$) δ=0.05 (s, 9, $OSiMe_3$), 1.60—2.50 (m, 7, CH_2, CH_2CO, CHCO), 5.20 (d, J=1 Hz, 1, CH-O), 6.10 (m, 1, CH=C), 6.21 (m, 1, CH=C), 7.25 (m, 1, CH=C); ^{13}C NMR ($CDCl_3$) δ=0.2 (q), 21.1 (t), 23.3 (t), 39.4 (t), 54.2 (d), 67.3 (d), 106.3 (d), 110.2 (d), 141.7 (d), 156.4 (s), 219.0 (s).

***threo*·7b:** IR (neat) 2920, 2880, 1740 (C=O), 1503, 1405, 1250, 1160, 1044, 1015, 924, 890, 840, 760 cm^{-1}; ^1H NMR ($CDCl_3$) δ=0.10 (s, 9, $OSiMe_3$), 1.60—2.70 (m, 7, CH_2, CH_2CO, CHCO), 5.12 (d, J=4.5 Hz, 1, CH-O), 6.22 (m, 2, CH=C), 7.26 (m, 1, CH=C).

***erythro*·2·[(Trimethylsiloxy)phenylmethyl]cyclopentanone (7c):** Bp 53—54 °C/0.005 Torr; IR (neat) 3080, 3050, 3025, 1740 (C=O), 1600 (C=C), 1585, 1495, 1450, 1405, 1370, 1250, 1200, 1150, 1120, 1050, 1030, 990, 915, 862, 840, 755, 735, 700 cm^{-1}; ^1H NMR ($CDCl_3$) δ=0.40 (s, 9, $OSiMe_3$), 1.35—2.40 (m, 7, CH_2, CH_2CO, CHCO), 5.25 (d, J=1 Hz, 1, CH-O), 7.20 (s, 5, PhH). Found: C, 68.79; H, 8.41%. Calcd for $C_{15}H_{22}O_2Si$: C, 68.65; H, 8.45%.

***threo*·7c:** IR (neat) 3080, 3050, 3025, 1740 (C=O), 1605, 1585, 1495, 1450, 1400, 1365, 1250, 1203, 1150, 1122, 1050, 1030, 990, 860, 840, 740, 700 cm^{-1}; ^1H NMR ($CDCl_3$) δ=0.70 (s, 9, $OSiMe_3$), 1.40—2.40 (m, 7, CH_2, CH_2CO, CHCO), 5.12 (d, J=5 Hz, 1, CH-O), 7.20 (s, 5, PhH).

2·[(4·Methoxyphenyl)(trimethylsiloxy)methyl]cyclopentanone (7d): IR (neat) 2840, 2815, 1740 (C=O), 1619, 1590, 1515, 1462, 1405, 1250, 1050, 990, 915, 870, 850 cm^{-1}; ^1H NMR ($CDCl_3$) δ=−0.05 (s, 9, $OSiMe_3$), 1.35—2.55 (m, 7, CH_2, CH_2CO, CHCO), 3.70 (s, 3, OCH_3), 5.15 (m, 1, CH-O), 6.11, 6.71 (d, J=9 Hz, 4, PhH). Found: C, 65.55; H, 8.48%. Calcd for $C_{16}H_{24}O_3Si$: C, 65.71; H, 8.27%.

3·Trimethylsiloxy·1,3·diphenyl·1·propanone (7e): IR (neat) 3080, 3050, 3020, 1695 (C=O), 1600, 1581, 1498, 1363, 1255, 1207, 1180, 1100, 1075, 1050, 1030, 980, 958, 925, 890, 845, 750, 700cm^{-1}; ^1H NMR ($CDCl_3$) δ=−0.05 (s, 9, $OSiMe_3$), 2.98 (dd, J=16, 4 Hz, 1, CH_2CO), 3.57 (dd, J=16, 8 Hz, 1, CH_2CO), 5.31 (dd, J=8, 4 Hz, 1, CH-O), 7.03—7.98 (m, 10, PhH); ^{13}C NMR ($CDCl_3$) δ=2.0 (q), 27.6 (q), 54.3 (t), 76.9 (s), 125.1 (d, 2c), 126.9 (d), 128.0 (d, 4c), 129.1 (d, 2c), 132.5 (d), 138.5 (s), 148.4 (s), 198.9 (s).

3·(Trimethylsiloxy)·1,3·diphenyl·1·butanone (7f): IR (neat) 3045, 3020, 1680 (C=O), 1600 (C=C), 1582, 1495, 1450, 1380, 1320, 1300, 1250, 1210, 1080, 1040, 1000, 840, 760, 738, 700 cm^{-1}; ^1H NMR ($CDCl_3$) δ=−0.1 (s, 9, $OSiMe_3$), 1.85 (s, 3, CH_3), 3.30 (AB_q, J=13 Hz, Δ_{AB}=30.3 Hz, 2, CH_2), 7.10—8.10 (m, 10, PhH); ^{13}C NMR ($CDCl_3$) δ=2.0 (q), 27.5 (q), 54.1 (t), 76.8 (s), 125.0 (d, 2c), 126.8 (d), 128.0 (d, 4c), 128.9 (d, 2c), 132.5 (d), 138.4 (s), 148.2 (s), 198.9 (s). Found: C, 72.89; H, 7.76%. Calcd for $C_{19}H_{24}O_2Si$: C, 73.03; H, 7.74%.

Preparation of Homoallyl Alcohol Methyl Ether 9 from Acetal 1 and Allyltrimethylsilane (8); General Procedure. A mixture of $LiClO_4$ (11 mg, 0.10 mmol) and n-Bu_4NClO_4 (35 mg, 0.10 mmol) in the same electrolysis vessel as described above was dried under reduced pressure over P_2O_5 for 1 h and then purged with argon. To this mixture were added acetal **1a** (154 mg, 1.0 mmol), allyltrimethylsilane (117 mg, 1.0 mmol), and CH_2Cl_2 (3 ml). The mixture was electrolyzed using platinum foil electrodes (1.5 cm^2) at a constant current of 4 mA (applied voltage: 9—11 V) with external cooling at 0 °C. After passing 0.07 F mol^{-1} of electricity (for about 27 min), the reaction was quenched with Et_3N (2 drops), and the resulting mixture was concentrated in vacuo. The residue was purified by column chromatography (SiO_2, hexane-AcOEt 5:1) to give 135 mg (82%) of **9a**[2] as an oil: bp 75.0 °C/2.5 Torr; IR (neat) 3060, 2830, 2810, 1638 (C=C), 1475, 1460, 1362, 1080, 993, 913, 850, 740 cm^{-1}; ^1H NMR ($CDCl_3$) δ=2.45 (m, 2, CH_2), 3.19 (s, 3, OCH_3), 4.12 (t, J=6.5 Hz, 1, CH-O), 4.72—6.10 (m, 3, CH_2=CH), 7.22 (s, 5, PhH).

4·(4·*t*·Butylphenyl)·4·methoxy·1·butene (9f): Bp 110.5 °C/4 Torr; IR (neat) 3060, 2855, 2802, 1640 (C=C), 1616 (C=C), 1507, 1460, 1362, 1262, 1190, 1100, 920, 834 cm^{-1}; ^1H NMR ($CDCl_3$) δ=1.32 (s, 9, CH_3), 2.49 (m, 2, CH_2), 3.20 (s, 3, OCH_3), 4.12 (t, J=6.5 Hz, 1, CH-O), 4.80—6.25 (m, 3, CH_2=CH), 7.05—7.40 (m, 4, PhH). Found: C, 81.51; H, 10.19%. Calcd for $C_{15}H_{22}O$: C, 82.52: H, 10.16%.

4·Methoxy·4·(4·methoxyphenyl)·1·butene (9g): Bp 105.5 °C/4.5 Torr; IR (neat) 3050, 2820, 2800, 1639 (C=C), 1610 (C=C), 1580, 1504, 1460, 1440, 1350, 1300, 1242, 1163, 1030, 990, 917, 826, 803 cm^{-1}; ^1H NMR ($CDCl_3$) δ=2.20—2.65 (m, 2, CH_2), 3.15 (s, 3, OCH_3), 3.75 (s, 3, OCH_3), 4.15 (t, J=6.5 Hz, 1, CH-O), 4.70—6.10 (m, 3, CH_2=CH), 6.77, 7.13 (d, J=9 Hz, 4, PhH).

4·Methoxy·4·(3,4,5·trimethoxyphenyl)·1·butene (9h): Bp 142.0 °C/3 Torr; IR (neat) 3075, 2815, 1644 (C=C), 1600 (C=C), 1505, 1463, 1420, 1358, 1330, 1240, 1191, 1130, 1110, 1024, 934, 843 cm^{-1}; ^1H NMR ($CDCl_3$) δ=2.42 (m, 2, CH_2), 3.20 (s, 3, OCH_3), 3.81, 3.82 (s, 9, OCH_3), 4.15 (t, J=6.5 Hz, 1, CH-O), 4.72—6.00 (m, 3, CH_2=CH), 6.45 (s, 2, PhH); ^{13}C NMR ($CDCl_3$) δ=42.6 (t), 56.1 (q, 2c), 56.7 (q), 60.7 (q), 83.9 (d), 103.5 (d, 2c), 116.8 (t), 134.9 (d), 137.3 (s), 137.6 (s), 153.3 (s, 2c). Found: C, 66.80; H, 7.95%. Calcd for $C_{14}H_{20}O_4$: C, 66.65; H, 7.99%.

4·(4·Cyanophenyl)·4·methoxy·1·butene (9i): Bp 118.0 °C/4 Torr; IR (neat) 3080, 2810, 2242 (C≡N), 1640 (C=C), 1615 (C=C), 1502, 1415, 1360, 1310, 1282, 1240, 1200, 1110, 1100, 920, 840 cm^{-1}; ^1H NMR ($CDCl_3$) δ=2.44 (m, 2, CH_2), 3.21 (s, 3, OCH_3), 4.19 (t, J=6 Hz, 1, CH-O), 4.70—6.10 (m, 3, CH_2=CH), 7.32, 7.60 (d, J=7 Hz, 4, PhH); ^{13}C NMR ($CDCl_3$) δ=42.1 (t), 57.0 (q), 83.0 (d), 117.7 (t), 118.7 (s), 127.4 (d, 2C), 132.2 (d, 2C), 133.6 (s), 133.6 (d), 147.4 (s).

3·Methoxy·1·phenyl·1,5·hexadiene (9j):[19] Bp 100.5 °C/2.5 Torr; IR (neat) 3072, 3014, 2805, 1640 (C=C), 1600 (C=C), 1579, 1492, 1448, 1360, 1190, 1100, 965, 916, 747, 690 cm^{-1}; ^1H NMR ($CDCl_3$) δ=2.39 (m, 2, CH_2), 3.30 (s, 3, OCH_3), 3.75 (m, 1, CH-O), 4.81—5.22 (m, 2, CH_2=C), 5.52—6.68 (m, 3, CH=C, CH=CH), 7.00—7.50 (m, 5, PhH).

3·(1·Methoxy·4·*t*·butylcyclohexyl)·1·propene (9k):[19] IR (neat) 3060, 2820, 2810, 1638 (C=C), 1390, 1360, 1080, 993, 910, 850, 810, 738 cm^{-1}; ^1H NMR ($CDCl_3$) δ=0.83 (s, 9, CH_3), 0.95—2.00 (m, 8, CH_2), 2.15 (d, J=6 Hz, 2, CH_2), 3.13 (s, 3, OCH_3), 4.75—6.10 (m, 3, CH=C).

Cyanation of Acetals 1 with Trimethylsilyl Cyanide (10) to α·Alkoxyalkanenitriles 11; General Procedure. A mixture of heptanal dimethyl acetal (**1c**, 541 mg, 3.38 mmol), trimethylsilyl cyanide (**10**, 0.7 ml, 5.26 mmol), $LiClO_4$ (23 mg, 0.22 mmol), and Et_4NClO_4 (52 mg, 0.18 mmol) in CH_2Cl_2 (5 ml) was electrolyzed with platinum electrodes (1.5 cm^2) in an

undivided cell at an applied voltage of 15 V (current: 12—13 mA). After electrolysis for 32 min (passed electricity: 0.077 F mol^{-1} based on the acetal **1c**) and an additional stirring for 5 min at room temperature, the reaction was quenched with pyridine (2 drops). Concentration of the mixture under vacuum followed by either column chromatography (SiO_2, hexane-AcOEt, 50 : 1) or bulb to bulb distillation gave 430 mg (89%) of **11c** as an oil.

2-Methoxy-2-phenylethanenitrile (11a):[4] Bp 105 °C/9 Torr; IR (neat) 3060, 3040, 3005, 2835, 2260 (C≡N), 1601 (C=C), 1590, 1500, 1458, 1320, 1284, 1207, 1100, 1037, 1008, 975, 918, 843, 760, 700 cm^{-1}; ^1H NMR ($CDCl_3$) δ=3.50 (s, 3, OCH_3), 5.17 (s, 1, CH-O), 7.40 (br, 5, PhH).

2-(2-Furyl)-2-methoxyethanenitrile (11b): Bp 105 °C/9 Torr; IR (neat) 3153, 3120, 3000, 2830, 1500, 1460, 1390, 1320, 1303, 1243, 1235, 1195, 1180, 1150, 1140, 1080, 1018, 962, 958, 910, 890, 880, 822, 797, 750 cm^{-1}; ^1H NMR ($CDCl_3$) δ=3.47 (s, 3, OCH_3), 5.30 (s, 1, CH-O), 6.41 (m, 1, CH=C), 6.62 (d, J=4 Hz, 1, CH=C), 7.47 (d, J=2 Hz, 1, CH=C).

2-Methoxyoctanenitrile (11c):[4] Bp 85 °C/9 Torr; IR (neat) 2970, 2900, 2810, 2800, 1465, 1370, 1330, 1130, 1100 cm^{-1}; ^1H NMR ($CDCl_3$) δ=0.97 (m, 3, CH_3), 1.31 (br, 10, CH_2), 3.46 (s, 3, OCH_3), 3.95 (t, J=6 Hz, 1, CH-O).

2-Methoxy-4-phenyl-3-butenenitrile (11j): Bp 90 °C/3 Torr; IR (neat) 3040, 3020, 3002, 2800, 2240 (C≡N), 1598, 1570, 1485, 1440, 1330, 1190, 1120, 1090, 960, 900, 740, 690 cm^{-1}; ^1H NMR ($CDCl_3$) δ=3.50 (s, 3, OCH_3), 4.81 (dd, J=6, 1 Hz, 1, CH-O), 6.13 (dd, J=16, 6 Hz, 1, CH=C), 6.92 (dd, J=16, 1 Hz, CH=C), 7.33 (br, 5, PhH).

2-Methoxy-3-phenylpropanenitrile (11l):[4] Bp 110 °C/9 Torr; IR (neat) 3075, 3040, 3005, 2840, 1600 (C=C), 1500, 1460, 1340, 1120, 1080, 750, 700 cm^{-1}; ^1H NMR ($CDCl_3$) δ=3.06 (d, J=7 Hz, 2, CH_2), 3.44 (s, 3, OCH_3), 4.18 (t, J=7Hz, 1, CH-O), 5.25 (s, 5, PhH).

2-(2-Methoxycarbonylethyl)-1-methoxycyclohexanecarbonitrile (11m): Bp 91 °C/3 Torr; IR (neat) 2840, 2803, 2240 (C≡N), 1730 (C=O), 1442, 1430, 1130, 1250, 1195, 1170, 1100, 1070, 1050, 1010, 980, 945, 922, 910, 884, 840, 725 cm^{-1}; ^1H NMR ($CDCl_3$) δ=1.00—2.08 (m, 10, CH_2), 2.08—2.60 (m, 3, CH_2CO, CH), 3.40 (s, 3, OCH_3), 3.65 (s, 3, CO_2CH_3).

3-Methoxycarbonyl-2-methoxypropanenitrile (11n): Bp 75 °C/5 Torr; IR (neat) 2815, 1740 (C=O), 1435, 1367, 1280, 1202, 1165, 1115, 1010, 982 cm^{-1}; ^1H NMR ($CDCl_3$) δ=2.87 (d, J=6 Hz, 2, CH_2), 3.51 (s, 3, OCH_3), 3.74 (s, 3, CO_2CH_3), 4.48 (t, J=6 Hz, 1, CH-O).

***N*-Ethoxycarbonyl-2-cyanopiperidine (11o):** Bp 83 °C/3 Torr; IR (neat) 2945, 2860, 1710 (C=O), 1420, 1260, 1180, 1040 cm^{-1}; ^1H NMR ($CDCl_3$) δ=1.25 (t, J=7 Hz, 3, CH_3), 1.30—2.20 (m, 7, CH_2, N-CH_2), 2.95 (m, 1, N-CH_2), 4.12 (q, J=7 Hz, 2, CO_2CH_2), 5.22 (m, 1, N-CH).

1-(Trimethylsiloxy)cyclododecanecarbonitrile (12e):[27] IR (neat) 2245 (C≡N), 1473, 1450, 1255, 1100, 1045, 1008, 863, 850 cm^{-1}; ^1H NMR ($CDCl_3$) δ=0.25 (s, 9, $OSiMe_3$), 1.36 (m, 18, CH_2), 1.61—2.11 (m, 4, CH_2).

2-Ethyl-2-(trimethylsiloxy)butanenitrile (12f):[26] IR (neat) 2240 (C≡N), 1460, 1250, 1160, 1130, 1077, 1018, 880, 845, 757 cm^{-1}; ^1H NMR ($CDCl_3$) δ=0.22 (s, 9, $OSiMe_3$), 1.11 (t, δ=7 Hz, 6, CH_3), 1.75 (q, J=7 Hz, 4, CH_2).

2-Methyl-2-(trimethylsiloxy)heptanenitrile (12g):[28] IR (neat) 2245 (C≡N), 1466, 1380, 1257, 1195, 1142, 1105, 1080, 1033, 850, 760 cm^{-1}; ^1H NMR ($CDCl_3$) δ=0.23 (s, 9, $OSiMe_3$), 0.90 (m, 3, CH_3), 1.30—1.85 (m, 8, CH_2), 1.55 (s, 3, CH_3).

Ethyl 2-Cyano-2-(trimethylsiloxy)propionate (12h): Bp 58—60 °C/2 Torr; IR (neat) 2280(C≡N), 1774 (C=O), 1458, 1383, 1262, 1200, 1156, 1008, 926, 860, 742 cm^{-1}; ^1H NMR ($CDCl_3$) δ=0.25 (s, 9, $OSiMe_3$), 1.32 (t, J=8 Hz, 3, CH_3), 1.75 (s, 3, CH_3), 4.26 (q, J=8 Hz, CH_2). Found: C, 49.96; H, 8.20; N, 6.34%. Calcd for $C_9H_{17}NO_3Si$: C, 50.20; H, 7.96; N, 6.51%.

2-Trimethylsiloxy-2-phenylpropanenitrile (12d):[28] IR (neat) 3043, 3010, 2240 (C≡N), 1600, 1490, 1445, 1370, 1250, 1223, 1150, 1120, 1000, 910, 843, 760, 695 cm^{-1}; ^1H NMR ($CDCl_3$) δ=0.17 (s, 9, $OSiMe_3$), 1.83 (s, 3, CH_3), 7.20—7.65 (m, 5, PhH).

5-Isopropenyl-2-methyl-1-trimethylsiloxy-2-cyclohexene-1-carbonitrile (12i): Bp 79—81 °C/2 Torr; IR (neat) 3070, 3020, 2960, 2240 (C≡N), 1645, 1450, 1260, 1135, 1055, 960, 910, 850, 760 cm^{-1}; ^1H NMR ($CDCl_3$) δ=0.20 (s, 9, $OSiMe_3$), 1.73 (s, 3, CH_3), 1.77 (s, 3, CH_3), 1.10—2.60 (m, 5, CH_2, CH), 4.72 (m, 2, CH_2=C), 5.60 (m, 1, CH=C). Found: C, 67.41; H, 7.96; N, 6.34%. Calcd for $C_{14}H_{23}NOSi$: C, 67.41; H, 9.29; N, 5.61%.

2-Hydroxyoctanenitrile (13j): IR (neat) 2920, 2840, 2240 (C≡N), 1460, 910, 730 cm^{-1}; ^1H NMR ($CDCl_3$) δ=0.90 (m, 3, CH_3), 1.10—2.10 (m, 10, CH_2), 2.60—3.40 (brs. 1, OH), 4.48 (t, J=6 Hz, 1, CH-O).

2-Hydroxy-2-phenylethanenitrile (13a): IR (neat) 3390 (OH), 3050, 2255 (C≡N), 1500, 1455, 1200, 1040, 1025, 940, 760, 700 cm^{-1}; ^1H NMR ($CDCl_3$) δ=3.72 (brs , 1, OH), 5.43 (s, 1, CH-O), 7.41 (s, 5, PhH).

2-Hydroxy-2-(4-methoxyphenyl)ethanenitrile (13c): IR (neat) 3400 (OH), 2840, 2235 (C≡N), 1620, 1595, 1520, 1260, 1180, 1035, 840 cm^{-1}; ^1H NMR ($CDCl_3$) δ=3.74 (s, 3, OMe), 3.50—4.00 (brs, 1, OH), 6.82 (d, J=10 Hz, 2, PhH), 7.32 (d, J=10Hz, 2, PhH).

2-Hydroxy-2-(4-cyanophenyl)ethanenitrile (13k): Mp 71—73 °C; IR ($CHCl_3$) 3400 (OH), 2245 (C≡N), 1420, 1200, 920, 740 cm^{-1}; ^1H NMR ($CDCl_3$) δ=3.5—4.5 (brs, 1, OH), 5.60 (s, 1, CH-O), 7.62 (s, 4, PhH). Found: C, 68.18; H, 3.80; N, 17.57%. Calcd for $C_9H_6N_2O$: C, 68.35, H, 3.82; N, 17.71%.

2-Hydroxy-4-phenyl-3-butenenitrile (13l): IR (neat) 3400 (OH), 3040, 3020, 2250 (C≡N), 1495, 1450, 970, 750, 690 cm^{-1}; ^1H NMR ($CDCl_3$) δ=3.70—4.30 (brs, 1, OH), 5.07 (d, J=6 Hz, 1, CH-O), 6.15 (dd, J=15, 6 Hz, 1, C=CH), 6.82 (d, J=15 Hz, 1, C=CH), 7.29 (s, 5, PhH).

Reaction of Acetals 1 with Triethylsilane (14); General Procedure. A mixture of acetal (**1a** 922 mg, 5.06 mmol) and Et_3SiH (**14**, 605.6 mg, 5.21 mmol) in CH_2Cl_2 (5 ml) containing $LiClO_4$ (42 mg, 0.39 mmol) and n-Bu_4NClO_4 (135.7 mg, 0.40 mmol) was electrolyzed at a constant current of 4 mA (applied voltage: 7—8 V) with platinum electrodes (1.5 cm^2) at 0 °C under argon. After passing 0.07 F mol^{-1} of electricity (it took about 25 min), the reaction was quenched with Et_3N (3 drops). Concentration followed by column chromatography (SiO_2, hexane-AcOEt, 5 : 1) gave 543 mg (88%) of **15a**[2] as an oil: IR (neat) 3080, 3060, 3020, 1605, 1450, 1380, 1100, 740 cm^{-1}; ^1H NMR ($CDCl_3$) δ=3.36 (s, 3, OCH_3), 4.43 (s, 2, CH_2-O), 7.29 (s, 5, PhH).

1-*t*-Butyl-4-(methoxymethyl)benzene (15f): Bp 88.5 °C/2 Torr; IR (neat) 2960, 2860, 2810, 1630, 1515, 1478, 1460, 1412, 1380, 1365, 1270, 1215, 1195, 1185, 1112, 1100, 1020, 970, 920, 855, 838, 818, 670, 660 cm^{-1}; ^1H NMR ($CDCl_3$) δ=1.30 (s, 9, CH_3), 3.35 (s, 3, OCH_3), 4.38 (s, 2, CH_2-O), 7.20—7.40 (m, 4, PhH).

1-Methoxy-4-(methoxymethyl)benzene (15g): Bp 91.5 °C/4 Torr; IR (neat) 2950, 2900, 2870, 2830, 1618, 1590, 1515, 1465, 1440, 1412, 1380, 1365, 1300, 1270, 1250, 1170, 1100, 1038, 1018, 1005, 960, 910, 850, 820, 740, 660 cm^{-1}; ^1H NMR

($CDCl_3$) δ=3.29 (s, 3, OCH_3), 3.72 (s, 3, OCH_3), 4.31 (s, 2, CH_2-O), 6.77, 7.16 (d, J=8.5 Hz, 4, PhH).

1,2,3-Trimethoxy-5-(methoxymethyl)benzene (15h): Bp 127.0 °C/4.5 Torr; IR (neat) 2930, 2830, 1600, 1510, 1470, 1430, 1390, 1370, 1340, 1240, 1190, 1130, 1110, 1050, 1020, 995, 925, 845, 795, 740, 705, 675 cm^{-1}; ^1H NMR ($CDCl_3$) δ=3.39 (s, 3, OCH_3), 3.82 (s, 9, OCH_3), 4.35 (s, 2, CH_2-O), 6.50 (s, 2, PhH).

4-(Methoxymethyl)benzonitrile (15i): Bp 104.0 °C/3.5 Torr; IR (neat) 2980, 2930, 2880, 2820, 2250 (C≡N), 1615, 1505, 1470, 1452, 1415, 1385, 1245, 1210, 1200, 1108, 1058, 1022, 990, 975, 925, 820 cm^{-1}; ^1H NMR ($CDCl_3$) δ=3.40 (s, 3, OCH_3), 4.47 (s, 2, CH_2-O), 7.35, 7.60 (d, J=8 Hz, 4, PhH).

References

1) a) T. H. Chan and I. Fleming, *Synthesis*, **1979**, 761; b) E. W. Colvin, "Silicon in Organic Synthesis," Butterworths, London (1981); c) W. R. Weber, "Silicon Reagents for Organic Synthesis," Springer-Verlag, Berlin, Heiderberg (1983).

2) R. Noyori, S. Murata, and M. Suzuki, *Tetrahedron*, **37**, 3899 (1981).

3) a) T. Mukaiyama, S. Kobayashi, and M. Murakami, *Chem. Lett.*, **1984**, 1759; b) *ibid.*, **1985**, 447.

4) K. Utimoto, Y. Wakabayashi, T. Horiie, M. Inoue, Y. Shishiyama, M. Obayashi, and H. Nozaki, *Tetrahedron*, **39**, 967 (1983).

5) S. Kobayashi, M. Murakami, and T. Mukaiyama, *Chem. Lett.*, **1985**, 953.

6) Preparation of $TrClO_4$: H. J. Dauben Jr., L. R. Honnen, and K. M. Harmon, *J. Org. Chem.*, **25**, 1442 (1960).

7) a) S. Torii, "Electroorganic Syntheses: Oxidations Methods and Applications;" Kodansha+Verlag Chemie: Tokyo+Weinheim, 1985; Part I, Chapter 13; b) K. Uneyama, *Yuki Gosei Kagaku Kyokai Shi*, **43**, 557 (1985).

8) a) K. Uneyama, A. Isimura, K. Fujii, and S. Torii, *Tetrahedron Lett.*, **24**, 2857 (1983); b) K. Uneyama, N. Nisiyama, and S. Torii, *ibid.*, **25**, 4137 (1984).

9) S. Torii, T. Inokuchi, K. Kondo, and H. Ito, *Bull. Chem. Soc. Jpn*, **58**, 1347 (1985).

10) K. Uneyama, Y. Masatsugu, T. Ueda, and S. Torii, *Chem. Lett.*, **1984**, 529.

11) K. Uneyama, A. Isimura, and S. Torii, *Bull. Chem. Soc. Jpn*, **58**, 1859 (1985).

12) S. Torii and T. Inokuchi, *Chem. Lett.*, **1983**, 1349.

13) T. Mukaiyama, *"Organic Reactions,"* Wiley & Sons, New York (1982), Vol. 28, p. 203.

14) a) S. Murata, M. Suzuki, and R. Noyori, *J. Am. Chem. Soc.*, **102**, 3248 (1980); b) E. Nakamura, M. Shimizu, I. Kuwajima, J. Sakata, Y. Yokoyama, and R. Noyori, *J. Org. Chem.*, **48**, 932 (1983).

15) a) T. Mukaiyama and M. Hayashi, *Chem. Lett.*, **1974**, 15; b) T. Mukaiyama and A. Ishida, *ibid.*, **1975**, 319; c) T. Mukaiyama, H. Ishihara, and K. Inomata, *ibid.*, **1975**, 527; d) *ibid.*, **1975**, 531.

16) a) J. Simada, K. Hashimoto, B. H. Kim, E. Nakamura, and I. Kuwajima, *J. Am. Chem. Soc.*, **106**, 1759 (1984); b) I. Kuwajima, "Gendai Kagaku Zokan;" Tokyo-Kagaku Dojin, (1985), Vol. 3, p. 108.

17) a) A. Hosomi and H. Sakurai, *Yuki Gosei Kagaku Kyokai Shi*, **43**, 406 (1985); b) Z. N. Parnes and G. I. Bolestova, *Synthesis*, **1984**, 991.

18) a) A. Hosomi, H. Sakurai, and M. Endo, *Chem. Lett., Gosei* **1976**, 941; b) A. Hosomi, M. Endo, and H. Sakurai, *ibid.*, **1978**, 499.

19) T. Tsunoda, M. Suzuki, and R. Noyori, *Tetrahedron Lett.*, **1980**, 71.

20) K. Kobayashi and T. Hiyama, *Tetrahedron Lett.*, **24**, 3509 (1983).

21) W. P. Wallace and H. R. Henze, *J. Am. Chem. Soc.*, **64**, 2882 (1942).

22) G. Stork and L. Maldonado, *J. Am. Chem. Soc.*, **93**, 5286 (1971).

23) M. Hudlický, "Reductions in Organic Chemistry;" Ellis Horwood Limited, Chichester, England (1984).

24) T. Tsunoda, M. Suzuki, and R. Noyori, *Tetrahedron Lett.*, **1979**, 4679.

25) a) H. O. House, L. J. Czuba, M. Gall, and H. D. Olmsted, *J. Org. Chem.*, **34**, 2324 (1969); b) J. K. Rasmussen, *Synthesis*, **1977**, 91.

26) K. Rühlmann, *Synthesis*, **1971**, 236.

27) D. A. Evans, G. L. Carroll, and L. K. Truesdale, *J. Org. Chem.*, **39**, 914 (1974).

28) D. A. Evans and L. K. Truesdale, *Tetrahedron Lett.*, **1973**, 4929.

Syntheses of Optically Active Pentaacetates of Pseudo-β-L-allopyranose and Pseudo-α-D-mannopyranose

Kin-ichi TADANO,* Chiyoko FUKABORI, Masayuki MIYAZAKI, Hiroshi KIMURA, and Tetsuo SUAMI*
Department of Applied Chemistry, Faculty of Science and Technology, Keio University,
Hiyoshi, Kohoku-ku, Yokohama 223
(Received November 13, 1986)

Diisobutylaluminium hydride reduction of D-glucose-derived chiral synthon, (1*R*,6*R*,8*R*,9*R*)-8,9-isopropylidenedioxy-7-oxabicyclo[4.3.0]non-4-en-3-one (**1**), gave a 7:1 mixture of (1*R*,3*S*,6*R*,8*R*,9*R*)- and (1*R*,3*R*,6*R*,8*R*,9*R*)-8,9-isopropylidenedioxy-7-oxabicyclo[4.3.0]non-4-en-3-ol, (**2**) and (**2'**). Introduction of cis-diol to the double bond of 3-*O*-acetyl derivatives of **2** and **2'** by osmium tetraoxide oxidation provided the diastereomeric mixture of (1*R*,3*S*,4*R*,5*S*,6*S*,8*R*,9*R*)-3-acetoxy-8,9-isopropylidenedioxy-7-oxabicyclo[4.3.0]-nonane-4,5-diol (**5**) and (1*R*,3*R*,4*S*,5*R*,6*S*,8*R*,9*R*) diastereomer. Compound **5** was transformed to optically active pseudo-β-L-allopyranose effectively via (1*R*)-1-[(1*S*,2*S*,3*S*,4*R*,5*S*)-3,4,5-tris(benzyloxy)-2-hydroxycyclohexyl]-1,2-ethanediol (**9**). Cyclohexanecarbaldehyde formed by glycol cleavage of **9** was treated with methanesulfonyl chloride and reduced with lithium aluminium hydride to give (3*S*,4*R*,5*S*)-3,4,5-tris(benzyloxy)-1-cyclohexene-1-methanol (**13**). Compound **13** was efficiently converted to pseudo-α-D-mannopyranose pentaacetate by stereoselective hydroboration as a key reaction. The Wharton reaction of (1*R*,4*S*,5*S*,6*S*,8*R*,9*R*)-4,5-epoxy-8,9-isopropylidenedioxy-7-oxabicyclo[4.3.0]nonan-3-one derived from **1** gave (1*R*,5*R*,6*S*,8*R*,9*R*)-8,9-isopropylidenedioxy-7-oxabicyclo[4.3.0]non-3-en-5-ol, into which (3*S*,4*S*)-diol was stereoselectively introduced by oxidation with osmium tetraoxide.

The pseudo-sugars, 1-hydroxymethyl-2,3,4,5-cyclohexanetetrols, are found in components of antibiotics and enzyme inhibitors.[1] Optically active pseudo-sugars have currently been investigated by several subtle approaches to these carbocyclic analogues of carbohydrates.[2] This situation made us use chiral synthon as a starting compound for the pseudo-sugar synthesis. In the previous papers,[3] we demonstrated a practicable access to the chiral synthon **1**, from which some optically active pseudo-sugars and pseudo-2-amino sugars were synthesized by stereoselective introduction of triol or azido diol on the cyclohexenone moiety of **1**. In our further study of synthesizing the optically active carbocyclic natural products and pseudo-sugars,[4] we described another approach to pseudo-sugars starting from synthon **1**. The approach features a stereoselective cis-diol introduction to the double bond of two allyl acetates **4** and **19**, both of which are easily prepared from **1**, to give (3*S*,4*R*,5*S*)- and (3*S*,4*S*,5*S*)- protected triols **5** and **20**. Compound **5** was transformed to pentaacetyl derivatives of pseudo-α-L-allopyranose and pseudo-α-D-mannopyranose, **11** and **15**, efficiently.

Results and Discussion

Synthesis of Pentaacetates of Pseudo-β-L-allopyranose and Pseudo-α-D-mannopyranose, (11) and (15) (Scheme 1). Diisobutylaluminium hydride (DIBAL-H) reduced chiral synthon **1**, which was prepared from 1,2:5,6-di-*O*-isopropylidene-α-D-glucofuranose by seven-steps reaction in an overall yield of 37%,[3] at −78 °C to give an inseparable mixture of allyl alcohols **2** and **2'** in 69% yield. The ratio of **2** to **2'** was 7:1 by conversion of the mixture to *t*-butyldimethylsilyl ethers **3** and **3'**, which were separated by silica-gel chromatography.[5] Although we were unable to confirm stereochemically C-3 (H-C-OH) of **2** and **2'** unambigously by ^{1}H NMR analysis of **3** and **3'**, the configuration of C-3 of the main product **2** was tentatively assigned to be (*S*), as was confirmed later. Osmium tetraoxide oxidation of an inseparable mixture of allyl acetates **4** and **4'**, which was prepared by acetylation of a mixture of **2** and **2'**, with aqueous hydrogen peroxide in *t*-butyl alcohol at room temperature gave (1*R*,3*S*,4*R*,5*S*,6*S*,8*R*,9*R*)- and (1*R*,3*R*,4*S*,5*R*,6*S*,8*R*,9*R*)-3-acetoxy-8,9-isopropylidenedioxy-7-oxabicyclo[4.3.0]nonane-4,5-diol, (**5**) and (**5'**), in 53 and 6% yield, respectively. The structure of main product **5** was verified by ^{1}H NMR spectrum of tri-*O*-acetyl derivative **6**, which was prepared in 96% yield. In the ^{1}H NMR spectrum of **6**, H-6 signal appeared at δ 3.85 as a double doublet with $J_{1,6}$=10.5 Hz and $J_{5,6}$=3 Hz, indicating that 5-acetoxyl group is axial. Three acetoxyl methyl signals of **6** appeared at δ 2.00, 2.03, and 2.12 indicate that acetoxyl groups on C-3, 4, and 5 are equatorial, equatorial, and axial, respectively.[6] The configurations at C-3 to C-5 are, therefore, (3*S*,4*R*,5*S*) as depicted. The structure of **5'**, (3*R*,4*S*,5*R*), was also confirmed by ^{1}H NMR spectrum of acetyl derivative **6'** obtained in 97% yield. In the ^{1}H NMR spectrum, H-6 of **6'** appeared at δ 4.02 as a triplet with $J_{1,6}$=$J_{5,6}$=9.5 Hz, indicating that 5-acetoxyl group is equatorial. Three acetoxyl methyl signals of **6'** appeared at δ 2.00 (3H) and 2.10 (6H), indicating that acetoxyl groups on C-3, 4, and 5 are axial, axial, and equatorial.[6] Stereoselective cis-diol introduction was thus achieved for both allyl acetates **4** and **4'**, and osmate formation in both cases occurred from the opposite side of acetoxyl group, providing **5** from **4** and **5'** from **4'**.[7]

Pseudo-sugar **11** was synthesized from **5** as follows. *O*-Deacetylation of **5** and successive benzylation with excess benzyl bromide in the presence of sodium

hydride gave tri-*O*-benzyl derivative **8** in 88% yield. Hydrolysis of **8** with 80% aqueous acetic acid to remove *O*-isopropylidene group, followed by reduction with sodium borohydride, gave pseudo-heptopyranose **9** in 56% yield. The glycol cleavage of **9** with sodium periodate, reduction of the resulting aldehyde group with sodium borohydride, and acetylation gave a fully protected pseudo-β-L-allopyranose **10** in 85% yield. Finally, hydrogenolysis of **10** in the presence of palladium-black to remove *O*-benzyl groups and successive acetylation gave compound **11** as crystals in 79% yield. The ^{1}H NMR spectrum of **11** was identical with that of authentic DL-**11**.[8]

The synthesis of pseudo-α-D-mannopyranose pen-

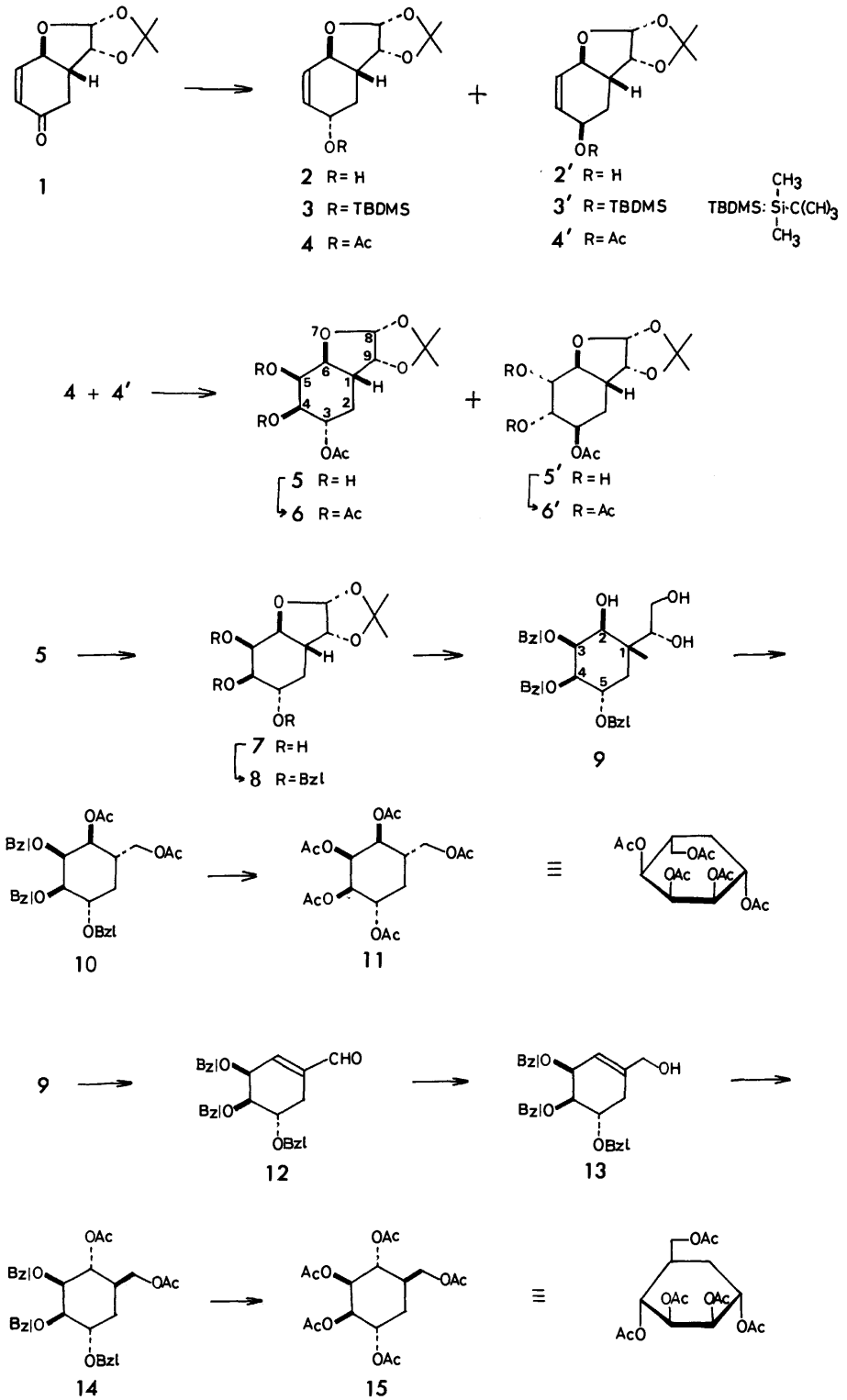

Scheme 1.

taacetate (**15**) from compound **9** was achieved as follows. The glycol cleavage of **9** as described above and successive treatment of the resulting cyclohexanecarbaldehyde with excess methanesulfonyl chloride at room temperature gave α,β-unsaturated 1-cyclohexene-1-carbaldehyde, which was reduced with lithium aluminium hydride to give 1-cyclohexene-1-methanol **13** in 37% yield from **9**. Hydroboration of **13** with borane-THF complex, treatment with alkaline hydrogen peroxide, and acetylation gave a fully protected pseudo-α-D-mannopyranose **14** in 47% yield. Since pseudo-β-L-allopyranose **10** was not detected in the reaction mixture, hydroboration of **13** seems to proceed stereoselectively from less-hindered side opposite to the benzyloxy groups on C-3 and C-4.[9] Hydrogenolysis of **14** in the presence of palladium-black followed by acetylation gave compound **15** as crystals in 56% yield. The ^{1}H NMR spectrum of **15** was identical with that of authentic DL-**15**.[10]

Synthesis of (1*R*,5*R*,6*S*,8*R*,9*R*)-8,9-Isopropylidenedioxy-7-oxabicyclo[4.3.0]non-3-en-5-ol (17) and Stereoselective Introduction of Two Hydroxyl Groups to the Double Bond in Acetate (19) of 17 (Scheme 2). Our next interest was to investigate stereoselectivity of introduction of two hydroxyl groups to the double bond located at C-3 and C-4 in the appropriate model **17**. Compound **17** was synthesized by the Wharton reaction[11] of known epoxy ketone **16**, which was obtained by stereoselective epoxidation of **1**.[3] Treatment of **16** in ethanol with each 5 molar equivalent of hydrazine hydrate and acetic acid at room temperature for 2.5 min gave compound **17** in 74% yield. Longer reaction time decreased the yield. In the ^{1}H NMR spectrum of **17**, H-6 signal appeared at δ 3.72 as a double doublet with $J_{1,6}$=10.5 Hz and $J_{5,6}$=4.5 Hz. Meanwhile, oxidation of **17** with pyridinium chlorochromate (PCC) gave (1*S*,6*S*,8*R*,9*R*)-8,9-isopropylidenedioxy-7-oxabicyclo[4.3.0]non-3-en-5-one (**18**) in 87% yield. In the ^{1}H NMR spectrum of **18**, H-6 signal appeared at δ 4.45 as a doublet with $J_{1,6}$=12 Hz. From these spectral data, it was concluded that hydroxyl group in the Wharton reaction product is at C-5 with (R)-configuration (a pseudo-axial orientation). Treatment of allyl acetate **19**, which was prepared by acetylation of **17** in 98% yield, with osmium tetraoxide in *t*-butyl alcohol in the presence of hydrogen peroxide gave cis diol **20** as a sole product in 35% yield. No stereoisomer was detected. The structure of **20** was estimated from the ^{1}H NMR spectrum of tri-*O*-acetyl derivative **21**, where H-6 signal appeared at δ 4.05 as a double doublet with $J_{1,6}$=10.5 Hz and $J_{5,6}$=3 Hz, indicating that 5-acetoxyl group is axial. Three acetoxyl methyl signals of **21** appeared at δ 1.99 (3H) and 2.10 (6H) and those signals were assigned to one equatorial and two axial acetoxyl groups.[6] Based on the results of oxidation of compound **4** and **4'** catalysed with osmium tetraoxide, cis diol introduction to compound **19** proceeded presumably from less-hindered side opposite to the 5-acetoxyl group to give solely (1*R*,3*S*,4*S*,5*S*,6*S*,8*R*,-9*R*)-5-acetoxy-8,9-isopropylidenedioxy-7-oxabicyclo-[4.3.0]nonane-3,4-diol (**20**). The possibility of formation of other stereoisomer possessing (1*R*,3*R*,4*R*,5*S*,6*S*,-8*R*,9*R*)-configuration, however, could not be excluded. To confirm the structure of **21**, we examined the sol-

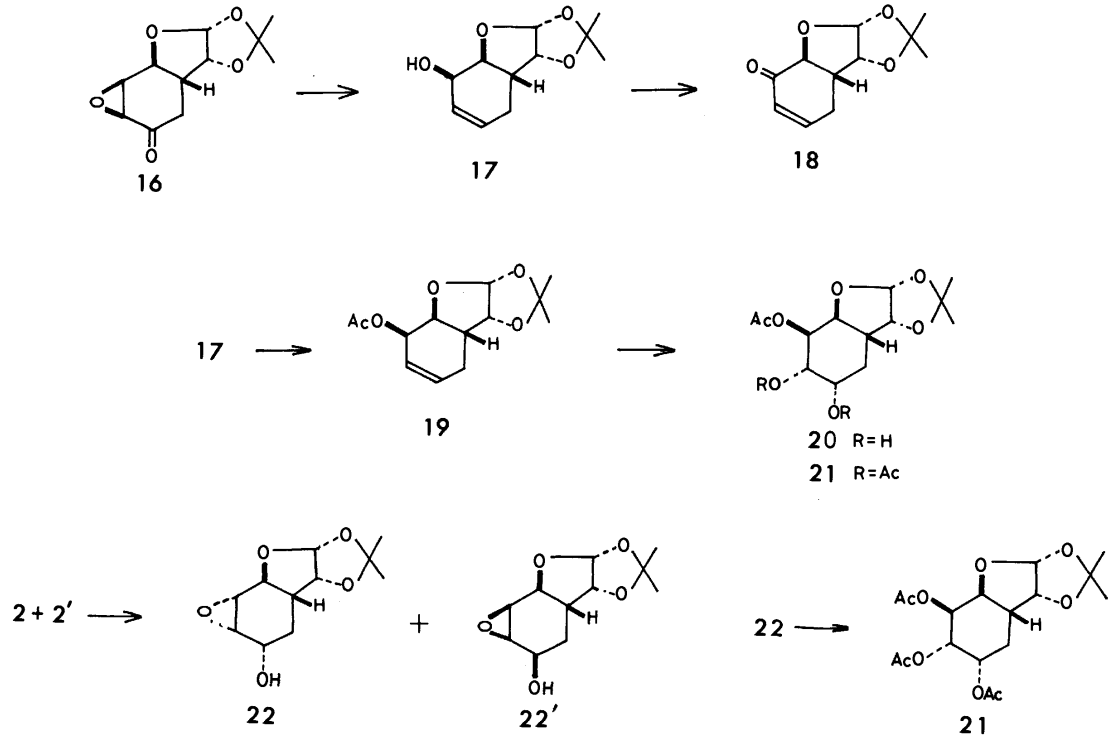

Scheme 2.

volysis of (1*R*,3*S*,4*S*,5*R*,6*S*,8*R*,9*R*)-4,5-epoxy-8,9-isopropylidenedioxy-7-oxabicyclo[4.3.0]nonan-3-ol (**22**). The solvolysis of **22** in aqueous solvent in the presence of sodium acetate was expected to give compound **21** via diaxial opening of epoxy ring by hydroxide ion and acetylation of the solvolytic product. The synthesis of **22** was carried out as follows. Epoxidation of an inseparable mixture of **2** and **2'** with *m*-chloroperbenzoic acid (MCPBA) in refluxing dichloromethane gave two products **22** and **22'** in 50 and 16% yield, respectively. The ^{1}H NMR spectrum of **22'**, which was derived from a minor allyl alcohol **2'**, was identical with that of authentic sample.[3] The ^{1}H NMR spectrum of **22** was apparently different from that of another possible epoxy alcohol possessing (3*S*,4*R*,5*S*)-configuration, which was prepared from **1** by (1) epoxidation and (2) sodium borohydride reduction.[3] The structure of **22** was confirmed. In epoxidation of **2** and **2'**, hydroxyl groups governed the direction of attack of the peroxy acid.[12] As expected, the solvolysis of **22** and successive acetylation gave compound **21**, which was identical with the compound derived from **19**, in 79% yield, and the structure of **21** was thus confirmed. The compound **20** seems to be a promising precursor for synthesizing pseudo-β-L-altropyranose and pseudo-α-D-glucopyranose.[13]

Experimental

General. Reactions were performed at room temperature unless otherwise stated. Evaporation was done under a reduced pressure at below 40 °C with a bath. Melting points were determined with a Mitamura Riken micro mp apparatus. Specific rotation was measured by a Jasco DIP-4 polarimeter with a 10 mm cell. Column chromatography was performed with Kieselgel 60 (Merck), and thin-layer chromatography (TLC) by a glass plate coated with Kieselgel 60 GF_{254} (Merck), followed by UV light detection and charring with sulfuric acid. IR spectra were recorded with a Hitachi 225 spectrometer by the KBr method or with a Jasco A-202 spectrometer by the $CHCl_3$ method. ^{1}H NMR spectra were recorded with a Varian EM-390 (90 MHz) for solutions in $CDCl_3$ with an internal standard of Me_4Si. High-resolution mass spectra were obtained by a Hitachi M-80 spectrometer.

Dichloromethane and *N*,*N*-dimethylformamide (DMF) were dried over CaH_2 and distilled. Pyridine was distilled over NaOH. Tetrahydrofuran (THF) was distilled over $LiAlH_4$ and then over benzophenone.

Mixture of (1*R*,3*S*,6*R*,8*R*,9*R*)- and (1*R*,3*R*,6*R*,8*R*,9*R*)-8,9-Isopropylidenedioxy-7-oxabicyclo[4.3.0]non-4-en-3-ol, (2) and (2'). To a solution of (1*R*,6*R*,8*R*,9*R*)-8,9-isopropylidenedioxy-7-oxabicyclo[4.3.0]non-4-en-3-one (**1**)[3] (1.20 g, 5.70 mmol) in dichloromethane (20 ml) was added with stirring DIBAL-H (1.5 mol dm^{-3} in toluene, 6.08 ml, 9.12 mmol) at −78 °C under an argon atmosphere. The mixture was stirred at the same temperature for 1 h, diluted with water (50 ml), and warmed to room temperature. The resulting insoluble materials were filtered with Celite pad, and the filtrate was condensed by evaporation. The residue was partitioned between dichloromethane (60 ml) and water (50 ml), and the aqueous layer was extracted with dichloromethane (60 ml×2). The organic layer was dried on Na_2SO_4 and condensed. The residue was chromatographed with silica gel (100 g, ethyl acetate-hexane=1 : 4), and the fraction corresponding to R_f 0.17 (ethyl acetate-hexane=1 : 2) was evaporated to give inseparable mixed crystals of **2** and **2'** (830 mg, 69% yield), mp 99—101.5 °C. IR ν_{max}^{KBr} 3500, 3000, 2950, 2900, 2845, 1450, 1400, 1385, 1375, 1315, 1265, 1240, 1210 cm^{-1}; ^{1}H NMR δ=1.33, 1.50 (3H×2, each s, $C(CH_3)_2$), 1.60—2.13 (3H, m, H-2,2', OH), 2.27—2.60 (1H, m, H-1), 4.07—4.50 (2H, m, H-3,6), 4.58 (1H, t, *J*=4.5 Hz, H-9), 5.87—5.97 (1H, m, H-4 or 5), 5.83 (1H, d, *J*=4.5 Hz, H-8), 6.00—6.33 (1H, m, H-4 or 5). Found: C, 62.51; H, 7.51%. Calcd for $C_{11}H_{16}O_4$: C, 62.25; H, 7.60%.

(1*R*,3*S*,6*R*,8*R*,9*R*)- and (1*R*,3*R*,6*R*,8*R*,9*R*)-3-(*t*-Butyldimethylsilyloxy)-8,9-isopropylidenedioxy-7-oxabicyclo[4.3.0]non-4-ene, (3) and (3'). To a solution of inseparable mixture of **2** and **2'** (24.8 mg, 0.12 mmol) in DMF (1 ml) were added *t*-butylchlorodimethylsilane (158.7 mg, 1.09 mmol) and imidazole (68.1 mg, 1.03 mmol) with stirring. The mixture was stirred at 70 °C for 72 h, and diluted with ethyl acetate (15 ml). The solution was washed with water (15 ml×3), and the organic layer was dried on Na_2SO_4 and condensed by evaporation. The residue was chromatographed with silica gel (4 g, ethyl acetate-hexane=1 : 50). The fraction corresponding to R_f 0.71 (ethyl acetate-hexane=1 : 4) was evaporated to give **3'** (3.4 mg, 9%) as a colorless syrup, and the fraction corresponding to R_f 0.60 was evaporated to give **3** (23.5 mg, 62% yield) as a colorless syrup. **3**: $[\alpha]_D^{25}$ −14.6° (*c* 1.14, $CHCl_3$); IR ν_{max}^{KBr} 2990, 2960, 2940, 2880, 1460, 1380, 1375, 1260, 1215 cm^{-1}; ^{1}H NMR δ=0.08 (6H, s, $OSiC(CH_3)_3(C\underline{H}_3)_2$), 0.90 (9H, s, $OSiC(C\underline{H}_3)_3(CH_3)_2$), 1.31, 1.49 (3H×2, each s, $C(CH_3)_2$), 1.60—1.78 (2H, m, H-2,2'), 2.18—2.37 (1H, m, H-1), 4.35—4.47 (2H, m, H-3,6), 4.54 (1H, t, *J*=3.5 Hz, H-9), 5.45—5.58 (1H, m, H-4 or 5), 5.81 (1H, d, *J*=3.5 Hz, H-8), 5.94—6.17 (1H, m, H-5 or 4). **3'**: ^{1}H NMR δ=0.08 (6H, s, $OSiC(CH_3)_3(C\underline{H}_3)_2$), 0.88 (9H, s, $OSiC(C\underline{H}_3)_3(CH_3)_2$), 1.31, 1.48 (3H×2, each s, $C(CH_3)_2$), 1.87—1.97 (3H, m, H-1, 2,2'), 4.03—4.39 (2H, m, H-3,6), 4.60 (1H, t, *J*=3.5 Hz, H-9), 5.47—5.65 (1H, m, H-4 or 5), 5.72 (1H, d, *J*=3.5 Hz, H-8), 6.03—6.22 (1H, m, H-5 or 4).

Mixture of (1*R*,3*S*,6*R*,8*R*,9*R*)- and (1*R*,3*R*,6*R*,8*R*,9*R*)-3-Acetoxy-8,9-isopropylidenedioxy-7-oxabicyclo[4.3.0]non-4-ene, (4) and (4'). An inseparable mixture of **2** and **2'** (596 mg, 2.81 mmol) was acetylated with acetic anhydride (6 ml) in pyridine (6 ml) for 4 h and the mixture was evaporated. The residue was chromatographed with silica gel (20 g, ethyl acetate-hexane=1 : 8), and the fraction corresponding to R_f 0.50 (ethyl acetate-hexane=1 : 2) was evaporated to give an inseparable mixed crystals of **4** and **4'** (683 mg, 96% yield), mp 63—66 °C°; IR ν_{max}^{KBr} 3000, 2980, 2965, 2940, 2840, 1735, 1370, 1325, 1300, 1265, 1240, 1210 cm^{-1}; ^{1}H NMR δ=1.35, 1.50 (3H×2, each s, $C(CH_3)_2$), 1.60—2.00 (2H, m, H-2, 2'), 2.05 (3H, s, $OCOCH_3$), 2.33—2.60 (1H, m, H-1), 4.10—4.50 (1H, m, H-6), 4.58 (1H, t, *J*=4.5 Hz, H-9), 5.30—5.70 (2H, m, H-3, H-4 or 5), 5.87 (1H, d, *J*=4.5 Hz, H-8), 6.13—6.43 (1H, m, H-5 or 4). Found: C, 61.55; H, 7.07%. Calcd for $C_{13}H_{18}O_5$: C, 61.40; H, 7.13%.

(1*R*,3*S*,4*R*,5*S*,6*S*,8*R*,9*R*)- and (1*R*,3*R*,4*S*,5*R*,6*S*,8*R*,9*R*)-3-Acetoxy-8,9-isopropylidenedioxy-7-oxabicyclo[4.3.0]nonane-4,5-diol, (5) and (5'). To a solution of the inseparable mixture of **4** and **4'** (675.8 mg, 2.66 mmol) in *t*-butyl alcohol (15 ml) were added osmium tetraoxide in *t*-butyl alcohol (0.02

mol dm^{-3} solution, 2.66 ml, 0.053 mmol) and aqueous hydrogen peroxide (35wt%, 1.5 ml) with stirring. The solution was stirred in dark for 38 h and evaporated. The residue was chromatographed with silica gel (50 g, ethyl acetate-hexane=2 : 3). The fraction corresponding to R_f 0.10 (ethyl acetate-hexane=1 : 1) was evaporated to give crystals of **5′** (49.5 mg, 6% yield). The fraction corresponding to R_f 0.06 was evaporated to give crystals of **5** (406.3 mg, 53% yield). **5**: Mp 154—155 °C; $[\alpha]_D^{21}$ +71.5° (*c* 1.57, $CHCl_3$); IR ν_{max}^{KBr} 3450, 2990, 2980, 2940, 2880, 1710, 1445, 1390, 1375, 1365, 1265, 1250, 1210 cm^{-1}; ^{1}H NMR δ=1.32, 1.50 (3H×2, each s, $C(CH_3)_2$), 1.95—2.40 (3H, m, H-1,2, 2′), 2.06 (3H, s, $OCOCH_3$), 3.20—3.78 (4H, m, H-4 or 5, 6, 2×OH), 4.32—4.50 (1H, m, H-5 or 4), 4.59 (1H, t, *J*=3 Hz, H-9), 4.99 (1H, dt, *J*=11 and 5 Hz, H-3), 5.88 (1H, d, *J*=3 Hz, H-8). **5′**: Mp 191—193 °C; $[\alpha]_D^{22}$ −7.9° (*c* 1.29, $CHCl_3$); IR ν_{max}^{KBr} 3450, 3300, 2980, 2930, 2890, 1730, 1450, 1370, 1350, 1330, 1305, 1250, 1220 cm^{-1}; ^{1}H NMR δ=1.32, 1.52 (3H×2, each s, $C(CH_3)_2$), 1.67—2.00 (3H, m, H-1, 2, 2′), 2.05 (3H, s, $OCOCH_3$), 2.70—3.20 (1H, br s, OH), 3.75—4.15 (4H, m, H-4, 5, 6, OH), 4.58 (1H, t, *J*=3.5 Hz, H-9), 5.22 (1H, q, *J*=3 Hz, H-3), 5.85 (1H, d, *J*=3.5 Hz, H-8).

Tri-*O*-acetyl Derivatives 6 and 6′ of 5 and 5′. Compounds **5** and **5′** were acetylated with acetic anhydride in pyridine. **6**: (96% yield): TLC R_f 0.61 (ethyl acetate-hexane=1 : 1); mp 66—67 °C; $[\alpha]_D^{23}$ +41.8° (*c* 0.97, $CHCl_3$); IR ν_{max}^{KBr} 2980, 2940, 1740, 1375, 1230, 1165, 1130, 1105 cm^{-1}; ^{1}H NMR δ=1.32, 1.50 (3H×2, each s, $C(CH_3)_2$), 2.00, 2.03, 2.12 (3H×3, each s, 3×$OCOCH_3$), 2.10—2.40 (3H, m, H-1, 2, 2′), 3.85 (1H, dd, $J_{1,6}$=10.5 Hz and $J_{5,6}$=3 Hz, H-6), 4.57 (1H, t, $J_{1,9}$=$J_{8,9}$=3 Hz, H-9), 4.90—5.20 (2H, m, H-3,5), 5.73—5.90 (2H, m, H-4, 8). Found: C, 54.95; H, 6.41%. Calcd for $C_{17}H_{24}O_9$: C, 54.83; H, 6.50%. **6′** (97% yield): TLC R_f 0.66 (ethyl acetate-hexane=1 : 1); mp 140—142 °C; $[\alpha]_D^{23}$ −25.5° (*c* 0.64, $CHCl_3$); IR ν_{max}^{KBr} 3000, 2960, 2940, 2900, 1750, 1735, 1435, 1375, 1305, 1285, 1275, 1250, 1235, 1220 cm^{-1}; ^{1}H NMR δ=1.32, 1.53 (3H×2, each s, $C(CH_3)_2$), 1.77—2.20 (3H, m, H-1, 2, 2′), 2.00, 2.10 (3H and 6H, each s, 3×$OCOCH_3$), 4.02 (1H, t, $J_{1,6}$=$J_{5,6}$=9.5 Hz, H-6), 4.58 (1H, t, $J_{1,9}$=$J_{8,9}$=3.5 Hz, H-9), 5.00—5.30 (2H, m, H-3, 5), 5.35 (1H, t, $J_{3,4}$=$J_{4,5}$=3 Hz, H-4), 5.85 (1H, d, $J_{8,9}$=3.5 Hz, H-8). Found: C, 54.97; H, 6.42%. Calcd for $C_{17}H_{24}O_9$: C, 54.83; H, 6.50%.

(1*R*,3*S*,4*R*,5*S*,6*S*,8*R*,9*R*)-3,4,5-Tris(benzyloxy)-8,9-isopropylidenedioxy-7-oxabicyclo[4.3.0]nonane (8). To a solution of **5** (302.5 mg, 1.05 mmol) in methanol (5 ml) was added sodium methoxide in methanol (1 mol dm^{-3} solution, 1.57 ml, 1.57 mmol) at 0 °C with stirring. The mixture was stirred at 0 °C for 30 min and neutralized by addition of Amberlite IR 120B (H^+). After removal of the resin by filtration, the filtrate was evaporated to give crude (1*R*,3*S*,4*R*,5*S*,6*S*,8*R*,9*R*)-8,9-isopropylidenedioxy-7-oxabicyclo[4.3.0]-nonane-3,4,5-triol (**7**) which was *O*-benzylated without purification. Sodium hydride (60% emulsion in mineral oil, 630 mg, 15.8 mmol) was washed with hexane (1 ml×2), dried, and suspended in DMF (5 ml). To the suspension was added a DMF (10 ml) solution of crude **7** and the mixture was stirred for 10 min. Benzyl bromide (1.87 ml, 15.8 mmol) was added. After the mixture was stirred for 12 h, ethanol (1 ml) was added and evaporated. The residue was dissolved in water (80 ml) and extracted with dichloromethane (80 ml×3). The extract was dried on Na_2SO_4 and evaporated. The residue was chromatographed with silica gel (90 g, ethyl acetate-hexane=1 : 15). The fraction corresponding to R_f 0.46 (ethyl acetate-hexane=1 : 3) was evaporated to give **8** (473.8 mg, 88% yield) as a colorless syrup, $[\alpha]_D^{21}$ +36.7° (*c* 1.15, $CHCl_3$); IR $\nu_{max}^{CHCl_3}$ 3060, 3000, 2930, 2880, 1490, 1455, 1385, 1375, 1360, 1305, 1260, 1200 cm^{-1}; ^{1}H NMR δ=1.28, 1.45 (3H×2, each s, $C(CH_3)_2$), 1.67—2.33 (3H, m, H-1, 2, 2′), 3.88 (1H, dd, *J*=9.5 and 3 Hz, H-6), 3.53—4.00 (2H, m, H-3, 4), 4.23 (1H, t, *J*=3 Hz, H-5), 4.52 (1H, t, *J*=4.5 Hz, H-9), 4.58—4.83 (6H, m, 3×$OCH_2C_6H_5$), 5.83 (1H, d, *J*=4.5 Hz, H-8), 7.13—7.52 (15H, m, 3×$OCH_2C_6H_5$). Found: *m/z* 516.2522. Calcd for $C_{32}H_{36}O_6$: M, 516.2510.

(1*R*)-1-[(1*S*,2*S*,3*S*,4*R*,5*S*)-3,4,5-Tris(benzyloxy)-2-hydroxycyclohexyl]-1,2-ethanediol (9). A solution of **8** (161 mg, 0.31 mmol) in a mixture of 80% aqueous acetic acid (32 ml) and dioxane (1.5 ml) was refluxed for 30 min and evaporated. The residue was dissolved in ethanol (4 ml) and sodium borohydride (24 mg, 0.64 mmol) was added. After stirring for 19 h, 35% aqueous hydrogen peroxide (1 ml) was added and stirred for further 15 min. The solution was neutralized with 1 mol dm^{-3} HCl and saturated aqueous sodium sulfite (1 ml) was added. The solution was diluted with water (20 ml) and extracted with dichloromethane (20 ml×3). The extract was dried on Na_2SO_4 and evaporated. The residue was chromatographed with silica gel (12 g, ethanol-toluene=1 : 25), and the fraction corresponding to R_f 0.26 (ethanol-toluene=1 : 7) was evaporated to give **9** (84 mg, 56% yield) as a colorless syrup, $[\alpha]_D^{22}$ +4.4° (*c* 1.09, $CHCl_3$); IR $\nu_{max}^{CHCl_3}$ 3300, 3050, 2900, 2850, 1600, 1580, 1490, 1400, 1360, 1300, 1200 cm^{-1}; ^{1}H NMR δ=1.67—2.17 (3H, m, H-1, 6, 6′), 2.83—3.25 (1H, m, 2×OH), 3.35 (1H, dd, *J*=10 and 3 Hz, H-2), 3.45—4.23 (7H, m, H-3, 4, 5, $CH(OH)CH_2OH$, OH), 4.57—5.15 (6H, m, 3×$OCH_2C_6H_5$), 7.28—7.47 (15H, m, 3×$OCH_2C_6H_5$). Found: *m/z* 479.2407. Calcd for $C_{29}H_{35}O_6$: M+H, 479.2430.

(1*S*,2*S*,3*S*,4*R*,5*S*)-2-Acetoxy-1-acetoxymethyl-3,4,5-tris(benzyloxy)cyclohexane (10). To a solution of **9** (77 mg, 0.16 mmol) in methanol (2 ml) was added an aqueous solution (0.5 ml) of sodium periodate (38 mg, 0.18 mmol) at 0 °C with stirring. The mixture was stirred at 0 °C for 2 h and evaporated. The residue was dissolved in water (10 ml) and extracted with dichloromethane (25 ml×5). The extract was dried on Na_2SO_4 and evaporated to give crude (1*R*,2*S*,3*S*,4*R*,-5*S*)-3,4,5-tris(benzyloxy)-2-hydroxycyclohexanecarbaldehyde, which was subjected to next step without purification. The residue was dissolved in ethanol (2 ml) and sodium borohydride (12 mg, 0.32 mmol) was added. The mixture was stirred for 1 h and 35% aqueous hydrogen peroxide (0.5 ml) was added, and stirred for 15 min. The solution was neutralized with 1 mol dm^{-3} HCl and saturated sodium sulfite (0.5 ml) was added. The solution was diluted with water (60 ml) and extracted with dichloromethane (60 ml×3). The extract was dried on Na_2SO_4 and evaporated. The residue (TLC R_f 0.37, ethanol-toluene=1 : 7) was acetylated with acetic anhydride (1 ml) in pyridine (1 ml) for 14 h. The mixture was evaporated and the residue was chromatographed with silica gel (5 g, ethyl acetate-hexane=1 : 5). The fraction corresponding to R_f 0.72 (ethanol-toluene=1 : 10) was evaporated to give **10** (73 mg, 85% yield) as a colorless syrup, $[\alpha]_D^{18}$ −40.2° (*c* 1.00, $CHCl_3$); IR $\nu_{max}^{CHCl_3}$ 3000, 2950, 2900, 2870, 1730, 1495, 1450, 1370, 1245, 1205 cm^{-1}; ^{1}H NMR δ=1.23—1.58 (2H, m, H-6, 6′), 1.97, 2.00 (3H×2, each s, 2×$OCOCH_3$), 2.08—2.45 (1H, m, H-1), 3.43 (1H, dd, $J_{3,4}$=3 Hz and $J_{4,5}$=9 Hz, H-4), 3.83—4.24 (4H, m, H-3,5, CH_2OAc), 4.57—4.92 (7H, m, H-2, 3×$OCH_2C_6H_5$), 7.29—7.47 (15H, m, 3×$OCH_2C_6H_5$). Found: *m/z* 533.2538. Calcd for $C_{32}H_{37}O_7$: M+H, 533.2537.

(1*S*,2*S*,3*S*,4*R*,5*S*)-2,3,4,5-Tetraacetoxy-1-(acetoxymethyl)-

cyclohexane, Pentaacetate of Pseudo-β-L-allopyranose (11). A solution of **10** (53.5 mg, 0.10 mmol) in methanol (2 ml) was hydrogenolyzed in the presence of palladium-black in the Parr apparatus for 14 h. The catalyst was removed by filtration and washed with methanol. The mixture of filtrate and washing methanol was evaporated to give crude *O*-debenzylated product, which was acetylated with acetic anhydride (1 ml) in pyridine (1 ml) for 46 h. The mixture was evaporated and the residue was chromatographed with silica gel (1 g, ethyl acetate-hexane=1 : 4). The fraction corresponding to R_f 0.29 (ethyl acetate-hexane=1 : 2) was evaporated to give crystals of **11** (30.5 mg, 79% yield). **11**: Mp 135—136 °C; $[\alpha]_D^{18}$ +3.7° (*c* 1.41, $CHCl_3$); IR ν_{max}^{KBr} 1750, 1740, 1425, 1375, 1225, 1095, 1075 cm^{-1}; ^1H NMR δ=1.10—2.60 (3H, m, H-1, 6, 6′), 2.00, 2.03, 2.05, 2.14 (6H, 3H, 3H, and 3H, each s, 5×$OCOCH_3$), 4.03—4.08 (2H, m, CH_2OAc), 4.91 (1H, dd, *J*=10 and 3 Hz, H-2 or 4), 5.03—5.43 (2H, m, H-4 or 2, 5), 5.59 (1H, t, *J*=3 Hz, H-3). The ^1H NMR spectrum of **11** was identical with that of authentic DL-**11**.[8] Found: C, 52.63; H, 6.15%. Calcd for $C_{17}H_{24}O_{10}$: C, 52.57; H, 6.23%.

(3*S*,4*R*,5*S*)-3,4,5-Tris(benzyloxy)-1-cyclohexene-1-methanol (13). Compound **9** (245 mg, 0.51 mmol) was converted to a glycol-cleaved compound as described in the preparation of **10**. The crude residue extracted with dichloromethane was dissolved in pyridine (10 ml) and methanesulfonyl chloride (0.32 ml, 4.1 mmol) was added. The mixture was stirred for 14 h and evaporated. The residue was partitioned between dichloromethane (60 ml) and water (30 ml). The aqueous layer was extracted with dichloromethane (60 ml×2). The organic layer was dried on Na_2SO_4 and evaporated to give crude (3*S*,4*R*,5*S*)-3,4,5-tris(benzyloxy)-1-cyclohexenecarbaldehyde (**12**) (256 mg). To a solution of crude **12** in THF (4 ml) was added a suspension of lithium aluminium hydride (39 mg, 1.0 mmol) in THF (4 ml) at 0 °C with stirring. The mixture was stirred at 0 °C for 4 h and ethyl acetate (1 ml) was added. The resulting solids were removed with Celite pad. The filtrate was evaporated and the residue was chromatographed with silica gel (10 g, ethyl acetate-hexane=1 : 4). The fraction corresponding to R_f 0.18 (ethyl acetate-hexane=1 : 2) was evaporated to give **13** (81 mg, 37% yield) as a colorless syrup, $[\alpha]_D^{21}$ +61.7° (*c* 0.85, $CHCl_3$); IR $\nu_{max}^{CHCl_3}$ 3580, 3000, 2910, 2860, 1490, 1450, 1360, 1140 cm^{-1}; ^1H NMR δ=1.20—1.63 (1H, OH), 1.90—2.65 (2H, m, H-6, 6′), 3.63—4.27 (5H, m, H-3, 4, 5, CH_2OH), 4.63—4.72 (6H, m, 3×$OCH_2C_6H_5$), 5.67—5.83 (1H, m, H-2), 7.35 (15H, s, 3×$OCH_2C_6H_5$). Found: *m/z* 430.2135. Calcd for $C_{28}H_{30}O_4$: M, 430.2141.

(1*R*,2*R*,3*S*,4*R*,5*S*)-2-Acetoxy-1-acetoxymethyl-3,4,5-tris(benzyloxy)cyclohexane (14). To a solution of **13** (81 mg, 0.19 mmol) in THF (2 ml) was added borane-THF complex (1 mol dm^{-3} in THF, 0.66 ml, 0.66 mmol) at 0 °C under an argon atmosphere with stirring. The mixture was stirred at 0 °C for 20 min, and at room temperature for 2 h. To the mixture were added water (1.8 ml), 3 mol dm^{-3} aqueous NaOH (0.6 ml), and hydrogen peroxide (35 wt% in water, 0.96 ml), successively. The mixture was stirred for 2 h and 1 mol dm^{-3} HCl was added for neutralization. The solution was evaporated, and the residue was dissolved in water (30 ml), extracted with dichloromethane (30 ml×3). The extract was dried on Na_2SO_4 and evaporated. The residue was acetylated with acetic anhydride (2 ml) in pyridine (2 ml) for 12 h. The mixture was evaporated and the residue was chromatographed with silica gel (7 g, ethyl acetate-hexane=1 : 10). The fraction corresponding to R_f 0.73 (ethyl acetate-hexane=1 : 2) was evaporated to give **14** (46 mg, 47% yield) as a colorless syrup, $[\alpha]_D^{19}$ +7.0° (*c* 0.97, $CHCl_3$); IR $\nu_{max}^{CHCl_3}$ 3000, 2920, 2860, 1730, 1490, 1450, 1365, 1240 cm^{-1}; ^1H NMR δ=1.75—2.10 (3H, m, H-1, 6, 6′), 2.00, 2.02 (3H×2, each s, 2×$OCOCH_3$), 3.60—4.07 (5H, m, H-3, 4, 5, CH_2OAc), 4.37—4.73 (6H, m, 3×$OCH_2C_6H_5$), 5.36 (1H, t, $J_{1,2}=J_{2,3}$=10 Hz, H-2), 7.17—7.47 (15H, m, 3×$OCH_2C_6H_5$). Found: *m/z* 532.2448. Calcd for $C_{32}H_{36}O_7$: M, 532.2458.

(1*R*,2*R*,3*S*,4*R*,5*S*)-2,3,4,5-Tetraacetoxy-1-(acetoxymethyl)cyclohexane, Pentaacetate of Pseudo-α-D-mannopyranose (15). A solution of **14** (44.5 mg, 0.08 mmol) in methanol (2 ml) was hydrogenolyzed in the presence of palladium black in the Parr apparatus for 45 h. After the catalyst was removed, the filtrate was evaporated. The residue was chromatographed with silica gel (2 g, chloroform-methanol=15 : 1), and the fraction corresponding to R_f 0.42 (chloroform-methanol=8 : 1) was evaporated. The colorless syrup was acetylated with acetic anhydride (0.5 ml) in pyridine (0.5 ml) for 2 h. The mixture was evaporated, and the residue was chromatographed with silica gel (1 g, ethyl acetate-hexane=1 : 4). The fraction corresponding to R_f 0.30 (ethyl acetate-hexane=1 : 2) was evaporated to give crystals of **15** (18 mg, 56% yield). **15**: Mp 80—81 °C; $[\alpha]_D^{19}$ +27.8° (*c* 0.84, $CHCl_3$); IR $\nu_{max}^{CHCl_3}$ 2950, 1740, 1430, 1370, 1220 cm^{-1}; ^1H NMR δ=1.50—2.70 (3H, m, H-1, 6, 6′), 1.97, 2.03, 2.05, 2.13 (3H, 3H, 3H, and 6H, each s, 5×$OCOCH_3$), 3.87—4.27 (2H, m, CH_2OAc), 5.03—5.40 (4H, m, H-2, 3, 4, 5). The ^1H NMR spectrum of **15** was identical with that of authentic DL-**15**.[10] Found: C, 52.79; H, 6.14%. Calcd for $C_{17}H_{24}O_{10}$: C, 52.57; H, 6.23%.

(1*R*,5*R*,6*S*,8*R*,9*R*)-8,9-Isopropylidenedioxy-7-oxabicyclo[4.3.0]non-3-en-5-ol (17). To a solution of (1*R*,4*S*,5*S*,6*S*,-8*R*,9*R*)-4,5-epoxy-8,9-isopropylidenedioxy-7-oxabicyclo-[4.3.0]nonan-3-one (**16**)[3] (373 mg, 1.65 mmol) in ethanol (54 ml) were added hydrazine hydrate (0.40 ml, 8.26 mmol) and acetic acid (0.47 ml, 8.26 mmol) with stirring. The mixture was stirred for 2.5 min, and added to a saturated aqueous $NaHCO_3$ solution (170 ml). The aqueous solution was extracted with chloroform (170 ml×5). The combined extract was dried on Na_2SO_4 and evaporated. The residue was chromatographed with silica gel (13 g, ethyl acetate-hexane=1 : 3), and the fraction corresponding to R_f 0.44 (ethyl acetate-hexane=1 : 1) was evaporated to give **17** (258 mg, 74% yield), mp 95—98 °C; $[\alpha]_D^{22.5}$ −136.4° (*c* 1.00, $CHCl_3$); IR $\nu_{max}^{CHCl_3}$ 3490, 3000, 2900, 1635, 1460, 1440, 1420, 1380, 1320, 1305, 1250 cm^{-1}; ^1H NMR δ=1.33, 1.50 (3H×2, each s, $C(CH_3)_2$), 1.80—2.50 (4H, m, H-1, 2,2′, OH), 3.72 (1H, dd, δ=10.5 and 4.5 Hz, H-6), 4.43 (1H, t, *J*=4.5 Hz, H-5 or 9), 4.61 (1H, t, *J*=4.5 Hz, H-9 or 5), 5.70—6.10 (3H, m, H-3, 4, 8). Found: C, 62.07; H, 7.54%. Cacld for $C_{11}H_{16}O_4$: C, 62.25; H, 7.60%.

(1*S*,6*S*,8*R*,9*R*)-8,9-Isopropylidenedioxy-7-oxabicyclo[4.3.0]non-3-en-5-one (18). To a solution of **17** (128.5 mg, 0.61 mmol) in dichloromethane (12 ml) were added PCC (521 mg, 2.42 mmol) and molecular sieves (4A powder, 150 mg) with stirring. The mixture was stirred for 1.5 h and evaporated. The residue charged on a silica-gel column (10 g) was eluted with ether to give crystals of **18** (110.4 mg, 87% yield; TLC R_f 0.57, ethyl acetate-hexane=3 : 2), mp 96—98 °C; $[\alpha]_D^{24}$ −141.0° (*c* 0.70, $CHCl_3$); IR $\nu_{max}^{CHCl_3}$ 2975, 2925, 2825, 1700, 1595, 1445, 1425, 1370, 1320, 1300, 1240, 1210 cm^{-1}; ^1H NMR δ=1.35, 1.52 (3H×2, each s, $C(CH_3)_2$), 2.00—2.50 (1H, m,

H-1), 2.55—2.80 (2H, m, H-2, 2′), 4.45 (1H, d, J=12 Hz, H-6), 4.69 (1H, t, J=4.5 Hz, H-9), 5.88 (1H, d, J=4.5 Hz, H-8), 5.98 (1H, d, J=12 Hz, H-4), 6.91 (1H, dt, J=12 and 4.5 Hz, H-3). Found: C, 62.96; H, 6.72%. Calcd for $C_{11}H_{14}O_4$: C, 62.85; H, 6.71%.

(1*R*,5*R*,6*S*,8*R*,9*R*)-5-Acetoxy-8,9-isopropylidenedioxy-7-oxabicyclo[4.3.0]non-3-ene (19). Acetylation of **17** (162 mg, 0.76 mmol) with acetic anhydride (5 ml) in pyridine (5 ml) for 14 h, and chromatographic purification with silica gel (4 g, ethyl acetate-hexane=1 : 3) gave **19** (191 mg, 98% yield), TLC R_f 0.47 (ethyl acetate-hexane=1 : 2); mp 121—122 °C; $[\alpha]_D^{24}$ −262.1° (c 0.62, $CHCl_3$); IR $\nu_{max}^{CHCl_3}$ 3040, 2975, 2925, 2875, 1730, 1630, 1450, 1370, 1330, 1290, 1250 cm^{-1}; ^{1}H NMR δ=1.33, 1.46 (3H×2, each s, $C(CH_3)_2$), 2.03 (3H, s, $OCOCH_3$), 2.10—2.50 (3H, m, H-1, 2, 2′), 3.86 (1H, dd, J=12 and 4.5 Hz, H-6), 4.60 (1H, t, J=4.5 Hz, H-9), 5.50 (1H, t, J=4.5 Hz, H-5), 5.70—6.20 (3H, m, H-3, 4, 8). Found: C, 61.16; H, 7.11%. Calcd for $C_{13}H_{18}O_5$: C, 61.40; H, 7.13%.

(1*R*,3*S*,4*S*,5*S*,6*S*,8*R*,9*R*)-5-Acetoxy-8,9-isopropylidenedioxy-7-oxabicyclo[4.3.0]nonane-3,4-diol (20). To a solution of **19** (190 mg, 0.74 mmol) in t-butyl alcohol (4 ml) were added osmium tetraoxide in t-butyl alcohol (0.02 mol dm^{-3} solution, 0.37 ml, 0.007 mmol) and hydrogen peroxide (35% in water, 0.26 ml) with stirring. The mixture was stirred for 88 h in dark. The mixture was evaporated and the residue was chromatographed with silica gel (15 g, ethyl acetate-hexane=1 : 2). The fraction corresponding to R_f 0.37 (ethanol-toluene=1 : 6) was evaporated to give crystals of **20** (75 mg, 35% yield), mp 174—175 °C; $[\alpha]_D^{22}$ −0.19 ° (c 0.90, MeOH); IR ν_{max}^{KBr} 3500, 3450, 2990, 1725, 1375, 1255 cm^{-1}; ^{1}H NMR δ=1.31, 1.52 (3H×2, each s, $C(CH_3)_2$), 1.70—2.10 (5H, m, H-1, 2, 2′,2×OH), 2.07 (3H, s, $OCOCH_3$), 3.66—4.35 (3H, m, H-3, 4, 6), 4.56 (1H, t, J=4.5 Hz, H-9), 5.43 (1H, t, J=3 Hz, H-5), 5.81 (1H, d, J=4.5 Hz, H-8). Found: C, 54.31; H, 6.83%. Calcd for $C_{13}H_{20}O_7$: C, 54.15; H, 6.99%.

(1*R*,3*S*,4*S*,5*S*,6*S*,8*R*,9*R*)-3,4,5-Triacetoxy-8,9-isopropylidenedioxy-7-oxabicyclo[4.3.0]nonane (21). Acetylation of **20** (23 mg, 0.08 mmol) with acetic anhydride (1 ml) in pyridine (1 ml), and chromatographic purification with silica gel (2 g, ethyl acetate-hexane=1 : 3) gave crystals of **21** (27 mg, 90% yield, TLC R_f 0.71 (ethanol-toluene=1 : 6); mp 135—137 °C; $[\alpha]_D^{22}$ +28.5° (c 0.94, $CHCl_3$); IR $\nu_{max}^{CHCl_3}$ 2990, 2930, 1745, 1370, 1250 cm^{-1}; ^{1}H NMR δ=1.30, 1.52 (3H×2, each s, $C(CH_3)_2$), 1.80—2.40 (3H, m, H-1, 2, 2′), 1.99, 2.10 (3H and 6H, each s, 3×$OCOCH_3$), 4.05 (1H, dd, J=10.5 and 3 Hz, H-6), 4.58 (1H, t, J=4.5 Hz, H-9), 4.90—5.56 (3H, m, H-3,4,5), 5.83 (1H, d, J=4.5 Hz, H-8). Found: C, 55.12; H, 6.50%. Calcd for $C_{17}H_{24}O_9$: C, 54.83; H, 6.50%.

(1*R*,3*S*,4*S*,5*R*,6*S*,8*R*,9*R*)- and (1*R*,3*R*,4*R*,5*S*,6*S*,8*R*,9*R*)-4,5-Epoxy-8,9-isopropylidenedioxy-7-oxabicyclo[4.3.0]nonan-3-ol, (22) and (22′). A solution of inseparable mixture of **2** and **2′** (106 mg, 0.50 mmol) in dichloromethane (4 ml) containing MCPBA (429 mg, 2.5 mmol) was refluxed for 41 h. The solution diluted with water (20 ml) was extracted with dichloromethane (20 ml×6). The combined extract was washed with saturated aqueous sodium sulfite (30 ml), dried on Na_2SO_4, and evaporated. The residue was chromatographed with silica gel (13 g, ethyl acetate-hexane=1 : 7). The fraction corresponding to R_f 0.29 (ethyl acetate-hexane=2 : 1) was evaporated to give **22′**[3] (18 mg, 16% yield), which was identical with authentic sample in TLC, mp, and ^{1}H NMR. The fraction corresponding to R_f 0.23 was evaporated to give crystals of **22** (57 mg, 50% yield), mp 159—161 °C; $[\alpha]_D^{21}$ −21.0° (c 1.00, $CHCl_3$); IR $\nu_{max}^{CHCl_3}$ 3560, 3000, 2850, 1460, 1380, 1300, 1265, 1255, 1215 cm^{-1}; ^{1}H NMR δ=1.30, 1.50 (3H×2, each s, $C(CH_3)_2$), 1.12—2.24 (3H, m, H-1, 2, 2′), 2.49—2.75 (1H, br, OH), 3.32 (1H, t, J=3 Hz, H-5), 3.58—3.83 (2H, m, H-4,6), 4.04—4.32 (1H, m, H-3), 4.51 (1H, t, J=4 Hz, H-9), 5.85 (1H, d, J=4 Hz, H-8). Found: C, 57.52; H, 6.90%. Calcd for $C_{11}H_{16}O_5$: C, 57.88; H, 7.07%.

Solvolysis of 22 and Successive Acetylation. Compound **21** from **22**. A solution of **22** (36 mg, 0.16 mmol) in a mixture of water and 2-methoxyethanol (3 : 10 v/v, 5 ml) in the presence of sodium acetate (39 mg, 0.48 mmol) was refluxed for 47 h and evaporated. The residue was acetylated with acetic anhydride (1.3 ml) in pyridine (1.3 ml) for 2 h. After the mixture was condensed by evaporation, the residue was partitioned between dichloromethane (10 ml) and water (10 ml). The aqueous layer was extracted with dichloromethane (10 ml×2). The organic layer was dried on Na_2SO_4 and evaporated. The residue was chromatographed with silica gel (5 g, ethyl acetate-hexane=1 : 4 to 1 : 3), and the fraction corresponding to R_f 0.59 (ethanol-toluene=1 : 6) was evaporated to give **21** (46 mg, 79%), which was identical with the compound prepared from **19** in TLC, mp, $[\alpha]_D$, and ^{1}H NMR.

The authors express their sincere thanks to Professor Seiichiro Ogawa of Keio University for his valuable discussion on the structural identification of the synthesized pseudo-sugars, and to Mr. Akio Takahashi for elemental analyses.

References

1) S. Ogawa, *Yuki Gosei Kagaku Kyokai Shi*, **43**, 26 (1985).

2) S. Ogawa, Y. Iwasawa, and T. Suami, *Chem. Lett.*, **1984**, 355; S. Ogawa, Y. Iwasawa, T. Nose, T. Suami, S. Ohba, M. Ito, and Y. Saito, *J. Chem. Soc., Perkin Trans. 1.*, **1985**, 903; S. Ogawa, K. Nakamura, and T. Takagaki, *Bull. Chem. Soc. Jpn.*, **59**, 2956 (1986); H. Paulsen, W. v. Deyn, and W. Roben, *Liebigs Ann. Chem.*, **1984**, 433; R. J. Ferrier and P. Prasit, *Pure Appl. Chem.*, **55**, 565 (1983) and references cited therein; C. S. Wilcox and J. J. Gaudino, *J. Am. Chem. Soc.*, **108**, 3102 (1986).

3) T. Suami, K. Tadano, Y. Ueno, and C. Fukabori, *Chem. Lett.*, **1985**, 1557; K. Tadano, Y. Ueno, C. Fukabori, Y. Hotta, and T. Suami, *Bull. Chem. Soc. Jpn.*, in press.

4) a) T. Suami, K. Tadano, Y. Kameda, and Y. Iimura, *Chem. Lett.*, **1984**, 1919; b) T. Suami, K. Tadano, Y. Ueno, and Y. Iimura, *Chem. Lett.*, **1985**, 37; c) K. Tadano, H. Maeda, M. Hoshino, Y. Iimura, and T. Suami, *Chem. Lett.*, **1986**, 1081; d) K. Tadano and T. Suami, *Yuki Gosei Kagaku Kyokai Shi*, **44**, 633 (1986).

5) Moderate stereoselectivity of the hydride attack was realized in the case of sodium borohydride reduction of compound **16**.[3] In this case, stereoselectivity was 5 : 1 with preferential formation of (3S)-4,5-epoxy-3-ol derivative. The direction of the preferential hydride attack was same as the case of DIBAL-H reduction of **1**.

6) In regard to the empirical rule for determining conformation of acetoxyl methyl signals on the six-membered ring systems by their ^{1}H NMR spetra: F. W. Lichtenthaler and P. Emig, *Carbohydr. Res.*, **7**, 121 (1968).

7) The similar cis-diol introduction catalyzed by osmium tetraoxide to cyclic allyl acetate for synthesis of pseudo-

sugars also appeared in the literatures: G. E. McCasland, S. Furuta, and L. J. Durham, *J. Org. Chem.*, **33**, 2835 (1968); S. Ogawa, T. Toyokuni, T. Kondoh, Y. Hattori, S. Iwasaki, M. Suetsugu, and T. Suami, *Bull. Chem. Soc. Jpn.*, **54**, 2739 (1981). In all cases, the osmate formation took place from the opposite side to acetoxy group(s). On the stereochemistry of osmium tetraoxide oxidation of acyclic and cyclic allyl alcohol systems, a wide range of examples are verified in the literatures: J. K. Cha, W. J. Christ, and Y. Kishi, *Tetrahedron Lett.*, **24**, 3943 (1983) and the accompanying paper; J. K. Cha, W. J. Christ, and Y. Kishi, *Tetrahedron*, **40**, 2247 (1984).

8) S. Ogawa, Y. Tsukiboshi, Y. Iwasawa, and T. Suami, *Carbohydr. Res.*, **136**, 77 (1985).

9) Hydroboration of some 1-hydroxymethyl-1-cyclohexene-3,4,5-triol derivatives, in general, took place from less hindered side with high to moderate stereoselectivity. For other examples of hydroboration of the above cyclic models, see References 3 and 4a, c, and d. On the theoretical aspects on stereoselective hydroboration of some acyclic allyl alcohols, a notable literature was published: K. N. Houk, N. G. Rondan, Y-D. Wu, J. T. Metz, and M. N. Paddon-Row, *Tetrahedron*, **40**, 2257 (1984).

10) S. Ogawa, M. Ara, T. Kondoh, M. Saitoh, R. Masuda, T. Toyokuni, and T. Suami, *Bull. Chem. Soc. Jpn.*, **53**, 1121 (1980).

11) P. S. Wharton and D. H. Bohlen, *J. Org. Chem.*, **26**, 3615 (1961).

12) A recent literature described on the stereoselectivity in the epoxidation of acyclic allyl alcohols with MCPBA: A. S. Narula, *Tetrahedron Lett.*, **24**, 5421 (1983).

13) Pseudo-β-L-altropyranose and pseudo-α-D-glucopyranose were synthesized by an independent approach employing L-arabinose as a chiral starting material in our laboratory, see reference 4a.

 © 1987 The Chemical Society of Japan Bull. Chem. Soc. Jpn., 60, 2197—2204 (1987)

Chemical Synthesis of a Biosynthetic Precursor of Lipid A with a Phosphorylated Tetraacyl Disaccharide Structure

Masahiro IMOTO, Hiroyuki YOSHIMURA, Michiharu YAMAMOTO, Tetsuo SHIMAMOTO, Shoichi KUSUMOTO, and Tetsuo SHIBA*

Department of Chemistry, Faculty of Science, Osaka University, Toyonaka, Osaka 560

(Received December 15, 1986)

2,2′-*N*:3,3′-*O*-Tetrakis[(*R*)-3-hydroxytetradecanoyl]-β(1-6)-D-glucosamine disaccharide 1,4′-bis(phosphate) and its dephospho derivatives were synthesized. The bisphosphate prepared was shown to be identical with a natural biosynthetic precursor of lipid A which corresponds to the lipophilic part of lipopolysaccharide (LPS) in bacterial cell wall. The synthetic bis- and monophosphates exhibited many of typical endotoxic activities of LPS. Consequently, this work established the chemical structure of the biosynthetic precursor of lipid A and elucidated the fundamental structure required for the expression of these activities.

Gram-negative bacteria contain in their cell surface a toxic principle which causes fever and lethal shock in higher animals. This toxin is called endotoxin since it is firmly bound to the cells in living bacteria and released only after the cells are destroyed. Endotoxin exhibits not only undesired toxic activities mentioned above but also beneficial ones such as stimulation of immune responses and induction of a tumor-necrotizing factor.[1] These toxic and beneficial biological activities have been shown to be attributed to the lipopolysaccharide (LPS) moiety which is a complex amphipathic molecule characteristic of the outer membrane of Gram-negative bacterial cells.[1] In 1954, Westphal and Lüderitz[2] isolated the lipophilic part of LPS by mild acidic hydrolysis and termed it "lipid A". They described that lipid A manifested most of the endotoxic activities of LPS. Although there had been some confusions due to the heterogeneous character of natural lipid A preparations,[3] this concept was unequivocally confirmed by our recent total synthesis of *Escherichia coli* lipid A (**1**).[4] In this paper we described in detail a total synthesis of a biosynthetic precursor (**2**) of lipid A and its dephospho derivatives. As reported previously in a preliminary form,[5] this synthetic work was the first successful chemical construction of a compound possessing definite endotoxic activities.[6]

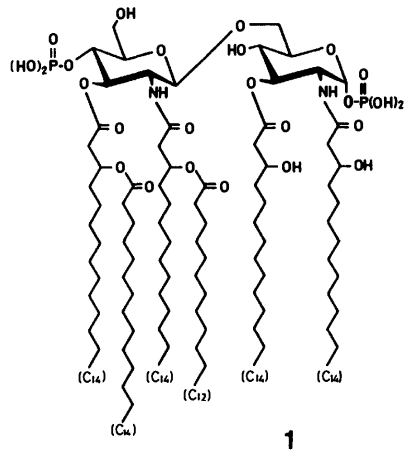

1

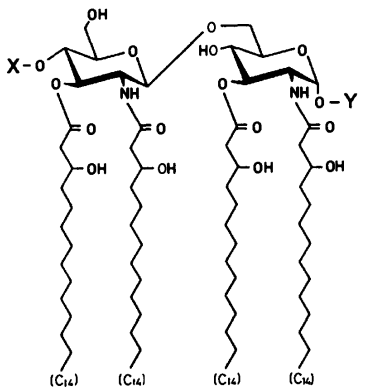

2 X = Y = PO(OH)$_2$
3 X = PO(OH)$_2$, Y = H
4 X = H, Y = PO(OH)$_2$
5 X = Y = H

The chemical structure of lipid A had been studied by the group of Westphal.[1] They demonstrated that lipid A's from many bacterial species share a common basic structure composed of polyacylated D-glucosamine β(1→6) disaccharide 1,4′-bis(phosphate). However, because of the heterogeneity of natural lipid A preparations studied before our synthetic work, the exact number and location of acyl groups could not be determined, the positions of acylation being rather tentatively assigned to the 2,2′-amino and 3,4,6′-hydroxyl groups. Since this assignment then proved incorrect by our synthesis of corresponding compounds,[7] we started a structural study on a purified main component of *E. coli* lipid A and elucidated that the bisphosphorylated disaccharide backbone is acylated at 2,2′-amino and 3,3′-hydroxyl groups with four moles of (*R*)-3-hydroxytetradecanoic acid[8] which is a typical constituent acid of LPS.

With this information, we took the structure **2** as the first target of our synthesis in order to confirm the newly proposed acylation pattern. We already knew that a biosynthetic precursor of lipid A which contained only four moles of 3-hydroxytetradecanoic acid possessed most of endotoxic activities.[9,10] The precursor designated "acidic precursor" and now renamed "precursor Ia"[11] was first isolated from a temperature-sensitive mutant of *Salmonella typhimurium*.[12] The location of the fatty acids in precursor Ia had not been determined but the structure **2** could be most reasonably assigned to it by taking our results on *E. coli* lipid A into consideration.[13]

The strategy for the synthesis was decided on the basis of our knowledges accumulated during the previous works[7] on the compounds with the incorrect old-type acylation pattern. Thus the target compound **2** was constructed via the following steps: 1) preparation of a $\beta(1\rightarrow6)$ disaccharide without long-chain acyl groups, 2) introduction of 3-benzyloxytetradecanoic acids to the two amino and two hydroxyl groups of the disaccharide, 3) phosphorylation of 4′-position, 4) phosphorylation of the glycosidic position, 5) hydrogenolytic deprotection. Phosphorylation of the glycosidic position had to be carried out at the last stage of the synthesis, since glycosyl phosphates are unstable. Thus, the 1-hydroxyl function was protected with allyl group which could be removed without affecting other functional and protecting groups. For persistent protection of other hydroxyl and 4′-phosphate groups were used benzyl and phenyl groups respectively.

In order to investigate the role of phosphate moieties for the biological activities, the corresponding monophosphates (**3** and **4**) and the dephospho derivative **5** were also prepared by slight modification of the synthetic route.

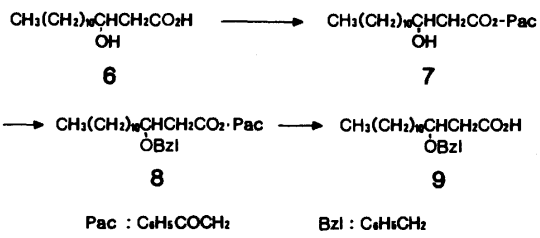

(*R*)-3-Benzyloxytetradecanoic acid (**9**) was prepared from optically pure (*R*)-3-hydroxytetradecanoic acid (**6**)[14] via the corresponding phenacyl ester **7**. For the next *O*-benzylation of **7**, strongly basic conditions should not be used since the 3-benzyloxy derivative formed was susceptible to base-induced β-elimination. Acid catalyzed *O*-benzylation by means of benzyl trichloroacetimidate-trifluoromethanesulfonic acid[15] proved to be preferable to the benzyl bromide-silver(I) oxide method employed in our previous work.[7] With the former method, a comparable yield of the benzylated product **8** could be obtained in a much shorter reaction time. The phenacyl group of **8** was removed with zinc dust in acetic acid to give the 3-benzyloxy acid **9**.

As the glycosyl acceptor was designed the compound **14**, whose 4-hydroxyl function was protected with persistent benzyl group and glycosidic position with allyl group for the reasons mentioned above. The starting material, β-allyl glycoside of *N*-acetyl-D-glucosamine (**11**), was prepared from D-glucosamine hydrochloride via peracetylated oxazoline **10** obtained by the new method, which is suitable for a large-scale preparation of the oxazoline **10**. Compound **11** thus obtained was selectively benzoylated with benzoyl chloride-pyridine at low temperature (−65 °C) to afford the 3,6-dibenzoate **12**.[16] Acid-catalyzed benzylation[15] of **12** gave 4-*O*-benzylated derivative **13**. Under these conditions, the *N*-acetyl group was partially converted into benzyl imidate, which could be reconverted to *N*-acetyl group via mild acidic hydrolysis and reacetylation. Compound **13** was purified by column chromatography on DIAION HP-20 (high-porous polystyrene gel). The recovered starting material **12** and trichloroacetamide formed from the reagent were readily removed by this chromatography. The benzoyl group on the primary hydroxyl function of **13** was selectively split off by transesterification to afford the glycosyl acceptor **14**.

Coupling of **14** with the oxazoline **10** yielded a disaccharide **15**. The β-configuration of the newly formed glycosidic linkage was confirmed by the coupling constant value (8 Hz) of the signal due to the anomeric proton in the ^{1}H NMR spectrum of **15**.

The next step in the synthesis was introduction of 3-benzyloxytetradecanoic acid (**9**) into the disaccharide backbone. Both *N*-acetyl groups of the disaccharide **15** were cleaved by an action of Meerwein's reagent, triethyloxonium tetrafluoroborate, followed by acid hydrolysis of the resultant imidates. The free amino functions were acylated with 3-benzyloxy acid **9** and dicyclohexylcarbodiimide (DCC) to give *N,N*′-diacylated disaccharide **16**. Thereafter all the ester-type protecting groups of **16** were removed and the 4′- and 6′-hydroxyl groups were protected by isopropylidenation. The remaining two hydroxyl functions on 3- and 3′-position of **18** were acylated with 3-benzyloxy acid **9**, DCC, and 4-dimethylaminopyridine (DMAP). Hydrolysis of the isopropylidene group afforded the product **19**, which possessed four acyl groups at the desired positions.

After protection of the primary hydroxyl function of **19** by benzyloxymethylation, the hydroxyl function on 4′-position of the product **20** was phosphorylated with diphenyl phosphorochloridate-pyridine-DMAP according to the procedure by Szabo et al.[17] to give **21**.

The final two steps of the synthesis were the introduction of the 1-α-phosphate moiety and deprotection.

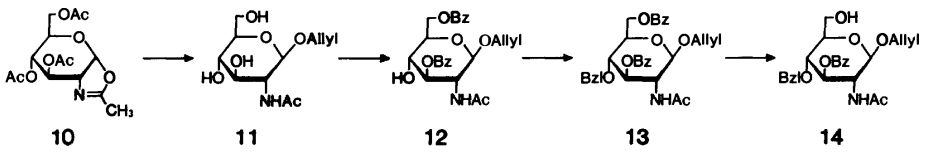

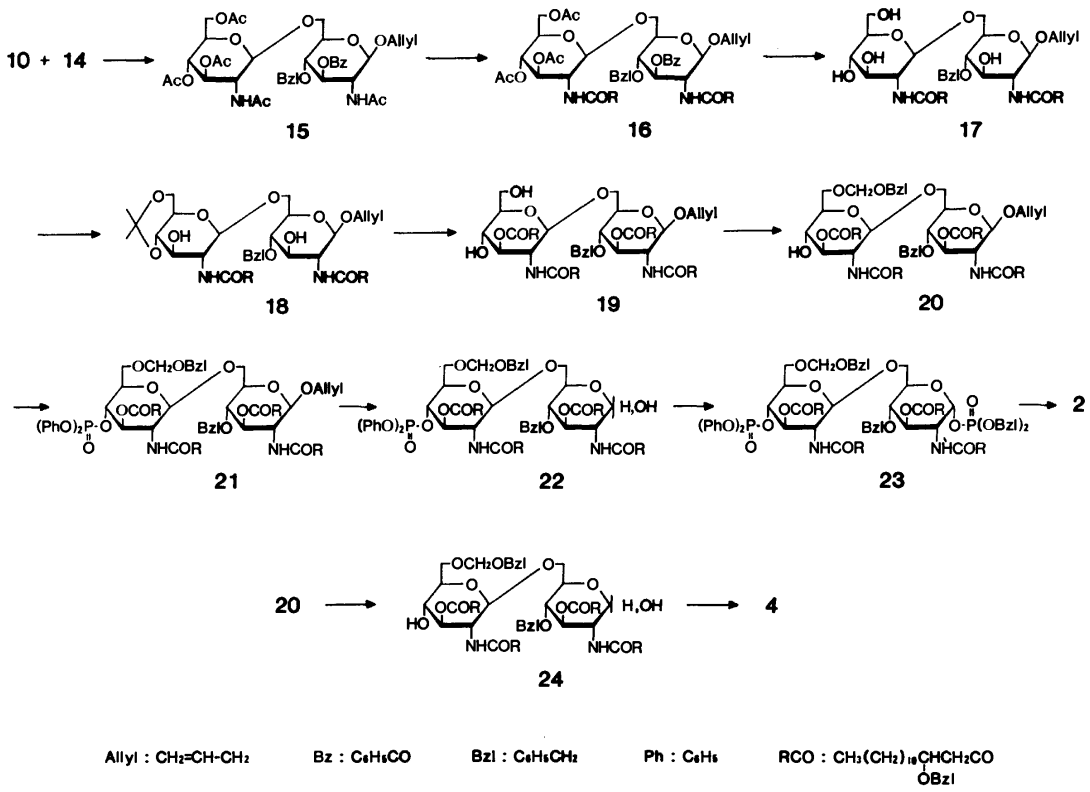

Thus, the glycosidic allyl group of **21** was removed by two-step conversion. It was first isomerized into 1-propenyl group with 1,5-cyclooctadienebis(methyldiphenylphosphine)iridium hexafluorophosphate[18] and then cleaved off by an action of iodine in aqueous THF[19] to afford the compound **22** with a free glycosidic position. 1-α-Phosphorylation of **22** was accomplished by using butyllithium-dibenzyl phosphorochloridate.[20] The protected 1-α,4′-bis(phosphate) **23** thus obtained was immediately hydrogenolyzed in order to prevent a decomposition of the labile dibenzyl ester of the glycosyl phosphate. After removal of all the benzyl-type groups with palladium catalyst, the phenyl groups on the 4′-phosphate were hydrogenolyzed with platinum.

The final product **2** was isolated by silica-gel column chromatography. Although **2** showed a behavior identical with that of natural precursor Ia in TLC analysis, the solubility of the former in water was lower than that of the natural compound. This seemed to be due to the formation of salts at the phosphate residues with inorganic cations from silica gel. It is known that the solubility as well as the biological activities of lipid A's are much influenced by counter cations of phosphate moieties.[21] Therefore the synthetic product was once converted into the free acid form and then to the triethylammonium salt, which is the most soluble form in water, by the following procedures. An aqueous suspension of synthetic **2**, the pH of which was adjusted to 9 with triethylamine, was electrodialyzed[21] under the conditions described in the experimental part. By this procedure, the solubility of the material increased considerably, but it was found that the phosphate groups still formed a monobasic salt as judged from TLC analysis after treatment with diazomethane. Removal of cations was completed by acidic precipitation method.[22] By addition of cold diluted hydrochloric acid to an aqueous solution of the electrodialyzed material under ice-cooling, pure **2** of free acid form was precipitated. The material thus obtained gave a satisfactory result in elemental analysis. The sample was supplied for biological tests as bis(triethylammonium) salt, which was prepared by lyophilization from aqueous solution of **2** after addition of a calculated amount of triethylamine.

The 4′-phosphate **3** was prepared by direct deprotection of the above intermediate **22**. Thus, the benzyl and phenyl groups of **22** were cleaved by hydrogenolysis with palladium and platinum respectively. In order to remove inorganic impurities resulted from catalyst, the product was subjected to the acidic precipitation method to afford the pure 4′-monophosphate **3**. This compound gave the same R_f value on silica-gel TLC with the corresponding 4′-monophosphate which was derived from natural precursor Ia by mild acidic hydrolysis of the unstable glycosyl phosphate. For more strict identification, synthetic and natural 4′-monophosphates were converted into the dimethyl esters by treatment with ethereal diazomethane. Both dimethyl esters of 4′-phosphate were indistinguishable on TLC as well as 360 MHz ^{1}H NMR spectrometry.

1-Monophosphate **4** was derived from the intermediate **20** by removal of the glycosidic allyl group followed by 1-*O*-phosphorylation. Since the reactivity of the hindered 4′-hydroxyl group is much lower than that of the glycosidic hydroxyl group, selective phos-

phorylation of the latter position of **24** was accomplished with a limited amount of butyllithium and dibenzyl phosphorochloridate.[7] Hydrogenolytic deprotection followed by column chromatography on silica gel afforded the desired 1-monophosphate **4**, which was purified by means of electrodialysis and acidic precipitation as described for **2**. Dephospho derivative **5** was prepared from the nonphosphorylated intermediate **19** by direct deprotection.

As had already been reported elsewhere,[6] the synthetic bisphosphate **2** showed fully identical biological activities with those of natural biosynthetic precursor obtained from *Salmonella*. The activities include lethal toxicity, B-cell mitogenicity, induction of interferon and so on.[23] These results together with the NMR spectroscopic and TLC identification of the synthetic and natural compounds described above led us to the following unequivocal conclusions. First, biosynthetic precursor Ia of lipid A has the structure formulated as **2**. Secondly, our new proposal of the location of the acyl groups on the disaccharide backbone[8] was correct. Finally, at least the most of the typical biological activities[23] of bacterial endotoxin can be attributed to this type of phosphorylated acyl disaccharide, which is now synthetically accessible.

Furthermore, this work demonstrated for the first time that a precise study became possible on the relationship between the chemical structures and biological activities of lipid A analogs by synthetic approaches. For example, the importance of the phosphate moieties was elucidated by a comparative study on the biological activities of the above synthetic derivatives: The two monophosphates **3** and **4** exhibited somewhat weaker than **2** but definite endotoxic activities whereas the dephospho derivative **5** was completely inactive.[6] Further synthetic studies in this line is described in the accompanying paper.

Experimental

All melting points are uncorrected. ^{1}H NMR spectra were measured on a Varian XL-100-15 spectrometer (100 MHz) or a JEOL PMX-60 spectrometer (60 MHz) for chloroform-*d* solutions unless noted otherwise. The chemical shifts are given in δ values with TMS as the internal standard. Optical rotations were measured with a Perkin-Elmer 141 polarimeter. High resolution EI-MS was obtained on a JEOL O1-SG mass spectrometer. Conventional and medium-pressure (2—4 kg cm^{-2}) column chromatography were carried out with Kieselgel 60 (E. Merck), 0.063—0.2 mm and 0.040—0.063 mm, respectively. Precoated Kieselgel F_{254} plates (0.5 mm thickness; E. Merck) were used for preparative TLC. For electrodialysis and acidic precipitation procedures was used a pyrogen-free water (Otsuka). Organic solutions were dried over magnesium sulfate and evaporated in vacuo.

Phenacyl (*R*)-3-Hydroxytetradecanoate (7). To a suspension of (*R*)-3-hydroxytetradecanoic acid (**6**) (21.8 g, 89.2 mmol) in ethyl acetate (400 ml) were added phenacyl bromide (19.1 g, 96.0 mmol) and triethylamine (10.6 g, 105 mmol) at 0 °C. The mixture was stirred at 0 °C for 10 min then at room temperature overnight. The precipitate was filtered off and the filtrate was washed with water, dried, and evaporated. The residue was recrystallized from hexane; yield 30.0 g (94%); mp 76—77 °C; $[\alpha]_D^{11}$ −5.1° (*c* 2.17, chloroform). Found: C, 72.88; H, 9.42%. Calcd for $C_{22}H_{34}O_4$: C, 72.89; H, 9.45%. ^{1}H NMR (60 MHz) δ=0.9 (3H, br t, CH_3), 1.1—1.7 (20H, br s, CH_2), 2.6 (2H, m, -$COCH_2$-), 3.1 (1H, s, -OH), 4.1 (1H, m, -C<u>H</u>(OH)-), 5.4 (2H, s, -$C\underline{H}_2COC_6H_5$), and 7.3—8.0 (5H, m, aromatic H).

Phenacyl (*R*)-3-Benzyloxytetradecanoate (8). To a solution of **7** (36.2 g, 100 mmol) and benzyl trichloroacetimidate (30.0 g, 119 mmol) in anhydrous dichloromethane (500 ml) was added dropwise trifluoromethanesulfonic acid (1.8 ml, 20 mmol) at 0 °C under argon atmosphere. After stirring at 0 °C for 2 h, the mixture was washed with a saturated aqueous solution of sodium hydrogencarbonate and water, dried, and concentrated. The residue was subjected to silica-gel column chromatography (1 kg). Elution with benzene gave a syrup; yield 33.3 g (74%). ^{1}H NMR (60 MHz) δ=0.9 (3H, br t, CH_3), 1.0—1.8 (20H, br s, CH_2), 2.8 (2H, AB-type, -$COCH_2$-), 3.9 (1H, m, -C<u>H</u>($OCH_2C_6H_5$)-), 4.5 (2H, s, -$C\underline{H}_2C_6H_5$), 5.3 (2H, s, -$COOCH_2$-), 7.1—7.9 (5H, m, -COC_6H_5), and 7.3 (5H, s, -$CH_2C_6\underline{H}_5$).

Further elution with benzene-ethyl acetate (9 : 1) gave the starting material **7**, which was recrystallized from hexane; 8.5 g (19 %).

(*R*)-3-Benzyloxytetradecanoic Acid (9). Zinc dust (30 g) was added to a solution of **8** (33.3 g, 73.6 mmol) in acetic acid (650 ml) and the mixture was stirred at 50 °C. After 2 h zinc dust (15 g) was added and the mixture was stirred for additional 1 h. Insoluble materials were filtered and washed with ethyl acetate. After evaporation of the solvent, the residue was dissolved in ethyl acetate, washed with water, dried, and concentrated. The residue was subjected to silica-gel column chromatography (500 g). The product eluted with chloroform–methanol (3 : 1) was dissolved in ethyl acetate, washed with 1 M† hydrochloric acid and water, and dried. Evaporation of the solvent gave a colorless syrup, which was used for the following reactions without further purification; yield 19.8 g (80%); $[\alpha]_D^{17}$ −6.6° (*c* 3.65, chloroform). EI-MS: *m/z* 334 (M^+). Found: C, 75.64; H, 10.10%. Calcd for $C_{21}H_{34}O_3$: C, 75.40; H, 10.34%. ^{1}H NMR (60 MHz) δ=0.9 (3H, br t, CH_3), 1.0—1.7 (20H, br s, CH_2), 2.6 (2H, d, J=7 Hz, -$COCH_2$-), 3.9 (1H, m, -C<u>H</u>($OCH_2C_6H_5$)-), 4.6 (2H, s, -$C\underline{H}_2C_6H_5$), and 7.3 (5H, s, aromatic H).

3,4,6-Tri-*O*-acetyl-2-amino-2-deoxy-1-α-*O*:2-*N*,*N*-ethylidyne-D-glucopyranose (10). 2-Acetamido-1,3,4,6-tetra-*O*-acetyl-2-deoxy-D-glucopyranose (100 g, 0.257 mol) was dissolved in anhydrous chloroform (1 l). The solution was saturated with dry hydrogen bromide at 0 °C and left overnight at room temperature in a stoppered flask. Pyridine (100 ml) was added dropwise to the mixture over 10 min at 0 °C with stirring. After stirring for additional 20 min at room temperature, the mixture was washed with water, dried, and evaporated. The residual pyridine was removed by coevaporation with toluene three times. The pale yellow syrup thus obtained was used for the following step without further purification; yield 79.4 g (94%). High resolution EI-MS Found: *m/z* 329.1092. Calcd for $C_{14}H_{19}NO_8$: M, 329.1111. ^{1}H NMR (60 MHz) δ=2.1 (12H, s, CH_3), 3.6 (1H, dt, $J_{5,4}$=8 Hz, $J_{5,6}$=4 Hz, H-5), 4.1 (1H, m, H-2), 4.2 (2H, d, $J_{6,5}$=4 Hz,

† 1 M=1 mol dm^{-3}.

H-6), 4.9 (1H, dd, $J_{4,3}$=2 Hz, $J_{4,5}$=4 Hz, H-4), 5.2 (1H, t, $J_{3,2}$=$J_{3,4}$=2 Hz, H-3), and 5.9 (1H, d, $J_{1,2}$=8 Hz, H-1).

Allyl 2-Acetamido-3,6-di-*O*-benzoyl-2-deoxy-β-D-glucopyranoside (12). Allyl 2-acetamido-2-deoxy-β-D-glucopyranoside (**11**) was prepared by heating a solution of oxazoline **10** in chloroform with allyl alcohol and *p*-toluenesulfonic acid followed by removal of *O*-acetyl groups with 0.01 M sodium methoxide; mp 173—175 °C.

To a solution of **11** (10.0 g, 76.0 mmol) in pyridine (200 ml) and THF (90 ml) was added benzoyl chloride (30.6 ml, 264 mmol) dropwise at −65 °C. The mixture was stirred at −60 °C for 1 h. After addition of water (150 ml), the mixture was concentrated. The residue was dissolved in ethyl acetate and worked up as usual, and the product was recrystallized from ethyl acetate; yield 24.7 g (69%); mp 194—195 °C; $[\alpha]_D^{19}$ +2.1° (*c* 1.02, chloroform). Found: C, 62.77; H, 5.80; N, 2.99%. Calcd for $C_{25}H_{27}NO_8 \cdot 0.5H_2O$: C, 62.75; H, 5.90; N, 2.93%. ^{1}H NMR (100 MHz) δ=1.82 (3H, s, NAc), 4.74 (1H, d, *J*=9 Hz, H-1), 5.04—5.35 (2H, m, $-OCH_2CH=C\underline{H}_2$), 5.66—6.04 (1H, m, $-OCH_2C\underline{H}=CH_2$), 6.12 (1H, d, *J*=9 Hz, NH), and 7.2—8.1 (10H, m, aromatic H).

Allyl 2-Acetamido-3,6-di-*O*-benzoyl-4-*O*-benzyl-2-deoxy-β-D-glucopyranoside (13). To a solution of **12** (30.0 g, 63.9 mmol) and benzyl trichloroacetimidate (56.5 g, 244 mmol) in anhydrous dichloromethane (1.5 l) was added trifluoromethanesulfonic acid (8.5 ml, 96 mmol) at −45 °C under argon atmosphere. The mixture was stirred overnight at 4 °C. After addition of saturated aqueous sodium hydrogencarbonate, the organic layer was washed with water, dried, and evaporated. The oily residue was dissolved in THF (300 ml) and treated with 1 M hydrochloric acid (130 ml) at room temperature for 1 h. To the solution were added triethylamine (30 ml) and acetic anhydride (13.5 ml). The mixture was stirred overnight at room temperature. After removal of the insoluble materials, the filtrate was concentrated. The residue was subjected to column chromatography on DIAION HP-20 (2 l). Elution by 70% aqueous methanol afforded first trichloroacetamide and then the starting material **12** which was recrystallized from ethyl acetate: 4.6 g (15%). The product was eluted by methanol and recrystallized from ethyl acetate; yield 17.2 g (48%); mp 160—162 °C; $[\alpha]_D^{15}$ +2.5° (*c* 1.21, chloroform). Found: C, 68.39; H, 5.96; N, 2.51%. Calcd for $C_{32}H_{33}NO_8$: C, 68.68; H, 5.94; N, 2.50%. ^{1}H NMR (100 MHz) δ=1.82 (3H, s, NAc), 5.02—5.34 (2H, m, $-OCH_2CH=C\underline{H}_2$), 5.58 (1H, dd, *J*=8 and 10 Hz, H-3), 5.68—6.07 (1H, m, $-OCH_2C\underline{H}=CH_2$), 7.06 (5H, s, $-CH_2C_6\underline{H}_5$), and 7.2—8.2 (10H, m, $-COC_6H_5$).

Allyl 2-Acetamido-3-*O*-benzoyl-4-*O*-benzyl-2-deoxy-β-D-glucopyranoside (14). Compound **13** (16.7 g, 30.0 mmol) was treated with 0.02 M sodium methoxide (600 ml) at 0 °C for 6 h. After neutralization with Dowex 50 (H^+ form) and silica-gel column chromatography (300 g, chloroform–methanol 9:1) the product was recrystallized from ethyl acetate–hexane; yield 10.8 g (79%); mp 165—167 °C (with sintering at 137 °C); $[\alpha]_D^{19}$ −54.1° (*c* 2.06, chloroform). Found: C, 66.01; H, 6.44; N, 3.06%. Calcd for $C_{25}H_{29}NO_7$: C, 65.92; H, 6.42; N, 3.07%. ^{1}H NMR δ=1.83 (3H, s, NAc), 4.60 (1H, d, *J*=8 Hz, H-1), 4.61 (2H, s, $-C\underline{H}_2C_6H_5$), 5.02—5.36 (2H, m, $-OCH_2-CH=C\underline{H}_2$), 5.51 (1H, dd, *J*=9 and 10 Hz, H-3), 5.68—6.08 (1H, m, $-OCH_2-C\underline{H}=CH_2$), 6.20 (1H, d, *J*=9 Hz, NH), 7.14 (5H, s, $-CH_2C_6\underline{H}_5$), and 7.3—8.1 (5H, m, $-COC_6H_5$).

Allyl 2-Acetamido-6-*O*-(2-acetamido-3,4,6-tri-*O*-acetyl-2-deoxy-β-D-glucopyranosyl)-3-*O*-benzoyl-4-*O*-benzyl-2-deoxy-β-D-glucopyranoside (15). A solution of **10** (13.0 g, 39.6 mmol), **14** (9.0 g, 19.8 mmol), and *p*-toluenesulfonic acid (1.5 g, 7.0 mmol) in anhydrous chloroform (450 ml) was heated under reflux for 7 h. After cooling, the mixture was washed with aqueous sodium hydrogencarbonate and water, dried, and concentrated. The residue was subjected to column chromatography on silica gel (500 g, chloroform–acetone 3:1) and recrystallized from methanol; yield 10.0 g (64% based on **10**); mp 222—224 °C (decomp); $[\alpha]_D^{17}$ −38.1° (*c* 0.43, chloroform). Found: C, 59.38; H, 6.16; N, 3.57%. Calcd for $C_{39}H_{48}N_2O_{15}$: C, 59.68; H, 6.16; N, 3.57%. ^{1}H NMR (100 MHz, $CDCl_3$–CD_3OD) δ=1.82 and 1.87 (each 3H, s, NAc), 2.02 (9H, s, OAc), 4.52 (1H, d, *J*=8 Hz, anomeric H), 4.52 (2H, s, $-C\underline{H}_2C_6H_5$), 4.82 (1H, d, *J*=8 Hz, anomeric H), 5.67—6.08 (1H, m, $-OCH_2C\underline{H}=CH_2$), 7.14 (5H, s, $-CH_2C_6\underline{H}_5$), and 7.3—8.1 (5H, m, $-COC_6H_5$).

Allyl 6-*O*-[3,4,6-Tri-*O*-acetyl-2-[(*R*)-3-benzyloxytetradecanoylamino]-2-deoxy-β-D-glucopyranosyl]-3-*O*-benzoyl-4-*O*-benzyl-2-[(*R*)-3-benzyloxytetradecanoylamino]-2-deoxy-β-D-glucopyranoside (16). To a solution of **15** (8.2 g, 10.4 mmol) in anhydrous dichloromethane (300 ml) were added anhydrous potassium carbonate and triethyloxonium tetrafluoroborate (6.0 g, 31.2 mmol). After stirring at room temperature for 13 h, insoluble materials were filtered off, the filtrate washed with aqueous sodium hydrogencarbonate and water, dried, and evaporated. To a solution of the residue in THF (180 ml) was added 1 M hydrochloric acid (20.8 ml). After stirring for 3 h at room temperature, the mixture was concentrated and coevaporated with anhydrous benzene three times. To a solution of the residue in anhydrous THF (250 ml), 3-benzyloxytetradecanoic acid (**9**) (10.5 g, 31.3 mmol) and DCC (6.47 g, 31.2 mmol) were added at 0 °C. The mixture was stirred for 19 h at room temperature, and then a small amount of acetic acid was added. After removal of the precipitate by filtration, ethereal diazomethane was added to the filtrate. The product was purified by silica-gel chromatography (300 g, chloroform–acetone 9:1) and recrystallized from ethyl acetate–hexane; yield 5.8 g (41%); mp 165—169 °C; $[\alpha]_D^{18}$ −13.2° (*c* 1.11, chloroform). Found: C, 68.99; H, 8.15; N, 2.01%. Calcd for $C_{77}H_{108}N_2O_{17} \cdot 0.5H_2O$: C, 68.88; H, 8.18; N, 2.09%. ^{1}H NMR (100 MHz) δ=0.90 (6H, t, *J*=6 Hz, CH_3), 1.1—1.5 (40H, br s, CH_2), 1.98 (3H, s, OAc), 2.01 (6H, s, OAc), 2.24—2.42 (4H, m, α-CH_2 of fatty acids), 6.31 (1H, d, *J*=9 Hz, NH), 6.41 (1H, d, *J*=9 Hz, NH), and 7.0—8.1 (20H, m, aromatic H).

Allyl 4-*O*-Benzyl-2-[(*R*)-3-benzyloxytetradecanoylamino]-6-*O*-[2-[(*R*)-3-benzyloxytetradecanoylamino]-2-deoxy-β-D-glucopyranosyl]-2-deoxy-β-D-glucopyranoside (17). To a solution of **16** (15.0 g, 11.2 mmol) in methanol (225 ml) and THF (225 ml) was added 1 M sodium methoxide (22.4 ml). After stirring at room temperature for 5 h, the mixture was neutralized with Dowex 50 (H^+ form). The solvent was evaporated and the residue recrystallized from methanol; yield 10.4 g (84%); mp 193—197 °C (decomp); $[\alpha]_D^{18}$ −18.3° (*c* 1.04, chloroform–methanol 3:1). Found: C, 68.04; H, 8.87; N, 2.42%. Calcd for $C_{64}H_{98}N_2O_{13} \cdot 1.5H_2O$: C, 68.00; H, 9.01; N, 2.48%. ^{1}H NMR (100 MHz, $CDCl_3$–CD_3OD) δ=0.90 (6H, br t, CH_3), 1.2—1.4 (40H, br s, CH_2), 2.34—2.56 (4H, m, α-CH_2 of fatty acids), 5.6—6.0 (1H, m, $-OCH_2C\underline{H}=CH_2$), and 7.25—7.4 (15H, br s, aromatic H).

Allyl 4-*O*-Benzyl-2-[(*R*)-3-benzyloxytetradecanoylamino]-6-*O*-[2-[(*R*)-3-benzyloxytetradecanoylamino]-2-deoxy-4,6-*O*-isopropylidene-β-D-glucopyranosyl]-2-deoxy-β-D-glucopyr-

anoside (18). A mixture of **17** (10.0 g, 9.06 mmol), 2,2-dimethoxypropane (1.66 ml, 13.5 mmol), and *p*-toluenesulfonic acid (345 mg, 1.81 mmol) in chloroform (150 ml) and THF (150 ml) was stirred at room temperature for 4 h. After neutralization with triethylamine and evaporation of the solvent, the residue was dissolved in chloroform, washed with water, and dried. The product was recrystallized from chloroform-methanol; yield 8.75 g (84%); mp 105—108 °C (with sintering at 95 °C); $[\alpha]_D^{19}$ −28.3° (*c* 1.12, chloroform). Found: C, 68.92; H, 8.98; N, 2.34%. Calcd for $C_{67}H_{102}N_2O_{13} \cdot 1.5H_2O$: C, 68.75; H, 9.04; N, 2.39%. ^{1}H NMR (100 MHz) δ=0.89 (6H, br t, CH_3), 1.2—1.4 (40H, br s, CH_2), 1.44 and 1.52 (each 3H, s, isopropylidene), 2.31—2.53 (4H, m, α-CH_2 of fatty acids), and 7.2—7.35 (15H, aromatic H).

Allyl 4-*O*-Benzyl-3-*O*-[(*R*)-3-benzyloxytetradecanoyl]-6-*O*-[3-*O*-[(*R*)-3-benzyloxytetradecanoyl]-2-[(*R*)-3-benzyloxytetradecanoylamino]-2-deoxy-β-D-glucopyranosyl]-2-[(*R*)-3-benzyloxytetradecanoylamino]-2-deoxy-β-D-glucopyranoside (19). To a solution of **18** (2.0 g, 1.8 mmol) in anhydrous dichloromethane (80 ml) were added **9** (1.8 g, 5.3 mmol), DCC (1.1 g, 5.3 mmol), and DMAP (107 mg, 0.88 mmol). The mixture was stirred at room temperature for 4 h. After addition of acetic acid (1 ml) and removal of the precipitate, the filtrate was washed with 1 M hydrochloric acid and water, dried, and evaporated to give a pale yellow solid. It was heated in 90% acetic acid (80 ml) at 90 °C for 2 h. After the evaporation of the solvent, the residue was recrystallized from methanol; yield 2.5 g (82 %); mp 117—119 °C; $[\alpha]_D^{17}$ −14.5° (*c* 0.40, chloroform). Found: C, 72.31; H, 9.32; N, 1.59%. Calcd for $C_{106}H_{162}N_2O_{17} \cdot H_2O$: C, 72.57; H, 9.42; N, 1.60%.

Allyl 4-*O*-Benzyl-6-*O*-[6-*O*-benzyloxymethyl-3-*O*-[(*R*)-3-benzyloxytetradecanoyl]-2-[(*R*)-3-benzyloxytetradecanoylamino]-2-deoxy-β-D-glucopyranosyl]-3-*O*-[(*R*)-3-benzyloxytetradecanoyl]-2-[(*R*)-3-benzyloxytetradecanoylamino]-2-deoxy-β-D-glucopyranoside (20). To a solution of **19** (7.78 g, 4.48 mmol) in anhydrous dichloromethane (150 ml) were added benzyloxymethyl chloride (1.40 g, 8.94 mmol) and *N,N*-diisopropylethylamine (1.56 ml, 8.95 mmol). The mixture was stirred for 23 h at room temperature with addition of benzyloxymethyl chloride (0.70 and 0.35 g) and *N,N*-diisopropylethylamine (0.78 and 0.39 ml) after 1 and 8 h, respectively. The mixture was worked up as usual and the product was recrystallized from methanol; yield 7.97 g (96%); mp 137—139 °C; $[\alpha]_D^{19}$ −12.3° (*c* 1.12, chloroform). Found: C, 73.12; H, 9.19; N, 1.48%. Calcd for $C_{114}H_{170}N_2O_{18} \cdot H_2O$: C, 73.04; H, 9.25; N, 1.49%.

Allyl 4-*O*-Benzyl-6-*O*-[6-*O*-benzyloxymethyl-3-*O*-[(*R*)-3-benzyloxytetradecanoyl]-2-[(*R*)-3-benzyloxytetradecanoylamino]-2-deoxy-β-D-glucopyranosyl]-3-*O*-[(*R*)-3-benzyloxytetradecanoyl]-2-[(*R*)-3-benzyloxytetradecanoylamino]-2-deoxy-β-D-glucopyranoside 4′-(Diphenyl Phosphate) (21). To a solution of **20** (1.70 g, 0.92 mmol) in anhydrous dichloromethane (70 ml) were added pyridine (0.24 ml, 3.0 mmol), DMAP (0.33 g, 2.7 mmol) and diphenyl phosphorochloridate (0.57 ml, 2.7 mmol). After stirring at room temperature for 7 h, the mixture was worked up as usual and the product was recrystallized from chloroform-methanol; yield 1.45 g (76%); mp 71—72 °C; $[\alpha]_D^{18}$ −7.3° (*c* 0.51, chloroform). Found: C, 72.50; H, 8.73; N, 1.40%. Calcd for $C_{126}H_{179}N_2O_{21}P$: C, 72.45; H, 8.64; N, 1.34%.

4-*O*-Benzyl-6-*O*-[6-*O*-benzyloxymethyl-3-*O*-[(*R*)-3-benzyloxytetradecanoyl]-2-[(*R*)-3-benzyloxytetradecanoylamino]-2-deoxy-β-D-glucopyranosyl]-3-*O*-[(*R*)-3-benzyloxytetradecanoyl]-2-[(*R*)-3-benzyloxytetradecanoylamino]-2-deoxy-D-glucose 4′-(Diphenyl Phosphate) (22). Compound **21** (1.39 g, 0.75 mmol) and 1,5-cyclooctadienebis(methyldiphenylphosphine)-iridium hexafluorophosphate (65 mg) were dissolved in degassed THF (50 ml). After activation of the iridium catalyst with hydrogen,[18] the mixture was stirred at 50 °C under nitrogen atmosphere for 80 min and then cooled to room temperature. Water (15 ml) and iodine (0.38 g. 1.50 mmol) were added and the mixture was stirred for 5 min. To the mixture were added 5% aqueous solution of sodium sulfite and chloroform. The organic layer was washed with water, dried and evaporated. The product was isolated by medium-pressure column chromatography on silica gel (83 g, chloroform-acetone 9:1) and recrystallized from chloroform-methanol; yield 750 mg (55%); mp 78—83 °C; $[\alpha]_D^{15}$ +10.6° (*c* 1.09, chloroform-methanol 3:1). Found: C, 71.88; H, 8.69; N, 1.39%. Calcd for $C_{123}H_{175}N_2O_{21}P$: C, 72.11; H, 8.61; N, 1.37%. ^{1}H NMR (100 MHz) δ=0.88 (12H, t, J=6 Hz, CH_3), 2.1—2.6 (80H, br s, CH_2), 2.06—2.60 (8H, m, α-CH_2 of fatty acids), and 7.0—7.3 (40H, m, aromatic H).

2-Deoxy-6-*O*-[2-deoxy-3-*O*-[(*R*)-3-hydroxytetradecanoyl]-2-[(*R*)-3-hydroxytetradecanoylamino]-β-D-glucopyranosyl]-3-*O*-[(*R*)-3-hydroxytetradecanoyl]-2-[(*R*)-3-hydroxytetracedanoylamino]-α-D-glucopyranose 1,4′-Bis(phosphate) (2). Compound **22** (500 mg, 0.24 mmol) was dissolved in anhydrous THF (15 ml) and cooled to −70 °C under argon atmosphere. The solution was treated with 1.6 M butyllithium in hexane (0.18 ml, 0.28 mmol) and then dibenzyl phosphorochloridate (70 μl, 0.28 mmol). The mixture was stirred at −70 °C for 5 min and then palladium black was added to it. The mixture was stirred under 6 kg cm^{-2} of hydrogen at room temperature for 17 h. After removal of palladium catalyst, platinum oxide was added and the mixture was stirred under 7 kg cm^{-2} of hydrogen at room temperature for 2 h. The catalyst was filtered off and the filtrate was neutralized with triethylamine. The product was isolated by medium-pressure column chromatography on silica gel (80 g, chloroform-methanol-water-triethylamine 50:50:10:1) as colorless solid (200 mg).

Electrodialysis and Acidic Precipitation of 2. Electrodialysis was carried out according to the method of Galanos and Lüderitz.[21] The apparatus for electrodialysis consisted of three compartments separated by two sheets of dialysis membrane (prepared by cutting Cellophane Tubings-Seamless, Union Carbide Co.). The two outer chamber were equipped with platinum electrodes and filled with distilled water (each 7 ml).

The crude product **2** (176 mg) obtained by the above silica-gel chromatography was suspended in pyrogen-free water (9 ml). The pH of the suspension was adjusted to 9 with triethylamine, sonicated and put in the middle chamber. Direct electric current was applied to the apparatus, voltage being increased gradually to 150 V, while current was maintained less than 30 mA. After 1 h, the pH value of the middle chamber dropped to 3 and some precipitate appeared, which was dissolved again by adjusting the pH of the solution to 9 with triethylamine. The temperature of the solution was kept below 20 °C by cooling water throughout the operations. A series of these operations was repeated three times. Thereafter the suspension in the middle chamber was lyophilized to afford a white powder (145 mg).

A suspension of the product in pyrogen-free water (40 ml)

was adjusted to pH 9 with triethylamine, sonicated and centrifugated at 17500 rpm for 10 min at 0 °C in order to remove insoluble materials. To the supernatant was added 1 M hydrochloric acid (4.4 ml) at 0 °C and then the resultant precipitate was collected by centrifugation under the same conditions as above. After centrifugal washing with 0.1 M hydrochloric acid and water, the substance was lyophilized to give a white powder; yield 69 mg (20% from **22**); $[\alpha]_D^{19}$ +2.1° (*c* 1.05, chloroform-methanol 3:1). Found: C, 56.33; H, 9.37; N, 2.01%. Calcd for $C_{68}H_{130}N_2O_{23}P_2 \cdot 2.5H_2O$: C, 56.30; H, 9.38; N, 1.93%.

2-Deoxy-6-*O*-[2-deoxy-3-*O*-[(*R*)-3-hydroxytetradecanoyl]-2-[(*R*)-3-hydroxytetradecanoylamino]-β-D-glucopyranosyl]-3-*O*-[(*R*)-3-hydroxytetradecanoyl]-2-[(*R*)-3-hydroxytetradecanoylamino]-D-glucose 4′-Phosphate (3). A solution of **22** (750 mg, 0.37 mmol) in THF (20 ml) and acetic acid (1.5 ml) was hydrogenolyzed for 38 h in the presence of palladium black under 6.5 kg cm^{-2} of hydrogen. After removal of the catalyst and addition of platinum oxide, the mixture was stirred for 15 h under 6.5 kg cm^{-2} of hydrogen. The catalyst was filtered and the filtrate was neutralized with triethylamine and then evaporated. Lyophilization from dioxane gave the crude product as a white powder (360 mg). A part of this material (149 mg) was purified further by means of acidic precipitation as described for compound **2**; yield 104 mg; $[\alpha]_D^{15}$ −13.6° (*c* 0.84, chloroform-methanol 3:1). Found: C, 59.47; H, 9.66; N, 2.17%. Calcd for $C_{68}H_{129}N_2O_{20} \cdot 2.5H_2O$: C, 59.59; H, 9.85; N, 2.04%.

Identification of Synthetic and Natural Dimethyl Ester of 3. Synthetic compound **3** (42.5 mg, 3.2×10^{-5} mol) in chloroform-methanol (9:1, 8 ml) was treated with ethereal diazomethane. The product was purified by preparative silica-gel TLC (chloroform-methanol 6:1) and lyophilized from dioxane; yield 27.3 mg (64%). This material is identical with the dimethyl ester of 4′-monophosphate prepared from natural precursor Ia as described below.

A suspension of crude natural precursor Ia (25 mg) in 2% aqueous acetic acid (10 ml) was heated at 95 °C for 1 h. The mixture was cooled and lyophilized to give a white powder, which was dissolved in chloroform-methanol (9:1, 15 ml). The solution was acidified with 1 M hydrochloric acid (1 ml), sonicated, and concentrated in vacuo. The residue was dissolved again in chloroform-methanol (9:1, 10 ml) and treated with ethereal diazomethane. Purification by preparative TLC and lyophilization from dioxane afforded a white powder; yield 3.0 mg.

4-*O*-Benzyl-6-*O*-[6-*O*-benzyloxymethyl-3-*O*-[(*R*)-3-benzyloxytetradecanoyl]-2-[(*R*)-3-benzyloxytetradecanoylamino]-2-deoxy-β-D-glucopyranosyl]-3-*O*-[(*R*)-3-benzyloxytetradecanoyl]-2-[(*R*)-3-benzyloxytetradecanoylamino]-2-deoxy-D-glucose (24). Compound **20** (990 mg, 0.53 mmol) was treated with the iridium complex (50 mg) then with iodine (270 mg, 1.06 mmol) as described for compound **22**. The product was isolated by medium-pressure column chromatography on silica gel (75 g, chloroform-acetone 5:1) and recrystallized from methanol; yield 660 mg (68%); mp 117—121 °C; $[\alpha]_D^{15}$ +3.1° (*c* 1.11, chloroform-methanol 3:1). Found: C, 72.64; H, 9.24; N, 1.47%. Calcd for $C_{111}H_{166}N_2O_{18}$: C, 72.67; H, 9.23; N, 1.53%.

2-Deoxy-6-*O*-[2-deoxy-3-*O*-[(*R*)-3-hydroxytetradecanoyl]-2-[(*R*)-3-hydroxytetradecanoylamino]-β-D-glucopyranosyl]-3-*O*-[(*R*)-3-hydroxytetradecanoyl]-2-[(*R*)-3-hydroxytetradecanoylamino]-α-D-glucopyranose 1-Phosphate (4). A solution of compound **24** (770 mg, 0.424 mmol) in THF (25 ml) was cooled to −70 °C under argon atmosphere and treated with 1.6 M butyllithium in hexane (0.30 ml, 0.47 mmol) and then with dibenzyl phosphorochloridate (0.12 ml, 0.48 mmol). After 20 min, palladium-black (500 mg) was added and the mixture was hydrogenolyzed under 6 kg cm^{-2} of hydrogen atmosphere at room temperature for 17 h. Isolation by medium-pressure column chromatography on silica gel (80 g, chloroform-methanol-water-triethylamine 250:100:15:1) gave a crude product as white solid (260 mg).

This material was purified by a combination of electrodialysis and acidic precipitation method as described for **2**; yield 183 mg (33%); $[\alpha]_D^{21}$ −5.1° (*c* 1.03, chloroform-methanol 9:1); Found: C, 60.21; H, 9.83; N, 2.14%. Calcd for $C_{68}H_{129}N_2O_{20}P \cdot 1.5H_2O$: C, 60.38; H, 9.83; N, 2.07%.

2-Deoxy-6-*O*-[2-deoxy-3-*O*-[(*R*)-3-hydroxytetradecanoyl]-2-[(*R*)-3-hydroxytetradecanoylamino]-β-D-glucopyranosyl]-3-*O*-[(*R*)-3-hydroxytetradecanoyl]-2-[(*R*)-3-hydroxytetradecanoylamino]-D-glucose (5). Compound **19** (700 mg, 0.40 mmol) was treated with the iridium complex (35 mg) and then with iodine (137 mg, 0.54 mmol) as described above for **22**. Isolation by medium-pressure column chromatography on silica gel (25 g, chloroform-acetone 2:1) gave a solid, which was dissolved in THF (20 ml) and acetic acid (1 ml). The solution was hydrogenolyzed with palladium-black under 7 kg cm^{-2} hydrogen. The product was recrystallized from methanol; yield 141 mg (28%); mp 210—212 °C (decomp). $[\alpha]_D^{18}$ −19.2° (*c* 1.02, chloroform-methanol 9:1). Found: C, 64.42; H, 10.40; N, 2.20%. Calcd for $C_{68}H_{128}N_2O_{17} \cdot H_2O$: C, 64.63; H, 10.37; N, 2.22%.

A part of this work was supported by Grant-in-Aid for Scientific Research from Ministry of Education, Science and Culture (Nos. 58122002, 59116004, and 60108004). The work was also partly supported by a Joint Research Project from Japan Society for Promotion of Science (JSPS). One of the authors (M. I.) thanks for the financial support by Fellowship for Japanese Junior Scientist from JSPS. The authors are grateful to Drs. Chris Galanos and Otto Lüderitz, Max-Planck-Institut für Immunbiologie, Freiburg, FRG, for the generous gift of natural precursor Ia. They also express their thanks to Dr. Yoshio Takai, Institute of Scientific and Industrial Research, Osaka University, for the measurement of 360 MHz ^{1}H NMR spectra.

References

1) C. Galanos, O. Lüderitz, E. Th. Rietschel, and O. Westphal, "International Review of Biochemistry, Biochemistry of Lipids II," Vol. 14, ed by T. W. Goodwin, University Park Press, Baltimore (1977), Chap. 6.

2) O. Westphal and O. Lüderitz, *Angew. Chem.*, **66**, 407 (1954).

3) Natural lipid A preparations from bacterial cells are always obtained as heterogeneous mixtures and their purification was very difficult. Consequently, a possibility could not completely be excluded that any impurity from bacteria might be still present and responsible for some of the activities attributed to lipid A.

4) M. Imoto, H. Yoshimura, N. Sakaguchi, S. Kusumoto,

and T. Shiba, *Tetrahedron Lett.*, **26**, 1545 (1985). See also the accompanying paper.

5) M. Imoto, H. Yoshimura, M. Yamamoto, T. Shimamoto, S. Kusumoto, and T. Shiba, *Tetrahedron Lett.*, **25**, 2667 (1984).

6) a) C. Galanos, V. Lehmann, O. Lüderitz, E. Th. Rietschel, O. Westphal, H. Brade, L. Brade, M. A. Freudenberg, T. Hansen-Hagge, T. Lüderitz, G. McKenzie, U. Schade, W. Strittmatter, K. Tanamoto, U. Zähringer, M. Imoto, H. Yoshimura, M. Yamamoto, T. Shimamoto, S. Kusumoto, and T. Shiba, *Eur. J. Biochem.*, **140**, 221 (1984); b) S. Kotani, H. Takada, M. Tsujimoto, T. Ogawa, K. Harada, Y. Mori, A. Kawasaki, A. Tanaka, S. Nagao, S. Tanaka, T. Shiba, S. Kusumoto, M. Imoto, H. Yoshimura, M. Yamamoto, and T. Shimamoto, *Infect. Immun.*, **45**, 293 (1984); c) S. Kanegasaki, Y. Kojima, M. Matsuura, J. Y. Homma, A. Yamamoto, Y. Kumazawa, K. Tanamoto, T. Yasuda, T. Tsumita, M. Imoto, H. Yoshimura, M. Yamamoto, T. Shimamoto, S. Kusumoto, and T. Shiba, *Eur. J. Biochem.*, **143**, 237 (1984).

7) M. Inage, H. Chaki, M. Imoto, T. Shimamoto, S. Kusumoto, and T. Shiba, *Tetrahedron Lett.*, **24**, 2011 (1983).

8) a) M. Imoto, S. Kusumoto, T. Shiba, H. Naoki, T. Iwashita, E. Th. Rietschel, H.-W. Wollenweber, C. Galanos, and O. Lüderitz, *Tetrahedron Lett.*, **24**, 4017 (1983); b) M. Imoto, S. Kusumoto, T. Shiba, E. Th. Rietschel, C. Galanos, and O. Lüderitz, *Tetrahedron Lett.*, **26**, 907 (1985).

9) O. Lüderitz, C. Galanos, V. Lehmann, H. Mayer, E. Th. Rietschel, and J. Weckesser, *Naturwissenschaften*, **65**, 578 (1978).

10) *E. coli* lipid A contains additional two nonhydroxylated acids whose locations were later determined to complete the structure **1**. (See Ref. 8). We had started the synthesis of **2** before their locations were fixed.

11) T. Hansen-Hagge, V. Lehmann, and O. Lüderitz, *Eur. J. Biochem.*, **148**, 21 (1985).

12) V. Lehmann, *Eur. J. Biochem.*, **75**, 257 (1977).

13) Strain et al. also isolated several biosynthetic precursors of lipid A from a similar mutant of *S. typhimurium*. With spectroscopic analysis they proposed the same structure **2** to the major compound. S. M. Strain, I. M. Armitage, L. Anderson, K. Takayama, N. Qureshi, and C. R. H. Raetz, *J. Biol. Chem.*, **260**, 16089 (1985).

14) A. Tai, M. Nakahata, T. Harada, Y. Izumi, S. Kusumoto, M. Inage, H. Chaki, and T. Shiba, *Chem. Lett.*, **1980**, 1125.

15) T. Iversen and D. Bundle, *J. Chem. Soc., Chem. Commun.*, **1981**, 1240.

16) S. Kusumoto, S. Imaoka, Y. Kambayashi, and T. Shiba, *Tetrahedron Lett.*, **23**, 2961 (1982).

17) P. Szabo, S. R. Sarfati, C. Diolez, and L. Szabo, *Carbohydr. Res.*, **111**, C9 (1983). This procedure was more convenient than the DCC method used in our previous works[7] in terms of the shorter reaction period and the facile work-up procedure.

18) J. J. Oltvoort, C. A. A. van Boeckel, J. H. de Koning, and J. H. van Boom, *Synthesis*, **1981**, 305.

19) N. A. Nashed and L. Anderson, *J. Chem. Soc., Chem. Commun.*, **1982**, 1274.

20) M. Inage, H. Chaki, S. Kusumoto, and T. Shiba, *Chem. Lett.*, **1982**, 1281.

21) C. Galanos and O. Lüderitz, *Eur. J. Biochem.*, **54**, 603 (1975).

22) The original procedure described in Ref. 6a) was modified according to U. Zähringer.

23) Interestingly, both synthetic and natural materials lack pyrogenicity which is one of the typical endotoxic activities. See the accompanying paper.

 © 1987 The Chemical Society of Japan Bull. Chem. Soc. Jpn., 60, 2205—2214 (1987)

Total Synthesis of *Escherichia coli* Lipid A, the Endotoxically Active Principle of Cell-Surface Lipopolysaccharide

Masahiro IMOTO, Hiroyuki YOSHIMURA, Tetsuo SHIMAMOTO, Nobuki SAKAGUCHI, Shoichi KUSUMOTO, and Tetsuo SHIBA*

Department of Chemistry, Faculty of Science, Osaka University, Toyonaka, Osaka 560

(Received December 15, 1986)

Chemical syntheses are described of polyacylated $\beta(1\rightarrow6)$ glucosamine disaccharide 1,4′-bis(phosphate), which corresponds to the proposed structure of *E. coli* lipid A, and of its dephospho derivatives. The synthetic bisphosphate proved to be identical with the corresponding natural specimen. The chemical structure of lipid A was thus established.

As described in the preceding paper,[1] lipopolysaccharide (LPS) which is located on the cell surface of gram-negative bacteria is called endotoxin and causes a diversity of toxic and beneficial biological responses in animals.[2] Its lipophilic part which could be liberated by mild acid hydrolysis of LPS was designated "lipid A" and has been believed to be responsible for most of the endotoxic activities.[2]

We recently elucidated the complete chemical structure **1** of lipid A isolated from *Escherichia coli* cells.[3] The structure contains a backbone of $1\alpha,4'$-bisphosphorylated $\beta(1\rightarrow6)$ disaccharide of D-glucosamine. The backbone is acylated at 2,2′- and 3,3′-positions with four moles of (*R*)-3-hydroxytetradecanoic acid. The 3-hydroxyl groups of amide- and ester-bound 3-hydroxytetradecanoic acid on the distal glucosamine residue are acylated with docosanoic and tetracosanoic acid respectively.

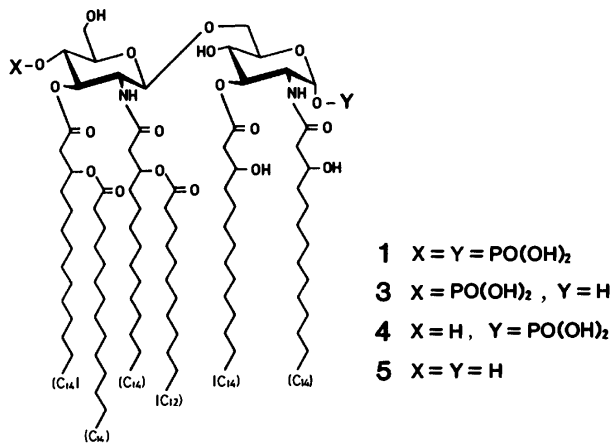

1 X = Y = $PO(OH)_2$
3 X = $PO(OH)_2$, Y = H
4 X = H, Y = $PO(OH)_2$
5 X = Y = H

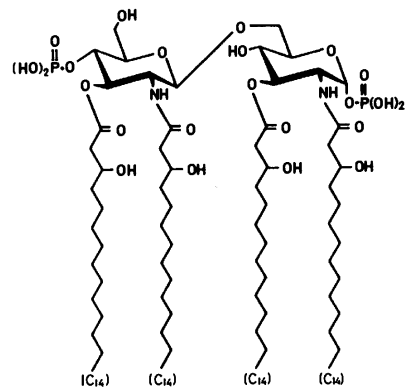

2

In the meantime we synthesized a biosynthetic precursor ("Precursor Ia") (**2**) of lipid A.[1,4] This compound contains four moles of 3-hydroxytetradecanoic acid but lacks the non-hydroxylated acids found in **1**. The results of biological tests showed that the precursor Ia (**2**) exhibits not all but many of definite endotoxic activities such as lethal toxicity.[5] This fact clearly demonstrates that an acyl disaccharide phosphate like **2** is certainly responsible for the activities of LPS. Simultaneously, it could be assumed that the 3-acyloxyacyl structure which is typical of *E. coli* and other natural mature lipid A's but absent in the biosynthetic precursor **2** is important for manifestation of pyrogenicity and Shwartzman reactivity[6] which are typical endotoxic activities not observed in both synthetic and natural precursor Ia (**2**).[5] In order to confirm this assumption as well as to construct chemically a compound with full endotoxic activity and finally to confirm the proposed structure of *E. coli* lipid A, we aimed at a total synthesis of **1**. As described in our preliminary communications,[7,8] the structure **1** was first confirmed by this synthesis and synthetic **1** proved to have identical biological activities with those of lipid A isolated from *E. coli* cells.[9] It could now be concluded that **1** is indeed the active structural principle of endotoxin thirty years after the report of Westphal and Lüderitz by whom lipid A was first described.[10] In this paper we describe the details of the synthesis of **1** and its dephospho derivatives (**3**, **4**, **5**).

Most of the problems in the synthetic approach to *E. coli*-type lipid A had been already solved in our previous works.[1,11] These include, for example, preparation of optically pure (*R*)-3-hydroxytetradecanoic acid, its protection and introduction of an α-glycosyl phosphate. The distinct feature of the present synthesis lies in the following point. As seen in the structural formula, the two glucosamine residues of *E. coli* lipid A (**1**) contain different acyl groups each other. For its synthesis, therefore, two appropriately acylated glucosamine units were first prepared and then coupled together to form an acylated disaccharide. This approach, which is different from that used in our previous synthesis of **2**, seemed to be advantageous to

minimize the use of temporary protecting groups for the attempted synthesis of **1**.[12] The phosphate moiety on 4′-position was also introduced at the monosaccharide stage for the same reason.

Among the four acyl groups bound to the disaccharide, however, 3-dodecanoyloxytetradecanoyl group on the 2′-amino function had to be introduced after the formation of the disaccharide. Preliminary model experiments revealed that *N*-bound 3-acyloxyacyl group on a glucosamine molecule underwent a β-elimination to form Δ^2-acyl group when the glycosidic position was activated for glycoside bond formation.[13]

Use of 2,2,2-trichloroethoxycarbonyl (Troc) group[14] was examined for the temporary protection of the particular amino group during the glycosidation reaction with a glycosyl halogenide. The carbonyl group of 2-Troc-amino function was expected to participate the neighboring glycosyl cation in a similar manner to a usual acyl group and thus to assist the formation of a desired 1,2-trans β-glycosidic bound. Furthermore, Troc was expected to be advantageous since this urethane type group does not form an oxazoline which is one of the main side products in the glycosidation reaction with 2-acylamino glycosyl halogenides. 2-*N*-Troc-glucosamine **6** as a model donor compound was prepared from *N*-Troc-glucosamine (**7**). Thus, peracetyl derivative of **7** was converted almost quantitatively to the bromide **6** on reaction with dry hydrogen bromide in dichloromethane as monitored by TLC. Coupling of **6** with a model acceptor **8** proceeded satisfactorily in the presence of mercury(II) cyanide in boiling chloroform to give a disaccharide **9**. The glycosyl bromide of *N*-Troc-glucosamine was less reactive and hence more stable than a corresponding *N*-acetyl-type derivative. Undesirable side reactions were not obvious in the coupling reaction of the former. The $\beta(1\rightarrow6)$ structure of **9** was ascertained at the corresponding acetyl derivative which was prepared by displacing the Troc of **9** with acetyl group. The resultant bis(*N*-acetyl) disaccharide **10** was identical with a sample obtained in our previous work.[1] As expected, Troc group proved to be suitable for the amino protection: It assures formation of the desired β-glycoside and is removable selectively after formation of the disaccharide.

In order to examine the synthetic strategy according to the above considerations, we first attempted to prepare the 4′-monophosphate derivative **3** of *E. coli* lipid A. This synthesis seemed to be urgently important for the purpose of confirming the structure of lipid A because the dimethyl ester of **3** was the sole chemical entity so far derived in a pure state from a natural source.[3a,15] Direct identification of the natural and synthetic dimethyl ester of **3** was expected to provide a decisive evidence for the structure **1**.

The glycosyl donor **11** for this synthesis was prepared from *N*-Troc-D-glucosamine (**7**). Reaction of **7** with allyl alcohol in the presence of hydrogen chloride gave predominantly the α-glycoside. The α/β ratio was approximately 5/1. Isopropylidenation of the glycoside mixture followed by a simple recrystallization afforded almost pure α-allyl glycoside **12** in an acceptable yield.[16] After 3-*O*-acylation of **12** with (*R*)-3-tetradecanoyloxytetradecanoic acid which was prepared via phenacyl (*R*)-3-hydroxytetradecanoate,[1] the isopropylidene group was removed to give **13**. Selective 6-*O*-mono(trichloroethoxycarbonylation) followed by phosphorylation with diphenyl phosphorochloridate and pyridine-4-dimethylaminopyridine (DMAP).[17,18] Gave a glucosamine derivative **15** which contained all required substituents for the glycosyl donor. The allyl group in **15** was then cleaved off via

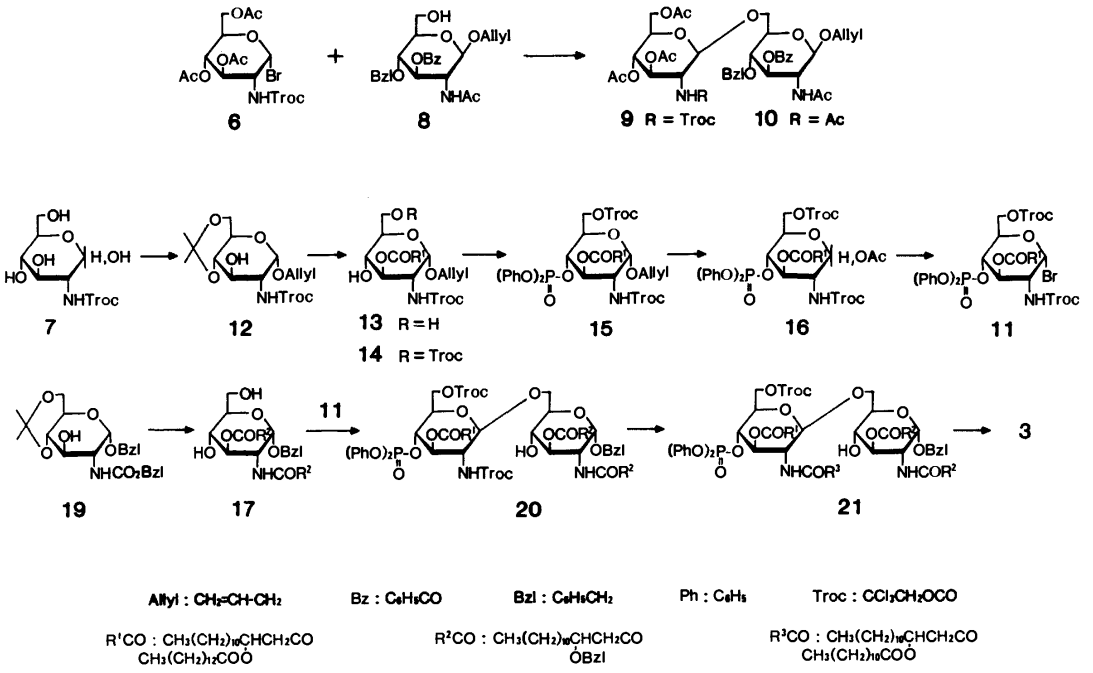

isomerization with an iridium complex to 1-propenyl group[19] followed by a reaction with iodine.[20] The product was converted via 1-*O*-acetate **16** to the glycosyl bromide **11** which was used for the coupling reaction without purification.

The glycosyl acceptor **17** was prepared from benzyl *N*-benzyloxycarbonyl-α-D-glucosaminide (**18**)[21] by 4,6-*O*-isopropylidenation, selective hydrogenolysis of *N*-benzyloxycarbonyl group[21] and simultaneous 3-*O*- and 2-*N*-acylation with (*R*)-3-benzyloxytetradecanoic acid[1] followed by deisopropylidenation. Because a primary 6-hydroxyl group has generally much higher reactivity than a 4-hydroxyl group in a glucopyranoside structure, preferential formation of the (1→6)-glycoside linkage was reasonably expected in the reaction of **17** without protecting the 4-position.[11] Furthermore, the 4-hydroxyl group becomes more hindered after formation of the β(1→6)disaccharide as observed in our previous work.[11] Therefore, a protection of this particular group seemed to be not necessary even during the further transformation of more reactive positions like 1- and 6′-hydroxyl groups of the disaccharide.

Coupling of the bromide **11** and the acceptor **17** was effected as the above model reaction with mercury(II) cyanide to give a sole disaccharide **20**, whose structure was confirmed by examination of its ^{1}H NMR spectrum. After cleavage of Troc groups of the disaccharide **20**, the last acyl group, i.e., (*R*)-3-dodecanoyloxytetradecanoyl group, was finally introduced to the 2′-amino function by use of 1-ethyl-3-(3-dimethylaminopropyl)carbodiimide hydrochloride. When dicyclohexylcarbodiimide was used for this step in place of the above water-soluble carbodiimide, the acylation reaction itself proceeded as well, but *N*-acyl-*N*,*N*′-dicyclohexylurea formed as a by-product made the chromatographic purification of the desired product difficult.

The acylation product **21** which contained all required functional groups on the respective positions was then subjected to two-step hydrogenolytic deprotection first with palladium and then with platinum. The deprotected compound **3** was identified by TLC with the corresponding 4′-monophosphate derived from *E. coli* lipid A.

For more strict identification by ^{1}H NMR, the product **3** was attempted to be converted to the dimethyl ester. However, the synthetic monophosphate was found to contain inorganic impurities and metal cations resulted from the hydrogenolysis catalysts. Some of cations formed salts with the phosphate group of **3**. Because the phosphate group must be converted to a free form prior to the reaction with diazomethane, removal of the inorganic contaminants was next tried. Removal of metal ions was also indispensable for preparation of triethylammonium salt which is a necessary form for biological tests.[22] Whereas the synthetic bisphosphate **2** and both its monophosphate analogs of the precursor-type could be freed from the contaminating cations by a combination of electrodialysis and acidic precipitation,[1] this method could not be applied to the present monophosphate **3** which has more lipophilic acyl groups and less solubility in water than the precursor-type derivatives. However, washing of a chloroform–methanol solution of **3** with cold hydrochloric acid under controlled conditions to avoid decomposition of the target compound was found to be effective to obtain salt-free **3**. It was then treated with diazomethane to give a compound which was identical on TLC with the corresponding dimethyl ester obtained from a natural source.[3] The synthetic and natural specimens were unequivocally identified by comparison of the 360 MHz ^{1}H NMR spectra of these dimethyl esters and their peracetates. Although the spectrum of the natural dimethyl ester still exhibited signals due to small amount of impurities, its peracetate purified and the corresponding synthetic one gave superimposable spectra.

Conclusively, the structure of *E. coli* lipid A proposed by us was confirmed by the present synthesis of 4′-monophosphate (**3**). The next step in our study was a chemical construction of the complete *E. coli* lipid A structure **1** containing both phosphate moieties. This could be performed in the same way as the above synthesis except that the glycosidic position of the disaccharide was protected with allyl group. This protecting group could be removed for the introduction of the unstable glycosyl phosphate just before the final hydrogenolysis. The corresponding glycosyl acceptor monosaccharide **23** was prepared from the same intermediate, 4,6-*O*-isopropylidenated allyl glycoside of *N*-Troc-D-glucosamine (**12**) described above. Condensation of **23** with the same glycosyl bromide (**11**) gave the disaccharide **24**. After removal of the two Troc group

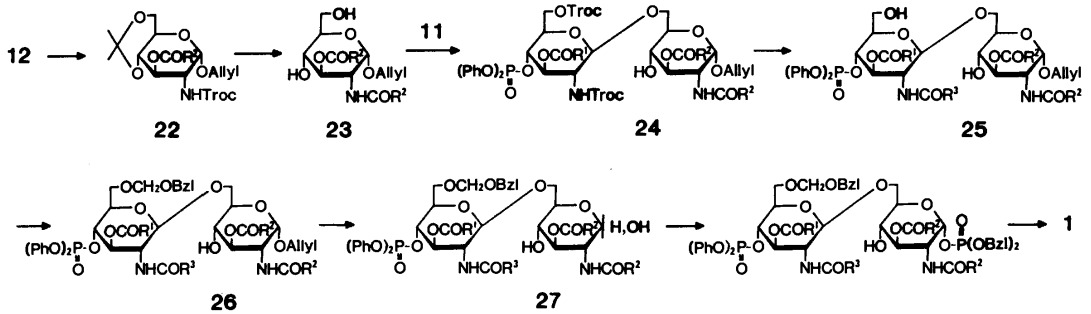

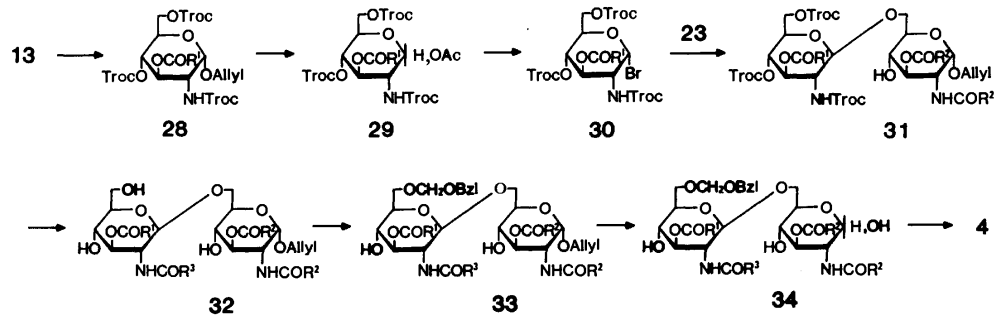

and introduction of (*R*)-3-dodecanoyloxytetradecanoyl group to the 2′-amino function, the 6′-hydroxyl group was protected by benzyloxymethylation for the subsequent glycosidic phosphorylation to give **26**.[23] Cleavage of the allyl group of **26**, glycosyl phosphorylation[11] and hydrogenolysis were successively performed in the same manner as described previously.[1]

The product (**1**) was purified by silica-gel column chromatography. Owing to the improved solubility in water compared to the 4′-monophosphate (**3**) above, the product (**1**) could be freed from inorganic contaminants by electrodialysis and precipitation with cold hydrochloric acid. This synthetic compound was identified on TLC with the main component of lipid A from *E. coli* Re cells. Further identification on TLC with the natural specimen was performed after cleavage of the glycosyl phosphate and methyl esterification.

As in the case of the biosynthetic precursor described in the preceding paper,[1] both 1-monophosphate (**4**) and dephospho derivative (**5**) of *E. coli*-type lipid A were also prepared. Comparison of the biological activities of a set of pure synthetic materials which have the same acyl disaccharide skeleton, but are only different in presence of phosphate groups, could give important informations particularly concerning the effect of the phosphates on the activities.

For the preparation of **4** and **5**, a glycosyl bromide **30** devoid of 4-phosphate moiety was prepared from **13** as a glycosyl donor. The 4-hydroxyl group of **30** was also protected with Troc group during the glycosidation. After coupling of the bromide **30** with the acceptor **23** to form a disaccharide **31**, the all Troc groups were removed and the 2′-amino group was acylated. Protection of 6′-position followed by glycosyl phosphorylation as above and deprotection afforded the 1-monophosphate (**4**). Chromatographic purification and washing with hydrochloric acid as described for 4′-monophosphate (**3**) gave pure **4**. The dephospho derivative **5** was obtained by direct deprotection of a intermediate **34** without phosphorylation.

Comparative studies were carried out on the biological activities of the synthetic products (**1**, **3**—**5**) and the corresponding natural lipid A. As already described,[9] the synthetic bisphosphate (**1**) manifested complete and identical activities including pyrogenicity and Shwartzman reactivity with the natural specimen. In conclusion, this work established first a synthetic route for lipid A and consequently provided the evidence that this structure should be certainly responsible to the active principle of endotoxin. Owing to these results, it becomes now possible to prepare any desired structural analogs of lipid A in a chemically pure forms by appropriate modification of the above synthesis. In addition, precise studies will be possible on the relationships between the biological activities and chemical structures of this type of unique glycolipid.

Experimental

All melting points are uncorrected. ^{1}H NMR spectra were measured for chloroform-*d* solutions on a Varian XL-100-15 spectrometer (100 MHz) unless noted otherwise. The chemical shifts are given in δ values with TMS as the internal standard. Optical rotations were measured with a Perkin-Elmer 141 polarimeter. Conventional and medium-pressure (2—4 kg cm^{-2}) column chromatography were carried out with Kieselgel 60 (E. Merck), 0.063—0.2 and 0.040—0.063 mm, respectively. Organic solutions were dried over magnesium sulfate.

2-Deoxy-2-(2,2,2-trichloroethoxycarbonylamino)-D-glucose (7). 2,2,2-Trichloroethoxycarbonyl chloride (50.0 g, 236 mmol) was added portionwise to an ice-cooled solution of 2-amino-2-deoxy-D-glucose hydrochloride (34.0 g, 158 mmol) and sodium hydrogencarbonate (34.0 g, 405 mmol) in water (500 ml). The mixture was stirred in an ice bath for 2 h and then at room temperature overnight. The colorless precipitate was collected by filtration, washed with water and ether, and then recrystallized from ethanol; yield 48.9 g (87%); mp 183—184 °C (decomp); $[\alpha]_D^{19}$ +50.4° (*c* 0.84, methanol). Found: C, 29.98; H, 4.19; N, 3.88; Cl, 29.20%. Calcd for $C_9H_{14}NO_7Cl_3 \cdot 0.5H_2O$: C, 29.73; H, 4.16; N, 3.85; Cl, 29.25%.

1,3,4,6-Tetra-*O*-acetyl-2-deoxy-2-(2,2,2-trichloroethoxycarbonylamino)-D-glucopyranosyl Bromide (6). A solution of the syrupy tetraacetate (500 mg, 0.96 mmol) obtained from **7** by the usual manner was dissolved in anhydrous dichloromethane (100 ml). The solution was saturated with dry hydrogen bromide at 0 °C and left at room temperature in a sealed flask for 18 h. After evaporation of the solvent in vacuo, the residual syrup was dried in vacuo over diphosphorus pentaoxide and sodium hydroxide; yield 520 mg. It was used for the following reaction without further purification.

Allyl 2-Acetamido-6-*O*-[3,4,6-tri-*O*-acetyl-2-deoxy-2-(2,2,2-trichloroethoxycarbonylamino)-β-D-glucopyranosyl]-3-*O*-benzoyl-4-*O*-benzyl-2-deoxy-β-D-glucopyranoside (9). A solution of the bromide **6** (520 mg, 0.96 mmol), allyl 2-acetamido-3-*O*-benzoyl-4-*O*-benzyl-2-deoxy-β-D-glucopyr-

anoside[1] (432 mg, 0.96 mmol) and mercury(II) cyanide (480 mg, 1.90 mmol) in anhydrous chloroform (10 ml) was heated under reflux for 40 min. After removal of the insoluble materials by filtration, the filtrate was washed successively with a saturated aqueous solution of sodium hydrogencarbonate and water, dried, and evaporated in vacuo. Purification by medium-pressure silica-gel column chromatography (90 g, chloroform–acetone 3:1) afforded a colorless solid; yield 390 mg (45%). ^{1}H NMR δ=1.81 (3H, s, NAc), 2.01 (6H, s, OAc), 2.04 (3H, s, OAc), and 7.1—8.2 (11H, m, aromatic H and NH).

Allyl 2-Acetamido-6-*O*-(2-acetamido-3,4,6-tri-*O*-acetyl-2-deoxy-β-D-glucopyranosyl)-3-*O*-benzoyl-4-*O*-benzyl-2-deoxy-β-D-glucopyranoside (10). Zinc powder (780 mg) was added to a solution of **9** (390 mg, 0.43 mmol) in acetic acid (10 ml). The mixture was heated at 50 °C with stirring for 30 min and then cooled to room temperature. After removal of the insoluble materials by filtration, the solvent was evaporated in vacuo. The residue was dissolved in chloroform, washed with water, and dried. The syrupy residue obtained after evaporation of the solvent in vacuo was again dissolved in chloroform and treated with triethylamine (67 μl, 0.48 mmol) and acetic anhydride (60 μl, 0.48 mmol). After usual work-up, the product was recrystallized from methanol–ether; yield 200 mg (59%); mp 220—223 °C (decomp). This product was identified with an authentic sample of **10** obtained in our previous work[1] by comparison of mps, TLC and ^{1}H NMR.

Allyl 2-Deoxy-4,6-*O*-isopropylidene-2-(2,2,2-trichloroethoxycarbonylamino)-α-D-glucopyranoside (12). Compound **7** (35.0 g, 98.7 mmol) was heated with stirring at 100 °C in allyl alcohol (230 ml) containing 2(w/v)% of dry hydrogen chloride for 20 min. The mixture was cooled and the solvent evaporated in vacuo. The residue dried by coevaporation with toluene three times was again dissolved in anhydrous acetone (400 ml). The solution was stirred with anhydrous calcium sulfate before 2,2-dimethoxypropane (37.8 ml, 296 mmol) and *p*-toluenesulfonic acid monohydrate (4.0 g, 19.7 mmol) were added to the solution. The mixture was stirred at room temperature for 3.5 h, neutralized by addition of aqueous sodium hydrogencarbonate and worked up as usual. The product was recrystallized from ethanol–ethyl acetate; yield 17.5 g (41%); mp 185—187 °C; $[\alpha]_D^{19}$ +59.8° (*c* 1.04, chloroform). Found: C, 41.57; H,4.93; N,3.20; Cl, 24.07%. Calcd for $C_{15}H_{22}NO_7Cl_3$: C, 41.45; H, 5.10; N, 3.22; Cl, 24.47%.

(*R*)-3-Tetradecanoyloxytetradecanoic Acid. Tetradecanoyl chloride (16.7 g, 67.6 mmol) was added dropwise to a solution of phenacyl (*R*)-3-hydroxytetradecanoate[1] (16.4 g, 45.3 mmol) in pyridine (100 ml) at room temperature. The mixture was stirred at room temperature for 1 h. Methanol (50 ml) was added and the mixture was stirred for additional 30 min. After evaporation of the solvent in vacuo, the residue was dissolved in benzene, and the solution was washed successively with 1 M† hydrochloric acid, saturated aqueous solution of sodium hydrogencarbonate, and water. The organic layer was treated with diazomethane and then dried. The syrupy residue obtained by evaporation of the solvent in vacuo was dissolved in acetic acid (300 ml). Zinc powder (45 g) was added and the mixture was stirred at 50 °C for 3 h. The mixture was filtered and the filtrate evaporated in vacuo. After coevaporation with toluene several times, the residue was subjected to column chromatography on silica gel (280 g, benzene) to give a colorless syrup; yield 17.6 g (86%); $[\alpha]_D^{17}$ −1.5° (*c* 4.99, chloroform). EI-MS: *m/z* 454 (M^+). Found: C, 73.99; H, 11.91%. Calcd for $C_{28}H_{54}O_4$: C, 73.99; H, 11.91%.

Allyl 2-Deoxy-3-*O*-[(*R*)-3-tetradecanoyloxytetradecanoyl]-2-(2,2,2-trichloroethoxycarbonylamino)-α-D-glucopyranoside (13). To a solution of **12** (10.0 g, 23.0 mmol) and (*R*)-3-tetradecanoyloxytetradecanoic acid (11.5 g, 25.3 mmol) in anhydrous dichloromethane (350 ml) were added 4-dimethylaminopyridine (DMAP) (1.41 g, 11.5 mmol) and dicyclohexylcarbodiimide (DCC) (5.22 g, 25.3 mmol). The mixture was stirred at room temperature for 2 h. The insoluble materials were removed by filtration and the filtrate was worked up as usual. After purification by silica-gel column chromatography (500 g, chloroform–acetone 30:1), the acylation product was heated in 90% acetic acid (200 ml) at 95 °C for 10 min. The solvent was evaporated in vacuo and the product recrystallized from hexane; yield 12.7 g (66%); mp 68—70 °C; $[\alpha]_D^{19}$ +43.7° (*c* 0.92, chloroform). Found: C, 57.90; H, 8.51; N, 1.75; Cl, 12.71%. Calcd for $C_{40}H_{70}NO_{10}Cl_3$: C, 57.79; H, 8.49; N, 1.68; Cl, 12.79%. ^{1}H NMR δ=0.87 (6H, t, *J*=6 Hz, CH_3), 1.1—1.45 (42H, br s, CH_2), 2.31 (2H, t, *J*=7 Hz, -COC$\underline{H}_2$CH$_2$-), 2.46—2.54 (2H, m, -COC$\underline{H}_2$CH-(OCOR)-), 4.73 (2H, s, CH_2 of Troc), and 4.94 (1H, d, *J*=4 Hz, H-1).

Allyl 2-Deoxy-3-*O*-[(*R*)-3-tetradecanoyloxytetradecanoyl]-6-*O*-(2,2,2-trichloroethoxycarbonyl)-2-(2,2,2-trichloroethoxycarbonylamino)-α-D-glucopyranoside (14). 2,2,2-Trichloroethoxycarbonyl chloride (0.89 ml, 6.5 mmol) was added to an ice-cooled solution of **13** (2.70 g, 3.25 mmol) in pyridine (60 ml). The mixture was stirred in an ice bath for 20 min. Then water was added and the mixture was stirred at room temperature. Usual work up and chromatographic purification on a silica-gel column (100 g, chloroform–acetone 30:1) gave a syrup; yield 2.00 g (61%). ^{1}H NMR δ=0.87 (3H, t, *J*=6 Hz, CH_3), 1.1—1.45 (42H, br s, CH_2), 2.27 (2H, t, *J*=7 Hz, -COC$\underline{H}_2$CH$_2$-), 2.52 (2H, d, *J*=6 Hz, -COC$\underline{H}_2$CH-(OCOR)-), 4.80 (2H, AB-type, CH_2 of Troc), and 4.88 (2H, s, CH_2 of Troc).

Allyl 2-Deoxy-3-*O*-[(*R*)-3-tetradecanoyloxytetradecanoyl]-6-*O*-(2,2,2-trichloroethoxycarbonyl)-2-(2,2,2-trichloroethoxycarbonylamino)-α-D-glucopyranoside 4-(Diphenyl Phosphate) (15). To a solution of **14** (2.00 g, 1.99 mmol) in anhydrous dichloromethane (60 ml) were added pyridine (0.24 ml, 3.0 mmol), DMAP (0.36 g, 3.0 mmol) and diphenyl phosphorochloridate (0.62 ml, 3.0 mmol). The mixture was stirred at room temperature for 2 h. The mixture was washed successively with 1 M hydrochloric acid, water, saturated aqueous sodium hydrogencarbonate, and water, and dried. After removal of the solvent, the residue was purified by medium-pressure chromatography on silica gel (90 g, chloroform–acetone 90:1) to give a syrup; yield 2.2 g (89%). ^{1}H NMR δ=0.87 (6H, t, *J*=6 Hz, CH_3), 1.1—1.6 (42H, br s, CH_2), 2.16 (2H, t, *J*=7 Hz, -COC$\underline{H}_2$CH$_2$-), 2.44 (2H, d, *J*=7 Hz, -COC$\underline{H}_2$-CH(OCOR)-), 4.66 and 4.70 (each 2H, s, CH_2 of Troc), 4.98 (1H, d, *J*=4 Hz, H-1), and 7.1—7.5 (10H, m, aromatic H).

1-*O*-Acetyl-2-deoxy-3-*O*-[(*R*)-3-tetradecanoyloxytetradecanoyl]-6-*O*-(2,2,2-trichloroethoxycarbonyl)-2-(2,2,2-trichloroethoxycarbonylamino)-α-D-glucopyranose 4-(Diphenyl Phosphate) (16). Compound **15** (17.9 g, 14.4 mmol) was dissolved in tetrahydrofuran (THF) (150 ml) and treated

† 1 M=1 mol dm^{-3}.

with 1,5-cyclooctadienebis(methyldiphenylphosphine)-iridium hexafuluorophosphate (200 mg) under nitrogen atmosphere at 50 °C for 40 min after activation of the iridium catalyst with hydrogen.[19] After cooling, water (8 ml) and iodine (7.3 g, 28 mmol) were added and the mixture was stirred for 10 min at room temperature. Purification by medium-pressure column chromatography on silica gel (500 g, chloroform-acetone 20 : 1) afforded a syrup. It was dissolved in anhydrous chloroform (120 ml) and treated with pyridine (3.3 ml, 42 mmol) and acetic anhydride (3.9 ml, 42 mmol). After usual work-up, the product was recrystallized from hexane; yield 8.00 g (45%); mp 77—80 °C $[\alpha]_D^{29}$ +35.6° (*c* 0.55, chloroform). Found: C, 52.32; H, 6.31; N, 1.13; Cl, 17.34%. Calcd for $C_{54}H_{78}NO_{16}Cl_6$: C, 52.27; H, 6.34; N, 1.13; Cl, 17.14%. ^{1}H NMR δ=0.88 (6H, t, *J*=6 Hz, CH_3), 1.1—1.5 (42H, br s, CH_2), 2.20 (3H, s, OAc), 2.20 (2H, t, *J*=7 Hz, $-COCH_2CH_2-$), 2.46 (2H, d, *J*=7 Hz, $-COCH_2CH(OCOR)-$), 4.45 (2H, AB-type, CH_2 of Troc), 4.72 (2H, s, CH_2 of Troc), 6.33 (1H, d, *J*=3.5 Hz, H-1), and 7.0—7.5 (10H, m, aromatic H).

Benzyl 2-Benzyloxycarbonylamino-2-deoxy-4,6-*O*-isopropylidene-α-D-glucopyranoside (19). Benzyl 2-benzyloxycarbonylamino-2-deoxy-α-D-glucopyranoside (**18**)[21] (20.0 g, 49.6 mmol) was dissolved in anhydrous acetone (700 ml) and treated with 2,2-dimethoxypropane (12.1 ml, 99.2 mmol) and *p*-toluenesulfonic acid monohydrate (1.89 g, 9.94 mmol) at room temperature for 4 h. Usual work-up followed by chromatographic purification on silica gel (500 g, chloroform-acetone 5 : 1) afforded a solid; yield 16.5 g (75%).

Benzyl 3-*O*-[(*R*)-3-Benzyloxytetradecanoyl]-2-[(*R*)-3-benzyloxytetradecanoylamino]-2-deoxy-α-D-glucopyranoside (17). Compound **19** (7.3 g, 16.5 mmol) was dissolved in methanol (80 ml) and hydrogenolyzed in the presence of palladium-black catalyst at room temperature under atmospheric pressure for 6 h. After usual work-up, the product was dissolved in dichloromethane (200 ml). To this solution were added (*R*)-3-benzyloxytetradecanoic acid (15.1 g, 45.1 mmol), DMAP (1.0 g, 8.3 mmol) and DCC (9.3 g, 45 mmol). The mixture was stirred at room temperature for 30 min. Usual work-up gave a syrup which was heated in 90% acetic acid at 90 °C for 20 min. After evaporation of the solvent in vacuo, the residue was recrystallized from methanol-ether-hexane; yield 7.00 g (47%); mp 88—89 °C; $[\alpha]_D^{27}$ +48.9° (*c* 0.50, chloroform). Found: C, 73.03; H, 9.13; N, 1.52%. Calcd for $C_{55}H_{83}NO_9$: C, 73.22; H, 9.27; N, 1.55%. ^{1}H NMR δ=0.89 (6H, t, *J*=6 Hz, CH_3), 1.1—1.5 (40H, br s, CH_2), 2.25—2.65 (4H, m, α-CH_2 of fatty acids), 4.88 (1H, d, *J*=4 Hz, H-1), 7.3 (15H, br s, aromatic H).

Benzyl 3-*O*-[(*R*)-3-Benzyloxytetradecanoyl]-2-[(*R*)-3-benzyloxytetradecanoylamino]-2-deoxy-6-*O*-[2-deoxy-3-*O*-[(*R*)-3-tetradecanoyloxytetradecanoyl]-6-*O*-(2,2,2-trichloroethoxycarbonyl)-2-(2,2,2-trichloroethoxycarbonylamino)-β-D-glucopyranosyl]-α-D-glucopyranoside 4′-(Diphenyl Phosphate) (20). Bromide **11** was prepared from **16** (4.00 g, 3.22 mmol) in anhydrous dichloromethane (800 ml) as described for the preparation of **6**.

To a solution of the bromide **11** in anhydrous chloroform (60 ml) were added anhydrous calcium sulfate (4.0 g), **17** (1.45 g, 1.61 mmol) and mercury(II) cyanide (1.63 g, 6.4 mmol). The mixture was heated under reflux for 22 h. After removal of the insoluble materials by filtration, the filtrate was washed successively with aqueous solution of potassium iodide and water, dried, and the solvent evaporated in vacuo. The residue was subjected to medium-pressure column chromatography on silica gel (90 g, chloroform-acetone 15 : 1) to give a syrup; yield 2.70 g (80% from **17**). Found: C, 60.81; H, 7.66; N, 1.28; Cl, 10.39%. Calcd for $C_{107}H_{157}N_2O_{23}PCl_6 \cdot 1.5H_2O$: C, 60.91; H, 7.64; N, 1.33; Cl, 10.08%. ^{1}H NMR δ=0.88 (12H, t, *J*=6 Hz, CH_3), 1.1—1.7 (82H, broad, CH_2), 2.1—2.7 (8H, m, α-CH_2 of fatty acids), 6.11 (1H, d, *J*=9 Hz, NH-2), and 7.0—7.4 (25H, m, aromatic H).

(*R*)-3-Dodecanoyloxytetradecanoic Acid. This compound was obtained as a syrup from phenacyl (*R*)-3-hydroxytetradecanoate and dodecanoyl chloride as described for the corresponding 3-tetradecanoyloxy derivative above; yield 6.1 g (95%); $[\alpha]_D^{11}$ −1.2° (*c* 5.54, chloroform). EI-MS: *m/z* 426 (M^+). Found: C, 73.23; H, 11.77%. Calcd for $C_{26}H_{50}O_4$: C, 73.19; H, 11.81%.

Benzyl 3-*O*-[(*R*)-3-Benzyloxytetradecanoyl]-2-[(*R*)-3-benzyloxytetradecanoylamino]-2-deoxy-6-*O*-[2-deoxy-2-[(*R*)-3-dodecanoyloxytetradecanoylamino]-3-*O*-[(*R*)-3-tetradecanoyloxytetradecanoyl]-β-D-glucopyranosyl]-α-D-glucopyranoside 4′-(Diphenyl Phosphate) (21). Zinc powder (5,4 g, 83 mmol) was added to a solution of **20** (2.70 g, 1.30 mmol) in acetic acid (75 ml). The mixture was stirred at room temperature for 30 min. After usual work-up, the crude product was dissolved in chloroform, and washed with 1 M hydrochloric acid and water, and dried. The solid obtained by evaporation of the solvent in vacuo was dissolved in dioxane. The solution was adjusted to pH 3 by addition of 1 M hydrochloric acid and then lyophilized to give colorless solid of hydrochloride of the 2′-amino derivative (2.18 g, 95%).

To a solution of a part of the solid (1.98 g, 1.12 mmol) in anhydrous dichloromethane (30 ml) was added triethylamine (0.16 ml, 1.15 mmol) and the solvent was evaporated. The residue was dissolved in anhydrous dichloromethane (30 ml) and dodecanoyloxytetradecanoic acid (716 mg, 1.68 mmol) and 1-ethyl-3-[3-(dimethylamino)propyl]carbodiimide hydrochloride (322 mg, 1.68 mmol) were added under ice-cooling. The mixture was stirred at room temperature for 22 h and worked up as usual. The crude product was dissolved in chloroform and treated with diazomethane and then subjected to medium-pressure chromatography on silica gel (90 g, chloroform-acetone 9 : 1) to give a syrup; yield 1.29 g (49%); $[\alpha]_D^{18}$ +19.5° (*c* 0.81, chloroform). Found: C, 70.96; H, 9.59; N, 1.36%. Calcd for $C_{127}H_{203}N_2O_{22}P$: C, 71.25; H, 9.56; N, 1.31%. ^{1}H NMR δ=0.88 (18H, t, *J*=6 Hz, CH_3), 1.1—1.8 (120H, broad, CH_2), 2.1—2.6 (12H, m, α-CH_2 of fatty acids), 6.12 (1H, d, *J*=9 Hz, NH), 6.25 (1H, d, *J*=8 Hz, NH), 7.0—7.4 (25H, m, aromatic H).

2-Deoxy-6-*O*-[2-deoxy-2-[(*R*)-3-dodecanoyloxytetradecanoylamino]-3-*O*-[(*R*)-3-tetradecanoyloxytetradecanoyl]-β-D-glucopyranosyl]-3-*O*-[(*R*)-3-hydroxytetradecanoyl]-2-[(*R*)-3-hydroxytetradecanoylamino]-D-glucose 4′-Phosphate (3). Compound **21** (860 mg, 0.402 mmol) was dissolved in a mixture of THF (22 ml) and acetic acid (1.4 ml) and hydrogenolyzed first in the presence of palladium black at room temperature under atmosphere of hydrogen (6.5 kg cm^{-2}) for 4 d. After removal of palladium and addition of platinum oxide, hydrogenolysis was continued under the same conditions for 6 h. Evaporation of the solvent followed by lyophilization from dioxane afforded colorless solid; yield 651 mg (94%).

The crude product obtained above (42.5 mg) was dissolved in chloroform-methanol (9 : 1, 6 ml). Cold 1 M hydrochloric acid (660 μl) was added and the homogeneous solution was

sonicated under ice-cooling for 5 min. The solvent was evaporated with stream of nitrogen, the residue dissolved in chloroform-methanol (9:1, 6 ml) and evaporated. The residue was again dissolved in the same solvent mixture and washed twice with water. Lyophilization from dioxane afforded a pure product; yield 39.2 mg; $[\alpha]_D^{18}$ −2.1° (*c* 0.58, chloroform). Found: C, 64.45; H, 10.31; N, 1.64%. Calcd for $C_{94}H_{177}N_2O_{22}P \cdot 2H_2O$: C, 64.35; H, 10.40; N, 1.60%.

Dimethyl Ester of 3 and Its Pentaacetate. Crude **3** (229 mg) was treated with 1 M hydrochloric acid as above and dissolved in chloroform-methanol (9:1, 9 ml). To the solution was added an ethereal solution of diazomethane. The product was purified by medium-pressure chromatography on silica gel (25 g, chloroform-methanol 15:1) and lyophilized from dioxane to give colorless solid; yield 68.2 mg (29%); $[\alpha]_D^{18}$ −2.5° (*c* 0.40, chloroform-methanol 9:1). Found: C, 65.15; H, 10.31; N, 1.55%. Calcd for $C_{96}H_{181}N_2O_{22}P \cdot 1.5H_2O$: C, 65.02; H, 10.46; N, 1.58%.

The dimethyl ester (30.0 mg, 0.017 mmol) was acetylated with acetic anhydride and pyridine in dichloromethane and purified by preparative TLC on silica gel (chloroform-acetone 5:1). The product was lyophilized from dioxane to give a colorless powder; yield 19.1 m (57%); $[\alpha]_D^{30}$ +17.9° (*c* 0.39, chloroform). Found: C, 65.17; H, 9.86; N, 1.46%. Calcd for $C_{106}H_{191}N_2O_{27}P$: C, 65.07; H, 9.84; N, 1.43%. The corresponding natural specimen: $[\alpha]_D^{30}$ +19.0.[3]

Allyl 3-*O*-[(*R*)-3-Benzyloxytetradecanoyl]-2-deoxy-4,6-*O*-isopropylidene-2-(2,2,2-trichloroethoxycarbonylamino)-α-D-glucopyranoside (22). To a solution of **12** (13.0 g, 29.9 mmol) in anhydrous chloroform (250 ml) were added (*R*)-3-benzyloxytetradecanoic acid[1] (10.0 g. 29.9 mmol), DCC (6.17 g, 29.9 mmol), and DMAP (731 mg, 5.98 mmol). The mixture was stirred at room temperature for 1 h and worked up as usual. Purification by silica-gel column chromatography (500 g, chloroform-acetone 30:1) afforded a colorless syrup; yield 14.5 g (64%). ^{1}H NMR δ=1.42 and 1.50 (each 3H, s, CH_3), 2.67 (1H, d, *J*=2 Hz, -OH), 4.70 (2H, AB-type, CH_2 of Troc), 4.86 (1H, d, *J*=3 Hz, H-1), 5.06—5.40 (3H, m, $-OCH_2-CH=C\underline{H}_2$ and NH), and 5.67—6.07 (1H, m, $-OCH_2-C\underline{H}=CH_2$).

Allyl 3-*O*-[(*R*)-3-Benzyloxytetradecanoyl]-2-[(*R*)-3-benzyloxytetradecanoylamino]-2-deoxy-α-D-glucopyranoside (23). Compound **22** (14.5 g, 19.3 mmol) was treated with zinc powder (29 g) in acetic acid (290 ml) as described for the preparation of **21**. After washing with hydrochloric acid and water, triethylamine (2.69 ml, 19.3 mmol) was added to a solution of the product in chloroform. The solvent was once evaporated in vacuo and the residue was again dissolved in anhydrous chloroform (250 ml). (*R*)-3-Benzyloxytetradecanoic acid (7.75 g, 23.2 mmol) and DCC (4.78 g, 23.2 mmol) were added to the solution. The mixture was stirred at room temperature for 30 min. After usual work-up, the crude product was heated in 90% acetic acid (250 ml) in a boiling water bath for 30 min. The product was purified by a silica-gel column (500 g, chloroform-acetone 5:1) and recrystallized from hexane; yield 9.53 g (58%); mp 80—82 °C; $[\alpha]_D^{19}$ +37.2° (*c* 1.02, chloroform). Found: C, 71.85; H, 9.67; N, 1.62%. Calcd for $C_{51}H_{81}NO_9$: C, 71.88; H, 9.58; N, 1.64%. ^{1}H NMR δ=0.88 (6H, t, *J*=6 Hz, CH_3), 1.1—1.5 (40H, br s, CH_2), 2.25—2.63 (4H, m, α-CH_2 of fatty acids), 4.47 (4H, s, $-C\underline{H}_2C_6H_5$), 4.75 (1H, d, *J*=3 Hz, H-1), 4.98—5.26 (2H, m, $-OCH_2-CH=C\underline{H}_2$), 5.50—5.92 (1H, m, $-OCH_2-C\underline{H}=CH_2$), 6.23 (1H, d, *J*=9 Hz, NH), and 7.22 (10H, s, aromatic H).

Allyl 3-*O*-[(*R*)-3-Benzyloxytetradecanoyl]-2-[(*R*)-3-benzyloxytetradecanoylamino]-2-deoxy-6-*O*-[2-deoxy-3-*O*-[(*R*)-3-tetradecanoyloxytetradecanoyl]-6-*O*-(2,2,2-trichloroethoxycarbonyl)-2-(2,2,2-trichloroethoxycarbonylamino)-β-D-glucopyranosyl]-α-D-glucopyranoside 4′-(Diphenyl Phosphate) (24). The glycosyl bromide (**11**) prepared from the acetate **16** (3.94 g, 3.18 mmol) as described above was dissolved in anhydrous chloroform (120 ml). Compound **23** (1.35 g, 1.58 mmol), mercury(II) cyanide (1.62 g, 6.33 mmol), and anhydrous calcium sulfate (4.0 g) were added to the solution and the mixture was heated under reflux. After 20 h, **23** (1.35 g, 1.58 mmol) was added and the mixture was heated for additional 13 h. Usual work-up followed by chromatography on a silica-gel column (110 g, chloroform-acetone 15:1) afforded a solid; yield 4.54 g (70%); $[\alpha]_D^{19}$ +18.4° (*c* 1.04, chloroform). Found: C, 60.74; H, 7.69; N, 1.29; Cl, 10.70%. Calcd for $C_{103}H_{155}N_2O_{23}Cl_6P$: C, 60.85; H, 7,68; N, 1.38; Cl, 10.46%. ^{1}H NMR δ=0.87 (12H, t, *J*=6 Hz, CH_3), 1.1—1.7 (82H, br s, CH_2), 2.12—2.84 (8H, m, α-CH_2 of fatty acids), 4.47 (4H, s, $-C\underline{H}_2C_6H_5$), 6.14 (1H, d, *J*=9 Hz, NH), and 7.0—7.4 (20H, m, aromatic H).

Allyl 3-*O*-[(*R*)-3-Benzyloxytetradecanoyl]-2-[(*R*)-3-benzyloxytetradecanoylamino]-2-deoxy-6-*O*-[2-deoxy-2-[(*R*)-3-dodecanoyloxytetradecanoylamino]-3-*O*-[(*R*)-3-tetradecanoyloxytetradecanoyl]-β-D-glucopyranosyl]-α-D-glucopyranoside 4′-(Diphenyl Phosphate) (25). Compound **24** (4.48 g, 2.20 mmol) was treated with zinc powder (9.0 g) in acetic acid (140 ml) and then with triethylamine (0.31 ml, 2.2 mmol) as described above for the preparation of **23**. To a solution of the product in anhydrous chloroform (80 ml) were added (*R*)-3-dodecanoyloxytetradecanoic acid (1.13g, 2.65 mmol) and DCC (546 mg, 2.65 mmol). The mixture was stirred at room temperature for 17 h. Usual work-up and chromatography on a silica-gel column (90 g, chloroform-acetone 9:1) afforded a colorless syrup; yield 3.25 g (71%). A part of the syrup was lyophilized from dioxane to give a colorless powder which was used for elemental analysis. Found: C, 69.97; H, 9.62; N, 1.43%. Calcd for $C_{123}H_{201}N_2O_{22}P \cdot H_2O$: C, 70.05; H, 9.70; N, 1.47%. ^{1}H NMR δ=0.87 (18H, t, *J*=6 Hz, CH_3), 1.0—1.7 (120H, br s, CH_2), 2.08—2.66 (12H, m, α-CH_2 of fatty acids) 4.47 (4H, s, $-C\underline{H}_2C_6H_5$), 6.18 (1H, d, *J*=9 Hz, NH), 6.36 (1H, d, *J*=8 Hz, NH), and 7.0—7.4 (20H, m, aromatic H).

Allyl 6-*O*-[6-*O*-Benzyloxymethyl-2-deoxy-2-[(*R*)-3-dodecanoyloxytetradecanoylamino]-3-*O*-[(*R*)-3-tetradecanoyloxytetradecanoyl]-β-D-glucopyranosyl]-3-*O*-[(*R*)-3-benzyloxytetradecanoyl]-2-[(*R*)-3-benzyloxytetradecanoylamino]-2-deoxy-α-D-glucopyranoside 4′-(Diphenyl Phosphate) (26). To a solution of **25** (3.14 g, 1.50 mmol) in anhydrous dichloromethane (100 ml) were added benzyloxymethyl chloride (352 mg, 2.25 mmol) and *N,N*-diisopropylethylamine (0.39 ml, 2.2 mmol). The mixture was stirred at room temperature for 48 h with portionwise addition of total 2.5 equivalent of each reagent. After usual work-up, the product was purified by silica-gel column chromatography (180 g, chloroform-acetone 15:1) to give a syrup; yield 2.17 g (65%). A part of the syrup was lyophilized from dioxane to give a colorless powder which was used for elemental analysis. Found: C, 70.80; H, 9.56; N, 1.30%. Calcd for $C_{131}H_{209}N_2O_{23}P \cdot 0.5H_2O$: C, 70.87; H, 9.53; N, 1.26%. $[\alpha]_D^{19}$ +18.3° (*c* 1.01, chloroform). ^{1}H NMR δ=0.88 (18H, t, *J*=6 Hz, CH_3), 1.1—1.7 (120H, br s, CH_2), 2.12—2.64 (12H, α-CH_2 of fatty acids), 6.11 (1H, d, *J*=9 Hz, NH), 6.24 (1H, d, *J*=8 Hz, NH), and 7.0—7.4 (25H, m,

aromatic H).

6-*O*-[6-*O*-Benzyloxymethyl-2-deoxy-2-[(*R*)-3-dodecanoyloxytetradecanoylamino]-3-*O*-[(*R*)-3-tetradecanoyloxytetradecanoyl]-β-D-glucopyranosyl]-3-*O*-[(*R*)-3-benzyloxytetradecanoyl]-2-[(*R*)-3-benzyloxytetradecanoylamino]-2-deoxy-D-glucose 4'-(Diphenyl Phosphate) (27). Compound **26** (2.11 g, 0.954 mmol) was treated with the iridium complex[19] (105 mg) in THF and then with water and iodine (500 mg) as described above for the preparation of **16**. Purification by medium-pressure column chromatography on silica gel (80 g, chloroform–acetone 10 : 1) followed by lyophilization from dioxane afforded a pale yellow powder; 1.31 g (63%). Found: C, 70.40; H, 9.44; N, 1.33%. Calcd for $C_{128}H_{205}N_2O_{23}P \cdot 0.5H_2O$: C, 70.52; H, 9,52; N, 1.29%. ^{1}H NMR δ=0.87 (18H, t, *J*=6 Hz, CH_3), 1.1—1.8 (120H, br s, CH_2), 2.10—2.62 (12H, m, α-CH_2 of fatty acids), 7.0—7.4 (25H, m, aromatic H).

2-Deoxy-6-*O*-[2-deoxy-2-[(*R*)-3-dodecanoyloxytetradecanoylamino]-3-*O*-[(*R*)-3-tetradecanoyloxytetradecanoyl]-β-D-glucopyranosyl]-3-*O*-[(*R*)-3-hydroxytetradecanoyl]-2-[(*R*)-3-hydroxytetradecanoylamino]-α-D-glucopyranose 1,4'-Bis(phosphate) (1). A solution of **27** (600 mg, 0.276 mmol) in anhydrous THF (12 ml) was cooled to −70 °C under argon atmosphere. To this solution were added 10(w/v)% hexane solution of butyllithium (210 μl, 0.33 mmol) and dibenzyl phosphorochloridate (85 μl) as described in our preceding paper.[1] After 20 min, palladium black was added to the cold mixture and the mixture was subjected to hydrogenolysis under 8 kg cm^{-2} of hydrogen at room temperature for 2 h. The catalyst was substituted with platinum oxide and then hydrogenolysis was continued under the same conditions. After purification by medium-pressure chromatography on silica gel (80 g, chloroform–methanol–water–triethylamine 200 : 100 : 20 : 1), the product was subjected to electrodialysis and acid precipitation as described previously[1] to afford colorless powder; yield 137 mg (27%). Found: C, 61.04; H, 10.05; N, 1.46%. Calcd for $C_{94}H_{178}N_2O_{25}P_2 \cdot 3H_2O$: C, 60.95; H, 10.01; N, 1.51%. $[\alpha]_D^{15}$ +11.3° (*c* 0.56, chloroform–methanol 9 : 1).

Allyl 2-Deoxy-3-*O*-[(*R*)-3-tetradecanoyloxytetradecanoyl]-4,6-bis[*O*-(2,2,2-trichloroethoxycarbonyl)]-2-(2,2,2-trichloroethoxycarbonylamino)-α-D-glucopyranoside (28). A solution of 2,2,2-trichloroethoxycarbonyl chloride (3.7 ml, 27 mmol) in THF (20 ml) was added to a solution of **13** (9.00 g, 10.8 mmol) in anhydrous pyridine (150 ml) cooled in an ice bath. The mixture was then stirred at room temperature for 50 min and worked up as usual. Chromatographic purification on a silica-gel column (500g, chloroform) afforded a colorless syrup; yield 12.8 g (quantitative). ^{1}H NMR δ=0.87 (6H, t, *J*=6 Hz, CH_3), 1.1—1.6 (42H, broad, CH_2), 2.24 (2H, t, *J*=7 Hz, -COC$\underline{H_2}$CH$_2$-), 2.50 (2H, d, *J*=6 Hz, -COC$\underline{H_2}$-CH(OCOR)-), 4.70 (2H, br s, CH_2 of Troc), and 4.72 and 4.73 (each 2H, s, CH_2 of Troc).

1-*O*-Acetyl-2-deoxy-3-*O*-[(*R*)-3-tetradecanoyloxytetradecanoyl]-4,6-bis[*O*-(2,2,2-trichloroethoxycarbonyl)]-2-(2,2,2-trichloroethoxycarbonylamino)-α-D-glucopyranose (29). Compound **28** obtained above (12.8 g) was treated with the iridium complex[19] (200 mg) in THF and then with iodine (5.5 g) and water as described for the preparation of **16**. Purification by column chromatography on silica gel (500 g, chloroform–acetone 50 : 1) afforded a pale yellow syrup (13.1 g), which was dissolved in anhydrous dichloromethane (200 ml) and treated with pyridine (3.7 ml) and acetic anhydride (2.2 ml, 23 mmol). Usual work-up and chromatographic purification on a silica-gel column (500 g, chloroform–acetone 100 : 1) gave colorless syrup; 12.6 g (93%). Found: C, 45.95; H, 6.06; N, 1.20; Cl, 27.16%. Calcd for $C_{45}H_{70}NO_{15}Cl_9$: C, 45.65; H, 5.96; N, 1.18; Cl, 26.95%. ^{1}H NMR δ=0.87 (6H, t, *J*=6 Hz, CH_3), 1.1—1.7 (42H, broad, CH_2), 2.15 (3H, s, OAc), 2.26 (2H, t, *J*=7 Hz, -COC$\underline{H_2}$CH$_2$-), 2.50 (2H, d, *J*=6 Hz, -COC$\underline{H_2}$CH(OCOR)-), 4.66 (2H, AB-type, CH_2 of Troc), 4.71 and 4.74 (each 2H, s, CH_2 of Troc), and 6.25 (1H, d, *J*=3 Hz, H-1).

Allyl 3-*O*-[(*R*)-3-Benzyloxytetradecanoyl]-2-[(*R*)-3-benzyloxytetradecanoylamino]-2-deoxy-6-*O*-[2-deoxy-3-*O*-[(*R*)-3-tetradecanoyloxytetradecanoyl]-4,6-bis[*O*-(2,2,2-trichloroethoxycarbonyl)]-2-(2,2,2-trichloroethoxycarbonylamino)-β-D-glucopyranosyl]-α-D-glucopyranoside (31). Syrupy **29** (12.6 g, 10.6 mmol) was converted to glycosyl bromide **30** and treated with **23** (5.50 g, 6.45 mmol) in the presence of mercury(II) cyanide (5.38 g) and anhydrous calcium sulfate in anhydrous chloroform (200 ml) under the same conditions as for the synthesis of **20**. Chromatography on a silica-gel column (500 g, chloroform–acetone 15 : 1) afforded a colorless syrup; yield 6.97 g (54% from **23**). A portion of the syrup was lyophilized to give colorless powder; $[\alpha]_D^{33}$ +19.3° (*c* 0.83, chloroform). Found: C, 56.82; H, 7.48; N, 1.44; Cl, 16.30%. Calcd for $C_{94}H_{147}N_2O_{22}Cl_9$: C, 57.13; H, 7.50; N, 1.42; Cl, 16.15%. ^{1}H NMR δ=0.88 (12H, t, *J*=6 Hz, CH_3), 1.1—1.7 (82H, broad, CH_2), 2.18—2.6 (8H, m, α-CH_2 of fatty acids), 4.47 (4H, s, $C_6H_5C\underline{H_2}$), 6.16 (1H, d, *J*=9 Hz, NH-2), and 7.22 (10H, br s, aromatic H).

Allyl 3-*O*-[(*R*)-3-Benzyloxytetradecanoyl]-2-[(*R*)-3-benzyloxytetradecanoylamino]-2-deoxy-6-*O*-[2-deoxy-2-[(*R*)-3-dodecanoyloxytetradecanoylamino]-3-*O*-[(*R*)-3-tetradecanoyloxytetradecanoyl]-β-D-glucopyranosyl]-α-D-glucopyranoside (32). This compound was prepared from **31** (6.97 g, 3.53 mmol) as described for the preparation of **21**, i.e., removal of Troc group with zinc (14 g) followed by acylation with (*R*)-3-dodecanoyloxytetradecanoic acid (2.26 g, 5.30 mmol) and DCC (1.09 g, 5.28 mmol) in dichloromethane. Purification by medium-pressure chromatography on silica gel (190 g, chloroform–acetone 6 : 1) followed by precipitation from methanol gave colorless solid; yield 3.00 g (46%); mp 99—102 °C (with sintering at 85 °C; $[\alpha]_D^{27}$ +15.1° (*c* 1.04, chloroform). Found: C, 71.27; H, 10.35; N, 1.51%. Calcd for $C_{111}H_{192}N_2O_{19} \cdot 0.5H_2O$: C, 71.38; H, 10.36; N, 1.50%. ^{1}H NMR δ=0.88 (18H, t, *J*=6 Hz, CH_3), 1.1—1.8 (122H, broad, CH_2), 2.2—2.65 (12H, m, α-CH_2 of fatty acids), 4.48 (4H, s, $C_6H_5C\underline{H_2}$), 5.96 (1H, d, *J*=9 Hz, NH), 6.14 (1H, d, *J*=8 Hz, NH), and 7.22 (10H, br s, aromatic H).

Allyl 6-*O*-[6-*O*-Benzyloxymethyl-2-deoxy-2-[(*R*)-3-dodecanoyloxytetradecanoylamino]-3-*O*-[(*R*)-3-tetradecanoyloxytetradecanoyl]-β-D-glucopyranosyl]-3-*O*-[(*R*)-3-benzyloxytetradecanoyl]-2-[(*R*)-3-benzyloxytetradecanoylamino]-2-deoxy-α-D-glucopyranoside (33). To a solution of **32** (3.00 g, 1.61 mmol) in anhydrous dichloromethane (100 ml) were added *N,N*-diisopropylethylamine (1,26 ml, 7.2 mmol) and benzyloxymethyl chloride (1.13 ml, 7.2 mmol). After 30 h at room temperature, the mixture was worked up as usual. The product was purified by medium-pressure chromatography on silica gel (90 g, chloroform–acetone 10 : 1) and recrystallized from methanol; yield 2.37 g (74%); mp 92—95 °C; $[\alpha]_D^{27}$ +14.5° (*c* 1.07, chloroform). Found: C, 71.51; H, 10.04; N, 1.42%. Calcd for $C_{119}H_{200}N_2O_{20}$: C, 71.58; H, 10.09; N, 1.40%. ^{1}H NMR δ=0.88 (18H, t, *J*=6 Hz, CH_3), 1.1—1.8 (122H, broad, CH_2), 2.2—2.5 (12H, m, α-CH_2 of fatty acids), 4.48

(4H, s, $C_6H_5C\underline{H}_2$), 4.58 (2H, s, $C_6H_5C\underline{H}_2OCH_2O$-), 4.76 (2H, s, $C_6H_5CH_2OC\underline{H}_2O$-), 7.1—7.4 (15H, aromatic H).

6-*O*-[6-*O*-Benzyloxymethyl-2-deoxy-2-[(*R*)-3-dodecanoyloxytetradecanoylamino]-3-*O*-[(*R*)-3-tetradecanoyloxytetradecanoyl]-β-D-glucopyranosyl]-3-*O*-[(*R*)-3-benzyloxytetradecanoyl]-2-[(*R*)-3-benzyloxytetradecanoylamino]-2-deoxy-D-glucose (34). This compound was prepared from **33** (3.30 g, 1.67 mmol) as described for **16** and purified by silica-gel column chromatography (90 g, chloroform–acetone 6 : 1) followed by recrystallization from methanol; yield 1.77 g (55%); mp 115—117 °C (with sintering at 81 °C); $[\alpha]_D^{19}$ +2.6° (*c* 0.66, chloroform). Found: C, 71.48; H, 10.19; N, 1.42%. Calcd for $C_{116}H_{196}N_2O_{20}\cdot 0.5H_2O$: C, 71.53; H, 10.14; N, 1.44%. ^{1}H NMR δ=0.88 (18H, t, *J*=6 Hz, CH_3), 1.1—1.8 (122H, broad, CH_2), 2.1—2.6 (12H, m, α-CH_2 of fatty acids), 4.45 and 4.47 (each 2H, s, $C_6H_5C\underline{H}_2$), 4.57 (2H, s, $C_6H_5C\underline{H}_2$-OCH_2O-), 4.76 (2H, s, $C_6H_5CH_2OC\underline{H}_2O$-), 7.1—7.4 (15H, aromatic H).

2-Deoxy-6-*O*-[2-deoxy-2[(*R*)-3-dodecanoyloxytetradecanoylamino]-3-*O*-[(*R*)-3-tetradecanoyloxytetradecanoyl]-β-D-glucopyranosyl]-3-*O*-[(*R*)-3-hydroxytetradecanoyl]-2-[(*R*)-3-hydroxytetradecanoylamino]-α-D-glucose 1-Phosphate (4). A solution of **34** (200 mg, 0.103 mmol) in anhydrous THF (10 ml) was treated under the same conditions as described for **1** with a solution of butyllithium in hexane (66 μl, 0.10 mmol) and dibenzyl phosphorochloridate (26 μl, 0.10 mmol). Hydrogenolysis with palladium black at room temperature at 6 kg cm^{-2} followed by medium-pressure chromatography on silica gel (15 g, chloroform–methanol–water–triethylamine 500 : 100 : 10 : 1) gave a crude product as colorless solid; 63.7 mg. A portion (58 mg) of the crude product was dissolved in chloroform–methanol (9 : 1, 5.8 ml) and treated with cold 1 M hydrochloric acid as described for the purification of **3** and lyophilized from dioxane; yield 43 mg. $[\alpha]_D^{18}$ +6.0° (*c* 0.42, chloroform–methanol 9 : 1). Found: C, 63.58; H, 10.27; N, 1.50%. Calcd for $C_{94}H_{177}N_2O_{22}P\cdot 3H_2O$: C, 63.70; H, 10.41; N, 1.58%.

2-Deoxy-6-*O*-[2-deoxy-2[(*R*)-3-dodecanoyloxytetradecanoylamino]-3-*O*-[(*R*)-3-tetradecanoyloxytetradecanoyl]-β-D-glucopyranosyl]-3-*O*-[(*R*)-3-hydroxytetradecanoyl]-2-[(*R*)-3-hydroxytetradecanoylamino]-D-glucose (5). Hydrogenolysis of **34** (217 mg) in THF (5 ml) and acetic acid (0.2 ml) under conditions described for **4** followed by recrystallization from methanol afforded the product; yield 155 mg (85%); mp 169—173 °C (decomp), $[\alpha]_D^{19}$ −5.5° (*c* 0.56, chloroform). Found: C, 68.29; H, 10.76; N, 1.70%. Calcd for $C_{94}H_{176}N_2O_{19}\cdot H_2O$: C, 68.16; H, 10.71; N, 1.69%.

A part of this work was supported by Grant-in-Aid for Scientific Research from Ministry of Education, Science and Culture (Nos. 58122002, 59116004, and 60108004). The work was also partly supported by a Joint Research Project from Japan Society for Promotion of Science (JSPS). One of the authors (M. I.) thanks for the financial support by Fellowship for Japanese Junior Scientist from JSPS. The authors are grateful to Mr. Hideo Naoki, Suntory Institute for Bioorganic Research, for his kind measurement of 360 MHz ^{1}H NMR spectra.

References

1) M. Imoto, H. Yoshimura, M. Yamamoto, T. Shimamoto, S. Kusumoto, and T. Shiba, *Bull. Chem. Soc. Jpn.*, **60**, 2197 (1987).

2) C. Galanos, O. Lüderitz, E. Th. Rietschel, and O. Westphal, "International Review of Biochemistry, Biochemistry of Lipids II," ed by T. W. Goodwin, University Park Press, Baltimore (1977), Vol. 14, Chap. 6.

3) a) M. Imoto, S. Kusumoto, T. Shiba, H. Naoki, T. Iwashita, E. Th. Rietschel, H.-W. Wollenweber, C. Galanos, and O. Lüderitz, *Tetrahedron Lett.* **24**, 4017 (1983); b) M. Imoto, S. Kusumoto, T. Shiba, E. Th. Rietschel, C. Galanos, and O. Lüderitz, *Tetrahedron Lett.*, **26**, 907 (1985).

4) M. Imoto, H. Yoshimura, M. Yamamoto, T. Shimamoto, S. Kusumoto, and T. Shiba, *Tetrahedron Lett.*, **25**, 2667 (1984).

5) a) C. Galanos, V. Lehmann, O. Lüderitz, E. Th. Rietschel, O. Westphal, H. Brade, L. Brade, M. A. Freudenberg, T. Hansen-Hagge, T. Lüderitz, G. McKenzie, U. Schade, W. Strittmatter, K. Tanamoto, U. Zähringer, M. Imoto, H. Yoshimura, M. Yamamoto, T. Shimamoto, S. Kusumoto, and T. Shiba, *Eur. J. Biochem.*, **140**, 221 (1984); b) S. Kotani, H. Takada, M. Tsujimoto, T. Ogawa, K. Harada, Y. Mori, A. Kawasaki, A. Tanaka, S. Nagao, S. Tanaka, T. Shiba, S. Kusumoto, M. Imoto, H. Yoshimura, M. Yamamoto, and T. Shimamoto, *Infect. Immun.*, **45**, 293 (1984).

6) Shwartzman reaction is a kind of tissue necrosis caused by endotoxin.

7) S. Kusumoto, H. Yoshimura, M. Imoto, T. Shimamoto, and T. Shiba, *Tetrahedron Lett.*, **26**, 909 (1985).

8) M. Imoto, H. Yoshimura, N. Sakaguchi, S. Kusumoto, and T. Shiba, *Tetrahedron Lett.*, **26**, 1545 (1985).

9) a) C. Galanos, O. Lüderitz, E. Th. Rietschel, O. Westphal, H. Brade, L. Brade, M. Freudenberg, U. Schade, M. Imoto, H. Yoshimura, S. Kusumoto, and T. Shiba, *Eur. J. Biochem.*, **148**, 1 (1985); b) H. Takada, S. Kotani, M. Tsujimoto, T. Ogawa, I. Takahashi, K. Harada, C. Katsukawa, S. Tanaka, T. Shiba, S. Kusumoto, M. Imoto, H. Yoshimura, M. Yamamoto, and T. Shimamoto, *Infect. Immun.*, **48**, 219 (1985); c) J. Y. Homma, M. Matsuura, S. Kanegasaki, Y. Kawakubo, Y. Kojima, N. Shibukawa, Y. Kumazawa, A. Yamamoto, K. Tanamoto, T. Yasuda, M. Imoto, H. Yoshimura, S. Kusumoto, and T. Shiba, *J. Biochem.*, **98**, 395 (1985).

10) O. Westphal and O. Lüderitz, *Angew. Chem.*, **66**, 407 (1954).

11) M. Inage, H, Chaki, S. Kusumoto, and T. Shiba, *Chem. Lett.*, **1982**, 1281.

12) In the synthesis of **2**, a disaccharide which contains no long-chain acyl group was prepared and then acylated (see Ref. 1). If this method was applied to the present synthesis of **1**, complicated manipulation of protecting groups would be required to differentiate the many functional groups of the disaccharide.

13) T. Shimamoto, S. Kusumoto, and T. Shiba, unpublished result. Elimination occurred at glycosyl activation both via oxazoline and via halogenide. Szabo et al. also observed the same elimination during glycosidation reactions with oxazoline: C. Diolez, S. R. Sarfati, and L. Szabo, *J. Chem. Soc., Perkin Trans. 1*, **1985**, 57, and the previous papers cited therein.

14) T. M. Windholz and B. R. Jonston, *Tetrahedron Lett.*, **1967**, 2555.

15) The unstable glycosyl phosphate in the natural lipid

A was cleaved off prior to the separation procedure (Ref. 3a).

16) A trace amount of the β-anomer was removed by the column chromatography after the subsequent acylation.

17) P. Szabo, S. R. Sarfati, C. Diolez, and L. Szabo, *Carbohydr. Res.*, **111**, C9 (1983).

18) The butyllithium-phosphorochloridate procedure was not applicable for this phosphorylation because of the presence of the base-labile Troc group.

19) J. J. Oltvoort, C. A. A. van Boeckel, J. H. de Koning, and J. H. van Boom, *Synthesis*, **1981**, 305.

20) M. A. Nashed and L. Anderson, *J. Chem. Soc., Chem. Commun.*, **1982**, 1274.

21) S. Kusumoto, M. Imoto, T. Ogiku, and T. Shiba, *Bull. Chem. Soc. Jpn*, **59**, 1419 (1986).

22) In order to obtain a clear result in a biological test, a water-soluble uniform salt form such as triethylammonium salt of a test compound is required, which can be obtained by neutralization of a compound in the free acid form with the corresponding amine. See the preceding paper.

23) Protection of secondary hydroxyl groups such as those on 4- and 4′-positions is not necessary during the phosphorylation of the glycosidic position with butyllithium-phosphorochloridate. By contrast, the reactive primary hydroxyl group on 6′-position had to be protected. See: M. Inage, H. Chaki, M. Imoto, T. Shimamoto, S. Kusumoto, and T. Shiba, *Tetrahedron Lett.*, **24**, 2011 (1983).

 © 1987 The Chemical Society of Japan Bull. Chem. Soc. Jpn., 60, 2215—2219 (1987)

Effect of Cationic Charge in Electrolyte-Amphoteric Ion-Exchange Membrane System

Yutaka HIRATA, Masashi DATE, Yukiko YAMAMOTO, Akira YAMAUCHI,* and Hideo KIMIZUKA
Department of Chemistry, Faculty of Science, Kyushu University 33, Hakozaki, Higashi-ku, Fukuoka 812
(Received October 4, 1986)

In order to clarify the membrane phenomena in an amphoteric membrane, four different experiments were carried out in a simple electrolyte-amphoteric membrane system. The ion transport numbers obtained from the membrane potential and electrodialysis were approximately in agreement with each other. It was indicated that the transport numbers strongly depended on the ionic valence in electrolyte solution. The membrane permeability coefficient representing the dynamic behavior of ion within membrane was evaluated in terms of membrane potential, transport number, and membrane conductance. In addition, the ionic concentrations within membrane equilibrated with outer electrolyte solution were measured to obtain the mobilities within membrane. The membrane phenomena were discussed on basis of the present experimental results.

The studies on an amphoteric membrane with cation- and anion-exchange sites have not been reported so many in comparison with those as to an ion-exchange membrane with homogeneous exchange sites. One of the reasons from physicochemical standpoint would be the complexity of ionic behavior within the membrane. However, the attractive possibilities concerning the amphoteric character have been predicted in various fields.[1-5] We also have recognized the valuable properties and investigated the fundamental membrane phenomena generated in simple electrolyte solution-amphoteric membrane system in which the amphoteric membranes developed by Central Research Laboratory of Kanegafuchi Chemical Industry Co., Ltd. were used.[6-8] The membrane phenomena have been examined through only the measurements of membrane potentials and membrane conductances in one of the works.[6] However, the membrane phenomena in the amphoteric membrane containing two kinds of exchange sites are too complicated to obtain the better understanding. More informations such as the experiments due to different amphoteric membrane or the determination of the concentration within membrane should be therefore accumlated.

Thus, the studies on the membrane having the different base membrane but the similar ion exchange sites as that of previous paper have been started in this series. In the previous reports of this series,[9,10] the membrane potential controlled by the ionic charge in the electrolyte solution was observed and was explained qualitatively by the apparent transport number, which can be obtained from the relation between the membrane potential and the activity in outer electrolyte solution. In order to confirm the results further, the alternative transport number which is evaluated from the measurement of ions transfered under the supplied currents, i.e., the electrodialysis experiment should be examined. Thus, the electrodialysis experiments were carried out, and the transport numbers were obtained about three species of electrolytes involving the cations of different valences. In addition, the ionic mobilities were estimated owing to know the ionic concentration within membrane. The details about the behavior of ion within membrane will be discussed in this work.

Experimental

Materials. The amphoteric ion exchange membrane used in the present study is coded as a "Neosepta CSV" and was supplied by Tokuyama Soda Co., Ltd., which was characterized with sulfonic acid group for cation-exchange site and *N*-methylpyridinium group for anion-exchange site. The characteristics of membrane were shown elsewhere.[9,10]

Before measurements, the membranes were conditioned by immersing successively in 0.1 M† aqueous ammonia, 0.5 M HCl, and 1.0 M NaCl aqueous solution, and the process was repeated a few times. The membranes thus obtained were washed with twice distilled water until the washing solutions did not contain any ions. The electrolytes(NaCl, $CaCl_2$, $LaCl_3$) were extra pure reagents and used without further purification. The aqueous electrolyte solutions indicated almost the same pH as that of distilled water equilibrated with carbon dioxides. For example, pH value of 10^{-2} mol dm^{-3} $LaCl_3$ solution was 5.46±0.05.

Apparatus. The cells for membrane potential, membrane conductance, and electrodialysis were made of glass, and consisted of two 20 cm^3 compartments. Two 1.57 cm^2 platinum black electrodes were equipped in the glass cells for membrane conductance. The membrane was placed between two compartments, and the available areas of membrane were 0.78 cm^2 for membrane potential and 3.14 cm^2 for membrane conductance and electrodialysis, respectively.

Measurements.

Membrane Potential: The membrane potential was measured according to the conventional method.[9,10] The results were obtained with the system in which the concentration of the electrolyte solution was kept constant in compartment(I) at 5.0×10^{-3} mol dm^{-3}, and was changed in compartment(II) from 1.0×10^{-3} to 1.0×10^{-1} mol dm^{-3}.

Electrodialysis: For the electrodialysis experiments, 10^{-2} mol dm^{-3} solutions of NaCl, $CaCl_2$, and $LaCl_3$ were used. In the electrodialysis experiment, a pair of silver-silver chloride electrodes with 2 cm^2 in area was inserted into aqueous electrolyte solutions at both sides of membrane. The currents of 0.1, 0.2, and 0.4 mA were supplied from phase(II) to phase(I) through Current Supply Equipment (Yokogawa

† 1 M=1 mol dm^{-3}.

Electric Works DC Voltage Current Standard Type 2853). After a passage of time, a constant volume (1 ml) was pipetted from both compartments and the concentration changes of ion from the initial electrolyte solutions were determined by the atomic absorption spectroscopy (Hitachi Co., Ltd., Model 180-50). In the case of La ion, the colorimeric method with arsenazo III reagent was employed because the sensitivity of atomic absorption was not effective.

Membrane Conductance: The membrane resistance was measured with Universal Bridge (Yokogawa-Hewlett-Packard Co., Model 4265B) through two platinum black electrodes in the sample solutions. After 10^{-2} mol dm^{-3} solutions of the respective electrolytes were poured into both compartments, the electrical resistances of the system with and without membrane were measured. The membrane resistance, R_m was obtained by subtracting the solution resistance without membrane from the total resistance. The membrane conductance, G_m was calculated by dividing $1/R_m$ with the available membrane area, 3.14 cm^2.

Ionic Concentration within Membrane: After the membrane (5×5 cm^2) was equilibrated with 10^{-2} mol dm^{-3} electrolyte solution for 72 h, the membrane was dipped into the distilled water for 72 h in order to remove the electrolyte due to donnan adsorption. Then, the ionic concentrations within membrane due to ion exchange with sites were eluted by 1.0 M HNO_3. The concentrations were determined by the same method as in electrodialysis experiment. The concentration of Cl ion was determined by Mohr's method. The total concentration of the electrolytes was taken as the concentration within membrane.

Throughout this study, the twice experiments for a single system were at least performed and the average value was taken as a reliable value. The solution phases were sufficiently stirred by the magnetic stirrers and the temperature of phases were kept at 25 °C.

Results and Discussion

Figure 1 shows the relations between the potentials and the mean activities of ions in the outer solutions for NaCl, $CaCl_2$, and $LaCl_3$. The mean activities were taken from the values in literature.[11] From dependence of the membrane potentials on activities in 1—1 valent electrolyte, NaCl, it was suggested that the membrane functions as a cation-exchange membrane regardless of having the anion-exchange site. On the other hand, in the case of 2—1 valent electrolyte, $CaCl_2$, the relation between the membrane potential and logarithmic mean activity of $CaCl_2$ deviated slightly from the linearity and the slope of potential per decade concentration decreased with suggesting the strong interaction of divalent cation with the cation-exchange site. Furthermore, in the system of $LaCl_3$ having tervalent cation, the inversion of the slope took place as seen in Fig. 1. In order to discuss the results quantitatively, it is convenient to use transport numbers which can be calculated from the membrane potential vs. mean activity relationships in Fig. 1.

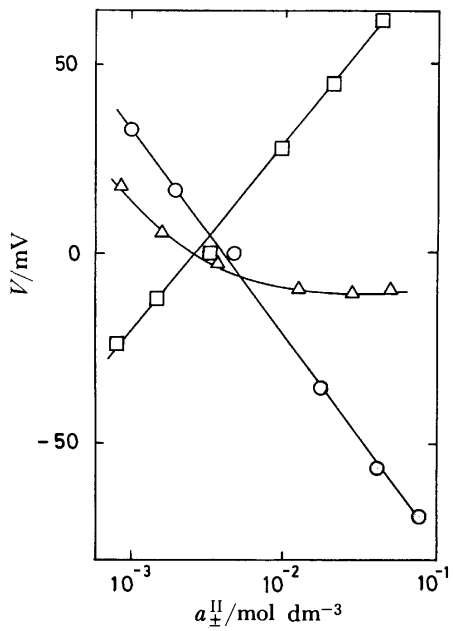

Fig. 1. Membrane potentials as a function of mean activities of electrolytes uni- to tervalent cations in phase (II). ○: NaCl, △: $CaCl_2$, □: $LaCl_3$.

Generally, the relationship between the membrane potential, V, and the mean activity of electrolyte, $a_\pm$, for amphoteric membrane was given as follows,

$$V = \left(\frac{t_M}{Z_M} + \frac{t_{Cl}}{Z_{Cl}}\right)\frac{RT}{F}\ln\frac{a_\pm(I)}{a_\pm(II)}, \quad (1)$$

where t_M and t_{Cl} indicate the transport numbers of cation and anion; Z_M and Z_{Cl}, the valences of M and Cl ions; respectively. Transport numbers were calculated from the slope in Fig. 1 by means of Eq. 1 and were summarized in Table 1. In the case of $CaCl_2$, the transport number was calculated from the tangent slope at 10^{-2} mol dm^{-3} $CaCl_2$ concentration.

As shown in Table 1, it is obvious that the transport numbers, t_M or t_{Cl}, correspond to the slopes in membrane potential vs. the activity of electrolyte solution relationships. In the case of $LaCl_3$, t_{La} was remarkably reduced to 0.13. The value means that Cl ion can be relatively transported more than La ion, and it may be supposed that La ion is trapped around the cation-exchange sites owing to the strong electrostatic attraction.

In order to confirm the results obtained above further, the transport number by electrodialysis method was estimated. A typical example for NaCl system (10^{-2} mol dm^{-3}, 0.2 mA) was shown in Fig. 2. Sodium ion in phase(I) increased and that in phase(II) decreased with a passage of time under the supplied

Table 1. Transport Numbers, t_M and t_{Cl} Evaluated from Membrane Potential and Electrodialysis

Salt	Membrane potential		Electrodialysis	
	t_M	t_{Cl}	t_M	t_{Cl}
NaCl	0.95	0.05	0.94	0.06
$CaCl_2$	0.82	0.18	0.83	0.17
$LaCl_3$	0.13	0.87	0.12	0.88

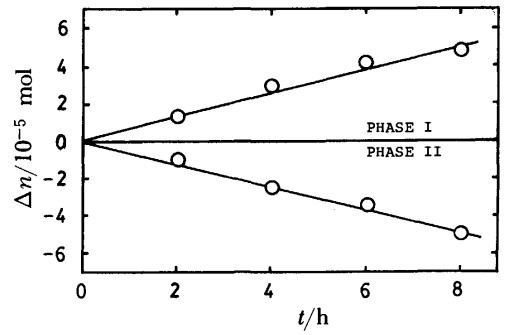

Fig. 2. The increase and decrease of Na ions in phase (I) and phase (II) against the passage of time for NaCl system (1.0×10^{-2} mol dm^{-3}, 0.2 mA).

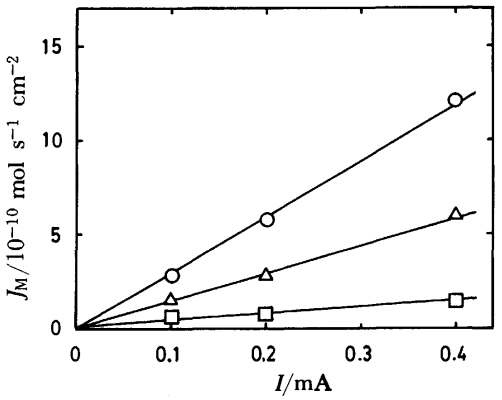

Fig. 3. The relationship between flux and current for each cation. ○: Na, △: Ca, □: La.

current of 0.2 mA. The concentration change from the initial Na ion concentration, Δn_{Na}, showed the straight line against time in both phases and the absolute values of the slope were approximately the same. The similar results were also obtained at the other systems. The absolute values of the concentration change in both phases were averaged, and the ion fluxes were evaluated with Eq. 2 from the slopes of the linear portion,

$$J_M = \frac{\Delta n}{sA}, \tag{2}$$

where Δn, s, and A denote moles of transfered ion, time in sec during the supplied currents and membrane area in cm^2, respectively. The relation between flux and current for each cation was shown in Fig. 3. The cationic current due to cation transfered, i_M, can be evaluated by the Eq. 3 taking account of the quantity of electricity on the flux,

$$i_M = Z_M F J_M A. \tag{3}$$

The transport number, t_M, can be obtained from the relationship between i_M and I according to the following relation,

$$t_M = \frac{i_M}{I}, \tag{4}$$

where I is the total supplied current. The transport numbers, t_M, due to the electrodialysis were shown together with t_{Cl} which were calculated by a relation, $t_M+t_{Cl}=1$, in Table 1. As seen in Table 1, the values of t_M decrease with increase of the cationic valences in accordance with t_M obtained by the membrane potential measurement.

In order to discuss the dynamic behavior of ions within the membrane in more detail, it would be effective to introduce the membrane permeability coefficients presented in previous papers.[6,12] The permeability coefficient reflects the dynamic behavior of ion within membrane and is a function of the membrane potential, V, membrane conductance, G_m, and transport number, t, and is expressed as follows,

$$P_M = \frac{t_M G_m RT}{Z_M^2 F^2 (a_M^I \cdot a_M^{II})^{1/2}} \cdot \frac{Z_M F(V-V_M)/2RT}{\sinh(Z_M F(V-V_M)/2RT)}, \tag{5}$$

$$P_{Cl} = \frac{t_{Cl} G_m RT}{Z_{Cl}^2 F^2 (a_{Cl}^I \cdot a_{Cl}^{II})^{1/2}} \cdot \frac{Z_{Cl} F(V-V_{Cl})/2RT}{\sinh(Z_{Cl} F(V-V_{Cl})/2RT)}, \tag{6}$$

where V_M and V_{Cl} denote the equilibrium potentials of ions, M and Cl, respectively, and $(a^I \cdot a^{II})^{1/2}$, geometrical mean activity in phase(I) and phase(II). On the

Table 2. Membrane Resistances, R_m and Membrane Conductances, G_m

Salt[a)]	R_m	G_m
	Ω	S cm^{-2}
NaCl	30	1.06×10^{-2}
$CaCl_2$	68	4.68×10^{-3}
$LaCl_3$	1050	3.03×10^{-4}

a) Concentration of salt solution: 1.0×10^{-2} mol dm^{-3}.

Table 3. Membrane Permeabilities, P_M and P_{Cl} Evaluated from Membrane Potential and Electrodialysis

Salt	Membrane potential			Electrodialysis		
	P_M	P_{Cl}	P_M/P_{Cl}	P_M	P_{Cl}	P_M/P_{Cl}
	cm s^{-1}	cm s^{-1}		cm s^{-1}	cm s^{-1}	
NaCl	4.14×10^{-4}	2.18×10^{-5}	18.99	2.97×10^{-4}	1.56×10^{-5}	19.04
$CaCl_2$	4.75×10^{-5}	4.17×10^{-5}	1.14	7.06×10^{-5}	2.90×10^{-5}	2.43
$LaCl_3$	2.27×10^{-7}	1.64×10^{-5}	0.017	5.77×10^{-7}	1.27×10^{-5}	0.045

other hand, G_m was measured in the same system as that of electrodialysis experiment. In calculation of P_M and P_{Cl}, the membrane potentials generated between 5×10^{-3} mol dm^{-3} in phase(I) and 1×10^{-2} mol dm^{-3} in phase(II), the respective mean activities, the transport numbers from membrane potentials and the membrane conductances in Table 2 were inserted into Eqs. 5 and 6. The results were shown in Table 3. The values of P_M were largely changed by the cationic valences while P_{Cl} showed almost constant values in three systems. For example, in the case of NaCl system, the membrane permeability coefficient of cation, P_{Na}, was approximately 20-fold larger than P_{Cl}. The large difference indicated that Na ion can be easily transported. In the case of $CaCl_2$, P_{Ca} decreased slightly. Contrary to former two cases, P_{La} in $LaCl_3$ was remarkably reduced, and as a result, Cl ion can be transported. The ratios, P_M/P_{Cl}, which were also given in Table 3, reflect the permselectivity of ions through membrane. The facts confirm again that membrane potential in the present system is determined by the difference of the membrane permeability coefficients for cation and anion. In other words, the membrane potentials strongly depend upon the cationic valences.

Here, it is interesting that the present result is compared with that of the previous paper at 10^{-2} mol dm^{-3} electrolyte solution.[6] The evaluated membrane permeabilities except for La ion in this study were almost the same order of magnitude as in previous one, but the membrane permeability ratios of cations to anions indicated large discrepancies between two kinds of the membranes. The values of present ratios were strongly dependent on the valency of electrolyte, and particularly, in the case of NaCl, the membrane indicated a high permselectivity to Na ion over Cl ion, while the permeability ratio of La ion to Cl ion was less than unity in the case of $LaCl_3$. On the other hand, the magnitude of cationic permeabilities exceeded that of anionic one as shown in Fig. 5 of previous paper though there is no result about $LaCl_3$. The reason is not clear at present, but it may be partly attributed to the difference of the membrane skeleton.

In the present electrodialysis and conductance experiments, the electrolyte solutions having the same concentration were placed at phase(I) and phase(II). Therefore, V, V_M, are V_{Cl} in Eqs. 5 and 6 are almost reduced to zero, and the potential terms can be dropped out. Furthermore, under the experimental conditions described above, $(a^{I}_{M}\cdot a^{II}_{M})^{1/2}$ and $(a^{I}_{Cl}\cdot a^{II}_{Cl})^{1/2}$ can be replaced by $a_{\pm M}$ and $a_{\pm Cl}$. Finally, taking account of $t_M G_m \delta = Z_M F^2 \bar{U}_M \bar{C}_M$, we can obtain Eqs. 7 and 8 as the alternative expression for P,

$$P_M = \frac{RT\bar{U}_M}{\delta}\cdot\frac{\bar{C}_M}{(a^{I}_{M}\cdot a^{II}_{M})^{1/2}}, \tag{7}$$

$$P_{Cl} = \frac{RT\bar{U}_{Cl}}{\delta}\cdot\frac{\bar{C}_{Cl}}{(a^{I}_{Cl}\cdot a^{II}_{Cl})^{1/2}}, \tag{8}$$

where δ denotes membrane thickness; $\bar{C}$, concentration of ion within membrane; $\bar{U}$, absolute mobility of ion within membrane. Equations of 7 and 8 are sufficiently applicable to the present systems in which the concentrations of electrolyte in both phases, I and II, were identical. The evaluated values of P were also shown in Table 3. The results were in good agreement with those obtained by means of Eqs. 5 and 6. Equations of 7 and 8 have the instructive expression for understanding of physicochemical meaning as to the membrane permeability coefficient, P. It is clear that P largely depends on a product of the mobility and the concentration within membrane under the present experimental conditions.

At present stage, it is possible to know the mobility of ion within membrane provided the ionic concentration within membrane, $\bar{C}$, is given. The ionic concentration, $\bar{C}$, was determined according to the method described in experimental section and given in Table 4. The ionic mobilities for three electrolyte systems examined were calculated in terms of Eqs. 7 and 8, and the results were summarized in Table 5 together with using mean activities. The mobilities indicated a similar tendency with membrane permeability coefficients. In the case of NaCl system, $\bar{U}_{Na}$ was larger than $\bar{U}_{Cl}$. In the system of $LaCl_3$ having tervalent cation, $\bar{U}_{La}$ was remarkably small. In this system, P_M and P_{Cl} could be mainly determined by the dynamic factor($\bar{U}$)

Table 4. Ionic Concentrations within Membrane

Salt	$\bar{C}_M$	$\bar{C}_{Cl}$
	mol dm^{-3}	mol dm^{-3}
NaCl	2.21	1.24
$CaCl_2$	5.76×10^{-1}	6.33×10^{-1}
$LaCl_3$	3.81×10^{-1}	5.81×10^{-1}

Table 5. Ionic Mobilities within Membrane, $\bar{U}_M$ and $\bar{U}_{Cl}$ Evaluated from Electrodialysis

Salt	$a_\pm$	$\bar{U}_M$	$\bar{U}_{Cl}$	$\bar{U}_M/\bar{U}_{Cl}$
	mol dm^{-3}	cm s^{-1} dyn^{-1}	cm s^{-1} dyn^{-1}	
NaCl	9.02×10^{-3}	5.81×10^{-12}	6.61×10^{-13}	8.79
$CaCl_2$	7.31×10^{-3}	4.34×10^{-12}	1.62×10^{-12}	2.69
$LaCl_3$	5.60×10^{-3}	4.08×10^{-14}	5.92×10^{-13}	0.07

rather than static factor($\bar{C}$). It is considered that La ion having large charge was trapped around the cation-exchange sites owing to the strong electrostatic attraction. It may be said that ionic permeability through membrane is controlled by the valence of cation.

The present work was partially supported by Grant-in-Aid for Scientific Research No. 58470007 from the Ministry of Education, Science and Culture.

References

1) K. Sollner, *Biochem. Z.*, **244**, 370 (1932).
2) O. Kedem and A. Katchalksy, *Trans. Faraday Soc.*, **59**, 1918 (1963).
3) C. R. Gardner, J. N. Weinstein, and S. R. Caplan, *Desalination*, **12**, 19 (1973).
4) J. Shorr and F. B. Leits, *Desalination*, **14**, 11 (1974).
5) I. Yamabe, J. Umezawa, S. Yoshida, and N. Takai, *Desalination*, **15**, 127 (1974).
6) A. Yamauchi, S. Tsuruyama, H. Masumori, Y. Nagata, K. Kaibara, and H. Kimizuka, *Bull. Chem. Soc. Jpn.*, **55**, 3297 (1982).
7) K. Kaibara, H. Sonoda, Y. Nagata, and H. Kimizuka, *Bull. Chem. Soc. Jpn.*, **56**, 1346 (1983).
8) H. Kimizuka, Y. Nagata, and K. Kaibara, *Bull. Chem. Soc. Jpn.*, **56**, 2371 (1983).
9) Y. Hirata, M. Sc. Thesis, Kyushu University, Fukuoka Japan, 1986.
10) A. Yamauchi, Y. Okazaki, R. Kurosaki, Y. Hirata, and H. Kimizuka, *J. Membr. Sci.* in Press.
11) "Electrochemical Data," ed by D. Dobos, Elsevier Scientific Pub. Co., Amsterdam-Oxford-New York (1975).
12) H. Kimizuka and Kaibara, *J. Colloid Interface Sci.*, **52**, 516 (1975).

 © 1987 The Chemical Society of Japan Bull. Chem. Soc. Jpn., 60, 2221—2226 (1987)

ESR Studies of the Dynamic Properties of Ion Radicals Captured by Surfactant Micelles

Kosaku SUGA,† Koushi MAEMURA,* Masamichi FUJIHIRA, and Shigeru AOYAGUI
Department of Chemical Engineering, Tokyo Institute of Technology, Ohokayama, Meguro-ku, Tokyo 152
(Received October 30, 1986)

ESR spectra of duroquinone anion radical (DQ^-), methyl viologen cation radical (MV^+), and 5,10-dimethyl-5,10-dihydrophenazine cation radical ($DMPZ^+$) were measured in various aqueous surfactant solutions. The line width of each peak of the ESR spectra for DQ^- in cationic and anionic surfactant solutions showed a quadratic dependence on the total nuclear quantum number, $M=\Sigma m_i$ (i=1 to 12), of methyl protons of DQ^-. The rotational correlation times, τ_c, of DQ^- determined from these dependences, were 10^{-9}—10^{-8} s in cationic surfactant (dodecyl-, tetradecyl-, and hexadecyltrimethylammonium bromide) solutions, and 10^{-10}—10^{-9} s in nonionic surfactant (Triton X-100) solution. ESR spectra of MV^+ and $DMPZ^+$ in anionic surfactant (sodium dodecyl sulfate; SDS) solution showed anomalous patterns as not exhibiting the hyperfine splittings due to the nitrogen nucleus. These anomalies were explained by the more significant broadening of the outer peaks due to nitrogen splitting compared with the broadening of the central peaks corresponding to the nuclear quantum number of nitrogen, $M_N=m_{N1}+m_{N2}=0$. From these results, the rotational correlation time for $DMPZ^+$ in SDS solution was estimated as about 10^{-10} s.

Many nitroxide radicals have been used as spin probes in order to study the dynamic properties of micelles and bilayers.[1-12] ESR spectra of nitroxide radicals solubilized into micelles have unsymmetric hyperfine structure mainly consisting of three peaks due to the nitrogen atom in the nitroxide radical. These unsymmetric properties of spectra are explained by the incomplete averaging of the anisotropic g tensor and the hyperfine coupling tensor. By the analysis of the unsymmetry of these spectra, dynamic properties of micelle and micelle solubilized substances have been determined.[1-12] We are studying the electron-transfer reactions of ion radicals captured by the micelle. In order to study the correlation between the reactivities and the dynamic properties of ion radicals, it is necessary to know the dynamic properties of these ion radicals. However, the ESR spectra of paramagnetic substances solubilized into a micelle other than nitroxide radicals have received little attention. In this paper, we report the characteristics of the ESR spectra of duroquinone anion radical (DQ^-), the 5,10-dimethyl-5,10-dihydrophenazine cation radical ($DMPZ^+$) and the methyl viologen cation radical (MV^+) in several surfactants solutions. Furthermore, we report the dynamic properties, as a rotational correlation time, of ion radicals captured by the micelle obtained from these ESR spectra.

Experimental

Duroquinone (DQ) and methyl viologen dibromide ($MV^{2+}Br_2^{2-}$) used were reagent grade and were used without further purification. 5,10-Dimethyl-5,10-dihydrophenazine (DMPZ) was provide by Dr. Y. Ohsawa in this laboratory. Sodium dodecyl sulfate (SDS), dodecyltrimethylammonium bromide (C_{12}TMAB), tetradecyltrimethylammonium bromide (C_{14}TMAB), hexadecyltrimethylammonium bromide (C_{16}TMAB) and Triton X-100 (TX-100) were reagent grade and used without further purification.

†Present address: Seiko Instruments Inc., Takatsuka, Matsudo, Chiba 271.

Sample solutions of DQ^- and MV^+ were prepared by the reduction of aqueous solutions of DQ and MV^{2+} with sodium dithionite ($Na_2S_2O_4$) in the presence or absence of a surfactant. Sample solutions of $DMPZ^+$ were prepared by the oxidation of aqueous micellar or acetonitrile solution of DMPZ with ceric sulfate ($Ce(SO_4)_2$).

Sample cells for ESR measurements were Pyrex glass capillary cells with about 1 mm inner diameter. ESR spectra were measured by a JEOL-FE3XI ESR spectrometer equipped with a variable temperature adapter. Computer simulation of ESR spectra were carried out with the Hitachi M-280H computer system at the Computer Center of Tokyo Institute of Technology.

Results and Discussion

ESR Spectra for DQ^- in Various Surfactant Solutions. Figure 1 shows the ESR spectra for DQ^- in various solutions. The ESR spectrum for an aqueous solution of DQ^- without surfactant was symmetric and the relative intensity of each peak agreed reasonably with those calculated theoretically. The observed hyperfine coupling constant for twelve equivalent methyl protons of DQ^- in this spectrum was 1.90 G (1G=10^{-4} T) and agreed well with the value for DQ^- in C_2H_5OH[13] and in CH_3OH-H_2O mixture.[14] The ESR spectrum for the DQ^- in 0.5 M (1 M=1 mol dm^{-3}) SDS solution was similar to that mentioned above. On the other hand, the ESR spectra for DQ^- in the nonionic and cationic surfactant solutions were unsymmetrical and the degree of dissymmetry was larger for those in the cationic surfactant solutions than that in the nonionic surfactant solution. Furthermore, for the cationic surfactant solutions, the longer the carbon chain of the surfactant molecule, the larger the degree of dissymmetry.

ESR Spectra of $DMPZ^+$ and MV^+ in SDS Solution. Figure 2 (a) shows the ESR spectrum of $DMPZ^+$ in 0.1 M SDS solution at 40 °C. This spectrum was analyzed as the hyperfine structure with A_1(6H)=6.15 G, A_2(4H)=1.68 G, and A_3(4H)=0.66 G. In fact, as shown

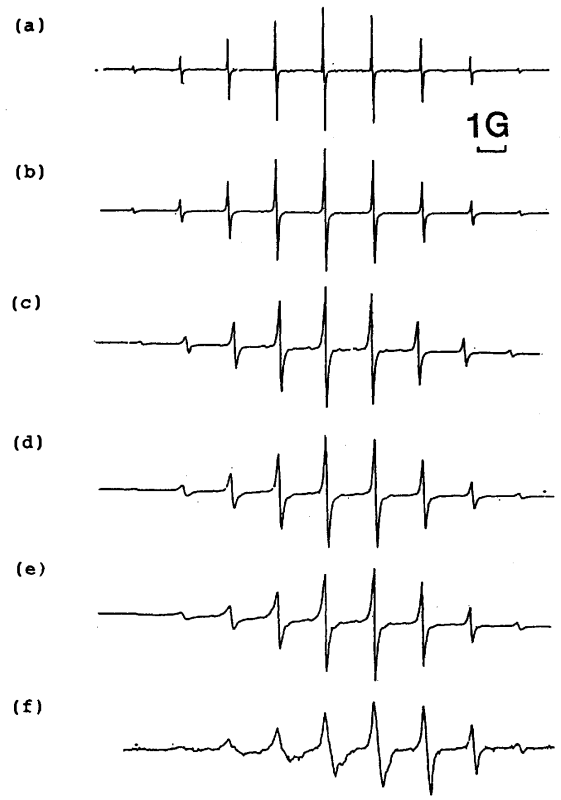

Fig. 1. The ESR spectra of DQ^- in aqueous solutions in the presence or absence of various surfactants at 20°C. (a) Without surfactant; (b) 0.5 M SDS; (c) 0.3 M TX-100; (d) 0.5 M C_{12}TMAB; (e) 0.5 M C_{14}TMAB; (f) 0.5 M C_{16}TMAB.

in Fig. 2 (b), the computer simulated spectrum with these parameters well-reproduced the experimental spectrum. Evidently, this spectrum appeared to have no hyperfine splitting due to the nitrogen nucleus in a $DMPZ^+$ ion. On the other hand, the ESR spectra of $DMPZ^+$ in AN and in aqueous solution without surfactant showed the hyperfine splittings due to the nitrogen nucleus.

Figure 3 (a) shows the ESR spectrum of MV^+ in 0.1 M SDS solution at 30°C. This spectrum also appears to have no hyperfine splittings due to the nitrogen nucleus, as shown by the comparison with the computer simulated spectrum with $A_1(6H)=3.99$ G, $A_2(4H)=1.57$ G, and $A_3(4H)=1.33$ G in Fig 3 (b). On the other hand, the ESR spectrum of MV^+ in aqueous solution agreed well with the computer simulated spectrum with $A(2N)=4.23$ G, $A_1(6H)=3.99$ G, $A_2(4H)=1.57$ G, and $A_3(4H)=1.33$ G.

Theoretical Basis for Line-Width Analysis. In order to simplify the analysis of the line width of the ESR spectrum, we assume that the g tensor and the hyperfine coupling tensor have cylindrical symmetry. Under this assumption, from the theory of Kivelson,[15] the line width of each hyperfine lines for an ESR spectrum of a free radical in a doublet state ($S=1/2$) is given by the following equation:

$$T_2^{-1} = \tau_c[(4/45)(\Delta\gamma H)^2+\sum(3/8)\sigma_{ii}^2[<J_i(J_i+1)>_{M_i}-M_i] + \sum\sigma_{ij}M_iM_j-(4/15)(\Delta\gamma H)b_iM_i] \quad (1)$$

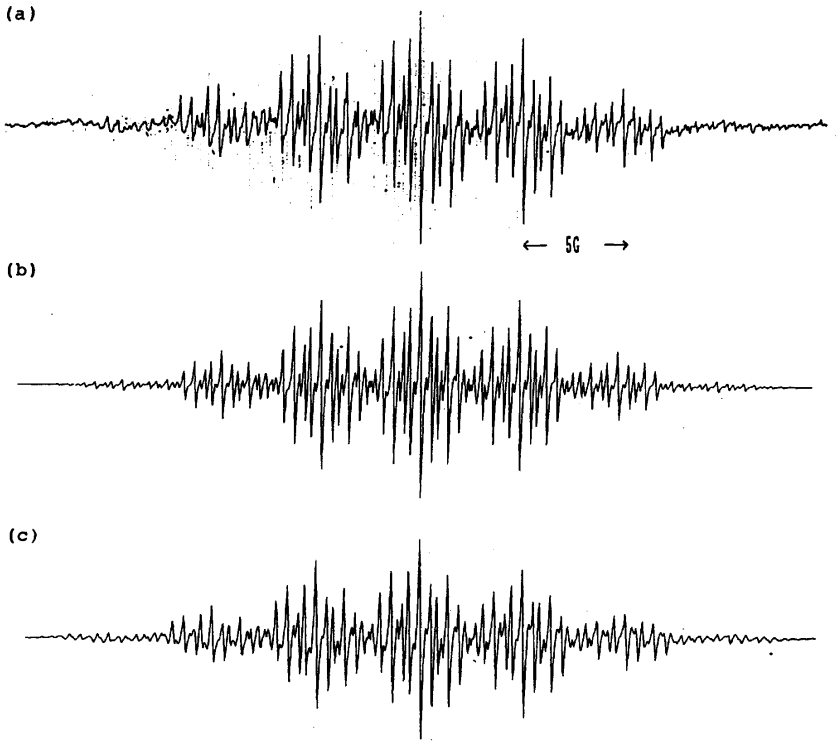

Fig. 2. The ESR spectra of $DMPZ^+$ (a) observed in 0.1 M SDS solution at 40°C; (b) simulated with $A_1(6H)=6.15$ G, $A_2(4H)=1.68$ G, $A_3(4H)=0.66$ G, and ΔH_{pp}(all peaks)=0.120 G; (c) simulated with $A(2N)=6.63$ G, $A_1(6H)=6.15$ G; $A_2(4H)=1.68$ G, $A_3(4H)=0.66$ G, $\Delta H_{pp}(M_N=\pm2)=0.570$ G, $\Delta H_{pp}(M_N=\pm1)=0.256$ G, and $\Delta H_{pp}(M_N=0)=0.120$ G.

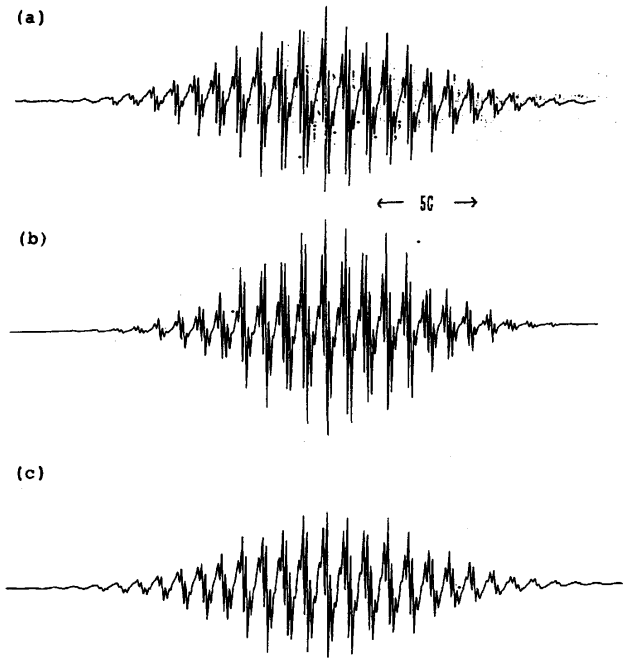

Fig. 3. The ESR spectra of MV^+ (a) observed in 0.1 M SDS solution at 30°C; (b) simulated with A_1(6H)=3.99 G, A_2(4H)=1.57 G, A_3(4H)=1.33 G, and ΔH_{pp}(all peaks)=0.120 G; (c) simulated with A(2N)=4.23 G, A_1(6H)=3.99 G; A_2(4H)=1.57 G, A_3(4H)=1.33 G, $\Delta H_{pp}(M_N=\pm 2)$=0.570 G, $\Delta H_{pp}(M_N=\pm 1)$=0.256 G, and $\Delta H_{pp}(M_N=0)$=0.120 G.

In this equation

$$\Delta\gamma=\gamma_{//}-\gamma_{\perp},$$
$$\sigma_{ij}=(1/5)b_ib_j,$$
$$b_i=(4\pi/3)\{(A_i)_{//}-(A_i)_{\perp}\}$$

and τ_c, H, M_i, and $\langle J_i(J_i+1)\rangle$ are the rotational correlation time, the value of the stationary magnetic field, the quantum number corresponding to the component of the stationary magnetic field of the ith group of equivalent nuclei, and the average value of $J_i(J_i+1)$ for a given value of M_i, respectively. And, $\gamma_{//}$, $\gamma_{\perp}$, $(A_i)_{//}$, and $(A_i)_{\perp}$ are the parallel and the perpendicular components of the principal values of gyromagnetic ratio tensor and hyperfine coupling tensors of the ith nuclear groups.

For one group of equivalent nuclei with I=1/2,

$$\langle J_i(J_i+1)\rangle=(1/2)n_i+M_i^2$$

where n_i is the number of nuclei in the group. When n_i=2 and I=1, $\langle J_i(J_i+1)\rangle$ is 6, 4, and 8/3 for M_i value of 2, 1, and 0, respectively.

Rotational Correlation Times for DQ^- in Micelle. The dissymmetry of the ESR spectra of DQ^- in nonionic and cationic micellar solutions may be explained by the incomplete averaging of the anisotropic g tensor and hyperfine coupling tensor for these radicals due to the restriction of the rotational Brownian motion by the solubilization to a micelle, as explained for nitroxide radicals solubilized into a micelle used as spin probe.

From the Eq. 1, the line width of each of the hyperfine lines for the ESR spectrum of DQ^- with equivalent twelve protons is expressed as follows,

$$(T_2)^{-1} = \tau_c\{[(9/20)b^2+(4/45)(\Delta\gamma H)^2] - (4/15)b\Delta\gamma HM + (b^2/5)M^2\}. \quad (2)$$

If the line width due to other relaxation mechanisms is given by ΔH_o, from Eq. 2 the total peak to peak line width, ΔH_{pp}, in the magnetic field unit is expressed as follows,

$$\Delta H_{pp} = a_1 + a_2M + a_3M^2 + \Delta H_o \quad (3)$$

where $a_1=(2\hbar\sqrt{3}g\beta)[9/20)b^2+(4/45)(\Delta\gamma H)^2]\tau_c$, $a_2=(2\hbar/\sqrt{3}g\beta)(4/15)b(\Delta\gamma H)\tau_c$, and $a_3=(2\hbar/\sqrt{3}g\beta)(b^2/5)\tau_c$.

Figure 4 shows the dependence of the observed line width for each peak of the ESR spectra of DQ^- in 0.5 M C_{12}TMAB solution at 10 and 20°C upon the value of M. These line width values agreed well with the quadratic fitted curves according to Eq. 3, and from these curves the parameters a_1, a_2, a_3, and ΔH_o were determined.

In order to determine the value of τ_c, however, the value of b and $\Delta\gamma$ must be known. Fortunately, as shown in Fig. 5, the ESR spectrum of DQ^- in C_{16}TMAB solution has marked unsymmetrical profile, and is similar to those in a solid matrix, especially at low temperature. The DQ^- molecule does not have exact cylindrical symmetry, but the spectrum in Fig. 5 shows that the principal values of the gyromagnetic ratio tensor and hyperfine coupling tensor of this

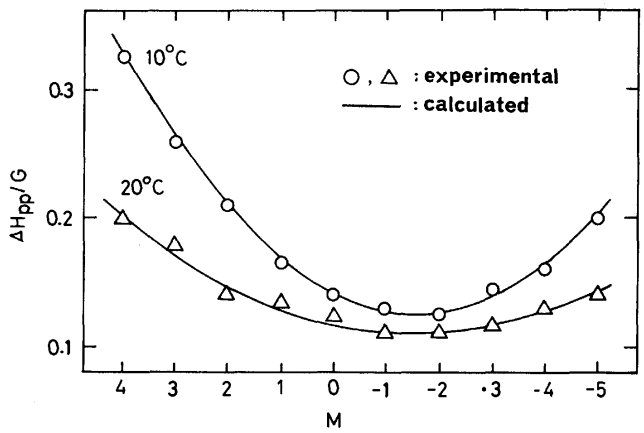

Fig. 4. The dependence of the line width, ΔH_{pp}, of the ESR spectrum of DQ^- in 0.5 M C_{12}TMAB solution on the total nuclear quantum number, M, of twelve hydrogens at 10 and 20°C.

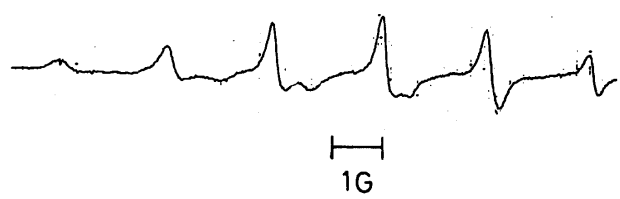

Fig. 5. The ESR spectrum of DQ^- in 0.5 M C_{16}TMAB solution at 10°C.

Table 1. Rotational Correlation Times of the Duroquinone Anion in Various Surfactant Micelles

Surfactant Solution	$\tau_c \times 10^9$/s			
	10°C	20°C	30°C	40°C
0.5 M C_{12}TMAB	3.4	1.5	—	—
0.5 M C_{14}TMAB	—	3.2	2.2	—
0.5 M C_{16}TMAB	>3	>3	>3	2.9
0.3 M TX-100	0.85	0.53	0.37	—

molecule are nearly cylindrically symmetric. From this spectrum, we have estimated the value of $|A_{//}-A_{\perp}|$ and $|g_{//}-g_{\perp}|$ as 0.225 G and 1.49×10^{-3}, respectively. The values of τ_c were determined from the values of a_1, a_2, and a_3 independently, and they agreed well with each other. Table 1 shows the values of τ_c for DQ^- in various micellar solutions. These values of τ_c decrease with the increase of temperature, and increase with the length of the alkyl chain of the surfactants. The τ_c of DQ^- in C_{16}TMAB solution at low temperature can not be determined because of the complexity of the ESR spectrum due to the large anisotropy as shown in Fig. 5. However, these values of τ_c may be nearly 10^{-8} s at 10 or 20 °C, because this large anisotropic character of the spectrum indicates the larger correlation time of DQ^- in this solution. In previous works, almost only the values of τ_c for nitroxide radicals in micellar solutions have been reported. Furthermore, the majority of these values were measured in anionic micellar solutions such as SDS. These values of τ_c for nitroxide radicals in anionic micellar solutions were about 10^{-10} s,[1,3,4,7,12] and those in nonionic micellar solutions were about 10^{-9} s.[6,8,11]

The values of τ_c for DQ^- in the nonionic surfactant solution was smaller than those of nitroxide radicals in nonionic surfactant solutions. This result may be due to the fact that DQ^- is not only in a micellar phase but also in an aqueous phase in the nonionic surfactant solution, because the diffusion coefficient of DQ^- in the nonionic surfactant solution determined by cyclic voltammogram was larger than those of micelle itself. On the other hand, it was shown by cyclic voltammetry that DQ^- in the cationic surfactant solutions was almost completely captured by the micelle. The values of τ_c for DQ^- in the cationic surfactant solutions measured in this experiment are larger by one or more orders than those for nitroxide radicals in anionic surfactant solutions cited in the literatures.[1,3,4,7,12] This result shows that the rotational diffusion of DQ^- in the cationic micelle was more strongly restricted by the micelle than the nitroxide radical in the anionic micelles.

Rotational Correlation Times for $DMPZ^+$ and MV^+ in the SDS Micelle. From the results for the ESR spectra of $DMPZ^+$ and MV^+ in SDS solution, it is suggested that the peaks of the ESR spectra of $DMPZ^+$ and MV^+ split by the hyperfine interaction with the nitrogen nucleus are extremely broadened except for the central peaks corresponding to the zero value of the total nuclear quantum number of nitrogen, $M_N=0$.

If the contribution to the line width of each hyperfine lines due to the anisotropy of the gyromagnetic ratio tensor and the hyperfine coupling tensors other than nitrogen nucleus are neglected, the line width of each peak is determined only by the value of M_N. In such a situation, from Eq. 1, the line width of the hyperfine lines corresponding to the value of M_N, which equals to 0, ±1, and ±2, are $(8/40)b_N^2\tau_c$, $(17/40)b_N^2\tau_c$, and $(38/40)b_N^2\tau_c$, respectively.

Figures 2 (c) and 3 (c) show the computer simulated spectra considering the hyperfine splitting by nitrogen nucleus: $A(2N)=6.63$ G ($DMPZ^+$),[16] $A(2N)=4.43$ G (MV^+),[17] and the contribution to the line width due to the anisotropy of the hyperfine coupling tensor of the nitrogen nucleus described above: $\Delta H_{pp}(M_N=\pm2)=0.570$ G, $\Delta H_{pp}(M_N=\pm1)=0.256$ G, and $\Delta H_{pp}(M_N=0)=0.120$ G. These spectra reproduced the observed spectra (Fig. 2 (a), 3 (a)) more exactly than the simulated spectra obtained by neglecting the hyperfine splitting due to the nitrogen nucleus.

These results show that the ESR spectra of $DMPZ^+$ and MV^+ in 0.1 M SDS solutions appear to have no nitrogen hyperfine splittings because of the larger anisotropy of the nitrogen hyperfine coupling tensor compared with those of the other coupling tensors and the g tensor.

In order to determine the rotational correlation times for $DMPZ^+$ and MV^+ captured by the SDS micelle, it is necessary to know the anisotropy parameter of the nitrogen hyperfine coupling tensors of these cation radical, b_N. Unfortunately, these values have not yet been determined experimentally. Therefore, we must estimate these values from those of nitrogen-containing paramagnetic compounds. Typical principal values of hyperfine coupling tensors for the nitrogen nucleus of nitroxide radicals are about 32, 6, and 6 G.[18] From these values, an anisotropy parameter, and an isotropic coupling constant are obtained: $b_N=26$ G, $A_N=15$ G. The relative anisotropy parameter defined here, $b_N/A_N=1.73$, of nitroxide radical is the largest among those of the nitrogen-containing paramagnetic compounds.[19] If we adopt this value as the relative anisotropy parameter for $DMPZ^+$ and MV^+, the calculated rotational correlation times of these cation radicals may be the lowest limit of these values. Assuming that the values of b_N's for $DMPZ^+$ and MV^+ are $6.63\times1.73=11.5$ G and $4.23\times1.73=7.3$ G, respectively, the rotational correlation times for these cation radicals can be evaluated from the following equation,

$$\Delta H_{pp}(M_N=0)=(2/\sqrt{3})(\hbar/g\beta)(38/40)b_N^2\tau_c. \quad (4)$$

Using the observed line width at 40 °C, i.e. 0.12 G for $DMPZ^+$ and MV^+, the calculated rotational correlation times are 1.4×10^{-11} and 3.4×10^{-11} s. These values are small compared with those for DQ^- in cati-

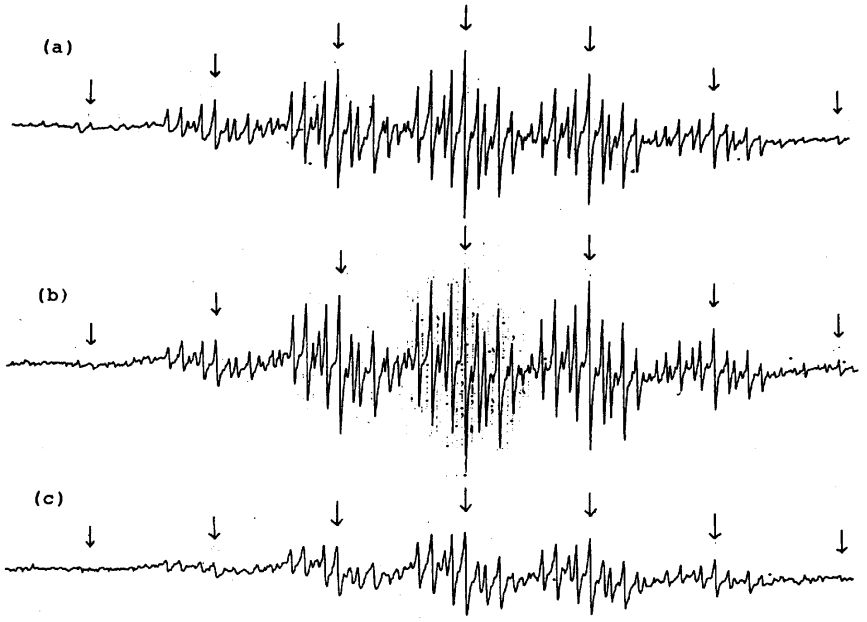

Fig. 6. The ESR spectra of $DMPZ^+$ in 0.1 M SDS solution at (a) 40 °C; (b) 20 °C; (c) 0 °C. Arrows shows the main peaks splitted by the hyperfine interaction of an electron spin with six methyl hydrogens.

onic micelles. However, these values are their lower limit, as described above. Therefore, it is desirable to determine their upper limit by the other method.

In the above discussion, we have neglected the effect of the anisotropy of the hyperfine coupling tensors of the hydrogen atoms. In fact, their anisotropy did slightly affect the ESR spectrum of $DMPZ^+$ at 40 °C, but appreciably more at lower temperatures. Figure 6 shows the temperature dependence of the ESR spectrum of $DMPZ^+$. Peaks indicated by arrows are the main peaks split by the hyperfine interactions of an electron spin with methyl hydrogens. Their intensities became more unsymmetrical with decreasing temperature. The degree of dissymmetry is smaller compared with that of DQ^- in cationic micelle at 20 °C (ref. Fig. 1). The twelve hydrogens of DQ^- is a β hydrogen with respect to an odd electron on the ring carbon atoms. Similarly, the methyl hydrogen of $DMPZ^+$ is also a β hydrogen with respect to an odd electron on the ring nitrogen atoms. The degree of anisotropy of the hyperfine coupling tensor for a β hydrogen is generally smaller compared to an α hydrogen. For DQ^-, the relative anisotropy parameter b_H/A_H is about 0.1. It is reasonable to assume that the relative anisotropy parameter for methyl hydrogens of $DMPZ^+$ is about 0.1. The isotropic hyperfine coupling constant of methyl hydrogens is 6.2 G, and about three times larger than that for the hydrogens of DQ^-. The contribution of an anisotropy parameter to the line width of an ESR spectrum is proportional to its square. Therefore, it is shown that the rotational correlation time (τ_c) of $DMPZ^+$ is at least smaller than a tenth of those for DQ^- in cationic micelles, i.e. about 10^{-9} s. The upper limit of the rotational correlation time of MV^+ in the SDS micelle can not be determined because of the complexity of the ESR spectrum of MV^+.

From the results shown above, it is concluded that the rotational coorrelation times (τ_c) of $DMPZ^+$ in the SDS micelle have a value between 10^{-9} and 10^{-11} s, and probably about 10^{-10} s. The large difference between the rotational correlation times for $DMPZ^+$ in the SDS micelle and DQ^- in a cationic micelle is a remarkable fact. The reason for this is not yet known, but it may be noteworthy that the cationic surfactant has three methyl groups at the positively charged hydrophilic part, $(CH_3)_3N^+$-, while the anionic surfactant (SDS) has only the $-SO_3^-$ group at the hydrophilic part.

We wish to thank Profs. Hiroshi Fukutomi and Hiroshi Tomiyasu for giving us facilities in ESR measurement at The Research Laboratory for Nuclear Reactor in Tokyo Institute of Technology.

References

1) A. S. Wagoner, O. H. Griffith, and C. R. Christensen, *Proc. Nat. Acad. Sci. U. S. A.*, **57**, 1198 (1967).
2) K. K. Fox, *Trans. Faraday Soc.*, **67**, 2802 (1971).
3) N. M. Atherton and S. J. Strach, *J, Chem. Soc., Faraday Trans. 2*, **68**, 374 (1972).
4) J. Oakes, *J. Chem. Soc., Faraday Trans. 2*, **68**, 1464 (1972).
5) K. K. Fox, *J. Chem. Soc., Faraday Trans. 2*, **72**, 220 (1976).
6) H. Yoshioka, *J. Colloid Interface Sci.*, **63**, 378 (1978).
7) H. Yoshioka, *Chem. Lett.*, **1977**, 1477.
8) H. Yoshioka, *J. Colloid Interface Sci.*, **66**, 352 (1978).

9) C. L. Kwan, S. Atik, and L. A. Singer, *J. Am. Chem. Soc.*, **100**, 4783 (1978).
10) Y. Y. Lim and J. H. Fendler, *J. Am. Chem. Soc.*, **101**, 4023 (1979).
11) H. Yoshioka, *J. Colloid Interface Sci.*, **83**, 214 (1981).
12) M. F. Ottaviani, P. Baglioni, and G. Martini, *J. Phys. Chem.*, **87**, 3146 (1983).
13) B. Venkataraman, B. G. Segal, and G. Fraenkel, *J. Chem. Phys.*, **30**, 1006 (1959).
14) J. K. Dohrmann, *Ber. Bunsenges. Phys. Chem.*, **74**, 575 (1970).
15) D. Kivelson, *J. Chem. Phys.*, **33**, 1094 (1960).
16) R. F. Nelson, D. W. Leedy, E. T. Seo, and R. N. Adams, *Z. Anal. Chem.*, **224**, 184 (1967).
17) C. S. Johnson Jr. and H. S. Gutowsky, *J. Chem. Phys.*, **39**, 58 (1963).
18) S. Schreier, C. F. Polnaszek, and I. C. P. Smith, *Biophys. Acta*, **515**, 375 (1978).
19) J. R. Rowlands and D. H. Whiffen, *Nature*, **193**, 61 (1962); T. Cole, *J. Chem. Phys.*, **35**, 1169 (1961); J. S. Hyde and E. S. Freeman, *J. Phys. Chem.*, **65**, 1636 (1961); H. Zeldes and R. Livingston, *J. Chem. Phys.*, **35**, 563 (1961).

 © 1987 The Chemical Society of Japan Bull. Chem. Soc. Jpn., 60, 2227—2230 (1987)

Catalase-Like Activity of Anion-Exchange Resin Modified with Metalloporphyrin in the Oxidation of Methyl Alcohol and Its Application to the Determination of Hydrogen Peroxide

Yutaka SAITO,* Mitsuko SATOUCHI, Masaki MIFUNE, Takaaki TAI, Junichi ODO, Yoshimasa TANAKA, Masahiko CHIKUMA,† and Hisashi TANAKA††

Faculty of Pharmaceutical Sciences, Okayama University, 1-1-1 Tsushima-Naka, Okayama 700
†Osaka College of Pharmacy, 2-10-65 Kawai, Matsubara-City 580
††Faculty of Pharmaceutical Sciences, Kyoto University, Sakyo-ku, Kyoto 606

(Received September 18, 1986)

The catalase-like activity of anion-exchange resins (Amberlite IRA 900) modified with various metalloporphyrins in the acceleration of reaction (1) was evaluated by efficiency in color reaction (2) based on dye formation:

$$H_2O_2 + CH_3OH \xrightarrow{\text{catalase}} 2H_2O + HCHO \quad (1)$$

$$HCHO + \text{4-amino-3-hydrazino-5-mercapto-1,2,4-triazole} + KIO_4 \xrightarrow{OH^-} \text{Dye } (\lambda_{max} = 550\ \text{nm}). \quad (2)$$

Amberlite IRA 900 modified with Mn^{3+}-tetrakis(sulfophenyl)porphine ($MnTPPS_r$) was found to exhibit the highest catalase-like activity among the resins tested and was applied as a mimesis of catalase to the determination of hydrogen peroxide by the use of reactions (1) and (2). The molar absorption coefficient for hydrogen peroxide was found to be $2.37\times10^4\ mol^{-1}\,dm^3\,cm^{-1}$, which is larger than twice that in the control catalase method ($0.97\times10^4\ mol^{-1}\,dm^3cm^{-1}$). Interferences by common foreign substances tested were found to be small. $MnTPPS_r$ gave a better result than catalase in the determination of hydrogen peroxide.

In clinical analyses, catalase has been used commonly for the determination of hydrogen peroxide released from some substances which are the target of the general clinical analyses. However, this enzyme is not stable and low reproducibility of its activity is a problem which we encounter sometimes. Attempts to develop stable and useful mimesis of catalase in the study of its model complex in solution did not give any success, for all investigations.[1-4] Previously, we have reported that some ion-exchange resins modified with metalloporphyrins (M-P resins) exhibit the catalase-like activity to accelerate the decomposition of hydrogen peroxide.[5,6] In order to apply the catalase-like activity of the M-P resins to the practical uses, we carried out the evaluation of their catalase-like activity in reaction (1) shown in Fig. 1, through the efficiency in the dye formation by reaction (2). In addition, we attempted to develop a new method for the determination of hydrogen peroxide by reactions (1) and (2) using an anion-exchange resin (Amberlite IRA 900) modified with Mn^{3+}-tetrakis(sulfophenyl)porphine ($MnTPPS_r$), which gave the highest activity.

Experimental

Material. Tetrakis(sulfophenyl)porphine (H_2TPPS), tetrakis(*p*-carboxyphenyl)porphine (H_2TCPP) and protoporphyrin (H_2PP) were purchased from Tokyo Kasei Co., Ltd., and used without further purification for the preparation of metalloporphyrins. Metalloporphyrins except for commercially available Fe^{3+}- and Cu^{2+}-chlorophyllins (M-CP) were prepared as aqueous solutions by the methods reported in the literatures.[7-10] Catalase (Type I, from beef liver) was purchased from Boeringer Co., Ltd. Other reagents were of analytical or reagent grade.

Modification of Amberlite IRA 900 with Metalloporphyrins. The resins modified with metalloporphyrins (M-P resins or $M\text{-}P_r$, subscript "r" indicates the resin modified with metalloporphyrin) were prepared by shaking 4 g of dry Amberlite IRA 900 (nitrate form) with the solutions of metalloporphyrin (100 μmol in 200 ml) in a 1 : 1 mixture of acetone and water as reported previously.[5,6] In all cases, metalloporphyrins were adsorbed on IRA 900 completely and not detected in the solution after adsorption.

The M-P resins were stable for at least one year at room temperature in the dark and the decrease of their activities was not observed.

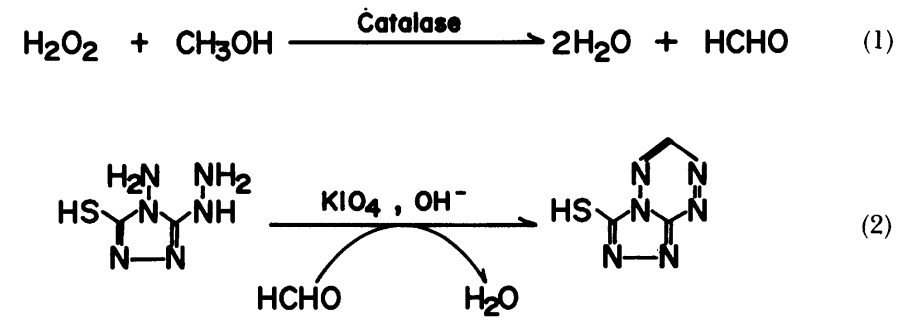

Fig. 1. Reactions.

Apparatus. The absorption spectra and the absorbances were measured on a Shimadzu UV-180 double beam spectrophotometer and a Shimadzu UV-100 spectrophotometer, respectively, with 10 mm quartz cells.

Procedure for the Examination of Catalase-Like Activity. The M-P resin was added into a mixture of hydrogen peroxide solution (0.5 ml), pH 11.0 carbonate buffer (4.0 ml, 0.2 M, 1 M=1 mol dm^{-3}) and distilled methyl alcohol (2.0 ml), and the mixture was incubated at 37 °C for 10 min. The supernatant taken (0.5 ml) was added to a mixture of 4-amino-3-hydrazino-5-mercapto-1,2,4-triazole (AHMT) solution (2.0 ml, 10 mg ml^{-1} in 0.5 M HCl) and 3 M KOH (2.0 ml), and the mixture was allowed to stand for 10 min. A solution of potassium periodate (2 ml, 0.02 M in 0.2 M KOH) was added to the mixture and the absorbance at 550 nm of the colored solution was measured against the reagent blank. The final solution corresponds to 0.888 μg ml^{-1} of hydrogen peroxide solution.

Procedure for the Determination of Hydrogen Peroxide. MnTPPS$_r$ was applied as a M-P resin to the solution of hydrogen peroxide (0.5 ml, 50—300 μg ml^{-1}, 0.296—1.776 μg ml^{-1} in the final solution) and the sample solutions were treated as described above.

Procedure for the Control Catalase Method.[11,12] A solution of hydrogen peroxide (0.1 ml, 5—60 μg ml^{-1}) was added to a mixture of 30% methyl alcohol (0.5 ml) and a solution of catalase (1.0 ml, 0.1 mg ml^{-1}) in 1/15 M phosphate buffer (pH 7.0). The mixture was incubated for 60 min at 37 °C, and 0.5 ml of the reaction mixture was taken and treated as described above.

Results and Discussion

Selection of Chromogen. In the clinical analyses, Hantzch[13] and AHMT[11] methods have been used for the determination of formaldehyde produced from methyl alcohol by reaction (1). In the present study, we selected the AHMT method, because of its higher sensitivity than that of the Hantzch method, although the reproducibility of the AHMT method was found to be a little lower in our preliminary examination by the use of standard formaldehyde solution.

Selection of Optimal Conditions. In MnTPPS$_r$, the absorbance of the dye formed from formaldehyde was the highest in the incubation for 10 min at pH 11.0 as shown in Fig. 2. The examination of the activity was carried out at pH 11.0, which seems to be the optimal pH for the catalase-like activity of these M-P resins.

Carbonate buffer gave the largest absorbance among the buffers tested, as shown in Table 1. Low activity caused by the use of glycinate buffer may be attributed to the coordinating property of glycinate ion to the central metal ion. We selected 0.2 M carbonate buffer (pH 11.0) for this study.

The activity did not vary so much at incubation temperatures from 20 to 45 °C except for MnTPPS$_r$ and CoPP$_r$. The activities of all the M-P resins were examined at 37 °C, which is also the optimal temperature for catalase, because MnTPPS$_r$ gave its highest activity at this temperature as shown in Fig. 3.

As seen in Fig. 4, reaction (1) proceeded fairly rapidly and attained its equilibrium in 10 min. It is of interest in the cases of Co- and Fe-TPPS$_r$, which

Table 1. Effect of Buffer (pH 11.0) on Absorbance[a,b]

	MnTPPS$_r$	MnTCPP$_r$	CoTPPS$_r$
Carbonate buffer	0.562 (100)	0.515 (100)	0.201 (100)
Borate buffer	0.555 (99)	0.497 (97)	0.126 (63)
Phosphate buffer	0.566 (101)	0.507 (98)	0.137 (68)
Ammonium buffer	0.525 (93)	0.442 (86)	0.150 (75)
Glycinate buffer	0.334 (60)	0.272 (53)	0.070 (35)

a) The values in parentheses indicate the ratios (%) to the values obtained by carbonate buffer. b) 150 μg ml^{-1} of H_2O_2 in the initial sample solution=0.888 μg ml^{-1} of H_2O_2 in the final solution; incubated at 37 °C for 10 min.

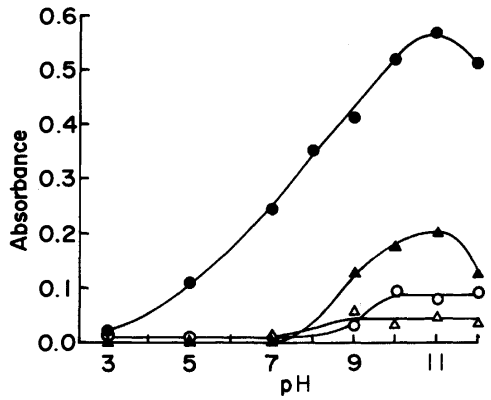

Fig. 2. Effect of pH. ●: MnTPPS$_r$, ○: FeTCPP$_r$, ▲: CoTPPS$_r$, △: H_2TPPS$_r$. Incubation temperature: 37 °C. Incubation time: 10 min.

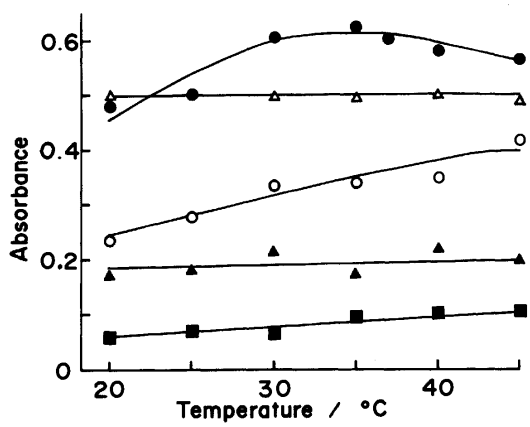

Fig. 3. Effect of temperature. ●: MnTPPS$_r$, △: MnTCPP$_r$, ○: CoPP$_r$, ▲: CoTPPS$_r$, ■: CuPP$_r$. Incubation for 10 min at pH 11.0.

exhibit a medium activity, that the amount of resulting formaldehyde did not increase in the incubation for more than 10 min, suggesting that reaction (1) comes to an end in spite of insufficient formation of the dye. We examined the activity of the M-P resins in the incubation for 10 min.

The absorbance increased in accord with the increase of the concentration of methyl alcohol as seen in Fig. 5. Pure methyl alcohol was then added in the present study, whereas 30% methyl alcohol was added in the catalase method.[11,12] Addition of methyl alcohol with high concentration caused the elution of metalloporphyrin in some cases.

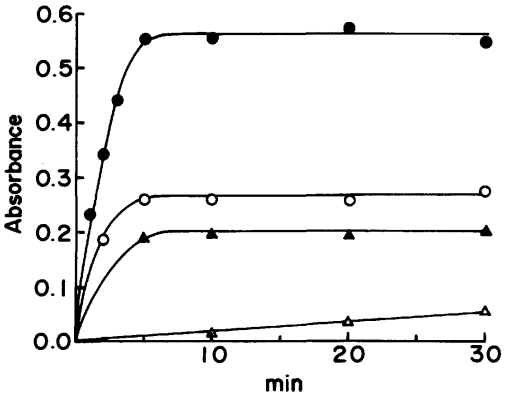

Fig. 4. Time courses. ●: MnTPPS$_r$, ▲: CoTPPS$_r$, ○: FeTPPS$_r$, △: H_2TPPS$_r$. Incubation temperature: 37°C (pH 11.0).

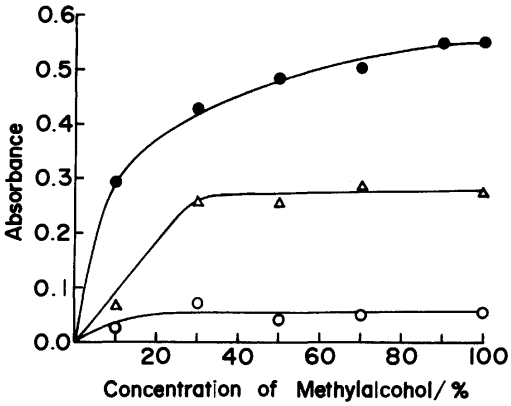

Fig. 5. Effect of concentration of methyl alcohol. ●: MnTPPS$_r$, △: FeTPPS$_r$, ○: CuTPPS$_r$. Incubation for 10 min at 37°C (pH 11.0).

Table 2. Absorbance of the Dye Formed from the Resulting HCHO by M-P Resins[a)]

Resin	Absorbance	Resin	Absorbance
MnTPPS$_r$	0.556	CuTPPS$_r$	0.030
MnTCPP$_r$	0.511	CuTCPP$_r$	0.094
MnPP$_r$	0.083*	CuPP$_r$	0.104
FeTPPS$_r$	0.276	CuCP$_r$	0.112
FeTCPP$_r$	0.082	ZnTPPS$_r$	0.034
FeCP$_r$	0.043	ZnTCPP$_r$	0.025
CoTPPS$_r$	0.202	ZnPP$_r$	0
CoTCPP$_r$	0.480	H_2TPPS$_r$	0.029
CoPP$_r$	0.398*	H_2TCPP$_r$	0.005

* A little elution of metalloporphyrin was observed.
a) 150 μg ml^{-1} of H_2O_2 in the sample solution = 0.888 μg ml^{-1} of H_2O_2 in the final solution; incubated in carbonate buffer (pH 11) at 37°C for 10 min.

Catalase-Like Activity of the M-P Resins. Table 2 represents the absorbance of the dye resulting from formaldehyde formed by the catalytic effect of the M-P resins. The resins containing Mn, Fe, and Co showed relatively high catalase-like activity, indicating that the activity seems to depend upon the presence of these metals. It is of interest that MnTPPS$_r$ exhibits the highest catalase-like activity in reaction (1) which is a kind of oxidation, similar to the case in the decomposition of hydrogen peroxide.[5] This result indicates the significance of Mn as a central atom in these reactions. Previously, we have found in the simple decomposition of hydrogen peroxide that the catalase-like activity of the resins modified with Co-porphyrins was approximately four times that of the resins modified with Fe-porphyrins.[5] In reaction (1), the activity of CoTPPS$_r$ is slightly smaller than that of FeTPPS$_r$, similar to the case of peroxidase-like activity of the M-P resins.[14] MnTPPS$_r$ is the best and is expected to be used as a mimesis of catalase in reaction (1). On the other hand, MnTPPS$_r$ exhibited the peroxidase-like

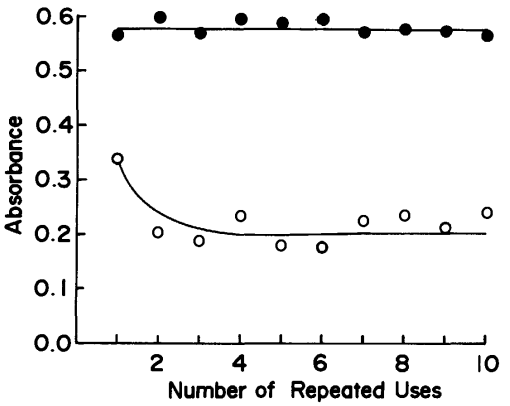

Fig. 6. Effect of repeated uses. ●: MnTPPS$_r$, ○: CoPP$_r$. Incubation for 10 min at 37°C (pH 11.0).

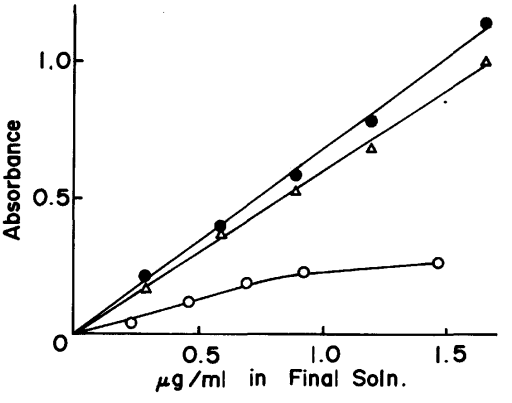

Fig. 7. Calibration curves. ●: MnTPPS$_r$, △: MnTCPP$_r$, ○: Catalase. 150 μg ml^{-1} of H_2O_2 in sample solution = 0.888 μg ml^{-1} of H_2O_2 in the final solution.

activity and the activity was the highest at around pH 7,[14] instead of pH 11 in the catalase-like activity as mentioned above. The difference of the optimal pH in these activities suggests that either catalase-like or peroxidase-like activity of the M-P resins can be utilized depending upon pH, and the mechanisms of these activities are different from each other.

Effect of Repeated Uses. In order to realize that $MnTPPS_r$ acts as a catalyst, the effect of repeated uses of $MnTPPS_r$ on the formation of formaldehyde was examined. As shown in Fig. 6, the decrease of the absorbance based on formaldehyde formed was slight in ten-times use. This result indicates that $MnTPPS_r$ acts as a catalyst like catalase in the oxidation of methyl alcohol.

Determination of Hydrogen Peroxide by the use of $MnTPPS_r$ as a Mimesis of Catalase. The calibration curve obtained by the use of $MnTPPS_r$ in place of catalase in reaction (1) is shown in Fig. 7, together with that obtained by the use of catalase as a control. Beer's law was applicable to the amount of hydrogen peroxide ranging from 0.296—1.776 $\mu g\,ml^{-1}$ in the final solution, whereas the catalase method was not applicable to the amount more than 0.80 $\mu g\,ml^{-1}$ of hydrogen peroxide, and in addition, the longer incubation time was required than $MnTPPS_r$ method. The molar absorption coefficient was $2.37\times10^4\,mol^{-1}\,dm^3\,cm^{-1}$, which is larger than twice the maximum value ($0.97\times10^4\,mol^{-1}\,dm^3\,cm^{-1}$) obtained by the control catalase method. The value of coefficient of variation (4.3%, $n=10$) was rather large in the AHMT method as pointed out above section.

Table 3. Effect of Foreign Substances[a]

Substance	μg	Error/%[b]
Heparin	500	3.5
EDTA	500	3.2
PO_4^{3-}	500	−4.9
Cl^-	500	−0.6
Ascorbic acid	500	−0.3
Na^+	500	−4.9
K^+	500	7.8
	50	−4.0
Ca^{2+}	500	0.3
Mg^{2+}	500	−17.0
	50	−3.0

a) 150 μg of H_2O_2 as the sample solution = 0.888 $\mu g\,ml^{-1}$ in the final solution; incubated in borate buffer (pH 11) at 37°C for 10 min. b) Error(%) = 100{H_2O_2(added) − H_2O_2 (found)}/H_2O_2(added).

The effect of foreign substances were summarized in Table 3. The presence of 500 μg of K^+ caused a slight increase of the absorbance and the presence of 500 μg of Mg^{2+} caused a decrease of the absorbance, but their interferences were negligible when their amounts were less than 50 μg. Any interference was not observed by other substances tested. It is noteworthy that the presence of 500 μg of ascorbic acid, which gives serious interference in the catalase method,[12] did not interfere at all in this method.

In conclusion, $MnTPPS_r$ is regarded as a good artificial mimesis of catalase, and exhibits higher sensitivity than the enzyme and hence is expected to be used practically in place of catalase or immobilized catalase for various purposes.

This work was supported in part by a Grant-in-Aid for Scientific Research from the Ministry of Education, Science and Culture.

References

1) S. B. Brown and P. Jones, *Trans. Faraday Soc.*, **64**, 999 (1982).
2) P. Waldmeier and H. Sigel, *Inorg. Chim. Acta*, **5**, 659 (1971).
3) P. Waldmeier and H. Sigel, *Inorg. Chem.*, **11**, 2174 (1972).
4) P. Jones and T. Robson, *Biochem. J.*, **135**, 353 (1973).
5) Y. Saito, M. Mifune, T. Kawaguchi, J. Odo, Y. Tanaka, M. Chikuma, and H. Tanaka, *Chem. Pharm. Bull.*, **34**, 2885 (1986).
6) Y. Saito, M. Mifune, J. Odo, Y. Tanaka, M. Chikuma, and H. Tanaka, *Reactive Polymers*, **4**, 243 (1986).
7) R. F. Pasternack, L. Francesconi, D. Raff, and E. Spiro, *Inorg. Chem.*, **12**, 2606 (1973).
8) R. F. Pasternack, P. R. Huber, P. Boyd, G. Engasser, L. Francesconi, E. Gibbs, P. Fasella, G. C. Venturo, and L. Dec. Hids, *J. Am. Chem. Soc.*, **94**, 4511 (1972).
9) A. Harriman and G. Porter, *J. Chem. Soc., Faraday Trans. 2*, **75**, 1532 (1979).
10) T. Yanetani and T. Aomura, *J. Biol. Chem.*, **244**, 4580 (1969).
11) R. G. Dickinson and N. W. Jocobson, *Chem. Commun.*, **1970**, 1719.
12) N. Kageyama, *Clin. Chim. Acta*, **31**, 421 (1971).
13) T. Nash, *Biochem. J.*, **55**, 416 (1953).
14) Y. Saito, M. Mifune, S. Nakashima, Y. Tanaka, M. Chikuma, and H. Tanaka, *Chem. Pharm. Bull.*, **34**, 5016 (1986).

 © 1987 The Chemical Society of Japan Bull. Chem. Soc. Jpn., 60, 2231—2235 (1987)

Comparison of Stability Constants of Alkaline Earth Chlorides between Conductometric and Potentiometric Studies

Hidekazu Doe,* Kenichi Wakamiya, and Toyokichi Kitagawa
Department of Chemistry, Faculty of Science, Osaka City University, Sumiyoshi-ku, Osaka 558
(Received October 3, 1986)

The stability constants of alkaline-earth metal chlorides, MCl^+ (M^{2+}=Ca, Sr, Ba), were determined by conductometric and potentiometric measurements in methanol. The conductometric study was made at 5, 15, 25, 35, and 45 °C; the potentiometric study was at 25 °C. The formation of MCl_2 was neglected in the conductometric study, while in the potentiometric study it was taken into account, though it was too slight to determine a reliable value of the stability constant of MCl_2. The stability constants of MCl^+, K_1, determined by conductometric measurements were compared with the previous conductometric results of the same metal(II) perchlorates, K_{1A}. The magnitudes of K_1 and K_{1A} increase in the orders Ca≃Sr<Ba and Ca<Sr<Ba, respectively. K_1 is larger than K_{1A} for calcium and strontium, though the K_1 and K_{1A} values for barium are similar to each other; that is, the degree of such an increase in K_{1A} is larger than that in K_1. Both enthalpy and entropy changes determined by conductometric measurements were positive for all the chlorides and perchlorates. However, the enthalpy changes of the chlorides were 1.2—1.4 times as large as those of the perchlorates. On the other hand, the K_1 from potentiometry was smaller for every chloride and also increased more steeply (in the order Ca< Sr<Ba) than that from conductometry. Therefore, the difference of K_1 between conductometry and potentiometry decreases in going from Ca to Ba.

We previously studied the stability constants of Ca(II), Sr(II), and Ba(II) chlorides in methanol with a potentiometric method.[1] Then, the K_1 of Sr(II) was about 4-times larger than those of Ca(II) and Ba(II). Regarding this abnormal results, we gave no explanation in the previous work, though we had a little doubt about the influence of impurities in the metal salts used on the stability constants. On the other hand, we were a little anxious about the accuracy of our potentiometric determination in the case of small stability constants, such as the alkaline-earth chlorides. Thus, with the main purpose of checking the abnormal result of Sr(II) chloride, we have made conductometric measurements. At the same time, the potentiometric experiment was repeated. However, the experimental method has been partly improved in order to determine the small stability constant more accurately. We also made a careful purification of the metal(II) salts, especially strontium perchlorate.

It is frequently thought that an ion pair, which is generally less stable than a highly covalent metal complex, does not exist as only one type of contact structure (contact ion pair) but also has various types of solvent-separated structures in which the cation and/or anion remain solvated (solvent-separated ion pair).[2] Therefore, in varying degrees of solvent-separation, if species detected as an ion pair vary according to experimental methods, it is natural that a different experiment yields a different stability constant of the ion pair. Being interested in the relation between ion pairing and solvation, we have carefully examined the results obtained by two quite different methods of conductometry and potentiometry in this study; the former showed an increase in the solution resistance but the latter showed a decrease in the concentration of the free anions caused by ion pairing.

Experimental

Materials. Conductometry: Calcium(II) and Strontium(II) chlorides hexahydrates were prepared by neutralizing the corresponding carbonates with hydrochloric acid and purifying by triple recrystallizations from distilled deionized-water. The calcium chloride was dried on a vacuum line over diphosphorus pentaoxide during heating under an infrared lamp for 1 day; the strontium chloride was vacuum dried in an oven over silica gel at 120 °C for 10 hours. After drying, these chlorides became nearly anhydrous salts. Barium(II) chloride anhydrous of a commercially available material (Rare Metallic, 99.99%-grade) was vacuum dried in an oven over silica gel at 120 °C for 10 h.

Potentiometry: By dissolving in perchloric acid, calcium(II) perchlorate trihydrate was prepared from calcium nitrate purified by double recrystallizations from distilled deionized-water and strontium(II) perchlorate dihydrate from strontium carbonate. The calcium perchlorate was recrystallized from distilled deionized-water and dried on a vacuum line over diphosphorus pentaoxide for 3 d and monohydrate was obtained. The strontium perchlorate was recrystallized from distilled deionized-water, and furthermore from purified methanol, and then vacuum dried in an oven over silica gel at 120 °C for 1 day and anhydrous perchlorate was obtained. Barium(II) perchlorate anhydrous (Wako, special grade) which was vacuum dried in an oven over silica gel at 120 °C for 1 day was used without any purification.

The purification of methanol has been described previously.[1,3] Stock solution of these metal(II) salts (except barium chloride) were standardized by titration with EDTA; the barium chloride stock solution was standardized by a gravimetric method.

Measurements. The detailed procedure of conductometric measurements has been described previously.[3] However, in this experiment temperatures were controlled within an accuracy of ±0.01 °C by a Neslab RTE-5 refrigerated circulating bath which was monitored by a Guildline digital platinum resistance thermometer (model 9535).

Outline of potentiometric measurements could be found in previous manuscripts.[4-6] All potentiometric measure-

ments were made at 25.0±0.1 °C, and ionic strength, I, was kept nearly constant at 0.05 M (M=mol dm^{-3}). In order to attain an accurate determination of a small K_1, measurements of the standard electromotive force, emf, were improved as follows. In the previous method, standardization was achieved by measuring the emf of a standard solution free from metal(II) ions (which were prepared aside) after every potentiometric titration was performed in the usual way. In this manner, a titrated sample solution must be replaced with a standard solution in a measuring cell when the standardization is carried out. It is possible that this displacement becomes a cause of experimental errors. In order to remove such a cause of errors, we rechecked the standard emf by measuring the emf of a solution which was prepared by the addition of an appropriate amount of metal(II) ions to the usual metal(II)-free standard solution already measured.

If K_2 is negligible relative to K_1, K_1 can be determined merely by the above standardization procedure. Using this procedure, the K_1 of Ca(II) and Ba(II) have been determined at several metal-ion concentrations, because it is assured by the previous study[1] and the present results of Sr(II) that K_2 of Ca(II), Sr(II), and Ba(II) chlorides are negligibly small.

Data Treatment

In a sample solution,

$$M^{2+} + Cl^- \rightleftarrows MCl^+ \quad (K_1) \tag{1}$$

$$MCl^+ + Cl^- \rightleftarrows MCl_2 \quad (K_2) \tag{2}$$

$$M^{2+} + ClO_4^- \rightleftarrows MClO_4^+ \quad (K_{1A}) \tag{3}$$

are major equilibria: However, the last case (Eq. 3) does not take place in the solution of conductometric measurements since no salts other than MCl_2 are contained in that solution.

Conductometry. Conductometric data were treated by a modified Fuoss and Edelson method[3] in which the equilibrium (Eq. 2) was not completely taken into account. The modified Fuoss and Edelson equation is

$$\Lambda F = \Lambda_0 - XK_1/\Lambda_0, \tag{4}$$

where

$$X = cy_{2+}\Lambda F(\Lambda F - \Lambda_0/2)$$

and

$$F = [\{1-\delta_c^{1/2}/(1+Ba I^{1/2})\}^{-1} + (\Lambda_0-\lambda_0)/2\Lambda]/\{1+(\Lambda_0-\lambda_0)/2\Lambda_0\}.$$

Here, Λ and Λ_0 are the molar and the limiting molar conductances of $1/2MCl_2$, respectively. λ_0 and c are the limiting molar conductance of Cl^- and the total concentration of Cl^-, respectively. Onsager's slope divided by Λ_0 is δ. The ion activity coefficient of M^{2+}, y_{2+}, was calculated by the Debye-Hückel second approximation:

$$\log y = -Az_i^2 I^{1/2}/(1+Ba I^{1/2}), \tag{5}$$

where a is an ion-size parameter which has been 5 Å (for Sr^{2+} and Ba^{2+}) or 6 Å (for Ca^{2+}). The ionic strength, I, is 1.5 times as large as the total concentration of Cl^-, c.

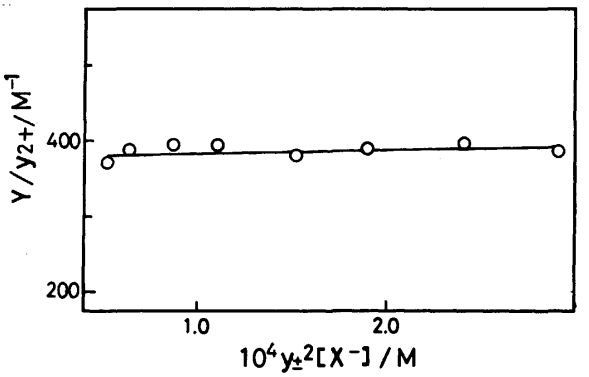

Fig. 1. The plot according to Eq. 6 for strontium chloride. $C°_M$=8.072×10^{-3} M, $C°_I$=0.035 M.

Potentiometry. Our latest treatment of potentiometric data was previously described in detail.[4] According to the treatment,

$$Y/y_{2+} = K_1 + 2K_1K_2(y_\pm^2[X^-]), \tag{6}$$

where

$$Y = (C°_X - [X^-])/([M^{2+}][X^-]),$$

is a key equation. Here, $C°_X$ is the total concentration of NaCl and $y_\pm$ is the ion activity coefficient of a monovalent ion which has been calculated by Eq. 5 at a=4 Å. In the present study, X^- is Cl^-. In order to plot Y/y_{2+} against $y_\pm^2[Cl^-]$, it is necessary to calculate the $[M^{2+}]$, $[Cl^-]$, and y's. The detailed procedure of the calculation could he found in a previous manuscript.[4]

If K_2 is negligible relative to K_1, we can determine the K_1 value from the data of a change in $[Cl^-]$ caused by the addition of M^{2+}, $C°_X$-$[Cl^-]$, and $[M^{2+}]$ after the M^{2+}-addition, which are obtained by the preceding standardization of emf.

Results and Discussion

Conductometry. From plots according to Eq. 3, Λ_0 and K_1 were determined (Tables 1 and 2). In the tables, K_{1A} of perchlorate salts is included; however, these values were determined by the recalculation of previous data[7] in the modified Fuoss and Edelson method. The difference between the modified and original Fuoss and Edelson methods was discussed in a previous manuscript.[3] Lee and Wheaton studied Ca, Sr, and Ba chlorides in methanol by using their original conductance equation; according to their results at 25 °C, K_1 were 410±2.6, 425±4.3, and 430±7.7 M^{-1} for Ca, Sr, and Ba, respectively (Λ_0 were 110.0, 112.2, and 112.9 S cm^{2}mol^{-1}, respectively).[8] Pethybridge recalculated these values using the data and calculation of Lee-Wheaton; K_1 were 450, 393, and 480 M^{-1} for Ca, Sr, and Ba, respectively.[9] In spite of our quite different data treatment, our K_1 are in relatively good agreement

Table 1. Limiting Molar Conductances ($S cm^2 mol^{-1}$) of $1/2MCl_2$ and $1/2M(ClO_4)_2$ in Methanol at 278.15—318.15 K

M(II)	278.15K	288.15K	298.15K	308.15K	318.15K
			MCl_2		
Ca	81.6±0.1	95.1±0.1	109.9±0.1	126.3±0.2	144.2±0.2
Sr	84.7±0.2	98.9±0.2	114.5±0.2	131.7±0.3	150.0±0.4
Ba	85.2±0.2	99.5±0.2	115.3±0.2	132.6±0.3	151.7±0.3
			$M(ClO_4)_2$[a]		
Ca	99.0±0.3	114.9±0.3	132.1±0.3	150.7±0.4	171.5±0.4
Sr	95.8±0.2	111.3±0.3	128.0±0.3	146.4±0.4	166.9±0.6
Ba	101.6±0.3	118.1±0.3	135.7±0.4	154.7±0.5	176.1±0.6

a) Recalculated from the previous data (Ref. 6) by the modified Fuoss and Edelson method.

Table 2. Stability Constants of MCl^+ and $MClO_4^+$, K_1 and K_{1A} (M^{-1}), in Methanol at 278.15—318.15 K

M(II)	278.15K	288.15K	298.15K	308.15K	318.15K
			MCl^+		
Ca	253± 7	309± 8	408± 7	549± 8	758±10
Sr	249±10	313±11	403±12	534±13	715±19
Ba	275± 8	353± 9	464±11	623±12	863±16
			$MClO_4^+$[a]		
Ca	173±10	209±11	254±12	309±12	386±14
Sr	227±10	277±11	345±12	430±15	551±21
Ba	293±13	363±15	451±17	562±20	717±24

a) Recalculated from the previous data (Ref. 6) by the modified Fuoss and Edelson method.

Table 3. Thermodynamic Functions of the Formation of MCl^+ and $MClO_4^+$ at 298.15 K

M(II)	$\Delta H_1^\ominus$	$\Delta S_1^\ominus$	$-\Delta G_1^\ominus$
	$kJ mol^{-1}$	$JK^{-1} mol^{-1}$	$kJ mol^{-1}$
		MCl^+	
Ca	20.6±0.5	119±2	14.90±0.04
Sr	19.7±0.8	116±3	14.87±0.07
Ba	21.2±0.6	122±2	15.21±0.06
		$MClO_4^+$	
Ca	14.8±1.1	96±4	13.72±0.11
Sr	16.4±0.9	104±3	14.49±0.09
Ba	16.5±0.9	106±3	15.15±0.10

with theirs. The λ_o of Cl^- is 52.35 $S cm^2 mol^{-1}$ at 25 °C.[10] The other λ_o, which have been evaluated proportionally to the λ_o of ClO_4^- in methanol.[3,7] are 39.5, 45.7, 59.8, and 67.9 $S cm^2 mol^{-1}$ at 5, 15, 35, and 45 °C, respectively.

According to the familiar Gibbs-Helmholtz equation, thermodynamic functions have been determined at 25 °C (Table 3). The results of perchlorates are also listed there for reference. The shapes of $\ln K_1$ vs. T^{-1} plots for the chloride systems were strikingly identical to those for the perchlorate systems, which were slightly concave downward (Fig. 2 in Ref. 7).

On the basis of previous discussions,[3,7] we wil give some explanations for the next two problems: 1) Why K_1 is larger than K_{1A} at Ca and Sr whereas those are similar to each other at Ba and 2) why both $\Delta H_1^\ominus$ and $\Delta S_1^\ominus$ of chlorides are larger than those of perchlorates. Relating to the problems, there are the following properties of M^{2+}, Cl^-, and ClO_4^- in methanol: a) The solvation of M^{2+} becomes strong in the order of Ba< Sr<Ca.[7] b) The solvation of Cl^- seems to be stronger than that of ClO_4^-, because of $\lambda_o(Cl^-)<\lambda_o(ClO_4^-)$: the hydration free energies, $\Delta G_h^\ominus$, of Cl^- and ClO_4^- are −317 and −190 $kJ mol^{-1}$, respectively.[11] c) The degree of covalency in MCl_2 bonding is in the order of Ca> Sr>Ba and the binding energy of MCl_2 is also in the same order in gas phase.[12] d) Cl^- has a greater preference for covalent bonding than ClO_4^-, because almost all metal perchlorates seem to be very unstable in solutions even if these metals are typical soft acids.[13]

As an important remark, here we propose from the previous discussion concerning the solvent-separated ion pair[7] that ion pairs separated with over one methanol molecule of solvent contribute little to their stabilities; that is, in this system we just consider the coexistence of ion pairs from a directly contacted one to a solvent-separated one with one methanol molecule though the two extremes may be major species on a time-average. Consequently, it means that anion (Cl^- or ClO_4^-) solvation is forced to reduce considerably by ion pairing since anion solvation is very weak relative to divalent cation solvation. This must be a direct cause of problem 2), because of property b).

Using property a), we previously explained why the stability of the perchlorate, K_{1A}, is of the order Ca< Sr<Ba.[7] That explanation can be simply summarized as: In the case that a cation is solvated more weakly than a certain limit, the cation forms a more stable ion

pair as the cation solvation becomes weaker. Examining problem 1) under the consideration of property d), we infer that the above rule regarding the stability of an ion pair depending on its cation solvation is more pronounced for an ion pair having a higher ionic bonding. Strictly speaking, since the bonding nature of Ba (Ba is the most ionic metal of them; Property c)) is so ionic, that Property d) has little effect on the stability constsnts. Hence, K_1 and K_{1A} are similar to each other for Ba. However, because, as shown in the binding energies of chlorides in gas phase, K_1 probably gains some larger contribution from covalency in $CaCl^+$ and $SrCl^+$ bonding than from that in $BaCl^+$ bonding (Property c)), the difference of K_1 and K_{1A} increases for Ca and Sr. Thus, problem 1) can be well explained by Properties a), c), and d).

Potentiometry. Since the slopes of plots according to Eq. 6 were very gentle (Fig. 1), K_2 of Sr was so small relative to K_1 that it was impossible to make an accurate determination of K_2. The K_1 values are summarized in Table 4; here the conductometric results at 25 °C are also listed. Only the reference a-value of Ca is 6 Å;[6,14] however, the stability constants calculated at a=5 Å are also indicated in the table in order to check the contribution of a to the results. According to the results, the values at a=5 Å are lower by 3% for conductometry and higher by 3.5% for potentiometry than those at a=6 Å. These differences will probably have little importance in our present discussion and, thus, even in comparison with their standard deviations.

Before the potentiometric and conductometric results are compared, we must explain the discrepancies between the previous[1] and present potentiometry results. In our potentiometry, stability constants are determined by measuring the concentration of free anions ($[Cl^-]$ in this study) which remain after combining with M^{2+}. Therefore, some metal compounds as impurities which form very stable chloride compounds have a considerably large influence on potentiometric data, even if the amount is so small that there is no problem in conductometric experiments. In fact, a measurement using a metal perchlorate of insufficient purification yielded a large stability constant; furthermore, the obtained stability constants varied with the total metal concentration, $C°_M$. Thus, the previous abnormally large K_1 of $SrCl^+$ was probably caused by some metal impurities. It is sure that the present K_1 of $CaCl^+$ and BaCl have also gained a higher reliability than the previous ones due to the experimental improvement.

Table 4. Comparison of Stability Constants between Potentiometry and Conductometry at 298.15 K

	a/Å	K_1/M^{-1} Poten.	K_1/M^{-1} Conduc.	K_{1A}/M^{-1} Conduc.
Ca	6	288± 8	408± 7	254±12
	5[a]	298± 8	398± 8	245±12
Sr	5	343±27	403±12	345±12
Ba	5	399±27	464±11	451±17

a) Calculated to know the effect of a.

As shown in Table 4, K_1 from potentiometry is smaller than that from conductometry for all the metals. This is a cause for neglecting K_2 in conductometry, though it may have only a negligibly small effect. That is to say, if the formation of MCl_2 is not taken into account in the data treatment, K_1 is evaluated to a higher value by a decrease in conductance caused by the MCl_2 formation than would be expected.

Regarding K_1(potentiometry)<K_1(conductometry), there is another general explanation which was slightly mentioned in the introduction: Simply expressed, a different measurement yields a different result. With this simple explanation our discussion may come to the end; however, it would be interesting to discuss the result that the difference in K_1 between conductometry and potentiometry increases in going from Ba to Ca. At least, here, we will be able to infer that the Ag-AgCl electrode responds to the Cl^- which weakly binds to M^{2+}, where the weak ion pair works to reduce the net conductance a little. That is, there is a weak ion pair which is potentiometrically detected as being dissociated, but conductometrically as being associated. Therefore, K_1(potentiometry)<K_1(conductometry). According to the previous discussion,[7] on the other hand, $CaCl^+$ is probably separated by solvent molecules more strongly than $BaCl^+$ because of the strong solvation and small K_1 of Ca^{2+} compared to Ba^{2+}. That is, Cl^- enters into the solvation shell of Ba^{2+} more deeply than into that of Ca^{2+}. Therefore, it is inferred that the fraction of weak ion pairs which may be detected as dissociated by other experimental methods is larger for Ca than for Ba. Consequently, if the solvent-separated species take a larger part of properties relating to ion pairing (that is, if the ion solvation is stronger and the stability of an ion pair is smaller) such an investigated system will have a higher possibility of yielding different results from other measurements.

This study has been partially supported by a Grant-in-Aid for Scientific Research from the Ministry of Education, Science and Culture.

References

1) H. Doe, A. Matsuda, and T. Kitagawa, *Bunseki Kagaku*, **33**, E511 (1984).

2) B. E. Conway, "Ionic Interactions and Activity Behavior of Electrolyte Solutions," in "Comprehensive Treatise of Electrochemistry," ed by B. E. Conway, J. O'M. Bockris, and E. Yeager, Plenum Press, New York (1983), Vol. 5, Chap. 2, p. 195.

3) H. Doe and T. Kitagawa, *Bull. Chem. Soc. Jpn.*, **58**, 2975 (1985).

4) H. Doe, K. Wakamiya, C. Yoshida, H. Ozaki, K. N. Soe, and T. Kitagawa, *Inorg. Chem.* in press.

5) H. Doe, A. Shibagaki, and T. Kitagawa, *Inorg. Chem.* **22**, 1639 (1983).
6) H. Doe and T. Kitagawa, *Inorg. Chem.*, **21**, 2272 (1982).
7) H. Doe, T. Kitagawa, and K. Sasabe, *J. Phys. Chem.*, **88**, 3341 (1984).
8) W. H. Lee and R. J. Wheaton, *J. Phys. Chem.*, **82**, 605 (1978).
9) A. D. Pethybridge, *Z. Physik. Chem. Neue Folge*, **133**, 143 (1982).
10) C. F. Mattina and R. M. Fuoss, *J. Phys. Chem.*, **79**, 1604 (1975).
11) H. Ohtaki, M. Tanaka, and S. Funahashi, "Yoekihanno-no-Kagaku," Gakkai-syuppan-center, Tokyo (1977), pp. 215, 216; D. R. Rosseinsky, *Chem. Rev.*, **65**, 467 (1965).
12) R. G. Pearson, H. B. Gray, *Inorg. Chem.*, **2**, 358 (1963).
13) R. M. Smith and A. E. Martell, "Critical Stability Constants," Plenum Press, New York (1976), Vol. 4; J. J. Christensen and R. M. Izatt, "Handbook of Metal Ligand Heats and Related Thermodynamic Quantities, 3rd Ed.," Marcel Dekker, New York (1983).
14) J. Kielland, *J. Am. Chem. Soc.*, **59**, 1675 (1937).

Hydrogenation of Carbon Monoxide over Solid Catalysts Dispersed in the Liquid Medium. I. Slurry-Phase Fischer-Tropsch Synthesis with Supported Ruthenium Catalysts

Kaoru FUJIMOTO* and Masahiko KAJIOKA
Department of Synthetic Chemistry, Faculty of Engineering, The University of Tokyo, Hongo, Bunkyo-ku, Tokyo 113
(Received October 31, 1986)

Fischer-Tropsch synthesis on supported ruthenium catalysts were operated successfully in the slurry phase, using ethyl cyclohexane solvent, in spite of the high selectivity of waxy products. Titania, fumed silica, and Nb_2O_5 were found to be excellent carriers for ruthenium. A Ru/SiO_2 catalyst yielded a hydrocarbon product with the rate as high as 600 mg(g-cat)$^{-1}$h^{-1} at 240 °C and 40 bar. The optimum metal loading was 2% by weight. Calcination of the catalyst precursor at 300 °C or above caused a marked decrease in the metal dispersion, which was essential for the high catalytic activity and chain-growth ability. The maximum chain-growth probability obtained on a calcined Ru/Al_2O_3 catalyst was 0.94.

Fischer-Tropsch synthesis (F-T synthesis), which produces hydrocarbon mixtures from synthesis gas, is one of the most promising coal liquefaction processes. Usually, the reaction is an exothermic reaction, which generates the heat from 54 to 39 kcal (1 cal_{th}=4.184 J) per mole of CO depending on the product. Therefore, it is quite important, in order to conduct the reaction on a large scale, to remove the heat of reaction effectively from the catalyst bed and to maintain its temperature at the suitable level. Typical reactor systems of the F-T synthesis are a multi-tube fixed bed reactor, a fluidized bed reactor, an ebulating bed reactor, and a slurry bed reactor. The multi-tube fixed bed reactor and the fluidized bed reactor are now in commercial operations.

The slurry bed reactor system was postulated and developed by Koelbel et al. since 1935.[1,2] The process utilizes fine powdery catalysts dispersed in a mineral oil medium, whereinto synthesis gas is fed in the bubble form to carry out the reaction. The characteristic features of the slurry bed reactor are: (1) The reactor structure is quite simple; (2) the removal of reaction heat can be effectively carried out to attain quite a flat temperature profile in the reactor;[2] and (3) it has no wax trouble because the high-boiling product on the catalyst surface is quickly removed by being dissolved into the liquid medium. Thus, the slurry-phase system is thought to be the most economical F-T synthesis reactor system.[3]

Almost all of the works on the slurry-phase F-T synthesis have been carried out by using precipitated iron catalyst or fused iron catalyst. In the present work the activities and selectivities of supported ruthenium catalysts were studied in the slurry-phase in comparing with the gas-phase reaction.

Experimental

Catalyst Preparation and Characterization. Several kinds of alumina were used as carrier materials in this study. γ-Al_2O_3-A (220 m^2g^{-1}) was prepared by hydrolyzing aluminium isopropoxide and calcining in air at 600 °C for 3 h. γ-Al_2O_3-B was a commercially available one (Tokai Konetsu, TKS-99651, 300 m^2mg^{-1}, and γ-Al_2O_3-C (Aerosil Al_2O_3-C, 100 m^2g^{-1}) was obtained from Japan Aerosil Co. γ-Al_2O_3-D was also a commercially available one (Sunbead AN, 340 m^2g^{-1}), γ-Al_2O_3-E (JRC-ALO-3, 123 m^2g^{-1}) and γ-Al_2O_3-F (JRC-ALO-4, 177 m^2g^{-1}) were obtained from Japan Catalyst Society. α-Al_2O_3 was a commercially available one (Tokai Konetsu, TAS-90337, <1 m^2g^{-1}). Other carrier materials than alumina were Aerosil SiO_2, Davison ID SiO_2, TiO_2, Nb_2O_5, ZrO_2, and Th_2O_5. These materials were commercially available ones and were already used by the present authors as carrier materials of ruthenium for the vapor-phase F-T synthesis.[5] Supported ruthenium catalysts were prepared by impregnating carrier materials with $RuCl_3 \cdot 3H_2O$ from its aqueous solution, drying up at 100 °C and then drying overnight at 120 °C in an air oven. The catalyst precursors thus obtained were ground to fine powders (under 150 mesh), calcined if needed, and then activated by reducing in flowing hydrogen at 150 °C for 1 h and 400 or 450 °C for 2 h in series. After the activation, the catalyst was directly introduced in the solvent which had been deoxygenated by bubbling CO_2 for 30 min, and then introduced into the F-T synthesis reactor as a slurry.

The dispersion of ruthenium metal was determined by means of CO chemisorption. Chemisorption was measured at room temperature by using a flow-through cell connected to a glass vacuum system. Catalyst samples were first activated in flowing hydrogen in situ, at 150 °C for 1 h and at 450 °C for 2 h, and then evacuated at 450 °C for 2 h. Chemisorption of CO was determined as the difference between the first isotherm and the second isotherm which was measured following the evacuation for 30 min at room temperature after the measurement of the first isotherm. The metal dispersion was calculated assuming one CO molecule was chemisorbed by one surface ruthenium atom.

Apparatuses and Procedures of Synthesis Gas Reaction and Analysis. The flow sheet of the reaction system is shown in Fig. 1. Synthesis gas reactions were conducted in a stainless steel autoclave reactor (volume 100 cm^3). Only gaseous substances were treated in a flow system, and the gas flow from the reactor was kept at 50 cm^3min^{-1} under the standard temperature and pressure. The effluent from the reactor was withdrawn in the gaseous state through a heated pressure regulator and analyzed by gas chromatographs. Most of the solvent and produced hydrocarbons were refluxed while small parts of product hydrocarbon and solvent came out of the reactor with the unreacted synthesis gas.

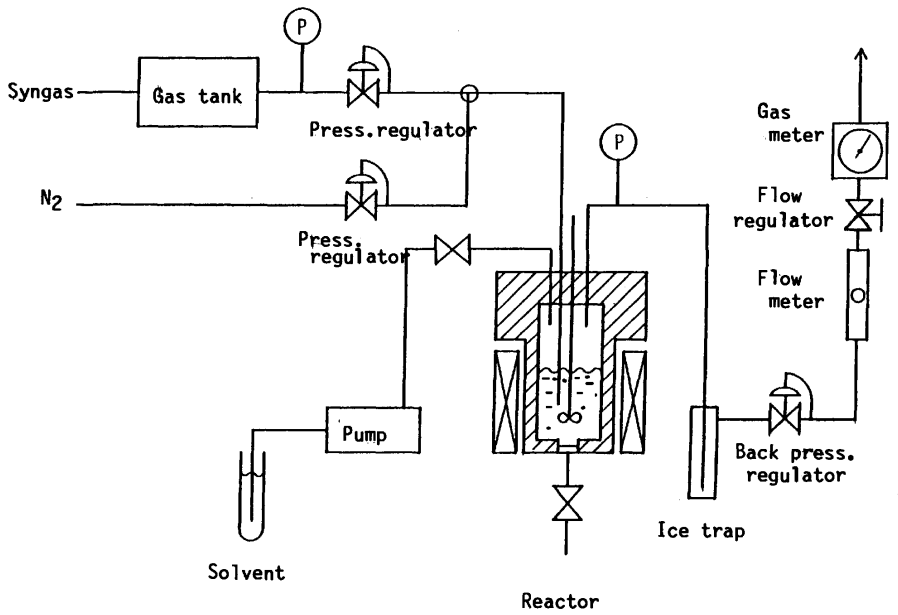

Fig. 1. Reaction apparatus for slurry-phase Fischer-Tropsch synthesis.

The volume of solvent (ethylcyclohexane) was 30 cm^3 and from 2 to 3 gram of catalyst was used for the reaction depending on its catalytic activity. The reaction pressure indicates the total pressure at the reaction temperature, including the vapor pressure of the solvent (about 10 bar). Synthesis gas was introduced from a cylinder through an activated carbon column. Activities and selectivities of the supported ruthenium catalysts were measured mainly under the following conditions: 240 °C, 40 bar, $H_2/CO=2$, and 4 h of reaction, and then the average formation rate of hydrocarbons and the hydrocarbon distribution were calculated.

Gaseous compounds were analyzed on line by gas chromatographs. CO, CH_4, and CO_2 were analyzed by an activated charcoal column using a TCD detector. Light hydrocarbons (C_1—C_6) were analyzed by a Porapak Q column using a FID detector. Liquid products dissolved in the solvent were analyzed after the reaction was over. Hydrocarbons with 2 to 21 carbon atoms were analyzed with a Silicone SE-30 column and hydrocarbons with 11 to 45 carbon atoms were analyzed with a Dexsil 300 GC column, respectively. Eicosane (n-$C_{20}H_{42}$) was used as an internal stan-dard material and a FID detector was used in each analysis

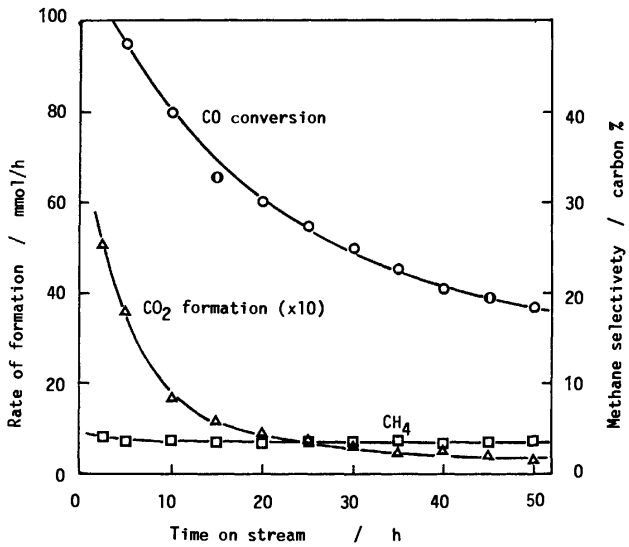

Fig. 2. Changes in the catalytic performance of a Ru/Al_2O_3 catalyst. 2 wt% Ru/γ-Al_2O_3-E, 400 °C calcined, temperature: 240 °C, pressure: 40 bar, H_2/CO: 2/1(mole ratio).

Results and Discussion

Catalyst Durability. In Fig. 2 are shown the changes in the rate of CO conversion, methane selectivity, and the rate of CO_2 formation for the synthesis gas reaction on a 2 wt% Ru/TiO_2 catalyst. It is clear that the catalytic activity (the rate of CO conversion) decreased constantly over 50 h of reaction. However, the methane selectivity was almost constant, irrespective of the catalytic activity. Although the reason of the decrease in the activity is not clear yet, it might be attributed to the coverage of ruthenium surface by carbon, as suggested by the marked decrease in the CO_2 formation, which should be attributed partly to the disproportionation of CO ($2CO \rightarrow C+CO_2$).

Effect of Carrier Materials. Tables 1 and 2 show the activities (formation rates of hydrocarbons and CO_2) and the selectivities (hydrocarbon distribution) of the slurry-phase F-T reaction using supported ruthenium catalysts which loaded 2 wt% ruthenium as metal. Most of the hydrocarbons were normal paraffins, and small amounts of isoparaffins and olefins were also produced. Formations of aldehydes and alcohols were quite small (less than 0.1% selectivity). The hydrocarbon distribution was well-simulated by the Anderson-Schulz-Flory (A-S-F) equation as demonstrated in Figs. 3 and 4. The plot is obviously divided into two straight lines. This fact has been observed also in the vapor-phase reaction, which has

Table 1. Activity and Selectivity of Supported Ruthenium Catalysts[a)]

Carrier	Dispersion	Formation rate		Product distribution/C-wt%					Chain-growth probability	
	%	H.C.[b)]	CO_2[c)]	C_1	C_2—C_4	C_5—C_{10}	C_{11}—C_{20}	C_{21}+	α_{15}+	α_{16}−
Aerosil SiO_2	26	626	0.92	8.8	8.6	27.0	30.0	25.7	0.89	0.93
TiO_2	88	350	3.06	9.1	17.1	30.3	26.5	17.0	0.86	0.92
Nb_2O_5	22	275	0.49	7.2	7.7	19.0	30.3	35.8	0.89	0.92
Aerosil-Al_2O_3	61	207	0.51	15.3	19.6	39.2	16.6	9.3	0.76	0.91
ZrO_2	10	172	0.42	8.5	9.5	21.6	36.1	24.3	0.92	0.92
γ-Al_2O_3-A	72	129	1.32	6.3	13.7	32.3	25.0	22.7	0.74	0.90
Ta_2O_5	10	86.8	0.29	12.5	12.4	21.0	21.7	32.5	0.85	0.93

a) 2 wt% loading of Ru; reaction temperature 240°C; total pressure 40 bar; $H_2/CO=2/1$ (mole ratio). b) mg-hydrocarbon $g^{-1}h^{-1}$. c) mmol-CO_2 $g^{-1}h^{-1}$.

Table 2. Activity and Selectivity of Alumina-Supported Ruthenium Catalysts[a)]

Carrier	Formation rate		Product distribution/C-wt%					Chain-growth probability	
	Hydrocarbon[b)]	CO_2[c)]	C_1	C_2—C_4	C_5—C_{10}	C_{11}—C_{20}	C_{21}+	α_{15}−	α_{16}+
γ-Al_2O_3-A	129	1.32	6.3	13.7	32.3	25.0	22.7	0.74	0.90
γ-Al_2O_3-B	23.5	0.21	31.9	31.9	22.3	10.3	3.6	0.55	0.88
γ-Al_2O_3-C	207	0.51	15.3	19.6	39.2	16.6	9.3	0.76	0.90
γ-Al_2O_3-D	190	0.55	10.8	14.6	35.3	23.9	15.4	0.82	0.91
γ-Al_2O_3-E	209	0.75	11.1	17.9	30.9	19.8	20.4	0.78	0.92
γ-Al_2O_3-F	232	0.99	12.5	17.1	35.0	21.0	14.4	0.77	0.90
α-Al_2O_3	16.8	0.05	21.7	25.7	28.3	16.5	7.8	0.78	0.88

a) 2 wt% loading of Ru; reaction temperature 240°C; total pressure 40 bar; $H_2/CO=2/1$ (mole ratio). b) mg-hydrocarbon $g^{-1}h^{-1}$. c) mmol-CO_2 $g^{-1}h^{-1}$.

been most likely attributed to the wide distribution of ruthenium particles.[7)]

As shown in Table 1 and Figs. 3 and 4, the activities and/or selectivities of the catalysts are markedly different from one another depending on the kind of the carrier materials even if they load the same amount of ruthenium. Especially, the ruthenium supported on TiO_2, Aerosil SiO_2 and Nb_2O_5 showed the high activities and the high chain-growth abilities when they

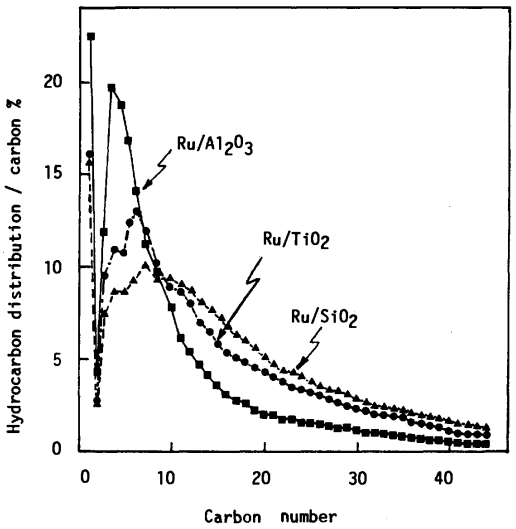

Fig. 3. Hydrocarbon distribution of the products on supported ruthenium catalyst. 2 wt% Ru on carriers, temperature: 240°C, pressure: 40 bar, H_2/CO: 2/1 (mole ratio).

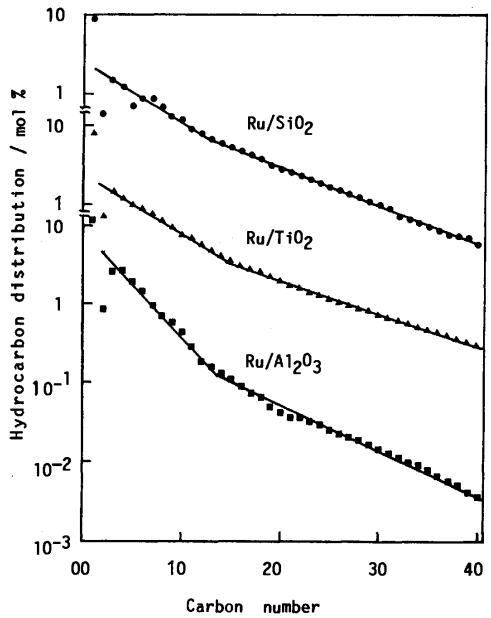

Fig. 4. Anderson-Schulz-Flory plot of the products. The same experiment as in Fig. 3.

were reduced without any pretreatment. This is the same trend which has been observed in the vapor-phase reaction over the same catalyst.[3)] It should be also noted that the Ru/TiO_2 catalyst made more CO_2 than other catalysts. The formation of CO_2 could be attributed mostly to the CO shift reaction of the product water. The high CO shift activity of the Ru/TiO_2 catalyst has been already reported by Kikuchi et al.[8)]

The high abilities of C-C chain growth of the Nb_2O_5-, ZrO_2-, and Ta_2O_5-supported catalysts have been observed also in the vapor-phase reaction.[7] As has been reported by us, the ruthenium particles with low dispersion are suitable for the production of high-molecular-weight hydrocarbons. The ruthenium dispersions on the carrier materials mentioned above are all lower than 20% (Table 1). Thus, their high chain-growth ability should be cased by the low dispersion of ruthenium particles.

The data in Table 2 shows that both the activity and selectivity vary with the kinds of the alumina carriers. Especially, the Ru/γ-Al_2O_3-B catalyst showed an extraordinary low activity and a low chain-growth ability. It could be attributed to sulfur-poisoning effect, because the carrier material which was prepared from aluminum sulfate contained SO_4^{2-} (about 2 wt%) and the sulfate ion is converted to hydrogen sulfide during the hydrogen treatment to poison the ruthenium. Although the reason why the chain-growth probability on the γ-Al_2O_3-B is lower than other alumina-supported ruthenium catalyst is not clear yet, the phenomenon itself is similar to that of a sulfur-poisoned cobalt catalyst,[9] Other γ-Al_2O_3-supported catalysts exhibited the similar activity and selectivity except the γ-Al_2O_3-based catalyst. Its reason will be discussed in the later chapter.

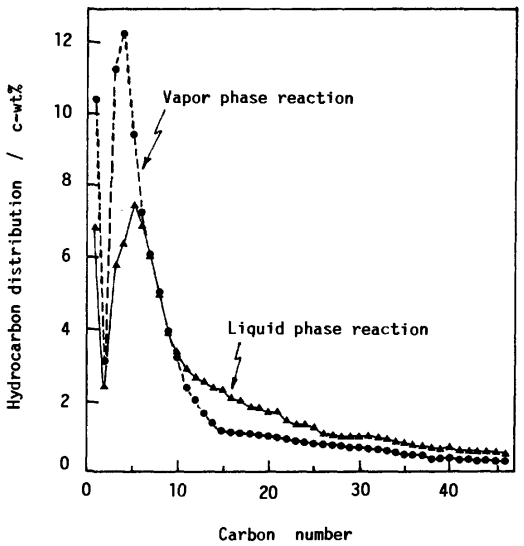

Fig. 5. Hydrocarbon distribution of the products from the vapor-phase reaction and the slurry-phase reaction. 2wt% Ru/TiO_2; noncalcined, temperature: 230°C (vapor phase); 240°C (slurry phase), pressure: 20 bar (vapor phase); 40 bar (slurry phase), H_2/CO: 2/1 (mole ratio).

In Fig. 5 are compared the difference in the hydrocarbon distribution between the products from the vapor-phase reaction and those from the liquid-phase reaction using the same catalyst. Obviously, the product from the vapor-phase reaction is rich in lower hydrocarbons. However, the degrees of chain-growth probability of both systems are very close, for example α_{15-} and α_{16+} are 0.72 and 0.88 for the vapor-phase reaction and 0.80 and 0.92 for the liquid-phase reaction. The higher selectivity of the high-molecular weight fraction in the liquid-phase reaction should be attributed to the fact that the higher fraction stays in the reactor and might grow further, whereas the lower fraction comes out of the reactor quickly.

Preparative Factors Which Control Catalytic Features. a. Metal Lording: As shown in Table 3, the rate of hydrocarbon formation increases with the increase in the metal loading on the catalyst weight base, while the dispersion of ruthenium decreases monotonously with increasing metal loading. It should be noted that the specific activity of ruthenium (the rate of hydrocarbon formation per unit weight of ruthenium) increases with increasing metal loading up to 2 wt%. It could be attributed to the decrease in the ruthenium dispersion. As previously reported by the present authors,[7] the catalytic activity of a low-dispersion-catalyst increases almost proportionally to the operating pressure up to 20 bar or higher in the vapor-phase reaction, while that of a high-dispersion catalyst levels off at 6 bar or lower. Thus, under the present reaction conditions where the operating pressure is 40 bar, the specific activity of the low-dispersion catalyst is higher than that of the high-dispersion catalyst.

Another charateristic feature wnich should be noted is that the chain-growth probility increased with the increase in the metal loading up to 2 wt% as shown in Table 3 and Fig. 6. This phenomenon is also attributable to their metal dispersions. It has been demon-

Table 3. Catalytic Features of Titania-Supported Ruthenium Catalysts[a]

Loading	Dispersion	Rate of formation		TOF[d]	Product distribution/C-wt%					Chain-growth probability	
wt%	%	H.C.[b]	CO_2[c]	$10^{-3}s^{-1}$	C_1	C_2—C_4	C_5—C_{10}	C_{11}—C_{20}	C_{21+}	α_{15-}	α_{16+}
0.2	87	9.8 (4.9)[e]	2.0	13	20.5	23.9	24.7	21.1	9.7	0.62	0.87
0.5	88	16.2 (3.2)	0.9	8	19.9	31.1	31.4	12.5	5.1	0.70	0.86
1.0	83	70.9 (7.1)	2.9	20	17.8	28.6	29.2	19.1	4.8	0.64	0.85
2.0	55	318 (16.0)	3.1	67	9.1	9.1	26.5	29.0	26.3	0.85	0.92
4.0	46	480 (12.0)	1.6	63	9.9	13.9	29.4	22.4	24.4	0.83	0.93

a) Reaction temperature 240°C; total pressure 40 bar; H_2/CO=2/1 (mole ratio). b) mg-hydrocarbon $g^{-1}h^{-1}$. c) mmol-CO_2 $g^{-1}h^{-1}$. d) Turnover frequency. e) g-hydrocarbon (g-Ru)$^{-1}h^{-1}$.

strated by several research groups that the chain growth probability on supported ruthenium catalysts increases with the decrease in the ruthenium dispersion.[7,10,11] However, the change of metal loading is less effective in changing its activity and selectivity than the air calcination treatment, which has been pointed out in the vapor-phase reaction[7] and also will be discussed in the later chapter of this report. It could be explained in terms of two reasons. One is that the change in the dispersion level with the change in the loading is not so remarkable as that of air calcination. For example, the dispersion of a 4 wt% Ru/TiO_2, which has the lowest dispersion (46%), is about half of the dispersion of a 0.2 wt% Ru/TiO_2 (88%), which has the highest dispersion, whereas the dispersion level of a 2 wt% Ru/γ-alumina decreases from 72 to 12% with the rise in the calcination temperature from 120 to 400 °C. The present authors have pointed out that the turnover frequency (TOF) and the chain-growing ability of a supported ruthenium catalyst are markedly promoted when the average dispersion of ruthenium particles (measured by CO chemisorption) is less than about 20%.[7] Another is a more important reason that the particles of ruthenium metal formed by the conventional impregnation method have a wide distribution in size.[2] Thus, the unlcined catalyst should have much small particles as well as large particles as demonstrated by an A-S-F plot of the product with a winding point (Fig. 6). As the result, the characters of large particles should be diluted by those of small particles.

b. Air Calcination: It is possible to change the activity and selectivity of the supported catalysts by means of air calcination before hydrogen reduction.[3,4] In Table 4 and Fig. 7 are shown the dispersion, the catalytic activity, the TOF, and the product selectivity of the 2 wt% Ru/γ-Al_2O_3 catalysts which have been

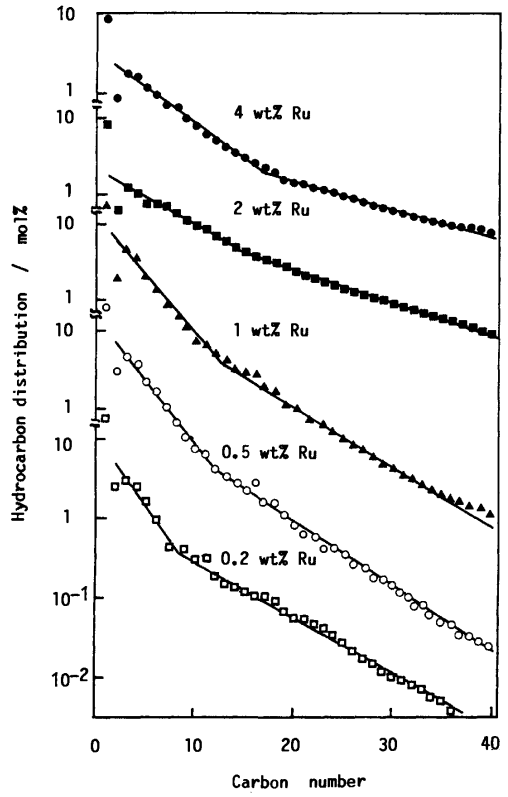

Fig. 6. Effect of metal loading on the hydrocarbon distribution of titania-supported ruthenium catalysts. The same reaction conditions as in Table 3.

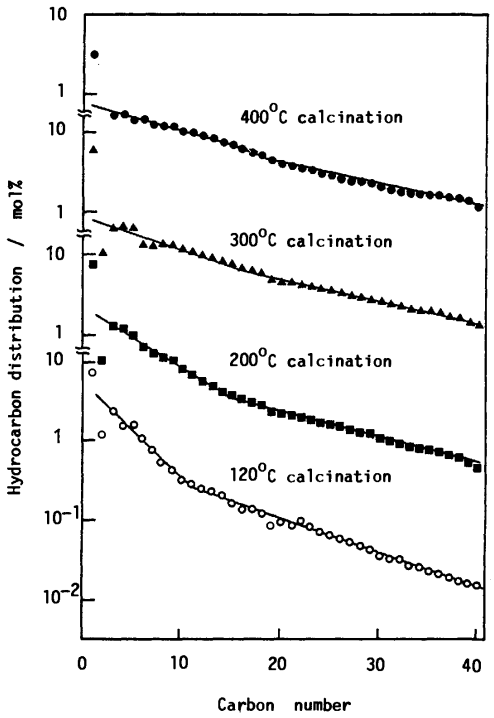

Fig. 7. Effect of calcination temperature on the hydrocarbon distribution of γ-alumina-supported ruthenium catalysts. 2 wt% Ru/γ-Al_2O_3-A, The same reaction conditions as in Table 4.

Table 4. Effect of Air Calcination on Physical and Catalytic Properties of γ-Alumina Supported Ruthenium Catalysts[a]

Calcination temperature	Rate of formation		Dispersion	TOF[d]	Product distribution/C-wt%					Chain-growth probability	
°C	H.C.[b]	CO_2[c]	%	$10^{-3}s^{-1}$	C_1	C_2—C_4	C_5—C_{10}	C_{11}—C_{20}	C_{21+}	α_{15-}	α_{16+}
120	129	1.32	72	25	6.3	13.7	32.3	25.0	22.3	0.74	0.91
200	227	1.75	78	40	7.6	9.8	23.9	26.2	32.6	0.86	0.93
300	250	0.77	36	98	5.9	5.0	17.1	30.0	42.0	0.91	0.94
400	218	0.37	12	246	3.2	4.1	17.6	31.6	43.5	0.93	0.94

a) 2 wt% loading of Ru; reaction temperature 240 °C; total pressure 40 bar; $H_2/CO=2/1$ (mole ratio). b) mg-hydrocarbon $g^{-1}h^{-1}$. c) mmol-CO_2 $g^{-1}h^{-1}$. d) Turnover frequency.

calcined in air at temperatures from 120 to 400 °C before reduction. The rate of hydrocarbon formation was promoted twice by calcining the virgin catalyst at 200 °C. Also the TOF was increased from 25×10^{-3} to 40×10^{-3} s^{-1} by calcining at 200 °C. Above 200 °C, the rate of hydrocarbon formation per unit weight of ruthenium is almost constant irrespective of the calcination temperature up to 400 °C. However, the TOF increased from 40×10^{-3} to 246×10^{-3} s^{-1} as the calcination temperature was increased from 200 to 400 °C. Concerning the product selectivity, the rate of CO_2 formation decreased and the chain growth-probability of the product was increased as the calcination temperature was increased. It should be attributed to the fact that the ruthenium dispersion decreased from 79 to 12% as the calcination temperature was increased from 200 to 400 °C. Also, it means that the surface character was changed as the ruthenium dispersion decreased.

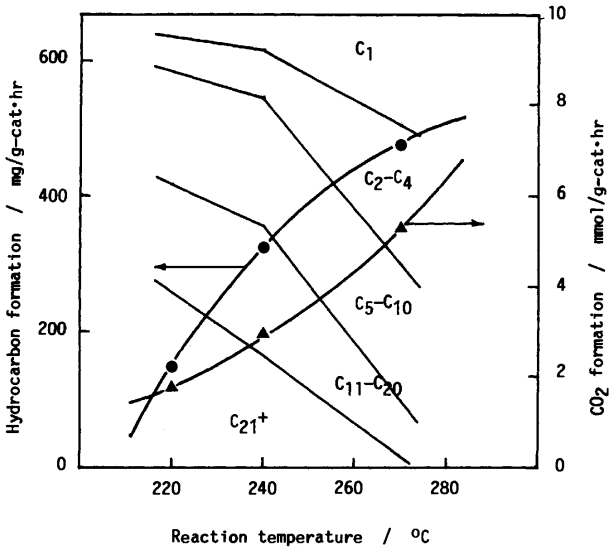

Fig. 8. Temperature effects on the slurry-phase Fischer-Tropsch synthesis on a 2wt% Ru/TiO_2 (non-calcined) catalyst. Pressure: 40 bar, H_2/CO: 2/1 (mole ratio).

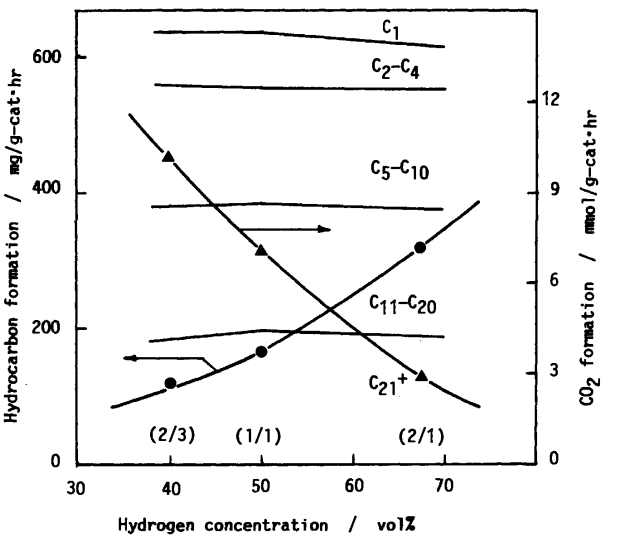

Fig. 9. Effects of feed gas composition on the slurry-phase Fischer-Tropsch synthesis on a 2wt% Ru/TiO_2 (noncalcined) catalyst. Temperature: 240 °C, pressure: 40 bar. Figures in parenthesis express the H_2/CO mole ratio in the feed gas.

Effect of Operating Factors on the Activity and Selectivity. Reaction Temperature: As is shown in Fig. 8, the rate of hydrocarbon formation on the Ru/TiO_2 catalyst was increased with increasing reaction temperature from 220 to 270 °C. The observed apparent activation energy for the hydrocarbon formation was about 12 kcal mol^{-1}. The rate of carbon dioxide formation was also increased with the rise of the reaction temperature, most likely due to the increase in the rate of water-gas shift reaction. In regard to the hydrocarbon distribution, the fraction of low-boiling hydrocarbons (C_1—C_4, especially methane) was increased drastically, which resulted in the change of the chain-growth probability (α) from 0.81 (220 °C) to 0.66 (270 °C).

H_2/CO Ratio of Feed Gas: Figure 9 also shows the effect of the H_2/CO ratio of the feed gas under the standard total pressure (40 bar). With the decrease in the H_2/CO ratio (2/1 to 2/3), the rates of hydrocarbon formation was decreased. These results are quite reasonable because the reaction rate on the ruthenium catalyst is usually first-order with respect to the partial pressure of hydrogen and zero or negative order with respect to the partial pressure of carbon monoxide[13] and because the solubility of either hydrogen or carbon monoxide in the solvent follows the Henry's law. As shown in Fig. 9, the hydrocarbon distribution obtained on a TiO_2-supported ruthenium catalyst was scarcely affected by the H_2/CO ratio. This result is in contrast to the characters on iron catalyst,[14] cobalt,[15] and ruthenium catalysts[16] in the vapor-phase reaction, which are markedly affected by the H_2/CO ratio. The fact that the hydrocarbon distribution is hardly affected by the H_2/CO ratio in the feed gas is one of the special features of the liquid-phase F-T synthesis with supported ruthenium catalysts, which should be studied further.

Conclusion

Highly active and selective ruthenium catalysts for Fischer-Tropsch synthesis were prepared by impregnating $RuCl_3$ on TiO_2, Nb_2O_5, or SiO_2 and then reducing in flowing hydrogen or by impregnating $RuCl_3$ on sulfur free γ-Al_2O_3, calcining at 300 °C or above, and then reducing. They were favorably used in the slurry-phase reaction.

The slurry-phase Fischer-Tropsch synthesis showed characters which was substantially similar to those of the vapor-phase reaction, but produced higher hydrocarbons with higher selectivity. However, no wax trouble was encountered under any conditions. The most effective condition could be chosen for the liquid

hydrocarbon synthesis. For instance, the highest selectivity of kerosene and gas oil (C_{11}—C_{20} hydrocarbons) calculated from the Anderson-Schulz-Flory distribution is 32.5% (α=0.87), while their highest selectivity value, 31.6%, was obtained in this study when the 2 wt% Ru/γ-Al_2O_3-A catalyst calcined in air at 400 °C was used with no troubles in spite of the high wax (C_{21}^+) selectivity, 43.5%.

Financial support by the Grant-in-Aid for Energy Research from the Ministry of Education, Science and Culture is greatly acknowledged.

References

1) H. Koelbel, P. Ackerman, and F. Engerhardt, *Erdoel Kohle*, **9**, 153, 225, 303 (1956).
2) H. Koelbel and M. Ralek, *Catal. Rev. Sci. Eng.*, **21**, 225 (1980).
3) M. L. Riekena, A. G. Vickers, E. C. Haun, and R. C. Koltz, *Chem. Eng. Prog.*, April 86 (1982).
4) C. C. Hall and D. Gall, *J. Inst. Petrol.*, **38**, 845 (1952).
5) T. Kunugi, T. Sakai, and N. Negishi, *J. Jpn. Petrol. Inst.*, **11**, 636 (1968).
6) M. Sclesinger, M. Crowel, and M. Leva, *Ind. Eng. Chem.*, **43**, 1474 (1951).
7) K. Fujimoto, T. Nobusawa, T. Fukushima and H. Tominaga, *Bull. Chem. Soc. Japan.*, **58**, 3164 (1985).
8) E. Kikuchi, H. Nomura, M. Matsumoto, and Y. Morita, *App. Catal.*, **7**, 1 (1983).
9) R. J. Madon and H. Shaw, *Catal. Rev.-Sci. Eng.*, **15**, 69 (1977).
10) C. S. Kellner and A. T. Bell, *J. Catal.*, **71**, 288 (1981).
11) R. C. Everson, K. J. Smith, and E. T. Woodburn, *Proc. Int. Mtg. S. Afr. Inst. Chem. Eng.*, (1980).
12) J. R. Anderson, "Structure of Metallic Catalysts," Academic Press (1975).
13) M. A. Vannice, *Catal. Rev. Sci. Eng.*, **14**, 153 (1976).
14) M. E. Dry, *Catalysis*, **1**, 159 (1981).
15) K. Fujimoto, H. Saima, and H. Tominaga, *J. Jpn. Petrol. Inst.*, **26**, 258 (1983).
16) F. S. Karn, J. F. Shultz, and R. B. Anderson, *Ind. Eng. Chem., Prod. Res. Dev.*, **4**, 265 (1965).

Direct Determination of Absolute Light Intensity in UV-Transmitting and UV-Dispersive Fluoro Polymer Tubes

Hitoshi FUNAYAMA* and Takuo SUGAWARA†

Department of Industrial Chemistry, Akita National College of Technology, 1-1 Bunkyo-cho, Iijima, Akita 011
†Department of Chemical Engineering for Resources, Mining College, Akita University, 1-1 Gakuen-cho, Tegata, Akita 010

(Received November 25, 1986)

To determine the absolute light intensity (including the reflective, scattered, and incident light intensity) in a UV-transmitting and UV-dispersive fluoro polymer tube, a new chemical actinometer, DPOF system, was introduced which was composed of dilute potassium tris(oxalato)ferrate(III), 0.03 mol m^{-3}; 1,10-phenanthroline, 0.135 mol m^{-3}; and potassium oxalate, 1.5 mol m^{-3}. The overall light intensity was determined with a simple procedure based on a precise analysis of the photochemical kinetics of a DPOF system. The absolute intensities at 366 nm in the UV-transmitting and UV-dispersive Teflon FEP and Folaflon PVdF tubes were detected to be higher than that in a fused-silica tube of similar size while the incident light intensities in the former tubes were always lower than that in the latter. In addition, the dispersive effect of a Teflon FEP tube was rather independent of the wall thickness and the tube diameter under the experimental conditions studied, owing to its high dispersibility of light. The dispersive effect was much more remarkable for the Folaflon PVdF tube. The property of light transmission with dispersion, with the characteristic of antifouling, would make the fluoro polymer tubes useful for novel photoreactors in various areas.

Photoreactions offer promising new processes for synthesis, conservation, and energy conversion. Sterilization by means of irradiation with ultraviolet rays(UV-sterilization process), for example, has recently attracted the attention not only of the pharmaceutical, biological and medical fields, but also the hygienic and electronic engineering fields concerning the antibacterial pretreatment.[1] The UV-sterilization may well be expected to play an important role in the future. However, UV-sterilizers and conventional photochemical reactors have an intrinsic problem in that they generally need restricted reactor-wall materials which are light-transmitting and resistant to fouling. In addition, a precise estimatiom of the light intensity is required for a design and performance evaluation for high quality-control standards. Even though it is permissible to estimate the incident intensity with the use of a conventional potassium tris(oxalato)ferrate (III) chemical actinometer[2] for a photoreactor with negligible reflection and dispersion, it is generally inconvenient to apply the system to other types of photoreactors which have considerable light reflection and dispersion at the reactor wall.[3] The estimation of light intensity is the characteristic and principal parameter required for the design of photoreactors (as stated above); thus, information concerning both hardware and software has long been desired. These include information concerning of new materials, other than fused-silica glass for the reactor wall, which are light-transmitting and resistive to fouling, and of new chemical actinometer system which readily determines the number of reflective and dispersive as well as the incident photons.

In the 1970's it was discovered that some fluoro polymers transmitted ultraviolet light and were stable under long-term irradiation.[4] In 1984, Funayama and coworkers developed a new chemical actinometer[5] (DPOF sysyem, named after the initial letters of dilute, potassium, oxalato, and ferrate) which detects the reflective and dispersive light as well as the incident absolute intensity in any type of photoreactor. The DPOF system has also the characteristic that the analytical procedure is very simple: the extent of conversion can be spectrophotometrically determined without any additional treatment for the reaction product. In the present paper, we determined the absolute light intensity at 366 nm in two kinds of UV-transmitting and UV-dispersive fluoro polymer tubes, compared with that in a fused-silica tube, with the use of the newly developed DPOF chemical actinometer to get fundamental information of novel wall-materials for photoreactors.

Experimental

Materials. All chemicals used were of special reagent grade distributed by Nakarai Chem. Co. Solutions were prepared with distilled and deionized water. Fluoro polymer tubes and sheets made of copolymer of tetrafluoroethylene with hexafluoropentene (denoted as Teflon FEP afterwards) and poly(vinylidene fluoride) (denoted as Folaflon PVdF afterwards) were supplied by Chiyoda Kohan Co. and Showa Denko Co., respectively.

DPOF Chemical Actinometer. The composition of DPOF chemical actinometer is listed in Table 1, as introduced in a previous paper.[5] The stoichiometry of this actinometer, Eq.1, holds in the photolysis of dilute potassium tris(oxalato)ferrate(III) (species A) aqueous solution with 1,10-phenanthroline (species B, denoted as phen afterwards), and potassium oxalate (species S), based on a preliminary

Table 1. Composition of DPOF Chemical Actinometer

Component	C_{j0} / mol m^{-3}
A : $K_3Fe(C_2O_4)_3$	0.03
B : 1,10-Phenanthroline(phen)	0.135
R : $Fe(phen)_3C_2O_4$	0.0
S : $K_2C_2O_4$	1.5

study[6] of the interaction of potassium tris(oxalato)ferrate(III) with phen and potassium oxalate:

$$A + 3B \longrightarrow R + (3/2)S + I_g. \quad (1)$$

Here, species R and I_g represent iron(II)oxalate-phen complex and carbon dioxide, respectively. Kinetics were examined at the wavelength 366 nm with the use of the apparatus combined with the batch-photochemical reactor and the spectrophotometric system which was a part of the stopped flow unit (as discussed in a previous paper).[5] The observed overall rate for reactant species A is

$$(-r_A) = 2\phi_1 I_a C_A/(C_A + k), \quad (2)$$

where ϕ_1, I_a, and k represent the primary quantum yield of DPOF chemical actinometer, the absorbed light, and the ratio of the rate constants of elementary two steps, respectively. Equation 2 holds for any light field irradiated from an arbitrary direction. When we use the DPOF system with a negligible optical thickness (within a few centimeters for the case of irradiation at 366 nm), we can obtain the overall light intensity I_1 in a general form,[5] as

$$I_1 = \{K(1/Z_A - 1) - \ln Z_A\}/(K_1'\theta), \quad (3)$$

where Z_A and θ represent the unconverted fraction of species A and the irradiation time, respectively. Values of K_1' and K, or ϕ_1 ($=K_1'/(2\alpha_A)$) and $k(=KC_{A0})$, experimentaly determined by changing the temperature from 20 to 40 °C are summarized in Fig. 1, (α_A and C_{A0} mean molar absorption coefficient and initial concentration of species A, respectively).

Experimental Apparatus and Procedures. To determine the absolute light intensity in fluoro polymer tubes, the monochromatic and parallel light of a 100 mm circular beam at 366 nm was irradiated on a sample tube by means of a parallel light irradiation unit L_1 (Ushio Electric Co., UI-501C) and a monochromator M_0 (JASCO, CT-25N) as shown in Fig. 2. The light source used was a 500 W superhigh-pressure mercury lamp(Ushio, USH-500D). The absolute light intensity (including the reflective and dispersive as well as incident light) was determined with the use of the DPOF chemical actinometer. On the other hand, the incident light intensity was determined with the use of the Parker's chemical actinometer.[2] The concentration of reaction product, iron(II)oxalate-phen complex, for the both chemical actinometers was quantitatively determined at the wavelength of 510 nm with the use of spectrophotometer (JASCO, UVIDEC-510). A neutral filter was used to change the radiant intensity. All of the procedures were carried out in a dark and constant-temperature room at 25 °C.

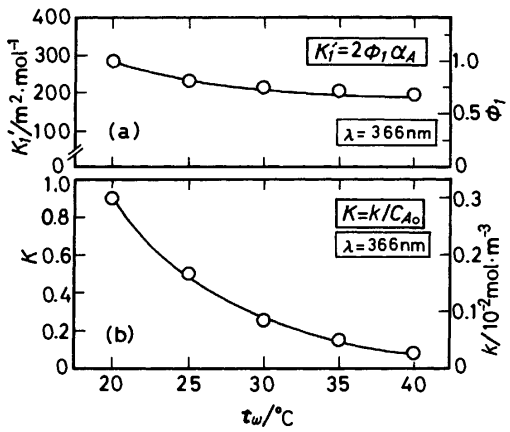

Fig. 1. Effect of temperature on (a) K_1' or ϕ_1, and (b) K or k for the irradiation at 366 nm.

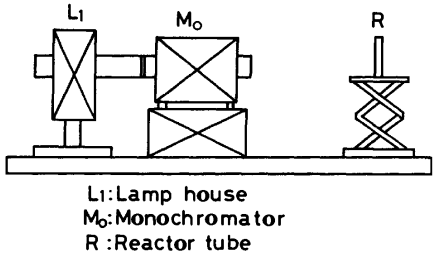

Fig. 2. Experimental apparatus for the measurement of overall and incident intensities in fluoro polymer tubes at 366 nm.

Results and Discussion

Light-Dispersibility of Fluoro Polymer Tubes. Figure 3 shows a spectral distribution of light transmitted through fluoro polymer films, where the transmitted intensity measured with a spectrophotometer (JASCO, UVIDEC-510) was restricted to a narrow beam in order to exclude most of the scattered light. We may well conclude from the figure that fluoro polymer is not as good a material as quartz for transmitting ultraviolet light, especially at shorter wavelengths. However, these fluoro polymer tubes are highly light-dispersive compared with a fused-silica tube as shown for the sample of a Teflon FEP tube in Fig. 4. The light-scattering patterns in a fused-silica tube and a fluoro polymer tube are schematically illustrated in Fig. 5. Figure 5(b) shows a more remarkable dispersion of light inside a fluoro polymer tube than a fused-silica tube in Fig. 5(a). We could not determine

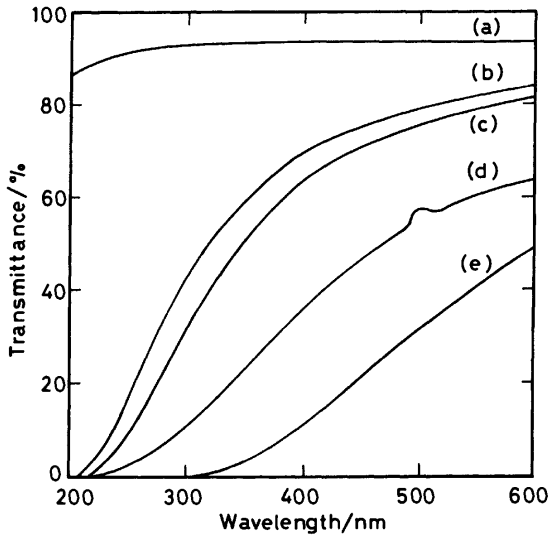

Fig. 3. Spectral distribution of light transmitted through a fluoro polymer film. (a) Fused-silica(thickness 1.0 mm), (b) Teflon FEP 1000 A(0.25), (c) Teflon FEP 1400 A(0.35), (d) Folaflon PVdF(1.0), (e) Teflon FEP 6000 L(1.75).

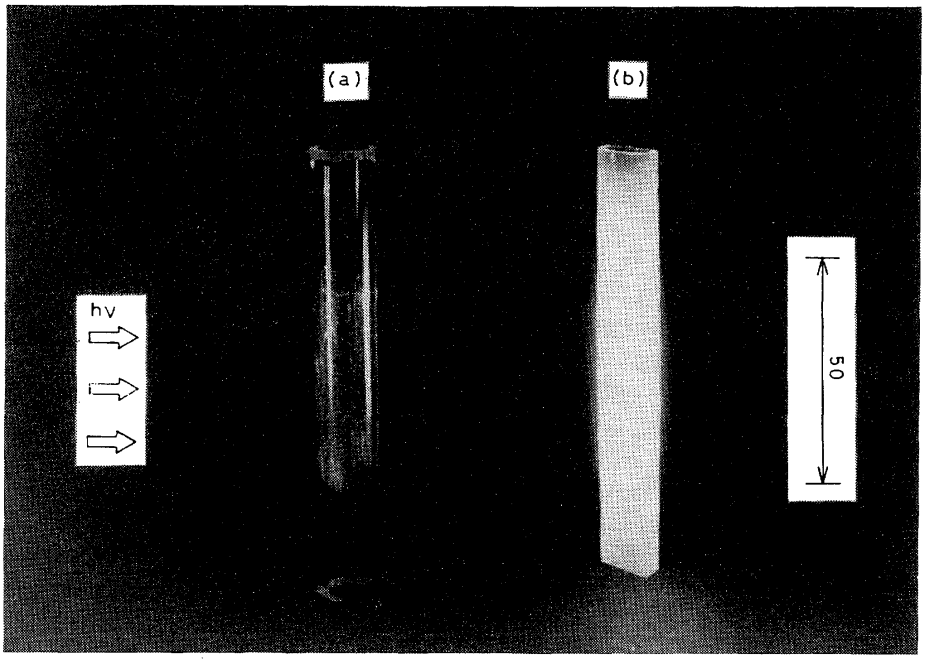

Fig. 4. Fused-silica tube (a) and Teflon FEP tube (b) irradiated with the parallel light from a superhigh-pressure mercury lamp.

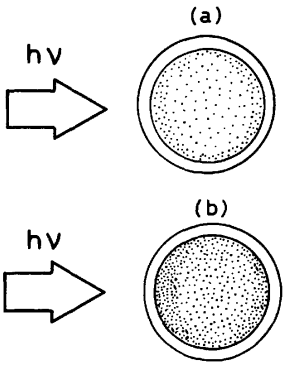

Fig. 5. Illustration of light-scattering pattern in a fused-silica (a) and a fluoro polymer tube (b).

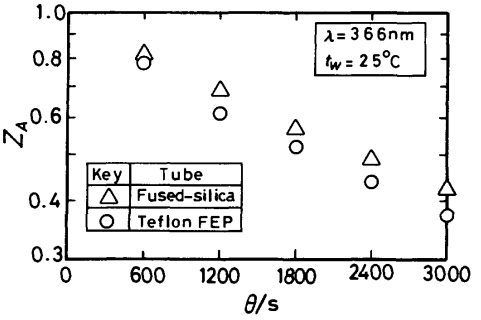

Fig. 6. Actinometry with the use of DPOF chemical actinometer in a fused-silica tube and a Teflon FEP tube having the same inside and outside diameters (10 mm×12 mm).

the absolute overall light intensity in this type of highly light-dispersive tube without the use of such a chemical actinometer as the DPOF system which detects reflective and dispersive as well as incident photons.

Determination of the Absolute UV-Intensity Involving the Effect of Dispersion. The overall light intensity, I_1, is obtained by substituting the relation of the fraction of A unconverted Z_A and irradiation time θ, and the values of K_1' and K into Eq. 3. An example of the experimental results of actinometry with the use of DPOF chemical actinometer is shown in Fig. 6. The figure indicates that the absolute light intensity I_1 is higher in a Teflon FEP tube than in a fused-silica tube having the same inside and outside diameters.

Determination of Incident UV-Intensity. The incident UV-intensity was determined with the use of conventional Parker's actinometer system. A batch analysis with the monochromatic irradiation (Fig. 7) gives

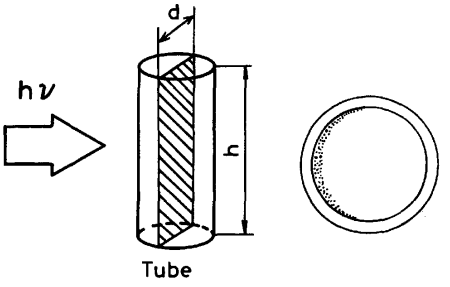

Fig. 7. Determination of incident intensity I_0 and illustration of light absorbed pattern.

Eq. 4 for the performance of the reaction

$$\phi_0 I_a = (S/V)\phi_0 I_0\{1-\exp(-\mu_l l)\} \fallingdotseq (S/V)\phi_0 I_0 \quad (\mu_l l \gg 1), \tag{4}$$

where $S(=h\cdot d)$, $V(=h\cdot \pi d^2/4)$, and ϕ_0 denote the irradiation area, the reaction volume, and the quantum yield of Parker's actinometer, respectively. The term,

$\mu_l l$, represents the optical thickness. The incident photons are perfectly absorbed near the incident wall under the condition of the conventional actinometry: $\mu_l l \gg 1$ as illustrated in Fig. 7. The incident light intensity I_0 was evaluated using

$$I_0 = \frac{(h \cdot \pi d^2/4)}{(h \cdot d)} \cdot \frac{1}{\phi_0} \cdot \frac{dC_R}{d\theta} = \frac{\pi d}{4} \cdot \frac{1}{\phi_0} \cdot \frac{C_R}{\theta}. \quad (5)$$

An example of the experimental results for the actinometry with the use of Parker's actinometer is shown in Fig. 8 for the same sample tubes as shown in Fig. 6. The figure indicates that the incident intensity I_0 is higher in a fused-silica tube than in a Teflon FEP tube having the same inside and outside diameters.

Absolute Light Intensity in Fluoro Polymer Tubes. A comparison of the overall intensity I_1 obtained from Fig. 6 through Eq. 3 and the incident intensity I_0 from Fig. 8 through Eq. 5 tells us that Teflon FEP is a UV-transmitting and highly UV-dispersive material: the characteristics of light scattering can be evaluated well by means of the DPOF actinometry by comparing it with the conventional Parker's actinometry (as discussed above). Table 2 shows an example of the data for the overall light intensity I_1 and the incident light intensity I_0 in both the Teflon FEP and the Folaflon PVdF tubes compared with those in a fused-silica tube as a reference. Three levels of incident intensity were achieved by means of the neutral filter (as mentioned in the experimental section).

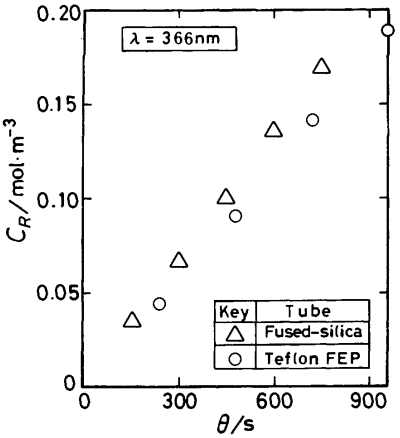

Fig. 8. Actinometry with the use of Parker's chemical actinometer in a fused-silica tube and a Teflon FEP tube having the same inside and outside diameters.

As for the case in the Teflon FEP tube, the overall light intensity I_1, is higher than in a fused-silica tube although Fig. 3 indicates the transmitted light apparently decreases to a considerable degree at 366 nm. In addition, it is noticeable that I_1 seems to be independent of the wall thickness and the tube diameter for the Teflon FEP tube. As for the Folaflon PVdF tube, the overall light intensity I_1 can also be inferred to be higher than that in a fused-silica tube of similar size, whereas it becomes lower as the wall gets thicker. The incident intensity I_0 in both the Teflon FEP and the Folaflon PVdF tubes is always lower than that in a fused-silica tube.

The characteristics of light transmission and dispersion of crystalline fluoro polymer are, in general, closely related to the crystallinity of polymer itself; the transmittance decreases with increasing crystallinity while dispersibility increases with it. First of all, from a comparison of the incident intensity I_0 in a Teflon FEP tube with that in a fused-silica tube having the same inside and outside diameters (Table 2), it is suggested that the crystallinity of fluoro polymer caused the decrease in transmittance in the former tube. Second, the fact that the overall intensity I_1 in a Teflon FEP tube is higher than that in a fused-silica tube whould indicate that the effect of dispersibility exceeds the effect of the decrease in the transmittance in the Teflon FEP tube. As for the Folaflon PVdF tubes, the effect of the decrease in transmittance owing to the crystallinity becomes more remarkable as the wall becomes thicker. Although the absolute values of data shown in Table 2 may slightly change with the sample tube selected, they would reflect the optical characteristics of fluoro polymer in general.

Figure 9 shows a comparison of the relative light intensities for the Teflon FEP and Folaflon PVdF tubes. The relative intensity in the fluoro polymer tubes studied is always higher than that in a fused-silica tube referred. It is remarkable that these effects seem to be practically independent of the wall thick-

Table 2. Overall Light Intensity I_1 and Incident Intensity I_0 in Fluoro Polymer Tubes at 366 nm Compared with Those in a Fused-Silica Tube

Tubes	Inside diameter	Wall thickness	I_1	I_0
	mm	mm	10^{-6} mol m^{-2} s^{-1}	
Teflon FEP	10	1.0	2.65	1.30
	10	0.5	2.51	1.35
	6	1.0	2.59	1.20
Fused silica	10	1.0	2.20	1.59
Folaflon PVdF	10	2.0	6.68	2.51
Fused silica	10	1.0	6.17	4.48
Folaflon PVdF	26	3.5	7.42	3.15
Fused silica	10	1.0	9.79	7.42

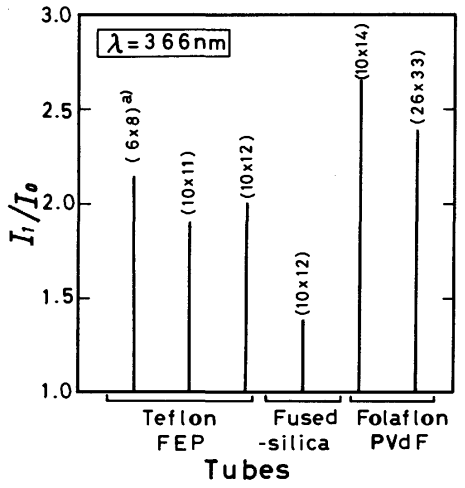

Fig. 9. Comparison of the relative light intensity in light dispersive fluoro polymer tubes.
(a) Inside diameter (mm)×outside diameter (mm).

ness and the tube diameter for a Teflon FEP tube under the experimental conditions studied. As for the Folaflon PVdF tube, the dispersive effect is much more considerable. Considering the observed results above, we conclude that UV-scattering effect is remarkable in these kinds of fluoro polymer tubes. The property of light transmission with dispersion, with the characteristic of antifouling, would make the fluoro polymer tubes useful for novel photoreactors in various areas.

Conclusion

To determine the reflective and scattered as well as the incident light intensity in UV-transmitting and UV-dispersive fluoro polymer tubes, a new chemical actinometer, the DPOF system, was introduced which was composed of dilute potassium tris(oxalato)ferrate, 0.03 mol m^{-3}; 1,10-phenanthroline, 0.135 mol m^{-3}; and potassium oxalate, 1.5 mol m^{-3}. The overall light intensity at 366 nm was determined with a simple procedure at 25 °C, based on the precise photochemical kinetics of the DPOF system.

The overall light intensities in UV-transmitting and UV-dispersive fluoro polymer tubes, Teflon FEP and Folaflon PVdF, were always higher than that in a fused-silica tube of similar size, although the transmitted light through the film apparently decreased to a considerable degree when observed with a restricted narrow beam. The incident intensity in the fluoro polymer tubes was always lower than that in a fused-silica tube. As for the Teflon FEP tube, the overall light intensity was practically independent of wall thickness and the tube diameter under the condition studied. The dispersive effect is much more remarkable for the Folaflon PVdF tube.

The authors wish to express their thanks to Associate Professor Nobumichi Ohno of Akita National College of Technology for his helpful discussion on the crystallinity of fluoro polymer. The present work was partially supported by a Grant-in-Aid for Scientific Research (59750752) from the Ministry of Education, Science and Culture. They would like to thank Chiyoda Cohan Co. for its financial assistance and offer of Teflon FEP tubes and sheets. Appreciation is also for Showa Denko Co. for the supply of Folaflon PVdF tubes and sheets. The assistance of student colleagues in Akita National College of Technology (Messrs. Hitoshi Kato, Yasumi Kaneya, Masayuki Watanabe, Shunji Tashiro, Katsuhiko Kikuchi, Akira Hashimoto, and Yoshikazu Yachi) is also appreciated.

References

1) J. E. Cruver, 25th Great Plains Wastewater Design Conference, Omaha, March 1981; T. Sugawara, H. Ohashi, H. Funayama, and K. Nakano, AIChE 1984 Annual Meeting, San Francisco, Octobor 1984, Abstr., No. 50f.

2) C. A. Parker, *Proc. R. Soc. London, Ser. A*, **220**, 104 (1953)

3) H. Funayama, K. Ogiwara, T. Sugawara, and H. Ohashi, *Kagaku Kogaku Ronbunshu*, **10**, 534 (1984)

4) A. Landry, U. S. Patents. 3634025 and 3700406 (1972)

5) H. Funayama, K. Ogiwara, T. Sugawara, and H. Ohashi, *Kagaku Kogaku Ronbunshu*, **10**, 446 (1984)

6) H. Funayama, K. Ogiwara, T. Sugawara, and H. Ohashi, *Research Reports of Akita National College of Technology*, **19**, 42 (1984).

Spectroelectrochemical Determination of Redox Potential of Cytochrome *c'* in *Rhodospirillum rubrum* Chromatophores

Tatsuo ERABI,* Yoshiharu YAMASHITA, Kumiko NISHIMURA, and Masanori WADA
Department of Industrial Chemistry, Faculty of Engineering, Tottori University, Koyama, Tottori 680
(Received December 22, 1986)

Synopsis. A spectroelectrochemical technique has been used for redox study of cytochrome *c'* in chromatophores in the presence of Toluidine Blue O as a mediator. The midpoint potential of cytochrome *c'* thus determined was 0 mV (n=1) at pH 7.0, which agreed well with the value determined by redox titration.

Studies of the redox properties of the components in photosynthetic and other several biological electron-transport chains become more important for understanding of their reaction mechanism, combined with the development of new disintegrating methods of biomembrane. Although the thin-layer spectroelectrochemistry[1] offers several advantages for the study of the redox chemistry of biological electron-transport components, many difficulties to be solved lies under our eyes. One of the difficulties is of measuring small absorbance change between oxidized and reduced forms of electroactive species due to the very short light path length in a thin-layer cell and extremely dilute suspension of the disintegrated membrane. So, few spectroelectrochemical studies on redox components in biomembrane have been reported so far except for study on fluorescence yield of chloroplast fragments,[2] whereas many studies on electron-transport components in soluble state[3-6] can be found. But this problem can be overcome to some extent by integrating the spectrum data with use of a microcomputer. This paper describes an attempt of such spectroelectrochemical measurement of indirect reduction of cytochrome *c'* in chromatophore membrane from *Rhodospirillum rubrum* (G-9).

Experimental

Chromatophores were prepared from the light grown cells of *Rs. rubrum* (G-9) according to the method described previously.[7] Chromatophores were suspended in 0.6 M (M=mol dm^{-3}) GTA buffer, consisting of a mixture of 0.2 M 3,3-dimethylglutaric acid, 0.2 M tris(hydroxymethyl)aminomethane and 0.2 M 2-amino-2-methyl-1,3-propanediol, which was adjusted to various pH by adding HCl or NaOH, and the concentration of chromatophores was expressed in terms of absorbance of bound bacteriochlorophyll at 873 nm (A_{873}). The sample solution was deoxygenated prior to use by vacuum-nitrogen cycling on a vacuum-purified nitrogen double manifold and loaded into a thin-layer cell by using rubber septum caps and syringe techniques,[6] because of the autooxidizability of cytochrome *c'*. The spectroelectrochemical thin-layer cell was used in a Hitachi Model 557 spectrophotometer equipped with Hitachi MB-6890 microcomputer at 25 °C. Our present spectroelectrochemical thin-layer cell design was reported previously.[8] The midpoint potential (E_m) was determined by sequentially applying a series of potentials (E_{appl}) against a micro Ag/AgCl electrode using a Hokuto Model HA-501 potentiostat. Each potential was maintained until electrolysis ceased so that the equilibrium of the ratio of the concentration of oxidized to reduced from ([Ox]/[Red]) was established as defined by the Nernst equation (for about 10—60 min), and each corresponding value of [Ox]/[Red] to the series of E_{appl}'s was estimated from the absorbance change at 430 nm. The absorbance spectra were recorded as the average of five times scanning for improvement the ratio of signal to noise.

Results and Discussion

It was suggested by a conventional electrochemical method that cytochrome *c'* in chromatophores could not directly exchange electrons at an electrode, presumably due to the insulation of redox site from the electrode by surrounding proteins. However, spectroelectrochemical measurement can be made on cytochrome *c'* in chromatophores by adding another redox species (a mediator-titrant[9]), which transports electrons between the electrode and cytochrome *c'*, to the suspension. The ideal properties for the mediator were discussed in detail.[9] Among the redox reagents tested, Toluidine Blue O (E_m=+34 mV at pH 7.0[10]) was finally chosen as the mediator, fulfilling some properties for mediator, and the properties were examined in some detail by means of conventional electrochemical and spectrophotometric techniques as described.[11] So, all the measurements described hereafter were carried out in the presence of 50 μM Toluidine Blue O and the concentration of cytochrome *c'* in chromatophores was adjusted to 4.2 μM (estimated from A_{873}=100[12]).

The computer-calculated reduced-minus-oxidized difference absorption spectra at several steps of electrolytic reduction are shown in Fig. 1.

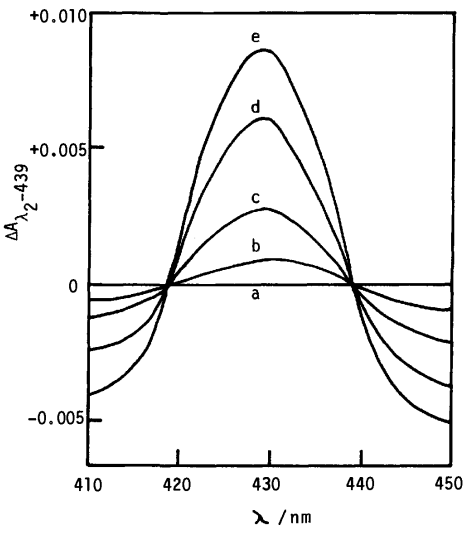

Fig. 1. Difference absorption spectra of cytochrome *c'* in chromatophores at thin-layer cell for series of applied potentials at pH 7.0.
E_{appl}; (a): +75, (b): +25, (c): 0, (d): −25, (e): −75 mV.

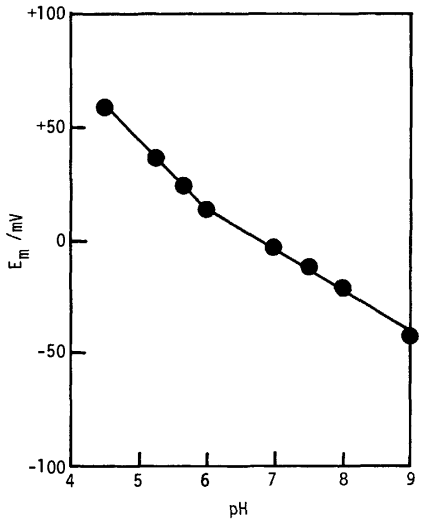

Fig. 2. Effect of pH on E_m values of cytochrome c' in chromatophores.

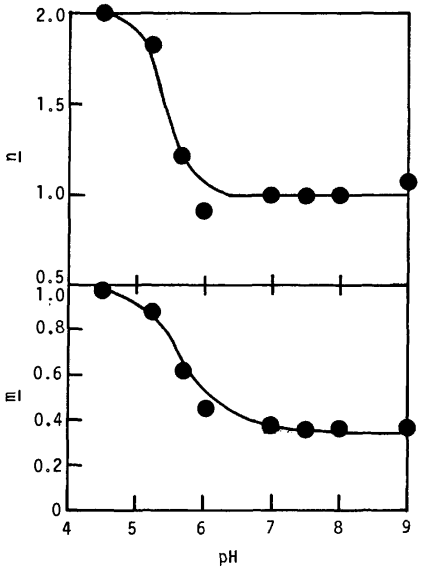

Fig. 3. Values of n and m at various pH's for cytochrome c' reduction.

The Nernst plots at various pH's showed good linear relationships. The E_m at pH 7.0 was 0 mV, which agreed well with the value determined by redox titration.[13] The pH-dependence of E_m was divided in two straight lines; one with a slope of −29 mV/pH in the acidic region below pH 6.0, and the other with −21 mV/pH in the more basic region. This result indicates the presence of a heme-linked ionization probably in the reduced form as described by Clark.[14] The ionization constant (K_{red}) became to be 1×10^{-6} M (pK_{red}=6.0). This result is supported by a spectrophotometric result on pH-dependence of absorbance at 430 nm for electro-reduced cytochrome c', where pK_{red} was estimated to be 5.95 according to the method by Moore et al.[15]

The number of electrons (n) involved in the reduction process was 2 in more acidic region than pH 5.0 and 1 in more basic region than pH 6.0 (Fig. 3). Values for the number of protons transferred (m) accompanying with cytochrome c' reduction are also shown in Fig. 3 as a function of pH. The value of m was about 1 near pH 5.0, and 0.4 in the more basic region. The small value of m may indicate the conformational change of cytochrome molecule or chromatophore membrane with pH change and/or the considerably slower rate of proton transfer than that of electron transfer probably due to hydrophobicity of the surrounding proteins.

In conclusion, it became clear that this spectroelectrochemical technique was very useful to determine the redox potential of the extremely small amounts of redox components in a biomembrane or the fragments such as photosynthetic reaction center, bc_1 and b_6f complexes.

The most parts of measurements were carried out at the Division of Enzymology, Institute for Protein Research, Osaka University. We wish to express our thanks to Professor Takekazu Horio and Dr. Tomisaburo Kakuno for their cordial guidance and helpful discussion.

References

1) W. R. Heineman, *Anal. Chem.*, **50**, 390A (1978).
2) F. M. Hawkridge and B. Ke, *Anal. Biochem.*, **78**, 76 (1977).
3) J. L. Anderson, T. Kuwana, and C. R. Hartzell, *Biochemistry*, **15**, 3847 (1976).
4) V. T. Taniguchi, W. R. Ellis, Jr., V. Cammarata, J. Webb, F. C. Anson, and H. B. Gray, *Adv. Chem. Ser.*, **210**, 51 (1982).
5) L. S. Reid, V. T. Taniguchi, H. B. Gray, and A. G. Mauk, *J. Am. Chem. Soc.*, **104**, 7516 (1982).
6) V. T. Taniguchi, B. G. Malmstrom, F. C. Anson, and H. B. Gray, *Proc. Natl. Acad. Sci. U. S. A.*, **79**, 3387 (1982).
7) N. Nishi, M. Kataoka, G. Soe, T. Kakuno, T. Ueki, J. Yamashita, and T. Horio, *J. Biochem.*, **86**, 1211 (1979).
8) T. Erabi, Y. Yamashita, and M. Tanaka, *Reps. Fac. Engn. Tottori Univ.*, **15**, 49 (1984).
9) R. Szentrimay, P. Yeh, and T. Kuwana, "Electrochemical Studies of Biological Systems," ed by D. T. Sawer, American Chemical Society, Washington, D. C. (1977), pp. 143—169.
10) W. M. Clark, "Oxidation-reduction Potentials of Organic Systems," Williams & Wilkins, Baltimore (1960), pp. 415—426.
11) E. Steckhan and T. Kuwana, *Ber. Bunsenges. Phys. Chem.*, **78**, 253 (1974).
12) T. Kakuno, R. G. Bartsch, K. Nishikawa, and T. Horio, *J. Biochem.*, **70**, 79 (1971).
13)T. Kakuno, K. Hosoi, T. Higuti, and T. Horio, *J. Biochem.*, **74**, 1193 (1973).
14) W. M. Clark, pp. 118—130 in Ref. 10.
15) G. R. Moore, G. W. Pettigrew, R. C. Pitt, and R. J. P. Williams, *Biochim. Biophys. Acta*, **590**, 261 (1980).

Mössbauer Spectroscopic Study on the Mixed-Valence States of 1′,1‴-Dimethyl-, 1′,1‴-Dipentyl-, 1′,1‴-Dihexyl-, and 1′,1‴-Didecylbiferrocenium Triiodide

Satoru NAKASHIMA, Motomi KATADA, Izumi MOTOYAMA,† and Hirotoshi SANO*
Department of Chemistry, Faculty of Science, Tokyo Metropolitan University, Fukasawa, Setagaya-ku, Tokyo 158
†Department of Chemistry, Faculty of Engineering, Kanagawa University, Rokkakubashi, Kanagawa-ku, Yokohama 221
(Received January 8, 1987)

Synopsis. 1′,1‴-Dimethyl-, 1′,1‴-dipentyl-, 1′,1‴-dihexyl-, and 1′,1‴-didecylbiferrocene were synthesized and Mössbauer spectroscopic measurements of their monocation salts were carried out at various temperatures in order to know the mixed-valence states. Effects of alkyl substituent on the valence states of iron atoms in the monocation salts of 1′,1‴-dialkylbiferrocenes are discussed.

Biferrocene derivatives are easily monooxidized to give the corresponding monocation salts, in which iron atoms are in a mixed-valence state. The electronic interaction and the electron-transfer process between the two metal sites in different oxidation states have been extensively investigated by means of Mössbauer spectroscopy. These compounds can be classified into two types of valence states of the iron atoms, a trapped-valence type and an averaged-valence type, by means of Mössbauer spectroscopy.[1] The former type has different states of iron atoms corresponding to ferrocene-like bivalent and ferricenium-like tervalent iron atoms, while the latter has an equivalent state of iron atom averaged over ferrocene-like bivalent and ferricenium-like tervalent iron atoms.

Iijima et al. first observed an interesting temperature-dependence of the mixed-valence state in 1′,1‴-diethyl- and 1′,1‴-dipropylbiferrocenium triiodide, which are of an averaged-valence type above ca. 200 K but of a trapped-valence type below ca. 200 K.[2] Similar temperature-dependences were also observed later in one crystal form of 1′,1‴-dibutylbiferrocenium triiodide[3] and in biferrocenium triiodide.[3,4]

In the present paper, the triiodide salts of other 1′,1‴-dialkylbiferrocene monocations shown in Fig. 1, such as 1′,1‴-dimethyl- (**1**), 1′,1‴-dipentyl- (**2**), 1′,1‴-dihexyl- (**3**), and 1′,1‴-didecylbiferrocene monocation (**4**), were synthesized and investigated by means of Mössbauer spectroscopy in order to clarify the effect of 1′,1‴-dialkyl substitution on the valence states of iron atoms.

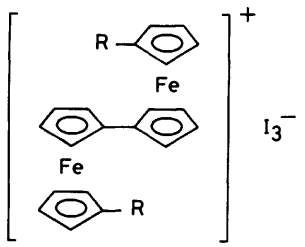

Fig. 1. Compounds of **1**, **2**, **3**, and **4**.
(**1**) 1′,1‴-Dimethylbiferrocenium triiodide (R=CH_3),
(**2**) 1′,1‴-Dipentylbiferrocenium triiodide (R=C_5H_{11}),
(**3**) 1′,1‴-Dihexylbiferrocenium triiodide (R=C_6H_{13}),
(**4**) 1′,1‴-Didecylbiferrocenium triiodide (R=$C_{10}H_{21}$).

Experimental

Materials. 1′,1‴-Dialkylbiferrocenes were prepared by the Ullmann coupling at 110—120 °C for 18 h of 1′-alkyl-1-bromoferrocenes. The triiodide salts were prepared by partial oxidation of the corresponding dialkylbiferrocenes in benzene with a stoichiometric amount of I_2. All the analytical data of the triiodide salts obtained in the present experiment are shown below. Found: C, 30.99; H, 2.71%. Calcd for $C_{22}H_{22}Fe_2I_3$: C, 33.93; H, 2.85%. Found: C, 40.56; H, 4.99%. Calcd for $C_{30}H_{38}Fe_2I_3$: C, 40.44; H, 4.30%. Found: C, 41.84; H, 4.64%. Calcd for $C_{32}H_{42}Fe_2I_3$: C, 41.82; H, 4.61%. Found: C, 47.46; H, 5.83%. Calcd for $C_{40}H_{58}Fe_2I_3$: C, 46.59; H, 5.67%.

Mössbauer Spectroscopic Measurements. A ^{57}Co(Pt) source moving in a constant-acceleration mode was used for Mössbauer spectroscopic measurements. The Mössbauer spectra were obtained by using an ELSCINT Mössbauer spectrometer with a proportional counter. The isomer shifts were referred to metallic iron foil. The Mössbauer parameters (isomer shift, *I. S.*, and quadrupole splitting, *Q. S.*) were obtained by least-squares fitting to Lorentzian peaks.

Results and Discussion

The Mössbauer parameters are summarized in Table 1, while typical spectra are shown in Fig. 2. The spectra of 1′,1‴-dimethylbiferrocenium triiodide (**1**) at 78 and 298 K consist of an inner- and an outer-doublet with nearly 1:1 ratio in areal intensity, which are

Table 1. Mössbauer Parameters

Compound	Temperature/K	*I.S.*[a]/ mm s^{-1}	*Q.S.*/ mm s^{-1}
1	298	0.43	1.74
		0.43	0.56
	78	0.49	1.82
		0.47	0.51
2	298	0.45	1.88
		0.44	0.54
	78	0.50	1.94
		0.49	0.55
3	298	0.45	1.80
		0.41	0.64
	78	0.47	1.91
		0.50	0.63
4	253	0.46	1.94
		0.46	0.48
	78	0.52	2.03
		0.52	0.49

a) Isomer-shift data are reported with respect to metallic iron foil.

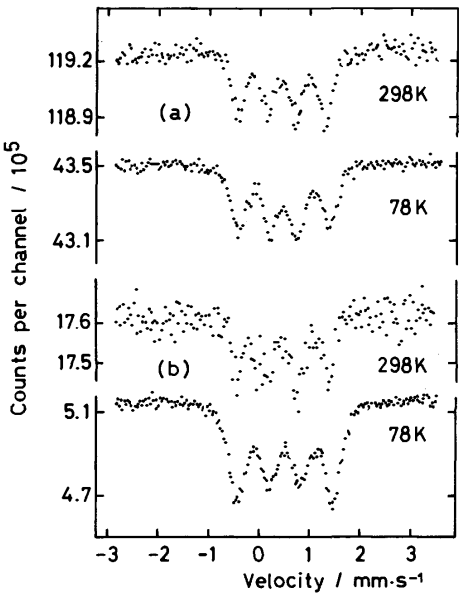

Fig. 2. Typical Mössbauer spectra of (a) 1′,1‴-dimethyl- and (b) 1′,1‴-dihexylbiferrocenium triiodide at 78 and 298 K.

ascribable to ferricenium-like tervalent and ferrocene-like bivalent states, respectively. Compound **1** is of trapped-valence type and temperature-independent. Table 1 shows that 1′,1‴-dipentyl- (**2**), 1′,1‴-dihexyl- (**3**), and 1′,1‴-didecylbiferrocenium triiodide (**4**) are classified into a trapped-valence type and are temperature-independent as well as **1**. The measurements of Mössbauer spectra of compound **4** were unsuccesful at room temperature because of its decreased recoil-free fraction.

The values of *Q. S.* of ferrocene-like bivalent iron atoms in these compounds are smaller than those of biferrocenium picrate (2.141 mm s^{-1} at 78 K and 2.053 mm s^{-1} at 298 K)[5] and biferrocenium triiodide (2.119 mm s^{-1} at 4.2 K and 2.013 mm s^{-1} at 300 K).[6] On the other hand, the values of *Q. S.* of ferricenium-like tervalent for these compounds are larger than those of biferrocenium picrate (0.288 mm s^{-1} at 78 K and 0.302 mm s^{-1} at 298 K)[5] and biferrocenium triiodide (0.381 mm s^{-1} at 4.2 K and 0.400 mm s^{-1} at 300 K).[6] Similar trends have been observed in 1′,1‴-diethyl-, 1′,1‴-dipropyl-, and 1′,1‴-dibutylbiferrocenium triiodide at low temperatures, although this effect seems to decrease in the case of 1′,1‴-didecylbiferrocenium triiodide.

As mentioned in the introduction, the Mössbauer spectra of 1′,1‴-diethyl- and 1′,1‴-dipropylbiferrocenium triiodide, and one crystal form of 1′,1‴-dibutylbiferrocenium triiodide show a remarkable temperature-dependence; i. e., iron atoms are in a trapped-valence state at low temperatures and in an averaged-valence state near room temperature. On the other hand, all the spectra obtained in the present study show the trapped-valence type from 78 K to room temperature. Although the Mössbauer parameters observed for the monocation salts in the present study at 78 K resemble those of 1′,1‴-diethyl-, 1′,1‴-dipropyl-, and 1′,1‴-dibutylbiferrocenium triiodide at 78 K, the temperature-dependences are not observed.

It was suggested that the environment surrounding each cation in a number of mixed-valence compounds in the solid state determines whether or not an intramolecular electron transfer occurs.[3,7] One of the most important factors controlling intramolecular electron transfer can be a symmetric structure of each binuclear mixed-valence cation experiencing weak or moderate electronic coupling between the two metal ions, associated with the positions of each anion. In the case of longer chain alkyl substituents, the possibility to have a center of symmetry for the dialkylbiferrocenium cation will also be reduced because of the increased possibility of having various kinds of conformational arrangements in the substituent.

The results suggest that the length of the chain of the alkyl substituent has an important effect on the mixed-valence states of 1′,1‴-dialkylbiferrocenium triiodides, probably because the alkyl substituents are too long or too short. The terminal atoms of the I_3^- anion will then be situated closer to one of the iron atoms of a given cation, even near room temperature. Detailed crystallographical studies of some of dialkylbiferrocenium triiodides are now being studied.

The authors wish to express their thanks to Dr. Sei'ichiro Iijima of the Research Institute for Polymer and Textiles for his helpful discussion.

References

1) "Mixed-Valence Compounds," ed by D. B. Brown, D. Reidel Publishing Company, Dordrecht (1980).

2) S. Iijima, R. Saida, I. Motoyama, and H. Sano, *Bull. Chem. Soc. Jpn.*, **54**, 1375 (1981).

3) T. -Y. Dong, D. N. Hendrickson, K. Iwai, M. J. Cohn, S. J. Geib, A. L. Rheingold, H. Sano, I. Motoyama, and S. Nakashima, *J. Am. Chem. Soc.*, **107**, 7996 (1985).

4) M. J. Cohn, T. -Y. Dong, D. N. Hendrickson, S. J. Geib, and A. L. Rheingold, *J. Chem. Soc., Chem. Commun.*, **1985**, 1095.

5) D. O. Cowan, R. L. Collins, and F. Kaufman, *J. Phys. Chem.*, **75**, 2025 (1971).

6) W. H. Morrison, Jr. and D. N. Hendrickson, *J. Chem. Phys.*, **59**, 380 (1973).

7) K. Sato, S. Nakashima, M. Watanabe, I. Motoyama, and H. Sano, *Nippon Kagaku Kaishi*, **1985**, 580; S. Nakashima, M. Katada, I. Motoyama, and H. Sano, *Bull. Chem. Soc. Jpn.*, **59**, 2923 (1986); M. Katada, S. Nakashima, Y. Uchida, I. Motoyama, H. Sano, H. Sakai, and Y. Maeda, *J. Radioanal. Nucl. Chem., Lett.*, **104**, 349 (1986); S. Nakashima, Y. Masuda, I. Motoyama, and H. Sano, *Bull. Chem. Soc. Jpn.*, **60**, 1673 (1987).

Activation of C-H Bonds of Heterocyclic and Alicyclic Compounds Using Calcium Atoms[1)]

Kunio MOCHIDA,* Kenji KOJIMA, and Yasuhiro YOSHIDA
Department of Chemistry, Faculty of Sciences, Gakushuin University, 1-5-1 Mejiro, Tokyo 171
(Received December 19, 1986)

Synopsis. Calcium atoms have been inserted into C-H bonds of heterocyclic (furans and thiophene) and alicyclic compounds (cyclohexanes and cyclopentane) to give the corresponding organocalcium hydrides. The organocalcium hydrides thus produced reacted with trimethylchlorosilane to give trimethylsilyl-substituted heterocyclic and alicyclic compounds, and a reduced product (trimethylsilane).

The study of metal-vapor reactions is of considerable interest in organometallic chemistry and organic synthesis because by these methods, it is possible to synthesize organometallic compounds which would be difficult, if not impossible, to prepare by other methods, and to study their reactive intermediates.[2)]

Activation of the C-H bond by metal atoms, clusters, and metal complexes is an area of intense research activity. In spite of this activation of the C-H bond by main group-metal atoms is still a rare phenomenon. Recently, we reported on the activation of the C-H bonds of substituted benzenes by calcium atoms.[3)] We have carried out the activation of the C-H bonds of heterocyclic and alicyclic compounds by calcium atoms.

In this paper, we describe the activation of the C-H bonds of heterocyclic and alicyclic compounds by calcium atoms.

Results and Discussion

Calcium atoms were generated by evaporation from a tungsten filament using essentially the same apparatus and conditions as have been described in the literature (ca. 900 °C and 5×10^{-3} Torr, 1 Torr=133.322 Pa).[3-7)] Calcium metal was evaporated at a rate of ca. 20 mg min^{-1} while excess of the heterocyclic or alicyclic compound was co-condensed on the walls of the reaction flask containing the crucible and a perforated inlet tube through which the heterocyclic or alicyclic compound was admitted. The reaction flask was immersed in liquid nitrogen during the calcium evaporation. After the calcium evaporation and admission of the organic substrate was completed, the reaction flask was warmed to room temperature and the excess of trimethylchlorosilane was admitted as vapor and the reaction flask left to stand for 1.5 h. After removal of the reaction flask from a vacuum line, the reaction mixture was slowly hydrolyzed with water. The organic layer was extracted with ether.

Table 1. Reactions of Calcium Atoms/Heterocyclic and Alicyclic Compound Vapors with Trimethylchlorosilane[a)]

Substrate	Products	(Yield/%[b)])	
	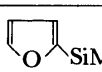	(3.0)	Me_3SiH (1.0)
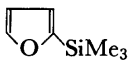	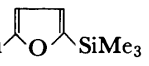	(4.0)	Me_3SiH (4.0)
	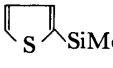	(1.0)	Me_3SiH (1.0)
	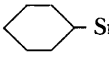	(1.0)	Me_3SiH (1.0)
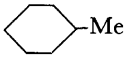	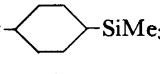	(1.0)	Me_3SiH (1.0)
	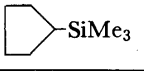	(1.0)	Me_3SiH (1.0)

a) Reactions were performed at room temperature for 1.5 h. b) Yields of products were based on the calcium metal consumed.

Hydrolysis of the products gave trimethylsilyl-substituted products, and a reduced product (trimethylsilane) (Eq. 1). All products were identified by comparing their GC-MASS and retention times on GLC with those of authentic samples. The results are summarized in Table 1.

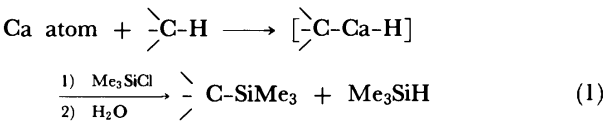

$$\text{Ca atom} + \text{-C-H} \longrightarrow [\text{-C-Ca-H}] \xrightarrow[2)\ H_2O]{1)\ Me_3SiCl} \text{-C-SiMe}_3 + Me_3SiH \quad (1)$$

As shown in Table 1, the reaction products of calcium atoms/furan, 2-trimethylsilylfuran, and thiophene vapors when treated with trimethylchlorosilane gave 2-trimethylsilylfuran, 2,5-bis(trimethylsilyl)furan, and 2-trimethylsilylthiophene, respectively, and trimethylsilane in very low yields. No 3-trimethylsilylfuran, 2,3-, 2,4-bis(trimethylsilyl)furan, and 3-trimethylsilylthiophene were produced. A theoretical calculation for anion radicals of five-membered ring compounds has been made.[8)] It appears that the position of calcium atom attack may be influenced by the unpaired spin density. Accordingly we suggest that the reaction sequence may be (1) electron transfer to form a Ca^+ five-membered ring compound$^-$, and (2) attack of the Ca^+ at the most electron-rich site. Thus selective insertion of calcium atoms into C-H bonds may depend upon the spin densities of the heterocyclic compound anion radicals.

The reaction products of calcium atoms/cyclohexane, methylcyclohexane, and cyclopentane vapors when treated with trimethylchlorosilane gave cyclohexyltrimethylsilane, 4-methylcyclohexyltrimethylsilane, and cyclopentyltrimethylsilane, respectively, and trimethylsilane in very low yields as shown in Table 1. The insertion mechanism of C-H bonds of alicyclic compounds with calcium atoms is not clear. It is not possible to predict whether electron transfer occurs between calcium atoms and the alicyclic compound in the vapor state.

Although the yields of products are very low as shown in Table 1, this is a first example of sp^3C-H bond activation with calcium metal.

Calcium hydride is known to be incapable of reducing trimethylchlorosilane. However, the organic calcium hydride thus prepared can reduce trimethylchlorosilane to give trimethylsilane.

The yields of trimethylsilyl-substituted products and reduced product (trimethylsilane) as shown in Table 1 are very low. The yields of these products were determined on the basis of the amount of calcium metal consumed on the assumption that all of the vaporized calcium metal reacted completely with the heterocyclic and alicyclic compound vapors. Therefore, taking into consideration that the calcium insertion products include a large amount of unreacted calcium metal, the yields of the products as shown in Table 1 may be considerably underestimated.

The co-condensation product which was formed by deposition of calcium atoms onto the frozen layer of heterocyclic and alicyclic compound or by condensation of the organic substrate vapor onto the layer of calcium atoms did not react with trimethylchlorosilane under these reaction conditions.

Experimental

GLC analyses were performed on a Shimazu GC-6A and 8A gas chromatograph with 2m 20% SE-30 and 2m 30% Apiezon L columns. GC-MASS spectra were obtained with JEOL JMS-DX 303 mass spectrometer. NMR spectra were obtained with a Varian FT-80A spectrometer using $CDCl_3$ as the solvent and TMS as the internal standard.

Materials. Calcium metal (granule, 99% pure, Wako chemicals) was commercially available. Furan, thiophene, cyclohexane, methylcyclohexane, and cyclopentane were dried and distilled prior to use. 2-Trimethylsilylfuran,[9] 2,5-bis(trimethylsilyl)furan,[10] 2-trimethylsilylthiophene,[9] cyclohexyltrimethylsilane,[11] 4-methylcyclohexyltrimethylsilane,[12] and cyclopentyltrimethylsilane[13] were prepared as described in the references cited.

Reactions of Calcium Atoms/Heterocyclic and Alicyclic Compound Vapors with Trimethylchlorosilane. As a typical example, the reaction of calcium atoms/furan vapor with trimethylchlorosilane is described. Calcium metal (200 mg, 5.0 mmol) was vaporized at a temperature of ca. 900 °C using a filament of tungsten in vacuo (ca. 5×10^{-3} Torr) at a rate of ca. 20 mg min^{-1}. During the vaporization of calcium metal, furan (20 cm^3, 276 mmol) was introduced into the reaction vessel as vapor. Calcium atoms/furan vapor condensed on the wall of the reaction vessel which was cooled to 77 K with liquid nitrogen. The initial product at 77 K was a muddy yellow. The reaction vessel was warmed to room temperature and trimethylchlorosilane (15 cm^3, 118 mmol) was then admitted as vapor. The reaction vessel was left to stand for 1.5 h. After removal of the reaction vessel from a vacuum line, the reaction mixture was slowly hydrolyzed with water. The organic layer was extracted with ether. The products were identified by comparing their GC-MASS and retention times on GLC with those of authentic samples. The yields of the products were determined by an internal-standard method.

Partial financial support of this research by a Grant-in-Aid from the Ministry of Education, Science and Culture.

References

1) Y. Yoshida, T. Yamanishi, and K. Mochida, 52nd National Meeting of the Chemical Society of Japan, Kyoto, April 1986, 1K29.

2) For examples; J. R. Blackborow, "Metal Vapor Synthesis in Organometallic Chemistry," Springer-Verlag, New York (1979); K. J. Klabunde, "Chemistry of Free Atoms and Particles," Academic Press, New York (1980); K. J. Klabunde, "Reactive Intermediates," ed by R. A. Abramovitch, Plenum Press, New York (1980), Chapt. 2; R. H. Crebtree, *Chem. Rev.*, **85**, 245 (1985).

3) K. Mochida, H. Takeuchi, Y. Hiraga, and H. Ogawa, *Chem. Lett.*, **1984**, 1989.

4) K. Mochida and H. Ogawa, *J. Organomet. Chem.*, **243**, 131 (1983).

5) K. Mochida and M. Manishi, *Chem. Lett.*, **1984**, 1077.

6) K. Mochida and Y. Mizuno, *Chem. Lett.*, **1986**, 1125.

7) K. Mochida and Y. Mizuno, *Bull. Chem. Soc. Jpn.*, **60**, 273 (1987).

8) M. M. Urberg and E. T. Kaiser, "Radical Ions," ed by E. T. Kaiser and L. Kevan, Interscience, New York (1968), Chapt. 8.

9) R. A. Benkeser and R. B. Currie, *J. Am. Chem. Soc.*, **70**, 1780 (1948).

10) C. S. Carman and G. F. Koser, *J. Org. Chem.*, **48**, 2534 (1983).

11) N. S. Nametkin, A. V. Topchiev, and T. I. Chernysheva, *Dokl. Akad. Nauk SSSR*, **110**, 97 (1956).

12) J. C. Saam and J. L. Speier, *J. Am. Chem. Soc.*, **83**, 1351 (1961).

13) G. A. Russell and K. L. Nagpal, *Tetrahedron Lett.*, **1961**, 421.

A Convenient Method for the Synthesis of Alkylsilyl Cyanides Using Potassium or Sodium Cyanide Impregnated on Amberlite XAD Resin

Kazuaki SUKATA
Nihon Tokushu Kagaku Kogyo Co., Ltd., 1 Takijiri-aza-hashimoto, Izumi-cho, Iwaki, Fukushima 970-04
(Received December 18, 1987)

Synopsis. Potassium and sodium cyanide impregnated on Amberlite XAD resin were found to be effective for converting alkylsilyl chloride to the corresponding alkylsilyl cyanide under mild conditions.

Alkylsilyl cyanides are versatile and important reagents for organic synthesis. Among these, trimethylsilyl cyanide (Me_3SiCN) has been most widely used for preparing useful nitriles and isonitriles: Carbonyl compounds[1] and imines[2] react with Me_3SiCN to give silylated cyanohydrins and aminonitriles, respectively. The reaction of acetals and orthoesters with Me_3SiCN gives alkoxynitriles.[3] The reaction of oxiranes with Me_3SiCN produces trimethylsilyloxynitriles in the presence of aluminium chloride[4] or diethylaluminium chloride,[5] whereas in the presence of zinc iodide it gives the corresponding isonitriles.[6] On the other hand, other alkylsilyl cyanides, *t*-butyldimethylsilyl cyanide (*t*-$BuMe_2SiCN$)[7] and dimethylsilyl dicyanide ($Me_2Si(CN)_2$),[8] also have recently been employed as cyanation agents.

A number of methods for the synthesis of Me_3SiCN have been reported.[1d,9] In many reported methods, however, there seem to be few methods that can be utilized for preparing other alkylsilyl cyanides in satisfactory yields. Although only the method reported by Mai and Patil[10] affords good yields of alkylsilyl cyanides, it requires the use of lithium cyanide which is prepared by the reaction of butyllithium and Me_3SiCN[10] or by the reaction of lithium hydride with hydrogen cyanide[1d] or acetone cyanohydrin.[9e]

In previous papers, it has been shown that potassium and sodium cyanide impregnated on macroporous polymer resins such as Amberlite XAD resins (KCN/XAD, NaCN/XAD) are effective reagents for some reactions.[11] This paper shows that the reaction of alkylsilyl chlorides with KCN/XAD or NaCN/XAD gives alkylsilyl cyanides in good yields under mild conditions.

$$R_{4-n}SiCl_n \xrightarrow{\text{KCN or NaCN/XAD}} R_{4-n}Si(CN)_n$$

In a preliminary experiment, the reaction of trimethylsilyl chloride (Me_3SiCl) with KCN/XAD-4 was carried out in various solvents. Table 1 shows the results. In *N*-methylpyrrolidone (NMP), the reaction was so fast that the complete conversion of Me_3SiCl occured within 0.5 h at room temperature giving Me_3SiCN in 92—94% yields (GLC). In acetonitrile, the reaction afforded 94—95% yield of Me_3SiCN at 60 °C after 1.5 h. Contrary to expectations, the yields in 1,2-dimethoxyethane (DME) and in tetrahydrofuran (THF) were very similar to that without any solvent. In a nonpolar solvent such as benzene or hexane, the

Table 1. Preparation of Me_3SiCN Using KCN/XAD-4 in Various Solvents[a]

Solvent	Time/h	Temp/°C	Yield/%[b]
NMP	<0.5	25	92[d]
c)	<0.5	25	94[d]
Acetonitrile	1.5	60	94[d]
c)	1.5	60	95[d]
DME	8.0	60	18
THF	8.0	60	22
Benzene	6.0	60	10
Hexane	8.0	60	11
None	8.0	60	19

a) Unless otherwise noted, reactions were carried out with KCN (15 mmol)/XAD-4 (3.75 g), Me_3SiCl (7.5 mmol), and a solvent (20 ml). b) Determined by GLC using toluene as the internal standard. c) NaCN (15 mmol)/XAD-4 (3.75 g) was used. d) The conversion of Me_3SiCl was completed.

Table 2. Alkylsilyl Cyanides[a]

Alkylsilyl cyanide	Alkali metal cyanide	Temp	Time	Yield[b]	Bp/mmHg (mp)		IR
		°C	h	%	Found	Reported	cm^{-1}
Me_3SiCN[c]	NaCN	25	0.5	61(94)	114—118/760	117—118/760[1d]	2190
$PhMe_2SiCN$	KCN	60	3.0	79(95)	79—81/3	228—235/760[10]	2185
t-$BuMe_2SiCN$	KCN	60	4.0	80(95)	77—79/45	163—167/760[10]	2185
	NaCN	60	4.0	85(95)	(79—81)	(82—84)[10]	
$Me_2Si(CN)_2$	KCN	60	6.0	73(85)	109—112/55	166—170/760[10]	2195
d)	NaCN	40	4.0	71(95)	(82—84)	(82—85)[10]	
$Et_2Si(CN)_2$	KCN	60	4.0	75(90)	89—92/9.5	210—215/760[10]	2195
d)	NaCN	40	4.0	77(95)	(35—37)		
$Ph_2Si(CN)_2$[d]	NaCN	40	4.0	70	121—122/0.35 (44—47)	110—115/0.1[10] (45—47)[10]	2185

a) Unless otherwise noted, reactions were carried out with alkylsilyl chloride (15 mmol), alkali metal cyanide (30 mmol)/XAD-4 (7.5 g), and acetonitrile (40 ml). b) Isolated yields. The values in parentheses are the yields determined by GLC. c) Me_3SiCl (24 mmol) and NMP (20 ml) were used. d) R_2SiCl_2 (10 mmol) was used.

reaction was very slow. The reaction of Me_3SiCl with KCN impregnated on alumina or silica gel was also performed. No Me_3SiCN was obtained, though the coversion of Me_3SiCl was very fast. Although NMP is an appropriate solvent for Me_3SiCN because of the ease in separating the product from the solvent, its use is limited in the preparation of other alkylsilyl cyanides having high boiling points. Table 1 shows that acetonitrile, which has a low boiling point, can be used for this purpose though the reaction is slower than that in NMP.

Table 2 shows the results of the preparation of alkylsilyl cyanides using KCN/XAD-4 or NaCN/XAD-4 in acetonitrile. These results are comparable to that using LiCN[10] and indicates that KCN/XAD-4 and NaCN/XAD-4 are very effective reagents for the synthesis of alkylsilyl cyanides. On the other hand, a small amount of siloxanes was produced because of the incomplete drying of the system. In particular, since the boiling points of Me_3SiCN and the by-product, hexamethyldisiloxane, are very similar, the isolated yield of Me_3SiCN was considerably lower than those of the other alkylsilyl cyanides.

For certain cyanosilylation, the use of isolated silyl cyanides will not be necessary. In fact, the one-pot cyanosilylation of aldehydes and ketones was found to proceed smoothly under mild conditions using KCN/XAD or NaCN/XAD producing silylated cyanohydrins in good yields.[12]

Experimental

Materials. Solvents were dried with molecular sieves 3A or 4A. Dimethylsilyl dichloride and Me_3SiCl (Toray Silicone Co.), *t*-$BuMe_2SiCl$, phenyldimethylsilyl chloride, diethylsilyl dichloride (Shin-Etsu Chemical Industries) and diphenylsilyl dichloride (Wako Pure Chemical Industries) were used without further purification. KCN/XAD and NaCN/XAD were prepared according to the method previously reported,[11] dried at 90 °C and 0.1 mmHg (1 mmHg=133.322Pa) for 5 h.

Typical Procedure for the Reaction of Alkylsilyl Chloride with KCN or NaCN/XAD-4. In all reactions, alkylsilyl chloride was added directly to the flask in which the KCN or NaCN/XAD-4 had been made and dried. All the products were known compounds.

The Reaction of Me_3SiCl with KCN/XAD-4 in Various Solvents. A mixture of KCN/XAD-4 made from KCN (15 mmol) and XAD-4 (3.75 g), Me_3SiCl (7.5 mmol), and a solvent (20 ml) was stirred under the conditions presented in Table 1. The yield of Me_3SiCN was determined by GLC using toluene as the internal standard.

Me_3SiCN: A mixture of NaCN (1.47 g, 30 mmol)/XAD-4 (7.5 g), Me_3SiCl (2.60 g, 24 mmol), and NMP (20 ml) was stirred for 0.5 h at 25 °C. The solid material was filtered and meticulously washed with dichloromethane. The filtrate and washings were combined. After the dichloromethane had been carefully removed, the residual solution was carefully distilled under reduced pressure (≈120 mmHg) giving the crude product. The total crude product obtained from triplicates was carefully redistilled with a 15 cm Vigreaux column, giving 4.33 g (61%) of Me_3SiCN, bp 114—118 °C (lit,[1d] bp 117—118 °C); IR (CCl_4) 2190 cm^{-1}.

***t*-$BuMe_2SiCN$:** A mixture of NaCN (1.47 g, 30 mmol)/XAD-4 (7.5 g), *t*-$BuMe_2SiCl$ (2.26 g, 15 mmol), and acetonitrile (40 ml) was stirred at 60 °C for 4 h. The solid material was filtered and meticulously washed with 100 ml of benzene-dichloromethane (2 : 1). The filtrate and the washings were combined. After removal of the solvent, the residual solid was distilled under reduced pressure, giving 1.80 g (85%) of *t*-$BuMe_2SiCN$, bp 77—79 °C/45 mmHg, mp 79—81 °C (lit,[10] bp 163—167 °C, mp 82—83 °C); IR (CCl_4) 2185 cm^{-1}.

Diethylsilyl Dicyanide ($Et_2Si(CN)_2$): A mixture of KCN (1.95 g, 30 mmol)/XAD-4 (7.5 g), diethylsilyl dichloride (2.36 g, 15 mmol) and acetonitrile (40 ml) was stirred at 60 °C for 4 h. The resulting mixture was treated according to the same method as *t*-$BuMe_2SiCN$. After removal of the solvent, the residual solid was distilled under reduced pressure giving 1.56 g (75%) of $Et_2Si(CN)_2$, bp 89—92 °C/9.5 mmHg, mp 35—37 °C (lit,[10] bp 210—215 °C); IR (CCl_4) 2195 cm^{-1}.

I thank Nihon Tokushu Kagaku Kogyo Co., Ltd., for permission to publish this article.

References

1) a) D. A. Evans, L. K. Truesdale, and G. L. Carroll, *J. Chem. Soc., Chem. Commun.*, **1973**, 55; b) D. A. Evans and L. K. Truesdale, *Tetrahedron Lett.*, **1973**, 4929; c) D. A. Evans, J. M. Hoffman, and L. K. Truesdale, *J. Am. Chem. Soc.*, **95**, 5822 (1973); d) D. A. Evans, G. L. Carroll, and L. K. Truesdale, *J. Org. Chem.*, **39**, 914 (1974); e) W. Lidy and W. Sundermeyer, *Chem. Ber.*, **106**, 587 (1973); f) H. Neef and R. Müller, *J. Prakt. Chem.*, **315**, 367 (1973).

2) I. Ojima, S. Inaba, and K. Nakatsugawa, *Chem. Lett.*, **1975**, 331; I. Ojima and S. Inaba, *ibid.*, **1975**, 737.

3) K. Utimoto, Y. Wakabayashi, Y. Shishiyama, M. Inoue, and H. Nozaki, *Tetrahedron Lett.*, **22**, 4279 (1981).

4) W. Lidy and W. Sundermeyer, *Tetrahedron Lett.*, **1973**, 1449.

5) J. C. Mullis and W. P. Weber, *J. Org. Chem.*, **47**, 2873 (1982).

6) G. O. Spessard, A. R. Ritter, D. M. Johnson, and A. M. Montgomery, *Tetrahedron Lett.*, **24**, 655 (1983); P. G. Gassman and T. L. Guggenheim, *J. Am. Chem. Soc.*, **104**, 5849 (1982); P. G. Gassman and R. S. Gremban, *Tetrahedron Lett.*, **25**, 3259 (1984); P. G. Gassman and L. M. Haberman, *ibid.*, **26**, 4971 (1985); P. G. Gassman and L. M. Haberman, *J. Org. Chem.*, **51**, 5010 (1986).

7) E. J. Corey, D. N. Crouse, and J. E. Anderson, *J. Org. Chem.*, **40**, 2140 (1975); A. S. Narula and S. P. Sethi, *Tetrahedron Lett.*, **25**, 685 (1984).

8) I. Ryu, S. Murai, A. Shinonaga, T. Horiike, and N. Sonoda, *J. Org. Chem.*, **43**, 780 (1978).

9) a) J. W. Zubrick, B. I. Dunbar, and H. D. Durst, *Tetrahedron Lett.*, **1975**, 71; b) S. Hünig and G. Wehner, *Synthesis*, **1979**, 522; c) J. K. Rasmussen and S. M. Heilmann, *ibid.*, **1979**, 523; d) M. T. Reetz and I. Chatziiosifidis, *ibid.*, **1982**, 330; e) T. Livinghouse, *Org. Synth.*, **60**, 126 (1981).

10) K. Mai and G. Patil, *J. Org. Chem.*, **51**, 3545 (1986).

11) K. Sukata, *J. Org. Chem.*, **50**, 4388 (1985); K. Sukata, *Bull. Chem. Soc. Jpn.*, **60**, 1085 (1987).

12) For example, the one-pot cyanosilylation of benzaldehyde with KCN/XAD and Me_3SiCl in acetonitrile gave the corresponding trimethylsilylated cyanohydrin in 98% yield (GLC) under mild conditions. The study of this reaction is now in progress.

Synthesis of Sterically Hindered Bicyclo[2.2.2]octanes by Lewis Acid Catalyzed Reaction of 2-(Trimethylsiloxy)-1,3-cyclohexadienes with 4-Methyl-3-penten-2-one

Morio ASAOKA,* Keiji ISHIBASHI, Wataru TAKAHASHI, and Hisashi TAKEI
Department of Life Chemistry, Tokyo Institute of Technology, Nagatsutacho, Midori-ku, Yokohama 227
(Received December 25, 1986)

Synopsis. Dienol silyl ethers of various 2-cyclohexenones reacted with 4-methyl-3-penten-2-one(mesityl oxide) or methyl acrylate in the presence of Lewis acid to give bicyclo[2.2.2]octanes in moderate yields.

In the course of the total synthesis of (±)-eremolactone,[1] we needed to develop a new method for the construction of crowded bicyclo[2.2.2]octane skeleton.

Some reports on the synthesis of bicyclo[2.2.2]octane skeleton starting from 2-cyclohexenones using sequential Michael reaction or thermal Diels-Alder reaction via enol silyl ethers are known,[2] however, none of these methods are applicable to the construction of crowded tricyclo[5.2.2.$0^{1,5}$]undecane derivative suitable for the synthesis of (±)-eremolactone.

Thus, we investigated the Lewis acid catalyzed reaction of the dienol silyl ether **2** prepared from 2-cyclohexenone **1** with various 3-methyl-2-butenoic acid derivatives.

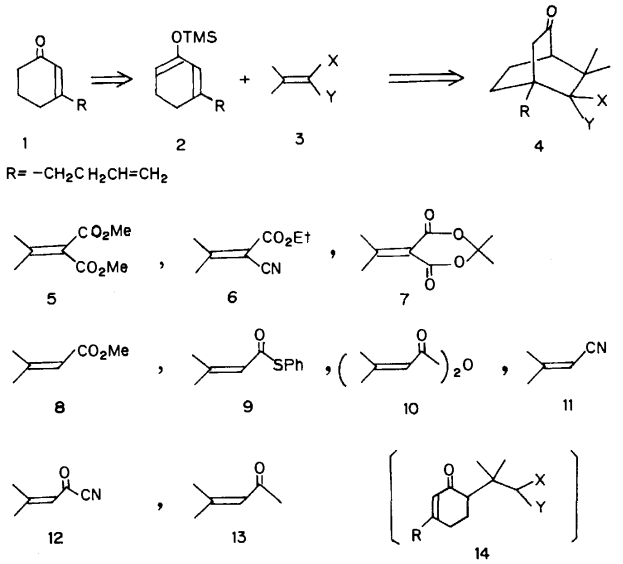

Scheme 1.

First, the reaction of dienol ether **2** with electron deficient tri- or tetra-substituted olefins (**5**—**13**) was examined in the presence of Lewis acid such as $SnCl_4$ or $TiCl_4$. In the case of the reaction of **5** or **6**, no bicyclo[2.2.2]octane but Michael adduct **14** was obtained as a major product and the attempts for the conversion of **14** to **4** under various (basic or acidic) conditions resulted in a failure. In the case of the reaction of other 3-methyl-2-butenoic acid derivatives **7**—**12**, none of desired products **4** nor **14** was obtained. When mesityl oxide (**13**) was used in the presence of $TiCl_4$, however **4** was successfully obtained in 44% yield. Then the reaction of mesityl oxide with some dienol silyl ethers derived from 2-cyclohexenones in the presence of $TiCl_4$ was carried out and the results are summarized in Table 1. The desired compounds were obtained except in the case of **15g**, in which case the reaction gave a complex mixture presumably due to the steric hindrance. As for the stereochemistry of the products, at least 2 isomers (endo- and exo-isomer) are possible, but only one isomer was isolated in the cases of **15a**, **15b**, **15e**, and **15f**, though the geometry of acetyl group is presently unknown. The dienol ether **15c** gave a mixture of two isomers and **15d** gave four isomers.[4] One of the tricyclic products synthesized from **15d** was used successfully for the synthesis of (±)-eremolactone.[1]

The mechanism of the reaction seems to involve a sequential Michael addition, because **14** was isolated when the reaction was quenched in the course of the process. For example, when the reaction of **15a** with

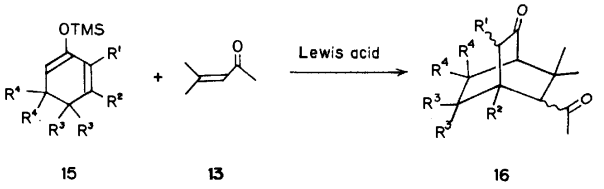

Scheme 2.

Table 1. Reaction of Dienol Silyl Ether (**15**) with Mesityl Oxide in the Presence of $TiCl_4$

Entry		R^1	R^2	R^3	R^4	Reaction condition		Yield
						temp/°C	time/h	**16** %
1	**15a**	H	$-CH_2CH_2CH=CH_2$	H	H	−78—−30	2.5	44[a]
2	**15b**	H	Me	H	H	−40	3	55[a]
3	**15c**	Me	Me	H	H	−78	1.5	32[b]
4	**15d**	$-CH(CH_3)CH_2CH_2-$		H	H	−78—−40	2	64[c]
5	**15e**	H	H	Me	H	−40	0.5	40[a]
6	**15f**	H	H	H	H	−78	2	12[a]
7	**15g**	H	Me	H	Me	−78—rt	6	—[d]

a) Single isomer. b) About one to one mixture of two geometric isomers. c) Mixture of four geometric isomers. d) Complex mixture.

Table 2. Reaction of Dienol Silyl Ether (**15**) with Methyl Acrylate in the Presence of $TiCl_4$

Entry		R_1	R_2	R_3	R_4	Reaction condition		Yield **18**[a]
						temp/°C	time/h	%
1	**15b**	H	Me	H	H	−78—−40	8	52[b]
2	**15c**	Me	Me	H	H	−78	6	55[c]
3	**15h**	H	H	H	Me	−78—−40	7	54[b]
4	**15i**	Me	H	H	H	−78	3	39[c]
5	**15g**	H	Me	H	Me	−78—rt	6	—[d]
6	**15f**	H	H	H	H	−78	5	10[b]

a) The structure was confirmed by comparison with authentic sample prepared by the method in Ref. 2. b) Single isomer. c) About two to one mixture of geometric isomers. d) Complex mixture.

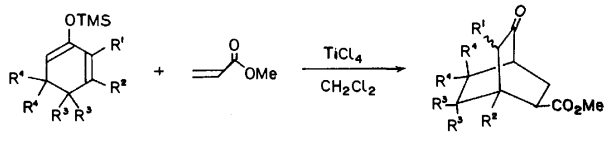

15 17 18

Scheme 3.

13 was carried out at −78 °C for 2 h, almost all the starting materials were consumed and 38% yield of **14** (X=Ac, Y=H) was obtained along with **16a** (29%). To make clear the scope and limitation, the reactions of dienol silyl ethers **15** with α,β-unsaturated esters were also examined. Although methyl crotonate gave no cyclo-adduct, methyl acrylate afforded the corresponding [2.2.2]bicyclo-products in moderate yields as shown in Table 2. We assigned all of the major products as endo-isomers by the comparison with authentic samples prepared by the methods[2] which are reported to give endo-isomers predominantly.

In conclusion, Lewis acid catalyzed reaction of dienol silyl ethers derived from 2-cyclohexenones with α,β-unsaturated carbonyl compounds is effective for the synthesis of crowded bicyclo[2.2.2]- or tricyclo-[5.2.2.$0^{1,5}$]-derivatives. In addition, this method is of importance especially when base labile compounds are subjected to such type of the reactions,[3] since this reaction proceeds under acidic conditions.

Experimental

Nuclear magnetic resonance spectra were taken on a JEOL PS-100 (100 MHz) or Hitachi R-24B (60 MHz). Infrared spectra were recorded on a Hitachi 260-50 spectrophotometer.

Typical Procedure: To a mixture of 1-methyl-3-trimethylsiloxy-1,3-cyclohexadiene **15b** (184 mg, 1 mmol), mesityl oxide (196 mg, 2 mmol) in dichloromethane (5 ml) was added $TiCl_4$ (2 mmol) in dichloromethane (5 ml) at −40 °C under an argon atmosphere. The solution was stirred at the temperature for 3 h, mixed with aqueous K_2CO_3 solution, and then extracted with dichloromethane. The extracts were dried over $MgSO_4$ and evaporated under reduced pressure. The residue was purified by silica-gel column chromatography to give **16b** (114 mg, 55%); mp 94—96 °C. IR (KBr) 1700 and 1720 cm^{-1} (C=O); ^1H NMR ($CDCl_3$) δ=0.84 (3H, s), 0.94 (3H, s), 1.34 (3H, s), 2.21 (3H, s), 2.58 (1H, d, J=2 Hz), 3.14 (1H, dd, J=2 and 18 Hz), 1.14—2.30 (6H, m). Found: C, 75.16; H, 9.69%. Calcd for $C_{13}H_{20}O_2$: C, 74.96; H, 9.68%.

16a: Mp 73—74 °C. IR (KBr) 1730, 1710 cm^{-1} (C=O) and 1640 cm^{-1} (C=C); ^1H NMR ($CDCl_3$) δ=0.71 (3H, s), 1.22 (3H, s), 2.18 (3H, s), 2.51 (1H, d, J=2 Hz), 2.95 (1H, dd, J=2 and 18 Hz), 4.60—5.12 (2H, m), 5.25—5.70 (1H, m), 0.55—2.63 (10H, m). Found: C, 77.45; H, 9.74%. Calcd for $C_{16}H_{24}O_2$: C, 77.37; H, 9.74%.

16c: IR (KBr) 1700 and 1718 cm^{-1} (C=O); ^1H NMR ($CDCl_3$) δ=0.85 (1.5H, s), 0.90 (1.5H, s), 1.33 (1.5H, s), 2.20 (1.5H, s), 1.05 (1.5H, d, 8 Hz), 1.15—3.36 (7H, m), 0.88 (1.5H, s), 1.02 (1.5H, s), 1.10 (1.5H, s), 2.18 (1.5H, s), 1.08 (1.5H, d, 8 Hz). Found: C, 75.61; H, 9.85%. Calcd for $C_{14}H_{22}O_2$: C, 75.63; H, 9.97%.

16e: Mp 87—88.5 °C. IR (KBr) 1695 and 1712 cm^{-1} (C=O); ^1H NMR ($CDCl_3$) δ=0.90 (3H, s), 0.98 (3H, s), 1.12 (3H, s), 1.38 (3H, s), 2.25 (3H, s), 1.50—2.10 (4H, m), 2.53 (1H, dd, J=2 and 4 Hz), 2.75 (1H, d, J=2 Hz), 2.98 (1H, m). Found: C, 75.69; H, 9.94%. Calcd for $C_{14}H_{22}O_2$: C, 75.63; H, 9.97%.

16f: Mp 68—70 °C. IR (KBr) 1700 and 1712 cm^{-1} (C=O); ^1H NMR ($CDCl_3$) δ=0.88 (3H, s), 1.38 (3H, s), 2.23 (3H, s), 0.80—3.20 (9H, m). Found: C, 74.22; H, 9.20%. Calcd for $C_{12}H_{18}O_2$: C, 74.19; H, 9.34%.

References

1) M. Asaoka, K. Ishibashi, N. Yanagida, and H. Takei, *Tetrahedron Lett.*, **24**, 5127 (1983); A. Uchida, Y. Ohashi, Y. Sasada, K. Ishibashi, M. Asaoka, and H. Takei, *Acta Crystallogr. Sect. C*, **42**, 1081 (1986).

2) K. B. White and W. Reusch, *Tetrahedron*, **34**, 2439 (1978); M. E. Jung and C. A. McCombs, *J. Am. Chem. Soc.*, **100**, 5207 (1978); G. I. Feutrill and R. N. Mirrington, *Aust. J. Chem.*, **31**, 1809 (1978); W. Weber, D. Spitzner, and W. Kraus, *J. Chem. Soc., Chem. Commun.*, **1980**, 1212; D. Spitzner, W. Weber, and W. Kraus, *Tetrahedron Lett.*, **23**, 2179 (1982); M. Ihara and K. Fukumoto, *Yuki Gosei Kagaku Kyokai Shi*, **44**, 96 (1986); H. Hagiwara and H. Uda, *J. Chem. Soc., Perkin Trans. 1*, **1986**; 629; Narula and A. J. Birch, *Tetrahedron Lett.*, **22**, 591 (1981).

3) Lewis acid catalyzed simple 1,4-addition of enol silyl ether to enones is reported; K. Narasaka, K. Soai, Y. Akikawa, and T. Mukaiyama, *Bull. Chem. Soc. Jpn.*, **49**, 7799 (1976). Recently, they also reported sequential Michael reaction of dienol silyl ethers; T. Mukaiyama, Y. Sagawa, and S. Kobayashi, *Chem. Lett.*, **1986**, 1821.

4) The X-ray analysis and the chemical transformation of **16d** proved that exo-products are formed predominantly in this case. The stereoselectivity is opposite to the results shown in Table 2, presumable due to the steric hindrance.

New Flavonoids Isolated from Infected Sugarbeet Roots

Hajime TAKAHASHI,* Teruji SASAKI, and Masaaki ITO
Chemistry Laboratory, Department of General Education, Higashi Nippon Gakuen University, Tobetsu, Hokkaido 061-02
(Received January 8, 1987)

Synopsis. New flavonoid compounds, 3,5-dihydroxy-6,7-methylenedioxyflavanone, 2′,5-dihydroxy-6,7-methylenedioxyisoflavone, and 5-hydroxy-6,7-methylenedioxyflavone were isolated from sugarbeet roots infected with *Rhizoctonia solani*.

Results

Phytoalexin, betagarin (**1**), and betavulgarin (**2**) have been recently isolated from the infected leaves of sugarbeet with *Corcospora beticola*.[1] We now report the isolation of some flavonoids from the sugarbeet roots infected with *R. Solani*. We also report that the compounds **3** and **4** have the weak inhibition effect of hypha growth, on the other hand, the compound **5**, being only the demethylated substance of betavulgarin (**2**), haven't that effect in the least.

The sliced and infected sugarbeet roots were extracted by a dipping in methanol at room temperature. The separation of the extracts by the column and preparative plates chromatographies on silica gel allowed an isolation of the pure six flavonoids. By the IR, UV, and ^{1}H NMR spectra datas, the compounds (**1**, 6.5×10^{-4}% yield), (**2**, 2.3×10^{-2}%), and (**3**, 7×10^{-4}%) were identified with the known betagarin, betavulgarin, and dihydrooroxylin A,[2] respectively.

It was indicated that each of the flavonoids (**4**, 4.5×10^{-5}% yield), (**5**, 7.5×10^{-4}%), and (**6**, 1.7×10^{-2}%) had one methylenedioxy group and one or some hydroxyl groups by IR, MS, and ^{1}H NMR spectra. In the each mass spectrum of **4**, **5**, and **6**, each peak (*m/z*, 180 or 181) due to a fragment ion $C_8H_4O_5$ via retro Diels Alder pathway[3] was observed and suggested that one hydroxyl group and one methylenedioxy group attached to each A-ring of these compounds. In the ^{1}H NMR spectra of **4**, **5**, and **6**, one proton signal (singlet) respectively appeared at δ 10.92, 12.15, and 12.83, and assigned as the chelated hydroxyl group. In the UV spectra of **4**, **5**, and **6**, the respective maximum of absorption was bathochromically shifted by addition of aluminium chloride, and then, the shifted maxima were not again moved by the addition of hydrochloric acid. These results indicated that the all hydroxyl groups attached to the A-rings of **4**, **5**, and **6** oriented to the 5-positions. The Gibbes tests (all positive) of **4**, **5**, and **6** suggested that all 8-positions were free, and so all methylenedioxy groups oriented to 6- and 7-positions.

In the ^{1}H NMR of **4**, signals of two protons appeared as an AB-quartet at δ 5.09 and 4.55 (J=12 Hz) were assigned as a C-2-H and a C-3-H (trans configuration), and indicated that **4** had a flavanonol structure. Two singlets and one multiplet were also observed at δ 6.14 (1H, C-8-H), 6.04 (2H, -OCH_2O-), and 7.50 (5H, W_H=8 Hz, B-ring's protons), separately, in the ^{1}H NMR. By these results, it was confirmed that **4** is 3,5-dihydroxy-6,7-methylenedioxyflavanone.

Two maxima (245 and 272 nm) in the UV of **5** and the appearance of C-2-H (δ 8.06, s) in the ^{1}H NMR indicated that **5** had an isoflavone structure. The position of B-ring's hydroxyl group of **5** was easily determined by the NMR. The splitting patterns of the aromatic four protons on the B-ring was characteristic of *ortho*-disubstituted benzene.[4] Two singlets also appeared at δ 6.61 (1H, C-8-H) and 6.15 (2H, -OCH_2O-) in the ^{1}H NMR. The compound **5** was ultimately derived by a demethylation of the known **2**. Thus, It was confirmed that **5** was 2′,5-dihydroxy-6,7-methylenedioxyisoflavone.

It was also estimated that the compound **6** was 5-hydroxy-6,7-methylenedioxyflavone by the followed data. In the UV spectrum of **6**, the maxima (275 and 316 nm) of the absorptions suggested that **6** had a flavone structure. In the ^{1}H NMR of **6**, the signals of the C-3-H (δ 6.61, s) and the five protons (δ 7.80, m, 2′6′-protons and δ 7.50, m, 3′4′5′-protons) also supported its structure.

The investigation of the inhibition effect of the isolated flavonoids allowed that the compounds **3** and **4** had more weak activities than **1** and **2**, and that **5** (the demethylated compound of the active **2**) and **6** haven't the activities in the least.

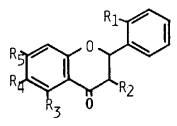

1: R_1=R_3=OCH_3, R_2=H, R_4,R_5=OCH_2O
3: R_1=R_2=H, R_3=R_5=OH R_4=OCH_3
4: R_1=H, R_2=R_3=OH, R_4,R_5=OCH_2O

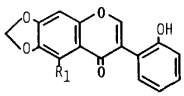

2: R_1=OCH_3
5: R_1=OH

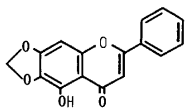

6

Experimental

All melting points are uncorrected. IR, UV, and ^{1}H NMR were determined with a Shimazu IR-400 spectrometer, with a Shimazu MPS-5000 spectrometer (solvent, ethanol), and with a JEOL-JNM-FX-90 spectrometer (solvent, chloroform-*d*; internal reference tetramethylsilane). MS spectra were taken with a Shimazu KLB-5000 spectrometer. High resolution MS spectra were taken by the staff of the Faculty of Agriculture, Hokkaido University, with a JEOL-D-500 spectrometer. TLC and column chromatographies were carried out on Merck kiesel gel and Cica silica gel.

Aphanomyces euteiches and *Rhizoctonia solani* were applied for screening test of growth inhibition properties. It was surely confirmed that methanol extract of the sliced and non-

infected sugarbeet roots had never the inhibition activity.

Isolation of the Flavoniods (1)—(6). Sliced sugarbeet roots (20 kg) were infected with *R. solani*, and stayed for 3 days at 25 °C, and dried at room temperature, and dipped in methanol (10 liters). After filtration of the extracts, the methanol solution was evaporated. Ethyl acetate solution of the obtained residue was washed with saturated water by sodium chloride, and dried (sodium sulfate). The produced residue by removal of solvent was washed with hexane (this hexane solution haven't the inhibition activity). The residue (20 g) was separated on column chromatography (solvent system; benzene, chloroform, and ethyl acetate). Further, the purification of the fractions was carried out by preparative TLC plates.

The known (**1**, 13 mg), (**2**, 450 mg), and (**3**, 14 mg) were identified with the standard compound **3** and the other data.

3,5-Dihydroxy-6,7-methlenedioxyflavanone (4): Yellow crystals (9 mg), mp 179—180 °C; Gibbes test (+); MS *m/z* 300 (M^+, 48%), 180 (M−120, 100); UV, λ_{max} (EtOH) 246 nm (ε 14150), 294 (ε 16500), λ_{max} (EtOH, $AlCl_3$ or $AlCl_3$, HCl) 245 nm (ε 6430), 322 (ε 20800); IR, 3450 cm^{-1} (OH), 1670 and 1620 (C=O); ^1H NMR δ=10.92 (1H, s, C-5-OH), 7.50 (5H, m, W_H=8 Hz, B-ring protons), 6.14 (1H, s, C-8-H), 6.04 (2H, s, $-OCH_2O-$),5.09 and 4.55 (2H, AB-q, J=12 Hz, C-2-H and C-3-H); High MS. Found: 300.0635. Calcd for $C_{16}H_{12}O_6$: 300.0634.

2',5-Dihydroxy-6,7-methylenedioxyisoflavone (5): Pale yellow crystals (15 mg), mp 230—233 °C; Gibbes Test (+); MS *m/z* 298 (M^+, 32%), 180 (M−118, 100); UV, λ_{max} (EtOH) 272 nm (ε 22600), 290 (shoulder), λ_{max} (EtOH, $AlCl_3$ or $AlCl_3$, HCl) 282 nm (ε 28000), 320 (ε 14000); IR, 3250 cm^{-1} (OH), 1670 and 1620 (C=O); ^1H NMR, δ 12.15 (1H, s, C-5-OH), 8.06 (1H, s, C-2-H), 7.30 (1H, m, C-6'-H), 7.10 (3H, m, C-3',4',5'-H), 6.61 (1H, s, C-8-H), 6.15 (2H, s, $-OCH_2O-$); High MS. Found: 298.0475. Calcd for $C_{16}H_{10}O_6$: 298.0477.

5 from 2: The mixture of **2** (100 mg), dry $AlCl_3$ (300 mg), and K_2CO_3 in ether (20 ml) was refluxed for 3 h. After an addition of acetic acid (10 ml) in the reaction mixture, removal of the solvent gave the residue. Chloroform solution of the residue was washed and dried (Na_2SO_4). Removal of solvent gave crystals **5**.

5-Hydroxy-6,7-methylenedioxyflavone (6): Yellow crystals (340 mg), mp 205 °C (decomp); Gibbes test (+); MS *m/z* 282 (M^+, 100%), 180 (M−102, 31), UV, λ_{max} (EtOH) 275 nm (ε 19700), 316 (ε 15200), λ_{max} (EtOH, $AlCl_3$ or $AlCl_3$, HCl) 284 nm (ε 20600), 292 (shoulder), 346 (ε 17800); IR, 3400 cm^{-1} (OH), 1670 and 1620 (C=O); ^1H NMR, δ=12.83 (1H, s, C-5-OH), 7.80 (2H, m, C-2',6'-H), 7.50 (3H, m, C-3',4',5'-H), 6.68 (1H, s, C-8-H), 6.61 (1H, s, C-3-H), 6.11 (2H, s, $-OCH_2O-$); High MS, Found: 282.0539. Calcd for $C_{16}H_{10}O_5$: 282.0529.

The authors wish to express their gratitude to Dr. Ryouzoh Yokosawa, Higashi Nippon Gakuen University, for infection and screening test by him, to Mr. Juichi Sugawara, Hokkaido Togyo co. LTD., for his supply of sugarbeet, to Dr. Akiyo Sakushima, Faculty of Pharmaceutical Sciences of Higashi Nippon Gakuen University for his valuable suggestions, and to Professor Shuzo Takagi, Faculty of Pharmaceutical Sciences, Mukogawa Women's University for his kind supply of dihydrooroxylin A.

References

1) J. Geigert, F. R. Stermitz, G. Johnson, D. D. Maag, and D. K. Johnson, *Tetrahedron*, **29**, 2703 (1973).

2) H. Sauer and R. Hansel, *Planta Med.*, **15**, 443 (1967); S. Takagi, M. Yamaki, and K. Inoue, *Yakugaku Zasshi*, **100** 1220 (1980).

3) H. Budzikiewicz, C. Djerassi, and D. H. Williams. "Structure Elucidation of Natural Products by Mass Spectrometry," Holden-Day (1964); A. Pelter, P. Stainton and M. Barber, *J. Heterocycl. Chem.*, **2**, 262 (1965).

4) M. Zanger, *Org. Magn. Reson.*, **4**, 1 (1972).

Silaethene in Pyrolysis of Spiro[silacyclobutane-1,9′-[9*H*-9]silafluorene]

Daiyo TERUNUMA,* Makoto NAKAMURA, Eiji MIYAZAWA, and Hiroyuki NOHIRA
Department of Applied Chemistry, Faculty of Engineering, Saitama University, Urawa, Saitama 338
(Received January 26, 1987)

Synopsis. A new silaspiro compound, i.e., spiro[silacyclobutane-1,9′-[9H-9]silafluorene](**1**) was synthesized in 75% yield. It was found that the pyrolysis of **1** at 650 °C under a reduced pressure gave a head-to-tail silaethene dimer in 15% yield. Copyrolysis of **1** in the presence of benzophenone gave 1,1-diphenylethene and a siloxane oligomer in 50 and 30% yield, respectively.

Current attention has been concentrated to the preparation and characterization of a silicon-carbon double bond.[1] It is suggested that 1-silafulvene systems have strong π stability and high reactivity, on the contrary 2-silafluvene systems have weak π stability and low reactivity.[2] In this connection, the generation of 1-silafluvene was already investigated.[3]

In the course of our studies on the synthesis of silicon-containing cyclic compounds,[4] we have interested in spiro[silacyclobutane-1,9′-[9H-9]silafluorene] (**1**). Because the generation of 2-silafluvene type intermediate would be expected with extrusion of ethene in the pyrolysis of **1**.

Results and Discussion

Compound **1** was obtained by treating 1,1-dichlorosilacyclobutane with biphenyl-2,2′-diyldilithium in 75% yield (Scheme 1).

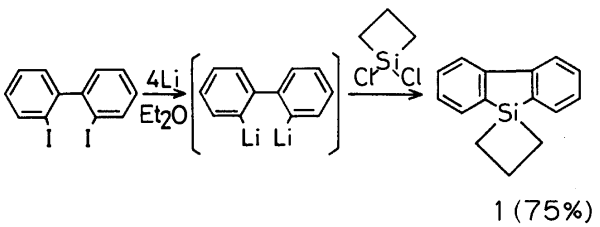

Scheme 1.

The mass spectrum of **1** shows relatively simple fragmentation including the base peak (m/z 194) corresponded to the silaethene fragment (Scheme 2).

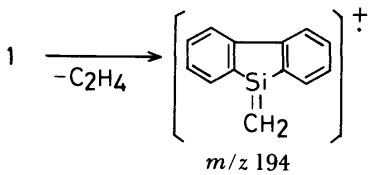

m/z 194

Scheme 2.

Then the pyrolysis of **1** was carried out at 650 °C under a reduced pressure (ca. 10^{-3} Torr†). A white crystalline product was obtained. The parent peak of the mass spectrum of the product was consistent with the molecular weight of a dimer of 2-silafluvene derivative (**2**) (m/z 388). Thus it is clear that **2** is generated under these reaction conditions and successive reaction of **2** occurs to give the dimer (Scheme 3).

†1 Torr=133.322Pa.

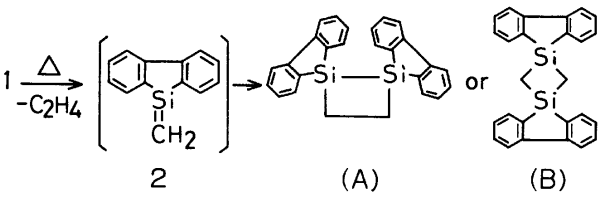

Scheme 3.

On the other hand, the silaethene can be dimerized in the two manners,[5] head-to-head (A) and head-to-tail (B).

NMR spectrum (^{29}Si) of the dimer (δ +2.1 based on TMS) suggests 1,3-disilacyclobutane structure (B).[6] The disilacyclobutane derivative has been known to undergo ring-openning reaction in the presence of lithium aluminum hydride (LAH).[7] The dimer was treated with LAH. The expected product from A and B are shown in Scheme 4.

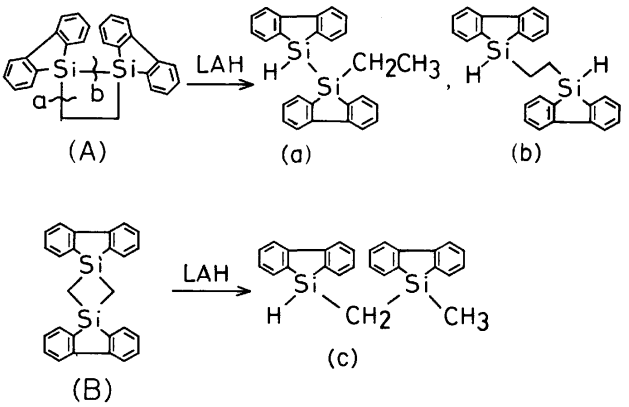

Scheme 4.

NMR spectra data of the product [^{13}C NMR ($CDCl_3$) δ −5.20 (t, CH_2), −2.27 (q, CH_3)] shows (c) in Scheme 4 which indicates the dimer structure of (B).

Furthermore, the reaction of the dimer with dimethylphenylsilane in the presence of platinum/carbon[8] afforded corresponding ring-opened product (d) (Scheme 5), but no reaction occurred with *m*-chloroperbenzoic acid (MCPBA).

These results show that the dimer has the structure of type B.

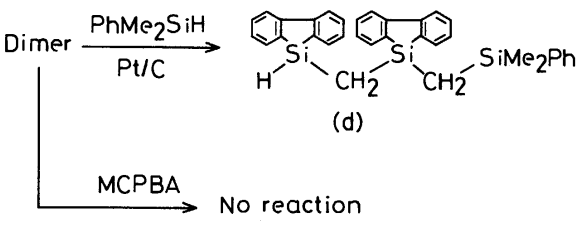

Scheme 5.

Then copyrolysis of **1** with benzophenone was investigated. The reaction was carried out at 540 °C under a

reduced pressure (ca. 10^{-3} Torr). 1,1-Diphenylethene and a siloxane oligomer were obtained in a 50 and 30% yield, respectively. Although we could not find out the direct evidence for the existence of the intermediates, it seems to be reasonable to consider that the reaction proceeds via a manner similar to that described in the copyrolysis of the silacyclobutane derivatives with benzophenone[9] (Scheme 6).

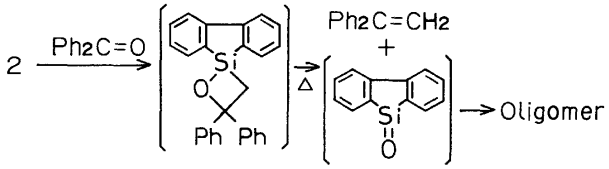

Scheme 6.

Experimental

The melting points and boiling points are uncorrected. The IR spectra were determined with a JASCO IR-A 302 spectrometer. The NMR spectra were determined at 90 MHz with a JEOL FX90Q and at 200 MHz with a JEOL FX200 spectrometers in $CDCl_3$ using TMS as an internal standard. The mass spectra were recorded on a JEOL-01SG instrument. Biphenyl-2,2′-diyldilithum was prepared in a manner similar to that described in the literature.[10]

Spiro[silacyclobutane-1,9′-[9H-9]silafluorene] (1). In a flask lithium (2.0 g, 0.29 gram-atoms) and dry ether (30 ml) were placed. A solution of 2,2′-diiodobiphenyl (12.0 g, 29.6 mmol) in dry ether (50 ml) was added to the mixture at reflux temperature with stirring under a dry nitrogen atmosphere. The mixture was refluxed for 1 h after the addition was complete. In another flask, a solution of 1,1-dichlorosilacyclobutane (4.0 g, 28.4 mmol) in dry ether (40 ml) was placed. The etheral solution of biphenyl-2,2′-diyldilithium was added to the solution of the chlorosilane by means of a syringe at 0 °C. The reaction mixture was stirred at 0 °C for 1 h, allowed to stand at room temperature for 1 h. The reaction mixture was hydrolyzed and the organic layer was separated and dried (Na_2SO_4). Evaporation and distilation gave **1** in 4.4 g (75%) yield. Bp 131 °C/0.25 Torr. n_D^{25} 1.6511. IR (neat) 2900, 1600, 1430, 1350, 1260, 1130, 1060, 850, 740, 720, 680, 540 cm^{-1}. ^1H NMR ($CDCl_3$) δ=1.56 (t, 4, Si-CH_2), 2.38 (quintet, CH_2), 7.1—7.8 (m, 8, Ar). ^{13}C NMR ($CDCl_3$) δ=15.0 (Si-CH_2), 19.29 (CH_2), 120.55, 127.48, 130.68, 133.11, 135.61, 147.58 (Ar). ^{29}Si NMR ($CDCl_3$) δ=12.9. UV (cyclohexane) ε_{max}(nm) 237 (4.51×10^4), 244 (3.84×10^4), 281 (1.40×10^4), 293 (1.21×10^4). Found: C, 81.00; H, 6.51%. Calcd for $C_{15}H_{14}Si$: C, 81.02; H, 6.34%.

Pyrorysis of 1. Pyrolysis was carried out using a vacuum flow system. Compound **1** (527 mg, 2.4 mmol) was added into a quartz tube (l=40 cm, d=0.8 cm) maintained at 640 °C through preheated tube (ca. 300 °C) under a reduced pressure (4×10^{-3} Torr). The products were collected in a liq. N_2 trap, and washed out with benzene. Evaporation and filtration gave crystalline product. It was purified by recrystallization from benzene. Yield 70 mg (15%). Mp 323—326 °C. MS M^+ 388. IR (KBr) 3050, 1600, 1435, 1340, 1260, 1130, 1080, 940, 770, 730, 710, 630 cm^{-1}. ^1H NMR ($CDCl_3$) δ=1.17 (s, 4H, Si-CH_2), 7.2—8.0 (m, 16H, Ar). ^{13}C NMR ($CDCl_3$) δ=1.10 (Si-CH_2), 121.1, 128.0, 131.0, 132.8, 137.5, 147.5 (Ar). ^{29}Si NMR ($CDCl_3$) δ=+2.1. UV (cyclohexane) ε_{max} (nm) 238 (9.65×10^4), 245 (1.02×10^5), 283 (3.44×10^4).

Copyrorysis of **1** (500 mg, 2.25 mmol) in the presence of benzophenone (410 mg, 2.25 mmol) was carried out at 540 °C in a manner similar to that described above. 1,1-Diphenylethene and the siloxane oligomer were separated from the reaction mixture by TLC (benzene-hexane 4 : 1) in 50% (200 mg) and 30% (130 mg) yield, respectively. 1,1-Diphenylethene; ^1H NMR (CCl_4) δ=5.35 (s, 2H, =CH_2), 7.20 (s, 10H, Ph). Oligomer IR (KBr) 3000, 1590, 1420, 1260, 1120, 1060, 740, 500 cm^{-1}. ^1H NMR (CCl_4) δ=7.0—8.2 (Ar).

Reaction of the Dimer with LAH. LAH (50 mg, 1.3 mmol) was added to a solution of the dimer (200 mg, 0.5 mmol) in dry ether (30 ml). The mixture was refluxed for 1 h with stirring. Usual work-up and purification by TLC (benzene) gave ring-opened product in 120 mg (60%) yield. ^1H NMR ($CDCl_3$) δ=0.40 (s, H, Si-CH_3), 0.61 (d, 2H, Si-CH_2-Si), 4.87 (t, 1H, Si-H), 7.1—7.8 (m, 16H, Ar). ^{13}C NMR ($CDCl_3$) δ=−5.20 (t, CH_2), −2.27 (q, Si-CH_3), 120.77, 127.33, 130.20, 130.33, 132.99, 133.64, 135.46, 138.19, 147.69, 148.34 (Ar).

Reaction of the Dimer with Dimethylphenylsilane in the Presence of Pt/C Catalyst. A mixture of the dimer (39.8 mg, 0.10 mmol), dimethylphenylsilane (1.00 g, 7.4 mmol), and 5% Pt/C (10 mg) was placed in a test tube. The tube was sealed under a dry nitrogen atmosphere, and it was kept at 100 °C for 55 h. After evaporation of excess dimethylphenylsilane, the product was separated by TLC (hexane-benzene 3 : 1) and recrystallized from pentane. Yield 16.1 mg (30%). ^1H NMR ($CDCl_3$) δ=−0.06 (s, 6H, Si-CH_3), 0.44 (s, 2H, Si-CH_2-Si), 0.58 (d, 2H, Si-CH_2), 4.82 (t, 1H, Si-H), 7.1—7.8 (m, 21H, Ar).

The authors are grateful to Professor Yasuhiro Nakadaira for help and advice in the determination of the structure of the dimer, and Asocciate Professor Sumio Tokita for letting us know the improved preparation method of 2,2′-diiodobiphenyl.

The authors also wish to thank the Shin-etsu Chemical Industry Co. for the gift of silanes.

References

1) H. Sakurai, *Kagaku No Ryoiki*, **29**, 742 (1975); L. E. Gusel'nikov and N. S. Nametkin, *Chem. Rev.*, **79**, 529 (1979); A. G. Brook, *J. Organomet. Chem.*, **300**, 21 (1986).

2) G. Bertrand, G. Trinquier, and P. Mazerolles, "Organometallic Chemistry Reviews" ed by D. Seyferth, Eksevier, Amsterdam (1981) Vol. 12, 1.

3) Y. Nakadaira, H. Sakaba, and H. Sakurai, *Chem. Lett.*, **1980**, 1071; T. J. Barton, G. T. Burns, E. V. Arnold, and J. Clardy, *Tetrahedron Lett.*, 7 (1981); T. J. Barton and C. R. Tully, *J. Organomet. Chem.*, **172**, 11 (1979).

4) D. Terunuma, N. Shibuya, and H. Nohira, *Bull. Chem. Soc. Jpn.*, **55**, 2287 (1982).

5) A. G. Brook, J. W. Harris, I. Lennon, M. ElSheikh, *J. Am. Chem. Soc.*, **101**, 83 (1979); M. Ishikawa, T. Fuchikami, M. Kumada, T. Higuchi, and S. Miyamoto, *J. Am. Chem. Soc.*, **101**, 1348 (1979); N. S. Nametkin, L. E. Gusel'nikov, V. M. Vdovin, P. L. Grinberg, V. I. Zav'yakov, and V. D. Oppengein, *Dokl. Akad. Nauk SSSR.*, **171**, 630 (1966).

6) A. M. Krapivin, M. Magi, V. I. Svergum, R. Z. Zaharjan, E. D. Babich, and N. V. Ushakov, *J. Organomet. Chem.*, **190**, 9 (1980).

7) A. M. Devine, P. A. Griffin, R. N. Haszeldine, M. J. Newlands, and A. E. Tipping, *J. Chem. Soc., Dalton Trans.*, **1975**, 1434.

8) D. R. Weyenberg and L. E. Nelson, *J. Org. Chem.*, **30**, 2618 (1965).

9) D. N. Roark and L. H. Sommer, *Chem. Commun.*, **1973**, 167; C. M. Golino, R. D. Bush, D. N. Roark, and L. H. Sommer, *J. Organomet. Chem.*, **66**, 29 (1974).

10) G. Wittig and W. Herwig, *Chem. Ber.*, **87**, 1511 (1954).

The ν_8 Infrared Band of Ethylidynephosphine $CH_3C{\equiv}P$ and Its Perdeuteride $CD_3C{\equiv}P$

Keiichi OHNO* and Hiroatsu MATSUURA
Department of Chemistry, Faculty of Science, Hiroshima University, Higashisenda-machi, Naka-ku, Hiroshima 730
(Received January 14, 1987)

Synopsis. The gas-phase infrared spectra of ethylidynephosphine $CH_3C{\equiv}P$ and its perdeuteride $CD_3C{\equiv}P$ were measured in the 50—400 cm^{-1} region with a resolution of 0.12 cm^{-1}. The molecular constants for the $\nu_8^{\pm1}$ and $2\nu_8^0-\nu_8^{\pm1}$ bands were determined by the $^{P,R}Q_K$ branch analysis.

Vibrational spectra of ethylidynephosphine (1-phosphapropyne)$CH_3C{\equiv}P$ and its perdeuteride $CD_3C{\equiv}P$ have been analyzed previously by infrared spectroscopy and the wavenumbers of the fundamental transitions have been determined.[1] Of the eight fundamentals, the $\nu_8^{\pm1}$ band, which is associated with the lowest vibrational level, has been detected only in the solid state, but no information has been available on this band for the gaseous state. In the present study, we have investigated the gas-phase infrared spectra of $CH_3C{\equiv}P$ and $CD_3C{\equiv}P$ in the 50—400 cm^{-1} region with a resolution of 0.12 cm^{-1} and the molecular constants for the $\nu_8^{\pm1}$ band have been determined. These constants will be eventually important for vibration-rotation analyses of the band systems in which the overtone and/or combination of $\nu_8^{\pm1}$ is involved.

Experimental

Samples of $CH_3C{\equiv}P$ and $CD_3C{\equiv}P$ were prepared by the pyrolyses of $C_2H_5PCl_2$ and $C_2D_5PCl_2$, respectively.[2] The far-infrared spectra were recorded on a JEOL JIR-40X Fourier transform infrared spectrometer. A globar source, a 6-μm Mylar beam splitter, and a TGS detector with a polyethylene window were used. The sample pressure was about 5 kPa in a 12-cm gas cell fitted with polyethylene windows. Dry nitrogen gas was continuously passed through the instrument during the measurement to get rid of water vapor.

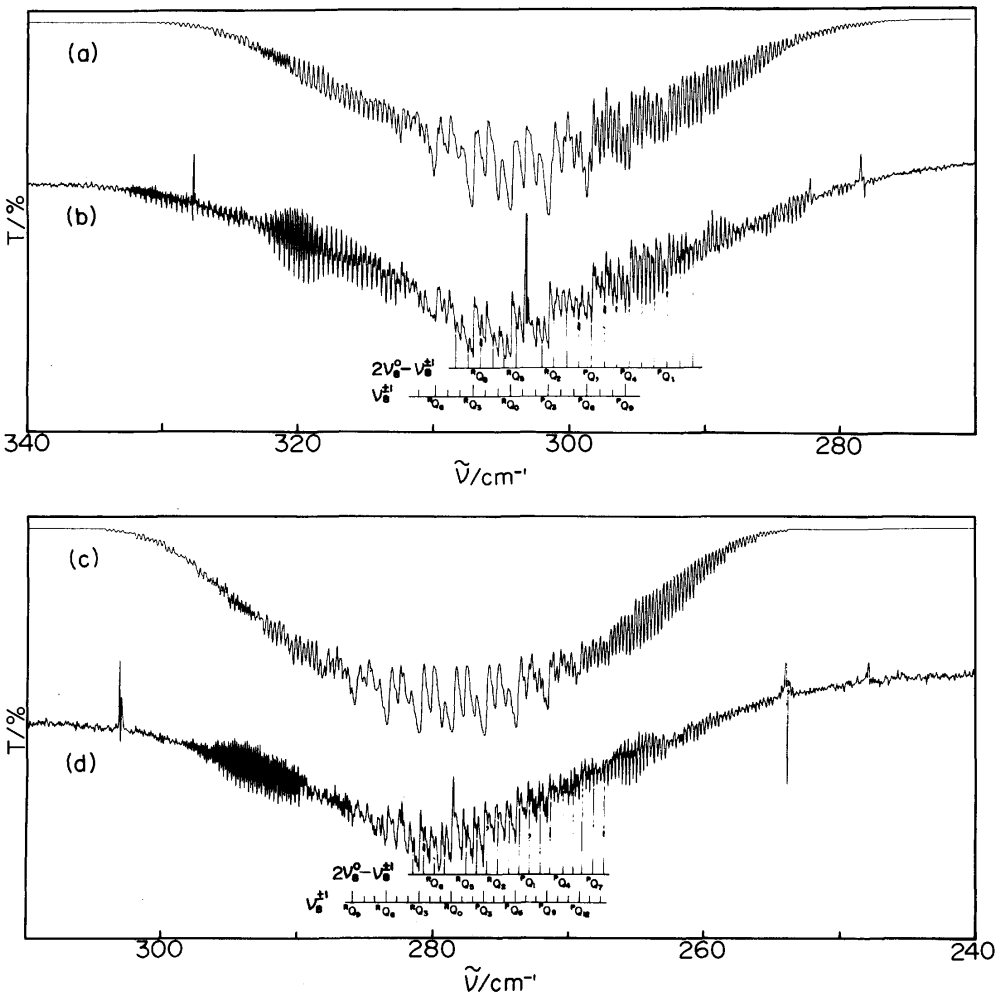

Fig. 1. Infrared spectra of the $\nu_8^{\pm1}$ and $2\nu_8^0-\nu_8^{\pm1}$ bands of $CH_3C{\equiv}P$ and $CD_3C{\equiv}P$. (a) Simulated spectrum of $CH_3C{\equiv}P$, (b) observed spectrum of $CH_3C{\equiv}P$, (c) simulated spectrum of $CD_3C{\equiv}P$, and (d) observed spectrum of $CD_3C{\equiv}P$.

Results and Discussion

Figure 1 shows the infrared spectra of the $\nu_8^{\pm 1}$ band region of $CH_3C{\equiv}P$ and $CD_3C{\equiv}P$. The $\nu_8^{\pm 1}$ band is due to the perpendicular transition of the prolate symmetric-top molecule. The wavenumbers for the $^{P,R}Q_K$ branches of $\nu_8^{\pm 1}$ are expressed by

$$ {}^{R}_{P}\nu^{Q}=\nu_0+[A'(1-2\zeta^z)-B']\pm 2[A'(1-\zeta^z)-B']K +[(A'-B')-(A''-B'')]K^2+(B'-B'')J(J+1), \quad (1) $$

where the centrifugal distortion terms are neglected. Thus, the $^{P,R}Q_K$ branches were easily assigned on the basis of a successive spacing of approximately $2[A'(1-\zeta^z)-B']=0.8$—0.9 cm^{-1} and the nuclear spin statistics, i.e., the $K=3|n|$ levels (n: integer) are stronger in intensity than the other K levels in the ground state. The assignments of the $^{P,R}Q_K$ branches are shown in Fig. 1. Definitive assignments of the $^{P,R}R_K$ and $^{P,R}P_K$ branch lines of individual subbands could not be made, because the small spacing of $2[A'(1-\zeta^z)-B']$ made the P and/or R branch lines overlap each other. The molecular constants ν_0, A', and $A'\zeta^z$ in the usual quadratic expression were determined by the least-squares method so as to fit the observed $^{P,R}Q_K$ branch wavenumbers, where other rotational and centrifugal distortion constants were constrained to the microwave values.[2] The observed line positions of the $^{P,R}Q_K$ branches are given in Table 1. The molecular constants determined are listed in Table 2.

The spectra of the $\nu_8^{\pm 1}$ band for $CH_3C{\equiv}P$ and $CD_3C{\equiv}P$ were simulated by using the molecular constants obtained. The simulation spectra have revealed the existence of additional series of lines in the experimental spectra. These lines may be ascribed to hot bands with which $\nu_8^{\pm 1}$ is associated. For the hot band $2\nu_8-\nu_8$, which is due to a transition from the most populated excited state, there are three possible cases; i.e., two perpendicular-type bands $2\nu_8^0-\nu_8^{\pm 1}$ and

Table 1. Observed $^{P,R}Q_K$ Line Positions of the $\nu_8^{\pm 1}$ and $2\nu_8^0-\nu_8^{\pm 1}$ Bands of $CH_3C{\equiv}P$ and $CD_3C{\equiv}P$[a]

	$CH_3C{\equiv}P$				$CD_3C{\equiv}P$			
	$\nu_8^{\pm 1}$		$2\nu_8^0-\nu_8^{\pm 1}$		$\nu_8^{\pm 1}$		$2\nu_8^0-\nu_8^{\pm 1}$	
	ν_{obsd} / cm^{-1}	$\Delta\nu$[b] / cm^{-1}	ν_{obsd} / cm^{-1}	$\Delta\nu$[b] / cm^{-1}	ν_{obsd} / cm^{-1}	$\Delta\nu$[b] / cm^{-1}	ν_{obsd} / cm^{-1}	$\Delta\nu$[b] / cm^{-1}
$^RQ_{10}$			308.287*	0.128			281.469	0.042
$^RQ_9$			307.383	0.046	285.748	−0.018	280.656	−0.017
$^RQ_8$			306.479	−0.013	285.055	0.062	279.902	−0.010
$^RQ_7$	310.668	0.056	305.545*	−0.083	284.272	0.057	279.119	−0.026
$^RQ_6$	309.794	0.040	304.732	−0.014	283.398	−0.034		
$^RQ_5$	308.860	−0.017	303.828	−0.022	282.674	0.028	277.552	−0.044
$^RQ_4$	307.926	−0.057			281.831	−0.026	276.768	−0.046
$^RQ_3$	307.022	−0.051	301.959	−0.061	281.017	−0.049	275.985	−0.043
$^RQ_2$	306.118	−0.033	301.055	−0.037	280.234	−0.038	275.202	−0.036
$^RQ_1$	305.184	−0.035	300.121	−0.037	279.451	−0.026	274.388	−0.058
$^RQ_0$	304.280	0.002	299.247	0.026	278.667	−0.015	273.665	0.013
$^PQ_1$	303.345	0.012	298.313	0.030	277.853	−0.033	272.912	0.056
$^PQ_2$	302.381	−0.004	297.349	0.001	277.070	−0.021	272.128	0.068
$^PQ_3$	301.477	0.042	296.445	0.029	276.286	−0.011	271.345	0.081
$^PQ_4$	300.543	0.056	295.541	0.051	275.503	−0.001	270.471	0.003
$^PQ_5$	299.579	0.036	294.607	0.035	274.750	0.037	269.687	0.015
$^PQ_6$	298.645	0.042	293.673	0.008	273.936	0.012	269.024*	0.147
$^PQ_7$	297.650	−0.022	292.767	−0.004	273.183	0.045	268.211*	0.126
$^PQ_8$	296.716	−0.035	291.775*	−0.117	272.399	0.043	267.427*	0.133
$^PQ_9$	295.812	−0.031	290.991	−0.040	271.616	0.039		
$^PQ_{10}$					270.832	0.029		
$^PQ_{11}$					270.049	0.016		
$^PQ_{12}$					269.265	−0.005		
$^PQ_{13}$					268.482	−0.030		
$^PQ_{14}$					267.699	−0.062		

a) The observed wavenumbers with asterisk are not included in the least-squares fit. J values were assumed to be $J=K+1$ for the ^RQ_K lines and $J=K$ for the ^PQ_K lines. b) $\nu_{obsd}-\nu_{calcd}$.

Table 2. Molecular Constants for the $\nu_8^{\pm 1}$ and $2\nu_8^0-\nu_8^{\pm 1}$ Bands of $CH_3C{\equiv}P$ and $CD_3C{\equiv}P$[a]

Molecular constant	$CH_3C{\equiv}P$		$CD_3C{\equiv}P$	
	$\nu_8^{\pm 1}$	$2\nu_8^0-\nu_8^{\pm 1}$	$\nu_8^{\pm 1}$	$2\nu_8^0-\nu_8^{\pm 1}$
$(\nu_0)_v$	308.338 (48)	294.217 (37)	280.330 (37)	271.207 (44)
A_v	5.1703 (14)	5.1692 (35)	2.58820 (53)	2.5878 (10)
$(A\zeta^z)_v$	4.5320 (31)	4.5320[b]	2.0470 (18)	2.0470[b]

a) In units of cm^{-1}. The three times standard deviations, given in parentheses, apply to the last significant figures. $A_0=5.17264$ cm^{-1} for $CH_3C{\equiv}P$ and $A_0=2.58826$ cm^{-1} for $CD_3C{\equiv}P$. b) Assumed.

$2\nu_8^{\pm2}-\nu_8^{\pm1}$ and one parallel-type band $2\nu_8^{\mp2}-\nu_8^{\pm1}$. Of these, only the $2\nu_8^{0}-\nu_8^{\pm1}$ band is likely to be observed in this region, since the microwave analysis of $CH_3C{\equiv}P$[2] has given the anharmonicity constant g_{88} to be 6.11±0.86 cm^{-1} which includes a Coriolis term $A_8(\zeta_8^z)^2$. The wavenumbers for the $^{P,R}Q_K$ branches of $2\nu_8^{0}-\nu_8^{\pm1}$ are given by

$$^{R}_{P}\nu^{Q}=\nu_0+A'-B'\pm2[A'-A''\zeta^z-B']K+[(A'-B')-(A''-B'')]K^2+(B'-B'')J(J+1). \quad (2)$$

The successive spacing of $2[A'-A''\zeta^z-B']$ is nearly equal to that for the $\nu_8^{\pm1}$ band. The transitions with the $|K-l|=3|n|$ levels in the lower vibrational state, i.e., ..., $^{R}Q_5$, $^{R}Q_2$, $^{P}Q_1$, $^{P}Q_4$, ... are stronger than the others. The assignments of the $^{P,R}Q_K$ branches of $2\nu_8^{0}-\nu_8^{\pm1}$ were made, as shown in Fig. 1, on the basis of the above criterion and the anharmonicity constant x_{88} for $CH_3C{\equiv}N$[3] and $x'_{88}\simeq(\omega'_8/\omega_8)x_{88}$. The observed line positions of the $^{P,R}Q_K$ branches are given in Table 1 and the molecular constants determined are given in Table 2.

The composite simulation spectrum of the $\nu_8^{\pm1}$ and $2\nu_8^{0}-\nu_8^{\pm1}$ bands is shown in Fig. 1(a) for $CH_3C{\equiv}P$ and in Fig. 1(c) for $CD_3C{\equiv}P$. It is seen that the $\nu_8^{\pm1}$ band is well simulated but the intensities of $2\nu_8^{0}-\nu_8^{\pm1}$ are not reproduced satisfactorily with the Boltzmann factor alone.

Table 3. Vibrational Parameters of the $\nu_8^{\pm1}$ Band of $CH_3C{\equiv}P$ and $CD_3C{\equiv}P$

Compound	ω_8^0/cm^{-1}	x_{88}/cm^{-1}	g_{88}/cm^{-1}
$CH_3C{\equiv}P$	303.18	−0.95	6.11[a]
$CD_3C{\equiv}P$	277.38	−0.81	3.75[b]

a) Microwave value (Ref. 2). b) The anharmonic terms in g_{88} are assumed to be the same as those for $CH_3C{\equiv}P$.

The determined band origins for $\nu_8^{\pm1}$ of $CH_3C{\equiv}P$ and $CD_3C{\equiv}P$ in the gaseous state are smaller by 8—7 cm^{-1} than those observed in the solid state: 316 cm^{-1} for the former and 287 cm^{-1} for the latter.[1] The band origins for $\nu_8^{\pm1}$ and $2\nu_8^{0}-\nu_8^{\pm1}$ and the microwave value[2] for g_{88} of $CH_3C{\equiv}P$ yield the vibrational parameters for $CH_3C{\equiv}P$ and $CD_3C{\equiv}P$ as given in Table 3. By using these parameters, the band origin for $3\nu_8^{\pm1}$ of $CD_3C{\equiv}P$ is estimated to be 828.6 cm^{-1}. An experimental value of 829.7±0.4 cm^{-1} has been obtained for this band origin from the $^{P,R}Q_K$ branch analysis of a Fermi-interacting band system $\nu_7^{\pm1}$ and $3\nu_8^{\pm1}$ with the assumption that $(\zeta_{eff}^z)_{888}=0.791$.[1] The Coriolis constant ζ_8^z was obtained to be 0.876 for $CH_3C{\equiv}P$ and 0.791 for $CD_3C{\equiv}P$, in good agreement with 0.865 and 0.772, respectively, calculated from the molecular force field.[1] The molecular parameters for $CH_3C{\equiv}P$ may also be compared with those for $CH_3C{\equiv}N$: $\omega_8^0=360.27$ cm^{-1}, $x_{88}=-0.963$ cm^{-1}, $g_{88}=5.75$ cm^{-1}, and $\zeta_8^z=0.874$.[3]

The authors wish to express their thanks to Miss Ikuko Shimooka for her assistance in the spectral analysis.

References

1) K. Ohno, H. Matsuura, D. McNaughton, and H. W. Kroto, *J. Mol. Spectrosc.*, **111**, 415 (1985).
2) H. W. Kroto, J. F. Nixon, and N. P. C. Simmons, *J. Mol. Spectrosc.*, **77**, 270 (1979).
3) Y. Mori, T. Nakagawa, and K. Kuchitsu, *J. Mol. Spectrosc.*, **104**, 388 (1984).

Topological Charge Stabilization Rule and Quasi-Aromaticity

Jun-ichi AIHARA
Department of Chemistry, Faculty of Science, Shizuoka University, Oya, Shizuoka 422
(Received January 26, 1987)

Synopsis. Stabilities of the oxocarbon dianions and some quasi-aromatic compounds can be rationalized in terms of Gimarc's topological charge stabilization rule. The term "quasi-aromatic" is recommended for describing those non-aromatic compounds which behave like aromatics owing to the operation of this rule.

Monocyclic oxocarbon dianions with the general formula $C_nO_n^{2-}$ (**1**—**4**) are fairly stable substances.[1,2] West et al.[1,3] and Herndon[4] considered them as a kind of aromatic species, stabilized by π electron delocalization around the ring. Two research groups, however, showed that extra stabilization energy scarcely arises from the cyclic conjugation in these ions.[5,6] So-called topological resonance energy (TRE) is very small except the deltate dianion (**1**).[5] Only $C_3O_3^{2-}$ seems to be aromatic with large TRE. Associating bond orders with aromaticity, Jug showed that for the oxocarbon dianions the aromaticity decreases rapidly as the ring size increases.[7]

In 1964 Lloyd and Marshall proposed that molecules should be called quasi-aromatic only if they contain an acyclic conjugated π-electron system and show chemical properties typical of aromatic compounds, especially reaction by substitution with retention of the original conjugated system.[8] They first used the term "quasi-aromatic" with this meaning to describe the behavior of the 2,3-dihydro-1,4-diazepinium salts (**5**).[8,9] The α,ω-diazapolymethinium salts (**6**)[10] and the transition-metal chelates of β-diketones (**7**)[11] can also be classified as quasi-aromatics. Although the metal chelates of acetylacetone apparently have a cyclic conjugated system, Musso et al. demonstrated that no ring currents are induced in these complexes.[12] This indicates that the π-electron conjugation is interrupted at the metal atom. All these quasi-aromatic species have no TRE since there are no cyclic paths for π electrons.

What then is the main origin of stability of the monocyclic oxocarbon dianions and the quasi-aromatic compounds? It is very true that their aromatic behavior and stability cannot be related to the cyclic conjugation of π electrons. The purpose of this note is to solve this problem using Gimarc's topological charge stabilization rule.[13-15]

In 1983 Gimarc stressed that the pattern of charge densities in a molecule is determined primarily by the connectivity or topology of the molecule.[13,14] Many examples showed that nature prefers to place atoms of greater electronegativity in those positions where the topology of the structure tends to pile up extra charge in the isoelectronic hydrocarbon.[13,15] Since such heteroatomic systems are preferentially stabilized by molecular topology, Gimarc called the effect the rule of topological charge stabilization.[13]

Oxocarbon Dianions

An oxocarbon dianion with n carbonyl groups is referred to as [n]oxocarbon dianion. Radialene with n exomethylenes is likewise referred to as [n]radialene. The [n]radialene dianion is iso-π-electronic with the [n]oxocarbon dianion. Such an iso-π-electronic hydrocarbon has been called a uniform reference frame (URF).[13] The [n]oxocarbon dianion and its URF have the same geometry with the same number of π electrons ($2n+2$). Charge densities were calculated for the URF's of **1**—**4**, (i.e., four radialene dianions) using the simple HMO model. They are shown in Fig. 1.

It is noteworthy that these radialene dianions have maximum charge densities at the exomethylene carbons. The oxocarbon dianions are formed by replacing all these carbons by more electronegative oxygens. Thus, the framework of every oxocarbon dianion is favored from the standpoint of the topological charge stabilization rule.[13] In other words, the stability of most oxocarbon dianions is largely due to the presence of oxygens at positions where, for purely geometrical reasons, the π electrons congregate.[13,14] This possibly constitutes the primary reason why the oxocarbon dianions have often been regarded as aromatics.

Many oxocarbon analogues have been synthesized by replacing one or more oxygens by other hetero atoms, such as nitrogens and sulfurs.[1,2] The topological charge stabilization rule necessarily operates in these compounds.

Oxocarbon acids of the general formula $C_nO_nH_2$ (**8**—**11**)[1,2] are acids conjugate to the oxocarbon dianions. The URF of each oxocarbon acid is identical with that of the corresponding oxocarbon dianion. A given oxocarbon acid is formed by replacing two of the exomethylene carbons in the URF by hydroxyl oxygens and the remaining ones by carbonyl oxygens. Thus, the carbons of maximum charge density in the URF are all replaced by electronegative oxygens. All oxocarbon acids are known indeed.

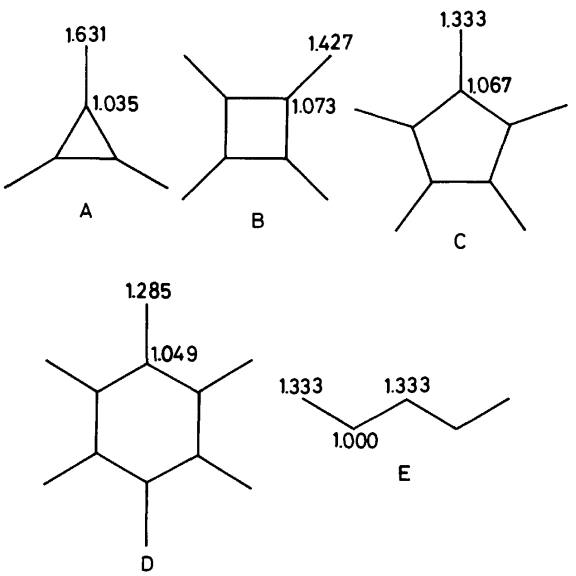

Fig. 1. Charge densities in: (A) the [3]radialene dianion (the URF of **1**); (B) the [4]radialene dianion (the URF of **2**); (C) the [5]radialene dianion (the URF of **3**); (D) the [6]radialene dianion (the URF of **4**); and (E) the pentadienide anion (the URF of **5** and **7**).

Unfortunately, the topological charge stabilization rule is not applicable to the neutral oxocarbons (C_nO_n). The URF of neutral [$2m$]oxocarbon is [$2m$]radialene. Since this is an alternant hydrocarbon, the charge distribution is uniform over the entire conjugated system. A similar situation is seen in the case of the URF of neutral [$2m+1$]oxocarbon. Although [$2m+1$]radialene is not an alternant hydrocarbon, the charge distribution is fairly uniform. These facts may not account for the instability of neutral oxocarbons, but coincide with it.

Quasi-Aromatic Compounds

Pentadienide ion ($C_5H_7^-$) is iso-π-electronic with the conjugated systems of the quasi-aromatic compounds **5** and **7**. As shown in Fig. 1, this URF has the maximum charge densities at one central and two edge carbons. If the two edge carbons are replaced by electronegative nitrogens, in such a manner that the entire conjugated system preserves the number of π electrons, we obtain the conjugated system of the 2,3-dihydro-1,4-diazepinium ion (**5**). If they are replaced by oxygens, we obtain the conjugated subsystem of the β-diketonate ion in **7**. Therefore, the stability of these quasi-aromatic systems can again be rationalized by the topological charge stabilization rule. A similar explanation applies to the quasi-aromaticity of other α,ω-polymethinium ions (**6**). We might safely say that the tendency of these compounds to retain the original conjugated system[8] arises primarily from such topological charge stabilization in the ground electronic state.

Concluding Remarks

The oxocarbon dianions and some acyclic systems have been classified as aromatics or quasi-aromatics although they have essentially zero TRE. It was shown that chemical behaviors and stability of these compounds can be rationalized well in terms of the topological charge stabilization rule. These compounds are thermodynamically favored since the constituent atoms are arranged such that their electronegativities match the pattern of charge densities of the iso-π-electronic hydrocarbon.[13,14] Considering that there have been no other widely accepted theories for the stability of these compounds, the present simple rationale seems to be the best one available.

It is suggested that to avoid confusion the term "aromatic" be restricted to compounds with relatively large TRE.[5] The term "quasi-aromatic" is instead recommended for describing those essentially non-aromatic conjugated compounds which tend to retain their own conjugated systems. The quasi-aromatic compounds defined here are those which are stabilized by the operation of the topological charge stabilization rule but not by cyclic conjugation. The oxocarbon dianions with $n>3$ should be classified as quasi-aromatic compounds, rather than as aromatic com-

pounds.

As already pointed out by Gimarc,[13] Y-aromaticity in guanidinium (**12**) and carbonate (**13**) ions[16] can also be rationalized in terms of the topological charge stabilization rule. These Y-aromatic compounds should again be classified as quasi-aromatic species.

References

1) R. West, Ed., "Oxocarbons," Academic Press, New York (1980).
2) A. H. Schmidt, *Janssen Chim. Acta*, **4**, 3 (1986).
3) R. West, H.-Y. Niu, D. L. Powell, and M. V. Evans, *J. Am. Chem. Soc.*, **82**, 6204 (1960).
4) W. C. Herndon, *J. Mol. Struct.*, **103**, 219 (1983).
5) J. Aihara, *J. Am. Chem. Soc.*, **103**, 1633 (1981).
6) A. Moyano and F. Serratosa, *J. Mol. Struct.*, **90**, 131 (1982).
7) K. Jug, *J. Org. Chem.*, **48**, 1344 (1983).
8) D. Lloyd and D. R. Marshall, *Chem. Ind. (London)*, **1964**, 1760; *Angew. Chem., Int. Ed. Engl.*, **11**, 404 (1972).
9) D. Lloyd, H. P. Cleghorn, and D. R. Marshall, *Adv. Heterocycl. Chem.*, **17**, 1 (1974).
10) J. Kučera and Z. Arnold, *Collect. Czech. Chem. Commun.*, **32**, 1704 (1967).
11) J. P. Collman, *Angew. Chem., Int. Ed. Engl.*, **4**, 132 (1965).
12) M. Kuhr and H. Musso, *Angew. Chem., Int. Ed. Engl.*, **8**, 147 (1969).
13) B. M. Gimarc, *J. Am. Chem. Soc.*, **105**, 1979 (1983).
14) H. C. Longuet-Higgins, C. W. Rector, and J. R. Platt, *J. Chem. Phys.*, **18**, 1174 (1950).
15) B. M. Gimarc and J. J. Ott, *J. Am. Chem. Soc.*, **108**, 4298 (1986); J. J. Ott and B. M. Gimarc, *ibid.*, **108**, 4303 (1986).
16) P. Gund, *J. Chem. Educ.*, **49**, 100 (1972).

The Preconcentration and Determination of a Trace Amount of Strontium in Fresh Water as Its 1-Phenyl-3-methyl-4-benzoyl-5-pyrazolone Chelate by Means of Solvent Extraction

Takaharu HONJO* and Takashi NAKATA
Department of Chemistry, Faculty of Science, Kanazawa University, Marunouchi, Kanazawa 920
(Received September 6, 1986)

Synopsis. The behavior of a trace amount of alkaline earth metals (magnesium, calcium, strontium, and barium) on solvent extraction has been examined with PMBP (1-phenyl-3-methyl-4-benzoyl-5-pyrazolone) in benzyl alcohol; the results have also been applied to the preconcentration and determination of a trace amount of strontium in ppb order in fresh water as its PMBP chelate by means of solvent extraction.

The content of strontium in fresh water is generally known to be in ppb order, and it must be concentrated up to ppm order, prior to its determination by means of a usual atomic absorption method. Solvent extraction, especially chelate extraction, is a simple and highly selective convenient method for the preconcentration and determination of a trace amount of metals like heavy metals[1-6,8] and alkaline earth metals[3,6,7] in natural waters. Among the extractive chelating agents of 8-hydroxyquinoline, β-isopropyltropolone, 2-thenoyltrifluoroacetone, and PMBP (1-phenyl-3-methyl-4-benzoyl-5-pyrazolone), PMBP has been reported to be most useful for the extraction of alkaline earth metals.[3,6-8]

In this investigation, the behavior of a trace amount of alkaline earth metals (magnesium, calcium, strontium, and barium) in solvent extraction has been examined with PMBP in benzyl alcohol; the results have been applied to the preconcentration and determination of a trace amount of strontium in ppb order in fresh water as its PMBP chelate by means of solvent extraction for the subsequent atomic absorption analysis.

Experimental

Apparatus. A model 323 Hitachi Recording Spectrophotometer; a model 239 Hitachi Digital Spectrophotometer; a model 170—50 Hitachi Atomic Absorption/Flame Spectrophotometer; a Hitachi-Horiba glass electrode pH meter, model M-5; an Iwaki shaking machine, model KM; a Kubota centrifuge machine, and a Tomi-Seiko Swing Type centrifuge, model CD-50R, were used.

Materials. PMBP (1-phenyl-3-methyl-4-benzoyl-5-pyrazolone) was synthesized by the condensation of 1-phenyl-3-methyl-5-pyrazolone with benzoyl chloride in dioxane, as described previously.[8] The PMBP was purified by recrystallization from a mixture of methanol and a dilute hydrochloric acid solution; it crystallizes in yellow plates (keto type) having the same reference value, melting point of 92 °C. The organic solvents used were all reagent-grade materials and if necessary were purified by an ordinary method. Benzyl alcohol was used within one week after opening the sealed bottle, because of its gradual degradation caused by air oxidation.

Distribution of PMBP. The distribution behavior of PMBP between various organic solvents and water was examined as follows: An equal volume (5 cm^3) of 5×10^{-5}—10^{-3} M (1M=1 mol dm^{-3}) each of various organic solutions of PMBP and buffer solutions of pH 1—12 adjusted to the desired value by mixing an appropriate amount of 0.1 M of hydrochloric acid, acetic acid, sodium acetate, boric acid, sodium borate, and sodium hydroxide, was equilibrated by shaking both phases for 30 min. After centrifugation at 2000 rpm for 15 min, the concentration of PMBP in the organic phase was determined spectrophotometrically by measuring its absorbance at 290—300 nm, around the absorption maxima of PMBP. The pH of the aqueous phase was checked again after the distribution.

Extraction of Alkaline Earth Metals. A 10 cm^3 of 10^{-3} M alkaline earth metal ion solution adjusted to the desired pH with buffer solutions described above and a 10 cm^3 of 10^{-2} M PMBP in organic solvent were placed in a 30 cm^3 glass-stoppered centrifuge tube and agitated on a shaking machine for 30 min. After the separation of the two phases by centrifugation at 2000—3000 rpm for 15—30 min, a 5 cm^3 of the organic phase was shaken with 0.1 M hydrochloric acid solution; the amount of metal ion stripped in the aqueous phase was determined by atomic absorption at 285.21 nm for magnesium, at 422.67 nm for calcium, and at 460.73 nm for strontium. The concentration of barium was determined by flame photometry at 553.6 nm. The pH of the aqueous phase was measured again after the extraction.

Results and Discussion

The distribution behavior of PMBP in various organic solvents was first studied in order to find the proper solvent having a higher distribution ratio and better phase separation in the basic region, where alkaline earth metals can be extracted quantitatively.[3,6-8] The preliminary experiments revealed that the distribution of PMBP expressed by percent extraction (%E) in an organic solution increased in the order of benzene, butyl acetate, isobutyl methyl ketone (0%) <chloroform (5%)<isopentyl alcohol, hexyl alcohol, decyl

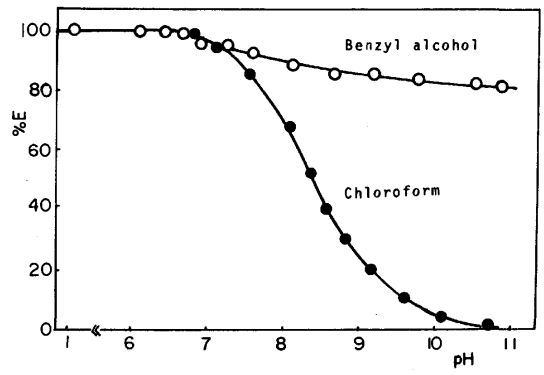

Fig. 1. Distribution of 5×10^{-5}—10^{-3} M PMBP in chloroform and benzyl alcohol as a function of pH.

alcohol, octyl alcohol (40—60%)<benzyl alcohol (83%) at pH 10 (Fig. 1). Judging from the higher distribution of PMBP in the organic phase and the better separation of the two phases by centrifugation at 2000 rpm for 15 min, it was evident that benzyl alcohol was most suitable for the extraction of alkaline earth metals with PMBP. Next, the pH dependence of the extractability of alkaline earth metals (magnesium, calcium, strontium, and barium) with 10^{-2} M PMBP in benzyl alcohol was examined in the region of pH 1.0 to 10.0. The results (Fig. 2) are shown in terms of percent extraction (%E) vs. pH plots of alkaline earth metals extracted in benzyl alcohol. The quantitative extraction of the PMBP chelate in benzyl alcohol was achieved in the pH region above 6 for magnesium, in the pH region above 7.0 for calcium, and in the pH region of 7.5—8.5 for strontium. Barium was not extracted completely in any pH region. The log D vs. pH plots gave straight lines having a slope of about 2, which gave the number of the PMBP molecule bound to alkaline earth metals. In general, the extractability of alkaline earth metals with PMBP in benzyl alcohol is better than in chloroform, benzene, and cyclohexane, without synergic extraction with the aid of TOPO (trioctylphosphine oxide).[3,6-8] On the basis of these results, it was decided that the extraction of strontium with 10^{-2} M PMBP in benzyl alcohol should be carried out at pH 8.0. Although the complete and quantitative extraction was achieved after 3 min of shaking, the two phases were shaken for 5—10 min. When the volume of the organic phase of 10^{-2} M PMBP in benzyl alcohol was kept at 10 cm^3, and when that of the aqueous phase was varied from 10 to 100 cm^3, almost the same extractability (100±1%) was obtained in each case. The effect of the presence of foreign ions, which exist in fresh water, on the extraction of strontium is given in Table

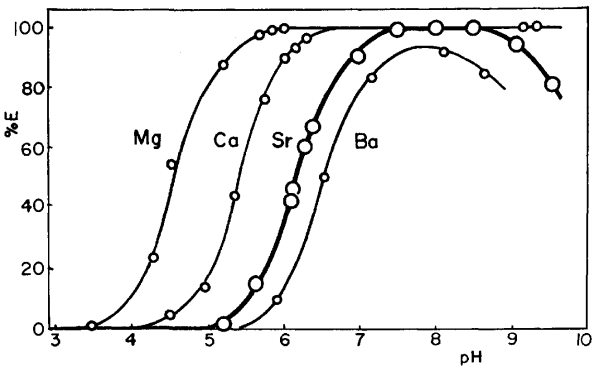

Fig. 2. Extraction of 10^{-3}M alkaline earth metals with 10^{-2}M PMBP in benzyl alcohol as a function of pH.

Table 1. Effect of Foreign Ions

Ion added		Sr^{2+} taken	Sr^{2+} found
ppm		ppm	ppm
Ca^{2+}	50	0.20	0.21
Mg^{2+}	10	0.20	0.20
Al^{3+}	1	0.20	0.21
HCO_3^-	100	0.20	0.20
SO_4^{2-}	20	0.20	0.20
PO_4^{3-}	1	0.20	0.20

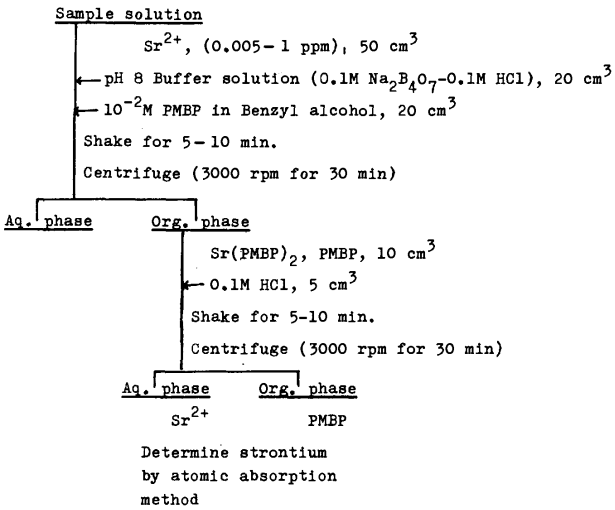

Fig. 3. Analytical scheme for the preconcentration and determination of a trace amount of strontium in fresh water.

Table 2. Content of Strontium, Calcium, and Magnesium Ions in Fresh Water near Kanazawa University

Sample	Solution volume	Sr^{2+} added	Sr^{2+} found	Sr^{2+} content[a]	Ca^{2+} content[b]	Mg^{2+} content[b]
	cm^3	μg	μg	ppb	ppm	ppm
Tap water	50	0	3.55	71±1	14.4	6.2
		0	3.65	73±1	14.4	6.2
		1.0	4.60	72±1	14.4	6.2
OHTEBORI moat water	50	0	3.65	73±1	14.1	5.5
Thawing water	50	1.0	1.35	7±1	1.6	1.2

a) Mean and relative standard deviation for at least three determinations. The experimental results obtained by adding a definite amount of strontium to fresh water revealed that the recovery of strontium was about 100±1%. In the case of thawing water, the absortance of atomic absorption of strontium gave very small value, and the result obtained by adding a definite amount of strontium to fresh water was shown in Table 2. b) The experimental results obtained by direct determinations of magnesium and calcium in fresh water with atomic absorption method without preconcentration.

1. The concentration of these ions was prepared so as to be somewhat larger than that of general fresh water as river water and underground water. None of the ions investigated interfered with the extractability of strontium with PMBP in benzyl alcohol. Finally, the systematic experimental procedures (Fig. 3) for the determination of strontium in natural waters based on the extraction and atomic absorption spectrophotometric determination of strontium with 10^{-2} M PMBP in benzyl alcohol have been applied to the preconcentration and determination of a trace amount of strontium in ppb order in fresh water in the vicinity of Kanazawa University.

The results are given in Table 2 together with the values obtained for calcium and magnesium in ppm order without preconcentration, showing that the proposed method was useful for the preconcentration and determination of strontium in ppb order (7—73±1 ppb) in fresh water.

The authors wish to thank Prof. Kikuo Terada of Kanazawa University for his valuable advice.

References

1) T. Honjo, S. Abe, and T. Kiba, *Bull. Chem. Soc. Jpn.*, **51**, 1239 (1978).
2) T. Honjo and M. Annen, *J. Soc. Eng. Mineral Springs*, **15**, 7 (1980); T Honjo, S. Hata, and A. Hatta, *ibid.*, **18**, 1 (1983).
3) M. Y. Mirza and F. I. Nwabue, *Talanta*, **28**, 49 (1981).
4) Y. Itoh, H. Kawamoto, and H. Akaiwa, *Anal. Sci.*, **2**, 43 (1986).
5) T. Honjo and T. Makino, *Bull. Chem. Soc. Jpn.*, **59**, 3273 (1986).
6) S. Umetani, M. Matsui, T. Kuzunishi, and Y. Nishikawa, *Bull. Inst. Chem. Res., Kyoto Univ.*, **60**, 254 (1982); S. Iwasaki, S. Umetani, K. Sasayama, and M. Matsui, *Anal. Lett.*, **15**, 1159 (1982).
7) M Sugiyama, O. Fujino, and M. Matsui, *Bunseki Kagaku*, **33**, E123 (1984).
8) B. S. Jensen, *Acta Chem. Scand.*, **13**, 1668 (1959); *Idem, ibid.*, **13**, 1980 (1959).

Synthetic Inorganic Ion-Exchange Materials. XXXXVI. Ion-Exchange Behavior of Titanium(IV) Antimonate Cation Exchanger for Alkali Metal Ions in Ammonium Nitrate Media

Ramesh CHITRAKAR and Mitsuo ABE*
Department of Chemistry, Faculty of Science, Tokyo Institute of Technology, 2-12-1 Ookayama, Meguro-ku, Tokyo 152
(Received November 27, 1986)

Synopsis. Titanium(IV) antimonate (TiSbA) showed an extremely high selectivity for lithium ions in ammonium nitrate media, the increased selectivity order for microamounts being $Rb^+<Na^+<Cs^+<K^+\ll Li^+$. The selective separation of lithium ions from other alkali metal ions can be achieved on small columns of TiSbA by a mixed solution of nitric acid and ammonium nitrate.

The synthesis and ion-exchange properties of tin(IV) antimonate and titanium(IV) antimonate (SnSbA and TiSbA) have been studied first by Abe et al.[1-3] Both of SnSbA and TiSbA behave as cation exchangers with high selectivity for lithium ions. The following unusual selectivities for microamounts of alkali metal ions in nitric acid media were observed: $Na^+<K^+<Rb^+<Cs^+\ll Li^+$ on SnSbA,[2] and $Na^+<K^+<Rb^+<Li^+<Cs^+$ on TiSbA[3,4] as compared to increased order of the selectivity with increasing ionic crystal radii for alkali metal ions on a strong acid type polystyrene resin. The high selectivity for lithium on SnSbA and TiSbA can be applied for the recovery of lithium ions from seawater and hydrothermal water.[5,6]

The ion-exchange behavior of various ions on SnSbA and TiSbA has been studied extensively.[7-10]

Isolation of lithium ions from other alkali metal ions on H^+ form TiSbA with nitric acid solution as an eluant is very difficult because of low values of separation factor for pairs of Rb^+-Li^+ and Li^+-Cs^+. It has been known that the selectivity depends much on a variety of solutions used as eluants.

The present work describes the adsorption of alkali metal ions by TiSbA in ammonium nitrate media and the chromatographic separation of lithium from other alkali metal ions.

Experimental

Chemicals. Chemical grade of antimony(V) chloride supplied by Yotsuhata Chemical Co. Ltd., and titanium(IV) chloride supplied by Wako Chemical Co. Ltd., (99% as metal) were used without further purification. The other chemicals were of analytical grade.

Preparation of TiSbA. A 4 M† antimony(V) chloride solution (80 cm^3) was mixed with a 4 M titanium(IV) chloride solution (120 cm^3) at 60 °C and the mixed solutions were immediately hydrolyzed in 4.8 dm^3 demineralized water at the same temperature. The precipitate obtained was kept in mother liquor overnight, filtered and washed with cold demineralized water using a centrifuge operated at 10000 rpm until the pH of supernatant solution was in the range of 1.5—1.8. The product obtained was dried at 60 °C for 4d, ground and sieved to 100—200 mesh size, washed with cold demineralized water in order to remove fine adherent particles, and conditioned with 1 M nitric acid until free from Na^+ ions. The sample was re-washed with demineralized water and air dried.

Preparation of TiSbA in Ammonium Ion Form. The hydrogen form of TiSbA was converted to ammonium form as follows: A solution containing 0.3% aq NH_3 and 0.1 M NH_4NO_3 was passed through a column packed with 10 g of TiSbA in H^+ form until the pH of the effluent was the same as that of the feed solution. Finally, the exchanger was washed with demineralized water and air dried.

pH Titration Curve. The pH titration curve was determined by equilibrating 0.10 g of TiSbA in H^+ form with 10.0 cm^3 of solution containing (NH_4NO_3+HNO_3) or (NH_4NO_3 +NH_3aq) at an ionic strength of 0.1 with intermittent shaking for one week at 30 °C. After equilibrium was attained, the pH of the supernatant solution was measured with a Toa Dempa pH meter, model HM-5B. The concentration of NH_4^+ in the solution was determined as described by Tsuji and Abe.[11]

Distribution Coefficients, (K_d). The K_d values of alkali metal ions were determined by equilibrating 0.10 g of TiSbA in NH_4^+ form with 10.0 cm^3 of 10^{-4} M alkali metal ions, except Li^+ at different concentrations of ammonium nitrate with intermittent shaking at 30 °C. The K_d of Li^+ at an initial concentration of 10^{-4} M showed extremely high values even at 5M NH_4NO_3 solution and could not be determined, because of the detection limit of atomic absorption analysis. Its K_d values were determined at the initial concentration 10^{-3} M of Li^+. The concentrations of metal ions in the solid and liquid phases were deduced from the concentration relative to the initial concentration in the solution. The K_d values were calculated at equilibrium using the following equation:

$$K_d = \frac{\text{Amount of metal ions in exchanger}}{\text{Amount of metal ions in solution}} \times \frac{\text{cm}^3 \text{ of solution}}{\text{g of exchanger}}$$

The concentrations of metal ions were determined by using a Varian Techtron 1100 Atomic Absorption Spectrometer.

Column Experiment. Relatively small columns (2 cm× 0.5 cm i.d.) of TiSbA in NH_4^+ form were used during column experiment. The flow rate was regulated by using a high pressure pump (Nihon Seimitsu Kagaku, model NSP-800-5UDX) and the effluents were collected by using a dropping-counting type fraction collector (Ohtaki Works, model UM-160).

Results and Discussion

Characterization of TiSbA. The TiSbA was characterized by X-ray diffraction and thermal analysis. The results showed a good agreement with the previous result.[4] The chemical composition of TiSbA used was determined by chemical analysis and weight loss at 700 °C by assuming that the ignition product was free from water. The empirical formula of TiSbA was $3.1TiO_2 \cdot Sb_2O_5 \cdot 4.9H_2O$.

pH Titration Curve. The pH titration curve of

†1 M=1 mol dm^{-3}.

NH_4^+ showed apparent monobasic acid behavior which was similar to that reported for alkali metal ions[4] (Fig. 1, top). The dependence of apparent capacity of NH_4^+ on pH (Fig. 1, bottom) is consistent with the titration curve. The uptake of NH_4^+ ions increased with increasing pH of the solution as reported for Na^+ and Li^+ ions. The uptakes of NH_4^+ correspond well to the difference between pH titration curve and blank titration curve, indicating that the ion-exchange reaction is predominant over the whole range of pH studied. Compared with the previous result,[4] the increased order of the uptakes was found to be $Cs^+ < Na^+ < NH_4^+ < Li^+$ at pH 9.

Distribution Coefficients, (K_d). The time dependence of adsorption of alkali metal ions on NH_4^+ form TiSbA in ammonium nitrate was measured in order to determine the equilibrium distribution coefficients. The exchange reaction in ammonium nitrate media was relatively fast and the equilibrium was attained within 24 h for all alkali metal ions studied (Fig. 2), while the reaction for Li^+ and Cs^+ in nitric acid media was slow, about 3 weeks being required for attainment of equilibrium. After equilibration, the K_d values were determined and shown in Fig. 3 as log-log plots of K_d vs. $a_{NH_4NO_3}$. A linear relationship with a slope of -1 was observed for all metal ions studied, indicating an ideal ion-exchange mechanism. The TiSbA in NH_4^+ form showed an extremely high selectivity for Li^+ ion in ammonium nitrate media, the selectivity order being $Rb^+ < Na^+ < Cs^+ < K^+ \ll {}^+Li$, which is not included in the 11 selectivity series predicted by Eisenman.[12] This selectivity is quite different from $Na^+ < K^+ <$

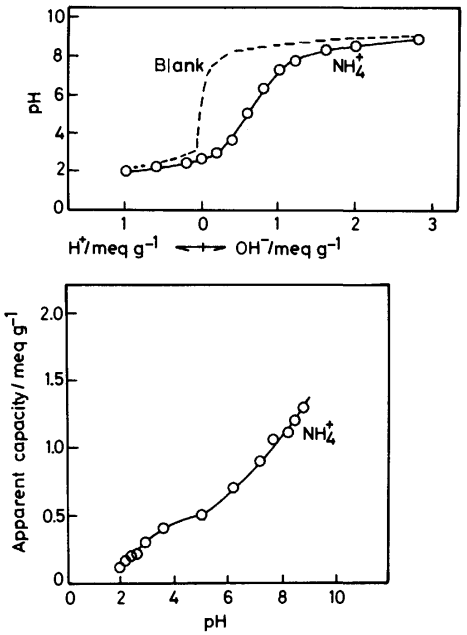

Fig. 1. pH Titration curve (top) and apparent capacity (bottom) of TiSbA.
TiSbA: 0.10 g. Soln.: 0.1 M (NH_4NO_3+HNO_3) or (NH_4NO_3+NH_3aq). Total vol: 10.0 cm^3. Temp: 30±0.5 °C.

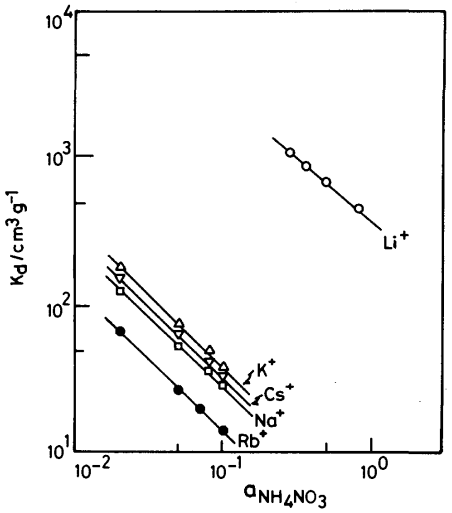

Fig. 3. Log-log plots of K_d values of alkali metal ions on NH_4^+ form TiSbA vs. activity of ammonium nitrate.
TiSbA: 0.10 g. Total vol: 10 cm^3. Other conditions are the same as in Fig. 2.

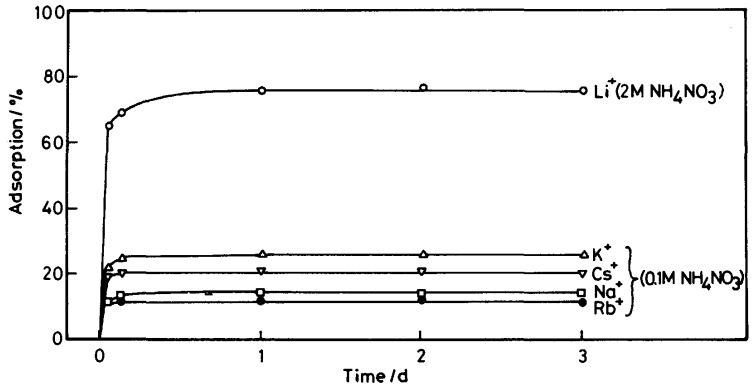

Fig. 2. Time dependence of adsorption of alkali metal ions on NH_4^+ form TiSbA.
TiSbA: 0.25 g. Initial concn of metal ions: 10^{-4} M for Na^+, K^+, Rb^+, and Cs^+, 10^{-3} M for Li^+. Total vol: 25.0 cm^3. Temp: 30±0.5 °C.

Table 1. K_d Values and Separation Factors(α) for Alkali Metal Ions on TiSbA and Bio-Rad AG 50W·X8

Ion exchanger	Media	Parameter					
			Rb^+	Na^+	Cs^+	K^+	Li^+
TiSbA (Ti/Sb=1.5)	0.1 M NH_4NO_3	K_d	14	18	31.3	35.4	$>10^5$
		α	1.3	1.7	1.1	>2800	
TiSbA[4] (Ti/Sb=1.5)	0.1 M HNO_3		Na^+	K^+	Rb^+	Li^+	Cs^+
		K_d	3.8	42	96	220	550
		α	11.1	2.3	2.3	2.5	
Bio-Rad AG 50W-X8[13]	0.1 M HNO_3		Li^+	Na^+	K^+	Rb^+	Cs^+
		K_d	33.1	54	99	118	148
		α	1.6	1.8	1.2	1.2	

$Rb^+<Li^+<Cs^+$ observed on H^+ form TiSbA in acid media.[3,4]

The K_d values and separation factors ($\alpha_A^B=K_{d_B}/K_{d_A}$), for a neighboring pair in NH_4NO_3 media, are summarized in Table 1, in which the K_d values on H^+ form of TiSbA and Bio-Rad AG 50W-X8[13] are included for comparison. The α value for neighboring pairs of alkali metals on H^+ form TiSbA are larger than those reported on Bio-Rad AG 50W-X8. But the values of α for neighboring pairs of alkali metals except Li^+ on NH_4^+ form TiSbA are comparable to Bio-Rad. However, the α value between Li^+ and other alkali metal ions are extremely high i.e. $>2.8\times10^3$.

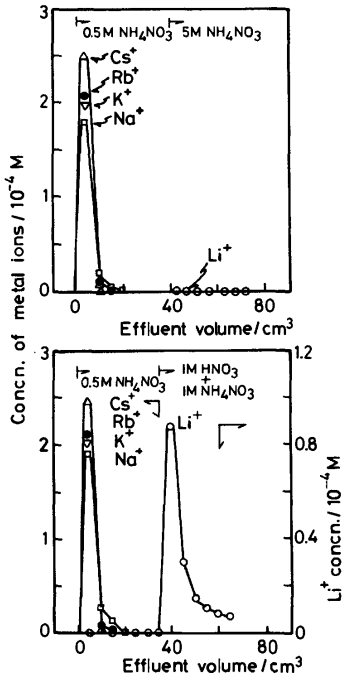

Fig. 4. Elution curves of alkali metals with NH_4^+ form TiSbA.
Column: 1.5 cm×0.5 cm i.d. (0.3 g of TiSbA), Metal ion loading: 1 μmol of each metal ion, Flow rate: 0.12 $cm^3\,min^{-1}$.

Ion-Exchange Separation. It is evident from the studies of K_d values that lithium can be separated from other alkali metals. A solution containing 1 μmol of alkali metal ions was added to the top of the small column (2 cm×0.5 cm i.d.) containing TiSbA in NH_4^+ form. The alkali metals except lithium were eluted with 100% recovery using 0.5 M NH_4NO_3 solution, while the adsorbed lithium could not be eluted even by using 5 M NH_4NO_3 solution as an eluant (Fig. 4, top). The elution of Li^+ was performed with 75% recovery upto 30 cm^3 of the eluant of 1M NH_4NO_3+1M HNO_3 solution (1+1) after elution of other alkali metal ions by a 0.5M NH_4NO_3 solution (Fig. 4, bottom). This procedure is very useful for isolation of lithium from other alkali metal ions.

References

1) M. Abe and T. Ito, *Kogyo Kagaku Zasshi*, **70**, 440 (1967).
2) M. Abe and K. Hayashi, *Solvent Extr. Ion Exch.*, **1**, 97 (1983).
3) M. Abe and M. Tsuji, *Chem. Lett.*, 1561 (1983).
4) M. Abe, R. Chitrakar, M. Tsuji, and K. Fukumoto, *Solvent Extr. Ion Exch.*, **3**, 149 (1985).
5) M. Abe and K. Hayashi, *Hydrometallurgy*, **12**, 83 (1984).
6) M. Abe, R. Chitrakar, and K. Hayashi, "Chemical Separation," ed by C. J. King and J. D. Navratil, Litervan Literature, Denever (1986), Vol. I, p. 187.
7) M. Abe and N. Furuki, *Solvent Extr. Ion Exch.*, **4**, 547 (1986).
8) M. Abe, "Lithium: Current Applications in Science, Medicine, and Technology," ed by R. O. Bach, Wiley-Interscience (1985), p. 1.
9) M. Abe, Y. Kanzaki, and R. Chitrakar, *J. Phys. Chem.*, in press.
10) R. Chitrakar and M. Abe, *Analyst*, **111**, 339 (1986).
11) M. Tsuji and M. Abe, *Bull. Chem. Soc. Jpn.*, **58**, 97 (1985).
12) G. Eisenman, *Biophys. J.*, **2**, 259 (1962).
13) F. W. E. Strelow, R. Rethemeyer, and C. J. C. Bothma, *Anal. Chem.*, **37**, 106 (1965).

X-Ray Structure of μ-Oxo-μ-sulfido-bis[(cysteinato)oxomolybdate(V)] Complex, $Ca[Mo_2O_3S(SCH_2CH(NH_2)CO_2)_2]\cdot 3H_2O$

Takashi SHIBAHARA,* Hisao KUROYA, Keiji MATSUMOTO,† and Shun'ichiro OOI†
Department of Chemistry, Okayama University of Science, 1-1 Ridai-cho, Okayama 700
†Department of Chemistry, Faculty of Science, Osaka City University, Sugimoto, Sumiyoshi-ku, Osaka 558
(Received December 15,1986)

Synopsis. The crystal structure of μ-oxo-μ-sulfido cysteinato Mo(V) dimer, $Ca[Mo_2O_3S(SCH_2CH(NH_2)CO_2)_2]\cdot 3H_2O$ has been determined from X-ray diffraction data. The structure of the complex anion is similar to those of di-μ-oxo- and di-μ-sulfido- Mo(V) dimers. The trans influence of sulfur atoms is observed.

As model compounds of some enzymes,[1] many molybdenum(V) complexes with di-μ-oxo, μ-oxo-μ-sulfido, or di-μ-sulfido bridges have been prepared and characterized. Cysteine (or its derivatives) is one of the ligands most frequently used in these investigations; Raman and resonance Raman spectra[2] and pulse-radiolysis study[3] on the cysteinato complexes have been reported and the X-ray structures of di-μ-oxo-[4] and di-μ-sulfido-bis[(cysteinato)oxomolybdate(V)][5] complexes have also been revealed. However, the X-ray structure of μ-oxo-μ-sulfido-bis [(cysteinato)oxomolybdate(V)], has not yet been determined. In view of the importance of this complex, we have carried out the X-ray crystal structure analysis of the title compound and we report here the result obtained.

Experimental

Preparation of Calcium μ-Oxo-μ-sulfido-bis[(cysteinato) oxomolybdate(V)] Trihydrate, $Ca[Mo_2O_3S(cys)_2]\cdot 3H_2O$. Corresponding sodium salt[6] (1 g) was dissolved in 10 mL of water and filtered. Solid $CaCl_2\cdot 2H_2O$ (ca. 1 g) was added to the filtrate. Cooling of the filtrate in a refrigerator gave red crystals (ca. 0.7 g). Anal. Found: N, 4.39; C, 11.54; H, 2.76%. Calcd for $C_6H_{12}O_{10}N_2S_3CaMo_2$: N, 4.66; C, 12.00; H, 2.01%.

X-Ray Data Collection. Crystal data: F. W.=600.3, orthorhombic, space group $P2_12_12_1$, a=16.430 (2), b=10.557 (2), c=9.782(2) Å, Z=4, D_c=2.35 g cm^{-3}, μ(Mo $K\alpha$)=21.4 cm^{-1}, λ(Mo $K\alpha$)=0.7107 Å, V=1696.7 (4) Å^3. The intensities were measured on a Philips PW1100 diffractometer. Crystal size: 0.20×0.26×0.45 mm^3; scan speed, 0.033° s^{-1}; scan range, 1.2°; back ground measurement at each side of the scan range, half of the scan time; maximam 2θ value, 50°; number of reflections ($F_o^2 \geqq 2\sigma(F_o^2)$), 2150. No correction was made for absorption. The refinement of the structure was performed by the block diagonal least-squares method. The function minimized was $w(|F_d|-|F_d|)^2$, where $w=1/\sigma^2(F_o)$ was used. The final R value was 0.026, $R_w=[\Sigma w\Delta F^2/\Sigma wF_o^2]^{1/2}=$ 0.036. In the final cycles of the refinement hydrogen atoms were included but their parameters were not refined. All the hydrogen atoms except for those bound to the water oxygens were located at the calculated positions. All the parameter shifts were less than 0.3σ. The maximum peak in the final difference synthesis was 1.0 e Å^{-3}. The atomic scattering factors, with corrections for anormalous scattering of Mo and S, were taken from Ref. 7. The F_o—F_c tables, anisotropic thermal parameters, and coordinates of the hydrogen atoms are preserved by the Chemical Society of Japan (Document No. 8744). The atomic coordinates are listed in Table 1. Computations were performed on a FACOM 230-60 computer at Osaka City University and on a ACOS 900 computer at the Crystallographic Research Center, Institute for Protein Research, Osaka University. The figure was drawn by the use of ORTEP.[8] The programs in the UNICS[9] were employed.

Results and Discussion

Recrystallization of the sodium salt gives only a

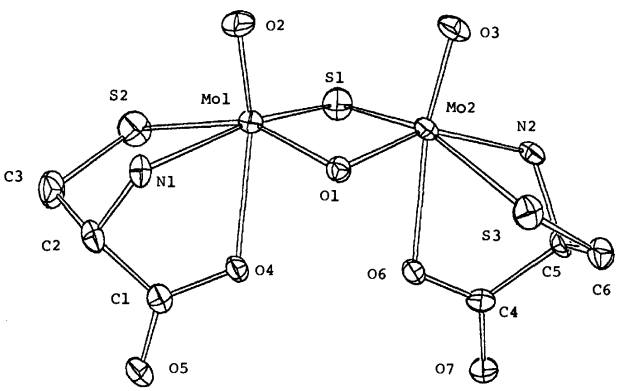

Fig. 1. Perspective view of $[Mo_2O_3S(cys)_2]^{2-}$.

Table 1. Fractional Coordinates and Temperature Factors[10] with Estimated Standard Deviations in Parentheses

Atom	x	y	z	B_{eq}/Å^2	Atom	x	y	z	B_{eq}/Å^2
Mo1	0.28734(2)	0.19550(4)	0.78538(4)	1.16	C5	0.4683(3)	0.4694(5)	1.1267(5)	1.4
Mo2	0.36778(3)	0.24974(4)	1.02107(4)	1.20	C6	0.5325(3)	0.3759(6)	1.1652(5)	1.9
Ca	0.4853(1)	0.7435(1)	0.7402(1)	1.40	O1	0.3973(2)	0.1484(3)	0.8608(3)	1.3
S1	0.2563(1)	0.3618(1)	0.9312(1)	1.80	O2	0.2325(2)	0.0698(4)	0.8396(4)	2.2
S2	0.1939(1)	0.3026(1)	0.6309(1)	2.11	O3	0.3214(3)	0.1524(4)	1.1341(4)	2.3
S3	0.5123(1)	0.2192(1)	1.0871(1)	1.90	O4	0.3813(2)	0.3040(3)	0.6545(3)	1.3
N1	0.3127(3)	0.0961(4)	0.5865(4)	1.5	O5	0.4052(3)	0.3688(4)	0.4425(4)	2.5
N2	0.3874(3)	0.4133(4)	1.1571(4)	1.4	O6	0.4401(2)	0.4082(3)	0.8996(3)	1.3
C1	0.3720(3)	0.2964(5)	0.5246(5)	1.4	O7	0.5037(2)	0.5938(4)	0.9286(4)	1.9
C2	0.3144(3)	0.1936(5)	0.4774(5)	1.6	WA1	0.3604(3)	0.8375(4)	0.6451(5)	2.6
C3	0.2284(4)	0.2466(6)	0.4637(5)	2.2	WA2	0.3919(3)	0.5764(4)	0.6874(5)	2.8
C4	0.4715(3)	0.4953(4)	0.9736(5)	1.3	WA3	0.4496(3)	0.9008(4)	0.9052(4)	2.2

Table 2. Interatomic Distances and Bond Angles with Estimated Standard Deviation in Parentheses

Bond distance	l/Å	Bond distance	l/Å	Bond distance	l/Å	Bond distance	l/Å
Mo1-S1	2.319(1)	Mo1-O2	1.689(4)	Mo2-O3	1.692(4)	C4-C5	1.523(7)
Mo1-S2	2.433(1)	Mo1-O4	2.310(3)	N1-C2	1.483(6)	C4-O6	1.278(6)
Mo1-N1	2.249(4)	Mo2-O1	1.959(3)	N2-C5	1.485(7)	C4-O7	1.247(6)
Mo2-S1	2.351(1)	Mo2-O3	1.692(4)	C1-C2	1.512(7)	C5-C6	1.493(8)
Mo2-S3	2.482(1)	Mo2-O6	2.372(3)	C1-O4	1.282(6)		
Mo2-N2	2.203(4)	Mo1-Mo2	2.718(1)	C1-O5	1.236(7)		
Mo1-O1	2.013(3)	Mo1-O2	1.689(4)	C2-C3	1.526(8)		

Short contact[a)]	l/Å	Short contact[a)]	l/Å	Short contact[a)]	l/Å	Short contact[a)]	l/Å
N2-O5^{I}	2.876(6)	Ca-O4^{II}	2.504(4)	WA1-N1^{III}	2.897(6)	WA3-O1^{III}	2.786(5)
Ca-O1^{II}	2.389(4)	Ca-O6^{II}	2.528(4)	WA1-O3^{IV}	2.990(6)	WA3-O5^{II}	2.832(6)

Bond angle	ϕ/°	Bond angle	ϕ/°	Bond angle	ϕ/°	Bond angle	ϕ/°
S1-Mo1-S2	83.77(5)	O1-Mo1-O2	99.7(2)	N2-Mo2-O1	151.0(2)	N1-C2-C1	106.9(4)
S1-Mo1-N1	157.8(1)	O1-Mo1-O4	74.1(1)	N2-Mo2-O3	98.5(2)	N1-C2-C3	107.5(4)
S1-Mo1-O1	99.1(1)	O2-Mo1-O4	156.9(2)	N2-Mo2-O6	71.1(1)	C1-C2-C3	110.1(5)
S1-Mo1-O2	106.5(1)	S1-Mo2-S3	155.22(5)	O1-Mo2-O3	107.6(2)	C5-C4-O6	114.5(4)
S1-Mo1-O4	96.4(1)	S1-Mo2-N2	86.9(1)	O1-Mo2-O6	82.0(1)	C5-C4-O7	120.7(4)
S2-Mo1-N1	78.2(1)	S1-Mo2-O1	99.7(1)	O3-Mo2-O6	169.2(2)	O6-C4-O7	124.8(5)
S2-Mo1-O1	155.3(1)	S1-Mo2-O3	101.5(2)	Mo1-S1-Mo2	71.20(4)	N2-C5-C4	107.4(4)
S2-Mo1-O2	103.0(1)	S1-Mo2-O6	81.2(1)	Mo1-N1-C2	107.6(3)	N2-C5-C6	108.5(4)
S2-Mo1-O4	81.2(1)	S3-Mo2-N2	78.7(1)	Mo2-N2-C5	108.8(3)	C4-C5-C6	110.0(4)
N1-Mo1-O1	92.0(1)	S3-Mo2-O1	84.3(1)	C2-C1-O4	115.0(4)	Mo1-O1-Mo2	86.4(1)
N1-Mo1-O2	90.2(2)	S3-Mo2-O3	100.5(2)	C2-C1-O5	121.5(4)	Mo1-O4-C1	116.0(3)
N1-Mo1-O4	68.2(1)	S3-Mo2-O6	75.1(1)	O4-C1-O5	123.5(5)	Mo2-O6-C4	115.2(3)

a) Roman numeral superscripts refer to atoms in the positions:
I x, y, 1+z; II 1−x, 1/2+y, 3/2−z; III x, 1+y, z; IV 1/2−x, 1−y, −1/2+z

Table 3. Comparison of the Bond Distances (l/Å) and Angles (ϕ/°)

	2[a)]	**1**[b)]	**3**[c)]		**2**[a)]	**1**[b)]	**3**[c)]
Mo-Mo	2.569(2)	2.718(1)	2.82(0.3)	Mo-$O_{cysteine}$	2.295(16)	2.310(3)	2.38(2.5)
Mo-O_{bridge}	1.946(15)[d)]	2.013(3)[d)]			2.295)14)	2.372(3)	2.35(2.5)
	1.954(15)[d)]	1.959(3)[e)]		Mo-N	2.260(16)	2.249(4)[f)]	2.31(2.5)
	1.907(15)[e)]				2.200(17)	2.203(4)[g)]	2.22(2.5)
	1.915(15)[e)]			Mo-$S_{cyseine}$	2.490(6)	2.482(1)[f)]	2.51(0.9)
Mo-$O_{terminal}$	1.706(18)	1.689(4)	1.69(2.5)		2.491(6)	2.433(1)[g)]	2.48(0.9)
	1.712(16)	1.692(4)	1.55(2.5)	Mo-O-Mo	83.6(6)	86.4(1)	
Mo-S_{bridge}		2.351(1)[d)]	2.34(0.9)[d)]		83.2(6)		
		2.319(1)[e)]	2.37(0.9)[d)]	Mo-S-Mo		71.20(4)	75
			2.32(0.9)[e)]				75
			2.30(0.9)[e)]	D[h)]	151	157.8(4)	155.6

a) Ref. 4. b) This work. c) Ref. 5. d) Trans to $S_{cysteine}$. e) Trans to N. f) Trans to S_{bridge}. g) Trans to O_{bridge}. h) Dihedral angle between the two MoS_2, MoOS, or MoO_2 planes.

powdery product. Addition of solid KCl or NH_4Cl to the aqueous solution of the sodium salt provides no precipitate, while that of $CaCl_2 \cdot 2H_2O$, $BaCl_2 \cdot 2H_2O$, or $MgCl_2 \cdot 6H_2O$ gives crystals of respective salts, of which calcium salt is best for the X-ray analysis. Perspective view of the complex anion, $[Mo_2O_3S(cys)_2]^{2-}$ (**1**), is shown in Fig. 1. The structure of the anion is similar to those of the di-μ-oxo- ($[Mo_2O_2(cys)_2]^{2-}$, (**2**)) and di-μ-sulfido ($[Mo_2O_2S_2(cys)_2]^{2-}$, (**3**)) complexes. Interatomic distances and bond angles are listed in Table 2. Comparison of dimensions is made in Table 3. The Mo-Mo distance and dihedral angle of the μ-oxo-μ-sulfido complex is closer to the respective values of the di-μ-sulfido complex than to those of the di-μ-oxo complex. The Mo-O-Mo angle of **2** is larger than the corresponding angles of **1**, while the Mo-S-Mo angle of **2** is smaller than those of **3**. The trans influence of sulfur atoms (S_{bridge} and $S_{cysteine}$) is observed in **1**, as is observed in **2** and **3**: Mo-N, Mo-O, and Mo-S bonds trans to the sulfur atom (S_{bridge} or $S_{cysteine}$) are longer than those trans to ligating N or O atom, respectively.

We are grateful to Mr. Motoji Akiyama for the help of the preparative work.

References

1) E. I. Stiefel, *Prog. Inorg. Chem.*, **22**, 1 (1977).
2) N. Ueyama, M. Nakata, T. Araki, A. Nakamura, S. Yamashita, and T. Yamashita, *Inorg. Chem.*, **20**, 1934 (1981).

3) J. D. Rush and B. H. J. Bielski, *Inorg. Chem.*, **24**, 3895 (1985).
4) J. R. Knox and C. K. Prout, *Acta Crystallogr., Sect. B*, **25**, 1857 (1969).
5) D. H. Brown and J. A. D. Jeffreys, *J. Chem. Soc., Dalton Trans.*, **1973**, 732.
6) V. R. Ott, D. S. Swieter, and F. A. Schultz, *Inorg. Chem.*, **16**, 2538 (1977).
7) "International Tables for X-Ray Crystallography," Kynoch Press, Birmingham (1974), Vol. IV, pp. 71 and 148.
8) C. K. Johnson, "ORTEP," Report ORLN-3794, Oak Ridge National Laboratory, Oak Ridge, Tenn. (1965).
9) "The Universal Crystallographic Computation Program System," The Crystallographic Society of Japan, Tokyo (1969).
10) W. C. Hamilton, *Acta Crystallogr.*, **12**, 609 (1959).

Photochemical Synthesis of η-Acetylene Complex of an Orthometalated Manganesecarbonyl Derivatives, $(PhO)_2P(OC_6H_4)Mn(CO)_3(PhC{\equiv}CPh)$, and Its Structural Study by ^{13}C and ^{31}P NMR Spectroscopies

Satoru ONAKA,* Nobuhiro FURUICHI, and Yukinobu TATEMATSU
Department of Chemistry, Nagoya Institute of Technology, Gokiso-cho, Showa-ku, Nagoya 466
(Received January 16, 1987)

Synopsis. Photochemical reaction of an orthometalated manganesecarbonyl derivative, $(PhO)_2P(OC_6H_4)Mn(CO)_4$ with PhC≡CPh in benzene yielded $(PhO)_2P(OC_6H_4)Mn(CO)_3(PhC{\equiv}CPh)$ and its structure was studied by ^{13}C and ^{31}P NMR spectroscopy based on ^{13}C and ^{31}P NMR data for relevant orthometalated metal carbonyl derivatives including $(o\text{-}CH_3C_6H_4O)_2P[OC_6H_3(CH_3)]Mn(CO)_3P[OC_6H_4(CH_3)]_3$ which was first synthesized in this study.

Previous reports from this labolatory revealed that orthometalated triphenyl phosphite manganesecarbonyl derivatives, $(PhO)_2P(OC_6H_4)Mn(CO)_4$ (**1**) and $(PhO)_2P(OC_6H_4)Mn(CO)_3P(OPh)_3$ (**2**) dissociate the ligand CO or L (L=$P(OPh)_3$) quite easily upon photolysis in solutions.[1,2]

$$(PhO)_2P(OC_6H_4)Mn(CO)_4 \xrightarrow{h\nu} (PhO)_2P(OC_6H_4)Mn(CO)_3\ (\mathbf{3}) + CO \quad (1)$$

$$(PhO)_2P(OC_6H_4)Mn(CO)_3L \xrightarrow{h\nu} (PhO)_2P(OC_6H_4)Mn(CO)_3\ (\mathbf{3}) + L \quad (2)$$

This observation prompted us to "trap" the 16 electron intermediate, $(PhO)_2P(OC_6H_4)Mn(CO)_3$ (**3**) by reacting with other nucleophiles such as diphenylacetylene. Present paper reports isolation of $(PhO)_2P(OC_6H_4)Mn(CO)_3(PhC{\equiv}CPh)$ (**4**) and its structural study by ^{13}C and ^{31}P NMR spectroscopies based on the spectral data for relevant orthometalated triphenyl phosphite metal carbonyl derivatives. Synthesis of $(o\text{-}CH_3C_6H_4O)_2P[OC_6H_3(CH_3)]Mn(CO)_3P[O(o\text{-}CH_3C_6H_4)]_3$ is also reported.

Experimental

Photolysis was performed under an argon atmosphere with a Riko 100 W high pressure Hg lamp. Solvent was purged with argon gas sufficiently before use. The sample of **1** was prepared according to the literature method[3] and other samples of **2** and $(PhO)_2P(OC_6H_4)Mn(CO)_2L_2$ (**5**) were obtained as was described in the previous papers.[1,2] IR spectra were measured with a Jasco 701G spectrometer for Nujol mull samples and ^{13}C and ^{31}P NMR were measured for ca. 0.5 mol dm^{-3} chloroform-*d* solutions at 30 °C on a Varian XL-200 spectrometer operated at 50.309 and 80.984 MHz respectively with Fourier transform mode for naturally abundant levels. The spectra were recorded using a 10 mm o.d. sample tube. Chemical shifts were referenced to internal Me_4Si standard for ^{13}C nucleus and to external H_3PO_4 standard contained in a 1 mm capillary for ^{31}P nucleus. A positive chemical shift designates a resonance to a lower field than that of the resonance of the respective standard.

Synthesis of $(C_6H_5O)_2P(OC_6H_4)Mn(CO)_3(C_6H_5C{\equiv}CC_6H_5)$ (4). A 0.996 g (2.1 mmol) sample of **1** and 0.372g (2.1 mmol) of diphenylacetylene, **dpa**, were dissolved into 50 ml of benzene and the mixture was photolyzed for 8 h. From the resulting yellow solution, the solvent was vacuum-stripped to leave an yellow oil. This oil was dissolved into a minimum amount of benzene and was loaded on a Florisil column. Unreacted starting materials (**1** and **dpa**) were eluted with petroleum ether. Then, mixed solvent of benzene and hexane (1 : 1) eluted a white product, which was recrystallized from mixed solvent of benzene and petroleum ether (1 : 1) to yield 200 mg of $(PhO)_2P(OC_6H_4)Mn(CO)_3(PhC{\equiv}CPh)$ (**4**). (Yield 15%). Retention of the orthometalated ring was exemplified by detection of three weak peaks at 1105, 960, and 795 cm^{-1} in IR which are characteristic of the orthometalated triphenyl phosphite.[1,2] Found: C, 66.76; H, 3.57; P, 4.70%. Calcd for $(PhO)_2P(OC_6H_4)Mn(CO)_3(PhC{\equiv}CPh)$, $C_{35}H_{24}O_6MnP$: C, 67.10; H, 3.86; P, 4.95%. IR ν(CO) (Nujol mull) 2080 (vs), 1995 (vs), and 1961(s) cm^{-1}.

Synthesis of $BrMn(CO)_3L'_2$ (L'=$(o\text{-}CH_3C_6H_4O)_3P$) (6). A 1.56 g (5.7 mmol) sample of $BrMn(CO)_5$ and 10 g (28 mmol) of $(o\text{-}CH_3C_6H_4O)_3P$, L', (hereafter L' denotes $(o\text{-}CH_3C_6H_4O)_3P$ and L denotes $P(OPh)_3$) were dissolved into 80 ml of choloroform and the mixture was stirred at 55 °C for 18 h. Then the solvent was almost vacuum-stripped and 50 ml of hexane was added to precipitate yellow crystals of $BrMn(CO)_3L'_2$ (**6**): Yield 2.6 g (53%). IR ν(CO) (Nujol mull) 2065 (m), 1990 (vs), and 1932 (vs) cm^{-1}.

Synthesis of $MeMn(CO)_3L'_2$ (7). A 2.0 g (2.2 mmol) sample of **6** in 40 ml of THF was reduced to $NaMn(CO)_3L'_2$ by stirring over Na amalgam for 3 h. To the supernatant THF solution of $NaMn(CO)_3L'_2$, 0.5 g (3.5 mmol) of CH_3I in 20 ml of THF was added and the mixture was stirred at room temperature overnight. Solvent was distilled off at reduced pressure to leave cleam yellow solid. This solid was extracted three times with each 20 ml of benzene. Then the benzene was almost distilled off at reduced pressure from the combined extracts and 10 ml of petroleum ether was added. The mixture was stored in a refrigerator to give pale yellow crystals of $MeMn(CO)_3L'_2$ (**7**). Yield 1.1 g (62%). IR ν(CO) (benzene solution) 2030 (w), 1953 (vs), and 1929 (s) cm^{-1}. Found: C, 64.30; H, 5.31%. Calcd for $CH_3Mn(CO)_3L'_2$, $C_{46}H_{45}MnO_9P_2$: C, 64.34; H, 5.28%.

Synthesis of $(o\text{-}CH_3C_6H_4O)_2P[OC_6H_3(CH_3)]Mn(CO)_3L'$ (8). A 0.9g (1 mmol) sample of **7** was dissolved into 50 ml of benzene and the solution was photolyzed for 4 h. The solution was concentrated to about 5 ml at reduced pressure and it was loaded on a Florisil column. After elution of unknown products and unreacted **7** with petroleum ether, pale yellow product of **8** was eluted with benzene. After

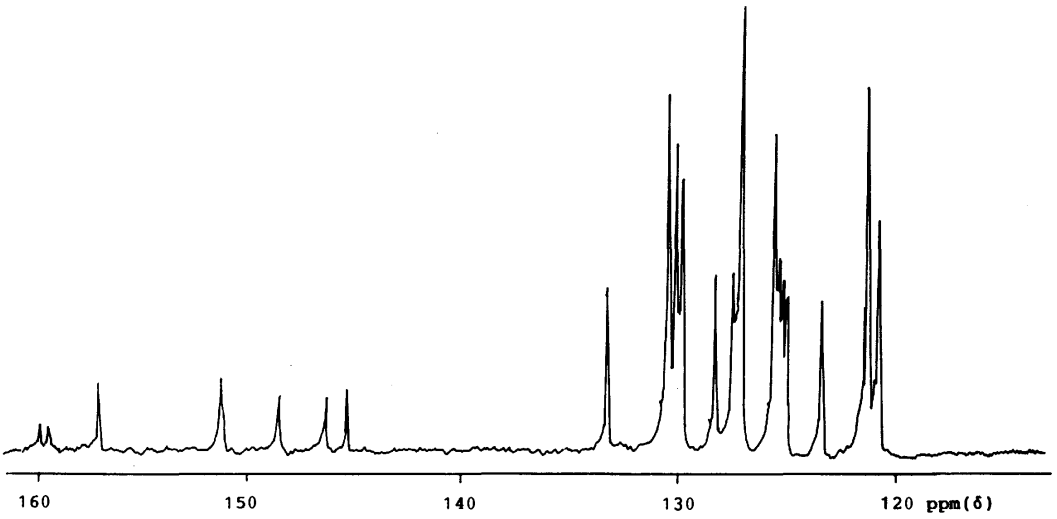

Fig. 1. ^{13}C NMR spectrum of $(PhO)_2\overline{P(OC_6H_4)}\overline{Mn(CO)_3}(PhC{\equiv}CPh)$ in $CDCl_3$.

recrystallization from mixed solvent of benzene-petroleum ether (1 : 1), 100 mg of pure product **8** was obtained. (Yield 12%) Found: C, 64.00; H, 5.09%. Calcd for $(o\text{-}CH_3C_6H_4O)_2\overline{P[OC_6H_3(CH_3)]Mn(CO)_3}L'$, $C_{45}H_{41}MnO_9P_2$: C, 64.14; H, 4.90%. IR ν(CO) (benzene solution) 2040 (w), 1970 (vs), and 1940 (s) cm^{-1}.

X-Ray Data Collection. A colorless crystal of **4** with approximate dimensions 0.30×0.35×0.70 mm^3, which was grown-up from cyclohexane-petroleum ether, was mounted on a Rigaku AFC-5 automated four circle diffractometer equipped with Mo $K\alpha$ radiation (λ=0.71073 Å). The crystal belongs to triclinic system with unit cell dimensions a=22.904(8), b=22.918(8), c=12.795(5) Å, α=106.32(3), β=106.28(3), γ=85.53(3)°, and V=6187(4) $Å^3$. A total of 8639 independent reflections with $|F_o|>3\sigma(|F_o|)$ were obtained at room temperature using the $\omega-2\theta$ scan technique up to 2θ=50°. The structure has so far been solved neither by the standard heavy atom method nor direct method based on $P\bar{1}$ space group (UNICS-III program package, MULTAN 78 program and a HITAC M-200H computer).

Spectral Assignments

As is shown in Fig. 1, ^{13}C NMR spectrum of **4** is very complex. Therefore, the assignment of each peak is rather laborious without the aid of ^{13}C NMR data of relevant orthometalated triphenyl phosphite derivatives. When the ^{13}C NMR spectrum of **4** is compared with those of $(PhO)_2\overline{P(OC_6H_4)}Fe(CO)Cp$ (**9**) and $(PhO)_2\overline{P(OC_6H_4)}Fe(L)Cp$ (L=$P(OPh)_3$) (**10**),[4] we are tempted to opt following assignments of peaks observed in the lower field than 140 ppm; the doublet at 159.6 ppm is assignable to C_2 carbon and the singlet at 151.2 ppm is assigned to P-O-C carbon of unmetalated benzene rings.[4,5] The doublet at 145.7 ppm is assignable to C_1 carbon and the signlet at 148.4 ppm to C_6 carbon (Scheme 1). The alkyne carbon resonance at 89.2 ppm for free PhC≡CPh disappears in **4** and a new resonance appears at 157.0 ppm instead, which is assignable to coordinated alkyne carbons to the Mn atom.[6,7] ^{13}C NMR spectrum of **4** is devoid of the doublet at around 111 ppm due to C_3 carbon resonance which is detected at 110.9 and 110.2 ppm in the spectra of **9** and **10**;[4,8] the doublet is not strong in **9** and **10** and this doublet is presumably hidden behind strong resonances around 120 ppm in **4**. The strong resonances between 120 and 133 ppm are so complex that it seems prudent to leave the assignment unsettled except just describing that these resonances are originated from phenyl carbon atoms of **dpa**, unmetalated phenyl carbons of P-O-Ph groups and phenyl carbons of metalated P-O-C_6H_4-groups. Thus, resonances due to C_4 and C_5 are not assigned but just pointing out that these resonances may be located at around 125 ppm.[4] Table 1 collates selected ^{13}C and ^{31}P NMR data of **4** together with those of relevant orthometalated manganesecarbonyl derivatives.

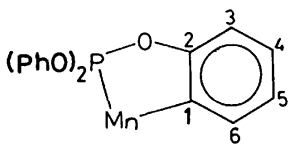

Scheme 1.

Results and Discussion

It is well recognized that ^{31}P NMR spectroscopy is very convenient and useful structural probe to discriminate between metalated and unmetalated triphenyl phosphite ligands;[9,10] that is, orthometalation of the ligand causes a large downfield chemical shift (≈30 ppm) compared to unmetalated coordinated $P(OPh)_3$. This criterion holds for present series of orthometalated manganese-carbonyl derivatives, **1**, **2**, **5**, and **8** except **4**, as is seen from Table 1; the internal ^{31}P-chemical shift between metalated and unmetalated phosphite ligands ranges from 30.5 to 36.5 ppm and the resonance of metalated phosphite ligand is detected at lower field than 190 ppm. However, ^{31}P chemical shift of **4** is observed at about 20—30 ppm upfield as for metalated phosphite and is close to those of unmetalated ligand(s) in **7**, **11**, and **12**. According to the ^{31}P NMR studies by Stewart's group,[10] the chemical shift of coordinated triphenyl phosphite is very sensitive to the nature of the trans ligand. Therefore, 21.4 ppm upfield shift for **4** compared to **1** seems to reflect the different trans effect of PhC≡CPh from that of CO. These lines of evidence prompt us to postulate the trans structure for **4** as is illustrated in Scheme 2, although definitive evidence of this issue must wait for future success of single crystal X-ray structure analysis.

Table 1. Selected ^{13}C and ^{31}P NMR Data

Compound	^{13}C Resonances (δ, ppm)					^{31}P Resonances (δ, ppm)	
	-C≡C-	C_1	C_2	C_3	C_6	Orthometalated	Unmetalated
$(PhO)_2P(OC_6H_4)Mn(CO)_3(PhC{\equiv}CPh)$ (**4**)	157.0	145.7	159.6		148.4	171.7	
$(PhO)_2P(OC_6H_4)Fe(CO)Cp$ (**9**)[4]		141.6	161.7	110.9	144.2	203.4	
$(PhO)_2P(OC_6H_4)Fe(L)Cp$ (**10**)[4]		143.0	163.2	110.2	146.0	200.0	166.4
$(PhO)_2P(OC_6H_4)Mn(CO)_4$ (**1**)						193.1	
$(PhO)_2P(OC_6H_4)Mn(CO)_3L$ (**2**)						194.4[a]	157.9[a]
$(PhO)_2P(OC_6H_4)Mn(CO)_2L_2$ (**5**)						196.5[b]	162.6[b]
$(o\text{-}MeC_6H_4O)_2P[OC_6H_3(Me)]Mn(CO)_3L'$ (**8**)						197.4[c]	166.9[c]
$MeMn(CO)_4L$ (**11**)							167.4
$MeMn(CO)_3L_2$ (**12**)							171.3
$MeMn(CO)_3L'_2$ (**7**)							169.9

a) J_{pp}=100.7 Hz. b) J_{pp}=103 Hz. c) J_{pp}=121 Hz. L denotes $P(OPh)_3$; L′ denotes $(o\text{-}CH_3C_6H_4O)_3P$; Cp denotes η-(C_5H_5).

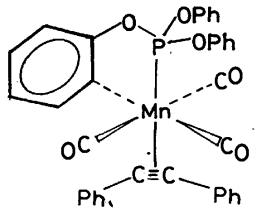

Scheme 2.

According to the previous report,[2] photolysis of $MeMn(CO)_3L_2$ yielded three kinds of orthometalated products, that is **1** (1 : 1), **2** (1 : 2), and **5** (1 : 3).[11] However, photolysis of $MeMn(CO)_3L'_2$ afforded only 1 : 2 type orthometalated compound **8**. Steric crowdness due to the methyl group located at another ortho position may partly be responsible for the lack of 1 : 3 type metalation product. However, the reason of the lack of 1 : 1 type metalation product is not clear at present. Presumably the yield of 1 : 1 type product is low and eluded isolation.

Carbonyl stretching pattern in IR of **8** is very close to that of **2**. This resemblance suggests that **8** has a similar cis structure to that of **2**.[1]

The present study was supported by Grant-in-Aid for Scientific Research No. 57470036 from the Ministry of Education, Science and Culture. Thanks are also due to the Institute for Molecular Science for permission to use the AFC-5 automated X-ray diffractometer (the Instrument Center) and the computer (the Computer Center).

References

1) S. Onaka, Y. Kondo, N. Furuichi, K. Toriumi, and T. Ito, *Bull. Chem. Soc. Jpn.*, **56**, 87 (1983).
2) S. Onaka, Y. Kondo, and N. Furuichi, *Bull. Chem. Soc. Jpn.*, **56**, 2296 (1983).
3) R. J. McKinney, R. Hoxmeier, and H. D. Kaesz, *J. Am. Chem. Soc.*, **97**, 3059 (1975).
4) R. P. Stewart, Jr., L. R. Isbrandt, J. J. Benedict, and J. G. Palmer, *J. Am. Chem. Soc.*, **98**, 3215 (1976).
5) Free $P(OPh)_3$ ligand shows this resonance at 152 ppm.
6) P. L. Watson and R. G. Bergman, *J. Am. Chem. Soc.*, **102**, 2698 (1980).
7) N. M. Boag, M. Green, D. M. Grove, J. A. K. Howard, J. L. Spencer, and F. G. A. Stone, *J. Chem. Soc., Dalton Trans.*, **1980**, 2170.
8) Indeed, this doublet is detected at around 111 ppm for **1**, **2**, and **5**.
9) R. P. Stewart, Jr., J. J. Benedict, L. R. Isbrandt, and R. S. Ampulski, *Inorg. Chem.*, **14**, 2933, (1975).
10) R. P. Stewart, Jr., L. R. Isbrandt, and J. J. Benedict, *Inorg. Chem.*, **15**, 2011 (1976) and references therein.
11) These abbreviation denote following metal to phosphite ligand ratios in orthometalated products; 1 : 1 means that Mn: phosphite is 1 : 1, 1 : 2 means Mn: phosphite is 1 : 2, and 1 : 3 means Mn: phosphite is 1 : 3.

Enantioselective Ion-Association Mode between the Tris(ethylenediamine)-cobalt(III) Cation and the Bis(μ-(−)$_{589}$-2,3-dimethyltartrato)-diantimonate(III) Anion in Solution

Hayami YONEDA,* Ushio SAKAGUCHI, and Hiroshi NAKAZAWA
Department of Chemistry, Faculty of Science, Hiroshima University, Higashisenda-machi, Naka-ku, Hiroshima 730
(Received January 20, 1987)

Synopsis. By analyzing the intensity changes in the circular dichroism spectra, the association constants of the Λ- and Δ-$[Co(en)_3]^{3+}$ ions with the bis(μ-(−)$_{589}$-2,3-dimethyltartrato)diantimonate(III) ion were determined to be 58.4±1.9 and 38.6±0.4 respectively in H_2O (mol^{-1} dm^3 at 25 °C and μ=0.1 ($NaClO_4$)). Based on these data together with the chromatographic data, the enantioselective association mode was discussed.

It is well-known that the bis(μ-*d*-tartrato)diantimonate(III) ion, $[Sb_2(d\text{-tart})_2]^{2-}$, is an effective chiral selector for chromatographic optical resolution of many types of octahedral metal chelate complexes.[1] Concerning the mechanism of chiral discrimination by this anion, we proposed previously the L-J model where attention was paid to an opening formed between chelate rings of a complex to be resolved.[2] An opening between chelate rings in the Λ configuration has a shape of L and is called an L-shaped channel. In contrast, an opening between chelate rings in the Δ configuration has a shape reverse to an L-shaped channel and is called a J-shaped channel. A counter ion which makes a good fit to an L-shaped channel does not make a good fit to a J-shaped channel. Such a counter ion associates more favorably with a complex having an L-shaped channel than with a complex having a J-shaped channel, and can be utilized as a chiral selector. The $[Sb_2(d\text{-tart})_2]^{2-}$ anion is considered to have a skeleton which makes a good fit to the L-shaped channel in a complex cation. Based on this idea the efficiency of chiral discrimination by this anion was successfully explained for a series of $[Co(N)_6]^{3+}$ complex cations having different numbers of L-shaped channels.[2]

The L-J model was originally born as a conceptual idea having no specified mode of association. However, using molecular models, we found that either one of the two tartrate backbones bridging the two Sb atoms makes a good fit to an L-shaped channel, and proposed a concrete mode of ion association for chiral discrimination in which the anion accepts a complex cation coming along the y direction in Fig. 1. This mode of association does not exclude any other possibilities for the $[Sb_2(d\text{-tart})_2]^{2-}$ anion to discriminate the chirality of the complex cation. In fact, it was shown by Sakaguchi et al. that the $[Sb_2(d\text{-tart})_2]^{2-}$ anion can discriminate the chirality of the $[Co(en)_3]^{3+}$ and its related complex cations coming along the x direction in Fig. 1.[3] In addition, the third concrete mode of association was put forward by Miyoshi et al., in which the two oxygen atoms of the $[Sb_2(d\text{-tart})_2]^{2-}$ anion participate in the double hydrogen bonding to two of the three axial N-H bonds directed along the C_3 axis of the complex, and the remaining part of the anion is disposed opposite to the third N-H bond which is not involved in hydrogen bonding.[4] In this third association mode, the $[Sb_2(d\text{-tart})_2]^{2-}$ anion accepts the complex cation coming along the x direction in Fig. 1.

All these modes of association basically explain the situation of chiral discrimination of $[Co(N)_6]^{3+}$ complex cations, but differ in the mode of orientation of the complex cation around the $[Sb_2(d\text{-tart})_2]^{2-}$ anion. To specify the direction of access of the complex cation toward the $[Sb_2(d\text{-tart})_2]^{2-}$ anion, we have prepared the methyl-substituted derivative of this anion, bis(μ-(−)$_{589}$-2,3-dimethyltartrato)diantimonate(III) anion (abbreviated as $[Sb_2((-)\text{-dmt})_2]^{2-}$) in which each tartrate backbone has two methyl substituents. According to the original L-J model, a good fit to an L-shaped channel is expected to be lost by such methyl substitution. Therefore, the efficiency of chiral discrimination should be markedly decreased with methyl substitution. In contrast, according to the other models, the methyl groups do not seem to effect any significant steric repulsion in ion-association, so that the efficiency of chiral discrimination should not be influenced greatly by methyl substitution. The results of the experiments in the present study imply that when the chiral anion discriminates the chirality of complex cations, it directs the x axis towards the complex cations.

Experimental

Material. The complexes used were the perchlorate salts of Λ- and Δ-$[Co(en)_3]^{3+}$. $Na_2[Sb_2((-)\text{-dmt})_2]\cdot 4H_2O$ was prepared according to the literature,[5] and purified by recrystallization from water.

Measurements of Ion-Association Constants and Chromatographic Resolution. The ion-association constants were

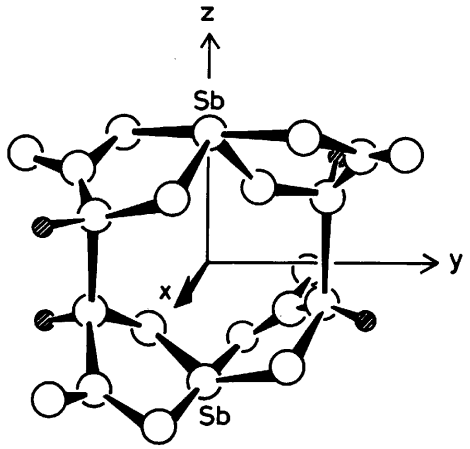

Fig. 1. Structure of $[Sb_2(d\text{-tart})_2]^{2-}$.

obtained by using CD intensity changes upon addition of chiral anions. The CD spectra were measured on a JASCO J-40CS recording spectropolarimeter. The sample cell was kept at 25±0.2 °C with a Haake circulator Model FK. For the Δ-$[Co(en)_3]^{3+}$ cation, the concentration of the cation, C_M, was fixed at 3.0×10^{-3} mol dm^{-3}, and that of the $[Sb_2((-)\text{-dmt})_2]^{2-}$ anion, C_A, was varied from 0 to 2.7×10^{-2} mol dm^{-3}. A sample cell of 1-cm length was used. In the case of the Λ-$[Co(en)_3]^{3+}$ cation, C_M was set to 6.0×10^{-4} mol dm^{-3} (C_A=0 to 1.5×10^{-2} mol dm^{-3}), because of the low solubility of the $[Sb_2((-)\text{-dmt})_2]^{2-}$ salt of this enantiomer, and the sample cell of 10-cm length was used for the CD measurement. The ionic strength was adjusted to μ=0.1 with sodium perchlorate. The CD intensity change of the chiral complex upon addition of $[Sb_2((-)\text{-dmt})_2]^{2-}$ salt was measured at 440 nm.

Chromatographic data were obtained as follows. The aqueous solution containing the racemic $[Co(en)_3]^{3+}$ complex was loaded on the IEX-510 cation-exchange resin (7.5×0.75 cm I. D.). The adsorbed complex was eluted with a 0.1 mol dm^{-3} aqueous solution of $Na_2[Sb_2((-)\text{-dmt})_2]$. Blue Dextran 2000 was used as a marker for the void volume measurememt of the column. The eluate was guided to a flow cell to detect the complex at 460 nm with a Shimadzu UV-140 spectrophotometer. The adjusted retention volumes were estimated from the elution curve thus recorded.

Results and Discussion

According to our recent X-ray analysis of Λ-$[Co(en)_3]$ $[Sb_2((-)\text{-dmt})_2]ClO_4\cdot7H_2O$, the absolute configuration of the 2 and 3 carbons of the 2,3-dimethyltartrate moiety in the $[Sb_2((-)\text{-dmt})_2]^{2-}$ was established to be R, R which corresponds to those of the 2 and 3 carbons of the *d*-tartrate moiety in $[Sb_2(d\text{-tart})_2]^{2-}$.[6]

The CD spectra of Λ-$[Co(en)_3]^{3+}$ with and without $[Sb_2((-)\text{-dmt})_2]^{2-}$ are shown in Fig. 2 together with their difference (DCD spectrum). The DCD spectrum is quite similar in shape to that obtained with the unmethylated anion used as an additive, and the both DCD spectra have the same sign.[3]

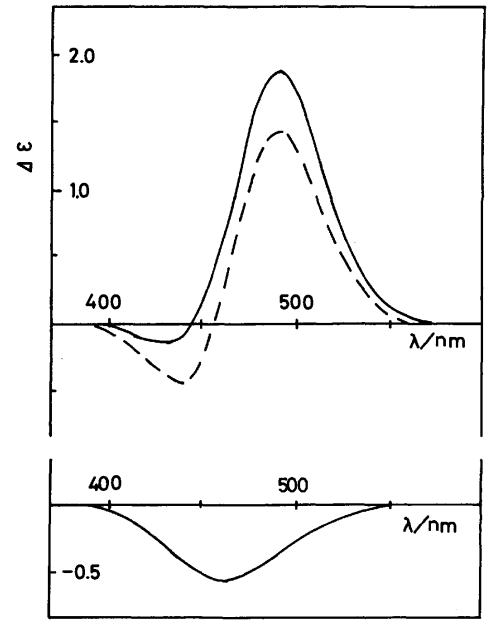

Fig. 2. Upper curves: CD spectra of Λ-$[Co(en)_3]^{3+}$ (——) and of the ion-pair with $[Sb_2((-)\text{-dmt})_2]^{2-}$ (----). Lower curve: the DCD spectrum.

Table 1. Association Constants at 25°C and μ=0.1 ($NaClO_4$)

System	K	D
Λ-$[Co(en)_3]^{3+}$ ..... $[Sb_2(d\text{-tart})_2]^{2-}$	47.3±0.6	29
Δ-$[Co(en)_3]^{3+}$ ..... $[Sb_2(d\text{-tart})_2]^{2-}$	26.0±0.3	
Λ-$[Co(en)_3]^{3+}$ ..... $[Sb_2((-)\text{-dmt})_2]^{2-}$	58.4±1.9	20
Δ-$[Co(en)_3]^{3+}$ ..... $[Sb_2((-)\text{-dmt})_2]^{2-}$	38.6±0.4	

$$D=\frac{K_\Lambda-K_\Delta}{K_\Lambda+K_\Delta}\times100$$

Table 2. Retention Volume(V) and Separation Factor(α) of $[Co(en)_3]^{3+}$

Eluent	V_1 (ml)	V_2 (ml)	α
$Na_2[Sb_2(d\text{-tart})_2]$	40.9 (Λ)	59.9 (Λ)	1.46
$Na_2[Sb_2((-)\text{-dmt})_2]$	27.9 (Λ)	38.6 (Λ)	1.38

The ion-association constants obtained by using the CD intensity changes upon addition of the chiral anion are listed in Table 1 with those for the $[Co(en)_3]^{3+}\cdots[Sb_2(d\text{-tart})_2]^{2-}$ system. Comparison of the corresponding values revealed the following two points. The first point noted is that the value of K_Λ is greater than that of K_Δ in both the methylated and unmethylated chiral anions. This suggests that the methyl substitution does not cause inversion of chiral discrimination. The second point noted is that the values of K for both Λ and Δ-$[Co(en)_3]^{3+}$ complexes are greater in $[Sb_2((-)\text{-dmt})_2]^{2-}$ than in $[Sb_2(d\text{-tart})_2]^{2-}$ (58.4 vs. 47.3 and 38.6 vs. 26.0). However, the value of D which is defined as $(K_\Lambda-K_\Delta)/(K_\Lambda+K_\Delta)\times100$ and is considered as a measure of the efficiency of chiral discrimination, shows only a slight decrease from the original chiral anion to the methyl-substituted chiral anion.

These features are reflected in the chromatographic data as shown in Table 2.[7] The values of V_1 and V_2 for $[Sb_2((-)\text{-dmt})_2]^{2-}$ are both smaller than the corresponding values for $[Sb_2(d\text{-tart})_2]^{2-}$. The value of the separation factor α for $[Sb_2((-)\text{-dmt})_2]^{2-}$ is smaller than that for $[Sb_2(d\text{-tart})_2]^{2-}$. However, the decrease in the values of α is not so great.

It can be concluded that the methyl substitution does not cause a significant influence upon the chiral discrimination on a chiral selector. Thus, we feel tempted to look with favor upon the models in which the chiral anion directs its x axis to the complex cation to recognize the chirality.

The preparation of the bis(μ-$(-)_{589}$-2,3-dimethyltartrato)diantimonate(III) salt was performed by U.S. in the laboratory of Prof. Yoshiharu Izumi, Director of Institute for Protein Research, Osaka University, under his instruction. His kind and helpful guidance is highly appreciated. The present work was partially supported by a Grant-in-Aid for Scientific Research No. 60470047 from the Ministry of Education, Science and Culture.

References

1) H. Yoneda, *J. Chromatogr.*, **313**, 59 (1985); H. Yoneda, *J. Liquid Chromatogr.*, **2**, 1157 (1979); Y. Yoshikawa and K.

Yamasaki, *Coord. Chem. Rev.*, **28**, 205 (1975).

2) H. Nakazawa and H. Yoneda, *J. Chromatogr.*, **160**, 89 (1978).

3) U. Sakaguchi, A. Tsuge, and H. Yoneda, *Inorg. Chem.*, **22**, 3735 (1983).

4) K. Miyoshi, S. Izumoto, and H. Yoneda, *Bull. Chem. Soc. Jpn.*, **59**, 3475 (1986); K. Miyoshi, S. Izumoto, K. Nakai, and H. Yoneda, submitted for publication.

5) S. Tatsumi, Y. Izumi, M. Imaida, Y. Fukuda, and S. Akabori, *Bull. Chem. Soc. Jpn.*, **39**, 602 (1966).

6) S. Izumoto, Y. Kushi, and H. Yoneda, under preparation for publication. Crystals of *Λ*-tris(ethylenediamine)-cobalt(III) bis(μ-$(-)_{589}$-2,3-dimethyltartrato)diantimonate(III) perchlorate heptahydrate, *Λ*-$[Co(en)_3][Sb_2((-)\text{-dmt})_2]\cdot ClO_4\cdot 7H_2O$, are bright orange, trigonal, space group $P3_121$, a=10.496(3), c=29.570(6) Å, Z=3, D_c=1.87 g cm^{-3}. The structure was solved from 1723 Mo K_α reflections ($F_o > 3\,\sigma\,F_o$). The final discrepancy factors were R=0.067 and R_w=0.072. In the $(-)_{589}$-2,3-dimethyltartrato groups, the absolute configuration of the two asymmetric carbon atoms are both having an R configuration from the comparison with that of the *Λ*-$[Co(en)_3]^{3+}$ cation.

7) The order of the ion-association constants in Table 1 and that of the retention volumes in Table 2 are not exactly the same, presumably because the entity of ion-associated species recognized by CD spectra and that by ion-exchange chromatography are not always the same.

(Acetylacetonato)(*N,N,N',N'*-tetramethylethylenediamine)copper(II) Tetraphenylborate as a Solvent Basicity Indicator

Rudolf Werner SOUKUP† and Kozo SONE*
Department of Chemistry, Faculty of Science, Ochanomizu University, Ohtsuka, Bunkyo-ku, Tokyo 112
†Institut für Anorganische Chemie, Technische Universität Wien, Getreidemarkt 9, A-1060 Vienna, Austria
(Received February 12, 1987)

Synopsis. The title complex, [Cu(acac)(tmen)]BPh_4, is a color indicator for solvent basicity which serves better than the corresponding perchlorate in very weak donor solvents owing to its reluctance in ion-pair formation. The complex cation $[Cu(acac)(tmen)]^+$ decomposes in very strong donor solvents, but these indicators may still be used in them with some care.

(Acetylacetonato)(*N,N,N',N'*-tetramethylethylenediamine)copper(II) perchlorate, abbreviated as [Cu(acac)(tmen)]ClO_4, is known to be strongly solvatochromic, owing to the subtle structure changes caused by the solvation processes.[1,2] The coordination center which determines the position of the visible d-d band is extremely sensitive to nucleophilic solvent attack; this fact led to the proposal to use it as a color indicator for solvent basicity, which is expressed in Gutmann's donor number (DN).[2,3]

The use of this complex to estimate the DN of solvents gives reasonably good results when the DN lies between 5 and 30. However, anomalies appear in very weak or very strong donor solvents. As can be seen from the first column of Table 1, the λ_{max} value of this complex decreases with the decrease of DN in going from pyridine to nitromethane, but when the basicity gets smaller it increases notably again. Moreover, in such very weak donor solvents, the λ_{max} values become slightly concentration dependent, decreasing by a few nanometers upon strong dilution. Concentration dependence of λ_{max} appears again, and much more strongly, in very strong donor solvents, but here the λ_{max} increases with dilution.

In order to understand these anomalies better, the tetraphenylborate of the same complex cation was prepared, and its spectral behavior was compared with that of the perchlorate.

Experimental

Preparation of [Cu(acac)(tmen)]BPh_4. 10 g (ca. 0.026 mol) of twice recrystallized [Cu(acac)(tmen)]ClO_4[1] was dissolved in 120 ml of water, and 50 ml of a warm aqueous solution containing 12 g (ca. 0.035 mol) of $NaBPh_4$ was added with stirring. The pale red violet precipitate obtained was filtered off, washed with warm water, and dried in vacuo for several hours at 30 °C. Found: C, 70.34; H, 7.27; N, 4.70%. Calcd for $C_{35}H_{43}BCuN_2O_2$: C, 70.29; H, 7.25; N, 4.68%.

Solvents. The solvents used were all purified according to the literature.

Spectral Measurements. Use was made of a Cary 17 spectrophotometer, with quartz cells of various path lengths. Measurements were made at room temperature (ca. 20 °C).

Results and Discussion

As can be seen from the second column of Table 1, the visible spectra of [Cu(acac)(tmen)]BPh_4 in various solvents of DN>5 are very similar to those of the perchlorate, but the anomalies in very weak donor solvents disappear. The λ_{max} value continues to decrease, even in these solvents, with the decrease of solvent basicity, which can be expressed in terms of Schmid's DN_B,[4] and its concentration dependence is nearly imperceptible. The difference in color between the tetraphenylborate and the perchlorate in such a solvent can be quite large; for example, they are red and blue, respectively, in chlorobenzene, and the difference in their λ_{max} amounts to ca. 100 nm.

Now the curves shown in Fig. 1 reveal that, in addition to the d-d band, there is a continuous background absorption in the blue part of the spectrum, which seems to be the tail of a strong CT band in the near

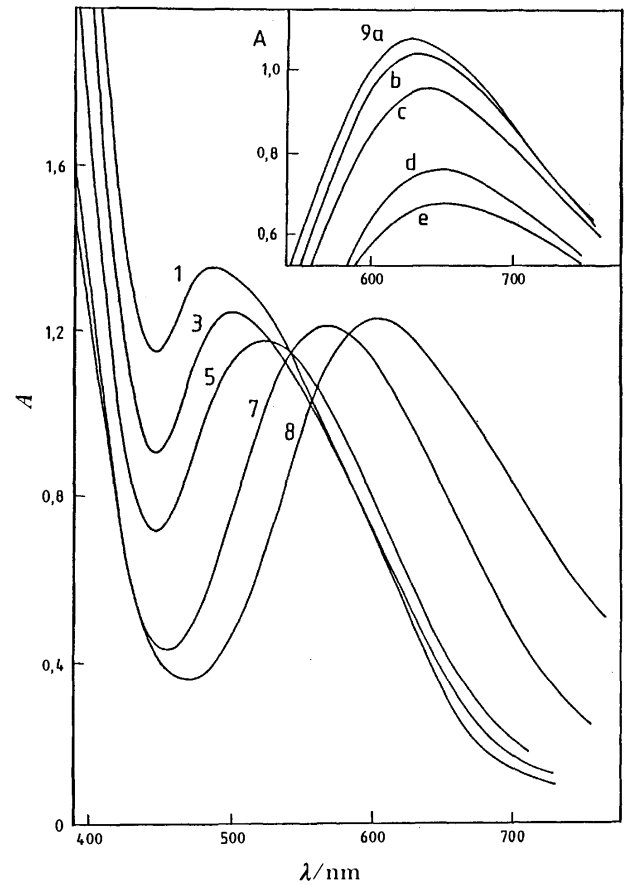

Fig. 1. Visible absorption spectra of [Cu(acac)(tmen)]BPh_4 in various solvents. Notations of the solvents: see Table 1. Concn/M: 0.1, path length/cm: 0.1. Inset: Concentration dependence of the spectrum of [Cu(acac)(tmen)]ClO_4 in pyridine. Concn/M: 0.092(a), 0.046(b), 0.023(c), 0.0092(d), 0.0046(e); path length/cm: 0.1(a), 0.2(b), 0.4(c), 1(d), 2(e). (A= absorbance).

Table 1. λ_{max} of the d-d Band of [Cu(acac)(tmen)]X in Various Solvents

	Solvent	λ_{max}/nm			DN/DN_B[a]
		X=ClO_4	X=BPh_4		
			Observed	Corrected	
1	Dichloromethane (10^{-2}M[b])	550[c]	488	515	(1.2)
2	Chlorobenzene (10^{-3}M)	≈572[c]	480	520	(2.2)
3	1,2-Dichloroethane (10^{-2}M)	≈543[c,d]	498	520	(2.9)
4	Nitrobenzene (10^{-3}M)	533	490	522	(3.7)
5	Nitromethane	532[d]	527	530	(4.8)
6	Acetonitrile	578[d]	573		14.1
7	Acetone	571[d]	569		17.0
8	N,N-Dimethylformamide	603[d]	602		26.6
9	Pyridine (10^{-1}M)	624[e]	623[e]	613[f]	33.1
10	2-Picoline (10^{-2}M)	624[e]	620[e]		—

a) DN_B in parentheses. b) 1 M=1 mol dm^{-3}. c) Slightly concentration dependent. d) From the literature.[1,3] e) Strongly concentration dependent. f) Cf. Table 2.

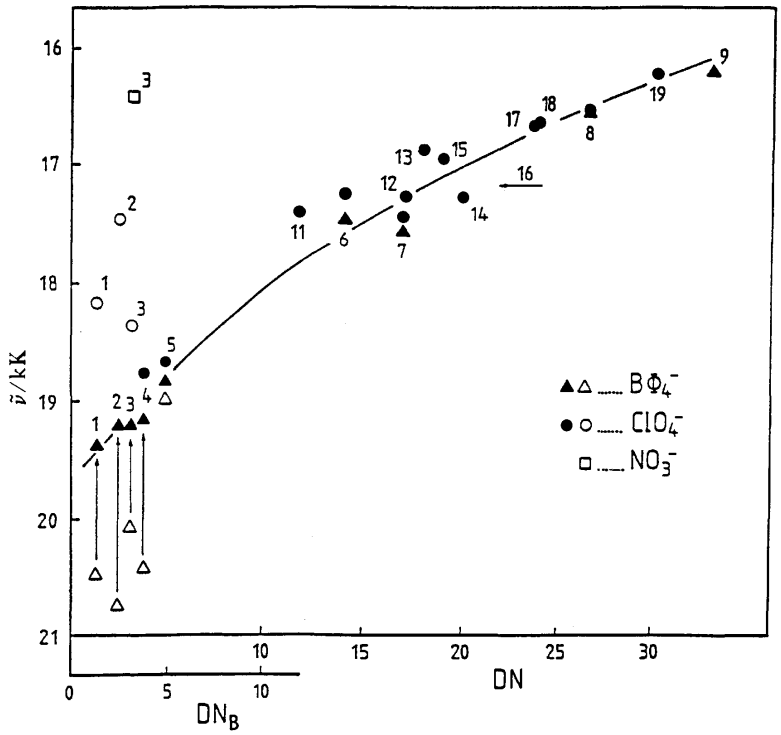

Fig. 2. A plot of the wavenumbers of the d-d band ($\tilde{\nu}_{max}$) against DN or DN_B. Notations of the solvents 1—9: see Table 1. Solvents 11 to 19 correspond, respectively, to benzonitrile, ethyl acetate, water, tetrahydrofuran, methanol, *t*-butyl alcohol, trimethyl phosphate, formamide, and DMSO. For solvents 1—5, DN_B values were used instead of DN. Full triangles 1 to 5 denote corrected values, while open triangles denote observed ones (cf. Table 1). Open circles, and a square for the nitrate, denote the cases where remarkable ion-pair formation takes place. The arrow for 16 indicates a range for its DN estimated from its DN_B.[4] (kK=10^3 cm^{-1}).

ultraviolet. With the decrease of DN or DN_B, this absorption is shifted toward the red, and overlaps remarkably with the d-d band in very weak donor solvents. So the λ_{max} values of the d-d band in such solvents should be corrected for this overlap. This correction was made by assuming that the d-d band in these solvents has the same $\tilde{\nu}$-symmetrical, pseudo-Gaussian shape as in other solvents; the obtained values are given in the third column of Table 1.

When the $\tilde{\nu}$-values corresponding to the λ_{max} values in Table 1 are plotted against DN or DN_B, it can be seen that the points for the tetraphenylborate (full triangles) and those for the perchlorate (full circles) lie along a smooth curve (Fig. 2). However, the points for the latter in three solvents 1—3 deviate strongly from the curve (open circles), confirming that the tetraphenylborate is a better solvent basicity indicator than the perchlorate.[5] The fact that this deviation tends to

Table 2. Variation of λ_{max} of [Cu(acac)(tmen)]BPh_4 in Pyridine with the Addition of tmen

[tmen]/M	0	0.033	0.13	0.27	0.40	∞[a]
λ_{max}/nm	623	619	616	615	614	613

a) Extrapolated by plotting λ_{max} against (1/[tmen]).

increase with the decrease of DN_B supports the view that ion-pair formation, i.e., weak coordination of ClO_4^- on the chelate plane, is responsible for it, which was formerly proposed by Fukuda et al.[6] to explain this type of spectral anomaly found in dichloroethane. In the case of the tetraphenylborate, such an ion-pair formation will not occur effectively since BPh_4^- is so large and inert; the regular spectral trend continues, therefore, in very weak donor solvents with no anomaly.

As to the anomaly in very strong donor solvents, there is no marked difference between the two complex salts. This anomaly is the result of the decomposition of the chelate cation caused by solvent attack. In the case of pyridine, it seems that the tmen ligand is driven off, since the addition of tmen to the solution apparently suppresses the decomposition, shifting λ_{max} to the blue (Table 2). With increasing tmen, the λ_{max} approaches a limit (613 nm); this may be taken as the λ_{max} value for the solvated complex cation [Cu(acac)(tmen)]$^+$ in pyridine, as the corresponding point on Fig. 2 is at a reasonable spot. The present indicators may still be used in such a strong donor solvent, therefore, by adding excess tmen to the solution.[7]

The solutions of the two complex salts in strong donor solvents are thermochromic, becoming more greenish on heating. This fact indicates that the decomposition equilibria in them, e.g.,

[Cu(acac)(tmen)]$^+$+$n$py $\rightleftarrows$ [Cu(acac)(py)$_n$]$^+$+tmen

are shifted to the right-hand side by heating.

References

1) Y. Fukuda and K. Sone, *Bull. Chem. Soc. Jpn.*, **45**, 465 (1972).

2) K. Sone and Y. Fukuda, "Ions and Molecules in Solution," ed by N. Tanaka, H. Ohtaki, and R. Tamamushi (Studies in Phys. and Theoret. Chem., Vol. 27), Elsevier, Amsterdam (1983), pp. 251—266.

3) R. W. Soukup and R. Schmid, *J. Chem. Educ.*, **62**, 459 (1985).

4) DN_B is a solvent polarity parameter derived from the linearity between DN and the frequency shift of the O-D vibration of CH_3OD in various solvents (Koppel and Palm's B value), and can be taken as a substitute for DN when the latter is unknown. Cf. R. Schmid, *J. Sol. Chem.*, **12**, 135 (1983); R. Schmid and V. N. Sapunov, "Non-formal Kinetics," Verlag Chemie, Weinheim (1982), Chap. 7.

5) Some authors are dubious about the significance of the concept of DN for protic solvents like water, formamide or alcohols (cf., e.g., L. L. Rusnak, E. S. Yang, and R. B. Jordan, *Inorg. Chem.*, **17**, 1810 (1978); M. Munakata, S. Kitagawa, and M. Miyazima, *ibid.*, **24**, 1638 (1985); M. H. Abraham, *Pure Appl. Chem.*, **57**, 1055 (1985)). In the present case, however, no remarkable deviation of such solvents from the general trend is observable. Of course, the donor ability of a highly structured solvent is always some function of the acceptor strength of the solute. Hence it seems that the acceptor ability of the cation [Cu(acac)(tmen)]$^+$ is essentially similar to that of $SbCl_5$, the reference compound for the DN scale.

6) Y. Fukuda, A. Shimura, M. Mukaida, E. Fujita, and K. Sone, *J. Inorg. Nucl. Chem.*, **36**, 1265 (1974); cf. also Fig. **1** in Ref. 2 and Footnote in Ref. 1.

7) I. Persson (*Pure Appl. Chem.*, **58**, 1153 (1986)) has collected more data on the λ_{max} of [Cu(acac)(tmen)]ClO_4 and [Cu(acac)(tmen)]BPh_4 in strong donor solvents, obtaining information on the latter complex from one of us (R. W. S.). He stated that there is a good correspondence between λ_{max} and DN even when the latter is very high (ca. 50), seemingly without taking the decomposition of the complexes into account.

Reactions of Trimethylsilyl Isothiocyanate with Aldehydes and Acetals. Synthesis of Symmetrically and Unsymmetrically Isothiocyanato-Substituted Ethers

Kozaburo NISHIYAMA* and Makoto OBA
Department of Chemistry, Tokyo Metropolitan University, 2-1-1 Fukasawa, Setagaya-ku, Tokyo 158
(Received November 28, 1986)

Synopsis. The reactions of trimethylsilyl isothiocyanate (TMSTC) with aldehydes catalyzed by Lewis acid gave α,α′-diisothiocyanato ethers in good to excellent yields. Similarly, unsymmetrical α-isothiocyanato ethers were obtained from the reactions of TMSTC with acetals in appropriate yields.

Silicon compounds carrying a functional group play important roles in organic synthesis.[1] For example, silyl cyanides and silyl azides have been shown to be highly versatile reagents, which converted carbonyl compounds into α-siloxy cyanides (**1a**),[1] α-siloxy azides (**1b**),[2] and *gem*-diazides (**2**).[3,4] As a part of our continuing studies on such silicon compounds, we investigated the synthetic utility of trimethylsilyl isothiocyanate (TMSTC) because there have been a few reports[5] on its reactivity to date. In this paper, we would like to describe $ZnCl_2$-promoted reactions of TMSTC with aldehydes and acetals to give α,α′-diisothiocyanato and α-isothiocyanato ethers, respectively.

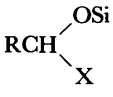

1a, X=CN; **1b**, X=N_3

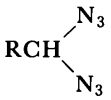

2

Results and Discussion

The Reaction of TMSTC with Aldehyde. Contrary to the reaction of silyl azide with aldehyde,[4] an 89% of bis(1-isothiocyanato-2-methylpropyl) ether (**4c**) was obtained by a reaction of 2-methylpropanal (**3c**) and TMSTC (2.2 equiv) in the presence of a catalytic amount of $ZnCl_2$ at room temperature for 24 h. Even when the reaction of **3c** with 1.2 equiv of TMSTC was carried out at room temperature for 4 h, the sole product was compound **4c** although the yield became poor. The reaction was also promoted by $SnCl_2$, giving the corresponding ether. By carrying out the reaction for other aldehydes under similar conditions, we obtained some symmetrically disubstituted ethers in good yields. The results and the spectral data of the products are summarized in Table 1. Trichloroethanal and benzaldehyde did not give any products under similar conditions and benzaldehyde was quantitatively recovered after the work-up. Such aldehydes reacted with silyl azide to afford adducts, **1b** and **2**.[4] By using hydrosilanes, several synthetic methods for ethers have been reported under various conditions.[6]

When the reaction of 2-methylpropanal (**3c**) with TMSTC in the presence of $ZnCl_2$ (catalytic amount) was carried out at 90 °C for 0.5 h, 2,4,6-tris(1-methylethyl)-1,3,5-trioxane (**5c**) along with ether **4c** (22%) was isolated in a 36% yield. The trioxane **5c** was also isolated in an 83% yield from the reaction of the aldehyd **3c** with $ZnCl_2$ (0.05 equiv) in the absence of TMSTC at room temperature for 1 h. In addition, a mixture of **5c**, TMSTC, and $SnCl_2$ was stirred for 1.5 h at room temperature, giving a 70% yield of **4c**, and 2,4,6-trimethyl-1,3,5-trioxne (**5f**) was also converted into bis(1-isothiocyanatoethyl) ether (**4f**) in a 73% yield. However, 1,3,5-trioxane (**5e**), 2,4-dimethyl-1,3-dioxane (**6a**), and 2,4,6-trimethyl-1,3-dioxane (**6b**) were recovered quantitatively under similar conditions.

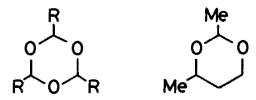

5e, R=H; **f**, R=Me

6a

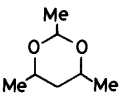

6b

On the basis of these findings, we propose that the reaction of TMSTC with aldehydes takes place as path A rather than path B of the Scheme, i.e. 1,3,5-trioxane **5** initially generated by $ZnCl_2$-catalyzed trimerization of the aldehyde is substituted by TMSTC to form ether **4** and bis(trimethylsilyl) acetal. The latter again trimerizes to trioxane **5** under these conditions. Otherwise, the yield of the product **4** should be at most 67%. As for path B, Mukaiyama et al. considered it a plausible reaction course of ether formation,[6d] i.e. 2:1-addition of aldehyde with silicon compound followed by condensation of the adduct with another silicon compound. That trichloroethanal and benzaldehyde were not converted into ether **4** shows that such aldehydes would not give trioxane **5** under the conditions employed.

Table 1. Yields and Spectral Properties of Ether **4**

Compd	Mp/(θ_m/°C)	Yield/%	FD-MS	IR/cm^{-1}	^{1}H NMR/δ
4a	liq	80[a]	216 (M^+)	2000	1.05 (t, 6H), 1.65—2.10 (m, 4H), 5.09 (t, 2H)
4b	liq	77[a]	244 (M^+)	2000	0.97 (t, 6H), 1.20—2.05 (m, 8H), 5.13 (t, 2H)
4c	liq	89[a]	244 (M^+)	2000	1.06 (d, 12H), 1.80—2.30 (m, 2H), 4.89 (d, 2H)
4d	45—46	84[a]	272 (M^+)	2050	1.03 (s, 18H), 4.72 (s, 2H)
4f	liq	73[b]	188 (M^+)	2000	1.59 (d, 6H), 5.27 (q, 2H)

a) Aldehyde/TMSTC=1/2.2. b) The compound was obtained from 2,4,6-trimethyl-1,3,5-trioxane (**5f**) and TMSTC.

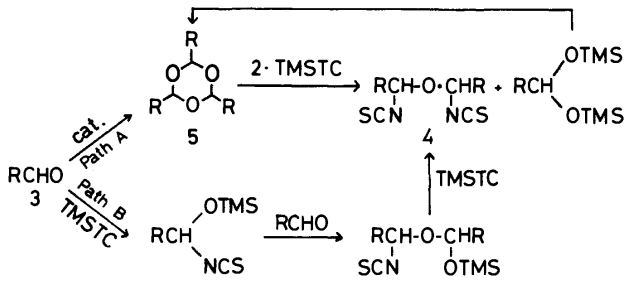

a, R=Et; b, R=n-Pr; c, R=i-Pr; d, R=t-Bu

Scheme 1.

The Reaction of TMSTC with Acetal. As described above, the substitution reaction of trioxane derivatives **5** by TMSTC occurred to give the corresponding ether **4** exclusively. This led us to examine a possibility of unsymmetrical ether formation from acetal with TMSTC.

When a mixture of propanal dimethyl acetal (**7b**), TMSTC, and $ZnCl_2$ was stirred for 4 h at room temperature, the desired ether **8b** was obtained in a 67% yield. This method could be applied to various acetals, and the results are compiled in Table 2. A conversion of acetals **7** into ethers **8** was achieved in good yields, but an isolation of the products depended upon their sensitivity to moisture. Notably, we could not isolate any of the *p*-methoxy derivative **8c** although compound **7c** was quantitatively converted into **8c**, determined by the ^1H NMR spectrum.

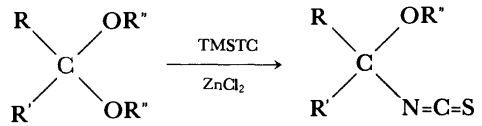

7 8

a) R=Me, R′=H, R″=Et; b) R=Et, R′=H, R″=Me; c) R=*p*-MeOC$_6$H$_4$, R′=H, R″=Et; d) R=*p*-MeC$_6$H$_4$, R′=H, R″=Et; e) R=C$_6$H$_5$, R′=H, R″=Me; f) R=*p*-ClC$_6$H$_4$, R′=H, R″=Et; g) R=*p*-O$_2$NC$_6$H$_4$, R′=H, R″=Et; h) R=R′=Et, R″=Me; i) R=Me, R′=*i*-Pr, R″=Me; j) R,R′=-(CH$_2$)$_4$-, R″=Me; k) R,R′=-(CH$_2$)$_5$-, R″=Me.

In conclusion, the synthesis of α-substituted and α,α′-disubstituted ethers was easily realized by using TMSTC, acetal, and aldehyde. While such ether synthesis is also considered to be achieved by a reaction of halogeno precursor with sodium thiocyanate, the applicability of the method as a general synthetic route to **4** and **8** is limited, due to the inaccessibility of the reagents.

Experimental

Materials. Trimethylsilyl isothiocyanate (TMSTC) was prepared from chlorotrimethylsilane and sodium thiocyanate according to the literature.[7] Acetals, except for commercial products, were synthesized by the reported methods.[8] Commercial products including aldehydes were purified if necessary.

The Reaction of Aldehyde 3 with TMSTC. As an example the reaction of 2-methylpropanal (**3c**) with TMSTC is shown. A mixture of **3c** (3.0 g, 42 mmol), TMSTC (12.0 g, 92 mmol), and $ZnCl_2$ (341 mg, 2.5 mmol) was stirred at room temperature for 24 h. After removal of low-boiling substances, the reaction mixture was triturated with hexane and the resulting precipitates ($ZnCl_2$) were filtered off. The filtrate was stirred with water for an additional 0.5 h. The extract with CH_2Cl_2 was dried over $MgSO_4$, the solvent were evaporated in vacuo, and the residual oil chromatographed on silica gel. Elution with hexane contained 4.6 g (89%) of bis(1-isothiocyanato-2-methylpropyl) ether (**4c**). ^{13}C NMR ($CDCl_3$) δ=17.04, 17.20, 35.10, 89.54, and 138.91. Other spectral data of **4c** and related compounds are shown in Table 1. **4a**: Found: C, 44.21; H, 5.63; N, 12.98%. Calcd for $C_8H_{12}N_2S_2O$: C, 44.41; H, 5.59; N, 12.95%. **4b**: Found: C, 49.00; H, 6.57; N, 11.51%. Calcd for $C_{10}H_{16}N_2S_2O$: C, 49.15; H, 6.60; N, 11.47%. **4c**: Found: C, 49.40; H, 6.75; N, 11.24%. Calcd for $C_{10}H_{16}N_2S_2O$: C, 49.15; H, 6.60; N, 11.47%. **4d**: Found: C, 52.93; H, 7.40; N, 10.23; S, 23.52%. Calcd for $C_{12}H_{20}N_2S_2O$: C, 52.90; H, 7.40; N, 10.29; S, 23.54%. **4f**: Found: C, 38.21; H, 4.26; N, 14.84%. Calcd for $C_6H_8N_2S_2O$: C, 38.28; H, 4.28; N, 34.06%.

Table 2. Yields and Spectral Properties of Ether **8**

Compd	Bp (θ_b/°C)/mmHg[a]	Yield/%	MS[b]	IR/cm^{-1}	^1H NMR/δ
8a	84—85/60	65	131	2025	1.28 (t, 3H), 1.55 (d, 3H), 3.30—4.15 (m, 2H), 4.98 (q, 1H)
8b	72—73/55	67	131	2050	1.02 (t, 3H), 1.64—2.15 (m, 2H), 3.47 (s, 4H), 4.70 (t, 1H)
8c		0 (100)[c]		2000	1.24 (t, 3H), 3.68 (q, 2H), 3.78 (s, 3H), 6.84, 7.34 (ABq, 4H)
8d	88/0.5	65 (100)[c]	162	2000	1.30 (t, 3H), 2.33 (s, 3H), 3.50—4.00 (m, 2H), 7.11, 7.31 (ABq, 4H)
8e	77—78/0.7	65 (100)[c]	148	2000	3.60 (s, 3H), 5.82 (s, 1H), 7.44 (m, 5H)
8f	83/0.25	76 (100)[c]	182	2000	1.30 (t, 3H), 3.50—4.05 (m, 2H), 5.85 (s, 1H) 7.38 (s, 4H)
8g	112/0.2	43 (65)[c]	193	2000	1.35 (t, 3H), 3.50—4.15 (m, 2H), 5.99 (s, 1H), 7.66, 8.27 (ABq, 4H)
8h	52—55/5	61	130	2025	0.97 (t, 6H), 1.87 (q, 4H), 3.32 (s, 3H)
8i	53/5	56	128	2050	0.99 (d, 3H), 1.03 (d, 3H), 1.49 (s, 3H), 1.60—2.20 (m, 1H), 3.37 (s, 3H)
8j	46—47/1.2	50	126	2025	1.50—2.25 (m, 8H), 3.40 (s, 3H)
8k	65/2	70	140	2025	1.40—2.10 (m, 10H), 3.35 (s, 3H)

a) 1 mmHg=133.322 Pa. b) The largest number of the fragment is shown. c) Yields determined by ^1H NMR spectrum are indicated in parenthesis.

The Reaction of Acetal 7 with TMSTC. When the boiling points of the products (unsymmetrically substituted ethers) were close to that of TMSTC, the following was representative of the reaction of acetal **7** with TMSTC. A mixture of propanal dimethyl acetal (**7b**, 6.3 g, 60 mmol), TMSTC (3.9 g, 30 mmol), and $ZnCl_2$ (0.4 g, 3 mmol) in dichloromethane (15 cm^3) was stirred at room temperature for 4 h. With aromatic derivatives, the quantities of compound **7** and TMSTC were altered to 30 and 60 mmol, respectively, and trimethylsilyl trifluoromethanesulfonate (TMSOTf) was used as a catalyst in order to avoid a complicated isolation. Work-up was similar to that for **4c** described above. 2.7 g (67%) of 1-isothiocyanatopropyl methyl ether (**8b**) was obtained by distillation at reduced pressure, bp 72—73 °C/55 mmHg. Physical and spectral data of compound **8** are listed in Table 2.

One of us (K. N.) wishes to thank the ministry of Education, Science and Culture for Grant-in-Aid (No 60540338).

References

1) W. P. Weber, "Silicon Reagents for Organic Synthesis," Springer-Verlag, New York (1983).

2) L. Birkofer, F. Müller, and W. Kaiser, *Tetrahedron Lett.*, **1967**, 2781; L. Birkofer and W. Kaiser, *Justus Liebigs Ann. Chem.*, **1975**, 266.

3) K. Nishiyama and A. Watanabe, *Chem. Lett.*, **1984**, 455.

4) K. Nishiyama, M. Oba, and A. Watanabe, *Tetrahedron*, **43**, 693 (1987).

5) For example, A. C. W. Curran and R. G. Shephered, *J. Chem. Soc., Perkin Trans. 1*, **1976**, 983; T. Sasaki, A. Nakanishi, and M. Ohno, *J. Org. Chem.*, **46**, 5445 (1981); R. F. Cunico and L. Bedell, *J. Organomet. Chem.*, **281**, 135 (1985).

6) a) D. N. Kursanov, Z. N. Parnes, and N. M. Loim, *Synthesis*, **1974**, 633; b) M. P. Doyle, C. T. West, S. J. Donnelly, and C. C. McOsker, *J. Organomet. Chem.*, **117**, 129 (1976); c) R. Noyori, S. Murata, and M. Suzuki, *Tetrahedron*, **37**, 3899 (1981); d) J. Kato, N. Iwasawa, and T. Mukaiyama, *Chem. Lett.*, **1985**, 743.

7) British Tomson-Houston Co. Ltd., Brit. Patent 643941 (1950); *Chem. Abstr.*, **45**, 7585 g (1951).

8) T. H. Fifi and L. K. Jao, *J. Org. Chem.*, **30**, 1492 (1965); S. R. Sandler and W. Karo, "Organic Functional Group Preparations," Academic Press, New York (1972), Vol. 3, Chap. 1, pp. 1—75.

Improved Synthesis of Dibenzo[*a,j*]perylene-8,16-dione

Kiyoichi HIRAKAWA,* Eriko OGIUE, Jiro MOTOYOSHIYA, and Toshio KAKURAI
Department of Chemistry, Faculty of Textile Science and Technology, Shinshu University, Ueda, Nagano 386
(Received January 5, 1987)

Synopsis. An improved method for the synthesis of the title compound **1** has been achieved through an application of the Scholl reaction. The key to the new approach is to use the dimeric compounds of 10-methyleneanthrone as the precursors of **1**.

Photochromic systems which are based on photoreversible addition of O_2 to arene derivatives have recently received much attention in connection with their potential use as photoresponsive materials.[1-12] The photochromic conversion of dibenzo[*a,j*]perylene-8,16-dione (heterocoerdianthrone) (**1**) into 4b,12b-epidioxy-4b,12b-dihydrodibenzo[*a,j*]perylene-8,16-dione (*endo*-peroxide) (**2**) is among the most extensively investigated reactions.[1-8,11] The self-sensitizing photooxidation of reddish violet **1** by visible light irradiation in air-saturated solution leads to the formation of colorless **2**, which reproduces the parent compound **1** and O_2 in a singlet state by ultraviolet light. The photochromic system consisting of **1** and **2** is highly reversible and thermally stable.[4,6,11]

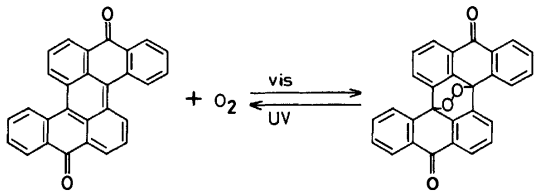

1 2

The methods reported to date for the synthesis of **1** are as follows: (a) Dehydration of 9,10-diphenyl-1,5-anthracenedicarboxylic acid which is prepared in four steps from the readily available starting material, 9,10-anthraquinone-1,5-dicarboxylic acid,[13] (b) thermolysis of 4-chloroanthrone whose preparation is difficult,[14] (c) reaction of 4-chloroanthrone with zinc chloride in pyridine,[15] and (d) the Scholl reaction of readily available 10-methyleneanthrone (**3**) with aluminium chloride.[16] The overall yield of **1** from the anthraquinonedicarboxylic acid by method (a), which is often employed, is low (ca. 23—25%). In method (d), **1** is prepared in one step from **3**. However, its detailed direction and yield have not been published. We have, therefore, examined the convenient synthesis of **1** using the Scholl reaction of **3** and its dimeric compounds.

Treatment of **3** with aluminium chloride-sodium chloride at 200 °C, in a modification of literature method,[16] gave very low yield of **1** (16%), together with anthraquinone (4%). The addition of a proper amount of the hydrogen acceptor, manganese dioxide, resulted in an increase in the yield of **1**. Similar treatment of **3** in the presence of manganese dioxide, 2—3 wt%/aluminium chloride, led to **1** in a 22% yield. However, addition of an organic base, e.g., pyridine, was without effect. The similar reaction of **3** at the reaction temperature of 150—170 °C afforded the intermediate, 4b,12b-dihydro-4b,12b-ethanodibenzo[*a,j*]perylene-8,16-dione (**4**), the structure of which followed from spectral data and thermolysis to **1**. Its IR spectrum indicates absorption for the carbonyl group at 1650 cm^{-1} and its ^1H NMR spectrum reveals an A_2B_2 multiplet due to the ethylene group at δ 1.92—2.26 and 2.40—2.74. Heating of **4** at its melting point gave **1** in a high yield, together with evolution of ethylene.

It seemed to us, based on the formation of **4**, that the dimeric compounds of **3**, dispiro[anthracene-9(10*H*), 1′-cyclobutane-2′,9″(10″*H*)-anthracene]-10,10″-dione (**5**) and 7′-acetoxy-1′,2′-dihydrospiro[anthracene-9(10*H*), 3′-[3*H*]benz[*de*]anthracene]-10-one (**6**),[17] would be favorable precursors for conversion to **1** via the Scholl reaction. The dimer **5** and its acetylated compound **6** were prepared from **3** in high yields according to the previously studied method (**5**: 97%; **6**: 89%), as shown in the scheme. The dimeric compounds **5** and **6** gave the expected dye **1** or its intermediate **4** under the Scholl reaction conditions (Table 1). The yields of **1** or **4** from **5** and **6** were much higher than those from **3**; under the optimum conditions, the reactions of **5** and **6** led to **1** in 33 and 26% yields, respectively. In addition, the Scholl reactions of **5** and **6** did not yield anthraquinone whose separation from **1** using the means of vatting process is troublesome, whereas **3** led to a significant amount of anthraquinone. Thus, the method involving the Scholl reaction of the dimer **5**, prepared from **3**, to **1** (**3**→**5**→**1**) is preferable to the other two (**3**→**1** and **3**→**5**→**6**→**1**) in terms both of convenience and yield. A similar treatment of **5** with zinc chloride as a Friedel-Crafts reagent did not give **1**, but, instead, gave spiro[anthracene-9(10*H*),3′-[3*H*]benz[*de*]anthracene]-7′,10(2′*H*)-dione (**7**).[17]

It seems likely that the formation of **1** occurs through **8** and its enol **9** and in turn **4**, since (a) all of

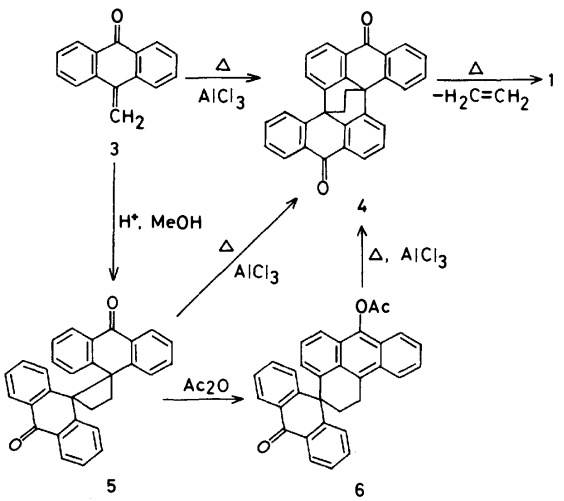

5 6

the reaction of **8**, **5**, and **6** with aluminium chloride at low temperature (150—170 °C) gave the intermediate **4** which yielded **1** by thermolysis, and (b) similar reactions at 135—140 °C led to **7** which probably arises from the dehydrogenation of **8** or **9**,[17] (c) the acid-catalyzed reaction of **3** in organic solvents readily gave **5**, which thermally rearranged with a synchronous ring expansion to give unstable **8** and/or **9**.[17] These peri-condensation reactions effected by aluminium chloride occured in the presence of a trace of water or hydrogen chloride.[18,19] In addition, hydrogen acceptors such as air, supplied by vigorous stirring of the reaction mixture, and manganese dioxide resulted in an increase in the yield of **1**. A conceivable mechanism for the formation of **1** from **3**, **5**, and **6** may be as follows: First, the formation of the enol **9** from **3**, **5**, and **6**, second, the protonation on the anthracene moiety of **9** by moist aluminium chloride to give σ complexes[20] which undergo the electrophilic substitution (cyclization) involving the C-11'b and C-4 atoms, third, the dehydrogenation promoted by air or manganese dioxide to lead to **4**, and finally, the retro Diels-Alder reaction of **4** to give **1** and ethylene. The low yields of these Scholl reactions might result from the deactivation at the 4-position by the inductive effect of the carbonyl group and the steric hindrance in the intramolecular electrophilic substitution of the σ complex. However, the synthetic method of **1** via the Scholl reaction of the dimer **5** can compete in terms of convenience and yield with those through 9,10-diphenyl-1,5-anthracenedicarboxylic acid.

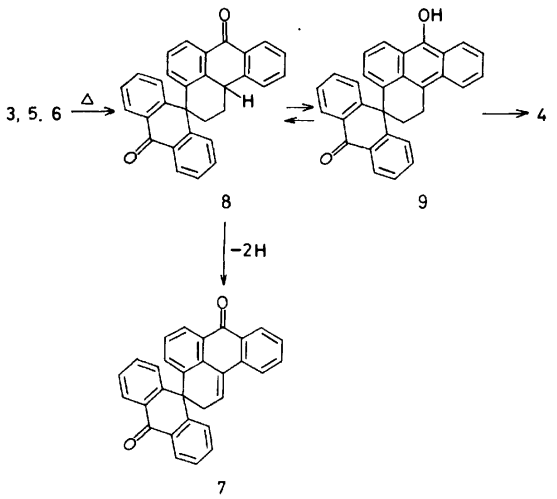

Experimental

The following compounds were prepared according to previously known procedures: **3**,[21] **5**,[17] and **6**.[17]

Dibenzo[*a,j*]perylene-8,16-dione (1). To a finely ground mixture of aluminium chloride (50 g), sodium chloride (15 g), and manganese dioxide (1.00 g), 5 (5.00 g) was added. The mixture was vigorously stirred and heated until TLC showed the absence of the intermediate **4**. The reaction temperature was kept at 160 °C during the first 10 min and then raised to 200 °C in 5—10 min, where it was kept for ca. 2 h. The resulting mixture was poured into ice-water (500 g) followed by addition of hydrochloric acid (100 ml). After boiling, the precipitate was filtered off and washed with water. The product mixture was extracted repeatedly with a hot alkaline sodium dithionite solution (NaOH, 10 g; $Na_2S_2O_4$, 10 g; H_2O, 500 ml). The alkali-soluble leuco product (deep green) was oxidized to the crude dye by contact with air. The dye was washed with water, dried, and recrystallized from chlorobenzene or pyridine to give pure **1** (33%) as reddish violet microcrystals, identical with an authentic specimen:[13] mp 363—365 °C (lit,[4] 361 °C); IR (KBr) 1643 cm^{-1} (C=O); ^1H NMR ($CDCl_3$) δ=7.55—7.95 (6H, m), 8.15—8.30 (2H, m), 8.50—8.65 (2H, m), 8.83 (2H, dd), and 9.00 (2H, d), MS *m/z* 382 (M^+); Anal. ($C_{28}H_{14}O_2$) C, H.

Results of the reactions of **3**, **5**, and **6** under the different conditions are summarized in Table 1.

4b,12b-Dihydro-4b,12b-ethanodibenzo[*a,j*]perylene-8,16-dione (4). The procedure for the Scholl reaction was similar to that for **1** except that the reaction was carried out without manganese dioxide at 160 °C for 1 h until TLC showed the absence of the starting material. The product mixture from **5** was chromatographed on silica (benzene as

Table 1. Scholl Reactions of **3**, **5**, and **6**

Reactant	Reaction Condition					Product/%	
	Reagent:Reactant/wt ratio			Temp	Time		
	$AlCl_3$	NaCl	MnO_2	°C	h	**1**	**4**
3	10	3	0	200	2	16[a]	0
3	10	3	0.2	200	2	22[a]	0
3	10	3	0	160[b]	1	Trace	16[a]
5	10	0	0	200	2	18	0
5	7	2.1	0	200	2	16	0
5	10	3	0	200	2	25	0
5	10	3	0.2	200	2	33	0
5	10	3	0.5	200	2	29	0
5	10	3	0.2	220	2	28	0
5	10	3	0.2	200	3	24	0
5	10	3	0	160[b]	1	Trace	24
6	10	3	0	210	2	21	0
6	10	3	0.2	210	2	26	0
6	10	3	0	160[b]	1	Trace	22

a) The reaction gave anthraquinone (ca. 4—5%) as by-product. b) At this reaction temperature, the addition of manganese dioxide resulted in an inadequate melting of aluminium chloride-sodium chloride medium. Consequently, it led to a decrease in the yield of **4**.

eluant). Recrystallization of the appropriate fraction from benzene-hexane gave **4** (24%) as nearly colorless microcrystals: TLC (Merck, silica gel 60 F_{254}, precoated plastic sheet, 0.2 mm, benzene) R_f 0.35; mp 319—321 °C; IR (KBr) 1650 cm^{-1} (C=O); ^1H NMR ($CDCl_3$) δ=1.92—2.26 (2H, m), 2.40—2.74 (2H, m), 7.15—7.40 (4H, m), 7.50—7.95 (6H, m), 8.15 (2H, dd), and 8.50—8.70 (2H, m); MS m/z 410 (M^+); Anal. ($C_{30}H_{18}O_2$) C, H.

Results for the similar reactions of **3** and **6** are shown in Table 1.

Thermolysis of 4. Compound **4** (2.05 g, 50 mmol) was heated at its melting point in a test tube for 5 min during which time gas was evolved. The violet product was recrystallized from chlorobenzene to give **1** (1.74 g, 89%). GLC analysis of the gas evolved in the thermolysis showed the presence of ethylene.

References

1) H. W. Wagener and H.-D. Brauer, *Mol. Photochem.*, **7**, 441 (1976).

2) W. Drews, R. Schmidt, and H.-D. Brauer, *J. Photochem.*, **6**, 391 (1977).

3) H.-D. Brauer, W. Drews, and R. Schmidt, *J. Photochem.*, **12**, 293 (1980).

4) R. Schmidt, W. Drews, and H.-D. Brauer, *J. Am. Chem. Soc.*, **102**, 2971 (1980).

5) H.-D. Brauer, W. Drews, R. Schmidt, G. Gauglitz, and S. Hubig, *J. Photochem.*, **20**, 335 (1982).

6) H.-D. Brauer and R. Schmidt. *Photochem. Photobiol.*, **37**, 587 (1983).

7) H.-D. Brauer and R. Schmidt, *Chem. Phys. Lett.*, **100**, 470 (1983).

8) H.-D. Brauer, A. Acs, W. Drews, R. Gabriel, S. Ghaeni, and R. Schmidt, *J. Photochem.*, **25**, 475 (1984).

9) R. Schmidt, *Z. Naturforsch., A*, **39**, 998 (1984).

10) R. Schmidt, W. Drews, and H.-D. Brauer, *J. Phys. Chem.*, **86**, 4909 (1982).

11) R. Schmidt and H.-D. Brauer, *J. Photochem.*, **25**, 489 (1984).

12) T. Kajiwara, S. Fujisawa, K. Ohno, and Y. Harada, *Bull. Chem. Soc. Jpn.*, **52**, 2771 (1979).

13) R. Scholl, H. K. Meyer, and W. Winkler, *Justus Liebigs Ann. Chem.*, **494**, 201 (1932).

14) I. M. Heilbrob and F. Irving, *Chem. Ind. (London)*, **1933**, 951.

15) E. Clar, *Chem. Ber.*, **82**, 46 (1949).

16) I. G. Farbenindustrie AG., British Patent, 373129 (1932).

17) K. Hirakawa and S. Nakazawa, *J. Org. Chem.*, **43**, 1804 (1978). More recently, the structure **7** has been probably erroneously assigned to the dimer obtained from **3** with acid catalyst: H.-D. Becker and D. Sanches, *J. Org. Chem.*, **44**, 1787 (1979).

18) C. D. Nenitzescu and A. T. Balaban, "Friedel-Crafts and Related Reactions," ed by G. A. Olah, Interscience, New York (1964), Vol. II, p. 979.

19) R. H. Thomson, "The Chemistry of the Quinonoid Compounds," ed by S. Patai, Interscience, New York (1974), Part 1, p. 140.

20) F. A. Vingiello, J. Yanez, and J. A. Campbell, *J. Org. Chem.*, **36**, 2051 (1971).

21) W. H. Starnes, Jr., *J. Org. Chem.*, **35**, 1974 (1970).

Favorskii-Type Rearrangement of α,α′-Dihalo Ketones with Sodiomalonates Leading to Conjugated Enone Derivatives

Takashi SAKAI,* Mutsumi ISHIKAWA, Eiichiro AMANO, Masanori UTAKA, and Akira TAKEDA
Department of Synthetic Chemistry, School of Engineering, Okayama University, Tsushima, Okayama 700
(Received January 14, 1987)

Synopsis. A new synthetic method of conjugated enones by the use of carbanion-induced Favorskii-type rearrangement is described. The reaction of α,α′-dihalo ketones $R^1R^2(X)CC(O)CH_2X$ with sodiomalonates $Na^+ {}^-CR^3(CO_2R^4)_2$ in THF at 0 °C—room temperature gave conjugated enones $R^1R^2C{=}CHC(O)CR^3(CO_2R^4)_2$ in 42—66% yields. The reaction can be also adaptable to the enolates of ethyl cyanoacetate or malononitrile to give the corresponding enones.

We recently reported that certain α,α′-dihalo ketones caused the Favorskii-type rearrangement by the action of enolate anions derived from β-keto esters[1] and ethyl (diethoxyphosphinyl)acetate,[2] giving dihydro-4-pyrones and α-(diethoxyphosphinyl) β-oxo γ,δ-unsaturated esters, respectively. In the previous communication,[1] we simply pointed out that the reaction of 1,3-dichloro-3-methyl-2-butanone (**1a**) with ethyl sodiomalonate (**2a**) gave diethyl (3-methyl-2-butenoyl)malonate (**3a**). Continuous interests to extend the synthetic utility stimulated us to apply the reaction to other α,α′-dihalo ketones and enolate anions.

The reaction of **1a** with two equivalents of **2a** in THF at 0 °C—room temperature gave **3a**[3] in a 52% yield exclusively (Scheme 1). The yield of **3a** was further improved up to 66% by the use of 3-bromo-1-chloro-3-methyl-2-butanone (**1b**) in place of **1a**. The mechanism for the formation of the unsaturated keto ester is explained in parallel with that described previously.[1]

Replacement of the chloro substituent at C-1 by bromine resulted in loss of the product selectivity. Thus the reaction of 1,3-dibromo-3-methyl-2-butanone (**1c**) with **2a** afforded diethyl (3-bromo-3-methyl-2-oxobutyl)malonate (**4**) (43% yield) in addition to the formation of **3a** (49% yield) (Scheme 2). These results

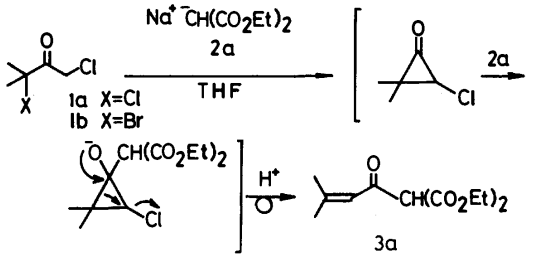

Scheme 1.

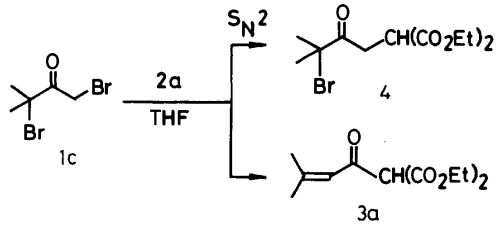

Scheme 2.

Table 1. Synthesis of Conjugated Enone Derivatives

Dihalo ketone	Enolate anion[a]	Product (Yield/%)
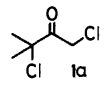 1a	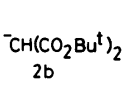 2b	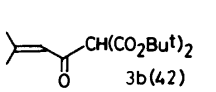 3b(42)
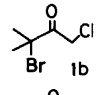 1b	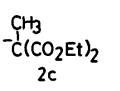 2c	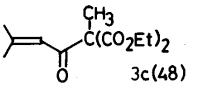 3c(48)
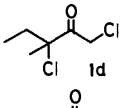 1d	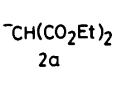 2a	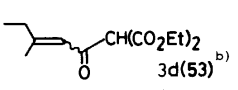 3d(53)[b]
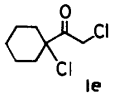 1e	2a	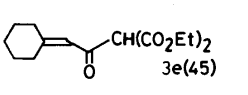 3e(45)
1a	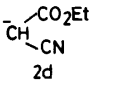 2d	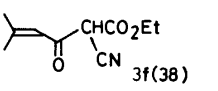 3f(38)
1b	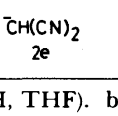 2e	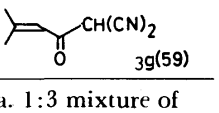 3g(59)

a) Sodium salt (NaH, THF). b) A ca. 1:3 mixture of cis- and trans-isomers on the basis of ^1H NMR analysis (see also Ref. 4).

suggest that the Favorskii-type rearrangement and the nucleophilic substitution of **2a** at C-1 occur competitively. The latter reaction would be accelerated in the case of **1c**.

Application of the reaction to the synthesis of various enones **3b—g** is summarized in Table 1. The reaction of 1,3-dichloro-3-methyl-2-pentanone (**1d**) with **2a** gave trans-enone **3d**[4] predominantly. It is worthwhile to note here that the reaction of **1a** with sodiocyanoacetate (**2d**) also gave **3f**, although the enolate gave only the S_N2 product in the reaction with 3-bromo-3-methyl-2-butanone (**5**).[5] The difference would come from the ease of abstraction of the C-1 proton of **1a**, **b**, as compared with that of **5**, by the less basic enolate **2d**. The present reaction provides synthetically useful conjugated enone derivatives (**3a—g**) by the use of the Favorskii-type rearrangement.

Furthermore, a similar reaction of **1b** with di-*t*-butyl sodiobenzylmalonate (**6**) afforded 5-methyl-1-phenyl-4-hexen-3-one (**7**) as a result of the decarboxylative decomposition of the Favorskii product in the course of vacuum distillation (Scheme 3).

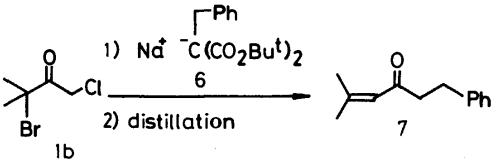

Scheme 3.

Experimental

Melting points were determined on a Yamato MP-21 apparatus and are uncorrected. The bulb-to-bulb distillation was done using a Büchi Kugelrohrofen at the pressure and the oven temperature indicated. IR spectra were taken on a JASCO A-102 spectrometer. ^{1}H NMR spectra were measured with a JEOL JNM PMX60-SI spectrometer. Both ^{1}H NMR (100 MHz) and ^{13}C NMR (25 MHz) spectra were taken on a JEOL FX-100 spectrometer using Me_4Si as an internal standard. HPLC analysis was performed by using Yanagimoto L-2000 apparatus. Elemental analyses were carried out with Yanagimoto MC-2 apparatus. Column chromatography was performed through silica gel (Wakogel C-200). TLCs were done on a silica gel (Kieselgel 60 PF_{254}).

Dihalo Ketones. Compound **1c**[6] was prepared by the bromination (Br_2, ether) of 3-methyl-2-butanone. Bromo chloro ketone **1b**[7] as well as dichloro ketones **1a**,[8] **1d**,[8] and **1e**[8] were prepared in a different way from that reported.[7,8]

1,3-Dichloro-3-methyl-2-butanone (1a).[8] Sulfuryl chloride (135 g, 1.0 mol) was added to 3-methyl-2-butanone (34.5 g, 0.41 mol) with stirring at room temperature. After being stirred for 25 h at 40—50 °C, the solution was poured into cold water carefully. The organic layer was separated and the aqueous layer was extracted with dichloromethane. The combined organic layer was washed with water, dried ($CaCl_2$), and concentrated under reduced pressure. The residual oil was distilled to give **1a** (44.7 g, 70%): bp 55—59 °C (9 mmHg, 1 mmHg=133.322 Pa).

Dichloro ketones **1d**[8] and **1e**[8] were prepared in a similar way in 53 and 40% yields, respectively.

3-Bromo-1-chloro-3-methyl-2-butanone (1b).[8] A mixture of 3-methyl-2-butanone (9.9 g, 0.115 mol), *N*-bromosuccinimide (20.4 g, 0.115 mol), benzoyl peroxide (2.1 g, 0.0087 mol), and CCl_4 (96 ml) was heated under reflux for 5 h. The mixture was filtered, washed with water and brine, dried ($CaCl_2$), and then concentrated. The residual oil was subjected to vacuum distillation to give 3-bromo-3-methyl-2-butanone,[9] (15.9 g, 84%): bp 73—77 °C (93 mmHg). The bromide was then treated with sulfuryl chloride (10.2 g, 0.076 mol) for 11 h at room temperature. Unreacted sulfuryl chloride was removed under reduced pressure. The resulting oil was treated in a manner similar to the foregoing experiment to give **1b** (13.1 g, 68%): bp 90—95 °C (24 mmHg); IR (neat) 1730 cm^{-1}; ^{1}H NMR (CCl_4) δ=1.90 (6H, s), 4.53 (2H, s).

Reaction of 1b with Diethyl Sodiomalonate (2a). Synthesis of Diethyl (3-Methyl-2-butenoyl)malonate (3a).[3] A mixture of diethyl malonate (3.04 g, 19.0 mmol), NaH (457 mg, 19.0 mmol), and THF (25 ml) was heated under reflux for 4 h and then cooled to 0 °C in an ice bath. To the suspension was added a solution of **1b** (1.90 g, 9.52 mmol) and THF (7 ml). After being stirred for 2 h at 0 °C and then for additional 20 h at room temperature, the mixture was acidified with 10% HCl, washed with water, dried ($MgSO_4$), and then concentrated under reduced pressure. The residual oil was purified by column chromatography (hexane-acetone, 10:1) to give **3a** (1.52 g, 66%). It was subjected to vacuum distillation to afford an analytical sample of **3a**: bp 120—140 °C (1.0 mmHg); IR (film) 1760, 1738, 1697, 1644, 1623 cm^{-1}; ^{1}H NMR (CCl_4) δ=1.25 (1.8 H, t, J=7Hz), 1.28 (1.2 H, t, J=7 Hz), 1.90 (3H, br s), 2.09 (3H, br s), 3.94—4.38 [4.4H, m, ester 2 CH_2 and $CH(CO_2Et)_2$], 6.00 (1H, m), 13.47 (0.6 H, s, enol OH).

A similar reaction of dichloro ketone **1a** with **2a** gave **3a** in a 52% yield.

Reaction of 1c with 2a. The crude product was separated by column chromatography (hexane-acetone, 15:1) to give **3a** (49%) and **4** (43%). **4**: IR (neat) 1760—1720 cm^{-1}; ^{1}H NMR (CCl_4) δ=1.28 (6H, t, J=7 Hz), 1.88 (6H, s), 3.42 (1H, d, J=8 Hz), 3.43 (1H, d, J=6.5 Hz), 3.77 (1H, dd, J=6.5 and 8 Hz), 4.26 (4H, q, J=7 Hz). Found: C, 44.46; H, 5.87%. Calcd for $C_{12}H_{19}O_5Br$: C, 44.59; H, 5.92%.

Di-*t*-butyl (3-Methyl-2-butenoyl)malonate (3b): Bp 125—145 °C (3 mmHg); IR (neat) 1730, 1690, 1625 cm^{-1}; ^{1}H NMR (CCl_4) δ=1.44 (18H, s), 1.91 (3H, br s), 2.13 (3H, br s), 3.98 (0.8H, s), 6.08 (1H, m), 13.16 (0.2H, s, enol OH). Found: C, 64.26; H, 8.85%. Calcd for $C_{16}H_{26}O_5$: C, 64.41; H. 8.78%.

Diethyl 5-Methyl-3-oxo-4-hexene-2,2-dicarboxylate (3c): Bp 125—145 °C (1.0 mmHg); IR (neat) 1735, 1697, 1623 cm^{-1}; ^{1}H NMR (CCl_4) δ=1.27 (6H, t, J=7 Hz), 1.51 (3H, s), 1.94 (3H, br s), 4.18 (4H, q, J=7 Hz), 6.09 (1H, m); ^{13}C NMR ($CDCl_3$) δ=13.7 (q), 18.0 (q), 20.9 (q), 27.7 (q), 61.7 (t), 66.8 (s), 120.8 (d), 158.1 (s), 168.6 (s), 191.0 (s). Found: C, 60.86; H, 7.72%. Calcd for $C_{13}H_{20}O_5$: C, 60.92; H, 7.87%.

Diethyl (3-Methyl-2-pentenoyl)malonate (3d). The crude product was purified by TLC (hexane-ether, 5:1) to give **3d**;[4] IR (neat) 1730, 1690, 1620 cm^{-1}; ^{1}H NMR ($CDCl_3$) δ=1.07 (3H, t, J=7 Hz), 1.27 (4.7H, t, J=7 Hz), 1.29 (1.3H, t, J=7 Hz), 1.89 (0.65H, br s, CH_3 of *cis*-**3d**), 2.10 (2.35H, br s, CH_3 of *trans*-**3d**), 2.02—2.72 (2H, m), 3.9—4.4 (4.46H, m, ester 2 CH_2 and OH), 5.95 (1H, m), 12.65 (0.54H, br s, enol OH). Found: C, 60.87; H, 7.62%. Calcd for $C_{13}H_{20}O_5$: C, 60.92; H, 7.87%.

Diethyl (Cyclohexylideneacetyl)malonate (3e). The crude product was purified by TLC (hexane-ether, 5:1) to give **3e**: IR (neat) 1730, 1640, 1560 cm^{-1}; ^{1}H NMR ($CDCl_3$) δ=1.28 (3.3H, t, J=7 Hz), 1.31 (2.7H, t, J=7 Hz), 1.50—2.94 (10H, m), 3.93—4.42 [4.45H, m, ester 2 CH_2 and $CH(CO_2Et)_2$], 5.94 (1H, s), 13.42 (0.55H, br s, enol OH). Found: C, 63.72; H, 8.03%. Calcd for $C_{15}H_{22}O_5$: C, 63.81; H, 7.85%.

Ethyl 2-Cyano-5-methyl-3-oxo-4-hexenoate (3f). The reaction of **1a** (1.55 g, 0.01 mol) with **2d** [ethyl cyanoacetate (1.94 g, 0.02 mol) and NaH (0.48 g, 0.02 mol) in THF (50 ml)] was done in a similar way. The crude product was purified by column chromatography (hexane-acetone, 5:1) to give **3f** (990 mg, 38%): mp 36—37 °C ($CHCl_3$); IR (KBr) 3700—3100, 2190, 1660, 1640 cm^{-1}; ^{1}H NMR (CD_3COCD_3) δ=1.13 (3H, t, J=7 Hz), 1.86 (3H, br s), 2.10 (3H, br s), 4.16 (2H, q, J=7 Hz), 3.6—4.5 (3H, br s), 6.31 (1H, m). Found: C, 61.49; H, 6.45%. Calcd for $C_{10}H_{13}O_3N$: C, 61.53; H, 6.71%.

(3-Methyl-2-butenoyl)malononitrile (3g). The reaction of **1a** (1.55 g, 0.01 mol) with **2e** [malononitrile (1.32 g, 0.02 mol) and NaH (0.48 g, 0.02 mol) in THF (40 ml)] was carried out in the usual manner. The crude product was purified by column chromatography (hexane-acetone, 5:1) to give **3g** (0.87 g, 59%): mp 162—163 °C ($CHCl_3$); IR (KBr) 2220, 2200 1624 cm^{-1}; ^{1}H NMR (CD_3COCD_3) δ=2.04 (3H, d, J=0.14 Hz), 2.08 (3H, d, J=1.5 Hz), 6.14 (1H, m), 9.28 (1H, br s, enol OH). Found: C, 64.72; H, 5.46%. Calcd for $C_8H_8ON_2$: C, 64.85; H, 5.44%.

5-Methyl-1-phenyl-4-hexen-3-one (7). The reaction of **1b** (1.99 g, 0.01 mol) with **6** [di-*t*-butyl benzylmalonate[10] (3.06 g, 0.01 mol) and NaH (0.528 g, 0.022 mol) in THF (100 ml)] was carried out in a usual manner. The crude product was subjected to vacuum distillation [bp 150—160 °C (0.3 mmHg)] and purified by column chromatography (hexane-acetone, 20:1) to give **7** (661 mg, 35%): IR (neat) 1693, 1625 cm^{-1}; ^{1}H NMR (CCl_4) δ=1.74 (3H, d, J=1.5 Hz), 2.11 (3H, d, J=1.5 Hz), 2.41—3.06 (4H, m), 5.94 (1H, m), 7.09 (5H, br s). Found: C, 82.86; H, 8.61%. Calcd for $C_{13}H_{16}O$: C, 82.94; H, 8.57%.

This research was supported in part by a Grant-in-Aid for Special Project Research No. 57218019 from the Ministry of Education, Science and Culture.

References

1) T. Sakai, K. Miyata, M. Ishikawa, and A. Takeda,

Tetrahedron Lett., **26**, 4727 (1985).

2) T. Sakai, E. Amano, K. Miyata, M. Utaka, and A. Takeda, *Bull. Chem. Soc. Jpn.*, **60**, 1945 (1987).

3) Preparation of **3a** by the reaction of 3-methyl-2-butenoyl chloride with $EtOMg^+ {}^-CH(CO_2Et)_2$: S. Gerin and R. Gerin, *Bull. Soc. Chim. Fr.*, **1970**, 340.

4) Attempts to separate the cis,trans-isomers resulted in failure. HPLC analysis (column packed with Yanagimoto SA-1, hexane-ether, 10:1) of this mixture showed a single peak.

5) T. Sakai, T. Katayama, and A. Takeda, *J. Org. Chem.*, **46**, 2924 (1981).

6) R. B. Wagner and J. B. Moore, *J. Am. Chem. Soc.*, **72**, 974 (1950).

7) A. A. Petrov, *J. Gen. Chem.*, **15**, 931 (1945).

8) N. Schamp, N. De Kimpe, and W. Coppens, *Tetrahedron*, **31**, 2081 (1975).

9) The reported procedure involves bromination of 3-methyl-2-butanone by Br_2 in the presence of $KClO_4$ under the irradiation of UV: J. W. Thorpe and J. Warkentin, *Can. J. Chem.*, **51**, 927 (1973).

10) A. Jonczyk, M. Ludwikow, and M. Makosza, *Rocz. Chem.*, **47**, 89 (1973).

Evidence for the Similarity Recognition Hypothesis. Structure Dependence of the Selectivity in Oxidation of a Pair of Associating Thiols Each Having an Alkyl Group

Tadashi ENDO,* Takeshi UEDA, Takashi ISAGO, Jun-ichi KATO, Takashi SUZUKI, Makoto MISAKA, and Masato M. ITO
Department of Chemistry, College of Science and Engineering, Aoyama Gakuin University, Chitosedai, Setagaya-ku, Tokyo 157
(Received January 17, 1987)

Synopsis. In base-catalyzed oxidation of a pair of associating thiols [$HSCH_2$-CONHCONH-R^1 and $HSCH_2CH_2$-NHCONHCO-R^2] (R^1=n-C_4H_9, R^2=n-C_nH_{2n+1}) with oxygen, the selectivity (a measure of molecular recognition) at 35.0 °C reached a maximum for R^1=R^2 (=n-C_4H_9) both in aqueous acetonitrile (n=2 to 6) and in aqueous ethanol (n=3 to 5).

The elucidation of factors controlling specific biological recognition is very significant in chemistry as well as in biology. In order to solve this problem, we have studied (i) the dependence of the selectivity in oxidation of a pair of associating thiols (**1** and **2**) on

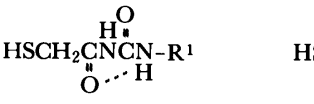

1a R^1=n-C_4H_9

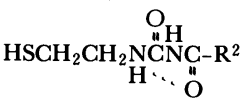

2a R^2=C_2H_5
b R^2=n-C_3H_7
c R^2=n-C_4H_9
d R^2=n-C_5H_{11}
e R^2=n-C_6H_{13}

the structures of R^1 and R^2,[1,2] (ii) the dependence of the crystalline 1 : 1 complex formation between a pair of acylurea derivatives on the structures of their substituents,[2,3] and (iii) the stacking mode of the substituents in the crystalline 1 : 1 complexes by X-ray diffraction.[2,3] From these studies using a pair of associating compounds, it has been proposed that the three dimensional shape similarity between interacting groups in reacting molecules is responsible for more specific and precise molecular recognition than would otherwise be achieved.[2] In the above investigations on the selectivity, one of the substituents (R^1 and R^2) was an aryl group: (i) R^1=p-$Me_2NC_6H_4$ and R^2=Me_2CH-$(CH_2)_m$ (m=0 to 4)[1a] and (ii) R^1=p-$Me_2NC_6H_4$ and R^2=p-ZC_6H_4 (Z=$CHMe_2$, NO_2, Me, and Cl).[2] We report here the experimental evidence to support the above "similarity recognition hypothesis," using straight-chain alkyl groups as both substituents.

Triethylamine-catalyzed oxidation of a pair of thiols (**1** and **2**) with oxygen gives one unsymmetrical (**4**) and two symmetrical disulfides (**3** and **5**). The selectivity (r, a measure of the degree of the recognition between **1** and **2**) is represented by the logarithmic ratio of the yield of **4** to twice that of **3**: r=ln([**4**]/(2[**3**])). The butyl group was chosen as R^1.

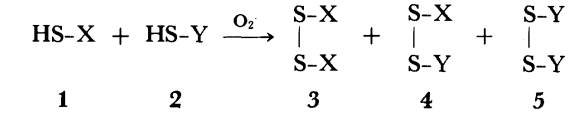

1 **2** **3** **4** **5**

Table 1 lists the yields of the disulfides (**4** and **3**) and the selectivity (r) in oxidation of **1a** and **2** at 35.0 °C in aqueous acetonitrile [mole fraction of water (x_w)=0.42]. In Fig. 1, r values are plotted against the structures of R^2. The selectivity (r) has proved to pass through a maximum at the butyl group, the same group used as R^1. Moreover, the selectivity was examined in another aqueous solvent, water-ethanol (x_w=0.75). The results are illustrated in Table 2 and Fig. 1.[4] Also in this case, the r has been found to reach a maximum for R^2=n-C_4H_9 (=R^1).

Table 1. Yields of Disulfides (**4** and **3**) and Selectivity (r) in Oxidation of **1a** and **2** at 35.0 °C in Aqueous MeCN (x_w=0.42)

R^2	Yield/%		r[a]
	4	**3**	
C_2H_5	18.4	32.9	−1.27±0.03
n-C_3H_7	76.8	9.2	1.4 ±0.1
n-C_4H_9	83.9	1.6	3.3 ±0.1
n-C_5H_{11}	85.5	2.6	2.8 ±0.1
n-C_6H_{13}	25.5	34.4	−0.99±0.06

a) Errors given are the standard deviations.

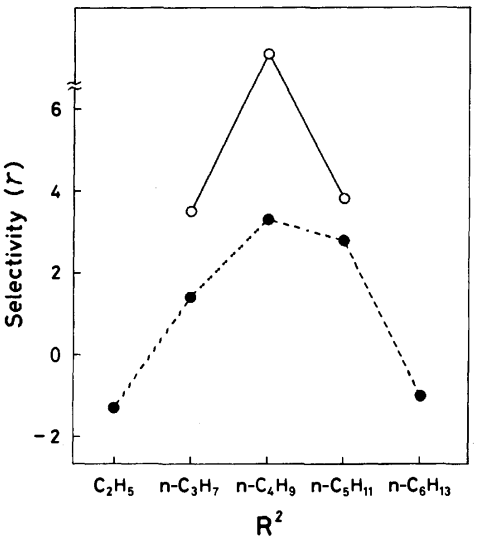

Fig. 1. Dependence of the selectivity (r) in oxidation of a pair of thiols (**1a** and **2**) on the structures of R^2 at 35.0 °C. ●, In aqueous acetonitrile [mole fraction of water (x_w)=0.42]; ○, in aqueous ethanol (x_w=0.75).

Table 2. Yields of Disulfides (**4** and **3**) and Selectivity (r) in Oxidation of **1a** and **2b—d** at 35.0 °C in Aqueous EtOH (x_w=0.75)

R^2	Yield/%		r[a]
	4	**3**	
n-C_3H_7	91.8	1.5	3.4±0.1
n-C_4H_9	88.1	<0.1	>6
n-C_5H_{11}	94.0	1.1	3.8±0.2

a) Errors given are the standard deviations.

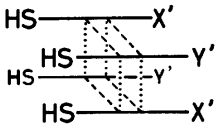

6

Fig. 2. Association scheme in a typical tetramer **6**. -----, Hydrogen bonds in dimers; ·····, noncovalent weak interactions responsible for stabilization of tetramers. The symbols X' and Y' represent R^1 and R^2, respectively.

In connection with the observations that the selectivity in the oxidation is sensitive to temperature,[1] we examined the temperature dependence of r values (R^1=n-C_4H_9) in aqueous acetonitrile (x_w=0.42). Unexpectedly, the r values at 20.0 °C remain almost unchanged with the structures of R^2: 3.7±0.1 (n-C_3H_7), 3.6±0.1 (n-C_4H_9), and 3.8±0.1 (n-C_5H_{11}). Furthermore, at a higher temperature (i.e., 50.0 °C), r values increase progressively with increasing number of carbon atoms in R^2: −0.59±0.04 (n-C_3H_7), 2.2±0.1 (n-C_4H_9), and 3.0±0.1 (n-C_5H_{11}).[5]

The findings shown in Fig. 1 are not understandable in terms of the following factors influencing chemical selectivity. First, electronic effects of R^2 fail to account for the selectivity data, because the order of σ_p values[7] for R^2 [−0.15 (C_2H_5), −0.13 (n-C_3H_7), −0.16 (n-C_4H_9), and −0.15 (n-C_5H_{11})] differs sharply from that of the corresponding r values (Fig. 1). Second, steric effects cannot explain the observed selectivity, because the order of E_s values for R^2 [−0.07 (C_2H_5), −0.36 (n-C_3H_7), −0.39 (n-C_4H_9), and −0.40 (n-C_5H_{11})][8] differs essentially from that of the corresponding r values (Fig. 1).[9] Third, the hydrophobic effect is not responsible for the selectivity data, because π values[11] increase with increasing number of carbon atoms in straight-chain alkyl groups, the π being a measure of the hydrophobic effect. Fourth, the reactivity differences between thiols **1a** and **2** cannot explain the selectivity. This is because r values should be negative, regardless of the structures of R^2, if the selectivity depends upon the reactivity differences: r values are largely positive for R^2=n-C_3H_7, n-C_4H_9, and n-C_5H_{11} (Fig. 1).

It has been shown that (i) the oxidation proceeds through tetramers (reaction intermediates) such as **6** (Fig. 2), which are formed by dimerization of dimers produced from **1** and **2** through two NH ··· O intermolecular hydrogen bonds between the inner -NHCO- units in the -CONHCONH- groups[12] and (ii) the product ratio in this type of oxidation is kinetically controlled.[1]

In conclusion, the experimental results and discussions presented here demonstrate that the similarity recognition hypothesis holds true for straight-chain alkyl groups at temperatures around 35 °C.

Experimental

The melting points were uncorrected. ^{1}H NMR (270 MHz) spectra were measured on a JEOL GX-270 spectrometer using tetramethylsilane as an internal standard. The mass spectra were taken on a Hitachi RMU-6M mass spectrometer.

Materials. Acetonitrile was dried, purified by distillation from calcium hydride and phosphorus pentaoxide, and stored over molecular sieves. Water was distilled after deionization. Ethanol was dried, purified by distillation from magnesium ethoxide,[13] and stored over molecular sieves.

Thiol **1a** was prepared as described before,[14] recrystallized from ether-hexane, and had the following properties: Mp 104—105 °C; ^{1}H NMR ($CDCl_3$) δ=0.94 (3H, t, J=7 Hz), 1.31—1.60 (4H, m), 2.09 (1H, t, J=9 Hz), 3.27—3.34 (4H, m), 8.29 (1H, s), 9.57 (1H, s). Found: C, 44.09; H, 7.56; N, 14.54; S, 17.30%; M^+, 190. Calcd for $C_7H_{14}N_2O_2S$: C, 44.19; H, 7.42; N, 14.72; S, 16.85%; M, 190.

Thiols **2** were synthesized as described before,[1b] recrystallized from ether-hexane, and had the following properties.

2a: Mp 117.5—119.0 °C; ^{1}H NMR ($CDCl_3$) δ=1.19 (3H, t, J=7 Hz), 1.43 (1H, t, J=8 Hz), 2.38 (2H, q, J=7 Hz), 2.67—2.75 (2H, m), 3.47—3.54 (2H, m), 8.79 (2H, s). Found: C, 41.16; H, 6.79; N, 15.98; S, 18.17%; M^+, 176. Calcd for $C_6H_{12}N_2O_2S$: C, 40.90; H, 6.87; N, 15.90; S, 18.17%; M, 176.

2b: Mp 119—120 °C; ^{1}H NMR ($CDCl_3$) δ=0.98 (3H, t, J=7 Hz), 1.42 (1H, t, J=9 Hz), 1.63—1.74 (2H, m), 2.31 (2H, t, J=7 Hz), 2.66—2.75 (2H, m), 3.46—3.53 (2H, m), 8.76 (2H, s). Found: C, 44.12; H, 7.51; N, 14.56; S, 17.11%; M^+, 190. Calcd for $C_7H_{14}N_2O_2S$: C, 44.19; H, 7.42; N, 14.72; S, 16.85%; M, 190.

2c: Mp 105.5—106.0 °C; ^{1}H NMR ($CDCl_3$) δ=0.94 (3H, t, J=7 Hz), 1.31—1.45 (3H, m), 1.59—1.70 (2H, m), 2.33 (2H, t, J=7 Hz), 2.66—2.74 (2H, m), 3.46—3.53 (2H, m), 8.79 (2H, s). Found: C, 47.18; H, 7.74; N, 13.66; S, 15.85%; M^+, 204. Calcd for $C_8H_{16}N_2O_2S$: C, 47.05; H, 7.90; N, 13.73; S, 15.67%; M, 204.

2d: Mp 107.5—108.5 °C; ^{1}H NMR ($CDCl_3$) δ=0.91 (3H, t, J=7 Hz), 1.30—1.45 (5H, m), 1.61—1.69 (2H, m), 2.32 (2H, t, J=8 Hz), 2.66—2.86 (2H, m), 3.46—3.53 (2H, m), 8.79 (2H, s). Found: C, 49.26; H, 8.38; N, 12.76; S, 14.74%; M^+, 218. Calcd for $C_9H_{18}N_2O_2S$: C, 49.52; H, 8.31; N, 12.83; S, 14.69%; M, 218.

2e: Mp 102—103 °C; ^{1}H NMR ($CDCl_3$) δ=0.86—0.91 (3H, m), 1.30—1.45 (7H, m), 1.60—1.68 (2H, m), 2.32 (2H, t, J=7 Hz), 2.66—2.74 (2H, m), 3.46—3.53 (2H, m), 8.73 (2H, s). Found: C, 51.89; H, 8.67; N, 12.08; S, 14.01%; M^+, 232. Calcd for $C_{10}H_{20}N_2O_2S$: C, 51.70; H, 8.68; N, 12.06; S, 13.78%; M, 232.

Symmetrical disulfide **3** (R^1=n-C_4H_9) was prepared as described before,[1b] and had the following properties: Mp 195—197 °C [tetrahydrofuran (THF)]; ^{1}H NMR (dimethyl-d_6 sulfoxide) δ=1.20 (6H, t, J=7 Hz), 1.56—1.79 (8H, m), 3.4—3.5 (4H, m), 3.97 (4H, s), 8.49 (2H, s), 10.75 (2H, s). Found: m/z 378.1380. Calcd for $C_{14}H_{26}N_4O_4S_2$: M, 378.1398.

Unsymmetrical disulfides **4** (R^1=n-C_4H_9) were synthesized as described before,[15] and had the following properties.

4a (R^2=C_2H_5): Mp 161.5—162.5 °C (MeCN); ^{1}H NMR ($CDCl_3$) δ=0.93 (3H, t, J=7 Hz), 1.18 (3H, t, J=8 Hz), 1.39—1.57 (4H, m), 2.36—2.41 (2H, m), 2.87—2.92 (2H, m), 3.28—3.30 (2H, m), 3.58 (2H, s), 3.61—3.70 (2H, m), 8.37 (1H, s), 8.74 (1H, s), 9.39 (1H, s), 9.83 (1H, s). Found: m/z 364.1205. Calcd for $C_{13}H_{24}N_4O_4S_2$: M, 364.1241.

4b (R^2=*n*-C_3H_7): Mp 171.0—173.5 °C (THF); ^{1}H NMR ($CDCl_3$) δ=0.91—1.00 (6H, m), 1.33—1.42 (2H, m), 1.50—1.58 (2H, m), 1.65—1.73 (2H, m), 2.34 (2H, t, J=7 Hz), 2.91 (2H, t, J=6 Hz), 3.27—3.34 (2H, m), 3.52 (2H, s), 3.65—3.72 (2H, m), 8.36 (1H, s), 8.76 (1H, s), 9.50 (1H, s), 10.18 (1H, s). Found: m/z 378.1410. Calcd for $C_{14}H_{26}N_4O_4S_2$: M, 378.1398.

4c (R^2=*n*-C_4H_9): Mp 174—176 °C (THF); ^{1}H NMR ($CDCl_3$) δ=0.91—0.96 (6H, m), 1.33—1.64 (8H, m), 2.36 (2H, t, J=7 Hz), 2.91 (2H, t, J=6 Hz), 3.29—3.31 (2H, m), 3.52 (2H, s), 3.69—3.71 (2H, m), 8.34 (1H, s), 8.73 (1H, s), 9.34 (1H, s), 10.08 (1H, s). Found: m/z 392.1567. Calcd for $C_{15}H_{28}N_4O_4S_2$: M, 392.1554.

4d (R^2=*n*-C_5H_{11}): Mp 168.0—169.5 °C (THF); ^{1}H NMR ($CDCl_3$) δ=0.88—0.96 (6H, m), 1.32—1.66 (10H, m), 2.35 (2H, t, J=7 Hz), 2.91 (2H, t, J=6 Hz), 3.29—3.31 (2H, m), 3.51 (2H, s), 3.68—3.70 (2H, m), 8.35 (1H, s), 8.76 (1H, s), 9.54 (1H, s), 10.24 (1H, s). Found: m/z 406.1725. Calcd for $C_{16}H_{30}N_4O_4S_2$: M, 406.1711.

4e (R^2=*n*-C_6H_{13}): Mp 174—175 °C (MeCN); ^{1}H NMR ($CDCl_3$) δ=0.89—0.96 (6H, m), 1.2—1.7 (12H, m), 2.3—2.4 (2H, m), 2.8—3.0 (2H, m), 3.2—3.4 (2H, m), 3.53 (2H, s), 3.6—3.8 (2H, m), 8.35 (1H, s), 8.73 (1H, s), 9.25 (1H, s), 9.99 (1H, s). Found: m/z 420.1859. Calcd for $C_{17}H_{32}N_4O_4S_2$: M, 420.1868.

Oxidation of a Pair of Thiols. A mixture of **1a** (0.50 mmol) and **2** (0.50 mmol) in 12.5 ml of the solvent was stirred vigorously under oxygen for 15 min in a well-stirred water bath which was thermostated to ±0.1 °C. To this mixture was added Et_3N (0.05 mmol), and vigorous stirring was continued for the time required to complete the oxidation. When the oxidation was completed, the reaction mixture was evaporated to dryness. The yields of **3** and **4** in the reaction mixture were determined exactly by an integrator after separation by HPLC using LiChrosorb CN [hexane–isopropyl alcohol (94 : 6—97 : 3)]. The r values are reproducible in two or more experiments within the errors described in Tables 1 and 2.

We thank Mr. Hajime Ishijima and Mr. Kazuo Tanaka, JEOL, for measuring high resolution mass spectra. We are grateful to Mr. Koki Tajima for his valuable assistance. This work was partly supported by a Grant-in-Aid for Scientific Research No. 61226012 from the Ministry of Education, Science and Culture.

References

1) a) T. Endo, A. Kuwahara, H. Tasai, T. Murata, M. Hashimoto, and T. Ishigami, *Nature*, **268**, 74 (1977); b) T. Endo, A. Okubo, Y. Kaneko, M. Uehara, H. Tasai, A. Sato, K. Nikki, N. Nakagawa, and S. Kamei, *Bull. Chem. Soc. Jpn.*, **55**, 2224 (1982).

2) T. Endo, H. Tasai, K. Miyazawa, M. Endo, K. Kato, A. Uchida, Y. Ohashi, and Y. Sasada, *J. Chem. Soc., Chem. Commun.*, **1983**, 636.

3) T. Endo, K. Miyazawa, M. Endo, A. Uchida, Y. Ohashi, and Y. Sasada, *Chem. Lett.*, **1982**, 1989.

4) The r value of larger than 6 implies that the oxidation gives **4** exclusively to such an extent that the yield of **3** exceeds the limitations of the determination.

5) Our previous work[6] showed that, in oxidation of **1** (R^1=*n*-C_5H_{11}) and **2c—e**, r values at 35.0 °C in aqueous acetonitrile (x_w=0.42) became positive (r=3.6 to 4.1) with a maximum for R^2=*n*-C_5H_{11} (=R^1).

6) T. Endo, H. Kasahara, S. Yagi, K. Tajima, M. M. Ito, M. Ogino, and K. Hagino, *Chem. Lett.*, **1986**, 705.

7) C. Hansch, A. Leo, S. H. Unger, K. H. Kim, D. Nikaitani, and E. J. Lien, *J. Med. Chem.*, **16**, 1207 (1973).

8) R. W. Taft, Jr., "Separation of Polar, Steric, and Resonance Effects in Reactivity," in "Steric Effects in Organic Chemistry," ed by M. S. Newman, Wiley, New York (1956), p. 598.

9) Another measure of steric effects, the v, also is not responsible for the data in Fig. 1, since v values [0.56 (C_2H_5), 0.68 (*n*-C_3H_7), 0.68 (*n*-C_4H_9), 0.68 (*n*-C_5H_{11}), and 0.73 (*n*-C_6H_{13})][10] slightly increase with increasing number of carbon atoms in straight-chain alkyl groups used as R^2.

10) M. Charton, *J. Am. Chem. Soc.*, **97**, 1552 (1975).

11) C. Hansch, A. R. Steward, J. Iwasa, and E. W. Deutsch, *Mol. Pharmacol.*, **1**, 205 (1965).

12) T. Endo, M. Hashimoto, T. Orii, and M. M. Ito, *Bull. Chem. Soc. Jpn.*, **57**, 1562 (1984) and the references cited therein.

13) J. A. Riddick and W. B. Bunger, "Organic Solvents," 3rd ed., Wiley, New York (1970).

14) T. Endo, K. Oda, and T. Mukaiyama, *Chem. Lett.*, **1974**, 443.

15) T. Endo, H. Tasai, and T. Ishigami, *Chem. Lett.*, **1975**, 813.

Partially Benzylated Derivatives of 6-Deoxy-D-glucose

Shinkiti KOTO,* Naohiko MORISHIMA,[1] Yoko MORI,[1] Hitoshi TANAKA, Seiichi HAYASHI, Yumi IWAI, and Shonosuke ZEN
School of Pharmaceutical Sciences, Kitasato University, Shirokane, Minato-ku, Tokyo 108
(Received January 24, 1987)

Synopsis. Several partially benzylated derivatives of 6-deoxy-D-glucose (D-quinovose) were synthesized from appropriate di-*O*-benzyl-D-glucosides whose primary hydroxyl group is unprotected, via unimolar tosylation and subsequent reduction with $LiAlH_4$.

6-Deoxy-D-glucose (D-quinovose, **1**) consititutes various sugar-clusters occurring in saponins, antibiotics, etc.[2] An attempt to synthesize such clusters by a direct coupling reaction[3] between a protected saccharide with a hemiacetal OH and that with the OH to be glycosylated requires various benzyl derivatives of **1**. This report describes the synthetic routes for several D-quinovosyl donors and glycosyl acceptors of **1** from the known di-*O*-benzyl derivatives of appropriate D-glucosides with unprotected 6-OH.

The acceptor **13** had been synthesized from **11**[4] via unimolar tosylation and reduction by $LiAlH_4$ (LAH).[5] This routine was carried out for **2**[6] and **5**[7] to give **4** and **7**, respectively. Compound **7** was also obtained by a controlled benzylation[8] of **10**.

As for donors, **17** was first synthesized from **14**[9] via benzylation with $PhCH_2Br$ and NaH in DMF,[10] reduction and hydrolysis. It was found that an analogous benzylation of **14** in DMSO[11] mainly gave the 2,4-dibenzyl ether **23**.

The replacement of one benzyl of **17** with participating Ac or non-participating allyl (AL) as a temporary protecting group[12] was then carried out. The 2-*O*-AL derivative **21** was synthesized from **18**[6] via tosylation and reduction, followed by allylation and hydrolysis. This process was also applied for the conversion of **22**[7] and **26**[13] into **25** and **29**, respectively.

The 2-*O*-Ac derivative **32** was synthesized from **31** by a through-process including orthoester formation.[14] The starting **31** was prepared from **14**[9] via LAH-reduction,[15] acetylation and acetolysis. On the other hand, the 3- and the 4-*O*-acetates **38** and **43** were syn-

Table 1. Physical and Analytical Data of Compounds

Cpd.	Mp (θ_m/°C) °C	$[\alpha]_D^{20}$ (*c*, $CHCl_3$) deg	Mol. Form.	Anal/% Calcd C	Calcd H	Found C	Found H
3	—	+73 (0.7)	$C_{34}H_{36}O_8S$	67.53	6.00	67.15	6.01
4	63—67	+117 (0.2)	$C_{27}H_{30}O_5$	74.63	6.96	74.81	6.88
6	65—69	+88 (0.7)	$C_{34}H_{36}O_8S$	67.53	6.00	67.56	6.06
7	41—43	+110 (1.4)	$C_{27}H_{30}O_5$	74.63	6.96	74.14	7.23
9	44—46	+72 (1.7)	$C_{20}H_{24}O_8S$	56.59	5.70	56.26	5.76
10	—	+130 (0.1)	$C_{13}H_{18}O_5$	61.40	7.28	60.59	7.08
12	—	+47 (1.4)	$C_{34}H_{36}O_8S$	67.53	6.00	67.50	6.01
13[a]	39—40	+72 (0.6)	$C_{27}H_{30}O_5$	74.63	6.96	74.34	6.96
15	—	+24 (4.5)	$C_{35}H_{38}O_8S$	67.74	6.19	67.85	6.15
16	—	+20 (2.2)	$C_{28}H_{32}O_5$	74.97	7.19	74.91	7.06
17	103—104	+13 (0.5)	$C_{27}H_{30}O_5$	74.63	6.95	74.37	6.90
19	59—61	+81 (2.0)	$C_{28}H_{32}O_8S$	63.62	6.10	63.23	6.09
20	106—109	+102 (1.0)	$C_{21}H_{26}O_5$	70.37	7.31	70.90	7.31
21	50—52	+19 (0.8)	$C_{23}H_{28}O_5$	71.85	7.34	71.02	7.28
23	—	+63 (1.1)	$C_{28}H_{32}O_8S$	63.62	6.10	64.34	6.49
24	—	+78 (1.2)	$C_{21}H_{26}O_5$	70.37	7.31	70.65	7.34
25	42—43	+35 (0.5)	$C_{23}H_{28}O_5$	71.85	7.34	71.27	7.34
27	—	+18 (2.0)	$C_{28}H_{32}O_8S$	63.62	6.10	63.76	6.14
28	—	+45 (0.5)	$C_{21}H_{26}O_5$	70.37	7.31	69.99	7.41
29	58—59	+38 (0.4)	$C_{23}H_{28}O_5$	71.85	7.34	71.60	7.26
32[b]	93—94	+63 (0.3)	$C_{22}H_{26}O_6$	68.38	6.78	68.16	6.85
34	55—57	−19 (1.5)	$C_{16}H_{24}O_9S$	48.97	6.16	48.17	6.34
35	41—42	−12 (0.8)	$C_{15}H_{24}O_9$	51.72	6.94	51.63	6.91
36	—	+18 (0.9)	$C_{23}H_{30}O_6$	68.64	7.51	68.90	7.65
38	100—101	+45 (0.3)	$C_{22}H_{26}O_6$	68.38	6.78	68.00	6.86
39	117—118[c]	−47 (0.5)	$C_{16}H_{21}O_7 \cdot 0.5H_2O$	57.48	6.63	57.68	6.87
40	65—66	−19 (0.3)	$C_{23}H_{30}O_7$	66.01	7.23	65.87	7.24
41	—	−10 (2.2)	$C_{30}H_{36}O_9S$	62.92	6.34	62.62	6.25
42	88	−36 (0.2)	$C_{23}H_{30}O_6$	68.64	7.51	68.45	7.37
43	100—103	+7 (0.3)	$C_{22}H_{26}O_6$	68.38	6.78	68.15	6.72

a) *Bull. Chem. Soc. Jpn.*, **54**, 2169 (1981); $[\alpha]_D$ +51.5° (*c* 0.84, $CHCl_3$). b) *Agr. Biol. Chem.* **47**, 2929 (1983); for L-form: mp 100—103 °C, $[\alpha]_D^{20}$ −54°—−48° (*c* 1.5, EtOH). c) Sintered at 98 °C.

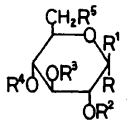

Cpd.	R	R^1	R^2	R^3	R^4	R^5	Cpd.	R	R^1	R^2	R^3	R^4	R^5
1	OH,	H	H	H	H	H	**23**	OMe	H	Bn	H	Bn	OTs
2	OBn	H	H	Bn	Bn	OH	**24**	OMe	H	Bn	H	Bn	H
3	OBn	H	H	Bn	Bn	OTs	**25**	OH,	H	Bn	AL	Bn	H
4	OBn	H	H	Bn	Bn	H	**26**	OMe	H	Bn	Bn	H	OH
5	OBn	H	Bn	H	Bn	OH	**27**	OMe	H	Bn	Bn	H	OTs
6	OBn	H	Bn	H	Bn	OTs	**28**	OMe	H	Bn	Bn	H	H
7	OBn	H	Bn	H	Bn	H	**29**	OH,	H	Bn	Bn	AL	H
8	OBn	H	H	H	H	OH	**30**	OMe	H	Ac	Ac	Ac	H
9	OBn	H	H	H	H	OTs	**31**	OAc	H	Ac	Ac	Ac	H
10	OBn	H	H	H	H	H	**32**	OH,	H	Ac	Bn	Bn	H
11	OBn	H	Bn	Bn	H	OH	**33**	H	OME	H	H	H	OH
12	OBn	H	Bn	Bn	H	OTs	**34**	H	OME	H	H	H	OTs
13	OBn	H	Bn	Bn	H	H	**35**	H	OME	Ac	Ac	Ac	H
14	OMe	H	H	H	H	OTs	**36**	H	OME	Bn	H	Bn	H
15	OMe	H	Bn	Bn	Bn	OTs	**37**	H	OME	Bn	Ac	Bn	H
16	OMe	H	Bn	Bn	Bn	H	**38**	OH,	H	Bn	Ac	Bn	H
17	OH,	H	Bn	Bn	Bn	H	**39**	H	OME	H	H		
18	OMe	H	H	Bn	Bn	OH	**40**	H	OME	Bn	Bn	H	OH
19	OMe	H	H	Bn	Bn	OTs	**41**	H	OME	Bn	Bn	H	OTs
20	OMe	H	H	Bn	Bn	H	**42**	H	OME	Bn	Bn	H	H
21	OH,	H	AL	Bn	Bn	H	**43**	OH,	H	Bn	Bn	Ac	H
22	OMe	H	Bn	H	Bn	OH							

AL=$-CH_2CH{=}CH_2$, Bn=$-CH_2Ph$, ME=$-CH_2CH_2OMe$, Ts=$-SO_2C_6H_4Me$(p).

thesized from the 2-methoxyethyl (ME) glucoside **33**.[16] The acetate **35** derived from **33** was directly converted into the 2,4-dibenzyl ether **36** by a controlled benzylation[8,17] with $PhCH_2Cl$ and KOH in a 37% yield. The structure of the acetate **37** was confirmed by the measurement of ^1H NMR at 400 MHz; the most deshielded (δ=5.19) was H-3 among five ring protons.[8] Regeneration of 1-OH[17] gave **38**. The dibenzyl ether **40** was transformed into **43** via tosylation and reduction, followed by acetylation and regeneration of 1-OH.

Experimental[3,6-8]

The solvent systems for gradient elusion for column chromatography on silica gel were toluene-2-butanone (TB), hexane-EtOAc (HE), and $CHCl_3$-MeOH (CM).

Benzyl 3,4-Di-*O*-benzyl-6-*O*-tosyl-α-D-glucopyranoside (3). To a flask containing **2**[6] (443 mg) and tosyl chloride (225 mg), pyridine (4.5 ml) was added under stirring at −10 °C. The mixture was stirred for 1 h and then left for 3 h at room temp. Work-up[9] and chromatography (TB) gave **3** (378 mg, 64%).

A similar procedure was applied for **5**,[7] **8**,[18] **11**,[4] **18**,[6] **22**,[7] **26**,[13] **33**,[16] and **40** to give **6** (71%), **9** (60%, CM instead of TB), **12** (82%), **19** (75%), **23** (91%), **27** (75%), **34** (75%, CM instead of TB), and **41** (65%), respectively.

Benzyl 3,4-Di-*O*-benzyl-6-deoxy-α-D-glucopyranoside (4). Compound **3** (269 mg) was refluxed in Et_2O (6 ml) containing LAH (70 mg) for 1 h. After quenching with EtOAc, filtration, and evaporation, chromatography (TB) gave **4** (179 mg, 92%).

A similar reduction was carried out for **6**, **12**, **15**, **19**, **23**, **27**, and **41** to afford **7** (74%), **13** (100%), **16** (98%), **20** (97%), **24** (84%), **28** (84%), and **42** (84%), respectively.

Methyl 2,3,4-Tri- and 2,4-Di-*O*-benzyl-6-*O*-tosyl-α-D-glucopyranosides (15 and 23). To a mixture of **14** (305 mg), $PhCH_2Br$ (1.2 ml) and DMF (3 ml), NaH in oil suspension (300 mg; 60% of NaH by wt) was added at 0 °C. The mixture was stirred for 50 min and then for 40 min at room temp. Work-up[10] and chromatography (HE) gave **15** (413 mg, 76%).

An analogous benzylation of **14** (154 mg) using $PhCH_2Br$ (0.45 ml), NaH in oil suspension (74 mg; 60% of NaH by wt), and DMSO (1.7 ml) for 45 min at 15 °C gave **15** (≈70 mg, ≈25%) and **23** (116 mg, 50%).

Benzyl 2,4-Di-*O*-benzyl-6-deoxy-α-D-glucopyranoside (7). Compound **10** (33.3 mg) was stirred in $PhCH_2Cl$ (0.7 ml) containing crushed KOH (22 mg) for 1 h at 120 °C, followed by work-up and chromatography (TB),[8] to give **7** (30.4 mg, 53%).

2,3,4-Tri-*O*-benzyl-6-deoxy-D-glucopyranose (17). A mixture of **16** (295 mg), AcOH (4 ml), and aq H_2SO_4 (3M (M=mol dm^{-3}), 0.05 ml) was stirred for 2 h at 90 °C. Work-up and chromatography (TB)[19] gave **17** (118 mg, 42%).

2-*O*-Allyl-3,4-di-*O*-benzyl-6-deoxy-D-glucopyranose (21). A mixture of **20** (80.4 mg), NaH in oil suspension (40.4 mg; 60% of NaH by wt), and ALBr (0.58 ml) was refluxed for 40 min. Filtration and evaporation gave a residue, which was stirred in a mixture of AcOH (1.6 ml) and aq H_2SO_4 (3M, 26

μl) for 1 h at 100 °C. Work-up and chromatography (TB)[19] gave **21** (39.3 mg, 46%).

A similar procedure was applied for **24** and **28** to furnish **25** (56%) and **29** (62%), respectively.

Methyl 2,3,4-Tri-*O*-acetyl-6-deoxy-α-D-glucopyranoside (30). A mixture of **14**[9] (500 mg), LAH (145 mg), and Et_2O (15 ml) was refluxed for 4 h. After quenching with EtOAc, filtration, and evaporation,[15] the solid obtained was acetylated with Ac_2O (10 ml) in pyridine (10 ml) for 2h at 80 °C. Evaporation and chromatography (TB) gave **30** (333 mg, 77% (Found: C, 51.50; H, 6.72%)), mp 73—75 °C, $[\alpha]_D^{20}$ +156° (*c* 0.8, $CHCl_3$) (lit,[20] mp 76—77 °C, $[\alpha]_D^{20}$ +153° (*c* 1.6, $CHCl_3$)).

A similar procedure was applied for **34** to give **35** (50%). The tosylate **9** was similarly reduced, followed by chromatography (CM) without acetylation, to give **10** (63%).

1,2,3,4-Tetra-*O*-acetyl-6-deoxy-α-D-glucopyranose (31). To a soln of **30** (107 mg) in Ac_2O (2.2 ml), a soln of H_2SO_4 in Ac_2O (10%, 1.2 ml) was added at 0 °C. The mixture was stirred for 1 h at room temp and then poured onto ice. Work-up and chromatography (TB) gave **31** (75.2 mg, 64% (Found: C, 50.68; H, 6.13%)), mp 116—118 °C, $[\alpha]_D^{20}$ +113° (*c* 0.3, $CHCl_3$) (lit,[21] mp 117 °C, $[\alpha]_D^{20}$ +122° (*c* 1.3, $CHCl_3$)).

2-*O*-Acetyl-3,4-di-*O*-benzyl-6-deoxy-D-glucopyranose (32). To a soln of **31** (72.4 mg) in $CHCl_3$ (1 ml) containing AcBr (86 μl), H_2O (15 μl) was added at 0 °C. The mixture was stirred for 1 h at room temp and then evaporated. The residue was treated with 2,6-dimethylpyridine (0.14 ml) and ethanol (0.17 ml) in $MeNO_2$ (0.26 ml) overnight at room temp. The soln was diluted with $CHCl_3$ and poured into aq $NaHCO_3$ (5%, 5 ml). The organic layer was evaporated and then stirred in $PhCH_2Cl$ (1.5 ml) containing KOH (0.63 g) for 2 h at 120 °C. The mixture was diluted with toluene and washed with H_2O. The organic layer was evaporated and then stirred in aq AcOH (80%, 2 ml) for 1 h at 50 °C. Work-up and chromatography (TB)[14] gave **36** (33.0 mg, 39%).

2-Methoxyethyl 2,4-Di-*O*-benzyl-6-deoxy-β-D-glucopyranoside (36). A mixture of **35** (63.6 mg), crushed KOH (71.6 mg) and $PhCH_2Cl$ (1.5 ml) was stirred for 3.5 h at 100 °C. Work-up and chromatography (TB)[8] gave **36** (27.6 mg, 38%).

3-*O*-Acetyl-2,4-di-*O*-benzyl-6-deoxy-D-glucopyranose (38). Acetylation of **36** (27.5 mg) with Ac_2O (1 ml) and pyridine (1 ml), followed by chromatography (TB), gave **37** (28.4 mg); ^1H NMR recorded with a Varian XL-400 spectrometer in H-H COSY mode (CCl_4) δ=1.31 (3H, d, $J_{5,6}$=6.0 Hz, $C\underline{H}_3$-5), 1.98 (3H, s, $C\underline{H}_3CO$), 3.17 (1H, t, $J_{3,4}$=$J_{4,5}$=9.5 Hz, H-4), 3.33 (1H, dd, $J_{1,2}$=8.0 Hz, $J_{2,3}$=9.5 Hz, H-2), 3.38 (3H, s, $C\underline{H}_3O$), 3.46 (1H, m, H-5), 4.48 (1H, d, H-1), 5.19 (1H, t, H-3). This was then treated with $TiCl_4$ (4.3 μl) in CH_2Cl_2 (0.6 ml) for 15 min at room temp, processed, and adsorbed on silica-gel column.[17] The column was left overnight and then eluted with TB to give **38** (18.9 mg, 72% form **36**).

A similar two-step routine for **42** gave **43** (74%).

2-Methoxyethyl 4,6-*O*-Benzylidene-β-D-glucopyranoside (39). Compound **33**[16] (6.28 g) was treated with PhCHO (45 ml) containing $ZnCl_2$ (7 g) for 5.5 h at room temp. Work-up and crystallization with diisopropyl ether furnished **39** (5.72 g, 66%).

2-Methoxyethyl 2,3-Di-*O*-benzyl-β-D-glucopyranoside (40). The acetal **39** (300 mg) was stirred in $PhCH_2Cl$ (6 ml) containing KOH (0.8 g) for 5 h at 100 °C. After filtration and evaporation, the residue was stirred in aq AcOH (80%, 6 ml) for 0.3 h at 100 °C. Work-up and chromatography (TB) gave **40** (314 mg, 82%).

List of characteristic signals (δ) of ^1H NMR recorded at 90 MHz with a Varian EM-390 spectrometer (T=CCl_4, C=$CDCl_3$, W=D_2O (ext. TMS)); MC=$C\underline{H}_3$-5 (3H, d, *J*=6.0 Hz), MA=$C\underline{H}_3CO$ (3H, s), MT=$C\underline{H}_3C_6H_4$ (3H, s), MO=$C\underline{H}_3O$ (3H, s), B=>C$\underline{H}$Ph (1H, s), L=-C$\underline{H}$=CH_2 (1H, m): **3** (T; 2.36 (MT)), **4** (T; 1.17 (MC)), **6** (T; 2.37 (MT)), **7** (T; 1.13 (MC)), **9** (C; 2.40 (MT)), **10** (W; 1.63 (MC)), **12** (T; 2.34 (MT)), **13** (T; 1.16 (MC)), **15** (T; 2.34 (MT), **3.24** (MO)), **16** (T; 1.13 (MC), 3.27 (MO)), **17** (T; 1.16 (MC-α), 1.24 (MC-β)), **19** (T; 2.37 (MT), 3.30 (MO)), **20** (T; 1.17 (MC), 3.34 (MO)), **21** (T; 1.17 (MC-α), 1.21 (MC-β), ≈5.9 (L)), **23** (T; 2.37 (MT), 3.20 (MO)), **24** (T; 1.14 (MC), 3.26 (MO)), **25** (T; 1.15 (MC-α), 1.23 (MC-β), ≈5.8 (L)), **27** (T; 2.36 (MT), 3.21 (MO)), **28** (T; 1.13 (MC), 3.28 (MO)), **29** (T; 1.17 (MC-α), 1.25 (MC-β), ≈5.8 (L)), **32** (T; 1.18 (MC-α), 1.20 (MC-β), 1.91 (MA-α), 2.06 (MA-β)), **34** (C; 2.40 (MT), 3.33 (MO)), **35** (T; 1.19 (MC), 1.94 (MA), 1.96 (2MA), 3.27 (MO)), **36** (T; 1.19 (MC), 3.28 (MO)), **38** (T; 1.20 (MC-α), 1.21 (MC-β), 1.87 (MA-α), 1.95 (MA-β)), **39** (C; 3.37 (MO), 5.51 (B)), **40** (T; 3.26 (MO)), **41** (T; 2.41 (MT), 3.32 (MO)), **42** (T; 1.22 (MC), 3.27 (MO)); **43** (T; 1.07 (MC-α), 1.13 (MC-β), 1.86 (MA-α and MA-β)).

References

1) Present address: School of Nursing, Kitasato University, Kitasato, Sagamihara 228.

2) I. Kitagawa, *Kagaku Sosetsu*, **25**, 201 (1979); K. Okano, T. Nakamura, Y. Kamiya, and S. Ikegami, *Agric. Biol. Chem.*, **45**, 805 (1981), G. R. Pettit, G. M. Cragg, D. Gust, and P. Brown, *Can. J. Chem.*, **60**, 544 (1982); K. Harada, S. Ito, and M. Suzuki, *Tetrahedron Lett.*, **23**, 2479 (1982); H. Seto, N. Otake, M. Koyama, H. Ogino, Y. Kodama, N. Nishizawa, T. Tsuruoka, and S. Inouye, *ibid.*, **24**, 497 (1983); M. Honda and H. Komori, *ibid.*, **27**, 3369 (1986).

3) S. Koto, N. Morishima, K. Takenaka, C. Uchida, and S. Zen, *Bull. Chem. Soc. Jpn.*, **58**, 1464 (1985), S. Koto, K. Yago, S. Zen, F. Tomonaga, and S. Shimada, *ibid.*, **59**, 411 (1986).

4) A. Lubineau, A. Thieffry, and A. Veyrières, *Carbohydr. Res.*, **46**, 143 (1976).

5) M. Matsuzawa, K. Kubo, H. Kodama, M. Funabashi, and J. Yoshimura, *Bull. Chem. Soc. Jpn.*, **54**, 2169 (1981).

6) S. Koto, N. Morishima, T. Yoshida, M. Uchino, and S. Zen., *Bull. Chem. Soc. Jpn.*, **56**, 1171 (1983).

7) S. Koto, S. Inada, T. Yoshida, M. Toyama, and S. Zen, *Can. J. Chem.*, **59**, 255 (1981).

8) S. Koto, K. Takenaka, N. Morishima, A. Sugimoto, and S.Zen, *Bull. Chem. Soc. Jpn.*, **57**, 3603 (1984) and the preceding reports.

9) F. Cramer, H. Otterbach, and H. Springmann, *Chem. Ber.*, **92**, 384 (1959).

10) J. S. Brimacombe, B. D. Jones, M. Stacey, and J. J. Willard, *Carbohydr. Res.*, **2**, 167 (1966).

11) T. Iwashige and H. Saeki, *Chem. Pharm. Bull.*, **15**, 1803 (1967).

12) C. A. A. van Boeckel and T. Beetz, *Recl. Trav. Chim. Pays-Bas*, **104**, 171 (1985).

13) K. Freudenberg and E. Plankenhorn, *Chem. Ber.*, **73**, 621 (1940).

14) S. Koto, N. Morishima, H. Sato, Y. Sato, and S. Zen, *Bull. Chem. Soc. Jpn.*, **58**, 120 (1985).

15) M. E. Evans, L. Long, Jr., and F. W. Parrish, *J. Org. Chem.*, **33**, 1074 (1968).

16) B. Helferich and H. H. Hiltmann, *Justus Liebigs Ann. Chem.*, **531**, 160 (1937).

17) N. Morishima, S. Koto, K. Kanemitsu, and S. Zen, *Chem. Lett.*, **1983**, 1189.

18) S. Koto, N. Morishima, C. Kusuhara, S. Sekido, T. Yoshida, and S. Zen., *Bull. Chem. Soc. Jpn.*, **55**, 2995 (1982).

19) S. Koto, N. Morishima, Y. Miyata, and S. Zen, *Bull. Chem. Soc. Jpn.*, **49**, 2639 (1976).

20) E. V. E. Roberts, J. C. P. Schwarz, and C. A. McNab, *Carbohydr. Res.*, **7**, 311 (1968).

21) S. Hardegger and R. M. Montavon, *Helv. Chim. Acta*, **29**, 1199 (1946).

Spin-Trapping of Alkyl Radicals by a Water-Soluble Nitroso Aromatic Spin-Trap, 3,5-Dibromo-4-nitrosobenzenesulfonate

Toshihiko OZAWA* and Akira HANAKI
National Institute of Radiological Sciences, 9-1 Anagawa-4-chome, Chiba 260
(Received January 29, 1987)

Synopsis. Some short-lived alkyl radicals generated by the oxidation with either Ti^{3+}-H_2O_2 or Fe^{2+}-H_2O_2 system were trapped by a water-soluble nitroso aromatic spin-trap, 3,5-dibromo-4-nitrosobenzenesulfonate (DBNBS, **1**), in aqueous solutions to yield the stable spin-adducts which could be easily detected and identified by electron spin resonance (ESR) spectroscopy.

The spin-trapping compounds react with the short-lived free radicals to form the more stable radical products, spin adducts, which can be detected and identified by electron spin resonance (ESR) technique.[1-6] Recently, a new water-soluble spin-trap, sodium 3,5-dibromo-4-nitrosobenzenesulfonate (DBNBS, **1**), was synthesized and was found to be an efficient radical trap in aqueous, or partially aqueous, solutions.[7] This new spin-trap does not yield observable spin adduct with hydroxyl radical (OH·) which is formed by the photolysis of hydrogen peroxide (H_2O_2), but dimethyl sulfoxide (DMSO) included in the aqueous H_2O_2 system gives the adduct with methyl radical which arises via hydroxyl radical attack on DMSO.[8]

In a previous paper,[9] we have reported that superoxide ion, O_2^-, can be easily trapped by DBNBS in aqueous solutions and that besides the intense signal due to O_2^- adduct, weak ESR signals assignable to methyl radical adduct are observed. Then, using DBNBS, we have further investigated the oxidation of some organic substrates by Fenton-type systems such as Ti^{3+}-H_2O_2 and Fe^{2+}-H_2O_2, both of which are known to be potent oxidizing agents,[10] and found that these Fenton-type systems give radical adducts similar to those obtained by the photolysis of the aqueous H_2O_2 system containing some organic substrates.

Experimental

Reagents. $TiCl_3$ (20% v/v), $FeCl_2$, and sulfuric acid (H_2SO_4) were purchased from Wako Pure Chemical Co. Ltd. and were used without further purification. H_2O_2 (30%) was obtained from Mitsubishi Gas Chemical Co. Ltd. Organic substrates were commercially available and were distilled prior to use. Deionized and triply distilled water was used throughout. Sodium 3,5-dibromo-4-nitrosobenzenesulfonate (DBNBS, **1**) was synthesized from 3,5-dibromosulfanilic acid by oxidation with H_2O_2 in glacial acetic acid.[7]

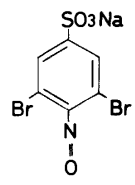

(1)

Procedure. Both 0.01 mol dm^{-3} metal ion (Ti^{3+} or Fe^{2+}) and 0.1 mol dm^{-3} H_2O_2 solutions were acidified by H_2SO_4 to pH 2.0. DBNBS (0.05 mol dm^{-3}) and organic substrates (0.1 mol dm^{-3}) were included in the aqueous H_2O_2 solutions. Reactions were started by adding the metal ion solutions to H_2O_2 solutions. The reaction solutions were immediately transferred to a JEOL quartz flat cell to measure ESR spectra. All the procedures were done in the air.

ESR Measurements. ESR spectra were obtained at room temperature on a JEOL-PE-1X (X-band) ESR spectrometer with 100 kHz field modulation. ESR parameters were calibrated by comparison with a standard Mn^{2+}/MgO marker and 2,2-diphenyl-1-picrylhydrazyl (DPPH, g=2.0036).

Results and Discussion

No ESR spectrum was observed from the following aqueous solutions: DBNBS, metal ion (Ti^{3+} or Fe^{2+}) with DBNBS, H_2O_2 with DBNBS.

When aqueous solutions of Ti^{3+} ion were mixed with aqueous solutions of H_2O_2 containing DBNBS, no ESR signal was observed. This result is consistent with the fact that DBNBS does not yield observable spin adduct with hydroxyl radical.[7,9,11] However, when DMSO was included in Ti^{3+}-H_2O_2-DBNBS system, an intensive ESR spectrum was observed as shown in Fig. 1. ESR parameters can be determined as follows: a^N (1)=13.9 G,[12] $a^H_{CH_3}$ (3)=12.8 G, a^H_{phenyl} (2)=0.7 G and g=2.0062 (1G=10^{-4} T). The ESR spectrum shown in Fig. 1 is almost identical with that of methyl radical adduct of DBNBS generated by the photolysis of aqueous solutions of H_2O_2 containing DMSO in the presence of DBNBS.[7] Therefore, the radical species observed in Fig. 1 can be assigned to the methyl radical adduct (**2**). In the Ti^{3+}-H_2O_2 system

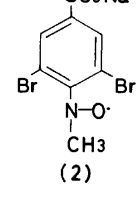

(2)

containing DMSO, methyl radical may be formed as follows:

$$Ti^{3+} + H_2O_2 \rightarrow Ti^{4+} + \cdot OH + OH^- \quad (1)$$

$$\cdot OH + (CH_3)_2SO \rightarrow CH_3SO_2H + CH_3\cdot \quad (2)$$

$$CH_3\cdot + \text{DBNBS} \rightarrow \text{methyl radical adduct (2)} \quad (3)$$

It is known that methyl radical is formed by the OH radical attack on DMSO (Eq. 2).[8] In Fig. 1, ESR spectrum is somewhat asymmetrical. Such a spectral pattern is often observed in even relatively small nitroxide molecules in aprotic media.[13] This phenomenon may be caused by anisotropic motion in isotropic media.[13]

When methyl alcohol was included in Ti^{3+}-H_2O_2-DBNBS system, ESR spectrum [a^N (1)=13.4 G, $a^H_{CH_2}$ (2)=7.4 G, a^H_{phenyl} (2)=0.8 G, and g=2.0064] was observed. Since these ESR parameters are almost identical with those

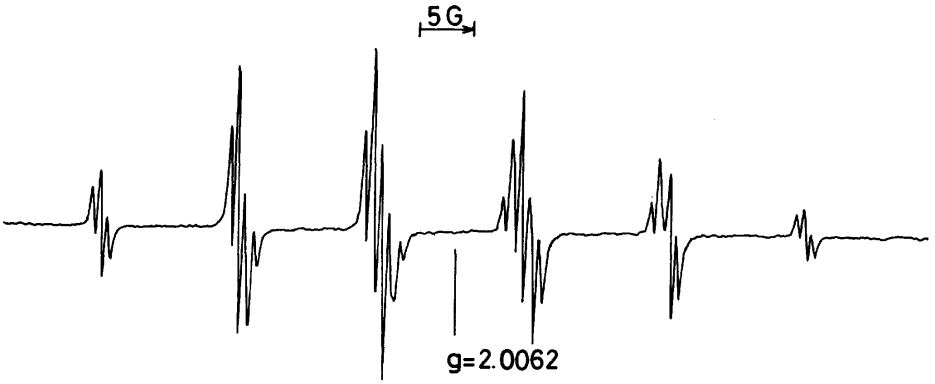

Fig. 1. ESR spectrum observed by the oxidation of DMSO with Ti^{3+}-H_2O_2 system in the presence of DBNBS in aqueous solutions.
Reaction conditions: 0.01 mol dm^{-3} Ti^{3+}, 0.1 mol dm^{-3} H_2O_2, 0.05 mol dm^{-3} DBNBS, 0.1 mol dm^{-3} DMSO. Instrument settings: microwave power, 10 mW; modulation amplitude, 0.5 G; amplitude, 10×100; time constant, 0.3 s; scan time, 8 min.

Table 1. ESR Parameters for Selected Spin Adducts of DBNBS

Substrate	Trapped radical	Method of generation of radical	Hyperfine splitting const (G)		
			a^N	a^H_{phenyl}	a^H_{other}
DMSO	CH_3·	Ti^{3+}-H_2O_2	13.9	0.7	12.8 (CH_3)
	CH_3·	Fe^{2+}-H_2O_2	14.1	0.7	13.3 (CH_3)
	CH_3·	$h\nu$-H_2O_2[a]	14.50		13.50(CH_3)
CH_3OH	$\dot{C}H_2OH$	Ti^{3+}-H_2O_2	13.4	0.8	7.4 (CH_2)
	$\dot{C}H_2OH$	Fe^{2+}-H_2O_2	13.6	—[b]	9.1 (CH_2)
	$\dot{C}H_2OH$	$h\nu$-H_2O_2[a]	13.70		9.20(CH_2)
C_2H_5OH	$\dot{C}H_2CH_2OH$	Ti^{3+}-H_2O_2	14.2	—[b]	12.2 (CH_2)
					—[b] (CH_2)
	$\dot{C}H_2CH_2OH$[c]	Fe^{2+}-H_2O_2	14.3	—[b]	13.6 (CH_2)
					9.2 (CH_2)
	$\dot{C}H_2CH_2OH$	$h\nu$-H_2O_2[a]	14.00		11.30(CH_2)
	$CH_3\dot{C}HOH$	$h\nu$-H_2O_2[a]	14.00		9.20(CH)

a) Deuteriated DBNBS was used as a spin-trap.[7] b) Not measured. c) A weak, unanalyzable signal was also observed.

of hydroxymethyl radical (·CH_2OH) adduct of DBNBS formed by the photolysis of aqueous solutions of H_2O_2 containing methyl alcohol in the presence of DBNBS,[2] the radical species observed can be assigned to the radical (**3**). In this reaction, hydroxymethyl radical is formed as follows:

(3)

$$\cdot OH + CH_3OH \rightarrow \cdot CH_2OH + H_2O \quad (4)$$

$$\cdot CH_2OH + DBNBS \rightarrow \text{hydroxymethyl radical adduct (3)} \quad (5)$$

When ethyl alcohol was included in Ti^{3+}-H_2O_2-DBNBS system, a weak ESR spectrum [a^N (1)=14.2 G, $a^H_{CH_2}$ (2)=12.2 G, and g=2.0063] which could be assigned to hydroxyethyl radical (·CH_2-CH_2OH) adduct of DBNBS (**4**) was observed.

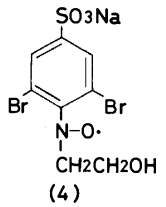

(4)

In this reaction system, another weak signal, which could not be analyzed, was also observed.

The same radical species were obtained from the Fe^{2+}-H_2O_2 system. These results are summarized in Table 1, along with the radical species observed by photolysis.

It is apparent from Table 1 that the same radical species were generated from both photolysis of H_2O_2 and Fenton-type reaction systems. However, the hyperfine coupling constants are somewhat different from each other, depending on the different reducing agents for H_2O_2.

The present experimental results indicate that a new water-soluble spin-trap, DBNBS, is an effective trapping agent for some alkyl radicals generated by the

oxidation with Fenton-type systems such as Ti^{3+}-H_2O_2 and Fe^{2+}-H_2O_2 in aqueous solutions. Recently, nitrone spin-traps such as 5,5-dimethyl-1-pyrroline *N*-oxide (DMPO) and *N*-*t*-butyl-α-phenylnitrone (PBN) are often used in biological systems. DBNBS may be compared with DMPO and PBN. DBNBS has a high solubility in aqueous solutions compared with PBN and, while DMPO is susceptible to decomposition by light,[6] DBNBS in aqueous solutions is stable under light. Further, DBNBS does not yield the observable spin-adduct with OH radical. From these facts, it is indicated that DBNBS is a useful spin-trap in aqueous reaction systems in which OH radical is formed as a first intermediate.

We wish to express our thanks to Prof. Yutaka Kirino, Faculty of Pharmaceutical Sciences, Kyushu University, for valuable discussions.

References

1) M. J. Perkins, *Adv. Phys. Org. Chem.*, **17**, 1 (1980).
2) E. G. Janzen, "Free Radicals in Biology," ed by W. A. Pryor, Academic Press, New York (1980), Vol. IV, pp. 116—154.
3) P. B. McCay, T. Noguchi, K.-L. Fong, E. K. Lai, and J. L. Poyer, "Free Radicals in Biology," ed by W. A. Pryor, Academic Press, New York (1980), Vol. IV, pp. 155—186.
4) E. Finkelstein, G. M. Rosen, and E. J. Rauckman, *Arch. Biochem. Biophys.*, **200**, 1 (1980).
5) E. G. Janzen, "Methods in Enzymology," ed by L. Packer, Academic Press, Orland, Florida (1984), Vol. 105, pp. 188—198.
6) G. M. Rosen and E. J. Rauckman, "Methods in Enzymology," ed by L. Packer, Academic Press, Orland, Florida (1984), Vol. 105, pp. 198—209.
7) H. Kaur, K. H. W. Leung, and M. J. Perkins, *J. Chem. Soc., Chem. Commun.*, **1981**, 142.
8) B. D. Flockhart, K. J. Ivin, R. C. Pink, and B. D. Sharma, *Chem. Commun.*, **1971**, 339.
9) T. Ozawa and A. Hanaki, *Biochem. Biophys. Res. Commun.*, **136**, 657 (1986).
10) M. J. Green and H. A. O. Hill, "Methods in Enzymology," ed by L. Packer, Academic Press, Orland, Florida (1984), Vol. 105, pp. 3—22.
11) T. Ozawa and A. Hanaki, *Biochem. Biophys. Res. Commun.*, **142**, 410 (1987).
12) In this paper, number of atom which interacts with unpaired electron is designated in parentheses.
13) S. Schreier, C. F. Polnaszenk and I. C. P. Smith, *Biochim. Biophys. Acta*, **515**, 375 (1978).

Optical Resolution and Absolute Configuration of Axially Dissymmetric 2,2′-Dihydroxy-6,6′-dimethylbiphenyl

Shigeyoshi KANOH, Nobuyuki TAMURA, Masatoshi MOTOI, and Hiroshi SUDA*
Department of Chemistry and Chemical Engineering, Faculty of Technology, Kanazawa University, 2-40-20 Kodatsuno, Kanazawa 920
(Received February 10, 1987)

Synopsis. 2,2′-Dihydroxy-6,6′-dimethylbiphenyl (**1**) was successfully resolved into its optically pure forms by the recrystallization of the diastereomeric salts derived from the hydrogenphosphate of **1** and cinchonidine or quinine. The dextrorotatory **1** was determined to have R-configuration.

It is well-known that axially dissymmetric biaryl compounds possess salient ability for chiral recognition. 1,1′-Binaphthyl unit has been very common in the design and construction of chiral auxiliaries,[1] while biphenyl[2,3] and 9,9′- or 4,4′-biphenanthryl units[4] have been applied as well. When biaryl derivatives, even though the nuclei of which are different from each other, have the same functional groups, they serve in most cases as quite similar catalysts for an asymmetric reaction with respect to stereochemistry.[3,5] In some cases, however, we have observed that the stereochemical outcomes are in disagreement.[3,6] Inspection of such results might provide an important clue of the consideration on the structure of active species or the steric factors operating in the reaction. It seems, therefore, to be important to compare the chiral catalysts derived from analogous biaryl compounds.

The most famous compound of a series of biaryls is 2,2′-dihydroxy-1,1′-binaphthyl, which is an important intermediate for the preparations of chiral crowns[7] and the *BINAL-H* reagent[8] as reported by Cram et al. and Noyori et al., respectively, and for the asymmetric Ullmann reaction as shown by Miyano.[9] More recently, its biphenanthryl analogs have been resolved on an optically active column in a preparative scale.[4]

Recently, we have reported briefly a synthesis of optically active 2,2′-dihydroxy-6,6′-dimethylbiphenyl (**1**) as a biphenyl analog and asymmetric reductions of alkyl phenyl ketones by using $LiAlH_4$- and borane-**1** complexes.[5,6] In this paper, we wish to describe the effective optical resolution of (*RS*)-**1** in more detail. In addition, each resolved **1** was confirmed to be optically pure, and the absolute configuration was determined.

The preparation of (*RS*)-**1** was carried out according to the method described in the literature.[10] The excellent method for the optical resolution of (*RS*)-2,2′-dihydroxy-1,1′-binaphthyl via its cyclic phosphate has been developed by Jacques et al.[11] The procedure is essentially applicable to the present case, as shown in the scheme. (*RS*)-**1** was easily converted to (*RS*)-6,6′-dimethylbiphenyl-2,2′-diyl hydrogenphosphate (**2**) by the reaction with phosphoryl chloride followed by hydrolysis in a high yield. We found that cinchonidine or quinine readily forms crystalline salt with the opposite enantiomer of **2** to each other. In the first step, the diastereomeric salts were prepared by mixing equimolar amounts of (*RS*)-**2** and cinchonidine in aqueous methanol. The crystalline salt deposited upon cooling, and the filtration afforded (*R*)-**2**·cinchonidine salt in a satisfactory yield of 45% based on (*RS*)-**2** used. The mother liquor containing the salt of (*S*)-enriched **2** was unsuitable for recrystallization. Crystallinity was greatly improved by employing quinine as a resolving reagent. Simple recrystallization of a mixture of the recovered **2** and an equimolar amount of quinine from aqueous methanol gave (*S*)-**2**·quinine salt in 40% yield. Further recrystallization of both salts of cinchonidine and quinine did not come about noticeable change in optical rotation. Decomposition of each salt with a diluted hydrochloric acid yielded (*R*)-(−)- and (*S*)-(+)-**2** in 42 and 38%, respectively. Each alkaloid used was recovered from the acidic filtrates. Reductive cleavage of (−)- and (+)-phosphates with $LiAlH_4$ yielded optically active **1** in 37 and 33%, respectively (overall yields based on the starting (*RS*)-**1**), whose specific rotations were $[\alpha]_D^{18}$ +91.5° and $[\alpha]_D^{20}$ −91.1° (*c* 1.0, ethanol), respectively.

The optical purity of each **1** thus resolved was determined from the ^1H NMR spectrum of the methyl 6,6′-dimethylbiphenyl-2,2′-diyl phosphate (**3**) derived from the intermediate **2**, in the presence of $Eu(tfc)_3$. The spectra are shown in Fig. 1. In the case of racemic **3**, the signals due to the aromatic methyl protons and the ester methyl protons split owing to the diastereomeric lanthanoide induced shift. On the other hand, each of the spectra, measured under the same conditions, of the optically active **3** shows the lack of the peaks due to opposed enantiomer. This fact reveals that each resolved **2** was optically pure.

The (R)-configuration of (+)-**1** was determined by

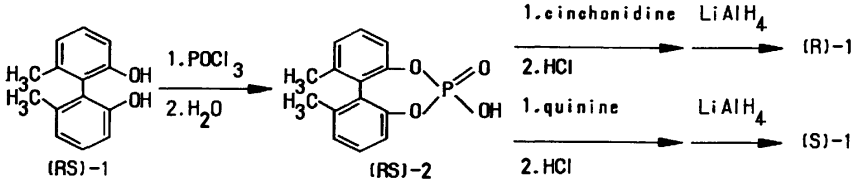

Scheme 1.

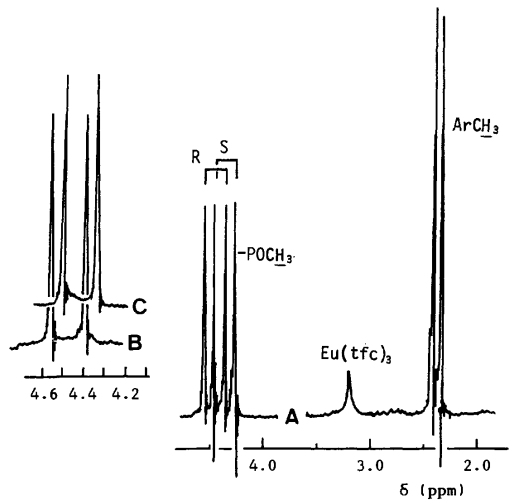

Fig. 1. ^{1}H NMR spectra of **3** (20 mg) in the presence of Eu(tfc)$_3$ (6 mg) in $CDCl_3$ (0.5 ml). A: (*RS*)-**3**, B: (*R*)-**3**, C: (*S*)-**3**.

chemical correlation with (+)-2,2′-diamino-6,6′-dimethylbiphenyl. The absolute configuration of the latter is known to be R from the X-ray crystallography of its *N,N′*-disalicylidene derivative,[12] and Sandmeyer-type reactions of biarylamines are known to proceed in a retention manner.[13] Thus, the optically pure (+)-diamine was treated with $NaNO_2$ in a diluted sulfuric acid. Thermal decomposition of the bis(diazonium) salt in an aqueous medium gave dextrorotatory **2**. The specific rotation ($[\alpha]_D^{19}$ +91.4° (*c* 1.0, ethanol)) is in good agreement with that observed for (+)-**1** resolved. This means that (+)-**1** has R-configuration.

More recently, Okamoto et al. have reported that racemic **1** of our sample can be directly resolved by a high performance liquid chromatography on optically active columns of cellulose tris(phenylcarbamate) derivatives.[14]

Experimental

Melting points are uncorrected. IR and NMR spectra were recorded on a JASCO A-202 and a JEOL JNM-PS-100 (100 MHz) spectrometer, respectively. Optical rotations were measured on a JASCO DIP-SL automatic polarimeter.

Racemic **1** was prepared through six-step reactions from *m*-cresol with slight modification of the reported method.[10] Mp 161.5—162.5 °C (lit,[10] 164 °C). IR (KBr) 3470, 3420, 1180 cm^{-1}. ^{1}H NMR (DMSO-d_6) δ=1.85 (s, 6H), 6.6—7.1 (m, 6H), 8.75 (s, 2H).

6,6′-Dimethylbiphenyl-2,2′-diyl Hydrogenphosphate (2). Fifty grams (0.23 mol) of (*RS*)-**1** and phosphoryl chloride (26 ml, 0.28 mol) were mixed in 230 ml of dichloromethane. Triethylamine (80 ml, 0.57 mol) was added dropwise to the stirred mixture under a gentle reflux. Reflux was continued for an additional 3 h. After cooling the precipitates were collected and washed thoroughly with cold water. The remaining solids were chlorophosphate of **1**. Extractive work-up of the filtrate led to an additional yield of the chloride. The combined crude chloride was hydrolyzed in a mixture of tetrahydrofuran (THF) (300 ml) and water (100 ml) with stirring at 50 °C for 3 h. The solution was freed from THF under reduced pressure, and the precipitates were collected. Recrystallization from aqueous methanol gave (*RS*)-**2** (61 g, 94% based on **1** used): mp 285—286 °C; IR (KBr) 3000—2000, 1255, 1215, 1020, 1000 cm^{-1}.

Optical Resolution of (*RS*)-2. All yields were based on (*RS*)-**2** used. Cinchonidine (68 g, 0.23 mol) and (*RS*)-**2** (61 g, 0.22 mol) were dissolved in 500 ml of boiling methanol. After the addition of 100 ml of water the solution was cooled in a refrigerator overnight. The crystals deposited were collected and washed with cold methanol to give (*R*)-**2**·cinchonidine salt (57 g, 45%): mp 185—188 °C (decomp); $[\alpha]_D^{24}$ −155° (*c* 0.5, methanol). The cinchonidine salt was decomposed in 6 mol dm^{-3} HCl (700 ml) with stirring at 50 °C for 1 h. After cooling the precipitates were collected. Recrystallization from aqueous methanol gave (*R*)-**2** (25.5 g, 42%): mp 299—305 °C (decomp); $[\alpha]_D^{19}$ −179° (*c* 0.5, methanol).

The (*S*)-enriched **2** was recovered by evaporating the mother liquor to dryness and subsequently treating the gamy residue with 6 mol dm^{-3} HCl. It was similarly reacted with an equimolar amount of quinine, and recrystallization from aqueous methanol gave (*S*)-**2**·quinine salt: mp 276—278 °C (decomp); $[\alpha]_D^{18}$ −43.0° (*c* 0.5, methanol). Decomposition of the salt followed by recrystallization in a similar way yielded (*S*)-**2** (23 g, 38%): mp 299—304 °C (decomp); $[\alpha]_D^{18}$ +177° (*c* 0.5, methanol).

Methyl 6,6′-Dimethylbiphenyl-2,2′-diyl Phosphate (3). In order to determine the optical purity of each resolved **2**, it was suspended in diethyl ether and treated with a large excess amount of diazomethane in ether. After standing overnight, removal of the solvent and drying under vacuum gave **3** in a nearly quantitative yield. The ^{1}H NMR spectrum of **3** (20 mg) was measured in a $CDCl_3$ solution (0.5 ml) containing Eu(tfc)$_3$ (6 mg) at room temperature. Crystalline **3** was obtained by recrystallizing from chloroform–ether in about 90% yield. (*RS*)-**3**: Mp 219—220 °C; IR (KBr) 2860, 1300, 1235, 1050, 1005 cm^{-1}; ^{1}H NMR ($CDCl_3$) δ=2.21 (s, 6H), 3.94 (d, 3H, J_{PH}=11 Hz), 7.0—7.5 (m, 6H). (*R*)-**3**: Mp 227—228 °C; $[\alpha]_D^{20}$ −119° (*c* 0.5, methanol). (*S*)-**3**: Mp 226—228 °C; $[\alpha]_D^{19}$ +117° (*c* 0.5, methanol).

(*R*)·/(*S*)-1. Powdered $LiAlH_4$ (8.4 g, 0.22 mol) was added in portions into a stirred suspension of the above phosphate (−)-**2** (25.5 g, 92 mmol) in dry THF (350 ml) at 0 °C. After the mixture was refluxed for 5 h, the reaction was quenched by successive additions of ethyl acetate, moist ether, and 6 mol dm^{-3} HCl with stirring at 0 °C. The organic layer was separated, washed with dil HCl and brine, and dried over Na_2SO_4. Evaporation of the solvents followed by recrystallization from benzene–petroleum ether gave (*R*)-**1** (18.4 g, 39% based on (*RS*)-**2** used): Mp 159—160 °C; $[\alpha]_D^{18}$ +91.5° (*c* 1.0, ethanol). Similarly, reduction of (+)-**2** led to (*S*)-**1** (16.5 g, 35%): Mp 159—160 °C; $[\alpha]_D^{20}$ −91.1° (*c* 1.0, ethanol).

Chemical Correlation between (+)-1 and (*R*)-2,2′-Diamino-6,6′-dimethylbiphenyl. A solution of the (*R*)-(+)-diamine (2.0 g, 9.3 mmol) ($[\alpha]_D^{25}$ +50.5° (*c* 1.0, ethanol))[15] in 25% aqueous sulfuric acid (25 ml) was cooled at 0 °C. To this was added an aqueous $NaNO_2$ (1.74 g, 25 mmol) with stirring at 0—5 °C. The resulting solution of the bis(diazonium) salt was occasionally dropped in small portions into a boiling solution of Na_2SO_4 (80 g) in 18 mol dm^{-3} H_2SO_4 (100 ml) over a period of 2 h. During the reaction, products were distilled away by bubbling steam into the reaction mixture. The distillate was extracted with ether. The organic layer was decolorized with charcoal and dried over Na_2SO_4. After the ether was removed, recrystallization gave (+)-**1** (0.17 g, 9%). The selected spectroscopic data were in agreement with those of the authentic sample. Mp 159—160 °C, $[\alpha]_D^{19}$ +91.4° (*c* 1.0, ethanol).

The authors are indebted to Dr. Yoshio Okamoto of Osaka University for the chromatographic separation of (*RS*)-**1** on the optically active cellulose column.

References

1) J. M. Wilson and D. J. Cram, *J. Am. Chem. Soc.*, **104**, 881 (1982), and references cited therein.

2) S. Kanoh, N. Kawaguchi, and H. Suda, *Makromol. Chem.*, **188**, 463 (1987), and references cited therein.

3) S. Kanoh, N. Kawaguchi, T. Sumino, Y. Hongoh, and H. Suda, *J. Polym. Sci., Polym. Chem. Ed.*, in press, and references cited therein.

4) K. Yamamoto, H. Fukushima, and M. Nakazaki, *J. Chem. Soc., Chem. Commun.*, **1984**, 1490; K. Yamamoto, K. Noda, and Y. Okamoto, *ibid*, **1985**, 1065.

5) H. Suda, S. Kanoh, N. Umeda, M. Ikka, and M. Motoi, *Chem. Lett.*, **1984**, 899. The $LiAlH_4$ complex modified with optically pure **1** had as high enantioselectivity as that observed for the *BINAL-H* reagent.[8] Both reagents provided the same chiral choice in the asymmetric reduction of prochiral ketones.

6) H. Suda, S. Kanoh, N. Umeda, T. Nakajo, and M. Motoi, *Tetrahedron Lett.*, **24**, 1513 (1983). The chiral hydride reagent prepared from borane and **1** had also an excellent enantioselectivity, whereas a similar type of borane complex with 2,2′-dihydroxy-1,1′-binaphthyl showed rather low selectivity. The configurations of the alcohols produced preferentially by these two chiral reagents were sometimes reversed to each other. With respect to the difference, the fact reported by Okamoto is interesting to us that 2,2′-dihydroxy-1,1′-binaphthyl cannot form the corresponding spiroborate compound; Y. Okamoto, *Yuki Gosei Kagaku Kyokai Shi*, **44**, 896 (1986).

7) For example, E. P. Kyba, G. W. Gokel, F. de Jong, K. Koga, L. R. Sousa, M. G. Siegel, L. Kaplan, G. D. Y. Sogah, and D. J. Cram, *J. Org. Chem.*, **42**, 4173 (1977).

8) R. Noyori, I. Tomino, Y. Tanimoto, and M. Nishizawa, *J. Am. Chem. Soc.*, **106**, 6709 (1984).

9) S. Miyano, S. Handa, M. Tobita, and H. Hashimoto, *Bull. Chem. Soc. Jpn.*, **59**, 235 (1986).

10) Y. Sugii, and H. Shindo, *J. Pharm. Soc. Jpn.*, **54**, 829 (1934).

11) J. Jacques, C. Fouquey, and R. Viterbo, *Tetrahedron Lett.*, **1971**, 4617.

12) L. H. Pignolet, R. P. Taylor, and W. D. Horrocks Jun., *J. Chem. Soc., Chem. Commun.*, **1968**, 1443.

13) E. L. Eliel, "Stereochemistry of Carbon Compounds," McGraw-Hill, 1962, p. 173.

14) Y. Okamoto, M. Kawashima, and K. Hatada, *J. Chromatogr.*, **363**, 173 (1986).

15) H. Suda, M. Motoi, M. Fujii, S. Kanoh, and H. Yoshida, *Tetrahedron Lett.*, **1979**, 4565.

Synthesis of Liquid Hydrocarbons from Carbon Monoxide and Water with a Hybrid Catalyst

Hiro-o TOMINAGA, Michiharu MIYAUCHI, and Kaoru FUJIMOTO*
Department of Synthetic Chemistry, Faculty of Engineering, The University of Tokyo, Bunkyo-ku, Hongo, Tokyo 113
(Received October 16, 1986)

Synopsis. Liquid hydrocarbons were produced from carbon monoxide and water at temperatures from 220 to 280 °C and under moderately pressurized conditions (3 atm), by utilizing a hybrid catalyst composed of a Co/SiO_2 catalyst and a CO shift conversion catalyst. Most of the steam, either added or formed, was converted to hydrogen in the reaction of H_2O with CO on the CO shift catalyst.

It has been known that the synthesis gas produced by modern coal gasifiers has CO/H_2 ratios between 1 and 2.[1] On the other hand the CO/H_2 ratio of feed gas for the Fischer-Tropsch (F-T) synthesis is about 0.5. In order to regulate the difference, a part of CO should be converted to CO_2 and H_2 by the reaction with added steam, and the CO_2 is removed from the product by a conventional method.[2] In this process a CO shift converter is necessary and a large amount of steam is consumed.

Koelbel et al.[3] have demonstrated that CO and H_2O are able to be directly utilized with a precipitated iron catalyst to produce a hydrocarbon mixture. Since iron catalysts are active for the $CO-H_2$ reaction as well, a synthesis gas with high CO/H_2 ratio can be used for hydrocarbon synthesis without any added steam. Because, the water produced by the $CO-H_2$ reaction could be utilized to form hydrocarbons.

$$CO + 2H_2 \rightarrow -CH_2- + H_2O \quad (1)$$
$$2CO + H_2O \rightarrow -CH_2- + CO_2 \quad (2)$$
$$3CO + 2H_2 \rightarrow 2\text{-}CH_2- + CO_2 \quad (3)$$

The present authors examined the same reaction with a fused iron catalyst and found that the catalyst is quickly carbulized by CO and oxidized by water during the reaction to lose its catalytic activity.[4]

The authors have developed a highly active supported cobalt catalyst for the Fischer-Tropsch synthesis.[5] Although the catalyst is highly resistant to oxidation with water, it has little activity for the CO shift reaction. Thus, if the cobalt catalyst mixed with a CO shift catalyst is subjected to the synthesis gas reaction, CO and H_2 should react on the cobalt catalyst to form hydrocarbons and H_2O, then the resultant water should react in situ with CO, on the CO shift catalyst to form CO_2 and H_2.

$$CO + 2H_2 \rightarrow -CH_2- + H_2O \quad (4)$$
$$CO + H_2O \rightarrow H_2 + CO_2 \quad (5)$$
$$2CO + H_2 \rightarrow -CH_2- + CO_2 \quad (6)$$

Experimental

The hybrid catalyst was prepared by physically mixing the granules (20—40 mesh) of a 10 wt% Co/SiO_2 catalyst with a commercial available Cu-Cr oxide catalyst (Nikki N-201). The Co/SiO_2 catalyst was prepared by impregnating a commercially available silica gel (Fuji Davison ID gel) with cobalt nitrate from its aqueous solution, calcining in air at 450 °C for 3 h, and then reducing the catalyst precursor in hydrogen flow at 400 °C for 15 h. The reduced Co/SiO_2 catalyst was mixed with the Cu-Cr oxide catalyst under nitrogen atmosphere and packed in a tubular reactor. The hybrid catalyst was activated by reducing, in situ, in flowing hydrogen at 250 °C for 3 h.

The reaction was conducted using a fixed bed flow type reaction apparatus under pressurized conditions. The details of this apparatus has been described elsewhere.[3] Water was fed by a micro-feeder and was evaporated in a container connected to the upper part of the reactor. All products effused from the reactor were withdrawn in the gaseous states from the pressurized zone and were analyzed by gas chromatographs. The details of analysis has been described elsewhere.[6]

Results and Discussion

The catalytic activity of Nikki N-201 for the CO shift reaction was tested under conditions: 240 °C, 1—5 atm, CO/H_2O=3/1 (mole ratio) and was shown to keep 100% H_2O conversion for more than 24 h.

In Fig. 1 are shown the yields of hydrocarbons, CO_2, and methane over the hybrid catalyst as a function of process time. The yield of CO_2 decreased gradually from the initial value, 50% (on CO base) to 30% within about 6 h and reached a steady state. Also the yields of product hydrocarbons and methane decreased in the similar manner as that of CO_2. The decrease in CO_2 yield could be attributed most probably due to the covering of active sites on the CO shift catalyst by high-boiling hydrocarbons, because a hybrid catalyst containing a supported ruthenium catalyst, which pro-

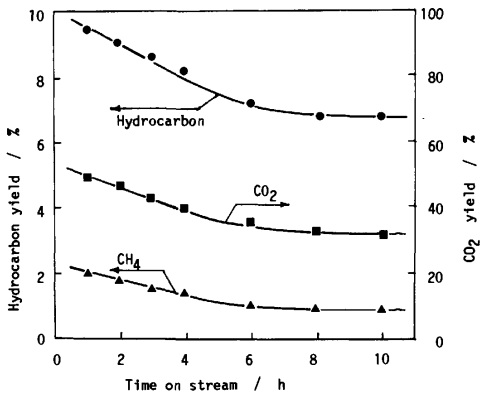

Fig. 1. Activity changes in the hybrid catalyst with time on stream CO/SiO_2+Cu-Cr (1/1 by weight), temp: 230 °C, press.: 1 atm, $CO/H_2/H_2O$: 2/1/1, W/F: 20 g-cat.h mol^{-1}.

Table 1. Yield and Hydrocarbon Distribution

Run No.	1	2	3	4[a)]
$CO/H_2/H_2O$ (mole ratio)	3/−/1	2/1/1	2/1/−	2/1/−
Yield (% carbon base)				
CO_2	33.9	56.0	6.0	0.1
Hydrocarbon	4.4	16.8	5.4	5.9
Distribution (C-wt%)				
C_1	4.2	8.7	6.2	5.0
C_2	1.7(29)[b)]	2.6(2)	1.7(12)	1.4(64)
C_3	4.5(76)	8.1(23)	5.5(49)	5.8(82)
C_4	5.2	9.6	6.5	7.0
C_5–C_9	32.9	49.6	41.9	42.5
C_{10}–C_{14}	30.6	19.7	29.0	25.7
C_{15}+	20.9	1.7	9.2	12.6

10wt% Co/SiO_2 plus Cu-Cr Cat.=1/1 (by weight). Temp: 230°C. Press.: 3atm. W/F: 19.5 g-cat. h mol^{-1}.
a) Co/SiO_2 only. b) Olefin content (mol%).

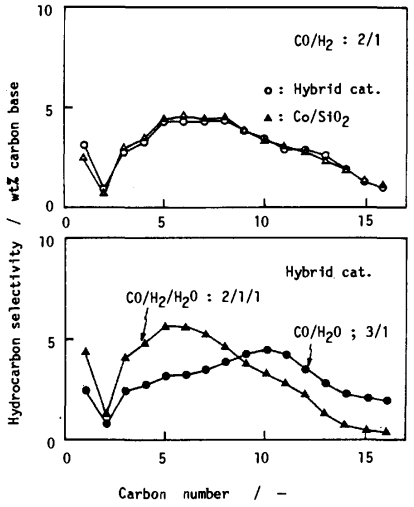

Fig. 2. Hydrocarbon distribution obtained from the reactions of water gas or synthesis gas. Temp: 230°C, press.: 3 atm, W/F: 20 g-cat.h mol^{-1}, hybrid catalyst; 10 g-cat.h mol^{-1} (Co/SiO_2 catalyst).

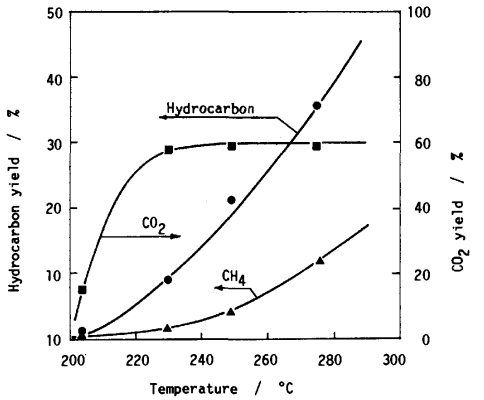

Fig. 3. Effects of temperature on the CO–H_2–H_2O reaction. Co/SiO_2+Cu-Cr (1/1 by weight), press.: 3 atm, $CO/H_2/H_2O$: 2/1/1, W/F: 20 g-cat.h mol^{-1}.

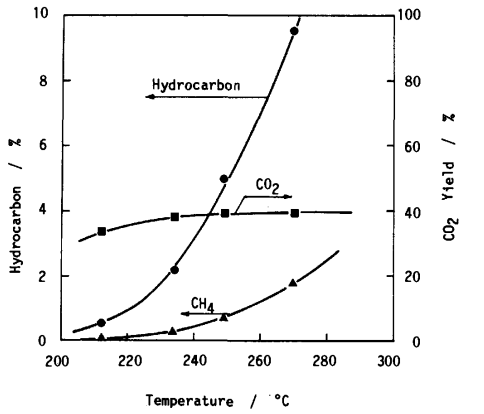

Fig. 4. Effects of temperature on the CO–H_2O reaction.
Co/SiO_2+Cu-Cr (1/1 by weight), press.: 3 atm, CO/H_2O: 3/1, W/F: 20 g-cat.h mol^{-1}.

duced higher hydrocarbons than the Co/SiO_2 catalyst, lost its activity more quickly. On the other hand, the decrease in the hydrocarbon formation should be attributed to the decrease in the partial pressure of hydrogen in the reaction mixture caused by the decrease in the conversion of CO and H_2O to hydrogen. All data described below were taken after the catalyst activity reached the steady state.

Some of the typical data of CO–H_2, CO–H_2O, and CO–H_2–H_2O reactions on the Co/SiO_2 catalyst or the hybrid catalyst are shown in Table 1 and Fig. 2. It is clear from the data in the table that while little CO_2 is formed on the Co/SiO_2 catalyst alone, almost all of water, irrespectively of that it is added or formed, reacted with CO to form CO_2 and hydrogen on the hybrid catalyst. For example, in experiments Nos. 2 and 3, the amount of CO_2 equal the sum of hydrocarbons (on carbon base) and added water. Since one molecule of water is formed for every one CO molecule reacted in the F-T synthesis reaction the sum of hydrocarbons and add water is the total amount of water supplied to the catalyst.

It should be also noted that the addition of steam to the system markedly accelerates its productivity of hydrocarbons, while the hydrocarbon productivity of the Co/SiO_2 catalyst was scarcely affected by the addition of CO shift catalyst only. It should be attributed to the increase in the practical partial pressure of hydrogen caused by CO shift reaction, because the rate of

hydrocarbon formation on the Co/SiO_2 catalyst is almost proportional to the partial pressure of hydrogen.[7]

The product pattern, shown in Fig. 2 and Table 1, is markedly affected by the CO shift catalyst and steam. The reaction of $CO-H_2O$ system gave a product rich in olefins and higher hydrocarbons (C_{15+}), whereas the $CO-H_2-H_2O$ reaction on the hybrid catalyst gave lower hydrocarbons rich in paraffins. The reaction of a synthesis gas ($2CO+1\ H_2$) on the Co/SiO_2 and the hybrid catalysts gave products with intermediate characters as compared with other two cases mentioned above. Although the carbon number distribution of the products from the Co/SiO_2 and the hybrid catalyst systems are fairly close to each other, the hybrid catalyst gave a product which is richer in methane and paraffins than that on the Co/SiO_2 catalyst.

The characteristic features mentioned above are well interpreted by the partial pressures of CO and H_2. As it has been well known high CO/H_2 ratio in the synthesis gas is favored for the production of high molecular weight hydrocarbons and high olefin content in the F-T synthesis. The CO/H_2 ratio in the reaction mixture is in the order: Run 2 > Run 3 > Run 4 > Run 1. The order is just the same as that of the average molecular weight and that of the olefin content in the product hydrocarbons.

Figures 3 and 4 illustrate the effects of reaction temperature on the product yields for the $CO-H_2-H_2O$ system and the $CO-H_2O$ system, respectively. In either system the yield of CO_2 reached the level which corresponds to 100% conversion of H_2O to H_2 and CO_2. The hydrocarbon yield increased monotonously with the increase in reaction temperature in the similar manner to that of the F-T synthesis on the same catalyst. The levels of hydrocarbon yield and space time yield were much higher for the $CO-H_2-H_2O$ system than the $CO-H_2O$ system because of the higher H_2 pressure and the lower CO pressure for the former system, as mentioned before.

This work was financially supported by the Special Grant for Energy Research from the Ministry of Education, Science and Culture, which is greatly appreciated.

References

1) S. A. Oader, "Coal Science and Technology," Elsevier (1985), Vol. 8, p. 198.
2) M. E. Dry, "Catalysis," Springer-Verlag (1981), Vol. 1, p. 159.
3) H. Koelbel, P. Ackerman, and F. Engelhardt, *Erdoel und Kohle*, **7**, 303 (1986).
4) K. Fujimoto, H. Saima, and T. Tominaga, *J. Jpn. Petrol. Inst.*, **26**, 258 (1983).
5) K. Fujimoto, K. Ejima, and T. Tominaga, 43rd National Meeting, Chemical Society of Japan (1981).
6) K. Fujimoto, T. Nobusawa, T. Fukushima, and H. Tominaga, *Bull. Chem. Soc. Jpn.*, **58**, 3164 (1985).
7) K. Fujimoto, O. Shimada, H. Saima, and H. Tominaga, 48th National Meeting, Chemical Society of Japan (1983).

Thermodynamic Study on Solvent Extraction of 18-Crown-6-Alkali Metal Ion Complexes and Tetraalkylammonium Ions with Picrate Anions into Benzene

Yasuyuki TAKEDA* and Yoshiki MATSUMOTO
Department of Chemistry, Faculty of Science, Chiba University,
Yayoi-chō, Chiba 260
(Received October 11, 1986)

Enthalpy and entropy changes for ion-pair extractions of tetraalkylammonium ions (Me_4N^+, Et_4N^+, n-Pr_4N^+, n-Bu_4N^+) with picrate anions, overall extractions of alkali metal (Na, K, Rb, Cs) picrates with 18-crown-6 (18C6), and distribution of 18C6 itself were determined between benzene and water, Me, Et, n-Pr, and n-Bu denoting methyl, ethyl, propyl, and butyl groups, respectively. All the extracted 18C6 complexes were 1:1:1 complexes (alkali metal ion:18C6:picrate anion). The values of enthalpy and entropy changes are negative for overall extractions of all the alkali metal picrates with 18C6. Plots of thermodynamic quantities for ion-pair extractions of R_4NA vs. the number of carbon atoms of R_4N^+ show a linear relationship, R_4N^+ and A^- being tetraalkylammonium ion and picrate anion, respectively. Enthalpy and entropy changes were calculated for ion-pair extractions of 18C6-alkali metal ion complexes with picrate anions. The thermodynamic parameters for ion-pair extractions of 18C6-alkali metal picrate complexes were compared with those of R_4NA, and were discussed in detail from the standpoint of molecular grounds. It was found from these data that the 18C6-K^+ complex acts as a structure breaker in water.

Numerous data have been presented on complexing power of crown compounds for metal ions. However, a few reports have been published on solvation properties of the crown compound complexes. Ion-pair extraction study of crown compound complexes provides very valuable information on solute-solvent interaction of the crown compound complexes in water.[1]

One of the principal objects of this paper is to investigate solvation behavior of the crown compound complexes in water. In the present work, enthalpy and entropy changes for ion-pair extraction of 18-crown-6 (18C6)-alkali metal ion complexes and tetraalkylammonium ions (R_4N^+) with picrate anions (A^-) have been determined between benzene and water. Thermodynamic quantities for ion-pair extraction of 18C6- and 15-crown-5 (15C5)-alkali metal picrate complexes were compared with those of R_4NA, and were discussed in detail from the standpoint of molecular grounds.

Experimental

Materials. Tetramethyl-, tetraethyl-, tetrapropyl-, and tetrabutylammonium hydroxides (Wako-Pure Chemicals Ltd.) were used as received. 18-Crown-6 (Nisso Co., Ltd.) was recrystallized from acetonitrile and, prior to use, dried at 80 °C in vacuo. Benzene, picric acid, $LiOH \cdot H_2O$, NaOH, and KOH were analytical grade reagents. Rubidium and caesium hydroxides were of reagent grade. Benzene was washed three times with distilled water.

Extraction Procedure. (1) Ion-pair extraction of tetraalkylammonium picrate. A benzene phase and an aqueous phase of R_4NOH (1.7×10^{-4}—3.2×10^{-2} M†), LiOH (0.1 M), and picric acid (4.2×10^{-5}—5.1×10^{-3} M) in stoppered glass tubes (30 ml) or Erlenmeyer flasks with stoppers (300 ml) were shaken for 2 h in a water bath thermostated at 20, 25, 30, 35, and 40±0.2 °C, and centrifuged. For Et_4NA, n-Pr_4NA, and n-Bu_4NA systems, the initial volume of each phase was 12 ml, whereas, for the Me_4NA system, those of benzene and aqueous phases were 200 and 20 ml, respectively. Extractions were conducted at pH 12.5—13.1. A portion of the benzene phase (10 ml for the former systems and 100 ml for the latter system) was transferred to a beaker and allowed to evaporate over several days. The residue was dissolved in 0.01 M NaOH aqueous solution (4 ml) and the picrate concentration was determined spectrophotometrically at 356 nm ($\varepsilon=1.45\times10^4$ cm^{-1} M^{-1}). (2) Extraction of alkali metal picrates with 18C6. Experimental procedures and concentrations of 18C6, alkali metal hydroxides, and picric acid were almost the same as those described in a previous paper.[2] Extractions were performed at pH 11.1—12.3 at 20, 30, 35, and 40±0.2 °C.

The Distribution Coefficient of 18C6. A 12 ml benzene solution of 18C6 (2.0×10^{-5}—9.3×10^{-4} M) and an equal volume of distilled water in a stoppered glass tube were shaken in a thermostated water bath for 1 h and centrifuged. A portion (11 ml) of the benzene phase and an equal volume of aqueous solution (pH 11.7—12.3) of KOH (3×10^{-2} M) and picric acid (8×10^{-3} M) were placed in a stoppered glass tube and agitated. After centrifuging, the picrate in the benzene phase was back-extracted into 8 ml of 0.01 M NaOH aqueous solution, and the picrate concentration was determined spectrophotometrically ($\lambda_{max}=356$ nm, $\varepsilon=1.45\times10^4$ cm^{-1} M^{-1}). Experiments were carried out at 20, 30, 35, and 40±0.2 °C. Each distribution coefficient value of 18C6 is the average of about seven measurements.

Results

Ion-Pair Extraction of R_4NA. In an equilibrium between benzene and an aqueous solution of R_4NA, the equilibrium constants are defined as

$$K_A(R_4NA) = [R_4NA]/[R_4N^+][A^-], \quad (1)$$

$$K_D(R_4NA) = [R_4NA]_o/[R_4NA], \quad (2)$$

† 1 M=1 mol dm^{-3}.

$$K_{ex,ip}(R_4NA) = [R_4NA]_o/[R_4N^+][A^-] = K_A(R_4NA)K_D(R_4NA), \quad (3)$$

where the subscript "o" and the lack of subscript denote the organic and aqueous phases, respectively. The distribution ratio of R_4N^+ is represented by

$$D = [R_4NA]_o/([R_4N^+] + [R_4NA]). \quad (4)$$

Combination of Eqs. 1—4 leads to

$$D^{-1} = K_D(R_4NA)^{-1} + (K_{ex,ip}(R_4NA)[A^-])^{-1}. \quad (5)$$

A plot of D^{-1} against $[A^-]^{-1}$ shows a straight line in every case. Values of $K_{ex,ip}(R_4NA)$ were calculated from the slopes of these straight lines. $K_D(R_4NA)$ and $K_A(R_4NA)$ values could be obtained only for the *n*-Bu_4NA system at 25 °C (K_D=4, K_A=1.4×10³). K_D values of *n*-Bu_4NA and K(18C6)A (3.7[3]) are almost the same, but, K_A value of *n*-Bu_4NA is one order of magnitude over that of K(18C6)A (140[3]).

$R\ln K_{ex,ip}(R_4NA)$ vs. T^{-1} plots are found to be linear in every system. Enthalpy change ($\Delta H_{ex,ip}(R_4NA)$) and entropy change ($\Delta S_{ex,ip}(R_4NA)$) for Eq. 3 were calculated from these data. The thermodynamic quantities are listed in Table 1.

Extraction of Alkali Metal Picrates with 18C6. When an equilibrium is established between an aqueous phase of alkali metal ion (M^+) and picrate ion, and a benzene phase of crown ether (L), the equilibrium constants are defined as

$$K_{ex} = [MLA]_o/[M^+][L]_o[A^-], \quad (6)$$
$$K_D(L) = [L]_o/[L], \quad (7)$$
$$K_{ML} = [ML^+]/[M^+][L], \quad (8)$$
$$K_{ex,ip}(MLA) = [MLA]_o/[ML^+][A^-]. \quad (9)$$

Thus, K_{ex} can be written as

$$K_{ex} = K_{ML} \cdot K_{ex,ip}(MLA) \cdot K_D(L)^{-1}. \quad (10)$$

The distribution ratio of the alkali metal is represented by

$$D = [MLA]_o/[M^+]. \quad (11)$$

Table 1. Thermodynamic Quantities for Ion-Pair Extraction of Tetraalkylammonium Picrates between Benzene and Water

	$\log(K_{ex,ip}$/ mol^{-1} dm^3) (at 25°C)	$\Delta H^\circ_{ex,ip}$/ kJ mol^{-1}	$T\Delta S^\circ_{ex,ip}$/ kJ mol^{-1} (at 25°C)
Me_4NA	−2.06	0	−12.1
Et_4NA	−0.60	5.3	1.8
n-Pr_4NA	1.61	10.3	19.5
n-Bu_4NA	3.67	15.1	35.8

Combination of Eqs. 6 and 11 leads to

$$D = K_{ex}[L]_o[A^-]. \quad (12)$$

Log (D/[A^-]) vs. log $[L]_o$ plots give a straight line with a slope of 1 in every case. This indicates that the K_{ex} can be described by Eq. 6. The values of $[L]_o$ and $[A^-]$ in Eq. 12 were calculated by

$$[L]_o = ([L]_t - [MLA]_o)/(1 + K_D(L)^{-1}), \quad (13)$$
$$[A^-] = [HA]_t - [MLA]_o, \quad (14)$$

where the subscript "t" refers to the total concentration.

$R\ln K_D(L)$ vs. T^{-1} and $R\ln K_{ex}$ vs. T^{-1} plots show a linear relationship in every system. Enthalpy and entropy change for Eqs. 6 and 7 were calculated from these data in the same manner as that mentioned above. The thermodynamic parameters are summarized in Table 2.

Discussion

Ion-Pair Extraction of R_4NA. It can be seen from log $K_{ex,ip}$ values in Table 1 that the larger the size of R_4N^+ is, the more extractable into benzene it is. Plots of log $K_{ex,ip}(R_4NA)$ against the number of carbon atoms of R_4N^+ give a straight line with a slope of

Table 2. Thermodynamic Quantities for Extraction of Alkali Metal Picrates with 18C6 between Benzene and Water

	$\log K_D(L)^{a,2)} = -1.19_8$		
	$\log K_{ex}{}^{a,2)}$	$\log K_{ML}{}^{a)}$	$\log K_{ex,ip}{}^{a,2)}$
Na	3.39	0.80[4]	1.39
K	5.97	2.03[4,5]	2.74
Rb	5.43	1.56[4]	2.67
Cs	4.38	0.99[4]	2.19
$\Delta H^\circ_D(L)$/kJ mol^{-1} = 37.6		$T\Delta S^\circ_D(L)$/kJ mol^{-1} a) = 30.4	
	ΔH°/kJ mol^{-1} b)		
	ΔH°_{ex}	ΔH°_{ML}	$\Delta H^\circ_{ex,ip}$
Na	−34.4	−9.41[4]	12.6
K	−77.3	−25.01[5]	−14.6
Rb	−77.6	−16.0[4]	−24.0
Cs	−66.3	−15.9[4]	−12.8
	$T\Delta S^\circ$/kJ mol^{-1} a,c)		
	$T\Delta S^\circ_{ex}$	$T\Delta S^\circ_{ML}$	$T\Delta S^\circ_{ex,ip}$
Na	−14.7	−4.6[4]	20.3
K	−42.8	−13.22[5]	0.8
Rb	−46.1	−7.1[4]	−8.6
Cs	−40.9	−10[4]	−0.5

a) at 25°C.
b) $\Delta H^\circ_{ex} = -\Delta H^\circ_D(L) + \Delta H^\circ_{ML} + \Delta H^\circ_{ex,ip}$.
c) $\Delta S^\circ_{ex} = -\Delta S^\circ_D(L) + \Delta S^\circ_{ML} + \Delta S^\circ_{ex,ip}$, where subscripts "ex, D, ML, and ex,ip" refer to reactions represented by Eqs. 6—9, respectively.

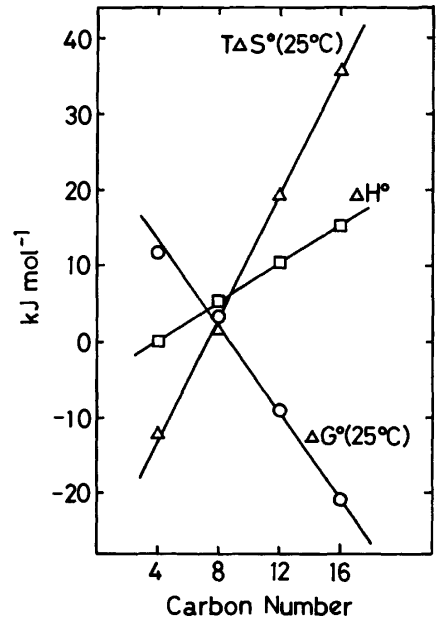

Fig. 1. Plots of thermodynamic parameters for ion-pair extraction of R_4NA vs. the number of carbon atoms of R_4N^+.

0.48_5. This indicates that the contribution of a methylene group to extraction constants of ion-pairs (Π_{CH_2}) at 25 °C between benzene and water is 0.48_5. The Π_{CH_2} value determined from the extraction of ion-pairs of alkanesulfonate ions with cationic dyes between benzene and water at 25 °C has been reported to be 0.64,[6] and is larger than that of this study. This may be due largely to the difference in the shape of tetraalkylammonium and alkanesulfonate ions.

Plots of thermodynamic parameters for ion-pair extraction of R_4NA vs. the number of carbon atoms of R_4N^+ in Fig. 1 show a linear relationship. Contributions of a methylene group to ΔH and ΔS of ion-pair extraction ($\Delta H_{ex,ip}(CH_2)$ and $\Delta S_{ex,ip}(CH_2)$) between benzene and water were found from the slopes to be 1.2_5 kJ mol^{-1} and 13.5 J K^{-1} mol^{-1}, respectively. Positive $\Delta H_{ex,ip}(CH_2)$ and $\Delta S_{ex,ip}(CH_2)$ values suggest that a methylene group may undergo hydrophobic hydration in the aqueous phase. From values of enthalpy and entropy changes of hydration of hydrocarbons (methane-butane),[7] enthalpy and entropy increments per methylene group were calculated to be -3.63 kJ mol^{-1} and -12.5 J K^{-1} mol^{-1}, respectively. Values of $\Delta H_{ex,ip}(CH_2)$ and $\Delta S_{ex,ip}(CH_2)$ determined in this work are comparable to the reported values. It follows from this finding that dehydration of CH_2 plays a very important role in the transfer equilibrium of CH_2 from water to benzene. The value of $T\Delta S_{ex,ip}(CH_2)$ at 25 °C is 3.2 times larger than that of $\Delta H_{ex,ip}(CH_2)$. This indicates that when the alkyl chain in R_4N^+ lengthens, an increase in extractability of R_4NA is largely entropy controlled.

Table 1 shows that the ion-pair extraction process of n-Pr_4NA and n-Bu_4NA is mostly entropy controlled, resulting in the positive $\log K_{ex,ip}$ values, whereas, for Me_4NA and Et_4NA, unfavorable entropy and enthalpy change cause the negative $\log K_{ex,ip}$ values, respectively.

The larger the size of R_4N^+, the greater the $\Delta S_{ex,ip}$ value and the more endothermic is the ion-pair extraction process of R_4NA ($\Delta H_{ex,ip}=0$ for Me_4NA). The negative $\Delta S_{ex,ip}$ value is observed only for Me_4NA. This tendency seems to reflect the change from structure-breaking effect of Me_4N^+ to structure-making effect of n-Bu_4N^+ in an aqueous solution.[8]

A plot of $\Delta H_{ex,ip}$ against reciprocal of the radius of R_4N^+ shows a better linear relationship compared to the case of $\Delta S_{ex,ip}$ (correlation coefficient $r=-0.992$ and -0.983 for $\Delta H_{ex,ip}$ and $\Delta S_{ex,ip}$, respectively). This indicates that $\Delta H_{ex,ip}$ is composed more largely of electrostatic interaction compared to $\Delta S_{ex,ip}$.

Distribution of Crown Ethers. Values of $\log K_D(L)$ at 25 °C of 12-crown-4 (12C4) and 15C5 between benzene and water are -0.82[9] and -0.80_6,[2] respectively. From $\log K_D(L)$ values of 12C4, 15C5, and 18C6, the contribution of an ether oxygen atom to $\log K_D(L)$ (Π_o) at 25 °C between benzene and water can be evaluated by means of Π_{CH_2} value determined in this work ($\Pi_o=(\log K_D(L)-\Pi_{CH_2}\times a)\div b$, a and b being the number of methylene groups and ether oxygen atoms, respectively). Values of Π_o are -1.17, -1.13_1, and -1.16_9 for 12C4, 15C5, and 18C6, respectively. They are almost the same. The Π_o value is -1.16 on the average. It can be seen from Π_{CH_2} and Π_o values that a methylene group is lipophilic, whereas an ether oxygen atom is hydrophilic. Values of $\log K_D(L)$ at 25 °C of crown ethers between benzene and water, which are unknown, can be estimated from these empirical parameters.

In a similar manner as above, the contribution of an ether oxygen atom to $\Delta H_D(L)$ ($\Delta H_D(o)$) and $\Delta S_D(L)$ ($\Delta S_D(o)$) between benzene and water was calculated from $\Delta H_D(L)$ and $\Delta S_D(L)$ of 15C5 (20.9 kJ mol^{-1} and 53.9 J K^{-1} mol^{-1}, respectively[10]) and 18C6 by use of $\Delta H_{ex,ip}(CH_2)$ and $\Delta S_{ex,ip}(CH_2)$ determined in this study ($\Delta H_D(o)=(\Delta H_D(L)-\Delta H_{ex,ip}(CH_2)\times a)\div b$, $\Delta S_D(o)=(\Delta S_D(L)-\Delta S_{ex,ip}(CH_2)\times a)\div b$). Values of $\Delta H_D(o)$ and $\Delta S_D(o)$ are 1.7 kJ mol^{-1} and -16 J K^{-1} mol^{-1} for 15C5, and 3.8 kJ mol^{-1} and -10 J K^{-1} mol^{-1} for 18C6, respectively. They are roughly equal. Values of $\Delta H_D(o)$ and $\Delta S_D(o)$ are 2.8 kJ mol^{-1} and -13 J K^{-1} mol^{-1} on the average, respectively. Positive $\Delta H_D(o)$ value and negative $\Delta S_D(o)$ value seem to reflect the interaction between the ether oxygen atom and water. The strong interaction of an ether oxygen atom with water has been reported.[11] By using these empirical thermodynamic parameters, $\Delta H_D(L)$ and $\Delta S_D(L)$ of crown ethers between benzene and water can be roughly estimated.

Transfer process of 18C6 from water to benzene is endothermic, and the ΔS_D(18C6) value between benzene and water is positive. Favorable $T\Delta S_D$(18C6) value at 25 °C for transfer of 18C6 from water to benzene is completely canceled by larger unfavorable ΔH_D(18C6) value, resulting in relatively large negative log K_D(18C6) value. A similar tendency is observed for partition of 15C5 itself between benzene and water.[10]

Extraction of Alkali Metal Picrates with 18C6. Table 2 shows that both ΔH_{ex} and ΔS_{ex} values of 18C6 for all the alkali metals are negative. The same trend is observed for 15C5,[10] benzo-15-crown-5,[12] and dibenzo-18-crown-6[13] between benzene and water, and for 15C5[14] and 18C6[15] between $CHCl_3$ and water. Differences in ΔH_{ex} values among K, Rb, and Cs are small, whereas ΔH_{ex} value of Na is much larger than the others. The same is true for $T\Delta S_{ex}$ values. The smallest ΔH_{ex} value of K is balanced by the second smallest $T\Delta S_{ex}$ value, leading to the largest log K_{ex}, and much the greatest ΔH_{ex} and $T\Delta S_{ex}$ values of Na compensate each other, resulting in the smallest log K_{ex}. Values of ΔH_D(18C6) and ΔS_D(18C6) play a major role in determining the magnitude of ΔH_{ex} and ΔS_{ex} values, respectively, whereas ΔH_{ML}, $\Delta H_{ex,ip}$, ΔS_{ML}, and $\Delta S_{ex,ip}$ values play a minor role.

Ion-Pair Extraction of Crown Ether-Alkali Metal Ion Complexes with Picrate Anions. Ion-pair extractability at 25 °C of M(18C6)A between benzene and water increases in the order, Na<Cs<Rb<K (Table 2). Much the largest $\Delta H_{ex,ip}$ and $\Delta S_{ex,ip}$ values of Na compensate each other, resulting in the lowest ion-pair extractability (Table 2). Ion-pair extraction of K(18C6)A and Cs(18C6)A is completely enthalpy controlled. The smallest $\Delta H_{ex,ip}$ and $\Delta S_{ex,ip}$ values of Rb balance each other, leading to the second greatest ion-pair extractability.

As can be seen from Table 2, both $\Delta H_{ex,ip}$ and $\Delta S_{ex,ip}$ values vary fairly with the alkali metal ion. This may reflect differences in interactions of 18C6-alkali metal ion complexes with picrate anions in an aqueous phase and water molecules.

Values[15] of log $K_{ex,ip}$, $\Delta H_{ex,ip}$, and $T\Delta S_{ex,ip}$ of 18C6-alkali metal picrate complexes between $CHCl_3$ and water are as follows.

	Na	K	Rb	Cs
$\log(K_{ex,ip}/\text{mol}^{-1}\,\text{dm}^3)$ (at 25°C)	3.46	4.83	4.88	4.42
$\Delta H^\circ_{ex,ip}$/kJ mol^{-1}	−18.8	−33.9	−45.6	−43.1
$T\Delta S^\circ_{ex,ip}$/kJ mol^{-1} (at 25°C)	0.6	−6.6	−17.8	−18.1

Log $K_{ex,ip}$(MLA) value of the $CHCl_3/H_2O$ system is about 2 larger than that of the benzene/H_2O system. The difference in log $K_{ex,ip}$(MLA) values between $CHCl_3$ and benzene systems (ca. 2) is smaller than that in individual extraction constants for solvents between $CHCl_3$ and benzene (3.4—4.2).[16] It is impossible to explain the large difference at the present time.

Both $\Delta H_{ex,ip}$ and $\Delta S_{ex,ip}$ of the 18C6-alkali metal picrate complex increase very much from $CHCl_3$ to benzene. This indicates that the interaction of the 18C6-alkali metal picrate complex with $CHCl_3$ is much stronger than that with benzene. It thus appears that ion-pair of the 16C6-alkali metal ion complex with picrate anion is extracted into $CHCl_3$ much more than into benzene.

Differences in $\Delta H_{ex,ip}$ and $\Delta S_{ex,ip}$ values of the 18C6-alkali metal picrate complex between benzene and $CHCl_3$ ($\Delta(\Delta H_{ex,ip})$ and $\Delta(\Delta S_{ex,ip})$) express enthalpy and entropy change of transfer of the 18C6 complex, respectively, from benzene (or $CHCl_3$) to $CHCl_3$ (or benzene). A large difference in $\Delta(\Delta H_{ex,ip})$ values of 18C6 complexes is found between a group of Na and Cs and that of K and Rb. The same is true for $\Delta(\Delta S_{ex,ip})$ values. This may reflect the difference in solute-solvent interactions caused by the difference in structures of the 18C6-alkali metal picrate complexes; namely, K^+ and Rb^+ have more suitable sizes for the 18C6 cavity than Na^+ and Cs^+.

Values[10] of log $K_{ex,ip}$, $\Delta H_{ex,ip}$, and $T\Delta S_{ex,ip}$ of 15C5-sodium picrate complex between benzene and water are 2.40 (at 25 °C), −18.1 kJ mol^{-1}, and −4.6 kJ mol^{-1} (at 25 °C), respectively. Since Na^+ and K^+ fit most nicely into 15C5 and 18C6 cavity, respectively, the metal ion trapped in the cavity is most effectively screened by the crown ether from environmental solvents. A nitrogen atom of tetraalkylammonium ion is well-shielded by four alkyl groups. Sizes of n-Pr_4N^+ and n-Bu_4N^+ ions are nearly equal to those of 15C5-Na^+ and 18C6-K^+ complexes, respectively.[17] Thus, it is interesting to compare the ion-pair-extraction process of 15C5-NaA and 18C6-KA complexes with that of n-Pr_4NA and n-Bu_4NA, respectively, from a thermodynamic point of view. A striking difference is found between the crown ether complexes and the tetraalkylammonium picrates. Values of $\Delta H_{ex,ip}$ and $\Delta S_{ex,ip}$ of 15C5-NaA and 18C6-KA complexes except for $\Delta S_{ex,ip}$ value of the 18C6-KA complex are negative, and $\Delta S_{ex,ip}$ value of the 18C6-KA complex is nearly equal to zero (Table 2). On the contrary, all the $\Delta H_{ex,ip}$ and $\Delta S_{ex,ip}$ values of n-Pr_4NA and n-Bu_4NA are positive. Values of $\Delta H_{ex,ip}$ and $\Delta S_{ex,ip}$ of the crown ether complex (18C6-KA, 15C5-NaA) are much smaller than those of the corresponding R_4NA (n-Bu_4NA, n-Pr_4NA). Ion-pair extraction of the crown ether complexes is enthalpy controlled, whereas, that of n-Pr_4NA and n-Bu_4NA is entropy controlled. Ion-pair extractability at 25 °C of the 18C6-KA complex is lower than that of n-Bu_4NA, and the contrary holds for the 15C5-NaA complex and n-Pr_4NA. From the above discussion and the fact that both n-Pr_4N^+ and n-Bu_4N^+ are structure makers in an aqueous solution,[8] it may be concluded that both

18C6-K^+ and 15C5-Na^+ complexes act as a structure breaker in water. In a series of our conductance studies,[5,18-20] it was reported that the 18C6-K^+ complex acts as a structure breaker in protic solvents. The result of this study for the 18C6-K^+ complex agrees with that of conductometry.

References

1) Y. Takeda, "The Solvent Extraction of Metal Ions by Crown Compounds, Host Guest Complex Chemistry III," Springer-Verlag, Topics in Current Chemistry, Vol. 121, Berlin, Heidelberg (1984), Chap. 1.

2) Y. Takeda and H. Gotō, *Bull. Chem. Soc. Jpn.*, **52**, 1920 (1979).

3) T. Iwachido, A. Sadakane, and K. Tōei, *Bull. Chem. Soc. Jpn.*, **51**, 629 (1978).

4) R. M. Izatt, R. E. Terry, B. L. Haymore, L. D. Hansen, N. K. Dalley, A. G. Avondet, and J. J. Christensen, *J. Am. Chem. Soc.*, **98**, 7620 (1976).

5) Y. Takeda and O. Arima, *Bull. Chem. Soc. Jpn.*, **58**, 3403 (1985).

6) S. Motomizu, A. Fujiwara, and K. Tōei, *Bunseki Kagaku*, **32**, 91 (1983).

7) T. J. Morrison and F. Billet, *J. Chem. Soc.*, **1952**, 3819.

8) C. V. Krishnan and H. L. Friedman, *J. Phys. Chem.*, **74**, 2356 (1970).

9) Y. Takeda, *Bull. Chem. Soc. Jpn.*, **53**, 2393 (1980).

10) Y. Takeda, T. Namisaki, and S. Fujiwara, *Bull. Chem. Soc. Jpn.*, **57**, 1055 (1984).

11) M. J. Harris, T. Higuchi, and J. H. Rytting, *J. Phys. Chem.*, **77**, 2694 (1973).

12) Y. Takeda, *Bull. Chem. Soc. Jpn.*, **56**, 931 (1983).

13) A. Sadakane, T. Iwachido, and K. Tōei, *Bull. Chem. Soc. Jpn.*, **48**, 60 (1975).

14) Y. Takeda, unpublished data.

15) Y. Takeda and A. Tanaka, *Bull. Chem. Soc. Jpn.*, **59**, 733 (1986).

16) I. Kasahara, Y. Ohgaki, K. Matsui, K. Kano, S. Taguchi, and K. Gotō, *Nippon Kagaku Kaishi*, **1986**, 894. $\log K_{ex,ip}=\log K_{cation}+\log K_{anion}+\log K_{solvent}$, where K_{cation}, K_{anion}, and $K_{solvent}$ are the individual extraction constants for the cation, anion, and solvent, respectively. The individual extraction constants were assigned to some ions and solvents on the assumption,

$$K_{Ph_4As^+}=K_{Ph_4B^-},\ K_{benzene}=1.0.$$

17) Y. Takeda, H. Yano, M. Ishibashi, and H. Isozumi, *Bull. Chem. Soc. Jpn.*, **53**, 72 (1980).

18) Y. Takeda, *Bull. Chem. Soc. Jpn.*, **56**, 866 (1983).

19) Y. Takeda, *Bull. Chem. Soc. Jpn.*, **58**, 1259 (1985).

20) Y. Takeda, *IONICS*, **11**, 49 (1985).

 © 1987 The Chemical Society of Japan Bull. Chem. Soc. Jpn., 60, 2319—2326 (1987)

Hydrates of Organic Compounds. XIII. The Confirmation of the Formation of Clathrate-Like Hydrates of Tetrabutylammonium and of Tetraisopentylammonium Polyacrylates

Haruo NAKAYAMA
Department of Chemistry, Faculty of Engineering, Yokohama National University, Tokiwadai, Hodogaya-ku, Yokohama 240
(Received December 1, 1986)

A thermal analytic method using a differential scanning calorimeter has been applied to aqueous solutions of a series of tetraalkylammonium polyacrylates ($(R_4NOOCCHCH_2)_n$; R=CH_3, C_2H_5, n-C_3H_7, n-C_4H_9, n-C_5H_{11}, and i-C_5H_{11}). It was found that only tetrabutylammonium polyacrylate and tetraisopentylammonium polyacrylate could form stable hydrates having a large number of moles of water per single $R_4NOOCCHCH_2$ unit of the polyacrylates (hydration numbers). The melting points and hydration numbers of these two hydrates were 11.2 °C, 30±1 for the tetrabutylammonium polyacrylate hydrate and 19.5 °C, 42±2 for the tetraisopentylammonium polyacrylate hydrate, respectively. Judging from the melting points, hydration numbers, and the concentration dependence of the dissolution temperatures, these hydrates were regarded as clathrate-like. The tetrabutylammonium polyacrylate hydrate seems to be iso-structural with $(n$-$C_4H_9)_4NF$ hydrate and the tetraisopentylammonium polyacrylate hydrate with $(i$-$C_5H_{11})_4NF$ hydrate.

A single-crystal X-ray examination by Jeffrey and his coworkers on the hydrates of tetraalkylammonium salts such as $(n$-$C_4H_9)_4NF$,[1] $(n$-$C_4H_9)_4NOOCC_6H_5$,[2] and $(i$-$C_5H_{11})_4NF$,[3] showed that these hydrates were clathrate-like hydrates similar to the so-called gas hydrates.[4] The water structure is a hydrogen-bonded framework and is essentially a regular arrangement of polyhedra like pentagonal dodecahedra, tetrakaidecahedra, and pentakaidecahedra. The latter two polyhedra enclose either a n-C_4H_9 or a i-C_5H_{11} group of the tetraalkylammonium cations, whereas pentagonal dodecahedra are empty. Fluoride ion and oxygen atoms of carboxylate anion are hydrogen-bonded to the water frameworks and form part of the polyhedral structure.

Although the tetraalkylammonium cation which can form a clathrate-like hydrate is almost exclusively limited either to tetrabutylammonium ion or to tetraisopentylammonium ion,[5-7] various types of anions are permissble. Of these anions, carboxylate anions are of interest since they can extend the diversity of the clathrate-like hydrates of tetraalkylammonium salts due to the variation of the alkyl groups of the carboxylate anions. The formation of a clathrate-like hydrate of tetrabutylammonium carboxylates has been confirmed for many carboxylates.[2,3,5,8-12] Experimental results found so far are briefly summarized as follows: (1) a series of tetrabutylammonium carboxylates, $(n$-$C_4H_9)_4NOOCR$, with R ranging from CH_3 to n-$C_{10}H_{21}$ can form clathrate-like hydrates whose hydration numbers are around 30;[10,12] and (2) a series of tetrabutylammonium dicarboxylates, $[(n$-$C_4H_9)_4N]_2(OOC(CH_2)_nCOO)$ (n=0—8), can also form clathrate-like hydrates with hydration numbers around 60 and the salt of n=3 forms the most stable hydrate whose melting point is 20.2 °C.[9]

The crystal structure of these carboxylate and dicarboxylate hydrates was assumed to be iso-structural with that of the $(n$-$C_4H_9)_4NF$ hydrate[1] from the fact that the hydration numbers (about 30 for one $(n$-$C_4H_9)_4N^+$ cation) and unit cell dimensions for some of the hydrates[12] are almost identical with those of the $(n$-$C_4H_9)_4NF$ hydrate. This speculation also means that the alkyl groups of carboxylate anions and methylene chains of dicarboxylate anions are enclosed in vacant pentagonal dodecahedra.

From such a versatile availability of vacant pentagonal dodecahedra and from the fact that, for dicarboxylate salts, the $-(CH_2)_3-$ methylene chain is the most suitable chain to form a stable clathrate-like hydrate, the formation of a clathrate-like hydrate of tetrabutylammonium polyacrylate and of tetraisopentylammonium polyacrylate may be anticipated, though such a hydrate has not been known previously.

In this paper, through a thermal analytic method using a differential scanning calorimeter for binary mixtures of a series of tetraalkylammonium polyacrylates ($(R_4NOOCCHCH_2)_n$; R=CH_3—n-C_5H_{11}, and i-C_5H_{11}) with water, an extensive study has been carried out in order to confirm the formation of clathrate-like hydrates of teraalkylammonium polyacrylates.

Experimental

Aqueous solutions of sodium polyacrylate and of tetraalkylammonium polyacrylates ($(R_4NOOCCHCH_2)_n$; R=CH_3, C_2H_5, n-C_3H_7, n-C_4H_9, n-C_5H_{11}, and i-C_5H_{11}) were obtained by the neutralization of an aqueous solution of polyacrylic acid with aqueous solutions of sodium hydroxide and of the corresponding tetraalkylammonium hydroxide. The aqueous solutions of tetraalkylammonium hydroxides were prepared by reacting tetraalkylammonium iodides with freshly prepared silver hydroxide in water with vigorous shaking, followed by filtration of resulting silver iodide in a CO_2-free atmosphere. Tetrabutylammonium

iodide, tetrapentylammonium iodide, and tetraisopentylammonium iodide were synthesized by reacting each trialkylamine with the corresponding alkyl iodide in ethyl acetate and were purified by recrystallization from ethyl acetate–acetone mixture.[7] Other iodides were purchased from the Tokyo Kasei Kogyo Co. and were recrystallized either from ethyl acetate–ethanol mixture or from ethanol. An aqueous solution of polyacrylic acid was purchased from Wako Pure Chemical Industries, Ltd. and was used without further purification. The mean degree of polymerization of polyacrylic acid was estimated to be about 2100 from viscosity measurements of the aqueous solutions of its sodium salt in 1 mol dm^{-3} NaCl solution at 25 °C using the equation proposed by Kagawa et al.[13]

The concentrations of each sample were determined either by measuring the water content using the Karl Fischer titration method on a MK-II apparatus (Kyoto Electronics Manufacturing Co.) for sodium polyacrylate and tetramethyl-, tetraethyl-, tetrapropyl-, and tetrapentylammonium polyacrylates or by measuring the amount of tetraalkylammonium cations by titration with a sodium tetraphenylborate solution which was standardized by pure tetrabutylammonium iodide for tetrabutyl- and tetraisopentylammonium polyacrylates.

The differential scanning calorimeter used was the model DSC-10 with SSC-580 thermal controller, manufactured by Seiko Instruments and Electronics Ltd. Each sample solution (about 15 mg) was sealed in a 15 μl aluminum pan and was either cooled or heated at the rate of 0.5 °C per minute. An empty 15 μl aluminum pan was used as a reference.

Results and Discussion

(1) Thermal Behavior of Aqueous Solutions of Sodium Polyacrylate and of Tetraalkylammonium Polyacrylates. The cooling and heating curves in the differential scanning calorimetry (DSC) for aqueous solutions of sodium polyacrylate (NaPA), tetramethylammonium polyacrylate ($(CH_3)_4NPA$), tetraethylammonium polyacrylate ($(C_2H_5)_4NPA$), tetrapropylammonium polyacrylate ($(n\text{-}C_3H_7)_4NPA$), tetrabutylammonium polyacrylate ($(n\text{-}C_4H_9)_4NPA$), tetrapentylammonium polyacrylate ($(n\text{-}C_5H_{11})_4NPA$) and tetraisopentylammonium polyacrylate ($(i\text{-}C_5H_{11})_4NPA$) are shown as a function of temperature for solutions of X=0.01 in Fig. 1 and of X=0.02 in Fig. 2 (X is the mole fraction of the polyacrylates based on the monomeric unit). It is obvious that in the cooling process steep exothermic peaks in the −15—−20 °C range indicate the solidification of supercooled water, and in the heating process endothermic peaks in the −10—0 °C

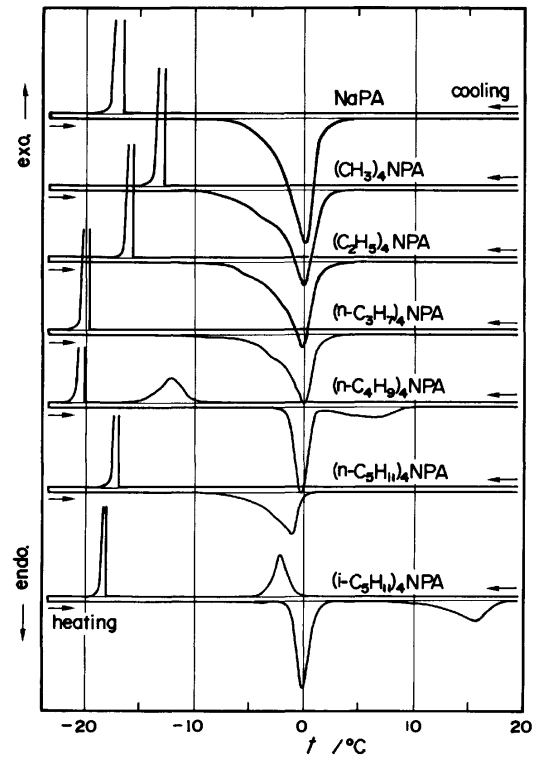

Fig. 1. Temperature dependence of the DSC signals, expressed in an arbitrary unit, for aqueous solutions of sodium polyacrylate (NaPA) and of a series of tetraalkylammonium polyacrylates (R_4NPA; R= CH_3, C_2H_5, n-C_3H_7, n-C_4H_9, n-C_5H_{11}, and i-C_5H_{11}). The mole fraction (X), based on the monomeric unit, is equal to 0.01 for all the solutions.

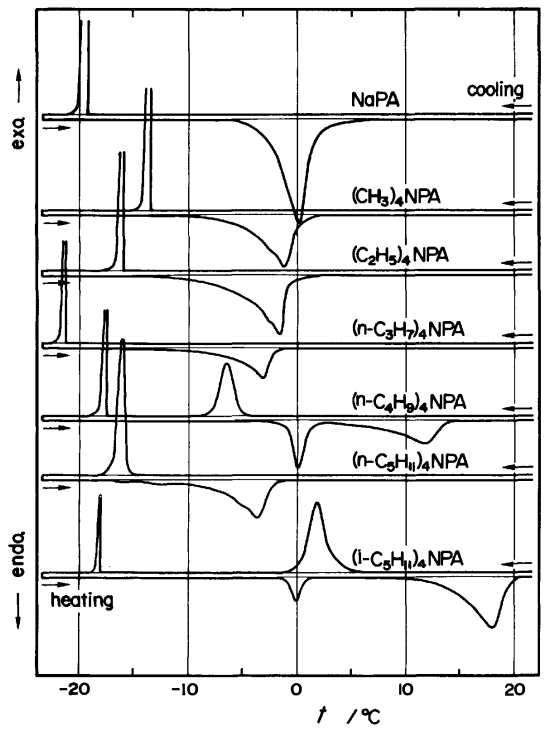

Fig. 2. Temperature dependence of the DSC signals, expressed in an arbitrary unit, for aqueous solutions of sodium polyacrylate (NaPA) and of a series of tetraalkylammonium polyacrylates (R_4NPA; R= CH_3, C_2H_5, n-C_3H_7, n-C_4H_9, n-C_5H_{11}, and i-C_5H_{11}). The mole fraction, based on the monomeric unit, is equal to 0.02 for all the solutions.

range are attributable to the melting of the ice phase.

However, the thermal behavior of $(n\text{-}C_4H_9)_4NPA$ and $(i\text{-}C_5H_{11})_4NPA$ solutions differs markedly from that of the other five solutions. In these two solutions, besides the peaks due to an ice phase exothermic peak occurs at around $-12\,^\circ C$ for $X=0.01$ and around $-7\,^\circ C$ for $X=0.02$ in the $(n\text{-}C_4H_9)_4NPA$ solutions and at around $-2\,^\circ C$ for $X=0.01$ and at around $+2\,^\circ C$ for $X=0.02$ in the $(i\text{-}C_5H_{11})_4NPA$ solutions and the endothermic peak occurs at temperatures above $0\,^\circ C$ depending both on the concentration and on the kind of salt. This clearly indicates that another solid phase other than ice is formed in these two systems and further that this solid phase contains some water, i.e., a hydrate, since the areas of both the exothermic peaks due to the solidification of supercooled water and of the endothermic peak due to the melting of the ice phase decrease markedly with increasing concentration of the salt. Further details of these hydrates will be discussed in the following sections.

Finally, the quantities $\Delta H/(6.0095\times10^3 n_0)$ for all the solutions examined are listed in Table 1, where ΔH (J unit) is the total endothermic enthalpy change in the heating process and n_0 is the total number of moles of water contained in each solution and the value 6.0095×10^3 is the molar heat of fusion (J unit) of pure water at $0\,^\circ C$.[14] This quantity may be regarded as an approximate index of the relative thermal stability of the solid phase as compared with that of pure ice. The values obtained are very small for the $X=0.02$ solution of $(n\text{-}C_3H_7)_4NPA$ and both $X=0.01$ and $X=0.02$ solutions of $(n\text{-}C_5H_{11})_4NPA$. At the same time, Figs. 1 and 2 show that the melting processes of the solid phase in these three solutions are completed at lower temperatures than those in the other solutions. These phenomena indicate that the degree of amorphousness of the ice phase formed around the $(n\text{-}C_3H_7)_4NPA$ and $(n\text{-}C_5H_{11})_4NPA$ molecules remarkably increases.

Table 1. The Quantity $\Delta H/(6.0095\times10^3 n_0)$ for Aqueous Solutions of Sodium Polyacrylate and of Tetraalkylammonium Polyacrylates

Polyacrylate	$\Delta H/(6.0095\times10^3 n_0)$	
	$X=0.01$	$X=0.02$
NaPA	0.98	0.99
$(CH_3)_4NPA$	0.96	0.80
$(C_2H_5)_4NPA$	1.00	0.75
$(n\text{-}C_3H_7)_4NPA$	0.82	0.50
$(n\text{-}C_4H_9)_4NPA$	0.88	0.77
$(n\text{-}C_5H_{11})_4NPA$	0.62	0.60
$(i\text{-}C_5H_{11})_4NPA$	0.85	0.87

All the notations are explained in the text. These values are averages of 3—5 measurements.

(2) The Confirmation of the Formation of a Clathrate-Like Hydrate of Tetrabutylammonium Polyacrylate. In a preliminary experiment it was found that when about 10 wt% aqueous solution of $(n\text{-}C_4H_9)_4NPA$ was cooled to about $-20\,^\circ C$, a white and powderly solid phase was formed which remained undissolved at $2\,^\circ C$. This suggests the formation of a solid phase other than ice. The cooling and heating curves for the $(n\text{-}C_4H_9)_4NPA$ solutions in various concentrations are shown in Fig. 3 as a function of temperature. The most important characteristic of both the cooling and heating curves is the occurrence of two kinds of peaks except for the solutions whose X's are either very small or very large. The areas of both the exothermic peaks corresponding to the solidification of ice and the endothermic peak corresponding to the melting of ice decrease markedly with increasing concentration and both peaks become very small when $X=0.0330$. Therefore, the solid phase other than ice seems to be a hydrate whose composition is approximately equal to $X=0.0330$, i.e., the hydration number of the hydrate is close to 29.

The thermal behavior shown in Fig. 3 shows a striking resemblance to that of the aqueous solutions

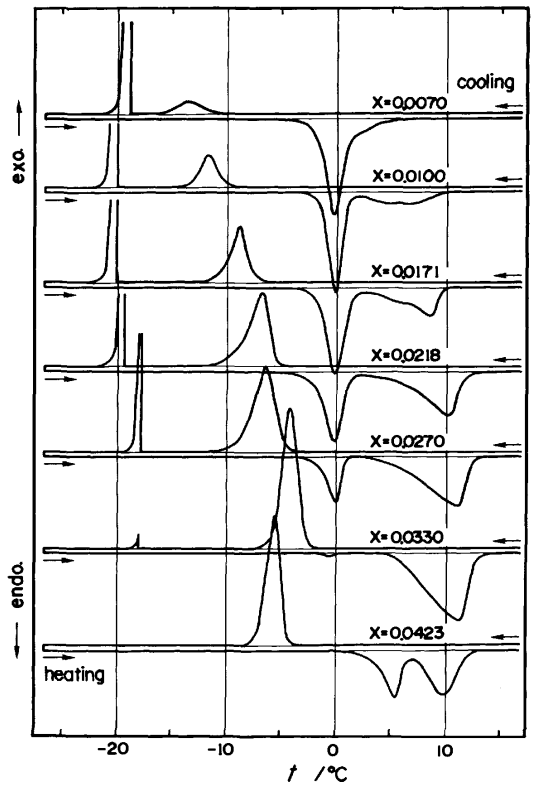

Fig. 3. Temperature dependence of the DSC signals, expressed in an arbitrary unit, for aqueous solutions of tetrabutylammonium polyacrylate ($(n\text{-}C_4H_9)_4NPA$) in various concentrations. The X is the mole fraction of the salt based on the monomeric unit.

of tetrabutylammonium chloride,[15] which is well-known to form a clathrate-like hydrate with hydration numbers around 30.[5,7,16] A thermal analytic procedure for obtaining hydration numbers and melting pont of a hydrate, and for determining the dissolution temperatures by DSC measurements has precisely been discussed in a previous paper.[15] The hydration numbers, m, of a hydrate can approximately be calculated by the following relation for solutions whose X's are equal to or smaller than the congruent composition:

$$m = \frac{1}{n_1}\left(n_0 - \frac{\Delta H_1 - \Delta H_2}{6.0095 \times 10^3}\right), \quad (1)$$

in which ΔH_1 (J unit) is the total enthalpy change during the whole heating processes for the solid phases which are solidified both by the first-step and by the second-step solidification; ΔH_2 (J unit) is the enthalpy change in the heating process for the solid phase which is solidified by the first-step solidification process only; n_0 and n_1 are the total number of moles of water and of (n-C_4H_9)$_4$NPA based on the monomeric unit, respectively. Some representative values of ΔH_1, ΔH_2, the dissolution temperatures observed, and the calculated hydration numbers m are listed in Table 2, together with some data for the solutions at concentrations higher than X=0.0330. These are briefly discussed in the last part of this section.

All the calculated values of m lie near 30 and the X=0.0330 solution has the highest dissolution temperature of 11.2 °C and almost the same values of ΔH_1 and ΔH_2, indicating that the congruent composition of the hydrate is close to X=0.0330 as observed above. In conclusion, the hydration numbers and the melting point of the (n-C_4H_9)$_4$NPA hydrate are determined to be 30±1 and 11.2 °C, respectively. The presence of the (n-C_4H_9)$_4$NPA hydrate has not been known previously. From the facts that the hydration numbers of the hydrate are 30±1, and the congruent melting pont is fairly high (11.2 °C), this hydrate seems to have a clathrate-like structure similar to such hydrates as (n-C_4H_9)$_4$NF·30H_2O and (n-C_4H_9)$_4$NCl·30H_2O.[15,16]

The solid-liquid phase diagram for the (n-C_4H_9)$_4$NPA-H_2O binary system, which is depicted by

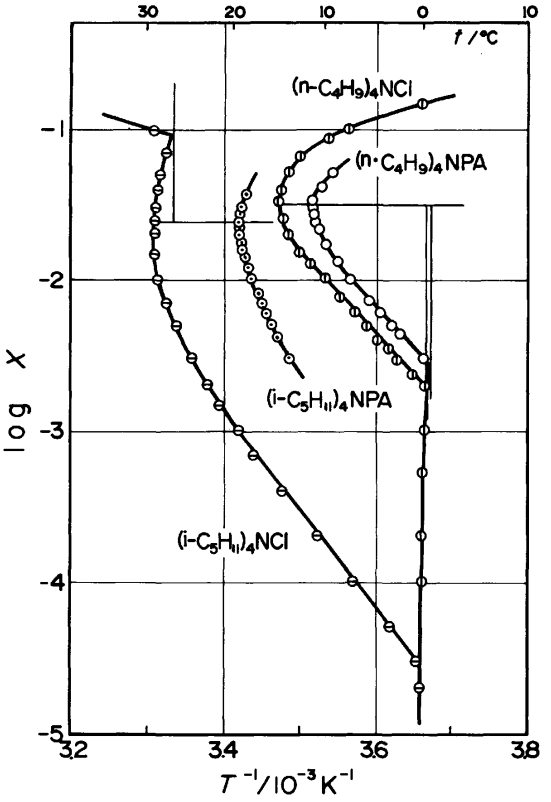

Fig. 4. The solid-liquid phase diagrams for binary systems of tetrabutylammonium polyacrylate ((n-C_4H_9)$_4$NPA)-water and of tetraisopentylammonium polyacrylate ((i-C_5H_{11})$_4$NPA)-water determined by the DSC experiments, together with those for binary systems of (n-C_4H_9)$_4$NCl-water and of (i-C_5H_{11})$_4$NCl-water determined previously by an ampoule method.[7,16]

Table 2. Dissolution Temperatures t, Enthalpy Changes ΔH_1 and ΔH_2, and Calculated Hydration Numbers m for Aqueous Solutions of Tetrabutylammonium Polyacrylate

X	n_0 / 10^{-4}mol	n_1 / 10^{-5}mol	t / °C	ΔH_1[a] / J	ΔH_2[a] / J	m
0.0070	8.8102	0.6214	5.2	4.81±0.08	0.64±0.03	30.1±2.3
0.0100	7.3641	0.7443	7.1	3.88±0.08	0.83±0.03	30.8±1.9
0.0171	6.9940	1.2153	9.7	3.38±0.05	1.44±0.04	31.0±0.9
0.0218	7.1983	1.6018	10.5	3.35±0.06	1.98±0.05	30.7±0.8
0.0270	6.3237	1.7535	11.0	2.89±0.03	2.26±0.05	30.1±0.5
0.0330	5.1716	1.7649	11.2	2.37±0.03	2.35±0.04	29.1±0.5
0.0423	5.3366	2.3590	10.0	2.31±0.12	1.43±0.10	—
0.0506	4.5584	2.4298	9.0	1.83±0.15	0.26±0.08	—

All the notations are explained in the text.

a) These values are averages of 3—5 measurements.

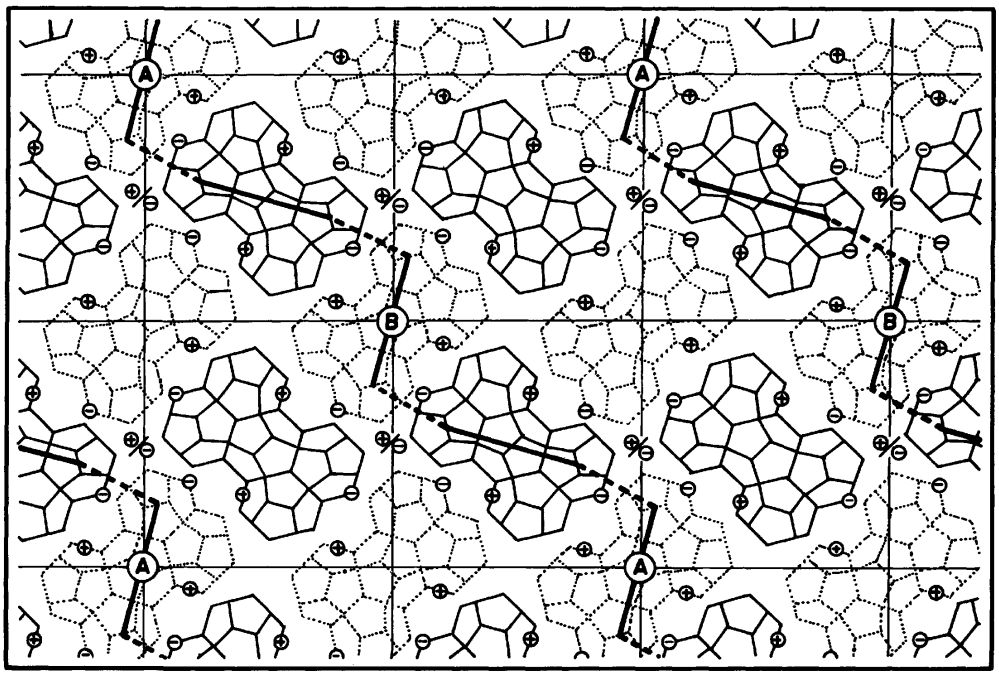

Fig. 5. One of the possible ways for polyacrylate chains (written by bold lines) to be accommodated within the structure which is iso-structural with $(n\text{-}C_4H_9)_4NF$ hydrate. Explanation is given in the text.

plotting the logarithm of the mole fraction X of each solution against their dissolution temperatures after conversion to the reciprocal of the absolute temperature, is shown in Fig. 4, together with that of the $(n\text{-}C_4H_9)_4NCl\text{-}H_2O$ system determined previously by an ampoule method.[16] A striking resemblance of both phase diagrams, especially a similar value of the slope of $-\partial \log X/\partial(1/T)$ in the concentration range between the eutectic composition and the congruent composition, provides another indication for the formation of a clathrate-like hydrate of $(n\text{-}C_4H_9)_4NPA$ similar to that of $(n\text{-}C_4H_9)NCl$. This slope has been proved to be approximately proportional to the hydration number of a hydrate.[17].

Although there is no information about the crystal structure of the $(n\text{-}C_4H_9)_4NPA$ hydrate, the most probable way of accommodating a polyacrylate chain within a water lattice is illustrated in Fig. 5 based on the assumptions that (1) the crystal structure is iso-structural with that of the $(n\text{-}C_4H_9)_4NF$ hydrate[1] and (2) the polyacrylate chain penetrates through associated, vacant pentagonal dodecahedra forming a hydrogen-bonded anionic host structure with water. In this figure only an arrangement of a block of vacant pentagonal dodecahedra in the planes perpendicular to the c-axis is shown. Each block represented by a solid line lies at the level of the $Z=0$ plane and the one represented by a dotted line lies at the level of the $Z=1/2$ plane. The marks $\oplus$ and $\ominus$ represent the positions of a nitrogen atom and of a fluorine atom, respectively, in the original $(n\text{-}C_4H_9)_4NF$ hydrate. The C-C main chain of the polyacrylate anion is illustrated by bold lines. The dotted portion of the bold line indicates the shift of the C-C chain between the $Z=0$ and $Z=1/2$ plane by breaking a single hydrogen-bond which connects two blocks of the pentagonal dodecahedra. The distance from position A to B in Fig. 5 is about 45 Å and the monomeric unit chain length of the polyacrylate chain is expected to be slightly shorter than 2.51 Å, which is the longest distance when the C-C chain is fully extended. This is because of the restriction that each carboxyl group must be incorporated within the water framework. Therefore, it will be reasonable to assume that 20 monomeric units of the polyacrylate chain are present between A and B. According to the structural analysis by Jeffrey et al.,[1] there exist 10 pentagonal dodecahedra (i.e., two blocks of pentagonal dodecahedra represented in Fig. 5) and five $(n\text{-}C_4H_9)_4NF$ molecules within a unit cell. Thus the above mentioned 20 units of negative charge are four times larger than the positive charge, leading the conclusion that only a fourth of all the pentagonal dodecahedra are used to accommodate the polyacrylate chain. This may be possible, for instance, if only the pentagonal dodecahedra existing within alternate unit cells arranged in the directions both perpendicular and parallel to the c-axis are used. Figure 5 is drawn according to this view.

In Fig. 6 two apparent quantities, $\Delta H_1/n_0$ and

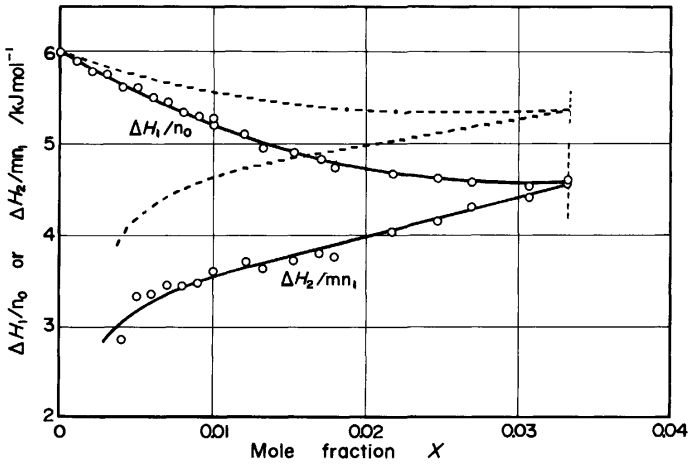

Fig. 6. The concentration dependence of the apparent total enthalpy change per mole of water, $\Delta H_1/n_0$, and of the apparent enthalpy change due to the dissolution of the hydrate solid per mole of water which forms hydrogen-bonded networks in the hydrate, $\Delta H_2/mn_1$, in the $(n\text{-}C_4H_9)_4NPA\text{-}H_2O$ binary system. Dotted lines represent similar quantities for the $(n\text{-}C_4H_9)_4NCl\text{-}H_2O$ system[15] for comparison.

$\Delta H_2/mn_1$, are plotted against the mole fraction X, together with the corresponding curves for the $(n\text{-}C_4H_9)_4NCl\text{-}H_2O$ system.[15] The quantity $\Delta H_1/n_0$ means apparent, total enthalpy change per mole of water and the quantity $\Delta H_2/mn_1$ means apparent enthalpy change due to the dissolution of the hydrate solid per mole of water which forms hydrogen-bonded networks in the hydrate solid. These two quantities become equal at the congruent composition as expected from Eq. 1. Although these curves cannot be analyzed in detail because of the lack of other thermodynamic information (especially of the data concerning the enthalpies of mixing of a hydrate melt with water), a striking resemblance of these curves between the $(n\text{-}C_4H_9)_4NPA$ hydrate and the $(n\text{-}C_4H_9)_4NCl$ hydrate suggests that the thermal behavior of water molecules in the $(n\text{-}C_4H_9)_4NPA$ hydrate is similar to that in the $(n\text{-}C_4H_9)_4NCl$ hydrate. However, the value of $\Delta H_2/mn_1$ (or $\Delta H_1/n_0$) at the congruent composition for the $(n\text{-}C_4H_9)_4NPA$ hydrate, 4.60 kJ mol^{-1}, is considerably smaller than that (5.47 kJ mol^{-1}) found for the $(n\text{-}C_4H_9)_4NCl$ hydrate.[15] This suggests that the hydrogen-bonded water frameworks in the $(n\text{-}C_4H_9)_4NPA$ hydrate are appreciably deformed as compared with those in the $(n\text{-}C_4H_9)_4NCl$ hydrate.

Finally, the thermal behavior of the solutions whose X's are larger than 0.0330 must be briefly discussed. Only two solutions with X=0.0423 and X=0.0506 have been examined and the results are included in Table 2. The thermal behavior of the X=0.0423 solution is represented in Fig. 3. The heating curve indicates the existence of two kinds of hydrates. The hydrate which melts at a higher temperature is the same as that discussed above (m=30±1) judging from the value of the dissolution temperature as well as from the concentration dependence of ΔH_2. The hydration numbers, m', of the other hydrate can approximately be estimated by the following equation using m=30:

$$m' = \left(n_0 - \frac{\Delta H_2}{4.60\times 10^3}\right) \Big/ \left(n_1 - \frac{\Delta H_2}{4.60\times 10^3 m}\right), \qquad (2)$$

where ΔH_2 is the second-step enthalpy change in the heating process, which is approximately separated from the total enthalpy change ΔH_1 (Table 2) and the value of 4.60×10^3 stands for the molar enthalpy of fusion (J unit) of the water which forms the hydrate of m=30 as determined above. The calculated values of m' are 16.8±1.9 for the X=0.0423 solution and 17.8±0.9 for the X=0.0506 solution, respectively. This hydrate seems to be a kind of clathrate-like hydrate since its melting point is high (about 6 °C) and its hydration number, m', is large (17—18) in comparison with that of ordinary hydrates of many other organic compounds.

(3) The Confirmation of the Formation of a Clathrate-Like Hydrate of Tetraisopentylammonium Polyacrylate. In a preliminary experiment it was found that when about 10 wt% aqueous solution of $(i\text{-}C_5H_{11})_4NPA$ was cooled to about −20 °C, a transparent crystalline phase was obtained as well-formed prisms which remained undissolved even at 10 °C. This phenomenon suggests the formation of a solid phase other than ice. The cooling and heating curves for $(i\text{-}C_5H_{11})_4NPA$ aqueous solutions are shown

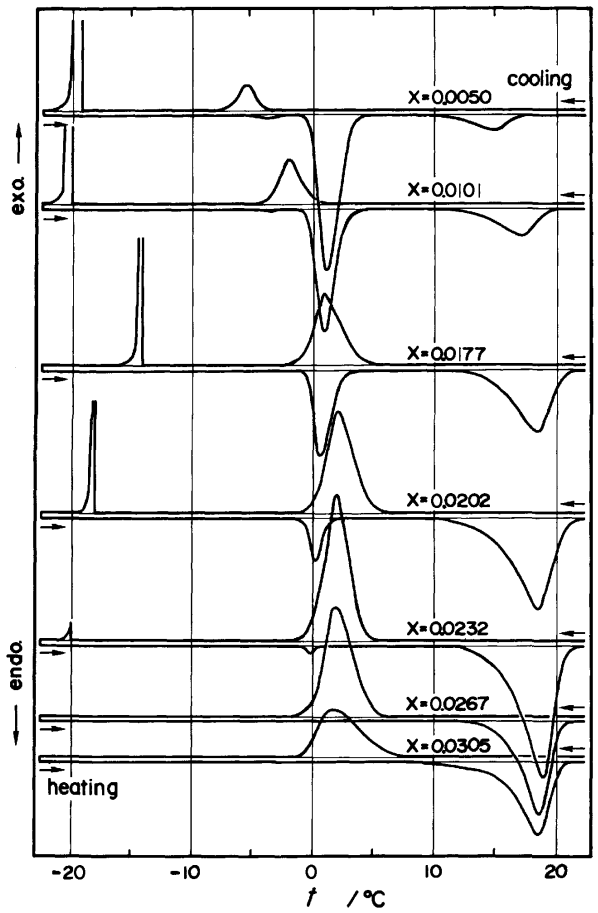

Fig. 7. Temperature dependence of the DSC signals, expressed in an arbitrary unit, for aqueous solutions of tetraisopenylammonium polyacrylate ((*i*-$C_5H_{11})_4$NPA) in various concentrations.

in Fig. 7 in a similar manner as in Fig. 3. The thermal behavior of these curves resembles that of the (*n*-$C_4H_9)_4$NPA solutions, suggesting the formation of a clathrate-like hydrate of (*i*-$C_5H_{11})_4$NPA. Thus, these curves can be analyzed in the same way as those of the (*n*-$C_4H_9)_4$NPA-H_2O system, giving each peak a similar physical meaning as before. Representative values of ΔH_1, ΔH_2, and dissolution temperatures observed, and the hydration numbers calculated by Eq. 1 are listed in Table 3.

The congruent composition, which gives the highest dissolution temperature (19.5 °C), is close to X=0.0232, indicating the hydration numbers of the (*i*-$C_5H_{11})_4$NPA hydrate are around 42. The hydration numbers calculated for the solutions in the concentration range of X=0.0121—0.0232 are also around 42, although those for the solutions with X's smaller than 0.0121 are larger than 42. It is not clear whether another kind of hydrate which has larger hydration numbers than 42 is formed in such dilute solutions. In conclusion, (*i*-$C_5H_{11})_4$NPA can form a clathrate-like hydrate with hydration numbers of 42±2 and melting point of 19.5 °C. The formation of such a hydrate has not been reported previously.

A solid-liquid phase diagram for the (*i*-$C_5H_{11})_4$NPA-H_2O system, determined in the same manner as in the case of the (*n*-$C_4H_9)_4$NPA-H_2O system, is also shown in Fig. 4, together with that of the (*i*-$C_5H_{11})_4$NCl-H_2O system which has been known to form a clathrate-like hydrate with hydration numbers around 40.[7] The striking resemblance of the phase diagrams of both systems affords an additional reason for concluding that the (*i*-$C_5H_{11})_4$NPA hydrate is a clathrate-like hydrate similar to the (*i*-$C_5H_{11})_4$NCl hydrate whose crystal structure is believed to be iso-

Table 3. Dissolution Temperatures t, Enthalpy Changes ΔH_1 and ΔH_2, and Calculated Hydration Numbers m for Aqueous Solutions of Tetraisopentylammonium Polyacrylate

X	n_0 / 10^{-4}mol	n_1 / 10^{-5}mol	t / °C	ΔH_1[a] / J	ΔH_2[a] / J	m
0.0060	8.3967	0.5068	16.1	4.45±0.06	0.86±0.04	47.8±2.4
0.0080	7.8194	0.6312	17.0	4.07±0.07	1.07±0.06	44.8±2.4
0.0101	6.8868	0.6989	17.8	3.52±0.05	1.23±0.04	44.0±1.5
0.0121	8.2880	1.0116	18.4	4.27±0.06	1.81±0.04	41.5±1.2
0.0160	6.8302	1.1106	18.9	3.55±0.04	2.24±0.02	41.9±0.7
0.0202	7.7283	1.5928	19.3	4.02±0.05	3.37±0.03	41.7±0.6
0.0232	6.3787	1.5147	19.5	3.48±0.02	3.44±0.02	41.7±0.3
0.0244	5.8726	1.4691	19.4	3.18±0.03 (3.20)[b]	3.18±0.03	—
0.0267	6.1725	1.6909	19.1	3.26±0.04 (3.36)[b]	3.26±0.04	—
0.0305	5.1569	1.6205	18.9	2.45±0.03 (2.81)[b]	2.45±0.03	—

All the notations are the same as those in Table 2.

a) These values are averages of 3—5 measurements. b) Calculated values from $5.45\times10^3 n_0$.

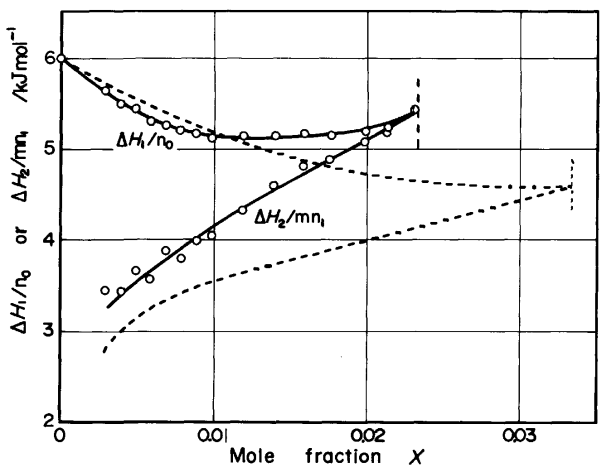

Fig. 8. The concentration dependence of $\Delta H_1/n_0$ and of $\Delta H_2/mn_1$ for the $(i\text{-}C_5H_{11})_4NPA\text{-}H_2O$ system. The physical meaning of these quantities are identical with those in Fig. 6. Dotted lines represent similar quantities for the $(n\text{-}C_4H_9)_4NPA\text{-}H_2O$ system (Fig. 6) for comparison.

structural with $(i\text{-}C_5H_{11})_4NF$ hydrate.

According to the crystal structure examination of the $(i\text{-}C_5H_{11})_4NF$ hydrate by Jeffrey et al.,[3] this hydrate consists of a regular arrangement of columns of tetrakaidecahedra extended in the c-axis direction by sharing hexagonal faces; these columns are connected by alternate layers of pentagonal dodecahedra and pentakaidecahedra which face-share congruently. A possible way to accommodate the polyacrylate chain in vacant pentagonal dodecahedra may be either to use the pentagonal dodecahedra layer extended in the direction perpendicular to the c-axis or to use pentagonal dodecahedra existing in the alternate layers in the c-axis direction by replacing fluorine atoms in the original $(i\text{-}C_5H_{11})_4NF$ hydrate by oxygen atoms of carboxyl groups of the polyacrylate chain. Precise structural analysis is awaited. A single-crystal X-ray examination will be possible since the $(i\text{-}C_5H_{11})_4NPA$ hydrate solid can be obtained as well-formed prisms.

In Fig. 8, the two apparent quantities, $\Delta H_1/n_0$ and $\Delta H_2/mn_1$, are plotted against the mole fraction X similarly to Fig. 6. The value of $\Delta H_2/mn_1$ (or of $\Delta H_1/n_0$) at the congruent composition is equal to 5.45 kJ mol^{-1}. This value is appreciably larger than that of the $(n\text{-}C_4H_9)_4NPA$ hydrate (4.60 kJ mol^{-1}), indicating that the water networks in the $(i\text{-}C_5H_{11})_4NPA$ hydrate are less deformed than those in the $(n\text{-}C_4H_9)_4NPA$ hydrate. This results coincides with a general trend that the water frameworks surrounding a $(i\text{-}C_5H_{11})_4N^+$ cation are more stable than those surrounding a $(n\text{-}C_4H_9)_4N^+$ cation if both cations have the same kind of anions.[17]

The thermal behavior of the solutions with X's higher than the congruent composition (X=0.0267 and 0.0305 in Fig. 7 and X=0.0244, 0.0267, and 0.0305 in Table 3) shows no formation of another kind of hydrate other than the one discussed above (m=42±2). In Table 3 the observed values of ΔH_1 (or of ΔH_2) are compared with the values calculated by a relation of $5.45\times10^3 n_0$. The quantity, $5.45\times10^3 n_0$, means the enthalpy of fusion of the hydrate (J unit) if we assume that all the water molecules participate in the hydrate formation and further that the enthalpy of fusion is equal to 5.45 kJ mol^{-1} as determined above. The observed value of ΔH_1 for X=0.0244 solution is almost compatible with the calculated one, whereas in more concentrated solutions (X=0.0267 and 0.0305) the observed values of ΔH_1 become small as compared with the calculated ones. At present a quantitative interpretation cannot be made because of a lack of information concerning the state of the solid-liquid mixture in such concentrated solutions.

The present work was supported by a Grant-in-Aid for Scientific Research No. 60470006 from the Ministry of Education, Science and Culture.

References

1) R. K. McMullan, M. Bonamico, and G. A. Jeffrey, *J. Chem. Phys.*, **39**, 3295 (1963).
2) M. Bonamico, G. A. Jeffrey, and R. K. McMullan, *J. Chem. Phys.*, **37**, 2219 (1962).
3) D. Feil and G. A. Jeffrey, *J. Chem. Phys.*, **35**, 1863 (1961).
4) W. F. Claussen, *J. Chem. Phys.*, **19**, 259, 662 (1951). M. von Stackelberg and H. R. Muller, *ibid.*, **19**, 1319 (1951). L. Pauling and R. E. Marsh, *Proc. Natl. Acad. Sci. U.S.A.*, **38**, 112 (1952).
5) R. McMullan and G. A. Jeffrey, *J. Chem. Phys.*, **31**, 1231 (1959).
6) H. Nakayama and K. Watanabe, *Bull. Chem. Soc. Jpn.*, **49**, 1254 (1976).
7) H. Nakayama, *Bull. Chem. Soc. Jpn.*, **54**, 3717 (1981).
8) G. Beurskens, G. A. Jeffrey, and R. K. McMullan, *J. Chem. Phys.*, **39**, 3311 (1963).
9) H. Nakayama and K. Watanabe, *Bull. Chem. Soc. Jpn.*, **51**, 2518 (1978).
10) H. Nakayama and S. Torigata, *Bull. Chem. Soc. Jpn.*, **57**, 171 (1984).
11) H. Nakayama and H. Usui, *J. Inclusion Phenomena*, **2**, 249 (1984).
12) Yu. A. Dyadin, L. S. Aladko, L. A. Gaponenko, and T. M. Polyanskaya, *Izv. Sib. Otd. Akad. Nauk SSSR, Ser. Khim. Nauk*, **1981**, 19.
13) A. Takahashi, Y. Hayashi, and I. Kagawa, *Kogyo Kagaku Zasshi*, **60**, 113 (1957).
14) D. Eisenberg and W. Kauzmann, "The Structure and Properties of Water," Oxford Univ. Press, London (1969).
15) H. Nakayama, *Bull. Chem. Soc. Jpn.*, **60**, 839 (1987).
16) H. Nakayama, *Bull. Chem. Soc. Jpn.*, **56**, 877 (1983).
17) H. Nakayama, *Bull. Chem. Soc. Jpn.*, **55**, 389 (1982).

 © 1987 The Chemical Society of Japan Bull. Chem. Soc. Jpn., 60, 2327—2333 (1987)

Studies of Collectors. VIII. The Flotation of the Gallium Ion with Oxine-Type Surfactants

Yoshifumi KOIDE,* Hisashi HOKONOHARA, Kuniaki JINNAI, and Kimiho YAMADA
Department of Applied Chemistry, Faculty of Engineering, Kumamoto University, Kurokami, Kumamoto 860
(Received December 8, 1986)

Oxine-type surfactants(5-alkanoyl-8-quinolinol, R_nOx, n=2, 8, 12, 18) and $R_{12}OOx$ were prepared and used as ion-flotation collectors. Cu^{2+}, Fe^{3+}, Zn^{2+}, and Pb^{2+} were floated with $R_{12}Ox$ around a neutral pH, and the selective removal of Cu^{2+} from the mixture of these four metal ions was observed at pH 1.0. The floatability of Ga^{3+} was also high around the neutral pH, and the selective Ga^{3+} flotation from an Al^{3+} (100 ppm)-Ga^{3+}(20 ppm) mixture was observed by using R_8Ox in the pH regions of 3—4 and 10—13.3 (0.2 M NaOH soln), while $R_{12}Ox$ did not float the Ga^{3+} so much at pH 10—13.3. By the addition of a small amount of R_nPy to the $R_{12}Ox$ or by the solvent sublation, an effective flotation of Ga^{3+} was observed in the pH range of 10—13.3. The Ga^{3+} flotation was superior to the Ga^{3+} extraction in pH 2—4. However, in a strong alkaline region the floatability was lower than the extractability.

The recovery of a metal ion from an acidic or a basic solution is usually difficult even if it is necessary to do so. The recovery by ion flotation from such a solution is considered to be more effective than that by extraction because the metal ion can be floated with the collector as a 1 : 1 complex, as has been reported in a previous paper.[1,2] In recent years, Ga^{3+} has drawn much attention in the electronics market as material of a Ga-As semiconductor. For the purpose of recovering the Ga^{3+} from a Bayer solution, 7-(3,3,5,5-tetramethyl-1-vinylhexyl)-8-quinolinol(KELEX 100) has been used as an extraction reagent.[3] The KELEX 100 has a large distribution coefficient. However, it is expensive and requires a larger amount for extraction than the collector used in ion flotation. In this connection, 8-quinolinol(Ox) is quite interesting since it is a well known as a chelating reagent, and 8-quinolinol with a long side chain can be expected to be useful as an ion-flotation collector for Ga^{3+}, just like alkylated acetylacetone.[2] In the present paper, a higher alkanoyl group was introduced to oxine, and the 5-alkanoyl-8-quinolinol(R_nOx, n denotes the carbon number of the alkanoyl group, 2, 6, 8, 12, 18) was used as an ion-flotation collector. The preparation of R_nOx is far easier than that of KELEX 100, and its hydrophile-lipophile balance(HLB) can be regulated by varying the alkyl group or by converting the carbonyl group into an oxime derivative. There are many reports concerning Ga^{3+} extraction.[4] However, no study of a Ga^{3+} flotation using an oxine-type surfactant has yet been reported as far as the present authors are aware, except for an ion flotation of Ga^{3+} in hydrochloric acid with cationic surfactants.[5]

Experimental

Materials. The Ox was obtained from Wako Pure Chemical Industries, Ltd. The R_nOx was prepared by the Fries rearrangement of the alkanoic acid Ox ester.[6,7] The preparation of $R_{12}Ox$ was as follows: Equimolar quantities (0.05 mol) of Ox and dodecanoyl chloride were dissolved in nitrobenzene below 5 °C, and then 0.1 mol of aluminium chloride was added to the nitrobenzene solution. The reaction mixture was heated at 80—85 °C for 15—16 h. After cooling to room temperature, 100 cm^3 of a 10% HCl solution was added to the reaction mixture, and then the nitrobenzene was steam-distilled. Twenty cm^3 of 35% HCl was then poured into the residue. The precipitant, crude $R_{12}Ox$, was filtered and recrystallized with methanol after neutralization. The R_2Ox, R_6Ox, R_8Ox, and $R_{18}Ox$ were obtained by the same procedure. The oxime derivative, $R_{12}OOx$, was prepared from $R_{12}Ox$ by reference to the phenylglyoxime preparation.[8] A 40-cm^3 portion of a 70% ethanol solution containing 0.02 mol of $R_{12}Ox$ and 0.1 mol of hydroxylamine was refluxed for 6 h. The solvent was evaporated, and the remainder, $R_{12}OOx$, was washed with cold water. The yields were: R_2Ox 67%, R_6Ox 12%, R_8Ox 39%, $R_{12}Ox$ 55%, $R_{18}Ox$ 50%, and $R_{12}OOx$ 90%. The structures were confirmed by means of their IR spectra (Shimadzu IR-408), ^1H NMR spectra (JEOL JMN-MH-100), and elementary analyses (Yanako CHN Corder MT-3). Mp: R_2Ox, 114.0—115.4 °C; $R_6Ox \cdot HCl$, 172.0—174.0 °C; R_8Ox, 63.5—64.2 °C; $R_{12}Ox$, 66.8—68.5 °C; $R_{18}Ox$, 83.2—85.0 °C; $R_{12}OOx$, 151.0—152.5 °C. IR(KBr): ν_{CH} 2900, 2850 cm^{-1}, $\nu_{C=O}$ 1670 cm^{-1}, $\nu_{C=C,C=N}$ 1620, 1570, 1510 cm^{-1}. ^1H NMR (CCl_4): δ=0.9 (3H, t, CH_3-C-C-), 1.3 (methylene in alkane), 3.0 (2H, t, -CH_2-CO-), 7.2, 7.8, 8.2, 9.0, 9.8 (5H, -C_9H_5NO). R_2Ox Found: C, 70.23; H, 4.77; N, 7.43%; Calcd for $C_{11}H_9O_2N$: C, 70.59; H, 4.81; N, 7.49%. $R_6Ox \cdot HCl$ Found: C, 64.29; H, 6.37; N, 4.98%; Calcd for $C_{15}H_{18}O_2NCl$: C, 64.40; H, 6.49; N, 5.01%. R_8Ox Found: C, 74.85; H, 7.67; N, 5.23%; Calcd for $C_{17}H_{21}O_2N$: C, 75.25; H, 7.80; N, 5.16%. $R_{12}Ox$ Found: C, 76.64; H, 9.00; N, 4.19%; Calcd for $C_{21}H_{29}O_2N$: C, 77.02; H, 8.93; N, 4.28%. $R_{18}Ox$ Found: C, 78.45; H, 10.27; N, 3.49%; Calcd for $C_{27}H_{41}O_2N$: C, 78.78; H, 10.04; N, 3.40%. $R_{12}OOx$ Found: C, 73.20; H, 8.73; N, 7.90%; Calcd for $C_{21}H_{30}N_2O_2$: C, 73.64, H, 8.83; N, 8.18%.

The surface tensions of a R_nOx solution and a $R_{12}OOx$ solution were measured by the use of a Du Noüy surface-tension balance. The surface tensions of aqueous solutions of R_8Ox, $R_{12}Ox$, and $R_{12}OOx$ at their critical micellar concentrations (cmc) are 47 dyn cm^{-1} (1 dyn=1×10^{-5}N) for 4×10^{-4} M (1 M=1 mol dm^{-3}) R_8Ox at pH 0.6, 39 dyn cm^{-1} for 2×10^{-4} M $R_{12}Ox$ at pH 0.6, and 41 dyn cm^{-1} for

7×10^{-4} M $R_{12}OOx$ at pH 0.6, 46 dyn cm^{-1} for 4×10^{-3} M R_8Ox at pH 13, and 44 dyn cm^{-1} for 4×10^{-3} M $R_{12}Ox$ at pH 13. $R_{18}Ox$ was scarcely soluble in water. The concentrations of these surfactants were kept below their cmc in the following ion flotation.

Apparatus and Procedures. The removals of seven metal ions (Ga^{3+}, Al^{3+}, Fe^{3+}, Cu^{2+}, Zn^{2+}, Pb^{2+}, and Ag^{+}) were measured by the methods of ion flotation, solvent sublation, and extraction. The apparatus and procedures of ion flotation and extraction were the same as those previously reported.[1] The apparatus used in the solvent sublation was the same as that used in the ion flotation; a cell made up of a glass cylinder containing 500 cm^3 of an aqueous solution (Cu^{2+})-25 cm^3 of benzene or 200 cm^3 of an aqueous solution (Ga^{3+})-50 cm^3 of benzene. The determined amount of R_nOx was added to the aqueous solution, the pH of which had been adjusted to the desired value. Nitrogen gas was introduced through a sintered-glass disk (No.4) into the aqueous solution. The rate of gas flow was kept at 36—40 $cm^3\ s^{-1}$. The concentrations of metal ions were determined with an atomic-absorption spectrophotometer (Hitachi 170-30).

The floatabilities of the metal ions in the ion flotation and in the solvent sublation or the extractabilities of the metal ions were calculated using this equation:

$$F(\%) = \frac{a_0 - a_1}{a_0} \times 100$$

where a_0 and a_1 denote the initial and final metal-ion concentrations in a solution respectively.

Results and Discussion

Flotation and Extraction from an Acidic Solution. The series of R_nOx's were used as ion-flotation collectors and extraction reagents in the acidic pH range. The effect of the removals of Cu^{2+}, Fe^{3+}, and Zn^{2+} are shown in Fig. 1. R_nOx bearing a long alkyl chain floated the metal ions. The Cu^{2+} flotation in the pH regions of 1—2 was more effective than the Fe^{3+} or Zn^{2+} flotation and than the metal extractions in that pH region. The floatabilities varied with the difference in the alkyl-chain length, resulting in the variation of their surface activities (HLB). Pb^{2+} and Ag^{+} didn't float in this acidic pH range, but these five metal ions were floated with R_nOx around a neutral pH. They are not shown in the figures except for Cu^{2+}. The Cu^{2+} floatabilities by using 4×10^{-5} M KELEX 100 were 0% at pH 1.0, 14% at pH 2.0, and 18% at pH 3.0. On the other hand, by using R_nOx the Cu^{2+} and Fe^{3+} were extracted into the benzene layer above the pH values of 3 and 5 respectively, and their extractabilities for the solution containing equimolar amounts of R_nOx and metallic ions were almost independent of the alkyl-chain length. It is likely that the extractabilities are affected by the alkyl group in the presence of an excess of R_nOx. Figure 2 shows the Cu^{2+} flotation and the Cu^{2+} extraction by using a molar amount of R_nOx double that of Cu^{2+}. The

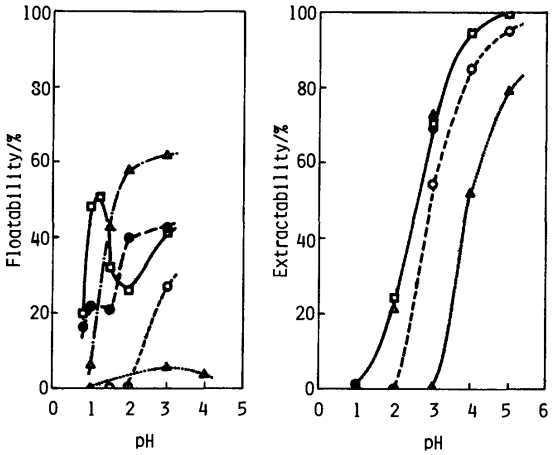

Fig. 2. Effects of alkyl-chain length on Cu^{2+} floatability and Cu^{2+} extractability. Initial concn: Cu^{2+} 1×10^{-5} M, R_nOx 2×10^{-5} M. ▲: Ox, ○: R_2Ox, △: R_8Ox, □: $R_{12}Ox$, ●: $R_{18}Ox$.

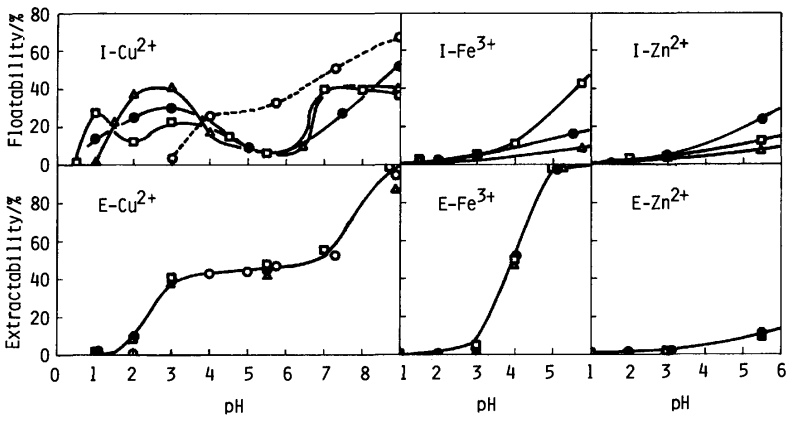

Fig. 1. Ion flotation and extraction. Initial concn: metal ion 1×10^{-5} M, R_nOx 1×10^{-5} M. I: ion flotation, E: extraction; ○: R_2Ox, △: R_8Ox, □: $R_{12}Ox$, ●: $R_{18}Ox$.

R_nOx bearing a long alkyl chain was far superior to the R_2Ox or Ox. The stability constants of Ox complexes are high (Cu^{2+} log K_{ML} 12.2, log K_{ML_2} 11.2, Fe^{3+} log K_{ML} 12.3, log K_{ML_2} 11.3).[2] The stability constants of the R_nOx complexes are presumed to be similar to the values of the Ox complexes. Therefore, the Cu^{2+} and Fe^{3+} could be complexed with equimolar R_nOx at a low concentration and a low pH. The 50% (Cu^{2+}) and 100% (Fe^{3+}) extractabilities in acidic pH indicate that the R_nOx/Cu^{2+} ratio in the extracted complex is 2:1 and the R_nOx/Fe^{3+} ratio is 1:1. These ratios were also confirmed by the method of continuous variation; e.g., for the $R_{12}Ox$-Cu complex, the concentration in benzene was measured with the absorbance at λ_{max} 415 nm. Their calculated HLB values, based on the Oda equation,[9] were $(R_{12}Ox)_2$-Cu 3.5 and $R_{12}Ox$-$Fe(OH)_2$ 6 respectively, so that they would have large distribution coefficients[10] and be extracted.

Then, the difference in the method of adding the collector in ion flotation was examined at pH 1.0, as may be seen in Fig. 3. A remarkable difference in the Cu^{2+} floatabilities was observed when 3—5×10^{-5} M $R_{12}Ox$ was added to the 1×10^{-5} M Cu^{2+}-mixed solution. The step-by-step addition was more effective than adding everything at one time, and the Cu^{2+} could be floated more selectively from a mixture of Cu^{2+}, Fe^{3+}, Zn^{2+}, and Pb^{2+} by the former method. The $R_{12}Ox/Cu^{2+}$ ratio in the scum was confirmed by the elementary analyses to be 1:1 (Found: C, 61.57; H, 7.57; N, 3.01%; Calcd for $C_{21}H_{28}O_2N \cdot Cu \cdot H_2O$: C, 61.66; H, 7.58; N, 3.44%). The complexes at pH 1.0 were surface-active $(R_nOx\text{-}M)^{m+}$, and their calculated HLB values[9] were $(R_{12}Ox\text{-}Cu)^+$ 9 and $(R_{12}Ox\text{-}Fe)^{2+}$ 15. Therefore, the hydrophobic Cu^{2+} complex would be floated selectively, and the hydrophilic Fe^{3+} complex thus produced would disperse the $(R_{12}Ox\text{-}Cu)^+$ complex into the solution. Actually, an excellent Cu^{2+}-selectivity from the mixture of all the metal ions except for Fe^{3+} was observed even when 3—5×10^{-5} M $R_{12}Ox$ was added all at one time. These results were similar to that shown in Fig. 3-(1) and so are not shown in the figures. The scum ($R_{12}Ox$-Cu complex) was dissolved in 20 cm^3 of benzene, and the benzene solution was shaken with 20 cm^3 of a 1 M or 3 M HCl solution. The recoveries of $R_{12}Ox$ from the benzene layer were 100% with 1 M HCl and 93% with 3 M HCl, while those of Cu^{2+} from the aqueous layer were 96% with 1 M HCl and 100% with 3 M HCl.

Ga^{3+} Flotation and Extraction from an Acidic Solution. The recovery of Ga^{3+} (20 ppm) was further examined. Figure 4 shows the pH effect on the floatability of Ga^{3+} from equimolar solutions (2.87×

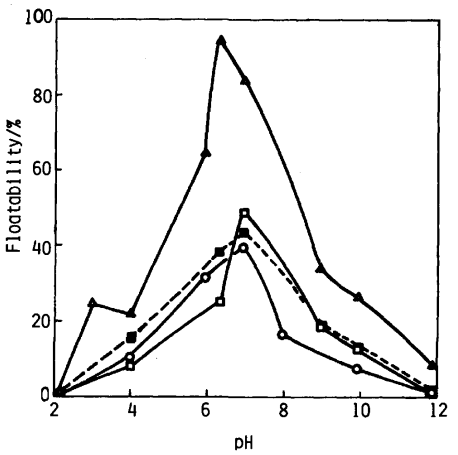

Fig. 4. Effect of pH on Ga^{3+} flotation. Initial concn: Ga^{3+} 2.87×10^{-4} M(20 ppm), R_nOx 2.87×10^{-4} M. O: R_2Ox, △: R_8Ox, □: $R_{12}Ox$, ■: $R_{12}OOx$.

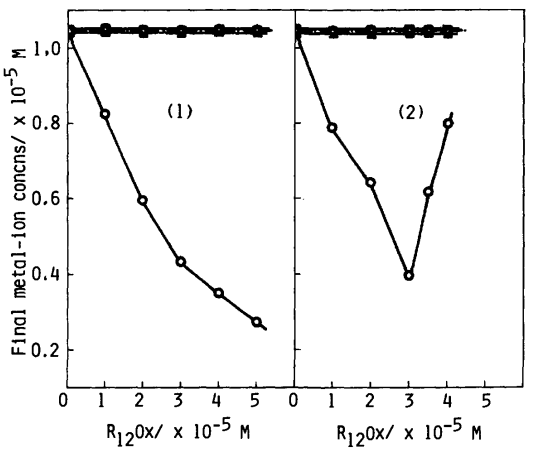

Fig. 3. Selective removal of Cu^{2+} at pH 1.0. Initial concn of metal ions mixture: Cu^{2+}, Fe^{3+}, Zn^{2+}, and Pb^{2+} 1×10^{-5} M, respectively. (1) Stepwise addition of $R_{12}Ox$. (2) Additions of $R_{12}Ox$ at a time. O: Cu^{2+}, ■: Fe^{3+}, △: Zn^{2+}, ▲: Pb^{2+}.

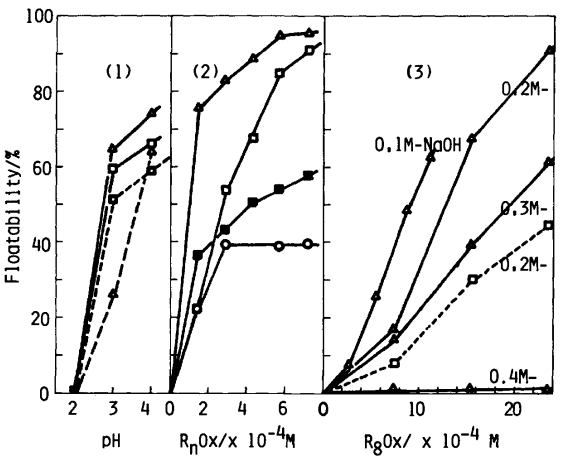

Fig. 5. Ga^{3+} flotation. Initial concn: Ga^{3+} 2.87×10^{-4} M(20 ppm). (1) R_nOx 5.74×10^{-4} M; ▲: extraction using R_8Ox, □: extraction using $R_{12}Ox$. (2) pH 7. (3) 0.1—0.4 M NaOH soln. O: R_2Ox; △: R_8Ox, □: $R_{12}Ox$, ■: $R_{12}OOx$.

10^{-4} M) of R_nOx and Ga^{3+}. A high floatability was observed around the neutral pH. R_8Ox was the most effective collector among the R_nOx homologues. The Ga^{3+} floatability increased as the concentration of R_nOx increased, as is shown in Fig. 5: The floatabilities for a 2.87×10^{-4} M Ga^{3+} solution were 65—72% in the pH regions of 3—4 with 5.74×10^{-4} M R_8Ox, and 96% at pH 7 with $5.7—7.2\times10^{-4}$ M R_8Ox. However, the Ga^{3+} floatability when R_2Ox or Ox was used was low: 40% at pH 7 with R_2Ox and 0% in the pH region of 0—14 with $0—5\times10^{-5}$ M Ox. The Ga^{3+} flotation at pH 3 was surperior in efficiency to the Ga^{3+} extraction at pH 3, but they were similar at pH 4. Furthermore, the Ga^{3+} was found to float selectively from a Ga^{3+}-Al^{3+} mixture in pH 3—4, but it was floated simultaneously with Al^{3+} at pH 7, as is shown in Fig. 6. The stability constants (log K_{ML}) of the Ox and the 8-hydroxy-5-quinolinesulfonic acid (OxS) complexes are Ox-Ga 14.51,[11] OxS-Ga 13.56,[12] and OxS-Al 9.76.[12] The values of the R_nOx complexes are presumed to be similar to those of the Ox and OxS complexes.[9] Therefore, the more stable Ga^{3+} must be floated selectively. The Ga^{2+} flotation and selectivity in the alkaline region will be discussed in the next section.

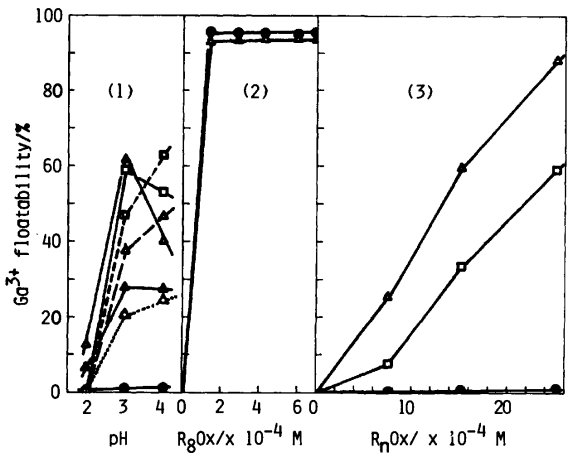

Fig. 6. Ga^{3+} selectivity from Ga^{3+}-Al^{3+} mixture. Initial concn of metal ions mixture: Ga^{3+} 2.87×10^{-4} M(20 ppm)-Al^{3+} 3.71×10^{-3} M(100 ppm). (1) R_nOx 5.74×10^{-4} M; ——△——: extraction using R_8Ox, ——□——: extraction using $R_{12}Ox$. ▲: ion flotation using 2.87×10^{-4} M R_8Ox, ---△---: extraction using 2.87×10^{-4} M R_8Ox. (2) pH 7. (3) 0.2 M NaOH soln. △: R_8Ox, □: $R_{12}Ox$, ●: floatability of Al^{3+} by using R_8Ox.

Flotation and Extraction from an Alkaline Solution. The Ga^{3+} floatabilities of 2.87×10^{-4} M Ga^{3+} at pH 10 were similar to those at pH 4, while the floatabilities at pH 11 were 63% with 5.74×10^{-4} M R_8Ox and 94% with 8.61×10^{-4} M R_8Ox. The amount of R_8Ox remaining after the Ga^{3+} flotation was below 10^{-5} M. Therefore, the R_8Ox/Ga^{3+} ratio in the scum was determined to be 2:1 from the elementary analyses{Found (pH 11): C, 65.61; H, 6.72; N, 5.05%; Found (pH 4): C, 66.76; H, 6.74; N, 4.70%; Calcd for R_8Ox-Ga: C, 60.04; H, 5.93; N, 4.12%; Calcd for $(R_8Ox)_2$-Ga: C, 66.90; H, 6.61; N, 4.59%; Calcd for $(R_8Ox)_3$-Ga: C, 69.54; H, 6.87; N, 4.77%}. Consequently, the equimolar R_8Ox is considered to float. The Ga^{3+} flotation from a strong alkaline solution is shown in Fig. 5-(3). The Ga^{3+} could be floated from the alkaline solution with a large excess of R_8Ox or $R_{12}Ox$. However, the R_nOx became insoluble in a strong NaOH solution (R_8Ox above 0.4 M, $R_{12}Ox$ above 0.3 M), while no flotation effect was observed when R_6Ox was used because of the soluble Ga^{3+} complex (yellow green). The Ga^{3+} flotation using KELEX 100 was less effective than those using R_8Ox and $R_{12}Ox$: The Ga^{3+} floatabilities from the 2.87×10^{-4} M (20 ppm) Ga^{3+} in a 0.1 M NaOH solution were 13% with 8.6×10^{-4} M KELEX 100, 31% with 17.2×10^{-4} M, 52% with 25.8×10^{-4} M, and 70% with 34.4×10^{-4} M. The R_nOx used as a collector was regenerated by the treatment of the scum with 5 M HCl, resulting in the precipitation of R_nOx and a Ga^{3+} solution. The Ga^{3+} selectivity from the Ga^{3+}-Al^{3+} mixture in a 0.2 M NaOH solution is shown in Fig. 6-(3). The Ga^{3+} was also found to float selectively. The complexes produced in the alkaline solution were presumed to be something like the hydroxo-Ga complexes, $\{(R_nOx)_2$-$Ga(OH)_2\}^-$, because the hydrolysis constants (pK_n) for the aqua-Ga complexes were pK_1 2.8—2.9, pK_2 3.5—4.4, pK_3 4.5, pK_4—, pK_5 10.3, and pK_6 11.7.[13] The flotation effect was evaluated first by the degree of the formation of a surface-active complex. The HLB

Table 1. HLB Values of R_nOx Complexes[a] in Alkaline Soln

Ligand	L^{b}-$Ga(OH)_2$ L-$Al(OH)_2$	L-CuOH	L_2-GaOH L_2-AlOH	$(L_2$-Ga$)^+\cdot\{L_2$-$Ga(OH)_2\}^-$ $(L_2$-Al$)^+\cdot\{L_2$-$Al(OH)_2\}^-$
Ox	13	10	9	13
R_2Ox	11	8	7	10
R_6Ox	8	6	5	8
R_8Ox	7	5	5	7
$R_{12}Ox$	6	4	4	5
$R_{12}OOx$	9	8	8	9

a) The HLB values based on the Oda equation.[9] b) L indicates ligand.

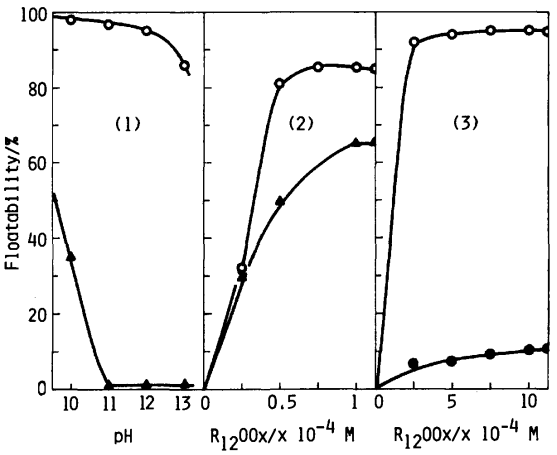

Fig. 7. Flotation of metal ion and coflotation with Cu^{2+} ion. (1) Cu^{2+} flotation: Cu^{2+} 1×10^{-4} M. $R_{12}OOx$ 3×10^{-4} M; Fe^{3+} flotation: Fe^{3+} 1×10^{-4} M, $R_{12}OOx$ 3×10^{-4} M. (2) Fe^{3+}-Cu^{2+} coflotation: 0.5×10^{-4} M Fe^{3+}-0.5×10^{-4} M Cu^{2+}; pH 13. (3) Ga^{3+}-Cu^{2+} coflotation: 2.87×10^{-4} M Ga^{3+}-1.5×10^{-4} M Cu^{2+}; pH 12. ○: Cu^{2+}, ▲: Fe^{3+}, ●: Ga^{3+}.

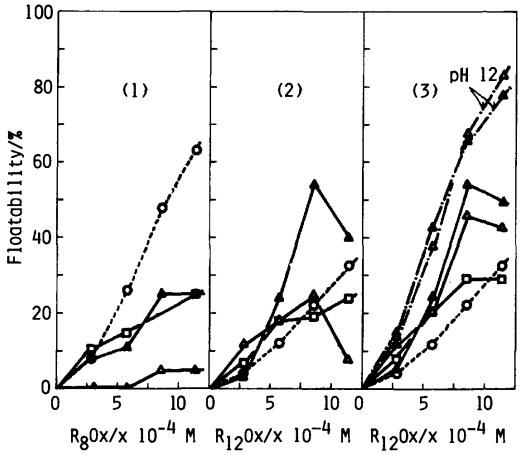

Fig. 8. Flotation of Ga^{3+} using $R_{12}Ox$-R_nPy at pH 13. Initial concn: Ga^{3+} 2.87×10^{-4} M(20 ppm). (1) R_nPy 1.44×10^{-4} M. (2) R_nPy 1.44×10^{-4} M. (3) R_nPy 2.87×10^{-4} M. △: $R_{12}Py$, ▲: $R_{18}Py$, □: $R_{22}Py$, ○: without R_nPy.

values of these complexes are in the range of 4—13, as is indicated in Table 1; the HLB value of the Ga^{3+} complex is the same as that of the Al^{3+} complex. However, the Ox, R_2Ox, and R_6Ox complexes were surface-inactive in spite of their HLB values being in the range of 5—13; the surface tension of a 2.87×10^{-4} M R_6Ox solution was 60 dyn cm^{-1} at 15 °C. Presumably they could not float the Ga^{3+} because of their structural characteristics. The reaction rate of the complex formation is considered to be another factor in the selectivity of ion flotation. Since the reaction rates of Al^{3+} with general chelating agents are known to be slow,[14] the Ga^{3+} selectivity from a Ga^{3+}-Al^{3+} mixture was examined after a sufficient time for the formation of the Al^{3+} complex. However, the Ga^{3+} was floated selectively at 60 °C or after it had stood for 24 h; therefore, the complex stability was considered to be a dominant factor in the Ga^{3+} selectivity. On the other hand, Cu^{2+} was effectively floated with the R_nOx or $R_{12}OOx$ below pH 13, but Fe^{3+} was not effectively floated above pH 10, as is shown in Fig. 7-(1). In this connection, we made coflotation experiments on the Fe^{3+}-Cu^{2+} and Ga^{3+}-Cu^{2+} systems in order to study the possibility of enhancing the floatabilities of Fe^{3+} and Ga^{3+} by the addition of Cu^{2+}. The Fe^{3+}-Cu^{2+} coflotation was done at pH 10 and 13, and the Ga^{3+}-Cu^{2+} coflotation was done at pH 10 and 12. The floatability of 5×10^{-5} M Fe^{3+} was 20% at pH 10 with 10^{-4} M $R_{12}Ox$ in the absence of Cu^{2+} and 80% in the presence of 5×10^{-5} M Cu^{2+}. The Fe^{3+}-Cu^{2+} coflotation at pH 13 was also effective, as is shown in Fig. 7-(2). However, the Ga^{3+}-Cu^{2+} coflotation was ineffective; the floatabilities of 2.87×10^{-4} M Ga^{3+} at pH 10 in the absence of Cu^{2+} and in the presence of 5×10^{-4} M Cu^{2+} were 55 and 43% respectively with 5×10^{-4} M $R_{12}Ox$, and 99 and 58% respectively with 10^{-3} M $R_{12}Ox$. The floatabilities at pH 12 when $R_{12}OOx$ was used were also high for Cu^{2+}, but low for Ga^{3+}, as is shown in Fig. 7-(3). Furthermore, the Ga^{3+} selectivity from a Ga^{3+} (2.87×10^{-4} M)-Al^{3+} (3.70×10^{-3} M)-Cu^{2+}(5×10^{-4} M) mixture was found to be less: The floatabilities of metal ions at pH 10 when 15×10^{-4} M $R_{12}OOx$ was used were Ga^{3+} 66%, Al^{3+} 49%, and Cu^{2+} 99%. The difference between the floatabilities of Fe^{3+} and Ga^{3+} may be due to the hydrophilic property caused by their hydrolysis.

Flotation with Cationic Surfactants. Ga^{3+} in an alkaline solution exists as an anionic polyhydroxo species, $Ga(OH)^{3-x}_{x(=4,5,6)}$, and the R_nOx probably forms an anionic hydroxo-gallium complex, e.g., $\{(R_nOx)_2\text{-}Ga(OH)_2\}^-$.[13] Therefore, the effects of the addition of a cationic surfactant were examined. Four *N*-alkylpyridinium bromides (R_nPy, n=8, 12, 18, 22) were prepared by the procedure of Knight et al.,[15] and their structures were identified by means of their melting points and the results of elementary analyses. The flotation of Ga^{3+} with the cationic R_nPy was examined in the absence of R_nOx. However, the R_8Py, $R_{12}Py$, $R_{18}Py$, and $R_{22}Py$ were not useful for Ga^{3+} flotation in the alkaline region. Then, both surfactants, the chelating R_nOx and the cationic R_nPy, were added to the Ga^{3+} solution. The Ga^{3+} floatabilities when R_8Ox-R_nPy was used were less than those without R_nPy; in the absence of the R_nPy, the R_8Ox was more effective than $R_{12}Ox$, as is shown by the dotted line in Fig. 8. On the other hand, the Ga^{3+} floatabilities when $R_{12}Ox$-R_nPy was used became higher than that without R_nPy, but were steeply lowered in a high concentration of $R_{12}Ox$, as is shown in Fig. 8-(2). The $R_{12}Ox$ in the presence of

2.87×10^{-4} M R_nPy enhanced the Ga^{3+} floatability more {Fig. 8-(3)}. These floatabilities varied a little with the difference in the alkyl-chain length of R_nPy. The cationic R_nPy was considered to be attracted to the anionic R_nOx-gallium complex or to the anionic R_nOx, resulting in a green suspension. Consequently, the colloidal $R_{12}Ox$-Ga complex may be floated with the surface-active R_nPy, but the Ga^{3+} floatability would be lowered in a high concentration of $R_{12}Ox$ (above 3-fold molar to Ga^{3+}) because of the complexation of R_nPy with the excess $R_{12}Ox$. On the other hand, the hydrophilic R_8Ox-Ga complex should be solubilized by the surface-active R_nPy. In addition, the more hydrophilic R_nOx, R_2Ox-R_nPy, R_6Ox-R_nPy, and $R_{12}OOx$-R_nPy did not show any flotation effect(these data are not shown in Fig. 8). The selective flotation of the Ga^{3+} at pH 13 from a Ga^{3+} (2.87×10^{-4} M, 20 ppm)-Al^{3+} (3.70×10^{-3} M, 100 ppm) mixture was also done, as is shown in Fig. 9. A highly selective flotation of Ga^{3+} at pH 13 is, of course, observed with the increase in the $R_{12}Ox$-R_nPy concentration, as is shown in Fig. 9-(2), (3); the floatabilities of metal ions when 11.5×10^{-4} M $R_{12}Ox$-5.76×10^{-4} M $R_{22}Py$ was used were Ga^{3+} 71% and Al^{3+} 0%. The Ga^{3+} selectivities when R_8Ox-R_nPy was used were almost identical with those without R_nPy, as is shown in Fig. 9-(1). Because the cationic R_nPy ions combine with the large excess of $Al(OH)^{3-x}_{x(=4,5,6)}$ ions, the Ga^{3+} floatabilities in the Ga^{3+}-Al^{3+} mixture are unaffected by the presence of R_nPy. The Al^{3+} did not float with any of the collectors used because of its lower stability.

Solvent Sublation. Solvent sublation is known as a nonfoaming, absorptive, bubble-separation process.[10] Trace amounts of metal ions were concentrated, by means of ion flotation with collectors, and then the ion-associates were dissolved in an organic solvent for their analyses, e.g., for Cr^{6+}, with diphenylcarbazide-sodium dodecyl sulfate;[16] for Fe^{3+}, with 1, 10-phenanthroline-sodium dodecyl sulfate,[17] and for Ge, with phenylfluorone-cyclohexane.[18] The collectors used in such flotation are generally a combination of complexing agents and oppositely charged surfactants or basic dyes.[19] However, a chelating surfactant has not yet been applied to a solvent-sublation collector.[20] Therefore, the R_nOx was examined as a solvent-sublation collector. Figure 10 shows the solvent sublation from an acidic (Cu^{2+}) and a basic solution (Ga^{3+}). The Cu^{2+} floatability when $R_{12}Ox$ was used at pH 1.0 varied with the aeration time and with the acid species. The Cu^{2+} could be floated initially as a 1:1 complex, and then the composition of the complex sublated, as well as that of that extracted, finally became 2:1. The formation of the Cu^{2+} complex with a small amount of $R_{12}Ox$ in a HCl solution was more difficult than that in a HNO_3 solution because of the formation of the stable Cu^{2+}-chloro complex.[2] The Ga^{3+} floatabilities by solvent sublation in the alkaline region (0.1, 0.3, 0.4 M NaOH) were superior to those by ion flotation, but inferior to the Ga^{3+} extractabilities. Thus, the R_nOx used as a solvent-sublation collector in the alkaline region showed properties intermediate between those of the ion-flotation collector and the extraction reagent. The solvent sublation using KELEX 100 was similar to that using R_8Ox, but the extraction was less: the floatabilities from the 2.87×10^{-4} M (20 ppm) Ga^{3+} in a 0.1 M NaOH solution were 45—47% with 8.6—14.3×10^{-4} M KELEX 100, while the extractabilities were 25% with

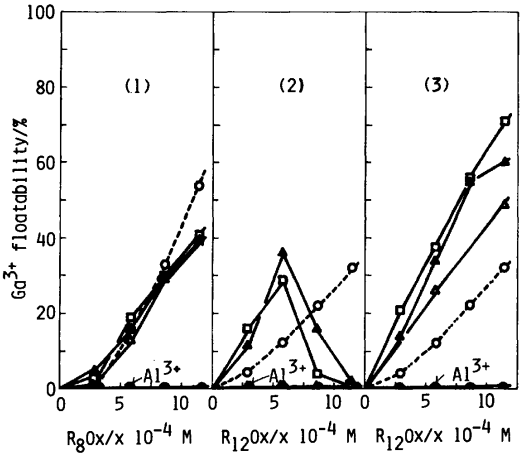

Fig. 9. Selectivity using R_nOx-R_nPy at pH 13. Initial concn of metal ions mixture: Ga^{3+} 2.87×10^{-4} M(20 ppm)-Al^{3+} 3.70×10^{-3} M(100 ppm). (1) R_nPy 1.44×10^{-4} M. (2) R_nPy 1.44×10^{-4} M. (3) R_nPy 4.31×10^{-4} M. △: $R_{12}Py$, ▲: $R_{18}Py$, □: $R_{22}Py$, ○: without R_nPy, ●: Al^{3+} floatability by using R_nOx-$R_{18}Py$.

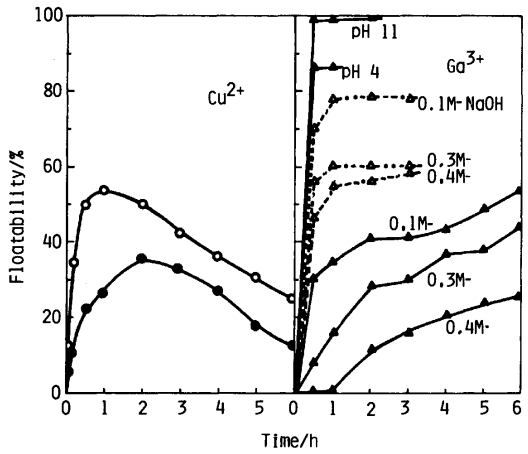

Fig. 10. Solvent sublation.
Cu^{2+} Initial concn: Cu^{2+} 1×10^{-5} M in acidic soln. $R_{12}Ox$ 2×10^{-5} M; volume: aq (500 cm^3)-benzene(25 cm^3). ○: 0.1 M HNO_3, ●: 0.1 M HCl.
Ga^{3+} Initial concn: Ga^{3+} 2.87×10^{-4} M(20 ppm) in 0.1—0.4 M NaOH soln and in soln of pH 4 or 11, R_8Ox 8.61×10^{-4} M; Volume: aq(200 cm^3)-benzene(50 cm^3). ▲: Solvent sublation. △: extraction.

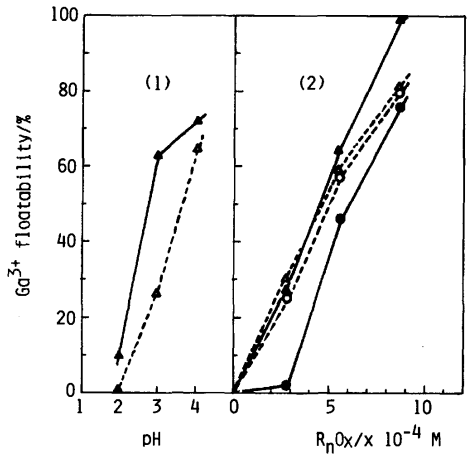

Fig. 11. Solvent sublation of Ga^{3+}. Initial concn: Ga^{3+} 2.87×10^{-4} M(20 ppm). (1) R_8Ox 5.74×10^{-4} M. ▲: Solvent sublation, △: extraction. (2) pH 11. ▲: Solvent sublation using R_8Ox, △: extraction using R_8Ox, ●: solvent sublation using $R_{12}Ox$, ○: extraction using $R_{12}Ox$.

8.6×10^{-4} M and 50% with 28.7×10^{-4} M. However, the gelation of a kerosene solution of R_nOx took place upon Ga^{3+} extraction from a Bayer solution, and KELEX 100 was still effective: 58% with 0.27 M KELEX 100 in kerosene (KELEX 100/$Ga^{3+}\approx80$). Therefore, the solvent sublation of Ga^{3+} using R_8Ox was superior to the Ga^{3+} extraction in the pH region from 3 to 11, as is shown in Fig. 11. As regards the solvent sublation for the Ga^{3+}-Al^{3+} system, the Ga^{3+} was floated selectively from the mixture at pH 3—4 and pH 11, but the Ga^{3+} and Al^{3+} were floated simultaneously in pH 5—10. Such a behavior of Ga^{3+} flotation from the mixture was similar to that for the solution of Ga^{3+} alone.

Thus, R_8Ox and $R_{12}Ox$ were confirmed to be more effective collectors than KELEX 100 for Cu^{2+} in an acidic solution and for Ga^{3+} in a basic solution and to favour the selective ion flotation of Cu^{2+} from a metal-ion mixture and that of Ga^{3+} from a Ga^{3+}-Al^{3+} mixture. These results prove that a useful collector in an acidic or a basic solution can be designed by the selection of a stronger complexing ligand and the regulation of its HLB, as well as by the preparation of a usual collector.[1)]

References

1) Y. Koide, S. Sato, and K. Yamada, *Bull. Chem. Soc. Jpn.*, **59**, 715 (1986).
2) H. Freiser and Q. Fernando, "Ion-heiko," translated by T. Fujinaga and E. Sekido, Kagakudojin (1970), p. 254.
3) J. Helgorsky and A. Leveque, German Patent 2530880 (1976); French Patent 2307047 (1976); German Patent 2743475 (1978); French Patent 2397464 (1979).
4) T. Sato, T. Nakamura, M. Yabuta, and H. Oishi, *Chem. Lett.*, **1982**, 591; K. Hagiwara, M. Nakane, Y. Osumi, E. Ishii, and Y. Miyake, *Bunseki Kagaku*, **10**, 1376 (1961).
5) T. Nozaki, K. Kato, M. Uchida, M. Doi, N. Mise, and Y. Soma, *Bunseki Kagaku*, **32**, 145 (1983).
6) D. V. Banthorpe, *Chem. Rev.*, **70**, 295 (1970).
7) G. Manecke and H. P. Aurich, *Makromol. Chem.*, **133**, 83 (1970).
8) J. V. Burakevich, A. M. Love, and G. P. Volpp, *J. Org. Chem.*, **36**, 1 (1971).
9) R. Oda and K. Teramura, "Kaimen-kasseizai No Gosei To Sonooyo," Maki Shoten, Tokyo (1962), p. 501; Y. Koide, K. Izumi, K. Okuzono, and K. Yamada, *Nippon Kagaku Kaishi*, **1980**, 742.
10) Y. Koide, S. Kitaoka, and K Yamada, *Bull. Chem. Soc. Jpn.*, **58**, 2456 (1985).
11) L. G. Sillen and A. E. Martell, "Stability Constants of Metal Complexes, Suppl. 1," The Chemical Society, London (1964), p. 1971.
12) T. Nishikawa, K. Hiraki, K. Morishige, and S. Katagi, *Bunseki Kagaku*, **26**, 365 (1977).
13) J. Burgess, "Metal Ions in Solution," John Wiley & Sons, New York (1978), p. 259.
14) K. Ueno, "Kireto-tekitei Hou," Nankoudou (1972), p. 246.
15) G. A. Knight and B. D. Shaw, *J. Chem. Soc.*, **1938**, 682.
16) M. Aoyama, T. Hobo, and S. Suzuki, *Anal. Chim. Acta*, **129**, 237 (1981).
17) K. Yamada, M. Aoyama, T. Hobo, and S. Suzuki, *Bunseki Kagaku*, **33**, 99 (1984).
18) J. Shida, Y. Takahashi, K. Ojima, and T. Matsuo, *Bunseki Kagaku*, **33**, E143 (1984).
19) Z. Marczenko and K. Kalinowski, *Anal. Chim. Acta.*, **153**, 219 (1983).
20) R. Lemlich, "Adsorptive Bubble Separation Techniques," Academic Press, New York and London (1972), p. 145.

Reaction Mechanism for Selective Synthesis of Gasoline-Range Isoalkanes from Syngas over RuPtHY Zeolites. II.[1] Role of Metals and Acid Sites

Yong-Gong SHUL, Yukari ARAI, Takashi TATSUMI,* and Hiro-o TOMINAGA
Department of Synthetic Chemistry, Faculty of Engineering, The University of Tokyo, Hongo, Bunkyo-ku, Tokyo 113
(Received December 16, 1986)

Role of metals and acid site in selective synthesis of gasoline-range isoalkanes from syngas catalyzed by zeolite Y supported Ru-Pt alloy has been studied. As a probe molecule 1-alkene was added into syngas over the various combination of catalysts. Alloying Ru with Pt enhanced 1-octene conversion as well as CO conversion. Reaction of 1-octene over metal-free DAHY (dealuminated HY) zeolite produced cracking products with high selectivity for isobutanes; C_{3+} carbon number distribution was similar to that from CO hydrogenation over DAHY2R2P (Ru and Pt 2 wt%, respectively), suggesting that the selective formation of isoalkanes in gasoline-range from CO–H_2 over DAHY2R2P could be essentially due to acid-catalyzed reactions on zeolites. Cracking of 1-octene was affected by the support and increased in the order: NaY2R2P<HY2R2P<DAHY2R2P. Products via disproportionation were predominant for NaY2R2P and HY2R2P and those via simple cracking prevailed in DAHY2R2P. This could account for shift to light side in carbon number distribution from simple CO hydrogenation over DAHY2R2P. From syngas H_2/CO ratio= 13/2, methane was the main product. However, methane production was virtually unchanged on addition of 1-octene, implying that the presence of CO suppressed the hydrogenolysis of 1-octene on RuPt bimetallic site. Effects of contact time and temperature on selectivity for products were also discussed.

Non-Schulz-Flory kinetics in Fischer-Tropsch synthesis has been studied by several authors.[2-8] Limitation on chain growth has been reported for RuNaY,[2] RuLaY,[3] FeNaY,[4] RuPtHY,[5] and Co-alumina[6] catalysts. With Co-alumina, a maximum in carbon number distribution was dependent on the pore size of the support. Over the ruthenium-encaged NaY or LaY zeolite, the product contained no hydrocarbons larger than C_{11}; the chain growth probability suddenly dropped as chain length increased. This product pattern was ascribed to particle size effect of the ruthenium metals in zeolite.[7]

In a previous paper, we reported the selective synthesis of gasoline-range products rich in isoalkanes over RuPt-HY or DAHY (dealuminated HY).[5] The deviation from the Schulz-Flory product pattern was attributed to secondary reactions rather than the effect of particle size,[7] since increasing the ruthenium particle size in HY had no effect on final products pattern.[5] The evidence for secondary reactions was obtained by adding 1-alkenes (C_n) in the range of C_3—C_{11} as probe molecules into synthesis gas.[1] Addition of light alkenes (n=3,4) resulted in a pronounced increase in the yield of C_{n+1} and heavier, which could be ascribed to the oligomerization of feed alkene followed by cracking. On the other hand, simple cracking predominated in the case of addition of heavy alkenes ($n \geq 7$).

In the present paper, we report a study of the role of acid sites and Ru-Pt bimetallic sites in the selective formation of gasoline-range isoalkanes from synthesis gas. The dependence of H_2/CO ratio, contact time and temperature on the product selectivity is also discussed from mechanistic viewpoints.

Experimental

Catalysts were prepared by simultaneous ion exchange with an aqueous solution containing $[Ru(NH_3)_6]Cl_3$ and $[Pt(NH_3)_4]Cl_2$, as described previously.[5] NaY (SiO_2/Al_2O_3= 4.8) was obtained from Nikka Seiko Co. HY was prepared by ion exchange of NaY with an aqueous solution of NH_4NO_3, followed by calcination at 400 °C. DAHY (dealuminated HY, SiO_2/Al_2O_3=7.6) was obtained from Shokubai Kasei Co. The designation of catalyst is, for example, DAHY2R2P which stands for a catalyst with 2% Ru and 2% Pt by weight supported on DAHY. Reaction was carried out with a continuous flow tubular reactor containing 1 g of catalyst. The standard reaction conditions were 240 °C, 1.5 MPa, H_2/CO=3/2, and W/F=12.5 g-cat. h mol.$^{-1}$ Liquid alkene was added by use of a high pressure microfeeder and homogeneously mixed with synthesis gas over the preheated quartz wool-packed bed before the reaction zone. Detailed analysis of hydrocarbon products was carried out on a gas chromatograph equipped with a chemically bonded OV-1 capillary column. Each product was identified with a Shimadzu QP-1000 mass spectrometer. Chemisorption of NH_3 was carried out by using a grease-free glass constant-volume adsorption system. The sample was evacuated at ambient temperature and then subjected to temperature-programmed desorption (TPD) analysis of NH_3. The heating rate was 7 °C min^{-1} and the amount of NH_3 was determined mass spectrometrically.

Results and Discussion

Effect of Metal Loadings. The catalyst activity substantially declined during the course of a catalytic run. Figure 1 shows the change of CO conversion with time on stream over DAHY2R and DAHY2R2P in the absence and presence of 1-octene. Deactivation proceeded faster in the presence of 1-octene than in its

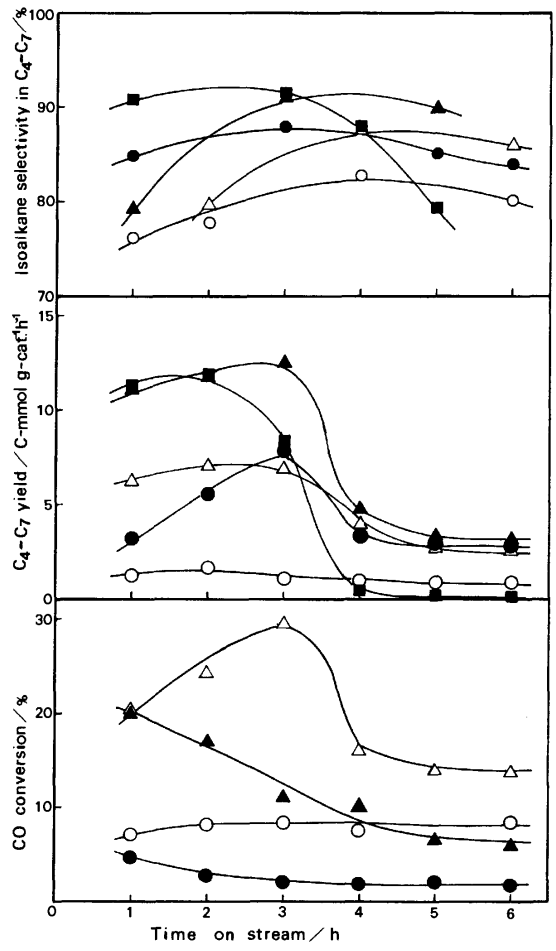

Fig. 1. Change of catalytic performance with time on stream. Reaction conditions: 240 °C, 1.5 MPa, $H_2/CO=3/2$, $W/F=12.5$ g-cat. h mol^{-1}, 1-octene feed rate=1.9 mmol g-cat.$^{-1}$ h^{-1}. Simple CO hydrogenation: △, DAHY2R2P; ○, DAHY2R. 1-Octene addition: ▲, DAHY2R2P; ●, DAHY2R; ■, DAHY (under He).

absence. In view of previous work,[8] this could be interpreted in terms of acceleration of coke deposition. Alloying of Ru with Pt enhanced CO conversion,as was observed with the HY-supported catalysts.[5] This was also the case in the presence of 1-octene.

The changes of the yield of and the isoalkane selectivity for C_4—C_7 fraction with time on stream are also shown in Fig 1. The effect of metal loadings on products is summarized in Table 1, where data obtained after 2—3 h on stream are adopted. The addition of 1-octene resulted in an increase in the yield of C_4—C_7, associated with the increase in their i/n ratios. Products in the C_4^+ range consisted mostly of branched alkanes. Alkanes with quaternary C-atoms were negligible for all the catalysts.[1,5] In most cases the fractions of monobranched alkanes in the range of C_4—C_6 were far above the equilibrium. Higher-than-equilibrium i/n ratios of C_4 and C_5 should be taken as evidence for the occurrence of carbenium ion cracking process.[1,9]

DAHY2R2P was similar to DAHY2R in the carbon number distribution of the products from CO-H_2 except for slightly increased selectivity for C_4—C_7.[5] The apparent conversion of 1-octene was considerably higher over DAHY2R2P than over DAHY2R. This higher cracking activity might be the cause of higher i/n ratios of C_4 and C_5 in simple CO hydrogenation over DAHY2R2P.[1] DAHY2P showed prolonged cracking activity of 1-octene than the other cases.

Cracking behavior of 1-octene under He flow over metal-free DAHY was also investigated. High initial selectivity for C_4 and no appreciable formation of C_1 and C_2 were observed, as would be expected for the acid-catalyzed cracking. As shown in Table 1, there were similarities between simple CO hydrogenation over DAHY2R2P and 1-octene cracking over DAHY in C_3^+ products distribution and selective formation of isoalkanes. Thus the selective formation of isoalkanes in gasoline-range from CO-H_2 over DAHY2R2P could be essentially due to acid-catalyzed reactions on zeolites. It should be noted that the metal-free DAHY support gave products exceptionally rich in branched isomers in C_4 and C_5 fractions, especially in the initial stage of the reaction. This could be caused by an increase in lifetime of carbenium ions associated with a low reactivity of hydrogen in the absence of metals,[10,11] resulting in the increased probability of isomerization before desorbing. The presence of metallic components should promote the hydrogenation of alkene to alkane and also may enhance hydrogen spillover to acid site,[12,13] leading to the formation of more normal isomers. In this regard, the proximity of metal and acid sites should be important to balancing these two functions.[5] On metal-free DAHY, decay of acid catalyzed cracking proceeded fast (Fig. 1) and the recovery of 1-octene added was ca. 60% after 2—3 h on stream, which suggested significant coke deposition.[8]

Effect of Support. Carbon number distribution of the products from CO-H_2 reaction was shifted to light side in the order: NaY2R2P[14,15]<HY2R2P<DAHY2R2P.[5] When 1-octene was added to syngas, product distribution was affected by concurrent cracking of 1-octene; apparent conversion[1] of 1-octene after 2—3 h on stream increased in the order: NaY2R2P (15%)< HY2R2P (26%)<DAHY2R2P (65%). As a result, yield of C_3—C_7 hydrocarbons increased by 1-octene addition in the same order: NaY2R2P<HY2R2P<DAHY2R2P.

TPD (temperature-programmed desorption) measurement of NH_3 revealed that the amounts of weak and strong acid, defined as the amount of ammonia desorbed below and above 350 °C, respectively, were as follows: NaY2R2P (1.51/0.20 mmol g-cat.$^{-1}$), HY2R2P (4.17/0.43 mmol g-cat.$^{-1}$), and DAHY2R2P (3.42/0.68 mmol g-cat.$^{-1}$). Therefore, the cracking tendency of 1-octene could be related to the amount of strong acid

Table 1. Effect of Metallic Composition on 1-Octene Cracking[a)]

Catalyst	DAHY2P	DAHY2R		DAHY2R2P		DAHY
Additive	1-Octene	None	1-Octene	None	1-Octene	1-Octene
CO conv./%	0.0	5.8	5.0	27.5	17.1	—
1-Octene Conv./%	97.3	—	42.1	—	65.0	95.7
Carbon number	Distribution/mmol g-cat.$^{-1}$ h^{-1}					
C_1	0.17	0.19	0.28	0.56	0.78	0.00
C_2	0.01	0.00	0.06	0.05	0.10	0.00
C_3	0.33	0.06	0.21	0.26	0.28	0.17
C_4	2.05	0.12	0.77	0.54	1.27	1.05
C_5	0.84	0.09	0.40	0.38	0.72	0.50
C_6	0.25	0.06	0.23	0.23	0.36	0.23
C_7	0.03	0.03	0.17	0.14	0.29	0.08
C_8	0.02	0.01	1.08	0.08	0.66	0.07
C_9	0.00	0.00	0.02	0.04	0.04	0.01
C_{10}	0.00	0.00	0.00	0.02	0.02	0.01
C_{11}	0.00	0.00	0.00	0.00	0.01	0.00
C_{12}^+	0.02	0.00	0.00	0.00	0.01	0.00
			i/n ratio (eq.[b)])			
C_4(1.1)	7.1	3.4	3.7	3.8	4.6	10.4
C_5(4.0)	18.8	5.1	16.0	14.9	15.6	135.0
C_6(5.9)	8.7	6.2	3.4	11.3	18.5	9.5
C_7(9.7)	3.2	6.3	31.0	15.6	28.0	4.6
C_8(7.1)	1.5	3.8	8.3	10.0	11.2	0.3

a) Reaction conditions : 240°C, 1.5 MPa, W/F=12.5 g-cat. h mol^{-1}, $H_2/CO=3/2$, 1-octene feed rate=1.9 mmol g-cat.$^{-1}$h^{-1}, data obtained after 2—3 h on stream, 1-octene cracking over support under flow of He b) Thermodynamic equilibrium at 240°C.

sites on the catalysts: NaY2R2P<HY2R2P<DAHY2R2P. It is generally known that cracking requires strong acid sites.[16] Selectivity for C_4 fraction and apparent 1-octene conversion are plotted against the amount of strong acid sites of the catalysts in Fig. 2. The content of isobutane amounted to more than 80% of C_4 fraction. The increase in isobutane should come from simple cracking of 1-octene following skeletal isomerization of carbenium ion on acid sites. This type of simple cracking was remarkable for DAHY2R2P, which possesses stronger acid sites than HY2R2P or NaY2R2P.

$$C_8 \rightarrow 2C_4 \quad (1)$$

The increase in the yield of C_7 and C_6 should originate from the disproportionation of feed 1-octene, since neither C_6 nor C_7 can be directly formed by β-scission of C_8 carbenium ions.

$$2C_8 \rightarrow [C_{16}] \begin{cases} \nearrow C_7 + C_9 \\ \searrow C_6 + C_{10} \end{cases} \quad (2)$$

An attempt was made to estimate the contribution of the disproportionation and the simple cracking to the carbon number distribution. Based on the Eqs. 1 and 2, the ratio of C_7/C_4 was taken as a crude measure of the ratio of disproportionation to simple cracking and shown in Fig. 2. The C_7/C_4 ratio decreased in the order: NaY2R2P>HY2R2P>DAHY2R2P. This indicates low selectivity for disproportionation with the catalysts with a large amount of strong acid sites, as was proposed by Corma et al.[17] Molar ratios

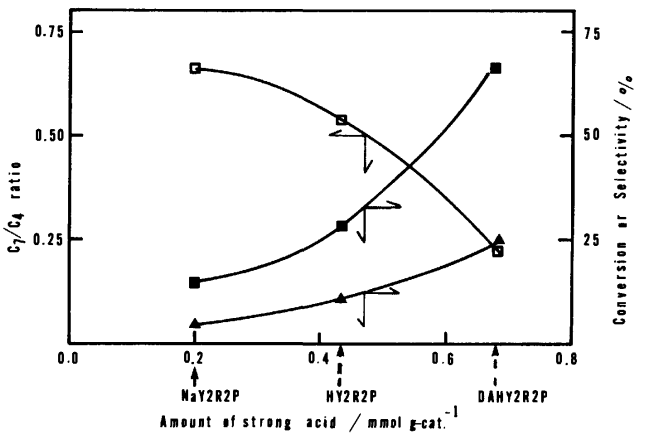

Fig. 2. 1-Octene conversion over NaY2R2P, HY2R2P, and DAHY2R2P. Reaction conditions: 240 °C, 1.5 MPa, $H_2/CO=3/2$, W/F=12.5 g-cat. h mol^{-1}, 1-octene feed rate=1.9 mmol g-cat.$^{-1}$ h^{-1}, after 2—3 h on stream. □, C_7/C_4 ratio; ■, 1-octene conversion;[1)] ▲, C_4 selectivity.

of C_7/C_9 and C_6/C_{10} are much larger than unity, suggesting subsequent cracking of heavy disproportionation products. The disproportionation/cracking ratio was also dependent on chain length of feed alkenes. With DAHY2R2P the ratio increased with decreasing the chain length as follows: $C_8<C_7<C_6$.[1]

Isomer distribution of C_8 fractions was scarcely dependent on the support, as shown in Fig. 3. The remaining C_8 feed consisted mostly of monobranched alkanes and dibranched alkanes. This suggests that relatively strong acid sites are not required for skeletal isomerization.[18] Cracking of alkanes and alkenes on large pore zeolite is considered to be preceded by conversion to readily formed branched isomers. With all this, it could be understood that the reaction path of 1-alkene should be strongly dependent on the acid properties of supports. The observed shift to the light side in carbon number distribution from simple CO hydrogenation over DAHY2R2P, compared to that over HY2R2P, was attributable to relatively large amount of strong acid sites.

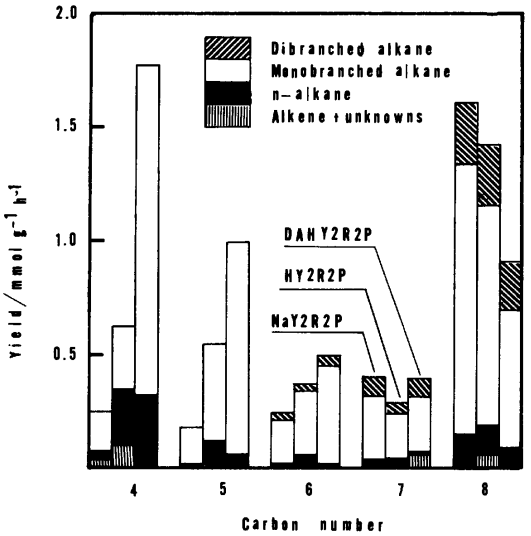

Fig. 3. Isomer distribution of product over NaY2R2P, HY2R2P, and DAHY2R2P. Reaction conditions: 240 °C, 1.5 MPa, $H_2/CO=3/2$, $W/F=12.5$ g-cat. h mol^{-1}, 1-octene feed rate=1.9 mmol g-cat.$^{-1}$ h^{-1}, after 2—3 h on stream.

Effect of H_2/CO Ratio. Effect of the partial pressure of H_2 and CO on products from DAHY2R2P was investigated by varying the H_2/CO ratio under the total pressure kept constant at 1.5 MPa. The obtained carbon number distribution is shown in Fig. 4. Isomer distribution is listed in Table 2. In the case of simple CO hydrogenation with high H_2/CO ratio large amount of methane was produced and the carbon number distribution shifted to light side. Activity decay was mitigated under these conditions, which was in agreement with the findings that the stabilized activity was obtained in case CH_4 was the main product.[8] Data obtained after 2—3 h on stream are shown in Table 2 and Fig. 4. Interestingly, only dimethyl isomers were detected for C_6 and C_7. Under these conditions the probability of skeletal isomerization could be high; the long chain alkenes and alkanes were virtually absent, resulting in the decrease in the rate of competitive adsorption and hydride transfer and hence prolonged lifetime of carbenium ion on acid site.[10,19]

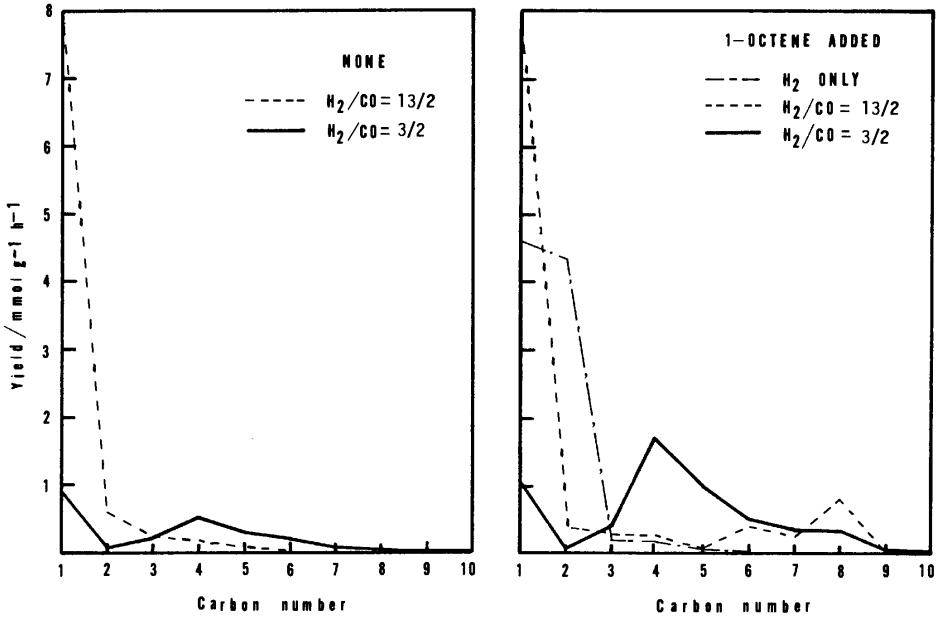

Fig. 4. Effect of H_2/CO ratio on carbon number distribution. Catalyst: DAHY2R2P; Reaction conditions: 240 °C, 1.5 MPa, $W/F=12.5$ g-cat. h mol^{-1}, 1-octene feed rate= 1.9 mmol g-cat.$^{-1}$ h^{-1}, after 2—3 h on stream.

Table 2. Effect of H_2/CO Ratio on Product Distribution[a)]

Reactant H_2/CO ratio		H_2/CO only		1-Octene addition[b)]		
		13/2	3/2	H_2 only	13/2	3/2
Carbon number	Product	Selectivity/%				
C_4	Butane	4.8	20.6	0.6	54.7	17.8
	Isobutane	94.0	78.9	95.1	45.2	81.3
	1-Butene	0.0	0.1	—	0.0	0.2
	t-2-Butene	1.2	0.3	4.3	0.1	0.5
	c-2-Butene	0.0	0.2	—	0.0	0.2
C_5	Pentane	1.4	6.3	—	41.2	6.0
	Isopentane	98.6	93.7	—	58.8	94.0
	Neopentane	0.0	0.0	—	0.0	0.0
	Alkenes + Unknown	0.0	0.0	—	0.0	0.0
C_6	Hexane	0.0	8.1	—	40.8	5.1
	2-M-pentane	0.0	51.5	—	35.4	56.9
	3-M-pentane	0.0	29.2	—	20.0	29.8
	2,2-DM-butane	17.7	0.0	—	0.2	0.0
	2,3-DM-butane	82.3	11.0	—	2.2	9.2
	Alkenes + Unknown	0.0	0.2	—	1.4	0.2
C_7	Heptane	0.0	8.4	—	17.4	3.3
	2-M-hexane	0.0	34.5	—	31.3	38.6
	3-M-hexane	0.0	31.3	—	33.7	31.5
	2,2-DM-pentane	0.0	0.0	—	1.6	0.0
	2,4-DM-pentane	100.0	8.4	—	6.2	9.5
	2,3-DM-pentane	0.0	10.7	—	5.1	9.5
	2,3,3-TM-butane	0.0	0.0	—	0.1	0.3
	Ethylpentane	0.0	6.3	—	2.5	2.8
	Alkenes + Unknown	0.0	1.3	—	2.1	4.5
C_8	Octane	—	8.0	—	12.2	8.0
	2-M-heptane	—	22.0	—	23.8	26.3
	3-M-heptane	—	26.1	—	27.3	32.8
	4-M-heptane (+3,4-DM-hexane)	—	8.2	—	8.5	9.8
	2,5-DM-hexane	—	7.8	—	8.6	7.3
	2,4-DM-hexane	—	10.4	—	9.6	9.5
	2,3-DM-hexane	—	5.2	—	3.1	4.9
	2,2-DM-hexane	—	0.0	—	1.6	0.0
	Alkenes + Unknown	—	12.3	—	5.5	1.4

a) Catalyst : DAHY2R2P; reaction conditions : 240°C, 1.5 MPa, W/F=12.5 g-cat. h mol^{-1}, data obtained after 2—3 h on stream, M : methyl, DM : dimethyl, TM : trimethyl, *c* : cis, *t* : trans. b) 1-Octene feed rate : 1.9 mmol g-cat.$^{-1}$h^{-1}.

Contribution of acid-catalyzed cracking to the carbon number distribution in the case of 1-octene addition seems to be less significant with H_2/CO= 13/2 than with H_2/CO=3/2. The addition of 1-octene to syngas with H_2/CO=13/2 resulted in the slight increase in the yield of C_6 and C_7, as shown in Fig. 4. In both cases, methane production was virtually unchanged on addition of 1-octene, suggesting methane formed mostly derived from CO hydrogenation directly. The higher H_2/CO ratio gave lower cracking conversion of 1-octene and larger portion of straight-chain products (Table 2). This would be caused by facile metal-promoted hydrogenation of 1-octene and other alkenes desorbed before hydrocracking since alkanes are less susceptible to hydrocracking than alkenes.[1)] One must also consider the desorption of alkanes from carbenium ions promoted by higher concentration of activated hydrogen,[12,13,19)] resulting in decrease in the chance of skeletal isomerization.

In the absence of CO, 1-octene converted to methane and ethane owing to hydrogenolysis on Ru-Pt bimetallic alloy (Fig. 4). It should be noteworthy that isobutane comprises most of the C_4 fraction. It was imagined that a large portion of 1-octene underwent carbenium ion type reactions on acid sites and the formed primary products were further hydrocracked to methane and ethane on metallic site. The relatively high yield of ethane can be accounted for by the

increasing order of activation energy of C-C bond breaking: $C_4<C_3\ll C_2$.[20] Small amount of CO (13%, $H_2/CO=13/2$) was sufficient to retard the hydrogenolysis of 1-octene. Further increase in CO fraction ($H_2/CO=3/2$) suppressed the methane formation during the courses of F-T synthesis. These findings imply negligible contribution of hydrogenolysis on metals to carbon number distribution of products in simple CO hydrogenation under standard conditions.

Effect of Contact Time. Effect of time factor on product distribution for DAHY2R2P was studied. The ratio of 2-M (2-methyl) and 3-M (3-methyl) isomers was employed as a measure of approach to equilibrium of the reaction products.[21,22] For simple CO hydrogenation, the short contact time (W/F=6.3 g-cat. h mol^{-1}) resulted in the 2-M/3-M ratios far below the equilibrium, as shown In Fig. 5. Low rate of 2-M isomers formation as primary products can be accounted for by a branching mechanism via protonated cyclopropanes.[22] With increasing contact time, the 2-M/3-M ratios increased.

The addition of 1-undecene resulted in the increase in 2-M/3-M ratios in C_6—C_8. This should come from the increased yield of 2-M isomers by cracking of 1-undecene and is in agreement with expectation based on carbenium ion-cracking mechanism.[23] These results suggest that there was only a minor contribution of cracking of heavy products to formation of C_6—C_8 fraction in the initial stage of CO-H_2 reaction. In the advanced stage, however, cracking of heavy fractions, which had been formed by oligomerization of light alkenes, seemingly occurred to a considerable extent.[1]

Effect of Temperature. Effect of temperature on the catalytic performance of DAHY2R2P is listed in Table 3. Simple CO hydrogenation at 300 °C exhibited remarkable increase in CO conversion and formation of methane and light hydrocarbons, compared to that at 240 °C. However, no significant change was observed for the *i/n* ratios of C_6—C_8 fractions. Slight decrease in the *i/n* ratios of C_4 and C_5 could result from contribution of cracking not preceded by formation of multibranched isomers. The addition of 1-undecene exhibited trends similar to simple CO hydrogenation. The yield of C_2 and C_3 was virtually unchanged on addition of 1-undecene at 300 °C, indicating little contribution of metal-promoted hydrogenolysis.

High temperature would lead to the promotion of CO hydrogenation on Ru-Pt alloy to produce light hydrocarbons. Simultaneously acid-catalyzed reaction should be also facilitated to give C_6—C_8 products rich in isoalkanes, although C_6—C_8 selectivity was significantly lowered. Thus the *i/n* ratios were kept at rather high levels while carbon number distribution

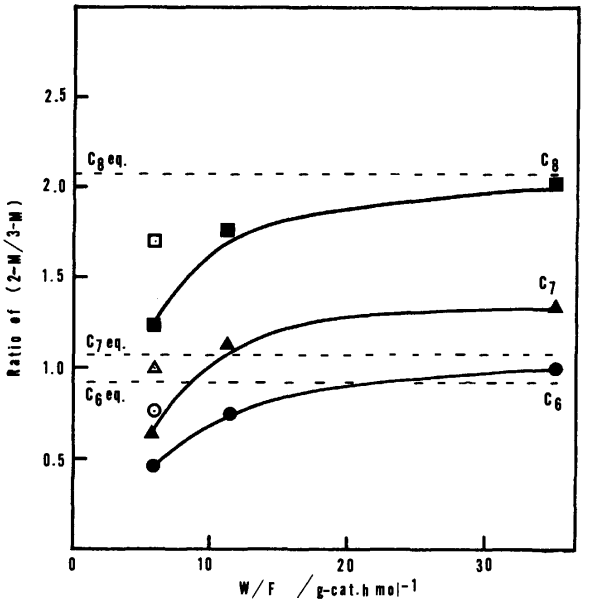

Fig. 5. Effect of time factor on 2-M/3-M ratio. Catalyst: DAHY2R2P; reaction conditions: 240 °C, 1.5 MPa, $H_2/CO=3/2$, 1-undecene feed rate=1.9 mmol g-cat.$^{-1}h^{-1}$, after 2—3 h on stream. 2-M/3-M ratio of products from simple CO hydrogenation: ●, C_6; ▲, C_7; ■, C_8. 2-M/3-M ratio of products from 1-undecene addition: ○, C_6; △, C_7; □, C_8. ···, 2-M/3-M ratio of thermodynamic equilibrium at 240 °C.

Table 3. Effect of Temperature on 1-Undecene Addition[a]

Additive	None		1-Undecene	
Temperature/°C	240	300	240	300
CO conv./%	15.5	42.2	12.9	52.8
Carbon number	Distribution/mmol g-cat$^{-1}h^{-1}$			
C_1	0.40	7.01	0.79	6.39
C_2	0.04	0.69	0.04	0.76
C_3	0.10	0.48	0.27	0.90
C_4	0.23	0.39	1.24	1.34
C_5	0.17	0.31	0.96	1.12
C_6	0.11	0.12	0.89	0.81
C_7	0.06	0.04	0.53	0.53
C_8	0.03	0.02	0.08	0.12
C_9	0.01	0.02	0.01	0.03
C_{10}	0.01	0.00	0.00	0.02
C_{11}	0.00	0.00	0.00	0.01
C_{12^+}	0.00	0.00	0.00	0.00
	i/n ratio			
C_4	3.8	1.3	5.9	1.6
C_5	14.0	9.0	19.4	10.9
C_6	11.3	11.2	3.2	17.3
C_7	10.0	13.2	15.6	26.6
C_8	8.2	9.2	7.9	21.9

a) Catalyst : DAHY2R2P; reaction conditions : 1.5 MPa, W/F=12.5 g-cat. h mol^{-1}, $H_2/CO=3/2$, 1-undecene feed rate=1.9 mmol g-cat.$^{-1}h^{-1}$. Data obtained after 2—3 h on stream.

was largely changed. The deactivation degree of the catalysts was strongly dependent on the operating temperature. High temperature seemed to be favorable to durability of cracking activity. In this respect, suppression of light alkane formation at high temperature on metallic site should be indispensable to develop a gasoline-forming catalyst with good activity, selectivity and life for practical use.

Conclusion

Addition of 1-alkenes has been successful to elucidate the role of acid site and metallic site in CO hydrogenation over RuPtHY and RuPtDAHY zeolite catalysts. Carbon number distribution and products composition are dependent on factors such as the activity for hydrogenation of CO and alkene as primary products on the metals, the amount of acid sites, and the acid strength distribution on the support as well as operating conditions such as partial pressure of H_2 and CO, H_2/CO ratio, temperature, and time factor.

Acid sites are crucial to producing isoalkanes in gasoline range products via secondary reactions. There is a dependence of major reaction path on acid strength; while simple β-cracking of carbenium ion is favorable on strong acid sites, disproportionation of carbenium ion is feasible on relatively weak ones, effecting changes in carbon number distribution of the products from CO-H_2.

References

1) Part I; T. Tatsumi, Y. G. Shul, Y. Arai, and H. Tominaga, "Proc. of 7 th International Zeolite Conference," ed by A. Iijima, Y. Murakami, and J. W. Ward, Kodansha-Elsevier, Tokyo (1986), pp. 891—898.

2) H. H. Nijs, P. A. Jacobs, J. J. Vendonck, and J. B. Uytterhoeven, *J. Chem. Soc., Chem. Commun.*, **1979**, 180.

3) H. H. Nijs, P. A. Jacobs, and J. B. Uytterhoeven, *J. Chem. Soc., Chem. Commun.*, **1979**, 1095.

4) D. Ballivet-Tkatchenko and I. Tkatchenko, *J. Mol. Catal.*, **13**, 1 (1981).

5) T. Tatsumi, Y. G. Shul, T. Sugiura, and H. Tominaga, *Appl. Catal.*, **21**, 119 (1986).

6) D. Vanhove, Z. Zhuyoung, L. Makambo, and M. Blanchard, *Appl. Catal.*, **9**, 327 (1984).

7) H. H. Nijs and P. A. Jacobs, *J. Catal.*, **65**, 328 (1980).

8) Y. G. Shul, T. Sugiura, T. Tatsumi, and H. Tominaga, *Appl. Catal.*, **24**, 131 (1986).

9) H. H. Voge, "Catalysis," ed by P.H. Emmett, Reinhold, New York (1958), Vol. 6, p. 425.

10) F. Ribeiro, C. Marcilly, and M. Guisnet, *J. Catal.*, **78**, 267 (1982).

11) R. V. Dmitriev, A. N. Detjuk, CH. M. Minachev, and K. H. Steinberg, "Spillover of Adsorbed Species," ed by G. M. Pajonk, S. J. Teichner, and J. E. Germain, Elsevier, Amsterdam (1983), pp. 17—29.

12) K. Fujimoto, M. Adachi, and H. Tominaga, *Chem. Lett.*, **1985**, 783.

13) B. K. Hodnett and B. Delmon, "Catalytic Hydrogenation," ed by L. Červený, Elsevier, Amsterdam (1986), pp. 53—76.

14) T. Tatsumi, Y. Takahashi, and H. Tominaga, *Sekiyu Gakkai Shi*, **28**, 114 (1985).

15) O. Okuda, T. Tatsumi, K. Fujimoto, and H. Tominaga, *Chem. Lett.*, **1983**, 1153.

16) A. Corma and B. W. Wojciechowski, *Catal. Rev.-Sci. Eng.*, **27**, 29 (1985).

17) A. Corma, J. B. Monton, and A. V. Orchilles, *Ind. Eng. Chem., Prod. Res. Dev.*, **23**, 404 (1984).

18) J. Abbot and B. W. Wojciechowski, *Ind. Eng. Chem., Prod. Res. Dev.*, **24**, 501 (1985).

19) D. J. Chick, J. R. Katzer, and B. C. Gates, *ACS Symp. Ser.*, **40**, 515 (1977).

20) B. A. Sarkany, K. Matusek, and P. Tetenyi, *J. Chem. Soc., Faraday Trans. 1*, **73**, 1699 (1977).

21) P. A. Jacobs, J. A. Martens, J. Weitkamp, and H. K. Beyer, *Discuss. Faraday Soc.*, **72**, 353 (1981).

22) J. Weitkamp, *Ind. Eng. Chem., Prod. Res. Dev.*, **21**, 550 (1982).

23) H. F. Schulz and J. H. Weitkamp, *Ind. Eng. Chem., Prod. Res. Dev.*, **11**, 46 (1972).

Cross Sections for the Quenching of Hg(6s6p$^1P_1$)

Hironobu UMEMOTO,* Akeo KASAKURA,† Jun KIKUMA, and Shin SATO†
Department of Applied Physics, Tokyo Institute of Technology, Ookayama, Meguro-ku, Tokyo 152
†Research Laboratory for Nuclear Reactors, Tokyo Institute of Technology, Ookayama, Meguro-ku, Tokyo 152
(Received December 27, 1986)

Absolute cross sections for the quenching of Hg(6s6p$^1P_1$) by simple molecules were measured by employing a Stern-Volmer type intensity measurement combined with a phase-shift measurement of effective radiative lifetime. The cross sections are approximately gas kinetic, except for rare gas atoms and tetrafluoromethane. The cross sections can be correlated with the C_6 long-range force parameter to the power 0.52.

Mercury is the most fundamental and widely used photosensitizer. Study on mercury-photosensitized reactions has the longest history in the field of photochemistry and relevant reactions have been dealt with in many review articles.[1-8] However, most of the study has been concentrated on the triplet excited-state mercury, the Hg(6s6p$^3P_1$) and Hg(6s6p$^3P_0$) states, and much less study has been made on Hg(6s6p$^1P_1$)-sensitized reactions.[9-15] No absolute values of cross section for the quenching of this state have been reported yet. Since the energy of Hg($^1P_1$) is 175 kJ mol^{-1} higher than that of Hg($^3P_1$), it is expected that some chemical exit channels which are not available in reactions of Hg($^3P_1$) or Hg($^3P_0$) are open in reactions of Hg($^1P_1$). For example, CO is not produced efficiently in the Hg($^3P_1$)-sensitized reaction of CO_2, while CO is one of main products in the Hg($^1P_1$)-sensitized decomposition of CO_2.[14] Quenching processes of the $^1P_1$ excited states of Cd, Zn, Mg, and Ca have been studied more extensively than reactions of Hg($^1P_1$).[7,8,16-26] It has been revealed that the $^1P_1$ states of these metal atoms are far less selective in quenching than the lower-energy ^3P_J states, and that the quenching cross sections are very large, comparable to those for gas kinetic collisions, except for rare gas atoms and perfluoroalkanes.[7,8,16-20,24-26] In other words, the quenching processes of these excited atoms are entrance-channel controlled. The cross sections for the deactivation of these $^1P_1$ states as well as the metastable $^3P_2$ and $^3P_0$ states of rare gas atoms can be correlated with the C_6 long-range force parameter to a power between 0.2 and 1.0, for cross sections larger than 50×10^{-20} m^2.[7,8,20] As for the Hg($^1P_1$) state, a similar relationship between cross sections and C_6 parameters has also been postulated on the basis of measurements of relative quenching efficiency obtained by Granzow et al.[7-9,27] In the present work, absolute cross sections for quenching of Hg(6s6p$^1P_1$) by simple molecules are determined and compared with those of analogous $^1P_1$ states of the other groups IIA and IIB metal atoms.

Experimental

The basic principle of lifetime measurement is the same as that described previously.[28] Resonance radiation at 184.9 nm from a microwave-powered mercury lamp was amplitude modulated at a frequency of 80, 100, or 120 kHz. This resonance radiation was used to irradiate a cylindrical reaction vessel made of Suprasil quartz, 31 mm in length and 27 mm in internal diameter, which contained a drop of mercury. The resonance fluorescence from the mercury vapor in the vessel as well as the exciting light from the lamp was detected alternately, with the aid of an aluminium mirror, with the same photomultiplier tube (Hamamatsu, R106) in conjunction with a vacuum ultraviolet monochromator (JASCO, VUV-1B). The phase difference between the photomultiplier signal and the internal reference signal of a lock-in amplifier (NF Circuit Design Block, 5610) was measured. The lifetime is given by the tangent of a phase delay angle of fluorescence relative to the excitation divided by the angular frequency of the modulation. In order to check the effect of the resonance radiation at 253.7 nm, some measurements were performed with a γ-ray irradiated LiF plate, which absorbed the 253.7 nm line more than 99% while transmitting the 184.9 nm line around 50%. It was confirmed that the lifetime is independent of the 253.7 nm light intensity.

In Stern-Volmer type experiments, the output of the mercury lamp was modulated at 70 Hz. At this frequency, steady-state can be assumed. The ratio of the fluorescence intensity in the absence of quencher, I_0, to that in the presence of quencher, I, was measured as a function of quenching gas pressure. The detection system was the same as that used for the lifetime measurement. The bimolecular rate constant for the quenching of Hg($^1P_1$), k_q, was determined by using:

$$\frac{I_0}{I} = 1 + k_q\tau_{eff}[Q], \quad (1)$$

where, τ_{eff} is the effective radiative lifetime of Hg($^1P_1$) in the absence of quencher as derived from the phase-shift measurement, and [Q] is the concentration of quencher. The validity of Eq. 1 will be discussed later. In order to avoid the effect of pressure broadening, measurements were performed in the presence of 8 kPa of He, which is much larger than the quencher gas pressure, except in the case of quenching by rare gas atoms. In the case of rare gas atoms, the total pressure was kept constant at 33 kPa. Since the quenching gases used in the present work do not absorb the 184.9 nm resonance line, no correction was necessary for direct absorption. The quenching cross section, σ_q, can be obtained by dividing k_q by the mean relative velocity,

$(8RT/\pi\mu)^{1/2}$, where R is the gas constant, T is the absolute temperature, and μ the reduced mass. The pressure of gases was measured with a mercury manometer. Low pressures, below 1 kPa, were estimated by the expansion technique using a known volume ratio. Experiments were performed at 306±2 K.

Similar experiments to determine the cross sections for the quenching of $Hg(^3P_1)$ by H_2 and D_2 were also performed. In this case, a glass cut-off filter was inserted between the lamp and the reaction vessel to remove the 184.9 nm resonance radiation.

Research-grade He (Japan Helium Center), N_2 (Toyo Sanso), H_2 (Showa Denko), D_2 (Takachiho Kako), and CO (Takachiho Kako) were used after being passed through a column of heated copper chips at 590 K and a trap filled with molecular sieve 4A cooled at 77 K. Ar (Nihon Sanso) and Xe (Takachiho Kako) were used after being treated in the same procedure of purification except that the temperature of the cold trap was raised properly. The organic compounds except n-C_4H_{10} (Tokyo Kasei) were products of Takachiho Kako and used without further purification. Hg was used after repeated distillation under vacuum.

Results

Quenching of $Hg(^3P_1)$ by H_2 and D_2. In advance of quenching measurements of $Hg(^1P_1)$, the cross sections for the quenching of $Hg(^3P_1)$ by H_2 and D_2 were measured. It was found that the apparent radiative lifetime of $Hg(^3P_1)$ in the absence of quencher is dependent on the modulation frequency. The measured lifetime in the presence of 8 kPa of He increased from 1.2 to 1.5 μs when the modulation frequency was changed from 30 to 120 kHz. A similar increase in lifetime with increase in modulation frequency has also been observed in the case of $Cd(^3P_1)$, and this has been attributed to the effect of radiation imprisonment.[29] On the other hand, the Stern-Volmer plots under the steady-state conditions in the presence of H_2 and D_2 were found to be linear. If we employ the average of the measured lifetimes between 30 and 120 kHz, 1.3 μs, as the effective radiative lifetime, the absolute quenching cross sections are calculated to be 28×10^{-20} and 29×10^{-20} m^2 for H_2 and D_2, respectively, by employing Eq. 1. These values agree well with the literature values.[30-32] Although there is an uncertainty in the estimation of effective lifetime, the above agreement should be enough for check of the present apparatus. In addition to this, it was found that the reciprocal of the measured lifetime of $Hg(^3P_1)$ in the presence of H_2, $1/\tau$, increased linearly with the H_2 pressure, and the slope did not show any marked dependence on the modulation frequency. If this value can be correlated with the quenching rate constant by the following equation, which is an exact expression when the radiation trapping can be ignored:

$$\frac{1}{\tau} = \frac{1}{\tau_{eff}} + k_q[Q], \qquad (2)$$

then, the quenching cross section for H_2 is calculated to be 29×10^{-20} m^2, which agrees well with that determined by the first procedure as well as the literature values.

Imprisonment Lifetime of $Hg(^1P_1)$. Because of the presence of radiation trapping, the effective radiative lifetime of $Hg(^1P_1)$ measured in the absence of quencher was much longer than the natural radiative lifetime, 1.4 ns,[7,8] but it showed no dependence on the modulation frequency between 80 and 120 kHz in contrast to the $Hg(^3P_1)$ case. On the other hand, the lifetime depended not only on the temperature of the system but also on the He pressure. Since the addition of a buffer gas is considered to broaden the spectral line, we supposed, at first, that the imprisonment lifetime would be shortened by the addition of a buffer gas even if the quenching efficiency by the gas is negligible. However, the lifetime in the absence of any buffer gas was found to be around 100 ns, which was shorter than that in the presence of a few kPa of He. The imprisonment lifetime increased with increase in the He pressure up to 0.5 kPa, and then began to decrease. Under the present experimental conditions, i.e., in the presence of 8 kPa of He and at 306±2 K, the effective radiative lifetime was around 160 ns. The fluctuation in the lifetime during the 1 or 2 h period necessary to perform a Stern-Volmer measurement for one species was less than the random error due to the uncertainty in the phase-angle measurement of the fluorescence, ±10 ns.

Quenching Cross Sections of $Hg(^1P_1)$. Figure 1 shows Stern-Volmer plots for four representative quenchers. Linearity of similar plots for the other quenchers was also good. The cross sections for the quenching of $Hg(^1P_1)$ were determined by employing

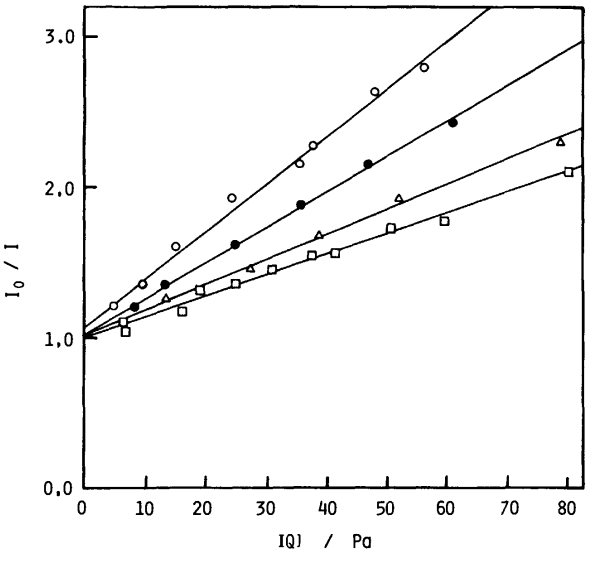

Fig. 1. Stern-Volmer plots for H_2(○), D_2(●), C_3H_8 (△), and N_2(□).

Table 1. Cross Sections for the Quenching of $Hg(^1P_1)$[a]

Quencher	Cross section $10^{-20}m^2$
Ar	<1
Xe	<1
N_2	79
H_2	44
D_2	44
CO	71
CH_4	52
C_2H_6	80
C_3H_8	132
n-C_4H_{10}	135
neo-C_5H_{12}	198
CF_4	<1

a) The error limits are ±9%; see text.

Eq. 1. In general, Eq. 1 is not a correct expression when the radiation trapping cannot be ignored.[33] However, according to the numerical calculation by Phillips,[34] under the condition of large optical depth, the effective radiative lifetime measured by the phase-shift method is nearly identical with that characteristic of the Stern-Volmer measurement. In other words, Eq. 1 may be used to evaluate quenching rate constants. Boxall et al.[35] have also shown experimentally that there is no significant difference between escape factors for pulsed and steady-state excitations at high opacities. The absolute quenching cross sections determined in this way are summarized in Table 1. These values are much larger than those for $Hg(^3P_1)$ or $Hg(^3P_0)$. The random statistical error from the least-squares best-fit slopes of the Stern-Volmer plots was around ±3%. Taking into account the uncertainty in the lifetime measurement, ±6%, the total uncertainty is estimated to be ±9%.

Discussion

Imprisonment Lifetime of $Hg(^1P_1)$. The increase in the imprisonment lifetime caused when a small amount of He was added, cannot be explained in terms of the concept of line broadening or quenching. In order to explain this increase, we considered that the decay of $Hg(^1P_1)$ in an evacuated system was controlled mainly by deactivation on walls. The mean free path in such a system is controlled by the vapor pressure of mercury and is about 2 cm. On the other hand, a simple calculation shows that, if the resonance radiation at 184.9 nm from the lamp has a Doppler broadened line shape at 1000 K and the hyperfine structure splitting of the $^1P_1$ state is much smaller than the Doppler width at 306 K, then 50% of the incident light is absorbed within 0.05 mm from the cell wall. Of course, the spectral line shape of the resonance radiation from the microwave-powered lamp we used must have been severely reversed, and the excitation in the reaction vessel should have been much more uniform, but the incident radiation from the lamp should still have been absorbed mainly within a thin layer near the cell wall. The addition of a small amount of a buffer gas decreases the mean free path and diffusion rate of $Hg(^1P_1)$ atoms, and increases the apparent lifetime. Similar deactivation processes of excited metal atoms at cell walls have also been reported recently with Zn and Cd.[24,36] The decrease in the imprisonment lifetime caused when more than 0.5 kPa of He was added can easily be explained by the increase in the escaping factor due to the change in the absorption line profile. The effective radiative lifetime without a buffer gas estimated by extrapolating the values above 0.5 kPa is 350 ns. This lifetime is a factor of 3 or 4 shorter than that predicted by the Holstein theory on the assumption of infinite slab or cylinder geometry.[37] This difference may be attributed to the difference in geometry of the reaction vessels. The effective radiative lifetime calculated numerically by Phillips for a realistic geometry is also one order of magnitude shorter than that calculated by the Holstein formula for infinite geometry.[34,37]

Table 2. Comparison of the Relative Quenching Cross Sections[a]

Quencher	This work	Granzow et al.[b]	Madhavan et al.[c]
N_2	(1.00)	(1.0)	(1.0)
Ar	<0.01	1.1	
H_2	0.56	0.2	
D_2	0.56		0.55
CO	0.89	1.0	2.3
CH_4	0.65	0.3	2.3
C_2H_6	1.01		4.8
C_3H_8	1.66		2.1

a) N_2 was chosen as a standard. b) Ref. 9. c) Ref. 10.

Comparison with the Literature Values. There have been no measurements of absolute cross section for the quenching of $Hg(^1P_1)$, but relative values have been reported by Granzow et al.[9] and Madhavan et al.[10] Granzow et al.[9] employed a Stern-Volmer measurement, while Madhavan et al.[10] estimated the cross sections by measuring production rates of $Hg(^3P_1)$ from $Hg(^1P_1)$. In Table 2, the results are compared. The agreement is very poor. If we choose N_2 as a standard, the value for CO reported by Granzow et al.[9] is in reasonable agreement with the present result, but their result for H_2 is a factor of 3 smaller than the present one. Granzow et al.[9] have described nothing about total pressure. Therefore, we suspect that they did not keep the total pressure constant. If they did not, this may be a cause of error, because the effective radiative lifetime as well as the

amount of light absorbed is considered to depend on the total pressure. It is more difficult to explain their result for Ar. Since the quenching of the $^1P_1$ states of Mg, Cd, and Zn by Ar is inefficient,[7,8,16,19,24,25] we are sure that the present result for Ar is much more reasonable. The quenching efficiency by Ar observed by Granzow et al.[9] is too large to be explained by effects of impurities in Ar, such as quenching and direct absorption of the 184.9 nm resonance line. Therefore, it is hard to give any reasonable explanation for this discrepancy. The agreement between the present results and those of Madhavan et al.[10] is still worse. The change in total pressure may also be a cause for the discrepancy in this case. However, in any cases, we suspect that their method is too indirect for quantitative determination of cross sections.

Recently, Callear and Du[13] have discovered three emission bands from a mixture of Hg($^1P_1$) and Xe. They have assigned the carrier of a broad band near 215 nm to a bound complex of Hg($^1P_1$) with Xe formed in a slow termolecular process, and the other carriers to excited complexes which are correlated to Hg($^3P_2$). They have also demonstrated that the production of Hg($^3P_2$) from Hg($^1P_1$) by Xe occurs in a bimolecular process with a considerably large cross section, 4×10^{-20} m^2. The former conclusion is consistent with the present results, while the cross section they obtained for the formation of Hg($^3P_2$) is fairly large compared with the present value for the quenching of Hg($^1P_1$).

Correlation with the C_6 Parameter. In the case of the $^1P_1$ states of Cd, Zn, Mg, and Ca, the quenching cross sections can be correlated with the proportionality constant for the attractive part of the Lennard-Jones 6—12 potential, C_6, to a power between 0.2 and 0.9.[7,8,16-20] Breckenridge and Renlund[18] have also pointed out that if only the quenching by simple alkane hydrocarbons are considered, the cross section increases rather linearly with increase in the C_6 parameter in the case of Cd($^1P_1$) and Zn($^1P_1$). In the present case, the cross sections are very large except for CF_4 and rare gas atoms and a good correlation could be obtained between $\log_{10}\sigma_q$ and $\log_{10}C_6$ as illustrated in Fig. 2. Figure 2 also suggests that a still better correlation can be obtained if only the cross sections by the alkane hydrocarbons are plotted. This will be discussed later. It should be noted that the cross sections for the quenching of Mg($^1P_1$) and Cd($^1P_1$) by CF_4 are also much smaller than those expected from the C_6 correlation.[16,19] The C_6 parameters were estimated by using the Slater-Kirkwood approximation. The procedure was the same as that employed by Breckenridge and Umemoto.[19,20] In general, for entrance-channel controlled quenching, net coupling to the final states must occur at a distance greater than

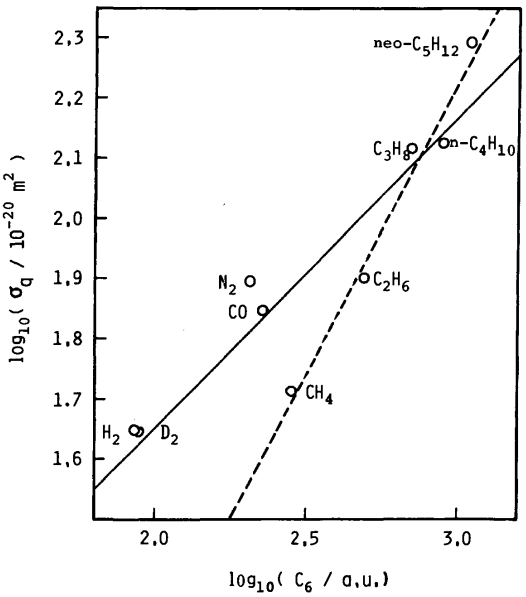

Fig. 2. A log-log plot of the cross sections for the quenching of Hg($^1P_1$) versus the long-range forces C_6 parameter. The solid line is the least-squares fit of the data, while the dashed line is the fit for only alkane hydrocarbons. The C_6 parameters are in atomic unit.

the hard-sphere collision distance. As for quenchers with positive or slightly negative electron affinities, such as N_2 and CO, the large quenching efficiencies have been explained in terms of the charge-transfer mechanism, in which it is assumed that facilitating potential surfaces with appreciable charge-transfer character are sufficiently low in energy.[7,8] On the other hand, in the case of saturated hydrocarbons, since the electron affinity is considerably negative, the above charge-transfer mechanism cannot be applied. It has been postulated that a strong chemical interaction of the $^1P_1$ states with individual C-H bonds provides necessary attractive potential surfaces.[7,8] Then, the inertness of CF_4 may be attributed to the lack of attractive chemical interaction between the $^1P_1$ states and the C-F bonds. In the reaction of Mg($^1P_1$) with alkyl C-H bonds, two processes have been postulated; insertion into C-H bonds and direct abstraction of H atoms.[22] Both of these chemical interactions should be less attractive in the case of C-F bonds because of the stronger bond strength,[38] as well as the heavier atomic weight of atom F. The least-squares slope of the log-log plot shown in Fig. 2 is 0.52 ± 0.08. Very similar results could also be obtained if the parameters for the dispersion forces were estimated from polarizabilities and ionization potentials according to the formula presented in Ref. 39. In this case, the slope is 0.54 ± 0.09. These values are smaller than those for Cd($^1P_1$) and Zn($^1P_1$) and nearly equal to the value for Mg($^1P_1$). It is interesting that

the empirical rule proposed by Breckenridge that the slope increases with increase in the electronic energy of the excited state, is not fulfilled in the present case.[7,8] On the other hand, if we restrict the discussion only to the quenching by the alkane hydrocarbons, the slope of the log-log plot shown in Fig. 2 is 0.96±0.10. Very similar results can be obtained for the other groups IIA and IIB metal atoms. The slopes are 0.85±0.16 for $Cd(^1P_1)$, 1.04±0.14 for $Zn(^1P_1)$, 0.86±0.06 for $Mg(^1P_1)$, and 0.78±0.17 for $Ca(^1P_1)$. These results are more consistent with the absorbing sphere model.[7,8]

The authors are grateful to Professor Toshihiro Ichimori of this Institute for permitting them to use the monochromator. They are indebted to Mr. Tadamasa Akutagawa of this Institute for the design of the microwave power generator. They are also grateful to Professor William H. Breckenridge of the University of Utah and one of the editors of this Bulletin for their suggestive comments.

References

1) H. E. Gunning and O. P. Strausz, *Adv. Photochem.*, **1**, 209 (1963).
2) R. J. Cvetanović, *Prog. React. Kinet.*, **2**, 39 (1964).
3) J. G. Calvert and J. N. Pitts, Jr., "Photochemistry," John Wiley & Sons, New York (1966).
4) L. F. Phillips, *Acc. Chem. Res.*, **7**, 135 (1974).
5) L. Krause, *Adv. Chem. Phys.*, **28**, 267 (1975).
6) D. L. King and D. W. Setser, *Ann. Rev. Phys. Chem.*, **27**, 407 (1976).
7) W. H. Breckenridge and H. Umemoto, *Adv. Chem. Phys.*, **50**, 325 (1982).
8) W. H. Breckenridge, "Reactions of Electronically Excited Atoms," in "Reactions of Small Transient Species," ed by A. Fontijn and M. A. A. Clyne, Academic, London (1983).
9) A. Granzow, M. Z. Hoffman, and N. N. Lichtin, *J. Phys. Chem.*, **73**, 4289 (1969).
10) V. Madhavan, N. N. Lichtin, and M. Z. Hoffman, *J. Phys. Chem.*, **77**, 875 (1973).
11) T. A. Gover and H. G. Bryant, Jr., *J. Phys. Chem.*, **70**, 2070 (1966); A. Granzow, M. Z. Hoffman, N. N. Lichtin, and S. K. Wason, *ibid.*, **72**, 3741 (1968).
12) A. B. Callear and K. Du, *Chem. Phys. Lett.*, **113**, 554 (1985).
13) A. B. Callear and K. Du, *Chem. Phys. Lett.*, **128**, 141 (1986).
14) Y. Mori, *Bull. Chem. Soc. Jpn.*, **34**, 1128 (1961); C. M. Wolff and R. Pertel, *J. Phys. Chem.*, **69**, 4047 (1965).
15) R. Holroyd and T. E. Pierce, *J. Phys. Chem.*, **68**, 1392 (1964); E. G. Spittler and G. W. Klein, *ibid.*, **72**, 1432 (1968); C. A. Heller and A. S. Gordon, *J. Chem. Phys.*, **42**, 1262 (1965); G. Liuti, S. Dondes, and P. Harteck, *ibid.*, **44**, 4051 (1966); N. L. Ruland and R. Pertel, *J. Am. Chem. Soc.*, **87**, 4213 (1965); R. Simonaitis and J. Heicklen, *J. Photochem.*, **1**, 181 (1972/73).
16) W. H. Breckenridge and A. M. Renlund, *J. Phys. Chem.*, **82**, 1474 (1978).
17) W. H. Breckenridge, R. J. Donovan, and O. K. Malmin, *Chem. Phys. Lett.*, **62**, 608 (1979).
18) W. H. Breckenridge and A. M. Renlund, *J. Phys. Chem.*, **83**, 1145 (1979).
19) W. H. Breckenridge and H. Umemoto, *J. Chem. Phys.*, **75**, 698 (1981).
20) W. H. Breckenridge and H. Umemoto, *Chem. Phys. Lett.*, **93**, 387 (1982).
21) W. H. Breckenridge and H. Umemoto, *J. Chem. Phys.*, **80**, 4168 (1984).
22) W. H. Breckenridge and H. Umemoto, *J. Chem. Phys.*, **81**, 3852 (1984).
23) W. H. Breckenridge, W. L. Nikolai, and D. Oba, *J. Phys. Chem.*, **90**, 5724 (1986).
24) M. Czajkowski, E. Walentynowicz, and L. Krause, *J. Quant. Spectrosc. Radiat. Transfer*, **28**, 493 (1982).
25) M. Czajkowski, E. Walentynowicz, and L. Krause, *J. Quant. Spectrosc. Radiat. Transfer*, **29**, 113 (1983).
26) P. D. Morten, C. G. Freeman, R. F. C. Claridge, and L. F. Phillips *J. Photochem.*, **3**, 285 (1974/75).
27) J. E. Velazco, J. H. Kolts, and D. W. Setser, *J. Chem. Phys.*, **69**, 4357 (1978).
28) H. Umemoto, S. Tsunashima, and S. Sato, *Chem. Phys.*, **43**, 93 (1979).
29) H. Umemoto, S. Tsunashima, and S. Sato, *Chem. Phys.*, **47**, 263 (1980).
30) J. S. Deech, J. Pitre, and L. Krause, *Can. J. Phys.*, **49**, 1976 (1971).
31) S. D. Gleditsch and J. V. Michael, *J. Phys. Chem.*, **79**, 409 (1975).
32) T. Hikida, M. Santoku, and Y. Mori, *Rev. Sci. Instrum.*, **51**, 1063 (1980).
33) G. van Volkenburgh and T. Carrington, *J. Quant. Spectrosc. Radiat. Transfer*, **11**, 1181 (1971).
34) L. F. Phillips, *J. Photochem.*, **4**, 407 (1975).
35) M. J. Boxall, C. J. Chapman, and R. P. Wayne, *J. Photochem.*, **4**, 435 (1975).
36) M. Czajkowski, A. Baczyński, and L. Krause, *J. Quant. Spectrosc. Radiat. Transfer*, **31**, 491 (1984); M. Czajkowski, E. Walentynowicz, and L. Krause, *ibid.*, **28**, 13 (1982).
37) T. Holstein, *Phys. Rev.*, **72**, 1212 (1947); *ibid.*, **83**, 1159 (1951).
38) R. C. Weast, ed., "CRC Handbook of Chemistry and Physics," CRC Press, 61st ed., Florida (1980/81), p. F-243.
39) J. O. Hirschfelder, C. F. Curtiss, and R. B. Bird, "Molecular Theory of Gases and Liquids," John Wiley & Sons, New York (1954), p. 963.

 © 1987 The Chemical Society of Japan Bull. Chem. Soc. Jpn., 60, 2349—2354 (1987)

ESR and Mass-Spectrometric Studies of Methanol Combustion. III. The Effect of CS_2 and CH_3NH_2 Additions on the Concentration Profiles of Chemical Species in a Methanol-Air Flame

Masayuki TANIGUCHI, Nobuhito HIRASAWA,† and Hiroshi YOSHIDA*
Faculty of Engineering, Hokkaido University, Kita-ku, Sapporo 060
(Received December 27, 1986)

The concentration profiles of chemical species (labile and stable) in methanol-air free-burning flames with and without the addition of CS_2 and CH_3NH_2 have been examined by means of the probe-sampling-ESR method, combined with mass-spectrometric measurements. In addition to the principal labile intermediates (H, O, and OH) and stable species (CH_3OH, O_2, H_2, CH_2O, CO_2, and H_2O), SO_2 and NO have been detected from the flame when it has been doped with CS_2 or CH_3NH_2 respectively. The observed results indicate that the addition of these dopants depresses the concentration of OH and raises the concentration of H_2 in the primary reaction zone, where SO_2 and NO are efficiently generated. The observed concentration profiles have been discussed in terms of the reaction mechanism of the oxidation of sulfur and nitrogen compounds.

In the previous works of this series,[1,2] we studied the concentration profiles of labile intermediates (H, O, and OH) and stable species (CH_3OH, O_2, CH_2O, CO, H_2, H_2O, and CO_2) in methanol-air premixed flames at atmospheric and low pressures by means of the probe-sampling-ESR method, combined with mass-spectrometric measurements. The chemical reactions during methanol combustion have been examined on the basis of the experimental results. The study will be extended here to the methanol-air flame doped with CS_2 and CH_3NH_2 in order to elucidate the chemical effects of these compounds on methanol combustion. CS_2 and CH_3NH_2 are examples of sulfur and nitrogen compounds which have simple chemical structures.

The chemical reactions of combustion involving sulfur and nitrogen compounds are interesting to study because their oxidation products, such as SO_x and NO_x, are the main sources of air pollution. In addition, sulfur compounds are believed to modify chemically the combustion processes in these flames. For example, it is known that SO_2 catalyzes the recombination of labile free radical intermediates in hydrogen,[3,4] hydrocarbon,[5] and carbon monoxide flames.[6] It is also known that the formation of NO from combustion is much affected by the presence of a sulfur compound in the flames.[4,7] However, there has been little investigation thus far reported on the chemical aspects of doping the flames with sulfur and nitrogen compounds.

As has been shown in the previous studies of our group[8,9] and others,[10] the concentration profiles of the labile intermediates in combustion flames can be examined comparatively easily by the ESR method. These previous studies have indicated that both the formation and the decay of the labile intermediates are sensitively dependent on the combustion conditions. Therefore, the chemical modification of combustion processes may be expected to be proven by observing the concentration profiles of the labile intermediates. With this expectation, the present study was planned. During the course of the preparation of this paper, Pauwels et al.[11] have reported the effect of H_2S addition on the concentration profiles of the labile intermediates in low-pressure methanol-air flames studied by the ESR method. In the present study, CS_2 and CH_3NH_2 are used as dopants. These studies as a whole will shed light on the chemical effects of doping the combustion of methanol under various combustion conditions.

Experimental

The burner used was made of brass and had a mouth 8 mm in diameter, as has been described previously.[1,9] Reagent-grade methanol was used as a fuel without further purification. Methanol with and without dissolved carbon disulfide, CS_2, and methylamine, CH_3NH_2, of reagent grade was continuously injected into the air stream supplied from a cylinder, regulated with a rotermeter, and preheated to 403 K. The composition of the premixed gas may be expressed by the equivalence ratio, ϕ, defined as: $\phi=([\text{fuel}]/[O_2])_{\text{actual}}/([\text{fuel}]/[O_2])_{\text{stoichiometric}}$. The flow rate of the premixed gas was kept constant at 1.0 l min^{-1}. The flame thus obtained was found to be axially symmetric. It consisted of a flat, bluish inner flame 1—2 mm above the burner mouth and a cone-shaped, faint-bluish outer flame 10 mm in height. The flame temperature was estimated by using a fine SiO_2-coated Pt/Pt-Rh thermocouple (0.1 mm in diameter) without correction for the radiative heat loss.

The concentration profiles of such labile intermediates as H, O, OH, and NO, together with O_2, in the flames were determined by means of the probe-sampling-ESR technique with an X-band ESR spectrometer previously described in detail.[1] About one-fifth of the reacting gas was continuously sampled through a pin hole (about 0.1 mm in diameter), and subjected to ESR measurements at 24 Pa. The residence time of the sampled gas in the sampling probe before reaching the ESR cavity was about 1.5 ms. A fraction of the sampled gas was then led to a quadrupole mass spectrometer to determine the concentration profiles of

† Present address: Marubeni, Ltd., Chiyoda-ku, Tokyo 100.

stable species (CH_3OH, CO_2, H_2O, H_2, CS_2, and SO_2). The mass spectrometric measurements were made at a total pressure of 10^{-3} Pa. The concentration profiles (all in mole fraction unit) were obtained on the center axis of the flame.

Results and Discussion

Observed ESR and Mass Spectra. ESR spectra due to H, O, OH, and O_2 were detected from both the doped and undoped flames. The features of the spectra were the same as has been reported previously.[1,8,9] When the fuel methanol was doped with a small amount of CH_3NH_2, an ESR spectrum with nine hyperfine lines centered at 830 mT (at 8.97 GHz) due to NO was additionally detected. The hyperfine splitting was found to be 2.7 mT, in agreement with that of NO($^2\Pi_{3/2}$) studied previously.[12] When the methanol was doped with CS_2, no additional spectrum was detected. Pauwels et al.[11] have recently observed the ESR spectrum due to SO and SH from low-pressure methanol flames doped with H_2S. The concentrations of SO and SH in the present atmospheric pressure flame are probably too low for ESR detection.

The intensity of the ESR spectra was calibrated with reference to the spectrum of O_2 (for H and O) and NO (for OH and NO) of known concentrations in the ESR cavity. The correction for the destruction of H, O, and OH in the sampling probe was made in the way described previously.[1]

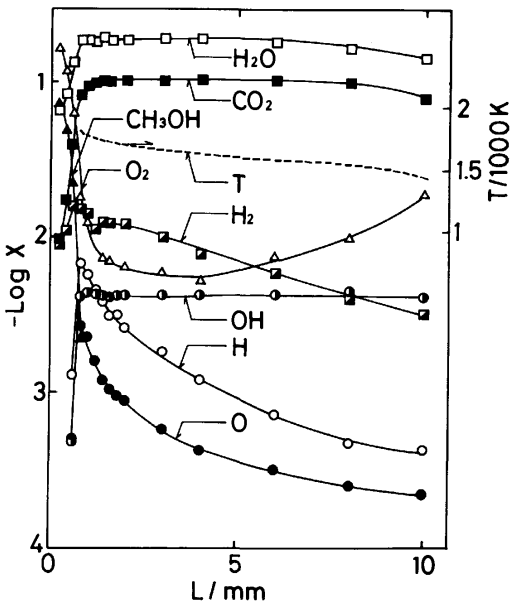

Fig. 1. The profiles of concentrations of stable and labile chemical species and temperature in a free-burning methanol-air flame of stoichiometric composition. The concentrations are presented in mole fraction units (X) on a logarithmic scale. The distance (L) is between the burner mouth and the sampling point on the center axis of the flame.

CH_3OH, H_2, CH_2O, CO_2, and H_2O were detected from both the doped and undoped flames by using the mass spectrometric method. When a small amount of CS_2 was added to the fuel methanol, additional intense spectra at m/z=64 and 76 were also detected. They are attributable to SO_2 and CS_2. The concentrations of these stable species were determined from the observed spectral intensities with reference to those of mixtures of known concentrations.

Concentration Profiles in the Undoped Flame. Figure 1 shows the concentration profiles of the labile intermediates and stable species in the flame of methanol-air premixed gas with the stoichiometric equivalence ratio: ϕ=1.0 (CH_3OH: 12.3%, O_2: 18.4%, and N_2: 69.3%). The concentration profile of CH_2O is not shown in Fig. 1 in order to avoid complexity of illustration, because the distribution of CH_2O was found to be limited to a restricted region in the inner flame. The concentration profiles in the inner flame region of the undoped methanol-air flame at atmospheric pressure were studied and reported in detail previously.[1]

The observed results in Fig. 1 show that O_2 and CH_3OH are consumed, while CO_2, H_2O, and H_2 are generated rapidly, in the inner-flame region. After the rapid generation, H_2O and CO_2 remain unchanged in concentration in the outer flame region. In contrast, H_2 decreases in concentration monotonously. The O_2 concentration shows a minimum value at about 4 mm above the burner mouth, and then it gradually increases. This increase is due to the diffusion of O_2 from the surrounding air into the flame.

The flame temperature reaches a maximum in the inner-flame region, after which it decreases monotonously downstream.

The concentrations of H, O, and OH increase rapidly and reach the maximum value in the inner flame region. The concentration of H and O then decrease continuously in the outer flame region, whereas the concentration of OH remains unchanged. Comparing the present results with those for the fuel-rich (ϕ=1.25) methane-air and fuel-lean (ϕ=0.75) methanol-air flames reported previously,[8,9] the overall features of the concentration profiles of the labile intermediates can be said to be little dependent on the equivalence ratio around ϕ=1.0, in both the inner- and outer-flame regions.

Effect of CS_2 Addition. Figure 2 shows the concentration profiles of CS_2 and SO_2 in the CS_2-doped flame. The premixed gas had a composition of CH_3OH: 11.6%, O_2: 18.5%, N_2: 69.4%, and CS_2: 0.46%. This composition gives almost a stoichiometric equivalence ratio, ϕ=1.02, if the combustion of CS_2 is expressed as $CS_2+3O_2 \rightarrow CO_2+2SO_2$. The concentration profiles of CH_3OH, H_2O, and CO_2 are also shown in Fig. 2 for the sake of comparison. CS_2 is rapidly consumed and SO_2 is concomitantly generated in the

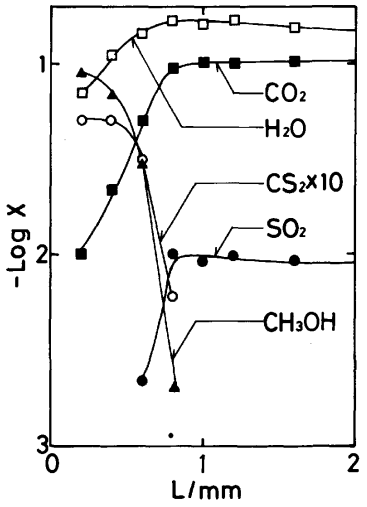

Fig. 2. Concentration profiles of CS_2, SO_2, CH_3OH, CO_2, and H_2O in a free-burning methanol-air flame doped with CS_2.

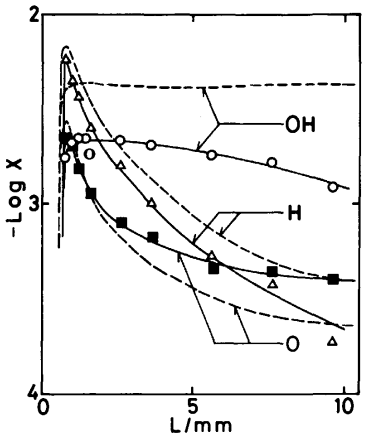

Fig. 3. Effects of CS_2 addition on the concentration profiles of labile intermediates in a free-burning methanol-air flame. The dashed lines and the solid lines denote the flame without and with addition of 0.46% CS_2.

inner-flame region, where CH_3OH is converted effectively and rapidly into H_2O and CO_2. The SO_2 thus-formed keeps a constant concentration throughout the downstream region of the flame, where almost all the S atoms exist in the form of SO_2.

The effect of the CS_2 addition on the concentration profiles of the labile intermediates is shown in Fig. 3. The maximum concentration of OH in the inner flame region is reduced by as much as 50%. In contrast, the maximum concentrations of H and O are not very much affected.

The dependence of the maximum concentration of the labile intermediates on the concentration of the added CS_2 was also studied. Qualitatively, the depression of the concentration of the labile inter-

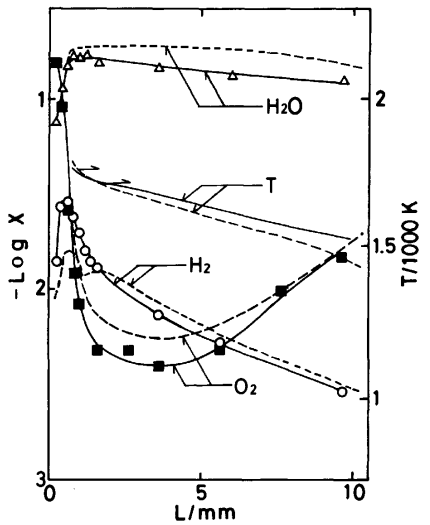

Fig. 4. Effects of CS_2 addition on the profiles of concentrations of stable species and temperature in a free-burning methanol-air flame. The dashed lines and the solid lines denote the flame without and with addition of 0.46% CS_2.

mediates becomes more remarkable with an increase in the CS_2 concentration. The effect of $(CH_3)_2SO$ as a dopant was also studied for comparison. The results were found to be qualitatively the same as those for CS_2.

The effect of CS_2 addition on the concentration profiles of the stable species is shown in Fig. 4. The concentration profiles of CH_3OH, CH_2O, and CO_2 are not affected significantly; therefore, they are not shown in Fig. 4. The flame temperature is lowered in the inner flame region and raised in the outer flame region by CS_2 addition.

One of the most remarkable effects of CS_2 addition is an increase in the H_2 concentration in the inner-flame region. According to the reaction model proposed by Westbrook and Dryer,[13] the main source of H_2 in the upstream region of the undoped methanol-air flame is the following reaction:

$$CH_3OH + H \longrightarrow H_2 + CH_2OH. \quad (1)$$

However, the rate of Reaction 1 in the inner-flame region is not promoted by the addition of CS_2, because the concentration of H is decreased, and the concentration of CH_3OH is not affected by the addition of CS_2.

Pauwels et al.[11] have recently studied the effect of the addition of H_2S to low-pressure methanol-air flames. They found an increase in the H_2 concentration as in the present case of the CS_2 addition. They have interpreted the increase as being due to the additional path of H_2 formation in the presence of H_2S:

$$H_2S + H \longrightarrow H_2 + SH. \quad (2)$$

However, the present results for CS_2 addition cannot be interpreted in the same way as those for H_2S addition; CS_2 cannot act as a primary source of H_2 because it has no H atoms. No hydrogen source, such as H_2S, originating from the added CS_2 could be observed in a concentration high enough to be responsible for the significant additional H_2 formation.

Another possible mechanism is that the increase in the H_2 concentration is attributable to the scavenging of OH by the added CS_2. The decrease in the OH concentration depresses the reaction;

$$H_2 + OH \longrightarrow H_2O + H, \quad (3)$$

which is otherwise an effective loss process of the H_2 generated by Reaction 1. Actually, the significant decrease in the OH concentration was observed in the inner-flame region on adding CS_2 to the flame.

The concentrations of H, O, and OH can be calculated by assuming a partial equilibrium in the flame based on the following rapid reactions:

$$H_2 + OH \rightleftharpoons H_2O + H \quad (3)$$
$$H_2 + O \rightleftharpoons OH + H \quad (4)$$
$$O_2 + H \rightleftharpoons O + OH \quad (5)$$

The partial equilibrium concentrations are given as:

$$X_e(OH) = [K_4K_5X(H_2)X(O_2)]^{1/2} \quad (6)$$
$$X_e(H) = K_3X(H_2)^{3/2}[K_4K_5X(O_2)]^{1/2}/X(H_2O) \quad (7)$$
$$X_e(O) = K_3K_5X(H_2)X(O_2)/X(H_2O) \quad (8)$$

By using the equilibrium constants in the literature[14]: $K_3=0.21\exp(7640/T)$, $K_4=2.27\exp(-938/T)$, and $K_5=300\cdot T^{-0.372}\exp(-8565/T)$, the observed concentrations of the corresponding stable species, and the observed flame temperatures, the equilibrium concentrations have been calculated to be $X_e(OH)=5.8\times10^{-3}$, $X_e(H)=7.0\times10^{-3}$, and $X_e(O)=2.2\times10^{-3}$ for the undoped flame and $X_e(OH)=5.5\times10^{-3}$, $X_e(H)=1.1\times10^{-2}$, and $X_e(O)=2.3\times10^{-3}$ for the CS_2-doped flame, both at a position 1.0 mm above the burner mouth. Considering the uncertainty in the observed flame temperatures caused by the radiative heat loss, the uncertainty of the calculated equilibrium concentrations is estimated to be within a factor of 1.5. The observed X values agree with the calculated X_e values in the undoped flame. In contrast, the observed X(H) and X(OH) values are significantly lower than the equilibrium concentrations for the CS_2-doped flame. These disagreements indicate that a decrease in the concentrations of labile intermediates upon the addition of CS_2 is not to be interpreted as being due to a decrease in the flame temperature. The decrease in the labile intermediates is probably caused by rapid reactions between the labile intermediates and sulfur species, such as CS_2, S, SO, and SO_2.

The comparison between calculated X_e and observed X values was originally made by Pauwels et al.[11] for undoped and H_2S-doped methanol flames: the observed X values of the labile intermediates were found to be generally lower than the calculated X_e values when the flame was doped with H_2S. This effect of H_2S addition is especially significant for H and OH. The present results are in general accordance with those reported by Pauwels et al.

As is shown in Fig. 3, the concentrations of H and OH are depressed by the addition of CS_2 in the outer flame region, where the added CS_2 has almost entirely been converted to SO_2. This effect can be interpreted in terms of the well-known function of SO_2 in catalyzing the recombination of the labile intermediates:[15]

$$X + SO_2 + M \longrightarrow XSO_2 + M \quad (9)$$
$$Y + XSO_2 \longrightarrow XY + SO_2 \quad (10)$$

where X and Y represent H, O, or OH. According to Reactions 9 and 10, the concentration of O can also be expected to be depressed by the existence of SO_2 in the outer-flame region. Actually, an enhancement of the O concentration was observed, as is shown in Fig. 3. Necessarily, an additional reaction path (or paths) of generating O can be expected in the outer-flame region when the flame is doped with CS_2, but it or they are not yet known. The diffusion of O_2 from the surrounding air into the present flame under the ambient conditions may play an important role in this.

Effect of CH_3NH_2 Addition. Figure 5 shows the effects of the addition of CH_3NH_2 on the concentration profiles of the labile intermediates. The composition of the premixed gas for this doped flame was CH_3OH: 11.6%, O_2: 18.4%, N_2: 69.4%, and CH_3NH_2: 0.58%. The equivalence ratio was 1.02, based on the presumed combustion reaction: $CH_3NH_2+(9/4)O_2\rightarrow$

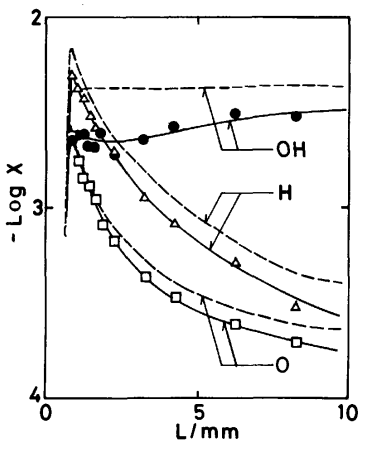

Fig. 5. Effects of CH_3NH_2 addition on the concentration profiles of labile intermediates in a free-burning methanol-air flame. The dashed lines and the solid lines denote the flame without and with addition of 0.58% CH_3NH_2.

CO_2+(5/2)H_2O+(1/2)N_2. The concentrations of the labile intermediates are qenerally lowered by the CH_3NH_2 addition. The effect is most significant for OH in the inner-flame region. It was also found that the depression of the concentrations of H and OH was more and more significant with an increase in the concentration of CH_3NH_2 added within the examined concentration range up to 1.2%, while the change in the concentration of O was rather insensitive in the higher CH_3NH_2-concentration range.

Dzotsenidze et al.[16] have studied the effect of the addition of CH_3NH_2 and NO on the H concentration in a rarefied H_2-O_2 flame at 700 K by using the ESR method: They have found a decrease in the H concentration upon the addition of CH_3NH_2 and NO. They have also found that the effect of added NO on the H concentration is significant. We examined also, in a separate experiment, the effect of adding NO to a methanol-air flame at atmospheric pressure. In this high-temperature flame, NO addition shows little effect on the concentrations of H, O, and OH. Thus, the effect of doping with CH_3NH_2 on the concentration of the labile intermediates seems to be the same for both high- and low-temperature flames, whereas the effect of doping with NO is not.

The effects of added CH_3NH_2 on the concentration profiles of stable species are shown in Fig 6. NO is rapidly formed from the added CH_3NH_2 in the inner-flame region, and it keeps a constant concentration downstream. About 50% of the N atoms of the added CH_3NH_2 exist in the form of NO in the flame after such a rapid NO formation. The concentration profiles of CH_3OH, H_2O, and CO_2 were found to be unchanged by the addition of CH_3NH_2 to the flame. The concentrations of CH_2O and CH_3NH_2 in the CH_3NH_2-doped flame could not be determined because of the overlap of their mass-spectral lines with those of NO (m/z=30) and CH_3OH (m/z=32) respectively.

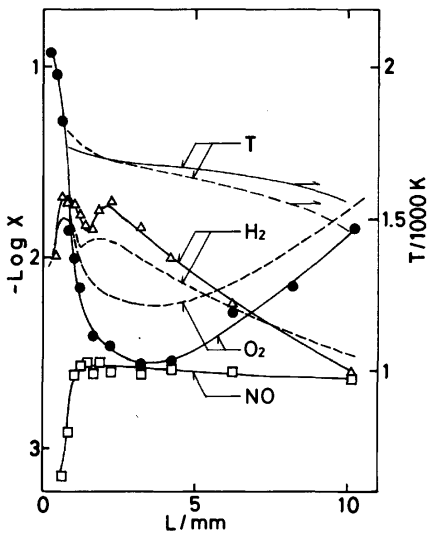

Fig. 6. Effects of CH_3NH_2 addition on the profiles of concentrations of H_2 and O_2, and temperature in a free-buring methanol-air flame. The dashed lines and the solid lines denote the flame without and with addition of 0.58% CH_3NH_2.

Two of the most significant effects of CH_3NH_2 addition are the enhancement of H_2 formation and the depression of the OH concentration occurring concomitantly in the inner-flame region. Such changes in the concentration of H_2 can be interpreted in the same way as for CS_2 addition: The decrease in OH caused by CH_3NH_2 addition depresses the oxidation of H_2 through Reaction 3.

Another possible mechanism is the formation of H_2 through the following reaction:

$$CH_3NH_2 + H \longrightarrow CH_3NH(\text{or } CH_2NH_2) + H_2. \quad (11)$$

According to the rate constant, $k_{11}=1.8\times10^7 \exp(-2670/T)$ m^3 mol^{-1} s^{-1}, reported by Blumberg and Wagner,[17] this reaction can have a rate constant of the same order of magnitude as that of the main H_2-forming reaction in the inner flame region (Reaction 1),[18] $k_1=4.0\times10^7 \exp(-3070/T)$ m^3 mol^{-1} s^{-1}, at the observed flame temperature. However, the enhancement of H_2 formation can not be attributed solely to Reaction 11, because the added concentration of CH_3NH_2 is not high enough for Reaction 11 to proceed at a significant rate.

The observed concentrations of H, O, and OH at the position 1 mm above the burner mouth were compared with the concentrations calculated by assuming a partial equilibrium based on Equations 6—8. It was found that the observed concentration is lower than the equilibrium concentration for H and OH in the CH_3NH_2-doped flame. This is the same trend as that observed in the CS_2-doped flame. The only different effect of doping between CH_3NH_2 and CS_2 is that the O concentration in the outer-flame region is lowered by CH_3NH_2 addition, whereas it is increased by the CS_2 addition. This may be due to the reaction of the NO oxidation, NO+O→NO_2, in the CH_3NH_2-doped flame.

Conclusion

The concentration profiles of the labile intermediates and the stable species in a methanol-air flame at atmospheric pressure with and without added carbon disulfide and methylamine were examined by means of a probe-sampling ESR method combined with mass-spectrometric measurements. The two dopants were found to be oxidized quickly into SO_2 and NO respectively. These products were comparatively stable, even in a high-temperature methanol-air flame. These dopants affect the chemical reactions in the inner-flame region by depressing the concentra-

tion of labile OH and by effectively enhancing the formation of H_2 from the principal fuel, CH_3OH. The effect of the H_2S-doping of the low-pressure methanol-air flame has very recently been studied by Pauwels et al.[11] The present results for the CS_2-doping are essentially the same as for H_2S-doping. These two studies by means of the ESR method show some of the general aspects of the chemical effects of sulfur compounds on the combustion reactions of methanol. They also show the usefulness of utilizing the ESR method for studies of the chemical modification of combustion. It should be stressed that the concentration profiles of labile intermediates are more sensitively dependent on the doping than are the concentration profiles of the stable intermediates.

References

1) M. Taniguchi, and H. Yoshida, *Bull. Chem. Soc. Jpn.*, **60**, 1249 (1987).

2) M. Taniguchi, T. Yoshioka, and H. Yoshida, *Bull. Chem. Soc. Jpn.*, **60**, 1617 (1987).

3) C. P. Fenimore and G. W. Jones, *J. Phys. Chem.*, **69**, 3593 (1965).

4) S. I. Tseregounis and O. I. Smith, *Symp. (Int.) Combust. [Proc.]*, **20**, 761 (1984).

5) R. McAndrew and R. Wheeler, *J. Phys. Chem.*, **66**, 229 (1962).

6) O. I. Smith, S.-N. Wang, S. Tseregounis, and C. K. Westbrook, *Combust. Sci. Technol.*, **30**, 241 (1983).

7) J. O. L. Wendt, J. T. Morcomb, and T. L. Corley, *Symp. (Int.) Combust. [Proc.]*, **17**, 671 (1979).

8) S. Noda, M. Miura, and H. Yoshida, *J. Phys. Chem.*, **84**, 3143, (1980).

9) S. Noda, H. Demise, O. Claesson, and H. Yoshida, *J. Phys. Chem.*, **88**, 2552 (1984).

10) J. F. Pauwels, M. Carlier, and L. R. Sochet, *J. Phys. Chem.*, **86**, 4330 (1982).

11) J. F. Pauwels, M. Carlier, P. Devolder, and L. R. Sochet, *J. Phys. Chem.*, **90**, 4377 (1986).

12) R. Beringer and J. G. Castle, Jr., *Phys. Rev.*, **78**, 581 (1950).

13) C. K. Westbrook and F. L. Dryer, *Combust. Flame*, **37**, 171 (1980).

14) G. Dixon-Lewis and D. J. Williams, "Comprehensive Chemical Kinetics," ed by C. H. Bamford and C. F. H. Tipper, Elsevier, Amsterdam (1977), Vol. 17, p. 91.

15) C. F. Cullis and M. F. R. Mulcahy, *Combust. Flame*, **18**, 225 (1972).

16) Z. G. Dzotsenidze, M. D. Museridze, M. M. Katsitadze, and R. G. Kobaladze, *Soobsch. Akad. Nauk Gruz. SSR*, **116**, 109 (1984).

17) V. B. Blumenberg and H. Gg. Wagner, *Ber. Bunsenges. Phys. Chem.*, **77**, 253 (1973).

18) J. Warnatz, "Combustion Chemistry," ed by W. C. Gardiner, Jr., Springer, New York (1984), p. 262.

 © 1987 The Chemical Society of Japan Bull. Chem. Soc. Jpn., 60, 2355—2360 (1987)

A Localized Molecular Orbital Approach to Bond Moment Theory. II. The Transferability of Bond Moment Derivatives

Hiroyuki SHINODA
Faculty of Pharmaceutical Science, Toyama Medical and Pharmaceutical University,
2630 Sugitani, Toyama 930-01
(Received February 2, 1987)

The transferability of bond moment derivatives(BMDs) in the bond moment theory was investigated by the use of localized molecular orbitals derived from INDO canonical orbitals. Five series of molecules were treated, two for a terminal C-H stretching motion and three for an O-H one. It is concluded that the transferability of BMDs with significant values is recognized among the molecules which have the same structure within the second neighbor bonds; it is also concluded that the changes in the molecular moiety beyond the third neighbor bonds slightly affect the BMDs of all the bonds, with the exception of the stretching one. These conclusions were confirmed by theoretical considerations, such as perturbation expansion.

It is well-known that the infrared-absorption intensity of a normal vibration described by the normal coordinate Q_j relates to the total dipole moment derivative with respect to Q_j, that is $(\partial\mu_{tot}/\partial Q_j)_o$, where μ_{tot} is the total dipole moment. Several methods of analyzing $(\partial\mu_{tot}/\partial Q_j)_o$ have thus far been presented;[1-6] they differ in the point of setting the intensity parameters. The bond moment theory has been of interest as one method of analyzing infrared intensities.[1] The theory is based on the assumption that the total dipole moment of a molecule is given as the sum of all the bond moments in the molecule. In using this theory, the bond moment derivatives(BMDs) with respect to the internal coordinates are used as intensity parameters, and $(\partial\mu_{tot}/\partial Q_j)_o$ is evaluated by means of their sum. Formally, a total dipole moment derivative with respect to any vibrational coordinate is a function of all the BMDs. In practice, however, their values can not be determined because the number of experimental information is less than the number of the BMDs. In order to overcome this difficulty, a large part of the BMDs are neglected and the transferability of a particular kind of BMD, e.g., C-H BMD, from one molecule to another has to be introduced. In a previous paper,[7] which will hereafter be called Part I, the bond moments and their derivatives with respect to a C-H stretching motion in some simple molecules were calculated by means of the localized molecular orbital approach, which is useful for discussing the bond moment theory because the approach can present the same situation as the basic assumption described above. In Part I the following two interesting results were obtained: The direction of each BMD is neither along the bond itself nor along the stretching bond, but the direction of the total dipole moment derivative is nearly along the stretching bond. Secondly, the change in a trans-sited bond moment is quite large. It was concluded from the results in Part I that the first-order approximation of the bond moment theory is inadequte to interpret an infrared-absorption intensity, since, in the first-order approximation, the direction of the BMD of a stretching bond was assumed to be parallel to the bond and the trans-sited BMD was never taken into account. Figeys et al. reached a similar interpretation.[8] They calculated the bond moments and their derivatives for cyanoacetylene and chloroacetonitrile by means of the ab initio molecular orbital method and said that there was quantum chemical evidence for the failure of the classical bond moment hypothesis for stretching modes.

In the present study, the BMDs with respect to C-H or O-H stretchings have been calculated for several series of molecules; their transferability will be discussed. The methods of calculation for localized molecular orbitals and the definition of bond moments are the same as those in Part I. In the calculation, the equilibrium geometries of molecules followed the data presented by Pople and Gordon.[9] Furthermore, the transferability of BMDs will be discussed along with considerations such as perturbation expansion.

Results and Discussion

Five series of molecules were considered in the present study, two for a C-H stretching and three for an O-H stretching; they are shown in Fig. 1. The numbering of the atoms and the designation of the lone-pair orbitals are also shown. The BMDs calculated for the molecules of the five series are listed in Tables 1—5. The BMDs of the bonds in the substituents X and Y in Fig. 1 were not included in the tables, since they were very small; most of them were smaller than 0.03D Å^{-1} (1D=3.33564×10^{-30} C m). Some exceptions were, however, found in the third neighbor bonds, which were connected with the trans-sited bond in a zigzag manner from a stretching bond.

Tables 1 and 2 include the BMDs with respect to a C-H stretching. In Table 1, the BMDs in any column resemble each other. The only exception is revealed in the BMDs of the stretching bond; they are roughly

divided into two groups by whether their values are larger or smaller than 0.14D Å^{-1}. The division of the BMDs seems to be attributable to the difference in the molecular fragments in the substituent X. Indeed, in the molecules which have an OH function directly connecting to the carbon atom of No. 5, the BMD of the stretching bond is less than 0.14D Å^{-1}. In the case of C^2-H^1 stretching, furthermore, the BMD of the stretching bond increases with the change in the substituent in X from -H to -C_2H_5, although the magnitude of the increase is small in comparison with that of the decrease in the presence of the OH function described above. On the other hand, in C^2-H^3 stretching the BMD of the stretching bond is only slightly affected by the substituent change from -H to -C_2H_5. Therefore, it can be said that the BMD of a stretching bond is very sensitive to the change in the substituent at a trans-sited position.

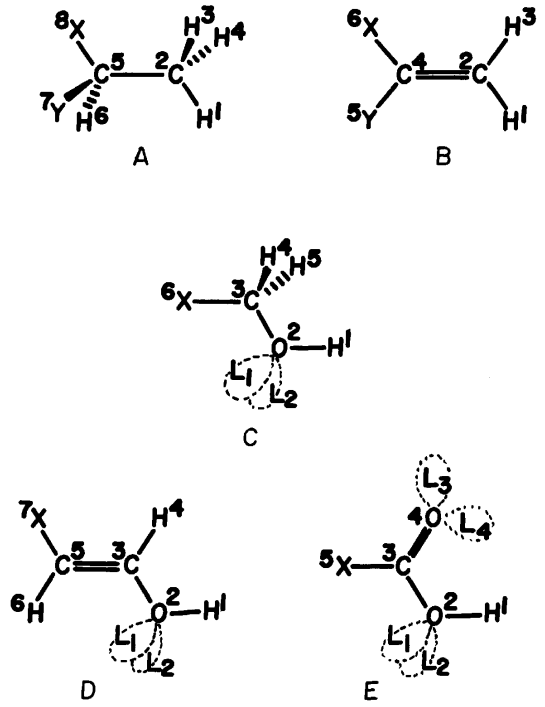

Fig. 1. The numbering of atoms and designation of lone pair orbitals for five series of molecules.

The results in Table 2 reveal the same tendency as those in Table 1, although the similarity of the BMDs in each type of bond is smaller than that shown in Table 1. The average of the BMDs for the adjacent C-H bond in Table 1 is 0.33D Å^{-1}; this is different from the corresponding value, 0.45D Å^{-1}, calculated from the results in Table 2. For the trans-sited C-H bonds, the averages from Tables 1 and 2 are also different from each other, their values being 0.21 and 0.29D Å^{-1} respectively. Such disparities are to be expected from the types of the adjacent carbon-carbon bonds, i.e., C-C or C=C, which bring different types of hybrids in the carbon atoms of the C-H bonds. On the basis of a study of the BMD of a stretching C-H bond for several hydrocarbons, Gussoni et al. pointed out that the hybridization of the carbon atom is the most important factor in deciding the BMD which increases with the increase in the s-character in the hybrid orbital.[4]

Tables 3—5 include the BMDs with respect to an O-H stretching. In Table 3 the similarity of the BMDs in each type of bond is recognized to some degree, and in the O-H stretching as well as the C-H stretchings, the spread of the BMDs for the stretching bond is wider than those of other bonds. Table 5 shows the same tendency. In Table 4 the similarity among the BMDs in each column is very well kept; it

Table 1. Bond Moment Derivatives with Respect to C-H Stretching in Series A[a] (D Å^{-1})[b]

Substituent[a]		Stretching bond		Adjacent bond		Trans-sited bond	Others	
X	Y			C-H	C-C			
C^2-H^1 stretching		1-2	2-3	2-4	2-5	5-8	5-6	5-7
-H	-H	0.144	0.333	0.333	0.347	0.213 (C-H)[c]	0.035	0.035
-CH_3	-H	0.168	0.333	0.333	0.360	0.222 (C-C)	0.027	0.027
-CH_2CH_3	-H	0.172	0.333	0.333	0.367	0.239 (C-C)	0.027	0.027
-CH_2OH	-H	0.148	0.333	0.333	0.351	0.224 (C-C)	0.033	0.033
-OH	-H	0.117	0.325	0.325	0.338	0.148 (C-O)	0.024	0.024
-OH	-CH_3	0.114	0.328	0.334	0.342	0.158 (C-O)	0.025	0.023
-OH	-CH_2CH_3	0.112	0.327	0.328	0.338	0.146 (C-O)	0.024	0.022
C^2-H^3 stretching		2-3	1-2	2-4	2-5	5-6	5-7	5-8
-CH_3	-H	0.144	0.330	0.331	0.349	0.210 (C-H)	0.031	0.032
-CH_2CH_3	-H	0.142	0.330	0.331	0.349	0.212 (C-H)	0.024	0.034
-CH_2OH	-H	0.141	0.337	0.331	0.334	0.207 (C-H)	0.031	0.027
-OH	-H	0.122	0.329	0.334	0.353	0.196 (C-H)	0.024	0.021
-OH	-CH_3	0.112	0.324	0.335	0.347	0.201 (C-H)	0.021	0.012
-OH	-CH_2CH_3	0.108	0.327	0.331	0.358	0.202 (C-H)	0.029	0.025

a) See Fig. 1. b) 1D=3.33564×10^{-30} Cm. c) Letters in parentheses indicate the type of trans-sited bond.

Table. 2. Bond Moment Derivatives with Respect to C-H Stretching in Series B[a] (D Å^{-1})[b]

Substituent[a] X	Substituent[a] Y	Stretching bond	Adjacent bond C-H	Adjacent bond C=C	Trans-sited bond	Others
C^2-H^1 stretching		1-2	2-3	2-4	4-6	4-5
-H	-H	0.161	0.451	0.426	0.300(C-H)[c]	0.067(C-H)[c]
-H	$-CH_3$	0.166	0.451	0.407	0.297(C-H)	0.064(C-C)
-H	$-CH_2CH_3$	0.156	0.445	0.409	0.300(C-H)	0.067(C-C)
-H	$-CH=CH_2$	0.152	0.445	0.409	0.300(C-H)	0.057(C-C)
-H	$-CH=CH-CH=CH_2$	0.152	0.447	0.407	0.300(C-H)	0.057(C-C)
-H	-OH	0.180	0.441	0.437	0.266(C-H)	0.042(C-O)
$-CH_3$	-OH	0.163	0.446	0.438	0.274(C-C)	0.032(C-O)
$-CH_2CH_3$	-OH	0.161	0.452	0.444	0.292(C-C)	0.034(C-O)
C^2-H^3 stretching		2-3	1-2	2-4	4-5	4-6
-H	$-CH_3$	0.175	0.458	0.427	0.303(C-C)	0.064(C-H)
-H	$-CH_2CH_3$	0.175	0.458	0.433	0.320(C-C)	0.064(C-H)
-H	$-CH=CH_2$	0.177	0.455	0.438	0.312(C-C)	0.065(C-H)
-H	$-CH=CH-CH=CH_2$	0.183	0.460	0.436	0.318(C-C)	0.064(C-H)
-H	-OH	0.150	0.433	0.408	0.197(C-O)	0.050(C-H)
$-CH_3$	-OH	0.152	0.441	0.394	0.190(C-O)	0.050(C-C)
$-CH_2CH_3$	-OH	0.148	0.441	0.391	0.199(C-O)	0.053(C-C)

a), b), c) See footnotes in Table 1.

Table 3. Bond Moment Derivatives with Respect to O-H Stretching in Series C[a] (D Å^{-1})[b]

Substituent[a] X	Stretching bond	Adjacent bond Lone-pair		Adjacent bond C-O	Trans-sited bond	Others	
	1-2	L_1	L_2	2-3	3-6	3-4	3-5
-H	0.917	0.860	0.860	0.216	0.184(C-H)[c]	0.025	0.025
$-CH_3$	0.850	0.870	0.870	0.231	0.194(C-C)	0.025	0.025
$-CH_2CH_3$	0.870	0.872	0.872	0.231	0.209(C-C)	0.025	0.025
$-CH_2CH_2CH_3$	0.832	0.877	0.877	0.226	0.216(C-C)	0.025	0.025
$-CH_2OH$	0.889	0.859	0.859	0.218	0.194(C-C)	0.025	0.025

a), b), c) See footnotes in Table 1.

Table 4. Bond Moment Derivatives with Respect to O-H Stretching in Series D[a] (D Å^{-1})[b]

Substituent[a] X	Strething bond	Adjacent bond Lone-pair		Adjacent bond C-O	Trans-sited bond(C=C)	Others		
	1-2	L_1	L_2	2-3	3-5	3-4	5-6	5-7
-H	0.924	0.831	0.831	0.236	0.126	0.038	0.007	0.067
$-CH_3$	0.915	0.839	0.839	0.231	0.129	0.043	0.007	0.072
$-CH_2CH_3$	0.914	0.838	0.838	0.251	0.142	0.043	0.007	0.071
$-CH=CH_2$	0.924	0.835	0.835	0.241	0.133	0.038	0.005	0.072

a), b), See footnotes in Table 1.

Table 5. Bond Moment Derivatives with Respect to O-H Stretching in Series E[a] (D Å^{-1})[b]

Substituent[a] X	Stretching bond	Adjacent bond Lone-pair		Adjacent bond C-O	Trans-sited bond	Others	
	1-2	L_1	L_2	2-3	3-5	3-4	L_3	L_4
-H	1.180	0.700	0.700	0.270	0.190(C-H)[c]	0.070	0.058	0.113
$-CH_3$	1.110	0.717	0.717	0.283	0.207(C-C)	0.071	0.067	0.130
$-CH_2CH_3$	1.095	0.721	0.721	0.283	0.218(C-C)	0.067	0.067	0.132

a), b), c) See footnotes in Table 1.

is better than those in Tables 3 and 5, and the molecules treated in the series D have quite the same structure within the second neighbor bonds. Therefore, it can be said that the BMDs with significant values are only slightly affected by the change in the structure beyond the third neighbor bonds. The BMDs of the adjacent C–O bond in Table 5 are considerably different from those in Tables 3 and 4; also, the BMDs of L_1 and L_2 in Table 5 are different from those in Tables 3 and 4. It can be said, on the basis of these results, that the type of second-neighbor bond affects not only the BMDs of the adjacent C–O bond, but also those of the L_1 and L_2 lone-pair orbitals. It is noticeable that the BMDs of L_4 in Table 5 are not so small as to be negligible, but those of L_3 are small. These facts give us a new insight to be added to the bond moment theory. That is, even when the number of the intervening bonds between a certain bond and a stretching one is larger than or equal to two, the BMD of the bond is not always small. In other words, if the direct separation between two bonds is not large, and if the relative orientation of the bond with respect to the stretching one is proper, the change in the bond moment is significant.

In part I, the number of BMDs which were needed to interpret an infrared-absorption intensity could not be offered, though it was pointed out that the first-order approximation is inadequate. The results shown in Tables 1—5 support the following several conclusions: (1) The stretching of a terminal bond always induces changes in the bond moments of the stretching bond, the adjacent bonds, and the adjacent lone-pair orbitals. In addition to them, the bond moments of the bonds which do not connect to the stretching bond, but which are located at any suitable position, especially at a trans-sited position, change with a considerably large magnitude. (2) The transferability of the BMDs with significant values is recognized among the molecules which have the same structure within the second neighbor bonds. (3) The change in the molecular structure beyond third neighbor bonds slightly affects the BMDs of all the bonds with the one exception of the stretching one.

In order to explain the results in Tables 1—5, we will now try to develop a theoretical consideration like the perturbation technique. When a Z–H stretching motion is the perturbation, only the hydrogen atom in the Z–H bond moves along the bond. Without the loss of generality, the stretching bond can be fixed on the z-axis. Therefore, the perturbation operator can be written as $(\partial H/\partial z_H)_o$, where H is the Hamiltonian of a system and where z_H is the z-component of the Cartesian coordinate of the hydrogen atom. Within the framework of the INDO method,[10] only two expressions are necessary to evaluate the matrix elements of $(\partial H/\partial z_H)_o$: $\partial S^{HA}_{\mu\nu}/\partial z_H$ and $\partial \gamma_{HA}/\partial z_H$, where $S^{HA}_{\mu\nu}$ is the overlap integral between the χ^H_μ and χ^A_ν atomic orbitals and where γ_{HA} is the two-center electronic repulsion integral between the electrons in the H and A atoms. The master formulas of the expressons are listed in Pancir's paper.[11] The distance dependency of $\partial S^{HA}_{\mu\nu}/\partial z_H$ was examined in the cases of typical atomic orbitals for χ^A_ν. The results are shown in Fig. 2, which shows that the derivatives of the overlap integrals are almost negligible at distances longer than 4.0 Å. The orientation dependency of $\partial S^{HA}_{\mu\nu}/\partial z_H$ is not simple. It was found in Part I that localized molecular orbitals are mainly constructed as linear combinations of two hybrid orbitals or of one hybrid orbital and one hydrogen 1 s orbital. In a special case, only one hybrid orbital itself becomes a localized molecular orbital. We will, therefore, examine two examples of the orientation dependency of $\partial S^{HA}_{\mu\nu}/\partial z_H$ in the cases of a carbon sp^3 hybrid orbital and a hydrogen 1s orbital as χ^A_ν. It is supposed that the A atom and also the hybrid orbital exist on the xz-plane of the Cartesian coordinate space, at the origin of which the H atom in the Z–H bond is fixed. The directions of the A atom and of the lobe of the hybrid orbital are symbolized by θ and α respectively; they are defined as is shown in Fig. 3. The orientation dependency of the hybrid orbital is shown in Fig. 4. It is found from the figure that the value of $\partial S^{HA}_{\mu\nu}/\partial z_H$ largely depends on the values of θ and α. It is easy to

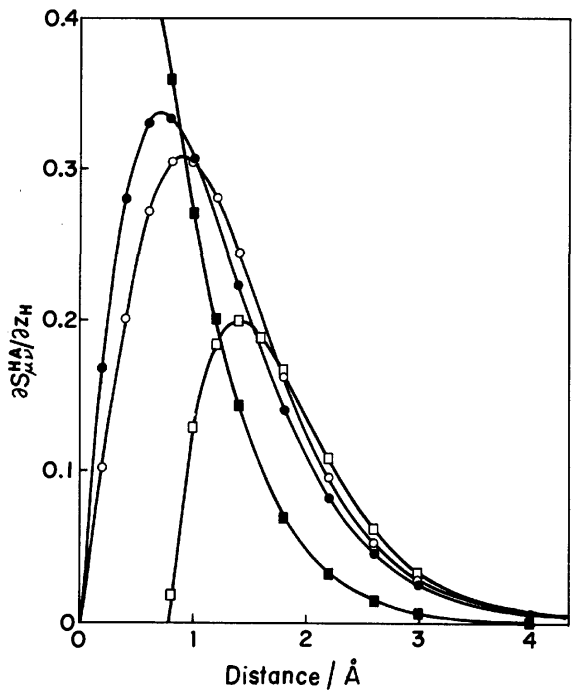

Fig. 2. The distance dependency of $\partial S^{HA}_{\mu\nu}/\partial z_H$ in a.u. (1a.u.=1.8898×10^{10} m^{-1}). The hydrogen 1s orbital, χ^H_μ, in H atom is located at the origin. (●): Hydrogen 1s orbital on z-axis for χ^A_ν, (○): carbon 2s orbital on z-axis for χ^A_ν, (■): carbon $2p_z$ orbital on x-axis for χ^A_ν, (□): carbon $2p_z$ orbital on z-axis for χ^A_ν.

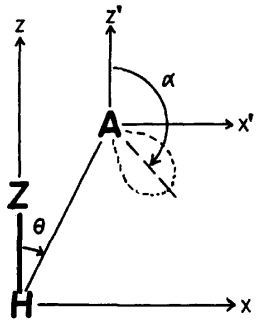

Fig. 3. The definition of θ and α. The z' and x' axes are parallel to z and x axes, respectively.

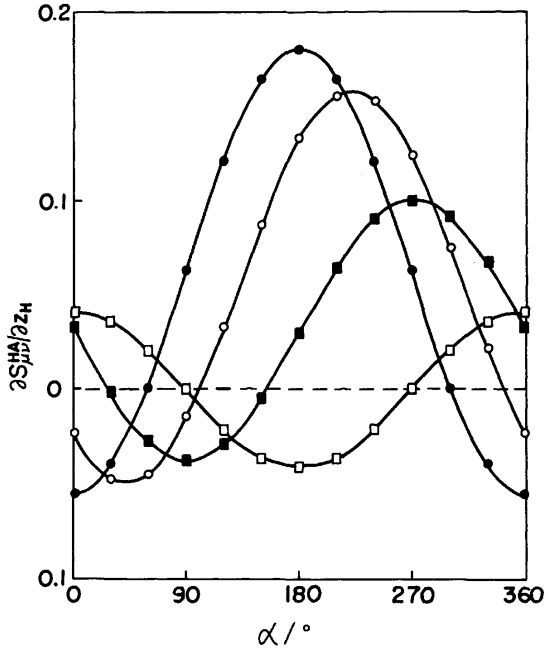

Fig. 4. The orientation dependency of $\partial S_{\mu\nu}^{HA}/\partial z_H$ in a.u. in the case of carbon sp^3 hydrid orbital for χ_ν^A. The distance between the H and A atoms is 2.0 Å. (●): θ=0°, (○): θ=30°, (■): θ=60°, (□): θ=90°.

derive that the variation of $\partial S_{\mu\nu}^{HA}/\partial z_H$ with respect to α at any constant value of θ corresponds to a *sin* curve as follows:

$$\frac{\partial}{\partial z_H}\int \chi_{1s}^H \chi_{sp^3}^A dv = \frac{1}{2}\left[\frac{\partial}{\partial z_H}\int \chi_{1s}^H \chi_{2s}^A dv + \sqrt{3}\,T\sin(\alpha+t)\right], \tag{1}$$

where:

$$T = \left[\left(\frac{\partial}{\partial z_H}\int \chi_{1s}^H \chi_{2p_z}^A dv\right)^2 + \left(\frac{\partial}{\partial z_H}\int \chi_{1s}^H \chi_{2p_x}^A dv\right)^2\right]^{1/2},$$

$$\sin(t) = \left(\frac{\partial}{\partial z_H}\int \chi_{1s}^H \chi_{2p_z}^A dv\right)/T,$$

and

$$\cos(t) = \left(\frac{\partial}{\partial z_H}\int \chi_{1s}^H \chi_{2p_x}^A dv\right)/T,$$

In these expressions, the derivatives of the overlap integrals with respect to z_H are the functions of θ. Therefore, the α_m value at which the maximum of Eq. 1 is given depends on the value of θ. In the results shown in Fig. 4, the α_m is 180° at θ=0°, and it continuously increases with the increase in θ until finally at θ=90° it becomes 360°. The maximum value of Eq. 1 also depends on the value of θ. The maximum at θ=0° is 0.18a.u.(1a.u.=1.8898×10^{10} m^{-1}), while at θ=90° it is 0.04a.u., which is small in comparison with that at θ=0°. However, we can not neglect it at θ=90° for the following two reasons. First, it can be seen from Fig. 4 that the value of Eq. 1 depends on α and becomes negligibly small in some regions of α, even at θ=0°. Second, in the localized molecular orbital which is constructed by a linear combination of two hybrid orbitals, their contributions to the derivative of the overlap integral are cancelled in some degree because the hybrid orbitals are located face-to-face. On the other hand, in the lone-pair orbital which is constructed by only one hybrid orbital, such a cancellation can never occur. The orientation dependency of $\partial S_{\mu\nu}^{HA}/\partial z_H$ in the case of a hydrogen 1 s orbital as χ_ν^A is very simple because of the spherical symmetry of the orbital. It is written as follows:

$$\partial S_{\mu\nu}^{HA}/\partial z_H = \cos(\theta)\left[\frac{\partial}{\partial z_H}\int \chi_{1s}^H \chi_{1s}^A dv\right]_{\theta=0}, \tag{2}$$

where the subscript θ=0 means that the A atom exists at θ=0° in Fig. 3. It is clear from Eq. 2 that the maximum of $\partial S_{\mu\nu}^{HA}/\partial z_H$, when χ_ν^A is the 1s orbital, is given at θ=0° and that $\partial S_{\mu\nu}^{HA}/\partial z_H$ continuously decreases until it reaches zero at θ=90°.

As is shown in Pancir's paper,[11] the orientation dependency of $\partial\gamma_{HA}/\partial z_H$ is the same as that of Eq. 2. The distance dependency of $\partial\gamma_{HA}/\partial z_H$ is shown in Fig. 5. It may be found from the figure that the derivatives are negligible at distances longer than 5.0 Å.

From the discussion of the distance and orientation dependencies of $\partial S_{\mu\nu}^{HA}/\partial z_H$ and $\partial\gamma_{HA}/\partial z_H$, it is concluded that the relative orientation of a bond with respect to the stretching one is an important facor in deciding the magnitude of the BMD of the bond. In other words, the BMDs of two bonds which are equidistant from the stretching bond are quite different if the orientaions of the bonds are different. It is also concluded that the bond moment of a bond separated from a stretching one by a distance of more than 5 Å changes slightly during the stretching motion. These conclusions do not contradict the results in Tables 1—5.

When the localized molecular orbitals of unperturbed and perturbed systems are denoted by $\{\phi_i^0\}$ and

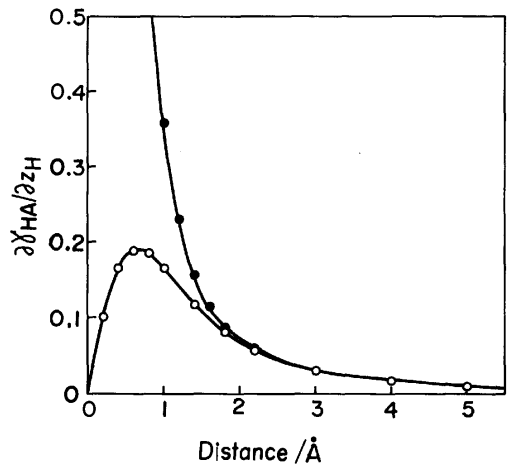

Fig. 5. The distance dependency of $\partial\gamma_{HA}/\partial z_H$ in a.u. (1a.u.=8.2390×10^{-8} J m^{-1}). The direction of A atom from H atom is parallel to z-axis. (●): The A atom is carbon, (O): the A atom is hydrogen.

$\{\phi_i\}$ respectively, ϕ_i is formally given by a linear combination of $\{\phi_i^\circ\}$ as follows:

$$\phi_i = \phi_i^\circ + \sum_{j\neq i} C_{ij} \langle \phi_j^\circ | \partial H/\partial z_H | \phi_i^\circ \rangle \phi_j^\circ, \quad (3)$$

where C_{ij} is the energy denominator in the first order perturbation expansion. The absolute value of the integral $\langle \phi_j^\circ | \partial H/\partial z_H | \phi_i^\circ \rangle$ is small unless ϕ_i° and/or ϕ_j° are localized on a stretching bond. Therefore, if ϕ_i° is localized on the stretching bond, all the terms in Eq. 3 remain more or less, but if ϕ_i° is not localized on the stretching bond, only the term with the ϕ_j° which is localized on the stretching bond remains. The above consideration fairly well explains the facts shown in Tables 1—5 that the influence of the changes of substituents beyond the second neighbor bond is found more in the BMD of a stretching bond than in those of other bonds.

Galabov and his coworkers have investigated the transferability of infrared intensity parameters by the method of bond polar parameters (BPPs), which are the derivatives of the total dipole moment with respect to the linear and angular coordinates, associated with individual bond vibrational distortions. In their study of F_2CO, Cl_2CO, F_2CS, and Cl_2CS,[12] it is shown that the transferability of BPPs does not hold among the molecules. Furthermore, from the results of their MO calculation for the series of C_1—C_5 normal paraffins and their 1-fluoro and 1-nitro derivatives, they concluded that the C-H BPPs are transferable between various hydrocarbon molecules and that the effect of polar substituents on BPPs may be quite significant because of intramolecular charge polarization; two methylene groups, however, almost entirely block their influence.[13] These conclusions from the investigations of Galabov et al. may also be well interpreted in terms of the theoretical discussion presented here.

The above theoretical consideration was performed along the INDO approximation. If the ab initio calculation is done, the number of kinds of the integrals which appear in the calculation is larger than that treated here. However, the distance dependency of the derivatives will be analogous to those in Figs. 2 and 5. Therefore, our qualitative conclusions derived from the results in Tables 1—5 will not be altered in the ab initio calculations. However, if a detailed and quantitative study of the infrared-absorption intensities is done, the selection of the basis set in the ab initio calculation becomes an important factor, since Miyazaki et al. pointed out, as a result of their investigation of carbon monoxide, that the expansion coefficients of the dipole moment with respect to the internal coordinate are highly sensitive to the selection of the basis sets.[14]

The calculation in this study was carried out at the Data Processing Center of Kyoto University.

References

1) D. F. Hornig and D. C. McKean, *J. Chem. Phys.*, **59**, 1133 (1955); P. R. Davies and W. J. Orville-Thomas, *J. Mol. Struct.*, **4**, 163 (1969); G. A. Thomas, J. A. Ladd, and W. J. Orville-Thomas, *ibid.*, **4**, 179 (1969); G. A. Thomas, G. Jalsovszky, J. A. Ladd, and W. J. Orville-Thomas, *ibid.*, **8**, 1 (1971); G. Jalsovszky and W. J. Orville-Thomas, *Trans. Faraday Soc.*, **67**, 1894 (1971).

2) W. B. Person and J. H. Newton, *J. Chem. Phys.*, **61**, 1040 (1974).

3) B. Galabov and W. J. Orville-Thomas, *J. Chem. Phys.*, **71**, 4716 (1979); B. Galabov, *ibid.*, **74**, 1599 (1981); B. Galabov, *J. Mol. Struct.*, **114**, 475 (1984).

4) M. Gussoni, P. Jona, and G. Zerbi, *J. Chem. Phys.*, **78**, 6802 (1983); M. Gussoni, C. Castiglioni, and G. Zerbi, *J. Phys. Chem.*, **88**, 600 (1984).

5) T. Koops and W. M. A. Smith, *J. Mol. Struct.*, **113**, 25 (1984).

6) For a review, see "Vibrational Intensities in Infrared and Raman Spectroscopy," ed by W. B. Person and G. Zerbi, Elsevier, Amsterdam (1982).

7) H. Shinoda and T. Miyazaki, *Bull. Chem. Soc. Jpn.*, **56**, 1924 (1983).

8) H. P. Figeys, P. Geerlings, and C. Van Alsenoy, *J. Chem. Soc., Faraday Trans. 2*, **75**, 528 (1979); *ibid.*, **75**, 542 (1979).

9) J. A. Pople and M. Gordon, *J. Am. Chem. Soc.*, **89**, 4253 (1967).

10) J. A. Pople and D. L. Beveridge, "Approximate Molecular Orbital Theory," McGraw-Hill, New York (1970).

11) J. Pancir, *Theoret. Chim. Acta (Berl.)*, **29**, 21 (1973).

12) B. Nikolova, B. Galabov, and C. Lozanova, *J. Chem. Phys.*, **78**, 4828 (1983).

13) B. Galabov, *J. Chem. Phys.*, **74**, 4744 (1981); B. Galabov, T. Dudev, and C. Lozanova, *J. Mol. Struct.*, **129**, 27 (1985).

14) T. Miyazaki, A. Matsuura, and H. Takeuchi, *Bull. Chem. Soc. Jpn.*, **57**, 1407 (1984).

 © 1987 The Chemical Society of Japan Bull. Chem. Soc. Jpn., 60, 2361—2365 (1987)

Adsorption of Dodecyltrimethylammonium Chloride from the Micellar Solution at Water/Air Interface

Makoto Aratono,* Toru Okamoto, and Kinsi Motomura
Department of Chemistry, Faculty of Science, Kyushu University 33, Fukuoka 812
(Received March 6, 1987)

The surface tension of the aqueous solution of dodecyltrimethylammonium chloride (DTAC) was measured as a function of temperature under atmospheric pressure at concentrations below and above the critical micelle concentration. The thermodynamic quantity changes associated with the adsorption of DTAC from its monomeric and micellar states were evaluated and proved to satisfy the thermodynamic relation derived on the assumption that the micelle formation can be treated as the appearance of a macroscopic bulk phase in the solution. Further their values were compared with those of the aqueous solution of dodecylammonium chloride and the influence of the chemical structure of the head group on the adsorption and micelle formation were discussed from the thermodynamic viewpoint.

It has been observed in the previous papers[1,2] that the entropy changes associated with surface adsorption and micelle formation of surfactant at concentrations around the critical micelle concentration (cmc) in its aqueous solution have negative values for dodecylammonium chloride and positive ones for 2-(octylsulfinyl)ethanol. Further the micelle has been proved to be treated thermodynamically as a macroscopic bulk phase in the solution when the thermodynamic quantities of micelle are replaced by the excess one with reference to the dividing surface chosen so that the excess number of moles of water equals zero. This treatment has been supported by measurements of the temperature and pressure dependence of interfacial tension of the aqueous solution of surfactant against oil.[3-6]

It is now interesting to investigate what influence the chemical structure of the polar head group of surfactant has on the thermodynamic quantity changes associated with adsorption and micelle formation. In this paper we are concerned with the adsorption of dodecyltrimethylammonium chloride (DTAC) at its aqueous solution/air interface at concentrations below and above the critical micelle concentration (cmc). The surface tension is measured as a function of temperature at fixed concentrations under atmospheric pressure and the thermodynamic quantity changes are evaluated by applying thermodynamic equations. The results are compared with those of dodecylammonium chloride (DAC).

Experimental

Dodecyltrimethylammonium chloride was synthesized and purified according to the method described previously[7] and its purity was checked by observing no minimum on the surface tension vs. concentration curve. Water was triply distilled from alkaline permanganate solution. The surface tension was measured by the drop volume technique described previously[8] and reproducible within 0.05 mN m^{-1}. The temperature was kept constant within 0.05 K by immersing the measuring cell in a thermostated water bath.

Results and Discussion

The surface tension γ was measured as a function of temperature under atmospheric pressure at various molalities m_1 of dodecyltrimethylammonium chloride in the aqueous solution. The surface tension vs. temperature curves are shown in Figs. 1a and 1b. It is seen that the value of γ decreases with increasing temperature and the curves at low concentrations are concave upward. At high concentrations, however, the curves seem to be linear. Therefore, it is expected that a break point will be observed on a surface tension vs. temperature curve at an intermediate concentration. Actually the curve 2 in Fig. 1b is found to have a break point, of which the concentration can be proved to be the critical micelle concentration.

Figure 2 illustrates the γ vs. m_1 curve depicted by picking up the γ values at a given temperature in Fig. 1. The sharp break is observed on the curve and its molality is referred to as the critical micelle concentration. The cmc values are shown as a function of temperature in Fig. 3 together with those of DAC. It is seen that the values depend remarkably on temperature and the cmc vs. T curve has a minimum. Comparing this curve with that of DAC, we notice that the chemical structure of the head group of surfactant has a considerable influence on the cmc value and temperature dependence of cmc. Making reference to our previous paper,[1] we also notice that the surface tension of DTAC at the cmc is considerably different from that of DAC.

The temperature derivative of surface tension obtained from Fig. 1 is plotted against molality at constant temperature in Fig. 4. It is seen that the value of $\partial\gamma/\partial T$ depends on temperature remarkably at concentrations below the cmc, while it is independent of temperature at concentrations above the cmc. Accordingly, the $-\partial\gamma/\partial T$ vs. m_1 curve is observed to vary discontinuously at the cmc. This observation supports the view that the micelle formation of DTAC is treated thermodynamically as if a macroscopic

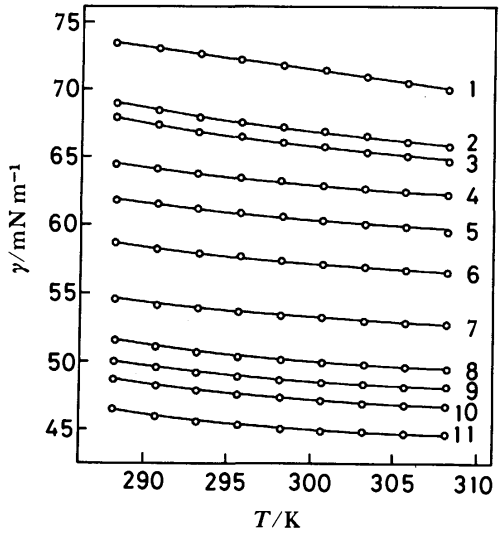

Fig. 1a. Surface tension vs. temperature curves at constant concentration under atmospheric pressure: (1) m_1=0 mmol kg^{-1}; (2) 2.18; (3) 2.76; (4) 4.18; (5) 5.83; (6) 7.76; (7) 11.32; (8) 14.59; (9) 16.45; (10) 18.32; (11) 21.57.

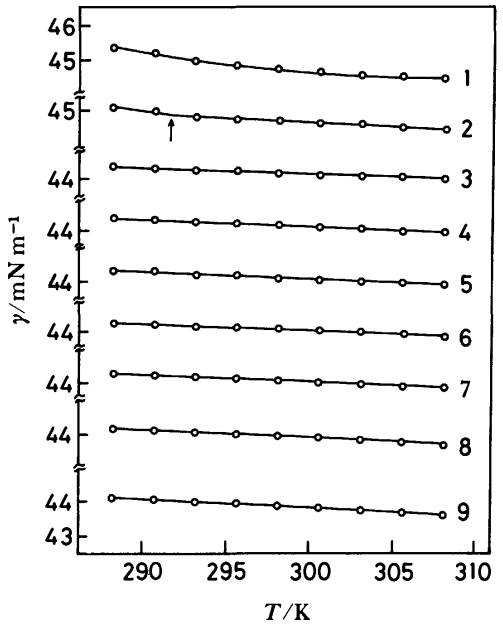

Fig. 1b. Surface tension vs. temperature curves at constant concentration under atmospheric pressure: (1) m_1=22.46 mmol kg^{-1}; (2) 23.40; (3) 25.47; (4) 27.76; (5) 28.50; (6) 29.43; (7) 31.70; (8) 37.29; (9) 48.76.

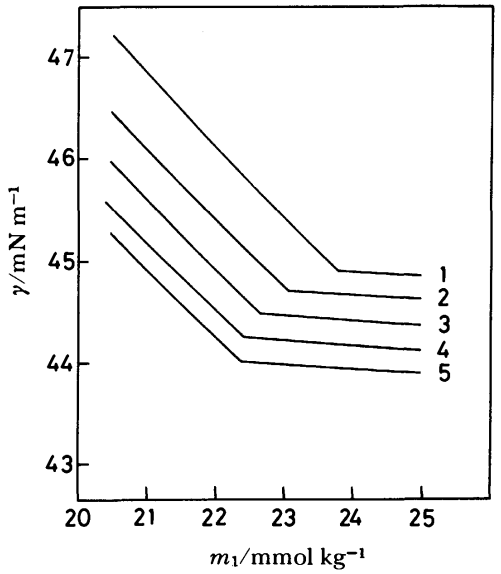

Fig. 2. Surface tension vs. concentration curves at constant temperature under atmospheric pressure: (1) 288.15 K; (2) 293.15 K; (3) 298.15 K; (4) 303.15 K; (5) 308.15 K.

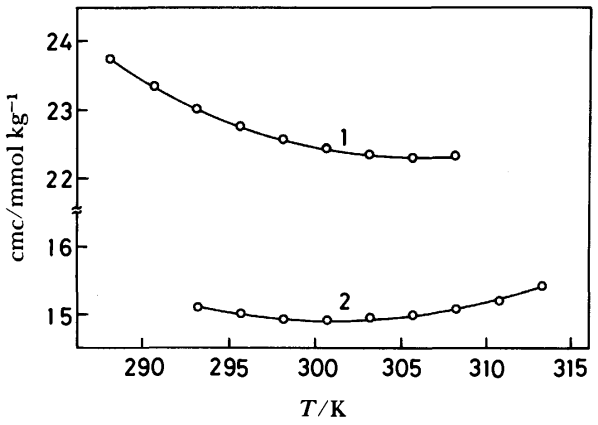

Fig. 3. Critical micelle concentration vs. temperature curves under atmospheric pressure: (1) DTAC; (2) DAC.

phase appears in the solution at the cmc.

It has been shown that the temperature dependence of surface tension of an aqueous micellar solution provides useful information upon the structures and properties of adsorbed films and micelles.[1-3] According to the thermodynamics of the adsorption of surfactant from its micellar solution,[1] the derivative of surface tension with respect to temperature under atmospheric pressure at a concentration below the cmc is related to the entropy change associated with the adsorption of surfactant from the aqueous solution $\Delta s(1)$:

$$(\partial\gamma/\partial T)_{p,m_1} = -\Delta s(1), m_1 < \text{cmc}, \quad (1)$$

while the derivative at a concentration above the cmc is related to the entropy change associated with the adsorption of surfactant from the micellar state $\Delta s(\text{M})$:

$$(\partial\gamma/\partial T)_{p,m_1} = -\Delta s(\text{M}), m_1 \geqq \text{cmc}, \quad (2)$$

on the assumption that the micelle formation may be treated thermodynamically like an appearance of a

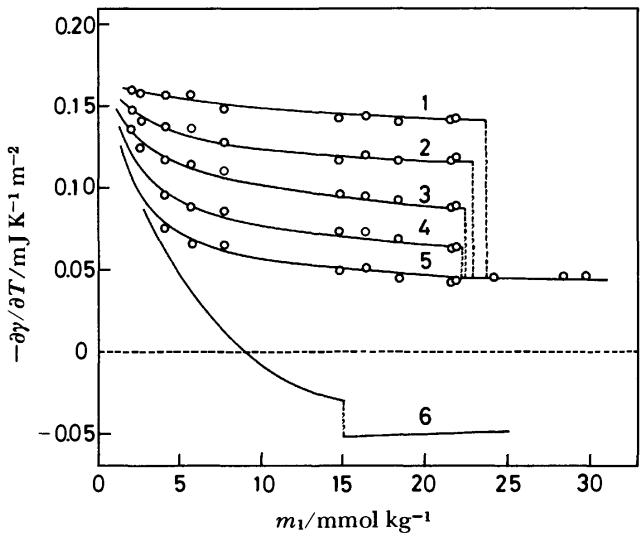

Fig. 4. Derivative of surface tension with respect to temperature vs. concentration curves under atmospheric pressure: (1) 288.15 K; (2) 293.15 K; (3) 298.15 K; (4) 303.15 K; (5) 308.15 K; (6) 298.15 K (DAC).

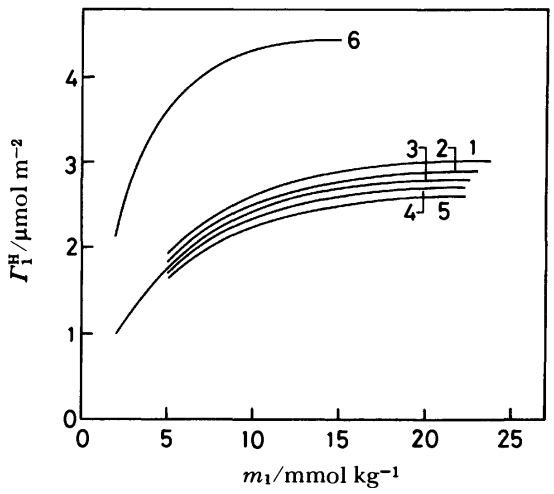

Fig. 5. Surface excess number of moles vs. concentration curves at constant temperature under atmospheric pressure: (1) 288.15 K; (2) 293.15 K; (3) 298.15 K; (4) 303.15 K; (5) 308.15 K; (6) 298.15 K (DAC).

new macroscopic phase and the behavior of micelle is determined only by temperature and pressure in a limited concentration range. Here $\Delta s(1)$ and $\Delta s(M)$ are respectively defined by

$$\Delta s(1) = \Gamma_1^H(s^H/\Gamma_1^H - s_1) \tag{3}$$

and

$$\Delta s(M) = \Gamma_1^H(s^H/\Gamma_1^H - s^M/N_1^M), \tag{4}$$

where Γ_1^H and s^H are the surface excess number of moles of surfactant and surface excess entropy with reference to the two dividing planes making the surface excess numbers of moles of air and water to be zero,[8,9] respectively, N_1^M and s^M are the number of surfactant ions in the micelle and the molar entropy of micelle defined with respect to the spherical dividing surface making the excess number of moles of water to be zero,[1] respectively, and s_1 is the partial molar entropy of monomeric surfactant in the solution.

Comparing the above equations with the results given in Fig. 4, it is found that $\Delta s(1)$ and $\Delta s(M)$ have positive values and accordingly the excess entropy of adsorbed film per mole of surfactant is larger than the partial molar entropy of monomeric surfactant and the excess entropy of micelle per mole of surfactant. This behavior is slightly different from that of DAC (curve 6). Further it is seen that the value of $\Delta s(1)$ decreases with increasing the concentration and depends on temperature remarkably, while that of $\Delta s(M)$ is almost independent of the concentration and temperature. On the other hand the discontinuous change of the $-\partial\gamma/\partial T$ vs. m_1 curve at the cmc, $\Delta s(1)-\Delta s(M)$, is correlated to the derivative of cmc

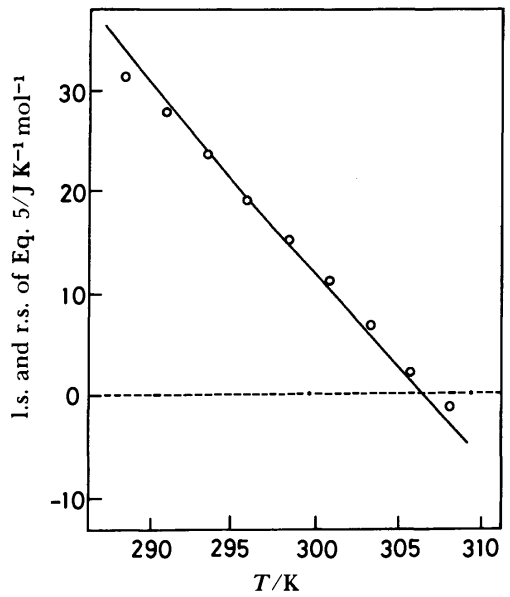

Fig. 6. Comparison between the left and the right side of Eq. 5: (O) left side; (—) right side.

with respect to T by the expression:[1]

$$[\Delta s(1) - \Delta s(M)]/\Gamma_1^H = -(2RT/\text{cmc})(\partial \text{cmc}/\partial T)_p. \tag{5}$$

The left side of Eq. 5 is numerically evaluated at the cmc by using the values of $\Delta s(1)$ and $\Delta s(M)$ given in Fig. 4 and the values of Γ_1^H which are calculated by applying the relation

$$\Gamma_1^H = -(m_1/2RT)(\partial\gamma/\partial m_1)_{T,p} \tag{6}$$

to the γ vs. m_1 curves and shown in Fig. 5 at constant temperature under atmospheric pressure. The right

side is calculated by the temperature dependence of the cmc values shown in Fig. 3. In Fig. 6, the values of the left side are plotted by circles and those of the right side are drawn by the full line. The values of both sides are in fair agreement with each other within the experimental error. Therefore, we can say that the present results concerning DTAC support the view that the micelle formation is treated like an appearance of a macroscopic phase in the solution in a limited concentration range.

It is now required to examine an effect of the head group of surfactant on the thermodynamic states of adsorbed film and micelle. This can be done by comparing the results of the DTAC system with those of the DAC system obtained in our previous paper.[1] Comparison between their temperature dependences of cmcs are made in Fig. 3. Looking at Fig. 4, the entropy change associated with the adsorption is found to be affected considerably by the difference in the head group. Since $\Delta s(1)/\Gamma_1^H$ gives the difference of the mean partial molar entropy of surfactant in the adsorbed film $\bar{s}_1^H$ from s_1 approximately at a large value of Γ_1^H,[2] the $\bar{s}_1^H$ value of DTAC may be said to be larger than that of DAC. This seems to be related to the fact that DTAC has fairly smaller Γ_1^H values than DAC as shown in Fig. 5. Further, it is noted that the $\Delta s(M)$ value of DTAC is positive, while that of DAC is negative. Taking into account that $\Delta s(M)/\Gamma_1^H$ is approximately equal in magnitude to $\bar{s}_1^H - \bar{s}_1^M$,[2] where $\bar{s}_1^M$ is the mean partial molar entropy of surfactant in the micelle, the value of $\bar{s}_1^H$ may be concluded to be larger than that of $\bar{s}_1^M$ in the case of DTAC in contrast with the case of DAC. Moreover, it is interesting that the corresponding entropy changes of 2-(octylsulfinyl)ethanol, which is a nonionic surfactant, behave similarly. These results indicate that the size and shape of the head group have a great influence on the packing of the surfactant molecules in the adsorbed film, the aggregation number of micelle,[10] and the distribution of counter ions.

Now we can obtain the thermodynamic quantities of micelle formation from the values of $\Delta s(1)$ and $\Delta s(M)$ at the cmc, because the adsorbed film, the micelle, and the monomeric surfactant in the solution are in equilibrium with each other when the adsorption takes place from the micellar solution. From Eqs. 3 and 4, we have

$$[\Delta s(1) - \Delta s(M)]/\Gamma_1^H = s^M/N_1^M - s_1. \quad (7)$$

The entropy change defined by the right side is referred to as the entropy of micelle formation $\Delta_W^M s$.[11] The values of $\Delta_W^M s$ evaluated by using the results in Figs. 4 and 5 are plotted against temperature with those of DAC in Fig. 7. It can be seen that the $\Delta_W^M s$ values of both systems decrease similarly with temperature and change their signs at high temperatures. Therefore we may say that the partial molar

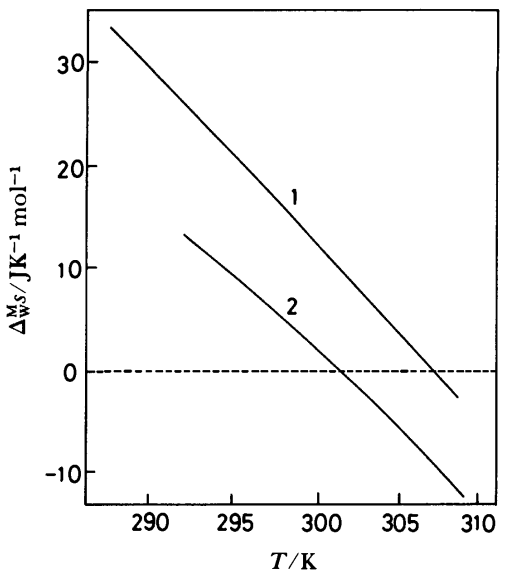

Fig. 7. Entropy change of micelle formation vs. temperature curves under atmospheric pressure: (1) DTAC; (2) DAC.

entropy of surfactant in the micelle is larger than that of monomeric surfactant at low temperature and is smaller at high temperature. Comparing the values of $\Delta_W^M s$ of DTAC with those of DAC, it is probable that the mean partial molar entropy of DTAC in the micelle is larger than that of DAC in conformity with the observation that the mean partial molar entropy of DTAC in the adsorbed film is larger than that of DAC.

Finally let us consider the micelle formation from an energetic point of view. The energy change associated with the adsorption of surfactant from the monomeric state $\Delta u(1)$ and that from the micellar state $\Delta u(M)$ are evaluated respectively by use of the relations

$$\Delta u(1) = \gamma + T\Delta s(1) - p\Delta v(1) \quad (8)$$

and

$$\Delta u(M) = \gamma + T\Delta s(M) - p\Delta v(M), \quad (9)$$

where $\Delta v(1)$ and $\Delta v(M)$ are the corresponding volume changes, respectively. The $\Delta u(1)$ and $\Delta u(M)$ values obtained by disregarding the pv terms on the right side[8] are illustrated in Fig. 8 at 298.15 K under atmospheric pressure. It is seen that $\Delta u(1)$ decreases with increasing concentration and is changed discontinuously at the cmc to $\Delta u(M)$ which is nearly constant for both surfactant systems. Comparing the $\Delta u(M)$ values of DTAC and DAC, though the $\Delta s(M)$ values of DTAC and DAC are opposite in sign as shown in Fig. 4, they are found to be positive, which suggests that the energy of the adsorbed state is larger than that of the micellar state for the two systems. It is further found that the $\Delta u(1)$ and $\Delta u(M)$ values of

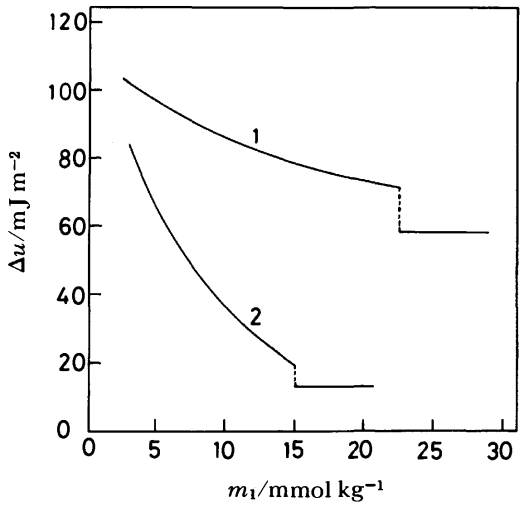

Fig. 8. Energy change associated with the adsorption vs. concentration curves at 298.15 K under atmospheric pressure: (1) DTAC; (2) DAC.

DTAC are larger than those of DAC. These results indicate that the energy states of the adsorbed film and micelle of surfactant are affected appreciably by the chemical structure of its head group. Further information regarding the effect of the head group will be obtained by investigating the systems of alkyldimethylammonium chloride and alkylmonomethylammonium chloride.

References

1) K. Motomura, S. Iwanaga, M. Yamanaka, M. Aratono, and R. Matuura, *J. Colloid Interface Sci.*, **86**, 151 (1982).
2) K. Motomura, S. Iwanaga, S. Uryu, H. Matsukiyo, M. Yamanaka, and R. Matuura, *Colloids Surf.*, **9**, 19 (1984).
3) M. Yamanaka, M. Aratono, H. Iyota, K. Motomura, and R. Matuura, *Bull. Chem. Soc. Jpn.*, **55**, 2744 (1982).
4) M. Yamanaka, H. Iyota, M. Aratono, K. Motomura, and R. Matuura, *J. Colloid Interface Sci.*, **94**, 451 (1983).
5) M. Yamanaka, M. Aratono, K. Motomura, and R. Matuura, *Colloid Polym. Sci.*, **262**, 338 (1984).
6) M. Yamanaka, M. Aratono, and K. Motomura, *Bull. Chem. Soc. Jpn.*, **59**, 2695 (1986).
7) M. Aratono, S. Uryu, Y. Hayami, K. Motomura, and R. Matuura, *J. Colloid Interface Sci.*, **98**, 33 (1984).
8) K. Motomura, S. Iwanaga, Y. Hayami, S. Uryu, and R. Matuura, *J. Colloid Interface Sci.*, **80**, 232 (1981).
9) K. Motomura, *J. Colloid Interface Sci.*, **64**, 348 (1978).
10) L. M. Kushner, W. D. Hubbard, and R. A. Parker, *J. Res. Nat. Bur. Stad.*, **59**, 113 (1957).
11) K. Motomura, M. Yamanaka, and M. Aratono, *Colloid Polym. Sci.*, **262**, 948 (1984).

Light-induced Electron-transfer Reactions. 5. Kinetics of the Oxidation of Ethylenediaminetetraacetatocobaltate(II) Complexes by Peroxodisulfate Ion, Induced by Irradiation with Visible Light of Aqueous Solutions Containing Tris(2,2′-bipyridine)ruthenium(II) Ion

Suzuko NISHIDA and Masaru KIMURA*
Department of Chemistry, Faculty of Science, Nara Women's University, Nara 630
(Received November 4, 1986)

The oxidation reaction of ethylenediaminetetraacetatocobaltate(II) ($[Co(edta)]^{2-}$) by peroxodisulfate ion ($S_2O_8^{2-}$) is greatly accelerated by irradiation with visible light of aqueous solutions containing tris(2,2′-bipyridine)ruthenium(II) ion ($[Ru(bpy)_3]^{2+}$). The overall reaction is $2[Co(edta)]^{2-}+S_2O_8^{2-} \rightarrow 2[Co(edta)]^{-}+2SO_4^{2-}$. The $[Ru(bpy)_3]^{2+}$ ion acts as a photosensitizer and -catalyst for this reaction, and the mechanism consists of a chain reaction being initiated by the quenching reaction of the photoexcited ruthenium(II) complex ion ($[Ru(bpy)_3]^{2+*}$) by $S_2O_8^{2-}$ ion. The mechanism of the reaction is presented to account for the results obtained.

There has been much interest in the photoinduced electron-transfer reactions containing $[Ru(bpy)_3]^{2+}$ from viewpoints of solar energy conversion.[1-3] In order to produce oxygen by the water photolysis, it is generally required to combine oxidative quenching reactions with redox catalytic steps with solid catalysts such as RuO_2, $RuO_2 \cdot xH_2O$, and IrO_2. Peroxodisulfate ion ($S_2O_8^{2-}$) is one of the most useful oxidative quenchers because $S_2O_8^{2-}$ decomposes to two sulfate ions upon photoreduction and thus, the reverse electron-transfer reaction can be completely prevented. Actually, there have been several reports using $S_2O_8^{2-}$ for the production of oxygen from water by use of $[Ru(bpy)_3]^{2+}$ as a photocatalyst.[4-13]

The photoexcited ruthenium(II) complex ($[Ru(bpy)_3]^{2+*}$), is quenched rapidly by the peroxodisulfate ion, generating $[Ru(bpy)_3]^{3+}$, $SO_4^{\cdot-}$, and SO_4^{2-}.[4] Both the species $[Ru(bpy)_3]^{3+}$ and $SO_4^{\cdot-}$ are strong oxidants and are able to oxidize various compounds. Thus, it is possible to design various kinds of light-induced oxidation reactions by using the peroxodisulfate ion containing $[Ru(bpy)_3]^{2+}$ as a photocatalyst. In previous works,[14,15] we studied the light-induced oxidation reactions of oxalate ions and formate ions by the peroxodisulfate ion. The present paper describes an experiment for the light-induced electron-transfer reaction between $[Co(edta)]^{2-}$ ($edta^{4-}$=ethylenediaminetetraacetate ion) and $S_2O_8^{2-}$ by employing $[Ru(bpy)_3]^{2+}$ as a photo-catalyst. This reaction hardly proceeded in the absence of $[Ru(bpy)_3]^{2+}$ under the conditions in the present paper and we demonstrate that the proposed scheme (v.i.) operates well in solutions over the pH range 1.9—7.0. Proposed scheme:

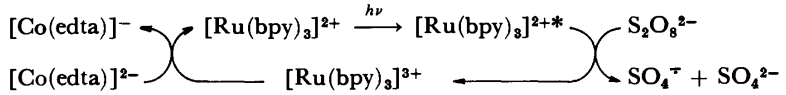

Hereafter, we use the abbreviation EDTA for all the forms of H_4edta, H_3edta^-, H_2edta^{2-}, $Hedta^{3-}$, and $edta^{4-}$.

Experimental

Chemicals. $[Ru(bpy)_3]Cl_2 \cdot 6H_2O$ and $K[Co(edta)] \cdot 2H_2O$ were prepared as described in the literature[16] and recrystallized twice from redistilled water. Reagent grade potassium peroxodisulfate (Wako Pure Chemicals Co.) was recrystallized twice from redistilled water and dried at room temperature in a vacuum desiccator. Sodium perchlorate used for adjusting ionic strength was recrystallized twice from redistilled water. Disodium dihydrogen ethylenediaminetetraacetate (Na_2H_2edta), cobalt sulfate($CoSO_4 \cdot 7H_2O$), and other chemicals were of guaranteed-reagent grade and used without further purification. Redistilled water was prepared from deionized water first by successive distillation from alkaline permanganate solution and then without addition of any reagents in a glass still.

Procedures. The reaction vessel was a colorless glass bottle (capacity 0.5 dm^3, diameter 80 mm, thickness 1 mm with 10 mm neck) and was placed in a thermostatted water bath made of colorless glass (2×3×3 dm^3, thickness 6 mm). Unless otherwise stated, the sample solution was irradiated with light from two 100-W tungsten lamps that were placed 3 dm to the right- and left-hand sides to the center of the reaction vessel. Irradiation was continued throughout the reaction. Oxygen was removed by bubbling pure nitrogen gas through the solution. Aliquot samples were withdrawn at appropriate times and mixed with a cation-exchange resin (Dowex 50W-X8, 200—400 mesh, hydrogen form, washed well with distilled water) in order to remove $[Ru(bpy)_3]^{2+}$ from the reaction solution and to stop the

reaction. After filtration, the concentration of $[Co(edta)]^-$ formed was determined spectrophotometrically by using the maximum molar absorption coefficient 295 $dm^3\ mol^{-1}\ cm^{-1}$ at 536 nm. The concentration of the peroxodisulfate ion remaining was determined polarographically at 0.1 V vs. SCE in a solution of 0.01 mol dm^{-3} perchloric acid, 0.1 mol dm^{-3} sodium perchlorate and 0.01% gelatine at 25 °C.

It was confirmed from the difference spectra between the reaction solution and the filtrate after removing $[Ru(bpy)_3]^{2+}$ with the cation-exchange resin (see above) that the concentration of $[Ru(bpy)_3]^{2+}$ maintained constant in the presence of $[Co(edta)]^{2-}$. The concentrations of $[Ru(bpy)_3]^{2+}$ and $[Ru(bpy)_3]^{3+}$ in the absence of $[Co(edta)]^{2-}$ were determined from the measurements of absorbance by using the values of molar absorption coefficients ($dm^3\ mol^{-1}\ cm^{-1}$) 1.1×10^4 and 3.3×10^3 at 420 nm, respectively, and 1.4×10^4 and 2.8×10^2 at 452 nm, respectively.[17] The Stern-Volmer plots were obtained from measurements of the luminescence of $[Ru(bpy)_3]^{2+*}$ by using a Hitachi 850 spectrofluorometer at an excitation energy of 452 nm after removing oxygen by bubbling pure argon gas through the solution.

Results and Discussion

As seen in Fig. 1, when the solutions containing $[Ru(bpy)_3]^{2+}$, $[Co(edta)]^{2-}$, and $S_2O_8^{2-}$ were irradiated with visible light, the concentration of $S_2O_8^{2-}$ decreased and that of $[Co(edta)]^-$ increased with the irradiation time (t). Both the kinetic curves in plots of $[S_2O_8^{2-}]$ vs. t and $[[Co(edta)]^-]$ vs. t were not influenced by the ratio of $[Co(II)]_{added}/[EDTA]_{added}$ over the range 1—3, but were seriously influenced at the ratio of 0.1.

Stoichiometry. When the light-induced reaction proceeded to large extent under the conditions $[Co(II)]_{added} \geq [EDTA]_{added}$, the concentrations of $[Co(edta)]^-$ and $S_2O_8^{2-}$ were determined. The ratio of $[[Co(edta)]^-]_{formed}/[S_2O_8^{2-}]_{decomposed}$ was 2.0±0.1 as an average of 7 runs. This indicates that the stoichiometry (and the overall reaction) is expressed by Eq. 1.

$$2[Co(edta)]^{2-} + S_2O_8^{2-} \longrightarrow 2[Co(edta)]^- + 2SO_4^{2-} \quad (1)$$

(in the case of $[Co(II)]_{added} \geq [EDTA]_{added}$)

On the other hand, when the concentration of cobalt(II) ion added was less than that of EDTA, the decomposition rate of $S_2O_8^{2-}$ became much faster, while the formation rate of $[Co(edta)]^-$ did not change so much. At the ratio $[Co(II)]_{added}/[EDTA]_{added}=0.1$, the rate of decomposition of $S_2O_8^{2-}$ became almost two times faster than that at the ratios of 1—3 (see the plots ▲ in Fig. 1). After the results and mechanisms of reaction under the conditions of $[Co(II)]_{added}=[EDTA]_{added}$ are presented, we discuss such behavior under the conditions of $[Co(II)]_{added} \ll [EDTA]_{added}$. As stated before, the concentration of $[Ru(bpy)_3]^{2+}$ remained constant during the reaction. However, after all the $[Co(edta)]^{2-}$ ion was oxidized to the $[Co(edta)]^-$ ion,

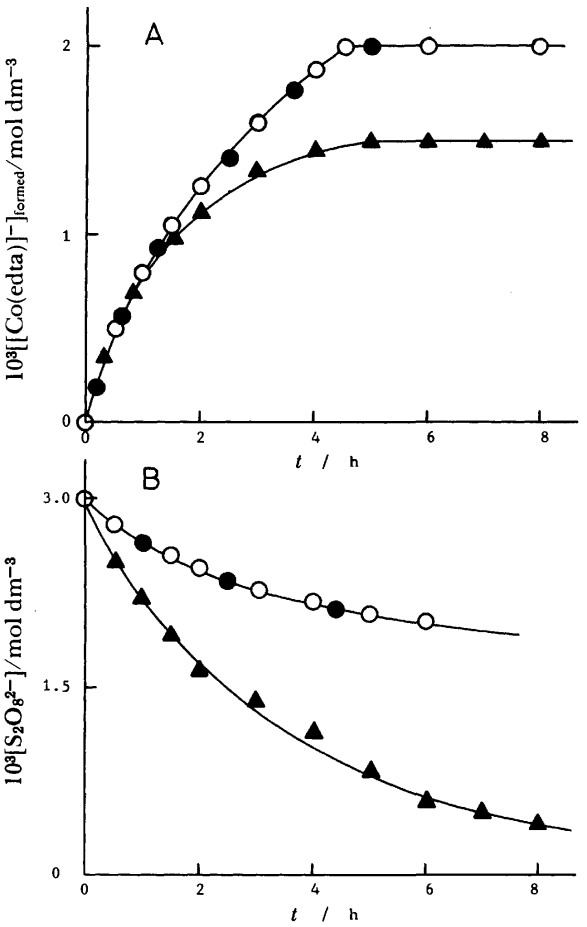

Fig. 1. Plots of $[[Co(edta)]^-]$ vs. t (A) and $[S_2O_8^{2-}]$ vs. t (B). Initial concentrations of $CoSO_4$ and EDTA are, respectively, 0.006 and 0.002 (-○-), 0.002 and 0.002 (-●-), and 0.002 and 0.020 mol dm^{-3} (-▲-), and those of $K_2S_2O_8$ and $[Ru(bpy)_3]Cl_2$ are 0.003 and 5×10^{-5} mol dm^{-3}, respectively. Reaction solution was irradiated with two 100-W tungsten lamps and saturated with nitrogen gas. pH 4.6. 30 °C. μ= 0.1 mol dm^{-3}.

the $[Ru(bpy)_3]^{2+}$ concentration began to decrease accompanying the formation of $[Ru(bpy)_3]^{3+}$. This fact is given in Fig. 2. After the complete change of $[Co(edta)]^{2-}$ to $[Co(edta)]^-$ the latter concentration remained constant, but the concentrations of $[Ru(bpy)_3]^{2+}$ as well as $[Ru(bpy)_3]^{3+}$ decreased gradually. The $[Ru(bpy)_3]^{3+}$ ion oxidizes slowly water, and some of $[Ru(bpy)_3]^{3+}$ appears to dissociate in such a solution without any reductants[9] and the dissociated bipyridine may be oxidized by the SO_4^- radical.

Effect of Hydrogen Ion Concentration. The effect of the hydrogen ion concentration on the reaction rates ($[S_2O_8^{2-}]$ vs. t and $[[Co(edta)]^-]$ vs. t) was examined over the pH range 1.1—7.0 under the conditions of the plots● in Fig. 1. The rate of the reaction was independent of the hydrogen ion concentrations over the pH range 1.9—7.0, and at pH 1.1, the rate of

the reaction became very slow, because $[Co(edta)]^{2-}$ in solution could dissociate to large extent at such a strong acidity.[18] Hereafter, all the experiments were carried out at pH 4.6.

Effect of Concentrations of Reactants, $[Co(edta)]^{2-}$ and $S_2O_8^{2-}$. Under the conditions of plots● in Fig. 1, i.e., $[Co(II)]_{added}=[EDTA]_{added}$, the rates of the reaction $-d[S_2O_8^{2-}]/dt$ and $d[[Co(edta)]^-]/dt$ were independent of the initial concentrations of $[Co(edta)]^{2-}$ over the range 0.001—0.005 mol dm^{-3}, and were, however, dependent on those of peroxodisulfate ion. The initial rate of the reaction $\Delta[[Co(edta)]^-]_i/\Delta t(=V_i)$ was determined at various concentrations of $S_2O_8^{2-}$, and the reciprocal V_i was plotted against the reciprocal of the initial concentration of $S_2O_8^{2-}$. As seen in Fig. 3, the plots of V_i^{-1} vs. $[S_2O_8^{2-}]_i^{-1}$ showed a straight line with an intercept, and the slope of the plot was dependent on the ionic strength(μ).

Thus the empirical rate law can be written as follows.

$$V_i^{-1}=\left(\frac{\Delta[[Co(edta)]^-]_i}{\Delta t}\right)^{-1}=\left(-\frac{2\Delta[S_2O_8^{2-}]_i}{\Delta t}\right)^{-1}$$
$$=\alpha+\beta[S_2O_8^{2-}]_i^{-1} \quad (2)$$

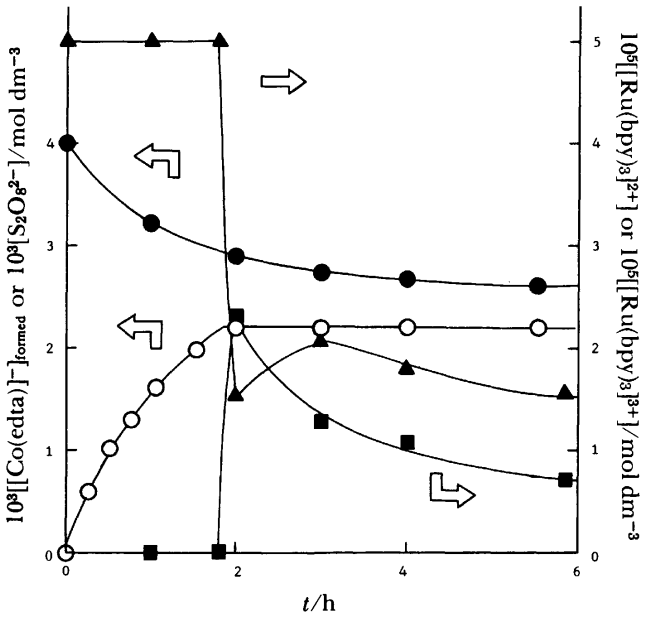

Fig. 2. Variations of the reactants' concentrations against reaction time. Plots ●, ○, ▲, and ■ indicate the variations of concentrations of $S_2O_8^{2-}$, $[Co(edta)]^-$, $[Ru(bpy)_3]^{2+}$, and $[Ru(bpy)_3]^{3+}$, respectively. Initial concentrations are 0.004 mol dm^{-3} in $K_2S_2O_8$, 2.2×10^{-3} mol dm^{-3} in $Na_2[Co(edta)]$, and 5×10^{-5} mol dm^{-3} in $[Ru(bpy)_3]Cl_2$. Reaction solution was irradiated with four 100-W tungsten lamps. μ=0.03 mol dm^{-3}. Other conditions are the same as in Fig. 1.

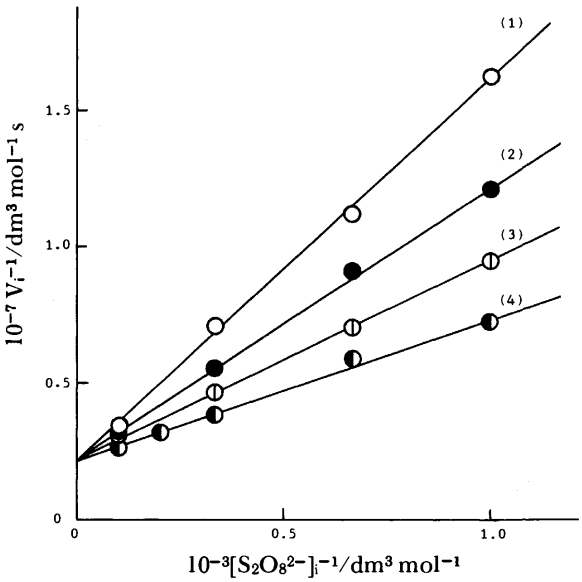

Fig. 3. Plots of Eq. 2. Conditions are the same as in Fig. 1, but $[Co(II)]_{added}=[EDTA]_{added}$=0.002 mol dm^{-3} and the ionic strengths(μ) are 0.5, 0.3, 0.2, and 0.1 mol dm^{-3} for lines(1), (2), (3), and (4), respectively.

Table 1. Values of α, β, k_q/k_0, k_q, and k_q' under Various Conditions[a]

Temp °C	μ mol dm^{-3}	$10^{-6}\alpha$ dm^3 mol^{-1} s	$10^{-3}\beta$ s	(k_q/k_0) dm^3 mol^{-1}	$10^{-8}k_q$ dm^3 mol^{-1} s^{-1}	$10^{-9}k_q'$ dm^3 mol^{-1} s^{-1}
30	0.1	2.13	5.13	416	6.30 7.00[b]	2.94[c]
30	0.2	2.32	7.08	328	4.97 4.77[b]	2.50[c]
30	0.3	2.30	9.82	234	3.55 3.26[b]	2.27[c]
30	0.5	2.14	14.0	153	2.32 2.02[b]	2.18[c]
10	0.1	2.00	5.01	381		
20	0.1	2.00	5.15	386		
40	0.1	2.11	5.94	355		
		Av. 2.13±0.11				

a) Conditions are as in Fig. 3. The k_q and k_q' values are calculated by using $\tau_0=660$ ns and $k_0=\tau_0^{-1}=1.52\times10^6$ s^{-1}.[20] b) Values obtained from the Stern-Volmer plots of the quenching of the luminescence from $[Ru(bpy)_3]^{2+*}$ by $S_2O_8^{2-}$(see Ref. 14)). c) Values obtained from the Stern-Volmer plots of the quenching of the luminescence from $[Ru(bpy)_3]^{2+*}$ by $[Co(edta)]^-$: the Stern-Volmer constants K_{sv} were 1.94×10^3, 1.65×10^3, 1.50×10^3, and 1.44×10^3 dm^3 mol^{-1} for ionic strengths 0.1, 0.2, 0.3, and 0.5 mol dm^{-3}, respectively.

The values of α and β in Eq. 2 obtained at various temperatures and ionic strengths are given in Table 1 together with the rate constants.

Effect of Incident Light. No appreciable formation of $[Co(edta)]^-$ and no appreciable decomposition of $S_2O_8^{2-}$ were found in the dark under the conditions given. It was found that the formation rate of $[Co(edta)]^-$(or twofold decomposition rate of $S_2O_8^{2-}$) was proportional to the number of lamps used: V_i in Eq. 2 was 1.18×10^{-7}, 2.27×10^{-7}, 3.50×10^{-7}, and 4.86×10^{-7} mol dm^{-3}s^{-1} at the number of lamps of 1, 2, 3, and 4, respectively.

Effect of Concentration of Photocatalyst. The initial rate (V_i in Eq. 2) increased with concentrations of $[Ru(bpy)_3]^{2+}$ and then reached a limiting value (see Fig. 4). This behavior is thought to be due to the change of the amount of light absorbed according to the concentation change of photo-catalyst $[Ru(bpy)_3]^{2+}$ and is accounted for by Eq. 3.

$$I_a = I_0(1-\exp(-A[[Ru(bpy)_3]^{3+}])), \tag{3}$$

where I_0 is the intensity of the incident light, I_a is the amount of light absorbed by $[Ru(bpy)_3]^{2+}$, and A is an empirical constant comprising the length of the light path and the molar absorption coefficient of $[Ru(bpy)_3]^{2+}$.

The rate of reaction (V_i) is proportional to I_a (see Eq. 10), and thus, a curve shown in Fig. 4 coincides with the expression of Eq. 3.

Mechanisms of the Reaction. The following mechanism of the reaction is presented to account for the results obtained.

$$[Ru(bpy)_3]^{2+} + h\nu \xrightarrow{I_a}$$
$$[Ru(bpy)_3]^{2+*} \xrightarrow{k_0} \begin{cases} \rightarrow [Ru(bpy)_3]^{2+} + h\nu'(\text{emission}) \\ \rightarrow [Ru(bpy)_3]^{2+} + \Delta(\text{thermal energy}) \end{cases} \tag{4}$$

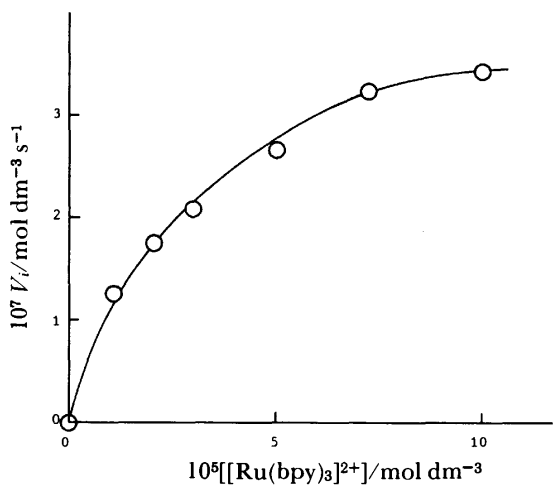

Fig. 4. Effect of the $[Ru(bpy)_3]^{2+}$ ion concentration on the reaction rate. Conditions as in Fig. 1, but $[Co(II)]_{added}=[EDTA]_{added}=0.002$ mol dm^{-3}.

$$[Ru(bpy)_3]^{2+*} + S_2O_8^{2-} \xrightarrow{k_q} [Ru(bpy)_3]^{3+} + SO_4^{\cdot-} + SO_4^{2-} \tag{5}$$
$$[Ru(bpy)_3]^{2+} + SO_4^{\cdot-} \xrightarrow{k_1} [Ru(bpy)_3]^{3+} + SO_4^{2-} \tag{6}$$
$$[Co(edta)]^{2-} + SO_4^{\cdot-} \xrightarrow{k_2} [Co(edta)]^- + SO_4^{2-} \tag{7}$$
$$[Co(edta)]^{2-} + [Ru(bpy)_3]^{3+} \xrightarrow{k_3} [Co(edta)]^- + [Ru(bpy)_3]^{2+} \tag{8}$$
$$[Ru(bpy)_3]^{2+*} + [Co(edta)]^- \xrightarrow{k_q'} [Ru(bpy)_3]^{3+} + [Co(edta)]^{2-} \tag{9}$$

Assuming the steady state concentrations of $SO_4^{\cdot-}$, $[Ru(bpy)_3]^{3+}$, and $[Ru(bpy)_3]^{2+*}$, the following rate law is obtained.

$$\frac{d[[Co(edta)]^-]}{dt} = \frac{2k_qI_a\phi[S_2O_8^{2-}]}{k_0 + k_q[S_2O_8^{2-}] + k_q'[[Co(edta)]^-]}, \tag{10}$$

where ϕ is the formation efficiency of the excited species, I_a is the amount of light absorbed by $[Ru(bpy)_3]^{2+}$ (see Eq. 3) and $I_a\phi$ corresponds to the formation rate of $[Ru(bpy)_3]^{2+*}$. Reaction 9 and the term $k_q'[[Co(edta)]^-]$ in Eq. 10 might be negligible at least for the initial period of the reaction, and thus, the following rate law can be applied under such conditions.

$$V_i^{-1} = \frac{1}{2I_a\phi} + \frac{k_0}{2I_a\phi k_q}[S_2O_8^{2-}]_i^{-1} \tag{11}$$

Equation 11 is equivalent to Eq. 2 obtained empirically, and is in agreement with all the results. The α and β values in Eq. 2 correspond to $(2I_a\phi)^{-1}$ and $k_0/(2I_a\phi k_q)$, respectively, and thus, the values of k_q/k_0 were obtained from the plots of V_i^{-1} vs. $[S_2O_8^{2-}]_i^{-1}$. It is to be noted that the reaction rate of the light-induced reaction was hardly dependent on temperature. The values of k_q/k_0 were almost independent of the temperature of solution, and thus, the activation energy of the quenching reaction(E_q) is almost equal to that of the nonradiative quenching of the photoexcited species(E_0=10.6 kJ mol^{-1} for k_0-path in Eq. 4[21]). The quenching rate constants k_q' and k_q were determined by the measurements of the luminescence of $[Ru(bpy)_3]^{2+*}$ in solutions of various concentrations of $[Co(edta)]^-$ and $S_2O_8^{2-}$. The k_q values determined by using Eq. 11 were in good agreement with those determined by the measurements of quenching luminescence. This fact supports the validity of the mechanism and the rate law proposed.

Confirmation of Rate Law (Eq. 11). The integral form of Eq. 10 is given by

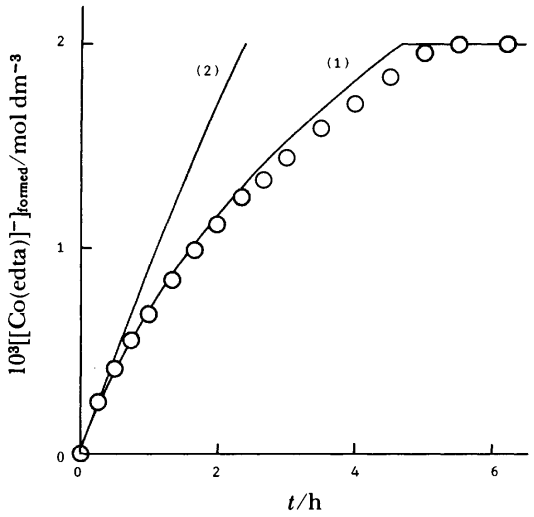

Fig. 5. Plots of Eq. 12. Conditions as in Fig. 1, but $[Co(II)]_{added}=[EDTA]_{added}=0.002$ mol dm^{-3}. The solid curve(1) indicates the calculated values using Eq. 12 and plots indicate the data obtained experimentally. Another solid curve(2) indicates the calculated values by using Eq. 12'.[22]

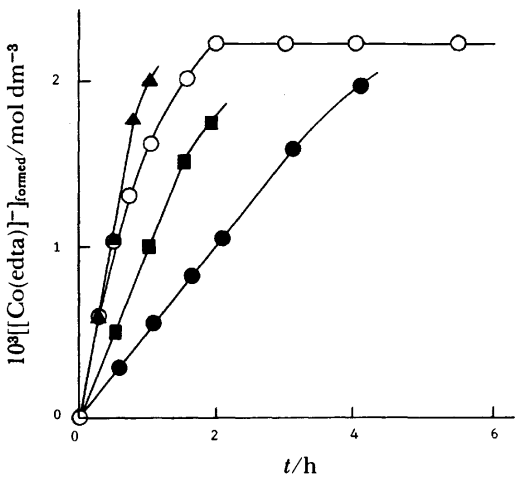

Fig. 6 Comparison with the silver(I) ion-catalyzed reaction. Plots O indicate the experimental data obtained under the same conditions as in Fig. 2. Plots ▲, ■, and ● indicate the silver(I) ion-catalyzed reaction. Conditions are 5×10^{-3} mol dm^{-3} in $AgClO_4$ and 30 °C (-▲-), 5×10^{-3} mol dm^{-3} in $AgClO_4$ and 20 °C (-■-), 1×10^{-3} mol dm^{-3} in $AgClO_4$ and 30 °C (-●-), and the other conditions are the same as in the plots O.

$$\left(\frac{1}{2}k_q - k_q'\right)[[Co(edta)]^-]_{t=t} - (k_0 + 2k_q'[S_2O_8^{2-}]_{t=0}) \times \ln\frac{[S_2O_8^{2-}]_{t=t}}{[S_2O_8^{2-}]_{t=0}} = k_q I_a \phi t \quad (12)$$

Using values of k_q, k_q', k_0, and $I_a\phi$, we can calculate a curve of the plots [[Co(edta)]$^-$] vs. t. The calculated curve was in good agreement with the data obtained experimentally (see curve(1) in Fig. 5). A slight deviation only near the completion of the reaction seems to be attributable to the inner-filter effect of [Co(edta)]$^-$ which is produced according to the progress of reaction time. It is to be noted that the calculated curve is greatly altered by neglecting the term k_q'[[Co(edta)]$^-$] in Eq. 10 (compare curve(2) to curve(1) in Fig. 5), and that the validity of Eq. 11 is limited to the reaction time less than 20 minutes.

As stated before and seen in Fig. 1, under the conditions of $[Co(II)]_{added}/[EDTA]_{added}=0.1$, the formation rate of [Co(edta)]$^-$ decreased to a small extent, while the decomposition rate of $S_2O_8^{2-}$ was accelerated greatly. These facts may indicate the occurrence of the following reactions.

$$EDTA + [Ru(bpy)_3]^{3+} \longrightarrow EDTA^{+} + [Ru(bpy)_3]^{2+} \quad (13)$$

$$S_2O_8^{2-} + EDTA^{+} \longrightarrow SO_4^{-} + SO_4^{2-} + \text{products} \quad (14)$$

$$EDTA + SO_4^{-} \longrightarrow EDTA^{+} + SO_4^{2-} \quad (15)$$

Reaction 13 is a competitive reaction with reaction 8, and thus, the formation rate of [Co(edta)]$^-$ might have been decreased. Successively, the EDTA radicals will react with peroxodisulfate and thus, the rate of decomposition of $S_2O_8^{2-}$ can be greatly accelerated (the reaction mechanisms might become more complex).

It is known that the oxidation reactions by the peroxodisulfate ion are catalyzed by the silver(I) ion.[23] We have compared the light-induced reaction using $[Ru(bpy)_3]^{2+}$ as a catalyst with the silver(I) ion-catalyzed reaction (see Fig. 6). The reaction rate of the silver(I) ion-catalyzed reaction was dependent on the pH[23] as well as the temperature of the solution. On the other hand, the reaction rate of the light-induced reaction using $[Ru(bpy)_3]^{2+}$ as a photo-catalyst was little dependent on both temperature and pH over the range of pH 1.9—7.0. It may be also simply stated that the activity of the light-induced reaction under four lamps is almost 100 times larger than that of the silver(I) ion-catalyzed reaction under the same concentration of each catalyst.

References

1) K. Kalyanasundaram, *Coord. Chem. Rev.*, **46**, 159 (1982).
2) N. Sutin, *J. Photochem.*, **10**, 19 (1979).
3) K. Kalyanasundaram, M. Grätzel, and E. Pelizzetti, *Coord. Chem. Rev.*, **69**, 57 (1986).
4) F. Bolletta, A. Juris, M. Maestri, and D. Sandrini, *Inorg. Chim. Acta*, **44**, L175 (1980).
5) M. Neumann-Spallart, K. Kalyanasundaram, C. Grätzel, and M. Grätzel, *Helv. Chim. Acta*, **62**, 1111 (1980).

6) M. Neumann-Spallart and K. Kalyanasundaram, *Ber. Bunsenges. Phys. Chem.*, **85**, 704 (1981).
7) J. N. Demas, *J. Chem. Educ.*, **60**, 803 (1983).
8) H. S. White, W. G. Becker, and A. J. Bard, *J. Phys. Chem.*, **88**, 1840 (1984).
9) G. Blondeel, A. Harriman, G. Porter, D. Arwin, and J. Kiwi, *J. Phys. Chem.*, **87**, 2629 (1983).
10) V. Ya Shafirovich and V. V. Strelets, *Nouv. J. Chim.*, **6**, 183 (1982).
11) D. H. M. W. Thewissen, N. Eeuwhorst-Reinten, K. Timmer, A. H. A. Tinnemans, and A. Mackor, *Recl. Trav. Chim. Pays-Bas.*, **101**, 79 (1982).
12) R. Humphry-Baker, J. Lilie, and M. Grätzel, *J. Am. Chem. Soc.*, **104**, 422 (1982).
13) N. K. Khannanov and V. Ya Shafirovich, *Dokl. Akad. Nauk. SSSR*, **260**, 1418 (1981).
14) M. Kimura and S. Nishida, *J. Chem. Soc., Dalton Trans.* **1985**, 355.
15) S. Nishida and M. Kimura, *J. Chem. Res. (S)*, **1986**, 336.
16) R. A. Palmer and T. S. Piper, *Inorg. Chem.*, **5**, 964 (1966); I. Fujita and H. Kobayashi, *Ber. Bunsunges. Phys. Chem.*, **76**, 115 (1972); T. Tachibana, M. Nakahara, and M. Shibata, "Shin Jikken Kagaku Koza 8," Maruzen, Tokyo (1977), pp. 1475 and 1533.
17) M. Kimura, M. Yamashita, and S. Nishida, *Inorg. Chem.*, **24**, 1527 (1985).
18) The equilibrium constants K_{II} (=[Co^{II}(Hedta)(H_2O)$^-$]/[Co^{II}(edta)$^{2-}$][H^+]) and K_{III}(=[Co^{III}(Hedta)(H_2O)]/[Co^{III}-(edta)$^-$][H^+]) are $10^{3.0}$ and $10^{2.98}$, respectively.[19] Thus, both [Co(Hedta)(H_2O)]$^-$ and [Co(Hedta)(H_2O)] will exist in strong acid solutions.
19) A. E. Martel and R. M. Smith, "Critical Stability Constant, Volume 1: Amino Acid," PLENUM PRESS, New York and London (1974), p. 206.
20) J. N. Demas and A. W. Adamson, *J. Am. Chem. Soc.*, **95**, 5159 (1973).
21) F. E. Lytle and D. H. Hercules, *J. Am. Chem. Soc.*, **91**, 253 (1969).
22) Assuming that reaction(9) is negligible, the integral form of Eq. 10 is:

$$\frac{1}{2}k_q[[Co(edta)]^-]_{t=t} - k_0 \ln \frac{[S_2O_8^{2-}]_{t=t}}{[S_2O_8^{2-}]_{t=0}} = k_q I_a \phi t \qquad (12')$$

23) K. Ohashi and K. Yamamoto, *Bull. Chem. Soc. Jpn.*, **50**, 3049 (1977).

 © 1987 The Chemical Society of Japan Bull. Chem. Soc. Jpn., 60, 2373—2380 (1987)

The Synthesis of CdTe by Means of Fused Salt Electrolysis and Its Characterization

Hideki MINOURA,* Masakazu KITAKATA, Takashi SUGIURA, Minoru MURAYAMA, and Yasusada UENO

Department of Synthetic Chemistry, Faculty of Engineering, Gifu University, 1-1 Yanagido, Gifu 501-11

(Received December 22, 1986)

Crystalline cadmium telluride layers of a cubic structure have been deposited potentiostatically on graphite cathodes by means of fused salt electrolysis employing $CdCl_2$ and TeO_2/Na_2TeO_3 in an LiCl-KCl eutectic melt at 450 °C. X-Ray diffraction and scanning-electron-microscope studies show that (i) these layers have a tendency to grow with a preferred orientation along the ⟨111⟩ direction and (ii) the surface morphology changes drastically with the change in the applied potential. Voltammetric analyses indicate two distinct mechanisms for cadmium telluride deposition; one is the codeposition of cadmium and tellurium occurring at potentials more negative than −0.2 V(vs. Ag/AgCl), and the other is the ionic reaction of the cathodically formed telluride ion with the cadmium ion occurring at potentials more negative than −0.7 V(vs. Ag/AgCl). As-deposited crystals are either n- or p-type, depending on the melt composition and the applied potential.

The electrodeposition from fused salts seems to be one of most promising of the new methods of obtaining semiconductor films. The important merits of this method are as follows; (i) it is easy to control the deposition conditions, as is common in the case of electrochemical deposition methods, and (ii) it enables us to obtain compound semiconductors with a high crystallinity since the deposition takes place at a relatively high temperature compared to that of aqueous solutions. In spite of its usefulness, however, no systematic studies of the preparation of semiconductor materials by means of fused salt electrolysis have been reported thus far, although a few reports dealing inadequately with this subject are available in the literature.[1-5] In the past decade our laboratory has been engaged in a major effort to produce polycrystalline cadmium chalcogenide films/layers by employing various methods aimed at their efficient use in photoelectrochemical cells.[6] As a part of this series of investigations, we have already reported the crystal growth of CdSe by means of fused salt electrolysis and its applicability in a photoelectrochemical cell.[7,8]

This paper deals with the electrodeposition of CdTe by means of fused salt electrolysis. CdTe is a promising material for solar photovoltaic devices because it possesses a direct bandgap of 1.44 eV, which is close to the maximum of the solar spectrum, and because it has a high absorption coefficient. Besides, with it both n-type and p-type forms can be conveniently prepared. Actually, polycrystalline CdTe has already been successfully used in a CdS/CdTe heterojunction solar cell for commercial use by Matsushita's group.[9] The electrodeposition of CdTe films from an aqueous solution and a nonaqueous solution has already been reported.[10-13] Electrodeposition is a low-temperature process (usually a room-temperature process) without resort to any vacuum technology and is subject to minimum losses of materials; thus, it offers a convenient and inexpensive method of film fabrication. However, as-deposited films obtained by this method generally have a poor crystallinity, a subsequent heat-treatment is required for its use in a photovoltaic device. In this particular aspect, the electrodeposition from fused salt has the advantage that no such subsequent heat-treatment is required because of the simultaneous occurrence of the electrodeposition and the crystal growth.

In this paper, the mechanism of CdTe deposition by means of fused salt electrolysis will be proposed on the basis of the previously proposed mechanism for the similarly deposited CdSe. We have also examined the possibility of getting n- and p-type samples of CdTe selectively by changing the deposition conditions, namely, the electrolytic potential and the salt composition.

Experimental

The experimental apparatus and procedures are nearly the same as those described in a previous paper.[7]

Almost all the electrodeposition procedures from the fused salts thus far reported have been carried out under galvanostatic condition in a two-electrode configuration.[1-4] In order to carry out the potentiostatic electrolysis, we adopted a three-electrode system consisting of a graphite working electrode (a substrate onto which CdTe is deposited), a graphite counter electrode, and an Ag/AgCl reference electrode. The potentiostatic electrolysis is required to examine the potential-dependent deposition, as has been emphasized earlier in the case of CdSe.[8] All the potential values in the present paper are expressed with respect to this reference electrode.

$CdCl_2$ and Na_2TeO_3/TeO_2 were added to the LiCl-KCl electrolyte of the eutectic composition as the source materials of cadmium and tellurium respectively. Electrolyses were carried out at 450 °C.

The crystal structure and the morphology of the deposits were examined by means of an X-ray diffractometer (Rigaku Denki) and a scanning electron microscope (Hitachi H-8010) respectively.

To determine the type of the majority carrier, the current-potential curves under illumination were recorded for the deposits in an aqueous sulfide solution.

Results and Discussion

According to our preliminary experiments, CdTe has been found to be deposited by electrolysis in the melts containing $CdCl_2$ and TeO_2 at the bath temperature of 450 °C. Therefore, prior to the analysis of the CdTe deposition reaction, the cathodic polarization curves of a cadmium-source material and tellurium-source materials have been examined separately in order to understand the CdTe deposition mechanism by using the same method as was reported previously for CdSe.[8] The results on the voltammetric curves of a cadmium source will be omitted in the present paper, as they have already been reported in a previous paper.[8]

Reduction of Te(+4). A voltammetric curve under cathodic polarization in Na_2TeO_3-containing melts is shown in Fig. 1. A cathodic current starts to flow at +0.2 V, reaches the saturation value at −0.3V, and rises again at −0.7 V. The deposit obtained at the first wave exhibits a metallic gray color and was identified as a metallic tellurium by means of the X-ray diffraction data. It has been noticed that, when polarized more cathodically than −0.7 V, the deposit on the substrate gradually disappears. These results indicate that the deposition of a metallic tellurium takes place at the first cathodic wave, while the further reduction of the metallic Te to Te(−2) proceeds at the second cathodic wave, analogous to the reduction of Se(+4) reported in the previous paper.[8] Bodewig and Plambeck[15] examined the electrochemical behavior of a tellurium electrode in the fused LiCl-KCl eutectic and reported the formation of a stable lithium-tellurium intermetallic compound, i.e,. Li_2Te, at −0.67 V. However, we could not detect such an intermetallic compound in our X-ray diffractograms. This particular result can perhaps be attributed to the difference in the electrodes used, i.e, a tellurium electrode in their work and a tellurium-deposited graphite electrode in our work.

In order to understand what reactions are taking place in the second-wave reduction process, cyclic voltammetric experiments were performed in the potential range between −0.6 and −0.9 V. Figure 2 shows cyclic voltammograms with different sweep rates. The peak potential is independent of the sweep rate within our experimental sweep rate range, and the oxidation-peak height is smaller than the reduction-peak height. The peak current density is proportional to the square root of the potential sweep rate and the concentration of Na_2TeO_3, as is indicated in Figs. 3 and 4. It follows that the cathodic reaction occurring in the potential region is a reversible reaction involving a soluble product. From the plot

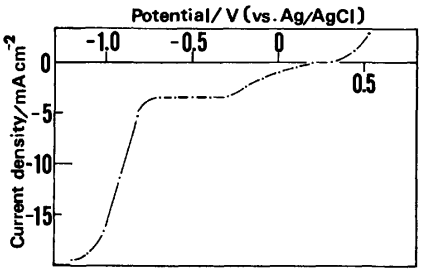

Fig. 1. Voltammogram for the reduction of Na_2TeO_3. Concentration of Na_2TeO_3 is 1.2×10^{-2} mol%.

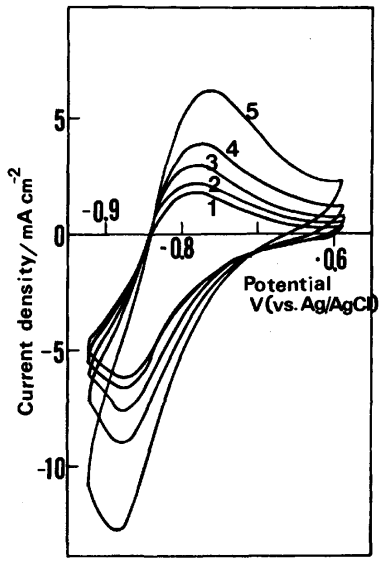

Fig. 2. Cyclic voltammograms for the reduction of Na_2TeO_3 at different sweep rates. Concentration of Na_2TeO_3 is 4.85×10^{-4} mol%. 1: 20 mV s^{-1}, 2: 25 mV s^{-1}, 3: 33.3 mV s^{-1}, 4: 50 mV s^{-1}, 5: 100 mV s^{-1}.

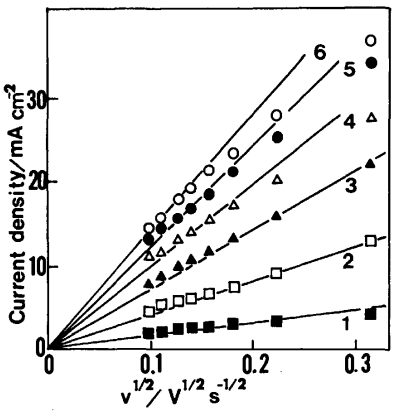

Fig. 3. Voltammetric peak current vs. square root of the sweep rate for the reduction of Te(0) in LiCl(0.236 mol)-KCl(0.172 mol) melts. Quantity of Na_2TeO_3 in melts; 1: 1.01×10^{-4} mol, 2: 1.98×10^{-4} mol, 3: 2.99×10^{-4} mol, 4: 3.92×10^{-4} mol, 5: 4.96×10^{-4} mol, 6: 5.95×10^{-4} mol.

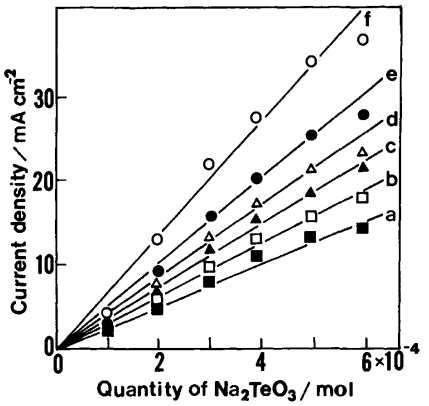

Fig. 4. Voltammetric peak current vs. Na_2TeO_3 concentration for the reduction of Te(0) in LiCl(0.236 mol)-KCl(0.172 mol) melts. Sweep rate; a: 10 mV s^{-1}, b: 16.7 mV^{-1}, c: 25 mV s^{-1}, d: 33.3 mV s^{-1}, e: 50 mV s^{-1}, f: 100 mV s^{-1}.

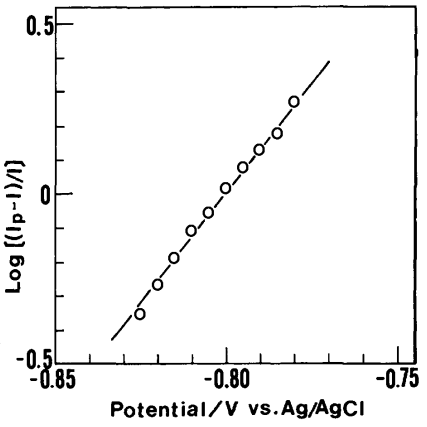

Fig. 5. Plots of log $[(i_p-i)/i]$ vs. electrode potential for the reduction of Na_2TeO_3. Na_2TeO_3 concentration: 4.85×10^{-4} mol%, Sweep rate: 16.7 mV s^{-1}.

shown in Fig. 5, and by applying Matsuda and Ayabe's equation,[16] the number of electrons involved in this cathodic process, n, was calculated by using the procedure reported in a previous paper.[8] This calculation yields the value of 1.89. In this way, it is confirmed that the reduction expressed as:

$$Te(0) + 2e \longrightarrow Te(-2)$$

proceeds at potentials more negative than −0.7 V.

Almost the same behavior was observed when a TeO_2-containing melt was used instead of an Na_2TeO_3-containing melt, with the only exception of a small increase in the cathodic current.

Deposition of CdTe. In the melt containing both $CdCl_2$ as a cadmium source and Na_2TeO_3 as a tellurium-source in an equimolar composition, the cathodic current starts to flow at around +0.2 V,

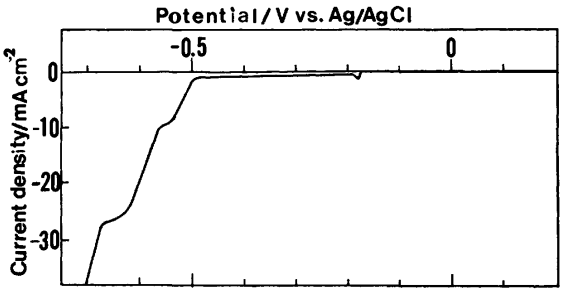

Fig. 6. Voltammograms for the deposition of CdTe in LiCl(0.236 mol)-KCl(0.172 mol)-$CdCl_2$(0.005 mol)-Na_2TeO_3(0.005 mol). Sweep rate: 0.1 mV s^{-1}.

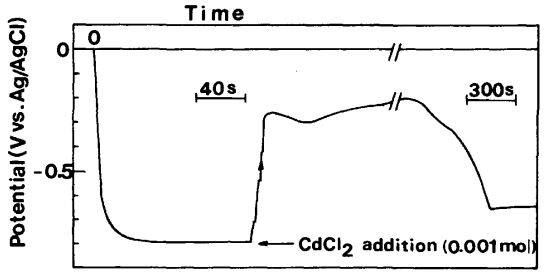

Fig. 7. Electrode potential change with time by the addition of $CdCl_2$ under galvanostatic electrolysis of −10 mA in LiCl(0.236 mol)-KCl(0.172 mol)-Na_2TeO_3(0.005 mol) melt. Electrode surface area: 3.4 cm^2.

which corresponds to the reduction of Te(+4) to Te(0). As is shown in the voltammogram of Fig. 6, a characteristic peak appears at about −0.2 V and the current remains constant with an increase in the cathodic polarization to −0.5 V. The CdTe deposit was observed at potentials more negative than −0.2 V. The appearance of the cathodic peak at around −0.2 V will be discussed later. The redox potential of Cd/Cd^{2+} was reported to be −0.589 V; our result implies that the deposition of cadmium metal starts to take place at −0.59 V. A comparison of the CdTe deposition onset potential of −0.2 V with this standard redox potential of Cd/Cd^{2+} clearly shows the occurrence of the underpotential deposition of CdTe.

The small peak at around −0.2 V in the voltammogram shown in Fig. 6 can be explained by assuming that the tellurium which had been deposited at the potentials more positive than −0.2 V was changed into CdTe at −0.2 V by the incorporation of cadmium, which starts to be deposited at this potential. In order to confirm this assumption, galvanostatic measurements were performed. Figure 7 presents the potential-time curve during the galvanostatic electrolysis. As can be seen from this curve, the electrode potential changes toward negative values and reaches the stationary value of −0.8 V when a

graphite electrode is polarized cathodically in melts containing only the tellurium source. After carrying out this electrolysis for 2 minutes and adding $CdCl_2$ to the melt, the potential suddenly changes to about −0.2 V. This potential corresponds to the small peak in Fig. 6. It is further seen that the potential gradually shifts to more negative values and then reaches the stationary value of −0.64 V. Taking into account the small peak at −0.2 V in Fig. 6, the transition time at −0.2 V in Fig. 7 can be regarded as the time for changing the deposited tellurium to CdTe by the incorporation of the deposited cadmium metal. Therefore, this transition time probably depends on the quantity of the deposited tellurium. Actually, this idea is supported by the results shown in Figs. 7 and 8, which demonstrate that halving the electrolysis time before $CdCl_2$ addition (Fig. 8) results in the reduction of the transition time at −0.2 V to about one-half of that in Fig. 7. The corresponding peak was not observed in the case of CdSe deposition, although a similar process can be expected to occur. This difference is attributable to the difference in the melting points of selenium(220.2 °C) and tellurium (449.8 °C). As the deposited selenium is in a liquified state, it is unlikely to stick to the graphite substrate.

The observation that the cathodic current rises again at −0.59 V suggests the occurrence of a usual cadmium deposition together with the above-mentioned underpotential deposition. The increase in the cathodic current at −0.7 V may be due to the reduction of Te(0) or Te(+4) to Te(−2). Thus, CdTe formation by a reaction of Te^{2-} with Cd^{2+} in the melt should take place in addition to the above-mentioned codeposition. Therefore, the deposition reactions at various potentials can be summarized in the manner shown in Fig. 9.

To get further information on the CdTe deposition process, the change in the surface morphology as the electrolysis progressed was monitored by means of a

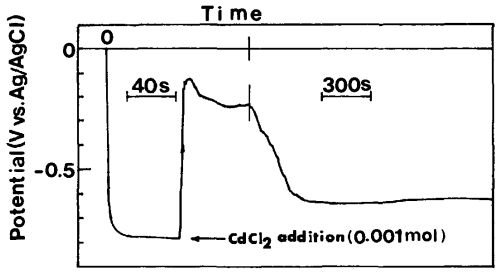

Fig. 8. Electrode potential change with time by the addition of $CdCl_2$ under galvanostatic electrolysis of −10 mA in LiCl(0.236 mol)-KCl (0.172 mol)-Na_2TeO_3(0.005 mol) melt. Electrode surface area: 1.9 cm^2. Electrolysis time before $CdCl_2$ is a half of that in Fig. 7.

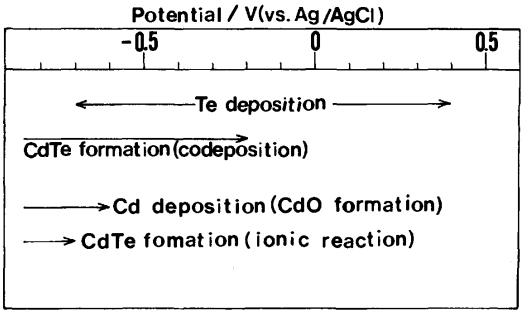

Fig. 9. Deposition reactions at different electrolytic potentials.

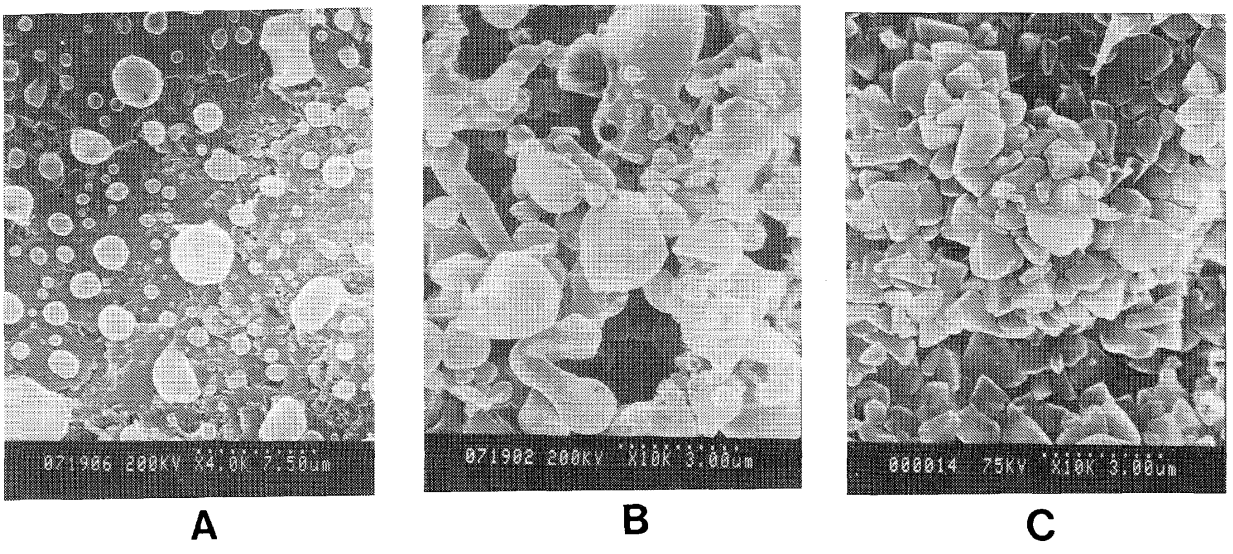

Fig. 10. SEM micrographs of the deposits obtained at −0.6 V. Quantity of electricity passed during electrodeposition; (A) 1.3 C cm^{-2}, (B) 1.3 C cm^{-2}, (C) 2.5 C cm^{-2}. (B) is a different place from (A) in the same sample.

scanning electron microscope. Figure 10 presents SEM micrographs of the deposits obtained at various stages of the electrolysis carried out at −0.6 V. Initially, spherical-shaped deposits appeared, as is shown in Fig. 10 (A). The EPMA results revealed that these deposits are metallic tellurium. This characteristic morphology becomes quite obvious if we consider the fact that the bath temperature is nearly the same as the melting point of tellurium. With the increase in the amount of electricity passed through, other deposits, but with a linear edge in contrast to the above-mentioned spherical-shaped ones, appear, as is shown in Fig. 10 (C). These deposits were identified as CdTe by means of the X-ray diffractograms and the EPMA results. The corresponding photographs show that tellurium is first deposited onto the substrate, and then cadmium is deposited and incorporated into tellurium deposits, resulting in CdTe formation. Thus, our SEM data further support the above-mentioned mechanism of CdTe codeposition.

Figure 11 shows the relationship between the weight gain and the amount of electricity passed through during fused salt electrolysis at −0.6 V. It is clear from these results that the weight of the deposits is directly proportional to the amount of electricity passed through; in other words, the current efficiency remains nearly constant during the electrolysis. Assuming that the overall reaction for CdTe deposition is expressed as:

$$Cd^{2+} + Te^{4+} + 6e \longrightarrow CdTe$$

the apparent current efficiency estimated on the basis of Faraday's law, is 43%. Such a low current efficiency may be attributable to a falling down of some deposited material while the cathode was dipped in a 1% HCl solution after electrolysis. This dipping procedure was employed to remove the solvents and solutes stuck to the deposits. Therefore, we feel that the real current efficiency must be higher than 43%.

Characterization of the Deposits. X-Ray diffractograms of the deposits obtained at the electrolytic potentials of −0.4 and −0.7 V are shown in Fig. 12. All these peaks match well with the ASTM data of cubic CdTe (zinc blende type). In the diffractograms of the deposit at −0.4—−0.6 V, there are some prominent peaks due to CdTe, the intensities of which are in good agreement with the standard powder diffraction data for CdTe. Interestingly, in the diffractogram of the deposits obtained at −0.7 V, only one strong peak corresponding to the (111) plane appears; it is indicative of the crystal growth with a preferred orientation along the ⟨111⟩ direction. This can be ascribed to a relatively high deposition rate at −0.7 V, in which the preferential growth of crystal nuclei with the most stable (111) plane may proceed.

We determined the conductivity type of our deposits by studying the current-potential curves under illumination in an aqueous solution. The deposit which exhibits an anodic photocurrent is referred to as the n-type, while that which exhibits a cathodic

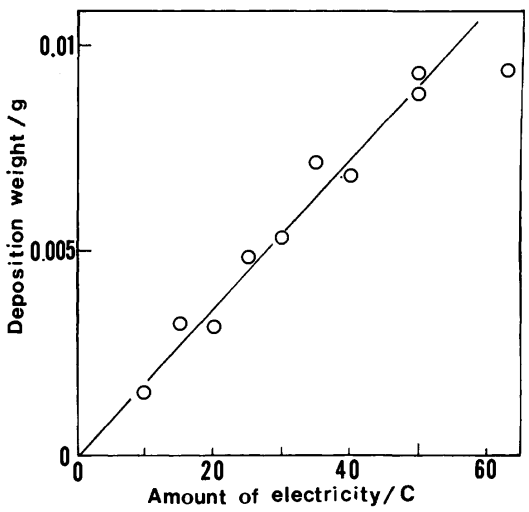

Fig. 11. Deposition weight vs. amount of electricity during electrodeposition from LiCl(0.236 mol)-KCl (0.172 mol)-$CdCl_2$(0.005 mol)-Na_2TeO_3(0.005 mol) melt at −0.7 V.

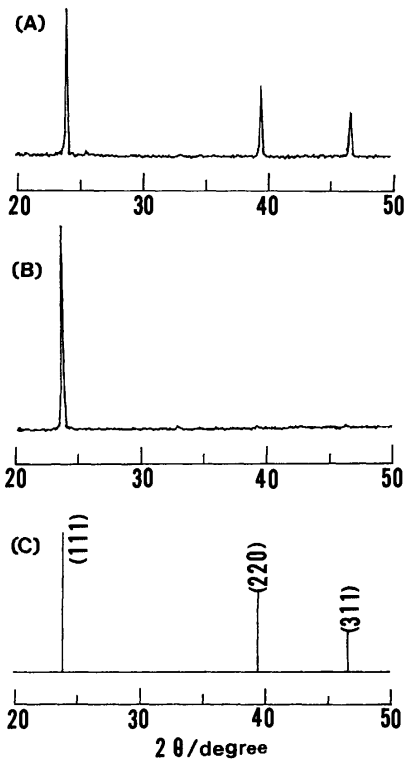

Fig. 12. X-Ray diffraction patterns of the deposits obtained from LiCl(0.236 mol)-KCl(0.172 mol)-$CdCl_2$(0.005 mol)-Na_2TeO_3(0.005 mol) melt. Deposition potential; (A) −0.4 V, (B) −0.7 V. (C) is the ASTM data for cubic CdTe.

photocurrent is referred to as the p-type, in the present paper.

Table 1 summarizes the electrical-conduction type as well as the chemical composition of the deposits obtained under various melt compositions and electrolytic potentials. The chemical compositions correspond to those estimated by means of X-ray diffractograms of the deposits.

From the melt with equimolar $CdCl_2$ and TeO_2, both n-type and p-type CdTe were obtained. At −0.1 V, no CdTe was deposited, however; only metallic tellurium was detected. At potentials more negative than −0.2 V, CdTe was deposited. It should be noted that both n-type and p-type are obtained by controlling the electrolytic potential applied. At potentials more negative than −0.6 V, only n-type CdTe was obtained. This interesting result seems quite reasonable if we consider that −0.59 V is the potential at which cadmium deposition starts to occur and that the n-type is associated principally with an excess of cadmium.

From the melt containing an excess of $CdCl_2$, an n-type sample is more likely to be deposited. Some weak peaks which can be assigned to CdO were found in the X-ray diffractograms. This indicates that a further excess of cadmium leads to the CdO formation. On the other hand, from a melt with an excess of a tellurium source, a p-type sample was found to be deposited, even at −0.7 V. In this case, the deposits were found to contain metallic tellurium, whereas no CdO was detectable. This is attributable to the slower rate of the deposition of cadmium compared to that of tellurium. Such an excess of tellurium in the deposits can be removed by subsequent heat-treatment, as has been reported in the case of CdTe films deposited from an aqueous solution.[13] These results are consistent with the above consideration of the deposition reaction.

When we add Na_2TeO_3 instead of TeO_2 as a tellurium-source material, an n-type is more likely to be deposited. This is attributable to a smaller cathodic current caused by a tellurium deposition, as was mentioned above.

Figure 13 displays SEM micrographs of the deposits obtained at various electrolytic potentials from KCl-LiCl melts containing 0.005 mol $CdCl_2$ and 0.005 mol Na_2TeO_3. As can clearly be seen from these photographs, the deposits at −0.4—−0.6 V have similar morphologies with tetrahedron-shaped crystals. However, it is interesting to note that, with the

Table 1. Chemical Composition of the Deposits under Various Conditions in LiCl (0.236 mol)-KCI (0.172 mol) Melts

Melt composition $CdCl_2$ / mol	Melt composition TeO_2 / mol	Deposition potential / V vs. Ag/AgCl	Cathode product[a] CdTe	Te	CdO	Photocurrent[b]
0.0067	0.0033	−0.1	—	W	—	—
0.0067	0.0033	−0.2	VS	W	—	p,(n)
0.0067	0.0033	−0.3	VS	W	—	p
0.0067	0.0033	−0.4	VS	—	—	p,(n)
0.0067	0.0033	−0.5	M	W	W	n,(p)
0.0067	0.0033	−0.6	W	—	W	n
0.0067	0.0033	−0.7	W	—	M	n
0.0067	0.0033	−0.8	W	—	W	n
0.0067	0.0033	−0.9	W	—	W	n
0.005	0.005	−0.1	—	M	—	—
0.005	0.005	−0.2	S	W	—	p
0.005	0.005	−0.3	M	—	—	p
0.005	0.005	−0.4	S	—	—	p
0.005	0.005	−0.5	S	—	—	p
0.005	0.005	−0.6	M	W	—	n
0.005	0·005	−0.7	M	VW	—	n
0.0033	0.0067	−0.2	M	M	—	p
0.0033	0.0067	−0.3	M	W	—	p
0.0033	0.0067	−0.4	M	W	—	p
0.0033	0.0067	−0.5	M	VW	—	p
0.0033	0.0067	−0.6	S	—	—	p
0.0033	0.0067	−0.7	W	W	—	p

The amount of electricity consumed during electrodeposition is 20 C cm^{-2}. a) Estimated from X-ray diffractograms: VS, very strong, S, strong, M, medium, W, weak, VW, very weak, —, undetectable. b) A deposit which shows an anodic photoresponse is termed "n", while that which shows a cathodic photoresponse is termed "p". When a deposit exhibits both anodic and cathodic photoresponses, the weaker one is shown in parentheses.

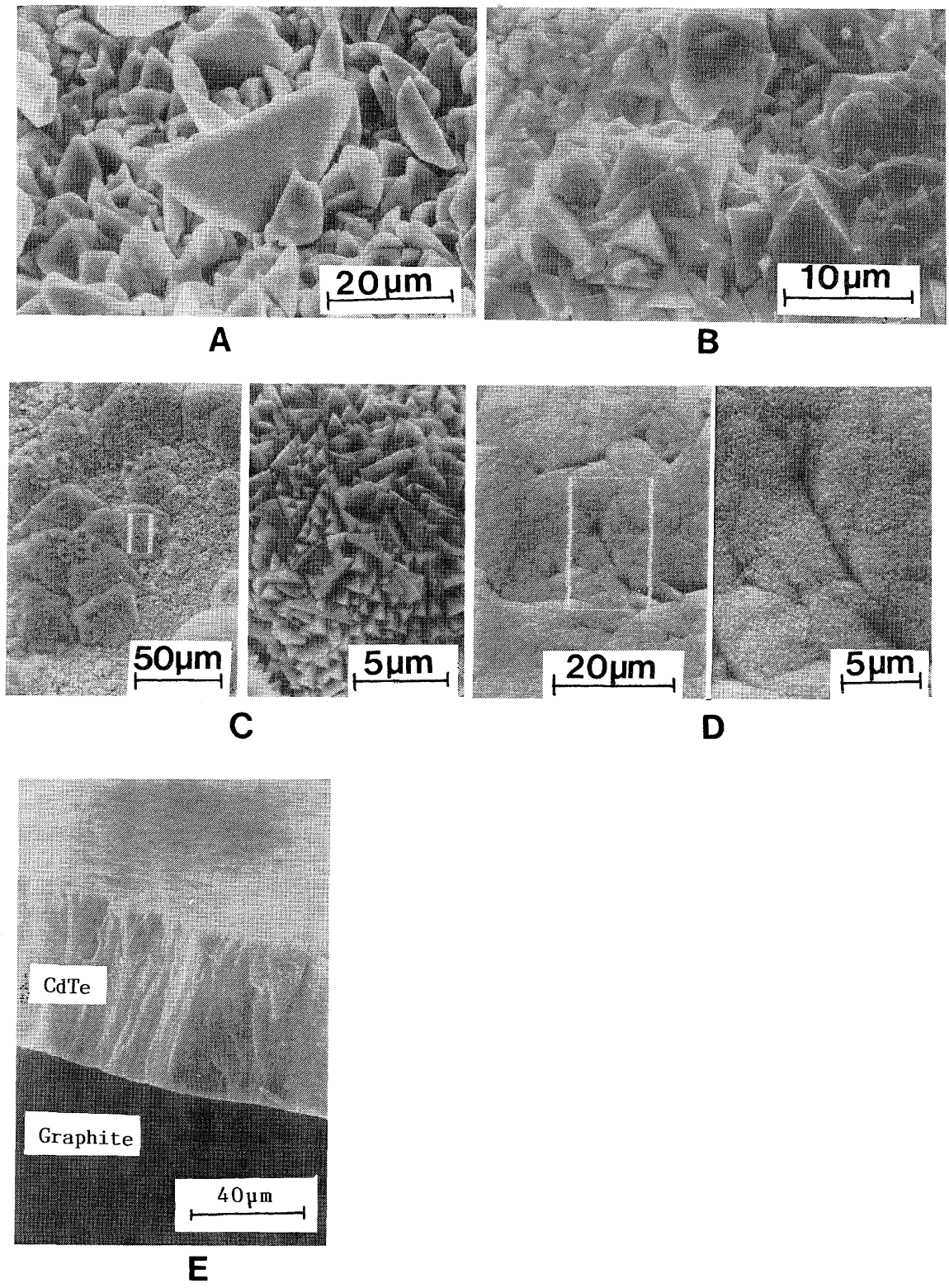

Fig. 13. SEM micrographs of the deposits obtained at different electrolytic potentials from LiCl(0.236 mol)-KCl(0.172 mol)-$CdCl_2$(0.005 mol)-Na_2TeO_3(0.005 mol) melt. Deposition potential; (A) −0.4 V, (B) −0.5 V, (C) −0.6 V, (D) −0.7 V. (E) is the cross section picture of the deposit obtained at −0.7 V.

more negative potentials, smaller crystals are deposited. The size of one crystal is 10—50 μm when deposited at −0.4 V, 5—10 μm at −0.5 V, and about 1 μm at −0.6 V. The deposits at −0.7 V have a slightly different morphology which seems to consist of very fine grains. Figure 13(E) shows a cross-section of the deposit at −0.7 V. The deposit has a columnar structure and a comparatively uniform thickness. We can conclude from this morphology that when a uniform coating of CdTe is required, −0.7 V is the optimum electrolytic potential. Deposition at less negative potentials, in contrast, may be useful for getting a single crystal of CdTe. A further study along these lines is now in progress.

This work was supported by a Grant-in-Aid for Energy Research No. 60045054 from the Ministry of Education, Science and Culture.

References

1) J. J. Cuomo and R. J. Gambino, *J. Electrochem. Soc.*, **115**, 755 (1967).
2) A. Yamamoto and M. Yamaguchi, *Jpn. J. Appl. Phys.*, **14**, 561 (1975).
3) I. Markov and M. Ilieva, *Thin Solid Films*, **74**, 109 (1980).
4) L. F. Schneemeyer and U. Cohen, *J. Electrochem. Soc.*, **130**, 1530 (1983).
5) R. Boen and J. Bouteillon, *J. Appl. Electrochem.*, **13**, 277 (1983).
6) H. Minoura, M. Tsuiki, and T. Oki, *Ber. Bunsenges. Phys. Chem.*, **81**, 588 (1977); M. Tsuiki, H. Minoura, T. Nakamura, and Y. Ueno, *J. Appl. Electrochem.*, **8**, 523 (1978); M. Tsuiki, Y. Ueno, T. Nakamura, and H. Minoura, *Chem. Lett.*, **1978**, 289; H. Minoura, K. Kobayashi, Y. Ueno, and M. Tsuiki, *Chem. Lett.*, **1982**, 505; Y. Ueno, H. Minoura, T. Nishikawa, and M. Tsuiki, *J. Electrochem. Soc.*, **130**, 43 (1983).
7) H. Minoura, T. Negoro, M. Kitakata, and Y. Ueno, *Solar Energy Mater.*, **12**, 335 (1985).
8) H. Minoura, T. Negoro, M. Kitakata, and Y. Ueno, *Thin Solid Films*, **147**, 65 (1987).
9) H. Uda, A.Nakano, K. Kuribayashi, Y. Komatsu, H. Matsumoto, and S. Ikegami, *Jpn. J. Appl. Phys.*, **22**, 1822 (1983); H. Matsumoto, K. Kuribayashi, H. Uda, Y. Komatsu, A. Nakano, and S. Ikegami, *Solar Cells*, 11, 367 (1984).
10) M. P. R. Panicker, M. Knaster, and F. A. Kroeger, *J. Electrochem. Soc.*, **125**, 566 (1978).
11) H. J. Gerritsen, *J. Electrochm. Soc.*, **131**, 136 (1984).
12) R. N. Bhattacharya and K. Rajeshwar, *J. Electrochem. Soc.*, **131**, 2032 (1984).
13) K. Uosaki, M. Takahashi, and H.Kita, *Electrochim. Acta*, **29**, 279 (1984); M. Takahashi, K. Uosaki, and H. Kita, *J. Appl. Phys.*, **55**, 3879 (1984); *J. Electrochem. Soc.*, **131**, 2304 (1984).
14) A. Darkowski and M. Cocivera, *J. Electrochem. Soc.*, **132**, 2768 (1985).
15) F. G. Bodewig and J. A. Plambeck, *J. Electrochem. Soc.*, **117**, 618 (1970).
16) H. Matsuda and Y. Ayabe, *Z. Elektrochem.*, **59**, 494 (1955).

 © 1987 The Chemical Society of Japan Bull. Chem. Soc. Jpn., 60, 2381—2386 (1987)

Application of Mössbauer Spectroscopy to a Structural Study of Superionic Conducting AgI-Ag_2O-B_2O_3 Glasses

Tetsuaki NISHIDA,* Michiko OGATA, and Yoshimasa TAKASHIMA
Department of Chemistry, Faculty of Science, Kyushu University 33,
Hakozaki, Higashiku, Fukuoka 812
(Received December 24, 1986)

A structural study of silver borate glasses containing 20 mol% AgI and 1 mol% $^{57}Fe_2O_3$ has been performed by Mössbauer spectroscopy. A Mössbauer spectrum of these glasses consists of an asymmetric quadrupole doublet with an isomer shift smaller than 0.4 mm s^{-1} with respect to metallic iron. This indicates that the individual Fe^{3+} ions are present at the substitutional sites of the tetrahedral boron atoms constituting BO_4 units as a network former. An increase in the Ag_2O content results in continuous decreases in the isomer shift and the quadrupole splitting when the Ag_2O content exceeds about 16 mol%, which corresponds to the Ag_2O/B_2O_3 ratio of 0.25 and the alkali oxide content of 20 mol% in the binary borate glasses. These results are ascribed to the formation of nonbridging oxygen atoms in the tetrahedral BO_4 and FeO_4 units. A glass transition temperature (T_g) of the glasses shows a distinct composition dependency, having a maximum around 16 mol% Ag_2O. These lead to the conclusions that planar BO_3 units are changed into the tetrahedral BO_4 units in the lower Ag_2O content region and that the nonbridging oxygen atoms are formed in the BO_4 and FeO_4 units when the Ag_2O content is higher than 16 mol%. These conclusions are well consistent with the composition dependency of the electric conductivity which shows a minimum when the Ag_2O content is 10—15 mol%.

Superionic conducting glasses have attracted much attention because of the scientific interest in the conduction mechanism as well as the high technological applicability. The electric conductivity of the superionic conducting glasses is known to reach the order of 10^{-2} S cm^{-1},[1-13] which is almost equivalent to that of the crystalline superionic conductor (solid state electrolytes) such as α-AgI and β-Al_2O_3. Comparing the magnitude of the electric conductivity of the superionic conducting glasses to that of ordinary oxide glasses such as borate and phosphate glasses, which is usually smaller than about 10^{-12} or 10^{-13} S cm^{-1},[14] it is easily understood that the former is extraordinary larger than the latter. The high electric conductivity of the superionic conducting glasses is assumed to be due to an "ion migration" of monovalent cations such as Ag^+, Li^+, and Na^+ which are present at the interstitial sites of the network structure. As for the role of the Ag^+ ions in the conduction mechanism of the superionic conducting glasses, Minami et al.[1,5,6] suggested the presence of two types of Ag^+ ions; those originated from AgX molecules (X=Cl, Br, and I) and those from Ag_2O molecules. The former is considered to be ionically bonded with the halide ions at the interstitial sites of the network structure, being primarily concerned with the electric (ionic) conduction. The latter is considered to be covalently bonded with oxygen atoms constituting a network structure and is less mobile than the former. Raman and EXAFS studies of the superionic conducting glasses revealed that the mobile Ag^+ ion is surrounded by four halide ions at the interstitial sites of network structure and is forming a microdomain or a distorted sublattice of α-AgI phase having a high electric conductivity.[9,10,12] On the other hand, Chiodelli et al.[13] ruled out the presence of the high electric conducting α-AgI phase dispersed in the glass network, for the electric conductivity of the silver borate glasses containing AgI shows a marked increase with increasing Ag_2O content when the AgI content is constant and also the conductivity of binary Ag_2O-B_2O_3 glasses is much higher than that of ordinary alkali borate glasses. The conductivity measurements of binary Ag_2O-B_2O_3 glasses performed by Matusita and Sakka[15] and Tsuchiya et al.[16] revealed that the conductivity of $30Ag_2O \cdot 70B_2O_3$ glass is about 10^{-6} S cm^{-1} at 100 °C and is higher than 10^{-8} S cm^{-1} at room temperature. These experimental results suggest that a part of the Ag^+ ions originating from Ag_2O also participate in the electric conduction. Tsuchiya et al.[16] ascribed the high conductivity of the Ag_2O-B_2O_3 glasses to an electron hopping from the colloidal Ag^0 to the Ag^+ ions. A structural study of the superionic conducting AgCl-Ag_2O-B_2O_3 glasses containing 1 mol% $^{57}Fe_2O_3$ has already been performed by means of Mössbauer spectroscopy,[17] where the present authors elucidated the relationship between the distinct composition dependency of the electric conductivity and the structural role of the Cl^- ions in those glasses. Namely the highest conductivity is observed when both the mobile and electric conducting Ag^+ ions and the Cl^- ions are present at the interstitial sites of the network structure, i.e. when the Ag_2O content is lower than about 10 mol% in the case of the silver borate glasses containing 20 mol% AgCl. Nishida et al.[17] also elucidated that the conductivity shows a distinct decrease when the Cl^- ions are incorporated into the network structure, as nonbridging chlorine atoms, of the borate glasses having the Ag_2O content higher than about 10 mol%. In these glasses, it was concluded

that the mobility of the Ag^+ ions is depressed because of the increased chemical bond strength between the Ag^+ ion and the Cl^- ion when the latter ion is present as a nonbridging chlorine atom. This conclusion is consistent with those given by Minami et al.[1,5,6] that only the Ag^+ ions originating from AgX molecules (X=Cl, Br, and I) contribute to the electric conduction and that the Ag^+ ions originating from Ag_2O molecules are almost immobile. This will be the case for the Ag^+ ions linked with the nonbridging chlorine atoms in the network structure. In contrast to the distinct composition dependency of the structural role of the Cl^- and Br^- ions in borate glasses,[18-20] all the I^- ions are known to be present at the interstitial sites of the network structure irrespective of the composition of the borate glasses.[20] The I^- ions are quite different from the Cl^- or Br^- ions in terms of the nature of the chemical bond with the Ag^+ ions; the chemical bond between the Ag^+ and the I^- ions is known to be always ionic and therefore the mobility of the Ag^+ ions is expected not to be affected by the structural role of the I^- ions.

Because of the background described above, the present Mössbauer study was performed in order to elucidate the local structure of the silver borate glasses containing 20 mol% AgI. Mössbauer spectroscopy has so far been applied to the structural study of several borate glasses.[17-19,21-25] As a result, several conclusions have been obtained such as a formation of nonbridging oxygen, chlorine, and bromine atoms and a structural change from glass to glass-ceramics. These structural studies by means of Mössbauer spectroscopy suggest that the Mössbauer spectroscopy is a very effective method for the structural study of glasses and that small amounts of iron (Fe^{3+} and Fe^{2+}), which are used as a Mössbauer probe, are easily incorporated into the glasses either as a network former or as a network modifier. DTA measurements of the silver borate glasses containing 20 mol% AgI and 1 mol% Fe_2O_3 were also performed because glass transition temperature (T_g) is known to reflect the structural changes such as a change in the coordination number of network-forming atoms (network former) and a destruction or a depolymerization of the network structure due to a formation of nonbridging oxygen atoms.[26-34]

Experimental

Silver borate glasses containing 20 mol% AgI and 1 mol% Fe_2O_3 were prepared by fusing the individual mixtures of commercially available AgI, Ag_2O, B_2O_3, and $^{57}Fe_2O_3$, of a guaranteed reagent grade, at 1020 °C for 3 h in an electric muffle furnace. After the fusion in the ambient atmosphere, each melt in a platinum crucible was immediately quenched with ice-cold water. Mössbauer measurements of pulverized samples were performed by a constant acceleration method at room temperature using a proportional counter and a 1024 channel multichannel analyzer. Cobalt-57 (10 mCi) diffused into a palladium foil was used as the Mössbauer source. As a standard material for the isomer shift, a metallic iron foil enriched with iron-57 was used. The iron foil was also used for the velocity-calibration of the spectrometer. Each Mössbauer spectrum was analyzed into a quadrupole doublet with the same linewidth. DTA measurements of these glasses were performed ranging from room temperature to 700 °C with a heating rate of 5 °C min^{-1}. An Al_2O_3 powder was used as a standard material in the DTA measurements. Electric-conductivity measurements were performed at room temperature by applying a DC voltage of 3 V. Before the measurement, each glass sample was pressed into a pellet at a net pressure of 2.6×10^6 g cm^{-2}.

Results and Discussion

All the transparent silver borate glasses prepared in the present study change their color from yellowish brown to reddish brown with increasing Ag_2O content. This is the same as the case of the silver borate glasses containing 20 or 30 mol% AgCl and 1 mol% $^{57}Fe_2O_3$.[17] The composition dependency of the color may be due to the different sizes of the colloidal Ag^0 present at the interstitial sites of the glass network.[16] A Mössbauer spectrum of the silver borate glass denoted by $20AgI\cdot25Ag_2O\cdot54B_2O_3\cdot1Fe_2O_3$ is shown in Fig. 1. It is seen from Fig. 1 that the spectrum consists of an asymmetric quadrupole doublet due to high spin Fe^{3+} species[35,36] and that the absorption intensity of the lower energy peak due to $\pm1/2\leftrightarrow\pm1/2$ transition is higher than that of the higher energy peak due to $\pm1/2\leftrightarrow\pm3/2$ transition. The asymmetric spectrum is known to be caused by the anisotropic recoil-free fraction referred to as the "Goldanskii-Karyagin effect."[37,38] In the case of the borate glasses, the asymmetric Mössbauer spectra are often observed especially in the borate glasses with lower alkali oxide contents, where the fraction of the planar BO_3 units is generally known to be large. The asymmetric Mössbauer spectra may be caused by the anisotropic chemical bond strength in the B-O or Fe-O bonds constituting the BO_4 or FeO_4 tetrahedra, brought about by the presence of the planar BO_3 units at the neighboring sites. It is seen from Fig. 1 that the doublet peaks are a little broadened around the base line. This will be due to a magnetic relaxation effect because of the relatively low Fe^{3+} concentration in the glasses, although the magnetic relaxation effect is not so strong as to exhibit a hyperfine spectrum composed of six absorption lines. All the Mössbauer parameters of the silver borate glasses studied in the present paper are summarized in Table 1, from which it is seen that the isomer shifts are located in a range of 0.32—0.25 mm s^{-1}. As for the coordination number of iron in glasses, earlier works are reviewed by Kurkjian[39] and Coey.[40] Recent Mössbauer results on the structure of glasses are reviewed by Müller-Warmuth

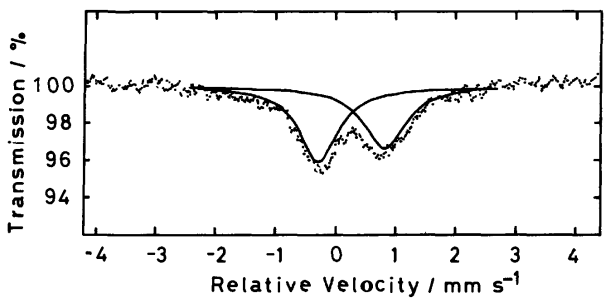

Fig. 1. Mössbauer spectrum of $20AgI \cdot 25Ag_2O \cdot 54B_2O_3 \cdot 1^{57}Fe_2O_3$ glass measured at room temperature.

Table 1. Mössbauer Parameters of the $AgI-Ag_2O-B_2O_3$ Glasses Containing 1 mol% $^{57}Fe_2O_3$

Composition	δ[a] / mm s^{-1}	Δ[b] / mm s^{-1}	Γ[c] / mm s^{-1}
$20AgI \cdot 5Ag_2O \cdot 74B_2O_3 \cdot 1Fe_2O_3$	0.31	1.20	0.88
$20AgI \cdot 10Ag_2O \cdot 69B_2O_3 \cdot 1Fe_2O_3$	0.31	1.19	0.93
$20AgI \cdot 13Ag_2O \cdot 66B_2O_3 \cdot 1Fe_2O_3$	0.32	1.17	0.91
$20AgI \cdot 15Ag_2O \cdot 64B_2O_3 \cdot 1Fe_2O_3$	0.31	1.15	0.97
$20AgI \cdot 20Ag_2O \cdot 59B_2O_3 \cdot 1Fe_2O_3$	0.28	1.14	0.93
$20AgI \cdot 25Ag_2O \cdot 54B_2O_3 \cdot 1Fe_2O_3$	0.26	1.10	0.82
$20AgI \cdot 30Ag_2O \cdot 49B_2O_3 \cdot 1Fe_2O_3$	0.25	1.11	0.83

a) Isomer shift. b) Quadrupole splitting. c) Linewidth.

and Eckert.[41] According to Coey,[40] most Fe^{3+} ions are known to occupy the tetrahedral sites in borate and silicate glasses. This is well consistent with the Mössbauer results of a series of alkali borate[17-19,21-25] and alkali borosilicate[42,43] glasses containing small amounts of Fe_2O_3, obtained by the present authors. In these Mössbauer studies,[17-19,21-25,42,43] all the isomer shifts proved to lie in a range of 0.38—0.22 mm s^{-1} with respect to metallic iron. (The experimental error for the isomer shift has usually been estimated to be $\pm$0.01 mm s^{-1}.) Judging from the experimental results shown in the reviews[39-41] and the recent Mössbauer results on the structure of glasses performed by the present authors,[17-19,21-25,42,43] the isomer shift of the Fe^{3+} ions is concluded to be smaller than about 0.40 mm s^{-1} when they are tetrahedrally coordinated. On the other hand, octahedrally coordinated Fe^{3+} ions have been observed in several phosphate glasses,[44-46] where all the isomer shifts proved to be larger than 0.42 mm s^{-1}. Those experimental results lead to the conclusion that the criterion of the isomer shift, with respect to metallic iron, lies at about 0.40 mm s^{-1} for the tetrahedrally and octahedrally coordinated Fe^{3+} ions. The symmetries refer to "distorted" tetrahedral or octahedral configurations, for the bond lengths and the bond angles are more or less distributed in glasses. This is well reflected in the large linewidth values summarized in Table 1, where the linewidth is much larger than that of the ordinary crystalline compounds containing iron.[35,36] The large linewidth of the glasses studied in the present paper is partially due to the magnetic relaxation effect described above. The present Mössbauer results therefore suggest that most of the Fe^{3+} ions are present at the tetrahedral environments in the silver borate glasses. This indicates the presence of the tetrahedral FeO_4 units at the substitutional sites of the tetrahedral BO_4 units. It is considered that the Fe^{3+} ions are easily incorporated into the matrix of borate glasses. The substitution of the iron for the other metal or metalloid ions will easily occur in the high energy and nonequilibrium states when the glass samples are prepared by fusion.

The composition dependencies of the isomer shift and the quadrupole splitting of the Fe^{3+} ions are shown in Figs. 2 and 3, respectively. It is seen from Fig. 2 that the isomer shift shows a distinct decrease when the Ag_2O content exceeds about 16 mol%. A distinct decrease in the isomer shift of the Fe^{3+} ions has already been observed in alkali borate[21-25] and borosilicate[42,43] glasses when the alkali oxide (K_2O) content is higher than 20 and 8—10 mol%, respectively. In these glasses,[21-25,42,43] the decrease in the isomer shift of the Fe^{3+} ion, which is present at the substitutional site of the tetrahedral boron or silicon atoms, was ascribed to the formation of nonbridging oxygen atoms ($-O^-$) in the BO_4 or SiO_4 tetrahedral units, because the formation of the nonbridging oxygen atoms results in decreased interatomic distances in the B-O or Si-O bonds. This will be the case for the chemical bond length in the Fe-O bond. On the other hand, germanate glasses,[30,47] of which network structure is composed of GeO_4 and GeO_6 units, showed a drastic increase in the isomer shift of Sn^{4+} ions when nonbriding oxygen atoms are formed in the tetrahedral GeO_4 units. In the case of the ^{119}Sn-Mössbauer spectroscopy, an increase in the s-electron density at the tin nucleus results in an increase in the isomer shift. This is apparently opposite to the case of the ^{57}Fe-Mössbauer spectroscopy.[35,36] It should be noted that the formation of the nonbridging oxygen atoms in the GeO_4 tetrahedra was concluded through an increase in the isomer shift of the Sn^{4+} ions present at the interstitial sites of the network structure composed of the GeO_4 tetrahedra and the GeO_6 octahedra. These experimental results lead to the conclusion that the distinct decrease in the isomer shift shown in Fig. 2, observed when the Ag_2O content is equal to or higher than about 16 mol%, is due to the formation of nonbridging oxygen atoms in the tetrahedral BO_4 or FeO_4 units. This conclusion is consistent with the distinct and continuous decrease in the quadrupole splitting in the similar Ag_2O content region (Fig. 3). It is seen from Fig. 3 that the quadrupole splitting shows a distinct decrease when the Ag_2O content is equal to or higher than 15 mol%. As to the composition dependency of the quadrupole

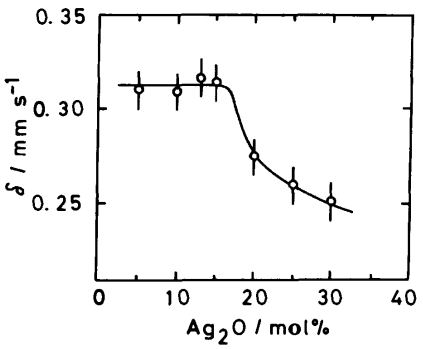

Fig. 2. Composition dependency of the isomer shift (δ) of the Fe^{3+} ions in the Ag_2O-B_2O_3 glasses containing 20 mol% AgI and 1 mol% $^{57}Fe_2O_3$.

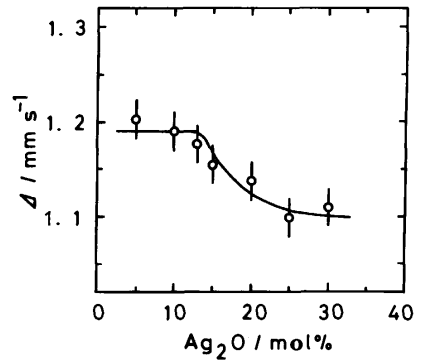

Fig. 3. Composition dependency of the quadrupole splitting (Δ) of the Fe^{3+} ions in the Ag_2O-B_2O_3 glasses containing 20 mol% AgI and 1 mol% $^{57}Fe_2O_3$.

splitting of the Fe^{3+} ions in glasses, distinct decreases have been observed when the nonbridging oxygen atoms are formed in alkali borate,[21-25] borosilicate,[42,43] and phosphate[45,46] glasses. The decrease in the quadrupole splitting of the Fe^{3+} ions is ascribed to an increased symmetry around the Fe^{3+} ions, because the Fe^{3+} ions of high spin state have a symmetric electron configuration of $3d^5$ in the outermost orbital and therefore only the electric field gradient brought about by the neighboring atoms or ions primarily affects the electric field gradient at the iron nucleus. Similar phenomenon has been observed in the case of potassium germanate glasses containing tin (Sn^{4+}), which also has a symmetric electron configuration of $4d^{10}$,[30,47] in spite that the Sn^{4+} ions are ionically present at the interstitial sites of the network structure. In the germanate glasses, the formation of nonbridging oxygen atoms was concluded to start when the alkali oxide content exceeds about 16 mol%. In the light of these reasons, the decrease in the quadrupole splitting of the Fe^{3+} ions observed in the present study is ascribed to the formation of nonbridging oxygen atoms in the tetrahedral BO_4 and FeO_4 units. (Each Fe^{3+} ion is concluded to be present at the substitutional site of the tetrahedral boron atom as described above.) These conclusions are well consistent with those obtained in the previous Mössbauer[21-25] studies of alkali borate glasses, i.e., the formation of nonbridging oxygen atoms in the BO_4 units starts when the alkali oxide content is equal to or higher than 20 mol%. The alkali oxide content of 20 mol% in the binary alkali borate glasses corresponds to about 16 mol% in the present ternary silver borate glass system containing 20 mol% AgI. (The Ag_2O/B_2O_3 ratio of 16/63 (=0.25) is consistent with the K_2O/B_2O_3 ratio of 20/80.) Effect of the Fe_2O_3 on the structure of the borate glasses can be neglected because the content is very low, i.e. 1 mol% in the present study and 0.33 mol% in the previous studies.[23,24] The same results have also been obtained in the borate glasses with the Fe_2O_3 content of 7 mol%.[21,22,25] These results suggest that the structure of the silver borate glasses is essentially the same as that of the alkali borate glasses and that the I^- ions are present at the interstitial sites of the network structure all over the compositional range studied in the present paper. This is obviously different from the case of the Cl^- and the Br^- ions which change their structural role from the interstitial anions to the nonbridging halogen atoms, depending on the composition.[17-20]

Each DTA curve of silver borate glasses containing 20 mol% AgI and 1 mol% Fe_2O_3 consists of a simple endothermic peak due to glass transition and one or two exothermic peak(s) due to crystallization. All the glass transition temperatures (T_g) obtained in the present study are shown in Fig. 4, where the T_g is plotted against the Ag_2O content of the glasses. DTA studies of several glasses have revealed that T_g shows a close relationship with a change in the coordination number of the network-forming atoms (network former) and with the formation of nonbridging oxygen or halogen atoms which means a destruction or depolymerization of the glass matrix.[17,26-34] In general. T_g shows a distinct increase when the coordination number of the network forming atoms increases. For example the change in the coordination

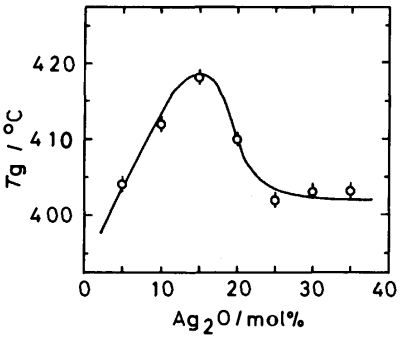

Fig. 4. Composition dependency of the glass transition temperature (T_g) of the Ag_2O-B_2O_3 glasses containing 20 mol% AgI and 1 mol% Fe_2O_3.

number of Ge from 4 to 6 in germanate glasses is observed as a continuous increase in the T_g.[27,28,30] The increase in the T_g, observed with increasing Ag_2O content of the silver borate glasses in the lower Ag_2O content region (Fig. 4), is therefore ascribed to the well-known structural change from the BO_3 triangles to the BO_4 tetrahedra in the ordinary borate glasses, i.e. an increase in the coordination number of boron from 3 to 4. Contrary to this, the formation of nonbridging oxygen atoms results in a decrease in the T_g.[27,28,30,34] These experimental results suggest that a decrease in the T_g, observed in the present silver borate glasses having the Ag_2O contents higher than 15 mol% (Fig. 4), is due to the formation of nonbridging oxygen atoms in the tetrahedral BO_4 or FeO_4 units. This is well consistent with the Mössbauer results described above.

Composition dependency of the electric conductivity is shown in Fig. 5a, from which it is seen that the conductivity of the silver borate glasses containing AgI shows a slight increase with increasing Ag_2O content when the Ag_2O content exceeds about 15 mol%. This is very contrary to the composition dependency of the silver borate glasses containing the same amount (20 mol%) of AgCl,[17] shown with a broken line (Fig. 5b). In the silver borate glasses containing 20 mol% AgCl and 1 mol% $^{57}Fe_2O_3$,[17] the drastic decrease in the conductivity was ascribed to the decreased number of the mobile Ag^+ ions present at the interstitial sites of the network structure, brought about as a result of the change in the structural role of the Cl^- ions. (Most of the Cl^- ions were concluded to change their structural role from the interstitial anions to the nonbridging chlorine atoms when the Ag_2O content exceeds about 10 mol%.[17]) Also, the decrease in the mobility of the electric conducting Ag^+ ions was concluded to be due to the increased chemical bond strength between the Ag^+ ions and the nonbridging chlorine atoms.[17] Judging from the structural information on the silver borate glasses containing 20 mol% AgI, obtained from the Mössbauer and DTA measurements in the present study, the slight increase in the conductivity observed with increasing Ag_2O content (Fig. 5a) is ascribed to the open structure of the borate glasses brought about as a result of the formation of nonbridging oxygen atoms in the tetrahedral BO_4 (or FeO_4) units. This means a destruction of the complicated network structure composed of the planar BO_3 and the tetrahedral BO_4 (and FeO_4) units linked with bridging oxygen atoms. In these glasses, the mobility of the Ag^+ ions will be enhanced because of the decreased physical and chemical interactions between the Ag^+ and the glass matrix. These results are well consistent with the general rule that the ionic conduction in solids is enhanced when the electric charge and the ionic radius of cations are small and the size of space or "tunnel," where the conducting ions actually pass through under an electric field, is large enough. This is also the case for the decrease in the electric conductivity observed in the Ag_2O content region lower than about 15 mol% (Fig. 5a), since the increase in the Ag_2O or alkali oxide contents results in a structural change from the planar BO_3 to the tetrahedral BO_4 units, as described above. This structural change will bring about a more complicated network structure of the borate glasses compared to that of the original boric (B_2O_3) glass having only the planar BO_3 units. The complicated structure will result in a decreased mobility of the electric conducting Ag^+ ions.

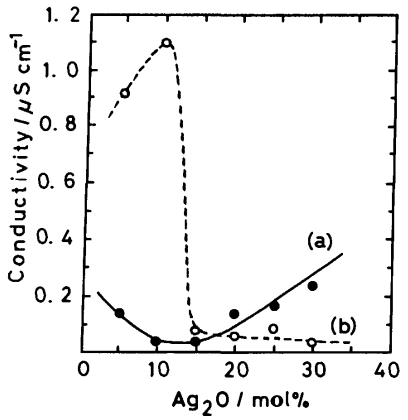

Fig. 5. Composition dependencies of the electric conductivity of the Ag_2O-B_2O_3 glasses containing (a) 20 mol% AgI and 1 mol% Fe_2O_3, and (b) 20 mol% AgCl and 1 mol% Fe_2O_3.[17]

The authors are indebted to Mr. Toshiharu Hirai of Chemical and Catalysis Industrial Corporation for his kind help in the electric conductivity measurements. One of the authors (TN) is grateful to the Itoh Science Foundation and Grants-in-Aid for Scientific Research (Nos. 60740234 and 61740350) from the Ministry of Education, Science and Culture, for the financial support.

References

1) T. Minami, Y. Takura, and M. Tanaka *J. Electrochem. Soc.*, **124**, 1659 (1977).
2) J. P. Malugani, A. Wasniewski, M. Doreau, G. Robert, and A. Rikabi, *Mater. Res. Bull.*, **13**, 427 (1978).
3) T. Minami and M. Tanaka, *Rev. Chim. Miner.*, **16**, 283 (1979).
4) A. Magistris, G. Chiodelli, and A. Schiraldi, *Electrochim. Acta*, **24**, 203 (1979).
5) T. Minami and M. Tanaka, *J. Non-Cryst. Solids*, **38/39**, 289 (1980).
6) T. Minami, K. Imazawa, and M. Tanaka *J. Non-Cryst. Solids*, **42**, 469 (1980).
7) J. P. Malugani, G. Robert, and R. Mercier, *Mater. Res. Bull.*, **15**, 715 (1980).

8) G. Chiodelli, A. Magistris, M. Villa, and J. L. Bjorkstam, *Mater. Res. Bull.*, **17**, 1 (1982).
9) A. Fontana, G. Mariotto, E. Cazzanelli, G. Carini, M. Cutroni, and M. Federico, *Phys. Lett. A*, **93**, 209 (1983).
10) G. Dalba, A. Fontana, P. Fornasini, G. Mariotto, M. R. Masullo, and F. Rocca, *Solid State Ionics*, **9/10**, 597 (1983).
11) J. P. Malugani, R. Mercier, B. Fahys, and G. Robert, *J. Solid State Chem.*, **45**, 309 (1982).
12) J. P. Malugani and R. Mercier, *Solid State Ionics*, **13**, 293 (1984).
13) G. Chiodelli, G. Camparivigano, G. Flor, A. Magistris, and M. Villa, *Solid State Ionics*, **8**, 311 (1983).
14) L. Murawski, *J. Mater. Sci.*, **17**, 2155 (1982).
15) K. Matusita and S. Sakka, *Yogyo Kyokai Shi*, **84**, 496 (1976).
16) T. Tsuchiya, T. Horiuchi, and T. Moriya, *Yogyo Kyokai Shi*, **87**, 223 (1979).
17) T. Nishida, M. Ogata, and Y. Takashima, *Bull. Chem. Soc. Jpn.*, **59**, 2401 (1986).
18) T. Nishida, N. Kai, Y. Takashima, *Phys. Chem. Glasses*, **22**, 107 (1981).
19) T. Nishida, T. Nonaka, T. Isobe, and Y. Takashima, *Phys. Chem. Glasses*, **24**, 88 (1983).
20) T. Maekawa, S. Satoh, and T. Yokokawa, *Yogyo Kyokai Shi*, **93**, 20 (1985).
21) T. Nishida and Y. Takashima, *J. Non-Cryst. Solids*, **37**, 37 (1980).
22) T. Nishida, Y. Takashima, and Y. Nakayama, *J. Solid State Chem.*, **33**, 141 (1980).
23) T. Nishida, T. Shiotsuki, and Y. Takashima, *J. Non-Cryst. Solids*, **41**, 161 (1980).
24) T. Nishida, T. Hirai, and Y. Takashima, *J. Non-Cryst. Solids*, **43**, 221 (1981).
25) T. Nishida and Y. Takashima, "Application of Mössbauer Effect on the Crystallization of Several Glasses," in "Industrial Applications of the Mössbauer Effect," ed by G. J. Long and J. Stevens, Plenum Publ. Corp., New York (1987), pp. 409—422.
26) E. M. Boulos and N. J. Kreidl *J. Am. Ceram. Soc.*, **54**, 368 (1971).
27) J. E. Shelby, *J. Am. Ceram. Soc.*, **57**, 436 (1974).
28) J. E. Shelby *J. Appl. Phys.*, **46**, 193 (1975).
29) R. M. Almeida and J. D. Mackenzie, *J. Chem. Phys.*, **74**, 5954 (1981).
30) T. Nishida, M. Katada, and Y. Takashima, *Bull. Chem. Soc. Jpn.*, **57**, 3566 (1984).
31) J. L. Piguet and J. E. Shelby, *J. Am. Ceram. Soc.*, **68**, 450 (1985).
32) T. Nishida, T. Nonaka, and Y. Takashima, *Bull, Chem. Soc. Jpn.*, **58**, 2255 (1985).
33) T. Nishida and Y. Takashima *Bull. Chem. Soc. Jpn.*, **59**, 2789 (1986).
34) T. Nishida and Y. Takashima, *Bull. Chem. Soc. Jpn.*, **60**, 941 (1987).
35) N. N. Greenwood and T. C. Gibb, "Mössbauer Spectroscopy," Chapman and Hall Ltd., London (1971) Chap. 3.
36) R. Ingalls, F. Van der Woude, and G. A. Sawatzky, "Iron and Nickel," in "Mössbauer Isomer Shifts," ed by G. K. Shenoy and F. E. Wagner, North-Holland Pub Co., Amsterdam (1978), Chap. 7.
37) V. I. Goldanskii, G. M. Gorodinskii, S. V. Karyagin, L. A. Korytko, L. M. Krizhanskii, E. F. Makarov, I. P. Suzdalev, and V. V. Khrapov, *Dokl. Akad. Nauk SSSR*, **147**, 127 (1962).
38) S. V. Karyagin, *Dokl. Akad. Nauk SSSR*, **148**, 1102 (1963).
39) C. R. Kurkjian, *J. Non-Cryst. Solids*, **3**, 157 (1970).
40) J. M. D. Coey, *J. Phys.*, **35**, C6—89 (1974).
41) W. Müller-Warmuth and H. Eckert, *Phys. Rep.*, **88**, 91 (1982).
42) T. Nishida, T. Hirai, and Y. Takashima, *Phys. Chem. Glasses*, **22**, 94 (1981).
43) T. Nishida, T. Hirai, and Y. Takashima, *Bull. Chem. Soc. Jpn.*, **54**, 3735 (1981).
44) M. F. Taragin, J. C. Eisenstein, and W. Heller, *Phys. Chem. Glasses*, **13**, 29 (1972).
45) T. Nishida, T. Shiotsuki, and Y. Takashima, *J. Non-Cryst. Solids*, **43**, 115 (1981).
46) T. Nishida, T. Shiotsuki, and Y. Takashima, *J. Non-Cryst. Solids*, **43**, 123 (1981).
47) T. Nishida, M. Katada, and Y. Takashima, *Bull. Chem. Soc. Jpn.*, **58**, 1745 (1985).

Preparation and Properties of Ammonium Hexachlorozirconate(IV) and Its Reaction with Gaseous Ammonia

Masao OHASHI,* Shoji YAMANAKA, Yuhki MORIMOTO, and Makoto HATTORI
Department of Applied Chemistry, Faculty of Engineering, Hiroshima University, Higashi-Hiroshima 724
(Received January 30, 1987)

Ammonium hexachlorozirconate $(NH_4)_2ZrCl_6$ was prepared by the direct reaction of $ZrCl_4$ with NH_4Cl. The X-ray powder diffraction and the density measurements showed that it has a face-centered cubic lattice with a=10.127(2) Å and is isostructural with K_2PtCl_6. The hexachlorozirconate undergoes ammonolysis in gaseous ammonia at room temperature, forming $ZrCl_3(NH_2)\cdot xNH_3$ and NH_4Cl. The ammonolysis product reverts to the initial $(NH_4)_2ZrCl_6$ on heating to 250 °C in the ammonia atmosphere. The hexachlorozirconate vaporizes at about 450 °C. The reaction of $ZrCl_4$ with gaseous ammonia was also studied in comparison with that of the hexachlorozirconate.

Most fine powders used for production of nitride ceramics are prepared by the reactions of metal chlorides with ammonia at elevated temperatures. Therefore, it is essentially important to understand these reaction mechanisms to obtain more refined powders for the production of improved nitride ceramics. In the reaction system of $ZrCl_4$–NH_3, a layer structured compound β-ZrNCl is formed in the intermediate temperature range prior to the formation of zirconium nitride at higher temperatures.[1] In previous papers,[2,3] we showed that this layer compound forms lithium intercalates Li_xZrNCl and could be a promising candidate for electrochromic electrode material.

Usually β-ZrNCl is prepared according to the method reported by Juza and Heners:[4] the solid sample of anhydrous $ZrCl_4$ is heated stepwise to 600 °C in dry ammonia. However, this method suffers the disadvantage of low yield. Yajima et al.[1] reported that in the reaction of $ZrCl_4$ vapor with ammonia, an adduct $ZrCl_4\cdot 2NH_3$ was formed in the temperature range below 400°C. The same ammonia adduct seems to be formed during the above preparation procedure for β-ZrNCl. It is very likely that the formation of this adduct is responsible for the low yield, because the adduct vaporizes easily at above 400 °C and is transported to the cooler part without decomposing to β-ZrNCl.

In the course of the present study for a better understanding of the properties of the adduct, we have found that the true composition of the adduct is $(NH_4)_2ZrCl_6$ rather than $ZrCl_4\cdot 2NH_3$. The same compound has been prepared by the direct reaction of $ZrCl_4$ with NH_4Cl and its thermal behavior in ammonia has been investigated.

Experimental

Preparation of $(NH_4)_2ZrCl_6$. Ammonium hexachlorozirconate(IV) $(NH_4)_2ZrCl_6$ was prepared by the dry method similar to that reported by Lister and Flengas[5] for K_2ZrCl_6 in the following procedure: Zirconium tetrachloride was purified by sublimation and mixed with ammonium chloride dried at 180 °C under vacuum in the molar ratio of 1:2 in a dry box. The mixture was placed in a Pyrex boat and heated to 400 °C in a stream of dry nitrogen. After the mixture was kept at the temperature for 5 h, the resulting residue in the Pyrex boat was taken out and vacuum sealed in a Pyrex tube, which was then placed in a two-zone furnace. The temperature of the residue was regulated at 400 °C, the other end of the sealed tube being at 100 °C. After standing for 5 h, white crystals of $(NH_4)_2ZrCl_6$ were transported to the lower temperature zone. Found: Zr, 27.4; N, 8.23; Cl, 62.6%. Calcd for $(NH_4)_2ZrCl_6$: Zr, 26.8; N, 8.24; Cl, 62.6%.

Analyses. Since most of the products treated in this study are sensitive to the humidity in air, those were manipulated in a dry box unless otherwise noted. X-Ray powder diffraction (XRD) patterns were measured under a dry argon atmosphere by using a cylindrical cover having thin polyethylene windows; nickel filtered Cu $K\alpha$ radiation was used.

Elemental analyses for zirconium, chlorine and nitrogen were carried out after the sample was dissolved in 2 mol dm^{-3} sulfuric acid. The nitrogen content was determined by Kjeldahl method; zirconium and chlorine were determined gravimetrically as ZrO_2 and AgCl, respectively. The density of $(NH_4)_2ZrCl_6$ was measured pycnometrically with toluene at 25 °C.

Thermogravimetric Study in Ammonia. The amount of ammonia taken up by $(NH_4)_2ZrCl_6$ was measured gravimetrically by using a quartz spring balance as a function of pressure of ammonia at 25 °C. The sample was heated in an ammonia stream (flow rate of 50 ml min^{-1}) to 650 °C for a heating rate of 3 °C min^{-1}. For comparison similar experiment was performed on $ZrCl_4$.

Results

X-Ray Diffraction Study. The XRD data of $(NH_4)_2ZrCl_6$ is shown in Table 1. The XRD pattern is very similar to that of K_2ZrCl_6 reported by Lister and Flengas[5] and all the diffraction peaks can be indexed on the basis of a cubic lattice with a=10.127(2) Å. Moreover, the lattice type of $(NH_4)_2ZrCl_6$ is face-centered cubic because the diffraction peaks are only present when h,k,l are all even or all odd. Engel[6] showed that a series of hexachloro complexes with the

general formula A_2MCl_6 (A=K, NH_4, Rb, Cs, Tl; M=Ti, Se, Zr, Sn, Te, Pt, Pb) has the K_2PtCl_6 structure and that for the complexes with an A ion in common, the lattice constants can be related with those of the corresponding Rb- salts by a linear relation as shown in Fig. 1. Although $(NH_4)_2ZrCl_6$ is not included in his plot, the value obtained above fits well on the line for the ammonium series. This fact indicates that $(NH_4)_2ZrCl_6$ has the K_2PtCl_6 structure. The density determined for the $(NH_4)_2ZrCl_6$ prepared by the direct method in this study is 2.14 g cm^{-3}, which is in good agreement with the value of 2.17 g cm^{-3} calculated on the basis of the K_2PtCl_6 structure with a=10.127 Å.

Ammonium hexachlorozirconate can be also prepared by the wet method from hot aqueous solutions of zirconium dichloride oxide and ammonium chloride.[7,8] If the solution is saturated with hydrogen chloride and gradually cooled, the crystals of $(NH_4)_2ZrCl_6$ precipitate. It is found that the crystals thus prepared exhibit the XRD pattern identical to that of the crystals obtained by the direct method. Toptygina and Barskaya[7] prepared $(NH_4)_2ZrCl_6$ by the wet method and reported its XRD data, which however, do not coincide with ours. Since their chemical analysis data are in agreement with ours for $(NH_4)_2ZrCl_6$, they probably used the sample hydrolyzed in air for the measurement of the XRD pattern. Yajima et al.[1] investigated the reaction of gaseous $ZrCl_4$ with ammonia at elevated temperatures, and reported that in the temperature range 300—400 °C, white crystals with composition $ZrCl_4 \cdot 2NH_3$ were formed. Strangely, the XRD pattern reported by them for the crystal is identical to that of $(NH_4)_2ZrCl_6$. Although the detailed procedures are not reported, it is likely that Yajima et al. analyzed the as-deposited sample without purification: the sample was probably a mixture of $(NH_4)_2ZrCl_6$ and noncrystalline zirconium amide trichloride $ZrCl_3(NH_2) \cdot xNH_3$ and the overall ratio of Zr:N:Cl of the mixture is 1:2:4. The formation of the zirconium amide trichloride will be discussed later in more details.

Table 1. X-Ray Diffraction Data of $(NH_4)_2ZrCl_6$

d_{obsd}/Å	d_{calc}/Å	hkl	I/I_0
5.844	5.847	111	100
5.068	5.064	200	65
3.577	3.580	220	15
3.050	3.053	311	50
2.923	2.923	222	60
2.534	2.532	400	100
2.320	2.323	331	20
2.263	2.264	420	50
2.070	2.067	422	5
1.947	1.949	333	25
1.791	1.790	440	60
1.712	1.712	531	20
1.687	1.688	600, 442	25
1.462	1.462	444	10

Uptake of Ammonia by $(NH_4)_2ZrCl_6$. Figure 2 shows the amounts of ammonia taken up by $(NH_4)_2ZrCl_6$ at 25 °C as a function of increasing-decreasing pressure of ammonia. The amount was recorded after standing for 2 d at each pressure although the rate of uptake or release of ammonia is so slow that it takes more than 2 d to attain complete equilibrium. As seen in the figure, the amount of uptake gradually increases with the pressure and approaches 9 mol per mole of $(NH_4)_2ZrCl_6$ at the pressure of about 1 atm. On reducing the pressure to 1.4×10^3 Pa, only 2 mol of ammonia are removed. By prolonged evacuation at the pressure of 10^{-1} Pa for 4 d, additional 5 mol of ammonia are removed, but 2 mol of ammonia are tenaciously retained.

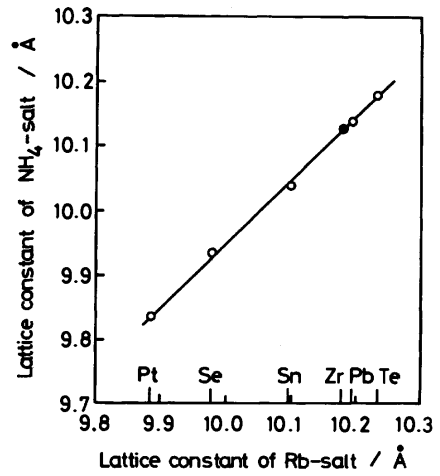

Fig. 1. Linear relationship between the lattice constants of NH_4-salts and those of Rb-salts. (●): This work, (○): results done by Engel.[6]

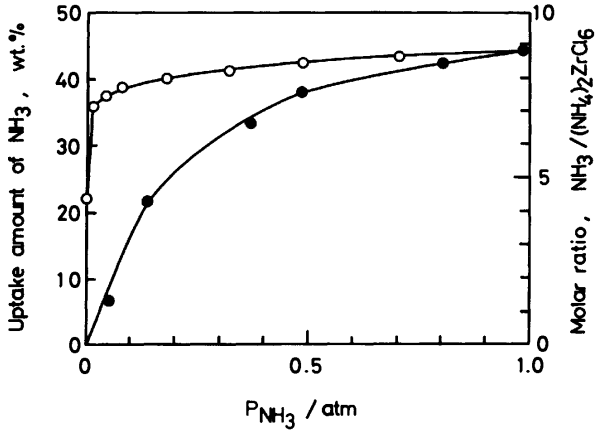

Fig. 2. Amount of ammonia taken up by $(NH_4)_2ZrCl_6$ at 25 °C as a function of the pressure of ammonia. (●), increasing pressure; (○), decreasing pressure.

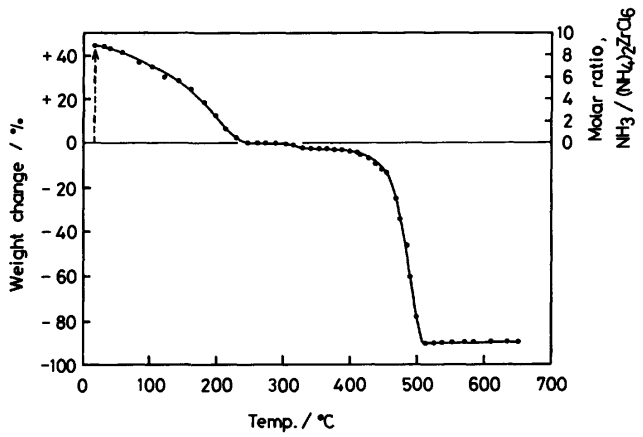

Fig. 3. Thermogravimetric curve for $(NH_4)_2ZrCl_6$ in an ammonia stream.

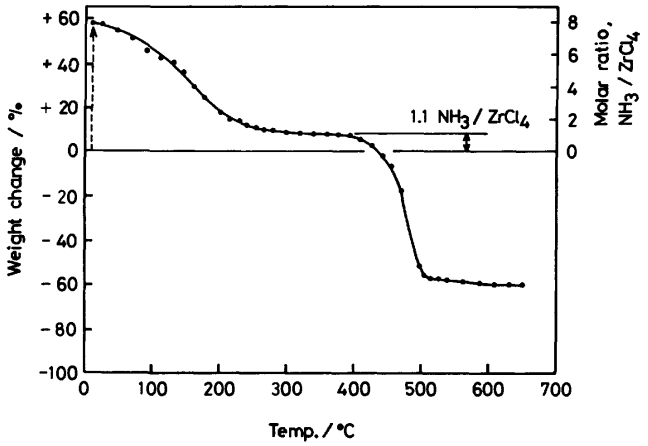

Fig. 4. Thermogravimetric curve for $ZrCl_4$ in an ammonia stream.

Separate samples of $(NH_4)_2ZrCl_6$ were also treated similarly and taken out to see the crystalline phases present at the different stages of uptake of ammonia. The XRD pattern of the sample equilibrated with 1 atm of ammonia exhibited the intense diffraction peaks due to NH_4Cl with the disappearance of the peaks due to $(NH_4)_2ZrCl_6$. The sample evacuated after the uptake of ammonia still exhibited only the peaks due to NH_4Cl.

The thermogravimetric analysis of $(NH_4)_2ZrCl_6$ was carried out in a stream of ammonia after about 9 mol of ammonia were taken up. As shown in Fig. 3, the ammonia is gradually removed with an increase in the temperature, and at 250 °C the sample reverts to the initial state in weight. The XRD pattern of the sample measured at this state indicated that the diffraction peaks of NH_4Cl extremely decreased in the intensity and, on the contrary, those of $(NH_4)_2ZrCl_6$ were almost completely recovered. The sample vaporized at about 450 °C and only 15% of the initial weight was left in the thermogravimetric analysis cell. The residue was found to be a mixture of α- and β-ZrNCl.

For comparison similar analysis was performed on $ZrCl_4$ in a stream of ammonia. During standing in ammonia of the pressure of 1 atm for 8 h, one mole of $ZrCl_4$ took up ammonia as much as 8 mol. Then, the temperature of the sample was raised in the manner similar to that of the analysis of $(NH_4)_2ZrCl_6$. Figure 4 shows the thermogravimetric curve observed. The curve is very similar to that observed for $(NH_4)_2ZrCl_6$ except that the weight does not revert to the initial state; as seen from the figure, about 1 mol of ammonia is retained up to 400 °C at which the vaporization of the sample begins. On heating to 650 °C, about 60% of the initial weight was lost and the residue was β-ZrNCl.

Discussion

Drake and Fowles[8] studied the ammonolysis of $(NH_4)_2ZrCl_6$ with liquid ammonia. They showed that $(NH_4)_2ZrCl_6$ behaves essentially like $ZrCl_4$. $ZrCl_4$ is subjected to ammonolysis to only one Zr–Cl bond in liquid ammonia, giving the zirconium amide chloride:[9]

$$ZrCl_4 \xrightarrow{NH_3} ZrCl_3(NH_2)\cdot xNH_3 + NH_4Cl. \quad (1)$$

Similarly $(NH_4)_2ZrCl_6$ undergoes ammonolysis to one Zr–Cl bond

$$(NH_4)_2ZrCl_6 \xrightarrow{NH_3} (NH_4)_2[ZrCl_5(NH_2)]\cdot xNH_3 + NH_4Cl. \quad (2)$$

On washing with liquid ammonia, the complex decomposes into ammonium chloride and zirconium amide trichloride:

$$(NH_4)_2[ZrCl_5(NH_2)]\cdot xNH_3 \longrightarrow 2NH_4Cl + ZrCl_3(NH_2)\cdot xNH_3. \quad (3)$$

The tensimetric study by Fowles and Pollard,[10] and our previous study[11] on the decomposition of the zirconium amide trichloride showed that x is about 6—7 in the above equations.

The results of thermogravimetric analyses seem to suggest that $(NH_4)_2ZrCl_6$ and $ZrCl_4$ are subjected to ammonolysis with gaseous ammonia in a similar manner:

$$(NH_4)_2ZrCl_6 + 9NH_3 \longrightarrow 3NH_4Cl + ZrCl_3(NH_2)\cdot 7NH_3, \quad (4)$$

$$ZrCl_4 + 8NH_3 \longrightarrow NH_4Cl + ZrCl_3(NH_2)\cdot 6NH_3. \quad (5)$$

In the reaction with gaseous ammonia, however the resulting NH_4Cl is not washed out, but remains in the product. The XRD pattern of the product indicates the formation of NH_4Cl with the disappearance of $(NH_4)_2ZrCl_6$. The zirconium amide trichloride $ZrCl_3(NH_2)\cdot xNH_3$ is likely a noncrystalline polymeric solid as suggested by Allbutt and Fowles.[12] The XRD results tell us that on heating, the reaction of Eq. 4 is reversed, and NH_4Cl reacts with $ZrCl_3(NH_2)$ and reforms $(NH_4)_2ZrCl_6$. A very small drop in weight is observed at 330 °C in the thermogravimetric curve of Fig. 3. This drop can be attributed to the sublimation of NH_4Cl remaining unreacted in the system.

In the case of $ZrCl_4$, one mole of ammonia remains in the system above 250 °C until the vaporization of the sample begins at 400 °C. This difference in the behavior of the ammonolysis products of $(NH_4)_2ZrCl_6$ and $ZrCl_4$ can be interpreted in terms of the insufficient NH_4Cl in the latter ammonolysis product. Since only one mole of NH_4Cl is present in the product (Eq. 5), only one third of $ZrCl_3(NH_2)$ is converted into $(NH_4)_2ZrCl_6$ according to the following reaction:

$$ZrCl_3(NH_2)\cdot 6NH_3 + NH_4Cl \longrightarrow \frac{1}{3}(NH_4)_2ZrCl_6 + \frac{2}{3}ZrCl_3(NH_2) + 6\frac{2}{3}NH_3. \quad (6)$$

It is interesting to note that the abrupt decreases in weight occur at the same temperature irrespective of the kinds of starting samples. It is apparent that the temperature of 450 °C corresponds to the vaporization of $(NH_4)_2ZrCl_6$, although the decomposition of $ZrCl_3(NH_2)$ to β-ZrNCl is also accompanied around this temperature.[11]

In summary, ammonium hexachlorozirconate $(NH_4)_2ZrCl_6$ can be prepared by the direct reaction of $ZrCl_4$ with NH_4Cl. $ZrCl_4$ and $(NH_4)_2ZrCl_6$ are subjected to ammonolysis with gaseous as well as liquidous ammonia and form the amide $ZrCl_3(NH_2)\cdot nNH_3$. The amide reverts to $(NH_4)_2ZrCl_6$ in the presence of NH_4Cl at elevated temperature. In the preparation procedure of β-ZrNCl from $ZrCl_4$ and NH_3, the formation of $(NH_4)_2ZrCl_6$ as a by-product is unavoidable, which is removed from the reaction system by vaporization above 400 °C. This should be responsible for the low yield of β-ZrNCl.

This work was supported in part by Grant-in-Aid for Developmental Scientific Research No.61850148 of the Ministry of Education, Science and Culture.

References

1) A. Yajima, Y. Segawa, R. Matsuzaki, and Y. Saeki, *Bull. Chem. Soc. Jpn.*, **56**, 2638 (1983).
2) S. Yamanaka, M. Ohasi, M. Sumihara, and M. Hattori, *Chem. Lett.*, **1984**, 1403.
3) M. Ohashi, S. Yamanaka, M. Sumihara, and M. Hattori, *J. Inclusion Phenomena*, **2**, 289 (1984).
4) R. Juza and J. Heners, *Z. Anorg. Allg. Chem.*, **332**, 159 (1964).
5) R. L. Rister and S. N. Flengas, *Can. J. Chem.*, **42**, 1102 (1964).
6) G. Engel, *Z. Krist.*, **90**, 341 (1935).
7) G. M. Toptygina and I. B. Barskaya, *Russ. J. Inorg. Chem.*, **10**, 1226 (1965).
8) J. E. Drake and G. W. A. Fowles, *J. Less-Common Met.*, **3**, 149 (1961).
9) J. E. Drake and G. W. A. Fowles, *J. Less-Common Met.*, **2**, 401 (1960).
10) G. W. A. Fowles and F. H. Pollard, *J. Chem. Soc.* **1953**, 4128.
11) M. Ohashi, S. Yamanaka, and M. Hattori, *Bull. Chem. Soc. Jpn.*, **59**, 2627 (1986).
12) M. Allbutt and G. W. A. Fowles, *J. Inorg. Nucl. Chem.*, **25**, 67 (1963).

The Pyrolysis of Heptathiazocine

Yoshiyuki KUDO and Shuichi HAMADA*
Department of Applied Chemistry, Faculty of Science, Science University of Tokyo, Kagurazaka, Shinjuku-ku, Tokyo 162
(Received March 5, 1987)

Heptathiazocine was pyrolyzed into ammonia, tetrasulfur tetranitride, and tetrasulfur dinitride above 383 K in an argon atmosphere; then, the latter two intermediates finally degraded into sulfur and nitrogen. According to the stoichiometric correlation among the final pyrolytic products, an overall pyrolysis can be expressed as: $S_7NH \rightleftharpoons 7/8\ S_8+1/3\ N_2+1/3\ NH_3$. The differential scanning calorimetry of heptathiazocine gave the standard enthalpy of the formation as 89.3 ± 1.1 kJ mol^{-1} by combining the enthalpy change of the pyrolysis with its molar heat capacity and known thermodynamic data of the concerned species. The standard enthalpies of the formation of this compound were also calculated as being 93 and 91 kJ mol^{-1} on the basis of Sanderson's method, assuming that hydrogen bonds were negligible in the crystal (which were comparable to that observed in this work).

Heptathiazocine (heptasulfur imide, S_7NH) is a stable compound at room temperature with a melting point of 386.7 K.[1,2] This compound is soluble in various organic solvents, of which the solubility parameter has been estimated in a previous paper.[1] Little information on the pyrolysis of this compound is available, though heptathiazocine decomposes above its melting point.[3] Becke-Goehring and Schwarz[4] have estimated its standard enthalpy of formation on the basis of pyrolysis in vacuo.

In this work, the pyrolysis of heptathiazocine was studied within the temperature range 353—513 K under an argon atmosphere in order to verify the thermal decomposition process and the thermodynamic quantities.

Experimental

Materials. The heptathiazocine was prepared by a method described by Heal and Kane,[5] followed by purification by repeated recrystallization and column chromatography.[1] Thin-layer chromatography (TLC) showed that the heptathiazocine, thus obtained, was sufficiently pure to use in this work.

Procedures. Differential thermal analysis (DTA) and thermal gravimetry (TG) on the heptathiazocine were carried out at heating rates of 3—15 K min^{-1} in an argon atmosphere with a Rigaku Denki Thermoflex (model 8002). Pyrolytic products of the heptathiazocine were identified by TLC[6] and with a Yanagimoto Seisakusho (model 80) gas chromatograph.

The stoichiometric correlation among the pyrolytic products was estimated as follows: The sample (≈300 mg) was heated at 433 K for 2 h in an argon flow (25 cm^3 min^{-1}). The ammonia produced was introduced together with argon into 4.04×10^{-2} mol dm^{-3} perchloric acid and then titrated with a 3.06×10^{-2} mol dm^{-3} sodium hydroxide solution. The quantity of nitrogen was estimated with an azotometer after the accompanying ammonia was removed by passing it through 0.5 mol dm^{-3} perchloric acid, while carbon dioxide was used as a carrier gas. Respective amounts of the residual heptathiazocine and solid pyrolytic products were determined spectrophotometrically at different wavelengths using their carbon tetrachloride solution.

The molar heat capacity of heptathiazocine and the enthalpy change of the decomposition were estimated at heating rates of 8 and 16 K min^{-1} with a Perkin-Elmer (model DSC-1B) differential scanning calorimeter. The sample was carefully weighed and sealed by the same method described in a previous paper.[7] The DSC instrument was calibrated with indium of 99.999% purity; quartz was used as a reference for the measurement of the molar heat capacity.

Results

Pyrolytic Products and Differential Thermal Analysis. The heptathiazocine (≈2 mg) sealed under the argon atmosphere was heated at the heating rate of 7.5 K min^{-1} up to the specified temperatures. The remaining solid was dissolved in carbon tetrachloride and identified by TLC (Table 1). Tetrasulfur tetranitride (S_4N_4) and tetrasulfur dinitride (S_4N_2) were observed as intermediates above 413 K under these conditions, whereas these two nitrides completely degraded into sulfur and nitrogen above 453 K. The heptathiazocine did not degrade below its melting point (386.7 K)[2] by rapid heating faster than 5 K min^{-1}. However, this compound obviously decomposed, even at 383 K, by prolonged heating for 1.5 h in an argon atmosphere.

Table 1. Solid Pyrolytic Products of Heptathiazocine at Different Temperatures[a]

T/K	Specie			
383	S_7NH			
393	S_7NH	S_8[b]		
403	S_7NH	S_8		
413	S_7NH	S_8	S_4N_4[b]	S_4N_2[b]
423	S_7NH	S_8	S_4N_4	S_4N_2
433	S_7NH	S_8	S_4N_4	S_4N_2
443	S_7NH	S_8	S_4N_4	S_4N_2
453	S_7NH	S_8		
463		S_8		

a) Heating rate of 7.5 K min^{-1}. b) Trace amount.

Nitrogen and ammonia were detected as gaseous products above 413 K by gas chromatography. Hydrogen sulfide was not detectable under the conditions applied in this work.

Table 2 shows the molar ratios of the final pyrolytic products to the original heptathiazocine upon heating at 433 K for 2 h. However, trace amounts of the tetrasulfur tetranitride and tetrasulfur dinitride were still detectable as $n(S_4N_4)/n(S_7NH)=5\times10^{-3}$ and $n(S_4N_2)/n(S_7NH)\approx1\times10^{-4}$, respectively, even under the conditions. As shown in Table 1, these two nitrides finally decomposed into sulfur and nitrogen.[8] Thus, the corresponding amounts of sulfur and nitrogen were taken into account to the molar ratios in Table 2. The stoichiometric correlation clearly indicated that the overall pyrolysis of heptathiazocine could be expressed as[9]

$$S_7NH = 7/8\ S_8 + 1/3\ N_2 + 1/3\ NH_3. \quad (1)$$

A differential thermal analysis of the heptathiazocine showed a sharp endothermic peak due to its fusion at 387 K and a broad exothermic peak at 430 K in an argon atmosphere at a heating rate of 10 K min^{-1} (as also shown in the DSC pattern (Fig. 1)). These peak temperatures shifted from 387 to 390 K and from 423 to 440 K, respectively, upon increasing the heating rate from 3 to 15 K min^{-1}. The TG curve obtained at a heating rate of 10 K min^{-1} showed a weight loss of about 6% between 398 and 443 K (Fig. 1). This weight loss approximately corresponded to a total mass of NH groups in the heptathiazocine molecules. As is also clearly shown in the gas-chromatographic analysis, these NH groups were partly converted to ammonia and nitrides.

Table 2. Molar Ratios of Final Pyrolytic Products of Heptathiazocine at 433 K

$n(S_7NH)$	Molar ratio of pyrolytic product		
mmol	$n(S_8)/n(S_7NH)$	$n(N_2)/n(S_7NH)$	$n(NH_3)/n(S_7NH)$
1.26	0.88_0	—	0.32_3
1.25	0.88_7	—	0.32_5
1.31	0.85_5	—	0.33_8
1.18	0.89_0	0.33_6	—
1.05	0.87_7	0.33_4	—
1.18	0.84_6	0.31_8	—
Average[a]	$0.87_3\pm0.02_2$	$0.32_9\pm0.01_7$	$0.32_9\pm0.01_4$

a) The uncertainty value was defined as $\pm3.0\,\sigma/\sqrt{n}$, where σ and n are the standard deviation and the number of data respectively.

Heat Capacity of Heptathiazocine. In order to determine the heat capacity, the sample was sealed in an aluminium container under an argon atmosphere. Measurements were carried out at a heating rate of 8 K min^{-1} between 328 and 368 K. The sample, thus heated, did not show any chemical change according to TLC, even after each run for 20 min. Figure 2 shows the molar heat capacity of heptathiazocine as a function of temperature. This procedure was confirmed to be reasonably reliable by comparing the molar heat capacities of α-sulfur[10] with those observed under the same conditions (±1.4%). The molar heat capacity of heptathiazocine at 298.15 K was deduced as 0.196±0.004 kJ mol^{-1}K^{-1} from a linear relationship in the given temperature range ($C_p=0.135+2.05\times10^{-4}T$) as shown in Fig. 2.

Enthalpy Change during Pyrolysis of Heptathiazocine in Argon Atmosphere. The enthalpy change during the overall pyrolysis of heptathiazocine was measured over a temperature range from 353 to 513 K in a closed system. Figure 1 shows the DSC pattern of the heptathiazocine obtained at a heating rate of 8 K min^{-1}, in addition to the base line (dotted line) taken in this work. Table 3 indicates the results of the enthalpy changes of the fusion, ΔH_{fus}, and of the thermal decomposition, ΔH, of the heptathiazocine, in which the average values were estimated as being 18.8±0.6 and −104.9±1.1 kJ mol^{-1}, respectively.

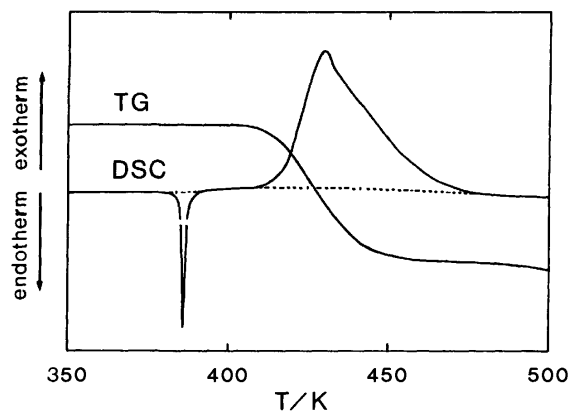

Fig. 1. DSC and TG patterns of heptathiazocine in argon atmosphere.

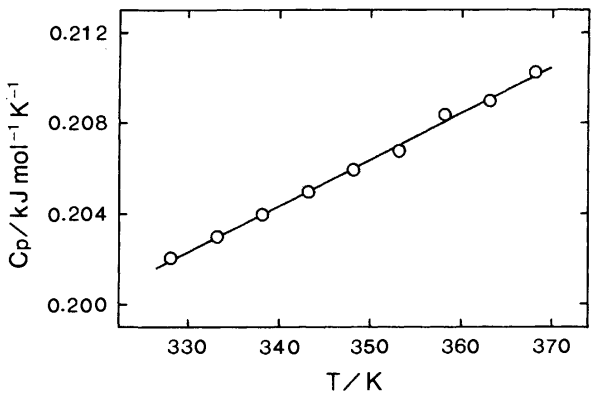

Fig. 2. Molar heat capacity of heptathiazocine observed at heating rate of 16 K min^{-1}.

Table 3. Enthalpy Changes of Fusion and Decomposition of Heptathiazocine

$n(S_7NH)$ / μmol	ΔH_{fus} / kJ mol^{-1}	$-\Delta H$ / kJ mol^{-1}
3.94	19.4	$105._0$
5.16	18.8	$104._2$
5.59	18.9	$107._2$
4.89	19.2	$105._7$
5.33	19.0	$104._7$
4.89	19.3	$104._1$
4.86	18.6	$104._7$
4.88	18.1	$103._5$
5.65	17.6	$104._8$
Average[a)]	18.8±0.6	$104._9$±$1._1$

a) The uncertainty value was shown in the same manner in Table 2.

On the basis of the stoichiometric correlation (Eq. 1), the standard enthalpy of the formation of heptathiazocine can be obtained by the following equation as:

$$\Delta H_f(S_7NH, s, 298.15\,K) = -\Delta H - \Delta H_{fus} + 2/3\,RT + 7/8(\Delta H_t(\alpha,\beta) + \Delta H_m(\beta,\lambda) + X\Delta H_p) + 1/3\,\Delta H_f(NH_3, g, 298.15\,K) - \int_{298.15}^{T} \Delta C_p dT \quad (2)$$

where $\Delta H_t(\alpha,\beta)$ and $\Delta H_m(\beta,\lambda)$ are the enthalpy changes of the transition from S_α to S_β (3.2 kJ mol^{-1})[10,11] and of the fusion of S_β (13.8 kJ mol^{-1}),[10,11] ΔH_p the enthalpy change of the polymerization from S_λ to S_μ (13.3 kJ mol^{-1}),[10,11] X the fraction of S_μ as the S_8 unit,[10,12] $\Delta H_f(NH_3, g, 298.15\,K)$ the standard enthalpy of the formation of ammonia (−45.9 kJ mol^{-1}),[11] and ΔC_p the difference in the molar heat capacities between the initial and final states, respectively. The reaction temperature, T, was taken as 429 K at the maximum of broad exothermic peak (Fig. 1). The integral term was calculated as 0.1 kJ mol^{-1} using the observed molar heat capacity of heptathiazocine. However, the peak temperature (429 K) was just below the initiation temperature (432 K)[12] of rapid polymerization of S_λ. Thus, the fraction of S_μ, X, was calculated to be 0.096 as that at 442.8 K: S_μ reaches the maximum degree of polymerization at this temperature.[12]

Accordingly, the standard enthalpy of the formation of heptathiazocine, $\Delta H_f(S_7NH,s,298.15\,K)$, was estimated to be $89._3$±$1._1$ kJ mol^{-1}, assuming that the formation of S_π was negligible.

Discussion

Pyrolytic Processes of Heptathiazocine. The heptathiazocine finally decomposed into sulfur, nitrogen, and ammonia above 383 K in the argon atmosphere through the tetrasulfur tetranitride and tetrasulfur dinitride as the intermediates. Hydrogen sulfide was undetectable as a gaseous pyrolytic product in this work, whereas Becke-Goehring[2] has reported its formation in vacuo. The thermal degradation of 1,3,5,7,2,4,6,8-tetrathiatetrazocine (tetrasulfur tetraimide, $S_4(NH)_4$), also took place step by step without the formation of hydrogen sulfide in the argon atmosphere.[6] The primary pyrolytic reaction of this compound can be expressed as[6]

$$S_4(NH)_4 = 1/6\,S_8 + 2/3\,S_4N_4 + 4/3\,NH_3. \quad (3)$$

According to these facts, the heptathiazocine may also release all the hydrogen atoms as in the form of ammonia during the first step of pyrolysis above 383 K in the argon atmosphere as

$$S_7NH = 19/24\,S_8 + 1/6\,S_4N_4 + 1/3\,NH_3. \quad (4)$$

The tetrasulfur tetraimide yielded a fairly large amount, $n(S_4N_4)/n(S_4(NH)_4)$=0.43, of the tetrasulfur tetranitride at 383 K for 1.5 h in an argon atmosphere, in addition to the tetrasulfur dinitride which was produced by a secondary degradation of tetrasulfur tetranitride in the presence of sulfur.[6] On the other hand, the heptathiazocine gave only small quantities of tetrasulfur tetranitride and tetrasulfur dinitride, $n(S_4N_4)/n(S_7NH)$=0.02 and $n(S_4N_2)/n(S_7NH)<0.01$ respectively, during pyrolysis under the same conditions.

The decomposition of tetrasulfur tetranitride can be promoted in the presence of sulfur as:[6]

$$S_4N_4 = S_4N_2 + N_2(\text{in the presence of sulfur}) \quad (5)$$

$$S_4N_2 = 1/2\,S_8 + N_2. \quad (6)$$

The decomposition degree of tetrasulfur tetranitride was examined in the presence of different amounts of sulfur using two kinds of sulfur-mixed samples. The compositions of the sample were specified as $n(S_8)/n(S_4N_4)$=0.25 and 4.0, where n refers to the initial number of moles (these molar ratios correspond approximately to those expressed in Eqs. 3 and 4 respectively). Figure 3 shows the decomposition degree, α, of the tetrasulfur tetranitride as a function of heating time at 413 K in the closed system (≈10 cm^3). The tetrasulfur tetranitride degraded slowly in the presence of a small amount of sulfur. On the other hand, the sulfur-rich sample was pyrolyzed much faster than the former sample through a pseudo first-order reaction. As clearly shown in Eq. 4, a large amount of sulfur is produced during primary pyrolysis; thus, the overall degradation of heptathiazocine would be greatly promoted. Thus, only small amounts of tetrasulfur tetranitride and tetrasulfur dinitride would be observed during the pyrolysis of heptathiazocine, in contrast to that of tetrasulfur tetraimide.

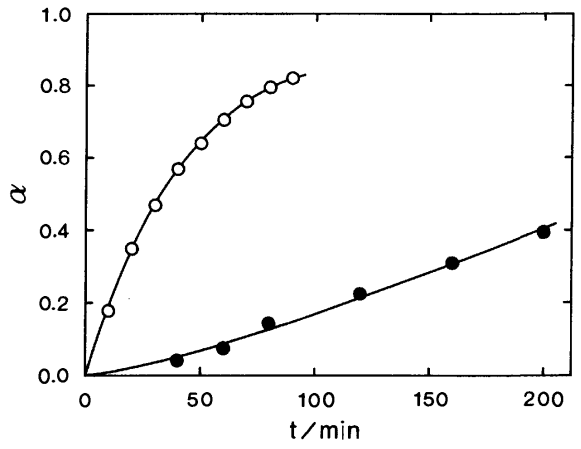

Fig. 3. Change in degradation degree of S_4N_4 in the presence of sulfur at 413 K in the closed system. Symbols: ○; $n(S_8)/n(S_4N_4)=4.0$ ●; $n(S_8)/n(S_4N_4)=0.25$.

Calculation of Standard Enthalpy of the Formation of Heptathiazocine. The heptathiazocine molecule consists of an eight-membered heterocyclic ring structure.[13] Its standard enthalpy of the formation can be deduced on the basis of the S-S, S-N, and N-H bond energies in the molecule and the standard enthalpies of the formation of atomic sulfur, nitrogen, and hydrogen, in addition to the enthalpy change of the sublimation of heptathiazocine. The standard enthalpies of the formation of these atomic species have been estimated as 277.4, 427.7, and 218.0 kJ mol^{-1},[14] respectively. The Sanderson method[15] gave the S-S, S-N, and N-H bond energies in the heptathiazocine molecule as 263, 245, and 363 kJ mol^{-1} based on their respective bond lengths.[13,16] Thus, the enthalpy of the formation of gaseous heptathiazocine, $\Delta H_f(S_7NH,g, 298.15\ K)$, was calculated to be 200 kJ mol^{-1} using the above values.

The solubility parameter, δ, and molar volume, V, of heptathiazocine have been reported to be 26.0 $J^{1/2}\,cm^{3/2}$ and 127 $cm^3\,mol^{-1}$, respectively.[1] The former term is defined as $(E_v/V)^{1/2}$, where E_v is the vaporization energy; thus, the enthalpy change of the vaporization, ΔH_v, of heptathiazocine can be estimated as 88.2 kJ mol^{-1} by

$$\Delta H_v = \delta^2 V + RT. \quad (7)$$

The enthalpy change of the fusion of this compound was obtained as 18.8±0.6 kJ mol^{-1} (Table 3). Thus, the enthalpy change of the sublimation is estimated to be 107 kJ mol^{-1}.

On the other hand, the enthalpy change of the sublimation was also deduced from the London dispersion force, calculated by means of the Slater-Kirkwood equation as described in the previous paper.[7] The interatomic distances were calculated on the basis of the coordinates of atoms in the crystal lattice[13] assuming the N-H bond length to be 108 pm.[16] The enthalpy change of the sublimation was estimated as 109.0 kJ mol^{-1} taking into account 123 interatomic distances less than 500 pm.

The standard enthalpies of the formation of heptathiazocine were estimated as 93 and 91 kJ mol^{-1} by combining the enthalpy of the formation of gaseous state (200 kJ mol^{-1}) with the enthalpy changes of the sublimation (107 and 109 kJ mol^{-1}). The value, thus calculated, were close to the experimental value determined in this work (89.3 ± 1.1 kJ mol^{-1}). Consequently, the standard enthalpy of the formation of heptathiazocine, $\Delta H_f(S_7NH,s,298.15\ K)$, obtained by the DSC measurement, is considered reasonable.

References

1) S. Hamada, Y. Kudo, and M. Kawano, *Bull. Chem. Soc. Jpn.*, **48**, 2963 (1975).
2) M. Becke-Goehring, "Advanced in Inorganic Chemistry and Radiochemistry," Vol. 2, (1960), p. 159.
3) M. S. Shahid, H. G. Heal, and H. Garcia-Fernandez, *J. Inorg. Nucl. Chem.*, **33**, 4364 (1971).
4) M. Becke-Goehring and R. Schwarz, *Z. Anorg. Allg. Chem.*, **296**, 3 (1958).
5) H. G. Heal and J. Kane, "Inorganic Syntheses," ed by L. R. Morss, J. Merbaum, and W. L. Jolly, McGraw-Hill, New York (1968), Vol. XI, p. 184.
6) S. Hamada and Y. Kudo, *Bull. Chem. Soc. Jpn.*, **52**, 1063 (1979).
7) Y. Kudo and S. Hamada, *Bull. Chem. Soc. Jpn.*, **59**, 1257 (1986).
8) Y. Kudo and S. Hamada, *Bull. Chem. Soc. Jpn.*, **56**, 2627 (1983).
9) It is assumed that sulfur produced in this process exists as cyclooctasulfur, S_8.
10) The thermodynamic quantities of sulfur are expressed as S_8 units.
11) "JANAF Thermochemical Tables," 2nd ed., Nat. Bur. Stand. (US), (1971).
12) A. V. Tobolsky and A. Eisenberg, *J. Am. Chem. Soc.*, **81**, 780 (1959).
13) H. J. Hecht, R. Reinhardt, R. Steudel, and H. Bradaczek, *Z. Anorg. Allg. Chem.*, **426**, 43 (1976).
14) M. W. Chase, Jr., J. L. Curnutt, J. R. Downey, Jr., R. A. McDonald, A. N. Syverud, and E. A Valenzuela, *J. Phys. Chem. Ref. Data*, **11**, 840 (1982).
15) R. T. Sanderson, *J. Inorg. Nucl. Chem.*, **28**, 1553 (1966).
16) The N-H bond length was taken as the same as that in the tetrasulfur tetraimide molecule. See, T. M. Sabine and G. W. Cox, *Acta Crystallogr.*, **23**, 574 (1967).

Action of Electron-Accepting Quenchers in Photoisomerization of Naphthylethylenes in Polar and Nonpolar Solvents

Takahisa Oguchi, Tatsuo Arai,* Hirochika Sakuragi, and Katsumi Tokumaru*
Department of Chemistry, University of Tsukuba, Sakura-mura, Ibaraki 305
(Received January 5, 1987)

The quantum yield of trans-cis isomerization of 3,3-dimethyl-1-(2-naphthyl)-1-butene was measured in the presence of various electron-accepting quenchers in benzene or in acetonitrile. In benzene the quantum yield was increased by addition of some of the quenchers; however, in acetonitrile it was decreased under similar conditions. This was attributed to more efficient formation of olefin triplets through an exciplex in benzene than through radical ion pairs in acetonitrile.

Recently, much attention has been paid to photoinduced electron transfer leading to characteristic reactions.[1-5] Among these reactions, isomerization of olefins by charge-transfer (CT) interaction with electron donors or acceptors were reported for stilbenes,[6-8] styrylnaphthalene,[9,10] and 1,2-dicyanoethylene.[11] Most studies on stilbenes in the presence of electron acceptors were carried out in very high concentrations of both components, and thus the reaction is usually initiated by excitation of ground state CT complexes. In these cases excitation of the CT complexes gives, by way of radical ion pairs, olefin triplets which play an important role in the isomerization. However, the reaction mechanism upon excitation of monomer olefins without exciting their ground state CT complex has scarcely been explored because of the short lifetime of the singlet excited state of most olefins. It has been reported that photochemical reactions on ground state CT excitation were often different from those on direct excitation of free molecules followed by diffusional CT quenching.[12] Since we have found that the singlet lifetime of an aromatic olefin, *trans*-3,3-dimethyl-1-(2-naphthyl)-1-butene (*trans*-DMNB), is as long as 63 ns in both polar and nonpolar solvents, we attempted to investigate the quenching effects of acceptors on behavior of the excited singlet *trans*-DMNB and also 2-styrylnaphthalene (SN) in acetonitrile and in benzene.

Experimental

Materials. *cis*- and *trans*-DMNB were obtained by the same method as described.[13] *cis*- and *trans*-SN were prepared and isolated as reported.[14] 1,2-Dicyanoethylene (FN) was purified by recrystallization in benzene followed by sublimation. Dimethyl terephthalate (TM), and *o*- (*o*-DCB), *m*- (*m*-DCB), and *p*-dicyanobenzene (*p*-DCB) were purified by recrystallization in ethanol. Benzene was distilled over calcium hydride. Acetonitrile was distilled over diphosphorus pentoxide followed by distillation over potassium carbonate.

Quantum Yield Measurements. Benzene or acetonitrile solutions of pure *trans*-DMNB (0.01 mol dm^{-3}) in the presence or absence of electron acceptors (0—0.02 mol dm^{-3}) in Pyrex tubes were degassed by bubbling argon for more than thirty minutes or by freeze-thaw cycles and were irradiated with 313-nm line of a 400 W high-pressure mercury lamp. The 313-nm mercury line was isolated by a Toshiba UV-D33S glass filter and a filter solution of potassium chromate.[15] Light intensity was determined by potassium tris(oxalato)ferrate(III) actinometry.[15] After irradiating for 1—2 h the conversion was determined by gas chromatography, a Shimadzu GC-4CM-PF gas chromatograph equipped with an FID. The experiments of *trans*-SN were carried out under similar conditions except olefin concentration (5×10^{-4} mol dm^{-3}) and an analytical procedure. The conversion was determined by both gas chromatography and by high-pressure liquid chromatography, a Shimadzu LC-6A and a spectro multichannel photodetector MCPD-350PC (Otsuka electronics).

Photostationary State Isomer Ratios. Photostationary state isomer ratios were determined in the presence of desired concentrations of a quencher and a sensitizer. The solutions were degassed using freeze-thaw cycles and irradiated with a 400W high-pressure mercury lamp. The compositions of the isomer were determined by gas chromatoraphy.

Fluorescence and Laser Photolysis Studies. Fluorescence spectra were obtained on a Hitachi MPF-2A or a Hitachi F-4000 fluorescence spectrophotometer. Fluorescence quantum yields were determined using anthracene (ϕ_f=0.27)[15] as a standard. Laser flash photolyses were performed as described elsewhere.[13] Sample solutions containing *trans*-DMNB (0.01 mol dm^{-3}) and acceptors (0.05 mol dm^{-3}) were deaerated by bubbling argon for 30 min. Fluorescence lifetimes of monomer and exciplex species were measured using a single photon counting apparatus, Applied Photophysics Model SP-3X.

Redox Potentials. Redox potentials were measured by cyclic voltammetry with a Hokuto-Denko Function Generator HB-104 and a Potentiostat/Galvanostat HA-201. Electrochemical measurements were carried out using a three-electrode cyclic voltammetric cell. The working electrode was a platinum wire. Tetraethylammonium perchlorate was used as a supporting electrolyte. The reference electrode was Ag/$AgNO_3$ (0.1 mol dm^{-3}) under an atmosphere of dried argon. The voltammograms were scanned at 100 mV s^{-1}. In some cases, the voltammograms showed no reversible peaks. In such cases, half-peak potentials were employed as half-wave redox potentials. Substrate concentrations were 5×10^{-3} mol dm^{-3}.

Results and Discussion

Fluorescence Quenching of DMNB by Various Electron Acceptors. The fluorescence quantum yield of *trans*-DMNB was determined as 0.61 in benzene and 0.60 in acetonitrile. The fluorescence lifetime of *trans*-DMNB was as long as 63 ns in both benzene and acetonitrile in contrast with those reported for other olefins, for example, 52 ps for *trans*-stilbene,[16] and the fluorescence of *trans*-DMNB was quenched efficiently by electron acceptors. In benzene, a new weak emission of exciplex appeared in longer wavelength. A typical example is shown in Fig. 1 for the case of *trans*-DMNB and *p*-dicyanobenzene. The emission maxima were in the range of 385—485 nm and the emission lifetimes were 5.2 to 27 ns as determined by single photon counting (Table 1). The exciplex lifetime in the case of a methoxycarbonyl-substituted acceptor, TM, is shorter than those in the cases of cyano-substituted acceptors, *o*-DCB, *m*-DCB, *p*-DCB, and FN.

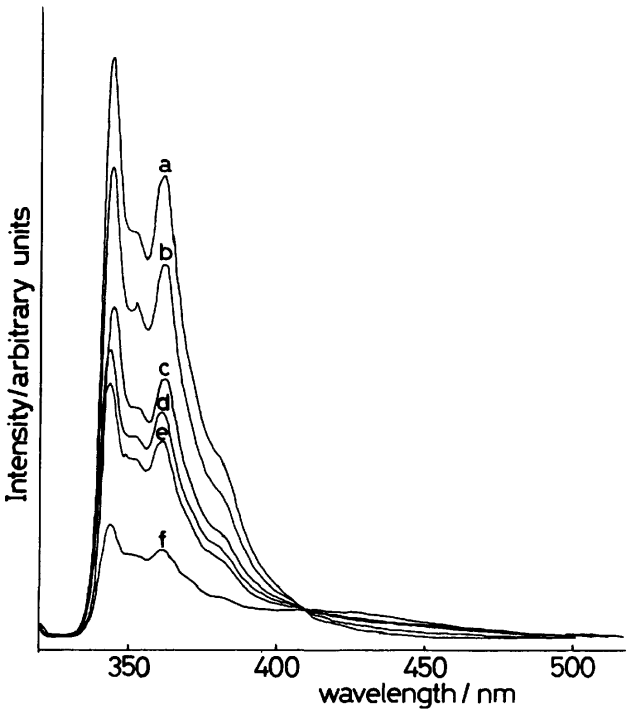

Fig. 1. Fluorescence spectra of *trans*-DMNB in the presence of different concentrations of *p*-DCB in benzene. The concentrations of *p*-DCB are a) 0, b) 4.7×10^{-3}, c) 1.4×10^{-2}, d) 1.9×10^{-2}, e) 2.4×10^{-2}, f) 8.2×10^{-2} mol dm^{-3}.

The rate constants for quenching by electron transfer in acetonitrile usually obey the well-known Weller equation (Eq. 1),[1,17] where ΔG° is the standard change of Gibbs free energy for the electron transfer from a singlet excited state to an electron acceptor calculated according to Eq. 2 and $\Delta G^{\circ *}$ denotes the Gibbs free energy of activation obtained from Eq. 3. The value $\Delta G^{\circ *}(0)$ is the Gibbs free energy of activation at $\Delta G^\circ=0$ kcal mol^{-1} (1 cal=4.184 J). The values for E_{red} and E_{ox} are the reduction potential of acceptors and the oxidation potential (1.23 V) of *trans*-DMNB, respectively, determined in acetonitrile and $E_{0,0}$ stands for the singlet excitation energy (83.6 kcal mol^{-1}) of *trans*-DMNB.

$$k_q = \frac{20\times10^9 \text{ mol}^{-1}\text{ dm}^3\text{ s}^{-1}}{1+0.25\{\exp(\Delta G^{\circ *}/RT)+\exp(\Delta G^\circ/RT)\}} \quad (1)$$

$$\Delta G^\circ = E_{ox} - E_{red} - 0.06 - E_{0,0}/\text{eV} \quad (2)$$

$$\Delta G^{\circ *} = \{(\Delta G^\circ/2)^2 + (\Delta G^{\circ *}(0))^2\}^{1/2} + \Delta G^\circ/2 \quad (3)$$

$$\Delta G^{\circ *}(0) = 2.4 \text{ kcal mol}^{-1} \quad (4)$$

Table 1 lists the observed quenching rate constants (k_q) of the fluorescence of *trans*-DMNB in both deaerated solvents, the reduction potentials (E_{red}), and ΔG° calculated by Eq. 2. Figure 2 plots the energies (E^{ex}_{max}) corresponding to the maximum wavelength of the exciplex emission (λ^{ex}_{max}) in benzene vs. ΔG°, and shows that the energies of the exciplexes over the ground state nearly linearly decrease with the decrease of ΔG°. This result shows that the larger the extent of charge transfer as revealed by the amount of ΔG°, the more stabilized the resulting exciplex.

In Fig. 3, the plot of the quenching rate constants of monomer fluorescence of *trans*-DMNB by electron acceptors in acetonitrile against ΔG° well fit the curve (curve a) calculated from Eqs. 1—4.[1,17] On the other hand, the plot of the quenching rate constants in benzene is shifted considerably from curve a, and best fit curve b, which is depicted

Table 1. Quenching Rate Constants, Exciplex Lifetimes, and Some Kinetic Values

Quencher	In acetonitrile				In benzene			
	E_{red}[a]	ΔG°[b]	$k_q\tau_0$[c]	k_q[d]/10^9	$k_q\tau_0$[c]	k_q[d]/10^9	λ^{ex}_{max}[e]	τ_{ex}[f]
m-DCB	−2.19	−6.12	535	8.49	71	1.13	385	12.6
TM	−2.11	−7.96	780	12.4	370	5.87	400	5.2
o-DCB	−2.09	−8.42	826	13.1	466	7.40	435	16.2
p-DCB	−2.07	−10.27	870	13.8	540	8.60	415	26.9
FN	−1.64	−18.80	1000	15.9	880	14.0	485	14.9

a) In V. b) In kcal mol^{-1}. c) In dm^3 mol^{-1}. d) In dm^3 mol^{-1} s^{-1}. e) In nm. f) In ns.

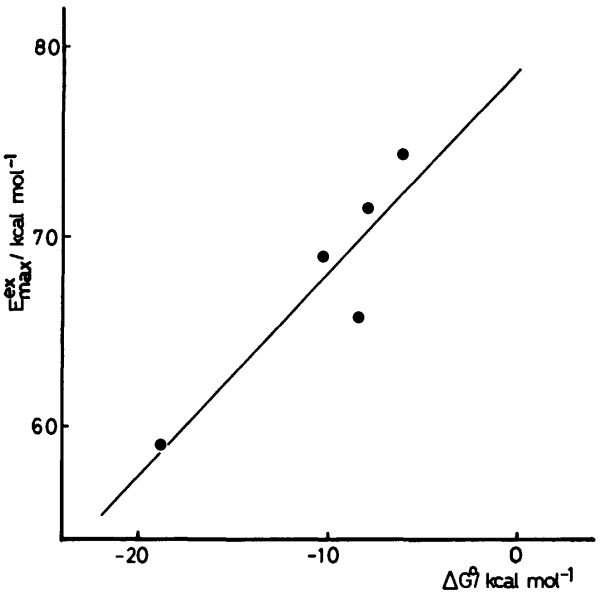

Fig. 2. The linear dependence of the exciplex emission maximum vs. the change of Gibbs free energy.

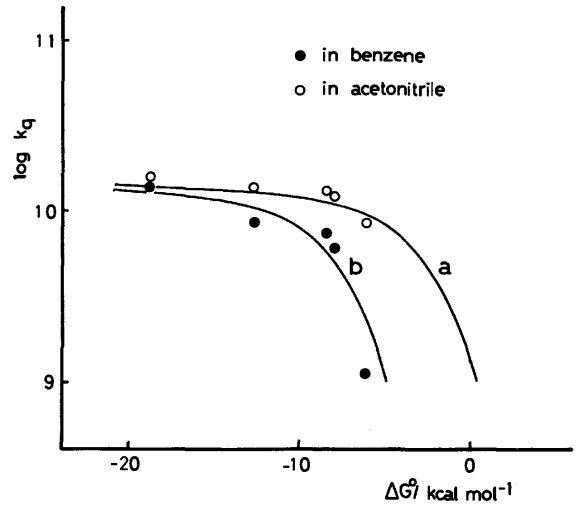

Fig. 3. The relation of the quenching rate constants vs. the change of Gibbs free energy. The curve a (in acetonitrile) is depicted according to Eqs. 1 and 2 (after Weller[17]) and the curve b (in benzene) is the best fitting one according to Eqs. 1 and 5.

by using Eq. 5 instead of Eq. 2. In Eq. 5, the value of 0.16 was chosen to give the best fitting. The energy of

$$\Delta G^\circ = E_{ox} - E_{red} + 0.16 - E_{0,0}/\text{eV} \quad (5)$$

$$E_e = E_{ox} - E_{red} + 0.15 \pm 0.10/\text{eV} \quad (6)$$

an exciplex (E_e) in nonpolar solvents can be generally expressed by Eq. 6,[1,17] which can lead to an equation similar to Eq. 5 showing the Gibbs free energy change in the electron transfer reaction in a nonpolar solvent. The above result means that the stabilization

Table 2. The Effect of Ferrocene on the Photostationary State Isomer Ratios $([t]/[c])_{pss}$ of DMNB on 2-Acetylnaphthalene Sensitization[a]

[ferrocene] / 10^{-3}mol dm^{-3}	$Trans_{pss}$ / %	$([t]/[c])_{pss}$
0	43.6±0.4	0.77±0.01
1.0	49.7±0.2	0.99±0.01
2.0	54.0±1.2	1.18±0.06
3.0	57.8±0.2	1.37±0.01

a) In the presence of 0.2 mol dm^{-3} of 2-acetylnaphthalene in benzene.

energy of the resulting radical ion pair solvated in acetonitrile is 0.22 eV larger than that in benzene. Therefore, it is safely concluded that the quenching of singlet excited state of *trans*-DMNB by electron acceptors proceeds by electron transfer.

Quantum Yields of Trans-Cis Isomerization. The quantum yields ($\phi_{t\to c}$) for the isomerization of *trans*- to *cis*-DMNB were 0.13 in benzene and 0.14 in acetonitrile, respectively, in the absence of quenchers. In benzene, $\phi_{t\to c}$ increased with increasing concentration of TM, *o*-DCB, and *p*-DCB, but slightly decreased with *m*-DCB and FN. The trans-cis isomerization was most effective through the exciplex with a quencher having moderate electron acceptability in benzene. On the other hand, in acetonitrile $\phi_{t\to c}$ was decreased on addition of any quenchers examined. These results indicate that behavior of the exciplex considerably changes with electron acceptors which control critically the efficiency of the isomerization.

Mechanism of Trans-Cis Isomerization in the Presence of Electron Acceptors. The isomerization of *trans*-DMNB on direct irradiation can occur in the singlet excited state as well as in the triplet excited state. If the isomerization proceeds on the triplet manifold, $\phi_{t\to c}$ should decrease with the increase of the concentration of an added triplet quencher such as ferrocene, because ferrocene can quench the transoid triplet state of DMNB. Actually, on benzophenone sensitization, the composition of the trans-isomer at the photostationary state of DMNB increased with the increase of ferrocene concentration (Table 2). However, $\phi_{t\to c}$ on direct excitation was not changed on addition of ferrocene. Therefore, it is clear that the isomerization of *trans*-DMNB on direct irradiation proceeds on the singlet manifold.

In view of the fact that $\phi_{t\to c}$ is much higher for triplet sensitization (0.46)[18] than $\phi_{t\to c}$ for direct irradiation, the increase of $\phi_{t\to c}$ in benzene by addition of some quenchers suggests that the triplet state of DMNB is produced in benzene possibly from the exciplex formed from the excited singlet DMNB and the acceptors. Actually, nitrogen laser excitation of *trans*-

$$t \xrightarrow{h\nu} {}^1t^* \quad \text{(a)}$$

$${}^1t^* \xrightarrow{k_f} t + h\nu_f \quad \text{(b)}$$

$${}^1t^* \xrightarrow{k_d} \beta t + (1-\beta)c \quad \text{(c)}$$

$${}^1t^* + Q \underset{k_{-en}}{\overset{k_{en}}{\rightleftharpoons}} {}^1t^*\cdots Q \quad \text{(d)}$$

encounter complex

A) in benzene

$$\text{(e)}\quad {}^1t^*\cdots Q \xrightarrow{k_{ex}} {}^1(t\cdots Q)^* \xrightarrow{k_T^e} {}^3t^* + Q$$

exciplex

$${}^1(t\cdots Q)^* \xrightarrow{k_f^e} t + Q + h\nu_{ef}$$

$${}^1(t\cdots Q)^* \xrightarrow{k_d^e} t + Q$$

B) in acetonitrile

$$\text{(f)}\quad {}^1t^*\cdots Q \xrightarrow{k_{rad}} (t^+\cdots Q^-) \xrightarrow{k_T^r} {}^3t^* + Q$$

radical ion pair

$$(t^+\cdots Q^-) \xrightarrow{k_d^r} t + Q$$

$$(t^+\cdots Q^-) \rightleftharpoons t^+ + Q^-$$

$$\text{(g)}\quad {}^3t^* \underset{}{\overset{K_{tp}}{\rightleftharpoons}} {}^3p^* \longrightarrow \alpha t + (1-\alpha)c$$

Scheme 1.

DMNB in the presence of the quenchers, e.g. *p*-DCB, gave the transient absorption due to the DMNB triplet (λ_{max}: around 420 and 580 nm)[13] in benzene. In acetonitrile the absorption due to DMNB radical cation (λ_{max}: 430, 640, and 700 nm)[19] was observed, although that of triplet DMNB was escaped from detection by interference of the absorption due to the radical ions. However, the intermediacy of the excited triplet state of DMNB was supported by the magnetic field effect on the photoisomerization in acetonitrile.[20] Therefore, it is reasonable to propose the preceding mechanism (Scheme 1) for photoisomerization of the olefin in the presence of the electron acceptors. According to Scheme 1, the quantum yield for trans-cis isomerization is described as Eq. 7 (in benzene) or 8 (in acetonitrile).

$$\phi_{t\to c} = \frac{(1-\beta)k_d + k_q[Q]\times\dfrac{(1-\alpha)k_T^e}{k_f^e + k_T^e + k_d^e}}{k_f + k_d + k_q[Q]}$$

$$= \frac{(1-\alpha)k_T^e}{k_f^e + k_T^e + k_d^e} + \frac{(1-\beta)k_d\tau_0 - \dfrac{(1-\alpha)k_T^e}{k_f^e + k_T^e + k_d^e}}{1 + k_q\tau_0[Q]}$$

$$\left(1/\tau_0 = k_f + k_d,\ k_q = \frac{k_{en}k_{ex}}{k_{-en} + k_{ex}}\right) \quad (7)$$

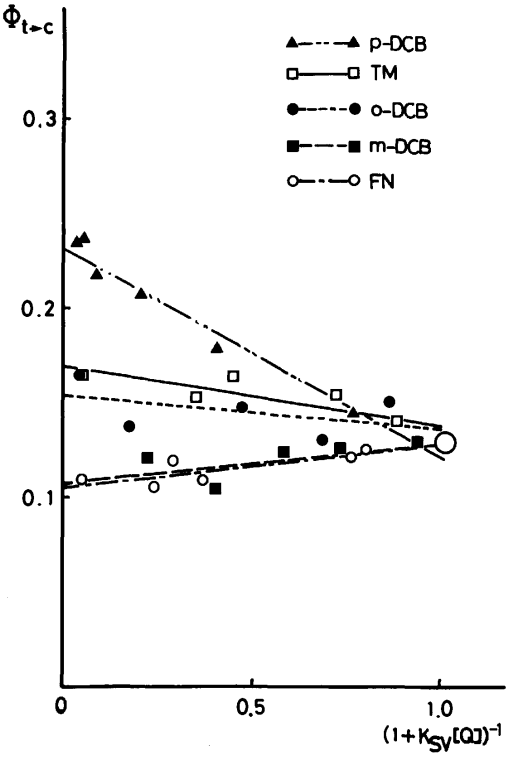

Fig. 4. Plots of the quantum yields for trans-cis isomerization vs. $(1+k_q\tau_0[Q])^{-1}$ in benzene.

Table 3. Quantum Yields for Trans-Cis Isomerization ($\phi_{t\to c}$) and Some Rate Constants

Quencher	In benzene			In acetonitrile
	$\phi^{\infty}_{t\to c}$	$k_T^{e\,a)}$	$k_d^e + k_f^{e\,a)}$	$\phi^{\infty}_{t\to c}$
m-DCB	0.11	1.7	6.3	0.06
TM	0.17	6.3	12	0.02
o-DCB	0.16	1.9	4.3	0.05
p-DCB	0.23	1.6	2.1	0.04
FN	0.11	1.4	5.3	0.01

a) In $10^7\ s^{-1}$.

$$\phi_{t\to c} = \frac{(1-\beta)k_d + k_q[Q]\times\dfrac{(1-\alpha)k_T^r}{k_d^r + k_T^r}}{k_f + k_d + k_q[Q]}$$

$$= \frac{(1-\alpha)k_T^r}{k_d^r + k_T^r} + \frac{(1-\beta)k_d\tau_0 - \dfrac{(1-\alpha)k_T^r}{k_d^r + k_T^r}}{1 + k_q\tau_0[Q]}$$

$$\left(1/\tau_0 = k_f + k_d,\ k_q = \frac{k_{en}k_{rad}}{k_{-en} + k_{rad}}\right) \quad (8)$$

Dependence of Charge-Transfer Interaction and Subsequent Steps on Quencher Properties. As Figs. 4 and 5 show, the quantum yields depend linearly upon $(1+k_q\tau_0[Q])^{-1}$. By extrapolating to the infinite quencher concentration, i.e. $(1+k_q\tau_0[Q])^{-1}\to 0$, one can obtain the quantum yields of trans-cis

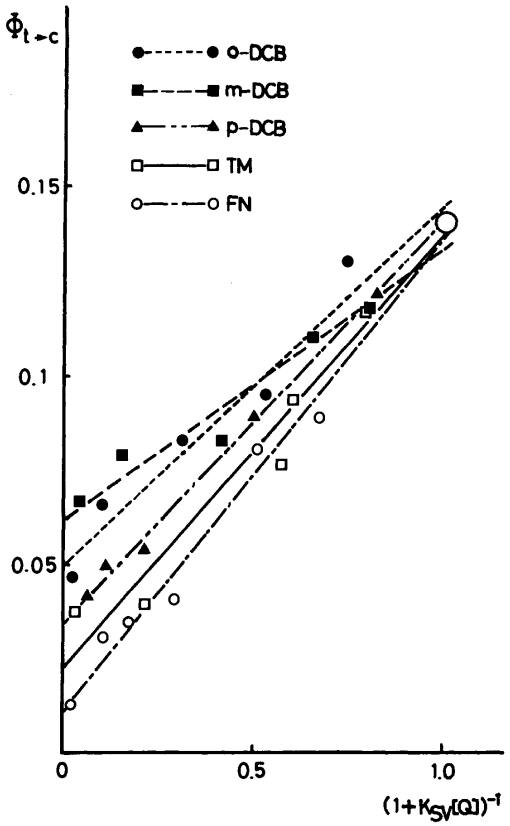

Fig. 5. Plots of the quantum yields for trans-cis isomerization vs. $(1+k_q\tau_0[Q])^{-1}$ in acetonitrile.

isomerization taking place solely through the exciplex or radical ion pairs ($\phi_{t\to c}^{\infty}$), as listed in Table 3. The $\phi_{t\to c}^{\infty}$ values are larger in benzene (0.11—0.23) than in acetonitrile (0.01—0.06). According to the Scheme 1, the quantum yield of triplet formation, ϕ_T, is expressed as $\phi_T=\phi_{t\to c}^{\infty}/(1-\alpha)$ where α, the decay fraction of the triplet DMNB producing the trans-isomer, is 0.48.[18] Accordingly, ϕ_T is obtained as 0.21—0.44 in benzene and 0.02—0.12 in acetonitrile varied with quenchers employed.

The trans-cis isomerization of 2-styrylnaphthalene (SN) was reported to be efficient in the presence of *p*-DCB in acetonitrile ($\phi_{t\to c}=0.53$) as well as in dichloromethane ($\phi_{t\to c}=0.25$).[10] The quantum yields for stilbene isomerization were also reported in the presence of FN in benzene ($\phi_{t\to c}=0.11$) and in acetonitrile ($\phi_{t\to c}=0.22$).[21] In those cases the quantum yields of the trans-cis isomerization increased with the increase of solvent polarity. This is in contrast with the present findings for DMNB. The reason for the difference in exciplex behavior is not certain. In the case of stilbene, however, because of the short lifetime of its excited singlet state, the experiments were done in very high concentrations of both stilbene and acceptors. Therefore, the excitation of a ground state CT complex cannot be ruled out at any wavelength and the isomerization mechanism must be rather complicated. For 2-styrylnaphthalene we have measured the quantum yields of the trans-cis isomerization at 313-nm irradiation and found that with the increase of *p*-DCB concentration in acetonitrile $\phi_{t\to c}$ decreased, while in benzene $\phi_{t\to c}$ increased. The $\phi_{t\to c}^{\infty}$ value was obtained from similar treatments using Eqs. 7 and 8 to be 0.18 (in benzene) and 0.04 (in acetonitrile).[22] The present results in acetonitrile are different from the previous one[10] in which irradiation was performed at 335 nm and trans-cis conversions were analyzed by a UV spectrometer. For analysis we used a gas chromatograph and a high-pressure liquid chromatograph with a multichannel photodiode detector to avoid contamination of side products. Actually, we observed in acetonitrile an unknown product which absorbs at similar wavelengths to *cis*- and *trans*-SN and this may be the reason of an overestimation of the quantum yield for its trans-cis isomerization.[10] Of course, the effect of the irradiation wavelength on the $\phi_{t\to c}^{\infty}$ value can also explain the above difference.

To examine the effects of acceptors on the decay process of exciplex, we have calculated the rate constant of the triplet DMNB production from the exciplex (k_T^e) and the sum of the rate constants for nonfluorescent and fluorescent decay $k_d^e+k_f^e$ as described below. The quantum yields of the triplet formation are expressed as $\phi_T=k_T^e\tau_{ex}$ in benzene and $\phi_T=k_T^r/(k_d^r+k_T^r)$ in acetonitrile. In the case of cyano-substituted compounds, as shown in Table 3, the k_T^e value seems constant regardless of the strength of charge-transfer interaction, $k_T^e=(1.7\pm0.3)\times10^7$ s^{-1}, while the $k_d^e+k_f^e$ value changed. To compare the efficiency of the isomerization among the isomeric cyanobenzenes for simplicity, it is to be noted that the apparent isomerization efficiency is not governed by the rate for triplet production from the exciplex (k_T^e) but by the rate for the deactivation of the exciplex ($k_d^e+k_f^e$). Among the dicyanobenzene isomers, the $k_d^e+k_f^e$ value tends to decrease as the exciplexes are more stabilized compared to the DMNB singlet excited state.

The low quantum yields in acetonitrile indicate that the ion pairs resulting from quenching of the singlet DMNB neither efficiently produce the triplet DMNB, though the radical ion pair (65—77 kcal mol^{-1}) lies sufficiently higher in energy than triplet-DMNB (52 kcal mol^{-1})[18], nor undergo isomerization in the form of the radical cation of DMNB. These results suggest that in acetonitrile the production of DMNB triplet by back electron transfer is not so efficient as in benzene. The radical ions of *cis*-β-methylstyrene and *cis*-stilbene were reported to isomerize effectively into the trans-isomer,[23,24] while the reverse process is inefficient. These facts are in accordance with our results and the assumption that $t^{+\cdot}$ should be thermodynamically more stable than $c^{+\cdot}$.

Conclusion

The quenching rate constants of the DMNB singlet state by various electron acceptors in acetonitrile and in benzene fit the curves for electron-transfer quenching mechanism. The electron-transfer process plays the key step for the trans-cis isomerization of *trans*-DMNB. However, once the exciplex is formed, the subsequent processes seem not to be linearly dependent on the reduction potentials of acceptors or the polarity of solvent. The trans-cis isomerization is more efficient in benzene than in acetonitrile, and also in benzene the exciplexes composed of the quenchers with moderate electron acceptability could efficiently produce the DMNB triplet state, the isomerization intermediate.

References

1) For example, M. Gordon and W. Ware, "The Exciplex," Academic Press, New York (1975).
2) F. D. Lewis, *Acc. Chem. Res.*, **12**, 152 (1979).
3) H. Masuhara and N. Mataga, *Acc. Chem. Res.*, **14**, 312 (1981).
4) S. L. Mattes and S. Farid, *Acc. Chem. Res.*, **15**, 80 (1982).
5) R. A. Caldwell and D. Creed, *Acc. Chem. Res.*, **13**, 45 (1980).
6) F. D. Lewis and J. T. Simpson, *J. Phys. Chem.*, **83**, 2015 (1979).
7) D. R. Arnold and P. D. Wong, *J. Am. Chem. Soc.*, **101**, 1894 (1979).
8) B. K. Adams and W. R. Cherry, *J. Am. Chem. Soc.*, **103**, 6904 (1981).
9) G. G. Aloisi, U. Mazzucato, J. B. Birks, and L. Minuti, *J. Am. Chem. Soc.*, **99**, 6340 (1977).
10) G. Gennari, G. Cauzzo, G. Galiazo, and M. Folin, *J. Photochem.*, **14**, 11 (1980).
11) H. Hayashi and S. Nagakura, *Chem. Phys. Lett.*, **53**, 201 (1978).
12) K. Onodera, G. Furusawa, M. Kojima, M. Tsuchiya, S. Aihara, R. Akaba, H. Sakuragi, and K. Tokumaru. *Tetrahedron*, **41**, 2215 (1985).
13) T. Arai, H. Sakuragi, K. Tokumaru, Y. Sakaguchi, J. Nakamura, and H. Hayashi, *Chem. Phys. Lett.*, **98**, 40 (1983).
14) G. S. Hammond, S. C. Shim, and S. P. Van, *Mol. Photochem.* **1**, 89 (1969).
15) S. L. Murov, "Handbook of Photochemistry," Marcel Dekker, New York, N. Y. (1973).
16) O. Teschke, E. O. Ippen, and G. R. Holton, *Chem. Phys. Lett.*, **52**, 233 (1977).
17) (a) D. Rehm and A. Weller, *Isr. J. Chem.*, **8**, 259 (1970). (b) A. Weller, *Z. Phys. Chem.* (Wiesbaden), **133**, 93 (1982).
18) T. Arai, H. Sakuragi, and K. Tokumaru, *Chem. Lett.*, **1980**, 1335.
19) We thank Prof. T. Shida, Kyoto University, for providing the spectrum of DMNB cation radical obtained by pulse radiolysis.
20) H. Sakuragi, R. Nakagaki, T. Oguchi, T. Arai, K. Tokumaru, and S. Nagakura, *Chem. Phys. Lett.*, **135**, 325 (1987).
21) W. Hub, U. Kluter, S. Schneider, F. Dorr, J. D. Oxman, and F. D. Lewis, *J. Phys. Chem.*, **88**, 2308 (1984).
22) The detailed results will be published elsewhere.
23) H. D. Roth and M. L. M. Schilling, *J. Am. Chem. Soc.*, **102**, 4303 (1980).
24) F. D. Lewis, J. R. Petisce, J. D. Oxwan, and M. J. Nepras, *J. Am. Chem. Soc.*, **107**, 203 (1985).

 © 1987 The Chemical Society of Japan Bull. Chem. Soc. Jpn., 60, 2401—2407 (1987)

The Synthesis of Ar-abietatrien-12,16-oxide and Its C-15 Epimer

Takashi MATSUMOTO,* Sachihiko IMAI, Takashi YOSHINARI, and Kazuaki TSURUTA
Department of Chemistry, Faculty of Science, Hiroshima University,
Higashisenda-machi, Naka-ku, Hiroshima 730
(Received January 10, 1987)

In order to elucidate the absolute configuration of C-15 in natural ar-abietatrien-12,16-oxide, (15*R*)-12,16-epoxy-8,11,13-abietatriene (**1a**) and its (15*S*)-epimer (**1b**) have been synthesized. Treatment of (15*R*)-8,11,13-abietatriene-12,16-diol with a mixture of chloromethyl methyl ether, dicyclohexano-18-crown-6, and potassium carbonate afforded **1a** as a minor product and (15*R*)-12-methoxymethyl ether as a major product. The latter was further converted into **1a**. A similar treatment of (15*S*)-8,11,13-abietatriene-12,16-diol gave **1b**. Catalytic hydrogenations of 12,16-epoxy-8,11,13,15-abietatetraene, methyl 12,16-epoxy-8,11,13,15-abietatetraen-19-oate (**5**), and methyl 12,16-epoxy-8,11,13,15-abietatetraen-18-oate (**7**) afforded the corresponding (15*R*)-dihydrobenzofuran derivatives and their (15*S*)-epimers. Conversions of the hydrogenation products from **5** and **7** into **1a** and **1b** were also carried out. The synthetic **1a** was identical with natural ar-abietatrien-12,16-oxide.

The two new abietane-type diterpenes, ar-abietatrien-12,16-oxide and 16-hydroxyferruginol, have been isolated from the seed of *Thujopsis dolabrata* Sieb. et Zucc. var. *dolabrata* by Hasegawa and Hirose.[1] On the basis of chemical and spectroscopic studies they deduced the structures of ar-abietatrien-12,16-oxide and 16-hydroxyferruginol to be 12,16-epoxy-8,11,13-abietatriene (**1**) and 8,11,13-abietatriene-12,16-diol (**2**), respectively. However, the absolute configurations of C-15 in both natural compounds remained unsettled. On the other hand, in the course of the synthetic work of coleon C tri-*O*-methyl ether (**3**) Burnell et al.[2] carried out the conversion of 12,16-epoxy-8,11,13,15-abietatetraene (**4**)[3] into a mixture of the C-15 epimeric dihydrobenzofuran derivatives (**1a** and **1b**) by catalytic hydrogenation. Although this mixture could not be separated at this stage, they assigned the stereochemistry of C-15 in the major product to be R-configuration from an examination of molecular models; that is, the hydrogenation is selectively from the convex β-face of **4**. The same assignment[4] was also reported on the catalytic hydrogenation products of methyl 12,16-epoxy-8,11,13,15-abietatetraen-19-oate (**5**).[5] However, it seems to be necessary to confirm the stereochemistry of the catalytic hydrogenation of these benzofuran derivatives by unambiguous methods. In a previous paper,[6] we reported the total syntheses of (15*R*)-8,11,13-abietatriene-12,16-diol (**2a**) and its (15*S*)-epimer (**2b**); synthetic **2a** was shown to be identical with natural 16-hydroxyferruginol. In order to elucidate the absolute configuration of C-15 in natural ar-abietatrien-12,16-oxide we have now attempted syntheses of the C-15 epimeric 12,16-epoxy-8,11,13-abietatrienes (**1a** and **1b**). This paper describes the syntheses of **1a** and **1b** starting from methyl 12-methoxy-8,11,13-abietatrien-18-oate (**6**),[7] and the stereochemistries of the catalytic hydrogenations of three benzofuran derivatives, **4**, **5**, and methyl 12,16-epoxy-8,11,13,15-abietatetraen-18-oate (**7**).

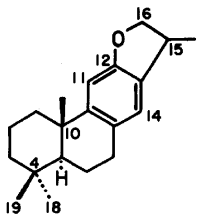

1

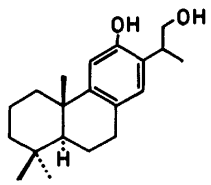

2

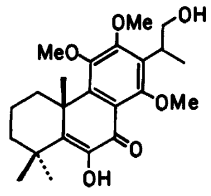

3

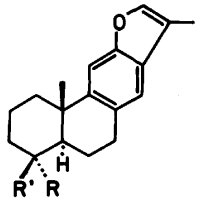

4 R=R'=Me
5 R=Me, R'=CO_2Me
7 R=CO_2Me, R'=Me

Reduction of **6** with lithium aluminium hydride in ether, followed by tosylation of the resulting alcohol **8** with *p*-toluenesulfonyl chloride in pyridine at 80—85 °C, afforded a tosylate **9**. This was treated with sodium iodide and zinc powder in *N*,*N*-dimethylformamide at 120—125 °C to give the corresponding 4,4-dimethyl compound **10** in 84.7% yield from **6**. According to the method of Akita and Oishi[8] with slight modifications, compound **10** was converted into 13-acetyl-8,11,13-podocarpatrien-12-ol (**11**: 4.2%) and its methyl ether (**12**: 74.5%) by a treatment with acetyl chloride and anhydrous aluminium chloride in dichloromethane at room temperature for 40 min. Demethylation of **12** with anhydrous aluminium chloride in refluxing dichloromethane afforded **11** (94.6%) which gave back **12** (88.2%) by methylation with methyl iodide and potassium *t*-butoxide in refluxing *t*-butyl alcohol. The acetyl methoxy compound **12** was further converted into (15*R*)-8,11,13-abietatriene-12,16-diol (**2a**) and its (15*S*)-epimer (**2b**) as reported in our previous papers.[9,10]

The (15*R*)-diol **2a** was then refluxed with a mixture

of chloromethyl methyl ether, dicyclohexano-18-crown-6, and anhydrous potassium carbonate in tetrahydrofuran–dichloromethane (1 : 1) to give (15*R*)-12,16-epoxy-8,11,13-abietatriene (**1a**: 10.3%) and 12-methoxymethyl ether (**13a**: 61.2%) along with small amounts of 16-methoxymethyl ether (**14a**: 8.5%) and 12,16-dimethoxymethyl ether (**15a**: 4.1%). The major product **13a** was mesylated with methanesulfonyl chloride in pyridine to give a mesylate **16a** which was converted into an iodide **17a** by refluxing with sodium iodide in ethyl methyl ketone. Hydrolysis of the methoxymethyl group in **17a** was carried out by refluxing with dilute hydrochloric acid in tetrahydrofuran; the resulting phenolic compound **18a** was cyclized with anhydrous potassium carbonate in refluxing ethyl methyl ketone to give the crystalline **1a**[11] in 60.2% yield from **13a**. Synthetic **1a** was identical with natural ar-abietatrien-12,16-oxide.

Similar methoxymethylation of (15*S*)-diol **2b** afforded (15*S*)-12,16-epoxy-8,11,13-abietatriene (**1b**: 8.4%), 12-methoxymethyl ether (**13b**: 60.1%), 16-methoxymethyl ether (**14b**: 10.3%), and 12,16-dimethoxymethyl ether (**15b**: 3.6%). The major product **13b** was further converted into an oily **1b** in 56.8% yield from **13b** via a mesylate **16b**, an iodide **17b**, and a phenol **18b**.

Subsequently, methyl 12,16-epoxy-8,11,13,15-abietatetraen-18-oate (**7**) was prepared as follows. Treatment of **6** with acetyl chloride and anhydrous aluminium chloride in dichloromethane at room temperature afforded three 13-acetyl compounds; **19** (15.9%), **20** (75.9%), and **21** (4.8%). Hydrolysis of **21** with dilute hydrochloric acid in refluxing ethanol produced **19** (97.9%), which was methylated to **20** (97.8%) by refluxing with methyl iodide and potassium *t*-butoxide in *t*-butyl alcohol. Demethylation of **20** with anhydrous aluminium chloride in refluxing dichloromethane afforded **19** (95.0%). The phenolic compound **19** was refluxed with ethyl bromoacetate and anhydrous potassium carbonate in ethyl methyl ketone, and the resulting ester **22** was then hydrolyzed with aqueous sodium hydroxide in refluxing ethanol to give the corresponding acid **23**.

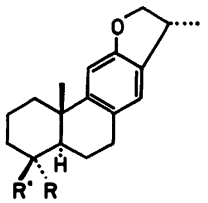

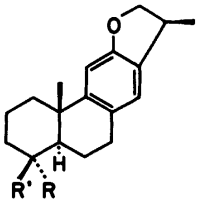

1a R=R'=Me **1b**
24a R=Me, R'=CO_2Me **24b**
25a R=Me, R'=CHO **25b**
26a R=CO_2Me, R'=Me **26b**

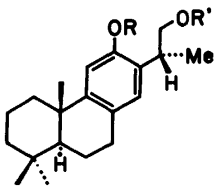

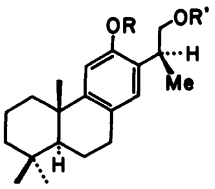

2a R=R'=H **2b**
13a R=CH_2OMe, R'=H **13b**
14a R=H, R'=CH_2OMe **14b**
15a R=R'=CH_2OMe **15b**
16a R=CH_2OMe, R'=Ms **16b**

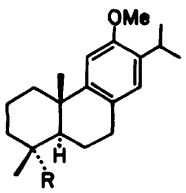

6 R=CO_2Me
8 R=CH_2OH
9 R=CH_2OTs
10 R=Me

11 R=Me, R'=H
12 R=R'=Me
19 R=CO_2Me, R'=H
20 R=CO_2Me, R'=Me
21 R=CO_2Me, R'=Ac
22 R=CO_2Me, R'=CH_2CO_2Et
23 R=CO_2Me, R'=CH_2CO_2H

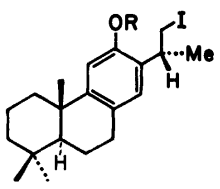

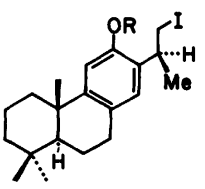

17a R=CH_2OMe **17b**
18a R=H **18b**

Table 1. Catalytic Hydrogenation of 12, 16-Epoxy-8, 11, 13, 15-abietatetraene Derivatives

Substrate	Condition		Product	
	Catalyst	Solvent[a]	(15R) : (15S)	Yield/%
4	10%Pd-C	AP	1 : 3	95
		A	1 : 4	91
		EA	1 : 5	93
	PtO_2	AP	2 : 3	74
		A	1 : 2	82
5	10%Pd-C	AP	1 : 5	97
		A	1 : 5	98
		EA	1 : 5	98
	PtO_2	AP	1 : 3	95
		A	1 : 3	91
7	10%Pd-C	AP	1 : 1	99
		A	2 : 3	97
		EA	1 : 2	96
	PtO_2	AP	1 : 1	92
		A	1 : 1	98

a) AP: AcOH+$HClO_4$, A: AcOH, EA: AcOEt

This was cyclized by refluxing with acetic anhydride and sodium acetate to yield **7** in 54.1% yield from **19**.

In order to ascertain the results of Burnell et al.[2,4] the catalytic hydrogenations of the three benzofuran derivatives **4**, **5**, and **7** were carried out at room temperature under an atmosphere of hydrogen. The conditions used and the results are summarized in Table 1. The ratio of the C-15 epimers was estimated by the intensities of doublet signals due to the C-15 methyls in the ^{1}H NMR spectrum[12] of the mixture. The hydrogenation mixture from **5** was separated by repeated column chromatography on silica gel and recrystallization to give the pure crystalline methyl (15*R*)-12,16-epoxy-8,11,13-abietatrien-19-oate (**24a**) and its (15*S*)-epimer (**24b**). The absolute configurations of C-15 in these epimers were determined by the following correlation. Reductions of **24a** and **24b** with lithium aluminium hydride in ether, followed by oxidation of the resulting alcohols with pyridinium chlorochromate in dichloromethane, afforded the corresponding aldehydes. These aldehydes, **25a** and **25b**, were converted, respectively, into the known **1a** and **1b** by Huang-Minlon reductions. The hydrogenation mixture from **7** was also separated to the pure methyl (15*R*)-12,16-epoxy-8,11,13-abietatrien-18-oate (**26a**) and its (15*S*)-epimer (**26b**), which were, respectively, converted into **1a** and **1b** by a series of reactions; reduction with lithium aluminium hydride in ether, tosylation with *p*-toluenesulfonyl chloride in pyridine, and treatment with sodium iodide and zinc powder in *N,N*-dimethylformamide. In the catalytic hydrogenations of **4** and **5** the major products were apparently the (15*S*)-epimers (**1b** and **24b**), but not the (15*R*)-epimers (**1a** and **24a**) as reported by Burnell et al.[2,4] The stereoselectivity can be explained as follows. Since the β-faces in these compounds are hindered by axial substituents at C-4 and C-10, hydrogen attacks predominantly the less hindered α-faces to give the (15*S*)-epimers as the major products. The less stereoselectivity of **7** is due to the presence of a bulky methoxycarbonyl group in the α-face; that is, the α-face approach of hydrogen is somewhat hindered by a methoxycarbonyl group. The hydrogenations over less active Pd-C catalyst were more stereoselective than those over more active PtO_2 catalyst.

From the present study, the stereochemistry of C-15 in natural ar-abietatrien-12,16-oxide was conclusively assigned as R-configuration.

Experimental

All melting points are uncorrected. The IR spectra and optical rotations were measured in chloroform, and the ^{1}H NMR spectra in carbon tetrachloride at 90 MHz with tetramethylsilane as an internal standard unless otherwise stated; s: singlet, bs: broad singlet, d: doublet, bd: broad doublet, dd: double doublet, t: triplet, m: multiplet. The column chromatography was performed using Merck silica gel (0.063 mm).

12-Methoxy-8,11,13-abietatriene (10). A solution of methyl 12-methoxy-8,11,13-abietatrien-18-oate (**6**)[7] (50.760 g) in dry ether (130 ml) was added dropwise to a stirred suspension of lithium aluminium hydride (3.635 g) in dry ether (180 ml) over a period of 20 min with cooling in an ice-water bath. The mixture was refluxed for 1 h. After the excess of lithium aluminium hydride had been decomposed with ethyl acetate, the mixture was poured into a mixture of ice and dilute hydrochloric acid, and extracted with ether. The ether extract was washed with brine, dried over sodium sulfate, and evaporated in vacuo to give 12-methoxy-8,11,13-abietatrien-18-ol (**8**) (47.547 g) which, without purification, was used in the next reaction.

A mixture of the crude **8** (47.547 g) and *p*-toluenesulfonyl chloride (33.710 g) in pyridine (200 ml) was heated at 80—85 °C for 3.5 h. The mixture was cooled, poured into a mixture of ice and dilute hydrochloric acid, and extracted with chloroform. The chloroform extract was washed with brine, dried over sodium sulfate, and evaporated in vacuo to give 12-methoxy-18-tosyloxy-8,11,13-abietatriene (**9**) (66.066 g) as a solid which, without purification, was used in the next reaction. The crude **9** obtained from another experiment was recrystallized from acetone-petroleum benzine, mp 147—149 °C. Found: C, 71.18; H, 7.97%. Calcd for $C_{28}H_{38}O_4S$: C, 71.45; H, 8.14%.

A stirred mixture of the crude **9** (66.066 g), sodium iodide (110.441 g), and zinc powder (48.170 g) in *N,N*-dimethylformamide (400 ml) was heated at 120—125 °C for 6 h. The mixture was cooled, diluted with benzene, and then filtered. The filtrate was poured into dilute hydrochloric acid and extracted with ether. The ether extract was washed successively with aqueous sodium thiosulfate and brine, dried over sodium sulfate, and evaporated in vacuo. The crude product was chromatographed on silica gel (350 g), using hexane-benzene (9:1) as eluent, to give **10** as an oil (37.481 g: 84.7% from **6**). ^{1}H NMR (60 MHz) δ=0.97 (6H, s, $-C(CH_3)_2$), 1.17 (6H, d, J=7 Hz, $-CH(CH_3)_2$), 1.18 (3H, s, $C_{10}-CH_3$), 3.75 (3H, s, $-OCH_3$), 6.58 (1H, s) and 6.69 (1H, s) (C_{11}-H and C_{14}-H). Found: C, 83.88; H, 10.84%. Calcd for $C_{21}H_{32}O$: C, 83.94; H, 10.73%.

13-Acetyl-8,11,13-abietatrien-12-ol (11) and 13-Acetyl-12-methoxy-8,11,13-abietatriene (12). Anhydrous aluminium chloride (10.982 g) was added to a stirred solution of **10** (12.373 g) and acetyl chloride (5.9 ml) in dichloromethane (80 ml) at 5—10 °C over a 10-min period. The mixture was further stirred at 5 °C for 10 min and at room temperature for 40 min, poured into a mixture of ice and dilute hydrochloric acid, and then extracted with ether. The ether extract was washed successively with aqueous sodium hydrogencarbonate and brine, dried, and evaporated in vacuo. The crude product was chromatographed on silica gel (250 g), using hexane-benzene (6:4) and ether-benzene (3:97) as eluents, to give **11** (0.500 g: 4.2%), mp 129—131 °C (from methanol), IR 1640 cm^{-1}, ^{1}H NMR (60 MHz) δ=2.52 (3H, s, $-COCH_3$), 6.73 (1H, s, C_{11}-H), 7.27 (1H, s, C_{14}-H), and **12** (9.222 g: 74.5%), mp 79—81 °C (from hexane), IR 1670 cm^{-1}, ^{1}H NMR (60 MHz) δ=2.48 (3H, s, $-COCH_3$), 3.86 (3H, s, $-OCH_3$), 6.72 (1H, s, C_{11}-H), 7.31 (1H, s, C_{14}-H). Anal. of **11**, Found: C, 79.51; H, 9.18%. Calcd for $C_{19}H_{26}O_2$: C, 79.68; H, 9.15%. Anal. of **12**, Found: C, 79.83; H, 9.53%.

Calcd for $C_{20}H_{28}O_2$: C, 79.95; H, 9.39%.

Demethylation of 12. A stirred mixture of **12** (2.240 g) and anhydrous aluminium chloride (1.988 g) in dichloromethane (25 ml) was refluxed for 2 h. The mixture was cooled, poured into dilute hydrochloric acid, and extracted with ether. The ether extract was washed with brine, dried, and evaporated in vacuo. The residue was chromatographed on silica gel (30 g), using benzene as eluent, to give **11** (2.019 g: 94.6%), mp 129—131 °C (from methanol).

Methylation of 11. A mixture of **11** (321 mg) and potassium *t*-butoxide (151 mg) in *t*-butyl alcohol (4.0 ml) was stirred at room temperature for 10 min. After the addition of methyl iodide (0.14 ml), the mixture was stirred at room temperature for 20 min and then refluxed for 2 h. The mixture was evaporated in vacuo, acidified with dilute hydrochloric acid, and extracted with ether. The ether extract was washed successively with water, aqueous sodium thiosulfate, and water. The dried solution was evaporated in vacuo. The residue was chromatographed on silica gel (10 g), using benzene as eluent, to give **12** (297 mg: 88.2%), mp 79—81 °C (from hexane).

Methoxymethylation of (15*R*)-8,11,13-Abietatriene-12,16-diol (2a). A mixture of **2a** (314.0 mg), dicyclohexano-18-crown-6 (54.9 mg), and anhydrous potassium carbonate (287.0 mg) in tetrahydrofuran–dichloromethane (1:1, 10 ml) was stirred at room temperature for 30 min. After the addition of chloromethyl methyl ether (0.16 ml), the mixture was refluxed for 3 h, cooled, and then diluted with ether. The ether solution was washed with brine, dried, and evaporated in vacuo. The residue was chromatographed on silica gel (30 g), using hexane–benzene (8:2) as eluent, to give (15*R*)-12,16-epoxy-8,11,13-abietatriene (**1a**) (30.4 mg: 10.3%), mp 54—56 °C (from ether), $[\alpha]_D$ +57.3° (*c* 0.89). Elution with ether–benzene (1:99) gave 12,16-dimethoxymethyl ether **15a** as an oil (16.5 mg: 4.1%) and 16-methoxymethyl ether **14a** as an oil (30.5 mg: 8.5%), IR 3600 and 3330 cm^{-1}. ^1H NMR ($CDCl_3$) of **15a** δ=0.91 (3H, s) and 0.93 (3H, s) (-C(CH$_3$)$_2$), 1.17 (3H, s, C_{10}-CH_3), 1.27 (3H, d, J=7 Hz, C_{15}-CH_3), 3.30 (3H, s, C_{16}-OCH_2OCH_3), 3.47 (3H, s, C_{12}-OCH_2OCH_3), 4.60 (2H, s, C_{16}-OCH_2O-), 5.13 (2H, s, C_{12}-OCH_2O-), 6.84 (1H, s) and 6.94 (1H, s) (C_{11}-H and C_{14}-H). ^1H NMR ($CDCl_3$) of **14a** δ=0.91 (3H, s) and 0.93 (3H, s) (-C(CH$_3$)$_2$), 1.17 (3H, s, C_{10}-CH_3), 1.31 (3H, d, J=7 Hz, C_{15}-CH_3), 3.30 (3H, s, C_{16}-OCH_2OCH_3), 4.63 (2H, s, C_{16}-OCH_2O-), 6.75 (1H, s) and 6.78 (1H, s) (C_{11}-H and C_{14}-H), 7.11 (1H, s, C_{12}-OH). Further elution with ether–benzene (1:9) gave 12-methoxymethyl ether **13a** (220 mg: 61.2%), $[\alpha]_D$ +66.6° (*c* 5.44), ^1H NMR ($CDCl_3$) δ=0.91 (3H, s) and 0.93 (3H, s) (-C(CH$_3$)$_2$), 1.17 (3H, s, C_{10}-CH_3), 1.23 (3H, d, J=7 Hz, C_{15}-CH_3), 3.47 (3H, s, C_{12}-OCH_2OCH_3), 3.69 (2H, bd, J=7 Hz, -CH_2OH), 5.14 (2H, s, C_{12}-OCH_2O-), 6.84 (1H, s) and 6.97 (1H, s) (C_{11}-H and C_{14}-H). Found: C, 76.18; H, 10.03%. Calcd for $C_{22}H_{34}O_3$: C, 76.26; H, 9.89%.

Methoxymethylation of (15*S*)-8,11,13-Abietatriene-12,16-diol (2b). A mixture of **2b** (283.0 mg), dicyclohexano-18-crown-6 (49.5 mg), anhydrous potassium carbonate (258.6 mg), and chloromethyl methyl ether (0.14 ml) in tetrahydrofuran–dichloromethane (1:1, 10.0 ml) was treated as described above. The crude product was chromatographed on silica gel to give four oily products, (15*S*)-12,16-epoxy-8,11,13-abietatriene (**1b**) (22.4 mg: 8.4%),$[\alpha]_D$ +60.7° (*c* 1.12), 12,16-dimethoxymethyl ether **15b** (13.2 mg: 3.6%), 16-methoxymethyl ether **14b** (33.4 mg: 10.3%), IR 3600 and 3330 cm^{-1}, and 12-methoxymethyl ether **13b** (194.7 mg: 60.1%), $[\alpha]_D$ +46.5°(*c* 4.59). Found: C, 76.42; H, 10.07%. Calcd for $C_{22}H_{34}O_3$: C, 76.26; H, 9.89%. ^1H NMR ($CDCl_3$) of **15b** δ=0.91 (3H, s) and 0.93 (3H, s) (-C(CH$_3$)$_2$), 1.17 (3H, s, C_{10}-CH_3), 1.24 (3H, d, J=7 Hz, C_{15}-CH_3), 3.30 (3H, s, C_{16}-OCH_2OCH_3), 3.47 (3H, s, C_{12}-OCH_2OCH_3), 4.60 (2H, s, C_{16}-OCH_2O-), 5.13 (2H, s, C_{12}-OCH_2O-), 6.84 (1H, s) and 6.94 (1H, s) (C_{11}-H and C_{14}-H). ^1H NMR ($CDCl_3$) of **14b** δ=0.92 (6H, s, -C(CH$_3$)$_2$), 1.17 (3H, s, C_{10}-CH_3), 1.31 (3H, d, J=7 Hz, C_{15}-CH_3), 3.30 (3H, s, C_{16}-OCH_2OCH_3), 4.63 (2H, s, C_{16}-OCH_2O-), 6.77 (1H, s) and 6.79 (1H, s) (C_{11}-H and C_{14}-H), 7.09 (1H, s, C_{12}-OH). ^1H NMR ($CDCl_3$) of **13b** δ=0.92 (6H, s, -C(CH$_3$)$_2$), 1.17 (3H, s, C_{10}-CH_3), 1.22 (3H, d, J=7 Hz, C_{15}-CH_3), 3.47 (3H, s, C_{12}-OCH_2OCH_3), 3.70 (2H, bd, J=7 Hz, -CH_2OH), 5.14 (2H, s, C_{12}-OCH_2O-), 6.84 (1H, s) and 6.97 (1H, s) (C_{11}-H and C_{14}-H).

Conversion of 13a into 1a. A mixture of **13a** (196 mg) and methanesulfonyl chloride (0.09 ml) in pyridine (1.5 ml) was heated at 75—80 °C for 2.5 h. The mixture was cooled, diluted with ether, and washed successively with dilute hydrochloric acid and brine. The dried solution was evaporated in vacuo to give a crude mesylate **16a** as an oil (225 mg), IR 1350 and 1170 cm^{-1}, ^1H NMR (60 MHz, $CDCl_3$) δ=0.96 (6H, s, -C(CH$_3$)$_2$), 1.18 (3H, s, C_{10}-CH_3), 1.35 (3H, d, J=7 Hz, C_{15}-CH_3), 2.84 (3H, s, -OSO_2CH_3), 3.49 (3H, s, -OCH_2OCH_3), 5.18 (2H, s, -OCH_2O-), 6.84 (1H. s) and 6.99 (1H, s) (C_{11}-H and C_{14}-H).

A mixture of the crude **16a** (225 mg) and sodium iodide (170 mg) in ethyl methyl ketone (5.0 ml) was refluxed for 4 h. The mixture was cooled, diluted with ether, and then washed successively with water, aqueous sodium thiosulfate, and brine. The dried solution was evaporated in vacuo to give a crude iodide **17a** (240 mg). ^1H NMR (60 MHz, $CDCl_3$) δ=0.95 (6H, s, -C(CH$_3$)$_2$), 1.18 (3H, s, C_{10}-CH_3), 3.48 (3H, s, -OCH_2OCH_3), 5.13 (2H, s, -OCH_2O-) 6.84 (1H, s) and 6.99 (1H, s) (C_{11}-H and C_{14}-H).

A mixture of the crude **17a** (240 mg) and dilute hydrochloric acid (15%: 0.2 ml) in tetrahydrofuran (5.0 ml) was refluxed for 3 h. The mixture was cooled, diluted with ether, and washed with brine. The dried solution was evaporated in vacuo to give a crude phenolic compound **18a** (234 mg), IR 3595 and 3325 cm^{-1}. ^1H NMR (60 MHz, $CDCl_3$) δ=0.96 (6H, s, -C(CH$_3$)$_2$), 1.17 (3H, s, C_{10}-CH_3), 1.39 (3H, d, J=6.5 Hz, C_{15}-CH_3), 6.61 (1H, s) and 6.79 (1H, s) (C_{11}-H and C_{14}-H).

A mixture of the crude **18a** (234 mg) and anhydrous potassium carbonate (600 mg) in ethyl methyl ketone (5.0 ml) was refluxed for 2.5 h. The mixture was cooled, diluted with water, and extracted with ether. The ether extract was washed with brine, dried, and evaporated in vacuo. The residue was chromatographed on silica gel (20 g), using hexane–benzene (3:1) as eluent, to give **1a** (97 mg: 60.2% from **13a**) which was recrystallized from ether, mp 54—56 °C, $[\alpha]_D$ +59.8° (*c* 3.33), IR (KBr) 1620, 1485, 1240, and 995 cm^{-1}; ^1H NMR ($CDCl_3$) δ=0.91 (3H, s) and 0.93 (3H, s) (-C(CH$_3$)$_2$), 1.17 (3H, s, C_{10}-CH_3), 1.27 (3H, d, J=7 Hz, C_{15}-CH_3), 3.44 (1H, m, C_{15}-H), 3.98 (1H, dd, J=7

and 8 Hz) and 4.61 (1H, t, J=8 Hz) ($-CH_2O-$), 6.70 (1H, s) and 6.80 (1H, s) (C_{11}-H and C_{14}-H). Found: C, 84.64; H, 10.21%. Calcd for $C_{20}H_{28}O$: C, 84.45; H, 9.92%. The synthetic **1a** was identical with natural ar-abietatrien-12,16-oxide (lit,[1] mp 49—52 °C).

Conversion of 13b into 1b. A mixture of **13b** (195 mg) and methanesulfonyl chloride (0.09 ml) in pyridine (1.5 ml) was heated at 75—80 °C for 2.5 h to give a crude mesylate **16b** (230 mg), IR 1350 and 1170 cm^{-1}, ^{1}H NMR (60 MHz, $CDCl_3$) δ=0.97 (6H, s, $-C(CH_3)_2$), 1.19 (3H, s, C_{10}-CH_3), 1.35 (3H, d, J=7 Hz, C_{15}-CH_3), 2.84 (3H, s, $-OSO_2CH_3$), 3.50 (3H, s, $-OCH_2OCH_3$), 5.19 (2H, s, $-OCH_2O-$) 6.86 (1H, s) and 7.00 (1H, s) (C_{11}-H and C_{14}-H).

A mixture of the crude **16b** (230 mg) and sodium iodide (169 mg) in ethyl methyl ketone (5.0 ml) was refluxed for 4 h to give a crude iodide **17b** (240 mg), ^{1}H NMR (60 MHz, $CDCl_3$) δ=0.97 (6H, s, $-C(CH_3)_2$), 1.19 (3H, s, C_{10}-CH_3), 3.50 (3H, s, $-OCH_2OCH_3$), 5.18 (2H, s, $-OCH_2O-$), 6.81 (1H, s) and 6.98 (1H, s) (C_{11}-H and C_{14}-H).

The crude **17b** (240 mg) was hydrolyzed with dilute hydrochloric acid (15%: 0.2 ml) in refluxing tetrahydrofuran (5.0 ml) for 3 h to give a crude phenolic compound **18b** (227 mg), IR 3600 and 3325 cm^{-1}, ^{1}H NMR (60 MHz, $CDCl_3$) δ=0.95 (6H, s, $-C(CH_3)_2$), 1.15 (3H, s, C_{10}-CH_3), 1.37 (3H, d, J=6.5 Hz, C_{15}-CH_3), 6.61 (1H, s) and 6.80 (1H, s) (C_{11}-H and C_{14}-H).

A mixture of the crude **18b** (227 mg) and anhydrous potassium carbonate (600 mg) in ethyl methyl ketone (5.0 ml) was refluxed for 2.5 h. The crude product was chromatographed on silica gel (30 g), using hexane–benzene (3:1) as eluent, to give an oily **1b** (91 mg: 56.8% from **13b**), $[\alpha]_D$ +61.3° (c 1.88), IR (KBr) 1620, 1485, 1240, and 995 cm^{-1}; ^{1}H NMR ($CDCl_3$) δ=0.92 (6H, s, $-C(CH_3)_2$), 1.17 (3H, s, C_{10}-CH_3), 1.28 (3H, d, J=7 Hz, C_{15}-CH_3), 3.45 (1H, m, C_{15}-H), 3.98 (1H, dd, J=7 and 8 Hz) and 4.61 (1H, t, J=8 Hz) ($-CH_2O-$), 6.70 (1H, s) and 6.80 (1H, s) (C_{11}-H and C_{14}-H). Found: C, 84.42; H, 10.21%. Calcd for $C_{20}H_{28}O$: C, 84.45; H, 9.92%.

Conversion of Methyl 12-Methoxy-8,11,13-abietatrien-18-oate (6) into 13-Acetyl Derivatives 19, 20, and 21. Anhydrous aluminium chloride (1.463 g) was added to a stirred solution of **6**[7] (1.260 g) and acetyl chloride (0.52 ml) in dichloromethane (10 ml) at 6—9 °C over a 7 min period. After stirring at this temperature for 13 min and at room temperature for 40 min, the mixture was poured into a mixture of ice and dilute hydrochloric acid, and then extracted with ether. The ether extract was washed with brine, dried, and evaporated in vacuo. The residue was chromatographed on silica gel (30 g), using benzene as eluent, to give methyl 13-acetyl-12-hydroxy-8,11,13-abietatrien-18-oate (**19**) (0.192 g: 15.9%) which was recrystallized from methanol, mp 154—155 °C, $[\alpha]_D$ +74.7° (c 5.25), IR 1723 and 1640 cm^{-1}. ^{1}H NMR (60 MHz) δ=1.20 (3H, s) and 1.23 (3H, s) (C_4-CH_3 and C_{10}-CH_3), 2.52 (3H, s, $-COCH_3$), 3.63 (3H, s, $-CO_2CH_3$), 6.70 (1H, s, C_{11}-H), 7.27 (1H, s, C_{14}-H), 11.77 (1H, s, C_{12}-OH). Found: C, 72.49; H, 8.24%. Calcd for $C_{20}H_{26}O_4$: C, 72.70; H, 7.93%.

Elution with ether-benzene (1:99) afforded methyl 13-acetyl-12-methoxy-8,11,13-abietatrien-18-oate (**20**) (0.956 g: 75.9%) which was recrystallized from hexane, mp 86—87 °C, $[\alpha]_D$ +62.0° (c 4.32), IR 1721 and 1670 cm^{-1}, ^{1}H NMR (60 MHz) δ=1.19 (3H, s and 1.22 (3H, s) (C_4-CH_3 and C_{10}-CH_3), 2.44 (3H, s, $-COCH_3$), 3.61 (3H, s, $-CO_2CH_3$), 3.83 (3H, s, $-OCH_3$), 6.67 (1H, s, C_{11}-H), 7.26 (1H, s, C_{14}-H).

Further elution with ether–benzene (5:95) afforded methyl 12-acetoxy-13-acetyl-8,11,13-abietatrien-18-oate (**21**) (0.066 g: 4.8%) which was recrystallized from acetone-hexane, mp 107—108 °C, $[\alpha]_D$ +71.7° (c 3.78), IR 1757, 1716, and 1680 cm^{-1}; ^{1}H NMR (60 MHz) δ=1.21 (3H, s) and 1.24 (3H, s) (C_4-CH_3 and C_{10}-CH_3), 2.23 (3H, s, $-OCOCH_3$), 2.40 (3H, s, $-COCH_3$), 3.62 (3H, s, $-CO_2CH_3$), 6.78 (1H, s, C_{11}-H), 7.34 (1H, s, C_{14}-H). Found: C, 71.07; H, 7.64%. Calcd for $C_{22}H_{28}O_5$: C, 70.94; H, 7.58%.

Hydrolysis of 21. A solution of **21** (2.587 g) and dilute hydrochloric acid (15%: 2.5 ml) in ethanol (20 ml) was refluxed for 1.5 h. After the usual work-up, the crude product was recrystallized from methanol to give **19** (2.248 g: 97.9%), mp 154—155 °C.

Methylation of 19. A mixture of **19** (5.148 g) and potassium t-butoxide (2.098 g) in t-butyl alcohol (60 ml) was stirred for 10 min. After the addition of methyl iodide (1.92 ml), the stirred mixture was refluxed for 2 h, and then treated as described above. The crude product was chromatographed on silica gel (35 g), using ether–benzene (5:95) as eluent, to give **20** (5.248 g: 97.8%), mp 86—87 °C (from hexane).

Demethylation of 20. A stirred mixture of **20** (200 mg) and anhydrous aluminium chloride (271 mg) in dichloromethane (4.0 ml) was refluxed for 3 h. After the work-up, as described above, the crude product was chromatographed on silica gel (10 g), using benzene as eluent, to give **19** (182 mg: 95.0%), mp 154—155 °C (from methanol).

Methyl 12,16-Epoxy-8,11,13,15-abietatetraen-18-oate (7). A mixture of **19** (4.00 g), ethyl bromoacetate (2.29 ml), and anhydrous potassium carbonate (10.0 g) in ethyl methyl ketone (30 ml) was refluxed for 8 h. The mixture was cooled, diluted with ether, and washed successively with water, aqueous sodium thiosulfate, and water. The dried solution was evaporated in vacuo to give a crude ester **22** (5.82 g), IR 1725 and 1665 cm^{-1}, ^{1}H NMR (60 MHz) δ=1.18 (3H, s, C_{10}-CH_3), 1.22 (3H, s, C_4-CH_3), 1.28 (3H, t, J=7 Hz, $-CO_2CH_2CH_3$), 2.55 (3H, s, $-COCH_3$), 3.61 (3H, s, $-CO_2CH_3$), 4.18 (2H, q, J=7 Hz, $-CO_2CH_2CH_3$), 4.61 (2H, s, $-OCH_2CO_2-$), 6.64 (1H, s, C_{11}-H), 7.29 (1H, s, C_{14}-H).

The crude **22** (5.82 g) was hydrolyzed with aqueous sodium hydroxide (10%: 10 ml) in refluxing ethanol (20 ml) for 1 h. The mixture was evaporated in vacuo, acidified with dilute hydrochloric acid, and extracted with chloroform. The chloroform extract was washed with brine, dried, and evaporated in vacuo to give a crude acid **23** (5.01 g), IR 3500—2400, 1720, and 1660 cm^{-1}; ^{1}H NMR (60 MHz, $CDCl_3$) δ=1.21 (3H, s) and 1.29 (3H, s) (C_4-CH_3 and C_{10}-CH_3), 2.65 (3H, s, $-COCH_3$), 3.68 (3H, s, $-CO_2CH_3$), 4.72 (2H, s, $-OCH_2CO_2H$), 6.78 (1H, s, C_{11}-H), 7.42 (1H, s, C_{14}-H), 10.32 (1H, bs, $-CO_2H$).

A mixture of the crude **23** (5.01 g) and sodium acetate (9.0 g) in acetic anhydride (20 ml) was refluxed for 7.5 h. The mixture was cooled, diluted with ether, and washed successively with water, aqueous sodium hydrogencarbonate, and water. The dried solution was evaporated in vacuo to give the crude benzofuran derivative (1.70 g). The alkaline washing was acidified with dilute hydrochloric acid, and extracted with chloroform. The chloroform extract was washed with brine, dried, and evaporated in

vacuo to give the recovered **23** (3.00 g). This was also submitted to cyclization to give the crude benzofuran derivative (1.04 g) and the recovered **23** (1.40 g). The combined crude benzofuran derivative was chromatographed on silica gel (30 g), using benzene as eluent, to give **7** (2.14 g: 54.1%) which was recrystallized from hexane, mp 123.5—124 °C, $[\alpha]_D$ +68.6° (*c* 9.50), IR 1721 cm^{-1}, ^1H NMR (60 MHz, $CDCl_3$) δ=1.23 (3H, s) and 1.30 (3H, s) (C_4-CH_3 and C_{10}-CH_3), 2.17 (3H, d, *J*=1 Hz, C_{15}-CH_3), 3.67 (3H, s, -CO_2CH_3), 7.12 (1H, s) and 7.29 (1H, s) (C_{11}-H and C_{14}-H), 7.24 (1H, m, overlap, C_{16}-H). Found: C, 77.21; H, 8.17%. Calcd for $C_{21}H_{26}O_3$:C, 77.27; H, 8.03%.

Catalytic Hydrogenation of 12,16-Epoxy-8,11,13,15-abietatetraene Derivatives 4, 5, and 7. a) A mixture of 12,16-epoxy-8,11,13,15-abietatetraene (**4**)[3] (303 mg) and 10% Pd-C (100 mg) in acetic acid (10 ml) containing four drops of 70% perchloric acid was hydrogenated at room temperature under an atmosphere of hydrogen for 7 h. After the usual work-up, the crude product was chromatographed on silica gel (20 g), using hexane-benzene (8:2) as eluent, to give a mixture (1:3) of (15*R*)-12,16-epoxy-8,11,13-abietatriene (**1a**) and its (15*S*)-epimer (**1b**) (291 mg: 95.4%).

b) A mixture of methyl 12,16-epoxy-8,11,13,15-abietatetraen-19-oate (**5**)[5] (100 mg: mp 130—131.5 °C) and PtO_2 (20 mg) in acetic acid (10 ml) was hydrogenated at room temperature under an atmosphere of hydrogen for 35 min. After the usual work-up, the crude product was chromatographed on silica gel (10 g), using benzene as eluent, to give a mixture (1:3) of methyl (15*R*)-12,16-epoxy-8,11,13-abietatrien-19-oate (**24a**) and its (15*S*)-epimer (**24b**) (91 mg: 90.7%). This mixture was separated by repeated column chromatography on silica gel using hexane-benzene (1:1) as eluent and recrystallization to give **24a**, mp 160—162 °C (from hexane), $[\alpha]_D$ +128.1° (*c* 0.96), and **24b**, mp 150—151.5 °C (from hexane), $[\alpha]_D$ +132.4° (*c* 3.70). Anal. of **24a**, Found: C, 76.63; H, 8.77%. Calcd for $C_{21}H_{28}O_3$: C, 76.79; H, 8.59%. Anal of **24b**, Found: C, 76.81; H, 8.81%. Calcd for $C_{21}H_{28}O_3$:C, 76.79; H, 8.59%. ^1H NMR ($CDCl_3$) of **24a** δ=1.01 (3H, s, C_{10}-CH_3), 1.25 (3H, s, C_4-CH_3), 1.27 (3H, d, *J*=7 Hz, C_{15}-CH_3), 3.64 (3H, s, -CO_2CH_3), 3.99 (1H, dd, *J*=7 and 8 Hz) and 4.62 (1H, t, *J*=8 Hz) (-OCH_2-), 6.67 (1H, s) and 6.79 (1H, s) (C_{11}-H and C_{14}-H). ^1H NMR ($CDCl_3$) of **24b** δ=1.01 (3H, s, C_{10}-CH_3), 1.25 (3H, s, C_4-CH_3), 1.28 (3H, d, *J*=7 Hz, C_{15}-CH_3), 3.64 (3H, s, -CO_2CH_3), 3.99 (1H, dd, *J*=7 and 8 Hz) and 4.62 (1H, t, *J*=8 Hz) (-OCH_2-), 6.67 (1H, s) and 6.79 (1H, s) (C_{11}-H and C_{14}-H).

c) A mixture of **7** (100 mg) and 10% Pd-C (30 mg) in ethyl acetate (10 ml) was hydrogenated at room temperature under an atmosphere of hydrogen for 6.5 h. After the usual work-up, the crude product was chromatographed on silica gel (10 g), using benzene as eluent, to give a mixture (1:2) of methyl (15*R*)-12,16-epoxy-8,11,13-abietatrien-18-oate (**26a**) and its (15*S*)-epimer (**26b**) (97 mg: 96.3%). This mixture was separated by repeated column chromatography on silica gel using hexane-benzene (4:6) as eluent and recrystallization to give **26a**, mp 142.5—143.5 °C (from hexane), $[\alpha]_D$ +63.7° (*c* 3.33), and **26b** as an oil, $[\alpha]_D$ +56.3° (*c* 2.90). ^1H NMR ($CDCl_3$) of **26a** δ=1.17 (3H, s) and 1.25 (3H, s) (C_4-CH_3 and C_{10}-CH_3), 1.27 (3H, d, *J*=7 Hz, C_{15}-CH_3), 3.66 (3H, s, -CO_2CH_3), 3.99 (1H, dd, *J*=7 and 8 Hz) and 4.62 (1H, t, *J*=8 Hz) (-OCH_2-), 6.67 (1H, s) and 6.78 (1H, s) (C_{11}-H and C_{14}-H). ^1H NMR ($CDCl_3$) of **26b** δ=1.17 (3H, s) and 1.25 (3H, s) (C_4-CH_3 and C_{10}-CH_3), 1.28 (3H, d, *J*=7 Hz, C_{15}-CH_3), 3.66 (3H, s, -CO_2CH_3), 3.99 (1H, dd, *J*=7 and 8 Hz) and 4.62 (1H, t, *J*=8 Hz) (-OCH_2-), 6.67 (1H, s) and 6.78 (1H, s) (C_{11}-H and C_{14}-H). Anal of **26a**, Found: C, 76.84; H, 8.80%. Calcd for $C_{21}H_{28}O_3$: C, 76.79; H, 8.59%. Anal. of **26b**, Found: C, 76.75; H, 8.74%. Calcd for $C_{21}H_{28}O_3$: C, 76.79; H, 8.59%. The other hydrogenations were summarized in Table 1.

(15*R*)-12,16-Epoxy-8,11,13-abietatrien-19-al (25a) and Its (15*S*)-Epimer (25b). a) A suspension of **24a** (128.0 mg) and lithium aluminium hydride (14.8 mg) in dry ether (5.0 ml) was stirred at room temperature for 1 h and then refluxed for 20 min. The mixture was poured into dilute hydrochloric acid and extracted with ether. The ether extract was washed with water, dried, and evaporated in vacuo to give a crude alcohol (120.0 mg).

A mixture of the crude alcohol (120.0 mg) and pyridinium chlorochromate (126.0 mg) in dichloromethane (5.0 ml) was stirred at room temperature for 1.5 h. After the addition of ether and aqueous sodium hydrogencarbonate, the mixture was extracted with ether. The ether extract was washed successively with aqueous sodium hydrogencarbonate and water, dried, and evaporated in vacuo. The residue was chromatographed on silica gel (10 g), using benzene as eluent, to give **25a** (94.4 mg: 81.2%) which was recrystallized from ethanol, mp 150—152 °C, $[\alpha]_D$ +89.4° (*c* 1.23), IR 2730 and 1716 cm^{-1}, ^1H NMR (60 MHz, $CDCl_3$) δ=1.03 (3H, s) and 1.09 (3H, s) (C_4-CH_3 and C_{10}-CH_3), 1.27 (3H, d, *J*=7 Hz, C_{15}-CH_3), 3.2—3.7 (1H, m, C_{15}-H), 3.97 (1H, dd, *J*=7 and 8 Hz) and 4.60 (1H, t, *J*=8 Hz) (-OCH_2-), 6.68 (1H, s) and 6.81 (1H, s) (C_{11}-H and C_{14}-H), 9.81 (1H, d, *J*=1.5 Hz, -CHO). Found: C, 80.51; H, 8.73%. Calcd for $C_{20}H_{26}O_2$: C, 80.49; H, 8.78%.

b) A suspension of **24b** (498.0 mg) and lithium aluminium hydride (57.5 mg) in dry ether (7.0 ml) was stirred at room temperature for 1 h and then refluxed for 20 min. The crude alcohol (503.0 mg) was immediately oxidized with pyridinium chlorochromate (490.3 mg) in dichloromethane (5.0 ml) at room temperature for 1.5 h. After the work-up, as described in **a)**, the crude product was chromatographed on silica gel (15 g), using benzene as eluent, to give **25b** (334.0 mg: 73.8%) which was recrystallized from ethanol, mp 138—140 °C, $[\alpha]_D$ +94.4° (*c* 3.13), IR 2730 and 1712 cm^{-1}, ^1H NMR (60 MHz, $CDCl_3$) δ=1.06 (3H, s) and 1.10 (3H, s) (C_4-CH_3 and C_{10}-CH_3), 1.30 (3H, d, *J*=7 Hz, C_{15}-CH_3), 3.2—3.7 (1H, m, C_{15}-H), 3.97 (1H, dd, *J*=7 and 8 Hz) and 4.60 (1H, t, *J*=8 Hz) (-OCH_2-), 6.65 (1H, s) and 6.78 (1H, s) (C_{11}-H and C_{14}-H), 9.78 (1H, d, *J*=1.5 Hz, -CHO). Found: C, 80.28; H, 9.00%. Calcd for $C_{20}H_{26}O_2$: C, 80.49; H, 8.78%.

Conversion of 25a into 1a. A mixture of **25a** (82.6 mg) and 80% hydrazine hydrate (0.42 ml) in diethylene glycol (4.0 ml) was refluxed for 2.5 h and powdered sodium hydroxide (443 mg) was then added. The mixture was heated at 185—190 °C for 3 h, cooled, diluted with water, and extracted with ether. The ether extract was washed with water, dried, and evaporated in vacuo. The residue was chromatographed on silica gel (10 g), using hexane-benzene (85:15) as eluent, to give **1a** (32.8 mg: 41.7%), mp 53—55 °C (from ether), $[\alpha]_D$ +58.0° (*c* 0.81).

Conversion of 25b into 1b. A mixture of **25b** (291.0 mg) and 80% hydrazine hydrate (1.8 ml) in diethylene glycol (10 ml) was refluxed for 2.5 h and powdered sodium

hydroxide (1.560 g) was then added. The mixture was heated at 185—190 °C for 3 h. The crude product was chromatographed on silica gel (10 g), using hexane–benzene (7:3) as eluent, to give **1b** as an oil (139.9 mg: 50.4%), $[\alpha]_D$ +61.6° (*c* 4.39).

Conversion of 26a into 1a. A suspension of **26a** (334 mg) and lithium aluminium hydride (39 g) in dry ether (10 ml) was stirred at room temperature for 1.5 h. The mixture was poured into dilute hydrochloric acid and extracted with ether. The ether extract was washed with water, dried, and evaporated in vacuo to give a crude alcohol (343 mg).

The crude alcohol was tosylated with *p*-toluenesulfonyl chloride (388 mg) in pyridine (3.0 ml) at 95—100 °C for 5.5 h. The mixture was cooled, poured into dilute hydrochloric acid, and extracted with chloroform. The chloroform extract was washed with aqueous sodium hydrogencarbonate and water, dried, and evaporated in vacuo to give a crude tosylate (650 mg).

A mixture of the crude tosylate, sodium iodide (762 mg), and zinc powder (333 mg) in *N,N*-dimethylformamide (5.0 ml) was heated at 120—125 °C for 7 h. The mixture was cooled, poured into dilute hydrochloric acid, and extracted with ether. The ether extract was washed successively with water, aqueous sodium thiosulfate, and brine. The dried solution was evaporated in vacuo and the residue was chromatographed on silica gel (10 g), using hexane–benzene (85:15) as eluent, to give **1a** (241 mg: 83.3%) which was recrystallized from ether, mp 52—55 °C, $[\alpha]_D$ +59.7° (*c* 0.75).

Conversion of 26b into 1b. The ester **26b** (198 mg) was reduced with lithium aluminium hydride (23 mg) in dry ether (3.0 ml) at room temperature for 1 h to give a crude alcohol (208 mg).

The above alcohol was tosylated with *p*-toluenesulfonyl chloride (345 mg) in pyridine (2.0 ml) at 95—100 °C for 5.5 h to afford a crude tosylate (400 mg).

A mixture of the crude tosylate, sodium iodide (452 mg), and zinc powder (197 mg) in *N,N*-dimethylformamide (3.0 ml) was heated at 120—125 °C for 7 h. The crude product was purified by column chromatography on silica gel (10 g), using hexane–benzene (7:3) as eluent, to give **1b** as an oil (90 mg: 52.4%), $[\alpha]_D$ +59.4° (*c* 0.96).

The authors are grateful to Professor Yoshiyuki Hirose, Science University of Tokyo, for kindly supplying the spectra of natural ar-abietatrien-12,16-oxide.

References

1) S. Hasegawa and Y. Hirose, *Phytochemistry*, **21**, 643 (1982).

2) R. H. Burnell, M. Neron-Desbiens, and S. Savard, *Synth. Commun.*, **12**, 11 (1982).

3) R. H. Burnell and M. Ringuet, *Can. J. Chem.*, **56**, 517 (1978).

4) R. H. Burnell, A. Andersen, M. Neron, and S. Savard, *Can. J. Chem.*, **63**, 2769 (1985).

5) G. D. Beresford, R. C. Cambie, and K. P. Mathai, *Aust. J. Chem.*, **26**, 1763 (1973).

6) T. Matsumoto, S. Imai, S. Miuchi, and H. Sugibayashi, *Bull. Chem. Soc. Jpn.*, **58**, 340 (1985).

7) R. C. Cambie and R. A. Franich, *Aust. J. Chem.*, **24**, 117 (1971).

8) H. Akita and T. Oishi, *Chem. Pharm. Bull.*, **29**, 1567 (1981).

9) T. Matsumoto, S. Imai, S. Takeda, and M. Mitsuki, *Bull. Chem. Soc. Jpn.*, **56**, 2013 (1983).

10) T. Matsumoto, S. Imai, and T. Yoshinari, *Bull. Chem. Soc. Jpn.*, **58**, 1165 (1985).

11) A personal communication from Professor Hirose informed us that the treatment of natural 16-hydroxyferruginol with *p*-toluenesulfonyl chloride in pyridine at room temperature for 39 h or in acetone in the presence of potassium carbonate, produced ar-abietatrien-12,16-oxide in 11 or 6% yields, respectively.

12) The ^{1}H NMR spectra (90 MHz) of the C-15 epimers were identical except doublet signals due to the C-15 methyls.

Peptide Synthesis in Aqueous Solution. I. Application of *p*-Dialkylsulfoniophenols as a Water-Soluble Coupling Reagent[1)]

Katsushige KOUGE, Tatsuya KOIZUMI, Hideo OKAI,†,* and Tetsuo KATO††
Sanshin Chemical Industrial Co. Ltd., 531 Nagahama, Hirao-cho, Kumage-gun, Yamaguchi 742-11
†Department of Fermentation Technology, Faculty of Engineering, Hiroshima University, Shitami, Saijo-cho, Higashihiroshima 724
††Laboratory of Biochemistry, Faculty of Science, Kyushu University, Higashi-ku, Fukuoka 812
(Received January 12, 1987)

(*p*-Hydroxyphenyl)dimethylsulfonium methyl sulfate(HODMSP·$MeSO_4^-$) was found to be an excellent coupling reagent having a water-soluble property and a high reactivity; it worked as satisfactory as usual active esters in regard to the reactivity, product purity, and racemization. The marked advantage of the HODMSP·$MeSO_4^-$ active ester method was the fact that bifunctional residues such as Arg, Lys, Cys, and Tyr could be selectively acylated when the pH of the reaction mixture was controlled. The molluscan neuropeptide FMRFamide(Phe-Met-Arg-Phe-NH_2) was synthesized by this new active ester method for an evaluation of this method to further applications involving peptide syntheses.

The active ester method, which allows the formation of an amide bond under a very mild condition, is known to be useful for peptide syntheses or chemical modifications of proteins. The reaction process of this active ester method proceeds by activating a carbonyl carbon atom in the carboxyl component, as shown in Fig. 1. In spite of many studies[2-5)] about the active ester method, most reactions require organic solvents since these active esters are not soluble in water due to the hydrophobic character of their molecules.

Recently, Kawasaki et al. applied *p*-trimethylammoniophenyl ester[6)] as a water-soluble active ester to peptide synthesis. They also reported that the active ester was advantageous for the removal of any unreacted active ester and resultant hydroxy compound from the reaction mixture. As a new application of the water-soluble active ester, we have considered applying it to the peptide forming reaction in an aqueous solution. The most notable effectiveness of a reaction in an aqueous solution seems to be that the selective aminolysis reaction of amino acids which have functional groups in their side chain (such as Arg, Glu, Lys, Cys, His, or Tyr) is possible only by controlling the pH of the reaction mixture. For this application, we focused on *p*-dialkylsulfoniophenols (HODASP·X^-) as water-soluble active ester reagents. These compounds generally exhibited high acidity[7)] and high solubility in water, due to the presence of the dialkylsulfonio group in the molecule which showed both hydrophilic and electron-withdrawing characteristics.

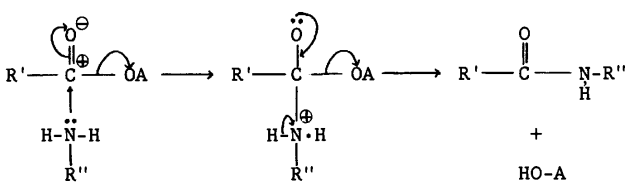

Fig. 1. Mechanism of aminolysis with active ester.

In this paper, we present such characteristic of HODASP·X^- as solubility in water or reactivity of their esters as well as fundamental information regarding applications to peptide syntheses, by making comparisons with other conventional HOSu or HONp active ester methods. Furthermore, the synthesis of FMRFamide, a molluscan neuropeptide, is also presented as an example application of the new method to a peptide synthesis in an aqueous solution.

Results and Discussion

pK_a of HODASP·X^- and Solubility of Their Esters in Water. Many kinds of HODASP·X^- were prepared in order to develop a water-soluble active ester reagent according to the procedure shown in Scheme 1. The pK_a values of HODASP·X^-, which have ClO_4^- as a counter anion (**1**—**7**), were measured in 30% aqueous ethanol and compared with that of HONp or other phenols having a sulfur group at the para position. Furthermore, the solubility in water of these compounds were examined (Table 1). The pK_a values of **1** and **2** were nearly the same level as that of HONp and their solubilities in water were more than 30%. Compounds **8**$_{a-d}$ were prepared by changing the counter anion of **1** (R_1=H, R_2=Me, and R_3=Me), and examined in the same manner described above. As shown in Table 1, these compounds (**8**$_{a-d}$) exhibited the same property as **1**. Owing to the pK_a and solubility in water, we judged **8**$_{a-d}$ and **1** to be

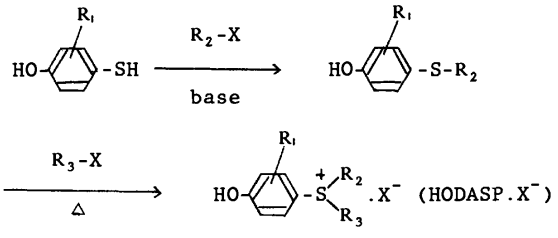

Scheme 1.

Table 1. Various Phenols Prepared

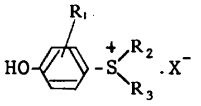

Run	R_1	R_2	R_3	X	Yield/%	Mp θ_m/°C (lit)[a]	Found(%) C	Found(%) H	Calcd(%) C	Calcd(%) H	R_{fs}[b]	pK_a	Solv.[c] (H_2O)
1	H	Me	Me	ClO_4	64	156—158 (157—159)	37.56	4.28	37.75	4.32	0.38	7.45	vs
2	H	Me	Et	ClO_4	49	79—83	40.41	4.78	40.25	4.84	0.38	7.45	vs
3	H	Et	Et	ClO_4	53	95—99	42.73	5.57	42.50	5.31	0.40	7.50	s
4	2-Me	Me	Me	ClO_4	64	111—114	40.54	4.53	40.25	4.84	0.41	7.75	s
5	3-Me	Me	Me	ClO_4	85	152—155	40.05	4.53	40.25	4.84	0.41	7.75	s
6	2,6-Me_2	Me	Me	ClO_4	73	174—176	42.17	5.47	42.50	5.31	0.45	7.85	s
7	2-Cl	Me	Me	ClO_4	74	128—131	33.54	3.23	33.24	3.46	0.38	5.80	s
8a	H	Me	Me	Cl	84	141—144	50.60	5.83	50.41	5.77	0.38	7.45	vs
8b	H	Me	Me	Br	81	145—146	40.64	4.81	40.88	4.68	0.36	7.41	vs
8c	H	Me	Me	TosO	74	77—79 (76—78)	52.78	5.94	52.33	5.81	0.42	7.43	vs
8d	H	Me	Me	$MeSO_4$	83	90—92 (92—93)	40.63	5.31	40.61	5.26	0.40	7.45	vs
9	HO-C$_6$H$_4$-SO_2Me				64	96—98 (96)	48.38	4.75	48.85	4.65	0.56	8.30	s
10	HO-C$_6$H$_4$-SCN				75	58—60 (62—63)	54.49	3.34	54.90	3.27	0.75	9.00	is
11	HO-C$_6$H$_4$-SMe				91	79—80 (76—79)	59.62	5.80	59.99	5.71	0.84	10.00	is
12	HO-C$_6$H$_4$-NO_2 (HONp)											7.40	is

Me=methyl, Et=ethyl, TosO=*p*-toluenesulfonate.

a) These literatures were described in Experimental. b) Solvent system: 1-Butanol-acetic acid-water (3 : 3 : 2).

c) Solubility in water at 25°C: vs: very soluble (above 30%), s: soluble, is: insoluble.

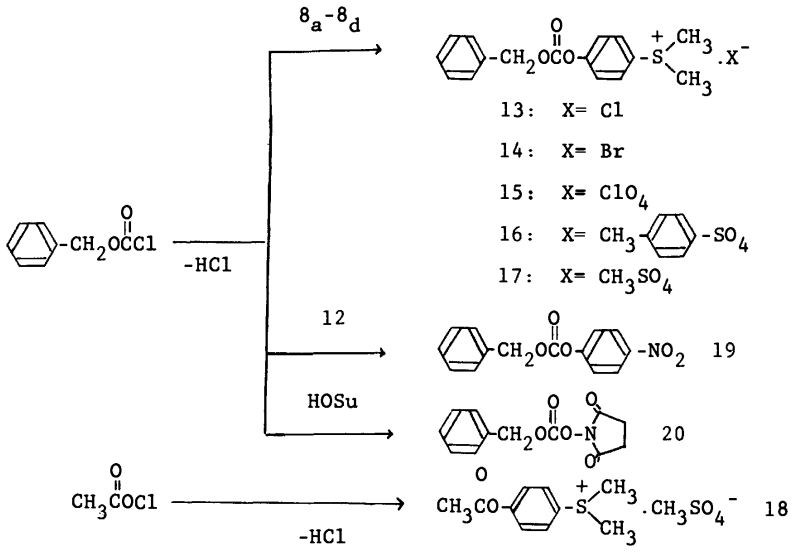

Scheme 2.

excellent reagents for the water-soluble active ester method. They were employed for the following investigation.

To examine the solubility of the esters derived from **1** and $\mathbf{8}_{a-d}$ in water, we prepared their benzyl carbonates using benzyloxycarbonyl chloride as benzyloxycarbonyl donor, according to the procedure shown in Scheme 2. The benzyl carbonates from HONp and HOSu were also prepared in the same procedure. The solubilities of these compounds in water and organic solvent are summarized in Table 2. A benzyl carbonate in which a methyl sulfate anion is present as a counter anion **17** exhibited a high solubility in water (more than 30%) in spite of the hydrophobic benzyl group in its molecule. Similarly, acetyl derivative **18** of $\mathbf{8}_d$, which was prepared from acetyl chloride and $\mathbf{8}_d$ was also very soluble in water. In addition, **17** and **18** were also very soluble in DMF, $CHCl_3$, and CH_3CN. These results indicate that the esters of $\mathbf{8}_d$ possess sufficient solubilities to be applied to a coupling reaction in an aqueous environment.

Reactivity of the Ester of HODMSP·$MeSO_4^-$($\mathbf{8}_d$) in Aminolysis. In order to compare the reaction of the benzyl carbonate (**17**) of HODMSP·$MeSO_4^-$ with that of the benzyl carbonates of HONp and HOSu, we examined their reaction rates with Gly in CH_3CN-H_2O at 25 °C (Fig. 2). As a result, it was found that **17** exhibited as a high reactivity as benzyl carbonates derived from HONp or HOSu. Furthermore, the water-soluble acylating agents derived from HODMSP·$MeSO_4^-$ were practically allowed to react with amino acids in aqueous solution (Table 3). As a result, the reaction of **17** or **18** with neutral amino acids proceeded in aqueous solution and the products were isolated in good yield. The acylation on the amino acids or peptides, which have a functional group on their side chain (such as Arg, Glu, Lys, Cys, or Gly-Tyr) was examined. The reaction with benzyl carbonate of HODMSP·$MeSO_4^-$ with Arg, Glu, His, Lys, or Gly-Tyr gave α-acylated compounds predominantly (at the controlled pH condition). Particularly, it was notable that reaction of **17** with Arg at pH 8.0 gave only an α-acylated derivative without any sub-reaction on guanidino group. However, the reaction of **17** with Cys or Lys gave an acylated product, mainly on a side functional group. This fact could explain why the reactivity of the functional group of the side chain was higher than that of the α-amino group. For the acylation of Tyr, Gly-Tyr was submitted to a test. As shown in Table 4, when the reaction proceeded at pH 6.0, the acylation was

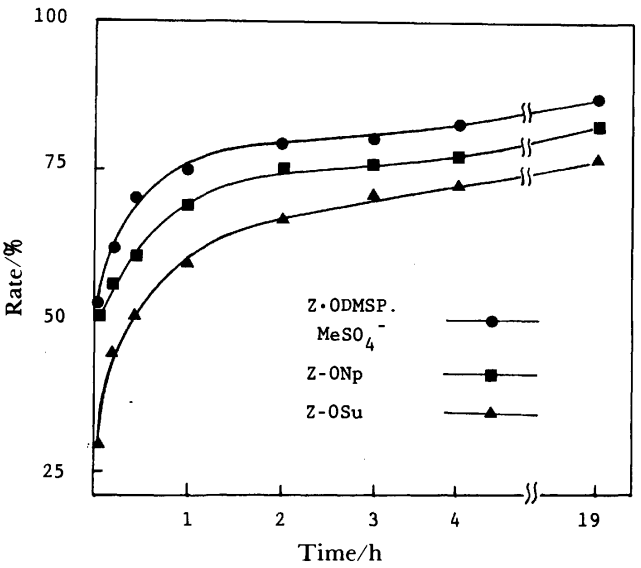

Fig. 2. Rates of aminolysis with Gly in CH_3CN-H_2O at 25 °C.

Table 2. Solubility of Esters Prepared

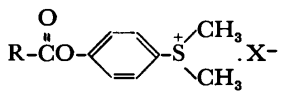

Run	R	X	Solubility	
			Water[a]	Organic solvent[b]
13	Benzyloxy	Cl	is	DMF, CH_3CN
14	Benzyloxy	Br	is	DMF, CH_3CN
15	Benzyloxy	ClO_4	is	DMF, CH_3CN
16	Benzyloxy	TosO	s(3%)	DMF, CH_3CN, $CHCl_3$
17	Benzyloxy	$MeSO_4$	vs(>30%)	DMF, CH_3CN, $CHCl_3$
18	Methyl	$MeSO_4$	vs(>30%)	DMF, CH_3CN, $CHCl_3$
19			is	Ether, AcOEt, THF
20			is	Ether, AcOEt, THF

TosO=*p*-toluensulfonate, Me=methyl, AcOEt=ethyl acetate.

a) Solubility in water at 25°C, vs=very soluble, s=soluble, is=insoluble (<1%). b) The solvents having solubility above 10% were listed.

predominantly inclined on the α-amino group of Gly moiety; while at pH 8.0, the acylation toward the phenolic hydroxy group of the Tyr moiety was increased. Because of the results described above, the esters of HODMSP·$MeSO_4^-$ were subjected to aminolysis in an aqueous solution to easily form an amide bond. In addition to this fact, a selective acylation was carried out at the suitable pH. We considered that the esters of HODMSP·$MeSO_4^-$ are quite useful as amino-protecting reagents.

Application of HODMSP·$MeSO_4^-$ Active Ester for Peptide Synthesis. In order to know whether the

Table 4. Acylation of Gly-Tyr with **17**

17 —(H-Gly-Tyr-OH; in 0.4 M phosphate buffer (pH 6 or 8) at 15°C, 10 h)→ Z-Gly-Tyr-OH **21** + Z-Gly-Tyr(Z)-OH **22**

pH	Product/% (HPLC)[a]		Yield of **21**/%
	21	**22**	
6	92.3	7.7	41
8	72.2	27.8	64

a) Product(%) means the ratio of **21** and **22** by HPLC.

Table 3. Preparation of Acylamino Acids

Acylating agent	Amino acid	Product	Reaction pH	Yield/%	Mpθ_m/°C(lit)	$[\alpha]_D$/°(c,solvent)(lit)	Ref.
17	Gly	Z-Gly-OH	10.0	72	118—120(120)	—	15
17	Ala	Z-Ala-OH	10.0	70	85—86(87)	−15(c2, AcOH) (−13.9)	16
18	Phe	Ac-Phe-OH	10.0	63	166—168(168)	+45(c2, AcOH) (+47)	17
17	Ser	Z-Ser-OH	9.0	85	118—119(119)	+6(c2, AcOH) (+5.9)	18
17	Arg	Z-Arg-OH	8.0	82	170—173(175)	−11(c2, 1M HCl) (−9.3)	19
17	Glu	Z-Glu-OH	9.0	62	120—122(120—121)	−10(c2, AcOH) (−7.9)	20
17	His	Z-His-OH	8.5	51	163—167(167)	−22(c2, 6M HCl) (−25)	21
17	Lys	H-Lys(Z)-OH	8.0	48	250—253(251—254)	+16(c1, 6M HCl) (+14.4)	22
17	Cys	H-Cys(Z)-OH	6.3	38	162—164(165)	−122(c1, DMF) (−134)	23

Table 5. Preparation of Protected Peptides

Active ester	Amine component	Product	Solvent (pH)	Yield/%	Mpθ_m/°C(lit)	$[\alpha]_D$/°(c,solvent)(lit)	Ref.
Z-Ala-ODMSP	Gly-OMe	Z-Ala-Gly-OMe	$CHCl_3$	74	99—100 (98—99)	−26(c1, MeOH) (−25)	24
Z-Phe-ODMSP	Leu-OMe	Z-Phe-Leu-OMe	$CHCl_3$	81	108—111 (110—111)	−23(c1, MeOH) (−25)	25
Boc-Leu-ODMSP	Gly-OMe	Boc-Leu-Gly-OMe	$CHCl_3$	63	128—130 (131)	−23(c1, DMF) (−21)	26
Z-Ala-ODMSP	Gly	Z-Ala-Gly-OH	H_2O(10.0)	62	132—134 (134—135)	−16(c1, EtOH) (−17)	27
Z-Ala-ONp	Gly	Z-Ala-Gly-OH	THF-H_2O	63	130—134 (134—135)	−16(c1, EtOH) (−17)	27
Z-Ala-OSu	Gly	Z-Ala-Gly-OH	THF-H_2O	47	132—134 (134—135)	−15(c1, EtOH) (−17)	27
Z-Phe-ODMSP	Pro	Z-Phe-Pro-OH	H_2O(10.0)	40	104—106 (105—106)	−63(c1, py) (−64)	28
Z-Phe-ONp	Pro	Z-Phe-Pro-OH	THF-H_2O	78	102—104 (105—106)	−58(c1, py) (−64)	28
Z-Phe-OSu	Pro	Z-Phe-Pro-OH	THF-H_2O	56	104—106 (105—106)	−70(c1, py) (−64)	28
Z-Ala-ODMSP	Ser	Z-Ala-Ser-OH	H_2O(9.0)	63	202—205 (205)	+27(c1, DMF) (+28)	29
Z-Ile-ODMSP	Glu	Z-Ile-Glu-OH	H_2O(9.0)	47	186—188 (189—190)	−23(c1, 0.5 M $KHCO_3$) (−21)	30
Z-Phe-ODMSP	His	Z-Phe-His-OH	H_2O(7.0)	43	181—184 (183—185)	−7(c1, DMF)	31
Z-Pro-ODMSP	Gly-Tyr	Z-Pro-Gly-Tyr-OH	H_2O(6.8)	41	102—103 (102)	−12(c1, EtOH) (−12)	32

-ODMSP= 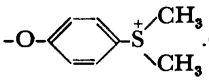 , py= pyridine.

active esters of HODMSP·$MeSO_4^-$ are applicable to peptide synthesis, some esters of the N-protected amino acids were prepared by direct condensation using DCC in CH_3CN. These esters, thus obtained, were very soluble in water, and were able to react with amine components for the formation of the amide bond (Table 5). When they were allowed to react with amine components in $CHCl_3$, the yield of the reaction products was always good and their purities were also quite satisfactory. In addition, the removal of unreacted active ester and the hydroxy compound resulting from the reaction was easy by an extraction procedure. Furthermore, these esters were also able to react with amino acids in aqueous solution in the presence of Et_3N at room temperature. The reaction proceeded smoothly, while the reaction of the HONp or HOSu active ester required an addition of THF. The products were isolated in good yield, and were comparable with those of HONp or HOSu active ester method. When HODMSP·$MeSO_4^-$ active esters were treated with Ser, His, Glu, and Gly-Tyr as amine components in aqueous solution, every reaction afforded the *N*-α-acylpeptides selectively.

Racemization Test. Izumiya et al. established the racemization test by ion-exchange chromatography.[33] We tried to determine the exact degree of racemization in the HODMSP·$MeSO_4^-$ active ester method by the same principle as their report. As a model peptide, L-Leu-L-Asp was prepared by this method and the ratio of diastereomeric dipeptide was measured by HPLC. The result was compared with that of the HONp or HOSu active ester method (Fig. 3). Figure 3 shows that racemization in our method, if any, was not detectable as well as in other methods. A further examination of the racemization was carried out in the coupling reaction of Z-Gly-L-Ala-OH and L-Leu (Table 6). The results suggested that the HODMSP·$MeSO_4^-$ active ester method is as useful as the existing active ester method in stepwise condensation using an N-protected amino acid with a urethane-type protecting group.

Application of HODMSP·$MeSO_4^-$ Active Ester for Synthesis of Biologically Active Peptide (Synthesis of FMRFamide). In order to evaluate the utility of the HODMSP·$MeSO_4^-$ active ester method, we tried to apply it to a synthesis of a tetra peptide amide, Phe-Met-Arg-Phe-NH_2 (FMRFamide) as an example of biologically active peptides.

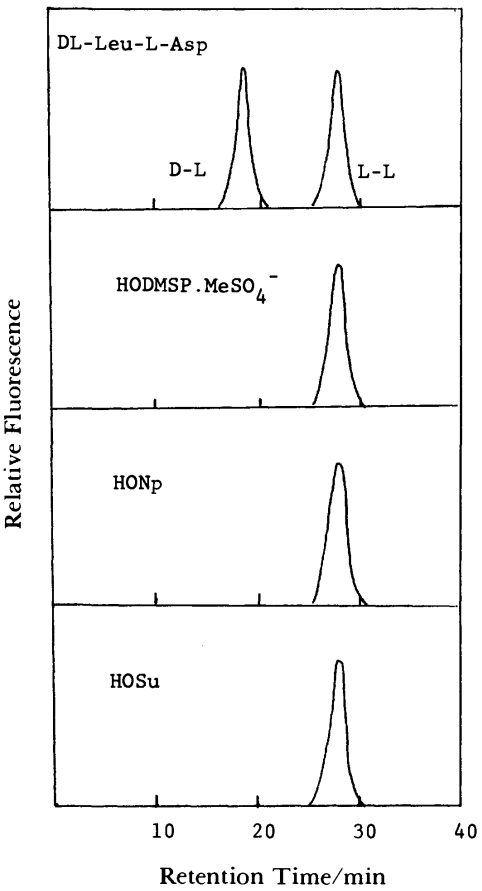

Fig. 3. Racemization test in Leu-Asp.

Table 6. Racemization Test in Gly-Ala-Leu

I. Z-Gly-L-Ala-OH + HO-A $\xrightarrow{DCC}$ Z·Gly-Ala-OA (L or D)

II. Z-Gly-Ala-OA (L or D) + L-Leu ⟶ Z-Gly-Ala-Leu-OH (L or D) $\xrightarrow{H_2/Pd}$ H-Gly-Ala-L-Leu-OH (L or D)

HO-A	I		II		D-L / L-L + D-L (%)
	Solv.	Temp/°C	Solv.	Temp/°C	
HOSu	THF	5	THF-H_2O	RT	16.4
HONp	THF	5	THF-H_2O	RT	50.9
HOPcp	THF	5	THF-H_2O	RT	40.7
HODMSP	CH_3CN	5	H_2O	RT	39.3

HODMSP= HO-C$_6$H$_4$-S$^+$(CH$_3$)$_2$.$CH_3SO_4^-$, Solv.= solvent, RT= room temperature.

FMRFamide was isolated from the ganglia of the clam *Macrocallista nimbosa* by Prince and Greenberg.[34] It has diverse effects on molluscan muscles and neurones.[35] For the synthesis of FMRFamide, the method of selective acylation to the Arg residue was employed. The synthetic route is shown in Fig. 4. Boc-Met-ODMSP·$MeSO_4^-$ (**25**), which was obtained by the esterification of Boc-Met-OH with HODMSP·$MeSO_4^-$, was allowed to react with H-Arg-Phe-NH_2·2AcOH (**24**), which was obtained

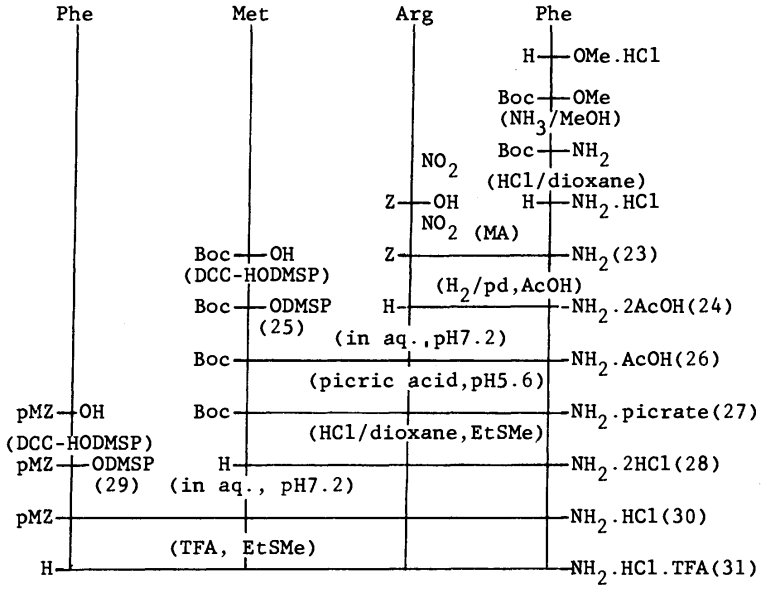

Fig. 4. Synthetic route of FMRFamide.

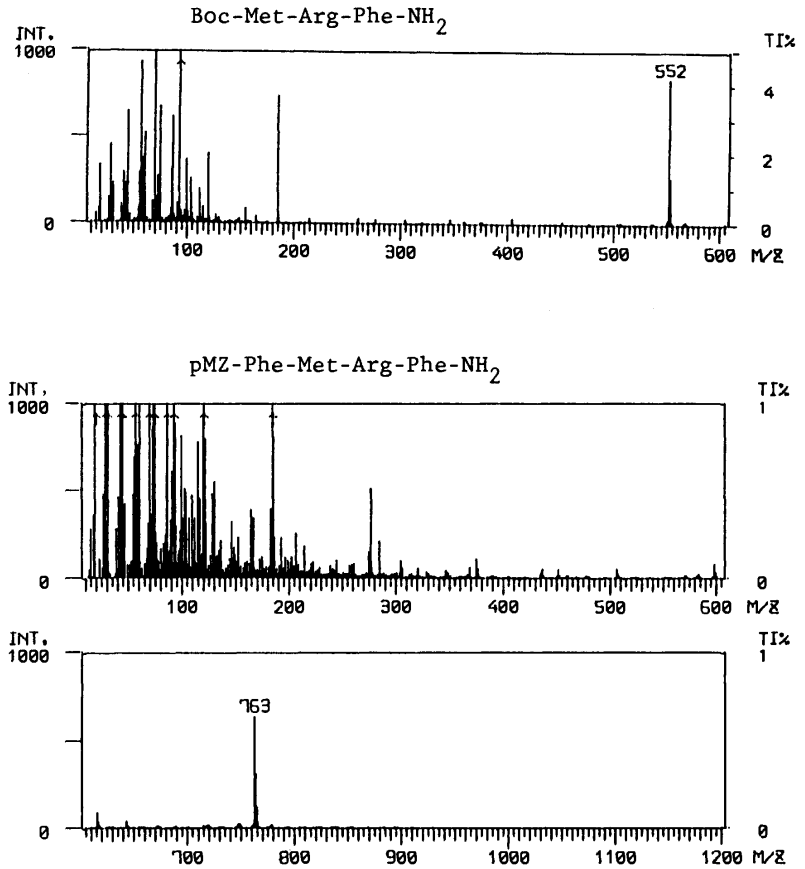

Fig. 5. Mass spectra in intermediates of FMRFamide.

from Z-Arg(NO_2)-OH and H-Phe-NH_2·2HCl by the conventional mixed anhydride method, followed by catalytic hydrogenation. The reaction proceeded on an aqueous solution with the presence of Et_3N at pH 7.2. After the isolation of Boc-Met-Arg-Phe-NH_2 as a picrate **27** by extraction with ethyl acetate from the reaction mixture, the Boc-group was removed by HCl in the presence of ethyl methyl sulfide, to yield tripeptide amide·2HCl (**28**). Then pMZ-Phe-ODMSP (**29**), which was obtained by the esterification of pMZ-Phe-OH with HODMSP·$MeSO_4^-$, was allowed to react with the tripeptide amide **28** (in the same manner as described regarding compound **26**) to yield pMZ-FMRFamide·HCl(**30**). After removing the pMZ-group of pMZ-FMRFamide (**30**) with trifluoroacetic acid in the presence of ethyl methyl sulfide, FMRFamide (**31**) was obtained. In the process of synthesizing **26** in aqueous solution, the product was not isolated, as such, owing to its high water-solubility. For this reason, this peptide was isolated and purified as a picrate. In the case of **30**, it could be extracted with ethyl acetate and purified smoothly. The homogeneity of these intermediates and the product was ascertained by TLC, elemental analysis, amino acid analysis, and mass spectra (Fig. 5).

The biological activity was measured on the anterior byssus retractor muscle of *Mytilus*, FMRFamide causes a relaxation or a contraction depending on its concentration.[36] At 10^{-8}—10^{-7} M (1 M=1 mol dm^{-3}), FMRFamide relaxes catch tension induced by acetylcholine (Ach). However, at a concentration higher than 10^{-7} M, it elicits a contraction by a direct action on the muscle fibers. From measurements of biological activity,[37] this synthesized FMRFamide was shown to possess the same activity as a natural one (Fig. 6).

All these results indicate that the HODMSP active ester method is promising for peptide syntheses in aqueous solution. We expect that our new active ester method will also be applicable for the chemical modifications of proteins.

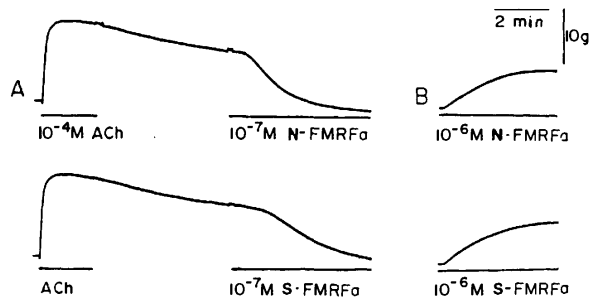

Fig. 6. Contractions and relaxations produced by synthesized FMRFamide and natural FMRFamide. A: Contractile effect, B: relaxing effect, N-FMRFa: natural FMRFamide, S-FMRFa: synthesized FMRFamide.

Experimental

All melting points were uncorrected. IR spectra were recorded on a Hitachi 269-30 infrared spectrometer. NMR spectra were measured on a Hitachi R-24B (60 MHz) spectrometer. The chemical shifts are given in δ (ppm) scale with tetramethylsilane as an internal standard. Mass spectra were obtained on a JEOL DX-300 spectrometer. The optical rotations were measured on a Union PM-101 polarimeter. TLC was carried out on Merck Silicagel G and Eastman chromagram sheet with solvent systems: R_{f_1}, 1-butanol-acetic acid-pyridine-water (4:1:1:2, v/v); R_{f_2}, $CHCl_3$-methanol (5:1, v/v); R_{f_3}, 1-butanol-acetic acid-water (3:3:2, v/v). Spots of materials possessing a free amino group on the TLC plate were detected by spraying with ninhydrin; those of amino group blocked materials were detected by spraying with 25% HBr in acetic acid and then ninhydrin. R_f spots of HODASP·X^- and its derivatives were visible with UV light. Amino acid analysis, detection of racemization, and other detection of substances were performed by HPLC using JASCO TRI ROTAR-V and UVIDEC-100V apparatus.

Preparation of HODASP·X^- and Other Phenols. **1**,[8] **8c**,[9] **8d**,[9] **9**,[10] **10**,[11] and **11**[12] were prepared by methods described in the literature. **2**—**7** and **8a**—**b** were prepared by reacting the corresponding thioether with a slight excess of dimethyl sulfate or diethyl sulfate. The reaction mixture was dissolved in ethanol; then, the ethanol solution was treated with an equimolar 70% $HClO_4$ below 5 °C. The resulting crystals were removed from the reaction mixture by filtration. The filter cake was washed with precooled ethanol and then recrystallized from ethanol or ethanol-ether. In the case of **8a** or **8d**, the ethanol solution was treated with 35% HCl or 15% HBr in place of 70% $HClO_4$. A white crystalline product was obtained. The precursor thioethers were prepared by the alkylation of the 4-mercaptophenols.

Preparation of Acylating Agents. Benzyl Carbonates: **19**[13] and **20**[14] were prepared by the methods described in the literature. **13**—**17** were prepared as follows. A mixture of the corresponding phenols and equimolar benzyloxycarbonyl chloride in CH_3CN was stirred at 5 °C. After 10 min, equimolar Et_3N was added. The reaction mixture was stirred at 5 °C for 1 h and then the precipitated triethylammonium chloride was removed from the reaction mixture by filtration. The filter cake was washed with CH_3CN, and combined filtrates were concentrated in vacuo to give the product either as a crystalline solid or as an oily residue, which was readily crystallized from ethyl acetate or ether.

13: Yield 84%; mp 68—69 °C; R_{f_3} 0.67; IR (KBr) 1762 cm^{-1} (ester C=O); ^{1}H NMR (DMSO-d_6) δ=3.15 (6H,s,-$\overset{+}{S}(CH_3)_2$), 5.28 (2H, s, -CH_2-), 7.44 (5H, s, C_6H_5), 7.63 (2H, d, J=8Hz, C_6H_4), 8.16 (2H, d, J=8Hz, C_6H_4); Found: C, 59.40; H, 5.19%; Calcd for $C_{16}H_{17}O_3SCl$: C, 59.19; H, 5.24%.

14: Yield 87%; mp 71—73 °C; R_{f_3} 0.65; IR (KBr) 1762 cm^{-1} (ester C=O); ^{1}H NMR (DMSO-d_6) δ=3.25 (6H, s, -$\overset{+}{S}(CH_3)_2$), 5.30 (2H, s, -CH_2-), 7.40 (5H, s, C_6H_5), 7.61 (2H, d, J=8Hz, C_6H_4), 8.12 (2H, d, J=8Hz, C_6H_4); Found: C, 52.21; H, 4.53%; Calcd for $C_{16}H_{17}O_3SBr$: C, 52.06; H, 4.61%.

15: Yield 72%; mp 141—143 °C; R_{f_3}, 0.54; IR (KBr) 1764 cm^{-1} (ester C=O); ^{1}H NMR (DMSO-d_6) δ=3.30 (6H, s, -$\overset{+}{S}(CH_3)_2$), 5.34 (2H, s, -CH_2-), 7.44 (5H, s, C_6H_5), 7.65 (2H, d, J=9Hz, C_6H_4), 8.15 (2H, d, J=8Hz, C_6H_4); Found: C, 49.21; H, 4.45%; Calcd for $C_{16}H_{17}O_7SCl$: C, 49.45; H, 4.37%.

16: Yield 80%; mp 155—157 °C; R_{f_3} 0.71; IR (KBr) 1770 cm^{-1} (ester C=O); ^1H NMR (DMSO-d_6) δ=2.20 (3H, s, CH_3-C_6H_5), 3.24 (6H, s, -$\overset{+}{S}(CH_3)_2$), 5.44 (2H, s, -CH_2-), 7.05—8.30 (13H, m, aromatic); Found: C, 60.31; H, 5.34%; Calcd for $C_{23}H_{24}O_6S_2$: C, 60.01; H; 5.21%.

17: Yield 81%; mp 78—80 °C; R_{f_3} 0.55; IR (KBr) 1760 cm^{-1} (ester C=O); ^1H NMR (DMSO-d_6) δ=3.30 (6H, s, -$\overset{+}{S}(CH_3)_2$), 3.42 (3H, s, CH_3SO_4), 5.35 (2H, s, -CH_2-), 7.41 (5H, s, C_6H_5), 7.60 (2H, d, J=9Hz, C_6H_4), 8.08 (2H, d, J=8Hz, C_6H_4); Found: C, 51.42; H, 4.58%; Calcd for $C_{17}H_{20}O_7S_2$: C, 51.51; H, 4.99%.

4-Acetoxyphenyldimethylsulfonium Methylsulfate: A mixture of **8**$_d$ and equimolar acetyl chloride in CH_3CN was stirred at 5 °C. After 10 min, equimolar Et_3N was added to it. A white crystalline product was obtained (as described for the preparation of benzyl carbonates). Yield 65%; mp 91—93 °C; R_{f_3} 0.56; IR (KBr) 1750 cm^{-1} (ester C=O); ^1H NMR (DMSO-d_6) δ=2.40 (3H, s, CH_3CO), 3.30 (6H, s, -$\overset{+}{S}(CH_3)_2$), 3.41 (3H, s, CH_3SO_4), 7.45 (2H, d, J=8Hz, C_6H_4), 8.10 (2H, d, J=8Hz, C_6H_4); Found: C, 42.43; H, 5.24%; Calcd for $C_{11}H_{16}O_6S_2$: C, 42.87; H, 5.19%.

Preparation of Active Ester of N-Protected Amino Acids. A typical example is as follows. **Z-Ala-ODMSP·$MeSO_4^-$**: Z-Ala-OH (2.23 g, 10 mmol) and **8**$_d$ (2.66 g, 10 mmol) were dissolved in CH_3CN and DCC (2.66 g, 10 mmol) was added to the solution below 0°C with stirring. After stirring overnight DCurea was filtered off and the filtrate was concentrated in vacuo to give an oily residue. The oily residue was washed with ether by decantation. Yield 87%; R_{f_1} 0.82; R_{f_2} 0.25; $[\alpha]_D^{20}$ −18° (*c*1, MeOH); IR (neat) 1760 cm^{-1} (ester C=O), 1700 cm^{-1} (amide C=O). **Z-Phe-ODMSP·$MeSO_4^-$**: Yield 90%; R_{f_1} 0.77; R_{f_2} 0.41; $[\alpha]_D^{20}$ −16° (*c*1, MeOH); IR (neat) 1764 cm^{-1} (ester C=O), 1700 cm^{-1} (amide C=O). **Boc-Leu-ODMSP·$MeSO_4^-$**: Yield 88%; R_{f_1} 0.77; R_{f_2} 0.38; $[\alpha]_D^{20}$ −29° (*c*1, MeOH); IR (neat) 1762 cm^{-1} (ester C=O), 1698 cm^{-1} (amide C=O). **Z-Pro-ODMSP·$MeSO_4^-$**: Yield 90%; R_{f_1} 0.61; R_{f_2} 0.30; $[\alpha]_D^{20}$ −62° (*c*1, MeOH); IR (neat) 1760 cm^{-1} (ester C=O), 1700 cm^{-1} (amide C=O). All these active esters were obtained as an oily product.

Reaction of 17 or 18 with Amino Acids or Peptide in Aqueous Solution. In the Case of Neutral Amino Acids: Amino acids and equimolar Et_3N were dissolved in water and equimolar **17** or **18** was added to the solution at room temperature with stirring. After 4 h, 20% citric acid was added to the solution and the pH of the solution was adjusted to 3.0. The mixture was extracted with ethyl acetate. The solution was washed with water and then dried over anhydrous sodium sulfate. The filtrate was concentrated in vacuo. The oily residue was crystallized with petroleum ether. **In the Case of Arg, Ser, His, Glu, Lys, Cys, and Gly-Tyr:** Each amino acid or peptide was dissolved in water and the pH of the solution was adjusted to 6.0—9.0 by addition of Et_3N. An equimolar amount **17** was added to a stirred solution below 20 °C, the pH being maintained automatically at the starting pH with Et_3N for 7 h. In the case of Ser or Glu, 20% citric acid was added to the solution and the pH of the solution was adjusted to 3.0. The mixture was extracted with ethyl acetate. The solution was washed with water and then dried over anhydrous sodium sulfate. The filtrate was concentrated in vacuo. The oily residue was crystallized with ether and petroleum ether. In the case of Arg, His, Lys, and Cys, each product was precipitated from the solution. The crystalline product was removed from the reaction mixture by filtration. Gly-Tyr was acylated using **17** in 0.4 M phosphate buffer (Na_2HPO_4-NaH_2PO_4) at pH 6.0 and 8.0 in a similar manner to the acylation of amino acids. The product which resulted from the reaction at each pH was isolated by extraction with ethyl acetate, respectively; then, the ratio of **21** and **22** in the product was determined by HPLC (column: Lichrosob PR-18; eluent: 85% MeOH). The results of acylation of amino acids and peptide in aqueous solution are shown in Tables 3 and 4.

Preparation of Protected Peptide Using HODMSP·$MeSO_4^-$ Active Ester. Reaction in $CHCl_3$: To a solution of HODMSP·$MeSO_4^-$ active ester of N-protected amino acid in $CHCl_3$, a solution of equimolar amino acid ester and Et_3N in $CHCl_3$ was added. The reaction mixture was stirred for 7 h at room temperature. After removing the solvent in vacuo, the residue was dissolved in ethyl acetate, and the solution was washed, successively, with water and 4% citric acid. The organic solution was dried over anhydrous sodium sulfate. The solution was concentrated to an oily residue which was crystallized by addition of ether and petroleum ether. **Reaction in H_2O: (A) In the Case of Neutral Amino Acid as Amine Component:** To a solution of HODMSP·$MeSO_4^-$ active ester of N-protected amino acid in water, a solution of equimolar amino acid and Et_3N in water was added. The reaction mixture was stirred at room temperature. After 12 h, 20% citric acid was added to the solution and the pH of the solution was increased to 3.0—4.0. The mixture was extracted with ethyl acetate. The solution was washed with water and dried over anhydrous sodium sulfate. The filtrate was concentrated in vacuo. The oily residue was crystallized with ether. **(B) In the Case of Ser, Glu, His, and Gly-Tyr as Amine Component:** These peptide were prepared with HODMSP·$MeSO_4^-$ active ester of N-protected amino acid in a similar manner to the acylation of amino acid having functional group in the side chain. Z-Ala-Ser-OH, Z-Ile-Glu-OH, and Z-Pro-Gly-Tyr-OH were obtained after extraction with ethyl acetate from the reaction mixture and crystallized from ether and petroleum ether. They were recrystallized from ethyl acetate. Z-Phe-His-OH was obtained after filtration from the reaction mixture. The results of these preparations are shown in Table 5.

Preparation of Protected Peptides Using HONp or HOSu Active Ester. To a solution of HONp or HOSu active ester of N-protected amino acid in THF, a solution of equimolar amino acid and Et_3N in water was added. The reaction mixture was stirred for 7 h at room temperature. After removing THF in vacuo, the aqueous solution was extracted with ethyl acetate to remove the unreacted active ester. 20% citric acid was added to the aqueous layer and the pH was adjusted to 3.0. The resulting oily product was extracted with ethyl acetate, and then washed with water. The organic solution was dried over anhydrous sodium sulfate. The filtrate was concentrated to an oily residue which was crystallized by the addition of ether.

Determination of the Rate of Aminolysis. Into a 50 ml volumetric flask was added a solution containing 2.0 mmol of an appropriate derivative **17**, **19**, or **20** in CH_3CN. To the solution having been heated at 25 °C was added a solution of 2.4 mmol of Gly in H_2O (50 ml). At predetermined time intervals, 1 ml aliquotes of the solution

were withdrawn and diluted with distilled water (total volume, 100 ml). The consumption of Gly was measured using HPLC (column: AApack Na; eluent: 0.1 M citrate buffer, pH 3.05, 60 °C). Each point in Fig. 3 represents a mean value of three runs.

Detection of Racemization. Leu-Asp: Boc-Lue-Asp-OH was prepared using HODMSP·$MeSO_4^-$ active ester, HONp active ester, or HOSu active ester. Each Boc-Leu-Asp-OH obtained was then treated with 4 M HCl in dioxane to afford Leu-Asp. A chromatographic detection of this diastereomeric dipeptide was carried out with HPLC (column: AApack Na; eluent: 0.1 M citrate buffer, pH 3.25, 60 °C). The detection of the dipeptide was performed by OPA detection system. Authentic samples of L-Leu-L-Asp and D-Leu-L-Asp were prepared by the usual manner. **Gly-Ala-Leu:** Z-Gly-D-Ala-OH and authentic samples of H-Gly-L-Ala-L-Leu-OH and H-Gly-D-Ala-L-Leu-OH were prepared by the methods described in the literature.[33] The dipeptide (Z-Gly-L-Ala-OH) was esterified with HODMSP·$MeSO_4^-$, HONp, HOSu, or HOPcp and DCC to afford the corresponding active ester. The conditions of esterification are summarized in Table 6. Each active ester, thus obtained, was allowed to react with L-Leu at room temperature overnight to give protected tripeptide. After catalytic hydrogenation to remove the protecting group, the tripeptide was analyzed according to the procedure in Leu-Asp.

Synthesis of FMRFamide. Z·Arg(NO_2)-Phe-NH_2 (23): A solution of Z-Arg(NO_2)-OH (3.53g, 10 mmol) and NMM (1.1 ml, 10 mmol) in THF (20 ml) was chilled to −5 °C, then ECF (1 ml,10 mmol) was added to it. After 10 min, a precooled solution of H-Phe-NH_2·HCl (2.00 g, 10 mmol) and Et_3N (1.4 ml, 10 mmol) in $CHCl_3$ (20 ml) was added. The reaction mixture was refrigerated for 1 h and then allowed to stand overnight at room temperature. The reaction mixture was concentrated in vacuo, and the residue was suspended in hot methanol (50 ml). The solid was filtered and washed with methanol; yield 4.24 g (85%); mp 218—221 °C; $[\alpha]_D^{20}$ −14° (*c* 0.5, DMF); R_{f_1} 0.91; R_{f_2} 0.41; Found: C, 55.56; H, 5.70; N, 19.38%; Calcd for $C_{23}H_{29}O_6N_7$: C, 55.34; H, 5.81; N, 19.63%. **H-Arg-Phe-NH_2·2AcOH (24):** Compound **23** (2.50 g, 5 mmol) in acetic acid (10 ml) was hydrogenated in the presence of palladium black. The filtrate was concentrated in vacuo and the residue was crystallized from ether as hygroscopic crystals; yield 1.08 g (98%); $[\alpha]_D^{20}$ +9° (*c* 1, H_2O); R_{f_1} 0.41; R_{f_3} 0.75. **Boc-Met-ODMSP·$MeSO_4^-$ (25):** To a chilled solution of Boc-Met-OH (2.49 g, 10 mmol) and HODMSP·$MeSO_4^-$ (2.66 g, 10 mmol) in CH_3CN (80 ml), DCC (2.06 g, 10 mmol) was added. The reaction mixture was kept overnight at 0 °C and the DCurea which formed was filtered off. The filtrate was concentrated in vacuo, and the residual oil was washed with ether by decantation; yield 3.93 g (80%); $[\alpha]_D^{20}$ −30° (*c* 1, MeOH); R_{f_1} 0.82; R_{f_2} 0.34. **Boc-Met-Arg-Phe-NH_2·picrate (27):** Compound **24** (0.88 g, 2 mmol) was dissolved in H_2O and the pH of the solution was adjusted to 7.2 by addition of Et_3N. Boc-Met-ODMSP·$MeSO_4^-$ (0.99 g, 2 mmol) was added to the stirred solution below 20 °C, the pH being automatically maintained at 7.2 with Et_3N. After 12 h, 1% picric acid was added to the solution and the pH of the solution was adjusted to 5.6. A yellow precipitate was filtered off and it was dissolved in ethyl acetate (100 ml). The solution was successively washed with 4% sodium hydrogencarbonate, 4% citric acid and water, and then dried over anhydrous sodium sulfate. The solution was concentrated to an oily residue which was crystallized by the addition of ether. It was recrystallized from $CHCl_3$; yield 0.75 g (45%); mp 110 °C (decomp); $[\alpha]_D^{20}$ −14° (*c* 0.5, DMF); R_{f_1} 0.83; R_{f_2} 0.32; Found: C, 46.84; H, 5.81; N, 17.95%; Calcd for $C_{25}H_{41}O_5N_7S·C_6H_3N_3O_7·1/2H_2O$: C, 47.17; H, 5.70; N, 17.74%; MS *m/z* 552 (M^+H); Amino acid ratios in acid hydrolyzate: Arg 0.94, Met 0.89, Phe 1.00. **H-Met-Arg-Phe-NH_2·2HCl (28):** To a solution of **27** (0.78 g, 1 mmol) and ethyl methyl sulfide (1 ml) in dioxane (5 ml), 4.1 M HCl in dioxane (5 ml) was added. The reaction mixture was allowed to stand at room temperature. After 2 h, the solution was concentrated in vacuo. The residue was crystallized with ether; yield 0.47 g (90%); mp 140 °C (decomp); $[\alpha]_D^{20}$ +10° (*c* 0.5, H_2O); R_{f_1} 0.52; R_{f_3} 0.74; Found: C, 49.03; H, 6.87; N, 20.01%; Calcd for $C_{20}H_{33}O_3N_7S.2HCl$: C, 49.25; H, 6.97; N, 20.09%. Amino acid ratios in acid hydrolyzate: Arg 0.96, Met 0.84, Phe 1.00. **pMZ-Phe-ODMSP·$MeSO_4^-$ (29):** pMZ-Phe-OH (3.29 g, 10 mmol) and HODMSP·$MeSO_4^-$ (2.66 g, 10 mmol) were coupled by the same method as **25**. The oily product was obtained; yield of the oily product 5.20 g (90%); $[\alpha]_D^{20}$ −7° (*c* 1, MeOH); R_{f_1} 0.85; R_{f_2} 0.51. **pMZ-Phe-Met-Arg-Phe-NH_2 (30):** Compound **28** (0.52 g, 1 mmol) was dissolved in H_2O (10 mmol) and the solution was adjusted to 7.2 by addition of Et_3N. pMZ-Phe-ODMSP.$MeSO_4^-$ (0.69 g, 1.2 mmol) was added to the stirred solution below 20 °C, the pH being maintained automatically at 7.2 with Et_3N. After 12 h, the mixture was extracted with ethyl acetate (100 ml). The solution was successively washed with 4% sodium hydrogencarbonate, 4% citric acid, and water, and then dried over anhydrous sodium sulfate. The solution was concentrated to a crystalline residue. It was recrystallized from methanol; yield 0.33 g (41%); mp 190 °C (decomp); $[\alpha]_D^{20}$ −20° (*c* 0.5, DMF); R_{f_1} 0.80; R_{f_3} 0.91; Found: C, 55.91; H, 6.31; N, 13.47%; Calcd for $C_{38}H_{50}O_7N_8S·HCl·H_2O$: C, 55.87; H, 6.49; N, 13.71%. MS *m/z* 763 (M^+H); amino acid ratios in acid hydrolyzate: Arg 0.95, Met 0.87, Phe 2.00. **H-Phe-Met-Arg-Phe-NH_2 (FMRFamide)·HCl·TFA (31):** Compound **30** (0.4 g, 0.5 mmol) and ethyl methyl sulfide (0.5 ml) were dissolved in TFA (5 ml). The reaction mixture was allowed to stand at room temperature. After 2 h, the solution was concentrated in vacuo. The residue was crystallized with ether; yield 0.37 g (92%); mp 164 °C (decomp); $[\alpha]_D^{20}$ +8° (*c* 0.5, H_2O); R_{f_1} 0.76; R_{f_3} 0.85; Found: C, 51.38; H, 5.94; N, 15.32%; Calcd for $C_{29}H_{42}O_4N_8S.CF_3COOH·HCl·1/2H_2O$: C, 51.62; H, 6.10; N, 15.53%; amino acid ratios in acid hydrolyzate: Arg 0.92, Met 0.90, Phe 2.00.

The authors wish to express their thanks to Professor Yojiro Muneoka of Hiroshima University for biological assays and helpful discussions. We also would like to thank Mr. Masataka Shoji of Ajinomoto Co. Inc., for the mass spectral data.

References

1) The abbreviations recommended by the IUPAC-IUB commission of Biochemical Nomenclature (*J. Biol. Chem.*, **247**, 977 (1972)) have been used. Amino acid symbols except

glycine denote the L-configuration. Additional abbreviations: DCC, dicyclohexylcarbodiimide; DCurea, *N,N'*-dicyclohexylurea; HONp, *p*-nitrophenol; HOSu, *N*-hydroxysuccinimide; ECF, ethyl chloroformate; THF, tetrahydrofuran; MeOH, methanol; Et_3N, triethylamine; NMM, *N*-methylmorpholine; MA,mixed anhydride; TFA, trifluoroacetic acid; py, pyridine.

2) M. Bodanszky and V. du Vigneaud, *J. Am. Chem. Soc.*, **81**, 5688 (1959).

3) J. Kovace, M. Q. Ceperini, C. A. Dupraz, and G. N. Schmit, *J. Org. Chem.*, **32**, 3696 (1967).

4) G. W. Anderson, J. E. Zimmerman, and F. Callahar, *J. Am. Chem. Soc.*, **85**, 3039 (1967).

5) M. Fujino, S. Kobayashi, M. Obayashi, T. Fukuda, S. Shinagawa, and O. Nishimura, *Chem. Pharm. Bull.*, **22**, 1857 (1974).

6) T. Tsuji, S. Okusada, M. Maeda, and K. Kawasaki, *Chem. Pharm. Bull.*, **34**, 2214 (1986).

7) S. Oae and C. C. Price, *J. Am. Chem. Soc.*, **80**, 3425 (1958).

8) J. K. Coward and W. D. Sweet, *J. Org. Chem.*, **36**, 2337 (1971).

9) F. G. Bordwell and P. J. Boutan, *J. Am. Chem. Soc.*, **78**, 87 (1956).

10) J. Yates and E. Haddock, Brit. Patent, 1128217 (1958).

11) F. G Bordwell and P. J. Bautan, *J. Am. Chem. Soc.*, **78**, 854 (1956).

12) Nippon Kayaku Co. Ltd., Jpn. Patent, 9134 (1967).

13) M. C. Khosla, F. M. Bumpus, and R. R. Smery, *Indian J. Chem.*, **5**, 279 (1967).

14) M. Frankel, D. Ladkany, C. Gilon, and Y. Wolman, *Tetrahedron Lett.*, **1966**, 4765.

15) M. Bergman and L. Zervas, *Ber.*, **65**, 1192 (1932).

16) M. Hunt and V. du Vigneaud, *J. Biol. Chem.*, **124**,699 (1938).

17) B. Weinstein and A. E. Pritchard, *J. Chem. Soc., Perkin Trans. 1*, **1972**, 1015.

18) E. Wünch and J. Jentsch, *Chem. Ber.*, **97**, 2490 (1964).

19) R. A. Boissonnas, S. Guttman, R. L. Huguenin, P. A. Jaquenoud, and E. Sandrin, *Helv. Chim. Acta*, **41**, 1867 (1958).

20) E. Wünch, and A. Zwick, *Chem. Ber.*, **97**, 2497 (1964).

21) A. Patchornik, A. Berger, and E. Katchalski, *J. Am. Chem. Soc.*, **79**, 6416 (1957).

22) S. Kuwata, and H. Watanabe, *Bull. Chem. Soc. Jpn.*, **38**, 676 (1965).

23) E. Scoffone, R. Rocchi, G. Vidal, A. Scatturine, and F. Marchiori, *Gazz. Chim. Ital.*, **94**, 743 (1964).

24) L. Zervas, D. Borovas, and E. Gazis, *J. Am. Chem. Soc.*, **85**, 3660 (1963).

25) Z. Pravda, K. Poduska, and K. Blaha, *Collect. Czech. Chem. Commun.*, **29**, 2626 (1964).

26) A. S. Dutta and J. S. Morley, *J. Chem. Soc. C*, **1971**, 2896.

27) F. H. C. Stewart, *Aust. J. Chem.*, **21**, 2543 (1968).

28) S. Sakakibara and M. Itoh, *Bull. Chem. Soc. Jpn.*, **40**, 656 (1967).

29) N. Yanaihara, C. Yanaihara, M. Sakagami, T. Nakajima, T. Nakayama, and K. Matsumoto, *Chem. Pharm. Bull.*, **21**, 616 (1973).

30) D. S. Kemp, S. J. Worbel, Jr., S. W. Wang, Z. Bernstein, and J. Rebek, Jr., *Tetrahedron*, **30**, 3677 (1974).

31) G. Losse and G. Muler, *Chem. Ber.*, **94**, 2768 (1961).

32) I. Z. Siemion, *Rczniki Chem.*, **38**, 811 (1964).

33) N. Izumiya, M. Muraoka, and H.Aoyagi, *Bull. Chem. Soc. Jpn.*, **44**, 3391 (1971).

34) A. D. Price and J. M. Greenberg, *Science*, **197**, 670 (1977).

35) S. D. Painter and J. M. Greenberg, *Biol. Bull.*, **162**, 311 (1982).

36) J. M. Greenberg and A. D. Price, *Am. Zool.*, **19**, 163 (1979).

37) We asked Professor Yojiro Muneoka of Hiroshima University to measured the biological activity. He measured these activities according to his report. Y. Muneoka and H. Saitoh, *Comp. Biochem. Physiol.*, **85c**, 207 (1986).

Redox-Photosensitized Reactions. XV.[1] Photosensitized and Direct Photolytic Isomerizations of the Tetrahydro Dimers of 1-Benzylnicotinamide

Osamu ISHITANI, Shozo YANAGIDA, Setsuo TAKAMUKU, and Chyongjin PAC*
Department of Chemical Process Engineering, Faculty of Engineering, Osaka University, Suita, Osaka 565
(Received January 16, 1987)

The photosensitization by either $[ReBr(bpy)(CO)_3]$ or $[Ru(bpy)_3]^{2+}$ (bpy=2,2′-bipyridine) resulted in the isomerization of 1,1′-dibenzyl-1,1′,4,4′-tetrahydro-4,4′-binicotinamide (**1**) and 1,1′-dibenzyl-1,1′,4,6′-tetrahydro-4,6′-binicotinamide (**2**) to give a common mixture of **1**, **2**, and the diastereoisomer of **2** (**3**) in a 2:2:1 ratio at a photostationary state, while either direct photoexcitation or thermal activation effected only the isomerization of **2** to **1** but not at all the retro isomerization.

The pyridine nucleotide coenzymes $(NAD(P)^+/NAD(P)H)$ reveal unique redox capabilities of undergoing specific transfer of a hydride equivalent (or two electrons) with a variety of substrates.[2] However, one-electron redox reactions can also very often occur with the coenzymes in the absence of oxido-reduction enzymes and particularly with their models in homogeneous solution, giving the corresponding tetrahydrobipyridines (NAD_2)[3-7] which are considered to be dead-end products incapable of undergoing two-electron redox reactions. Therefore, little has been investigated on chemical properties of NAD_2.

Nevertheless, it is certainly of chemical significance to explore chemistry of NAD_2 because of the unique dihydropyridyl structures and because of potential electron-donating nature. From this point of view, we have investigated chemical behaviors of NAD_2 using 1,1′-dibenzyltetrahydrobinicotinamides (**1**—**3**) which are selectively formed either by one-electron reduction of 1-benzylnicotinamide (BNA^+), a typical NAD^+ model, or by one-electron oxidation of 1-benzyl-1,4-dihydronicotinamide (BNAH), a typical NADH model. This paper deals with photochemical isomerizations of the 1,1′-dibenzyl-1,1′,4,4′-tetrahydro-4,4′-binicotinamide (**1**) and the diastereomeric isomers of 1,1′-dibenzyl-1,1′,4,6′-tetrahydro-4,6′-binicotinamide (**2** and **3**) (Scheme 1).

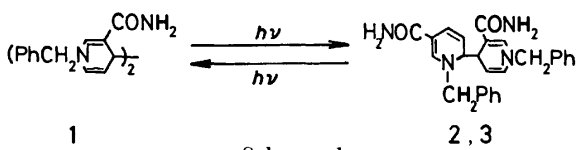

Scheme 1.

Results and Discussion

The zinc reduction of 1-benzylnicotinamide gave a mixture of the corresponding tetrahydrobinicotinamides,[3] from which one of the 4,4′-bonded diastereomers **1** and one of the 4,6′-bonded diastereomers **2** were obtained in purities enough for the present photochemical investigation, while another diastereomer of **2** (**3**) could be isolated only in a small amount. On the other hand, what appears to be the other isomer of **1**[3] was able to be detected by HPLC but not isolated because of its minor formation and difficulties of the isolation. Therefore, we used **1** and **2** as the starting materials and *N*,*N*-dimethylformamide (DMF) as the solvent.

Irradiation of a deaerated solution of **1** (2.5 mM†) and $[ReBr(bpy)(CO)_3]$ (0.8 mM) at 436 nm resulted in the isomerization of **1** to **2** and **3**, thus giving a 2:2:1 mixture of **1**, **2**, and **3** at a photostationary state (Fig. 1). The photosensitized isomerization of **2** to **1** and **3** again occurred to reach an identical photostationary state. Similarly, $[Ru(bpy)_3]^{2+}$ was effectively used as the photosensitizer for the isomerizations while the irradiation was carried at >470 nm. In all the runs, HPLC analyses showed the formation of a few common products in small amounts at retention times identical with those of the minor products in the zinc reduction of BNA^+.[3] Table 1 summarizes the photostationary-state ratios of **1**, **2**, and **3**.

The efficient photosensitized isomerization of **1** to **2**

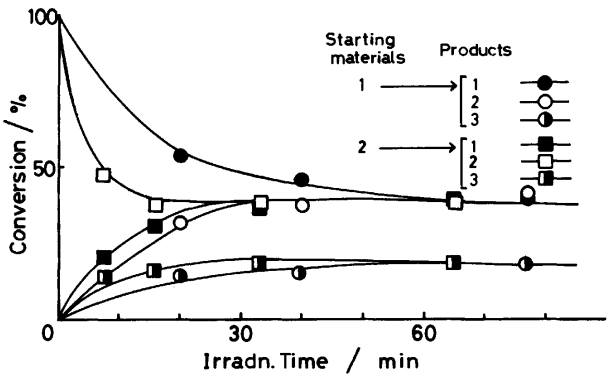

Fig. 1. Time-conversion plots for the $[ReBr(bpy)(CO)_3]$-photosensitized isomerization of **1** and **2** at 436 nm; [**1**] or [**2**]=2.5 mM and $[[ReBr(bpy)(CO)_3]]$= 0.8 mM.

† 1 M=1 mol dm^{-3}.

Table 1. Photosensitized Isomerization of **1** and **2** by $[ReBr(bpy)(CO)_3]$ and $[Ru(bpy)_3]^{2+}$ [a]

Starting Material	Sensitizer[b]	Irradn. Time/min	Yield[c]/%			$k_q\tau$[d]	k_q[e]
			1	**2**	**3**	M^{-1}	$M^{-1}\,s^{-1}$
1	$[ReBr(bpy)(CO)_3]$	35	40	40	19	182	3.7×10^9
1	$[Ru(bpy)_3]^{2+}$	90	25	28	12	1340	1.4×10^9
2	$[ReBr(bpy)(CO)_3]$	35	36	39	18	571	1.2×10^{10}
2	$[Ru(bpy)_3]^{2+}$	25	32	29	14	680	7.3×10^8

a) For deaerated DMF solutions containing **1** or **2** (2.5 mM) and the sensitizers (0.8 mM). b) Irradiated at 436 nm for the $[ReBr(bpy)(CO)_3]$ runs and at >470 nm for the $[Ru(bpy)_3]^{2+}$ runs. c) Based on the **1** or **2** used. d) Slopes of linear Stern-Volmer plots for quenching of the sensitizer-luminescence by **1** or **2** in deaerated DMF solutions at 20 °C. e) Calculated from the $k_q\tau$ values in DMF using the observed luminescence lifetimes of $[ReBr(bpy)(CO)_3]$ (49 ns) and $[Ru(bpy)_3]^{2+}$ (928 ns).

Table 2. Isomerization of **1** and **2** by Direct Photolysis and Thermal Activation[a]

Starting Material	Reaction[b] Condition	Reaction Time/min	Yield[c]/%		
			1	**2**	**3**
1	Photolysis	100	95	Trace	0
2	Photolysis	130	73	11	Trace
1	60°C	960	94	Trace	Trace
1	100°C	300	56	Trace	Trace
2	60°C	960	2	78	1
2	100°C	300	14	2	1

a) For deaerated DMF solutions containing **1** or **2** (2.5 mM). b) "Photolysis" means the reactions by direct photoexcitation at 436 nm, whereas the temperatures indicate the reaction temperatures for the thermal reactions in the dark. c) Based on the **1** or **2** used.

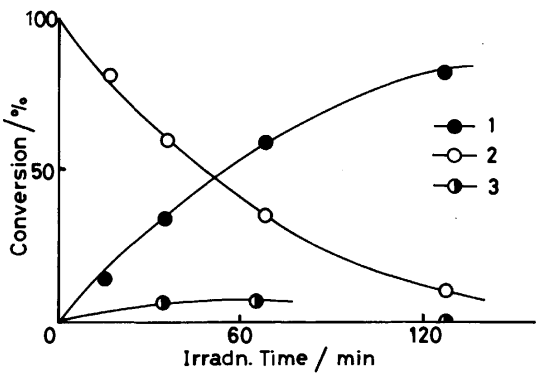

Fig. 2. Time-conversion plots for the direct photolytic isomerization of **2** at 436 nm; [**2**]=2.5 mM.

and **3** is of synthetic and mechanistic interest, since either thermal[3] or direct photoexcitation can effect the one-way isomerization from **2** to **1** for the most part. Upon heating a DMF solution of **2** at 60 or 100 °C, a reaction proceeded to give **1** only in poor yields along with substantial amounts of untractable materials, while little isomerization of **1** to either **2** or **3** occurred at 60 °C and even at 100 °C being accompanied by substantial consumption of **1**, as shown in Table 2. This means that the isomerization of **1** and **2** is only a negligible or minor pathway in the ground-state reactions. On the other hand, direct photoexcitation of **2** in DMF at 436 nm resulted in the isomerization to **1** along with very minor formation of **3** (Fig. 2), while **1** was found to be quite stable under the irradiation at 436 nm. In the excited state(s), **2** might cross to a reactive state or might give reactive intermediates while physical and chemical decays to the original ground state should predominantly occur with **1**.

For mechanistic elucidation, it shoud be noted that either chemical or electrochemical one-electron reduction of BNA^+ affords a mixture of **1**, **2**, and **3** in comparable amounts along with the other minor isomers in ratios depending on reaction conditions.[3] We also observed that a 2:2:1 mixture of **1**, **2**, and **3** is quantitatively formed by the photosensitized one-electron reduction of BNA^+ with triethylamine.[8] It is therefore conceivable that the formation of mixtures of **1**, **2**, and **3** should arise as the consequences of kinetic-controlled dimerization of the 1-benzyl-3-carbamoyldihydropyridyl radicals (BNA·), since BNA· is certainly a common intermediate in the chemical, electrochemical, and photochemical one-electron reductions of BNA^+.

These arguments strongly suggest that the photosensitized isomerizations of **1** and **2** involve BNA· as a key intermediate. In this regard, it should be

noted that the luminescence of [ReBr(bpy)(CO)$_3$] or [Ru(bpy)$_3$]$^{2+}$ is efficiently quenched by **1** and **2** at the rate constants listed in Table 1. In a previous paper,[9] we demonstrated that the luminescence of [Ru(bpy)$_3$]$^{2+}$ is quenched by BNAH at 2.0×10^8 M^{-1} s^{-1} in DMF by way of electron transfer from the quencher to the ruthenium(II) complex. Therefore, it is reasonable to assume that electron transfer from **1** and **2** to the luminescent excited-state sensitizers occurs to initiate the isomerizations, since **1** and **2** have the dihydronicotinamide chromophores. The dimeric structures of **1** and **2** imply that these compounds should be stronger electron donors compared with BNAH, a presumption being in accord with the greater quenching rate constants for **1** and **2**. Furthermore, the observation that the luminescence quenching is more efficient for [ReBr(bpy)(CO)$_3$] than for [Ru(bpy)$_3$]$^{2+}$ can be reasonably understood according to the electron-transfer mechanism, since the excited-state reduction potential of [ReBr(bpy)(CO)$_3$] is more positive by ca. 0.24 eV than that of [Ru(bpy)$_3$]$^{2+}$.[10,11] An alternative mechanism involving triplet-energy transfer from the sensitizers to **1** and **2** is unlikely to operate in the photosensitized isomerizations, since such organic triplet photosensitizers as coronene and chrysene were found to be totally ineffective.

According to the above discussion, we propose a possible mechanism for the photosensitized isomerizations in Eqs. 1—5. The key mechanistic sequence is the fragmentation of BNA$_2^{+\cdot}$ (**1**$^{+\cdot}$ and **2**$^{+\cdot}$) to BNA$\cdot$ and BNA$^+$ (Eq. 3) followed by back electron transfer from S$^{-\cdot}$ ([ReBr(bpy)(CO)$_3$]$^{-\cdot}$ or [Ru(bpy)$_3$]$^+$) to BNA$^+$ to generate BNA$\cdot$ (Eq. 4). It can be predicted that electron transfer from S$^{-\cdot}$ to BNA$^+$ (Eq. 4) rapidly occurs since the reduction potentials of [ReBr(bpy-(CO)$_3$] (-1.35 V vs. SCE in acetonitrile)[12] and [Ru-(bpy)$_3$]$^{2+}$ (-1.36 V)[13] are substantially more negative than that of BNA$^+$ (ca. -1.0 V).[14] The final products are thus formed by free-radical coupling of BNA$\cdot$ (Eq. 5). Since material balances are excellent in the photosensitized isomerizations, the fragmentation of BNA$_2^{+\cdot}$ (Eq. 3) appears to be efficient, thus predominating over Eq. 2.

$$S + BNA_2 \overset{h\nu}{\rightleftharpoons} S^{-\cdot} + BNA_2^{+\cdot} \quad (1)$$

$$BNA_2^{+\cdot} \longrightarrow \text{Others} \quad (2)$$

$$BNA_2^{+\cdot} \longrightarrow BNA^+ + BNA\cdot \quad (3)$$

$$S^{-\cdot} + BNA^+ \longrightarrow S + BNA\cdot \quad (4)$$

$$2BNA\cdot \longrightarrow \mathbf{1} + \mathbf{2} + \mathbf{3} \quad (5)$$

(S=[ReBr(bpy)(CO)$_3$] or [Ru(bpy)$_3$]$^{2+}$; BNA$_2$=**1**—**3**)

On the other hand, the participation of BNA$\cdot$ appears to be negligible or minor in the isomerizations of ground-state and excited-state BNA$_2$, since only the one-way isomerization from **2** to **1** can occur. Furthermore, the free-radical mechanism disagrees with the negligible formation of **3** from **2** upon either thermal activation or direct photoexcitation, since the isomerization of **2** to **3** should comparably occur, at least at an early stage of the reactions, by this mechanism. Presumably, the photoisomerization of **2** might mainly proceed via 1,3-sigmatropic migration of the 1,4-dihydropyridinyl moiety from the 6′ position to the 4′ position of the 1,6-dihydronicotinamide ring, which is an orbital-symmetry-allowed process in the excited state (Scheme 2).[15] The reverse sigmatropic migration (i.e. **1** to **2**) would be thermodynamically unfavorable. According to this mechanism, it can be reasonably understood that the thermal isomerization of **2** occurs only in poor yields, since a suprafacial 1,3-sigmatropic rearrangement is forbidden in the ground state.

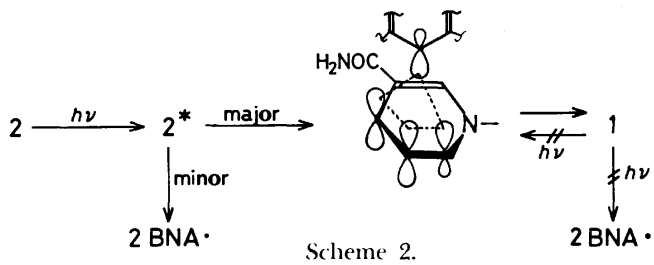

Scheme 2.

Summary

It was found that the isomerizations of **1** and **2** occur upon photosensitization by [ReBr(bpy)(CO)$_3$] or [Ru(bpy)$_3$]$^{2+}$ to give a common 2:2:1 mixture of **1**, **2**, and **3** at a photostationary state. On the other hand, direct photoexcitation resulted in the one-way isomerization from **2** to **1** along with only minor formation of **3**; **1** was found to be photostable. Although **2** was reported to isomerize to **1** by thermal activation,[3] we confirmed that the isomerization can occur only as a minor pathway in the ground-state reactions.

The photosensitized isomerzations of **1** and **2** were discussed in terms of the following chemical sequences; (1) electron transfer from **1** or **2** to the luminescent excited state sensitizers, (2) bond cleavage of **1**$^{+\cdot}$ and **2**$^{+\cdot}$ to generate BNA$\cdot$ and BNA$^+$, (3) back electron transfer from the one-electron reduced sensitizers to BNA$^+$, and (4) the free-radical dimerization of BNA$\cdot$ to give a mixture of **1**, **2**, and **3** for the most part. According to this mechanism, a significant point is that both **1**$^{+\cdot}$ and **2**$^{+\cdot}$ are chemically reactive to undergo the fragmentation to BNA$\cdot$ and BNA$^+$. On the other hand, a 1,3-sigmatropic mechanism was suggested for the direct photolytic isomerization of **2** to **1**.

Experimental

Materials. The sensitizers, [ReBr(bpy)(CO)$_3$][16] and [Ru-(bpy)$_3$]Cl$_2$·6H$_2$O,[17] were prepared and purified according to

the literature methods. The preparation and isolation of **1**, **2**, and **3** was carried out according to the Ohnishi's method[3] utilizing the reduction of 1-benzyl-3-carbamoylpyridinium chloride with activated zinc powder in the presence of copper(II) sulfate. The isolated tetrahydrobipyridines, particularly **2** and **3**, were carefully recrystallized from deaerated DMF-H_2O solution below room temperature in order to avoid the contamination of untractable materials due to thermal decomposition and oxidation. The ^1H NMR spectra of the isolated samples were essentially identical with the published data.[3]

Analytical Methods. Both the disappearance and the formation of 1, **2**, and **3** were followed by HPLC, which was carried out on a Chemicosorb 7-ODS-H column with a Yanaco M-315 spectromonitor working at 355 nm. The mobile phase was a 6:4 (v/v) mixture of methanol and an NaOH-KH_2PO_4 buffer solution (pH 7) at a flow rate of 0.8 $cm^3\ min^{-1}$. A Hitachi 850 spectrofluorometer was used for luminescence-quenching experiments; the ruthenium complex (0.25 mM) in DMF was excited at 550 nm and intensities of the luminescence were monitored at 610 nm, whereas the luminescence of the rhenium complex (0.75 mM) excited at 420 nm was monitored at 600 nm.

Photoreactions. Deaerated DMF solutions of **1** or **2** (2.5 mM) in the presence or absence of the sensitizers (0.8 mM) were irradiated under cooling with water (20±2 °C), and the progress of the reactions was followed by HPLC. It was confirmed that no reaction of 1 and **2** occurred in the dark under the conditions. The $[Ru(bpy)_3]^{2+}$-photosensitized reactions were run by the irradiation with a tungsten-halogen lamp (300W) using a 1-cm pathlength filter solution of K_2CrO_4 (20 g dm^{-3}), $NaNO_3$ (200 g dm^{-3}), and NaOH (6.7 g dm^{-3}) which cuts off the light shorter than 470 nm.[9] In both the $[ReBr(bpy)(CO)_3]$-photosensitized runs and the direct photolyses, an Eikosha high-pressure mercury arc (300W) was used; the 436-nm resonance line was isolated by the passage through a 1-cm pathlength solution of $CuSO_4$ in 28% ammonium hydroxide.[18] In the $[ReBr(bpy)(CO)_3]$-photosensitized reactions, contributions of reactions due to direct light absorption of the reactants are negligible, since the optical density of the sensitizer at 436 nm is 7—8 times greater than that of each reactant and since the photosensitized reactions are much more efficient than the direct photolyses.

Thermal Reactions. Deaerated DMF solutions of **1** or **2** (2.5 mM) were heated at 60±0.5 °C or at 100±0.5 °C in a dark room. The progress of the reactions was followed by HPLC. All the procedures were done with care in order to avoid exposure of the reactant solutions to scattering light.

This work was partly supported by Grant-in-Aid for Special Project Research No. 61123001 from the Ministry of Education, Science and Culture.

References

1) Part XIV. O. Ishitani, S. Yanagida, S. Takamuku, and C. Pac, *Bull. Chem. Soc. Jpn.*, **60**, 1801 (1987).

2) T. C. Bruice, "Progress in Bioorganic Chemistry," ed by F. T. Kaiser and F. J. Kendy, Wiley, New York (1976), Vol. IV.

3) Y. Ohnishi and M. Kitami, *Bull. Chem. Soc. Jpn.*, **52**, 2674 (1979).

4) C. O. Schmakel, K. S. V. Sonthanan, and P. J. Elving, *J. Am. Chem. Soc.*, **97**, 3083 (1975); K. Kano and T. Matsuo, *Bull. Chem. Soc. Jpn.*, **49**, 3269 (1976); H. Nezu, N. Kaneko, and S. Wakabayashi, *Denki Kagaku*, **47**, 559 (1979); M. A. Jensen and P. J. Elving, *Biochem. Biophys. Acta*, **764**, 310 (1984).

5) F. T. McNamara, J. W. Nieft, J. F. Ambrose, and E. S. Huyser, *J. Org. Chem.*, **42**, 988 (1977).

6) C. Pac, M. Ihama, M. Yasuda, Y. Miyauchi, and H. Sakurai, *J. Am. Chem. Soc.*, **103**, 6495 (1981).

7) O. Ishitani, C. Pac, and H. Sakurai, *J. Org. Chem.*, **48**, 2941 (1983).

8) O. Ishitani and C. Pac, unpublished results.

9) C. Pac, Y. Miyauchi, O. Ishitani, M. Ihama, M. Yasuda, and H. Sakurai, *J. Org. Chem.*, **49**, 26 (1984).

10) J. C. Luong, L. Nadjo, and M. S. Wrighton, *J. Am. Chem. Soc.*, **100**, 5790 (1978).

11) R. Ballardini, G. Varani, M. T. Indelli, F. Scandola, and V. Balzani, *J. Am. Chem. Soc.*, **100**, 7219 (1978).

12) B. P. Sullivan, C. M. Bolinger, D. Conrad, W. J. Vining, and T. J. Meyer, *J. Chem. Soc., Chem. Commun.*, **1985**, 1414.

13) C. R. Bock, J. A. Connor, A. R. Gutierrez, T. J. Meyer, D. G. Whitten, B. P. Sulliron, and J. K. Nagle, *J. Am. Chem. Soc.*, **101**, 4815 (1979).

14) W. J. Blaedel and R. G. Haas, *Anal. Chem.*, **42**, 918 (1965).

15) R. B. Woodward and R. Hoffman, *J. Am. Chem. Soc.*, **87**, 2511 (1965).

16) M. S. Wrighton and D. L. Morse, *J. Am. Chem. Soc.*, **96**, 998 (1974).

17) J. A. Broomhead and C. G. Yang, *Inorg. Synth.*, **22**, 127 (1983).

18) N. J. Turro and R. Engel, *J. Am. Chem. Soc.*, **91**, 7113 (1969).

NAD(P)$^+$-NAD(P)H Model. 63. Regioselective Reduction of Dienoic Ketones and Aldehydes with an NAD(P)H Model on Silica Gel

Masayuki Fujii, Kaoru Nakamura, Shinro Yasui,† Shinzaburo Oka, and Atsuyoshi Ohno*
Institute for Chemical Research, Kyoto University, Uji, Kyoto 611
†Tezukayama College, Gakuen-Minami, Nara 631
(Received January 20, 1987)

The Hantzsch ester reduces carbon-carbon double bonds in α,β-unsaturated ketones and aldehydes under the catalysis of silica gel. The 1,4-selectivity is satisfactorily high even in the reductions of polyenes conjugated to a carbonyl group. Methyl substituent at an olefinic position (α or β to the carbonyl group) retards the reduction. The reduction can be used as a useful tool in obtaining building blocks for the syntheses of terpenoids and their derivatives.

Quite a few reports have been published concerning to the mechanism of reduction with NADH, NADPH, and their analogs.[1] Stereochemistry for the reduction of carbonyl function in both biological and mimetic systems has been documented as well.[2] On the other hand, studies on synthetic application of the reduction with dihydropyridine derivatives has attracted little attention from organic chemists.[3] Namely, the mimetic reduction of carbon-carbon double bonds has been studied much less extensively than the reduction of carbon-oxygen double bonds, and reducible olefins in mimetic systems are limited to those that are substituted by a strongly electron-withdrawing substituent(s).[4] In some cases, photoirradiation is also effective for the reduction of olefins.[5] The reduction of carbon-carbon double bonds may have more value in synthetic organic chemistry than the reduction of carbon-oxygen double bonds and should be studied much more seriously.

Contrary to the mimetic systems, however, there are several biological systems that reduce carbon-carbon double bonds with the catalyses of NAD$^+$- or NADP$^+$-dependent dehydrogenases or reductases.[6] Since most NAD(P)H models so far studied have redox potentials comparable to that of NADH or NADPH[7] and these coenzymes reduce olefins in enzymatic systems, our effort should be concentrated on finding a suitable catalyst that behaves as a *mimetic enzyme* in order to undergo the organic reduction under mild conditions.

In previous papers of the series, we reported that silica gel is indeed a good catalyst for the reduction of carbon-carbon double bonds in α,β-unsaturated ketones and aldehydes,[8] and those in α-nitro olefins.[9] We now wish to report that the reduction with Hantzsch ester (HEH) in the presence of silica gel proceeds with very high chemoselectivity and regioselectivity under mild conditions, and that the reduction can be employed as a useful tool for wide variety of organic syntheses.

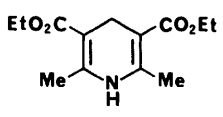

HEH

Experimental

Instruments. ^{1}H NMR spectra were measured at 100 and 400 MHz with a JEOL JNM-FX100 and a JEOL GX400 Fourier transform NMR spectrometers. IR spectra were recorded on a Hitachi EPI-S2 infrared spectrometer. Elemental analyses were performed with a Yanaco MT-3 elemental analyzer. Gas chromatographic data were recorded on a Yanaco G-1800 gas chromatograph (OV330, 1 m).

Materials. Hantzsch ester (HEH), and HEH-4,4-d_2 were prepared as reported in a previous paper.[10] The deuterium content in HEH-4,4-d_2 was confirmed to be 98% by 400 MHz ^{1}H NMR analysis. Citral (**3**), 2,4-nonadienal (**4c**), and β-ionone (**15**) are commercially available (Nakarai Chemicals Ltd.).

Other substrates were prepared according to literature methods.[11]

Silica gel (Nakarai Silica Gel 60, 35—70 mesh) was activated at about 80 °C in an oven for a few days. Anhydrous benzene was freshly distilled over calcium hydride immediately before the use.

Reduction of Benzylideneacetone (1a). In a 20 ml flask equipped with a magnetic stirrer and a reflux condenser, were placed 288 mg (2 mmol) of **1a**, 760 mg (3 mmol) of HEH, 2.0 g of silica gel, and 10 ml of anhydrous benzene. The mixture was heated to reflux for about 20 h under an argon atmosphere in the dark. The reaction mixture was cooled to room temperature, filtered, and washed with 30 ml of benzene. The filtrate was washed with 2 M†† hydrochloric acid (2×20 ml), water (2×20 ml), and 20 ml of brine, then dried on anhydrous sodium sulfate. Filtration and evaporation left a crude product, which was subjected to column chromatography on silica gel with benzene eluent to give 280 mg (96% yield) of the pure product, 4-phenyl-2-butanone (**2a**). The yield measured on gas chromatography was 100%.

†† 1 M=1 mol dm^{-3}.

^{1}H NMR ($CDCl_3$) δ=2.07 (s, 3H, CH_3CO), 2.74—2.81 (m, 4H, CH_2), 7.14—7.27 (m, 5H, Ph). IR (neat) 3000 (m) and 1717 (s) cm^{-1}. Found: C, 80.94; H, 8.31%. Calcd for $C_{10}H_{12}O$: C, 81.04; H, 8.31%.

Reduction of Cinnamaldehyde (1b). Reduction of 264 mg (2 mmol) of **1b** with 760 mg (3 mmol) of HEH and 2.0 g of silica gel afforded 192 mg (72% yield) of 3-phenylpropanal (**2b**). The yield on gas chromatography was 100%.

^{1}H NMR ($CDCl_3$) δ=2.64—3.04 (m, 4H, CH_2), 7.04—7.35 (m, 5H, Ph), and 9.76 (t, 1H, CHO). IR (neat) 3000 (m) and 1730 (s) cm^{-1}. Found: C, 80.38; H, 7.62%. Calcd for $C_9H_{10}O$: C, 80.56; H, 7.51%.

Reduction of Ethyl Cinnamate (1c). Starting with 2 mmol of **1c**, 3 mmol of HEH, and 2.0 g of silica gel, no product was detected, and the starting materials were obtained from the reaction mixture in 100% recovery, respectively.

Reduction of β-Nitrostyrene (1d). A mixture of 151 mg (1 mmol) of **1d**, 280 mg (1.1 mmol) of HEH, and 1.0 g of silica gel in 5 ml of anhydrous benzene was heated to reflux for 5 h under an argon atmosphere in the dark. The reaction mixture was worked up as described above giving 129 mg (84% yield) of 2-phenyl-1-nitroethane, (**2d**).

^{1}H NMR ($CDCl_3$) δ=3.30 (t, 2H, J=7 Hz, $PhCH_2$), 4.58 (t, 2H, J=7 Hz, CH_2NO_2), and 7.11—7.33 (m, 5H, Ph). IR (neat) 3000 (m), 1530 (s), and 1380 (s) cm^{-1}. Found: C, 63.90; H, 6.10; N, 9.16%. Calcd for $C_8H_9NO_2$: C, 63.56; H, 6.00; N, 9.27%.

Reduction of Citral (3). Reduction of 152 mg (1 mmol) of **3** with 380 mg (1.5 mmol) of HEH and 1.0 g of silica gel under the same conditions as described above gave 103 mg (67% yield) of citronellal.

^{1}H NMR ($CDCl_3$) δ=0.97 (d, 3H, J=7 Hz, CH_3CH), 1.20—1.44 (m, 3H, $-CH_2CH(CH_3)-$), 1.60 (s, 3H, $(CH_3)_2C=$), 1.68 (s, 3H, $(CH_3)_2C=$), 2.00 (q, 2H, J=7 Hz, $-CH_2CH=$), 2.24—2.50 (m, 2H, CH_2CHO), 5.00—5.17 (m, 1H, C=CH), and 9.74 (t, 1H, J=1 Hz, CHO). IR (neat) 3000 (m) and 1740 (s) cm^{-1}. Found: C, 77.62; H, 11.74%. Calcd for $C_{10}H_{18}O$: C, 77.86; H, 11.74%.

Reduction of (3*E*,5*E*)-6-Phenyl-3,5-hexadien-2-one (4a). After the reaction of 172 mg (1 mmol) of **4a** with 380 mg (1.5 mmol) of HEH and 1.0 g of silica gel in 10 ml of anhydrous benzene followed by usual work-up, column chromatography on silica gel with benzene eluent gave 153 mg (88% yield) of a mixture of two products, **5a** and **6a**. The ratio of **5a** to **6a** was determined by ^{1}H NMR analysis. The integration of signals for allylic C_α (C_3) protons (2H) in **6a** which appeared at δ 3.12 (d, J=5 Hz) and δ 3.25 (d, J=5 Hz)[12] was compared with that of signals for acetyl protons (3H) at δ 2.11 and the ratio was calculated as 73:27 (*E*:*Z* of **6a**=63:37).

^{1}H NMR ($CDCl_3$) δ=2.11 (s, CH_3CO-), 2.42—2.60 (m, CH_2 of **5a**), 3.12 (d, J=5 Hz, $-CH_2CO-$ of (*E*)-**6a**), 3.25 (d, J=5 Hz, $-CH_2CO-$ of (*Z*)-**6a**), 3.36 (d, J=5 Hz, $PhCH_2-$ of **6a**), 5.56—5.76 (m, H_β and H_γ of **6a**), 6.12 (dt, J=15, 6 Hz, H_γ of **5a**), 6.38 (d, J=15 Hz, H_δ of **5a**), and 7.04—7.41 (m, Ph). IR (neat) 3025 (m), 2925 (m), 1715 (s), and 1660 (w) cm^{-1}.

Reduction of 86 mg (0.5 mmol) of **4a** with 191 mg (0.75 mmol) of HEH-4,4-d_2 (98% purity in deuterium) and 0.5 g of silica gel afforded 75 mg of a mixture of the two products. The analysis of the 400 MHz ^{1}H NMR spectrum of the mixture revealed that the deuterium was incorporated in the 4-position of **5a** and in the 6-position of **6a**. The deuterium content in each product was 98%. The ratio of **5a**-4-*d*:**6a**-6-*d* was calculated to be 88:12.

400 MHz ^{1}H NMR ($CDCl_3$) δ=2.15 (s, CH_3CO-), 2.45 (q, J=6.8 Hz, -CHD- of **5a**-4-*d*), 2.59 (d, J=7.3 Hz, $-CH_2CO-$ of **5a**-4-*d*), 3.14 (d, J=5.9 Hz, $-CH_2CO$ of (*E*)-**6a**-6-*d*), 3.28 (d, J=7.3 Hz, $-CH_2CO-$ of (*Z*)-**6a**-6-*d*), 3.36 (bs, PhCHD- of **6a**-6-*d*), 5.60—5.72 (m, H_β and H_γ of **6a**-6-*d*), 6.18 (dd, J=16.1, 6.8 Hz, H_γ of **5a**-4-*d*), 6.40 (d, J=16.1 Hz, H_δ of **5a**-4-*d*), and 7.17—7.37 (m, Ph). IR (neat) 3030 (w), 2975 (s), 2170 (w), 1715 (s), and 1652 (w) cm^{-1}.

Reduction of (3*E*,5*E*)-3,5-Nonadien-2-one (4b). The reduction of 138 mg (1 mmol) of **4b** with 380 mg (1.5 mmol) of HEH and 1.0 g of silica gel gave 132 mg (94% yield) of a mixture of two compounds, **5b** and **6b**. The ratio of **5b**:**6b** was determined as 75:25 by comparing the integration for allylic C_α (C_3) protons (2H) at δ 3.16 (d, J=7 Hz) and 3.28 (d, J=8 Hz)[12] with the integration for the whole vinylic protons at δ 5.30—6.36 (m). The ratio thus determined was consistent with the ratio of the integration for vinylic protons of **5b** at δ 5.44—5.52 to that of vinylic protons of **6b** at δ 5.31—5.40.

IR (neat) 2925 (s), 1720 (s), and 1680 (m) cm^{-1}.

Reduction of (2*E*,4*E*)-2,4-Nonadienal (4c). The reduction of 158 mg (1.0 mmol) of **4c** with 380 mg (1.5 mmol) of HEH and 1.0 g of silica gel afforded 85 mg of **5c** and 21 mg of **6c** as pure compounds, respectively, after a routine column chromatography. The ratio of **5c**:**6c** was 80:20.

IR (neat) 2930 (s), 1715 (s), and 1660 (w) cm^{-1}.

Reduction of α-Methylcinnamaldehyde. The reduction of 14.6 mg (0.1 mmol) of α-methylcinnamaldehyde with 38.0 mg (0.15 mmol) of HEH, 150 mg of silica gel, and 2 ml of dry benzene gave the corresponding alcohol in 20% yield after 3 h and in 60% yield after 20 h.

Reduction of β-Methylcinnamaldehyde. The reduction of 14.6 mg (0.1 mmol) of β-methylcinnamaldehyde with 38.0 mg (0.15 mmol) of HEH was carried out under the same conditions as described above. The GLC analysis indicated that the chemical yields of the corresponding alcohol were 39% after 3 h and 79% after 20 h.

Reduction of 6-Phenyl-3,5-heptadien-2-one (7). The reduction of 186 mg (1 mmol) of **7** with 380 mg (1.5 mmol) of HEH and 1.0 g of silica gel afforded 175 mg (93% yield) of a mixture of two products, **9** and **10**. The ratio of **9**:**10** was calculated to be 92:8 from the ratio of integration for the allylic C_α (C_3) protons (2H) of **10** at δ 3.09 (d, J=6 Hz) to that for the trisubstituted vinylic proton (1H) of **9** at δ 5.32—5.76 (m).

^{1}H NMR ($CDCl_3$) δ=1.28 (d, J=8 Hz, CH_3CH of **10**), 2.00 (s, CH_3CH of **9**), 2.10 (s, CH_3CO- of **9** and **10**), 2.34—2.65 (m, CH_2 of **9**), 2.58—2.86 (m, PhCH- of **10**), 3.09 (d, J=6 Hz, $-CH_2CO-$ of **10**), 5.32—5.76 (m, H_γ of **9**), 6.00—6.33 (m, H_β and H_γ of **10**), and 7.12—7.60 (m, Ph). IR (neat) 3050 (m), 2980 (s), 1715 (s), and 1680 (m) cm^{-1}.

Reduction of 6,10-Dimethyl-3,5,9-undecatrien-2-one (8). The reduction of 192 mg (1 mmol) of **8** with 380 mg (1.5 mmol) of HEH and 1.0 g of silica gel afforded 167 mg (86% yield) of a mixture of two products, **11** and **12**. The ratio of **11**:**12** was calculated to be 95:5 by examining the integration for the trisubstituted vinylic protons of **11** (2H) and **12** (1H) at δ 4.96—5.20 (m), and that for allylic C_α (C_3)

protons (2H) of **12** at δ 3.09 (d, J=6 Hz). The ratio was also confirmed by comparison of the integration for trisubstituted vinylic protons of **11** and **12** and that for disubstituted vinylic protons of **12** at δ 5.38—5.59 (m).

^{1}H NMR ($CDCl_3$) δ=0.98 (d, J=6 Hz, CH_3CH of **12**), 1.58 (s, $(CH_3)_2C$= of **11** or **12**, and CH_3C of **11**), 1.67 (s, $(CH_3)_2C$= of **12** or **11**), 1.92—2.08 (m, CH_2 of **11** and **12**, and CH_3CH of **12**), 2.11 (s, CH_3CO- of **11** and **12**), 2.12—2.36 (m, CH_2 of **11**), 3.09 (d, J=6 Hz, -CH_2CO- of **12**), 4.96—5.20 (m, C=CH- of **11** and **12**), and 5.38—5.59 (m, -CH=CH- of **12**). IR (neat) 2980 (s), 1740 (s), and 1670 (m) cm^{-1}. Found: C, 80.60; H, 11.53%. Calcd for $C_{13}H_{22}O$: C, 80.35; H, 11.41%.

Preparation of Farnesol (14). Geranylacetone (**11**) (194 mg, 1 mmol) was converted into 172 mg (65% yield) of the corresponding α,β-unsaturated ester, **13**, as shown in Eq. 7.

The E:Z ratio of the new olefinic double bond was confirmed to be larger than 20:1 by ^{1}H NMR analysis; the signals for the allylic methyl protons trans to the carboethoxy group appeared at δ 2.12, whereas those cis to the carboethoxy group could not be detected at higher field.

^{1}H NMR ($CDCl_3$) δ=1.28 (t, J=7 Hz, 3H), 1.59 (s, 6H), 1.67 (s, 3H), 1.80—2.40 (m, 4H), 2.12 (s, 3H), 2.40 (t, J=6 Hz, 2H), 4.14 (q, J=7 Hz, 2H), 4.96—5.20 (m, 2H), and 5.65 (s, 1H). IR (neat) 2980 (s), 1740 (s), and 1670 (m) cm^{-1}. Found: C, 77.48; H, 10.53%. Calcd for $C_{17}H_{28}O_2$: C, 77.22; H, 10.68%.

The reduction of 150 mg (0.57 mmol) of **13** was carried out with 21.7 mg (0.28 mmol) of lithium aluminium hydride to give 111 mg (88% yield) of farnesol (**14**).

^{1}H NMR ($CDCl_3$) δ=1.60 (s, 9H), 1.68 (s, 3H), 1.82—2.36 (m, 8H), 4.15 (d, J=7 Hz, 2H), 4.97—5.24 (m, 2H), and 5.41 (t, J=7 Hz, 1H). IR (neat) 3355 (s), 2925 (s), and 1668 (m) cm^{-1}. Found: C, 81.11; H, 12.00%. Calcd for $C_{15}H_{26}O$: C, 81.02; H, 11.79%.

Reduction of β-Ionone (15). The reduction of 192 mg (1 mmol) of **15** with 380 mg (1.5 mmol) of HEH and 1.0 g of silica gel gave 136 mg of **16** as a sole product. The structure of **16** was confirmed by ^{13}C and ^{1}H NMR spectra.

^{1}H NMR ($CDCl_3$) δ=0.95 (s, 6H), 1.25—1.68 (m, 4H), 1.56 (s, 3H), 1.90 (t, J=6 Hz, 2H), 2.12—2.60 (m, 4H), and 2.13 (s, 3H). ^{13}C NMR ($CDCl_3$) δ=19.54 (q), 19.72 (q), 22.41 (t), 28.49 (q), 29.72 (t), 32.82 (t), 35.10 (s), 39.90 (t), 44.56 (t), 127.83 (s), 136.14 (s), and 208.68 (s). IR (neat) 2960 (s), 1715 (s), and 1665 (s) cm^{-1}. Found: C, 80.12; H, 11.56%. Calcd for $C_{13}H_{22}O$: C, 80.35; H, 11.41%.

Results and Discussion

Chemoselectivity. Benzylideneacetone (**1a**) and cinnamaldehyde (**1b**) were reduced quantitatively into 4-phenyl-2-butanone (**2a**) and 1-phenylpropanal (**2b**), respectively, after 20 h at the temperature of refluxing benzene, whereas ethyl cinnamate (**1c**) remained entirely unchanged (Eq. 1). The result indicates that the reduction discriminates the carbon-carbon double

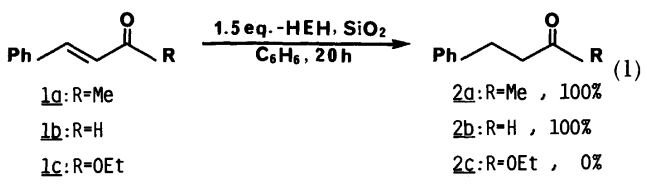

(1)

bond adjacent to a carbonyl group from that adjacent to an alkoxy-carbonyl group. The discrimination can also be seen between the double bonds adjacent to acetyl and nitro groups; under the conditions where 95% of β-nitrostyrene (**1d**) was reduced, only 5% of **1a** was converted into 4-phenyl-2-butanone (**2a**) (Eq. 2).

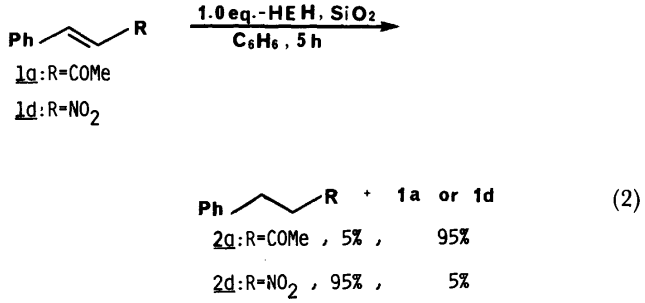

(2)

Under the same conditions, where **1b** afforded **2b** in quantitative yield, α- and β-methylcinnamaldehydes yielded the corresponding product alcohols in only 60 and 71% yields, respectively. Apparently, the methyl substituent at an olefinic position retards the reduction.

The isolated double bond is not affected by the reduction; only 1,4-reduction took place for citral (**3**) (Eq. 3).

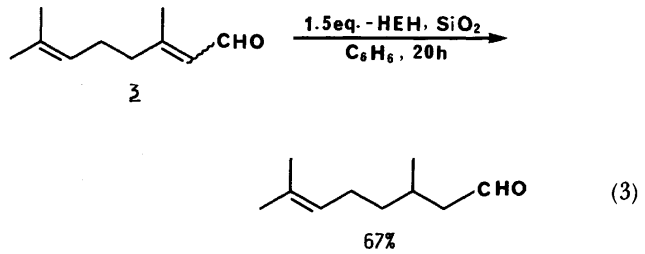

(3)

Reduction of Conjugated Dienones and Dienals. Reduction of conjugated dienoketones and aldehydes proceeded smoothly and afforded the products in good yields (Eq. 4). Although 1,4- and 1,6-type reductions are competitive here, the regioselectivity observed was reasonably satisfactory with the predominance of the 1,4-type reduction;[13] **5a**:**6a**=73:27, **5b**:**6b**=75:25, and **5c**:**6c**=80:20.

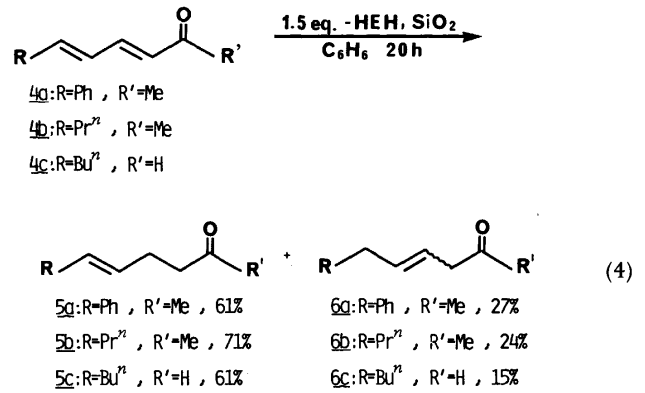

(4)

The ratio was determined by the ^1H NMR analysis comparing the sum of integration of signals for the vinylic protons with that for the allylic α-protons. The latter signal is inherent to the 1,6-reduction product, **6**, and usually appear at around δ 3.05—3.15 as a doublet. It should be noted that the predominance of the 1,4-reduction over the 1,6-reduction shows a sharp contrast to the predominant 1,6-selectivity exerted by the reduction with sodium dithionite under phase-transfer conditions[14] or with diisobutylaluminium hydride in the presence of methylcopper.[15] When the 6-position of conjugated carbon-carbon double bonds is substituted by a methyl group, the ratio of 1,4- vs. 1,6-reduction becomes much higher as a consequence of steric inhibition. For example, the reduction of 6-phenyl-3,5-heptadien-2-one (**7**) and 6,10-dimethyl-3,5,9-undecatrien-2-one (**8**) afforded **9** and **10** in 92:8 ratio and **11** and **12** in 95:5 ratio, respectively (Eqs. 5 and 6).

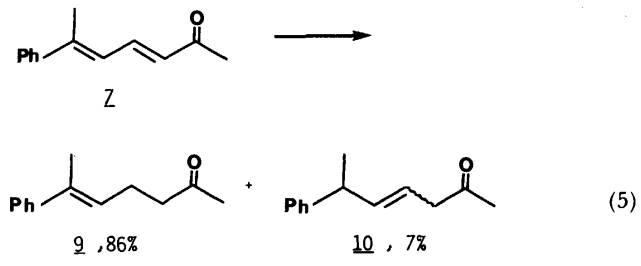

(5)

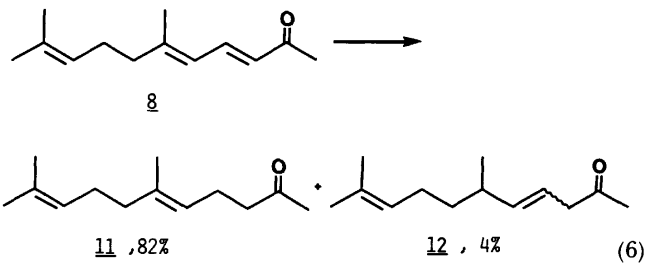

(6)

The reduction of **4a** with HEH-4,4-d_2 afforded **5a**-4-*d* and **6a**-6-*d*, which clearly demonstrated that a deuterium was directly incorporated into the 4- and 6-positions of the 1,4- and 1,6-reduction products, respectively.

Application to Syntheses. Geranylacetone (**11**) thus obtained is an important component for the syntheses of terpenoids; a straightforward synthesis of farnesol (**14**) is one of examples (Eq. 7).[16]

The significance of the steric effect on the regioselectivity was clearly exaggerated by the reduction of β-ionone (**15**) which has three methyl groups on the cyclohexenyl moiety. In addition to the methyl

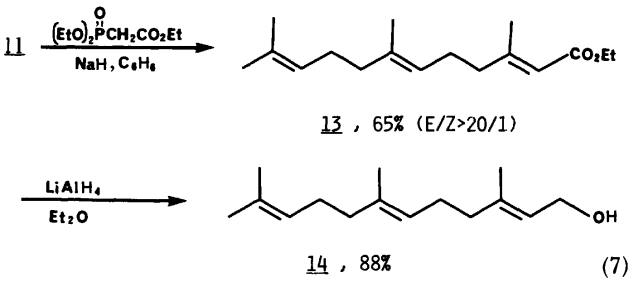

(7)

substituent on the endo-double bond, two methyl groups on the cyclohexenyl ring also plays a role to decrease the reactivity of this double bond, and the sole product obtained in this reduction is **16**, the 1,4-reduction product (Eq. 8). Recently, we came to the conclusion that the silica gel-catalyzed reduction with

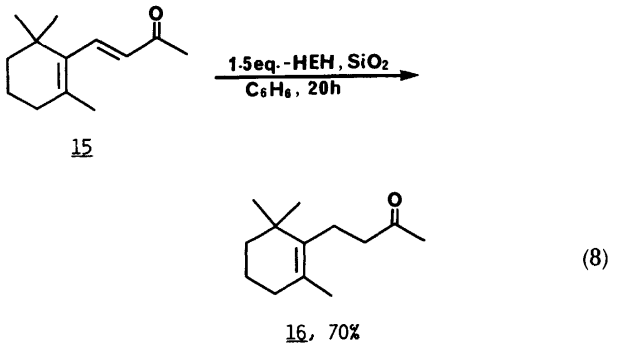

(8)

HEH proceeds with the HEH absorbed on silica gel instead of the intermediacy of a substrate-silica gel complex.[17] Consequently, the reacting HEH is sterically highly blocked by a huge silica-gel component, and a small difference in steric effects in the substrate may differentiate the reactivity of certain carbon-carbon double bond quite sensitively. A CPK molecular model shows that the axial methyl group at the 1-position of the cyclohexenyl ring of **15** prevents the (formal) hydride from attacking the endo-double bond from the axial side, whereas the attack from the equatorial side results in the 1,3-diaxial repulsion between 1- and 3-methyl groups in the product. Thus, this endo-double bond in **15** is sterically set unreactive remaining the exo-double bond as the sole reacting function.

The product, **16**, is a component of natural products. For example, it is an important precursor of manoalides (Eq. 9), a series of natural marine products (e.g., 17—19) with strong biological activities.[18]

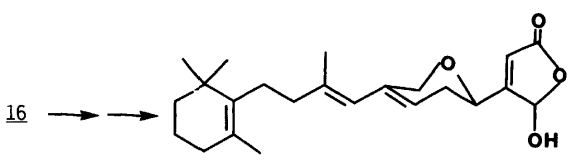

manoalide(17)

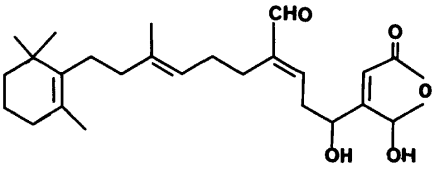

seco-manoalide(18)

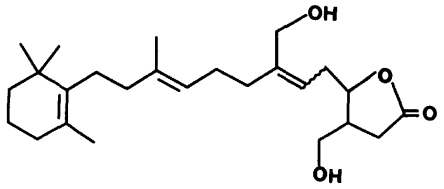

(E)and(Z)-neomanoalide(19) (9)

In conclusion, HEH is a very mild reducing agent, which, in turn, can be employed as an efficient device to sharply differentiate the susceptibilities of functional groups in the reduction. Namely, it has been demonstrated that HEH on silica gel is a useful tool to synthesize γ,δ-unsaturated ketones and aldehydes that are important building blocks for the syntheses of terpenoids and other natural products.

References

1) For a recent review, see S. Yasui and A. Ohno, *Bioorg. Chem.*, **14**, 70 (1986).

2) A. Ohno and S. Ushida, *Lecture Notes in Bio-Organic Chemistry*, 1, (1986) Springer-Verlag, Heidelberg, F. R. D.

3) For one of rare examples, see S. H. Mashraqui and R. M. Kellogg, *J. Am. Chem. Soc.*, **105**, 7792 (1983).

4) B. E. Norcross, P. E. Klinedist Jr., and F. H. Westheimer, *J. Am. Chem. Soc.*, **84**, 797 (1962); Y. Ohnishi, M. Kagami, T. Numakunai, and A. Ohno, *Chem. Lett.*, **1976**, 915; S. Fukuzumi, Y. Kondo, and T. Tanaka, *J. Chem. Soc., Perkin Trans. 2*, **1984**, 673.

5) Y. Ohnishi, M. Kagami, and A. Ohno, *Chem. Lett.*, **1975**, 125; C. Pac, M. Ihama, M. Yasuda, Y. Miyauchi, and H. Sakurai, *J. Am. Chem. Soc.*, **103**, 6495 (1981).

6) For example: (3-Keto steroid Δ^4-dehydrogenase) J. S. McGuire and G. M. Tompkins, *Fed. Proc.*, **19**, A29 (1960); (Melilotate dehydrogenase) C. C. Levy and G. D. Weinstein, *Biochemistry*, **3**, 1944 (1964); (β-Nitroacrylate reductase) P. D. Show, *Biochemistry*, **6**, 2253 (1967); (Acyl-CoA dehydrogenase) W. Hinsch, C. Klages, and W. Seubert, *Eur. J. Biochem.*, **64**, 45 (1976).

7) R. M. Kellogg and O. Piepers, *J. Chem. Soc., Chem. Commun.*, **1982**, 402.

8) K. Nakamura, M. Fujii, A. Ohno, and S. Oka, *Tetrahedron Lett.*, **25**, 3983 (1984).

9) K. Nakamura, M. Fujii, S. Oka, and A. Ohno, *Chem. Lett.*, **1985**, 523.

10) A. Singer and S. M. McElvain, *Org. Synth.*, Coll. Vol. II, 214 (1966).

11) M. Schlosser and K. F. Christmann, *Justus Liebigs Ann. Chem.*, **708**, 1 (1967).

12) Two couples of doublets refer to E and Z forms, respectively.

13) For 1,4- vs. 1,2-selectivity, see A. Ohno, T. Yasuma, K. Nakamura, and S. Oka, *Bull. Chem. Soc. Jpn.*, **59**, 2905 (1986).

14) F. Camps, J. Coll, A. Guerrero, J. Guitart, and M. Riba, *Chem. Lett.*, **1982**, 715.

15) T. Tsuda, T. Hayashi, H. Satomi, T. Kawamoto, and T. Saegusa, *J. Org. Chem.*, **51**, 537 (1986).

16) O. P. Vig, J. C. Kapur, C. K. Khurana, and B. Vig, *J. Ind. Chem. Soc.*, **46**, 505 (1965).

17) S. Yasui, M. Fujii, K. Nakamura, and A. Ohno, *Bull. Chem. Soc. Jpn.*, **60**, 963 (1987).

18) S. Isoe, T. Takemoto, H. Inaba, K. Kon, K. Nakatani, S. Katsumura, K. Yamamoto, N. Fujiwara, and K. Hori, Abstracts of Papers of "27 th Symposium on the Chemistry of Natural Products," 1985, pp. 160—167.

Synthesis of (*E,E*)- and (*Z,Z*)-1,5-Cycloalkadienes by Means of the Electrochemical Cyclization of Allylic 1,ω-Dibromides

Masao Tokuda,* Kuniaki Satoh, and Hiroshi Suginome*
Division of Organic Synthesis, Department of Chemical Process Engineering,
Faculty of Engineering, Hokkaido University, Sapporo 060
(Received January 21, 1987)

Electrolysis of (*E,E*)-1,*n*-dibromo-2,(*n*-2)-alkadienes (*n*=12, 14) in tetrahydrofuran gave the corresponding twelve or fourteen-membered (*E,E*)-1,5-cycloalkadienes, albeit in low yields, together with (*E*)-4-vinylcycloalkenes and isomeric alkadienes. Similar electrolysis of (*Z,Z*)-1,*n*-dibromo-2,(*n*-2)-alkadienes (*n*=10, 12, 14) gave the corresponding ten, twelve, or fourteen-membered (*Z,Z*)-1,5-cycloalkadienes in 11 to 13% yields, with the accompanying formation of (*Z*)-4-vinylcycloalkenes and isomeric alkadienes.

Electroreductive cyclization of 1,3-dihalides has been reported to be useful for the preparation of substituted[1-5] and strained cyclopropanes.[1] Cyclobutane derivatives[1,4] have also been prepared by the electrochemical reduction of 1,4-dihalides. However, higher cycloalkanes have not been prepared by the electrolysis of simple aliphatic dihalides. We ourselves have previously reported that the three to seven-membered cycloalkanes are obtained by the electrochemical reductive cyclization of 1,ω-dibromides with alkoxycarbonyl groups at their terminal carbons.[6] A similar cyclization of 1,5-dibromopentanes with an electron-withdrawing group at their one termini was also reported recently.[7] As one of the extensions of our study of the electroreductive cyclization of 1,ω-dibromides we studied the preparation of even higher cycloalkanes by means of the electrochemical cyclization of (*E,E*)- or (*Z,Z*)-1,*n*-dibromo-2,(*n*-2)-alkadienes. We now report that ten, twelve, and fourteen-membered (*E,E*)- or (*Z,Z*)-1,5-cycloalkadienes can be prepared by the electrolysis of the corresponding (*E,E*)- or (*Z,Z*)-allylic dibromides, albeit in low yields.

A transition metal-catalyzed cyclization of allylic dibromides has been reported to lead generally to more stable (*E,E*)-1,5-cycloalkadiene rather than to (*Z,Z*)-dienes, regardless of the geometry of the double bonds of the starting allylic dibromides.[8,9] For the preparation of (*Z,Z*)-1,5-cycloalkadienes only a few methods have been reported, however, (*Z,Z*)-1,5-Cyclotetradecadiene was prepared by partial hydrogenation of 1,5-cyclotetradecadiynes with a Lindler catalyst.[10] (*Z,Z*)-1,5-Cyclododecadiene was formed, as one of several isomers, either in the photochemical isomerization of its (E,E)-isomer[11] or in the hydrogenation of 1,5,9-cyclododecatriene.[12] (*Z,Z*)-1,5-Cyclodecadiene was similarly formed either in the photochemical isomerization of its (E,Z)-isomer[13] or in the partial hydrogenation of cyclodecatrienes.[14] Of these (*Z,Z*)-1,5-cycloalkadienes, (*Z,Z*)-1,5-cyclododecadiene has not been isolated in a pure form and the stereochemistries of (*Z,Z*)-1,5-cyclotetradecadiene and (*Z,Z*)-1,5-cyclododecadiene have not been established in an unambiguous manner.

Results and Discussion

The starting (*E,E*)-allylic dibromides **1**, **5**, and **10** were readily prepared by reduction of the corresponding 2,(*n*-2)-alkadiyn-1,*n*-diols with lithium aluminum hydride, followed by bromination.[8,9] On the other hand, the (*Z,Z*)-allylic dibromides **11**, **15**, and **19** were prepared by partial hydrogenation of the corresponding alkadiyne diols with a Lindler catalyst.[8,9]

Electrochemical reduction of (*E,E*)- and (*Z,Z*)-allylic dibromides was carried out at a constant current in tetrahydrofuran (THF) containing 0.1 M† tetrabutylammonium perchlorate (*n*-Bu_4NClO_4) as a supporting electrolyte. Each allylic dibromide was gradually added to the cathodic solution with a microfeeder. The electricity passed was 2.2 Faradays per mole of the dibromide. The electrochemical reduction of (*E,E*)-1,14-dibromo-2,12-tetradecadiene (**1**) afforded three major products **2** (8%), **3** (5%), and **4** (19%) which could be separated by preparative GLC (Scheme 1). High resolution mass spectrometry indicated that **2** and **3** were isomeric and had the molecular formula $C_{14}H_{24}$. The ^1H NMR spectrum of **2** exhibited overlapped multiplets due to the four olefinic protons of the two unconjugated vinyl groups at δ 5.28. The geometry of the double bonds of **2** was deduced from the IR spectrum. (E)-Double bonds of the medium-sized cycloalkenes give rise to a medium to a strong band at 965—980 cm^{-1} while (Z)-double bonds at 700—710 cm^{-1}.[15,16] (E)-Double bonds of several 1,5-cycloalkadienes give a characteristic band at 960—970 cm^{-1} while (Z)-double bonds at 695—710 cm^{-1}.[8,9,16,17] A strong band at 980 cm^{-1} in the IR spectrum of cycloalkadiene **2** indicated that the configurations of the two double bonds are (E).

The ^1H NMR spectrum of **3** showed characteristic signals due to a vinyl group and its IR spectrum showed a characteristic band due to an (E) double bond at 970—980 cm^{-1}. On the basis of these results an (*E*)-4-vinylcyclododecene structure was assigned to **3**. The alkadiene **4** isolated was a mixture of two

† 1 M=1 mol dm^{-3}.

isomers and the structure of the major isomer was determined to be (*E,E*)-2,12-tetradecadiene (**4a**) as described in the experimental section.

Similar electrolysis of (*E,E*)-1,12-dibromo-2,10-dodecadiene (**5**) gave (*E,E*)-1,5-cyclododecadiene (**6**) (10%), (*E*)-4-vinylcyclodecene (**8**) (3%), (*E,Z*)-1,5-cyclododecadiene (**7**) (2%), and a mixture of isomeric dodecadienes (**9**) (21%) (Scheme 1). The structures of these products [including the geometries of their double bonds] were determined by MS, IR, and ^{1}H NMR spectra; the details are described in the experimental section. The structure of **7** was confirmed additionally by a direct comparison with an authentic specimen prepared by the selective reduction of (*E,E,Z*)-1,5,9-cyclododecatriene with hydrazine.[16]

Electrochemical reduction of (*E,E*)-1,10-dibromo-2,8-decadiene (**10**), however, gave a complex mixture of products that contained a large amount of isomeric decadienes.

We then turned our attention to the electrolysis of (*Z,Z*)-allylic bromides **11**, **15**, and **19**. Electrochemical reductions of (*Z,Z*)-1,14-dibromo-2,12-tetradecadiene (**11**), (*Z,Z*)-1,12-dibromo-2,10-dodecadiene (**15**), and (*Z,Z*)-1,10-dibromo-2,8-decadiene (**19**) afforded (*Z,Z*)-1,5-cycloalkadienes (**12**, **16**, and **20**) in 11—13% yields and (*Z*)-4-vinylcycloalkenes (**13**, **17**, and **21**) in 4—7% yields as outlined in Scheme 2. The structures of the above products [including their geometries] were deduced by MS, IR, and ^{1}H NMR spectroscopy. Thus, cycloalkadienes **12**, **16**, and **20** showed bands 715, 720, and 700 cm^{-1} respectively in their IR spectra, indicating (Z,Z)-geometries of their isolated double bonds. The ^{1}H NMR of **16** exhibited a double triplet at δ 5.26 and a multiplet at δ 5.60 that were due to the olefinic protons as well as two multiplets at δ 2.10 and δ 1.35. Irradiation at δ 2.10 collapsed the former two olefinic signals to two doublets each with J=10.7 Hz. Since the coupling constants of the olefinic protons of seven to ten-membered (*Z*)-cycloalkenes are in the range of 10.3—10.8 Hz,[18] we assigned Z-configurations to the geometry of the double bonds of **16**. Similar decoupling studies on the ^{1}H NMR spectra of **12** and **20** by 400 MHz NMR spectrometer indicated that the coupling constants of the four olefinic protons of **12** were 10.7 Hz in each case while those of two pairs of olefinic protons of **20** were 10.7 and 11.2 Hz. On the basis of these results, (Z)-configuration is assigned to all the double bonds of **12** and **20**. The IR showed that 4-vinylcycloalkenes **13**, **17**, and **21** have bands at 690—705 cm^{-1}; (Z)-configuration is therefore also assigned to their double bonds. The coupling constant of the olefinic protons of the internal double bond of **13** was found to be 10.0 Hz; this was consistent with its (Z)-geometry. In addition to these cyclic olefins, electrolysis of **15** gave (*E,Z*)-cyclic diene **7** in a 4% yield. It was identical with **7** obtained by the electrolysis of **5**. Electrolysis of **11** and **15** also gave a mixture of the isomeric alkadienes **14** and **18** in 18% and 16% yields. The major isomers of **14** and **18**, separated by preparative GLC, were shown to be (*Z,Z*)-2,12-tetradecadiene (**14c**) and (*Z,Z*)-2,10-dodecadiene (**18c**), respectively.

Cyclic voltammetry of the starting dibromides and the electrode potential during the electrolysis indicated that such an electrolysis as the one we have described involves a two-electron reduction of the carbon-bromine bond. Cyclic voltammetry has shown that the reduction peaks of **5**, **15**, and crotyl bromide in an *N,N*-dimethylformamide (DMF) solution are −2.00, −2.00, and −1.81 V vs. Ag/AgI and the reduction peak of crotyl bromide in a THF solution is −1.65 V vs. Ag/AgI. Although the present elec-

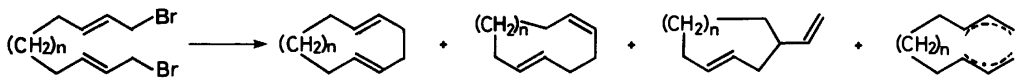

1 n = 6 **2** (8%) **3** (5%) **4** (19%)
5 n = 4 **6** (10%) **7** (2%) **8** (3%) **9** (21%)
10 n = 2

Scheme 1.

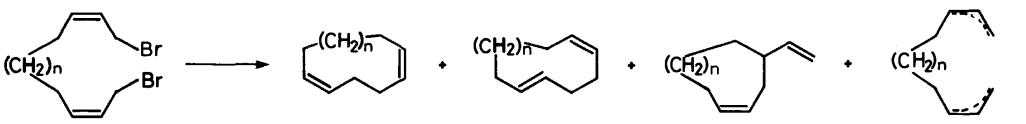

11 n = 6 **12** (11%) **13** (7%) **14** (18%)
15 n = 4 **16** (11%) **7** (4%) **17** (6%) **18** (16%)
19 n = 2 **20** (13%) **21** (4%) **22**

Scheme 2.

trochemical reduction was carried out at a constant current in a THF solution, the working electrode in the electrolysis of **15** was kept at the potential ranging from −1.6 V to −1.8 V, which nearly corresponded to the reduction potential of **15**. These results suggest that the electroreductive cyclization described above proceeds via an intramolecular nucleophilic attack at a bromine-bearing allylic carbon atom by the allylic carbanion which is generated by a two-electron reduction of the carbon-bromine bond.[19] In agreement with this mechanism the geometry of at least one of the double bonds in each of the starting dibromide was retained in all the cycloalkadienes obtained.

During such cyclizations as these, a partial interconversion between (E) and (Z) geometries may take place,[20] as the formation of (*E,Z*)-cycloalkadiene **7** from (*E,E*)-dibromide **5** and (*Z,Z*)-dibromide **15** indicates. Vinylcycloalkenes **3**, **8**, **13**, **17**, and **21** are likely to be formed via either an intramolecular nucleophilic attack on the bromine-carrying carbon atom by an allylic carbanion centered on the C-3 or by an intramolecular attack on the C-3 carbon by an allylic carbanion centered on the terminal carbon with allylic rearrangement.

Experimental

Tetrahydrofuran (THF) was dried over sodium benzophenone ketyl and distilled before use. The IR spectra were obtained with a Hitachi Model 285 spectrometer. The ^{1}H NMR spectra in $CDCl_3$ were measured with a JEOL FX 100 (100 MHz) and a JEOL FX 400 (400 MHz) (Faculty of Science of this University), using tetramethylsilane as an internal reference. Mass spectra were obtained with a JEOL JMS-D300 mass spectrometer (Faculty of Agriculture). Quantitative GLC analyses were carried out with a Hitachi 063 instrument by the internal standard method.

Preparation of Allylic Dibromides. (*E,E*)-Allylic dibromides **1**, **5**, and **10** were prepared according to an established procedure.[8,9] Since purification of these dibromides by distillation or column chromatography led to decomposition, the prepared dibromides were therefore immediately subjected to electrolysis without further purification. The spectral data of the (*E,E*)-allylic dibromides are recorded below.

(*E,E*)-1,14-Dibromo-2,12-tetradacadiene (1): n^{20} 1.5089; IR (neat) 3030, 1660, 965 cm^{-1}; ^{1}H NMR ($CDCl_3$)[9] δ=1.28 (bs, 12H), 2.02 (m, 4H), 3.94 (d, 4H, J=5.9 Hz), 5.71 (m, 4H); MS *m/z* (rel intensity) 273 (M^+ −Br, 1.0), 271 (M^+ −Br, 1.3), 109 (75), 97 (41), 95 (100), 83 (69), 81 (63), 69 (47), 67 (73), 55 (92).

(*E,E*)-1,12-Dibromo-2,10-dodecadiene (5): n^{20} 1.5237; IR (neat) 3030, 1660, 963 cm^{-1}; ^{1}H NMR ($CDCl_3$)[9] δ=1.32 (m, 8H), 2,06 (m, 4H), 3.95 (d, 4H, J=5.9 Hz), 5.72 (m, 4H); MS *m/z* (rel intensity) 326 (0.23), 324 (0.40), 322 (0.22), 163 (29), 109 (29), 95 (84), 81 (100), 69 (36), 67 (90), 55 (70). Found: *m/z* 323.9932. Calcd for $C_{12}H_{20}Br_2$: M, 323.9913.

(*E,E*)-1,10-Dibromo-2,8-decadiene (10): n^{20} 1.5291; IR (neat) 3030, 1660, 965 cm^{-1}; ^{1}H NMR ($CDCl_3$) δ=1.39 (m, 4H), 2.04 (m, 4H), 3.94 (d, 4H), 5.72 (m, 4H). MS *m/z* (rel intensity) 296 (0.17), 135 (56), 93 (40), 81 (79), 79 (38), 67 (100), 53 (48). Found: *m/z* 295.9621. Calcd for $C_{10}H_{16}Br_2$: M, 295.9599.

(*Z,Z*)-Allylic dibromides **11**, **15**, and **19** were prepared by bromination of (*Z,Z*)-alkadiene diols; these were obtained by hydrogenation of the corresponding 2, (*n*-2)-alkadiyn-1, *n*-diols by a Lindler catalyst.[8,9] The dibromides were subjected to electrolysis without any further purification.

(*Z,Z*)-1,14-Dibromo-2,12-tetradacadiene (11): n^{20} 1.5199; IR (neat) 3030, 1645, 720—750 (br) cm^{-1}; ^{1}H NMR ($CDCl_3$) δ=1.31 (bs, 12H), 2.13 (m, 4H), 4.00 (d, 4H), 5.66 (m, 4H); MS *m/z* (rel intensity) 273 (M^+ −Br, 0.9), 271 (M^+ −Br, 1.2), 109 (65), 97 (32), 95 (100), 83 (58), 81 (71), 69 (44), 67 (85).

(*Z,Z*)-1,12-Dibromo-2,10-dodecadiene (15): n^{20} 1.5310; IR (neat) 3030, 1645, 720—750 (br) cm^{-1}; ^{1}H NMR ($CDCl_3$) δ=1.33 (bs, 8H), 2.11 (m, 4H), 3.88 (d, 4H), 5.61 (m, 4H); MS *m/z* (rel intensity) 326 (0.20), 324 (0.38), 322 (0.21), 163 (26), 109 (32), 95 (80), 81 (100), 69 (41), 67 (91), 55 (70), 54 (35), 53 (41). Found: *m/z* 323.9890. Calcd for $C_{12}H_{20}Br_2$: M, 323.9913.

(*Z,Z*)-1,10-Dibromo-2,8-decadiene (19): n^{20} 1.5381; IR (neat) 3030, 1645, 720—750 (br) cm^{-1}; ^{1}H NMR ($CDCl_3$) δ=1.44 (m, 4H), 2.12 (m, 4H), 3.98 (d, 4H), 5.65 (m, 4H); MS *m/z* (rel intensity) 298 (0.15), 296 (0.29), 294 (0.17), 135 (54), 93 (34), 81 (63), 79 (30), 67 (100), 53 (40). Found: *m/z* 295.9576. Calcd for $C_{10}H_{16}Br_2$: M, 295.9599.

General Procedure for Electrolysis. For most of the electrolyses, we used a normal undivided cell (2.8 cm dia.) equipped with a magnetic stirrer, a reflux condenser, and a serun cap for the introduction of nitrogen gas. Electrolysis was carried out under a nitrogen atmosphere at a constant current (20 mA cm^{-2}) using two platinum electrodes (2×2 cm^2). Allylic dibromide (0.6—1.0 mmol) dissolved in 1 ml of THF was added to a 20 ml of THF solution containing 0.1 M Bu_4NClO_4 over a period of 3—4 h with a micro-feeder. The electricity passed was 2.2 Faradays per mole of the dibromide. After electrolysis, most of THF had been evaporated and the residue was dissolved in diethyl ether. The ethereal solution was washed with water and dried over magnesium sulfate. A column chromatography (silica gel; hexane) of the reaction mixture gave a mixture of cycloalkadienes and alkadienes which was subjected to a preparative GLC (Carbowax 20M 15%, 150—170 °C) to give pure products. Yields of the products were determined by GLC using an internal standard method and were based on the starting allylic dibromides employed. An amount of the unreacted allylic dibromides was not determined because of their instability in the GLC column.

Spectral data of the products obtained by electrolysis are recorded below.

(*E,E*)-1,5-Cyclotetradecadiene (2):[9] IR (neat) 3070, 980 cm^{-1}; ^{1}H NMR ($CDCl_3$) δ=1.29 (bs, 12H), 1.96 and 2.11 (bs and m, total 8H), 5.28 (m, 4H); MS *m/z* (rel intensity) 192 (M^+, 7), 95 (57), 82 (54), 81 (100), 80 (95), 68 (62), 67 (97), 55 (50), 54 (99). Found: *m/z* 192.1859. Calcd for $C_{14}H_{24}$: M, 192.1876. An attempt to determine the coupling constant between olefinic protons of **2** by decoupling technique was unsuccessful.

(*E*)-4-Vinylcyclododecene (3): IR (neat) 990, 978, 915 cm^{-1}; ^{1}H NMR ($CDCl_3$) δ=1.30 (s, 14H), 2.07 (m, 5H), 4.9—5.1 (m, 2H), 5.41 (m, 2H), 5.6—6.0 (m, 1H); MS *m/z* (rel intensity)

192 (M^+, 2), 95 (22), 82 (49), 81 (92), 80 (77), 68 (72), 67 (95), 55 (65), 54 (100). Found: *m/z* 192.1905. Calcd for $C_{14}H_{24}$: M, 192.1878.

A Mixture of Isomeric Tetradecadiene (4): IR (neat) 3020, 1640, 965, 910 cm^{-1}; ^1H NMR ($CDCl_3$) δ=1.27 (bs, CH_2), 1.64 (d, CH_3), 1.97 (bs, $=CHCH_2-$), 4.8—5.1 (m, $=CH_2$), 5.41 (m, $-CH=CH-$), 5.5—6.1 (m, $-CH=CH_2$); MS *m/z* (rel intensity) 194 (M^+, 4), 96 (26), 95 (25), 82 (39), 81 (37),69 (32), 68 (100), 67 (31), 55 (96). Found: *m/z* 194.2045. Calcd for $C_{14}H_{26}$: M, 194.2035. Tetradecadiene **4** was proved to be a 74:26 mixture of (*E,E*)-2, 12-tetradecadiene (**4a**) and (*E*)-1,12-tetradecadiene (**4b**).

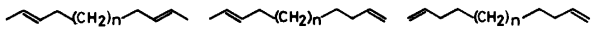

n=6 **4a** **4b**
n=4 **9a** **9b** **9c**

(*E,E*)-1,5-Cyclododecadiene (6):[9] IR (neat) 3025, 973, 927 cm^{-1}; ^1H NMR ($CDCl_3$) δ=1.19 (m, 4H), 1.42 (bs, 4H), 2.03 and 2.12 (m and bs, total 8H), 5.10 (m, 4H); MS *m/z* (rel intensity) 164 (M^+, 4), 121 (65), 81 (81), 67 (100), 54 (99). Found: *m/z* 164.1569. Calcd for $C_{12}H_{20}$: M, 164.1564.

(*E,Z*)-1,5-Cyclododecadiene (7): IR (neat) 3030, 977, 970, 703 cm^{-1}; ^1H NMR ($CDCl_3$) δ=1.26 and 1.56 (m and bs, total 8H), 2.09 (m, 8H), 5.0—5.8 (m, 4H); MS *m/z* (rel intensity) 164 (M^+, 2), 121 (45), 81 (61), 80 (41), 68 (41), 67 (100), 54 (63). Found: *m/z* 164.1558. Cacld for $C_{12}H_{20}$: M, 164.1564. Various spectra of **7** were identical with those of (*E,Z*)-1,5-cyclododecadiene which was prepared by means of a selective reduction of (*E,E,Z*)-1,5,9-cyclododecatriene with hydrazine. Reduction of the triene (77 mmol scale) was carried out according to an established procedure[16] but in order to obtain a best yield of **7**, the reduction was discontinued after a shorter reaction time (20 min.). GLC analysis showed that the reaction mixture consisted of **7** (50%), a starting cyclododecatriene (30%), and (*Z*)-cyclododecene (20%). These three products were separated by a preparative GLC (Carbowax 20M 15% on Uniport B).

(*E*)-4-Vinylcyclodecene (8): IR (neat) 3030, 970, 913 cm^{-1}; ^1H NMR ($CDCl_3$) δ=1.38 and 1.57 (m and m, 10H), 2.12 and 2.25 (m and m, 5H), 4.8—5.2 (m, 2H), 5.48 (m, 2H), 5.6—6.1 (m, 1H); MS *m/z* (rel intensity) 164 (M^+, 3), 121 (66), 93 (26), 81 (94), 80 (46), 68 (30), 67 (100), 54 (59). Found: *m/z* 164.1560. Calcd for $C_{12}H_{20}$: M, 164.1562.

A Mixture of Isomeric Dodecadienes (9): IR (neat) 3020, 1640, 967, 910 cm^{-1}; ^1H NMR ($CDCl_3$) δ=1.30 (bs, CH_2), 1.64 (d, $=CHCH_3$), 1.97 (bs, $=CHCH_2-$), 4.8—5.2 (m, $=CH_2$), 5.44 (m, $-CH=CH-$), 5.5—6.1 (m, $-CH=CH_2$); MS *m/z* (rel intensity) 166 (M^+, 2), 95 (31), 82 (50), 81 (51), 69 (44), 68 (100), 67 (67), 55 (88), 54 (40). Found: *m/z* 166.1736. Calcd for $C_{12}H_{22}$: M, 166.1721. GLC analysis and ^1H NMR spectrum of the mixture showed that it consisted of **9a** (90%), **9b** (8%), and **9c** (2%).

(*Z,Z*)-1,5-Cyclotetradecadiene (12): IR (neat) 3003, 1650, 945, 715 cm^{-1}; ^1H NMR ($CDCl_3$) δ=1.32 (m, 12H), 2.05 (m, 8H), 5.43 (m, 4H, J=7.3 Hz, J=10.7 Hz); MS *m/z* (rel intensity) 192 (M^+, 10), 135 (35), 121 (31), 95 (67), 87 (100), 67 (96), 59 (70), 54 (71). Found: *m/z* 192.1883. Calcd for $C_{14}H_{24}$: M, 192.1878. Irradiation of the multiplet due to the allylic protons at δ 2.05 using a 400 MHz machine caused the multiplet of the olefinic protons at δ 5.43 to collapse into two doublets (each J=10.7 Hz).

(*Z*)-4-Vinylcyclododecene (13): IR (neat) 3060, 1650, 985, 945, 905, 690 cm^{-1}; ^1H NMR ($CDCl_3$) δ=1.34 and 1.57 (bs and s, 14H), 1.8—2.5 (m, 5H), 4.9—5.2 (m, 2H), 5.35 (m, 2H), 5.7—6.2 (m, 1H); MS *m/z* (rel intensity) 192 (M^+, 2), 135 (25), 121 (29), 95 (67), 81 (100), 67 (92), 54 (75). Found: *m/z* 192.1879. Calcd for $C_{14}H_{24}$: M, 192.1878. Irradiation of the multiplet due to the allylic protons at δ 2.2 caused the multiplet of the olefinic protons at δ 5.35 to collapse into two doublets (each J=10.0 Hz).

(*Z*)-1,12-Tetradecadiene (14a): IR (neat) 3030, 985, 910, 695 cm^{-1}; ^1H NMR ($CDCl_3$) δ=1.28 (s, 14H), 1.60 (d, 3H), 2.00 (m, 4H), 4.8—5.1 (m, 2H), 5.39 (m, 2H), 5.7—6.04 (m, 1H); MS *m/z* (rel intensity) 194 (M^+, 3), 96 (33), 95 (28), 82 (47), 81 (42), 68 (100), 55 (70). Found: *m/z* 194.2069. Calcd for $C_{14}H_{26}$: M, 194.2035. Tetradecadienes **14a** and **14c** were obtained in a ratio of 17:83.

(*Z,Z*)-2,12-Tetradecadiene (14c): IR (neat) 3003, 1655, (w), 965, 690 cm^{-1}; ^1H NMR ($CDCl_3$) δ=1.28 (s, 12H), 1.60 (d, 6H), 2.03 (m, 4H), 5.39 (m, 4H); MS *m/z* (rel intensity) 194 (M^+, 2), 96 (34), 82 (65), 81 (45), 68 (100), 55 (63). Found: *m/z* 194.2051. Calcd for $C_{14}H_{26}$: M, 194.2035.

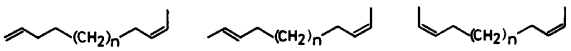

n=6 **14a** **14c**
n=4 **18a** **18b** **18c**

(*Z,Z*)-1,5-Cyclododecadiene (16): IR (neat) 3005, 855, 805, 720 cm^{-1}; ^1H NMR ($CDCl_3$) δ=1.32 and 1.42 (bs and m, total 8H), 2.10 (m, 8H), 5.27 (m, 2H, J=10.7 Hz, J=8.2 Hz), 5.57 (m, 2H, J=10.7 Hz, J=8.2 Hz); MS *m/z* (rel intensity) 164 (M^+, 3), 81 (60), 67 (100), 54 (66). Found: *m/z* 164.1564. Calcd for $C_{12}H_{20}$: M, 164.1564. Irradiation of the multiplet due to the allylic protons at δ 2.10 caused the multiplets at δ 5.27 and δ 5.57 to collapse into the doublets (each J=10.7 Hz).

(*Z*)-4-Vinylcyclodecene (17): IR (neat) 3060, 1635, 990, 968, 915, 705 cm^{-1}; ^1H NMR ($CDCl_3$) δ=1.43 and 1.56 (m and s, total 10H), 2.11 and 2.25 (m and m, 5H), 4.8—5.2 (m, 2H), 5.44 (m, 2H), 5.7—6.2 (m, 1H); MS *m/z* (rel intensity) 164 (M^+, 3), 81 (86), 67 (100), 54 (88). Found: *m/z* 164.1563. Calcd for $C_{12}H_{20}$: M, 164.1563.

A Mixture of Isomeric Dodecadiene (18): IR (neat) 3020, 1650, 968, 910, 700 cm^{-1}; ^1H NMR ($CDCl_3$) δ=1.32 (bs, 8.2H), 1.59 (d, 5.3H), 2.02 (m, 4.0H), 5.41 (m, 4.1H). GLC analysis of the mixture showed the presence of three isomers in a ratio of 14:36:50. Each of these isomers of nearly 80% purity was separated by a preparative GLC (Ucon oil 150 15% on Uniport HB 7000; 120 °C). The first peak was identified to be (*Z*)-1,10-dodecadiene (**18a**): IR (neat) 3030, 990, 910, 700 cm^{-1}; ^1H NMR ($CDCl_3$) δ=1.30 (m, 10H), 1.59 (d, 3H), 1.93—2.05 (m, 4H), 4.9—6.0 (m, 5H); MS *m/z* (rel intensity) 166 (M^+, 4), 81 (40), 68 (100), 55 (56). Found: *m/z* 166.1713. Calcd for $C_{12}H_{22}$: M, 166.1719. The second peak was identified to be (*E,Z*)-2,10-dodecadiene (**18b**): ^1H NMR ($CDCl_3$) δ=1.31 (m, 8H), 1.60 (d, 6H), 1.93—2.05 (m, 4H), 5.42 (m, 4H), MS *m/z* (rel intensity) 166 (M^+, 4), 81 (43), 68 (100), 55 (78). Found: *m/z* 166.1731. Calcd for $C_{12}H_{22}$: M, 166.1721. The third peak was identified to be (*Z,Z*)-2,10-dodecadiene (**18c**): IR (neat) 3030, 700 cm^{-1}; ^1H NMR ($CDCl_3$) δ=1.32 (m, 8H), 1.60 (d, 6H, J=5.0 Hz), 1.93—2.05 (m, 4H), 5.42 (m, 4H); MS *m/z* (rel intensity) 166 (M^+, 4), 81

(34), 68 (100), 55 (65). Found: *m/z* 166.1727. Calcd for $C_{12}H_{22}$: M, 166.1721.

(*Z,Z*)-1,5-Cyclodecadiene (20): IR (neat) 3005, 1650, 945, 700 cm^{-1}; ^1H NMR ($CDCl_3$; 400 MHz) δ=1.50 (m, 4H), 2.16 (m, 4H), 2.35 (m, 4H), 5.33 (m, 4H, J=11.2 Hz), 5.45 (dt, 4H, J=10.7 Hz, J=8.3 Hz); MS *m/z* (rel intensity) 136 (M^+, 38), 107 (34), 95 (64), 94(56), 93 (62), 81 (27), 80 (54), 79 (82), 67 (100), 54 (61). Found: *m/z* 136.1270. Calcd for $C_{10}H_{16}$: M, 136.1253. Irradiation of the multiplet due to the allylic protons at δ 2.35 caused the multiplet at δ 5.33 to collapse into a doublet (J=11.2 Hz). While irradiation of the multiplet at δ 2.16 caused the multiplet at δ 5.45 to collapse into a doublet (J=10.7 Hz).

(*Z*)-4-Vinylcyclooctene (21): IR (neat) 3060, 1660, 990, 910, 700 cm^{-1}; ^1H NMR ($CDCl_3$) δ=1.56 (m, 6H), 2.17 (m, 5H), 4.8—5.2 (m, 2H), 5.40 (m, 1H), 5.6—6.1 (m, 2H); MS *m/z* (rel intensity) 136 (M^+, 17), 121 (35), 107 (32), 95 (49), 94 (44), 93 (43), 82 (40), 81 (37), 80 (45), 79 (71), 67 (100), 54 (63). Found: *m/z* 136.1236. Calcd for $C_{10}H_{16}$: M, 136.1249.

Cyclic Voltammetry. Cyclic voltammetry was carried out with a Nichia potentiostat HP-E_{500H} in combination with a Nichia linear potential scanner. The sweep rate was 0.2 V s^{-1} and a platinum disc (1 mm dia.) was used as a working electrode. Reduction peaks of **5**, **15**, and crotyl bromide in DMF containing 0.1M *n*-Bu_4NClO_4 were observed at −2.00, −2.00, and −1.81 V vs. Ag/AgI. Another reduction peak was observed at −1.32 V only in the case of **15**. The reduction peak of crotyl bromide shifted to −1.65 V when a cyclic voltammetry was carried out in THF containing 0.1M *n*-Bu_4NClO_4.

References

1) M. R. Rifi., *Org. Synth.*, **52**, 22 (1972) and references cited therein.

2) R. Gerdil, *Helv. Chim. Acta*, **53**, 2100 (1970).

3) A. J. Fry and W. E. Britton, *J. Org. Chem.*, **38**, 4016 (1973).

4) K. B. Wiberg and G. A. Epling, *Tetrahedron Lett.*, **1974**, 1119.

5) M. Mitani, Y. Yamamoto, and K. Koyama, *J. Chem. Soc., Chem. Commun.*, **1983**, 1446.

6) S. Satoh, M. Itoh, and M. Tokuda, *J. Chem. Soc., Chem. Commun.*, **1978**, 481; S. Satoh, M. Itoh, H. Suginome, and M. Tokuda, *Bull. Fac. Eng. Hokkaido Univ.*, **102**, 33 (1981).

7) M. Mitani, H. Takeuchi, and K. Koyama, *Chem. Lett.*, **1986**, 2125.

8) E. J. Corey and E. K. W. Wat, *J. Am. Chem. Soc.*, **89**, 2757 (1967).

9) P. J. M. Reijnders, H. R. Fransen, and H. M. Buck., *Recl. Trav. Chim. Pays-Bas.*, **98**, 511 (1979).

10) A. J. Hubert and J. Dale, *J. Chem. Soc.*, **1963**, 4091.

11) J. Graefe, M. Muehlstaedt, and T. Welsch, *Z. Chem.*, **11**, 19 (1971).

12) J. Hanika, I. Svobota, and V. Ruzicka, *Coll. Czech. Chem. Commun.*, **46**, 1039 (1981).

13) J. G. Traynham and H. H. Hsieh, *Tetrahedron Lett.*, **1969**, 3905,; H. Gotthardt and G. S. Hammond, *Chem. Ber.*, **109**, 3767 (1976).

14) I. M. Takakis and W. G. Agosta, *J. Org. Chem.*, **44**, 1294 (1979).

15) A. T. Blomquist, R, E. Burge, Jr., and A. C. Suesy, *J. Am. Chem. Soc.*, **74**, 3636 (1952).

16) M. Ono and M. Okamoto, *Org. Synth.*, **49**, 30 (1969).

17) W. Stumpt and K. Rombusch, *Justus Liebigs Ann. Chem.*, **687**, 136 (1965); G. Haufe, *Synthesis*, **1983**, 235.

18) G. V. Smith and H. Kriloff, *J. Am. Chem. Soc.*, **85**, 2016 (1963).

19) A. J. Bard and A. Merz, *J. Am. Chem. Soc.*, **101**, 2959 (1979).

20) N. S. Isaacs, "Reactive Intermediates in Organic Chemistry," John Wiley and Sons, Ltd., London (1974), pp. 255, 277.

 © 1987 The Chemical Society of Japan Bull. Chem. Soc. Jpn., 60, 2435—2443 (1987)

The Synthesis of (15*R*)-Coleon C and (15*S*)-Coleon C

Takashi MATSUMOTO,* Sachihiko IMAI, and Takashi YOSHINARI
Department of Chemistry, Faculty of Science, Hiroshima University,
Higashisenda-machi, Naka-ku, Hiroshima 730
(Received January 21, 1987)

(15*R*)-11,16-Dihydroxy-12-methoxymethoxy-8,11,13-abietatrien-7-one and its (15*S*)-epimer prepared from a C-15 epimeric mixture of 12-methoxy-8,11,13-abietatrien-16-ol, were transformed into (15*R*)-6,11,12,14,16-pentahydroxy-5,8,11,13-abietatetraen-7-one and its (15*S*)-epimer; these were identical with natural (15*R*)-coleon C and (15*S*)-coleon C, respectively.

Coleon C was first isolated as a mixture of the C-15 epimers from the leaves of *Coleus aquaticus* Gürcke (Labiatae) by Eugster et al.;[1] they[2] later separated the mixture into (15*R*)-coleon C (**1a**) and (15*S*)-coleon C (**1b**). Recently, Burnell et al.[3] reported the synthesis of (15*R*)-coleon C tri-*O*-methyl ether (**2a**) via a (15*R*)-quinone intermediate (**3a**) which was prepared from 12,16-epoxy-8,11,13,15-abietatetraene (**4**) by the following series of reactions. Stereoselective catalytic hydrogenation of **4** gave a mixture of the C-15 epimeric 12,16-epoxy-8,11,13-abietatrienes (**5**) which was oxidized with chromium trioxide in acetic acid to give the epimeric 7-oxo compounds **6**. Further oxidation of **6** with hydrogen peroxide in acetic anhydride containing concentrated sulfuric acid produced two quinones, **3a** and its C-15 epimer **3b**, in a ratio of 5:2. Their stereochemical assignments of C-15 in **3a** and **3b** were based on the stereochemistries of C-15 in the catalytic hydrogenation products **5**, whose stereochemistries were assigned to be 15R for the major product and 15S for the minor product (from examinations of molecular models). However, it seemed to be necessary to confirm the stereochemistries of the hydrogenation products **5** by unambiguous methods. Very recently,[4] we also carried out the catalytic hydrogenation of **4** and assigned the stereochemistry of C-15 in the major product to have a S configuration in contrast to the assignment of Burnell et al. As an extension of our previous work,[4] we here describe the successful syntheses of (15*R*)-coleon C (**1a**) and (15*S*)-coleon C (**1b**) starting from a C-15 epimeric mixture of 12-methoxy-8,11,13-abietatrien-16-ol (**7**)[5] which was previously prepared from (+)-dehydroabietic acid.

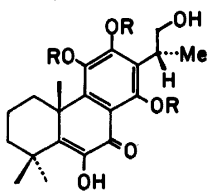

1a R=H
2a R=Me

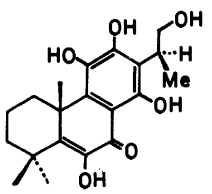

1b

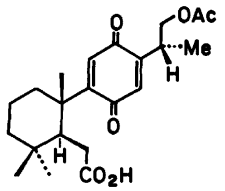

3a

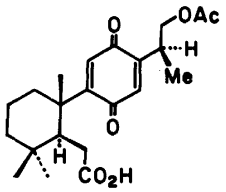

3b

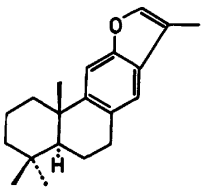

4

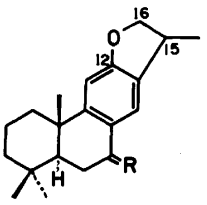

5 R=H_2
6 R=O

Mixture **7** was demethylated with anhydrous aluminium chloride and ethanethiol in dichloromethane to give a mixture of the corresponding diols **8** (90.3%). To introduce an oxygen function at the C-11 position, mixture **8** was submitted to a series of reactions: oxidation with benzoyl peroxide in refluxing chloroform, reduction with lithium aluminium hydride in ether, and acetylation with acetic anhydride in pyridine. Purification of the crude product by column chromatography on silica gel afforded a mixture of the C-15 epimeric triacetates **9** (50.6%) along with a mixture of the C-15 epimeric diacetates **10** (24.8%) which gave back the starting **8** (95.1%) by reduction with lithium aluminium hydride. Oxidation of **9** with chromium trioxide in acetic acid yielded a mixture of the 7-oxo compounds **11a** and **11b** (61.4%). This mixture was then hydrolyzed with dilute hydrochloric acid in refluxing methanol and the crude product was immediately methoxymethylated with a mixture of chloromethyl methyl ether, anhydrous potassium carbonate, and dicyclohexano-18-crown-6 in tetrahydrofuran–dichloromethane (1:1) at room temperature to give 12-methoxymethyl ethers **12a** and **12b** (73.6%) and 12,16-bis(methoxymethyl) ethers **13** (14.3%). The C-15 epimeric mixture of 12-methoxymethyl ether was carefully separated by repeated column chromatography on silica gel and recrystalliza-

tion to afford the pure crystalline 11,16-dihydroxy-12-methoxymethoxy-8,11,13-abietatrien-7-one (**12a**), mp 135—136 °C, and its C-15 epimer **12b**, mp 140—142 °C. In order to assign the absolute configurations of C-15 in these epimers, the compound **12a** was hydrolyzed with dilute hydrochloric acid in refluxing tetrahydrofuran and the resulting triol was acetylated with acetic anhydride in pyridine to give a triacetate (88.5%) which was identical with authentic (15*R*)-11,12,16-triacetoxy-8,11,13-abietatrien-7-one (**11a**).[5] On the other hand, the authentic (15*S*)-triacetate **11b**[5] was hydrolyzed with dilute hydrochloric acid in refluxing methanol and then partially methoxymethylated as described above. Purification of the crude product yielded (15*S*)-11,16-dihydroxy-12-methoxymethoxy-8,11,13-abietatrien-7-one (70.7%) which was identical with **12b**. Thus, the absolute configurations of C-15 in **12a** and **12b** were assigned to be R and S respectively.

Subsequently, conversion of **12a** into (15*R*)-coleon C (**1a**) was carried out as follows. Hydrolysis of **12a** with dilute hydrochloric acid followed by methylation with diazomethane afforded 11,16-dihydroxy-12-methoxy-8,11,13-abietatrien-7-one (**14a**: 64.4%) together with small amounts of 11-hydroxy-12,16-methylenedioxy-8,11,13-abietatrien-7-one (**15a**: 19.8%) and 11-hydroxy-12,16-dimethoxy-8,11,13-abietatrien-7-one (**16a**: 13.9%). For the protection of the hydroxyl groups, **14a** was acetylated with acetic anhydride in pyridine to give a diacetate **17a** (93.9%). This was reduced with sodium borohydride in methanol and the resulting mixture of the epimeric 7-hydroxy compounds was immediately subjected to dehydration with *p*-toluenesulfonic acid in refluxing benzene to give 11,16-diacetoxy-12-methoxy-6,8,11,13-abietatetraene (**18a**: 86.8%). Epoxidation of **18a** with *m*-chloroperbenzoic acid in dichloromethane followed by treatment with *p*-toluenesulfonic acid in refluxing benzene afforded 11,16-diacetoxy-12-methoxy-8,11,13-abietatrien-6-one (**19a**: 79.6%). To introduce an oxygen function at the C-14 position, the 6-oxo compound **19a** was reduced with lithium aluminium hydride in ether and the resulting mixture of the epimeric 6-hydroxy compounds **20a** was immediately oxidized with *m*-chloroperbenzoic acid in methanol to give two *p*-quinones, **21a** (42.5%) and **22a** (6.6%). In the ^{1}H NMR spectrum of **21a**, the downfield shift of a signal (δ=1.69) due to the methyl group at C-10 relative to the corresponding signal (δ=1.36) for **22a** suggested a 1,3-diaxial-*cis*-relationship between the methyl group and the hydroxyl group at C-6. Thus, the structures of **21a** and **22a** were assigned to be 6β,16-dihydroxy-12-methoxy-8,12-abietadiene-11,14-dione and its 6α-hydroxy isomer respectively. Hydrolysis of **21a** with dilute hydrochloric acid in refluxing methanol afforded a trihydroxy quinone, which was partially acetylated with acetic anhydride in pyridine at 0—5 °C to give a 12,16-diacetoxy compound. This was further subjected to reductive acetylation with zinc powder and acetic anhydride in pyridine. The crude product

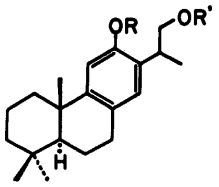

7 R=Me, R'=H
8 R=R'=H
10 R=R'=Ac

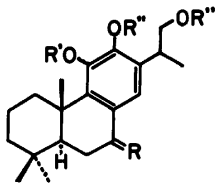

9 R=H$_2$, R'=R''=Ac
13 R=O, R'=H, R''=CH$_2$OMe

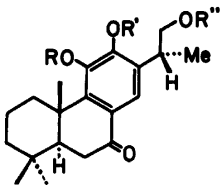

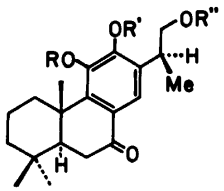

11a	R=R'=R''=Ac	11b
12a	R=R''=H, R'=CH$_2$OMe	12b
14a	R=R''=H, R'=Me	14b
15a	R=H, R'·R''=-CH$_2$-	15b
16a	R=H, R'=R''=Me	16b
17a	R=R''=Ac, R'=Me	17b

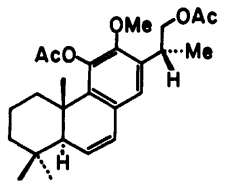

18a

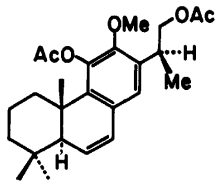

18b

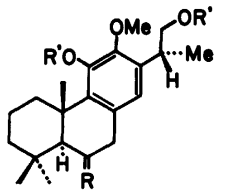

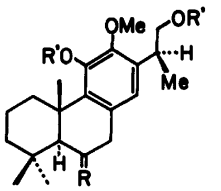

19a	R=O, R'=Ac	19b
20a	R=H·OH, R'=H	20b

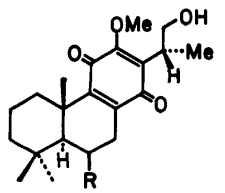

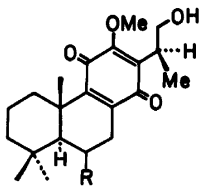

21a	R=β-OH	21b
22a	R=α-OH	22b

was then oxidized with Jones reagent at 0—5 °C to give 11,12,14,16-tetraacetoxy-8,11,13-abietatrien-6-one (**23a**: 21.9% from **21a**) and 11,12-diacetoxy-14,16-epoxy-8,11,13-abietatrien-6-one (**24a**: 23.5% from **21a**). The ^{1}H NMR spectrum of **23a** showed singlet (3H) signals at δ=2.00, 2.27, 2.29, and 2.32 due to four acetoxyl groups, while that of **24a** showed the corresponding signals at δ 2.25 and 2.27 ppm due to two acetoxyl groups and signals at δ=1.23 (3H, doublet), ca. 3.6 (1H, multiplet), 4.10 (1H, double doublet), and 4.69 (1H, triplet) due to a dihydrofuran moiety. The structure of **24a** was further supported from a similarity to its (15*S*)-epimer **24b** which is described later. To introduce a final oxygen function at the C-7 position, the tetraacetate **23a** was oxidized with Jones reagent at room temperature to afford 11,12,16-triacetoxy-14-hydroxy-8,11,13-abietatriene-6,7-dione [(15*R*)-coleon D triacetate] (**25a**: 27.4%). The presence of a hydroxyl group at C-14 in **25a** was supported by its ^{1}H NMR spectrum which showed a singlet signal due to a hydrogen-bonded hydroxyl group at δ 13.33. Compound **25a** was then hydrolyzed with dilute hydrochloric acid in refluxing methanol to give the desired 6,11,12,14,16-pentahydroxy-5,8,11,13-abietatetraen-7-one (**1a**: 98.9%) which was identical with natural (15*R*)-coleon C.

Similar conversion of (15*S*)-12-methoxymethyl ether **12b** into (15*S*)-coleon C (**1b**) was also carried out as follows. Hydrolysis of **12b** with dilute hydrochloric acid followed by methylation with diazomethane afforded 11,16-dihydroxy-12-methoxy-8,11,13-abietatrien-7-one (**14b**: 73.7%) along with small amounts of 12,16-methylenedioxy (**15b**: 13.9%) and 12,16-dimethoxy (**16b**: 12.1%) compounds. The 12-methoxy compound **14b** was acetylated and the resulting diacetate **17b** (90.2%) was transformed into 11,16-diacetoxy-12-methoxy-6,8,11,13-abietatetraene (**18b**: 83.0%) by sodium borohydride reduction and acid-catalyzed dehydration. Oxidation of **18b** with *m*-chloroperbenzoic acid followed by treatment with *p*-toluenesulfonic acid led to the corresponding 6-oxo compound **19b** (79.4%). This was converted into 6β,16-dihydroxy-12-methoxy-8,12-abietadiene-11,14-dione (**21b**: 38.7%) and its 6α-hydroxy isomer **22b** (9.1%) by reduction with lithium aluminium hydride and subsequent oxidation of the epimeric 6-hydroxy compounds **20b** with *m*-chloroperbenzoic acid. The *p*-quinone **21b** was then converted into tetraacetoxy ketone **23b** (66.1%) and diacetoxy ketone **24b** (31.8%) by a series of reactions; hydrolysis with dilute hydrochloric acid in methanol, acetylation with acetic anhydride in pyridine, reductive acetylation with zinc powder and acetic anhydride in pyridine, and oxidation with Jones reagent at 0—5 °C. The ^{1}H NMR spectrum of **24b** showed signals at δ 2.27 (6H, singlet) due to two acetoxyl groups and at δ 1.23 (3H, doublet), ca. 3.6 (1H, multiplet), 4.09 (1H, double doublet), and 4.69 (1H, triplet) due to a dihydrofuran moiety. For a structure determination of **24b**, the following conversion was carried out. Oxidation of the C-7 position in **24b** with Jones reagent afforded a mixture of the 6,7-dioxo compound **28b** and the diosphenol derivative **27b** which was hydrolyzed with dilute hydrochloric acid to give a phenolic compound **29b**. Since the ^{1}H NMR spectrum of **29b** showed no signal in the low field (δ=10—15) due to a hydrogen-bonded hydroxyl group at the C-14 position, the phenolic hydroxyl groups must be located at the C-11 and C-12 positions. Thus, the structure of **24b** was assigned to be 11,12-diacetoxy-14,16-epoxy-8,11,13-abietatrien-6-one. Further oxidation of **23b** with Jones reagent at room temperature produced 11,12,16-triacetoxy-14-hydroxy-8,11,13-abietatriene-6,7-dione [(15*S*)-coleon D triacetate] (**25b**: 54.4%). This was hydrolyzed with dilute hydrochloric acid in

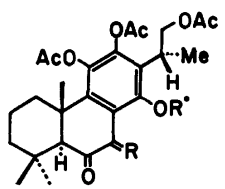

23a R=H$_2$, R'=Ac
25a R=O, R'=H

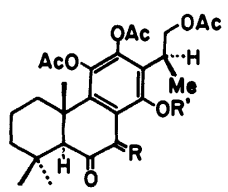

23b
25b

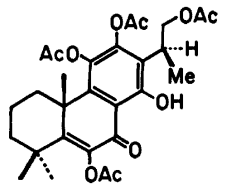

26b

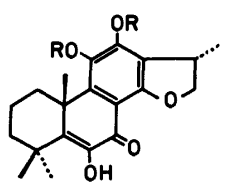

27b R=Ac
29b R=H

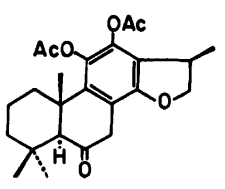

24a

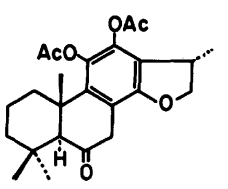

24b

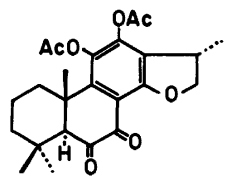

28b

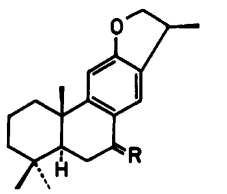

5b R=H$_2$
6b R=O

refluxing methanol to give the desired 6,11,12,14,16-pentahydroxy-5,8,11,13-abietatetraen-7-one (**1b**: 99.7%) which gave the corresponding 6,11,12,16-tetraacetoxy compound **26b** with acetic anhydride in pyridine. The synthetic **1b** was also identical with natural (15*S*)-coleon C.

Finally, in order to confirm the absolute configuration of C-15 in the reported coleon C tri-*O*-methyl ether,[3] (15*S*)-12,16-epoxy-8,11,13-abietatriene[4] (**5b**) prepared by unambiguous methods in our laboratory was converted into the (15*S*)-*p*-quinone **3b**, mp 148—150 °C, via (15*S*)-12,16-epoxy-8,11,13-abietatrien-7-one (**6b**) by the method of Burnell et al.[3] As we would expect, the physical and spectral data of the synthetic **3b** are in good agreement with those of the reported (15*R*)-*p*-quinone (mp 143—145 °C),[3] but different from those of the reported (15*S*)-*p*-quinone (mp 119—120 °C).[3] Therefore, the reported 15R configuration for coleon C tri-*O*-methyl ether and all other compounds derived from the major *p*-quinone in the articles of Burnell et al.[3] must be corrected to the reverse configuration (15*S*).

Experimental

All melting points are uncorrected. The IR spectra and optical rotations were measured in chloroform, and the ^{1}H NMR spectra in deuteriochloroform at 60 MHz, with tetramethylsilane as an internal standard, unless otherwise stated; s: singlet bs: broad singlet, d: doublet, bd: broad doublet, dd: double doublet, t: triplet, m: multiplet. The column chromatography was performed using Merck silica gel (0.063 mm).

8,11,13-Abietatriene-12,16-diol (8). Anhydrous aluminium chloride (8.407 g) was added to a stirred solution of 12-methoxy-8,11,13-abietatrien-16-ol (**7**)[5] (6.651 g) and ethanethiol (9.4 ml) in dichloromethane (67 ml) at 4—10 °C with cooling in an ice-water bath over a 12-min period. After stirring at this temperature for 10 min and at room temperature for 2 h, the mixture was poured into ice-dilute hydrochloric acid and extracted with ether. The ether extract was washed with brine, dried over sodium sulfate, and evaporated in vacuo. The residue was chromatographed on silica gel (60 g), using ether–benzene (4:96) as eluent, to give a mixture of the C-15 epimeric diols **8** (5.739 g: 90.3%).

11,12,16-Triacetoxy-8,11,13-abietatriene (9). A solution of **8** (12.062 g) and benzoyl peroxide (15.078 g) in chloroform (240 ml) was refluxed for 5 h, cooled, and diluted with ether (250 ml). After the addition of acetic acid (60 ml) and aqueous potassium iodide (30%: 200 ml), the mixture was stirred at room temperature for 2 h and then washed successively with water, aqueous sodium thiosulfate, aqueous sodium hydrogencarbonate, and brine. The dried solution was evaporated in vacuo to give the crude product, which was used, without purification, in the next reaction.

A solution of the above crude product in dry ether (80 ml) was added dropwise to a stirred suspension of lithium aluminium hydride (2.876 g) in dry ether (100 ml) with cooling in an ice-water bath over a 20-min period. The mixture was refluxed for 80 min, cooled; the excess lithium aluminium hydride was decomposed with ethyl acetate (20 ml). The mixture was poured into ice-dilute hydrochloric acid and extracted with ether. The ether extract was washed with brine, dried, and evaporated in vacuo. The residue was acetylated with acetic anhydride (15 ml) in pyridine (15 ml) at 75—80 °C for 2 h. After the usual work-up, the crude product was chromatographed on silica gel (200 g), using ether–benzene (1:99) as eluent, to give 12,16-diacetoxy-8,11,13-abietatriene (**10**) (3.824 g: 24.8%). Further elution with ether–benzene (1:9) gave **9** (8.964 g: 50.6%). The IR and ^{1}H NMR spectra of **9** and **10** were identical with those of the corresponding (15*R*)-isomers or (15*S*)-isomers.[5]

A solution of **10** (3.782 g) in dry ether (25 ml) was added dropwise to a stirred suspension of lithium aluminium hydride (483 mg) in dry ether (25 ml) with cooling in an ice-water bath over a 10-min period. The mixture was refluxed for 1 h, poured into ice-dilute hydrochloric acid, and extracted with ether. The ether extract was washed with brine, dried, and evaporated in vacuo to give **8** (2.815 g: 95.1%).

11,12,16-Triacetoxy-8,11,13-abietatrien-7-one (11a,b). Chromium trioxide (4.177 g) was added to a stirred solution of **9** (9.771 g) in acetic acid (80 ml) with cooling in a water bath over a period of 1 h. The mixture was stirred at room temperature for 22 h, diluted with water, and extracted with ether. The ether extract was washed successively with water, aqueous sodium hydrogencarbonate, and brine. The dried solution was evaporated in vacuo. The residue was chromatographed on silica gel (250 g), using ether–benzene (4:96) as eluent, to give the recovered **9** (0.504 g: 5.2%) and a mixture of **11a** and **11b** (6.183 g: 61.4%).

11,16-Dihydroxy-12-methoxymethoxy-8,11,13-abietatrien-7-one (12a,b) and 11-Hydroxy-12,16-dimethoxymethoxy-8,11,13-abietatrien-7-one (13). A mixture of the triacetate (**11a,b**: 8.374 g) and dilute hydrochloric acid (15%: 15 ml) in methanol (80 ml) was refluxed for 2 h. After removal of the methanol in vacuo, the residue was extracted with ether. The ether extract was washed with water, dried, and evaporated in vacuo to give the crude triol (5.603 g).

A mixture of the crude triol (5.603 g), anhydrous potassium carbonate (3.028 g), and dicyclohexano-18-crown-6 (0.282 g) in tetrahydrofuran–dichloromethane (1:1, 100 ml) was stirred at room temperature for 30 min. After the addition of chloromethyl methyl ether (1.65 ml), the mixture was stirred at room temperature for 20 h and then diluted with ether. The ether solution was washed with brine, dried, and evaporated in vacuo. The residue was chromatographed on silica gel (250 g), using ether–benzene (1:9) as eluent, to give **13** (1.095 g: 14.3%) and a mixture of **12a** and **12b** (5.060 g: 73.6%). ^{1}H NMR of **13**: δ=0.94 (3H, s) and 0.97 (3H, s) (-C(CH$_3$)$_2$), 1.19 (d, J=7 Hz) and 1.23 (d, J=7 Hz) (3H, C$_{15}$-CH$_3$), 1.40 (3H, s, C$_{10}$-CH$_3$), 3.26 (3H, s, C$_{16}$-OCH$_2$OCH$_3$), 3.62 (3H, s, C$_{12}$-OCH$_2$OCH$_3$), 4.56 (2H, s, C$_{16}$-OCH$_2$OCH$_3$), 5.03 (2H, s, C$_{12}$-OCH$_2$OCH$_3$), 7.56 (1H, s, C$_{14}$-H).

The mixture (**12a,b**) was separated into the pure **12a**, mp 135—136 °C (from acetone–hexane), $[\alpha]_D$ +44.1° (c 3.93), IR: 3620, 3480, and 1678 cm^{-1}, and **12b**, mp 140—142 °C (from acetone–hexane), $[\alpha]_D$ +5.7° (c 21.98), IR: 3620, 3480, and 1678 cm^{-1}, by repeated column chromatography on silica

gel and recrystallization. ^{1}H NMR of **12a**: δ=0.94 (3H, s) and 0.98 (3H, s) (-C(CH$_3$)$_2$), 1.22 (3H, d, J=6.5 Hz, C$_{15}$-CH$_3$), 1.42 (3H, s, C$_{10}$-CH$_3$), 3.62 (3H, s, -OCH$_3$), 5.02 (2H, s, -OCH$_2$O-), 7.28 (1H, s, C$_{11}$-OH), 7.52 (1H, s, C$_{14}$-H). ^{1}H NMR of **12b**: δ=0.97 (3H, s) and 0.99 (3H, s) (-C(CH$_3$)$_2$), 1.19 (3H, d, J=6.5 Hz, C$_{15}$-CH$_3$), 1.42 (3H, s, C$_{10}$-CH$_3$), 3.63 (3H, s, -OCH$_3$), 5.07 (2H, s, -OCH$_2$O-), 7.32 (1H, s, C$_{11}$-OH), 7.56 (1H, s, C$_{14}$-H). Anal. of **12a**; Found: C, 70.46; H, 8.66%. Calcd for $C_{22}H_{32}O_5$: C, 70.18; H, 8.57%. Anal. of **12b**; Found: C, 70.40; H, 8.82%. Calcd for $C_{22}H_{32}O_5$: C, 70.18; H, 8.57%.

Conversion of 12a into (15*R*)-11,12,16-Triacetoxy-8,11,13-abietatrien-7-one (11a). A mixture of **12a** (155.0 mg) and dilute hydrochloric acid (15%: 0.2 ml) in tetrahydrofuran (1.0 ml) was refluxed for 3 h. The mixture was cooled, diluted with ether, and then washed with brine. The dried solution was evaporated in vacuo to give (15*R*)-11,12,16-trihydroxy-8,11,13-abietatrien-7-one which was recrystallized from acetone-hexane, mp 250—252 °C. ^{1}H NMR (acetone-d_6) δ=0.95 (3H, s) and 0.99 (3H, s) (-C(CH$_3$)$_2$), 1.29 (3H, d, J=7 Hz, C$_{15}$-CH$_3$), 1.41 (3H, s, C$_{10}$-CH$_3$), 7.33 (1H, s, C$_{14}$-H).

The above trihydroxy ketone was acetylated with acetic anhydride (0.5 ml) in pyridine (0.5 ml) at 85—90 °C for 2 h. After the usual work-up, the crude product was chromatographed on silica gel (10 g), using ether-benzene (5:95) as eluent, to give **11a** (167.0 mg: 88.5%), $[\alpha]_D$ +65.0° (c 2.77). The IR and ^{1}H NMR spectra of **11a** were identical with those of authentic (15*R*)-11,12,16-triacetoxy-8,11,13-abietatrien-7-one.[5]

Conversion of (15*S*)-11,12,16-Triacetoxy-8,11,13-abietatrien-7-one (11b) into 12b. A mixture of **11b**[5] (3.251 g) and dilute hydrochloric acid (15%: 5.0 ml) in methanol (30 ml) was refluxed for 2 h. After removal of the methanol in vacuo, the residue was extracted with ether. The ether extract was washed with brine, dried, and evaporated in vacuo to give (15*S*)-11,12,16-trihydroxy-8,11,13-abietatrien-7-one which was recrystallized from acetone-hexane, mp 228—230 °C, ^{1}H NMR (acetone-d_6) δ=0.97 (3H, s) and 1.01 (3H, s) (-C(CH$_3$)$_2$), 1.30 (3H, d, J=7 Hz, C$_{15}$-CH$_3$), 1.44 (3H, s, C$_{10}$-CH$_3$), 7.42 (1H, s, C$_{14}$-H).

A mixture of the above trihydroxy ketone (2.500 g), anhydrous potassium carbonate (1.274 g), and dicyclohexano-18-crown-6 (187 mg) in tetrahydrofuran-dichloromethane (1:1, 40 ml) was stirred at room temperature for 30 min. After the addition of chloromethyl methyl ether (0.69 ml), the mixture was stirred at room temperature for 18 h and then diluted with ether. The ether solution was washed with brine, dried, and evaporated in vacuo. The residue was chromatographed on silica gel (100 g), using ether-benzene (2:8) as eluent, to give (15*S*)-11,16-dihydroxy-12-methoxymethoxy-8,11,13-abietatrien-7-one (1.886 g: 70.7%), mp 140—142 °C (from acetone-hexane), whose IR and ^{1}H NMR spectra were identical with those of **12b**.

Hydrolysis and Methylation of 12a. A mixture of **12a** (1.580 g) and dilute hydrochloric acid (15%: 1.0 ml) in tetrahydrofuran (10 ml) was refluxed for 1.5 h. After removal of the tetrahydrofuran in vacuo, the reidue was extracted with ether. The ether extract was washed with brine, dried, and evaporated in vacuo to give the crude trihydroxy ketone.

A suspension of the above trihydroxy ketone in acetone-ether (1:4, 25 ml) was methylated with diazomethane in ether at room temperature for 3 h. After the usual work-up, the crude product was recrystallized from acetone-hexane to give (15*R*)-11,16-dihydroxy-12-methoxy-8,11,13-abietatrien-7-one (**14a**) (650 mg: 44.7%), mp 199—200.5 °C, $[\alpha]_D$ +41.2° (c 2.50), IR: 3490 and 1675 cm^{-1}; ^{1}H NMR δ=0.95 (3H, s) and 0.99 (3H, s) (-C(CH$_3$)$_2$), 1.26 (3H, d, J=7 Hz, C$_{15}$-CH$_3$), 1.42 (3H, s, C$_{10}$-CH$_3$), 3.73 (2H, bd, J=7 Hz, -CH$_2$OH), 3.84 (3H, s, -OCH$_3$), 6.29 (1H, s, C$_{11}$-OH), 7.58 (1H, s, C$_{14}$-H). Found: C, 72.71; H, 8.64%. Calcd for $C_{21}H_{30}O_4$: C, 72.80; H, 8.73%. The mother liquor of recrystallization was evaporated in vacuo and the residue was chromatographed on silica gel (50 g), using ether-benzene (1:9) as eluent, to give (15*R*)-11-hydroxy-12,16-methylenedioxy-8,11,13-abietatrien-7-one (**15a**) (286 mg: 19.8%) which was recrystallized from acetone-hexane, mp 182.5—183 °C, $[\alpha]_D$ +94.8° (c 1.54), IR: 3510 and 1675 cm^{-1}; ^{1}H NMR δ=0.95 (3H, s) and 0.99 (3H, s) (-C(CH$_3$)$_2$), 1.32 (3H, d, J=7 Hz, C$_{15}$-CH$_3$), 1.40 (3H, s, C$_{10}$-CH$_3$), 4.77 (1H, d, J=7 Hz) and 5.37 (1H, d, J=7 Hz) (-OCH$_2$O-), 6.24 (1H, s, C$_{11}$-OH), 7.49 (1H, s, C$_{14}$-H). MS (m/z): 344 (M$^+$). Found: C, 73.32; H, 8.28%. Calcd for $C_{21}H_{28}O_4$: C, 73.22; H, 8.19%.

Subsequent elution gave (15*R*)-11-hydroxy-12,16-dimethoxy-8,11,13-abietatrien-7-one (**16a**) (210 mg: 13.9%) which was recrystallized from hexane, mp 181—182.5 °C, $[\alpha]_D$ +20.0° (c 2.00), IR: 3505 and 1676 cm^{-1}, ^{1}H NMR δ=0.95 (3H, s) and 0.99 (3H, s) (-C(CH$_3$)$_2$), 1.23 (3H, d, J=6.5 Hz, C$_{15}$-CH$_3$), 1.41 (3H, s, C$_{10}$-CH$_3$), 3.31 (3H, s, C$_{16}$-OCH$_3$), 3.82 (3H, s, C$_{12}$-OCH$_3$), 6.11 (1H, s, C$_{11}$-OH), 7.59 (1H, s, C$_{14}$-H). Found: C, 73.17; H, 9.24%. Calcd for $C_{22}H_{32}O_4$: C, 73.30; H, 8.95%.

Further elution with ether-benzene (1:4) gave an additional **14a** (287 mg: 19.7%).

Hydrolysis and Methylation of 12b. The 12-methoxymethyl ether **12b** (690 mg) was hydrolyzed with dilute hydrochloric acid (15%: 0.5 ml) in refluxing tetrahydrofuran (5.0 ml) for 1.5 h. The crude trihydroxy ketone was then methylated with diazomethane in ether at room temperature for 4 h to give the following three compound **14b**, **15b**, and **16b**.

(15*S*)-11,16-Dihydroxy-12-methoxy-8,11,13-abietatrien-7-one (**14b**) (468 mg: 73.7%), mp 240—241 °C (from acetone-hexane), $[\alpha]_D$ −18.8° (c 0.59), ^{1}H NMR δ=0.94 (3H, s) and 0.98 (3H, s) (-C(CH$_3$)$_2$), 1.22 (3H, d, J=7 Hz, C$_{15}$-CH$_3$), 1.40 (3H, s, C$_{10}$-CH$_3$), 3.70 (2H, bd, J=7 Hz, -CH$_2$OH), 3.82 (3H, s, -OCH$_3$), 6.09 (1H, s, C$_{11}$-OH), 7.59 (1H, s, C$_{14}$-H). Found: C, 72.58; H, 8.67%. Calcd for $C_{21}H_{30}O_4$: C, 72.80; H, 8.73%.

(15*S*)-11-Hydroxy-12,16-methylenedioxy-8,11,13-abietatrien-7-one (**15b**) (88 mg: 13.9%), mp 210—211 °C (from acetone-hexane), $[\alpha]_D$ −41.0° (c 1.88), ^{1}H NMR: δ=0.97 (3H, s) and 1.00 (3H, s) (-C(CH$_3$)$_2$), 1.35 (3H, d, J=7 Hz, C$_{15}$-CH$_3$), 1.42 (3H, s, C$_{10}$-CH$_3$), 4.80 (1H, d, J=7 Hz) and 5.38 (1H, d, J=7 Hz) (-OCH$_2$O-), 6.35 (1H, s, C$_{11}$-OH), 7.53 (1H, s, C$_{14}$-H). Found: C, 73.24; H, 7.91%. Calcd for $C_{21}H_{28}O_4$: C, 73.22; H, 8.19%.

(15*S*)-11-Hydroxy-12,16-dimethoxy-8,11,13-abietatrien-7-one (**16b**) (80 mg: 12.1%), mp 169.5—171 °C (from hexane), $[\alpha]_D$ +9.2° (c 1.20), ^{1}H NMR δ=0.97 (3H, s) and 1.00 (3H, s)

(-C(CH$_3$)$_2$), 1.24 (3H, d, J=6.5 Hz, C$_{15}$-CH$_3$), 1.42 (3H, s, C$_{10}$-CH$_3$), 3.35 (3H, s, C$_{16}$-OCH$_3$), 3.84 (3H, s, C$_{12}$-OCH$_3$), 6.18 (1H, s, C$_{11}$-OH), 7.60 (1H, s, C$_{14}$-H). Found: C, 73.29; H, 8.93%. Calcd for $C_{22}H_{32}O_4$: C, 73.30; H, 8.95%.

(15*R*)-11,16-Diacetoxy-12-methoxy-8,11,13-abietatrien-7-one (17a) and Its (15*S*)-Epimer (17b). *a*): A mixture of **14a** (1.441 g) and acetic anhydride (3.0 ml) in pyridine (4.0 ml) was heated at 75—80 °C for 2 h. After the usual work-up, the crude product was chromatographed on silica gel (30 g), using ether-benzene (1:9) as eluent, to give **17a** (1.681 g: 93.9%), $[\alpha]_D$ +51.9° (*c* 10.01), IR: 1767, 1733, and 1680 cm^{-1}; ^{1}H NMR δ=0.98 (3H, s) and 1.00 (3H, s) (-C(CH$_3$)$_2$), 1.31 (3H, d, J=7 Hz, C$_{15}$-CH$_3$), 1.37 (3H, s, C$_{10}$-CH$_3$), 2.03 (3H, s, C$_{16}$-OCOCH$_3$), 2.38 (3H, s, C$_{11}$-OCOCH$_3$), 3.48 (1H, m, C$_{15}$-H), 3.79 (3H, s, C$_{12}$-OCH$_3$), 4.13 (2H, bd, J=7 Hz, -CH$_2$OAc), 7.98 (1H, s, C$_{14}$-H). Found: C, 69.86; H, 7.85%. Calcd for $C_{25}H_{34}O_6$: C, 69.74; H, 7.96%.

b): A mixture of **14b** (410.0 mg) and acetic anhydride (2.0 ml) in pyridine (3.0 ml) was heated at 75—80 °C for 2 h to give **17b** (459.6 mg: 90.2%), $[\alpha]_D$ +13.0° (*c* 2.77), IR: 1767, 1733, and 1680 cm^{-1}; ^{1}H NMR δ=0.98 (3H, s) and 1.00 (3H, s) (-C(CH$_3$)$_2$), 1.28 (3H, d, J=7 Hz, C$_{15}$-CH$_3$), 1.37 (3H, s, C$_{10}$-CH$_3$), 2.03 (3H, s, C$_{16}$-OCOCH$_3$), 2.38 (3H, s, C$_{11}$-OCOCH$_3$), 3.46 (1H, m, C$_{15}$-H), 3.78 (3H, s, C$_{12}$-OCH$_3$), 4.16 (2H, bd, J=7 Hz, -CH$_2$OAc), 7.97 (1H, s, C$_{14}$-H). Found: C, 69.54; H, 8.21%. Calcd for $C_{25}H_{34}O_6$: C, 69.74; H, 7.96%.

(15*R*)-11,16-Diacetoxy-12-methoxy-6,8,11,13-abietatetraene (18a) and Its (15*S*)-Epimer (18b). *a*): A mixture of **17a** (915.5 mg) and sodium borohydride (40.2 mg) in methanol (5.0 ml) was stirred at 0—5 °C for 30 min and at room temperature for 1 h. The mixture was diluted with ether, acidified with dilute hydrochloric acid, and then extracted with ether. The ether extract was washed with brine, dried, and evaporated in vacuo. The residue was refluxed with *p*-toluenesulfonic acid (100 mg) in dry benzene (10 ml) for 1 h, cooled, and diluted with ether. The ether solution was washed with water, dried, and evaporated in vacuo. The crude product was chromatographed on silica gel (40 g), using ether-benzene (5:95) as eluent, to give **18a** (765.2 mg: 86.8%). This was recrystallized from hexane, mp 79.5—81 °C, $[\alpha]_D$ −76.9° (*c* 4.85), IR: 1745sh and 1730 cm^{-1}; ^{1}H NMR δ=0.98 (3H, s) and 1.02 (3H, s) (-C(CH$_3$)$_2$), 1.12 (3H, s, C$_{10}$-CH$_3$), 1.26 (3H, d, J=7 Hz, C$_{15}$-CH$_3$), 2.01 (3H, s, C$_{16}$-OCOCH$_3$), 2.31 (3H, s, C$_{11}$-OCOCH$_3$), 3.71 (3H, s, C$_{12}$-OCH$_3$), 4.08 (2H, d, J=7 Hz, -CH$_2$OAc), 5.89 (1H, dd, J=9.5 and 3 Hz, C$_6$-H), 6.43 (1H, dd, J=9.5 and 3 Hz, C$_7$-H), 6.78 (1H, s, C$_{14}$-H). Found: C, 72.20; H, 8.30%. Calcd for $C_{25}H_{34}O_5$: C, 72.43; H, 8.27%.

b): The ketone **17b** (437.0 mg) was treated as described in *a*) to give **18b** (349.4 mg: 83.0%), $[\alpha]_D$ −74.0° (*c* 2.65), IR: 1745sh and 1730 cm^{-1}, ^{1}H NMR δ=0.98 (3H, s) and 1.02 (3H, s) (-C(CH$_3$)$_2$), 1.12 (3H, s, C$_{10}$-CH$_3$), 1.22 (3H, d, J=7 Hz, C$_{15}$-CH$_3$), 2.03 (3H, s, C$_{16}$-OCOCH$_3$), 2.32 (3H, s, C$_{11}$-OCOCH$_3$), 3.72 (3H, s, C$_{12}$-OCH$_3$), 4.15 (2H, d, J=7 Hz, -CH$_2$OAc), 5.92 (1H, dd, J=9.5 and 3 Hz, C$_6$-H), 6.45 (1H, dd, J=9.5 and 3 Hz, C$_7$-H), 6.78 (1H, s, C$_{14}$-H). Found: C, 72.51; H, 8.18%. Calcd for $C_{25}H_{34}O_5$: C, 72.43; H, 8.27%.

(15*R*)-11,16-Diacetoxy-12-methoxy-8,11,13-abietatrien-6-one (19a) and Its (15*S*)-Epimer (19b). *a*): A mixture of **18a** (1.335 g) and *m*-chloroperbenzoic acid (80%: 1.042 g) in dichloromethane (10 ml) was stirred at 0—5 °C for 30 min and at room temperature for 2.5 h. The mixture was diluted with ether (30 ml) and washed successively with aqueous potassium iodide, aqueous sodium thiosulfate, aqueous sodium hydrogencarbonate, and brine. The dried solution was evaporated in vacuo. The residual oil was refluxed with *p*-toluenesulfonic acid (100 mg) in dry benzene (10 ml) for 1 h, cooled, and diluted with ether. The ether solution was washed successively with water, aqueous sodium hydrogencarbonate, and water. The dried solution was evaporated in vacuo. The crude product was chromatographed on silica gel (30 g), using ether-benzene (1:9) as eluent, to give an oily **19a** (1.104 g: 79.6%), $[\alpha]_D$ +92.1° (*c* 6.17), IR: 1767 and 1720 cm^{-1}, ^{1}H NMR δ=1.06 (3H, s), 1.23 (3H, s), and 1.33 (3H, s) (-C(CH$_3$)$_2$ and C$_{10}$-CH$_3$), 1.28 (3H, d, J=7 Hz, C$_{15}$-CH$_3$), 2.03 (3H, s, C$_{16}$-OCOCH$_3$), 2.36 (3H, s, C$_{11}$-OCOCH$_3$), 2.59 (1H, s, C$_5$-H), 3.72 (3H, s, C$_{12}$-OCH$_3$), 4.10 (2H, d, J=7 Hz, -CH$_2$OAc), 6.78 (1H, s, C$_{14}$-H). Found: C, 69.84; H, 7.91%. Calcd for $C_{25}H_{34}O_6$: C, 69.74; H, 7.96%.

b): The tetraene **18b** (1.019 g) was treated as described in *a*) to give an oily **19b** (840 mg: 79.4%), $[\alpha]_D$ +84.7° (*c* 2.36), IR: 1765 and 1720 cm^{-1}, ^{1}H NMR δ=1.06 (3H, s), 1.23 (3H, s), and 1.33 (3H, s) (-C(CH$_3$)$_2$ and C$_{10}$-CH$_3$), 1.23 (3H, d, J=7 Hz, C$_{15}$-CH$_3$), 2.03 (3H, s, C$_{16}$-OCOCH$_3$), 2.36 (3H, s, C$_{11}$-OCOCH$_3$), 2.58 (1H, s, C$_5$-H), 3.72 (3H, s, C$_{12}$-OCH$_3$), 4.14 (2H, d, J=7 Hz, -CH$_2$OAc), 6.79 (1H, s, C$_{14}$-H). Found: C, 69.59; H, 7.68%. Calcd for $C_{25}H_{34}O_6$: C, 69.74; H, 7.96%.

Conversion of 19a into (15*R*)-6β,16-Dihydroxy-12-methoxy-8,12-abietadiene-11,14-dione (21a) and Its 6α-Hydroxy Isomer (22a). A mixture of **19a** (1.074 g) and lithium aluminium hydride (142 mg) in dry ether (10 ml) was refluxed for 1.5 h. The mixture was poured into ice-dilute hydrochloric acid and extracted with ether. The ether extract was washed with brine, dried, and evaporated in vacuo to give a mixture of the C-6 epimeric triols **20a** (822 mg). This was recrystallized from acetone-hexane to give (15*R*)-12-methoxy-8,11,13-abietatriene-6β,11,16-triol, mp 201—203 °C, IR (KBr): 3515 and 3490—3350 cm^{-1}, ^{1}H NMR (acetone-d_6) δ=1.02 (3H, s) and 1.30 (3H, s) (-C(CH$_3$)$_2$), 1.20 (3H, d, J=7 Hz, C$_{15}$-CH$_3$), 1.72 (3H, s, C$_{10}$-CH$_3$), 3.69 (3H, s, C$_{12}$-OCH$_3$), 4.57 (1H, m, $W_{1/2}$=7 Hz, C$_6$-H), 6.35 (1H, s, C$_{14}$-H). Found: C, 72.47; H, 9.34%. Calcd for $C_{21}H_{32}O_4$: C, 72.38; H, 9.26%.

A mixture of **20a** (503 mg) and *m*-chloroperbenzoic acid (80%: 623 mg) in methanol (7.0 ml) was stirred at room temperature for 4 h and then diluted with ether (50 ml). The ether solution was washed successively with aqueous potassium iodide, aqueous sodium thiosulfate, aqueous sodium hydrogencarbonate, and brine. The dried solution was evaporated in vacuo. The residue was chromatographed on silica gel (30 g), using ether-chloroform (1:9) as eluent, to give **21a** (235 mg: 42.5%) which was recrystallized from acetone-hexane, mp 178—180 °C, $[\alpha]_D$ −73.8° (*c* 0.65). IR: 3600, 3450, 1658, and 1638 cm^{-1}; ^{1}H NMR δ=1.01 (3H, s) and 1.27 (3H, s) (-C(CH$_3$)$_2$), 1.18 (3H, d, J=7 Hz, C$_{15}$-CH$_3$), 1.69 (3H, s, C$_{10}$-CH$_3$), 3.72 (2H, bd, J=7 Hz, -CH$_2$OH), 3.91 (3H, s, C$_{12}$-OCH$_3$), 4.62 (1H, $W_{1/2}$=8 Hz, C$_6$-H). Found: C, 69.81; H, 8.37%. Calcd for $C_{21}H_{30}O_5$: C, 69.58; H, 8.34%. Further elution with ether-chloroform (1:4) gave **22a** as an

oil (37 mg: 6.6%), ^{1}H NMR δ=1.13 (3H, s) and 1.20 (3H, s) (-C(CH$_3$)$_2$), 1.16 (3H, d, J=7 Hz, C$_{15}$-CH$_3$), 1.36 (3H, s, C$_{10}$-CH$_3$), 3.87 (3H, s, C$_{12}$-OCH$_3$).

Conversion of 19b into (15*S*)-6β,16-Dihydroxy-12-methoxy-8,12-abietadiene-11,14-dione (21b) and Its 6α-Hydroxy Isomer (22b). A mixture of **19b** (725.0 mg) and lithium aluminium hydride (95.9 mg) in dry ether (8.0 ml) was refluxed for 1.5 h. The crude product **20b** (533.8 mg) was recrystallized from acetone-hexane to give (15*S*)-12-methoxy-8,11,13-abietatriene-6β,11,16-triol, mp 186—188 °C, IR (KBr): 3480 and 3370 cm^{-1}, ^{1}H NMR (acetone-d_6) δ=1.03 (3H, s) and 1.31 (3H, s) (-C(CH$_3$)$_2$), 1.19 (3H, d, J=7 Hz, C$_{15}$-CH$_3$), 1.73 (3H, s, C$_{10}$-CH$_3$), 3.71 (3H, s, C$_{12}$-OCH$_3$), 4.60 (1H, $W_{1/2}$=7 Hz, C$_6$-H), 6.38 (1H, s, C$_{14}$-H). Found: C, 72.25; H, 9.18%. Calcd for C$_{21}$H$_{32}$O$_4$: C, 72.38; H, 9.26%.

A mixture of **20b** (310.4 mg) and *m*-chloroperbenzoic acid (80%: 384.3 mg) in methanol (5.0 ml) was stirred at room temperature for 4 h. The crude product was chromatographed on silica gel (20 g), using ether-chloroform (1:4) as eluent, to give **21b** (137.3 mg: 38.7%) which was recrystallized from acetone-hexane, mp 183—185 °C, [α]$_D$ −63.6° (c 2.06), IR: 3615, 3450, 1660, 1642, and 1602 cm^{-1}; ^{1}H NMR δ=0.99 (3H, s) and 1.25 (3H, s) (-C(CH$_3$)$_2$), 1.14 (3H, d, J=7 Hz, C$_{15}$-CH$_3$), 1.67 (3H, s, C$_{10}$-CH$_3$), 3.72 (2H, bd, J=7 Hz, -CH$_2$OH), 3.91 (3H, s, C$_{12}$-OCH$_3$), 4.60 (1H, $W^1_{/2}$=8 Hz, C$_6$-H). Found: C, 69.31; H, 8.48%. Calcd for C$_{21}$H$_{30}$O$_5$: C, 69.58; H, 8.34%. Further elution gave **22b** as an oil (32.3 mg: 9.1%), IR: 3600, 3450, 1660, and 1640 cm^{-1}; ^{1}H NMR δ=1.12 (3H, s) and 1.20 (3H, s) (-C(CH$_3$)$_2$), 1.15 (3H, d, J=7 Hz, C$_{15}$-CH$_3$), 1.36 (3H, s, C$_{10}$-CH$_3$), 3.88 (3H, s, C$_{12}$-OCH$_3$).

(15*R*)-11,12,14,16-Tetraacetoxy-8,11,13-abietatrien-6-one (23a) and (15*R*)-11,12-Diacetoxy-14,16-epoxy-8,11,13-abietatrien-6-one (24a). A mixture of **21a** (341.5 mg) and dilute hydrochloric acid (5%: 0.3 ml) in methanol (3.0 ml) was refluxd for 30 min and then diluted with ethyl acetate. The solution was washed with water, dried, and evaporated in vacuo to give a crude triol, ^{1}H NMR δ=1.01 (3H, s) and 1.27 (3H, s) (-C(CH$_3$)$_2$), 1.63 (3H, s, C$_{10}$-CH$_3$), 4.60 (1H, $W_{1/2}$=7 Hz, C$_6$-H).

The crude triol was acetylated with acetic anhydride (1.0 ml) in pyridine (3.0 ml) at 0—5 °C for 1 h. The mixture was diluted with ethyl acetate and washed successively with dilute hydrochloric acid, aqueous sodium hydrogencarbonate, and brine. The dried solution was evaporated in vacuo to give a crude diacetate, ^{1}H NMR δ=1.01 (3H, s) and 1.27 (3H, s) (-C(CH$_3$)$_2$), 1.67 (3H, s, C$_{10}$-CH$_3$), 1.99 (3H, s, C$_{16}$-OCOCH$_3$), 2.31 (3H, s, C$_{12}$-OCOCH$_3$), 4.21 (2H, d, J=7 Hz, -CH$_2$OAc), 4.62 (1H, $W_{1/2}$=7 Hz, C$_6$-H).

A mixture of the crude diacetate, acetic anhydride (1.0 ml), and zinc powder (90 mg) in pyridine (3.0 ml) was stirred at 0—5 °C for 1 h. After the addition of ether, zinc powder was removed and the organic solution was washed successively with dilute hydrochloric acid, aqueous sodium hydrogencarbonate, and brine. The dried solution was evaporated in vacuo. The residue was oxidized with Jones reagent (2.5 mol dm^{-3}: 0.57 ml) in acetone (2.0 ml) with cooling in an ice-water bath for 3 min. After the addition of ether, the mixture was washed with water, dried, and evaporated in vacuo. The crude product was chromatographed on silica gel (12 g), using ether-benzene (1:99) as eluent, to give **24a** (91.9 mg: 23.5%), [α]$_D$ +53.2° (c 1.32), IR: 1770 and 1719 cm^{-1}, ^{1}H NMR (90 MHz) δ=1.01 (3H, s), 1.22 (3H, s), and 1.33 (3H, s) (-C(CH$_3$)$_2$ and C$_{10}$-CH$_3$), 1.23 (3H, d, J=7 Hz, C$_{15}$-CH$_3$), 2.25 (3H, s) and 2.27 (3H, s) (C$_{11}$-OCOCH$_3$ and C$_{12}$-OCOCH$_3$), 2.60 (1H, s, C$_5$-H), 3.18 (1H, d, J=21 Hz) and 3.57 (1H, d, J=21 Hz) (-COCH$_2$-), 4.10 (1H, dd, J=7 and 8 Hz) and 4.69 (1H, t, J=9 Hz) (-OCH$_2$-). Found: C, 69.67; H, 7.43%. Calcd for C$_{24}$H$_{30}$O$_6$: C, 69.54; H, 7.30%. Further elution with ether-benzene (1:9) gave **23a** (106.6 mg: 21.9%) which was recrystallized from methanol, mp 214.5—217.5 °C, [α]$_D$ +37.4° (c 1.23), IR: 1776 and 1725 cm^{-1}, ^{1}H NMR (90 MHz) δ=1.01 (3H, s), 1.19 (3H, s), and 1.31 (3H, s) (-C(CH$_3$)$_2$ and C$_{10}$-CH$_3$), 1.18 (3H, d, J=7 Hz, C$_{15}$-CH$_3$), 2.00 (3H, s, C$_{16}$-OCOCH$_3$), 2.27 (3H, s), 2.29 (3H, s), and 2.32 (3H, s) (C$_{11}$-OCOCH$_3$, C$_{12}$-OCOCH$_3$, and C$_{14}$-OCOCH$_3$), 2.62 (1H, s, C$_5$-H), 3.16 (1H, d, J=21 Hz) and 3.42 (1H, d, J=21 Hz) (-COCH$_2$-), 4.03 (1H, dd, J=8 and 9.5 Hz) and 4.30 (1H, dd, J=8 and 9.5 Hz) (-CH$_2$OAc). Found: C, 65.38; H, 7.29%. Calcd for C$_{28}$H$_{36}$O$_9$: C, 65.10; H, 7.03%.

(15*S*)-11,12,14,16-Tetraacetoxy-8,11,13-abietatrien-6-one (23b) and (15*S*)-11,12-Diacetoxy-14,16-epoxy-8,11,13-abietatrien-6-one (24b). The quinone **21b** (19.0 mg) was hydrolyzed with dilute hydrochloric acid (5%: 0.1 ml) in refluxing methanol (1.0 ml) for 30 min to give a crude triol (19.0 mg), ^{1}H NMR δ=1.01 (3H, s) and 1.25 (3H, s) (-C(CH$_3$)$_2$), 1.28 (3H, d, J=7 Hz, C$_{15}$-CH$_3$), 1.61 (3H, s, C$_{10}$-CH$_3$), 4.60 (1H, $W_{1/2}$=7 Hz, C$_6$-H).

The crude triol (19.0 mg) was acetylated with acetic anhydride (0.5 ml) in pyridine (0.5 ml) at 0—5 °C for 1 h to give a crude diacetate (20.0 mg), ^{1}H NMR δ=1.00 (3H, s) and 1.25 (3H, s) (-C(CH$_3$)$_2$), 1.64 (3H, s, C$_{10}$-CH$_3$), 1.97 (3H, s, C$_{16}$-OCOCH$_3$), 2.30 (3H, s, C$_{12}$-OCOCH$_3$), 4.20 (2H, d, J=7 Hz, -CH$_2$OAc), 4.62 (1H, $W_{1/2}$=7 Hz, C$_6$-H).

A mixture of the crude diacetate (20.0 mg), acetic anhydride (0.5 ml), and zinc powder (50 mg) in pyridine (0.5 ml) was stirred at 0—5 °C for 1 h. After the addition of ether, zinc powder was removed and the ether solution was washed successively with dilute hydrochloric acid, aqueous sodium hydrogencarbonate, and brine. The dried solution was evaporated in vacuo to give an oil (26.0 mg).

The above oil (26.0 mg) in acetone (1.0 ml) was oxidized with Jones reagent (2.5 mol dm^{-3}: 0.03 ml) at 0—5 °C for 3 min. After the addition of ether and water, the ether solution was washed with brine, dried, and evaporated in vacuo. The residue was chromatographed on silica gel (5 g), using ether-benzene (5:95) as eluent, to give **24b** (6.9 mg: 31.8%) which was recrystallized from acetone-hexane, mp 186.5—188.5 °C, [α]$_D$ +107.2° (c 2.92), IR: 1769 and 1720 cm^{-1}, ^{1}H NMR (90 MHz) δ=1.02 (3H, s), 1.20 (3H, s), and 1.32 (3H, s) (-C(CH$_3$)$_2$ and C$_{10}$-CH$_3$), 1.23 (3H, d, J=7 Hz, C$_{15}$-CH$_3$), 2.27 (6H, s, C$_{11}$-OCOCH$_3$ and C$_{12}$-OCOCH$_3$), 2.63 (1H, s, C$_5$-H), 3.18 (1H, d, J=21 Hz) and 3.57 (1H, d, J=21 Hz) (-COCH$_2$-), 4.09 (1H, dd, J=7 and 8 Hz) and 4.69 (1H, t, J=9 Hz) (-OCH$_2$-). Found: C, 69.81; H, 7.59%. Calcd for C$_{24}$H$_{30}$O$_6$: C, 69.54; H, 7.30%. Further elution with ether-benzene (1:9) gave **23b** as an oil (17.9 mg: 66.1%), [α]$_D$ +77.4° (c 0.84), IR: 1771 and 1721 cm^{-1}, ^{1}H NMR (90 MHz) δ=1.01 (3H, s), 1.20 (3H, s), and 1.32 (3H, s) (-C(CH$_3$)$_2$ and C$_{10}$-CH$_3$), 1.18 (3H, d, J=7 Hz,

C_{15}-CH_3), 2.00 (3H, s, C_{16}-$OCOCH_3$), 2.27 (3H, s), 2.29 (3H, s), and 2.33 (3H, s) (C_{11}-$OCOCH_3$, C_{12}-$OCOCH_3$, and C_{14}-$OCOCH_3$), 2.63 (1H, s, C_5-H), 3.16 (1H, d, J=21 Hz) and 3.42 (1H, d, J=21 Hz) (-$COCH_2$-), 4.03 (1H, dd, J=8 and 9.5 Hz) and 4.30 (1H, dd, J=8 and 9.5 Hz) (-CH_2OAc). Found: C, 65.40; H, 6.81%. Calcd for $C_{28}H_{36}O_9$: C, 65.10; H, 7.03%.

(15*R*)-11,12,16-Triacetoxy-14-hydroxy-8,11,13-abietatriene-6,7-dione (25a) and Its (15*S*)-Isomer (25b). *a*): A solution of **23a** (103.6 mg) in acetone (2.0 ml) was oxidized with Jones reagent (2.5 mol dm^{-3}: 0.40 ml) at 0—5 °C for 5 min and then at room temperature for 2.5 h. The mixture was diluted with ether and washed with water. The dried solution was evaporated in vacuo. The residue was chromatographed on silica gel (10 g), using ether-benzene (1:9) as eluent, to give (15*R*)-coleon D triacetate (**25a**) as an oil (26.9 mg: 27.4%), $[\alpha]_D$ +92.8° (*c* 0.83), IR: 1779, 1732, 1634, and 1606 cm^{-1}; ^1H NMR (90 MHz) δ=1.06 (3H, s), 1.36 (3H, s), and 1.38 (3H, s) (-$C(CH_3)_2$ and C_{10}-CH_3), 1.31 (3H, d, J=7 Hz, C_{15}-CH_3), 1.97 (3H, s, C_{16}-$OCOCH_3$), 2.28 (3H, s) and 2.30 (3H, s) (C_{11}-$OCOCH_3$ and C_{12}-$OCOCH_3$), 3.03 (1H, s, C_5-H), 4.37 (2H, d, J=7 Hz, -CH_2OAc), 13.33 (1H, s, C_{14}-OH). Found: C, 63.63; H, 6.71%. Calcd for $C_{26}H_{32}O_9$: C, 63.92; H, 6.60%.

b): A solution of **23b** (86.5 mg) in acetone (2.0 ml) was oxidized with Jones reagent (2.5 mol dm^{-3}: 0.34 ml) at 0—5 °C for 5 min and then at room temperature for 2.5 h. The crude product was chromatographed on silica gel (7 g), using ether-benzene (1:9) as eluent, to give (15*S*)-coleon D triacetate (**25b**) as an oil (44.5 mg: 54.4%), $[\alpha]_D$ +100.0° (*c* 1.44), IR: 1777, 1733, 1636, and 1610sh cm^{-1}; ^1H NMR (90 MHz) δ=1.05 (3H, s), 1.37 (3H, s), and 1.39 (3H, s) (-$C(CH_3)_2$ and C_{10}-CH_3), 1.32 (3H, d, J=7 Hz, C_{15}-CH_3), 1.97 (3H, s, C_{16}-$OCOCH_3$), 2.28 (3H, s) and 2.30 (3H, s) (C_{11}-$OCOCH_3$ and C_{12}-$OCOCH_3$), 3.02 (1H, s, C_5-H), 4.37 (2H, d, J=7 Hz, -CH_2OAc), 13.31 (1H, s, C_{14}-OH). Found: C, 64.19; H, 6.88%. Calcd for $C_{26}H_{32}O_9$: C, 63.92; H, 6.60%.

(15*R*)-Coleon C (1a) and (15*S*)-Coleon C (1b). *b*): A mixture of **25a** (24.0 mg) and dilute hydrochloric acid (15%: 0.1 ml) in methanol (1.0 ml) was refluxed for 2 h. After the addition of ether, the mixture was washed with brine, dried, and evaporated in vacuo. The residue was chromatographed on silica gel (Mallinckrodt CC-4, 5 g), using hexane-chloroform (3:7) as eluent, to give **1a** (17.6 mg: 98.9%) which was recrystallized from methanol, mp 230—232.5 °C, $[\alpha]_D$ +39.0° (MeOH, *c* 0.21), IR (KBr): 3525, 3350sh, 1623, 1594, and 1576 cm^{-1}; ^1H NMR (90 MHz, acetone-d_6) δ=1.28 (3H, d, J=7 Hz, C_{15}-CH_3), 1.43 (3H, s) and 1.45 (3H, s) (-$C(CH_3)_2$), 1.68 (3H, s, C_{10}-CH_3), 3.89 (1H, dd, J=11 and 2 Hz) and 4.08 (1H, dd, J=11 and 4 Hz) (-CH_2OH), 13.12 (1H, s, C_{14}-OH). Found: C, 66.49; H, 7.15%. Calcd for $C_{20}H_{26}O_6$: C, 66.28; H, 7.23%. The synthetic **1a** was identical with natural (15*R*)-coleon C (mp 236—238 °C, $[\alpha]_D$ +46.8° (MeOH)).[2]

b): A mixture of **25b** (38.8 mg) and dilute hydrochloric acid (15%: 0.15 ml) in methanol (1.5 ml) was refluxed for 1 h. The crude product was chromatographed on silica gel (Mallinckrodt CC-4, 6 g), using hexane-chloroform (3:7) as eluent, to give **1b** (28.7 mg: 99.7%) which was recrystallized from methanol, mp 199.5—201.5 °C, $[\alpha]_D$ −41.0° (MeOH, *c* 0.39), IR (KBr): 3470, 3330sh, 1622, 1596, and 1574 cm^{-1}; ^1H NMR (90 MHz acetone-d_6) δ=1.31 (3H, d, J=7 Hz, C_{15}-CH_3), 1.43 (3H, s) and 1.45 (3H, s) (-$C(CH_3)_2$), 1.68 (3H, s, C_{10}-CH_3), 3.87 (1H, dd, J=11 and 2 Hz) and 4.08 (1H, dd, J=11 and 4 Hz) (-CH_2OH), 13.10 (1H, s, C_{14}-OH). Found: C, 66.53; H, 7.38%. Calcd for $C_{20}H_{26}O_6$: C, 66.28; H, 7.23%. The synthetic **1b** was identical with natural (15*S*)-coleon C (mp 202—204 °C, $[\alpha]_D$ −34.7° (MeOH)).[2]

(15*S*)-Coleon C Tetraacetate (26b). The synthetic **1b** (19.7 mg) was acetylated with acetic anhydride (0.5 ml) in pyridine (0.5 ml) at 75—80 °C for 2 h. The crude product was chromatographed on silica gel (5 g), using ether-benzene (1:9) as eluent, to give **26b** (22.2 mg: 77.1%) which was recrystallized from acetone-hexane, mp 222—224 °C, $[\alpha]_D$ +28.6° (*c* 0.63), IR: 1771, 1729, 1631sh, and 1611 cm^{-1}; ^1H NMR (90 MHz) δ=1.32 (3H, d, J=7 Hz, C_{15}-CH_3), 1.36 (6H, s, -$C(CH_3)_2$), 1.63 (3H, s, C_{10}-CH_3), 1.97 (3H, s, C_{16}-$OCOCH_3$), 2.28 (3H, s), 2.29 (3H, s), and 2.33 (3H, s) (C_6-$OCOCH_3$, C_{11}-$OCOCH_3$, and C_{12}-$OCOCH_3$), 3.37 (1H, m, C_{15}-H), 4.37 (2H, bd, J=7 Hz, -CH_2OAc), 13.51 (1H, s, C_{14}-OH). Found: C, 63.68; H, 6.51%. Calcd for $C_{28}H_{34}O_{10}$: C, 63.38; H, 6.46%.

(15*S*)-11,12-Diacetoxy-14,16-epoxy-6-hydroxy-5,8,11,13-abietatetraen-7-one (27b) and (15*S*)-11,12-Diacetoxy-14,16-epoxy-8,11,13-abietatriene-6,7-dione (28b). A solution of **24b** (86.0 mg) in acetone (3.0 ml) was oxidized with Jones reagent (2.5 mol dm^{-3}: 0.41 ml) at 0—5 °C for 5 min and then at room temperature for 2 h. The crude product was chromatographed on silica gel (10 g), using ether-benzene (1:9) as eluent, to give **27b** (21.9 mg: 24.6%) which was recrystallized from acetone-hexane, mp 248—250 °C, $[\alpha]_D$ +44.6° (*c* 0.56), IR: 3377, 1780, and 1631 cm^{-1}; ^1H NMR (90 MHz) δ=1.24 (3H, d J=7 Hz, C_{15}-CH_3), 1.42 (3H, s) and 1.44 (3H, s) (-$C(CH_3)_2$), 1.56 (3H, s, C_{10}-CH_3), 2.28 (3H, s) and 2.33 (3H, s) (C_{11}-$OCOCH_3$ and C_{12}-$OCOCH_3$), 4.32 (1H, dd, J=7 and 8 Hz) and 4.92 (1H, t, J=9 Hz) (-OCH_2-), 7.22 (1H, s, C_6-OH). Found: C, 67.53; H, 6.81%. Calcd for $C_{24}H_{28}O_7$: C, 67.27; H, 6.59%. Further elution gave a mixture of **27b** and **28b** (11.6 mg: 13.1%). Elution with ether-benzene (1:1) gave **28b** (13.0 mg: 14.6%) which was recrystallized from acetone-hexane, mp 220—223 °C decomp, $[\alpha]_D$ +177.5° (*c* 0.36), IR: 1779, 1747, and 1680 cm^{-1}; ^1H NMR (90 MHz) δ=1.07 (3H, s), 1.43 (3H, s), and 1.46 (3H, s) (-$C(CH_3)_2$ and C_{10}-CH_3), 1.25 (3H, d, J=7 Hz, C_{15}-CH_3), 2.28 (6H, s, C_{11}-$OCOCH_3$ and C_{12}-$OCOCH_3$), 2.54 (1H, bs, C_5-H), 4.32 (1H, dd, J=7 and 8 Hz) and 4.90 (1H, t, J=9 Hz) (-OCH_2-). Found: C, 67.48; H, 6.76%. Calcd for $C_{24}H_{28}O_7$: C, 67.27; H, 6.59%.

The diacetate **27b** (11.6 mg) was refluxed with dilute hydrochloric acid (15%: 0.1 ml) in ethanol (1.0 ml) for 3 h to give a triol **29b**, whose ^1H NMR spectrum showed no signal at δ=10—15 due to a hydrogen-bonded hydroxyl group at the C-14 position.

2-[4-[(*S*)-2-Acetoxy-1-methylethyl]-2,5-dioxo-1(6),3-cyclohexadienyl]-2,6,6-trimethylcyclohexaneacetic Acid (3b). A solution of (15*S*)-12,16-epoxy-8,11,13-abietatriene (**5b**)[4] (132 mg) in acetic acid (3.0 ml) was oxidized with chromium trioxide (69.6 mg) at room temperature for 1 h. The crude product was chromatographed on silica gel (10 g), using benene as eluent, to give (15*S*)-12,16-epoxy-8,11,13-abietatrien-7-one (**6b**) as an oil (87.2 mg: 63.0%), $[\alpha]_D$ +18.4° (*c* 2.99), IR: 1658 cm^{-1}; ^1H NMR δ=0.92 (3H, s) and 0.97 (3H, s)

(-C(CH$_3$)$_2$), 1.20 (3H, s, C$_{10}$-CH$_3$), 1.31 (3H, d, J=7 Hz, C$_{15}$-CH$_3$), 4.08 (1H, dd, J=7 and 9 Hz) and 4.71 (1H, t, J=9 Hz) (-OCH$_2$-), 6.71 (1H, s, C$_{11}$-H), 7.89 (1H, s, C$_{14}$-H). Found: C, 80.28; H, 8.94%. Calcd for $C_{20}H_{26}O_2$: C, 80.49; H, 8.78%.

According to the method of Burnell et al.,[3] the ketone **6b** (87.2 mg) in acetic anhydride (1.0 ml) was oxidized with peracetic acid prepared from hydrogen peroxide (30%: 0.5 ml), acetic anhydride (1.5 ml), and concentrated sulfuric acid (0.01 ml). The crude product was chromatographed on silica gel (10 g), using hexane-ethyl acetate (7:3 and then 1:1) as eluents, to give **3b** (74.4 mg: 65.2%) which was recrystallized from ethanol, mp 148—150 °C, $[\alpha]_D$ −52.4° (*c* 1.26), IR: 3200, 1726, and 1651 cm^{-1}; ^{1}H NMR δ=0.92 (3H, s) and 0.99 (3H, s) (-C(CH$_3$)$_2$), 1.21 (3H, d, J=7 Hz, C$_{15}$-CH$_3$), 1.29 (3H, s, C$_{10}$-CH$_3$), 2.09 (3H, s, -OCOCH$_3$), 3.76 (1H, dd, J=11 and 4 Hz) and 4.87 (1H, dd, J=11 and 3 Hz) (-CH$_2$OAc), 6.36 (1H, d, J=1.5 Hz, C$_{14}$-H), 6.58 (1H, s, C$_{11}$-H). The physical and spectral data of the synthetic (15*S*)-quinone **3b** were identical with those of the reported major quinone (mp 143—145 °C, $[\alpha]_D$ −50°), whose stereochemistry at the C-15 position was assigned to be R configuration by Burnell et al.[3]

References

1) P. Rüedi and C. H. Eugster, *Helv. Chim. Acta*, **54**, 1606 (1971).

2) P. Rüedi, J. M. Schmid, and C. H. Eugster, *Helv. Chim. Acta*, **65**, 2181 (1982).

3) R. H. Burnell, M. Neron, and S. Savard, *Synth. Commun.*, **12**, 11 (1982); R. H. Burnell, A. Andersen, M. Neron, and S. Savard, *Can. J. Chem.*, **63**, 2769 (1985).

4) T. Matsumoto, S. Imai, T. Yoshinari, and K. Tsuruta, *Bull. Chem. Soc. Jpn.*, **60**, 2401 (1987).

5) T. Matsumoto, S. Imai, and T. Yoshinari, *Bull. Chem. Soc. Jpn.*, **58**, 1165 (1985).

Infrared Absorption Study of Peptide Fragments of Human Hemoglobin α-Chain (123-136) in the Solid State[1)]

Mitsuaki NARITA,* Masamitsu DOI, and Hitoshi TAKEGAHARA
Department of Industrial Chemistry, Faculty of Technology,
Tokyo University of Agriculture and Technology, Koganei, Tokyo 184
(Received January 22, 1987)

In order to evaluate the influence of polar amino acid residues on peptide conformations, IR absorption spectroscopic analysis of peptide fragments of human hemoglobin α-chain (123-136) and Boc-Leu$_n$-OBzl (n=3—6, 9, and 12) was performed in the solid state. The polar amino acid residues involved in the peptide fragments are in the following: Asp(OBzl), Lys(Z), Ser(Bzl), and Thr(Bzl). Regardless of the amino acid composition, all of the peptides equal to or larger than a pentapeptide level exhibited a high potential for the formation of a β-sheet structure in the solid state. Conformational behaviors of peptides having polar amino acid residues are similar to those of Boc-Leu$_n$-OBzl, indicating that polar side chains can not cause disturbance of the formation of β-sheet structures. The fine relationship among the conformation, solubility, and $\langle P_c \rangle$ value of the peptide fragments strongly supports the propriety of the solubility prediction method for peptide intermediates. The influence of shear stress on peptide conformations in the solid state was also investigated precisely, and it was suggested that a heptapeptide size had the potential for the development of a helical structure in the solid state.

In previous papers,[2-6)] we have demonstrated that the insolubility of peptide intermediates in high-polar solvents is essentially caused by a β-sheet aggregation formed by peptides equal to or larger than an octapeptide sequence level and that their solubility is independent of their amino acid sequences and compositions. The insolubility of peptide intermediates is a serious problem in protein synthesis. The relationship between the conformation and the solubility of peptide having polar amino acid residues has received little attention,[5,6)] since their role in the conformational behavior of the peptides is complicated.

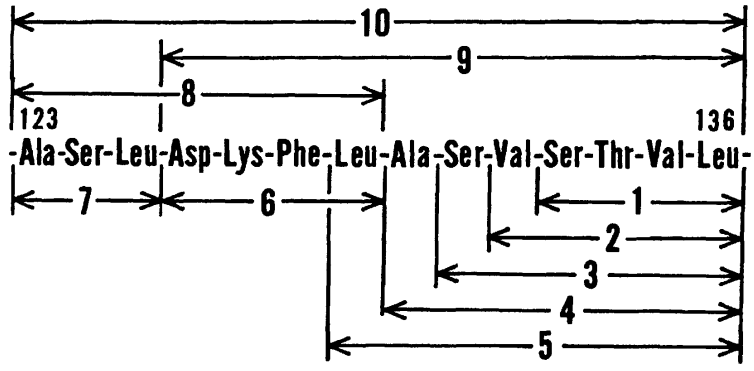

1. Boc·Ser(Bzl)·Thr(Bzl)·Val-Leu-OBzl
2. Boc·Val-Ser(Bzl)-Thr(Bzl)-Val-Leu·OBzl
3. Boc-Ser(Bzl)·Val·Ser(Bzl)-Thr(Bzl)-Val·Leu·OBzl
4. Boc·Ala-Ser(Bzl)·Val·Ser(Bzl)·Thr(Bzl)-Val-Leu-OBzl
5. Boc·Leu·Ala-Ser(Bzl)-Val·Ser(Bzl)-Thr(Bzl)-Val-Leu-OBzl
6. Boc-Asp(OBzl)-Lys(Z)·Phe·Leu-OPac
7. Boc·Ala-Ser(Bzl)·Leu·OPac
8. Boc-Ala·Ser(Bzl)-Leu·Asp(OBzl)·Lys(Z)-Phe·Leu·OPac
9. Boc·Asp(OBzl)-Lys(Z)-Phe-Leu-Ala·Ser(Bzl)-Val-Ser(Bzl)·Thr(Bzl)-Val-Leu-OBzl
10. Boc·Ala-Ser(Bzl)-Leu-Asp(OBzl)-Lys(Z)·Phe-Leu-Ala·Ser(Bzl)·Val·Ser(Bzl)·Thr(Bzl)-Val·Leu·OBzl
11. Boc·Leu$_3$·OBzl
12. Boc-Leu$_4$-OBzl
13. Boc-Leu$_5$-OBzl
14. Boc-Leu$_6$-OBzl
15. Boc-Leu$_9$-OBzl
16. Boc-Leu$_{12}$-OBzl

Fig. 1. The amino acid sequence of human hemoglobin α-chain (123-136) and peptides **1**—**16** used in this study.

This is in contrast to the fact that conformational analyses of homo- and sequential peptides have been widely carried out.[7-9]

On the other hand, in a study of the relationship between the conformation and solubility of human proinsulin C-peptide fragments,[5] we have shown that the average coil conformation $\langle P_c \rangle$ value of each peptide fragment was effective for estimating the potential for the formation of a β-sheet structure of peptide fragments below the critical size for the development of an α-helical structure in the solid state. The result also clearly showed that a synthetic route for peptides and proteins could be designed on the basis of the solubility prediction method which we previously proposed.[3] Human proinsulin C-peptide fragments previously investigated include the polar amino acids, Asp (OBzl), Gln, Glu (OBzl), and Ser (Bzl), and their conformational analysis was performed using IR absorption spectra in the solid state and in dichlormethane solution.

In this study, we performed IR absorption spectroscopic analysis of peptide fragments of human hemoglobin α-chain (123-136) in the solid state and investigated the influence of polar amino acid residues on peptide conformdtions. For the IR analysis, we also examined the influence of shear stress on peptide conformation. Human hemoglobin α-chain (123-136) shown in Fig. 1 corresponds to the partial sequence of the helical region H of the α-chain.[10,11] Figure 1 also illustrates the protected peptide fragments **1**—**10** and Boc-Leu$_n$-OBzl ($n=3$—6, 9, and 12) **11**—**16** used in this study.

Experimental

Materials. Samples of human hemoglobin α-chain (123-136) fragments **1**—**10** and Boc-Leu$_n$-OBzl **11**—**16** are those described in previous papers.[2,6] The solid samples of the peptides **1**—**4**, **6**—**8**, and **11**—**14** were obtained by repeated recrystallization from appropriate solvents.[2,6] Those of the peptides **5**, **9**, **10**, **15**, and **16** were obtained by repeated washing with hot methanol. The purity of the peptides was confirmed by elemental and amino acid analyses. The peptides soluble in *N,N*-dimethylformamide also gave a single peak on high-performance liquid chromatography.

IR Measurements. The IR absorption spectra of the solid samples were recorded with a JEOL Model JIR-100 FT-IR spectrometer in a Nujol mull. IR spectra (Figs. 2—4) of the peptides **1**—**16** under a slight shear stress were

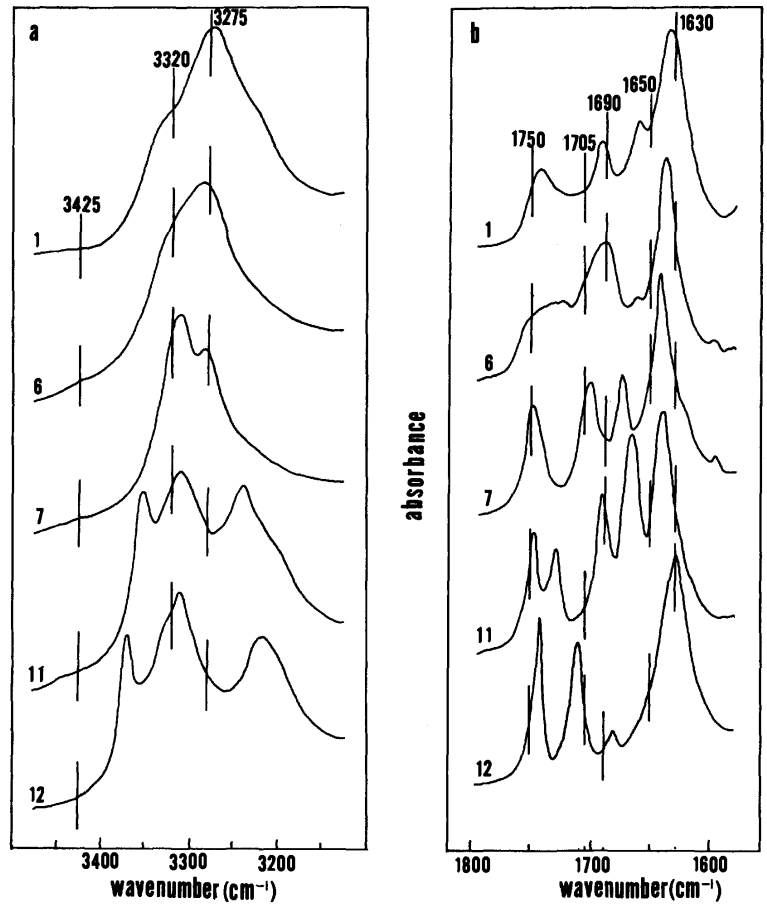

Fig. 2. IR absorption spectra of the tri- and tetrapeptides **1**, **6**, **7**, **11**, and **12** in the solid state. a: The amide A region; b: the amide I region.

obtained after the solid samples were pulverized with Nujol by weak shear stress. IR spectra (Figs. 5—7) of the peptides after application of shear stress were also obtained in a Nujol mull after the solid samples were pulverized without Nujol by strong shear stress.

Results

IR Absorption Spectra of the Tri- and Tetrapeptides 1, 6, 7, 11, and 12 in the Solid State. Figure 2 shows the IR absorption spectra of the peptides **1**, **6**, **7**, **11**, and **12** in the most significant spectral regions for the conformational assignments (3500—3100 cm^{-1}, amide A; 1800—1600 cm^{-1}, amide I). All of the peptides show a few of strong bands at 3371—3215 cm^{-1} and a negligibly small band around 3425 cm^{-1} in the amide A region, suggesting that the Boc- and Z-urethane N-H bonds and peptide N-H bonds are mostly subjected to hydrogen bonding in the solid state. The spectra in the amide A region further indicate that hydrogen bonding patterns of the peptides are different from those of helical and β-sheet structures.[7-9,12,13] However, the spectra of the tetrapeptides **1** and **6** still show the strong bands at 3284—3271 and 1641—1635 cm^{-1}, indicative of a large contribution of β-sheet-like structure.[8,9,13] The assignment of each band in the amide I region is as follows: The bands around 1750 cm^{-1} are assigned to the Pac- and Bzl-ester carbonyl groups, the bands at 1736—1705 cm^{-1} to the Boc- and Z-urethane-carbonyl groups and the bands at 1695—1630 cm^{-1} mainly to hydrogen-bonded amide-carbonyl groups. The Pac ketone carbonyl group is presumed to show the band around 1685 cm^{-1}, overlapped with the amide carbonyl group.[5]

IR Absorption Spectra of the Peptides 2—5, 8—10, and 13—16 Equal to or Larger than a Pentapeptide in the Solid State. Figure 3 shows the IR absorption spectra of the pentapeptides **2** and **13** through the heptapeptides **4** and **8**. Figure 4 also presents those of the octapeptide **5** through the tetradecapeptide **10**. All of the peptides have the strong bands at 3280—3265 cm^{-1} in the amide A region, at 1635—1625 cm^{-1} in the amide I region and the weak band at 1699—1689 cm^{-1} in the amide I region, being indicative of typical antiparallel β-sheet structures, although most of them are accompanied by weak shoulder bands around 1650 cm^{-1}, assigned to other conformations. The shoulder bands around 3320

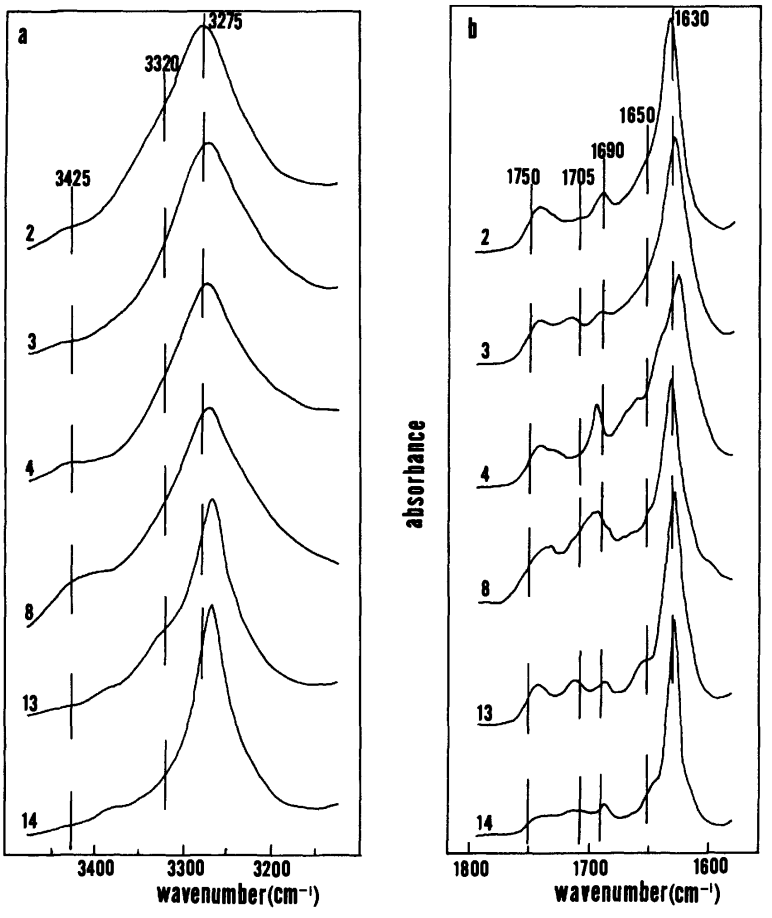

Fig. 3. IR absorption spectra of the pentapeptides **2** and **13** through the heptapeptides **4** and **8** in the solid state. a: The amide A region; b: the amide I region.

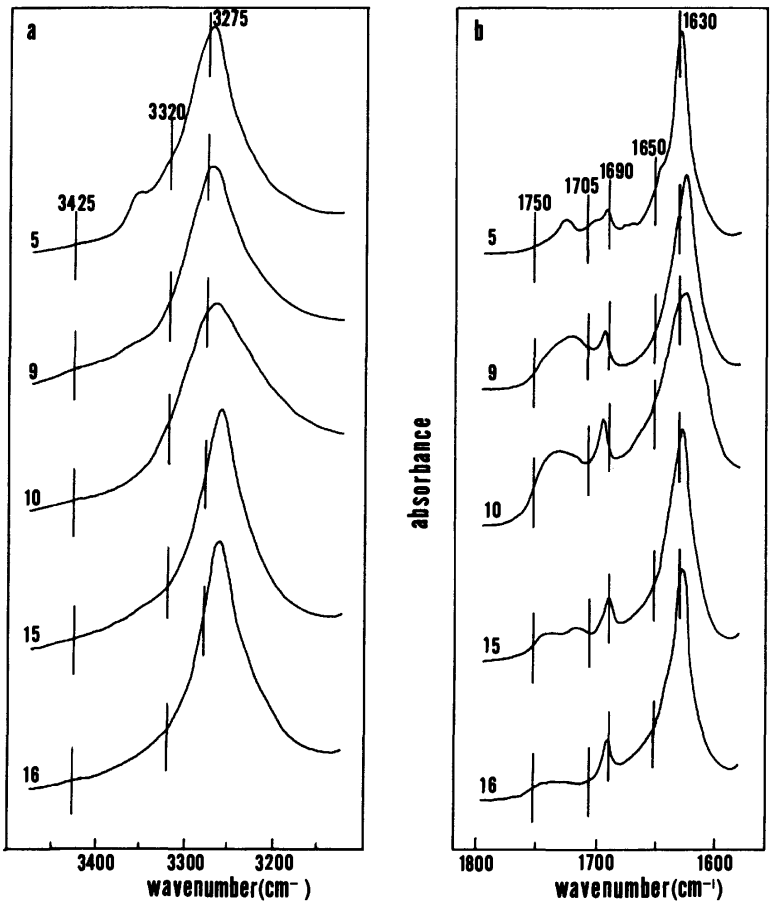

Fig. 4. IR absorption spectra of the octapeptide **5** through the tetradecapeptides **10** in the solid state. a: The amide A region; b: the amide I region.

cm^{-1} of peptides also indicate a small contribution of other conformations. The intensity of both shoulder bands increases with increasing shear stress when solid samples are pulverized with Nujol.

The Influence of Shear Stress on Peptide Conformations in the Solid State. It has been reported that β-sheet→α-helix conformational change occurs in the solid state on application of shear stress at the decapeptide level.[14] Figure 5 shows the IR absorption spectra of the tri- and tetrapeptides **1**, **6**, **7**, **11**, and **12** after application of strong shear stress and illustrates the influence of shear stress on peptide conformations in the solid state although it is difficult to estimate their specific conformational changes. For the peptides **1**—**16**, the influence of shear stress on their conformation is observed to a small or large extent. Conformational changes of the penta- and hexapeptides are relatively small although not negligible (not shown). Figures 6 and 7 exhibit the IR absorption spectra of the hepta- and octapeptides **4** and **5** and the peptides **8**—**10** after application of strong shear stress. The former spectra (Fig. 6) exhibit the influence of shear stress to a small extent, and the conformations of both peptides are essentially antiparallel β-sheet structures. On the other hand, the latter spectra (Fig. 7) are in contrast to the former. Especially, the conformational change of the heptapeptide **8** is quite drastic. The shoulder band at 3320 cm^{-1} in the amide A region and the band at 1657 cm^{-1} in the amide I region strongly suggest a β-sheet → α-helical transformation to a considerable extent. The onset of helical conformation, although to a small extent, is also evident in the undeca- and tetradecapeptides **9** and **10**.

Discussion

As pointed out, application of shear stress for solid peptides brings about a small or large extent of conformational transformation. IR spectra (Figs. 2—4) of the peptides **1**—**16** under a slight influence of shear stress are reproducibly obtained when solid samples are pulverized with Nujol by weak shear stress. Regardless of the amino acid composition, all of the peptides equal to or larger then a pentapeptide exhibit a high potential for the formation of β-sheet structures in the solid state. The conformational behavior of peptides having polar amino acid residues is essential-

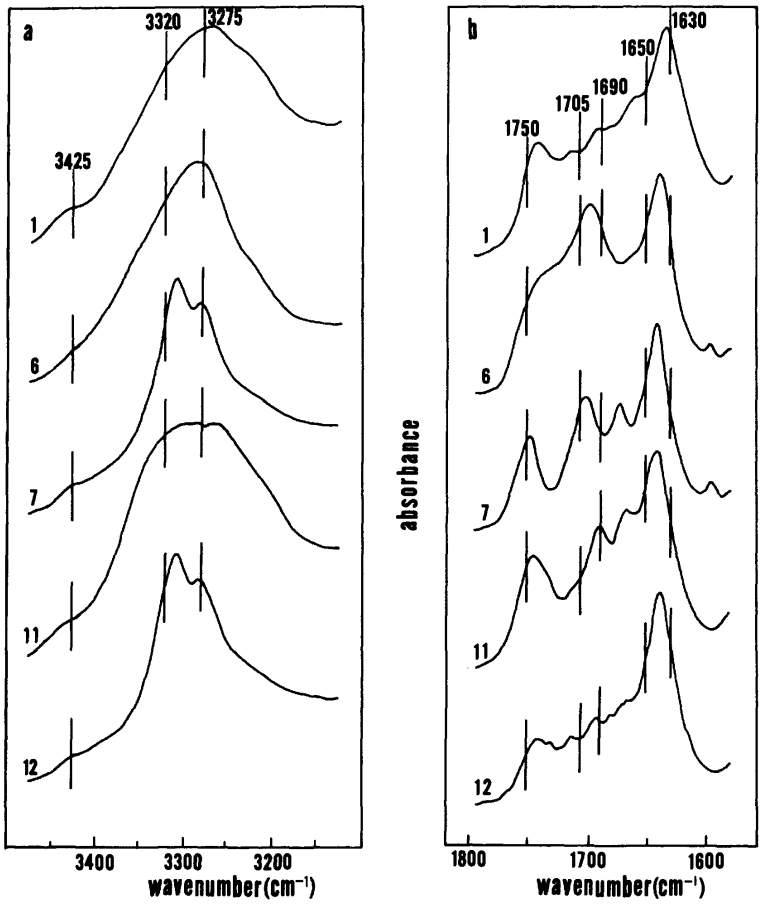

Fig. 5. IR absorption spectra of the tri- and tetra-peptides **1**, **6**, **7**, **11**, and **12** in the solid state after application of strong shear stress. a: The amide A region; b: the amide I region.

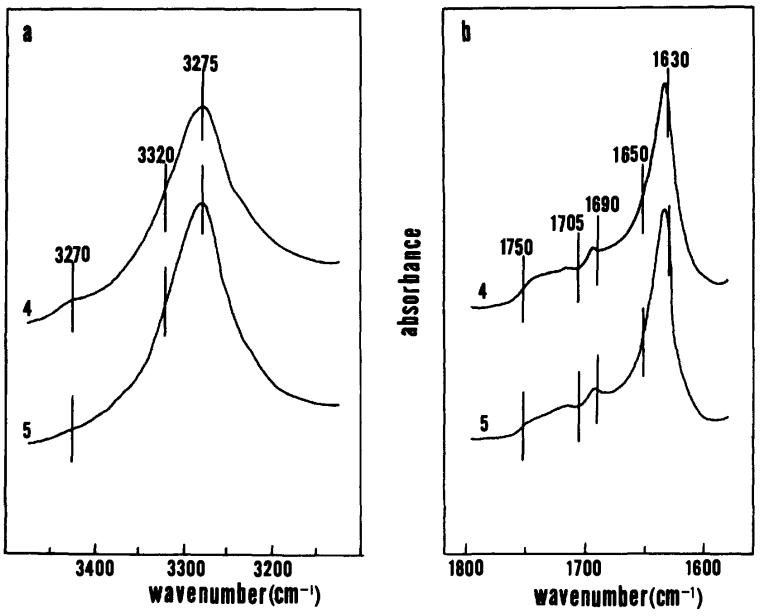

Fig. 6. IR absorption spectra of the hepta- and octapeptides **4** and **5** in the solid state after application of strong shear stress. a: The amide A region; b: the amide I region.

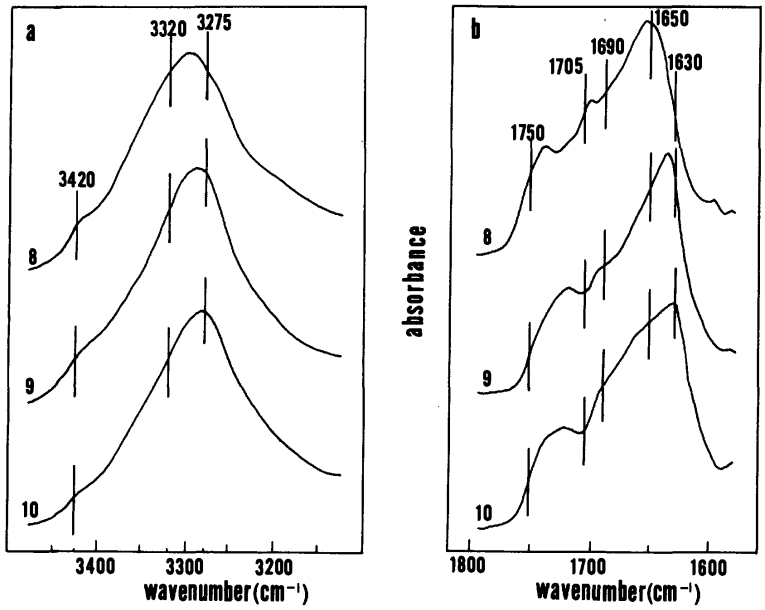

Fig. 7. IR absorption spectra of the peptides **8**—**10** in the solid state after application of strong shear stress. a: The amide A region; b: the amide I region.

ly similar to those of Boc-Leu$_n$-OBzl, indicating that polar side chains can not disturb the formation of β-sheet structures. Furthermore, as in the case of hydrophobic peptides and human proinsulin C-peptide fragments,[2-5] the peptides **5**, **9**, **10**, **15**, and **16** equal to or larger than an octapeptide are notably less soluble in high polar solvents.[2,6] These results strongly support our previous findings that the insolubility of peptide intermediates in highly polar solvents is principally caused by β-sheet aggregation formed by peptides equal to or larger than an octapeptide sequence level and that their insolubility is independent of their amino acid sequences and composition. However, apparently, this conclusion is not applicable to peptide intermediates including a Pro residue.[2,3,15]

In the Table 1, the average conformation $\langle P_c \rangle$, $\langle P_\alpha \rangle$, and $\langle P_\beta \rangle$ values of each peptide are summarized. The values of $\langle P_c \rangle$, $\langle P_\alpha \rangle$, and $\langle P_\beta \rangle$ were determined according to the literature.[3,16] The average coil conformation $\langle P_c \rangle$ values of the peptides **1**—**16** are below 0.9, suggseting that these peptides are highly structured. In fact, the peptides **2**—**5**, **8**—**10**, and **13**—**16** exhibit a high potential for the formation of β-sheet structures. This indicates that, even when the polar side chains of the Asp, Lys, Ser, and Thr residues are protected by suitable groups, the coil conformational parameters, P_c, obtained for intact amino acid residues[3] are useful for estimating the potential for the formation of a β-sheet structure of peptides smaller than critical size[14] for the development of an α-helical structure in the solid state. This result is also in good accord with our previous findings.[5] The fine relationship among the conformation, solubility,

Table 1. The Average Conformation $\langle P_c \rangle$, $\langle P_\alpha \rangle$, and $\langle P_\beta \rangle$ Values of Each Peptide

Compound	$\langle P_c \rangle$	$\langle P_\alpha \rangle$	$\langle P_\beta \rangle$
1	0.92	1.02	1.20
2	0.86	1.05	1.29
3	0.94	1.00	1.19
4	0.90	1.07	1.16
5	0.88	1.10	1.17
6	0.89	1.13	1.01
7	0.90	1.19	0.97
8	0.90	1.16	0.99
9	0.90	1.09	1.11
10	0.90	1.11	1.08
11—16	0.68	1.34	1.22

and $\langle P_c \rangle$ value of the peptide fragments **1**—**10** of human hemoglobin α-chain (123-136) also strongly supports the correctness of our solubility prediction method for peptide intermediates.[3]

IR spectra (Figs. 5—7) of peptides after application of shear stress are also reproducibly obtained when solid samples are pulverized without Nujol by strong shear stress. The effect of shaer stress on the conformational behavior of the peptides **4**, **5**, and **8**—**10** may directly reflect their potential for the formation of an α-helical structure, and the tendency of the β-sheet $\rightarrow\alpha$-helix transformation is clearly estimated using the average helix conformation $\langle P_\alpha \rangle$ values of each peptide. In fact, the heptapeptide **8** has the high $\langle P_\alpha \rangle$ value, 1.16, and the most significant transformation is observed. The minimum size for the development of

an α-helical structure in the solid state has hitherto been recognized to be not less than the decapeptide level,[14] but this result suggests that a helical structure can be held at a heptapeptide size level in the solid state as well as in dichloromethane solution.[17] On the other hand, the average $\langle P_\alpha \rangle$ and $\langle P_\beta \rangle$ values of the heptapeptide **4** are 1.07 and 1.16, and those of the octapeptide **5** are 1.10 and 1.17, respectively. This suggests that the peptides **4** and **5** have a high potential for the formation of a β-sheet structure. In fact, no tendency for the β-sheet→α-helix transformation is observed in the solid state as well as in dichloromethane solution.[17] Therefore, the partial β-sheet→α-helix transformanion of the peptides **9** and **10** probably takes place at their N-terminal portions, while their C-terminal portions remain β-sheet structures.

References

1) This paper forms Part VI of "Design of the Synthetic Route for Peptides and Proteins Based on the Solubility Prediction Method" series. For part V of this series, see M. Narita, M. Doi, K. Kudo, and Y. Terauchi, *Bull. Chem. Soc. Jpn.*, **59**, 3553 (1986). The abbreviations for amino acids are those recommended by the IUPAC-IUB Commission on Biochemical Nomenclature, *J. Biol. Chem.*, **247**, 977 (1972). Amino acid symbols denote the L-configuration. Additional abbreviations used are the following: IR, infrared Bzl, benzyl; Z, benzyloxycarbonyl; Boc, *t*-butoxycarbonyl; Pac, phenacyl.

2) M. Narita, T. Fukunaga, A. Wakabayashi, K. Ishikawa, and H. Nakano, *Int. J. Pept. Protein Res.*, **23**, 306 (1984); M. Narita, K. Ishikawa, H. Nakano, and S. Isokawa, *ibid.*, **24**, 14 (1984).

3) M. Narita, K. Ishikawa, J.-Y. Chen, and Y. Kim, *Int. J. Pept. Protein Res.*, **24**, 580 (1984).

4) M. Narita, J.-Y. Chen, H. Sato, and Y. Kim, *Bull. Chem. Soc. Jpn.*, **58**, 2494 (1985).

5) M. Narita, T. Ogura, K. Sato, and S. Honda, *Bull. Chem. Soc. Jpn.*, **59**, 2433, 2439, 2445 (1986).

6) M. Narita, M. Doi, and T. Nakai, manuscript in preparation.

7) R. Katakai, *Biopolymers*, **25**, 1 (1986) and references cited therein.

8) U. Narayanan, T. A. Kederling, G. M. Bonora, and C. Toniolo, *J. Am. Chem. Soc.*, **108**, 2431 (1986) and references cited therein.

9) K.-H. Altmann, A. Flörsheimer, and M. Mutter, *Int. J. Pept. Protein Res.*, **27**, 314 (1986), and references cited therein.

10) G. Braunitzer, R. Gehring-Muller, N. Hilschmann, K. Hilsen, G. Hobom, V. Rudloff, and B. Wittmann-Liebold, *Z. Phys. Chem.*, **325**, 283 (1961).

11) M. F. Perutz, M. G. Rossmann, A. F. Cullis, H. Muirhead, G. Will, and A. C. T. North, *Nature*, **185**, 416 (1960); E. J. Heidner, R. C. Ladner, and M. F. Perutz, *J. Mol. Biol.*, **104**, 707 (1976).

12) T. Miyazawa and E. J. Blout, *J. Am. Chem. Soc.*, **83**, 712 (1961); Yu. N. Chirgadze and N. A. Nevskaya, *Biopolymers*, **15**, 627 (1976).

13) M. Narita, S. Isokawa, Y. Tomotake, and S. Nagasawa, *Polymer J.*, **15**, 25 (1983), and references cited therein.

14) R. Katakai and Y. Nakayama, *J. Chem. Soc., Chem. Commun.*, **1977**, 924; R. Katakai, *J. Chem. Soc., Perkin Trans. 1*, **1979**, 905.

15) M. Narita, S. Nagasawa, J.-Y. Chen, H. Sato, and Y. Tanaka, *Makromol. Chem.*, **185**, 1069 (1984); M. Narita, N. Ohkawa, S. Nagasawa, and S. Isokawa, *Int. J. Pept. Protein Res.*, **24**, 129 (1984); S. Isokawa, T. Asakura, and M. Narita, *Macromolecules*, **18**, 871 (1985); S. Isokawa, I. Tominaga, T. Asakura, and M. Narita, *ibid.*, **18**, 878 (1985); M. Narita, S. Isokawa, M. Doi, and R. Wakita, *Bull. Chem. Soc. Jpn.*, **59**, 3547 (1986).

16) P. Y. Chou and G. D. Fasman, *Biochemistry*, **13**, 211 (1974).

17) M. Narita, M. Doi, and T. Nakai, *Bull. Chem. Soc. Jpn.*, in press.

 © 1987 The Chemical Society of Japan Bull. Chem. Soc. Jpn., 60, 2453—2461 (1987)

Synthesis of Some Five- and Six-Membered Oxasteroids of Cholestane Series by Ring Contraction and the Mass Spectrometric Fragmentations of Oxasteroids[1)]

Hiroshi SUGINOME* and Shinji YAMADA
Organic Synthesis Division, Department of Chemical Process Engineering,
Faculty of Engineering, Hokkaido University, Sapporo 060
(Received January 30, 1987)

Synthesis of several new five- and six-membered oxasteroids of the cholestane series by the ring contraction of those oxasteroids whose oxygen-containing ring is larger by one member has been achieved. Ring contraction utilizes a series of reactions recently developed by us for the transformation of cyclic ketones into cyclic ethers; it involves a regioselective β-scission of the alkoxyl radical generated by irradiation of the lactol hypoiodite derived from the starting oxasteroid to give the iodoformate followed by its cyclization. The present work demonstrates the versatility of our new method for the synthesis of cyclic ethers and extends the scope of its application. The mass spectral fragmentation of some oxasteroids synthesized in the present and previous work is discussed.

We have recently reported a new, efficient and versatile method for transforming steroidal cyclic alcohols and ketones into cyclic ethers with the same ring size.[2-5)] The essential steps of the transformation of cyclic ketones into cyclic ethers are outlined as a sequence **A** to **E** in Scheme 1. The transformation involves four steps: a), the Baeyer-Villiger oxidation of cyclic ketones (**A**) to give the corresponding lactones (**B**); b), the reduction of these lactones with DIBAL (diisobutylaluminium hydride) to the corresponding lactols (**C**); c), a regioselective β-scission of the C-C bond of the corresponding hypoiodites generated in situ with mercury(II) oxide, iodine and pyridine, by irradiation to give an iodoformate (**D**); and d), the cyclization of the iodoformate to cyclic ether (**E**) with sodium borohydride or methyllithium.

By this method, a variety of steroidal ketones,[2,3)] camphor,[4)] and adamantanone[5)] have been transformed into the corresponding oxasteroids and cyclic ethers.

As will be apparent from Scheme 1, the oxasteroid (**E**) can be further transformed into oxasteroids with oxygen-containing rings smaller by one member if oxasteroid (**E**) can be oxidized to the corresponding lactone (**F**).

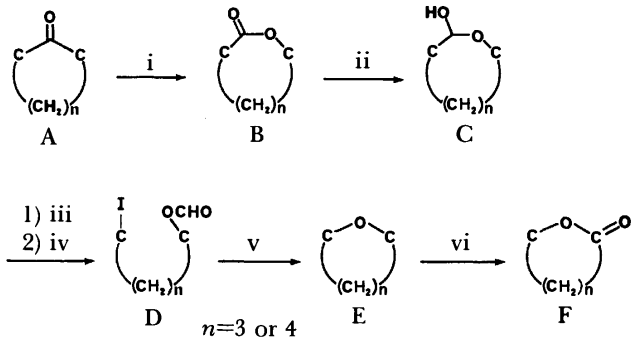

Scheme 1. Reagents: i, MCPBA: ii, DIBAL-toluene: iii, HgO-I_2-pyridine-benzene: iv, *hν*: v, MeLi-THF or $NaBH_4$-THF: vi, RuO_2-$NaIO_4$-CCl_4 or CrO_3-CH_3CO_2H-H_2O.

We therefore used this ring contraction sequence to undertake the synthesis of several more new five- and six-membered oxasteroids of the cholestane series in order to broaden the applicability of our method to include the synthesis of this group of chiral molecules of biological interest.

We chose three six-membered oxasteroids, 4-oxa-5α-cholestane (**1**),[3,6-9)] 4-oxa-5β-cholestane (**5**)[7)] and 4,4-

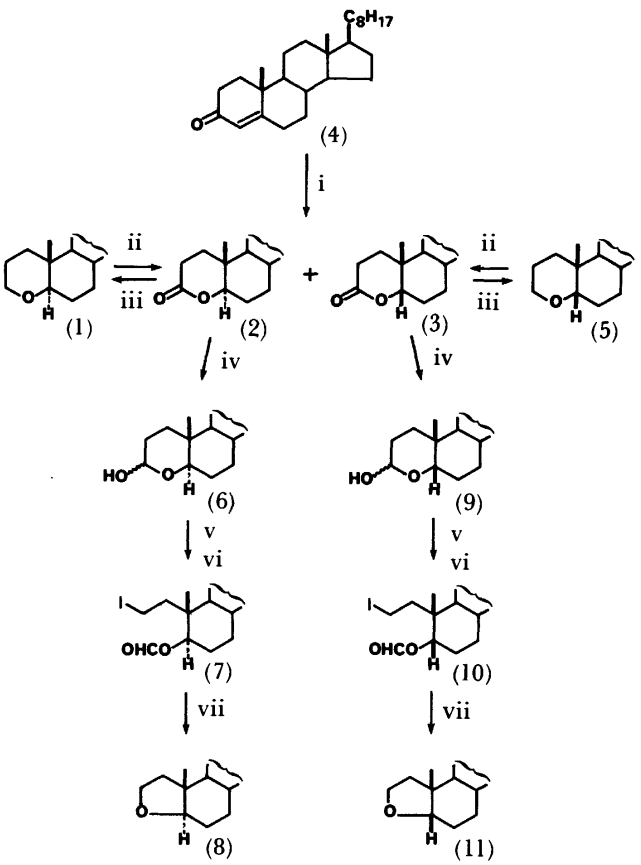

Scheme 2. Reagents: i, $K_2S_2O_8$-H_2SO_4-CH_3COOH: ii, RuO_2-$NaIO_4$-CCl_4: iii, $LiAlH_4$-BF_3-diethyl ether: iv, DIBAL-toluene: v, HgO-I_2-pyridine-benzene: vi, *hν*: vii, MeLi-THF.

dimethyl-3-oxa-5α-cholestane (**12**)[2] and a seven-membered oxasteroid, 6-oxa-*B*-homo-5β-cholestane (**17**).[12]

Oxidation of 4-oxa-5α-cholestane (**1**) with ruthenium tetraoxide[10] in THF gave 4-oxa-5α-cholestan-3-one (**2**)[7,9,11] in a good yield. Lactone **2** can be directly prepared by means of oxidation with peroxodisulfuric acid of cholest-4-en-3-one (**4**), as Pettit and Kasturi report.[9] Reduction of lactone **2** with DIBAL at $-78°C$ gave a mixture of the corresponding α- and β-lactols **6**.[9] Irradiation of the hypoiodites of the lactol mixture generated in situ with mercury(II) oxide-iodine and pyridine in benzene with a Pyrex-filtered light readily gave an iodoformate **7**. Its cyclization to *A*-nor-3-oxa-5α-cholestane (**8**) was achieved with methyllithium at $-78°C$ in an almost quantitative yield.

The isomeric 4-oxa-5β-chloestane (**5**), prepared after Edward and Morand,[7] was similarly oxidized to give 4-oxa-5β-cholestan-3-one (**3**)[7,11] with ruthenium tetraoxide (84%). Lactone **3** was then successively transformed into the lactols **9** (81%) and iodoformate **10** (59%). The cyclization of **10** with $NaBH_4$ gave *A*-nor-3-oxa-5β-cholestane (**11**). In the course of our study of the oxidation of cholest-4-en-3-one (**4**) with peroxodisulfuric acid after Pettit and Kasturi,[9] we found that lactone **3** can be obtained as a by-product (8% yield) along with the isomeric 5α-lactone **2**[7,9,11] (32% yield) reported by them. Although the yield is low, the formation of lactone **3** by one step from a readily available cholest-4-en-3-one may be useful in bringing about a quicker synthesis of lactone **3**.

We were also able to transform 4,4-dimethyl-3-oxa-5α-cholestane (**12**)[2] into 3,3-dimethyl-*A*-nor-2-oxa-5α-cholestane (**16**) through a lactone **13**, an α-lactol **14**, and an iodoformate **15** in a good overall yield (Scheme 3).

We then turned our attention to the preparation of six-membered oxasteroids. Oxidation of *B*-homo-6-oxa-5β-cholestane (**17**)[12] with ruthenium tetraoxide in THF gave *B*-homo-6-oxa-5β-cholestan-6-one (**18**) in an 88% yield. This new lactone was also prepared by stereospecific photo-rearrangement of 5-hydroxy-5α-cholestan-6-one (**19**)[13] according to the method reported by Cookson et al.[14] Reduction of lactone (**18**) with DIBAL gave a mixture of *B*-homo-6-oxa-5β-cholestan-7α- and 7β-ols **20** in a 90% yield. Preparation of the corresponding hypoiodites with mercury(II) oxide, iodine and pyridine in benzene followed by the irradiation of the solution gave an iodoformate **21** in a 45% yield. Its cyclization with methyllithium gave a new oxasteroid, 6-oxa-5β-cholestane (**22**) in an 87% yield (Scheme 4).

The present results broaden the applicability of our method for the transformation of cyclic ketones into cyclic ethers and will extend its scope for application to synthetic problems. It should also be noted that since we have recently shown that the iodoformates in the sequence outlined in Scheme 1 can be transformed into thia- and azasteroids,[15] the present results imply

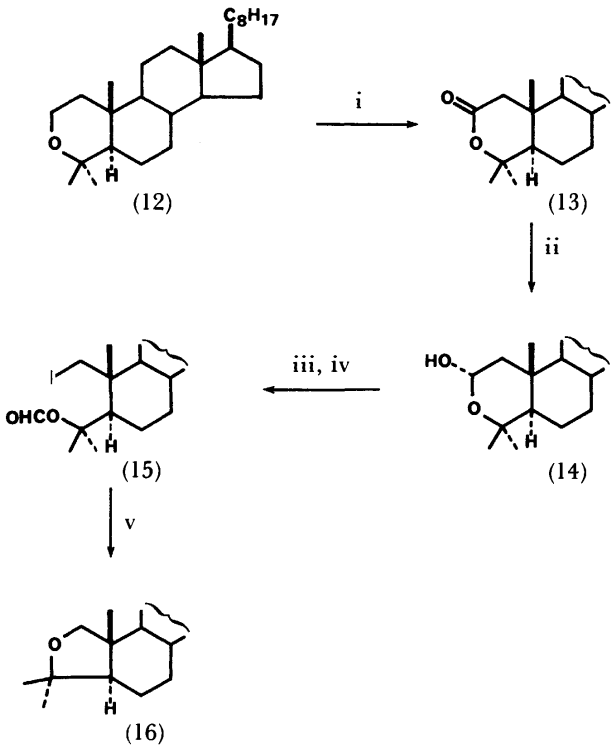

Scheme 3. Reagents i, CrO_3CO_2H-H_2O: ii, DINBAL-toluene: iii, HgO-I_2-pyridine-benzene: iv, *hν*: v, MeLi-THF.

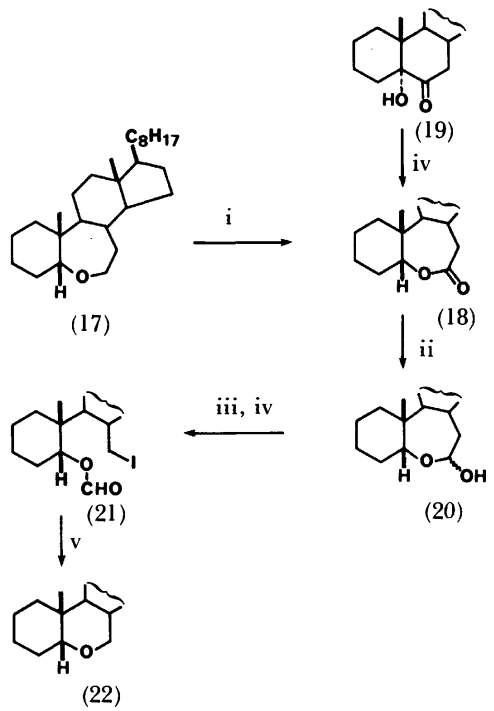

Scheme 4. Reagents: i, RuO_2-$NaIO_4$-CCl_4: ii, DIBAL-toluene: iii, HgO-I_2-pyridine-benzene: iv, *hν*: v, MeLi-THF.

that the transformation of 6- or 7-membered oxasteroids into 5- or 6-membered cyclic sulfides as well as amines is now achievable.

The Mass Spectrometric Fragmentations of the Oxasteroids. The synthesis of a number of oxasteroids, steroidal lactones, and steroidal lactols reported in previous papers[2,3] as well as in the present ones has provided us with a good opportunity to examine the pattern of their mass spectral fragmentations.

In the following part, the structures and the probable genesis of the major fragment ions in the mass spectra of steroidal lactones, lactols, and cyclic ethers described in this and the previous papers,[2,3] are briefly discussed.

a) **Steroidal Lactones.** The mass spectral fragmentation of certain steroidal lactones has already been reported.[16] Our studies have revealed that the lactone-directed fragmentation and the general fragmentation of a complex hydrocarbon framework take place competitively after the electron impact of steroidal lactones.

We examined the mass spectra of four lactones **2**, **3**, **13**, and **18**, prepared in the present work, as well as the mass spectra of four lactones, 17*a*-oxa-*D*-homo-5*α*-androstan-17-one (**23**), 3*α*,5-cyclo-6-oxa-*B*-homo-5*α*-cholestan-7-one (**24**), 7*a*-oxa-*B*-homo-5*α*-cholestan-7-one (**25**), and 6-oxa-*B*-homo-5*α*-cholestan-7-one (**26**) reported in our previous paper.[3] We found that the mass spectra of these 8 lactones can be divided into two categories according to their mode of fragmentation. Thus, the mass spectra of lactones **2** and **3** are grouped in a category that exhibits a fragmentation pattern similar to that of the corresponding steroidal hydrocarbons. One of the distinct features of the mass spectra of the C-17 substituted steroidal hydrocarbons is the expulsion of the ring-D; this is of diagnostic importance. The genesis of this expulsion that involves both single and reciprocal electron transfers has been established by Djerassi and his colleagues.[16,17] The intensities of the molecular ions and fragment ions that arise from the ring-D cleavage of lactones **2** and **3** are listed in Table 1. Although no appreciable ions arising from the fragmentation of the oxygen-containing A-rings are present in the mass spectra of lactones **2** and **3**, the comparison of the mass spectra of the two isomeric lactones shows an interesting difference in the intensities of the fragment ions that arise from their ring-D cleavage. Thus, while the intensity of the fragment ions corresponding to the elimination of the ring-D involving both a single electron transfer and a reciprocal electron transfer were 100 and 70%, the intensity of the fragment ions corresponding to the elimination of the ring-D of the mass spectrum of the isomer was only 14 and 11%. It is thus apparent that the geometry of the remote ring can exert an appreciable effect on the elimination of the ring-D of these isomeric steroids during the electron impact.

Table 1. Intensities of the Molecular Ions and the Fragment Ions Corresponding to the Elimination of the Ring-D of Isomeric Lactones **2** and **3**

Lactone	M^+ ion/%	M^+-155 ion/%	M^+-154 ion/%
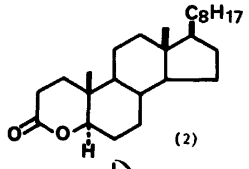 (2)	72	100	70
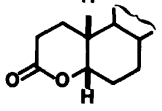 (3)	100	14	11

This seems to be a clear example of "conformational transmission"[18] in the mass spectrometric fragmentation. The mass spectra of the six other lactones revealed lactone-directed fragmentation. Thus, lactone **13** exhibited the fragment ion of m/z 316 that arose from the elimination of the ring-A as the base peak while the parent ion was very weak (2%). Accurate mass measurement indicated that the elemental composition of the ion at m/z 316 is $C_{23}H_{40}^+$ (316.31407). The probable structure of the ion

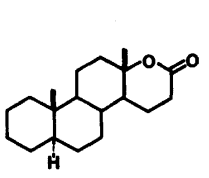
(23)

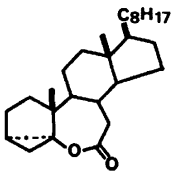
(24)

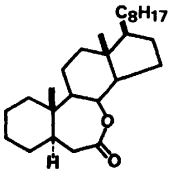
(25)

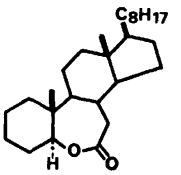
(26)

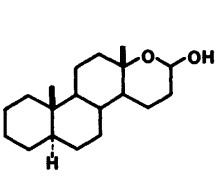
(27)

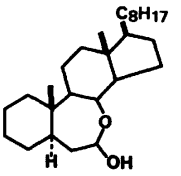
(28)

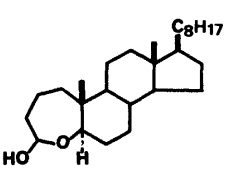
(29)

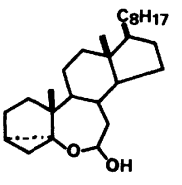
(30)

together with its genesis is outlined in Scheme 5.

The mass spectrum of lactone **23**[3] exhibited a fragment ion at m/z 218 as the base peak and an oxonium ion at m/z 275 (32%) arising from the expulsion of 13β-Me from the molecular ion (Scheme 6). The intensity of the oxonium ion at m/z 275 was only 32% and this low intensity contrasts with the ion that arises from the expulsion of 13α-Me in the mass spectrum of a 17-oxasteroid,[19] which has been reported to be very prominent. Accurate mass measurement showed that the elemental composition of the base peak is $C_{16}H_{26}^+$ (218.20296). A probable structure of the ion at m/z 218 and its genesis involving the elimination of the ring-D is outlined in Schceme 7.

The mass spectra of isomeric seven-membered lactones **18** and **26** exhibited almost identical patterns of fragmentation, with a fragment ion at m/z 318 as their base peak. Accurate mass measurement of the ion that arises from lactone **18** indicated that the elemental composition of the ion is $C_{22}H_{38}O^+$ (318.29253). Scheme 8 illustrates a probable structure of the ion and its genesis.

Although lactone **24** is structurally analogous to lactones **18** and **26**, its mass spectral fragmentation, nevertheless differed considerably from those of lactones **18** and **26**. It showed an ion at m/z 95 as the base peak and the intense ion at m/z 400 ($M^+ - CO$, 54.9%). A probable genesis of the ion at m/z 95, which was proved to have the elemental composition $C_7H_{11}^+$ by accurate mass measurement, is outlined in Scheme 9. An ion at m/z 95 was again the base peak in the mass spectrum of lactones **25**. A probable structure and the genesis of the ion is outlined in Scheme 10.

b) **Steroidal Lactols.** We examined the mass spectra of seven steroidal lactols, 17a-oxa-*D*-homo-5α-androstan-17α- and 17β-ols (**27**), 7a-oxa-*B*-homo-5α-cholestan-7α- and 7β-ols (**28**), 4a-oxa-*A*-homo-5α-cholestan-4α- and 4β-ols (**29**), 3α,5-cyclo-6-oxa-*B*-homo-5α-cholestan-7α- and 7β-ols (**30**), 4-oxa- 5α- and 5β-cholestan-3α- and 3β-ols (**6**) and (**9**), and 4,4-dimethyl-3-oxa-5α-cholestan-2α-ol (**14**). Most of these lactols showed that the decomposition of their oxygen-containing ring is predominant over the decomposition of their hydrocarbon framework. Thus, the mass spectrum of lactol **27** exhibited the base peak at m/z 218; this is equivalent to the ion from the corresponding lactone **23** (Scheme 7), which is attributable to the ion arising from the expulsion of the ring-D.

The mass spectrum of steroidal lactol **28** exhibited the base peak at m/z 95. Accurate mass measurement indicated that its elemental composition was $C_7H_{11}^+$ (95.0858). The ion probably arises from the breakdown of the oxygen-containing ring as outlined in

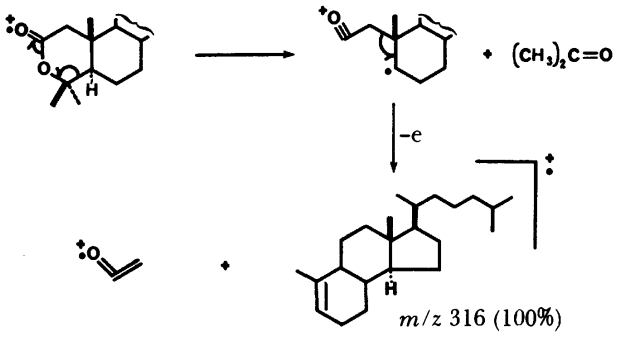

Scheme 5.

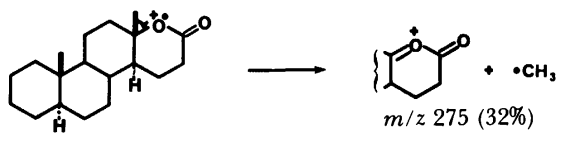

Scheme 6.

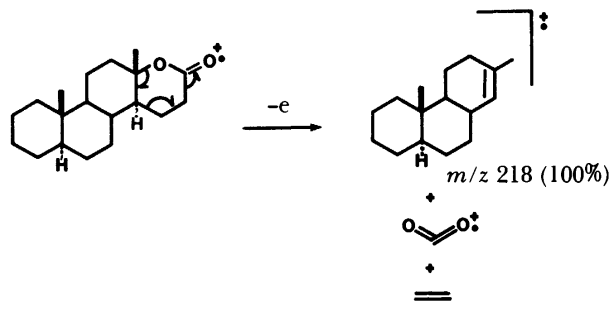

Scheme 7.

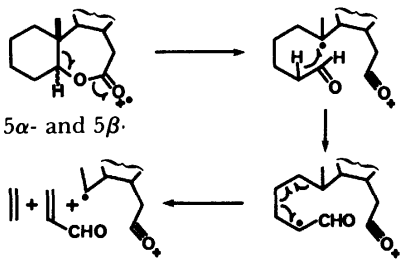

Scheme 8.

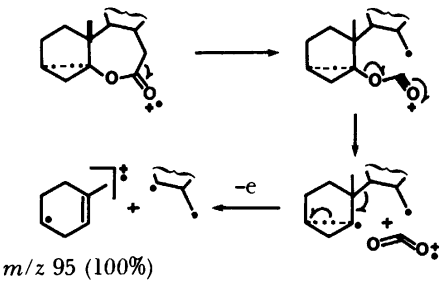

Scheme 9.

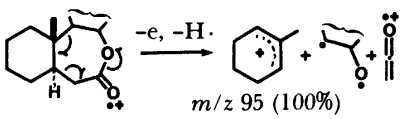

Scheme 10.

Scheme 11.

The base peak in the mass spectrum of steroidal lactol **29** appeared at m/z 332. Accurate mass measurement indicated that the elemental composition was $C_{23}H_{40}O^+$ (332.3092). The outline formation of this ion is rationalized in Scheme 12. It can be formed by the loss of the ring-A with a transfer of the angular hydrogen to the ethereal oxygen.

The mass spectrum of lactol **30** exhibited the base peak at m/z 111. Accurate mass measurement indicated that the elemental composition was $C_7H_{11}O^+$ (m/z 111.0826). The genesis of this ion, which involved a breakdown of its oxygen-containing ring, is outlined in Scheme 13.

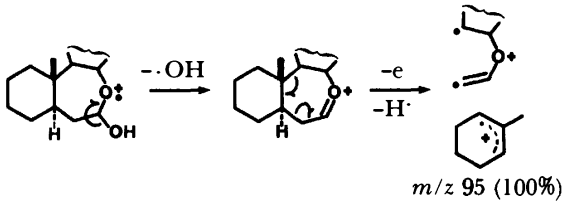

Scheme 11.

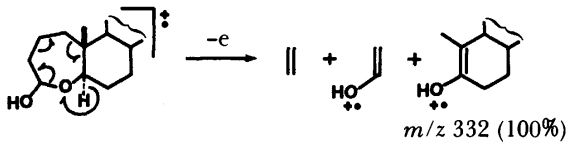

Scheme 12.

Table 2. Intensities of the Molecular Ion and the Fragment Ions Corresponding to the Elimination of the Ring-D of Some Oxasteroids of Cholestane Series

Substrate	M+ ion/%	M+−155 ion/%	M+−154 ion/%
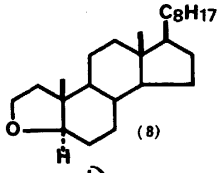 (8)	75	100	74
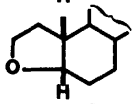 (11)	100	13	16
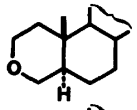 (31)	79	100	76
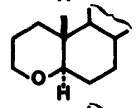 (1)	54	100	48
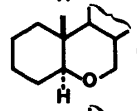 (32)	37	100	28
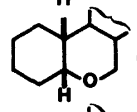 (22)	36	100	20
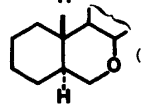 (33)	7	100	6

The mass spectra of isomeric lactols **6** and **9** both exhibited their base peaks at m/z 372, owing to a loss of water.

Finally, the mass spectrum of 4,4-dimethyl-3-oxa-5α-cholestan-2-ol (**14**) exhibited the base peak at m/z 385; this is assignable to the loss of the element of water and the 4-methyl group.

c) **Steroidal Ethers.** We examined the mass spectra of 12 steroidal cyclic ethers prepared in our present and the previous work. As in the case of the steroidal lactones the mass spectra of these cyclic ethers can be divided into two categories according to their type of the fragmentation.

The mass spectra of seven steroidal cyclic ethers listed in Table 2 are grouped in the first category which shows fragmentation similar to that of the steroidal hydrocarbons. The mass spectra of these oxasteroids with an oxygen atom in their ring-A or B showed, with only one exception, normal fragmentation arising from the elimination of their ring-D. The mass spectrum of *A*-nor-3-oxa-5β-cholestane (**11**) showed the molecular ion as the base peak while the intensity of the fragment ions that corresponded to the elimination of the ring-D with a single electron transfer and a reciprocal electron transfer were only 13 and 16%. The 5α-isomer **8**, on the other hand, gave the mass 205 ion as the base peak and the ion at m/z 206 was very intense (74%). This is another example of what has been called the "conformational transmission" in the mass spectrometric fragmentation which we have already found in the mass spectra of the isomeric pair of lactones **2** and **3**. The geometry of the remote ring exerts a notable effect on the elimination of the ring-D of these oxasteroids during the electron impact.

The mass spectra of the five further oxasteroids listed in Table 3 exhibited fragmentation directed by their oxygen-containing ring. The mass spectrum of 16-oxa-5α-androstane (**34**) exhibited its base peak at m/z 231. The probable genesis, which is based on an

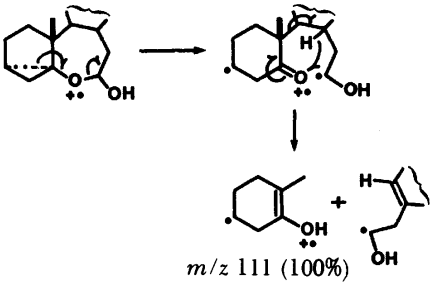

Scheme 13.

Table 3. The Base Peak and the Intensities of the Molecular Ions of Some Oxasteroids

Substrate	M+ ion/%	M+−155 ion/%	M+−154 ion/%
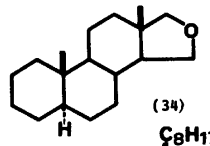 (34)	10	—	100
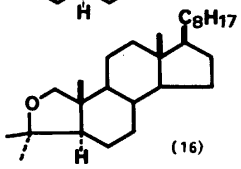 (16)	0.4	85	100
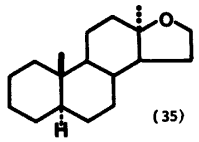 (35)	0.2	100	—
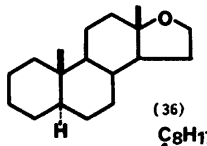 (36)	1.5	100	—
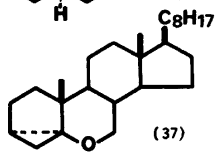 (37)	100	—	*m/z* 111 (89%)

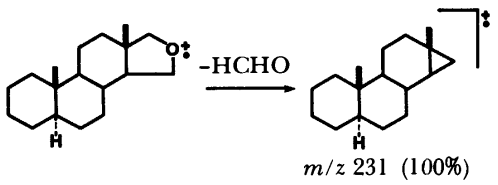

m/z 231 (100%)

Scheme 14.

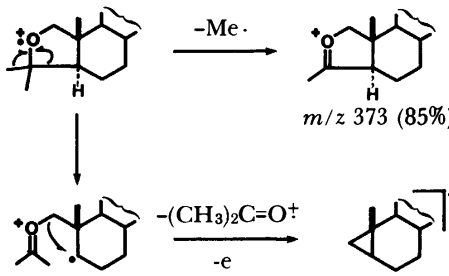

m/z 373 (85%)

m/z 330 (100%)

Scheme 15.

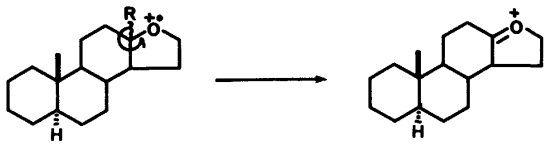

R=α- and β-Me

m/z 247 (100%)

Scheme 16.

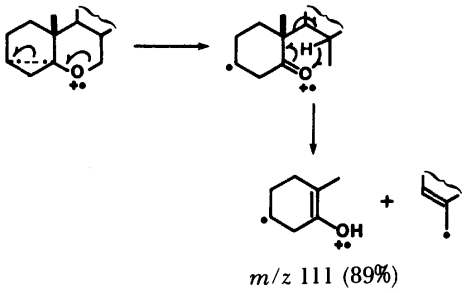

m/z 111 (89%)

Scheme 17.

analogy with the loss of formaldehyde from tetrahydrofuran, [20] is outlined in Scheme 14.

The mass spectrum of 3,3-dimethyl-2-oxa-*A*-nor-5α-cholestane (**16**) exhibited the base peak at *m/z* 330 and an intense fragment ion at *m/z* 373 (85%). The base peak arises as the result of a similar loss of the element of acetone while the latter is generated by the expulsion of the 3-methyl-group as outlined in Scheme 15.

The mass spectra of 17-oxa-5α-androstane (**35**) and its 13-epimer (**36**) exhibited their base peak at *m/z* 247; this arises from the expulsion of 13α- and 13β-methyl group, as expected (Scheme 16).

The mass spectrum of 3α,5-cyclo-6-oxa-5α-cholestane (**37**) exhibited the molecular ion as the base peak and an intense fragment ion at *m/z* 111 (89%). Accurate mass measurement indicated that the molecular composition of the latter was $C_7H_{11}O^+$ (*m/z* 111.0828). Its formation is rationalized as outlined in Scheme 17.

Experimental

Mps were recorded with a Yanagimoto micro mp apparatus. IR spectra were determined for Nujol mulls with a Hitachi Model 285 infrared spectrophotometer. ^{1}H NMR spectra were determined with a JEOL PS 200 high-resolution FT-NMR spectrometer (200 MHz) (Solvent, $CDCl_3$: $SiMe_4$ as an internal standard) (Faculty of Pharmaceutical Sciences of this University). TLC was carried out on a Merck Kiesel gel 60 PF_{254}. All the high and low resolution mass spectra were recorded with a JEOL JMS-D 300 spectrometer (70 eV) (Faculty of Agriculture). Elemental analysis was performed by the staff of the Laboratory for Microanalysis of the Faculty of Pharmaceutical Sciences of this University.

4-Oxa-5α-cholestan-3-one (2). An aqueous $NaIO_4$ solution (300 mg $NaIO_4$ in water 1 ml) was added dropwise to carbon tetrachloride (4 ml) containing $RuO_2 \cdot X\,H_2O$ (15 mg) while stirring at about 0°C. 4-Oxa-5α-cholestane (**1**)[3,6-9] (65 mg) in carbon tetrachloride (4 ml) was added dropwise at room temperature to the solution containing RuO_2. The solution was stirred for 4 h and a further amount of aq $NaIO_4$ solution (100 mg $NaIO_4$ in water 0.3 ml) was added. The solution was stirred 20 h. After the addition of isopropyl alcohol to the solution, RuO_2 was removed by filtration. The solution was washed with water and dried over anhydrous Na_2SO_4. The work-up as usual gave crystals (60 mg) which were subjected to preparative TLC with

a 5 : 1 mixture of benzene and diethyl ether. Two fractions were obtained. The more mobile TLC fraction (13 mg) was the starting material. The less mobile fraction (35 mg, 65% based on the converted material) was lactone **2** which was recrystallized from pet. ether. Mp 111—118°C (lit,[7] mp 114—115°C; lit,[9] mp 118—119°C; lit,[11] mp 116—116.5°C). ^{1}H NMR (90 MHz) δ=0.67 (3H, s, 18-H), 0.93 (3H, s, 19-H), 3.95 (1H, dd, J=11.20 and 4.61 Hz, 5α-H), and 2.55—2.68 (2H, m, 2-H), MS m/z (rel intensities) 388 (M^+, 72%), 233 (100), 81 (48), 55 (60), and 43 (97).

4-Oxa-5α-cholestan-3-ols (6).[9] A solution of DIBAL (1.8 ml) was added dropwise to a solution of the lactone **2** (570 mg) in dry toluene (40 ml) at −78°C. The solution was stirred for 3 h at −78°C and poured into iced water. After the solution had been filtered, the filtrate was extracted with dichloromethane. The organic layer was washed with water and dried over anhydrous Na_2SO_4. The usual work-up gave a product (540 mg) which was recrystallized from acetone-dichloromethane to yield a 1 : 1 mixture of α- and β-lactols **6**, mp 185—187°C (lit,[9] β-lactol, 197—199°C). ^{1}H NMR δ=0.65 (3H, s, 18-H of α- and β-ols), 0.91 and 0.94 (each s, 19-H of α- and β-ols), 3.01 (dd, J=11.23 and 4.40 Hz, 5α-H of 3β-ol), 3.71 (J=10.74 and 5.37 Hz, 5α-H of 3α-ol), 4.73 (m, 3α-H of 3β-ol), and 5.25 (m, 3β-H of 3α-ol), MS, m/z (rel intensity) 390 (M^+, 0.5%), 372 [$(M-H_2O)^+$, 100], and 83 (83).

Irradiation of the Hypoiodite of 4-Oxa-5α-cholestan-3-ols in the Presence of Mercury(II) Oxide and Iodine. Lactols **6** (300 mg) were added to dry benzene (39 ml) containing pyridine (0.5 ml), mercury(II) oxide (332 mg), and iodine (391 mg). The solution in a Pyrex vessel was irradiated for 2 h in an atmosphere of nitrogen. The solution was filtered and the filtrate was worked up as usual to give an oily product (419 mg) which was subjected to preparative TLC with benzene. Three fractions were obtained. The most mobile TLC fraction (200 mg) was crystalline formate **7**. The next fraction (17 mg) was an intractable mixture. The least mobile fraction (120 mg) was lactone **2**. The formate **7** was recrystallized from methanol-acetone. Mp 99 — 100°C. (Found: C, 60.42; H, 8.76 %. Calcd for $C_{26}H_{45}IO_2$: C, 60.46; H, 8.78%). IR 1718 (CHO), 1210 and 1183 cm^{-1} (OCHO), ^{1}H NMR δ=0.65 (3H, s, 18-H), 0.92 (3H, s, 19-H), 2.95—3.19 (2H, m, 2-H), 4.86 (1H, dd, J = 11.23 and 4.89 Hz, 5α-H), 8.10 (1H, s, OCHO); MS m/z (rel intensity) 516 (M^+, 0.4%), 470 [$(M-OCH_2O)^+$, 8.2], 389 [$(M-I)^+$, 31], 343 (53), 315 (39), 287 (62), and 55 (100).

3-Oxa-A-nor-5α-cholestane (8). A solution of formate **7** (140 mg) in THF (30 ml) was cooled to −78°C by Dry Ice-methanol. Methyllithium (1.05 M† diethyl ether solution) (0.7 ml) was added to this stirred solution. The solution was stirred for 30 min at that temperature and then stirred for further 1 h at room temperature and then extracted with diethyl ether. The ethereal solution was worked up as usual. A crystalline product (98 mg) was recrystallized from methanol-acetone to yield a pure specimen (89 mg), mp 77—78°C. (Found: C, 83.11; H, 12.42%. Calcd for $C_{25}H_{44}O$: C, 83.27; H, 12.30%). IR 1124, 1010, and 975 cm^{-1}; ^{1}H NMR δ=0.67 (3H, s, 18-H), 0.81 (3H, s, 19-H), 3.04 (1H, dd, J=12.21 and 3.91 Hz, 5α-H), 3.85—3.93 (2H, m, 2-H); MS m/z (rel intensity) 360 (M^+, 75%), 345 [$(M-Me)^+$, 35], and 205 (100).

Oxidation of Cholest-4-en-3-one with Peroxodisulfuric Acid. Potassium peroxodisulfate (3 g) and concd sulfuric acid (3.3 g) were dissolved in glacial acetic acid (50 ml). The mixture was added to a solution of cholest-4-en-3-one (3 g) in glacial acetic acid (50 ml). The solution was stirred for two weeks at room temperature in the absence of light. The mixture was treated with aqueous 50% potassium hydroxide (14 ml). Precipitated salts were removed by filtration and the filtrates evaporated. The residue was extracted with diethyl ether. The ether solution was washed with water and dried over anhydrous Na_2SO_4. The solution was worked up as usual. The product (2.5 g) was subjected to column chromatography (Merck Kiesel gel 60; 70—230 mesh, 40 g). Elutions with benzene gave a major fraction (1.38 g) which was a crystalline mixture of lactones. Recrystallization with pet. ether gave 4-oxa-5α-cholestan-3-one (620 mg). The filtrate of the recrystallization was evaporated to yield a mixture of 5α- and 5β-lactones. An attempted separation of the mixture to its two components by preparative TLC with a variety of solvents was unsuccessful. The mixture was therefore subjected to fractional crystallization with methanol-pet. ether 6 times to give almost pure 5β-lactone **3**, (40 mg). This lactone was subjected to DIBAL reduction. A pure lactone melted at 106 — 107°C (pet. ether) (lit,[11] 109.5 — 110°C, lit,[7] 107 — 107.5°C). ^{1}H NMR δ=0.68 (3H, s, 18-H), 0.99 (3H, s, 19-H), 2.39—2.56 (2H, m, 2-H), and 4.14 (1H, dd, J=3.3 and 2.4 Hz), MS m/z (rel intensity) 388 (M^+, 100%), 315 (6), 233 (14), and 55 (19).

Reduction of 4-Oxa-5β-cholestan-3-one. Lactone **3** (38 mg) was dissolved in dry toluene (5 ml) and the solution was cooled to −78°C by Dry Ice-methanol. A DIBAL solution (0.13 ml) was added to this solution and the solution was stirred for 2 h at −78°C. The solution was poured into water and the inorganic precipitates were removed by filtration. The solution was washed with water and dried. The usual work-up gave 4-oxa-5β-cholestan-3-ols (40 mg) which were purified by preparative TLC with a 5 : 1 benzene-diethyl ether to yield an oily mixture of 4-oxa-5β-cholestan-3α- and 3β-ols. (Found: m/z 390.3533. Calcd for $C_{26}H_{46}O_2$: M, 390.3498). IR (neat) 3365 (OH) and 1015 cm^{-1}; ^{1}H NMR δ=0.65 (3H, s, 18-H of 3α- and 3β-ols), 0.88 and 0.92 (each 3H, each s, 19-H of 3α- and 3β-ols), 3.30 and 3.84 (each 1H, each, brs, 5β-H of 3α- and 3β-ols), and 4.72 and 5.32 (each 1H, each brs, 3α- and 3β-H of 3α- and 3β-ols); MS m/z (rel intensity) 390 (M^+, 7%), 372 [$(M-H_2O)^+$, 100], and 315 (14).

Irradiation of the Hypoiodite of 4-Oxa-5β-cholestan-3-ols in the Presence of Mercury(II) Oxide and Iodine. Lactols **9** (68 mg) were added to a dry benzene (9 ml) containing pyridine (0.1 ml), mercury(II) oxide (75 mg) and iodine (89 mg). The solution in a Pyrex vessel was irradiated for 2 h in an atmosphere of nitrogen. The solution was filtered and the filtrate was worked up as usual to give a crystalline product (98 mg) which was subjected to preparative TLC with benzene. Of the two fractions, the more mobile TLC fraction was a crystalline formate **10** (53 mg). After recrystallization from acetone-methanol, the formate melted at 112 — 117°C. (Found: m/z 516.2490. Calcd for $C_{26}H_{45}IO_2$: M, 516.2465). IR (Nujol) 1728 (CHO) and

† 1M=1 mol dm^{-3}.

1190 cm^{-1} (OCHO); ^1H NMR δ= 0.66 (3H, s, 18-H), 0.95 (3H, s, 19-H), 3.00—3.15 (2H, m, $-CH_2I$), 4.88 (1H, br. s, 5 β-H) and 8.11 (1H, s, CHO); MS *m/z* (rel intensity) 516 (M^+, 0.7%), 470 [$(M-OCH_2O)^+$, 14], 389 [$(M-I)^+$, 48], and 343 [$(M-OCH_2O-I)^+$, 100].

3-Oxa-*A*-nor-5β-cholestane (11). A solution of formate **10** (51 mg) in THF (10 ml) was cooled to −78°C. To this stirred solution, there was added methyllithium (1.05 M diethyl ether solution) (0.24 ml). The solution was stirred for 30 min and then the temperature of the solution was raised to room temperature. The solution was stirred for 1 h at room temperature and extracted with diethyl ether. The usual work-up of the solution gave a crude crystalline oxasteroid **11**. This was then recrystallized from methanol-acetone. Mp 91.5—92.5°C. (Found: C, 83.09; H, 12.31%. Calcd for $C_{25}H_{44}O$: C, 83.27; H, 12.30%). IR (Nujol) 1039 and 1017 cm^{-1} (C-O); ^1H NMR δ= 0.67 (3H, s, 18-H), 0.93 (3H, s, 19-H), 3.43 (1H, dd, J= 2.9 and 2.4 Hz, 5β-H), and 3.75—3.94 (2H, m, 2-H), MS *m/z* (rel intensity) 360 (M^+, 100%), 345 [$(M-Me)^+$, 3], 315 (6), 206 (16), and 43 (34).

4,4-Dimethyl-3-oxa-5α-cholestan-2-one (13). A solution of aqueous acetic acid (0.5 ml of water plus 5 ml of acetic acid) containing chromium trioxide (200 mg) was added dropwise to an acetic acid solution (10 ml) of 4,4-dimethyl-3-oxa-5α-cholestane (103 mg) at room temperature. The solution was stirred overnight and then heated at 40°C for 2 h. The solution was extracted with dichloromethane and the organic layer was neutralized with aqueous sodium hydrogencarbonate. The usual work-up of the solution gave an oily product which was subjected to preparative TLC to give a crystalline lactone **13** (35 mg). This was recrystallized from acetone-methanol to yield a pure material, mp 171—173°C. (Found: C, 80.62; H, 11.60%. Calcd for $C_{28}H_{48}O_2$: C, 80.71; H, 11.61%). IR 1720 (C=O), 1114, 1100, 989, and 950 cm^{-1}; ^1H NMR δ= 0.65 (3H, s, 18-H), 1.00 (3H, s, 19-H), 1.34 and 1.40 (each 3H, each s, *gem* dimethyl), and 1.92 and 2.65 (each 1H, each d, J= 16.8 Hz, 1-H), MS *m/z* (rel intensity) 416 (M^+, 2%), 401 [$(M-Me)^+$, 1.5], 358 (1.5), and 316 [(M−ring-A)$^+$, 100].

4,4-Dimethyl-3-oxa-5α-cholestan-2α-ol (14). A solution of DIBAL (0.1 ml) was added dropwise to a solution of lactone **13** (31 mg) in dry toluene (5 ml) at −78°C. The solution was stirred for 3 h and poured into iced water. After the solution was filtered, the solution was washed with water and dried over anhydrous Na_2SO_4. The work-up by the usual method gave a product (32 mg) which was recrystallized from acetone to yield 2α-lactol **14**. Mp 166—170°C. (Found: C, 80.07; H, 12.05%. Calcd for $C_{28}H_{50}O_2$: C, 80.32; H, 12.04%). IR 3375 (OH), 1130, and 1048 cm^{-1} (C-O); ^1H NMR δ= 0.63 (3H, s, 18-H), 1.01 (3H, s, 19-H,), 1.18 and 1.24 (each 3H, each s, *gem* dimethyl), 2.75 (1H, d, J= 7.3 Hz, OH), and 5.06 (1H, ddd, J= 9.0, 7.3, and 2.0 Hz, 2β-H); MS *m/z* (rel intensity) 400 [$(M-H_2O)^+$, 9%], 385 [$(M-H_2O-Me)^+$, 100], 316 (51), 95 (35), and 43 (94).

Irradiation of the Hypoiodite of 4,4-Dimethyl-3-oxa-5α-cholestan-2α-ol (14). The lactol (14 mg) was added to a dry benzene (3 ml) containing pyridine (0.05 ml), mercury(II) oxide (15 mg) and iodine (17 mg). The solution in a Pyrex vessel was irradiated for 2 h in an atmosphere of nitrogen. The solution was filtered and the filtrate was worked up as usual to give oily formate (20 mg). The product was subjected to preparative TLC with benzene. Of the two fractions, the more mobile TLC fraction was an oily formate **15** (11 mg). (Found: *m/z* 417.3760. Calcd for $C_{28}H_{49}IO_2-I$: M, 417.3732). IR (neat) 1720 (CHO), 1180 and 1143 cm^{-1} (OCHO); ^1H NMR δ= 0.63 (3H, s, 18-H), 1.13 (3H, s, 19-H), 1.56 and 1.63 (each 3H, each s, *gem* dimethyl), 3.35 and 3.94 (each 1H, each d, J= 10.25 Hz, CH_2I), and 8.12 (1H, s, CHO); MS *m/z* (rel intensity) 417 [$(M-I)^+$, 0.8%], 371 [$(M-I-OCH_2O)^+$, 81], 301 (18), and 95 (100).

3,3-Dimethyl-*A*-nor-2-oxa-5α-cholestane (16). A solution of formate **15** (10 mg) in THF (3 ml) was cooled to −78°C. To this stirred solution, there was added methyllithium (0.57 M diethyl ether solution) (0.08 ml). The solution was stirred for 1 h at that temperature and thereafter stirred for further 1 h at room temperature and extracted with diethyl ether. The usual work-up of the solution gave an almost pure crystalline oxasteroid **16** (7 mg). It was recrystallized from methanol. Mp 106—107°C. (Found: C, 83.21; H, 12.38%. Calcd for $C_{27}H_{48}O_2$: C, 83.43; H, 12.45%). IR 1019 and 1014 cm^{-1} (C-O); ^1H NMR δ= 0.66 (3H, s, 18-H), 1.01 (3H, s, 19-H), 1.13 and 1.19 (each 3H, each s, *gem* dimethyl), 3.27 and 3.58 (each 1H, each d, J= 7.33 Hz, 1H), MS *m/z* (rel intensity) 388 (M^+, 0.4%), 373 [$(M-Me)^+$, 85], 330 [$(M-(CH_3)_2CO)^+$, 100], 288 (39), 217 (38), 175 (34), 95 (38), and 43 (42).

***B*-Homo-6-oxa-5β-cholestan-7-one (18).** Aqueous $NaIO_4$ solution (200 mg $NaIO_4$ in water 1 ml) was added dropwise to carbon tetrachloride (3 ml) containing $RuO_2 \cdot X\,H_2O$ (20 mg) while stirring at about 0°C . The *B*-homo-6-oxacholestane (**17**) (23 mg) in carbon tetrachloride (3 ml) was added dropwise to the solution containing ruthenium tetraoxide at 0°C. The solution was stirred for 5 h at room temperature. After the addition of isopropyl alcohol to the solution, RuO_2 was removed by filtration. The solution was washed with water and dried over anhydrous Na_2SO_4. The usual work-up gave crystals (25 mg) which were recrystallized from methanol to yield a specimen for analysis, mp 119—121°C. (Found: C, 80.50; H, 11.61%. Calcd for $C_{27}H_{46}O_2$: C, 80.55; H, 11.51%). IR 1735 (C=O), 1310, 1253, 1144, 1106, and 1024 cm^{-1}; ^1H NMR δ= 0.65 (3H, s, 18-H), 0.95 (3H, s, 19-H), 2.44 (1H, br.d, J= 14.7 Hz, 7a-H), 2.97 (1H, m, 7a-H), and 4.17 (1H, br.s, 5β-H). MS *m/z* (rel intensity) 402 (M^+, 2%) and 318 (100).

Preparation of *B*-Homo-6-oxa-5β-cholestan-7-one (18) by the Photo-Rearrangement. 5-Hydroxy-5α-cholestan-6-one[10] (240 mg) in ethanol (50 ml) in a Pyrex vessel was irradiated with a 450-W high pressure Hg arc (Eikosha-PIH 450) in an atmosphere of nitrogen for 50 h. The solvent was removed under reduced pressure and the residue was recrystallized from methanol to yield *B*-homo-6-oxa-5β-cholestan-7-one (174 mg). This lactone was identical with the lactone obtained by the oxidation of *B*-homo-6-oxa-5β-cholestane with ruthenium tetraoxide.

***B*-Homo-6-oxa-5β-cholestan-7α- and 7β-ols (20).** A solution of DIBAL (0.25 ml) was added dropwise to a solution of lactone **18** (90 mg) in dry toluene (10 ml) at −78°C. The solution was stirred for 5 h at −78°C and poured into iced water. After the solution was filtered, the filtrate was washed with water and dried over anhydrous Na_2SO_4. The usual work-up gave an oily product. This was purified once by preparative TLC with a 10 : 1 benzene-diethyl ether to

yield a mixture of 7α- and 7β-ols **20**. (Found: m/z 404.3663. Calcd for $C_{27}H_{48}O_2$: M, 404.3655). IR 3260 (OH) and 1018 cm^{-1} (C-O); ^{1}H NMR δ= 0.65 and 0.66 (each 3H, each s, 18-H of 7α- and 7β-ols), 2.61 and 2.75 (each 1H, each d, J= 3.9 Hz, OH of 7α- and 7β-ols), 3.41 and 3.93 (each 1H, each t, J=6.6 and 4.2 Hz, 5β-H of 7α- and 7β-ols), 5.07 and 5.33 (each 1H, m, 7-H of 7α- and 7β-H); MS m/z (rel intensity) 404 (M^+, 2%), 386 [$(M-H_2O)^+$, 43], 249 (35), 140 (36), 112 (82), and 43 (100).

Irradiation of the Hypoiodite of *B*-Homo-6-oxa-5β-cholestan-7-ols in ths Presence of Mercury(II) Oxide and Iodine. Lactols **20** (24 mg) were dissolved in dry benzene (3 ml) containing pyridine (0.1 ml), mercury (II) oxide (26 mg) and iodine (31 mg). The solution in a Pyrex vessel was irradiated for 2 h in an atmosphere of nitrogen. After the removal of inorganic precipitates, the filtrate was worked up as usual to give an oily product (35 mg). This was subjected to preparative TLC with benzene to give two fractions. The less mobile fraction (10 mg) was lactone **18**. (Found: m/z 530.2614. Calcd for $C_{27}H_{47}IO_2$: M, 530.2619). IR (neat) 1714 (CHO) and 1177 cm^{-1} (OCHO); ^{1}H NMR δ=0.69 (3H, s, 18-H), 1.02 (3H, s, 19-H), 3.33 (1H, dd, J= 10.74 and 2.92 Hz, CH_2I), 3.51 (1H, dd, J= 10.74 and 1.95 Hz, CH_2I), 4.87 (1H, br.s, 5β-H), and 8.23 (1H, s, CHO); MS m/z (rel intensity) 530 (M^+, 0.2%), 403 (M^+-I, 0.7), 357 [$(M-I-OCH_2O)^+$, 48], 261 (18), 149 (36), 95 (96), and 83 (100).

6-Oxa-5β-cholestane (22). A solution of formate **21** (9 mg) in THF (3 ml) was cooled at −78°C. Methyllithium (0.57 M diethyl ether solution 0.08 ml) was added to this stirred solution. The solution was stirred for 2 h and the temperature of the solution was then raised to room temperature. The solution was then stirred for 1 h at room temperature and extracted with diethyl ether. The ethereal solution was worked up as usual to yield an oily product. This was purified by preparative TLC with benzene to yield a pure material (5.5 mg) (Found: m/z 374.3564. Calcd for $C_{26}H_{46}O$: M, 374.3549). IR 1102 and 1086 cm^{-1} (C-O); ^{1}H NMR δ= 0.67 (3H, s, 18-H), 1.07 (3H, s, 18-H), 3.34 (1H, dd, J= 12.2 and 4.40 Hz, 5β-H), 3.36 (1H, dd, J= 11.5 and 11.5 Hz, 7α-H), and 3.53 (1H, dd, J= 11.5 and 5.4 Hz, 7β-H); MS m/z (rel intensity) 374 (M^+, 36%), 219 (100), 201 (19), and 164 (16).

References

1) Photoinduced Molecular Transformations. Part 91. Part 90. H. Suginome and S. Yamada, *Tetrahedron*, in press.

2) H. Suginome and S. Yamada, *J. Org. Chem.*, **49**, 3753 (1984).

3) H. Suginome and S. Yamada, *J. Org. Chem.*, **50**, 2489 (1985).

4) H. Suginome and S. Yamada, *Bull. Chem. Soc. Jpn.*, **58**, 3055 (1985).

5) H. Suginome and S. Yamada, *Synthesis*, **1986**, 741.

6) L. F. Fieser, T. Goto, and B. K. Bhattacharyya, *J. Am. Chem. Soc.*, **82**, 1700 (1960).

7) J. T. Edward and P. F. Morand, *Can. J. Chem.*, **38**, 1325 (1960).

8) N. J. Doorenbos and M. T. Wu, *J. Org. Chem.*, **26**, 4550 (1961).

9) B. R. Pettit and T. R. Kasturi, *J. Org. Chem.*, **26**, 4557 (1961).

10) L. M. Berkowitz and P. N. Rylander, *J. Am. Chem. Soc.*, **80**, 6682 (1958); A. B. Smith, III and R. M. Searborough, Jr., *Synth. Commun.*, **10**, 205 (1980).

11) R. B. Turner, *J. Am. Chem. Soc.*, **72**, 579 (1950).

12) H. Lettré and D. Hotz, *Liebigs Ann. Chem.*, **620**, 63 (1959).

13) H. Reich, F. E. Walker, and R. W. Collins, *J. Org. Chem.*, **16**, 1753 (1951); D. N. Jones, J. R. Lewis, C. W. Shoppee, and G. H. R. Summers, *J. Chem. Soc.*, **1955**, 2876; T. Suga, T. Shishibori, and T. Matsuura, *J. Chem. Soc., Perkin Trans. 1*, **1972**, 171.

14) R. C. Cookson, R. P. Gandhi, and R. M. Southam, *J. Chem. Soc. C*, **1968**, 2494.

15) H. Suginome and S. Yamada, *Chem. Lett.*, **1984**, 2479.

16) For reviews, see H. Budzikiewicz, C. Djerassi, and D. H. Williams, "Mass Spectrometry of Organic Compounds," Holden-Day, Inc., San Francisco (1967), p. 205.

17) L. Tökés, G. Jones, and C. Djerassi, *J. Am. Chem. Soc.*, **90**, 5465 (1968).

18) D. H. R. Barton, A. J. Head, and P. J. May, *J. Chem. Soc.*, **1957**, 935; For reviews, see E. L. Eliel, N. L. Allinger, S. J. Angyal, and G. A. Morrison, "Conformational Analysis," Interscience Publ., New York (1965) p. 345; R. Bucourt, in "Topics in Stereochemistry," ed by, E. L. Eliel and N. L. Allinger, Wiley, New York (1974), Vol. 8, p. 159.

19) H. Budzikiewicz, J. Buchler, and G. Quinkert. The work cited in Ref. 16.

20) A. M. Duffield, H. Budzikiewicz, and C. Djerassi, *J. Am. Chem. Soc.*, **87**, 2920 (1965).

 © 1987 The Chemical Society of Japan Bull. Chem. Soc. Jpn., 60, 2463—2473 (1987)

Synthesis of (Diethoxyphosphoryl)acetonitrile Oxide and Its Cycloaddition to Olefins. Synthetic Applications to 3,5-Disubstituted 2-Isoxazolines

Otohiko Tsuge,* Shuji Kanemasa, Hiroyuki Suga, and Norihiko Nakagawa
Institute of Advanced Material Study, and Department of Molecular Science and Technology, Interdisciplinary Graduate School of Engineering Sciences, Kyushu University, Kasugakoen, Kasuga 816
(Received February 5, 1987)

(Diethoxyphosphoryl)acetonitrile oxide undergoes regioselective cycloaddition to olefins leading to 3-[(diethoxyphosphoryl)methyl]-2-isoxazolines or -isoxazole. The phosphorus-stabilized carbanions generated by deprotonation of the cycloadducts can be utilized for the condensation with carbonyl compounds, alkylation, and oxidation with oxygen to provide 3,5-disubstituted 2-isoxazolines as useful synthetic building blocks. Raney nickel hydrogenolysis of 3-[(diethoxyphosphoryl)methyl]-2-isoxazolines gives β-hydroxy-β′-phosphoryl ketones bearing a variety of functional groups, which can be further converted into α,β-unsaturated β′-phosphoryl ketones.

High synthetic versatility of isoxazoles and 2-isoxazolines is based on their potentiality as flexible synthetic equivalents of 1,3-diketones, β-hydroxy ketones, γ-amino alcohols, α,β-unsaturated ketones, and other related functions.[1] One of the most general preparation methods of these heterocycles is regioselective cycloaddition of nitrile oxides.[2] Use of monosubstituted acetylenes or olefins furnishes isoxazoles or 2-isoxazolines bearing a 5-substituent. As nitrile oxides undergo smooth cycloadditions to electron-poor to -rich dipolarophiles,[3] a wide variety of substituents may be introduced at the 5-position by the regioselective cycloaddition route. Accordingly it is soon realized that these cycloadducts will become synthetically versatile building blocks which involve masked complex functionalities.[4]

From this point of view, a functionalized nitrile oxide must be important because the cycloaddition reaction of this 1,3-dipole produces isoxazoles or 2-isoxazolines with this newly added functionality which can be then utilized to introduce these heterocycles as talent synthetic blocks into other molecules.[5] We recently started our project on the synthetic applications of a phosphorus-functionalized nitrile oxide, (diethoxyphosphoryl)acetonitrile oxide (**1**).

The present report describes the first preparation of **1** and some examples of its synthetic applications: Regioselective cycloaddition of **1** to monosubstituted olefins leading to 2-isoxazolines or isoxazole; reactions of the phosphorus-stabilized carbanions with electrophiles; reductive cleavage of the heterocycles on Raney Ni.[6]

Results and Discussion

Among several preparation methods of nitrile oxides,[7] the halogenation and dehydrohalogenation sequence of aldoximes as well as the direct oxidation method was applied to *N*-[2-(diethoxyphosphoryl)-ethylidene]hydroxylamine (**3**) because **3** is available in large quantities from bromoacetaldehyde diethyl acetal and triethyl phosphite. Thus, known (diethoxyphosphoryl)acetaldehyde (**2**)[8] was prepared by Arbuzov reaction of the acetal and further converted into oxime **3** in 95% yield (a 3 : 4 mixture of syn and anti forms).

The direct oxidative conversion of aldoxime **3** into nitrile oxide **1** was unsuccessful: Both the reaction of **3** with lead tetraacetate/triethylamine[7c] and the treatment of **3** with sodium hypochlorite/triethylamine,[7b] both in dichloromethane solution, failed in the generation of nitrile oxide **1**. Complex mixture of many products was only formed.

The chlorination and dehydrochlorination method[7d] was next applied. When **3** was treated with *N*-chlorosuccinimide (NCS) in DMF, chlorination took place not only at the oxime carbon but also at the adjacent methylene carbon to give a mixture of *N*-[1-chloro-2-(diethoxyphosphoryl)ethylidene]hydroxylamine (**4**) and its isomer **5** (Scheme 1). Both combined yield (**4** + **5**) and isomer ratio were found to depend upon the reaction temperature as shown in Table 1. Although the desired chloro oxime **4** could be separated from **5** through column chromatography over silica gel, the maximum yield of isolated **4** was only less than 50% even under the optimum conditions

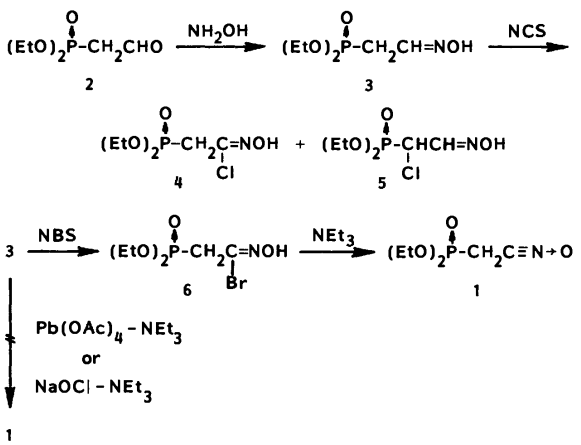

Scheme 1.

Table 1. Chlorination of Oxime **3** with NCS Leading to **4** and **5**[a]

Run	Reaction condition		Total yield/%[b]	Isomer ratio (**4**:**5**)[c]
	Addition of NCS	Reaction with NCS		
1	0 °C, 5 min	rt, 5 h	60	1:1
2	0 °C, 5 min	0 °C, 1 h	71	10:3
3	−15 °C, 5 min	−15 °C, 30 min	34	17:7
4	0 °C, 40 min	0 °C, 2 h	71	16:3

a) Carried out in DMF with 1 equiv amount of NCS. b) Yield of the isolated mixture of **4** and **5** based on **3**. c) Determined by ^{1}H NMR spectrum of the mixture of **4** and **5**.

Table 2. Generation of Nitrile Oxide **1** and Its Trapping with *N*-(*p*-Tolyl)maleimide[a]

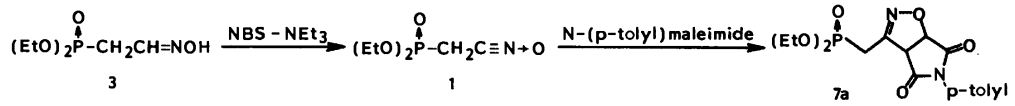

3 1 7a

Run	Reaction with NBS		NEt_3 (equiv)[c]	Cycloaddition[b] time/h	Yield of **7a**/%[d]
	NBS (equiv)	Condition[e]			
1	1	0 °C, 30 min	1	15	54
2	1	−20 °C, 5 min then 0 °C, 30 min	1	12	63
3	1	−20 °C, 1 h then 0 °C, 30 min	1	12	67
4	2	−20 °C, 5 min then 0 °C, 30 min	1	21	71
5	2	0 °C, 30 min	2	21	41
6	2	−20 °C, 1 h then 0 °C, 30 min	1	18	80

a) Carried out in DMF. b) Reaction temperature; room temperature. c) After the reaction with NBS was over, a mixture of *N*-(*p*-tolyl)maleimide and triethylamine was added. d) Yield of isolated **7a** based on **3**. e) NBS in DMF was added to **3** in a period of 5 min.

(Run 4, total yield: 71%; **4** : **5** = 16 : 3) to let us discard this chlorination route.

An alternative is bromination of oxime **3**. Thus, **3** was treated with *N*-bromosuccinimide (NBS) in DMF according to the Steven's method.[7d] As bromo oxime **6** was not isolable, **6** was in situ dehydrobrominated with triethylamine. The nitrile oxide **1** generated was trapped by *N*-(*p*-tolyl)maleimide as cycloadduct **7a** (Table 2). It should be noted that all procedures for the bromination of **3**, the dehydrobromination of **6**, and the cycloaddition trapping could be conveniently carried out in one flask.

When oxime **3** was treated with two equivalents of NBS at −20 °C in a period of 5 min and then one equivalent of triethylamine at room temperature (run 6 of Table 2), the desired nitrile oxide **1** was generated in an excellent yield and successfully captured by *N*-(*p*-tolyl)maleimide to give **7a** in 80% yield.

Cycloadditions of nitrile oxide **1** with a variety of olefins were next investigated. Under similar conditions, **1** underwent smooth cycloadditions to such a wide variety of olefins as electron-poor olefins (*N*-(*p*-tolyl)maleimide, methyl acrylate, 3-buten-2-one, acrylonitrile, phenyl vinyl sulfone), an electron-rich olefin

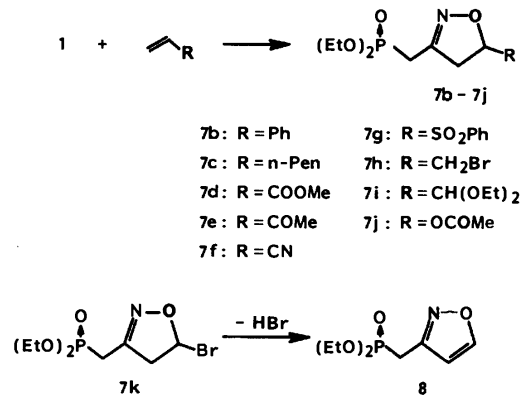

Scheme 2.

(vinyl acetate), and nonactivated olefins (styrene, 1-heptene, 3-bromopropene, 3,3-diethoxypropene) all in regioselective manners to give 5-substituted 3-[(diethoxyphosphoryl)methyl]-2-isoxazolines **7a—j** (Scheme 2 and Table 3). Better yields of **7** were generally obtained if more than 1 equivalent amount of dipolarophiles was employed. Accordingly some of low-boiling or volatile olefins were used as much as 5 equivalents. The reaction of **1** with bromoethene pro-

Table 3. Cycloaddition of Nitrile Oxide **1** to Olefins[a)]

Olefin (equiv)	Time/h[b)]	Product	Yield/%[c)]
N-(*p*-Tolyl)maleimide (1)	18	**7a**	80
Styrene (5)	18	**7b**	81
1-Heptene (5)	18	**7c**	75
Methyl acrylate (1)	18	**7d**	84
3-Buten-2-one (2)	48	**7e**	70
Acrylonitrile (5)	27	**7f**	77
Phenyl vinyl sulfone (1)	18	**7g**	25
3-Bromopropene (5)	18	**7h**	62
3,3-Diethoxypropene (5)	18	**7i**	54
Vinyl acetate (5)	18	**7j**	73

a) Carried out in DMF. b) Bromo oxime **6** was first generated by treatment of oxime **3** with NBS (2 equiv) at −20 °C for 1 h and then 0 °C for 30 min. A mixture of olefin and triethylamine (1 equiv) was added. The mixture was stirred at room temperature for the reaction time listed in this table. c) Yield of isolated cycloadduct **7** based on **3**.

duced 3-[(diethoxyphosphoryl)methy]isoxazole (**8**) in 47% yield by the elimination of hydrogen bromide of the initial cycloadduct, 5-bromo-3-[(diethoxyphosphoryl)methyl]-2-isoxazoline (**7k**).

Regioselective deprotonation of 3-alkyl-2-isoxazolines is quite difficult. Thus, it is known that 3-methyl-5-phenyl-2-isoxazoline can be deprotonated, at a low temperature, with LDA both at the 3-methyl group (exo) and the 4-position (endo).[9] At an elevated temperature the endo carbanion causes a ring opening via a β-elimination leading to α,β-unsaturated ketone. The regioselectivity depends upon the substituents[10] as well as the polarity of reaction solvent.[11] Although a few successful cases of the trapping of exo carbanions have been recently reported,[12] the exclusive utilization of exo carbanion is still difficult. The phosphorus-functionalized 2-isoxazolines **7** are expected to generate stable phosphoryl-stabilized carbanions.

The 2-isoxazoline **7b** as a representative was first treated with butyllithium at −78 °C in THF. The resulting yellow carbanion **A** is so highly stabilized that it can servive even at room temperature. It was

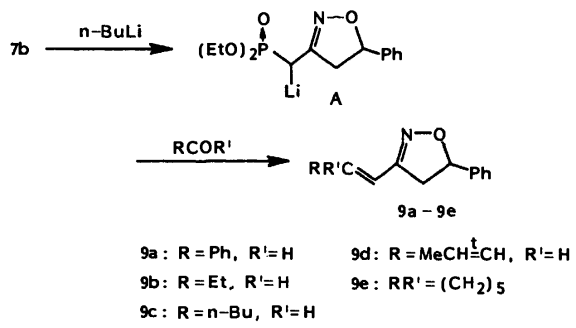

Scheme 3.

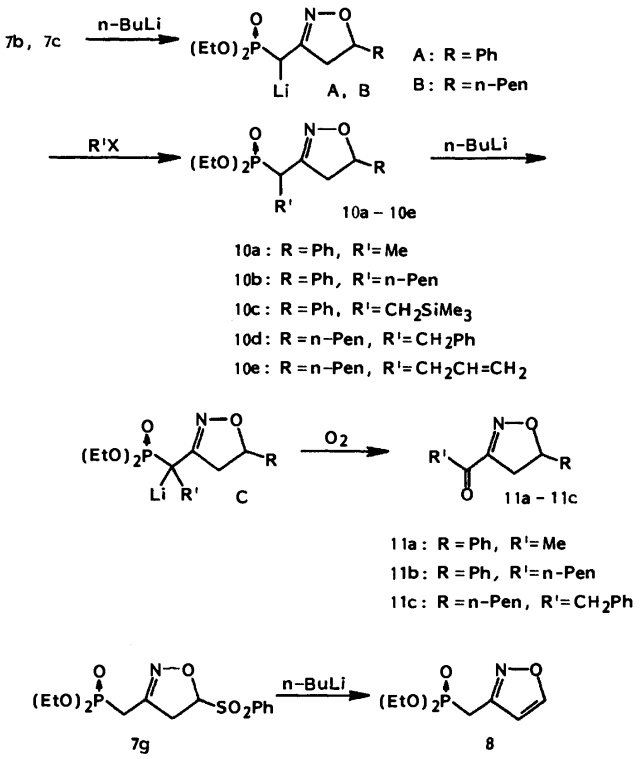

Scheme 4.

then treated with carbonyl compounds at room temperature to succeed in reacting with aromatic, aliphatic, α,β-unsaturated aldehydes, and a ketone to give 3-(1-alkenyl)-2-isoxazolines **9a**—**e** (Scheme 3 and Table 4). The Horner-Emmons olefination products **9** were mostly E-isomers as expected. The carbanions derived from 2-isoxazolines **7d** and **7e** which carry a carbonyl group failed in reacting with aldehydes.[13]

Under similar conditions, the above carbanion **A** as well as **B** which was derived from 5-alkyl-2-isoxazoline **7c** by deprotonation reacted with alkyl halides to give 3-(1-phosphorylalkyl)-2-isoxazolines **10a**—**e** in good yields (Scheme 4 and Table 4). Alkyl iodides (methyl, pentyl, and trimethylsilylmethyl iodides) were sufficiently reactive toward **A** or **B**. Although activated bromides such as benzyl and 2-propenyl bromides are exceptions, less reactive alkyl bromides such as pentyl and 1-methylpropyl bromides were recovered intact.

The 3-(1-phosphorylalkyl)-2-isoxazolines **10** thus prepared could be again deprotonated with butyllithium at the same carbon to generate carbanions **C**. These anions **C** were oxidized with dry oxygen gas at −78 °C to furnish 3-(1-oxoalkyl)-2-isoxazolines **11a**—**c** (Scheme 4 and Table 4). The silylmethyl-substituted 2-isoxazoline **10c** led to desilylated ketone **11a** which was also accessible from **10a**.

When the cycloadduct **7g** obtained from the cycloaddition to phenyl vinyl sulfone was treated with butyllithium, deprotonation took place at the 4-position causing the elimination of benzenesulfinic acid

Table 4. Reaction of 2-Isoxazolines **7** and **10** with Electrophiles[a]

2-Isoxazoline		Electrophile	Temp/°C	Time/h	Product		Yield/%[b]
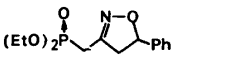	7b	PhCHO	rt	12.5	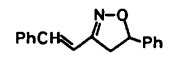	9a	99[c]
7b		EtCHO	rt	12.5	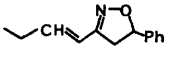	9b	75[d]
7b		*n*-BuCHO	rt	16	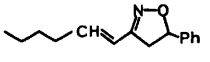	9c	66[e]
7b		$MeCH=\overset{t}{C}HCHO$	rt	17	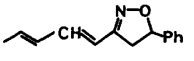	9d	81[c]
7b		Cyclohexanone	rt	16	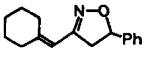	9e	94
7b		MeI	rt	17	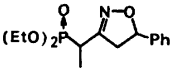	10a	80
7b		*n*-PenI	rt	11	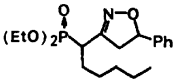	10b	72
7b		Me_3SiCH_2I	rt	15	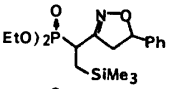	10c	70
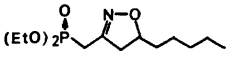	7c	$PhCH_2Br$	rt	15	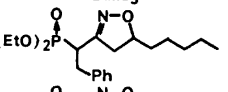	10d	75
7c		$CH_2=CHCH_2Br$	rt	15.5	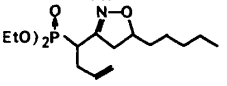	10e	91
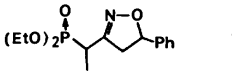	10a	Oxygen	−78	1	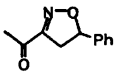	11a	70[f]
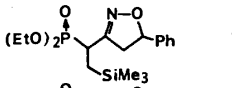	10c	Oxygen	−78	1	11a		78[g]
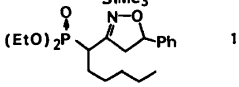	10b	Oxygen	−78	1	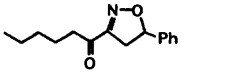	11b	83[h]
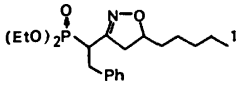	10d	Oxygen	−78	1	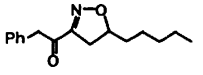	11c	57[i]

a) Carbanions **A**—**C** were first generated by the action of butyllithium in THF at −78 °C and the reactions with electrophiles were followed under the conditions shown above. b) Yield of isolated product. c) E only (^{1}H NMR). d) E:Z=75:25 (GLC). e) E:Z=72:28 (GLC). f) Recovered **10a**: 16%. g) Recovered **10c**: 12%. h) Recovered **10b**: 15%. i) Recovered **10d**: 39%.

to give 3-phosphorylmethyl-2-isoxazole **8** whose formation was already mentioned above.

The phosphoryl moiety of **7** was found to servive on the reductive N-O bond fission and the subsequent hydrolysis. Thus, 3-phosphorylmethyl-2-isoxazolines **7** bearing a variety of substituents at the 5-position were hydrogenated on Raney-Ni (W-2) in aqueous ethanol in the presence of acetic acid or boric acid to give good yields of β-hydroxy ketones **12a** — **f** bearing phosphoryl and R moieties (Scheme 5). Such functional groups as ester, ketone, halogen, and acetal are also safe under the conditions of hydrogenolysis. Instability of **12d** may arise from its 1,4-dicarbonyl or α-hydroxy ketone structure.[14]

Although the Raney Ni reduction of **7e** in H_3BO_3-H_2O gave β-hydroxy ketone **12d** as described above, a similar reduction in AcOH-H_2O procuced 2-methyl-5-[(diethoxyphosphoryl)methyl]pyrrole (**13**) in a fair yield. The intermediary β-hydroxy imine, initially formed by the N-O bond reduction of 2-isoxazoline **7e**, was presumably overreduced to lead to 4-amino-2-hydroxy ketone intermediate **D** whose intramolecular dehydration gave **13**.

The alkylated derivative **10a** prepared above by methylation of the phosphorus-stabilized carbanion **A** was similarly converted into 1-phosphorylethyl 2-hydroxyalkyl ketone **12g** (Scheme 5).

The phosphorus-functionalized β-hydroxy ketones **12** could be further converted into phosphorus-functionalized α,β-unsaturated ketones **14a** and **14b**

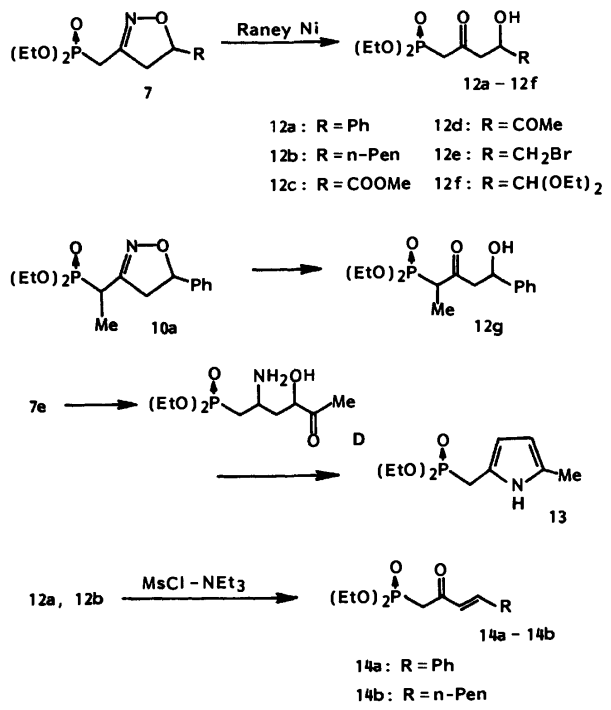

Scheme 5.

in quantitative yields through the initial mesylation with methanesulfonyl chloride and triethylamine and the subsequent chromatography over silica gel (Scheme 5).

Synthetic utilization of the phosphoryl moiety of the compounds newly prepared herein is now under progress. The results will be soon published elsewhere.

Experimental

General. Melting points were determined on a Yanagimoto melting point apparatus and are uncorrected. IR spectra were taken with a JASCO IRA-1 or a JASCO A-702 spectrometer. ^{1}H NMR spectra were recorded on a Hitachi R-40 (90 MHz) or a JEOL FX-100 instrument (100 MHz) and ^{13}C NMR on a JEOL FX-100 spectrometer at 25.05 MHz. Chemical shifts are expressed in parts per million downfield from tetramethylsilane as an internal standard. Mass spectra were measured with a JEOL-01SG-2 spectrometer at 70 eV of ionization energy. High resolution mass spectra were obtained on the same instrument. Elemental analyses were performed on a Hitachi 026 CHN analyzer. Thin-layer chromatography (TLC) was accomplished on 0.2 mm precoated plates of silica gel 60 F-254 (Merck). Visualization was made with ultraviolet light (254 and 365 nm), iodine, molybdophosphoric acid (5% in ethanol), or *p*-anisaldehyde (5% in ethanol containing 5% of sulfuric acid). For preparative column chromatography, Wakogel C-200, C-300 (Wako), and Silicagel 60 (Merck) were employed. Flash chromatography was carried out on an EYELA EF-10 apparatus using a column (20 × 180 mm) packed with Silicagel 60 (Merck, size: 0.04—0.063 mm). Preparative high performance liquid chromatography (HPLC) was performed on a Kusano KHLC-201 apparatus with a UV-detector Uvilog-III using a column (22 × 300 mm) packed with silica gel (Wakogel LC-50H). Gas liquid chromatography (GLC) was accomplished on a Yanaco G-2800 gas chromatograph (Yanagimoto) with an ionization flame detector using a glass column (SE-30, 3 × 2000 mm) or a glass capillary column (Silicone GE, SE-30, 0.25 × 5000 mm). Micro vacuum distillation was carried out on a Sibata GTO-250R Kugelrohr distilling apparatus. Solvents were evaporated with a Tokyo Rikakikai rotary evaporator type-V at about 50 °C unless otherwise stated.

***N*-[2-(Diethoxyphosphoryl)ethylidene]hydroxylamine (3).** To a solution of aldehyde **2**[8] (0.5 g, 2.78 mmol) in ethanol (5 ml) was added an aqueous hydroxylamine hydrochloride (0.386 g, 5.56 mmol in 2 ml of water). The mixture was stirred at room temperature for 11.5 h, poured into water (50 ml), and extracted with dichloromethane (25 ml × 2). The combined extracts were dried over magnesiun sulfate and evaporated in vacuo to give **3** (0.513 g, 95%) as a 3 : 4 mixture of syn and anti isomers, which was purified through a column chromatography (silica gel/ethyl acetate): Colorless liquid; IR (neat) 3200, 1600, and 1240 cm^{-1}; ^{1}H NMR ($CDCl_3$) δ = 1.30 (6H, t, J = 7.0 Hz, OEt), 2.77 (3/7 × 1H, dd, J = 6.3 and 21.8 (HP) Hz, CH_2 (syn)), 3.04 (4/7 × 1H, dd, J = 6.0 and 22.0 (HP) Hz, CH_2 (anti)), 4.12 (4H, dq, J = 7.0 and 7.5 (HP) Hz, OEt), 6.75 (4/7 × 1H, dt, J = 6.0 and 5.0 (HP) Hz, CH=N (anti)), 7.35 (3/7 × 1H, dt, J = 6.3 and 5.0 (HP) Hz, CH=N (syn)), and 10.10 (1H, br, OH); ^{13}C NMR ($CDCl_3$) δ = 16.32 (qd, J_{cp} = 7.4 Hz, OEt), 23.56 (td, J_{cp} = 139.7 Hz, OEt (anti)), 28.18 (td, J_{cp} = 141.2 Hz, OEt (syn)), 62.62 (td, J_{cp} = 7.4 Hz, CH_2), 140.74 (dd, J_{cp} = 7.4 Hz, CH=N (anti)), and 142.27(dd, J_{cp} = 10.3 Hz, CH=N (syn)); MS (rel intensity, %) 195 (M^+, 13), 167 (17), 139 (39), 122 (49), 111 (25), 109 (56), 104 (19), 99 (64), 96 (23), 93 (32), 82 (27), 81 (base peak), and 65 (72). HRMS Found: m/z 195.0603. Calcd for $C_6H_{14}NO_4P$: M, 195.0660.

Reaction of Oxime 3 with NCS Leading to 4 and 5. A mixture of **3** (1 mmol) and NCS (1 mmol) in DMF (1 ml) was stirred under the conditions shown in Table 1. The mixture was poured into water (20 ml) and extracted with diethyl ether (20 ml × 2). The combined extracts were washed with water, dried over magnesium sulfate, and evaporated in vacuo. The residue was chromatographed over silica gel. The fraction eluted with hexane-ethyl acetate (1 : 2 v/v) gave *N*-[1-chloro-2-(diethoxyphosphoryl)-ethylidene]hydroxylamine (**4**) and with hexane-ethyl acetate (1 : 5 v/v) *N*-[2-chloro-2-(diethoxyphosphoryl)ethylidene]-hydroxylamine (**5**). Results obtained under several conditions are listed in Table 1. Both **4** and **5** are too labile to be highly purified as analytical samples.

4: Yellow liquid; IR (neat) 3200, 1625, 1220, 1020, and 800 cm^{-1}; ^{1}H NMR ($CDCl_3$) δ = 1.31 (6H, t, J = 7.0 Hz, OEt), 3.06 (2H, d, J = 21.0 (HP) Hz, CH_2P), 4.10 (4H, qd, J = 7.0 and 7.5 (HP)Hz, OEt), and 10.66 (1H, br, OH); MS m/z (rel intensity, %) 229 (M^+, 4), 138 (11), 137 (16), 122 (21), 109 (51), 104 (19), 91 (21), 81 (86), 77 (18), 65 (42), and 43 (base peak).

5 (A 7 : 5 mixture of syn- and anti-isomers): Pale yellow liquid; IR (neat) 3200, 1625, 1240, and 1020 cm^{-1}; ^{1}H NMR ($CDCl_3$) δ = 1.34 (6H, t, J = 7.0 Hz, OEt), 4.23 (4H, qd, J = 7.0 and 7.4 (HP) Hz, OEt), 4.61 (7/12 × 1H, dd, J = 8.5 and 13.0 (HP) Hz, CH (syn)), 5.42 (5/12 × 1H, dd, J = 8.0 and

13.0 (HP) Hz, CH (anti)), 6.77 (5/12×1H, dd, J=8.0 and 3.0 (HP) Hz, CH=N (anti)), and 7.38 (7/12×1H, dd, J=8.5 and 4.0 (HP) Hz, CH=N (syn)); ^{13}C NMR ($CDCl_3$) δ= 16.38 (qd, J_{cp}=6.1 Hz, OEt), 40.89 (dd, J_{cp}=159.9 Hz, OEt (anti)), 48.83 (dd, J_{cp} = 163.6 Hz, OEt (syn)), 64.74 (td, J_{cp}=7.3 Hz, CH), 142.26 (dd, J_{cp}=3.7 Hz, CH=N (anti)), and 143.89 (dd, J_{cp}=2.4 Hz, CH=N (syn)); MS m/z(rel intensity, %) 229 (M^+, 8), 130 (10), 127 (14), 109 (61), 99 (33), 91 (27), 81 (56), 73 (14), 65 (69), and 43 (base peak).

General Procedure for the Generation of Nitrile Oxide 1 and Its Cycloaddition to Olefins Leading to 7a—j. To a solution of oxime **3** (0.195 g, 1 mmol) in dry DMF (2 ml) was added NBS (0.356 g, 2 mmol in 2 ml of DMF) at −20 °C. The mixture was stirred at the same temperature for 1 h and then at 0 °C for 30 min. A mixture of triethylamine (0.101 g, 1 mmol) and an olefin (1 to 5 mmol) in dry diethyl ether (2 ml) was added. The mixture was stirred at room temperature, poured into water (20 ml), and extracted with dichloromethane (20 ml × 2) or diethyl ether (20 ml × 2). The combined extracts were dried over magnesium sulfate and evaporated in vacuo. The residue was chromatographed over silica gel to give cycloadduct **7**. The eluents used are as follows: **7a**, **7b**, **7d**, and **7j**: ethyl acetate; **7c**, **7e**, **7f**, **7g**, **7h**, and **7i**: hexane-ethyl acetate (1 : 5 v/v). The yields of **7**, the amounts of olefin used, and the reaction times are summarized in Table 3. The reaction with *N*-(*p*-tolyl)maleimide under various conditions is shown in Table 2.

7a: Colorless prisms (diethyl ether); mp 88—89 °C; IR (KBr) 1720, 1240, and 1020 cm^{-1}; ^{1}H NMR ($CDCl_3$) δ= 1.32 (6H, t, J=7.0 Hz, OEt), 2.34 (3H, s, *p*-Me), 3.00 (1H, d, J = 15.5 (gem) and 22.5 (HP) Hz, one of CH_2P), 4.13 (1H, d, J = 15.5 (gem) and 21.0 (HP) Hz, the other of CH_2P), 4.14 (4H, qd, J=7.0 and 7.3 (HP) Hz, OEt), 4.75 (1H, dd, J=9.5 and 4.0 (HP) Hz, 3a-H), 5.43 (1H, d, J= 9.5 Hz, 6a-H), and 7.0—7.3 (4H, m, Ar); ^{13}C NMR ($CDCl_3$) δ=16.35 (qd, J_{cp}=5.9 Hz, OEt), 21.23 (q, *p*-Me), 24.35 (td, J_{cp} = 138.3 Hz, CH_2P), 52.82 (d, 3a-C), 63.18 (td, J_{cp} = 5.9 Hz, OEt), 79.77 (d, 6a-C), 126.24 (d), 128.54 (s), 130.07 (d), 139.48 (s), 148.54 (d, J_{cp} = 8.8 Hz, 3-C), 170.67, and 171.95 (each s, CON); MS m/z(rel intensity, %) 380 (M^+, 3), 353 (18), 352 (90), 246 (base peak), 218 (46), 190 (67), 133 (72), 132 (46), 109 (60), 107 (28), 105 (22), 104 (39), 91 (34), 81 (68), 78 (24), and 77 (26). Found: C, 53.86; H, 5.61; N, 7.46%. Calcd for $C_{17}H_{21}N_2O_6P$: C, 53.67; H, 5.57; N, 7.37%.

7b: Pale yellow liquid; IR (neat) 1620, 1250, 1020, and 825 cm^{-1}; ^{1}H NMR ($CDCl_3$) δ=1.2—1.4 (6H, m, OEt), 2.98 (2H, d, J=21.8 (HP) Hz, CH_2P), 3.07 (1H, ddd, J=17.5 (gem), 8.0, and 4.2 (HP) Hz, one of 4-H), 3.50 (1H, ddd, J= 17.5 (gem), 10.8, and 4.2(HP) Hz, the other of 4-H), 3.9—4.3 (4H, m, OEt), 5.56 (1H, dd, J = 10.8 and 8.0 Hz, 5-H), and 7.28 (5H, s, Ph); ^{13}C NMR ($CDCl_3$) δ=16.38 (qd, J_{cp}=6.1 Hz, OEt), 26.24 (td, J_{cp}=140.4 Hz, CH_2P), 45.26 (t, 4-C). 62.62 (td, J_{cp} = 6.1 Hz, OEt), 82.37 (d, 5-C), 126.02, 128.32, 128.51 (each d), 141.06 (s), and 151.27 (d, J_{cp}=9.8 Hz, 3-C); MS m/z (rel intensity, %) 297 (M^+, 2), 109 (16), 105 (11), 104 (13), 81 (15), 77 (19), and 43 (base peak). HRMS Found: m/z 297.1120. Calcd for $C_{14}H_{20}NO_4P$: M, 297.1128.

7c: Pale yellow liquid; IR (neat) 1630, 1260, 1025, and 825 cm^{-1}; ^{1}H NMR ($CDCl_3$) δ= 0.88 (3H, t, J=7.0 Hz, *n*-Pen), 1.1—1.8 (8H, m, *n*-Pen), 1.33 (6H, t, J=7.0 Hz, OEt), 2.72 (1H, ddd, J=17.0 (gem), 8.2, and 4.2 (HP) Hz, one of 4-H), 2.93 (2H, d, J=21.5 (HP) Hz, CH_2P), 3.14 (1H, ddd, J = 17.0 (gem), 10.0, and 4.2 (HP) Hz, the other of 4-H), 4.12 (4H, qd, J=7.0 and 7.5 (HP) Hz, OEt), and 4.52 (1H, m, 5-H); ^{13}C NMR ($CDCl_3$) δ= 14.00 (q), 16.41 (qd, J_{cp} = 5.8 Hz, OEt), 22.59, 25.06 (each t), 26.41 (td, J_{cp}=141.2 Hz, CH_2P), 31.71, 35.12 (each t), 42.36 (t, 4-C), 62.59 (td, J_{cp}= 5.8 Hz, OEt), 81.42 (d, 5-C), and 151.48 (d, J_{cp}=8.8 Hz, 3-C); MS m/z(rel intensity, %) 291 (M^+, 8), 220 (base peak), 192 (28), 164 (43), 146 (10), 109 (14), 81 (17), and 44 (29). HRMS Found: m/z 291.1587. Calcd for $C_{13}H_{26}NO_4P$: M, 291.1598.

7d: Pale yellow liquid; IR (neat) 1730, 1620, 1220, 1020, and 825 cm^{-1}; ^{1}H NMR ($CDCl_3$) δ=1.33 (6H, t, J=7.0 Hz, OEt), 2.98 (2H, d, J=21.5 (HP) Hz, CH_2P), 3.39 (2H, dd, J=9.0 and 4.0 (HP) Hz, 4-H), 3.76 (3H, s, COOMe), 4.13 (4H, qd, J= 7.0 and 7.4 (HP) Hz, OEt), and 5.04 (1H, t, J = 9.0 Hz, 5-H); ^{13}C NMR ($CDCl_3$) δ=16.35 (qd, J_{cp}= 5.9Hz, OEt), 25.83 (td, J_{cp} = 141.2 Hz, CH_2P), 41.24 (t, 4-C), 52.77 (q, COOMe), 62.80 (td, J_{cp} = 7.4 Hz, OEt), 77.77 (d, 5-C), 151.48 (d, J_{cp} = 8.8 Hz, 3-C), and 170.77 (s, COOMe); MS m/z(rel intensity, %) 220 (M^+ −COOMe, 52), 192 (28), 164 (92), 146 (44), 109 (49), 91 (16), 83 (20), 82 (19), 81 (80), 65 (40), 59 (base peak), and 54 (89). Found: C, 43.25; H, 6.26; N, 4.74%. Calcd for $C_{10}H_{18}NO_6P$: C, 43.01; H, 6.50; N, 5.02%.

7e: Pale yellow liquid; IR (neat) 1725, 1625, 1250, 1025, and 800 cm^{-1} ^{1}H NMR ($CDCl_3$) δ=1.33 (6H, t, J=7.0 Hz, OEt), 2.27 (3H, s, COMe), 2.96 (2H, d, J=21.5 (HP) Hz, CH_2P), 3.1—3.5 (2H, m, 4-H), 4.13 (4H, qd, J=7.0 and 7.5 (HP) Hz, OEt), and 4.90 (1H, dd, J=10.0 and 8.0 Hz, 5-H); ^{13}C NMR ($CDCl_3$) δ=16.41 (qd, J_{cp}=5.9 Hz, OEt), 25.97 (td, J_{cp}=139.7 Hz, CH_2P), 26.12 (q, COMe), 39.71 (t, 4-C), 62.77 (td, J_{cp}=5.9 Hz, OEt), 84.18 (d, 5-C), 152.07 (d, J_{cp} = 8.8 Hz, 3-C), and 207.37 (s, COMe); MS m/z(rel intensity, %) 220 (M^+ −COMe, 54), 192 (25), 164 (base peak), 152 (18), 146 (30), 125 (15), and 42 (43). Satisfactory elemental analysis was not obtained because of its hygroscopic property.

7f: Pale yellow liquid; IR (neat) 2230, 1625, 1250, 1025, and 800 cm^{-1}; ^{1}H NMR ($CDCl_3$) δ=1.35 (6H, t, J=7.0 Hz, OEt), 3.01 (2H, d, J=22.0 (HP) Hz, CH_2P), 3.2—3.7 (2H, m, 4-H), 4.15 (4H, qd, J=7.0 and 7.6 (HP) Hz, OEt), and 5.27 (1H, dd, J = 9.0 and 7.2 Hz, 4-H); ^{13}C NMR ($CDCl_3$) δ= 16.35 (qd, J_{cp}=5.9 Hz, OEt), 25.71 (td, J_{cp}=141.2 Hz, CH_2P), 43.24 (t, 4-C), 63.03 (td, J_{cp}=7.3 Hz, OEt), 66.59 (d, 5-C), 117.30 (s, CN), and 152.33 (d, J_{cp}=10.3 Hz, 3-C); MS m/z(rel intensity, %) 246 (M^+, 62), 220 (17), 218 (35), 192 (17), 190 (58), 164 (40), 146 (40), 122 (47), 109 (67), 108 (21), 97 (19), 96 (45), 83 (88), 82 (23), 81 (base peak), 79 (20), 64 (45), and 54 (63). HRMS Found: m/z 246.0745. Calcd for $C_9H_{15}N_2O_4P$: M, 246.0768.

7g: Colorless prisms (benzene-hexane); mp 108—110 °C; IR (KBr) 1590, 1300, 1250, 1150, 1020, and 810 cm^{-1}; ^{1}H NMR ($CDCl_3$) δ=1.32 (6H, t, J=7.0 Hz, OEt), 2.71 (1H, dd, J = 17.5 (gem) and 21.5 (HP) Hz, one of CH_2P), 3.10 (1H, dd, J = 17.5 (gem) and 20.5 (HP) Hz, the other of CH_2P), 3.3—3.9 (2H, m, 4-H), 4.12 (4H, qd, J=7.0 and 7.5 (HP) Hz, OEt), 5.42 (1H, dd, J=10.0 and 6.0 Hz, 5-H), and 7.4—8.0 (5H, m, Ar); ^{13}C NMR ($CDCl_3$) δ=16.35 (qd, J_{cp}=5.9 Hz, OEt), 25.62 (td, J_{cp}=141.2 Hz, CH_2P), 39.00 (t,

4-C), 62.95 (td, J_{cp}=5.9 Hz, OEt), 93.18 (d, 5-C), 129.48, 129.83, 134.72 (each d), 135.60 (s), and 152.75 (d, J_{cp}=10.3 Hz, 3-C); MS *m/z* (rel intensity, %) 220 (M^+, 78), 192 (36), 164 (base peak), 146 (36), and 76 (32). Found: C, 46.42; H, 5.58; N, 3.89%. Calcd for $C_{14}H_{20}NO_6PS$: C, 46.54; H, 5.58; N, 3.88%.

7h: Pale yellow liquid; IR (neat) 1625, 1250, 1020, and 825 cm^{-1}; ^1H NMR ($CDCl_3$) δ=1.33 (6H, t, J=7.0 Hz, OEt), 2.93 (2H, d, J=21.8 (HP) Hz, CH_2P), 2.9—3.6 (4H, m, 4-H and CH_2Br), 4.13 (4H, qd, J=7.0 and 7.4 (HP) Hz, OEt), and 4.84 (1H, m, 5-H); ^{13}C NMR ($CDCl_3$) δ=16.41 (qd, J_{cp}=5.9 Hz, OEt), 26.15 (td, J_{cp}=139.7 Hz, CH_2P), 33.24 (t, CH_2Br), 41.82 (t, 4-C), 62.74 (td, J_{cp}=5.9 Hz, OEt), 79.60 (d, 5-C), and 151.51 (d, J_{cp}=10.3 Hz, 3-C); MS *m/z* (rel intensity, %) 314 (M^+, 1), 220 (base peak), 192 (26), 164 (65), and 146 (17). HRMS Found: *m/z* 313.0055. Calcd for $C_9H_{17}NO_4BrP$: M, 313.0078.

7i: Pale yellow liquid; IR (neat) 1675, 1250, 1025, and 830 cm^{-1}; ^1H NMR ($CDCl_3$) δ=1.1—1.3 (6H, m, OEt), 1.33 (6H, t, J=7.0 Hz, OEt), 2.93 (2H, d, J=22.0 (HP) Hz, CH_2P), 2.9—3.3 (2H, m, 4-H), 3.4—3.9 (4H, m, OEt), 4.14 (4H, qd, J=7.0 and 7.5 (HP) Hz, OEt), and 4.3—4.7 (2H, m, 5-H and CH); ^{13}C NMR ($CDCl_3$) δ=14.65 (q, OEt), 15.71 (qd, J_{cp}=5.9 Hz, OEt), 25.41 (td, J_{cp}=141.2 Hz, CH_2P), 37.83 (t, 4-C), 61.83 (td, J_{cp}=5.9 Hz, OEt), 62.53, 63.48 (each t, OEt), 80.48 (d, 5-C), 101.65 (d, $CH(OEt)_2$), and 151.16 (d, J_{cp}=10.3 Hz, 3-C); MS *m/z* (rel intensity, %) 278 (M^+−OEt, 9), 103 (base peak), 75 (45), and 47 (27), Satisfactory elemental analysis was not available because of its hygroscopic property.

7j: Pale yellow liquid; IR (neat) 1750, 1230, 1020, and 825 cm^{-1}; ^1H NMR ($CDCl_3$) δ=1.34 (6H, t, J=7.0 Hz, OEt), 2.04 (3H, s, COMe), 2.9—3.6 (2H, m, 4-H), 3.05 (2H, d, J=22.0 (HP) Hz, CH_2P), 4.15 (4H, qd, J=7.0 and 7.5 (HP) Hz, OEt), and 6.64 (1H, dd, J=6.2 and 2.0 Hz, 5-H); ^{13}C NMR ($CDCl_3$) δ=16.41 (qd, J_{cp}=5.9 Hz, OEt), 21.00 (q, COMe), 25.83 (td, J_{cp}=141.2 Hz, CH_2P), 43.53 (t, 4-C), 62.83 (td, J_{cp}=5.9 Hz, OEt), 96.01 (d, 5-C), 152.89 (d, J_{cp}=8.8 Hz, 3-C), and 169.83 (s, OCOMe); MS *m/z* (rel intensity, %), 220 (M^+−OCOMe, base peak), 209 (39), 192 (40), 164 (78), 146 (24), 83 (21), 81 (28), 64 (20), 54 (23), and 44 (75). Found: C, 42.93; H, 6.57; N, 5.08%. Calcd for $C_{10}H_{18}NO_6P$: C, 43.01; H, 6.50; N, 5.02%.

Reaction of Nitrile Oxide 1 with Bromoethene Leading to 8. To a solution of oxime **3** (0.39 g, 2 mmol) in dry DMF (4 ml) was added at −20 °C NBS (0.712 g, 4 mmol in 4 ml of DMF) in a period of 5 min. The mixture was stirred at −20 °C for 1 h, at 0 °C for 30 min, and then again cooled to −20 °C. Dry diethyl ether (4 ml) and triethylamine (0.28 ml, 2 mmol in 4 ml of diethyl ether) were added. After bromoethene (5 ml, 71 mmol) was added, the resulting mixture was stirred at room temperature for 18 h, poured into ice water, and extracted with dichloromethane (100 ml × 2). The combined extracts were dried over magnesium sulfate and evaporated in vacuo. The residue was chromatographed over silica gel by using hexane-ethyl acetate (3 : 1 v/v) to give **8** (0.205 g, 47%): Colorless liquid; IR (neat) 1650, 1565, 1250, 1020, and 800 cm^{-1}; ^1H NMR ($CDCl_3$) δ=1.30 (6H, t, J=7.0 Hz, OEt), 3.27 (2H, d, J=20.8 (HP) Hz, CH_2P), 4.09 (4H, qd, J=7.0 and 7.4 (HP) Hz, OEt), 6.45 (1H, t, J=1.5 Hz, 4-H), and 8.36 (1H, dd, J=1.5 and 0.8 Hz, 5-H); ^{13}C NMR ($CDCl_3$) δ=16.35 (qd, J_{cp}=5.9 Hz, OEt), 24.47 (td, J_{cp}=141.2 Hz, CH_2P), 62.68 (td, J_{cp}=7.3 Hz, OEt), 105.36 (d, 4-C), 159.07 (d, 5-C), and 155.12 (d, J_{cp}=6.8 Hz, 3-C); MS *m/z* (rel intensity, %) 219 (M^+, 92), 192 (31), 176 (28), 174 (34), 164 (67), 163 (31), 149 (37), 148 (25), 146 (70), 112 (23), 111 (20), 110 (67), 83 (base peak), 82 (48), 81 (53), 65 (30), and 55 (35). HRMS Found: *m/z* 219.0658. Calcd for $C_8H_{14}NO_4P$: M, 219.0660.

General Procedure for the Horner Emmons Olefination of 7b Leading to 9a—e. To a solution of isoxazoline **7b** (1 mmol) in dry THF (3 ml) was added butyllithium (1.6 M† in hexane, 0.66 ml, 1.06 mmol) at −78 °C under nitrogen. After 1 h an aldehyde or a ketone (1 mmol) was added. The mixture was stirred under the conditions shown in Table 4, poured into ice water (30 ml), and extracted with dichloromethane (20 ml × 2). The combined extracts were dried over magnesium sulfate and evaporated in vacuo. The residue was crystallized or chromatographed over silica gel by using the following eluent: **9a**: crystallization; **9b** and **9d**: hexane-ethyl acetate (20 : 1 v/v); **9c** and **9e**: hexane-ethly acetate (30 : 1 v/v). All the results are summarized in Table 4.

9a: Colorless needles (diethyl ether-hexane); mp 109—111 °C; IR (KBr) 1600 and 950 cm^{-1}; ^1H NMR ($CDCl_3$) δ=3.10 (1H, ddd, J=16.5 (gem), 8.5, and 0.7 Hz, one of 4-H), 3.54 (1H, ddd, J=16.5 (gem), 10.8, and 0.7 Hz, the other of 4-H), 5.59 (1H, dd, J=10.8 and 8.5 Hz, 5-H), 6.64 (1H, d, J=16.0 Hz, CH=), 7.07 (1H, d, J=16.0 Hz, CHPh), and 7.2—7.4 (10H, m, Ph); ^{13}C NMR ($CDCl_3$) δ=41.65 (t, 4-C), 82.76 (d, 5-C), 117.96 (d, CH=), 126.02, 127.14, 128.41, 128.91, 129.00, 135.88 (s), 136.81 (d), 141.02 (s), and 157.52 (s, 3-C); MS *m/z* (rel intensity, %) 249 (M^+, 10), 248 (18), 143 (20), 130 (23), 128 (20), 115 (81), 105 (23), 104 (43), 103 (42), 102 (25), 91 (55), 89 (30), 78 (45), 77 (base peak), 76 (19), and 65 (25). Found: C, 82.00; H, 6.21; N, 5.66%. Calcd for $C_{17}H_{15}NO$: C, 81.90; H, 6.21; N, 5.62%.

9b (A 75 : 25 mixture of E- and Z-isomers): Pale yellow liquid; IR (neat) 1640, 1610, and 970 cm^{-1}; ^1H NMR ($CDCl_3$) δ=1.01 (2/9×3H, t, J=7.5 Hz, Et (Z)), 1.03 (7/9×3H, t, J=7.0 Hz, Et (E)), 2.18 (2H, m, Et), 2.97 (7/9×1H, dd. J=16.5 (gem) and 8.5 Hz, one of 4-H (E)), 3.07 (2/9×1H, dd, J=16.5 (gem) and 8.5 Hz, one of 4-H (Z)), 3.46 (7/9×1H, dd, J=16.5 (gem) and 11.0 Hz, the other of 4-H (E)), 3.55 (2/9×1H, dd, J=16.5 (gem) and 11.0 Hz, the other of 4-H (Z)), 5.53 (1H, dd, J=11.0 and 8.5 Hz, 5-H), 5.7—6.5 (2H, m, CH=CH), and 7.26 (5H, s, Ph); ^{13}C NMR ($CDCl_3$) δ=12.84 (q, Et (E)), 14.06 (q, Et (Z)), 22.90 (t, Et (Z)), 25.92 (t, Et (E)), 42.09 (t, 4-C (E)), 45.36 (t, 4-C (Z)), 82.13 (d, 5-C (E)), 82.32 (d, 5-C (Z)), 117.19, 119.14, 125.97, 128.22, 128.80, 141.21, 142.04 (each d), 155.71 (s, 3-C (Z)), and 157.23 (s, 3-C (E)); MS *m/z* (rel intensity, %) 201 (M^+, 6), 129 (22), 128 (39), 127 (17), 115 (36), 105 (30), 104 (63), 91 (39), 78 (76), 77 (base peak), and 65 (30). Found: C, 77.65; H, 7.52; N, 6.93%. Calcd for $C_{13}H_{15}NO$: C, 77.58; H, 7.51; N, 6.96%.

9c (A 72 : 28 mixture of E- and Z-isomers): Colorless liquid; IR (neat) 1640, 1600, and 960 cm^{-1}; ^1H NMR ($CDCl_3$) δ=0.89 (3H, m, *n*-Bu), 1.1—1.6 (4H, m, *n*-Bu), 2.0—2.4 (2H, m, *n*-Bu), 2.98 (7/10×1H, dd, J=16.5 (gem) and 8.5 Hz, one of 4-H (E)), 3.07 (3/10×1H, dd, J=16.5 and 8.5 Hz, one of 4-H (Z)), 3.46 (7/10×1H, dd, J=16.5 (gem) and

† 1M=1 mol dm^{-3}.

11.0 Hz, the other of 4-H (E)), 3.56 (3/10×1H, dd, J=16.5 (gem) and 11.0 Hz, the other of 4-H (Z)), 5.53 (1H, dd, J= 11.0 and 8.5 Hz, 5-H), 5.6−6.5 (2H, m, CH=CH), and 7.26 (5H, s, Ph); ^{13}C NMR ($CDCl_3$) δ=13.82 (q), 22.18, 29.29, 30.83, 31.71, 32.59, 42.12, 45.42 (each t), 82.12 (d, 5-C (E)), 82.36 (d, 5-C (Z)), 117.71, 120.07, 126.01, 128.25, 128.83, 139.83, 140.72 (each d), 141.30, 155.78 (s, 3-C (Z)), and 157.19 (s, 3-C (E)); MS m/z(rel intensity, %) 229 (M^+, 36), 212 (17), 200 (25), 168 (17), 129 (18), 128 (20), 115 (25), 105 (20), 104 (base peak), 103 (23), 91 (43), 78 (36), 77 (49), and 51 (30). Found: C, 78.28; H, 8.37; N, 6.12%. Calcd for $C_{15}H_{19}NO$: C, 78.56; H, 8.35; N, 6.11%.

9d: Colorless prisms (diethyl ether-hexane); mp 62—64 °C; IR (KBr) 1650, 1625, and 975 cm^{-1}; ^{1}H NMR ($CDCl_3$) δ=1.76 (3H, d, J=6.0 Hz, Me), 2.96 (1H, dd, J=16.5 (gem and 8.5 Hz, one of 4-H), 3.43 (1H, dd, J=16.5 (gem) and 11.0 Hz, the other of 4-H), 5.50 (1H, dd, J=11.0 and 8.5 Hz, 5-H), 5.6—6.6 (3H, m, CH=), and 7.24 (5H, s, Ph); ^{13}C NMR ($CDCl_3$) δ=18.41 (q, Me), 41.70 (t, 4-C), 82.42 (d, 5-C), 118.71, 126.01, 128.25, 128.83, 131.13, 134.48, 137.42 (each d), 141.13 (s), and 157.42 (s, 3-C); MS m/z (rel intensity, %) 213 (M^+, 30), 198 (base peak), 180 (25), 115 (19), 105 (18), 104 (46), 103 (26), 91 (36), 78 (39), 77 (68), and 65 (26). Found: C, 78.73; H, 7.05; N, 6.71%. Calcd for $C_{14}H_{15}NO$: C, 78.84; H, 7.09; N, 6.57%.

9e: Colorless needles (hexane); mp 82—84 °C; IR (KBr) 1640 cm^{-1}; ^{1}H NMR ($CDCl_3$) δ=1.54 (6H, m, c-Hex), 2.15, 2.41 (each 2H, m, c-Hex), 2.99 (1H, dd, J=16.5 (gem) and 8.5 Hz, one of 4-H), 3.50 (1H, dd, J=16.5 (gem) and 11.0 Hz, the other of 4-H), 5.47 (1H, dd, J=11.0 and 8.5 Hz, 5-H), 5.83 (1H, s, CH=), and 7.24 (5H, s, Ph); ^{13}C NMR ($CDCl_3$) δ=26.27, 27.78, 28.56, 30.81, 38.28, 45.90 (each t), 81.88 (d, 5-C), 111.18 (d, CH=), 125.93, 128.12, 128.76 (each d), 141.50, 151.56 (each s), and 155.71 (s, 3-C); MS m/z(rel intensity, %) 241 (M^+, 21), 224 (18), 135 (25), 134 (base peak), 128 (24), 107 (31), 106 (42), 105 (27), 104 (55), 103 (30), 91 (76), 79 (43), 78 (50), 77 (84), 67 (28), and 65 (41). Found: C, 79.52; H, 7.90; N, 5.94%. Calcd for $C_{16}H_{19}NO$: C, 79.63; H, 7.94; N, 5.80%.

Geneal Procedure for the Alkylation of 7b, 7c Leading to 10a—e. To a solution of isoxazoline **7b** or **7c** (1 mmol) in dry THF (3 ml) was added butyllithium (1.6M in hexane, 0.62 ml, 0.989 mmol) at −78 °C under nitrogen. After 1 h, an alkyl halide (2 mmol) was added. The mixture was stirred at −78 °C for 1 h, at 0 °C for 1 h, and then at room temperature for the time shown in Table 4. Ice water (30 ml) was added and the mixture was extracted with dichloromethane (20 ml×2). The combined extracts were dried over magnesium sulfate and evaporated in vacuo. The residue was chromatographed over silica gel by using the following eluent: **10a**: hexane-ethyl acetate (1 : 5 v/v); **10b**, **10c**, **10d**: hexane-ethyl acetate (1 : 1 v/v); **10e**: hexane-ethyl aceate (2 : 3 v/v). All alkylated isoxazolines **10** were mixtures of two diastereoisomers. The results are summarized in Table 4.

10a: Pale yellow liquid; IR (neat) 1600, 1250, 1020, and 800 cm^{-1}; ^{1}H NMR ($CDCl_3$) δ=1.2—1.6 (9H, m, OEt and Me), 2.8—3.7 (3H, m, CH and 4-H), 3.8—4.3 (4H, m, OEt), 5.55 (1H, dd, J=11.0 and 8.5 Hz, 5-H), and 7.27 (5H, s, Ph); ^{13}C NMR ($CDCl_3$) δ=12.35 (qd, J_{cp}=5.9 Hz, Me), 16.41 (qd, J_{cp}=5.9 Hz, OEt), 32.30, 32.47, (each dd, J_{cp}=141.2 Hz, CH), 43.71, 44.00 (each t), 62.69 (d, J_{cp}=7.4 Hz, 4-C), 82.24 (d, 5-C), 126.10, 128.30, 128.83 (each d), 141.13, 141.24 (each s), and 156.19 (d, J_{cp}=8.9 Hz, 3-C); MS m/z (rel intensity, %) 311 (M^+, 62), 310 (base peak), 248 (28), 234 (41), 220 (14), 206 (21), 178 (34), 156 (25), 129 (21), 128 (23), 109 (29), 105 (23), 104 (49), 103 (23), 91 (25), 81 (34), 78 (20), and 77 (31). HRMS Found: m/z 311.1268. Calcd for $C_{15}H_{22}NO_4P$: M, 311.1285.

10b: Pale yellow liquid; IR (neat) 1610, 1250, 1025, and 830 cm^{-1}; ^{1}H NMR ($CDCl_3$) δ=0.83, 0.89 (3H, each t, n-Pen), 1.1—2.1 (8H, m, n-Pen), 1.26 (6H, m, OEt), 2.7—3.7 (3H, m, 4-H and CH), 3.8—4.3 (4H, m, OEt), 5.56, 5.59 (1H, each dd, J=10.5 and 8.0 Hz, 5-H), and 7.27 (5H, s, Ph); ^{13}C NMR ($CDCl_3$) δ=13.87, 13.96 (each q, n-Pen), 16.38 (qd, J_{cp}=6.1 Hz, OEt), 22.31, 26.37, 26.56, 27.10, 27.29, 27.69, 27.88, 31.10, 31.25 (each t), 37.70 (dd, J_{cp}=139.2 Hz, CH), 43.21, 43.66 (each t), 62.35 (td, J_{cp}=4.7 Hz, 4-C), 62.57 (td, J_{cp}=6.1 Hz, 4-C), 81.98 (d, 5-C), 125.78, 126.02, 128.22, 128.80 (each d), 141.30 (s), and 155.13 (d, J_{cp}=7.3 Hz, 3-C); MS m/z (rel intensity, %) 367 (M^+, 53), 366 (66), 290 (19), 230 (24), 137 (31), 128 (21), 109 (base peak), 105 (33), 104 (43), 91 (35), 81 (68), 78 (20), and 77 (41). HRMS Found: m/z 367.1904. Calcd for $C_{19}H_{30}NO_4P$: M, 367. 1911.

10c: Pale yellow liquid; IR (neat) 1600, 1250, 1025, 850 and 800 cm^{-1}; ^{1}H NMR ($CDCl_3$) δ=0.02, 0.07 (9H, each s, $SiMe_3$), 1.0—1.4 (8H, m, OEt and CH_2SiMe_3), 2.8—3.6 (3H, m, 4-H and CH), 3.9—4.3 (4H, m, OEt), 5.53 (1H, dd, J=11.0 and 8.0 Hz, 5-H), and 7.28 (5H, s, Ph); ^{13}C NMR ($CDCl_3$) δ=−1.37 (q, $SiMe_3$), 13.38 (t, CH_2SiMe_3), 16.38 (qd, J_{cp}=6.1 Hz, OEt), 33.50 (dd, J_{cp}=139.1 Hz, CH), 33.72 (dd, J_{cp}=137.9 Hz, CH), 43.41, 43.90 (each t), 62.50 (td, J_{cp}=7.3 Hz, 4-C), 62.60 (td, J_{cp}=7.3 Hz, 4-C), 82.22 (dd, J_{cp}=7.3 Hz, 5-C), 126.07, 128.22, 128.76 (each d), 140.72, 141.30 (each s), 155.95 (d, J_{cp}=9.8 Hz, 3-C), and 156.32 (d, J_{cp}=8.5 Hz, 3-C); MS m/z(rel intensity, %) 383 (M^+, base peak), 382 (72), 368 (29), 156 (19), and 73 (46). HRMS Found: m/z 383.1654. Calcd for $C_{18}H_{30}NO_4PSi$: M, 383.1680.

10d: Pale yellow liquid; IR (neat) 1600, 1250, 1025, and 800 cm^{-1}; ^{1}H NMR ($CDCl_3$) δ=0.85 (3H, t, n-Pen), 1.1—1.7 (8H, m, n-Pen), 1.30 (6H, t, J=7.0 Hz, OEt), 2.3—3.7 (5H, m, 4-H, CH, and CH_2Ph), 4.11 (4H, qd, J=7.0 and 7.5 (HP) Hz, OEt), 4.40 (1H, m, 5-H), and 7.17 (5H, s, Ph); ^{13}C NMR ($CDCl_3$) δ=13.96 (q, n-Pen), 16.43 (qd, J_{cp}=6.2 Hz, OEt), 22.51, 24.91, 31.60, 32.76, 34.72, 34.91 (each t), 39.09 (dd, J_{cp}=137.9 Hz, CH), 39.38 (dd, J_{cp}=137.9 Hz, CH), 40.77, 41.02 (each t), 62.77 (td, J_{cp}=6.7 Hz, 4-C), 81.09 (d, 5-C), 126.96, 128.76 (each d), 137.74, 138.37 (each s), and 154.64 (d, J_{cp}=6.6 Hz, 3-C); MS m/z(rel intensity, %) 381 (M^+, 15), 311 (19), 310 (base peak), 254 (23), 91 (29), and 43 (45). HRMS Found: m/z 381.2062. Calcd for $C_{20}H_{32}NO_4P$: M, 381.2067.

10e: Colorless liquid; IR (neat) 1640, 1250, 1025, 980, and 800 cm^{-1}; ^{1}H NMR ($CDCl_3$) δ=0.89 (3H, t, n-Pen), 1.1—1.9 (8H, m, n-Pen), 1.33 (6H, t, J=7.0 Hz, OEt), 2.3—3.4 (5H, m, 4-H, CH, and $CH_2CH=CH_2$), 4.12 (4H, qd, J=7.0 and 7.4 (HP) Hz, OEt), 4.52 (1H, m, 5-H), 5.05 (1H, dd, J=10.0 and 1.7 Hz, one of $=CH_2$), 5.09 (1H, dd, J=17.5 and 1.7 Hz, the other of $=CH_2$), and 5.70 (1H, m, CH=); ^{13}C NMR ($CDCl_3$) δ=14.00 (q, n-Pen), 16.47 (qd, J_{cp}=5.9 Hz, OEt), 22.59, 25.07, 25.18, 30.88, 31.00, 31.71, 35.06 (each t), 37.56 (dd, J_{cp}=139.7 Hz, CH), 40.36 (t), 62.71 (td,

J_{cp}=5.9 Hz, 4-C), 81.12 (d, 5-C), 117.54 (t, =CH_2), 134.77 (dd, J_{cp}=17.6 Hz, CH=), and 154.98 (d, J_{cp}=7.3 Hz, 3-C); MS *m/z* (rel intensity, %) 331 (M^+, 6), 260 (34), 204 (20), 109 (21), 94 (29), 93 (21), 91 (24), 82 (23), 81 (52), 80 (24), 79 (25), and 43 (base peak). HRMS Found: *m/z* 311.1902. Calcd for $C_{16}H_{30}NO_4P$: M, 311.1911.

General Procedure for Oxidation of the Carbanions Derived from 10a—d Leading to 3-(1-Oxoalkyl)-2-isoxazolines 11a — c. Butyllithium (1.6 M in hexane, 0.63 ml, 1 mmol) was added, at −78 °C under nitrogen, to the solution of isoxazoline **10** (1 mmol) in dry THF (5 ml) and stirred for 1 h. Dry oxygen was slowly bubbled into this solution for 1 h at the same temperature. The mixture was poured into ice water (20 ml) and extracted with dichloromethane (20 ml×2). The combined extracts were dried over magnesiun sulfate and evaporated in vacuo. The residue was chromatographed over silica gel with the following eluent: **11a**: hexane-ethyl acetate (10 : 1 v/v); **11b**, **11c**: hexane-ethyl acetate (20 : 1 v/v). Unreacted **10** was recovered from the fraction eluted with ethyl acetate. The results are listed in Table 4.

11a: Colorless liquid; IR (neat) 1680 and 1575 cm^{-1}; ^1H NMR ($CDCl_3$) δ=2.52 (3H, s, COMe), 3.09 (1H, dd, J= 17.7 (gem) and 9.0 Hz, one of 4-H), 3.53 (1H, dd, J=17.7 (gem) and 11.5 Hz, the other of 4-H), 5.73 (1H, dd, J=11.5 and 9.0 Hz, 5-H), and 7.31 (5H, s, Ph); ^{13}C NMR ($CDCl_3$) δ=26.71 (q, COMe), 39.77 (t, 4-C), 85.59 (d, 5-C), 126.01, 128.77, 129.01 (each d), 139.78 (s), 158.06 (s, 3-C), and 193.19 (s, COMe); MS *m/z* (rel intensity, %) 189 (M^+, 3), 115 (17), 105 (15), 104 (13), 78 (17), 77 (38), 51 (32), and 43 (base peak). Found: C, 69.90; H, 5.93; N, 7.37%. Calcd for $C_{11}H_{11}NO_2$: C, 69.83; H, 5.86; N, 7.40%.

11b: Colorless needles (hexane); mp 43—44 °C; IR (KBr) 1660 and 1560 cm^{-1}; ^1H NMR ($CDCl_3$) δ=0.89 (3H, t, *n*-Pen), 1.1—1.9 (6H, m, *n*-Pen), 2.90 (2H, t, J=7.0 Hz, *n*-Pen), 3.07 (1H, dd, J=17.8 (gem) and 9.0 Hz, one of 4-H), 3.51 (1H, dd, J=17.8 (gem) and 11.2 Hz, the other of 4-H), 5.69 (1H, dd, J=11.2 and 9.0 Hz, 5-H), and 7.27 (5H, s, Ph); ^{13}C NMR ($CDCl_3$) δ=13.88 (q, *n*-Pen), 22.41, 23.71, 31.36, 39.30, 40.00 (each t), 85.24 (d, 5-C), 126.01, 128.71, 129.01 (each d), 139.89 (s), 157.59 (s, 3-C), and 196.02 (s, CO); MS *m/z* (rel intensity, %) 245 (M^+, base peak), 244 (24), 228 (43), 129 (21), 128 (16), 115 (20), 105 (19), 104 (83), 99 (49), 91 (20), 76 (26), and 71 (35). Found: C, 73.57; H, 7.85; N, 5.78%. Calcd for $C_{15}H_{19}NO_2$: C, 73.44; H, 7.81; N, 5.71%.

11c: Colorless prisms (hexane); mp 33—34 °C; IR (KBr) 1680 and 1580 cm^{-1}; ^1H NMR ($CDCl_3$) δ=0.88 (3H, t, J=7.0 Hz, *n*-Pen), 1.2—1.8 (8H, m, *n*-Pen), 2.67 (1H, dd, J=17.5 (gem) and 9.0 Hz, one of 4-H), 3.10 (1H, dd, J= 17.5 (gem) and 10.5 Hz, the other of 4-H), 4.13 (2H, s, CH_2Ph), 4.67 (1H, m, 5-H), and 7.22 (5H, s, Ph); ^{13}C NMR ($CDCl_3$) δ=13.94 (q, *n*-Pen), 22.47, 24.88, 31.53, 35.18, 36.89, 45.65 (each t), 85.06 (d, 5-C), 127.19, 128.72, 129.89 (each d), 133.90 (s), 157.95 (s, 3-C), and 193.07 (s, CO); MS *m/z* (rel intensity, %) 259 (M^+, 71), 258 (base peak), 168 (38), 91 (89), and 65 (11). Found; C, 74.31; H, 8.26; N, 5.65%. Calcd for $C_{16}H_{21}NO_2$: C, 74.10; H, 8.16; N, 5.40%.

Reaction of 7k with Butyllithium Leading to 8. Butyllithium (1.6 M in hexane, 0.23 ml, 0.37 mmol) was slowly added, at −78 °C under nitrogen, to the solution of isoxazoline **7k** (0.133 g, 0.37 mmol) in dry THF (2 ml). After 1 h at −78 °C, pentyl iodide (0.146 g, 0.74 mmol) was added. The mixture was stirred at 0 °C for 1 h, at room temperature for 12 h, and then poured into ice water. The product was extracted with dichloromethane (30 ml × 2). The combined extracts were dried over magnesium sulfate and evaporated in vacuo. The residue was chromatographed over silica gel by using hexane-ethyl acetate (1 : 5 v/v) to give **8** (0.059 g, 73%) which was characterized above.

General Procedure for the Raney Ni Hydrogenolysis of 7 or 10a Leading to 12a—g. The following two procedures were applied: A mixture of **7** or **10a** (1 mmol), Raney Ni (W-2, suspension in ethanol, 1 ml), acetic acid (0.5 ml), and water (0.5 ml) in ethanol (5 ml) -Method A- or a mixture of **7** or **10a** (1 mmol), Raney Ni (1 ml), boric acid (0.13 g, 2 mmol), and water (1 ml) in ethanol (5 ml) -Method B- was stirred under an atmosphere of hydrogen (1 atm) at room temperature. The insoluble materials were removed off by filteration through celite 545 and the filtrate was evaporated in vacuo. The residue was dissolved in dichloromethane (20 ml). The solution was washed with water, dried over magnesium sulfate, and evaporated in vacuo to give **12**. The methods applied, the reaction times, the yields of **12**, and the purification methods are as follows: **12a**: B, 12 h, 80%, a silica-gel chromatography with ethyl acetate; **12b**: B, 13 h, 91%, a silica-gel chromatography with ethyl acetate; **12c**: B, 13 h, 63%, a silica-gel chromatography with ethyl acetate; **12d**: B, 13 h, 63%, decomposed in a silica-gel column; **12e**: A, 20 h, 77%, a silica-gel chromatography with hexane-ethyl acetate (5 : 1 v/v); **12f**: B, 13 h, 88%, a silica-gel chromatography with ethyl acetate. **12g**: B, 12 h, 73%, a silica-gel chromatography ethyl acetate.

12a: Colorless liquid: IR (neat) 3360, 1710, 1240, 1020, and 790 cm^{-1}; ^1H NMR ($CDCl_3$) δ=1.28 (6H, t, J=7.0 Hz, OEt), 2.7—3.2 (2H, m, $COCH_2$), 3.08 (2H, d, J=23.0 (HP) Hz, CH_2P), 3.8—4.3 (1H, br, OH), 4.08 (4H, qd, J=7.0 and 7.5 (HP) Hz, OEt), 5.12 (1H, dd, J=8.0 and 4.5 Hz, CHPh), and 7.0−7.5 (5H, m, Ph); ^{13}C NMR ($CDCl_3$) δ= 16.29 (qd, J_{cp}=5.9 Hz, OEt), 43.06 (td, J_{cp}=126.5 Hz, CH_2P), 53.06 (t, $COCH_2$), 62.83 (td, J_{cp}=5.9 Hz, OEt), 69.95 (d, CH), 125.95, 127.77, 128.65 (each d), 143.48 (s), and 202.02 (d, J_{cp}=5.9 Hz, CO); MS *m/z* (rel intensity, %) 300 (M^+, 1), 125 (14), 123 (20), 109 (37), 107 (33), 105 (29), 97 (20), 96 (22), 81 (48), 79 (84), 78 (33), and 77 (base peak). HRMS Found: *m/z* 300.1121. Calcd for $C_{14}H_{21}O_5P$: M, 300.1125.

12b: Colorless liquid IR (neat) 3400, 1710, 1240, 1025, and 790 cm^{-1}; ^1H NMR ($CDCl_3$) δ=0.88 (3H, t, J=6.0 Hz, *n*-Pen), 1.33 (6H, t, J=7.0 Hz, OEt), 1.1—1.7 (8H, m, *n*-Pen), 2.72 (2H, d, J=6.0 Hz, $COCH_2$), 3.16 (2H, d, J=22.5 (HP) Hz, CH_2P), 3.82 (1H, br, OH), 4.04 (1H, m, CH), and 4.13 (4H, qd, J=7.0 and 7.5 (HP) Hz, OEt); ^{13}C NMR ($CDCl_3$) δ=14.06 (q, *n*-Pen), 16.29 (qd, J_{cp}=5.9 Hz, OEt), 22.65, 25.24, 31.83, 37.00 (each t), 43.00 (d, J_{cp}=126.5 Hz, CH_2P), 51.36 (t), 62.77 (td, J_{cp}=5.9 Hz, OEt), 67.77 (d, CH), and 202.89 (d, J_{cp}=5.9 Hz, CO); MS *m/z* (rel intensity, %) 294 (M^+, 3), 223 (base peak), 195 (33), 194 (42), 179 (19), 167 (17), 152 (18), 139 (19), 125 (20), 123 (25), and 97 (16). HRMS Found: *m/z* 294.1546. Calcd for $C_{13}H_{27}O_5P$: M, 294.1595.

12c: Colorless liquid; IR (neat) 3340, 1730, 1710, 1240,

1020, 970, and 790 cm^{-1}; ^1H NMR ($CDCl_3$) δ=1.33 (6H, d, J=7.0 Hz, OEt), 3.10 (2H, d, J=5.0 Hz, $COCH_2$), 3.15 (2H, d, J=22.5 (HP) Hz, CH_2P), 3.73 (3H, s, COOMe), 4.13 (4H, qd, J=7.0 and 7.5 (HP) Hz, OEt), 4.51 (1H, t, J=5.0 Hz, CH), and 4.65 (1H, s, OH); ^{13}C NMR ($CDCl_3$) δ=16.30 (qd, J_{cp}=5.9 Hz, OEt), 42.80 (td, J_{cp}=128.0 Hz, CH_2P), 47.71 (t, $COCH_2$), 52.42 (q, COOMe), 62.89 (td, J_{cp}=5.9 Hz, OEt), 66.89 (d, CH), 174.19 (s, COOMe), and 199.89 (d, J_{cp}=5.9 Hz, CO); MS m/z (rel intensity, %) 282 (M^+, 2), 223 (base peak), 195 (16), 194 (22), 179 (29), 152 (21), 151 (23), 139 (21), 125 (34), and 123 (54). HRMS Found: m/z 282.0864. Calcd for $C_{10}H_{19}O_7P$: M, 282.0867.

12d: Labile colorless liquid; ^1H NMR ($CDCl_3$) δ=1.33 (6H, J=7.0 Hz, OEt), 2.25 (3H, s, COMe), 3.06 (2H, dd, J=6.2 and 4.2 Hz, $COCH_2$), 3.15 (2H, d, J=22.6 (HP) Hz, CH_2P), 4.13 (4H, qd, J=7.0 and 7.4 (HP) Hz, OEt), 4.37 (1H, dd, J=6.2 and 4.2 Hz, CH), and 4.34 (1H, br, OH); ^{13}C NMR ($CDCl_3$) δ=16.32 (qd, J_{cp}=7.4 Hz, CH_2P), 25.53 (q, COMe), 42.97 (td, J_{cp}=125.0 Hz, OEt), 47.12 (t, $COCH_2$), 62.98 (td, J_{cp}=8.3 Hz, OEt), 73.53 (d, CH), 200.37 (d, J_{cp}=5.9 Hz, CO), and 209.72 (s, COMe); MS m/z (rel intensity, %) 223 (M^+−COMe, 77), 195 (26), 179 (22), 167 (26), 152 (34), 151 (26), 139 (48), 125 (40), 123 (73), 121 (20), 109 (23), 97 (33), and 43 (base peak). This compound was too labile to be purified as an authentic sample.

12e: Colorless liquid; IR (neat) 3400, 1700, 1240, 1025, and 800 cm^{-1}; ^1H NMR ($CDCl_3$) δ=1.33 (6H, t, J=7.0 Hz, OEt), 2.93 (2H, d, J=6.0 Hz, CH_2Br), 3.16 (2H, d, J=22.5 (HP) Hz, CH_2P), 3.46 (2H, d, J=5.0 Hz, $COCH_2$), 3.72 (1H, s, OH), 4.12 (4H, qd, J=7.0 and 7.3 (HP) Hz, OEt), and 4.24 (1H, tt, J=6.0 and 5.0 Hz, CH); ^{13}C NMR ($CDCl_3$) δ=16.30 (qd, J_{cp}=5.9 Hz, OEt), 37.82 (t, CH_2Br), 43.03 (td, J_{cp}=128.0 Hz, CH_2P), 48.94 (t, $COCH_2$), 62.95 (td, J_{cp}=5.9 Hz, OEt), 67.01 (d, CH), and 201.19 (d, J_{cp}=5.9 Hz, CO); MS m/z (rel intensity, %) 319, 317 (M^+, 17), 223 (base peak), 219 (47), 195 (23), 194 (60), 179 (40), 167 (22), 163 (19), 151 (33), 139 (34), 125 (36), 123 (59), 109 (32), 97 (26), and 80 (41). Found: C, 33.87; H, 5.65%. Calcd for $C_9H_{18}O_5BrP$: C, 34.09; H, 5.72%.

12f: Colorless liquid; IR (neat) 3370, 1710, 1245, 1025, and 965 cm^{-1}; ^1H NMR ($CDCl_3$) δ=1.1—1.4 (12H, m, OEt), 2.79 (2H, d, J=5.8 Hz, $COCH_2$), 3.12 (2H, d, J=21.6 (HP) Hz, CH_2P), 3.20 (1H, br, OH), 3.4—3.8 (4H, m, OEt), 3.9—4.2 (1H, m, CH), 4.07 (4H, qd, J=7.0 and 7.5 (HP) Hz, OEt), and 4.30 (1H, d, J=5.8 Hz, $CH(OEt)_2$); ^{13}C NMR ($CDCl_3$) δ=15.35 (q, OEt), 16.29 (qd, J_{cp}=5.9 Hz, OEt), 43.15 (td, J_{cp}=128.0 Hz, CH_2P), 46.06 (t, $COCH_2$), 62.65 (td, J_{cp}=5.9 Hz, OEt), 63.36, 64.00 (each t, OEt), 68.77 (d, CHOH), 104.36 (d, $CH(OEt)_2$), and 201.60 (s, CO); MS m/z (rel intensity, %) 281 (M^+-OEt), 223 (16), 179 (7), 152 (6), 123 (9), 104 (6), 103 (base peak), 75 (31), and 47 (21). Found: C, 47.85; H, 8.24%. Calcd for $C_{13}H_{27}O_7P$: C, 47.85; H, 8.44%.

12g (A mixture of two diastereomers): Pale yellow liquid; IR (neat) 3360, 1710, 1240, 1020, and 790 cm^{-1}; ^1H NMR ($CDCl_3$) δ=1.26 (6H, t, J=7.0 Hz, OEt), 1.4—1.5 (3H, m, Me), 2.8—3.6 (3H, m, CH_2CO and CH), 4.04 (4H, qd, J=7.0 and 8.0 (HP) Hz, OEt), 5.12 (1H, dd, J=7.0 and 5.0 Hz, CHPh), and 7.1—7.5 (5H, m, Ph); ^{13}C NMR ($CDCl_3$) δ=10.24 (q, Me), 16.00 (qd, J_{cp}=5.9 Hz, OEt), 46.65, 47.12 (each td, J_{cp}=126.5 Hz, CH_2P), 52.12, 52.89 (each d), 62.30 (td, J_{cp}=5.9 Hz, OEt), 69.59, 69.89 (each d, CHPh), 125.60, 127.13, 128.13 (each d), 143.78 (s), 204.87, and 205.34 (each d, J_{cp}=4.4 Hz, CO); MS m/z (rel intensity, %) 314 (M^+, 4), 208 (16), 190 (23), 180 (32), 166 (28), 139 (21), 138 (29), 137 (26), 123 (30), 109 (79), 107 (47), 105 (52), 103 (24), 91 (26), 81 (68), 79 (86), 78 (30), 77 (base peak), 51 (24), and 43 (22). HRMS Found: m/z 314.1276. Calcd for $C_{15}H_{23}O_5P$: M, 314.1282.

2-[(Diethoxyphosphoryl)methyl]-5-methylpyrrole (13). The Raney Ni reduction of **7e** (0.270 g, 1.03 mmol) was carried out for 19 h according to the method A mentioned above and followed by the usual work-up and the column chromatography over silica gel (hexane-ethyl acetate (1 : 1 v/v)) to give **13** (0.056 g, 24%): Pale yellow liquid; IR (neat) 3220, 1590, 1225, 1020, and 790 cm^{-1}; ^1H NMR ($CDCl_3$) δ=1.24 (6H, t, J=7.0 Hz, OEt), 2.17 (3H, d, J=1.5 Hz, Me), 3.11 (2H, d, J=20.0 (HP) Hz, CH_2P), 4.00 (4H, qd, J=7.0 and 14.0 (HP) Hz, OEt), 5.6—5.9 (2H, m, 3- and 5-H), and 8.90 (1H, br, s, NH); ^{13}C NMR ($CDCl_3$) δ=13.00 (q, Me), 16.41 (qd, J_{cp}=5.3 Hz, OEt), 25.88 (td, J_{cp}=141.2 Hz, CH_2P), 62.50 (td, J_{cp}=7.4 Hz, OEt), 106.02 (d, 4-C), 108.33 (dd, J_{cp}=10.3 Hz, 3-C), 118.89 (d, J_{cp}=11.8 Hz, 2-C), and 128.33 (s, 5-C); MS m/z (rel intensity, %) 231 (M^+, 6), 95 (15), 94 (base peak), and 93 (12). HRMS Found: m/z 231.1019. Calcd for $C_{10}H_{18}NO_3P$: M, 231.1023.

General Procedure for the Dehydration of Hydroxy Ketones 12a, 12b Leading to 14a, 14b. To a solution of **12** (1 mmol) and triethylamine (0.3 g, 3 mmol) in dichloromethane (5 ml) was added dropwise methanesulfonyl chloride (0.14 g, 1.2 mmol) at −20 °C. The mixture was stirred at −20 °C for 0.5 h and at room temperature for 1 h. Ice water (20 ml) was added and the product was extracted with diethyl ether (20 ml × 2). The combined extracts were washed with 1 M hydrochloric acid (20 ml), aqueous sodium hydrogencarbonate (20 ml), and water (20 ml × 2). After dried over magnesium sulfate, the solvent was evaporated in vacuo. The residue was chromatographed over silica gel by using hexane-ethyl acetate (1 : 5 v/v).

14a: Yield 87%; pale yellow liquid; IR (neat) 1650, 1600, 1240, 1020, and 790 cm^{-1}; ^1H NMR ($CDCl_3$) δ=1.30 (6H, t, J=7.0 Hz, OEt), 3.30 (2H, d, J=23.0 (HP) Hz, CH_2P), 4.14 (4H, qd, J=7.0 and 8.0 (HP) Hz, OEt), 6.84 (1H, d, J=16.0 Hz, CH=), 7.60 (1H, d, J=16.0 Hz, CH=), and 7.2—7.6 (5H, m, Ph); ^{13}C NMR ($CDCl_3$) δ=16.29 (qd, J_{cp}=5.9 Hz, OEt), 40.97 (td, J_{cp}=128.0 Hz, CH_2P), 62.68 (td, J_{cp}=7.4 Hz, OEt), 125.95, 128.77, 129.13, 131.01 (each d), 134.06 (s), 144.89 (d), and 191.30 (d, J_{cp}=5.9 Hz,CO); MS m/z (rel intensity, %) 282 (M^+, 31), 253 (14), 224 (66), 197 (96), 180 (47), 179 (base peak), 169 (35), 152 (62), 151 (70), 144 (49), 131 (32), 125 (43), 123 (88), 109 (44), 97 (24), 88 (38), and 81 (38). HRMS Found: m/z 282.1019. Calcd for $C_{14}H_{19}O_4P$: M, 282.1020.

14b: Yield 93%; pale yellow liquid; IR (neat) 1690, 1660, 1250, 1025, 960, and 790 cm^{-1}; ^1H NMR ($CDCl_3$) δ=0.89 (3H, t, J=6.0 Hz, *n*-Pen), 1.1—1.7 (6H, m, *n*-Pen), 1.32 (6H, t, J=7.0 Hz, OEt), 2.24 (2H, q, J=7.0 Hz, *n*-Pen), 3.20 (2H, d, J=22.0 (HP) Hz, CH_2P), 4.13 (4H, qd, J=7.0 and 7.5 (HP) Hz, OEt), 6.20 (1H, dt, J=15.0, 1.0, and 1.0 Hz, CH=), and 6.94 (1H, dt, J=15.0, 7.0, and 7.0 Hz, CH=); ^{13}C NMR ($CDCl_3$) δ=13.94 (q, *n*-Pen), 16.35 (qd, J_{cp}=5.9 Hz, OEt), 22.41, 27.71, 31.41, 32.59 (each t), 40.18 (tq, J_{cp}=129.4 Hz, CH_2P), 62.59 (td, J_{cp}=5.9 Hz, OEt),

130.25, 150.72 (each d), and 191.57 (d, $J_{cp} = 7.4$ Hz, CO); MS m/z (rel intensity, %) 276 (M^+, 6), 244 (73), 173 (40), 136 (24), 121 (base peak), 81 (23), 65 (70), and 55 (30). HRMS Found: m/z 276.1487. Calcd for $C_{13}H_{25}O_4P$: M, 276.1489.

References

1) These heterocycles can be converted into: 1,3-Diketones and 3-imino ketones: R. Stevens, C. G. Christensen, W. L. Edmonson, M. Kaplan, E. B. Reid, and M. P. Wentland, *J. Am. Chem. Soc.*, **93**, 6629 (1971). β-Hydroxy ketones: R. H. Wollenberg and J. E. Goldstein, *Synthesis*, **1980**, 757; A. P. Kozikowski and M. Adamczyk, *Tetrahedron Lett.*, **23**, 3123 (1982); D. P. Curran, *J. Am. Chem. Soc.*, **105**, 5826 (1983). γ-Amino alcohols: G. W. Perold and F. V. K. von Reiche, *J. Am. Chem. Soc.*, **79**, 465 (1957); V. Jäger, V. Buss, and W. Schwab, *Tetrahedron Lett.*, **1978**, 3133. α,β-Unsaturated ketones: G. Buchi and J. C. Vederas, *J. Am. Chem. Soc.*, **94**, 9128 (1972); V. Jäger and H. Grund, *Angew. Chem.*, **88**, 27 (1976); H. Grund and V. Jäger, *Liebigs Ann. Chem.*, **1980**, 80. Other functionalities: A. P. Kozikowski and M. Adamczyk, *J. Org. Chem.*, **48**, 366 (1983); A. Hosomi, H. Shoji, and H. Sakurai, *Chem. Lett.*, **1985**, 1049.

2) P. Caramella and P. Grunanger, "Nitrile Oxides and Imines," in "1,3-Dipolar Cycloaddition Chemistry," ed by A. Padwa, John Wiley and Sons, New York, Chichester, Brisbane, Toronto, Singapore (1984), Vol. 1, Chap. 3, pp. 291—392; C. Grundmann and P. Grunanger, "Nitrile Oxides," Springer Verlag, New York, Heidelberg (1971).

3) E. J. McAlduff, P. Caramella, and K. N. Houk, *J. Am. Chem. Soc.*, **100**, 105 (1980); K. N. Houk and K. Yamaguchi, "Theory of 1,3-Dipolar Cycloaddition," in "1,3-Dipolar Cycloaddition Chemistry," ed by A. Padwa, John, Willey and Sons, New York, Chichester, Brisbane, Toronto, Singapore (1984), Vol. 2, Chap. 13, pp. 407—450.

4) As reviews: A. P. Kozikowski, "Comprehensive Heterocyclic Chemistry," ed by A. R. Katrizky, C. W. Rees, Pergamon Press, Oxford, New York, Toronto, Sydney, Paris, Frankfurt (1984), Vol. 1, Chap. 1—16, pp. 413—491; A. P. Kozikowski, *Acc. Chem. Res.*, **17**, 410 (1984); G. Desimoni, G. Tacconi, A. Barco, G. P. Pollini, "Natural Product Synthesis through Pericyclic Reactions," ed by M. C. Caserio, American Chemical Society, Washington, D. C. (1983), Chap. 4, pp. 89—117.

5) As functionalized nitrile oxides: R. V. Stevens, C. G. Christensen, R. M. Cory, and E. Thorsett, *J. Am. Chem. Soc.*, **97**, 6865 (1975); P. A. Wade and H. R. Hinney, *ibid.*, **101**, 1319 (1979); T. Kametani, S.-P. Huang, and M. Ihara, *Heterocycles*, **12**, 1183 (1979); A. P. Kozikowski and A. K. Ghosh, *J. Am. Chem. Soc.*, **104**, 5788 (1982); A. P. Kozikowski and A. K. Ghosh, *Tetrahedron Lett.*, **24**, 2623 (1983); A. P. Kozikowski and C.-S. Li, *J. Org. Chem.*, **50**, 778 (1985).

6) Part of the this work was already published as a preliminary communication (O. Tsuge, S. Kanemasa, and H. Suga, *Chem. Lett.*, **1986**, 183).

7) a) Dehydration of nitroalkanes: T. Mukaiyama and T. Hoshino, *J. Am. Chem. Soc.*, **82**, 5339 (1960). b) Hypochlorite or -bromite oxidation of aldoximes: C. Grundmann and J. M. Dean, *J. Org. Chem.* **30**, 2809 (1965); G. A. Lee, *Synthesis*, **1982**, 508. c) Lead tetraacetate oxidation of aldoximes: G. Just and K. Dahl, *Tetrahedron*, **24**, 5251 (1968); R. N. Butler, F. L. Scott, and T. A. F. O'Mahony, *Chem. Rev.*, **73**, 93 (1973). d) Via bromination or chlorination of aldoximes: C. Grundman and R. Richter, *J. Org. Chem.*, **33**, 476 (1968); R. V. Stevens, C. G. Christensen, R. M. Cory, and E. Thorsett, *J. Am. Chem. Soc.*, **97**, 5940 (1975); R. V. Stevens, *Tetrahedron*, **32**, 1599 (1976); K.-C. Liu, B. R. Shelton, and R. K. Howe, *ibid.*, **45**, 3916 (1980).

8) A. I. Razumov and V. V. Moskva, *Zh. Obshch. Khim.*, **34**, 2589 (1964) and *Chem. Abstr.*, **70**, 140707a (1964).

9) V. Jäger and W. Schwab, *Tetrahedron Lett.*, **1978**, 3129.

10) V. Jäger and H. Grund, *Angew. Chem.*, **88**, 27 (1976) and *Liebigs Ann. Chem.*, **1980**, 80.

11) S. Shatzmiller, E. Shalom, R. Lidor, and E. Tartkovski, *Liebigs Ann. Chem.*, **1983**, 906.

12) M. Cinquini, F. Cozzi, and A. Gilardi, *J. Chem. Soc., Chem. Commun.*, **1984**, 551; R. Annunziata, M. Cinquini, F. Cozzi, and A. Restelli, *ibid.*, **1984**, 1253; R. Annunziata, M. Cinquini, F. Cozzi, and L. Raimondi, *ibid.*, **1985**, 403; R. Annunziata, M. Cinquini, F. Cozzi, A. Gilardi, and A. Restelli, *J. Chem. Soc., Perkin Trans. 1*, **1985**, 2289.

13) 3-Phenylthiomethyl-2-isoxazoline-5-carboxylic acid can be deprotonated with LDA (2 equiv) to generate the dianion which is then smoothly alkylated with aldehydes and alkyl halides (Our unpublished results). Accordingly the carboxylic acid derived from **7d** would be similarly utilized.

14) S. H. Andersen, N. B. Das, R. D. Jorgensen, G. Kjeldsen, J. S. Knudsen, S. C. Sharma, and K. B. G. Torssell, *Acta Chim. Scand.*, **B 36**, 1 (1982).

Reinvestigation of Base-Catalyzed Condensation of Ethyl α,α-Dichloroacetoacetate with Aldehydes. A New Synthesis of (±)-Disparlure

Sadao Tsuboi,* Hiroyuki Furutani, Akira Takeda, Kayoko Kawazoe,† and Sadao Sato†
Department of Synthetic Chemistry, School of Engineering, Okayama University, Tsushima, Okayama 700
†Analytical and Metabolic Research Laboratories, Sankyo Co. Ltd., Hiromachi-1, Shinagawa-ku, Tokyo 140
(Received February 5, 1987)

The titled reaction gave ethyl 2-chloro-2,3-epoxyalkanoates (**2**) and ethyl 3-chloro-2-oxoalkanoates in improved yields. The structure of the by-product was revised as 1,5-dichloro-4,8-dialkyltricyclo[5.1.0.0^{3,5}]octane-2,6-dione by means of the ^{13}C-^{1}H two-dimensional NMR spectrum and an X-ray crystallographic analysis. Compound **2** was applied to the synthesis of (±)-disparlure, the pheromone of the gypsy moth, in 49% overall yield via 6 steps.

As our continuing study on α-halo carbonyl compounds,[1] we have reported the reaction of ethyl α,α-dichloroacetoacetate (**1**) with aldehydes in the presence of sodium ethoxide.[2] This novel reaction involving a retro acetoacetate reaction[3] gave ethyl 2-chloro-2,3-epoxyalkanoate (**2**) or ethyl 3-chloro-2-oxoalkanoate (**3**) in low or moderate yields together with a small amount of crystalline by-products, one of which was identified as 2,5-bis(1-chloroalkylidene)-1,4-cyclohexanedione (**4′**).[2]

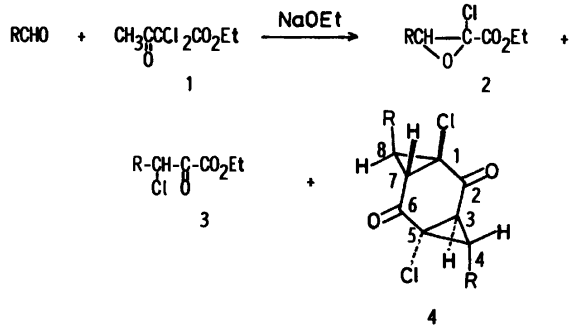

Recently, we reinvestigated this reaction in order to improve the yields of **2** and **3**; we also reexamined the structure of the by-product by means of the ^{13}C-^{1}H two-dimensional NMR spectrum and an X-ray crystallographic analysis. In the present paper we describe the results, which involve a revision of the previously assigned structure **4′** to 1,5-dichloro-4,8-dialkyltricyclo[5.1.0.0^{3,5}]octane-2,6-dione (**4**) as well as a highly stereoselective synthesis of the racemate of (+)-disparlure[(7*R*,8*S*)-7,8-epoxy-2-methyloctadecane] (**5**),[4] the pheromone of the gypsy moth.

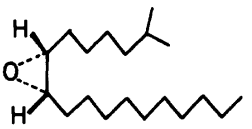

(+)-Disparlure **5**

When we carried out the present reaction under an absolutely dry conditions,[5] the yields of the products **2** and **3** (R=C_6H_5) were dramatically improved, as shown in Table 1, although the crystalline by-product

Table 1. Products from the Reaction of **1** with Aldehydes

No.	R	Yield[a,b]/% of **2** and/or **3**		Bp (θ_b/°C)/Torr[c] of **2** and/or **3**	Yield[a]/% of **4**
a	CH_3	**2a**	(30.4)		
b	C_2H_5	**2b**	73.9 (68.6)	115—130/2.5	**4b** 0 (6.1)
c	*n*-C_3H_7	**2c**	96.0	135/4	
d	$(CH_3)_2CH$	**2d**	83.2 (24.7)	130/2.5	**4d** 0 (3.7)
e	$(CH_3)_2CHCH_2$	**2e**	66.7	140/2	
f	*n*-C_6H_{13}	**2f**/**3f** (2/1)	54.7 (14.4)	200/3	**4f** 0 (7.9)
		2f	90[d]		
g	C_6H_5	**3g**	77.1 (16.4)	190/3	**4g** 0 (5.9)
		2g	100		
h	*n*-C_8H_{17}	**2h**	69.7[d]		
i	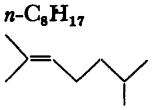	**2i**	80.7[d]		
j	*n*-$C_{10}H_{21}$	**2j**	73.6[d]	200/0.3	**4j** 5.5

a) Previously reported values[3] are given in parenthesis. b) Isolated yields by distillation unless otherwise indicated. c) Bath temperature of bulb-to-bulb tube oven. d) Isolated yield by column chromatography.

4 produced before[2] was not isolated. All of the reactions gave the epoxide **2** in good yields. The epoxides **2a—e** (R=CH_3, C_2H_5, n-C_3H_7, $(CH_3)_2CH$, $(CH_3)_2CHCH_2$) bearing small alkyl groups were thermally stable, while the epoxides (**2f** and **2g**) (R=n-C_6H_{13}, C_6H_5) bearing larger groups were isomerized to keto esters (**3f** and **3g**) by distillation via halo-epoxy rearrangement.[1a,b] On the other hand, the reaction of **1** with 3-methylbutanal in the presence of commercial, old sodium ethoxide gave **4e** (R=$(CH_3)_2CHCH_2$) in 4.8% yield besides **2e** (R=$(CH_3)_2CHCH_2$) (18%) and ethyl 2,2-dichloro-3-hydroxy-5-methylhexanoate (**6**) (30%). Similarly, the reaction of **1** with undecanal under the same conditions gave **2j** (R=n-$C_{10}H_{21}$) in 73.6% yield and **4j** (R=n-$C_{10}H_{21}$) in 5.65% yield. Measurement of the ^{13}C NMR spectra of **4** coupled with that of the heteronuclear ^{13}C-^1H chemical shift correlated spectrum (HETCOR), led us to assign all the carbon signals (Table 2). The result indicated that the structure of **4'** was incorrect owing to the absence of signals due to olefinic carbons.

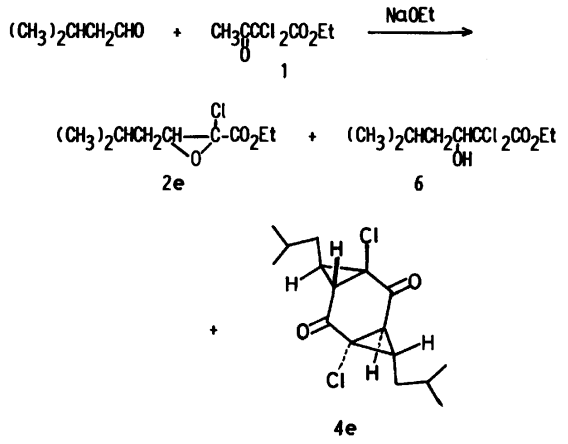

The structure of **4** was absolutely verified by a representative X-ray crystallographic analysis of **4b** (R=C_2H_5) to be 1,5-dichloro-4,8-diethyltricyclo[5.1.0.$0^{3,5}$]-octane-2,6-dione. ORTEP drawing in Fig. 1 illustrates the geometrical aspect of the molecule and explains the chemical structure reasonably. The molecule is located about a crystallographic center and the asymmetric unit contains half of the molecule.

Although the accurate mechanism is not clear, the formation of **4** can be explained by assuming intermediates **A**, **B**, C, and **D**. Aldol condensation product **A** between aldehydes and **1** would give an anion **C** via the intermediate **B**. Two molecules of the anion **C** would undergo a Michael addition each other to afford a cyclized product **D**. The subsequent double dehydrochlorinations of **D** would give the final product **4**.

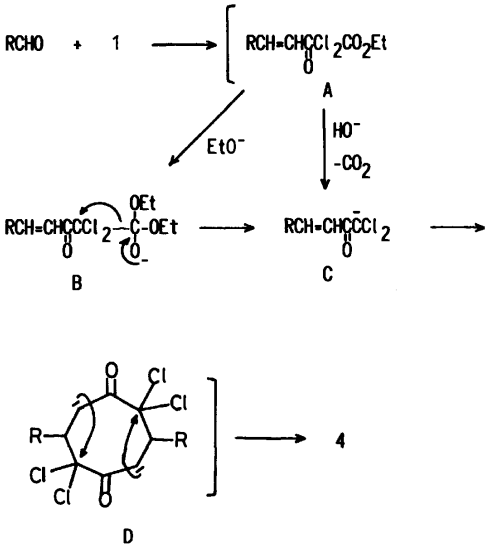

Furthermore, compound **2j** was utilized for the synthesis of the racemate of (+)-disparlure **5**. Since (±)-**5** and (+)-**5** are effective as an attractant against the harmful forest pest like gypsy moth, their syntheses

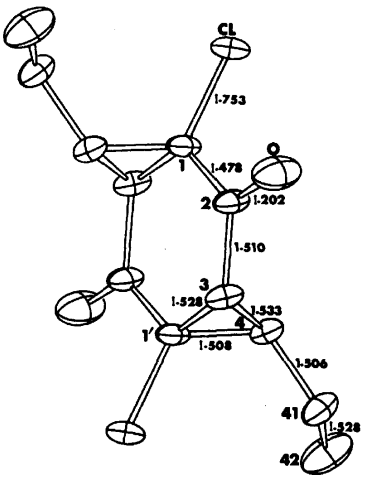

Fig. 1. ORTEP drawing of **4b**.

Table 2. ^{13}C NMR Data of **4**

No.	C-1	C-2	C-3	C-4	C-5	C-6	C-7	C-8	Others				
4b[a]	50.3	192.5	39.8	33.9	50.3	192.5	39.8	33.9	22.4	12.6			
4d[a]	50.4	192.2	39.6	39.3	50.4	192.2	39.6	39.3	30.0	21.5	21.2		
4e	50.3	192.7	39.8	32.8	50.3	192.7	39.8	32.8	31.5	28.7	28.1	22.5	14.0
4j	50.3	192.5	39.8	32.7	50.3	192.5	39.8	32.7	31.8	29.4	29.3	29.0	28.7
									28.1	22.6	14.0		

a) Prepared in the previous paper. See Ref. 2.

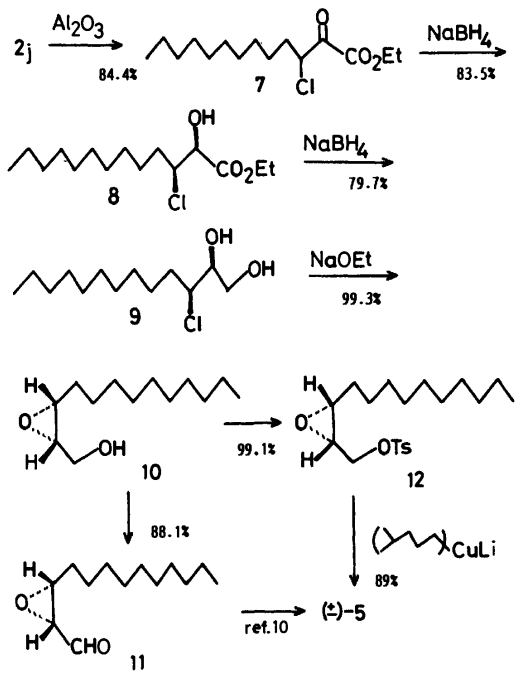

Scheme 1.

have been reported repeatedly to date.[6,7] Our synthetic sequence is shown in Scheme 1. A thermal treatment of **2j** with alumina in xylene induced a chlorocarbonyl rearrangement[1c] to give ethyl 3-chloro-2-oxotridecanoate (**7**) in 84.4% yield. Reduction of **7** with sodium borohydride in ethanol at 0°C afforded ethyl 3-chloro-2-hydroxytridecanoate (**8**) in 83.5% yield with high stereoselectivity (threo/erythro = 93/7). Purification of a stereoisomeric mixture with preparative HPLC afforded pure *threo*-**8**, which was reduced again with sodium borohydride at room temperature to give *threo*-3-chloro-1,2-tridecanediol (**9**) in 79.7% yield. Dehydrochlorination of **9** with sodium ethoxide in ethanol gave *cis*-2,3-epoxy-1-tridecanol (**10**)[8] in a quantitative yield. Reaction of **10** with tosyl chloride afforded tosylate **12** in 99.1% yield. Treatment of **12** with lithium bis(4-methylpentyl)cuprate(I) gave (±)-disparlure **5** in 89% yield. A total synthesis of (±)-**5** was established in 49% overall yield via 6 steps starting from **2j**. Furthermore, the oxidation of **10** with a Collins reagent afforded *cis*-2,3-epoxytridecanal (**11**) in 88.1% yield; this could be converted to (±)-**5** via a Wittig reaction and hydrogenation.[8]

Experimental

Melting and boiling points are uncorrected. Elemental analyses were carried out by Mr. Eiichiro Amano in our laboratory. Infrared (IR) spectra were obtained with a JASCO Model A-102 infrared spectrophotometer. ^{1}H NMR (100 MHz) and ^{13}C NMR spectra (25 MHz) were obtained with a JEOL JNM-FX100 apparatus, using $CDCl_3$ as a solvent. Two-dimensional NMR spectra were acquired on a Varian VXR 300 spectrometer operating at 300 and 75 MHz for ^{1}H and ^{13}C observation, respectively. Spectra were obtained for solutions in 5-mm NMR sample tubes in the ^{1}H-^{13}C switchable probe. Heteronuclear correlation spectra (HETCOR)[9] were run with the standard Varian 6.1-version software and obtained with sweep widths dictated by the appearance of the ^{13}C and ^{1}H spectra by using a 1024×512 data matrix and 128 increments in the first dimension.

Unless otherwise indicated, solvent (ether) was dried by distillation in the presence of sodium-benzophenone complex. Aldehydes were distilled prior to use.

Some representative examples of reactions of **1** with aldehydes are shown below.

Ethyl 2-Chloro-4-methyl-2,3-epoxypentanoate (2d) was prepared according to the procedure previously reported.[2] Sodium ethoxide was freshly prepared by dissolving sodium (250 mg, 11 mg-atom) in absolute ethanol (8 ml). After concentration of the solvent in vacuo, dry ether (50 ml) was added. To a stirred mixture was added dropwise ethyl α,α-dichloroacetoacetate (2.00 g, 10.1 mmol) at 0°C and then isobutyraldehyde (0.70 g, 0.9 ml, 9.5 mmol) was added dropwise. The mixture was stirred for 30 min at 0°C; it was then heated at the reflux temperature for 4 h, and poured into ice water. After the mixture was neutralized with 10% HCl, the organic materials were extracted with ethyl acetate. The combined extracts were washed with water and dried over $MgSO_4$. Removal of the solvent gave 2.01 g of an oil, which was distilled with bulb-to-bulb tube oven, giving 1.52 g (83.2%) of **2d**: Bp 130°C/2.5 Torr (1 Torr = 133.322 Pa). The IR and ^{1}H NMR data were consistent with those of an authentic sample.[2]

Reaction of 1 with 3-Methylbutanal. 1,5-Dichloro-4,8-diisobutyltricyclo[5.1.0.0^{3,5}]octane-2,6-dione (4e). Commercial sodium ethoxide (1.6 g, 24 mmol) in ether (50 ml) was added in several portions to a solution of **1** (4.0 g, 20.1 mmol) in dry ether (50 ml) with stirring at 0°C. The mixture was stirred for 10 min and then 3-methylbutanal (1.6 g, 2.0 ml, 19 mmol) was added dropwise. After being stirred for 30 min at 0°C and for 30 min at 25°C, the mixture was heated under reflux for 4 h and then poured into ice water. The mixture was neutralized with 10% HCl, and the organic materials were extracted with ethyl acetate. The combined extracts were washed with water, dried over $MgSO_4$, and concentrated. The residual oil containing crystals was filtered and washed with hexane to give 287 mg (4.8%) of **4e**: Mp 175—176°C (from hexane-ether); IR (KBr) 3050, 2960, 1699, 1285, 1100, and 875 cm^{-1}; ^{1}H NMR ($CDCl_3$) δ = 0.98 (d, 12H, J = 6 Hz, 2(CH_3)$_2$CH), 1.4—2.1 (m, 8H, 2(CH_3)$_2$CHCH_2CH<), and 2.23 (d, 2H, J=5.5 Hz, 2COCH). Found: C, 60.62; H, 7.14%. Calcd for $C_{16}H_{22}Cl_2O_2$: C, 60.57; H, 6.99%.

Concentration of the filtrate gave an oil which was chromatographed on SiO_2 (hexane-acetone, 20 : 1—2 : 1) to afford 2.07 g of a mixture of **2e**[1c] (18%) and **6** (30%): 1 : 2 ratio by ^{1}H NMR analysis; TLC (hexane-acetone, 5 : 1), R_f = 0.34.

Compound **6** was prepared independently by the reaction of ethyl dichloroacetate with 3-methylbutanal in the presence of commercial sodium ethoxide: 35% yield; bp 100—108°C/2 Torr; IR (neat) 3500, 1745 cm^{-1}; ^{1}H NMR (CCl_4) δ = 0.95 (d, 3H, J = 6 Hz, (CH_3)$_2$CH), 0.98 (d, 3H, J = 6 Hz, (CH_3)$_2$CH), 1.35 (t, 3H, J = 6.5 Hz, $CO_2CH_2CH_3$), 1.3—2.2

(m, 3H, $(CH_3)_2CHCH_2$), 3.0 (br. s, 1H, OH), 4.12 (t, 1H, J = 5 Hz, CHOH), and 4.26 (q, 2H, J=6.5 Hz, $CO_2CH_2CH_3$). Found: C, 44.16; H, 6.69%. Calcd for $C_9H_{16}Cl_2O_3$: C, 44.45; H, 6.63%.

Ethyl 2-Chloro-2,3-epoxytridecanoate (2j) and 1,5-Dichloro-4,8-didecyltricyclo[5.1.0.0^{3,5}]octane-2,6-dione (4j). A mixture of undecanal (3.40 g, 4.12 ml, 20 mmol) and ethyl α,α-dichloroacetoacetate (4 g, 20.1 mmol) in the presence of commercial sodium ethoxide (1.6 g, 24 mmol) was heated under reflux for 17 h, and then worked up. The crude products containing crystals were filtered and washed with hexane to give 536 mg (5.50%) of **4j**: Mp 93.5—94.0°C, IR (KBr) 1700, 1458, 1298, 1280, 1140, and 875 cm^{-1}; ^{1}H NMR ($CDCl_3$) δ=0.90 (br. t, 6H, J=5Hz, CH_3), 1.28 (m, 36H, 2(CH_2)$_8$), and 1.50—2.30 (m, 4H, 4 >CH-). Found: C, 69.46; H, 9.39%. Calcd for $C_{28}H_{46}Cl_2O_2$: C, 69.26; H, 9.55%.

Concentration of the filtrate gave an oil which was chromatographed on SiO_2 (hexane-acetone, 20 : 1) to afford 4.30 g (73.6% yield) of **2j**: TLC (hexane-acetone, 5 : 1), R_f=0.32; IR (neat) 1750, 1465, 1255, 1020, and 715 cm^{-1}; ^{1}H NMR (CCl_4) δ=0.90 (br. t, 3H, J=5 Hz, CH_3), 1.27 (m, 18H, (CH_2)$_9$), 1.30 (t, 3H, $CO_2CH_2CH_3$), 3.30 (m, 1H, >CH-O-CCl), and 4.25 (m, 2H, $CO_2CH_2CH_3$). Found: C, 61.90; H, 9.26%. Calcd for $C_{15}H_{27}ClO_3$: C, 61.95; H, 9.35%.

Compounds **2h** and **2i** were also obtained according to the same procedure as described above.

Ethyl 3-Chloro-2-oxoundecanoate (2h): IR (neat) 2950, 1750, 1470, 1255, 1030, and 870 cm^{-1}; ^{1}H NMR (CCl_4) δ=0.90 (br, t, 3H, J=5 Hz, CH_3), 1.30 (q, 3H, J=7 Hz, $CO_2CH_2CH_3$), 1.20—2.40 (m, 14H, (CH_2)$_7$), 3.25 (t, 1H, J =3 Hz, >CH-O-), and 4.20 (m, 2H, $CO_2CH_2CH_3$). Found: C, 59.61; H, 8.75%. Calcd for $C_{13}H_{23}ClO_3$: C, 59.42; H, 8.82%.

Ethyl 2-Chloro-5,9-dimethyl-2,3-epoxy-8-decenoate (2i): IR (neat) 2950, 1750, 1450, 1380, 1270, and 1030 cm^{-1}; ^{1}H NMR (CCl_4) δ=0.85—2.40 (m, 10H, (CH_2)$_2$-$CHCH_3CH_2$), 1.33 (t, 3H, J=7 Hz, $CO_2CH_2CH_3$), 1.56 (s, 3H, $(CH_3)_2C$=CH), 1.65 (s, 3H, $(CH_3)_2C$=CH), 3.35 (t, 1H, J=7 Hz, >CHO-), 4.25 (q, 2H, J=7 Hz, $CO_2CH_2CH_3$), and 5.05 (m, 1H, $(CH_3)_2C$=CH). Found: C, 61.33; H, 8.26%. Calcd for $C_{14}H_{23}ClO_3$: C, 61.20; H, 8.44%.

Ethyl 3-Chloro-2-oxotridecanoate (7) was prepared by the procedure reported previously.[4c] A mixture of **2j** (9.71 g, 33.4 mmol), alumina (10 g), and xylene (25 ml) was heated under reflux with stirring for 2 h. After filtration, the solvent was evaporated to give an oil which was chromatographed on SiO_2 (hexane-acetone, 20 : 1), giving 8.20 g (84.4%) of **7**: IR (neat) 2950, 1735, 1470, 1300, 1070, and 790 cm^{-1}; ^{1}H NMR (CCl_4) δ=0.90 (br. t, 3H, J=5.5 Hz, CH_3), 1.27 (m, 18H, (CH_2)$_9$), 1.38 (t, 3H, J=7 Hz, $CO_2CH_2CH_3$), 4.21 (q, 2H, J=7 Hz, $CO_2CH_2CH_3$), and 4.82 (t, 1H, J=6 Hz, CHCl). Found: C, 61.94; H, 9.12%. Calcd for $C_{15}H_{27}ClO_3$: C, 61.95; H, 9.36%.

Ethyl *threo*-3-Chloro-2-hydroxytridecanoate (8). To a stirred mixture of $NaBH_4$ (52 mg, 1.37 mmol) and dry ethanol (3 ml) was added a solution of **7** (1.19 g, 4.10 mmol) in dry ethanol (2 ml) at 0°C. The mixture was stirred for 10 min at 0°C, then poured into ice water and neutralized with dilute HCl. The organic materials were extracted with dichloromethane, washed with water, and dried over $MgSO_4$. Concentration of the solvent gave a crude product (1.23 g) which was chromatographed on SiO_2 (hexane-acetone, 10 : 1) to give 1.00 g (84%) of **8**: threo/erythro (93 : 7) by HPLC analysis [column, SA-I (6 mmϕ × 250 mm); eluent, hexane-ethyl acetate (10 : 1), 1.25 ml min^{-1}]. Preparative HPLC gave 603 mg of *threo*-**8**: R_t=13.5 min; IR (neat) 3430, 1745, 1465, 1270, and 1135 cm^{-1}; ^{1}H NMR (CCl_4) δ=0.86 (br. t, 3H, J=5 Hz, CH_3), 1.28 (br. s, 18H, (CH_2)$_9$), 1.30 (t, 3H, J=7 Hz, $CO_2CH_2CH_3$), 4.16 (m, 2H, CHCl-CHOH-), and 4.25 (q, 2H, J=7 Hz, $CO_2CH_2CH_3$). Found: C, 61.72; H, 9.92%. Calcd for $C_{15}H_{29}ClO_3$: C, 61.52; H, 9.98%. The component of R_t=21.6 min gave 64.4 mg of *erythro*-**8**: IR (neat) 3500, 1745, 1470, 1220, and 1130 cm^{-1}; ^{1}H NMR (CCl_4) δ=0.86 (br. t, 3H, J=5 Hz, CH_3), 1.28 (br. s, 18H, (CH_2)$_9$), 1.30 (t, 3H, J=7 Hz, $CO_2CH_2CH_3$), 4.16 (m, 2H, CHClCHOH), and 4.25 (q, 2H, J=7 Hz, $CO_2CH_2CH_3$). Found: C, 61.70; 9.85%. Calcd for $C_{15}H_{29}ClO_3$: C, 61.52; H, 9.98%.

***threo*-3-Chloro-1,2-tridecanediol (9).** To a stirred mixture of $NaBH_4$ (266 mg, 7.0 mmol) and absolute ethanol (6 ml) was added a solution of **8** (1.64 g, 5.61 mmol) in absolute ethanol (4 ml) at 0°C. The mixture was stirred for 5 h at room temperature, then poured into ice water and neutralized with dilute HCl. The organic materials were extracted with dichloromethane. The combined extracts were washed with water, dried over $MgSO_4$, and the solvent was evaporated. The residual oil (1.40 g) was chromatographed on SiO_2 (hexane-acetone, 3 : 1) to give 1.12 g (79.7%) of **9**: TLC (hexane-acetone, 3 : 1), R_f = 0.37; mp 60 — 60.5°C (from pentane); IR (KBr) 3260, 2920, 1461, 1040, 1009, 882, and 690 cm^{-1}; ^{1}H NMR (CCl_4) δ=0.90 (br. t, 3H, J=5.5 Hz, CH_3), 1.28 (br. s, 16H, (CH_2)$_8$), 1.5—2.7 (m, 4H, 2OH, CH_2CHCl), and 3.5—4.2 (m, 4H, $CHClCHOHCH_2OH$). Found: C, 62.36; H, 10.92%. Calcd for $C_{13}H_{27}ClO_2$: C, 62.26; H, 10.85%.

***cis*-2,3-Epoxy-1-tridecanol (10).**[8] Sodium (104 mg, 4.5 g-atom) was dissolved in 6 ml of absolute ethanol; a solution of **7** (1.01 g, 4.03 mmol) in absolute ethanol (4 ml) was added at 0°C. The mixture was stirred for 7 h at room temperature and then poured into ice water. After neutralization with dilute HCl, the organic materials were extracted with dichloromethane. The combined extracts were washed with water and dried over $MgSO_4$. The solvent was removed and the residual oil (1.12 g) was chromatographed on SiO_2 (hexane-acetone, 5 : 1), giving 856 mg (99.3%) of **10**: TLC (hexane-acetone, 3 : 1), R_f=0.30. Recrystallization from pentane gave 838 mg (97.2%) of **10**: mp 59.5—60.0°C (lit,[8b] 62.5—63.0°C for (−)-**10**; IR (KBr) 3500, 3400, 1461, 1103, 1027, 880, and 845 cm^{-1}; ^{1}H NMR ($CDCl_3$) δ=0.89 (br. t, 3H, J=5 Hz, CH_3), 1.05—1.95 (m, 19H, (CH_2)$_9$ and OH), 3.1 (m, 2H, -CH-CH-), and 3.73 (m, 2H, CH_2OH).

***cis*-2,3-Epoxytridecanal (11).**[8b] In a 50 ml two-necked flask was charged chromium trioxide (0.625 g, 6.25 mmol) and dried in vacuo under nitrogen. A solution of dry pyridine (1.97 g, 2 ml, 12.5 mmol) in dry CH_2Cl_2 (11 ml) was slowly added and the mixture was stirred for 30 min. After a solution of **10** (0.149 mg, 0.69 mmol) in dry CH_2Cl_2 (4 ml) was added dropwise, the mixture was stirred for 2.4 h and the organic materials were extracted with ether. The combined extracts were washed with 5% NaOH (10 ml), dilute HCl (10 ml), neutralized with aqueous $NaHCO_3$, washed with brine, and dried over $MgSO_4$. Evaporation of the sol-

vent gave 0.151 g of an oil which was chromatographed on SiO_2 (hexane-acetone, 15 : 1) to give 0.128 g (88.1 %) of **11**:[8b] IR (neat) 2950, 1730, 1470, and 840 cm^{-1}; ^1H NMR (CCl_4) $\delta = 0.86$ (br. t, 3H, $J = 5$ Hz, CH_3), 1.26 (m, 18H, $(CH_2)_9$), 3.15 (d, 2H, $J = 3.2$ Hz, >CH-O-CH<), and 9.30 (d, 1H, $J = 6.0$ Hz, CH=O).

2,3-Epoxytridecyl *p*-Toluenesulfonate (12). To 251 mg (1.32 mmol) of *p*-toluenesulfonyl chloride was added a solution of **10** (109 mg, 0.51 mmol) in pyridine (2 ml) at 0°C under an atmosphere of nitrogen. The mixture was stirred for 12 h and then poured into ice-water. The organic materials were extracted with ether. The combined extracts were washed with saturated $CuSO_4$, brine, and water successively, and dried over $MgSO_4$. Removal of the solvent gave 467 mg of an oil which was purified by preparative TLC (hexane-acetone, 3 : 1) to give 187 mg (99.1 %) of **12**: TLC (hexane-acetone, 3 : 1), $R_f = 0.33 - 0.46$: IR (neat) 2940, 1595, 1365, 1180, 1095, 970, 815, and 660 cm^{-1}; ^1H NMR (CCl_4) $\delta = 0.90$ (br. t, 3H, $J = 5$ Hz, CH_3), 1.30 (m, 18H, $(CH_2)_9$), 2.45 (s, 3H, $CH_3C_6H_4$), 2.70—3.15 (m, 2H, >CH-O-CH<), 4.03 (d, 2H, $J = 6$ Hz, CH_2OTs), 7.25 (d, 2H, $J = 8$ Hz, $CH_3C_6H_4$), and 7.73 (d, 2H, $J = 8$ Hz, $CH_3C_6H_4$). Found: C, 65.08; H, 8.76%. Calcd for $C_{20}H_{32}O_4S$: C, 65.18; H, 8.75%.

(±)-Disparlure (5). To a mixture of CuI (209 mg, 1.1 mmol) and dry ether (10 ml) was slowly added 2.3 ml (2.2 mmol) of 0.96 M 4-methylpentyllithium in ether at −22°C. After the mixture was stirred for 20 min at −20°C, a solution of **12** (76 mg, 0.21 mmol) in dry ether (4 ml) was added dropwise. The mixture was stirred for 20 min; then the ice bath was removed. After saturated NH_4Cl (15 ml) was added, the mixture was stirred for 30 min. The organic materials of the filtrate were extracted with ether three times and the combined extracts were washed with brine and dried over $MgSO_4$. Removal of the solvent gave 101 mg of an oil which was chromatographed on SiO_2 (hexane-acetone, 30 : 1) to afford 53 mg (89 %) of **5**: TLC (hexane-acetone, 3 : 1), $R_f = 0.81$. The IR and ^1H NMR data were identical with those of the literature.[7]

X-Ray Analysis of 4b. A crystal of dimensions 0.4×0.3×0.2 mm obtained from ethyl acetate-ether, was used for intensity measurement. Intensity data were obtained on a Rigaku AFC-5R diffractometer with graphite monochromatized Cu$K\alpha$ radiation, and using the $\theta - 2\theta$ scan technique ($2\theta \leqslant 128°$). The space group was approximated to be close to $P2_1/c$; however, a small number of very weak $0\,k\,0$ and $h\,0\,l$ reflections were observed for which $k \neq 2n$ and $1 \neq 2n$. The data were corrected for Lorentz and polarization effects but not for absorption. Among the 1014 unique reflection collected, 926 were considered to be observed at the 2.0 σ (F_o) level. Crystal data: $C_{12}H_{14}O_2Cl_2$, $Mr = 261.2$. Monoclinic, $P2_1/c$, $a = 6.858$ (1), $b = 9.630$ (3), $c = 9.307$ (4) Å, $\beta = 92.74$ (3)°, $U = 614.0$ Å^3, $Z = 2$, $Dx = 1.41$ g cm^{-3}. The structure was solved by direct method with MULTAN78 and refined by block-diagonal least-square methods. Positions of the hydrogen atoms were estimated from standard geometry. Final refinements with anisotropic temperature factors for the non-hydrogen atoms were reduced the R to 0.096.

The final atomic parameters, the full list of bond lengths and angles, and the F_o-F_c data have been deposited at the Chemical Sodiety of Japan (Document No. 8742).

We thank Mr. Shinichi Ninomiya for some experiments. We are grateful to Drs. Hajime Kato and Kazuhiko Kushida of Varian Instrument Ltd. for the measurement of two dimensional NMR spectra.

References

1) a) A. Takeda, S. Wada, and T. Uno, *Mem. School. Eng., Okayama Univ.*, **2**, 80 (1967). b) A. Takeda, S. Wada, M. Fujii, and H. Tanaka, *Bull. Chem. Soc. Jpn.*, **43**, 2997 (1970). c) S. Tsuboi, H. Furutani, and A. Takeda, *Synthesis*, **1987**, 292. d) A. Takeda, S. Tsuboi, and T. Hongo, *Bull. Chem. Soc. Jpn.*, **46**, 1844 (1973). e) A. Takeda, S. Tsuboi, and Y. Oota, *J. Org. Chem.*, **38**, 4148 (1973). f) A. Takeda, S. Tsuboi, and S. Sakai, *ibid.*, **39**, 2601 (1974).

2) A. Takeda, S. Tsuboi, and I. Nakashima, *Bull. Chem. Soc. Jpn.*, **48**, 1067 (1975).

3) S. K. Gupta, *J. Org. Chem.*, **38**, 4081 (1973).

4) B. A. Bierl, M. Beroza, and C. W. Collier, *Science*, **170**, 88 (1970).

5) In the previous paper, the solvent (ether) was dried over calcium chloride. The reaction was carried out under an atmosphere of air by using calcium chloride tube.

6) S. Iwaki, S. Marumo, T. Saito, M. Yamada, and K. Katagiri, *J. Am. Chem. Soc.*, **96**, 7842 (1974).

7) K. Mori and T. Ebata, *Tetrahedron*, **42**, 3471 (1986).

8) Optically active **10** is known although the spectral data is not reported: a) T. Katsuki and K. B. Sharpless, *J. Am. Chem. Soc.*, **102**, 5975 (1980); b) B. E. Rossiter, T. Katsuki, and K. B. Sharpless, *ibid.*, **103**, 464 (1981).

9) A. Bax and G. Morris, *J. Magn. Reson.*, **42**, 501 (1981).

Structure-Activity Relationship of a Heat-Stable Enterotoxin Produced by *Yersinia enterocolitica*†

Shoko YOSHIMURA, Yuji HIDAKA, Saburo AIMOTO, Yasutsugu SHIMONISHI,*
Tae TAKEDA,††,** Toshio MIWATANI,†† and Yoshifumi TAKEDA§
Institute for Protein Research, Osaka University, Yamada-oka 3-2, Suita, Osaka 565
††Research Institute for Microbial Diseases, Osaka University,
Yamada-oka 3-1, Suita, Osaka 565
§The Institute of Medical Science, The University of Tokyo, Shirokanedai, Minato-ku, Tokyo 108
(Received February 17, 1987)

Several shorter analogues of heat-stable enterotoxin (ST) produced by *Yersinia enterocolitica* were synthesized by a conventional method and their toxicities were examined by using suckling mice. The full enterotoxigenic activity of ST of *Y. enterocolitica* was found to be carried on a peptide, which consists of 13 amino acid residues from the 18th Cys to the C-terminal Cys and has a similar amino acid sequence to those of ST's produced by enterotoxigenic *Escherichia coli* (S. Aimoto et al., *Eur. J. Biochem.*, **129**, 257 (1982)) and *Vibrio cholerae* non-01 (T. Takao et al., *FEBS Lett.*, **193**, 250 (1985)). The results imply that the structural elements for expression of the toxicity are present in the common amino acid sequences of ST's of *Y. enterocolitica*, *E. coli*, and *V. cholerae* non-01.

Some strains of *Yersinia enterocolitica* produce a heat-stable enterotoxin that is responsible for gastroenteritis in children.[1,2] Recently, we isolated six molecular species of the enterotoxin (named *Yersinia*-ST) from the culture supernatant of the bacteria,[3,4] purified them to homogeneity by high-performance liquid chromatography (HPLC) and determined their amino acid sequences, as shown in Fig. 1. These peptides had a common sequence from Asp at position 15 from the N-terminus to the C-terminal residue, although their N-terminal sequences differed in length. This finding suggested that peptides 2—6 in Fig. 1 were not synthesized individually in the cells, but derived from peptide **1** by proteolytic cleavage in the cells or after excretion from the cells. The amino acid sequence of *Yersinia*-ST from the 18th amino acid residue from the N-terminus to the C-terminal residue was very similar to those of STI's of enterotoxigenic *Escherichia coli*.[5,6] However, in *Yersinia*-ST the C-terminal residue is Cys without the additional Tyr residue present in STI's of *E. coli*. Moreover, the N-terminal portion of the sequence of *Yersinia*-ST from the 17th residue is quite different from those of STI's of *E. coli*. The homology and differences in the primary structures of STI's of *E. coli* and *Yersinia*-ST suggest common biological properties of the two but differences in their degrees of activity and physicochemical properties. These observations raised the question of whether most, or all

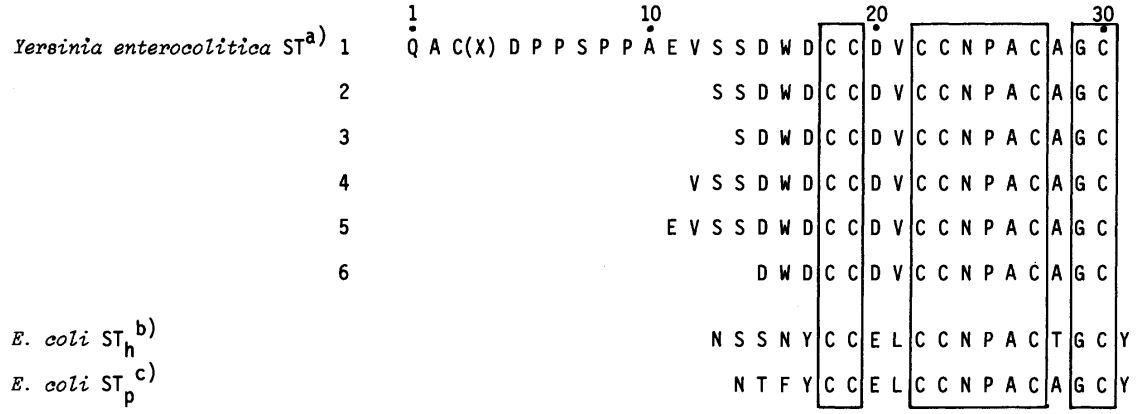

Fig. 1. Amino acid sequences of *Yersinia*-ST's and their comparison with those of ST_h and ST_p of enterotoxigenic *E. coli*. Amino acid residues in boxes are common to all sequences. a) Cited from Refs. 3 and 4. b) Cited from Ref. 5. c) Cited from Ref. 6. The single letter notations of amino acid residues are according to *J. Biol. Chem.*, **261**, 1 (1986).

† Part of this work was reported at the 21st Joint Conference on Cholera of the US-Japan Cooperative Medical Science Program at the National Institutes of Health, Oct. 21—23, 1985.

** Present address: National Children's Medical Research Center, Taishido, Setagaya-ku, Tokyo 154.

the toxicities of these ST's are due to the common sequence while the divergent sequences in the N-terminal and C-terminal regions merely represent the result of mutation, or whether these latter regions are responsible for the specific toxicities of the respective enterotoxins.

To elucidate the structure-activity relationship of *Yersinia*-ST, in this work we synthesized several shorter analogues of *Yersinia*-ST that had no N-terminal sequence or had an additional Tyr at the C-terminus, and examined their properties.

Experimental

The general and analytical methods used were as described previously.[7] All chemicals used for synthetic experiments were of reagent grade, while those used for analysis were of guaranteed grade and solvents were distilled before use. Carboxypeptidase B was obtained from Boehringer-Yamanouchi (Tokyo). A reversed-phase resin (YMC-ODS, S-5) was purchased from Yamamura Chemical Laboratories Co. (Kyoto) and packed in our laboratory into columns of 4×250 mm and 6×150 mm and 8×300 mm for analytical and preparative purposes. The abbreviations used in this paper are those recommended by the IUPAC-IUB [*J. Biol. Chem.*, **261**, 1 (1986)]. Additional abbreviations are: MBzl, *p*-methylbenzyl; TFA, trifluoroacetic acid; DMF, *N,N*-dimethylformamide; TEA, triethylamine; DMSO, dimethyl sulfoxide; HONSu, *N*-hydroxysuccinimide.

Peptide Synthesis. The protected linear peptides with the amino acid sequences of *Yersinia*-ST(16-30), *Yersinia*-ST(15-30), *Yersinia*-ST(14-30), Tyr^{31}-*Yersinia*-ST(18-30), and Thr^{28}, Tyr^{31}-*Yersinia*-ST(18-30) were synthesized according to the scheme shown in Fig. 2. Their experimental detail is described below.

Boc-Trp-Asp-Cys(MBzl)-Cys(MBzl)-Asp-Val-Cys(MBzl)-Cys(MBzl)-Asn-Pro-Ala-Cys(MBzl)-Ala-Gly-Cys(MBzl)-OBzl (1). Boc-Asp(OBu')-Cys(MBzl)-Cys(MBzl)-Asp-Val-Cys(MBzl)-Cys(MBzl)-Asn-Pro-Ala-Cys(MBzl)-Ala-Gly-Cys(MBzl)-OBzl[7] (0.42 g, 0.19 mmol) was dissolved in TFA (5 ml) and stirred at room temperature for 2 h. The solution was concentrated to a syrup, which was triturated in ether. The resulting powder was dissolved with Boc-Trp-ONSu (0.12 g, 0.28 mmol) in a mixture of DMF (1 ml) and 1-methyl-2-pyrrolidone (1 ml) and stirred at room temperature for 2 d. The solution was concentrated under reduced pressure to a solid, which was recrystallized from a mixture of EtOH and ether; 0.43 g (95.6%), mp 179—181 °C, $[\alpha]_D^{25}$ −38.0° (*c* 0.5, DMSO).

Found: C, 59.62; H, 6.41; N, 10.00; S, 8.00%. Calcd for $C_{119}H_{149}O_{23}N_{17}S_6 \cdot H_2O$: C, 59.66; H, 6.35; N, 9.94; S, 8.01%.

Z-Asp(OBu')-Trp-N_2H_3 (2). Z-Asp(OBu')-Trp-OMe[7] (2.62 g, 5.0 mmol) was dissolved in MeOH (100 ml) and mixed with 100% hydrazine hydrate (10 ml) in an ice-water bath. The mixture was stirred at room temperature for 2.5 h, concentrated under reduced pressure, and mixed with water. The resulting precipitate was recrystallized from a mixture of EtOH and ether; 1.8 g (68.7%), mp 195 °C (decomp), $[\alpha]_D^{20}$ −12.2° (*c* 1.0, DMF).

Found: C, 56.66; H, 6.73; N, 20.28%. Calcd for $C_{27}H_{33}O_6N_5 \cdot 3/2H_2O$: C, 56.72; H, 6.87; N, 19.60%.

Z-Asp(OBu')-Trp-Asp-Cys(MBzl)-Cys(MBzl)-Asp-Val-Cys(MBzl)-Cys(MBzl)-Asn-Pro-Ala-Cys(MBzl)-

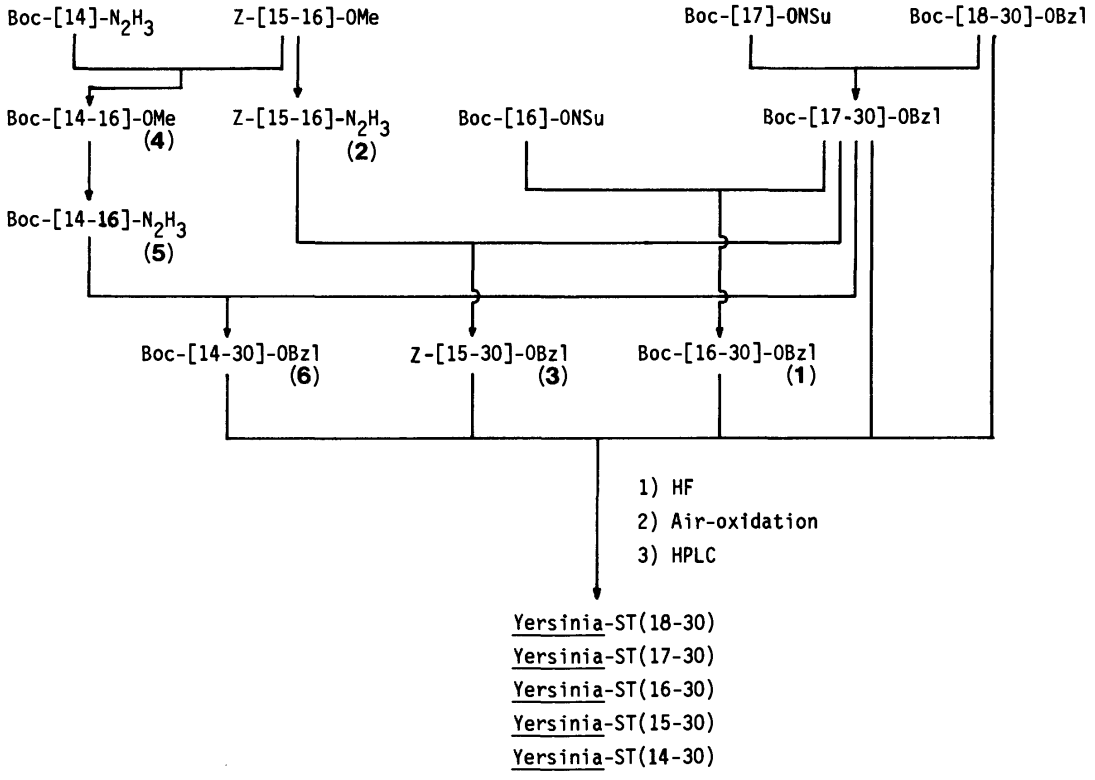

Fig. 2. Scheme for syntheses of shorter analogues of a heat-stable enterotoxin of *Y. enterocolitica*.

Ala-Gly-Cys(MBzl)-OBzl (3). Boc-Asp(OBu')-Cys-(MBzl)-Cys(MBzl)-Asp-Val-Cys(MBzl)-Cys(MBzl)-Asn-Pro-Ala-Cys(MBzl)-Ala-Gly-Cys(MBzl)-OBzl[7] (1.12 g, 0.5 mmol) was dissolved in TFA (10 ml) and stirred at room temperature for 2.5 h. The residue was triturated in ether. Meanwhile, compound **2** (0.31 g, 0.6 mmol) was dissolved in DMF (4 ml), cooled below −20 °C, and treated with 6.72 M HCl (1 M≒1 mol dm^{-3}) in dioxane (0.7 ml) and isopentyl nitrite (0.1 ml, 0.7 mmol) at −20 °C for 30 min. The solution was then mixed with the above powder and TEA (0.87 ml) and stirred at 0 °C for 1 d. The solid isolated from the reaction mixture was recrystallized from a mixture of EtOH, DMF, and ether; 1.1 g (85.3%), mp 194 °C (decomp), $[\alpha]_D^{25}$ −69.4° (*c* 0.5, DMSO).

Found: C, 59.35; H, 6.15; N, 10.09; S, 7.40%. Calcd for $C_{130}H_{160}O_{26}N_{18}S_6 \cdot 2H_2O$: C, 59.62; H, 6.31; N, 9.63; S, 7.33%.

Boc-Ser-Asp(OBu')-Trp-OMe (4). Z-Asp(OBu')-Trp-OMe[7] (3.93 g, 7.5 mmol) was dissolved in MeOH (150 ml) and hydrogenated at room temperature for 40 min over 5% palladium-charcoal in the presence of a solution of 6.72 M HCl in dioxane (1.2 ml). The catalyst was filtered off and the filtrate was concentrated to a syrup under reduced pressure. Meanwhile, Boc-Ser-N_2H_3 (1.98 g, 9.0 mmol) was dissolved in DMF (20 ml) and cooled below −20 °C. The chilled solution was treated with 6.72 M HCl in dioxane (3.5 ml) and isopentyl nitrite (1.4 ml, 11 mmol) at the same temperature for 25 min. The solution was mixed with a solution of the above syrup in DMF (15 ml) and TEA (4.34 ml) and stirred at 0 °C for 1 d. The precipitate was filtered off and the filtrate was concentrated under reduced pressure to a syrup, which was dissolved in ethyl acetate and washed with 0.2 M HCl, 5% aq $NaHCO_3$, and water. The washed solution was dried over anhydrous Na_2SO_4 and then concentrated to dryness; 4.32 g (100%).

Boc-Ser-Asp(OBu')-Trp-N_2H_3 (5). Compound **4** (4.32 g, 7.5 mmol) was dissolved in MeOH (150 ml) and mixed with 100% hydrazine hydrate (15 ml) under cooling. The solution was stirred at room temperature for 2 h and concentrated under reduced pressure to a syrup, which was crystallized from EtOH and ether; 3.4 g (79.1%), mp 200 °C (decomp), $[\alpha]_D^{20}$ −13.7° (*c* 1.0, DMF).

Found: C,53.16; H,7.64; N,18.99%. Calcd for $C_{27}H_{40}O_8N_6 \cdot N_2H_4 \cdot H_2O$: C, 53.27; H, 7.28; N, 18.41%.

Boc-Ser-Asp(OBu')-Trp-Asp-Cys(MBzl)-Cys(MBzl)-Asp-Val-Cys(MBzl)-Cys(MBzl)-Asn-Pro-Ala-Cys-(MBzl)-Ala-Gly-Cys(MBzl)-OBzl (6). Boc-Asp(OBu')-Cys(MBzl)-Cys(MBzl)-Asp-Val-Cys(MBzl)-Cys(MBzl)-Asn-Pro-Ala-Cys(MBzl)-Ala-Gly-Cys(MBzl)-OBzl[7] (0.99 g, 0.44 mmol) was dissolved in TFA (10 ml) and stirred at room temperature for 2 h. The solution was concentrated under reduced pressure to a syrup, which was triturated in ether. Meanwhile, compound **5** (0.32 g, 0.55 mmol) was dissolved in DMF (5 ml) and mixed with 6.72 M HCl in dioxane (0.87 ml) and isopentyl nitrite (0.78 ml, 0.6 mmol) below −20 °C. The mixture was stirred at the same temperature for 30 min, mixed with a solution of the above powder in DMF (10 ml), and stirred at 0 °C for 1 d. The mixture was concentrated to dryness under reduced pressure. The residue was washed with water and then recrystallized from EtOH and ether: 1.0 g (86.2%), mp 185 °C (decomp), $[\alpha]_D^{25}$ −55.4° (*c* 0.35, DMSO).

Found: C, 57.36; H, 6.11; N, 10.57; S, 7.28%. Calcd for $C_{130}H_{167}O_{28}N_{19}S_6 \cdot 4H_2O$: C, 57.63; H, 6.51; N, 9.83; S, 7.09%.

Boc-Cys(MBzl)-Cys(MBzl)-Asp(OBu')-Val-Cys-(MBzl)-Cys(MBzl)-Asn-Pro-Ala-Cys(MBzl)-Ala-Gly-Cys(MBzl)-Tyr-OBzl (7). Boc-Cys(MBzl)-Cys(MBzl)-Asn-Pro-Ala-Cys(MBzl)-Ala-Gly-Cys(MBzl)-Tyr-OBzl[8] (0.32 g, 0.2 mmol) was dissolved with anisole (0.07 ml) in TFA (2 ml) at 0 °C and stirred at room temperature for 50 min. The solution was concentrated under reduced pressure to a syrup, which was triturated in ether. Meanwhile, Boc-Cys(MBzl)-Cys(MBzl)-Asp(OBu')-Val-N_2H_3[7] (0.20 g, 0.25 mmol) was dissolved in DMF (2 ml) and cooled below −20 °C. The solution was treated with 6.72 M HCl in dioxane (0.14 ml) and isopentyl nitrite (0.04 ml) at −20 °C for 60 min. Then the mixture was mixed with *N*-methylmorpholine (0.2 ml) and a solution of the above powder in DMF (1 ml) and stirred at 0 °C for 6 d. The resulting precipitate was filtered off and the filtrate was concentrated under reduced pressure to a solid, which was washed with water and recrystallized from DMF and EtOH: 0.35 g (76.0%), mp 218—220 °C (decomp), $[\alpha]_D^{19}$ −55.6° (*c* 1.0, DMF).

Found: C, 61.03; H, 6.57; N, 9.27; S, 8.24%. Calcd for $C_{117}H_{151}O_{21}N_{15}S_6$: C, 61.20; H, 6.63; N, 9.15; S, 8.38%.

Boc-Cys(MBzl)-Cys(MBzl)-Asp(OBu')-Val-Cys-(MBzl)-Cys(MBzl)-Asn-Pro-Ala-Cys(MBzl)-Thr-Gly-Cys(MBzl)-Tyr-OBzl (8). Boc-Cys(MBzl)-Cys-(MBzl)-Asn-Pro-Ala-Cys(MBzl)-Thr-Gly-Cys(MBzl)-Tyr-OBzl[9] (1.64 g, 1.0 mmol) was treated with TFA (3.5 ml) and allowed to react with Boc-Cys(MBzl)-Cys(MBzl)-Asp-(OBu')-Val-N_3, which was prepared from Boc-Cys-(MBzl)-Cys(MBzl)-Asp(OBu')-Val-N_2H_3[7] (1.0 g, 1.2 mmol) according to the procedure described in **7**. The crude product was recrystallized from DMF and EtOH: 1.96 g (84.3%), mp 207.5—208.5 °C, $[\alpha]_D^{18}$ −46.5° (*c* 1.0, DMF).

Found: C, 60.76; H, 6.66; N, 8.89; S, 8.42%. Calcd for $C_{118}H_{153}O_{22}N_{15}S_6$: C, 60.93; H, 6.63; N, 9.03; S, 8.27%.

Removal of Protecting Groups and Air Oxidation. The protected peptides (Boc-Cys(MBzl)-Cys(MBzl)-Asp-(OBu')-Val-Cys(MBzl)-Cys(MBzl)-Asn-Pro-Ala-Cys-(MBzl)-Ala-Gly-Cys(MBzl)-OBzl,[7] Boc-Asp(OBu')-Cys-(MBzl)-Cys(MBzl)-Asp-Val-Cys(MBzl)-Cys(MBzl)-Asn-Pro-Ala-Cys(MBzl)-Ala-Gly-Cys(MBzl)-OBzl,[7] and compounds **1**, **3**, **6**, **7**, and **8**) (25 μmol) were each treated with anhydrous liquid hydrogen fluoride[10] and air-oxidized by the procedure described in Ref. 8. The solutions containing the deprotected and air-oxidized peptides were lyophilized and purified by HPLC, as described below.

High-Performance Liquid Chromatography (HPLC). The HPLC column was equilibrated with 10% CH_3CN in 0.05% TFA or 0.01 M ammonium acetate (pH 5.7) and after injection of the sample solution, was developed with a linear gradient of 10—40% CH_3CN with increase in CH_3CN concentration of 1% min^{-1} at a flow rate of 1 ml min^{-1}. Eluates were monitored for absorbance at 220 and 280 nm using a double-wavelength flow-through spectrophotometer.

Carboxypeptidase Digestion. The sample peptide (ca, 60 μg) was dissolved in 0.01 M pyridine acetate (pH 7.0) (50 μl) and mixed with carboxypeptidase B at a substrate; enzyme ratio (w/w) of 36 : 1. The solution was kept for 17 h at 37 °C and then the digested peptide was separated by HPLC.

Amino Acid Analysis and Fast Atom Bombardment

(FAB) Mass Spectrometry. The amino acid compositions and molecular weights of purified peptides were determined as described in a previous paper.[4]

Biological Assay. Toxicity was assayed in suckling mice of 2—4 d old as described previously.[11]

Heat Stability. The purified peptide was dissolved at a concentration of 200 μg ml^{-1} in 0.01 M phosphate buffered saline (pH 7.2), sealed in a capillary tube and heated for a given period at 100 or 120 °C. Then the solution was cooled in an ice bath and analyzed by HPLC, as described above.

Results and Discussion

Chemical Synthesis. To elucidate the structure-activity relationship of *Yersinia*-ST, in this work we tried to synthesize shorter analogues of *Yersinia*-ST with progressively fewer N-terminal amino acid residues or an additional Tyr residue at the C-terminus or with a replacement by Thr at position 28. In previous work,[7] we synthesized *Yersinia*-ST(13-30) (peptide **2** in Fig. 1), which has the sequence from the 13th residue from the N-terminus to the C-terminal residue, and found that the peptide had the same biological properties as those of the corresponding native peptide. This indicated that the procedure for synthesis of *Yersinia*-ST(13-30) is suitable for the syntheses of *Yersinia*-ST peptides. Therefore, we used this procedure for the syntheses of protected linear peptides **1**, **3**, and **6** which had 15, 16, and 17, respectively, of the amino acid residues in the C-terminal portion of *Yersinia*-ST as shown in Fig. 2. All the protecting groups in these protected peptides **1**, **3**, and **6** were removed by their treatment with anhydrous liquid hydrogen fluoride. Boc-[18-30]-OBzl and Boc-[17-30]-OBzl in Fig. 2, which were intermediates in the syntheses of **1**, **3**, and **6** and had 13 and 14 of the amino acid residues in the C-terminal region of *Yersinia*-ST, were also deprotected by treatment with hydrogen fluoride. The resulting free linear peptides were spontaneously oxidized by air in dilute solution (5×10^{-5} M) until no free mercapto groups were detectable.[12] All the *Yersinia*-ST peptides thus synthesized except *Yersinia*-ST(14-30) were obtained as main products by HPLC after deprotection and air-oxidation, suggesting that peptides with the same disulfide linkages as those

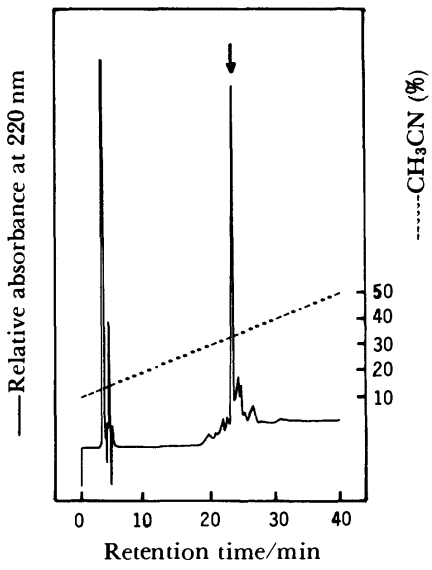

Fig. 3. HPLC profiles on a reversed-phase column (YMC-ODS S-5, 8×300 mm) of a deprotected and air-oxidized solution of compound **1**. The peak fraction marked by an arrow was separated as *Yersinia*-ST(16-30).

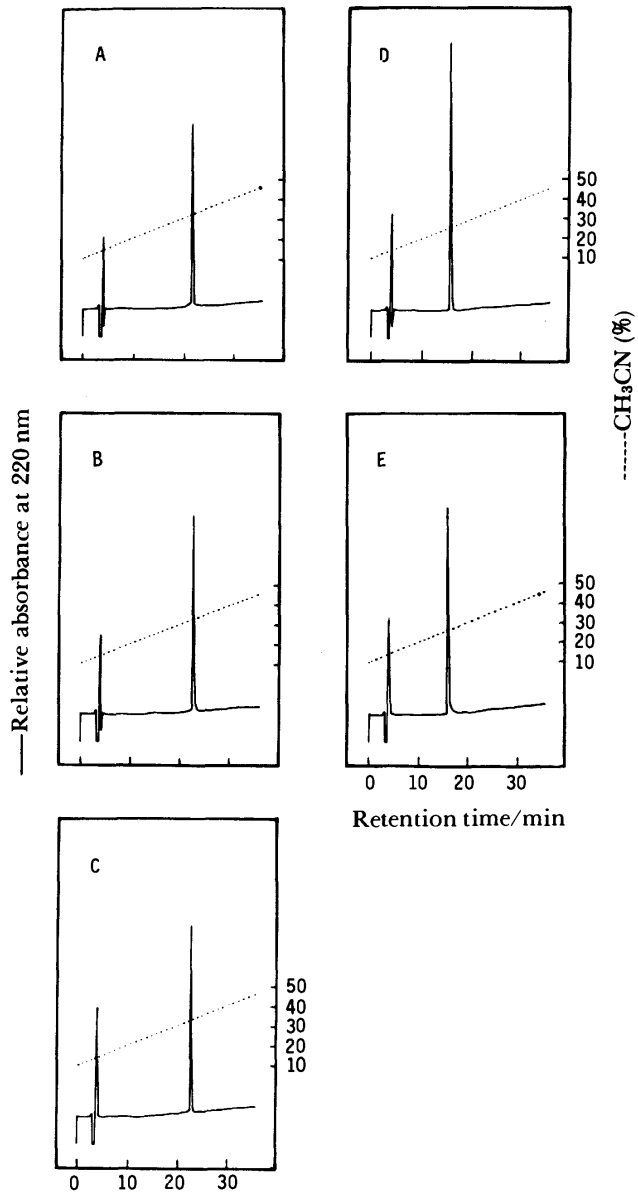

Fig. 4. HPLC profiles of purified synthetic *Yersinia*-ST peptides on a reversed-phase column (YMC-ODS S-5, 6×150 mm): A) *Yersinia*-ST(14-30); B) *Yersinia*-ST(15-30); C) *Yersinia*-ST(16-30); D) *Yersinia*-ST-(17-30); E) *Yersinia*-ST(18-30).

of native *Yersinia*-ST are thermodynamically most stable, as described below. Typical examples of the HPLC profiles of the air-oxidized products are shown in Fig. 3. *Yersinia*-ST(14-30) could be recovered by HPLC only as a minor peak, and it was very difficult to identify its peak on HPLC. Therefore, a deprotected and air-oxidized solution of synthetic *Yersinia*-ST(14-30) was coeluted with the corresponding native peptide (peptide **3** in Fig. 1), and in this way synthetic *Yersinia*-ST(14-30) was isolated. The low yield of *Yersinia*-ST(14-30) after deprotection and air-oxidation is probably due to various side-reactions in the deprotection, because the air-oxidized solution of *Yersinia*-ST(14-30) showed various unidentified peaks on an HPLC (not shown). The HPLC profiles of the purified synthetic peptides are depicted in Fig. 4.

The protected peptides with an additional Tyr residue at the C-terminal position (**7** and **8**) were also synthesized by the same way as that shown in Fig. 2. After treatment of **7** and **8** with hydrogen fluoride, the deprotected peptides were air-oxidized and purified by HPLC, to give Tyr^{31}-*Yersinia*-ST(18-30) and Thr^{28}, Tyr^{31}-*Yersinia*-ST(18-30), respectively (Fig. 5). Thr^{28}-*Yersinia*-ST(18-30) was prepared by digestion of Thr^{28}, Tyr^{31}-*Yersinia*-ST(18-30) with carboxypeptidase B. The amino acid compositions, mass values, and yields of the purified synthetic peptides are summarized in Table 1.

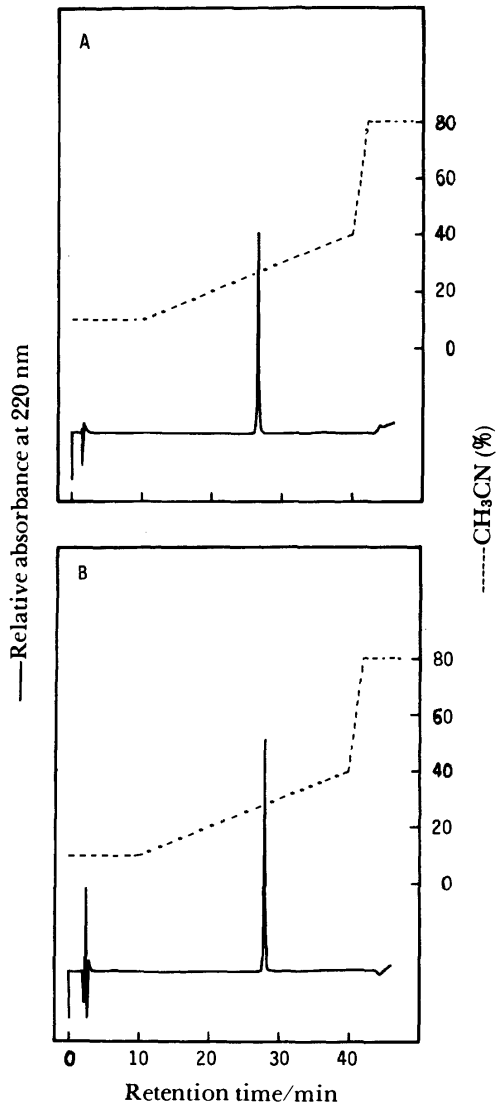

Fig. 5. HPLC profiles of A) purified Tyr^{31}-*Yersinia*-ST(18-30) and B) purified Thr^{28}, Tyr^{31}-*Yersinia*-ST-(18-30) on a reversed-phase column (YMC-ODS S-5, 4X250 mm).

Identification of Synthetic *Yersinia*-ST Peptides with Native Peptides. In a previous paper,[7] we presented evidence that synthetic *Yersinia*-ST(13-30) had the same structure as native peptide **2** in Fig. 1. To confirm that the *Yersinia*-ST peptides synthesized in this work had the same structure as native *Yersinia*-ST, we compared their retention times on HPLC with those of the corresponding native *Yersinia*-ST peptides. One-step Edman degradation of synthetic *Yersinia*-ST(13-30), which had the same structure as native *Yersinia*-ST(13-30),[7] gave a peptide with the same retention time on HPLC as synthetic *Yersinia*-ST(14-30). Synthetic *Yersinia*-ST(15-30) had the same retention time on HPLC as not only native peptide **3** in Fig. 1 but also *Yersinia*-ST(15-30), which was derived from synthetic *Yersinia*-ST(13-30) by digestion with aminopeptidase M. On HPLC synthetic *Yersinia*-ST(16-30) was eluted at the same position as preparations of *Yersinia*-ST(16-30) obtained both from synthetic *Yersinia*-ST(15-30) by the Edman reaction and from synthetic *Yersinia*-ST(17-30) by coupling with Boc-Trp-ONSu. Synthetic *Yersinia*-ST (18-30) was identical on HPLC with synthetic *Yersinia*-ST(17-30) degraded by the Edman reaction. Furthermore, digestions with carboxypeptidase B of synthetic Tyr^{31}-*Yersinia*-ST(18-30) and Thr^{28}, Tyr^{31}-*Yersinia*-ST(18-30), which were prepared from compounds **7** and **8**, gave *Yersinia*-ST(18-30) and Thr^{28}-*Yersinia*-ST(18-30), respectively. The former peptide was identical on HPLC with synthetic *Yersinia*-ST(18-30), which was obtained directly from Boc-[18-30]-OBzl, indicating that Tyr^{31}-*Yersinia*-ST(18-30) had the same structure as *Yersinia*-ST(18-30). A typical example of the correlation of the HPLC profiles of *Yersinia*-ST peptides with each other is shown in Fig. 6. These results demonstrate clearly that the synthetic *Yersinia*-ST peptides had the same structure as the native *Yersinia*-ST peptides. The correlations between these synthetic and native *Yersinia*-ST peptides are summarized in Fig. 7.

Biological Activity. The toxic activities of *Yersinia*-ST peptides synthesized in this paper were examined by the fluid accumulation test in suckling mice.[11] The minimum effective doses of *Yersinia*-ST(14-30), *Yersinia*-ST(15-30), *Yersinia*-ST(16-30), *Yersinia*-ST(17-30), and *Yersinia*-ST(18-30) were all be-

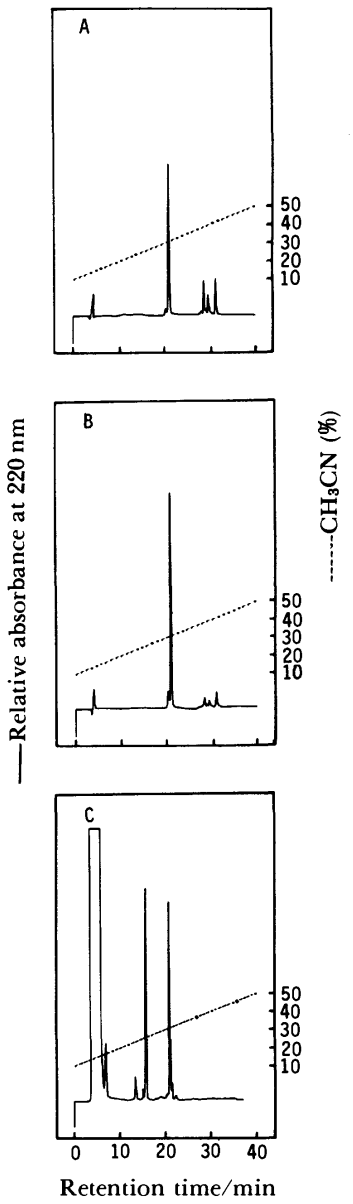

Fig. 6. HPLC profiles on a reversed-phase column (YMC-ODS S-5, 6×150 mm): A) synthetic *Yersinia*-ST(15-30) after one-step Edman degradation, B) a mixture of A) and synthetic *Yersinia*-ST(16-30), C) synthetic *Yersinia*-ST(17-30) after coupling with Boc-Trp-ONSu and removal of the Boc group.

tween 12.5 and 25 ng, as shown in Table 1, indicating that the N-terminal amino acid sequence from the 17th amino acid residue is not concerned in expression of the toxicities of *Yersinia*-ST. Namely, the enterotoxigenic activity of *Yersinia*-ST is carried on *Yersinia*-ST(18-30), which consists of 13 amino acid residues from the 18th Cys to the C-terminal Cys. This observation suggests that the divergency of the amino acid sequences in the N-terminal regions of ST's of *Y. enterocolitica* and *E. coli* is not related to their toxicities, but that the structural elements for expression of their toxicities are present in the commom amino acid sequences of ST's of *Y. enterocolitica* and *E. coli*.

Previously, we synthesized various analogues of ST's of enterotoxigenic *E. coli* and found that the minimum effective doses of their 13 amino acid peptides, which correspond to the sequence of *Yersinia*-ST from Cys at position 18 to the C-terminus, were 0.6 ng.[13] The activity of *Yersinia*-ST(18-30) was one-twentieth to one-thirtieth of those of *E. coli* peptides. The lower toxicity of *Yersinia*-ST(18-30) is considered to be due to the differences of amino acid residues in the common sequences of ST's of *Y. enterocolitica* and *E. coli*, that are at positions 20, 21, and 28 of *Yersinia*-ST(18-30).

The amino acid residue at position 28 is Ala in *Yersinia*-ST, but Thr in ST_h of *E. coli*, as shown in Fig. 1. To elucidate the effect of this amino acid residue on the biological activity of *Yersinia*-ST, we examined the activity of an analogue of *Yersinia*-ST(18-30), Thr^{28}-*Yersinia*-ST(18-30), in which Ala at position 28 is replaced by Thr. As shown in Table 1, Thr^{28}-*Yersinia*-ST(18-30) showed almost the same activity as *Yersinia*-ST(18-30). This result indicated that the toxicity of *Yersinia*-ST is not influenced by replacement of the amino acid residue at position 28 of *Yersinia*-ST by Thr.

The C-terminal amino acid residue, which is Tyr in ST's of *E. coli*, is not related to their toxicities.[13] Since this amino acid residue does not exist in *Yersinia*-ST, it was supposed that the addition of this residue to the C-terminus of *Yersinia*-ST would not effect the toxicity of *Yersinia*-ST. However, we synthesized two analogues of *Yersinia*-ST(18-30) with an additional Tyr at the C-terminus, Tyr^{31}-*Yersinia*-ST(18-30) and Thr^{28}, Tyr^{31}-*Yersinia*-ST(18-30), and found that these peptides had twice and four times the activity of *Yersinia*-ST(18-30), respectively. A monoclonal antibody (ST_h 8G7) raised against native ST_h of *E. coli* recognizes an epitope including the C-terminal Tyr residue of ST_h of *E. coli*, but does not react with synthetic analogues of ST_h lacking its C-terminal Tyr residue.[14,15] Synthetic *Yersinia*-ST peptides do not react with this monoclonal antibody over the range of their concentrations from 0.5 to 0.03 $\mu g\ ml^{-1}$ in an enzyme-linked immunosorbent assay system. However, Tyr^{31}-*Yersinia*-ST(18-30) and Thr^{28}, Tyr^{31}-*Yersinia*-ST(18-30) bind with this antibody. These results suggest that the addition of a Tyr residue to the C-terminus of *Yersinia*-ST(18-30) makes the tertiary structure around the Tyr residue in Tyr^{31}-*Yersinia*-ST(18-30) and Thr^{28}, Tyr^{31}-*Yersinia*-ST(18-30) somewhat similar to that of ST_h of *E. coli*, with resulting increase in toxicity.

The results discussed above imply that the lower toxicity of *Yersinia*-ST(18-30) than of ST_h(6-18) of *E. coli*, which consists of the sequence from position 6 to 18 in ST_h of *E. coli*, is mainly due to the difference in the amino acid residues at positions 20 and 21 of *Yersinia*-ST. In fact, a preliminary experiment showed

Table 1. Amino Acid Compositions[a], Mass Values[b], Yields, and Biological Activities[c] of Synthetic Peptides

	Yersinia-ST (14–30)	*Yersinia*-ST (15–30)	*Yersinia*-ST (16–30)	*Yersinia*-ST (17–30)	*Yersinia*-ST (18–30)	Tyr^{31}-*Yersinia*-ST (18–30)	Thr^{28}, Tyr^{31}-*Yersinia*-ST (18–30)	Thr^{28}-*Yersinia*-ST (18–30)
Asp	3.89(4)	3.84(4)	2.97(3)	3.14(3)	2.10(2)	1.99(2)	2.00(2)	1.97(2)
Thr							1.02(1)	0.97(1)
Ser	1.00(1)							
Pro	1.16(1)	0.99(1)	1.05(1)	1.18(1)	0.99(1)	1.22(1)	1.12(1)	0.96(1)
Gly	1.04(1)	1.05(1)	1.02(1)	0.91(1)	1.03(1)	1.01(1)	1.04(1)	1.05(1)
Ala	2.00(2)	2.00(2)	2.00(2)	2.00(2)	2.00(2)	2.00(2)	1.00(1)	1.00(1)
Cys	4.63(6)	4.34(6)	4.42(6)	4.56(6)	4.72(6)	4.83(6)	4.66(6)	4.54(6)
Val	0.73(1)	0.69(1)	0.71(1)	0.74(1)	0.67(1)	0.87(1)	0.67(1)	0.70(1)
Trp	0.83(1)	0.86(1)	0.94(1)					
Tyr						1.00(1)	0.98(1)	
$[M+H]^+$	1758.1 (1758.5)	1671.2 (1671.4)	1556.2 (1556.4)	1370.2 (1370.3)	1255.3 (1255.3)	1418.3 (1418.4)	1447.9 (1448.4)	1285.0 (1285.3)
Yield/%	0.5	8.3	6.5	8.0	11.8	10.3	14.2	85.8
MED/ng	25	25	25	12.5	12.5	6.25	3.12	12.5

a) Values were calculated as mol/mol of Ala; numbers in parentheses indicate theoretical values. b) $[M+H]^+$, mass value of quasi-molecular ion. c) MED, minimum effective dose.

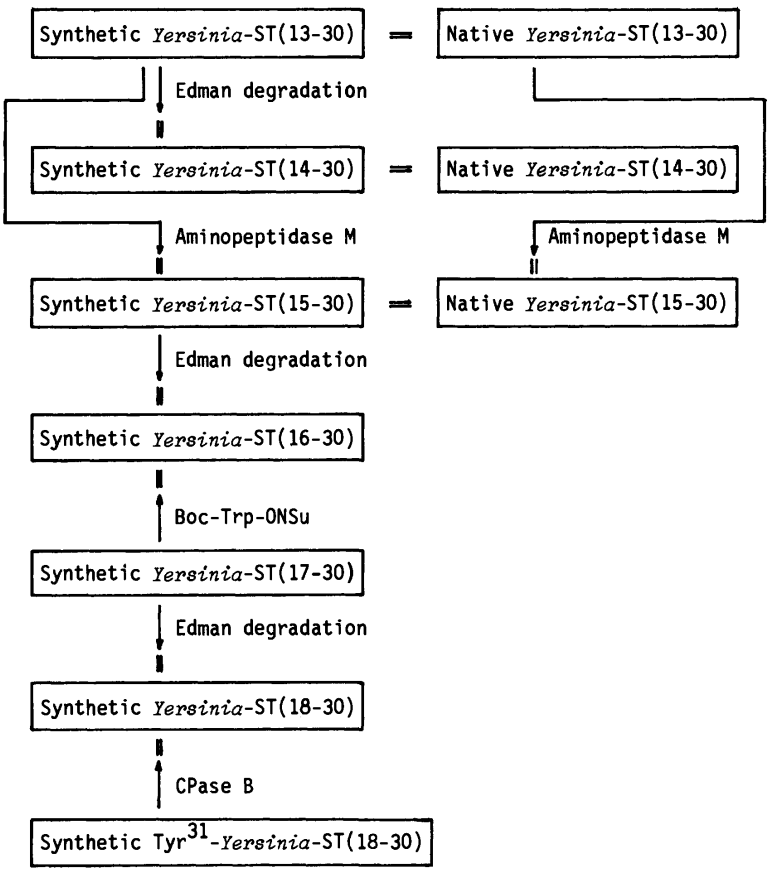

Fig. 7. Structural relationships of synthetic and native *Yersinia*-ST peptides.→=denotes that for example the reaction product of synthetic *Yersinia*-ST(13-30) obtained by Edman degradation is identical as judged by HPLC with synthetic *Yersinia*-ST(14-30).

that substitution of the amino acid residues at positions 20 and 21 in *Yersinia*-ST(18-30) by other amino acid residues influenced the toxicity, as will be reported elsewhere.

Heat Stability. Previously, a crude preparation of *Yersinia*-ST was found to be more heat-stable than a preparation of ST of *E. coli*.[6] In this work, to obtain detailed information about the heat-stability of *Yersinia*-ST peptides, we examined the heat-stabilities of synthetic shorter analogues. Figure 8 shows the HPLC profiles of synthetic *Yersinia*-ST(18-30) after its treatment at 100 and 120 °C for various times. After treatment at 100 °C for 30 min, the peak area of synthetic *Yersinia*-ST(18-30) on HPLC was reduced to about three-quarters of that of the untreated peptide. Under the same conditions the peak area of ST_h of *E. coli* is decreased drastically.[7] Furthermore, after heating at 100 °C for 60 min or at 120 °C for 10 min about two-thirds of the synthetic peptide remained unchanged, and on heating at 120 °C for 60 min the peptide was almost completely destroyed. This heat-stability of *Yersinia*-ST(18-30) was similar to that of synthetic *Yersinia*-ST(13-30) reported previously,[7] indicating that the N-terminal region from position 17 of *Yersinia*-ST does not affect its heat-stability.

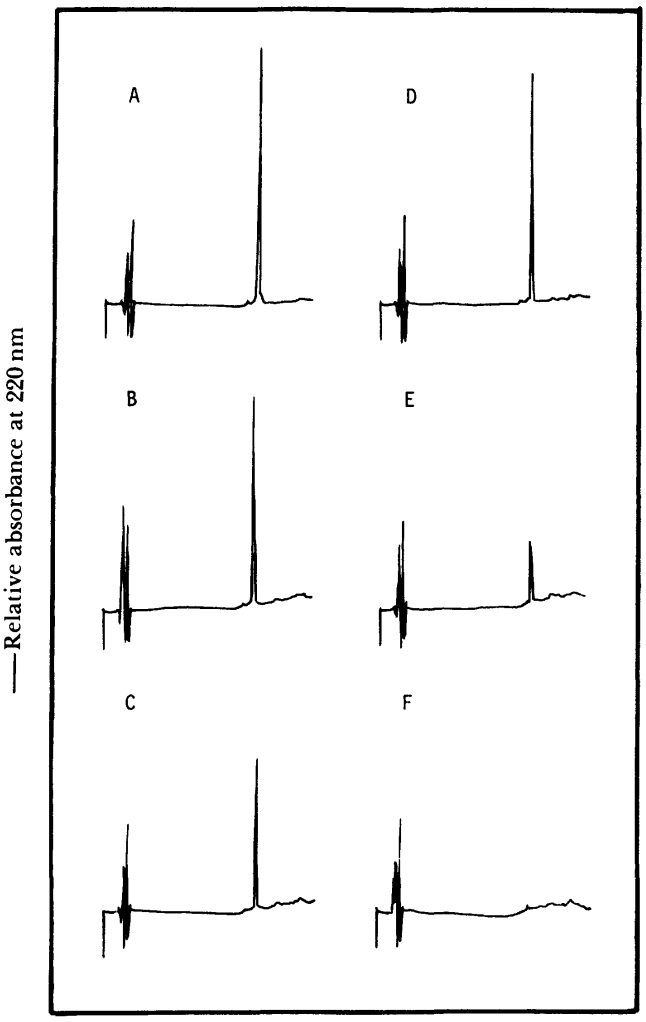

Fig. 8. HPLC profiles on a reversed-phase column (YMC-ODS S-5, 6×150 mm) of synthetic *Yersinia*-ST (18-30) treated under the following conditions: A) at 100 °C for 10 min, B) at 100 °C for 30 min, C) at 100 °C for 60 min, D) at 120 °C for 10 min, E) at 120 °C for 30 min, and F) at 120 °C for 60 min.

Recently, we reported that ST_h(6-19) of *E. coli*, which lacks the five N-terminal amino acid residues of ST_h of *E. coli*, has higher heat-stability than ST_h of *E. coli* with the whole amino acid sequences or ST_h(5-19) of *E. coli*, which lacks the four N-terminal amino acid residues of ST_h of *E. coli*.[7] These results imply that removal of the amino acid residues located at the N-terminal region from Tyr at position 5 results in increase of heat-stability of ST_h of *E. coli*. Moreover, the C-terminal Tyr residue is not related to the heat-stability of ST_h of *E. coli*, because ST_h(6-18) of *E. coli*, which lacks the C-terminal Tyr of ST_h(6-19) of *E. coli*, showed almost the same heat-stability as the latter.

The heat-stabilities of synthetic *Yersinia*-ST(13-30)[7] and *Yersinia*-ST(18-30) were higher than that of ST_h of *E. coli* and comparable with that of synthetic ST_h(6-19) of *E. coli*. Thus the degrees of heat-stability of heat-stable enterotoxins, in other words, the effects of heating in perturbation of their molecules, are due to differences in their N-terminal amino acid sequences.

This study was supported in part by a Grant-in-Aid for Scientific Research (No. 59340034 to Y. S.) from the Ministry of Education, Science and Culture. We are indebted to Mrs. Aiko Kobatake for elemental analysis and preparation of the manuscript.

References

1) J. Delorme, L. Michel, B. Martineau, and L. Lafleur, *Can. Med. Assoc. J.*, **11**, 281 (1974).

2) S. Kohl, J. A. Jacobson, and A. Nahmias, *J. Pediatr.*, **89**, 77 (1977).

3) T. Takao, N. Tominaga, Y. Shimonishi, S. Hara, T. Inoue, and A. Miyama, *Biochem. Biophys. Res. Commun.*, **125**, 845 (1984).

4) T. Takao, N. Tominaga, S. Yoshimura, Y. Shimonishi, S. Hara, T. Inoue, and A. Miyama, *Eur. J. Biochem.*, **152**, 199 (1985).

5) S. Aimoto, T. Takao, Y. Shimonishi, S. Hara, T. Takeda, Y. Takeda, and T. Miwatani, *Eur. J. Biochem.*, **129**, 257 (1982).

6) T. Takao, T. Hitouji, S. Aimoto, Y. Shimonishi, S. Hara, T. Takeda, Y. Takeda, and T. Miwatani, *FEBS Lett.*, **152**, 1 (1983).

7) S. Yoshimura and Y. Shimonishi, *Bull. Chem. Soc. Jpn.*, **58**, 2805 (1985).

8) S. Yoshimura, M. Miki, H. Ikemura, S. Aimoto, Y. Shimonishi, T. Takeda, Y. Takeda, and T. Miwatani, *Bull. Chem. Soc. Jpn.*, **57**, 125 (1984).

9) H. Ikemura, S. Yoshimura, S. Aimoto, Y. Shimonishi, S. Hara, T. Takeda, Y. Takeda, and T. Miwatani, *Bull.*

Chem. Soc. Jpn., **57**, 2543 (1984).
10) S. Sakakibara, Y. Shimonishi, Y. Kishida, M. Okada, and H. Sugihara, *Bull. Chem. Soc. Jpn.*, **40**, 2164 (1967).
11) Y. Takeda, T. Takeda, T. Yano, K. Yamamoto, and T. Miwatani, *Infect. Immun.*, **25**, 978 (1979).
12) G. L. Ellman, *Arch. Biochem. Biophys.*, **82**, 70 (1959).
13) S. Yoshimura, H. Ikemura, H. Watanabe, S. Aimoto, Y. Shimonishi, S. Hara, T. Takeda, T. Miwatani, and Y. Takeda, *FEBS Lett.*, **181**, 138 (1985).
14) W. Hemelhof, P. Retore, P. de Mol, J.-P. Butzler, T. Takeda, T. Miwatani, and Y. Takeda, *Lancet* i: 1011 (1984).
15) T. Takeda, T. Miwatani, S. Yoshimura, H. Watanabe, H. Ikemura, S. Aimoto, Y. Shimonishi, Y. Takeda, W. Hemelhof, and J.-P. Butzler, "Advances in Research on Cholera and Related Diarrheas," ed by S. Kuwahara and N. F. Pierce, **4**, in press (1986).
16) J. M. Boyce, D. J. Evans, Jr., D. G. Evans, and H. L. Dupont, *Infect. Immun.*, **25**, 532 (1979).
17) S. Aimoto, H. Watanabe, H. Ikemura, Y. Shimonishi, T. Takeda, Y. Takeda, and T. Miwatani, *Biochem. Biophys. Res. Commun.*, **112**, 320 (1983).

 © 1987 The Chemical Society of Japan Bull. Chem. Soc. Jpn., 60, 2491—2496 (1987)

Pyrolysis of Sulfoxide Bearing Electron-Withdrawing Substituents on β-Position in *S*-Ethyl Group of Ethyl Phenyl Sulfoxide

Toshiaki YOSHIMURA, Masaki YOSHIZAWA, and Eiichi TSUKURIMICHI*
Department of Industrial Chemistry, Faculty of Engineering, Toyama University, Gofuku, Toyama 930
(Received October 24, 1986)

In order to obtain information concerning the reaction mechanism of the pyrolysis of a sulfoxide bearing an electron-withdrawing substituent on the β-position in the *S*-ethyl group of ethyl phenyl sulfoxide, 2-(substituted phenyl)ethyl aryl sulfoxides(**1**) and 2-cyanoethyl (substituted phenyl) sulfoxides(**2**) were pyrolyzed. The rate-enhancing effect of the β-phenyl group of **1** was small. The activation enthalpy and entropy of **1** were found to be 110 kJ mol^{-1} and -45 JK^{-1} mol^{-1}, respectively. Hammett plots for **1** gave positive trends for the substituents, both on the β-phenyl group (ρ=0.76) and on the *S*-phenyl group (ρ=0.32), though the ρ-value of the latter was about half of the former. On the other hand, the Hammett plot for **2** did not give a straight line, but a concave curve in which a series of substituents from the *p*-OCH_3 to *p*-Cl groups gave a negative trend (ρ=$-$0.49), while the *p*-NO_2 group afforded a positive trend. The pyrolytic rate of **2** was found to be about 23-times faster than that of **1** at 100 °C. The kinetic isotope effect for β-position hydrogen in the β-phenylethyl group of **1** was considerably large (k_H/k_D=4.3). From the obtained results, it was suggested that the pyrolysis of **1** and **2** proceeds via a nearly carbanion-like mechanism in a five-membered cyclic transition state.

Sulfoxides having at least one hydrogen atom on the β-position carbon in the *S*-alkyl group are easily decomposed to give olefins, like *N*,*N*-dimethyl-2-phenylethylamine oxide,[1] at relatively lower temperatures than those in the pyrolysis of xanthates, i.e., a Chugaev elimination reaction.[2] From studies on the pyrolysis of various sulfoxides, it has been suggested that the reaction proceeds through a five-membered cyclic transition state:[6] That is, a concerted cis-elimination process, like a Cope reaction.[1,8] Three types of the Ei reaction mechanisms (an ideal cis-concerted[3] (i.e., the electron-delocarized state), an El-like[4,5] and a radical pair[6] process) have been observed in the pyrolysis of various sulfoxides of different molecular structures. For example, Emerson et al.[3] concluded that the pyrolysis of *s*-butyl propyl sulfoxide proceeds via an ideal concerted mechanism from observations of the product distribution. In contrast, phenyl propyl sulfoxide[4] and phenyl *t*-butyl sulfoxide[5] are considered to decompose thermally via an El-like process from observations of Hammett substituent effects.

On the other hand, Kingsbury and Cram[6] found that a stereospecific cis-elimination of 1,2-diphenylpropyl phenyl sulfoxides (**7**) is accompanied by a concomitant radical C-S bond cleavage. It is of interest to determine the mechanism regarding the pyrolysis of the sulfoxide bearing an electron-withdrawing group on the β-position in the *S*-ethyl group of ethyl phenyl sulfoxide; this has not yet been investigated kinetically.

Thus, 2-(substituted phenyl)ethyl phenyl sulfoxides (**1**) and 2-cyanoethyl (substituted phenyl) sulfoxides (**2**) were prepared and subjected to pyrolysis. In the present paper, we give a detailed account of a kinetic study of the pyrolysis of the reaction system as well as a possible mechanism.

Results and Discussion

Reaction Products. Pyrolysis was carried out by heating a solution of the sulfoxide in dioxane in a sealed tube in a thermostat adjusted to within the range ± 0.05 °C of the desired temperature. Though the reaction products were not actually isolated, the products were identified by comparing their HPLC and GLPC with those of authentic samples. Thus, under these reaction conditions, the resultant products were found to be both substituted styrene (**3**) and substituted diphenyl disulfide (**4**); **2** produced both **4** and acrylonitrile (**5**). The disulfide **4** is probably formed via an initial formation of arenesulfenic acid followed by a dimerization process.[14,15]

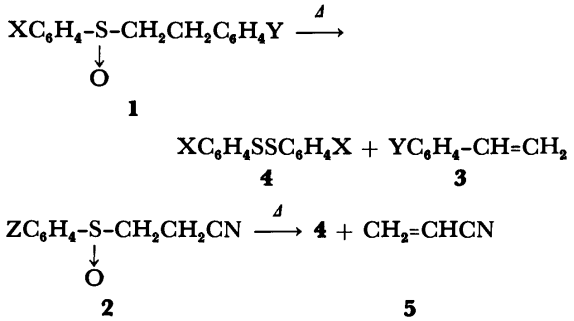

The NMR spectra of the product mixtures that resulted from the pyrolysis of sulfoxides **1** and **2** in CCl_4 in sealed tubes at 100 °C showed that the yields of **3** and **5** are nearly quantitative.

Kinetics. Kinetic measurements were carried out by following the intensity of the UV absorption (254 nm) by means of HPLC. In order to obtain pyrolytic information concerning the sulfoxide bearing a stronger electron-withdrawing group than the phenyl group

Table 1. The Kinetic Data for Pyrolysis of 2-Arylethyl Aryl Sulfoxides(**1**) and 2-Cyanoethyl Aryl Sulfoxides(**2**)

XC_6H_4-S(O)-$CH_2CH_2C_6H_4Y$ (**1**)

Sulfoxide X	Sulfoxide Y	Temp °C	Rate constant[a] $k\times10^5$ s^{-1}	
H	*p*-OCH_3	120.0	5.54±0.12	
H	*p*-CH_3	120.0	6.34±0.87	
H	*m*-CH_3	120.0	7.56±0.15	
H	H	100.0	1.41±0.03	$\Delta H^{\ddagger}=(110\pm3)$ kJ mol^{-1}
H	H	110.0	3.65±0.13	$\Delta S^{\ddagger}=(-45\pm9)$ J K^{-1} mol^{-1}
H	H	120.0	10.5 ±0.3	(at 100 °C)
H	H	130.0	22.3 ±0.3	
H	H	140.0	46.6 ±2.2	$\rho_X=+0.32$ ($\gamma=0.963$)
H	*p*-Cl	120.0	11.2 ±0.3	
H	*p*-NO_2	120.0	36.0 ±0.3	$\rho_Y=+0.76$ ($\gamma=0.987$)
p-CH_3	H	120.0	8.14±0.16	
m-CH_3	H	120.0	10.6 ±0.2	
p-Cl	H	120.0	11.1 ±0.6	
p-NO_2	H	120.0	18.2 ±0.2	
PhS(O)CH_2CD_2Ph		120.0	2.46±0.04	$k_H/k_D=4.3$

ZC_6H_4-S(O)-CH_2CH_2CN (**2**)

Z	Temp °C	$k\times10^4$ s^{-1}	
p-OCH_3	100.0	5.03±0.53	
p-CH_3	100.0	4.38±0.17	
H	100.0	3.30±0.22	
p-Cl	100.0	2.92±0.15	$\rho_Z=-0.49$ ($\gamma=0.971$)[b]
p-NO_2	100.0	4.96±0.20	

a) The rate constants were calculated by the least-squares method and the errors are standard diviations. b) The datum for *p*-nitro derivative is not included in calculation.

on the β-position, **2** was also subjected to pyrolysis. The reaction rates of the sulfoxides were all correlated in a fine manner with a first-order equation with respect to the concentration of the substrate.

The kinetic data obtained are summarized in Table 1.

An Arrhenius plot for 2-phenylethyl phenyl sulfoxide afforded a good straight line; the activation enthalpy (110 kJ mol^{-1}) and a considerably small activation entropy (−45 J K^{-1} mol^{-1}) were obtained. A comparison of the pyrolytic rate of **1** to that of other sulfoxides are listed in Table 2.

The pyrolytic rate of 2-cyanoethyl phenyl sulfoxide (**2**) was found to be 200-times faster than that of ethyl phenyl sulfoxide (**6**), while that of **1** was only 8-times faster than that of **6**. This finding reveals that the rate-enhancing effect of the β-phenyl group in the reaction system is rather small.

Kinetic Isotope Effect. The kinetic isotope effect using 2-phenylethyl-2,2-d_2 phenyl sulfoxide was measured and the effect was found to be $k_H/k_D=4.3$ (120 °C). The large kinetic isotope effect apparently reveals that the reaction process involves C-H bond breaking in a rate-determining step.

Table 2. The Relative Rates of Pyrolysis of Sulfoxides at 100 °C in Dioxane

Sulfoxide	Rate constant $k\times10^5$ s^{-1}	Relative rate
PhS(O)CH_2CH_3	0.165	1
PhS(O)$CHCH_3$ (threo)	43.5	264
Ph (erythro)	83.9	508
PhS(O)CH_2CH_2Ph	1.41	8.55
PhS(O)CH_2CH_2CN	33.0	200

The magnitude of the effect is larger than those for the pyrolysis of heptyl-2-*d* phenyl sulfoxide ($k_H/k_D=2.9$)[10] and *cis*- and *trans*-*N*,*N*-dimethylcyclooctyl-2-

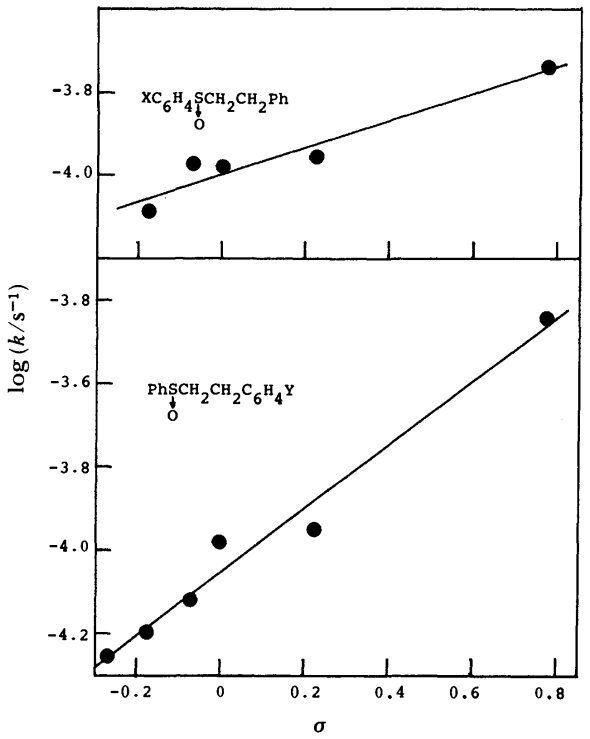

Fig. 1. Hammett relations for the pyrolysis of 2-(substituted phenyl)ethyl phenyl sulfoxides and 2-phenylethyl (substituted phenyl) sulfoxides (**1**).

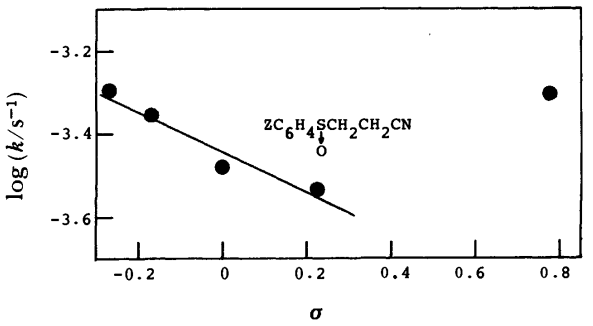

Fig. 2. Hammett relation for the pyrolysis of 2-cyanoethyl (substituted phenyl) sulfoxides (**2**).

Table 3. Solvent Effect on Pyrolysis of 2-Phenylethyl Phenyl Sulfoxide at 120 °C

Solvent	Dielectric constant	Rate constant $k\times10^5$ / s^{-1}	Relative rate
Dioxane	2.21	10.5 ±0.3	1
Benzene	2.27	9.00±0.34	0.86
DMSO	48.9	6.02±0.22	0.57
Acetonitrile	37.5	4.13±0.08	0.39
Ethanol	24.3	1.73±0.08	0.16

d-amine oxide ($k_H/k_D = 3.5$) in benzene,[7] which proceed via a five-membered cyclic transition state.[8]

Substituent Effect. The substituent effects for the pyrolysis of **1** and **2** were studied in dioxane. Figure 1 shows Hammett plots for **1** with both β-aryl and *S*-aryl substituents at 120 °C.

As is apparent from Fig. 1, log *k* nicely correlates with σ-values, showing a positive trend for both the X-side ($\gamma = 0.96$) and the Y-side ($\gamma = 0.99$). The ρ-value for the Y-side was +0.76, while that for the X-side ($\rho = +0.33$) was only about half of the Y-side. Thus, in the pyrolysis of **1**, electron-withdrawing substituents are apparently more favorable than electron-releasing types. On the other hand, the Hammett relation for **2** did not afford a straight line, but a concave curve in which a series of the substituents from the *p*-OCH_3 to *p*-Cl groups gave a negative trend ($\rho = -0.49$, $\gamma = 0.97$), while the *p*-NO_2 group, as a strong electron-withdrawing substituent, afforded a positive trend. The effect for **2** is shown in Fig. 2.

It appears at first sight that, due to the negative trend, that pyrolysis proceeds via another mechanism than that for **1**. However, since the effect corresponding to that of X-substituents in **1** is small, the pyrolysis mechanism should also be the same as that for **1**. The result of a Hammett relation for **2** together with the behavior of the *p*-NO_2 substituent will be discussed later.

Solvent Effects. Pyrolysis was carried out in five kinds of solvents; the obtained rate constants are summarized in Table 3. The pyrolysis was not much affected by solvent change. Though it seems that an increase in the solvent polarity tends to cause a retardation of pyrolysis, the rates of pyrolysis are not correlated to the dielectric constants and the effect is small. This indicates that the transition state of the reaction is not ionic. This observation is similar to those for the pyrolysis of sulfilimines[11] and sulfoxides **7**,[6] except for reactions in protic solvents. The small decrease in the rate for reactions in dipolar aprotic solvents is interpreted in view of the more solvation in the starting state by a dipole-dipole interaction than in the transition state. Meanwhile, a large rate retardation in the pyrolysis of sulfoxides and sulfilimines in protic solvents has been shown.[8] Kingsbury and Cram reported that the pyrolysis of sulfoxide **7** in methanol is 1000-times slower than that in dioxane.[6] Though the rate difference in both solvents is not so large, hydrogen-bonding to the sulfoxide oxygen in the starting state apparently prevents pyrolysis. Recently, we demonstrated the effect of hydrogen-bonding in the pyrolysis of aryl ethyl sulfilimines in protic solvents.[16]

From the above results the following conclusion can be obtained. In the first place, the considerably large β-hydrogen kinetic isotope effect rules out a radical pair mechanism, since the free radical mechanism involving the rate-determining C-S bond cleavage is not in accord with the large kinetic isotope effect.

Secondarily, an E1-like mechanism is also ruled out because of the positive ρ-value for Y-substituents and the small ρ-value for X-substituents. For example, recently it has been found that the pyrolysis of 1-phenylethyl phenyl sulfoxide, which has been revealed to proceed via an E1-like mechanism, gives relatively large positive ρ-values for *S*-phenyl substituents and negative ρ-values for electron-releasing substituents on 1-phenyl group.[9]

Oae et al.[11] proposed that the pyrolysis of *S*-(1- and 2-phenylethyl)-*S*-phenyl-*N*-tosylsulfilimines proceeds via an E1-like cis-concerted mechanism in view of the following results: A small kinetic isotope effect ($k_H/k_D=2.9$), a substituent effect of the opposite relation giving a positive ρ-value for *S*-aryl substituents against a negative one for 1-aryl substituents, a large rate acceleration by α-phenyl group and a small rate-enhancing effect of β-phenyl group [$k_{Ph}/k_H=2000$ for $PhS(NTs)CH(R)CH_3$, $k_{Ph}/k_H=1.5$ for $PhS(NTs)-CH_2CH_2R$ (R=H and Ph)].

However, in system **1**, the substituent effect on the β-phenyl group gave a positive Hammett correlation in both ρ_Y and ρ_X; also, the kinetic isotope effect for β-hydrogen gave a large value. Thus, the present data suggest that the pyrolysis of both **1** and **2** proceed via a nearly carbanion-like internal concerted cis-elimination.

The small rate-enhancing effect of the β-phenyl group might reveal that pyrolysis proceeds via an E1-like mechanism, since some E2 reactions[12] and Cope eliminations,[13] which are presumed to proceed via a nearly carbanion like mechanism, show large rate-enhancements by the β-phenyl group.[12,13] For the above reason, the small enhancement effect appears to be somewhat inconsistent with the nearly carbanion like mechanism; however, it may be explaind as follows. In general, the pyrolysis of the alkyl aryl sulfoxides tends to proceed, essentially, via an E1-like mechanism, which should give a positive Hammett ρ-value in the substituent effect on the *S*-phenyl group. On the other hand, in the nearly carbanion-like mechanism, the basicity of a sulfoxide-oxygen atom should affect the rate of the reaction giving a negative Hammett ρ-value for the substituent effect on the *S*-phenyl group. In the pyrolysis of **1** the ρ-value still shows a positive trend like other sulfoxides,[4] though the trend becomes considerably small. This small positive ρ-value is attributed to the substituent effect on the *S*-phenyl group being more susceptible to C-S bond cleavage than proton abstraction. In other words, the 2-phenyl group as a relatively weak electron-withdrawing substituent is insufficient to give a negative trend in the Hammett relation for *S*-phenyl substituents.

Therefore, the sulfoxide bearing a stronger electron-withdrawing group at the β-position can be expected to give a negative Hammett ρ-value. Thus, the

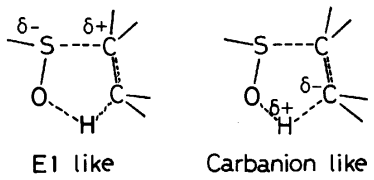

Fig. 3. El-like and Carbonion-like cyclic transition states.

Hammett relation on the pyrolysis of **2** indicated a negative trend. The result reveals that the transition state is apparently changed to a nearly carbanion-like type by the CN group as a stronger electron-withdrawing group than the phenyl type. Meanwhile, the positive trend for the *p*-Cl to the *p*-NO_2 group in the Hammett plot may be explained as follows. The substituent, the *p*-NO_2 group, is so strong in electron-withdrawing that the rate-enhancing effect by the CN group on the β-position might be weakened; thus, the reaction was conversely accelerated.

The Hammett relation for **2** apparently suggests that the transition state is gradually changed from a nearly carbanion-like to an E1-like type in going from *p*-CH_3 to *p*-NO_2 substituents (Fig. 2). Thus, it can be concluded that the pyrolysis of sulfoxides bearing electron-withdrawing substituents on the β-position carbon in the *S*-ethyl group proceeds via a nearly carbanion-like mechanism in a five-membered cyclic transition state (Fig. 3).

Experimental

Measurements. All the melting points are uncorrected. The IR spectra were determined on a JEOL-810 spectrometer. The ^1H NMR spectra were recorded with a Hitachi R-24B spectrometer in $CDCl_3$ or CCl_4 using TMS as an internal standard. The HPLC analysis were carried out with a JASCO FAMILIC-100N and UVIDEC-100 SYSTEM apparatus by using silica gel (SS-10) and styrene-divinylbenzene copolymer (HP-01) columns (CH_3CN/H_2O, hexane/THF as eluting solution). The peak area were mesured by a TAKEDA-RIKEN TR-2217 integrater. The MS spectra were taken with JEOL-JMS-D 300 mass spectrometer.

Procedures and Materials. All the reactions were monitored by TLC (MERCK, Kieselgel 60 GF), and the substrates were separated by column chromatography using Merck kieselgel 60 silica gel, Wako Activated Alumina (200 mesh). All the substrates obtained were identified by IR, ^1H NMR, GC, MS, and elemental analyses. The computations were performed on the NEC 9801-F computer. Elemental analyses were carried out by Chemical Analysis Center in Toyama Medical and Pharmaceutical University. All reagents were obtained from Wako Pure Chemical Industries Ltd., Tokyo Kasei Co. Ltd., or Aldrich Chemical Co. The reagents and solvents used were further purified by general methods.

Preparation of Sulfoxides. 2-(Substituted phenyl)-ethyl phenyl sulfoxides were prepared by treating methyl

phenyl sulfoxide with LDA and with substituted benzyl chlorides in dry ether at −78 °C, and were extracted with chloroform. The extracts were dried and evaporated. The residues were purified by column chromatography (a mixture of ether and hexane as eluent). Ethyl phenyl sulfoxide and 2-phenylethyl (substituted phenyl) sulfoxides were prepared by oxidizing the corresponding sulfides with hydrogen peroxide in acetic acid, and was isolated through SiO_2-column chromatography (chloroform as eluent), or was recrystallized from ether-methanol. 2-Cyanoethyl (substituted phenyl) sulfoxides (**2**) were prepared by oxidizing the corresponding sulfides obtained in the method described below with hydrogen peroxide, and was worked up as described above. The sulfides were prepared by treating acrylonitrile and substituted benzenethiol in benzene under the presence of a minute amount of triethylamine.

Preparation of 2-Phenylethyl-2,2-d_2 Phenyl Sulfoxide. 2-Phenylethyl-2,2-d_2 phenyl sulfoxide were prepared by treating methyl phenyl sulfoxide with LDA and with benzyl-α,α-d_2 chloride in dry ether at −78 °C.

Benzyl-α,α-d_2 Alcohol: Methyl benzoate was treating by lithium aluminium deuteride in the usual way; after the solution was extracted with ether and the solvent evaporated, the residue was distilled under reduced pressure. Yield 60%.

Benzyl-α,α-d_2 Chloride: The deuterated alcohol was converted into the corresponding chloro compound with thionyl chloride. Yield 60%.

2-(Substituted Phenyl) ethyl Phenyl Sulfoxides (1): ***p*-OCH$_3$:** ^{1}H NMR ($CDCl_3$) δ=2.89—3.25 (4H, m, CH_2-CH_2), 3.58 (3H, s, OCH_3), 6.57—7.65 (9H, m, C_6H_5, C_6H_4); IR (neat) 1030 cm^{-1} (S=O). Found: C, 68.32; H, 6.18%. Calcd for $C_{15}H_{16}O_2S$: C, 69.20; H, 6.19%.

***p*-CH$_3$:** ^{1}H NMR ($CDCl_3$) δ=2.20 (3H, s, CH_3), 2.56—2.98 (4H, m, CH_2CH_2), 6.85 (5H, s, C_6H_5), 7.26—7.53 (4H, m, C_6H_4); IR (KBr) 1040 cm^{-1} (S=O). Found: C, 73.00; H, 6.54%. Calcd for $C_{15}H_{16}OS$: C, 73.73; H, 6.60%. Mp 46.0—47.5 °C.

***m*-CH$_3$:** ^{1}H NMR ($CDCl_3$) δ=2.30—2.80 (4H, m, CH_2-CH_2), 2.58 (3H, s, CH_3) 7.09—7.60 (9H, m, C_6H_5, C_6H_4); IR (neat) 1040 cm^{-1} (S=O).

***p*-Cl:** ^{1}H NMR ($CDCl_3$) δ=2.70—3.30 (4H, m, CH_2-CH_2), 7.20 (5H, s, C_6H_5), 7.06—7.61 (4H, m,C_6H_4); IR (KBr) 1040 cm^{-1} (S=O). Found: C, 63.71; H, 5.04%. Calcd for $C_{14}H_{13}ClOS$: C, 63.51; H, 4.95%. Mp 62.5—63.5 °C.

***p*-NO$_2$:** ^{1}H NMR ($CDCl_3$) δ=2.85—3.45 (4H, m, CH_2CH_2), 8.22—9.15 (9H, m, C_6H_5, C_6H_4); IR (KBr) 1040 cm^{-1} (S=O). Found: C, 61.24; H, 4.69; N, 4.60%. Calcd for $C_{14}H_{13}NO_3S$: C, 61.07; H, 4.76; N, 5.09%. Mp 111.5—113.0 °C.

2-Phenylethyl (Substituted Phenyl) Sulfoxides (1). ***p*-CH$_3$:** ^{1}H NMR ($CDCl_3$) δ=2.32 (3H, s, CH_3), 2.37—2.98 (4H, m, CH_2CH_2), 7.05 (5H, s, C_6H_5), 6.92—7.50 (4H, m, C_6H_4); IR (neat) 1050 cm^{-1} (S=O). Found: C, 72.60; H, 6.44%. Calcd for $C_{15}H_{16}OS$: C, 73.73; H, 6.60%.

***m*-CH$_3$:** ^{1}H NMR ($CDCl_3$) δ=2.35 (3H, s, CH_3), 2.62—3.35 (4H, m, CH_2CH_2), 7.09 (5H, s, C_6H_5), 6.90—7.63 (4H, m, C_6H_4); IR (neat) 1055 cm^{-1} (S=O). Found: C, 72.95: H, 6.50%. Calcd for $C_{15}H_{16}OS$: C, 73.73; H, 6.60%.

***p*-Cl:** ^{1}H NMR ($CDCl_3$) δ=2.70—3.30 (4H, m, CH_2CH_2), 7.20 (5H, s, C_6H_5), 7.06—7.61 (4H, m, C_6H_4); IR (neat) 1050 cm^{-1} (S=O). Found: C, 62.57; H, 4.97%. Calcd for $C_{14}H_{13}ClOS$: C, 63.51; H, 4.95%.

***p*-NO$_2$:** ^{1}H NMR ($CDCl_3$) δ=2.75—3.68 (4H, m, CH_2CH_2), 7.18 (5H, s, C_6H_5), 7.69—8.39 (4H, m C_6H_4); IR (KBr) 1055 cm^{-1} (S=O). Found: C, 61.09; H, 4.84; N 5.38%. Calcd for $C_{14}H_{13}NO_3S$: C, 61.07; H, 4.76; N, 5.09%. Mp 101.5—103.0 °C.

2-Cyanoethyl (Substituted Phenyl) Sulfoxides (2). ***p*-OCH$_3$:** ^{1}H NMR ($CDCl_3$) δ=3.90 (3H, s, OCH_3), 2.50—3.30 (4H, m, CH_2CH_2), 7.05—7.70 (4H, m, C_6H_4); IR (neat) 1050 cm^{-1} (S=O).

***p*-CH$_3$:** ^{1}H NMR ($CDCl_3$) δ=2.48 (3H, s, CH_3), 2.39—3.35 (4H, m, CH_2CH_2), 7.55 (4H, s, C_6H_4); IR (KBr) 1050 cm^{-1} (S=O). Found: C, 62.29; H, 5.63; N, 7.29%. Calcd for $C_{10}H_{11}NOS$: C, 62.15; H, 5.74; N, 7.25%. Mp 49.5—50.1 °C.

H: ^{1}H NMR ($CDCl_3$) δ=2.24—3.35 (4H, m, CH_2CH_2), 7.58 (5H, s, C_6H_5); IR (KBr) 1045 cm^{-1} (S=O). Found: C, 60.47; H, 5.01; N, 7.59%. Calcd for C_9H_9NOS: C, 60.31; H, 5.60; N, 7.81%. Mp 64.0—65.0 °C.

***p*-Cl:** ^{1}H NMR ($CDCl_3$) δ=2.52—3.50 (4H, m, CH_2CH_2), 7.62 (4H, s, C_6H_4); IR (KBr) 1045 cm^{-1} (S=O). Found: C, 50.62; H, 4.00; N, 6.66%. Calcd for C_9H_8NClOS: C, 50.59; H, 3.77; N, 6.55%. Mp 66.8—67.5 °C.

***p*-NO$_2$:** ^{1}H NMR ($CDCl_3$) δ=2.62—3.25 (4H, m, CH_2CH_2), 7.79—8.58 (4H, m, C_6H_4); IR (KBr) 1050 cm^{-1} (S=O). Found: C, 47.95; H, 3.61; N, 12.59%. Calcd for $C_9H_8N_2O_3S$: C, 48.21; H, 3.60; N, 12.49%. Mp 114.0—115.0 °C.

Kinetics. A pre-cooled solution of desired amount of a sulfoxide (7.0×10^{-3} mol dm^{-3}) in an anhydrous solvent was prepared and devided into a number of 10 μl of sealed capillary tubes, which were immersed in a constant temperature silicone oil bath (±0.05°C), at appropriate time intervals, the tubes were taken out and frozen in ice bath to stop the reaction. The reaction rate was then calculated by following the decreasing peak area at UV 254 nm due to the recovered sulfoxide, which was separated from the reaction mixture by HPLC (column; HP-01, eluent; CH_3CN : H_2O=5 : 2) using diphenyl ether or diphenyl sulfide as an internal standard. The rate constants were calculated by a least-squares method using the 8—12 points accumulated during 70% completion of reaction. When the data were plotted as ln (V_0/V_0-V_t) vs. time (where V_0 is the initial volume of sulfoxide and V_t is the volume of sulfoxide at a particular time), a linear correlation was observed suggesting that the kinetics is of first order. Activation parameters were computer calculated by a least-squares method using ln k vs. $1/T$. The Hammett ρ-value was computed by the least-squares method using σ-values and the logarithmus of the rate constants.

The authors are grateful to Professor Shigeru Oae of Okayama University of Science, and Professor Naomichi Furukawa, the University of Tsukuba, for their helpful discussions.

References

1) A. C. Cope, T. T. Foster, and P. H. Toole, *J. Am. Chem. Soc.*, **71**, 3729 (1949).

2) D. V. Banthorpe, "Elimination Reaction," Elsvier, New York (1963), P. 167.
3) D. W. Emerson, A. R. Craig, and J. W. Potts, Jr., *J. Org. Chem.*, **32**, 102 (1967).
4) D. W. Emerson and T. J. Korniski, *J. Org. Chem.*, **34**, 4115 (1969).
5) J. R. Shelton and K. E. Davis, *Int. J. Sulfur Chem.*, **8**, 197 (1973).
6) C. A. Kingsbury and D. J. Cram, *J. Am. Chem. Soc.*, **82**, 1810 (1960).
7) R. D. Bach, D. Andrzejewski, and L. R. Dusold, *J. Org. Chem.*, **38**, 1742 (1973).
8) S. Oae and N. Furukawa, *Tetrahedron*, **33**, 2359 (1977).
9) T. Yoshimura, T. Sekioka, H. Mizuno, Y. Iizuka, M. Yoshizawa, and E. Tsukurimichi, 24th Symposium on Organic Radical Reactions and 34th Symposium on Organic Reaction Mechanisms, Sapporo, Japan, August 1983, Abstr., No. 3G08.
10) H. Kwart and T. J. George, *J. Am. Chem. Soc.*, **100**, 3927 (1978).
11) S. Oae, K. Harada, K. Tsujihara, and N. Furukawa, *Bull. Chem. Soc. Jpn.*, **46**, 3842 (1973).
12) E. D. Hughes and C. K. Ingold, *J. Chem. Soc.*, **1948**, 2038, 2044.
13) A. C. Cope, N. A. Lebel, H. H. Lee, and W. R. Moor, *J. Am. Chem. Soc.*, **79**, 4720 (1957).
14) F. A. Davis and R. H. Jenkins, Jr., *J. Am. Chem. Soc.*, **102**, 7967 (1980).
15) T.-L. Ju and J. L. Kice, *J. Org. Chem.*, **44**, 610 (1979).
16) E. Tsukurimichi, T. Yoshimura, and M. Kanda, *Nippon Kagaku Kaishi*, **1987**, 202.

Synthesis and Electrochemical Properties of 3-(3,6-Dioxo-1,4-cyclohexadienyl)methyl-*p*-tropoquinone. Analysis of a Four-Electron Redox System by Cyclic Voltammetry

Akira MORI, Yasutomo GOTO,† and Hitoshi TAKESHITA*
Research Institute of Industrial Science, 86, Kyushu University, Kasuga-koen, Kasuga, Fukuoka 816
†Graduate School of Engineering Sciences, 39, Kyushu University, Kasuga-koen, Kasuga, Fukuoka 816
(Received January 26, 1987)

A methylene-linked bisquinone, 3-(3,6-dioxo-1,4-cyclohexadienyl)methyl-*p*-tropoquinone, was prepared from 2,5-bis(arylmethoxy)tropone by consecutive reaction, a homolytic rearrangement, subsequent debenzylation, and a DDQ-dehydrogenation. According to cyclic voltammetry, this four-electron redox system was operative, in sharp contrast to the case of the benzenoid bisquinones, via four successive one-electron transfer processes. Two other tropolone derivatives carrying *p*-benzoquinone segment were also prepared by a similar procedure. The first reduction potentials of these benzoquinones showed a slight enhancement by intramolecular hydrogen bonding.

Recently, we have measured an enhancement of the half-wave potentials due to an electron-attractive substituent of the *p*-tropoquinones;[1] in the case of 3-(*p*-hydroxybenzyl)-*p*-tropoquinone, the hydroxyl group considerably enhanced the redox potentials by an intermolecular hydrogen bonding.[2]

As one part of an electrochemical study of *p*-tropoquinones, we synthesized 3-(3,6-dioxo-1,4-cyclohexadienyl)methyl-*p*-tropoquinone (**1**), a methylene-linked bisquinone, together with 3-[(3,6-dioxo-1,4-cyclohexadienyl)methyl]tropolone and 5-methoxy-3-[(3,6-dioxo-1,4-cyclohexadienyl)methyl]tropolone (**2** and **3**). As described below, cyclic voltammetry (CV) of **1** indicated occurrence of four-times one-electron transfer processes.

When 2,5-bis(2,5-dimethoxybenzyloxy)tropone (**4**), prepared in 70% yield from 5-hydroxytropolone (**5**) and 2,5-dimethoxybenzyl chloride (**6**), was heated in decalin,[3] the thermally-transformed isomer, 3-(2,5-dimethoxybenzyl)-5-(2,5-dimethoxybenzyloxy)tropolone (**7**) was obtained in 55% yield. A debenzylation of **7** by 48% hydrobromic acid in acetic acid afforded 5-hydroxy-3-(2,5-dihydroxybenzyl)tropolone (**8**), and its DDQ (2,3-dichloro-5,6-dicyano-*p*-benzoquinone)-dehydrogenation gave desired **1**. The overall yield of **1** from **7** was 70%.

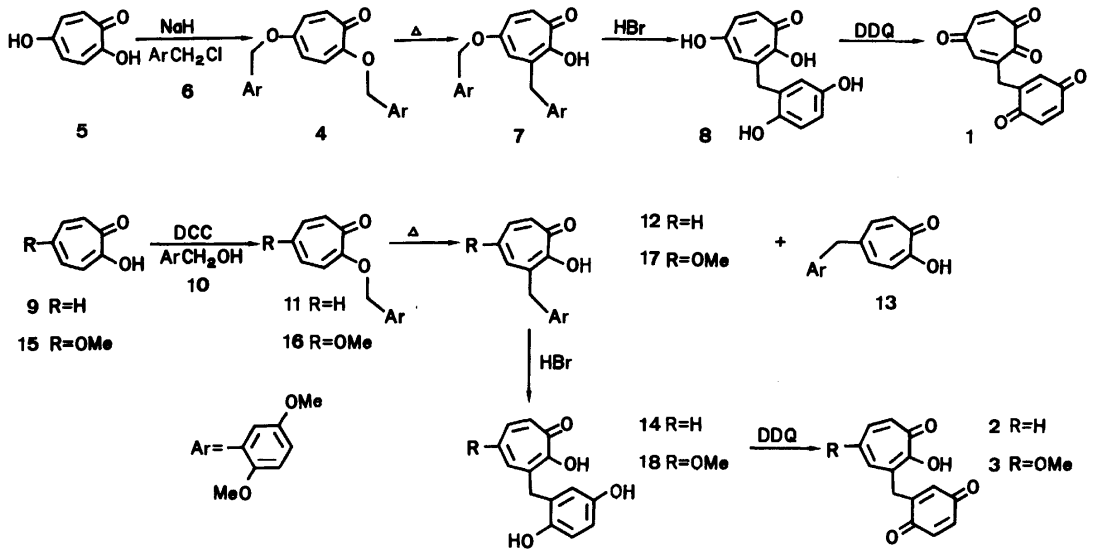

The condensation[4] of tropolone (**9**) with 2,5-dimethoxybenzyl alcohol (**10**) in the presence of dicyclohexylcarbodiimide (DCC) and copper(I) chloride gave 2-(2,5-dimethoxybenzyloxy)tropone (**11**), which was converted to 3-(2,5-dimethoxybenzyl)tropolone (**12**) and 5-(2,5-dimethoxybenzyl)tropolone (**13**) in refluxing decalin. Subsequent demethylation of **12** with concd hydrobromic acid in acetic acid afforded the hydroquinone derivative, 3-(2,5-dihydroxybenzyl)-tropolone (**14**), which was dehydrogenated with DDQ to **2**, a tropolonated *p*-benzoquinone.

Similarly, a condensation of 5-methoxytropolone

(**15**) and **10** gave the corresponding arylmethoxytropone (**16**) in 71% yield. Heating of **16** in refluxing decalin afforded 5-methoxy-3-(2,5-dimethoxybenzyl)-tropolone (**17**) in 93% yield. Hydrobromic acid-demethylation of **17** in acetic acid formed only a 5-methoxytropolone derivative, 3-(2,5-dihydroxybenzyl)-5-methoxytropolone (**18**). The dehydrogenation of **18** with DDQ gave **3**, another tropolonated *p*-benzoquinone.

The CV of **1** showed four waves. The first half-wave potential ($E_1 = -0.20$ V vs. Ag/AgCl) was just the same as the E_1 of *p*-tropoquinone (**19**),[4] indicating a negligible substituent effect due to a methylene-linked electronegative *p*-benzoquinone moiety; the second wave ($E_2 = -0.51$ V) was also similar to the $E_1 = -0.50$ V of methyl-*p*-benzoquinone (**20**).

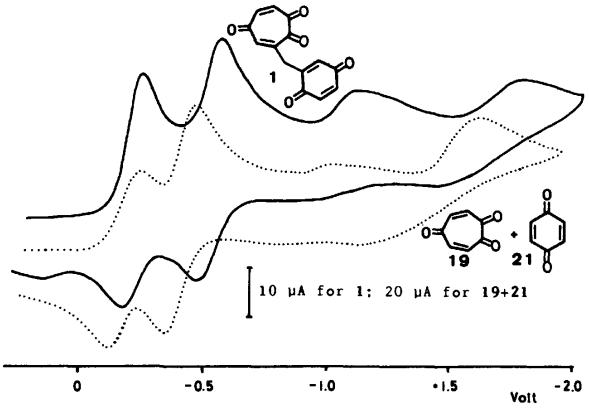

Fig. 1. The CV curve (working electrode, Pyrex-glass-sealed Pt wire; reference electrode, standard Ag/AgCl) of **1** (1.56×10^{-3} mol dm^{-3}, solid line) and a 1 : 1-mixture of **19** and **21** (1.49×10^{-3} mol dm^{-3}, dotted line) at 22—23 °C in anhydrous DMF with 0.1 M TBAF under N_2 with a scan rate of 100 mV s^{-1}.

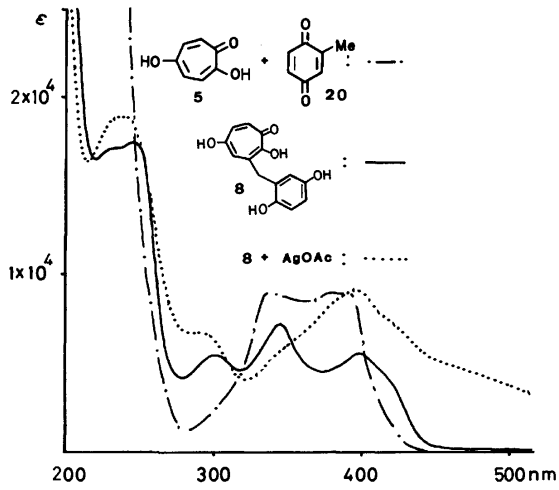

Fig. 2. Effect of AgOAc to the UV Spectrum of **8** in methanol: (——) without AgOAc; (------) in the presence of stoichiometric amount of AgOAc to produce the "Half-quinone" (**E**); (-·-·) equimolar amounts of **5** and **20**.

However, the intensities of the E_3 and E_4 peaks (−1.10 and −1.68 V) of **1** gradually decreased upon multiple-sweeping; finally, only the E_1 and E_2 remained at −0.21 and −0.52 V. This might be due to both or either the further chemical reaction and/or the instability of the intermediate species (**A** — **D**). On the other hand, a CV measurement of a 1 : 1-mixture of **19** and *p*-benzoquinone (**21**) showed four reproducible waves at $E_1 = -0.21$, $E_2 = -0.41$, $E_3 = -0.89$, and $E_4 = -1.46$ V. Consequently, **1** behaved as a combination of **19** and **21** in respect to CV.

The UV spectrum of **8** in the presence of silver acetate, whose amount was just equivalent to two-electron oxidation, showed a new absorption band around 430 nm. The UV spectrum of a 1 : 1-mixture of **5** and **20** showed no band around this region. Therefore, the occurrence of this absorption band indicated a charge-transfer character of the half quinone equivalent (**E**) formed in situ. Since the concentrations for the UV measurement were ca. 10^{-5} to 10^{-6} mol dm^{-3}, this must be an intramolecular charge-transfer absorption.[5] Should the two-electron reduced species (**B**) disproportionate to the deprotonated species of a half-quinone equivalent, **E**, the CV of **1** might reveal an irreversible intervention of subsequent processes due to an intramolecular side reaction. To date, there is no UV spectral evidence for the formation of either "quinhydrone" or charge-transfer complex in tropoquinones.

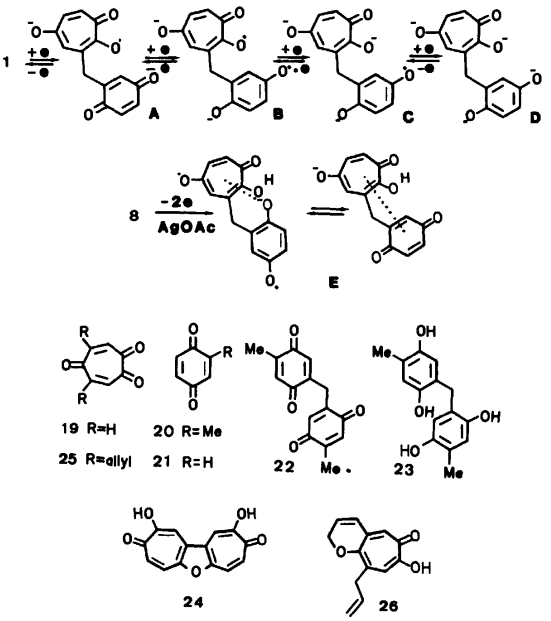

The peak potintials of **2** and **3** are shown in Table 1 together with those of **20** and **21**. Both show irreversible waves; particularly, their oxidation waves are hardly discernible. Nevertheless, their first reduction peaks move to a slightly more positive side than that

Table 1. The Peak Potentials/V of **2** and **3** together with Reference Quinones[a)]

Compds.	**2**	**3**	**20**	**21**
Ep1	−0.47	−0.46	−0.50	−0.44
Ep2	−1.23	−1.27	−1.58	−1.55

a) CV was measured in anhydrous DMF with 0.1 M TBAF using Pyrex glass-sealed Pt-wire as working electrode and standard Ag/AgCl as reference electrode at 22—23 °C under N_2 with a scan rate of 100 mv s^{-1}.

of **20**. This is attributable to an intramolecular hydrogen bonding.[2)]

Interestingly, bis(4-methyl-3,6-dioxo-1,4-cyclohexadienyl)methane, a bisquinone (**22**),[6)] is known to reveal two one-electron paths and one two-electron path in the formation of fully reduced bis[(2,5-dihydroxy-4-methyl)phenyl]methane (**23**); a marked difference in the reduction mode should be attributable to the structural difference of the two bisquinones.

In conclusion, this conversion of **1** to **8** via the four single-electron reduction processes constitutes a new redox system; its CV data suggested that the present bisquinone is as a strong oxidizing agent as **19**. At the same time, the appearance of a charge-transfer band in the UV spectrum might suggest a possible formation of a side product from the intermediate species, such as **B**.[7)] In fact, the electrolysis of **19** gave 2,10-dihydroxycyclohepta[*b*,*d*]furan-3,9-dione (**24**)[8)] in 44% yield under the same conditions as the CV measurement; moreover, we observed that 4,6-diallyl-*p*-tropoquinone (**25**) was electrolyzed to a cyclized derivative, 9-allyl-7-hydroxycyclohepta[*b*]pyran-6(2*H*)-one (**26**).[9)]

Experimental

The elemental analyses were performed by Miss S. Hirashima, of the Research Institute of Industrial Science, Kyushu University. The CV measurements were carried out in a standard three-electrode cell (working electrode; Pyrex glass-sealed Pt wire, reference electrode; standard Ag/AgCl) at 23°C in an anhydrous *N*,*N*-dimethylformamide (DMF) with 0.1 M tetrabutylammonium tetrafluoroborate (TBAF) under an N_2 stream with a scan rate of 100 mV s^{-1}; the values were corrected with an internal standard for the redox of a ferrocenium/ferrocene couple at +0.465 V vs. Ag/AgCl. The NMR spectra were measured by a JEOL FX 100 spectrometer in $CDCl_3$ solutions (unless otherwise specified) and the chemical shifts were expressed in δ units. The mass spectra were measured with a JEOL 01SG-2 spectrometer. The IR spectra were taken as KBr disks using a Jasco IR-A 102 spectrometer.

Preparation of 2,5-Bis(2,5-dimethoxybenzyloxy)-tropone (4). To an HMPA solution (4.5 cm^3) of **5** (300 mg), NaH (50%, 256 mg) was added under an N_2 atmosphere at 0—5°C. The mixture was then warmed to room temperature and stirred for a further 2 h at 60°C. After again cooling mixture to room temperature, an HMPA solution (2 cm^3) of **6** (853 mg) was added and stirring continued for 19 h; then, the mixture was diluted with water and the precipitates were collected by filtration and recrystallized from aqueous acetone to give **4** [yellow brown crystals, mp 123.5—125.5°C (decomp), 669 mg; 70%. Found: C, 68.20; H, 6.14%. Calcd for $C_{25}H_{26}O_7$: C, 68.48; H, 5.98%. ^{1}H NMR δ=3.72 (3H, s), 3.76 (3H, s), 3.79 (3H, s), 3.81 (3H, s), 4.97 (2H, s), 5.22 (2H, s), 6.35 (1H, d, J=11.5 Hz), 6.76 (1H, d, J=11.5 Hz), 6.7—7.0 (6H, m), 7.10 (1H, d, J=13 Hz), and 7.26 (1H, d, J=13 Hz). ^{13}C NMR δ=55.7 (2C), 55.9 (2C), 65.4, 65.8, 109.1, 111.3 (2C), 113.5, 113.8 (2C), 114.6, 116.5, 124.9, 125.3, 132.7, 137.6, 150.5, 150.8, 153.6, 153.8, 158.6, 158.9, and 179.5. IR ν: 1572, 1520, 1242, 1220, 1185, and 1042 cm^{-1}. UV λ_{max}^{MeOH}: 227 nm (ε=37900), 251 (10100, sh), 308 (11300), 329 (12400), 361 (9100, sh), and 379 (5900, sh)].

Thermal Rearrangement of 4 to 3-(2,5-Dimethoxybenzyl)-5-(2,5-dimethoxybenzyloxy)tropolone (7). A decalin solution (40 cm^3) of **4** (800 mg) was refluxed for 2 h under an N_2 atmosphere. Silica-gel column chromatography of the mixture gave **7** [pale yellow crystals, mp 101—104°C, 482 mg; 55%. Found: C, 68.31; H, 5.96%. Calcd for $C_{25}H_{26}O_7$: C, 68.48; H, 5.98%. ^{1}H NMR δ=3.68 (3H, s), 3.70 (3H, s), 3.72 (3H, s), 3.74 (3H, s), 4.10 (2H, s), 4.93 (2H, s), 6.7—7.0 (6H, m), and 7.0—7.3 (3H, m). ^{13}C NMR δ=35.0, 55.7 (2C), 55.8 (2C), 65.8, 111.4 (2C), 112.1, 113.4, 114.5, 117.1, 120.5, 120.9, 124.2, 125.1, 128.3, 128.9, 140.2, 150.8, 151.8, 153.6, 157.7, 163.8, and 170.0. IR ν: 1605, 1502, 1400, 1230, 1218, 1200, and 1049 cm^{-1}. UV λ_{max}^{MeOH}: 229 nm (ε=35100), 251 (21100, sh), 298 (8900), 333 (10800), 370 (7400), and 387 (7100)].

Hydrobromic Acid Treatment of 7 to 3-(2,5-Dihydroxybenzyl)-5-hydroxytropolone (8). An AcOH solution (15 cm^3) of **7** (576 mg) and aq HBr (48%, 15 cm^3) was refluxed for 2 h. The mixture was then diluted with water and extracted with AcOEt. The organic extract was washed with an aqueous NaCl solution, dried on Na_2SO_4, and heated in vacuo to give a residue which, by recrystallization from $CHCl_3$, gave **8** [brown crystals, mp 167—170°C, 331 mg; 97%. Found: M.W., 260.0673. Calcd for $C_{14}H_{12}O_5$: 260.0683. ^{1}H NMR (CD_3OD) δ=4.00 (2H, s), 6.4—6.7 (3H, m), 6.92 (1H, dd, J=11.5, 3 Hz), 7.31 (1H, d, J=11.5 Hz), and 7.34 (1H, d, J=3 Hz). ^{13}C NMR (CD_3OD) δ= 36.7, 115.8, 118.0, 118.4, 122.6, 124.0, 127.8, 131.2, 145.6, 149.6, 151.7, 160.2, 163.9, and 171.9. IR ν: 3600—2400, 1375, and 1210 cm^{-1}. UV λ_{max}^{MeOH}: 231 nm (ε=17000), 244 (17200), 300 (5400), 344 (7100), 398 (5500), and 413 (4600, sh)].

DDQ-Oxidation of 8 to 3-[(3,6-Dioxo-1,4-cyclohexadienyl)methyl]-*p*-tropoquinone (1). To an acetone solution of **8** (25.4 mg) was added DDQ (48 mg) at room temperature. After stirring for 18 h, the mixture was evaporated in vacuo, and the residue was chromatographed on a silica-gel column; **1** [yellow crystals, mp 122—125°C (decomp), 17.9 mg; 72%. Found: M.W., 256.0368. Calcd for $C_{14}H_8O_5$: 256.0369. ^{1}H NMR δ=3.64 (2H, dd, J=1.5, 1 Hz), 6.65 (1H, tt, J=1.5, 1 Hz), 6.76 (2H, d, J=1 Hz), 6.82 (1H, quint, J=1 Hz), and 6.84 (2H, d, J=1 Hz). ^{13}C NMR δ=32.8, 134.2, 135.2, 136.8, 137.0, 138.5, 139.5, 144.0, 144.5, 186.6, 187.0, 187.5, 188.3, and 188.7. IR ν: 1655 cm^{-1}. UV λ_{max}^{MeOH}: 245 nm (ε= 21100)] was obtained from the elution with benzene: AcOEt (10 : 1).

AgOAc-Oxidation of 8 to 1. To an acetone solution (3 cm^3) of **8** (30 mg) was added AgOAc (79 mg) at room temperature. After 5 h, the insoluble materials were filtered off, and the filtrate was evaporated in vacuo and chromatographed on a silica-gel column to give **1** [10 mg; 34%].

Preparation of 2-(2,5-Dimethoxybenzyloxy)tropone (11). To an anhydrous benzene solution (0.5 cm^3) of **10** (895 mg) was added DCC (1.13 g) and CuCl (3 mg). After being stirred at 60°C for 11 h, an anhydrous benzene solution (0.5 cm^3) of **9** (436 mg) was added to the mixture and kept at 60°C for another 18 h. The resultant precipitates were filtered off and washed with AcOEt. The combined organic portion was evaporated in vacuo and the residue was chromatographed on a silica-gel column to give **11** [pale yellow crystals, mp 71—72.5°C, 806 mg; 83%. Found: C, 70.73; H, 6.06%. Calcd for $C_{16}H_{16}O_4$: C, 70.57; H, 5.92%. ^{1}H NMR δ=3.70 (3H, s), 3.80 (3H, s), 5.24 (2H, s), and 6.6—7.2 (8H, m). ^{13}C NMR δ=55.9, 56.1, 65.9, 111.7, 114.1, 114.3, 114.7, 124.8, 128.2, 133.0, 136.6, 137.4, 150.9, 154.2, 164.8, and 181.0 IR ν: 1594, 1580, 1515, 1498, and 1284 cm^{-1}. UV λ_{max}^{MeOH}: 227 nm (ε=24900), 303 (7900), 318 (7200), 347 (5400), and 365 (3600)].

Thermal Rearrangement of 11 to 3-(2,5-Dimethoxybenzyl)tropolone (12) and 5-(2,5-Dimethoxybenzyl)-tropolone (13). A decalin solution (16 cm^3) of **11** (353 mg) was refluxed for 11.5 h under an N_2 atmosphere. The resultant mixture was chromatographed on a silica-gel column to give **12** [yellow brown crystals, mp 65—67°C, 270 mg; 93%. Found: C, 70.67; H, 5.92%. ^{1}H NMR δ=3.70 (3H, s), 3.72 (3H, s), 4.12 (2H, s), 6.7—7.0 (4H, m), and 7.2—7.4 (3H, m). ^{13}C NMR δ=34.6, 55.7, 56.1, 111.7, 112.1, 117.5, 121.0, 127.4, 128.7, 136.0, 139.6, 140.3, 152.1, 153.8, 168.2, and 173.0. IR ν: 1612, 1600, 1522, 1500, 1425, 1380, 1226, 1050, and 750 cm^{-1}. UV λ_{max}^{MeOH}: 231 nm (ε=26000), 243 (24700, sh), 304 (6900, sh), 322 (7600), 356 (5900), and 367 (5800)] and **13** [yellow crystals, mp 108.5—111°C, 8.8 mg; 3%. Found: C, 70.68; H, 6.01%. ^{1}H NMR δ=3.72 (6H, s), 3.88 (2H, s), 6.6—6.8 (3H, m), 7.18 (2H, d, J=12 Hz), and 7.30 (2H, d, J=12 Hz). ^{13}C NMR δ=40.1, 55.8, 56.0, 111.8, 112.1, 117.2, 124.1 (2C), 129.4, 138.8 (2C), 142.0, 151.8, 153.9, and 171.1 (2C). IR ν: 3200, 1560, 1495, 1460, 1420, 1270, 1238, and 1214 cm^{-1}. UV λ_{max}^{MeOH}: 228 nm (ε=26500), 325 (10300), and 372 (4800, sh)] together with **3** [61.7 mg; 17%].

Demethylation of 12. An AcOH solution (10 cm^3) of **12** (378 mg) and HBr (48%, 10 cm^3) was refluxed for 1.5 h. The mixture was then diluted with water and extracted with AcOEt. The organic extract was dried on $MgSO_4$ and heated in vacuo. The residue was purified by repeated recrystallizations from a mixture of AcOEt and hexane to give **14** [yellow crystals, mp 134—136°C, 267 mg; 79%. Found: C, 68.67; H, 5.24%. Calcd for $C_{14}H_{12}O_4$: C, 68.84; H, 4.95%. ^{1}H NMR (CD_3OD) δ=4.01 (2H, s), 6.47 (1H, dd, J=8.5, 2.5 Hz), 6.56 (1H, dd, J=2.5, 1 Hz), 6.63 (1H, dd, J=8.5, 1 Hz), and 6.8—7.7 (4H, m). ^{13}C NMR (CD_3OD) δ=36.8, 115.7, 117.8, 118.4, 122.7, 127.9, 129.4, 137.9, 141.5, 143.4, 149.6, 151.7, 169.5, and 175.0. IR ν: 3600—2500, 1542, 1510, 1482, 1476, 1380, and 1210 cm^{-1}. UV λ_{max}^{MeOH}: 237 nm (ε=20000), 331 (7700), 375 (5900), and 392 (4700, sh)].

The DDQ-Oxidation of 14. An acetone solution (10 cm^3) of **14** (99.1 mg) and DDQ (105 mg) was stirred at room temperature for 4 h. The solvent was then removed by evaporation and the residue was briefly chromatographed on a silica-gel column. Yellow crystals obtained by elution from hexane-AcOEt (10 : 1) and removal of the solvent were recrystallized from benzene to give **2** [mp 99.5—101.5°C, 65.2 mg; 66%. Found: C, 69.16; H, 4.11%. Calcd for $C_{14}H_{10}O_4$: C, 69.42; H, 4.16%. ^{1}H NMR δ=3.90 (2H, d, J=1.5 Hz), 6.53 (1H, dtd, J=2, 1.5, 1 Hz), 6.65 (1H, dd, J=10, 2 Hz), 6.77 (1H, dd, J=10, 1 Hz), 6.9—7.3 (3H, m), and 7.57 (1H, d, J=9.5 Hz). ^{13}C NMR δ=34.6, 120.7, 127.7, 128.7, 133.8, 136.7, 137.0, 137.3, 141.4, 146.4, 168.1, 173.6, 187.4, and 188.0. IR ν: 3600—3300, 3200, 1650, 1548, 1420, 1295, and 1236 cm^{-1}. UV λ_{max}^{MeOH}: 243 nm (ε=37600), 327 (8600), 333 (8700), 373 (6000), and 391 (4300, sh)].

Preparation of 2-(2,5-Dimethoxybenzyloxy)-5-methoxytropone (16). A benzene solution (0.3 cm^3) of **10** (357 mg), DCC (428 mg), and CuCl (5 mg) was stirred at 60°C for 16 h under an N_2 atmosphere, to which, a benzene solution (0.5 cm^3) of **15** (213 mg) was introduced and stirred further for 10 h. The precipitates formed were filtered off and washed with AcOEt, and the residue obtained by removing organic solvents in vacuo was recrystallized from AcOEt to give **16** [yellow crystals, mp 131—132°C, 300 mg; 71%. Found: C, 67.76; H, 6.05%. Calcd for $C_{17}H_{18}O_5$: C, 67.54; H, 6.00%. ^{1}H NMR δ=3.72 (6H, s), 3.81 (3H, s), 5.23 (2H, s), 6.21 (1H, dd, J=11, 2.5 Hz), 6.74 (1H, d, J=8 Hz), 6.77 (1H, d, J=11 Hz), 6.84 (1H, d, J=8 Hz), 7.02 (1H, dd, J=13, 2.5 Hz), 7.03 (1H, br s), and 7.21 (1H, d, J=13 Hz). ^{13}C NMR δ=55.5, 55.8, 56.0, 65.8, 107.3, 111.4, 113.8 (2C), 116.5, 125.3, 132.5, 137.6, 150.6, 153.8, 158.8, 159.5, and 179.7. IR ν: 1566, 1507, 1220, 1200, and 1102 cm^{-1}. UV λ_{max}^{MeOH}: 227 nm (ε=31600), 252 (7600, sh), 310 (9600, sh), 328 (11300), 347 (9900), 362 (3900, sh), and 378 (6300, sh)].

Thermolysis of 16. Formation of 3-(2,5-Dimethoxybenzyl)-5-methoxytropolone (17). A decalin solution (5 cm^3) of **16** (128 mg) was refluxed under an N_2 atmosphere for 3 h. A silica-gel column chromatography of the mixture afforded **17** [pale yellow crystals, mp 101—103°C, 96.3 mg; 93%. Found: C, 67.69; H, 6.01%. ^{1}H NMR δ=3.66 (3H, s), 3.69 (3H, s), 3.73 (3H, s), 4.11 (2H, s), 6.72 (1H, dd, J=11, 3 Hz), 6.7—6.9 (3H, m), 7.09 (1H, d, J=3 Hz), and 7.26 (1H, d, J=11 Hz). ^{13}C NMR δ=34.9, 55.6 (2C), 55.9, 111.4, 112.0, 117.2, 117.7, 120.3, 122.9, 124.2, 140.7, 151.8, 153.5, 158.5, 162.8, and 170.6. IR ν: 1610, 1540, 1498, 1451, 1226, 1205, and 1055 cm^{-1}. UV λ_{max}^{MeOH}: 230 nm (ε=21500), 250 (16200, sh), 300 (5200), 341 (7800), 388 (5200), and 416 (2300, sh)] and **16** [23.9 mg; 19%].

Demethylation of 17. An AcOH solution (7.5 cm^3) of **17** (328 mg) and HBr (48%, 7.5 cm^3) was refluxed for 2 h. The mixture was then diluted with water and extracted with AcOEt. After evaporation of the solvent, the residue was recrystallized from $CHCl_3$ to give **18** [yellow crystals, mp 162—165°C (decomp), 276 mg; 93%. Found: M.W., 274.0856. Calcd for $C_{15}H_{14}O_5$: 274.0841. ^{1}H NMR (CD_3OD) δ=3.73 (3H, s), 4.02 (2H, s), 6.45—6.7 (3H, m), 6.92 (1H, dd, J=11, 3 Hz), 7.33 (1H, d, J=11 Hz), and 7.34 (1H, d, J=3 Hz). ^{13}C NMR (CD_3OD) δ=36.4, 56.4, 115.7, 117.7, 118.4, 119.3, 122.7, 127.6, 130.6, 144.1, 149.4, 151.5, 160.7, 163.9, and 172.4. IR ν: 3300—3100, 1618, 1504, 1452, 1398, and 1208 cm^{-1}. UV λ_{max}^{MeOH}: 228 nm (ε=19600, sh), 249 (25400), 339 (11800), and 395 (9100)].

The DDQ-Oxidation of 18. To an acetone solution (9

cm^3) of **18** (93.2 mg), DDQ (85.6 mg) was added stirred at room temperature for 2 h. A brief silica-gel column chromatography of the mixture afforded **3** [deep yellow crystals, mp 105—107°C (decomp), 52 mg; 56%. Found: C, 65.78; H, 4.42%; M.W., 272.0682. Calcd for $C_{15}H_{12}O_5$: C, 66.17; H, 4.44%; M.W., 272.0682. ^{1}H NMR δ=3.79 (3H, s), 3.89 (2H, d, J=1.5 Hz), 6.52 (1H, dtd, J=2, 1.5, 1 Hz), 6.65 (1H, dd, J=10, 2 Hz), 6.77 (1H, dd, J=11, 3 Hz), 6.78 (1H, dd, J=10, 1 Hz), 7.46 (1H, d, J=11 Hz), and 7.47 (1H, d, J=3 Hz). ^{13}C NMR δ=34.9, 56.1, 118.4, 120.6, 130.7, 133.7, 136.6, 136.8, 137.2, 146.3, 158.8, 163.1, 171.0, 187.2, and 187.8. IR ν: 3600—3300, 1652, 1208, and 1200 cm^{-1}. UV λ_{max}^{MeOH}: 246 nm (ε=30800), 338 (11900), and 400 (7400)].

Electrolysis of 19 to 24. An anhydrous DMF solution (30 cm^3) of **19** (616 mg) was electrolyzed in the presence of TBAF (1 g) at −1.30 V for 22 h. After evaporation of the solvent in vacuo, the residue was diluted with AcOEt to precipitate **24** [258 mg; 44%], which was identical with the authentic sample.[9]

The authors wish to thank the Ministry of Education, Science and Culture for a financial assistance, a Grant-in-Aid for Scientific Research to A. M. (No. 60470025).

References

1) A. Mori, T. Kusaba, Y. Isayama, and H. Takeshita, *Chem. Lett.*, **1986**, 155.

2) H. Takeshita, A. Mori, and Y. Goto, *Bull. Chem. Soc. Jpn.*, **59**, 1125 (1986).

3) H. Takeshita, H. Mametsuka, A. Chisaka, and N. Matsuo, *Chem. Lett.*, **1981**, 73; H. Takeshita and H. Mametsuka, *Heterocycles*, **22**, 663 (1984).

4) E. Vowinckel, *Chem. Ber.*, **99**, 1479 (1966).

5) R. Carruthers, F. M. Dean, L. E. Houghton, and A. Ledwith, *Chem. Commun.*, **1967**, 1206.

6) A. S. Lindsey, H. E. Peover, and N. G. Savill, *J. Chem. Soc.*, **1962**, 4558.

7) The electrolysis was carried out by Hokuto Denko Potentiostat/Galvanostat HA-301.

8) Stoichiometric amount of one-electron oxidizing agents causes only a dimerizations of *p*-tropoquinones to dicyclohepta[*b*,*d*]furandiones. See H. Takeshita, T. Kusaba, and A. Mori, *Chem. Lett.*, **1982**, 710.

9) H. Takeshita, A. Mori, Y. Goto, and T. Nagao, *Bull. Chem. Soc. Jpn.*, **60**, 1747 (1987).

 © 1987 The Chemical Society of Japan Bull. Chem. Soc. Jpn., 60, 2503—2507 (1987)

The Structure of Graucin A, a New Bitter Limonoid from *Evodia grauca* Miq. (Rutaceae)

Munehiro NAKATANI,* Hideki TAKAO, Takashi IWASHITA,† Hideo NAOKI,† and Tsunao HASE

Department of Chemistry, Faculty of Science, Kagoshima University, 1-21-35 Koorimoto, Kagoshima 890

†Suntory Institute for Bioorganic Research, Shimamoto-cho, Mishima-gun, Osaka 618

(Received January 31, 1987)

Graucin A, a new bitter limonoid, has been isolated from the root bark of *Evodia grauca* Miq. as well as the known limonoids limonin, rutaevin and limonin diosphenol. Its structural and stereochemical assignments were made using NMR (COSY and NOESY), and CD spectroscopy, which indicated the uncommon 5β-H configuration of this new compound. Rutaevin was also recognized to be a 5β-H limonoid.

In the course of our studies on the biologically active limonoids,[1] we isolated a new limonoid graucin A (**1**) along with the known limonoid limonin (**2**),[2] rutaevin (**3**)[3] and limonin diosphenol (**4**)[3,4] as bitter components of the root bark of *Evodia grauca* Miq.(Rutaceae). The structure **1** was assigned on the basis of COSY and NOESY NMR spectra of **1** and the acetate **5**, and by the CD study on the benzoate **6**. Both graucin A and the structurally similar limonoid rutaevin (**3**) have been assigned the 5β-H configuration, which is opposite to that of many other known Rutaceae limonoids including limonin.

Some biological activities of the limonoids (**1**—**4**) were also examined.

Results and Discussion

The ether extract of the root bark contained a variety of limonoids which were detected by the characteristic color with Ehrlich's reagent on TLC. Fractionation by extensive silica-gel column chromatography followed by the final HPLC purification on a normal phase column using 0.4—1.0% methanol in dichloromethane as an eluant gave the new compound **1** named graucin A along with three known limonoids previously isolated from various Rutaceae plants: limonin (**2**), rutaevin (**3**) and limonin diosphenol (**4**).

Graucin A (**1**), $C_{26}H_{30}O_{10}$, mp > 310 °C (prisms from acetonitrile), exhibited the following spectral data. SI-MS: m/z 503 $(M+1)^+$; $[\alpha]_D^{15}$ −150° (c 0.0005, CH_3CN); UV (MeOH): 209 nm (ε 6300, π-π^* of furan). The IR spectrum showed the presence of hydroxyl (3450 cm^{-1}), γ-lactone (1765 cm^{-1}), δ-lactone (1740 cm^{-1}) and ketone groups (1700 cm^{-1}) and the CD spectrum also showed the presence of furan (228 nm, $\Delta\varepsilon$ −5.3; π-π^*) and ketone groups (297 nm, $\Delta\varepsilon$ −1.7; n-π^*). The ^{1}H NMR spectrum showed signals of four tertiary methyl groups at δ 0.61 (8-Me), 1.23 (4α-Me), 1.35 (13-Me), and 1.44 (4β-Me), a singlet at δ 4.15 (15-H), a AB quartet (J=12 Hz) at δ 4.10 (19-H_a) and 4.28 (19-H_b), and a signal at δ 5.51 (s, 17-H) weakly coupling with furan

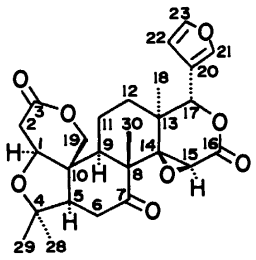

limonin (**2**)

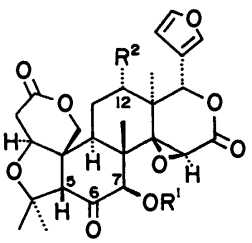

	R^1	R^2
1:	H	OH
3:	H	H
5:	Ac	OAc
6:	Bz	OBz
7:	Ac	H
8:	Bz	H

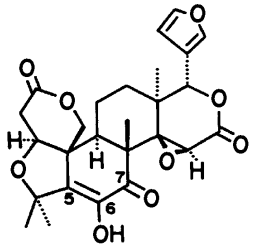

4

protons,[1,5] along with the usual limonoid furan signals at δ 7.29 (21-H), 6.46 (22-H), and 7.29 (23-H). The 19-H_b signal showed a W-type long-range coupling with a signal at δ 4.45 (br t, 1-H), which revealed the 1-H to be in α. Furthermore, the chemical shift of the deshielded 15-epoxide proton suggested the presence of a 7β-OH group.[6] The ^{1}H NMR spectrum of **1** also showed a signal for a carbinol methine proton at δ 4.34 (d, 7α-H), which collapsed to a singlet by addition of deuterium oxide (D_2O). Another carbinol methine signal was observed at δ 4.04 (12-H) as a multiplet, which also collapsed to a doublet by the addition of D_2O. The above ^{1}H NMR spectral feautures closely resembled to those of rutaevin (**3**) except for the presence of the signals due to an additional hydroxyl group (see experimental).

Because of the low solubility of the natural compound **1** in all common NMR solvents, the acetate **5**, obtained by treating with acetic anhydride/pyridine, was used for detailed NMR studies. The ^{1}H NMR spectrum of **5** also showed close similarity to that of rutaevin acetate (**7**) except for the additional acetyl signal at 1.83 (12α-OAc), which was heavily shielded by a paramagnetic anisotropy of the furan ring (Table 1). 2D-Homonuclear J-correlation (COSY) indicated the coupling protons on the linked carbons (C-1 and 2, and C-9, 11, and 12). No couplings were observed between 11α- and 9α-H and 11α- and 12β-H, showing their dihedral angles to be close to 90°. A skew boat conformation of the C ring was suggested by that the 11α-proton showed only geminal coupling (J=15 Hz).

The configuration of the 7- and 12-hydroxyl groups in **1** was also clarified from exciton-split CD curves arising from interaction between benzoate and furan chromophores.[7] The 7,12-dibenzoate **6** exhibited a positive split CD spectrum at 242 ($\Delta\varepsilon$+4.0) and 227 nm ($\Delta\varepsilon$−4.9) like rutaevin 7-benzoate (**8**), arised from the positively coupled oscillator of furan and 7-benzoate (Fig. 2). Since both interactions of 7-OBz/12-OBz (dihedral angle is *ca.* 180°) and 12-OBz/furan (dihedral angle is *ca.* 0°) are not appreciated, the configuration of the 12-hydroxyl group could be determined to be α.

In the ^{1}H NOE experiments of **5**, irradiation of the 8-Me protons at δ 0.78 induced 19.9, 10.0 and 2.9% peak enhancements on the 15α-H, 19-H_b and 5-H signals, respectively. The NOE on 5-H revealed its configuration to be in β opposite to that of limonin (**2**), in the spectrum of which irradiation of the 8-Me protons at δ 1.07 showed following NOEs: 5.5 (6β-H), 13.5 (15-H), 2.5 (19-H_a), and 6.7% (19-H_b). Therefore, graucin A should be the 7β,12α-dihydroxy-6-oxo-5β-*H* analog of limonin. The ^{1}H NMR spectrum of **5**

Table 1. ^{1}H NMR Data of Graucin A Acetate (**5**) and Rutaevin Acetate (**7**)

H	Compound **5**					Compound **7**				
	δ	Mult	J/Hz	Coupled to[a]	NOE[b]	δ	Mult	J/Hz	Coupled to[a]	NOE[b]
1	4.21	brt	3	2a, 2b, (19b)	9, 28	4.37	brt	2	2a, 2b, (19b)	28
2a	2.55	dd	16, 3	2b, 1	2b	2.64	dd	16.5, 3	2b, 1	2b
2b	2.88	dd	16, 3	2a, 1	2a	2.91	dd	16.5, 3	2a, 1	2a
5	3.10	s			29, 30	3.06	s			29, 30
7	5.63	brs		30	18	5.61	brs		30	18
9	3.08	d	12	11β	1, 7, 18	2.90	d	12	11β	18
11α	1.67	brd	15	11β, (12β)		1.75	brdd	13, 7.5	11β, 12α, (12β)	
11β	2.18	ddd	15, 12, 5	11α, 9, 12		1.83	m		9, 11α, 12α, 12β	
12α						1.6	m		11α, 11β, 12β	
12β	5.00	brd	5	11β, (11α)	17	1.95	brdd	13.5, 7	12α, 11β, (11α)	
15	3.81	s			30, 7-OAc	3.82	s			30
17	5.52	brs		(21, 22)	12β, 21, 22	5.48	brs		(21, 22)	21, 22
19a	4.04	d	12.5	19b	19b	4.15	d	12.5	19b	19b
19b	4.30	brd	12.5	19a, (1)	5, 19a, 30	4.37	brd	12.5	19a, (1)	19a, 30
21	7.41	m		22, 23, (17)	17, 18	7.42	m		22, 23, (17)	18
22	6.46	m		21, 23, (17)	17, 18, 23	6.35	m		21, 23, (17)	18
23	7.42	m		21, 22	22	7.43	m		21, 22	22
18	1.41	s			7, 9, 21, 22	1.32	s			7, 9, 21, 22
28	1.32	s			1	1.30	s			1
29	1.42	s			5	1.40	s			5
30	0.78	brs		7	5, 15, 19b	0.78	brs		7	5, 15, 19b
OAc	2.30	s			15	2.29	s			
	1.83	s								

a) Distinguished couplings are listed and numerals in parenthesis denote small coupling. b) Numerals denote the proton exhibiting the NOE based on 2D-NOE.

(Table 1) well supports the structure **1** and the cross-relaxation correlated 2D-^{1}H NOE (NOESY) of **5** (4α-Me/1-H, 4β-Me/5-H, 8-Me/5-H, 19-H$_b$, 15-H, 13-Me/7-H, 9-H, 21-H, 22-H, 7-OAc/15-H, and 9-H/1-H, 7-H) revealed the gross conformation (Fig. 1).

The mutual similarities of the ^{1}H NMR spectra of graucin A (**1**) and rutaevin (**3**) and their acetates **5** and **7** suggested that rutaevin was also a 5β-H limonoid in contrast to the previously formulated structure. It had been determined by Dreyer as 6-oxoepilimonol possessing a 5α-H from the correlation with limonin (**2**) via limonin diosphenol (**4**), $\Delta^{5,6}$-6-hydroxylimonin, and analogy with other many Rutaceae limonoids.[3] The NOE different spectra of **3** and **7** showed 2.8% and 3.1% NOEs between 8-Me and 5-H, respectively, which assigned a 5β-H configuration to **3** as pointed out from the ^{13}C NMR study by Bennett and Hasegawa.[8] Further NOE data also supported the revised structure; NOEs between methyl and proton in **3**: 4α-Me/1-H (9.5%), 4β-Me/5-H (12.0%), 8-Me/15-H (18.4%), 19-H$_a$ (3.6%), 19-H$_b$ (11.3%), and 13-Me/7-H (5.8%), 9-H (6.1%), 21-H (4.2%), 22-H (6.1%); and Table 1 for **7**. The 5β-H configuration is apparently favored in **1** and **3** because a cis-fusion of the 5-membered A ring allows a less strained conformation.

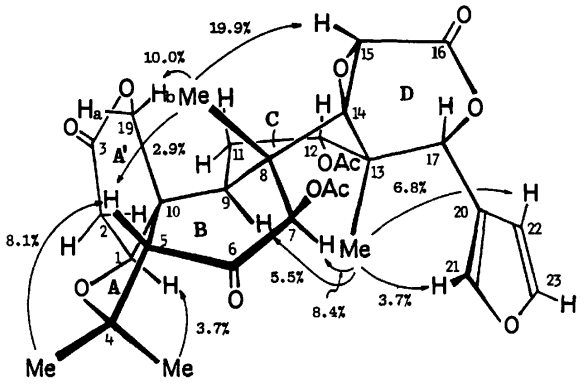

Fig. 1. Graucin A acetate (**5**), stereochemistry and NOEs between methyl and proton.

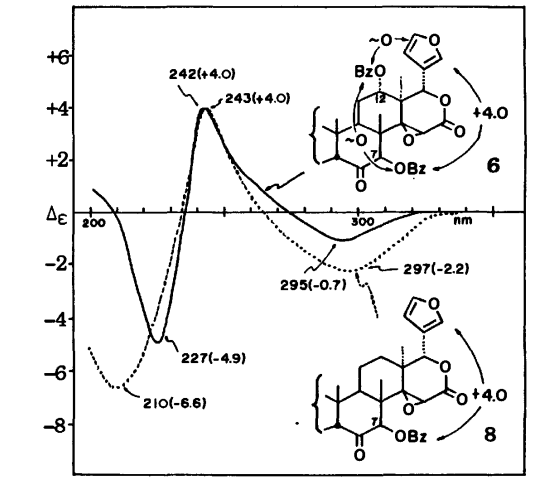

Fig. 2. CD spectra of 7,12-dibenzoylgraucin A (**6**) and 7-benzoylrutaevin (**8**).

Although there have been reported many Rutaceae limonoids, the 5β-H compounds are rare.[8] Among the compounds isolated in this work, limonin (**2**) and limonin diosphenol (**4**) were active as insect antifeedant against the larvae of *Spodoptera litura* Fab. with the leaf disk choice test. On the other hand, in antimicrobial tests against bacteria, yeasts and fungi rutaevin (**3**) showed weak antibacterial activity against *Bacillus subtilis*.

Experimental

Mps are uncorrected. UV spectra were measured in methanol (MeOH) and ^{1}H NMR spectra in chloroform-*d* with TMS as internal standard ($\delta = 0$ ppm) were measured at 360 MHz.

Plant Material. Roots of the plant were collected at Kagoshima University and identified by Dr. Sako, Kagoshima University.

Extraction and Isolation. Fresh root bark (1.0 kg) was extracted with MeOH (3×31). After concn to 200 ml, water (300 ml) was added to afford 5.2 g of a ppt which was applied onto a silica-gel column. The column was eluted with a dichloromethane (CH_2Cl_2)-MeOH gradient to yield a complex limonoid mixture and compound **1** (42 mg). The mixture was separated by repeated passage through a HPLC, semiprep silica-gel column, using 0.4—1% MeOH-CH_2Cl_2 as the solvent to give **2** (320 mg), **3** (26 mg) and **4** (21 mg).

Graucin A (1). Prisms from acetonitrile; mp >310 °C; $[\alpha]_D^{15}$ −150° (*c* 0.0005, CH_3CN); UV 209 nm (ε 6200); IR (Nujol) 3450, 1765, 1740, 1700, 1503, 1110, 1050, 1010, 875 cm^{-1}; CD(MeOH) 228 ($\Delta\varepsilon$ −5.3), 297 nm ($\Delta\varepsilon$ −1.7); SIMS *m/z*503 $(M+H)^+$, 645, 595, 553, 461, 277, 185, 93, 75, 57; ^{1}H NMR δ=0.61 (3H, s; 8-Me), 1.23 (3H, s; 4α-Me), 1.35 (3H, s; 13-Me), 1.44 (3H, s; 4β-Me), 2.63 (1H, dd, J= 15 and 3 Hz; 2-H$_a$), 2.91 (1H, dd, J=15 and 3 Hz; 2-H$_b$), 2.98 (1H, br d, J=12 Hz; 9-H), 3.13 (1H, s; 5-H), 3.87 (1H, d, J =3 Hz; -OH), 4.04 (1H, m; 12β-H), 4.10 (1H, d, J=12 Hz; 19-H$_a$), 4.15 (1H, s; 15-H), 4.28 (1H, d, J=12 Hz; 19-H$_b$), 4.34 (1H, m; 7-H), 4.37 (1H, d, J=7 Hz; -OH), 4.45 (1H, m; 1-H), 5.51 (1H, s; 17-H), 6.46 (1H, m; 22-H), 7.29 (2H, m; 21- and 23-H). Found: C, 62.12; H, 6.04%. Calcd for $C_{26}H_{30}O_{10}$: C, 62.14; H, 6.02%.

Limonin (2). Prisms from MeOH; mp 289 — 293 °C; $[\alpha]_D^{24}$ −136° (*c* 0.004, acetone); UV 208 nm (ε 7300); IR (Nujol) 1760, 1705, 1503, 878 cm^{-1}; CD (MeOH) 230 ($\Delta\varepsilon$ −4.9), 293 nm ($\Delta\varepsilon$ −2.3); EIMS *m/z*470 (M^+), 455, 426, 413, 347, 135, 108, 94; ^{1}H NMR δ=1.07 (3H, s; 8-Me), 1.18 (3H, s; 4β-Me), 1.18 (3H, s; 13-Me), 1.30 (3H, s; 4α-Me), 1.52 (1H, m; 12α-H), 1.78 (1H, m; 12β-H), 1.83 (1H, m; 11α-H), 1.90 (1H, m; 11β-H), 2.23 (1H, dd, J=16 and 3 Hz; 5-H), 2.47 (1H, dd, J=14.5 and 3.5 Hz; 6α-H), 2.55 (1H, dd, J=12 and 2.5 Hz; 9-H), 2.68 (1H, dd, J=17 and 2 Hz; 2-Ha), 2.86 (1H, dd, J=15.5 and 14.5 Hz; 6β-H), 2.98 (1H, dd, J=17 and 4 Hz; H-2$_b$), 4.03 (1H, m; 1-H), 4.03 (1H, s; 15-H), 4.47 (1H, d, J=13; 19-H$_a$), 4.77 (1H, br d, J

$=13$; 19-H_b), 5.47 (1H, br s; 17-H), 6.34 (1H, ddd, $J=2$, 1, and 1Hz; 22-H), 7.40 (1H, dd, $J=2$ and 1.5 Hz; 23-H), 7.42 (1H, dd, $J=1.5$ and 1 Hz; 21-H). NOEs (no indication in parentheses based on 2D-NOE): 9-H/1-H, 5-H, 13-Me, 13-Me/9-H (5.8%), 21-H (4.3%), 22-H (5%), 4α-Me/5-H (6.9%), 1-H (2.5%), 4β-Me/19-H_b, 8-Me/6β-H (5.5%), 15-H (13.5%), 19-H_a (2.5%), 19-H_b (6.7%).

Rutaevin (3). Needles from MeOH; mp >300 °C; $[\alpha]_D^{24}$ −146° (*c* 0.0005, MeOH); UV 208 nm (ε 9400); IR (Nujol) 3420, 1770, 1740, 1710, 1504, 880 cm^{-1}; CD (MeOH) 230 ($\Delta\varepsilon$−4.1), 295 nm ($\Delta\varepsilon$−1.0); FDMS *m/z* 487 (M^+), 410, 369, 327, 244, 190, 127, 85; ^1H NMR $\delta=0.65$ (3H, s; 8-Me), 1.21 (3H, s; 4α-Me), 1.36 (3H, s; 13-Me), 1.44 (3H, s; 4β-Me), 1.6 (1H, m; 12α-H), 1.73 (1H, br dd, $J=13$ and 8 Hz; 11α-H), 1.85 (1H, m; 11β-H), 1.95 (1H, m; 12β-H), 2.64 (1H, dd, $J=15$ and 3 Hz; 2-H_a), 2.79 (1H, br d, $J=12$ Hz; 9-H), 2.92 (1H, dd, $J=15$ and 3 Hz; 2-H_b), 3.12 (1H, s; 5-H), 3.89 (1H, d, $J=3$ Hz; -OH), 4.15 (1H, d, $J=12.5$ Hz; 19-H_a), 4.16 (1H, s; 15-H), 4.28 (1H, br d, $J=12.5$ Hz; 19-H_b), 4.35 (1H, br d, $J=3$ Hz; 7-H), 4.37 (1H, br t, $J=3$ Hz; 1-H), 5.48 (1H, br s; 17-H), 6.35 (1H, m; 22-H), 7.43 (1H, m; 23-H), 7.44 (1H, m; 21-H). NOEs: 13-Me/7-H (5.8%), 9-H (6.1%), 21-H (4.2%), 22-H (6.1%), 4α-Me/1-H (9.5%), 4β-Me/5-H (12.0%), 8-Me/15-H (18.4%), 19-H_a (3.6%), 19-H_b (11.3%).

Limonin Diosphenol (4). Needles from acetone; mp 273—278 °C; $[\alpha]_D^{24}$ −193° (*c* 0.002, acetone); UV 207 (ε 7900), 278 nm (ε 7900); IR (Nujol) 3450, 1740, 1690, 1660, 880 cm^{-1}; CD (MeOH) 208 ($\Delta\varepsilon$−4.2), 275 ($\Delta\varepsilon$+10.7), 320 nm ($\Delta\varepsilon$−8.5); ^1H NMR $\delta=1.04$ (3H, s; 8-Me), 1.16 (3H, s; 4β-Me), 1.49 (3H, s; 13-Me), 1.54 (3H, s; 4α-Me), 2.64 (1H, dd, $J=13$ and 3 Hz; 9-H), 2.84 (1H, dd, $J=17$ and 5 Hz; 2-H_a), 2.91 (1H, dd, $J=17$ and 3 Hz; 2-H_b), 4.07 (1H, br t, $J=3$ Hz; 1-H), 4.12 (1H, s; 15-H), 4.62 (1H, d, $J=13$ Hz; 19-H_a), 4.66 (1H, d, $J=13$ Hz; 19-H_b), 5.43 (1H, s; 17-H), 6.23 (1H, s; -OH), 6.38 (1H, m; 22-H), 7.40 (1H, m; 23-H), 7.41 (1H, m; 21-H).

7, 12-Diacetylgraucin A (5). Graucin A (**1**) (8 mg) was acetylated with Ac_2O-pyridine at room temperature and the product was purified by chromatography over SiO_2. Recrystallization from MeOH afforded diacetate **5** (6 mg) as needles, mp >300 °C. UV 213 nm (ε 8000); IR (CH_2CI_2) 1770—1740, 1720, 1700, 1225, 1060, 875 cm^{-1}; SIMS *m/z* 587 $(M+H)^+$, 609, 551, 527, 418, 207, 185, 115, 93, 61, 43.

7,12-Dibenzoylgraucin A (6). Graucin A (**1**) (3 mg) was benzoylated with benzoyl chloride in pyridine at 60 °C and the product was chromatographed over SiO_2 and purified by HPLC to give **6** (2 mg). 7,12-dibenzoylgraucin A (**6**): UV 207 (ε 9400), 232 nm (ε 18000); IR (CH_2Cl_2) 1770, 1750, 1720, 1600, 1245, 1180, 1100, 880 cm^{-1}; CD (MeOH) 227 ($\Delta\varepsilon$−4.9), 242 ($\Delta\varepsilon$+4.0), 295 nm ($\Delta\varepsilon$−0.7); SIMS *m/z* 711 $(M+H)^+$.

7-Acetylrutaevin (7). Rutaevin (**3**) (20 mg) was acetylated with Ac_2O-pyridine and the product was purified by chromatography. Recrystallization from MeOH afforded **7** (18 mg) as needles, mp 184—188 °C; $[\alpha]_D^{24}$ −101° (*c* 0.0005, MeOH); UV 209 nm (ε 9400); IR (CH_2Cl_2) 1770—1740, 1715, 1700, 1220, 1055, 875 cm^{-1}; CD (MeOH) 297 nm ($\Delta\varepsilon$−0.56), 227 nm ($\Delta\varepsilon$−2.29).

7-Benzoylrutaevin (8). Rutaevin (**3**) (15 mg) was benzoylated with benzoyl chloride in pyridine at 60 °C. Final purification of the product by HPLC afforded **8** (11 mg). Compound **8**, mp 285—288 °C; UV 209 (ε 9700), 234 nm (ε 14000); IR (CH_2Cl_2) 1780, 1750, 1730, 1605, 1503, 885 cm^{-1}; CD (MeOH) 210 ($\Delta\varepsilon$−6.6), 243 ($\Delta\varepsilon$+4.0), 297 nm $\Delta\varepsilon$−2.2); ^1H NMR $\delta=0.92$ (3H, s; 8-Me), 1.36 (3H, s; 4α-Me), 1.40 (3H, s; 13-Me), 1.42 (3H, s; 4β-H), 1.6 (1H, m; 12α-H), 1.8 (1H, m; 11α-H), 1.85 (1H, m; 11β-H), 1.95 (1H, m; 12β-H), 2.66 (1H, dd, $J=15$ and 3 Hz; 2-H_a), 2.93 (1H, dd, $J=15$ and 3 Hz; 2-H_b), 3.00 (1H, br d, $J=12$ Hz; 9-H), 3.12 (1H, s; 5-H), 3.79 (1H, s; 15-H), 4.20 (1H, d, $J=12$ Hz; 19-H_a), 4.36 (1H, br d, $J=12$ Hz; 19-H_b), 4.41 (1H, br t, $J=3$ Hz; 1-H), 5.47 (1H, s; 17-H), 5.90 (1H, s; 7-H), 6.35 (1H, m; 22-H), 7.40 (1H, m; 21-H), 7.42 (1H, m; 23-H), 7.52 (2H, t, $J=7$ Hz; 3′-and 5′-H), 7.65 (1H, tt, $J=7.5$ and 1.5 Hz; 4′-H), 8.06 (2H, dd, $J=7$ and 1.5 Hz; 2′-and 6′-H).

Limonin Diosphenol (4) from Limonin (2). Limonin (**2**) (100 mg) suspended in *t*-butyl alcoholic *N*-potassium *t*-butoxide (20 ml) was shaken with oxygen in a hydrogenetion apparatus for 2 h. After addition of water, the soln was acidified with 6M-hydrochloric acid (1 M=1 mol dm^{-3}) and extracted with chloroform ($CHCl_3$). The $CHCl_3$ soln was washed with aq sodium hydrogencarbonate and water, and then shaken with aq 4M-sodium hydroxide. Acidification of this extract with 6M-hydrochloric acid gave a ppt which was extracted with $CHCl_3$ again. The $CHCl_3$ soln was washed with water, and the solvent was removed. Recrystallization from acetone gave **4** (43 mg) as needles, mp 273—278 °C.[9]

Limonin Diosphenol (4) from Rutaevin (3). Pyridinium chlorochromate (80 mg) was added to a stirred soln of rutaevin (**3**) (44 mg) in CH_2Cl_2. After stirring over night at room temperature, MeOH was added and stirred for additional 1 h, and then the soln was evapolated in vacuo to yield a brown residue which was chromatographed over SiO_2 to give **4** (30 mg).

Biological Activities. Insect Antifeedant Activity. The limonoids **1**—**4** were tested against the larvae of the pest insect *Spodoptera litura* Fab. with the leaf disk method.[10] Limonin (**2**) and limonin diosphenol (**4**) showed the activity at 1000 ppm concn. **Antimicrobial Activity.** Effects of the compound **1**—**4** on growth of microorganisms were tested by the broth dilution method by Dr. M. Taniguchi (Osaka City University). Among the compounds rutaevin (**3**) was active against a bacterium *Bacillus subtilis* at 100 μg ml^{-1} concn. Test organisms; bacterium; *S. aureus, B. subtilis, E. coli* and *Ps. aeruginosa*: fungus; *Mucor mucedo, Rh. chinensis, Asp. niger* and *P. crustosum*: yiest; *S. cerevisiae, C. utilis, Schiz. pombe* and *H. anomala*.

We are grateful to Dr. Shizuo Sako (Kagoshima University) for the identification of the plant and to Mr. Mitsuo Tahara (Sankei Chemical Co. LTD.) for the supply of the insect. Our thanks are also due to Dr. Makoto Taniguchi (Osaka City University) for the antimicrobial test and Dr. Kozo Shibata (Osaka City University) for the elemental analysis.

References

1) M. Nakatani, J. C. James, and K. Nakanishi, *J. Am. Chem. Soc.*, **103**, 1228 (1981); M. Nakatani, M. Okamoto, T. Iwashita, K. Mizukawa, H. Naoki, and T. Hase, *Heterocycles*, **22**, 2335 (1984); M. Nakatani, T. Iwashita, H. Naoki, and T.

Hase, *Phytochemistry,* **24**, 195 (1985).
2) D. Arigoni, D. H. R. Barton, E. J. Corey, O. Jeger, L. Coglioti, S. G. Ferrini, E. R. Glazier, A. Melera, S. K. Pradhan, K. Schaffner, S. Stemhell, J. E. Templeton, and S. Tobinaga, *Experimentia,* **16**, 41 (1960).
3) D. L. Dreyer, *J. Org. Chem.,* **32**, 3442 (1967).
4) Y. Hirose, *Chem. Pham. Bull. Tokyo,* **11**, 535 (1963).
5) S. D. Jodad, J. J. Hoffmann, K. H. Schram, J. R. Cole, M. S. Tempesta, and R. B. Bates, *J. Org. Chem.,* **46**, 641 (1981).
6) D. L. Dreyer, *Tetrahedron,* **21**, 75 (1965).
7) R. S. Stonard, D. A. Trainor, M. Nakatani, and K. Nakanishi, *J. Am. Chem. Soc.,* **105**, 130 (1983).
8) R. D. Bennett and S. Hasegawa, *Tetrahedron,* **37**, 17 (1981).
9) D. H. R. Barton, S. K. Pradhan, S. Sternhell, and J. F. Templeton, *J. Chem. Soc.,* **1961**, 255.
10) I. Kubo, M. Taniguchi, A. Chapya, and K. Tsujimoto, *Planta Med.,* **1980**, 185.

 © 1987 The Chemical Society of Japan Bull. Chem. Soc. Jpn., 60, 2509—2515 (1987)

Preparation of 2-Alkenylsilanes and 2-Alkenylstannanes by the Reaction of 2-Alkenyl-1,1-cyclopropanedicarboxylate Esters with $PhMe_2SiAlEt_2$ and $(Ph_3Sn)_2Zn$. Generation of 2-Alkenyl-3-cyclopentene-1,1-dicarboxylates via Alkenyl-Substituted π-Allylpalladium Complexes Derived from Dienylsilanes and $[PdCl_2(CH_3CN)_2]$

Keigo FUGAMI, Koichiro OSHIMA,* Kiitiro UTIMOTO, and Hitosi NOZAKI
Department of Industrial Chemistry, Faculty of Engineering, Kyoto University, Yoshida, Kyoto 606
(Received February 26, 1987)

Reaction of 2-vinyl-1,1-cyclopropanedicarboxylate with $PhMe_2SiAlEt_2$, $PhMe_2SiZnEt_2Li$, or $(Ph_3Sn)_2Zn$ gave 1,7-homoconjugate addition products, 2-alkenylsilanes or 2-alkenylstannanes. In a similar fashion, 2-(1,3-butadienyl)-1,1-cyclopropanedicarboxylate provided the corresponding 1,9-homoconjugate adducts, dienylsilanes or dienylstannanes. The adducts were converted into π-allylpalladium complexes by means of $[PdCl_2(CH_3CN)_2]$. Treatment of the alkenyl-substituted π-allylpalladium complexes derived from dienylsilanes and $[PdCl_2(CH_3CN)_2]$ with bases such as PPh_3 or Na_2CO_3 gave 2-alkenyl-3-cyclopentene-1,1-dicarboxylates. In contrast, the reaction of the π-allylpalladiums generated from 2-alkenylsilanes and $[PdCl_2(CH_3CN)_2]$ with the bases resulted in the formation of original vinylcyclopropane derivatives.

Scheme 1 refers to the reaction of organoaluminum reagents with vinylcyclopropanes activated by two electron-withdrawing group. The regiochemistry in the homoconjugate addition of an alkyl group to 2-vinyl-1,1-cyclopropanedicarboxylic ester (**1**) is controlled by the nature of organoaluminum reagents.[1] Here we wish to report the reactions of Scheme 2, in which organometallic reagents such as $PhMe_2SiAlEt_2$,[3] $PhMe_2SiZnEt_2Li$,[3] and $(Ph_3Sn)_2Zn$[4] react with vinylcyclopropanes regioselectively to give 1,7-homoconjugate addition products, 2-alkenylsilanes and 2-alkenylstannanes. Similarly, 2-(1,3-butadienyl)cyclopropanes provide the corresponding dienylsilanes upon treatment with silylmetal reagents.

For example, the vinylcyclopropane **1** was allowed to react with 2.0 equivalents of $PhMe_2SiAlEt_2$ derived from $PhMe_2SiLi$ and Et_2AlCl in tetrahydrofuran. The reaction took place smoothly and was completed usually in 1 h at 0 °C. Dilution of the reaction mixture with dichloromethane, followed by workup (NaF and H_2O) and isolation by silica-gel column chromatography, gave a stereoisomeric mixture of (*E*)-2-alkenylsilane and the (Z)-isomer (**2a**, E : Z = 81 : 19, Run 1 in Table 1). Ate complexes such as $PhMe_2SiAlMe_3Li$,[3] $PhMe_2SiZnEt_2Li$,[3] $PhMe_2SiBEt_3Li$,[5] $(PhMe_2Si)_3MnMgMe$,[6] and $Ph_3SiAlMe_3Li$ are also effective for the regioselective formation of 1,7-homoconjugate adducts with an exception of the reaction of 2-styryl-1,1-cyclopropane dicarboxylate (**8**) (Run 10 in Table 1). The use of $(Ph_3Sn)_2Zn$ instead of silyl reagents produced 2-alkenylstannanes (Runs 6 and 7 in Table 1). In the same way, 2-(1,3-butadienyl)cyclopropanes gave the corresponding dienylsilanes upon treatment with these silylmetal reagents. The regiochemisty of the reaction heavily depends on the nature of the substrates. The 2-(1,3-butadienyl)-cyclopropane (**12**) gave 1,9-homoconjugate adduct mainly, whereas the 2-(4-phenyl-1,3-butadienyl)-cyclopropane (**14**) and 2-(3-methyl-1,3-butadienyl)-cyclopropane (**17**) afforded regioisomeric mixtures. The new method was successfully extended to the ring opening of vinylaziridines and dienylaziridines.

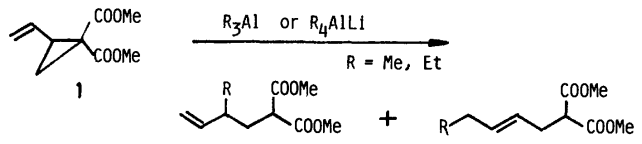

Scheme 1.

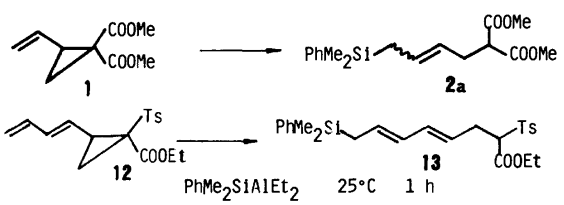

Scheme 2.

Two necessary factors for successful homoconjugate addition are as follows: (a) The presence of two activating groups and (b) a vinyl or dienyl group on the cyclopropane ring. Ethyl chrisanthemate did not undergo conjugate addition, and the attempted reaction of dimethyl 1,1-cyclopropanedicarboxylic ester resulted in the recovery of the starting material. Dimethyl 2-(2-methyl-1-propenyl)-1,1-cyclopropanedicarboxylate remained unchanged upon treatment with $PhMe_2SiAlEt_2$ (Run 11 in Table 1). Steric hindrance of geminal dimethyl groups explains the absence of the attack of $PhMe_2Si$ anion on the vinyl moiety.

Table 1. Homoconjugate Addition of Silylmetal Reagents to Vinylcyclopropanes and Dienylcyclopropanes

Run	Substrate	Reagent	Product	Y/% (E/Z)
1	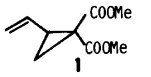 1	$PhMe_2SiAlEt_2$	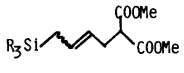	100 (81/19)
2		$PhMe_2SiBEt_3Li$		100 (88/12)
3		$(PhMe_2Si)_3MnMgMe$	**2a** $R_3 = PhMe_2$	78 (90/10)
4		$Ph_3SiAlEt_2$	**2b** $R_3 = Ph_3$	100 (69/31)
5		$Ph_3SiAlMe_3Li$	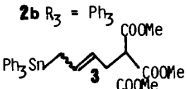 **3**	70 (70/30)
6	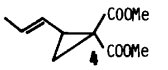 **4**	$(Ph_3Sn)_2Zn$		81 (82/18)
7		$(Ph_3Sn)_2Zn$	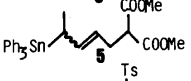 **5**	74 (90/10)
8	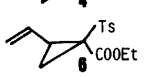 **6**	$PhMe_2SiAlEt_2$	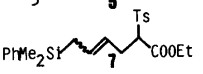 **7**	98 (79/21)
9		$PhMe_2SiAlBu_3Li$		93 (73/27)
10	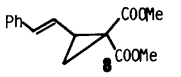 **8**	$PhMe_2SiAlEt_2$	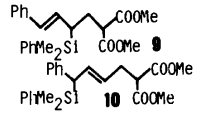 **9** **10**	60 9/10=28/72
11	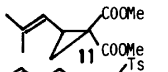 **11**	$PhMe_2SiAlEt_2$	No Reaction	
12	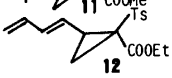 **12**	$PhMe_2SiZnEt_2Li$	**13**	75
13	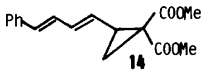 **14**	$PhMe_2SiZnEt_2Li$	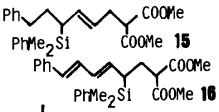 **15** **16**	48 15/16=1/1
14	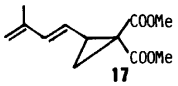 **17**	$PhMe_2SiAlMe_3Li$	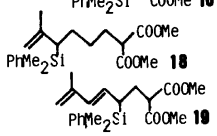 **18** **19**	37 18/19=31/69
15	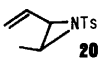 **20**	$PhMe_2SiAlMe_3Li$	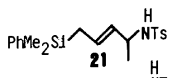 **21**	81 (100/0)
16	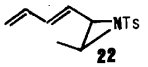 **22**	$PhMe_2SiAlMe_3Li$	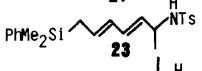 **23**	82 E, E only
17	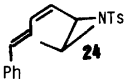 **24**	$PhMe_2SiAlEt_3Li$	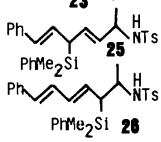 **25** **26**	86 25/26=4/6

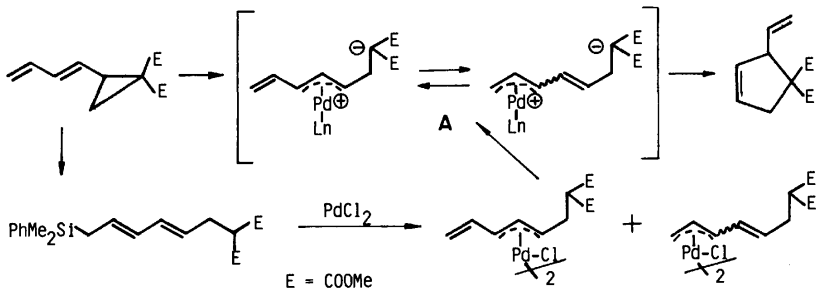

Scheme 3.

Previously, we reported[7,8] that 1,3-butadienylcyclopropanes in Scheme 3 activated by two electron-withdrawing groups smoothly rearranged to vinylcyclopentenes in the presence of a Pd(0) catalyst. 1-Tosyl-2-(1,3-butadienyl)aziridines reacted similarly to give pyrroline derivatives. A zwitterion **A** plays a critical role in the rearrangement. We next examined the synthesis of five-membered ring compounds via the π-allylpalladium complexes which were readily prepared from the above-mentioned alkenylsilanes and $[PdCl_2(CH_3CN)_2]$.

Treatment of the 2-alkenylsilanes **3**, **7**, **9(10)**, and

Table 2. Synthesis of π-Allylpalladium Complexes

Alkenylsilane (Alkenylstannane)	Product	Y/%
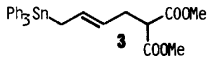 **3**	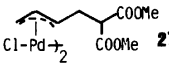 **27**	21
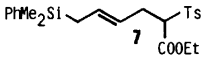 **7**	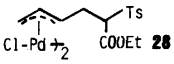 **28**	46
9, 10 (9/10 = 72/28)	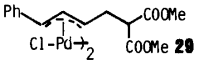 **29**	80
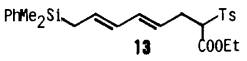 **13**	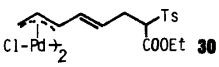 **30**	40
15, 16 (15/16 = 1/1)	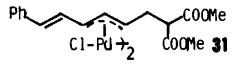 **31**	35
18, 19 (18/19 = 31/69)	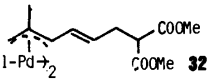 **32**	50
	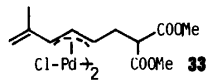 **33**	32/33 = 3/1
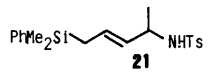 **21**	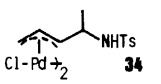 **34**	47
25, 26 (25/26 = 40/60)	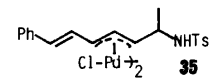 **35**	—

21 and 2,4-dienylsilanes **13**, **15(16)**, **18(19)**, and **25(26)** with one equivalent of $[PdCl_2(CH_3CN)_2]$ in tetrahydrofuran at 25 °C provided π-allylpalladium complexes[9] after purification by silica-gel column chromatography[10] (Table 2).

Exposure of the π-allylpalladiums **28** and **29** to PPh_3 resulted in the formation of the original alkenylcyclopropane derivatives **6** (40%) and **8** (46%) along with unidentified complex products containing isomeric methyl 2-methoxycarbonyl-6-phenylhexadienoate or ethyl 2-tosylhexadienoate. No trace of cyclopentene derivatives was observed. In contrast, treatment of a mixture of **32** and **33** in DMSO with PPh_3 or Na_2CO_3 gave the cyclopentene derivative **36** in 70% or 80% yield, respectively. Similarly, treatment of the crude π-allylpalladium **35** generated from a mixture of **25** and **26** with PPh_3 also produced the pyrroline derivative **38**. Naturally, the prerequisite to the cyclization into five-membered rings should be a U shaped configuration of the zwitterion **A** as shown in Scheme 4. The simple π-allylpalladium complexes such as **27**, **28**, and **29** can not take this form but give vinylcyclopropanes only. On the other hand, the conjugation of C=C bond to the π-allylpalladium moiety enables the aliphatic chain to assume the U shape and leads to the cyclization to five-membered rings. The observed behavior of the isolated π-allylpalladium complexes in the present work does support this idea.

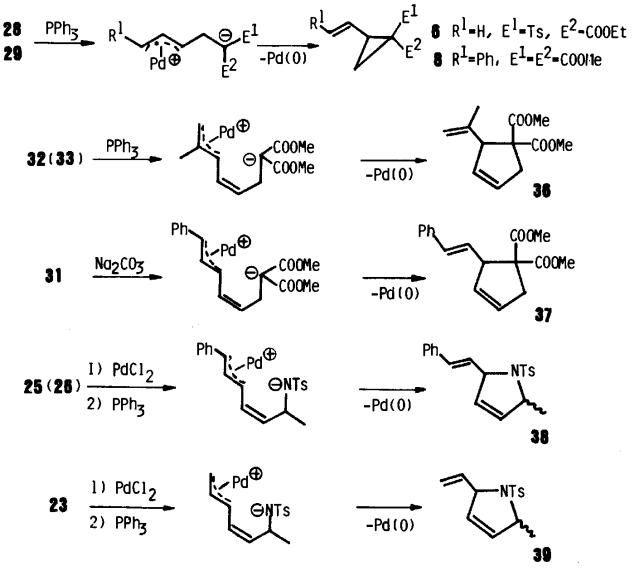

Scheme 4.

Experimental

Distillation of the products was performed by use of Kugelrohr (Büchi), and boiling points are indicated by an airbath temperature without correction. All melting points were obtained on a Yanaco MP-50929 melting point apparatus and are uncorrected, too. ^{1}H NMR and ^{13}C NMR spectra were taken on a Varian XL-200 spectrometer, $CDCl_3$ was used as solvent unless otherwise noted, chemical shifts being given in δ with tetramethylsilane as an internal standard. IR spectra were determined on a JASCO IR-810 spectrometer. The analyses were carried out by the staff at the Elemental Analyses Center of Kyoto University. Tetrahydrofuran (THF) was freshly distilled from sodium benzophenone ketyl. Purification of 2-alkenylstannanes was performed by column chromatography on neutral alumina (Merck Art. 1077 (95 g), H_2O (5 g)), and other products were purified by silica-gel column chromatography.

Dimethyl 2-Vinyl-1,1-cyclopropanedicarboxylate (1). The compound was prepared by the reported procedure.[11]

Syntyesis of *cis*-1-Tosyl-3-methyl-2-vinylaziridine (20). This was synthesized in 40% overall yield from 1,3-pentadiene by oxyamination:[12] Mp 90—92 °C (crystallizes after distillation at 110 °C/0.2 Torr (1 Torr = 133.322 Pa)); ^{1}H NMR δ = 1.20 (d, J = 5.8 Hz, 3H), 2.44 (s, 3H), 3.03 (dq, J = 7.0, 5.8 Hz, 1H), 3.33 (d, J = 7.0, 6.9 Hz, 1H), 5.30 (dd, J = 9.9, 1.8 Hz, 1H), 5.39 (dd, J = 17.2, 1.8 Hz, 1H), 5.61 (ddd, J = 17.2, 9.9, 6.9 Hz, 1H); ^{13}C NMR δ = 12.2, 21.6, 40.8, 45.7, 121.3, 127.2, 127.6, 129.5, 129.6, 144.3; IR (nujol) 1596, 1323, 1161, 1091, 927, 841, 678 cm^{-1}; Found: C, 60.69; H, 6.35; N, 5.64%. Calcd for $C_{12}H_{15}NO_2S$: C, 60.73; H, 6.37; N, 5.90%.

General Procedure for the Preparation of Cyclopropanecarbaldehydes and Aziridinecarbaldehyde. These materials were prepared by means of oxidative cleavage of the corresponding olefinic compounds.[13] In a typical procedure a hexane solution of OsO_4 (0.06 mmol) was added to a solution of **20** (2.1 g, 9.0 mmol) in THF (55 ml) and water

(18 ml) at room temperature under argon atmosphere. The color of the solution turned dark brown after stirring for 5 min. Then powdered sodium periodate (5.2 g, 24.3 mmol) was added and the stirring was continued overnight. The mixture was diluted with hexane and the precipitate was filtered off. The filtrate was washed twice with aqueous sodium thiosulfate solution (1 M, 1 M = 1 mol dm^{-3}, 50 ml × 2), and aqueous layer was extracted with dichloromethane (30 ml). Combined organic layers were dried over anhydrous sodium sulfate and concentrated in vacuo. Purification by column chromatography (hexane-ethyl acetate, 3 : 1) afforded 1.7 g (80%) of *cis*-2-formyl-3-methyl-1-tosylaziridine: Mp 50 °C (crystallizes after distillation at 120 °C/0.2 Torr); ^{1}H NMR δ = 1.41 (d, J = 6.0 Hz, 3H), 2.48 (s, 3H), 3.0—3.4 (m, 1H), 3.20 (dq, J = 7.0, 6.0 Hz, 1H), 7.43 (d, J = 8.3 Hz, 2H), 7.89 (d, J = 8.3 Hz, 2H), 9.35 (d, J = 5.5 Hz, 1H); ^{13}C NMR δ = 12.9, 21.5, 40.8, 46.4, 127.8, 129.7, 129.8, 145.1, 195.3; IR (neat) 1727, 1595, 1326, 1162, 1090, 878, 714, 670 cm^{-1}.

Dimethyl 2-Formyl-1,1-cyclopropanedicarboxylate. Ozonolysis of **1** following the reported procedure[5] gave the title compound in 65% yield.

Ethyl 2-Formyl-1-tosyl-1-cyclopropanecarboxylate. This material was prepated in 87% yield from ethyl 1-tosyl-2-vinyl-1-cyclopropanecarboxylate[14] with $NaIO_4$ and OsO_4.

***cis*-3-Methyl-2-(4-phenyl-1,3-butadienyl)-1-tosylaziridine (24) (General Method for the Preparation of Dienylcyclopropanes[5] and Dienylaziridines).** To an ethereal suspension of cinnamyltriphenylphosphonium chloride (0.62 g, 1.5 mmol) was added potassium *t*-butoxide (0.12 g, 1.1 mmol) at 0 °C under argon atmosphere. The resulting red suspension was stirred for additional 10 min and then allowed to stand still. The supernatant was transferred using a hypodermic syringe into an ethereal solution of 1-tosyl-2-formyl-3-methylaziridine. After stirring for 30 min, the reaction mixture was poured into aqueous ammonium chloride (30 ml), extracted with hexane, and washed with water. The organic layer was dried over anhydrous sodium sulfate and evaporated in vacuo. Purification by column chromatography afforded **24** as a colorless oil (0.12 g, 54% yield): Bp 140 °C/760 Torr (decomp); ^{1}H NMR δ = 1.22 (d, J = 5.7, 3H), 2.37 (s, 3H), 3.14 (dq, J = 5.7, 7.2 Hz, 1H), 3.74 (ddd, J = 8.1, 7.2, 1.0 Hz, 1H), 5.21 (dd, J = 10.9, 8.1 Hz, 1H), 6.41 (dd, J = 11.1, 10.9 Hz, 1H), 6.61 (d, J = 15.5 Hz, 1H), 7.12 (ddd, J = 15.5, 11.1, 1.0 Hz, 1H), 7.2—7.5 (m, 7H), 7.85 (d, J = 8.3 Hz, 2H); ^{13}C NMR δ = 12.7, 21.5, 41.1, 41.9, 121.7, 123.1, 126.7, 127.6, 128.1, 128.6, 129.7, 135.4, 135.5, 135.7, 136.7, 144.3; IR (neat) 3026, 1591, 1493, 1450, 1396, 1323, 1156, 1091, 1046, 935, 875, 713, 693, 669 cm^{-1}; Found: C, 70.66; H, 6.48; N, 3.83%. Calcd for $C_{20}H_{21}NO_2S$: C, 70.77; H, 6.24; N, 4.13%.

***cis*-2-(1,3-Butadienyl)-3-methyl-1-tosylaziridine (22).** (E : Z = 22 : 78): Mp 78—80 °C (crystallizes after distillation at 150 °C/0.1 Torr); ^{1}H NMR δ = 1.19 (d, J = 5.9 Hz, 0.66H), 1.21 (d, J = 5.9 Hz, 2.34H), 2.43 (s, 3H), 3.0—3.2 (m, 1H), 3.37 (dd, J = 7.3, 7.3 Hz, 0.22H), 3.64 (ddd, J = 8.3, 7.1, 1.2 Hz, 0.78H), 5.1—5.7 (m, 3.22H), 6.2—6.5 (m, 0.22H), 6.25 (dd, J = 11.9, 10.1 Hz, 0.78H), 6.68 (dddd, J = 16.6, 11.2, 10.1, 1.1 Hz, 0.78H), 7.33 (d, J = 8.4 Hz, 2H), 7.82 (d, J = 8.4 Hz, 2H); ^{13}C NMR δ = 12.6, 21.5, 40.9, (41.2), 41.6, (45.2), (118.6), 120.7, 122.2, (124.6), (127.0), (127.2), 127.6, (129.5), 129.6, (131.1), 135.5, 135.6, (136.7), 144.3; IR (Nujol) 1596 (w), 1319, 1159, 1090, 910, 868, 677; Found: C, 63.61; H, 6.70; N, 5.58%. Calcd for $C_{14}H_{17}NO_2S$: C, 63.85; H, 6.51; N, 5.32%.

A Typical Procedure for Generation of Silylmetal Reagents. A THF solution of $PhMe_2SiLi$ (1.0 mmol) was added to a solution of Et_2AlCl (1.0 mmol) in THF (2 ml) at 0 °C under argon atmosphere and the resulting solution was stirred for 10 min. Other silylmetal reagents such as $PhMe_2SiBEt_3Li$,[6] $(PhMe_2Si)_3MnMgMe$,[7] and $PhMe_2SiAlEt_3Li$ were also prepared according to the procedures described before.

Reaction of Dimethyl 2-Vinyl-1,1-cyclopropanedicarboxylate (1) with $PhMe_2SiAlEt_2$. To a THF solution of $PhMe_2SiAlEt_2$ (0.94 mmol) was added a solution of **1** (80 mg, 0.43 mmol) in THF (2 ml) at 0 °C under argon atmosphere. After stirring for 1 h, the reaction mixture was diluted with dichloromethane (15 ml) and anhydrous sodium fluoride (0.42 g) was added. Then water (0.2 ml) was added dropwise and the resulting white suspension was vigorously stirred for 10 min. Filtration through a short column of anhydrous sodium sulfate and concentration followed by column chromatography gave 80 mg (100%) of dimethyl 5-(dimethylphenylsilyl)-3-pentene-1,1-dicarboxylate (**2a**) (E : Z = 81 : 19): Bp 125 °C/0.1 Torr; ^{1}H NMR δ = 0.21 (s, 4.9H), 0.28 (s, 1.1H), 1.66 (dd, J = 7.9, 0.8 Hz, 1.62H), 1.75 (dd, J = 8.7, 1.1 Hz, 0.38H), 2.53 (dd, J = 7.6, 7.6 Hz, 0.38H), 2.57 (dd, J = 7.6, 7.6 Hz, 1.62H), 3.25 (t, J = 7.6 Hz, 0.19H), 3.66 (t, J = 7.6 Hz, 0.81H), 3.70 (s, 4.9H), 3.71 (s, 1.1H), 5.1—5.3 (m, 1H), 5.4—5.6 (m, 1H), 7.3—7.6 (m, 5H); ^{13}C NMR δ = −3.6, (−3.4), (17.7), 21.8 (26.4), 32.0, (47.8), 51.6, (52.2), 52.3, (122.7), 124.2, 127.7, (127.8), (128.3), 128.9, (129.0), (129.1), 129.5, 133.5, 138.5, (143.0), 169.3, (169.5); IR (neat) 2952, 1752, 1737, 1437, 1249, 1156, 837, 731, 699 cm^{-1}; Found: C, 63.98; H, 7.71%. Calcd for $C_{17}H_{24}O_4Si$: C, 63.72; H, 7.55%.

Preparation of Dimethyl 5-(Triphenysilyl)-3-pentene-1,1-dicarboxylate (2b). (E : Z = 70 : 30). This compound was obtained (78 mg, 70%) by the reaction between vinylcyclopropane **1** (92 mg, 0.50 mmol) and $Ph_3SiAlMe_3Li$ (1.0 mmol) prepared from Ph_3SiLi[15] and Me_3Al: Bp 250 °C/0.1 Torr; ^{1}H NMR δ = 2.29 (d, J = 7.9 Hz, 1.4H), 2.37 (d, J = 7.4 Hz, 0.6H), 2.46 (dd, J = 7.3, 7.3 Hz, 0.6H), 2.50 (dd, J = 7.3, 7.3 Hz, 1.4H), 3.07 (t, J = 7.3 Hz, 0.3H), 3.23 (t, J = 7.3 Hz, 0.7H), 3.59 (s, 4.2H), 3.66 (s, 1.8H), 5.2—5.4 (m, 1H), 5.5—5.8 (m, 1H), 7.3—7.7 (m, 15H); ^{13}C NMR δ = (13.8), 19.4, (25.8), 32.1, 51.9, 52.3, 125.8, 127.8, 128.6, 129.5, 134.5, 135.7, 169.3; IR (neat) 3066, 3046, 3018, 2950, 1753, 1736, 1429, 1234, 1156, 1111, 967, 734, 700 cm^{-1}; Found: C, 73.09; H, 6.23%. Calcd for $C_{27}H_{28}O_4Si$: C, 72.94; H, 6.23%.

Preparation of Dimethyl 5-(Triphenylstannyl)-3-hexene-1,1-dicarboxylate (5). A hexane solution of diethylzinc (1.5 M, 0.24 ml, 0.35 mmol) was added to a THF solution of triphenylstannane (0.25 g, 0.70 mmol) at 0 °C under argon atmosphere. After stirring for 15 min, a solution of **4** (70 mg, 0.35 mmol) in THF (2 ml) was added. The reaction mixture was stirred for 30 min and poured into aqueous ammonium chloride (10 ml). Aqueous layer was extracted with dichloromethane. Organic layers were combined, washed with aqueous ammonium chloride and dried over anhydrous sodium sulfate. The solvent was removed and the residue was submitted to preparative TLC on silica

gel (hexane-ethyl acetate, 5 : 1) to give **5** (0.14 g, 74%, E : Z = 90 : 10) as a white solid: mp 63—66 °C (CH_2Cl_2); ^{1}H NMR δ=1.32 (dd, J=7.3, 1.5 Hz, 0.3H), 1.48 (d, J=7.3 Hz, 2.7H), 2.5—2.9 (m, 3H), 3.63 (s, 2.7H), 3.64 (s, 2.7H), 3.66 (s, 0.3H), 3.72 (s, 0.3H), 5.2—5.4 (m, 1H), 5.9—6.2 (m, 1H), 7.3—7.5 (m, 15H); ^{13}C NMR δ=16.9, 26.6, 32.1, 52.2, 52.3, 120.2, (128.0), 128.5, (128.8), 128.9, (136.9), 137.2, (137.4), 137.6, (137.8), 137.9, 138.1, 169.4; IR (neat) 2920, 2825, 1750, 1727, 1460, 1426, 1237, 1207, 1071, 971, 723, 697 cm^{-1}; Found: C, 61.29; H, 5.42%. Calcd for $C_{28}H_{30}O_4Sn$: C, 61.23; H, 5.51%.

Ethyl 6-(Dimethylphenylsilyl)-2-tosyl-4-hexenoate (7). (E : Z = 79 : 21): Bp 190 °C/0.1 Torr; ^{1}H NMR δ=0.21 (s, 4.74H), 0.27 (s, 1.26H), 1.12 (t, J=7.1 Hz, 2.37H), 1.13 (t, J=7.1 Hz, 0.63H), 1.63 (d, J=8.3 Hz, 1.58H), 1.73 (d, J=8.3 Hz, 0.42H), 2.44 (s, 3H), 2.5—2.8 (m, 2H), 3.75 (dd, J=8.6, 6.9 Hz, 0.21H), 3.88 (dd, J=11.2, 4.0 Hz, 0.79H), 4.0—4.2 (m, 2H), 5.0—5.2 (m, 1H), 5.4—5.6 (m, 1H), 7.1—7.6 (m, 9H); ^{13}C NMR δ=−3.6, 13.8, 21.6, 21.9, 30.1, 61.9, 70.8, 121.7, 127.7, 129.0, 129.3, 129.6, 131.1, 133.4, 134.1, 138.2, 145.3, 165.5; IR (neat) 2954, 1739, 1597, 1427, 1370, 1326, 1249, 1248, 1085, 837, 815, 731, 664, 572 cm^{-1}; Found: C, 64.33; H, 7.13%. Calcd for $C_{23}H_{30}O_4SSi$: C, 64.15; H, 7.02%.

A Mixture of Dimethyl (*E*)-3-(Dimethylphenylsilyl)-5-phenyl-4-pentene-1,1-dicarboxylate (9) and Dimethyl (*E*)-5-(Dimethylphenylsilyl)-5-phenyl-3-pentene-1,1-dicarboxylate (10) and (9 : 10= 72 : 28): Bp 190 °C/0.1 Torr; ^{1}H NMR δ=0.21 (s, 0.84H), 0.24 (s, 0.84H), 0.33 (s, 2.16H), 0.35 (s, 2.16H), 1.9—2.1 (m, 1.44H), 2.25 (dd, J=11.0, 10.0 Hz, 0.72H), 2.62 (dd, J=7.5, 7.3 Hz, 0.56H), 3.08 (d, J=10.0 Hz, 0.28H), 3.37 (t, J=7.3 Hz, 0.72H), 3.49 (dd, J=9.5, 4.5 Hz, 0.28H), 3.61 (s, 2.16H), 3.65 (s, 0.84H), 3.70 (s, 2.16H), 3.71 (s, 0.84H), 5.29 (dt, J=15.2, 7.5 Hz, 0.28H), 5.88 (dd, J=15.2, 10.0 Hz, 0.28H), 5.97 (dd, J=15.6, 9.0 Hz, 0.72H), 6.23 (d, J=15.6 Hz, 0.72H), 7.0—7.7 (m, 10H); ^{13}C NMR δ=−5.2, −4.5, (−4.41), (−4.36), 28.6, (32.05), 32.14, (42.5), 51.1, (52.0), 52.3, 52.4, (77.7), (124.2), (124.7), 125.7, 126.7, (127.3), 127.4, 127.8, 128.1, (128.4), 128.4, (129.1), 129.3, 129.6, 130.1, (132.9), 134.0, 134.2, (136.5), 137.7, 141.7, (169.3), (169.45), 169.54, 170.1; IR (neat) 2952, 1751, 1736, 1435, 1250, 1153, 832, 814, 700 cm^{-1}; Found: C, 69.78; H, 7.14%. Calcd for $C_{23}H_{28}O_4Si$: C, 69.66; H, 7.12%.

Ethyl 8-(Dimethylphenylsilyl)-2-tosyl-4,6-octadienoate (13): Bp 210 °C/0.1 Torr; ^{1}H NMR δ=0.2—0.3 (m, 6H), 1.1—1.2 (m, 3H), 1.6—1.9 (m, 2H), 2.46 (s, 3H), 2.5—2.9 (m, 2H), 3.8—4.3 (m 3H), 4.7—6.3 (m, 4H), 7.2—7.9 (m, 9H); ^{13}C NMR δ=−3.4, 13.9, 13.9, 21.7, 22.6, 30.1, 62.1, 70.4, 70.5, 73.0, 121.7, 127.0, 127.6, 127.7, 127.8, 128.6, 128.95, 129.04, 129.2, 129.3, 129.4, 129.5, 129.6, 131.2, 132.5, 133.9, 134.1, 134.9, 145.3, 165.5; IR (neat) 2956, 1738, 1598, 1428, 1327, 1148, 1085, 989, 835, 815, 700, 667 cm^{-1}; Found: C, 65.51; H, 7.10%. Calcd for $C_{25}H_{32}O_4SSi$: C, 65.75; H, 7.06%.

A Mixture of Dimethyl 5-(Dimethylphenylsilyl)-7-phenyl-3,6-heptadiene-1,1-dicarboxylate (15) and Dimethyl 3-(Dimethylphenylsilyl)-7-phenyl-4,6-heptadiene-1,1-dicarboxylate (16) (15 : 16 = 1 : 1): Bp 200 °C/0.2 Torr; ^{1}H NMR δ=0.30 (s, 1.5H), 0.31 (s, 1.5H), 0.31 (s, 1.5H), 0.33 (s, 1.5H), 1.8—2.0 (m, 1.0H), 2.20 (dd, J=11.4, 9.9 Hz, 0.5H), 2.62 (dd, J=7.3, 7.0 Hz, 1.0H), 2.76 (ddd, J=8.8, 4.4, 4.2 Hz, 0.5H), 3.38 (t, J=7.3 Hz, 0.5H), 3.4−3.5 (m, 0.5H), 3.64 (s, 1.5H), 3.68 (s, 3.0H), 3.70 (s, 1.5H), 5.21 (dt, J=16.2, 7.0 Hz, 0.5H), 5.5—5.6 (m, 0.5H), 5.63 (dd, J=16.2, 6.7 Hz, 0.5H), 6.04 (dd, J=15.2, 10.2 Hz, 0.5H), 6.1—6.2 (m, 1.0H), 6.39 (d, J=15.6 Hz, 0.5H), 6.73 (dd, J=15.6, 10.2 Hz, 0.5H), 7.0—7.6 (m, 10H); ^{13}C NMR δ=−5.2, −4.8, 28.6, 32.2, 39.6, 51.1, 52.1, 52.4, 52.5, 123.7, 125.7, 126.0, 126.5, 127.1, 127.6, 127.7, 127.8, 128.4, 128.6, 129.2, 129.48, 129.53, 130.6, 132.0, 134.05, 134.10, 134.7, 169.3, 169.5, 170.2; IR (neat) 3020, 2952, 1752, 1736, 1434, 1249, 1154, 1114, 832, 812, 735, 698 cm^{-1}; Found: C, 70.53; H, 7.22%. Calcd for $C_{25}H_{30}O_4Si$: C, 71.05; H, 7.16%.

Reaction of Dimethyl 2-(3-Methyl-1,3-butadienyl)-1,1-cyclopropanedicarboxylate (17) with $PhMe_2SiAlEt_3Li$. Treatment of **17** (0.13 g, 0.58 mmol) with $PhMe_2SiAlMe_3Li$ (1.5 mmol) afforded a mixture of dimethyl (3*E*)-5-(dimethylphenylsilyl)-6-methyl-3,6-heptadiene-1,1-dicarboxylate (**18**) and (4*E*)-3-(dimethylphenylsilyl)-6-methyl-4,6-heptadiene-1,1-dicarboxylate (**19**) (**18** : **19** = 31 : 69, 76 mg, 37%): bp 130 °C/0.1 Torr; ^{1}H NMR δ=0.28 (s, 0.93H), 0.28 (s, 0.93H), 0.29 (s, 2.07H), 0.30 (s, 2.07H), 1.58 (s, 0.93H), 1.78 (s, 2.07H), 1.80 (d, J=10.1 Hz, 0.31H), 1.8—2.0 (m, 0.69), 2.1—2.3 (m, 0.69H), 2.5—2.7 (m, 1.31H), 3.3—3.5 (m, 1H), 3.66 (s, 2.07H), 3.70 (s, 2.07H), 3.71 (s, 0.93H), 3.72 (s, 0.93H), 4.47 (bs, 0.31H), 4.66 (m, 0.31H), 4.81 (bs, 1.38H), 5.17 (dt, J=15.1, 7.1 Hz, 0.31H), 5.34 (dd, J=15.8, 9.3 Hz, 0.69H), 5.64 (dd, J=15.1, 10.1 Hz, 0.31H), 5.97 (d, J=15.8 Hz, 0.69H), 7.3—7.6 (m, 5H); ^{13}C NMR δ=−5.2, −4.5, (−4.3), 18.8, 28.5, 31.6, (32.1), (43.7), 52.0, (52.1), (52.3), 52.4 (108.5), 113.9, (123.4), 127.5, 127.7, (128.8), 128.95), (129.02), 129.2, 129.8, (129.9), (132.6), 132.7, (133.5), 134.0, 134.1, (136.6), 141.9, 169.4, (169.6), 170.2; IR (neat) 2954, 1754, 1737, 1435, 1250, 1155, 1115, 833, 816, 776, 735, 701 cm^{-1}; Found: C, 66.43; H, 7.87%. Calcd for $C_{20}H_{28}O_4Si$: C, 66.63; H, 7.83%.

(2*E*)-1-(Dimethylphenylsilyl)-4-tosylamino-2-pentene (21): Bp 170—180 °C/0.1 Torr; ^{1}H NMR δ=0.20 (s, 6H), 1.11 (d, J=6.7 Hz, 3H), 1.54 (d, J=7.9 Hz, 2H), 2.40 (s, 3H), 3.77 (ddq, J=7.0, 6.7, 6.7 Hz, 1H), 4.62 (d, J=7.0 Hz, 1H), 5.02 (ddt, J=15.2, 6.7, 1.2 Hz, 1H), 5.38 (ddt, J=15.2, 7.9, 1.0 Hz, 1H), 7.25 (d, J=8.1 Hz, 1H), 7.3—7.5 (m, 5H), 7.73 (d, J=8.1 Hz, 2H); ^{13}C NMR δ=−3.6, 21.4, 21.5, 22.3, 51.6, 127.1, 127.6, 127.7, 129.0, 129.4, 129.7, 133.5, 138.0, 138.2, 143.0; IR (neat) 3272, 2956, 1657, 1598, 1426, 1325, 1249, 1159, 1113, 1095, 1066, 965, 836, 813, 698, 663 cm^{-1}; Found: C, 64.11; H, 7.33; N, 3.68%. Calcd for $C_{20}H_{27}NO_2SSi$: C, 64.30; H, 7.28; N, 3.75%.

(2*E*,4*E*)-1-(Dimethylphenylsilyl)-6-tosylamino-2,4-heptadiene (23): Bp 220 °C/0.1 Torr (partially decomposed); ^{1}H NMR δ=0.26 (s, 6H), 1.18 (d, J=6.7 Hz, 3H), 1.74 (d, J=7.8 Hz, 2H), 2.40 (s, 3H), 3.94 (ddq, J=7.2, 6.5, 6.7 Hz, 1H), 4.28 (d, J=7.2 Hz, 1H), 5.20 (dd, J=15.1, 6.5 Hz, 1H), 5.59 (dt, J=15.0, 7.8 Hz, 1H), 5.74 (dd, J=15.0, 9.5 Hz, 1H), 5.92 (dd, J=15.1, 9.5 Hz, 1H), 7.28 (d, J=8.2 Hz, 2H), 7.3—7.6 (m, 5H), 7.75 (d, J=8.2 Hz, 2H); IR (neat) 3270, 2956, 1736, 1427, 1327, 1249, 1158, 1116, 1094, 833, 813, 700, 665 cm^{-1}; Found: C, 65.70; H, 7.38; N, 3.30%. Calcd for $C_{22}H_{29}NO_2SSi$: C, 66.12; H, 7.31; N, 3.50%.

Reaction of 2-(4-Phenyl-1,3-butadienyl)-3-methyl-1-tosylaziridine (24) with $PhMe_2SiAlEt_3tLi$. Reaction between **24** (89 mg, 0.26 mmol) and $PhMe_2SiAlEt_3Li$ (1.0 mmol)

afforded a mixture of 3-(dimethylphenylsilyl)-1-phenyl-6-tosylamino-1,4-heptadiene (**25**) and 5-(dimethylphenylsilyl)-1-phenyl-6-tosylamino-1,3-heptadiene (**26**) (**25** : **26** = 40 : 60, 63 mg, 46%): bp 250 °C/0.1 Torr; ^{1}H NMR δ = 0.24 (s, 2.4H), 0.26 (s, 1.8H), 0.27 (s, 1.8H), 1.11 (d, J = 6.7 Hz, 1.8H), 1.13 (d, J = 6.7 Hz, 1.2H), 2.2—2.4 (m, 0.4H), 2.32 (s, 1.8H), 2.43 (s, 1.2H), 2.61 (dd, J = 7.8, 6.7 Hz, 0.6H), 3.5—3.7 (m, 0.4H), 3.84 (ddq, J = 7.2, 6.7, 6.7 Hz, 0.6H), 4.30 (d, J = 7.2 Hz, 0.6H), 4.50 (d, J = 8.9 Hz, 0.4H), 4.93 (ddd, J = 15.4, 6.7, 1.0 Hz, 0.6H), 5.3—5.5 (m, 0.4H), 5.51 (ddd, J = 15.4, 8.9, 1.0 Hz, 0.6H), 5.9—6.2 (m, 1.2H), 6.2—6.6 (m, 1.2H), 7.1 — 7.8 (m, 9.0H); ^{13}C NMR δ = −5.2, −4.7, (−4.2), (−3.9), (19.7), 21.4, (21.5), 22.2, (36.5), 39.6, (50.4), 51.6, (123.9), 124.0, (125.6), 125.7, (126.5), 126.6, (127.0), 127.1, (127.5), 127.7, (127.9), 128.5, 128.8, 128.9, 129.4, 129.5, (129.59), (129.64), 130.1, (131.7), (133.0), (133.3), (133.8), 134.1, 136.4, (136.5), (137.3), 137.9, 138.1, (138.2), (139.1), 143.0, (143.1); IR (neat) 3446 (br, w), 3270, 2956, 1736, 1598, 1427, 1325, 1249, 1160, 1114, 1094, 1071, 969, 812, 698, 664; Found: C, 70.08; H, 7.08; N, 2.78%. Calcd for $C_{28}H_{33}NO_2SSi$: C, 70.69; H, 6.99; N, 2.94%.

General Method for the Preparation of π-Allylpalladium Complexes from 2-Alkenylsilanes and 2,4-Dienylsilanes with $[PdCl_2(CH_3CN)_2]$. The preparation of di-μ-chloro-bis{1,3-η-[5,5-bis(methoxycarbonyl)-2-pentenyl]-palladium(II)} (**27**) is representative. To a THF solution (2 ml) of dimethyl 5-(triphenylstannyl)-3-pentene-1,1-dicarboxylate (**3**) (0.20 g, 0.37 mmol) was added in one portion bis(acetonitrile)dichloropalladium(II) (0.10 g, 0.40 mmol) at room temperature under argon atmosphere. The resulting orange-yellow suspension was stirred for 1 h. The reaction mixture was subjected to column chromatography[15] (hexane-ethyl acetate, 1 : 1). Crude product was repurified by column chromatography to give 26 mg (0.07 mmol, 21% yield) of **27** as yellow crystals from CH_2Cl_2: mp 153.5—154 °C; ^{1}H NMR δ = 2.1—2.4 (m, 2H), 2.87 (d, J = 12.0 Hz, 1H), 3.6—3.8 (m, 2H), 3.73 (s, 3H), 3.75 (s, 3H), 3.94 (d, J = 6.7 Hz, 1H), 5.35 (ddd, J = 12.0, 6.9, 6.7 Hz, 1H); ^{13}C NMR δ = 31.2, 50.3, 52.6, 52.6, 59.8, 80.0, 111.2, 168.6, 168.8; IR (Nujol): 1731, 1294, 1212, 1154, 1025 cm^{-1}; Found: C, 33.35; H, 4.06%. Calcd for $C_{18}H_{26}Cl_2O_8Pd_2$: C, 33.05; H, 4.01%.

Di-μ-chloro-bis[1-3-η-(5-ethoxycarbonyl-5-tosyl-2-pentenyl)palladium(II)] (28) (Mixture of Diastereomers (6 : 4)): Mp 60 °C (CH_2Cl_2); ^{1}H NMR δ = 1.14 (t, J = 7.3 Hz, 1.2H), 1.18 (t, J = 7.2 Hz, 1.8H), 2.1—2.6 (m, 2H), 2.46 (s, 3H), 2.87 (d, J = 11.9 Hz, 0.6H), 2.92 (d, J = 11.9 Hz, 0.4H), 3.54 (dt, J = 11.1, 6.3 Hz, 0.6H), 3.83 (dt, J = 11.1, 6.3 Hz, 0.4H), 3.95 (d, J = 6.3 Hz, 0.6H), 3.98 (d, J = 6.3 Hz, 0.4H), 4.13 (q, J = 7.3 Hz, 0.8H), 4.15 (q, J = 7.2 Hz, 11.2H), 4.26 (dd, J = 7.3, 6.7 Hz, 0.4H), 4.36 (dd, J = 11.0, 3.9 Hz, 0.6H), 5.33 (ddd, J = 11.9, 11.1, 6.3 Hz, 0.6H), 5.36 (ddd, J = 11.9, 11.1, 6.3 Hz, 0.4H), 7.39 (d, J = 8.3 Hz, 2H), 7.78 (d, J = 8.3 Hz, 2H); ^{13}C NMR δ = (13.8), 13.9, 21.7, (29.2), 29.4, 60.3, (60.4), 62.4, 68.5, (69.0), 76.3, 77.8, (78.8), (111.0), 111.4, 129.2, (129.3), 129.8, (134.1), 145.6, 165.2; IR (neat) 2980, 2934, 1736, 1597, 1446, 1370, 1325, 1247, 1148, 1084, 1046, 814, 716, 668 cm^{-1}; Found: C, 41.16; H, 4.29%. Calcd for $C_{30}H_{38}Cl_2O_8S_2Pd_2$: C, 41.20; H, 4.38%.

Di-μ-chloro-bis{1-3-η-[5,5-bis(methoxycarbonyl)-1-phenyl-2-pentenyl]palladium(II)} (29, 80% from a mixture of **9** and **10**): Mp 195 °C (decomp) (CH_2Cl_2); ^{1}H NMR δ = 2.2—2.4 (m, 2H), 3.6—3.9 (m, 2H), 3.73 (s, 6H), 4.47 (d, J = 11.4 Hz, 1H), 5.70 (dd, J = 11.4, 10.8 Hz, 1H), 7.2—7.4 (m, 5H); ^{13}C NMR δ = 31.3, 50.5, 52.7, 52.7, 77.7, 78.8, 106.9, 128.0, 128.4, 129.0, 168.7, 168.9; IR (Nujol) 1750, 1733, 1282, 1222, 1147, 690 cm^{-1}; Found: C, 44.67; H, 4.31%. Calcd for $C_{30}H_{34}O_8Cl_2Pd_2$: C, 44.69; H, 4.25%.

Di-μ-chloro-bis[1-3-η-(7-ethoxycarbonyl-7-tosyl-2,4-heptadienyl)palladium(II)] (30) (1 : 1 Diastereomeric Mixture, Very Unstable): Mp 80 °C (decomp) (CH_2Cl_2); ^{1}H NMR δ = 1.14 (t, J = 7.0 Hz, 1.5H), 1.16 (t, J = 7.0 Hz, 1.5H), 2.46 (s, 3H), 2.5—2.7 (m, 2H), 2.89 (d, J = 11.7 Hz, 1H), 3.86 (d, J = 6.7 Hz, 1H), 3.98 (dd, J = 9.1, 6.0 Hz, 1H), 4.0—4.5 (m, 3H), 5.23 (ddd, J = 11.7, 10.2, 6.7 Hz, 1H), 5.73 (dd, J = 15.5, 9.5 Hz, 1H), 5.8—6.1 (m, 1H), 7.37 (d, J = 7.9 Hz, 2H), 7.75 (d, J = 7.9 Hz, 2H); IR (benzene) 1736, 1597, 1326, 1147, 1084 cm^{-1}.

Di-μ-chloro-bis{3-5-η-[7,7-bis(methoxycarbonyl)-1-phenyl-1,3-hephadienyl]palladium(II)} (31) (from a mixture of 15 and 16): Mp 80 °C (decomp) (CH_2Cl_2); ^{1}H NMR δ = 1.5—1.7 (m, 1H), 2.1—2.3 (m, 1H), 3.5—3.8 (m, 2H), 4.47 (dd, J = 15.6, 10.3 Hz, 1H), 5.31 (dd, J = 11.5, 10.3 Hz, 1H), 6.31 (dd, J = 15.6, 10.3 Hz, 1H), 6.99 (d, J = 15.6 Hz, 1H), 7.2—7.6 (m, 5H); IR (CH_2Cl_2) 2922, 2842, 1730, 1433, 1261 cm^{-1}.

A Mixtrure of Di-μ-chloro-bis{1-3-η-[7,7-bis(methoxycarbonyl)-2-methyl-2,4-heptadienyl] palladium(II)} (32) and Di-μ-chloro-bis{3-5-η-[7,7-bis(carbomethoxy)-2-methyl-1,3-heptadienyl]palladium(II)} (33) (32 : 33 = 3 : 1): Mp 80 °C (decomp) (CH_2Cl_2); ^{1}H NMR δ = 1.97 (s, 0.75H), 2.1—2.4 (m, 0.25H), 2.13 (s, 2.25H), 2.46 (dd, J = 7.3, 7.3 Hz, 0.25H), 2.53 (dd, J = 7.3, 7.1 Hz, 1.50H), 2.74 (s, 0.75H), 3.49 (t, J = 7.3 Hz, 0.75H), 3.5—3.6 (m, 0.25H), 3.7—3.8 (m, 0.25H), 3.74 (s, 0.75H), 3.75 (s, 4.50H), 3.77 (s, 0.75H), 3.80 (s, 0.75H), 4.19 (d, J = 10.3 Hz, 0.75H), 4.25 (d, J = 11.1 Hz, 0.25H), 5.26 (dd, J = 11.4, 11.1 Hz, 0.25H), 5.42 (s, 0.25H), 5.53 (s, 0.25H), 5.89 (dd, J = 15.4, 10.4 Hz, 0.75H), 6.12 (dt, J = 15.4, 7.1 Hz, 0.75H); ^{13}C NMR δ = 18.8, 32.8, 49.3, 50.5, 50.9, 52.58, 52.63, 52.7, 60.2, 67.2, 76.6, 83.8, 102.6, 120.1, 129.6, 135.0, 135.1, 169.0, 169.1; IR (neat) 2952, 2254, 2236, 1732, 1436, 1343, 1266, 1230, 1157, 1026, 969, 914, 731 cm^{-1}; Found: C, 39.15; H, 4.83%. Calcd for $C_{24}H_{34}Cl_2O_8Pd_2$: C, 39.26; H, 4.67%.

Di-μ-chloro-bis[1-3-η-(4-tosylamino-2-pentenyl)palladium(II)] (34) (55 : 45 Diastereomeric Mixture): Mp 58 °C (CH_2Cl_2); ^{1}H NMR δ = 1.21 (d, J = 7.0 Hz, 1.65H), 1.26 (d, J = 6.7 Hz, 1.35H), 2.43 (s, 3H), 2.94 (d, J = 11.8 Hz, 0.45H), 2.97 (d, J = 12.2 Hz, 0.55H), 3.3—3.6 (m, 1H), 3.60 (dd, J = 10.8, 2.2 Hz, 0.55H), 3.73 (dd, J = 11.1, 3.1 Hz, 0.45H), 4.01 (d, J = 6.7 Hz, 0.45H), 4.07 (d, J = 6.7 Hz, 0.55H), 4.96 (d, J = 8.8 Hz, 0.55H), 5.33 (ddd, J = 11.8, 11.1, 6.7 Hz, 0.45H), 5.38 (d, J = 8.0 Hz, 0.45H), 5.60 (ddd, J = 12.2, 10.8, 6.7 Hz, 0.55H), 7.32 (d, J = 8.3 Hz, 2H), 7.79 (d, J = 8.3 Hz, 1.10H), 7.80 (d, J = 8.3 Hz, 0.90H); ^{13}C NMR (benzene) δ = 14.7, 20.0, 21.3, 21.6, 50.4, 50.8, 60.6, 60.9, 61.3, 87.9, 88.9, 108.6, 109.1, 127.3, 127.7, 127.8, 128.3, 128.8, 130.4, 139.7, 140.2, 143.5, 143.6; IR (benzene) 3274 (br.m), 1597, 1412, 1332, 1158, 1091, 967, 814 cm^{-1}; Found: C, 39.38; H, 4.59; N, 4.01%. Calcd for $C_{24}H_{32}Cl_2N_2O_4S_2Pd_2$: C, 37.91; H, 4.24; N, 3.68%.

Di-μ-chloro-bis[3-5-η-(1-phenyl-6-tosylamino-1,3-heptadienyl)palladium(II)] and Its Unidentified Isomers

(35): The compound is so unstable and the crude product was used directly for further transformation (see below).

4,4-Bis(methoxycarbonyl)-3-isopropenylcyclopentene (36). Treatment of **32** (36 mg, 0.08 mmol) with PPh_3 (87 mg, 0.3 mmol) in DMSO (2 ml) at 60 °C for 1 h gave **36** (15 mg, 70% yield) which was identical with a sample prepared by the Pd(0) promoted vinylcyclopropane-cyclopentene rearrangenent method.[5] The use of Na_2CO_3 (10 equiv) and anhydrous LiCl (10 equiv)[16] instead of PPh_3 also gave **36** in 80% yield.

4,4-Bis(methoxycarbonyl)-3-styrylcyclopentene (37). Na_2CO_3 (35 mg, 0.35 mmol) and LiCl (15 mg, 0.35 mmol) were added to a solution of **31** (15 mg, 0.035 mmol) in DMSO (1 ml) and the resulting mixture was heated at 60 °C for 3 h to give **37**[5] (11 mg, 95% yield).

General Procedure for the Transformation of Dienylsilanes into Pyrroline Derivatives via Alkenyl-substituted π-Allylpalladiums. The crude product **35** (^{1}H NMR δ=1.5—1.7 (m, 1H), 2.1—2.3 (m, 1H), 3.5—3.8 (m, 2H), 4.47 (dd, J=11.5, 10.3 Hz, 1H), 5.31 (dd, J=11.5, 10.3 Hz, 1H), 6.31 (dd, J=15.6, 10.3 Hz, 1H), 6.99 (d, J=15.6 Hz, 1H), 7.2—7.6 (m, 5H)) derived from a mixture of **25** and **26** (32 mg, 0.07 mmol) and $[PdCl_2(CH_3CN)_2]$ (20 mg, 0.08 mmol) was dissolved in 2 ml of dimethyl sulfoxide under argon atmosphere. To this yellow solution was added triphenylphosphine (15 mg, 0.057 mmol). The reaction mixtrure was heated at 63 °C overnight. Resulting dark brown suspension was poured into water and extracted with ether. Purification by preparative TLC on silica gel (hexane-ethyl acetate, 5 : 1) gave 1-tosyl-2-(*E*)-2-styryl-5-methyl-3-pyrroline (**38**, cis : trans = 85 : 15, 0.012 mmol, 18% overall yield from dienylsilane) as colorless crystals: mp 145 °C (CH_2Cl_2); ^{1}H NMR δ=1.42 (d, J=6.5 Hz, 2.55H), 1.55 (d, J=6.3 Hz, 0.45H), 2.33 (s, 0.45H), 2.37 (s, 2.55H), 4.58 (ddq, J=1.8, 0.9, 6.5 Hz, 0.85H), 4.6—4.8 (m, 0.15H), 5.05 (dm, J=7.1 Hz, 0.85H), 5.1—5.2 (m, 0.15H), 6.06 (dd, J=15.9, 7.1 Hz, 1H), 6.50 (d, J=15.9 Hz, 0.15H), 6.51 (d, J=15.9 Hz, 0.85H), 7.10 (d, J=8.0 Hz, 0.30H), 7.1—7.4 (m, 6.7H), 7.64 (d, J = 8.0 Hz, 0.30H), 7.74 (d, J = 8.4 Hz, 1.70H); ^{13}C NMR δ= 21.5, 23.8, 63.5, 68.9, 126.6, 127.4, 127.5, 127.7, 128.4, 129.6, 120.0, 131.0, 131.3, 135.8, 136.4, 143.3; IR (CCl_4) 2990, 1740, 1720, 1587, 1492, 1444, 1344, 1167, 1091 cm^{-1}; Found: C, 70.70; H, 6.29; N, 3.88%. Calcd for $C_{20}H_{21}NO_2S$: C, 70.77; H, 6.24; N, 4.13%.

2-Ethenyl-5-methyl-1-tosyl-3-pyrroline (39). (cis: trans = 84 : 16): Mp 63—64 °C (crystallizes after distillation at 150 °C/0.1 Torr); ^{1}H NMR δ=1.38 (d, J=6.5 Hz, 2.52H), 1.43 (d, J=6.3 Hz, 0.48H), 2.41 (s, 3H), 5.51 (ddq, J=1.9, 3.6, 4.5 Hz, 0.84H), 4.6—4.8 (m, 0.16H), 4.8—4.9 (m, 0.84H), 4.9—5.0 (m, 0.16H), 5.13 (dt, J=10.1, 1.1 Hz, 1H), 5.29 (dt, J=10.1, 1.1 Hz, 1H), 5.4—5.7 (m, 2H), 5.83 (ddd, J=17.1, 10.1, 6.7 Hz, 1H), 7.29 (d, J=8.0 Hz, 2H), 7.72 (d, J = 8.0 Hz, 2H); ^{13}C NMR δ= (20.1), 21.5, (21.7), 23.8, (63.0), 63.6, 69.2, (69.8), 115.8, (116.0), (116.7), (117.0), 127.3, 127.4, (127.6), (127.7), 129.2, 129.6, 131.0, (131.6), (135.4), 138.8, 143.3; IR (Nujol) 1343, 1182, 1163, 1126, 1091, 1044, 926, 806, 668, 656, 595 cm^{-1}; Found: C, 63.64; H, 6.60; N, 5.09%. Calcd for $C_{14}H_{17}NO_2S$: C, 63.85; H, 6.51; N, 5.32%.

References

1) T. Hiyama, Y. Morizawa, H. Yamamoto, and H. Nozaki, *Bull. Chem. Soc. Jpn.*, **54**, 2151 (1981).

2) H. Hayami, M. Sato, S. Kanemoto, Y. Morizawa, K. Oshima, and H. Nozaki, *J. Am. Chem. Soc.*, **105**, 4491 (1983); Y. Okuda, M. Sato, K. Oshima, and H. Nozaki, *Tetrahedron Lett.*, **24**, 2051 (1983); Y. Morizawa, M. Oda, K. Oshima, and H. Nozaki, *ibid.*, **25**, 1163 (1984).

3) K. Wakamatsu, T. Nonaka, Y. Okuda, W. Tückmantel, K. Oshima, K. Utimoto, and H. Nozaki, *Tetrahedron*, **42**, 4427 (1986).

4) T. Nonaka, Y. Okuda, S. Matsubara, K. Oshima, K. Utimoto, and H. Nozaki, *J. Org. Chem.*, **51**, 4716 (1986); S. Matsubara, T. Nonaka, Y. Okuda, S. Kanemoto, K. Oshima, and H. Nozaki, *Bull. Chem. Soc. Jpn.*, **58**, 1480 (1985).

5) K. Nozaki, K. Wakamatsu, T. Nonaka, W. Tückmantel, K. Oshima, and K. Utimoto, *Tetrahedron Lett.*, **27**, 2007 (1986).

6) J. Hibino, S. Nakatsukasa, K. Fugami, S. Matsubara, K. Oshima, and H. Nozaki, *J. Am. Chem. Soc.*, **107**, 6416 (1985); K. Fugami, K. Oshima, K. Utimoto, and H. Nozaki, *Tetrahedron Lett.*, **27**, 2161 (1986); K. Fugami, S. Nakatsukasa, K. Oshima, K. Utimoto, and H. Nozaki, *Chem. Lett.*, **1986**, 869.

7) Y. Morizawa, K. Oshima, and H. Nozaki, *Israel. J. Chem.*, **24**, 149 (1984). Palladium catalyzed [3+2] cycloaddition reaction of vinylcyclopropanes with α,β-unsaturated esters or ketones has been reported. I. Shimizu, Y. Ohashi, and J. Tsuji, *Tetrahedron Lett.*, **26**, 3825 (1985).

8) K. Fugami, Y. Morizawa, K. Oshima, and H. Nozaki, *Tetrahedron Lett.*, **26**, 857 (1985).

9) T. Hayashi, M. Konishi, and M. Kumada, *J. Chem. Soc., Chem. Commun.*, **1983**, 736; K. Itoh, M. Fukui, and Y. Kurachi, *ibid.*, **1977**, 500; J. M. Kliegman, *J. Organomet. Chem.*, **29**, 73 (1971).

10) π-Allylpalladiums derived from dienylsilanes were fairly unstable. Prolonged contact with silica gel caused partial decomposition. Compounds containing nitrogen such as **34** and **35** were especially sensitive to silica gel, so that chromatographic columns were cooled with Dry ice.

11) K. C. Murdock and R. B. Angier, *J. Org. Chem.*, **27**, 2395 (1962).

12) J. E. Bäckvall, K. Oshima, R. E. Palermo, and K. B. Sharpless, *J. Org. Chem.*, **44**, 1953 (1977).

13) K. Mori and M. Matsui, *Tetrahedron*, **24**, 3095 (1968).

14) A. Michael, *Justus Liebigs Ann. Chem.*, **5**, 116 (1883).

15) Prepared from Ph_3SiCl (5.2 ml, 25.0 mmol) and Li (0.7 g, 100 mmol) in THF.

16) L. S. Hegedus and J. M. McKearin, *J. Am. Chem. Soc.*, **104**, 2444 (1982).

 © 1987 The Chemical Society of Japan Bull. Chem. Soc. Jpn., 60, 2517—2522 (1987)

Selective Formation of Formic Acid, Oxalic Acid, and Carbon Monoxide by Electrochemical Reduction of Carbon Dioxide

Shoichiro IKEDA,* Takehiko TAKAGI, and Kaname ITO
Department of Applied Chemistry, Nagoya Institute of Technology,
Gokiso-cho, Showa-ku, Nagoya 466
(Received October 8, 1986)

Selective formation of formic acid, oxalic acid, and carbon monoxide by electrochemical reduction of carbon dioxide (CO_2) is demonstrated using several metallic electrodes in aqueous and nonaqueous electrolytes. The electrode metals catalyze the electrochemical reduction of CO_2 and are classified to three groups according to their main products from CO_2. In and Pb electrodes as well as Hg electrodes are useful for the selective formation of formic acid by electrochemical reduction of CO_2 in aqueous electrolytes. In the case of nonaqueous electrolytes, Pb, Hg, and Tl are useful for oxalic acid, and In, Zn, Au, and Sn electrodes are useful for carbon monoxide. Also, reaction mechanisms of CO_2 electrochemical reduction are discussed.

We have studied the electrochemical reduction of carbon dioxide, CO_2, to organic compounds using solid-state metallic electrodes. Then, we have also indicated that the reduction product of CO_2 in aqueous electrolytes is only formic acid at all electrodes examined such as Zn, In, Sn and Pb,[1-3] as well as at Hg as previously reported by other authors.[4-6] In the previous papers,[7,8] we reported that oxalic acid and carbon monoxide were mainly produced by the electroreduction of CO_2 at some metallic electrodes in nonaqueous electrolytes.

In the present work, a gastight cell with a cyclic gas flow system was used for electrolytic experiments, and the gaseous products in the gas phase were then determined in a manner similar to that used for the products in the electrolytes. According to the results in this work and those reported in the previous papers, we will discuss on the electrochemical reduction of CO_2 in aqueous and nonaqueous electrolytes, and also we will summarize the selective formation of formic acid, oxalic acid, and carbon monoxide from CO_2 by the electrochemical method.

Experimental

The working electrodes were prepared from solid-state metals such as Ti (99.3%), Cr (99.2%), Fe (99.9%), Ni (99.3%), Cu (99.99%), Zn (99.9999%), Nb (99.2%), Mo (99.95%), Pd (99.9%), Ag (99.99%), Cd (99.9999%), In (99.999%), Sn (99.999%), Pt (99.99%), Au (99.99%), Tl (99.99%), and Pb (99.99%) which were as pure as possible. These have employed as plate electrodes described in the previous papers[1-3] except for Au having a string shape. Hg was also used in liquid-state after distillation. A silver-silver chloride electrode and a bright platinum plate served as a reference electrode and an anode, respectively.

An electolytic cell for electroreduction of CO_2 in this work was almost the same structure as that reported in a previous paper[9] except for lacking of a quartz window. Namely, the cell made of Teflon was designed to separate the cathode chamber from the anode one with a cation-exchange membrane, Nafion 315, and also to be able to operate with a small volume of electrolyte, that is, 10 ml, for easy determination of the products. The cell was gastight and CO_2 gas was supplied with the cyclic gas flow system,[9] which was assembled from a mini peristaltic pump, a manometer, a gas sampler, and glass tubes.

Carbon dioxide gas was at first supplied into the catholyte of the cell from a CO_2 gas cylinder and exhausted through the cyclic gas flow system for 30 min. After the electrolytes was sufficiently saturated with CO_2 gas and the system was filled with CO_2, the line was closed to make it gastight. Thereafter, the gas in the system was circulated by the mini peristaltic pump at a rate of 1 ml min^{-1}.

Aqueous electrolytes, namely 0.1 M TEAP/H_2O (1 M = 1 mol dm^{-3}), were prepared from the synthesized tetraethylammonium perchlorate, TEAP, which was prepared from tetraethylammonium bromide, TEABr, and perchloric acid, and twice distilled water.

In order to prepare the nonaqueous electrolytes, propylene carbonate, PC, acetonitrile, AN, and dimethyl sulfoxide, DMSO, were employed as an aprotic solvent. The nonaqueous electrolytes, namely 0.1 M TEAP/PC, were prepared from synthesized TEAP and PC purified by Jasinski and Kirkland's method.[10] AN and DMSO were dried with unhydrous sodium sulfate (1.5 g l^{-1}) and then with Molecular sieve-4A (40 g l^{-1}). They were used without the other purification, although a little amount of the reduction products of some impurities in AN was found by high performance liquid chromatography.

The electrolytic experiment for CO_2 reduction was potentiostatically performed using a potentiostat and an electronic coulometer, Hokuto Denko; PS-303 and HF-201, respectively. Mainly, 100 coulombs were passed through the working electrode for each experiment.

The products in the gas phase were quantitatively determined using a gas chromatograph, Shimadzu; GC-3AH, having a TC detector on a column of activated charcoal using He gas as the carrier gas. On the other hand, the products in the electrolytes were sampled after the line was exposed to the atmosphere and then were determined using a high performance liquid chromatograph, Mitsumi (Atto); HSLC-022, having a RI detector and an UV detector on a column of Shodex Ion-Exchanger HC-125S using 1% H_3PO_4 aqueous solution as an eluent solution. Also a steam chromatograph, Ohkura Riken; SSC-1, having a FID detector on a column of G-0 (Chlomosolb 101), was used for determination of alcohols and aldehydes, although they were not observed at all in the present work.

Results and Discussion

In Aqueous Electrolytes. Table 1 shows all products obtained by electroreduction of CO_2 at potentials of −2.0 and −2.4 V vs. Ag/AgCl/sat'd KCl, using Zn, In, Sn, and Pb electrodes in 0.1 M TEAP aqueous electrolytes. It is evident from this table that carbon monoxide is produced even in aqueous electrolytes. Also the sum of the current efficiencies for formic acid, carbon monoxide, and hydrogen as a by-product is approximately 100%, so that they must represent all of the products obtained in this experiment.

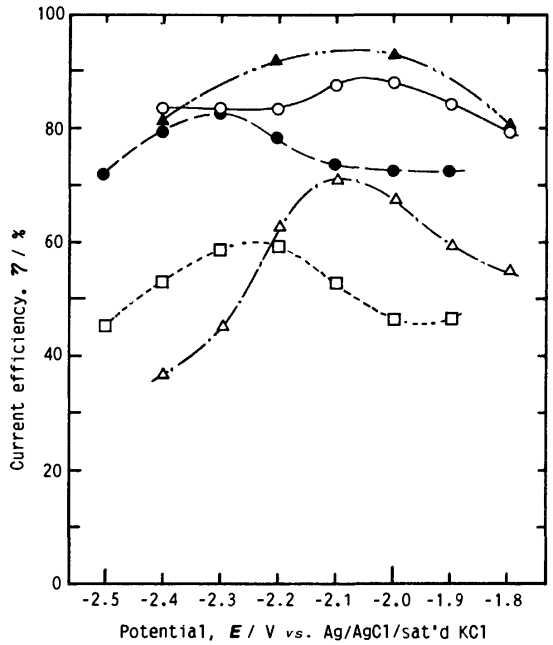

Fig. 1. Current efficiencies for formic acid formation at various metallic electrodes in 0.1 M TEAP/H_2O. Quantity of electricity passed: 100 C. ▲: Hg, ○: In, ●: Pb, △: Sn, □: Zn.

The current efficiencies for formic acid formation with respect to electrode potentials, when CO_2 has been reduced at various electrodes in 0.1 M TEAP aqueous electrolytes is shown in Fig. 1. In the case of In electrodes, the current efficiency went up to about 90% in the potential range of −2.0 to −2.1 V. Therefore, In electrode will be the most useful of the solid-state metallic electrodes for formic acid formation.

Figure 2 shows the current efficiencies for carbon monoxide formation under the same conditions as in Fig. 1. In the case of Zn electrodes, the current efficiency went up to about 36% in the potential range of −1.9 to −2.0 V even in the aqueous electrolyte.

In Nonaqueous Electrolytes. The brief results of electroreduction products of CO_2 obtained at In, Pb, Sn, and Zn electrodes in 0.1 M TEAP/PC electrolytes were already reported in the previous paper.[8] In the case of In electrodes, the efficiency for carbon

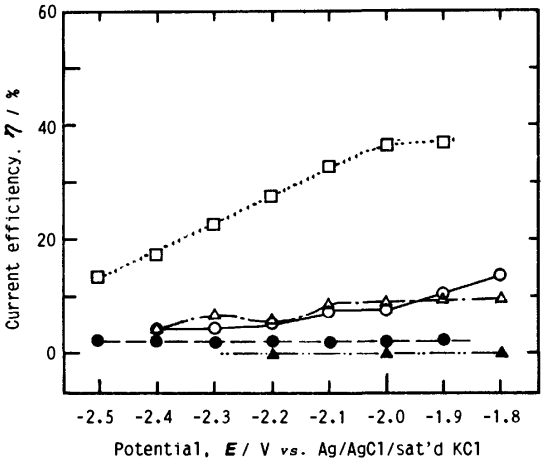

Fig. 2. Current efficiencies for carbon monoxide formation at various metallic electrodes in 0.1 M TEAP/H_2O. Quantity of electricity passed: 100 C. ▲: Hg, ○: In, ●: Pb, △: Sn, □: Zn.

Table 1. Electrochemical Reduction Products of CO_2 at Various Electrodes in 0.1 M TEAP/H_2O under Normal Pressure
Quantity of Electricity; 100 C

Cathode	Potential	HCOOH		CO		H_2		$\eta_1+\eta_2$	$\eta_1+\eta_2+\eta_3$
	V	n_1/μmol	η_1/%	n_2/μmol	η_2/%	n_3/μmol	η_3/%	%	%
In	−2.0	454	87.6	35	6.8	25	4.9	94.4	99.1
	−2.4	431	83.2	22	4.2	69	13.2	87.4	100.6
Pb	−2.0	377	72.9	10	2.0	81	15.6	74.9	90.5
	−2.4	409	78.9	11	2.1	74	14.3	81.0	95.3
Zn	−2.0	241	46.6	185	35.6	64	12.4	82.2	94.6
	−2.4	277	53.4	89	16.8	183	35.2	70.2	105.4
Sn	−2.0	350	67.5	47	9.1	155	29.9	76.5	106.4
	−2.4	192	37.1	22	4.2	329	61.6	41.3	102.9

n and η represent the produced amount and the current efficiency of each product, respectively.

Table 2. Relationship between Water Content and Current Efficiency of Products Obtained by CO_2 Electroreduction at −2.6 V vs. Ag/AgCl/(0.01 M LiCl+0.1 M TEAP)/PC in 0.1 M TEAP/PC Quantity of Electricity; 100 C

Cathode	Water added Weight %	Current efficiency/%				$\eta_1+\eta_2+\eta_3+\eta_4$ %
		Oxalic acid, η_1	Glyoxylic acid, η_2	Formic acid, η_3	Carbon monoxide, η_4	
Pb	0.0	73.3	3.4	2.2	11.0	89.9
	0.83	9.8	0.0	56.9	14.4	81.1
	4.2	trace	0.0	72.8	8.6	81.4
In	0.0	0.1	0.0	1.3	85.3	86.7
	0.83	0.0	0.0	33.3	57.8	91.1
	4.2	0.0	0.0	63.6	20.0	83.6

Initial water content of 0.1 M TEAP/PC is 0.032%.

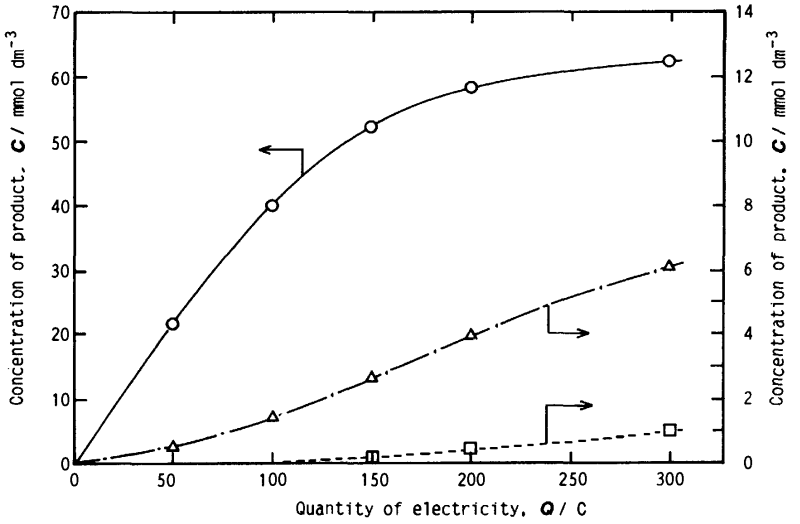

Fig. 3. Carboxylic acid formation at Pb electrode in 0.1 M TEAP/PC at −2.8 V vs. Ag/AgCl/(0.01 M LiCl+0.1 M TEAP)/PC. ○: Oxalic acid, △: glyoxylic acid, □: glycolic acid.

monoxide went up to 90% at −2.8 V, while the efficiency for formic acid and oxalic acid were very small. Therefore, an In electrode was suitable for selective production of carbon monoxide from CO_2 in nonaqueous electrolyte.

On the other hand, at a Pb electrode, the main product became oxalic acid, and the current efficiencies increased at more negative potentials and went up to 84% at −3.0 V. In this case, detectable amount of glyoxylic acid was produced and the efficiency went up to 7% at −3.0 V, while carbon monoxide increased at relatively noble potentials and the efficiency went up to 13% at −2.2 V. These results indicated that Pb electrodes were suitable for selective production of oxalic acid.

Figure 3 shows the concentration of oxalic acid, glyoxylic acid, and glycolic acid, with respect to the quantity of electricity passed, when electrolytic reduction of CO_2 has been performed at −2.8 V, using Pb electrodes in 0.1 M TEAP/PC nonaqueous electrolytes. The concentration of oxalic acid increased almost linearly up to 150 C and thereafter the rate of increase slowed. The concentration of glyoxylic acid then progressively increased, and after 150 C passed, glycolic acid also began to be produced.

These facts suggest that glyoxylic acid and glycolic acid are psoduced by the further reduction of oxalic acid obtined in the electrochemical reduction of CO_2.

Table 2 shows the relationship between the water content in nonaqueous electrolytes and the electroreduction products of CO_2. In the case of Pb electrodes, as mentioned above, oxalic acid was the main product in 0.1 M TEAP/PC electrolyte having an initial water content of 0.032%, while increasing the water content to 0.83 or 4.2% causes an extreme decrease in oxalic acid and an increase in formic acid.

In the case of In electrodes, increasing the water content causes a decrease in carbon monoxide and also an increase in formic acid. In both cases of 4.2% water content, formic acid becomes the main product in-

stead of oxalic acid or carbon monoxide.

The above mentioned results demonstrate that the main products of CO_2 electroreduction in nonaqueous electrolytes are oxalic acid at Pb electrodes and carbon monoxide at In electrodes. In order to clarify the function of these electrode metals, various electrodes were prepared from many kinds of metals and the current efficiencies for oxalic acid and carbon monoxide production were measured using these electrodes in 0.1 M TEAP/PC, 0.1 M TEAP/DMSO, and 0.1 M TEAP/AN nonaqueous electrolytes, respectively. The water content of each electrolyte determined by Karl Fischer's method was 294, 883, and 206 ppm, respectively.

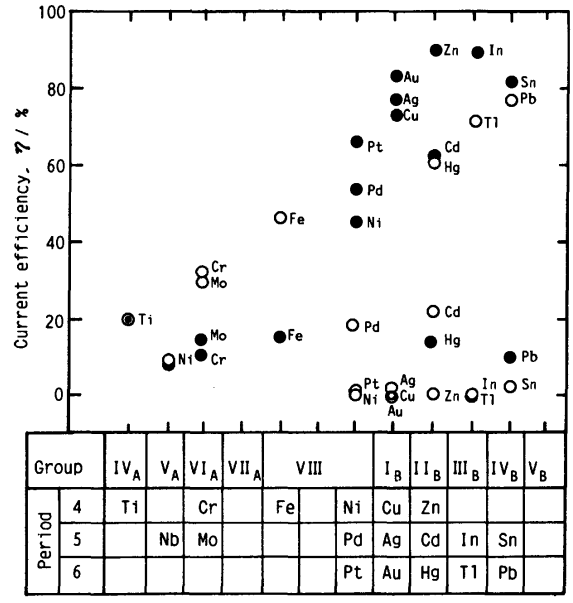

Fig. 4. Current efficiencies for oxalic acid or carbon monoxide formation from CO_2 at various electrodes in 0.1 M TEAP/PC at −2.8 V vs. Ag/AgCl/(0.01 M LiCl+0.1 M TEAP)/PC. Quantity of electricity passed: 100 C. O: Oxalic acid, ●: carbon monoxide.

Figures 4, 5, and 6 show the relationships between the position on the periodic table for the metals employed and the current efficiencies for oxalic acid and carbon monoxide formations in these electrolytes, respectively. These figures indicate that these metals are divided into three groups. The first group is the metals of Group A in the periodic table, such as Fe, Cr, Mo, and Ti; the electrodes prepared from such metals contribute to the production of substantial amounts of oxalic acid and carbon monoxide. The second group is VIII and B group metals except for Pb, Tl, and Hg; the electrodes of these metals contribute to the selective production of carbon monoxide, of which the current efficiencies at In and Zn electrodes go up to 90% and oxalic acid production is very small. The third group consists of Pb, Tl, and Hg, and such metal electrodes contribute to selective production of oxalic acid in spite of the B group metal. The current efficiency for oxalic acid production at the Pb electrode goes up to 80% and carbon monoxide production is very small. The Hg electrode belongs to this group, because it does not produce hydrogen at all similarly to the other IIB, IIIB, and IVB group metals as shown in Table 3, although its production rates of ox-

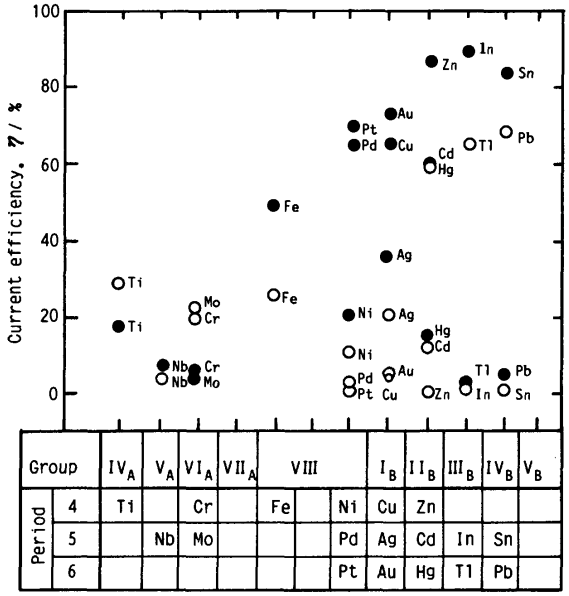

Fig. 5. Current efficiencies for oxalic acid or carbon monoxide formation from CO_2 at various electrodes in 0.1 M TEAP/DMSO at −2.8 V vs. Ag/AgCl/(0.01 M LiCl+1 M $LiClO_4$+ 0.1 M TEAP)/DMSO. Quantity of electricity passed: 100 C. O: Oxalic acid, ●: carbon monoxide.

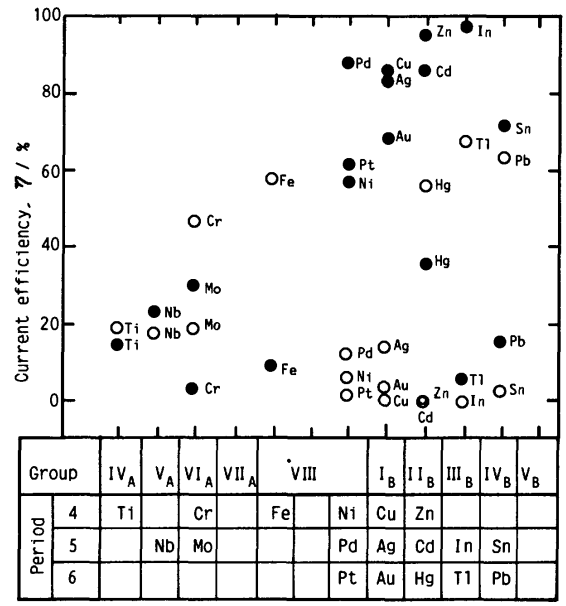

Fig. 6. Current efficiencies for oxalic acid or carbon monoxide formation from CO_2 at various electrodes in 0.1 M TEAP/AN at −2.6 V vs. Ag/AgCl/(0.01 M LiCl+0.1 M TEAP)/AN. Quantity of electricity passed: 100 C. O: Oxalic acid, ●: carbon monoxide.

Table 3. Electrochemical Reduction Products of CO_2 at Various Electrodes at −2.8 V vs. Ag/AgCl/(0.01 M LiCl+0.1 M TEAP)/PC in 0.1 M TEAP/PC. Quantity of Electricity; 100 C

Group	Cathode	Amount of products, n/μmol				
		Oxalic acid	Glyoxalic acid	Formic acid	Carbon monoxide	Hydrogen
IV_A	Ti	103	6	22	104	235
V_A	Nb	39	4	42	35	256
VI_A	Cr	165	5	23	58	189
	Mo	153	Trace	28	72	212
VIII	Fe	239	None	7	81	115
	Ni	1	None	43	237	228
	Pd	113	None	16	269	None
	Pt	5	None	40	345	90
I_B	Cu	3	None	Trace	388	Trace
	Ag	7	Trace	11	401	10
	Au	1	None	19	431	72
II_B	Zn	2	None	Trace	465	None
	Cd	112	20	8	327	None
	Hg	312	5	6	92	None
III_B	In	1	None	12	462	None
	Tl	365	5	11	16	None
IV_B	Sn	10	5	18	424	None
	Pb	397	15	13	54	None

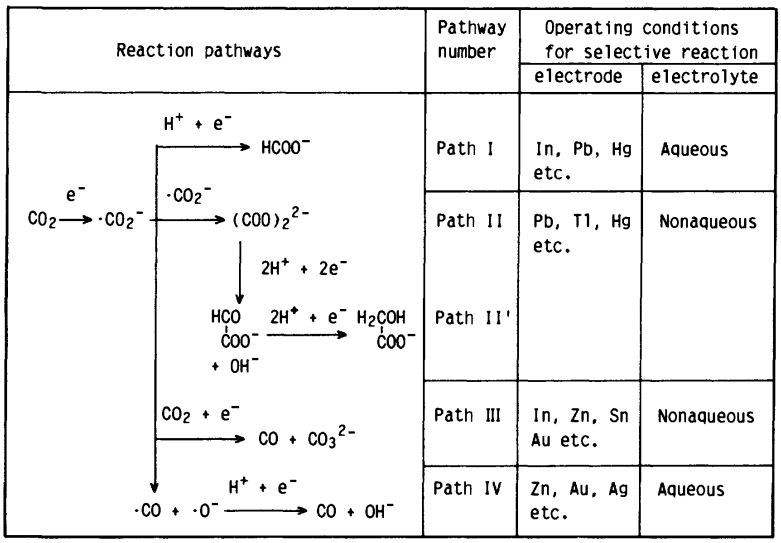

Fig. 7. Reaction pathways in electrochemical reduction of CO_2 under various conditions.

alic acid and carbon monoxide are like to those of the Fe electrode of which hydrogen production is in the order of 100 μmol for 100 C passed.

Such behavior of these metal electrodes has also been observed in the other nonaqueous electrolytes using AN and DMSO as aprotic solvents. Results were almost similar to that in the case of PC. Slight differences are thought to be due to the water content of them and electrode potentials.

Reaction Pathways. Figure 7 shows the reaction pathways in the electroreduction of CO_2 and the operating conditions for each pathway to proceed selectively. These reaction pathways may proceed competitively, but the reaction rate of each pathway is dependent upon the electrode metals and the electrolytes.

Namely, in Pass I, the reduced CO_2 anion radical reacts with proton or water molecule in aqueous electrolytes to produce formic acid. This reaction is competitive with the hydrogen evolution reaction (HER), so metals having higher overvoltages for HER, such as In, Pb, and Hg, are useful for the formic acid formation by Pass I.[1,2,11]

In nonaqueous electrolytes, if CO_2 anion radicals remained for a somewhat longer time at the surface of electrode metals such as Pb, Hg, and Tl, they would react together on the surface to produce an oxalate ion.[2,3,7,8] Thereafter the oxalate ion will be further reduced to produce glyoxalate, glycolate anions, etc. (Pass II′). These passes also observed at Pb electrodes in aqueous electlolytes.[3] If CO_2 anion radicals easily desorb from the surface of metals, such as Zn, Sn, and Au, they are attacked by CO_2 molecules near at the surface or in the bulk to disproportionate producing carbon monoxide and carbonate ion passing an intermediate anion radical (Pass III).[8,12] This mechanism also accounts for the production of carbon monoxide at some metals, such as Zn, in aqueous electrolytes.[13]

If metals are more attractive to CO_2 anion radicals, such as Zn, Au, and Ag, a dissociative adsorption mechanism of CO_2 anion radicals or molecules, Pass IV, may also be proposed to account for the carbon monoxide production in aqueous electrolytes.[9,13]

References

1) K. Ito, T. Murata, and S. Ikeda, *Bull. Nagoya Inst. Tech.*, **27**, 209 (1975).
2) K. Ito, S. Ikeda, and M. Okabe, *Denki Kagaku*, **48**, 247 (1980).
3) K. Ito, S. Ikeda, T. Iida, and H. Niwa, *Denki Kagaku*, **49**, 106 (1981).
4) F. Fischer and O. Prziza, *Ber. Dtsch. Chem. Ges.*, **47**, 256 (1914).
5) T. E. Teeter and P. Van Rysselberghe, *J. Chem. Phys.*, **22**, 759 (1954).
6) K. S. Udupa, G. S. Subramanian, and H. V. K. Udupa, *Electrochim. Acta*, **16**, 1593 (1971).
7) K. Ito, S. Ikeda, T. Iida, and A. Nomura, *Denki Kagaku*, **50**, 463 (1982).
8) K. Ito, S. Ikeda, N. Yamauchi, T. Iida, and T. Takagi, *Bull. Chem. Soc. Jpn.*, **58**, 3027 (1985).
9) S. Ikeda, M. Yoshida, and K. Ito, *Bull. Chem. Soc. Jpn.*, **58**, 1353 (1985).
10) R. J. Jasinski and S. Kirkland, *Anal. Chem.*, **39**, 1663 (1967).
11) Yu. B. Vassiliev, V. S. Bagotzky, N. V. Osetrova, O. A. Khazova, and N. A. Mayorova, *J. Electroanal. Chem.*, **189**, 271 (1985).
12) Yu. B. Vassiliev, V. S. Bagotzky, O. A. Khazova, and N. A. Mayorova, *J. Electroanal. Chem.*, **189**, 295 (1985).
13) Y. Hori, K. Kikuchi, and S. Suzuki, *Chem. Lett.*, **1985**, 1695.

 © 1987 The Chemical Society of Japan Bull. Chem. Soc. Jpn., 60, 2523—2529 (1987)

Novel Effect of Additives on the Quenching Mechanism of the Excited State of Copolymer-Pendant $[Ru(bpy)_3]^{2+}$ by Methylviologen in Methyl Alcohol

Masao KANEKO,* Xiao-Huai HOU, and Akira YAMADA
The Institute of Physical and Chemical Research, Wako-shi, Saitama 351-01
The Institute of Chemistry, Beijin, Chinese Academia Sinica, Beijin, China
(Received December 24, 1986)

The quenching of the excited state of acrylic acid copolymer-pendant $[Ru(bpy)_3]^{2+}$ by methylviologen (MV^{2+}) was studied in methyl alcohol. The Stern-Volmer plots for the quenching showed a line or a curve (downward or upward) depending on the additive such as acid, alkali, or neutral salt in methyl alcohol. This behavior in methyl alcohol is entirely different from that in water where only dynamic quenching occurs. The behaviors in alcohol were analyzed by assuming stepwise binding of MV^{2+} into the domains around the Ru complex formed by the dissociated carboxylates and by considering dynamic as well as static quenching models. The one kind of photochemical reaction system showed four different quenching mechanisms induced by the additives.

Photochemical reactions in polymer[1,2] and molecular assembly[3,4] systems are receiving intense interest as an approach to solar energy conversion.[5] Microenvironment of polymer systems very often affects remarkably photochemical reaction through electrostatic[6-8] or hydrophobic[9] interaction with quencher molecule. Tris(2,2′-bipyridine)ruthenium(II) complex ($[Ru(bpy)_3]^{2+}$) is attracting much attention as a sensitizer for visible light energy conversion.[2,4,5] Quenching of the excited state of $[Ru(bpy)_3]^{2+}$ by methylviologen (MV^{2+}) has been studied in the presence of anionic polymers[7,8] showing that an electrostatic interaction enhances the reaction rate. In such cases where polymer is present as a separate molecule in a sensitizer solution, the sensitizer should interact with the polymer in order that the polymer affects the sensitizing reaction. When a sensitizer is covalently attached to a polymer molecule, however, the microenvironmental effect of the polymer chain upon the photochemical reaction of the sensitizer can easily be studied independent of the interaction between sensitizer and polymer. The influencing factor is then only the interaction between polymer and quencher.

The present authors have prepared copolymer-pendant $[Ru(bpy)_3]^{2+}$, where copolymer is prepared from 4-methyl-4′-vinyl-2,2′-bipyridine and comonomer such as styrene, acrylic acid, etc.[10] These copolymer-pendant $[Ru(bpy)_3]^{2+}$ complexes have their characteristics in that the microenvironment around the Ru complex can drastically be changed by changing the comonomer compound. It means that the chemical as well as the physicochemical properties of the attached Ru complex can be changed with ease by choosing a proper comonomer. Taking solubility of a copolymer-pendant $[Ru(bpy)_3]^{2+}$, for example, a copolymer complex containing styrene comonomer is well soluble in many organic solvent such as benzene or chloroform, but entirely insoluble in water in contrast to the conventional low-molecular $[Ru(bpy)_3]^{2+}$ which is well soluble in water but insoluble in benzene or chloroform. This styrene-copolymer-pendant $[Ru(bpy)_3]^{2+}$ could be used as a stable membrane in water for fabricating photoresponsive graphite electrode[11,12] or stabilizing liquid-junction n-GaAs[13] and n-CdS[14].

When acrylic acid (AA) was used as a comonomer, the excited state of the water-soluble copolymer-pendant $[Ru(bpy)_3]^{2+}$ showed a remarkably pH-dependent activity toward MV^{2+} quencher due to the dissociation of the AA.[6] At neutral and alkaline regions in water, the quenching of the excited state of the AA-copolymer complex by MV^{2+} was remarkably enhanced due to the polyanionic domain formed around the Ru complex by the dissociation of the AA groups. It was concluded that electrostatic interaction brought about the enhancement of the quenching reaction, however, the linear relationship of the Stern-Volmer plots showed that the quenching is understood to occur via dynamic process in water.[6] Since the interaction is an electrostatic one, the reaction in a less polar solvent must present an aspect different from an aqueous system. It was found in the further study that static quenching occurs in methyl alcohol and that the mechanism is different depending on the additives such as base, acid, and neutral salt. This is the first example as far as the present authors know that one photochemical reaction system exhibits various quenching mechanisms as a function of additives. The mechanisms will be interpreted in terms of binding of MV^{2+} to polyanionic domain formed around Ru complex and of static quenching therein, and reported in this paper.

Experimental

Copolymer-pendant $[Ru(bpy)_3]^{2+}$ was prepared by reaction of a copolymer of 4-methyl-4′-vinyl-2,2′-bipyridine and acrylic acid (mol wt 4000) with *cis*-$[Ru(bpy)_2Cl_2]$ at the molar ratio of [bpy unit of the copolymer]/[Ru]=3.5 in n-BuOH under reflux for 2.5 h.[6] The polymer complex was

purified by dialysis in water. The composition of the copolymer-pendant complex **1** was as follows.

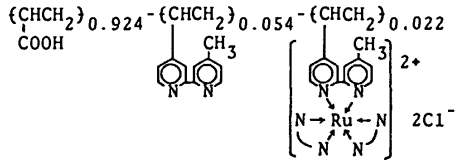

1 N⌒N=2,2′-bipyridine

Methylviologen (MV^{2+}) was purified by recrystallization in methyl alcohol–acetone mixture. The quenching of the excited state of the copolymer-pendant $[Ru(bpy)_3]^{2+}$ by methylviologen (MV^{2+}) was measured in methyl alcohol under the addition of various salts. Emission intensities were measured by the fluorimeter (Hitachi MPF-4). The emission decay was measured by a single-photon counting method with 1-ns pulsed light from a 12-atm hydrogen lamp.

Results and Discussion

The Stern–Volmer plots of the quenching of the excited state of the copolymer complex **1** by MV^{2+} in methyl alcohol were shown in Fig. 1. The plots without any additive show a downward curve. The plots of the quenching with the addition of HCl showed a linear relationship which almost coincides with those of conventional low molecular $[Ru(bpy)_3]^{2+}$. When neutral salt (Et_4NBr) is further added to this HCl-containing system, the quenching has become more efficient, and the slope of the plots is almost equal to the initial slope of the plots without additives. The solution in the presence of NaOH showed a very efficient quenching, and the plots gave a downward curve. The presence of thiourea in addition to HCl brought about an upward-curved plots.

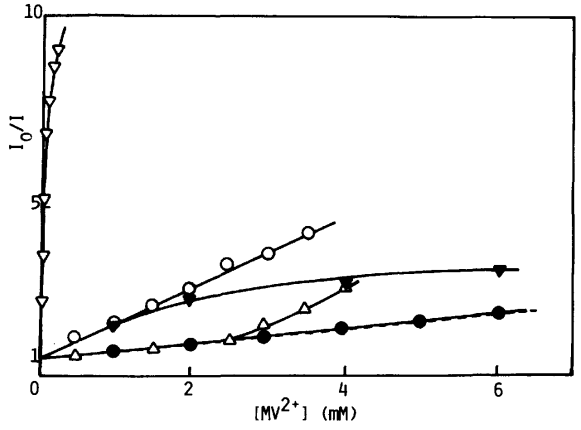

Fig. 1. Stern–Volmer plots for the quenching of excited **1** by MV^{2+} in methyl alcohol. Ru complex, 10^{-5} M (1 M=1 mol dm^{-3}). ▼, With no additive; ●, 0.5 mM HCl added; ○, 0.5 mM HCl and 0.1 M Et_4NBr added; ▽, 1 mM NaOH added; △, 0.5 mM HCl and 0.1 M H_2NCSNH_2 added; ------, $Ru(bpy)_3^{2+}$.

In the aqueous solution system reported before,[6] the quenching by MV^{2+} showed a remarkably pH-dependent behavior, indicating electrostatic interaction between carboxylate anions and MV^{2+}, but the linear Stern–Volmer plots showed a dynamic quenching. In the present system in methyl alcohol, the curved plots in Fig. 1 indicate the occurrence of static quenching. Since electrostatic interaction is enhanced in less polar medium as alcohol than in water, the behaviors of Fig. 1 are reasonable.

The polymer complex **1** contains both acid and base groups, i.e., carboxylic acid and free bpy pendant groups. These groups can interact and form hydrogen bonds as was reported.[6] Such interaction must be more enhanced in alcohol than in water and provide ionic environment around Ru complex. The much longer lifetime (843 ns) of the excited state of the polymer-pendant Ru complex in methyl alcohol than that of the monomeric complex (664 ns) supports a rigid and compact structure of the polymer complex which is possibly caused by such acid–base interactions between the pendant groups.

The plots of the emission quenching in the absence of any additive in Fig. 1 shows the occurrence of static quenching. The ionic microenvironment formed by acid–base interaction described above would attract the cationic substrate (MV^{2+}), and cause static quenching. Hydrogen chloride added to this solution destroys such interaction by protonating free bpy groups, thus making the plots linear. The quenching efficiency in the presence of HCl for the polymer system is almost the same as the monomeric complex. The cationic protonated bpy groups as well as the divalent Ru complex species attached to the polymer chain would bring about expanded macromolecular structure due to electrostatic repulsion, which would make the reactivity of the pendant Ru complex almost the same as an isolated monomeric complex. The quenching rate constants (k_q) for the polymer complex with HCl additive as well as for the monomeric complex were shown in Table 1. They have almost the same k_q values.

The addition of Et_4NBr to the HCl-added system enhanced the quenching efficiency, the Stern-Volmer plots still being linear. The neutral salt not only weakens the electrostatic repulsion between the pendant cationic groups, but also can enhance the reaction between the cationic Ru complex and MV^{2+} through shielding effect. The result of Fig. 1 shows that the latter effect prevails to make the quenching more efficient in the presence of Et_4NBr than in its absence for the HCl-added polymer system. The k_q value was also shown in Table 1 for the Et_4NBr-added system which is five times as high as that without Et_4NBr.

The addition of NaOH remarkably enhanced the quenching efficiency. This is understood as due to the

Table 1. Quenching Parameters for the Systems That Can Be Analyzed by a Conventional Dynamic Model

Complex	Additive	k_{sv}/M^{-1}	$\tau/ns^{a)}$	$k_{q,2}/M^{-1}s^{-1}$
1	HCl	1.97×10^2	680	2.90×10^8
1	HCl+Et_4NBr	9.31×10^2	622	1.50×10^9
$[Ru(bpy)_3]^{2+}$	HCl	2.00×10^2	664	3.01×10^8

Ru; 10^{-5} M. a) Measured by a single photon counting method.

anionic domain formed around the Ru complex by the dissociation of the acrylic acid.[6] The Stern-Volmer plots in methyl alcohol show a downward curve different from the behavior in water for which the plots show a linear relationship. Static quenching must occur in methyl alcohol. The Stern-Volmer plots with the addition of thiourea shows an upward-curve, also indicating static quenching. The quenching of the excited state of the polymer complex **1** by MV^{2+} in methyl alcohol is therefore entirely depending on the additives. Both the dynamic and static quenching mechanisms have to be considered. The quenching mechanisms were analyzed as follows.

The occurrence of static quenching in the present system shows that we should consider some specific microenvironment (called "domain") around the pendant Ru complex to which the substrate (MV^{2+}) is bound and quenches the excited Ru complex statically. Such a domain which affects specifically catalytic reactions of polymeric compounds have often been studied.[15] The domain formed around pendant Ru complex is represented by [Ru]. Quencher molecule (MV^{2+}), Q is bound to this domain. Multistep reaction should be considered for such binding. It is assumed now that the rate constant of the forward binding reaction is equal for all the binding steps, but the backward rate constant of the binding is proportional to the number of Q bound to the domain. The stepwise bindings can then be expressed by Eqs. 1 to 3 where $[Ru\text{-}Q_i]$ represents the domain to which i molecules of Q are bound.

$$[Ru] + Q \underset{k_{-a}}{\overset{k_a}{\rightleftharpoons}} [Ru\text{-}Q_1] \qquad K_1 = k_a/k_{-a} \tag{1}$$

$$[Ru\text{-}Q_1] + Q \underset{2k_{-a}}{\overset{k_a}{\rightleftharpoons}} [Ru\cdot Q_2] \qquad K_2 = K_1/2 \tag{2}$$

$$\vdots \qquad\qquad \vdots$$

$$[Ru\text{-}Q_{i-1}] + Q \underset{ik_{-a}}{\overset{k_a}{\rightleftharpoons}} [Ru\text{-}Q_1] \qquad K_1 = K_1/i \tag{3}$$

According to this assumption, the number of Q molecule bound to the domain obeys the Poisson distribution. Such a Poisson distribution of quencher molecule to the microenvironment around sensitizer has often been considered for micellar[16,17] or polymeric[9] systems. The total concentration of the domain, $[Ru]_t$, is expressed by Eq. 4. The concentration of the Q bound to the domain, $[Q]_b$, is:

$$[Q]_b = \sum_{i=0}^{\infty} i[Ru\text{-}Q_i] = [Ru]K_1[Q]\exp(K_1[Q]) = [Ru]_tK_1[Q] \tag{5}$$

where [Q] is the concentration of the free Q and expressed by the following Eq.

$$[Q] = [Q]_t/(K_1[Ru]_t+1) \tag{6}$$

Under these situations the next four quenching models were considered where dynamic and static quenchings are concerned.

In model 1 are considered both the dynamic quenching of [Ru*] by the bulk Q and the static quenching in the domain, in the latter of which the quenching rate is independent of the number of the Q in the domain.

Model 1

$$[Ru] \xrightarrow{h\nu} [Ru^*] \begin{cases} \xrightarrow{k_{q,2}[Q]} [Ru] & (7) \\ \xrightarrow{k_d} [Ru] & (8) \\ \xrightarrow{k_f} [Ru] & (9) \end{cases}$$

$$[Ru\text{-}Q_i] \xrightarrow{h\nu} [Ru^*\text{-}Q_i] \begin{cases} \xrightarrow{k_{q,1}} [Ru\cdot Q_i] & (10) \\ \xrightarrow{k_d} [Ru\text{-}Q_i] & (11) \\ \xrightarrow{k_f} [Ru\cdot Q_i] & (12) \end{cases}$$

In these equations k_d and k_f are the rate constants of the nonluminescent and luminescent decays of the excited state of the Ru complex, respectively. It should be reasonable to assume that these photochemical processes of Eqs. 7 to 12 are much faster than the binding processes of Eqs. 1 to 3. It means that the equilibrium processes of Eqs. 1 to 3 etc. should be kept constant during the time period when the photochemical processes of Eqs. 7 to 12 occur. The total rate of light absorption at the excitation of the Ru complex, I_t is expressed by the following equation, when steady state is assmued for the Reactions 7 to 12.

$$I_t = [Ru^*](k_d+k_f+k_{q,2}[Q]) + \sum_{i=1}^{\infty}[Ru^*\cdot Q_i](k_d+k_f+k_{q,1}) \tag{13}$$

The rate of light absorption by [Ru] is,

$$I_t \times \frac{[Ru]}{[Ru]_t} = [Ru^*](k_d + k_f + k_{q,2}[Q]). \quad (14)$$

The relative emission intensity, I_0/I, from the excited state of the Ru complex in the absence and the presence of Q is,

$$I_0/I = (k_f/(k_d + k_f)) \div (k_f \sum_{i=0}^{\infty} [Ru^*\text{-}Q_i]/I_t). \quad (15)$$

From Eq. 13,

$$\sum_{i=0}^{\infty} [Ru^*\text{-}Q_i] = \frac{I_t + [Ru^*](k_{q,1} - k_{q,2}[Q])}{k_d + k_f + k_{q,1}}, \quad (16)$$

and from Eq. 14,

$$[Ru^*] = \frac{I_t}{k_d + k_f + k_{q,2}[Q]} \cdot \frac{[Ru]}{[Ru]_t}. \quad (17)$$

Therefore, from Eqs. 16 and 17,

$$\sum_{i=0}^{\infty} [Ru^*\text{-}Q_i] = I_t \cdot \frac{(k_1 + k_{q,2}[Q]) + (k_{q,1} - k_{q,2}[Q])[Ru]/[Ru]_t}{(k_1 + k_{q,2}[Q])(k_1 + k_{q,1})}, \quad (18)$$

where

$$k_d + k_f = k_1, \quad \text{Lifetime } \tau_0 = 1/k_1. \quad (19)$$

Since the lifetime in the absence of Q (τ_0) equals $1/k_1$, Eq. 15 becomes as Eq. 20.

$$I_0/I = \frac{\tau_0 I_t}{\sum_{i=0}^{\infty} [Ru^*\cdot Q_i]} = \frac{(1 + \tau_0 k_{q,1})(X + Y[Q]_t)}{X + Y[Q]_t + \tau_0 (X k_{q,1} - k_{q,2}[Q]_t) \exp(-K_1[Q]_t/X)} \quad (20)$$

$$X = K_1[Ru]_t + 1 \quad (21) \qquad Y = \tau_0 k_{q,2} \quad (22)$$

Although Eq. 20 contains too many parameters to be determined, it is shown by differentiation that the I_0/I vs. [Q] plots fall on a downward curve.

In model 2, no dynamic quenching by the bulk Q is considered, so that the reactions can be expressed by Eqs. 23 to 27.

Model 2

$$[Ru] \xrightarrow{h\nu} [Ru^*] \quad \begin{cases} \xrightarrow{k_d} [Ru] & (23) \\ \xrightarrow{k_f} [Ru] & (24) \end{cases}$$

$$[Ru\text{-}Q_i] \xrightarrow{h\nu} [Ru^*\cdot Q_i] \quad \begin{cases} \xrightarrow{k_{q,1}} [Ru\text{-}Q_i] & (25) \\ \xrightarrow{k_d} [Ru\cdot Q_i] & (26) \\ \xrightarrow{k_f} [Ru\text{-}Q_i] & (27) \end{cases}$$

In this model, $k_{q,2}=0$ and $Y=0$ in comparison to the model 1, so Eq. 28 can be derived from Eq. 20.

$$I_0/I = \frac{(1 + \tau_0 k_{q,1})}{1 + \tau_0 k_{q,1} \exp(-K_1[Q]_t/X)} \quad (28)$$

According to this model, the I_0/I vs. $[Q]_t$ plots show a downward curve as the model 1. The method to distinguish between the models 1 and 2 is described later.

In the next model 3 both the dynamic and the static quenchings were considered, but the rate of the static quenching in the domain is proportional to the number of the Q molecule bound to the domain. This is different from the model 1 where the rate of the static quenching is independent of the number of the Q molecule bound. The reactions are expressed by the Eqs. 29 to 34.

Model 3

$$[Ru] \xrightarrow{h\nu} [Ru^*] \quad \begin{cases} \xrightarrow{k_{q,2}[Q]} [Ru] & (29) \\ \xrightarrow{k_d} [Ru] & (30) \\ \xrightarrow{k_f} [Ru] & (31) \end{cases}$$

$$[Ru\text{-}Q_i] \xrightarrow{h\nu} [Ru^*\text{-}Q_i] \quad \begin{cases} \xrightarrow{ik_{q,1}} [Ru\text{-}Q_i] & (32) \\ \xrightarrow{k_d} [Ru\text{-}Q_i] & (33) \\ \xrightarrow{k_f} [Ru\text{-}Q_i] & (34) \end{cases}$$

In this model, the total rate of light absorption is expressed by Eq. 35 when steady state is assumed for the Reactions 29 to 34.

$$I_t = [Ru^*](k_1 + k_{q,2}[Q]) + \sum_{i=1}^{\infty} [Ru^*\cdot Q_i](k_1 + ik_{q,1}) = k_1 \sum_{i=0}^{\infty} [Ru^*\cdot Q_i] + k_{q,2}[Q][Ru^*] + k_{q,1} \sum_{i=0}^{\infty} i[Ru^*\text{-}Q_i] \quad (35)$$

The rate of light absorption by [Ru] is,

$$I_t \times \frac{[Ru]}{[Ru]_t} = [Ru^*](k_1 + k_{q,2}[Q]). \quad (36)$$

Therefore,

$$[Ru^*] = \frac{I_t[Ru]}{(k_1 + k_{q,2}[Q])[Ru]_t}. \quad (37)$$

The relative emission intensity, I_0/I, is,

$$I_0/I = (k_f/k_1) \div (k_f \sum_{i=0}^{\infty} [Ru^*\text{-}Q_i]/I_t) = \frac{\tau_0 I_t}{\sum_{i=0}^{\infty} [Ru^*\text{-}Q_i]}. \quad (38)$$

From Eq. 35,

$$\sum_{i=0}^{\infty} [Ru^*\text{-}Q_i] = \frac{I_t - k_{q,2}[Q][Ru^*] - k_{q,1} \sum_{i=0}^{\infty} i[Ru^*\text{-}Q_i]}{k_1} \quad (39)$$

From Eq. 5,

$$\sum_{i=0}^{\infty} i[Ru^*\text{-}Q_i] = [Ru^*]K_1[Q] \exp(K_1[Q]) \quad (40)$$

Therefore Eq. 39 becomes

$$\sum_{i=0}^{\infty}[Ru^*\text{-}Q_i] = \frac{1}{k_1}[I_t-(k_{q,2}[Q] + k_{q,1}K_1[Q]\exp(K_1[Q]))[Ru^*]]. \quad (41)$$

By using Eqs. 14 and 4, Eq. 41 becomes Eq. 42

$$\sum_{i=0}^{\infty}[Ru^*\cdot Q_i] = \frac{I_t}{k_1}\left[1-\frac{1}{k_1+k_{q,2}[Q]}\cdot\frac{[Ru]}{[Ru]_t} \times (k_{q,2}[Q]+k_{q,1}K_1[Q]\exp(K_1[Q]))\right] = \frac{I_t}{k_1}\cdot\frac{k_1+k_{q,2}[Q](1-\exp(-K_1[Q]))-k_{q,1}K_1[Q]}{k_1+k_{q,2}[Q]}. \quad (42)$$

Therefore, from Eqs. 15 and 42,

$$I_0/I = \frac{I_t\tau_0}{\sum_{i=0}^{\infty}[Ru^*\cdot Q_i]} = \frac{k_1+k_{q,2}[Q]}{k_1+k_{q,2}[Q](1-\exp(-K_1[Q]))-k_{q,1}K_1[Q]}. \quad (43)$$

Since

$$[Q] = [Q]_t/(K_1[Ru]_t+1) = [Q]_t/X, \quad (44)$$

Eq. 45 is concluded.

$$I_0/I = \frac{k_1+k_{q,2}[Q]_t/X}{k_1+k_{q,2}[Q]_t(1-\exp(-K_1[Q]_t/X)/X)-k_{q,1}K_1[Q]_t/X}. \quad (45)$$

The I_o/I vs. $[Q]_t$ plots of the model 3 thus show a downward curve.

In model 4, no dynamic quenching by the bulk Q is considered, and only the static quenching in the domain is assumed whose rate constant is proportional to the number of the bound Q (see Eqs. 46 to 50).

Model 4

$$[Ru] \xrightarrow{h\nu} [Ru^*] \begin{cases} \xrightarrow{k_d} [Ru] & (46) \\ \xrightarrow{k_f} [Ru] & (47) \end{cases}$$

$$[Ru\cdot Q_i] \xrightarrow{h\nu} [Ru^*\text{-}Q_i] \begin{cases} \xrightarrow{ik_{q,1}} [Ru\cdot Q_i] & (48) \\ \xrightarrow{k_d} [Ru\cdot Q_i] & (49) \\ \xrightarrow{k_f} [Ru\text{-}Q_i] & (50) \end{cases}$$

By substituting $k_{q,2}=0$ in the Eq. 45 (model 3), the next relation is obtained.

$$I_0/I = \frac{k_1}{k_1-k_{q,1}K_1[Q]_t/X} = \frac{1}{1-k_{q,1}\tau_0K_1[Q]_t/X} \quad (51)$$

The I_o/I vs. $[Q]_t$ plots should show an upward curve, and the I/I_o vs. $[Q]_t$ plots be linear.

The models 1 and 2 can be distinguished by emission decay profile. The patterns of the emission decay for the models 1 and 2 are illustrated as Fig. 2.

Since in the model 1 both dynamic and static quenching occur, the emission decay should be nonexponential, and both the shorter and the longer lifetime components should decay faster than the system without Q. In the model 2 only static quenching occurs, indicating that the emission decay is also nonexponential, but that the [Ru] which does not bind Q even in the presence of Q in the system emits just as the system without Q. It means that the longer lifetime components in the presence of Q decay at the same rate as the decay in the absence of Q. The decay profile of the model 2 can therefore be shown as Fig. 2.

In Fig. 1 the quenchings in the absence of additive as well as in the presence of NaOH showed downward curves, so that they should obey either the model 1 or 2. The emission decay in the absence of any additive was studied and shown in Fig. 3. The relative emission decays in the absence and the presence of MV^{2+} shown in Fig. 3 are corresponding to the decay profile of the model 1 shown in Fig. 2. The quenching with no additive should therefore obey the model 1. The emission decay in the presence of NaOH was shown in Fig. 4. This shows the same

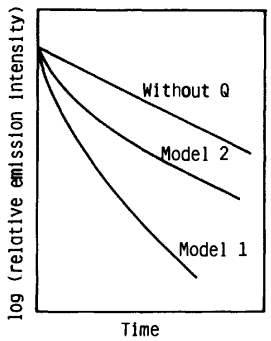

Fig. 2. Profiles of emission decay in the models 1 and 2.

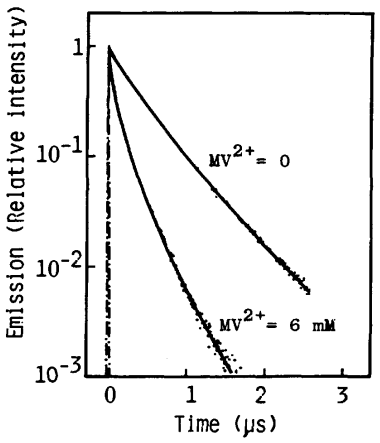

Fig. 3. Emission decay of excited **1** in MeOH with no additive under Ar at 25 °C.

Table 2. Quenching Mechanism of the Excited Copolymer-Pendent $[Ru(bpy)_3]^{2+}$ (**1**) by MV^{2+} in Methyl Alcohol

Model	Rates of quenching by		Stern-Volmer plot based on emission intensity	Additive
	Bulk Q	Bound Q		
1	$k_{q,2}[Q]$	$k_{q,1}$	Downward curve	None
2	—	$k_{q,1}$	Downward curve	NaOH
3	$k_{q,2}[Q]$	$ik_{q,1}$	Upward curve	$HCl+H_2NCSNH_2$
4	—	$ik_{q,1}$	Upward curve	
Conventional dynamic model	$k_{q,2}[Q]$	—	Linear relationship	HCl or $HCl+Et_4NBr$

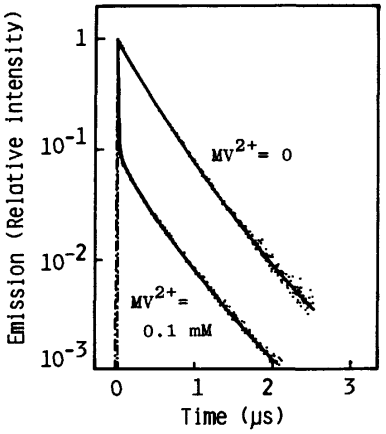

Fig. 4. Emission decay of excited **1** in MeOH containing 1 mM NaOH measured under Ar at 25 °C.

decay profile as the model 2 (see Fig. 2). The quenching in the presence of NaOH should therefore obey the model 2.

The quenching in the presence of HCl and H_2NCSNH_2 showed an upward curve (Fig. 1), indicating that it should obey either the model 3 or 4. Since the I/I_0 vs. $[Q]_t$ plots did not give a straight line, this should not obey the model 4, but the model 3.

The quenching mechanism of the systems shown in Fig. 1 can therefore be summarized as Table 2. It was already described that the quenching of the system containing HCl or both HCl and Et_4NBr is explained by a conventional dynamic model. In the system with no additive, both the dynamic quenching by the bulk Q and the static quenching in the domain occur, the rate of the latter being independent of the number of the bound Q.

In the presence of NaOH, no dynamic quenching occurs and only static quenching is involved whose rate is independent of the number of the bound Q. This situation is entirely different from the alkaline aqueous system[6] for which the Stern-Volmer plots showed a linear relationship indicating that the quenching in water can be explained by a dynamic model even in the presence of NaOH. In the present MeOH system, the quenching specificity of the NaOH-added system would be due to the less polarity of the medium than water. In MeOH the binding of MV^{2+} to the anionic domain composed by the dissociated carboxylato groups would be much stronger than in water, which would make the quenching static.

In the system containing HCl and H_2NCSNH_2, both the dynamic quenching by the bulk Q and the static quenching in the domain occur, the rate of the latter being proportional to the number of the bound Q. Some specific anionic domain formation might be suggested to occur due to acid-base interaction between carboxylic groups of the polymer chain and H_2NCSNH_2.

The quenching mechanism of the acrylic acid-copolymer pendant $[Ru(bpy)_3]^{2+}$ by MV^{2+} is thus strongly dependent on the conditions of the MeOH medium. This is the first example in which one photochemical reaction system exhibits different quenching mechanisms depending on the additives.

References

1) B. H. Milosavljevic and J. K. Thomas, *J. Chem. Soc., Faraday Trans. 1*, **81**, 735 (1985).
2) M. Kaneko and A. Yamada, *Adv. Polym. Sci.*, **55**, 1 (1984).
3) K. Kalyanasundaram and M. Graetzel, *Photochem. Photobiol.*, **40**, 807 (1984).
4) J. H. Fendler, *J. Chem. Education*, **60**, 872 (1983).
5) "Photochemical Conversion and Storage of Solar Energy," ed by J. S. Connolly, Academic Press, New York (1981).
6) M. Kaneko, A. Yamada, E. Tsuchida, and Y. Kurimura, *J. Phys. Chem.*, **88**, 1061 (1984).
7) R. E. Sasoon and J. Rabani, *J. Phys. Chem.*, **84**, 1319 (1980).
8) R. E. Sassoon and J. Rabani, *Isr. J. Chem.* **22**, 138 (1982).
9) Y. Morishima, Y. Itoh, and S. Nozakura, *Chem. Phys. Lett.*, **91**, 258 (1982).
10) M. Kaneko, A. Yamada, E. Tsuchida, and Y. Kurimura, *J. Polym. Sci., Polym. Lett. Ed.*, **20**, 1011 (1982).
11) M. Kaneko, S. Moriya, A. Yamada, H. Yamamoto, and N. Oyama, *Electrochim. Acta*, **29**, 115 (1984).
12) M. Kaneko, A. Yamada, N. Oyama, and S.

Yamaguchi, *Makromol. Chem., Rapid Commun.* **3**, 769 (1982).
13) K. Rajeshwar, M. Kaneko, and A. Yamada, *J. Electrochem. Soc.*, **130**, 38 (1983).
14) K. Rajeshwar, M. Kaneko, A. Yamada, and R. Noufi, *J. Phys. Chem.*, **89**, 806 (1985).
15) M. Kaneko and E. Tsuchida, *J. Polym. Sci., Macromol. Rev.*, **16**, 397 (1981).
16) A. Yekta, M. Aikawa, and N. J. Turro, *Chem. Phys. Lett.*, **63**, 543 (1979).
17) P. P. Infelta, *Chem. Phys. Lett.*, **61**, 88 (1979).

 © 1987 The Chemical Society of Japan Bull. Chem. Soc. Jpn., 60, 2531—2534 (1987)

Electronic Structure of (BEDT-TTF)$CuCl_2$ Complex

Masashi TANAKA,* Atsushi KAWAMOTO,† Jiro TANAKA,† Mitsuru SANO, Toshiaki ENOKI,†† and Hiroo INOKUCHI††
Department of Chemistry, College of General Education, Nagoya University, Chikusa-ku, Nagoya 464
†Department of Chemistry, Faculty of Science, Nagoya University, Chikusa-ku, Nagoya 464
††Institute for Molecular Science, Myodaiji, Okazaki 444
(Received January 20, 1987)

The X-ray photoelectron spectra and the ESR spectra of the (BEDT-TTF)$CuCl_2$ complex were taken. The analysis of the X-ray photoelectron spectra shows that the Cu atoms in (BEDT-TTF)$CuCl_2$ are in a mixed-valence state consisting of mono and bivalent cations and the concentration ratio of Cu(I) and Cu(II) is determined to be 2:1. The ESR signals show the presence of the BEDT-TTF cation radical and Cu(II)Cl_2. The temperature dependence of the magnetic susceptibility of these components were obtained from the ESR data.

A new family of organic conductors, based on 3,4;3′,4′-bis(ethylenedithio)-2,2′,5,5′-tetrathiafulvalene (BEDT-TTF), has been synthesized[1] and some of them are the first sulfur-based organic superconductors, (BEDT-TTF)$_2ReO_4$(T_c=2 K) at 0.4 GPa pressure[2] and (BEDT-TTF)$_2I_3$(T_c=1.5 K) at ambient pressure.[3] Following these complexes, a large number of BEDT-TTF salts have been synthesized in an attempt to obtain an organic superconductor with a high critical temperature. Many BEDT-TTF salts ever known have compositions (BEDT-TTF)$_2$X or (BEDT-TTF)$_3X_2$ where X is a monovalent anion such as PF_6^-,[4] AsF_6^-,[5] $InBr_4^-$,[6] ClO_4^-,[7] I_3^-,[8-10] or other polyhalide series. (BEDT-TTF)X(THF)$_{0.5}$ (X=ReO_4^- and IO_4^-) salts form 1:1 salts which consist of four independent complex units in the unit cell.[11] The new type of the 1:1 salt of (BEDT-TTF)$CuCl_2$ was recently found by us.[12] In this paper, we report the results of the measurement of the X-ray photoelectron and ESR spectra of the (BEDT-TTF)$CuCl_2$ complex.

Experimental

Black prism crystals were prepared by the diffusion method of BEDT-TTF and $CuCl_2 \cdot 2H_2O$ in 1,1,2-trichloroethane. The X-ray photoelectron spectra were recorded on a JEOL model JESCA-3A spectrometer. Aluminium $K_{\alpha 1,2}$ radiation (1486.6 eV) was used as the X-ray excitation source and the measurements were carried out at 5×10^{-8} Torr or below. The ESR spectra were taken by a Varian E112 at X-band with a continuous helium flow cryostat and a rectangular microwave cavity.

Results and Discussion

Figure 1 shows the X-ray photoelectron spectra (ESCA) of the (BEDT-TTF)$CuCl_2$ complex together with $CuCl_2 \cdot 2H_2O$ and CuCN. The cupric compound has intense satellites on the higher binding energy sides of the $2p_{1/2}$ and $2p_{3/2}$ peaks, however, the cuprous compound has no satellite associated with these bands.[13] Such a satellite pattern may be explained by the difference in the electronic structures of $3d^9$ for Cu(II) and $3d^{10}$ for Cu(I), respectively. The half-width (γ_ω) and intensity (γ_i) ratios of the satellite to the main $2p_{3/2}$ peak are estimated to be γ_ω=1.66 and γ_i=0.4 for $CuCl_2 \cdot 2H_2O$. However, these values are γ_ω=1.4 and γ_i=0.15 for the (BEDT-TTF)$CuCl_2$ complex. Accordingly, the ESCA spectrum of (BEDT-TTF)$CuCl_2$ is considered as the overlap of the signals of Cu(I) and Cu(II) in the 2p energy region. The dashed line of the $2p_{3/2}$ peak shows the contribution of Cu(II) to the ESCA line shape of the (BEDT-TTF)$CuCl_2$ complex and the ratio of area of the dashed line part and the remaining part of the $2p_{3/2}$ peak is estimated to be 1:2. That is, the Cu atoms in (BEDT-TTF)$CuCl_2$ are in a mixed-valence state consisting of mono and bivalent

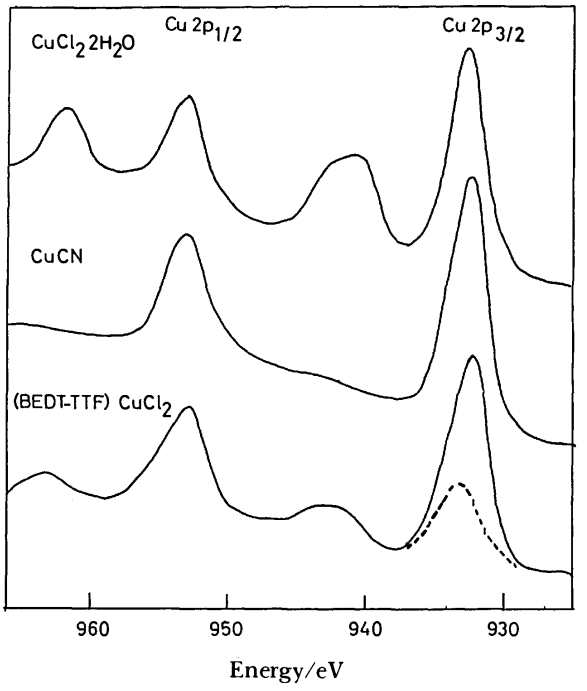

Fig. 1. X-Ray photoelectron spectra of $CuCl_2 \cdot 2H_2O$, CuCN, and (BEDT-TTF)$CuCl_2$.

cations and the concentration ratio of $[Cu(I)Cl_2]^-$: $[Cu(II)Cl_2]$ or $[BEDT\text{-}TTF\cdot]^+$:[BEDT-TTF] is determined to be 2:1.

The ESR spectra of (BEDT-TTF)$CuCl_2$ were measured over a temperature range of 4—300 K as is shown in Fig. 2. The numbers in parenthesis mean the relative intensity ((peak value/gain value)$\times 10^6$) of the maximum ESR peak. Bands I and II are the ESR signals of the impurity of $CuCl_2\cdot 2H_2O$.[14] The sharp band III with g=2.009 can be assigned to the unpaired π-electron of the BEDT-TTF cation radical[15] and the broad band IV with g=2.003 to the d electron of $Cu(II)Cl_2$.

The ESR spectra can be expressed by the following equation:

$$I = \sum_i \frac{2B_i A_i^2 (H_i - H)}{[1 + A_i^2 (H_i - H)^2]^2}. \quad (1)$$

The parameters A_i, B_i, and H_i are determined by the best fit of Eq. 1 to the observed ESR spectra and the magnetic susceptibility $X_i(T)$ of the i-th component at temperature T is given by the absolute intensity of $(\pi B_i/A_i)_T$ of the ESR signal,

$$X_i(T) = C\left(\frac{\pi B_i}{A_i}\right)_T. \quad (2)$$

The coefficient C is estimated with the observed static magnetic susceptibility at room temperature of $X(290\text{ K})=9\times 10^{-4}$ emu mol^{-1} by the following equation:

$$X(290\text{K}) = C\sum_i \left(\frac{\pi B_i}{A_i}\right)_{T=290\text{K}}. \quad (3)$$

The value of $X(290\text{ K})$ was corrected by considering the diamagnetic effect of the constituting atoms. The temperature dependences of the susceptibilities X_{III} and X_{IV} are shown in Figs. 3 and 4.

Band III is the ESR signal of the BEDT-TTF radicals with g=2.009 at room temperature and with the temperature-independent line-width of $\Delta H \approx 20$G. The susceptibility X_{III} seems to be independent of temperature above 240 K and decreases gradually from

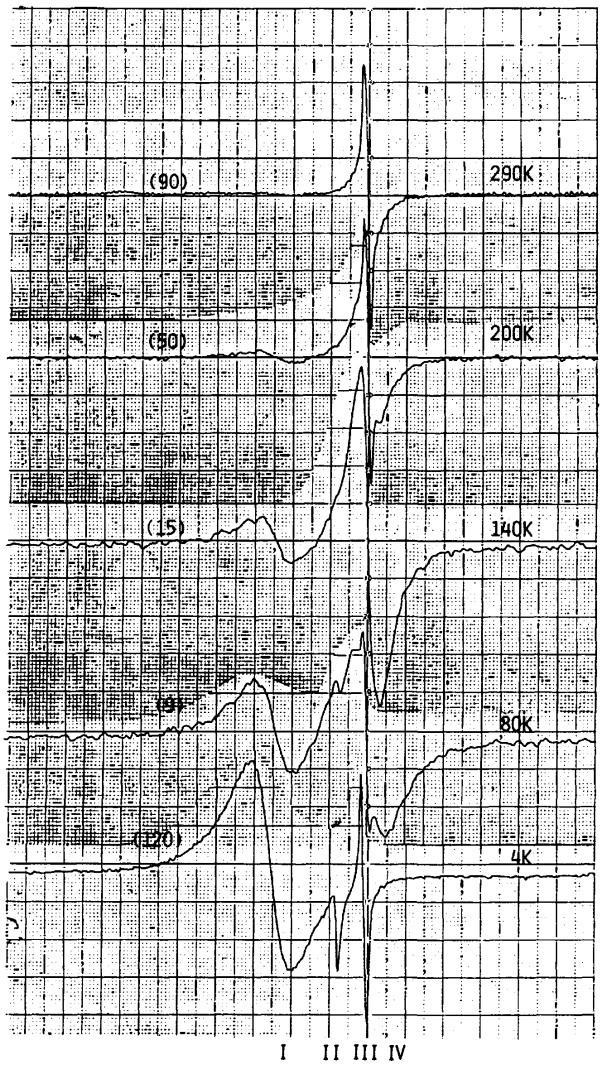

Fig. 2. ESR spectra of (BEDT-TTF)$CuCl_2$. The numbers in parenthesis mean the relative intensity.

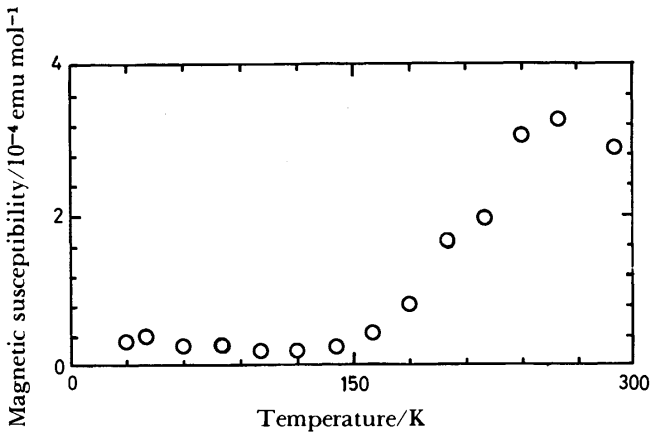

Fig. 3. Temperature dependence of the magnetic susceptibility X_{III} obtained by the analysis of the ESR signal of the band III.

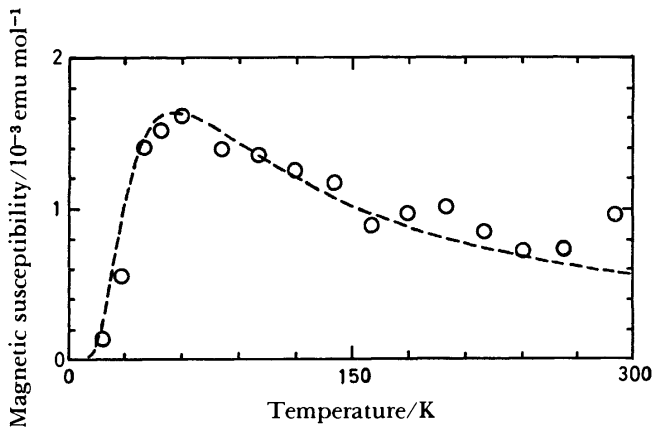

Fig. 4. Temperature dependence of the magnetic susceptibility X_{IV} obtained by the analysis of the ESR signal of the band IV. (°°°°: Obsd., ------: Calcd.)

240 to 140 K. After that, X_{III} remains constant down to 10 K. Then, the susceptibility below 240 K is described by the singlet-triplet model as follows:[16]

$$X(T) = \frac{0.750\,g^2}{T} n_{III} \exp(-J/kT), \quad (4)$$

where g=2 and J=850 K. n_{III}=0.78 is the mole number of the BEDT-TTF cation radical per one mole of (BEDT-TTF)$CuCl_2$. This value (≈3/4) is in agreement with the value (2/3) determined by the ESCA experiment. However, the calculated susceptibility above 240 K increases with the temperature and has no maximum peak below 300 K although the observed susceptibility does not change with temperature. Such temperature-independent susceptibility from 240 to 300 K may be described by the Pauli paramagnetism of the one-dimensional model. As BEDT-TTF molecules form the one-dimensional stacking column along the c axis (Fig. 5) and the overlap between the π- molecular orbitals along the stacking column forms the one-electron tight-binding band with a bandwidth 4t, the calculated X(T) is given by the simple Pauli susceptibility[17],

$$X = \frac{No\,\mu_B^2}{\pi t \sin(\rho\pi/2)}, \quad (5)$$

where N_o is Avogadro's number, μ_B is the Bohr magneton and ρ=4/3 is the number of carrier electrons per BEDT-TTF molecule. Accordingly, the observed susceptibility of ca. 3×10^{-4} emu mol^{-1} at room temperature gives t≈0.19 eV. Such large value of the transfer integral may be explained by the short interplanar distance of 3.39 A and the two-dimensional interaction of BEDT-TTF molecules.[12] The above-mentioned change of the magnetic susceptibility in the vicinity of 240 K may be explained by the metal-insulator transition due to the Peierls instability.

The temperature dependence of the susceptibility X_{IV} of band IV can be depicted by the following Bleaney-Bowers equation[16] for the dimerization of Cu(II)Cl_2,

$$X(T) = \frac{0.125\,g^2}{T} \frac{2\,n_{IV}}{1+\frac{1}{3}\exp(J/kT)}, \quad (6)$$

where g=2 and J=90 K. The magnitude of the g value obtained (g≈2.00) is almost similar to that of Cu(II).[18] n_{IV}=0.245 is the mole number of Cu(II)Cl_2 per one mole of (BEDT-TTF)$CuCl_2$. This value (≈1/4) is comparable with the value (1/3) determined by the ESCA experiment. The difference between these two values obtained by the ESCA and the magnetic susceptibility measurements may be due to the presence of the impurity of $CuCl_2\cdot2H_2O$. These facts mean that the crystal of the (BEDT-TTF)$CuCl_2$ complex consists of the columns of the stack of BEDT-TTF and the dimers of $[Cu(II)Cl_2]_2$ and $[Cu(I)Cl_2]^{2-}_2$. However, the crystal belongs to the space group of $P\bar{1}$ (Z=1) and the projection of the structure along the c axis is shown in Fig. 5.[12] Accordingly, all of BEDT-TTF molecules and $CuCl_2$ molecules are crystallographically equivalent and the charge carrier delocalizes along each column of BEDT-TTF and $CuCl_2$.

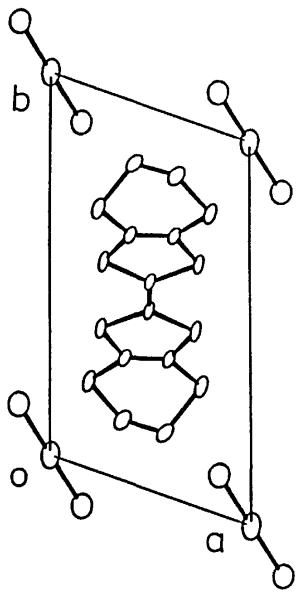

Fig. 5. Projection of the structure of (BEDT-TTF)-$CuCl_2$ along the c axis.[12]

The authors would like to thank Dr. Tetsuo Asaji of Nagoya university for the measurement of the static magnetic susceptibility.

References

1) G. Saito, T. Enoki, K. Toriumi, and H. Inokuchi, *Solid State Commun.*, **42**, 557 (1982).

2) S. S. Parkin, E. M. Engler, R. R. Schumaker, R. Lagier, V. Y. Lee, J. C. Scott, and R. L. Greene, *Phys. Rev. Lett.*, **50**, 270 (1983).

3) E. B. Yagubskii, I. F. Shchegolev, V. N. Laukhin, P. A. Kononovich, M. V. Kartsovnik, A. V. Zvarykina, and L. I. Buravov, *Zh. Eksp. Teor. Fiz., Pis'ma Red.* **39**, 12 (1984); *JETP Lett.*, **39**, 12 (1984).

4) H. Kobayashi, R. Kato, T. Mori, A. Kobayashi, Y. Sasaki, G. Saito, and H. Inokuchi, *Chem. Lett.*, **1983**, 759.

5) P. C. W. Leung, M. A. Beno, G. S. Blackman, B. R. Coughlin, C. A. Miderski, W. Joss, G. W. Crabtree, and J. M. Williams, *Acta Crystallogr., Sect. C*, **40**, 1334 (1984).

6) M. A. Beno, D. D. Cox, J. M. Williams, and J. F. Kwak *Acta Crystallogr., Sect. C*, **40**, 1334 (1984).

7) H. Kobayashi, R. Kato, T. Mori, A. Kobayashi, Y. Sasaki, G. Saito, T. Enoki, and H. Inokuchi, *Chem. Lett.*, **1984**, 179.

8) K. Bender, I. Hennig, D. Schweitzer, K. Dietz, H. Endres, and H. J. Keller, *Mol. Cryst. Liq. Cryst.*, **108**, 359 (1984).

9) P. C. W. Leung, T. J. Emge, M. A. Beno, H. H. Wang, and J. M. Williams, *J. Am. Chem. Soc.*, **106**, 7644 (1984).
10) R. P. Shibaeva, V. F. Kaminskii, and E. B. Yagubskii, *Mol. Cryst. Liq. Cryst.*, **119**, 361 (1985).
11) H. Kobayashi, A. Kobayashi, Y. Sasaki, G. Saito, and H. Inokuchi, *Chem. Lett.*, **1984**, 183.
12) A. Kawamoto, J. Tanaka, and M. Tanaka, *Acta Crystallogr., Sect. C*, **43**, 205 (1987).
13) D. C. Frost, A. Ishitani, and C. A. McDowell, *Mol. Phy.*, **24**, 861 (1972).
14) F. K. Kneubuhl, *J. Chem. Phys.*, **33**, 1074 (1960).
15) T. J. Emge, H. H. Wang, P. C. W. Leung, P. R. Rust, J. D. Cook, P. L. Jackson, K. D. Carlson, J. M. Williams, M.-H. Whangbo, E. L. Venturini, J. E. Schirrber, L. T. Azevedo, and J. R. Ferraro, *J. Am. Chem. Soc.*, **108**, 695 (1986).
16) B. Bleaney and K. D. Bowers, *Proc. R. Soc. London, Ser. A*, **214**, 451 (1952).
17) J. B. Torrance, Y. Tomkiewicz, and B. D. Silverman, *Phys. Rev. B*, **15**, 4738 (1977).
18) M. Inoue and M. B. Inoue, *Inorg. Chem.*, **25**, 37 (1986).

 © 1987 The Chemical Society of Japan Bull. Chem. Soc. Jpn., 60, 2535—2537 (1987)

Preferential Solvation of Ni(II) in Water-Solvent Mixtures from ^{13}C NMR Paramagnetic Relaxation Rate

Kanya KOBAYASHI, Masatoki YOKOI,* Shigeki KURODA,† and Eiji KUBOTA
Department of Chemistry, Faculty of Science, Shinshu University,
Asahi, Matsumoto 390
(Received February 2, 1987)

^{13}C NMR spin-lattice relaxation time of carbon atom on methanol, ethanol, 1-propanol, and dimethyl sulfoxide molecules has been measured for solutions of $Ni(ClO_4)_2$ in these solvents and their mixtures with water. The comparison of the NMR data for solutions with aqueous mixtures and pure solvents gave the number of organic solvent molecules that locate in the first coordination sphere of Ni^{2+} ion. The result shows that Ni^{2+} ion is preferentially hydrated in water-alcohol systems, while in water-dimethyl sulfoxide system, the ion is solvated preferentially with dimethyl sulfoxide.

The preferential solvation of an ion in mixed solvents is an interesting subject in the electrolyte solution chemistry. The detailed information on the structure of solvated ion in a mixed solvent is expected to gain a better understanding of the behavior of ion. The NMR spectroscopy has provided a useful method for investigating local structure in the vicinity of ion. If the signal arising from the solvated solvent molecules is distinguished from that of bulk molecules, the solvation number can be determined directly from integration of the both signals.[1-3] The application of the direct NMR method is, however, confined to systems of high electrolyte concentration and of low rate of solvent exchange. On the other hand, the exchange rate of most ions with moderate number of charge is so high that the NMR spectrum gives a coalesced signal of both the coordinated and bulk molecules. In this case, chemical shift and relaxation rate are utilized to get information on the constitution of coordination sphere of ion.[4-7] This paper reports ^{13}C NMR paramagnetic relaxation rates for carbon atoms of organic solvent molecules caused by Ni^{2+} ion in Ni $(ClO_4)_2$ solution with water-solvent mixtures. The dependence of relaxation rate on concentration was analyzed to deduce the number of organic molecules that locate in the first coordination sphere of Ni^{2+} ion.

Experimental

Commercially available nickel perchlorate hexahydrate was recrystallized from water. The content of water was determined as six mole per formula from cation analysis using a cation-exchange column. The hydrated crystal was used to prepare solutions. Since the mole fraction of Ni(II) was less than 0.001 for solutions in pure organic solvents, a small amount of water accompanied with the crystal will give only a negligible effect on the ^{13}C NMR T_1 (spin-lattice relaxation time) of the solvent molecules. Methanol, ethanol, 1-propanol, and dimethyl sulfoxide (DMSO) were of reagent grade and used without further purification. ^{13}C NMR T_1 was measured by a JEOL FX90Q-FT NMR spectrometer at 35 °C with a standard inversion-recovery technique. The NMR frequency was 22.5 MHz. The error in measuring T_1 was leas than 5%.

Results and Discussion

If we denote the ^{13}C NMR relaxation rate of carbon atoms of solvent molecules located in the first coordination sphere of a paramagnetic ion as $1/T_{1M}$, and that of the bulk solvent as $1/T_{1B}$, then the observed relaxation rate $1/T_1$ is expressed by

$$\frac{1}{T_1} = \frac{X_M}{T_{1M}} + \frac{1-X_M}{T_{1B}}, \quad (1)$$

where X_M denotes the fraction of solvent molecule in the first coordination sphere. X_M is given by

$$X_M = n\frac{C_i}{C_s}, \quad (2)$$

where n is the number of coordinated solvent molecules to Ni^{2+} ion, C_i and C_s are the molar concentrations of ion and solvent molecule, respectively. If we assume that the rate $1/T_{1M}$ and coordination number of Ni^{2+} ion are unchanged in pure and mixed solvent, and that the relationship

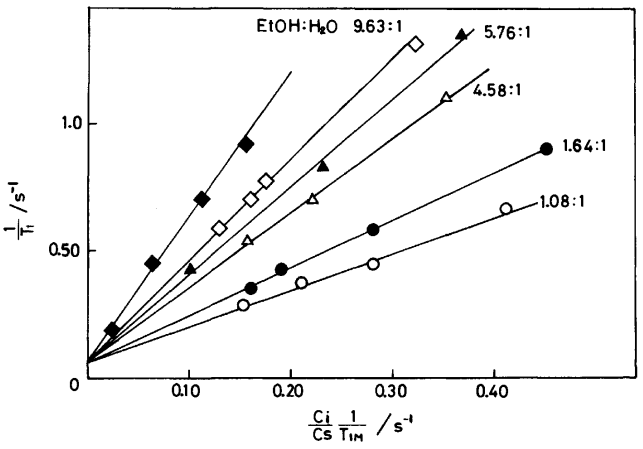

Fig. 1. Relationship between the ^{13}C spin-lattice relaxation rate in Ni-EtOH-H_2O at 35 °C and $C_i/(C_s T_{1M})$.

† Present address: Oki Electric Industry Co. Ltd., 550-1 Higashiasakawa-cho, Hachioji 193.

Table 1. ^{13}C Spin-Lattice Relaxation Time in $Ni(ClO_4)_2$-CH_3OH-H_2O System

$X(H_2O)$	Ni :	CH_3OH :	H_2O	T_1/s	Slope
0.70	0.00148	0.430	1	1.05	0.78
	0.00113	0.430	1	1.43	
	0.000603	0.430	1	2.48	
	0.000448	0.430	1	3.21	
0.50	0.000930	0.992	1	2.27	1.9
	0.000521	0.992	1	3.56	
	0.000352	0.992	1	4.71	
0.40	0.00102	1.51	1	2.46	2.5
	0.000585	1.51	1	3.61	
	0.000358	1.51	1	5.28	
0.30	0.00188	2.35	1	1.83	3.4
	0.00143	2.35	1	2.32	
	0.000874	2.35	1	3.37	
0.21	0.00351	3.67	1	1.32	3.8
	0.00306	3.67	1	1.50	
	0.00251	3.67	1	1.84	
	0.00121	3.67	1	3.25	
0.13	0.00582	6.70	1	1.19	4.7
	0.00346	6.70	1	1.94	
	0.00317	6.70	1	2.13	
	0.00152	6.70	1	3.64	
0	0.000877	1	0	0.89	
	0.000688	1	0	1.06	
	0.000447	1	0	1.67	
	0.000228	1	0	2.62	
	0.000111	1	0	4.09	

Table 2. ^{13}C Spin-Lattice Relaxation Time in $Ni(ClO_4)_2$-C_2H_5OH-H_2O System

$X(H_2O)$	Ni :	C_2H_5OH :	H_2O	T_1/s	Slope
0.48	0.00315	1.08	1	1.50	1.5
	0.00219	1.08	1	2.23	
	0.00159	1.08	1	2.67	
	0.00118	1.08	1	3.44	
0.38	0.00529	1.64	1	1.10	1.8
	0.00333	1.64	1	1.69	
	0.00224	1.64	1	2.33	
	0.00162	1.64	1	2.84	
0.18	0.0116	4.58	1	0.90	2.9
	0.00715	4.58	1	1.39	
	0.00510	4.58	1	1.82	
0.15	0.0153	5.76	1	0.73	3.5
	0.00953	5.76	1	1.19	
	0.00317	6.76	1	2.13	
0.094	0.0232	9.63	1	0.75	4.2
	0.0119	9.63	1	1.28	
	0.0111	9.63	1	1.40	
	0.00895	9.63	1	1.69	
0	0.00103	1	0	1.07	
	0.000775	1	0	1.39	
	0.000361	1	0	2.19	
	0.000132	1	0	4.94	

Table 3. ^{13}C Spin-Lattice Relaxation Time in $Ni(ClO_4)_2$-n-C_3H_7OH-H_2O System

$X(H_2O)$	Ni :	n-C_3H_7OH :	H_2O	T_1/s	Slope
0.50	0.00199	1.00	1	2.80	0.61
	0.00128	1.00	1	3.32	
	0.00100	1.00	1	3.74	
	0.000647	1.00	1	4.27	
0.40	0.00325	1.51	1	2.07	0.96
	0·00252	1.51	1	2.56	
	0.00172	1.51	1	3.05	
	0.00139	1.51	1	3.29	
0.30	0.00506	2.30	1	1.63	1.3
	0.00281	2.30	1	2.45	
	0.00220	2.30	1	2.80	
0.21	0.0632	3.77	1	1.62	1.8
	0.0352	3.77	1	2.58	
	0.00262	3.77	1	2.78	
0.099	0.0150	9.08	1	1.22	2.8
	0.00952	9.08	1	1.83	
	0.00831	9.08	1	1.93	
0	0.00150	1	0	0.66	
	0.00110	1	0	0.92	
	0.000627	1	0	1.32	
	0.000263	1	0	2.45	
	0.000158	1	0	3.64	

Table 4. ^{13}C Spin-Lattice Relaxation Time in $Ni(ClO_4)_2$-$(CH_3)_2SO$-H_2O System

$X(H_2O)$	Ni :	$(CH_3)_2SO$:	H_2O	T_1/s	Slope
0.60	0.00158	0.660	1	0.97	2.9
	0.00102	0.660	1	1.40	
	0.000707	0.660	1	1.75	
0.50	0.00240	1.02	1	0.81	3.9
	0.00190	1.02	1	0.96	
	0.00106	1.02	1	1.51	
	0.000735	1.02	1	1.98	
0.35	0.00723	1.86	1	0.43	4.7
	0.00300	1.86	1	0.92	
	0.00161	1.86	1	1.58	
0.21	0.00978	3.81	1	0.57	5.2
	0.00620	3.81	1	0.86	
	0.00309	3.81	1	1.50	
0.10	0.0162	8.96	1	0.76	5.5
	0.0112	8.96	1	1.07	
	0.00783	8.96	1	1.45	
	0.00536	8.96	1	1.85	
0	0.00119	1	0	1.04	
	0.000782	1	0	1.46	
	0.000598	1	0	1.81	
	0.000325	1	0	2.80	

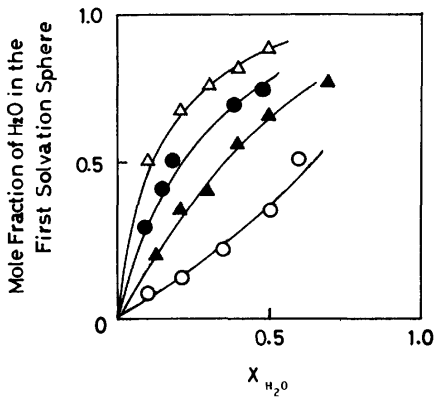

Fig. 2. Relationship between the mole fraction of H_2O in the first solvation sphere and H_2O mole fraction of the solvent at 35 °C. ○: DMSO-H_2O, ▲: MeOH-H_2O, ●: EtOH-H_2O, △: *n*-PrOH-H_2O.

between $1/T_1$ and $C_i/(C_sT_{1M})$ is linear at low concentration of Ni^{2+} ion, slope gives n directly. The coordination number, n, of Ni^{2+} ion in pure solvent was assumed to be six,[9-11] then $1/T_{1M}$ values were obtained from data for pure organic solvent solution. Figure 1 shows the plots for ethanol (Cl) carbon in water-ethanol systems, which appear to be linear. Tables 1—4 give the observed T_1 and the slopes for water-methanol, -ethanol (Cl), -1-propanol (Cl), and -DMSO, respectively. The variation of the composition of the first coordination sphere is shown in Fig. 2 as a function of the composition of bulk solvent. Figure 2 shows that Ni^{2+} ion is preferentially solvated with DMSO in water-DMSO system, while Ni^{2+} in water-alcohol mixture is preferentially hydrated. The magnitude of the preferential hydration increases with the increase in the chain length of alcohol molecules. The behavior of this preferential solvation in water-methanol system is consistent qualitatively with the result obtained by a kinetic study of solvated Ni^{2+} ion reacting with ammonia in water-methanol system.[12] The tendency of solvation in water-methanol mixture has been reported for other ions: Preferential solvation of Eu^{3+} was investigated by luminesence lifetime method[13] and those of Na^+ and Rb^+ were examined by ^{23}Na and ^{87}Rb spin-lattice relaxation rate.[5,6] A coordination ability of DMSO competing with water was demonstrated in $Al(ClO_4)_3$-DMSO-water system by direct ^1H NMR peak integration method.[1-3] ^{23}Na chemical shift and spin-lattice relaxation rate showed that Na^+ ion is solvated preferentially with DMSO in water-DMSO system.[5,7] Luminesence lifetime study of Eu^{3+} in water-DMSO system resulted in preferential solvation with DMSO.[13] ^{23}Na and ^1H NMR chemical shift studies also showed that Na^+ is solvated preferentially with DMSO in binary mixtures of DMSO with nitromethane, acetonitrile, pyridine, and 1-propanol.[7,8] It seems that solvation tendency is not expressed by the Gutmann donor number.[14,15] As for the solvation of Ni^{2+} ion, Munakata et al. have proposed the coordination power to express the solvent donor ability from electronic spectra of Ni^{2+} ion in various binary mixed solvents.[16] The present results agree qualitatively with the order proposed by them. The solvent used in our experiments is confined to solvent rich compositions because of the difficulty of ^{13}C NMR T_1 measurement in low contents of organic species. The measurement by a high field NMR spectrometer or the use of ^{13}C-enriched solvent will overcome the difficulty. The effect of perchlorate counter ion is completely ignored. Since the measurement was carried out in low electrolyte concentration, the effect of counter ion is considered to be small. The measurement with other counter ions will confirm the assumption.

References

1) A. Fratiello, R. E. Lee, V. M. Nishida, and R. E. Schuster, *J. Chem. Phys.*, **47**, 4951 (1967); *ibid.*, **48**, 3705 (1968); *Inorg. Chem.*, **8**, 69 (1961).

2) S. Thomas and W. L. Reynolds, *Inorg. Chem.*, **9**, 78 (1970).

3) A. Fratiello, G. A. Vidulich, C. Cheng, and V. Kubo, *J. Solution Chem.*, **1**, 433 (1971).

4) L. S. Frankel, C. H. Langford, and T. R. Stengle, *J. Phys. Chem.*, **74**, 1376 (1970).

5) M. Holz, *J. Chem. Soc., Faraday Trans. 1*, **74**, 644 (1978).

6) M. Holz, H. Weingärtner, and H. G. Hertz, *J. Chem. Soc., Faraday Trans. 1*, **73**, 71 (1977).

7) R. H. Erlich, M. S. Greenberg, and A. I. Popov, *Spectrochim. Acta*, **29A**, 543 (1973).

8) B. W. Maxey and A. I. Popov, *J. Am. Chem. Soc.*, **90**, 4470 (1968).

9) H. Ohtaki, T. Yamaguchi, and M. Maeda, *Bull. Chem. Soc. Jpn.*, **49**, 701 (1976).

10) J. W. Neely and R. E. Connick, *J. Am. Chem. Soc.*, **94**, 3419 (1972).

11) R. Caminiti, G. Licheri, G. Piccaluga, and G. Pinna, *Faraday Discuss. Chem. Soc.*, **64**, 62 (1977).

12) W. J. Mackellar and D. B. Rorabacher, *J. Am. Chem. Soc.*, **93**, 4379 (1971).

13) F. Tanaka, Y. Kawasaki, and S. Yamashita, 9th Solution Chemistry Symposium, Nagoya, December 1986, Abstr., 1A12.

14) V. Gutmann, "The Donor-Acceptor Approach to Molecular Interactions," Plenum Press, New York (1978), Chap. 2.

15) Y. Marcus, *J. Solution Chem.*, **13**, 599 (1984).

16) M. Munakata, S. Kitagawa, and M. Miyazima, *Inorg. Chem.*, **24**, 1638 (1985).

^{1}H and ^{13}C NMR Studies of Formation and Molecular Dynamics of Methylated-Cyclodextrin Inclusion Complexes with Phenylalanine

Yoshio INOUE,* Fu-Hua KUAN, and Riichiro CHÛJÔ
Department of Polymer Chemistry, Tokyo Institute of Technology,
O-okayama 2-12-1, Meguro-ku, Tokyo 152
(Received February 10, 1987)

The formation and the molecular dynamics of the host-guest inclusion complexes in aqueous solution have been studied for hosts α- and permethylated α-cyclodextrin and permethylated β-cyclodextrin and guest phenylalanine by ^{1}H and ^{13}C NMR spectroscopy. The changes in ^{1}H chemical shift, ^{1}H spin-coupling constant, and ^{13}C spin-lattice relaxation time for the guest phenylalanine on addition of the host cyclodextrin show that they form the inclusion complexes in a similar manner, that is, by insertion of the guest's phenyl ring into the host's cavity. The strength of the host-guest dynamic coupling varies with the cavity size of cyclodextrins.

The cyclodextrins are a series of cyclic oligosaccharides composed of at least six(1→4)-linked α-D-glucosyl residues. Each cyclodextrin molecule has a toroidal, hollow, trancated cone with primary and secondary hydroxyl groups crowning the narrower and wider rims, respectively. The interior of the cavity of each cyclodextrin contains two bands of C-H groups and a band of glucosidic oxygens. Hence the interior of the cavity is relatively hydrophobic, whereas the exterior is relatively hydrophilic.

Cyclodextrins can admit various guest molecules into the cavity, without any covalent bonds being formed, and in some cases they catalyze reactions of included guest compounds.[1-4] Because of these properties, cyclodextrins serve as models for studying topochemical aspects and catalytic reactions of enzymes. In particular, cyclodextrins are good models for such hydrolytic enzymes as esterases and proteases in which the hydroxyl group of serine residue attacks the acyl group of a bound substrate.[5] It is well known that a typical serine protease, chymotrypsin, cleaves selectively at a significant rate the peptide bonds on the carboxyl side of residues with bulky side chain such as phenylalanine, tryptophan, and tyrosine. In these residues, the bulky side chains are assumed to be fitted neatly into a nonpolar pocket of chymotrypsin. Cyclodextrins also exhibit specificity for the guest inclusion.

The complexation and catalytic properties of chemically modified cyclodextrins have been extensively investigated.[2,3] Partially and fully methylated cyclodextrins can also form inclusion complexes in aqueous solution,[2,6] some of which are more stable than those of the parent cyclodextrins. Recently, these derivatives have become of great interest as their solubility in water as well as in organic solvents is very high and inclusion behaviors of them are not always the same as those of parent cyclodextrins.[7]

In order to characterize the inclusion behaviors, it is relevant to investigate the stoichiometry, the host-guest orientation, and the molecular dynamics of inclusion complex. In preceding papers,[8-11] the molecular dynamics of the inclusion complexes of α-, β-, and γ-cyclodextrin(α-, β-, and γ-CD, which are composed of **6**, **7**, and **8** glycosyl residues respectively) with some amino acids and dipeptides having aromatic side chain have been studied in aqueous solution by ^{13}C NMR. It was found that the strength of the host-guest dynamic coupling depends on the cavity size of the host cyclodextrin. We now report on the formation and molecular dynamics of inclusion complexes of methylated cyclodextrins with L-phenylalanine(Phe) in aqueous solution by the measurements of ^{1}H NMR parameters and ^{13}C spin-lattice relaxation times. The influence of the methylation of hydroxyl groups of cyclodextrins on the formation and the molecular dynamics of the complexes may be investigated by comparing the results with those obtained for unmodified cyclodextrin-Phe systems. As hosts we chose α-CD, hexakis(2, 3, 6-tri-*O*-methyl)-α-cyclodextrin(α-TMCD), and heptakis(2, 3, 6-tri-*O*-methyl)-β-cyclodextrin(β-TMCD). β-CD could not be studied because its solubility in neutral water is too poor to observe its natural abundance ^{13}C NMR spectrum with high quality.

Experimental

Materials α-CD, β-CD, and Phe were purchased from Nakarai Chemicals Ltd., Kyoto. α-TMCD and β-TMCD were synthesized by the procedure of Casu et al.[12] from α-CD and β-CD, respectively. They were recrystallized twice from hot water. Their structures and purities were confirmed by ^{1}H and ^{13}C NMR spectra as well as by thin-layer chromatography. Their ^{1}H NMR spectra were shown in Fig. 1, in which the previous assignments[13] were partly revised based on the ^{1}H-^{1}H and ^{1}H-^{13}C COSY spectra. The details of assignments will be published elsewhere.[14] $^{2}H_2O$ was purchased from Merck Sharp & Dohme, Canada, Ltd.

Methods. ^{1}H NMR spectra were recorded with a JEOL GX-500 spectrometer operated at 500 MHz. ^{13}C NMR spectra were recorded with a JEOL JNM PS-100 spectrometer operated at 25.1 MHz. The ^{13}C spin-lattice relaxation

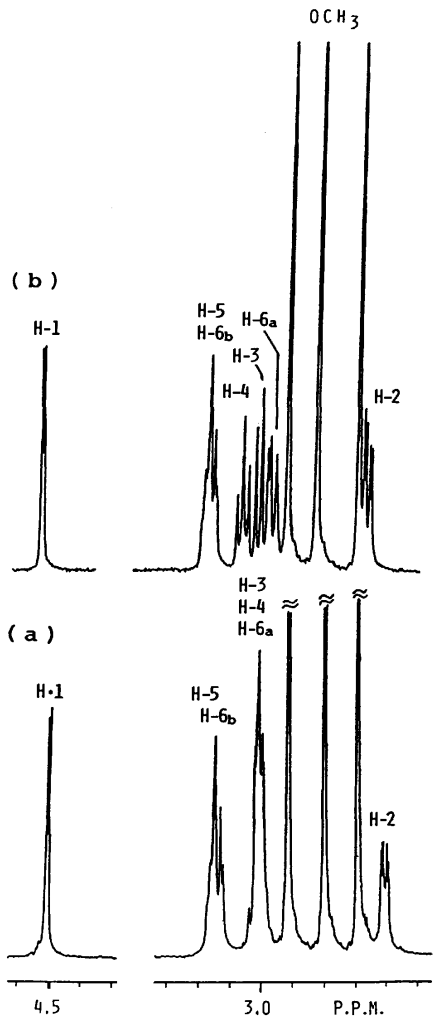

Fig. 1. 500 MHz ^{1}H NMR spectra of α-TMCD(a) and β-TMCD(b) in 0.01 M solution in ^2H_2O. The previous assignments[13] are partly revised[14] in this figure.

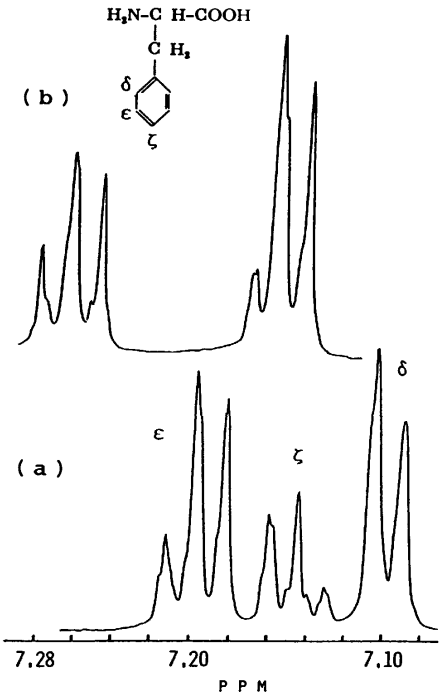

Fig. 2. 500 MHz ^{1}H NMR resonances of phenyl ring protons of phenylalanine(0.01 M) in the absence(a) and in the presence of α-TMCD(0.07 M)(b) in ^2H_2O.

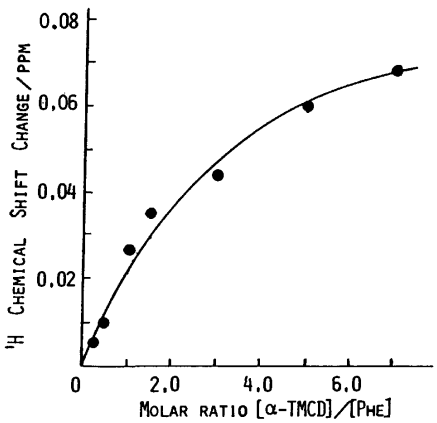

Fig. 3. ^{1}H chemical shift change of phenylalanine ε-proton on addition of α-TMCD in deuterium oxide, as a function of the molar ratio[α-TMCD]/[Phe]. The solid line indicates theoretically calculated chemical shift changes.

time (T_1) was measured by the inversion-recovery method using a 180°-t-90° pulse sequence, where t is the time interval between the 180° and 90° pulses. The estimated error in the ^{13}C-T_1 values was approximately ±10%. The ^{1}H- and ^{13}C-chemical shifts were referenced to external tetramethylsilane. The digital resolution of ^{1}H shift was 0.0006 ppm. The macroscopic viscosity of solution was measured with a Cannon-Finske viscometer.[9] The temperature was kept at 30±2 °C for all measurements.

Results

Cyclodextrin-Induced ^{1}H-Chemical Shifts in Phe and Dissociation Constants. As found previously,[8-11] ^{1}H as well as ^{13}C NMR spectra of each cyclodextrin-Phe system consist of only one set of resonances, indicating that only one type of complexation occurs and/or the chemical exchange of the type

$$CD + S \rightleftarrows [CD, S] \quad (1)$$

is rapid process compared with the NMR time scale, where CD, S, and [CD, S] are host cyclodextrin, guest (substrate) Phe, and complex between them, respectively. The phenyl proton resonances of Phe in the 500 MHz ^{1}H NMR spectra were well resolved and were assigned easily as shown in Fig. 2. On addition of cyclodextrin, the phenyl proton resonances showed remarkably large changes, the example of which is also shown in Fig. 2. By plotting these cyclodextrin-induced ^{1}H chemical shift changes against the molar

ratio [CD]/[S], it is possible to determine the value of dissociation constant K_d (reciprocal of the association constant K_a) for CD-Phe complexation as shown in Fig. 3. In these experiments, the concentration of Phe was kept constant at 0.01 M and that of cyclodextrin was varied between 0 and ca. 0.07—0.10 M (1 M=1 mol dm^{-3}), depending on the solubility of cyclodextrins. The K_d value was estimated by fitting of the modified Hildebrand-Benesi equations[9,15,16] to the chemical shift change vs. [CD]/[S] curve. Here, it was assumed that a 1:1 complex between each CD and Phe was formed and that complexation was reversible as represented by Eq. 1. In Fig. 3 theoretically calculated shifts are also shown by the solid line, reproducing adequately the observed shift changes. Examination of the residuals obtained by subtraction observed shift changes from calculated ones revealed random but not systematic trends and the standard deviation was 0.003 ppm. The reversible dimerization has been suggested for α-TMCD in aqueous solution from its ^{13}C chemical shifts[17], but influence of dimerization was not found in the plot of ^1H shift change of guest Phe against [CD]/[S] molar ratio. That influence has also not been found for *p*-nitrophenol-α-TMCD system.[6]

The values of K_d and the cyclodextrin-induced ^1H chemical shift change $\Delta\delta$ were summerized in Table 1. Here, $\Delta\delta$ is defined as chemical shift difference between the shifts found in the fully complexed and in the uncomplexed states and was estimated from the chemical shifts at known concentrations of cyclodextrin and Phe, in conjunction with the predetermined K_d value.

The large chemical shift changes of phenyl proton resonances suggest that the Phe molecule forms the complex with each cyclodextrin by insertion of its phenyl ring into the cyclodextrin cavity.

The K_d values for three cyclodextrin-Phe systems are practically the same, although that for the α-CD-Phe system is the smallest and that for the β-TMCD one the largest.

Conformational Change of Phe by Complexation with Cyclodextrins. In order to investigate the steric host-guest interaction, a conformational change of the guest Phe on the occasion of complexation with cyclodextrin was analyzed by observing ^1H spin coupling constants.[18] The 500 MHz ^1H NMR resonances of the Phe α- and β-protons could be analyzed as an ABX three spin system. The ^1H coupling constants were observed at the host and guest concentrations of 0.07 and 0.01 M (in ^2H_2O solution), respectively. The coupling constants for Phe in the fully complexed states were estimated from the observed ones with the aid of K_d values. The results were given in Table 2, in which the rotamer populations for the side chain estimated with the use of the Feeney's approximation[19] were also included.

In the free as well as in the complexed states, the most stable rotamer is the gt one with the aromatic ring trans to the carboxyl group. These results are in agreement with the general observations that the aromatic side chain has a tendency to orient itself toward the amino group of the same residue.[20] Thus, the most stable rotamer, gt, in the free state is still the one in the complexed state.

The complexation with α-TMCD induces a small but a notable increase of gt rotamer population with a decrease of gg one. The influence of β-TMCD on the conformation is negligibly small. In the case of α-CD,

Table 1. Dissociation Constants K_d and Complexation-Induced ^1H Chemical-Shift Changes $\Delta\delta$ for Cyclodextrin-Phenylalanine System in Deuterium Oxide[a]

Compound	K_d/M[b]	$\Delta\delta$/ppm[c]		
		H_δ	H_ε	H_ζ
[Phe, α-CD]	3.0×10^{-2}	0.112	0.106	0.052
[Phe, α-TMCD]	3.3×10^{-2}	0.080	0.103	0.023
[Phe, β-TMCD]	3.5×10^{-2}	0.045	0.039	0.032

a) Assignments of carbon atoms of phenylalanine are as follows.

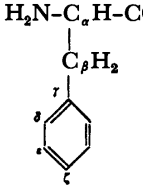

b) Estimated error is less than ±15%. c) $\Delta\delta$ is chemical shift difference between free and fully complexed states, and positive value indicates lowfield shift.

Table 2. ^1H Coupling Constants and Populations of Rotamers about C_α-C_β Bond of Phenylalanine in Free State and Complexed State with Cyclodextrin in Deuterium Oxide

Compound	Coupling constant/Hz			Rotamer population[a]		
	J_{AB}	J_{AX}	J_{BX}	gt	tg	gg
[Phe]	14.5	7.9	5.2	0.53	0.26	0.21
[Phe, α-CD]	14.5	7.5	5.5	0.49	0.28	0.23
[Phe, α-TMCD]	14.5	8.5	5.0	0.60	0.26	0.14
[Phe, β-TMCD]	14.5	8.0	5.1	0.54	0.25	0.21

a) Caluculated by Freeney's relation. Rotamer notations are as follows.

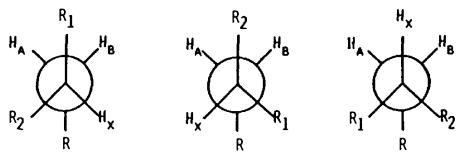

g t t g g g

where R=C_6H_5, R_1=COOH, and R_2=NH_2.

the complexation induces a small decrease of gt population. These results indicate that the steric perturbation of the host cyclodextrins on the conformation of the guest Phe is the largest in the α-TMCD system.

^{13}C Spin-Lattice Relaxation Times of Phe. The measurements of ^{13}C-T_1 values are particularly useful for the investigation of molecular dynamics of cyclodextrin inclusion complexes.[8-11] In Table 3 are given the values of ^{13}C-T_1 for Phe in the free state and in the cyclodextrin-Phe mixed systems in aqueous solution. In the limit of rapid exchange process of Eq. 1, one measures an average relaxation rate

$$\frac{1}{T_1} = p_f\frac{1}{T_{1f}} + p_c\frac{1}{T_{1c}} \tag{2}$$

where T_{1f} and T_{1c} are intramolecular spin-lattice relaxation times for a spin in the free and complexed states, and p_f and p_c ($=1-p_f$) are the probabilities that Phe is found in the free and complexed states, respectively.

For the complexation reaction of Eq. 1, the p_c value can be expressed by[8,9]

$$p_c = \frac{1}{2}(1+r)\left\{1-\left[1-\frac{4K_a}{K_a+1}\cdot\frac{r}{(1+r)^2}\right]^{1/2}\right\} \tag{3}$$

where r is the molar ratio of Phe to cyclodextrin and K_a is the association constant ($=1/K_d$).

The viscosity of the cyclodextrin solution varies widely, depending on the type and concentration of cyclodextrin.[9-11] In order to compare the ^{13}C-T_1 values of Phe in different solutions, a correction for the viscosity difference between the solutions is needed. For a molecule of medium size whose motion is rapid enough on the ^{13}C NMR time scale, it is likely that the ^{13}C-T_1 value of the carbon atom having at least one directly-bonded proton is governed by ^{13}C-^{1}H dipole-dipole relaxation brought about by a rotational motion.[21,22] In this case, if the overall molecular motion is isotropic, ^{13}C-T_1 is given by

$$\frac{1}{T_1} = \hbar^2\gamma_C^2\gamma_H^2 N r_{CH}^{-6}\tau_{eff} \tag{4}$$

where τ_{eff} is the effective correlation time for the overall molecular motion, r_{CH} is the carbon-hydrogen bond length, γ_H and γ_C are the gyromagnetic ratios of ^{1}H and ^{13}C nuclei, and N is the number of directly bonded proton. The τ_{eff} can be related to the viscosity of solution, η, by assuming the Brownian diffusion model.[21-23] As the result, ^{13}C-T_1 is given as follows

$$\frac{1}{NT_1} = \hbar^2\gamma_C^2\gamma_H^2 r_{CH}^{-6}\eta f_r V_m/kT. \tag{5}$$

where k is the Boltzman's constant, T is the absolute temperature, f_r is a microviscosity factor, and V_m is the molecular volume. We have shown in the previous paper[8] that the isotropic diffusion model expressed by Eq. 5 was applicable to the analysis of overall molecular motion of Phe in aqueous solution. According to Eq. 5, $NT_1\eta$ value for a given carbon nucleus must be constant, if all situations except the viscosity of solution remain unchanged. The expected

Table 3. Values of ^{13}C NT_1[a] for Free Phenylalanine and Its Inclusion Complexes with Cyclodextrins in Deuterium Oxide

Compound	Concn/10^{-1} M	^{13}C NT_1/s±10%				
		C_α	C_β	C_δ	C_ε	C_ζ
[Phe]	1.0	1.60	1.82	1.85	1.86	1.33
[Phe, α-CD]	1.0, 1.2	0.45	0.58	0.56	0.58	0.38
[Phe, α-TMCD]	0.83, 1.0	0.74	0.81	0.72	0.71	0.40
[Phe, β-TMCD]	0.83, 1.0	0.76	0.82	0.80	0.81	0.56

a) Here, N is the number of proton(s) attached to the carbon and T_1 is the spin-lattice relaxation time.

Table 4. Values of ^{13}C NT_1 and ^{13}C $NT_1\eta$ (in parenthesis) for Phenylalanine in Free State and in Fully Comlexed State with Cyclodextrins in Deuterium Oxide

Compound	Viscosity η/cp	^{13}C NT_1 (^{13}C $NT_1\eta$)/s(s cp)				
		C_α	C_β	C_δ	C_ε	C_ζ
[Phe]	0.94	(1.50)	(1.71)	(1.74)	(1.75)	(1.25)
[Phe, α-CD]	1.27	0.42	0.54	0.52	0.54	0.35
		(0.53)	(0.69)	(0.66)	(0.69)	(0.44)
[Phe, α-TMCD]	1.43	0.71	0.77	0.68	0.67	0.37
		(1.02)	(1.10)	(0.97)	(0.96)	(0.53)
[Phe, β-TMCD]	1.70	0.75	0.80	0.78	0.79	0.54
		(1.28)	(1.36)	(1.33)	(1.34)	(0.92)

constancy of $NT_1\eta$ values has been certainly observed for aqueous solutions of Phe,[9] where the solution viscosity was controlled by adding various amounts of D-glucose. Thus, the ^{13}C-T_1 values of free Phe molecule in the cyclodextrin-Phe mixture can be estimated by multipling the ^{13}C-T_1 values observed in the solution containing only Phe by the value of viscosity ratio η(solution of cyclodextrin-Phe mixture)/η(solution of Phe). By using these T_1 values in Eq. 2 as T_{1f} values of Phe in the cyclodextrin-Phe solution, the T_{1c} values are calculated for each system. The results are shown in Table 4 with the values of solution viscosity.

The NT_{1c} values for phenyl ring C_ζ are always shorter than those of other ring protonated carbons. These results indicate the existence of rapid internal rotation of the Phe ring in addition to the overall molecular motion even in the complexed states. The rotational motion of Phe ring about the C_β–C_γ bond makes lengthen the NT_1 values of C_δ and C_ε. This motion, however, cannot affect that of C_ζ, since the C_ζ–H bond is on the extension line of rotational axis.[9]

To investigate strictly the influence of complexation on the molecular motion of the guest Phe, we used the $NT_1\eta$ values, which are shown also in Table 4 (in parenthesis). According to the theoretical prediction expressed by Eq. 5, a decrease in $NT_1\eta$ value corresponds to an increase in molecular volume Vm. For cyclodextrin-Phe inclusion systems, the greater the dynamic coupling between them, the greater is the increase in the apparent molecular volume of the Phe and hence the greater is the decrease in the $NT_1\eta$ value, as the molecular volume of cyclodextrins is about 6—9 times larger than that of Phe.[8] Thus, the extent of the decrease in the $NT_1\eta$ value may be used as a measure of the strength of dynamic coupling of Phe with cyclodextrins. As can be seen from the data in Table 4, all of the $NT_1\eta$ values show a decrease, to greater or lesser extents, on the addition of cyclodextrins. These results clearly indicate that the molecular motion of Phe is restricted by the cyclodextrins.

The degree of restriction can be clarified by estimating the ratios of $NT_1\eta$ values for the complexed and free states of Phe, which are shown in Table 5. It is noticeable that almost all phenyl-ring carbons in the three cyclodextrin-Phe systems show larger decreases in the $NT_1\eta$ values than those for other carbons in the same systems, indicating a larger slow-down of the internal rotation of the phenyl ring than that of the other part or of the overall molecular motion. The results clearly show that the Phe molecule forms truly the inclusion complexes with three cyclodextrins by insertion of its phenyl ring into the cyclodextrin cavities. This conclusion is supported by the large chemical shift changes of phenyl protons as shown in the preceding section.

Table 5. Values of ^{13}C $NT_1\eta$ Ratios for the Complexed and Free States of Phenylalanine[a]

Compound	$(NT_1\eta)_{complex}/(NT_1\eta)_{free}$				
	C_α	C_β	C_δ	C_ε	C_ζ
[Phe, α-CD]	0.35	0.40	0.38	0.39	0.36
[Phe, α-TMCD]	0.68	0.64	0.56	0.55	0.42
[Phe, β-TMCD]	0.85	0.80	0.76	0.77	0.74

a) The corresponding $NT_1\eta$ values are given in Table 4.

The $NT_1\eta$ values of the phenyl carbons suffer the largest reduction on complexing with α-CD. In this case, the values of C_α and C_β also suffer the largest reductions. On the other hand, the $NT_1\eta$ values of Phe show the intermediate and the smallest reductions by comlexation with α- and β-TMCD, respectively.

Discussion

The changes of chemical shifts and ^{13}C-T_1 of the guest Phe on addition of the hosts α-CD, α-TMCD, and β-TMCD show clearly that they form the inclusion complexes in a similar manner, namely, by insertion of the guest's phenyl ring into the host's cavity. The results that the NT_1 values of C_δ and C_ε in Phe phenyl ring agree well with each other and they are always larger than those of C_ζ indicate that all cyclodextrins investigated here favor the axial inclusion in which the internal rotation axis C_γ–C_ζ of the phenyl ring is parallel or nearly parallel to the axis of the cyclodextrin cavity. Thus, it is concluded that the permethylation of hydroxyl groups of cyclodextrin does not modify essentially the mode of Phe inclusion. It is generally accepted that many benzene derivatives form 1:1 complexes with α-CD by inserting their benzene rings into the α-CD's cavity from its secondary hydroxyl side, namely from the wider side of cavity. The same type inclusion has been also found for α-TMCD–*p*-nitrophenol system in aqueous solution.[6] The phenyl ring of Phe may be also inserted into the cavities of α- and β-TMCD as well as into that of α-CD[8–11] from the wider side with C_α as the head.

Several mechanisms have been proposed to interpret the formation of cyclodextrin inclusion complexes; such as van der Waals interactions between the guest and cyclodextrin, hydrogen bonding between the guest and the hydroxyl groups of cyclodextrins, release of strain energy in the macrocycle of cyclodextrin and so on.[1,2] But the driving force(s) for formation of cyclodextrin inclusion complexes is(are) still unclear and a matter of speculation.

In the general cases of the enzyme-substrate complex formation the binding force is supposed to be provided, at least partly, by hydrophobic interaction. The methylation of the hydroxyl groups of cyclodextrin is expected to increase the extent of the low

polar or apolar sphere of its cavity. In fact, heptakis (2,6-di-*O*-methyl)-β-cyclodextrin is found to be a hydrophobic solute in contrast with α-CD which is hydrophilic.[24,25] Thus, the permethylation may result an increasing the binding tendency of the Phe's apolar phenyl ring to the cyclodextrin cavity, if the hydrophobic interaction is the major mechanism for the formation of the inclusion complexes. The values of K_d and ^{13}C relaxation time do not support this expectation. Instead, the K_d values for both permethylated cyclodextrin-Phe systems are more or less larger than that for the α-CD-Phe system. The strength of dynamic coupling between the host and the guest estimated from the ^{13}C-T_1 is the largest also in the α-CD complex. Thus; only the hydrophobic interaction, although it may play some role, may not be the major driving force for the formation of inclusion complexes between Phe and permethylated cyclodextrins investigated here.

The X-ray crystallographic studies of the inclusion complexes of α-CD[26] and α-TMCD[27] with *p*-nitrophenol have shown that the size of the secondary hydroxyl side of the cyclodextrin cavity is widened by the methylation of all hydroxyl groups. In these cases, the intermolecular hydrogen-hydrogen distances indicate that the benzene ring of the guest *p*-nitrophenol has weaker van der Waals contacts with the inside of the α-TMCD cavity than with that of the α-CD cavity. Similar situations must hold for the cyclodextrin-Phe systems investigated here. The orders of stability of complex manifested in K_d values and the strength of host-guest dynamic coupling estimated from the ^{13}C relaxation times are related to that of cavity sizes of cyclodextrins. Namely, according to the CPK space-filling molecular models, the cavity size of α-CD is the smallest and that of β-TMCD is the largest. α-TMCD has the cavity of intermediate size. The steric contacts between the host and the guest molecules are expected to become the greatest and the smallest in the α-CD and β-TMCD systems, respectively. Therefore, the van der Waals interactions seem to play a significant role for the formation of cyclodextrin inclusion complexes with Phe in aqueous solution. This is also supported by the facts that the greatest and the smallest $\Delta\delta$ values were observed for the Phe aromatic proton resonances in the α-CD and β-TMCD systems, respectively, although it is not easy to interpret the signs and the magnitudes of the complexation-induced shifts.

The formation of hydrogen bond between the peripheral secondary hydroxyl groups of α-CD and the carboxyl group of Phe may also contribute, more or less, to the stabilization of complex, as the population of gt rotamer decreased and those of tg and gg rotamers increased slightly, on complexation with α-CD. In the α-CD inclusion complex, where the phenyl ring or Phe is inserted into the cyclodextrin cavity from its secondary hydroxyl side, the carbonyl group of Phe can form the hydrogen bond with the cyclodextrin's hydroxyl groups when the Phe side chain takes the tg and gg rotamers. The existence of this hydrogen bond is also suggested from the ^{13}C $NT_1\eta$ values for Phe C_α and C_β, which reveal significant decrease on complexation with α-CD (Table 5), indicating the reduction of mobility of these carbons in the complexed state. This reduction may be due to the anchoring effect of the hydrogen bond on the molecular motion.[28]

In the case of α-TMCD complex, the tg and gg rotamers may become unfavorable because of the repulsive interactions between the Phe's carbonyl and α-TMCD's methoxyl groups. Thus, the gt rotamer, in which the carbonyl group is far away from the methoxyl groups, becomes more probable. On complex formation with β-TMCD, which has the largest cavity size, the rotamer populations of Phe side chain remain unchanged. The cavity size of β-TMCD may be large enough to avoid severe contact between the Phe carboxyl and β-TMCD's rim even in the tg and gg rotamers. This conclusion is supported again by the ^{13}C $NT_1\eta$ values of C_α and C_β in the complexed state, which are comparable to those in the free state.

In conclusion, permethylated cyclodextrins form inclusion complexes with phenylalanine in a manner similar to parent cyclodextrins, but stability and strength of host-guest dynamic coupling change significantly by methylation. The NMR is useful method for studies of formation and molecular dynamics of cyclodextrin inclusion complexes.

The authors thank Dr. Yoshiyuki Nakamura of Research Laboratory of Resources Utilization, Tokyo Institute of Technology for the measurements of 500 MHz ^1H NMR spectra.

References

1) M. L. Bender and M. Komiyama, "Cyclodextrin Chemistry," Springer-Verlag, New York (1978).
2) J. Szejtli, "Cyclodextrins and Their Inclusion Complexes," Akademiai Kiado, Budapest (1982).
3) I. Tabushi, *Acc. Chem. Res.*, **15**, 66 (1982).
4) Y. Inoue, *Kagaku (Tokyo)*, **55**, 710 (1985).
5) L. Stryer, "Biochemistry," W. H. Freeman and Co., San Francisco (1975).
6) Y. Inoue, Y. Takahashi, and R. Chûjô, *Carbohydr. Res.*, **144**, C9 (1985).
7) K. Harata, K. Uekama, M. Otagiri, and F. Hirayama, *J. Incl. Phenom.*, **1**, 279 (1984).
8) Y. Inoue, Y. Katôno, and R. Chûjô, *Bull. Chem. Soc. Jpn.*, **52**, 1692 (1979).
9) Y. Inoue and Y. Miyata, *Bull. Chem. Soc. Jpn.*, **54**, 809 (1981).
10) Y. Inoue, T. Okuda, and Y. Miyata, *Carbohydr. Res.*, **101**, 187 (1982).
11) Y. Inoue, Y. Yamamoto, and R. Chûjô, *Carbohydr.*

Res., **118**, 37 (1983).
12) B. Casu, M. Reggiani, G. G. Gallo, and A. Vigevani, *Tetrahedron*, **24**, 803 (1968).
13) Y. Inoue, Y. Takahashi, and R. Chûjô, *Carbohydr. Res.*, **148**, 109 (1986).
14) Y. Yamamoto, M. Onda, Y. Takahashi, Y. Inoue, and R. Chûjô, *Carbohydr. Res.*, in Press.
15) Y. Inoue, T. Okuda, Y. Miyata, and R. Chûjô, *Carbohydr. Res.*, **125**, 65 (1984).
16) R. J. Bergeron, M. A. Channing, G. J. Gibeily, and D. M. Pillor, *J. Am. Chem. Soc.*, **99**, 5146 (1977).
17) R. I. Gelb, L. M. Schwartz, J. E. Markinac, and A. Laufer, *J. Am. Chem. Soc.*, **101**, 1864 (1979).
18) Y. Inoue, T. Okuda, and Y. Miyata, *J. Am. Chem. Soc.*, **103**, 7393 (1981).
19) J. Feeney, *J. Magn. Reson.*, **21**, 473 (1976).
20) K. Wüthrich and A. de Marco, *Helv. Chim. Acta*, **59**, 2228 (1976).
21) A. Allerhand, D. Doddrell, and R. Komoroski, *J. Chem. Phys.*, **55**, 189 (1971).
22) R. D. Deslauries, A. C. M. Paiva, K. Schaumburg, and I. C. P. Smith, *Biochemistry*, **14**, 878 (1975).
23) R. D. Deslauries, Z. Grzonka, K. Schaumburg, T. Shiba, and R. Walter, *J. Am. Chem. Soc.*, **97**, 5093 (1975).
24) K. Miyajima, M. Sawada, and M. Nakagaki, *Bull. Chem. Soc. Jpn.*, **56**, 3556 (1983).
25) K. Miyajima, T. Mukai, M. Nakagaki, M. Otagiri, and K. Uekama, *Bull. Chem. Soc. Jpn.*, **59**, 643 (1986).
26) K. Harata, *Bull. Chem. Soc. Jpn.*, **50**, 1416 (1977).
27) K. Harata, K. Uekama, M. Otagiri, and F. Hirayama, *Bull. Chem. Soc. Jpn.*, **55**, 3904 (1982).
28) D. Doddrell and A. Allerhand, *J. Am. Chem. Soc.*, **93**, 1558 (1971).

 © 1987 The Chemical Society of Japan Bull. Chem. Soc. Jpn., 60, 2547—2553 (1987)

Study of One-Dimensional Metal Complexes: $K[Ni(mnt)_2]\cdot H_2O$ and $K[Pt(mnt)_2]\cdot H_2O$

Shoichi KUTSUMIZU,* Norimichi KOJIMA, Toshiro BAN, and Ikuji TSUJIKAWA
Department of Chemistry, Faculty of Science, Kyoto University,
Kitashirakawa-oiwake-cho, Sakyo-ku, Kyoto 606
(Received February 20, 1987)

The crystal structure, electrical conductivity and electronic and IR absorption spectra of two metal complexes, $K[Ni(mnt)_2]\cdot H_2O$ and $K[Pt(mnt)_2]\cdot H_2O$ (mnt=1,2-dicyano-1,2-ethylenedithiolato, $C_4N_2S_2^{2-}$) were investigated. These two metal complexes belong to orthorhombic system and the lattice constants are a=12.00 Å, b=28.85 Å, and c=3.90 Å for the Ni complex and a=12.11 Å, b=29.23 Å, and c=7.73 Å for the Pt complex. Despite the same stoichiometries and similar crystal structures, the conductivity of Pt complex is 10^3 times as high as that of the Ni complex. The difference in the conductivity between the Ni and Pt complexes may be explained from the density of the unpaired electron on the central metal. The effects of the central metal on the electrical conduction properties may not be negligible for this type of complexes.

In the last decade, many quasi-one-dimensinal (1-D) compounds have been synthesized and intensively studied[1] in order to look for new materials having novel properties. Furthermore, these 1-D systems have stimulated theoretical investigations.

Among these 1-D compounds, typical examples are the 1-D platinum complexes, such as $K_2Pt(CN)_4Br_{0.3}\cdot 3H_2O$ (KCP(Br)) and the selenium donor organic metals, such as $(TMTSF)_2ClO_4$ (TMTSF=tetramethyltetraselenafulvalene). In these complexes, the constituent planar molecules form columnar stack structures, which lead to highly directional intermolecular d_{z^2} or π orbital interaction and, consequently, 1-D electronic nature.

As mentioned above, the planarity of molecule is necessary to form a stack with large intermolecular interactions. For this reason, the metal dithiolate complex can be used as a constituent planar molecule and expected to form a 1-D electrical conductor. In addition, these metal dithiolate complexes have unusual redox properties,[2-5] whereas we have taken notice of following two characteristic features:

i) This system has the capacity for structural modifications through changes in the central metal, the ligand substituent, and the counter cation; these chemical modifications are expected to produce a rich variety of new compounds with interesting electrical properties.

ii) The planar molecules have both metal d_{z^2} and ligand p_z orbitals; from this reason, Little suggested that this system is one possible example of the model of excitonic superconductors.[6] Although the real system is not necessarily satisfied with his criterion, this possibility cannot be perfectly excluded.

In fact, Underhill and Ahmad[7] have succeeded in synthesizing a new type of 1-D metallic complex with the mnt ligand; $Li_{0.8}(H_3O)_{0.3}[Pt(mnt)_2]\cdot 1.7H_2O$ (mnt= 1,2-dicyano-1,2-ethylenedithiolato, $C_4N_2S_2^{2-}$). The crystal structure and physical properties[8-13] of this salt have indicated that it is similar to the sulfur donor organic metals rather than to the 1-D platinum complexes. This conduction pathway is attributed to the overlap of delocalized MO's within the whole anions in which S p_z orbitals in the ligands play a dominant role and the central metal Pt plays a minor role in its conduction. The contribution of the central metal to its physical properties are still uncertain and the partial oxidation state of this system is not fully described.

We intended to elucidate the role of the central metal in the electrical conduction of these metal dithiolate complexes. For this purpose, we chose the cyano-substituted complex (Fig. 1) from a following reason: In the metal dithiolate complexes the electron density is always larger on the ligand than on the metal, but in this cyano-substituted Ni complex the density on the metal is not so small compaired with that on the ligand; these results were suggested by Schläpfer and Nakamoto.[14] We synthesized two metal complexes, $K[Ni(mnt)_2]\cdot H_2O$ and $K[Pt(mnt)_2]\cdot H_2O$, which will be abbreviated as KNi(mnt) and KPt(mnt), respectively. Because the metal d orbitals of KPt(mnt) are more extended than those of KNi(mnt), it is expected that the differences of two central metal are reflected in those of electrical properties.

In this paper, we report the syntheses, crystal structures, electrical conductivity behaviors, optical absorption spectra, and IR spectra of KNi(mnt) and KPt(mnt). From these data, we have considered the central metal effects on the electrical conduction properties for this type of complexes.

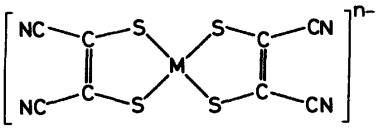

Fig. 1. $[M(mnt)_2]^{n-}$ complex.

Experimental

Preparation. The mnt^{2-} ligand was prepared following a procedure which is the combination of those described by Bray et al.[15] and Davison and Holm.[16] $[Et_4N]_2[Ni(mnt)_2]$ was prepared following a procedure described by Billig et al.[17] KNi(mnt) was prepared by use of a similar procedure of Ahmad and Underhill[8] described below. Slow O_2 oxidation of a solution of $K_2[Ni(mnt)_2]$ (ca. 10^{-3} mol dm^{-3}) in acetone-water (1:1) or (2:1) gave a black microcrystalline product. Oxidation by oxidant of H_2O_2 or slow evaporation on a steam bath gave the same results. KPt(mnt) may be prepared in a similar method described above, but we used a direct mixing at 50—70 °C of K_2PtCl_4 in aqueous solution and $Na_2(mnt)$ in EtOH-water (1:1). Obtained green-black precipitate was filtered off and washed with cold water.

The needle-like crystals of both KNi(mnt) and KPt(mnt) are dichroic with dark brown and green for polarized light parallel and perpendicular to the needle axis, respectively, under microscope. Both samples were stored in a moist (81% relative humidity) atmosphere to prevent dehydration.

Calcd for $KNiS_4C_8N_4H_2O$: C, 24.25; H, 0.51; N, 14.14; K, 9.9; Ni, 14.81; H_2O, 4.55%. Found: C, 24.32; H, 0.55; N, 14.05; K, 9.9; Ni, 13.8; H_2O, 4.35%. Calcd for $KPtS_4C_8N_4H_2O$: C, 18.04; H, 0.38; N, 10.52; K, 7.34; Pt, 36.63; H_2O, 3.49%. Found: C, 17.99; H, 0.38; N, 10.22; K, 7.0; Na, 0.08; Pt, 33; H_2O, 3.44%. Carbon, hydrogen, and nitrogen analyses were carried out by the Laboratory for Organic Elemental Microanalysis of Kyoto University.

Structure. The space group and lattice constants of KNi(mnt) were determined from X-ray oscillation photographs around the needle axis and X-ray Weissenberg photographs. The lattice constants were more accurately determined from X-ray powder diffraction patterns. The lattice constants of KPt(mnt) were determined from X-ray powder diffraction patterns by using those of KNi(mnt) as a guide.

Electrical Conductivity. The d.c. electrical conductivity measurements were performed on polycrystalline samples with two-probe method. Samples were prepared by pressing powders under pressure of (2.0—2.9)×10^8 GPa into cylindrical pellets, 10 mm in diameter and typically 0.5 mm in thickness. Electrical contacts to the disc planes by wetting gold wires with gold-paste (Tokuriki Chemical Research, No. 8560-1A). In order to prevent dehydration, samples were thinly covered with Apiezon N grease. For KPt(mnt), measurements parallel to the disc planes were also performed by cutting a pellet into a rectangular slice in order to evaluate the anisotropy in the conductivity. It is possible in such a case that microcrystalline needles are not oriented randomly but arranged nearly parallel to the disc planes in the compressed pellets. All samples gave ohmic behavior under the conditions of measurement.

IR and Electronic Spectra. The IR spectra were recorded on a Jasco Model IRA-1 (650—4000 cm^{-1}) in KBr pellets. Frequency reading was calibrated by recording the spectra of polystyrene film and the accuracy was about ±1 cm^{-1}.

The solid-state electronic spectra were recorded on a Cary 17D grating spectrometer (4000—33000 cm^{-1}) in KBr pellets.

DSC Measurement. The DSC measurements were performed with a Rigaku DSC-10A apparatus between 110K and 450K, scanning rate 3 or 5 °C min^{-1}.

Results and Discussion

Crystal Structure. Structural Analysis of KNi(mnt). Single crystals (typical size: 0.5×0.14×0.01 mm) coated with a thin layer of paraffin were used for the measurements. A careful inspection of the intensities of oscillation and Weissenberg photographs showed the Laue group *mmm*. The systematic absences $hk0$, $h=2n+1$ and $0kl$, $k+l=2n+1$ indicated two possible space groups: $Pn2_1a$ or *Pnma*. Unfortunately, because of the smallness in size of the crystals it has not been possible to obtain information on the space group for KPt(mnt).

Crystal Structure. The lattice constants of KNi(mnt) and KPt(mnt) are shown in Table 1 together with the values of $[NH_4][Ni(mnt)_2]\cdot H_2O$ reported by Isett et al.[18] They belong to orthorhombic system and have similar crystal structures. For KNi(mnt), there were no diffuse lines in oscillation photographs, which indicates that uniform spacing of the $[Ni(mnt)_2]^-$ anions along the c-axis. However, the $[Ni(mnt)_2]^-$ planes are probably tilted with respect to the c-axis as is often seen for other dithiolate complexes so that the plane-to-plane separation is decreased from 3.90 Å. On the other hand, the X-ray powder diffraction pattern and broadening of the C=C stretching modes on KPt(mnt) (see the section of IR Spectra) suggest a dimerization of the unit cell in the chain direction, the c-axis, which is similar to the fact that $Rb[Pt(mnt)_2]\cdot 2H_2O$[19] posesses a dimerized stack structure. In order to clarify this, the single crystal measurements are necessary and now in progress. Anyway, KPt(mnt) and KNi(mnt) have similar crystal structures, except the possibility of dimerization.

From Table 1, it is clear that there are significant similarities in the crystal structure between KNi(mnt) and $[NH_4][Ni(mnt)_2]\cdot H_2O$, which seems reasonable considering the comparable size of the cations (K^+, 1.33 Å; NH_4^+, 1.48 Å[20]). However, the conductivity for compressed pellets of NH_4 salt (5×10^{-3} S cm^{-1}) is 10^4 times as high as that of K salt (ca. 10^{-7} S cm^{-1}, vide infra). Although the space group of NH_4 salt is unknown, it is probable that the ability of NH_4^+ ions to form hydrogen-bonding networks causes some

Table 1. Crystal Data of KNi(mnt), KPt(mnt) and $[NH_4][Ni(mnt)_2]\cdot H_2O$

	KNi(mnt)	KPt(mnt)	α-NH_4-Ni(mnt)[18]
Chemical Formula	$K[Ni(mnt)_2]\cdot H_2O$	$K[Pt(mnt)_2]\cdot H_2O$	$[NH_4][Ni(mnt)_2]\cdot H_2O$
a/Å	12.00	12.11	12.10
b/Å	28.85	29.23	29.26
c/Å	3.90	7.73	3.92
Space Group	$Pn2_1a$ or *Pnma*	—	—
Z	4	8	4

subtle change in arrangement of the $[Ni(mnt)_2]^-$ monoanions, which causes large difference in the conductivity between NH_4 salt and K salt.

Electrical Conductivity. The experimental results of the electrical conductivity σ are shown in Fig. 2. In both complexes, thermally activated semiconducting behaviors were observed at all temperature. At room temperature, the value of KNi(mnt) is ca. 10^{-7} S cm^{-1}, whereas that of KPt(mnt) is 10^{-4} S cm^{-1}. The activation energy E_a was obtained by a least-squares fit to the usual equation, $\sigma=\sigma_0\exp(-E_a/k_BT)$, with E_a=0.33—0.37 eV (between 300—230 K) for KNi(mnt), whereas E_a=0.18 eV (between 300—200 K) for KPt(mnt). The value of KNi(mnt) is in agreement with that obtained by Underhill et al. ($\sigma_{r.t.}$=*ca.* 10^{-6} S cm^{-1}. E_a=0.346 eV)[21] on single crystals. In addition, observed anisotropy in the conductivity for KPt(mnt) was 10—20, which is considered as a lower limit (see Experimental section).

First, we will discuss the dependence of the conductivity on the central metal. Despite the same stoichiometries and similar crystal structures, the conductivity of KPt(mnt) differs significantly from that of KNi(mnt). However, caution must be paid in interpretation of these results because our measurements were made on compressed pellets; Rosseinsky and Malpas[22] have found that in some intervalence mixtures of more conductive $[Ni(mnt)_2]^-$ monoanion and less conductive $[Ni(mnt)_2]^{2-}$ dianion salts, the conductivities are enhanced; in the mixture with the best conduction, 10^3 times higher conductivity relative to the $[Ni(mnt)_2]^-$ monoanion salt was observed. In order to confirm this, we studied the IR spectra of KPt(mnt), which showed no evidence of the presence of $[Pt(mnt)_2]^{2-}$ dianions (see Fig. 4). Therefore, the sample of KPt(mnt) obtained was not such a mixture but was a genuine compound having the formula of $K[Pt(mnt)_2]\cdot H_2O$. Furthermore, very recently, similar results have been obtained for other metal complexes with the sulfur containing ligands, such as $Li_x[M(mnt)_2]\cdot nH_2O$ (M=Ni, Pd, Pt; for M=Pt, $Li_{0.8}(H_3O)_{0.3}[Pt(mnt)_2]\cdot 1.7H_2O$)[23] and TTF$[M(dmit)_2]_n$ (for M=Ni and Pd, n=2; for M=Pt, n=3; TTF=tetrathiafulvalene; H_2dmit=4,5-dimercapto-1,3-dithiol-2-thione),[24] which indicate that their central metals have considerable effects on conductivity. Our results show that it is inappropriate to ignore the role of the central metals of the metal mnt complexes with integral oxidation states as well as those with non-integral oxidation states.

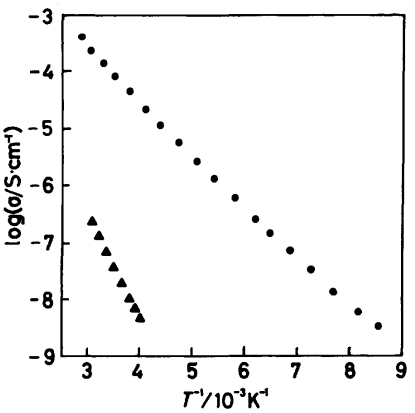

Fig. 2. Electrical conductivity of KNi(mnt) (▲) and KPt(mnt) (●).

Next, we will mention that effects of the ligand substituent R are important in the metal dithiolate complexes of the form $[M(S_2C_2R_2)_2]^-$. Table 2 shows the conductivity of alkali metal salts containing monoanions. Although for R=H and Ph (Ph=C_6H_5) the crystal structures are unknown and an exact comparison cannot be made, it is possible to point out that only the cyano-substituted complexes, namely the metal mnt complexes, show significant dependence of the conductivity on the central metals. This can be explained in terms of the difference of the electron distribution within the whole anion. From the IR spectra of $[Ni(S_2C_2R_2)_2]^z$ series (R=H, Ph, CF_3, and CN; z=0, 1− and 2−) and their normal coordinate analyses, Schläpfer and Nakamoto[14] have argued that in monoanion salts the density of the unpaired electron on the Ni atom increases in the order of R=H<Ph<CF_3<CN. Therefore, it can be interpreted that in R=CN the role of the central metal in the conductivity is significantly large compared with those in other complexes and the difference between Ni and Pt atom is directly reflected in the conductivity; on the other hand, in R=H and Ph the central metals have minor roles in determining the conductivity.

At this point, one question that arises is why the conductivity of the Pt complex, KPt(mnt), is higher than that of the Ni complex. We will discuss this problem in the section of General Discussion.

Electronic Spectra. The solid-state and solution electronic spectra of KNi(mnt) and KPt(mnt) are shown in Fig. 3. Our result of the solution spectra of KNi(mnt) is in agreement with that of [n-Bu_4N][Ni(mnt)$_2$] by Shupack et al.[27] For both Ni and Pt complexes, the spectra of a very dilute solution were

Table 2. Conductivity of $[M(S_2C_2R_2)_2]^-$ Monoanions with Alkali Metal Cations

Compound	$\sigma_{r.t.}$/S cm^{-1} a)	
	M=Ni	M=Pt
$Cs[M(S_2C_2H_2)_2]$	1.4×10^{-7} [25]	8.3×10^{-7} [25]
$K[M(S_2C_2Ph_2)_2]$	1×10^{-7} [26]	$\sim10^{-6}$ [26]
$K[M(S_2C_2(CN)_2)_2]\cdot H_2O$	$\sim10^{-7}$	1×10^{-4}

a) All measurements were made on compressed pellets.

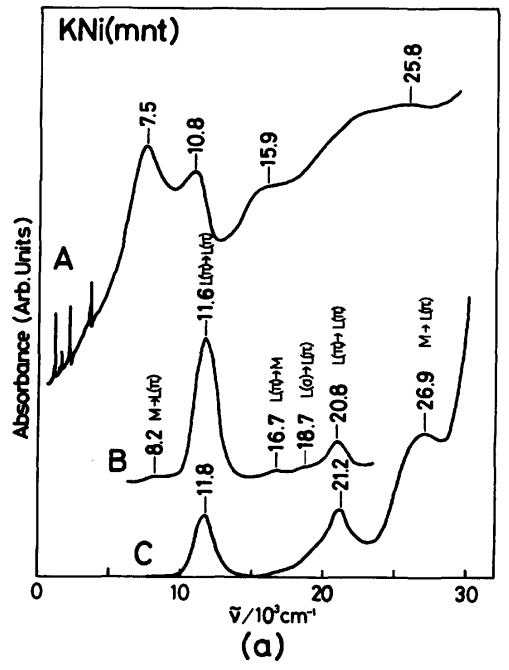

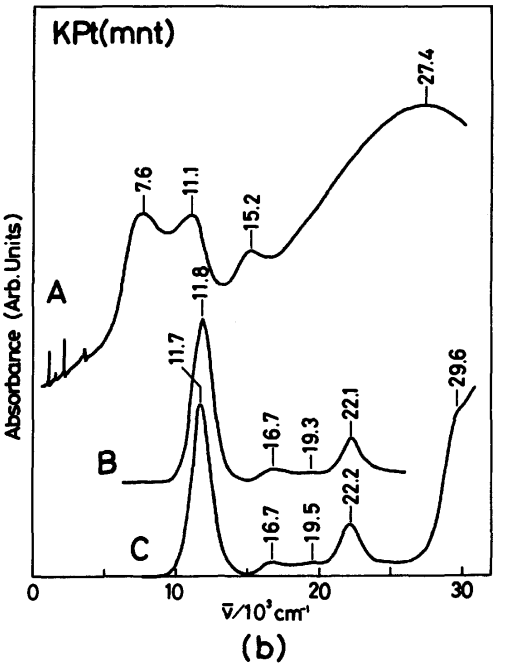

Fig. 3. Electronic spectra of (a) KNi(mnt) and (b) KPt(mnt): A, Solid-state spectra in KBr pellets; B, in acetonitrile solution; C, in acetone-water (1:1) solution. In the acetone-water (1:1) solution, very intense absorptions due to solvent made it impossible to measure below ca. 8000 cm^{-1}. In the case of the Ni complex, the assignments of solution spectra by Schrauzer and Mayweg[28] are also shown: L(π)=ligand π orbital dominant MO, L(σ)=ligand σ orbital dominant MO, M=metal d orbital dominant MO.

almost the same with Fig. 3, suggesting the presence of monomeric $[M(mnt)_2]^-$ species in solution. Moreover, the band positions are essentially the same in both acetone-water (1:1) and acetonitrile solutions. In the solution spectra of $[Ni(mnt)_2]^-$ monoanion, the assignments by Schrauzer and Mayweg[28] are also shown in Fig. 3 (a).

First, we will look at the results of the solid-state spectra of KNi(mnt) and KPt(mnt). In contrast with the significant differences in the conductivity, the solid-state spectra of both complexes are very similar. This is partly due to the intense absorptions involving the ligand-dominant orbitals, such as L(π)→L(π) transition. The differences of both Ni and Pt complexes which appear in solution spectra are smeared in the solid-state spectra. From the solid-state spectra, we could not find any marked differences in contrast to the conductivity.

Next, we compare the solid-state spectra of both complexes with their solution spectra. As the solid-state electronic bands are appreciably diffused and continuously overlap with each other, it is difficult to find the correspondence between the bands of the solid-state spectra and of solution spectra. However, in the solution spectra of both complexes there is no band observed corresponding to the lowest-energy bands around 7500 cm^{-1} in solid-state, except a very weak band at 8200 cm^{-1} in KNi(mnt). Therefore, these lowest-energy bands probably correspond to the intermolecular charge-transfer (CT) bands. Similar observations have been made on TCNQ anion radical salts[29] (TCNQ=tetracyanoquinodimethane); they have several electronic transitions from near-IR to visible region, among which the lowest-lying one or two peaks result from intermolecular CT transitions and higher-energy peaks correspond to the localized excitations within a single anion. In order to clarify the character of this band, the polarized optical measurements and photoconduction measurements are useful and now in progress.

IR Spectra. The frequencies of the bands observed in the IR spectra of KNi(mnt) and KPt(mnt) are given in Table 3, together with the assignments based on those of Schläpfer and Nakamoto.[14] A comparison of the IR spectra of both complexes indicates a surprising similarity.

As is well-known, IR spectra of the metal dithiolate complexes have following important features:

i) The frequencies of some modes, such as the C=C and C-S stretching modes, are dependent on the net charge of the $[M(S_2C_2R_2)_2]^z$ molecule; when the complex is oxidized and then the net charge is decreased, the frequencies of the C=C and C-S modes decreases and increases, respectively. In other words, the HOMO of the monoanion is bonding with respect to the C=C bond but antibonding with respect to the C-S bond.

ii) In the case of the isolated molecule in solid state,

such as in the dianion salts,[30] the dependence of the frequencies on the central metal M is very little, except for the M-S modes; the mass of the metal little affects the frequencies of modes arising principally from the ligand vibrations.

The most significant difference between KNi(mnt) and KPt(mnt) is that the band associated with the C=C modes in KPt(mnt) is much broad and energetically lower compared with the corresponding peak in KNi(mnt)(Fig. 4); the band of KPt(mnt) seems to comprise two C=C modes, whereas the band of KNi(mnt) is observed as a sharp single peak. In addition, the C-S mode of KPt(mnt) is seen at higher frequency than that of KNi(mnt)(see Table 3), which is consistent with the fact that the C=C modes of KPt(mnt) are observed at lower frequency than that of KNi(mnt).

These results can be interpreted as follows: Firstly,

Table 3. Observed IR Frequencies of KNi(mnt) and KPt(mnt) (cm^{-1})

KNi(mnt)	KPt(mnt)	Assignment
3628 m	3632 m	$\nu_3(H_2O)$
3552 vw	3558 vw	$\nu_1(H_2O)$
2208 s	2211 s	ν(C≡N)
2196 sh	2200 sh	
1609 m	1607 m	$\nu_2(H_2O)$
1426 w	1422 ~1396 b	ν(C=C)
1155 vs	1154 vs	ν(C-C)+ν(C-S)
1142 sh	1138 sh	?
1112 w	1108 w	π(C-CN)
1064 vw	1063 vw	ν(C-C)+ν(C-S)
869 vw	876 vw	ν(C-S)

s: Strong, vs: very strong, m: medium w: weak, vw: very weak, b: broad, sh: shoulder.

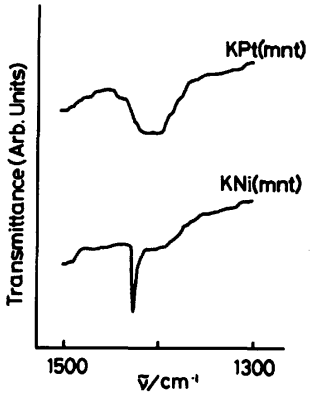

Fig. 4. The C=C stretching modes of KNi(mnt) (bottom curve) and KPt(mnt) (top curve). It can be pointed out that the C=C stretching modes around 1480 cm^{-1} which show the presence of the dianions are not observed for both complexes (see text).

the lower shift in frequency of the C=C bands in KPt(mnt) than in KNi(mnt) results from the differences in the electron distribution within the whole anion; the electron density on the ligand in KPt(mnt) is smaller than that in KNi(mnt). Secondly, the broadening or splitting of the C=C bands in KPt(mnt) reflects a lower symmetry around the anion than in KNi(mnt), which suggests the dimerization of the anion stack. Although the electron density and symmetry mentioned above are complicatedly related to each other, it is probable that both of these two factors more or less affect the C=C modes of both two metal complexes.

Thermal Properties and Crystal Water. No anomalies can be detected in thermal analyses by DSC for both complexes except irreversible heat anomalies corresponding to the loss of crystal water. The loss of crystal water occured slightly higher in temperature (80—160 °C) in both complexes compared with the cases of $Li_{0.8}(H_3O)_{0.3}[Pt(mnt)_2]\cdot 1.7H_2O$ (50—133 °C)[8] or KCP(Br) (30—110 °C).[31] However, close inspection of the stretching and bending motions of crystal water indicates that the ν_1 and ν_3 modes occur at rather high frequencies for a solid[32] and the ν_2 mode occurs at a low frequency, which suggests that there are only weak hydrogen bondings in both complexes, similar in KCP(Br)(ν_1 or ν_3=3490 cm^{-1}).[33]

General Discussion. The measured thermal activation energies from the conductivity for both complexes would indicate 'band gaps' which are ca. 0.7 eV for KNi(mnt) and 0.36 eV for KPt(mnt). The electronic spectra, on the other hand, shows that the lowest-energy bands have peaks at higher energies, 0.93 eV (7500 cm^{-1}) for KNi(mnt) and 0.94 eV (7600 cm^{-1}) for KPt(mnt). This discrepancy indicates that the simple band model is not appropriate for the conduction mechanism and a hopping mechanism must be taken into account, as proposed by Ahmad et al. in the cases of $Rb[Pt(mnt)_2]\cdot 2H_2O$[19] and other dithiolate complexes.[26] Moreover, similar behaviors have been reported for alkali TCNQ salts, such as K(TCNQ).[29]

At this point, we must consider the polycrystalline nature of the samples; in this case grain boundary effects are not negligible. However, although it cannot be a priori determined whether the observed activation energies from the conductivity measurements correspond to the true values for the single-crystal samples or activation energies for electron hopping through the grain boundary, the 'band gaps' estimated from the conductivity data are lower than those from the solid-state spectra. Hence, it is certain that true band gaps for conduction, if any, are lower than the electronic band gaps; we can conclude that a hopping model is appropriate for the conduction mechanism. In the case of the hopping mechanism, repulsive Coulomb interactions are important in

determining the conductivity behavior because the orbital for conduction is half-filled; the less Coulomb interactions lead to the higher conductivity.

On the basis of the hopping mechanism, we can understand the origin of the differences in the conductivity between KNi(mnt) and KPt(mnt). The IR spectra indicate a possibility that in KPt(mnt) the density of the unpaired electron on the ligand is lower than that of KNi(mnt). This possibility is also supported from the following consideration. In general, the metal d orbitals are raised in energy in the heavier transition metals, whereas the ligand-based orbitals are relatively unaffected. Although there is no detailed information about the mode of $[M(mnt)_2]^-$ stacking in both complexes, the structural similarities indicate that the ligand-dominant orbitals of both complexes are energetically equal. Following Schrauzer's MO scheme,[3,4,28] the HOMO of $[Ni(mnt)_2]^-$ monoanion salts is an antibonding combination of the ligand π and metal d_{xz} orbitals and the ligand π orbital associated with the HOMO lies energetically higher than the metal d orbital. The latter implies that the electron density is larger on the ligand (60%)[14] than on the metal. If one replaces Ni by a heavier atom Pt, the metal d orbitals rise in energy. As a result, one can expect larger mixing of the ligand π and metal d_{xz} orbitals compared with that in KNi(mnt), which leads lower density on the ligand in KPt(mnt). This lower density on the ligand of KPt(mnt) reduces the Coulomb interactions between anions, which facilitates higher conductivity. Although the differences in the electron distribution within the whole anion of both complexes may not be so large, this effect on the conduction arising from the hopping mechanism is possibly large.

In the above discussion, we have assumed that there is no contribution of structural difference between KNi(mnt) and KPt(mnt). In order to confirm whether or not above tentative explanation is true, further structural studies are necessary.

The authors wish to thank Professor Tsuyoshi Murao and Dr. Masako Tanaka of Kyoto University for their helpful discussions. Some measurements and calculations were carried out using the programs developed by Mr. Kazuya Suzuki and Mr. Naohilo Watanabe of Kyoto University.

We are indebted to Professor Tadamasa Shida and Dr. Tatsuhisa Kato of Kyoto University for the measurements of near-IR spectra; Dr. Eiichiro Nakayama of Research Center of Instrumental Analyses of Kyoto University offered an atomic absorption and flame emission spectrophotometer; Dr. Katsutoshi Tomita of Kyoto University offered a Weissenberg camera. We are grateful to Professor Allan E. Underhill for communicating their results on $M'[Ni(mnt)_2]\cdot H_2O$ (M'=Na, K, Rb, Cs, and NH_4) prior to publication.

References

1) "Extended Linear Chain Compounds Vol. 1—3," ed by J. S. Miller, Plenum Press, New York (1982,83).
2) J. A. McCleverty, "Progress in Inorganic Chemistry, Vol. 10," ed by F. A. Cotton, Interscience, New York (1968), p. 49.
3) G. N. Schrauzer, "Transition Metal Chemistry," ed by R. C. Carlin, Marcel Dekker, New York (1968), Vol. 4, p. 299.
4) G. N. Schrauzer, *Acc. Chem. Res.*, **2**, 72 (1969).
5) L. Alcácer and H. Novais, in Ref. 1, Vol. 3, p. 319.
6) W. A. Little, *J. Phys. (Paris)*, **44**, C3-819 (1983).
7) A. E. Underhill and M. M. Ahmad, *J. Chem. Soc., Chem. Commun.*, **1981**, 67.
8) M. M. Ahmad and A. E. Underhill, *J. Chem. Soc., Dalton Trans.*, **1982**, 1065.
9) A. Kobayashi, Y. Sasaki, H. Kobayashi, A. E. Underhill, and M. M. Ahmad, *J. Chem. Soc., Chem. Commun.*, **1982**, 390.
10) J. R. Cooper, M. Miljak, M. M. Ahmad, and A. E. Underhill, *J. Phys. (Paris)*, **44**, C3-1391 (1983).
11) M. M. Ahmad, D. J. Turner, A. E. Underhill, C. S. Jacobsen, K. Mortensen, and K. Carneiro, *Phys. Rev.*, B**29**, 4796 (1984).
12) A. Kobayashi, T. Mori, Y. Sasaki, H. Kobayashi, M. M. Ahmad, and A. E. Underhill, *Bull. Chem. Soc. Jpn.*, **57**, 3262 (1984).
13) K. Carneiro, J. Vazquez, A. E. Underhill, and P. I. Clemenson, *Phys. Rev.*, B**31**, 1128 (1985).
14) C. W. Schläpfer and K. Nakamoto, *Inorg. Chem.*, **14**, 1338 (1975).
15) J. Bray, J. Locke, J. A. McCleverty, and D. Coucouvanis, *Inorg. Synth.*, **13**, 187 (1972).
16) A. Davison and R. H. Holm, *Inorg. Synth.*, **10**, 8 (1967).
17) E. Billig, R. Williams, I. Bernal, J. H. Waters, and H. B. Gray, *Inorg. Chem.*, **3**, 663 (1964).
18) L. C. Isett, D. M. Rosso, and G. L. Bottger, *Phys. Rev.*, B**22**, 4739 (1980).
19) M. M. Ahmad, D. J. Turner, A. E. Underhill, A. Kobayashi, Y. Sasaki, and H. Kobayashi, *J. Chem. Soc., Dalton Trans.*, **1984**, 1759.
20) G. S. G. Philips and R. J. P. Williams, "Inorganic Chemistry Vol. 1—Principles and Non-Metals," Oxford University Press (1965), p. 152.
21) A. E. Underhill, P. I. Clemenson, and M. B. Hursthouse, International Conference on Science and Technology of Synthetic Metals, Japan, Kyoto, June 1986, Abstr., No. P6-29; *Synth. Metals*, in press.
22) D. R. Rosseinsky and R. E. Malpas, *J. Chem. Soc., Chem. Commun.*, **1977**, 455.
23) A. E. Underhill, M. M. Ahmad, D. J. Turner, P. I. Clemenson, K. Carneiro, S. Yueqiuan, and K. Mortensen, *Mol. Cryst. Liq. Cryst.*, **120**, 369 (1985).
24) M. Bousseau, L. Valade, J.-P. Legros, P. Cassoux, M. Carbauskas, and L. V. Interrante, *J. Am. Chem. Soc.*, **108**, 1908 (1986).
25) K. W. Browall and L. V. Interrante, *J. Coord. Chem.*, **3**, 27, (1973).
26) M. M. Ahmad and A. E. Underhill, *J. Chem. Soc., Dalton Trans.*, **1983**, 165.

27) S. I. Shupack, E. Billig, R. J. H. Clark, R. Williams, and H. B. Gray, *J. Am. Chem. Soc.*, **86**, 4594 (1964).
28) G. N. Schrauzer and V. P. Mayweg, *J. Am. Chem. Soc.*, **87**, 3585 (1965).
29) D. B. Tanner, in Ref. 1, Vol. 2, p. 205.
30) R. J. H. Clark and P. C. Turtle, *J. Chem. Soc., Dalton Trans.*, **1977**, 2142
31) J. M. Williams, P. L. Johnson, A. J. Schultz, C. C. Coffey, *Inorg. Chem.*, **17**, 834 (1978).
32) K. Nakamoto, "Infrared Specra of Inorganic and Coordination Compounds," John Wiley & Sons, New York (1963), p. 155.
33) E. F. Steigmeier, R. Loudon, G. Harbeke, H. Auderset, and G. Scheiber, *Solid State Commun.*, **17**, 1447 (1975).

 © 1987 The Chemical Society of Japan Bull. Chem. Soc. Jpn., 60, 2555—2560 (1987)

Relations between Gas-Phase Stepwise and Bulk Solvation of Cl^- with Water and Aliphatic Alcohols

Kenzo HIRAOKA
Faculty of Engineering, Yamanashi University, Takeda-4, Kofu 400
(Received February 26, 1987)

Higher order clustering reactions of Cl^- with H_2O and ROH for ROH=CH_3OH, C_2H_5OH, and n-C_3H_7OH were measured in the gas phase with the pulsed electron-beam mass spectrometer. The general trend is found that the obtained $-\Delta H^\circ_{n-1,n}$ and $-\Delta S^\circ_{n-1,n}$ increase in the order $H_2O<CH_3OH<C_2H_5OH<n$-C_3H_7OH. This order is just the opposite to the free energies of solvation of Cl^-. This is due to the increasingly more unfavorable entropy changes for the solvation of Cl^- in the order $H_2O<CH_3OH<C_2H_5OH<n$-C_3H_7OH. This is clearly manifested on the increasing entropy changes $-\Delta S^\circ_{n-1,n}$ for the measured gas-phase clustering reactions for higher alcohols.

Cluster ions represent an aggregated state of matter, having properties midway between gaseous and condensed phase. Investigation into the formation and the properties of increasingly larger clusters offers a deep insight into the mode of the molecular interactions and a way of studying the molecular details of the course of change between gaseous and condensed phase.[1-4]

Equilibria for the ion-solvent molecule clustering reactions involving positive or negative ions can be measured in the gas phase. The van't Hoff plots of the equilibrium constants lead to the determination of thermochemical data $\Delta G°$, $\Delta H°$, and $\Delta S°$ for the stepwise addition of solvent molecules to the ion. In our laboratory, we have been making an effort to obtain some information which may bridge between gas and condensed phase by measuring the higher-order solvation reactions of ions in the gas phase. In our previous work,[5] we studied the stabilities and structures of cluster ions $X^-(M)_n$ for X^-=halide ions and M=protic solvents. In the present work, a study was made to extrapolate the thermochemical data obtained in the gas phase to those in the condensed phase. The obtained results give some insight for the elucidation of the ion solvation in the condensed phase.

Experimental

The measurements were made with a pulsed electron-beam mass spectrometer which has been described previously.[6,7] About 20—100 mTorr† of H_2O or aliphatic alcohols and 1 mTorr of electron capture agent CCl_4 were introduced into 2—3 Torr of CH_4 major (buffer) gas through stainless steel capillaries. The equilibrium constants were found to be independent on the change of solvent vapor pressure in the range 20—100 mTorr.

The equilibrium constants for the clustering reactions were obtained from the expression

$$K_{n-1,n} = \frac{I_n}{I_{n-1}} \cdot \frac{1}{P},$$

where I_n/I_{n-1} is the ratio of ion intensities of the clusters $Cl^-(ROH)_n$ and $Cl^-(ROH)_{n-1}$ in equilibrium and P is the sample pressure. The measurements of I_n/I_{n-1} were made using a mass spectrometer (ULVAC, MSQ-400) with a pulsed electron beam. Pulsing permits one to follow the kinetics of the approach to equilibrium. The enthalpy and entropy changes for each clustering reactions ($n-1$, n) are determined from van't Hoff plots based on the equation

$$\ln K_{n-1,n} = -\frac{\Delta H^\circ_{n-1,n}}{RT} + \frac{\Delta S^\circ_{n-1,n}}{R},$$

where the standard state is 1 atm.

Results

The enthalpy and entropy changes for the clustering reactions

$$Cl^-(H_2O)_{n-1} + H_2O = Cl^-(H_2O)_n, \quad (1)$$
$$Cl^-(CH_3OH)_{n-1} + CH_3OH = Cl^-(CH_3OH)_n, \quad (2)$$
$$Cl^-(C_2H_5OH)_{n-1} + C_2H_5OH = Cl^-(C_2H_5OH)_n, \quad (3)$$
$$Cl^-(n\text{-}C_3H_7OH)_{n-1} + n\text{-}C_3H_7OH = Cl^-(n\text{-}C_3H_7OH)_n. \quad (4)$$

obtained from the van't Hoff plots are summarized in Tables 1 and 2. The experimental errors for the $\Delta H^\circ_{n-1,n}$ and $\Delta S^\circ_{n-1,n}$ values are about ±0.5 kcal mol^{-1}†† and ±2 cal mol^{-1} K^{-1}, respectively. The obtained data are generally in good agreement with those obtained in other laboratories. The measurements for higher-order clustering reactions in the low temperature region were limited by the condensation of the sample vapor on the wall of the ion source. The values of $\Delta H^\circ_{n-1,n}$ and $\Delta S^\circ_{n-1,n}$ for Reactions 1—4 were measured down to temperatures just above the condensation of sample vapor.

Discussion

Referring to Table 1, the bond energies of $ROH\cdots Cl^-(-\Delta H^\circ_{0,1})$ increase in the order $H_2O<CH_3OH<C_2H_5OH<n$-C_3H_7OH. Interestingly, as shown in Table 3, the polarizabilities for H_2O, CH_3OH, C_2H_5OH, and n-C_3H_7OH follow the same order and the permanent dipole moments are just the opposite

† 1 Torr=133.322 Pa.

†† 1 cal=4.184 J.

Table 1. Experimentally Determined Enthalpy Changes $-\Delta H^\circ_{n-1,n}$ (kcal mol^{-1}) for Clustering Reactions $Cl^-(ROH)_{n-1}+ROH=Cl^-(ROH)_n$

n	1	2	3	4	5	6	7	8	9	10	11
H_2O	14.7 13.1[a] 14.9[b] 14.4[d] 14.9[e]	13.0 12.7[a] 12.6[b]	11.8 11.7[a] 11.5[b]	10.6 11.1[a] 10.9[b]	9.5	8.8	≈8.1[f]				
CH_3OH	17.4 14.2[c] 16.8[d] 17.5[e]	14.1 13.0[c]	11.8 12.3[c]	10.5 11.2[c]	9.2 10.5	8.9	8.0	7.6	7.6	7.4	≈7.3[f]
C_2H_5OH	17.6 17.3[d]	16.1	12.8	12.0	11.5	11.1	9.8	9.2	≈9.0[f]	≈8.9[f]	
n-C_3H_7OH	20.4 17.7[d]	15.8	14.2	13.3	12.6	11.6	11.0	≈10.8[f]			

a) Reference 10. b) Reference 11. c) Reference 12. d) Reference 9. Enthalpy value calculated from experimentally determined ΔG° and estimated ΔS° from statistical dynamics. e) Reference 13. f) Value obtained using the assumed entropy change. See Table 2.

Table 2. Experimentally Determined Entropy Changes $-\Delta S^\circ_{n-1,n}$ (cal mol^{-1} K^{-1}) for Clustering Reactions $Cl^-(ROH)_{n-1}+ROH=Cl^-(ROH)_n$. Standard State 1 atm

n	1	2	3	4	5	6	7	8	9	10	11
H_2O	19.7 16.5[a] 19.7[b] 20.1[d] 19.7[e]	21.4 20.8[a] 20.5[b]	22.3 23.2[a] 22.4[b]	22.7 25.8[a] 24.8[b]	21.7	21.2	(20)[f]				
CH_3OH	24.1 14.8[c] 22.9[d] 24.1[e]	24.2 19.4[c]	22.9 23.6[c]	22.9 26.4[c]	21.7 25.5[c]	22.2	20.1	19.7	20.6	20.1	(20)[f]
C_2H_5OH	23.7 23.1[d]	25.9	25.8	29.5	30.6	31.0	26.9	25.2	(25)[f]	(25)[f]	
n-C_3H_7OH	29.0 23.2[d]	25.4	31.2	32.1	32.9	31.0	30.2	(30)[f]			

a) Reference 10. b) Reference 11. c) Reference 12. d) Reference 9. Entropy value estimated from statistical dynamics. e) Reference 13. f) Entropy value assumed.

Table 3. Dipole Moments (debye) and Polarizabilities (Å^3) of H_2O, CH_3OH, C_2H_5OH, n-C_3H_7OH, and Cl^-

Compound	Dipole moment[a]	Polarizability[b]
H_2O	1.84	1.45
CH_3OH	1.75	3.25
C_2H_5OH	1.69	5.01
n-C_3H_7OH	1.68	6.81
Cl^-	0	3.5

a) Reference 14. b) Reference 15.

to the observed bond energies. Polarization must be one of the crucial factors in the determination of the bond energy of the cluster ROH···Cl$^-$. This may be due to the ability of the ligand to approach close to the ion, and thereby become more influenced by the ionic electric field with the attendant result of a larger induced dipole. Qualitatively, consideration of the polarizabilities partially explains the increased bonding strength of CH_3OH, C_2H_5OH, and n-C_3H_7OH over that of H_2O in clustering to the Cl^- ion.

It has been already pointed out that there is a good correlation between the gas-phase acidity and the bond energy ROH···Cl$^-$.[8,9] With increase of the

polarizability, the acidity of oxygen acid ROH increases, i.e., the decrease of the heterogeneous bond energy ROH→RO^-+H^+. The binding energy in ROH···Cl^- can be considered as a partial proton transfer, [RO···H···Cl]$^-$, in which the strength of the interaction increases with the acidity of ROH. This is an alternative explanation for the order of the bond strengths of ROH···Cl^-.

The bond energy of n-C_3H_7OH···Cl^- is larger than expected from its polarizability since it is appreciably larger than those of CH_3OH···Cl^- and C_2H_5OH···Cl^-. The strong bond may be explained by the head-and-tail interaction in n-C_3H_7OH···Cl^- as shown below.

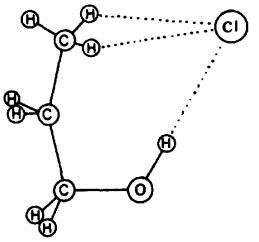

Structure I

In such a configuration, acidic hydrogen atoms of -OH and $-CH_3$ can realize the most favorable interaction with Cl^- by adjusting the rotations around the C-O and two C-C bond axes. In the structure I, the C_3H_7OH ligand suffers a considerable restriction of internal rotations. This may explain the exceptionally large negative entropy change for Reaction 4 with n=1 (Table 2).

Castleman et al. measured the clustering reactions of Cl^- with H_2O and SO_2 in the gas phase. They found that the bond energy ($-\Delta H^\circ_{0,1}$) of Cl^-···SO_2 (21.8 kcal mol^{-1}) is much larger than that of Cl^-···H_2O (14.9 kcal mol^{-1}). However, the $-\Delta H^\circ_{n-1,n}$ values for SO_2 show a much a faster fall-off than those for H_2O with n and the cross-over of the values $-\Delta H^\circ_{n-1,n}$ was observed between n=3 and 4. A similar trend was also observed for the clustering reactions of alkali positive ions with H_2O and CH_3CN.[17] The bond energies $-\Delta H^\circ_{n-1,n}$ of $M^+(CH_3CN)_n$ for M=Na and Cs are considerably higher than those of $M^+(H_2O)_n$ for small n. However, much faster decrease of $\Delta H^\circ_{n-1,n}$ for the formers than those for the latters with n leads to the cross-over of $-\Delta H^\circ_{n-1,n}$ between n=4 and 5. Generally, the bond energies of the ionic clusters of aprotic solvents show faster decrease than those of protic solvents and the crossover of the bond energies are observed at relatively small n. Such a trend is not observed for the clusters $Cl^-(ROH)_n$ between ROH=H_2O and aliphatic alcohols (see Table 1). The ionic clusters of higher alcohols have increasingly stronger bonds compared to $Cl^-(H_2O)_n$ up to the largest n measured. This indicates that in the cluster $Cl^-(ROH)_n$, aliphatic alcohols in the inner shell maintain the stronger bonds with the core ion Cl^- at the expense of the more unfavorable entropy changes (see Table 2) than in the cluster $Cl^-(H_2O)_n$.

In Table 4, free energies (ΔG°_s), enthalpies (ΔH°_s), and entropies (ΔS°_s) of transfer of Cl^- from the gas phase into ROH solvents are summarized. These values are calculated from the free energies, enthalpies, and entropies of transfer of Cl^- from the gas phase into the aqueous solution[18] and those from the aqueous solution to CH_3OH, C_2H_5OH, and n-C_3H_7OH solvents.[19] The free energies of solution of Cl^- ($-\Delta G^\circ_s$) decrease in the order H_2O>CH_3OH>C_2H_5OH>n-C_3H_7OH, i.e., the solvating power of ROH solvents for Cl^- decreases in that order. Since the values of enthalpies of solution ($-\Delta H^\circ_s$) are more or less the same, the observed weaker solvating power for higher alcohols are mainly due to the increase of entropies of solution ($-\Delta S^\circ_s$). Interestingly, there is a similar trend in the gas phase clustering reactions as the case of entropies of solution, i.e., the greater $-\Delta S^\circ_{n-1,n}$ values for higher alcohols (see Table 2). It is evident that ligands of higher alcohols are highly immobilized in the inner shell of the clusters $Cl^-(ROH)_n$. The observed greater entropy changes $-\Delta S^\circ_{n-1,n}$ for the gas-phase clustering reactions may partly explain the more unfavorable entropies of solution for higher alcohols.

Recently Swain et al. have evaluated the anion and cation solvation components based on rate constants, product ratios, equilibrium constants, and electronic, IR, ESR, and NMR spectra.[25] They found that the solvating power for ion can be represented by the two factors, the acity (anion-solvating tendency) and the basity (cation-solvating tendency). It would be informative to compare the bond energy of single-molecule solvated Cl^-, D(ROH···Cl^-), with the acity which represents the solvating power of the bulk ROH solvent toward anions. Figure 1 shows the correlation between the bond energies D(ROH···Cl^-) and the solvent acity for H_2O, CH_3OH, C_2H_5OH, and n-C_3H_5OH. The solvent with larger value of acity is a better solvent for anion. As shown in Fig. 1, H_2O which is the best solvent for anion has the smallest bond energy D(HOH···Cl^-), and D(ROH···Cl^-) increases with decrease of solvent acity for higher

Table 4. Free Energies (ΔG°_s), Enthalpies (ΔH°_s), and Entropies (ΔS°_s) of Transfer of Cl^- from Gas Phase into Solvents

	$-\Delta G^\circ_s$ / kcal mol^{-1}	$-\Delta H^\circ_s$ / kcal mol^{-1}	$-\Delta S^\circ_s$ / cal mol^{-1} K^{-1}
H_2O	75.8	81.3	18.2
CH_3OH	72.6	79.3	22.3
C_2H_5OH	70.9	78.8	26.1
n-C_3H_7OH	69.6	79.2	32.1

alcohols. Since the enthalpies of solution of Cl^- are about the same for the four solvents (Table 4), the reverse order observed in Fig. 1 suggests that for solvents with larger acities, greater number of solvent molecules participate in the ion solvation and contribute to stabilize the anion in solution.

Some more detailed discussion on the stepwise solvation into the ultimate solvation may be given as follows.

In the interaction of ROH with Cl^-, the ROH molecule is polarized, $RO^{\delta-}$-$H^{\delta+}\cdots Cl^-$. For hard Brönsted acids, like H_2O and CH_3OH, the negative charge in the polarized ROH is mainly localized on the oxygen atom. The negatively polarized oxygen atom in ROH would enhance further hydrogen bonding with the ROH molecules in the outer solvation shell. This effect would extend from inner ligands to outer ligands in the shells surrounding the core ion and thus make the solvation energy ultimately large (enhancement effect).[4,20] When the size of alkyl group R gets larger, the ROH ligands in the inner shell of the cluster $Cl^-(ROH)_n$ bind more strongly due to their larger polarizabilities. However, the negative charge will be more delocalized in the rest parts of the acidic hydrogen atom, and the enhancement effect will become less effective than the case of harder ROH solvents. Such a cancellation may explain about the same enthalpies of solvation of Cl^- for H_2O, CH_3OH, C_2H_5OH, and n-C_3H_7OH.

In our previous paper,[3] gas-phase stepwise hydration and single-ion enthalpies and free energies of solution in water were studied. Here, the similar but some more detailed examination will be given. The stepwise solvation free energies $\Delta G^\circ_{n-1,n}$ and the free energies of solution ΔG°_s, or the stepwise solvation enthalpies $\Delta H^\circ_{n-1,n}$ and the enthalpies of solution ΔH°_s, or the stepwise solvation entropies $\Delta S^\circ_{n-1,n}$ and the entropies of solution ΔS°_s are related as[3,21,22]

$$\Delta G^\circ_s = \sum_{n=1}^{n=N} \Delta G^\circ_{n-1,n}(\text{ion(solvent)}_n) - \sum_{n=2}^{n=N} \Delta G^\circ_{n-1,n}(\text{solvent})_n \quad (5)$$

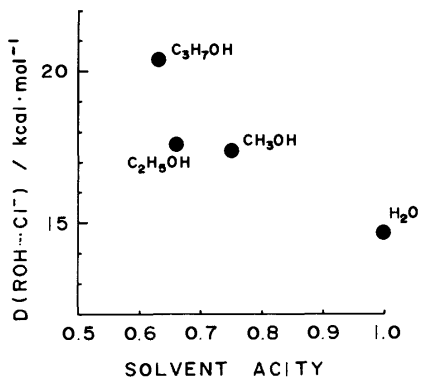

Fig. 1. Correlation between the bond energy D-(ROH···Cl^-) and the solvent acity.

$$\Delta H^\circ_s = \sum_{n=1}^{n=N} \Delta H^\circ_{n-1,n}(\text{ion(solvent)}_n) - \sum_{n=2}^{n=N} \Delta H^\circ_{n-1,n}(\text{solvent})_n, \quad (6)$$

$$\Delta S^\circ_s = \sum_{n=1}^{n=N} \Delta S^\circ_{n-1,n}(\text{ion(solvent)}_n) - \sum_{n=2}^{n=N} \Delta S^\circ_{n-1,n}(\text{solvent})_n. \quad (7)$$

The values of $\Delta G^\circ_{n-1,n}(\text{ion(solvent)}_n)$ and $\Delta G^\circ_{n-1,n}(\text{solvent})_n$, or $\Delta H^\circ_{n-1,n}(\text{ion(solvent)}_n)$ and $\Delta H^\circ_{n-1,n}(\text{solvent})_n$, or $\Delta S^\circ_{n-1,n}(\text{ion(solvent)}_n)$ and $\Delta S^\circ_{n-1,n}(\text{solvent})_n$ converge at $n=N$. In this section, relationships between $\Delta G^\circ_{0,n}$ and ΔG°_s, or $\Delta H^\circ_{0,n}$ and ΔH°_s, or $\Delta S^\circ_{0,n}$ and ΔS°_s are studied on the ground of Eqs. 5—7 with use of the presently available experimental $\Delta G^\circ_{n-1,n}$, $\Delta H^\circ_{n-1,n}$, and $\Delta S^\circ_{n-1,n}$ values.

Unfortunately not much thermochemical data are available for neutral solvent clusters. As a crude approximation, we assume that the enthalpy and entropy changes of stepwise Reaction 8

$$(H_2O)_{n-1} + H_2O = (H_2O)_n \quad (8)$$

are the same as that for $n=2$ for small n, $\Delta H^\circ_{1,2}(H_2O)_2$. In water, an H_2O molecule has four hydrogen bonds with neighboring H_2O molecules. Upon vaporization, each H_2O molecule dissociates these four hydrogen bonds. If one assumes that the strength of each hydrogen bond in water is the same as $-\Delta H^\circ_{1,2}(H_2O)_2$, the relation, $4\times\Delta H^\circ_{1,2}(H_2O)_2\times 1/2 = -\Delta H^\circ_{evap}$, holds. The factor 1/2 comes from the fact that two H_2O molecules participate in each hydrogen bond. Thus $\Delta H^\circ_{1,2}(H_2O)_2$ may be approximated to be $-1/2\Delta H^\circ_{evap}$. Similarly, the entropy change $\Delta S^\circ_{1,2}(H_2O)_2$ may also be approximated to be $-1/2\ \Delta S^\circ_{evap}$. The values of ΔH°_{evap}=10.5 kcal mol^{-1} and ΔS°_{evap}=35.2 cal mol^{-1} K^{-1} for water at the standard state lead to the approximated values $\Delta H^\circ_{1,2}(H_2O)_2$=−5.3 kcal mol^{-1} and $\Delta S^\circ_{1,2}(H_2O)_2$=−18 cal mol^{-1}K^{-1}.

For the clustering reactions of alcohols,

$$(ROH)_{n-1} + ROH = (ROH)_n, \quad (9)$$

$\Delta H^\circ_{n-1,n}(ROH)_n$ values are also assumed to be equal to $-1/2\Delta H_{evap}$. Since the standard state ΔS°_{evap} values are not available for alcohols, the $\Delta S^\circ_{n-1,n}(ROH)_n$ values are assumed to be the same as that of Reaction 8, i.e., −18 cal mol^{-1} K^{-1}.

Figures 2—5 show the n dependences of the right-hand side of Eqs. 5—7, $-[\Delta G^\circ_{0,n}(Cl^-(ROH)_n)-\Delta G^\circ_{0,n}(ROH)_n]$, (denoted as $-\Delta\Delta G^\circ_n$), $-[\Delta H^\circ_{0,n}(Cl^-(ROH)_n)-\Delta H^\circ_{0,n}(ROH)_n]$, (denoted as $-\Delta\Delta H^\circ_n$), and $-T[\Delta S^\circ_{0,n}(Cl^-(ROH)_n)-\Delta S^\circ_{0,n}(ROH)_n]$, (denoted as $-T\Delta\Delta S^\circ_{0,n}$) at T=298 K for ROH=H_2O, CH_3OH, C_2H_5OH, and n-C_3H_7OH. In these figures, the values of $-\Delta\Delta G^\circ_n$, $-\Delta\Delta H^\circ_n$, and $-T\Delta\Delta S^\circ_n$ with n=0 are taken as values of ΔG°_s, ΔH°_s, and $T\Delta S^\circ_s$, respectively. Since the values of the right-hand side of Eqs. 5—7 converge to ΔG°_s, ΔH°_s, and $T\Delta S^\circ_s$ with $n\to N$, all curves which start from the values ΔG°_s, ΔH°_s, and $T\Delta S^\circ_s$ at n=0

converge to the value 0 with an increase of n. Such a representation is useful because one can see how the stepwise solvation thermochemical data approach the ultimate values with an increase of n.

In Fig. 2, $-\Delta\Delta G_n^\circ$ and $-\Delta\Delta H_n^\circ$ converge to zero only very gradually. This suggests that a greater number of H_2O solvent molecules take part in the hydration of Cl^- in aqueous solution (enhancement effect). The small positive values of $-T\Delta\Delta S_n^\circ$ with n=1—7 suggest that H_2O ligands in the inner shell of $Cl^-(H_2O)_n$ are only slightly more immobilized than that of $(H_2O)_n$. The interaction of H_2O ligands with Cl^- does not

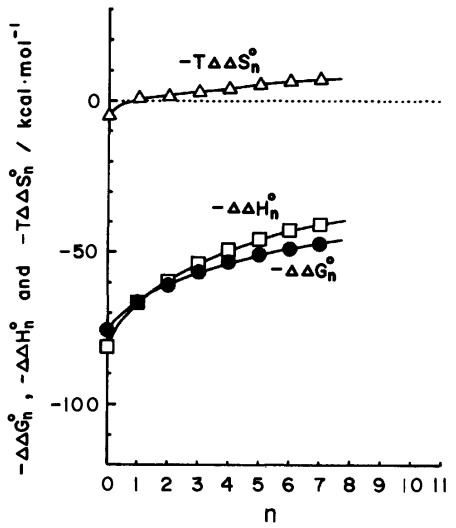

Fig. 2. The n dependence of the values of $-\Delta\Delta G_n^\circ$, $-\Delta\Delta H_n^\circ$, and $-T\Delta\Delta S_n^\circ$ (T=298 K) for reaction $Cl^-(H_2O)_{n-1}+H_2O=Cl^-(H_2O)_n$. The values of $-\Delta\Delta G_n^\circ$, $-\Delta\Delta H_n^\circ$, and $-\Delta\Delta S_n^\circ$, with n=0 are taken as those for the free energy of hydration, the enthalpy of hydration, and the entropy of hydration for Cl^-, respectively.

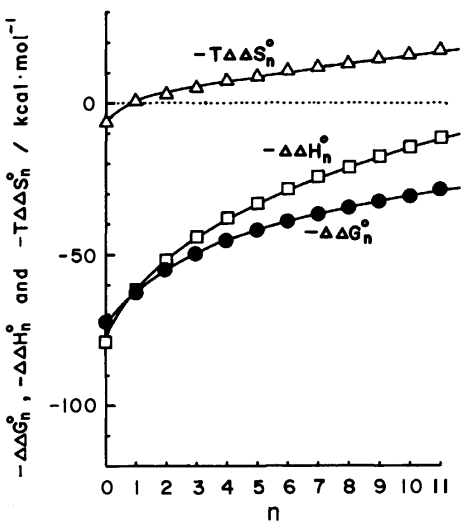

Fig. 3. The n dependence of the values of $-\Delta\Delta G_n^\circ$, $-\Delta\Delta H_n^\circ$, and $-T\Delta\Delta S_n^\circ$ (T=298 K) for reaction $Cl^-(CH_3OH)_{n-1}+CH_3OH=Cl^-(CH_3OH)_n$. The values of $-\Delta\Delta G_n^\circ$, $-\Delta\Delta H_n^\circ$, and $-\Delta\Delta S_n^\circ$ with n=0 are taken as those for the free energy of solution, the enthalpy of solution, and the entropy of solution for Cl^-, respectively.

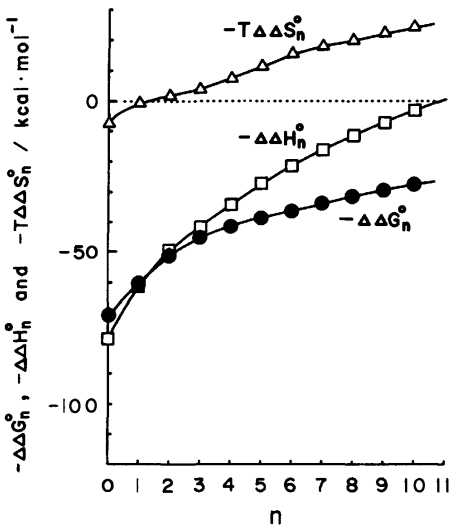

Fig. 4. The n dependence of the values of $-\Delta\Delta G_n^\circ$, $-\Delta\Delta H_n^\circ$, and $-T\Delta\Delta S_n^\circ$ (T=298 K) for reaction $Cl^-(C_2H_5OH)_{n-1}+C_2H_5OH=Cl^-(C_2H_5OH)_n$. The values of $-\Delta\Delta G_n^\circ$, $-\Delta\Delta H_n^\circ$, and $-\Delta\Delta S_n^\circ$ with n=0 are taken as those for the free energy of solution, the enthalpy of solution, and the entropy of solution for Cl^-, respectively.

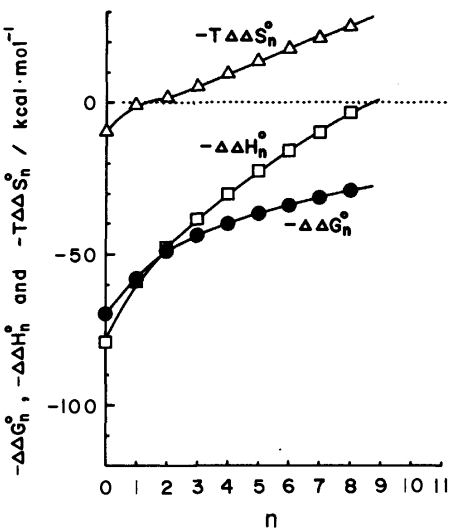

Fig. 5. The n dependence of the values of $-\Delta\Delta G_n^\circ$, $-\Delta\Delta H_n^\circ$, and $-T\Delta\Delta S_n^\circ$ (T=298 K) for reaction $Cl^-(C_3H_7OH)_{n-1}+C_3H_7OH=Cl^-(C_3H_7OH)_n$. The values of $-\Delta\Delta G_n^\circ$, $-\Delta\Delta H_n^\circ$, and $-\Delta\Delta S_n^\circ$ with n=0 are taken as those for the free energy of solution, the enthalpy of solution, and the entropy of solution for Cl^-, respectively.

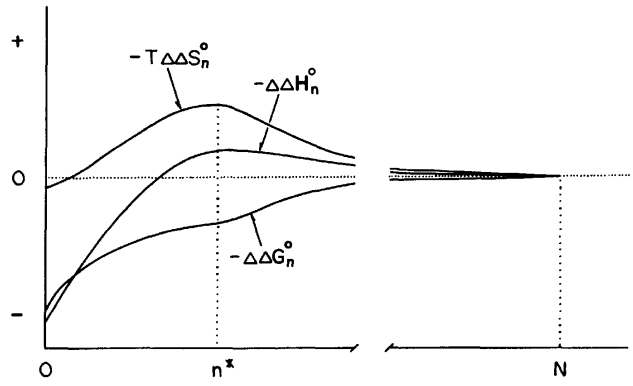

Fig. 6. Schematic representation of n-dependence of $-\Delta\Delta G_n^\circ$, $-\Delta\Delta H_n^\circ$, and $-T\Delta\Delta S_n^\circ$ for n=0→N.

seem to induce a serious restriction of freedoms of motion. In fact, the libration motion of the H_2O molecule with a large amplitude in the cluster is suggested by a theoretical molecular orbital calculation.[23]

In Fig. 3, $-\Delta\Delta H_n^\circ$ and $-\Delta\Delta G_n^\circ$ deviate from each other progressively with an increase of n, and the deviation of $-T\Delta\Delta S_n^\circ$ from zero is larger than the case of H_2O. Such a tendency gets more prominent in the order $CH_3OH<C_2H_5OH<n$-C_3H_7OH as shown in Figs. 3—5. For n-C_3H_7OH, $-\Delta\Delta H_n^\circ$ seems to cross the ultimate value zero and become positive after n=8. The rapid increase of both of $-\Delta\Delta H_n^\circ$ and $-T\Delta\Delta S_n^\circ$ up to n=8 clearly indicates that strong bonds are formed between the Cl^- ion and the ligand molecules at the expense of the unfavorable entropy changes in the inner shell of the cluster ion $Cl^-(n\text{-}C_3H_7OH)_n$. Since all the values of $-\Delta\Delta G_n^\circ$, $-\Delta\Delta H_n^\circ$, and $-T\Delta\Delta S_n^\circ$ converge to zero at n=N, the latter two must decrease at certain value of n=n^*. With this n^*, $\Delta H^\circ_{n-1,n}(\text{ion-(ROH)}_n)\approx\Delta H^\circ_{n-1,n}(\text{ROH})_n$ and $\Delta S^\circ_{n-1,n}(\text{ion(ROH)}_n)\approx\Delta S^\circ_{n-1,n}(\text{ROH})_n$. The decrease in $-\Delta\Delta H_n^\circ$ and $-T\Delta\Delta S_n^\circ$ may begin at the same time when the tight inner shells are completed and the loose outer shells start to be formed. Figure 6 shows the predicted conceptional idea of n-dependence of $-\Delta\Delta G_n^\circ$, $-\Delta\Delta H_n^\circ$, and $-T\Delta\Delta S_n^\circ$ for n=0→N. After the completion of the tight inner shells at n=n^*, the $-\Delta\Delta H_n^\circ$ and $-T\Delta\Delta S_n^\circ$ value start to decrease and the $-\Delta\Delta G_n^\circ$ value to increase more steeply at n^* where the outher shell formation begins. The values of n^* and N may increase in the order n-$C_3H_7OH<C_2H_5OH<CH_3OH<H_2O$ since the enhancement effect becomes more effective in that order. On the version of Frank and Wen,[24] the ligands with $n<n^*$ and $n>n^*$ may be regarded as those belonging to the structure making and structure breaking region, respectively.

The financial supports of the Grant-in-Aid from the Ministry of Education and of the first Morino Trust for Molecular Science are gratefully acknowledged.

References

1) A. W. Castleman, Jr. and I. N. Tang, *J. Chem. Phys.*, **57**, 3629 (1972).
2) T. F. Magnera, G. Caldwell, J. Sunner, S. Ikuta, and P. Kebarle, *J. Am. Chem. Soc.*, **106**, 6140 (1984).
3) K. Hiraoka, H. Takimoto, and K. Morise, *J. Am. Chem. Soc.*, **108**, 5683 (1986).
4) K. Hiraoka, *Bull. Chem. Soc. Jpn.*, **59**, 2571 (1986).
5) K. Hiraoka and S. Mizuse, *Chem. Phys.*, in press.
6) K. Hiraoka, K. Morise, T. Nishijima, S. Nakamura, M. Nakazato, and K. Ohkuma, *Int. J. Mass Spectrom. Ion Processes*, **68**, 99 (1986).
7) K. Hiraoka, H. Takimoto, and S. Yamabe, *J. Phys. Chem.*, **90**, 5910 (1986).
8) R. Yamdagni and P. Kebarle, *J. Am. Chem. Soc.*, **93**, 7139 (1971).
9) J. W. Larson and T. B. McMahon, *J. Am. Chem. Soc.*, **106**, 517 (1984).
10) M. Arshadi, R. Yamdagni, and P. Kebarle, *J. Phys. Chem.*, **74**, 1475 (1970).
11) R. G. Keesee and A. W. Castleman, Jr., *Chem. Phys. Lett.*, **74**, 139 (1980).
12) R. Yamdagni, J. D. Payzant, and P. Kebarle, *Can. J. Chem.*, **51**, 2507 (1973).
13) S. Yamabe, Y. Furumiya, K. Hiraoka, and K. Morise, *Chem. Phys. Lett.*, **131**, 261 (1986).
14) A. W. McClellan, "Tables of Experimental Dipole Moments," W. H. Freeman and Company, San Francisco (1963).
15) R. J. W. Le Fèbre, *Adv. Phys. Org. Chem.*, **3**, 1 (1963).
16) A. W. Castleman, Jr., P. M. Holland, and R. G. Keesee, *Radiat. Phys. Chem.*, **20**, 57 (1982).
17) W. R. Davidson and P. Kebarle, *J. Am. Chem. Soc.*, **98**, 6125 (1976).
18) D. R. Rosseinsky, *Chem. Rev.*, **65**, 467 (1965).
19) Y. Marcus, *Pure Appl. Chem.*, **55**, 977 (1983); **57**, 1103 (1985).
20) V. Gutmann, "The Donor-Acceptor Approach to Molecular Interactions," Plenum, New York (1978).
21) Y. K. Lau, P. P. S. Saluja, and P. Kebarle, *J. Am. Chem. Soc.*, **102**, 7492 (1980).
22) C. E. Klots, *J. Phys. Chem.*, **85**, 3585 (1981).
23) A. Karpfen and P. Schuster, "The Chemical Physics of Solvation. Part A. Theory of Solvation," ed by R. R. Dogonatze, E. Kalman, A. A. Kornyshev, and J. Ulstrup, Elsevier, Amsterdam (1985), p. 298.
24) H. S. Frank and W.-Y. Wen, *Disc. Faraday Soc.*, **24**, 133 (1957).
25) C. G. Swain, M. S. Swain, A. L. Powell, and S. J. Alunni, *J. Am. Chem. Soc.*, **105**, 502 (1983).

Ylide-Metal Complexes. XIII.[1] An X-Ray Photoelectron Spectroscopic Study of Bis(dimethylsulfoxonium methylide)gold Chloride

Hidetaka KONNO† and Yoshihisa YAMAMOTO*
Faculty of Pharmaceutical Sciences, Higashi Nippon Gakuen University, Ishikari-Tobetsu, Hokkaido 061-02
†Faculty of Engineering, Hokkaido University, Sapporo 060
(Received January 5, 1987)

Bis(dimethylsulfoxonium methylide)gold chloride, $[(CH_3)_2S(O)CH_2AuCH_2S(O)(CH_3)_2]Cl$, has been studied by X-ray photoelectron spectroscopy. The C 1s spectrum was separated into two peaks at E_B=284.0 and 285.1 eV in a ratio of 1:2. The peak at 285.1 eV corresponds to the methyl carbons, and that at 284.0 eV is assigned to the electron-rich methylene carbon (or carbanion). The E_B of Cl $2p_{3/2}$ agreed with that for chlorobis(triphenylphosphine)gold(I) and chlorobis(triphenylmethylenephosphorane)gold(I). The E_B of Au $4f_{7/2}$ was 84.4 eV, suggesting the oxidation number +1. These results indicate that the structure of the title complex is $(CH_3)_2S(O)CH_2Au(Cl)CH_2S(O)(CH_3)_2$, and different from that reported previously.

A previous paper[2] in this series reported an X-ray photoelectron spectroscopic study of methylenetriphenylphosphorane, $(C_6H_5)_3P{=}CH_2$, chlorobis(methylenetriphenylphosphorane)gold(I), $(C_6H_5)_3PCH_2Au(Cl)CH_2P(C_6H_5)_3$, and the corresponding copper(I) complex. However, the separation and assignment of the carbanion peak and the normal carbon peak for the bonded ylide in the complexes have been difficult, because the carbon ratio is 1:18. Only few XPS studies of ylide-metal complexes have been reported, and the separation and assignment of the carbanion and normal carbons remain uncertain. We surveyed ylides from the sulfonium, phosphonium, and arsonium ylides for XPS measurements, and found a dimethylsulfoxonium methylide to be suitable for the assignment, since the carbanion to the normal carbon ratio is 1:2. This paper deals with the XPS measurements and the structure of bis(dimethylsulfoxonium methylide)gold(I) chloride, $[(CH_3)_2S(O)CH_2AuCH_2S(O)(CH_3)_2]Cl$; the results are compared with those[2] from the chlorobis(methylenetriphenylphosphorane)gold(I) previously reported.

Experimental

Preparation of bis(dimethylsulfoxonium methylide)gold(I) chloride, $[(CH_3)_2S(O)CH_2]_2AuCl$ (**1**), was done as reported previously.[1] Sample handling was always carried out in a 99.9995% pure nitrogen atmosphere to prevent possible decomposition. The instrument was a VG ESCA 3 electron spectrometer.

For the XPS measurements, samples were placed on a nickel mesh holder and introduced into the spectrometer in a 99.9995% pure nitrogen atmosphere. After evacuating to a vacuum better than 2.7×10^{-5} Pa (2×10^{-7} Torr), the sample was cooled to 180—200 K, and irradiated with Mg $K\alpha$ X-ray (50—120 W). The analyzer energy was set to give a half width at half maximum [FWHM] of the Au $4f_{7/2}$ peak of 1.18 eV (high resolution) or 1.80 eV (low resolution) for vacuum evaporated gold on a smooth nickel plate. Peak separation of the spectra was made by the Gauss-Newton least-squares method, where a mixed Gaussian-Lorentzian curve shape was utilized. The electron binding energies, E_B, were calibrated by assigning 284.8 eV to the C 1s peak of the contamination from the spectrometer, 285.0 eV to the C 1s peak of the normal phenyl carbons, and 67.5 eV to the Br 3d peak of the bromide in $[(C_6H_5)_3PCH_3]Br$ and $[(C_6H_5)_3AsCH_3]Br$. This calibration is self-consistent (as shown in the results section).

Results and Discussion

We have reported[1] that dimethylsulfoxonium methylide, $(CH_3)_2S(O)CH_2$ (**L**),[3-5] in complex **1** was bonded to the metal atom through the carbanion donor atom[6-8] from the result of the ^1H NMR measurements. The elemental analysis of **1** and NMR results agreed with the proposed structure $(CH_3)_2S(O)CH_2Au(Cl)CH_2S(O)(CH_3)_2$ (**1a**) or $[(CH_3)_2S(O)CH_2{\cdot}AuCH_2S(O)(CH_3)_2]Cl$ (**1b**). Complex **1** has a free anion[1] judging from the molar conductance (Λ=100 S

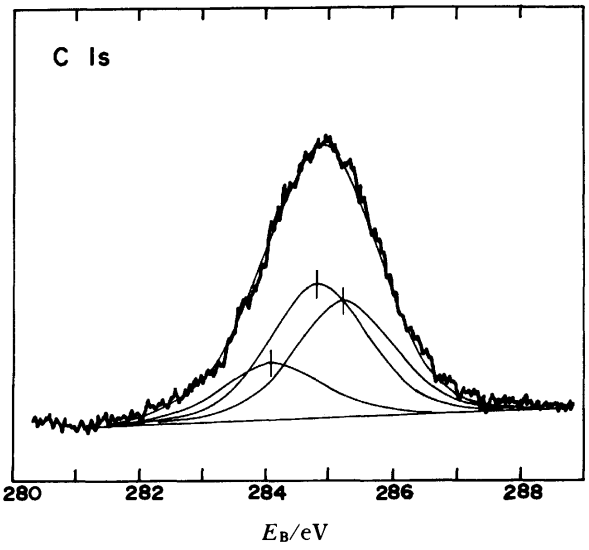

Fig. 1. The C 1s spectrum of $(CH_3)_2S(O)CH_2Au(Cl)CH_2S(O)(CH_3)_2$.

Table 1. Binding Energies for Ylide Metal Complexes and Relative Compounds

	Compound	Binding energies of electrons, E_B/eV												
		C 1s			O	S	N	P	As	Cl	Br	Au	
		(a)	(b)	(c)	1s	2p	1s	2p	3d	$2p_{3/2}$	3d	$4f_{7/2}$	$4f_{5/2}$
1	$[(CH_3)_2S(O)CH_2]_2AuCl$	284.0 (±0.1)	285.1 (±0.2)	284.8[a]	531.5 (±0.6)	167.7 (±0.2)				197.7 (±0.5)		84.4 (±0.2)	88.1 (±0.1)
2	$[(CH_3)_3S{=}O]Br$		285.4 (±0.2)	284.8[a]	532.3 (±0.3)	168.4 (±0.4)					67.5[a]		
3	$[(C_6H_5)_3PCH_2]_2AuCl$	283.8	285.0[a]					132.4 (±0.4)		197.5 (±0.3)		84.9 (±0.3)	88.6 (±0.1)
	$[(C_6H_5)_3PCH_3]Br$		285.0[a]					132.6 (±0.4)			67.5[a]		
	$[(C_6H_5)_3AsCH_3]Br$		285.0[a]						44.4 (±0.3)		67.5[a]		
	$[(CH_3)_4N]Cl$		285.4[b]				402.3			197.1			

Uncertainties shown in parentheses are 90% confidence limits.
a) Reference peaks: E_B[Contamination C 1s]=284.8 eV, E_B[Phenyl C 1s]=285.0 eV, E_B[Br 3d]=67.5 eV. b) E_B of C 1s for methyl carbons was tentatively taken as 285.4 eV.

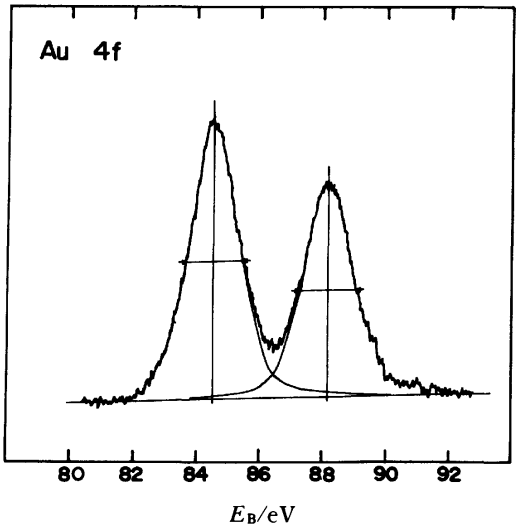

Fig. 2. The Au 4f spectrum of $(CH_3)_2S(O)CH_2Au(Cl)CH_2S(O)(CH_3)_2$ (this spectrum was measured together with the C 1s spectrum in Fig. 1).

$cm^2\ mol^{-1}$) in dry methanol. Thus, we suggested that the structure of **1** is $[(CH_3)_2S(O)CH_2AuCH_2S(O)(CH_3)_2]Cl$ (**1b**).[1]

With the XPS, the C 1s peak of **1** can be separated into three peaks having an intensity ratio of $1:x:2$ (Fig. 1). The peak separation was carried out under only two limiting conditions: One that the peak intensity ratio between methylene carbons, methyl carbons, and carbonaceous contamination from the spectrometer is $1:2:x$, and the other that the three peaks have the same FWHM. After the separation, the peak with an intensity x changed slightly in each measurement and could be assigned as a contamination carbon peak at 284.8±0.2 eV (with our instrument). The reproducibility of the E_B for carbonaceous contamination, when no other organic materials contaminate the sample surface, has been established by data accumulated over the 10-year operation of the instrument. The peak at 285.1 eV (C 1s (b) in Table 1) is assigned to methyl carbon and the peak at 284.0 eV to methylene carbon (C 1s (a)). The spectrum in Fig. 1 was taken in the high-resolution mode; the FWHM of the separated carbon peaks was 1.85 eV. The FWHM of the Au $4f_{7/2}$ peak for **1** taken under the same conditions was 1.81 eV (Fig. 2). Fig. 2 also indicates that there were no distortions of the spectra due to the charge-up effect. It should be noted that the symmetric peak shape for the contamination peak is a first approximation. Usually, the contamination peak shows a slight tailing at the higher E_B side: The degree of asymmetry is about 12:13 in a half width at half maximum. The asymmetric peak shape can be expressed by the superposition of a few symmetric peaks; but this introduces more parameters for the peak separation, leading to the arbitrary convergence in the calculation. The above approximation may not

Table 2. Relative Peak Intensities of XPS

	Compound		Au 4f / S 2p	C 1s / S 2p (a)	C 1s / S 2p (b)	O 1s / S 2p	Cl 2p / S 2p	C 1s / Br 3d
1	$[(CH_3)_2S(O)CH_2]_2AuCl$	Atomic ratio	0.5	1	2	1	0.5	
		Intensity ratio	5.72 (±0.76)	0.78 (±0.03)	1.57 (±0.06)	2.25 (±0.20)	0.74 (±0.07)	
2	$[(CH_3)_3S{=}O]Br$	Atomic ratio			3	1		3
		Intensity ratio			2.23 (±0.28) [0.74]	2.24 (±0.62)		1.42 (±0.18) [0.47]
	$[(C_6H_5)_3PCH_3]Br$ / $[(C_6H_5)_3AsCH_3]Br$	Atomic ratio						19
		Intensity ratio						9.59[a] (±1.76) [0.50]

Uncertainties shown in parentheses are 90% confidence limits. Values in brackets are per one carbon atom.
a) The contributions from the contaminated carbons are not excluded.

lead to a serious error in the E_B values of the separated peaks. The validity of the peak separation is supported by the good reproducibility of the relative peak intensities, as shown in Table 2. Further, C 1s/S 2p and O 1s /S 2p relative intensities for **1** agree well with those for trimethylsulfoxonium bromide, $[(CH_3)_3S{=}O]Br$ (**2**), and C 1s/Br 3d relative intensity per carbon atom for **2** (0.47) agrees with the 0.50 for $[(C_6H_5)_3PCH_3]Br$ and $[(C_6H_5)_3AsCH_3]Br$ as well. In Table 2, the intensity due to the contaminated carbons is excluded by the peak separation, except for $[(C_6H_5)_3PCH_3]Br$ and $[(C_6H_5)_3AsCH_3]Br$. For these two compounds, the peak separation could not be performed precisely due to the large number of phenyl carbons. In this case, however, the contribution from the contaminated carbon is negligible compared with the intrinsic intensity. The results imply that the peak separation is correct and that the stability of **1** during the measurements was comparable to that of **2** and the others in Table 2. The E_B[S 2p] for **2** coincides with that for trimethylsulfoxonium iodide, $[(CH_3)_3S{=}O]I$, reported in Ref. 9.

The E_B value of the ylide methylene carbons for chlorobis(methylenetriphenylphosphorane)gold(I),[2] $(C_6H_5)_3PCH_2Au(Cl)CH_2P(C_6H_5)_3$ (**3**), was not very reliable (as mentioned in the introduction). The E_B value for the ylide methylene carbons in **3**, however, is very close to that of ylide methylene carbons in **1** (Table 1). The E_B of the ylide methylene carbon of **3** strongly suggests that the carbon is anionic (or possibly a carbanion).

The E_B[Au $4f_{7/2}$] for **1** is lower than that for **3** or chlorobis(triphenylphosphine)gold(I), $(C_6H_5)_3PAu(Cl)P(C_6H_5)_3$ (**4**),[2,10] but higher than that (E_B=84.2—84.4 eV) for tetraethylammonium dibromoaurate(I), $[(C_2H_5)_4N][Au(I)Br_2]$ (**5**),[10] which leads to the conclusion that the oxidation number of gold in **1** is +1. The E_B[Cl $2p_{3/2}$] for **1** agrees well with those for **3** and **4**,[2,10] and is higher than that for the unbound chloride ion in tetramethylammonium chloride, $[(CH_3)_4N]Cl$, and others.[11] The bond between the chlorine atom and gold atom in **4** has been established by X-ray diffraction.[12] Thus, the chlorine atom in **1** is bonding to the gold atom. Consequently, the structure of **1** must be similar to **3** and **4**, and the trigonal structure as shown in Scheme 1.

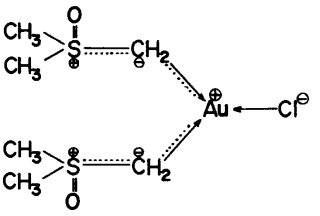

Scheme 1.

In the previous paper,[1] the structure of **1** was suggested to be bis(dimethylsulfoxonium methylide)-gold(I) chloride (**1b**) from the results of the electric conductivity (Λ=100 S cm^2 mol^{-1}) in dry methanol. Later, however, it was found that the compound **4** in which chlorine is bonding to gold[12] also shows the electric conductivity in dry methanol and it is 75 S cm^2 mol^{-1} (similar to the value for **1**). This indicates that the chlorine atom in **4** dissociates in the methanol, and so does the one in **1**.

Both E_B[O 1s] and E_B[S 2p] for **1** are lower than those for **2**, indicating that the density of electrons on the S=O group of **1** is higher than that for **2**. As E_B[Au $4f_{7/2}$] for **1** is lower than for **3**, the electrons on the ylide methylene carbons in **1** may be delocalizing over the molecular orbitals of O=S-C-Au-C-S=O as shown in Scheme 1.

References

1) Part XII. Y. Yamamoto, *Bull. Chem. Soc. Jpn.*, **60**, 1189 (1987).
2) Y. Yamamoto and H. Konno, *Bull. Chem. Soc. Jpn.*,

59, 1327 (1986).

3) H. Schmidbaur and W. Richter, *Z. Anorg. Allg. Chem.*, **429**, 222 (1977).

4) E. J. Corey and M. Chaykovsky, *J. Am. Chem. Soc.*, **87**, 1333 (1965).

5) H. Schmidbaur and W. Tronich, *Tetrahedron Lett.*, **1968**, 5335.

6) Y. Yamamoto and H. Schmidbaur, *J. Organomet. Chem.*, **97**, 479 (1975).

7) Y. Yamamoto and Z. Kanda, *Bull. Chem. Soc. Jpn.*, **52**, 2560 (1979).

8) Y. Yamamoto and H. Sugimoto, *Bull. Chem. Soc. Jpn.*, **53**, 3176 (1980).

9) B. J. Lindberg, K. Hamrin, G. Johansson, U. Gelius, A. Fahlman, C. Nordberg, and K. Siegbahn, *Physica Scripta*, **1**, 286 (1970).

10) A. McNeillie, D. H. Brown, W. E. Smith, M. Gibson, and L. Watson, *J. Chem. Soc., Dalton Trans.*, **1980**, 767.

11) J. Escard, G. Mavel, J. E. Guerchais, and R. Kergoat, *Inorg. Chem.*, **13**, 695 (1974).

12) N. C. Baenziger, K. M. Dittemore, and J. R. Doyle, *Inorg. Chem.*, **13**, 805 (1974).

 © 1987 The Chemical Society of Japan Bull. Chem. Soc. Jpn., 60, 2565—2571 (1987)

Effect of Lattice Anions on the Ligand Substitution Reaction of Tris-(1,10-phenanthroline)metal(II) Complexes: $[M(phen)_3]SO_4$ and $[M(phen)_3]X_2$ (M: Fe(II), Co(II), Ni(II); X: Cl^-, Br^-, I^-)

Shoji YAMASAKI, Terufumi FUJIWARA,* and Yuroku YAMAMOTO†
Department of Chemistry, Faculty of Science, Hiroshima University, Higashisenda, Naka-ku, Hiroshima 730
†Environmental and Safety Engineering Department, Fukui Institute of Technology, Gakuen, Fukui 910
(Received January 28, 1987)

The kinetics of the ligand substitution reaction of the title complexes in the solid state have been studied using thermogravimetry (TG) and differential scanning calorimeter (DSC) techniques. For these complex salts, an exothermic peak appears in the DSC curve which correlates with a ligand substitution in which anionatobis(1,10-phenanthroline)metal(II) complexes are formed. The heats of the exothermic reaction for ligand substitution of the sulfates decrease in the order Co(II)>Ni(II)>Fe(II). Isothermal and nonisothermal kinetic analyses were carried out using the exothermic peak. Activation energies of the ligand substitution for the same counterion generally increase with the metal in the order Co(II)<Ni(II)<Fe(II) and for the same metal, Ni(II) or Fe(II), increase with the counterion in the order Cl^-<Br^-<I^-<SO_4^{2-}. However, for the cobalt complex, the activation energies are almost identical for this series of counterions. From the trends in activation parameters for the ligand substitution, we propose a dissociative mechanism for the sulfates of all complexes studied and for the cobalt complex halides studied. For the halides of the iron(II) and nickel(II) complexes studied, a mechanism involving nucleophilic attack of the halide ions is important.

The ligand substitution reaction and the solvent exchange reaction of complex compounds in solution media have been studied by many workers.[1] However, only a few studies concerning such reactions in the solid phase have been done. One reason for this lack of effect is because it is difficult to estimate contributions from the lattice anions.

Counterions play an important role in reactions such as catalysis, due to their donicity. For example, the racemization of $[Ni(phen)_3]^{2+}$ is accelerated by the pairing of the complex ion with a counterion in water-*t*-BuOH. The rate increases in the order[2] ClO_4^-<I^-<Br^-<Cl^-. Moreover, we showed that since lattice anions in the solid state are in contact with the complex ion, the mechanism of the racemization could be determined by studying the effect of the donicity of lattice anions on the kinetic parameters.[3] We reported that such lattice anions affect the ligand substitution reaction in the solid state[4] as well as the racemization.

In this paper, the mechanism of the ligand substitution reaction of tris(1,10-phenanthroline) iron-(II), nickel(II), and cobalt(II) salts (chloride, bromide, iodide, and sulfate) is investigated from the point of view of the effect of lattice anions on the kinetic paramaters. By comparing kinetic information on the racemization mentioned above with that of ligand substitution, it was found that two types of mechanisms operate, depending on the donicity of the counterion, and M-N bond strengths.

Experimental

Materials. The complex salts, $[M(phen)_3]X_2 \cdot nH_2O$ (M: Fe(II), Co(II), Ni(II); X: Cl^-, Br^-, I^-; n=7 for chloride, 6 for bromide, and 2 for iodide) and $[M(phen)_3]SO_4 \cdot 10H_2O$, were prepared by the usual procedures.[4] The crude products were recrystallized three times from water, and dried in air. All the complexes were powdered by grinding with an agate mortar and pestle (200—270 mesh). Found: C, 53.26; H, 4.13; N, 10.36%. Calcd for $C_{36}H_{38}O_7N_6Cl_2Fe$: C, 54.49; H, 4.83; N, 10.59%. Found: C, 54.15; H, 4.50; N, 10.34%. Calcd for $C_{36}H_{38}O_7N_6Cl_2Co$: C, 54.28; H, 4.81; N, 10.55%. Found: C, 54.51; H, 4.25; N, 10.37%. Calcd for $C_{36}H_{38}O_7N_6Cl_2Ni$: C, 54.30; H, 4.81; N, 10.55%. Found: C, 52.13; H, 3.71; N, 10.01%. Calcd for $C_{36}H_{36}O_6N_6Br_2Fe$: C, 50.02; H, 4.20; N, 9.72%. Found: C, 48.74; H, 3.69; N, 9.74%. Calcd for $C_{36}H_{36}O_6N_6Br_2Co$: C, 49.85; H, 4.18; N, 9.69%. Found: C, 50.16; H, 3.64; N, 9.58%. Calcd for $C_{36}H_{36}O_6N_6Br_2Ni$: C, 49.86; H, 4.18; N, 9.69%. Found: C, 48.80; H, 3.10; N, 9.39%. Calcd for $C_{36}H_{28}O_2N_6I_2Fe$: C, 48.79; H, 3.18; N, 9.48%. Found: C, 48.69; H, 2.91; N, 9.54%. Calcd for $C_{36}H_{28}O_2N_6I_2Co$: C, 48.62; H, 3.17; N, 9.45%. Found: C, 51.38; H, 3.34; N, 10.21%. Calcd for $C_{36}H_{28}O_2N_6I_2Ni$: C, 48.63; H, 3.17; N, 9.45%. Found: C, 49.70; H, 4.26; N, 9.49%. Calcd for $C_{36}H_{44}O_{14}N_6SFe$: C, 49.55; H, 5.08; N, 9.63%. Found: C, 49.94; H, 4.50; N, 9.67%. Calcd for $C_{36}H_{44}O_{14}N_6SCo$: C, 49.37; H, 5.06; N, 9.60%. Found: C, 47.64; H, 5.86, N, 9.20%. Calcd for $C_{36}H_{44}O_{14}N_6SNi$: C, 49.36; H, 5.07; N, 9.60%.

Kinetic Methods. Under linear heating conditions, the Reich-Stivala method[5] and the direct Arrhenius method were used. The Reich-Stivala method is based on the well-known expression involving mechanisms for homogeneous kinetics, i.e.

$$\ln [g(\alpha)T^{-2}] = -E_a R^{-1}T^{-1} + \ln[ARP(RH)^{-1}E_a^{-1}] \quad (1)$$

where, P=1−2X+6X^2−24X^3+120X^4−⋯; X=RT/E_a; (RH)= heating rate; α=fractional conversion; the symbols, T, R, A, E_a, have their usual meanings.[5] The following equation can readily be obtained from Eq. 1.

$$U(1) \ln [g(\alpha_1)g(\alpha_2)^{-1}T(1)] = E_a/R, \quad (2)$$

where $T(1)=(T_2/T_1)^2$; $U(1)=T_1T_2/(T_1-T_2)$. Data were fitted to Eq. 2 by interative calculations and the most probable function $g(\alpha)$ can be obtained when the minimum standard deviation of E_a/R is attained. The reaction rate $d\alpha/dt$ is given directly from differential scanning calorimeter (DSC) and thermogravimetric (TG) experiments.

Under isothermal conditions, the Arrhenius method was used. In this study, the conversion coefficient α corresponding to the concentration of the reactant in the liquid or gas phase, can be derived from the ratio of the area corresponding to heat evolved up to a certain heating time (t_1) to the integral area of the total reaction heat obtained by DSC (Fig. 1), or the mass lost up to a time (t_1), divided by the total mass loss, determined by TG analysis. More than 5 runs for each system were carried out, and the average and the standard deviation were calculated.

Measurements. DSC and TG measurements were performed using a Sinku-Riko Model ULBAC DSC-1500L and Sinku-Riko Model TGD-3000RHN instruments, respectively. The DSC instrument was calibrated[6] from the heat of fusion of indium (99.999%), mp 156 °C, ΔH(fusion)=3.26 kJ mol^{-1}. Dry nitrogen flowed through the system. The finely ground samples (200—270 mesh) were placed in an aluminium cell for the DSC measurement. The sample mass was varied until a linear relationship between mass and peak area or height was obtained. Table 1 presents the average activation energy obtained by more than 5 runs of the ligand substitution reaction at various heating rates. No significant change of the activation energy with different heating rates was appeared. In this study, a heating rate of less than 6 K min^{-1} was used throughout the experiment unless otherwise stated. Infrared spectra were obtained by the nujol method with a JASCO Model A-102 Infrared spectrometer.

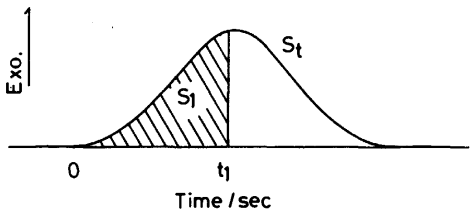

Fig. 1. Determination of reaction kinetics based on a part of the DSC curves. S_t: total area of this peak; S_1: the area evolved up to the heating time t_1. Conversion coefficient $\alpha_1=S_1/S_t$.

Results

Typical TG and DSC curves for $[M(phen)_3]SO_4 \cdot 10H_2O$ [M=Fe(II), Co(II), Ni(II)] are shown in Fig. 2. An exothermic peak is observed on the DSC curves and the TG curve shows that there is no loss of mass during this process. This is similar to the results already reported for the bromides of the iron and nickel complexes.[4] The heat of this exothermic reaction ($-\Delta H$) was determined from the area of the peak. The results obtained for the sulfates and the halides are given in Table 2, with the temperatures

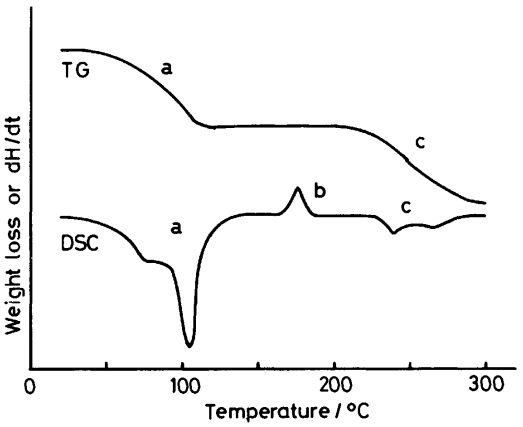

Fig. 2. Typical TG and DSC curves for $[Co(phen)_3]SO_4 \cdot 10H_2O$. Heating rate is 6 K min^{-1}. a: Vaporization of H_2O; b: exothermic peak with ligand substitution; c: vaporization of 1,10-phenanthroline.

Table 1. Effect of Heating Rate on Activation Energy of 1,10-Phenanthroline Substitution of Tris(1,10-phenanthroline)nickel(II) Sulfate Decahydrate

Heating rate/K min^{-1}	10	8	6	4	2
E_a/kJ mol^{-1}	236±60	201±21	227±28	235±12	200±52

Table 2. The Heat of Reaction, $-\Delta H$ of 1,10-Phenanthroline Substitution and the Peak Temperature, T_p,[a] for $[M(phen)_3]SO_4$ and $[M(phen)_3]X_2$

M=	Fe(II)		Ni(II)		Co(II)	
Counterion	$-\Delta H$/kJ mol^{-1}	T_p/°C	$-\Delta H$/kJ mol^{-1}	T_p/°C	$-\Delta H$/kJ mol^{-1}	T_p/°C
SO_4^{2-}	13.9±1.1	175	31.9±1.5	183	51.9±4.2	179
Cl^-	10.8±0.9	155	6.3±0.2	194	13.5±0.7	139
Br^-	12.7±0.9	194	24.7±2.7	234	7.7±0.5	187
I^-	—	—	—	—	4.5±0.5	170

a) T_p: The temperature at which the exothermal peak appears on the DSC curves.

(T_p) at which the exothermic peak appears. The $-\Delta H$ values for the sulfates decrease with the metal in the order Co(II)>Ni(II)>Fe(II), although the peak temperatures are almost equal for this series of metals. The amount of heat evolved at any time divided by the total heat corresponds to the degree of progress of the phen substitution for the complex salts except for the iodides of the iron and nickel complexes. The iodides undergo phen substitution at a temperature higher than 220 °C, which is the boiling point of 1,10-phenanthroline. 1,10-Phenanthroline molecules therefore evaporate rapidly out of the system as soon as they are released from the complexes.[4] The result is that the mass loss is related to the degree of progress of the phen substitution.

The sulfatobis(1,10-phenanthroline)metal(II) complexes, $[M(phen)_2SO_4]\cdot nH_2O$ [M=Fe(II), n=1; M=Co(II), n=0; M=Ni(II), n=0], were obtained as products of the ligand substitution by using the TG techniques for the sulfates. Found: C, 54.36; H, 3.07; N, 10.66%. Calcd for $C_{24}H_{18}O_5N_4SFe$: C, 54.36; H, 3.42; N, 10.56%. Found: C, 55.29; H, 3.14; N, 10.85%. Calcd for $C_{24}H_{16}O_4N_4SCo$: C, 55.93; H, 3.13; N, 10.87%. Found: C, 55.73; H, 3.15; N, 10.78%. Calcd for $C_{24}H_{16}O_4N_4SNi$: C, 55.95; H, 3.13; N, 10.88%.

The Freeman-Carrol,[7] Coats-Redfern,[8] and Reich-Stivala[5] methods were applied to the data obtained from the ligand substitution observed here. Preliminary experiments showed that the Freeman-Carrol method involving the n order reaction gave unfavorable fits to the data curves. Analysis by the Coats-Redfern method or the Reich-Stivala method involving the function $g(\alpha)$ depending on processes controlling the reaction rates of solids, gave the best fits, using computer simulations. In this study, we employed the Reich-Stivala method as described above, due to its greater convenience. Avrami-Erofeyev functions based on the different nucleation and growth mechanisms[9] were selected to give the best possible fits of the substitution kinetic data for most of the complex salts, under linear heating conditions. However, the best fitting function could not be obtained only by the linear heating method because of a lack of significant differences in the relative errors obtained using the different functions (Table 3). Therefore the isothermal method was also applied and the best fitting function of a group of Avrami-Erofeyev functions was found. Figure 3 shows the degree of fitting for each function. A straight line is

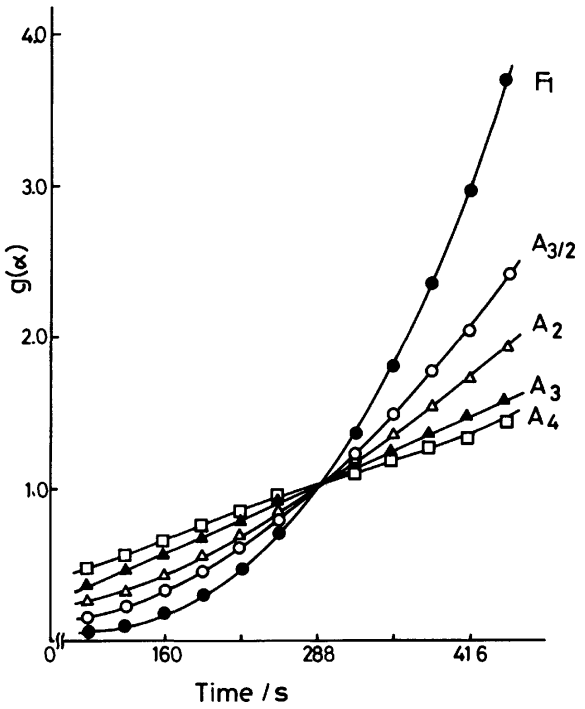

Fig. 3. Kinetic analysis for $[Co(phen)_3]SO_4\cdot 10H_2O$ under isothermal conditions at 150 °C. Notation of Sharp and co-workers (Ref. 10) is used.

Table 3. Estimation of Activation Energy Using the Reich-Stivala Method for Tris(1,10-phenanthroline)-cobalt(II) Sulfate Decahydrate

Function		E_a/kJ mol^{-1}	% Error
Notation[a]	$g(\alpha)$		
F_1	$-\ln(1-\alpha)$	334.4±8.19	2.45
$A_{3/2}$	$[-\ln(1-\alpha)]^{2/3}$	220.5±5.45	2.47
A_2	$[-\ln(1-\alpha)]^{1/2}$	163.6±4.09	2.50
A_3	$[-\ln(1-\alpha)]^{1/3}$	106.6±2.72	2.55
A_4	$[-\ln(1-\alpha)]^{1/4}$	78.1±2.03	2.60
R_1	α	236.4±18.96	8.02
R_2	$1-(1-\alpha)^{1/2}$	278.1±10.74	3.86
R_3	$1-(1-\alpha)^{1/3}$	295.1±7.45	2.52
D_1	α^2	480.1±37.90	7.89
D_2	$(1-\alpha)\ln(1-\alpha)+\alpha$	582.4±29.43	5.57
D_3	$[1-(1-\alpha)^{1/3}]^2$	597.5±14.88	2.49
D_4	$(1-2\alpha/3)-(1-\alpha)^{2/3}$	550.7±24.46	4.44

a) Notation of Sharp and co-workers (Ref. 10) is used.

Table 4. Comparison of Activation Parameters Calculated by the Reich-Stivala and Arrhenius Methods[a] for 1,10-Phenanthroline Substitution of $[M(phen)_3]SO_4$

Metal		Reich-Stivala method	Arrhenius method
Fe(II)	ΔH^*/kJ mol^{-1}	361±32	350±0.8[b]
	E_a/kJ mol^{-1}	368±32	352±0.8[b]
Ni(II)	ΔH^*/kJ mol^{-1}	219±28	254±0.7[b]
	E_a/kJ mol^{-1}	227±28	262±0.7[b]
Co(II)	ΔH^*/kJ mol^{-1}	94±7	97±3.3[c]
	E_a/kJ mol^{-1}	102±7	105±3.3[c]

a) The best fitting function, A_3, for the sulfates (Table 5) is used. b) Isothermal conditions. c) Linear heating conditions.

Table 5. The Best Fitting Function[a] and Kinetic Parameters for 1,10-Phenanthroline Substitution of the Sulfates and Halides of Tris(1,10-phenanthroline)metal(II) Complexes in the Solid State

Metal		Counterion			
		Cl^-	Br^-	I^-	SO_4^{2-}
Fe(II)	Function	A_3	F_1	D_1	A_3
	E_a/kJ mol^{-1}	164±13	239±20	335±35	368±32
	ΔH^*/kJ mol^{-1}	157±13	231±20	325±35	361±32
	ΔS^*/J K^{-1} mol^{-1}	98±30	284±46	266±69	515±89
Ni(II)	Function	A_3	A_3	D_2	A_3
	E_a/kJ mol^{-1}	98±24	183±20	206±9	227±28
	ΔH^*/kJ mol^{-1}	90±24	177±20	197±9	219±28
	ΔS^*/J K^{-1} mol^{-1}	−70±52	72±39	101±12	279±33
Co(II)	Function	A_3	A_3	A_3	A_3
	E_a/kJ mol^{-1}	123±1	119±20	133±4	102±7
	ΔH^*/kJ mol^{-1}	113±1	111±20	126±4	94±7
	ΔS^*/J K^{-1} mol^{-1}	5±32	−34±45	−15±7	−57±8

Kinetic Parameters of Racemization in the Solid State

	$[Ni(phen)_3]I_2$[b]	$[Ni(phen)_3](ClO_4)_2$[c]
ΔH^*/kJ mol^{-1}	203±4	268±36
ΔS^*/J K^{-1} mol^{-1}	99±8	240±20

a) Notation of Sharp and co-workers (Ref. 10) is used. b) Ref. 3. c) Ref. 18.

expected to be obtained using the best function. The activation parameters obtained by the linear heating method and the isothermal method are in good agreement with each other, and the activation energy and enthalpy, E_a and ΔH^*, by the Reich-Stivala method are in good agreement with those by the Arrhenius method under linear heating conditions (Table 4). The kinetic parameters obtained are given in Table 5 with the functions which gave the best fits for the sulfates and halides of the complexes. The enthalpy and entropy of activation were calculated by the relationship: $E_a=\Delta H^*+2RT$, $\Delta S^*=R(\ln A-\ln(kT/h)-2)$ where the parameter, E_a and $\ln A$, were obtained by the Arrhenius equation and other parameters have their usual meanings.

The ΔH^* values for the same counterion increase with the metal in the order Co(II)<Ni(II)<Fe(II) for the bromides, iodides, and sulfates and for the chlorides, in the order Co(II)≃Ni(II)<Fe(II). For the same metal, the ΔH^* values increase with the counterion in the order $Cl^-<Br^-<I^-<SO_4^{2-}$ for the nickel and iron complexes while the values for the cobalt complexes are almost identical for this series of counterions.

Discussion

The ligand substitution reaction of $[M(II)(phen)_3]X_2$ in the solid state have been reported.[4] The scheme of the reaction is as follows.

$$[M(phen)_3]X_2(s) \longrightarrow [M(phen)_2X_2](s) + phen(g \text{ or } l),$$

where M is Fe or Ni, X^- is I^-, Br^-, or Cl^-, and s, l, and g indicate the solid, liquid, and gaseous states, respectively. A similar reaction occurs in the case of the sulfates of all the metal complexes studied and all the cobalt complex halides studied. The coordination of the SO_4^{2-} ion to the central metal ion was confirmed by IR measurements after heating under dynamic or constant temperature conditions. If the SO_4^{2-} ion is coordinated to a metal ion, the symmetry is lowered and splitting of degenerated vibrations occurs, together with the appearance of new bands in the IR spectrum, which correspond to Raman active

Fig. 4. Infrared spectra of sulfate ion for the complex salt, $[Fe(phen)_3]SO_4$. a: before heating; b: after dehydration; c: after exothermic reaction; d: product.

bands in the free ion.[11] These changes in SO stretching bands are observed when the sulfates are heated to the temperature where the exothermic DSC peak described above appears (Fig. 4).

It is interesting to note that the function based on nucleation and three- or one-dimensional growth, A_3 or F_1, respectively, gives best fits for the ligand substitution of most of the complex salts while for that of the nickel(II) or iron(II) complex iodides the D_2 or D_1 function based on two- or one-dimensional diffusion, respectively, is the best fitting function (Table 5). Many mathematical models have been advanced relating nucleation and nuclei growth rates to the kinetics of phase transformation and decomposition:[12] The solid-state reaction models have been based on the assumption that the nucleation of products at active sites and subsequent growth of the nuclei occurs. In the case where all the nuclei are initially present and the growth rate of the product phase is phase-boundary controlled, the three- and one-dimensional nuclei growth equations take the forms of A_3 and F_1, respectively. According to Laidler,[13] when a discontinuous product phase occurs, the rate-determining step may be the chemical process occurring at the phase boundary: The rate is controlled by the chemical reaction itself-that is, the breaking and re-forming of bonds at the interface. On the other hand, when material transport is the rate-controlling process (or the chemical reaction at the phase boundary is considerably faster than the transport process and thus the solid-state reaction is diffusion controlled), the functions, D_2 and D_1, ought to be applicable in two and one dimension(s), respectively.

The defect-diffusion mechanism proposed for solid-state reactions of coordination compounds by House[14] may be applicable to this diffusion process. If the reaction begins with the loss of a ligand from a complex ion in a lattice site, the ligand must be placed in an interstitial position in the lattice with the formation of a Frenkel type defect. Interstitial diffusion of Frenkel defects through the lattice is enhanced by a greater difference in size between cation and anion because the volume of free space is greater when the cations and anions are of greatly differing sizes. Thus, if the dissociation occurs, the diffusion of interstitial phenanthroline would be more difficult for the iodide owing to the smaller free volume: The expected difficulty should decrease in the order $SO_4^{2-}>I^->Br^->Cl^-$. On the other hand, Table 5 shows the same order of anion effects on activation energies for the phase-boundary controlled nuclei growth (A_3 and F_1: the chemical reaction itself), where the anion effects are attributed to the donicity of the lattice anions as discussed below. In the case of the iodides alone, the activation energy for the diffusion may be slightly larger than that for the chemical reaction and thus this leads to the ligand substitution through a diffusion controlling process for the iodides.

A dissociative mechanism has been proposed for ligand substitution of several transition metal complexes in solution.[15] If the dissociative mechanism is also operative in the solid state, the activation parameters, ΔH^* and ΔS^*, of ligand substitution should be independent of the donicity of lattice anions. This is demonstrated by the data on ΔH^* and ΔS^* for the cobalt complex salts (Table 5).

For the nickel and iron complexes, on the other hand, changes in the lattice anion were found to alter the activation parameters, indicating an interaction of the complex cations with the anions in the transition state. Moreover, the ΔH^* and ΔS^* values of ligand substitution for the iodide of the nickel complex, 197 ± 9 kJ mol^{-1} and 101 ± 12 J K^{-1} mol^{-1}, are almost equal to those of the solid-state racemization,[3] 203 ± 4 kJ mol^{-1} and 99 ± 8 J K^{-1} mol^{-1}, respectively (Table 5). This implies that the mechanism of ligand substitution should be the same as proposed in our previous paper for the solid-state racemization of the nickel complex.[3] The mechanism involves expansion of M-N bonds to a 7-coordinate transition state with one lattice anion. If so, the rate should be controlled by the donicity of the lattice anion in the same manner as the racemization rate. Table 5 shows that the ΔH^* values for the nickel and iron complexes decrease with the anion in the order $I^->Br^->Cl^-$. This sequence is the same as observed for the solid-state racemization of $[Ni(bpy)_3]X_2$[3] and $[Co(phen)_3]X_3$,[16] and lies in the order of increasing donicity of the anions.[17] Thus, the trend in ΔH^* is attributable to the ability of the anions to stabilize the transition state by donation. In such a mechanism, a metal-anion distance will shorten with lengthening of a M-N bond(s). The interaction of the anion with the metal leads to the stabilization of the transition state and thus to a lower energy of the activation for the ligand substitution. For the iron complex, we can note that the mechanism of ligand substitution discussed above is different from that of the solid-state racemization,[3] ΔH^* values for the racemization of all the iron complex halides are identical within experimental errors (174—178 kJ mol^{-1}), which can be explained by a twist mechanism.

Table 5 shows another interesting fact that the ΔH^* values for the sulfates of the nickel and iron complexes are larger than those for the corresponding iodides, respectively, despite the greater negative charge of the lattice anion, SO_4^{2-}, compared with the I^- ion. This indicates that the donicity of the SO_4^{2-} ion is lower than that of the I^- ion. Moreover, the ΔH^* and ΔS^* values of ligand substitution for the sulfate of the nickel complex, which are 219 ± 28 kJ mol^{-1} and 279 ± 33 J K^{-1} mol^{-1} ($\Delta H^*=254$ kJ mol^{-1} by Arrhenius method in Table 4), are comparable to those of the solid-state racemization for the corresponding per-

chlorate,[18] 268±36 kJ mol^{-1} and 240±20 J K^{-1}mol^{-1}, respectively (Table 5). It is reasonable to infer that the perchlorate racemizes in the solid state by a mechanism involving expansion of M-N bonds without donation of the ClO_4^- ion since the ion has negligible donor ability. The transition state for the phen substitution of the sulfate is assumed to be similar to that for the solid-state racemization of the perchlorate; thus a dissociative mechanism involving such an expansion of M-N bonds leading to bond breaking is most likely. Support for this is furnished by the relationship between E_a for ligand substitution in the solid state and the third stability constant, logK_3, for the following formation reaction in aqueous media:[19]

$$[M(phen)_2(H_2O)_2]^{2+}_{aq} + phen_{aq} \rightleftharpoons [M(phen)_3]^{2+}_{aq}$$

logK_3 can be taken as a measure of the strength of M-N bonds in the tris(1,10-phenanthroline)complexes.[20] If the rate determining step of the ligand substitution in the solid state is dominated by the ability to release a phen ligand, a linear relationship with a positive slope between E_a and log K_3 for these complexes would be expected. In fact, good linearity was obtained for the sulfates (Fig. 5). Furthermore, the logK_3 data show that the cobalt complex is less stable than the nickel and iron complexes and thus strength of the M-N bonds should be lower. This seems to be the reason for the change from an associative to a dissociative mechanism for the phen substitution of the cobalt complex salts.

The resultant exothermic heat of reaction for the ligand substitution of the complex salts in the solid state can be divided into two components. One is the release of one phen ligand molecule from the complex which is endothermic, and the other is the coordination of anions to the central metal which is exothermic. The heats of the exothermic reaction for the ligand substitution of the sulfates in the solid state also show a linear relationship with log K_3 (Fig. 5); the reaction heat decreases with increasing log K_3 (Table 5). This result implies that the release of phen is an important factor in lowering the reaction heat and the heat due to coordination of the SO_4^{2-} ion to all the metals is nearly identical, where there should be only an electrostatic effect. These results are consistent with the operation of a dissociative mechanism for the ligand substitution of the sulfates, suggesting negligible ability of the SO_4^{2-} ion to stabilize the transition state by donation.

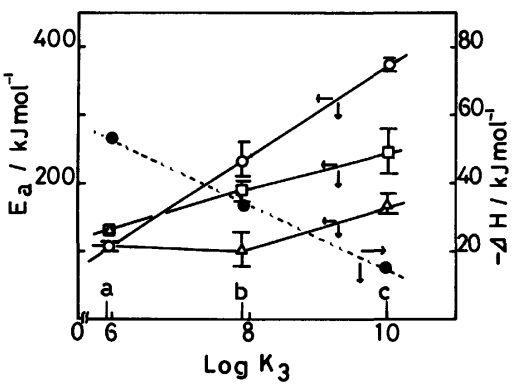

Fig. 5. Plots of activation energy (E_a: O, sulfate; Δ, chloride; □, bromide) and heat of reaction of ligand substitution ($-\Delta H$: ●, sulfate) vs. log of consecutive stability constant (log K_3) for the tris(1,10-phenanthroline)metal(II) complexes [a, cobalt(II); b, nickel(II); c, iron(II)].

In addition, the plots of E_a against logK_3 for the halides for the nickel and iron complexes show that the slopes for the chlorides and bromides are nearly half the slopes for the sulfates (Fig. 5). This result may suggest that expansion of two M-N bonds to the transition state is likely for the sulfates while for the bromides and chlorides, only one M-N bond expansion occurs, although the large, rigid, flat phenanthroline ligands seem to impose considerable steric constraints on one-ended phen dissociation.[3]

The heats of the exothermic reaction for the halides are smaller than those for the sulfate. This may be attributed to more difficulty of the migration of anions to the complex in the case of the halides compared to the sulfates since the process of substitution of one phenanthroline ligand in the solid state for the halides would require that two anions leave their lattice sites and enter the coordination sphere of the metal ion while for the sulfate only one lattice site is vacated. Although there is a good relationship between the activation energies for ligand substitution of the halides and the third stability constant, log K_3, no correlation of the reaction heats with log K_3 is observed for the halides. Factors such as covalency of M-X bonds in the products, crystal structures of the products, etc., other than strength of M-N bonds in the reactants, may be responsible for the differences in ΔH. Further research on other complexes and studies of crystal structures are required in order to understand this phenomenon. In addition, main differences in ΔS^* for the cobalt complex salts (Table 5) seem to arise from differences in the volume of free space in the lattice but at this time we have no clear explanation of the results and it is hoped that the studies of crystal structures will clarify the situation.

The present work was partially supported by a Grant-in-Aid for Scientific Research No. 57740317 from the Ministry of Education, Science and Culture.

References

1) See, for example, F. Basolo and R. G. Pearson, "Mechanisms of Inorganic Reactions," 2nd ed, John Wiley

& Sons, New York (1967).
2) M. Yamamoto, T. Fujiwara, and Y. Yamamoto, *Inorg. Nucl. Chem. Lett.*, **5**, 37 (1979).
3) T. Fujiwara and Y. Yamamoto, *Inorg. Chem.*, **19**, 1903 (1980).
4) K. Akabori, H. Matsuo, and Y. Yamamoto, *J. Inorg. Nucl. Chem.*, **35**, 2679 (1973); Y. Yamamoto, K. Akabori, and T. Seno, *Inorg. Nucl. Chem. Lett.*, **9**, 195 (1973).
5) L. Reich and S. S. Stivala, *Thermochim. Acta*, **34**, 287 (1979).
6) G. Beech, C. T. Mortimer, and E. G. Tyler, *J. Chem. Soc. A*, **1967**, 925.
7) E. S. Freeman and B. Carrol, *J. Phys. Chem.*, **62**, 394 (1958).
8) A. W. Coats and J. P. Redfern, *Nature*, **201**, 68 (1964).
9) M. Avrami, *J. Chem. Phys.*, **9**, 177 (1941); B. V. Erofeyev, *C. R. (Dolk.) Acad. Sci. U.R.S.S.*, **52**, 511 (1946).
10) J. H. Sharp, G. W. Brindley, and B. N. N. Achar, *J. Am. Ceram. Soc.*, **49**, 379 (1966).
11) K. Nakamoto, "Infrared Spectra of Inorganic and Coordination Compounds," 2nd ed, John Wiley & Sons, New York (1970), pp. 173—175.
12) S. F. Hulbert, *J. British Ceram. Soc.*, **6**, 11 (1969).
13) K. J. Laidler, "Chemical Kinetics," McGraw-Hill, Inc., New York (1965), pp. 316—318.
14) J. E. House, Jr., *Thermochim. Acta*, **38**, 59 (1980).
15) See, for example, J. Burgess, "Metal Ions in Solution," Ellis Horwood Limited, Chichester (1978), pp. 349—404, the references cited therein, and also in Ref. 1.
16) T. Fujiwara, *Bull. Chem. Soc. Jpn.*, **56**, 122 (1983).
17) V. Gutmann and R. Schmid, *Coord. Chem. Rev.*, **12**, 263 (1974).
18) A. Tatehata, T. Kumamaru, and Y. Yamamoto, *J. Inorg. Nucl. Chem.*, **33**, 3427 (1971).
19) W. A. E. McBryde, "Critical Evaluation of Equilibrium Constants in Solution: Part A," Pergamon Press, Oxford (1978), No. 17; H. M. Irving and D. H. Mellor, *J. Chem. Soc.*, **1962**, 5222.
20) The effect of hydration on the formation reaction is almost equal for the Co(II), Fe(II), and Ni(II) complexes since the complex ions have the same charge and the same ligand. In addition, the coordination ability of water molecules is much weaker than that of 1,10-phenanthroline.

Preparation, Structure, and Circular Dichroism Spectra of $[Co(L_1)(L_2)]^+$-Type Complexes (L_1=Iminodiacetato or *N*-Methyliminodiacetato and L_2=3-Azapentane-1,5-diamine or 3-Methyl-3-azapentane-1,5-diamine)

Takaji YASUI,* Ken-ichi OKAMOTO,† Jinsai HIDAKA,† Tomoharu AMA, and Hiroshi KAWAGUCHI

Department of Chemistry, Faculty of Science, Kochi University, Akebono-cho, Kochi 780
†Department of Chemistry, University of Tsukuba, Sakura, Ibaraki 305

(Received January 29, 1987)

Three geometrical isomers (mer, u-fac, and s-fac) possible in each of $[Co(ida)(mdien)]^+$ and $[Co(mida)(mdien)]^+$ and u-fac isomer of $[Co(mida)(dien)]^+$ (ida=iminodiacetate, mida=*N*-methyliminodiacetate, mdien=3-methyl-3-azapentane-1,5-diamine, and dien=3-azapentane-1,5-diamine) were newly prepared, and the u-fac isomers were optically resolved. The geometrical structures of these isomers were assigned on the basis of their absorption and ^{13}C NMR spectral data. The crystal structure of $(+)^{CD}_{550}$-*u-fac*-$[Co(ida)(mdien)]\cdot(+)^{CD}_{575}$-$[Co(ox)_2(en)]\cdot 6H_2O$ was determined by X-ray diffraction method. The crystal is monoclinic, space group $P2_1$, a=15.793(6), b=12.855(3), c=7.070(2) Å, β=96.80(5)°, and Z=2. Both of the absolute configurations of the two complex ions take Λ configuration. The relationship between the absolute configurations and the CD spectral behaviors of the u-fac isomers is also discussed.

The mixed-ligand complexes of cobalt(III) with imino-diacetate (ida) or *N*-methyliminodiacetate (mida) and 3-azapentane-1,5-diamine (dien) or 3-methyl-3-azapentane-1,5-diamine (mdien) as the terdentate ligands can exist in three geometrical isomeric forms (mer, u-fac, and s-fac), as shown in Fig. 1. All of the three isomers have been first isolated for $[Co(ida)(dien)]^+$, while the mer and s-fac isomers except for u-fac have been isolated for $[Co(mida)(dien)]^+$.[1] The structures of these isomers were assigned based on their visible absorption and ^1H NMR spectra.[1] The u-fac isomer of $[Co(ida)(dien)]^+$, which has a chiral structure, was optically resolved by Yoshikawa et al., and the absolute configuration was assigned as ΛΔΛ for the $(-)_{589}$ isomer on the basis of the CD spectrum.[2] Koine et al. reported optical resolution of the mer isomer for $[Co(mida)(dien)]^+$.[3] Gailey et al.[4] and Kawamoto et al.[5] studied, respectively, the ^{13}C NMR spectra and the Raman spectra of the $[Co(ida)_n(dien)_{2-n}]$-type complexes.

Previously, we reported the methods to prepare all the geometrical isomers possible in $[Co(ida)_2]^-$,[6] $[Co(mida)_2]^-$,[7] $[Co(ida)(mida)]^-$,[6,8] $[Co(edma)_2]^+$,[9] $[Co(ida)(edma)]$,[10] and $[Co(mida)(edma)]$.[11] All the preparative reactions were performed under weakly acidic conditions.[6-11]

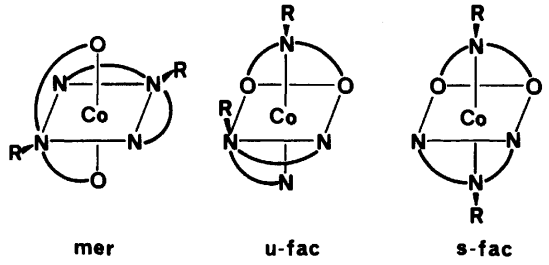

Fig. 1. Three geometrical isomers possible in $[Co(Rida)(Rdien)]^+$ (R=H or CH_3).

In the present paper, the preparations of the mixed-ligand type complexes, $[Co(ida)(mdien)]^+$ and $[Co(mida)(mdien)]^+$, will be described, and all the isomers isolated will be characterized on the basis of their absorption and ^{13}C NMR spectral data. In addition, we report the crystal structure of $(+)^{CD}_{550}$-*u-fac*-$[Co(ida)(mdien)]\cdot(+)^{CD}_{575}$-$[Co(ox)_2(en)]\cdot 6H_2O$ and will discuss on the relationship between the CD spectral behaviors of the u-fac isomers and the absolute configurations.

Experimental

Ligands. Iminodiacetic acid (H_2ida) and 3-azapentane-1,5-diamine (dien) were obtained commercially from Wako Pure Chemical Industries, Ltd. and used without further purification. *N*-Methyliminodiacetic acid[12] (H_2mida) and 3-methyl-3-azapentane-1,5-diamine trihydrochloride[13] (mdien·3HCl) were synthesized by the methods described in the literatures.

Preparation of Complexes. Three Isomers (mer, u-fac, and s-fac) of $[Co(mida)(mdien)]^+$: An aqueous solution containing 4.5 g (0.02 mol) of mdien·3HCl in 100 cm^3 of water was passed through a short Dowex 1×8 (OH^- form) column. The column was washed with ca. 100 cm^3 of water. Three grams (0.02 mol) of H_2mida and 4.8 g (0.02 mol) of $CoCl_2\cdot 6H_2O$ were added to the combined solution of eluate and washings, and the resulting solution was adjusted to pH 6 with 1 mol dm^{-3} NaOH solution. Lead dioxide (15 g, excess) was added into the solution with stirring. After stirring for 30 min at 50 °C, the solution was filtered to remove insoluble materials. The filtrate was poured onto an SP-Sephadex C-25 column (ϕ4.7 cm×50 cm, K^+ form). The adsorbed band, which was not eluted with water, was separated into two bands of purplish-red and orange colors by elution with 0.2 mol dm^{-3} KCl solution. The purplish-red band containing desired complexes was transferred into another SP-Sephadex C-25 column (ϕ4.7 cm×90 cm, K^+

form) and developed with the same eluent. The band separated into two bands of reddish-purple (first-eluted isomer: mer) and pinkish-red (a mixture of u-fac and s-fac isomers) colors. The reddish-purple band was eluted out. The pinkish-red band was transferred into another SP-Sephadex column (ϕ4.7 cm×90 cm, NH_4^+ form) and developed with 0.1 mol dm^{-3} $(NH_4)_2SO_4$ solution. The band easily separated into two bands of red (second-eluted isomer: s-fac) and purple (third-eluted isomer: u-fac) colors.

The reddish-purple eluate containing mer isomer was concentrated under reduced pressure and a large amount of methanol was added to the concentrated solution to eliminate potassium chloride. After methanolic solution was again concentrated, a crude complex was obtained by addition of methanol to the concentrated solution. The crude complex was recrystallized from a small amount of water by addition of a mixture (1:3) of methanol and ethanol. The crude crystals of the u-fac and s-fac isomers were also obtained as sulfate salts from the eluates of the red and purple bands, respectively, by the procedure similar to that described for the mer isomer above. By the use of a short QAE-Sephadex A-25 (Cl^- form) column, the sulfate salts of the u-fac and s-fac isomers were changed to the chloride salts, which were recrystallized from a small amount of water by addition of methanol. The formation molar ratio of the three isomers was mer:u-fac:s-fac=3:7:90. Found for the mer isomer: C, 30.44; H, 6.80; N, 14.31%. Calcd for [Co(mida)(mdien)]Cl·2H_2O=$C_{10}H_{26}N_4O_6ClCo$: C, 30.58; H, 6.67; N, 14.27%. Found for the u-fac isomer: C, 29.26; H, 6.84; N, 13.56%. Calcd for [Co(mida)(mdien)]Cl·3H_2O=$C_{10}H_{28}N_4O_7ClCo$: C, 29.24; H, 6.87; N, 13.64%. Found for the s-fac isomer: C, 31.30; H, 6.61; N, 14.75%. Calcd for [Co(mida)(mdien)]Cl·1.5H_2O=$C_{10}H_{25}N_4O_{5.5}ClCo$: C, 31.30; H, 6.57; N, 14.60%.

Three Isomers of [Co(ida)(mdien)]$^+$: The mer, u-fac, and s-fac isomers of this complex were obtained by the same method as that used for [Co(mida)(mdien)]Cl, except that the crystals of the u-fac isomer were obtained by converting the chloride salt to the bromide salt. The formation molar ratio was mer:u-fac:s-fac=4:42:54. Found for the mer isomer: C, 28.71; H, 6.33; N, 15.02%. Calcd for [Co(ida)(mdien)]Cl·2H_2O=$C_9H_{24}N_4O_6ClCo$: C, 28.54; H, 6.39; N, 14.79%. Found for the u-fac isomer: C, 26.52; H, 5.57; N, 13.78%. Calcd for [Co(ida)(mdien)]Br·H_2O=$C_9H_{22}N_4O_5BrCo$: C, 26.68; H, 5.47; N, 13.83%. Found for the s-fac isomer: C, 29.28; H, 6.28; N, 15.02%. Calcd for [Co(ida)(mdien)]Cl·1.5H_2O=$C_9H_{23}N_4O_{5.5}ClCo$: C, 29.24; H, 6.27; N, 15.16%.

Three Isomers of [Co(mida)(dien)]$^+$ and [Co(ida)(dien)]$^+$: Two isomers (mer and s-fac) of [Co(mida)(dien)]$^+$ and three isomers of [Co(ida)(dien)]$^+$ were already reported, but there is no report for the u-fac isomer of [Co(mida)(dien)]$^+$. In the present work all the three isomers of these complexes were obtained by the same method as that described above. The formation molar ratios were mer:u-fac:s-fac=23:18:59 for [Co(mida)(dien)]$^+$ and 24:46:30 for [Co(ida)(dien)]$^+$. Found for the newly prepared u-fac isomer: C, 29.34; H, 6.04; N, 15.03%. Calcd for [Co(mida)(dien)]Cl·1.5H_2O=$C_9H_{23}N_4O_{5.5}ClCo$: C, 29.24; H, 6.27; N, 15.16%. The chemical formulas of the other isomers were as follows: *mer*-[Co(mida)(dien)]Cl·1.5H_2O, *s-fac*-[Co(mida)(dien)]Cl, *mer*-[Co(ida)(dien)]Cl·H_2O, and *u-fac*- and *s-fac*-[Co(ida)(dien)]Cl·0.5H_2O.

Optical Resolution. The racemic u-fac isomers of the four complexes were optically resolved on an SP-Sephadex column using K_2Sb_2(*d*-tart)$_2$ aqueous solution as an eluent.

(+)$^{CD}_{564}$-*u-fac*-[Co(mida)(mdien)]Cl·3H_2O: A solution containing ca. 1.0 g of racemic *u-fac*-[Co(mida)(mdien)]Cl·3H_2O in a small amount of water was poured onto an SP-Sephadex C-25 column (ϕ4.7 cm×90 cm, K^+ form). The adsorbed band was developed with a 0.05 mol dm^{-3} K_2Sb_2(*d*-tart)$_2$ solution. After the band had been separated completely into two, each band was eluted out with a 0.1 mol dm^{-3} KCl solution. Each eluate was concentrated under reduced pressure and then ethanol was added to the concentrated solution. Potassium chloride which deposited out was removed by filtration and the filtrate was concentrated to a small volume. Ethanol was added to the concentrated solution and the ethanolic solution was kept in a refrigerator overnight. Violet crystals which deposited were collected by filtration and recrystallized from water by addition of ethanol. The (+)$^{CD}_{564}$ and (−)$^{CD}_{564}$ isomers were obtained from the front and rear eluates, respectively. Found for the (+)$^{CD}_{564}$ isomer: C, 29.37; H, 6.69; N, 13.64%. Calcd for [Co(mida)(mdien)]Cl·3H_2O=$C_{10}H_{28}N_4O_7ClCo$: C, 29.24; H, 6.87; N, 13.64%.

(+)$^{CD}_{550}$-*u-fac*-[Co(ida)(mdien)]Cl·1.5H_2O, (+)$^{CD}_{544}$-*u-fac*-[Co(mida)(dien)]Cl·0.5H_2O, and (+)$^{CD}_{538}$-*u-fac*-[Co(ida)(dien)]Cl·2H_2O: The racemates were also optically resolved in the same manner as that described for [Co(mida)(mdien)]$^+$. Found for the early eluted (+)$^{CD}_{550}$ isomer: C, 29.34; H, 6.25; N, 15.13%. Calcd for [Co(ida)(mdien)]Cl·1.5H_2O=$C_9H_{23}N_4O_{5.5}ClCo$: C, 29.24; H, 6.27; N, 15.16%. Found for the late eluted (+)$^{CD}_{544}$ isomer: C, 31.08; H, 6.05; N, 16.05%. Calcd for [Co(mida)(dien)]Cl·0.5H_2O=$C_9H_{21}N_4O_{4.5}ClCo$: C, 30.74; H, 6.02; N, 15.93%. Found for the late eluted (+)$^{CD}_{538}$ isomer: C, 26.59; H, 6.05; N, 15.49%. Calcd for [Co(ida)(dien)]Cl·2H_2O=$C_8H_{22}N_4O_6ClCo$: C, 26.35; H, 6.08; N, 15.36%. Previously, Okamoto et al. isolated this isomer as a monohydrate.[14]

X-Ray Analysis of (+)$^{CD}_{550}$-*u-fac*-[Co(ida)(mdien)]·(+)$^{CD}_{575}$-[Co(ox)$_2$(en)]·6H_2O. This diastereomer was prepared by adding methanol to the solution obtained by passing an aqueous solution of (+)$^{CD}_{550}$-*u-fac*-[Co(ida)(mdien)]Cl through a short QAE-Sephadex column of (+)$^{CD}_{575}$-[Co(ox)$_2$(en)]$^-$ form.

Unit cell parameters and intensity data for the single crystal (ca. 0.09×0.22×0.40 mm^3) were measured on a Rigakudenki four-circle diffractometer (AFC-5) with graphite-monochromatized Mo $K\alpha$ radiation. The unit cell parameters were determined by a least-squares refinement based on 25 reflections ($20<2\theta<30°$). Systematic absences led to the space group $P2_1$. Crystal Data: $Co_2C_{15}H_{40}N_6O_{18}$, M.W.=710.4, monoclinic, space group $P2_1$, a=15.793(6), b=12.855(3), c=7.070(2) Å, β=96.80(5)°, V=1425.3(8) Å^3, D_x=1.655 g cm^{-3}, D_m=1.66(1) g cm^{-3}, Z=2, and μ(Mo $K\alpha$)=1.303 mm^{-1}.

The intensity data were collected by the ω—2θ scan technique up to 2θ=60° with scan rate of 3° min^{-1}. The intensity data were converted to the Fo data in the usual manner. Absorption corrections were not applied. A total of 3864 independent reflections with $|F_o|>3\sigma(|F_o|)$ of the measured 4664 reflections were considered as 'observed' and used for the structure analysis.

The position of one cobalt atom was determined from a three-dimensional Patterson function. The difference-Fourier maps based on the cobalt position revealed the other cobalt position and then all non-hydrogen atoms. The structure was refined by a full-matrix least-squares refinement using the positional parameters, the anisotropic thermal parameters of the non-hydrogen atoms of the complex ions, and the isotropic thermal parameters of the non-hydrogen atoms of the water molecules (program RFINE by L. W. Finger[15] was used). The neutral atomic scattering factors for all the non-hydrogen atoms were taken from the literatures.[16,17] The final residual values were R=0.061 and R_w=0.066, respectively. We attempted to determine the absolute configurations of the complex ions by an anomalous-scattering technique. When the refinements were carried out by use of a set of the atomic parameters containing the Λ configuration of the complex ions (*Λ*- or *ΔΔΛ-u-fac*-[Co(ida)(mdien)]+ and *Λ*-[Co(ox)$_2$(en)]$^-$), the residual values converged to R=0.058 and R_w=0.059, respectively. On the contrary, the refinements in the enantiomeric atomic parameters (*Δ*- or *ΔΔΔ-u-fac*-[Co(ida)(mdien)]+ and *Δ*-[Co(ox)$_2$(en)]$^-$) resulted in the residual values of R=0.060 and R_w=0.062, respectively. These facts suggest that the former is probably the correct choice. This absolute configuration coincides with the result that $(+)^{CD}_{575}$-[Co(ox)$_2$(en)]$^-$, which was used as an internal reference, has been assigned to the Λ configuration based on the CD spectral behavior.[18]

The final positional parameters are listed in Table 1. A list of structure factors (Table A) and anisotropic thermal parameters of non-hydrogen atoms of the complex ions (Table B) are kept at the Chemical Society of Japan as Document No. 8745.

Measurements. The X-ray analysis calculations were carried out on a FACOM M-382 computer at the University of Tsukuba. The absorption and CD spectra were measured by a Hitachi 557-type spectrometer and a JASCO J-22 spectropolarimeter, respectively. The ^{13}C NMR spectra at 25 MHz were recorded on a JEOL JNM-FX 100 spectrometer. The peak positions were measured relative to internal dioxane (δ=67.40).

Results and Discussion

Formation Ratio of the Geometrical Isomers. In the previous studies concerning the reactivity of the [Co(ida)$_2$]$^-$ (and [Co(ida)(mida)]$^-$)[8] and [Co(mida)$_2$]$^-$[7] complexes, it was revealed that the mer isomer of the first complex easily isomerizes to u-fac and s-fac isomers in a basic aqueous solution and that the u-fac isomer of the third complex decomposes accompanying reduction of Co(III) to Co(II).

In the bis(terdentate) complexes, the formation ratio of the possible geometrical isomers varied largely with the stereochemistry of the chelate rings and reaction conditions (pH, temperature, etc.). The preparative reaction under basic conditions or using a catalyst such as activated carbon restricted the formation of less stable isomers.[1] As described in the Experimental section, however, the preparation of the present complexes under weakly acidic conditions provided all of the possible isomers. The formation ratios of the three isomers were mer:u-fac:s-fac=24:46:30 for [Co(ida)(dien)]+, 23:18:59 for [Co(mida)(dien)]+, 4:42:54 for [Co(ida)(mdien)]+, 3:7:90 for [Co(mida)-

Table 1. Position and Thermal Parameters (with e.s.d.'s)

Atom	X	Y	Z	B_{eq}/Å^2 a)	Atom	X	Y	Z	B_{eq}/Å^2 a)
CoA	0.08995(5)	0.25000	0.1395(1)	1.70	OB1	0.2804(3)	0.4286(4)	0.7990(7)	2.97
NA1	−0.0205(3)	0.1759(4)	0.1314(7)	1.82	OB2	0.3308(4)	0.2654(5)	0.8152(9)	4.88
NA2	0.1984(3)	0.3144(5)	0.1031(8)	2.45	OB3	0.4292(3)	0.5057(5)	0.7596(7)	3.19
NA3	0.1507(3)	0.1910(5)	0.3798(7)	2.39	OB4	0.4868(4)	0.3467(5)	0.7375(10)	5.17
NA4	0.0578(4)	0.3648(5)	0.2939(8)	2.50	OB5	0.3008(3)	0.5415(4)	0.4823(6)	2.69
OA1	0.1261(3)	0.1373(4)	−0.0049(6)	2.42	OB6	0.1912(3)	0.5350(4)	0.2538(7)	3.05
OA2	0.0853(3)	−0.0109(4)	−0.1448(7)	3.05	OB7	0.2082(3)	0.6160(4)	0.7294(6)	2.94
OA3	0.0384(3)	0.3166(4)	−0.0841(6)	2.26	OB8	0.0913(3)	0.6147(5)	0.5211(7)	3.71
OA4	−0.0882(3)	0.3532(5)	−0.2472(7)	3.53	CB1	0.3405(5)	0.3608(6)	0.7946(11)	3.38
CA1	0.0718(4)	0.0672(5)	−0.0475(8)	2.12	CB2	0.4262(5)	0.4036(6)	0.7599(11)	3.17
CA2	−0.0126(4)	0.0738(6)	0.0335(10)	2.74	CB3	0.2243(4)	0.5562(6)	0·4179(9)	2.38
CA3	−0.0866(4)	0.2427(6)	0.0241(9)	2.43	CB4	0.1665(4)	0.5982(5)	0.5642(9)	2.20
CA4	−0.0432(4)	0.3085(5)	−0.1167(9)	2.15	CB5	0.3512(7)	0.7071(9)	1.0516(15)	5.79
CA5	0.2674(4)	0.2872(7)	0.2597(11)	3.44	CB6	0.4075(6)	0.7413(9)	0.8985(14)	5.20
CA6	0.2438(4)	0.1838(7)	0.3511(11)	3.18	OW1	0.4674(6)	0.4672(9)	0.2364(14)	10.19b)
CA7	0.1221(5)	0.0859(7)	0.4286(12)	4.02	OW2	0.2518(5)	0.8461(7)	0.4442(11)	6.92b)
CA8	0.1380(5)	0.2683(7)	0.5377(10)	3.89	OW3	0.2480(5)	0.9294(7)	0.8046(11)	7.02b)
CA9	0.0580(5)	0.3280(7)	0.4912(10)	3.60	OW4	0.3810(6)	0.0632(10)	0.9303(15)	10.60b)
CoB	0.32075(6)	0.5644(1)	0.7523(1)	2.37	OW5	0.4765(6)	0.1783(10)	0.4669(16)	10.39b)
NB1	0.3351(4)	0.5930(5)	1.0221(8)	3.31	OW6	0.3804(7)	0.9808(10)	0.3219(16)	12.04b)
NB2	0.3691(4)	0.6995(5)	0.7142(10)	3.52					

a) $B_{eq}=8\pi^2(U_{12}+U_{22}+U_{33})/3$. b) Isotropic temperature factor.

(mdien)]+. When activated carbon was used as a catalyst,[1] the ratios for the first and second complexes (12:29:59 for [Co(ida)(dien)]+ and 20:0:80 for [Co(mida)(dien)]+) differ from the above ratios. These differences suggest that the formation ratios of the isomers depend not only on a thermodynamic factor but also largely on a kinetic factor. The small ratio of the u-fac isomer in [Co(mida)(mdien)]+ is surely attributed to a strong intramolecular repulsion between the coordinating mida and mdien ligands. However, the small ratios of the mer isomers in [Co(ida)(mdien)]+ and [Co(mida)(mdien)]+ can not be explained only by such the repulsion.

Geometrical Structure. Previously, the structures of three geometrical isomers of [Co(ida)(dien)]+ have been assigned on the basis of the visible absorption and ^{1}H NMR spectral data.[1] Figure 2 shows the absorption spectra of the mer, u-fac, and s-fac isomers of [Co(ida)(dien)]+ and the newly isolated isomers of [Co(mida)(mdien)]+, and their spectral data are summarized in Table 2, together with those of [Co(mida)(dien)]+ and [Co(ida)(mdien)]+.

For the four complexes, the geometrical isomers which were obtained in the same elution order on a column-chromatographic separation showed quite similar spectral behaviors to one another in the visible absorption region. Such spectral behaviors suggest that the isomers correspond to one another in geometry. All the first-eluted isomers exhibited the first bands with a shoulder (or broad band) in the shorter wavelength side (Fig. 2), which is generally observed for the *trans(O)*-[Co(N)$_4$(O)$_2$]-type complex.[19] This indicates that the structure of these isomers may be assigned to mer.

The structural assignments for the second- and third-eluted isomers of the new complexes can be made on the basis of their ^{13}C NMR data. Figure 3 shows a stick diagram of the ^{13}C resonance position for all the isomers. The most simple resonance patterns of the third-eluted isomers are due to two equivalent chelate rings in each of terdentate ligands and indicate that the third-eluted isomers take the s-fac structure having a mirror plane.

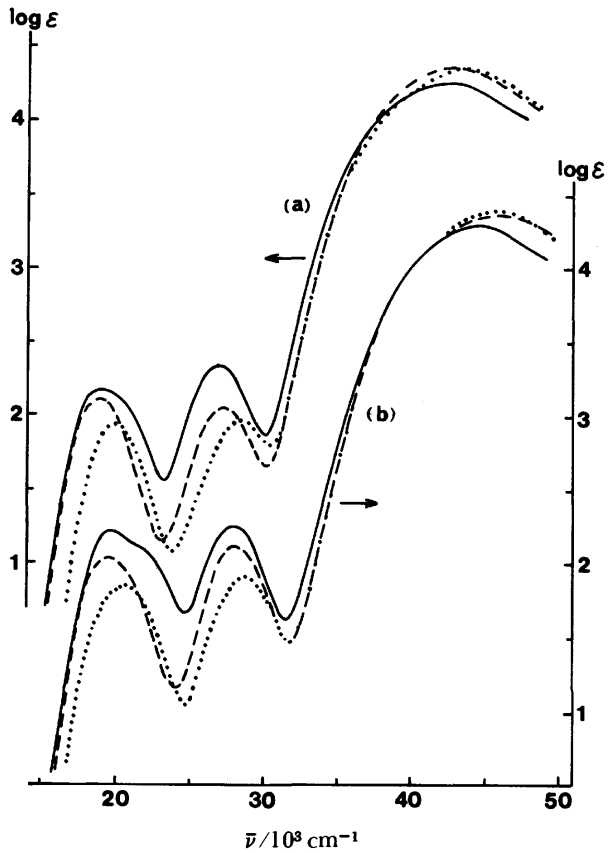

Fig. 2. Absorption spectra of the first-eluted (mer) ——, second-eluted (u-fac) ------, and third-eluted (s-fac) ····· isomers of (a) [Co(mida)(mdien)]+ and (b) [Co(ida)(dien)]+.

Table 2. Absorption Spectral Data of the [Co(L$_1$)(L$_2$)]+-Type Complexes

Complex	Structure	First band[a]	Second band[a]	CT band[a]
[Co(ida)(dien)]+	mer	19.65 (2.22)	27.93 (2.25)	44.25 (4.29)
		sh. 21.8 (2.08)		
	u-fac	19.57 (2.03)	28.17 (2.11)	46.08 (4.35)
	s-fac	20.70 (1.84)	28.82 (1.90)	45.66 (4.38)
[Co(mida)(dien)]+	mer	19.53 (2.20)	27.25 (2.33)	43.67 (4.30)
	u-fac	19.46 (2.03)	28.09 (2.02)	44.25 (4.36)
	s-fac	20.41 (1.81)	28.57 (1.87)	44.64 (4.35)
[Co(ida)(mdien)]+	mer	19.16 (2.26)	27.55 (2.32)	43.48 (4.30)
	u-fac	19.23 (2.03)	27.70 (2.11)	44.44 (4.32)
	s-fac	20.24 (1.97)	28.17 (2.00)	44.64 (4.37)
[Co(mida)(mdien)]+	mer	18.87 (2.19)	26.88 (2.34)	42.55 (4.24)
	u-fac	18.90 (2.11)	27.32 (2.06)	42.55 (4.35)
	s-fac	19.96 (1.95)	28.33 (1.98)	43.48 (4.34)

a) Wave numbers and log ε values (in parentheses) are given in 10^3 cm^{-1} and mol^{-1} dm^3 cm^{-1}, respectively. sh) Shoulder band.

The single peaks observed for the third-eluted isomers (s-fac), however, appear as doublet peaks in the second-eluted isomers except for the resonance peaks of methyl carbons. These doublet peaks for the second-eluted isomers indicate that the two chelate rings of each terdentate ligand are nonequivalent, as expected for the unsymmetrical (u-fac) structure. This structure was confirmed by X-ray crystal analysis (vide post).

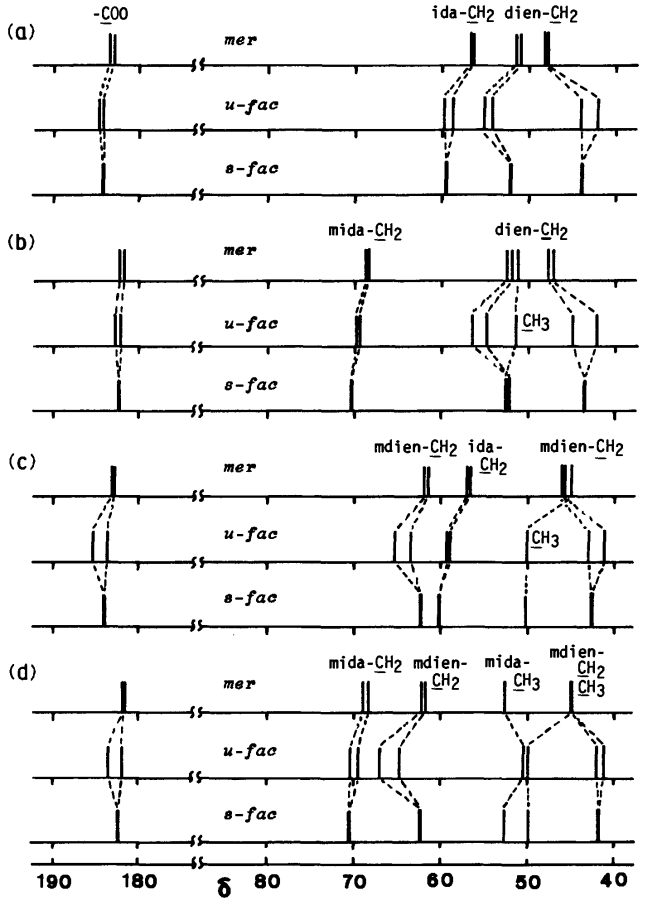

Fig. 3. ^{13}C NMR spectral patterns of the first-eluted (mer), second-eluted (u-fac), and third-eluted (s-fac) isomers of $[Co(L_1)(L_2)]^+$-type complexes: (a) [Co(ida)(dien)]+, (b) [Co(mida)(dien)]+, (c) [Co(ida)(mdien)]+, and (d) [Co(mida)(mdien)]+.

Crystal Structure of $(+)^{CD}_{550}$-*u-fac*-[Co(ida)(mdien)]·$(+)^{CD}_{575}$-[Co(ox)$_2$(en)]·6H$_2$O. Perspective drawings of the complex cation and anion obtained are given in Figs. 4 and 5 respectively, together with numbering scheme. The bond lengths and angles with their standard deviations are summarized in Table 3. In the complex cation (Fig. 4), the cobalt atom is surrounded octahedrally by two cis oxygen atoms and four nitrogen ones. Both of the ida and mdien ligands, which act as terdentate, take a facial form, and the tertiary amine, NA3, in the mdien ligand is located on the cis position of the nitrogen atom, NA1, in the ida one. As a result, the complex cation, [Co(ida)(mdien)]+, takes an unsymmetric facial configuration, u-fac. The absolute configuration of the complex anion, $(+)^{CD}_{575}$-[Co(ox)$_2$(en)]$^-$ (Fig. 5), was determined as Λ (see Experimental section) and this result confirms the suggestion made on the basis of the CD spectra.[18] Therefore, the absolute configuration of $(+)^{CD}_{550}$-*u-fac*-[Co(ida)(mdien)]+ can be assigned to ΛΔΛ (net Λ) configuration based on that of $(+)^{CD}_{575}$·*Λ*-[Co(ox)$_2$(en)]$^-$. This assignment for the $(+)^{CD}_{550}$ isomer coincides with that made by the ^1H NMR method using stereospecific deuteration.[20]

In the complex cation, the fused five-membered chelate rings in the ida and mdien ligands are not symmetrically equivalent. The ethylenediamine chelate ring in the mdien ligand, NA2-CA5-CA6-NA3, takes similar asymmetric gauche form with λ conformation (displacement from the NA2-CoA-NA3 plane: CA5=0.027 and CA6=0.640 Å) to those of *s-fac*- and *u-fac*-[Co(dien)$_2$]$^{3+}$.[21,22] The other chelate ring, NA3-CA8-CA9-NA4, takes the unusual form with λ conformation (displacement from the NA3-CoA-NA4

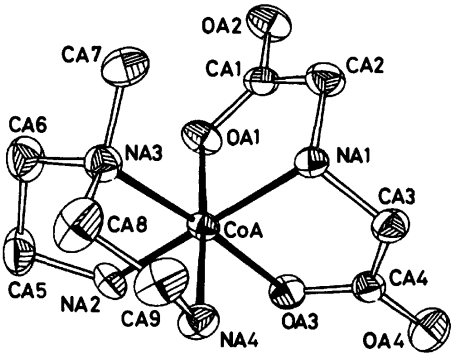

Fig. 4. Perspective view of $(+)^{CD}_{550}$-*u-fac*-[Co(ida)(mdien)]+ ion.

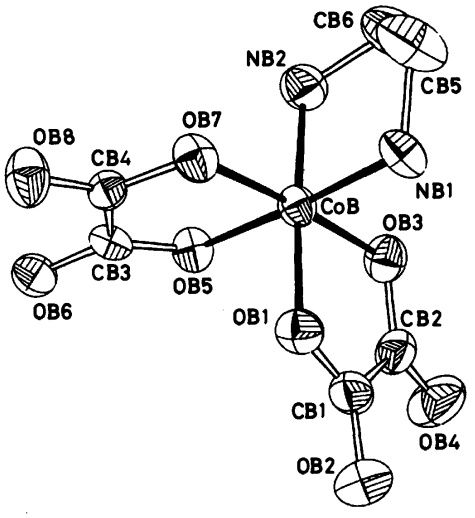

Fig. 5. Perspective view of $(+)^{CD}_{575}$-[Co(ox)$_2$(en)]$^-$ ion.

Table 3. Interatomic Distances and Bond Angles (with e.s.d.'s)

(a) Bond distance (l/Å)

$[Co(ida)(mdien)]^+$:			
CoA-NA1	1.983(5)	CoA-NA2	1.947(6)
CoA-NA3	1.999(5)	CoA-NA4	1.939(6)
CoA-OA1	1.899(5)	CoA-OA3	1.895(4)
NA1-CA2	1.495(9)	NA2-CA5	1.500(9)
NA3-CA6	1.511(9)	NA3-CA7	1.479(11)
NA3-CA8	1.525(10)	NA4-CA9	1.473(9)
OA1-CA1	1.257(8)	OA2-CA1	1.250(8)
OA3-CA4	1.286(8)	OA4-CA4	1.237(8)
CA1-CA2	1.514(9)	CA3-CA4	1.528(10)
CA5-CA6	1.543(12)	CA8-CA9	1.481(12)
$[Co(ox)_2(en)]^-$:			
CoB-NB1	1.930(6)	CoB-NB2	1.929(7)
CoB-OB1	1.901(5)	CoB-OB3	1.867(5)
CoB-OB5	1.920(4)	CoB-OB7	1.887(5)
NB1-CB5	1.499(13)	NB2-CB6	1.472(12)
OB1-CB1	1.292(10)	OB2-CB1	1.246(10)
OB3-CB2	1.314(10)	OB4-CB2	1.229(10)
OB5-CB3	1.253(8)	OB6-CB3	1.245(8)
OB7-CB4	1.291(8)	OB8-CB4	1.210(8)
CB1-CB2	1.508(12)	CB3-CB4	1.555(10)
CB5-CB6	1.544(15)		

(b) Bond angle (ϕ/°)

$[Co(ida)(mdien)]^+$:			
NA1-CoA-NA2	170.2(2)	NA1-CoA-NA3	100.1(2)
NA1-CoA-NA4	95.4(2)	NA1-CoA-OA1	86.4(2)
NA1-CoA-OA3	84.4(2)	NA2-CoA-NA3	86.1(2)
NA2-CoA-NA4	92.5(3)	NA2-CoA-OA1	85.9(2)
NA2-CoA-OA3	89.7(2)	NA3-CoA-NA4	86.7(2)
NA3-CoA-OA1	91.3(2)	NA3-CoA-OA3	174.9(2)
NA4-CoA-OA1	177.5(2)	NA4-CoA-OA3	90.6(2)
OA1-CoA-OA3	91.3(2)	CoA-NA1-CA2	108.3(4)
CoA-NA1-CA3	107.4(4)	CA2-NA1-CA3	111.2(5)
CoA-NA2-CA5	112.1(5)	CoA-NA3-CA6	106.6(4)
CoA-NA3-CA7	114.6(4)	CoA-NA3-CA8	106.5(4)
CA6-NA3-CA7	107.7(6)	CA6-NA3-CA8	110.7(5)
CA7-NA3-CA8	110.7(6)	CoA-NA4-CA9	108.5(5)
CoA-OA1-CA1	115.8(4)	CoA-OA3-CA4	115.8(4)
OA1-CA1-OA2	123.5(6)	OA1-CA1-CA2	118.4(6)
OA2-CA1-CA2	118.0(6)	NA1-CA2-CA1	110.5(6)
NA1-CA3-CA4	108.1(5)	OA3-CA4-OA4	124.8(6)
OA3-CA4-CA3	116.4(5)	OA4-CA4-CA3	118.7(6)
NA2-CA5-CA6	108.7(6)	NA3-CA6-CA5	106.8(6)
NA3-CA8-CA9	111.0(6)	NA4-CA9-CA8	106.4(6)
$[Co(ox)_2(en)]^-$:			
NB1-CoB-NB2	87.9(3)	NB1-CoB-OB1	90.3(3)
NB1-CoB-OB3	92.8(3)	NB1-CoB-OB5	176.6(2)
NB1-CoB-OB7	91.0(2)	NB2-CoB-OB1	176.1(2)
NB2-CoB-OB3	89.5(3)	NB2-CoB-OB5	91.2(3)
NB2-CoB-OB7	93.2(3)	OB1-CoB-OB3	87.1(2)
OB1-CoB-OB5	90.7(2)	OB1-CoB-OB7	90.3(2)
OB3-CoB-OB5	90.5(2)	OB3-CoB-OB7	175.4(2)
OB5-CoB-OB7	85.8(2)	CoB-NB1-CB5	108.8(5)
CoB-NB2-CB6	109.5(6)	CoB-OB1-CB1	110.7(5)
CoB-OB3-CB2	111.8(5)	CoB-OB5-CB3	112.1(4)
CoB-OB7-CB4	112.9(4)	OB1-CB1-OB2	124.1(8)
OB1-CB1-CB2	115.7(7)	OB2-CB1-CB2	120.2(8)
OB3-CB2-OB4	124.4(7)	OB3-CB2-CB1	113.5(7)
OB4-CB2-CB1	122.1(8)	OB5-CB3-OB6	125.9(6)
OB5-CB3-CB4	115.3(5)	OB6-CB3-CB4	118.7(6)
OB7-CB4-OB8	125.2(6)	OB7-CB4-CB3	112.8(5)
OB8-CB4-CB3	122.0(6)	NB1-CB5-CB6	106.5(8)
NB2-CB6-CB5	107.8(8)		

plane: CA8=−0.019 and CA9=0.599 Å) (Fig. 4). This conformation displacement seems to arise from the result that the NA3-NA4 chelate ring and the amine group, NA1, in the ida ligand repel each other. Similarly, the chelate ring, NA1-CA3-CA4-OA3, in the ida ligand takes an envelope form with λ conformation (displacement from the NA1-CoA-OA3 plane: CA3=−0.591 and CA4=−0.318 Å) similar to those of *u-fac*-$[Co(ida)_2]^-$.[23] While, the other chelate ring, OA1-CA1-CA2-NA1, takes nearly planar (displacement from the OA1-CoA-NA1 plane: CA1=−0.014 and CA2=0.097 Å). This planarity seems to depend on the steric repulsion between the OA1-NA1 chelate ring and the methyl group in the mdien ligand. In the complex anion, the ox ligands take similar conformation to those of $[Co(ox)_3]^{3-}$[24] and $[Co(ox)(en)_2]^+$.[25,26] The ethylenediamine takes a reasonable gauche form with δ(lel) conformation.[25-27]

The bond lengths and angles of the complex cation and anion are similar to those of the cobalt(III) complexes with the ida, dien, ox, and en ligands.[22-27] In the complex cation, the Co-N (tertiary) bond of 1.999(5) Å in the mdien ligand is considerably longer than the Co-N (terminal) bond of 1.943(6) Å, and this difference is more remarkable than those in the *u-fac*-$[Co(dien)_2]^{3+}$ [Co-N (secondary) 1.971 and Co-N (terminal) 1.961 Å].[22] The Co-N bond, 1.983(5) Å, in the ida ligand is longer than those of *u-fac*-$[Co(ida)_2]^-$ [1.946(4) and 1.936(4) Å].[23] These results seem to depend mainly on the arrangement of the terdentate ligands around the cobalt atom.

Absolute Configuration and CD Spectra of the u-fac Isomers. The CD spectral curves of the u-fac isomers in this work are shown in Fig. 6 and their CD data are summarized in Table 4. All the optically active u-fac isomers isolated from the later eluates on the column chromatographic resolution show similar CD patterns to one another in the first absorption band region. Since the absolute configuration of $(+)^{CD}_{550}$-*u-fac*-$[Co(ida)(mdien)]^+$ is ΛΔΛ (net Λ), we assign the remaining three u-fac isomers, which show the same

Table 4. CD Spectral Data of the $[Co(L_1)(L_2)]^+$-Type Complexes

Complex	First band region[a)]	Second band region[a)]	CT band region[a)]
$(+)^{CD}_{538}$-*u-fac*-[Co(ida)(dien)]+	18.59(+2.014)	sh 26.5 (+0.282)	43.86(−6.405)
	21.05(−1.472)	28.49(+0.398)	
$(+)^{CD}_{544}$-*u-fac*-[Co(mida)(dien)]+	18.38(+2.441)	sh 26.0 (+0.322)	38.46(+0.560)
	20.62(−1.757)	28.17(+0.425)	43.67(−10.27)
$(+)^{CD}_{550}$-*u-fac*-[Co(ida)(mdien)]+	18.18(+1.804)	25.91(+0.417)	37.59(+0.145)
	20.45(−0.946)	28.25(+0.419)	43.29(−2.138)
			46.95(+3.592)
$(+)^{CD}_{564}$-*u-fac*-[Co(mida)(mdien)]+	17.70(+1.658)	27.70(+0.507)	41.67(−7.334)
	19.88(−1.280)		45.87(+9.825)

a) Wave number and $\Delta\varepsilon$ values (in parentheses) are given in $10^3\,cm^{-1}$ and $mol^{-1}\,dm^3\,cm^{-1}$, respectively. sh) Shoulder band.

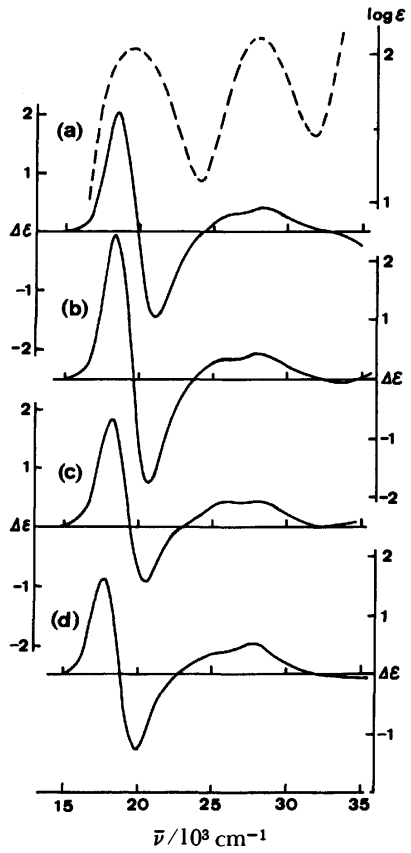

Fig. 6. Absorption and CD spectra of the u-fac isomers: (a) $(+)^{CD}_{538}$-[Co(ida)(dien)]+, (b) $(+)^{CD}_{544}$-[Co(mida)(dien)]+, (c) $(+)^{CD}_{550}$-[Co(ida)(mdien)]+, and (d) $(+)^{CD}_{564}$-[Co(mida)(mdien)]+.

CD pattern as that of $(+)^{CD}_{550}$-*u-fac*-[Co(ida)(mdien)]+, to be the ΛΔΛ configuration.

For the cobalt(III) complexes with bidentate ligands such as ethylenediamine, glycinate, oxalate, and so on, their CD spectral patterns in the first absorption band region have successfully been related with their absolute configurations.[28] However, the CD spectral behaviors of the cobalt(III) complexes with linear terdentate-*N,N,N*, -*N,N,O*, and -*O,N,O* ligands differ significantly from those of the cobalt(III) complexes with the bidentate one. In other words, the cobalt(III) complexes with the terdentate ligands, which take the same absolute configuration (for example, ΛΔΛ in this case), exhibit similar CD pattern in the first absorption band region, in spite of a difference in the type of chromophore. For example, $(+)_{589}$-*u-fac*-[Co(dien)$_2$]$^{3+}$ ([Co(N)$_6$]),[22] $(+)^{CD}_{514}$-*fac*(N_t)*cis*(N_c)- and $(+)^{CD}_{527}$-*mer*(N_t)*cis*(N_c)-[Co(edma)(dien)]$^{2+}$ ([Co(N)$_5$(O)]),[29] $(+)^{CD}_{543}$-*trans*(*O*)- and $(+)^{CD}_{534}$-*C*$_1$-*cis*(*O*)-[Co(edma)$_2$]$^+$ ([Co(N)$_4$(O)$_2$]),[9] $(+)^{CD}_{572}$-*mer*(*O*)*cis*(N_c)- and $(+)^{CD}_{565}$-*fac*(*O*)-[Co(ida)(edma)] ([Co(N)$_3$(O)$_3$]),[11] and $(-)_{546}$-*u-fac*-[Co(ida)$_2$]$^-$ ([Co(N)$_2$(O)$_4$]),[2,30] which have been determined to be the ΛΔΛ configuration, exhibited in common a positive and a negative CD bands from the lower energy in the first absorption band region, as in the case of the present ΛΔΛ-u-fac isomers. These facts suggest that the empirical treatment[28] applied favorably for the cobalt(III) complexes with the bidentate ligands can not be directly applied for those with the terdentate ones. In order to discuss these CD spectral behaviors, however, more data will be needed.

References

1) J. I. Legg and D. W. Cooke, *Inorg. Chem.*, **5**, 594 (1966).
2) Y. Yoshikawa, A. Kondo, and K. Yamasaki, *Inorg. Nucl. Chem. Lett.*, **12**, 351 (1976).
3) N. Koine, T. Tanigaki, J. Hidaka, and Y. Shimura, *Chem. Lett.*, **1980**, 871.
4) K. Gailey, K. Igi, and B. E. Douglas, *J. Coord. Chem.*, **5**, 171 (1976).
5) T. Kawamoto, T. F. Maruyama, T. Yasui, K. Okamoto, J. Hidaka, and H. Einaga, *Bull. Chem. Soc. Jpn.*, **59**, 2393 (1986).
6) T. Yasui, H. Kawaguchi, N. Koine, and T. Ama, *Bull. Chem. Soc. Jpn.*, **56**, 127 (1983).
7) T. Ama, H. Kawaguchi, and T. Yasui, *Chem. Lett.*, **1981**, 323.
8) H. Kawaguchi, T. Ama, and T. Yasui, *Bull. Chem. Soc. Jpn.*, **57**, 2422 (1984).

9) T. Ama, H. Kawaguchi, T. Yasui, K. Matsumoto, and S. Ooi, *Bull. Chem. Soc. Jpn.*, **58**, 2561 (1985).
10) T. Ama, H. Kawaguchi, and T. Yasui, *Bull. Chem. Soc. Jpn.*, **59**, 1471 (1986).
11) T. Ama, R. Niiyama, H. Kawaguchi, and T. Yasui, *Bull. Chem. Soc. Jpn.*, **60**, 119 (1987).
12) M. Mori, M. Shibata, E. Kyuno, and F. Maruyama, *Bull. Chem. Soc. Jpn.*, **35**, 75 (1962).
13) M. Kojima, M. Iwagaki, Y. Yoshikawa, and J. Fujita, *Bull. Chem. Soc. Jpn.*, **50**, 3216 (1977).
14) K. Okamoto, J. Hidaka, and Y. Shimura, *Bull. Chem. Soc. Jpn.*, **48**, 2456 (1975).
15) L. W. Finger, RFINE-2, Geophysical Lab. Carnegie Institution, Washington, D. C., 1972.
16) International Tables for X-Ray Crystallography, Kynoch Press, Birmingham (1974), Vol. IV.
17) D. T. Cromer and J. B. Mann, *Acta Crystallogr., Sect. A*, **24**, 321 (1968).
18) B. E. Douglas, R. A. Haines, and J. C. Brushimiller, *Inorg. Chem.*, **2**, 1194 (1963).
19) N. Matsuoka, J. Hidaka, and Y. Shimura, *Bull. Chem. Soc. Jpn.*, **40**, 1868 (1967).
20) T. Ama, S. Kaizaki, H. Kawaguchi, and T. Yasui, *Chem. Lett.*, **1987**, 441.
21) M. Kobayashi, F. Marumo, and Y. Saito, *Acta Crystallogr., Sect. B*, **28**, 470 (1972).
22) M. Konno, F. Marumo, and Y. Saito, *Acta Crystallogr., Sect. B*, **29**, 739 (1973).
23) A. B. Corradi, C. G. Palmieri, M. Nardelli, M. A. Pellinghelli, and M. E. V. Tani, *J. Chem. Soc., Dalton Trans.*, **1973**, 655.
24) K. R. Butler and M. R. Snow, *J. Chem. Soc. A*, **1971**, 565.
25) T. Aoki, K. Matsumoto, S. Ooi, and H. Kuroya, *Bull. Chem. Soc. Jpn.*, **46**, 159 (1973).
26) K. Toriumi, S. Sato, and Y. Saito, *Acta Crystallogr., Sect. B*, **33**, 1378 (1977).
27) C. J. Hawkins, "Absolute Configuration of Metal Complexes," John-Wiley & Sons, Inc., New York (1971).
28) Y. Saito, "Inorganic Molecular Dissymmetry," in series of Inorganic Chemistry Concepts, Springer-Verlag, Berlin Heidelberg (1979), Vol. 4, pp. 132—148.
29) T. Yasui, T. Shikiji, N. Koine, T. Ama, and H. Kawaguchi, *Bull. Chem. Soc. Jpn.*, **60**, 595 (1987).
30) C. W. Van Saun and B. E. Douglas, *Inorg. Chem.*, **8**, 1145 (1969).

 © 1987 The Chemical Society of Japan Bull. Chem. Soc. Jpn., 60, 2581—2592 (1987)

Stereochemical Properties of Copper(II) Complexes of (*RS*)-3-Aminohexahydroazepine: Crystal and Molecular Structures of [(*R*)-3-Aminohexahydroazepine][(*S*)-3-aminohexahydroazepine]copper(II) Diperchlorate, [Cu(*R*-ahaz)(*S*-ahaz)]$(ClO_4)_2$ and Related Complexes

Masahiko Saburi,* Kazuo Miyamura, Masatoshi Morita, Sadao Yoshikawa, Sei Tsuboyama,*,† Tosio Sakurai,†† Hiroshi Yamazaki,† and Kaoru Tsuboyama†

Department of Synthetic Chemistry, Faculty of Engineering, The University of Tokyo, Hongo, Bunkyo-ku, Tokyo 113
†Institute of Physical and Chemical Research, Wako, Saitama 351-01
††Faculty of Education, Shinshu University, Nishinagano, Nagano 380

(Received February 9, 1987)

Orange-red copper(II) complexes of (*RS*)-3-aminohexahydroazepine (=*RS*-ahaz), Cu(*RS*-ahaz)$_2X_2\cdot nH_2O$ (X^-=ClO_4^-, BF_4^-, NO_3^-, Br^-, I^-) were prepared, and the molecular structures of complex **1** (X^-=ClO_4^-; n=0) and complex **2** (X^-=Br^-; n=2) were determined by the single-crystal X-ray diffraction method. The complex **1** has centrosymmetry, and the complex cation in **1** involves a pair of *R*- and *S*-ahaz (*R*- and *S*-ahaz refer to (*R*)- and (*S*)-3-aminohexahydroazepine) and takes a strict four-coordination geometry, so that **1** is formulated as [Cu(*R*-ahaz)(*S*-ahaz)]$(ClO_4)_2$. The complex cation in **2** resembles closely that of **1**, and **2** can be represented as [Cu(*R*-ahaz)(*S*-ahaz)]$Br_2\cdot 2H_2O$. The other orange-red complexes of *RS*-ahaz (X^-=BF_4^-, NO_3^-, I^-) were concluded to take similar strict four-coordinated structures. Blue-violet hetero-anion complexes Cu(*RS*-ahaz)$_2$X(ClO_4) were obtained from complex **1** and LiX (X^-=Cl^-, Br^-). The crystal structure determination of Cu(*RS*-ahaz)$_2$Br(ClO_4) (=complex **3**) revealed that **3** involves a pair of enantiomeric five-coordinated cations, $[CuBr(R\text{-ahaz})_2]^+$ and $[CuBr(S\text{-ahaz})_2]^+$, in the single crystal, whereby the ligand exchange which proceeds during the transformation from **1** to **3** is indicated.

3-Aminohexahydroazepine abbreviated as ahaz is a unique chiral 1,2-diamine having C- and N-substituents which are connected to form a seven-membered monoazaheterocycle. The R- and S-enantiomers and racemic form will be indicated hereafter by *R*-ahaz, *S*-ahaz, and *RS*-ahaz, respectively.

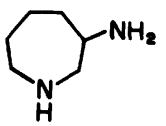

ahaz

In a previous paper we demonstrated through the X-ray crystallographic structure determination of a copper(II) complex of *S*-ahaz, [CuBr(*S*-ahaz)$_2$]ClO_4, that ahaz functions as a bidentate ligand, and that its ring carbon chain directs nearly perpendicular to the five-membered chelate ring as illustrated in Fig. 1 (I) (X^-=Br^-).[1] Evidently, the ring carbon chain of S-ahaz hangs over the central metal ion and blocks effectively the sixth coordination site from the access of a further ligand to maintain the square-pyramidal geometry of (I).

We noticed, further, that the copper(II) complex prepared from $Cu(ClO_4)_2$ and *RS*-ahaz was orange-red, while the corresponding complex with the single enantiomer (*S*-ahaz) was violet.[1] The latter was supposed to take a four-coordinated geometry such as

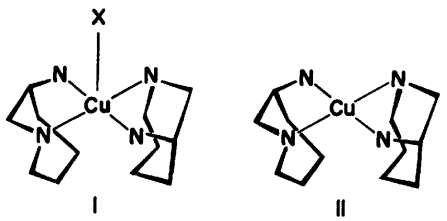

Fig. 1. Stereochemistries of copper(II) complexes of *S*-ahaz; five-coordinated $[CuX(S\text{-ahaz})_2]^+$ ion, (I) and four-coordinated $[Cu(S\text{-ahaz})_2]^{2+}$ ion, (II).

Fig. 1 (II),[1] but the structure of the former remained unsolved. To our surprise, the copper(II) complexes of *RS*-ahaz with certain anions other than perchlorate are thoroughly orange-red, which is rather exceptional color for bis(diamine)copper(II) complexes.[2] The coexistence of both *R*- and *S*-ahaz seems to be necessary to give these orange-red complexes, because no copper(II) complex of *S*-ahaz exhibits reddish color.[1] With a view to elucidate the common structural features of orange-red *RS*-ahaz copper(II) complexes, the crystal structures of Cu(*RS*-ahaz)$_2$-$(ClO_4)_2$[3] (**1**) and Cu(*RS*-ahaz)$_2Br_2\cdot 2H_2O$ (**2**) were determined by the X-ray diffraction method. This paper describes the structural characteristics of complexes **1** and **2** and other *RS*-ahaz complexes, Cu(*RS*-ahaz)$_2X_2$.

In addition we isolated the hetero-anion complexes[4] of *RS*-ahaz having the formula Cu(*RS*-ahaz)$_2$X(ClO$_4$)[3] (X$^-$=Cl$^-$, Br$^-$) from complex **1** and LiX. The crystal structure determination of Cu(*RS*-ahaz)$_2$Br(ClO$_4$) (complex **3**) revealed that a pair of enantiomeric five-coordinated cations, [CuBr(*R*-ahaz)$_2$]$^+$ and [CuBr(*S*-ahaz)$_2$]$^+$, are involved in the single crystal and suggested a possibility of interesting ligand exchange during the conversion of **1** into **3**. Besides the stereochmical features of complex **3**, the pathway for formation of five-coordinated **3** from four-coordinated **1** in solution will be discussed in the present paper.

Experimental

Measurements. Spectroscopic and electric conductivity data were obtained in the same way as in the previous paper.[1]

(*RS*)-3-Aminohexahydroazepine (*RS*-ahaz). This was obtained by the same procedure for preparing *S*-ahaz,[1] except the use of (*RS*)-3-aminohexahydro-2-azepinone hydrochloride in place of the *S*-enantiomer. The product was purified by distillation. Bp, 92—94 °C 27 mmHg (1 mmHg=133.322 Pa).

Preparation of Cu(*RS*-ahaz)$_2$X$_2$·*n*H$_2$O (*n*=0 for X$^-$=ClO$_4^-$, NO$_3^-$, BF$_4^-$, and I$^-$; *n*=2 for X$^-$=Br$^-$). The complexes (X$^-$=ClO$_4^-$, NO$_3^-$, or Br$^-$) were obtained from CuX$_2$·*n*H$_2$O and *RS*-ahaz in the same way for preparing the corresponding *S*-ahaz complexes.[1] Cu(*RS*-ahaz)$_2$(BF$_4$)$_2$ was prepared by using 45% aqueous solution of Cu(BF$_4$)$_2$ in a similar method of obtaining Cu(*S*-ahaz)$_2$(BF$_4$)$_2$.[1] Cu(*RS*-ahaz)$_2$I$_2$ was obtained by adding a methanol solution of LiI to an aqueous methanol solution of Cu(*RS*-ahaz)$_2$(ClO$_4$)$_2$. Found (complex **1**; X$^-$=ClO$_4^-$): C, 29.05; H, 5.60; N, 11.40. Calcd for $C_{12}H_{28}Cl_2CuN_4O_8$: C, 29.36; H, 5.75, N, 11.42%. Found (complex **2**; X$^-$=Br$^-$): C, 29.68; H, 6.56; N, 11.55. Calcd for $C_{12}H_{32}Br_2CuN_4O_2$: C, 29.54; H, 6.63; N, 11.49%. Found (X$^-$=NO$_3^-$): C, 34.59; H, 6.74; N, 20.16. Calcd for $C_{12}H_{28}CuN_6O_6$: C, 34.65; H, 6.78, N, 20.21%. Found (X$^-$=BF$_4^-$): C, 31.21; H, 6.04; N, 11.69. Calcd for $C_{12}H_{28}B_2CuF_8N_4$: C, 30.96; H, 6.06; N, 12.04%. Found (X$^-$=I$^-$): C, 26.22; H, 5.22; N, 10.47. Calcd for $C_{12}H_{28}CuI_2N_4$: C, 26.28; H, 5.14; N, 10.24%.

Table 1 summarizes the spectral and conductivity data of copper(II) complexes prepared in this study.

Preparation of Cu(*RS*-ahaz)$_2$X(ClO$_4$) (X$^-$=Cl$^-$, Br$^-$). Complex **1** (0.93 g, 2 mmol) was dissolved in hot aqueous methanol (methanol-water=4:1) and mixed with a methanol solution of LiX (3 mmol). The crystals which appeared were collected, washed with ethanol and diethyl ether, and air-dried. The crude product was recrystallized from aqueous methanol containing LiX. The bromo complex **3** (X$^-$=Br$^-$) was also obtained by adding a slight excess of LiClO$_4$ to a solution of complex **2**. Found (X$^-$=Cl$^-$): C, 33.44; H, 6.60; N, 12.77%. Calcd for $C_{12}H_{28}Cl_2CuN_4O_4$: C, 33.77; H, 6.61, N, 13.13%. Found (X$^-$=Br$^-$): C, 30.49; H, 5.85; N, 11.77%. Calcd for $C_{12}H_{28}BrClCuN_4O_4$: C, 30.58; H, 5.99; N, 11.89%.

X-Ray Diffraction. Diffraction data for the orange-red complexes **1** and **2** and blue-violet complex **3** were collected on a Rigaku AFC-5 four-circle diffractometer with graphite-monochromatized Mo *K*α radiation (λ=0.71073 Å) at 296 K. Details of crystal data and experimental conditions are listed in Table 2. Intensity data were collected by ω and ω—2θ (2θ>30°) scan mode and at scan rate, 4.0° min^{-1}. For each of the complexes, the intensities of three standard reflections

Table 1. Electronic Spectral and Electric Conductivity Data of Copper(II) Complexes of *RS*- and *S*-ahaz

Complex	Reflectance ν_{max} / cm^{-1}	Absorption[a] $\nu_{max}(\varepsilon_{max})$[c] / cm^{-1}	Conductivity[b] / 10^{-3} S m^2 mol^{-1}
Cu(*RS*-ahaz)$_2$(ClO$_4$)$_2$	21100	19340 (96)	161
		19230 (84)[d]	
Cu(*S*-ahaz)$_2$(ClO$_4$)$_2$	18950	19420 (97)	152
		19050 (86)[d]	
Cu(*RS*-ahaz)$_2$Br$_2$·2H$_2$O	20900	17300	75
Cu(*S*-ahaz)$_2$Br$_2$	18700	17120 (117)	81
Cu(*RS*-ahaz)$_2$(BF$_4$)$_2$	21100	19490 (96)	179
Cu(*S*-ahaz)$_2$(BF$_4$)$_2$	19200	19530 (103)	174
Cu(*RS*-ahaz)$_2$(NO$_3$)$_2$	21550	e)	71
Cu(*S*-ahaz)$_2$(NO$_3$)$_2$	18950	e)	88
Cu(*RS*-ahaz)$_2$I$_2$	21280	e)	96
Cu(*RS*-ahaz)$_2$Br(ClO$_4$)	18300	17270 (115)	97
		18660 (90)[d]	
Cu(*S*-ahaz)$_2$Br(ClO$_4$)	18300	17210 (113)	97
		18520 (91)[d]	
Cu(*RS*-ahaz)$_2$Cl(ClO$_4$)	17900	17060 (107)	97
Cu(*S*-ahaz)$_2$Cl(ClO$_4$)	18200	17120 (107)	97

a) Obtained for nitromethane solution using 5 cm cells unless otherwise noted. b) Obtained for nitromethane solution (4×10^{-4} mol dm^{-3}) at 19 °C. c) Given in mol^{-1} dm^3 cm^{-1} unit. d) Obtained for methanol solution using 5 cm cells. e) Unmeasurable due to insufficient solubility of the complex in the solvent.

Table 2. Crystallographic Parameters and Experimental Conditions

Compound	1	2	3	4[a]
Color	Orange-red	Orange-red	Blue-violet	Blue-violet
Formula	$C_{12}H_{28}Cl_2CuN_4O_8$	$C_{12}H_{32}Br_2CuN_4O_2$	$C_{12}H_{28}BrClCuN_4O_4$	$C_{12}H_{28}BrClCuN_4O_42$
M	490.83	487.77	471.28	471.28
Crystal system	Monoclinic	Orthorhombic	Orthorhombic	Orthorhombic
Space group	$P2_1/a$	$Iba2$	$Pna2_1$	$P2_12_12_1$
a/Å	8.849(3)	11.087(5)	13.655(4)	13.449(6)
b/Å	16.869(5)	23.64(3)	17.480(9)	17.411(11)
c/Å	6.649(3)	14.67(1)	7.863(3)	7.937(2)
β/°	99.36(3)			
U/Å^3	979.3(6)	3848(6)	1877(1)	1859(2)
Z	2	8	4	4
D_m/g cm^{-3} [b]	1.66	1.69	1.67	1.66
D_c/g cm^{-3}	1.665	1.684	1.671	1.684
$F(000)$	510	1976	964	964
μ(Mo $K\alpha$)/cm^{-1}	14.4	52.6	34.5	34.7
Crystal size(mm)	0.30×0.30×0.50	0.20×0.40×0.60	0.20×0.20×0.40	0.20×0.38×0.57
No. of reflections obsd[c]	3973	1563	1188	1906
No. of unique reflections	1874	1437	1137	1853
R[d]	0.054	0.100	0.151	0.068
Rw[e]	0.056	0.107	0.140	0.079
Largest shift/error value on final cycle	0.14	0.35	0.21	0.13

a) Ref. 1. b) Obtained at 293 K by the floating method in CBr_4-CCl_4 mixture. c) Critetion: $|F_o|>3\sigma(|F_o|)$. d) $R=\Sigma(||F_o|-|F_c||)/\Sigma|F_o|$. e) $Rw=[\Sigma w(|F_o|-|F_c|)^2/\Sigma w|F_o|^2]^{1/2}$.

Table 3. Positional Parameters (×10^4) and Equivalent Isotropic Temperature Factors for Complex 1

Atom	x	y	z	B_{eq}/Å^2
Cu	0	0	0	2.6(0.03)
N(1)	690(5)	968(3)	1739(7)	4.1(0.1)
C(2)	2332(7)	917(3)	2452(8)	4.3(0.1)
C(3)	3138(6)	496(3)	835(8)	3.7(0.1)
C(4)	3241(6)	1008(3)	−1020(8)	4.1(0.1)
C(5)	1764(7)	1392(3)	−2057(8)	4.3(0.1)
C(6)	1131(7)	2020(3)	−787(9)	4.4(0.2)
C(7)	212(7)	1730(3)	783(9)	4.3(0.1)
N(8)	2218(5)	−228(2)	267(7)	4.1(0.1)
Cl	−2724(2)	1330(1)	−5340(2)	4.0(0.05)
O(1)	−1605(5)	704(3)	−5292(7)	5.9(0.1)
O(2)	−3566(7)	1376(3)	−7296(7)	8.0(0.2)
O(3)	−3621(9)	1217(5)	−3889(11)	13.3(0.3)
O(4)	−1892(8)	2052(4)	−5051(13)	12.0(0.3)

Table 4. Positional Parameters (×10^4) and Equivalent Isotropic Temperature Factors for Complex 2

Atom	x	y	z	B_{eq}/Å^2
Cu	2420(3)	1290(1)	1434(3)	2.6(0.1)
Br(1)	287(3)	2806(2)	2587(3)	5.1(0.1)
Br(2)A	0	0	0	4.5(0.1)
Br(2)B	0	5000	740(5)	6.5(0.2)
N(1)	3447(28)	1858(13)	814(25)	6.1(1.0)
C(2)	3953(30)	1572(18)	0(26)	5.2(1.1)
C(3)	3024(35)	1193(17)	−448(23)	5.4(1.1)
C(4)	1949(35)	1481(17)	−908(23)	5.6(1.1)
C(5)	1250(42)	1913(22)	−336(40)	8.8(1.9)
C(6)	1992(53)	2451(23)	−176(33)	10.2(2.0)
C(7)	2967(33)	2451(23)	585(24)	5.6(1.1)
N(8)	2644(36)	824(11)	306(21)	5.6(0.9)
N(1)′	1338(25)	696(12)	1992(23)	5.3(0.9)
C(2)′	926(32)	959(17)	2858(22)	4.9(1.0)
C(3)′	1894(35)	1350(18)	3266(24)	5.8(1.2)
C(4)′	2963(32)	1047(15)	3727(23)	4.4(0.9)
C(5)′	3660(31)	633(15)	3118(26)	4.6(1.0)
C(6)′	2916(37)	108(20)	2876(25)	6.8(1.4)
C(7)′	2064(42)	170(23)	2058(37)	9.4(1.9)
N(8)′	2278(26)	1746(10)	2533(23)	4.9(0.8)
O(W)1	1705(27)	3843(15)	1462(35)	9.4(1.1)
O(W)2	4094(30)	3843(16)	1033(20)	9.0(1.2)

were measured after every 150 reflections, but they showed no appreciable changes. The intensities were corrected for Lorentz and polarization factors, but not for absorption.

Structure Analysis. Atomic scattering factors are taken from International Table for X-ray Crystallography.[5] All structures were refined by a block diagonal least-squares procedure based on $|F_o|$ including H atoms. Unit weight was used for all reflections. H atom coordinates were obtained by calculation. All non-hydrogen atoms are anisotropic and H atoms isotropic. The crystallographic calculations were performed on a FACOM M-380 computer of The Institute of Physical and Chemical Research using UNICS III program system.[6] The maximum heights in the final difference Fourier maps were 1.2, 1.5, and 0.9 e/Å^3 near

Table 5. Positional Parameters ($\times 10^4$) and Equivalent Isotropic Temperature Factors for Complex **3**

Atom	x	y	z	B_{eq}/Å^2
Cu	1383(3)	859(2)	0	4.6(0.1)
Br	−392(3)	−39(3)	3(18)	7.6(0.1)
N(1)	2014(28)	−40(27)	1322(52)	8.0(1.4)
C(2)	2174(36)	−657(25)	206(139)	7.9(1.7)
C(3)	2576(38)	−331(27)	−1537(72)	7.5(1.8)
C(4)	3704(38)	−111(33)	−1299(75)	8.9(2.0)
C(5)	3958(32)	489(26)	137(130)	8.1(1.6)
C(6)	3833(38)	143(34)	1895(78)	9.1(2.1)
C(7)	2828(41)	159(38)	2525(69)	8.7(2.0)
N(8)	1985(21)	350(18)	−1927(35)	4.0(0.8)
N(1)′	659(30)	1643(25)	−1239(60)	8.0(1.5)
C(2)′	17(24)	2076(21)	−182(77)	4.5(1.1)
C(3)′	597(44)	2247(38)	1522(81)	10.4(2.4)
C(4)′	1362(41)	2859(32)	1330(82)	9.6(2.1)
C(5)′	2096(42)	2745(34)	−294(151)	11.0(2.8)
C(6)′	1629(44)	2831(33)	−1866(79)	9.2(2.1)
C(7)′	1146(45)	2166(36)	−2490(74)	9.5(2.2)
N(8)′	969(27)	1483(21)	2075(44)	6.0(1.1)
Cl	3647(11)	1988(9)	5115(48)	11.6(0.6)
O(1)	3462(37)	2719(28)	4690(117)	15.7(2.5)
O(2)	2785(38)	1542(30)	5280(161)	17.5(2.7)
O(3)	4115(93)	1949(69)	6425(169)	43.2(9.7)
O(4)	4160(59)	1635(47)	3875(109)	25.6(4.4)

the heavy atoms for **1**, **2**, and **3**, respectively. The atomic coordinates for complexes **1**, **2**, and **3** are listed in Tables 3, 4, and 5.[7]

Complex **1**: Since Z is 2 in space group $P2_1/a$, Cu atom is at the origin. Thus, the structure was solved by the heavy atom method. The R index gave 0.054.

Complex **2**: Two space groups *Iba*2 and *Ibam* are possible from the systematic extinction. Independent structure analyses were attempted for both space groups using MULTAN 78 program.[8] The satisfactory solution was obtained only for *Iba*2. During the refinement, however, Br(2) was found to be disordered in two positions with equal population. Then, a half atomic multiplicity was given to these positions. The final R index gave 0.10.

Complex **3**: Two space groups $Pna2_1$ and *Pnam* are possible from the systematic extinction. Independent structure analyses were attempted for both space groups using MULTAN 78. It was found that all three heavy atoms, Cu, Br, and Cl, are happened to be on the ab plane, and the mirror symmetry appeared in both cases. However, the structure could not be refined for space group *Pnam*. After several trials, the structure was solved by assuming the space group $Pna2_1$ and carefully eliminating the ghost atoms due to the pseudo mirror operation.[6] The structure was refined to R=0.11. However, oxygen atoms of perchlorate and some of the carbon atoms in the ligands were disordered. Therefore, at the last stage the ligand was refined by using the molecular mechanical calculation (MM2 program described by Allinger[10]). The final R factor constrained by MM2 was 0.151.

Results

Preparation of Orange-Red Homo-Anion Copper(II) Complexes of *RS*-ahaz. The copper(II) complexes obtained by adding $CuX_2 \cdot nH_2O$ (X^-=ClO_4^-, NO_3^-, Br^-, BF_4^-) to twice the molar of *RS*-ahaz were found to be orange-red without exception. The diiodide prepared by mixing $[Cu(RS\text{-ahaz})_2](ClO_4)_2$ and LiI in methanol solution was also orange-red. It was found, however, that the product with $CuCl_2 \cdot 2H_2O$ was a mixture of red and blue complexes. We did not examine the dichloride further.

These orange-red homo-anion complexes had the general composition $Cu(C_6H_{14}N_2)_2X_2 \cdot nH_2O$ (n=0 for X^-=ClO_4^-, NO_3^-, BF_4^-, and I^-; n=2 for X^-=Br^-). Although the complex **2**, prepared from *RS*-ahaz and $CuBr_2$, was found to contain two water molecules per one complex molecule, it exhibited the visible reflectance spectrum closely similar to those of the others. The spectral data are summarized in Table 1.

As described in introduction, it is rather unusual[2] that a series of copper(II) complexes of bis(diamine) type is thoroughly orange-red and shows the reflectance spectral maximum around 21000 cm^{-1} regardless of the sort of counter ion. Hence, the crystal structures of complexes **1** and **2** were examined by the X-ray diffraction method.

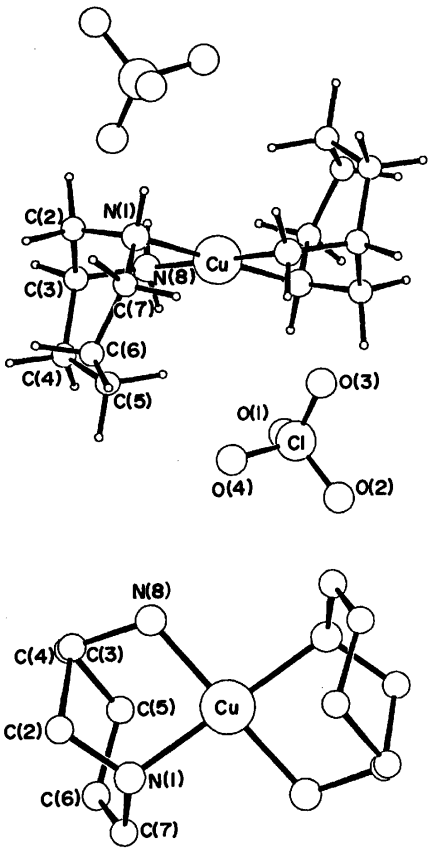

Fig. 2. Perspective views of complex **1**.

Molecular Structure of Complex 1. As is indicated by the crystal parameters, the molecular structure of the complex **1** has the strict C_i symmetry, where the Cu^{2+} ion occupies the center of inversion. The perspective views of **1** are shown in Fig. 2. The selected bond parameters are listed in Table 6. The bond distances and angles are in the normal range. It is noticed that one of two ahaz ligands has the R- and the other has the S-configuration.

Obviously the seven-membered rings of both ahaz stand perpendicular to the respective five-membered chelate rings. The primary and secondary amino groups of both diamines are located at the trans positions around the Cu^{2+} ion, and the seven-membered rings extend towards the opposite sides of the CuN_4 plane. Thus, the C(5) methylene group of *S*-ahaz and C(5)′ methylene of *R*-ahaz prevent completely the approach of the perchlorate, respectively, to the top and bottom apical sites of the central metal ion. The interatomic distance Cu-O(1), the shortest distance between Cu atom and the perchlorate group, is 3.77 Å and the Cu-O(1) vector intersects the CuN_4 plane at 62.8°, indicating no appreciable coordination of the anion to the Cu^{2+}. It is apparent, therefore, that the complex cation of **1** takes the strict four-coordination geometry with C_i symmetry, and that the cation can be expressed by the formula $[Cu(R\text{-ahaz})(S\text{-ahaz})]^{2+}$.

The five-membered chelate and the seven-membered ring of *S*-ahaz in **1** is depicted in Fig. 3 (i) and (ii). The chelate ring adopts a λ conformation, and the seven-membered ring takes a twist-chair conformation. The coordinating secondary N center has the S-configuration. The structural characteristics for *R*-ahaz are exactly antipodal to those for *S*-ahaz, reflecting the C_i symmetry of **1**.

The hydrogen bonding modes and intermolecular short contacts in complex **1** are summarized in Table 7. The nitrogen atoms of the ligands of **1** are hydrogen-bonded to the oxygen atoms of the perchlorate ions. Therefore, the shape of perchlorate is fairly normal in **1**.

Molecular Structure of Complex 2. The perspective views of complex **2** are shown in Fig. 4, and the selected bond parameters are given in Table 6. Each complex cation contains an *R*-ahaz and an *S*-ahaz as the ligands, in the same manner as **1**, but **2** no longer has the true centrosymmetry. The distances between Cu^{2+} and Br^- or O of water molecules, Cu-Br(1), Cu-Br(2)A, Cu-O(2)B, Cu-O(1), and Cu-O(2) are respectively, 4.6, 4.6, >7.0, 6.1, and 6.3 Å. Thus, neither the bromides nor the water molecules coordinate to

Table 6. Bond Lengths (l/Å) and Bond Angles (ϕ/°) for Complexes **1**, **2**, and **3**

	1	**2**	**3**		**1**	**2**	**3**
N(8)-Cu	1.979(5)	2.00(3)	1.94(3)	Cu-N(1)-C(2)	109.2(3)	106(2)	109(4)
N(8)′-Cu		1.95(3)	2.04(4)	Cu-N(1)′-C(2)′		104(2)	113(3)
Cu-N(1)	2.036(4)	1.98(3)	2.07(4)	N(1)-C(2)-C(3)	110.3(4)	111(3)	109(4)
Cu-N(1)′		2.02(3)	1.95(4)	N(1)′-C(2)′-C(3)′		112(3)	107(4)
N(1)-C(2)	1.456(7)	1.48(5)	1.41(9)	C(2)-C(3)-N(8)	104.9(4)	103(3)	106(4)
N(1)′-C(2)′		1.49(5)	1.43(6)	C(2)′-C(3)′-N(8)′		107(3)	104(4)
C(2)-C(3)	1.555(8)	1.52(5)	1.6(1)	C(3)-N(8)-Cu	111.0(3)	109(2)	116(3)
C(2)′-C(3)′		1.54(5)	1.59(8)	C(3)′-N(8)′-Cu		106(2)	110(3)
C(3)-N(8)	1.482(6)	1.47(5)	1.47(6)	C(7)-N(1)-C(2)	113.3(4)	111(3)	117(4)
C(3)′-N(8)′		1.49(5)	1.49(7)	C(7)′-N(1)′-C(2)′		117(3)	109(4)
C(3)-C(4)	1.521(8)	1.53(5)	1.60(7)	C(2)-C(3)-C(4)	113.3(4)	117(3)	109(4)
C(3)′-C(4)′		1.54(5)	1.50(8)	C(2)′-C(3)′-C(4)′		115(3)	113(5)
C(4)-C(5)	1.519(8)	1.53(7)	1.58(9)	C(3)-C(4)-C(5)	116.7(5)	117(3)	117(4)
C(4)′-C(5)′		1.54(5)	1.6(1)	C(3)′-C(4)′-C(5)′		115(3)	115(5)
C(5)-C(6)	1.517(8)	1.53(8)	1.5(1)	C(4)-C(5)-C(6)	114.4(4)	111(4)	111(4)
C(5)′-C(6)′		1.53(6)	1.4(1)	C(4)′-C(5)′-C(6)′		112(3)	113(5)
C(6)-C(7)	1.505(9)	1.56(6)	1.46(8)	C(5)-C(6)-C(7)	116.7(4)	116(4)	114(5)
C(6)′-C(7)′		1.53(6)	1.42(9)	C(5)′-C(6)′-C(7)′		116(4)	115(4)
C(7)-N(1)	1.465(7)	1.46(5)	1.50(7)	C(6)-C(7)-N(1)	115.8(5)	118(3)	119(5)
C(7)′-N(1)′		1.49(6)	1.50(7)	C(6)′-C(7)′-N(1)′		118(4)	119(5)
Cl-O(1)	1.445(5)		1.34(6)	O(1)-Cl-O(2)	108.8(3)		113(3)
Cl-O(2)	1.392(5)		1.42(6)	O(1)-Cl-O(3)	111.1(4)		111(7)
Cl-O(3)	1.358(8)		1.2(1)	O(1)-Cl-O(4)	106.6(4)		111(6)
Cl-O(4)	1.421(7)		1.35(9)	O(2)-Cl-O(3)	112.7(4)		109(8)
Cu-Br			2.888(9)	O(2)-Cl-O(4)	105.3(4)		104(5)
N(8)-Cu-N(1)	84.5(2)	86(1)	82(1)	O(3)-Cl-O(4)	111.9(5)		108(7)
N(8)′-Cu-N(1)′		90(1)	83(2)				

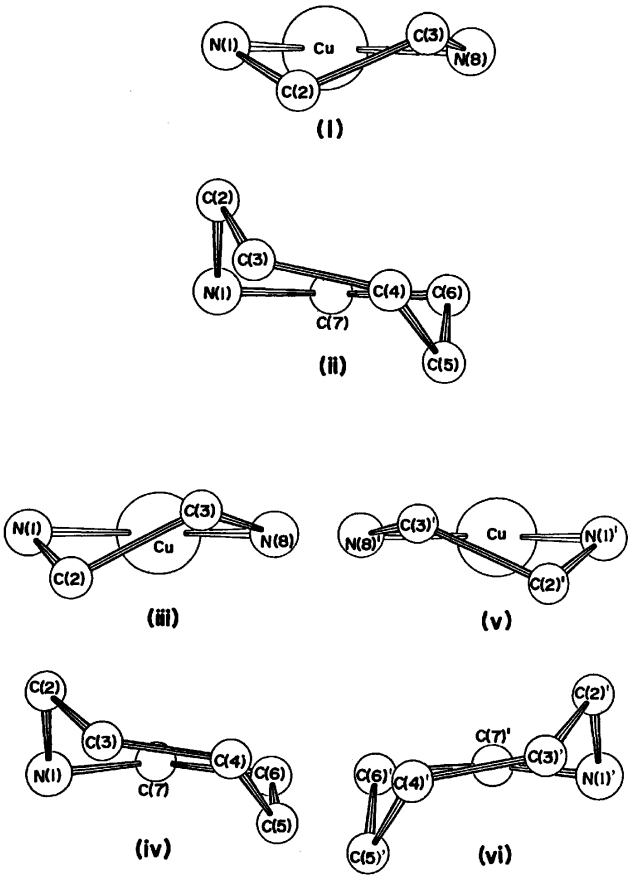

Fig. 3. Fiv-membered chelate rings (i), (iii), (v), and seven-membered rings (ii), (iv), (vi) in **1** and **2**. (i) and (ii) for *S*-ahaz in **1**; (iii) and (iv) for *s*-ahaz in **2**; (v) and (vi) for *R*-ahaz in **2**.

Table 7. Hydrogen Bond Distances and Intermolecular Contacts (Å)

Atom 1	Atom2	Distance	Symmetry[a]
		Complex **1**	
Hydrogen bond			
N(1)	-O(1)	3.086(7)	I
N(8)	-O(1)	3.361(6)	II
N(8)	-O(2)	3.138(7)	II
N(8)	-O(3)	3.025(8)	III
Intermolecular contact (<3.5 Å)			
C(3)	-O(2)	3.329(7)	IV
		Complex **2**	
Hydrogen bond			
Br(1)	-N(1)	3.40(3)	V
Br(2)A	-O(2)	3.29(4)	V
Br(2)B	-N(8)	3.32(4)	V
N(1)′	-O(2)	3.06(4)	V
Intermolecular contact (<3.5 Å)			
C(2)′	-O(2)	3.39(5)	V
		Complex **3**	
Hydrogen bond			
Br	-N(8)	3.30(3)	VI

a) Symmetry of atom 2,
I: $x, y, z+1$, II: $-x, 1-y, -1-z$, III: $-x, 1-y, -z$, IV: $x+1, y, z+1$, V: $x-1/2, -y+1/2, z$, VI: $1-x, 1-y, z+1/2$.

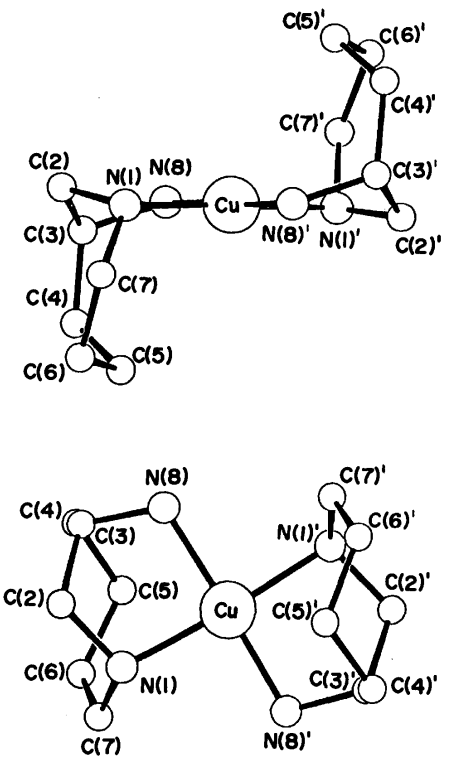

Fig. 4. Perspective views of complex **2**.

the central Cu^{2+} ion, showing that the complex cation also holds the strict four-coordination geometry as found in complex **1**, and that **2** can be represented with the formula $[Cu(R\text{-ahaz})(S\text{-ahaz})]Br_2 \cdot 2H_2O$.

The conformations of five-membered chelates and those of seven-membered rings of *S*-ahaz and *R*-ahaz in **2** are shown in Fig. 3 (iii)—(vi). The chelate rings of *S*-ahaz and *R*-ahaz take a λ and a δ gauche conformation respectively, and the seven-membered rings of these ligands adopt twist-chair conformations. Because of lacking the exact C_i symmetry, the conformation of *S*-ahaz is not the exact antipode of that of *R*-ahaz in **2** as indicated in Fig. 3, in contrast to the case of complex **1**. Despite of this fact, the conformation of *S*-ahaz (or *R*-ahaz) in **1** is quite similar to that of *S*-ahaz (or *R*-ahaz) in **2**, though slight deformations are recognized between them (Fig. 3).

The hydrogen bonding modes and intermolecular short contacts in **2** are also listed in Table 7. For complex **2**, the bromide ions are situated on the two fold axis and form rectangular parallelepiped with one-eighth of the unit cell as shown in Fig. 5. The Br(1) atom is near the center of bc plane of the parallelepiped. The complex cation is surrounded by Br^- ions. Although the Cu^{2+} ion is situated at a

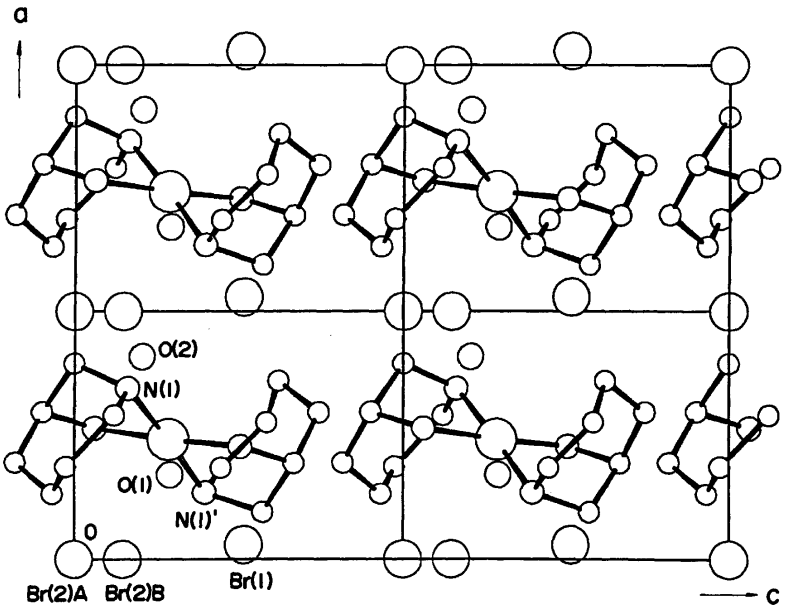

Fig. 5. Crystal packing of complex **2**.

general position, the complex has an approximate centrosymmetry similar to the complex **1**.

Preparation of Hetero-Anion Copper(II) Complexes of *RS*-ahaz. It was found that the orange-red complexes of *RS*-ahaz are classified into two categories based on their electric conductivity behaviors. The complexes with X^-=ClO_4^- and BF_4^- were bi-univalent electrolytes in nitromethane solution, while those of X^-=Br^-, I^-, and NO_3^- dissociated uni-univalently in the same solvent (Table 1). With regard to the latter family, the coordination of an X^- to the central Cu^{2+} seems to take place in the solution, generating new mono-positively charged five-coordinated Cu^{II} species. In spite of the clear difference in the conductivity behaviors, these two families showed no significant differences in their solution spectra (Table 1). Further, it was noticed that the visible absorption spectra of Cu(*RS*-ahaz)$_2$X$_2$ resemble closely those of Cu(*S*-ahaz)$_2$X$_2$ taken in the same solvent (Table 1). For example, the absorption curve of complex **2** is similar to that of Cu(*S*-ahaz)$_2$Br$_2$ and, further, to that of five-coordinated [CuBr(*S*-ahaz)$_2$]-ClO_4 (Fig. 6).

It was demonstrated previously[1] that a series of hetero-anion complexes of *S*-ahaz, Cu(*S*-ahaz)$_2$X-(ClO_4) were obtained by adding LiX or NaX to a solution of Cu(*S*-ahaz)$_2$(ClO_4)$_2$ or, alternatively, adding $LiClO_4$ to Cu(*S*-ahaz)$_2$X$_2$. Similarly the addition of $LiClO_4$ to a methanol solution of complex **2** resulted in the formation of blue-violet crystals having the composition Cu($C_6H_{14}N_4$)$_2$Br(ClO_4). The addition of LiX to a solution of Complex **1** afforded hetero-anion complexes more generally, but in a slightly limited manner compared with the case of *S*-ahaz complexes. The hetero-anion complexes

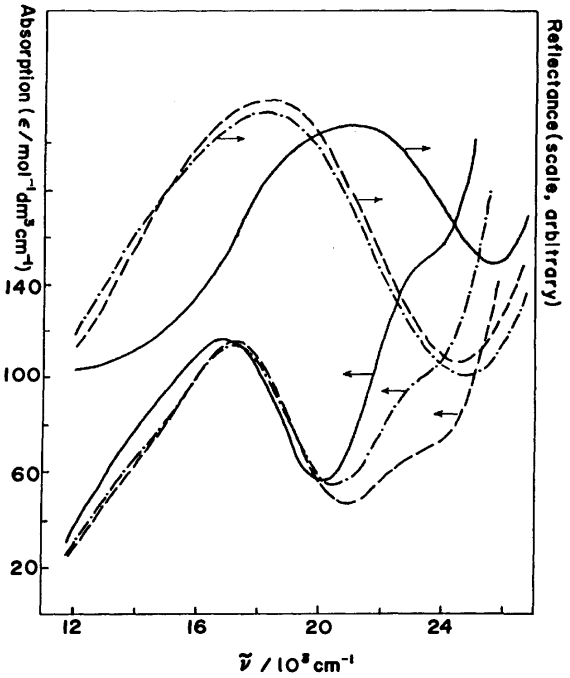

Fig. 6. Reflectance and absorption spectra in nitromethane solution for complexes **2**: (——), **3**: (------), and **4**; (-·-·-).

Cu(*RS*-ahaz)X(ClO_4) were obtained only for X^-=Cl^- and Br^-, while the addition of LiI resulted in the precipitation of orange-red [Cu(*R*-ahaz)(*S*-ahaz)]I_2 as described previously.

The reflectance and absorption spectral as well as electronic conductivity features of the hetero-anion complexes of *RS*-ahaz resembled indistinguishably those of the corresponding *S*-ahaz complexes (Table 1

and Fig. 6). This implies that both *RS*- and *S*-ahaz complexes of the hetero-anion type took stereochemistries closely similar to one another. Since the structure of $[CuBr(S\text{-ahaz})_2]ClO_4$, referred hereafter as to complex **4**, has already been clarified crystallographically,[1] the structure determination of the corresponding *RS*-ahaz complex **3** was performed by the X-ray diffraction method with a view to compare the stereochemical characteristics of **3** and **4** and to examine the ligand exchange mode for the formation of **3** from **1** or **2**.

Molecular and Crystal Structure of Complex 3. Although complex **3** has been represented as $Cu(RS\text{-ahaz})_2Br(ClO_4)$ for simplicity, the X-ray analysis result demonstrated that a racemic pair of five-coordinated complex ions, $[CuBr(R\text{-ahaz})_2]^+$ and $[CuBr(S\text{-ahaz})_2]^+$, exists in the single crystal, and so **3** is represented with the formula $[CuBr(R\text{-ahaz})_2]$-$[CuBr(S\text{-ahaz})_2](ClO_4)_2$. The perspective views shown in Fig. 7 are those for the complex cation comprised with *S*-ahaz, which is exactly antipodal to the counterpart involving *R*-ahaz. We will consider the stereochemical characteristics of the cation with *S*-ahaz as the representative, in relation to that of complex **4**. The selected bond parameters of **3** are listed in Table 6.

The $[CuBr(S\text{-ahaz})_2]^+$ ion in **3** (Fig. 7) is similar to that in **4**[1]. Both complex ions adopt typical square-pyramidal geometries, in which four amino nitrogens of ahaz ligands occupy the basal plane and a bromide at the apex, and the five-membered chelate rings take λ conformations. Seven-membered rings thoroughly assume preferable twist-chair conformations. A noticeable difference between **3** and **4** is found with regard to the cyclic sequences of dihedral angles of both seven-membered rings; i.e. those are nearly identical for **3**, but evidently different for **4**.[1] Thus, the complex ion of **3** appears to have a pseudo C_2 axis perpendicular to CuN_4 plane (Fig. 7), though that of **4** seems not to have such symmetry axis at all.[1]

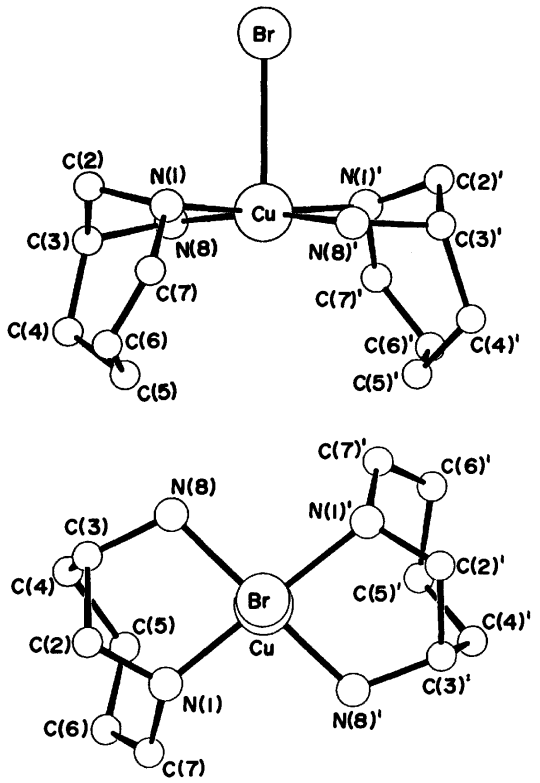

Fig. 7. Perspective views of complex **3**.

The crystal packings and lattice constants of complexes **3** and **4**, as well as their molecular structures, are fairly similar to each other, as shown in Fig. 8 and Table 2. Each complex forms zigzag chains consisting of the complex of the same chirality along c axis through two fold screw operation. Each chain is surrounded by four similar chains as in polyethylene packing.[11] For complex **3**, the neighboring chains, indicated by the broken line rectangles, have the chirality opposite to the chain shown with the solid line rectangle as indicated in Fig. 8 (a). On the other hand, all the chains for complex **4** in Fig. 8 (b) have the same chirality.

Discussion

Structural Characteristics of Reddish Bis(diamine)-copper(II) Complexes. The X-ray diffraction study revealed that $[Cu(R\text{-ahaz})(S\text{-ahaz})]^{2+}$ ion in **1** adopts the strictly rhombic-coplanar CuN_4 stereochemistry, and that the complex cation in **2** is intrinsically identical with that in **1**, though slight deformations from the centrosymmetric geometry take place. The fact that the reflectance spectra of other orange-red homo-anion complexes of *RS*-ahaz resemble those of **1** and **2** strongly suggests that these complexes also assume similar coplanar configurations represented as the structure (III) in Fig. 9 and can be formulated as $[Cu(R\text{-ahaz})(S\text{-ahaz})]X_2$ (X^-=BF_4^-, NO_3^-, I^-).

However, the existence of rhombic- or square-coplanar CuN_4 chromophore in copper(II) complexes has been considered to be unusual.[2] One of the rare examples of such chromophore has been established for $[Cu(deen)_2]^{2+}$ ion (deen=*N*,*N*-diethyl-1,2-ethanediamine) in the diperchlorate[12] or dinitrate.[2] In these deen complexes the coordination of the anions (ClO_4^- or NO_3^-) is disturbed by the *N*-ethyl groups, which orient axially with regard to the respective chelate rings as indicated by Fig. 9 (IV). It is noticeable that $[Cu(deen)_2]X_2$ (X^-=ClO_4^-, NO_3^-) are also reddish-colored and have centrosymmetric rhombic-coplanar structures in a similar manner as **1**.

In addition, it was demonstrated that the wine-red complexes $[Cu(1,3\text{-chxn})_2]X_2$ (1,3-chxn=*cis*-1,3-cyclohexanediamine; X^-=NO_3^-, Br^-) also took square-coplanar stereochemistries.[13,14] The established

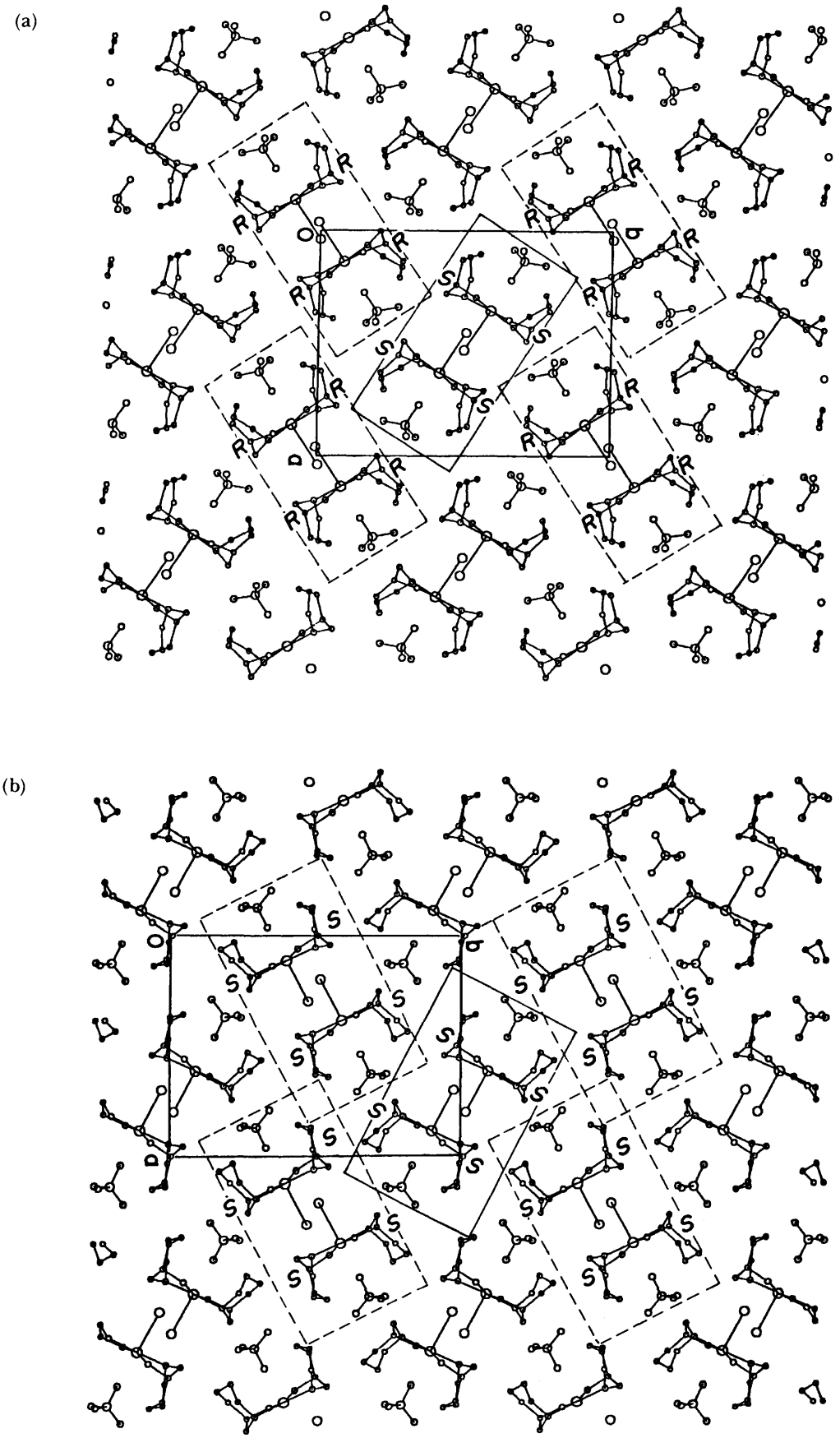

Fig. 8. Comparative views of the crystal structures (projection along c axis); (a) for complex **3** and (b) for complex **4**.

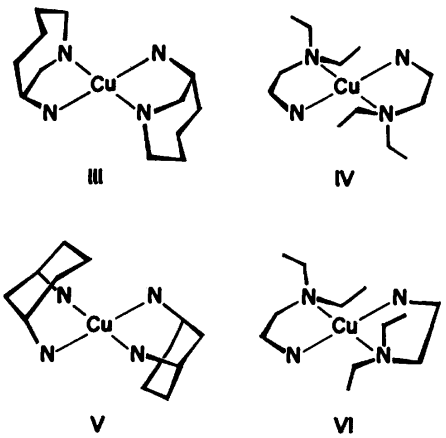

Fig. 9. Stereochemistries of copper(II) complexes having the CuN_4 chromophore. [Cu(*R*-ahaz)(*S*-ahaz)]$^{2+}$ ion, (III); [Cu(deen)$_2$]$^{2+}$ ion (red-form), (IV)[2,12]; [Cu(1,3-chxn)$_2$]$^{2+}$ ion, (V)[14]; [Cu(deen)$_2$]$^{2+}$ ion (blue-form), (VI).[12]

structure of [Cu(1,3-chxn)$_2$]$^{2+}$ ion in these wine-red complexes is illustrated in Fig. 9 (V), where the contact of anions to the apical coordination sites is completely prevented by the ring methylene chains of the ligands in quite a similar manner as that in (III). It can be concluded, therefore, that the common structural features of reddish-colored copper(II) complexes with diamine ligands are the strict four-coordination geometries with C_i or closely similar molecular symmetry and the absence of the coordination of anions to the central ion.

It is noteworthy that the production of reddish-colored bis(diamine)copper(II) complex with the square- or rhombic-coplanar stereochemistry is rather delicate phenomena, being influenced with some complicated factors. For example, Cu(1,3-chxn)$_2$Br$_2$ was found to form violet crystals from ethanol, in spite that it afforded wine-red crystals from methanol.[13] In the case of *RS*-ahaz complexes, the dibromide gave only orange-red crystals, but the dichloride was a mixture of orange-red and blue-violet forms. For deen complex, the dibromide was no longer reddish-colored, but blue-violet.[15] For the violet or blue-violet modifications of these diamine complexes, some intrinsic changes from the strictly four-coordinated centrosymmetric structure should be effected within the complex ion, though the details of such structural changes are uncertain.

Pathway for Formation of [CuBr(*R*-ahaz)$_2$]$^+$ and [CuBr(*S*-ahaz)$_2$]$^+$ Ions from [Cu(*R*-ahaz)(*S*-ahaz)]$^{2+}$ Ion. The X-ray diffraction study of complex **3** clarified the formation of the five-coordinated [CuBr(*S*-ahaz)$_2$]$^+$ and its antipode from [Cu(*R*-ahaz)(*S*-ahaz)]$^{2+}$ ion, indicating that not only the coordination of Br^- but certain ligand exchanges of ahaz take place during such transformation in solution. Moreover, the pair of **1** and **3** exemplifies two typical coordination modes possible for metal complexes containing the racemic modification of a chiral bidentate ligands; the first involves both of the R- and S-enantiomers in each complex ion, giving a meso type compound as **1**, while in the second case each complex ion comprises two molecules of the single enantiomer and becomes chiral as in **3**. The formation of **3** can therefore be regarded as a process of chiral discrimination; that is, the first *R*-ahaz (or *S*-ahaz) coordinated to Cu^{2+} ion chooses the same enantiomer as the second ligand to form the chiral five-coordinated complex.

The ligand exchange which occurs upon the dissolution of ahaz complexes is presumed by comparing the electronic spectral data of a series of copper(II) complexes of *RS*- and *S*-ahaz. Thus, the absorption spectrum of complex **1** obtained in nitromethane solution was found to be markedly different from its reflectance spectrum, while it closely resembles the solution spectrum of Cu(*S*-ahaz)$_2$(ClO$_4$)$_2$ (Table 1). Taking into consideration that these complexes dissociate uni-bivalently, it is supposed that such ligand exchanges as those shown in Scheme 1 occur in nitromethane solution, at least in part, to generate a racemic pair of [Cu(*R*-ahaz)$_2$(Sol)]$^{2+}$ and [Cu(*S*-ahaz)$_2$(Sol)]$^{2+}$ ((Sol) denotes the coordinating solvent molecule). When all the complexes take exclusively the square-pyramidal structures in solution, the spectra for the *RS*-ahaz complex should

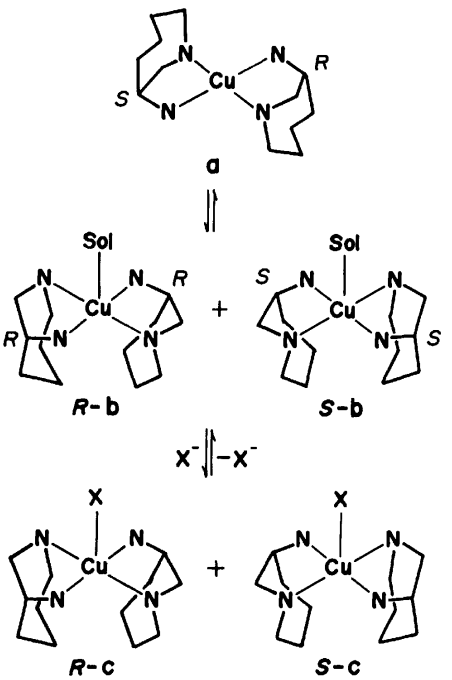

Scheme 1. Equilibria for copper(II) complexes of *RS*-ahaz in the presence of X^-: **a**, [Cu(*R*-ahaz)(*S*-ahaz)]$^{2+}$; *R*-**b**, [Cu(*R*-ahaz)$_2$(Sol)]$^{2+}$; *S*-**b**, [Cu(*S*-ahaz)$_2$(Sol)]$^{2+}$; *R*-**c**, [Cu(*R*-ahaz)$_2$X]$^+$; *S*-**c**, [Cu(*S*-ahaz)$_2$X]$^+$.

coincide with that for the *S*-ahaz complex. In methanol, the absorption spectra of the above complexes of racemic and optically active ahaz actually become almost identical with each other, probably due to that most part of the racemic complex takes the solvent-coordinated square-pyramidal structures.

In the presence of anions such as Cl^-, Br^-, or I^-, the solvent-coordinated species tend to be converted into the five-coordinated $[CuX(S\text{-ahaz})_2]^+$ and its enantiomer as shown in Scheme 1. It is interesting to note that $[Cu(R\text{-ahaz})(S\text{-ahaz})]X_2$ (X^-=Br^-, I^-) dissociates uni-univalently in nitromethane, in contrast to that $[Cu(R\text{-ahaz})(S\text{-ahaz})]X_2$ (X^-=ClO_4^-, BF_4^-) behaves as uni-bivalent electrolytes in the same solvent. These facts suggest that the halide complexes transform almost completely into $[CuX(R\text{-ahaz})_2]^+$ and $[CuX(S\text{-ahaz})_2]^+$ in nitromethane.

Alternatively, when halides or pseudohalides (NCS^- or ONO^-) were added in excess to a solution of **1**, most part of the complex species would adopt the five-coordinated structures with a coordinating X^-. In the case where ClO_4^- and X^- coexist, the product that crystallized from an equilibrated mixture in Scheme 1 is likely to depend on the relative concentrations of ClO_4^- and X^- and the solubilities of individual species as the perchlorate or halide.

Thus, under the conditions where X^- is Cl^- or Br^- and sufficient amounts of both X^- and ClO_4^- coexist in aqueous methanol solution, the hetero-anion complex $Cu(RS\text{-ahaz})_2X(ClO_4)$ is the least soluble species and crystallizes out as the sole product. But in the case where X^- is I^-, $[Cu(R\text{-ahaz})(S\text{-ahaz})]I_2$ is the least soluble one in methanol, so that the addition of NaI to a solution of **1** results in the precipitation of $[Cu(R\text{-ahaz})(S\text{-ahaz})]I_2$. When X^- is ONO^-, a mixture of blue-violet crystals, probably the hetero-anion complex $Cu(RS\text{-ahaz})_2(ONO)(ClO_4)$, and orange-red **1** precipitated out of a solution of **1** containing $NaNO_2$. When X^- is NCS^-, the precipitation of blue-violet crystals no longer resulted, but complex **1** recovered.

It was found, further, that complex **1** crystallized out of an aqueous methanol solution of complex **3**. It was necessary for the recrystallization of the hetero-anion complex to add a small amount of LiBr to the solution. But the addition of a large excess of bromide to a solution of **3** resulted in the precipitation of complex **2**. We observed actually that the lattice constants of an orange-red crystal obtained from **3** by the treatment with excess KBr solution were the same as those of complex **2**. These facts demonstrate that the coordinating bromide is easily replaced with a solvent molecule in aqueous methanol solution, and that the equilibrium shown in Scheme 1 actually exists.

Stereochromism: Dichromism Due to Enantiomeric Composition of Chiral Ligand. Since the structural characteristics of orange-red homo-anion complexes of *RS*-ahaz has been clarified as mentioned above, it becomes possible to consider the interesting phenomenon caused by employing either the racemate or the pure single enantiomer of ahaz; i.e. $Cu(RS\text{-ahaz})_2X_2\cdot nH_2O$ are thoroughly orange-red, while the corresponding *S*-ahaz complexes $Cu(S\text{-ahaz})_2X_2$ are violet or blue-violet.[1] Although no exact structures of *S*-ahaz complexes have been established by the crystallographic method owing to poor quality of crystals, we have postulated them to be (I) or (II).[1] Whichever structures the *S*-ahaz complexes assume, they are intrinsically chiral, so that it is impossible for them to adopt any meso type structures such as centrosymmetric (III). Therefore, it is reasonable that no orange-red form was found for *S*-ahaz complexes, because it is concluded necessary for reddish bis(diamine)copper(II) complexes to adopt the centrosymmetric strict coplanar geometry.

Such color change depending on the enantiomeric composition of a chiral ligand, the racemate or the pure single enantiomer, may be termed "stereochromism" in analogy with thermochromism[16] or other dichromic phenomena. As far as bis(diamine)copper(II) complexes concern, the thermochromism exhibited by deen complexes is one of the most well known and thoroughly examined cases, i.e., $Cu(deen)_2X_2$ interconverts reversibly between the red lower temperature form and the blue higher temperature form, when X^- is of low coordinating ability as ClO_4^- or BF_4^-.[12,15,17-21] The structural change which may accompany with the color change has been studied from various aspects.[12,15,18-21] The hexagonal distortion involving the Cu-N bond lengthening and the synchronous access of anions to the apical sites of Cu^{2+} had been suggested to be responsible for the color change.[15,18-20] However, it was conclusively demonstrated for the diperchlorate[12] that in the course of the transformation from red to blue form no obvious Cu-N bond lengthening took place, and that the most apparent stereochemical change was the conformation inversion of one of the deen chelates. The structures of the red and blue forms thus determined[12] are illustrated in Fig. 9 (IV) and (VI), respectively. It should be pointed out that both chelate rings in (VI) adopt λ conformations (or δ conformations for the antipode of (VI)), so that the complex cation of the blue form (VI) is chiral, even though it has a C_2 axis perpendicular to the CuN_4 plane. As previously noted, (IV) in the red form is strictly centrosymmetric.[2,12] Thus, we can deduce common stereochemical features between the stereochromism of ahaz complexes and the thermochromism of deen complexes; the complex ions in the red forms has the C_i molecular symmetry and are strictly four-coordinated, and in the blue or violet forms they assume certain kind of chiral structures, irrespective of its coordination number being four or

five.

It is apparent that the interconversion between (II) and (III) requires the configurational inversion at the asymmetric carbon center of ahaz. Such conversion is difficult under ordinary condition, so that it is reasonable that orange-red Cu(*RS*-ahaz)$_2$X$_2$ does not show any sign of thermochromism. Alternatively, stereochromism can be realized by using *S*-ahaz in place of *RS*-ahaz as the ligand. More examples of stereochromism will probably be observed among copper(II) complexes by employing both racemic and optically pure forms of certain N-substituted diamines, an example of which will be presented in a following paper.[22]

References

1) M. Saburi, K. Miyamura, M. Morita, Y. Mizoguchi, S. Yoshikawa, S. Tsuboyama, T. Sakurai, and K. Tsuboyama, *Bull. Chem. Soc. Jpn.*, **60**, 141 (1987).

2) A. Walsh and B. J. Hathaway, *J. Chem. Soc., Dalton Trans.*, **1984**, 15.

3) For simplicity, copper(II) complexes of *RS*-ahaz are indicated with the formula such as Cu(*RS*-ahaz)$_2$X$_2$ or CuX(*RS*-ahaz)$_2$ClO$_4$ throughout the text regardless of the actual formulae which will be clarified in the following part.

4) The terms "hetero-anion" and "homo-anion" are used in the same sense as in Ref. 1.

5) "International Tables for X-Ray Crystallography," Kynoch Press, Birmingham (1974), Vol. IV.

6) T. Sakurai and K. Kobayashi, *Rikagaku Kenkyusho Hokoku*, **55**, 69 (1979).

7) Tables of the coordinates of hydrogen atoms, the anisotropic thermal parameters of the non-hydrogen atoms, and observed and calculated structure factors are kept as Document No. 8746 at the Chemical Society of Japan.

8) P. Main, S. E. Hull, L. Lessinger, G. Germain, J.-P. Declercq, and M. M. Woolfson, (1978), MULTAN. A Computer Program for the Automatic Solution of Crystal Structures of X-ray Diffraction Data. Univ. of York, England and Louvain, Belgium.

9) T. Sakurai, K. Kobayashi, and Y. Iinuma, *Rikagaku Kenkyusho Hokoku*, **61**, 142 (1985).

10) N. L. Allinger, *J. Am. Chem. Soc.*, **99**, 8127 (1977).

11) C. W. Bunn, *Trans. Faraday Soc.*, **35**, 482 (1939).

12) I. Grenthe, P. Paoletti, M. Sandsstrom, and S. Glikberg, *Inorg. Chem.*, **18**, 2687 (1979).

13) R. Saito and Y. Kidani, *Bull. Chem. Soc. Jpn.*, **52**, 57 (1979).

14) K. Kamisawa, K. Matsumoto, S. Ooi, R. Saito, and Y. Kidani, *Bull. Chem. Soc. Jpn.*, **54**, 1072 (1981).

15) A. P. B. Lever and E. Mantovani, *Inorg. Chem.*, **10**, 817 (1971).

16) D. R. Bloomquist and R. D. Willett, *Coord. Chem. Rev.*, **47**, 125 (1982).

17) P. Pfeiffer and H. Glaser, *J. Prakt. Chem.*, **151**, 134 (1938).

18) A. P. B. Lever, E. Mantovani, and J. C. Donini, *Inorg. Chem.*, **10**, 2424 (1971).

19) L. Fabbrizzi, M. Micheloni, and P. Paoletti, *Inorg. Chem.*, **13**, 3019 (1974).

20) J. R. Ferraro, L. J. Basilè, L. R. Garcia-Ineguez, P. Paoletti, and L. Fabbrizzi, *Inorg. Chem.*, **15**, 2342 (1976).

21) R. J. Pylkki, R. D. Willett, and H. W. Dodgen, *Inorg. Chem.*, **23**, 594 (1984).

22) K. Miyamura, M. Saburi, Y. Gohshi, S. Tsuboyama, T. Sakurai, and K. Tsuboyama, to be submitted.

 © 1987 The Chemical Society of Japan Bull. Chem. Soc. Jpn., 60, 2593—2598 (1987)

Development of Functionalized Materials Using Organometallic Compounds. IV.[1] Thermal Residual Stresses during the Fabrication of a Ni-Coated Continuous Carbon Fiber Aluminum Composites

Yozo MIKATA,† Tamotsu TAKAHASHI, Shuenn-Kung SU, and Yasuzo UCHIDA*
Department of Industrial Chemistry, Faculty of Engineering,
The University of Tokyo, Hongo, Bunkyo-Ku, Tokyo 113
†Department of Civil Engineering, Technological Institute, Northwestern University,
Evanston, IL 60201, U.S.A.
(Received December 18, 1986)

The thermal residual stresses during the fabrication of a Ni-coated carbon fiber composite are calculated by using two- and four-concentric-circular-cylinders models. The advantage of the CDL (chemical deposition in liquid phase) coating method at low temperature (200 °C), which is using organonickel compounds such as $Ni(cod)_2$ (cod=1,5-cyclooctadiene), over the conventional melted Ni-coating method (1453 °C) has been definitely confirmed from the crack prevention viewpoint.

There has been a growing interest in coated fiber composites such as electric composites or metal matrix composites. For such composites, the purpose of the coating on fiber is to develop a functionalized fiber or to serve as a chemical reaction barrier between the metal matrix and the fiber. We have recently reported that carbon materials were uniformly coated with metals such as Al,[2] Fe,[3] Co,[1] or Ni[1] at low temperature by the CDL method using organometallic compounds. Advantages of this CDL method have been investigated. This CDL method for an aluminum coating improved the wetting of carbon by aluminum metal and obviated the formation of aluminum carbide.[2] $Ni(cod)_2$ and $Co_2(CO)_8$, which do not have low boiling points, can be used by this CDL method for Co- and Ni-coating of carbon fibers, respectively, in sharp contrast to the CVD (chemical vapor deposition) method.

In order to evaluate the effect of the low coating temperature of the CDL method (ca. 200 °C) compared with the conventional nickel coating using melted nickel metal (1453 °C), we calculated the thermal residual stresses due to the mismatch of thermal expansion coefficients of its constituents. The thermal stresses in a coated short fiber composite[4] and in a coated continuous fiber composite[5] have been recently discussed by one of the authors. There have been a number of other works for a continuous fiber (not coated) composite,[6,7] and for a composite cylinder.[8,9] However, none of these works considered the thermal residual stresses of the coated continuous fiber composite during the fabrication process.

In this paper, specific emphasis will be given to the feasibility study of Ni-coated carbon fiber and its aluminum composite from the fabrication viewpoint. Two nickel coating methods were compared. One is the CDL method using organonickel compounds we recently reported.[1] The big advantage of this method is that the temperature at the time of coating is very low (about 200 °C) and to be controlled. The other is a conventional method in which nickel metal is heated up to its melting point (1453 °C) and coated on the carbon fiber. We will focus on the effect of the difference of these two temperatures on thermal residual stresses built up during the fabrication process.

Thermal Residual Stress. In the following analysis, we largely rely on the formulation presented in Ref. 4. For the sake of self containedness, however, we review some of the results reported before.[4]

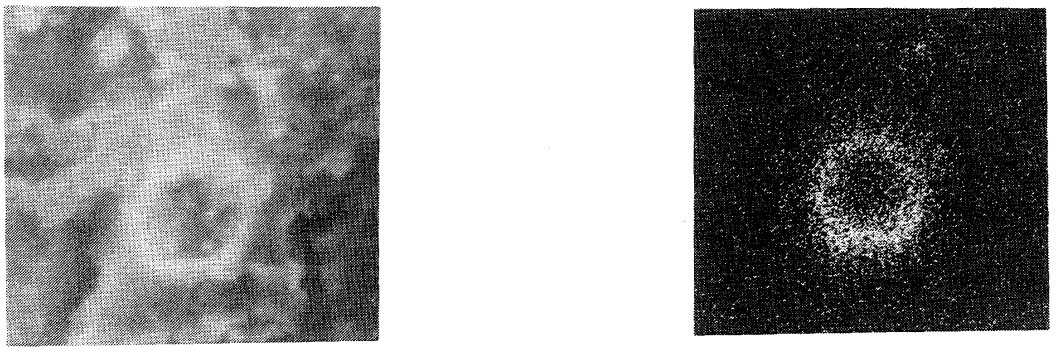

(A) SEM picture (B) Characteristic X-ray picture

Fig. 1. Cross section of Ni coated carbon fiber.

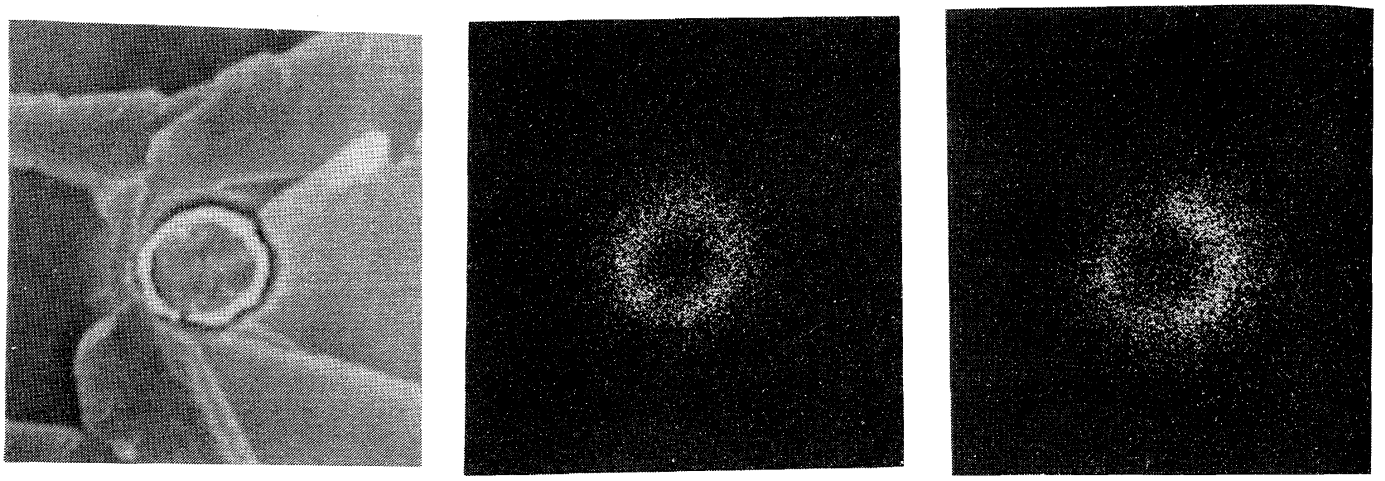

(A) SEM picture (B) Ni characteristic X-ray picture (C) Al characteristic X-ray picture

Fig. 2. Cross section of Al/Ni coated carbon fiber.

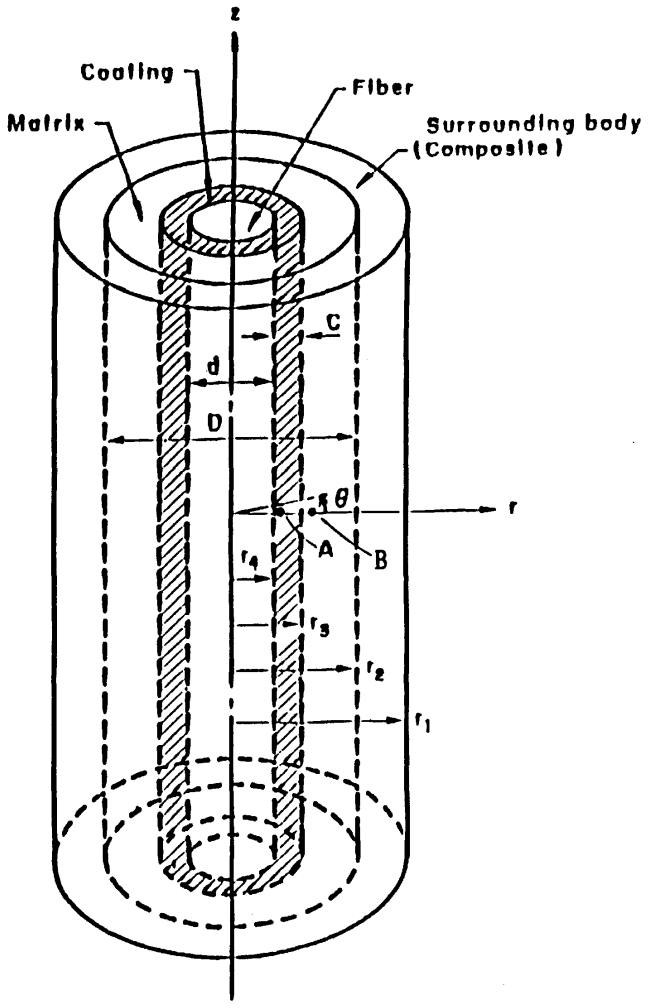

Fig. 3. Four phase model.

In order to evaluate the thermal residual stresses during the fabrication process, we need to consider two stages, stage-1: making the coated fiber, and stage-2: making the composite by combining the coated fiber and the matrix. At each stage, there are thermal residual stresses. The final thermal residual stresses are the sum of those stresses at stage 1 and 2.

Cross section of nickel-coated carbon fiber by the CDL method and that surrounded with aluminum are shown in Figs. 1 and 2. To simplify the calculations a coated continuous fiber composite is modeled as four concentric infinitely long circular cylinders (four phase model) as shown in Fig. 3. The surrounding body with the composite properties (outermost cylinder), matrix, coating and fiber (innermost cylinder) are denoted by domain 1, 2, 3, and 4, respectively, and their radii by r_1, r_2, r_3, and r_4, respectively. The diameters of fiber and matrix (including a coated fiber) are denoted by d and D, respectively, and the coating thickness by c. Since the surrounding body is infinite, r_1 will be made infinity at the end of the formulation.

To compute the thermal residual stresses at stage 1, we only need to consider two concentric circular cylinders, which consists of the fiber and the coating. Thermal residual stresses at stage 2 can be computed by using the four phase model described above.

Let us first obtain the thermal residual stresses at stage 1. The coating and the fiber are denoted as the domain 3 and 4, respectively, and the radii of the coating and the fiber as r_3 and r_4, respectively. Their surface of the coating is stress free at this stage. The constant temperature change is denoted as ΔT_1. The stress field is obtained in a similar manner as reported before[4] and given by

$$\sigma_{rr}^{(m),1} = C_{11}^{(m)}\left(A_m^1 - \frac{B_m^1}{r^2}\right) + C_{12}^{(m)}\left(A_m^1 + \frac{B_m^1}{r^2}\right) + C_{13}^{(m)}E^1 - \beta_1^{(m)}\Delta T_1$$
$$\sigma_{\theta\theta}^{(m),1} = C_{12}^{(m)}\left(A_m^1 - \frac{B_m^1}{r^2}\right) + C_{11}^{(m)}\left(A_m^1 + \frac{B_m^1}{r^2}\right) + C_{13}^{(m)}E^1 - \beta_1^{(m)}\Delta T_1 \quad (1)$$
$$\sigma_{zz}^{(m),1} = 2C_{13}^{(m)}A_m^1 + C_{33}^{(m)}E^1 - \beta_3^{(m)}\Delta T_1 \qquad m=3,4$$

with $B_4^1=0$, and where

$$\beta_1^{(m)} = (C_{11}^{(m)}+C_{12}^{(m)})\alpha_{mT} + C_{13}^{(m)}\alpha_{mL}$$
$$\beta_3^{(m)} = 2C_{13}^{(m)}\alpha_{mT} + C_{33}^{(m)}\alpha_{mL}, \qquad m=3,4 \quad (2)$$

$C_{ij}^{(m)}$ are elastic constants of the m-th material, and α_{mT} and α_{mL} are the thermal expansion coefficients of the m-th material along the transverse (r) and longitudinal (z) direction, respectively. The unknown coefficients A_3^1, A_4^1, B_3^1, E^1 are determined by solving the following simultaneous equations.

$$\begin{pmatrix} a_{11}^1 & a_{12}^1 & a_{13}^1 & 0 \\ a_{21}^1 & 0 & a_{23}^1 & a_{24}^1 \\ a_{31}^1 & a_{32}^1 & a_{33}^1 & a_{34}^1 \\ a_{41}^1 & a_{42}^1 & 0 & a_{44}^1 \end{pmatrix} \begin{pmatrix} A_3^1 \\ A_4^1 \\ B_3^1 \\ E^1 \end{pmatrix} = \begin{pmatrix} b_1^1 \\ b_2^1 \\ b_3^1 \\ b_4^1 \end{pmatrix} \quad (3)$$

where the explicit expressions of elements in the square matrix a_{ij}^1 and column vector b_i^1 are given in the Appendix A.

The thermal residual stresses in the stage 2 are obtained by using the four phase model.[4] Let us denote the constant temperature change as ΔT_2. Then we find the stress field as

$$\sigma_{rr}^{(n),2} = C_{11}^{(n)}\left(A_n^2 - \frac{B_n^2}{r^2}\right) + C_{12}^{(n)}\left(A_n^2 + \frac{B_n^2}{r^2}\right) + C_{13}^{(n)}E^2 - \beta_1^{(n)}\Delta T_2$$
$$\sigma_{\theta\theta}^{(n),2} = C_{12}^{(n)}\left(A_n^2 - \frac{B_n^2}{r^2}\right) + C_{11}^{(n)}\left(A_n^2 + \frac{B_n^2}{r^2}\right) + C_{13}^{(n)}E^2 - \beta_1^{(n)}\Delta T_2$$
$$\sigma_{zz}^{(n),2} = 2C_{13}^{(n)}A_n^2 + C_{33}^{(n)}E^2 - \beta_3^{(n)}\Delta T_2, \qquad n=1\text{—}4 \quad (4)$$

Table 1. Material Properties of Constituents of Coated Fiber Composite

Material	Matrix Al 6009	Fiber Graphite T300	Coating Ni
E_T (GPa)	69.0	22.0	207
E_L (GPa)	69.0	226	207
ν_{12}	0.33	0.42	0.31
ν_{13}	0.33	0.30	0.31
α_T (1/°C)	24.3×10^{-6}	27.0×10^{-6}	13.3×10^{-6}
α_L (1/°C)	24.3×10^{-6}	-1.50×10^{-6}	13.3×10^{-6}
σ_{ult} (GPa)	0.342	3.04	0.317
Mp (θ_m/°C)	650		1453

with $B_4^2=0$, and where

$$\beta_1^{(n)} = (C_{11}^{(n)}+C_{12}^{(n)})\alpha_{nT} + C_{13}^{(n)}\alpha_{nL}$$
$$\beta_3^{(n)} = 2C_{13}^{(n)}\alpha_{nT} + C_{33}^{(n)}\alpha_{nL}, \qquad n=1\text{—}4 \quad (5)$$

The simultaneous equations for the eight unknowns A_1^2, A_2^2, A_3^2, A_4^2, B_1^2, B_2^2, B_3^2, E^2 in (4) are given by

$$\begin{pmatrix} a_{11}^2 & a_{12}^2 & 0 & 0 & a_{15}^2 & a_{16}^2 & 0 & 0 \\ 0 & a_{22}^2 & a_{23}^2 & 0 & 0 & a_{26}^2 & a_{27}^2 & 0 \\ 0 & 0 & a_{33}^2 & a_{34}^2 & 0 & 0 & a_{37}^2 & 0 \\ a_{41}^2 & 0 & 0 & 0 & 0 & 0 & 0 & a_{48}^2 \\ a_{51}^2 & a_{52}^2 & 0 & 0 & a_{55}^2 & a_{56}^2 & 0 & a_{58}^2 \\ 0 & a_{62}^2 & a_{63}^2 & 0 & 0 & a_{66}^2 & a_{67}^2 & a_{68}^2 \\ 0 & 0 & a_{73}^2 & a_{74}^2 & 0 & 0 & a_{77}^2 & a_{78}^2 \\ a_{81}^2 & 0 & 0 & 0 & 0 & 0 & 0 & a_{88}^2 \end{pmatrix} \begin{pmatrix} A_1^2 \\ A_2^2 \\ A_3^2 \\ A_4^2 \\ B_1^2 \\ B_2^2 \\ B_3^2 \\ E^2 \end{pmatrix} = \begin{pmatrix} 0 \\ 0 \\ 0 \\ b_4^2 \\ b_5^2 \\ b_6^2 \\ b_7^2 \\ b_8^2 \end{pmatrix} \quad (6)$$

where the explicit expressions of elements in the square matrix a_{ij}^2 and column vector b_i^2 are given in the Appendix B.

The final thermal residual stresses are computed as

$$\sigma_{ij}^{(l),f} = \sigma_{ij}^{(l),1} + \sigma_{ij}^{(l),2}, \qquad l=1\text{—}4 \quad (7)$$

where we have the following specifications.

$$\sigma_{ij}^{(1),1} = \sigma_{ij}^{(2),1} = 0 \quad (8)$$

Results and Discussion

Two Ni-coating methods are compared from 'mechanics viewpoint. Let us call the conventional melted nickel coating method at 1453 °C as the method I, and the CDL method at 200 °C as the method II.

The representative material properties of the Ni-coated graphite fiber/aluminum 6009 are given in Table 1,[10] where the tensile strength is denoted by σ_{ult}. It should be noted in Table 1 that the engineering elastic constants, E_T, E_L, ν_{12}, ν_{13}, G_L, are given instead of C_{ij}. The elastic constants C_{ij} are related to the engineering elastic constants.[11] Material properties of the surrounding body (composite) are obtained by using a rule of mixture,

$$C_{ij}^{(1)} = V_m C_{ij}^{(2)} + V_c C_{ij}^{(3)} + V_f C_{ij}^{(4)}$$
$$\alpha_{1T} = V_m\alpha_{2T} + V_c\alpha_{3T} + V_f\alpha_{4T} \quad (9)$$
$$\alpha_{1L} = V_m\alpha_{2L} + V_c\alpha_{3L} + V_f\alpha_{4L}$$

where V_m, V_c, V_f are the volume fraction of the matrix, coating and fiber, respectively, and they are given by

$$V_m = 1 - \left(\frac{r_3}{r_2}\right)^2, \quad V_c = \left(\frac{r_3}{r_2}\right)^2 - \left(\frac{r_4}{r_2}\right)^2,$$
$$V_f = \left(\frac{r_4}{r_2}\right)^2 = \left(\frac{d}{D}\right)^2 \quad (10)$$

In the following figures, the stresses in the surrounding body are omitted, because they are either 0 ($=\sigma_z$) or so small (σ_r, σ_θ) to draw in those scales.

Thermal residual stresses of the coated fiber along the radial direction (r-axis) which are caused by the method I and II are shown in the Figs. 4 and 5, respectively. It is assumed in both cases that the coated fiber is cooled down to room temperature (25 °C) after completing the Ni-coating. The ratio of coating thickness to fiber diameter c/d is set to be 0.2143. It is easily seen from Fig. 4 that σ_z in the coating (Ni) is far greater than the tensile strength of Ni (317 MPa). Thus it is very likely that the Ni-coating will be completely cracked, if we use the method I. Whereas, in the Fig. 5, it is seen that the maximum tensile stress (σ_z) in the Ni-coating is less than its tensile strength.

The final thermal residual stresses of the composite caused by the method II are shown in the Fig. 6. The

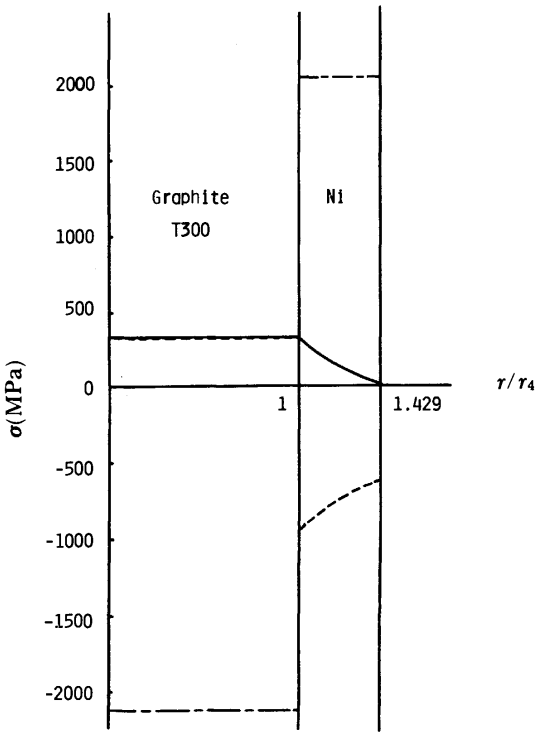

Fig. 4. Thermal residual stresses of the fiber caused by the method I (1453 °C—25 °C). $\Delta T \fallingdotseq -1428$ °C, $c/d \fallingdotseq 15/70$. ——σ_r, ------σ_θ, —·—σ_z.

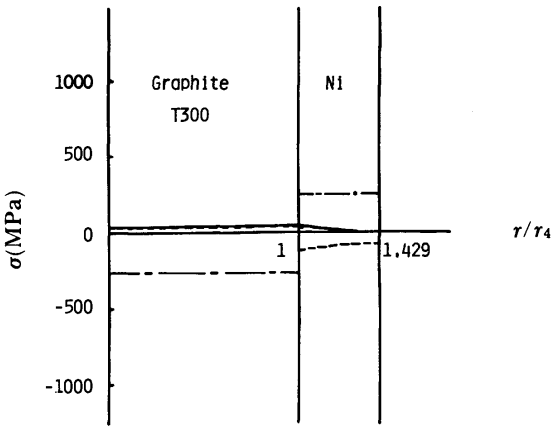

Fig. 5. Thermal residual stresses of the coated fiber caused by the method II. (200 °C—25 °C) $\Delta T \fallingdotseq -175$ °C, $c/d \fallingdotseq 15/70$, ——σ_r, ------σ_θ, —·—σ_z.

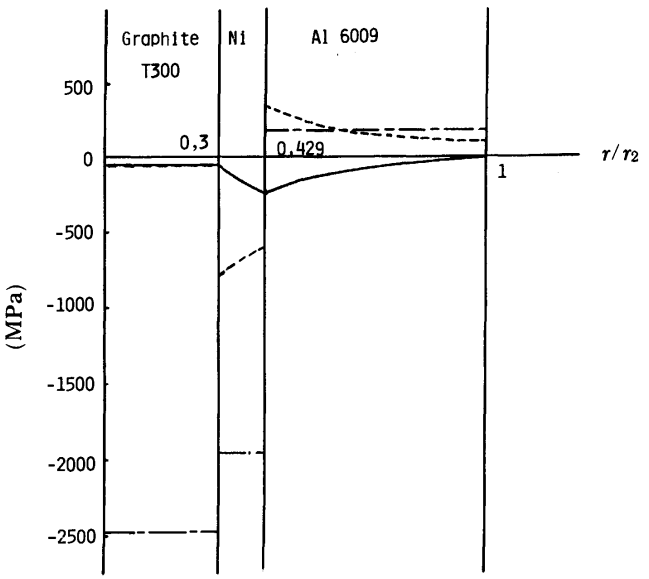

Fig. 6. Final thermal residual stresses of the composite by the method II. Coated fiber: 200 °C—(25 °C)—650 °C—25 °C, composite: 650 °C—25 °C. $V_f = 0.09$, $c/d \fallingdotseq 15/70$, ——σ_r, ------σ_θ, —·—σ_z.

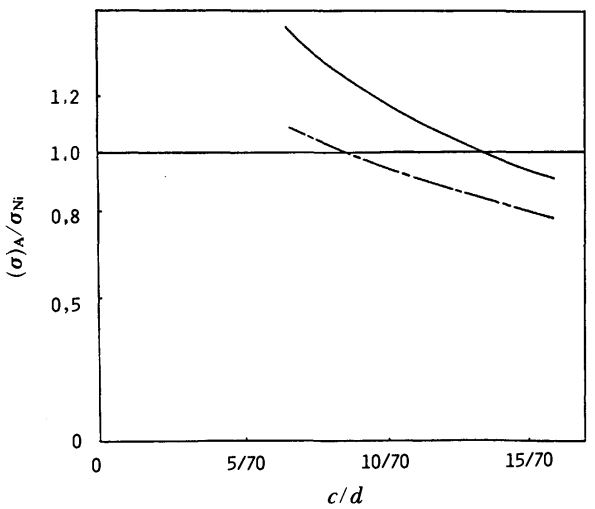

Fig. 7. Residual tensions of the coated fiber at a point A caused by the method II as a function of c/d. The stresses are normalized by the tensile strength of Ni. ——$(\sigma_\theta)_A/\sigma_{Ni}$, $\Delta T \fallingdotseq 450$ °C, 200 °C—(25 °C)—650 °C; —·—$(\sigma_z)_A/\sigma_{Ni}$, $\Delta T \fallingdotseq -175$ °C, 200 °C—25 °C; $\sigma_{Ni} \fallingdotseq 317$ MPa.

volume fraction of the fiber V_f and the ratio of coating thickness to fiber diameter c/d set to be 0.09 and 0.2143, respectively. These values have been determined so as to make the maximum tensile stress occurring in each phase of the composite less than its tensile strength. It is observed in the Fig. 6 that the highest tensile residual stress (σ_θ) is formed at a point B (see Fig. 3). Even though this stress ($(\sigma_\theta)_B$=341.69 MPa) is almost reaching the tensile strength (342 MPa) of Al 6009, it is expected that the stress is somewhat relaxed by a possible plastic deformation of Al 6009, which our elastic calculation cannot predict. It is generally true that our elasticity assumption of the model gives rise to a higher stress value than expected in reality.

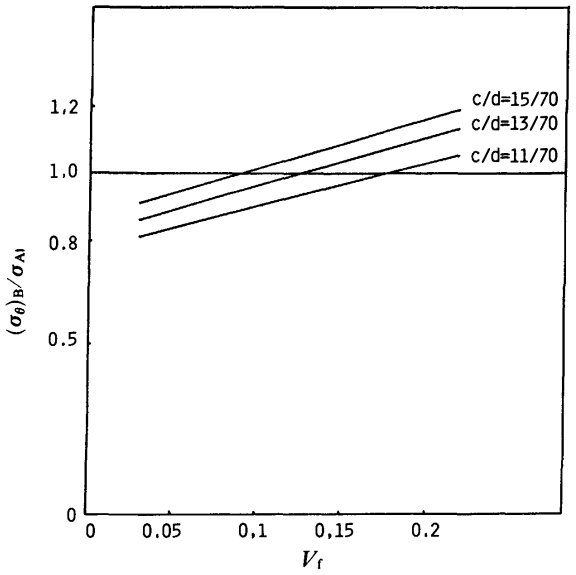

Fig. 8. Residual tension σ_θ of the composite at a point B caused by the method II as a function of V_f for various values of c/d. The stresses are normalized by the tensile strength of Al. ΔT=−625 °C, 650 °C—25 °C, σ_{Al}=342 MPa.

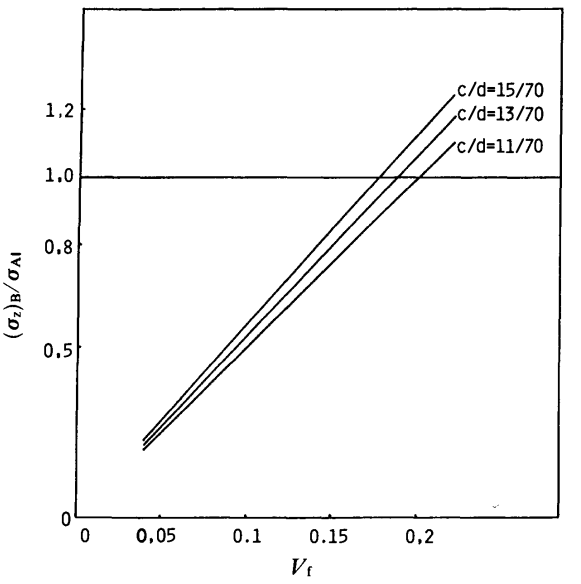

Fig. 9. Residual tension σ_z of the composite at a point B caused by the method II as a function of V_f for various values of c/d. The stresses are normalized by the tensile strength of Al. ΔT=−625 °C, 650 °C—25 °C, σ_{Al}=342 MPa.

A parametric study has been conducted by changing two parameters, i.e. V_f=0.04, 0.09, 0.16, and c/d= 11/70, 13/70, 15/70. Some of the highest tensile stresses occurring at each stage of the fabrication of the composite are drawn in the Figs. 7—9. In the Fig. 7, residual tensions of the coated fiber at a point A (see Fig. 3) caused by the method II are shown as a function of c/d. It is seen in this Figure that the residual tensions decrease as the ratio of coating thickness to fiber diameter c/d increases. In the Figs. 8 and 9, residual tensions σ_θ and σ_z of the composite at a point B caused by the method II are shown as a function of V_f for various values of c/d. It follows from Figs. 8 and 9 that the residual tensions increase as V_f and c/d increase.

Conclusion

(1) It was found that the melted Ni-coating method (method I) gives rise to a tremendous amount of tension (σ_z) in Ni phase, which presumably leads to cracking of Ni coating. Thus the method I is not desirable as a coating method of Ni on a carbon fiber.

(2) With suitable choices of geometrical parameters, it was found possible to make a Ni-coated graphite fiber/Al 6009 composite without cracking in any phase of the composite by the CDL method using organonickel compound (method II). It has been shown from this parametric study that, in general, the residual tension may be kept below the tensile strength of the material, if we design the composite so as to have sufficiently large c/d and sufficiently small V_f.

(3) Coupled with a possible applied stress field, however, the residual tension (σ_θ and σ_z) in Al phase may reach the tensile strength of Al rather easily. To reduce the residual tension, it would be desirable to lower the fabrication temperature of the composite by the CDL method using triisobutylaluminum for Al.[2]

(4) It should be also noted that since our calculation is based on the elasticity assumption of the model, it tends to give rise to a higher residual tension. Thus we may be able to fabricate a flawless composite even with a slightly smaller ratio of coating thickness to fiber diameter c/d, and with a slightly larger volume fraction of the fiber V_f than prescribed by our calculation.

Appendix A

$$a^1_{11} = r_4,\quad a^1_{12} = -r_4,\quad a^1_{13} = \frac{1}{r_4}$$

$$a^1_{21} = -(C^{(3)}_{11}+C^{(3)}_{12}),\quad a^1_{23} = \frac{1}{r_3^2}(C^{(3)}_{11}-C^{(3)}_{12}),\quad a^1_{24} = -C^{(3)}_{13}$$

$$a^1_{31} = C^{(3)}_{11} + C^{(3)}_{12},\quad a^1_{32} = -(C^{(4)}_{11}+C^{(4)}_{12}),$$

$$a^1_{33} = -\frac{1}{r_4^2}(C^{(3)}_{11}-C^{(3)}_{12}),\quad a^1_{34} = C^{(3)}_{13} - C^{(4)}_{13}$$

$$a^1_{41} = 2C^{(3)}_{13}(r_3^2-r_4^2),\quad a^1_{42} = 2C^{(4)}_{13}r_4^2,\quad a^1_{44} = C^{(3)}_{33}(r_3^2-r_4^2) + C^{(4)}_{33}r_4^2$$

and

$$b^1_1 = 0,\quad b^1_3 = -\beta^{(3)}_1\Delta T_1,\quad b^1_4 = (\beta^{(3)}_1-\beta^{(4)}_1)\Delta T_1$$

$$b^1_4 = \beta^{(3)}_3(r_3^2-r_4^2)\Delta T_1 + \beta^{(4)}_3 r_4^2\Delta T_1$$

Appendix B

$$a^2_{11} = r_3,\quad a^2_{12} = -r_3,\quad a^2_{15} = \frac{1}{r_3},\quad a^2_{16} = -\frac{1}{r_3}$$

$$a^2_{22} = r_5,\quad a^2_{23} = -r_5,\quad a^2_{26} = \frac{1}{r_5},\quad a^2_{27} = -\frac{1}{r_5}$$

$$a^2_{33} = r_4,\quad a^2_{34} = -r_4,\quad a^2_{37} = \frac{1}{r_4},$$

$$a^2_{41} = -(C^{(1)}_{11}+C^{(1)}_{12}),\quad a^2_{48} = -C^{(1)}_{13},$$

$$a^2_{51} = C^{(1)}_{11} + C^{(1)}_{12},\quad a^2_{52} = -(C^{(2)}_{11}+C^{(2)}_{12})$$

$$a^2_{55} = -\frac{C^{(1)}_{11}-C^{(1)}_{12}}{r_3^2},\quad a^2_{56} = \frac{C^{(2)}_{11}-C^{(2)}_{12}}{r_3^2},\quad a^2_{58} = C^{(1)}_{13}-C^{(2)}_{13}$$

$$a^2_{62} = C^{(2)}_{11} + C^{(2)}_{12},\quad a^2_{68} = -(C^{(2)}_{11}+C^{(2)}_{12})$$

$$a^2_{66} = -\frac{C^{(2)}_{11}-C^{(2)}_{12}}{r_3^2},\quad a^2_{67} = \frac{C^{(2)}_{11}-C^{(2)}_{12}}{r_3^2},\quad a^2_{68} = C^{(2)}_{13} - C^{(4)}_{13}$$

$$a^2_{73} = C^{(3)}_{11} + C^{(3)}_{12},\quad a^2_{74} = -(C^{(4)}_{11}+C^{(4)}_{12})$$

$$a^2_{77} = -\frac{(C^{(3)}_{11}-C^{(3)}_{12})}{r_4^2},\quad a^2_{78} = C^{(3)}_{13} - C^{(4)}_{13}$$

$$a^2_{81} = 2C^{(1)}_{13},\quad a^2_{88} = C^{(1)}_{33}$$

and

$$b^2_4 = -\beta^{(1)}_1\Delta T_2,\quad b^2_5 = (\beta^{(1)}_1-\beta^{(2)}_1)\Delta T_2,\quad b^2_6 = (\beta^{(2)}_1-\beta^{(3)}_1)\Delta T_2$$

$$b^2_7 = (\beta^{(3)}_1-\beta^{(4)}_1)\Delta T_2,\quad b^2_8 = \beta^{(1)}_3\Delta T_2$$

References

1) Part 3. S.-K. Su, M. Akiba, T. Takahashi, M. Saburi, M. Hidai, and Y. Uchida, *Chem. Lett.*, **1987**, 337.

2) S.-K. Su, T. Takahashi, T. Kodama, M. Hidai, and Y. Uchida, *Nippon Kagaku Kaishi*, **1985**, 629.

3) S.-K. Su, T. Takahashi, T. Kodama, M. Hidai, and Y. Uchida, *Nippon Kagaku Kaishi*, **1987**, 877.

4) Y. Mikata and M. Taya, *J. Comp. Mater.*, **19**, 554 (1985).

5) Y. Mikata and M. Taya, *J. Appl. Mech.*, **53**, 681 (1986).

6) T. Ishikawa, K. Koyama, and S. Kobayashi, *J. Comp. Mater.*, **12**, 153 (1978).

7) M. Uemura, H. Iyama, and Y. Yamaguchi, *J. Thermal Stress*, **2**, 393 (1979).

8) D. Iesan, *J. Thermal Stress*, **3**, 495 (1980).

9) Y. Takeuchi, T. Furukawa, and Y. Tanigawa, "The effect of thermoelastic coupling for transient thermal stresses in a composite cylinder," ASME, WAM, DE-2 (1983).

10) "Metals Handbook," 9th ed, ed by T. Lyman, American Society for Metals, Vol. 2 (1979).

11) H. A. Elliot, *Proc. Camb. Phil. Soc.*, **44**, 522 (1948).

Behavior of the Heat of Formation in the Bismuth-Antimony System

Walid Ahmad BADAWI
Department of Chemistry, Faculty of Science, Al-Fateh University, Tripoli, Libya
(Received December 2, 1985)

Calorimetric studies on the behavior of the heat of formation in the bismuth-antimony system have been carried out at eight different compositions (10—80 at-% Sb). Values of the enthalpy and excess enthalpy at those compositions have been determined and tabulated at even temperature intervals of 10 °C in the range 50 to 650 °C. The heat of formation at 200 °C is given through the equation:

$$H^F = 11.658x_2 - 14.436x_2^2 + 2.778x_2^3$$

The heat of formation is positive and takes a maximum value (2556±11) J mol^{-1} at 50 at-% Sb. The heat of formation is larger than the heat of mixing. The excess over the value of the heat of mixing is attributed to the larger excess volume in the solid state.

There has been considerable interest in the study of thermodynamic properties of binary systems of metals and metalloids. One such system, namely bismuth-antimony has been studied by some researchers e.g. phase diagram by Hansen and Anderko[1] and heat of mixing at 700 °C by Wittig and Gehring.[2]

The present study has been undertaken with the purpose of studying the behavior of the heat of formation in the bismuth-antimony system and of obtaining the ratio of the heats of formation to those of mixing. This would facilitate interpolation of the behavior of the heat of formation at positions having indefinite structures in other binary systems.

Experimental

Sample. The samples were prepared at eight different mole fractions of antimony between 0.1 and 0.8. The metals in the form of bars were procured from E. Merck Company. These were of chemically pure grade. The alloy samples were produced in a melting device operating as "Zintl funnel" system (Fig. 1). By this melting device, while the clean liquid metal flows down into the lower tube of quartz, the oxide layer remains apart in the first one. The mixture of metals was stirred mechanically with a stirrer made of ceramic for 30 min at 700 °C. In order to reduce the effect of oxidation, argon gas was used as a protector during the melting process.

The samples of 10—40 at-% Sb were tempered for 70 h at 200 °C, those of 50—80 at-% Sb at 280, 300, 320, and 380 °C for 70 h at each temperature. The homogeneity of all the compositions studied was established through testing the polished pictures prepared as described by Czochralsky and Przyjemski.[3]

Apparatus. The measurements of enthalpies were carried out using the calorimeter described and utilized by Wittig and co-workers.[4] Modifications on the calorimeter, alteration to the suitable dimensions, regulation of the furnace temperature by means of a p-regulator[5] and using a digital millivoltmeter for measurement of the potential of the thermocouples, revealed satisfactory result.

Procedure. The procedure used depended on the method of primary indirect provision of energy under adiabatic conditions. (see Ref. 6).

The heat of formation can be computed through the equations:

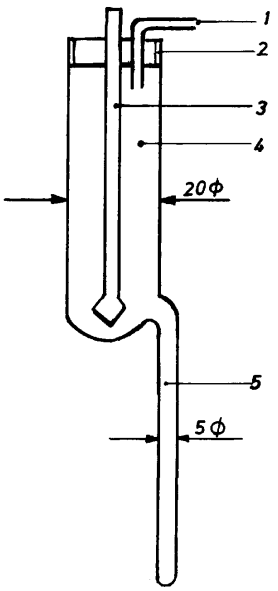

Fig. 1. Melting device.
1 : Gas supply, 2 : sealing, 3 : stirrer, 4 : quartz tube, 5 : quartz tube.

$$(1-x_2)\cdot Bi_{(l)} + x_2\cdot Sb_{(s)} \longrightarrow Bi_{1-x_2}Sb_{x_2(s)} - H^{F,M}$$
$$(1-x_2)\cdot Bi_{(s)} \longrightarrow (1-x_2)\cdot Bi_{(l)} - H_{Bi}^{s}$$

$$(1-x_2)\cdot Bi_{(s)} + x_2\cdot Sb_{(s)} \longrightarrow Bi_{1-x_2}Sb_{x_2(s)} - [H^{F,M} + (1-x_2)H_{Bi}^{s}]$$

$$H^F = H^{F,M} + (1-x_2)\cdot H_{Bi}^{s} \quad (1)$$

where H^F is the heat of formation of solid bismuth and antimony, $H^{F,M}$ the heat of formation at the temperature of mixing, H_{Bi}^{s} the heat of fusion of bismuth and x_2 the mole fraction of antimony. $H^{F,M}$ can be calculated with reference to the Helmholtz equation:

$$H^F(T_1) - H^F(T_0) = {}^eH(T_1) - {}^eH(T_0) \quad (2)$$

T_0 refers to the initial temperature, T_1 to any higher temperature and ${}^eH(T_1)-{}^eH(T_0)$ to the difference of the excess enthalpy which is given by

$${}^eH(T_1) - {}^eH(T_0) = [H_3(T_1)-H_3(T_0)] - (1-x_2)\cdot[H_1(T_1)-H_1(T_0)] - x_2\cdot[H_2(T_1)-H_2(T_0)] \quad (3)$$

Table 1. Enthalpy Values ($H_{50}{}^{t}$/J mol^{-1}) in the System Bi-Sb

t/°C	At-% Sb							
	10	20	30	40	50	60	70	80
60	258	258	250	260	270	250	250	250
70	522	522	513	522	540	513	488	501
80	782	782	771	791	808	771	752	798
90	1048	1038	1029	1058	1088	1038	1005	1008
100	1321	1300	1290	1318	1360	1290	1252	1260
110	1589	1569	1553	1592	1652	1553	1508	1518
120	1862	1840	1820	1860	1908	1820	1758	1782
130	2128	2100	2082	2134	2180	2108	2018	2041
140	2415	2375	2348	2408	2458	2375	2280	2305
150	2684	2654	2618	2685	2730	2644	2535	2558
160	2962	2922	2888	2948	3005	2912	2788	2835
170	3245	3203	3172	3228	3268	3180	3055	3092
180	3518	3473	3450	3500	3450	3328	3364	3364
190	3800	3750	3728	3777	3818	3720	3590	3618
200	4083	4033	4012	4058	4104	4002	3861	3888
210	4368	4308	4290	4340	4379	4268	4122	4160
220	4652	4600	4579	4618	4658	4548	4388	4421
230	4944	4884	4870	4900	4920	4832	4658	4690
240	5220	5167	5141	5179	5218	5101	4918	4957
250	5517	5456	5408	5472	5508	5379	5188	5228
260	5785	5760	5682	5748	5762	5171	5472	5505
270	6151	6048	5959	6039	6092	5959	5740	5775
280	9265	7025	6245	6325	6495	6285	6015	6055
290	13460	8450	6540	6620	6950	6640	6320	6330
300	16665	10085	7075	6910	7285	6950	6610	6600
310	17795	13740	7940	7240	7610	7300	6920	6890
320	18200	16040	10350	7620	8020	7680	7240	7180
330	18610	17530	12720	10020	8470	8050	7570	7480
340	19010	18500	14310	12160	9790	8430	7900	7790
350	19370	19220	15610	13770	11400	8950	8230	8100
360	19710	19810	16700	14960	12680	10080	8560	8410
370	20040	20330	17610	16010	13760	11210	8900	8710
380	20360	20790	18420	16790	14740	12160	9500	9010
390	20670	21220	19120	17920	15650	13050	10300	9310
400	20980	21620	19740	18850	16580	13900	11070	9610
410	21270	22000	20320	19700	17460	14730	11830	9940
420	21560	22360	20860	20480	18490	15560	12570	10380
430	21840	22720	21380	21200	19360	16440	13340	10910
440	22130	23070	21880	21830	20340	17320	14120	11490
450	22410	23410	22360	22420	21290	18370	14930	12120
460	22680	23750	22820	22990	22190	19320	15780	12790
470	22960	24080	23260	23530	23040	20540	16710	13490
480	23230	24410	23680	24070	23890	21610	17720	14260
490	23510	24720	24090	24570	24680	22790	18830	15080
500	23780	25010	24480	25060	25370	23930	20090	16000
510	24050	25280	24840	25520	25990	25020	21500	17010
520	24330	25650	25180	25940	26540	26020	23050	18170
530	24600	25910	25500	26320	27000	26910	24660	19460
540	24870	26170	25800	26640	27400	27710	26210	20830
550	25140	26420	26090	26930	27760	28410	27380	22500
560	25410	26680	26380	27230	28080	29020	28310	24270
570	25680	26940	26670	27510	28360	29560	29130	26110
580	25950	27190	26960	27790	28636	29990	29850	27690
590	26210	27450	27250	28070	28910	30330	30420	29190
600	26480	27710	27850	28350	29190	30590	30870	30450
610	26760	27960	27870	28360	29460	30850	31190	31500
620	27030	28220	28170	28910	29740	31110	31480	32320
630	27310	28470	28460	29190	30010	31360	31760	32980
640	27590	28730	28750	29470	30290	31610	23040	33430
650	27870	28980	29040	29760	30570	31870	32320	33760

Table 2. Excess Enthalpies (${}^{e}H_{50}{}^{t}$/J mol^{-1}) in the System Bi-Sb

t/°C	At-% Sb							
	10	20	30	40	50	60	70	80
60	0	0	−10	0	10	0	−10	−10
70	0	0	−10	0	10	0	−10	−10
80	10	−10	−30	0	20	0	−20	−30
90	10	−10	−40	0	30	0	−30	−40
100	10	−10	−50	0	30	0	−40	−50
110	10	−20	−60	0	40	0	−50	−60
120	10	−20	−60	0	40	0	−60	−70
130	20	−30	−70	0	50	0	−60	−70
140	20	−30	−70	0	50	0	−70	−80
150	20	−30	−80	0	60	0	−80	−90
160	20	−30	−80	0	60	0	−90	−90
170	20	−40	−80	0	60	0	−100	−90
180	30	−40	−80	0	60	0	−100	−100
190	30	−40	−80	0	70	0	−110	−100
200	30	−40	−80	0	70	0	−120	−100
210	30	−40	−80	0	70	0	−130	−110
220	30	−50	−80	0	70	0	−140	−110
230	40	−50	−80	10	70	0	−140	−120
240	40	−50	−70	10	80	0	−150	−120
250	40	−50	−70	10	80	0	−160	−130
260	40	−50	−60	−10	100	0	−170	−140
270	−10120	−9160	−8020	−6850	−5560	−4520	−3580	−2410
280	−7100	−8480	−8010	−6850	−5510	−4500	−3580	−2420
290	−3210	−7360	−8000	−6850	−5440	−4460	−3570	−2430
300	−300	−6100	−7740	−6850	−5350	−4400	−3550	−2430
310	+540	−2870	−7170	−6810	−5250	−4320	−3530	−2430
320	750	−970	−5060	−6730	−5120	−4230	−3430	−2420
330	870	+220	−2980	−4610	−4960	−4140	−3450	−2400
340	970	+900	−1680	−2760	−3920	−4030	−3400	−2370
350	1040	1330	−680	−1440	−2600	−3850	−3350	−2340
360	1090	1640	+120	−530	−1600	−3000	−3290	−2320
370	1130	1860	740	+220	−780	−2200	−3220	−2300
380	1160	2040	1270	900	−110	−1550	−2930	−2280
390	1190	2200	1670	1570	+530	−950	−2410	−2270
400	1200	2310	2010	2020	1150	−380	−1920	−2240
410	1220	2410	2300	2770	1780	+170	−1450	−2170
420	1230	2490	2560	3270	2430	710	−990	−2040
430	1230	2570	2790	3700	3120	1270	−520	−1790
440	1230	2630	3000	4050	3850	1850	−40	−1500
450	1230	2690	3200	4360	4480	2500	+490	−1150
460	1234	2742	3371	4642	5112	3252	1112	−772
470	1234	2792	3532	4902	5702	4082	1820	−355
480	1234	2845	3675	5120	6265	4965	2625	+135
490	1234	2875	3805	5385	6765	5855	3525	665
500	1224	2885	3905	5595	7175	6685	4485	1295
510	1224	2885	3985	5765	7485	7435	5585	2015
520	1224	2875	4045	5905	7725	8095	6805	2885
530	1222	2865	4085	5995	7885	8665	8125	3885
540	1212	2840	4095	6035	7995	9165	9365	5115
550	1212	2825	4105	6045	8065	9575	10255	6335
560	1202	2805	4115	6055	8095	9905	10925	7755
570	1202	2785	4125	6045	8095	10105	11495	9205
580	1202	2765	4125	6045	8085	10245	11975	10635
590	1192	2745	4135	6035	8075	10215	12275	11745
600	1192	2725	4145	6035	8055	10185	12425	12805
610	1185	2705	4145	6025	8045	10155	12425	13485
620	1185	2685	4155	6025	8025	10125	12415	14085
630	−815	−1325	−1795	−1935	−1955	−1845	−1535	−1505
640	−805	−1355	−1785	−1945	−1975	−1875	−1555	−1395
650	−805	−1375	−1785	−1945	−1995	−1910	−1575	−1305

The indices 1, 2, and 3 indicate bismuth, antimony, and the alloy, respectively. The enthalpies of the alloys were measured at even temperature intervals of 10 °C in the region 50 to 650 °C. The enthalpy differences between T_0 and T_1 for bismuth and antimony are reported and tabulated (see Ref. 7). The heat of mixing values are reported by Wittig and Gehring.[2)]

Results and Discussion

Results of the enthalpy measurements are presented in Table 1 at even temperature intervals of 10 °C in the range 50 to 650 °C. The values of the excess enthalpy are listed in Table 2 at even temperature intervals of 10 °C in the same region of temperature.

The data in Table 3 represent the integral and partial heat of formation at 200 °C. The error of the individual measurement was found to be about 1%. The experimental result is in good agreement with the calculated value. Table 3, also illustrate the ξ-values. For $\xi(T)$, the following equation was used:

$$\xi(T) = H^F(T)/x_2 \cdot (1-x_2) \quad (4)$$

The experimentally determined H^F-values were used to obtain a polynomial function for $H^F(T)$. The $H^F(T)$ function was employed together with Eq. 4 to derive the following relation for ξ:

$$\xi = 11.658 - 2.778x_2 \quad (5)$$

Using the ξ-function (Eq. 5) and Eq. 4, the heat of formation is given as a function of x_2 through the equation:

$$H^F(200\,°C) = 11.658x_2 - 14.436x_2^2 + 2.778x_2^3 \quad (6)$$

This equation represents the curve shown in Fig. 3. Table 3 illustrate the H^F-values, calculated with the aid of Eq. 6. These values are presented in brackets.

Table 3. Integral and Partial Molar Heats of Formation; ξ-Values in the Bi-Sb System at 200 °C

x_{Sb}	H^F / kJ mol^{-1} Found (Calcd)	$H_{Bi}{}^F$ / kJ mol^{-1}	$H_{Sb}{}^F$ / kJ mol^{-1}	ξ / kJ mol^{-1}
0.1	1.035 (1.024)	0.139	8.993	11.369
0.2	1.760 (1.770)	0.533	6.750	11.119
0.3	2.294 (2.273)	1.149	4.896	10.805
0.4	2.544 (2.531)	1.954	3.398	10.531
0.5	2.556 (2.567)	2.915	2.222	10.251
0.6	2.378 (2.398)	3.997	1.335	9.972
0.7	2.056 (2.398)	5.168	0.703	9.693
0.8	1.519 (1.501)	6.394	0.294	9.453

The partial molar heats of formation of bismuth and antimony are given by

$$H_{Bi}{}^F = H^F - x_2 \cdot (\partial H^F/\partial x_2)_{T,p} \quad (7)$$

$$H_{Sb}{}^F = H^F - (x_2-1) \cdot (\partial H^F/\partial x_2)_{T,p} \quad (8)$$

Using Eq. 6, we obtain

$$H_{Bi}{}^F = 14.436x_2^2 - 5.556x_2^3 \quad (9)$$

$$H_{Sb}{}^F = 11.658 - 28.872x_2 + 22.778x_2^2 - 5.556x_2^3 \quad (10)$$

The calculated partial molar heats of formation of bismuth and antimony are presented in Table 3.

The data in Table 3 clearly indicate that the heat of formation in the bismuth-antimony system is positive and larger than the heat of mixing. This leads to the

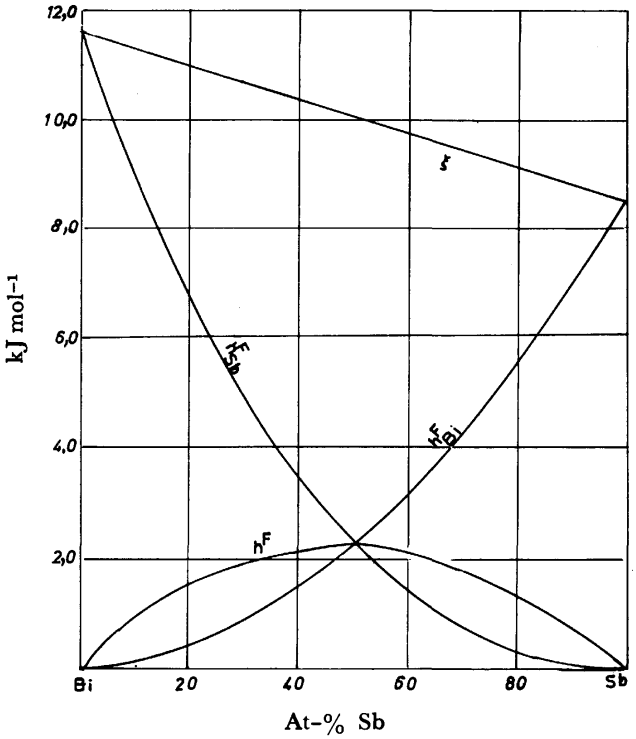

Fig. 2. The heat of formation, ξ-function and partial heats of formation of Bi and Sb in Sb–Bi system at 200 °C.

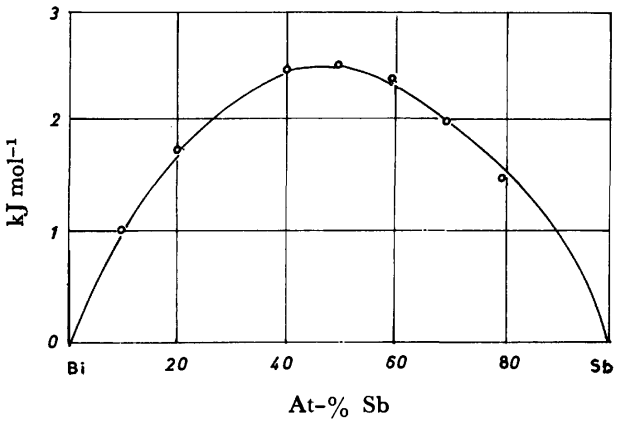

Fig. 3. Heat of formation in Bi–Sb system at 200 °C.

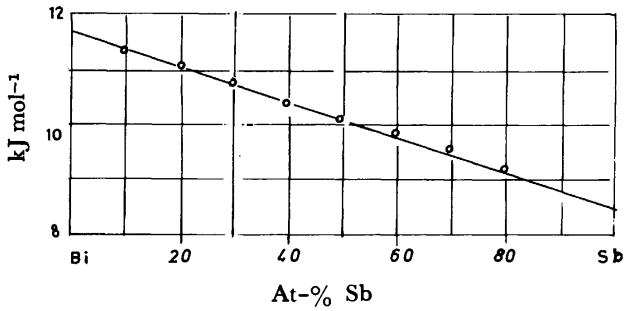

Fig. 4. ξ-Values in Bi-Sb system at 200 °C.

conclusion that there is a larger excess volume in the solid state. Bismuth expands more than antimony on solidification. As a result of this, the maximum of expansion lies at larger bismuth concentration.

Figure 2 shows the curves of the partial molar heats of formation of bismuth and antimony. These curves indicate that the partial heat of formation of bismuth is positive and increases with the increase of antimony mole fraction. The partial molar heat of formation of antimony is also positive but decreases with the increase of antimony mole fraction.

The heat of formation increases with the increase of the antimony mole fraction to reach a maximum at the point $x_{Sb}=0.5$ (Fig. 3); after that the heat of formation decreases with the increase of antimony mole fraction.

With reference to Eq. 5, ξ (200 °C) exhibits a linear function of x_2. Figure 4 represents the experimentally determined ξ-values at 200 °C.

References

1) M. Hansen and K. Anderko, "Constitution of Binary Alloys," 2nd Ed, McGraw Hill, New York-Toront-London (1958), pp. 1175/7.

2) F. E. Wittig and E. Gehring, *Naturwissenschaften*, **46**, 200 (1959).

3) J. Czochralski and E. Przyjemski, *Wiadomsci. Inst. Metallurg. Metaloznawstwa*, **3**, 113 (1936).

4) F. E. Wittig and F. E., u. F. Huber, *Ber. Bunsen Ges. Phys. Chem.*, **60**, 1181 (1956).

5) F. E. Wittig and F. E., u. G. Kemeny, *Chem. Ing.-Technik.*, **32**, 685 (1960).

6) F. E. Wittig and A. Stingle, *Z. Angew. Phys.*, **23**, 35 (1967).

7) R. L. Hulgren, R. L. Orr, P. D. Anderson, and K. K. Kelley, "Selected Values of the Thermodynamic Properties of Metals and Alloys," John Wiley, New York (1965, 1969, 1973).

 © 1987 The Chemical Society of Japan Bull. Chem. Soc. Jpn., 60, 2605—2610 (1987)

Dissociation Constants of Some Amino Acid and Pyridinecarboxylic Acids in Ethanol-H_2O Mixtures

M. S. K. Niazi* and J. Mollin†
Department of Chemistry, Quaid-i-Azam University, Islamabad, Pakistan
(Received December 24, 1985)

The dissociation constants of nicotinic, picolinic, benzoic, and *o*-, *m*-, and *p*-aminobenzoic acids and those of glycine, *dl*-alanine, β-alanine, aniline, and pyridine were determined potentiometrically and spectrophotometrically in 0, 10, 30, 50, and 72% (w/w) ethanol-water mixtures at 25 °C at various ionic strengths (0.01—0.5 mol dm^{-3}). The pK's of benzoic, *o*-, *m*-, and *p*-aminobenzoic acids increased with increase of EtOH contents while those of nicotinic acid, picolinic acid, glycine, *dl*-alanine, and β-alanine passed through minimum (upto 30% w/w EtOH contents). The pK's of aniline and pyridine were almost the same as those found in literature. The variation in pK's with the solvent composition is discussed in terms of the free energy of transfer from H_2O to EtOH-H_2O mixtures. The zwitterion to neutral molecule ratio of these acids is also discussed in terms of variation of composition of mixtures.

There has been increasing interest during past few years in properties of mixed solvent systems such as water+organic solvent or mixtures of organic solvent themselves.[1] While there have been many physicochemical studies in these mixed solvents, relatively few data are available on the effect of these mixed solvent systems on the dissociation of weak acids or bases.[2-10,20]

Acid-base equilibria of pyridine monocarboxylic acid monoaminobenzoic acids and simple aliphatic amino acids like glycine, *dl*-alanine, β-alanine are well known in aqueous medium[11-13,15,21] as in the following;

$$\begin{array}{ccc} N^+H_3CHRCO_2^- & \underset{-H^+}{\overset{H^+}{\rightleftharpoons}} & N^+H_3CHRCO_2H \\ -H^+\downarrow\uparrow H^+ & \diagdown\!\!\diagup & -H^+\downarrow\uparrow H^+ \\ NH_2CHRCO_2^- & \underset{-H^+}{\overset{H^+}{\rightleftharpoons}} & NH_2CHRCO_2H \end{array} \quad (1)$$

Mostly these substances exist as dipolar zwitterions with varying percentage in aqueous medium. These acids while titrated with strong base and acid dissociate according to Eqs. 2 and 3.

$$K_1 = \frac{[H^+][(N^+H_3CHRCO_2^- + (NH_2CHRCO_2H)]}{[N^+H_3CHRCO_2H]} \quad (2)$$

and

$$K_2 = \frac{[H^+][(NH_2CHRCO_2^-)]}{[(NH_3^+CHRO_2^-) + (NH_2CHRCO_2H)]} \quad (3)$$

Generally, these dissociation constants (K_1 and K_2) have been determined potentiometrically and spectrophotometrically in the UV region.[21]

Protonation of aniline and pyridine and dissociation of acetic and benzoic acids are also known in aqueous medium as well as in some mixed solvents.[6,7]

Some measurement on dissociation, thermodynamic properties and viscosities of glycine, *dl*-alanine and β-alanine are also available in literature.[9,17] We have chosen ethanol (EtOH)-water mixtures of composition 0, 10, 30, 50, and 71.98% weight (w/w) of EtOH. We have determined dissociation constants of pyridine monocarboxylic, benzoic, and acetic acids, aniline, and pyridine in these mixtures titrimetrically and by emf measurements of cells (I) and (II) and spectrophotometrically using the known procedures.[2,14,15,19]

Pt, H_2(1 atm)/HA(m_1), NaA(m_2), NaCl(m_3)/AgCl-Ag (I)

Pt, H_2(1 atm)/B+H(m_1), B(m_2), NaCl(m_3)/AgCl-Ag (II)

From these pK values, the free energy of transfer $-\Delta G_{tr}$(dis) of these substances have been calculated and are discussed in terms of the effect of composition of solvent mixtures. Some attempts have been made for evaluation of the ratio of (dipolar) zwitterionic form to neutral molecular form of these amino acids in these EtOH-H_2O mixtures.

Experimental

All the substances under study were reagent grade product from Lachema BRNO. Ethanol was of a spectral grade purity from Lachema BRNO and was used without further purification. Doubly distilled conductivity water was used as aqueous medium as well as for preparation of EtOH-H_2O mixtures in a weight by weight composition.

For the determination of pK's, ethanolic and aqueous solutions of the substances under investigation were prepared. The ionic strengths (μ=0.1, 0.2, 0.3, and 0.5 mol dm^{-3}) were maintained with sodium perchlorate (reagent grade, Lachema, BRNO). Titrations were performed with 0.1 M†† sodium hydroxide or perchloric acid (both reagent grade, from Lachema BRNO and Jenapharm respectively) in the same solvent. The pH's were measured using a glass electrode with calomel electrode in aqueous medium and with 0.1 M silver-silver chloride electrode in EtOH-H_2O mixtures at 25 °C. A titration vessel was kept in a thermostat at 25±0.01 °C. The electrode assembly was

† Present address: Department of Inorganic and Physical Chemistry, Palacky University, Olomouc, Czechoslovakia 77000.

†† 1 M=1 mol dm^{-3}.

calibrated with buffer solutions prepared according to literature.[2,7,19] The UV spectra for 10^{-4}—5×10^{-5} mol dm^{-3} solutions in water or mixtures were obtained with a Pye Unicam SP 1800 spectrophotometer. For spectrophotometric determination of pK's, solutions of the substances were mixed with solutions of perchloric acid of various concentrations or with mixtures of 0.1 M perchloric acid and 0.1 M KH_2PO_4 (reagent grade Lachema, BRNO) in water or ethanolic mixtures. During these experiments pH was measured with a hydrogen electrode against references as mentioned above. The emf's of cells (I) and (II) were also measured with the same pH meter. Solutions of the substances were half neutralized with 0.1 NaOH or 0.1 M $HClO_4$ before putting in cell (I) and cell (II).

Calculations and Results

The pK's of weak acid (HA) and a base (BH^+) with the dissociation processes $HA \overset{K_1}{\rightleftharpoons} H^+ + A^-$ and $BH^+ \overset{K_2}{\rightleftharpoons} B + H^+$ were evaluated from the following equations:

$$pK_1 = pH - \log\frac{[A^-]}{[HA]} - \log\gamma_{A^-} = pK_1' - \log\gamma_{A^-} \quad (4)$$

$$pK_2 = pH - \log\frac{[B]}{[BH^+]} + \log\gamma_{BH^+} = pK_2' + \log\gamma_{BH^+} \quad (5)$$

Here, $\log\gamma_{A^-}$ and $\log\gamma_{BH^+}$ were calculated from the Debye-Hückel limiting law (DHLL).[14,15] The values of densities and dielectric constants of water and EtOH-H_2O mixtures at 25 °C were taken from literature.[2,7,19] The values of the radii of these substances used in DHLL were from 3—10 Å. The pK's measured at different μ were plotted against $\mu^{1/2}$ and extrapolated to μ=0, the values being listed in Table 1.

For the evaluation of pK's by the emf method, Eqs. 6 and 7 were used.[2,19,22]

$$E = E^\circ_{Ag\text{-}AgCl} + \frac{2.303}{F}RT\log[(m_{H^+}\cdot\gamma_{H^+})\cdot(m_{Cl^-}\cdot\gamma_{Cl^-})] \quad (6)$$

$$pK = p\overset{*}{a}_H = -\log m_{H^+}\cdot\gamma_{H^+} = \frac{E - E^\circ_{Ag\text{-}AgCl}}{0.0591} + \log\gamma_{Cl^-} + \log m_{Cl^-} \quad (7)$$

where values of $E^\circ_{Ag\text{-}AgCl}$ in these mixtures and water were taken from literature.[2,19] These pK'a calculated by Eq. 7 were plotted against $\mu^{1/2}$ and extrapolated to μ=0 and are given in Table 1. It was found that these pK's are in accord within ±0.02 pK units with those determined by the potentiometric titration method.

The spectrophotometric data were used in Eq. 8 for calculations of pK's.

$$pK = pH + \log\frac{(A - A_2)}{(A_1 - A)} \quad (8)$$

where A_1 and A_2 are absorbances of substance in acidic and basic media while A is absorbance at some other

Table 1. Thermodynamic Dissociation Constants, pK_1, pK_2, or pK of Amino Carboxylic Acids in EtOH-H_2O Mixtures at 298 °K and Zero Ionic Strength (μ=0)

Acids %EtOH	Benzoic p$K\pm\delta$	Nicotinic		Picolinic		o-Aminobenzoic		m-Aminobenzoic		p-Aminobenzoic	
		p$K_2\pm\delta$	p$K_1\pm\delta$	p$K_2\pm\delta$	p$K_1\pm\delta$	p$K_2\pm\delta$	p$K_1\pm\delta$	p$K_2\pm\delta$	p$K_1\pm\delta$	p$K_2\pm\delta$	p$K_1\pm\delta$
0	4.18±0.02	4.83±0.02	2.09±0.04	5.47±0.02	1.82±0.04	4.92±0.02	2.14±0.04	4.78±0.02	3.11±0.04	4.91±0.02	2.39±0.04
10	4.29±0.02	4.58±0.02	1.98±0.04	5.30±0.02	1.74±0.04	5.03±0.02	2.05±0.02	4.88±0.02	3.02±0.04	5.08±0.02	2.21±0.04
30	5.24±0.02	4.37±0.02	1.89±0.04	5.06±0.02	1.63±0.04	5.43±0.02	1.82±0.04	5.14±0.02	2.85±0.04	5.64±0.02	2.05±0.04
50	5.67±0.02	4.60±0.02	1.77±0.04	5.24±0.02	1.54±0.04	6.15±0.02	1.43±0.04	5.51±0.02	2.72±0.04	6.47±0.02	1.80±0.04
72[a]	6.24±0.02	5.03±0.02	1.70±0.04	5.42±0.02	1.61±0.04	6.75±0.02	1.37±0.04	6.18±0.02	2.54±0.04	7.04±0.02	1.71±0.04

Substance %EtOH	Glycine		dl-Alanine		β-Alanine		Pyridine p$K\pm\delta$	Aniline p$K\pm\delta$	Ethyl nicotinate p$K\pm\delta$	Trigonelline p$K\pm\delta$
	p$K_1\pm\delta$	p$K_2\pm\delta$	p$K_1\pm\delta$	p$K_2\pm\delta$	p$K_1\pm\delta$	p$K_2\pm\delta$				
0	9.78±0.02	2.38±0.02	9.85±0.02	2.39±0.02	10.23±0.02	3.57±0.02	5.13±0.02	4.59±0.03	3.18±0.06	2.92±0.07
10	9.64±0.02	2.47±0.02	9.72±0.02	2.48±0.02	10.03±0.02	3.65±0.02	4.89±0.02	4.42±0.03	2.92±0.06	2.97±0.07
30	9.37±0.02	2.68±0.02	9.55±0.02	2.77±0.02	9.84±0.02	3.88±0.02	4.36±0.02	4.19±0.03	2.64±0.06	3.00±0.07
50	9.41±0.02	3.03±0.02	9.62±0.02	3.13±0.02	9.80±0.02	4.12±0.02	3.92±0.02	3.86±0.03	1.78±0.06	2.99±0.07
72[a]	9.58±0.02	3.21±0.02	9.78±0.02	3.47±0.02	9.99±0.02	4.51±0.02	3.54±0.02	3.73±0.03	1.68±0.06	3.00±0.07

a) 71.98=72.

Table 2. The $\Delta pK_a = pK_a^s(HA) - pK_a^w(HA)$ and $\Delta G_{tr}(dis)$ (kJ mol^{-1}) Values for Aminocarboxylic Acids in EtOH-H_2O Mixtures at 298 K

Acids %EtOH	Benzoic		Nicotinic		Picolinic		*o*-Aminobenzoic		*m*-Aminobenzoic	
	ΔpK	ΔG_{tr}(dis)	ΔpK	ΔG_{tr}(dis)	ΔpK	ΔG_{tr}(dis)	ΔpK	ΔG_{tr}(dis)	ΔpK	ΔG_{tr}(dis)
10	0.11	0.627	−0.25	−1.425	−0.17	−0.969	0.11	0.627	0.10	0.570
30	1.06	6.042	−0.46	−2.622	−0.41	−2.337	0.51	2.907	0.36	2.052
50	1.49	8.493	−0.23	−1.311	−0.23	−1.311	1.23	7.011	0.73	4.161
72	2.06	11.742	+0.20	−1.14	−0.05	−0.285	1.83	10.431	1.40	7.98
	p-Aminobenzoic		Glycine		*dl*-Alanine		*β*-Alanine		Aniline	
	ΔpK	ΔG_{tr}(dis)	ΔpK	ΔG_{tr}(dis)	ΔpK	ΔG_{tr}(dis)	ΔpK	ΔG_{tr}(dis)	ΔpK	ΔG_{tr}(dis)
10	0.17	0.969	−0.14	−0.798	−0.13	−0.741	−0.20	−1.14	−0.17	−0.969
30	0.73	4.161	−0.41	−2.337	−0.30	−1.71	−0.39	−2.223	−0.40	−2.28
50	1.56	8.892	−0.37	−2.109	−0.13	−0.741	−0.43	−2.451	−0.73	−4.161
72	2.13	12.141	−0.20	−1.14	−0.07	−0.399	−0.24	−1.368	−0.86	−4.902

%EtOH	10		30		50		72	
	ΔpK	ΔG_{tr}(dis)	ΔpK	ΔG_{tr}(dis)	ΔpK	ΔG_{tr}(dis)	ΔpK	ΔG_{tr}(dis)
Pyridine	−0.24	−1.368	−0.77	−4.389	−1.21	−6.897	−1.59	−9.063

pH of medium.[14,15,21] The pK's found by this method agree within ±0.03 units of pK with those obtained by the emf method. Therefore, Table 1 gives the average values of pK's of these substances obtained by three methods.

The free energy change in the transfer of these substances from H_2O(w) to EtOH-H_2O(s) mixtures was evaluated from Eq. 9 at 25 °C and are given in Table 2.

$$\left.\begin{aligned}\Delta G_{tr}(dis) &= 2.303\,RT(pK_a^s - pK_a^w)\\ &= 5.70(\Delta pK_a)\end{aligned}\right\} \quad (9)$$

Where pK_a^s and pK_a^w are dissociation constants in EtOH-H_2O mixtures and in H_2O respectively. The change in proton affinity ΔP_a of conjugate base ($\bar{A}$) of these acids on transfer from H_2O to H_2O+cosolvent were calculated by Eq. 10 at 25 °C and are given in Table 3.

$$\Delta P_a = 5.70\ (\Delta pK_a) + \Delta G_{tr}(H^+) - C \quad (10)$$

Here constant C=5.70 log (18.01 d_s/$M_s \cdot d_w$) in molar scale. The average mass M_s of EtOH-H_2O mixtures were calculated from Eq. 11.

$$M_s = 100/(\text{wt\% EtOH}/46.00) + (\text{wt\% } H_2O/18.016) \quad (11)$$

and $\Delta G_{tr}^{\circ}(H+)$ are free energies of transfer of proton from H_2O to EtOH-H_2O mixtures and were taken from literature.[23]

Discussion

The reproducibility of the measurements was ±0.01 both in the titrimetric as well as in the emf measurements and was ±0.03 in the spectrophotometric measurements. The pK values of all substances determined are in good agreement with earlier reported values in some EtOH-H_2O mixture.[2,7,9,19,24]

In Fig. 1, pK's of nicotinic and picolinic acids, glycine, *dl*-alanine, and *β*-alanine have been plotted against the reciprocal of dielectric constants (ε^{-1}) of EtOH-H_2O mixtures. These pK's decrease as the concentration of EtOH increases upto 30% (w/w) in the EtOH-H_2O mixtures and increase again in mixtures of higher EtOH contents. On the other hand pK's of *o*-, *m*-, and *p*-aminobenzoic acids (Table 1) and those of acetic acid[6] increase with increase in

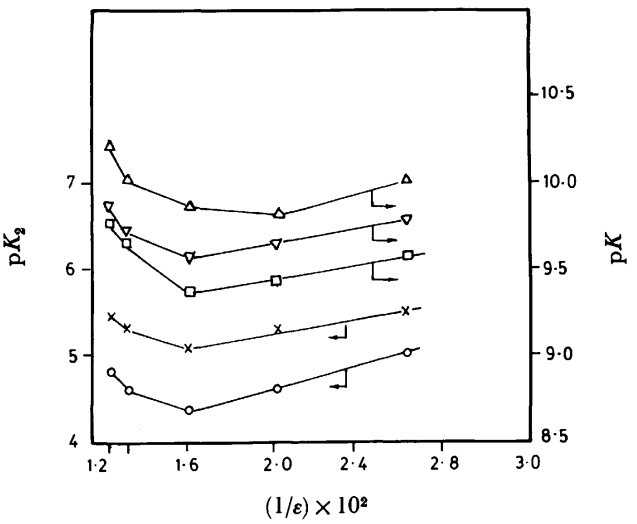

Fig. 1. Dependence of pK of Glycine (□) *dl*-alanine (▽), *β*-alanine (△), nicotinic acid (○), and picolinic acid (×) on inverse of permitivities (ε^{-1}) of EtOH-H_2O mixtures.

Table 3. Change in Proton Affinity ΔP_a (kJ mol^{-1}) in Transfer $H_2O \rightarrow EtOH\text{-}H_2O$ System: Values of $-\Delta P_a$ at 25 °C

%EtOH	$\bar{A}$=Conjugate base/Benzoate	Nicotinate	Picolinate	*o*-Amino-benzoate	*m*-Amino-benzoate	*p*-Amino-benzoate	Glycinate	*dl*-Alaninate	*β*-Alaninate	Aniline	Pyridine
10	2.635	0.578	1.038	2.6384	2.578	2.978	2.517	2.517	2.464	1.038	0.638
30	13.623	4.971	5.251	10.491	9.631	11.741	9.291	9.747	9.348	5.301	3.191
50	17.819	8.016	8.016	16.336	13.486	18.216	13.03	13.544	12.351	5.166	2.446
72	20.387	7.505	8.365	19.075	16.625	20.785	13.375	14.801	14.003	3.745	−0.415

%EtOH	$\Delta pK_2 = (pK^s - pK^w)$				$RT \ln (\Delta pK_2) = 5.7(\Delta pK_2)$			
	Glycinium	*dl*-Alaninium	*β*-Alaninium		Glycinium	*dl*-Alaninium	*β*-Alaninium	
10	0.09	0.09	0.08		0.513	0.513	0.456	
30	0.30	0.38	0.31		1.71	2.166	1.767	
50	0.65	0.74	0.55		3.705	4.218	3.025	
72	0.83	1.08	0.94		4.731	6.156	5.358	

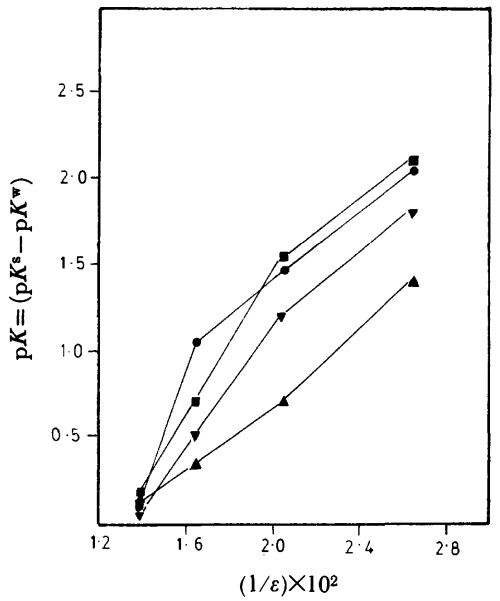

Fig. 2. Dependence of ΔpK of benzoic (●), *o*-(▲), *m*-(▼), and *p*-aminobenzoic acid (■) on inverse of permitivities (ε^{-1}) of EtOH-H_2O mixtures.

EtOH contents in EtOH-H_2O mixtures in a similar way as observed in case of benzoic acid (Fig. 2). It means that these aminobenzoic acids exist with stable structure as benzoic acid in EtOH-H_2O mixtures when ethanol contents are more than 10% (w/w). Further pK_1's of three aminobenzoic acids go on decreasing with increase of EtOH percentage in the same way as observed in case of aniline (Table 1). Therefore, one can postulate that *o*-, *m*-, and *p*-aminobenzoic acids exist as neutral molecules in EtOH-H_2O mixture rather than zwitterions as found in aqueous medium.

The anomalous dependence of pK_2's of glycine, *dl*-alanine, *β*-alanine, nicotinic, and picolinic acids on composition of EtOH-H_2O mixtures (Fig. 1) can be attributed to changes in structures of these acids when they transfer from H_2O to EtOH-H_2O media. Chattopadhyay et al.[9] have determined pK's of glycine, *dl*-alanine, *β*-alanine in some EtOH-H_2O mixtures and have evaluated K_Z (ratio of zwitterions to neutral molecules) of these acids with conclusion that this ratio (K_Z) decreases with increase of EtOH contents inferring preferential solvation of zwitterions with water and neutral molecules with alcohol. Wada et al.[20] have also determined the K_Z values of glycine in various water+organic solvent mixtures and have concluded that the K_Z value of glycine decreases with increase in the mole fraction of organic solvent. Khan et al.[3] have also postulated these results for nicotinic acid using ^{1}H NMR spectroscopy in DMSO-H_2O media and have pointed out that nicotinic acid exists in a neutral from in 80:20% DMSO-H_2O mixture.

In the present work, we have also chosen not only

nicotinic acid but its ethyl ester and trigonelline as model compounds. Table 1 shows that pK's of trigonelline almost did not change with change in composition of EtOH-H_2O mixtures. However, pK's of ethyl nicotinate and nicotinic acid decreased with increase of EtOH and become almost equal in 50 and 72% EtOH-H_2O mixtures. This decrease in pK values of nicotinic acid and its ethyl ester follows from the same course of decreasing as observed in case of pyridine with increase in EtOH (Table 1). As it has been assumed in literature[9,11,13] $K_Z=(K_1-K_E)/K_E$, one can verify that from the present values of K_1 and K_E of nicotinic acid and its ethyl ester, K_Z is equal to zero in 50% EtOH-H_2O mixtures. This procedure was also followed by Chattopadhyay et al.[9] in case of glycine and *dl*-alanine, etc.

Figure 3 (I—IV) are UV absorption curves of nicotinic acid, its ethyl ester and trigonelline at isoelectric points in 10, 30, 50, and 72% EtOH-H_2O mixtures at 25 °C. The UV spectra of these compounds show that nicotinic acid and its ethyl ester have similar absorption curves in 50 and 72% EtOH-H_2O mixtures but differ in H_2O and 10% EtOH-H_2O mixture. These spectra further assist in concluding that nicotinic acid exists as in a neutral form in EtOH-H_2O mixtures rather than zwitterions as found in aqueous medium.

Table 2 gives the values of free energy change ($-\Delta G_{tr}$(dis)) of dissociation on transfer of these acids from H_2O to EtOH-H_2O mixture. As shown in Fig. 2, the pK's of aminobenzoic acids and benzoic acid are not linear with variation of composition of EtOH-H_2O mixtures. Almost all compounds studied in the present work show remarkable deviation from $\Delta pK_a'$ calculated by using Born's equation.

$$pK_a = 122\left(\frac{1}{\varepsilon_r} - 0.0128\right)[(1/r_{H^+} + 1/r_{A^-})]$$

These deviations suggest that the effect of the EtOH-H_2O mixtures on the acidity of these amino

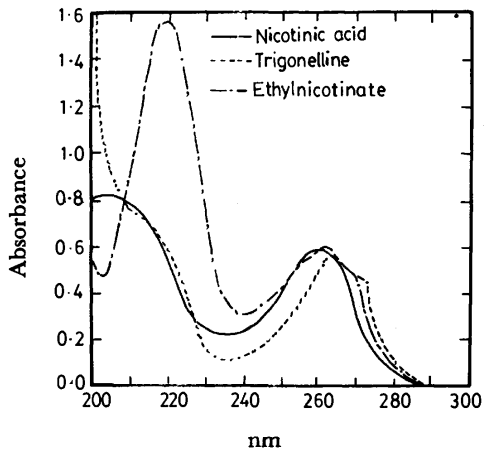

Fig. 3(I). UV spectra of nicotinic acid and its ethylester and trigonelline in 10% EtOH-H_2O mixture, at 25 °C, pH 3.43.

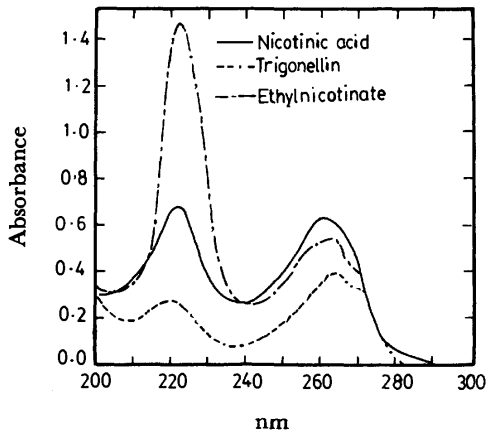

Fig. 3(II). UV spectra of nicotinic acid and its ethylester and trigonelline in 30% EtOH-H_2O mixture, of pH 3.22, at 25 °C.

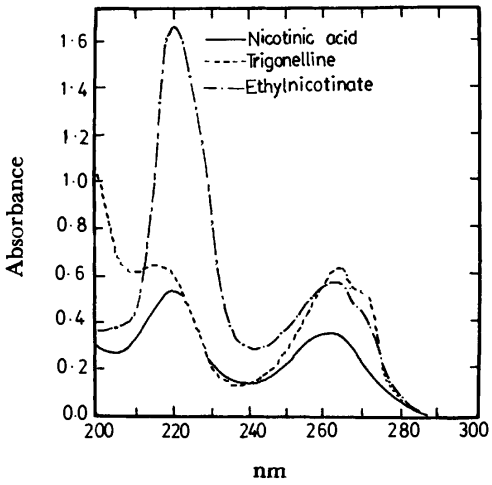

Fig. 3(III). UV spectra of nicotinic acid and its ethylester and trigonelline in 50% EtOH-H_2O mixture, 25 °C, pH 3.04.

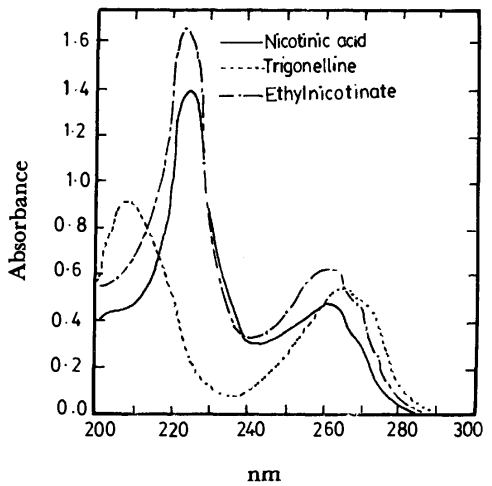

Fig. 3(IV). Same as above in 70% EtOH-H_2O mixture of pH 3.25, at 25 °C.

acids does not depend solely on electrostatic features, as predicated by Born's theory. It may also be caused by ignoring the variation in dielectric constant of the solvent molecules in the vicinity of an ion[25] and of specific change in $RH^{\mp} \rightleftharpoons RH$ i.e. from zwitterions to to neutral molecular form of these acid. If one divides G_{tr}(dis) into ΔG_{tr}(el) - electrostatic free energy and ΔG_{tr}(chem) - the non-electrostatic chemical free energy parts, of all these compounds, it is found that the contribution of the chemical free energy increases as the EtOH concentration is raised in case of aminobenzoic and benzoic acids but it passes through minimum in case of glycine, *dl*-alanine, *β*-alanine, and pyridine monocarboxylic acids. Again previous conclusion can be drawn.

The calculations of proton affinities ($-\Delta P_a$) of the corresponding conjugate bases of these amino acids are given in Table 3 in kJ mol^{-1}. These values show that again glycine, *dl*-alanine, *β*-alanine, and pyridinecarboxylic acids are grouped together giving similar trend in variation of ΔP_a with composition of EtOH–H_2O mixtures. While aminobenzoic acids are grouped together. Therefore, the present study fully supports the conclusion that these amino acids exist as in neutral molecular form in low polarity organic solvent mixtures with water rather than zwitterions as observed in aqueous medium.

Similar results are being found in some methanol-water mixtures and free enthalpy and entropy changes on dissociation of these amino acids are being measured in EtOH–H_2O mixture. These results will be published elsewhere in a near future.

References

1) O. Popovych and R. P. T. Tomkins, "Nonaqueous Solution Chemistry," John Wiley, New York, Chrichester, Brisbane, Toronto (1981).

2) W. J. Gelsema, C. L. De Ligny, and M. G. F. Visserman, *Recl. Trav. Chim. Pays-Bas*, **84**, 1129 (1965).

3) T. Khan, J. C., Halle, M. P. Simonin, and R. Schaal, *J. Phys. Chem.*, **81**, 587 (1977).

4) J. Mollin, *Collect. Czech. Chem. Commun.*, **40**, 2266 (1975).

5) B. Nowak and Z. Pawlak, *J. Chem. Soc., Faraday Trans. 1*, **78**, 2693 (1982).

6) J. C. Coupez and C. Madec, *Bull. Soc. Chim. Fr.*, **1971**, 4621.

7) J. Mollin and T. Kucerova, *Chem. Zvesti*, **33**, 52 (1979).

8) M. Georgieva, *Anal. Chim. Acta*, **101**, 139 (1978).

9) A. K. Chattopadhyay and S. C. Lahiri, *Electrochim. Acta*, **27**, 271 (1982); *Indian J. Chem.*, **15A**, 930 (1977).

10) F. Rodante, G. Ceccarani, and F. Fantanzzi, *Thermochim. Acta*, **72**, 335 (1984).

11) R. W. Green and H. K. Tong, *J. Am. Chem. Soc.*, **78**, 4896 (1956).

12) J. J. Christensen, D. P. Wrathal, R. M. Izatt, and D. O. Tolman, *J. Phys. Chem.*, **71**, 3001 (1967).

13) J. J. Christensen, R. M. Izatt, D. P. Wrathal, and L. D. Harsen, *J. Chem. Soc., A*, **1969**, 1212.

14) R. F. Cookson, *Chem. Rev.*, **74**, 5 (1974) and references therein.

15) E. J. King, "Acid-Base Equilibria," Pergamon Press, Oxford (1965).

16) M. Booij and G. Somsen, *J. Chem. Soc., Faraday Trans. 1*, **78**, 2851 (1982).

17) A. K. Mishra and J. C. Ahluwalia, *J. Chem. Soc., Faraday Trans. 1*, **77**, 1169 (1981).

18) N. C. Dey and B. K. Saikia, *Can. J. Chem.*, **58**, 1512 (1980).

19) M. Yu. Gorina and L. N. Seregina, *Electrokhimiya*, **8**, 829 (1972).

20) G. Wada, E. Tamura, M. Okina, and M. Nakamura, *Bull. Chem. Soc. Jpn.*, **55**, 3064 (1982).

21) A. Bryson, *J. Am. Chem. Soc.*, **82**, 4858, 4871 (1960).

22) R. G. Bates, "pH Its Determination and Practice," Wiley, New York (1973), Chap. 3.

23) C. F. Wells, *J. Chem. Soc., Faraday Trans. 1*, **80**, 2445 (1984).

24) G. K. W. Vogel K. Andrussow, "Dissociation Constant of Organic Acids in Aqueous Solution," Butterworth, London (1961): D. D. Perrin, "Dissociation Constants of Organic Bases in Aqueous Solution," Butterworth, London (1965).

25) M. Paabo, R. G. Bates, and R. A. Robinson, *J. Phys. Chem.*, **70**, 247 (1966).

 © 1987 The Chemical Society of Japan Bull. Chem. Soc. Jpn., 60, 2611—2614 (1987)

Approximate Formulas for Hosoya's Topological Index

Ivan GUTMAN* and Zoran MARKOVIĆ
Faculty of Science, University of Kragujevac, P.O.Box 60,
YU-34000 Kragujevac, Yugoslavia
(Received June 30, 1986)

Approximate formulas for Hosoya's topological index (Z) are reported for the first time. These formulas reproduce ln Z with an error of some 1—2% and require the knowledge of only a few easily obtainable invariants of the molecular graph.

The topological index Z was introduced by Hosoya[1] in 1971. Since then numerous scientific results on this quantity have accumulated[1-11] revealing the importance of Z in various branches of theoretical chemistry and theoretical physics. In particular, the relations between Z and several physicochemical properties of alkanes are nowadays well established.[3,5,7,10] Hosoya also showed[2] that Z and the closely related nonadjacent numbers play a significant role in the molecular orbital theory of conjugated π-electron systems.

This later resulted in the introduction of the modified topological index,[12] topological bond order,[13,14] matching polynomial,[15-17] a novel theory of aromaticity,[18,19] novel approach to total π-electron energy,[12,20] π-electron charge distribution[21] etc.

A detailed account of various applications of the index Z and especially of its mathematical properties can be found in Chapter 11 of the book.[11]

In spite of such a great interest towards Hosoya's topological index, no attempts seem to have been made to find approximate methods for its calculation. This is even more surprising if one knows that the evaluation of Hosoya's index is a very hard combinatorial task, especially in the case of large polycyclic molecules. In the present paper we wish to fill this gap and to provide a class of reliable approximate formulas for Z, enabling its estimation from a number of easily obtainable invariants of the molecular graph.

Preliminaries

Hosoya's topological index is defined as[1]

$$Z = Z(G) = \sum_{k=0}^{h} m(G,k),$$

where $m(G,k)$ is the number of k-matchings of the molecular graph G. This means that one can select k independent edges in G in $m(G,k)$ distinct ways; therefore $m(G,k)$ is often called the k-th nonincident number of G.

In what follows the molecular graph considered will be assumed to possess n vertices and m edges, whereas h will denote the size of the maximal matching (i.e. $m(G,h)\neq 0$, $m(G,h+1)=0$). Note that $m(G,1)=m$ and $h\leqslant n/2$. Besides, by definition, $m(G,0)=1$ for all graphs G.

The Z-counting polynomial

$$Q(x) = \sum_{k=0}^{h} m(G,k)x^k$$

is an auxiliary quantity, introduced within the theory of Hosoya's index,[1] with the immediate property

$$Q(1) = Z.$$

A less obvious property of $Q(x)$ is that all its zeros are real and negative numbers.[17] Therefore we can write the Z-counting polynomial as

$$Q(x) = \prod_{i=1}^{h} (1+p_i x)$$

where $p_i>0$ and $-1/p_i$ is a root of $Q(x)=0$, $i=1,2,\cdots,h$. Consequently,

$$Z = \prod_{i=1}^{h} (1+p_i).$$

The Approximation

The basic idea of the present consideration is to approximate the Z-counting polynomial $Q(x)$ by means of another polynomial $Q^{\times}(x)$,

$$Q^{\times}(x) = (1+Ax)^t(1+Bx)^{h-t} \tag{1}$$

and to adjust the parameters A and B so that the first three coefficients of $Q^{\times}(x)$ and $Q(x)$ coincide:

$$Q^{\times}(x) = 1 + m(G,1)x + m(G,2)x^2 + \cdots . \tag{2}$$

$Q^{\times}(1)$ would then provide an approximate expression for Z.

Combining Eqs. 1 and 2 we arrive at

$$tA + (h-t)B = m(G,1) \tag{3a}$$

$$\binom{t}{2}A^2 + \binom{h-t}{2}B^2 + t(h-t)AB = m(G,2). \tag{3b}$$

It is easily seen that the approximation $Q(x)\approx Q^{\times}(x)$ is equivalent to the assumption that among the zeros of $Q(x)$, t of them are mutually equal and the remaining $h-t$ zeros are also mutually equal. The problems arising in connection with the choice of the third parameter in Eq. 1, namely t, will be discussed in the subsequent section.

Bearing in mind that

$$m(G, 1) = m,$$

and

$$m(G, 2) = (m^2+m-d)/2,$$

where d denotes the sum of the squares of the vertex degrees of the graph G, we can transform the Eqs. 3a and 3b into the form

$$tA + (h-t)B = m \tag{4a}$$

$$tA^2 + (h-t)B^2 = d-m. \tag{4b}$$

The solution of the system (4) in which we are interested in is

$$A = (m+RS)/h, \tag{5}$$

$$B = (m-R/S)/h, \tag{6}$$

where

$$R = \sqrt{hd-m^2-hm}, \tag{7}$$

$$S = \sqrt{(h-t)/t}.$$

We show now that R is necessarily a real quantity. In order to do this note that the right-hand sides of Eqs. 4a and 4b are equal to the sum of the numbers $p_1, p_2, \cdots, p_h$ and $p_1^2, p_2^2, \cdots, p_h^2$, respectively. Since the inequality

$$\left(\frac{1}{n}\sum_{i=1}^{n} x_i\right)^2 \leqslant \frac{1}{n}\sum_{i=1}^{n} x_i^2$$

holds for arbitrary numbers $x_1, x_2, \cdots, x_n$, we conclude that

$$\left(\frac{1}{h}\sum_{i=1}^{h} p_i\right)^2 \leqslant \frac{1}{h}\sum_{i=1}^{n} p_i^2$$

i.e.

$$\left(\frac{1}{h}m\right)^2 \leqslant \frac{1}{h}(d-m)$$

i.e.

$$hd - m^2 - hm \geqslant 0$$

which is a sufficient condition for the reality of R.

It is now immediate to conclude that A is positive for all $1 \leqslant t \leqslant h-1$ whereas B is positive for $1 \leqslant t \leqslant T$; where T stands for the integer part of $m^2/(d-m)$.

Substituting Eqs. 5 and 6 back into Eq. 1 and setting $x=1$, we arrive at

$$Z^x = Z^x(t) = [1+(m+RS)/h]^t[1+(m-R/S)/h]^{h-t} \tag{8}$$

which is the required algebraic expression for our approximate formulas for Hosoya's index Z.

As a matter of fact, it can be shown[23] that $Z^x(t)$ is a monotonously decreasing function of the parameter t and that for $t=1$, $Z^x(t)$ is an upper bound for Z.

The Function Z^x of Some Series of Graphs

In order to illustrate Eq. 8 we have examined the function Z^x for three classes of graphs, namely for the star S_n, the path P_n, and the comb C_n:

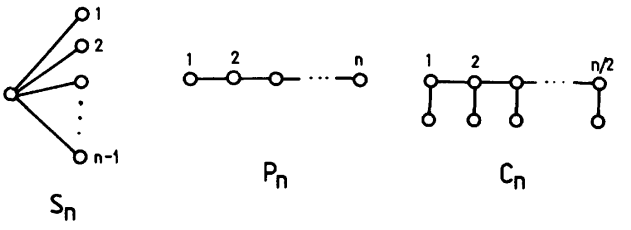

Both S_n, P_n, and C_n have n vertices and $n-1$ edges. Their topological indices are given as

$$Z(S_n) = n$$

$$Z(P_n) = \frac{1}{\sqrt{5}}\left[\left(\frac{1+\sqrt{5}}{2}\right)^{n+1} - \left(\frac{1-\sqrt{5}}{2}\right)^{n+1}\right]$$

$$Z(C_n) = \frac{1}{\sqrt{8}}[(1+\sqrt{2})^{n/2+1} - (1-\sqrt{2})^{n/2+1}].$$

For the star S_n we have $h=1$ and $d=(n-1)\cdot 1^2+1\cdot(n-1)^2=n(n-1)$ and therefore $R=0$. Consequently, $Z^x(S_n)=Z(S_n)$ for all values of n.

In the case of the path P_n, $h=n/2$ if n is even and $h=(n-1)/2$ if n is odd. Furthermore, $d=2\cdot 1^2+(n-2)\cdot 2^2=4n-6$. Substituting this back into Eqs. 7 and 8 we obtain an expression for $Z^x(P_n)$ whose form considerably differs from that of $Z(P_n)$. However, for large values of n,

$$Z^x(P_n) \approx t^{-t/2}(4n/9)^{t/2}(\sqrt{3})^n$$

whereas

$$Z(P_n) \approx \frac{1+\sqrt{5}}{2\sqrt{5}}\left(\frac{1+\sqrt{5}}{2}\right)^n.$$

This means that for large n, the logarithms of $Z(P_n)$ and $Z^x(P_n)$ are linearly proportional and, in particular,

$$\lim_{n\to\infty} \ln Z(P_n)/\ln Z^x(P_n) = [\ln(1+\sqrt{5})-\ln 2]/[(\ln 3)/2]$$

$$= 0.88$$

The above limit is independent of the parameter t and is not very different from the value 0.91, estimated for alkanes by least squares fitting (see later).

The case of the comb C_n is similar. Here $h=n/2$, $d=5n-10$ and for large values of n,

$$Z^x(C_n) \approx t^{-t/2}(5n/9)^{t/2}3^{n/2}$$

whereas

$$Z(C_n) \approx \frac{1+\sqrt{2}}{\sqrt{8}}(1+\sqrt{2})^{n/2}.$$

Therefore also the logarithms of $Z(C_n)$ and $Z^x(C_n)$ are linearly proportional and

$$\lim_{n\to\infty} \ln Z(C_n)/\ln Z^x(C_n) = \ln(1+\sqrt{2})/\ln 3 = 0.80.$$

The above examples can be generalized. Let G_1, G_2, $\cdots$, G_n, $\cdots$ be a series of graphs, such that G_{i+1} has

more vertices than G_i. Suppose that the parameter $d(G_n)$ is a linear function of n, say

$$d(G_n) = pn + q. \quad (9)$$

Suppose further that the limit L,

$$L = \lim_{n\to\infty} m(G_n)/h(G_n) \quad (10)$$

exists. Then for large values of n, the function $Z^x(G_n)$ behaves asymptotically as

$$Z^x(G_n) \approx t^{-t/2}\left(\frac{\sqrt{p}}{1+L}\right)^t (1+L)^{h(G_n)}.$$

Note that the conditions (9) and (10) are fulfilled for practically all molecular graphs. Furthermore, in almost all cases of chemical interest, the limit L equals to 2 and $h(G_n)\sim n(G_n)/2$.

Numerical Work

As already indicated in the previous section, a good linear correlation exists between ln Z and ln Z^x. We have examined this correlation on two samples of molecules—the hexanes, heptanes, octanes, and decanes from the book[24] (a total of 141 alkanes) and the benzenoid hydrocarbons from the paper[25] (a total of 116 benzenoid molecules). The results obtained are presented in Tables 1 and 2. Two approximate formulas have been investigated, viz.

$$\ln Z = a_0 \ln Z^x \quad (11)$$

$$\ln Z = a_1 \ln Z^x + b_1 \quad (12)$$

and the coefficients a_0, a_1, and b_1 calculated by least squares fitting.

The parameter t in Eq. 8 needs not be necessarily considered as an integer and we have examined the correlations of the type (11) and (12) for both integer and noninteger values of t, $0<t\leqq T$. Our calculations show, however, that the accuracy and the reliability of the approximations (11) and (12) are not very sensitive to the choice of t. If t is set to be a constant, then $t=1$ in the case of alkanes, and $t=2$ in the case of benzenoids gave the best results. For benzenoids a somewhat better correlation between Z and Z^x is found when t is adjusted to be equal to $T/2$.

The choice $t=T$ gave the worst correlation in both cases.

Table 1. Correlation between Hosoya's Index and $Z^x(t)$ in the Case of Alkanes with 6, 7, 8, 9, and 10 Carbon Atoms[24]

t	Formula	a_0 or a_1	b_1	Correlation coefficient	Mean error %	Max. error observed %
1	11	0.9707	—	0.995	1.4	3.0
1	12	0.9145	0.2224	0.995	1.1	3.0
$T/2$	11	0.9698	—	0.993	1.4	3.6
$T/2$	12	0.9507	0.0757	0.993	1.3	3.9
T	11	1.0200	—	0.984	2.0	6.1
T	12	1.0144	0.0212	0.984	2.0	6.2

Discussion

Our final conclusion is that in the case of alkanes

$$\ln Z = 0.914 \ln Z^x(t) + 0.222;\ t = 1,$$

whereas in the case of benzenoid hydrocarbons (as well as other polycyclic conjugated molecules)

$$\ln Z = 0.951 \ln Z^x(t) + 0.082;\ t = T/2$$

should be used for the approximate calculation of Hosoya's topological index. These formulas estimate ln Z with an error of some 1—2%, which is an acceptable accuracy for all practical applications of Hosoya's index.

The above formulas have been designed so to reproduce the topological indices of medium sized molecular graphs. However, in view of the three examples examined in a previous section, one may expect that formulas of the type (11) are capable to estimate the (logarithms of the) Hosoya indices of very large molecular graphs and infinite networks.

The right-hand sides of the above approximate expressions depend on the following invariants of the molecular graph: Number of edges (m), vertex degree sequence and size of the maximal matchings (h). The number of vertices and the number of maximal matchings play no (explicit) role in the present approach.

All the required invariants are easily obtained by inspection of the molecular graph. In particular, in the case of acyclic molecular graphs (i.e. molecular graphs of alkanes), $h=(n-n_0)/2$, where n is the number of vertices and n_0 is the number of isolated vertices which are obtained from the molecular graph by deleting from it a vertex of degree one and its first neighbor, and by repeating this deletion procedure

Table 2. Correlation between Hosoya's Index and $Z^x(t)$ in the Case of Benzenoid Hydrocarbons[25]

t	Formula	a_0 or a_1	b_1	Correlation coefficient	Mean error %	Max. error observed %
1	11	0.9166	—	0.9992	0.7	5.0
1	12	0.8917	0.3355	0.9992	0.6	4.0
2	11	0.9359	—	0.9995	0.8	10.2
2	12	0.9015	0.4554	0.9995	0.4	2.2
$T/2$	11	0.9574	—	0.9996	0.4	1.4
$T/2$	12	0.9511	0.0818	0.9996	0.4	1.4
T	11	1.0410	—	0.997	0.9	3.6
T	12	1.0282	0.1569	0.997	1.0	4.7

as long as it is possible. For practically all benzenoid hydrocarbons, $h=n/2$ if n is even and $h=(n-1)/2$ if n is odd.

References

1) H. Hosoya, *Bull. Chem. Soc. Jpn.*, **44**, 2332 (1971).
2) H. Hosoya, *Theor. Chim. Acta*, **25**, 215 (1972).
3) H. Hosoya, K. Kawasaki, and K. Mizutani, *Bull. Chem. Soc. Jpn.*, **45**, 3415 (1972).
4) H. Hosoya, *Fibonacci Quart.*, **11**, 255 (1973).
5) H. Narumi and H. Hosoya, *Bull. Chem. Soc. Jpn.*, **53**, 1228 (1980).
6) I. Gutman, *Croat. Chem. Acta*, **54**, 81 (1981).
7) H. Narumi and H. Hosoya, *Bull. Chem. Soc. Jpn.*, **58**, 1778 (1985).
8) H. Hosoya and A. Motoyama, *J. Math. Phys.*, **26**, 157 (1985).
9) H. Hosoya, *Comput. Math.*, **12B**, 271 (1986).
10) I. Gutman, *Z. Phys. Chem. (Leipzig)*, **267**, 1152 (1986).
11) I. Gutman and O. E. Polansky, "Mathematical Concepts in Organic Chemistry," Springer-Verlag, Berlin (1986).
12) H. Hosoya, K. Hosoi, and I. Gutman, *Theor. Chim. Acta*, **38**, 37 (1975).
13) H. Hosoya and M. Murakami, *Bull. Chem. Soc. Jpn.*, **48**, 3512 (1975).
14) H. Hosoya and K. Hosoi, *J. Chem. Phys.*, **64**, 1065 (1976).
15) I. Gutman, *Publ. Inst. Math. (Beograd)*, **22**, 63 (1977).
16) I. Gutman and H. Hosoya, *Theor. Chim. Acta*, **48**, 279 (1978).
17) C. D. Godsil and I. Gutman, *J. Graph Theory*, **5**, 137 (1981).
18) J. Aihara, *J. Am. Chem. Soc.*, **98**, 2750 (1976).
19) I. Gutman, M. Milun, and N. Trinajstić, *J. Am. Chem. Soc.*, **99**, 1692 (1977).
20) J. Aihara, *J. Org. Chem.*, **41**, 2488 (1976).
21) I. Gutman, T. Yamaguchi, and H. Hosoya, *Bull. Chem. Soc. Jpn.*, **49**, 1811 (1976).
22) I. Gutman, *Croat. Chem. Acta*, **46**, 209 (1974).
23) I. Gutman and J. Ciosłowski, *Z. Naturforsch.*, **42a**, 438 (1987).
24) R. R. Dreisbach, "Physical Properties of Chemical Compounds," Am. Chem. Soc., Washington (1959), Vol. I.
25) T. Yamaguchi, M. Suzuki, and H. Hosoya, *Nat. Sci. Rept. Ochanomizu Univ.*, **26**, 39 (1975).

 © 1987 The Chemical Society of Japan Bull. Chem. Soc. Jpn., 60, 2615—2617 (1987)

Activation Parameters of Bromoacetate-Thiosulfate Reaction in Ethylene Glycol-Water Mixtures

Prasanta Kumar Biswas, Anwarul Maula, and Mihir Nath Das*
Department of Chemistry, Jadavpur University, Calcutta 700032, India
(Received July 3, 1986)

The activation parameters for the reaction between bromoacetate ($\bar{R}$) and $S_2O_3^{2-}$ ions in water and aqueous mixtures of ethylene glycol (5—50% by weight) have been evaluated from the rate constants, corresponding to zero ionic strength, at 15, 25, and 35 °C. The standard free energies of transfer (ΔG_{tr}°) of the reacting ions and hence of the transition state ($\Delta G_{tr}^{\neq}$) from water to the mixed media at 25 °C have been determined from the measured solubilities of AgR, TlCl, and $Tl_2S_2O_3$ in the different media, using the reported values of ΔG_{tr}° of Ag^+ and Cl^- ions. Attempts have been made to interpret the kinetic results in the light of solvent properties and free energies of transfer. Although both the reacting ions are destabilized, on adding glycol to the medium, the larger destabilization of the transition state, arising from decreased dielectric constant as well as solvating capacity of the medium, outweighs the combined effects on the reactants leading to reduced reaction rates.

The kinetics of the reaction between bromoacetate and thiosulfate ions

$$BrCH_2COO^- + S_2O_3^{2-} = S_2O_3CH_2COO^{2-} + Br^-$$

has been and is still being used as a probe for studying the effects of various factors influencing reaction rates. Medium effects on the kinetics of the reaction have been studied in different types of water-organic mixtures[1-7] as well as in anhydrous methanol and ethylene glycol.[8] Results of kinetic studies on the reaction in aqueous mixtures of ethylene glycol (5—50% by weight) at different temperatures were reported earlier.[7] The free energies of transfer (ΔG_{tr}°) of the two reacting ions and hence of the transition state from water to the water-glycolic media have now been evaluated from solubility measurements, using TlCl, $Tl_2S_2O_3$, and silver bromoacetate (AgR) in the different media at 25 °C. The medium effects on the rates and activation parameters have been discussed in the light of solvent properties and transfer free energies.

Experimental

Ethylene glycol was purified by a standard procedure.[9] Sodium bromoacetate was prepared by the method of Kappana and Patwardhan.[10] Silver bromoacetate (AgR) was prepared by precipitation on adding $AgNO_3$ to sodium bromoacetate solution followed by filtration and thorough washig with cold water. TlCl and $Tl_2S_2O_3$ were similarly prepared by precipitation on adding NaCl and $Na_2S_2O_3$ respectively to saturated solutions of $TlNO_3$.

The solubilities of the three salts in water and the water-glycolic media at 25 °C were determined by titrating measured volumes of the saturated solutions as described below:

For AgR: The titrant was 0.01 M(1 M≡1 mol dm^{-3}) KCNS, and the indicator iron(III) alum,

For TlCl: The titrant was 0.08 M $AgNO_3$, and the indicator K_2CrO_4.

For $Tl_2S_2O_3$: Measured volumes of the saturated solutions were added to measured excess of standard iodine solutions followed by back titration with 0.03 M $Na_2S_2O_3$ using starch as the indicator. The solubilities of TlCl and $Tl_2S_2O_3$ were reproducible within ±2%. For AgR, the solubilities being very low in the glycol-rich media, the errors are higher, but the order of the magnitude is definitely reproducible.

Results and Discussion

The values of the rate constants (k_o) in water and the mixed media[7] at 25 °C corresponding to zero ionic strength, as obtained by extrapolation, and the ratios k_s/k_w are recorded in Table 1, where k_w and k_s are the respective values of k_o in water and any water-glycolic medium. The activation parameters for 25 °C were evaluated from the rate constants (k_o) at 15, 25, and 35 °C, as reported earlier,[7] by the usual method, and recorded in Table 1.

The rate constant decreases with increase in the glycol content in the medium, i.e. with decrease in the dielectric constant, as expected for a reaction between two ions of like charge, $\Delta H^{\neq}$ for the reaction is found to increase with increasing glycol concentration, and so does the value of $\Delta S^{\neq}$ (which is negative for each medium, as expected). Thus, there occurs a reasonable degree of compensation between $\Delta H^{\neq}$ and $T\Delta S^{\neq}$, but the larger effect of $\Delta H^{\neq}$ predominates leading to a monotonic decrease in the reaction rate.

The medium effect on $\Delta H^{\neq}$ may be examined on the basis of the classification of solvents into typically

Table 1. Variation of Rate Constants ($dm^3\ mol^{-1}\ min^{-1}$) and Activation Parameters (kJ mol^{-1}) at Zero Ionic Strength at 25 °C (Molar Scale)

Wt./% EG	k_0	k_s/k_w	$\Delta H^{\neq}$	$T\Delta S^{\neq}$	$\Delta G^{\neq}$	$m\delta\Delta G^{\neq}$	$\Delta G_{tr}^{\neq}$
0	0.72	—	50.5	−33.5	84.0	—	—
5	0.69	0.96	52.7	−31.4	84.1	0.1	2.4
20	0.59	0.82	53.3	−31.2	84.5	0.5	5.7
30	0.53	0.74	55.0	−29.8	84.8	0.8	8.2
50	0.43	0.60	56.2	−29.1	85.3	1.3	11.1

aqueous (TA) and typically nonaqueous (TNA) groups.[11,12] The excess functions, G^E and H^E, for aqueous mixtures of ethylene glycol are negative.[12-14] However, ethylene glycol in its aqueous mixtures is considered to form a borderline between the two groups, but leaning more towards TA.[12] On the basis of the model of Caldin and Bennetto,[15,16] the process of the formation of an 'encounter complex' between the reacting ions involves the movement of solvent molecules from the second zone of solvation to the bulk. This second zone is more or less disordered, approximating to an ideal mixture. Hence the excess functions correspond to the changes in the respective thermodynamic quantities occurring in the process of the transfer of the solvent molecules from the second zone to the bulk. If G^E and H^E are negative as for water-glycolic mixtures, this step should tend to decrease $\Delta G^{\neq}$ and $\Delta H^{\neq}$. The experimental results (Table 1) are, however, just the reverse. Obviously other factors predominate. The electrostatic factor definitely operates, leading to increasing $\Delta H^{\neq}$ and $\Delta G^{\neq}$, for the reaction between similarly charged ions, with decreasing dielectric constant. Moreover, decreasing solvation of the transition state may also cause its destabilization. The decreasing magnitude of negative value of $\Delta S^{\neq}$ (Table 1) may be taken to indicate progressive desolvation of the transition state, in comparison with the reacting ions. The desolvation may arise from an overall reduction in the solvating capacity of the mixed medium, as glycol molecules are gradually substituted for water molecules, because of intramolecular hydrogen bond formation between the adjacent OH groups in the glycol molecule.[17,18]

For a better insight into the medium effect on the rates and activation parameters, the results should be examined in the light of the free energies of transfer of the reactants and the transition state.

The standard free energies of transfer (ΔG°_{tr}) of AgR, TlCl, and $Tl_2S_2O_3$ from water to the mixed media were evaluated from the solubility products (K_{sp}) of the salts (Tables 2 and 3) by Eq. 1.

$$\Delta G^\circ_{tr}(\text{salt}) = RT \ln \frac{K_{sp}(w)}{K_{sp}(s)} \quad (1)$$

where w and s refer to water and any mixed medium respectively. The results are recorded in Tables 2 and 3.

The standard free energies of transfer of the bromoacetate ($\bar{R}$) ion from water to the mixed media at 25 °C were calculated by subtracting from ΔG°_{tr} (AgR) the corresponding literature values[19] for the Ag^+ ion (Table 2).

The ΔG°_{tr} values for the $S_2O_3^{2-}$ ion were obtained as described below. The ΔG°_{tr} (Tl^+) values were first calculated by subtracting from the ΔG°_{tr}(TlCl) values (Table 3) the reported values[18] of ΔG°_{tr} for the Cl^- ion. The ΔG°_{tr} values for the $S_2O_3^{2-}$ ion were then evaluated by subtracting the free energies of transfer of two moles of Tl^+, i.e. $2\Delta G^\circ_{tr}$ (Tl^+) from the corresponding values of ΔG°_{tr} ($Tl_2S_2O_3$), as determined in the present work and recorded in Table 3.

The single ion free energies of transfer for Ag^+ and Cl^-, used above, are based on the familiar extrathermodynamic TATB assumption that ΔG°_{tr} for the tetraphenylarsonium (TA^+) ion is the same as that for the tetraphenylborate (TB^-) ion for any particular medium. Wells[17,20] has used a different extrathermodynamic assumption for evaluating single ion free energies of transfer, and his values are in general appreciably different. The TATB assumption is, however, considered to be more sound.[21] Although uncertainties are unavoidably involved in the ΔG°_{tr} values for the single ions because of the extrathermodynamic assumption, some conclusions of a semiquantitative nature can definitely be drawn

Table 2. Solubility Products (K_{sp}) of Silverbromoacetate (AgR) and Standard Free Energies of Transfer (kJ mol^{-1}) of AgR, Ag^+, and R^- at 25 °C (Molar Scale)

Wt./ % EG	K_{sp}(AgR) $\times 10^8$	ΔG°_{tr} (AgR)	ΔG°_{tr} (Ag^+)[a]	ΔG°_{tr} (R^-)
0	13.3	—	—	—
5	7.0	1.6	−0.10	1.7
20	3.9	3.0	−0.40	3.4
30	2.7	3.9	−0.70	4.6
50	1.3	5.8	−1.40	7.2

a) Ref. 19.

Table 3. Solubility Products (K_{sp}) of TlCl and $Tl_2S_2O_3$ and Standard Free Energies of Transfer, ΔG°_{tr} (kJ mol^{-1}) of the Salts and Single ions at 25 °C (Molar Scale)

Wt./% EG	K_{sp}(TlCl) $\times 10^4$	ΔG°_{tr}(TlCl)	ΔG°_{tr}[a] (Cl^-)	ΔG°_{tr} (Tl^+)	$K_{sp}(Tl_2S_2O_3) \times 10^7$	$\Delta G^\circ_{tr}(Tl_2S_2O_3)$	$\Delta G^\circ_{tr}(S_2O_3^{2-})$
0	4.58	—	—	—	4.36	—	—
5	3.99	0.3	0.3	0	3.33	0.6	0.6
20	3.00	1.1	1.0	0.1	1.96	2.0	1.8
30	2.72	1.3	1.4	−0.1	1.54	2.6	2.8
50	2.40	1.6	1.1	0.5	1.03	3.6	2.6

a) Ref. 18.

therefrom in respect of the medium effect.

The medium effect on the free energy of activation ($m\delta\Delta G^{\#}$) is given by Eq. 2.

$$m\delta\Delta G^{\#} = \Delta G^{\#}(s) - \Delta G^{\#}(w) \quad (2)$$

where w and s denote water and any mixed medium respectively. The standard free energy of transfer of the transition state ($\Delta G^{\#}_{tr}$) is given by Eq. 3.

$$\Delta G^{\#}_{tr} = m\delta\Delta G^{\#} + \Delta G^{\circ}_{tr}(\overline{R}) + \Delta G^{\circ}_{tr}(S_2O_3^{2-}) \quad (3)$$

The values of $m\delta\Delta G^{\#}$ and $\Delta G^{\#}_{tr}$ are shown in Table 1.

From Tables 1—3 it will be seen that for both the reacting ions as well as the transition state, ΔG°_{tr} values are positive, increasing with the proportion of glycol in the medium. The effect on the $\overline{R}$ ion (Table 2) is distinctly larger than that on the $S_2O_3^{2-}$ ion (Table 3). For the transition state (Table 1), however, the transfer free energy ($\Delta G^{\#}_{tr}$) is not only larger than the corresponding value of either of the reacting ions, but preponderates over the combined effect on the two reactants taken together, leading to a reduced rate. Thus, basically it is the large destabilization of the transition state which dictates the resultant medium effect on the reaction rate. The effect, however, is not as pronounced as it might have been, because of the simultaneous destabilization of the reacting, ions, although occurring to a smaller extent.

We thank the University Grants Commission, New Delhi, for the award of fellowships to P. K. B. and A. M. and the authorities of R. B. C. College, Naihati, West Bengal for granting P. K. B. leave of absence.

References

1) A. N. Kappana, *J. Indian Chem. Soc.*, **6**, 419 (1929).
2) V. K. LaMer and M. E. Kamner, *J. Am. Chem. Soc.*, **57**, 2669 (1935)
3) D. Straup and E. J. Cohn, *J. Am. Chem. Soc.*, **57**, 1794 (1935).
4) V. K. LaMer, *J. Frank. Inst.*, **225**, 709 (1938).
5) S. Eagle and J. C. Warner, *J. Am. Chem. Soc.*, **58**, 2335 (1936).
6) H. G. Davis and V. K. LaMer, *J. Chem Phys.*, **10**, 585 (1942).
7) Anwarul Maula, *Indian J. Chem.*, **16A**, 1049 (1978).
8) L. D. Clements, Jr., *Ind. Eng. Chem., Process Des. Dev.*, **10**, 401 (1971).
9) "Techniques of Organic Chemistry," 2nd ed, ed by J. A. Riddick and E. E. Toops, Jr., Interscience, New York (1955), Vol. 7, p. 362.
10) A. N. Kappana and H. W. Patwardhan, *J. Indian Chem. Soc.*, **9**, 379 (1932).
11) M. J. Blandamer and J. Burges, *Chem. Soc. Rev.*, **4**, 55 (1975).
12) M. J. Blandamer, "Advances in Physical Organic Chemistry," ed by V. Gold and D. Bethel, Academic Press, New York (1977), Vol. 14, p. 327.
13) H. M. Trimble and W. Potts, *Ind. Eng. Chem.*, **27**, 66 (1935).
14) H. G. Konneke, H. Steinert, and E. Leibnitz, *Z. Phys. Chem. (Leipzig)*, **208**, 148 (1957).
15) E. F. Caldin and H. P. Bennetto, "The Physical Chemistry of Aqueous Systems," ed by R. L. Kay, Plenum, New York (1973), pp. 129—131.
16) P. P. Tejeda, J. R. Velasco, and F. S. Burgos, *J. Chem. Soc., Dalton Trans.*, **1983**, 2679.
17) C. F. Wells, *J. Chem. Soc., Faraday Trans. 1*, **71**, 1868 (1975).
18) A. K. Das and K. K. Kundu, *Indian J. Chem.*, **16A**, 467 (1978).
19) K. K. Kundu and A. J. Parker, *J. Solution Chem.*, **12**, 847 (1981).
20) C. F. Wells, *J. Chem. Soc., Faraday Trans. 1*, **77**, 1515 (1981).
21) J. I. Kim, *J. Phys. Chem.*, **82**, 191 (1978).

 © 1987 The Chemical Society of Japan Bull. Chem. Soc. Jpn., 60, 2619—2626 (1987)

Zirconium-Bis(triethylamine): A New Class of Chelate Ion and Anion Exchanger

Jagdish Prasad RAWAT,* Masood ALAM,† Hasan M. Abdul AZIZ, and Balbir SINGH††
Department of Chemistry, Aligarh Muslim University, Aligarh-202001, India
(Received August 12, 1985)

A new inorganic ion exchanger, zirconium-bis(triethylamine) has been synthesized. The material has been studied for its anion exchange capacity, sorption capacity, K_d values, composition, infrared spectrum and thermodynamic behavior. Analytically important separation of anions have been achieved. Ion exchange equilibria of $Cr_2O_7^{2-}$, CrO_4^{2-}, SO_4^{2-}, $S_2O_3^{2-}$, and MnO_4^- systems have been studied at 30, 40, 45, and 60 °C. The exchange isotherms have been measured for both forward and backward reactions with solutions of ionic strength 0.10 by batch process. The isotherms showed S shaped curves. The overall thermodynamic data are also calculated.

In the continued effort to synthesize a new inorganic anion exchanger based on metal hydroxides with amino groups, some materials of this kind have been tried: Tin(IV)-bis(diethanolamine),[1] titanium-bis(diethanolamine),[2] aluminium triethanolamine,[3] and thorium triethanolamine.[4] The studies on these materials pave the way to develop some analytically important separations on the basis of their anion exchange behavior and for sorption of metal ions on the basis of their chelating action. Therefore the studies were extended to synthesize another material of this kind, zirconium-bis(triethylamine). The material has been studied for its anion exchange capacity, sorption capacity and distribution of different anions to measure selectivity. Composition and IR studies are made to characterize the exchanger. Thermodynamic study is actually the study of ion exchange equilibrium, which tells the possibility of an ion exchange process, it's spontaneity for different exchange systems can be compared by the free energy concept. Therefore, such a study was made on this exchanger, zirconium-bis(triethylamine).

Experimental

Apparatus. An electric temperature controlled SICO shaker, a Bausch and Lomb Spectronic 20 (USA) and an Elico pH-meter model Li-10 (India) were used for shaking, spectrophotometric determination and pH measurements, respectively.

Reagents. Zirconium dichloride oxide (BDH) and triethylamine (E. Merck) were used. The other chemicals were of analytical grade.

Synthesis. Zirconium-bis(triethylamine) was prepared by mixing 0.10 mol dm^{-3} zirconium dichloride oxide solution with 0.10 mol dm^{-3} solution of triethylamine in the ratio of 1:2 (Table 1). The precipitate thus obtained was kept standing for 24 h at room temperature (25±1 °C). The precipitate was then filtered and washed with deionized water. It was dried in an air oven at 40 °C and then kept in the air for 12 h. The dried material on immersion in water broke down in small pieces. The exchanger granules were converted into nitrate form by keeping in 1.0 mol dm^{-3}

Table 1. Conditions of Preparation and Properties of Zirconium-Bis(triethylamine) Exchanger

Sample	Conditions of synthesis		Mixing volume ratio	Nature of precipitate	Propertie	
	Molarity of reagent					
	Zirconium dichloride oxide	Triethylamine			Ion exchange capacity ($Cr_2O_7^{2-}$)	Sorption capacity [Cu(II)]
	mol dm^{-3}	mol dm^{-3}			meq g^{-1}	meq g^{-1}
S-1	0.10	0.10	1 : 1	Precipitate appears but dissolves on shaking.	—	—
S-2	0.10	0.10	2 : 1	Precipitate appears but dissolves on shaking.		
S-3	0.10	0.10	1 : 2	A thick precipitate.	3.20	0.42
S-4	0.10	0.10	1 : 3	Precipitate appears but dissolves.	—	—
S-5	0.10	0.10	3 : 1	Precipitate appears but dissolves.	—	—

† Present address: Engineering College, Jamia Millia Islamia, New Delhi-110 025, India.
†† Present address: Envirotech Instruments (P) Ltd. A-239 Okhala Industrial Complex Phase-I, New Delhi, India.

sodium nitrate solution overnight intermittently replacing the supernatant liquid with fresh solution of sodium nitrate. It was finally washed and dried at 40 °C. The anion exchange capacity of zirconium-bis(triethylamine) was determined by column method. The anion exchanger weighing one gram was poured in a glass column measuring 20 cm in length and 0.60 cm diameter with a glass wool support. The capacity was calculated for different anions, namely chromate, dichromate, chloride, bromide, iodide, thiosulfate, sulfate, and thiocyanate by converting the exchanger in the required form with sodium or potassium salts of the required ions. The column was washed with deionized water. The eluent used was 1.0 mol dm^{-3} sodium nitrate. The elution rate was fixed at 0.5 cm^3 min^{-1}. Anion exchange capacities for Cl^-, Br^-, I^-, SO_4^{2-}, $S_2O_3^{2-}$, SCN^-, CrO_4^{2-}, and $Cr_2O_7^{2-}$ were 0.20, 0.16, 0.10, 1.00, 0.27, 0.15, 2.50, and 3.20 meq g^{-1}, respectively.

For sorption capacity 1.0 g of the exchanger was taken in the column, 10.0 cm^3 of 0.10 mol dm^{-3} copper(II) solution was poured over the column at a rate of 0.5 cm^3 min^{-1}. The effluent was then titrated and copper ions were determined. A fresh sample of 10.0 cm^3 of 0.01 mol dm^{-3} copper(II) nitrate was added over the column and the effluent was again titrated. The readings of EDTA consumed for total effluent was subtracted from the reading of EDTA consumed for total influent (0.01 mol dm^{-3} copper nitrate). The sorption capacity was then calculated from these readings. For the determination of copper(II) ions, the solution was titrated against 0.01 mol dm^{-3} EDTA solution using buffer of pH 3.6 and 1-(2-pyridylazo)-2-naphthol (PAN).

The composition of zirconium-bis(triethylamine) was determined by dissolving 1.0 g exchanger in 50.0 cm^3 aqua regia. Heating was avoided for preparing solution. It was then made upto the mark in a 100 cm^3 volumetric flask with deionized water. The amount of zirconium present in the sample was determined by chelometric titrations using copper PAN indicator while quantitative determination of triethylamine in another portion of the sample was done spectrophotometrically by ninhydrin.[5]

To check the chemical stability of the exchanger, zirconium-bis(triethylamine), 0.5 g of the exchanger was shaken with different solvents for 4 h. The amount of zirconium present in the supernatant liquid was determined by titrating a known volume of the solution against EDTA and the amount of triethylamine was determined spectrophotometrically in another sample by ninhydrin. The stability of the exchanger in different solvent systems reveal that the exchanger is stable in deionized water, methyl alcohol, ethyl alcohol, aqueous ammonia (10.0 mol dm^{-3}). However, the exchanger is less stable in concentrated solutions of acids.

Different samples of zirconium-bis(triethylamine) were heated in a muffle furnace for 4 h. The capacity of the exchanger at 60, 100, 150, 200, 300, and 400 °C were determined, respectively.

To characterize the exchanger infrared studies were performed. The spectrum of zirconium-bis(triethylamine) was observed by using KBr disc. The results are presented in Fig. 1.

IR spectrum of zirconium-bis-(triethylamine) exchanger shows the absorption peaks at different values of wave number as given below: (a) A broad peak ranging from 3300—3550 cm^{-1} is due to O-H stretching vibrations. (b) A strong peak at 1380 cm^{-1} is due to C-N vibrations and C-H bending vibrations. (c) A medium peak lies at 2930 cm^{-1} due to C-H stretching vibrations. (d) A strong C-C stretching vibration is observed in the frequency range of 1620—1660 cm^{-1}. (e) A medium C-N bending frequency lies in the frequency range 1070—1080 cm^{-1}, and (f) A medium peak in the frequency range of 800—840 cm^{-1} is observed due to metal oxygen bending vibrations.

pH Titrations of the exchanger were performed by shaking 0.50 g of the exchanger with solution of 0.01 mol dm^{-3} HCl and its salts of 0.01 mol dm^{-3} concentration by Topp and Pepper method.[6] The volume of the reaction mixture was kept 50.0 cm^3 in each case. The pH of the solution was noted after equilibrating the solution for 4 h. Results are plotted in Fig. 2.

K_d Values for anions were determined by batch process.

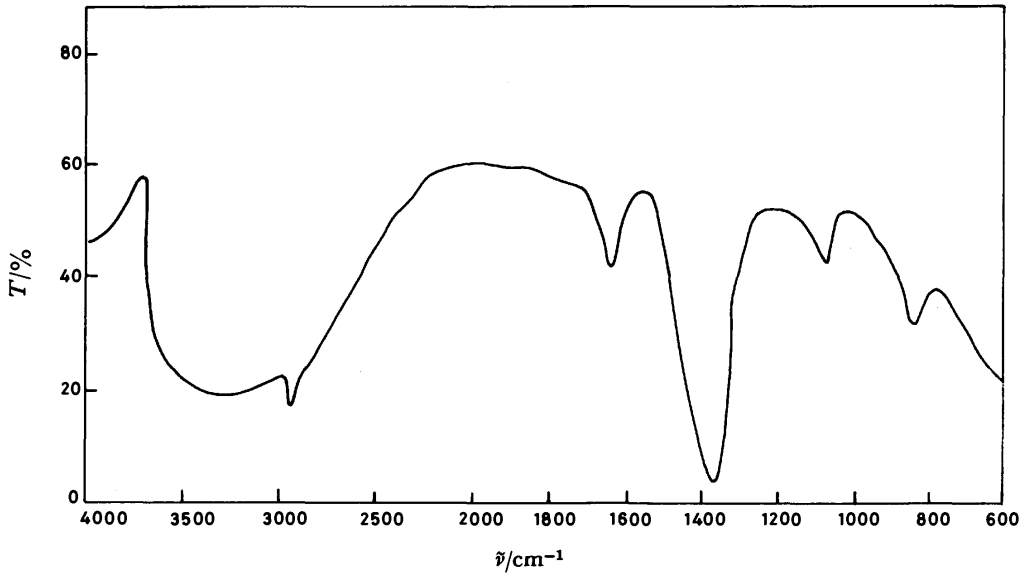

Fig. 1. IR spectrum of zirconium-bis(triethylamine) exchanger.

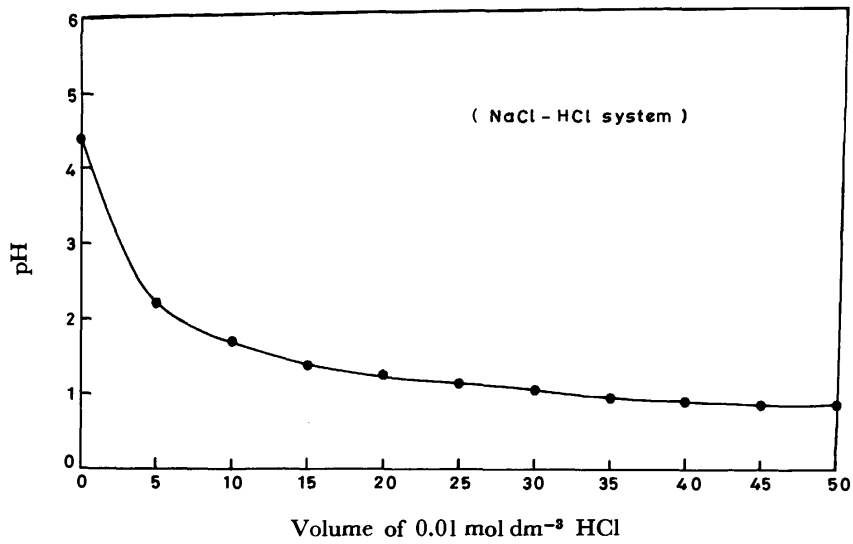

Fig. 2. Potentiometric titration curve for zirconium-bis(triethylamine) exchanger.

Table 2. K_d Values for Different Anions in Different Solvents

Sample No.	Anion	K_d value in				
		Water	NaOH 10^{-4} mol dm^{-3}	NaOH 10^{-3} mol dm^{-3}	NaOH 10^{-2} mol dm^{-3}	NaOH 10^{-1} mol dm^{-3}
1	Chloride	267±5	256±4	171±3	48±2	42±3
2	Bromide	200±3	175±2	153±4	20±2	8±2
3	Iodide	115±4	79±3	72±2	43±3	34±3
4	Dichromate	T.A.	T.A.	T.A.	4±1	0
5	Chromate	T.A.	T.A.	271±3	60±1	0
6	Thiosulfate	T.A.	T.A.	T.A.	11±4	2±1
7	Thiocyanate	132±2	116±3	108±2	10±1	0
8	Iodate	800±2	620±4	414±5	56±6	0
9	Peroxodisulfate	566±5	263±6	100±2	54±1	5±1
10	Bromate	1114±8	466±6	372±5	31±5	11±2
11	Sulfate	T.A.	T.A.	T.A.	0	0
12	Sulfite	T.A.	T.A.	T.A.	34	23
13	Hexacyanoferrate(III)	T.A.	T.A.	300±4	0	0
14	Hexacyanoferrate(II)	T.A.	T.A.	150±3	4±1	0
15	Arsenite	T.A.	T.A.	T.A.	1750±6	58±2
16	Phosphate	T.A.	2750±5	230±2	125±2	20±2
17	Vanadate	570±3	340±2	120±3	25±2	25±2

T.A. = Total adsorption.

1.0 cm^3 of anionic solution was taken in a 50.0 cm^3 volumetric flask. The remaining volume was filled up with NaOH solution in which its distribution studies were to be studied. This solution was then shaken for 4 h with the exchanger weighing 0.50 g in a shaker. The anions which remained in the solution after equilibration were then determined. Total amount of anions were also determined without equilibration. Results of the K_d values in deionized water and different concentrations of sodium hydroxide solutions are summarized in Table 2.

The anions having large differences in K_d values were tried for the separations. The column was prepared using 2.0 g of the exchanger (150—200 mesh size) in nitrate form in a glass column having a height of 30 cm and diameter 0.60 cm. A mixture of anionic solutions was poured on to the column. The solution was allowed to flow down very slowly through the column. These anions were adsorbed at the top of the exchanger bed forming initial zone. Column was washed with deionized water. The anions were then eluted by appropriate eluting reagent. The amount of anions were then determined by standard methods.

To study the thermodynamic behavior of the exchanger, the material (50—100 mesh) was converted to other anionic form by placing the material in a column and passing 1.0 mol dm^{-3} potassium or sodium salts of the respective anions until the concentration of anions in the eluent and eluate was identical. The sample was washed with deionized water until it was free from anions. After drying

the exchanger it was stored in the stoppered bottle.

The equilibrium experiments were performed by taking 20 cm^3 solution containing sodium or potassium nitrate solution and appropriate anion solution. The ionic strength of the total content was kept 0.10 mol dm^{-3} in the stoppered conical flasks. To this 0.20 g of the exchanger in nitrate form was added and flasks were shaken thoroughly in a temperature controlled shaker for 4 h at desired temperatures. Equilibrium was attained within this period and aliquots from supernatant solutions were analyzed for anions.

Experiments were also performed by equilibrating the exchanger in the particular anionic form with sodium nitrate solution at 30 °C.

Results and Discussion

The results of Table 1 show that for complete precipitation to occur, zirconium dichloride oxide to triethylamine ratio must be kept 1:2.

Anion Exchange Capacity. Anion exchange capacity of the exchanger is quite high. The capacity for dichromate, chromate, and sulfate is 3.20, 2.50, and 1.00 meq g^{-1}, respectively. A very high value of ion exchange capacity towards chromate ion (3.2 meq g^{-1}) is in accordance with the results of zirconia. The order for capacity for halides is $Cl^->Br^->I^-$. The capacity of the exchanger decreases as the ionic size of the halide increases and for some other ionic species the capacity decreases in the order $Cr_2O_7^{2-}>SO_4^{2-}>S_2O_3^{2-}$. Thus the exchanger behaves a chelating as well as an anion exchanger. On the basis of the above discussions it is concluded that zirconium-bis-(triethylamine) shows anion exchange capacity due to the presence of $-N^+-$ group and chelating properties due to the presence of $-\ddot{N}-$ group.

Sorption Capacity. The sorption capacity of copper(II) was found to be 0.42 meq g^{-1} of zirconium-bis(triethylamine). When zirconium-bis(triethylamine) in H^+ form was kept in contact with a solution of sodium nitrate, no release of H^+ was observed. When exchanger was kept in Cu(II) solution it turned blue in appearance. Copper(II) ions were so strongly attached to zirconium-bis(triethylamine) exchanger that even strong chelating group EDTA did not completely detach copper(II) from the exchanger. Hence sorption capacity was calculated by column method. Due to this great affection of exchanger for metal ions like copper(II), K_d values were not calculated for the metal ions.

Composition. The results of composition studies show that zirconium and triethylamine are present in the molar ratio of 1:2 in the exchanger. Results show that the exchanger is quite stable in aqueous and basic media. The use of acidic solutions of greater concentrations must be avoided.

Effect of Heating. The results of effect of temperature on the capacity of the exchanger, show that the capacity decreases with the increase in temperature. At higher temperatures the water molecules and amine molecules are lost from the exchanger thereby decreasing the capacity. As a result the capacity at higher temperatures is much low. Loss in weight per gram of the exchanger at different temperatures shows that at 100 °C the weight loss is because of loss in water molecules and amine molecules upto 300 °C. Above 300 °C there is no appreciable weight loss since all the amine is lost. These results are in accordance with the results of capacity at different temperatures.

Structural Studies. It is quite clear that the exchanger, zirconium-bis(triethylamine), contains amino group and the metal oxygen bond. It confirms that in the formation of this type of exchanger the amine is incorporated with the metal oxide forming the matrix.

Potentiometric Titrations. pH titrations of the exchanger, zirconium-bis(triethylamine) were performed by shaking 0.50 g of the exchanger with solution of 0.10 mol dm^{-3} HCl and its salts of 0.01 mol dm^{-3} concentration by Topp and Pepper method. The volume of reaction mixture was kept 50 cm^3 in each case. The pH of the solution was noted after equilibration of the solution for 4 h. Results plotted in Fig. 2 show that the exchanger behaves as monofunctional anion exchanger.

Table 3. Quantitative Separations of Anions on Zirconium-Bis(triethylamine)

Sample No.	Mixture	Eluent	Eluate ml	Amount loaded mg	Amount found mg	Percent recovery
1	Br^-	0.0001 mol dm^{-3} NaOH	90	2.640	2.480	93.93
	CrO_4^{2-}	0.1 mol dm^{-3} NaOH	120	11.078	10.846	97.90
2	I^-	0.001 mol dm^{-3} NaOH	90	2.667	2.603	97.60
	CrO_4^{2-}	0.1 mol dm^{-3} NaOH	100	11.078	10.904	98.42
3	Cl^-	0.001 mol dm^{-3} NaOH	120	2.023	1.917	94.76
	AsO_2^-	0.1 mol dm^{-3} NaOH	90	3.050	2.890	94.75
4	SCN^-	0.0001 mol dm^{-3} NaOH	120	3.509	3.422	97.52
	$Cr_2O_7^{2-}$	0.1 mol dm^{-3} NaOH	120	13.068	12.852	98.34

Distribution Studies. The distribution behavior of anions given in Table 2 indicates that the K_d values were high when deionized water was used as a medium. Distribution values were less when sodium hydroxide solution was used for studies. Distribution values decreased as the concentration of sodium hydroxide solution was increased. Being a weak anion exchanger, zirconium-bis(triethylamine) has a high affinity for hydroxide ions, hence anions other than hydroxide ion showed less uptake in the presence of hydroxide ions.

Separations. Separations of $Cr_2O_7^{2-}$ from Br^-, I^-; AsO_2^- from Cl^-; CrO_4^{2-} from I^-, Br^-; and $Cr_2O_7^{2-}$ from SCN^- were successfully achieved. The quantitative separations of anions on zirconium-bis-(triethylamine) exchanger given in Table 3, also show a high selectivity towards CrO_4^{2-} and $Cr_2O_7^{2-}$ as predicted by capacity.

The exchange isotherms for various anions at different temperatures are plotted in Figs. 3—7. From these results equivalent fractions of anions, selectivity coefficients and thermodynamic equilibrium constants can be evaluated.

The plot of $\ln K_c$ versus equivalent fraction of anion in exchanger phase are presented in Figs. 8—12.

The results of enthalpy change $\Delta H°$, free energy

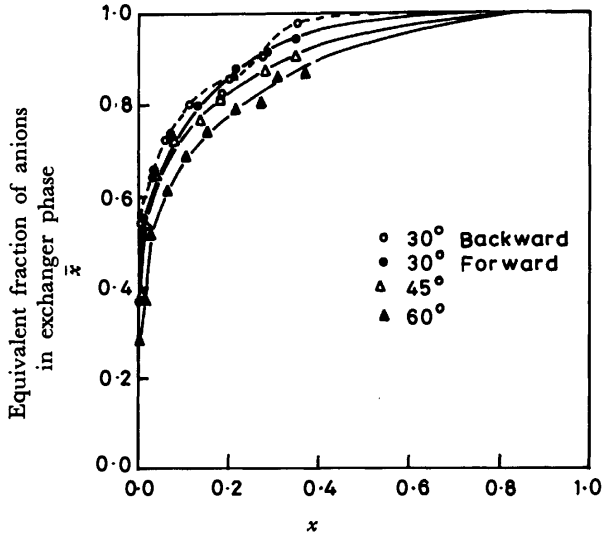

Equivalent fraction of anion in solution phase

Fig. 3. Ion exchange isotherm of dichromate ions on zirconium-bis(triethylamine).

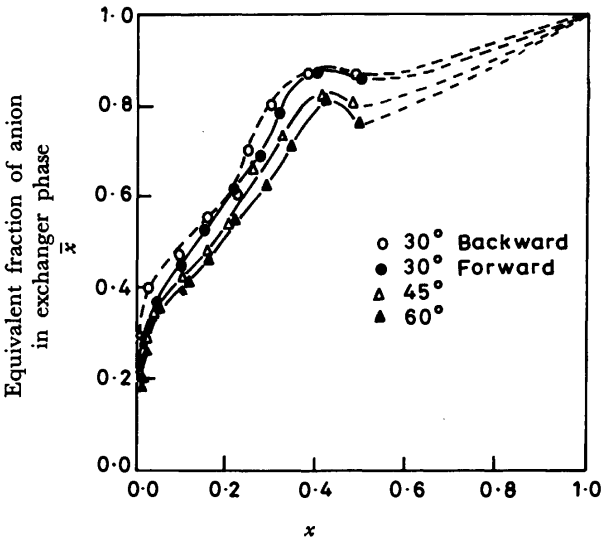

Equivalent fraction of anion in solution phase

Fig. 4. Ion exchange isotherm of chromate ions on zirconium-bis(triethylamine).

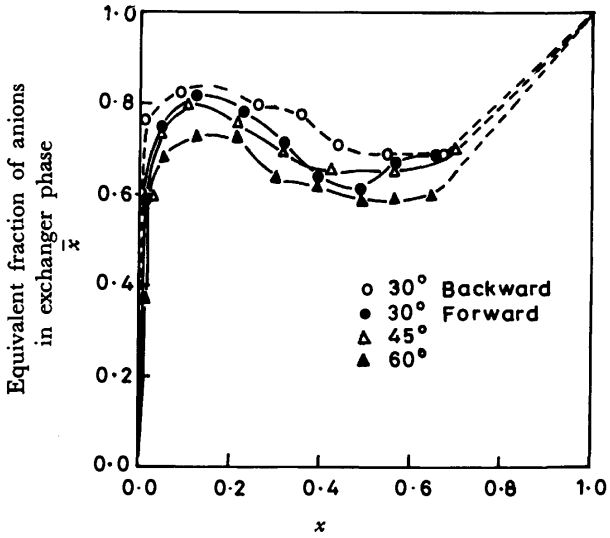

Equivalent fraction of anions in solution phase

Fig. 5. Ion exchange isotherm of thiosulfate ions on zirconium-bis(triethylamine).

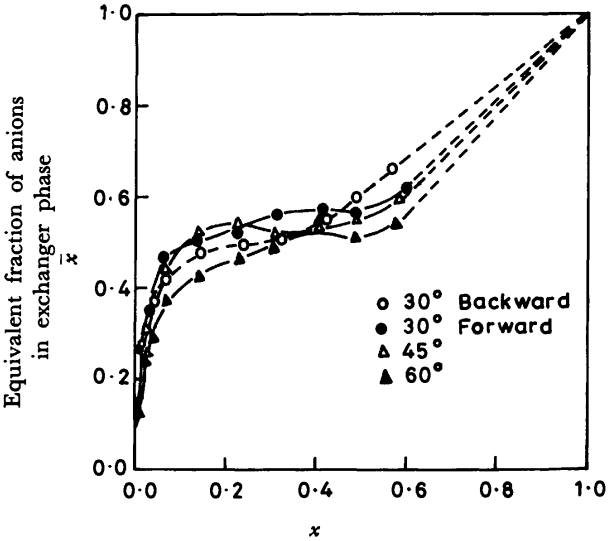

Equivalent fraction of anions in solution phase

Fig. 6. Ion exchange isotherm of sulfate ions on zirconium-bis(triethylamine).

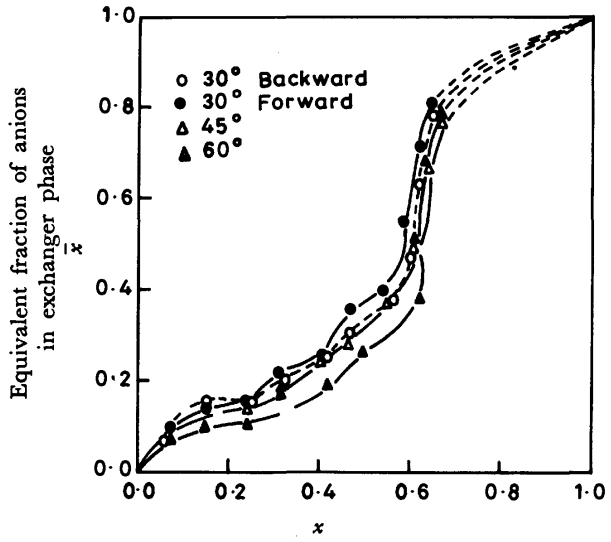

Fig. 7. Ion exchange isotherm of permanganate ions on zirconium-bis(triethylamine).

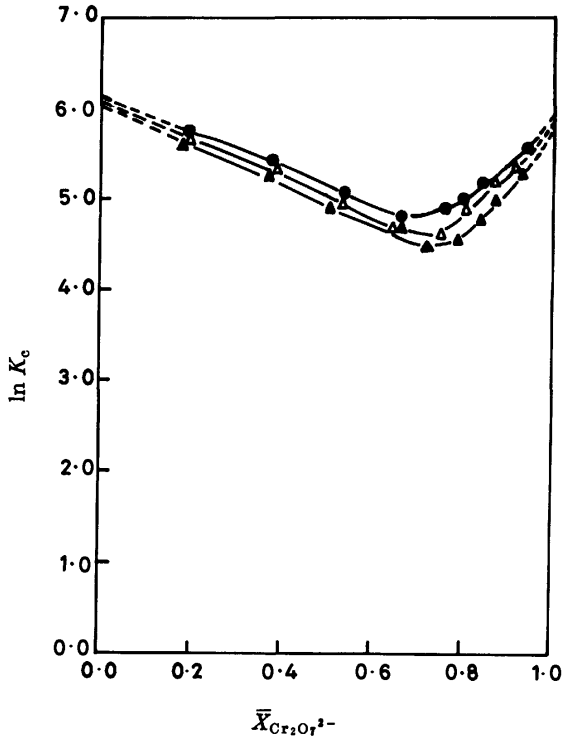

Fig. 8. Selectivity coefficients vs. equivalent fractions of $Cr_2O_7^{2-}$ in exchanger, phase.

change $\Delta G°$, and entropy change $\Delta S°$ were calculated and are reported in Table 4.

The ion exchange equilibria with certain ion exchangers, especially inorganic ion exchangers can be studied by the application of mass-action law modified in terms of activities. For the exchanger in nitrate form and solution having univalent counter ion A^- at equilibrium the exchange may be represented as:

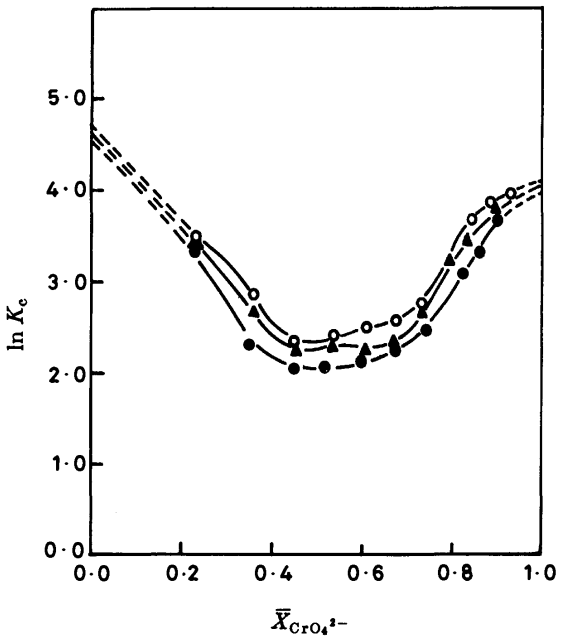

Fig. 9. Selectivity coefficients vs. equivalent fractions of CrO_4^{2-} in exchanger phase.

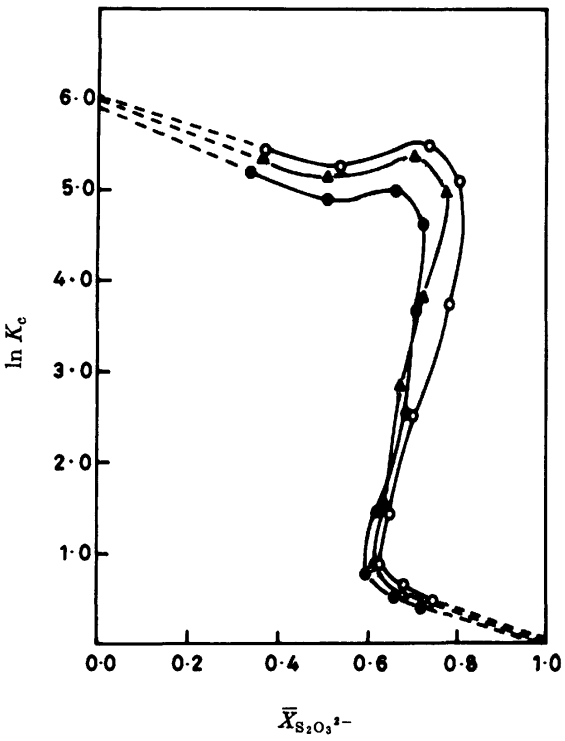

Fig. 10. Selectivity coefficients vs. equivalent fractions of $S_2O_3^{2-}$ in exchanger phase.

$$\overline{NO_3^-} + A^-_{(aq)} \rightleftharpoons \overline{A^-} + NO_3^-{}_{(aq)} \quad (1)$$

and for bivalent counter ion

$$\overline{2NO_3^-} + A^{2-}_{(aq)} \rightleftharpoons \overline{A^{2-}} + 2NO_3^-{}_{(aq)} \quad (2)$$

The thermodynamic equilibrium constant for the above reactions may be written for uni-univalent

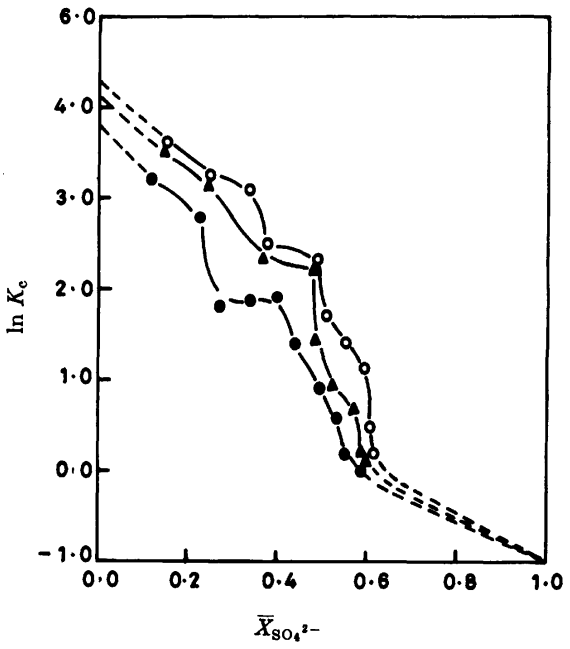

Fig. 11. Selectivity coefficients vs. equivalent fractions of SO_4^{2-} in exchanger phase.

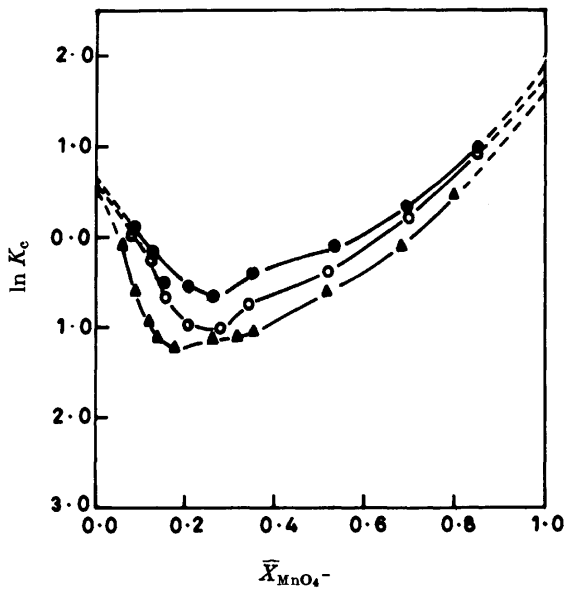

Fig. 12. Selectivity coefficients vs. equivalent fractions of MnO_4^- in exchanger phase.

exchange as:

$$K_a = \frac{\overline{a_{A^-}} a_{NO_3^-}}{\overline{a_{NO_3^-}} a_{A^-}} = \frac{[\overline{A^-}][NO_3^-]}{[\overline{NO_3^-}][A^-]} \times \frac{\gamma_{A^-} f_{NO_3^-}}{\gamma_{NO_3^-} f_{A^-}} \quad (3)$$

and uni-bivalent exchange as:

$$K_a = \frac{(\overline{a_{A^{2-}}})(a_{NO_3^-})^2}{(\overline{a_{NO_3^-}})^2 (a_{A^{2-}})} = \frac{[\overline{A^{2-}}][NO_3^-]^2}{[\overline{NO_3^-}]^2[A^{2-}]} \times \frac{\gamma_{A^{2-}} f^2_{NO_3^-}}{\gamma^2_{NO_3^-} f_{A^{2-}}} \quad (4)$$

where γ represents activity coefficients in the exchanger phase and f the activity coefficient in the aqueous phase.

An examination of the ion exchange isotherms, Figs. 3—7, show that the isotherms are above the diagonal except for MnO_4^- indicating that bivalent anions are strongly preferred in comparison to nitrate by the zirconium-bis(triethylamine) exchanger. The

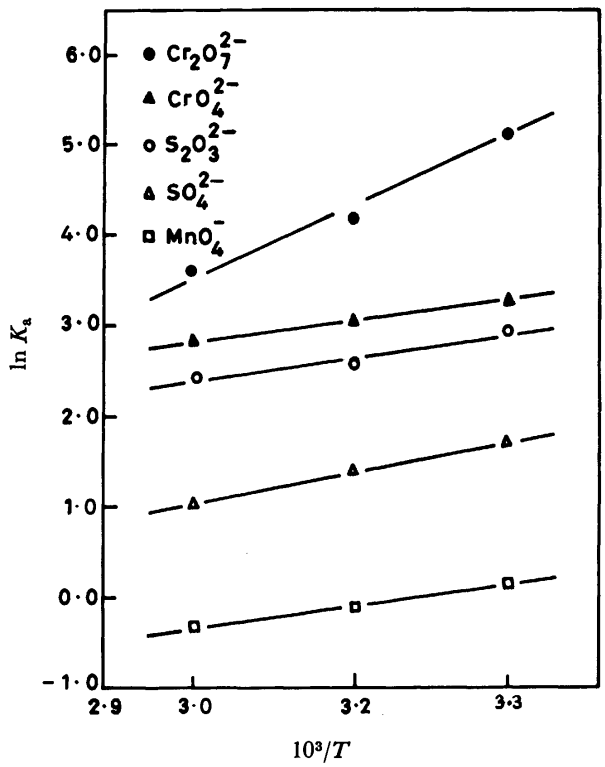

Fig. 13. Temperature dependece of the thermodynamic equilibrium constant.

Table 4. Thermodynamic Parameters on Zirconium-Bis(triethylamine) at Anionic Strength of 0.1 and Various Parameters

Anion	K_a			$\Delta G°$			$\Delta H°$/kJ equiv^{-1}	$\Delta S°$/J equiv^{-1} deg^{-1}
	30 °C	45 °C	60 °C	30 °C	45 °C	60 °C	30—60 °C	30—60 °C
$Cr_2O_7^{2-}$	170.28	64.08	39.25	−12.94	−10.99	−10.16	−4.80	20.80
CrO_4^{2-}	26.31	21.04	17.68	−8.21	−8.06	−7.94	−1.33	21.23
$S_2O_3^{2-}$	19.21	13.88	11.19	−7.43	−6.95	−6.67	−1.50	17.40
SO_4^{2-}	5.59	4.16	2.73	−4.33	−3.75	−2.77	−1.92	5.41
MnO_4^-	1.18	0.89	0.74	−0.40	0.32	0.83	−1.39	−5.09

affinity for the anions decreases as the temperature increases. Figures 3—7 show that all the studied isotherms were reversible whereas the selectivity sequence was

$$Cr_2O_7^{2-} > CrO_4^{2-} > S_2O_3^{2-} > SO_4^{2-} > MnO_4^-$$

If K_c is the selectivity coefficient, then for univalent exchange

$$K_c = \frac{\bar{X}_{A^-} X_{NO_3^-}}{\bar{X}_{NO_3^-} X_{A^-}} \times \frac{f_{NO_3^-}}{f_{A^-}} \quad (5)$$

and for uni-bivalent exchange

$$K_c = \frac{\bar{X}_{A^{2-}} X^2_{NO_3^-}}{\bar{X}^2_{NO_3^-} X_{A^{2-}}} \times \frac{f^2_{NO_3^-}}{f_{A^{2-}}} \quad (6)$$

where $\bar{X}_{NO_3^-}$ and $\bar{X}_{A^-}$ are equivalent fractions of competing anions in exchanger phase, $X_{NO_3^-}$ and X_{A^-} the equivalent fractions of the nitrate and competing anion in solution phase respectively. $f_{NO_3^-}$ and f_{A^-}, the activity coefficients of nitrate and the competing anion, respectively in solution. The activity coefficients of the anions in solution phase were calculated using Debye-Hückel equation:

$$-\log f_i = \frac{Az_i^2\sqrt{\mu}}{1+Ba_i\sqrt{\mu}} \quad (7)$$

where A and B are constants, a_i the ion size parameter, μ the ionic strength and z_i the charge of the ion i. The values of A and B at appropriate temperatures are taken from the table given earlier.

The results of the selectivity coefficients indicate that as the temperature increases the value of the selectivity coefficient decreases. The results plotted (Figs. 8—12) reveal that the selectivity coefficient K_c does not remain constant at all with the varying concentrations of anions in solution and therefore K_a should be calculated.

K_a, The thermodynamic equilibrium constant can be obtained according to Gaines and Thomas, from the equation:

$$\ln K_a = (Z_{X^-} - Z_{NO_3^-}) + \int_0^i \ln K_c \, d\bar{X}_{A^-} \quad (8)$$

The values of thermodynamic equilibrium constant are calculated by integration under the curves of Figs. 8—12 applying Eq. 8. Variation of $\ln K_c$ with loading, X, is given in Figs. 8—12. The values of the changes in thermodynamic quantities are calculated from the respective thermodynamic equilibrium constants as follows:

$$\Delta G^\circ = -RT \ln K_a \quad (9)$$

$$\Delta H^\circ = -R\frac{d(\ln K_a)}{d(1/T)} \quad (10)$$

and

$$\Delta S^\circ = (\Delta H^\circ - \Delta G^\circ)/T \quad (11)$$

ΔH° is obtained from Fig. 13 (expressing the variation of $\ln K_a$ with $1/T$). The results indicate that during the exchange of anions over zirconium-bis-(triethylamine) in nitrate form, the free energy change is negative in all cases except for MnO_4^- at higher temperatures. It reveals that for bivalent anions the exchange process is spontaneous and is in accordance with, mainly, on charge relations. However, for univalent anion exchange with MnO_4^- the charge being same it may depend on other factors.

The results (Table 4) giving enthalpy change in all the exchange reactions indicate that process is exothermic, i.e. the binding energy of one competing anion is lower than the two anions of nitrate. Thus nitrate ion is less tightly bound to the zirconium-bis-(triethylamine) matrix than any of the other anions studied except MnO_4^-.

The results of enthalpy changes given in Table 4 indicate that during the forward reaction the competing anionic species are more orderly arranged than that of nitrate form of zirconium-bis(triethylamine).

The authors are thankful to Professor M. S. Ahmad, Chairman, Department of Chemistry, Aligarh Muslim University, Aligarh for providing research facilities. Two of the authors (M.A. and B.S.) are thankful to C.S.I.R. and H.M.A.A. is grateful to Cultural Department, Ministry of Foreign Affairs, Govt. of India for financial assistance.

References

1) J. P. Rawat and M. Iqbal, *Ann. Chim.*, **1981**, 431.
2) J. P. Rawat, M. Iqbal, and S. Ali, *J. Indian Chem. Soc.*, **61**, 185 (1984).
3) J. P. Rawat, M. Iqbal, and M. Alam, *Ann. Chim.*, **75**, 87 (1985).
4) J. P. Rawat and M. Alam, *J. Indian Chem. Soc.*, in press.
5) F. D. Snell and C. T. Snell, "Colorimetric Methods of Analysis," 3rd ed, D. Van Nostrand, Princeton, New Jersey (1954), Vol. 4, p. 37.
6) N. E. Topp and K. W. Pepper, *J. Chem. Soc.*, **1949**, 3299.

 © 1987 The Chemical Society of Japan Bull. Chem. Soc. Jpn., 60, 2627—2633 (1987)

Synthesis and Characterization of New Three-Component Ion-Exchange Material: Zirconium(IV) Selenophosphate

Saidul Zafar QURESHI* and Nafisur RAHMAN
Department of Chemistry, Aligarh Muslim University, Aligarh-202001, India
(Received October 7, 1985)

Zirconium(IV) selenophosphate has been prepared by adding a mixture which is 0.05 M in sodium selenite and 0.05 M in orthophosphoric acid to a 0.05 M solution of zirconium(IV) bis(nitrate) oxide in different volume ratios at pH 1. Its ion-exchange capacity, thermal and chemical stability, pH titration curves, and chemical composition were studied. Adsorption of some of the metal ions in different solvent systems has been studied. The effect of particle size on the sorption behavior of metal ions has also been studied. The analytical importance of this material has been demonstrated by achieving the eleven quaternary separations of metal ions. A comparison of ion-exchange properties of this material has also been made with some other ion-exchangers.

The most intensively studied group of synthetic inorganic ion-exchangers are the acidic salts of multivalent metals (especially quadrivalent metals) prepared in combination with the anions of phosphate, arsenate etc. as two-component ion-exchangers.[1-3] Three-component inorganic ion-exchangers which consist of a combination of zirconium phosphate compound with other organic or inorganic salts such as zirconium arsenate, molybdate, tungstate, tellurate, oxalate, silicate etc. have been prepared. Attempts were made to increase the ion-exchange capacity by increasing degree of polymerization of the component materials.[4] However, a higher content of polyphosphate in the exchanger is considered to effect the kinetics of absorption[5] and therefore, the conditions are set within optimum limits.[6] A study of the literature shows the preparation of a large number of three-component ion-exchangers with increased ion-exchange capacity and selectivity of these materials.[7-16] In this manuscript, we describe the preparation and properties of zirconium(IV) selenophosphate. Some analytically important separation of metal ions of quaternary systems have been successfully achieved.

Experimental

Reagents. Zirconium(IV) bis(nitrate) oxide (B.D.H.), sodium selenite (B.D.H.), and orthophosphoric acid (B.D.H.) were used for the synthesis of ion-exchangers. All other chemicals were of analytical grade.

Apparatus. An Elico model Li-10 pH meter was used for pH measurement. A Bausch and Lomb Spectronic 20 colorimeter and a Perkin Elmer 137 spectrophotometer were used for spectrophotometric and IR studies respectively. An electric temperature-controlled shaker (SICO) was used for shaking.

Synthesis. Samples of zirconium(IV) selenophosphate ion-exchangers were synthesized by adding an aqueous solution which is 0.05 M (1 M=1 mol dm^{-3}) in sodium selenite and 0.05 M in orthophosphoric acid to an aqueous solution of zirconium(IV) bis(nitrate) oxide. The desired pH was adjusted by adding dilute HNO_3 or NaOH solution. The gel so formed was allowed to settle down for 24 h, washed several times with demineralized water to remove excess reagents and finally filtered under suction. It was

Table 1. Synthesis and Properties of Zirconium(IV) Selenophosphate

Sample No.	Zirconium(IV) bis(nitrate) oxide	Sodium selenite	Orthophosphoric acid	Mixing ratio	pH	Appearance of precipitate	Appearance of beads after drying at 40 °C	Ion-exchange capacity for K^+ (meq g^{-1}-dry exchanger)
	M	M	M	v/v/v				
ZSP_1	0.05	0.05	0.05	1 : 1 : 1	1.0	White gelatinous	White opaque	1.51
ZSP_2	0.05	0.05	0.05	2 : 1 : 1	1.0	White gelatinous	White opaque	1.07
ZSP_3	0.05	0.05	0.05	1 : 2 : 1	1.0	White gelatinous	White opaque	1.13
ZSP_4	0.05	0.05	0.05	1 : 1 : 2	1.0	White gelatinous	White opaque	1.15
ZSP_5	0.05	0.05	0.05	1 : 1 : 2	<0	White gelatinous	White opaque	0.95
ZP	0.05	—	0.05	1 : 1	1.0	White gelatinous	White opaque	0.64
ZS_1	0.05	0.05	—	1 : 1	1.0	No precipitation		—
ZS_2	0.05	0.05	—	1 : 1	4.0	White gelatinous	White opaque	0.44

then dried at 40 °C for 7 d in an oven. The dried material was then treated with demineralized water, which resulted in cracking of the substance into smaller particles with slight evolution of heat. To convert the sample into H^+ form, the material was kept for 24 h in 1.0 M HNO_3 solution. It was then washed with demineralized water to remove excess acid.

Ion-Exchange Capacity. A half gram of the exchanger in H^+ form was taken into the column with the glass wool support. One molar solutions of different uni- and bivalent metal salts were passed through the column and the H^+ ion liberation capacity was determined as usual.[17] The ion-exchange capacities thus determined were therefore those at neutral pH conditions (pH ≈6.5).

Chemical Stability. A 0.50 gram exchanger material (ZSP_1, Table 1) was equilibrated with 50 ml of the solution or solvent of interest at room temperature and kept for 24 h with occasional shaking. Zirconium and selenium in the solution was determined spectrophotometrically using Alizarin Red-S[18] and 3,3′,4,4′-tetraaminobiphenyl tetrahydrochloride[19] as coloring reagents respectively. The phosphate was determined titrimetrically.[20]

pH-Titration. pH-Titrations for NaCl-NaOH and KCl-KOH systems, (using 0.1 M solution of NaCl and KCl each) of sample ZSP_1 were performed by the method of Topp and Pepper.[21]

Thermal Treatment. Thermogravimetric analysis of sample ZSP_1 in the H^+ form was performed at a heating rate of 10 °C min^{-1}. To examine the effect of drying temperature on the ion-exchange capacity the materials were heated at different temperatures in a muffle furnace for 1 h.

Chemical Composition. For the determination of chemical composition of zirconium(IV) selenophosphate sample ZSP_1, 0.10 g of exchanger was dissolved in hot concentrated sulfuric acid. Then the solution was diluted to 100 ml with water. Zirconium and selenium were determined gravimetrically[22,23] while phosphate was determined titrimeterically.[20] The mole ratio of Zr, Se, and P was found to be 5.06:2.0:4.05.

Infrared Spectrum. Infrared analysis of zirconium(IV) selenophosphate was performed using KBr technique.

Distribution Coefficient. The distribution coefficients of metal ions in various aqueous solutions were determined. A quarter gram of exchanger in H^+ form (30—50, 50—100, 100—150, 150—200 mesh sizes) was treated with 25.0 ml of 2.0×10^{-4} M metal salt solution in 250 ml Erlenmeyer flask. The mixture was then shaken for 6 h at 25±2 °C in a shaker incubator. The amount of metal species left in the solution was then determined by titrating against the standard solution of EDTA. The K_d values were calculated according to the formula.

$$K_d = \frac{\text{mmoles of metal species/gram of exchanger}}{\text{mmoles of metal species/ml of the total volume of the resultant solution.}}$$

Separation of Metal Ions. Quantitative separations of metal ions were achieved on a 0.6 cm diameter (i.d.) glass column using 2.0 g exchanger (50—100 mesh) in H^+ form. A metal ion mixture was poured on the top of the column. The flow rate of the effluent was maintained at 1 ml min^{-1} throughout the elution process.

Results and Discussion

Table 1 describes the preparations of samples of Zr(IV) selenophosphate. It is apparent from the table that the ion-exchange capacity of the mixed salt is greater when compared with other simple salts such as zirconium phosphate and zirconium selenite. The ion-exchange capacities for alkali and alkaline earth metals are shown in Table 2. It is clear from the table that the capacity increases with the decrease of hydrated ionic radii for both the alkali and alkaline earth metals.

The effect of heating on the ion-exchange capacities of Zr(IV) selenophosphate and other ion-exchange materials[5,13,15] at different temperatures has been shown in Fig. 1 and interpreted. A 300, 500, and 600 °C, the decreasing orders of the ion-exchange capacities are [Zr(IV) selenophosphate, Sn(IV) selenoarsenate, Sn(IV) selenite, Cr(III) arsenophosphate, Sn(IV) arsenophosphate], [Sn(IV) selenite, Sn(IV) selenoarsenate, Zr(IV) selenophosphate, Cr(III) arsenophosphate, Sn(IV) arsenophosphate], and [Sn(IV)

Table 2. Ion-Exchange Capacity (meq g^{-1}-dry exchanger) of Zirconium(IV) Selenophosphate Sample ZSP_1 for Various Cations at pH 6.5 and 25 °C

Sample No.	Cation	Hydrated ionic radius/Å	Ion exchange capacity (meq g^{-1}-dry exchanger)
1	Li^+	10	1.11
2	Na^+	7.9	1.23
3	K^+	5.3	1.51
4	Rb^+	—	0.71
5	Mg^{2+}	10.8	1.21
6	Ca^{2+}	9.6	1.31
7	Sr^{2+}	9.4	1.42
8	Ba^{2+}	8.8	1.44

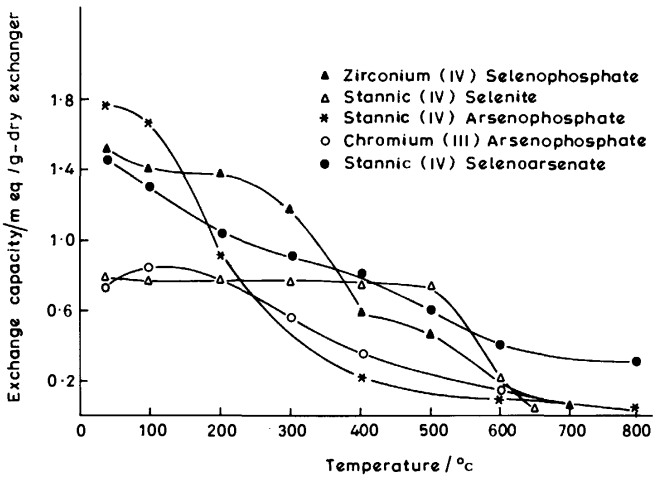

Fig. 1. Plot of exchange capacity vs. drying temperature.

selenoarsenate, Sn(IV) selenite, Zr(IV) selenophosphate, Cr(III) arsenophosphate, Sn(IV) arsenophosphate] respectively. The ion-exchange capacity of Zr(IV) selenophosphate for K^+ was found to be 1.51 meq g^{-1} when the sample was dried at 40 °C. However, a decreasing trend in ion-exchange capacities was observed when the drying temperature was elevated. The ion-exchange capacity became negligible i.e., 0.05 meq g^{-1} at 700 °C.

It is apparent from Table 3 that Zr(IV) selenophosphate is quite stable in water. It is fairly stable in dilute mineral acids such as hydrochloric acid, perchloric acid, nitric acid, and sulfuric acid. The material is also fairly stable in organic acids like formic acid, oxalic acid, acetic acid, citric acid, and tartaric acid and in organic solvents such as ethanol, 1-butanol, DMSO, and dioxane but is highly soluble in 2 M sodium hydroxide.

The titration curves with added salts have been shown in Fig. 2. The curve in the presence of added sodium salt showed a slight difference from that in the presence of potassium salt and the ion-exchange capacities calculated from these curves are 1.20 and 1.50 meq g^{-1} for sodium and potassium salts and those obtained from column operation are 1.23 and 1.51 meq g^{-1} respectively. Further the titration curves showed a monofunctional behavior of the exchanger.

Berardelli and coworkers[24] have synthesized a single crystalline phase, a layered mixed inorganic ion-exchanger, $Zr(HAsO_4)(HPO_4)\cdot H_2O$, containing two anions. The X-ray diffraction studies and differential thermal analysis of the crystalline product showed a great similarity with those of α-$Zr(HPO_4)_2\cdot H_2O$ and α-$Zr(HAsO_4)_2\cdot H_2O$ and possessed an interlayer spacing of 7.73Å intermediate between those of the last two compounds. It was, therefore, concluded that the mixed crystalline product possessed an α-type layered structure. Taking the example of this product we have tried to explain the increased ion-exchange capacity and tentatively extending this concept on synthesized material, zirconium(IV) selenophosphate (assuming that it possessed an α-type layered structure). Its ion-exchange capacity was reported to be 5.80 meq g^{-1}. In describing the structure of zirconium phosphate in terms of three-dimensional skeleton which composed of Zr, P, and O, Clearfield[25] suggested that each phosphate group is bonded to three different zirconium atoms through oxygen forming a sheet-like structure. The remaining phosphate oxygen atoms bear the hydrogen atoms. Half of these P-OH groups are believed to form hydrogen bonds with phosphate oxygen atoms in the adjacent layers (P-O-H·····O-P) and form a zigzag array of weak interlayers running parallel to the *b*-axis. The other half of the P-OH groups are thought to be hydrogen bonded to the water molecules to form interlayer bonds $\left(\text{P-OH}\cdots\text{O}\begin{matrix}\nearrow\text{H}\\ \searrow\text{H}\end{matrix}\right)$. These differences in hydrogen bonding give rise to different acidities or ion-exchange sites for the two hydrogen atoms. The ion-exchange capacity has been measured as the amount of the total H^+ ions available from the

Table 3. Chemical Stability of Zirconium(IV) Selenophosphate (sample ZSP_1, 0.5 g) in Solution (50 ml)

No.	Solution or solvent[a]	Zr released mg/50 ml	Se released mg/50 ml	PO_4^{3-} released mg/50 ml
1	Water	0.00	0.00	0.00
2	1 M HNO_3	0.18	0.15	0.13
3	2.0 M HNO_3	0.54	0.23	0.21
4	1.0 M H_2SO_4	0.41	0.18	0.29
5	2.0 M $HClO_4$	0.54	0.16	0.24
6	1.0 M Acetic acid	0.18	0.12	0.20
7	1.0 M Citric acid	0.11	0.13	0.21
8	1.0 M Tartaric acid	0.12	0.19	0.24
9	1.0 M Oxalic acid	0.11	0.18	0.21
10	1.0 M Formic acid	0.13	0.15	0.22
11	0.1 M NaOH	0.98	0.39	0.54
12	2.0 M NaOH	Complete dissolution		
13	4.0 M NH_4NO_3	0.11	0.21	0.18
14	4.0 M NH_4Cl	0.12	0.17	0.21
15	0.1 M HCl	0.20	0.13	0.23
16	2.0 M HCl	0.28	0.22	0.26
17	2.0 M DMSO	0.11	0.13	0.17
18	2.0 M Dioxane	0.17	0.12	0.19
19	Ethanol	0.13	0.12	0.21
20	1-Butanol	0.12	0.14	0.19

a) No. 2—18, aqueous solution.

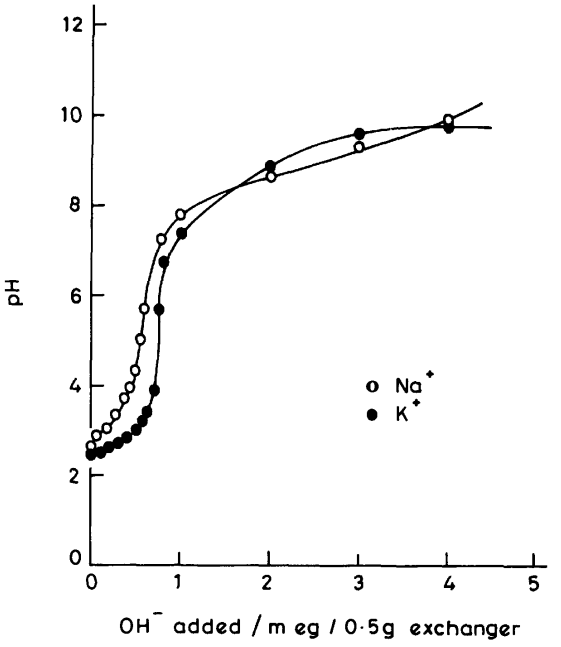

Fig. 2. pH Titration curves of zirconium(IV) selenophosphate.

two different interlayer bonds of P-OH groups. In case of three-component materials e.g., $Zr(HAsO_4)(HPO_4)\cdot H_2O$, X-ray diffraction studies revealed the existance of a mixed exchanger to give solid solutions because of the presence in the lattice layer of atoms (P and As) with analogous chemical characteristics but with different dimensions. Moreover, the substitution of P with As provided strength of their acidic sites when employed as acid catalysts.[24] On the basis of these studies, it can be suggested that in addition to the two different P-OH groups there should also be a third exchange site (in case of three-component materials) formed by mixed interlayer bonds (As-OH$\cdots\cdots$O-P), whose existance was supported by mixed ion-exchanger to give solid solution. The ion-exchange capacity is therefore a total contribution from all these different exchange sites. new let P-OH and As-OH represent dihydrogenphosphate ($-H_2PO_4$) and dihydrogenarsenate ($-H_2AsO_4$) groups corresponding to the second dissociation constant of the phosphoric and arsenic acid. The magnitude of the dissociation constants of these groups ($H_2PO_4^- \overset{K_2}{\rightleftharpoons} H^+ + HPO_4^{2-}$; $K_2=6.2\times10^{-8}$ and $H_2AsO_4^- \overset{K_2'}{\rightleftharpoons} H^+ + HAsO_4^{2-}$; $K_2'=8.3\times10^{-8}$) are almost of the same order and therefore the hydrogen ions released from these ion-exchange sites should be the sum from the above two groups. The total hydrogen ions released from all three different sources must be greater than the hydrogen ions released from the two ion-exchange sites.

The IR spectrum of Zr(IV) selenophosphate shows the presence of usual characteristic groups such as lattice water, free water and phosphates at corresponding frequencies. On the other hand, the separate identity of $-SeO_3$ group is indicated by a strong band at a frequency of 720 cm^{-1}.[26]

The combined studies of thermogram of Zr(IV) selenophosphate in H^+ form (Fig 3) and its exchange capacity at different temperatures compared with other exchange materials (Fig. 1) reveal some interesting results. At 200 °C about 8.6% of the total capacity is lost due to the loss of water molecules and start of the formation of pyrophosphate groups. The corresponding weight loss of exchanger is about 2.58%. At 560 °C, there is a complete conversion to pyrophosphate with a decrease in capacity equal to 72% of the starting value and the corresponding weight loss is about 4.6%. Further decrease in capacity may be attributed due to the condensation of $-HSeO_3$ group to $(Se_2O_5)H_2O$. After 800 °C the weight becomes constant and the capacity decreases, is 96% of the original value.

On the basis of the exchange capacity, pH titration curve, chemical composition and thermogravimetric analysis, the following formula for Zr(IV) seleno-

Table 4. Distribution Coefficients (ml g^{-1}) of Metal Ions on Zirconium(IV) Selenophosphate (sample ZSP_1, 50—100 mesh) at 25±2 °C

No.	Metal ion	Water	0.001 M HNO_3	0.01 M HNO_3	0.1 M HNO_3	1.0 M NH_4NO_3	0.01 M HNO_3 + 1.0 M NH_4NO_3 (1 : 1)
1	Mg^{2+}	2	2	2	2	8	8
2	Ca^{2+}	52	26	90	375	3700	3700
3	Ba^{2+}	17	11	8	5	2	5
4	Sr^{2+}	22	3	8	3	4800	30
5	Al^{3+}	109	27	9	2	27	35
6	Zn^{2+}	40	20	12	5	425	180
7	Cu^{2+}	15	22	15	2	8	2
8	Co^{2+}	5	10	28	4800	28	22
9	Ni^{2+}	6	6	12	28	20	6
10	Fe^{3+}	4300	780	340	214	144	17
11	Pb^{2+}	780	780	340	17	340	486
12	VO^{2+}	100	77	25	3900	33	23
13	Zr^{4+}	560	1220	560	340	3200	3200
14	Th^{4+}	3400	3400	3400	3400	3400	3400
15	Gd^{3+}	69	61	42	36	27	11
16	Y^{3+}	30	15	20	24	11	7
17	Sm^{3+}	82	93	138	244	12	161
18	Eu^{3+}	45	7	12	40	3	12
19	Er^{3+}	8	8	11	23	3	6
20	Nd^{3+}	37	12	24	3000	12	3
21	Pr^{3+}	7	10	7	8500	1	14
22	Tb^{3+}	16	16	16	22	5	3
23	Yb^{3+}	1	8	1	1	1	8

phosphate is tentatively suggested.

$$[(ZrO)_5(OH)_4(HSeO_3)_2(H_2PO_4)_4]_n \cdot 2nH_2O$$

If it is assumed that the weight loss (2.58%) up to 200 °C is due to the removal of water molecules, then the number of water molecules (n) per molecule of exchanger, calculated from the formula given by Alberti[27] is 2. If two hydrogen ions in the tentative formula above are exchanged at pH 6.5, the ion-exchange capacity calculated from the above formula is 1.55 meq g^{-1} which is in accordance with the experimental value (1.51 meq g^{-1}). The mole ratio of Zr, Se, and P, which is calculated from the above formula is found to be 5.04:2.00:4.01.

It is clear from Table 4 that the K_d values vary with

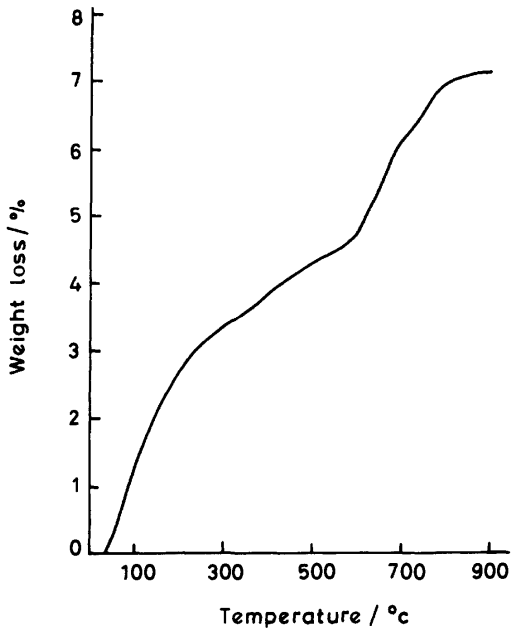

Fig. 3. Thermogram of Zr(IV) selenophosphate in H^+ form.

Table 5. Distribution Coefficient (ml g^{-1}) of Metal Ions on Zirconium(IV) Selenophosphate of Different Particle Sizes at 25±2 °C in 0.1 M Acetic Acid

No.	Metal ion	30—50 mesh	50—100 mesh	100—150 mesh	150—200 mesh
1	Mg^{2+}	8	15	29	35
2	Ca^{2+}	5	22	32	70
3	Sr^{2+}	6	13	23	36
4	Ba^{2+}	29	52	65	68
5	Cu^{2+}	2	12	24	142
6	Zn^{2+}	8	16	32	69
7	Hg^{2+}	147	666	820	1050
8	Th^{4+}	25	89	106	164
9	Zr^{4+}	560	560	840	1220
10	Pb^{2+}	14	137	170	175
11	Cd^{2+}	5	38	72	127
12	Al^{3+}	10	80	100	300

Table 6. Separations of Metal Ions Achieved on Zirconium(IV) Selenophosphate Columns

No.	Separation achieved	Amount loaded (μg)	% of metal ions eluted	Volume of effluent (ml)	Eluent used
1	Y^{3+}	138	99	40	0.001 M HNO_3
	Al^{3+}	24	100	40	0.01 M HNO_3
	Pb^{2+}	190	96	40	0.05 M HNO_3
	Fe^{3+}	49	98	30	1.0 M HNO_3
2	Yb^{3+}	132	100	30	H_2O
	Gd^{3+}	280	100	50	0.01 M HNO_3
	Pb^{2+}	190	97	40	0.05 M HNO_3
	Th^{4+}	177	92	40	1.0 M HNO_3
3	Cu^{2+}	58	98	30	H_2O
	Al^{3+}	24	100	40	0.01 M HNO_3
	Pb^{2+}	186	98	40	0.05 M HNO_3
	Fe^{3+}	49	98	30	1.0 M HNO_3
4	Eu^{3+}	94	97	50	H_2O
	Gd^{3+}	280	99	50	0.01 M HNO_3
	Pb^{2+}	190	96	40	0.05 M HNO_3
	Th^{4+}	177	93	40	1.0 M HNO_3
5	Pr^{3+}	242	99	40	H_2O
	Gd^{3+}	280	100	50	0.01 M HNO_3
	Pb^{2+}	190	96	40	0.05 M HNO_3
	Th^{4+}	177	92	40	1.0 M HNO_3
6	Er^{3+}	381	99	40	H_2O
	Gd^{3+}	280	99	50	0.01 M HNO_3
	Pb^{2+}	190	97	40	0.05 M HNO_3
	Th^{4+}	177	93	40	1.0 M HNO_3
7	Tb^{3+}	181	100	40	H_2O
	Gd^{3+}	280	99	50	0.01 M HNO_3
	Pb^{2+}	190	97	40	0.05 M HNO_3
	Th^{4+}	177	93	40	1.0 M HNO_3
8	Mg^{2+}	23	96	40	H_2O
	Al^{3+}	24	100	40	0.01 M HNO_3
	Pb^{2+}	190	96	40	0.05 M HNO_3
	Zr^{4+}	64	97	50	1.0 M HNO_3
9	Ca^{2+}	40	98	40	H_2O
	Al^{3+}	24	100	40	0.01 M HNO_3
	Pb^{2+}	190	96	40	0.05 M HNO_3
	Zr^{4+}	64	95	50	1.0 M HNO_3
10	Sr^{2+}	86	98	40	H_2O
	Al^{3+}	24	100	40	0.01 M HNO_3
	Pb^{2+}	190	96	40	0.05 M HNO_3
	Zr^{4+}	64	97	50	1.0 M HNO_3
11	Ba^{2+}	115	98	40	H_2O
	Al^{3+}	24	96	40	0.01 M HNO_3
	Pb^{2+}	190	96	40	0.05 M HNO_3
	Zr^{4+}	64	95	50	1.0 M HNO_3

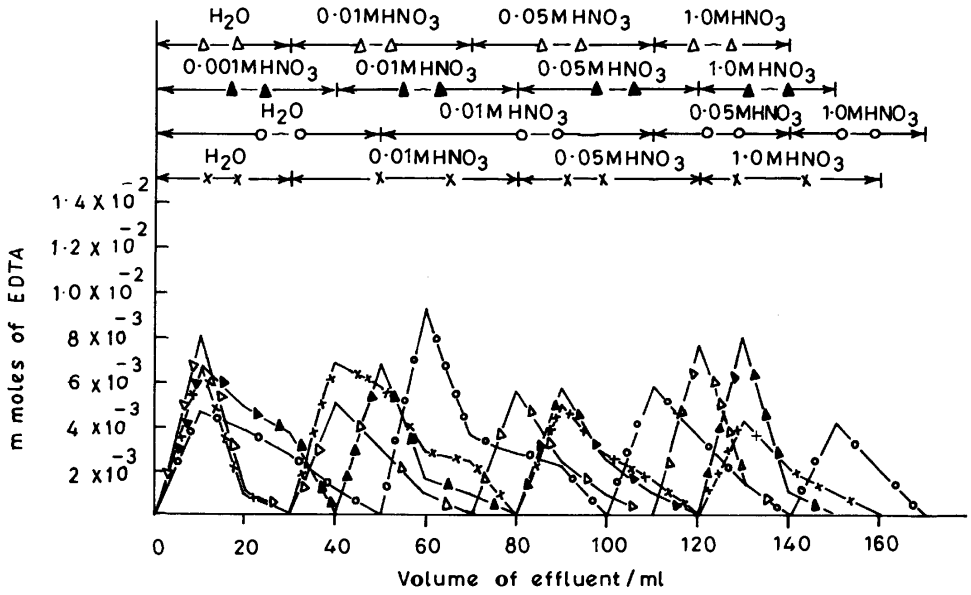

Fig. 4(a) Separation of (—△—) Cu^{2+}–Al^{3+}–Pb^{2+}–Fe^{3+}, (—○—) Eu^{3+}–Gd^{3+}–Pb^{2+}–Th^{4+}, (—▲—) Y^{3+}–Al^{3+}–Pb^{2+}–Fe^{3+}, and (—×—) Yb^{3+}–Gd^{3+}–Pb^{2+}–Th^{4+} on Zirconium(IV) selenophosphate column.

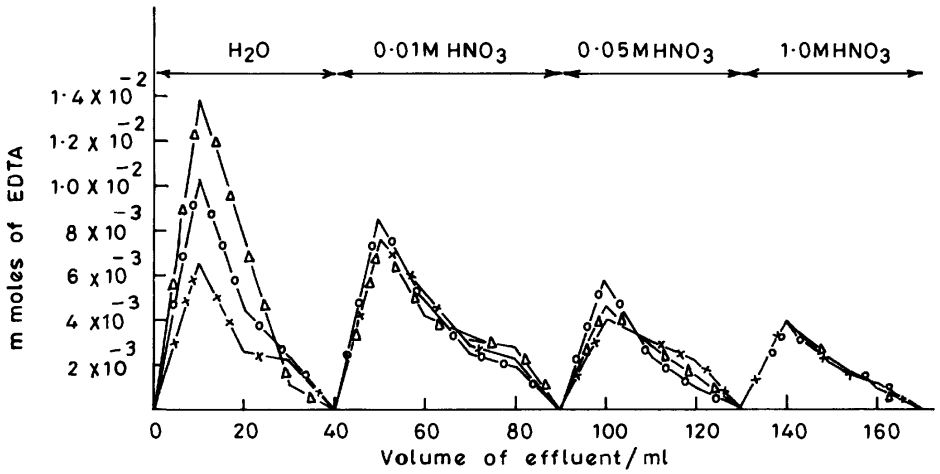

Fig. 4(b) Separation of (—△—) Er^{3+}–Gd^{3+}–Pb^{2+}–Th^{4+}, (—○—) Pr^{3+}–Gd^{3+}–Pb^{2+}–Th^{4+}, and (—×—) Th^{4+}–Gd^{3+}–$Pb^{2+}Th^{4+}$ on zirconium(IV) selenophosphate column.

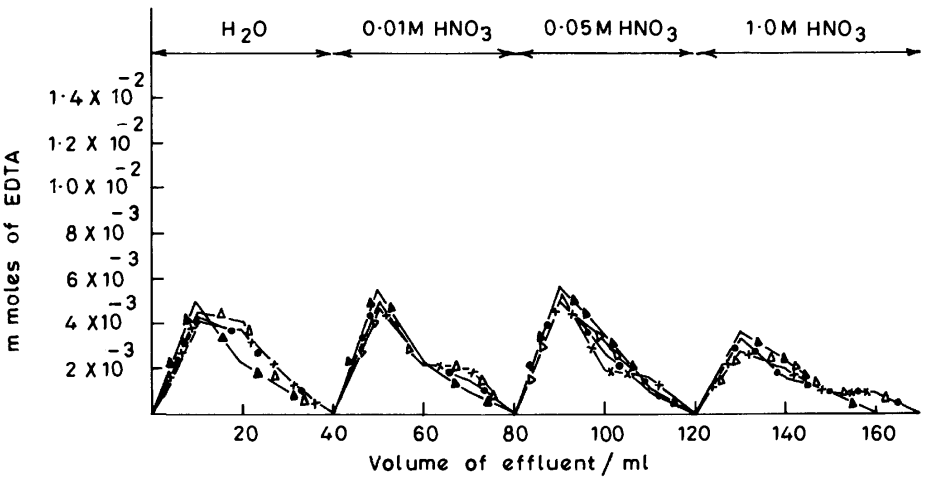

Fig. 4(c) Separation of (—○—) Mg^{2+}–Al^{3+}–Pb^{2+}–Zr^{4+}, (—△—) Ca^{2+}–Al^{3+}–Pb^{2+}–Zr^{4+}, (—▲—) Ba^{2+}–Al^{3+}–Pb^{2+}–Zr^{4+}, and (—×—) Sr^{2+}–Al^{3+}–Pb^{2+}–Zr^{4+} on Zirconium(IV) selenophosphate column.

the composition and the nature of the contacting solution. The K_d value for Th^{4+} is very high showing a high affinity of Zr(IV) selenophosphate to Th^{4+}, whereas the rare earth metals are least strongly adsorbed in almost all the solution systems studied. An increase in the concentration of nitric acid has significant effect on the adsorption of Pb^{2+} and Fe^{3+} but has a little effect on the behavior of rare earth metals. Kd values are increasing as the mesh size of the exchanger increases (Table 5). The sorption studies on Zr(IV) selenophosphate for different metal ions reveal some important separations. As a result, eleven quaternary separations were performed by using small column (30 cm length and 0.6 cm internal diameter) of Zr(IV) selenophosphate. Results are summarized in Table 6. The elution profiles are shown in Fig. 4a—c.

The authors are thankful to Professor M. S. Ahmad, Chairman, Department of Chemistry for providing research facilities. Department of Atomic Energy, Government of India is also acknowledged for financial assistance to N. Rahman.

References

1) C. B. Amphlett, "Inorganic Ion Exchangers," Elsevier, New York (1964).
2) Y. Inoue, *J. Inorg. Nucl. Chem.*, **26**, 2241 (1964).
3) M. Qureshi, R. Kumar, V. Sharma, and T. Khan, *J. Chromatogr.*, **118**, 175 (1976).
4) E. S. Boichinova and T. I. Podgorelova, *Zh. Prikl. Khim. (Leningrad)*, **40**, 1837 (1967).
5) E. S. Boichinova and D. A. Sokolova, *Zh. Prikl. Khim. (Leningrad)*, **38**, 1732, (1965).
6) V. Pekarek and V. Vesley, *Talanta Rev.*, **19**, 224 (1972).
7) K. G. Varshney and Asif A. Khan, *J. Inorg. Nucl. Chem.*, **41**, 241 (1979).
8) M. Qureshi and R. C. Kaushik, *Anal. Chem.*, **49**, 165 (1977).
9) M. Qureshi, R. Kumar, and R. C. Kaushik, *Sep. Sci. Technol.*, **13**, 185 (1978).
10) K. G. Varshney, U. Sharma, and S. Rani, *Indian J. Technol.*, **22**, 99 (1984).
11) K. G. Varshney, R. Pal Singh, and S. Rani, *J. Indian Chem. Soc.*, **61**, 220 (1984).
12) K. G. Varshney and A. Premadas, *J. Liq. Chromatogr.*, **4**, 1245 (1981).
13) P. S. Thind, S. S. Sandhu, and J. P. Rawat, *Chim. Anal. (Warsaw)*, **24**, 65 (1979).
14) S. A. Nabi, R. A. K. Rao, and W. A. Siddiqui, *J. Liq. Chromatogr.*, **6**, 777 (1983).
15) S. A. Nabi, R. A. K. Rao, and A. R. Siddiqui, *Z. Anal. Chem.*, **311**, 505 (1982).
16) K. G. Varshney and A. Premadas, *J. Liq. Chromatogr.*, **4**, 915 (1981).
17) M. Qureshi and S. A. Nabi, *Talanta*, **19**, 1033 (1972).
18) F. D. Snell and C. T. Snell, "Colorimetric Methods of Analysis," D. Van Nostrand, Princeton, New Jersey (1959), Vol. IIA, p. 235.
19) Ref. 18, p. 679.
20) N. H. Furman, "Standard Methods of Chemical Analysis," 6 th ed, D. Van Nostrand, Princeton, New Jersey (1962), Vol. 1, p. 814.
21) N. E. Topp and K. W. Pepper, *J. Chem. Soc.*, **1949**, 3299.
22) Ref. 18, p. 1270.
23) Ref. 18, p. 929.
24) M. L. Berardelli, P. Galli, A. L. Ginestra, M. A. Massucci, and K. G. Varshney, *J. Chem. Soc., Dalton Trans.*, **1985**, 1741.
25) A. Clearfield and J. A. Stynes, *J. Inorg. Nucl. Chem.*, **26**, 128 (1964).
26) F. A. Miller and C. H. Wilkins, *Anal. Chem.*, **24**, 1281 (1952).
27) G. Alberti, E. Torracca, and A. Conte, *J. Inorg. Nucl. Chem.*, **28**, 607 (1966).

Titanium Determination under High-Sensitivity Conditions with 2-(5-Chloro-2-pyridylazo)-5-dimethylaminophenol. II. Ternary Compounds of Ti(IV)-H_2O_2-5-ClDMPAP

Héctor José MARINI, Rosa Isabel ANTÓN, and Roberto Antonio OLSINA*
Departamento de Quimica Analitica "Dr. Carlos B. Marone," Universidad Nacional de San Luis, Argentina
(Received April 8, 1986)

Ti(IV) together with pyridylazo-type reagents and other molecular compounds form ternary complexes that may stand as the basis for analytical methods designed for the quantitative determination of the metal. This paper reports the results obtained by the use of the system Ti(IV)-H_2O_2-5-ClDMPAP in aqueous ethanolic solutions, and application to routine analyses of Ti(IV) in various types of samples. The spectral characteristics of the complexes formed, the pH ranges appropriate for their formation, ethanol influence, composition and stability have been studied. The complex selected for this analytical work is formed between pH 2.5 and 6.5 with a 1:2:2 Ti(IV)-H_2O_2-5-ClDMPAP molar ratio. The system fulfils Beer's law up to a Ti(IV) concentration of 0.7 ppm, working at λ_{max} 534 nm. The molar absorptivity and Sandell index are 4.59×10^4 dm^3 mol^{-1} cm^{-1} and 0.0010 μg cm^{-2} respectively.

Reactions involving ternary compounds are important in determination and separation methods, specially in absorptiometric analysis, liquid-liquid extraction and masking. Babko[1] describes four basic types of ternary compounds which form the following systems: a) Lewis' metallic ion-electronegative ligand-base; b) metallic ion-two different electronegative ligands; c) ternary heteropolyacids; d) two different metallic ions-one ligand. According to the general qualities of each of these types, our Ti(IV)-H_2O_2-2-(5-chloro-2-pyridylazo)-5-dimethylaminophenol, system, belongs to type b). Ternary compounds belonging to this type have been extensively studied and applied to absorptiometric determinations, as well as to complexometric titrations.[1] In the latter case, one of the complexing reagents helps in the process's kinetics for it destroys the existing hydroxopolynuclear complexes, and it usually activates the forming reaction of the ternary complex.

In the spectrometric determination of titanium, Ozawa[2] adds H_2O_2 together with 4-(2-pyridylazo)resorcinol, thus forming a ternary complex Ti(IV)-H_2O_2-PAR of 1:3:3 stoichiometry, and a molar absorptivity of 5.10×10^4 dm^3 mol^{-1} cm^{-1} at pH 7.9. When no H_2O_2 is addes, the complex formed at pH 3.2—3.8, Ti(IV)-PAR (1:2) has an absorptivity rate of 2.1×10^4 dm^3 mol^{-1} cm^{-1}. Nevertheless, no method to solve severe interferences caused by Cu(II), Fe(III), Co(II), Ni(II), Sn(II), Bi(III), V(V), and Zr(IV) is suggested.

Tsurumi and Furuya[3] have determined Ti(IV) by spectrometry, using 2-(2-thiazolylazo)-5-dimethylaminophenol (TAM) as a reagent of the azo group. This reagent together with Ti(IV) at a 1:2 (Ti(IV)-TAM) molar ratio, formed a complex capable of being quantitatively removed as an ionic association compound by means of 1,3-diphenylguanidine (DPG) in benzyl alcohol at pH 4.2—5.2. This proposed method becomes interesting due its relatively high molar absorptivity, but the interferences caused, in this case, by Fe(III), Co(II), Ta(V), and Zr(IV) are not solved. Cd(II), Co(II), Ni(II), Cr(VI), UO_2(II), Fe(III), Zr(IV), and Hf(IV) are severe interferers in most Ti(IV) spectrometric determination. These interferers could be drawn by means of an extraction technique with 8-quinolinol[4] and cupferron[5] when Ti(IV), under high sensitivity conditions, was determined by spectrometric with 5-ClDMPAP.[6] Although this method yields a relatively high molar absorptivity, its drawback is the complex's limited stability in solution. In order to solve this limitation, a method involving hydrogen peroxide was developed so as to greater stability to the system. The results attained by the use of ternary system Ti(IV)-H_2O_2-5-ClDMPAP in aqueous ethanolic solutions are shown in the present paper, as well as the studies on the spectral characteristics of the three species developed, proper pH ranges for forming them, the influence of the organic solvent used, stability and composition. An increase in both sensitivity and stability has been observed to occur when pyridylazo reagents are used and hydrogen peroxide is added to the reaction medium.

Experimental

Reagents. A 5-ClDMPAP solution was prepared by coupling *m*-dimethylaminophenol with sodium 5-chloro-2-pyridinediazotate, according to the method described by Shibata et al.[7] Purification was carried out by means of repeated cycles of dissolution-reprecipitation starting from ethanol-water mixtures. A 0.25% (w/v) solution of the pure material was prepared. Lower concentration solutions of the above one, were prepared by dilution with ethanol. All solutions were kept away from light. A 5×10^{-4} mol dm^{-3} solution can be kept unaltered for at least 25 d. The Ti(IV) solution was prepared according to that described by Roseman and Thornton.[8] Its titer was determined by complexometric titration.[9] To obtain reproducible results, the solution must be prepared daily. The hydrogen peroxide solution was prepared by dilution from H_2O_2 of 200 vol. All the other chemicals were also of an analytical-

reagent grade.

Apparatus. A Varian 634 UV-Vis. spectrophotometer with 10 mm optical path cell to obtain the absorption spectra an absorbance measures was used. An Orion 701-A pH meter for pH measurements was used. Volumes in Ti(IV) complexometric titrations were obtained by means of an automatic Metrohn Dosimat E412P buret.

Results and Discussion

Study on Ti(IV)-H_2O_2-5-ClDMPAP. Influence of pH. In the presence of 5-ClDMPAP and H_2O_2, Ti(IV) forms three ternary complex species with compositions varying according to the pH value of the

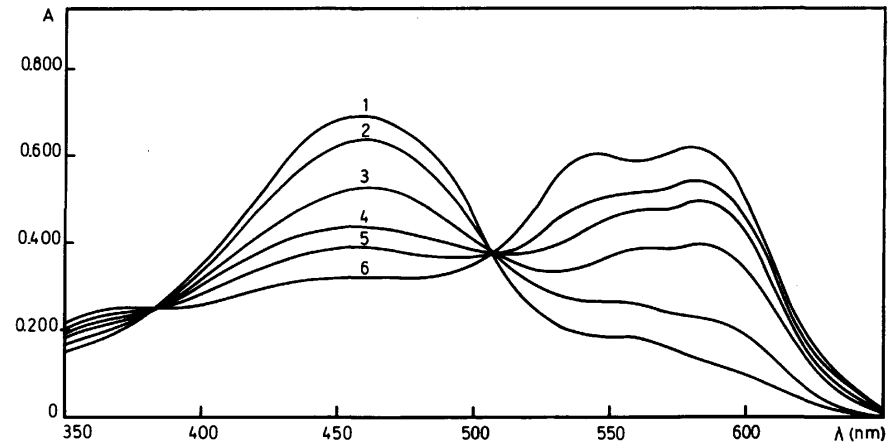

1: pH=1, 2: pH=1.13, 3: pH=1.27, 4: pH=1.5, 5: pH=1.8, 6: pH=2

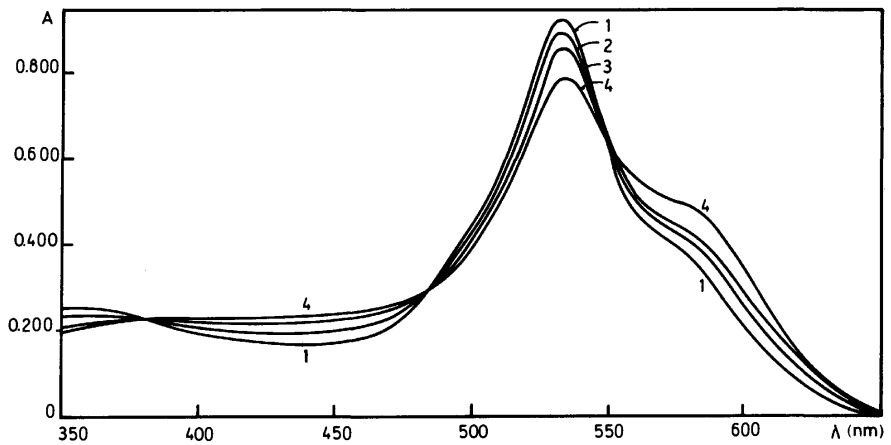

1: pH=4—5—6, 2: pH=3.5, 3: pH=3, 4: pH=2.5

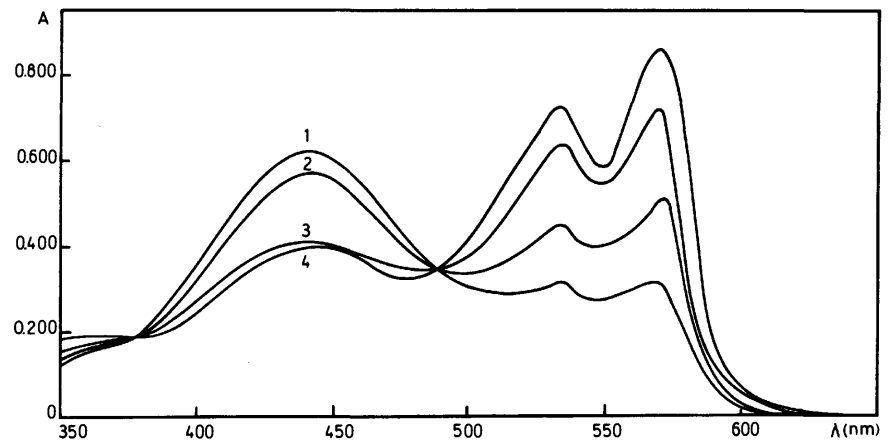

1: pH=10, 2: pH=9, 3: pH=8.5, 4: pH=8

Fig. 1. Ternary complex's isosbestic point formed to different values of pH in presence of metal excess. $C_{Ti}=7.7\times10^{-5}$ M; $C_R=2.2\times10^{-4}$ M.

medium. For values ranging from 2.5 to 6.5 the prevailing species has λ_{max} at 534 nm; while the two other species are formed at pH values ranging from 1—2 to 7—9 with λ_{max} at 580 and 570 nm respectively.

The ternary species spectra formed show isosbestic points at different wavelengths, depending on the range (Figs. 1a, 1b, and 1c). For the analytical work, a ternary complex quantitatively formed between pH 2.5 and 6.5 was singled out bacause of its higher absorptivity values, stability and pH range of formation.

Stoichiometry of the Selected Ternary Species. Stoichiometry of the ternary complex was studied at pH 5.4. In order to determine Ti(IV)-5-ClDMPAP molar ratio, the method of continuous variations (Job)[10] was used, keeping H_2O_2 concentration constant at a rate of 0.3%. This methods proved to be uncapable of determining Ti(IV)-H_2O_2 molar ratio, so that the equilibrium shift methods[11] had to be employed (Fig. 2). Ti(IV)-H_2O_2-5-ClDMPAP molar ratio happened to be 1:2:2.

The order in which the reagents are added is very important. First, the reaction between Ti(IV) and H_2O_2 is caused at low pH values (<2), second a reaction between the Ti(IV)-H_2O_2 complex and 5-ClDMPAP is caused; and then a 5.4 pH buffer is added in order to select the wanted complex.

If it is accepted that the predominant Ti(IV) species at low pH values (2—3), is $[Ti(OH)_2]^{2+}$,[12,13] and that the reaction with H_2O_2 leads to the formulation of $[Ti(OH_2)_2]^{2+}$[15,16] the following equilibria can be written:

$$[Ti(HO)_2]^{2+} + 2H_2O_2 \rightleftharpoons [Ti(HO_2)_2]^{2+} + 2H_2O$$
$$[Ti(HO_2)_2]^{2+} + RH \rightleftharpoons [Ti(HO_2)_2R]^{+} + H^{+}$$
$$[Ti(HO_2)_2R]^{+} + RH \rightleftharpoons [Ti(HO_2)_2R_2] + H^{+}$$

The validity of the above formulation is guaranteed by the results obtained applying the equilibrium shift method[11] (Fig. 3). The equilibrium constant of the ternary compounds formation was studied by means of absorptiometric measurements,[14] the value obtained was 2.77×10^{13} at 25 °C.

Influence of the Solvent and the Hydrogen Peroxide Concentration. The influence of methanol, ethanol, dioxane, and acetone on the absorbance value was studied; whichever the solvent may be, the λ_{max} is the same. As the maximum absorptivity is attained when using methanol or ethanol, the latter was singled out for the present experiment. The best ethanol concentration is between 5 and 25% (v/v) (Fig. 4). The

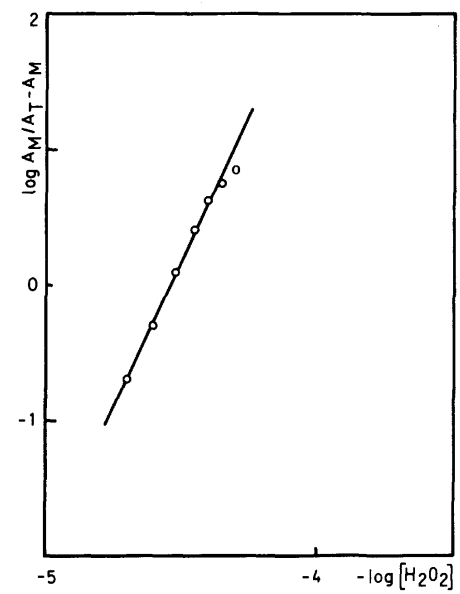

Fig. 2. Equilibrium shift method for the determination of the Ti(IV)-H_2O_2 molar ratio.
$C_{Ti}=1.3\times10^{-5}$ M; $C_R=2.2\times10^{-4}$ M; $C_{H_2O_2}$=Variable $\lambda=534$ nm. A_M=Absorbance read at unfavorable hydrogen peroxide concentration for the ternary complex formation. A_T=Absorbance corresponding to a $C_{H_2O_2}=5.5\times10^{-5}$ M and to a 1.3×10^{-5} M of the ternary complex formation.

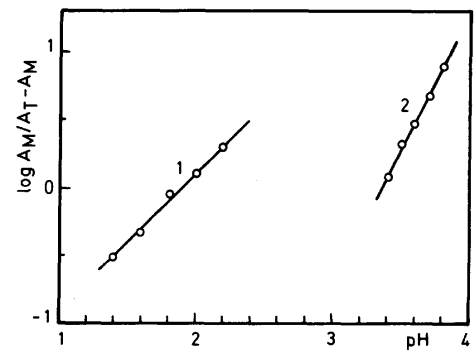

Fig. 3. Equilibrium shift method for determining hydrogen ions released during ternary complex formation.
$C_{Ti}=1.6\times10^{-5}$ M; $C_R=2.2\times10^{-4}$ M. A_M=Absorbance read at unfavorable pH values for the ternary complex formation. A_T=Absorbance corresponding to a 1) pH 2.4; 2) pH 3.9 solution and to 1.6×10^{-5} M of the ternary complex.

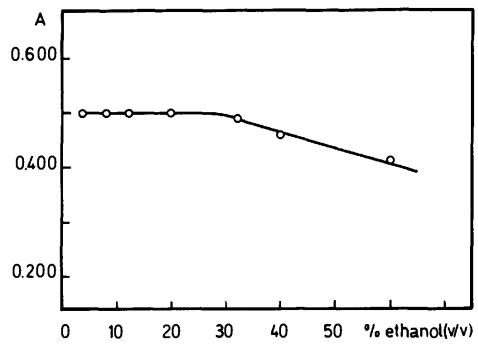

Fig. 4. Influence of the concentration of ethanol on the absorbance of ternary complex.
pH 5.4; $\lambda=534$ nm; $C_{Ti}=1.1\times10^{-5}$ M; $C_{H_2O_2}$= 0.3%(v/v); $C_R=2.2\times10^{-4}$ M.

minimum H_2O_2 concentration needed to get a maximum absorbance is 0.25%, and no transformations take place for concentration up to 1.2% (Fig. 5).

Reagent Concentration and Calibration Curve. The reagent concentration appropriate for the quantitative work was evaluated by plotting the saturation curve (Fig. 6) at pH 5.4. Ti(IV) concentration was kept constant (1.1×10^{-5} mol dm^{-3}), that one corresponding to 5-ClDMPAP was changed between 1×10^{-6} and 5.5×10^{-4} mol dm^{-3}, while H_2O_2 concentration remained constant (0.3% v/v). Absorbance was read at λ_{max} 534 nm and the ethanol concentration remained constant at 16% (v/v).

For a 1:10 Ti(IV):5-ClDMPAP molar ratio, the complete development of a complex is achieved, and this is kept unaltered for proportions up to 1:50. The ternary complex solutions at pH 5.4, keeping a 1:20:10000 metal-ligand-H_2O_2 ratio, change neither their absorption spectrum nor their absorptivity at λ_{max} 534 nm, during 1 h. Aqueous ethanolic solutions of the studied ternary species obey Beer's law up to a concentration of 0.7 ppm when they are made up in a medium with a pH 5.4 and are controlled by means of acetic acid-sodium acetate. The outstanding aspects referring to Ti(IV) absorptiometric determination are stated in Table 1.

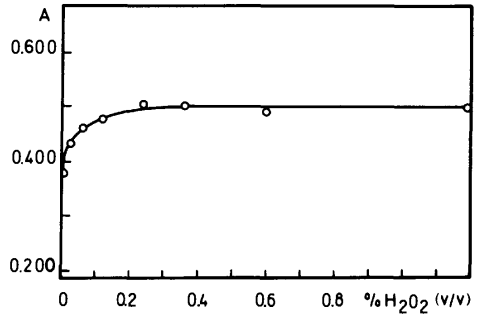

Fig. 5. Influence of the concentration of hydrogen peroxide on the absorbance of ternary complex. pH 5.4; λ=534 nm; ethanol-water 16% (v/v); $C_{Ti}=1.1\times10^{-5}$ M; $C_R=2.2\times10^{-4}$ M.

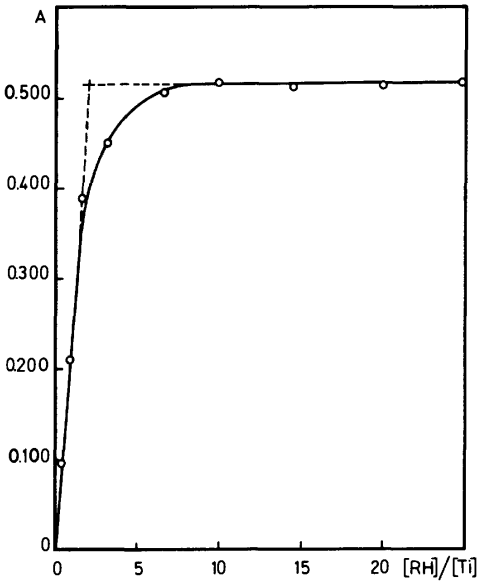

Fig. 6. Saturation curve. $C_{Ti}=1.1\times10^{-5}$ M; $C_{H_2O_2}=0.3\%$(v/v); pH 5.4; λ= 534 nm; ethanol-water 16%(v/v).

Effect of Foreign Ions. The reagent used reacts with ions different from Ti(IV) and produces various colors, depending upon the experimental complexation conditions. The interferences brought about by Fe(III), Cu(II), Ni(II), Co(II), W(VI), Nb(V), Ta(V),

Table 1. Experimental Variables of Ti(IV) Absorptiometric Determination

pH range	2.5—6.5
Solvent	Ethanol-Water 16% v/v
Stoichiometry	1 : 2 : 2 (Ti(IV)-H_2O_2-R)
Maximum absorption of ternary complex:	534 nm
Maximum absorption of reagent	: 440 nm
	$\Delta\lambda$: 94 nm
Stability of ternary complex:	1 h
Beer's law-sensitivity	
Acidity (pH):	5.4
Molar absorptivity:	4.59×10^4 dm^3 mol^{-1} cm^{-1}
$\left(s=2400;\ Cl\ \begin{matrix}43381-48418\\ \alpha=0.05\end{matrix}\right)$	
Optimum concentration range (Ringbom)	0.05—0.7 ppm
Sensitivity of sandell:	0.0010 μg/cm^2
Beer's law fulfilment:	Up to 0.7 ppm

Table 2. Tolerances for Some Common Anions

Ion	Ion/Ti(IV) tolerated molar ratio	Ion/Ti(IV) tolerated mass ratio
Acetate	10000	12.3×10^3
Hydrogen phthalate	5000	17.1×10^3
Bromide	5000	8.3×10^3
Chloride	5000	3.7×10^3
Thiourea	5000	7.9×10^3
Nitrate	4000	5.1×10^3
Thiosulfate	3000	7.0×10^3
Perchlorate	3000	6.2×10^3
Sulfate	2000	4.0×10^3
Sulfamic acid	2000	6.6×10^3
CDTA	500	3.6×10^3
EDTA	500	3.8×10^3
Fluoride	100	40
Tetraborate	30	77
Citrate	10	40
Phosphate	Int	—
Oxalate	Int	—
Iodide	Int	—
Tartrate	Int	—
Ascorbic acid	Int	—

and V(V) have severe effects on the systems and they cannot always be controlled by masking. Zn(II), Mn(II), Mo(VI), and Cr(VI) ions are tolerated in a 10:1 ratio (foreign ion:Ti(IV)). The tolerated ratio for Al(III) and Mg(II) is a 50:1 and for Na(I) and K(I) is 1000:1. Table 2 shows the tolerances for anions, coming from strong acids, used to dissolve samples, as well as for other anions or compound added as possible masking agents. In order to finish with the negative effects of the differents interferers the liquid-liquid extractions method was applied, using 8-quinolinol[4,6] as a removing reagent and chloroform as a solvent, and adjusting pH value in the presence of adequate complexing agents.

Methods and Applications. The method proposed by Cheng,[5] makes use of EDTA and cupferron. Adequately varying the concentration of both species, the selective and quantitative extraction of Ti(IV) present in complex samples as *cast iron* and *nickel bases Alloy* can be obtained. It is important to take into account that EDTA and cupferron concentration will be in agreement with the Ti(IV) concentration and to the other metal interferents concentration in the sample (Fe, Cu, Ni, Cr, and Mo).

Determination of Titanium in Standard Samples. The methodology developed was applied to two kinds of samples.

1. Nodular Cast Iron (NBS 342): A sample of 1 g was digested with 20 cm^3 of hydrochloric acid on a hot plate until action ceased. The insoluble matter was filtered while still hot and washed with 1% hydrochloric acid (Fl). After drying, the paper and residue were ignited in an uncovered platinum crucible. 1 cm^3 of 48% hydrofluoric acid and 1 cm^3 of to sulfuric acid were added and the solution was evaporated to dryness. The residue was fused with 1 to 2 g of sodium carbonate. The melt was dissolved in 50 cm^3 of water and digested for 15 min at 90 to 95 °C. The remaining residue was filtered and washed with water. The residue was ignited with 1 g of potassium disulfate for 10 min. The melt was cooled and dissolved with a minimum amount of 2 mol dm^{-3} sulfuric acid. This solution was added to the original (Fl) filtrate and diluted to approximately 250 cm^3. To a 25 cm^3 aliquot a slight excess of the disodium salt of EDTA (1 g) was added, followed by sufficient 6 M aqueous ammonia to adjust the solution to pH 5.4. The solution was boiled for 2 min and cooled. Then it was transferred to 125 cm^3 separatory funnel, and diluted to approximately 50 cm^3. 5 cm^3 of 0.4% freshly prepared cupferron were added dropwise with swirling. After standing for 5 min, the solution was extracted with 10 cm^3 of methylisobutylketone. Separate the organic phase, put it dry into a porcelain

Table 3. Results in the Determination of Ti(IV) in Samples

Sample	Composition/%(w/w)		Found/%(w/w)	Error/%
Nodular cast	C	2.450		
iron	Mn	0.369		
	P	0.020		
(NBS 342)	S	0.014		
	Si	2.850		
	Cu	0.140		
	Ni	0.023		
	Cr	0.032		
	V	0.005		
	Mo	0.009		
	Ti	0.019	$0.0187\ \left(s=7.53\times10^{-5};\ \mathrm{Cl}\ {}^{0.0186-0.0188}_{\alpha=0.05}\right)$	1.6
	Mg	0.053		
	Fe	Rem.		
Nickel based	C	0.015		
alloys	Mg	0.007		
	Si	0.150		
Monel-alloy-400	Cu	31.700		
	Fe	0.130		
(BNF B. 7002)	Mn	2.650		
	Cr	0.100		
	Ti	0.015	$0.0152\ \left(s=6.44\times10^{-4};\ \mathrm{Cl}\ {}^{0.0144-0.0159}_{\alpha=0.05}\right)$	1.3
	Al	0.060		
	Co	0.100		
	Ni	Rem.		

crucible on sand bath and melt it with 0.4 g of potassium hydrogensulfate. Cool it take it with 3 cm^3 of 3% (v/v) hydrogen peroxide and pour it into a 25 cm^3 flask; then add 2 cm^3 of reagent, 2 cm^3 of ethanol, buffer acetic-acetate up to pH 5.4 and bring it to gauging. Read the solution absorbance at λ_{max} 534 nm against a reference prepared as usual. Results are shown in Table 3.

2. Synthetic Nickel Based Alloys Sample Corresponding to Metals Technology Center (BNF B. 7002 MONEL-ALLOY 400): To an aliquot of 25 cm^3 of synthetic sample, 0.5 g of the disodium salt of EDTA was added for masking purposes. The solution was made slightly acid and heated for a few minutes to hasten the reaction of EDTA and chromium. The solution was cooled and adjusted to pH 5.4. 5 cm^3 of 1.5% freshly-prepared cupferron were added and the solution was extracted with 25 cm^3 of the solvent. After the extraction, the method used for the *cast iron sample* is applied. Results and shown in Table 3.

The authors are gratefully indebted to CONICET and CyT of UNSL for financial support.

References

1) A. K. Babko, *Talanta*, **15**, 721 (1968).
2) T. Ozawa, *Bunseki Kagaku*, **16**, 435 (1967).
3) C. Tsurumi and K. Furuya, *Bunseki Kagaku*, **26**, 149 (1977).
4) J. Starý, *Anal. Chim. Acta*, **28**, 132 (1963).
5) K. L. Cheng, *Anal. Chem.*, **30**, 1941 (1958).
6) H. Marini, R. Antón, S. Boeris, and R. Olsina, *Bull. Chem. Soc. Jpn.*, **59**, 3951 (1986).
7) S. Shibata and M. Furukawa, *Jpn Analyst*, **23**, 1420 (1974).
8) R. Roseman and W. M. Thornton, *Am. J. Sci.*, **20**, 14 (1930).
9) D. H. Wilkins, *Anal. Chim. Acta*, **20**, 113 (1959).
10) P. Job, *Ann. Chem.*, **9**, 113 (1982).
11) Yu A. Zolotov, "Extraction of Chelate Compounds," Ann Arbor-Humphrey Science Publishers Inc., London (1970).
12) J. Kragten, "Atlas of Metal-Ligand Equilibria in Aqueous Solution," John Wiley & Sons, N.Y. (1978).
13) J. Selbin, *J. Chem. Educ.*, **41**, 86 (1964).
14) F. J. C. Rossotti and H. Rossotti, "The Determination of Stability Constants in Solution," McGraw-Hill, N.Y. (1961).
15) A. K. Babko and A. I. Volkova, *Zh. Obshch. Khim.*, **21**, 1949 (1951).
16) M. Mori, M. Shibata, E. Kyuno, and S. Ito, *Bull. Chem. Soc. Jpn.*, **29**, 904 (1956).

 © 1987 The Chemical Society of Japan Bull. Chem. Soc. Jpn., 60, 2641—2650 (1987)

The Reactions of Alkoxyl Radicals with O_2. IV. n-C_4H_9O Radicals†

Paul MORABITO and Julian HEICKLEN*
Department of Chemistry and Center for Air Environment Studies, The Pennsylvania State University, University Park, PA 16802, U.S.A.
(Received December 2, 1985)

n-C_4H_9ONO was photolyzed with 366 nm radiation at −8, 23, 55, 88, and 120 °C in the presence of NO, O_2, and N_2. The quantum yields of n-C_3H_7CHO, C_2H_5CHO, and CH_3CHO were measured as a function of reaction conditions. The primary photolytic act produces n-$C_4H_9O\cdot$ radicals which can react with NO by two routes

$$n\text{-}C_4H_9O\cdot + NO \longrightarrow n\text{-}C_4H_9ONO \quad (2a)$$
$$\longrightarrow n\text{-}C_3H_7CHO + HNO \quad (2b)$$

or isomerize via an internal H-atom abstraction

$$n\text{-}C_4H_9O\cdot \longrightarrow I\cdot \quad (4)$$

where I· is the $HOCH_2CH_2CH_2CH_2\cdot$ radical, and $\ln(k_4/k_2, \text{mol dm}^{-3})=1.93\pm1.60-(4014\pm509)/T$. If k_2 is taken as 2.6×10^{10} dm^3 mol^{-1} s^{-1}, then $\log(k_4, \text{s}^{-1})=11.25\pm0.69-(4014\pm509)/2.303T$. In the presence of O_2, n-$C_4H_9O\cdot$ radicals can also react with O_2

$$n\text{-}C_4H_9O\cdot + O_2 \longrightarrow n\text{-}C_3H_7CHO + HO_2 \quad (6)$$

with $\ln(k_6/k_2)=(-4.09\pm0.54)-(1178\pm176)/T$. If $k_2=2.6\times10^{-10}$ dm^3 mol^{-1} s^{-1}, then $k_6=4.5\times10^8 \exp\{(-1178\pm176)/T\}$ dm^3 mol^{-1} s^{-1}. The radical I· is removed via

$$I\cdot \longrightarrow CH_3CHO + 2CH_2O + HO \quad (12a)$$
$$\longrightarrow \text{Undetected aldehydes} + HO \quad (12b)$$
$$I\cdot + O_2 \longrightarrow n\text{-}C_3H_7CHO + HO \quad (13a)$$
$$\longrightarrow C_2H_5CHO + HO \quad (13b)$$

where these reactions are composites of a series of steps. The ratio $k_{13a}/k_{13b}\simeq1.3\pm0.2$ nearly independent of temperature. The ratio k_{12}/k_{13} was not found very accurately, but is $\simeq3\times10^{-3}$ mol dm^{-3}. There was no evidence for the oxidation of I· leading to dioxygenated products.

Alkoxyl radicals are important intermediates in the atmospheric photooxidation of NO to NO_2. These radicals are produced in the atmosphere from the oxidation of hydrocarbons. Over the past few years studies have been undertaken to determine the rate coefficient for the alkoxyl radical oxidation reaction since these reactions have considerable importance in both photochemical smog and combustion.

Extensive rate coefficient studies have been made only for the $CH_3O\cdot$ radical oxidation.[1-9] Only three studies report rate coefficients for the $C_2H_5O\cdot+O_2$ reaction[9-11] while one report is given for higher homologs such as the n-$C_3H_7O\cdot+O_2$[12] and i-$C_4H_9O\cdot+O_2$[13] systems.

In this study, we investigate the reaction of n-$C_4H_9O\cdot+O_2$. Unlike the other radicals that have been studied, the n-$C_4H_9O\cdot$ radical can undergo a rapid intramolecular hydrogen abstraction to form a new radical:

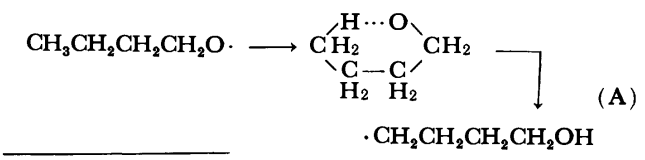

(A)

Such isomerizations are well known in gas phase studies and occur when a δ-carbon atom is present which contains a hydrogen atom.[14] However very few measurements have been made on the isomerization reaction (A) because both reactant and product are free radicals.

The radical produced in step A could now decompose, or in the presence of O_2 and NO, form a new alkoxyl radical, $HO(CH_2)_4O\cdot$. This radical would have a variety of reaction paths available to it and has been subjected to speculation.[15] There are only three experimental studies which report processes involving the isomerization pathway.[16-18] Unfortunately these studies lack detailed qualitative and quantitative information concerning the isomerization pathway. The Arrhenius expressions for reaction A were estimated to be $k_A=10^{11.8}\exp(-8900/RT)$ and $k_A=10^{11.4}\exp(-7700/RT)$ s^{-1}, respectively, by Carter et al.[16] and Baldwin and Golden,[17] where the activation energies are in cal mol^{-1} (1 cal=4.184 J). Niki et al.[18] showed that at 298 K in 700 Torr (1 Torr=133.322 Pa) of air the ratio of reaction of n-$C_4H_9O\cdot$ with O_2 compared to isomerization was 0.23. In this study we not only report the rate coefficient for n-$C_4H_9O\cdot$ isomerization reaction but also report some of the

† CAES Report No. 744-85.

products that are formed from the isomerization pathway.

Experimental

Mixtures of n-C_4H_9ONO with NO, O_2, and N_2 were photolyzed with 366 nm radiation, and the products analyzed using gas chromatography and mass spectrometry. In the gas chromatography system, two reaction cells were used. A 765-cm^3 spherical Pyrex reaction vessel was used for the temperature range of 23 to 120 °C. The reaction vessel was enclosed in an aluminum furnace, resistively-heated in which temperature regulation was achieved by an Omega proportional temperature controller model type 1522. For low-temperature photolysis at −8 °C, a 413 cm^3 cylindrical Pyrex reaction vessel was used. The low temperature was obtained by circulating ethanol cooled by dry ice through a Pyrex jacket that surrounds the reaction vessel. This procedure has been previously described.[11]

After irradiation was terminated, n-C_3H_7CHO, C_2H_5CHO, and CH_3CHO were analyzed on a Varian 1520B gas chromatograph using a FID detector. The products were separated using a 9-foot by 1/4″-diameter stainless-steel column containing GP 20%, SP-2100/0.1% Carbowax 1500 on Supelcoport. All analyses were carried out at 23 °C with a helium flow rate of 25 $cm^3\ min^{-1}$. In experiments with added NO, N_2, or O_2 the excess reactants were removed by condensing a portion of the photolysis mixture in a gas sample loop at −196 °C and pumping off the non-condensable gases prior to analysis.

In the mass spectrometry system a 329-cm^3 cylindrical Pyrex reaction vessel was used for the temperature range of 23 to 120 °C. The heating and regulation of the cell temperature was the same as mentioned earlier. Photolyses at −8 °C were not performed using the mass spectrometer due to the difficulty involved in adapting the low temperature cell to the instrument. The performance and operating parameters of the mass spectrometer have been described in previous studies.[19-20]

In both systems a conventional Pyrex vacuum line was employed. The line was kept grease free by the use of Teflon stopcocks with Viton "O" rings. The source of radiation was a medium pressure mercury lamp (Hanovia type 30620), used in conjunction with a 0—52 and 7—54 Corning glass filters to isolate the 366 nm line.

Quantum yields were based on light intensities measured by the photolysis of azomethane which has also been previously described.[19] The azomethane was prepared as before.[19] Absorption cross-sections were determined by using the lamp/filter combination as a light source and an RCA 935 phototube to measure the radiation. The absorption cross-sections were found to be (to base 10) 5.94×10^{-20} cm^2 for n-C_4H_9ONO which was independent of temperature from −8 to 120 °C and 4.54×10^{-21} cm^2 for azomethane at 23 °C.

The butyl nitrite was prepared as before and stored over mercury and Drierite in the dark at −196 °C.[19] Ninety-nine percent acetaldehyde, propionaldehyde, and butyraldehyde were obtained from Aldrich and used without purification. Extra dry oxygen (>99.6%) was obtained from Airco and used without purification. Matheson NO and N_2 was used; only the NO was purified trap-to-trap from −186 to −196 °C prior to use. All compounds condensable at −196 °C were degassed at this temperature before use.

Results

n-C_4H_9ONO was photolyzed by 366-nm radiation in the presence of NO, N_2, and O_2. The photolysis products n-C_3H_7CHO, C_2H_5CHO, and CH_3CHO were measured. In experiments performed at 88 and 120 °C, product growth occurred even without irradiation. At these elevated temperatures the thermal decomposition of the nitrite starts to become significant thus explaining the dark growth. To obtain correct quantum yields at these temperatures each photolysis was performed along with an identical dark run in which the dark growth was subtracted from the photolytic run. The correction was usually small and always less than 15% of the total amount of each product produced.

Initially experiments were performed in the absence of O_2 with a constant pressure of NO and the total pressure was varied by the addition of N_2. The results are presented in Table 1. At 23 °C, the total density was varied from $\approx2.8\times10^{-4}$ n-C_4H_9ONO mol dm^{-3} (≈5.0 Torr) to 1.7×10^{-2} mol dm^{-3} (300 Torr) while the concentration of NO and n-C_4H_9ONO remained constant at $\approx1.6\times10^{-7}$ NO mol dm^{-3} (≈30 mTorr) and 2.8×10^{-4} n-C_4H_9ONO mol dm^{-3} (≈5.0 Torr) respectively. The quantum yield of C_3H_7CHO, $\Phi\{n$-$C_3H_7CHO\}$, essentially remained constant over the entire pressure range, and was equal to 0.012±0.001.

As the temperature increases from −8 to 120 °C, the value of $\Phi\{n$-$C_3H_7CHO\}$ at low NO pressures decreases. However if additional NO is added the value of $\Phi\{n$-$C_3H_7CHO\}$ increases to the same limiting value at high [NO] for every temperature. These results are presented in Table 2. Experiments were performed at constant total pressure of 400 Torr while the NO pressure was varied from ≈30 mTorr to ≈55 Torr.

We next introduced oxygen into our system. First mixtures of n-C_4H_9ONO, NO, and O_2 were photolyzed to illustrate the effect of irradiation time on $\Phi\{n$-

Table 1. Effect of Total Gas Density on the Photolysis of n-C_4H_9ONO-NO Mixtures[a]

Total density[b]/10^{-4} mol dm^{-3}	$\Phi\{n$-$C_3H_7CHO\}$
2.8	0.011
27.4	0.013
54.6	0.012
82.0	0.011
109.4	0.012
164.0	0.011

a) $I_a=7.08\times10^{-5}$ Einsteins/s-mol n-C_4H_9ONO, [NO]=$(1.62\pm0.03)\times10^{-6}$ mol dm^{-3}. T=23 °C, irradiation time=45.00 min, [n-C_4H_9ONO]=$(2.77\pm0.05)\times10^{-4}$ mol dm^{-3}. b) Diluent is N_2.

Table 2. Effect of NO Concentration on the Photolysis of n-C_4H_9ONO-NO Mixtures at 400 Torr Total Pressure[a)]

[NO]/10^{-6} mol cm^{-3}	Irradiation time/min	$\Phi\{n$-$C_3H_7CHO\}$
$T=-8$ °C, low temp cell, $I_a=6.87\times10^{-5}$ Einsteins/s-mol n-C_4H_9ONO, $[n$-$C_4H_9ONO]=(3.02\pm0.10)\times10^{-4}$ mol dm^{-3}, Total density $=2.42\times10^{-2}$ mol dm^{-3}		
1.88	10.00	0.025
6.13	10.00	0.036
15.16	12.00	0.049
32.5	12.00	0.052
66.7	8.00	0.054
114.6	10.00	0.057
$T=23$ °C, high temp cell, $I_a=7.08\times10^{-5}$ Einsteins/s-mol n-C_4H_9ONO, $[n$-$C_4H_9ONO]=(2.74\pm0.08)\times10^{-4}$ mol dm^{-3}, Total density $=2.16\times10^{-2}$ mol dm^{-3}		
2.82	15.00	0.014
6.28	12.00	0.023
13.42	12.00	0.033
26.9	12.00	0.037
50.5	12.00	0.047
102.3	12.00	0.052
140.8	10.00	0.052
553	12.00	0.054
1710	10.00	0.054
$T=55$ °C, high temp cell, $I_a=1.08\times10^{-4}$ Einsteins/s-mol n-C_4H_9ONO, $[n$-$C_4H_9ONO]=(2.51\pm0.08)\times10^{-4}$ mol dm^{-3}, Total density $=1.96\times10^{-2}$ mol dm^{3}		
3.75	20.00	0.008
7.22	12.00	0.009
16.04	10.00	0.016
24.7	10.00	0.030
49.8	8.00	0.037
98.1	8.00	0.050
264	7.00	0.059
272	7.00	0.059
$T=88$ °C, high temp cell, $I_a=1.10\times10^{-4}$ Einsteins/s-mol n-C_4H_9ONO, $[n$-$C_4H_9ONO]=(2.24\pm0.07)\times10^{-4}$ mol dm^{-3}, Total density $=1.78\times10^{-2}$ mol dm^{-3}		
2.22	25.00	0.001
6.16	15.00	0.003
13.64[b)]	12.00	0.011
22.4	10.00	0.015
45.7	10.00	0.022
94.5	8.00	0.034
239[c)]	8.00	0.051
$T=120$ °C, high temp cell, $I_a=1.14\times10^{-4}$ Einsteins/s-mol n-C_4H_9ONO, $[n$-$C_4H_9ONO]=(2.04\pm0.08)\times10^{-4}$ mol dm^{-3}, Total density $=1.63\times10^{-2}$ mol dm^{-3}		
20.8	20.00	0.0023
41.7	15.00	0.0047
77.5	10.00	0.0073
206	8.00	0.012
628	10.00	0.037
910	6.00	0.044
1680	5.00	0.050
2260	5.00	0.051

a) Mixtures brought to total density by adding N_2. b) $[n$-$C_4H_9ONO]=1.88\times10^{-4}$ mol dm^{-3}. c) $[n$-$C_4H_9ONO]=2.03\times10^{-4}$ mol dm^{-3}.

$C_3H_7CHO\}$. Photolyses were performed at 23 °C for mixtures containing $\approx2.8\times10^{-4}$ n-C_4H_9ONO mol dm^{-3} (≈5.0 Torr), $\approx1.6\times10^{-6}$ NO mol dm^{-3} (30 mTorr), and 5.5×10^{-3} O_2 mol dm^{-3} (100 Torr). These data are presented in Table 3 and show that the quantum yield drops slightly with irradiation time between 1.00 and 5.00 min. However it can be observed from a plot of n-C_3H_7CHO produced vs. irradiation time in Fig. 1 that a nearly linear plot is obtained up to ≈5.5 min of irradiation time. This corresponds to the production ≈14.0 mTorr of n-C_3H_7CHO. Thus as long as irradiations are short enough to produce $\leqslant14$ mTorr of n-C_3H_7CHO, accurate initial quantum yields will be obtained. In all subsequent runs, the amount of n-C_3H_7CHO produced was kept below this value.

Next a series of runs was performed at five temperatures (−8 °C to 120 °C) in which n-C_4H_9ONO and NO pressures were kept constant at ≈5.0 Torr and ≈30 mTorr respectively while the O_2 pressure varied from 25 to 200 Torr. In each experiment the total pressure was kept constant at 400 Torr by adding N_2 gas. The general trend at each temperature is that $\Phi\{n$-$C_3H_7CHO\}$ and $\Phi\{C_2H_5CHO\}$ increase while

Table 3. Effect of Irradiation Time on the Photolysis of n-C_4H_9ONO-NO-O_2 Mixtures[a)]

Irradiation time/min	$[C_3H_7CHO]$/ 10^{-7} mol dm^{-3}	$\Phi\{n$-$C_3H_7CHO\}$
1.00	1.64	0.140
1.50	2.27	0.130
3.00	3.37	0.128
5.00	7.04	0.120
7.00	8.67	0.106
9.00	9.80	0.093
10.50	10.01	0.080

a) $I_a=7.08\times10^{-5}$ Einsteins/s-mol n-C_4H_9ONO. $[O_2]=5.41\times10^{-3}$ mol dm^{-3}. $[NO]=(1.61\pm0.05)\times10^{-6}$ mol dm^{-3}. $T=23$ °C. $[n$-$C_4H_9ONO]=(2.76\pm0.05)\times10^{-4}$ mol dm^{-3}.

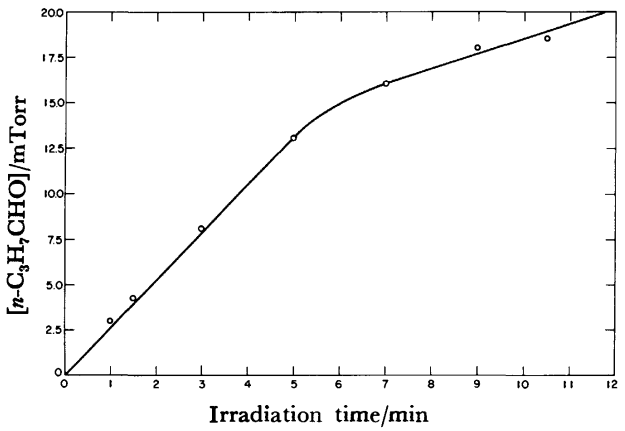

Fig. 1. Plot of $[n$-$C_3H_7CHO]$ vs. irradiation time at 23 °C for data in Table 3.

$\Phi\{CH_3CHO\}$ decreases with increasing O_2 pressure. The results are presented in Table 4.

Finally experiments were performed to check if any higher molecular weight products were being formed from the isomerization pathway. In these experiments n-C_4H_9ONO and NO were kept constant at ≈5.0 Torr and ≈30 mTorr, respectively, while the O_2 pressure was varied from 30 to 300 Torr. The total pressure in each experiment was kept constant at 400 Torr with N_2. Continuous recording of the mass spectra in the range of m/z 65—130 was obtained by allowing the contents of the cell to bleed through a small pinhole

Table 4. Photolysis of n-C_4H_9ONO-NO-O_2 Mixtures[a)]

$[O_2]/10^{-4}$ mol dm^{-3}	$[NO]/10^{-7}$ mol dm^{-3}	Irradiation time/min	$\Phi\{CH_3CHO\}$	$\Phi\{C_2H_5CHO\}$	$\Phi\{n\text{-}C_3H_7CHO\}$	$\frac{(\Phi\{n\text{-}C_3H_7CHO\}_{corr}-\rho)^{b)}}{\Phi\{C_2H_5CHO\}_{corr}}$
$T=-8$ °C, low temp cell, $I_a=6.87\times10^{-5}$ Einsteins/s-mol n-C_4H_9ONO						
16.9	21.3	5.00	—	0.017	0.066	1.35
30.4	18.3	5.00	—	0.016	0.073	1.19
45.5	19.4	4.50	—	0.023	0.110	2.03
60.6	18.8	4.00	—	0.026	0.130	2.13
75.7	18.3	4.00	—	0.029	0.159	2.65
91.0	18.8	3.00	—	0.031	0.174	2.65
106.1	19.9	3.00	—	0.028	0.192	3.36
121.2	18.3	2.50	—	0.032	0.212	3.28
$T=23$ °C, high temp cell, $I_a=7.08\times10^{-5}$ Einsteins/s-mol n-C_4H_9ONO						
13.6	16.4	4.00	≤0.01	0.024	0.064	1.84
19.4	16.4	4.00	≤0.01	0.039	0.077	1.35
27.1	16.8	4.00	≤0.01	0.030	0.085	1.84
40.7	16.6	4.00	≤0.01	0.031	0.092	1.93
54.1	17.3	4.00	≤0.01	0.046	0.115	1.52
81.2	16.4	4.00	≤0.01	0.045	0.123	1.41
108.3	15.9	4.00	≤0.01	0.045	0.151	1.65
$T=55$ °C, high temp cell, $I_a=1.08\times10^{-4}$ Einsteins/s-mol n-C_4H_9ONO						
12.3	15.1	4.00	0.048	0.048	0.048	0.72
12.3	15.1	4.00	0.050	0.053	0.057	0.86
24.4	15.6	4.00	0.037	0.062	0.068	0.83
36.7	15.1	4.00	0.035	0.067	0.086	0.93
48.8	15.6	4.00	0.035	0.062	0.094	1.05
61.1	15.1	4.00	0.034	0.068	0.099	0.95
61.1	15.1	4.00	0.036	0.069	0.097	0.89
73.2	15.6	4.00	0.031	0.070	0.107	0.97
73.2	16.6	4.00	0.029	0.063	0.105	1.04
85.5	15.1	4.00	0.025	0.069	0.113	1.01
85.1	15.1	4.00	0.026	0.060	0.109	1.12
97.1	15.1	4.00	0.023	0.062	0.119	1.23
97.1	19.1	4.00	0.024	0.062	0.115	1.06
$T=88$ °C, high temp cell, $I_a=1.10\times10^{-4}$ Einsteins/s-mol n-C_4H_9ONO						
11.1	13.8	4.50	0.134	0.047	0.039	0.70
22.2	13.8	4.00	0.107	0.061	0.059	0.87
33.2	13.8	4.00	0.101	0.075	0.078	0.88
44.3	14.1	4.00	0.075	0.077	0.086	0.97
55.5	13.8	4.00	0.062	0.080	0.092	0.97
66.6	14.1	4.00	0.072	0.093	0.101	0.91
88.7	13.8	4.00	0.069	0.091	0.110	0.98
$T=120$ °C, high temp cell, $I_a=1.14\times10^{-4}$ Einsteins/s-mol n-C_4H_9ONO						
10.3	1.31	4.00	0.205	0.031	0.030	0.94
20.4	1.23	4.00	0.155	0.045	0.044	0.95
30.7	1.27	4.00	0.150	0.059	0.065	1.07
40.8	1.23	4.00	0.133	0.066	0.078	1.18
51.1	1.27	4.00	0.126	0.068	0.082	1.18
61.3	1.31	4.00	0.121	0.076	0.087	1.10
81.7	1.18	4.00	0.113	0.082	0.093	1.08

a) All runs at 400 Torr total pressure (mainly O_2 and N_2). b) $\rho\equiv(k_{2b}[NO]+k_6[O_2])/k_4$.

into the mass spectrometer. Other techniques such as GC/CI mass spectrometry and high resolution mass spectrometry were also utilized to determine any higher molecular weight products. In all cases the only mass spectral peak that grew was the 76 m/z peak. Relative quantum yields were obtained by assuming a calibration factor since we could not determine the identity of the 76 m/z peak. The results are presented in Table 5 and indicate that $\Phi\{76\}$, the relative quantum yield of the product with m/z 76, remains nearly constant as the O_2 pressure increases at lower temperatures. However at 120 °C, $\Phi\{76\}$ drops as the O_2 pressure increases.

Discussion

O_2 Absent. The mechanism for the photolysis of n-C_4H_9ONO-NO mixtures is:

Table 5. Effect on 76 m/z Peak in the Photolysis of n-C_4H_9ONO-NO-O_2 Mixture[a)]

$[O_2]$/Torr	$\Phi\{76\}$[b)]
T=23 °C, $I_a=1.88\times10^{-4}$ Einsteins/s-mol n-C_4H_9ONO	
30	0.262
30	0.270
100	0.330
300	0.277
T=55 °C, $I_a=1.88\times10^{-4}$ Einsteins/s-mol n-C_4H_9ONO	
30	0.154
100	0.167
100	0.142
300	0.133
T=88 °C, $I_a=1.88\times10^{-4}$ Einsteins/s-mol n-C_4H_9ONO	
30	0.101
100	0.088
300	0.081
T=120 °C, $I_a=1.88\times10^{-4}$ Einsteins/s-mol n-C_4H_9ONO	
30	0.091
30	0.097
100	0.070
100	0.064
300	0.048
300	0.048

a) $[n$-$C_4H_9ONO]=5.0$ Torr. $[NO]\simeq30$ mTorr. N_2 added to give a total pressure of 400 Torr. b) Relative quantum yield for product with m/z 76.

$$n\text{-}C_4H_9ONO + h\nu \longrightarrow n\text{-}C_4H_9O\cdot + NO, \quad (1)$$

$$n\text{-}C_4H_9O\cdot + NO \longrightarrow n\text{-}C_4H_9ONO, \quad (2a)$$

$$\longrightarrow n\text{-}C_3H_7CHO + HNO, \quad (2b)$$

$$2HNO \longrightarrow N_2O + H_2O, \quad (3)$$

$$n\text{-}C_4H_9O\cdot \longrightarrow I\cdot, \quad (4a)$$

$$\longrightarrow \text{Decomposition}, \quad (4b)$$

$$R\cdot + NO \longrightarrow RNO, \quad (5)$$

where I· is the $HOCH_2CH_2CH_2CH_2\cdot$ radical resulting from the internal abstraction of an H atom by the n-$C_4H_9O\cdot$ radical, and R· can be I· or any radical produced in Reaction 4b.

In addition, there is the possibility that vibrationally-excited n-$C_4H_9O\cdot$ radicals are being produced by photolysis. McMillan et al.[21] have shown that the production of these "hot" alkoxyl radicals is probably not very important in the photolysis of alkyl nitrites at 366 nm. If present, these hot radicals would be expected to rapidly decompose to yield the same products as in the decomposition of the thermally-equilibrated alkoxyl radicals, Reaction 4b.

The data in Table 1 indicate that at 23 °C there is no change in $\Phi\{n$-$C_3H_7CHO\}$ with an increase in total pressure. This leads to the conclusion that Reaction 2a is in its second-order regime at our working pressures (>5 Torr) and that "hot" alkoxyl radicals are not present to any significant extent in this sytem.

The Arrhenius expression for k_{4a} has been estimated to be $k_{4a}=10^{11.8}\exp\{-8900/RT\}$ s^{-1} by Carter et al.[16] and $k_{4a}=10^{11.4}\exp\{-7700/RT\}$ s^{-1} by Baldwin and Golden[17], where the activation energies are in cal mol^{-1}. As we will show our result is in good agreement with these estimates. No measurement exists for k_{4b}, but Baldwin and Golden[17] estimate a high-pressure value for $k_{4b}=10^{13.6}\exp\{-19100/RT\}$ s^{-1}. Furthermore Batt[22] has reported that for a series of alkoxyl radical decompositions log (A_∞ s^{-1}) is $\simeq$15 with high-pressure activation energies $\geqslant$13.8 kcal mol^{-1}. Thus Reaction 4b is very much slower than Reaction 4a at temperatures $\leqslant$120 °C and can be neglected.

The reaction mechanism then predicts that

$$\Phi\{n\text{-}C_3H_7CHO\}^{-1} = \frac{k_2}{\phi_1 k_{2b}}\left(1+\frac{k_2}{k_2[NO]}\right). \quad (a)$$

Plots of $\Phi\{n$-$C_3H_7CHO\}^{-1}$ vs. $[NO]^{-1}$ are given in

Table 6. Values of k_4/k_2 at Various Temperatures[a)]

Temp/°C	Intercept[b)]	Slope/Torr[b)]	k_4/k_2/Torr	k_4/k_2/mol dm^{-3}
−8	18.10±0.66	0.72±0.05	0.040±0.004	(2.39±0.25) × 10^{-6}
23	18.52±0.90	2.95±0.12	0.159±0.010	(8.60±0.55) × 10^{-6}
55	20.74±5.93	9.40±0.90	0.452±0.140	(2.21±0.68) × 10^{-5}
88	21.95±6.70	34.0±1.7	1.55 ±0.80	(6.87±3.55) × 10^{-5}
120	19.11±4.94	210±10	11.1 ±3.2	(4.52±1.31) × 10^{-4}

a) Uncertainties are one standard deviation. b) From Figs. 2—4.

Figs. 2—4 for the five temperatures studied. The plots are linear, and the intercepts and slopes are listed in Table 6. The slope increases with increasing temperature while the intercept remains essentially constant at 20.0±2.0. The data at 23 and 120 °C were taken to much higher values of [NO] than at the other temperatures and should give more reliable values for the intercept. However the uncertainty at 120 °C is quite large. Thus we adopt the value of 18.5 obtained at 23 °C for the intercept, independent of temperature. The intercept gives $k_2/k_{2b}\phi_1$. Previously we have shown that $k_{2b}/k_2=0.29\pm0.05$.[20] Thus $\phi_1=0.19\pm0.04$. The ratio of slope to intercept gives k_4/k_2 and these values are given in Table 6. An Arrhenius plot for k_4/k_2 is shown in Fig. 5. The data show some curvature, but the least-squares straight line gives $\ln(k_4/k_2,\ \text{mol dm}^{-3})=1.93\pm1.60-(4014\pm509)/T$. A value of k_2 has never been determined for butoxyl, but Batt[22] has shown that k_2 is essentially constant and independent of temperature for a series of alkoxyl radicals from methoxyl to *t*-pentoxyl. His value for k_2 for the ethoxyl radical is 2.6×10^{10} dm^3 mol^{-1} s^{-1}. With this value for k_2, $\log(k_4,\ \text{s}^{-1})=11.25\pm0.69-(4014\pm509)/2.303T$. Our activation energy of 8.0 kcal mol^{-1} is in good agreement with the estimates of 8.9[16] and 7.7[17] kcal mol^{-1}, while our pre-exponential factor of 11.25 is somewhat lower than the estimates of 11.8[16] and 11.4[17].

O_2 Present. In the presence of O_2, the following additional reactions occur.

$$n\text{-}C_4H_9O\cdot + O_2 \longrightarrow n\cdot C_3H_7CHO + HO_2\cdot \quad (6)$$

$$HO_2\cdot + NO \longrightarrow NO_2 + HO\cdot \quad (7)$$

$$HO\cdot + n\cdot C_4H_9ONO \longrightarrow H_2O + n\cdot C_3H_7CHO + NO \quad (8a)$$

$$\longrightarrow n\cdot C_4H_9O\cdot + HONO \quad (8b)$$

$$\longrightarrow \text{Termination } (+76) \quad (8c)$$

$$\longrightarrow \text{Termination } (-76) \quad (8d)$$

$$HO\cdot + NO + M \longrightarrow HONO + M \quad (9)$$

$$HO\cdot + NO_2 + M \longrightarrow HONO_2 + M \quad (10)$$

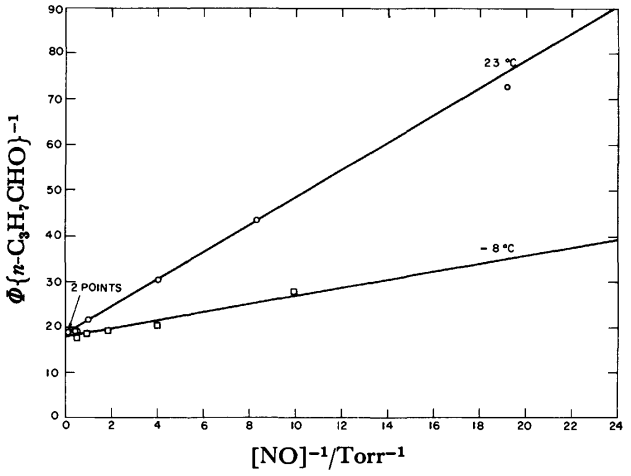

Fig. 2. Plots of $\Phi\{n\text{-}C_3H_7CHO\}^{-1}$ vs. $[NO]^{-1}$ at temperatures of −8 and 23 °C.

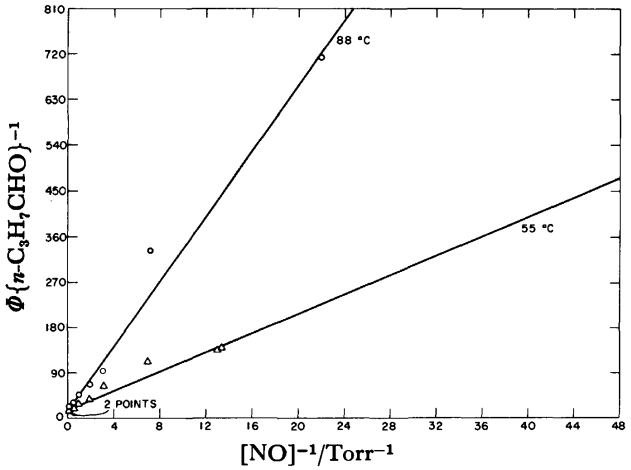

Fig. 3. Plots of $\Phi\{n\text{-}C_3H_7CHO\}^{-1}$ vs. $[NO]^{-1}$ at temperatures of 55 and 88 °C.

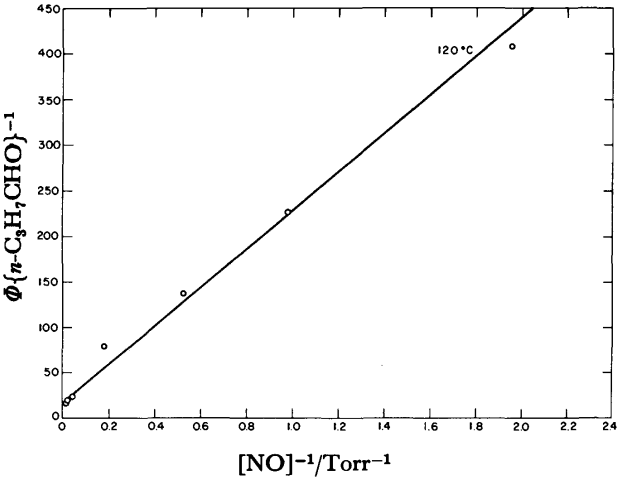

Fig. 4. Plot of $\Phi\{n\text{-}C_3H_7CHO\}^{-1}$ vs. $[NO]^{-1}$ at 120 °C.

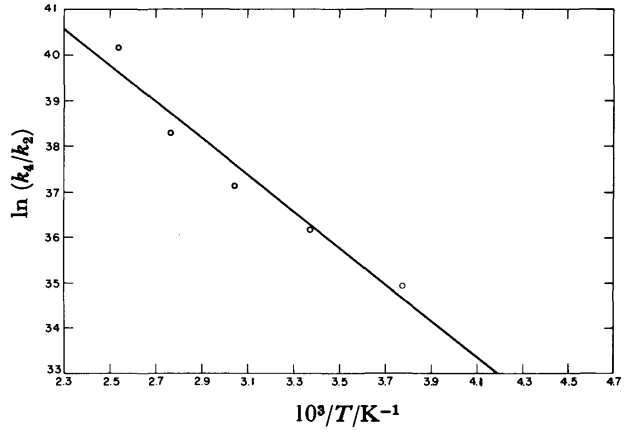

Fig. 5. Arrhenius plot for k_4/k_2.

$$n\text{-}C_4H_9O\cdot + NO_2 \longrightarrow n\text{-}C_4H_9ONO_2 \quad (11a)$$
$$\longrightarrow n\text{-}C_3H_7CHO + HONO, \quad (11b)$$

where Reactions 8c and 8d are some unspecified radical termination steps that either produce the high-molecular weight product with m/z 76 (Reaction 8c) or do not produce it (Reaction 8d). Some termination steps are required in Reaction 8 since other termination steps are too slow to account for the results. We believe that the unidentified product with m/z 76 may be formed in a termination step since its quantum yield is independent of O_2 pressure (except at 120 °C). In principle the reaction of $HO_2\cdot$ with NO_2 should be included, but it is very much slower than Reaction 7 under our reaction conditions so that it can be ignored.

The rate coefficients at 23 °C for k_9 and k_{10} are, respectively, 2.4×10^{11} dm^3 mol^{-1} s^{-1} and 9.4×10^{11} dm^3 mol^{-1} s^{-1}[23] for N_2 or O_2 as a chaperone. k_8 has been measured for butyl nitrite, and it is 2.9×10^9 dm^3 mol^{-1} s^{-1} at 295 K.[24] Furthermore k_8, k_9, and k_{10} are not very sensitive to temperature changes. Thus under all of our conditions 98% of the HO· radicals react with n-C_4H_9ONO, and Reactions 9 and 10 can be ignored. In principal Reaction 11 must be included in the reaction scheme, since NO is converted to NO_2, but Reaction 11 behaves just like Reaction 2, so that ignoring it does not affect the analysis.

The fate of the radical I· formed in Reaction 4b must be considered. It must lead to the aldehyde products which are observed. $\Phi\{CH_3CHO\}$ decreases but $\Phi\{C_2H_5CHO\}$ and $\Phi\{n\text{-}C_3H_7CHO\}$ increase with increasing O_2 pressure. Thus a competition exists to produce these aldehydes, and the implied reactions are

$$I\cdot \longrightarrow CH_3CHO + 2CH_2O + HO, \quad (12a)$$
$$\longrightarrow \text{Undetected aldehydes} + HO, \quad (12b)$$
$$I\cdot + O_2 \longrightarrow n\text{-}C_3H_7CHO + HO, \quad (13a)$$
$$\longrightarrow C_2H_5CHO + HO, \quad (13b)$$

where all the reactions are composite reactions. It is not clear how Reaction 12 proceeds. It may involve an internal rearrangement, a bond cleavage, or reaction with NO. Reaction 12b is included for generality, and appears to be needed. The undetected aldehydes may be $CH_2O\cdot$ or other carbonyl compounds. A corresponding reaction could be written for the I·+O_2 reaction, and it may occur to some extent. However for simplicity we shall ignore it.

Reaction 13a probably proceeds via

$$I\cdot + O_2 \longrightarrow HO_2\cdot + \cdot OCH_2CH_2CH_2CH_2\cdot$$

followed by Reaction 7 and rearrangement of the diradical to give n-C_3H_7CHO. The rearrangement may proceed through an excited cyclic tetrahydrofuran intermediate. Reaction 13b probably occurs by addition of O_2 to the radical site

$$I\cdot + O_2 \longrightarrow HOCH_2CH_2CH_2CH_2O_2\cdot$$

followed by

$$HOCH_2CH_2CH_2CH_2O_2\cdot + NO \longrightarrow HOCH_2CH_2CH_2CH_2O\cdot + NO_2$$
$$HOCH_2CH_2CH_2CH_2O\cdot \longrightarrow HOCH_2CH_2CH_2\cdot + CH_2O$$
$$HOCH_2CH_2CH_2\cdot + O_2 \longrightarrow HO_2\cdot + \cdot OCH_2CH_2CH_2\cdot$$

followed by Reaction 7 and rearrangement of the diradical to C_2H_5CHO.

At 120 °C, the ratio $\Phi\{n\text{-}C_3H_7CHO\}/\Phi\{C_2H_5CHO\}$ is constant at 1.40±0.07 independent of O_2 pressure. This indicates that all of the n-C_3H_7CHO is produced in reaction 13a, and that neither Reactions 6 nor 8a are important at 120 °C. Since Reactions 8a and 8b both have small and similar activation energies, then if Reaction 8a is unimportant at 120 °C, it will also be unimportant at all temperatures. This differs markedly from the situation with the lower alkyl nitrites, where it was found that Reactions 8a and 8b were of comparable importance at all temperatures.[11-13] Reaction 8a is really a two-step reaction; i.e. an H-atom abstraction followed by a decomposition of the resulting radical. Possibly with n-C_4H_9ONO, the radical formed from the abstraction isomerizes and undergoes further oxidation before decomposition. Thus Reaction 8a transforms into Reactions 8c and 8d.

The mechanism predicts that

$$\frac{\phi_1(k_{2b}[NO]+\varepsilon k_4+k_6[O_2])}{\sum\Phi\{ald\}(k_2[NO]+k_4+k_6[O_2])} = \frac{(k_{8c}+k_{8d}+\Gamma k_{8b})}{k_8} \quad (b)$$

where $\Gamma \equiv k_2[NO]/(k_2[NO]+k_4+k_6[O_2])$

$\varepsilon \equiv (k_{12a}+k_{13}[O_2])/(k_{12}+k_{13}[O_2])$

$\sum\Phi\{ald\} \equiv \Phi\{CH_3CHO\} + \Phi\{C_2H_5CHO\} + \Phi\{n\text{-}C_3H_7CHO\}$

At 120 °C, $\sum\Phi\{ald\}=0.27\pm0.01$ independent of O_2 pressure. This means that k_{12b} is unimportant so that $\varepsilon=1.0$, and that Reaction 2 is negligible compared to Reaction 4. Γ is essentially zero, and Eq. b simplifies to

$$\phi_1/\sum\Phi\{ald\} = (k_{8c}+k_{8d})/k_8. \quad (c)$$

Since $\phi_1=0.19$, $(k_{8c}+k_{8d})/k_8=0.70\pm0.03$ at 120 °C. At lower temperatures, the correction terms become more important, but they are still small at 88 °C. Here $\sum\Phi\{ald\}$ increases from 0.22 at low $[O_2]$ to 0.27 at high $[O_2]$ indicating that ε is not constant. However at high $[O_2]$, $\varepsilon\simeq1.0$, and Eq. c can be used. Thus at 88 °C, $(k_{8c}+k_{8d})/k_8$ also is $\simeq0.70$. This is in accord with the findings for lower alkyl nitrites that the branching ratios for k_8 are independent of temperature.[11-13] Thus we assume that $(k_{8c}+k_{8d})/k_8=0.70$ at

all temperatures and thus $k_{8b}/k_8=0.30$. This can be compared with the values of 0.57±0.13, 0.44±0.24, and 0.66±0.12 found, respectively, for $C_2H_5O\cdot$,[11] n-$C_3H_7O\cdot$,[12] and i-$C_4H_9O\cdot$.[13]

The mechanism gives a rate law for butyraldehyde production which can be cast into two forms:

$$(\Phi\{n\text{-}C_3H_7CHO\}_{corr}-\rho)^{-1}=\frac{k_{13}}{k_{13a}}+\frac{k_{12}}{k_{13a}[O_2]}, \quad (d)$$

$$\Phi\{n\text{-}C_3H_7CHO\}_{corr}-\frac{k_{2b}[NO]}{k_4}-\frac{k_{13a}[O_2]}{(k_{12}+k_{13}[O_2])}=\frac{k_6[O_2]}{k_4}, \quad (e)$$

where $\Phi\{n\text{-}C_3H_7CHO\}_{corr}\equiv\theta\Phi\{n\text{-}C_3H_7CHO\}/\phi_1\xi$

$\rho\equiv(k_{2b}[NO]+k_6[O_2])/k_4$

$\theta\equiv(\Gamma k_{8b}+k_{8c}+k_{8d})/k_8$

$\xi\equiv k_4/(k_2[NO]+k_4+k_6[O_2])$.

All of the rate coefficient ratios needed to compute the parameters in Eqs. d and e are known except for k_6/k_4, k_{12}/k_{13a}, and k_{13}/k_{13a}. Thus at each temperature we assume a value for k_6/k_2, compute the left-hand-side of Eq. d, and plot it vs. $[O_2]^{-1}$. From the slope and intercept of the plot, we obtain k_{12}/k_{13a} and k_{13}/k_{13a}, respectively. These values are then used to compute the left-hand-side of Eq. e, which is then plotted vs. $[O_2]^{-1}$ to get a new value for k_6/k_4. This value is then used for the next calculation of the parameters in Eq. d, and the process is repeated until consistent values of k_6/k_4, k_{13}/k_{13a}, and k_{12}/k_{13a} are obtained. This method works well at all temperatures except at −8 and 120 °C. At 120 °C, Eq. e fails because Reaction 6 makes a negligible contribution to $\Phi\{n\text{-}C_3H_7CHO\}$ under all conditions. At this temperature k_6/k_2 is obtained from an extrapolation of the Arrhenius plot of the values at lower temperatures. At −8 °C, Eq. d fails because the results suggest an excess production of n-C_3H_7CHO not accounted for in the mechanism. At this temperature k_{12}/k_{13a} and k_{13}/k_{13a} are obtained from an extrapolation of their Arrhenius plots of the values at higher temperatures.

The final plots based on Eqs. d and e are shown in Figs. 6 and 7, respectively, at each temperature. The values of the slopes and intercepts are listed in Table 7. The intercepts of Fig. 7 have been forced to zero as predicted. Regression analyses of the Arrhenius plots (not shown) give the Arrhenius expressions tabulated in Table 8. If k_2 is taken to be 4.4×10^{-11} cm^3 s^{-1},[22] then $k_6=4.5\times10^8\exp\{(-1178\pm176)/T\}$ dm^3 mol^{-1} s^{-1}. Both the pre-exponential factor and activation energy are slightly larger than those found for the lower alkoxyl radicals.[11-13] However, this difference probably just represents uncertainties since k_6 was determined over a small temperature range (23—88 °C) in this study.

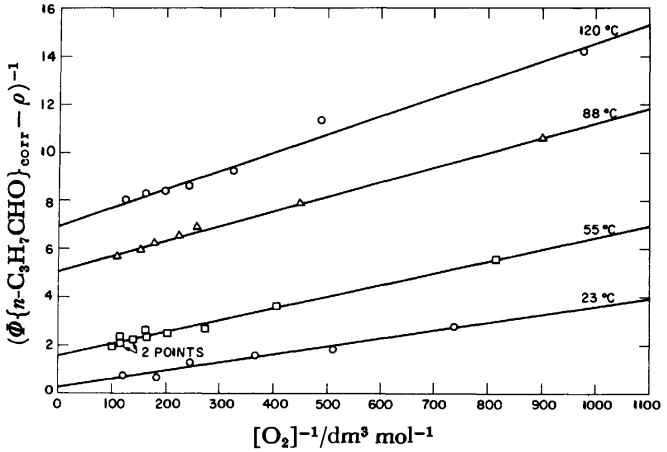

Fig. 6. Plots of $(\Phi\{n\text{-}C_3H_7CHO\}_{corr}-\rho)^{-1}$, computed using values of k_6/k_2 in Table 7, vs. $[O_2]^{-1}$. The plots are displaced upwards by 5, 3, −1, and −2 units, respectively, for 120, 88, 55, and 23 °C for clarity.

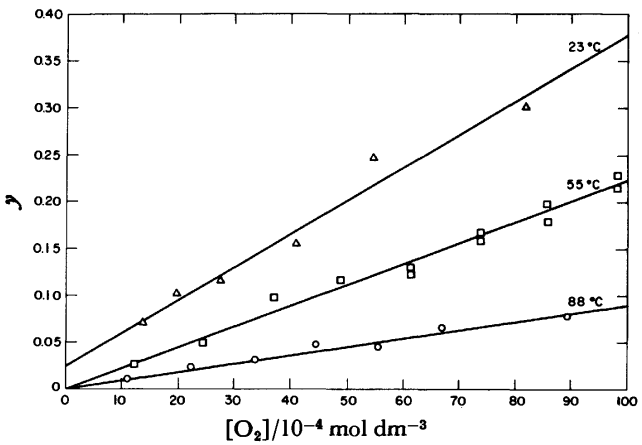

Fig. 7. Plots of y=left-hand side of Eq. e as computed using values of k_{13a}/k_{13} and k_{13a}/k_{12} in Table 7, vs. $[O_2]$. The plot at 23 °C is dispaced upward by 0.025 unit for clarity.

Table 7. Rate Coefficient Ratios from $\Phi\{n\text{-}C_3H_7CHO\}$ Analysis[a,b]

Temp/°C	$10^3\,k_{12}/k_{13a}$/mol dm^{-3}	k_{13a}/k_{13}	$10^3\,k_{12}/k_{13}$/mol dm^{-3}	k_6/k_2
−8	2.29[c]	0.38[c]	0.88[c]	1.97×10^{-4} [c]
23	3.37±0.30	0.444±0.016	1.49±0.22	$(3.05\pm0.20)\times10^{-4}$
55	4.90±0.17	0.394±0.080	1.93±0.30	$(4.92\pm0.17)\times10^{-4}$
88	6.19±0.15	0.489±0.050	3.02±0.18	$(6.21\pm0.40)\times10^{-4}$
120	7.57±0.45	0.508±0.052	3.85±0.23	$(8.35\pm0.55)\times10^{-4}$ [c]

a) Uncertainties are one standard deviation. b) Results tabulated using $k_{8b}/k_8=0.30$. c) Values were determined by extrapolation from Arrhenius plots.

A simpler analysis is obtained from examination of C_2H_5CHO production. The rate law for $\Phi\{C_2H_5CHO\}$ is

$$\Phi\{C_2H_5CHO\}_{corr}^{-1} = \frac{k_{13}}{k_{13b}} + \frac{k_{12}}{k_{13b}[O_2]}, \qquad (f)$$

where

$$\Phi\{C_2H_5CHO\}_{corr} \equiv \Phi\{C_2H_5CHO\}\theta/\phi_1\xi.$$

The left-hand-side of Eq. f is computed from the rate coefficient ratios already determined including those for k_6/k_2, though reaction 6 makes only a trivial correction. The left-hand side of Eq. f is plotted vs. $[O_2]^{-1}$ in Figs. 8 and 9. The values of k_{13b}/k_{13}, k_{12}/k_{13b}, and k_{12}/k_{13} obtained from the plots are listed in Table 9. Respective Arrhenius parameters are listed in Table 8.

The sum of $k_{13a}/k_{13}+k_{13b}/k_{13}$ should be 1.0 according to the mechanism. It is listed in Table 10 and varies from 0.74 to 0.90, indicating that another channel to Reaction 13, perhaps giving CH_2O, might also occur. The ratio k_{13a}/k_{13b} found from the individual values of k_{13a}/k_{13} and k_{13b}/k_{13} is also listed in Table 10. It is about 1.3 independent of temperature.

Another way to obtain k_{13a}/k_{13b} is directly from the following equation predicted by the mechanism:

$$(\Phi\{n\text{-}C_3H_7CHO\}_{corr}-\rho)/\Phi\{C_2H_5CHO\}_{corr} = k_{13a}/k_{13b} \qquad (g)$$

The values of the left-hand side of Eq. g are listed in

Table 8. Regression Equations[a)]

A) From $\Phi\{n\text{-}C_3H_7CHO\}$ analysis
$\ln(k_{13a}/k_{13}) = -0.17\pm0.49-(209\pm165)/T$
$\ln(k_{13a}/k_{12}) = -2.42\pm0.15+(963\pm49)/T$
$\ln(k_{12}/k_{13}) = -2.61\pm0.36-(1194\pm66)/T$
$\ln(k_6/k_2) = -4.09\pm0.54-(1178\pm176)/T$

B) From $\Phi\{C_2H_5CHO\}$ analysis
$\ln(k_{13b}/k_{13}) = -0.60\pm0.41-(139\pm131)/T$
$\ln(k_{12}/k_{13b}) = -6.35\pm1.77+(324\pm566)/T$
$\ln(k_{12}/k_{13}) = -7.12\pm1.87+(230\pm597)/T$

C) Others
$\ln(k_4/k_2) = 1.92\pm1.60-(4014\pm509)/T$[b)]
$\ln(k_{13a}/k_{13b}) = -2.03\pm0.68+(738\pm217)/T$[c)]

a) Uncertainties are 1 standard deviation. Units of rate coefficient ratios are in mol dm^{-3} to the appropriate power. b) From data in absence of O_2. c) From mean values listed in Table 10.

Table 9. Rate Coefficient Ratios from $\Phi\{C_2H_5CHO\}$ Analysis[a,b)]

Temp/°C	k_{13b}/k_{13}	$10^3\,k_{12}/k_{13b}$/ mol dm^{-3}	$10^3\,k_{12}/k_{13}$/ mol dm^{-3}
−8	0.361±0.074	7.01±1.99	2.52±0.17
23	0.295±0.079	6.22±2.17	1.96±0.12
55	0.334±0.010	2.16±0.23	7.31±0.10
88	0.413±0.022	3.82±0.30	1.39±0.12
120	0.385±0.016	6.33±0.25	2.42±0.12

a) Uncertainties are one standard deviation. b) Results tabulated using $k_{8b}/k_8 = 0.30$.

Table 10. Comparison of k_{13a}/k_{13} and k_{13b}/k_{13}

Temp/°C	$(k_{13a}+k_{13b})/k_{13}$[a)]	k_{13a}/k_{13b}[b)]	k_{13a}/k_{13b}[c)]
−8	0.74	1.06	2.32±0.81
23	0.74	1.51	1.65±0.25
55	0.73	1.18	0.97±0.11
88	0.90	1.18	0.90±0.10
120	0.89	1.32	1.07±0.10

a) Sum of values obtained individually from $\Phi\{n\text{-}C_3H_7CHO\}$ and $\Phi\{C_2H_5CHO\}$ as listed in Tables 7 and 9, respectively b) Ratio of values obtained individually from $\Phi\{n\text{-}C_3H_7CHO\}$ and $\Phi\{C_2H_5CHO\}$ as listed in Tables 7 and 9, respectively. c) Obtained from mean value of k_{13a}/k_{13b} obtained from $(\Phi\{n\text{-}C_3H_7CHO\}_{corr}-\rho)/\Phi\{C_2H_5CHO\}_{corr}$ from Table 4.

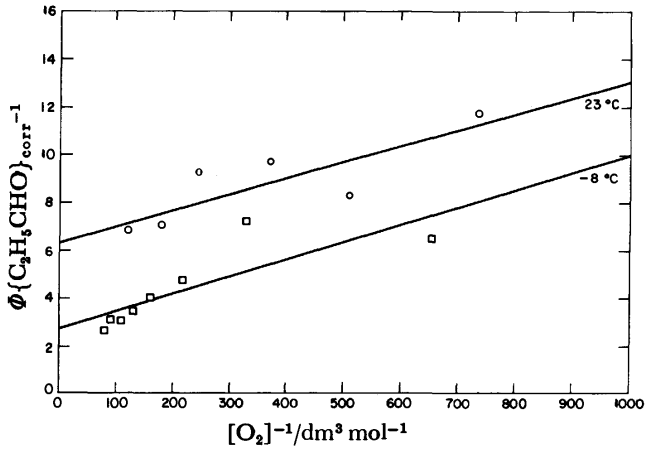

Fig. 8. Plots of $\Phi\{C_2H_5CHO\}_{corr}^{-1}$ computed using values of k_6/k_2 in Table 7, vs. $[O_2]^{-1}$ at −8 and 23 °C. The plot at 23 °C is displaced upward by 3 units for clarity.

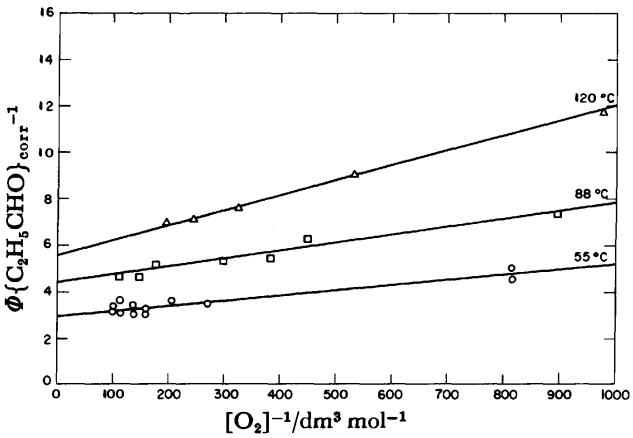

Fig. 9. Plots of $\Phi\{C_2H_5CHO\}_{corr}^{-1}$, computed using values of k_6/k_2 in Table 7, vs. $[O_2]^{-1}$ at 55, 88, and 120 °C. The plots at 88 and 120 °C are displaced upward by 2 and 3 units, respectively, for clarity.

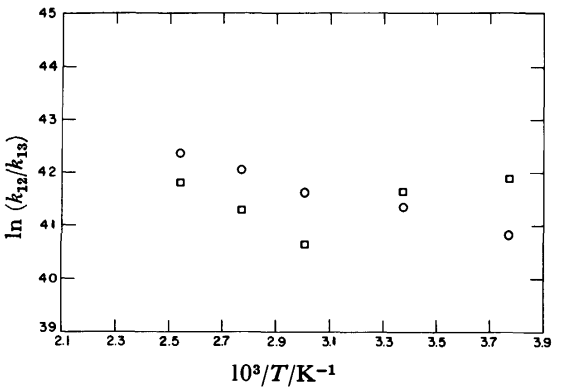

Fig. 10. Arrhenius plot for $\ln(k_{12}/k_{13})$ vs. reciprocal temperature.
○, from $\Phi\{n\text{-}C_3H_7CHO\}$; and □, from $\Phi\{C_2H_5CHO\}$.

Table 4 for every run. The values are nearly independent of O_2 pressure, as they should be, except at −8 °C, where they increase with $[O_2]$. It is not clear why this trend occurs at −8 °C, but an additional source of n-C_3H_7CHO, not given by the mechanism, is indicated. The mean values at any temperature are listed in Table 10, and they are consistent with the values obtained from analysis of the individual aldehyde quantum yields.

In principle additional information can be found from the rate law for CH_3CHO formation. However this is not feasible here since the details of the rate law are unknown. The values of k_{12}/k_{13} obtained from $\Phi\{n\text{-}C_3H_7CHO\}$ and $\Phi\{C_2H_5CHO\}$ are plotted in an Arrhenius plot in Fig. 10. The agreement between the values obtained from the two aldehydes is good only to within a factor of three. The values obtained from $\Phi\{n\text{-}C_3H_7CHO\}$ give a good linear Arrhenius plot, whereas those from $\Phi\{C_2H_5CHO\}$ do not. Thus we prefer the value of k_{12}/k_{13} obtained from $\Phi\{n\text{-}C_3H_7CHO\}$.

For the quantum yield of termination product of Reaction 8c, $\Phi\{76\}$, the mechanism predicts that

$$\Phi\{76\} = \phi_1(1-\Gamma)k_{8c}/(k_{8c}+k_{8d}+\Gamma k_{8b}) . \qquad (i)$$

Since $\Gamma \approx 0$, Eq. i simplifies to:

$$\Phi\{76\} = \phi_1 k_{8c}/(k_{8c}+k_{8d}) . \qquad (j)$$

Thus $\Phi\{76\}$ should be independent of O_2 pressure at any temperature, which it is, except at 120 °C. Perhaps at 120 °C, some secondary oxidation of this product occurs which reduces its primary quantum yield. However it decreases with increasing temperature indicating that both Reaction 8c and 8d must be playing a role in termination. Since only relative values are known for $\Phi\{76\}$, the relative importance of Reactions 8c and 8d cannot be found.

We appreciate helpful comments and suggestions by S. Zabarnick. This work was supported by the Environmental Protection Agency through Grant. No. R808528 for which we are grateful.

References

1) H. A. Wiebe, A. Villa, T. M. Hellman, and J. Heicklen, *J. Am. Chem. Soc.*, **95**, 7 (1973).
2) W. Glasson, *Environ. Sci. Technol.*, **9**, 1048 (1975).
3) W. A. Alcock and B. Mile, *Combust. Flame*, **24**, 125 (1975).
4) J. R. Barker, S. W. Benson, and D. M. Golden, *Int. J. Chem. Kinet.*, **9**, 31 (1977).
5) L. J. Kirsch and D. A. Parkes, Presented at 5th International Symposium on Gas Kinetics, Manchester, Great Britain, 1977.
6) L. Batt and G. N. Robinson, *Int. J. Chem. Kinet.*, **11**, 1045 (1979).
7) K. Selby and D. J. Waddington, *J. Chem. Soc., Perkin Trans. 2*, **1979**, 1259.
8) R. A. Cox, R. G. Derwent, S. V. Kearsey, L. Batt, and K. G. Patrick, *J. Photochem.*, **13**, 149 (1980).
9) D. Gutman, N. Sanders, and J. E. Butler, *J. Phys. Chem.*, **86**, 66 (1982).
10) L. Batt, K. G. Patrick, and G. A. Reid, Presented at International Symposium on Chemical Kinetics Related to Atmospheric Chemistry, Tsukuba, Ibaraki, Japan (June, 1982), Paper No. 39.
11) S. Zabarnick and J. Heicklen, *Int. J. Chem. Kinet.*, **17**, 455 (1985).
12) S. Zabarnick and J. Heicklen, *Int. J. Chem. Kinet.*, **17**, 477 (1985).
13) S. Zabarnick and J. Heicklen, *Int. J. Chem. Kinet.*, **17**, 503 (1985).
14) A. Fish, *Quart. Rev. Chem. Soc.*, **18**, 243 (1964).
15) A. C. Baldwin, J. R. Barker, D. M. Golden, and D. G. Hendry, *J. Phys. Chem.*, **81**, 2483 (1977).
16) W. P. L. Carter, K. R. Darnall, A. C. Lloyd, A. M. Winer, and J. N. Pitts, Jr., *Chem. Phys. Lett.*, **42**, 22 (1976).
17) A. C. Baldwin and D. M. Golden, *Chem. Phys. Lett.*, **60**, 108 (1978).
18) H. Niki, P. D. Maker, C. M. Savage, and L. P. Breitenbach, *J. Phys. Chem.*, **85**, 2698 (1981).
19) P. Morabito and J. Heicklen, *Int. J. Chem. Kinet.*, **17**, 535 (1985).
20) P. Morabito and J. Heicklen, *J. Phys. Chem.*, **89**, 2914 (1985).
21) G. R. McMillan, J. Kumari, and D. L. Snyder, "Chemical Reactions in Urban Atmospheres," ed by C. S. Tuesday (1971), p. 35.
22) L. Batt, *Int. J. Chem. Kinet.*, **11**, 977 (1979).
23) R. F. Hampson, DOT Report No. FAA-EE-80-17 (1982) "Chemical Kinetic and Photochemical Data Sheets for Atmospheric Reactions."
24) D. L. Baulch, I. M. Campbell, and S. M. Saunders, *Int. J. Chem. Kinet.*, **17**, 355 (1985).

 © 1987 The Chemical Society of Japan Bull. Chem. Soc. Jpn., 60, 2651—2655 (1987)

Preparation, Absolute Configuration and Conformation of Some α-Aryl-2-pyridylmethanols

Stefan E. Bojadziev, Dimiter T. Tsankov, Petko M. Ivanov,* and Nikolina D. Berova*,†
Institute of Organic Chemistry with Centre of Phytochemistry, Bulgarian Academy of Sciences, 1113 Sofia, Bulgaria
†Faculty of Chemistry, University of Sofia, 1126 Sofia, Bulgaria
(Received December 6, 1985)

The syntheses of five optically active α-aryl-2-pyridylmethanols **1**—**5** are described. It is shown by means of chemical correlation with the known (−)-(α *R*,2*S*)-α-phenyl-2-piperidylmethanol **6** that all levo-rotatory isomers of **1**—**4** are of R configuration. It is also found via the relative integral intensities in the infrared spectra of the bands due to free and intramolecularly bonded hydroxyl groups in the compounds **1**—**4** and the free hydroxyl groups in the model compounds **7**—**10**, that the population of the conformers with an intramolecular OH···N bond in compounds **1**—**4** exceeds 80%.

In continuation of our investigations on the preparation, absolute stereochemistry and chiroptical properties of chiral 1,2-disubstituted 1,2-diarylethanes[1,2] were recently undertaken studies employing as models compounds containing two geminal aromatic carbo- or hetero-cyclic chromophores.

We presently wish to report the results from the preparation of a series of chiral α-aryl-2-pyridylmethanols **1**—**5** as well as data on their absolute configuration and preferred conformations obtained by means of chemical correlation and infrared spectroscopy. Our circular dichroism investigations require the stereochemical structure of the above mentioned compounds to be reliably known as the aim is the elucidation of some general relationships between molecular chirality and aromatic Cotton effects in compounds with geminal phenyl and pyridyl chromophores at the chiral center. It is known that such molecular moieties are present in important biologically active compounds with clearly observable biostereoselectivity.[3]

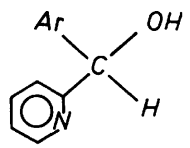

1 Ar = C_6H_5
2 Ar = 2-ClC_6H_4
3 Ar = 4-ClC_6H_4
4 Ar = 2,6-$Cl_2C_6H_3$
5 Ar = 4-$CH_3OC_6H_4$

Scheme 1.

Results and Discussion

Synthesis of the Racemic Methanols 1—5. Various approaches exist in the literature regarding the preparation of the racemic methanols **1**—**5**.[4-10] Among the most convenient ones is the procedure developed by Gilman and Spatz[10a] based on the interaction of 2-pyridyllithium with the corresponding aromatic aldehyde. In the present case the reaction was conducted at −78 °C, a temperature considerably lower than the recommended, leading to the racemic methanols **1**—**5** in yields significantly better than those reported for analogous compounds (see Experimental).

Preparation of the Optically Active Methanols. Among all presently considered methanols **1**—**5** only compound **1** was found described in an optically active form.[11-13] This compound resolved by Davies with (+)-tartaric acid[11] and considered as the pure levo-rotatory isomer[12-14] was found in the present investigations to be optically impure (see below).

The racemic methanols **2** and **4** were successfully resolved by means of (+)-tartaric acid, while the racemic **3** was resolved by means of (−)-*O*,*O*′-dibenzoyltartaric acid.

The optically active methanol **1** was obtained by dehalogenating samples of (+)-**2**, (−)-**3**, and (+)-**4** of highest purity by treatment acc. ref.[15] with hydrazine hydrate in the presence of palladium over charcoal. In all three cases the obtained samples of **1** showed at λ=589 nm in chloroform practically the same absolute value of the specific rotation i.e. +162.9°, −161.5°, and +162.8°. It can be seen that these values agree very well among themselves while on the other hand they considerably exceed the reported ones for **1** by other authors i.e. $[\alpha]_{589}=-86.2°$ [11] and $[\alpha]_{589}=-108°$.[12]

It can thus be concluded that in the present investigations the racemates of **2**, **3**, and **4** were completely resolved, while the previously reported resolution of (±)-**1** with (+)-tartaric acid[11,12] indeed afforded a product of 50—70% optical purity.

The resolution of (±)-**5** offered considerable difficulties, the best result being obtained with (+)-camphor-10-sulfonic acid. Repeated recrystallization of the diastereoisomeric sulfonates afforded insufficiently pure free base **5** which had to be subjected to additional fractional recrystallization in order to remove the less soluble (±)-**5** finally leading to the desired optically pure **5**.

Absolute Configuration. The possibilities for the application of chemical correlation are rather restricted since only a few chiral compounds with geminal aryl and pyridyl groups with reliable absolute configuration have hitherto been reported.[3a,16]

Employing the chemical transformation approach and circular dichroism Pohl and Wollweber recently compared the absolute configuration of (−)-ephedrine and (−)-*erythro*-α-phenyl-2-piperidylmethanol **6**.[17] In this much more reliable way they corroborated the earlier assumption made by Fauley and LaPidus[18] that (−)-*erythro*-**6** is of (α*R*,2*S*) configuration. On the ground of this conclusion and the earlier results[12,14] regarding the conversion of (−)-α-phenyl-2-pyridylmethanol on catalytic hydrogenation into (−)-*erythro*-**6** it can be assumed that the chiral center in (−)-**1** is of R configuration.

In the conversion of (−)-**1** into (−)-**6** carried out by other researchers[12,14] samples of low optical purity have been used and the absence of *threo*-**6** in the products had not been experimentally determined. For this reason we subjected the presently obtained (−)-**1** with $[\alpha]_{578}=-169.5°$ (chloroform) to catalytic hydrogenation. The thin-layer chromatographic analysis of the crude reaction mixture revealed indeed the presence of the two expected diastereoisomers. From this mixture was successfully isolated in pure form only the predominating *erythro*-**6** isomer with $[\alpha]_{578}=-53.2°$(chloroform). The comparison of the data obtained in the present study for (−)-**1** and (−)-*erythro*-**6** with the reported ones[14] for (−)-**1** $[\alpha]_{578}=-113°$(chloroform) and for (−)-*erythro*-**6** $[\alpha]_{578}=-35.3°$(chloroform) shows that the two samples described earlier have been only of about 65% optical purity. The (α*R*, 2*S*) absolute configuration of the (−)-*erythro*-**6** is in agreement with data obtained recently in circular dichroism studies conducted on molybdenum and rhodium complexes of (−)-**6** formed in situ.[19]

On the other hand the chemical conversions conducted of (+)-**2** to (+)-**1**, of (−)-**3** to (−)-**1**, and of (+)-**4** to (+)-**1**, respectively, which obviously proceed without affecting the absolute configuration,[1b,15] allow the correlation of the absolute configurations also of the three presently obtained chlorine-containing methanols **2**—**4**. In this manner to all the levo-rotatory isomers of **1**—**4** should be assigned R configuration.

For the correlation of the absolute configuration of (−)-**5** CD method turned out to be the most convenient way. On the basis of the observed exciton coupling between the benzene and 2-pyridine chromophores of a series α-aryl-2-pyridylmethane derivatives we ascribed recently to the levo-rotatory isomer of **5** also the R configuration.[20]

Infrared Spectra. The infrared spectra of the compounds studied (**1**—**4**) give evidence for the existence of at least two conformations, one of them being intramolecularly hydrogen bonded. The task of this study consists in calculating statistical weights of these two conformations in order to give preference to one of them.

The relative populations of mobile conformational equilibria between conformers with bonded and nonbonded hydroxyl groups can be evaluated from the integral intensities (*B*) of the free OH band whose molar absorptivity has been taken from suitably chosen model compounds without intramolecular hydrogen bond.[21] Many reasons reject the use of the bonded OH band.[22] The mole percentage of the bonded conformation is simply derived by subtracting the mole percentage of the free one from 100%.

The IR spectral data are listed in Table 1. Besides the presently studied α-aryl-2-pyridylmethanols it also includes the corresponding 3- and 4-pyridyl-containing compounds used as models. The spectra were taken in 1×10^{-3} mol dm^{-3} carbon tetrachloride solutions in a 5 mm NaCl cell.

The relative error in the determination of the mole percentage of the free and bonded conformations mainly reflects the accuracy of the *B* values for the

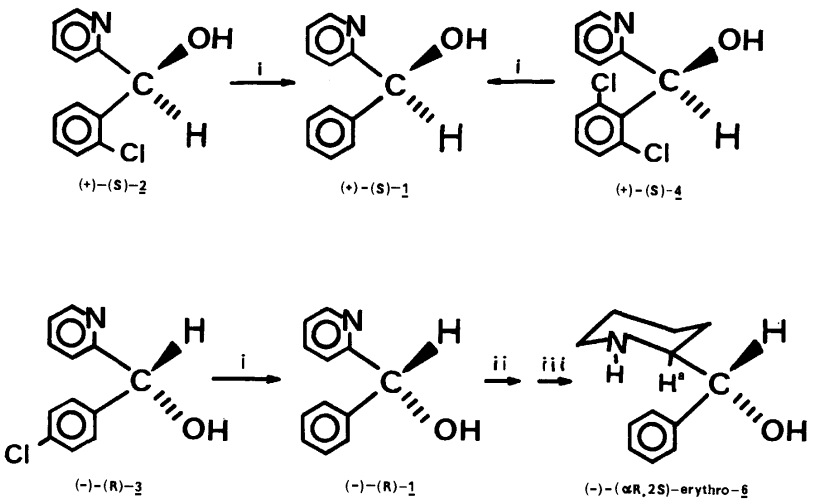

Scheme 2. i $NH_2NH_2\cdot H_2O$, Pd/C; ii H_2, PtO_2; iii Separation of mixture erythro+threo, TLC analyse.

Table 1. IR Spectral Data from Diluted (1×10^{-3} mol dm^{-3}) CCl_4 Solutions of α-Aryl-2-pyridylmethanols

Intramolecularly Bonded α-Aryl-2-pyridylmethanols								α-Aryl-3- or 4-Pyridylmethanols		
Compd No.	ν_{OH}/cm^{-1} Free	ν_{OH}/cm^{-1} Bonded	Band area(B) l mol^{-1} cm^{-2} free OH	Band area(B) l mol^{-1} cm^{-2} bonded OH	% free OH	% OH···N	% OH···Cl	Compd[b] No.	ν_{OH}/cm^{-1} free	Band area(*B*) l mol^{-1} cm^{-2} free OH
1	3620	3408	508	2689	22	78	—	7	3618	2280
2	3616	3398	142	1837	9	91	—	8	3618	2276
3	3620	3404	292	2067	15	85	—	9	3616	1642
4	3618	3413	104	3370	6	91	3	10	3618	1912
		3579[a]		128				11[c]	3618	634

a) Bond OH···Cl. b) α-Phenyl-3-pyridylmethanol (**7**), α-Phenyl-4-pyridylmethanol (**8**), α-(2-Chlorophenyl)-3-pyridylmethanol (**9**), α-(4-Chlorophenyl)-3-pyridylmethanol (**10**), α-(2,6-Dichlorophenyl)-3-pyridylmethanol (**11**). c) The *B* value for OH···Cl band is 2570.

studied sample and the reference model compounds. The structural isomers containing 3- and 4-pyridyl groups **7**—**11** were chosen as standard compounds free of intramolecular OH···N bonding. The conformational distribution of compound **1** was determined employing **7** and **8** as models. The difference between the calculated B values of these two compounds was 4 units which renders the error in the evaluation of the conformational distribution below 1%. For this reason the conformational populations of the remaining compounds **2**—**4** were evaluated using one standard compound with free hydroxyl group — the corresponding α-aryl-3-pyridylmethanols.

The study of the mole percentage of the conformational populations of compounds **1**—**4** given in Table 1 leads to the conclusion that the greatest statistical weight (above 80%) should be ascribed to conformations with bonded hydroxyl functions. The introduction of a chlorine atom in an ortho position, compound **2**, increases the statistical weight of the intramolecularly bonded conformer by 13%. The effect of the chlorine atom in para position, compound **3**, in comparison with the ortho isomer appears to be less pronounced because of the lack of steric hindrance. The difference in the conformational populations of compound **1** and **3** is too small to seek for an explanation. They have been expected to give rise to nearly equal populations. The corresponding differences for **1** and **2** (respectively, 4) obviously reflect the presence of the voluminous chlorine atoms in the ortho positions. The helical (I) and the perpendicular (II) conformations are the two

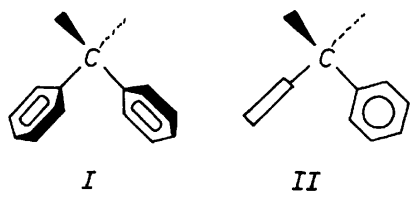

I *II*

Scheme 3.

conformations that diarylmethanes may assume. The helical conformation is considered to be the preferred one in the solid state, while the data in solution are ambiguous.[23] Most probably the helical conformations are the preferred ones for compounds **1**—**4**, and the ortho substitution further diminishes the population of perpendicular and other forms.[24]

Compound **4** with two chlorine atoms in ortho positions deserves a special attention. Its IR spectrum shows weakening of the OH···N bonding and a presence of a second weak OH···Cl bond at 3579 cm^{-1},[27,28] thus indicating the existence of three conformations: A - without intramolecular hydrogen bonding, B - with an OH···N bonding and C - with an OH···Cl bonding. The contributions of these three conformations will be separately considered for the sake of clarity.

The IR spectrum of compound **11** used as a reference, however, contains two bands: A free OH band at 3618 cm^{-1} and a second one at 3579 cm^{-1} due to OH···Cl bonding. The correct use of these bands as standards requires an estimation of their relative populations. Firstly we calculated the mole percentage of the free OH population. This quantity could be determined employing the *B* value of compound **9** as a 100% free OH standard. A value of 39% free OH population for compound **11** was obtained in this way. Using this value and the *B* values of the free OH bands of compounds **4** and **11** we found 6% for the population of the conformation A of compound **4**. The remaining quantity of 94% is distributed among the conformations B and C. The contribution of the conformation C could be approximately estimated using the *B* value (2570) for the OH···Cl band of compound **11** taken as a standard. The relative population of this bonded conformation was found to be 61%. On this basis a value of ca. 3% is obtained for the conformation C in compound **4**. The remaining 91% should be ascribed to the OH···N bonded conformation B which appears to be the most populated one.

Experimental

The mp (on a Kofler apparatus) are uncorrected. Optical rotations were measured with a Perkin-Elmer 241 instrument. IR spectra were recorded on a Bruker IFS 113V instrument. TLC analyses of compound **1—5** were performed on plates coated with silica gel DG (Riedel de Haën, Hanover) using benzene: chloroform: methanol=6:4:1 as a solvent system.

Syntheses of the Racemic α-Aryl-2-pyridylmethanols (1—5) and Their Resolution. General Procedure. To a stirred ethereal solution of 2-pyridyllithium prepared by the halogen-interconversion method (see Refs. 9, 10) from 2-bromopyridine (38 g, 240 mmol) and butyllithium (4.25 g, 600 mmol Li and 41 g, 300 mmol butyl bromide) at −78 °C was added dropwise during 45 min (while the temperature was allowed to rise to −30 °C) the freshly-distilled aromatic aldehyde (120 mmol) dissolved in about 150 ml dry ether. The mixture was stirred for another 1.5 h at the same temperature, hydrolyzed carefully with 25 ml water and worked-up as usual. The isolated crude reaction product was purified as a base or after conversion into hydrochloride.

α-Phenyl-2-pyridylmethanol (1). (±)-**1**: Prepared according to the general procedure. Recrystallization from methanol of the crude base gave the pure (±)-**1** (16.4 g, 74%), mp 74—76 °C (lit,[4,5] mp 76—78 °C).

α-(2-Chlorophenyl)-2-pyridylmethanol (2). (±)-**2**: The crude hydrochloride was recrystallized from MeOH-Et_2O affording 25.4 g (83%) pure (±)-**2**·HCl, mp 170—174 °C (with decomposition) (lit,[4] mp 174—175 °C). Mp of free base 62—64.5 °C (lit,[5,8] mp 63—65 °C).

(+)-**2**: A hot solution of 10.98 g (±)-**2** and 7.50 g (+)-tartaric acid in 130 ml *i*-PrOH was allowed to cool slowly to room temp and then kept at this temp for another 24 h. The resulting crystalline product (10.10 g, mp 133—144 °C) was recrystallized three times with 8 ml *i*-PrOH for each gram of salt to give 5.11 g of crystals, mp 145—147 °C and $[\alpha]_D^{17}$ +28.2° (*c* 1.2, MeOH). After two additional recrystallizations the samples of the corresponding free base (oil) possess practically the same $[\alpha]_D^{17}$ values: +242.8° (*c* 0.5, $CHCl_3$). Yield of (+)-**2** was 2.20 g (40%).

α-(4-Chlorophenyl)-2-pyridylmethanol (3). (±)-**3**: After one recrystallization of the crude **3**·HCl from MeOH-Et_2O and one of the free base from EtOAc 20.2 g (77%) pure (±)-**3** was obtained with mp 82.5—84 °C (lit, mp 80—81 °C,[5] 83 °C[6]).

(−)-**3**: From a solution of 3.30 g (±)-**3** and 5.37 g (−)-*O,O'*-dibenzoyltartaric acid in 25 ml hot *i*-PrOH after slow cooling and standing for 24 h at room temp 3.14 g salt (mp 141—144 °C) was collected and subjected to two additional recrystallizations from 7 resp. 6 ml *i*-PrOH. Yield of the crystalline salt was 1.80 g, mp 145—148 °C, $[\alpha]_D^{17}$ −80.1° (*c* 0.6, MeOH). The corresponding free base mp 95—97 °C, $[\alpha]_D^{17}$ −123.2° (*c* 0.5, $CHCl_3$). After two further recrystallizations of the salt the optical rotation of the liberated base reached $[\alpha]_D^{13}$ −131.1° (*c* 0.5, $CHCl_3$), which value increased after two more recrystallizations of the salt to $[\alpha]_D^{16}$ −132.5° (*c* 0.7, $CHCl_3$).

α-(2,6-Dichlorophenyl)-2-pyridylmethanol (4). (±)-**4**: The pure **4**·HCl after recrystallization of the crude salt from MeOH-Et_2O (yield 28.7 g, 83%, Anal. ($C_{12}H_{10}Cl_3NO$) C, H, Cl) was converted into the free base (±)-**4**, mp 76—78 °C (lit,[7,8] mp 79.5—82 °C).

(+)-**4**: 5.08 g (±)-**4** and 3.00 g (+)-tartaric acid were dissolved in 75 ml of refluxing *i*-PrOH and then allowed to stand. After about 10 d by spontaneous crystallization at room temp 1.27 g crystals were collected. The further recrystallization of this crystalline product from *i*-PrOH (15 ml) afforded after 1 d at room temp 0.12 g of salt (3%), mp 105—108 °C and $[\alpha]_{546}^{19}$ +189.1° (*c* 0.4, MeOH). The corresponding free base (oil) with $[\alpha]_D^{19}$ +182.9° (*c* 1.0, $CHCl_3$) on hydrogenolysis to (+)-**1** found to be optically pure.

α-(4-Methoxyphenyl)-2-pyridylmethanol (5). (±)-**5**: After recrystallization of the crude base from EtOAc 12.94 g (50%) (±)-**5** with mp 131.5—133 °C (lit,[3] mp 133—134 °C) was obtained.

(−)-**5**: 4.30 g (±)-**5** and 4.00 g (+)-camphor-10-sulfonic acid were dissolved in 50 ml refluxing *i*-PrOH. After six recrystallizations from *i*-PrOH (salt(g): *i*-PrOH(ml)=1:6) the resulting crystalline salt with mp 144—147 °C and $[\alpha]_D^{16}$ −0.1° (*c* 0.5, MeOH) was found to be only partially resolved. The corresponding optically impure base with $[\alpha]_D^{16}$ −24.8° (*c* 0.7, $CHCl_3$) was recrystallized several times from EtOAc by which procedure only from the third mother liquor 90 mg (4%) of the levo-rotating isomer, mp 70.5—72 °C and $[\alpha]_D^{16}$ −139.2° (*c* 0.7, $CHCl_3$) was isolated.

Convesion of the Optically Active Chlorine-Containing Methanols 2—4 into α-Phenyl-2-pyridylmethanol 1. General Procedure. The chlorine containing methanol (1 mmol) dissolved in 10 ml dry EtOH was refluxed for 5 min in the presence of 2 ml of hydrazine hydrate (98%) and 70 mg of Pd/C (10%).[15] The catalyst was filtered off, washed with EtOH and the combined filtrates evaporated to dryness. The resulting oil was taken up in $CHCl_3$ and washed with water. The residue after removing the chloroform is the practically TLC pure methanol **1**. A recrystallization from light petroleum afforded **1** as colorless crystals.

Conversion of (+)-2 into (+)-1. From 450 mg (+)-**2** with $[\alpha]_D^{17}$ +242.8° (*c* 0.5, $CHCl_3$) according to the general procedure 266 mg (70%) of pure (+)-**1**, mp 63—67 °C and $[\alpha]_D^{17}$ +162.9° (*c* 0.4, $CHCl_3$), was obtained after recrystallization.

Conversion of (−)-3 into (−)-1. 220 mg (−)-**3** with $[\alpha]_D^{17}$ −132.5° (*c* 0.7, $CHCl_3$) in the same manner afforded 132 mg (71%) pure (−)-**1**, mp 64.5—66 °C and the following values for the optical rotation in chloroform: $[\alpha]_D^{16}$ −161.5° (lit, −86.2°,[11] −108°[12]), $[\alpha]_{578}^{16}$ −169.5° (lit,[14] −113°), $[\alpha]_{546}^{16}$ −197.0° (lit,[11] −104.7°).

Conversion of (+)-4 into (+)-1. From 221 mg of (+)-**4** with $[\alpha]_D^{23}$ +182.9° (*c* 0.5, $CHCl_3$) according to the general procedure after recrystallization pure (+)-**1** (62 mg, 39%), mp 64—67 °C and $[\alpha]_D^{17}$ +162.8° (*c* 0.4, $CHCl_3$), was obtained.

Catalytic Hydrogenation of (−)-1 to (−)-*erythro*-(*αR, 2S*)-α-Phenyl-2-piperidylmethanl (6). 2.44 g (11 mmol) of (−)-**1**·HCl ($[\alpha]_D^{17}$ −215.0° (*c* 0.4, MeOH), corresponding base: $[\alpha]_D^{17}$ −162.8° (*c* 0.4, $CHCl_3$)) dissolved in 100 ml dry EtOH in the presence of 70 mg of PtO_2 was hydrogenated according to Ref. 12a in a rotating laboratory autoclave at 5.5 atm and room temp. After the consumption of 36.3 mmol of H_2 (in about two hours and a half) the catalyst and the

solvent were removed. The resulting mixture containing the two optically active diastereoisomeric α-phenyl-2-piperidylmethanol hydrochlorides was subjected to separation by twofold recrystallization from abs EtOH–Et_2O[29] to give 1.24 g (51%) of (−)-*erythro*-**6**, mp 212—216 °C and $[\alpha]_D^{17}$ −32.2° (*c* 0.6, H_2O), $[\alpha]_D^{17}$ −12.4° (*c* 0.3, $CHCl_3$). TLC analysis of the corresponding free base: One spot (silica gel; Et_2O:MeOH=17:3) was found to be free from the threo isomer. At the same conditions TLC analysis of the crude reaction mixture gave two spots with $R_{f(erythro)}$=0.13 and $R_{f(threo)}$=0.21.

The free base of (−)-*erythro*-**6** had mp 127—130 °C and $[\alpha]_D^{17}$ −50.8°, $[\alpha]_{578}^{17}$ −53.2° (*c* 0.4, $CHCl_3$). Lit mp and optical rotation for (−)-*erythro*-**6**·HCl 213.5—215 °C, $[\alpha]_D$ −22.0° (H_2O),[18] $[\alpha]_D$ +7.0° ($CHCl_3$)[12] and for (−)-*erythro*-(α*R*,2*S*)-**6**-base −132—133°C, $[\alpha]_{578}$ −35.3° ($CHCl_3$).[14,17]

We thank the referees for thoroughly examining the paper and making critical comments which we feel have greatly contributed to its improvement. Thanks are also due to Dr. B. Jordanov for helpful discussions.

References

1) a) N. Berova and B. Kurtev, *Tetrahedron*, **25**, 2301 (1969); b) N. Berova, S. Bojadziev, and R. Rakovska, *Commun. Dept. Chem. Bulg. Acad. Sci.*, **14**, 487 (1981); c) N. Berova, S. Spassov, and R. Rakovska, *ibid.*, **15**, 217 (1982).

2) a) N. Berova, B. Kurtev, and G. Snatzke, *Tetrahedron*, **39**, 1371 (1983); b) *Croat. Chem. Acta*, **58**, 189 (1985).

3) a) A. Shafiée and G. Hite, *J. Med. Chem.*, **12**, 266 (1969); b) B. Testa, "Molecular and Quantum pharmacology," ed by E. Bergmann and B. Pullman, D. Reidel Publishing Company, Dordrecht-Holland (1974), pp. 241—259; c) C. Kook, A. Karim, D. Shappelon, and J. Sanner, Annual Meeting of the Academy of Pharmaceutical Sciences, 27th, A. Ph. A., Washington, D.C., 84 (1979); d) M. Mirro, A. Watanabe, and J. Bailey, *Circulation*, **60** (Suppl. II), II-89 (1979); e) A. Harms, W. Hespe, W. Nauta, R. Rekker H. Timmerman, and J. de Vries, "Drug Design" (Medicinal chemistry, a series of monographs) ed by E. Ariens, Academic Press, New York, (1976), Vol. 6, pp. 2—77.

4) Ch. H. Tilford, R. S. Shelton, and M. G. VanCampen, *J. Am. Chem. Soc.*, **70**, 4001 (1948).

5) N. Sperber, D. Papa, E, Schwenk, and M. Sherlock, *J. Am. Chem. Soc.*, **71**, 887 (1949).

6) N. H. Cantwell and E. U. Brown, *J. Am. Chem. Soc.*, **75**, 1489 (1953).

7) G. E. Hardtmann, W. J. Houlihan, and E. I. Takesue, *J. Med. Chem.*, **12**, 1093 (1969).

8) F. H. Pinkerton and S. F. Thames, *J. Organomet. Chem.*, **24**, 623 (1970).

9) D. W. Adamson and J. W. Billinghurst, *J. Chem. Soc.*, **1950**, 1039.

10) a) H. Gilman and S. M. Spatz, *J. Org. Chem.*, **16**, 1485 (1951); b) J. P. Wibaut, A. P. DeJonge, H. G. Van der Voort, and H. Otto, *Recl, Trav. Chim.*, **70**, 1054 (1951).

11) A. G. Davies, J. Kenyon, and K. Thaker, *J. Chem. Soc.*, **1956**, 3394.

12) R. M. Jacob and N. M. Joseph, a) U. S. Patent 2928835; Mar 15 (1960); b) Brit. Patent 850826; Oct 5 (1960).

13) A. Ohno, M. Ikeguchi, T. Kimura, and S. Oka, *J. Am. Chem. Soc.*, **101**, 7036 (1979).

14) H. Wollweber and R. Hiltmann, *Arch. Pharm.*, **306**, 284 (1973) and ref. 4 therein.

15) A. Collet and J. Jacques, *Bull. Soc. Chim. Fr.*, **1972**, 3857.

16) T. R. Burke, W. L. Nelson, M. Mangion, G. J. Hite, C. M. Mokler, and P. C. Ruenitz, *J. Med. Chem.*, **23**, 1044 (1980).

17) H. U. Pohl and H. Wollweber, *Eur. J. Med. Chem.-Chim. Ther.*, **13**, 127 (1978).

18) J. J. Fauley and J. B. LaPidus, *J. Org. Chem.*, **36**, 3065 (1971).

19) G. Snatzke, N. Berova, S. Bojadziev, and J. Frelek, unpublished results.

20) N. Berova, S. Bojadziev, and G. Snatzke, Procedings of International Conference on Circular Dichroism, Sofia (1985), Publishing House Bulg. Acad. Sci., Vol. 6, pp. 303—311.

21) H. Aaron, "Topics in Stereochemistry," ed by E. Eliel and N. Allinger, J. Wiley & Sons, New York (1979), Vol. 11, pp. 1—52.

22) H. Aaron and C. Ferguson, *Tetrahedron*, **30**, 803 (1974).

23) D. Gust and K. Mislow, *J. Am. Chem. Soc.*, **95**, 1535 (1973) and references cited therein.

24) A molecular mechanics study of the basic compound **1** revealed that *helical* conformers also are the most populated local minima of 1 in the absence of intramolecular hydrogen bonding.[25] Two among three of them possess an N-C(Py)-C^{al}-O skeleton suitably dispositioned for an intramolecular hydrogen bond formation. *Perpendicular* and other local minima are of energy higher than 0.7 kcal mol^{-1}(1 cal=4.184 J) above the global minimum helical conformer.

25) The calculations were carried out with the MM2 force field.[26] A potential function to simulate intramolecular hydrogen bond formation is not included in the present version of MM2, and the results has to be considered only as an approximate estimation of the conformational preferences in the absence of intramolecular hydrogen bonding. Calculational details are available on request from the authors.

26) a) N. L. Allinger, *J. Am. Chem. Soc.*, **99**, 8127 (1977); b) N. L. Allinger and Y. H. Yuh, Q. C. P. E., **13**, 395 (1981).

27) H. Hallam, "Infrared Spectroscopy and Molecular Structure," ed by M. Davies, Elsevier, Amsterdam (1963), p. 415.

28) P. Krueger and H. Mettee, *Can. J. Chem.*, **42**, 326 (1964).

29) K. E. Crook and S. M. McElvain, *J. Am. Chem. Soc.*, **52**, 4006 (1930).

 © 1987 The Chemical Society of Japan Bull. Chem. Soc. Jpn., 60, 2657—2662 (1987)

Synthesis and Fluorescence Analysis of 3-Substituted 7-Dialkylamino-2*H*-1,4-benzoxazin-2-ones

Claude TREBAUL, Jean RONCALI,† Francis GARNIER*,† and Robert GUGLIELMETTI††
Laboratoire de Synthèse Organique, Université de Bretagne Occidentale,
6, rue le Gorgeu, 29283 Brest, France
†Laboratoire de Photochimie Solaire, ER 241, C.N.R.S., 2-8, rue Henry Dunant, 94320 Thiais, France
††Laboratoire de Chimie Organique et Bioorganique, Faculté des Sciences de Luminy,
70, Route L. Lachamp, 13258 Marseille, France
(Received December 19, 1985)

New benzoxazinone type dyes have been synthesized by the reaction of α-keto esters on 2-amino-5-(dialkylamino)phenols. The obtained 7-dialkylamino-2*H*-1,4-benzoxazin-2-ones show a strong fluorescence and a large Stokes shift, reaching 183 nm. An effect of 15 various substituents in position 3, together with a solvent effect have been characterized on their absorption and emission bands. Linear free energy relationships allow the tuning of their spectroscopic characteristics over a large spectral range.

The 2*H*-1,4-benzoxazin-2-ones, abusively called "azacoumarins," have been described by Wislicenus[1] in 1897, and more recently by Biekert[2] and Moffett.[3] They have synthesized many heterocyclic compounds of this kind by the reaction of an acid or a keto ester with an *o*-aminophenol. Actually, only a few derivatives of benzoxazinones with an amino group in the position 7 have been described in the literature.[4] These compounds (**A**) show a strong fluorescence which, due to the bathochromic effect of the heterocyclic nitrogen, is shifted towards the red when compared to the analogous 7-aminocoumarins (**B**). In order to better understand the spectroscopic properties of these highly fluorescent dyes (**A**), we have synthesized a large serie of 3-substituted 7-aminobenzoxazinones, and analyzed the substituent effect together with the solvent effect on their absorption and emission spectra.

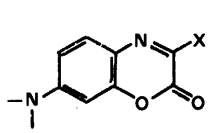

A

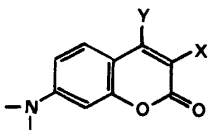

B

Synthesis of 2*H*-1,4-Benzoxazin-2-ones. The 7-amino derivatives of benzoxazinones are poorly described because of the difficulty to synthesize the starting 2,5-diaminophenols. These compounds are easily oxidized, and their fast degradation leads to highly-blue-colored products, whose structure is still unknown. Nevertheless, taking great care to avoid this oxidation, we isolated 2-amino-5-(dialkylamino)-phenols **1a,b** by reducing 5-dialkylamino-2-nitrosophenols with sodium dithionite in basic medium (**a**, R=Me; **b**, R=Et).

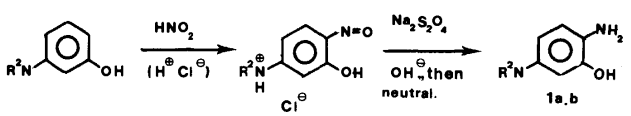

The 7-dialkylamino-2*H*-1,4-benzoxazin-2-ones, **3a,b** substituted in the position 3, have been obtained by the action of α-keto esters **2** on the 2-amino-5-(dialkylamino)phenols **1a,b**, or on the corresponding dihydrochloride **1a,b**, in the presence of a tertiary amine.

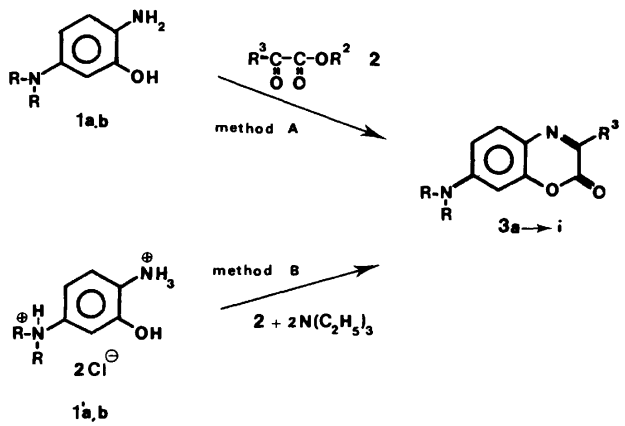

The reactivity of the methyl group on the position 3 in the 7-dimethylamino-3-methyl-2*H*-1,4-benzoxazin-2-ones **3a** allows the formation of 3-styrylbenzoxazinone **5**, by using the method described by Le Bris[4d] which involves the condensation of aromatic aldehydes.

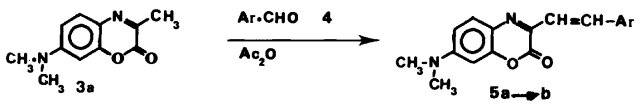

Moreover, a Lewis acid such as anhydrous zinc chloride allows the condensation of a few α-keto esters **2** on the activated methyl group on the position 3.

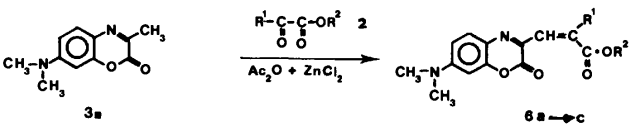

An ester function on the position 3 can also be easily substituted into an amide function, the unsubstituted amide leading to the corresponding nitrile by dehydration.

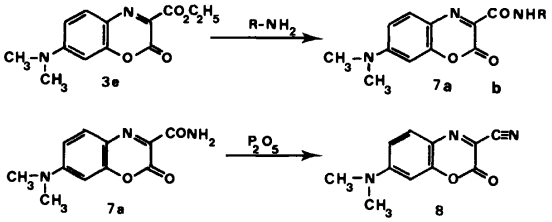

Spectral Properties of 3-Substituted Benzoxazinones. As shown on Table 1, 3-substituted benzoxazinones (**A**) thus obtained showed very interesting fluorescence properties, which can be explained on the basis of the following mesomeric forms (**I**) and (**II**).

In the ground state, the π-electron distribution in this essentially neutral molecule closely relates to the form (**I**), with a minor contribution of the dipolar form (**II**). On the other hand, the first excited singlet state S_1 can be described by a predominant dipolar

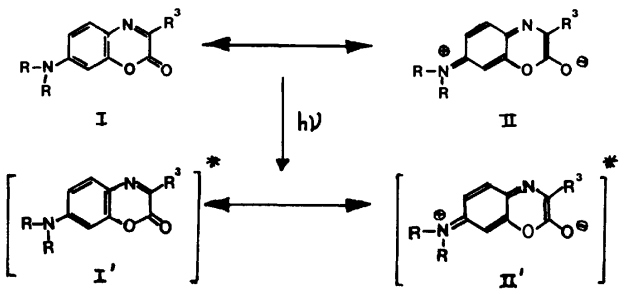

form (**II'**). Consequently, a large increase in the dipole moment of the molecule can be expected during the excitation $S_0 \rightarrow S_1$, which will result in a large rearrangement of the surrounding solvent molecule around the excited state. Thus the energy level of this excited state will be markedly lowered before the emission takes place, with regard to the energy level of its Franck-Condon excited state. These considerations explain the unusually large Stokes shift observed for these molecules (**A**), as compared to others dyes such as xanthenes or even the parent coumarins (**B**).

The dipolar moment variation will be controlled by

Table 1. Effect of R^3 Substituent on the Spectral Properties of Compounds of Type **3**

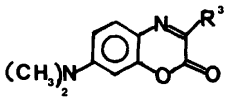

R^3	Solvents								
	$(C_2H_5)_2O$			$CHCl_3$			DMF		
	Abs	Em (nm)	SS	Abs	Em (nm)	SS	Abs	Em (nm)	SS
CH_3	384	484	100	400	502	102	395	525	130
CH_2-C($CO_2C_2H_5$)($OCOCH_3$)-$CO_2C_2H_5$	408	486	78	422	502	80	423	525	102
$C_6H_4OCH_3$(*p*-)	428	512	84	444	530	86	445	550	105
α-$C_{10}H_7$	429	510	81	445	528	83	449	557	108
C_6H_5	427	506	79	440	520	80	443	551	108
CH=C($CO_2C_2H_5$)($CO_2C_2H_5$)	475	546	71	500	557	57	510	592	82
CH=C(CH_3)(CO_2CH_3)	450	521	71	469	536	67	476	572	96
CH=C(C_6H_5)(CO_2CH_3)	464	533	69	483	551	68	488	583	85
$C_6H_4N(CH_3)_2$(*p*-)	450	548	98	467	584	117	468	586	118
$CO_2C_2H_5$	426	502	76	457	517	60	455	538	83
$CONH_2$	502	578	76	470	513	43	445	540	95
$CONHC_6H_5$	446	511	65	476	524	48	454	522	68
CN	457	512	55	476	523	47	478	548	70
CH=CH-$C_6H_4N(CH_3)_2$(*p*-)	472	560	88	500	616	116	499	634	135
CH=CH-$C_6H_4NO_2$(*p*-)	475	566	91	496	591	95	499	682	183

Abs=absorption maximum, Em=emission maximum, SS=Stokes Shift

Table 2. Effect of Solvent on Spectroscopic Properties of Compound **3a**

Solvent	Abs/nm	Em/nm	SS/cm^{-1}	Parameter E_T
Benzene	390	478	4721	34.5
Diethyl ether	384	484	5381	34.6
Dioxane	383	482	5363	36
Chloroform	400	502	5080	39.1
Pyridine	398	506	5363	40.2
Acetone	391	510	5968	42.2
DMF	395	525	6269	43.8
DMSO	399	532	6266	45
Acetonitrile	392	519	6242	46
Methanol	398	558	7204	55.5

the extent of the contribution of the dipolar forms (**II, II'**) to the S_0 and S_1 states, and thus governed by external parameters which are able to modify the electronic distribution in the molecule. For instance substituent as well as solvent can be expected to affect on the position of the absorption and emission bands. For instance, if the small contribution of the polar form (**II**) in the ground state is increased by an electronic effect of the R^3 substituent, a shift of the main absorption band to longer wavelength will occur. A stabilization of (**II**) can also be achieved by the increase of the solvent polarity. The energy level of the S_1 excited state will also be affected by these effects, resulting in an even larger shift of the emission band towards longer wavelength.

In order to go into more details, we have analyzed the effects of the R^3 substituent and of the solvent on the spectral properties of this class of compounds (Tables 1 and 2). The R^3 substituent effect determined in three different solvents shows that shifts of the absorption band higher than 100 nm can be obtained by varying the electronic distribution in the molecule. Using the parameter σ_I which represents the polar nature of a substituent,[5] a satisfying correlation with absorption frequency is obtained for a few substituents for which σ_I is given (Fig. 1). The emission maximum is also shifted by the substituents but to a smaller extent, as could be expected for a state in which the dipolar form (**II'**) is predominant, even for unsubstituted molecule.

Solvents can also affect on the energy levels of the S_0 and S_1 states. As already shown in the literature, the spectroscopic properties of such type of molecules possessing two limit forms, a neutral and a dipolar one, are governed by the solvent polarity.[6] Solvent parameters have been proposed for representing this effect, as for instance E_T on the basis of the spectral behavior of the pyridinium derivative (**C**).[7] Ten solvents of varying polarity have been used to analyze the solvent effect on the absorption and emission bands of one representative molecule of (**A**), with

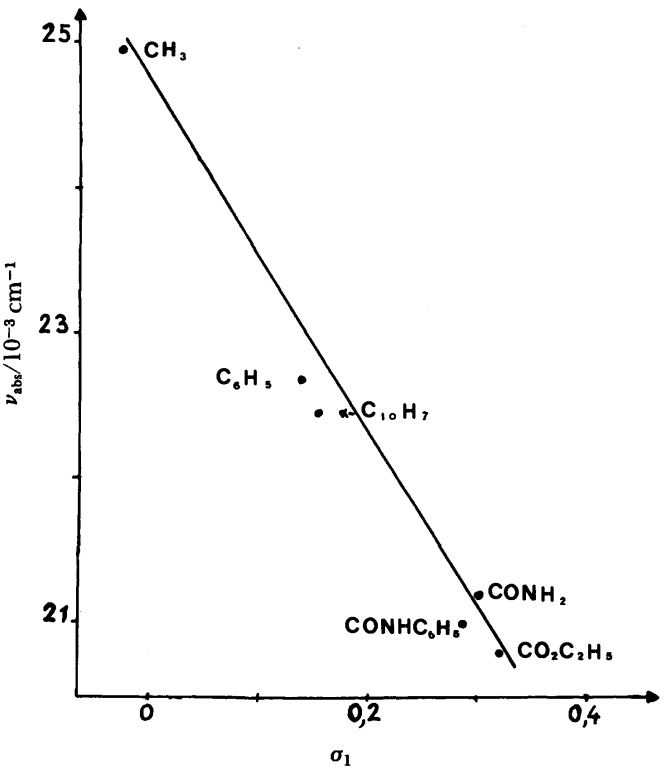

Fig. 1. Free energy relationship between absorption frequency ν_{abs} and substituent parameter σ_I. Solvent: $CHCl_3$.

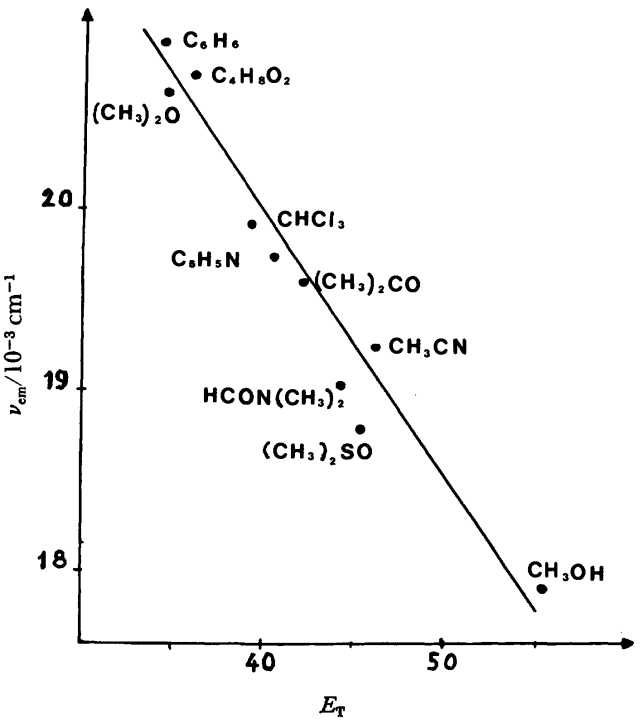

Fig. 2. Relationship between emission frequency (cm^{-1}) and the polarity parameter E_T in various solvents.

R=Me. The very large shift observed, which obey to a linear relationship with E_T (Fig. 2), emphasizes the significance of the dipolar form contribution to the

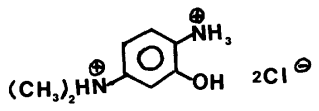

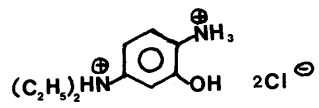

structure of these molecules. The observed Stokes shift reaches unusual value as high as 183 nm, compared with the 100 nm obtained with the parent coumarin dyes (**B**) when studied in the same range of solvent polarity. Furthermore, these benzoxazinone dyes possess a high fluorescence yield, as shown by the quantum yield η=0.93 obtained for R=CH_3 in chloroform, using Rhodamine 101 as standard.

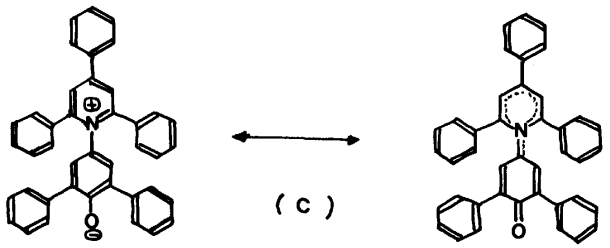

In conclusion, the position of the absorption and emission bands of these news benzoxazinone dyes can be tuned over a very large spectral range by the use of a substituent and (or) a solvent effect. Taking also account for their strong fluorescence, this new class of material appears promising for a large field of applications and particularly as laser dyes.

Experimental

Melting points were not corrected and were determined on a Koffler apparatus. The IR spectra were recorded on a Pye Unicam SP 200 spectrophotometer, the ^{1}H NMR spectra on a JNM-FX 100 JEOL spectrometer (the chemical shifts were reported as δ values in parts per million employing tetramethylsilane as an internal standard). The absorption spectra were obtained on a Cary 219 spectrophotometer and the fluorescence spectra on a MPF-44R Perkin Elmer spectrophotometer. Elemental analyses were carried out by the CNRS Microanalysis Laboratory.

Preparation of 2-Amino-5-(dialkylamino)phenols (1a,b). The hydrochloride of 5-dialkylamino-2-nitrosophenols have been obtained in yields of 90% following Ref. 8, then reduced into 2-amino-5-(dialkylamino)phenols by sodium dithionite in basic medium.[9]

We have isolated the compounds **1a** and **1b** by operating under nitrogen atmosphere to avoid of oxidative degradation, and using them readily for subsequent cyclization into benzoxazinones **3**. Besides, the dihydrochlorides **1'a** and **1'b** are stable under solid state. **1'a**: Gray crystals; mp 230 °C (decomp). ^{1}H NMR (D_2O) δ=3.37 (s, 6H, $N(C\underline{H}_3)_2$), 7.20—7.37 (m, 2H, H_4+H_6), 7.63 (d, J=9 Hz, 1H, H_3). **1'b**: Slightly blue crystals; mp 220 °C (dec). ^{1}H NMR (D_2O) δ=1.10 (t, J=7 Hz, 6H, $N(CH_2C\underline{H}_3)_2$), 3.57 (q, J=7 Hz, 4H, $N\text{-}(C\underline{H}_2\text{-}CH_3)_2$), 6.80—7.10 (m, 3H, H_3+H_4+H_6).

Preparation of 3-Substituted 7-Dialkylamino-2*H*-1,4-benzoxazin-2-ones. Metod A. To a solution of 20 mmol of α-ketoester **2**† in 50 ml of dry toluene and under nitrogen atmosphere, 20 mmol of 2-amino-5-(dialkylamino)phenols (**1**) were added with stirring. This reaction mixture was refluxed for 1 h and the water produced during the cyclization was eliminated by azeotropic distillation. After cooling, the organic layer was separated and concentrated to dryness. The benzoxazinone **3** was purified by chromatography on deactivated alumina or on silica gel, then by recrystallization. **2d** p-$(CH_3)_2N$-C_6H_4-CO-$CO_2C_2H_5$: Yellow-green crystals, mp 95 °C (lit,[10] mp 95 °C), **2e** p-CH_3O-C_6H_4-CO-$CO_2C_2H_5$: Slightly yellow oil, bp 195 °C/2 mmHg,†† **2f** $C_{10}H_7$-CO-$CO_2C_2H_5$: Yellow oil, bp 155—160 °C/1 mmHg, (lit,[11] bp 213—215°/23 mmHg).

Method B. Under a nitrogen atmosphere and while stiring, a mixture of 20 mmol of dihydrochloride **1'** and 20 mmol of α-keto ester **2** in 50 ml of dry toluene was refluxed; then 40 mmol of triethylamine were gradually added. The reflux was continued for 1 h with elimination of water as azeotrope. The cooled solution was filtered, the solid triethylammonium chloride was washed two times by 15 ml of toluene. All the organic layers were then treated as above.

7-Dimethylamino-3-methyl-2*H*-1,4-benzoxazin-2-ones (3a). Orange yellow crystals mp 125—126 °C (benzene-ethanol), yield 60% (method A); 70% (method B). Found: C, 64.59; H, 5.97; N, 13.81%. Calcd for $C_{11}H_{12}N_2O_2$: C, 64.69; H, 5.92; N, 13.72%. ^{1}H NMR ($CDCl_3$) δ=2.47 (s, 3H, CH_3-3), 3.02 (s, 6H, $N(CH_3)_2$-7, 6.32 (d, J=2.5 Hz, 1H, H_8), 6.60 (dd, J=9 and 3 Hz, 1H, H_6), 7.42 (d, J=^{1}H, H_5). UV-visible: λ_{max} 400 ($CHCl_3$), 395 nm (DMF); fluorescence: 502 ($CHCl_3$), 525 nm (DMF). IR (KBr): 1725 (s), 1624 cm^{-1} (s) (s=strong).

7-Diethylamino-3-methyl-2*H*-1,4-benzoxazin-2-one (3b). Yellow crystals mp 63—64 °C (cyclohexane). Yield: 50% (Method A); 54% (Method B). Found: C, 67.35; H, 5.94; N, 12.18. Calcd for $C_{13}H_{16}N_2O_2$: C, 67.22; H, 6.94; N, 12.06. ^{1}H NMR ($CDCl_3$) δ=1.16 (t, J=7 Hz, 6H, $N(CH_2C\underline{H}_3)_2$-7), 2.37 (s, 3H, CH_3-3), 3.29 (q, J=7 Hz, 4H, $N(C\underline{H}_2CH_3)_2$-7), 6.16 (d, J=3 Hz, 1H, H_8), 6.39 (dd, J=9 and 3 Hz, 1H, H_6), 7.47 (d, J=9 Hz, 1H, H_5). UV-visible: λ_{max} 397 ($CHCl_3$), 402 nm (DMF); fluorescence: 500 ($CHCl_3$), 520 nm (DMF). IR (KBr): 1733 (s), 1633 cm^{-1} (s).

7-Dimethylamino-3-phenyl-2*H*-1,4-benzoxazin-2-one (3c). Orange crystals, mp 182 °C ($CHCl_3$-ethanol). Yield 40% (method A). Found: C, 72.14; H, 5.15; N, 10.51%. Calcd for $C_{16}H_{14}N_2O_2$: C, 72.16; H, 5.30; N, 10.52%. ^{1}H NMR ($CDCl_3$) δ=3.07 (s, 6H, $N(C\underline{H}_3)_2$-7), 6.33 (d, J=3 Hz, 1H, H_8), 6.68

† α-Ketoesters **2** used are commercial (methyl pyruvate **2a**, methyl benzoylformate **2b**, diethyl mesoxalate **2c**) or have been prepared by a Friedel-Crafts reaction between the ester chloride of oxalic acid ($ClCOCO_2C_2H_5$) and the appropriate aromatic derivative. The structure of these α-keto esters has been verified by ^{1}H NMR.

†† 1 mmHg=133.322 Pa.

(dd, J=9 and 3 Hz, 1H, H_6), 7.37—7.50 (m, 3H, $H_3'+H_4'+H_5'$), 7.62 (d, J=9 Hz, 1H, H_5), 8.17—8.33 (m, 2H, $H_2'+H_6'$). UV-visible: λ_{max} 440 ($CHCl_3$), 443 nm (DMF); fluorescence: 520 ($CHCl_3$), 551 nm (DMF). IR (KBr): 1728 (s), 1620 cm^{-1} (s).

7-Diethylamino-3-phenyl-2*H*-1,4-benzoxazin-2-one (3d). Yield: 60% (Method B). Yellow crystals, mp 101 °C (cyclohexane). Found: C, 73.22; H, 6.21; N, 9.48%. Calcd for $C_{18}H_{18}N_2O_2$: C, 73.45; H, 6.16; N, 9.52%. ^1H NMR ($CDCl_3$) δ=1.19 (t, J=7 Hz, 6H, $N(CH_2CH_3)_2$-7), 3.35 (q, J=7 Hz, 4H, $N(CH_2CH_3)_2$-7), 6.25 (d, J=3 Hz, 1H, H_8), 6.47 (dd, J=9 and 3 Hz, 1H, H_6), 7.15—7.37 (m, 5H, H aromatic phenyl-3), 7.40 (d, J=9 Hz, 1H, H_5). UV-visible: λ_{max} 450 ($CHCl_3$), 462 nm (DMF); fluorescence: 520 ($CHCl_3$), 550 nm (DMF). IR (KBr): 1730 (s), 1620 cm^{-1} (s).

7-Dimethylamino-3-ethoxycarbonyl-2*H*-1,4-benzoxazin-2-one (3e). Yield: 70% (Method A); red crystals, mp 153—154 °C (ethanol). Found: C, 59.77; H, 5.39; N, 10.65% Calcd for $C_{13}H_{14}N_2O_4$: C, 59.53; H, 5.38; N, 10.68%. ^1H NMR ($CDCl_3$) δ=1.43 (t, J=7 Hz, 3H, $CO_2CH_2CH_3$-3), 3.15 (s, 6H, $N(CH_3)_2$-7), 4.43 (q, J=7 Hz, 2H, $CO_2CH_2CH_3$), 6.35 (d, J=3 Hz, 1H, H_8), 6.72 (dd, J=9 and 3 Hz, 1H, H_6), 7.64 (d, J=9 Hz, 1H, H_5). UV-visible: λ_{max} 457 ($CHCl_3$), 455 nm (DMF); fluorescence: 517 ($CHCl_3$), 538 nm (DMF). IR (KBr): 1760 (s), 1625 cm^{-1} (s).

7-Diethylamino-3-ethoxycarbonyl-2*H*-1,4-benzoxazin-2-one (3f). Yield: 27% (Method B); orange crystals, mp 68—69 °C (ethanol-water). Found: C, 62.13; H, 6.28; N, 9.33%. Calcd for $C_{15}H_{18}N_2O_4$: C, 62.06; H, 6.26; N, 9.65%. ^1H NMR ($CDCl_3$) δ=1.22 (t, J=7 Hz, 6H, $N(CH_2CH_3)_2$-7), 1.39 (t, J=7 Hz, 3H, $CO_2CH_2CH_3$-3), 3.47 (q, J=7 Hz, 4H, $N(CH_2CH_3)_2$-7), 4.47 (q, J=7 Hz, 2H, $CO_2CH_2CH_3$-3), 6.40 (d, J=3 Hz, 1H, H_8), 6.75 (dd, J=9 and 3 Hz, 1H, H_6), 7.65 (d, J=9 Hz, 1H, H_5). UV-visible: λ_{max} 420 ($CHCl_3$), 462 nm (DMF); fluorescence: 450 ($CHCl_3$), 538 nm (DMF). IR (KBr): 1770 (s), 1628 cm^{-1} (s).

7-Dimethylamino-3-(*p*-(dimethylamino)phenyl)-2*H*-1,4-benzoxazin-2-one (3q). Yield: 75% (Method A); red crystals, mp 222 °C ($CHCl_3$-ethanol). Found: C, 69.18; H, 6.17; N, 13.44%; Calcd for $C_{18}H_{19}N_3O_2$: C, 69.88; H, 6.99; N, 13.58%. ^1H NMR ($CDCl_3$) δ=3.07 (s, 12H, $N(CH_3)_2$-7 and -4'); 6.37 (d, J=3 Hz, 1H, H_8), 6.60 (dd, J=9 and 3 Hz, 1H, H_6), 6.70 (d, J=9 Hz, 2H, $H_3'+H_5'$), 7.52 (d, J=9 Hz, 1H, H_5), 8.25 (d, J=9 Hz, 2H, $H_2'+H_6'$). UV-visible: λ_{max} 467 ($CHCl_3$), 468 nm (DMF); fluorescence: 584 ($CHCl_3$), 586 nm (DMF). IR (KBr): 1725 (s), 1615 cm^{-1} (s).

7-Dimethylamino-3-(*p*-methoxyphenyl)-2*H*-1,4-benzoxazin-2-one (3h). Yield: 40% (Method A); red crystals, mp 177—178 °C ($CHCl_3$-ethanol). Found: C, 68.40; H, 5.45; N, 9.35%. Calcd for $C_{17}H_{16}N_2O_3$: C, 68.91; H, 5.44; N, 9.35%. ^1H NMR ($CDCl_3$) δ=3.07 (s, 6H, $N(CH_3)_2$-7), 3.87 (s, 3H, OCH_3-4'), 6.40 (d, J=3 Hz, 1H, H_8), 6.63 (dd, J=9 and 3 Hz, 1H, H_6), 5.97 (d, J=9 Hz, 2H, $H_3'+H_5'$), 7.55 (d, J=9 Hz, 1H, H_5), 8.23 (d, J=9 Hz, 2H, $H_2'+H_6'$). UV-visible: λ_{max} 444 ($CHCl_3$), 445 nm (DMF); fluorescence: 530 ($CHCl_3$), 550 nm (DMF). IR (KBr): 1726 (s), 1630 (s), 1605 cm^{-1} (s).

7-Dimethylamino-3-(naphthyl)-2*H*-1,4-benzoxazin-2-one (3i). Yield: 59% (Method A); orange red crystals, mp 182 °C ($CHCl_3$-ethanol). Found: C, 75.90; H, 5.08; N, 8.75%. Calcd for $C_{20}H_{16}N_2O_2$: C, 75.93; H, 5.10; N, 8.86%. ^1H NMR ($CDCl_3$) δ=3.05 (s, 6H, $N(CH_3)_2$-7); 6.42 (d, J=9 Hz, 1H, H_5), 6.66 (dd, J=9 and 3 Hz, 1H, H_6), 7.64 (d, J=9 Hz, 1H, H_5), 8.35 (dd, J=9 and 3 Hz, 1H, H_2), 7.40—8.12 (m, 6H, $H_3'+H_4'+H_5'+H_6'+H_7'+H_8'$). UV-visible: λ_{max} 445 ($CHCl_3$), 449 nm (DMF); fluorescence: 528 ($CHCl_3$), 557 nm (DMF). IR (KBr): 1728 (s); 1625 cm^{-1} (s).

Preparation of 7-dimethylamino-3-styryl-2*H*-1,4-benzoxazin-2-ones (5). A solution of 10 mmol of **3a** and 20 mmol of aromatic aldehyde **4** in 20 ml of acetic anhydride was refluxed for 7 h. In the case of *p*-nitrobenzaldehyde **4b**, the compound **5b** was obtained by filtration of the cooled mixture. In the case of the *p*-(dimethylamino)benzaldehyde **4a**, the compound **5a** was isolated after concentration and chromatography on silica gel using the chloroform as eluent.

7-Dimethylamino-3-(*p*-(dimethylamino)styryl)-2*H*-1,4-benzoxazin-2-one (5a). Yield: 6%; red crystals, mp 252 °C ($CHCl_3$-ethanol). Found: C, 71.53; H, 6.28; N, 12.58%. Calcd for $C_{20}H_{21}N_3O_2$: C, 71.62; H, 6.31; N, 12.53%. ^1H NMR ($CDCl_3$) δ=3.02 (s, 6H, $N(CH_3)_2$-4'), 3.07 (s, 6H, $N(CH_3)_2$-7), 6.43 (d, J=3 Hz, 1H, H_8), 6.67 (dd, J=9 and 3 Hz, 1H, H_6), 6.68 (d, J=9 Hz, 2H, $H_3'+H_5'$), 7.25 (d, J=16 Hz, 1H, H_β), 7.53 (d, J=9 Hz, 3H, $H_5+H_2'+H_6'$), 7.92 (d, J=16 Hz, 1H, H_α). UV-visible: λ_{max} 500 ($CHCl_3$), 495 nm (DMF); fluorescence: 616 ($CHCl_3$), 634 nm (DMF). IR (KBr): 1730 (s), 1632 (m), 1600 cm^{-1} (s).

7-Dimethylamino-3-(*p*-nitrostyryl)-2*H*-1,4-benzoxazin-2-one (5b). Yield: 64%; dark red crystals, mp 260 °C ($CHCl_3$). Found: C, 64.10; H, 4.54; N, 12.44%. Calcd for $C_{18}H_{15}N_3O_4$: C, 64.59; H, 4.48; N, 12.46%. This compound is nearly insoluble in NMR solvents and the spectrum cannot be registered. UV-visible: λ_{max} 496 ($CHCl_3$), 499 nm (DMF); fluorescence: 591 ($CHCl_3$), 682 nm (DMF). IR (KBr): 1737 (s), 1630 (s), 1615 (s), 1595 cm^{-1} (s).

Condensation of 3a with α-Ketoesters 2. A mixture of 5 mol of **3a**, 10 mmol of α-keto ester **2** and 5 mmol of anhydrous zinc chloride in 10 ml of acetic anhydride was refluxed for 1 h. After the removal of the solvent, the residue was washed with boiling methanol; the methanolic solution was evaporated and the residual oil was submitted to column chromatography on silica gel using the dichloromethane as eluent.

Methyl 3-(7-Dimethylamino-2-oxo-2*H*-1,4-benzoxazin-3-yl)-2-methylpropenoate (6a). Yield: 42%; red crystals, mp 174—175 °C ($CHCl_3$-methanol). Found: C, 62.27; H, 5.52; N, 9.22%. Calcd for $C_{15}H_{16}N_2O_4$: C, 62.49; H, 5.59; N, 9.72%. ^1H NMR ($CDCl_3$) δ=2.42 (d, J=1.6 Hz, 3H, C=C-CH_3): 3.08 (s, 6H, $N(CH_3)_2$-7), 3.82 (s, 3H, CO_2CH_3), 6.37 (d, J=3 Hz, 1H, H_8), 6.66 (dd, J=9 and 3 Hz, 1H, H_6), 7.52 (d, J=9 Hz, 1H, H_5), 7.88 (q, J=6 Hz, 1H, HC=C-CH_3). UV-visible: λ_{max} 469 ($CHCl_3$), 476 nm (DMF); fluorescence: 536 ($CHCl_3$), 572 nm (DMF). IR (KBr): 1730 (s), 1710 (s), 1630 cm^{-1} (s).

Methyl 3-(7-Dimethylamino-2-oxo-2*H*-1,4-benzoxazin-3-yl)-2-phenylpropenoate (6b). Yield: 21%; red crystals, mp 188 °C ($CHCl_3$-methanol). Found: C, 67.92; H, 5.17; N, 7.96%. Calcd for $C_{20}H_8N_2O_4$: C, 68.56; H, 5.18; N, 8.00%. ^1H NMR ($CDCl_3$) δ=3.08 (s, 6H, $N(CH_3)_2$-7), 3.95 (s, 3H, CO_2CH_3), 6.38 (d, J=3 Hz, 1H, H_8), 6.65 (dd, J=9 and 3 Hz, 1H, H_6), 7.20—7.70 (m, 7H, 5H aromatic+H_5+HC=C-3). UV-visible: λ_{max} 483 ($CHCl_3$), 488 nm (DMF); fluorescence: 551 ($CHCl_3$), 583 nm (DMF). IR (KBr): 1740 (s), 1730 (s), 1620 cm^{-1} (s).

Diethyl (7-Dimethylamino-2-oxo-2*H*-1,4-benzoxazin-3-yl)-methylenemalonate. Yield: 47%; red crystals, mp 175 °C ($CHCl_3$-methanol). Found: C, 60.00; H, 5.57; N, 7.61%.

Calcd for $C_{18}H_{20}N_2O_6$: C, 59.59; H, 5.59; N, 7.77%. ^{1}H NMR ($CDCl_3$) δ=1.35 (t, J=7 Hz, 6H, $C(CO_2CH_2C\underline{H}_3)_2$), 3.13 (s, 6H, $N(C\underline{H}_3)_2$-7), 4.38 (q, J=7 Hz, 4H, $C(CO_2C\underline{H}_2CH_3)_2$), 6.38 (d, J=3 Hz, 1H, H_8), 6.67 (dd, J=9 and 3 Hz, 1H, H_6), 7.33 (d, J=9 Hz, 1H, H_5), 7.96 (s, 1H, $\underline{H}$-C=C$(CO_2C_2H_5)_2$). UV-visible: λ_{max} 500 ($CHCl_3$), 510 nm (DMF); fluorescence: 557 ($CHCl_3$), 592 nm (DMF). IR (KBr): 1745 (s), 1700 (s), 1628 cm^{-1} (s).

Reactivity of the Ester Group on the 3 Position of the 1,4-Benzoxazin-2-one. 3-Carbamoyl-7-dimethylamino-2*H*-1,4-benzoxazin-2-one (7a). A solution of 10 mmol of **3e** in a mixture of 50 ml of methanol and 5 ml of concentrated aqueous ammonia was refluxed during 15 min.

The amide **7a** was obtained by filtration of the cooled mixture. Yield: 86%; red crystals, mp>280 °C. Found: C, 56.82; H, 4.73; N, 18.16%. Calcd for $C_{11}H_{11}N_3O_3$: C, 56.65; H, 4.75; N, 18.02%. This compound is nearly insoluble in NMR solvents and so the spectrum cannot be registered. UV-visible: λ_{max} 470 ($CHCl_3$), 445 nm (DMF); fluorescence: 530 ($CHCl_3$), 540 nm (DMF). IR (KBr): 3420 and 3285 (-NH), 1710, 1620, 1595 cm^{-1} (s).

7-Dimethylamino-3-phenylcarbamoyl-2*H*-1,4-benzoxazin-2-one (7b). To a refluxed solution of 5 mmol of **3e** in 10 ml of xylene, 10 mmol of aniline were slightly added while azeotrope ethanol-xylene issued from the reaction is eliminated. After cooling the compound **7b** is isolated by filtration. Yield: 50%; red crystals, mp 241 °C ($CHCl_3$-methanol). Found: C, 65.77; H, 4.68; N, 13.54%. Calcd for $C_{17}H_{15}N_3O_3$: C, 66.01; H, 4.89; N, 13.59%. ^{1}H NMR ($CDCl_3$) δ=3.18 (s, 6H, $N(C\underline{H}_3)_2$-7), 6.46 (d, J=3 Hz, 1H, H_8), 6.80 (dd, J=9 and 3 Hz, 1H, H_6), 7.0—7.6 (m, 3H, H_5+2H (o)N-aromatic group), 7.7—8.0 (m, 3H, 2H(m)+1H(p)N-aromatic group), 10.60 (s, large, 1H, $N\underline{H}C_6H_5$). UV-visible: λ_{max} 476 ($CHCl_3$), 474 nm (DMF): fluorescence: 524 ($CHCl_3$), 522 nm (DMF). IR (KBr): 3285 (s, -NH), 1710 (s), 1625 (s), and 1598 cm^{-1} (s).

3-Cyano-7-dimethylamino-2*H*-1,4-benzoxazin-2-one (8). A mixture of 10 mmol of amide **7a** and of 10 mmol of P_2O_5 was heated cautiously on the flame until near 100 °C. At this temperature the reaction starts violently and it can be slowed by rapid cooling. The residue was then extracted by boiling chloroform, the compound **8** then purified by submitting to column chromatography on silica gel, using the chloroform as eluent. Yield: 23%; red crystals, mp 260 °C. Found: C, 61.30; H, 4.31; N, 19.02%. Calcd for $C_{11}H_9N_3O_2$: C, 61.39; H, 4.22; N, 19.53%. ^{1}H NMR (DMSO-d_6) δ=3.22 (s, 6H, $N(C\underline{H}_3)_2$-7), 6.43 (d, J=3 Hz, 1H, H_8), 6.77 (dd, J=9 and 3 Hz, 1H, H_6), (7.68 (d, J=9 Hz, 1H, H_5). UV-visible: λ_{max} 476 ($CHCl_3$), 478 nm (DMF); fluorescence: 523 ($CHCl_3$), 548 nm (DMF). IR (KBr) 2212 (s, C=N), 1722 (s), 1625 cm^{-1} (s).

References

1) W. Wislicenus and W. Beckh, *Justus Liebigs Ann. Chem.*, **295**, 339 (1987): W. Wislicenus and F. Schultz, *ibid.*, **436**, 55 (1924): W. Wislicenus and E. Mundinger, *ibid.*, **436**, 62 (1924): W. Wislicenus and H. Bubeck, *ibid.*, **436**, 113 (1924).

2) E. Biekert, D. Hoffmann, and F. J. Meyer, *Chem. Ber.*, **94**, 1664 (1961).

3) R. B. Moffett, *J. Med. Chem.*, **9**, 475 (1966).

4) a) P. Sokorin, *Sci. Amer.*, **220**, 30 (1969); b) R. Srinivasan, *IEFE J. Quant. Electron. QE-5*, 552 (1969); c) K. H. Drexhage, *Laser Focus*, **9**, 35 (1973); d) M. T. Le Bris, *J. Heterocycl. Chem.*, **21**, 551 (1984); e) G. A. Reynolds and K. H. Drexhage, *Opt. Commun.*, **13**, 222 (1975); f) M. T. Le Bris, J. Mugnier, J. Bourson, and B. Valeur, *Chem. Phys. Lett.*, **106**, 124 (1984).

5) R. D. Topson, "Progress in Physical Organic Chemistry," ed by R. W. Taft, John Wiley, New York (1976), Vol. 12, p. 1.

6) C. Reichardt, "Lösumgsmittel-Effekte in der Organischen Chemie," Verlag Chemie, GmbH, Weinheim (1969).

7) K. Dimroth and C. Reichardt, *Justus Liebigs Ann. Chem.*, **727**, 93 (1969).

8) G. M. Bennett and E. V. Bell, *Org. Synth.* Coll. Vol. II, p. 223.

9) J. B. Conant and B. B. Corson, *Org. Synth.* Coll. Vol. II, p. 33.

10) W. Michler and U. Handhardt, *Ber.*, **10**, 2081 (1877).

11) J. Rousset, *Bull. Soc. Chim. Fr.*, **3**, 301 (1871); *Beilstein*, X, p. 745.

Support Effect of Zinc Oxide Catalyst on Synthesis of Methanol from CO_2 and H_2

Takashi INOUE, Tokio IIZUKA, and Kozo TANABE*
Department of Chemistry, Faculty of Science, Hokkaido University, Sapporo 060
(Received January 5, 1987)

Synopsis. The synthesis of methanol from CO_2+H_2 was carried out at 340—400 °C under total pressure of 10 atm over ZnO supported on MgO, Al_2O_3, SiO_2, TiO_2, ZrO_2, and Nb_2O_5. The ZnO/ZrO_2 catalyst showed high activity and selectivity for methanol formation. The hydrogenation of CO_2 was more selective for methanol synthesis than that of CO.

The hydrogenation of CO has been extensively studied for the synthesis of hydrocarbons and alcohols.[1] For the production of methanol from $CO+H_2$, several catalysts such as $ZnO-Cr_2O_3$, $CuO-ZnO-Al_2O_3$, $CuO-ZnO-Cr_2O_3$ are known to be efficient.[2] However, the study of CO_2 hydrogenation has been much less extensive than those of CO hydrogenation. Although, for the synthesis of methanol from CO_2+H_2, several catalysts such as CuO,[3] Pd,[4] Re,[5] or Pt[6] supported on metal oxides are reported, no study has been made of ZnO supported on metal oxides. Thus, the support effect of ZnO catalyst on CO_2 hydrogenation has been examined in the present work.

Experimental

Zinc oxides supported on various oxides were prepared by impregnating ZrO_2, TiO_2, SiO_2, Al_2O_3, or Nb_2O_5 with an aqueous solution of zinc nitrate followed by calcining at 500 °C for 3 h and reducing at 400 °C in a stream of hydrogen before use. In the case of ZnO/MgO, a methanol solution of zinc nitrate was used to avoid the partial dissolution of MgO in water. The content of ZnO was 10 wt % for all catalysts. Zinc oxide itself was prepared by hydrolyzing an aqueous solution of zinc nitrate with aqueous ammonia followed by treating similarly as above. Commercial catalysts of methanol synthesis from CO and H_2 used for comparison were Toyo CCI, KMA ($ZnO-Cr_2O_3$), and MDC-02 ($CuO-ZnO-Al_2O_3$) which were treated similarly as above.

The reaction was carried out at 340—400 °C under 10 atmospheric pressure by use of a conventional flow reactor. The molar ratio of CO_2/H_2 or CO/H_2 in the premixed gas obtained from Nippon Sanso Co. was 1/3. The flow rate of the gas was 12.5 mmol h^{-1} under standard condition, GHSV being 600—1200 h^{-1}. The reaction products were analyzed by gas chromatography.

Results and Discussion

Table 1 shows the results of the hydrogenation of CO_2 over supported ZnO catalysts. Main products were, besides CO, methanol and dimethyl ether. The ZnO and ZnO/MgO catalysts showed 100 % selectivity for methanol formation, but their activities (rate of methanol formation) were low. On the other hand, the activities of ZnO/Al_2O_3, ZnO/SiO_2, and ZnO/TiO_2 were higher, but their selectivities were lower. The ZnO/ZrO_2 catalyst exhibited not only high activ-

Table 1. Hydrogenation of CO_2 over Supported ZnO Catalysts
($CO_2/H_2=1/3$, Total Pressure = 10 atm)

Catalyst (weight)	Reaction temp / °C	Rate of MeOH+Me_2O formation / 10^{-4} mol h^{-1} g^{-1}	Selectivity/% MeOH	Selectivity/% Me_2O	Rate of CO formation / 10^{-4} mol h^{-1} g^{-1}
ZnO (3.0 g)	360	0.07	100.0	—	0.8
	400	0.08	100.0	—	2.5
ZnO/MgO (1.5 g)	360	0.02	100.0	—	0.1
	400	0.08	100.0	—	0.6
ZnO/Al_2O_3 (1.0 g)	360	0.18	40.8	59.2	1.3
	380	0.5	38.0	62.0	3.7
ZnO/SiO_2 (1.0 g)	360	0.13	97.8	2.2	0.3
	400	0.35	86.9	13.1	1.3
ZnO/TiO_2 (2.0 g)	340	0.3	86.9	13.1	0.6
	360	0.7	77.0	23.0	1.2
ZnO/ZrO_2 (2.0 g)	340	0.4	99.9	trace	0.4
	360	0.8	99.2	0.8	1.1
ZnO/Nb_2O_5 (2.0 g)	360	trace	—	—	1.5
KMA[a] (2.0 g)	360	0.8	99.8	0.2	10.6
MDC-2[a] (2.0 g)	340	0.5	89.7	(10.3)[b]	10.2

a) Commercial catalysts of Toyo CCI. The composition of KMA and MDC-2 are known to be $ZnO-Cr_2O_3$ and $CuO-ZnO-Al_2O_3$, respectively. b) No ether is formed, the selectivities of CH_4 and C_2^+ being 5.7 and 4.6%, respectively.

Table 2. Hydrogenation of CO over ZnO/TiO_2 ($CO/H_2=1/3$, Total Pressure = 10 atm)

Catalyst	Reaction temp °C	Rate of $MeOH+Me_2O$ formation 10^{-4} mol h^{-1} g^{-1}	Selectivity/%		Rate of CO_2 formation 10^{-4} mol h^{-1} g^{-1}
			MeOH	Me_2O	
ZnO/TiO_2	340	0.7	29.2	70.7	0.8
	360	2.2	9.9	90.0	1.0

ity, but also high selectivity. Little activity was found in the case of ZnO/Nb_2O_5.

These results can be interpreted in terms of acid-base properties of the catalyst supports. Dimethyl ether which is known to be formed by dehydration of methanol was formed over the acidic catalyst supports (Al_2O_3, TiO_2, and SiO_2). The stronger the acid strength of the oxides, the larger the amount of dimethyl ether. Thus, the high selectivity for formation of methanol was obtained over basic or less acidic catalyst or supports (ZnO, MgO, and ZrO_2). In the hydrogenation of CO over Rh supported on various metal oxides, Ichikawa[7] reported that the selectivity for methanol formation was high over Rh supported on basic oxides such as BeO, MgO, CaO, and ZnO. In the case of Pt supported on metal oxides, the selectivity for methanol formation was also high over Pt supported on a basic MgO in the hydrogenations of both CO and CO_2.[6] Hence, the use of basic supports seem to be advantageous for methanol synthesis regardless of the kinds of metals and the difference between CO and CO_2.

Commercial catalysts of methanol synthesis from $CO + H_2$ showed considerably high activities and KMA gave a high selectivity for methanol formation. However, the rate of CO formation was much higher over both KMA ($ZnO-Cr_2O_3$) and MDC-2 ($CuO-ZnO-Al_2O_3$) than over the other catalysts.

The rate of formation of methanol and dimethyl ether from CO_2+H_2 was low in the initial stage of the reaction, but gradually increased and reached steady states in 2—4 h over all the catalysts. The selectivity for methanol formation gradually increased as the reaction proceeded. This suggests the gradual change of surface active species to favor methanol formation. In fact, the activity and the selectivity of ZnO/TiO_2 for methanol formation in the initial stage of the reaction increased when treated with the mixture gas of H_2O+H_2. Therefore, water molecules are one of the factors to enhance the catalytic activity.

To clarify the difference in reactivity between CO_2 and CO, the reaction of CO_2+H_2 was compared with that of $CO+H_2$ over the ZnO/TiO_2 catalyst. As seen from the comparison of Table 2 with Table 1, the reactivity of CO was higher than that of CO_2, however the selectivity for methanol formation in the reaction of $CO+H_2$ was much lower than that in the reaction of CO_2+H_2. Denise and Sneeden[8] made a comparison of methanol synthesis from CO with that of CO_2 over CuO/ZnO and found that the hydrogenation of CO_2 is more reactive than that of CO at lower temperatures, though the latter is more reactive than the former at higher temperatures. These indicate that the superiority of CO_2 hydrogenation to CO hydrogenation for methanol synthesis depends on the kinds of catalysts and reaction conditions.

References

1) C. K. Rofer-DePoorter, *Chem. Rev.*, **81**, 447 (1981).
2) K. Klier, *Advan. Catal.*, **31**, 243 (1982).
3) R. Bardet, J. Cazat, and Y. Trambouze, *J. Chim. Phys.*, **78**, 135 (1981).
4) E. Ramaroson, R. Kieffer, and A. Kienneman, *J. Chem. Soc., Chem. Commun.*, **1982**, 645.
5) T. Iizuka, K. Kojima, and K. Tanabe, *J. Chem. Soc., Chem. Commun.*, **1983**, 638.
6) T. Inoue and T. Iizuka, *J. Chem. Soc., Farady Trans. 1*, **82**, 1681 (1986).
7) M. Ichikawa, *Bull. Chem. Soc. Jpn.*, **51**, 2268 (1978).
8) B. Denise and R. P. Sneeden, *J. Mol. Catal.*, **17**, 359 (1982).

Electrochemical Preparation of Tetrakis(isocyanide)-dipalladium(I) Dichloride[1)]

Yasuhiro YAMAMOTO,* Katsuo TAKAHASHI,* and Hiroshi YAMAZAKI
RIKEN (The Institute of Physical and Chemical Research), Wako, Saitama 351-01
(Received January 8, 1987)

Synopsis. The electrochemical behavior of $PdCl_2(RNC)_2$ (1) has been investigated in acetonitrile at Pt and Hg electrodes. The cyclic voltammogram of **1** showed a reduction wave at ca. −1.2 V, corresponding to a two-electron transfer. Coulometric reduction of **1** at the Pt electrode gave a binuclear complex, $Pd_2Cl_2(RNC)_4$ (**2**). A similar reaction at the Hg electrode gave **2** in a relatively low yield. A Pt electrode was superior to a Hg one in the electrochemical synthesis of **2**. The polarogram of **1** at a Hg electrode suggested a CE mechanism of the electrode reaction.

Binuclear complexes having a metal-metal bond are of interest in areas of photo- and catalytic chemistry.[2)] Recently we described electrochemical preparation of $Pt_2Cl_2(RNC)_4$ from $PtCl_2(RNC)_2$.[3)] Analogous binuclear palladium(I) complexes of isocyanide have been prepared by the metathesis reactions between Pd(II) and Pd(0) complexes.[4)] We report here the electrochemical preparation of dichlorotetrakis(isocyanide)dipalladium(I).

The cyclic voltammogram (CVM) of $PdCl_2(2,6\text{-}Me_2C_6H_3NC)_2$ (**1a**) was measured in acetonitrile by means of a Pt electrode to determine the preparative condition of a macroscopic electroreduction (Fig. 1). The CVM showed reduction waves at ca. −1.1 V (current peak potential, E_{pc}) for aryl isocyanide complexes and at ca. −1.4 V for alkyl isocyanide complex. In comparison with the CVM of $PtCl_2(RNC)_2$,[5)] these waves were assigned to a two-electron reduction of the Pd(II) complexes.

When a charge-controlled electrolysis of **1a** consumed 1F (1F=96.5 kC) of charge per mole of the Pd(II) complex at −1.5 V, binuclear complex, $Pd_2Cl_2(2,6\text{-}Me_2C_6H_3NC)_4$ **2a** was obtained in a 73% yield. Similar binuclear complexes were obtained in a relatively high yield by the electroreduction of $PdCl_2(RNC)_2$ (R=2,6-Me_2-4-BrC_6H_2, 2,4-*t*-Bu_2-6-MeC_6H_2, 2,4,6-*t*-$Bu_3C_6H_2$, and *t*-Bu), as shown in Table 1.

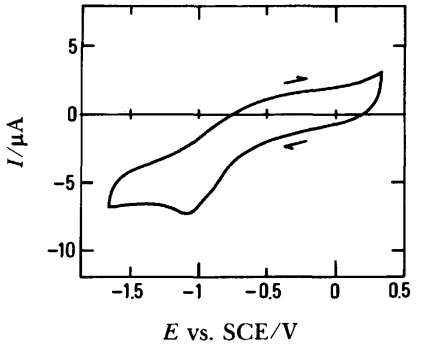

Fig. 1. Cyclic voltammogram of $PdCl_2(2,6\text{-}Me_2C_6H_3NC)_2$ (0.2 mM) on a Pt-tip electrode (surface area= 0.078 cm^2) in a 0.1 M *n*-Bu_4NClO_4-CH_3CN solution at 22 °C. Sweep rate=0.1 Vs^{-1}.

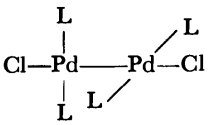

2
L=RNC

The charge-controlled electrolysis of **1a** consumed 1 F of charge per mole of complex at −1.4 V carried out at a mercury pool electrode and gave **2a** in a 23% yield. In this reaction, palladium metal was liberated as a precipitate, showing decomposition of a part of the palladium complexes. Yields of **2** at a mercury electrode were lower than those at a platinum one. In an attempt to reveal the origin of the low yields of **2** at a mercury electrode, a d.c. polarogram of **1a** was measured in a 0.1 M (mol dm^{-3}) *n*-Bu_4NClO_4-CH_3CN solution, using a dropping mercury electrode (Fig. 2). The polarogram showed a reduction wave at $E_{1/2}$ = 0.05 V where $E_{1/2}$ is an apparent halfwave potential. This was significantly different from that at the CVM. The shape of this wave and the reduction potential agreed resonably with those of the polarogram of $HgCl_2$ (Fig. 1).

These results suggest that the CE (chemical-electrochemical) reaction is operative at the Hg electrode surface, in which an initial chemical reaction of 1a with Hg proceeds to give $HgCl_2$ (Eq. 1), followed by an electrochemical reduction of $HgCl_2$ to Hg(0)

Table 1. Cathodic Current Peak Potential (E_{pc}) of $PdCl_2(RNC)_2$ (**1**) on the CVM and Yields of $Pd_2Cl_2(RNC)_4$ (**2**)[a)]

	R	Electrode	E_{pc}/V[b)]	Yield/%
1a	2,6-$Me_2C_6H_3$	Pt	−1.19	73
		Hg		23
1b	2,6-Me_2-4-BrC_6H_2	Pt	−1.13	83
		Hg		38
1c	2,4-*t*-Bu_2-6-MeC_6H_2	Pt	−1.18	87
		Hg		49
1d	2,4,6-*t*-$Bu_3C_6H_2$	Pt	−1.15	70
		Hg		52
1e	*t*-Bu	Pt	−1.41	69

a) Reactions were carried out at −1.5 V except **1e** (−1.6 V) in a 0.1 M $NaClO_4$-CH_3CN solution (ca. 30 cm^3) containing ca. 0.25 mmol of a sample. Charge, ca. 1 F per mole of a sample, was passed. b) A Pt-tip electrode was used for the CVM measurement in a 0.1 M *n*-Bu_4NClO_4-CH_3CN solution. The potentials are shown against a saturated calomel electrode. Sample concentration: ca. 0.1—0.5 mM; scan rate: 0.2 Vs^{-1}.

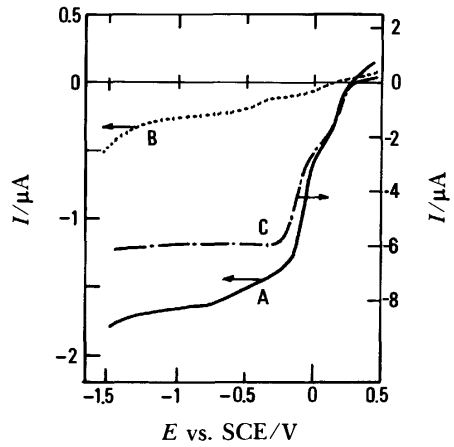

Fig. 2. d.c. Polarograms on a dropping mercury electrode (m=0.864 mg s^{-1}, drop time=4 s) in a 0.1 M n-Bu_4NClO_4-CH_3CN solution at 23 °C. A: $PdCl_2(2,6\text{-}Me_2C_6H_3NC)_2$ (0.2 mM). B: Blank (suppoting electrolyte solution). C: $HgCl_2$ (0.5 mM).

(Eq. 2).[6]

$$Hg(metal) + Pd(II) \longrightarrow Hg(II) + Pd(metal) \quad (1)$$

$$Hg(II) + 2e \longrightarrow Hg(metal) \quad (2)$$

Relatively high yields of complexes having bulky isocyanide ligands showed less interaction with mercury than that in the complex **1a**.

In conclusion, a Pt electrode was superior to a Hg electrode in the electrochemical synthesis of the Pd complex (Table 1).

The reaction path leading to the formation of $Pd_2Cl_2(RNC)_4$ was considered to be similar to that in a platinum complex.[5] The electrochemical reaction was initiated by a two-electron transfer to **1** to give a zerovalent species **3**. The chemical reaction of the zerovalent species (or a trinuclear complex, $Pd_3(RNC)_6$) and **1** led to a formation of **2**.

$$PdCl_2(RNC)_2 \xrightarrow{2e} \underset{\mathbf{3}}{\text{"}Pd(RNC)_2\text{"}} \text{ (or } Pd_3(RNC)_6\text{)}$$

$$\xrightarrow{PdCl_2(RNC)_2} \underset{\mathbf{2}}{Pd_2Cl_2(RNC)_4}$$

Experimental

The electrochemical apparatus has been already descrbed.[5] 2,6-Xylyl, 2,6-dimethyl-4-bromophenyl, 2,4,6-tri-t-butylphenyl, and t-butyl isocyanides were prepared according to the literature.[7] $PdCl_2(RNC)_2$ (R = 2,6-$Me_2C_6H_3$, 2,6-Me_2-4-BrC_6H_2) was prepared according to the literature.[3]

2,4-Di-t-methylphenyl isocyanide was prepared by a modification of the method described in the literature.[7b] IR (Nujol) 2109 cm^{-1},

^1H NMR($CDCl_3$) δ = 1.32 (s, 4-t-Bu), 1.52 (s, 2-t-Bu), 2.43 (s, 6-Me), ca. 7.2 (aromatic protons). Anal. ($C_{46}H_{23}N$) C, H, N.

$PdCl_2(2,4,6\text{-}t\text{-}Bu_3C_6H_2NC)_2$: IR (Nujol) 2229, 2195 cm^{-1}. Anal. ($C_{38}H_{58}N_2Cl_2Pd$) C, H, N.

$PdCl_2(2,4\text{-}t\text{-}Bu_2\text{-}6\text{-}MeC_6H_2NC)_2$: IR (Nujol) 2205 cm^{-1}. ^1H NMR ($CDCl_3$) δ = 1.30 (4-t-Bu), 1.48 (2,-t-Bu), 2.50 (6-Me), ca. 7.3(aromatic protons). Anal. ($C_{32}H_{46}N_2Cl_2Pd$) C, H, N.

$Pd_2Cl_2(2,4,6\text{-}t\text{-}Bu_3C_6H_2NC)_4$: IR (Nujol) 2144 cm^{-1}. ^1H NMR ($CDCl_3$) δ = 1.29 (s, 4-t-Bu), 1.65 (bs, 2 and 6-t-Bu), 7.32 (s, aromatic protones, 3- and 4-H). Found: C, 66.66: H, 8.54; N, 4.09%. Calcd for $C_{76}H_{116}N_4Cl_2Pd_2$: C, 66.71; H, 8.91; N, 3.90%.

$Pd_2Cl_2(2,4\text{-}t\text{-}Bu_2\text{-}6\text{-}MeC_6H_2NC)_4$: IR (Nujol): 2187, 2147 cm^{-1}. ^1H NMR ($CDCl_3$) δ = 1.27 (4-t-Bu), 1.46 (2-t-Bu), 2.47 (6-Me), ca. 7.3(aromatic protons). Anal. ($C_{64}H_{92}N_4Cl_2Pd_2$) C, H, N.

The authors (Y.Y and K.T) with to express their thanks for a Grant-in-Aid for Scientific Research 59540332 from the Ministry of Education, Science and Culture.

References

1) A part of this paper was presented at the 32nd Symposium on Organometallic Chemistry, November (1985), Osaka. Electrochemical studies of organometallic compounds, Part 4. Part 1: Y. Yamamoto, K. Takahashi, and H. Yamazaki, *Chem. Lett.*, **1984**, 201. Part 2: Y. Yamamoto, K. Takahashi, and H. Yamazaki, *J. Am. Chem. Soc.*, **108**, 2458 (1986). Part 3: Y. Yamamoto, K. Takahashi, K. Matsuda, and H. Yamazaki, *J. Chem. Soc., Dalton Trans.*, in press.

2) G. L. Geoffroy and M. S. Wrighton, "Organometallic Photochemistry," Academic Press (**1979**); M. P. Brown, J. R. Fisher, S. J. Franklin, R. J. Puddephatt, M. A. Thomson, *Adv. Chem. Ser.*, **196**, 231 (1982) and references therein.

3) Y. Yamamoto, K. Takahashi, and H. Yamazaki, *Chem. Lett.*, **1985**, 201.

4) Y. Yamamoto and H. Yamazaki, *Bull. Chem. Soc. Jpn.*, **58**, 1843 (1985).

5) Y. Yamamoto, K. Takahashi, K. Matsuda, and H. Yamazaki, *J. Chem. Soc., Dalton Trans.*, in press.

6) Mechanistic study of the electrochemical reactions is now in progress and details will be reported in the future.

7) H. M. Walborsky and G. E. Niznik, *J. Org. Chem.*, **37**, 187 (1972); Y. Yamamoto, K. Aoki, and H. Yamazaki, *Inorg. Chem.*, **18**, 1681 (1979).

Synthesis of Dibromoacetyl Derivatives by Use of Benzyltrimethylammonium Tribromide

Shoji KAJIGAESHI,* Takaaki KAKINAMI,† Hajime TOKIYAMA,† Takahiro HIRAKAWA,† and Tsuyoshi OKAMOTO†

Department of Industrial Chemistry, Faculty of Engineering, Yamaguchi University, Tokiwadai, Ube 755

†Department of Industrial Chemistry, Ube Technical College, Tokiwadai, Ube 755

(Received December 24, 1986)

Synopsis. The reaction of acetyl derivatives with double the molar quantity of benzyltrimethylammoniun tribromide in dichloromethane-methanol solution at room temperature gave dibromoacetyl derivatives in fairly good yields.

Organic ammonium tribromides are considered to be mild and selective brominating agents.[1] These reagents have a merit in that they can be quantitatively treated, compared with liquid bromine, because of their solid character. Previous work in this series[2] has shown that monobromoacetyl derivertives are readily obtained from reactions of acetyl derivatives with tetrabutylammonium tribromide (TBA Br_3) under mild conditions. In the present paper, we wish to report the syntheses of dibromoacetyl derivatives (**1**) by the use of a new reagent, benzyltrimethylammonium tribromide (BTMA Br_3).

Results and Discussion

The reaction of benzyltrimethylammonium chloride with bromine in dichloromethane gave BTMA Br_3. BTMA Br_3 was also prepared by the addition of hydrobromic acid to an aqueous solution of benzyltrimethylammonium chloride and sodium bromate in good yield.

The reaction of acetyl derivatives (**2**) with double the molar quantity of BTMA Br_3 in a dichloromethane-methanol solution for 2—7 h at room temperature gave **1** readily. The results are summarized in the Table 1.

$$\underset{\mathbf{2}}{RCOCH_3} \xrightarrow[\text{in } CH_2Cl_2\text{-}CH_3OH \text{ rt}]{2PhCH_2(CH_3)_3N^+Br_3^-} \underset{\mathbf{1}}{RCOCHBr_2}$$

Table 1. Dibromoacetyl Derivatives (1) from Acetyl Derivatives (2)

	Starting material (2)	Product (1)	Reaction time/h	Yield[a] %	IR (KBr) ν(CO) cm^{-1}	Mp θ_m/°C Found	Mp θ_m/°C Reported
a		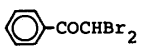	2	86	1695	33.5—34.5	36[3]
b	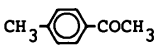	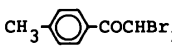	2	88	1690	99—99	100[4]
c	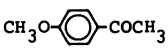	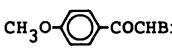	2	87	1680	93—94	93—94[5]
d	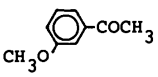	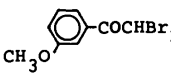	2	89	1690	67—68	—
e	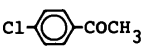	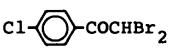	7	89	1695	92.5—93.5	92.5[6]
f	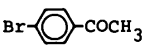	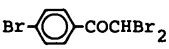	7	82	1700	92—93	92—93[7]
g	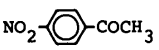	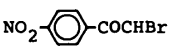	7	83	1700	63—65	67.4[8]
h	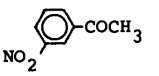	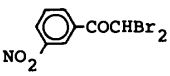	7	88	1710	56—57	59[9]
i	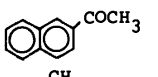	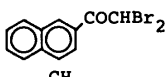	4	89	1695	100—101	101[10]
j	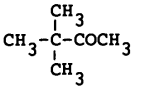	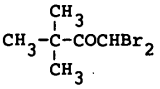	7	75	1725	73.5—74	74.5[11]

a) Yield of isolated product.

When an equimolecular amount of BTMA Br_3 was used with **2**, monobromoacetyl derivatives **3** were obtained in the same manner as when using TBA Br_3.[2] However, the reaction of **2**, with double the molar quantity of TBA Br_3 gave **1** as a byproduct, together with the main product **3**.[12] Therefore, it turned out that the brominating effect of BTMA Br_3 is stronger than that of TBA Br_3. Nevertheless, BTAM Br_3 could not further brominate **1** to tribromoacetyl derivatives at room temperature.

Because the presence of methanol markedly facilitated the bromination of **2**, it can be presumed that active species which generate Br^+ is probably methyl hypobromite produced from the reaction of BTMA Br_3 with methanol. In fact, we confirmed the evolution of hydrogen bromide by the addition of methanol to BTMA Br_3 at room temperature.

$$PhCH_2(CH_3)_3N^+Br_3^- + CH_3OH \longrightarrow PhCH_2(CH_3)_3N^+Br^- + CH_3OBr + HBr$$

$$\mathbf{2} + 2CH_3OBr \longrightarrow \mathbf{1} + 2CH_3OH$$

In general, derivatives **1** such as phenacylidene dibromide (a material for mandelic acid), were prepared from acyl derivatives and bromine.[3] By our method, **1** was easily obtained under mild conditions.

Experimental

Benzyltrimethylammonium Tribromide (BTMA Br_3). To a solution of benzyltrimethylammonium chloride (11.1 g, 60 mmol) and sodium bromate (4.5 g, 30 mmol) in water (100 ml) was added hydrobromic acid (47%, 180 mmol) under stirring at room temperature. A precipitated solid was extracted with dichlormethane (50 ml×4). The organic layer was dried with magnesium sulfate and evaporated in vacuo to leave a residue which was recrystallized from dichloromethane-ether (10 : 1) to give BTMA Br_3 as orange crystals; yield 18.2 g (78%); mp 100—101 °C. Found: C, 30.69; H, 4.11; N, 3.76; Br, 61.44%. Calcd for $C_{10}H_{16}NBr_3$: C, 30.80; H, 4.14; N, 3.59; Br, 61.47%.

Phenacylidene Dibromide (1a): Typical procedure. To a solution of acetophenone (**2a**) (0.5 g, 4.16 mmol) in dichloromethane (50 ml)-methanol (20 ml) was added BTMA Br_3 (3.4 g, 8.74 mmol) at room temperature. The mixture was stirred for 2 hr until a decoloration of the orange solution took place. The solvent was distilled; the obtained precipitate was extracted with ether (40 ml × 4). The ether layer was then dried with magnesium sulfate and evaporated in vacuo to give a residue which was recrystallized from methanol-water (1 : 2) affording **1a** as colorless crystals; yield 1.0 g (86%); mp 33.5—34.5 °C (lit,[3] mp 36 °C).

2,2-Dibromo-3′-methoxyacetophenone (1d). Compound **1d** was obtained as colorless needles; mp 67—68 °C. ^1H NMR ($CDCl_3$) δ=3.82 (3H, s, OCH_3), 6.70 (1H, s, $CHBr_2$), and 6.9—7.75 (4H, m, H_{arom}). Found: C, 35.00; H, 2.78; Br, 51.80%. Calcd for $C_9H_8O_2Br_2$: C, 35.10; H, 2.62; Br, 51.89%.

References

1) L. F. Fieser and M. Fieser, "Reagents for Organic Synthesis," John Wily and Sons, New York (1967), Vol. 1, p. 967.
2) S. Kajigaeshi, T. Kakinami, T. Okamoto, and S. Fujisaki, *Bull. Chem. Soc. Jpn.*, **60**, 1159 (1987).
3) H. Hunius, *Ber.*, **10**, 2010 (1877).
4) A. Michaelis, *Ber.*, **15**, 186 (1882).
5) F. Kröhnke and K. Ellegast, *Chem. Ber.*, **86**, 1556 (1953).
6) A. Collet, *Bull. Soc. Chim. Fr.*, [3] **21**, 70 (1899).
7) A. Collet, *Bull. Soc. Chim. Fr.*, [3] **31**, 68 (1899).
8) C. Engler and O. Zielke, *Ber.*, **22**, 204 (1889).
9) C. Engler and E. Hassenkamp, *Ber.*, **18**, 2240 (1885).
10) R. Schweitzer, *Ber.*, **24**, 547 (1891).
11) R. Scholl, *Liebigs Ann. Chem.*, **338**, 24 (1905).
12) For example, the reaction of 4-methylacetophenone (**2b**) with double the molar quantity of TBA Br_3 in dichloromethane-methanol at room temperature gave a mixture of 2,2-dibromo-4′-methylacetophenone (**1b**) and 2-bromo-4′-methylacetophenone (**3b**) in the ratio of 1:2.5 on NMR spectra. The same treatment of 4-methoxyacetophenone (**2c**) afforded 2,2-dibromo-4′-methoxyacetophenone (**1c**) and 2-bromo-4′-methoxyacetophenone (**3c**) in the ratio of 1:2.

Evaluation of the Hydrogen Shuttling Ability of Coal Liquefaction Solvents

Koji CHIBA,* Hideyuki TAGAYA,* Tohru SUZUKI, and Takashi SUZUKI
Department of Chemical Engineering, Faculty of Engineering, Yamagata University, Johnan, Yonezawa 992
(Received January 24, 1987)

Synopsis. The hydrogen-shuttling ability of coal liquefaction solvents were evaluated using benzophenone and dibenzyl ether as hydrogen acceptors. Hydrogen-transfer reactions from tetralin to acceptors were accelerated by shuttlers and the ranking of the shuttling ability was determined to be as follows:
anthracene > fluorene > pyrene≅triphenylmethane > phenanthrene > 1-methylnaphthalene

It is generally well-accepted that the hydrogen-donation of solvents plays an important role in the noncatalytic dissolution of coal.[1] Therefore, many researchers have attempted to evaluate the hydrogen donor ability of coal liquefaction solvents.[2] Hydroaromatic compounds, such as tetralin, are known as donors. On the other hand, polynuclear fused aromatics, such as pyrene, have been identified as being effective solvent components in spite of their low donor abilities. For example, when mixtures of pyrene and tetralin were used in the presence of hydrogen, coal conversions almost as high as that in pure tetralin were achieved at 30% tetralin.[3] Pyrene is not a donor; however, the ability of condensed aromatics to assist in liquefaction by physical solvation has been well recognized,[4] and an important role of pyrene as the hydrogen shuttler is suggested. In order to fully understand the function and importance of liquefaction solvents, an evaluation of the hydrogen-shuttling ability must be undertaken. We have developed a method by which the relative hydrogen-shuttling ability of liquefaction solvents can be evaluated using two different types of model hydrogen acceptors.

Experimental

Benzophenone and dibenzyl ether were used as hydrogen acceptors. An acceptor (1 g), tetralin (10 g) and a solvent (1 g) were placed in a magnet-driven autoclave and pressurized to 3 MPa with nitrogen. When benzophenone was used as an acceptor, the autoclave was heated to 430 °C and maintained at this temperature for 1 hour. The yields of diphenylmethane and benzhydrol were determined by gas chromatography (GC). Dibenzyl ether was unstable and decomposed completely at 430 °C. Therefore, the reaction was carried out at 375 °C for 1 h when dibenzyl ether was used as an acceptor. The yields of toluene, benzaldehyde and benzyl alcohol were determined by GC. Benzene was scarcely produced.

Results and Discussion

It has already been reported that benzophenone accepted hydrogen from tetralin as follows:[5]

$$2Ph_2CO \xrightarrow{\text{donor}} 2Ph_2CHOH \longrightarrow Ph_2CO + Ph_2CH_2 + H_2O. \quad (1)$$

Table 1. The Effect of Hydrogen Shuttlers on the Hydrogen Transfer Reaction[a] from Tetralin to Benzophenone (BZP)

Shuttler	Conv. of BZP/mol%	Yield of DPM[b]/mol%	Yield of BZH[b]/mol%
None	36.3	32.9	2.0
None	37.5	33.5	2.0
1-Methylnaphthalene	35.5	32.9	2.6
Anthracene	59.8	56.4	≈0
Phenanthrene	35.1	27.5	2.1
Pyrene	44.6	36.0	5.5
Fluorene	49.2	39.2	8.6
Triphenylmethane	40.2	33.1	5.0

a) Shuttler (1 g), tetralin (10 g) and benzophenone (1 g) were used. Reaction temperature 430 °C; initial nitrogen pressure 3MPa; reaction time 1 h. b) DPM=Diphenylmethane, BZH=benzhydrol.

In this work 36—38% of the benzophenone was hydrogenated by tetralin at 430 °C for 1 h (Table 1). Diphenylmethane is thermally stable, whereas benzhydrol is considered to be an unstable intermediate. When the mixture of benzhydrol and 1-methylnaphthalene was heated at 270 °C in a nitrogen atmosphere for 1 h, over 50% of the benzhydrol disproportionated to diphenylmethane and benzophenone. Actually, in the reaction of tetralin with benzophenone, the yield of benzhydrol was only 2%. Polyaromatic nondonor solvents such as 1-methylnaphthalene, anthracene, phenanthrene, pyrene, and fluorene were used to rank their shuttling ability. Triphenylmethane was also used because we had already confirmed that it accelerated the decomposition of bibenzyl in spite of a nondonor.[6] The ranking according to the degree of the reduction of benzophenone is as follows:

Anthracene > fluorene > pyrene > triphenylmethane > 1-methylnaphthalene≅phenanthrene.

We must pay attention to the fact that the two benzhydrol molecules disproportionate and produce one benzophenone molecule. Therefore, the total yield of products must be considered as the summation of the yield of diphenylmethane and one half of the yield of benzhydrol. The total yield of the products was 1.3 to 6.6% lower than the conversion of benzophenone. This indicates the presence of undetermined compounds. The high shuttling ability of anthracene is closely related to the fact that anthracene can be readily hydrogenated to dihydroanthracene. When anthracene was reacted with tetralin at 430 °C for 1 h,

Table 2. The Effect of Hydrogen Shuttlers on the Hydrogen Transfer Reaction[a] from Tetralin to Dibenzyl Ether (DBE)

Shuttler	Conv. of DBE /mol%	Yield of TOL[b] /mol%/2	Yield of BZA[b] /mol%/2	Yield of BYA[b] /mol%/2
None	21.4	8.7	7.5	3.5
None	21.8	7.2	5.8	5.1
1-Methylnaphthalene	21.3	8.8	6.9	5.6
Anthracene	60.4	21.6	22.4	7.1
Phenanthrene	33.4	14.5	12.0	5.9
Pyrene	36.9	8.5	8.7	3.5
Fluorene	41.4	17.4	15.8	8.2
Triphenylmethane	38.3	9.3	12.8	4.8

a) Shuttler (1 g), tetralin (10 g) and dibenzyl ether (1 g) were used. Reaction temperature 375 °C; initial nitrogen pressure 3MPa; reaction time 1 h. b) TOL= Toluene, BZA=benzaldehyde, BYA=benzyl alcohol.

26% of the anthracene was hydrogenated to dihydroanthracene. Dihydroanthracene is a hydrogen donor which was confirmed in a reaction with benzophenone. When dihydroanthracene (1 g) was heated with benzophenone (1 g) in 1-methylnaphthalene (10 g), 31.3% of the benzophenone was reduced. In blank tests (Table 1), 36—38% of the benzophenone was reduced by tetralin; however, the injection weight of tetralin was 10 times that of dihydroanthracene. The same mechanism, including the dihydroaromatic compound, may be applied to pyrene.

The high conversions noted for fluorene and triphenylmethane can possibly account for the high reactivity of their benzylic hydrogen.[7]

It is well-known that intermolecular (2) and intramolecular (3) reactions are involved in the dibenzyl ether thermolysis.[8]

$$PhCH_2OCH_2Ph \longrightarrow PhCH_2\cdot + \cdot OCH_2Ph \xrightarrow{\text{donor}} PhCH_3 + HOCH_2Ph \quad (2)$$

$$PhCH_2OCH_2Ph \longrightarrow PhCH_3 + OHCPh. \quad (3)$$

That two free radicals resulting from the fission of a C-O bond possess a higher dehydrogenation ability than benzophenone. Table 2 shows the effect of the hydrogen shuttler on the hydrogenation reaction of dibenzyl ether in tetralin. The yield of benzaldehyde is higher and the yield of toluene is lower than that expected from Reactions 2 and 3. This may be due to further reactions of benzyl alcohol and the benzyl radical to benzaldehyde and undetermined compounds.[9] The ranking for the dibenzyl ether conversion is

anthracene > fluorene > triphenylmethane > pyrene > phenanthrene > 1-methylnaphthalene.

This is almost similar to that of Table 1, except for triphenylmethane and phenanthrene. It is considered that triphenylmethane readily donates hydrogen and that the resulting triphenylmethyl radical initiates the bond fission of dibenzyl ether as a molecule-induced homolysis.[7] This indicates the possibility of an overestimation of the triphenylmethane shuttling ability if the ability is estimated only from the ranking for the dibenzyl ether conversion. Although the mixture of phenanthrene and tetralin was heated at 430 °C for 1 h, dihydrophenanthrene was scarcely produced. Furthermore, only 9.8% of the benzophenone was reduced when dihydrophenanthrene (1 g) was heated with benzophenone (1 g) in 1-methylnaphthalene (10 g). This indicates that the hydrogen-shuttling mechanism through dihydrophenanthrene is minor. Another mechanism, in which phenanthrene donates hydrogen to a free radical and the resulting phenanthryl radical abstracts hydrogen from tetralin, is possible.

From these results, using different types of hydrogen acceptors, the hydrogen-shuttling ability of the liquefaction solvent could be evaluated as follows:

anthracene > fluorene > pyrene ≅ triphenylmethane > phenanthrene > 1-methylnaphthalene.

It appears that the presence of the hydrogen shuttler constitutes a necessary and important component of coal conversion. A more effective solvent for coal liquefaction can be prepared by determining the capabilities of various solvents.

References

1) M. L. Gorbatty, J. W. Larsen, and I. Wender, "Coal Science," Academic Press (1983), Vol 2, p. 65; C. W. Curtis, J. A. Guin, M. A. Hale, and N. L. Smith, *Fuel*, **64**, 461 (1985); K. Chiba, H. Tagaya, S. Sato, and K. Ito, *Fuel*, **64**, 68 (1985).

2) B. C. Bockrath, E. Bittner, and J. McGrew, *J. Am. Chem. Soc.*, **106**, 135 (1984); B. C. Bockrath and R. P. Noceti, *Am. Chem. Soc. Div. Fuel Chem. Preprints*, **26**, 94 (1981); C. W. Curtis, J. A. Guin, M. A. Hale, and N. L. Smith, *Fuel*, **64**, 461 (1985); J. W. Clarke, T. D. Rantell, and C. E. Snape, *Fuel*, **61**, 707 (1982); D. C. Cronauer, D. M. Jewell, Y. T. Shah, and K. A. Kueser, *Ind. Eng. Chem. Fundam.*, **17**, 291 (1978); K. Chiba, H. Tagaya, T. Kobayashi, and Y. Shibuya, *Ind. Eng. Chem. Research*, in press.

3) F. J. Derbyshire and D. D. Whitehurst, *Fuel*, **60**, 655 (1981).

4) R. C. Neavel, *Fuel*, **55**, 237 (1976).

5) V. F. Raaen and W. H. Roark, *Fuel*, **57**, 650 (1978).

6) K. Chiba, H. Tagaya, T. Yamauchi, and Y. Tsukahara, *Chem. Lett.*, **1985**, 945.

7) H. H. King and L. M. Stock, *Fuel*, **61**, 257 (1982); *ibid*, **63**, 810 (1984).

8) M. B. Simmons and M. T. klein, *Ind. Eng. Chem. Fundam.*, **24**, 55 (1985).

9) K. Chiba, H. Tagaya, S. Sato, and S. Ohgi, *Bull. Chem. Soc. Jpn.*, **60**, 653 (1987).

The Addition Reaction of Benzynes Generated Electrochemically from Dihalobenzenes with Tertiary Amines

Naoyoshi EGASHIRA,* Jun TAKENAGA, and Fumiaki HORI
Department of Environmental Chemistry and Engineering, Faculty of Engineering, Oita University, 700 Dannoharu, Oita 870-11
(Received January 8, 1987)

Synopsis. The electroreduction of dihalobenzenes was carried out in the presence of tertiary amines as benzyne acceptors in DMF-TBAP, giving the addition products in yields of more than 10%. For *o*-dibromobenzene, the yield of the addition product, *N*-phenylpiperidine, increased to 21% in the presence of *N*-ethylpiperidine.

Benzynes which undergo many types of addition reactions are uaually generated on the photolysis or pyrolysis of reactive reagents.[1] An electrolytic method can be expected to generate benzynes under mild conditions from reagents which are readily available. Wawzonek et al.[2] have reported on the generation of a benzyne in the electrolysis of *o*-dibromobenzene (**1**) in the presence of furan as a benzyne acceptor and have obtained the addition product derived from the benzyne in a 1% yield. This has been the sole report on the electrolytic generation of benzyne. We have previously reported that the yield of the addition product of the benzyne from **1** increased to 10% when *N*-ethylpiperidine (**2**) was used instead of furan.[3] In the present work, five dihalobenzenes are electrolyzed in a sufficiently dried electrolyte containing five tertiary amines; they are examined in detail for the addition products.

Compound **1** showed an irreversible cathodic peak at −3.00 V vs. Ag/Ag^+ in the presence of **2**. The electrolysis of **1** in the presence of a large excess of **2** was thus carried out at −3.20 V. The resulting products were bromobenzene, benzene, and an unknown compound. The unknown compound was isolated from the catholyte after electrolysis and confirmed to be *N*-phenylpiperidine (**3**) since it gave an IR spectrum identical with that of the authentic sample. The time-course of the products is shown in Fig. 1, which represents the simultaneous formation of each product. Three gaseous products containing ethylene were also detected by gas chromatography, and their amounts increased gradually. The electrolysis of bromobenzene at −3.20 V in the presence of **2** gave simply benzene; the consumption rate of bromobenzene was low, since the cathodic peak potential of bromobenzene (−3.30 V) was higher than the electrolysis potential of **1**. Furthermore, **3** was not detected in the electrolysis of **1** at −3.20 V when **2** was not added to the electrolyte. These results indicate that bromobenzene does not participate in the formation of **3** and that benzene is formed in part from **1** directly and in part through bromobenzene. It has been reported that **3** was produced through the reaction of benzyne generated in a homogeneous reaction with **2**.[1] Compound **3** is thus presumed to be produced through benzyne as depicted in Scheme 1.

The yield of **3** (14%) is larger than that of the product through benzyne reported by Wawzonek et al.[2] Table 1 shows the effects of the electrolyte temperature, the electrolysis potential, the benzyne acceptors, and the electrode materials on the electrolysis of **1**. An appropriate potential for the electrolysis is determined to be −3.20 V because of the higher yields obtained in three experiments (Runs 1—3). A decrease in the electrolyte temperature to 20 °C lowered the yield of **3** (Run 4). When SCE was used instead

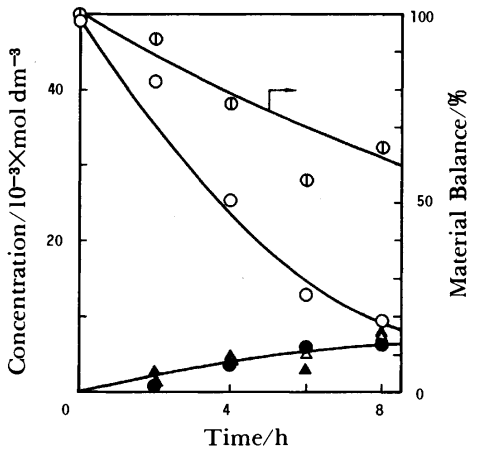

Fig. 1. Time-course of products in electrolysis of **1** in the presence of **2**. ○: material balance, ○: **1**, ●: **3**, ▲: bromobenzene, △: benzene.

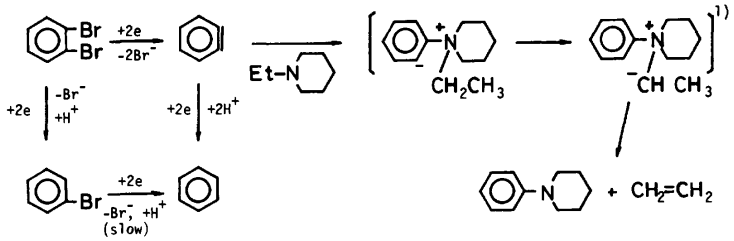

Scheme 1.

Table 1. Electrolytic Results of Dihalobenzenes[a)]

Run	Substrate	Benzyne acceptor	Working electrode	−E/V vs. Ag/Ag^+	Yield/% Addition product	Yield/%	Yield/%	Electricity F mol^{-1}
1	**1**	**2**	Pt	3.20	14 (**3**)[f)]	15	16	3.7
2	**1**	**2**	Pt	3.00	10 (**3**)	10	21	4.2
3	**1**	**2**	Pt	3.40	11 (**3**)	6.9	15	4.0
4	**1**	**2**	Pt	3.20[b)]	12 (**3**)	7.0	27	2.6
5	**1**	**2**	Pt	2.80[c)]	6.0 (**3**)	9.0	70	9.0
6	**1**	**2**[d)]	Pt	3.20	21 (**3**)	16	22	2.8
7	**1**	**2**	Hg	3.20	2.6 (**3**)	4.0	10	2.7
8	**1**	**2**	GC	3.80	0.8 (**3**)	2.0	5.0	1.6
9	**1**	*N*-Ethylmorpholine	Pt	3.20	12 (*N*-Phenylmorpholine)[e)]	15	18	4.0
10	**1**	*N*-Methylpiperidine	Pt	3.20	11 (**3**)	5.5	45	2.0
11	**1**	*N*-(2-Hydroxyethyl)piperidine	Pt	3.20	14 (**3**)	25	36	3.1
12	**1**	Triethylamine	Pt	3.20	13 (*N*,*N*-Diethylaniline)[e)]	9.5	25	3.4
13	*o*-Dichlorobenzene	**2**	Pt	3.60	2.0 (**3**)	27	11	2.6
14	*o*-Diiodobenzene	**2**	Pt	3.20	14 (**3**)	16	14	4.1
15	*m*-Dibromobenzene	**2**	Pt	3.20	tr (**3**)	54	22	2.5
16	*p*-Dibromobenzene	**2**	Pt	3.20	0.3 (**3**)	23	19	4.6
17	**1**	—	Pt	3.20	—	2.0	24	3.0

a) Electrolysis was carried out in DMF solutions containing 5.0 cm^3 of the benzyne acceptor at 40 °C unless otherwise noted. b) The temperature was 20 °C. c) SCE was used as the reference electrode. d) 20 cm^3 of **2** was used. e) The retention time of each product, as determined by HPLC, agreed with that of an authentic sample. f) Ethylene was detected by means of gas chromatography.

of the Ag/Ag^+ reference electrode, the yield of **3** remarkably decreased (Run 5). This was due to a large increase in the water concentration of the electrolyte from the beginning of the electrolysis (0.010 M: 1 M = mol dm^{-3}) to the end (0.080 M); the use of an Ag/Ag^+ reference electrode hardly increased the water concentration at all. The further addition of **2** (20 cm^3) resulted in an increase in the yield of **3** to 21% (Run 6). Benzyne can exit in the vicinity of the electrode, as it has a short lifetime. The amount of benzyne available for the formation of the addition products may thus be smaller than that in a conventional homogeneous reaction. The disadvantage can be reduced by the use of a high concentration of a benzyne acceptor. The use of Hg and glassy carbon (GC) as working electrodes considerably decreases the yields of the products containing **3** (Runs 7 and 8). These products are perhaps attributable to the formation of mercury compounds and polymers respectively. The reaction of benzyne with several tertiary amines similarly gave the corresponding addition products, the yields of which were in the range of 11—14% (Runs 9—12). This fact suggests that the steric hindrance around nitrogen atoms of the tertiary amines against benzyne is of the same degree. Electrolysis in the presence of *N*-methylpiperidine and *N*-(hydroxyethyl)-piperidine produced methane and an unknown gaseous product respectively; the evolution mechanisms remain ambiguous. *o*-Dichlorobenzene and *o*-diiodobenzene gave the same addition product as **3** in moderate yields, while *o*-dichlorobenzene gave it in a very low yield (Runs 13 and 14). *o*-Dibromobenzene and *o*-diiodobenzene are thus thought to be suitable for the electrolytic generation of benzyne. The fact that *m*- and *p*-dibromobenzenes also give **3** is interesting, since it suggests the generation of *m*- and *p*-benzynes (Runs 15 and 16). Unfortunately, the yields of **3** for both the compounds were very low. Each electrolysis requires about 3 F mol^{-1} of electricity, except for Run 5, indicating that dihalobenzenes undergoes electroreduction with a good efficiency. The ratio of the total moles of the products containing the starting material to the original moles of the starting material, the material balance, gradually decreased (Fig. 1). This suggests that the generated intermediates, such as benzyne, radical anions, and free radicals, follow complex reactions.

Experimental

DMF was purified by a conventional method.[4)] Cyclic voltammetry was carried out in the same way as in a previous work.[5)] A DMF solution containing **1** (0.050 M), **2** (5.0 cm^3), and tetrabutylammonium perchlorate (TBAP, 0.10 M) was prepared. A large-scale electrolysis of the DMF solution was performed on a platinum electrode (25.5 cm^2) at 40 °C in a two-compartment cell after 6.4 g molecular sieve 4A (heated at 350 °C for 3 h) had been added to the catholyte in order to dry it. The counter and reference electrodes used were a platinum plate (1.0 cm^2) and an Ag/Ag^+ electrode. The outlet of nitrogen of the electrolytic cell was cooled with

water in order to collect any benzene produced in the cell. After the electrolysis has finished, the catholyte was concentrated under reduced pressure, and then the residue was extracted with diethyl ether. The product was separated with TLC (SiO_2, chloroform : benzene = 8 : 2) after the ethereal solution had been evaporated. Compound **3** as an authentic sample was synthesized in the way reported by Bunnett et al.:[6] ^1H NMR ($CDCl_3$) δ = 1.7—1.9 (6H, *m*, $-CH_2-$), 3.2—3.4 (4H, *m*, $N-CH_2-$), 6.9—7.5 (5H, *m*, Arom). The catholyte was analyzed by using HPLC (ODS, CH_3CN : H_2O = 55 : 45) in order to determine the concentrations of the products.

References

1) R. W. Hoffman, "Dehydrobenzene and Cycloalkynes," Academic Press, New York (1967), p. 171.
2) S. Wawzonek and J. H. Wagenknecht, *J. Electrochem. Soc.*, **110**, 420 (1963).
3) N. Egashira, I. Sakurai, and F. Hori, *Denki Kagaku*, **54**, 282 (1986).
4) S. Wawzonek, E. W. Blaha, R. Berkey, and M. E. Runner, *J. Electrochem. Soc.*, **102**, 235 (1955).
5) N. Egashira, S. Tomishige, Y. Takita, and F. Hori, *Denki Kagaku*, **50**, 909 (1982).
6) J. F. Bunnett and T. K. Brotherton, *J. Am. Chem. Soc.*, **22**, 832 (1957).

An Explanation of the Temperature Dependence of the Mössbauer Spectra of Mixed Valence Biferrocenium Derivatives with a (Valence-State) Order-Disorder Transition

Yuichi MASUDA* and Hirotoshi SANO
Deparment of Chemistry, Faculty of Science, Tokyo Metropolitan University, Fukasawa, Setagaya-ku, Tokyo 158
(Received January 16, 1987)

Synopsis. The temperature dependence of the quadrupole splitting values in the Mössbauer spectra for monooxidized biferrocenium derivatives is well explained in term of an order-disorder transition with regard to the valence state of two iron atoms in the cations.

It has been reported that several kinds of triiodide salts of monooxidized 1′,1‴-dialkylbiferrocenium derivatives [Fe(II)·Fe(III)] ($R_2bfc \cdot I_3$) show a characteristic temperature dependence in their Mössbauer spectra,[1,3-5] where two well resolved doublets are observed at low temperatures. With an increase in the temperature, the quadrupole splitting (*Q.S.*) values of the outer and inner doublets decrease and increase respectively, until finally these two doublets are superimposed on each other, giving only one doublet, as is shown in Figs. 1 and 2. No line-broadening is observed in the process of the temperature dependence of *Q.S.*, although it might be expected for a relaxation process. There has thus far been no explanation for the characteristic temperature dependence of the quadrupole split lines commonly observed in the triiodide salts of ethyl, propyl, butyl, and benzyl derivatives.[5] In the present paper, this characteristic temperature dependence of the Mössbauer spectra is explained in terms of an order-disorder transition of the valence state of two iron atoms in the biferrocenium cations caused by a cooperative intermolecular interaction in a crystal.

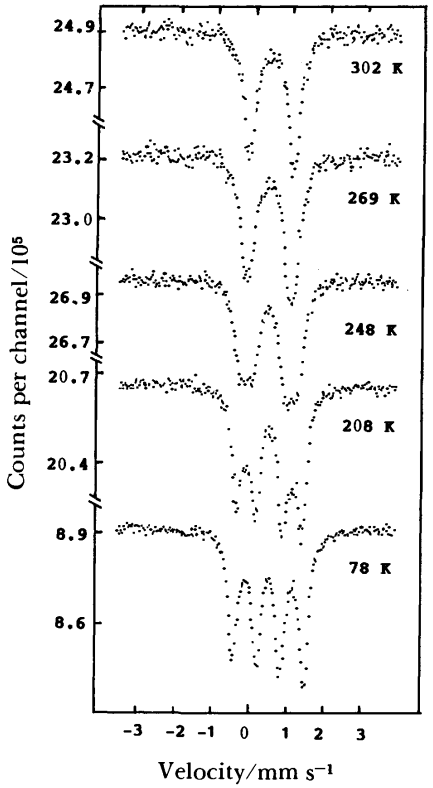

Fig. 1. Variable temperature ^{57}Fe Mössbauer spectra for 1′,1‴-dibutylbiferrocenium triiodide. The data are taken from Ref. 4.

I. Explanation of the Temperature Dependence of the Mössbauer Spectra. In order to explain the temperature dependence characteristic of the dialkylbiferrocenium triiodides, the following two hypotheses are assumed:

(i) The two iron atoms, Fe_A and Fe_B, in a cation are inequivalent in the crystal state, i.e., the potential energies between State I, [Fe_A(II)·Fe_B(III)], and State II, [Fe_A(III)·Fe_B(II)], differ from each other.

(ii) The electrontransfer rate between the two iron atoms becomes much faster than the Mössbauer time scale, $\approx 10^{-7}$ s, at higher temperatures, where the two ΔE_Q values start to change.

The (i) assumption is supported by the crystal structure of dipropylbiferrocenium triiodide.[2,3] The two iron atoms in the cation are found not to be

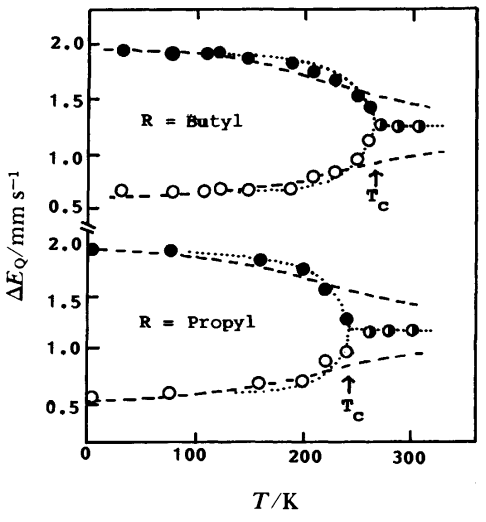

Fig. 2. Temperature dependence of quadrupole splitting for 1′.1‴-dialkylbiferrocenium triiodide ($R_2bfc \cdot I_3$). The open and closed circle corresponds to ferrocene and ferrocenium potion, respectively. The data were taken from Refs. 1 and 4 and the meanings of the dotted and broken lines in the figure are given in the text.

equivalent in the crystal packing. The (ii) assumption is important in explaining why no line-broadening is observed upon a change in the ΔE_Q values (see below). An intramolecular electron exchange rate faster than the Mössbauer time scale, as assumed above, has actually been found in, for example, 1′,1‴-dibromo and diiodobiferrocenium triiodides, even at 4.2 K, in the crystal state.[6,7]

At a sufficiently low temperature, if State I, [Fe_A(II)·Fe_B(III)], is assumed to be predominant, the two *Q. S.* values for iron A and B, atoms $\Delta E_{Q,A}$ and $\Delta E_{Q,B}$, will the approximately equal to those for the ferrocene and ferrocenium species corresponding to an outer doublet and an inner doublet in the Mössbauer spectrum respectively. At increased temperatures, the population of State II, [Fe_A(III)·Fe_B(II)], can be expected to increase. If the intramolecular valence exchange occurs sufficiently faster than the Mössbauer time scale, as assumed in the (ii) hypothesis, the observed $\Delta E_{Q,A}$ and $\Delta E_{Q,B}$ values can be represented by using the populations of State I, P_I, and State II, P_{II};

$$\Delta E_{Q,A} = P_I \cdot \Delta E_Q(\text{Fe(II)}) + P_{II} \cdot \Delta E_Q(\text{Fe(III)}) = P_I \cdot \Delta E_Q(\text{Fe(II)}) + (1-P_I) \cdot \Delta E_Q(\text{Fe(III)}) \quad (1)$$

because:

$$P_I + P_{II} = 1$$

and:

$$\Delta E_{Q,B} = P_I \cdot \Delta E_Q(\text{Fe(III)}) + (1-P_I) \cdot \Delta E_Q(\text{Fe(II)}) \quad (1)'$$

where ΔE_Q(Fe(II)) and ΔE_Q(Fe(III)) stand for the *Q. S.* values for the ferrocene-like and ferrocenium-like moieties in the R_2bfc·I_3 respectively; those values are determined by extrapolating the temperature dependences of the $\Delta E_{Q,A}$ and $\Delta E_{Q,B}$ values to 0 K. With an increase in the temperature, P_I decreases from unity, accompanied by both a decrease in the $\Delta E_{Q,A}$ value and an increase in the $\Delta E_{Q,B}$ value because $\Delta E_Q(\text{Fe(II)}) > \Delta E_Q(\text{Fe(III)})$. At sufficiently high temperatures, both the P_I and P_{II} populations both approach 0.5, and the values of $\Delta E_{Q,A}$ and $\Delta E_{Q,B}$ both also approach a mean value of ΔE_Q(Fe(II)) and ΔE_Q(Fe(III)), showing only one doublet just superimposed by the two doublets of the Fe_A and Fe_B absorbances in the Mössbauer spectrum. In this process, if the valence-exchange rate between the two iron atoms is sufficiently faster than the Mössbauer time scale, no line-broadening is observed in the Mössbauer absorptions. The observed Mössbauer spectra shown in Fig. 1 are qualitatively explained by the above consideration.

At 110 K and room temperature, the X-ray structure of the *n*-propyl derivative also supports this consideration. In the X-ray structure of Pr_2bfc·I_3 at 110 K, the cations have two kinds of inequivalent ferrocene and ferrocenium units, of which one corresponds to the Fe(II) unit, and the other, to the Fe(III) unit. These two units in the cations are aligned in the crystal in an orderly manner, as is schematically illustrated in Fig. 3(a). On the contrary, these two ferrocene and ferrocenium units become equivalent at room temperature; i.e., the configuration of the ferrocene or ferrocenium units in the cation is aligned in a disorderly manner at room temperature, as is demonstrated in Fig. 3(b).[3,7] If this disordering is dynamic, the time averaged population in the divalent and trivalent state for all the iron atoms will become nearly 0.5 in the crystal at room temperature.

II. Simple Model for the Order-Disorder Transition of the Valence State by Means of Cooperative Intermolecular Interaction. In the previous section, an energy difference between the states of [Fe_A(II)·Fe_B(III)] and [Fe_A(III)·Fe_B(II)] was assumed to explain the temperature dependence of the *Q.S.* values. If this energy difference remains constant over the temperature range where the Mössbauer spectra are observed, the population of State I or II, P_I or P_{II}, is related to the free-energy difference between State I and II, ΔG, as is expressed in the following equation:

$$P_I = (\exp(-\Delta G/RT) + 1)^{-1} \quad (2)$$

Table 1. Transition Temperatures and Interaction Energies

R	T_c/K	ε/kJ mol^{-1}		ΔG/kJ mol^{-1} c)
		2-Dimensional a)	3-Dimensional b)	
Butyl	262	1.08	0.72	2.6
Propyl	242	1.01	0.67	2.4
Ethyl	272	1.13	0.75	2.8
Benzyl	262	1.08	0.72	2.7

a) The values assuming a square lattice. b) The values assuming a cubic lattice. c) See Eq. 2 in the text.

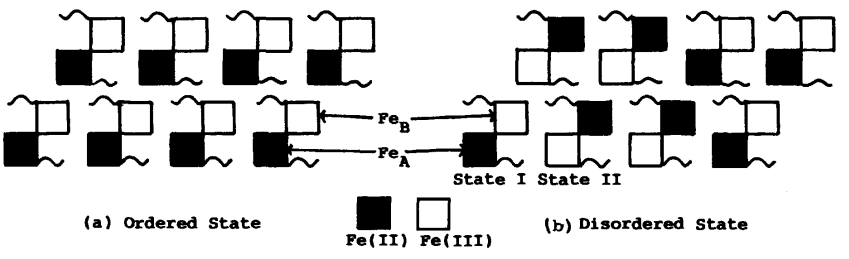

Fig. 3. Schematic representation of ordered (a) and disordered (b) state with regard to valence state of 1′,1‴-dialkylbiferrocenium triiodide.

The calculated temperature dependence of the ΔE_Q values for Fe_A and Fe_B, based on Eq. 1 and Eq. 2 with the ΔG values listed in Table 1, are shown in Fig. 2 by the broken lines. For all the cases, the calculated values do not fit well to the temperature dependence of the observed ΔE_Q values, especially the sudden change of ΔE_Q at 200—270 K.

This sudden change in the observed ΔE_Q values suggests an abrupt change in the population of the State I or II (see the previous section); i.e., an ordered state in which most cations remain in either one of the two states (I or II) changes to a disordered state, in which the populations of the two state of the cations are approximately equal, within a narrow temperature range, as is schematically illustrated in Fig. 3. This feature of the temperature dependence of the population in the valence states resembles the well-known order-disorder phase transitions, such as a ferro-to-para magnetic or electric transition. The small endothermic peak observed in the DSC measurements near the temperature showing a sudden change in the ΔE_Q value (e.g., several hundred J mol^{-1} for dipropylbiferrocenium triiodide) also indicates that change can be regarded as an order-disorder transition with regard to the valence state of the cations. In the crystal, the valence state of a cation may be affected by that of the neighboring cations, i.e., the energy difference between the two valence states, e.g., States I and II, of a cation are affected by those of the neighboring cations. This cooperative intermolecular interaction between cations is considered to cause an order-disorder transition. It seemed worthwhile to examine whether or not the Ising model could be applied to this system in order to explain such a cooperative intermolecular interaction. The states of I and II are represented by $\sigma_i=1$ and $=-1$ respectively, and an interaction Hamiltonian, H_{ij}, for the Ising model is geven with an intermolecular interaction energy, ε, that is:

$$H_{ij}=-(\varepsilon/2)\sum_{ij}\sigma_i\sigma_j \qquad (\sigma_i, \sigma_j=\pm 1) \tag{3}$$

where the intermolecular interaction, ε, is defined by considerig the interaction with the first neighboring cations, neglecting any anisotropic interaction. The values of P_I and P_{II} at various temperatures are obtained by using a molecular field approximation.[8] The ΔE_Q values for Fe_A and Fe_B can also be obtained by using the P_I and P_{II} values estimated based on Eq. (1). The results for butyl and propyl derivatives with ε values satisfactorily reproduce the observed ΔE_Q values at various temperature as is shown in Fig. 2 by dotted lines. The estimated interaction energies, ε, assuming a two- and three- dimensional interaction and the (second order) transition temperature, T_C, are listed in Table 1. Similarly good coincidences between the theoretical curves and the experimental data are also obtained for the ethyl and benzyl derivatives.

In this treatment, an isotropic interaction between neighboring cations placed on the square (for a two dimensional alignment) or the cubic (for a three dimensional alignment) lattice points is assumed, although the environment of a cation is not actually isotropic. For example, in the X-ray structure of $Pr_2bfc{\cdot}I_3$, the alignment of the cations shows a step-by-step slipping π-π stack between cycropentadienyl rings in one direction, while those same cations are aligned across one triiodide anion in two directions.[2] In spite of the different interaction in different direction in an actual crystal, the results show a fairly good coincidence between the experimental and theoretical results in which an isotropic interaction is assumed. This means that the valence state of the cations is determined by the alignment of the neighboring cations and by their interaction and that two- or three-dimensional[9] intermolecular interactions have a similar interaction energy value, ε, as is tabulated in Eq. 3.

We wish to thank Professor Hendrickson and Professor Kambara for their encouraging discussions. This work was partially supported by a Grant-in-Aid for Scientific Research (No. 60430014).

References

1) S. Iijima, I. Motoyama, R. Saida, and H. Sano, *Bull. Chem. Soc. Jpn.*, **54**, 1375 (1981).

2) M. Konno, S. Hyodo, and S. Iijima, *Bull. Chem. Soc. Jpn.*, **55**, 2327 (1982).

3) T.-Y. Dong, D. N. Hendrickson, K. Iwai, M. J. Cohn, S. J. Geib, A. L. Rheingold, H. Sano, I. Motoyama, and S. Nakashima, *J. Am. Chem. Soc.*, **107**, 7996 (1985).

4) S. Nakashima, M. Katada, I. Motoyama, and H. Sano, *Bull. Chem. Soc. Jpn.*, **59**, 2923 (1986).

5) S. Nakashima, Y. Masuda, I. Motoyama, and H. Sano, *Bull. Chem. Soc. Jpn.*, **60**, 1673 (1987).

6) I. Motoyama, K. Suto, M. Katada, and H. Sano, *Chem. Lett.*, **1983**, 1215.

7) W. H. Morrison, Jr., and D. N. Hendrickson, *Inorg. Chem.*, **19**, 2331 (1975).

8) The calculation of P_I and P_{II} based on the molecular field approximation at various temperatures is equivalent to that of spontaneous magnetization for a 1/2 spin system. Regarding States I ($\sigma_i=1$) and II ($\sigma_i=-1$) as the +1/2 and −1/2 spin states respectively, the values (P_I-P_{II}) at various temperatures correspond to the values proportional to the spontaneous magnetization of the spin system. Such calculation of the magnetization based on the molecular-field approximation is carried out according to the procedure in such textbooks as "Introduction to Solid State Physics," ed by C. Kittel, Jhon Willey & Sons Inc., New York (1975), Chap. 15, and "The Structures and Properties of Solids. **6**, The Magnetic Properties of Solids," ed by J. Crangle, Edward Arnold, London (1976), Chap. 2.

9) It has been theoretically proved that one dimensional interaction in the Ising model shows no phase transition: in the exact solution for the one-dimensional Ising model, the population of the two states does not show any such steep temperature dependence as is shown in Fig. 2.

An Application of Factor Analysis to the Electronic Spectra of Iodine in Mixed Solvents

Koichiro NAKANISHI,* Kenkichi MAYA, and D. G. HOWERY†
Department of Industrial Chemistry, Kyoto University, Sakyo-ku, Kyoto 606
†Department of Chemistry, City University of New York, Brooklyn College, Brooklyn, N. Y. 11210, U.S.A.
(Received January 20, 1987)

Synopsis. The electronic spectra of iodine diluted in three kinds of mixed solvents, ethanol-heptane, 1,4-dioxane-cyclohexane, and tetrahydrofuran-cyclohexane have been measured as a function of molar composition in mixed solvents and a factor analysis technique has been applied to interpret the results. The number of different iodine-solvent complexes in ethanol solutions is smaller than that in ether solutions.

It is well-known that iodine molecule can form charge-transfer complex with many organic molecules which act as an electron donor (e.g., benzene, alcohols, etc.) and its color becomes brown or red. In nonpolar solvents such as aliphatic hydrocarbons, however, the color of iodine remains purple just as in the vapor or solid phase. We may classify these solvents into complexing(C) and non-complexing(NC) solvents to iodine.

Now, what happen when we use mixed solvents? If we adopt a combination of C and NC solvents, there should be a preferential solvation of C solvent to iodine molecules because of stronger intermolecular interaction. The purpose of the present study is to investigate the behavior of iodine in some kinds of mixed solvents from the spectroscopic point of view.

When we adopt an associated liquid as the C solvent, we have again a preferential solvation because associated liquids are usually a strong C solvent and in addition, possible change in the state of the association of the solvent in mixed solvents may result anomalous behavior in some physical properties. We have already studied diffusion, solubility, and their temperature dependence of iodine in various kinds of mixed solvents.[1-3] In this paper, we will describe the results on the electronic spectra of iodine in the visible light region as a function of molar composition of some typical mixed solvents and an analysis of these spectra by a factor analysis technique developed by one of us.[4]

Spectral Measurements

Electronic spectra of iodine in three kinds of mixed solvents have been measured by using a Shimadzu multipurpose spectrophotometer. The mixed solvents used are ethanol-heptane, 1,4-dioxane-cyclohexane, and tetrahydrofuran-cyclohexane. Sample solutions were prepared by dissolving certain amounts of spectrograde iodine into mixed solvents which consist of two kinds of spectrograde reagents. The concentration of iodine which is near 1×10^{-3} M (1 M = 1 mol dm^{-3}) was determined by conventional iodometry and the molar composition of C solvent in mixed solvents is 0, 0.025, 0.05, 0.10, 0.15, 0.2, 0.4, 0.6, 0.8, or 1.0, respectively.

The wavelength range used is between 410 and 600 nm. Reproducibility of the spectra is ±0.003 for 100% absorbance and ±0.0005 for 0% absorbance and the effect of titration error on the absorbance is estimated to be ±0.0010. Total experimental error is thus as large as ±0.0025.

The spectra of iodine in the three mixed solvents obtained in the present study are shown in Fig. 1. Each absorbance value is corrected to that for a concentration of 1×10^{-3} M. Qualitative feature of the results is as follows: in the case of iodine in ethanol-heptane solutions, one can observe the presence of a rather clear isosbestic point, whereas there is no specific isosbestic point for 1,4-dioxane-cyclohexane and tetrahydrofuran-cyclohexane solutions. Note that the present measurement is different from that normally adopted when the charge-transfer complex between iodine and ethers is to be studied in dilute solution of inert solvents.[5] In this case, we would have a definite isosbestic point.

Factor Analysis

The Lambert-Beer law in the absorption spectra may be written as

$$A = \sum_{k=1}^{n_c} \varepsilon_k c_k \tag{1}$$

where A, ε, c, and n_c stand for the absorbance, molar extinction coefficient, the concentration of each component and the number of components, respectively. If we measure the absorbance in the wavelength between λ_1 and λ_r for some number(s) of solutions with different molar compositions, we obtain an absorbance matrix [A]

$$[A] = \begin{bmatrix} A_{11} \cdots\cdots A_{1s} \\ \vdots \qquad\quad \vdots \\ A_{r1} \cdots\cdots A_{rs} \end{bmatrix} \tag{2}$$

which has the elements A_{ij} given below.

$$A_{ij} = \sum_{k=1}^{n_c} \varepsilon_{ik} c_{kj} = \sum_{k=1}^{n_c} f_k \tag{3}$$

Here i and j refer to the number of wavelength used and of solutions with different molar composition, respectively.

The application of main component analysis in the factor analysis technique will permit us to determine the number of the factor n_c whenever the data matrix can be expressed by a linear summation of the factor f_k as in Eq. 3. This number n_c is equal to that of the component to be evaluated. Further details are referred to literature.[4]

We have prepared the data matrix which consist of the absorbance at each 10 nm for each finite molar composition

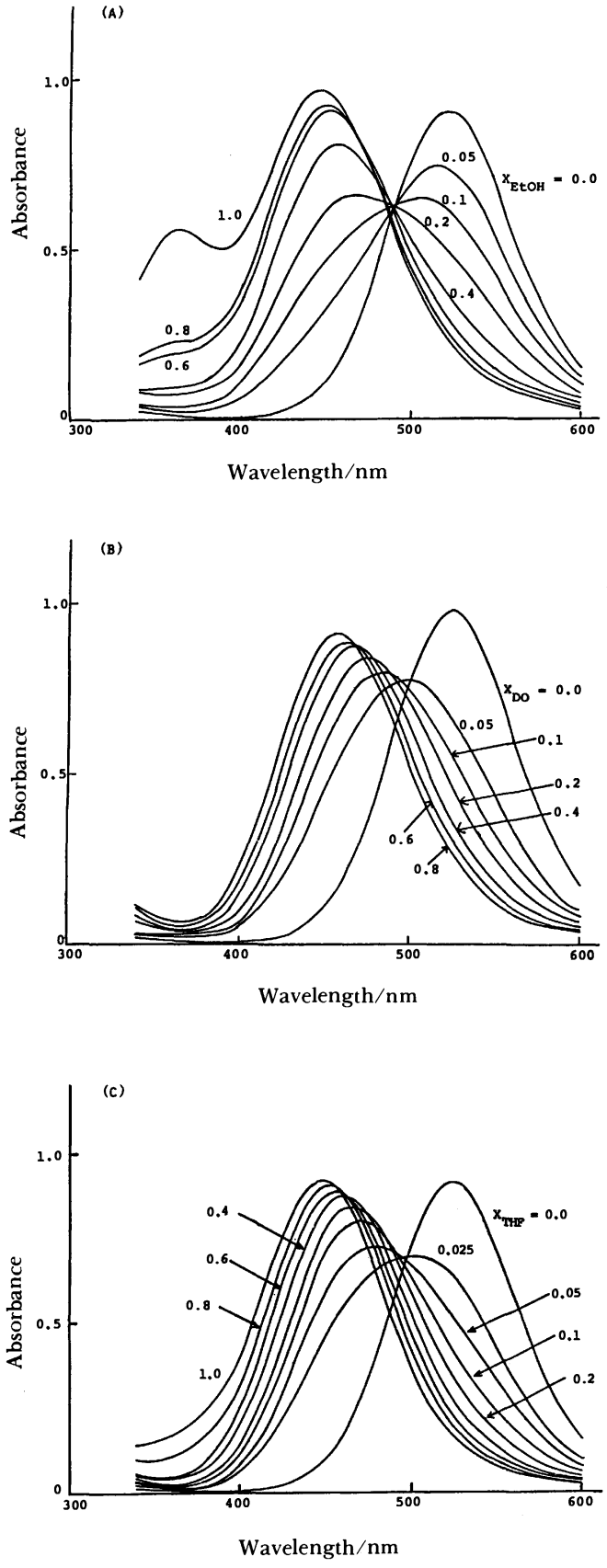

Fig. 1. Absorption spectra of iodine in mixed solvents at 293 K. (A): Ethanol-heptane, (B): 1,4-dioxane-cyclohexane, (C): tetrahydrofuran-cyclohexane.

Table 1. Factor Analysis of the Absorbances of Visible Spectra of Iodine in Mixed Solvents at 293 K

Factor	Eigenvalue	RMS Error	Error 1	Error 2
	1,4-Dioxane + Cyclohexane			
1	41.858549	0.16830	−0.5486	−0.5408
2	5.592714	0.03044	−0.1022	−0.0940
3	0.198604	0.00305	−0.0103	−0.0070
4	0.001504	0.00107	−0.0038	0.0035
5	0.000101	0.00078	−0.0027	0.0020
6	0.000055	0.00055	−0.0020	0.0017
7	0.000035	0.00036	0.0010	−0.0010
	Tetrahydrofuran + Cyclohexane			
1	39.410261	0.15932	−0.6422	−0.6147
2	5.210475	0.03421	−0.1292	−0.1214
3	0.254358	0.00243	0.0125	−0.0098
4	0.001134	0.00071	0.0022	−0.0020
5	0.000049	0.00050	0.0014	0.0014
6	0.000018	0.00038	−0.0012	0.0011
7	0.000016	0.00027	−0.0009	0.0009
	Ethanol + Heptane : case 1.[a]			
1	20.240611	0.11935	0.3328	0.3152
2	1.157937	0.00233	−0.0061	0.0056
3	0.000292	0.00115	−0.0031	0.0028
4	0.000083	0.00042	0.0019	−0.0017
	Ethanol + Heptane : case 2.[a]			
1	34.498014	0.17106	0.4951	0.4925
2	4.576991	0.00983	−0.0435	−0.0347
3	0.015547	0.00146	−0.0063	0.0043
4	0.000197	0.00088	−0.0026	0.0025
5	0.000049	0.00062	0.0023	−0.0021
6	0.000028	0.00043	0.0014	0.0013
7	0.000012	0.00030	−0.0011	0.0011

a) Case 1: $x_{EtOH} < 0.20$. Case 2: $1 > x_{EtOH} > 0$.

c. By using these data matrix, we have made factor analysis explained above. Necessary computer program has been written by one of us(D.G.H.).

The results of the main component analysis are given in Table 1. The value for RMS error is based on the following equation.

$$\mathrm{RMS} = [\sum_{i=1}^{r} \sum_{j=1}^{s} (d_{ij} - d^*_{ij})^2 / rs]^{1/2} \quad (4)$$

where r is the number of the wavelengths examined, s the number of solutions used, d^*_{ij} the raw data, and d_{ij} the reproduced data. Error 1 and Error 2 refer to the largest and second largest $(d_{ij} - d^*_{ij})$ values, respectively.

It is clear from the table that the RMS error becomes comparable with experimental uncertainty, ±0.0025, when the number of the factor is 3 for tetrahydrofuran-cyclohexane solution, 4 for 1,4-dioxane-cyclohexane solution, 2 or 3 for ethanol-heptane solution, respectively. More careful inspection of the table leads to the conclusion that the number of the factor for the first solution should be 4 rather than 3, because both Error 1 and Error 2 are as large as 0.01 for the factor number of 3.

We have made two analyses for ethanol-haptane solution with each different composition range. As shown in Table 1. the factor number is 3 for the whole composition range. This may be an effect of a small peak at 360 nm which is

ascribed to the presence of I_3^- in the solution. If we confine the composition range to the heptane-rich region, the factor number becomes 2, namely the presence of the only one isosbestic point. This suggests that there should be only the 1 : 1 complex in ethanol solutions.

The above analysis clearly shows that ether solutions are more complex environment for iodine than ethanol solution and that the present results coincide with the tendency in the magnitude of molar enthalpy of complex formation between iodine and electron donors.[6] There is thus essentially no difference between 1,4-dioxane and tetrahydrofuran as electron donor or a partner in complex formation, suggesting that the mode of complex formation with iodine is independent of the number of ether oxygens in the molecule.

Finally, we point out that the present results should be taken into account in the interpretation of the diffusion behavior in mixed solvents.

The authors thank the Data Processing Center of Kyoto University for the permission to use the facility.

References

1) K. Nakanishi and Y. Furusawa, *J. Chem. Eng. Data*, **23**, 101 (1978).

2) K. Nakanishi and S. Asakura, *J. Phys. Chem.*, **81**, 1745 (1977).

3) K. Nakanishi and Y. Nishimoto, *J. Chem. Soc., Faraday Trans. 1*, **73**, 1840 (1977).

4) E. R. Malinowski and D. G. Howery, "Factor Analysis in Chemistry," John Wiley, New York (1980).

5) G. Kortum and M. Kortum-Seller, *Z. Naturforsch.*, **59**, 544 (1950).

6) P. A. D. de Maine, *J. Chem. Phys.*, **26**, 1192 (1957).

Raman Spectra of the Organic Conductor, (TTM-TTF)$I_{2.47}$

Kikujiro Ishii,* Hideyuki Nakayama, Peiji Wu,† Takehiko Mori,†
Toshiaki Enoki,† Kenichi Imaeda,† Gunzi Saito,††
and Hiroo Inokuchi†
Department of Chemistry, Faculty of Science, Gakushuin University,
Mejiro, Toshimaku, Tokyo 171
†Institute for Molecular Science, Myodaiji, Okazaki 444
††Institute for Solid State Physics, The University of Tokyo,
Roppongi, Minatoku, Tokyo 106
(Received February 16, 1987)

Synopsis. The Raman spectra of a highly conductive molecular complex of the title were measured. The I_3^- symmetric stretching band and its well-known overtones were observed, indicating that the formula for this complex should be written as (TTM-TTF)$(I_3)_{0.823}$. A brief discussion is given comparing the spectra of the present complex with those of TMA-I-TCNQ and (BEDT-TTF)$_2I_3$ complexes.

Organic conductors containing trihalide ions have attracted the attention of many workers[1] since the discovery of the ambient pressure organic superconductor, β-(BEDT-TTF)$_2I_3$.[2] The intermolecular interactions through the sulfur atoms of BEDT-TTF(hereafter, ET) may, of course, be important in endowing this crystal with high conductivity. However, the role played by I_3^- ions should not be overlooked, since some similar ET complexes containing similar halide ions have been found to become superconducting.[3]

The structure and various properties of the iodine complex of TTM-TTF, tetrakis(methylthio)tetrathiafulvalene, were previously reported.[4] TTM-TTF has eight sulfur atoms, similarly to ET. The iodine complex, (TTM-TTF)$I_{2.47}$, is metal-like at room temperature, but becomes insulating at low temperatures below 100 K. The iodine atoms were found to make a fairly ordered sublattice which is incomensulate to the TTM-TTF lattice. However, the structure of the iodine sublattice has not yet been clarified.

In this note, we report on the Raman spectra of (TTM-TTF)$I_{2.47}$. The results comprise essentially the typical resonance Raman spectra of I_3^- ions.[5] Thus, the formula for the present complex should be written as (TTM-TTF)$(I_3)_{0.823}$. The frequencies and the band structures found for the I_3^- bands of the present complex are significantly different from those of the ET-complexes.[6] A brief discussion is given regarding the vibrational state of I_3^- ions.

Experimental

Black thin plate crystals of (TTM-TTF)$I_{2.47}$ were obtained by previously described methods.[4] These were apparently bundles of needle crystals. The crystal b axis is known to correspond to the needle axis.[4]

The Raman spectra were measured with a SPEX 1403 monochromater equipped with a Hamamatsu R-649 photomultiplier. Data were recorded with a convensional photoncounter in combination with a personal computer. An Oxford DN1704 cryostat was used between 89 K and room temperature. The samples were mounted in a nitrogen atmosphere. The 501.7 nm line from an NEC GLG-3201 Ar-ion laser was used as the excitation source with a grazing angle of about 20°. The Raman light was collected in the direction perpendicular to the incident light. To avoid any decomposition of the sample by the local heating, the incident light was attenuated to a power below 3 mW for measurements at low temperatures and below 1 mW at room temperature. The sample temperature was estimated with an alumel-chromel thermocouple which was placed near the sample surface.

Results and Discussion

Figure 1 shows the wide-scan spectrum at 89 K with the incident-light polarization parallel to the b axis and a spectral resolution of 1.8 cm^{-1}. A series of bands (No. 1—5) are seen with almost the same separations of about 108 cm^{-1}; the wavenumber of each band is listed in Table 1. For bands 1 and 2, solid curves were drawn for eyes guides. Some strong and sharp bands observed in addition to bands 1—5 are the plasma lines coming from the Ar-ion laser.

Bands 1—5 can obviously be assigned to the fundamental and overtone bands of the symmetric stretching mode of I_3^- ions.[5] The unusually strong intensities of the overtone bands, and the fact that

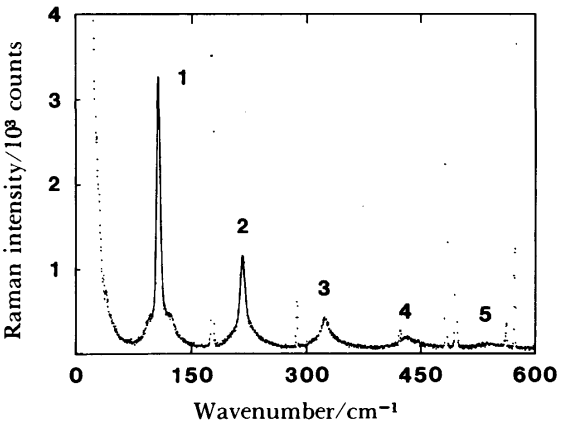

Fig. 1. Raman spectrum of (TTM-TTF)$I_{2.47}$ complex at 89 K.

Table 1. Raman Frequencies of the Fundamental and Overtone Bands (cm^{-1})

(TTM-TTF)$I_{2.47}$ (89K)	107.0 109.7	216.7	324	432	≈538
TMA-I-TCNQ (15K)[7]	110	218	327	435	544

only the I_3^- bands and no TTM-TTF band was observed, are attributed to the resonance Raman effect.[5] The fact that the spectra were observed with b-polarized incident light and not with the polarization perpendicular to this, indicates that the I_3^- ions exist with their molecular axis parallel to the b axis. This is because the intensity is enhanced by resonance with the electronic transition $\sigma_g \rightarrow \sigma_u^*$.[7] These results are in accordance with the result of the X-ray analysis.[4]

Details of band 1, measured with a spectral resolution of 0.6 cm^{-1}, is presented in Fig. 2. Band 1 apparently comprises two substructures. By assuming Lorentzian shapes, their frequencies were estimated to be 107.0 and 109.7 cm^{-1}, respectively, and the apparent width of either substructure to be 2.8 cm^{-1}. One possibility of the cause of this splitting is a factor-group splitting due to intermolecular interactions between I_3^- ions in the iodine sublattice. However, the polarization behaviors of the above substructures are almost the same, and we could not obtain any experimental evidence of this possibility. The fact that the structure of the iodine sublattice is inferred to be complicated, with 16 I_3^- ions in the unit cell and incommensurate to the TTM-TTF sublattice,[4] also excludes the above possibility of a simple factor-group splitting. Another possibility is that there exist roughly two kinds of I_3^- ions in the crystal, although a variety of environments of I_3^- ions must exist owing to the incommensuration. The relative ratio of the intensities of the substructures is about 2.5. This is not a ratio simply related to the structure of the iodine sublattice, and might manifest slightly different resonance effects for the different I_3^- ions.

The overtone frequencies are almost multiples of that of band 1. However, these frequencies are slightly larger than the multiples of the frequency of the main substructure of band 1. Bandrauk et al.[8] observed a regular sequence of overtone frequencies of I_3^- bands for TMA-I-TCNQ with a slight indication of anharmonicity (Table 1). In their case, the higher-order Raman processes could be assigned to multi-quantum excitations in the same vibrational mode. However, for explaining the frequencies of our overtones, we must assume that not the main substructure of band 1 but the smaller substructure gives the second-order band, or that the second-order process involves both the two modes which give these two substructures, respectively. Note that the peak frequency of band 2, 216.7 cm^{-1}, is comparable with the sum of 107.0 and 109.7 cm^{-1}, the frequencies of the substructures of band 1. An example, in which the peak of a second-order Raman band is located at a frequency higher than twice the most prominent fundamental band, is found for crystalline iodine.[9] In this case, the apparent shape of the second-order band is interpreted by a double phonon generation on the factor-group-splitted two phonon branches in the whole area of the Brillouin zone. In our case, the vibrations participating the higher-order Raman processes might not be those arising from the factor-group splitting. However, it is very likely that these processes involve the vibrations on different molecules or the vibrations delocalized over the molecules.

Figure 3 shows the temperature dependences of the frequencies of bands 1 and 2. As the temperature is raised, both bands decrease their frequecies almost monotonically within the experimental error. Such temperature shifts of low-frequency intramolecular vibrations are considered to occur by a coupling with the lattice vibrations and sometimes seen for molecular crystals. It has been inferred in connection with the metal-insulator transition around 100 K that the degree of the charge transfer would be slightly changed depending on the temperature.[4] The present Raman results do not answer this problem, but we can say that the vibrational states are not greatly affected by the temperature change.

The frequency of the fundamental band observed here is slightly smaller than of I_3^- in solution[5] or in TMA-I-TCNQ,[8] but it is not unusual as compared with other semicondutive iodine complexes.[7] Recently, the corresponding frequencies of the α and β forms of ET-iodine complexes were found to be 117 and 122 cm^{-1}, respectively at 80 K.[6] These are remarkably larger than those of other I_3^- complexes, and considered to manifest a tight crystal field around the I_3^- ions in these complexes.

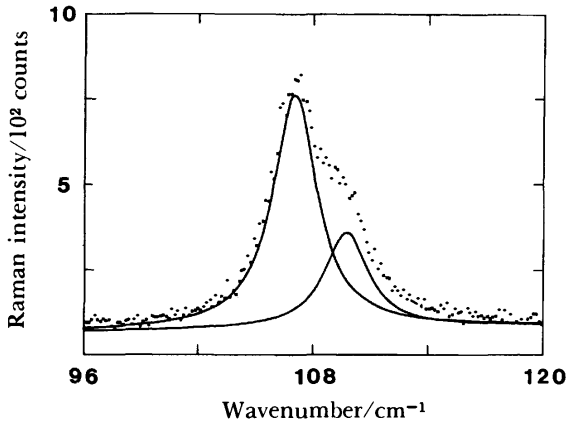

Fig. 2. Detail of band 1 with the resolution of 0.6 cm^{-1}. Solid lines are the assumed substructures.

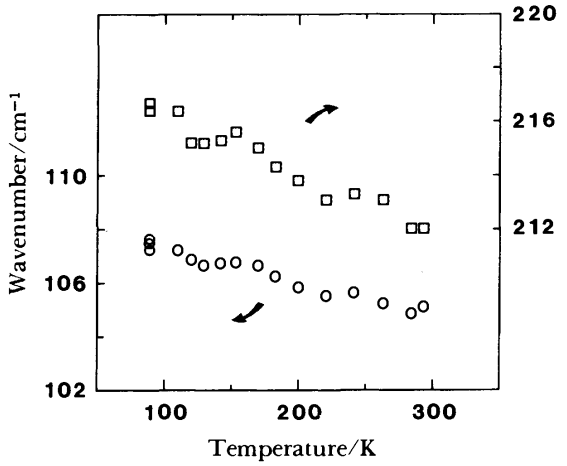

Fig. 3. Temperature dependences of the frequencies of bands 1 and 2.

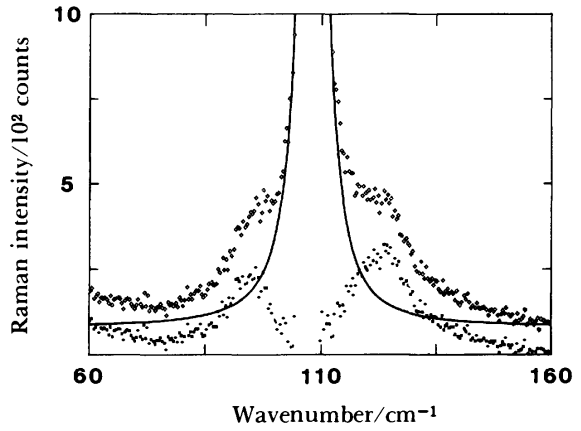

Fig. 4. Structure of the side bands accompanying band 1. Solid line is the assumed band shape of band 1, and closed squares are the difference spectrum giving the side bands.

Two side bands appear at the tail of band 1 (Fig. 1). This feature is very similar to that of TMA-I-TCNQ.[8] Similar side bands were also observed for the ET-complexes, and were attributed to the coupled excitations between the stretching and librational modes of I_3^- ions.[6] These assignments are plausible since the separations of the bands from the fundamental band are almost the same as the low-frequency bands appearing around 30 cm^{-1} in their spectra. In the cases of (TTM-TTF)$I_{2.47}$ and TMA-I-TCNQ, the separations of the side bands from the fundamental band are much smaller. Details of the side bands of our complex at 89 K are presented in Fig. 4, in which the spectrum is decomposed by assuming a Lorentzian shape for the fundamental band. The frequencies of these side bands were estimated to be 94 and 123 cm^{-1}, respectively. Then, the separations from the main substructure of band 1 are 13 and 16 cm^{-1}, respectively. No band appears in the 30 cm^{-1} region in both the (TTM-TTF)$I_{2.47}$ and TMA-I-TCNQ spectra. Thus, it is very likely that the librational frequencies of I_3^- ions in these complexes are as small as 15 cm^{-1}, much smaller than those in the ET-complexes. This indicates a large difference between the crystal fields in these two types of complexes.

The superconduction mechanism in the ET-complexes has not yet been clarified. However, it is likely that the Coulomb field produced by the halide ions or their large polarizability play important roles in the superconduction. Thus, it is worth noting that the frequencies of the optical phonons involving I_3^- ions in the ET-complexes are much larger than those in (TTM-TTF)$I_{2.47}$ or TMA-I-TCNQ, which are insulating at low temperatures.

References

1) See for instance, P. C. W. Leung, T. J. Emge, A. J. Schultz, M. A. Beno, K. D. Carlson, H. H. Wang, M. A. Firestone, and J. M. Williams, *Solid State Commun.*, **57**, 93 (1986).

2) E. B. Yagubskii, I. F. Shchegolev, V. N. Laukhin, and L. I. Buravov, *Pis'ma Zh. Eksp. Teor. Fiz.*, **39**, 12 (1984); see also, K. Murata, M. Tokumoto, H. Anzai, H. Bando, G. Saito, K. Kajimura, and T. Ishiguro, *J. Phys. Soc. Jpn.*, **54**, 2084 (1985).

3) H. H. Wang, M. A. Beno, U. Geiser, M. A. Firestone, K. S. Webb, L. Nunez, G. W. Crabtree, K. D. Carlson, J. M. Williams, L. J. Azevedo, J. F. Kwak, and J. E. Schirber, *Inorg. Chem.*, **24**, 2465 (1985).

4) P. Wu, T. Mori, T. Enoki, K. Imaeda, G. Saito, and H. Inokuchi, *Bull. Chem. Soc. Jpn.*, **59**, 127 (1986).

5) W. Kiefer and H. J. Bernstein, *Chem. Phys. Lett.*, **16**, 5 (1972); K. Kaya, N. Mikami, Y. Udagawa, and M. Ito, *ibid.*, **16**, 151 (1972).

6) S. Sugai and G. Saito, *Solid State Commun.*, **58**, 759 (1986).

7) M. Mizuno, J. Tanaka, and I. Harada, *J. Phys. Chem.*, **85**, 1789 (1981).

8) A. D. Bandrauk, K. D. Truong, C. Carlone, and S. Jandl, *Chem. Phys. Lett.*, **95**, 78 (1983).

9) B. V. Shanabrook and J. S. Lannin, *Solid State Commun.*, **38**, 49 (1981).

Crystal Structure of $(+)^{CD}_{490}$*mer*-Bis{bis(3-aminopropyl)amine-cobalt(III)} Hexacyanocobaltate(III) Dihydrate, $(+)^{CD}_{490}$*mer*-$[Co(dpt)_2][Co(CN)_6]\cdot 2H_2O$

Minoru Ishii,* Michiko Umehara, Kazumasa Harada, and Masayoshi Nakahara
Department of Chemistry, College of Science, Rikkyo (St. Paul's) University,
Nishiikebukuro 3, Toshima-ku Tokyo 171
(Received November 11, 1986)

Synopsis. The structure of optically active title compound was determined by X-ray diffraction. The absolute configuration is *trans*-δ-NH. A pair of two-fused six-membered rings is extended. The geometry of the octahedron is distorted by the presence of the six-membered chelate rings.

The linear triamine bis(3-aminopropyl)amine ($NH_2CH_2CH_2CH_2NHCH_2CH_2CH_2NH_2$, abbreviated as dpt) acts as a terdentate ligand and coordinates to the central metal ion in two topological modes. The cobalt complex, $[Co(dpt)_2]^{3+}$, which contains four six-membered chelate rings, can exist in three geometrical isomers, mer-, sym-fac-, and unsym-fac-isomers. As for the mer-isomers, an optical isomer due to the alternative disposition of N-H bond of the secondary nitrogen atom in dpt ligands is presumed (Fig. 1). The *mer*-$[Co(dpt)_2]^{3+}$ has been prepared and resolved by the present authors,[1] and the structure of optically nonactive complex, $[Co(dpt)_2](ClO_4)_3$, was determined by X-ray analysis by Hambley et al.[2] However, no report has been published on an optically active one. This paper reports the molecular structure of $(+)^{CD}_{490}$*mer*-$[Co(dpt)_2][Co(CN)_6]\cdot 2H_2O$.

Experimental

The $[Co(dpt)_2]^{3+}$ complex was prepared by the method described in a previous paper.[1] The product was dissolved in a small amount of water, and the solution was poured into a column of 2 cm diameter and 120 cm length containing SP-Sephadex C-25 resin (H^+ form). When the elution was carried out with a sodium bis[$(+)_{589}$tartrato]-diantimonate(III) solution of 0.20 mol dm^{-3} at pH≈2, adjusted with HCl,[2] and at a temperature below 7 °C, two reddish purple bands were separated as shown in Fig. 2. These bands were optically active.[3] The elute corresponding to the faster layer was collected and poured into a column (2×ca. 25 cm) of SP-Sephadex C-25 (H^+ form). After the column was washed with 1.0 dm^3 of 0.1 mol dm^{-3} hydrochloric acid, an elute with 1.0 mol dm^{-3} hydrochloric acid was obtained. Crystals were allowed to grow from the elute on addition of equivalent $K_3[Co(CN)_6]$.

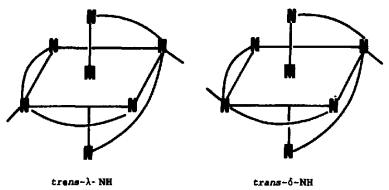

Fig. 1. Two optical isomers of *mer*-$[Co(dpt)_2]^{3+}$.

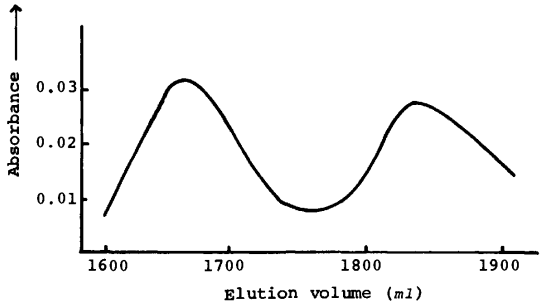

Fig. 2. Elution curve of *mer*-$[Co(dpt)_2]^{3+}$ (516 nm).

Crystal Structure Determination. The crystal is reddish purple, transparent hexagonal prism and of monoclinic structure. The absence of systematic ($0k0$) patterns for $k=2n+1$ indicated that the possible space group is $P2_1$ or $P2_1/m$. Since the crystal is optically active, the space group seems to be $P2_1$.

Crystal Data: $(+)^{CD}_{490}$*mer*-$[Co(dpt)_2][Co(CN)_6]\cdot 2H_2O$, $Co_2C_{18}H_{38}N_{12}O_2$ *F.W.* = 572.44, monoclinic, space group $P2_1$, $a=9.528(2)$, $b=16.464(2)$, $c=8.997(2)$ Å, $\beta=113.50(2)°$, $V=1294.3(5)$ Å^3, $Z=2$, $D_m=1.45$ Mg m^{-3}, $D_c=1.47$ Mg m^{-3}.

A crystal with dimensions of ca. 0.4 × 0.2 × 0.4 mm was used for X-ray diffraction intensity measurements. The intensity was determined by a Rigaku AFC-5 four-circle diffractometer with graphite-monochromated Mo $K\alpha$ radiation ($\lambda=0.7107$ Å) up to 2θ of 55°. Independent 3634 reflections containing Bijvoet pairs with $|F_o|>3\sigma(|F_o|)$ were used for the structure determination. The usual corrections were made for the Lorentz and polarization effects, but no correction was applied for absorption. The calculation was carried out on a FACOM M-360 computer at Rikkyo University. The structure was solved by the Patterson-Fourier method with UNICS III computation program system.[4] The positions of cobalt atoms were deduced from three-dimensional Patterson maps and those of other non-hydrogen atoms were derived from the Fourier map. The scattering factors were taken from Ref. 5). The refinements by the block diagonal least-squares with anisotropic thermal parameters gave R of 0.032. The absolute structure was de-

Table 1. Determination of the Absolute Configuration

$h\ k\ l$	$\lvert F_c(hkl)\rvert$	Obs.	$\lvert F_c(\bar{h}\bar{k}\bar{l})\rvert$
0 8 0	45	>	43
0 6 0	39	<	42
2 5 0	21	<	23
3 5 0	57	>	54
−8 1 2	21	<	23
−8 3 4	15	>	12
−5 1 6	36	>	33
−4 1 1	40	>	37
−4 4 4	15	>	13
−3 2 4	58	<	59

Table 2. Final Atomic Coordinates ($\times 10^4$ for Co, N, C, and O, $\times 10^3$ for H) and Their Equivalent Isotropic Thermal Parameters

Atom	x	y	z	B_{eq}/Å^2
Co(1)	6171(1)	7500(0)	3098(1)	1.4
Co(2)	281(1)	4732(0)	596(1)	1.6
N(1)A	4537(3)	7418(2)	3999(4)	1.9
N(2)A	7779(4)	6845(2)	4932(4)	1.9
N(3)A	7536(3)	7568(2)	1925(4)	2.3
N(4)A	5430(4)	6416(2)	2029(4)	2.1
N(5)A	4614(4)	8164(2)	1264(4)	2.1
N(6)A	6947(4)	8488(2)	4447(4)	2.0
C(1)A	4831(5)	7148(3)	5680(5)	2.8
C(2)A	5995(5)	6484(3)	6267(5)	3.1
C(3)A	7556(5)	6781(3)	6473(5)	2.6
C(4)A	9436(4)	7054(3)	5381(5)	2.8
C(5)A	9940(5)	7034(3)	3989(6)	3.6
C(6)A	9232(5)	7702(3)	2792(6)	3.4
C(7)A	4411(5)	6305(3)	297(5)	2.9
C(8)A	3215(5)	6961(3)	−330(5)	3.2
C(9)A	3902(5)	7787(3)	−365(5)	3.1
C(10)A	5007(5)	9027(3)	1007(6)	3.0
C(11)A	5530(5)	9538(2)	2501(6)	3.1
C(12)A	7043(5)	9285(3)	3747(6)	3.2
C(1)C	−1147(4)	4031(3)	−920(5)	2.1
C(2)C	628(4)	5159(2)	−1184(5)	2.2
C(3)C	1845(4)	3951(2)	934(5)	2.0
C(4)C	−136(4)	4264(2)	2305(5)	2.1
C(5)C	−1271(4)	5510(2)	397(5)	2.1
C(6)C	1794(4)	5444(2)	2022(5)	2.2
N(1)C	−1965(4)	3610(3)	−1866(5)	3.5
N(2)C	813(5)	5381(2)	−2302(5)	3.4
N(3)C	2808(5)	3495(2)	1155(5)	3.1
N(4)C	−425(4)	3976(2)	3304(5)	3.3
N(5)C	−2182(4)	5960(2)	379(5)	3.7
N(6)C	2723(5)	5873(3)	2830(5)	3.7
O(1)W	8033(4)	5053(2)	4675(4)	4.0
O(2)W	5374(5)	4116(3)	4281(5)	5.7
N(2)AH	762(4)	629(2)	460(5)	2.4
N(5)AH	397(5)	824(3)	168(6)	4.3

termined by the anomalous-scattering technique. The enantiomeric structure was refined in the same way at this stage and converged at residuals R of 0.042. As is shown in Table 1, the comparison of the observed and calculated differences between $|F(hkl)|$ and $|F(h\bar{k}l)|$ indicated that $(+)^{CD}_{490}$-isomer has the absolute configuration illustrated in Fig. 3.

The final refinement was carried out using the block diagonal least-squares with anisotropic thermal parameters for non-hydrogen atoms and isotropic ones for hydrogen atoms. The positions of twenty-nine hydrogen atoms among thirty-four, except those of water, were found from a difference synthesis. The final R and R_2 values were 0.022 and 0.028, respectively. The final atomic parameters and thermal parameters are given in Table 2.[6]

Results and Discussion

A perspective drawing of the complex cation is shown in Fig. 3. Two molecules of dpt ligands coordinate with six nitrogen atoms to form an octahedral complex. Each ligand occupies a meridional position as expected. The absolute structure shown in Fig. 3 was assigned to *trans*-δ-NH[7]($\vec{\Lambda}$).[8]

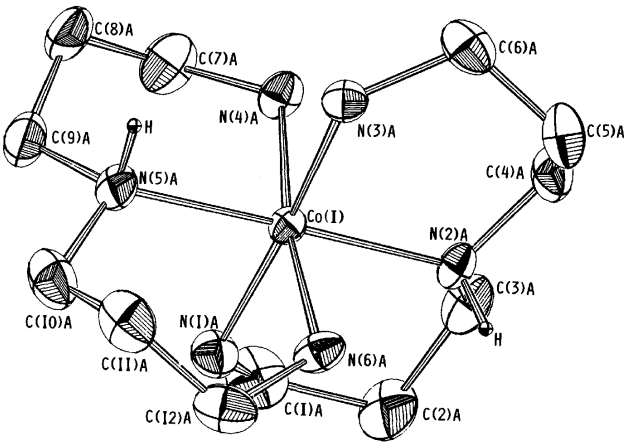

Fig. 3. Perspective drawing of the $[Co(dpt)_2]^{3+}$. The hydrogen atoms except for the secondary amine are not shown.

The bond lengths and angles in the complex cation are listed in Table 3. The Co-N bond lengths (the longest value is 2.053(3) Å for Co(1)-N(2) and the shortest is 1.979(4) Å for Co(1)-N(3)) agreed with the observations for the $[Co(diamine)_3]^{3+}$- and $[Co(triamine)_2]^{3+}$-type complexes containing six-membered chelate rings.[9] Co(1)-N(secondary) length is, however, longest in other values, in contrast to the cases of $(+)_{589}$*mer*-$[Co(dien)_2]Br_3\cdot 1.6H_2O$[6] and $(-)_{589}$*unsym*·*fac*-$[Co(dien)_2][Co(CN)_6]\cdot 2H_2O$.[10] All of the N(secondary)-Co-N(terminal) angles in the dpt chelates are larger than 90°. These results indicate that the six-membered chelate rings are considerably extended. As for the $[Co(triamine)_2]^{3+}$-type complexes containing six-membered chelate ring, such as $[Co(chta)_2]I_3$[11] and $(-)^{CD}_{474}$*mer*-$[Co(aepn)(dien)]I_3\cdot H_2O$[12] (chta: *r*-1,*c*-3,*c*-5-cyclohexanetriamine, aepn: *N*-(2-aminoethyl)-1,3-propanediamine), octahedrons of chromophores are not distorted, although these complexes have many six-membered chelate rings. In contrast to these complexes, a pair of two-fused six-membered chelates coordinate to form a distorted octahedral complex in $[Co(dpt)_2]^{3+}$. The reddish purple coloration of $[Co(dpt)_2]^{3+}$ is unusual as CoN_6 chromophores. The maxima of the absorption spectra (19400 and 27200 cm^{-1}) are at lower energy sides than other CoN_6 complexes, and imply that this octahedron is distorted. The structure described above is consistent with the speculations based on the absorption spectrum.

References

1) S. Yamada, M. Umehara, M. Ishii, and M. Nakahara, *Nippon Kagaku Kaishi*, **1983**, 1733.
2) T. W. Hambley, G. H. Searle, and M. R. Snow, *Aust. J. Chem.*, **35**, 1285 (1982).
3) The values reported in the Ref. 1 should be corrected

Table 3. Bond Distances and Angles within the Complex Cation, *mer*-$[Co(dpt)_2]^{3+}$, with Their Estimated Standard Deviations in Parentheses

Bond distance	l/Å	Bond angle	ϕ/°
Co(1)-N(1)A	2.026(4)	N(1)A-Co(1)-N(2)A	95.2(1)
Co(1)-N(2)A	2.053(3)	N(1)A-Co(1)-N(3)A	172.1(2)
Co(1)-N(3)A	1.979(4)	N(1)A-Co(1)-N(4)A	87.7(2)
Co(1)-N(4)A	2.016(4)	N(1)A-Co(1)-N(5)A	86.1(1)
Co(1)-N(5)A	2.042(4)	N(1)A-Co(1)-N(6)A	88.2(2)
Co(1)-N(6)A	1.987(4)	N(2)A-Co(1)-N(3)A	91.1(2)
		N(2)A-Co(1)-N(4)A	85.7(1)
N(1)A-C(1)A	1.493(6)	N(2)A-Co(1)-N(5)A	178.6(1)
N(2)A-C(3)A	1.489(6)	N(2)A-Co(1)-N(6)A	87.9(1)
N(2)A-C(4)A	1.505(6)	N(3)A-Co(1)-N(4)A	88.6(2)
N(3)A-C(6)A	1.504(7)	N(3)A-Co(1)-N(5)A	87.6(2)
N(4)A-C(7)A	1.483(6)	N(3)A-Co(1)-N(6)A	96.6(2)
N(5)A-C(9)A	1.483(6)	N(4)A-Co(1)-N(5)A	94.9(1)
N(5)A-C(10)A	1.510(6)	N(4)A-Co(1)-N(6)A	171.8(2)
N(6)A-C(12)A	1.474(6)	N(5)A-Co(1)-N(6)A	91.7(1)
C(1)A-C(2)A	1.495(7)	Co(1)-N(1)A-C(1)A	124.2(3)
C(2)A-C(3)A	1.504(7)	Co(1)-N(2)A-C(3)A	116.6(3)
C(4)A-C(5)A	1.510(7)	Co(1)-N(2)A-C(4)A	117.6(3)
C(5)A-C(6)A	1.499(8)	Co(1)-N(3)A-C(6)A	122.0(3)
C(7)A-C(8)A	1.506(7)	Co(1)-N(4)A-C(7)A	124.7(3)
C(8)A-C(9)A	1.515(7)	Co(1)-N(5)A-C(9)A	118.3(3)
C(10)A-C(11)A	1.494(7)	Co(1)-N(5)A-C(10)A	118.9(3)
C(11)A-C(12)A	1.490(8)	Co(1)-N(6)A-C(12)A	122.7(3)
		N(1)A-C(1)A-C(2)A	112.9(4)
		N(2)A-C(3)A-C(2)A	114.2(4)
		N(2)A-C(4)A-C(5)A	114.7(4)
		N(3)A-C(6)A-C(5)A	110.3(4)
		N(4)A-C(7)A-C(8)A	112.7(4)
		N(5)A-C(9)A-C(8)A	112.8(4)
		N(5)A-C(10)A-C(11)A	114.0(4)
		N(6)A-C(12)A-C(11)A	111.4(4)
		C(1)A-C(2)A-C(3)A	111.4(4)
		C(4)A-C(5)A-C(6)A	112.3(4)
		C(7)A-C(8)A-C(9)A	112.5(4)
		C(10)A-C(11)A-C(12)A	113.3(4)

as follows: at 490 nm, in 1 mol dm^{-3} HCl: *trans*-δ-NH, $\Delta\varepsilon$=+0.16; *trans*-λ-NH, $\Delta\varepsilon$=−0.13.

4) T. Sakurai and K. Kobayashi, *Rikagaku Kenkyusho Hokoku*, **55**, 69 (1979).

5) "International Tables for X-Ray Crystallography," Kynoch Press, Birmingham (1974), Vol. IV, pp. 72, 73, and 78.

6) The observed and calculated structure factors, anisotropic thermal parameters for non-hydrogen atoms, and atomic parameters for hydrogen atoms are deposited at Bull. Chem. Soc. Jpn. (Document No. 8743).

7) K. Okiyama, S. Sato, and Y. Saito, *Acta Crystallogr., Sect. B*, **35**, 2389 (1979).

8) T. Dambus and G. Shaffer, *Inorg. Chem.*, **22**, 2406 (1983).

9) R. Nagao, F. Marumo, and Y. Saito, *Acta Crystallogr., Sect. B*, **29**, 2438 (1973).

10) M. Konno, F. Marumo, and Y. Saito, *Acta Crystallogr., Sect. B*, **29**, 739 (1973).

11) M. Ishii, M. Umehara, T. Nomura, and M. Nakahara, *Chem. Lett.*, **1983**, 541.

12) M. Ishii, S. Sato, Y. Saito, and M. Nakahara, *Bull. Chem. Soc. Jpn.*, **57**, 3094 (1984).

The Synthesis of Heteroaromatic Cations Containing Sulfur or Selenium Atoms

Isao SHIBUYA* and Hiroshi NAKANISHI
National Chemical Laboratory for Industry, Yatabe, Ibaraki 305
(Received December 26, 1986)

Synopsis. The dialkylamino-substituted heteroaromatic cations, such as 1,2,4-diselenazolium, 1,2-diselenolium, 1,3,5-selenadiazinium, and 1,3-selenazinium cations, were newly synthesized, and their *S*-analogs were also obtained through similar procedures.

Heteroaromatic cations containing sulfur atoms, **1, 3, 5,** and **7,** (Fig. 1), have been accessible; they are very reactive toward various nucleophiles to give many kinds of heterocyclic derivatives.[1-5] On the other hand, the synthetic routes of heteroaromatic cation compounds containing selenium atoms, such as **2, 4, 6,** and **8,** (Fig. 1), are so far unexplored.

Since it is of interest to examine the reactivities of these seleno-compounds and to compare them with the corresponding *S*- and *Se*-analogs regarding their chemical and physical properties, we attempted to synthesize these seleno-compounds, and have succeeded, as described below.

3,5-Bis(dimethylamino)-1,2,4-dithiazolium perchlorate (**1a**) and the corresponding *Se*-analog (**2a**) were prepared in the manner shown in Scheme 1.

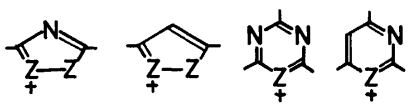

Fig. 1. Heteroaromatic cations containing *S*- or *Se*-atoms.

1,3-Bis(dimethylamino)-1,3-dichloro-2-azapropenylium chloride (**9**), obtained by treating (dichloromethylene)dimethylammonium chloride with dimethylcyanamide,[6] afforded tetramethyldithiobiuret by treating it with sodium hydrogensulfide. Then, without separating the biuret, a successive addition of perchloric acid and oxidation by hydrogen peroxide or *m*-chloroperbenzoic acid led to **1a** almost quantitatively. Similarly, the use of sodium hydrogen selenide, instead of sodium hydrogensulfide, gave **2a** as a stable white crystalline salt in 51 % yield. The results of their yields, mps, elemental analyses, and UV spectral data are summarized in Table 1.

3,5-Bis(dimethylamino)-1,2-dithiolium perchlorate (**3a**) and the 1,2-selenolium perchlorate (**4a**) were prepared when 1,3-bis(dimethylamino)-1,3-dichloropropenylium chloride[7] (**10**) was treated in a similar manner as **1a** and **2a**. Their characterization data are collected in Table 1.

As for the six-membered heteroaromatic cations, **5, 6, 7,** and **8** (Fig. 1), 2-substituted 4,6-bis(dimethylamino)-1,3,5-thiadiazinium perchlorates (**5a, b**) and the corresponding 1,3,5-selenadiazinium perchlorates (**6a—c**) were prepared by the reaction of **9** with thiocarbamoyl or selenocarbamoyl compounds, respectively (see Scheme 2). Similarly, the 1,3-thiazinium perchlorates (**7a, b**) and the 1,3-selenazinium perchlorates (**8a, b**) were also derived from **10** in good yields.

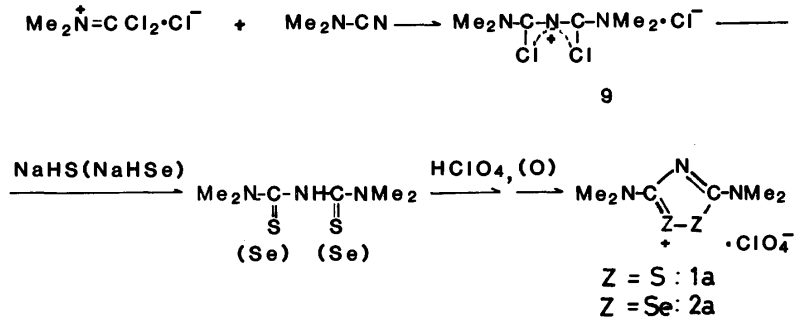

Scheme 1.

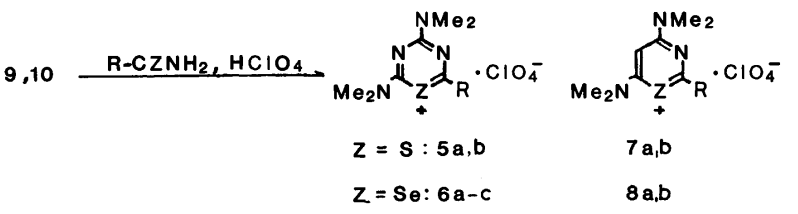

Scheme 2.

Table 1. Preparation of Dimethylamino-Substituted Heteroaromatic Cations, **1a**—**8b**

Compd	R-	Z	Mp θ_m/°C	Yield/%	λ_{max}/nm (ε)	Found (Calcd)/%		
						C	H	N
1a		*S*	210	95	266 (25000)	24.62 (24.87)	4.07 (4.17)	14.53 (14.50)
2a		*Se*	239	51	275 (22900)	18.78 (18.79)	3.15 (3.15)	10.96 (10.96)
3a		*S*	260	78	312 (33000)	29.09 (29.12)	4.47 (4.54)	9.67 (9.70)
4a		*Se*	212	43	322 (32000)	21.72 (21.98)	3.30 (3.42)	7.26 (7.32)
5a	$(CH_3)_2N$-	*S*	>300	73	275 (22500)	32.39 (32.98)	5.52 (5.53)	21.44 (21.36)
5b	Ph-	*S*	286	47		43.21 (43.28)	4.72 (4.75)	15.62 (15.53)
6a	$(CH_3)_2N$-	*Se*	>300	63	285 (24900)	32.26 (32.14)	5.19 (5.12)	14.95 (14.99)
6b	Ph-	*Se*	281	44		38.25 (38.30)	4.17 (4.20)	13.85 (13.74)
6c	$(CH_2)_4N$-	*Se*	294	53		32.95 (32.97)	5.06 (5.03)	17.47 (17.48)
7a	$(CH_3)_2N$-	*S*	>300	55	332 (19400)	36.79 (36.75)	5.84 (5.86)	17.24 (17.15)
7b	Ph-	*S*	303	64		46.73 (46.73)	4.97 (5.04)	11.58 (11.68)
8a	$(CH_3)_2N$-	*Se*	>300	51	341 (20100)	31.96 (32.14)	5.06 (5.12)	14.80 (14.99)
8b	$(CH_2)_4N$-	*Se*	>300	60		36.12 (36.02)	5.23 (5.30)	14.03 (14.02)

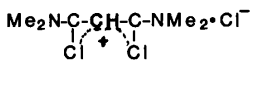

10

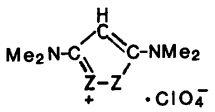

Z = S : 3a
Z = Se : 4a

The synthetic methods of heteroaromatic cations containing selenium atoms, as well as sulfur atoms, have thus been developed systematically, and their procedures could be performed at room temperature.

The results (summarized in Table 1) show that all *S*-analogs have better yields than the corresponding *Se*-analogs, and that, in many cases, they have a higher melting point. These facts suggested that the *S*-analogs are more stable than the corresponding *Se*-analogs.

Giving attention to the spectral data of dimethylamino-substituted cations, **1a**—**8a**, we found several interesting points to be noted. Namely, the IR spectra of **1a** and its *Se*-analog, **2a**, were almost the same, (Fig. 2); these phenomena were also observed between the other *S* and *Se*-analogs: (**3a**, **4a**), (**5a**, **6a**), and (**7a**, **8a**), respectively. In their UV spectra, the *Se*-analogs (**2a**, **4a**, **6a**, and **8a**), have their absorption maxima shifted to about 10 nm longer than that of the corresponding *S*-analogs. In the ^{1}H NMR spectra of **1a** and **2a**, the signals assignable to the dimethylamino group appear as two peaks in the range $\delta = 3.281 - 3.407$ at room temperature. This fact indicates that the rotation of their dimethylamino groups around the C(3)-N bond is restricted or stopped. Similar phenomena were also observed among **5a**—**8a**. A NMR study of these phenomena will be further discussed in our next report.

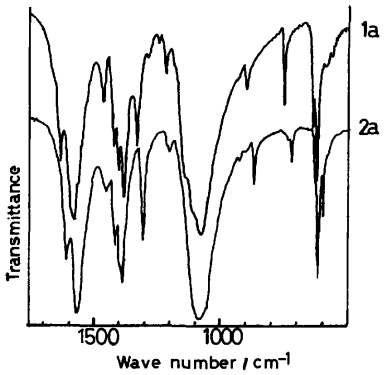

Fig. 2. IR spectra of **1a** and **2a**.

Experimental

All melting points are uncorrected. The IR spectra were recorded on a JASCO A-302 spectrometer using KBr disks. The UV spectra were taken in ethanol solutions using a Hitachi 200-10 spectrometer. The ^{1}H NMR spectra were measured on JEOL GX400 (399.65 MHz) spectrometer; solvent: DMSO-d_6, ca 7 mM (1 M = 1 mol dm^{-3}), δ: ppm from TMS.

3,5-Bis(dimethylamino)-1,2,4-dithiazolium Perchlorate (1a) and the 1,2,4-Diselenazolium Perchlorate (2a). A solution of 1,3-bis(dimethylamino)-1,3-dichloro-2-azapro-

penylium chloride (**9**) in dichloromethane (20 ml) was previously prepared by mixing dimethylcyanamide (0.70 g, 0.01 mol) and (dichloromethylene)dimethylammonium chloride (1.63 g, 0.01 mol).[6] Then, the solution of **9** was added to a solution of sodium hydrogensulfide (1.70 g, 0.03 mol) in ethanol (20 ml) drop by drop for 1 h with stirring; successively, 70% perchloric acid (2 ml) and 30% hydrogen peroxide (1 ml) or *m*-chloroperbenzoic acid (1.73 g, 0.01 mol) were added to it at room temperature. After the solvent was distilled away under reduced pressure, the residue was dissolved in hot acetonitrile (20 ml), and filtered in order to remove any insoluble substances. White crystals of **1a** were obtained from the mixed solution of the acetonitrile filtrate and the same volume of ethyl acetate after cooling overnight at 0—5 °C. Its *Se*-analog, **2a**, was obtained by a similar manner as follows. The solution of **9** was slowly added to a solution of sodium hydrogenselenide, which was obtained by the reaction of selenium powder (2.40 g, 0.03 mol) with sodium boron tetrahydride (1.15 g, 0.03 mol) in absolute ethanol (70 ml) under an argon atomosphere;[8] then, the reaction mixture was treated in the same procedure as described in **1a**. Their yields, mps, UV data, and elemental analyses results are listed in Table 1, and their IR spectra are shown in Fig. 2.

^{1}H NMR, **1a**: δ=3.281 and 3.395; **2a**: δ=3.286 and 3.407.[9]

3,5-Bis(dimethylamino)-1,2-dithiolium Perchlorate (3a) and the 1,2-Diselenolium Perchlorate (4a). The solution of 1,3-bis(dimethylamino)-1,3-dichloropropenylium chloride[7] (**10**) (2.32 g, 0.01 mol) in dichloromethane (20 ml) was treated with sodium hydrogensulfide or sodium hydrogenselenide using similar procedures as in the cases of **1a** and **2a**. Their characterization data are shown in Table 1.

3a IR: 3100, 1558, 1413, 1276, 1064, and 617 cm^{-1};
^{1}H NMR: δ=3.264 and 6.176.

4a IR: 3080, 1551, 1411, 1290, 1085, and 619 cm^{-1};
^{1}H NMR: δ=3.269 and 6.637.

2-Substituted 4,6-Bis(dimethylamino)-1,3,5-thiadiazinium Perchlorates (5a, b) and the 1,3,5-Selenadiazinium Perchlorates (6a—c). To the solution of **9** (0.01 mol) in dichloromethane (20 ml) was added 0.01 mol of thiocarbamoyl or selenocarbamoyl compounds with stirring at room temperature for 1 h; 70% perchloric acid (1 ml) was added to it. The resulting mixture was evaporated and recrystallized from ethanol to give **5a, b** and **6a—c**, respectively.

5a IR: 1603, 1577, 1551, 1413, 1176, 1091, and 619 cm^{-1};
^{1}H NMR: δ=3.279, 3.285, and 3.332.

6a, IR: 1621, 1580, 1545, 1411, 1197, 1091, and 619 cm^{-1};
^{1}H NMR: δ=3.332 and other very broad signals.

2-Substituted 4,6-Bis(dimethylamino)-1,3-thiazinium Perchlorates (7a, b) and the 1,3-Selenazinium Perchlorates (8a, b). The solution of **10** (0.01 mol) in dichloromethane (20 ml) was treated with 0.01 mol of thiocarbamoyl or selenocarbamoyl compounds and perchloric acid (as mentioned above). The resulting mixtures were recrystallized from ethanol to afford **7a, b**, and **8a, b**. Their characterization data are shown in Table 1.

7a, IR: 1613, 1577, 1545, 1414, 1317, 1089, and 617 cm^{-1};
^{1}H NMR: δ=3.285, 3.323, 3.352, and 3.368.

8a, IR: 1603, 1558, 1536, 1409, 1315, 1088, and 615 cm^{-1};
^{1}H NMR: δ=3.234, 3.285, and 3.338.

References

1) W. R. Diveley, U. S. Patent, 3166564 (1965); *Chem. Abst.*, **62**, 9145g (1965).
2) J. E. Oliver, *J. Org. Chem.*, **36**, 3465 (1971); J. E. Oliver, B. A. Bierl, and J. M. Ruth, *ibid.*, **37**, 131 (1972).
3) J. Liebscher and H. Hartmann, *Z. Chem.*, **15**, 438 (1975).
4) J. Liebscher and H. Hartmann, *D. D. R. Pat.*, 129,447 (1977).
5) I. Shibuya, *Bull. Chem. Soc. Jpn.*, **55**, 2158 (1982); **57**, 605 (1984).
6) Z. Janousek and H. G. Viehe, *Angew. Chem.*, **85**, 90 (1973).
7) Z. Janousek and H. G. Viehe, *Angew. Chem.*, **83**, 615 (1971).
8) A. Moradpour, V. Peyrussan, I. Johansen, and K. Bechgaard, *J. Org. Chem.*, **48**, 388 (1983).
9) The results of the NMR spectra analyses of these dimethylamino signals will be submitted somewhere soon.

Clay Montmorillonite-Catalyzed Aldol Reactions of Silyl Ketene Acetals with Carbonyl Compounds

Makoto ONAKA,* Ryosuke OHNO, Motomitsu KAWAI, and Yusuke IZUMI
Department of Synthetic Chemistry, Faculty of Engineering, Nagoya University, Furo-cho, Chikusa-ku, Nagoya 464
(Received January 10, 1987)

Synopsis. Al^{3+} ion-exchanged montmorillonite efficiently catalyzes the aldol reactions of silyl ketene acetals with carbonyl compounds and acetals. The optimum preparation of the effective montmorillonite catalyst is described.

The use of silicon reagents in organic synthesis has been expanding rapidly in recent years.[1] During the course of our investigation on the application of solid acids as efficient catalysts to carbon-carbon bond formation reactions in a liquid phase, we discovered that the reactions of allylic silanes[2] and silyl enol ethers[3] with aldehydes and acetals are catalyzed by clay montmorillonite to afford the corresponding adducts in high yields. We describe herein catalytic efficiency of Al^{3+} ion-exchanged montmorillonite (Al-Mont) for aldol reactions of silyl ketene acetals (1-alkoxy-1-silyloxy-1-alkenes) with carbonyl compounds, and also the optimum preparation of the effective Al-Mont catalyst.

The cross-aldol reactions of silyl ketene acetals with aldehydes and acetals are generally conducted in the presence of a stoichiometric amount of various Lewis acids.[4,5] Recently the use of effective homogeneous catalysts such as Ph_3CClO_4,[6] Me_2AlCl,[7] and ZnX_2[8] was reported.

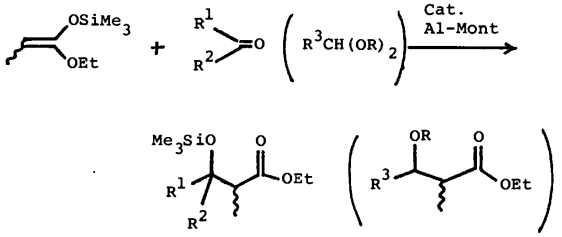

Table 1 summarizes reactions of 1-ethoxy-1-[(trimethylsilyl)oxy]propene with carbonyl compounds and acetals catalyzed by Al^{3+}-montmorillonite.

The Al-Mont-catalyzed aldol reaction of silyl ketene acetals is characterized as follows. 1) Aldehydes and ketones are more reactive than acetals. 2) The catalytic activities of Al-Mont are sensitive to reaction solvent; 1,2-dimethoxyethane (DME) is superior to

Table 1. Al^{3+}-Montmorillonite-Catalyzed Aldol Reactions of Silyl Ketene Acetals with Electrophiles[a]

Run	Silyl ketene acetal	Electrophile	Solv.	Condition: Temp °C	Condition: Time min	Yield %	Diastereomer ratio[b]
1	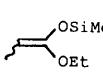 [c]	$C_5H_{11}CHO$	Toluene	0	60	70	49 : 51
2			CH_2Cl_2	−30	145	75	53 : 47
3			DME	−50	50	88	49 : 51
4[d]		PhCHO	Toluene	−78	120	89	52 : 48[e]
5[d]			CH_2Cl_2	−50	90	91	50 : 50[e]
6[d]			DME	−78	45	95	51 : 49[e]
7		*c*-$C_6H_{11}CHO$	CH_2Cl_2	0	60	78	50 : 50
8			DME	−50	40	93	50 : 50
9[d]		$(C_2H_5)_2CO$	CH_2Cl_2	−78	55	97	—
10		$C_5H_{11}CH(OEt)_2$	Toluene	0	200	68	52 : 48
11			CH_2Cl_2	0	120	56	51 : 49
12			DME	0	30	94	51 : 49
13		$PhCH(OMe)_2$	DME	−50	45	94	50 : 50[f]
14[d]	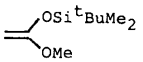	$C_5H_{11}CHO$	DME	−78	25	86	—
15[d]	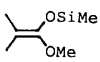	$C_5H_{11}CHO$	DME	−50	90	86	—

a) The reaction of the silyl ketene acetal (1 mmol) with an electrophile (0.8 mmol) was carried out in the presence of Al-Mont (0.05 g). b) Determined by GLC. c) E/Z=80 : 20. d) Al-Mont*(0.2 g) was used as a catalyst. e) Determined by NMR on the basis of the integral of the C-3 proton (δ=4.70, 4.98). f) Determined by NMR on the basis of the integral of methoxy protons (δ=3.18, 3.27).

dichloromethane and toluene. 3) Simple distillation, after removal of Al-Mont by filtration, is all that is required to furnish pure products. 4) Aldol products are obtained from aldehyde and ketone in the form of β-trimethylsiloxy esters owing to a non-aqueous work-up procedure, and no formation of α,β-unsaturated esters is observed. 5) In all cases mixtures of diastereomers are produced in good yields but with little or no apparent stereoselectivity.

The reactions of hexanal with silyl ketene acetals derived from acetate and isobutyrate were also catalyzed by Al-Mont catalyst (Runs 14 and 15). In each case the corresponding aldol adduct was readily obtained in the form of β-siloxy ester in high yield.

Clay montmorillonite is easily available and handled. The careful drying pretreatment of the clay is responsible for the attainment of high catalytic activity and good reproducibility in the present reactions because the clay structure changes irreversibly at high temperature.[9]

It should be noted that the present heterogeneous catalyst system of Al-Mont has several advantages and is an alternative to existing homogeneous catalyst systems in aldol reactions by use of silyl ketene acetals.

Experimental

Materials and Measurements. All reactions were performed under nitrogen atmosphere. Solvents were purified by distillation over an appropriate drying agent. Silyl ketene acetals were prepared according to procedures reported in the literature.[10] Aldehydes and ketone were purchased commercially. Acetals were prepared from aldehyde and trialkyl orthoformate by use of Amberlyst-15. Infrared spectra were obtained on a JASCO IRA-2 spectrometer. ^{1}H NMR spectra were recorded in $CDCl_3$ with a Hitachi R-600 spectrometer at 60 MHz. All chemical shifts were reported in relative to tetramethylsilane. GLC was performed with a Shimadzu GC-8A gas chromatograph with a capillary column (PEG-HT, 25 m).

Preparation of Al^{3+} Ion-Exchanged Montmorillonite (Al-Mont). Cation exchange was effected[11] by adding the powdered montmorillonite (100 g) (Purified Na^+ ion-exchanged montmorillonite "Kunipia-F" (cation exchange capacity = 1.19 meq./g) supplied by Kunimine Industries Co. Japan) to an aqueous solution (800 ml) of $Al(NO_3)_3 \cdot 9H_2O$ (150 g, 0.4 mol) with vigorous stirring at r.t. for 2 h. The resultant suspension was filtered on a Büchner funnel by suction. The clay was collected, suspended again in deionized water (500 ml) with stirring at r.t. for 1 h, filtered on a suction funnel, and washed with deionized water (200 ml). The clay collected was again suspended in a mixture of deionized water (200 ml) and methanol (200 ml) with stirring at r.t. for 1 h and filtered. This procedure was repeated twice. The washed clay was pre-dried at 20 °C/1 Torr (1 Torr = 133.322 Pa) for 6 h, and the agglomerated clay was then ground and passed through a 60 mesh screen. The resultant powdered clay was dried at 20 °C/0.5 Torr for 24 h, and stored in a desiccator over anhydrous silica gel until use.

Reaction Procedures. Al^{3+} ion-exchanged montmorillonite (0.05 — 0.2 g) was placed in a 30-ml round-bottomed flask equipped with a magnetic stirrer and dried at 120 °C/0.4 Torr for 3 h. To a suspended Al-Mont in a solvent (3 ml) at −78 °C were added an electrophile (0.8 mmol) in solvent (1 ml) and silyl ketene acetal (1 mmol) in solvent (1 ml) successively. The resulting mixture was stirred vigorously at the temperature shown in Table 1, and the reaction was monitored by TLC or GLC. As work-up, the suspended mixture was passed through a Celite pad and the organic filtrate was evaporated. Aldol products were purified by distillation on a Kugelrohr apparatus and diastereomer ratio of the products was determined by NMR, or by GLC after desilylation of the products.

Ethyl 2-Methyl-3-[(trimethylsilyl)oxy]octanoate. (A mixture of diastereomers): Distilled at 122 °C(bath temp)/0.5 Torr; IR (CCl_4) 1725 cm^{-1} (C=O); ^{1}H NMR ($CDCl_3$) δ = 0.08 (s, CH_3Si), 0.86 (t, J=5.8 Hz, CH_3), 1.06 (d, J=6.8 Hz, $C\underline{H}_3CH$), 1.13 (d, J=6.8 Hz, $C\underline{H}_3CH$), 1.25 (t, J=7.0 Hz, $C\underline{H}_3CH_2O$), 1.00—1.60 (br, $(CH_2)_4$), 2.30—2.75 (m, $CH_3C\underline{H}$), 3.80—4.20 (br, CHOSi), 4.10 (q, J = 7.0 Hz, $CH_3C\underline{H}_2O$).

Ethyl 2-Methyl-3-phenyl-3-[(trimethylsilyl)oxy]propanoate. (A mixture of diastereomers): Distilled at 125 °C(bath temp)/0.3 Torr; IR (CCl_4) 1720 cm^{-1} (C=O); ^{1}H NMR ($CDCl_3$) δ = −0.05 (s, CH_3Si), 0.02 (s, CH_3Si), 0.85 (d, J=7.0 Hz, CH_3), 1.15 (d, J=7.2 Hz, CH_3), 1.09 (t, J= 7.2 Hz, CH_3), 1.28 (t, J=7.2 Hz, CH_3), 2.40 — 3.00 (m, $C\underline{H}CH_3$), 3.98 (q, J=7.2 Hz, CH_2), 4.16 (q, J=7.2 Hz, CH_2), 4.70 (d, J=9.6 Hz, CHOSi), 4.98 (d, J = 7.0 Hz, CHOSi), 7.20—7.40 (br, Ph).

Ethyl 3-Cyclohexyl-2-methyl-3-[(trimethylsilyl)oxy]propanoate. (A mixture of diastereomers): Distilled at 128 °C(bath temp)/0.6 Torr; IR (CCl_4) 1725 cm^{-1} (C=O); ^{1}H NMR ($CDCl_3$) δ=0.00 (s, CH_3Si), 0.90—2.00 (br, cyclohexyl), 0.97 (d, J=7.8 Hz, $C\underline{H}_3CH$), 1.03 (d, J=6.4 Hz, $C\underline{H}_3CH$), 1.18 (t, J=7.4 Hz, CH_3), 2.30—2.85 (m, $C\underline{H}CH_3$), 3.50—3.85 (br, CHOSi), 4.07 (q, J=7.4 Hz, CH_2).

Ethyl 3-Ethyl-2-methyl-3-[(trimethylsilyl)oxy]pentanoate. Distilled at 130 °C(bath temp)/38 Torr; IR (CCl_4) 1730 cm^{-1} (C=O); ^{1}H NMR ($CDCl_3$) δ = 0.02 (s, CH_3Si), 0.78 (t, J=6.8 Hz, CH_3), 1.03 (d, J=6.8 Hz, $C\underline{H}_3CH$), 1.18 (t, J=7.2 Hz, $C\underline{H}_3CH_2O$), 1.44 (q, J=6.8 Hz, CH_2), 2.55 (q, J=6.8 Hz, CH), 4.05 (q, J=7.2 Hz, $CH_3C\underline{H}_2O$).

Ethyl 3-Ethoxy-2-methyloctanoate. (A mixture of diastereomers): Distilled at 107 °C(bath temp)/0.3 Torr; IR (CCl_4) 1730 cm^{-1} (C=O); ^{1}H NMR ($CDCl_3$) δ=0.83 (t, J= 6.0 Hz, CH_3) 1.02 (d, J=7.2 Hz, $C\underline{H}_3CH$), 1.10 (d, J=7.2 Hz, $C\underline{H}_3CH$), 1.20 (t, J=6.8 Hz, $C\underline{H}_3CH_2O$, $C\underline{H}_3CH_2OCO$), 0.95—1.55 (br, $(CH_2)_4$), 2.35—2.95 (m, $CH_3C\underline{H}$), 3.47 (q, J =6.8 Hz, $CH_3C\underline{H}_2O$), 3.30−3.75 (br, CHOEt), 4.10 (q, J= 6.8 Hz, $CH_3C\underline{H}_2OCO$).

Ethyl 3-Methoxy-2-methyl-3-phenylpropanoate. (A mixture of diastereomers): Distilled at 130 °C(bath temp)/0.5 Torr; IR (CCl_4) 1720 cm^{-1} (C=O); ^{1}H NMR ($CDCl_3$) δ=0.88 (d, J = 6.6 Hz, $C\underline{H}_3CH$), 1.14 (d, J=6.4 Hz, $C\underline{H}_3CH$), 1.30 (t, J=7.0 Hz, CH_3), 2.45—2.95 (m, $C\underline{H}CH_3$), 3.18 (s, CH_3O), 3.27 (s, CH_3O), 4.02 (q, J=7.0 Hz, $CH_3C\underline{H}_2O$), 4.26 (d, J=6.8 Hz, $C\underline{H}OCH_3$), 4.45 (d, J=6.8 Hz, $C\underline{H}OCH_3$), 7.20—7.60 (br, Ph).

Methyl 3-[(*t*-Butyldimethylsilyl)oxy]octanoate. Distilled at 127 °C(bath temp)/0.6 Torr; IR (CCl_4) 1735 cm^{-1} (C=O); ^{1}H NMR ($CDCl_3$) δ = −0.03 (s, CH_3Si), −0.01 (s, CH_3Si), 0.80 (s, $(CH_3)_3C$), 0.70—1.00 (br, CH_3), 1.00—1.70 (br, $(CH_2)_4$), 2.39 (d, J=6.6 Hz, CH_2CO_2), 3.61 (s, CH_3O), 3.80—4.25 (br, CHOSi).

Methyl 2,2-Dimethyl-3-[(trimethylsilyl)oxy]octanoate. Distilled at 120 °C(bath temp)/0.4 Torr; IR (CCl_4) 1730 cm^{-1} (C=O); ^{1}H NMR ($CDCl_3$) δ = 0.04 (s, CH_3Si), 0.75—0.95 (br, CH_3), 1.02 (s, CH_3), 1.09 (s, CH_3), 1.10—1.55 (br, $(CH_2)_4$), 3.62 (s, CH_3O), 3.70—4.05 (br, CHOSi).

The authors gratefully acknowledge financial support for this research by the foundation "Hattori-Hokokai."

References

1) E. Colvin, "Silicon in Organic Synthesis," Butterworths, London (1981); W. P. Weber, "Silicon Reagents for Organic Synthesis," Springer-Verlag, New York (1983); P. Brownbridge, *Synthesis*, **1983**, 1, 85.

2) M. Kawai, M. Onaka, and Y. Izumi, *Chem. Lett.*, **1986**, 381.

3) M. Kawai, M. Onaka, and Y. Izumi, *Chem. Lett.*, **1986**, 1581.

4) K. Saigo, M. Osaki, and T. Mukaiyama, *Chem. Lett.*, **1975**, 989; **1976**, 769.

5) Y. Kita, O. Tamura, and Y. Tamura, *Yuki Gosei Kagaku Kyokai Shi*, **44**, 1118 (1986).

6) T. Mukaiyama, S. Kobayashi, and M. Murakami, *Chem. Lett.*, **1984**, 1759.

7) Y. Naruse, J. Ukai, N. Ikeda, and H. Yamamoto, *Chem. Lett.*, **1985**, 1451.

8) B. D. Gray and J. D. White, *J. Chem. Soc., Chem. Commun.*, **1985**, 20; Y. Kita, H. Yasuda, O. Tamura, F. Itoh, Y. Y. Ke, and Y. Tamura, *Tetrahedron Lett.*, **26**, 5777 (1985).

9) For example, R. E. Grim, "Clay Mineralogy," McGraw-Hill, New York (1953), p. 190.

10) C. Ainsworth, F. Chen, and Y.-N. Kuo, *J. Organomet. Chem.*, **46**, 59, 73 (1972); C. H. Heathcock, S. K. Davidsen, K. T. Hug, and L. A. Flippin, *J. Org. Chem.*, **51**, 3027 (1986).

11) Minor modification of Ballantine's procedure: J. A. Ballantine, J. H. Purnell, M. Rayanakorn, and K. J. Williams, *J. Mol. Catal.*, **30**, 373 (1985).

Substitution Reaction of Organic Halide by Trimethylsilyl Isothiocyanate: Formation of Thiocyanate and Its Rearrangement to Isothiocyanate†

Kozaburo NISHIYAMA* and Makoto OBA
Department of Chemistry, Tokyo Metropolitan University,
2-1-1, Fukasawa, Setagaya, Tokyo 158
(Received January 31, 1987)

Synopsis. The reaction of organic halide with trimethylsilyl isothiocyanate (TMSTC) gave thiocyanate **1** and its isomerized isothiocyanate **2**. Details of the substituion and the isomerization reactions were examined.

Recently, the application of silicon reagents has increased regarding organic synthesis. For example, a variety of silyl cyanides and silyl azides have been widely employed as synthetic tools.[1] Although trimethylsilyl isothiocyanate (TMSTC) is one of these silyl pseudo-halides, there have been only a few reports on its reactivity: Our previous report[2] concerning the formation of symmetrically and unsymmetrically isothiocyanato-substituted ethers is one of them. As the substitution reaction by TMSTC, Sasaki et al. explored the reaction of adamantyl chloride in the presence of $TiCl_4$.[3] For introducing NCS group into an organic molecule, the use of metal thiocyanate has been generalized,[4] but no detailed discussion has been given. As one part of our studies on silicon chemistry, we report here on the substitution reaction of organic halide by TMSTC and the rearrangement of thiocyanate into isothiocyanate.

Results and Discussion

When a solution of benzyl bromide and TMSTC in hexamethylphosphoric triamide (HMPA) was stirred at 60 °C for 24 h, a mixture of benzyl thiocyanate **1** and benzyl isothiocyanate **2** was obtained in a ratio of 32 : 68. On the other hand, only *S*-benzylation product **1** was yielded from a reaction which was carried out at room temperature. The effects of the solvent, leaving group, and substituent were examined and the results are summarized in Table 1. The results using sodium thiocyanate are also shown in the parentheses of Table 1. Both isomer ratios of **1** and **2** were very similar. The reaction occured favorably in HMPA or DMF. With benzyl chroride (harder alkylating agent than the bromide), compound **1** resulted as the sole product when the reaction was performed at 60 °C. This result could not be accounted for by "the principle of hard and soft acids and bases" which was often applied to the alkylation of ambident nucleophile.[5] The reactions of other *p*-substituted benzyl bromides, similarly, gave a mixture of **1** and **2**. The *N*-benzylation product was relatively increased by an electron-donating group. Coupled with the result of benzyl chloride, this indicates that *N*-benzylation can be rationalized by the consideration that the carbon-halogen bond breaking is more important than the carbon-nitrogen bond making in a transition state, i.e. the stability of the corresponding benzyl cation.

Furthermore, we investigated the substitutent effects on the *S*-benzylation. Plotting the $\log(k_X/k_H)$ values vs. the Hammett's σ constant gave a nonlinear relationship (Fig. 1). Both the electron-attracting and electron-donating substituents accelerated the rate of substitution, suggesting that a gradual change in mechanism occurs. This has been discussed by Swain and Langsdorf[6] in terms of the relative importance of bond-making and bond-breaking in the transition state. This behavior is commonly characteristic for a benzyl-type S_N2 reaction.

For a mechanistic study, the time dependency of the

Table 1. Reaction of Benzyl Bromides and Trimethylsilyl Isothiocyanate

$$R\text{-}X \xrightarrow[24\,h]{TMSTC} \underset{\mathbf{1}}{R\text{-}SCN} + \underset{\mathbf{2}}{R\text{-}NCS}$$

Substrate	Solvent	Temp/ °C	Yield/ %[a]	Ratio 1 : 2
$C_6H_5CH_2Br$	HMPA	RT	89	100 : 0
			(100)[b]	(100 : 0)
$C_6H_5CH_2Br$	HAPA	60	83	32 : 68
			(100)[b]	(23 : 77)
$C_6H_5CH_2Br$	DMF	60	68	94 : 6
$C_6H_5CH_2Br$	MeCN	60	0	
$C_6H_5CH_2Cl$	HMPA	60	50	100 : 0
p-$MeOC_6H_4CH_2Br$	HMPA	60	100	11 : 89
p-$MeC_6H_4CH_2Br$	HMPA	60	85	25 : 75
p-$NCC_6H_4CH_2Br$	HMPA	60	92	37 : 63
p-$O_2NC_6H_4CH_2Br$	HMPA	60	95	46 : 54

a) Determined by ^1H NMR and no by-product was detected. b) Obtained from NaSCN.

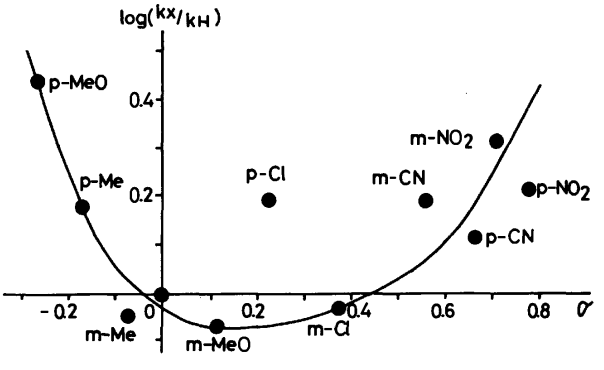

Fig. 1. Hammet's plot for the reaction between benzyl bromides and TMSTC.

† Dedicated to Professor Yoichiro Nagai on the Occasion of his 60th birthday.

product distributions was examined at 60 °C. Compound **1** was predominant during the early stages of the reaction and the molar ratios were gradually changed. After 120 h, the mixture consisted of **1** (9%), **2** (87%), and benzyl bromide (4%). *S*-Benzylation product **1** is the kinetically controlled product and **1** is isomerized to the *N*-benzylation product **2** which is thermodynamically more stable. A treatment of **1** with bromotrimethylsilane gave a mixture of isomerized **2** (55%) and benzyl bromide (16%), and chlorotrimethylsilane converted **1** into only benzyl chloride (51%). In the absence of bromosilane, no isomerization occurred. From these experiments, it is likely that the coexistent bromide ion catalyzes the isomerization of **1** to **2** and *S*-benzylation should be reversible. As shown in the equation, isothiocyanate **2** may be explained as being produced by the competitive *N*-attack of TMSTC on benzyl bromide, not by the direct isomerization of **1** to **2**

$$ArCH_2Br + Me_3SiNCS \rightleftharpoons ArCH_2SCN + Me_3SiBr$$
$$\searrow^{slow} \qquad \mathbf{1}$$
$$ArCH_2NCS + Me_3SiBr$$
$$\mathbf{2}$$

Allyl halide, 1-bromo-3-methyl-2-butene, was also reactive toward TMSTC, giving a mixture of three products. This reaction pathway is supported by the time dependency of the product distribution (Table 2). The intramolecular rearrangement between (A) and (B) was known,[7] and the rearrangement was postulated to take place via a cyclic mechanism:

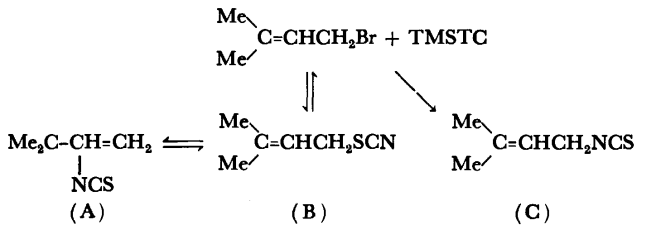

Table 2. Reaction of 1-Bromo-3-methyl-2-butene with TMSTC[a]

Time/h	Product/%		
	(A)	(B)	(C)
24	37	34	29
48	27	25	48
72	23	23	54
120	15	22	63

a) The reaction was carried out in HMPA at room temperature.

These results led us to examine the reactions of vinyl, aryl, and aliphatic halides. As expected, alkyl halide was converted to thiocyanate or isothiocyanate but vinyl and aryl halides were unreactive.

$$PhCH_2CH_2Br + TMSTC \longrightarrow PhCH_2CH_2SCN \quad (56\%)$$
$$Me_2CHCH_2Br + TMSTC \longrightarrow Me_2CHCH_2SCN \quad (12\%)$$
$$EtOCOCH_2Br + TMSTC \longrightarrow EtOCOCH_2NCS \quad (68\%)$$
$$NCCH_2Cl + TMSTC \longrightarrow NCCH_2SCN \quad (39\%)$$

From these results, it has become clear that TMSTC may be a useful reagent for introducing an NCS group under homogeneous and neutral conditions in nonaqueous solvent. Moreover, details concerning *S*- and *N*-benzylation were distinctly observed.

Experimental

Infrared spectra were measured on a Hitachi 260-10 infrared spectrometer. ^{1}H NMR spectra were determined with a Hitachi R-600 or a Varian XL-300 spectrometer using tetramethylsilane as an internal standard. Mass spectra were obtained using a JEOL DX-300 spectrometer. Trimethylsilyl isothiocyanate (TMSTC) was prepared by the reaction of sodium thiocyanate with chlorotrimethylsilane, bp 144 °C (lit,[8] bp 141.8—142 °C). Organic halides were commercial products and were purified if necessary. Some benzyl bromides were obtained from the corresponding toluenes and *N*-bromosuccinimide in the presence of benzoyl peroxide in CCl_4.

Reaction of Organic Halides with TMSTC. A solution of benzyl bromide (1.71 g, 10 mmol) and TMSTC (1.31 g, 10 mmol) in HMPA (6.7 cm^3) was heated at 60 °C for 24 h. The reaction mixture was poured into water and extracted with dichloromethane. The organic layer was washed five times with water and dried over $MgSO_4$. After the removal of solvent, fast elution with hexane on silica gel contained benzyl isothiocyanate (0.45 g, 30%), IR (neat) ν 2100 cm^{-1} (NCS); ^{1}H NMR ($CDCl_3$) δ=4.70 (s, 2H) and 7.35 (s, 5H) and benzene eluted benzyl thiocyanate (0.44 g, 30%), mp 42—43 °C, IR (KBr) ν 2150 cm^{-1} (SCN); ^{1}H NMR ($CDCl_3$) δ=4.17 (s, 2H) and 7.38 (s, 5H). The conversion and the ratio were determined by ^{1}H NMR spectra before the chromatographic separation. All the products were identified by a comparison with the authentic samples by at least two of the following methods: Mixed melting point, IR, NMR, and retention time of HPLC.

Kinetic Measurement. A competitive reaction was carried out at −20 °C for 6 min. For example, a solution of benzyl bromide (0.513 g, 3 mmol) and *p*-methoxybenzyl bromide (0.603 g, 3 mmol) in HMPA (4 cm^3) was cooled at −20 °C, and then TMSTC (0.79 g, 6 mmol) was added. The mixture was stirred for 6 min at the temperature. Work-up was similar to that described above. The relative rate of the substitution reaction was determined by ^{1}H NMR spectrum (at 300 MHz) of the products. All competitive reactions were carried out at least twice and the results were obtained from the averaged values.

Rearrangement of Benzyl Thiocyanate to Benzyl Isothiocyanate. An HMPA solution of benzyl thiocyanate (0.22 g, 1.5 mmol) and bromotrimethylsilane (0.31 g, 2 mmol) was stirred at 60 °C for 24 h. Similar work-up gave a mixture of benzyl isothiocyanate (55%), benzyl bromide (16%), and the starting material (29%). The product distribution was determined by ^{1}H NMR spectrum.

Reaction of 1-Bromo-3-methyl-2-butene with TMSTC. A mixture of 1-bromo-3-methyl-2-butene (1.49 g, 10 mmol), TMSTC (1.31 g, 10 mmol), and HMPA was treated at room temperature for 24 h. A similar work-up gave a mixture of 3-isothiocyanato-3-methyl-1-butene (A), 1-thiocyanato- (B), and 1-isothiocyanato-3-methyl-2-butene (C) in a ratio of 37 : 34 : 29, determined by ^{1}H NMR spectrum. An attempt to separate a mixture failed because of the intramolecular rearrangement during the separation on silica gel. Each structure was confirmed by ^{1}H NMR and IR spectra. ^{1}H NMR signals were assigned by their intensities. The time de-

pendency of the product distribution is given in Table 2. 3-Isothiocyanato-3-methyl-1-butene (A), IR (neat) ν 2080 cm^{-1} (NCS); ^1H NMR ($CDCl_3$) δ=1.49 (s, 6H) and 4.99—6.09 (m, 3H). 1-Thiocyanato-3-methyl-2-butene (B), IR (neat) ν 2150 cm^{-1} (SCN); ^1H NMR ($CDCl_3$) δ=1.79 (d, 6H), 3.61 (d, 2H), and 5.32 (t, 1H). 1-Isothiocyanato-3-methyl-2-butene (C), IR (neat) ν 2060 cm^{-1} (NCS); ^1H NMR ($CDCl_3$) δ=1.74 (d, 6H), 4.05 (d, 2H), and 5.30 (t, 1H).

References

1) W. P. Weber, "Silicon Reagents for Organic Synthesis," Springer-Verlag, New York (1983).

2) K. Nishiyama and M. Oba, *Bull. Chem. Soc. Jpn.*, **60**, 2289 (1987).

3) T. Sasaki, A. Nakanishi, and M. Ohno, *J. Org. Chem.*, **46**, 5445 (1981).

4) R. G. R. Bacon, "Organic Sulfur Compounds," ed by N. Kharasch, Pergamon Press, New York (1961), Vol. 1, Chap. 27, pp. 306.

5) T.-L. Ho, "Hard and Soft Acids and Bases Principle in Organic Chemistry," Academic Press, New York (1977).

6) C. G. Swain and W. P. Langsdorf, *J. Am. Chem. Soc.*, **73**, 2813 (1951).

7) O. Mumm and H. Richter, *Chem. Ber.*, **73**, 843 (1940).

8) British Thomsom-Houston Co Ltd., Brit. Partent 643941 (1950); *Chem. Abstr.*, **45**, 7585g (1951).

Normal- and High-Pressure Diels-Alder Reactions of *p*-Tropoquinone with Furans

Tohru TSUDA, Shigeru SUGIYAMA,† Akira MORI,† and Hitoshi TAKESHITA†,*
Graduate School of Engineering Sciences, 39, Kyushu University,
Kasuga-koen, Kasuga, Fukuoka 816
†Research Institute of Industrial Science, 86, Kyushu University,
Kasuga-koen, Kasuga, Fukuoka 816
(Received February 10, 1987)

Synopsis. The Diels-Alder reactions of *p*-tropoquinone with furans were investigated under normal- and high-pressure conditions. With furan or 2-methylfuran, no cycloadduct was obtained at all, but with 2-methoxyfuran, a double Michael adduct was isolated from the reaction under the atmospheric pressure, and its structure was elucidated mainly by ^{1}H NMR analysis. With 3,4-dimethoxyfuran, an exo-1 : 1-adduct and its further reacted 2 : 1-adduct were isolated.

Because of the poor reactivity of furan (**1**) towards dienophiles,[1] there is no successful example of a reaction with simple *p*-benzoquinone (**2a**) and its derivatives (such as **2b** and **2c**) under atmospheric pressure. However, furans became accessible to the reaction under the high-pressure conditions; with 3,4-dimethoxyfuran (**3**), formations of the endo- and exo-adducts were exemplified in the reaction with various dienophiles.[2-4] Recently, we have succeeded in obtaining the Diels-Alder adducts of tropone (**4**) with **1** under high-pressure conditions,[5] and with a continuing interest to the chemistry of tropoquinones as well as high-pressure cycloaddition reactions in troponoids, we have carried out the reaction with *p*-tropoquinone (**5**), and the results obtained therefrom are described briefly as illustrated in Scheme 1.

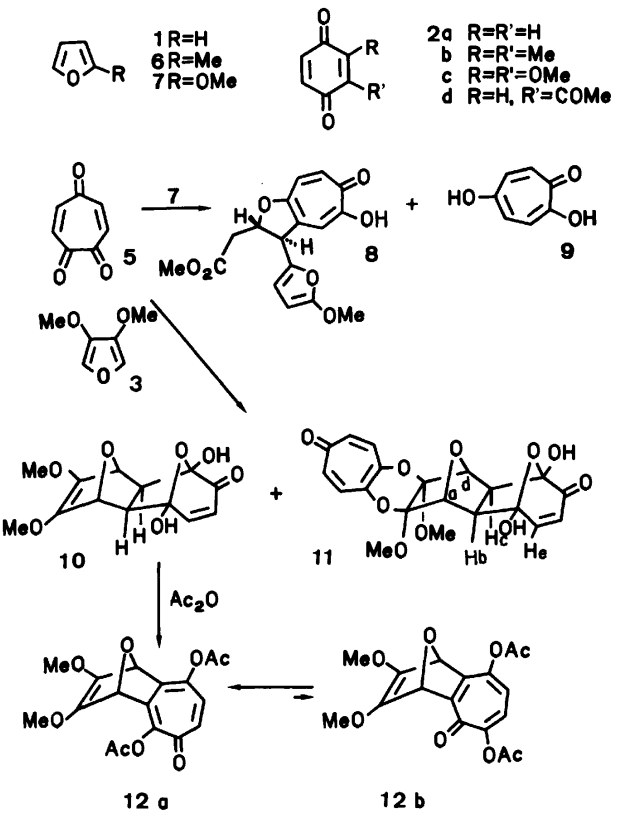

Scheme 1.

When the reaction of **5** with **1** or 2-methylfuran (**6**) was performed under 2800 bar at 40 °C, no identifiable product was formed. The reaction of **5** with 2-methoxyfuran (**7**) at room temperature gave a single adduct (**8**) in 24% yield with some amounts of 5-hydroxytropolone (**9**), which was inevitably formed by reduction of **5**. The molecular ion peak of **8** at m/z= 332, in the mass spectrum was indicated as being a 2 : 1-adduct of **7** with **5**. The IR spectrum of **8** still disclosed the presence of a tropone ring system and a newly-formed ester carbonyl function. The ^{1}H NMR spectrum revealed the signals ascribable to the ester methyl, at δ = 3.80, ethereal methyl on the furan ring, 3.69, and two furan ring protons, at 5.08 and 6.17, as well as four aliphatic proton signals, at 2.83 (2H), 4.41, and 5.11. In addition to these, there were three troponoid proton signals; at 7.12, which only spin-coupled to a proton on a sp^3-carbon, and an *AB*-pair at 6.94 and 7.24 (J=11 Hz). Analyses of these observations led to the assignment of the structure, 3-(5-methoxy-2-furyl)-5-hydroxy-2-methoxycarbonylmethyl-2,3-dihydro-1-oxaazulen-6-one. Presumably, the formation of **8** could be explained by a Michael-type addition of **7** to **5**, a furan-ring-cleavage, and a further Michael addition of **7** (as illustrated in Scheme 2).

This preferential occurrence of a Michael addition over a Diels-Alder reaction is of interest; since a distinct coloration occurred immediately after mixing **7** and **5** a charge-transfer complex should have been formed. Also, the recombination of the cation radical and the anion radical initiated a series of the subsequent C-C bond formations.[6] In this case, 5-hydroxytropolone was isolated in 33% from the reaction mixture. In this respect, a Michael addition of furans and thiophenes had a precedence in a benzenoid quinone, acetyl-*p*-benzoquinone (**2d**).[7]

On the other hand, the reaction of **5** with **3** under ordinary pressures afforded a 1 : 1-adduct (**10**) in 49% yield. Under 3000 bar at room temperature, the reac-

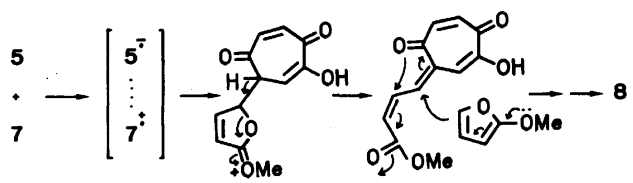

Scheme 2.

tion afforded an additional product (**11**) in 17% yield together with **10** in 59% yield. However, the yield of **11** under 2900 bar at 40 °C improved to 58% and that of **10** decreased to 18%. Hence, **10** is a precursor of **11**. The ^{1}H NMR spectrum of **10** immediately identified its structure to be an exo-Diels-Alder product on the basis of a lack of the vinyl protons on the furan ring: The proton signals ascribable to the ethereal carbons were doublets (J=1 Hz) at δ=4.90 and 4.99 which indicated the exo-orientation, and two mutually-coupled (J=9.5 Hz) olefinic proton signals at 5.97 and 7.33 were appropriate for the α,β-unsaturated keto group. These NMR data closely resembled those of 8-oxabicyclo[3.2.1]oct-3-en-2-one derivatives,[8] and suggested the formation of the same framework via an intramolecular hemiacetalization.[9] This was verified when **10** was treated with acetic anhydride in pyridine, a diacetate **12** was obtained and it possessed a 2,5-diacetoxytropone structure. The proton signals on the ethereal carbons caused a down-field shift, δ=5.31 and 5.49, and the observed magnitude of the coupling constant for the vicinal protons on the troponoid ring was J=13 Hz, from which, the α-acetoxy keto function could be expressed as depicted (**12a**).[10] It is interesting to point out that **12** showed no tendency of an "acetotropy" which is common in the 2-acetoxytropones.[11] Probably, a bond strain from the fused oxanorbornene framework might disfavor the contribution of the isomeric form, **12b**. Indeed, the ^{13}C NMR of **12** has not revealed any appreciable broadening of the signals at room temperature.

The structure of **11** was also elucidated by the NMR spectral data: Its ^{1}H NMR spectrum resembled that of **10**, other than the additional signals at 6.94 (2H) and 7.40 (2H), ascribable to the overlapped tropone ring protons. Furthermore, the methoxyl signal moved to an up-field region. Therefore, **11** was assumed to be a secondary adduct of **5** with the dimethoxyethylene moiety of **10**. In this case, the α-dioxo group of **5** worked as the 4π component in the Diels-Alder reactions; as a cyclic α-diketone, this also has a precedence.[12] The stereochemistry of the methoxyl groups was assigned to be anti to two ether bridges on the basis of the positive nuclear Overhauser effect (NOE)[13] between the methoxyl and the methine proton signals (H_b and H_c), and between the β-proton (H_e) of the enone part and the H_b, respectively. This stereopreferential formation was parallel to other examples of the 7-oxabicyclo[2.2.1]heptene system.[14]

Consequently, the Diels-Alder reaction of **5** with **3** under normal- and high-pressure conditions gave a single exo-[4+2]π adduct, which was a thermodynamically controlled product. In the case of **2a** with **3**, the endo-[4+2]π adduct was the sole product under the ordinary pressure, but under the high-pressure conditions, e.g., 7000 to 19000 bar, the exo-[4+2]π adduct gradually increased.[4] This contrast in the stereoselectivity is noteworthy.

Experimental

Reaction of 5 with 7 under Ordinary Pressure. A benzene solution (1 cm^3) of **5** (68 mg) and **7** (213 mg) was kept at room temperature for 1 h. The resultant precipitate was filtered to collect **9** [22.8 mg; 33%], whose identity with the authentic sample was confirmed by direct comparisons. Silica-gel column chromatography of the filtrate afforded **8** [yellow crystals, mp 138—139 °C, 26.1 mg; 24%. Found: C, 61.62; H, 4.92%; M.W., 332.0938. Calcd for $C_{17}H_{16}O_7$: C, 61.44; H, 4.85%; M.W., 332.0895. ^{1}H NMR δ[15]=2.83 (2H, d, J=6 Hz), 3.69 (3H, s), 3.80 (3H, s), 4.41 (1H, dd, J=9, 1.5 Hz), 5.08 (1H, d, J=3.5 Hz), 5.11 (1H, dt, J=9, 6 Hz), 6.17 (1H, d, J=3.5 Hz), 6.94 (1H, d, J=11 Hz), 7.12 (1H, d, J=1.5 Hz), and 7.24 (1H, d, J=11 Hz). ^{13}C NMR δ=38.7, 50.6, 52.1, 57.8, 80.2, 81.9, 110.9, 118.4, 123.0 (2C), 139.0, 139.8, 158.6, 162.4, 166.5, and 170.2 (2C). IR ν 1740, 1585, 1460, and 1260 cm^{-1}. UV λ_{max}^{MeOH} 232 nm (ε=26600), 238 (27100), 342 (10700), 386 (7000), 400 (7600), and 425 (3700)].

Reaction of 5 with 3 under Ordinary Pressure. A benzene solution (1.5 cm^3) of **5** (30 mg) and **3** (70.4 mg) was kept at room temperature for 5 h. Silica-gel column chromatography of the mixture afforded **10** [colorless crystals, mp 129 — 131 °C (decomp), 30.5 mg; 49%. Found: C, 55.24; H, 5.11%. Calcd for $C_{13}H_{14}O_7$: C, 55.31; H, 5.01%. ^{1}H NMR (CD_3OD) δ=2.44 (1H, d, J=6.5 Hz), 2.70 (1H, d, J=6.5 Hz), 3.66 (3H, s), 3.68 (3H, s), 4.90 (1H, d, J=1 Hz), 4.99 (1H, d, J=1 Hz), 5.97 (1H, d, J=9.5 Hz), and 7.33 (1H, d, J=9.5 Hz). ^{13}C NMR (CD_3OD) δ=52.2, 57.2, 59.5 (2C), 78.4, 79.1, 101.4, 102.6, 127.4, 141.6, 142.3, 159.4, and 197.6. IR ν 3370, 3170, 1690, 1175, 1160, 1015, and 1005 cm^{-1}. UV λ_{max}^{MeOH} 218 nm (ε=8350)].

Reaction of 5 with 3 under High-Pressure. a) An isopropylbenzene (IB) solution (2.5 cm^3) of **5** (55.2 mg) and **3** (53.7 mg) was kept at room temperature under 3000 bar for 5 h. The silica-gel column chromatography of the mixture afforded **10** [67.4 mg; 59%] and **11** [colorless crystals, mp 223 °C (decomp), 14.2 mg; 17%. Found: C, 57.47; H, 4.58%. Calcd for $C_{20}H_{18}O_{10}$: C, 57.41; H, 4.35%. ^{1}H NMR (CD_3OD) δ=2.58 (1H, d, J=7 Hz), 2.86 (1H, d, J=7 Hz), 3.39 (3H, s), 3.43 (3H, s), 5.02 (1H, d, J=1 Hz), 5.07 (1H, d, J=1 Hz), 6.09 (1H, d, J=10 Hz), 6.94 (2H, d, J=12.5 Hz), 7.36 (1H, d, J=10 Hz), and 7.40 (2H, d, J=12.5 Hz). ^{13}C NMR (CD_3OD) δ=48.5, 49.4, 51.4, 52.9, 83.2, 84.4, 101.9, 103.3, 108.4 (2C), 128.3, 135.1 (2C), 137.6 (2C), 148.2, 148.5, 159.3, 187.8, and 197.0. IR ν 3020, 1705, 1550, 1510, 1212, 1180, 1110, and 1015 cm^{-1}. UV λ_{max}^{MeOH} 232 nm (ε=19500) and 337 (12000)].

b) An IB solution (3 cm^3) of **5** (54 mg) and **3** (62 mg) was kept at 40 °C under 2900 bar for 5 h. The silica-gel column chromatography of the mixture afforded **10** [19.9 mg; 18%] and **11** [48.2 mg; 58%].

Acetic Anhydride Treatment of 10. An Ac_2O solution (2.5 cm^3) of **10** (100.4 mg) and pyridine (2.5 cm^3) was kept at room temperature for 1 d. Evaporation of the solvent in vacuo revealed the formation of **12** [pale yellow crystals, 134 — 136 °C, 84.4 mg; 68%. Found: C, 58.45; H, 4.68%. Calcd for $C_{17}H_{16}O_8$: C, 58.62; H, 4.63%. ^{1}H NMR δ=2.29 (3H, s), 2.34 (3H, s), 3.71 (3H, s), 3.73 (3H, s), 5.31 (1H, d, J=2 Hz), 5.49 (1H, d, J=2 Hz), 6.77 (1H, d, J=13 Hz), and 6.94 (1H, d, J=13 Hz). ^{13}C NMR δ=20.4, 20.5, 59.2 (2C), 80.0, 80.5, 135.2, 136.3, 138.7, 142.1, 142.9, 143.7, 144.2, 147.2, 167.8, 168.8, and 177.9. IR ν 1770, 1675, 1600, 1230, 1185, 1165, 1115, and 1085 cm^{-1}. UV λ_{max}^{MeOH} 216 nm (ε=23650) and 302 (13800)].

Attempted Reaction of 5 with 1. A mixture of **5** (62 mg) and **1** (332 mg) was kept at 40 °C under 2800 bar for 12 h, no appreciable change occurred, and 21.8 mg (35%) of **5** was recovered.

Attempted Reaction of 5 with 6. A mixture of **5** (62 mg) and **6** (391 mg) was similarly kept at 40 °C under 2800 bar for 12 h. TLC of the mixture indicated no formation of

the adduct, and silica-gel column chromatography furnished no isolable material.

We thank The Ministry of Education, Science, and Culture for a financial support by a Grant-in-Aid for Scientific Research to S. S. (No. 61740294).

References

1) W. G. Dauben, C. R. Kessel, and K. H. Takemura, *J. Am. Chem. Soc.*, **102**, 6893 (1980).

2) J. Jurczak, T. Kozluk, S. Filipek, and C. H. Eugster, *Helv. Chim. Acta*, **66**, 222 (1983).

3) K. Matsumoto, Y. Ikemi, S. Hashimoto, H. S. Lee, and Y. Okamoto, *J. Org. Chem.*, **51**, 3729 (1986).

4) J. Jurczak, T. Kozluk, M. Takacz, and C. H. Eugster, *Helv. Chim. Acta*, **66**, 218 (1983).

5) S. Sugiyama, T. Tsuda, A. Mori, H. Takeshita, and M. Kodama, *Chem. Lett.*, **1986**, 1315.

6) A UV spectroscopic detection of the charge-transfer band has failed.

7) N. Baumann, S. Fumagalli, G. Weisgerben, and C. H. Eugster, *Helv. Chim. Acta*, **49**, 1794 (1966).

8) A. Mori, Y. Isayama, and H. Takeshita, *Bull. Chem. Soc. Jpn.*, **59**, 511 (1986).

9) We observed an easy intramolecular acetalization of a Diels-Alder adduct from **5** with cyclopentadiene; Hirama et al.[12] obtained a 1:1-adduct, **i**, at room temperature and a 1:2-adduct, **ii**, at 60 °C. However, when we carried out the reaction at 5 °C, another 1:2-adduct, **iii** (a hemiacetal) [colorless needles, mp 156—157 °C. Found: C, 71.31; H, 6.36%. Calcd for $C_{17}H_{18}O_4$: C, 71.30; H, 6.35%. ^{1}H NMR δ=1.2—1.4 (2H, m), 1.4—1.6 (2H, m), 2.50 (1H, dd, J=7.5, 4 Hz), 2.52 (1H, s, OH), 2.67 (1H, dd, J=8, 3 Hz), 2.87 (1H, dd, J=7.5, 3.5 Hz), 2.9—3.3 (3H, m), 3.30 (1H, dd, J=7.5, 4 Hz), 3.3—3.5 (1H, m), 4.00 (1H, s, OH), 5.85 (1H, dd, J=5, 2.5 Hz), 6.08 (1H, dd, J=5, 2.5 Hz), 6.12 (1H, dd, J=5, 2.5 Hz), and 6.31 (1H, dd, J=5, 2.5 Hz). ^{13}C NMR δ(DMSO-d_6)=43.9, 44.5 (2C), 46.4, 47.3, 48.3, 49.1, 49.9, 51.5, 54.4, 100.9, 101.4, 133.6, 133.9, 134.8, 135.6, and 204.8. IR ν 3425, 3370, 3325, and 1712 cm^{-1}], was isolated in 50% yield.

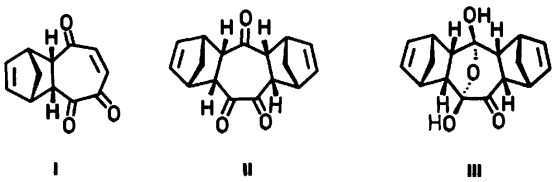

I II III

10) M. Sato, S. Ebine, and J. Tsunetsugu, *J. Chem. Soc., Chem. Commun.*, **1978**, 215.

11) S. Masamune, A. V. Kemp-Jones, J. Green, D. L. Rabenstein, M. Yasunami, K. Takase, and T. Nozoe, *Chem. Commun.*, **1973**, 283; H. Takeshita, A. Mori, H. Watanabe, T. Kusaba, S. Sugiyama, and M. Kodama, in preparation.

12) M. Hirama, Y. Koyama, Y. Shoji, and S. Itô, *Tetrahedron Lett.*, **1978**, 2289.

13) We thank Prof. Mitsuaki Kodama, Tokushima Bunri University, Tokushima, for these NOE experiments by a high-resolution instrument, a GX 400 spectrometer, JEOL Co.

14) P. A. Grieco, R. Lis, R. E. Zelle, and J. Finn, *J. Am. Chem. Soc.*, **108**, 5908 (1986).

15) Unless otherwise stated, the NMR spectra were measured in $CDCl_3$ solutions with an FX 100 spectrometer, JEOL Co.

Substitution-Type Thermal 1,2-Rearrangement. Synthesis of Chiral β-Aryl(or Alkenyl) α-Oxo Nitrile Acetal

Yutaka HONDA* and Gen-ichi TSUCHIHASHI*
Department of Chemistry, Faculty of Science and Technology, Keio University,
3-14-1 Hiyoshi, Kohoku-ku, Yokohama 223
(Received March 13, 1987)

Synopsis. Title compound was synthesized via a substitution-type thermal 1,2-rearrangement accompanied by introduction of a cyano group, and derived into the corresponding aldehyde, alkanoic acid, and amide.

In the last five years, we have studied on 1.2-rearrangement accompanied by introduction of hydroxide,[1-3] hydride,[4] alkanide, and alkynide anion[5] to give chiral α-substituted alkanoic ester, aldehyde acetal, and ketone acetal, respectively. They were promoted by elimination of sulfonyloxy group caused by heating or activation with Lewis acids (Eq. 1).

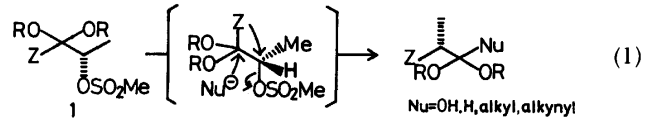

(1)

Now, we report a new thermal rearrangement accompanied by introduction of a cyano group.

Results and Discussion

Since cyanide anion is a strong nucleophile compared with hydroxide anion, cyano group was expected to be introduced even when chiral α-sulfonyloxy ketone acetal (**1**) is treated with sodium cyanide in aqueous solution. In practice, however, the corresponding alkanoic ester (**3**, Fig. 1) was formed quantitatively instead of the desired β-substituted α-oxo nitrile acetal (**2**). Under reflux conditions in anhydrous methanol, **2** was yielded in 11%, but the main product was also **3**. It is concluded that the attack of a large excess of methanol has occurred predominantly. As the results, **1** was treated with two equivalents of sodium cyanide in anhydrous dimethyl sulfoxide to yield chiral α-oxo nitrile acetal (**2**) in a good yield (Eq, 2, Table 1).

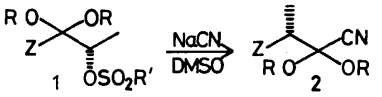

(2)

Obtained **2** was sensitive to light. Many by-products were generated in Entries 1—3, because the rate of migration of a phenyl group was extremely low. Taking into consideration of the reaction temperature and time, the migratory aptitudes are enhanced by the migrating groups in the order alkenyl≧*p*-methoxyphenyl>phenyl and by the acetal groups in the order dimethyl>trimethylene>2,2-dimethyltrimethylene.

α-Oxo nitrile acetal (**2**) can be transformed into the variety of the corresponding derivatives. At first **2** was treated with DIBAL (*i*-Bu_2AlH) to give an imino derivative quantitatively,[6] and then with oxalic acid dihydrate to give α,α-dialkoxy aldehyde (**4**) (Eq. 3,

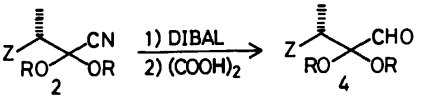

(3)

Table 1. Introduction of a Cyano Group

Entry	Z	R	R′	Temp/°C	Time/h	Yield/%	$[\alpha]_D$/° (*t*/°C, *c*, in $CHCl_3$)
1	Ph-		Me	130	54	38	+ 7.5 (24, 0.77)
2	〃		〃	〃	48	29	+ 5.8 (22, 0.89)
3	〃	Me	Br-C_6H_4-	〃	24	43	+ 7.4 (22, 0.82)
4	MeO-C_6H_4-		Me	〃	18	90	+ 5.6 (24, 1.00)
5	〃		〃	〃	16	85	+10.9 (21, 1.06)
6	〃	Me	〃	110	12	86	− 2.3 (21, 1.06)
7			〃	130	9	84	+68.8 (17, 1.20)
8	〃		〃	120	20	93	+69.2 (17, 1.34)
9	〃	Me	〃	120	4	75	+38.0 (17, 1.13)
10	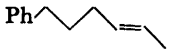		〃	130	11	76	+ 4.8 (20, 0.92)

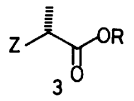

Fig. 1.

Table 2. Synthesis of α,α-Dialkoxy Aldehyde (**4**)

Z	R	Yield/%	$[\alpha]_D$/° (t/°C, c, in $CHCl_3$)
MeO-C_6H_4-		81	−15.7 (21, 1.00)
〃		71	−16.8 (20, 0.71)
〃	Me	78	− 7.0 (21, 0.99)
Ph		80	+17.5 (22, 0.74)
〃		75	+ 9.3 (21, 0.97)
〃	Me	78	+15.3 (21, 0.84)

Table 3. Synthesis of α,α-Dialkoxy Carboxylic Acid (**5**)

Z	R	Yield/%	$[\alpha]_D$/° (t/°C, c, in $CHCl_3$)
MeO-C_6H_4		95[a]	−19.1 (24, 0.79)
〃		91[a]	−16.1 (22, 0.68)
Ph		79[b]	+35.7 (21, 0.74)

a) $KMnO_4$-10% KOH. b) CrO_3-H_2SO_4-Acetone.

Table 2), which would be capable to be a useful building block for acyclic stereoselective synthesis of chiral compounds.

Aldehyde (**4**) was easily oxidized by treatment with $KMnO_4$-KOH[7] or Jones reagent in acetone to yield α,α-dialkoxy carboxylic acid (**5**) (Eq. 4, Table 3).

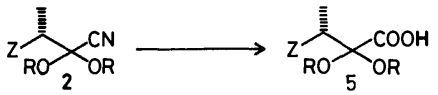

(4)

The absolute configuration of **2** was determined to be *S* from the sign of the specific rotation of the corresponding dithioacetal (**6**); $[\alpha]_D^{21} = -20.7°$ (c 0.34, $CHCl_3$), prepared from **5** in 88% yield by treatment with 1,3-propanedithiol in the presence of catalytic amount of $BF_3 \cdot OEt_2$ in dichloromethane at rt. An authentic **6**; $[\alpha]_D^{21} = -21.3°$ (c 0.35, $CHCl_3$), was prepared from (*S*)-aldehyde acetal (**7**)[4] by dithioacetalization, followed by lithiation and carboxylation with CO_2 (Fig. 2).

Table 4. Synthesis of α,α-Dialkoxy Amide (**8**)

R	Yield/%	$[\alpha]_D$/° (t/°C, c, in $CHCl_3$)
	95	−54.9 (22, 0.81)
Me	62	+ 8.8 (23, 0.64)

The enantiomeric excess was determined to be over 98% by HPLC analysis[8] of α,α-dimethoxy amide (**8**), which was prepared from **2** (R = $CH_2CMe_2CH_2$, Z = $MeOC_6H_4$) in 95% yield by treatment with 30% H_2O_2-NaOH in ethanol[9] (Eq. 5, Table 4).

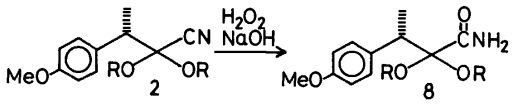

(5)

Consequently, it was concluded that the optical purity of the starting material, ethyl (*S*)-lactate,[10] was remained through the rearrangenent and the follwing derivation.

Experimental

General Synthetic Procedure of α-Oxo Nitrile Acetal (2). Under an argon atmosphere, **1** (1.00 mmol) was dissolved in anhydrous dimethyl sulfoxide (10 ml) containing sodium cyanide (2.00 mmol) in a sealed tube. The mixture was heated in dark, and allowed to cool to rt. It was poured into a vigorously stirred ice-water, and extracted with ethyl acetate (30 ml×2). The residual syrup was purified by using silica-gel column chromatography (hexane-ethyl acetate-pyridine) to give **2** as a colorless oil.

(*S*)-3-(*p*-Methoxyphenyl)-2-oxobutanenitrile 2,2-Dimethyltrimethylene Acetal: IR (film) $\nu = 2230\ cm^{-1}$; ^1H NMR (CCl_4) $\delta = 0.78$ (s, 3H), 0.99 (s, 3H), 1.42 (d, $J = 7.2$ Hz, 3H), 3.05 (q, $J = 7.2$ Hz, 1H), 3.46 (d, $J = 11.4$ Hz, 2H), 3.72 (d, $J = 11.4$ Hz, 2H), 3.73 (s, 3H), 6.69 (d, $J = 9.0$ Hz, 2H), 7.58 (d, $J = 9.0$ Hz, 2H) ppm. HRMS; Found: m/z 275.1539. Calcd for $C_{16}H_{21}NO_3$: M^+, m/z 275.1522.

(3*S*,4*Z*)-3-Methyl-2-oxo-8-phenyl-4-heptenenitrile 2,2-Dimethyltrimethylene Acetal: IR (film) $\nu = 2230\ cm^{-1}$; ^1H NMR (CCl_4) $\delta = 0.83$ (s, 3H), 1.10 (d, $J = 6.3$ Hz, 3H), 1.17 (s, 3H), 1.5—2.2 (m, 4H), 2.58 (t, $J = 7.5$ Hz, 2H), 2.83 (dq, $J = 8.3$ Hz, $J = 6.3$ Hz, 1H), 3.48 (d, $J = 10.8$ Hz, 2H), 3.76 (d, $J = 10.8$ Hz, 2H), 5.1—5.7 (m, 2H), 6.9—7.3 (m, 5H) ppm. HRMS; Found: m/z 313.2018. Calcd for $C_{20}H_{27}O_2N$: M^+, m/z 313.2043.

General Synthetic Procedure of α,α-Dialkoxy Aldehyde (4). Into a solution of α-oxo nitrile acetal (**2**, 1.00 mmol) in toluene (10 ml), DIBAL (1.20 mmol, in hexane) was added at −78 °C. After 30 min, THF (10 ml) and oxalic acid dihydrate (5 mmol) were added at 0 °C. The mixture was extracted with ethyl acetate (30 ml×2). Obtained residue was purified by using silica-gel column chromatography to give **4** as a colorless oil.

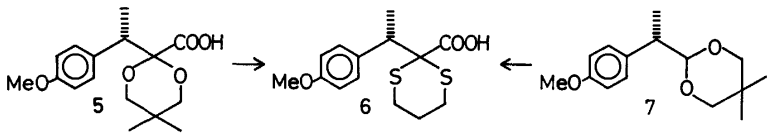

Fig. 2. Determination of the absolute configuration of **2**.

(*S*)-5,5-Dimethyl-2-formyl-2-[2-(*p*-methoxyphenyl)-propyl]-1,3-dioxane: IR (film) ν=1740 cm^{-1}; ^{1}H NMR (CCl_4) δ=0.65 (s, 3H), 1.04 (s, 3H), 1.32 (d, J=7.2 Hz, 3H), 2.89 (q, J=7.2 Hz, 1H), 3.43 (m, 4H), 3.73 (s, 3H), 6.65 (d, J=9.0 Hz, 2H), 7.08 (d, J=9.0 Hz, 2H), 9.20 (s, 1H) ppm. HRMS; Found: m/z 278.1515. Calcd for $C_{16}H_{22}O_4$, M^+: m/z 278.1519.

(*S*)-5,5-Dimethyl-2-formyl-2-[(*Z*)-1-methyl-6-phenyl-2-hexenyl]-1,3-dioxane: IR (film) ν=1735 cm^{-1}; ^{1}H NMR (CCl_4) δ=0.68 (s, 3H), 1.00 (d, J=7.2 Hz, 3H), 1.17 (s, 3H), 1.4—2.2 (m, 4H), 2.59 (t, J=7.5 Hz, 2H), 2.66 (dq, J=9.5 Hz, J=7.2 Hz, 1H), 3.2—3.5 (m, 4H), 5.1—5.5 (m, 2H), 6.9—7.3 (m, 5H), 9.36 (s, 1H) ppm. HRMS; Found: m/z 316.2026. Calcd for $C_{20}H_{28}O_3$, M^+: m/z 316.2036.

(*S*)-2-Carboxy-5,5-dimethyl-2-[2-(*p*-methoxyphenyl)-propyl]-1,3-dioxane (5): Colorless oil: IR (film) ν=1729 cm^{-1}; ^{1}H NMR (CCl_4) δ=0.67 (s, 3H), 0.96 (s, 3H), 1.32 (d, J=7.2 Hz, 3H), 3.43 (br m, 4H), 3.73 (s, 3H), 6.65 (d, J=8.4 Hz, 2H), 7.12 (d, J=8.4 Hz, 2H), 10.17 (br s, 1H) ppm. HRMS; Found: m/z 249.1502. Calcd for $C_{15}H_{21}O_3$, M^+-COOH: m/z 249.1491.

(*S*)-2-Carboxy-5,5-dimethyl-2-[(*Z*)-1-methyl-6-phenyl-2-hexenyl]-1,3-dioxane (5): Colorless oil: IR (film) ν=3070, 1715 cm^{-1}; ^{1}H NMR (CCl_4) δ=0.70 (s, 3H), 1.04 (d, J=6.9 Hz, 3H), 1.19 (s, 3H), 1.4—2.2 (m, 4H), 2.55 (t, J=7.5 Hz, 2H), 2.86 (dq, J=9.0 Hz, J=6.9 Hz, 1H), 3.2—3.7 (m, 4H), 5.1—5.5 (m, 2H), 6.9—7.3 (m, 5H), 10.92 (br s, 1H) ppm. HRMS; Found: m/z 287.1998. Calcd for $C_{19}H_{27}O_2$, M^+-COOH: m/z 287.2009.

(*S*)-2-Carboxy-2-[2-(*p*-methoxyphenyl)propyl]-1,3-dithiane (6): Colorless oil: IR (film) ν=1720 cm^{-1}; ^{1}H NMR ($CDCl_3$) δ=1.57 (d, J=7.2 Hz, 3H), 1.8—2.2 (m, 2H), 2.5—2.9 (m, 2H), 2.9—3.3 (m, 2H), 3.53 (q, J=7.2 Hz, 1H) 3.79 (s, 3H), 6.83 (d, J=9.0 Hz, 2H), 7.33 (d, J=9.0 Hz, 2H), 10.23 (br s, 1H) ppm. HRMS; Found: m/z 253.0715. Calcd for $C_{13}H_{17}OS_2$, M^+-COOH: m/z 253.0722.

(*S*)-2-Carbamoyl-5,5-dimethyl-2-[2-(*p*-methoxyphenyl)propyl]-1,3-dioxane (8): Colorless oil: IR (film) ν=1685 cm^{-1}, ^{1}H NMR ($CDCl_3$) δ=0.68 (s, 3H), 1.01 (s, 3H), 1.40 (d, J=6.9 Hz, 3H), 3.00 (q, J=6.9 Hz, 1H), 3.77 (s, 3H), 5.86 (br s, 1H), 6.02 (s, 1H), 6.76 (d, J=8.4 Hz, 2H), 7.21 (d, J=8.4 Hz, 2H) ppm. HRMS; Found: m/z 249.1517. Calcd for $C_{15}H_{21}O_3$, M^+-CONH_2: m/z 249.1491.

References

1) G. Tsuchihashi, S. Mitamura, K. Kitajima, and K. Kobayashi, *Tetrahedron Lett.*, **23**, 5427 (1982).

2) The detail of the general synthetic procedure of chiral α-arylalkanoic ester had been reported; Y. Honda, A. Ori, and G. Tsuchihashi, *Bull. Chem. Soc. Jpn.*, **60**, 1027 (1987).

3) Synthesis of chiral α-methyl-β-alkenoic esters had been reported; Y. Honda, A. Ori, and G. Tsuchihashi, *Chem. Lett.*, **1986**, 13.

4) Y. Honda, M. Sakai, and G. Tsuchihashi, *Chem. Lett.*, **1985**, 1153.

5) Y. Honda, E. Morita, and G. Tsuchihashi, *Chem. Lett.*, **1986**, 277.

6) J. A. Marshall, N. H. Andersen, and J. W. Schlicher, *J. Org. Chem.*, **35**, 858 (1970).

7) J. A. Marshall and J. L. Belletire, *Tetrahedron Lett.*, **1971**, 871.

8) Chiralcel OB offered from Daicel Chemical Industries, LTD. was used; MeOH/H_2O=9/1 (v/v), flow rate 0.4 ml min^{-1}, k'_S=8.10, α=k'_R/k'_S=1.64.

9) J. G. Wallace, "Hydrogen peroxide in organic chemistry", E. I. Du Pont Co., 42 (1962).

10) Determined to be over 98% ee by HPLC measurement of the corresponding (*R*)-MTPA ester by using Develosil (Nomura Chemical Co., LTD.); hexane/dichloromethane/methanol=6/1/0.007 (v/v/v), flow rate 0.4 ml min^{-1}, k'_S=3.24, α=k'_R/k'_S=1.21. Methyl (*R*)-lactate is also available (Aldrich, >98% ee), which can be converted into (*R*)-**2**.

Some Unusual Phase Transitions of Nickel(II) Diamine Complexes

Sukumar Roy, Goutam De, and Nirmalendu Ray Chaudhuri*
Department of Inorganic Chemistry, Indian Association for the Cultivation of Science, Calcutta 700 032, India
(Received December 26, 1985)

Synopsis. $[NiX_2(tn)_2]$, (tn=1,3-propanediamine; X_2=Br_2, SO_4, or SeO_4) undergoes phase transitions upon heating and reverts to their original structure upon cooling. These transitions have been investigated by differential scanning calorimetry and infrared spectroscopy.

Earlier, we reported the thermally induced phase transitions of nickel(II) diamine complexes.[1-5] Most of these phase transitions are time dependent reversible type and the extent of reversibility are found to be catalyzed by humid atmosphere. $[Ni(tn)_3]X_2$[6] and $[NiX_2(tn)_2]\cdot H_2O$[7,8] (X_2=Cl_2, Br_2, SO_4 etc.) were found to decompose through bis and monodiamine steps. We isolated and characterized all the possible intermediates. But we did not carry out thermal studies of these intermediates from the room temperature. This communication reports some new and interesting reversible phase transitions of $[NiX_2(tn)_2]$ (X_2=Br_2, SO_4, or SeO_4).

Experimental

Preparation of the Complexes: The complexes $[NiBr_2(tn)_2]$ (**1**) and $[Ni(SO_4)(tn)_2(H_2O)]$ (**3**) were prepared following the method reported earlier.[6,7]

The complex $[Ni(SeO_4)(tn)_2(H_2O)]$ (**8**) was prepared by mixing $NiSeO_4$ and the diamine in 1:2 molar ratio in water and subsequent precipitation by adding ethanol. This complex was recrystallized from water–ethanol (2:1) mixture.

Elemental analyses of these samples are in good conformity with their compositions. Infrared spectra were recorded in KBr matrices (pellets) on a Perkin Elmer 783 IR spectrophotometer. Temperatures of the samples were varied using a variable temperature cell with a temperature controller. C, H, and N were analyzed using a Perkin-Elmer 240C elemental analyzer. Electronic spectra were recorded in a Pye Unicam SP8-150 and Hitachi 330 spectrophotometer. Thermal measurements were carried out with a Perkin-Elmer DSC-2 differential scanning calorimeter. The enthalpy of melting of indium was used for the calculation of enthalpy changes associated with the phase transition.

Results and Discussion

Earlier, we reported the synthesis of $[NiBr_2(tn)_2)]$ from $[Ni(tn)_3]Br_2\cdot H_2O$ in solid state and its spectral properties.[6] This complex is slightly hygroscopic. It is very difficult to distinguish the cis or trans form of the nickel(II) octahedral complexes by usual spectral data. We have taken the electronic spectra (Table 1) of *trans*-$[Ni(NCS)_2(tn)_2]$,[1] $[NiBr_2(tn)_2]$, $[Ni(SO_4)(tn)_2(H_2O)]$,[7] and found hardly any difference. But the IR spectra of these three are quite different. Splitting of $\rho(CH_2)$ and $\delta(NH_2)$ of the latter two complexes suggest probably cis-structure (C_2 symmetry) of $[NiBr_2(tn)_2]$ (**1**).[9,10] Figure 1 and Table 2 show the thermal behavior of $[NiBr_2(tn)_2]$ (**1**) which shows one phase transition upon heating accompanied by no color change. The species **2**, after phase transition reverts to **1** upon cooling. IR spectra of **1** and **2** are taken at 380 K (room temperature IR spectrum of this complex is faulty owing to its hygroscopic nature) and 450 K, respectively (Table 3). It is found that **2** shows a simpler spectrum than **1**. Splitting of $\delta(NH_2)$, ν(C–N), ν(C–C), and $\rho_r(CH_2)$ bands occurs in **1**. This is absent or reduced in **2** (Table 3). This suggests **2** exists in more symmetrical form than **1**.

Earlier, we reported[7] thermal behavior of $[Ni(SO_4)(tn)_2(H_2O)]$ (**3**) where we presumed that water molecule in **3** was not coordinated to nickel as we were unable to record the IR spectrum of the dehydrated complex due to its hygroscopic nature. With the new technique of IR measurements, it was found that water molecule is coordinated in **3** as it shows $\rho_r(H_2O)$ at 731 cm^{-1} and $\rho_w(H_2O)$ at 700 cm^{-1}. These bands are found to be absent in the anhydrous species. With the help of IR the prediction about the mode of coordination of SO_4 in $[Ni(SO_4)(tn)_2(H_2O)]$ (**3**) and its dehydrated form **4** is not possible due to the serious overlapping of diamine and SO_4 bands.

Table 1. Electronic Spectral Data

Compound	$\frac{\lambda_{max}}{nm}$
$[NiBr_2(tn)_2]$	≈965 wbr,[a] 563, 362
$[Ni(SO_4)(tn)_2(H_2O)]$	≈955 wbr,[a] 680 sh,[b] 560, 360
trans-$[Ni(NCS)_2(tn)_2]$	≈965 wbr,[a] 563, 362

a) wbr=weak and broad. b) sh=shoulder.

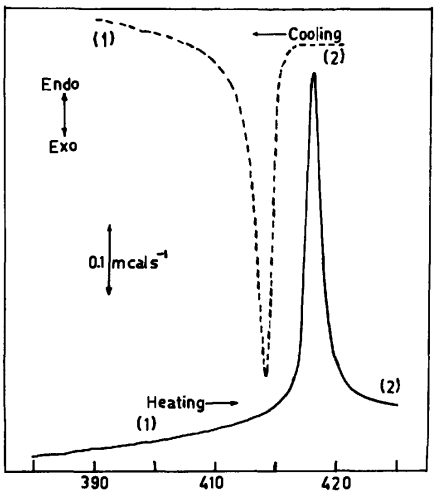

Fig. 1. DSC curves showing the transformations of: complex **1** (wt taken=12.73 mg) into **2**, heating curve (——); **2** into **1**, cooling curve (----).

But SO_4 appears to be unidentate in **3**, which exists in octahedral geometry as is evident from its electronic spectral data (Table 1) and magnetic moment reported by us.[7] However, on comparison of the geometry attained by the analogous species $[Ni(SeO_4)(tn)_2]$,[7] bidentacy of SO_4 may be predicted indirectly in **4**. It is interesting to note that the dehydrated complex $[Ni(SO_4)(tn)_2]$ (**4**) undergoes three successive reversible phase transitions (Table 2; Fig. 2). Earlier,[7] we could not notice these phase transitions in DTA curve because the first two peaks were hidden in the endothermic peak associated with the elimination of water and the third peak was weak in nature which was not possible to detect by DTA. Differential scanning calorimetry traces of the phase transitions (both heating and cooling curve) are shown in Fig. 2. These phase transitions are not associated with any color change. On comparison the IR spectra of **3**,

Table 2. Thermal Data

Phase transition	Heating		Cooling		ΔH
	Temp range / K	Peak temp / K	Temp range / K	Peak temp / K	kJ mol^{-1}
$[NiBr_2(tn)_2]$ (**1**) $\underset{\text{Cooling}}{\overset{\text{Heating}}{\rightleftarrows}}$ $[NiBr_2(tn)_2]$ (**2**)	411.0—438.5	426.5	434.5—393.5	418.0	1.53
$[Ni(SO_4)(tn)_2(H_2O)]$ (**3**) $\xrightarrow[-H_2O]{\text{Heating}}$ $[Ni(SO_4)(tn)_2]$ (**6**)	353.0—403.0	388.0			
$[Ni(SO_4)(tn)_2]$ (**4**) $\underset{\text{Cooling}}{\overset{\text{Heating}}{\rightleftarrows}}$ $[Ni(SO_4)(tn)_2]$ (**5**)	353.0—375.5	368.7	362.0—342.5	355.5	0.96
$[Ni(SO_4)(tn)_2]$ (**5**) $\underset{\text{Cooling}}{\overset{\text{Heating}}{\rightleftarrows}}$ $[Ni(SO_4)(tn)_2]$ (**6**)	376.2—401.0	385.7	396.0—364.0	382.0, 373.5	0.29
$[Ni(SO_4)(tn)_2]$ (**6**) $\underset{\text{Cooling}}{\overset{\text{Heating}}{\rightleftarrows}}$ $[Ni(SO_4)(tn)_2]$ (**7**)	403.0—433.0	417.8	422.5—401.7	412.5	0.25
$[Ni(SeO_4)(tn)_2(H_2O)]$ (**8**) $\xrightarrow[-H_2O]{\text{Heating}}$ $[Ni(SeO_4)(tn)_2]$ (**10**)	320.0—375.0	354.0			
$[Ni(SeO_4)(tn)_2]$ (**9**) $\underset{\text{Cooling}}{\overset{\text{Heating}}{\rightleftarrows}}$ $[Ni(SeO_4)(tn)_2]$ (**10**)	362.0—376.0	372.5	391.0—378.5	360.5	
$[Ni(SeO_4)(tn)_2]$ (**10**) $\underset{\text{Cooling}}{\overset{\text{Heating}}{\rightleftarrows}}$ $[Ni(SeO_4)(tn)_2]$ (**11**)	376.0—406.5	392.0	378.5—346.5	383.5	0.67

Table 3. IR Data

Compound	$\delta(NH_2)$	$\delta(CH_2)$	$\rho_w(CH_2)$	$\nu(C\text{-}N)+\nu(C\text{-}C)$	$\rho_r(CH_2)$
$[NiBr_2(tn)_2]$ (**1**)	1587 sh,	1462 sh,	1397 m,	1087 w,	910 s,
	1583 sh,	1455 w,	1381 m,	1069 ms,	869 w,
	1577 s	1448 vw,		1009 s	864 w
		1428 w			
$[NiBr_2(tn)_2]$ (**2**)	1583 sbr	1467 sh,	1395 wbr	1100 vw,	913 s,
		1461 w,		1073 m,	874 vw
		1451 vw,		1014 msbr	
		1432 w			
$[Ni(SO_4)(tn)_2(H_2O)]$ (**3**)[a]	1584 vs,	1468 m,	1403 m,	1070 s,	908 s,
	1560 s,	1455 w,	1392 m,	1023 s	880 w,
	1554 s	1439 m	1358 vw		805 vw
$[Ni(SO_4)(tn)_2]$ (**4**)	1578 s	1458 m,	1396 m,	1075 s,[b]	918 s,
		1450 w,	1383 ms,	1019 s	878 m, 874 m,
		1433 w,	1346 vw		800 vw
		1428 w			
$[Ni(SO_4)(tn)_2]$ (**7**)	1576 sbr	1460 w,	1394 m,	1075 s,[b]	915 s,
		1452 w,	1386 m,	1016 s,	876 m,
		1448 w,	1382 m,	1012 sh	800 vw
		1430 w	1347 vw		

a) (**3**) shows $\delta(HOH)$, $\rho_r(H_2O)$, and $\rho_w(H_2O)$ bands at 1628 s, 731 s, and 700 s cm^{-1}. b) Spectra complicated due to overlapping of diamine vibration with ν_3 of SO_4. Some diamine vibrations are masked by SO_4 vibration.

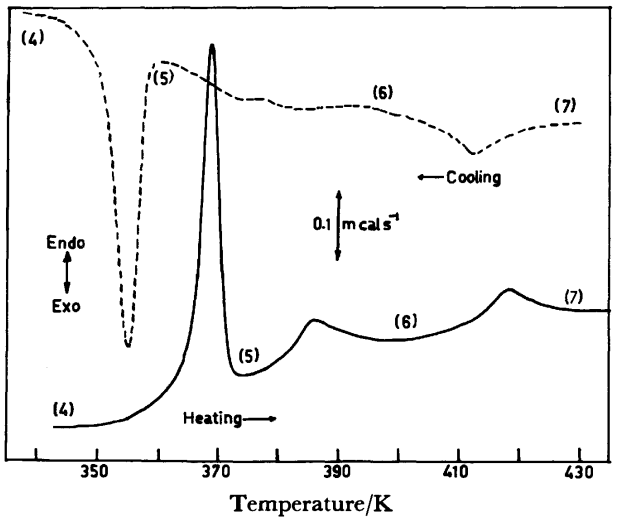

Fig. 2. DSC curves showing the transformations of: complex **4** (wt taken=16.08 mg) into **5**, **6**, and **7**, heating curve (——), **7**, into **6**, **5**, and **4**, cooling curve (----).

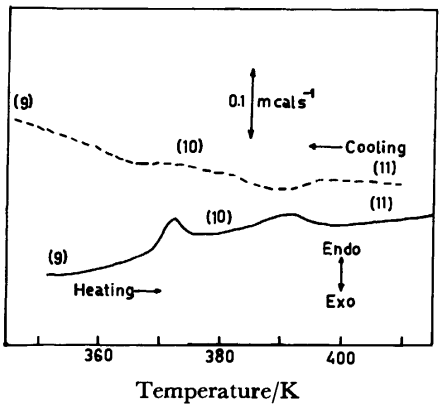

Fig. 3. DSC curves showing the transformations of: complex **9** (wt taken=11.85 mg) into **10** and **11**, heating curve (——), **11** into **10** and **9**, cooling curve (----).

4, and **7** taken at 303, 340, and 435 K respectively (Table 2), it is noticed that complex **3** possesses more infrared active bands than **4** and **7**. IR spectra of **4** and **7** differ in the $\delta(NH_2)$, $\delta(CH_2)$, $\rho_w(CH_2)$, ν(C-N), ν(C-C), and $\rho_r(CH_2)$ regions (Table 3). These data indicate that the six-membered chelate conformations in **4** and **7** are different.

$[Ni(SeO_4)(tn)_2(H_2O)]$ (**8**) shows similar IR and electronic spectra to its corresponding sulfato complex **3**. Its dehydration and phase transition phenomena are tabulated in Table 2. Figure 3 shows the differential scanning calorimetry traces of the phase transitions of $[Ni(SeO_4)(tn)_2]$ (**9**). It shows two overlapping endothermic peaks during heating and transforms to **11** via **10**. Here, the enthalpy changes for the transformation of **9**→**11** is low in comparison to the bromo and sulfato complexes. This is probably due to the presence of large anion SeO_4^{2-} (ionic size of which is larger than SO_4^{2-} and Br^-). Regarding IR spectra of **9** and **11**, we observe only a little difference.

The occurrence of phase changes in $[NiX_2(tn)_2]$ (X_2=Br_2, SO_4, or SeO_4) but not in $[NiCl_2(tn)_2]$ is probably due to the intramolecular interaction of the large anion with hydrogen atoms of the six-membered chelate owing to its unfavorable entropy effect.[11] Experiments have been carried out with large anion like halogenoacetates. But any phase transition phenomena were not noticed due to the decomposition of halogenoacetates at appreciably low temperatures.

References

1 G. De, P. K. Biswas, and N. Ray Chaudhuri, *J. Chem. Soc., Dalton Trans.*, **1984**, 2591.
2) G. De and N. Ray Chaudhuri, *Trans. Met. Chem.*, **10**, 476 (1985).
3) A. Ghosh, G. De, and N. Ray Chaudhuri, *J. Therm. Anal.*, **30**, 471 (1985).
4) A. Ghosh, G. De, and N. Ray Chaudhuri, *Thermochim. Acta*, **92**, 747 (1985).
5) A. Ghosh, G. De, and N. Ray Chaudhuri, *Trans. Met. Chem.*, **11**, 81 (1986).
6) G. De, P. K. Biswas, and N. Ray Chaudhuri, *Bull. Chem. Soc. Jpn.*, **56**, 3145 (1983).
7) S. Mitra, G. De, and N. Ray Chaudhuri, *Thermochim. Acta*, **71**, 107 (1983).
8) S. Mitra, G. De, and N. Ray Chaudhuri, *Thermochim. Acta*, **66**, 187 (1983).
9) M. E. Baldwin, *J. Chem. Soc.*, **1960**, 4369.
10) M. L. Morris and D. H. Busch, *J. Am. Chem. Soc.*, **82**, 1521 (1960).
11) E. J. Correy and J. C. Bailar, Jr., *J. Am. Chem. Soc.*, **81**, 2620 (1959).

 © 1987 The Chemical Society of Japan Bull. Chem. Soc. Jpn., 60, 2705—2711 (1987)

The Brillouin Scattering of Highly Viscous Mixtures

Ryuki HASHITANI, Shinobu KODA, and Hiroyasu NOMURA*
Department of Chemical Engineering, School of Engineering, Nagoya University, Chikusa-ku, Nagoya 464
(Received November 28, 1986)

The sound velocities of mixtures of tri-*o*-tolyl phosphate and diisobutyl phthalate were measured by means of the Brillouin scattering method in the temperature range from 214 to 333 K. The velocity dispersion was observed in the mixtures at temperatures from 273 to 323 K in the gigahertz region. The velocity dispersion was attributed to the structural relaxation, as in the case of pure highly viscous liquids. The reduced variable method proposed by Lamb et al. could not be applied to the storage moduli over wide frequency and temperature ranges. The relaxation curves of the reduced storage modulus obtained at room temperature, where the viscosity obeyed the Arrhenius equation, were well expressed by a single relaxation equation. The structural relaxation mechanism of the highly viscous liquids investigated here is related to the weak cooperative motions of molecules in the liquid state. The activation energy, ΔE_τ, obtained from the temperature dependences of the relaxation times was about a third of those estimated from the Arrhenius plots of the shear viscosities of the mixtures.

Generally, liquids cannot support shear stress, no matter how small it may be. They yield or flow in response to the applied shear stress. However, on a short time scale, liquids can show elastic properties. Therefore, in the liquid state relaxations exist which are related to the collective motion of molecules. Such relaxations are called viscoelastic and/or structural relaxations. In order to study the dynamical aspects of the local structure in liquids and solutions, information on the mechanism of structural relaxation is highly desirable. Highly viscous liquids, such as glycerol and 1,3-butanediol, are suitable for the investigation of these relaxations, since they have long relaxation times as a result of their high viscosities at low temperatures and their relaxation times can be easily determined by experiments.

Such highly viscous liquids, which have no definite freezing point, are called "supercooled liquids." The viscoelastic and/or structural relaxations of supercooled liquids have been extensively investigated by means of ultrasonic methods, and the studies have been summarized.[1] In the studies by Lamb's school, the relaxation curves were obtained by superimposing the data at different temperatures on the basis of a reduced variable method. i.e., the frequency-temperature superposition method, applied to the elastic modulus, since measurable ultrasonic frequencies were limited to a narrow range. Besides, in the experiments on ultrasonic methods, measurements were made only at low temperatures, since, at room temperature, the relaxation times are too short to be measured in the megahertz region. In view of this situation, direct measurements of relaxation behavior in higher temperature ranges are indispensable to elucidate the structural relaxation mechanism of highly viscous liquids in detail.

The Brillouin scattering method is also very useful for investigating the structural relaxation of highly viscous liquids. The Brillouin spectra which arise from the local thermal density fluctuation provide information about the dynamic properties of liquids in the GHz region.

Previously, we investigated the relaxation behavior of two pure highly viscous liquids, tri-*o*-tolyl phosphate[2] and diisobutyl phthalate,[3] by means of Brillouin scattering method. Assuming that the reduced variable method can be applied to the data obtained from Brillouin scattering, as well as those from the ultrasonic method, the master curves obtained were analyzed by means of the generalized B.E.L. (Barlow, Erginsav, and Lamb) model.[1] The values of the parameter K in the generalized B.E.L. equation were found to be around 0.3—0.5, within the limits of experimental error, although, in ultrasonic studies, the K's of these materials have been found to be nearly unity.[1] Besides, the data on the master curves deviated systematically from the curves calculated by the B.E.L. model, even if experimental errors were taken into account. These results suggested that a reduced variable method might be invalid for the superposition of elastic moduli over such wide frequencies as from MHz to GHz regions. However, the differences in K values obtained by the two methods were not so large that we could not conclude clearly whether or not the reduced variable method was useful.

In order to ascertain the validity of the reduced variable method for analyzing the data in the GHz region, and in order to discuss the relaxation mechanism in detail, careful experiments are required.

Large deviations in the parameter K from unity were observed by Barlow et al.[4] for several binary mixtures of supercooled liquids in their ultrasonic studies. The values of the parameter K have varied widely, from about 0.2 to about 2.0, depending on the mole fraction of the components of the binary mixtures. Besides, these composition dependences of the parameter K have been expressed by a universal curve, independent of the species of the supercooled liquids.

In this paper, the structural relaxation of binary mixtures of diisobutyl phthalate and tri-*o*-tolyl phosphate are investigated by means of the Brillouin scattering method. The compositions of the binary mixtures were chosen as 0.20 mole fraction and 0.78 mole fraction of diisobutyl phthalate. In these composi-

tions, the parameter K takes the minimum and maximum values. The spectra were observed over wide frequency ranges at various temperatures, especially in the relaxation regions. The dependences of the relaxation behavior on the temperature and/or the frequency are discussed by comparing the data in the GHz region with those in the MHz region. The structural relaxation mechanism of highly viscous liquids in the higher-temperature range is also discussed.

Experimental

The diisobutyl phthalate (DIBP), which was of a guaranteed grade, was obtained from the Nakarai Chemicals Co., Ltd., while a practical grade of tri-*o*-tolyl phosphate(TOTP) was obtained from Eastman Organic Chemicals. They were distilled under reduced pressure. Mixtures with composition of 0.78 and 0.20 mole fraction of DIBP were prepared. For pure DIBP, some measurements were carried out in addition to those previously reported.,[3] The sample liquids were poured into the scattering cells through a millipore filter with a pore size of 1.0 μm.

The Rayleigh-Brillouin spectra were obtained by the use of a pressure-scanning Fabry-Perot interferometer, using a He-Ne laser (NEC, GLG 5800, output 50 mW). Measurements were done over the temperature range from 214 to 331 K (0.78 DIBP mole fraction) and from 223 to 333 K (0.20 DIBP mole fraction). At 263, 273, 298, and 323 K, spectra were obtained over scattering angles from 40 to 145°. The experimental procedures were described in detail previously.[2,5]

The sound velocity and density were measured by means of an ultrasonic interferometer operating at 5 MHz and by means of the buoyancy balance method respectively. The viscosity measurements were carried out using a rotational viscometer, which was calibrated using standard sample liquids with known viscosities. The refractive indexes were measured by the use of an Abbe refractometer, manufactured by the Erma Optical Co., Ltd. All measurements were carried out within the temperature range from about 260 to 340 K. The values needed for the data analysis at the lower temperature were estimated by means of the extrapolation method.

Results

Typical Rayleigh-Brillouin scattering spectra of the 0.78 DIBP mole fraction mixture are shown in Fig. 1 at a constant scattering angle (θ=90°) as a function of the temperature. The sound velocity, V, can be calculated from the Brillouin shift, Δf, and the scattering angle, θ, by the use of the following relation;

$$V = \frac{\lambda_i \, \Delta f}{2n \sin(\theta/2)} \tag{1}$$

where λ_i is the wavelength of the incident light, and n, the refractive index of the sample.

Figure 2 shows the frequency dependence of the sound velocities of the samples obtained. The data measured at 273, 298, and 323 K all show clear sound velocity dispersions. These velocity dispersions can be attributed to the structural relaxation, much as in the

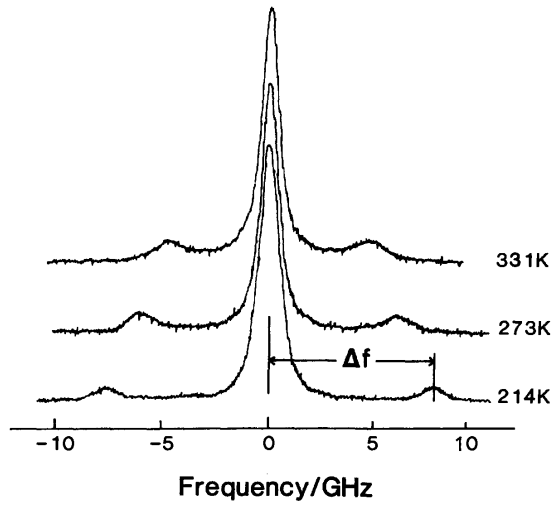

Fig. 1. Representative Rayleigh-Brillouin spectra of 0.78 mole fraction mixture at the scattering angle at 90°.

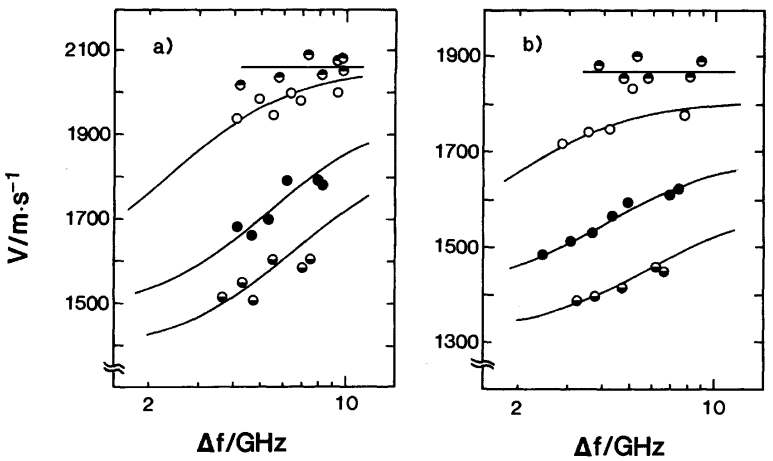

Fig. 2. Frequency dependence of sound velocities. a) 0.2 DIBP mole fraction, b) 0.78 DIBP mole fraction. ◓: −10°C, ○: 0°C, ●: 25°C, ◒: 50°C.

cases of pure DIBP[3] and TOTP.[2] The temperature dependences of the sound velocity obtained from the Brillouin scattering spectra at the scattering angle of 90° are shown in Figs. 3 and 4. In those figures, the temperature dependences of the sound velocities are different in the lower and higher temperature ranges. The sound velocities in the higher temperature region belong to those in the relaxation range, as is shown in Fig. 2. Besides, the sound velocities for the 0.20 DIBP mole fraction and 0.78 DIBP mole fraction mixtures below 260 K were almost independent of the frequencies investigated, as is shown in Fig. 2. Therefore, we can consider that the sound velocities below 260 K shown in Figs. 3 and 4 correspond to the velocities of the high-frequency limit. These limiting values were fitted to the following Doolittle type equation;

$$V_\infty = \frac{a}{T} + b \tag{2}$$

where T is the absolute temperature. The following values were obtained for the fitting parameters: a=4.00×10^5 (m s^{-1} K^{-1}), b=339 (m s^{-1}) for the 0.78 DIBP mole fraction and a=3.59×10^5 (m s^{-1} K^{-1}), b=739 (m s^{-1}) for the 0.20 DIBP mole fraction.

The sound velocities measured at 5 MHz by means of an ultrasonic interferometer were used as the low-frequency limiting sound velocities, as is usually done. The temperature dependences of these data were reproduced by the following linear relations;

V_0=−3.410×T+2420 for the 0.20 DIBP mole fraction (3)

and;

V_0=−3.573×T+2538 for the 0.78 DIBP mole fraction. (4)

In order to discuss the viscoelastic behavior of highly viscous liquids, the storage modulus, M', which is the real part of the complex longitudinal modulus, M^* ($=M'+iM''$), was calculated by the use of $M'=\rho V^2$ assuming that $(\alpha V/\omega)^2 \ll 1$, where ρ is the density and α is the absorption coefficient of the sound wave in a sample.

Discussion

The Validity of the Reduced Variable Method. First, we will discuss the value of making a composed relaxation curve, a master curve, by means of the reduced variable method for structural relaxation, as was proposed by Lamb's school. According to the reduced variable method, proposed by Lamb, a reduced elastic modulus, $(M'-M_0)/(M_\infty-M_0)$, should be plotted against $\omega\eta_s/G_\infty$, where ω is the angular frequency ($\omega=2\pi f$) and where G_∞ is the shear modulus at the high frequency limit. In our mixed systems, no values of G_∞ were found at any temperature in any literature. For this reason, we used the parameter $\omega\eta_s/M_2$ ($M_2=M_\infty-M_0$) instead of $\omega\eta_s/G_\infty$. According to Litovitz and Davis,[6] the relation $(1/M_2)(\partial M_2/\partial T)=(1/G_\infty)(\partial G_\infty/\partial T)$ holds over a wide temperature range and the quantity G_∞/M_2 is independent of the temperature.

Therefore, a reduced plot of $(M'-M_0)/(M_\infty-M_0)$ against $\omega\eta_s/M_2$ should provide the same distribution of relaxation times as those obtained by plotting the reduced modulus against $\omega\eta_s/G_\infty$. The master curves obtained are shown in Figs. 5 and 6 for the 0.20 DIBP mole fraction mixture and 0.78 DIBP mole fraction mixture, respectively.

Assuming the generalized B.E.L. equation for complex shear and bulk moduli,[1,4] the expression for complex longitudinal modulus can be given as follows;

$$\frac{M^*-M_0}{M_\infty-M_0} = C\left[1+\left(\frac{1}{i\zeta\omega\tau_s}\right)+2K\left(\frac{1}{i\zeta\omega\tau_s}\right)^{1/2}\right]^{-1} + (1-C)\left[1+\left(\frac{1}{i\omega\tau_s}\right)+2K\left(\frac{1}{i\omega\tau_s}\right)^{1/2}\right]^{-1} \tag{5}$$

and

$$C=\frac{K_\infty-K_0}{M_\infty-M_0}=1-\frac{4}{3}\frac{G_\infty}{M_\infty-M_0},\quad \tau_s=\frac{\eta_s}{G_\infty}$$

$$\zeta=\frac{\tau_v}{\tau_s}=\frac{\eta_v}{\eta_s}\frac{G_\infty}{K_\infty-K_0}=\frac{3}{4}\frac{\eta_v}{\eta_s}\frac{1-C}{C}$$

where η_s and η_v are the shear and bulk viscosities and where K is an adjustable parameter which represents a measure of the distribution of the relaxation times. As has been mentioned previously, the estimation of the parameters, C and ζ, of our experimental systems is impossible, since the data on G_∞ are lacking. However, the values of C and ζ exert little effect on the shape of the relaxation curve calculated from Eq. 5. The broken lines in Figs. 5 and 6 are those calculated using Eq. 5 with the same values of C=0.35, and ζ=2.64 as were used for pure DIBP. The values of K

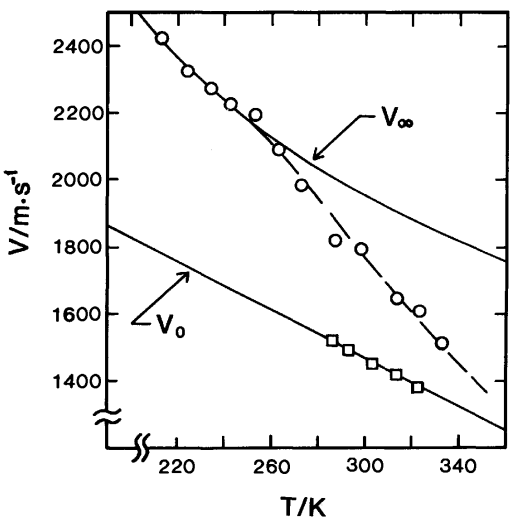

Fig. 3. Temperature dependence of sound velocities for 0.2 DIBP mole fraction. ○: Brillouin scattering (scattering angle at 90°), □: ultrasonic interferometer (5 MHz).

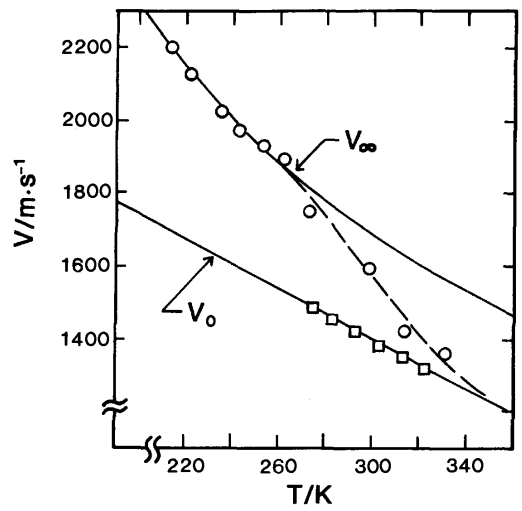

Fig. 4. Temperature dependence of sound velocities for 0.78 DIBP mole fraction. O: Brillouin scattering (scattering angle at 90°), □: ultrasonic interferometer (5 MHz).

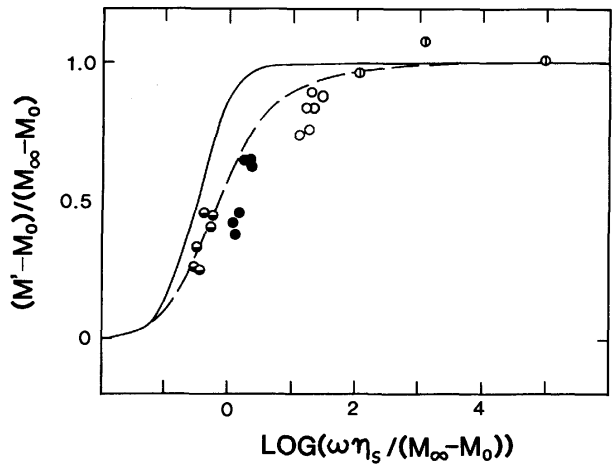

Fig. 5. Plots of $(M'-M_0)/(M_\infty-M_0)$ against log $(\omega\eta_s/(M_\infty-M_0))$ for 0.2 DIBP mole fraction. The solid and broken lines were drawn by the generalized B.E.L. Eq. 5 with $K=0$ and $K=0.28$, respectively. O: 0°C, ●: 25°C, ◒: 50°C, Φ: others.

used in Figs. 5 and 6 were 0.28 and 1.8 respectively; they were determined by experiments in the ultrasonic region.[4] The solid lines in Figs. 5 and 6 correspond to the Maxwell equation with $K=0$ in Eq. 5.

As is shown clearly in Figs. 5 and 6, the data obtained in the GHz region do not agree with the broken lines in either case. This indicates that the reduced variable method fails in the superposition of elastic moduli over such a wide frequency range as from the MHz to the GHz region. Besides, the data in the GHz region deviate systematically from the curve calculated using Eq. 5. Consequently, we can not draw a master relaxation curve for both systems. Moreover, the data at each constant temperature form a group which seems to be parallel to a Maxwellian relaxation curve.

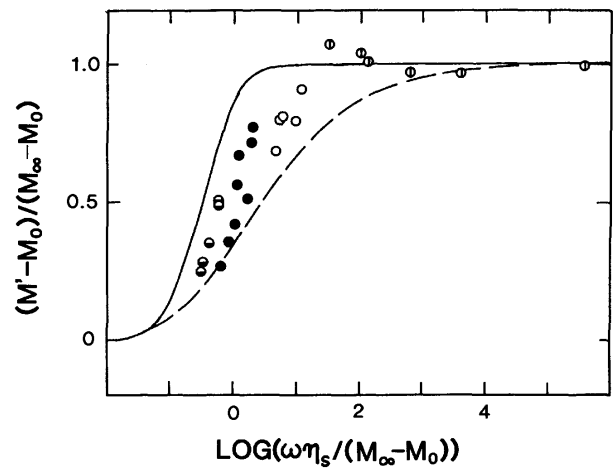

Fig. 6. Plots of $(M'-M_0)/(M_\infty-M_0)$ against log $(\omega\eta_s/(M_\infty-M_0))$ for 0.78 DIBP mole fraction. The solid and broken lines were drawn by the generalized B.E.L. Eq. 5 with $K=0$ and $K=1.8$, respectively. O: 0°C, ●: 25°C, ◒: 50°C, Φ: others.

As is shown in Fig. 6, the data corresponding to $(M'-M_0)/(M_\infty-M_0)=0.5$, can be measured at 298 K with an angular frequency, $\omega=2.5\times10^{10}$ (rad s^{-1}), that is, $f=\omega/2\pi=3.99$ (GHz). In order to obtain the same plot based on the ultrasonic method working at $f=50$ (MHz), and considering the temperature dependence of V_0, V_∞, η_s, and ρ, the temperature must be controlled at about 242 K. Brillouin scattering provides information about the relaxation behavior at room temperature, while the ultrasonic methods provide information in the low temperature region.

Therefore, we can clearly conclude that the reduced variable method for the relation between $(M'-M_0)/(M_\infty-M_0)$ and $\omega\eta_s/M_2$ may hold for the behavior at low temperatures, but that it breaks down at room temperature.

Relaxation Spectrum Obtained by Brillouin Scattering. Apart from the generalized B.E.L. model and the reduced variable method, we would like to examine Figs 5 and 6 carefully. As has been mentioned previously, we can recognize in Figs. 5 and 6 that the data at the same temperature are located on the line parallel to the Maxwellian curve in both cases. If the reduced elastic modulus, $(M'-M_0)/(M_\infty-M_0)$, in the GHz region could be expressed by the following single relaxation equation;

$$\frac{M'-M_0}{M_\infty-M_0}=\frac{\omega^2\tau^2}{1+\omega^2\tau^2} \tag{6}$$

where τ is the relaxation time, the plot of $((M'-M_0)/(M_\infty-M_0))^{-1}$ against $1/\omega^2$ should be linear and its slope should show the square of the reciprocal relaxation time, $1/\tau^2$. As an example, Fig. 7 shows this relationship between $((M'-M_0)/(M_\infty-M_0))^{-1}$ and $1/\omega^2$ for the case of 0.78 DIBP mole fraction at each temperature. As may be seen in Fig. 7, linear relationships are obtained within the limits of experimental error. Sim-

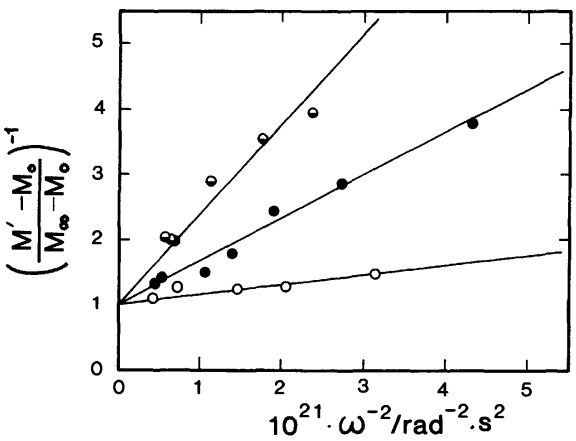

Fig. 7. Plots of $((M'-M_0)/(M_\infty-M_0))^{-1}$ against $1/\omega^2$ for 0.78 DIBP mole fraction.
○: 0°C, ●: 25°C, ◒: 50°C.

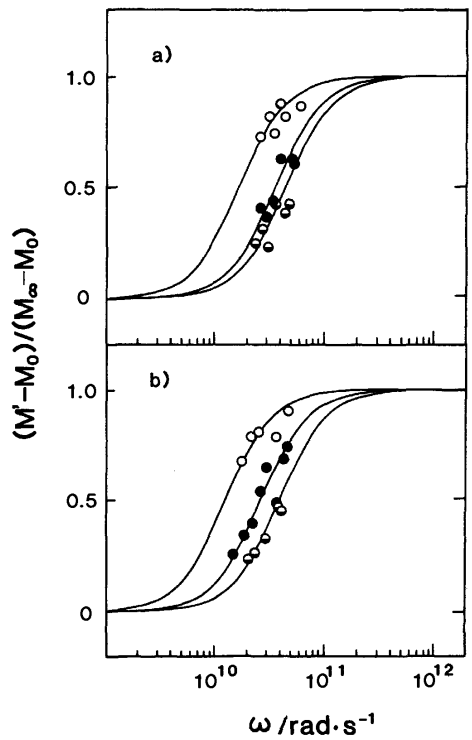

Fig. 8. Plots of $(M'-M_0)/(M_\infty-M_0)$ against angular frequency ω. a): 0.2 DIBP mole fraction, b): 0.78 DIBP mole fraction. ○: 0°C, ●: 25°C, ◒: 50°C. Solid lines were drawn by single relaxation Eq. 6.

ilar linear relationships are also obtained for the case of the 0.2 mole fraction at each temperature. Using the relaxation times thus obtained, the reduced elastic moduli, $(M'-M_0)/(M_\infty-M_0)$, in the GHz region can be well expressed by a single relaxation equation (Eq. 6) within the measured frequency and temperature ranges, as is shown in Fig. 8.

Previously, we also analyzed the Brillouin scattering data of pure DIBP[3] and TOTP[2] by the use of the generalized B.E.L. equation, on the basis of the reduced variable method. However, as has been mentioned above, the elastic moduli measured over a wide frequency range and at several constant temperatures suggested that the reduced variable method might be invalid for analyzing the Brillouin scattering data. Therefore, the previous experimental data for the pure systems of DIBP and TOTP were re-analyzed using a single relaxation equation by means of the method described above. Figure 9 shows plots of $(M'-M_0)/(M_\infty-M_0)$ against the observed Brillouin frequency. A single relaxation process can reproduce very well the experimental results at any temperature of our experiments. Thus, it is confirmed that the viscoelastic behavior of highly viscous liquids at higher temperatures, (that is, around room temperature) can be expressed well by a single relaxation process.

Similar single relaxation behavior in viscoelastic and/or structural relaxations have previously been reported. Tauke, Litovitz, and Macedo[7] reported that the B_2O_3 in the liquid state behaves as a simple Maxwellian liquid in the temperature ranges where its viscosity obeys the Arrhenius viscosity equation, while the liquid of B_2O_3 showed relaxation processes with a wide distribution of relaxation times in the temperature ranges where its viscosity is expressed in terms of the free volume type, namely, the Doolittle-type equation. For the molten zinc chloride, a single relaxation time was also observed for the absorption of the longitudinal wave in the frequency range from 5 to 95 MHz at temperature ranges from 582 to 673 °C.[8] Madigosky and Warfield,[9] who carried out ultrasonic relaxation

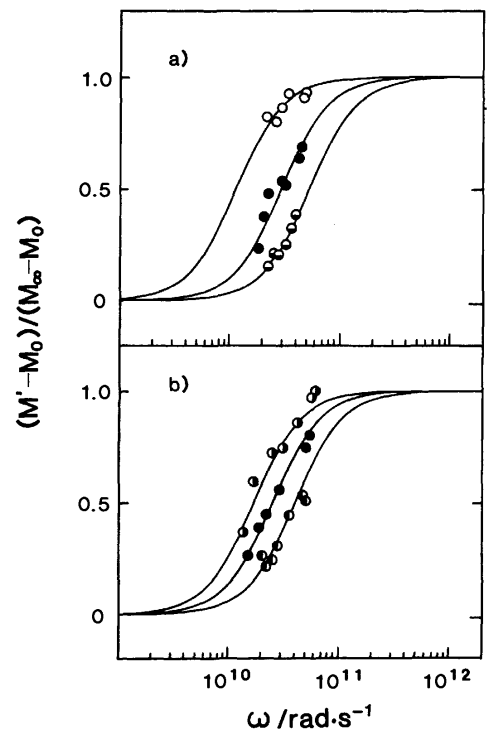

Fig. 9. Plots of $(M'-M_0)/(M_\infty-M_0)$ against angular frequency ω. a): Pure DIBP, b): pure TOTP.
○: 0°C, ◑: 10°C, ●: 25°C, ◐: 40°C, ◒: 50°C.
Solid lines were drawn by single relaxation Eq. 6.

measurements in the frequency range from 5.5 to 200 MHz, concluded that the mixture of water and dimethyl sulfoxide (DMSO) shows structural relaxation behavior at temperatures below −55 °C. This relaxation behavior can also be expressed by a single relaxation equation, while the viscosities of these mixtures can be fitted well by Arrhenius equation in the temperature ranges investigated. In these papers, it was suggested that single relaxation behavior is observed if the viscosity obeys the Arrhenius viscosity equation.

Figure 10 shows the temperature dependence of the viscosities of the 0.20 and 0.78 DIBP mole fraction mixtures. As may be seen in Fig. 10, in the high temperature region the relationship between ln η and $1/RT$ is almost linear for the liquid mixtures involved here. This also indicates that, in the temperature range where the temperature dependence of the viscosity is expressed by the Arrhenius equation, the relaxation spectrum of the elastic modulus of liquids shows a single relaxation.

Litovitz and McDuffie[10] considered that, in a liquid

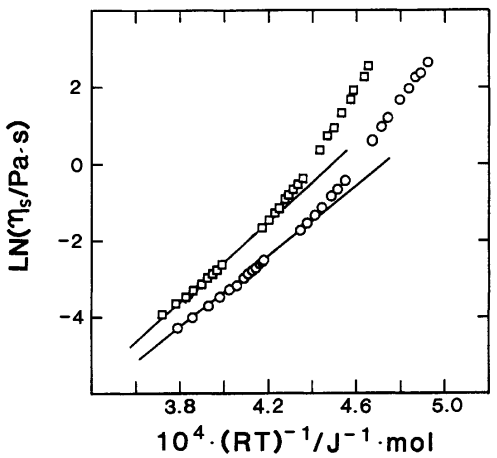

Fig. 10. Plots of ln η_s against $1/RT$. □: 0.2 DIBP mole fraction, ○: 0.78 DIBP mole fraction. The lines were drawn by fitting the data in the higher temperature region to linear relation between ln η_s against $1/RT$.

obeying a free volume type equation for viscosity, a molecule moves in a manner cooperative with the surrounding ones, while in a liquid obeying Arrhenius viscosity equation, the motions of molecules have a non-cooperative character. They proposed that the distribution of the relaxation time arises from the cooperative motions of molecules. From this point of view, the relaxation behavior of the reduced elastic moduli of highly viscous liquids obtained from Brillouin scattering are considered to be related to the weak cooperative motions of molecules.

The relaxation times of pure TOTP, the 0.20 DIBP mole fraction, the 0.78 DIBP mole fraction, and pure DIBP at various temperatures, and the activation energies obtained from the linear plot of ln τ against $1/RT$, are summarized in Table 1. In view of the experimental errors, it is difficult to discuss the concentration dependence of ΔE_τ. The activation energy for viscosity, ΔE_η, obtained from the slope in Fig. 10 is also listed in Table 1. The values of ΔE_τ are about a third those of ΔE_η. Also, the concentration dependence of ΔE_η can not be found clearly.

The composition of a mixture should affect the cooperative motions of molecules very much because of the large differences in their molecular size and in their intermolecular interaction. As for the low-temperature behavior which corresponds to that of the free volume type liquids, the relaxation curves (broken lines in Figs. 5 and 6) depend largely on the composition of the mixture. The values of the parameter K in the generalized B.E.L. equation vary largely, from 1.8 for the 0.78 DIBP mole fraction to 0.28 for the 0.2 DIBP mole fraction.[4] On the contrary, in the case of high-temperature behavior obtained from the Brillouin scattering investigated here, all the relaxation curves can be reproduced well by the use of the single relaxation equation. This fact also confirms that the cooperative character involved is weak in this relaxation mechanism.

Very recently, Oh et al.[11] have reported the experimental results on the Rayleigh-Brillouin spectra of bis(2-ethylhexyl)sebacate (hereafter abbreviated as DOS) and tetracosane at temperatures higher than their

Table 1. Relaxation Times at Various Temperatures and Activation Energies

Temperature	DIBP	0.78 DIBP mole fraction	0.20 DIBP mole fraction	TOTP
K	ps	ps	ps	ps
273	88.0	81.7	62.8	
283				58.7
293				56.1
298	34.6	38.9	29.1	32.5
303				30.2
313				24.8
323	19.0	26.9	23.6	
ΔE_τ (kJ mol^{-1})	22.5±1.3	14.5±2.6	16.3±1.6	23.5±3.7
ΔE_η (kJ mol^{-1})	50.2[a]	46.6	48.3	60.3[b]

a) Ref. 13. b) Ref. 14.

melting points. They analyzed the temperature dependences of the Brillouin spectra, using the generalized hydrodynamic theory proposed by Lin and Wang,[12] and concluded that these spectra were attributable to the single relaxation of the longitudinal stress modulus. The relaxation times estimated by them are 49 and 67 ps at 325 K, while the activation energies are 16.1 and 12.7 kJ mol^{-1} for DOS and tetracosane respectively. Their experimental results are in close agreement with ours. They have pointed out that this relaxation is related to the structural relaxation of liquids, but they did not present any detailed relaxation picture.

Conclusion

According to the experimental results obtained in this investigation, the following conclusions can be drawn. 1) The reduced variable method proposed by Lamb et al. does not hold over the wide temperature and frequency ranges. 2) The relaxation spectra of the elastic moduli of highly viscous liquids and mixtures at higher temperature and in the GHz region can be well expressed by a single relaxation equation. 3) In the temperature range where the single relaxation spectrum is obtained, the viscosity of liquids and mixtures can be expressed by the Arrhenius equation. 4) The activation energies obtained by the relation between ln τ and $1/RT$ were a third of those obtained from the Arrhenius plot of viscosity. These facts indicate that this structural relaxation mechanism is related to the weak cooperative motions and the elementary dynamic properties of liquids.

References

1) G. Harrison, "The Dynamic Properties of Supercooled Liquids," Academic Press, London (1976).
2) S. Koda, H. Nomura, M. Nakamura, and Y. Miyahara. *Bull. Chem. Soc. Jpn.*, **58**, 1484 (1985).
3) S. Koda, R. Hashitani, and H. Nomura. *Bull. Chem. Soc. Jpn.*, **58**, 3465 (1985).
4) A. J. Barlow, A. Erginsav, and J. Lamb. *Proc. R. Soc. London, Ser. A*, **309**, 473 (1969).
5) H. Nomura, H. Shimizu. Y. Tanaka. S. Koda. T. Okunishi, S. Kato, and Y. Miyahara, *Bull. Chem. Soc. Jpn.*, **55**, 3899 (1982).
6) T. A. Litovitz and C. M. Davis, "Physical Acoustics," ed by W. P. Mason, Academic Press. New York (1965), Vol. IIA, pp. 329—331.
7) J. Tauke, T. A. Litovitz, and P. B. Macedo, *J. Am. Ceram. Soc.*, **51**, 158 (1968).
8) G. J. Gruber and T. A. Litovitz, *J, Chem. Phys.*, **40**, 13 (1964).
9) W. M. Madigosky and R. W. Warfield, *J. Chem. Phys.*, **78**, 1912 (1983).
10) T. A. Litovitz and G. E. McDuffie, Jr., *J. Chem. Phys.*, **39**, 729 (1963).
11) T. G. Oh, E. W. Fischert, G. P. Hellmann, T. P. Russell. and C. H. Wang, *Polymer.* **27**, 261 (1986).
12) Y.-H. Lin and C. H. Wang, *J. Chem. Phys.*, **70**, 681 (1979).
13) A. J. Barlow, J. Lamb, and J. Matheson, *Proc. R. Soc., London, Ser. A*, **292**, 322 (1966).
14) A. J. Barlow, A. Erginsav, and J. Lamb, *Proc. R. Soc., London, Ser. A*, **298**, 481 (1967).

 © 1987 The Chemical Society of Japan Bull. Chem. Soc. Jpn., 60, 2713—2718 (1987)

Homogeneous and Electrochemical Electron-Transfer Reaction of Nitrobenzene Anion Radical Dissolved in Nitrobenzene

Kosaku SUGA* and Shigeru AOYAGUI
Department of Chemical Engineering, Tokyo Institute of Technology, Ohokayama, Meguro-ku, Tokyo 152
(Received November 28, 1986)

Nitrobenzene anion radical was stably prepared by the electrolytic reduction of nitrobenzene solution containing various kinds and amounts of tetraalkylammonium perchlorates. The rate constants of homogeneous electron-transfer reactions of these nitrobenzene anion radicals with nitrobenzene molecules as a solvent were determined by ESR method at various temperatures. These rate constants at 25 °C were about 10^7 dm^3 mol^{-1} s^{-1} and comparable with the rate constant of electron-transfer reation between nitrobenzene and its anion radial in *N,N*-dimethylformamide. The quasi-first order rate constants evaluated from these rate constants were about 10^8 s^{-1} and were larger than the rate constants of the intramolecular electron-transfer reactions of the anion radical of bis(*p*-nitrophenyl) compounds except for bis(*p*-nitrophenyl)methane. The absorption spectrum of the solution of nitrobenzene anion radical in nitrobenzene containing 0.1 M tetrabutylammonium perchlorate or 0.1 M tetraethylammonium perchlorate showed an additional weak peak at about 800 or 900 nm as well as the ordinary peak. The light energies of these additional peaks were in good agreement with the energy values of the optical electron-transfer reactions evaluated according to the theory of Hush from the activation energies of corresponding thermal electron-transfer reactions. The rate constants of electrochemical electron-transfer reactions and the diffusion coefficients of nitrobenzene anion radical in nitrobenzene were also measured.

Nitrobenzene (NB) is well-known to be reduced to a stable anion radical in an aprotic solvent as *N,N*-dimethylformamide (DMF),[1] and also can be used as a solvent at room temperature. An anion radical molecule dissolved in a solvent composed of its parent molecules such as NB^- in NB, can exchange its electron with contiguous parent molecules. Such an electron-exchange reaction is different from usual electron-exchange reactions in the following points: Anion radical and its parent molecules are always in contact with one another, and therefore do not require their encounter prior to the electron transfer between them. This would be expected to cause the following unique behavior of such a system. According to Hush,[2] electron-transfer reactions can be caused not only by thermal energy but also by optical energy when two reactants are in the immediate neighbourhood of each other. He discussed the relation between the activation energy of a thermal electron-transfer reaction and the light energy of the corresponding optical electron-transfer reaction. In the electron-transfer systems examined by them, however, only one of the values of the electron-transfer rate and the absorption maximum was determined. Therefore, the theory about the relation between them has not yet been proved experimentally. Since NB^- molecules are always in the immediate neighbourhood of NB molecules in the considering NB^-/NB system, the possibility of the occurrence of the optical electron-transfer reaction between them may be very high. Furthermore, the rate constant of thermal electron-transfer reaction between them can be easily determined by ESR.

On the other hand, as suggested by Levich,[3] Dahms,[4] and Ruff and Friedrich,[5] the large increase of the apparent diffusion coefficient of anion radicals due to an electron-hopping mechanism may be expected to occur in these systems.

In this paper, we report the rate constants and the activation energies of homogeneous electron-transfer reactions, the absorption spectra, the rate constants of electrochemical electron-transfer reactions, and the diffusion coefficients of NB^- prepared by electrolytic reduction of NB containing various tetraalkylammonium perchlorates. Furthermore, we will examine the possibility of the occurrence of an optical electron-transfer reaction and the increase of the diffusion coefficients of NB^- in this system by making use of these results.

Experimental

Reagents. Nitrobenzene commercially obtained was purified by passing through a column packed with activated alumina from ICN Pharmaceuticals GmbH & Co. Tetrabutylammonium perchlorate (TBAP) and tetraethylammonium perchlorate (TEAP) used as supporting electrolytes were prepared and purified as described in the previous paper.[6]

Cell and Electrodes. Electrolytic cell used for electrochemical measurements was an air-tight Pyrex glass cell composed of three compartments. For voltammetric measurements, a platinum gauze and a platinum sphere were used as the counter and working elctrodes respectively. The reference electrode used for the measurements of cyclic voltammogram (CV) for a NB solution without NB^- was composed of a silver wire dipped in the NB solution which was saturated with $AgNO_3$ and contained the same supporting elctrolyte as the test solution. The reference and the counter electrode used for the measurements of CV for a NB solution containing NB^- was the platinum gauze electrode in the test solution. For bulk electrolysis, the platinum gauze electrode was used as the working electrode, and a platinum spiral wire was used as the counter electrode. Bulk electrolysis was carried out while stirring the solution with a magnetic stirrer.

Electrochemical Measurements. The anion radical of NB

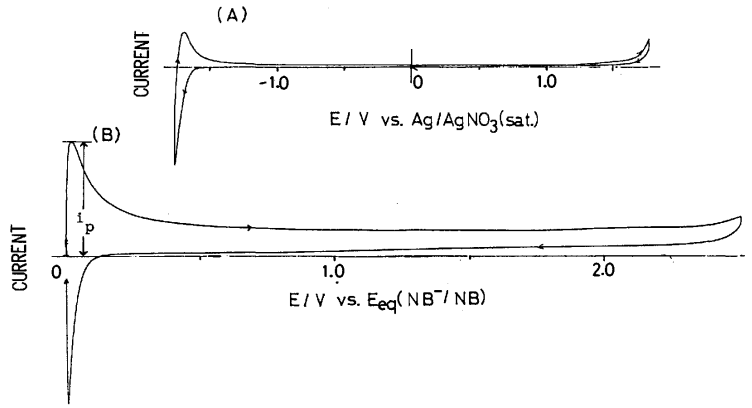

Fig. 1. Cyclic voltammograms of NB containing 0.1 M TEAP; (A) without NB^-, (B) with 0.8 mM NB^-. Scan rate: 0.1 V s^{-1}.

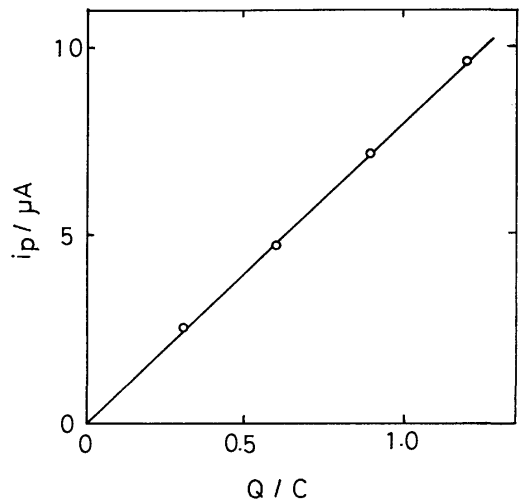

Fig. 2. Dependence of peak current, i_p, on the quantity of electricity, Q, consumed during the electrolytic reduction of NB containing 0.1 M TEAP.

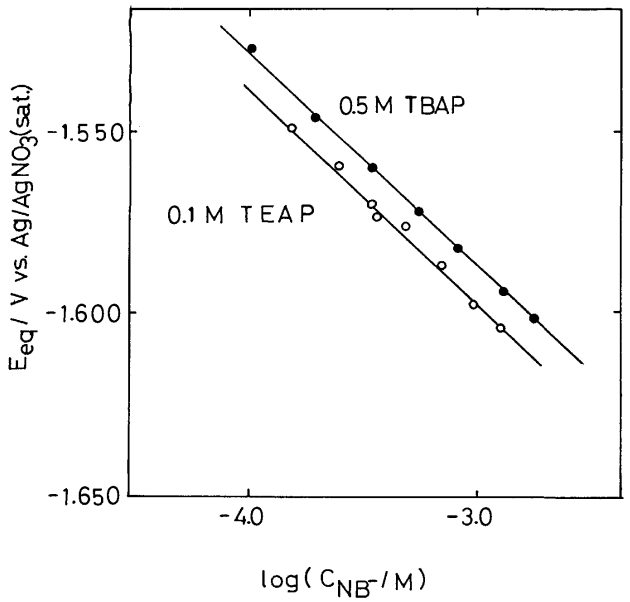

Fig. 3. Nernst plots for the NB^-/NB systems in NB containing 0.1 M TEAP and 0.5 M TBAP.

was prepared by electrochemical reduction. The concentration of NB^- was determined by the quantity of electricity passed during the electrolysis. Diffusion coefficients were determined by potential step chronoamperometry. Standard rate constants of the electrochemical electron transfer reactions were determined by the galvanostatic double pulse (gdp) method. A conventional potentiostat and function generators assembled from operational amplifiers were used for linear sweep voltammetry. Galvanostatic double pulse measurements were performed on an apparatus devised in this laboratory.[7]

ESR Measurements. ESR spectra were measured with a JEOL JES3BSX ESR spectrometer equipped with a variable temperature adapter.

Results and Discussion

Electrochemical Preparation of NB^- in NB. Figure 1 (a) shows the CV of a solution of NB containing 0.1 M TEAP (1 M=1 mol dm^{-3}). This CV showed a sharp cathodic current rise corresponding to the reduction of NB to NB^-, and an anodic peak corresponding to the oxidation of NB^- at about −1.6 V. During the bulk electrolysis with constant current, the solution gradually became brown coloured. Figure 1 (b) shows the CV of a solution of NB^- in NB containing 0.1 M TEAP prepared by the eletrolytic reduction as described above. This CV was obtained by scanning from the equilibrium potential of NB^-/NB. It shows an anodic peak current (illustrated as i_p in Fig. 1 (b)) corresponding to the oxidation of NB^- existing in the test solution, at the potential about 25 mV positive from the equilibrium potential.

Figure 2 shows the dependence of i_p for such solution on the quantity of electricity (Q) consumed during the electrolytic preparation of the solution. Good linearity was attained between i_p and Q. Moreover, the values of i_p, which are proportional to the concentration of NB^- in NB containing various tetraalkylammonium perchlorates, decreased only 10—20% after a period of one night from the end of the preparation. These results show that NB^- in NB prepared electrolytically is fairly stable.

Table 1. Standard Redox Potentials, $E°$, of NB^-/NB Systems in NB Containing Various Kinds and Amounts of Tetraalkylammonium Perchlorates

Supporting electrolyte	$E°(NB^-/NB)$/V vs. $Ag/AgNO_3$(sat.)	
	Potentiometry	Potential sweep method
0.1 M TEAP	−1.782	−1.782
0.17 M TEAP	−1.778	−1.757
0.1 M TBAP	−1.775	−1.757
0.5 M TBAP	−1.764	−1.783

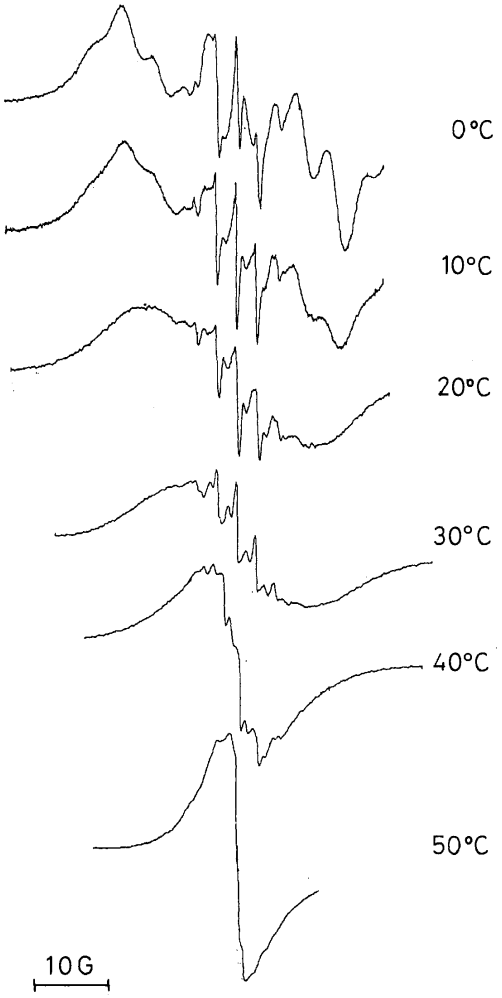

Fig. 4. ESR spectra of NB^- prepared by the electrolytic reduction of NB containing 0.5 M TBAP at various temperatures. Concentration of NB^- is about 1 mM.

In Fig. 3, we show the Nernstian plots between equilibrium potentials and the logarithm of the concentrations of NB^- determined from Q for the solution of NB^- in NB containing 0.1 M TEAP or 0.5 M TBAP. These plots showed good linearity. The solutions of NB^- in NB containing other supporting electrolyte also showed linear Nernstian plots. All of the slopes of these Nernstian plots were close to 60 mV per decade of concentration. This result shows that the electrode reactions of NB^- in NB containing several tetraalkylammonium perchlorates are the reversible ones accompanying the transfer of one electron. Table 1 shows the value of the standard redox potentials for NB^-/NB couples determined from these Nernstian plots in NB containing several kinds and amounts of tetraalkylammonium perchlorates, together with those determined by the potential sweep method according to the literatures.[8] The values determined by both methods agreed well with each other.

Homogeneous Electron-Transfer Reaction of NB^- in NB. Figure 4 shows the ESR spectra of the solutions of NB containing about 1 mM of NB^- and 0.5 M TBAP at various temperatures. Each spectrum was composed of one group of intense broad lines corresponding to NB^- superposed by another group of weak and sharp lines corresponding to a small amount of paramagnetic impurity probably formed by the decomposition of NB^-. The ESR signal due to NB^- at low temperature has a hyperfine structure, but this hyperfine structure disappeared and the ESR lines changed to a single broad one at higher temperature. ESR spectra of the solutions of NB containing NB^- and other tetraalkylammonium perchlorates are similar to these spectra.

These ESR signals due to NB^- can be well reproduced by computer simulation by the use of a modified Bloch equation. By these simualations we can determine the rate constant (k) of the homogeneous electron-exchange reactions between NB^- and NB. In these simulations we have used the values of hyperfine coupling constants for NB^- produced electrolytically in *N,N*-dimethylformamide (DMF) containing TEAP.[1] Figure 5 shows the Arrhenius plots for the rate constants of homogeneous electron-exchange reactions between NB^- and NB in the solutions containing 0.1 M TEAP or 0.5 M TBAP determined as described above. The respective rate constants at the same temperature are different from each other, and their activation energies are equal to 31 and 35 kJ mol^{-1} for the solutions containing 0.1 M TEAP or 0.5 M TBAP, respectively. This difference may be due to the ion pairing of NB^- with the different tetraalkylammonium ions as well as in the case of anthracene anion radical.[6]

Table 2 shows the homogeneous rate constants for the electron-exchange reactions at 25 °C between NB^- and NB determined in this experiment together with the value determined in DMF by Malachesky et al.[9] It is noteworthy that the values in this experiment are nearly equal to that in DMF. In this experiment, the

molecule of NB^- is always in contact with NB molecules, but such a situation did not affect the rate of the electron-exchange reaction. The reason for this result may be based on the fact that these reactions are slow and not diffusion limited.

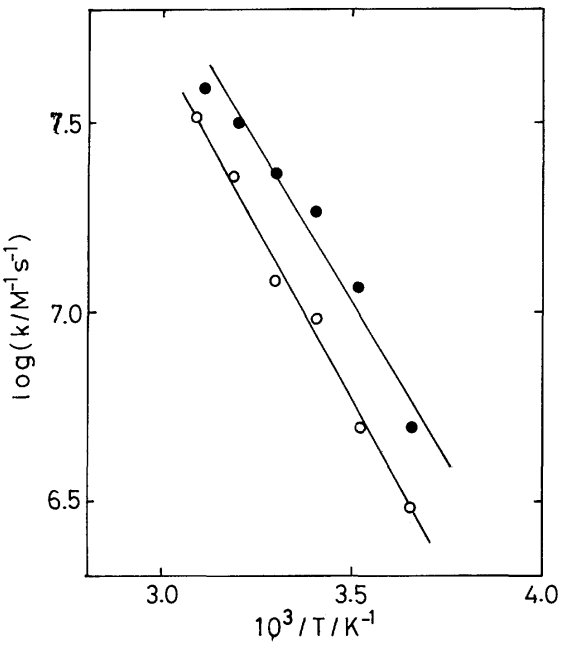

Fig. 5. Arrhenius plots for homogeneous electron-transfer reactions of NB^-/NB systems in NB containing (—○—) 0.5 M TBAP or (—●—) 0.1 M TEAP.

Table 2. Rate Constants of Homogeneous Electron-Transfer Reactions between NB^- and NB at 25 °C

Solvent	Supporting electrolyte	$k/M^{-1}s^{-1}$
NB	0.1 M TEAP	1.9×10^{7} a)
NB	0.5 M TBAP	1.5×10^{7} a)
DMF	0.01 M TEAP	3.0×10^{7} b)

a) This experiments. b) Ref. 9.

However, such a situation is interesting from another view point. Since the NB^- molecule are always in contact with NB molecules, the quasi-first order rate constant, $k_1=k[NB]$, may be closely related to the rate constants of the following intramolecular electron-transfer reactions,

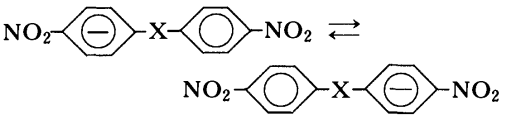

(1)

where X represents some bifunctional groups. Table 3 shows the quasi-first order rate constant, k_1, determined in this experiment and the rate constants of intramolecular electron-transfer reactions of such compounds measured by Harriman and Maki.[10] The fact that the quasi-first order rate constant is larger than the rate constants of intramolecular electron-transfer reactions except bis(*p*-nitrophenyl)methane is based on the follwing points: (a) A molecule of NB^- in this experiment is surrounded by several NB molecules, (b) the overlap of the orbitals of NB^- and NB in which the transfering electrons exist or will exist, is larger than those for the intramolecular electron-transfer reactions.

Examination of the Optical Electron-Transfer Reaction of NB^- in NB. Hush discussed the intervalence-transfer absorption of mixed valent compounds.[2] In his papers, he derived the relations between the light energy of such optical electron-transfer reaction, E_{op}, and the activation energy of the corresponding thermal electron-transfer reaction, E_{th} and between the wavenumber of the intervalence-transfer absorption maximum, $\bar{\nu}_{max}$, and the half width of the absorption band, $\Delta\bar{\nu}_{1/2}$, according to the theory of Kubo and Toyozawa.[11] When the Gibbs energy of the thermal

Table 3. Comparison between the Quasi-First Order Rate Constant of Electron-Transfer Reaction of NB^- in NB and the Rate Constants of Intramolecular Electron-Transfer Reactions of Bis(*p*-nitrophenyl) Compounds

A. Quasi-First Order Rate Constant (This Experiment)

System	$k_1=k[NB]/s^{-1}$
NB^-/NB	$1-2\times10^{8}$

B. Rate Constants of Intramolecular Electron-Transfer Reactions[a]

Reactant	k_1/s^{-1}	
	In acetonitrile	In dimethyl sulfoxide
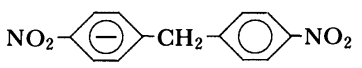	$>10^{8}$	$>10^{8}$
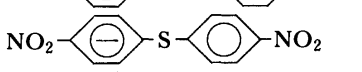	2×10^{6}	9×10^{6}
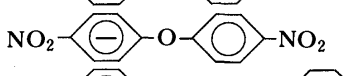	1×10^{6}	3×10^{6}
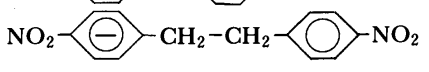	1×10^{6}	2×10^{6}

a) Ref. 10.

electron-transfer reaction, $\Delta G°$, is zero as in the NB^-/NB system, these relations are represented by the following equations.

$$E_{op}=4E_{th} \quad (2)$$

$$\bar{\nu}_{max}=(\bar{\nu}_{1/2})^2/2310 \ (\bar{\nu} \text{ in } cm^{-1}) \quad (3)$$

Figure 6 shows the absorption spectra of NB^- prepared by the electrolytic reduction of NB containing 0.1 M TBAP (A) and 0.1 M TEAP (B), together with that of NB^- in DMF containing 0.1 M TEAP (C). The absorption spectrum (A) has a large peak at about 460 nm and an additional small peak at about 790 nm. The spectrum (B) has a large peak at about 580 nm and an additional small peak at about 930 nm. The spectrum (C), however, has only one peak at about 460 nm in the visible range. Chambers and Adams reported that the absorption spectrum of NB^- in DMF containing 0.1 M TEAP has a single peak at 465 nm.[12] Lyons and Mackie reported that the absorption spectrum of NB^- in DMF containing 0.2 M $NaNO_3$ has two adjacent peaks at 435 and 465 nm.[13] However, Ishitani et al. reported that the absorption spectrum of NB^- prepared by potassium reduction in 1,2-dimethoxyethane has a peak at 560 nm.[14] Therfore, the absorption peak of the spectra (A) and (C) at 460 nm can be attributed to the NB^-. Although the reason of the shift of the peak is not clear, the peak of the spectrum (B) at 580 nm may also be attributed to NB^-. If the additional small peak of (A) at 790 nm and that of (B) at 930 nm, which do not exist in the spectrum (C), were the peak due to an optical electron-transfer reaction, there must be a relation represented by Eq. 3. From the values of the activation energies of homogeneous thermal electron-transfer reactions between NB^- and NB described above, we can estimate the values of E_{op} as 140 and 125 kJ mol^{-1} for 0.5 M TBAP and 0.1 M TEAP solutions, respectively. The values of these energies correspond to wavelengths of 850 and 960 nm, respectively. These values are in good agreement with the experimental wavelengths of the additional small peaks of the spectra (A) and (B). This result suggests that these absorption peaks may be attributable to the optical electron-transfer reactions between NB^- molecules and adjacent NB molecules.

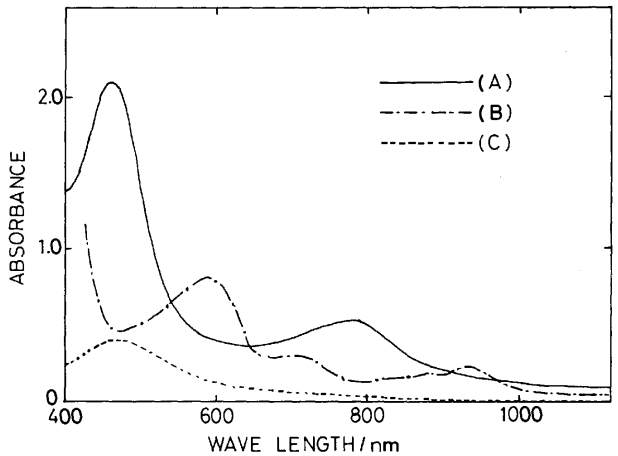

Fig. 6. Absorption spectra of solutions containing NB^- prepared by the electrolytic reduction of (A) NB containing 0.1 M TBAP; (B) NB containing 0.1 M TEAP; (C) DMF solution of NB containing 0.1 M TEAP.

On the other hand, the half width of these additional peaks were smaller than the half values of those predicted by the Eq. 3. This discrepancy may be attributed to the limitation of the applicability of Eq. 3 to this system, or the disturbance of the exact determination of $\Delta\bar{\nu}_{1/2}$ by the impurity formed by the decomposition of NB^-. Therefore, a more carefull experimental and theoretical examination is required for the complete confirmation of the occurence of optical electron-transfer reaction in this system.

Electrochemical Electron-Transfer Reaction Rates of NB^- in NB. Figure 7 shows the plots of log (I_o/Fc_O/cm s^{-1}) vs. log (c_R/c_O) for NB^-/NB couples in NB containing various kinds and amounts of tetraalkylammonium perchlorates determined by the gdp method, where I_o, F, c_O, and c_R are the exchange current density, the Faraday constant, the concentration of oxidant, and the concentration of reductant, respectively. I_o/Fc_O corresponds to the rate constant of electrochemical electron-transfer reaction at various reductant/oxidant ratios. The standard rate constants were determined by the extrapolation of these plots to the zero value of the abscissa. These rate constants in various solutions are different from each other, but even the largest value in 0.17 M TEAP, 7×10^{-3} cm s^{-1}, is smaller by about two orders than that in a DMF solu-

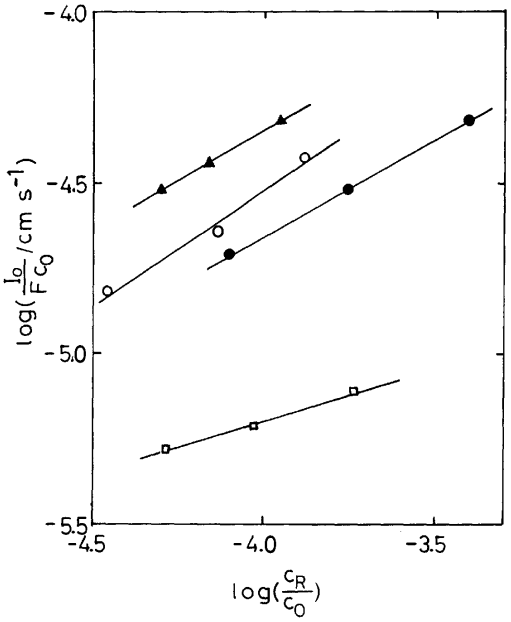

Fig. 7. Plots of log(I_o/Fc_O/cm s^{-1}) vs. log(c_R/c_O) for NB^-/NB systems in NB containing various kinds and amounts of tetraalkylammonium perchlorates determined by gdp method at 25 °C. (—▲—) 0.17 M TEAP; (—○—) 0.1 M TBAP; (—●—) 0.5 M TBAP; (—□—) 0.1 M TAAP.

Table 4. Diffusion Coefficients, D, of NB^- in NB and DMF Containing Various Tetraalkylammonium Perchorates at 25 °C

Supporting electrolyte	Solvent(viscosity/Pa s)	D/cm^2 s^{-1}
0.1 M TEAP	NB(1.81×10^{-3})	3.6×10^{-6}
0.17 M TEAP	NB(1.81×10^{-3})	3.6×10^{-6}
0.1 M TBAP	NB(1.81×10^{-3})	3.6×10^{-6}
0.5 M TBAP	NB(1.81×10^{-3})	3.2×10^{-6}
0.1 M TEAP	DMF(0.80×10^{-3})	10.8×10^{-6} [a]

a) Ref. 15.

tion.[15] NB molecules which have formed compact double layer in contact with the electrode surface may act as oxidants for this electrode reaction. These molecules are considered to be specifically adsorbed oxidants in a sense. The reason for the retardation of the electron-transfer reaction in these system is not clear, but such unique structure of the electrical double layer of these systems as described above may be attributed to these phenomena.

Diffusion Coefficients of NB^- in NB. Dahms,[4] and Ruff and Friedrich[5] derived an expression for the contribution of an exchange reaction to the diffusion coefficient of species which participate in the exchange reaction. When the rate constant of the electron-exchange reaction between NB^- and NB is expressed by k, the apparent diffusion coefficient of NB^- in NB, D_{NB^-}, is represented by the following equation.[5]

$$D_{NB^-}=D^{\circ}_{NB^-}+(\pi\delta^2k/4)c_{NB} \quad (4)$$

where $D^{\circ}_{NB^-}$ is the intrinsic diffusion coefficient of NB^- in NB when the value of k is assumed to be zero, δ is the jumping distance of an electron from NB^- to NB, and c_{NB} is the concentration of NB. The second term represents the contribution of the electron-exchange reaction.

Table 4 shows the diffusion coefficients of NB^- in NB containing various kinds of tetraalkylammonium perchlorates determined by the potential step method, together with that in DMF. If the contribution of the electron-transfer reaction between NB^- and NB to an apparent diffusion coefficient of NB^- predicted by the Eq. 4 would be larger than the intrinsic diffusion coefficient of NB^-, $D^{\circ}_{NB^-}$, a large apparent diffusion coefficient might be observed. However, this result shows that the diffusion coefficients of NB^- in NB is smaller than the value in DMF, even if we corrected the value considering the difference of the viscosities of these solvents. These results can probably be attributed to the small rate constant of the homogeneous electron-transfer reaction of these systems and ion pairing of NB^- with tetraalkylammonium ions. In fact, although the rate constant of the electron-transfer reaction between anthracene (An) and its anion radical (An^-) is larger by about two orders than these system, its contribution to the electric conductivity of anthracene anion radical is only a few percent.[16] Even when we consider the large concentration of NB in these system compared with that of An, the contribution of the electron-transfer reaction between NB and NB^- may be not so large as to be detectable by this experiment. Moreover, it is considered that NB^- in this system will usually be ion paired with tetraalkylammonium ions, because the odd electrons in free NB^- molecules tend to transfer to NB molecules in the vicinity of tetraalkylammonium ions. In a separate paper, we will report the electrical conductivity of solid NB containing NB^- and tetraalkylammonium salts in order to detect only the contribution of electron hopping to the electric conductivity.

References

1) A. H. Maki and D. H. Geske, *J. Chem. Phys.*, **39**, 609 (1960).
2) N. S. Hush, "Progress in Inorganic Chemistry," ed by F. A. Cotton, Interscience, New York (1967), Vol. 8, p. 391; N. S. Hush, *Electrochim. Acta*, **13**, 1005 (1968).
3) V. G. Levich, *Adv. Electrochem. Elecrochem. Eng.*, **4**, 314 (1966).
4) H. Dahms, *J. Phys. Chem.*, **72**, 362 (1968).
5) I. Ruff and V. J. Friedrich, *J. Phys. Chem.*, **75**, 3277 (1971); **76**, 2954 (1972).
6) K. Suga and S. Aoyagui, *Bull. Chem. Soc. Jpn.*, **55**, 358 (1982).
7) M. Kogoma, Y. Kanzaki, and S. Aoyagui, *Chem. Instrum.*, **7**, 193 (1976).
8) Y. Kanzaki and S. Aoyagui, *J. Electroanal. Chem.*, **36**, 297 (1972); T. Teherani, K. Itaya, and A. J. Bard, *Nouv. J. Chim.*, **2**, 481 (1978); Y. Harima and S. Aoyagui, *Isr. J. Chem.*, **18**, 81 (1979).
9) P. A. Malachesky, T. A. Miller, T. Layloff, and R. N. Adams, *Exch. React., Proc. Symp.*, 157 (1965).
10) J. H. Harriman and A. H. Maki, *J. Chem. Phys.*, **39**, 778 (1963).
11) R. Kubo and Y. Toyozawa, *Prog. Theor. Phys.*, **13**, 160 (1955).
12) J. Q. Chambers and R. N. Adams, *Mol. Phys.*, **8**, 413 (1965).
13) J. E. Lyons and J. C. Mackie, *Nature*, 197, 588 (1963).
14) A. Ishitani, K. Kuwata, H. Tsubomura and S. Nagakura, *Bull. Chem. Soc. Jpn.*, **36**, 1357 (1963).
15) H. Kojima and A. J. Bard, *J. Electroanal. Chem.*, **63**, 117 (1975).
16) K. Suga, T. Yorifuji, S. Aoyagui, and T. Saji, *Electrochim. Acta.*, **27**, 1259 (1982).

 © 1987 The Chemical Society of Japan Bull. Chem. Soc. Jpn., 60, 2718—2725 (1987)

A Light-Scattering Study of Temperature Effect on Micelle Formation of *N*-Alkanoyl-*N*-methylglucamines in Aqueous Solution

Makoto Ōkawauchi, Mayumi Hagio, Yoshitomi Ikawa,† Gohsuke Sugihara,*
Yoshio Murata, and Mitsuru Tanaka
Department of Chemistry, Faculty of Science, Fukuoka University, Nanakuma, Jonan-ku, Fukuoka 814-01
†San-Ei Chemical Industries, Ltd., 1-1-11 Sanwa-cho, Toyonaka 561
(Received December 10, 1986)

The physicochemical properties of *N*-alkanoyl-*N*-methylglucamine in aqueous solution have been studied by applying a Debye plot and small-system thermodynamics to an analysis of static light scattering data in the temperature range from 25 to 55 °C. A small minimum was found in a plot of the critical micelle concentration vs. temperature, instead of the monotonously decreasing tendency, as in the case of poly(oxyethylene) alkyl ether. The temperature dependence of the aggregation number of the micelle and the spread of the aggregation number distribution of micelle are both very small. The standard enthalpy change associated with micelle formation varies from positive to negative as the temperature is raised. The micellization of *N*-alkanoyl-*N*-methylglucamine surfactants is discussed separately in terms of the respective contributions from the hydrophilic and hydrophobic groups.

N-Alkanoyl-*N*-methylglucamines (MEGA-n; the chemical structure is shown in Fig. 1), nonionic surfactants, have been utilized to solubilize membrane proteins[1-3] since the time it was synthesized by Hildreth[4] in 1982. However, the physicochemical properties, such as the critical micelle concentration (cmc) and the aggregation number of micelle, at various temperatures have not yet been accurately determined. In the present study, we investigated the physicochemical properties of *N*-octanoyl-, *N*-nonanoyl-, and *N*-decanoyl-*N*-methylglucamine (MEGA-8, MEGA-9, MEGA-10) in aqueous solution at temperatures ranging from 25 to 55 °C by using a static light-scattering technique.

Ikeda et al.[5-13] have extensively studied various ionic surfactants by means of a light-scattering technique and have clearly revealed the interesting behaviors of the size and shape of surfactant aggregates. Some light-scattering studies have been made for poly(oxyethylene)-type nonionic surfactants.[14-20] For other nonionic surfactants, especially for the present MEGA-n, however, few light-scattering studies have been made in spite of the usefulness of MEGA-n in the special field of biochemistry. Thus, we have investigated the light-scattering behavior of aqueous solutions of the homologues series, MEGA-n. To analyze light-scattering data, not only Debye plots, but also small-system thermodynamics[21] have been applied. As partly described elsewhere,[20,25,26] the treatment of micelle formation by small-system thermodynamics constitutes a general theory which partly includes treatments of both mass-action and phase-separation models and can be used to clarify the thermodynamical meaning of the application of both models.

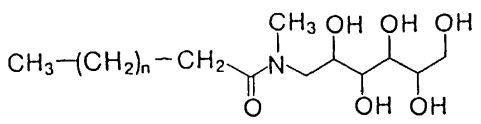

Fig. 1. The structures of *N*-octanoyl- (n=7), *N*-nonanoyl- (n=8), and *N*-decanoyl-*N*-methylglucamine (n=9).

Experimental

Materials. MEGA-8, MEGA-9, and MEGA-10 were purchased from Dojindo Laboratories and recrystallized several times from a methanol–dimethyl ether mixture and acetone. The purities of the surfactants were examined by the surface tension method. No minimum around cmc was observed for the surface tension vs. concentration curve of their aqueous solutions. Solvent water was redistilled from alkaline $KMnO_4$ after being passed through a column of an ion-exchange resin.

Methods. The light-scattering measurement was carried out using a JASCO Light Scattering Photometer LSP-1 with the unpolarized light of a mercury lamp at 436 nm. The intensities of light scattered at scattering angles, 45, 90, and 135° were measured for sample solutions in a semioctagonal cell. The semioctagonal cell was placed in a cell housing whose temperature was controlled within ±0.1 °C by circulating water around it. The reduced intensity of scattered light at 90° was calculated by

$$R_{90} = \frac{I_{90}}{I_0} \phi_{90}^{B} \frac{n_0}{n_B}, \quad (1)$$

where I_0 and I_{90} are, respectively, the intensities of the incident and scattered light at 90°; n_0 and n_B are the refractive indices of the solvent and benzene, respectively. The calibration constant, ϕ_{90}^{B}, was determined by using purified benzene at 25 °C.[22] We assumed in this study that the ϕ_{90}^{B} was independent of the temperature. The angular dissymmetry Z_{45} of light scattering was determined by

$$Z_{45} = \frac{I_{45}}{I_{135}}, \quad (2)$$

where I_{45} and I_{135} are the intensities of scattered light at 45 and 135°, respectively. A surfactant solution was directly filtered into the semioctagonal cell by using the cell-filling apparatus shown in Fig. 2. All parts of the cell-filling apparatus were cleaned in a sonicater. A membrane filter (Advan-

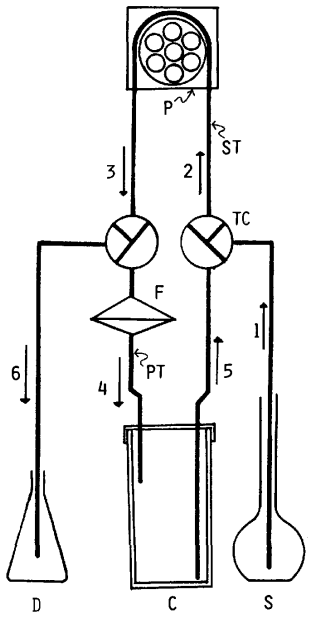

Fig. 2. Schematic diagram of cell filling system; S: sample solution, C: semioctagonal cell, D: drain solution, TC: three ways stopped cock, F: filter, P: pump, ST: silicon tube, PT: polyethylene tube.

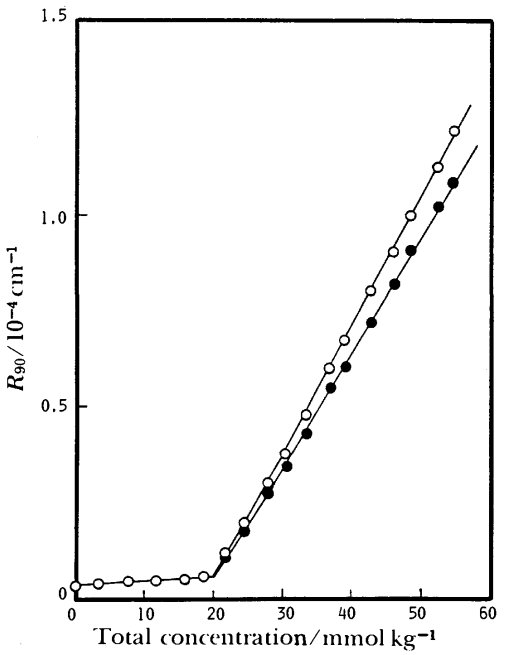

Fig. 3. Reduced scattered intensity of MEGA-9 solution as a function of total concentration at 30°C (○) and 55°C (●).

Table 1. The cmc of MEGA-n at Various Temperatures

T	cmc/mmol kg^{-1}		
°C	MEGA-8	MEGA-9	MEGA-10
25	69.0	21.4	6.7
30	66.6	20.9	6.6
35	64.9	20.5	6.5
40	63.8	20.4	6.5
45	63.2	20.3	6.6
50	63.2	20.5	6.7
55	63.7	20.8	6.9

tec) having a pore size of 0.1 μm was washed with boiling redistilled water; these parts were then arranged as shown in the figure. Firstly, the cell was filled with a sample solution or solvent which came from S through paths 1, 2, 3, F, and 4; after that, the solution or solvent was drained through paths 5, 2, 3, and 6. By repeating this procedure several times, the cell and other parts of the apparatus could be completely washed. Finally, the cell was again filled with a sample solution by the same procedure as described above and the sample solution in the cell was repeatedly circulated through path 5 to 4. A concentration change of the sample solution before and after filteration was not detected in the refractive index.

The specific refractive index increment at temperatures ranging from 25 to 55 °C was measured by means of an Otsuka Electronics Differential Refractometer R102 at 436 nm of a tungsten-halogen lamp. The calibration of the apparatus was carried out with an aqueous solution of KCl at 25 °C;[23] we assumed in this study that the calibration constant of the apparatus was independent of the temperature. The specific refractive index increment was constant over the whole concentration range measured and was almost constant at temperatures ranging from 25 to 55 °C.

Results and Discussion

The angular dissymmetry, Z_{45}, was found to be very close to unity for all the MEGA-n solutions over the whole range of the temperatures and concentrations investigated. Figure 3 shows a plot of the reduced intensity, R_{90} vs. total surfactant concentration in molality of MEGA-9 at 30 and 55 °C. Each curve has a break point indicating the beginning of micelle formation. Thus, the cmc is determined as the concentration at the break point. The values of the cmc's of MEGA-8, MEGA-9, and MEGA-10 are listed in Table 1 and the temperature dependence of the cmc's are shown in Fig. 4. It is noteworthy that a minimum appears in the cmc vs. temperature curve for MEGA-n, since the

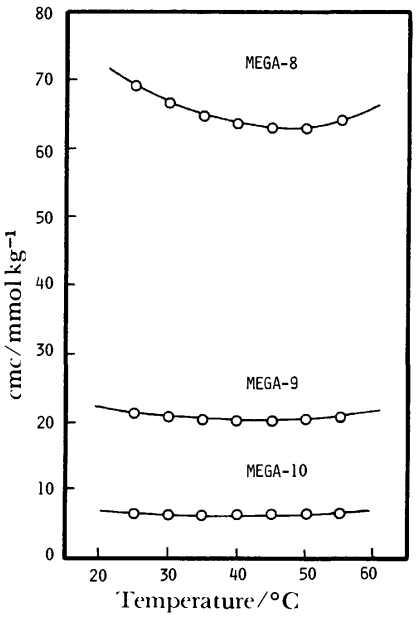

Fig. 4. Temperature dependence of cmc of MEGA-n.

existence of such a minimum has been considered to be characteristic of ionic surfactants. The cmc of poly (oxyethylene) alkyl ethers had been found to decrease monotonously with increasing temperature.[24]

From the data of R_{90} and cmc a Debye plot of MEGA-n could be made. In the absence of angular dissymmetry, the scattered light intensity at 90° from a dilute micellar solution irradiated by unpolarized light can be represented by Debye's equation:

$$\frac{K_D(C-\mathrm{cmc})}{R_{90}-R_{90,\mathrm{cmc}}} = \frac{1}{\bar{N}_w M_n} + 2B(C-\mathrm{cmc}), \quad (3)$$

where K_D, the optical constant, is

$$K_D = \frac{2\pi^2 n^2}{N_A \lambda^4}(\partial n/\partial C)^2. \quad (4)$$

Further, C is the total surfactant concentration (g ml^{-1}), $R_{90,\mathrm{cmc}}$ the reduced intensity of the solution at cmc, $\bar{N}_w$ the weight-average aggregation number of micelle, M_n the molecular weight of MEGA-n and B the second virial coefficient. n_0 and n are, respectively, the refractive indices of solvent and solution, λ the wavelength of the incident radiation and N_A Avogadro's number. Debye plots of MEGA-9 at various temperatures are shown in Fig. 5. If we draw an approximate straight line which threads through the plotted points by a least-square method, we can obtain the weight-average aggregation number of micelle as well as the second virial coefficient from the intercept and slope of this straight line, respectively. It can be seen from Fig. 5 that the respective second virial coefficients have small and negative values (2×10^{-3} mol ml g^{-2}) with a small temperature dependence. The same trends were also found for MEGA-8 and MEGA-10. It should be noted that the second virial coefficients of poly(oxyethylene) alkyl ethers change from positive to negative[16,17] in the same temperature range as the present case.

The application of small-system thermodynamics to the analysis of light-scattering data[24-27] allowed us to determine the monomeric concentration, C_1, micellar concentration, C_m, number-average and mean-square aggregation number of micelle $\bar{N}_1$, $\bar{N}_1^2$ and spread of the aggregation number distribution of micelle of MEGA-n.

In the absence of angular dissymmetry, the R_{90} of a micellar solution is given by

$$R_{90}-R_{90,0} = K_s(C_1+\bar{N}_1^2 C_m), \quad (5)$$

where

$$K_s = \frac{2\pi^2 n^2}{N_0 \lambda^4}(\partial n/\partial C_1^t)^2. \quad (6)$$

Here, $R_{90,0}$ is the reduced scattered intensity at 90° from solvent water, C_1^t the total surfactant concentration and N_0 the number of solvent molecules per unit volume. Equation 5 can be easily derived from Eq. 3 when B=0 in Eq. 3.

C_1 and C_m can be determined from the following equations:

$$\ln C_1 = \int_{\mathrm{cmc}}^{C_1^t} K_s/(R_{90}-R_{90,0})\mathrm{d}C_1^t + \ln \mathrm{cmc} \quad (7)$$

and

$$C_m = \int_{\mathrm{cmc}}^{C_1^t} K_s C_1^t/(R_{90}-R_{90,0})\mathrm{d}C_1^t - C_1 + \mathrm{cmc}. \quad (8)$$

From C_1 and C_m, thus obtained, $\bar{N}_1$, and $\bar{N}_1^2$ can be determined using

$$\bar{N}_1 = (C_1^t - C_1)/C_m \quad (9)$$

and

$$\bar{N}_1^2 = [(R_{90}-R_{90,0})/K_s - C_1]/C_m. \quad (10)$$

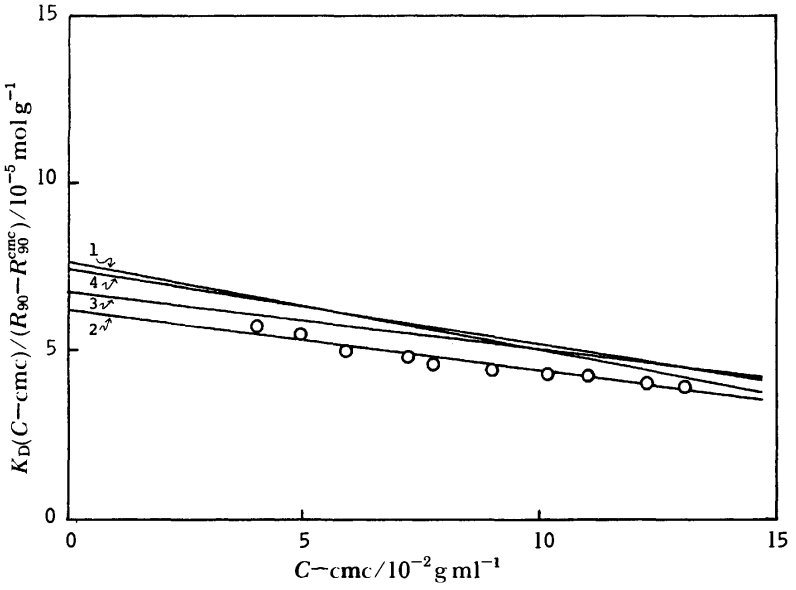

Fig. 5. The Debye plots of MEGA-9 at various temperatures; 1: 25 °C, 2: 35 °C, 3: 45 °C, 4: 55 °C.

In these calculations, the concentration (C_1^t, C_1, and C_m) units are the solute molecular number per solvent molecular number (in figures, concentrations are represented by molality).

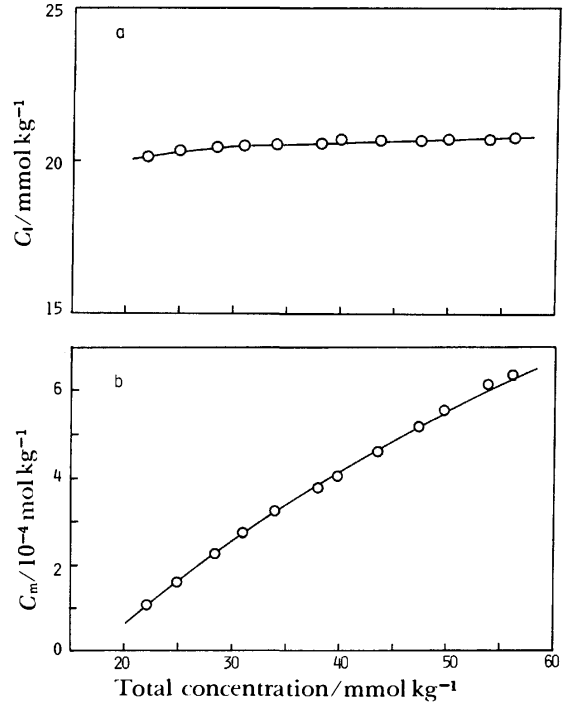

Fig. 6. Monomer concentration, C_1 and micellar concentration, C_m of MEGA-9 as a function of total concentration at 45°C.

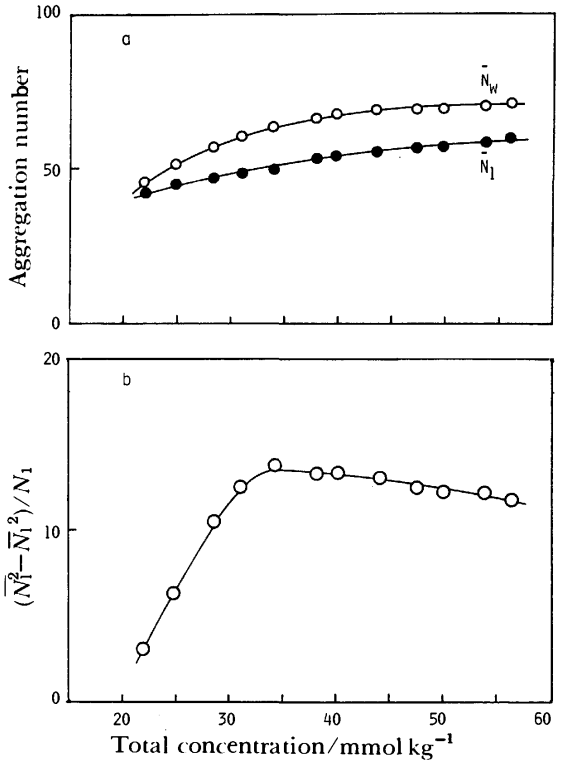

Fig. 7. Number-average and mean square aggregation number of MEGA-9 micelle (a) and the spread of aggregation number of micelle of MEGA-9 (b) at 45°C.

Figure 6 shows the dependence of C_1 and C_m on C_1^t in the case of MEGA-9 at 45 °C. C_1 increases only slightly from cmc with increasing C_1^t, and is regarded approximately as equal to the cmc. The same trend can be seen in the cases of MEGA-8 and MEGA-10 at various temperatures. This shows that the micellization of these nonionic surfactants can be approximately treated by the phase separation model. C_m increases with an increase of C_1^t and has a value of the order of 0.01 C_1^t in the total concentration range.

Figure 7-a shows the dependence of $\bar{N}_1$ and the weight-averaged aggregation number $\bar{N}_w$ ($=\bar{N}_1^2/\bar{N}_1$) of the micelle of MEGA-9 on C_1^t at 45 °C. Both $\bar{N}_1$ and $\bar{N}_w$ increase with an increase in C_1^t. The same trend can be seen in the cases of MEGA-8 and MEGA-10 at various temperatures. The increasing tendency of $\bar{N}_1$ with C_1^t is consistent with the Eq. 11, which has been derived using a treatment based on small-system thermodynamics:[26]

$$(\partial\bar{N}_1/\partial C_1^t)=(\bar{N}_1^2-\bar{N}_1^{\,2})/(C_1+\bar{N}_1^2C_m)\geqq 0. \quad (11)$$

Corkill et al.[28] have also derived a similar equation from the multiequilibrium model. They found that $\bar{N}_1$ of the 3-(dimethyloctylammonio)-1-propanesulfonate micelle increases with C_1^t. We also found that $\bar{N}_1$ of penta- and hexa(oxyethylene) dodecyl ether micelles increase with C_1^t under various pressures[20] at 25 °C.

The spread of the aggregation number of MEGA-9 micelle, $(\bar{N}_1^2-\bar{N}_1^{\,2})/\bar{N}_1$, obtained from the difference between $\bar{N}_w$ and $\bar{N}_1$, is shown in Fig. 7-b, where $(\bar{N}_1^2-\bar{N}_1^{\,2})/\bar{N}_1$, increases initially with C_1^t and then reaches an almost constant value. The same trend was observed for MEGA-8 and MEGA-10 at various temperatures. The spread of the aggregation number of the micelle of MEGA-n is much smaller than that of polyoxyethylene alkyl ether, and its C_1^t dependence is also smaller.[20]

In order to analyze the results based on small-system thermodynamics, we assumed an ideal condition for

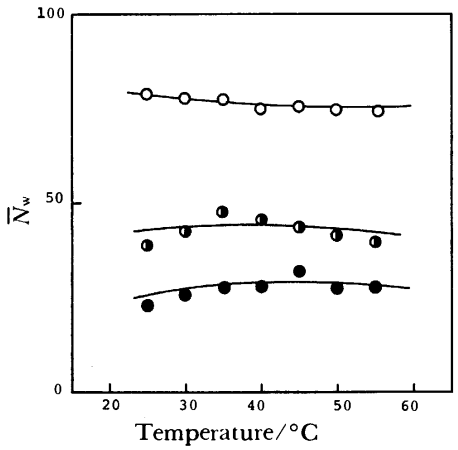

Fig. 8. Temperature dependence of weight averaged aggregation numbers of micelle of MEGA-8 (●), MEGA-9 (◑), and MEGA-10 (○).

very dilute micellar solutions of MEGA-n. This assumption can be regarded as reasonable owing to the very small value of the second virial coefficient obtained from the Debye plot.

The value of $\overline{N}_w$ extrapolated to cmc in Fig. 7 agrees well with the weight-average aggregation number obtained from the Debye plot. Figure 8 shows the temperature dependence of $\overline{N}_w$. The extrapolated $\overline{N}_w$ of MEGA-8, MEGA-9, and MEGA-10 may be regarded as being almost constant, irrespective of the temperature change, which differs remarkably from the strikingly increasing trend of $\overline{N}_w$ of poly(oxyethylene) alkyl ethers.[15] The temperature dependence of C_m and the $(\overline{N_1^2}-\overline{N}_1^2)/\overline{N}_1$ of MEGA-8, MEGA-9, and MEGA-10 are also very small.

From the temperature dependence of C_1, C_m, and $\overline{N}_1$, the standard Gibbs free energy, enthalpy and entropy change on micelle formation, ΔG_m°, ΔH_m°, and ΔS_m° can be estimated by the use of the following equations from small-system thermodynamics:[27]

$$\Delta G_m^\circ \simeq RT \ln C_1 - RT/\overline{N}_1 \ln C_m, \quad (12)$$

$$\Delta H_m^\circ \simeq -RT^2 (\partial \ln C_1/\partial T)_p - RT^2/\overline{N}_1 (\partial \ln C_m/\partial T)_p, \quad (13)$$

and

$$\Delta S_m^\circ \simeq -RT (\partial \ln C_1/\partial T)_p + RT/\overline{N}_1 (\partial \ln C_m/\partial T)_p - R \ln C_1 + R/\overline{N}_1 \ln C_m. \quad (14)$$

These equations are (formally) the same equations as derived from the mass-action model. However, the second terms of Eqs. 12—14 and the 4 th term of Eq. 14 are much smaller than the other terms in the respective equations because of the factor $1/\overline{N}_1$; also, the smaller temperature dependence of ln C_m than that of ln C_1. C_1 is nearly equal to the cmc (as described above). The equations obtained from the elimination of the terms on the respective equations described above are consistent with the equations derived from the phase-separation model. We have taken the standard states of monomer and micelle as the states of an infinite dilute solution; therefore, their standard free energies consist of self free energies as well as their interaction with water. Then, ΔG_m° represents the change of the interaction (hydrophobic and hydrophilic) of the monomer and water accompanied by the transfer of a mole of the monomer from the solution bulk into the micelle.

The temperature dependence of ΔG_m°, ΔH_m°, and ΔS_m° thus obtained, are shown in Fig. 9. The ΔG_m°, ΔH_m°, and ΔS_m° of MEGA-n decreases monotonously with the temperature. ΔG_m° is always negative and ΔS_m° positive. On the other hand, ΔH_m° changes sign from positive to negative at a lower temperature, since the hydrocarbon chain is longer. However, ΔH_m° is always positive and decreases to zero with temperature in the case of poly(oxyethylene) alkyl ether.[29-32]

In order to investigate these features of MEGA-n in detail, let us try to separate these thermodynamic parameters into contributions from the hydrophilic and hydrophobic parts of a MEGA-n molecule, assuming the additivity. ΔG_m° can be divided into three parts:

$$\Delta G_m^\circ \simeq \Delta G_m^\circ(w) + (N_c - 1)\Delta G_m^\circ(CH_2) + \Delta G_m^\circ(CH_3), \quad (15)$$

where $\Delta G_m^\circ(w)$ is the contribution of the hydrophilic part, $\Delta G_m^\circ(CH_2)$ the methylene group, and $\Delta G_m^\circ(CH_3)$ the terminal methyl group; N_c should be taken as 7, 8, and 9, respectively, for MEGA-8, MEGA-9, and MEGA-10. Similar equations are valid for ΔS_m° and ΔH_m°.

From the linear plots of ΔG_m°, ΔH_m°, and ΔS_m° vs. the number of carbon atoms in alkyl chain of MEGA-n at various temperatures, $\Delta G_m^\circ(CH_2)$, $\Delta H_m^\circ(CH_2)$, and $\Delta S_m^\circ(CH_2)$, can be determined (as listed in Table 2). These are the same values as those of poly(oxyethylene) alkyl ethers.[33]

$\Delta G_m^\circ(w)$ can be obtained by substituting the values of $\Delta G_m^\circ(CH_2)$ and $\Delta G_m^\circ(CH_3)$ (=2100 cal mol^{-1} (1 cal= 4.184 J))[24] into Eq. 15. The $\Delta H_m^\circ(w)$ and $\Delta S_m^\circ(w)$ can be determined from Eqs. 16 and 17 (see Table 3):

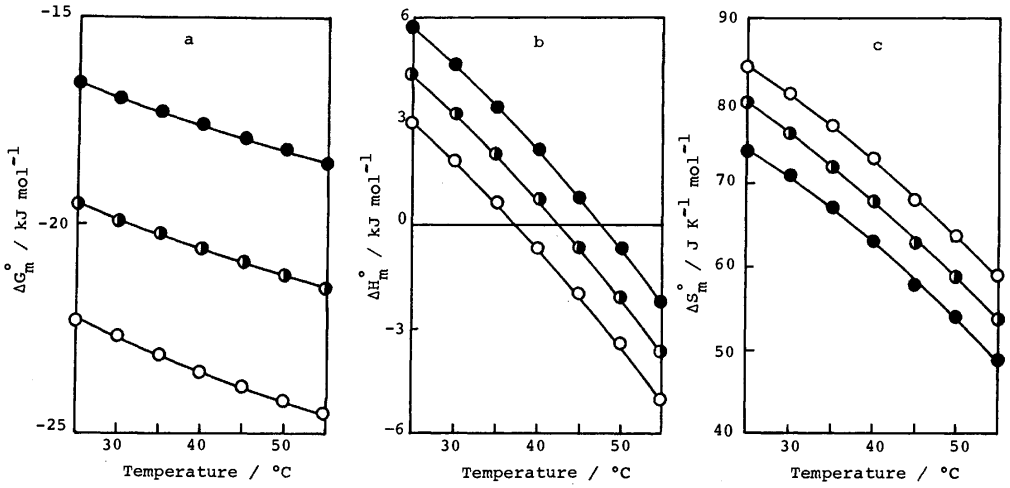

Fig. 9. Thermodynamic parameter changes on micelle formation of MEGA-8 (●), MEGA-9 (◑), and MEGA-10 (○) as a function of temperature.

Table 2. The Thermodynamic Parameters per Methylene Group of MEGA-n on Micelle Formation at Various Temperatures

T	$\Delta G_m^\circ(CH_2)$	$\Delta H_m^\circ(CH_2)$	$\Delta S_m^\circ(CH_2)$
°C	kJ mol^{-1}	kJ mol^{-1}	J K^{-1} mol^{-1}
25	−2.88	−1.40	4.96
30	−2.91	−1.40	4.98
35	−2.93	−1.40	4.98
40	−2.96	−1.40	4.97
45	−2.98	−1.40	4.95
50	−3.00	−1.41	4.93
55	−3.03	−1.42	4.90

Table 3. The Thermodynamic Parameters of Contribution of Hydrophilic Parts on Micelle Formation of MEGA-n at Various Temperatures

T	$\Delta G_m^\circ(w)$	$\Delta H_m^\circ(w)$	$\Delta S_m^\circ(w)$
°C	kJ mol^{-1}	kJ mol^{-1}	J K^{-1} mol^{-1}
25	9.48	21.9	41.6
30	9.26	21.5	40.4
35	9.09	20.7	37.9
40	8.88	19.7	34.4
45	8.73	18.2	29.9
50	8.59	16.6	24.7
55	8.48	14.6	18.7

$$\Delta H_m^\circ(w) = \partial(\Delta G_m^\circ(w)/T)/\partial(1/T) \quad (16)$$

and

$$T\Delta S_m^\circ(w) = \Delta H_m^\circ(w) - \Delta G_m^\circ(w). \quad (17)$$

Let us compare the contribution of $\Delta H_m^\circ(w)$ to $\Delta G_m^\circ(w)$ between poly(oxyethylene) alkyl ether and MEGA-n. In the case of MEGA-n, the enthalpy term, $\Delta H_m^\circ(w)$, is superior to the entropy term, $T\Delta S_m^\circ(w)$, while in the case of poly(oxyethylene) alkyl ether both terms are comparable.[33] This difference can be interpreted in terms of the interaction between water and the respective hydrophilic parts. The relatively large contribution of $T\Delta S_m^\circ(w)$ to $\Delta G_m^\circ(w)$ in the poly (oxyethylene) group compared to the case of the hydrophilic part of MEGA-n seems to be caused by a relatively large degree of weakening of the hydration of poly(oxyethylene) group on micellization.

The experimental results are summarized as follows. The cmc vs. temperature curve has a small minimum in the temperature range from 25 to 55 °C; also, the temperature dependence of micellar aggregation numbers, the spread of its distribution and the micellar concentration of MEGA-n are very small. The standard enthalpy change on micelle formation, ΔH_m°, changes sign from positive to negative with increasing temperature. Further, a cloud point was not observed for MEGA-8, MEGA-9, or MEGA-10, even if their solutions were heated to the boiling point and a large amount of NaCl was added into the solutions of MEGA-n (on the basis of the fact that addition of NaCl depress the cloud point of poly(oxyethylene) alkyl ethers).[34]

A suggestion concerning the solution properties of MEGA-n resulted through a comparison with those of poly(oxyethylene) alkyl ethers. The hydrophilicity of poly(oxyethylene) alkyl ether arises from the formation of two hydrogen bonds per oxyethylene group with water.[35] On the other hand, a hydroxyl group of the hydrophilic part of MEGA-n can possibly make three hydrogen bonds with water. However, by taking into account the fact that a cloud point was not observed for MEGA-n and that cmc has a shallow minimum at a certain temperature (instead of monotonous decreasing with temperature like the cmc of poly (oxyethylene) alkyl ether), it may be concluded that there is a considerable difference between the interaction of hydroxyl groups of MEGA-n with water and that of the oxyethylene groups of poly(oxyethylene) alkyl ether with water. The minimum in the temperature dependence of the cmc, as observed in ionic surfactants with ion-water dipole interaction, may result from the predominant role of the electrostatic dipole-dipole interaction of the hydrophilic part of MEGA-n with water. Further, the amide group may also play an important role in the hydrophilicity of MEGA-n. The hydrogen bond formation between hydroxyl groups in the micellar state cannot be considered as an important factor of micelle formation, since it should cause the micelle size to be much larger than the observed values.

It seems, however, that it is not always reasonable to regard the character of hydrophilic group of MEGA-n as attributable to each separate hydroxyl group. It has been well-known that for such a molecule (having several hydroxyl groups) that the steric configuration of the hydroxyl groups plays a more important role than the nature of each hydroxyl group itself. For instance, galactaric acid and D-glucaric acid are only different in the stereochemical configuration of a certain hydroxyl group; however, the former is very soluble in water and the latter is insoluble.

Finally, one should pay attention to the fact that the micellization behavior of poly(oxyethylene)-type nonionic surfactants is not common to all other types of nonionic surfactants.[31,36,37]

Thanks are due for the partial support by a research grant from the Ministry of Education (No. 60470011) and partial support of a fund from the Central Research Institute of Fukuoka University.

References

1) M. Hanatani, K. Nishifuji, M. Futani, and T. Tsuchiya, *J. Biochem.*, **95**, 1349 (1984).

2) M. Kidrič, J. Petrović V. Šoškić, and D. Trajković, *Br. J. Pharmac.*, **83**, 687 (1984).

3) F. Yu and R. E. McCarty, *Arc. Biochem. Biophys.*, **61**, 238 (1985).

4) J. E. K. Hildreth, *Biochem. J.*, **363**, 207 (1982).

5) S. Ikeda, S. Ozeki, and M. Tsunoda, *J. Colloid Interface Sci.*, **73**, 27 (1980).
6) S. Ikeda, S. Hayashi, and T. Imae, *J. Phys. Chem.*, **85**, 106 (1981).
7) S. Ozeki and S. Ikeda, *J. Colloid Interface Sci.*, **77**, 219 (1981).
8) S. Ozeki and S. Ikeda, *J. Colloid Interface Sci.*, **87**, 424 (1982).
9) T. Imae and S. Ikeda, *Colloid Polym. Sci.*, **262**, 497 (1984).
10) T. Imae and S. Ikeda, *Colloid Polym. Sci.*, **263**, 765 (1985).
11) S. Ozeki and S. Ikeda, *Colloid Polym. Sci.*, **262**, 409 (1984).
12) T. Imae, R. Kamiya, and S. Ikeda, *J. Colloid Interface Sci.*, **108**, 215 (1985).
13) T. Imae and S. Ikeda, *J. Colloid Interface Sci.*, **98**. 363 (1984).
14) D. Attwood, *J. Phys. Chem.*, **72**, 339 (1968).
15) D. Attwood, P. H. Elworthy, and S. B. Kayne, *J. Phys. Chem.*, **74**, 3529 (1970).
16) H. Fujimatsu, K. Takagi, H. Mastuda and S. Kuroiwa, *J. Colloid Interface Sci.*, **94**, 237 (1983).
17) S. Kuroiwa, H. Matsuda, and H. Fujimatsu, *Nippon Kagaku Kaishi*, **1980**, 362.
18) N. Nishikido, M. Shinozaki, G. Sugihara, and M. Tanaka, *J. Colloid Interface Sci.*, **74**, 474 (1980).
19) N. Nishikido, M. Shinozaki, G. Sugihara, and M. Tanaka, *J. Colloid Interface Sci.*, **82**, 352 (1981).
20) M. Ōkawauchi, M. Shinozaki, Y. Ikawa, and M. Tanaka, *J. Phys. Chem.*, **91**, 109 (1987).
21) T. L. Hill, "Thermodynamics of Small Systems," W. A, Benjamin, New York (1963).
22) H. Utiyama, "Calibration and Correction Factors" in "Light Scattering from Polymer Solutions," ed by M. B. Huglin, Academic Press, New York (1972); Chap. 4, pp. 61—88.
23) M. B. Huglin, "Specific Refractive Index Increments" in "Light Scattering from Polymer Solutions;" ed by M. B. Huglin, Academic Press, New York (1972); Chap. 6, pp. 165—331.
24) C. Tanford, "The Hydrophobic Effect," 2nd ed, Wiley-Interscience, New York (1980).
25) D. G. Hall, *Trans. Faraday Soc.*, **66**, 1351 (1970).
26) D. G. Hall, *Trans. Faraday Soc.*, **66**, 1359 (1970).
27) D. G. Hall and B. A. Pethica, "Thermodynamics of Micelle Formation" in "Nonionic Surfactants;" ed by M. J. Schick, Marcel Dekker, New York (1967); Chap. 16, pp. 516—557.
28) J. M. Corkill, J. F. Goodman, T. Walker, and J. Wyer, *Proc. R. Soc. London, Ser. A*, **312**, 243 (1969).
29) J. M. Corkill, J. F. Goodman, and S. P. Harrold, *Trans. Faraday Soc.*, **60**, 202 (1964).
30) J. M. Corkill, J. F. Goodman and S. P. Harrold, *Trans. Faraday Soc.*, **60**, 996 (1964).
31) J. M. Corkill, J. F. Goodman, R. Robson, and J. R. Tate, *Trans. Faraday Soc.*, **62**, 987 (1966).
32) N. Muller and F. E. Platko, *J. Phys. Chem.*, **75**, 547 (1971).
33) K. Meguro, Y. Takasawa, N. Kamahashi, Y. Tabata, and M. Ueno., *J. Colloid Interface Sci.*, **83**, 50 (1981).
34) W. N. Macley, *J. Colloid Sci.*, **11**, 272 (1956).
35) K. Shinoda, "Yōeki to yōkaido," Maruzen, Tokyo (1974), pp. 201.
36) K. Shinoda, T. Yamaguchi, and R. Hori, *Bull. Chem. Soc. Jpn.*, **34**, 273 (1961).
37) K. Shinoda, T. Yamanaka, and K. Kinoshita, *J. Phys. Chem.*, **63**, 648 (1959).

 © 1987 The Chemical Society of Japan Bull. Chem. Soc. Jpn., 60, 2727—2735 (1987)

Ion/Molecule Reactions in Gaseous Isopropyl Alcohol

Kenzo HIRAOKA,* Hajime TAKIMOTO, and Shinichi YAMABE†,*
Faculty of Engineering, Yamanashi University, Takeda-4, Kofu 400
†Department of Chemistry, Nara University of Education, Takabatake-cho, Nara 630
(Received December 25, 1986)

The ion/molecule reactions observed in 4 Torr CH_4 containing known small amounts of i-C_3H_7OH or i-C_3H_7OH/H_2O mixture were studied over the temperature range 40—400 °C. The experiments were carried out using a pulsed electron beam mass spectrometer. At low temperatures (<150 °C), the major ions are i-$C_3H_7OH_2^+(i\text{-}C_3H_7OH)_n$. By increasing the temperature, the slow growth of ions with m/z=59, 85, and 101 is observed. These ions are assigned to $(CH_3)_2COH^+$, $(CH_3)_2CHC^+(CH_3)_2$, and $C_6H_{13}O^+$, respectively. They are probably produced from reactions of i-$C_3H_7^+$ with isopropyl alcohol. The $(CH_3)_2COH^+$ ion may be produced from the electrophilic attack of i-$C_3H_7^+$ onto the secondary carbon atom of i-C_3H_7OH. At high temperatures (≈400 °C), the $(CH_3)_2COH^+$ ion becomes dominant. Acid-catalyzed dehydration of isopropyl alcohol, i-$C_3H_7OH_2^+ + H_2O \rightarrow H_3O^+(H_2O) + C_3H_6$, is also observed. Ion/molecule reactions involved in the present experiment are discussed according to the frontier-orbital theory.

The kinetics of the gas-phase ion/molecule reactions of aliphatic alcohols have been studied in various respects. The condensation reactions of protonated alcohols ROH_2^+ leading to the formation of protonated ethers R_2OH^+have been observed.[1-7]

$$ROH_2^+ + ROH \rightarrow R_2OH^+ + H_2O \quad (1)$$

The γ-radiation-sensitized pyrolysis of isopropyl alcohol vapor has been studied by Freeman and coworkers.[7-9] At temperatures about 250 °C, chain reactions were found to be important in isopropyl alcohol vapor. Four modes of radiation-induced chain decomposition were found.[9] The stoichiometric representation of the modes, with G values at 380 °C are $2i$-$C_3H_7OH \rightarrow H_2O + (i\text{-}C_3H_7)_2O$, 300; i-$C_3H_7OH \rightarrow H_2O + C_3H_6$, 1200; i-$C_3H_7OH \rightarrow CH_4 + CH_3CHO$, 43; i-$C_3H_7OH \rightarrow H_2 + (CH_3)_2CO$, 600. For the formation of diisopropyl ether, radiation-induced cationic chain reactions 2—4 have been proposed.[8]

$$i\text{-}C_3H_7OH_2^+ + i\text{-}C_3H_7OH \rightarrow (i\text{-}C_3H_7)_2OH^+ + H_2O \quad (2)$$

$$(i\text{-}C_3H_7)_2OH^+ + i\text{-}C_3H_7OH \rightarrow (i\text{-}C_3H_7)_2OH^+(i\text{-}C_3H_7OH) \quad (3)$$

$$(i\text{-}C_3H_7)_2OH^+(i\text{-}C_3H_7OH) + i\text{-}C_3H_7OH \rightarrow i\text{-}C_3H_7OH_2^+(i\text{-}C_3H_7OH) + (i\text{-}C_3H_7)_2O \quad (4)$$

Reaction 2 has the mechanism of the bimolecular nucleophilic substitution (S_N2).

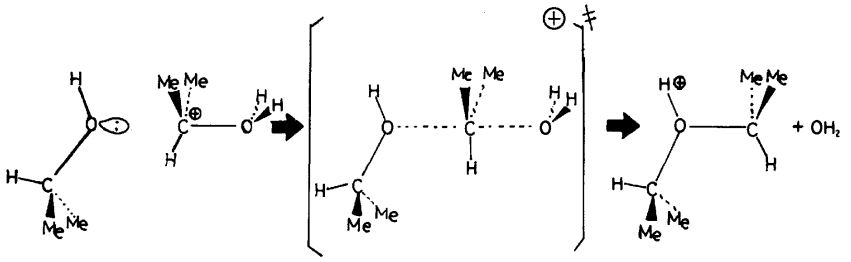

Back side attack of i-PrOH to cation S_N2

Reaction 3 is the standard clustering, and reaction 4 is the displacement reaction.

Van der Linde and Freeman[9] suggested the radical chain reactions 5—8 for the formation of H_2, $(CH_3)_2CO$, and C_3H_6.

$$H + i\text{-}C_3H_7OH \longrightarrow H_2 + (CH_3)_2\dot{C}OH \quad (5)$$

$$(CH_3)_2\dot{C}OH \longrightarrow (CH_3)_2CO + H \quad (6)$$

$$OH + i\text{-}C_3H_7OH \longrightarrow H_2O + \dot{C}H_2(CH_3)CHOH \quad (7)$$

$$CH_2(CH_3)CHOH \longrightarrow C_3H_6 + OH \quad (8)$$

Hiraoka and Kebarle found the acid-catalyzed dehydration reaction 9 of t-butyl alcohol in the gas phase.[10] It is a unimolecular elimination (E1).

$$t\text{-}C_4H_9OH_2^+ + H_2O \rightarrow H_3O^+(H_2O) + i\text{-}C_4H_8 \quad (9)$$

So far the gas-phase ion/molecule reactions in isopropyl alcohol have not been studied before. In the present work, some detailed examination of the same reactions were done using a pulsed electron beam mass spectrometer. It was found that several unique ions were produced from the ion/molecule reactions in isopropyl alcohol such as i-$C_3H_7^+$, $(CH_3)_2COH^+$, $C_6H_{13}^+$, $C_6H_{11}O^+$, $C_6H_{13}O^+$, $(i\text{-}C_3H_7)_2OH^+$, and $C_6H_{13}O_2^+$ in addition to the proton-bound cluster ions i-$C_3H_7OH_2^+$ $(i\text{-}C_3H_7OH)_n$. The mechanisms for the

formation of these ions were proposed on the grounds of the thermochemical data and the frontier-orbital theory. The evidence for the occurrence of the acid-catalysed dehydration reaction analogous to reaction 9 was obtained for isopropyl alcohol.

Experimental

The measurements were made with the pulsed electron beam mass spectrometer which has been described previously.[11-13] A small amount of isopropyl alcohol or isopropyl alcohol/water vapor mixture was introduced into 4 Torr[14] CH_4 carrier gas through stainless steel capillaries.

Two keV electron beam was pulsed on for 100 μs and off for 3 ms. The electron beam entered the ion source through the electron entrance slit made of stainless steel razor blades. The width and the length of the slit were 15 μm and 1 mm, respectively. The incident electron current at non-pulsed mode was about 5×10^{-9} A. The ions produced were sampled through an ion exit slit made of razor blades. The width and the length of the slit were the same as those of the electron entrance slit. Under the present experimental conditions, the mean free paths of ions and molecules are greater than the slit width. Thus the ions pass through the slit by molecular flow and the adiabatic cooling of the escaping gas is negligible. The lifetime of ions due to the diffusive loss to the wall was more than a few ms under the present experimental conditions. They were dependent on the ion source temperature and the gas pressure. The loss of ions due to the electron-positive ion recombination reaction is negligible under the present experimental conditions. About 2 ms after the electron pulse, a short positive pulse (+25 V) was applied to the ion repeller electrode in order to annihilate all ions produced in the ion source. The ions escaping from the field-free ion source into an evacuated region were mass analysed by a quadrupole mass spectrometer (ULVAC MSQ-400) and collected in a multichannel analyser as a function of their arrival time after the electron pulse. The intensities of all ions are normalized on the measurements so that they correspond to their relative concentrations in the ion source. The ion counts collected in a multichannel analyser were transferred to the microcomputer and the time profiles of the calculated per cent of the total ionization of observed ions were recorded on the x-y plotter.

Structural data were obtained by the ab initio MO calculation with the 3-21G and STO-3G basis sets. The GAUSSIAN 80 program was used.[15]

Results

When the ion source temperature is low (<150 °C), the observed major ions are $i\text{-}C_3H_7OH_2^+(i\text{-}C_3H_7OH)_n$. That is, the standard clustering reaction takes place. When the ion source temperature is raised, several new ions are formed. Figure 1 shows the temporal profile of ions observed in 4.05 Torr of CH_4 containing 2.3 mTorr of $i\text{-}C_3H_7OH$ and 0.116 Torr of H_2O at 302.0 °C. The primary ion H_3O^+ is produced from reactions of the added H_2O with CH_5^+ and $C_2H_5^+$. These major ions are produced from the methane ion/molecule reactions. The rapid increase of $H_3O^+(H_2O)$ (mass 37) and $i\text{-}C_3H_7^+$ (mass 43) is observed at the expense of the H_3O^+ ion. The onsets of appearance of ions with m/z=59 and higher masses are slower than those of $H_3O^+(H_2O)$ and $i\text{-}C_3H_7^+$ ions. This indicates that the ions with m/z=59 and higher masses are the

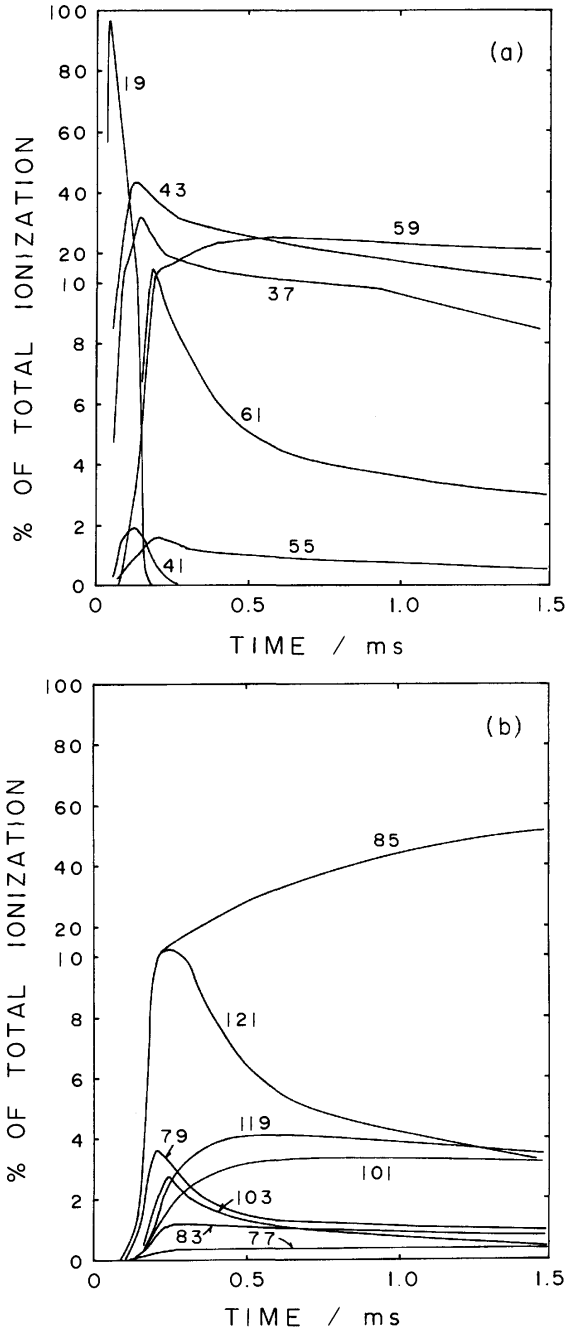

Fig. 1. Positive ions observed after electron pulse ionization in a gas mixture containing 4.05 Torr of CH_4, 0.116 Torr of H_2O, and 2.3 mTorr of $i\text{-}C_3H_7OH$ at 302.0 °C.
(a) Mass 19: H_3O^+, mass 37: $H_3O^+(H_2O)$, mass 41: $C_3H_5^+$, mass 43: $i\text{-}C_3H_7^+$, mass 55: $H_3O^+(H_2O)_2$, mass 59: $(CH_3)_2COH^+$, mass 61: $i\text{-}C_3H_7OH_2^+$.
(b) Mass 77: $(CH_3)_2COH^+(H_2O)$, mass 79: $i\text{-}C_3H_7OH_2^+(H_2O)$, mass 83: $C_6H_{11}^+$, mass 85: $C_6H_{13}^+$, mass 101: $C_6H_{13}O^+$, mass 103: $(i\text{-}C_3H_7)_2OH^+$, mas 119: $(CH_3)_2COH^+(i\text{-}C_3H_7OH)$, mass 121: $i\text{-}C_3H_7OH_2^+(i\text{-}C_3H_7OH)$.

secondary ions mainly produced from $H_3O^+(H_2O)_n$ or i-$C_3H_7^+$ as precursor ions.

Figure 2 shows the temporal profiles of ions observed in 4.08 Torr of CH_4 and 2.0 mTorr of i-C_3H_7OH at 307.3 °C. The CH_5^+ (mass 17) and $C_2H_5^+$ (mass 29) ions which are the primary ions produced from the ion/molecule reactions in methane are quickly converted to ions with m/z=41, 43, and 61. The slower onsets of appearance of ions with m/z=83 and higher masses suggest that these ions are secon-

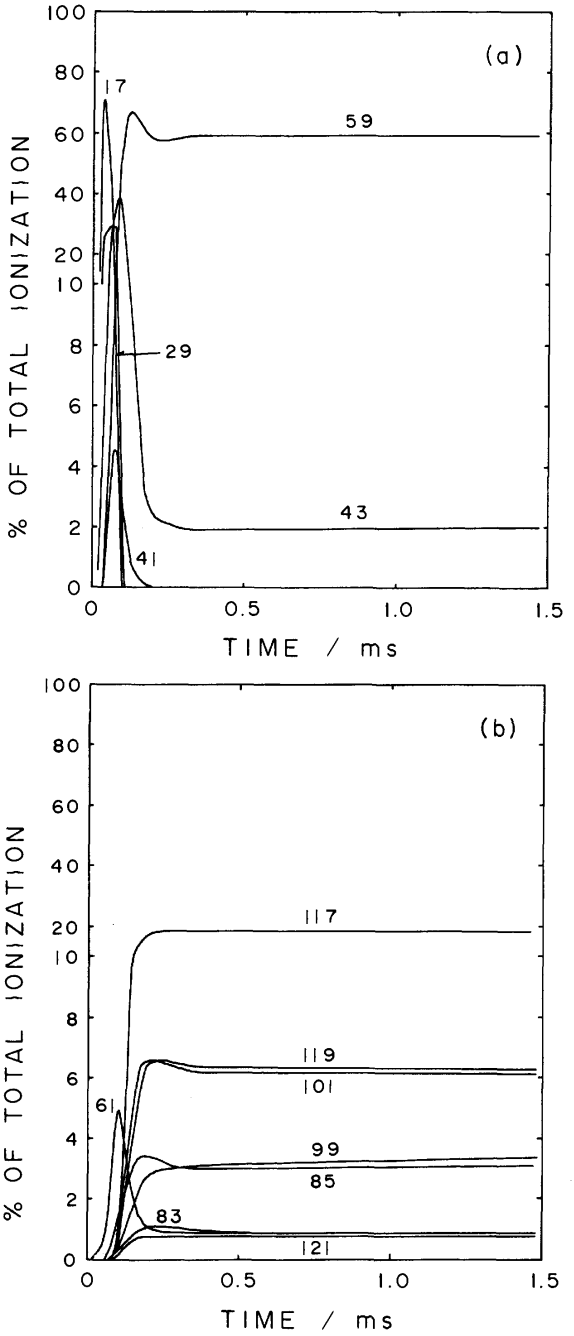

Fig. 2. Positive ions observed after electron pulse ionization in a gas mixture containing 4.08 Torr of CH_4 and 2.0 mTorr of i-C_3H_7OH at 307.3 °C.
(a) Mass 17: CH_5^+, mass 29: $C_2H_5^+$, mass 41: $C_3H_5^+$, mass 43: i-$C_3H_7^+$, mass 59: $(CH_3)_2COH^+$.
(b) Mass 61: i-$C_3H_7OH_2^+$, mass 83: $C_6H_{11}^+$, mass 85: $C_6H_{13}^+$, mass 99: $C_6H_{11}O^+$, mass 101: $C_6H_{13}O^+$, mass 117: $(CH_3)_2COH^+((CH_3)_2CO)$, mass 119: $(CH_3)_2COH^+(i$-$C_3H_7OH)$, mass 121: i-$C_3H_7OH_2^+(i$-$C_3H_7OH)$.

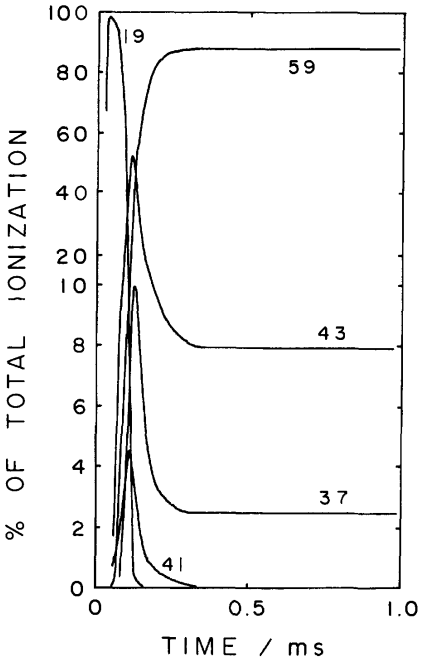

Fig. 3. Positive ions observed after electron pulse ionization in a gas mixture containing 4.06 Torr of CH_4, 0.12 Torr of H_2O, and 2.4 mTorr of i-C_3H_7OH at 413.0 °C.
Mass 19: H_3O^+, mass 37: $H_3O^+(H_2O)$, mass 41: $C_3H_5^+$, mass 43: i-$C_3H_7^+$, mass 59: $(CH_3)_2COH^+$.

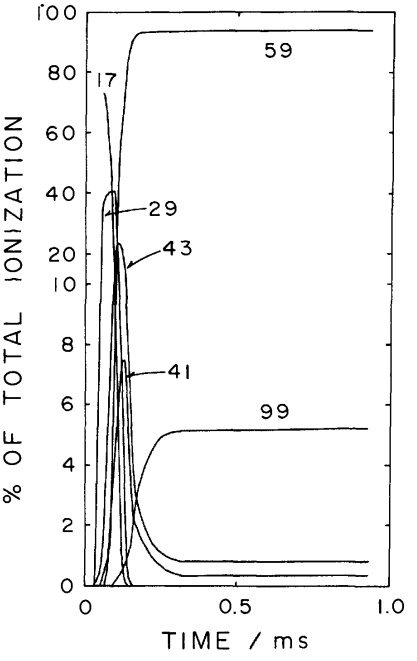

Fig. 4. Positive ions observed after electron pulse ionization in a gas mixture containing 4.1 Torr of CH_4 and 2.0 mTorr of i-C_3H_7OH at 403.0 °C.
Mass 17: CH_5^+, mass 29: $C_2H_5^+$, mass 41: $C_3H_5^+$, mass 43: i-$C_3H_7^+$, mass 59: $(CH_3)_2COH^+$, mass 99: $C_6H_{11}O^+$.

dary product ions in gaseous i-PrOH. The ions with m/z=99 and 117 are formed which are not detected in Fig. 1. The H_2O vapor seems to suppress the formation of these ions.

Figure 3 shows the temporal profiles of ions observed in 4.06 Torr of CH_4, 0.12 Torr of H_2O, and 2.4 mTorr of i-PrOH at 413 °C. The strong growth of the ion with m/z=59 is observed.

In Fig. 4 are shown the temporal profiles of ions observed in 4.1 Torr of CH_4 and 2.0 mTorr of i-PrOH at 403.0 °C. In this case, the ion with m/z=99 as well as that with m/z=59 are observed as major product ions.

Discussion

$C_3H_7^+$ Ion m/z=43. In Fig. 1, the rapid increase of the i-$C_3H_7^+$ ion, at the expense of the H_3O^+ ion is observed. This indicates that the i-$C_3H_7^+$ ion is produced by reaction 10.

$$H_3O^+ + i\text{-}C_3H_7OH \rightarrow i\text{-}C_3H_7^+ + 2H_2O \qquad \Delta H^\circ = -0.9 \text{ kcal mol}^{-1} \quad (10)$$

(1 cal=4.184 J)

The thermochemically estimated bond energy of the species i-$C_3H_7^+ \cdots OH_2$ is 23.8 kcal mol^{-1}. Since the proton transfer reaction 11

$$H_3O^+ + i\text{-}C_3H_7OH \rightarrow i\text{-}C_3H_7OH_2^+ + H_2O \qquad \Delta H^\circ = -24.7 \text{ kcal mol}^{-1} \quad (11)$$

is exothermic by −24.7 kcal mol^{-1}, the protonated isopropyl alcohol produced from reaction 11 has more than enough energy to dissociate toward i-$C_3H_7^+$ and OH_2.

As is shown later in reactions 13, 16, 17, and 23, i-$C_3H_7^+$ reacts with i-PrOH in various patterns. It is of interest to examine its electronic structure with the theoretically optimized geometry. i-PrOH and i-$PrOH_2^+$ are also investigated. Three carbon atoms and H_α are in the common plane. As an electrophile, i-$C_3H_7^+$ has two reactive sites. The reactivity is demonstrated by the shape of the lowest unoccupied MO (LUMO) and the next lowest unoccupied one (LU+1)MO. Anions or bases attack $C_3H_7^+$ potentially from two directions. These are indicated by bold arrows in the figure above.

Geometries of i-PrOH and i-$PrOH_2^+$ are shown below.

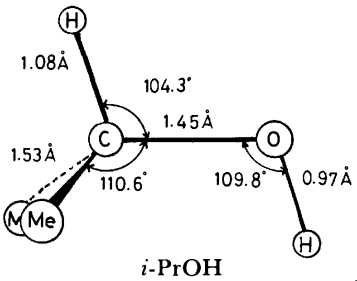

i-PrOH

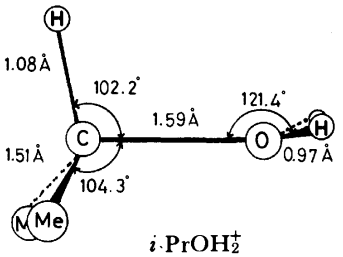

i-$PrOH_2^+$

By protonation of i-PrOH, the C-O bond is elongated, 1.45 Å→1.59 Å. The decrease of the C-O bond population, 0.24→0.05, is remarkable. This bond weakening suggests that the thermal decomposition of i-$PrOH_2^+$ to i-$C_3H_7^+$ and H_2O in reaction 15 shown later is likely as well as the proton transfer in reaction 11. It is natural that the proton should attack the oxygen atom of i-PrOH. However, it is a question whether the attacking pattern is exclusive or not. To examine this, the shape of the highest occupied MO, HOMO, and the next highest occupied MO, (HO−1)-MO of i-PrOH is drawn. The shape indicates that

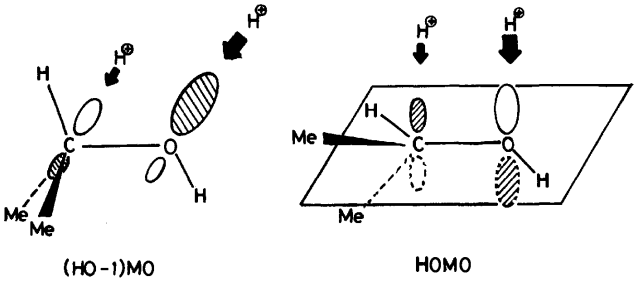

the oxygen lone-pair electron is the best target for an electrophile (e.g., proton) and the next favorable site is the secondary carbon atom. The carbon may be

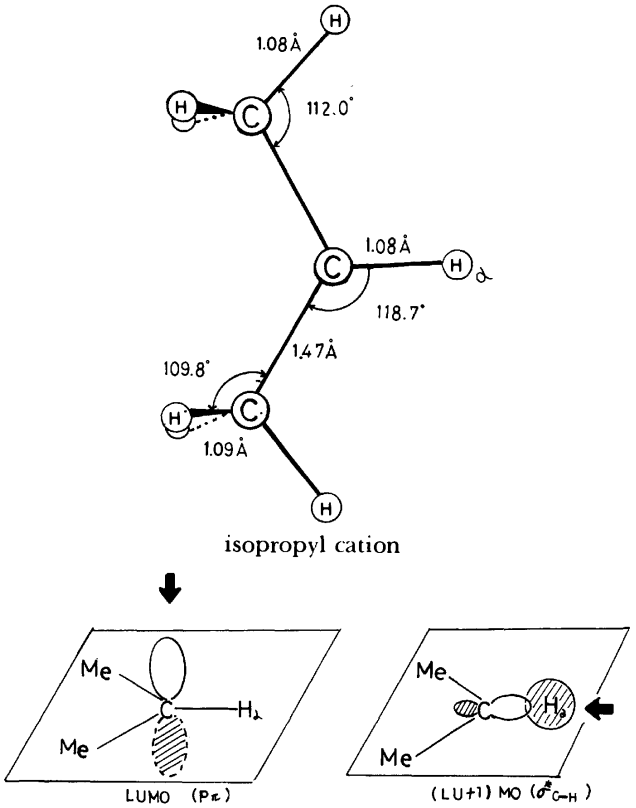

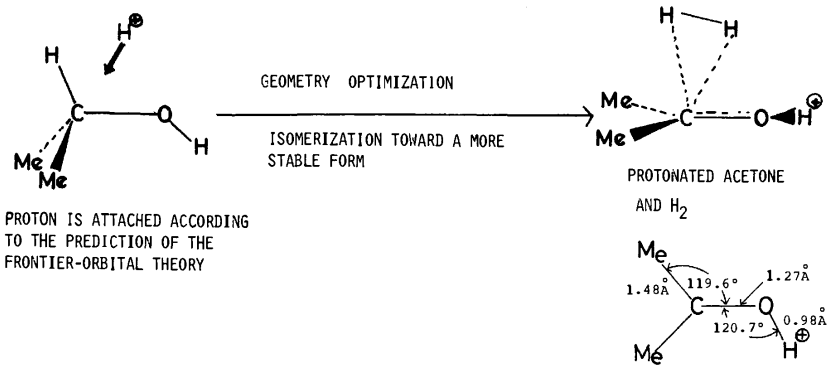

attacked by a proton. In the next sub-section, this reactivity is described.

$(CH_3)_2COH^+$ Ion m/z=59. The production of the ion m/z=59 from the ion/molecule reaction of i-PrOH is stated. As the case of i-$C_3H_7^+$, the initial rapid increase of this ion is due to the proton transfer reaction. What kind of species is formed by the protonation on the secondary carbon of i-PrOH? To answer this question, the geometry of the species is optimized with the MO of the 3-21G basis set. A following isomerization reaction is found during the optimization. That is, two C-H bonds begin to be cleaved to give a hydrogen molecule. This geometric change occurs without the energy barrier. The secondary carbon gets the electronic density from two methyl groups through the hyperconjugation and pushes out H_2 by the exchange repulsion. Thus, the ion m/z=59 is the protonated acetone. Three reactions, 12—14, are possible to form the protonated acetone. Their difference lies in the source of the proton.

$$H_3O^+ + i\text{-}C_3H_7OH \rightarrow (CH_3)_2COH^+ + H_2 + H_2O \qquad \Delta H^\circ = -17 \text{ kcal mol}^{-1} \quad (12)$$

$$i\text{-}C_3H_7^+ + i\text{-}C_3H_7OH \rightarrow (CH_3)_2COH^+ + H_2 + C_3H_6 \qquad \Delta H^\circ = -3.9 \text{ kcal mol}^{-1} \quad (13)$$

$$i\text{-}C_3H_7OH_2^+ + i\text{-}C_3H_7OH \rightarrow (CH_3)_2COH^+ + H_2 + i\text{-}C_3H_7OH \qquad \Delta H^\circ = 7.3 \text{ kcal mol}^{-1} \quad (14)$$

Reaction 12 is more exothermic than reaction 10, however, the frontier orbital [(HO−1)MO or HOMO] of i-PrOH suggests that reaction 10 is more favorable than reaction 12. The ion-permanent dipole interaction between H_3O^+ and i-PrOH also favors reaction 10. This explains the greater initial increase of i-$C_3H_7^+$ than $(CH_3)_2COH^+$ (Fig. 1,a). Since reaction 14 is endothermic by 7.3 kcal mol^{-1}, the contribution of the reaction for the formation of protonated acetone is negligible under the present experimental conditions.

The gradual increase of the m/z=59 ion following the initial rapid growth is also observed (Fig. 1,a). Since the reactive ion which survives after 0.2 ms is i-$C_3H_7^+$, this ion is a possible precursor for the gradual formation of the m/z=59 ion in reaction 13.

The gradual decrease of i-$C_3H_7OH_2^+$ (mass 61) and i-$C_3H_7OH_2^+$ (i-C_3H_7OH) (mass 121) may be due to the consumption of these ions by the unimolecular decomposition reaction 15 of i-$C_3H_7OH_2^+$ at high temperatures.

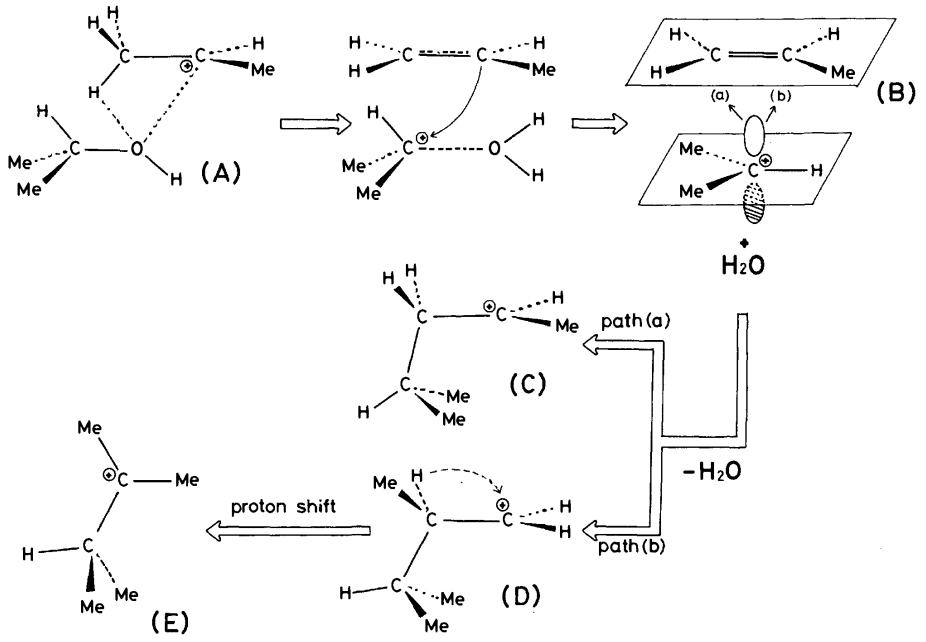

Scheme 1.

$$i\text{-}C_3H_7OH_2^+ \rightarrow i\text{-}C_3H_7^+ + OH_2$$
$$\Delta H^\circ = 23.8 \text{ kcal mol}^{-1} \quad (15)$$

$C_6H_{13}^+$Ion m/z=85. The gradual growth of the m/z=85 ion, probably $C_6H_{13}^+$, is also observed as shown in Fig. 1,b. As in the case of the m/z=59 ion, no other probable candidates are conceivable for the precursor ions except for the i-$C_3H_7^+$ ion. It seems likely that the reaction of i-$C_3H_7^+$ with i-C_3H_7OH produces the $C_6H_{13}^+$ ion.

$$i\text{-}C_3H_7^+ + i\text{-}C_3H_7OH \rightarrow C_6H_{13}^+ + H_2O$$
$$\Delta H^\circ = -27 \text{ kcal mol}^{-1} \quad (16)$$

The mechanism for the $C_6H_{13}^+$ formation by reaction 16 may be described in Scheme 1. In the process of the elimination of H_2O in the associated complex **A**, the intermediate complex may have the structrure **B** in which i-$C_3H_7^+$ is interacting with propylene. According to the Markownikov rule, the less substituted sp^2 carbon in propylene may be attacked by the cation, i.e., the path (a). This leads to the formation of the secondary carbonium ion C. The enthalpy change of reaction 16 leading to the formation of C is calculated to be -9.7 kcal mol^{-1}. Here, the heat of formation of C is estimated to be 174 kcal mol^{-1} by the method proposed by Nakata and Kobayashi.[16] The species C has the structure of protonated 4-methyl-1-pentene, CH_2=CH-CH_2-$CH(CH_3)_2$. The proton affinity of this compound is expected to be much lower than that of i-PrOH.[17] Thus the rate constant of the proton transfer reaction $C_6H_{13}^+ + i\text{-PrOH} = i\text{-PrOH}_2^+ + C_6H_{12}$ may be of the order of 10^{-9} cm^3/molecule·s. From this value, the lifetime of the decay of the $C_6H_{13}^+$ ion due to the proton transfer reaction can be calculated to be $\approx$20 μs under the present experimental conditions. Since the condensation reactions such as reaction 16 are usually much slower than the collision rate ($\approx 10^{-9}$ cm^3/molecule·s), the steady state concentration of the ion C would become very low under the present experimental conditions. However, as shown in Fig. 1,b, $C_6H_{13}^+$ shows a gradual increase. This indicates that $C_6H_{13}^+$ has a much more stable structure than **C**. If the central sp^2 carbon of propylene is attacked by i-$C_3H_7^+$ and the hydrogen atom on it migrates to the terminal sp^2 carbon of propylene (path b), the tertiary carbonium ion **E** would be formed. From the calculated heat of formation of **E**, 156.7 kcal mol^{-1},[16] the enthalpy change of reaction 16 can be estimated to be -27 kcal mol^{-1}. E is about 17 kcal mol^{-1} more stable than C. **E** has the structure of protonated 2,3-dimethyl-1-butene, CH_2=$C(CH_3)CH(CH_3)_2$. Since the proton transfer reaction of $C_6H_{13}^+$(**E**) with i-PrOH is endothermic by about 7 kcal mol^{-1}, the long lifetime of $C_6H_{13}^+$(**E**) can be expected under the present experimental conditions. This explains the time profile of $C_6H_{13}^+$ shown in Fig. 1,b. Thus we would like to conclude that $C_6H_{13}^+$ has the structure E. It would be worthwhile noting that the nominal Markownikov rule may not be applied to the reactions of propylene (or terminal olefins) with the secondary carbonium ions. The rule is concerned usually with the orientation of the proton (electrophilic) addition to the double bond. However, when the electrophile is a large species with the secondary carbon, the rule would become exceptionally invalid. The present reaction seems to favor the formation of thermochemically more stable tertiary carbonium ions (by the anti-Markownikov rule) through the hydrogen migration in the intermediate complex.

The $C_6H_{13}^+$ ion starts to be observed at $\approx$180 °C and becomes a dominant ion at $\approx$300 °C. At higher temperature, its intensity decreases and becomes nil at $\approx$400 °C. Some finite lifetime for the intermediate complex of (i-$C_3H_7^+ \cdots i$-C_3H_7OH)* seems indispensable for the formation of $C_6H_{13}^+$ in the condensation reaction 16.

$C_6H_{13}O^+$ Ion m/z=101. The slow production of the m/z=101 ion in Figs. 1 and 2 may be explained by reaction 17.

$$i\text{-}C_3H_7^+ + i\text{-}C_3H_7OH \rightarrow C_6H_{13}O^+ + H_2 \quad (17)$$

Reaction 17 would consist of two steps. One is the H_2 elimination leading to the formation of the tertiary carbonium ion, $(CH_3)_2C^+$-$C(CH_3)_2OH$. The other is

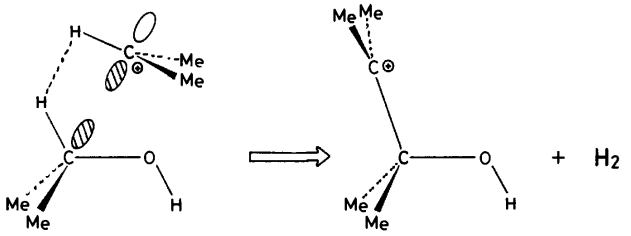

the closure of the epoxide ring. During the optimization, the open cation is found to be converted smoothly to the protonated epoxide. The hydroxyl group cannot stay alone due to the intramolecular charge transfer.

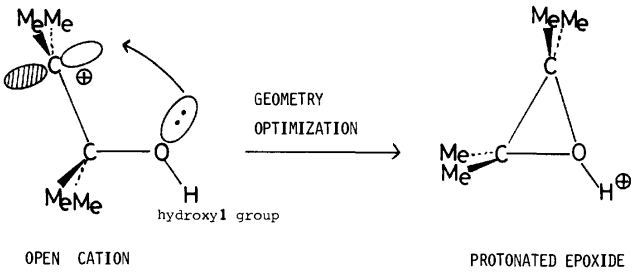

The minor product ion with m/z=83 may be produced from the dehydration of $C_6H_{13}O^+$.

$$C_6H_{13}O^+ \rightarrow C_6H_{11}^+ + H_2O \quad (18)$$

$(i\text{-}C_3H_7)_2OH^+$ Ion m/z=103. The $(i$-$C_3H_7)_2OH^+$ ion (mass 103) shows the initial rapid increase which is followed by the slow decrease (Fig. 1,b). Freeman[8] proposed the cationic chain reactions 2—4 for the formation of diisopropyl ether. The obtained experi-

mental results can be interpreted by the Freeman's proposal. The initial rapid increase of the $(i\text{-}C_3H_7)_2OH^+$ ion may be mainly due to reaction 2 and partly to reaction 19.

$$i\text{-}C_3H_7^+ + i\text{-}C_3H_7OH \xrightarrow{M} (i\text{-}C_3H_7)_2OH^+ \quad (19)$$

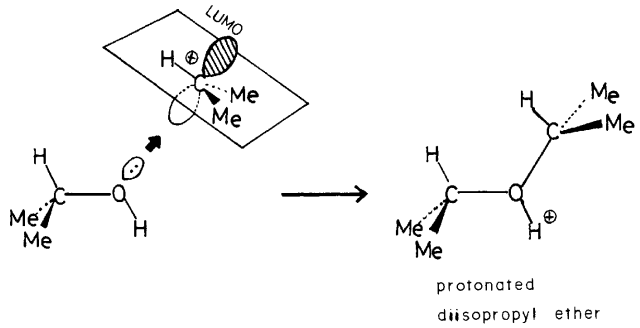

The slow decrease of $(i\text{-}C_3H_7)_2OH^+$ may be due to reactions 3 and 4. The contribution of the direct proton transfer reaction 20 may be negligible, because the reaction is highly endothermic.

$$(i\text{-}C_3H_7)_2OH^+ + i\text{-}C_3H_7OH \rightarrow i\text{-}C_3H_7OH_2^+ + (i\text{-}C_3H_7)_2O$$
$$\Delta H^\circ = 15.2 \text{ kcal mol}^{-1} \quad (20)$$

$C_6H_{13}O_2^+$ and $C_6H_{11}O^+$ Ions m/z=117 and 99. Strong growths of m/z=117 and 99 ions are observed in Fig. 2,b. The $(CH_3)_2COH^+$ ion as a precursor may explain the formation of these ions.

$$(CH_3)_2COH^+ + i\text{-}C_3H_7OH \rightarrow C_6H_{13}O_2^+ + H_2 \quad (21)$$
$$(CH_3)_2COH^+ + i\text{-}C_3H_7OH \rightarrow C_6H_{11}O^+ + H_2 + H_2O \quad (22)$$

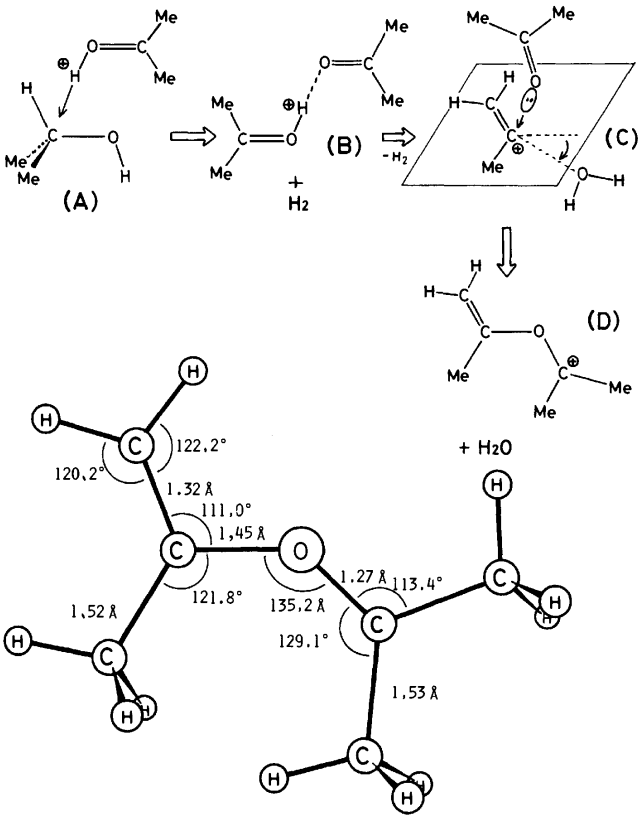

The attack of the secondary carbon of i-PrOH by the protonated acetone yields the proton-held acetone dimer cation (m/z=117) (**A**→**B**). This reaction may be followed by the dehydration to give the m/z=99 ion. The dehydration involves two mechanisms. One is the keto-enol isomerization of the protonated acetone. The other is the subsequent attack of acetone onto the unsaturated carbon of the enol form in C. The latter reaction is similar to the nucleophilic displacement on the carbonyl carbon. It is well known that the $C_6H_{11}O^+$ ion with m/z=99 is formed from the ion/molecule reactions in gaseous acetone.[18-20] We think that this ion D is produced by the same mechanism as shown above. It is noteworthy that the length of the C$^+$-O bond is 1.27 Å in the optimized geometry of D. The double bond makes the cationic nature small, leading to the stability of the species. The geometry of the m/z=99 ion is described by the resonance structure.

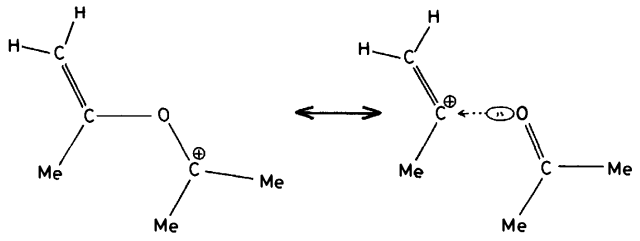

Freeman[8,9] found that the isopropyl alcohol vapor starts to suffer the thermal decomposition on the wall of the reaction vessel above ≈300 °C. It would be possible that $(CH_3)_2COH^+$ (mass 59) and $(CH_3)_2COH^+ \cdots OC(CH_3)_2$ (mass 117) ions observed in Fig. 2 originate from the acetone produced from the thermal decomposition of i-PrOH in the reaction chamber. If this was the case, acetone should exist in the system regardless of the presence or absence of the H_2O vapor. However, the m/z=117 ion could not be detected in Fig. 1 where the H_2O vapor is present in the system. This clearly indicates that the m/z=59 and 117 ions in Fig. 2 are produced from the ion/molecule reactions in gaseous i-PrOH. In Figs. 3 and 4, the situation is more serious since the ion source temperature is high (≈400 °C). If an appreciable amount of acetone were produced, all the protonated species should be quickly converted to the protonated acetone due to the high proton affinity of acetone. However, the steady concentrations of ions such as $H_3O^+(H_2O)$ and i-$C_3H_7^+$ are established in Fig. 3. It is likely that the thermal decomposition of i-PrOH toward acetone is negligible under the present experimental conditions.

It is of interest to note that the $C_6H_{11}O^+$ ion (mass 99) is observed in Fig. 4, but not in Fig. 3. The presence of H_2O vapor seems to suppress the formation of this ion. It is described that the $C_6H_{11}O^+$ ion is produced through the formation of several intermediate complexes such as **A**—**C**. When such intermediate complexes are formed in the atmosphere of highly polar H_2O vapor, the neutral species in the

complex may suffer the displacement reaction with an H_2O molecule. For example, the loose complex of $(CH_3)_2COH^+ \cdots i\text{-}C_3H_7OH$ (A) may be converted to $(CH_3)_2COH^+ \cdots OH_2$ by the displacement reaction, $(CH_3)_2COH^+ \cdots i\text{-}C_3H_7OH + H_2O \rightarrow (CH_3)_2COH^+ \cdots OH_2 + i\text{-}C_3H_7OH$. Such reactions of intermediate complexes may interrupt the formation of the $C_6H_{11}O^+$ ion. This also explains the absence of the m/z=99 and 117 ions in Fig. 1. This kind of reactions may become important when the lifetimes of the intermediate complexes are long enough that the complexes suffer multiple collisions with third-body gas molecules. The destruction of the complex, A, B, or C by a water molecule may be regarded as a solvent effect in the gas-phase ion/molecule reactions.

$C_3H_7^+$ Ion Re-Visited. After the rapid decrease, the intensity of $i\text{-}C_3H_7^+$ becomes time-independent as shown in Figs. 1—4. The rapid consumption of the ion is mainly due to reaction 23, proton transfer.

$$i\text{-}C_3H_7^+ + i\text{-}C_3H_7OH \rightarrow i\text{-}C_3H_7OH_2^+ + C_3H_6 \qquad \Delta H^\circ = -11.7 \text{ kcal mol}^{-1} \quad (23)$$

The contribution of reactions 13, 16, 17, and 19 may be relatively minor compared to that of reaction 23. The lifetime of $i\text{-}C_3H_7^+$ due to reaction 23 is estimated to be less than 20 μs under the present experimental conditions. Since the steady-state concentration is established for $i\text{-}C_3H_7^+$, the rate of the regeneration of $i\text{-}C_3H_7^+$ by reaction 15 must be comparable to that of the consumption by reaction 23.

Van der Linde and Freeman[9] proposed the radical chain reactions 5—8 for the formation of H_2, $(CH_3)_2CO$, and C_3H_6 in the γ-radiation-sensitized pyrolysis of gaseous i-PrOH. In the present experiments, the strong growth of $(CH_3)_2COH^+$ is observed at high temperatures in ion/molecule reactions in gaseous i-PrOH. Alternative cationic chain reactions 13, 24, and 15 may be possible for the formation of $(CH_3)_2CO$ and H_2 in the γ-radiation-sensitized pyrolysis of gaseous i-PrOH.

$$(CH_3)_2COH^+ + i\text{-}C_3H_7OH \rightarrow i\text{-}C_3H_7OH_2^+ + (CH_3)_2CO \qquad \Delta H^\circ = 5.5 \text{ kcal mol}^{-1} \quad (24)$$

Besides, the rapid chain reactions 23 and 15 for the formation of C_3H_6 are established at high temperatures in gaseous i-PrOH. The formation of C_3H_6 in the γ-radiation-sensitized pyrolysis of i-PrOH could also be accounted for by the cationic chain reactions 23 and 15.

It would be of great interest to measure the temperature dependences of the rate constants of reactions 13, 16, etc., and determine the energy barriers for the corresponding reactions. However, the measurements of the rate constants for these reactions are difficult due to the regeneration of the $i\text{-}C_3H_7^+$ ion by reaction 15. Besides, the product ions such as $(CH_3)_2COH^+$ and $C_6H_{13}^+$ are slowly consumed by the proton transfer reactions with i-PrOH. This also makes the kinetic measurements difficult. Thus we are discouraged to perform the detailed measurements of rate constants to obtain the meaningful information on the reaction kinetics.

Acid-Catalyzed Dehydration Reaction of $i\text{-}C_3H_7OH$. It should be noted that the steady-state concentration of $H_3O^+(H_2O)$ (m/z=37) is established in Fig. 3. If the $H_3O^+(H_2O)$ ion establishes the equilibrium with H_3O^+, the concentration ratio of $H_3O^+(H_2O)/H_3O^+$ can be estimated to be about 3 to 1 under the present experimental conditions. Thus, the $H_3O^+(H_2O)_n$ ions should be rapidly converted to $i\text{-}C_3H_7OH_2^+$ by the proton transfer reaction 11. The expected lifetime of $H_3O^+(H_2O)_n$ is less than 100 μs under the present experimental conditions. The steady appearance of $H_3O^+(H_2O)$ indicates that the $H_3O^+(H_2O)$ ion is quickly reproduced from some ion/molecule reactions. The regeneration of $H_3O^+(H_2O)$ may be due to reaction 25.

$$i\text{-}C_3H_7OH_2^+ + H_2O \rightarrow H_3O^+(H_2O) + C_3H_6 \qquad \Delta H^\circ = 2 \text{ kcal mol}^{-1} \quad (25)$$

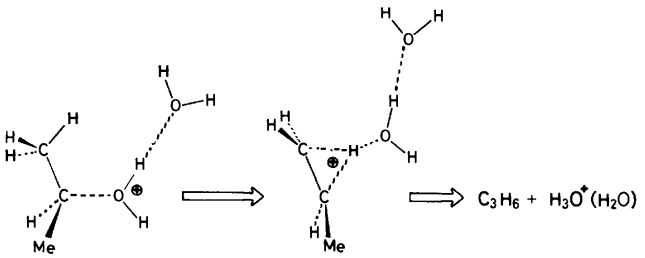

The $i\text{-}C_3H_7OH_2^+$ ion produced from reaction 23 decomposes unimolecularly to produce $i\text{-}C_3H_7^+$. When the $i\text{-}C_3H_7OH_2^+$ ion collides with an H_2O molecule within its lifetime, the dehydration of $i\text{-}C_3H_7OH_2^+$ may take place. Since the product ion $H_3O^+(H_2O)$ from reaction 25 reproduces the $i\text{-}C_3H_7OH_2^+$ ion by reaction 11, H_2O acts as a catalyst for the formation of propylene. Reaction 25 is analogous to acid-catalyzed dehydration of alcohols in solution. A similar reaction is also found for t-butyl alcohol in the gas phase.[10]

Summary and Conclusion

The positive ion/molecule reactions in gaseous isopropyl alcohol were studied in detail. The new information obtained in the present work may be summarized as follows.

1) The isopropyl alcohol has two reactive sites for the nucleophilic reactions, i.e., the oxygen atom and the secondary carbon atom. The protonations onto the O and s-C atom yield $i\text{-}C_3H_7^+$ and $(CH_3)_2COH^+$ ion, respectively. The condensation reactions of $i\text{-}C_3H_7^+$ with i-PrOH leads to the formation of $C_6H_{13}^+$ and $C_{16}H_{13}O^+$ ion. The reactions of $i\text{-}C_3H_7^+$ with i-PrOH may be summarized as the Scheme 1.

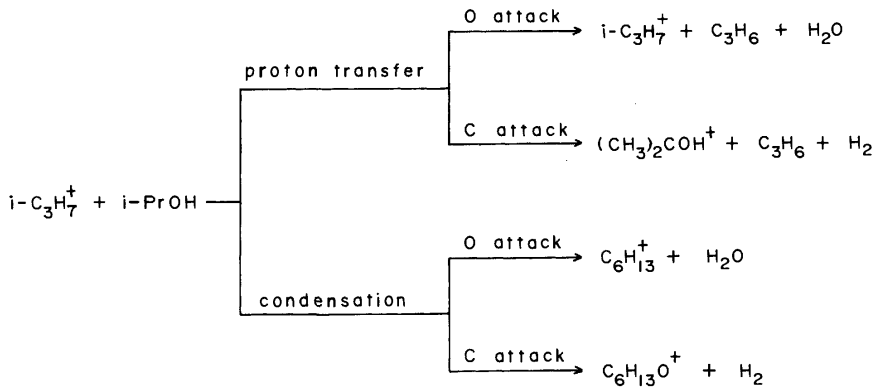

2) The condensation reactions of the secondary product ion $(CH_3)_2COH^+$ with *i*-PrOH produce $C_6H_{13}O_2^+$ and $C_6H_{11}O^+$ ion. The $C_6H_{13}O_2^+$ ion may have the structure of the proton-bound acetone dimer cations. The dehydration of $C_6H_{13}O_2^+$ yields $C_6H_{11}O^+$ through the keto-enol isomerization of the protonated acetone molecule in the complex $C_6H_{13}O_2^+$. The $C_6H_{11}O^+$ ion (m/z=99) is known to be one of the major product ions from the gas-phase ion/molecule reactions in acetone.[18-21] We think that this ion has the same structure as the one produced in the present system. It was found that the presence of H_2O in the system greatly suppresses the formation of $C_6H_{13}O_2^+$ and $C_6H_{11}O^+$ ion. This may be due to the displacement reactions of the intermediate ions with the H_2O molecule. This may be regarded as the solvent effect in the gas-phase ion/molecule reactions.

3) The acid-catalyzed dehydration reaction, $i\text{-}C_3H_7OH_2^+ + H_2O \rightarrow H_3O^+(H_2O) + C_3H_6$, was observed. The similar reaction has also been observed for *t*-C_4H_9OH but at much lower temperature.[10]

4) Acetone and propylene are produced with high *G* values from the γ-radiation-sensitized pyrolysis of *i*-PrOH vapor.[7-9] The formation of these compounds may be explained by the cationic chain reactions 13, 24, 23, and 15. The radical chain reactions 5—8 suggested by van der Linde and Freeman[9] for the formation of these compounds are not unique because the rate constants of hydrogen abstraction reactions such as reactions 5 and 7 are relatively small.[22]

5) The Markownikov rule may not be applied to the reactions of terminal olefins with the secondary carbonium ions. When the electrophile is a large secondary carbonium ion, the reaction seems to favor the formation of thermochemically more stable tertiary carbonium ion through the hydrogen migration in the intermediate complex.

One of the authors (KH) thanks Mr. Yukio Chino of the Yamanashi University for making the ion source used in this experiment. The financial supports of the Grant-in-Aid from the Ministry of Education and of the 1st Morino Trust for Molecular Science are gratefully acknowledged.

MO calculations were carried out on the FACOM M-382 computer at the Data Processing Center of Kyoto University and on the HITAC M-200H computer at the Institute for Molecular Science.

References

1) K. R. Ryan, L. W. Sieck, and J. H. Futrell, *J. Chem. Phys.*, **41**, 111 (1964).
2) S. K. Gupta, E. G. Jones, A. G. Harrison, and J. J. Myher, *Can. J. Chem.*, **45**, 3107 (1967).
3) J. M. S. Henis, *J. Am. Chem. Soc.*, **90**, 844 (1968).
4) E. P. Grimsrud and P. Kebarle, *J. Am. Chem. Soc.*, **95**, 7939. (1973).
5) T. B. McMahon and J. L. Beauchamp, *J. Phys. Chem.*, **81**, 593. (1977).
6) K. M. Bansal and G. R. Freeman, *J. Am. Chem. Soc.*, **92**, 4173 (1970).
7) K. M. Bansal and G. R. Freeman, *Radiation Res. Rev.*, **3**, 209. (1971).
8) H. J. van der Linde, and G. R. Freeman, *J. Am. Chem. Soc.*, **92**, 4417 (1970).
9) H. J. van der Linde and G. R. Freeman, *J. Phys. Chem.*, **75**, 20 (1971).
10) K. Hiraoka and P. Kebarle, *J. Am. Chem. Soc.*, **99**, 360 (1977).
11) K. Hiraoka, K. Morise, and T. Shoda, *Int. J. Mass Spectrom. Ion Process.*, **67**, 11 (1985).
12) K. Hiraoka, K. Morise, T. Nishijima, S. Nakamura, M. Nakazato, and K. Ohkuma, *Int. J. Mass Spectrom. Ion Process*, **68**, 99 (1986).
13) K. Hiraoka, H. Takimoto, and S. Yamabe, *J. Phys. Chem.*, **90**, 5910 (1986).
14) 1 Torr is 133.322 Pa.
15) J. S. Binkley, R. A. Whiteside, R. Krishnan, R. Seeger, D. J. DeFrees, H. B. Schlegel, S. Topiol, L. R. Kahn, and J. A. Pople, *QCPE*, **13**, 406 (1981).
16) H. Nakata and T. Kobayashi, *Mass Spectroscopy (Tokyo)*, **32**, 381 (1984).
17) Proton affinities of propylene and *i*-PrOH are 179 and 194 kcal mol^{-1}, respectively.
18) K. A. G. MacNeil, and J. H. Futrell, *J. Phys. Chem.*, **76**, 409 (1972).
19) Z. Luczynski, and H. Wincel, *Int. J. Mass Spectrom. Ion Phys.*, **23**, 37 (1977).
20) A. J. Stace, and A. K. Shukla, *J. Phys. Chem.*, **86**, 865. (1982).
21) K. Hiraoka, H. Takimoto, K. Morise, T. Shoda, and S. Nakamura, *Bull. Chem. Soc. Jpn.*, **59**, 2247 (1986).
22) F. Westly, NSRDS-NBS 67, 1980.

 © 1987 The Chemical Society of Japan Bull. Chem. Soc. Jpn., 60, 2737—2742 (1987)

Structure Study of Supermonomolecular Layers in Langmuir-Blodgett Films. Surface Active Squarylium Dye-Fatty Acid Binary Mixed System

Mutsuyoshi MATSUMOTO,* Takayoshi NAKAMURA, Motoo TANAKA, Tatsuo SEKIGUCHI, Hideo KOMIZU, Sanae Y. MATSUZAKI, Eiichiro MANDA, Yasujiro KAWABATA, Mitsuyoshi SAITO,† Sigeru IIZIMA,† and Michio SUGI†

National Chemical Laboratory for Industry, Yatabe, Ibaraki 305

†Electrotechnical Laboratory, Sakura-mura, Ibaraki 305

(Received December 25, 1986)

The structures of the Langmuir-Blodgett (LB) films of the ordinary mixed monolayer (LPF) and the supermonomolecular layer (HPF) of a surface active squarylium dye-icosanoic acid binary mixed system were examined by absorption spectroscopy. The absorption spectra of one unit layer of LPF with a molar mixing ratio ranging from 1/10 to 1/1 were almost the same, strongly suggesting that each component exists separately in the films. The LB films of two unit layers of LPF showed two peaks at 590 and 560 nm ascribed to intralayer and interlayer aggregates, respectively, besides the monomeric peak at 640 nm. The absorption spectra of one unit layer of HPF indicated a critical value of the mixing ratio 1/3.5 above which the 700-nm peak is observed. This peak is an indication of a multilayer consisting of pure **1** due to the interlayer interaction. The 560-nm peak observed for LPF is caused by a hindered interlayer interaction of the chromophores between the mixed monolayers.

Recently, the vacuum-deposited films of squarylium dyes have been investigated from the viewpoint of photovoltaic properties, whose quantum yields are high and depend not only upon the structure of the chromophore itself but also upon the packing of molecules involving intermolecular interaction and aggregate formation.[1-4] Two polymorphs are observed for a squarylium dye.[5,6] A change in the crystal form is considered to be the reason for the quick deterioration of the high solar energy conversion efficiency.[1] It is therefore important to develop a technique to obtain the desired aggregate structure.

In order to construct a system with the desired structure, i.e., suitable arrangement of molecules and aggregate formation, the Langmuir-Blodgett (LB) technique is one of the most powerful tools.[7] This technique contains a process in which a condensed phase at the air-water interface is deposited onto a substrate. Consequently, it is quite important to obtain a condensed phase with the desired structure. The desired structure is not necessarily limited to the typical condensed monolayer. In a previous paper,[8] we pointed out the technical importance of the supermonomolecular layer defined as an ordered multilayer at the gas-liquid interface.

Indeed, many studies have been categorized as concerning the supermonomolecular layer. For instance, the formation of ordered multilayers of some polypeptides at the air-water interface was observed when compressed under appropriate surface pressures.[9-11] As for 1-octadecanol, octadecanoic acid, and substituted phthalocyanine, the use of different spreading solvents leads to various structures of the condensed phases at an air-water interface.[12-15] A stable multilayer is obtained when a class of water-soluble azobenzene amphiphiles form complexes with polyanion.[16] Even more interesting are the cases where surface active azo dyes were squeezed out of the fatty acid matrices.[17,18] Selective squeezing-out of dye molecules from the mixed layer was, however, estimated mainly from *F-A* isotherms and molecular models, and the structure of the subsequent supermonomolecular layer has not yet been fully understood.

We have found, for surface active squarylium dye-fatty acid binary mixed system, that an ordinary mixed monolayer is formed under lower surface pressures (ca. 25 $mN\,m^{-1}$), and that higher surface pressures (ca. 40 $mN\,m^{-1}$) result in the supermonomolecular structure.[8,19] The structure of the supermonomolecular layer with the mixing ratio of 1/5 is characterized as a bilayer stack of a cadmium icosanoate monolayer and monolayer islands of the dye molecules squeezed out under the icosanoate monolayer. The dye molecules exist in such a manner that they are attached to the icosanoate matrix with their hydrophobic carbon chains and that the long axis of the chromophore is parallel to the film surface.

In this report, LB films with various mixing ratios were examined by absorption spectroscopy in order to clarify the supermonomolecular structure.

Experimental

The surface active squarylium dye, 2,4-bis[3,3-dimethyl-1-octadecyl-2(3*H*)-indolylidenemethyl]-1,3-cyclobutadienediylium-1,3-diolate, (**1**) was synthesized as previously described.[20] Icosanoic acid was purchased from Eastman Kodak Co. and used without further purification. Experimental conditions where LB films were prepared were the same as those in the previous reports.[8,19] Icosanoic acid was converted to cadmium icosanoate (**2**) upon the subphase containing 4.0×10^{-4} mol dm^{-3} of $CdCl_2$ and 5.0×10^{-5} mol dm^{-3} of $KHCO_3$. Mixed LB films deposited at 25 $mN\,m^{-1}$ and at 40 $mN\,m^{-1}$ are hereafter referred to as LPF and HPF, respectively. The molar mixing ratio r of mixed LB films of **1** and **2** was in the range of 1/10 to 1/1. Absorption spectra of the deposited films were taken by differential spectroscopy,

using the method of Kuhn et al.[21] Polarized absorption spectra were measured under four conditions described previously;[22] an incident angle of 45 or 90° to the film surface, and the electric field of the incident light parallel or normal to the dipping direction. The polarized spectra showed that all the transition moments discussed below were alomst parallel to the film surface. Absorption spectra of the solutions were measured by use of the Cary 17 DX spectrometer.

Results and Discussion

Two Condensed Phases at Air-Water Interface. Figure 1 shows *F-A* isotherms of **1** (curve g), **2** (curve a), and mixed layers of **1** and **2** with the mixing ratio r ranging from 1/10 to 1/1 (curves b—f). A common feature is observed for mixed layers: the first condensed phase at ca. 20—30 mN m^{-1}, the plateau region at ca. 30 mN m^{-1}, the second condensed phase at ca. 30—60 mN m^{-1}, and finally the collapse point at ca. 60 mN m^{-1}. The observed plateau region can be attributed to a transition from a monolayer in the first condensed phase to a multilayer in the second condensed phase.[9]

The mean area per molecule, s, is expressed as

$$s=(rs_1+s_2)/(r+1), \quad (1)$$

where s_1 and s_2 are the areas per molecule of **1** and **2**, respectively. On the plausible assumption of s_2 as 0.020 nm^2, even in the mixed layers,[8,19] the values of s_1 obtained were independent of the mixing ratio: 0.70 and nearly 0 nm^2 at 25 and 40 mN m^{-1}, respectively.

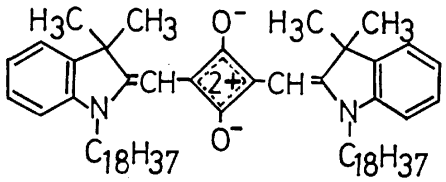

1

The former value is consistent with the molecular model when the chromophore is oriented with the long axis parallel and the short axis perpendicular to the surface. This fact indicates that an ordinary mixed monolayer is formed in the first condensed phase. In other words, the occupied area is governed by both **1** and **2**.

On the other hand, the value of s_1 (0 nm^2) under higher surface pressures indicates that the occupied area is governed by **2** alone. This strongly suggests the presence of a monolayer of **2**, which is supported by the same collapse pressure of the mixed layers with that of the monolayer of **2** (curve a). Absorption spectra of HPF with r=1/5 gave the model for the supermonomolecular structure.[19] This model for the squeezing-out is supported by the fact that the *F-A* isotherm of pure **1** (curve g) also shows a plateau region at ca. 30 mN m^{-1} which is almost identical with that for the onset of the plateau region for the mixed layers. The large plateau region for pure **1** (curve g) suggests that the molecules **1** tend to form a multilayer at air-water interface without any detectable rise in surface pressure.

The area occupied by HPF is ns_2' where n is the number of the molecule **2** in the mixed films and s_2' is the area per molecule of **2** at 25 mN m^{-1} (0.20 nm^2). If the squeezed-out molecules of **1** in the above film form a monolayer under the monolayer of **2**, the area occupied by **1** will be nrs_1' where s_1' is the area per molecule of **1** at 25 mN m^{-1} (0.70 nm^2). The fact that the area is governed by ns_2' suggests that the layer of the squeezed-out molecules of **1** becomes a multilayer when $nrs_1'>ns_2'$ ($r>s_2'/s_1'$=1/3.5).

Four Types of LB Films. In order to examine the supermonomolecular structure more precisely, four types of mixed LB films were prepared for each mixing ratio. Figure 2 shows a schematic view of one or two unit layers of LPF in the first condensed phase or HPF

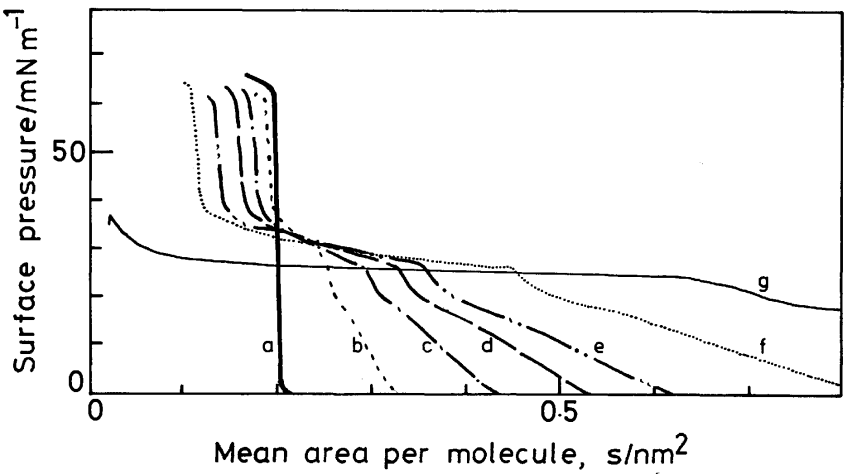

Fig. 1. Surface pressure-area isotherms of **1**, **2**, and mixed layers of **1** and **2**. a: r=0 (pure **2**), b: r=1/10, c: r=1/5, d: r=1/3, e: r=1/2, f: r=1/1, g: pure **1**. The data of a—f were reproduced from Ref. 19 by permission of Elsevier Sequoia, Lausanne.

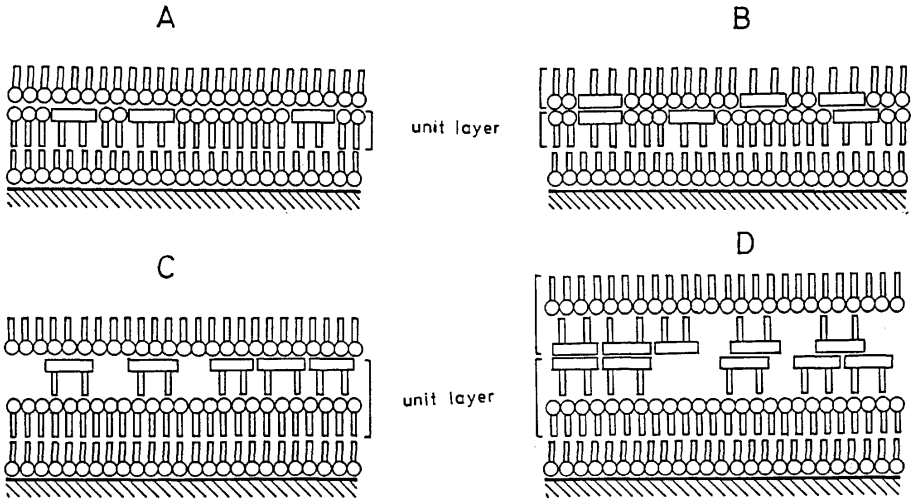

Fig. 2. Schematic view of the LB films of LPF and HPF with the mixing ratio of 1/5 deposited on a glass slide precoated with five monolayers of **2**. Only one monolayer of **2** is drawn in each case for simplicity. A: One unit layer of LPF followed by deposition of one monolayer of **2**, B: two unit layers of LPF, C: one unit layer of HPF followed by deposition of one monolayer of **2**, D: two unit layers of HPF.

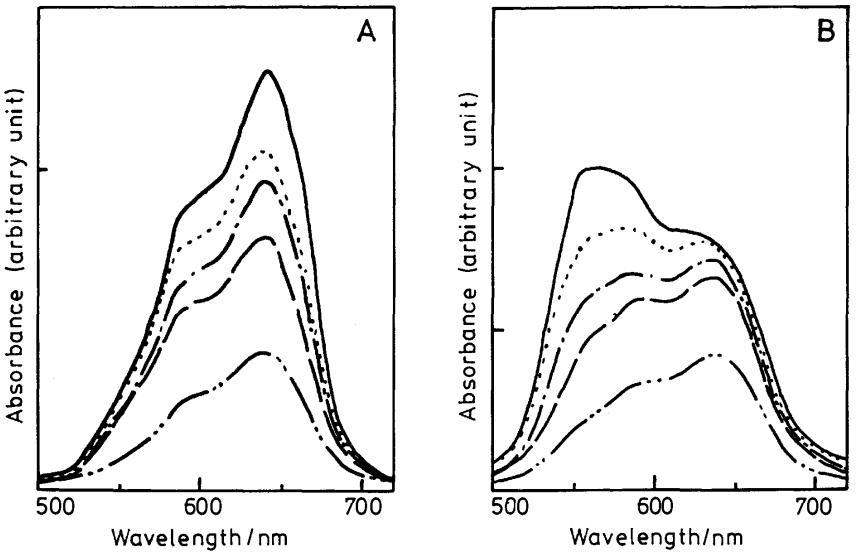

Fig. 3. Absorption spectra of one unit layer (A) and two unit layers (B) of LPF with various mixing ratios.
——: r=1/1, ·····: r=1/2, -·-·-: r=1/3, ----: r=1/5, -·····-: r=1/10.

in the second condensed phase with the mixing ratio of 1/5 deposited on a glass slide precoated with five monolayers of **2**. Only one monolayer of **2** is drawn in each case in Fig. 2 for simplicity.

In case A, where one unit layer of LPF is deposited on a substrate followed by deposition of one monolayer of **2**, the formation of chromophore aggregates is restricted within the same plane. Therefore, isolated molecules and intralayer aggregates with their characteristic spectra may be detected. In the case B, where two unit layers of LPF are deposited, there is a possibility of interlayer chromophore aggregation. Consequently, interlayer aggregates may be observed in addition to isolated molecules and intralayer aggregates. As is seen in this figure, LPF is an ordinary mixed monolayer whose occupied area is governed by both **1** and **2**.

In the cases C and D where one and two unit layers of HPF are deposited, respectively, the structures are quite different from those in the above two. HPF consists of dye and cadmium icosanoate segregated from each other into different layers. This gives rise to aggregates different from those in the cases A and B. The occupied area of HPF is, as is seen, governed by **2** alone.

One Unit Layer of LPF (Case A). Figure 3A shows the absorption spectra of one unit layer of LPF. Almost the same spectral patterns were observed for

LPF with r ranging from 1/10 to 1/1. This fact strongly suggests that the molecules **1** are immiscible with the molecules **2** and that each component exists separately in the form of domains.

Each peak value of absorbance,I, was proportional to the area fraction of **1** in the film plane (Fig. 4). This is expressed by

$$I=I_0 rs_1'/(rs_1'+s_2'), \quad (2)$$

where I_0 is the limiting value of I when the area fraction approaches unity. This proportional relationship indicates that **1** was not dissolved into the subphase and supports the structure of the ordinary mixed monolayer.

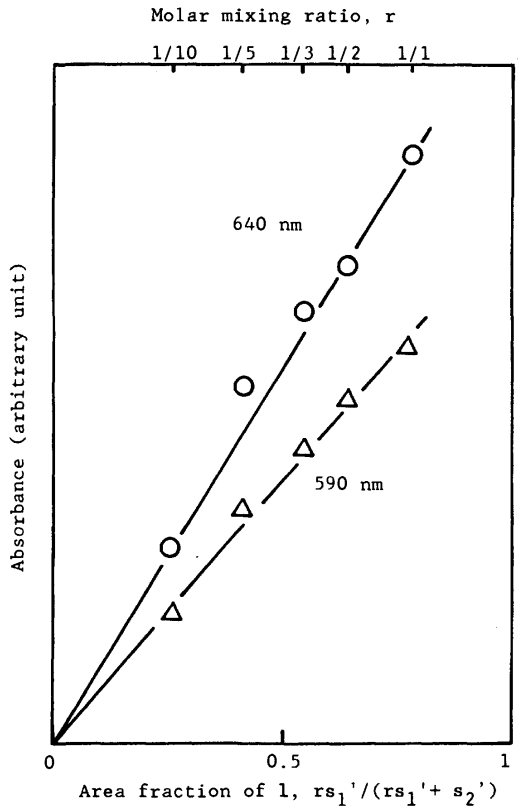

Fig. 4. Absorbance of one unit layer of LPF at each peak position as a function of area fraction of **1**. The molar mixing ratio is also shown.
○: 640 nm, △: 590 nm.

The absorption spectra of **1** in $CHCl_3$ solution ranging in concentration from 4.5×10^{-8} to 1.0×10^{-3} mol dm^{-3} show a main peak at ca. 640 nm (The full width at half maximum is ca. 20 nm.) and a shoulder at ca. 590 nm. The 640-nm peak and the 590-nm peak as well are attributed to isolated molecules. The absorbance ratio of the latter to the former is ca. 0.2 irrespective of concentration. This indicates that these two peaks are a vibronic progression.[23,24]

In contrast to the case of chloroform solutions, the 590-nm peak observed for LB films will be ascribed to an aggregate by the following reasons, although we cannot deny the contribution from the vibronic state. Firstly, the 590-nm peak is also observed even when the monomeric peak at 640 nm is hardly found (shown later in Fig. 5B). Secondly. the absorbance ratio of the 590-nm peak to the 640-nm peak is ca. 0.7, which is much larger than the value observed in solution. Therefore, we assume that the 590-nm peak mainly originates from the side-by-side structure of the aggregate[25] formed through intralayer interaction, since the origin of the 590-nm peak does not change the context significantly.

Studies with polarized light indicated that the transition moments for both 590-nm and 640-nm peaks lie statistically in the layer plane.

Two Unit Layers of LPF (Case B). The absorption spectra of two unit layers of LPF are depicted in Fig.

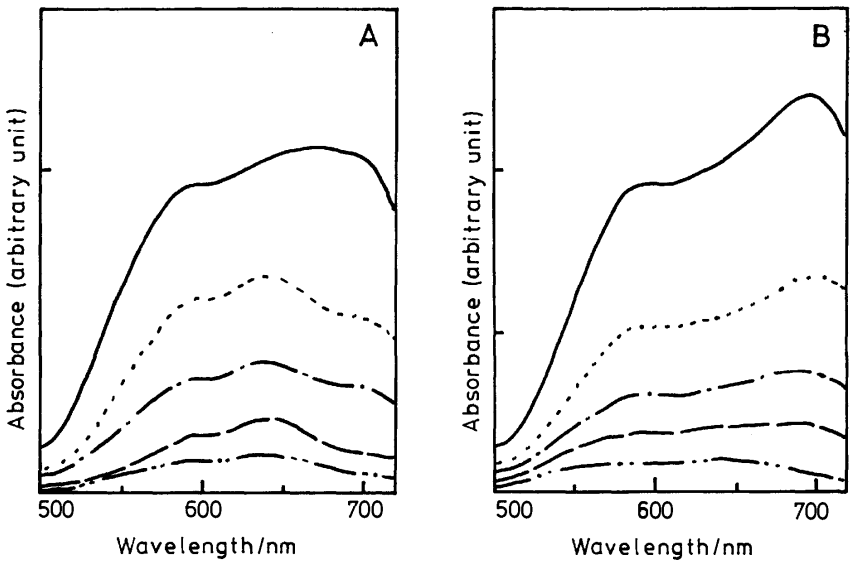

Fig. 5. Absorption spectra of one unit layer (A) and two unit layers (B) of HPF with various mixing ratios.
——: r=1/1, ·····: r=1/2, -·-·-: r=1/3, – – –: r=1/5, -·····-: r=1/10.

3B. In this case, both intralayer and interlayer aggregates have the possibility of being formed. Actually, evidence for an interlayer aggregate is clearly shown in the spectra. The 560-nm peak becomes prominent with an increase in the r value, which is presumably caused by the increasing occurrence of the interlayer interaction between two chromophores located in adjacent unit layers. Therefore, this peak is ascribed to the side-by-side structure of the aggregate through interlayer interaction.[26]

Polarized spectra indicated that the transition moments for the 590-nm and the 640-nm peaks lie statistically in the film plane, whereas that of the interlayer aggregate prefers the arrangement parallel to the dipping direction (absorbance ratio of 1.2—1.3). This suggests that the chromophores are slightly rearranged during or after the deposition process when the interlayer interaction of the chromophores occurs.

One Unit Layer of HPF (Case C). Figure 5A shows the absorption spectra of one unit layer of HPF. In the case of $r>s_2'/s_1'=1/3.5$, the excessive **1** should be squeezed out of the monolayer of **1** to form a complicated multilayer, since otherwise the area must be governed by nrs_1'. This structural change with r value is schematically shown in Fig. 6.

This change is clearly detected in the absorption spectra, which is strong evidence for the validity of the supermonomolecular structure. With an increase in the r value, the monomeric peak at 640 nm is relatively suppressed and the 700-nm peak emerges instead of the 560-nm peak observed for LPF. The 700-nm peak is observed only when r is higher than the critical value of 1/3.5. This peak is an indication of a multilayer consisting of pure **1**. The 700-nm peak indicates the aggregate involving end-to-end interaction[25] or J-aggregate[27] induced by interlayer interaction within the multilayer region consisting of pure **1**.

Studies with polarized light showed that the transition moment of the above aggregate also has the tendency to be oriented parallel to the dipping direction (absorbance ratio of 1.3—1.4). This again suggests a slight rearrangement of the chromophores during or after the deposition process. The transition moments for the other peaks lie statistically in the film plane.

Two Unit Layers of HPF (Case D). The absorption spectra of two unit layers of HPF are shown in Fig. 5B. The feature of the similar spectral patterns for samples with r ranging from 1/5 to 1/1 should be noted. Two peaks are observed at 590 and 700 nm, whereas the monomeric peak at 640 nm and the 560-nm peak are hardly to be seen.

The supermonomolecular structure is supported by the absorbances at peak positions for samples with r ranging from 1/5 to 1/1. If the structures shown in Fig. 6 are valid, the absorbances should be proportional to the number of the molecule **1** per unit area because the spectral patterns are similar for these samples. The number of the molecule **1** per unit area is nr/ns_2'. Therefore, the absorbances I' should obey the following equation:

$$I'=rI_0', \tag{3}$$

where I_0' is the absorbance when r equals unity. This relationship is clearly seen in Fig. 7. This figure includes the points for the sample with r=1/10. It is noted that the point for the 700-nm peak is signifi-

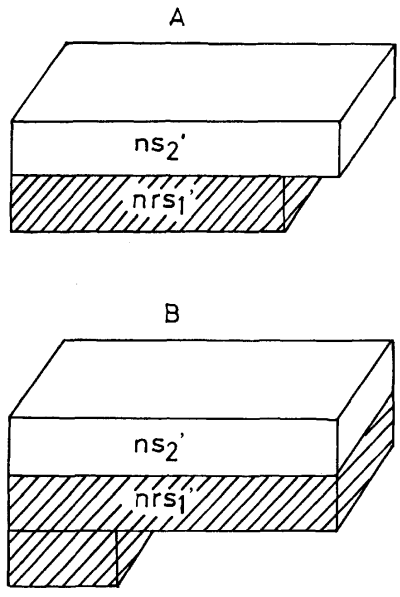

Fig. 6. Schematic view of the structural change of one unit layer of HPF with r value. The portions with and without hatches represent the layers composed of pure dye **1** and pure **2**, respectively. A: $nrs_1' \leqq ns_2'$ ($r \leqq 0.20/0.70$), B: $nrs_1' > ns_2'$ ($r > 0.20/0.70$). When r is small, the supermonomolecular structure is a bilayer as shown in A, while the excessive **1** and the bilayer should form a complicated multilayer in the case of $r>1/3.5$.

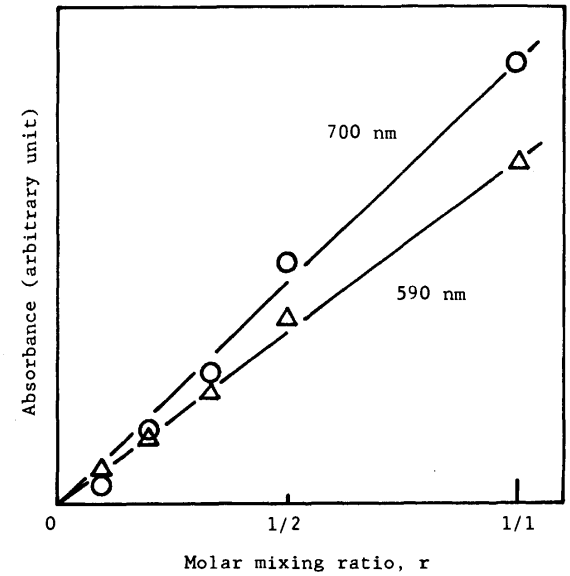

Fig. 7. Absorbance of two unit layers of HPF at each peak position as a function of the mixing ratio r. O: 700 nm, Δ: 590 nm.

cantly deviated under the straight line. Equation 3 also indicates that **1** was not dissolved into the subphase even when compressed under higher surface pressures.

The two observed peaks are attributed to two different aggregates, as opposed to the single herringbone structure whose unit cell contains two chromophores and which possesses two allowed transitions.[24,28] This is concluded by the fact that the 590-nm peak is also observed for the case of intralayer interaction in LPF, while the 700-nm peak is found only when the multilayer consisting of pure **1** is formed. Furthermore, the transition moment for the 590-nm peak lies statistically in the film plane, while that for the 700-nm peak has a preference of being oriented to the dipping direction (absorbance ratio of 1.3—1.4). This is quite contradictory to a herringbone structure, where two allowed transitions are governed by one and the same distribution of the aggregate. In other words, if a random distribution in a plane is the case with one transition moment, this applies also to the other.

The relationship of Eq. 3 suggests that the relative ratio of occurrence of the two aggregates remains invariant for HPF with higher mixing ratios (1/5—1/1), i.e., the equilibrium between the two aggregates is held in the multilayer region consisting of pure **1**. As for HPF with r=1/10, the 700-nm peak is almost extinguished and the broad band covering from 550 to 650 nm remains. This suggests that the 700-nm peak is attributable to a larger aggregate than the 590-nm peak since HPF with r=/10 would have a considerable fraction of area which is not occupied by **1** in the mutilayer region of pure **1**.

The aggregates in HPF containing multilayers of pure **1** (case C with $r \geqq 1/3$ and case D with $r \geqq 1/5$) are not the same as those in LPF consisting of multilayers diluted by **2** (case B with all values of r studied). This is reflected in the fact that the 700-nm peak emerges only for the former films and that the 560-nm peak is observed only for the latter films. The chromophores of the dyes are subjected to interlayer interaction for both cases. In contrast to the former films, however, this is more or less hindered by the molecules **2** for the latter films.

In conclusion, the desired aggregates can be obtained by the control of mixing ratio and surface pressure, which is useful in constructing molecular organizates. The method employed in this work will serve as means for clarifying other supermonomolecular structures involving interlayer interaction between chromophores.

We would like to thank Professor Kiyoshige Fukuda and Dr. Hiroo Nakahara of Saitama University for helpful comments. We also acknowledge Dr. Shinichi Kuroda, Dr. Keiichi Ikegami, and Dr. Koichi Honda for stimulating discussions.

References

1) P. Yamln, A. P. Piechowski, G. R. Bird, and D. L. Morel, *J. Phys. Chem.*, **86**, 3796 (1982).
2) R. O. Loufty, C. K. Hsiao, and P. M. Kazmaier, *Photogr. Sci. Eng.*, **27**, 5 (1983).
3) D. L. Morel, E. L. Stogryn, A. K. Ghosh, T. Feng, P. E. Purwin, R. F. Shaw, C. Fishman, G. R. Bird, and A. P. Piechowski, *J. Phys. Chem.*, **88**, 923 (1984).
4) A. P. Piechowski, G. R. Bird, D. L. Morel, and E. L. Stogryn. *J. Phys. Chem.*, **88**. 934 (1984).
5) M. Tristani-Kendra, C. J. Eckhardt, J. Bernstein, and E. Goldstein, *Chem. Phys. Lett.*, **98**, 57 (1983).
6) M. Tristani-Kendra and C. J. Eckhardt, *J. Chem. Phys.*, **81**, 1160 (1984).
7) For example, D. Möbius, *Acc. Chem. Res.*, **14**, 63 (1981), and references therein.
8) Y. Kawabata, T. Sekiguchi, M. Tanaka, T. Nakamura, H. Komizu, K. Honda, E. Manda, M. Saito, M. Sugi, and S. Iizima, *J. Am. Chem. Soc.*, **107**, 5270 (1985).
9) T. Takenaka, K. Harada, and M. Matsumoto, *J. Colloid Interface Sci.*, **73**, 569 (1980).
10) F. Takeda, M. Matsumoto, T. Takenaka, and Y. Fujiyoshi, *J. Colloid Interface Sci.*, **84**, 220 (1981).
11) F. Takeda, M. Matsumoto, T. Takenaka, Y. Fujiyoshi, and N. Uyeda, *J. Colloid Interface Sci.*, **91**, 267 (1983).
12) H. E. Ries Jr., *Nature (London), Phys. Sci.*, **243**, 14 (1973).
13) S. Baker, M. C. Petty, G. G. Roberts, and M. V. Twigg, *Thin Solid Films*, **99**, 53 (1983).
14) G. J. Kovacs, P. S. Vincett, and J. H. Sharp, *Can. J. Phys.*, **63**, 346 (1985).
15) J. R. Fryer, R. A. Hann, and B. L. Eyres, *Nature*, **313**, 382 (1985).
16) M. Shimomura and T. Kunitake, *Thin Solid Films*, **132**, 243 (1985).
17) E. E. Polymeropoulos, D. Möbius, and H. Kuhn, *J. Chem. Phys.*, **68**, 3918 (1978).
18) J. Heeseman, *J. Am. Chem. Soc.*, **102**, 2176 (1980).
19) Y. Kawabata, T. Sekiguchi, M. Tanaka, T. Nakamura, H. Komizu, M. Matsumoto, and E. Manda, *Thin Solid Films*, **133**, 175 (1985).
20) M. Tanaka, T. Sekiguchi, Y. Kawabata, T. Nakamura, and E. Manda, *Nippon Kagaku Kaishi*, **1985**, 1516.
21) H. Kuhn, D. Möbius, and H. Bücher, "Physical Methods of Chemistry," ed by A. Weisserberger and B. W. Rossiter, John Wiley & Sons, Inc., New York (1972), Vol. 1 Part IIIB, p. 577.
22) T. Fukui, M. Saito, M. Sugi, and S. Iizima, *Thin Solid Films*, **109**, 247 (1983).
23) W. West, S. P. Lovell, and W. Cooper, *Photogr. Sci. Eng.*, **14**, 52, (1970).
24) G. R. Bird, G. Debuch, and D. Möbius, *J. Phys. Chem.*, **81**, 2657 (1977).
25) For example, J. N. Murrel, "The Theory of the Electronic Spectra of Organic Molecules," John Wiley & Sons,
26) R. Steiger, R. Kitzing, and P. Junod, *J. Photogr. Sci.*, **21**, 107 (1973).
27) For example, H. Bücher and H. Kuhn, *Chem. Phys. Lett.*, **6**, 183 (1970).
28) C. Reich, *Photogr. Sci. Eng.*, **18**, 335 (1974).

 © 1987 The Chemical Society of Japan Bull. Chem. Soc. Jpn., 60, 2743—2746 (1987)

Time-Resolved Unimolecular Fragmentations of $C_3H_7O^+$ Ions

Ryuichi ARAKAWA* and Yozaburo YOSHIKAWA
Institute of Chemistry, College of General Education, Osaka University, Osaka 560
(Received December 26, 1986)

The unimolecular dissociations of the $C_3H_7O^+$ ions produced by the dissociative ionization of *t*-butyl and *s*-butyl alcohols have been studied by means of trapped ion mass spectrometry(TIMS). The metastable peak intensities for two competing formations of $C_3H_5^+$ and CH_3O^+ have been measured for the ion lifetimes of 0—50 μs. Also, the shifts of the electron-ionization-efficiency(EIE) curves for these ions have been observed between the ion-storage times of 2 and 800 μs. These data have then been fitted by means of QET model calculations. The dissociation paths of $C_3H_7O^+$ can be interpreted without any assumption of a rate-determining isomerization process.

The potential energy profiles have been of much interest in understanding the reaction mechanism. One of the problems is the experimental uncertainty concerning a rate-determining isomerization process or its barrier height on the potential surface. In a $C_3H_7O^+$ system, most of the studies have employed electron-impact(EI) ionization,[1-5] isotope labeling techniques,[6,7] and chemical ionization(CI)[8,9] for metastable fragmentations. Collision-induced dissociation(CID) spectra of ions have been used for the identification of ion structures.[10] The molecular orbital calculations[11] have provided accurate knowledge about the relative energies of the various $C_3H_7O^+$ ions involved on the potential energy surface. In the reaction paths for water and ethylene elimination (Scheme 1), several structures of $C_3H_7O^+$ ions have been postulated to lie on the same potential energy surface. Detailed potential energy surfaces for the fragmentations of $(CH_3)_2C{=}OH^+$ [**I**] and $CH_3CH_2CH{=}OH^+$ [**II**] have been studied by Williams and his co-workers.[2,3] Their results for the ratios of the metastable peak intensity or kinetic energy releases showed that the fragmentation of **I** by either reaction, 1 or 2, involves a rate-determining isomerization to **II** prior to fragmentation. Harrison et al.[9] have obtained the same conclusion from the fact that the ratios of metastable peak intensities for **I** are essentially insensitive to activation modes, such as the EI, CI, and CID methods. However, measurements of the metastable appearance energies for $C_3H_5^+$ and CH_3O^+ with energy-selected electrons have shown that the fragmentations of the **I** and **II** isomers, which were formed from *t*-butyl and *s*-butyl alcohols respectively, take place at the thermochemical threshold.[4]

There is no consistent explanation for the rate-determining isomerization of **I**→**II**. Therefore, our present study examines in more detail the fragmentations of the **I** and **II** ions by means of time-resolved measurements of the metastable peak intensities and the EIE curves. In particular, an experiment for long-lifetime ions can study the lower internal energy fragmentation than have previous studies. A wide variation in ion lifetimes permits a close comparison of the metastable peak intensity with the calculated intensity by assuming the rate models. The TIMS experiment can change the ion residence time up to several milliseconds, so that the unimolecular reaction of 10^3—10^6 s^{-1} can be sampled.

$$\underset{\mathbf{I}}{(CH_3)_2C{=}OH^+} \longrightarrow \underset{\mathbf{II}}{CH_3CH_2CH{=}OH^+}$$

$$CH_2{=}CHCH_2OH_2^+ \longrightarrow C_3H_5^+ + H_2O \quad (1)$$

$$\longrightarrow CH_3\overset{+}{C}HCH_2OH \longrightarrow {}^+CH_2CH_2CH_2OH \longrightarrow CH_3O^+ + C_2H_4 \quad (2)$$

Scheme 1.

Experimental

The ion-trapping technique has been described in detail elsewhere.[12] The space charge formed by a continuous 5-eV electron beam was used to trap ions produced when a negative pulse was applied to a filament. At a known delay time after the ionizing pulse, a positive pulse 5 μs in duration and 4 eV high was applied to a repeller electrode in order to remove ions for mass analysis. Argon ions were stored far up to several milliseconds without any serious decrease in the trapped ion concentration, as is shown in Fig. 1. An ionizing pulse 2 μs in duration was applied to the filament at 1ms-intervals. The nominal electron energy was varied by changing the pulse height applied to the filament.

A home-built tandem-type mass spectrometer was used to measure the EIE curves and the metastable fragmentation. The parent ions, which are selected by the first magnet,

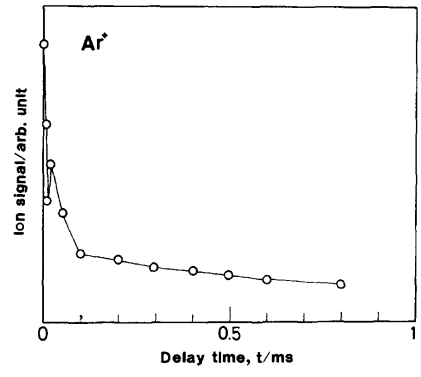

Fig. 1. Argon ion signals as a function of the delay time, *t*.

decompose in the second field free region between two magnets. The product ions are analyzed by the second magnet. A data accumulation of about an hour was statistically needed for both the EIE and metastable peak measurements. The temperature of the ion source was 423 K. The ion-accelerating voltage was 1.5 kV. The ion-source pressure was kept at 2×10^{-6} Torr (1 Torr=133.32 Pa). The collision-induced reactions were negligible, because the pressure in the field free region was always less than 1×10^{-6} Torr. Samples were commercially obtained.

Results and Discussion

Figure 2 shows the time-resolved EIE curves for the $C_3H_5^+$ and CH_3O^+ fragments produced from *t*-butyl and *s*-butyl alcohols. The argon EIE curve was used for the EIE curve normalization between different ion storage times, because the ion trapping efficiency decreases with the delay time, as is shown in Fig. 1. The EIE shifts observed at V=13.5 eV are about 0.4 eV for $C_3H_5^+$ and zero for CH_3O^+. These shifts are due to the so-called "kinetic shift," the excess energy required to produce a detectable dissociation (usually 10^5 s^{-1}) of a polyatomic ion. The molecular ions for both samples were very low in intensity in the present energy range, while the $C_3H_7O^+$ fragment is very abundant on both mass spectra. The EIE shifts with the delay times are, therefore, believed to be caused by the slow dissociation, not for the molecular ions, but for the $C_3H_7O^+$ precursor ions.

The time-dependent EIE for the *i*-th daughter ion at a nominal electron energy V can be written in this form:[13]

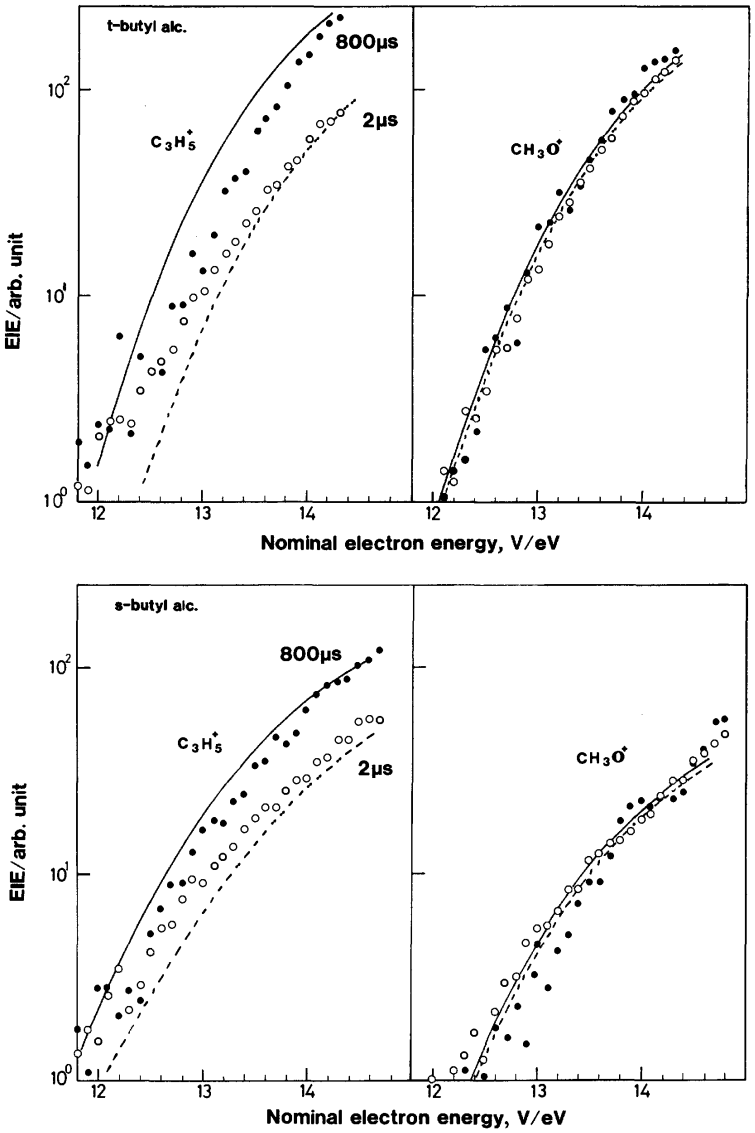

Fig. 2. Time-resolved electron-ionization-efficiency(EIE) curves for $C_3H_5^+$ and CH_3O^+ daughter ions vs. nominal electron energy V: (a) *t*-butyl alcohol, (b) *s*-butyl alcohol. ● (——) and ○ (----) indicate the experimental (calculated) EIEs of t=800 and 2 μs, respectively.

$$\mathrm{EIE}_i(V,t) \propto \int_0^\infty m(E'-V)\left[\int_{AE_0}^{E'} f(E',E)\times (k_i(E)/\sum k_j(E))w(E)\mathrm{d}E\right]\mathrm{d}E' \quad (3),$$

where t is the ion-source-residence time, $m(E'-V)$ is the instrumental electron-energy distribution, E' is the total electron energy, $f(E',E)$ is the internal energy distribution of $C_3H_7O^+$, AE_0 is the 0 K appearance energy for the daughter ion, $k_i(E)$ is the unimolecular rate constant for the i-th path, and $w(E)$ is the fraction of dissociation given by $1-\exp(-t\sum k_j(E))$. The $m(E'-V)$ distribution was obtained from the second derivatives of a helium experimental EIE curve on the basis of Morrison's method[14]; its half-width was 0.8 eV. The $f(E',E)$ distribution for the ionized $C_3H_7O^+$ was assumed to be equal to that for the molecular ions. From the ionization-threshold law,[15] the energy distribution for molecular ions can be given by $p(E)(E'-E)$, where $p(E)$ is the energy-deposition function. The photoelectron spectra of t-butyl and s-butyl alcohols were assumed to represent $p(E)$.[16]

The decay rates were obtained from a simple form[17] of $k(E)=v(1-E_0/E)^s$, where v is the frequency factor, E_0 is the activation energy, and s is the effective number of oscillators. In the same reaction system, Tsang and Harrison[1] have investigated, by means of model calculation, the effect of change in the internal energy distribution on the metastable peak ratio of $C_3H_5^+/CH_3O^+$. Their adjusted parameters of the frequency factor were $v_a=10^{8-9}$ and $v_b=10^{11}-10^{12}$ for reactions 1 and 2 respectively. In the present calculation, we employed similar parameters of the frequency factor, as are summarized in Table 1. Moreover, for the sake of simplicity, the frequency factors for **I** and **II** were assumed to be the same. The s value was taken to be 9, corresponding to a third of the number of vibrational degrees of freedom of $C_3H_7O^+$. The activation energies were obtained from the potential energy diagram illustrated in Ref. 9, assuming that the dissociations occur at their thermochemical onsets. The calculated EIE curves are in fair agreement with the experimental curves. The amount of the EIE shift between different delay times depends principally on the rising steepness of the $k(E)$ vs. E curves. As may be seen in Fig. 2, the EIE shift is greater for $C_3H_5^+$ formation than for CH_3O^+. This is because the $k(E)$ curve of $C_3H_5^+$, having the smaller frequency factor, rises more slowly with the energy.

The metastable peak intensities relative to the parent ions, $m^*/C_3H_7O^+$, for the **I** and **II** ions are shown in Fig. 3 for the range of t=0—50 μs. Our ratios of the peak intensities, $C_3H_5^+/CH_3O^+$, at t=0 μs agree with those of the literature.[9] The experimental errors estimated were, at most, 20%. After a careful consideration of the reproducibility and error limits, we obtained the significant result for **I** that the peak intensities between $C_3H_5^+$ and CH_3O^+ are reversed at a long delay time. This result is inconsistent with the previous results[3,9] indicating that the metastable peak ratios are insensitive to ion formation and to ion lifetime of several microseconds. Its lifetime was varied by change in an accelerating voltage. The ratios of $C_3H_5^+/CH_3O^+$ are not affected by the ion lifetime if there is the rate-determining isomerization of **I**→**II**. The metastable peak intensities were calculated assuming the direct fragmentation of **I** and **II** to products. For the calculation, Eq. 3 was modified in such a way that $w(E)$ was replaced by $\exp(-t_1\sum k_j(E))-\exp(-t_2\sum k_j(E))$. Therefore, $w(E)$ means the fraction of dissociation occurring in the second field-free region. t_1 and t_2 are the entrance and exit times relative to the time of ion formation (t_1=5.8+t and t_2=10.1+t μs).

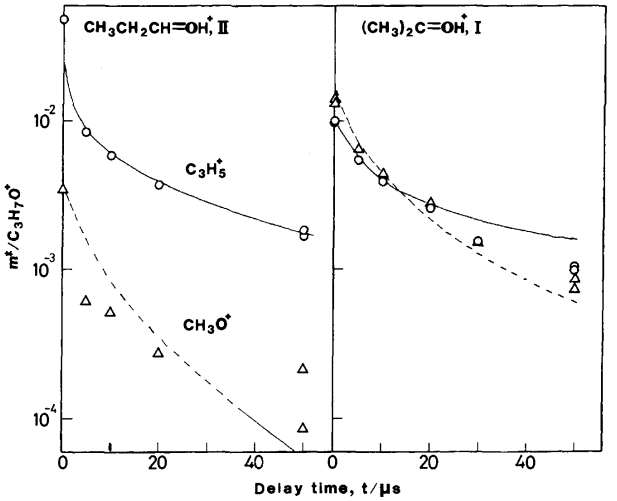

Fig. 3. A plot of metastable peak intensities relative to the parent ion, $m^*/C_3H_7O^+$, against delay time when V=40 eV. Experimental (calculated) data; $C_3H_5^+$, ○ (——) and CH_3O^+, △ (----). The ions **I** and **II** were produced by dissociative ionization from t-butyl and s-butyl alcohols, respectively.

The smooth lines in Fig. 3 are the fragmentation curves calculated by the use of the same rate models as in Table 1. The overall agreement with the experimental curves is fairly satisfactory. The rate-determining isomerization of **I**→**II** was supported by the experimental evidence that the metastable-peak ratios for **I** were independent of the activation modes. In other words, the relative rates were essentially constant over the internal-energy range generated. Accordingly, the rate-determining isomerization mechanism may be ruled out by the presence of curve crossing for **I**.

Table 1. Activation Energies and Frequency Factors Used in the Rate Model of the $C_3H_7O^+$ Dissociation

Ion	$C_3H_5^+$		CH_3O^+	
	E_0	v_a	E_0	v_b
	eV	s^{-1}	eV	s^{-1}
I	2.08	$10^{8.5}$	2.66	10^{11}
II	1.56	$10^{8.5}$	2.14	10^{11}

A collisional deactivation and an infrared radiative decay are nondissociative processes particularly important for long-lived ions. However, these processes proved to have no effect on the EIE curves or the metastable fragmentations at the present pressure of the sample. This has previously been discussed in detail in the case of pyridine dissociation.[13]

The time-resolved measurements of EIEs and metastable fragmentations lead to the conclusion that the dissociations of **I** and **II** require no hypothesis of the rate-determining isomerization or the barrier on their paths. This conclusion is exclusively valid for the dissociation of ions whose internal energy is close to the threshold. In the case of t=50 μs, for example, the rate of $k(E)=1.7\times10^4$ s^{-1} corresponding to a peak of $w(E)$ contributes principally to metastable fragmentation.

References

1) C. W. Tsang and A. G. Harrison, *Org. Mass Spectrom.*, **7** 1377 (1973).

2) G. Hvistendahl, R. D. Bowen, and D. H. Williams, *J. Chem. Soc., Chem. Commun.*, **1976**, 294.

3) R. D. Bowen, J. R. Kalman, and D. H. Williams, *J. Am. Chem. Soc.*, **99**, 5481 (1977); R. D. Bowen, D. H. Williams, G. Hvistendahl, and J. R. Kalman, *Org. Mass Spectrom.*, **13**, 721 (1978).

4) J. L. Holmes and J. K. Terlouw, *Org. Mass Spectrom.*, **15**, 383 (1980).

5) G. Hvistendahl and D. H. Williams, *J. Am. Chem. Soc.*, **97**, 3097 (1975).

6) C. W. Tsang and A. G. Harrison, *Org. Mass Spectrom.*, **5**, 877 (1971).

7) J. H. Holmes, R. T. B. Rye, and J. K. Terlouw, *Org. Mass Spectrom.*, **14**, 606 (1979).

8) R. D. Bowen and A. G. Harrison, *Org. Mass Spectrom.*, **16**, 159 (1981).

9) A. G. Harrison, T. Gaumann, and D. Stahl, *Org. Mass Spectrom.*, **18**, 517 (1983).

10) F. W. McLafferty and I. Sakai, *Org. Mass Spectrom.*, **7**, 971 (1973).

11) R. H. Nobes and L. Radom, *Org. Mass Spectrom.*, **19**, 385 (1984).

12) A. A. Herod and A. G. Harrison, *Int. J. Mass Spectrom. Ion Phys.*, **4**, 415 (1970); C. Lifshitz, *Mass Spectrom. Rev.*, **1**, 309 (1982).

13) R. Arakawa and Y. Yoshikawa, *Bull. Chem. Soc. Jpn.*, **60**, 49 (1987).

14) J. D. Morrison, *J. Chem. Phys.*, **21**, 1767 (1953).

15) M. R. H. Rudge, *Rev. Mod. Phys.*, **40**, 564 (1968); M. R. H. Rudge and M. J. Seaton, *Proc. Phys. Soc.*, **83**, 680 (1964).

16) A. D. Baker, D. Betteridge, N. R. Kemp, and R. E. Kirby, *Anal. Chem.*, **43**, 375 (1971).

17) H. M. Rosenstock, M. B. Wallenstein, A. L. Wahrhaftig, and H. Eyring, *Proc. Natl. Acad. Sci. U.S.A.*, **38**, 667 (1952).

 © 1987 The Chemical Society of Japan Bull. Chem. Soc. Jpn., 60, 2747—2750 (1987)

Electrical Double Layer Formed on the Monolayer of Crown Ether Compounds

Hideo MATSUMURA,* Tsutomu WATANABE,† Kunio FURUSAWA,† Seiichi INOKUMA,†† and Tsunehiko KUWAMURA††
Electrotechnical Laboratory, Umezono, Sakura-mura, Ibaraki 305
†Department of Chemistry, The University of Tsukuba, Tennoudai, Sakura-mura, Ibaraki 305
††Faculty of Technology, Gunma University, Kiryu, Gunma 376
(Received January 12, 1987)

The binding behavior of metal ions to the monolayers of a crown ether compound has been studied by the surface potential measurements. The obtained data are analyzed from the viewpoint of interfacial electrochemistry, i.e., the electrical double layer theory at the interfaces. The analysis reveals that the generated double layer at a membrane-solution interface after the complexing of metal ions with crown ethers is well described by the Stern model for the electrical double layer; it shows that there exists a possibility to evaluate the binding constants of metal ions with crown ethers under interfacial circumstances.

The transport behavior across biological membranes or oil liquid film is one of the attractive problems in colloid and surface chemistry. A lot of compounds which mediate ion transport through membranes have been found in biological systems (e.g. antibiotics) and have been manufactured artificially.[1-3] These compounds are called "ionophores" and are classified approximately into two categories from their functional characteristics, (carrier type and channel type). Crown ethers are the most attractive synthetic ionophores, which can complex with various metal ions with a characteristic selectivity.[2,3] Since these complexes are lipophilic, arising from crown's hydrophobic rings, they can dissolve in nonaqueous media. Thus, the crown ether can transport metal ions through oil liquid films or lipid bilayer membranes. Despite the fact that a lot of studies have been performed on this subject, details concerning the transport mechanisms, whether carrier type or channel type, have been incompletely revealed. For the purpose of understanding the transport mechanism, it is desirable to clarify fundamental factors of the transport process, e.g. the binding characteristics of metal ions with crown ethers, the adsorption and desorption equilibrium between oily phase and aqueous phases, etc.[4,5] In the case of amphiphilic crown ethers, binding with metal ions can occur both in the bulk aqueous phase and at the interface of the membrane-aqueous phase. On the other hand, some lipophilic crown ethers hardly dissolve in the aqueous phase; therefore, they make complexes with metal ions only at the interface of the oil-aqueous phase or the membrane-aqueous phase. At such interfaces, the binding behavior of metal ions with crown ether are influenced by various interfacial properties, especially an electrical double layer at the interface.

In this work, the binding behavior of metal ions with a crown ether under interfacial circumstances has been studied from the viewpoint of interfacial electrochemistry. To find the fundamental feature of binding at the interface, simple systems have been employed, i.e., monolayers of a water-insoluble crown compound and the change in the surface potential of the monolayers caused by ion-binding to them has been studied.[6]

Experimental

Materials. To make a monolayer on a water surface, a crown ether which had a long hydrocarbon chain was prepared. The compound was octadecyloxymethyl 18-crown-6 (see Fig. 1) and is hereafter abbreviated as C18-18-crown-6.

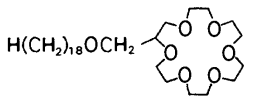

Fig. 1. Molecular structure of octadecyloxymethyl 18-crown-6.

C18-18-crown-6 was synthesized from octadecyl glycidyl ether and pentaethylene glycol by the same method as that reported in the literature.[7,8] The product was purified by column chromatography on silica gel or repeated Kugelrohr distillation (bp 230—235 °C/0.002 Torr (1 Torr=133.322 Pa)) and then recrystallized from methanol (mp 46—47 °C). The purity (>99%) was confirmed by GLC, TLC, NMR, IR, and elemental analyses. To make mixed monolayers with C18-18-crown-6, stearyl alcohol (Tokyo Kasei Kogyo Co.) was employed.

Surface Potential Measurement. A monolayer of C18-18-crown-6 was spread from a hexane solution on pure water. The packing density of the membrane was about 1/100 (molecule/Å^2). This value is comparable to the density of this compound in a close-packed state of a two-dimensional array. After the addition of a concentrated metal chloride aqueous solution to the subphase solution in a 80-ml Teflon trough, the solution was stirred for more than 30 min; the change in the surface potential ($\Delta\Delta V$) caused by a binding of the metal ions was measured by the vibrating-electrode method[9] at 23 °C. The 1:1 mixed monolayer of C18-18-crown-6 with stearyl alcohol was also employed and the experiment was carried out according to the same procedure as that for the pure monolayer, except for the packing density (in this case: ca. 1/100 molecular pair/Å^2).

Results and Discussion

The monolayer of C18-18-crown-6 has no electrical charges when it is spread on distilled water. The addition of metal ions to the subphase solution causes the formation of an electrical double layer at the membrane-water interface by binding to the crown

rings, leaving counter ions (Cl^-) in the aqueous phase. The generation of the electrical double layer can be observed by measuring the surface potential of the monolayer. Strictly speaking, the surface potential of the monolayer is described as a combination of the potential arising from the oriented dipoles of polar head groups of crown ether molecules and the ionic double-layer potential. In the present analysis, the change in the surface potential is assumed to be caused by a structural change in the ionic double layer; this has no serious disadvantage judging from the following fact. The change in the molecular orientation of this type crown ether, caused by a variation in the molecular packing density in the monolayer, shows a rather drastic potential change (Details will be published elsewhere). In Fig. 2, the change in the surface potential is plotted against the concentration of several kinds of metal ions. As can be seen, the contribution of these ions to $\Delta\Delta V$ is of the order of $K^+ > Na^+$ for alkali ions and $Ba^{2+} > Ca^{2+}$ for alkaline earth ions. These orders are the same as those of the complexing stability constant of these ions with 18-crown-6 in water or methanol.[10] For a mixed monolayer of C18-18-crown-6 with steary alcohol (1 : 1 molar ratio), plots of $\Delta\Delta V$ vs. the concentrations of various metal ions are shown in Fig. 3. A similar tendency to those in Fig. 2 is observed regarding $\Delta\Delta V$; however, the apparent ion-selectivity is lower than that for the pure membrane. All these facts suggest that there exists the same ion-selectivity of crown ethers at the membrane-solution

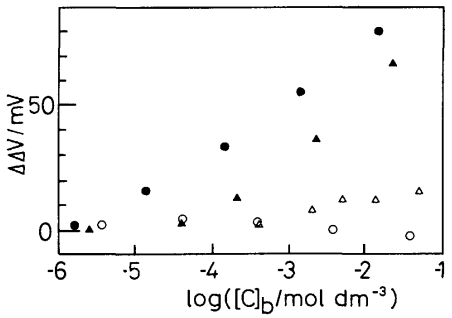

Fig. 2. Surface potential change of C18-18-crown-6 monolayer vs. concentration of various ions, (●) Ba^{2+}, (▲) K^+, (△) Na^+, (○) Ca^{2+}.

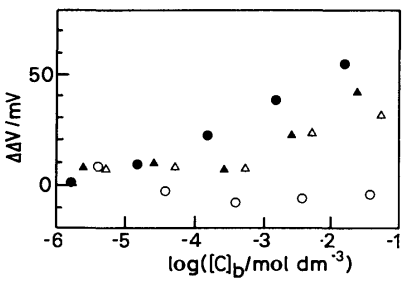

Fig. 3. Surface potential change of mixed monolayer of C18-18-crown-6 and stearyl alchol (molar ratio=1/1) vs. concentration of various ions, (●) Ba^{2+}, (▲) K^+, (△) Na^+, (○) Ca^{2+}.

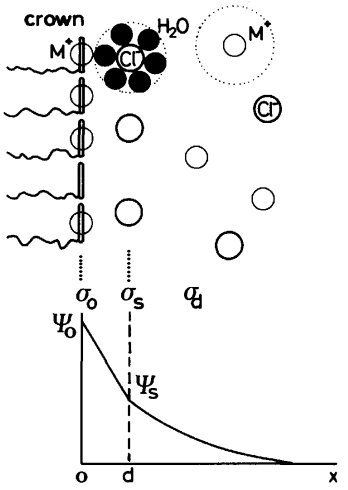

Fig. 4. Schematic representation of the distribution of ions and the profile of electrostatic potential across the double layer at the interface of crown ether monolayer and aqueous solution.

interface to that in the bulk phase.

To know further details regarding the binding behavior, the obtained data are analyzed using the concepts of interfacial electrochemistry.[11] Figure 4 shows a schematic representation of an electrical double layer at the interface between the monolayer of a crown ether and aqueous salt solution. In this system, the charges on the membrane-surface arise from the binding of metal ions with crown rings after dehydration, while the hydrated chloride ions remaining in the solution become counter ions. Therefore, the Gouy-Chapman-Stern model may be adequate for describing this elctrical double layer. However, a slight modification is required to describe the feature of surface charges. That is, the charges are localized at each of the crown rings; then the number of binding sites for metal ions is limited. This corresponds to the number of crown ether molecules in the monolayer. Therefore, the Langmuir adsorption isotherm is adopted to represent the binding behavior of metal ions to the membrane. The relations between the potential and the charges are described in the following way.

(1) The electroneutrality requires the following relation:

$$\sigma_0 + \sigma_s + \sigma_d = 0, \tag{1}$$

where σ_0 is the charge density on the membrane surface, σ_s the charge density on the Stern plane, and σ_d the charge density in the diffuse double layer.

(2) σ_0 is represented by a Langmuir-type equation:

$$\sigma_0 = z|e| \frac{KC_0[M^+]_b \exp(-z|e|\Phi/kT)}{1 + K[M^+]_b \exp(-z|e|\Phi/kT)} \tag{2}$$

where K is the binding constant, C_0 the density of crown ether on the monolayer (in the present experiment, $C_0 = 1/100$ number/Å^2), $[M^+]_b$ the concentration of metal ion in the bulk solution, z the valency of

metal ions, and Φ the micropotential which influences the binding of metal ions.[12] Φ is represented by the following simple formula:

$$\Phi = \alpha \cdot \psi_0, \tag{3}$$

where ψ_0 is the surface potential of the membrane and α is a constant ($0<\alpha<1$).

(3) σ_s is also represented by a Langmuir-type equation:

$$\sigma_s = -|e| \frac{K^*C_0^*[Cl^-]_b \exp(|e|\psi_s/kT)}{1+K^*C_0^*[Cl^-]_b \exp(|e|\psi_s/kT)}, \tag{4}$$

where K^* is the binding constant of Cl^- to the Stern plane, C_0^* the maximum binding density of Cl^- ions, $[Cl^-]_b$ the concentration of Cl^- ion in the bulk, and ψ_s the electrostatic potential at the Stern plane.

(4) The electrical charge density in a diffuse double layer is expressed by the Gouy-Chapman theory, as follows:

$$\sigma_d = -\left(\frac{2N[Cl^-]_b \varepsilon kT}{\pi}\right) \sinh\left(\frac{\psi_s|e|}{2kT}\right), \tag{5}$$

where N is Avogadoro's number and ε is the dielectric constant of bulk water (ε=80).

(5) The potential at the Stern plane is related to the surface potential as

$$\psi_0 - \psi_s = \frac{4\pi d\sigma_0}{\varepsilon^*}, \tag{6}$$

where d is the distance between the membrane surface and the Stern plane and ε^* is the dielectric constant in the Stern layer.

When the counter ions are completely distributed in the diffuse double layer, i.e., when the existence of the Stern plane can be ignored, the relation $\sigma_0+\sigma_d=0$ can hold by replacing ψ_s in Eq. 5 by ψ_0. On the other hand, when the counter ions are completely localized on the Stern plane, the relation $\sigma_o+\sigma_s=0$ holds. For the intermediate states, K^* and C_0^* in Eq. 4 can be expressed by the following equations:

$$K^* = AK\exp(-z|e|(\Phi+\psi_s)/kT) \tag{7a}$$

$$C_0^* = C_0, \tag{7b}$$

where A is a parameter representing the mixed ratio of Stern model and Gouy-Chapman model ($0<A<1$). For monovalent ions, the potential change ($\Delta\Delta V=\psi_0$) is calculated using the above equations; the results are drawn against the concentration of metal ions in Fig. 5. In these calculations, several parameters are assumed to be consistent with the physical meaning. That is, ε^*=32, which corresponds to a partially immobilized water layer and d=7 Å, which is calculated from $d=r_M+\phi_w+r_{Cl}$, where r_M is the radius of metal ions (for K^+ $r_M\simeq$1.3, for Ba^{2+} $r_M\simeq$1.4 Å), ϕ_w is the diameter of a water molecule (ϕ_w=3—4 Å), and r_{Cl} is the radius of a chloride ion (r_{Cl}=1.8 Å). In Fig. 5, the experimental data of $\Delta\Delta V$ for K^+ are also plotted. As can be seen from the figure, the data are fit the Stern model better than the Gouy-Chapman model. That is, a condenser-type double layer is adequate for describing the present double layer. Next, the same analysis is carried out for divalent ions. In Fig. 6, analytical curves are presented together with experimental data for Ba^{2+}. As can be seen, the Stern model is more suitable for describing the double layer on the membrane of crown ethers than the Gouy-Chapman model. Further, in Figs. 7 and 8, the experimental data for K^+ and Ba^{2+} are plotted along with the analytical curves from the Stern model calculated using "α" as a parameter. In these calculations, we assumed that α is a parameter which correlates the micropotential (Φ) with macropotential ($\Delta\Delta V=\psi_0$) and takes a value between 0 and 1, where α=0 indicates that the adsorbing ions are not influenced by electrostatic potential generated by the already adsorbed ions, while α=1 indicates that the electrostatic potential influences the adsorption of next adsorbing ions completely. As can

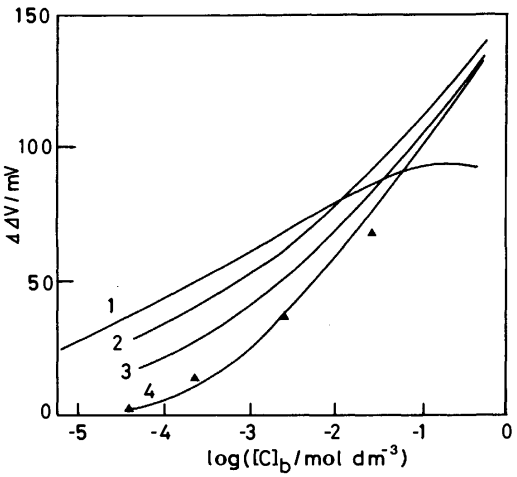

Fig. 5. Calculated curves from Eqs. 1—6 for the change of surface potential caused by mono-valent metal ions in various cases: (1) Gouy-Chapman model, (2) A=0.5, (3) A=0.8, and (4) Stern model; $\log K$=2.3, α=1. Experimental data (▲) of KCl are also plotted as to fit to one of these curves.

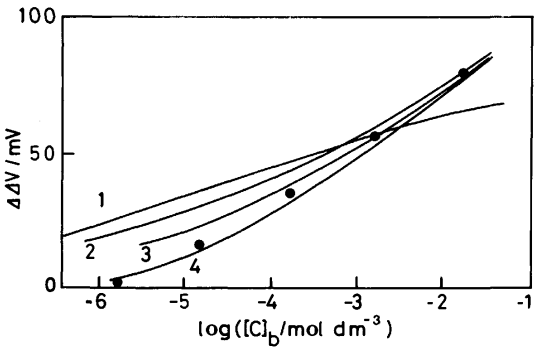

Fig. 6. Calculated curves from Eqs. 1—6 for the change of surface potential caused by di-valent metal ions in various cases: (1) Gouy-Chapman model, (2) A=0.5, (3) A=0.8, and (4) Stern model; $\log K$=3.6, α=1. Experimental data (●) of $BaCl_2$ are also plotted as to fit to one of these curves.

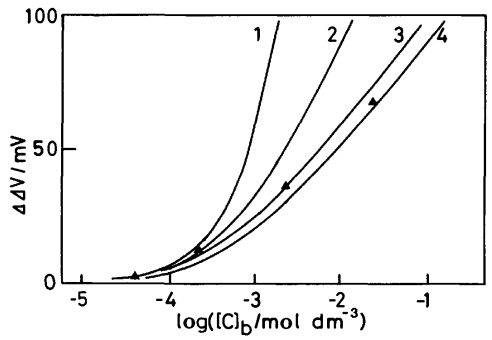

Fig. 7. Calculated curves of the change of surface potential for mono-valent ions from the Stern model with various values of parameters: (1) α=0, (2) α=0.5, (3) α=1, (d=7 Å); and (4) α=1, (d=5 Å). Experimental data (▲) of KCl are also plotted as to fit to one of the curves.

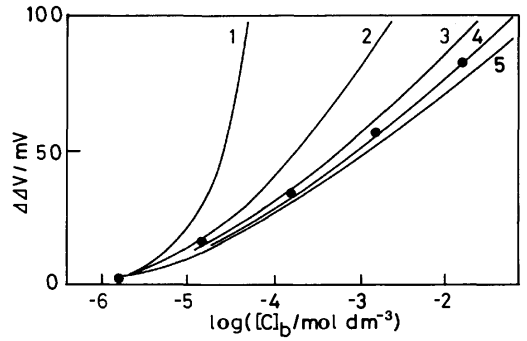

Fig. 8. Calculated curves of the change of surface potential for di-valent ions from the Stern model with various values of parameters: (1) α=0, (2) α=0.5, (3) α=0.8, (4) α=0.9, and (5) α=1. Experimental data (●) of $BaCl_2$ are also plotted as to fit to one of the curves.

be seen in Fig. 7, the experimental data for K^+ are well fitted to the analytical curve of α=1, in the range of low salt concentration. However, in the range of high salt concentration, $\Delta\Delta V$ changes more slowly than the analytical curve against the salt concentration. This phenomenon may arise from the fact that either the thickness of the Stern layer is smaller than that of this model (7 Å); in Fig. 7 the analytical curve of $\Delta\Delta V$ (assuming d=5 Å) is also drawn; or the diffuse double layer may be combined with the Stern layer to some extent in the high salt concentration range, i.e., an incomplete condenser type-double layer is formed and some counter ions are distributed over the diffuse double layer. The experimental data for Ba^{2+}, on the contrary, are well fitted to the theoretical curve for α=0.9—1. These results indicate that the mutual electrostatic repulsion among adsorbed metal ions is stronger for K^+ than for Ba^{2+}. This difference may arise from a difference in the discreteness of the charge distribution on the membrane surface. That is, the charges on di-valent metal ions are more localized than those on mono-valent ions on the membrane surface. In the case of di-valent ions, the one site for adsorption on the membrane can carry two electrical charges, while the site for mono-valent ions can carry only one charge.

Also, it is possible to obtain the value of the binding constant (K) in Eq. 2 by fitting the data to analytical curves. The estimated values for K^+ and Ba^{2+} are log $K\simeq$2 and log $K\simeq$4, respectively. These values are compared with the ones of 18-crown-6 appearing in the literatures, which were obtained by various kinds of experiments in the bulk liquid phase. Some typical examples are as follows: for K^+, log K=2.03—2.15 in H_2O and log K=5.93—6.20 in MeOH, while for Ba^{2+}, log K=3.87 in H_2O and log K=7.04 in MeOH.[10] As can be seen from these data, the estimated values of K in the present study are not so different from the values determined experimentally in bulk water.

In the present study, we can indicate that the electrical double layer generated by the complex-formation of a crown ether membrane with metal ions is of the type of the Stern model and that the binding constants of metal ions with the crown ethers under the interfacial circumstances can be evaluated by a simple electrical double layer theory.

This work was supported in part by a Grant-in-Aid from the Ministry of Education, Science and Culture (Nos. 61470084 and 61550586).

References

1) G. Stark, "Membrane Transport in Biology," I, Springer-Verlag, New York/Berlin (1978), p. 447.
2) C. J. Pedersen, *J. Am. Chem. Soc.*, **89**, 7017 (1967).
3) H. K. Frensdorff, *J. Am. Chem. Soc.*, **93**, 600 (1971).
4) G. Eisenman, S. M. Sergio, and G. Szabo, *Fed. Proc.*, **27**, 1289 (1968).
5) S. G. A. McLaughlin, G. Szabo, S. Ciani, and G. Eisenman, *J. Membr. Biol.*, **9**, 3 (1972).
6) Preliminary work has been reported previously; H. Matsumura, K. Furusawa, S. Inokuma, and T. Kuwamura, *Chem. Lett.*, **1986**, 453.
7) I. Ikeda, S. Yamamura, Y. Nakatsuji, and M. Okahara, *J. Org. Chem.*, **45**, 5355 (1980).
8) I. Ikeda, H. Emura, and M. Okahara, *Bull. Chem. Soc. Jpn.* **57**, 1612 (1984).
9) H. Matsumura and K. Furusawa, *Nippon Kagaku Kaishi*, **1985**, 1216.
10) R. M. Izatt, J. S. Bradshaw, S. A. Nielsen, J. D. Lamb, J. J. Christensen, and D. Sen, *Chem. Rev.*, **85**, 271 (1985).
11) S. Usui, "Electrical Phenomena at Interface," ed by A. Kitahara and A. Watanabe, Marcel Dekker, Inc., New York and Basel (1984), p. 15.
12) C. A. Barlow and J. R. MacDonald, "Advances in Electrochemistry and Electrochemical Engineering," Vol. 6 Interscience, New York (1967).

 © 1987 The Chemical Society of Japan Bull. Chem. Soc. Jpn., 60, 2751—2756 (1987)

Fluorenone Monomer Dianion Studied by ^1H and ^{13}C NMR and Charge Density Distribution

Masatoshi HIRAYAMA* and Hiroshi OHHATA
Department of Chemistry, Faculty of Science, Ibaraki University, 2-1-1 Bunkyo, Mito 310
(Received January 17, 1987)

The diamagnetic monomer dianion of fluorenone was prepared from 1,2-dimethoxyethane solution of neutral molecule in contact with excess sodium metal at −5 °C for 5 days and its ^1H and ^{13}C NMR spectra were measured. The possibility that a pinacolate-type dimer dianion occurs in an equilibrium system was ruled out from reactivity with oxygen, water, deuterium oxide, and reducible aromatics in addition to the analysis of NMR spectra. The charge density distribution of neutral and dianion molecules was estimated by MO calculations. Comparison between experimental and theoretical ^{13}C shifts suggested a strong interaction of sodium ions with carbonyl group. It is presumed that an anormalous diamagnetic ring current in 14π-peripheral structure is responsible for poor correlation between theoretical and observed ^1H shifts.

It was demonstrated by Hirota et al.[1] from ESR and optical measurements that when aromatic ketones (fluorenone, benzophenone, and xanthone) were in contact with alkali metal in a dilute solution, a ketyl monomer (**1**) and a paramagnetic ketyl dimer (**2**) mainly coexisted in equilibrium in an etherial solvent, while in a nonpolar solvent there mainly existed an equilibrium between **2** and a diamagnetic ketyl dimer (**3**). These authors further studied in detail ion-pair structures of **1** and **2** and the equilibrium between **1** and **2**.[2] On the other hand, Herold et al. discussed in

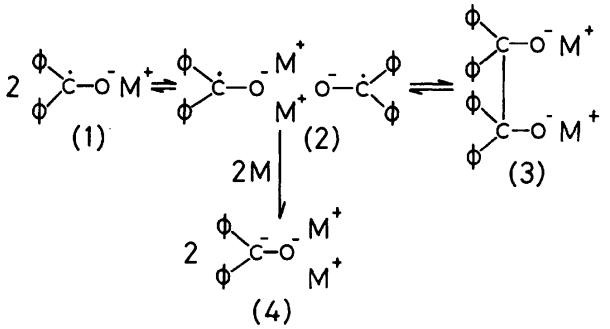

detail the substituent effect on the spin density distribution (or hfs patterns) of free anion radical and sodium ketyl of fluorenone by means of ENDOR technique and ESR.[3] Hirota et al. further proposed from optical spectra that when fluorenone of approximately 10^{-2} mol dm^{-3} was in contact with excess sodium in 2-methyltetrahydrofuran (2MTHF) **2** was further reduced into diamagnetic monomer dianion (**4**)[1a] and the concentration of **3** was extremely small.

A direct evidence for the occurrence of **3** and **4** has been required, because their existence was proposed only indirectly by optical measurements. Although the best method to identify a diamagnetic species in solution will be NMR analysis, it seems that NMR measurement of these systems at high-resolution is difficult due to line broadening by fast spin exchange between diamagnetic species and paramagnetic ketyl monomer or dimer. Moreover, it is difficult to discuss the same equilibrium state as that for optical measurements by NMR method, which requires a much higher concentration of species than that in optical measurements.

The present paper demonstrates that a diamagnetic green species formed from fluorenone and excess sodium metal in 0.15 mol dm^{-3} 1,2-dimethoxyethane (DME) solution is ascribed to its monomer dianion (**4**) on the basis of ^1H and ^{13}C NMR spectra and calculated electron density distribution.[4]

Experimental

Fluorenone was contacted with sodium metal in DME-d_{10} in high vacuum by standard technique for preparing hydrocarbon anion radicals. Fluorenone (Tokyo Kasei Co. Ltd.) was used without further purification. DME-d_{10} (Canada MSD Co. Ltd.) was dried, degassed, and stored over sodium/potassium alloy in vacuo. 0.6 ml of DME-d_{10} was transferred into an NMR tube containing 10 mg of fluorenone at its bottom and connecting with a high-vacuum line. Sodium mirror was previously made in the upper part of the sample tube, so that the solution could be in contact with metal even after the sample tube was cut off from the vacuum line. The solution was contacted with sodium mirror by turning upside down the sealed tube. ^1H and ^{13}C NMR spectra were measured on Varian VXR-300 at 300 MHz on the FT mode. ESR spectra were measured on JEOL JES-FE1XG, in order to confirm the disappearance of anion radical. The MO calculation of charge density was performed on HITAC M-240H at Ibaraki University, the program used for the CNDO calculation being Y4CB04[5] in library programs of the University of Tokyo.

Results and Discussion

The color of fluorenone solution in DME-d_{10} changed to reddish-yellow immediately after contact with sodium at −5 °C. The resulting solution gave a well-resolved ESR spectrum of sodium fluorenide after dilution. The ESR signal gradually disappeared upon continued contact, and the color of the solution turned to green. Several new lines gradually grew up in ^1H NMR spectrum. This green species was stable even at room temperature for several days. ^1H and ^{13}C NMR spectra observed after 5 days of contact are shown in

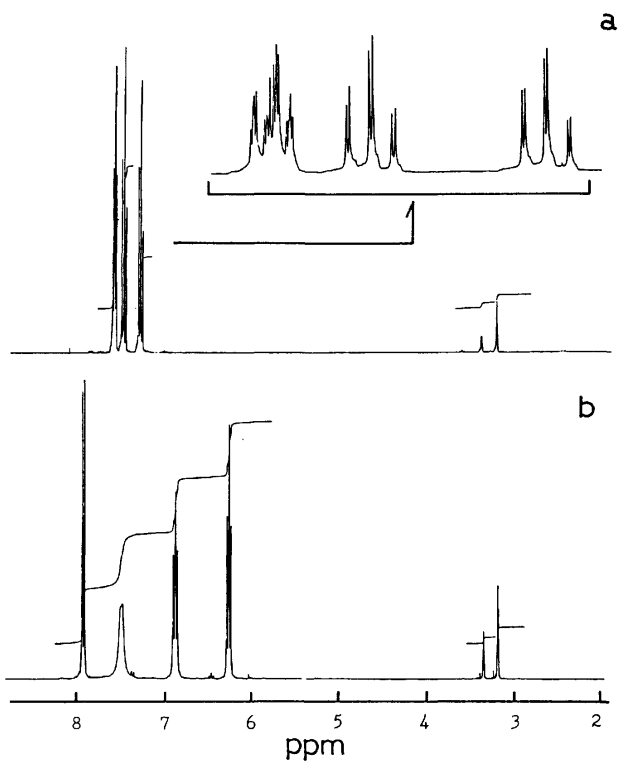

Fig. 1. ^{1}H NMR spectra (300 MHz) of fluorenone in DME-d_{10} (a) and of the diamagnetic green species formed by sodium reduction in DME-d_{10} (b). In (b), the high-field one of two doublets is considerably broadened by the spin exchange with a slight amount of the fluorenone ketyl.

Figs. 1 and 2, respectively, together with that of the precursor. The ^{1}H spectrum consisted of two triplets and two doublets which were separated well. Its center of gravity shifted toward higher field by 0.39 ppm than that of neutral molecule. The pattern of ^{13}C spectrum of this species was identical with that of neutral molecule, suggesting that the spectrum arises from four carbons bonded to a hydrogen and three quaternary carbons, one of which has particularly long T_1. The high-field shift of center of gravity in ^{13}C spectrum was 20.9 ppm relative to that in neutral molecule.

The assignment of ^{1}H and ^{13}C spectra of neutral molecule was made by literature,[7] which was confirmed here by the H-C shift correlation 2D NMR (Fig. 3). For the green species, the smallest ^{13}C line was assigned to C_9 by its very large T_1. This is consistent with the intramolecular distribution of calculated excess charge density of a monomer dianion mentioned later. The residual two carbon lines with weak intensity were assigned to C_{10} and C_{11} due to their long T_1 values, the higher-field one being tentatively assigned to C_{10} by the comparison of observed shifts with excess charge density of the dianion. In the ^{1}H spectrum, the line at a higher field of two doublets became much broader than the other in the existence of a small amount of ketyl radical. This is considered to be due to an electron spin exchange between diamagnetic green species and paramagnetic ketyl. From the fact that the hfs constant a_1^H is much larger than a_4^H,[3] the higher-field doublet could be assigned to H_1, and the lower-field one to H_4. The lower-field triplet was assigned to H_2 using the same technique. The assignment of four ring carbons was made by combining the above ^{1}H assignment with the 2D correlation NMR between ^{1}H and ^{13}C shifts (Fig. 4). The results are listed in Table 1.

By introducing oxygen into this green solution fluorenone was regenerated. Contacting this solution with a reducible aromatics, methyl *m*-nitrobenzoate, in vacuo, gave ESR of sodium salt of anion radical of this compound. From these experimental results, it may be reasonable to determine that a pinacolate-type compound (diamagnetic ketyl dimer, **3**) is not formed by bonding between ketyl monomers. It was further confirmed by analysing ^{1}H and ^{13}C NMR that addition of water to this species in oxygen-free conditions gave 9-fluorenol and that deuterium oxide treatment gave the corresponding deuterated 9-fluorenol. This result supports the assumption that dimer dianion is not formed. This is also consistent with the fact that C_9 appeared at much lower field than that of pinacol. It can thus be said that an adequate evidence for the formation of diamagnetic monomer dianion (**4**) was obtained. As seen from Figs. 1 and 2, no other diamagnetic species were observed from this green solution and line broadening completely disappeared during contact with sodium metal. Monomer dianion (**4**) is the final product at a high concentration (1.5×10^{-1} mol dm^{-3}) by complete reduction with excess sodium in etherial solvent, similarly as the reduction at a low concentration (4×10^{-2}—5×10^{-3} mol dm^{-3}) in 2MTHF discussed by Hirota et al.[1a] A direct formation of **4** from **1** may be expected in the present system in DME in addition to the process through **2**, from larger dissociation constant in $\mathbf{2} \rightleftarrows 2\cdot\mathbf{1}$ in DME than that in 2MTHF.[1a] One may expect that monomer dianion observed here is of an ion pair form $A^{=}2M^{+}$ or solvated ion pair $A^{=}2M^{+}(S)_n$, where A and S are fluorenone and solvent, respectively, but not of a solvent-separated ion pair $A^{=}(S)_n2M^{+}$,[8] from analogy with the ion pair structures of monomer ketyl proposed by Hirota et al.[2a]

Reduction of fluorenone with excess sodium or potassium metal in THF also gave the green species, which was insoluble in THF and precipitated. On the reduction with potassium in DME, paramagnetic reddish-yellow solution initially formed did not change to green even after a long time. These results are consistent with the order of solvation power of solvents for alkali metals, DME>THF. It may be considered that the ionic interaction between ion pairs, $A^{=}2Na^{+}$, is so strong as to overcome solvation of THF to $A^{=}2Na^{+}$, while the ionic interaction between ion pairs $A^{\cdot-}Na^{+}$ is relatively weaker than solvation power of THF to $A^{\cdot-}Na^{+}$. The ionic bonding of potassium

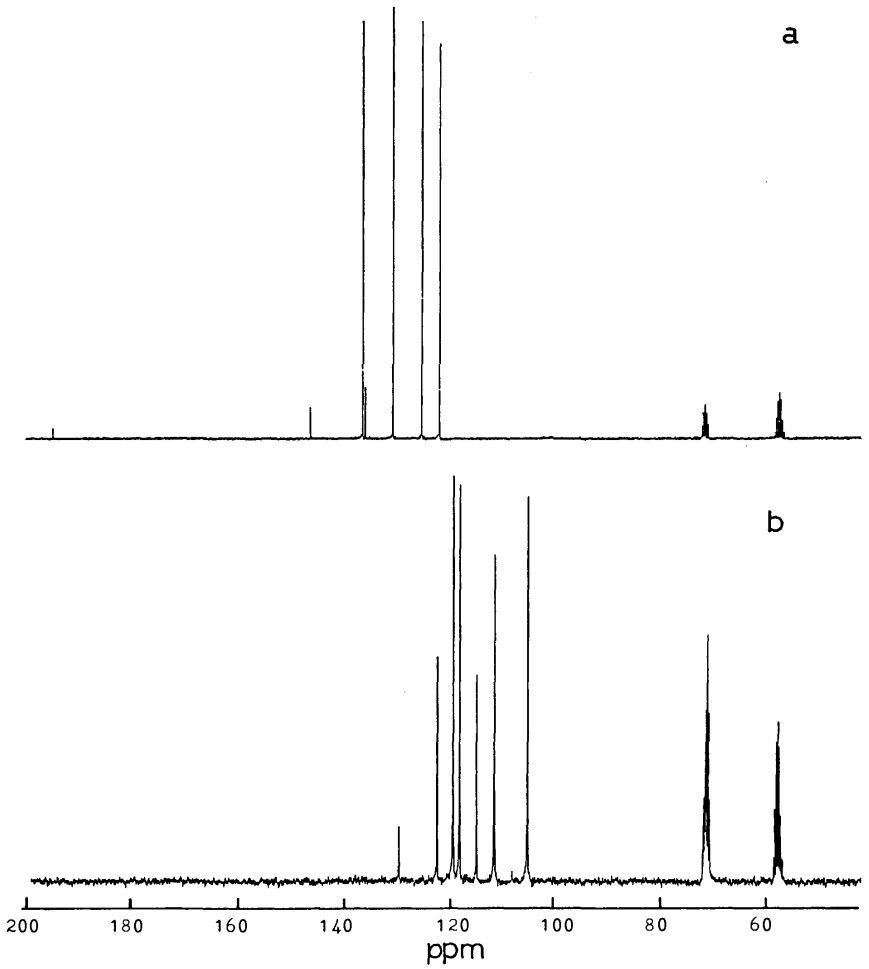

Fig. 2. ^{13}C NMR spectra (75 MHz) of fluorenone in DME-d_{10} (a) and of the diamagnetic green species formed by sodium reduction in DME-d_{10} (b).

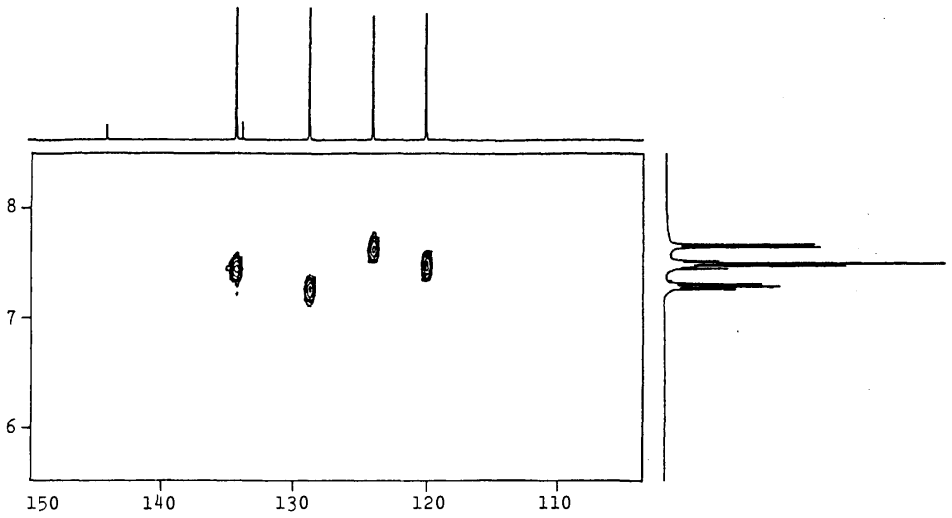

Fig. 3. ^{1}H-^{13}C shift correlation 2D NMR spectrum of fluorenone in $CDCl_3$.

ion to the carbonyl group (perhaps a carbonyl oxygen) is generally considered to be weaker than that of sodium ion owing to the difference in ionic radius. This may explain the experimental result that an ion pair structure $A^{=}2K^{+}$ doesn't exist as a stable species in DME, but exists in THF of which solvation power is weaker than that of DME.

Several workers have previously noted a linear relationship between proton chemical shift $\Delta\delta_H$ and excess local π-charge density at a carbon bonded to proton, Δq_C^{π}, according to the formula,[9] $\Delta\delta_H = k_H \cdot \Delta q_C^{\pi}$. The gradient k_H amounts to 10.7 ppm per unit charge. A

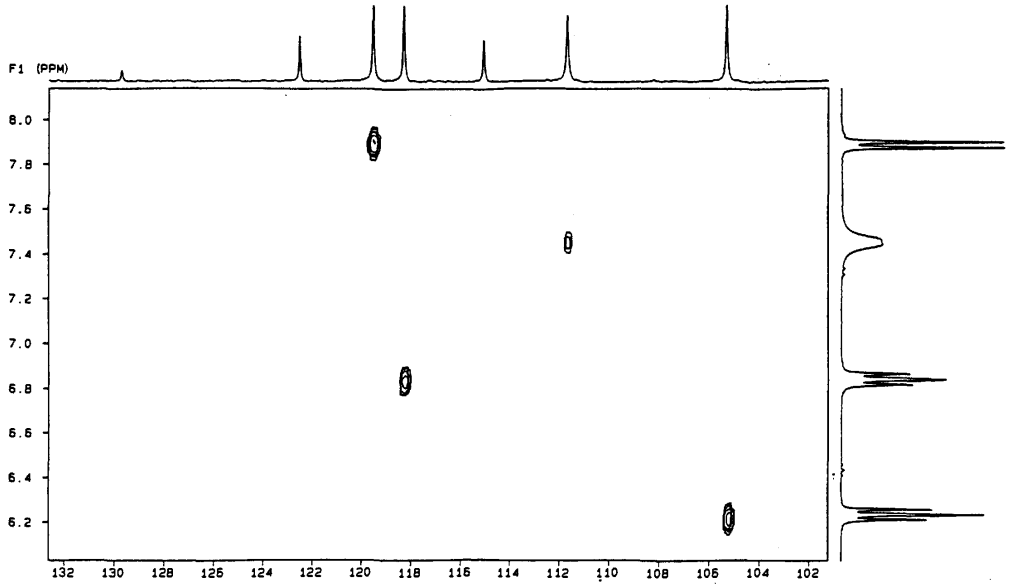

Fig. 4. ^{1}H-^{13}C shift correlation 2D NMR spectrum of the green species formed by sodium reduction in DME-d_{10}.

Table 1. Observed ^{1}H and ^{13}C Chemical Shifts

	δ_N [a]	δ_D [a]	$\Delta\delta$ [b]
H_1	7.60	7.46	0.14
H_2	7.30	6.84	0.46
H_3	7.49	6.24	1.25
H_4	7.59	7.89	−0.30
C_1	124.53	111.69	12.84
C_2	129.86	118.29	11.57
C_3	135.41	105.31	30.10
C_4	121.25	119.51	1.74
C_9	193.38	129.70	63.68
C_{10}	134.90	115.09	19.81
C_{11}	145.17	122.53	22.64

a) In ppm relative to TMS. All chemical shifts were determined relative to the high-field multiplet of DME. (3.22 ppm from TMS for ^{1}H and 57.8 ppm from TMS for ^{13}C.) b) Shifts of dianion relative to those of neutral molecule. (Positive signs denote high-field shifts. $\Delta\delta_{obsd}=-(\delta_D-\delta_N)$.)

similar correlation, $\Delta\delta_C=k_C\cdot\Delta q_{\pi}$, was later found for ^{13}C chemical shifts with $k_C\approx160$ ppm per electron.[10] Although one should be aware that such empirical dependence of δ_H and δ_C on charge density has no firm theoretical foundation, such relations are applicable to the closely related compounds, provided that one accounts for ion pairing, ring current effect, and magnetic anisotropy of neighboring atoms or substituent groups. The neutral precursor was used as a reference of shift (Table 1)[11] for estimating charge-induced shifts ($\Delta\delta_{obsed}$), and these three effects were considered as follows. It has been predicted from theoretical consideration that two excess electrons in the lowest vacant π-orbital of dianion doesn't contribute to the ring current.[12] The ^{13}C chemical shift is particularly insensitive to ring-current effect as long as carbons are within a π-periphery. No correction of the observed shifts for ring current effect was, therefore, applied for comparing the observed shifts with calculated ones. Although the anisotropy of carbonyl bond in dianion is different from that of neutral molecule, the difference may be ignored as a small correction of charge-induced shifts for all the protons and carbons except for C_9. The ^{1}H and ^{13}C chemical shifts of π-dianion may be affected by ion pairing effect of counter ions, as will be mentioned later.

The charge density on carbon 2pz orbitals, q_{2p_z}, was calculated by both the CNDO[6] and semi-empirical SCF π-MO (PPP) methods. The averaged crystallographic data[13] were used for geometric parameters. The changes of π-charge Δq_{2p_z} and calculated shift $\Delta\delta$ on going from the neutral molecule to dianion are listed in Table 2 together with the corresponding observed changes of δ_H and δ_C. It is found that the $\Delta\delta$(obsd) pattern of ^{13}C correlates, though roughly, with those of $\Delta\delta$(calcd) estimated by both the CNDO and PPP methods. However, the comparison between observed and theoretical shifts at each position showed very poor agreement: At C_9 $\Delta\delta$(obsd) is extraordinarily larger than $\Delta\delta$(calcd), at C_1 larger, at C_3 slightly smaller, at C_2 very smaller, and at C_4 the comparison was vague, because the theoretical values obtained from CNDO and PPP are widely different. For fluorenone ketyl, the ion-pair effect on electron-spin-density distribution has successfully been explained by INDO calculations.[14] Also for the present dianion, the ionic bonding of sodium ions to carbonyl group may affect largely the shift pattern. Then, in order to make a rough estimate of the change of $\Delta\delta$(calcd) pattern caused by ion pairing, the dependence of Δq_{2p_z} on the Coulomb integral parameter of carbonyl oxygen, h_O, was calculated by the Hückel approximation.[15] With

Table 2. Comparisons of Observed and Calculated Differences of ^1H and ^{13}C Shifts of Dianion from Those of Neutral Molecule[a)]

	CNDO				PPP		$\Delta\delta_{obsd}$
	Δq_{2pz}[b)]	$\Delta\delta_{calcd}$[c)]	Δq_{1s}[d)]	$\Delta\delta_{calcd}$[e)]	Δq_{2pz}[b)]	$\Delta\delta_{calcd}$[c)]	
H_1		0.34	0.0725	1.21		0.37	0.14
H_2		1.54	0.0844	1.41		2.48	0.46
H_3		2.13	0.0820	1.37		2.16	1.25
H_4		−0.03	0.0766	1.28		0.60	−0.30
C_1	0.0316	5.06			0.0344	5.50	12.84
C_2	0.1441	23.06			0.2321	37.14	11.57
C_3	0.1986	31.78			0.2017	32.27	30.10
C_4	−0.0029	−0.46			0.0564	9.02	1.74
C_9	0.1492	23.87			0.2124	33.98	63.68
C_{10}	0.1262	20.19			0.0717	11.47	19.81
C_{11}	0.1797	28.75			0.1371	21.94	22.64

a) In ppm. See Table 1 for the numbering system. b) Excess charge density at carbon 2pz orbitals in dianion relative to those in neutral molecule. c) Estimated using 10.7 ppm/electron as k_H and 160 ppm/electron as k_C. d) Excess charge density at proton 1s orbitals in dianion relative to those in neutral molecule. e) Estimated using 16.7 ppm/electron as k'_H.

increasing h_O from 1.45, Δq_{2pz} at C_9 considerably increased, at C_1 next largely increased, at C_4 and C_3 slightly increased, at C_2 largely decreased, and at C_{10} and C_{11} almost unchanged. It appears that the result implies the calculated ^{13}C shift pattern changing toward the experimental one and that it suggests formation of strong ionic interaction of sodium ions with carbonyl group. However, the extraordinarily large high-field shift at C_9 will be ascribed to a possible difference of bond anisotropy of carbonyl group in dianion from neutral molecule, in addition to the ion-pair effect. The experimental fact that the shift value of C_9, 129.7 ppm, is much smaller than those of pinacolate-type compounds supports the conclusion that no diamagnetic dimer dianion is formed in the present system. It is generally said that the PPP method explains better the observed ^{13}C shift pattern rather than the CNDO method for hydrocarbon dianions having no hetero atoms or substituents. Since several factors other than charge-induced effect may affect the ^{13}C shift pattern in the present case, it is indefinite which method is more favorable.

As shown in Table 2, ^1H $\Delta\delta$(obsd) of dianion is fairly smaller on the overall ring than $\Delta\delta$(calcd) predicted by both methods and its pattern doesn't correlate well with that of ^{13}C $\Delta\delta$(obsd). This allows us to consider that the observed ring proton shifts may contain another effect in addition to the counter ion effect. It may be prossible for polycyclic systems that an anormalous peripheral ring current affects ring proton shifts,[16)] although it doesn't affect the shifts of carbons which are members of the ring itself. One of the most probable structures of fluorenone dianion is that at which one of two excess π-electrons is occupied by C_9. Since this structure has a 14π-periphery, an induced-diamagnetic ring current may be found in the fluorenone dianion. Thus, one may consider that the anormalous ring current is responsible for the decrease in ring proton shifts.

An attempt was made further to calculate $\Delta\delta$ of protons directly from excess charges at proton 1s-orbitals, Δq_{1s}. A value of 16.7 ppm per electron obtained simply from the character of a hydrogen 1s-orbital was used as the proportionality constant k'_H in the relation, $\Delta\delta_H = k_H' \cdot \Delta q_{1s}$. The resulting values of $\Delta\delta_H$ were on the whole larger than $\Delta\delta$(obsd) values as well as those obtained from $\Delta\delta_{2p_z}$ and were more uniform through all protons. One must, therefore, depend on the peripheral ring current model.

References

1) a) N. Hirota and S. I. Weissman, *J. Am. Chem. Soc.*, **86**, 2538 (1964); b) N. Hirota, *ibid.*, **89**, 32 (1967).

2) a) K. S. Chen, S. W. Mao, K. Nakamura, and N. Hirota, *J. Am. Chem. Soc.*, **93**, 6004 (1971); b) T. Takeshita and N. Hirota, *ibid.*, **93**, 6421 (1971).

3) B. J. Herold and J. M. A. Empis, *J. Chem. Soc., Perkin Trans. 2*, **1986**, 431; J. M. A. Empis and B. J. Herold, *ibid.*, **1986**, 425; J. C. Evans, C. C. Rowlands, and B. J. Herold, *ibid.*, **1984**, 389.

4) M. Hirayama, H. Suzuki, and H. Ohhata, *Chem. Lett.*, **1987**, 413.

5) This program was prepared on the basis of Ref. 6.

6) J. A. Pople, D. C. Beveridge, and P. A. Dobosh, *J. Am. Chem. Soc.*, **90**, 4201 (1968).

7) J. B. Stothers, C. T. Tan, and N. K. Wilson, *Org. Magn. Reson.*, **9**, 408 (1977).

8) The formation of solvated Li-ketyl in DME $A^{\cdot-}Li^+DME$ was supported also by INDO calculations.[14)] The ionic bond of alkali ion (Li, Na, K, and Cs) to carbonyl oxygen has been known to be so strong that a solvent-separated ion pair $A^{\cdot-}DMF \cdot M^+$ is not formed even in the mixture of DME or THF and DMF.[2a)] We have measured that the ESR spectrum of tightly bound ion pair $A^{\cdot-}Na^+$ remains unchanged by the addition of dibenzo 18-crown-6 to sodium ketyl solution in DME, and that an effect of dibenzo 18-crown-6 cannot be sufficiently observed in NMR spectrum of monomer dianion disodium salt owing to poor solubility of the ether.

9) T. Schaefer and W. G. Schneider, *Can. J. Chem.*, **41**, 966 (1963).

10) H. Spiesecke and W. G. Schneider, *Tetrahedron Lett.*, **1961**, 468; G. A. Olah and G. D. Matteeseu, *J. Am. Chem. Soc.*, **92**, 1430 (1970).

11) Although the use of benzene as a reference for the estimation of charge-induced shifts has generally been made, the correction of ring current and anisotropy of substituents must be precisely made. On the other hand, if the corresponding neutral precursor is used as a reference, it may be considered that such corrections need not be made as mentioned in the text, when one doesn't take into account an anormalous ring current effect and a possible change of anisotropy of substituents induced by excess charges.

12) J. A. Pople, *Mol. Phys.*, **1**, 175 (1958).

13) J. P. Reboul, J. C. Soyfer, B. Cristau, N. Darbon, Y. Oddon, and G. Pepe, *Acta Crystallogr., Sect. C*, **39**, 600 (1983).

14) W. Lubitz, M. Plato, K. Mubius, and R. Biehl, *J. Phys. Chem.*, **83**, 3402 (1979).

15) The CNDO calculation containing sodium atom as a counter ion has tentatively been performed using the atomic parameters of sodium within the Pople's program. However, this attempt resulted in large negative charges on two sodium ions. An attempt is now being made to find some sodium parameters appropriate to explain $\Delta\delta$(obsd).

16) It has been suggested that $4n+2$ polycyclic systems can be treated in terms of their peripheries by considering the cross links as small perturbations.[17] Therefore, the aromatic protons in these systems may undergo an anormalous induced diamagnetic ring current.

17) J. R. Platt, *J. Chem. Phys.*, **22**, 1448 (1954); J. A. Pople and K. G. Untch, *J. Am. Chem. Soc.*, **88**, 4811 (1966) and references therein.

 © 1987 The Chemical Society of Japan Bull. Chem. Soc. Jpn., 60, 2757—2762 (1987)

Oxidation of Ketones over Metal Oxide Catalysts. II. Biacetyl Synthesis over Co_3O_4-Lanthanoid Oxide Catalysts

Yusaku TAKITA,* Fumiaki HORI, Noboru YAMAZOE,† and Tetsuro SEIYAMA†
Department of Environmental Chemistry and Engineering, Faculty of Engineering, Oita University, Dannoharu, Oita 870-11
†Department of Materials Science and Technology, Graduate School of Engineering Science, Kyushu University, Kasuga, Fukuoka 816
(Received January 29, 1987)

The effects of the addition (10 atomic%) of lanthanoid oxides into Co_3O_4 on the oxidation of methyl ethyl ketone (MEK) were studied. The addition of La_2O_3 brought about marked enhancement of the rate of biacetyl (BA) formation. MEK conversion increased by a factor of 2.8 and the BA selectivity was improved at 450—500K owing to the suppression of deep oxidation. The addition of CeO_2 much improved the MEK conversion but BA selectivity decreased to less than 50% and the scission reaction leading to acetaldehyde and acetic acid was enhanced. The addition of Pr_6O_{11} improved MEK conversion but the addition of Nd_2O_3, Gd_2O_3, or Er_2O_3 showed little effect on MEK conversion. The reduction of both scission reaction and deep oxidation and the compensative increase in BA selectivities were observed. An approximately linear relationship was found between the specific rate of BA formation of the catalysts and logarithmic solubitity product constants of hydroxides of tervalent lanthanoid elements added, suggesting that the basicity of the catalysts is one of major factors for BA formation. The maximum efficiency (23.4%) of BA formation was attained at a La content of ca. 10 at.%.

In the previous papers,[1,2] we have been studied the gas phase oxidation of methyl ethyl ketone over the various metal oxides. In part I of this series,[2] the following findings were reported. Two types of competitive partial oxidation, i.e., biacetyl formation and oxidative scission reaction leading to acetaldehyde and acetic acid took place on every oxide studied at 400—500K.

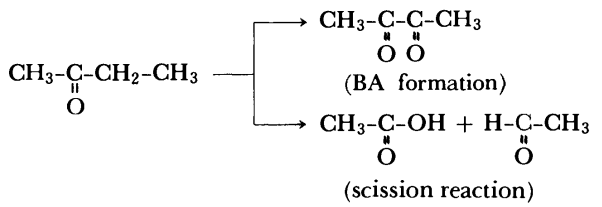

The former reaction was accelerated on the basic or amphoteric oxides such as Co_3O_4, NiO, ZnO, and CuO, while the latter reaction became predominant on the acidic oxides such as MoO_3, V_2O_5, WO_3, and Cr_2O_3. The addition of Li_2O or Na_2O into Co_3O_4, the most effective biacetyl former of the single component oxides, improved BA selectivity by depressing the scission reaction and deep oxidation. The addition of K_2O or Rb_2O brought about negative effects on BA formation, however, it was somewhat effective to depress the scission reaction and successive complete oxidation at higher temperatures. These results suggest that basic oxides added diminish acidic sites of the catalysts on which scission reaction proceeds.

Lanthanoid oxides are known to belong to a group of basic oxides. Basisity of La_2O_3, Pr_2O_3, and Gd_2O_3 are comparable to that of CaO.[3] So that provided that the oxides of lanthanoid elements are added into Co_3O_4, the lanthanoid oxides added can be expected to induce the desirable effects for BA formation.

In the present paper, we describe the effects of lanthanoid oxide addition into Co_3O_4 on the methyl ethyl ketone oxidation.

Experimental

Catalysts. Binary oxide cataltysts used in this work were prepared by the following procedure. Aqueous solutions of $Co(NO_3)_2 \cdot 6H_2O$ and either of lanthanoid nitrates, phosphoric acid, telluric acid, or selenous acid were mixed and evaporated to dryness on a hot plate with stirring. The powder obtained was submitted to calcination at 673 K for 3 h followed by pressing at 500 kg cm^{-2}. 24—32 mesh granules of the oxides were finally calcined at 823 K for 4 h in the air.

Apparatus and Method. Experimental procedures and analyses of reactants and products were the same as described in the previous paper.[2]

The oxidation reaction was carried out in a conventional flow type reaction system using a 17-mm-i.d. Pyrex glass tubular reactor with a fixed catalyst bed inside. An aqueous solution of MEK was introduced by means of a microliquid feeder to a glass wool bed which was located at the entrance of the reactor and heated at 473 K, where the solution was evaporated and mixed with oxygen and nitrogen. Before every experimental run, prereaction was carried out for 10 h at the temperature where MEK conversion reached about 10% for the stabilization of activity of catalyst.

The effluent gas was led into a cold trap kept at ca. 290 K, to condense the products having high boiling points along with water vapor. Both trapped products and the gas that passed through the trap were analyzed by gas chromatography. The column packings used were PEG No. 1000 (3 m, 313 K) for aldehydes, ketones, and alcohols, silica gel (1.5 m, r.t.) for carbon dioxide, molecular sieves 5A (1.5 m, r.t.) for oxygen, nitrogen, and carbon monoxide, and DOS (dioctyl sebacate, 2 m, 363 K) for carboxylic acids. The selectivity of a product A is defined as

$$\frac{\text{Moles of MEK converted to A}}{\text{Total moles of MEK consumed}} \times 100\ (\%).$$

Table 1. Oxidation of MEK over Co_3O_4 Catalysts Promoted by Lanthanide Oxide

Catalyst[a]	Temperature	Conversion	Selectivity[b]/%					Specific surface area
	K	%	$(CH_3CO)_2$	CH_3CHO	CH_3COOH	CH_3COCH_3	$CO+CO_2$	$m^2 g^{-1}$
(a) Co_3O_4-La_2O_3	423	5.2	75.5	5.2	15.4	1.1	1.9	12.9
	454	16.9	65.0	6.8	19.8	1.7	5.9	
	472	28.4	62.6	8.1	16.8	2.3	9.5	
	493	43.0	54.5	9.9	19.0	3.2	12.2	
	524	68.5	6.6	1.7	0.4	3.8	74.2	
(b) Co_3O_4-CeO_2	425	10.0	44.7	4.3	45.8	0.9	3.6	20.3
	450	29.6	45.7	4.7	40.6	1.7	6.1	
	473	51.2	33.6	5.0	43.1	3.0	13.4	
	499	50.1	15.6	7.7	32.0	8.3	34.0	
(c) Co_3O_4-Pr_6O_{11}	444	11.2	66.4	4.8	15.1	2.4	10.8	17.8
	473	25.2	55.3	6.3	13.4	5.2	19.2	
	492	41.9	43.7	8.3	9.6	9.9	27.8	
	507	48.7	14.7	4.1	1.0	7.4	66.0	
(d) Co_3O_4-Nd_2O_3	422	2.4	77.5	5.3	6.9	3.2	4.1	12.3
	453	6.2	72.6	5.4	9.3	3.2	8.0	
	495	18.1	58.2	6.7	5.8	10.2	18.1	
	533	35.4	28.5	9.2	4.4	17.3	39.6	
(e) Co_3O_4-Gd_2O_3	428	2.7	71.2	6.3	16.1	4.4	—	8.4
	473	9.3	64.4	7.0	12.8	5.4	9.4	
	503	21.2	44.0	8.0	8.1	10.1	28.9	
	524	38.2	23.5	7.9	4.5	15.3	47.9	
(f) Co_3O_4-Er_2O_3	426	3.7	68.7	5.9	11.8	5.4	5.3	12.9
	471	12.4	53.5	6.7	20.2	5.4	13.7	
	496	21.1	40.0	8.6	11.3	9.4	29.5	
	518	32.8	20.0	10.3	4.6	19.3	42.8	
(g) Co_3O_4-Yb_2O_3	453	5.75	36.5	19.8	36.0	0.8	4.8	11.0
	473	9.33	42.6	18.2	30.2	1.1	6.1	
	492	21.2	39.6	18.8	31.9	1.4	7.2	
	518	38.2	34.6	19.8	34.9	1.2	8.6	

a) Ten atomic% Lanthanoid oxide. b) Normalized to MEK; $W/F=2.00$ sg-cat. cm^{-3}; feed gas composition: 1.5 mol% MEK, 8.5 mol% O_2, 30.0 mol% H_2O, 60.0 mol% N_2.

Results and Discussion

The Oxidation of MEK over Binary Oxides of Cobalt-Lanthanoid Elements. Modification of Co_3O_4 by the addition of lanthanoid oxides was examined to develop more effective catalysts for BA synthesis. The results of the MEK oxidation are shown in Fig. 1 and Table 1. The results of Co_3O_4 containing no lanthanoid oxide are also shown in Fig. 2 for comparison although the reaction conditions are somewhat different.

The addition of lanthanoid oxides into Co_3O_4 more or less affected the activities of the catalysts and the product distributions, however, gave rise to the formation of no new compound other than formed in the oxidation over Co_3O_4.

The addition of La_2O_3 into Co_3O_4 brought about the increase of MEK conversion by a factor of 2.5—2.8 (Table 1(a)). It can be seen from the comparison of Fig. 1 with Fig. 2 that the addition of La_2O_3 into Co_3O_4 gave no significant influence on the selectivity of scission reaction but depressed the deep oxidation over the whole temperature range examined, especially at below 500 K. Consequently the selectivity of BA was improved at 450—500 K. In the previous paper we noted the maximum efficiency of 13% in BA formation over Co_3O_4-Li_2O (Co/Li=93/7) catalyst.[2] The much higher BA yield (17.7 and 23.4% at 472 and 493 K, respectively) was attained over Co_3O_4-La_2O_3 (Co/La=90/10) catalyst.

The activity of Co_3O_4-CeO_2 was 4—5 times as high as that of Co_3O_4 (Table 1(b)). Almost equimolar BA and acetic acid were formed at 425—450K as the major products and the selectivities of both products decreased monotonously with increasing the reaction temperature. Acetaldehyde and acetone were also formed, the selectivity of the both products remained less than 10% at all temperatures examined.

Co_3O_4-Pr_6O_{11} also showed higher activity for MEK oxidation (Table 1(c)). The selectivity of acetic acid

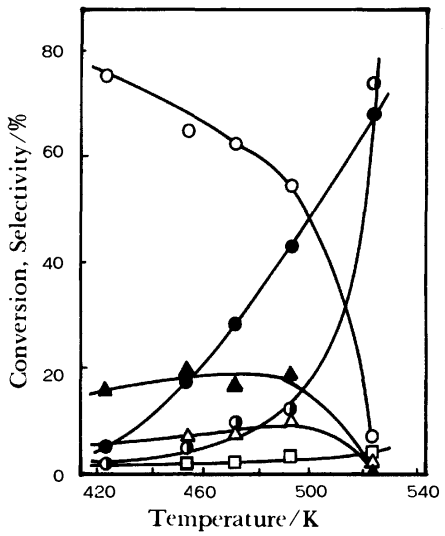

Fig. 1. The oxidation of MEK over Co_3O_4-La_2O_3 catalyst. Catalyst: 10 at.% La_2O_3, 2.48 g. W/F=2.00 (s.g-cat.cm^{-3}). Feed gas composition is the same as in Table 1. Symbols: ●, MEK conversion; ○, BA; △, acetaldehyde; ▲, acetic acid; ◑, carbon oxides; □, acetone.

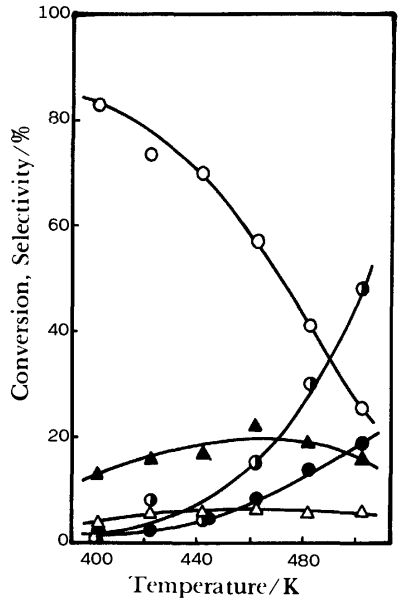

Fig. 2. The oxidation of MEK over Co_3O_4 catalyst. W/F=2.65 (s.g-cat.cm^{-3}). Feed gas composition: 1.62 mol% MEK, 32.8 mol% each of N_2, O_2, and H_2O. Symbols are the same as in Fig. 1.

was reduced at >460 K and the selectivity of deep oxidation was also suppressed at 470—490 K and compensatory increase in BA selectivity was observed at 460—490 K.

The activities of the catalysts containing Nd_2O_3, Gd_2O_3, and Er_2O_3 were comparable to that of Co_3O_4. Comparing the results of Table 1(d)—(f) with Fig. 2, it emerges that the addition of these oxides brought about the inhibition of scission reaction and deep oxidation at relatively high reaction temperatures. Therefore, BA selectivities were improved compensatively at above 440 K.

The addition of Yb_2O_3 gave negative effects on BA formation as shown in Table 1 (g). In this catalyst, since scission reaction was much promoted the BA selectivity remained low value even at low conversion level although the deep oxidation was much suppressed over the whole temperature range examined. A very small amount of acetone was formed over the Co_3O_4 catalyst whereas the Co_3O_4 catalysts containing lanthanoid oxides gave no neglectable extent of acetone and the catalysts containing Nd, Gd, and Er were somewhat peculiar in its ability to form acetone.

It is well-known that the decomposition of metal acetate gives acetone. Alternatively, lanthanoid oxides have been reported to be effective catalysts for vapor phase synthesis of ketones from C_2-C_4 alcohols and carboxylic acids.[4-7] According to mechanistic investigations for 1-butanol, at first 1-butanol was dehydrogenated to corresponding aldehyde which was rapidly succeively converted to aldol and then final ketone.[4,8] In latter case, feed gas contained no molecular oxygen. In the previous work,[2] a large amount of acetone formation (20—55% selectivity) from MEK was observed on the Co_3O_4 catalysts supported on MgO and CaO and it was presumed that acetone plausibly originates from acetate ions adsorbed on the basic supports. Although acetaldehyde was actually formed during the oxidation over every lanthanoid oxide containing catalyst, its selectivities were less than those of acetic acid. It appears that there is no correlation between the selectivities of acetaldehyde and those of acetone.

In addition, in this study feed gas contained 8.5 mol% O_2 which was larger than the stoichiometric concentration of complete oxidation of MEK. It is

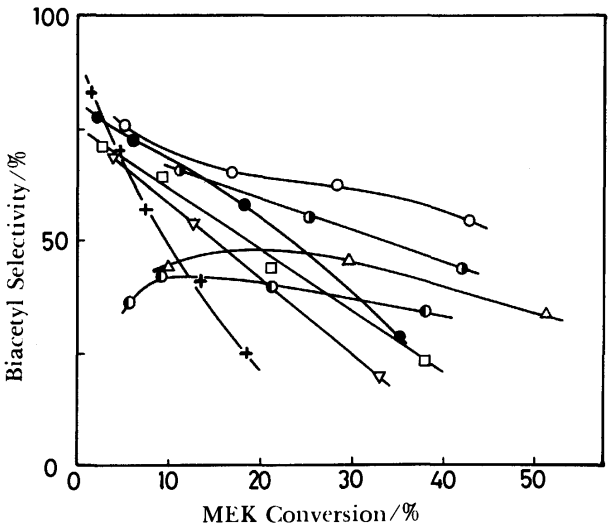

Fig. 3. Improvement in BA selectivity of Co_3O_4 catalyst by the addtion of lanthanoid oxide.
○: La_2O_3, ●: Nd_2O_3, ◑: Pr_6O_{11}, ◐: Yb_2O_3, △: CeO_2, ▽: Er_2O_3, □: Gd_2O_3, +: none (Co_3O_4 only).

confirmed by IR that only the bands arising from surface acetate and carbonate appeared when acetaldehyde was introduced on a wafer of Co_3O_4 at 373 K. So that it is believed that acetone was formed through the carboxylate intermediate on the surface. The activity-selectivity profiles of the catalysts are shown in Fig. 3. In case of Co_3O_4, BA selectivity decreased steeply with increase in conversion. This figure explicitly shows the improvement in the BA selectivity at higher MEK conversion by the addition of lanthanoid oxides especially by the addition of La_2O_3. Specific surface area of the Co_3O_4 catalyst was determined to be 8.4 m^2g^{-1} by BET method and those of the catalysts containing lanthanoid oxides are listed in Table 1. The values were distributed 8.4—20.3 m^2g^{-1} and the active catalysts in general had relatively large specific surface area, however, there is no simple correlation between the catalytic activities per unit weight and the specific surface areas of the catalysts. Specific activities of the catalysts for the MEK consumption (rate per unit surface area at 443—483 K) decreased in the order of

$$Ce > La > Pr > none > Gd > Er > Nd, Yb.$$

While the specific activities of BA formation decreased in the order of

$$La > Ce, Pr, Gd > none > Nd, Er, Yb.$$

It can be roughly said from these orders that the addition of lighter lanthanoid oxides into Co_3O_4 are favorable to BA formation.

The specific rates of BA formation of the catalysts were plotted in Fig. 4 against logarithmic solubility product constants (log K) of hydroxides of tervalent lanthanoid elements[9] as a measure of basicity of the catalysts. The figure shows an approximately linear relationship, suggesting that the basicity of the catalysts in one of the major factors for BA formation.

The Effects of Composition in Co_3O_4-La_2O_3 System. In foregoing section, it has become apparent that the Co_3O_4-La_2O_3 catalyst exceeds the Co_3O_4-Li_2O catalyst in the activity of BA formation. So that the effects of La content of the catalysts on the activity and BA selectivity were examined. At first, the oxidation of MEK was examined over La_2O_3 catalyst (9.0 m^2g^{-1}) under the same reaction conditions as those in Table 1. Oxidation took place with measurable rate at above 500 K, MEK conversion, however, reached only 1.5% even at 558 K. BA selectivity was less than 15% and acetaldehyde, acetone and methyl vinyl ketone were formed as major products. The MEK oxidation was examined over four Co_3O_4-La_2O_3 catalysts with different compositions at 423—493 K. No new kind of products appeared in the reactions over these catalysts.

Figure 5 shows specific surface areas and specific rates of BA formation of the catalysts. The catalysts showed almost similar surface areas except the catalyst of 10% La content (5.8 m^2g^{-1}). While BA formation rates have taken sharp peaks at 10% La content in the different reaction temperatures. Since it has been well known the compounds $LnCoO_3$ (Ln: lanthanoid elements) with perovskite structure[10,11] in Co_3O_4-Ln_2O_3 systems, the catalyst powder with 10% La content was examined by X-ray diffractmeter. However only the diffractions characteristic of Co_3O_4 crystallites of spinel structure were observed. The absence of the perovskite type compounds may be due to the relatively low calcination temperature in the catalyst preparation process. The thickness of La_2O_3 layer is calculated to be about 4.9 nm from its density (6.51 gcm^{-3}) assuming that the whole amount of La_2O_3 covered the surface of Co_3O_4 in the Co_3O_4-La_2O_3 (Co/La=9/1) catalyst. This thickness is sufficient to be detected by XRD. Absence of diffraction arising from La_2O_3 in the XRD measurement suggests that the catalyst composed of no simple mixture of the component oxides.

In summary, it has become apparent that the addition of ca. 10 atomic% of La oxide into Co_3O_4 is much preferable to BA formation.

Effect of the Addition of Acidic Oxides. So far, it

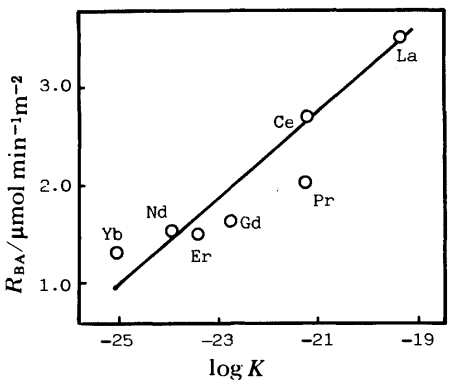

Fig. 4. The effect of acid-base properties of lanthanoid oxides promotors on the activity of BA formation. R_{BA}: Specific rate of BA formation. K: See text.

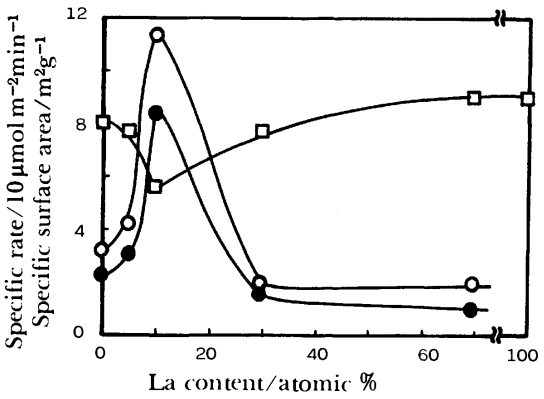

Fig. 5. The effects of La content on the specific surface area and specific rate of BA formation.
□: Specific surface area, ●: specific rate at 453 K, ○: specific rate at 473 K.

Table 2. Oxidation of MEK

Catalyst[a]	Temperature	Conv.	Selectivity[b]/%				
	K	%	$(CH_3CO)_2$	CH_3CHO	CH_3COOH	MVK	$CO+CO_2$
Co_3O_4-P_2O_5	403	11.4	1.3	46.3	22.6	8.2	21.2
	443	21.9	6.7	42.5	22.4	Tr.	26.9
	463	25.8	16.6	35.1	20.1	Tr.	26.9
Co_3O_4-TeO_2	373	3.4	5.2	28.3	60.1	3.3	—
	403	14.1	2.0	39.5	36.4	0.1	18.2
	463	28.4	17.3	33.8	19.9	0.5	27.7
Co_3O_4-SeO_2	403	9.6	29.9	29.2	9.1	17.3	13.6
	423	16.1	39.7	35.7	9.1	0.6	14.1
	463	29.4	39.9	33.7	8.0	0.4	16.4
Co_3O_4-SeO_2-Li_2O	423	2.4	41.0	40.7	6.3	—	11.5
	443	3.9	39.3	37.5	7.1	—	15.4
	463	5.0	52.9	24.1	8.1	—	13.9

a) Ten atomic% P_2O_5, TeO_2, SeO_2, Li_2O. b) Normalized to MEK; $W/F=4.27$ s g-cat. cm^{-3}; feed gas composition: 1.16 mol% MEK, 32.9 mol% each of N_2, O_2, and H_2O.

has been examined the effects of basic additives on MEK oxidation. The effects of some acidic additives were studied in this section.

The addition of P_2O_5 brought about exceeding acceleration of scission reaction as it is expected (Table 2). The selectivity of scission reaction went up over 55% and BA selectivity remained very low value at the all temperatures examined. MEK conversion of the catalyst was presumed to be higher than that of the Co_3O_4-La_2O_3 catalyst even if the difference of W/F is taking into account.

Scission reaction was also enhanced over Co_3O_4-TeO_2 catalyst and the product distribution was closely similar to that of Co_3O_4-P_2O_5.

In case of Co_3O_4-SeO_2 catalyst, activity of the catalyst was somewhat lower than the P_2O_5 or TeO_2 containing catalyst and both BA formation and acetaldehyde formation proceeded with comparable rates and substantially the selectivities did not vary at between 423—463K.

According to Sanderson,[3] SeO_2 do not act as a base since the partial negative charge of the oxide ions in SeO_2 is very low (0.07), on one hand, TeO_2 possessing relatively high partial charge (0.13) is rather amphoteric. So that Co_3O_4-TeO_2 catalyst is expected to be more efficient in BA formation than Co_3O_4-SeO_2 catalyst. The specific activity of Co_3O_4-SeO_2 catalyst, however, was far beyond that of Co_3O_4-TeO_2 catalyst both for MEK conversion and for BA formation. Selective inhibition of scission reaction was attempted by the addition of Li_2O into the Co_3O_4-SeO_2 catalyst (Table 2). MEK conversion was significantly reduced by the addition of Li_2O, and the oxidative dehydrogenation to methyl vinyl ketone was completely inhibited. Although the scission reaction was somewhat depressed at higher reaction temperatures, the improvement in BA selectivity was rather small.

When scission reaction takes place, a part of acetaldehyde molecules formed can be successively oxidized to acetic acid and a part of acetic acid molecules formed can likewise be oxidized to carbon oxides. Then the selectivity of acetaldehyde (normalized to reactant) never surpasses the sum of the selectivities of acetic acid and carbon oxides. In practice, that is the case in all catalysts except for the catalysts containing SeO_2. In case of Co_3O_4-SeO_2 catalyst the selectivity of acetaldehyde was greater than that of acetic acid but also corresponding to the sum of selectivities of acetic acid and carbon oxides. This may suggests that there is another path of acetaldehyde formation expressed by

$$MEK + 1/2\ O_2 = 2\ CH_3CHO.$$

The reason of the complicated behavior of Co_3O_4-SeO_2 catalyst in MEK oxidation is obscure at the present stage. Measurement of the concentrations of surface acidic and basic sites, observation of surface structure, and detailed study on the reaction mechanism will be required for understanding the result of Co_3O_4-SeO_2.

It can be said from the results in this section that the addition of acidic oxides into Co_3O_4 generally enhance the activity of the Co_3O_4 catalyst for scission reaction.

References

1) Y. Takita, K. Iwanaga, N. Yamazoe, and T. Seiyama, *Oxidation Commun.*, **1**, 135 (1980).

2) Y. Takita, K. Inokuchi, O. Kobayashi, F. Hori, N. Yamazoe, and T. Seiyama, *J. Catal.*, **90**, 232 (1984).

3) R. T. Sanderson, "Inorganic Chemistry." Reinhold Pub. Corp., New York (1967).

4) M. A. Markov, Kh. M. Minachev, and G. A. Loginov, *Neftekhimya*, **7**, 76 (1967).

5) M. B. Turova-Polyak and N. T. Thuan, *Zh. Org. Khim.*, **1**. 1771 (1965).

6) M. B. Turova-Polyak, C. Huang, and I. E. Susnina, *Neftekhimya*, **4**, 603 (1964).

7) I. E. Sosnina and E. P. Denisova, *Kinet. Katal.*, **11**, 1437 (1970).
8) G. A. Loginov, M. A. Markov, and Kh. M. Minachev, *Neftekhimya*, **10**, 393 (1970).
9) Bjerrum, Shuwarzenbach, Sillen, "Stability Constants of Metal Complexes," Chemical Society, Lodon (1958), Part II.
10) A. Wold and R. Ward, *J. Am. Chem. Soc.*, **76**, 1029 (1954).
11) A. Wold, B. Post, and E. Banks, *J. Am. Chem. Soc.*, **79**, 6365 (1957).

 © 1987 The Chemical Society of Japan Bull. Chem. Soc. Jpn., 60, 2763—2767 (1987)

The Structure of the Cyclodextrin Complex. XX. Crystal Structure of Uncomplexed Hydrated γ-Cyclodextrin

Kazuaki HARATA
Research Institute for Polymers and Textiles, 1-1-4 Yatabe-Higashi, Tsukuba, Ibaraki 305
(Received February 9, 1987)

Crystal structure of uncomplexed γ-cyclodextrin, $C_{48}H_{80}O_{40}\cdot 14.1H_2O$, was determined by the X-ray method. The crystal is monoclinic and the space group is $P2_1$ with cell dimensions; $a=16.847(2)$, $b=11.098(2)$, $c=20.271(2)$ Å, and $\beta=104.97(1)°$. The structure was solved by the inspection of a Patterson map and the R-map method combined with the rigid-body least-squares technique and refined by the block-diagonal least-squares method to the R-value of 0.061 for 5099 reflections ($\sin\theta/\lambda\geqq 0.57$). γ-Cyclodextrin is in a round shape and somewhat distorted from the regular octagonal symmetry. Intramolecular hydrogen bonds are formed between adjacent glucose residues and maintain the round structure of γ-cyclodextrin. γ-Cyclodextrin molecules are arranged in a cage-type packing, and 7.1 water molecules, occupying 14 sites, are located within the host cavity.

Cyclodextrins are cyclic oligosaccharides consisting of six or more D-glucose residues, which are connected to form a macrocycle by the α-1,4-linkage. Because of the cylindrically-shaped intramolecular cavity, cyclodextrins form inclusion complexes with a wide variety of molecules and ions,[1] which can be fitted into the cavity, even if only partially. X-Ray studies of a number of crystalline complexes of α-cyclodextrin and β-cyclodextrin have revealed the geometrical feature of the host-guest interaction as well as the conformation of the macrocyclic ring,[2] and chemical and physical properties of the inclusion complexes have been interpreted on that basis. On the other hand, only a few crystal structures have been reported for γ-cyclodextrin[3] and its complexes.[4,5] Maclennan and Stezowski have reported the crystal structure of uncomplexed γ-cyclodextrin at 120 K,[3] and suggested that one glucose residue is statistically disordered. The low accuracy of their structure analysis, however, has prevented them from discussing the detailed bonding geometry and the conformation of the macrocycle in comparison with other cyclodextrins. We have been investigating the crystal structure of uncomplexed γ-cyclodextrin at room temperature, and have elucidated the structure with the accuracy comparable to that of other cyclodextrins. The preliminary report of this study[6] has shown the round structure of γ-cyclodextrin having no disordered glucose residue. We here report details of the crystal structure of γ-cyclodextrin in comparison with the structure of α-cyclodextrin and β-cyclodextrin.

Experimental

Materials and Measurements. γ-Cyclodextrin was purchased from Nihon Shokuhin Kako Co., Ltd., and recrystallized three times from water. Crystals were obtained at room temperature by the slow evaporation of an aqueous solution containing γ-cyclodextrin and D-xylose in ca. 1:1 molar ratio. Lattice parameters and diffraction intensities were measured at 22 °C on a Nicolet P3/F diffractometer with graphite-monochromated Cu $K\alpha$ radiation. The crystal was sealed in a thin glass capillary with a drop of mother solution. By using θ—2θ scan mode, 5099 independent reflections with $|F_o|\geqq 3\sigma(F)$ were obtained up to 118° in 2θ. No corrections were made for absorption or extinction effects.

Crystal Data: $C_{48}H_{80}O_{40}\cdot 14.1H_2O$, F.W.=1551.2, monoclinic, space group $P2_1$, $Z=2$, $a=16.847$ (2), $b=11.098$ (2), $c=20.271$ (2) Å, $\beta=104.97$ (1)°, $V=3661.4$ Å^3, $D_x=1.415$ g·cm^{-3}.

Determination and Refinement of the Structure. The orientation of the pseudo octagonal axis of γ-cyclodextrin was deduced from a Patterson map. The rotation around the molecular axis and the position in the unit cell were determined by the R-map method by using the model structure with the regular octagonal symmetry. After the correction of the positional and orientational parameters of each glucose residue, the structure was refined by the usual least-squares method. Water molecules were found on a difference-Fourier map. The final block-diagonal least-squares refinement of the structure, including 87 hydrogen atoms, achieved the R-value of 0.061. The quantity minimized was $\sum w(|F_o|-|F_c|)^2$, with $w=1.0$ for all the reflections. Atomic coordinates and B_{eq} values of non-hydrogen atoms are given in Table 1. Tables of observed and calculated structure factors, anisotropic temperature factors of non-hydrogen atoms, and atomic parameters of hydrogen atoms, are deposited to the Chemical Society of Japan (Document No. 8749). The computation was carried out on a FACOM M380 computer at the Center of Research Information Processing System (RIPS), Agency of Industrial Science and Technology, Tsukuba.

Description of the Structure

γ-Cyclodextrin is in the shape of a nearly regular octagon as shown in Fig. 1. Each glucose unit has the $^4C_1$ chair conformation and is connected to the next residue by the α-1,4-linkage. Average bond distances and angles are shown in Fig. 2. These values are in good agreement with the corresponding values of α-cyclodextrin[7] and β-cyclodextrin.[8] The C(6)-O(6) bonds show two types of orientations; gauche-gauche (to the C(5)-O(5) bond and to the C(4)-C(5) bond, respectively) in the G2, G3, G4, and G7 residues and gauche-trans in the G1, G5, and G8 residues. The C(6)-O(6) bond in the G6 residue is disordered and the occupancy factor of the O(6,G6) atom is 0.76 for the

Table 1. Atomic Coordinates ($\times 10^4$) and B_{eq} Values[a] of Non-Hydrogen Atoms[b]

	OC	x	y	z	B_{eq}/Å^2		OC	x	y	z	B_{eq}/Å^2
C(1,G1)	1.0	−4005(4)	929(8)	2816(4)	4.76	C(2,G6)	1.0	4169(4)	1699(9)	5063(3)	4.84
C(2,G1)	1.0	−3974(4)	985(9)	3572(4)	4.65	C(3,G6)	1.0	3812(4)	2725(8)	4582(3)	4.34
C(3,G1)	1.0	−3132(4)	612(8)	4030(3)	4.15	C(4,G6)	1.0	3866(4)	2382(8)	3855(3)	4.02
C(4,G1)	1.0	−2812(4)	−505(8)	3775(4)	4.61	C(5,G6)	1.0	3418(5)	1198(8)	3645(3)	4.40
C(5,G1)	1.0	−2817(5)	−365(9)	3043(4)	5.29	C(6,G6)	1.0	3327(6)	771(9)	2924(4)	6.38
C(6,G1)	1.0	−2527(6)	−1450(12)	2736(5)	7.99	O(2,G6)	1.0	4034(3)	1930(7)	5712(2)	6.26
O(2,G1)	1.0	−4201(3)	2149(6)	3754(3)	5.46	O(3,G6)	1.0	4224(4)	3825(6)	4790(3)	5.18
O(3,G1)	1.0	−3206(3)	433(6)	4708(2)	4.85	O(4,G6)	1.0	3490(3)	3353(5)	3412(2)	3.81
O(4,G1)	1.0	−1997(3)	−682(5)	4207(3)	5.09	O(5,G6)	1.0	3850(3)	286(6)	4109(3)	5.26
O(5,G1)	1.0	−3656(3)	−151(6)	2659(3)	5.44	O(6,G6)	0.76	4056(4)	529(7)	2796(3)	5.08
O(6,G1)	1.0	−2403(6)	−1020(10)	2065(5)	13.50	O(6′,G6)	0.24	3257(15)	−182(18)	2775(10)	4.98
C(1,G2)	1.0	−3882(4)	4501(9)	1109(4)	5.02	C(1,G7)	1.0	1433(4)	−1994(9)	5445(4)	5.07
C(2,G2)	1.0	−4101(4)	4889(9)	1765(4)	4.89	C(2,G7)	1.0	1983(5)	−1231(9)	5986(4)	5.14
C(3,G2)	1.0	−3752(4)	3989(8)	2333(4)	4.18	C(3,G7)	1.0	2315(5)	−155(9)	5672(4)	4.94
C(4,G2)	1.0	−3994(4)	2717(8)	2102(3)	4.58	C(4,G7)	1.0	2760(4)	−621(8)	5149(3)	4.45
C(5,G2)	1.0	−3772(5)	2419(8)	1443(4)	4.94	C(5,G7)	1.0	2162(5)	−1408(9)	4608(4)	5.09
C(6,G2)	1.0	−4117(7)	1251(10)	1111(4)	6.86	C(6,G7)	1.0	2543(6)	−2004(10)	4103(4)	6.12
O(2,G2)	1.0	−3819(4)	6068(6)	1960(3)	6.91	O(2,G7)	1.0	1516(4)	−805(7)	6438(3)	7.22
O(3,G2)	1.0	−4046(3)	4227(6)	2920(2)	5.20	O(3,G7)	1.0	2895(3)	514(6)	6191(2)	5.26
O(4,G2)	1.0	−3562(3)	1931(5)	2644(2)	4.64	O(4,G7)	1.0	3000(3)	412(5)	4841(2)	4.52
O(5,G2)	1.0	−4093(3)	3324(6)	930(2)	5.25	O(5,G7)	1.0	1866(3)	−2396(6)	4966(3)	5.35
O(6,G2)	1.0	−5024(4)	1295(8)	942(3)	8.59	O(6,G7)	1.0	3252(4)	−2697(6)	4450(3)	6.20
C(1,G3)	1.0	−1391(4)	6298(8)	252(3)	3.98	C(1,G8)	1.0	−1809(5)	−1826(10)	4497(6)	7.27
C(2,G3)	1.0	−2014(4)	7109(8)	462(4)	4.10	C(2,G8)	1.0	−1427(5)	−1716(12)	5266(5)	7.70
C(3,G3)	1.0	−2384(4)	6496(7)	972(3)	3.77	C(3,G8)	1.0	−557(5)	−1156(11)	5374(5)	6.62
C(4,G3)	1.0	−2731(4)	5276(7)	695(3)	3.57	C(4,G8)	1.0	−58(6)	−1923(9)	5008(6)	6.31
C(5,G3)	1.0	−2067(4)	4515(8)	514(4)	4.43	C(5,G8)	1.0	−486(5)	−1927(11)	4248(6)	7.72
C(6,G3)	1.0	−2392(5)	3370(8)	151(5)	5.56	C(6,G8)	1.0	−53(7)	−2810(17)	3841(7)	13.43
O(2,G3)	1.0	−1635(3)	8238(5)	728(3)	5.26	O(2,G8)	1.0	−1908(3)	−964(9)	5577(3)	9.11
O(3,G3)	1.0	−3010(3)	7253(5)	1117(3)	4.78	O(3,G8)	1.0	−164(4)	−1198(11)	6090(3)	10.43
O(4,G3)	1.0	−3005(3)	4675(5)	1222(2)	3.98	O(4,G8)	1.0	732(3)	−1320(6)	5108(3)	5.38
O(5,G3)	1.0	−1741(3)	5197(5)	25(2)	4.38	O(5,G8)	1.0	−1296(4)	−2511(7)	4188(4)	8.50
O(6,G3)	1.0	−3016(4)	3558(6)	−463(3)	6.29	O(6,G8)	1.0	−431(6)	−2689(15)	3137(6)	20.71
C(1,G4)	1.0	1833(4)	6627(8)	1274(4)	4.35	O(W1)	1.0	−3888(5)	218(9)	−543(4)	9.93
C(2,G4)	1.0	1332(5)	7684(8)	1427(5)	5.87	O(W2)	1.0	−2323(5)	366(8)	310(4)	9.62
C(3,G4)	1.0	466(5)	7252(8)	1447(4)	5.08	O(W3)	1.0	−4656(4)	3222(7)	−3409(5)	11.00
C(4,G4)	1.0	66(4)	6638(7)	777(4)	3.94	O(W4)	1.0	−5744(4)	3068(8)	−41(4)	8.71
C(5,G4)	1.0	607(4)	5565(7)	671(4)	4.07	O(W5)	1.0	−5182(6)	2891(10)	−2156(5)	12.81
C(6,G4)	1.0	284(4)	4929(11)	5(5)	7.66	O(W6)	1.0	−1727(10)	5900(15)	2630(6)	21.08
O(2,G4)	1.0	1761(4)	8213(7)	2047(4)	8.72	O(W7)	0.82	−4539(5)	2559(9)	−722(4)	7.77
O(3,G4)	1.0	−20(4)	8334(7)	1495(4)	7.51	O(W8)	0.18	−4553(24)	3781(40)	−697(19)	8.17
O(4,G4)	1.0	−705(3)	6153(5)	841(2)	4.26	O(W9)	0.82	3618(5)	560(8)	1360(3)	6.79
O(5,G4)	1.0	1401(3)	6084(5)	657(2)	4.37	O(W10)	0.18	2831(24)	−38(31)	1421(14)	7.05
O(6,G4)	1.0	136(4)	5748(11)	−553(3)	11.18	O(W11)	0.56	1310(7)	694(12)	1713(7)	8.55
C(1,G5)	1.0	3950(4)	3833(7)	2984(4)	4.00	O(W12)	0.44	1185(17)	114(28)	2744(13)	16.98
C(2,G5)	1.0	3984(4)	5229(8)	3076(4)	4.81	O(W13)	0.44	1039(18)	1597(46)	1799(22)	30.04
C(3,G5)	1.0	3143(4)	5751(7)	2768(4)	4.25	O(W14)	0.27	343(33)	3507(65)	2116(28)	24.94
C(4,G5)	1.0	2823(4)	5359(7)	2039(3)	3.73	O(W15)	0.25	1388(17)	3251(81)	3109(13)	23.19
C(5,G5)	1.0	2793(4)	3958(7)	2013(3)	3.88	O(W16)	0.56	−247(19)	−552(27)	2583(11)	21.71
C(6,G5)	1.0	2526(5)	3467(8)	1287(4)	4.97	O(W17)	0.56	−138(26)	1106(28)	3354(16)	28.37
O(2,G5)	1.0	4275(3)	5541(6)	3783(3)	6.21	O(W18)	0.56	1072(11)	4854(33)	2986(9)	22.01
O(3,G5)	1.0	3197(3)	7042(6)	2815(3)	5.90	O(W19)	0.29	−835(37)	1996(57)	1285(18)	31.78
O(4,G5)	1.0	1990(3)	5809(5)	1813(2)	4.05	O(W20)	0.71	−1512(17)	890(30)	1832(14)	27.20
O(5,G5)	1.0	3616(3)	3522(5)	2295(2)	4.28	O(W21)	0.38	−466(19)	4367(44)	2154(15)	20.95
O(6,G5)	1.0	2370(4)	2210(6)	1281(3)	6.15	O(W22)	0.44	1058(22)	1536(55)	2937(18)	28.36
C(1,G6)	1.0	3834(4)	479(9)	4800(3)	4.87	O(W23)	0.62	−1376(13)	3060(30)	2386(11)	23.34

a) $B_{eq}=8\pi^2(u_1^2+u_2^2+u_3^2)/3$, where u_i is the root-mean-square deviation in the i-th principal axis of the thermal ellipsoid.
b) *OC* indicates the occupancy factor.

former and 0.24 for the latter. Some geometrical parameters describing the macrocyclic conformation are summarized in Table 2. Eight glycosidic oxygen atoms (O(4)) form a nearly regular octagon with the radius of 5.81—5.94 Å and the side length of 4.43—4.59 Å. These O(4) atoms are coplanar within the maximum deviation of 0.192 Å. The torsion-angle index of 97.0—120.4° is somewhat larger than those of other two cyclodextrins. Since the O(4)···O(4′) distance is in rather narrow region, the correlation

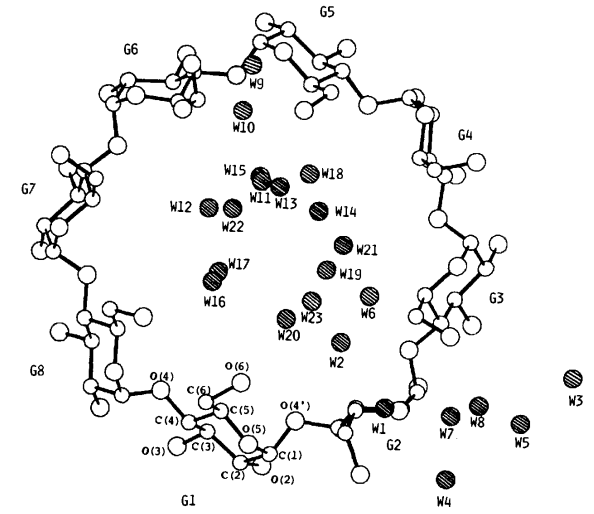

Fig. 1. The Structure and numbering scheme of γ-cyclodextrin hydrate. Water molecules are shaded.

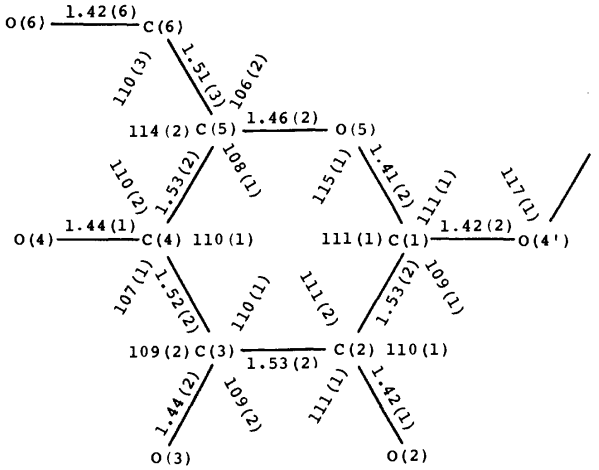

Fig. 2. Average bond distances and angles for the eight glucose residues. Standard deviations in parentheses were estimated according to the equation: $\sigma=[\sum_{i=1}^{8}(x_i-\bar{x})^2/7]^{1/2}$ where x_i refers to the bond distance or angle of the i-th residue and $\bar{x}$ is the average value.

between the O(4)···O(4′) distance and the torsion-angle index is less obvious than the correlation found in α-cyclodextrin,[9] β-cyclodextrin,[10] or in mono- and disaccharides.[11] The tilt-angle is distributed in the range form −2.5° to 23.8°. The G2 and G4 residues are almost normal to the plane through the eight O(4) atoms, while the other residues incline with their O(6) side turning to the inside of the macrocycle. The average value of 13.9° is similar to that of β-cyclodextrin (12.5°), but smaller than that of α-cyclodextrin (19.2°). The O(2)···O(3′) distances of 2.76—2.91 Å between adjacent residues indicate that adjacent two residues are linked by the O(2)···O(3′) hydrogen bond. Although no hydrogen bond is observed between O(2,G7)H and O(3,G8)H hydroxyl groups, four O(2)-H···O(3) and three O(3)-H···O(2) hydrogen

Table 2. Geometrical Parameters Describing the Macrocyclic Conformation of γ-Cyclodextrin

I. Distance from the Center of Gravity of Eight O(4) Atoms to Each O(4) Atom[a)]

Residue	Distance (l/Å)	Residue	Distance (l/Å)
G1	5.84	G5	5.88
G2	5.88	G6	5.81
G3	5.90	G7	5.94
G4	5.84	G8	5.94

a) The estimated standard deviation is 0.01 Å.

II. O(4)···O(4′) Distance between Adjacent Glucose Residues[a)]

Distance (l/Å)		Distance (l/Å)	
O(4,G1)···O(4,G8)	4.54	O(4,G4)···O(4,G5)	4.48
O(4,G1)···O(4,G2)	4.59	O(4,G5)···O(4,G6)	4.48
O(4,G2)···O(4,G3)	4.46	O(4,G6)···O(4,G7)	4.58
O(4,G3)···O(4,G4)	4.46	O(4,G7)···O(4,G8)	4.43

a) The estimated standard deviation is 0.01 Å.

III. O(2)···O(3′) Distances between Adjacent Glucose Residues[a)]

Distance (l/Å)		Distance (l/Å)	
O(2,G1)···O(3,G2)	2.91	O(2,G4)···O(3,G5)	2.83
O(3,G1)···O(2,G8)	2.88	O(2,G5)···O(3,G6)	2.81
O(2,G2)···O(3,G3)	2.77	O(2,G6)···O(3,G7)	2.84
O(2,G3)···O(3,G4)	2.76	O(2,G7)···O(3,G8)	2.77

a) The estimated standard deviation is 0.01 Å.

IV. Torsion Angle Index[a)]

Residue	Index (ϕ/°)	Residue	Index (ϕ/°)
G1	99.8	G5	112.0
G2	107.0	G6	97.0
G3	113.1	G7	120.4
G4	119.9	G8	116.5

a) The torsion angle index is defined as follows: $\phi=|\phi(C(1)\text{-}C(2))|+|\phi(C(2)\text{-}C(3))|+|\phi(C(5)\text{-}O(5))|+|\phi(O(5)\text{-}C(1))|-|\phi(C(3)\text{-}C(4))|-|\phi(C(4)\text{-}C(5))|$, where the conformation angle, C(1)-C(2)-C(3)-C(4), is expressed as ϕ(C(2)-C(3)).

V. Tilt Angle[a)]

Residue	Tilt angle (ϕ/°)	Residue	Tilt angle (ϕ/°)
G1	16.6	G5	18.4
G2	−2.5	G6	13.4
G3	23.8	G7	12.7
G4	4.8	G8	23.6

a) The tilt angle is defined as the angle made by the plane through the eight O(4) atom and the plane through C(1), C(4), O(4), and O(4′) of each residue.

VI. Deviation of O(4) Atoms from Their Least-Squares Plane

Atom	Deviation (d/Å)	Atom	Deviation (d/Å)
O(4,G1)	0.054	O(4,G5)	−0.077
O(4,G2)	−0.173	O(4,G6)	−0.046
O(4,G3)	−0.005	O(4,G7)	−0.056
O(4,G4)	0.192	O(4,G8)	0.126

bonds are found. These hydrogen bonds may maintain the round structure of γ-cyclodextrin.

The crystal structure is shown in Figs. 3 and 4. γ-Cyclodextrin molecules are stacked along the crystallographic b axis, showing a packing feature similar to the cate-type packing found in the crystal of uncomplexed β-cyclodextrin.[10] The plane through eight O(4) atoms makes an angle of 46.5° with the b axis. As the result, adjacent two molecules along the b axis are laterally shifted each other by about half a molecule.

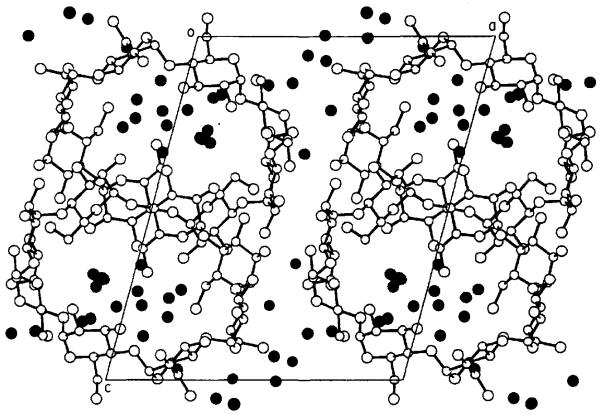

Fig. 3. The crystal structure viewed along the b axis. Water molecules are shown by full circles.

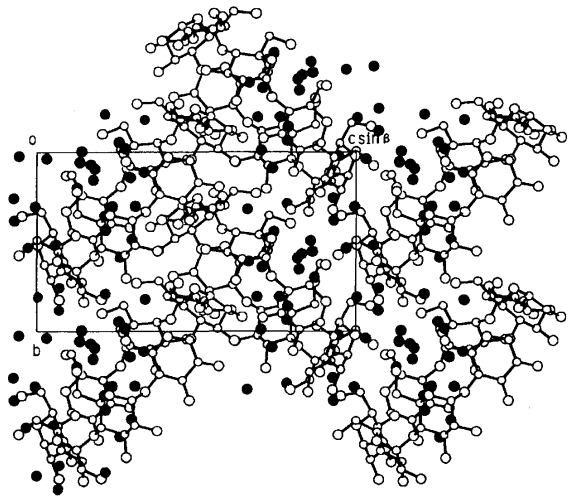

Fig. 4. The crystal structure viewed along the a axis. Water molecules are shown by full circles.

Both ends of the γ-cyclodextrin cavity are blocked by adjacent molecules. Owing to the incomplete blockade, however, the cavity is not closed. A narrow channel runs through the inside of the macrocycle stacked along the b axis. This channel is filled with water molecules as shown in Fig. 4. The G7 and G8 residues are partially inserted into the adjacent γ-cyclodextrin ring from the O(2), O(3) side, and form hydrogen bonds with included W6, W15, W18, and W23 water molecules.

The asymmetric unit of the crystal contains 14.1 water molecules, which are distributed over 23 sites. γ-Cyclodextrin includes 7.1 water molecules which occupy 14 sites. It is obvious that water molecules within the cavity can not fully form hydrogen bonds. These water molecules are arranged in the limited accommodation space so that they can form no ideal geometry of hydrogen bonding. Although it is not possible to discuss the details of hydrogen-bonding scheme because most of hydrogen atoms of water molecules were not located on the difference-Fourier map, most of hydroxyl groups of γ-cyclodextrin are hydrogen-bonded to water molecules located outside the cavity and form hydrogen-bond network in the crystal.

Discussion

The present X-ray analysis has shown that the γ-cyclodextrin molecule is round and rather symmetrical. When compared this structure with the structure reported by Maclennan and Stezowski,[3] a major difference is that one glucose residue is disordered in the structure at 120 K. In the structure at room temperature, however, all glucose residues are well ordered although the average temperature factor of the G8 residue is ca. twice greater than the average value of the other residues. This difference may be ascribed to the different conditions of data measurements and/or crystallization.

Table 3 gives some geometrical parameters to compare the macrocyclic conformation among three cyclodextrins. The glycosidic oxygen angle does not significantly change among these cyclodextrins, and is in good agreement with the O(4) angle found in maltosides.[12-14] This indicates that the effect of cyclization on the O(4) angle is small. A difference is found in the

Table 3. Comparison of Average Values of Some Geometrical Parameters Describing the Macrocyclic Conformation[b]

	α-Cyclodextrin	β-Cyclodextrin	γ-Cyclodextrin
O(2)···O(3′) distance (l/Å)	3.3(0.6)	2.9(0.1)	2.8(0.1)
O(4)···O(4′) distance (l/Å)	4.3(0.1)	4.4(0.1)	4.5(0.1)
O(4) angle (ϕ/°)	118(1)	118(1)	117(1)
Planarity of the O(4) polygon (d/Å)[a]	0.084	0.178	0.110
Torsion-angle index (ϕ/°)	127(9)	120(7)	111(9)
Tilt-angle (ϕ/°)	19(12)	12(10)	14(9)

a) The root-mean-square deviation from the least-squares plane through the O(4) polygon. b) Standard deviations are given in parentheses.

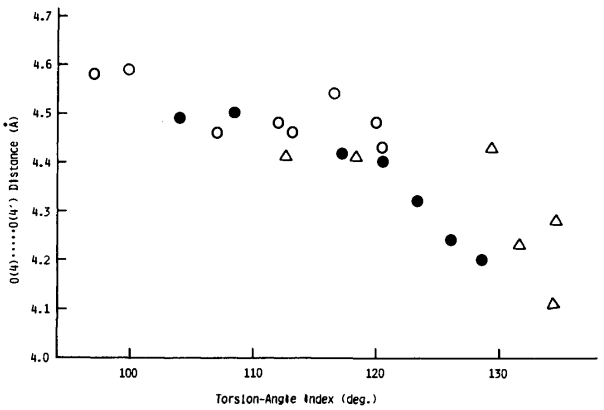

Fig. 5. Plot of the O(4)···O(4′) distance between adjacent glucose residues against the torsion angle index: α-cyclodextrin (△), β-cyclodextrin (●), and γ-cyclodextrin (○).

O(4)··· O(4′) distance and the torsion-angle index. The average O(4)··· O(4′) distance increases with the increasing number of the glucose residues, while the average torsion-angle index decreases. Figure 5 shows that the O(4)··· O(4′) distance and the torsion angle index are in the limited region depending on the size of the macrocycle. Since the O(4) atoms of γ-cyclodextrin are aligned on a circle with the radius larger than the radius of the other cyclodextrins, the greater O(4)··· O(4′) distance is necessary to avoid the unfavorable distortion of the glycosidic linkage. The change of the O(4)··· O(4′) distance can be easily derived by the small change of the endocyclic conformation angle of the pyranose ring, as indicated by the correlation between the O(4)··· O(4′) distance and the torsion-angle index.

The O(2)··· O(3′) distance indicates that the intramolecular hydrogen bond becomes stronger in order of α-, β-, and γ-cyclodextrin. The α-cyclodextrin ring is remarkably distorted and two intramolecular hydrogen bonds are disrupted because of the sharp inclination of glucose residues. Chako and Saenger[15] have also reported that the uncomplexed α-cyclodextrin, crystallized in the presence of $BaCl_2$, is more symmetrical with the six O(2)··· O(3′) hydrogen bonds. In that case, however, the average O(4)··· O(4′) distance is decreased to 4.234 Å and the glycosidic oxygen angle is somewhat increased (118.4°), suggesting that the strain is imposed on the macrocycle although such strain energy may be compensated by the formation of additional two hydrogen bonds. In β-cyclodextrin and γ-cyclodextrin, the radius of the macrocycle is so large that the macrocyclic ring can be symmetrical and also in the relaxed state.

The G7 and G8 residues are found to be partially inserted into the cavity of the adjacent γ-cyclodextrin, which is related by the two-fold screw axis. Such close contact between host molecules has not been observed in other cyclodextrin crystals since the diameter of the cavity is too small to allow the penetration of the glucose moiety. The effective space of the γ-cyclodextrin cavity to accommodate water molecules becomes considerably smaller than the expected space from the radius of the macrocycle. The interesting fact is that the temperature factor of the G8 residue is significantly larger than the temperature factor of the other residues. This may be ascribed to the limited hydrogen-bonding contacts of the G8 residue in the hydrophobic environment. The O(2,G8)H and O(3,G8)H hydroxyl groups form hydrogen bonds with W15 and W18, respectively, which have relatively low occupation factor (0.25 and 0.55, respectively). Moreover, no intramolecular hydrogen bond is observed between O(2,G7)H and O(3,G8)H hydroxyl groups. This indicates that hydrogen bonds, especially intramolecular hydrogen bonds, play an important role to maintain the rigid structure of cyclodextrins.

This work was supported in part by a Grant from the Science and Technology Agency.

References

1) J. Szejtli, "Cyclodextrins and their Inclusion Complexes," Academiai Kiado, Budapest (1982).
2) W. Saenger, "Inclusion Compounds," ed by J. L. Atwood, J. E. D. Davies, and D. D. MacNicol, Academic Press, London (1984), Vol. 2, pp. 231—259.
3) J. M. Maclennan and J. J. Stezowski, *Biochem. Biophys. Res. Commun.*, **92**, 926 (1980).
4) K. Lindner and W. Saenger, *Biochem. Biophys. Res. Commun.*, **92**, 933 (1980).
5) S. Kamitori, K. Hirotsu, and T. Higuchi, *J. Chem. Soc., Chem. Commun.*, **1986**, 690.
6) K. Harata, *Chem. Lett.*, **1984**, 641.
7) P. C. Manor and W. Saenger, *J. Am. Chem. Soc.*, **96**, 3630 (1974).
8) K. Lindner and W. Saenger, *Carbohydr. Res.*, **99**, 103 (1982).
9) K. Harata, *Bull. Chem. Soc. Jpn.*, **50**, 1416 (1977).
10) K. Harata, *Bull. Chem. Soc. Jpn.*, **55**, 2315 (1982).
11) A. D. French and V. G. Murphy, *Carbohydr. Res.*, **27**, 391 (1973).
12) S. S. C. Chu and G. A. Jeffrey, *Acta Crystallogr.*, **23**, 1038 (1967).
13) G. J. Quigley, A. Sarko, and R. H. Marchessault, *J. Am. Chem. Soc.*, **92**, 5834 (1970).
14) I. Tanaka, N. Tanaka, T. Ishida, and M. Kakudo, *Acta Crystallogr., Sect. B*, **32**, 155 (1976).
15) K. K. Chako and W. Saenger, *J. Am. Chem. Soc.*, **103**, 1708 (1981).

 © 1987 The Chemical Society of Japan Bull. Chem. Soc. Jpn., 60, 2769—2774 (1987)

Polarized Raman and Infrared Spectra of 2-Amino- and 2-Amino-d_2-pyrimidines

Masayoshi MAEHARA, Sekiichiro NAKAMA,† Yoshinori NIBU, Hiroko SHIMADA,* and Ryoichi SHIMADA††
Department of Chemistry, Faculty of Science, Fukuoka University, Nanakuma, Jonan-ku, Fukuoka 814-01
†Department of Chemistry, Faculty of Liberal Arts, University of Yamaguchi, Yoshida, Yamaguchi 753
††Department of Chemistry, Faculty of Science, Kyushu University 33, Hakozaki, Higashi-ku, Fukuoka 812
(Received February 16, 1987)

An assignment of the normal vibrations of 2-aminopyrimidine was made through the vibrational analyses of the polarized Raman and infrared spectra and also through the normal coordinate calculation. The assignment was confirmed by the same study made on 2-amino-d_2-pyrimidine.

Lafaix and Lebas studied the infrared and Raman spectra of various amino-substituted pyrimidines and gave tentative assignments for some normal vibrations of these molecules.[1] Kydd studied the amino inversion vibration of 2-aminopyrimidine through observation of the infrared spectrum in vapor and showed that the molecule is planar in the vibrational ground state.[2] Scheinbeim and Schempp[3] and Furberg et al.[4] determined the crystal structure of 2-aminopyrimidine and pointed out that the molecules form hydrogen-bonded dimer-like pairs in crystal.

Since the orientation of the 2-aminopyrimidine molecule in crystal has been known, the vibrational analyses of the polarized Raman and infrared spectra in single crystals became possible. In this paper, the assignment of the normal vibrations of 2-aminopyrimidine is discussed based on polarization behavior of the Raman and infrared bands observed in single crystals and also the normal coordinate calculation. The same study is made on 2-amino-d_2-pyrimidine and the assignment is confirmed.

Experimental

Material. 2-Amino-d_2-pyrimidine was synthesized by the exchange reaction of 2-aminopyrimidine obtained from Tokyo Kasei Chemical Company with D_2O. Isotopic purity of the product was determined by the nuclear magnetic resonance measurement. The samples were purified by zone-refining of about 100 passages.

Optical Measurements. Polarization measurement of the Raman spectrum was made in molten and single crystal phases with a JEOL 400 T Laser Raman Spectrophotometer. The sample was excited with the 514.5 nm line from an Ar^+ ion laser. A well grown single crystal of 2-aminopyrimidine obtained by the Bridgman method was cut along the cleavage bc plane and then cut along the ab and ac planes. Samples with cubic shape of about 5 mm^3 were prepared. The crystal axes were determined by observing the birefringence under the polarization microscope. The crystal growth direction was found to be the c axis. 2-Amino-d_2-pyrimidine changes quite rapidly into 2-amino- and 2-amino-d_1-pyrimidines by the exchange reaction with moisture in atmosphere, and thus the polarized Raman spectrum of the 2-amino-d_2-pyrimidine crystal was observed for a single crystal grown in a capillary glass tube of about 50 mm in length and 3 mm in diameter. The method of measurement of the polarized Raman spectrum was exactly the same as that described previously.[5,6]

The infrared spectrum of 2-aminopyrimidine was observed in vapor and single crystal phases with a Hitachi Infrared Spectrophotometer Model 345. The single crystal sample was grown between two KRS-5 plates in the same way as that described previously.[7] A well grown single crystal portion of the crystal sample was selected under polarized light and other portion was covered with aluminum foil. The polarized infrared spectrum was measured with an AgBr wire-grid polarizer. The incident infrared light was polarized by the polarizer in such a way that the electric vector pointed in the direction of 45° from both the vertical and horizontal directions. The polarizer is rotatable by 90°. Although the spectrophotometer had some preferential sensitivity to vertically polarized light, the two components of the diagonally polarized light beam behaved equally concerning the intensity. The sample crystal sandwiched between two KRS-5 plates was held in a cell holder adjusting the orientation of the crystal, so that the spectrum showed the most remarkable polarization behavior by rotating the polarizer by 90°. The spectrum observed with polarized light which gives the maximum intensity for the strong and narrow band at 1210 cm^{-1} is referred to as the $\perp$ spectrum and that giving the minimum intensity is to as the // spectrum. In this orientation of the sample crystal, the crystal growth direction (c axis) was found to point roughly in the vertical direction. The infrared spectrum of the 2-amino-d_2-pyrimidine single crystal could not be observed because the deuterium atoms were replaced by the hydrogen atoms with moisture in atmosphere.

Normal Coordinate Calculation

A normal coordinate calculation was performed through the standard GF matrix methods with a FACOM M-200 computer at the Computer Center of Fukuoka University. The geometric parameters of the 2-aminopyrimidine molecule were taken from the data determined by Scheinbeim and Schempp.[3] The F matrix elements for the in-plane vibrations were evaluated with the potential field of an improved modification of the Urey-Bradley force field described previously.[5-7] For the out-of-plane vibrations the valence force field and ϕ type torsional coordinates were used. Values of the force constants used for the calculation of the in-plane and out-of-plane normal vibrations of 2-amino- and 2-amino-d_2-pyrimidines are listed in Table 1. The notation of the force constants are exactly the same as those used previously[5-7] and the symbols given for atoms and internal coordinates are shown in Fig. 1. The calculated frequencies and modes of the normal vibrations are given in Table 4.

Table 1. Force Constants for the In-Plane and Out-of-Plane Vibrations of 2-Aminopyrimidine[a)]

$K_{C'-N}$[b)]	5.2 hNm^{-1}	$F_{N\cdots N}$	0.8 hNm^{-1}	$Q_{C'-N}$	0.17 aNmrad^{-2}
K_{C-N}	5.4	$F_{C'\cdots C}$	0.5	Q_{N-C}	0.18
K_{C-C}	4.5	$F_{N\cdots C}$	0.3	Q_{C-C}	0.2
$K_{N'-C'}$	4.3	$F_{C\cdots C}$	0.7	$Q_{N'-C'}$	0.1
K_{C-H}	4.4	$F_{N\cdots N}$	0.9	$P_{N'}$	0.13
$K_{N'-H'}$	5.9	$F_{H\cdots C'}$	0.5	P_H	0.32
$H_{N-C'-N}$	0.75	$F_{H\cdots H'}$	0.1	$q^o_{N'}$[c)]	−0.15
$H_{C'-N-C}$	0.5	$F_{N\cdots H}$	0.75	$q^o_{C'}$[c)]	−0.1
H_{N-C-C}	0.6	$F_{C\cdots H}$	0.45	$q^{o\,c)}_{C}$	−0.06
H_{C-C-C}	0.4	ρ	0.35	$q^m_{N'}$	0.04
$H_{N'-C'-N}$	0.4	k^o_{rr}	0.06	q^m	0.03
H_{N-C-H}	0.18	k^m_{rr}	−0.06	q^p	0.04
H_{C-C-H}	0.18	$h^m_{R\alpha}$	−0.7 nNrad^{-1}	p^o	0.02
$H_{H'-N'-H'}$	0.43	$h^m_{R\beta}$	0.5	$p^m_{H,H}$	0.02
$H_{H'-N'-C'}$	0.28			$t^o_{N'}$[d)]	−0.01
				t^o_H[d)]	−0.06
				t^m_H	0.02

a) The same values of the force constants were used for the calculation made on 2-amino-d_2-pyrimidine, where H′ atom of the amino group is replaced by D atom. b) See Fig. 1 for notation of atoms. c) Torsional vibration involving N′, C, or C′ atom. d) Wagging vibration involving N′ or H atom.

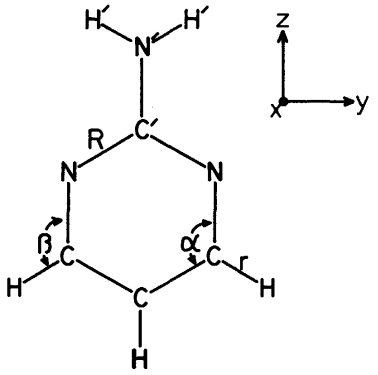

Fig. 1. Symbols for the atoms and internal coordinates.

Calculation of Relative Intensities of the Raman and Infrared Bands in Single Crystals

2-Aminopyrimidine crystallizes in orthorhombic space group D^{15}_{2h} with eight molecules in the unit cell, where the structure contains centrosymmetrically related hydrogen-bonded dimer-like pairs separated by hydrophobic regions and the dihedral angle between the planes of the amino group and pyrimidine ring is about 22°.[3,4)] The projection of the crystal structure on the bc plane is shown in Fig. 2. No factor group splitting was observed for the Raman bands due to molecular vibrations in crystal and thus the relationship between the Raman tensors for the free molecule and the crystal was derived based on the simple oriented gas model. Evaluation of the matrix elements of the Raman tensor of 2-aminopyrimidine was made in the same way as that made for maleic anhydride[5)] and tetramethylpyrazine.[6)] The direction cosines between the crystal and molecular axes were calculated using the crystal data given by Scheinbeim and Schempp.[3)] The squares of relative values of the elements of the Raman tensor, which are proportional to the relative intensities of the Raman bands, are given in Table 2, where the molecular structure of 2-aminopyrimidine is assumed to belong to point group C_{2v}.

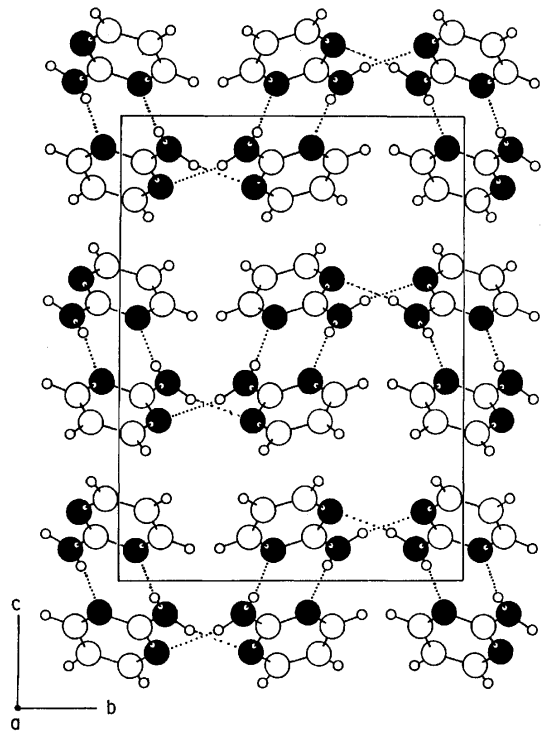

Fig. 2. Projection of the 2-aminopyrimidine crystal on the bc plane.

In order to carry out the vibrational analysis of the polarized infrared spectrum, the crystal axes in the sample crystal sandwiched between two KRS-5 plates have to be determined. Since the crystal growth direction (c axis) was found in a plane of the sample crystal,

Table 2. Squares of the Relative Values of Elements of the Raman Tensors for 2-Aminopyrimidine

	b_2	b_1	a_2
$(A_{aa})^2$	0.31	0.68	0.18
$(A_{bb})^2$	0.81	0.11	0.17
$(A_{cc})^2$	0.12	0.25	0.70
$(A_{ab})^2$	0.10	0.02	0.28
$(A_{ac})^2$	0.27	0.15	0.0
$(A_{bc})^2$	0.0	0.31	0.20

Table 3. Proportionality Factors of the Intensity of the Infrared Bands in the // and ⊥ Spectra

θ[a)]	Pol[b)]	a_1	b_2	b_1
0°	//	0.42	0.02	0.55
	⊥	0.04	0.83	0.13
10°	//	0.45	0.10	0.45
	⊥	0.01	0.76	0.23
20°	//	0.46	0.21	0.33
	⊥	0.00	0.65	0.35

a) θ is the angle between the c axis and the vertical line. The plane of the sample crystal was assumed to be the cleavage bc plane. b) For the definition of the // and ⊥ polarized spectra, see text.

the plane would be the cleavage bc or ac plane. Proportionality factors of the intensity of the infrared bands in the // and ⊥ spectra were calculated for the bands assigned to the vibrations belonging to symmetry species a_1, b_2, and b_1 assuming that the sample crystal plane is the bc or ac plane, in the same way as calculated for pyrazine.[9] The calculation was made varying the angle between the c axis and the vertical line and the values obtained for the angles of 0, 10, and 20° for the bc plane are listed in Table 3.

Results and Discussion

2-Aminopyrimidine. The polarized Raman spectrum of 2-aminopyrimidine observed in single crystal is shown in Fig. 3. The polarized spectrum was denoted by two characters such as ab in the same manner as described previously.[5,6] The first letter refers to the direction of polarization of the excitation light and the latter to that of the scattering light. It is expected from Table 2 that the relative intensity of the b_2 vibrations is strongest in the bb polarized spectrum, the b_1 vibrations in the aa spectrum and the a_2 vibrations in the cc spectrum.

The polarized infrared spectrum of 2-aminopyrimidine in single crystal is shown in Fig. 4, where the // and ⊥ spectra are drawn with the solid and dotted lines, respectively. As can be seen in the figure, polarization behavior of the infrared bands in crystal can be classified into three types. The bands showing the first type polarization are almost missing in the ⊥ spectrum, while the second type bands are observed much strongly in the ⊥ spectrum. The intensity of the third type bands observed in the // spectrum is about 1.5

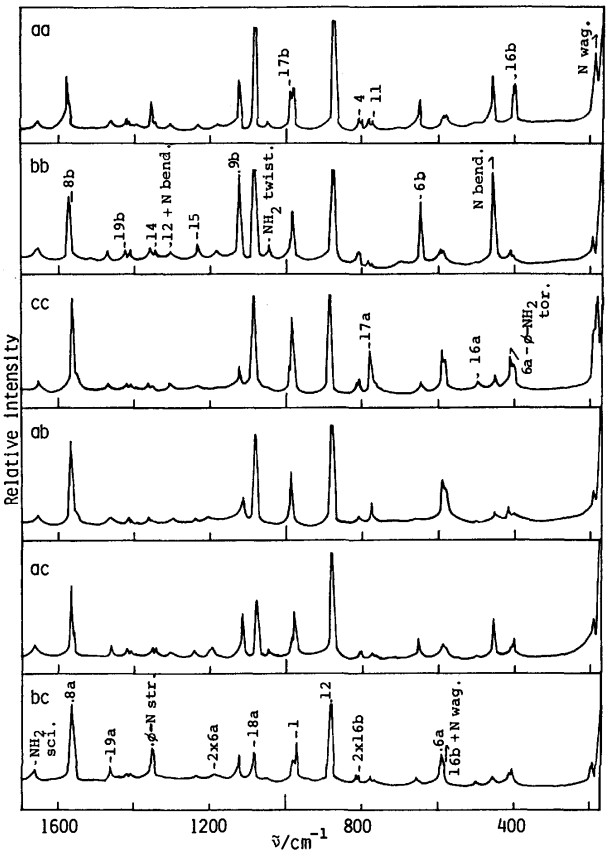

Fig. 3. Polarized Raman spectra of the 2-aminopyrimidine crystal. For the definition of the symbols of the spectra such as aa, see text.

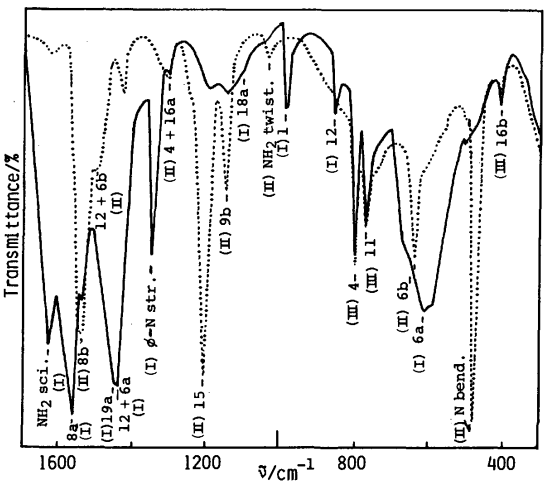

Fig. 4. Polarized infrared spectrum of the 2-aminopyrimidine crystal.

times strong as that in the ⊥ spectrum. These three types of polarization behavior are referred to as the types I, II, and III, respectively. The proportionality factors of the intensity of the bands calculated for the bc plane, which is given in Table 3, indicate that the spectra can be well explained by the values calculated for the crystal orientation with the c axis pointing in the direction of 10° from the vertical line. This means

that the propagation direction of the incident light was along the a axis and the direction of the electric vector deviated from the c axis by 35° in our polarization measurement. The calculation was also made for the ac plane, but the result was not consistent with the observed polarization behavior even if the sample crystal assumes to be in any orientation. Thus the infrared bands showing the type I, II, and III polarization behavior could be assigned to the vibrations belonging to the symmetry species a_1, b_2, and b_1, respectively.

The vibrational modes were determined through the normal coordinate calculation. Since the 2-aminopyrimidine molecule forms hydrogen-bonded dimer-like pairs in crystal, the infrared bands whose frequencies largely shift in crystal from those in vapor could be assigned to the vibration involving the NH_2 group.

Species a_1: The strongly polarized Raman bands observed at 3330, 3025, 1580, 1448, 1360, 1080, 990, and 870 cm^{-1} in molten phase were directly ascribed to the a_1 vibrations and assigned to the N-H stretching, ν_2, ν_{8a}, ν_{19a}, ϕ-N stretching, ν_{18a}, ν_1, and ν_{12} vibrations, respectively. Where ϕ refers to the pyrimidine ring. The corresponding infrared bands showed the type I polarization as predicted. The Raman band observed at 1650 cm^{-1}, whose corresponding infrared band was observed strongly in crystal but was not in vapor and showed the type I polarization, was ascribed to the NH_2 scissoring vibration of the hydrogen-bonded molecule. The strong infrared band observed at 1597 cm^{-1} in vapor was assigned to the NH_2 scissoring vibration of the free molecule. The band at 605 cm^{-1} showing the type I polarization was assigned to the ν_{6a} vibrations, although the corresponding Raman band showed low depolarization factor in molten phase.

Species b_2: The relative intensities of the Raman bands observed at 1558, 1425, 1355, 1230, 1130, 1040, 642, and 457 cm^{-1} were strongest in the bb spectrum and decreased in the aa and ac spectra in order. This polarization behavior is consistent with the assignment to the b_2 vibrations and thus these bands were assigned to the ν_{8b}, ν_{19b}, ν_{14}, ν_{15}, ν_{9b}, NH_2 twisting, ν_{6b}, and N bending vibrations, respectively. The corresponding infrared bands showed the type II polarization.

Species b_1: The relative intensities of the Raman bands observed at 997, 802, 765, 410, and 187 cm^{-1} were strongest in the aa spectrum and medium in the bc and cc spectra. Thus these bands were assigned to the ν_{17b}, ν_4, ν_{11}, ν_{16b}, and N wagging vibrations belonging to the species b_1, respectively. The corresponding infrared bands showed the type III polarization. The NH_2 wagging vibration could not be resolved.

Species a_2: The relative intensities of the Raman bands observed at 782, 516, and 417 cm^{-1} were strongest in the cc spectrum and decreased in the ab, bc, aa, and bb spectra in order. Thus these bands were assigned to the ν_{17a}, ν_{16a}, ν_{6a}—ϕ-NH_2 torsional vibrations of the species a_2, respectively. The very weak infrared band observed at 514 cm^{-1} in crystal was assigned to the ν_{16a} vibration of the species a_2. An appearance of the infrared inactive a_2 band may be due to the distortion of the molecular structure in crystal.

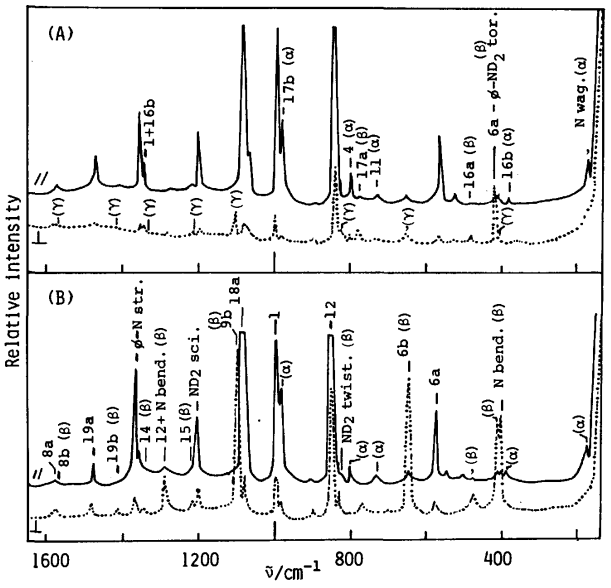

Fig. 5. Polarized Raman spectrum of the 2-amino-d_2-pyrimidine crystal. For the definition of the spectra of (A) and (B), see text.

2-Amino-d_2-pyrimidine. The polarized Raman spectrum of 2-amino-d_2-pyrimidine is given in Fig. 5. A single crystal of 2-amino-d_2-pyrimidine grown in a capillary tube was held in a cell holder in such a way that the crystal growth direction was along the polarization direction of the excitation light and the scattering light was observed at the direction perpendicular to the excitation light beam. The polarized Raman spectra were observed in two crystal orientations, in which the spectra showed drastically different polarization behaviors with each other. These crystal orientations are referred to as the orientations A and B. The narrow band at 648 cm^{-1} gave the minimum intensity in the orientation A and the maximum intensity in the orientation B.

The Raman spectra observed for the scattering lights polarized parallel and perpendicular to the crystal growth direction are referred to as the // and ⊥ spectra, respectively. The polarized Raman bands can be classified into three types α, β, and γ as indicated in Fig. 5. The type α refers to the band whose intensity is stronger in the // spectrum than in the ⊥ spectrum, the type β to the band whose intensity is stronger in the ⊥ spectrum than in the // spectrum, and the type γ to the band whose intensity is nearly equal in the // and ⊥ spectra. Polarization behavior of the Raman band is represented by two symbols such as $\gamma\beta$, where the first and second letters refer to the types of polarization behavior observed in the crystal orientations A and B, respectively. Observed polarization behavior of the non-totally symmetric Raman bands can be classi-

Table 4. Normal Vibrations of 2-Amino- and 2-Amino-d_2-pyrimidines

Sym	Mode	2-Aminopyrimidine							2-Amino-d_2-pyrimidine				
		L.L[a]	Raman			Infrared		Calcd	L.L[a]	Raman			Calcd
		$\tilde{\nu}$/cm^{-1}	$\tilde{\nu}$/cm^{-1}	Pol		$\tilde{\nu}$/cm^{-1}	Pol Cry	$\tilde{\nu}$/cm^{-1}	$\tilde{\nu}$/cm^{-1}	$\tilde{\nu}$/cm^{-1}	Pol		$\tilde{\nu}$/cm^{-1}
				Liq	Cry						Liq	Cry	
	N-H str.[b]		3330	p				3327		2410	p		2399
	ν_2		3025	p				3038		3027	p		3038
	ν_{13}							2993		2995			2993
	NH_2 sci.[b]		1650			1630	I	1650		1205			1209
	ν_{8a}	1576	1580	p		1560	I	1562	1597	1578	p		1563
a_1	ν_{19a}	1440	1448	p		1460	I	1466	1421	1475	p		1470
	ϕ-N str.		1360	p		1348	I	1336		1363	p		1347
	ν_{18a}	1087[c]	1080	p		1090	I	1103	1081[c]	1078	p		1103
	ν_1	997	990	p		990	I	1008	997	983	p		1002
	ν_{12}	870	870	p		862	I	878	853	848	p		863
	ν_{6a}		587	p?		605	I	602		578	p?		585
	N-H str.[b]		3395					3391		2520	dp	$\gamma\beta$	2512
	ν_{7b}		3050	dp				3058		3053	dp	$\gamma\beta$	3058
	ν_{8b}	1556	1558	dp	bb	1544	II	1563	1556	1557	dp	$\gamma\beta$	1550
	ν_{19b}	1472	1425	dp	bb			1415	1495	1420	dp	$\gamma\beta$	1415
b_2	ν_{14}	1320	1355	dp	bb			1350	1290	1350	dp	$\gamma\beta$	1331
	ν_{15}	1224[c]	1230	dp	bb	1210	II	1225	1219[c]	1220	dp	$\gamma\beta$	1223
	ν_{9b}	1176[c]	1130	dp	bb	1155	II	1139	1168[c]	1102	dp	$\gamma\beta$	1122
	NH_2 twist.[b]		1040	dp	bb	1040	II	1039		823	dp	$\gamma\beta$	838
	ν_{6b}	644	642	dp	bb	640	II	655	643	648	dp	$\gamma\beta$	655
	N bend.		457	dp	bb	472	II	462		407	dp	$\gamma\beta$	423
	ν_{17b}		997	dp	aa			990		975	dp	$\alpha\alpha$	990
	ν_4	804[c]	802	dp	aa	798	III	814	801[c]	798	dp	$\alpha\alpha$	824
b_1	ν_{11}		765	dp	aa	768	III	730		745	dp	$\alpha\alpha$	737
	ν_{16b}	524	410	dp	aa	410	III	415	539	390	dp	$\alpha\alpha$	408
	NH_2 wag.[b]							377					315
	N wag.		187	dp	aa			187		173		$\alpha\alpha$	174
	ν_{17a}	788[c]	782	dp	cc			781	788[c]	780	dp	$\beta\beta$	781
a_2	ν_{16a}	411	516	dp	cc	514		526	405	480	dp	$\beta\beta$	480
	ϕ-NH_2 tor.[b]		172[d]					190		163[d]			149

a) See Ref. 1. b) H is replaced by D in 2-amino-d_2-pyrimidine. Vibrational modes for the NH_2 group are determined on referring to Ref. 8. c) Lafaix and Lebas presented the modes of H bending and H wagging vibrations instead of individual modes such as ν_{18a} and ν_{11} vibrations for these frequencies. d) Frequency obtained from difference band.

fied into three types $\gamma\beta$, $\alpha\alpha$, and $\beta\beta$ through which each Raman band can be experimentally assigned to the certain symmetry species.

Species a_1: The strongly polarized Raman bands observed at 3027, 2410, 1578, 1475, 1363, 1078, 983, and 848 cm^{-1} in molten phase were assigned to the ν_2, N-D stretching, ν_{8a}, ν_{19a}, ϕ-N stretching, ν_{18a}, ν_1, and ν_{12} vibrations, respectively. The Raman band observed at 578 cm^{-1} in molten with low depolarization factor and the band clearly observed at 1205 cm^{-1} in crystal were assigned to the ν_{6a} and ND_2 scissoring vibrations, respectively, because these bands showed no $\gamma\beta$, no $\alpha\alpha$, and no $\beta\beta$ polarization behavior in crystal.

Species b_2: The depolarized Raman bands observed at 3053, 2520, 1557, 1420, 1350, 1220, 1102, 823, 648, and 407 cm^{-1} in molten phase showed the type $\gamma\beta$ polarization in crystal and were assigned to the ν_{7b}, N-D stretching, ν_{8b}, ν_{19b}, ν_{14}, ν_{15}, ν_{9b}, ND_2 twisting, ν_{6b}, and N bending vibrations, respectively, because the frequencies of the out-of-plane vibrations are lower than 1000 cm^{-1} in pyrimidine derivatives.

Species b_1: The depolarized Raman bands observed at 975, 798, 745, 390, and 173 cm^{-1} in molten phase showed the type $\alpha\alpha$ polarization in crystal and were assigned to the ν_{17b}, ν_4, ν_{11}, ν_{16b}, and N wagging vibrations, respectively.

Species a_2: The depolarized Raman bands observed at 780, 480, and 415 cm^{-1} in molten phase showed the type $\beta\beta$ polarization in crystal and thus were assigned to the ν_{17a}, ν_{16a}, and ν_{6a}—ϕ-ND_2 torsional vibrations, respectively.

The normal vibrations thus assigned are summarized in Table 4. The table shows that the assignment of the normal vibrations given for 2-amino-d_2-pyrimidine is consistent with the assignment given for 2-aminopyrimidine, and this fact confirms the reasonability of the assignments.

The normal coordinate calculation indicates that the ν_{19a},ν_{12}, and ν_{6a} vibrations mix largely with the ϕ-N stretching vibration. This mixing is supported by the experimental fact that the ν_{19a} vibration increases in frequency and the ν_{12} and ν_{6a} vibrations decrease com-

pared with the corresponding vibrations of pyrimidine (1402, 1068, and 677 cm^{-1}).[10] The normal coordinate calculation shows that the ν_{16b} and ν_{16a} vibrations mix with the N wagging and ϕ-NH_2 torsional vibrations, respectively. The fact that the ν_{16b} and ν_{16a} vibrations increase in frequency compared with the corresponding vibrations of pyrimidine (344 and 394 cm^{-1}) justifies the mixing. The ν_{17a} vibration decreases in frequency compared with the ν_{17a} vibration of pyrimidine (1004 cm^{-1}). This fact may be caused by the mixing of the ν_{17a} and NH_2 twisting vibrations as indicated by the normal coordinate calculation. The out-of-phase displacements of the H atoms of the NH_2 group from the plane of the pyrimidine ring are calculated to be fairly large in the NH_2 twisting vibration because of the nonplanality of the planes of the amino group and the ring. The same frequency shifts due to vibrational mixing were also found in the normal vibrations of 2-amino-d_2-pyrimidine. The vibrational analysis of the polarized sublevel phosphorescence spectra of 2-aminopyrimidine, which will be reported soon, also confirms the validity of the assignments made in this work.[11]

References

1) A. J. Lafaix and J. M. Lebas, *Spectrochim. Acta*, **26A**, 1243 (1970).
2) R. A. Kydd, *Chem. Phys. Lett.*, **61**, 183 (1979).
3) J. S. Scheinbeim and E. S. Schempp, *Acta. Cryst.*, **B32**, 607 (1976).
4) S. Furberg, J. Grφgaard, and B. Smedsrud, *Acta. Chem. Scand.*, **B33**, 715 (1979).
5) Y. Ishibashi, R. Shimada, and H. Shimada, *Bull. Chem. Soc. Jpn.*, **55**, 2765 (1982).
6) Y. Ishibashi, F. Arakawa, H. Shimada, and R. Shimada, *Bull. Chem. Soc. Jpn.*, **56**, 1327 (1983).
7) S. Kizuki, Y. Ishibashi, H. Shimada, and R. Shimada, *Mem. Fac. Sci. Kyushu Univ. Ser. C*, **13**, 7 (1981).
8) A. K. Kalkar and C. C. Ars, *Bull. Chem. Soc. Jpn.*, **59**, 3223 (1986).
9) S. Califano, G. Adembri, and G. Sbrana, *Spectrochim. Acta*, **20**, 385 (1964).
10) G. Sbrana, G. Adembri, and S. Califano, *Spectrochim. Acta*, **22**, 125 (1966).
11) M. Maehara, H. Shimada, and R. Shimada, Symposium on the Molecular Structure and Molecular Electronic Structure, Osaka, November 1986, Abstr. No. 1B08.

Radiolysis of Methanol Adsorbed on Zeolite

Chiyoko NAKAZATO,* Ryoji MURAYAMA, Masayoshi AOKI, and Takahiro MASUDA
Department of Chemistry, Faculty of Science, Tokyo Metropolitan University, Fukasawa, Setagaya-ku, Tokyo 158
(Received February 26, 1987)

Radiolysis of methanol adsorbed on synthesized zeolite was investigated by means of product analysis. Molecular hydrogen, formaldehyde, and ethylene glycol are produced as major products. The *G*-value for the formation of H_2 increases with increasing amount of methanol adsorbed on zeolite and approaches ca. 2.1 at about 10^{-2} mol of methanol per g of zeolite, where the coverage of methanol is approximately unity and *G*-values of ca. 1.0 are observed for formaldehyde and ethylene glycol. Addition of an electron scavenger causes decrease in $G(H_2)$. However, the hydrogen formation is not completely suppressed by N_2O, SF_6, or CCl_4. Kinetics in solution is useful for the interpretation of results and allows the estimation of the *G*-value for the generation of electron in zeolite and of its relative reactivity toward methanol and some electron scavengers.

Radiolysis of compounds adsorbed on the surface of solid has been extensively investigated because of much interest in the mechanism of energy transfer from adsorbent to adsorbate and in reaction specificity possibly observed in the adsorbed state.[1-6] In an irradiated solid such as silica gel or zeolite, formation of electron and positive hole has been confirmed by experiments using electron or hole scavenger.[7-12] Recently, we found that a part of electrons generated in an irradiated zeolite (Molecular Sieve 13X; abbreviated to MS) are very similar to quasi-free electrons produced in irradiated liquid 2,2-dimethylpropane with respect to reactivity toward some electron scavengers.[13,14] The result suggests that rate constants for reactions of electrons produced in irradiated MS with a substrate adsorbed on the solid may be estimated by competition kinetics using electron scavengers. The synthetic zeolite, MS, is characterized by the possession of many cages and channels. Especially, the supercavity of MS is known to allow passage of molecules below 1 nm in effective diameter. A variety of compounds, therefore, can be used as substrates or scavengers to clarify the detailed profile of radiolysis in heterogeneous systems.

This paper deals with a kinetic study on reactions of methanol adsorbed on MS with electrons or positive holes generated in irradiated MS. Yields of radiolytic products, molecular hydrogen, formaldehyde, and ethylene glycol, were discussed in terms of a mechanism which resembles one operative in solution.

Experimental

Zeolite (MS) was obtained from Nippon Kuromatokogyo K. K. The specific surface area is 1030 $m^2 g^{-1}$. Dinitrogen monoxide and sulfur hexafluoride were purchased from Takachiho Kagakukogyo K. K. Methanol (Uvasol) and carbon tetrachloride were obtained from Merck.

Samples were evacuated at 600 °C for 24 h prior to introduction of adsorbate(s). The experimental procedures were described in detail elsewhere.[13,14] Irradiation was carried out by ^{60}Co with a total dose of 1.34×10^4 Gy at room temperature. The amounts of molecular hydrogen and nitrogen were determined by gas chromatography according to the method employed in previous works.[11-14] Formaldehyde was determined colorimetrically by using chromotropic acid. Ethylene glycol was oxidized with periodic acid to formaldehyde after being extracted from the irradiated sample with methanol and subjected to the colorimetry.

Results

As shown in Fig. 1, the *G*-value for the formation of molecular hydrogen increases with increasing amount of methanol adsorbed on MS, but the increase rate is gradually reduced in the range of adsorbed amount above 5×10^{-3} mol of methanol per g of MS (the adsorbed amount on MS will be expressed in mol g^{-1} hereafter). $G(H_2)$ was observed to be ca. 2.1 at 1×10^{-2} mol g^{-1} where the coverage of methanol is unity approximately. On the other hand, the formation of H_2 was hardly observed in the region below 1×10^{-3} mol g^{-1}. This suggests that a limited amount of H_2 or H atom produced by irradiation is chemisorbed on MS or otherwise that some active sites of MS may consume a limited amount of methanol without irradiation, since chemisorption of ethanol was reported to proceed on high-surface silica (Cabosil) by Abrams and Allen.[3]

In the presence of an electron scavenger such as N_2O, $G(H_2)$ decreases with increasing amount of the scavenger. Figures 2 and 3 show the dependence of $G(H_2)$ on amounts of N_2O and CCl_4, respectively. The adsorbed amount of methanol is 9×10^{-3} mol g^{-1}. In

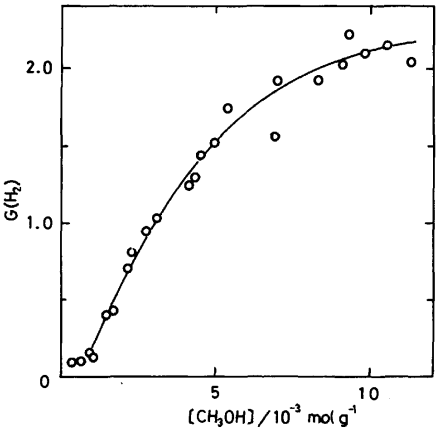

Fig. 1. $G(H_2)$ vs. $[CH_3OH]$.

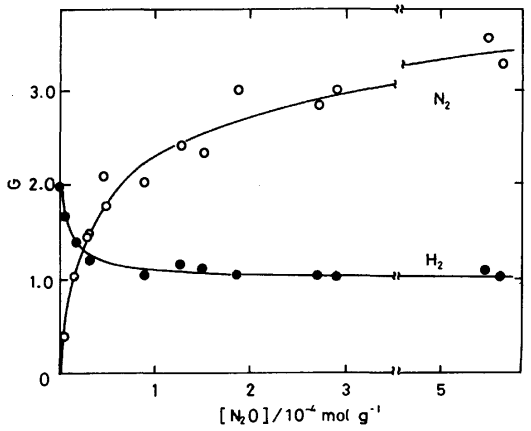

Fig. 2. $G(H_2)$ and $G(N_2)$ vs. $[N_2O]$. $[CH_3OH]=9\times10^{-3}$ mol g^{-1}.

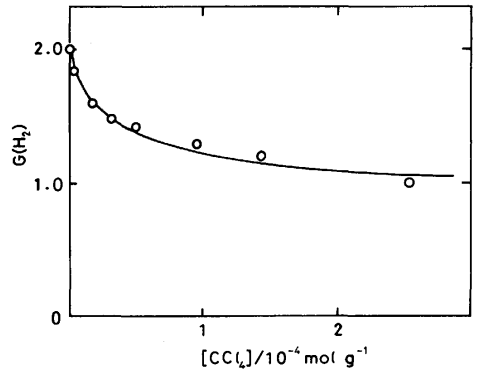

Fig. 3. $G(H_2)$ vs. $[CCl_4]$. $[CH_3OH]=9\times10^{-3}$ mol g^{-1}.

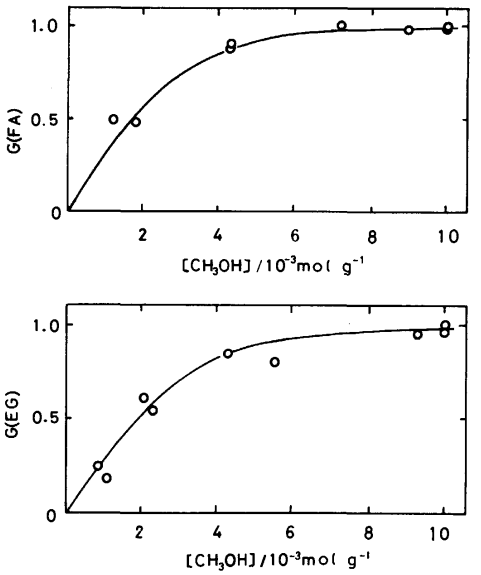

Fig. 4. $G(FA)$ and $G(EG)$ vs. $[CH_3OH]$.

both cases, $G(H_2)$ approaches to 1 and appears to be fixed over the region above 1×10^{-4} mol g^{-1} for N_2O and 2×10^{-4} mol g^{-1} for CCl_4. In the MS-CH_3OH-N_2O system, N_2 is produced from N_2O as expected. $G(N_2)$ increases also with increasing amount of N_2O and a small increase continues even in the region where $G(H_2)$ appears to be constant. At 5.5×10^{-4} mol g^{-1}

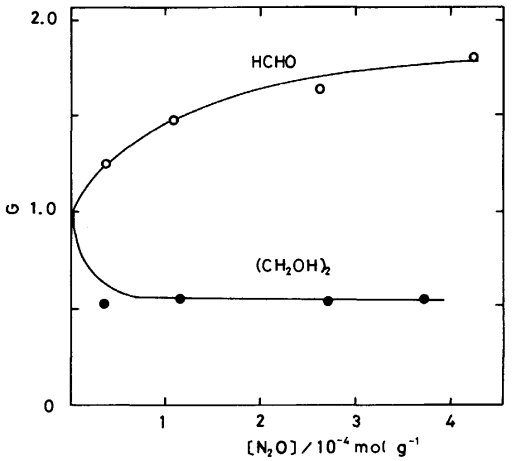

Fig. 5. $G(FA)$ and $G(EG)$ vs. $[N_2O]$. $[CH_3OH]=9\times10^{-3}$ mol g^{-1}.

N_2O, $G(N_2)$ amounts to 3.4. On the contrary, in the MS—N_2O system $G(N_2)$ is constant, 2.8, at amounts above 1×10^{-4} mol g^{-1} N_2O, as already reported.[14] With SF_6, the behavior of $G(H_2)$ is similar to that in the case of CCl_4, but not suitable for quantitative treatment because of a deviation of experimental points.

As in liquid methanol, a considerable amount of formaldehyde or ethylene glycol has been detected and their G-values increase with increasing amount of methanol similarly to the case of $G(H_2)$ (Fig. 4). At 9×10^{-3} mol g^{-1}, the G-values for formaldehyde, $G(FA)$, and ethylene glycol, $G(EG)$, are ca. 1.0, as seen in Fig. 4. In the presence of N_2O, $G(EG)$ is reduced to 0.57 and $G(FA)$ increases with increasing amount of N_2O as seen in Fig. 5. At 4.2×10^{-4} mol g^{-1} of N_2O, $G(FA)$ was observed to be 1.87.

Discussion

In this study, G-values are calculated on the basis of the total energy absorbed by adsorbent and adsorbate, because the energy absorbed by adsorbate cannot be neglected for such a large amount of methanol as 1×10^{-2} mol g^{-1}. In the range of adsorbed amount of methanol below 1×10^{-2} mol g^{-1}, the coverage is kept within unity and an adsorbed methanol molecule is allowed barely to have a limited number of neighbors. In consideration of the highly developed network structure of MS, the situation can be approximated to a dilute solution where solvent is immovable. Therefore, an attempt was made to use a kinetic treatment usually applied to dilute solution so as to interpret the experimental results obtained in the present heterogeneous systems. The formation of molecular hydrogen will be explained by the following reactions:

$$MS \wedge\!\!\vee MS^+ + e^-, \quad (1)$$

$$e^- + MS^+ \longrightarrow MS^*, \quad (2)$$

$$e^- + CH_3OH_{ad} \longrightarrow CH_3O^- + H, \quad (3)$$

$$H + CH_3OH_{ad} \longrightarrow H_2 + CH_2OH, \quad (4)$$

where CH_3OH_{ad} represents an adsorbed methanol molecule and MS^+ designates a positive hole. In this system, electrons produced in Reaction 1 will be consumed by Reactions 2 and 3. Thus the following equation is derived:

$$1/G(H_2)=1/G_e(1+k_2[MS^+]/k_3[CH_3OH_{ad}]). \quad (I)$$

As shown in Fig. 6, plots of $1/G(H_2)$ vs. $1/[CH_3OH_{ad}]$ give a straight line with a slope of 1.56×10^{-3}, an intercept of 0.371, and a correlation coefficient of 0.9683, if correction is made for the adsorbed amount of CH_3OH ineffective in the formation of H_2 by shifting the origin of Fig. 1 to (1×10^{-3}, 0.13). From the intercept, G_e is obtained to be 2.7, which is close to the $G(N_2)$ of 2.8 obtained in the MS-N_2O system. This indicates that methanol reacts with N_2O-scavengeable electrons to produce H_2. The slope gives the ratio, $k_2[MS^+]/k_3$, of 4.2×10^{-3} mol g^{-1}.

In the presence of N_2O, the following reaction occurs:

$$e^- + N_2O \longrightarrow N_2O + O^-. \quad (5)$$

For the MS-CH_3OH-N_2O system, therefore, $G(H_2)$ will be expressed by

$$1/G(H_2)=1/G_e(1+k_2[MS^+]/k_3[CH_3OH_{ad}] + k_5[N_2O]/k_3[CH_3OH_{ad}]). \quad (II)$$

Plots of $1/G(H_2)$ vs. $[N_2O]$ with data shown in Fig. 2 should give a straight line. As shown in Fig. 7, however, they give a curve dependent on the amount of N_2O. In a limited region below 1.5×10^{-5} mol g^{-1} N_2O where the formation of hydrogen is effectively suppressed by N_2O, a straight line with a slope of 1.03×10^4, an intercept of 0.556, and a correlation coefficient of 0.9954 is obtained. At amounts above 1.5×10^{-5} mol g^{-1}, the decrease in $G(H_2)$ is slowed down and $G(H_2)$ becomes constant. The partial depression will be interpreted in terms of either a precursor of hydrogen other than electron or decrease in effective amount of N_2O on MS due to the coexistence of methanol. In the MS-N_2O system, $G(N_2)$ was observed to be 2.8 at amounts of N_2O above 2×10^{-4} mol g^{-1} and a partial depression of $G(N_2)$ by SF_6 or CCl_4 was observed similarly with the present case of $G(H_2)$. If a precursor of hydrogen other than electron exists and N_2O does not react with it, a good agreement between the saturated $G(N_2)$, 2.8, and the G_e estimated by extrapolation of plots of $1/G(H_2)$ vs. $1/[CH_3OH_{ad}]$, cannot be interpreted. Furthermore, CCl_4 was observed to behave similarly to N_2O with respect to the partial depression of the hydrogen formed from methanol, in spite of the fact that it lowers only a part of $G(N_2)$ in the MS-N_2O system. These results suggest that the partial depression of hydrogen formation is caused by decrease in effective amount of scavenger due to competition with methanol for limited adsorption sites. From the linear relation between $1/G(H_2)$ and $[N_2O]$ obtained in the region of small amount of N_2O, G_e can be estimated. Since the intercept is equal to $1/G_e(1+k_2[MS^+]/k_3[CH_3OH_{ad}])$ and $k_2[MS^+]/k_3$ is 4.2×10^{-3} mol g^{-1} as described above, 2.6 is obtained as G_e, which is consistent with that obtained in the MS-CH_3OH and MS-N_2O systems. Thus, the ratio of rate constants, k_5/k_3, is estimated to be 2.5×10^2 from the slope, which is equal to $1/G_e(k_5/k_3 \cdot [CH_3OH_{ad}])$.

In the MS-MeOH-CCl_4 system, the same kinetic treatment is also applicable if the following reaction is considered:

$$e^- + CCl_4 \longrightarrow \text{product}. \quad (6)$$

Plots of $1/G(H_2)$ vs. $[CCl_4]$ give the curve as shown in Fig. 8. From the experimental data in the limited amount region, G_e is obtained as 2.9 and the ratio of rate constants, k_6/k_3, as 2.0×10^2. It should be noticed

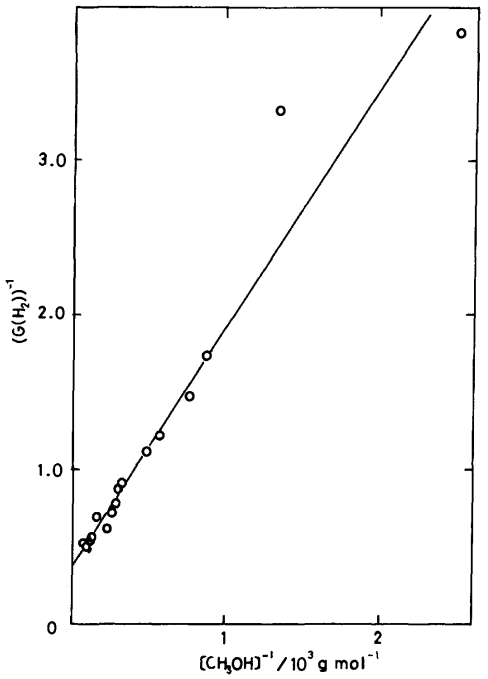

Fig. 6. $1/G(H_2)$ vs. $1/[CH_3OH]$. $[CH_3OH]$ and $G(H_2)$ are corrected by moving the origin of Fig. 1 to (1×10^{-3}, 0.13), respectively.

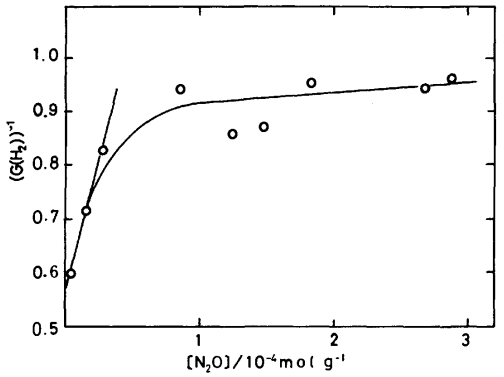

Fig. 7. $1/G(H_2)$ vs. $[N_2O]$. Calculated from the data shown in Fig. 2.

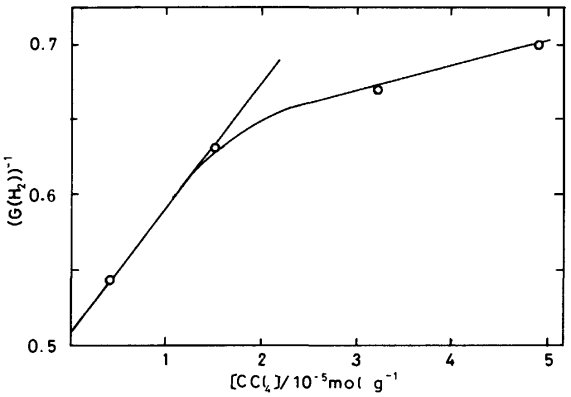

Fig. 8. $1/G(H_2)$ vs. $[CCl_4]$. Calculated from the data shown in Fig. 3.

that the ratio of k_6/k_5, 0.8, is quite different from that obtained in the MS-N_2O-CCl_4 system, 12.8.[14] The ratio obtained in the present system is close to that obtained for electrons generated in nonpolar liquid such as hexane or cyclohexane rather than in 2,2-dimethylpropane. This suggests that an energy state of excess electrons in MS, probably the conduction band of MS, may be affected by the adsorption of methanol. If the rate constant of electron for its reaction with N_2O in hexane, 1.09×10^{12} dm^3 mol^{-1} s^{-1}, or in cyclohexane, 2.4×10^{12} dm^3 mol^{-1} s^{-1},[15] is applied to k_5, 4.4×10^9 or 9.6×10^9 dm^3 mol^{-1} s^{-1} is obtained, respectively, as the rate constant of methanol for its reaction with the electron produced in MS.

The formation of formaldehyde and ethylene glycol may be explained by a mechanism which has been composed of Reactions 1, 4, 7, 8, and 9 by assuming processes similar to those of the radiolysis of liquid methanol:

$$MS^+ + CH_3OH_{ad} \longrightarrow MS + CH_3OH^+, \quad (7)$$

$$CH_3OH^+ + CH_3OH \longrightarrow CH_3OH_2^+ + \cdot CH_2OH, \quad (8)$$

$$2\cdot CH_2OH \longrightarrow HCHO + CH_3OH \quad (9a)$$

$$\longrightarrow (CH_2OH)_2. \quad (9b)$$

From these reactions we obtain

$$2\{G(FA) + G(EG)\} = G_e + G(MS^+), \quad (III)$$

where $G(FA)$ and $G(EG)$ designate the G-values for the formation of formaldehyde and ethylene glycol, respectively. Since electrons and positive holes which have escaped from Reaction 2 produce these products and the G-value for such electrons or positive holes can be taken as $G(H_2)$, the relation expressed by Eq. III holds. The above mechanism appears to be very simple despite the complexity of adsorbed state. However, the formation of methane was observed to be negligible (G-value below 0.1) and no other products including carbon have been found. Furthermore, the yield of ethylene glycol decreases in the presence of N_2O, whereas formaldehyde increases as shown in Fig. 5. The result may be explained by addition of Reaction 10 to the above reactions:

$$O^- + \cdot CH_2OH \longrightarrow HCHO + OH^-. \quad (10)$$

At 4.2×10^{-4} mol g^{-1} N_2O, $G(FA)$ of 1.87 and $G(EG)$ of 0.57 were obtained. If the ratio of Reactions 9a to 9b is not affected by N_2O, the formaldehyde produced through Reaction 9a is 0.57 and hence 1.3 is estimated as the G-value for the formaldehyde through Reaction 10. Therefore, the G-value for $\cdot CH_2OH$, which is a precursor radical of formaldehyde and ethylene glycol, is calculated to be 3.58. On the other hand, $\cdot CH_2OH$ is produced through Reactions 4 and 8. Thus $G(\cdot CH_2OH)$ is equal to the sum of $G(H_2)$ in Reaction 4 and $G(MS^+)$ in Reaction 7. In the presence of ca. 10^{-2} mol g^{-1} methanol and 4.2×10^{-4} mol g^{-1} N_2O, Reaction 2 may be neglected. Therefore, the total $G(\cdot CH_2OH)$ is calculated to be 3.8. This is considerably close to the value calculated on the basis of $G(FA)$ and $G(EG)$. The above mechanism, therefore, seems to be reliable.

The formation of N_2 is hard to understand in the presence of methanol. $G(N_2)$ increases with increasing amount of N_2O even in the region where $G(H_2)$ reaches a plateau value. It amounts to 3.4 at ca. 5×10^{-4} mol g^{-1} N_2O in spite of the incomplete suppression of H_2 formation. Although these results suggest that a short chain mechanism works, it needs another study to find a consistent mechanism.

References

1) J. M. Caffrey, Jr. and A. O. Allen, *J. Phys. Chem.*, **62**, 33 (1958).
2) J. W. Sutherland and A. O. Allen, *J. Am. Chem. Soc.*, **83**, 1040 (1961).
3) L. Abrams and A. O. Allen, *J. Phys. Chem.*, **73**, 2741 (1969).
4) R. I. Zalevskaya and Yu. D. Tsvetkov, *Kinet. Catal.*, **8**, 468 (1967).
5) G. R. Joppien and J. E. Willard, *J. Phys. Chem.*, **76**, 3158 (1972).
6) N. H. Sagert, J. A. Reid, and R. W. Robinson, *Can. J. Chem.*, **48**, 17 (1970).
7) J. W. Sutherland and R. Goodrich, *J. Am. Chem. Soc.*, **89**, 6779 (1967).
8) P. K. Wong and J. E. Willard, *J. Phys. Chem.*, **72**, 2623 (1968).
9) N. H. Sagert and R. W. Robinson, *Can. J. Chem.*, **46**, 2075 (1968).
10) H. Ogura, Y. Tachika, Y. Suzuki, C. Nakazato, M. Kondo, T. Sawai, and T. Sawai, *J. Nucl. Sci. Technol.*, **12**, 167 (1975).
11) H. Ogura, M. Hinata, C. Nakazato, M. Kondo, T. Sawai, and T. Sawai, *J. Nucl. Sci. Technol.*, **15**, 433 (1978).
12) H. Ogura, C. Nakazato, M. Kondo, T. Sawai, and T. Sawai, *J. Nucl. Sci. Technol.*, **16**, 57 (1979).
13) C. Nakazato and T. Masuda, *Chem. Lett.*, **1984**, 731.
14) C. Nakazato and T. Masuda, *Bull. Chem. Soc. Jpn.*, **59**, 2237 (1986).
15) A. O. Allen and R. A. Holroyd, *J. Phys. Chem.*, **78**, 796 (1974).

 © 1987 The Chemical Society of Japan Bull. Chem. Soc. Jpn., 60, 2779—2783 (1987)

Effects of Some Additives on Proton-Transfer Reaction Studied by Ultrasonic Methods

Yukio YOSHIDA and Sadakatsu NISHIKAWA*
Department of Chemistry, Faculty of Science and Engineering, Saga University, Saga 840
(Received March 5, 1987)

Ultrasonic absorption and velocity were measured in aqueous solutions of propylamine at 25 °C both in the absence and in the presence of 2 g dm^{-3} PVA(poly(vinyl alcohol)), 5 mol dm^{-3} urea and 1 mol dm^{-3} NaCl. No excess absorption was observed in these solutions without propylamine. A single relaxational absorption was observed in the concentration range from 0.0196 to 0.719 mol dm^{-3} of propylamine both in the presence and absence of the additives. The ultrasonic parameters have been found to be quite dependent on the concentration of propylamine and also on the structure of additives. This relaxational absorption has been attributed to the perturbation of an equilibrium associated with a proton-transfer reaction. The rate constants and the standard volume change of the reaction have been determined from the concentration dependences of the relaxation frequency and the maximum excess absorption per wavelength. As a result, it was discovered that the forward rate in a solution with PVA increased and those with urea and NaCl, on the other hand, decreased; also, the standard volume change associated with the reaction increased in a series of the solutions with urea, no additive, NaCl, and PVA. The data have been interpreted by means of the structural changes of the solvent water.

Any mechanism by which protons get carried along particularly quickly has important implications for a large area of molecular biology. The proton-transfer reaction is directly followed by the ultrasonic absorption technique.[1] So far, investigations for the proton-transfer in aqueous solutions of various amines have been performed;[1,2] the present authors[3] have also reported some results of the rate constants with a revised analysis of the reaction mechanism. Recently, Yamashita et al.[4] have examined the effect of an additive on this reaction in the presence of the surfactant micelle; also, the decreasing effect on the proton-transfer rates has been reported. They have interpreted the effect as restricted reaction fields owing to the charged surface of the micelles. On the other hand, it is expected that the proton-transfer reaction in an aqueous solution of amine may be closely related to the water structure since the reaction is hydrolysis. From this view, the present study was undertaken in order to clarify this speculation by adding nonelectrolyte and electrolyte using ultrasonic methods. Propylamine was chosen as the solute since another type relaxation which is observed in the solutions of some amines with larger hydrophobic groups[5] was not expected to be observed. The phenomenon that the reaction rate is accelerated or decelerated by additives is also interesting from a pharmacological point of view.

Experimental

All reagents, i.e. propylamine, urea, PVA(poly(vinyl alcohol)), and NaCl, were purchased from Wako Pure Chemical Industries Ltd. Propylamine was distilled once; however, the other reagents which were of the purest grade obtainable were used without further purification. Solutions were prepared by weight with doubly distilled water. The additive concentrations were fixed to be 2 g dm^{-3}, 1 mol dm^{-3}, and 5 mol dm^{-3} for PVA (number-average molecular weight; 22000), NaCl and urea, respectively.

A semiautomatic pulse method was used for ultrasonic absorption measurements over a frequency range from 15 to 220 MHz. Two cells with fundamental crystals of 5 and 20 MHz were utilized at their odd harmonic frequencies. Details of the apparatus are described elsewhere.[6] The sound velocity was determined using an interferometer at 2.5 MHz. The ultrasonic cells were immersed in a water bath which was controlled within ±0.002 °C. The density of the solutions was measured by using a standard pycnometer, the volume of which was about 4 cm^3. The measurement of pH was performed using a HITACHI-HORIBA pH meter with a glass electrode. The standard buffer solutions at 9.18 and 11.88 were used as the standard references of the electrode. All pH and ultrasonic measurements were carried out under a dry nitrogen atmosphere because of the high basicity of the solution. They were all measured at 25 °C.

Results

No excess absorption was observed in any aqueous solutions of urea, PVA, or NaCl at the concentrations used in this work. However, the value of the absorption coefficient, α, divided by the square of the frequency, f, has been found to be frequency dependent in all of aqueous solutions of propylamine both in the presence and in the absence of the additives. If an observed spectrum is due to a single relaxational process, it may be generally well expressed by[7]

$$\alpha/f^2 = A/(1+(f/f_r)^2)+B, \quad (1)$$

where A is the excess absorption amplitude, f_r the relaxation frequency and B the back ground absorption. Figure 1 shows some representative absorption spectra in an aqueous solution of propylamine. The ultrasonic parameters have been determined in terms of a nonlinear least mean square method by microcomputer, and the solid curves in the figure represent the theoretical values. The fact that the agreements between experimental and theoretical values are excellent indicates that the relaxation phenomenon observed in the measured frequency range can be associated with a clear single relaxation process.

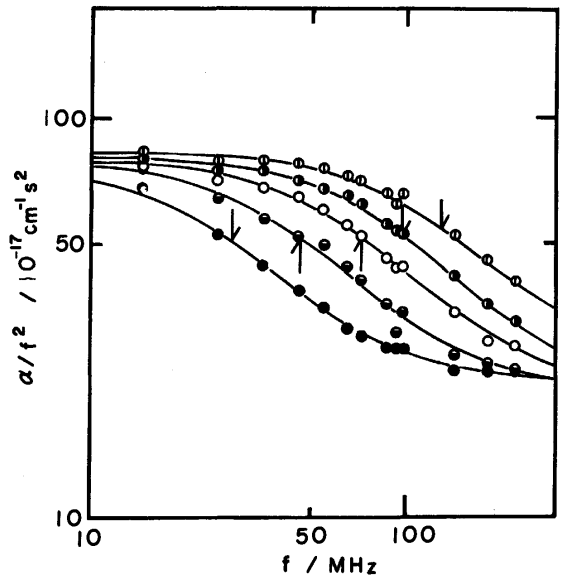

Fig. 1. The representative ultrasonic absorption spectra in aqueous solutions of propylamine at 25 °C. ●: 0.0196 mol dm^{-3}, ◒: 0.0491 mol dm^{-3}, ○: 0.114 mol dm^{-3}, ◑: 0.236 mol dm^{-3}, ⦶: 0.631 mol dm^{-3}.

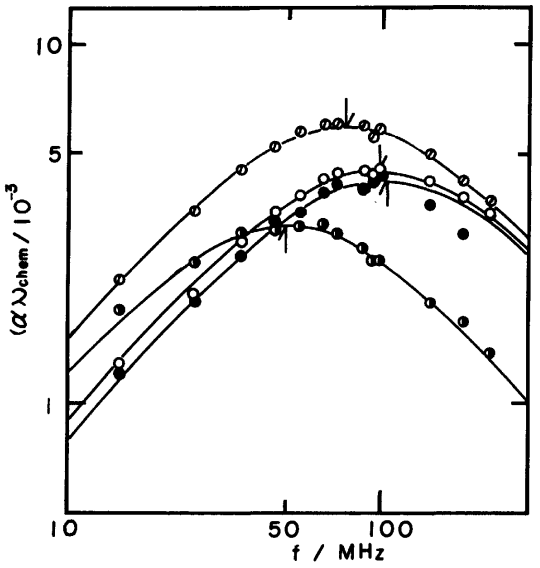

Fig. 2. The ultrasonic absorption spectra for aqueous solutions of propylamine at 0.236 mol dm^{-3} in the absence and in the presence of additive. ○: No additive, ●: PVA, ⦶: NaCl, ◑: urea.

Table 1. Ultrasonic and Thermodynamic Parameters for Aqueous Solutions of Propylamine with Additives at 25 °C

Concn	pH	ρ	c	f_r	A	B
mol dm^{-3}		g cm^{-3}	m s^{-1}	MHz	10^{-17} s^2 cm^{-1}	
			(No additive)			
0.0196	11.30	0.9970	1498	28	56	22
0.0491	11.90	0.9966	1500	46	60	21
0.114	11.83	0.9959	1503	72	60	21
0.236	12.05	0.9943	1513	97	61	21
0.476	12.26	0.9911	1526	120	62	23
0.631	12.38	0.9887	1536	130	60	24
0.719	12.41	0.9873	1539	134	58	26
			(PVA)			
0.0196	10.91	0.9970	1497	39	24	22
0.0491	11.34	0.9968	1499	58	38	22
0.114	11.47	0.9964	1504	76	52	21
0.236	11.65	0.9953	1510	103	54	21
0.476	11.87	0.9924	1525	132	57	22
0.631	11.95	0.9903	1533	143	59	22
0.719	11.98	0.9890	1541	146	56	24
			(Urea)			
0.0196	11.55	1.0740	1620	23	37	18
0.0491	11.90	1.0738	1620	27	66	18
0.114	12.20	1.0735	1621	38	68	17
0.236	12.38	1.7025	1626	49	79	18
0.479	12.59	1.0677	1637	61	82	19
0.631	12.72	1.0669	1643	65	80	20
0.719	12.86	1.0657	1645	68	80	20
			(NaCl)			
0.114	11.92	1.0366	1567	60	95	19
0.236	12.10	1.0357	1571	76	100	21
0.476	12.29	1.0318	1584	95	101	23
0.631	12.38	1.0306	1592	106	103	21
0.719	12.42	1.0301	1596	110	106	21

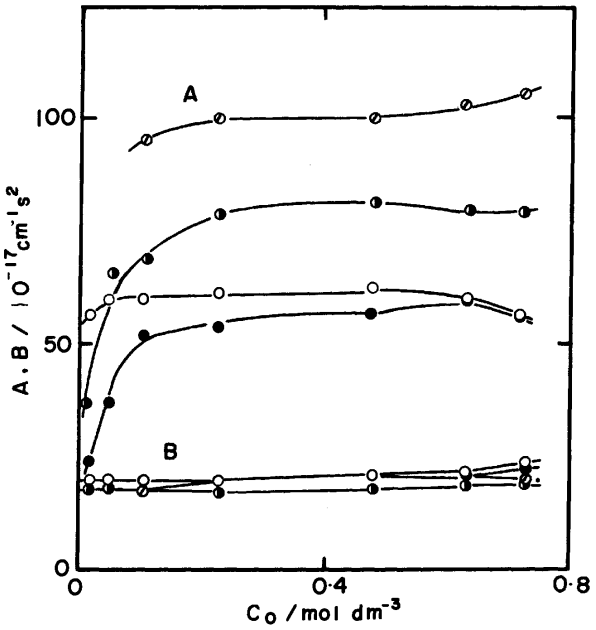

Fig. 3. Concentration dependence of the amplitude of the excess absorption, A, and the background absorption, B, for aqueous solutions of propylamine in the absence and in the presence of additives. O: No additive, ●: PVA, ∅: NaCl, ◑: urea.

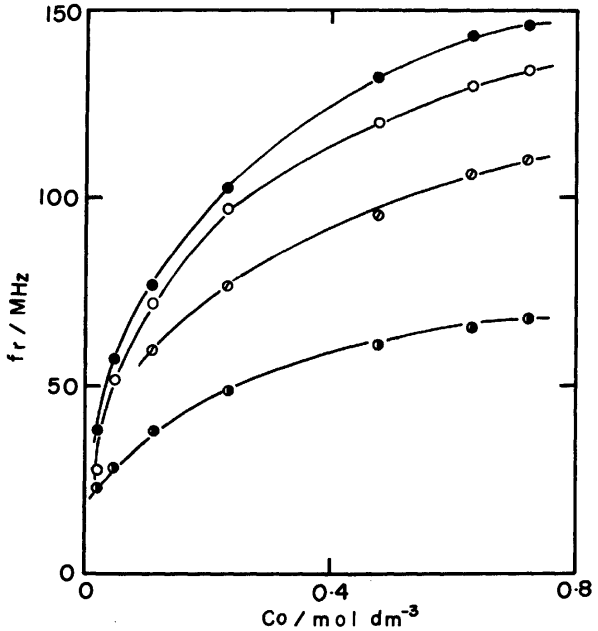

Fig. 4. Concentration dependence of the relaxation frequency for aqueous solutions of propylamine at 25 °C. O: Without additive, ●: with PVA, ∅: with NaCl, ◑: with urea.

Another relation, which is a modification of Eq. 1, is the plot of the chemical absorption per wavelength, $(\alpha\lambda)_{chem}$ against the frequency:

$$(\alpha\lambda)_{chem} = Afc/(1+(f/f_r)^2). \quad (2)$$

Here, $(\alpha\lambda)_{chem}$ is calculated from the relation $(\alpha\lambda)_{chem} = (\alpha/f^2 - B)fc$, where c is the sound velocity. Figure 2 shows the spectra observed in the aqueous solutions in the absence and in the presence of additives at 0.236 mol dm^{-3} of propylamine. The spectra can also be well expressed by a single relaxational equation. It can clearly be seen that the absorption amplitude and the relaxation frequency strongly depend on the additives. The obtained excess absorption amplitude, A, and the background absorption, B, are shown in Fig. 3 as a function of propylamine concentration. In Table 1, they are also tabulated along with other values obtained in this study. The background absorptions are close to those of solvent water, though they decrease slightly when NaCl and urea are added. On the other hand, the excess absorption amplitudes differ from each other, depending upon the additives. They increase at a low-concentration range and tend to show a plateau. These concentration dependences are very similar to the result for the ultrasonic absorption due to proton-transfer reaction reported previously.[3,5] Figure 4 shows the analytical concentration dependence of the relaxation frequency, f_r for the solutions in the absence and the in presence of additives. Obviously, f_r shifts to higher or lower values, and its degree depends upon the additives. These results imply that the additives affect the dynamic properties

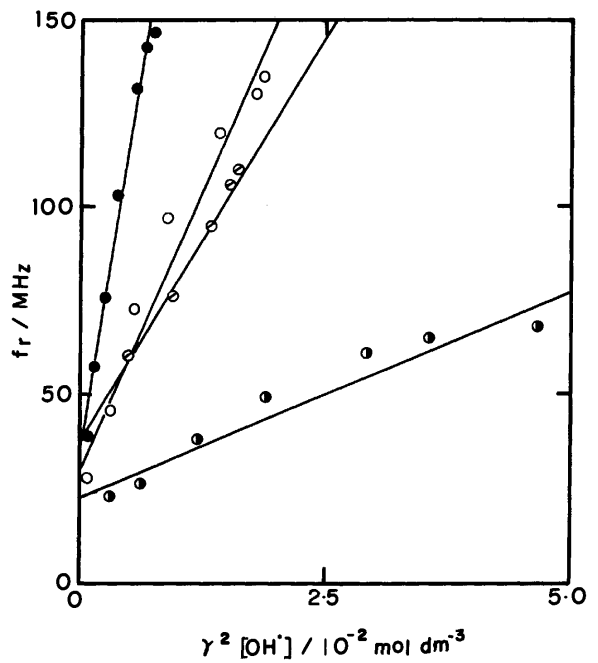

Fig. 5. The plots of f_r vs. $\gamma^2[OH^-]$ for aqueous solutions of propylamine at 25 °C. O: No additive, ●: PVA, ∅: NaCl, ◑: urea.

of the aqueous solutions. However, these similar concentration dependences of the ultrasonic parameters, that is, the plateau of the excess absorption amplitude and the monotonical increase of the relaxation frequency, have let us to predict that the cause of the relaxation in all of the solutions is the same and that it may be associated with the hydrolysis of amine. A detailed reaction mechanism has been proposed origi-

Table 2. The Rate and Thermodynamic Constants for the Hydrolysis of Propylamine in the Absence and in the Presence of Additives at 25 °C

Additive	k_{12}	k_{21}	K_b^1	K_b^2	ΔV
	10^{10} mol^{-1} dm^3 s^{-1}	10^8 s^{-1}	10^{-4} mol dm^{-3}		cm^3 mol^{-3}
a)	1.8±0.1	1.9±0.3	5.1±2.0	4.8±1.3	33±8
PVA	4.8±0.2	2.1±0.2	0.78±0.24	0.84±0.18	45±8
Urea	0.34±0.03	1.5±0.2	25±12	25±10	21±7
NaCl	1.4±0.1	2.5±0.1	4.0±0.7	5.3±0.6	27±3

K_b^1: The calculated values from Eq. 5. K_b^2: Those from the pH measurements. a) The obtained rate constants without additives are slightly different from those reported previously.[5] This is because the present study was undertaken in the wider concentration range of propylamine than the previous one.

nally by Eigen,[1] and is expressed by

$$\text{R-NH}_3^+ + \text{OH}^- \underset{k_{21}}{\overset{k_{12}}{\rightleftharpoons}} \text{R-NH}_3^+ \cdots \text{OH}^- \underset{k_{32}}{\overset{k_{23}}{\rightleftharpoons}} \text{R-NH}_2 + \text{H}_2\text{O}, \quad (3)$$

where k_{ij} is the rate constant at each step. Usually, the relation between the relaxation frequency and the reactant concentrations is derived on the bases of the coupled reactions;[8] that is, the faster process influences the slower one. However, as has been reported in a previous paper,[3] the analysis based on the assumption that the only first step is associated with the observed relaxation process gives us a reasonable result. This means that the second step in Eq. 3 may not so affects on the observed process even if the relaxation associated with the second step may exist in other time region. Then, the relation between the relaxation frequency and the reactant concentrations is simply represented by

$$\tau^{-1} = 2\pi f_r = \gamma^2 k_{12}([\text{R-NH}_3^+] + [\text{OH}^-]) + k_{21}, \quad (4)$$

where τ is the relaxation time and γ a mean activity coefficient which is calculated using Davies equation.[9] Figure 5 shows plots of f_r vs. $\gamma^2[\text{OH}^-]$. The linearity of these plots confirms that the cause of the relaxational sound absorption is due to the hydrolysis of propylamine. The rate constants, k_{12} and k_{21}, were determined from the slope and intercept of the straight lines, respectively. The obtained results are listed in Table 2. These results enable us to determine the dissociation constant, K_b.[3] The relation between K_b and the analytical concentration, C_o, is derived as

$$K_b = [(\tau^{-1})^2 + k_{21}^2 - 2\tau^{-1} k_{21}] / [k_{12}(4\gamma^2 C_o k_{12} + 2k_{21} - 2\tau^{-1})]. \quad (5)$$

The calculated K_b values for each solution are listed in Table 2.

The dissociation constants for these solutions have been estimated from the results of pH measurements using the relation $K_b = \gamma^2[\text{OH}^-]/(C_o - \gamma[\text{OH}^-])$, which are also listed in Table 2. The value for a solution without any additives is very close to that in the literature.[10] The smaller K_b value in the solution with PVA indicates the smaller concentrations of the ionic species in Eq. 4. The larger value in the solution with urea, on the other hand, shows the opposite condition. It should be noticed that the relaxation frequency in the PVA solution is higher than that in the urea solution.

Another parameter obtained from ultrasonic absorption measurement along with the sound velocity is the maximum excess absorption per wavelength, μ_{max}. It is related to the thermodynamic parameters as

$$\mu_{max} = Af_r c/2 = \pi\rho c^2 \Gamma \Delta V^2/2RT. \quad (6)$$

where ρ is the density, ΔV the standard volume change of the reaction, and Γ the concentration term which is expressed for the reaction under consideration as

$$\Gamma = (1/[\text{R-NH}_3^+] + 1/[\text{OH}^-] + 1/[\text{R-NH}_3^+ \cdots \text{OH}^-])^{-1} \quad (7)$$

With the help of Eqs. 6 and 7, standard volume changes could be calculated at each concentration (listed in Table 2).

Discussion

As has been described previously, it is certain that the cause of the relaxation process observed by the ultrasonic absorption measurement in the aqueous solutions of propylamine with some additives is due to the hydrolysis of the amine. The additives have been found to considerably affect the rate processes. The micellar effect on the hydrolysis seems to be associated with the restricted reaction field by micelles.[4] However, the present additive effects are not associated with such a microscopic heterogenious reaction field. They seem to be associated with structural changes of the solvent water.

First, the effect of PVA on the hydrolysis is considered. When PVA is added, the relaxation frequency shifts to a higher frequency range and the reactant concentration, i.e. $[\text{OH}^-]$ decreases, even if the analytical concentration of propylamine is identical (Table 1). Therefore, as a result, the forward rate constant, k_{12} has been found to increase considerably when PVA is added. This may be considered as follows. Adding a small amount of the polymer with the hydroxyl groups to the solution, the water structure may be changed by an extension of the hydrogen-bond network. Consequently, it can be expected that hydrogen or hydroxide ion mobility increases. It is said that the

proton-transfer rate in a more hydrogen-bonded network is faster than that in less hydrogen-bonded types.[11] The above experimental evidence is consistent with the proton-transfer proposed reaction mechanism so far. The obtained standard volume change for the reaction also reflects the solvent structural change by an addition of PVA. That is, it is larger than that in only water (Table 2). The considerably large volume change may be caused by a breaking of the constructed water hydrogen-bonds by PVA.

Second, the additive effect of urea on the hydrolysis is now considered. Urea is a so-called water structure-breaker.[12] When it is added to water, it breaks the water hydrogen bonds; then, the sound velocity increases, the absorption decreases and the solution density increases. These trends are also observed in aqueous solutions of propylamine (Table 1). This means that the solvent water may be in a less structured state. Then, the diffusion-controlled reaction rate may decrease. This expectation has been supported by the concentration dependence of the relaxation frequency. That is, the relaxation frequency shifts to a lower range when it is compared wiht that in the absence of additive. The smaller volume change for the reaction has also reflected this situation. The reaction may proceed through breaking hydrogen bonds just around the reaction site.

Third, in a solution with NaCl, it has been observed that the relaxation frequency is lower than that without additives (Fig. 4). The recent investigation[13] for the proton-transfer reaction by a fluorimetry has shown that the effect of NaCl on the decreasing rate is due to the structure breaking for solvent water. This seems to be sonsistent with the result obtained in our study. However, it is not so reasonable to compare the rate constants with those obtained in the solutions with urea and PVA because they are at quite different ionic strengths each other. In order to obtain more information concerning the effect of electrolytes on the proton-transfer reaction, it should be necessary to clarify the concentration dependence of the salts on the rate.

In conclusion, the additive effects on the proton-transfer reaction have been well interpreted on the bases of the structural changes of solvent water. This is, when the water structure is promoted by the addition of PVA, the rate for the proton transfer is accelerated. On the other hand, when water hydrogen-bonds are partly broken by the addition of urea, the proton-transfer rate is diminished. It may be expected that the fast proton-transfer reactions are now utilized in order to investigate the structural properties of liquids and solutions. The concentration dependences of the additives on the hydrolysis of various amines are now under investigation and the results will be reported in due course.

This work was partly supported by The Naito Foundation.

References

1) M. Eigen, L. DeMaeyer, "Technique of Organic Chemistry," ed by A. Weissberger, Jr. Wiley, New York N. Y. (1961), Vol. VIII, Part 2.

2) R. D. White, L. J. Slutsky, and S. Pattison, *J. Phys. Chem.*, **75**, 161 (1971).

3) Y. Yoshida and S. Nishikawa, *Bull. Chem. Soc. Jpn.*, **59**, 1941 (1986).

4) T. Yamashita, H. Yano, S. Harada, and T. Yasunaga, *J. Phys. Chem.*, **88**, 2671 (1984).

5) S. Nishikawa, T. Yasunaga, and K. Takahashi, *Bull. Chem. Soc. Jpn.*, **46**, 2992 (1973).

6) S. Nishikawa and K. Kotegawa, *J. Phys. Chem.*, **89**, 2896 (1985).

7) M. J. Blandamer, "Introduction to Chemical Ultrasonics," Academic Press, New York (1973).

8) G. H. Czerlinski, "Chemical Relaxation," Marcel Dekker Inc., New York (1966).

9) C. W. Davies, "Ion Association," Butterworths, London (1962).

10) J. J. Christennsen, R. M. Izatt, D. P. Wrathall, and L. D. Hansen, *J. Chem. Soc. A*, 1212 (1969).

11) J. O. Bockris and A. K. N. Reddy, "Modern Electrochemistry," Plenum, (1970).

12) For examples: H. F. Frank and F. Frank, *J. Chem. Phys.*, **48**, 4746 (1968); J. C. MacDonald, J. Serphillips, and J. J. Grenera, *J. Phys. Chem.*, **77**, 370 (1973).

13) H. Shizuka, T. Ogiwara, A. Narita, M. Sumitani, and K. Yoshihara, *J. Phys. Chem.*, **90**, 6708 (1986).

 © 1987 The Chemical Society of Japan Bull. Chem. Soc. Jpn., 60, 2785—2789 (1987)

Effect of an Ionic Surfactant on the Kinetic Properties of an Aqueous Nonelectrolyte Solution Studied by Ultrasonic Methods

Sadakatsu NISHIKAWA
Department of Chemistry, Faculty of Science and Engineering, Saga University, Saga 840
(Received March 12, 1987)

In order to investigate the effect of ionic surfactant on the dynamic properties of nonelectrolyte aqueous solutions, the ultrasonic absorption, velocity and the conductivity have been measured for aqueous solutions of triethylene glycol monobutyl ether (TGBE) in the presence of sodium dodecyl sulfate (SDS) at 25 °C. In aqueous solution of TGBE, a clear single relaxational ultrasonic absorption is observed in the MHz frequency range. When SDS is added the relaxation process is observed in the more dilute solutions, the relaxation frequency shifts to lower frequency and the amplitude of the excess absorption increases in the TGBE concentration range of less than 1.0 mol dm^{-3}. Further, for TGBE concentration greater than 1.0 mol dm^{-3}, the relaxation frequency is found to be almost independent of SDS concentration and the amplitude of the excess absorption decreases with increasing SDS concentration. The observed relaxation is well accounted for by a kinetic scheme involving the interaction between the nonelectrolyte and water. From the concentration dependence of TGBE, the rate and thermodynamic parameters have been determined as a function of SDS concentration. The obtained data have been interpreted in terms of the structural changes of the solvent water by SDS molecules. As the results, it has been proposed that the hydrophobic parts of SDS have a considerable effect on water structure.

It has been proposed that the MHz frequency ultrasonic absorptions in aqueous solutions of nonelectrolytes containing hydroxyl groups are well accounted for the two relaxations by mechanisms involving an interaction between the solute and solvent and a molecular aggregation of the solutes.[1-4] The former process is observed in most of the solutions studied, whereas the latter is limited to solutions of solutes containing large hydrophobic groups.

On the other hand, it is generally accepted that micellar surfactant solutions solubilize sparingly water-soluble compounds. Many nonelectrolytes are not soluble enough to allow examination of their dynamic properties by ultrasonic methods. The ability of the surfactant to solubilize the nonelectrolyte provides an apparent homogeneous aqueous nonelectrolyte system and also allows studies of the phenomena associated with cosurfactants, which are very important in understanding microemulsions.

Zana et al.[5,6] have measured ultrasonic absorptions in aqueous solutions of butanol and hexanol in the presence of surfactants. They have interpreted the observed relaxation by a model involving an exchange reaction of the nonelectrolyte between the micellar and bulk phase in these solutions. Hall et al.[7-9] have also analyzed the relaxation process observed in aqueous alcohol solutions of other surfactants using a similar kinetic model and also a phenomenological treatment. In addition, an ultrasonic study concerning the effect of surfactant on the relaxation properties of aqueous solutions of 2-butoxyethanol (ethylene glycol monobutyl ether) was also performed by Verrel et al.[10] and they also accounted for the observations by the same analysis as Zana's. A very recent study by Verrall's[11] group showed that there exist a clathrate aggregate of alcohol with water in aqueous solution of 2-butoxyethanol and a surfactant. However, it is evident that the excess absorption or relaxational absorption of the ultrasound in the MHz frequency range exists in aqueous solutions of highly soluble alcohols. In the solution of 2-butoxyethanol, for example, a clear excess absorption is observed even at 0.7 mol dm^{-3}.[12] It is very important to prove if the observed relaxation corresponds to the interconversion of such nonelectrolytes between micelles and the bulk phase. For this purpose, we have chosen triethylene glycol monobutyl ether (TGBE) and sodium dodecyl sulfate (SDS) as solutes. In aqueous solutions of TGBE,[4] a clear single relaxational absorption is observed in the frequency range of 6.5 to 220 MHz, while in aqueous SDS solution, no excess absorption is found in the same frequency range up to 0.1 mol dm^{-3} concentration.[13] Therefore, such a ternary system may be very suitable for studying the effect of surfactant on the ultrasonic properties. Though too much time has been required to accumulate such desirable ultrasonic data by a pulse method, our recent semiautomatic equipment[2] has made it possible to perform such experiments much faster.

Experimental

Triethylene glycol monobutylether (TGBE) was purchased from TOKYO Kasei Co. Ltd. and was distilled once. Sodium dodecyl sulfate (SDS) was from BDH Chemicals Ltd. and was used without further purification. Doubly distilled water was used as a solvent. The concentrations of TGBE were determined by weighing. A stock solution of SDS was prepared and it was added to TGBE solutions in order to obtain the desired concentrations of SDS.

Ultrasonic absorption measurements were performed by the computerized pulse method in the frequency range from 6.5 to 220 MHz using three cells with 0.5, 5, and 20 MHz fundamental x-cut transducers. The detailed description of the apparatus was reported elsewhere.[2] Sound velocity was measured by means of an interferometer at 2.5 MHz and by a sing around method at 1.92 MHz. By both methods, the absolute values of the sound velocity were obtainable with a

precision of ±1 m s^{-1} and the relative values by the sing around method were reproducible to within ±5 cm s^{-1}. All ultrasonic measurement cells were immersed in a water bath which was controlled to within ±0.002 °C. Conductivity measurements were carried out on a conductivity meter (Yanagimoto Model MY-7). All measurements were made at 25 °C.

Results and Interpretation

Figure 1 shows a representative ultrasonic absorption spectrum in aqueous solutions of TGBE with SDS present at 25 °C. In the concentration range of TGBE from 0.2 to 1.7 mol dm^{-3} and that of SDS from 1 to 100 mmol dm^{-3}, the observed spectra are all satisfactorily fitted to an equation which is characteristic of a single relaxation process:

$$\alpha/f^2 = A/[1+(f/f_r)^2]+B, \quad (1)$$

where α is the absorption coefficient, f the frequency, A the amplitude of the excess absorption, f_r the relaxation frequency and B the background absorption including the classical absorption.[14] These parameters, f_r, A, and B, have been determined by a least mean square method described in detail elsewhere.[4] Figure 2 shows the TGBE concentration dependence of the relaxation frequency at various concentrations of SDS. At low concentrations of SDS (less than 5 mmol dm^{-3}), the plot indicates a minimum, while it seems to increase monotonically when SDS is present at a concentration greater than 20 mmol dm^{-3}. Another interesting feature is that the relaxation frequency at more than 1.0 mol dm^{-3} of TGBE falls on almost a same line even if the concentration of SDS is changed.

The excess absorption amplitudes as a function of TGBE are shown in Fig. 3 at various concentrations of SDS and it is seen that they indicate maxima, i.e. the peak sound absorption concentrations. Without SDS, the excess absorption is only observed in the TGBE concentration range of more than 0.60 mol dm^{-3}. However, when SDS is added the excess absorption is found in more dilute solutions of TGBE. For example when the SDS concentration is 100 mmol dm^{-3}, the

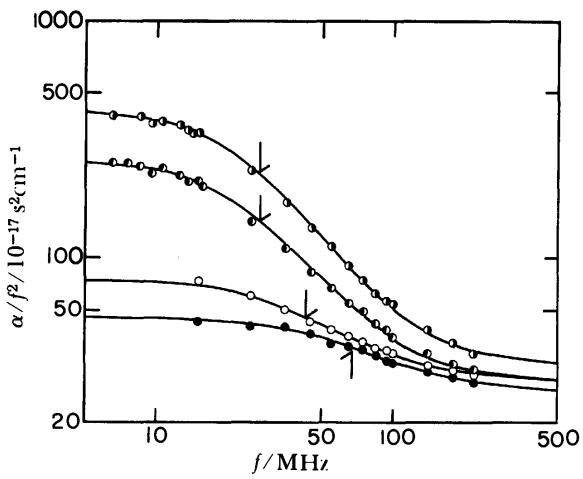

Fig. 1. Representative ultrasonic absorption spectra in 0.60 mol dm^{-3} TGBE aqueous solution at various SDS concentration at 25 °C. The arrows show the positions of the relaxation frequencies. ●; 0 mmol dm^{-3}, ○; 1.5 mmol dm^{-3}, ◐; 20 mmol dm^{-3}, ◑; 100 mmol dm^{-3}.

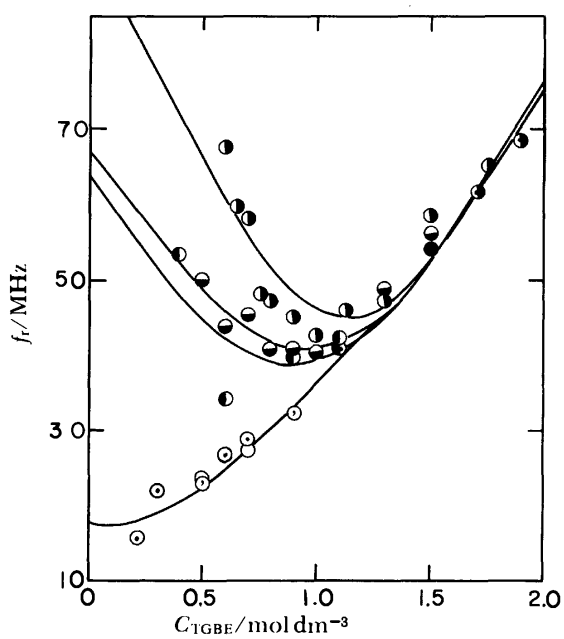

Fig. 2. TGBE concentration dependence of the relaxation frequency as a function of SDS at 25 °C. The solid curves are those calculated using the determined β, k_b, K_{12} values. The calculated values at 20 and 100 mmol dm^{-3} SDS solutions are almost same. ◑; 0 mmol dm^{-3}, ◒; 1.5 mmol dm^{-3}, ◐; 5 mmol dm^{-3}, ⊙; 20 and 100 mmol dm^{-3}.

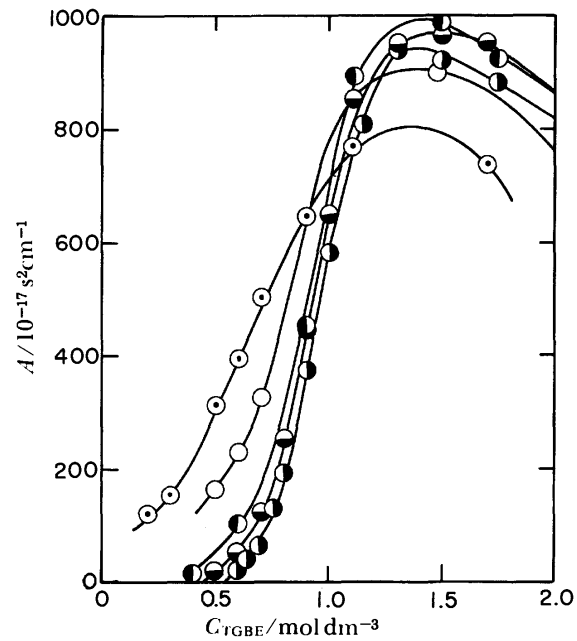

Fig. 3. TGBE concentration dependence of the amplitude of the excess absorption at different SDS concentrations. ◑; 0 mmol dm^{-3}, ◒; 1.5 mmol dm^{-3}, ◐; 5 mmol dm^{-3}, ○; 20 mmol dm^{-3}, ⊙; 100 mmol dm^{-3}.

excess absorption is clearly observed even at 0.20 mol dm^{-3} of TGBE. The amplitude of the excess absorption depends on the concentrations of both SDS and TGBE.

In order to see if micelles are formed in the solutions, sound velocity and conductivity measurements have been carried out. The former results are shown in Fig. 4 and the latter in Fig. 5. In 0.60 mol dm^{-3} solution of TGBE, a break point has been found in the sound velocity at 6.2 mmol dm^{-3} SDS concentration and in the conductivity at about 7 mmol dm^{-3}. These results indicate that the addition of TGBE decreases the critical micelle concentration (cmc) because the cmc for SDS solution is 8.3 mmol dm^{-3}.[15]

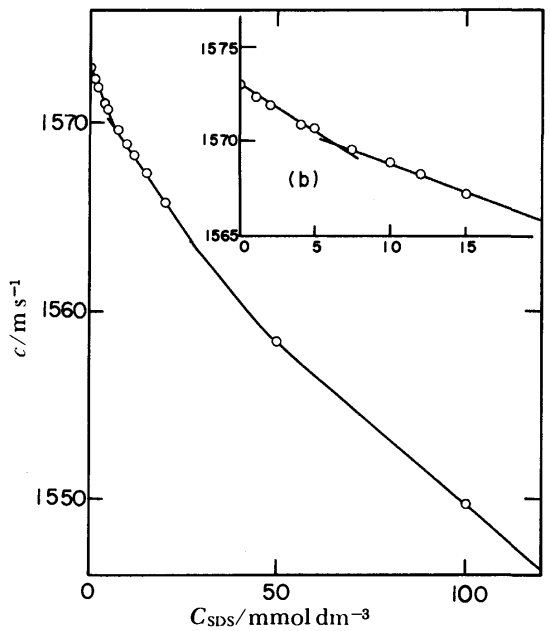

Fig. 4. SDS concentration dependence of the sound velocity at 0.60 mol dm^{-3} TGBE. The break point has been seen at about 6.2 mmol dm^{-3}. In (b), the scale of the concentration is expanded.

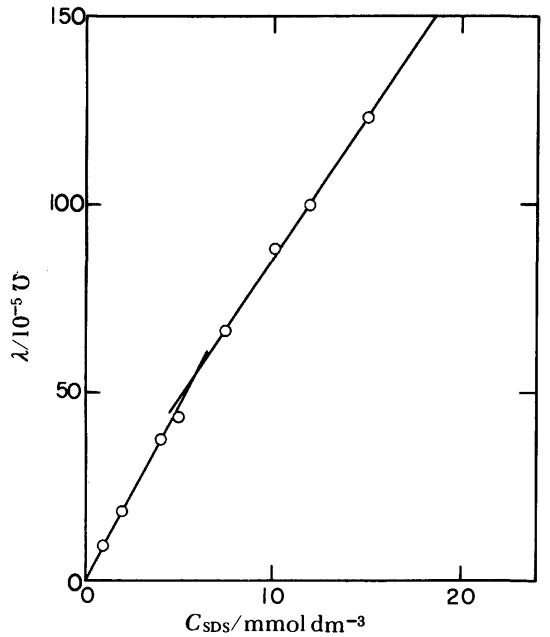

Fig. 5. SDS concentration dependence of the conductivity at 0.60 mol dm^{-3} at 25°C. At 7 mmol dm^{-3} SDS, the two straight lines intercect.

In aqueous solution of SDS it has been reported that the ultrasonic relaxational absorption is observed far below the MHz frequency range.[13] Even if the surfactant is added to the aqueous solutions of TGBE, the ultrasonic spectra can be well expressed by a single relaxational equation and the ultrasonic relaxation parameters change gradually with the concentration of SDS. Therefore, it may be considered that the cause of the excess absorption in the TGBE solutions with SDS present is associated with the same mechanism as that observed in the absence of SDS. Therefore, we may interpret the relaxation phenomena in terms of a similar reaction mechanism. It is represented as follows:[3]

$$AB \underset{k_f}{\overset{k_r}{\rightleftharpoons}} A+B \qquad (2)$$

where k_f and k_b are the forward and reverse rate constants, A the solute and B the solvent, and AB the complex formed between the solute and the solvent. In order to analyze the relaxation process, it is a reasonable assumption that water exists in hydrogen honded and nonhydrogen bonded states. Only the latter molecules may participate in the reaction. The relationship between the relaxation frequency and the analytical concentrations is derived to be[3]

$$2\pi f_r = k_b[(C_{TGBE} - \beta C_w + K_{12})^2 + 4\beta C_w K_{12}]^{1/2}, \qquad (3)$$

where C_{TGBE} and C_w are the analytical concentrations of TGBE and water, β the fraction of nonhydrogen bonded water and K_{12} is defined as $K_{12}=k_f/k_b$. Under the assumption that the rate and thermodynamic parameters in Eq. 3 are independent of TGBE concentration, a nonlinear least mean square computer program has been used in order to determine the three parameters, β, k_b, and K_{12} at the various concentrations of SDS. In Table 1, the experimental results are shown and the solid lines in Fig. 2 represent f_r's which are calculated according to Eq. 3 and using these values.

The excess absorption amplitude is related to the reaction parameters as follows:[16]

$$A = (\rho c/f_r)(\Gamma/RT)(\Delta V - \alpha_p \Delta H/\rho C_p)^2(C_P^\infty/C_p), \qquad (4)$$

Table 1. Rate and Thermodynamic Constants for Aqueous Solutions of Triethylene Glycol Monobutyl Ether with Sodium Dodecyl Sulfate at 25°C

SDS	k_f	k_b	β
mmol dm^{-3}	10^7 s^{-1}	10^8 mol^{-1}dm^3 s^{-1}	
0	4.6±0.3	3.5±0.2	0.0285±0.0006
1.5	5.3±0.4	3.1±0.2	0.0225±0.0004
5.0	5.1±0.4	2.9±0.2	0.0216±0.0011
20	4.9±1.5	2.2±0.7	0.0051±0.0019
100	5.0±2.0	2.2±0.7	0.0046±0.0011

where ρ is the solution density, c the sound velocity, ΔV the standard reaction volume change, α_P the thermal expansion coefficient in the high frequency limit, C_P^∞ the specific heat in the high frequency limit, ΔH the standard enthalpy change of the reaction, C_p the specific heat in the low frequency limit, and Γ the concentration term expressed by,

$$\Gamma=(1/[A]+1/[B]+1/[AB]-1/([A]+[B]+[AB]))^{-1}. \quad (5)$$

The relaxational specific heat and the relaxational thermal expansion coefficient are very small compared with those values in the low frequency limit, and the concentration dependences of these two values are not expected to contribute so much to the dependence of the amplitude of the excess absorption, A. Therefore, the most important term that controls the dependence of the excess absorption amplitude may be $\rho c\Gamma/f_r$. In order to see how they depend on the analytical concentration, the terms have been calculated as a function of TGBE concentrations at various concentrations of SDS and they are shown in Fig. 6. These calculations indicate that the amplitude of the excess absorption should increase in the low concentration range of TGBE when SDS is added, and the calculated results are consistent with the experimental data shown in Fig. 3. However, we are reluctant to make the quantitative analysis for the amplitude of excess absorption because of the lack of the definitive thermodynamic constants, e.g. the specific heat and the thermal expansion coefficient.

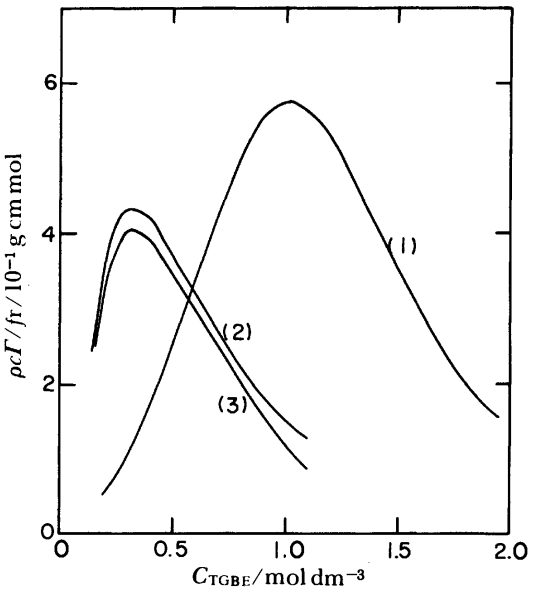

Fig. 6. The calculated $\rho c\Gamma/f_r$ values as a function of TGBE concentration. Those at 0, 1.5, and 5 mmol dm^{-3} SDS are almost identical. When SDS increases, the position of the maximum decreases. (1): 0, 1.5, and 5 mmol dm^{-3} SDS, (2): 20 mmol dm^{-3} SDS, (3): 100 mmol dm^{-3} SDS.

Discussion

Previous investigations[5-9] by ultrasonic relaxation methods for aqueous solution containing both surfactants and alcohols as solutes seem to have been focussed on the findings that no relaxation was observed for either pure surfactant solutions or for alcohol solutions, and that a relaxational absorption appears when the surfactant and alcohol are mixed. Those experiments were carried out above cmc of the surfactants because the solubilities of the solutes were limited. The relaxation time depends on the concentrations of both surfactant and alcohol. From these results the source of the relaxation was attributed to the perturbation of the equilibrium involving the exchange process of the alcohols between micelles and bulk solvent.[5-8,11] However, our ultrasonic studies[1,4] for aqueous solutions of various nonelectrolytes bearing a hydroxyl group have indicated that the water structure may be changed when a certain amount of nonelectrolyte is added, and then the relaxational absorption appears suddenly and the cause of the relaxation is due to the interaction between the solute and solvent. Under these circumstances, the present experimental study indicates that when SDS is added to the aqueous solution of TGBE the ultrasonic parameters are affected considerably by the surfactant as is seen in Figs. 2 and 3. However, the observed ultrasonic spectra are all characterized by a single relaxation process in the concentration range employed of both TGBE and SDS, and the ultrasonic parameters seem to change gradually with concentration. These experimental results lead us to believe that the cause of the excess absorption in aqueous solution of TGBE in the presence of SDS is the same as that observed when SDS is absent. That is, the equilibrium associated with the solute-solvent (TGBE-water) interaction is perturbed. The exchange reaction of the nonelectrolyte between the micellar and bulk phase may be ruled out as the cause of the observed excess absorption, though such process does exist in an other frequency range. It is worth noting that when the SDS concentration is greater than 10 mmol dm^{-3} the dependence of the relaxation frequency on TGBE concentration is quite similar to those reported so far for aqueous solutions of some alcohols in the presence of some surfactants. That is, the relaxation frequency increases approximately linearly with TGBE concentration. However, it might be expected that the exchange reaction may be observed in the pulse frequency range if the appropriate system had been chosen. That is, we do not deny the analysis for other systems studied so far.

It is easily seen that the concentration dependences of the relaxation frequency and the amplitude of the relaxational absorption are controled by the reactant concentration according to Eqs. 3—5. The reason why the relaxation frequency look to increase

monotonically with TGBE concentration when SDS is more than 10 mmol dm^{-3} may be speculated as follows. The concentration of water participating in the reaction may decrease when SDS is added, and then the dominant variable for the relaxation frequency becomes the concentration of TGBE. This situation is reflected in the change of β value. The β representing the fraction of nonhydrogen bonded water or less structured water decreases with increasing concentration of SDS. This means that the SDS may also act as a water structure promoter. It should be noted that the difference in the value of parameter, β above and below cmc is remarkable.

Next, it is examined the kinetic results obtained by this investigation in light of the reaction kinetics of solute-solvent interaction. The rate constant for the dissociation of the solute-solvent complex seems to be SDS concentration independent, while the association rate constant decreases with increasing SDS concentration. This result may imply that some of the nonelectrolytes are bound to the SDS micelles and the electrorepulsive force may hinder the interaction between the water and nonelectrolyte, or that the mobility of the cosurfactants may decrease because of the existence of the micelles.

A similar micelle effect has also been observed in the kinetics of a proton-transfer reaction: the rate constant diminished when the ionic surfactants formed micelles.[17] In order to interpret the observations more quantitatively, other surfactants should be selected and such studies are now under investigation.

The author acknowledges Professor Frank Jordan of Rutgers University for discussions and reading the manuscript. This work was partly supported by Naito Foundation and the author thanks also to Mr. Ryutaro Shinohara for assistance with parts of this research.

References

1) S. Nishikawa, G. Tanaka, and R. Shinohara, *Bull. Chem. Soc. Jpn.*, **59**, 827 (1986).
2) S. Nishikawa and K. Kotegawa, *J. Phys. Chem.*, **89**, 2896 (1985).
3) S. Nishikawa, M. Mashima, and T. Yasunaga, *Bull. Chem. Soc. Jpn.*, **48**, 661 (1975).
4) S. Nishikawa and R. Shinohara, *J. Soln. Chem.*, **15**, 221 (1986).
5) R. Zana, S. Yiv, C. Strazielle, and P. Lianos, *J. Colloid Interface Sci.*, **80**, 208 (1981).
6) S. Yiv and R. Zana, *J. Colloid Interface Sci.*, **80**, 224 (1981).
7) D. Hall, P. L. Jobling, E. Wyn-Jones, and J. E. Rassing, *J. Chem. Soc., Faraday Trans. 2*, **73**, 1582 (1977).
8) J. Gettins, D. Hall, P. L. Jobling, J. E. Rassing, and E. Wyn-Jones, *J. Chem. Soc., Faraday Trans. 2*, **74**, 1957 (1978).
9) J. Gormally, B. Sztuba, E. Wyn-Jones, and D. Hall, *J. Chem. Soc., Faraday Trans. 2*, **81**, 395 (1985).
10) N. P. Rao and R. E. Verrall, *J. Phys. Chem.*, **86**, 4777 (1982).
11) S. Kato, D. Jobe, N. P. Rao, C. H. Ho, and R. E. Verrall, *J. Phys. Chem.*, **90**, 4167 (1986).
12) S. Nishikawa, M. Tanaka, and M. Mashima, *J. Phys. Chem.*, **85**, 686 (1981).
13) T. Yasunaga, T. Oguri, and M. Miura, *J. Colloid Interface Sci.*, **23**, 352 (1967).
14) A complete set of the absorption coefficients and frequencies is available for various conditions from the author on request.
15) M. Miura and M. Kodama, *Bull. Chem. Soc. Jpn.*, **45**, 428 (1972).
16) G. G. Hammes and W. Knoche, *J. Chem. Phys.*, **45**, 4041 (1966).
17) T. Yamashita, H. Yano, S. Harada, and T. Yasunaga, *Bull. Chem. Soc. Jpn.*, **57**, 2352 (1984).

 © 1987 The Chemical Society of Japan Bull. Chem. Soc. Jpn., 60, 2791—2801 (1987)

A Linear Response Polarizability Theory for an Extended Fano-DeVoe Model with Comments on the Joint Use of Both Short- and Long-Range Inter(sub)molecular Interaction Approximations

Hirotoshi Ito and Yasumasa J. I'haya*
Department of Materials Science, The University of Electro-Communications, Chofu, Tokyo 182
(Received March 5, 1987)

An approach to extend the Fano-DeVoe model is presented for copolymer systems by making use of the Green's operator method within the dipole-dipole approximation. We derive a model Hamiltonian for a system by expanding its primitive Hamiltonian in terms of a bare complete basis set consisting of zero-order one-site and two-site excitation states in the first-order perturbation theory. A generalized extension of the Fano-DeVoe theory can be given by the polarizability tensor derived for this model Hamiltonian. As a more refined way, we derive another model Hamiltonian by expanding the primitive Hamiltonian of the system in terms of the corrected complete basis set consisting of the first-order excitation states. With such model Hamiltonians, we can fabricate polarizability theories on the same footing with the exciton wave function approaches based on the usual perturbation theory. Simplified schemes for the latter model Hamiltonians are applied to the copolymer system consisting of such chromophores that have permanent dipole moments in their ground states. Even if the constituent chromophores do not have permanent moments, extension of the Fano-DeVoe model is made by allowing for the total polymer ground state wave function corrected in terms of two-site excitation states. To circumvent the deficiency of the dipole approximation in the region of short separations of submolecules, we show a recipe as to how to make use of the monopole approximation together with the dipole approximation in conformity with the compromized idea of Moffitt.

When predicting the UV absorption as well as the CD and ORD spectra for free molecules[1] and molecular aggregates,[2] polarizability tensors afford their bandshape functions. In the previous paper,[2] we presented such a polarizability tensor theory for the real DNA molecules, which have the highly repeating sequences of base pairs. This formulation for copolymer systems is essentially the same as the decorrelation approximation[3] for homogeneous systems and the polarizability theory for homopolymer systems sketched by Herzenberg and Modinos[4] as a Fano-DeVoe model.[5-7] Also, DeVoe's coupled oscillator theory[8] which was semiclassically derived for copolymers and has been applied successfully to various biomolecules[9,10] falls under the cetegory of this model. We showed that the polarizability tensor equation[2] is of the same form as the matrix equation for the scalar polarizability in DeVoe's theory. However, if the kth submolecule for a copolymer (N-mer) has k_f oscillators, the size of the latter matrix equation is $(\sum_{k=1}^{N} k_f)\times(\sum_{k=1}^{N} k_f)$, whereas the size of our tensor matrix is always limited to be $3N\times3N$. This means that for the large N-mer with large number of k_f transitions, the oscillator formalism comes to require extremely longer computing time than the tensor formalism needs. Furthermore, we can use in our formalism the Green's operator methos which offers a convenient tool capable of expanding the polarizability theory in different ways by use of model Hamiltonians designed on the same footing with the usual exciton wave function approaches.

Herzenberg and Modinos[4] first used the terminology of the Fano-DeVoe model for the polarizability theory of homopolymers. However, in this paper, both DeVoe's scalar polarizability theory[8] and our polarizability theory[2] for copolymers are referred to as the original Fano-DeVoe model. The theories on the optical properties of molecular aggregates have often been developed by the usual perturbation theory on the basis of the exciton-state wave function approaches, in which we can find analogous treatments useful for the present purpose. For instance, some of the wave function approaches[13,14,19] can refine the polymer-state wave functions by taking into account the static field effect of permanent moment $\boldsymbol{\mu}_{00}^{(\mathrm{site})}$ of a certain chromophore onto the rest of constituent chromophores for the polymer system. We hope to develop polarizability theories in parallel with the works made by such perturbational approaches; we extend our previous polarizability tensor theory for the UV absorption and CD spectra by designing a model Hamiltonian on the same footing with the exciton theory given in Tinoco's review[19] on optical activity. Also, it is another concern to consider how the interactions between transition and permanent dipole moments are involved in the present theory.

Most of polarizability theories were not able to involve the effect of permanent dipole moments of submolecules. However, by making use of the so-called transition matrix method[14,15] based on a Green's operator approach, Rebenold has presented the linear response theory which contains the static effect,[16,17] i.e., the static interaction terms of the inner excited f→g transitions of a certain submolecule with the ground states of the rest of submolecules such as $|fm\rangle\{\sum_{g\neq f}\sum_{k\neq m}\boldsymbol{\mu}_{fg}^{(m)}\cdot\boldsymbol{U}_{mk}\cdot\boldsymbol{\mu}_{00}^{(k)}\langle gm|$. Having a glance at the original Fano-DeVoe model Hamiltonian,[2] one may perhaps be apt to judge it impossible to bring the static effect in the polarizability tensor theory in a usual way rather than in an artificial way. This is

because, in the expansion[20] of inter(sub)molecular interaction in terms of Legndre's polynomials, the terms including the point charge defined as the sum of net charges on nuclei vanish for neutral submolecules with permanent moments. However, we must note that even if there are no such point charges in permanent-polarized submolecules, each atom of these submolecules has nonzero net charge which exerts the static field effect to other submolecules. In this paper, we will derive such a model Hamiltonian that can involve the static effect in a natural fashion.

We build the polarizability theory within the dipole-dipole approximation. However, the dipole approximation is valid only for large separations between charge clouds, so that it is better to introduce the monopole-monopole approximation[18-20] at least for the nearest neighbors of monomer units and the dipole-dipole approximation for the remaining neighbors, following Moffitt.[18] In this joint use of the two approximations for the Fano-DeVoe type of polarizability tensor theory, it is impossible to use the monopole approximation without changing its present form,[2] as will be shown in the following section. In order to make use of the monopole approximation, it is of course necessary to obtain the transition and permanent monopole densities at each atom in the monomers. For the case where the sizes of chromophores in a copolymer are larger than or nearly equal to the separations of adjacent monomers, it is expected that the monopole approximation between the near neighbors becomes operative to remedy the dipole approximation. DNA and protein molecules are certainly the cases.[18,24-26]

In the next section, we first present a new scheme to extend the Fano-DeVoe model. Then, we simplify this scheme and apply it to the copolymer system of such constituent chromophores that have permanent dipole moments. Finally, we show a recipe as to how to make use of the short-range-oriented monopole approximation together with the long-range-oriented dipole approximation.

An Extended Fano-DeVoe Model Hamiltonian and the Polarizability

We will develop a polarizability tensor theory for describing the UV absorption and CD bandshapes of nucleic acids, in which the subunits of the purine and pryrimidine bases have the permanent dipole moments that are as large as the transition moments in magnitude.[24-25]

To begin with, let us assume that for the electronic Hamiltonian of the mth monomer H_m°, we know the eigenfunctions of the fth excitation states $\xi_f^{(m)}$ with the eigenvalues $E_f^{(m)}$ (f=0; ground state). Let V_{mn} be an interaction operator between the two submolecules located at sites m and n. The total Hamiltonian of the copolymer(N-mer) is then given by

$$H=\sum_{m=1}^{N} H_m^\circ+\sum_{n=1}^{N-1}\sum_{m>n}^{N} V_{mn}=H^\circ+V, \tag{1}$$

in which V_{mn} involves all the Coulomb interactions among electrons and nuclei of both submolecules separated by the distance R_{mn}. Neglecting higher-order terms in the expansion of V_{mn}, we approximate it for the two neutral submolecules by the dipole-dipole term:

$$V_{mn}=\boldsymbol{\mu}_m\cdot(R_{mn}^2\mathbf{1}-3\,\boldsymbol{R}_{mn}\boldsymbol{R}_{mn})R_{mn}^{-5}\cdot\boldsymbol{\mu}_n=\boldsymbol{\mu}_m\cdot\boldsymbol{U}_{mn}\cdot\boldsymbol{\mu}_n, \tag{2}$$

where $\boldsymbol{U}_{mn}$ defines the unit dipole interaction tensor, and $\boldsymbol{\mu}_m$ is the electric dipole moment operator centered at site m:

$$\boldsymbol{\mu}=\sum_{\mathrm{A}}^{\mathrm{Nuc}} Z_{\mathrm{A}}\,e\,\boldsymbol{r}_{m\mathrm{A}}-\sum_{i}^{\mathrm{Elec}} e\,\boldsymbol{r}_{mi}. \tag{3}$$

Z_{A} is the effective nuclear charge on nucleus A. In relation with Eq. 2, we dropped lower-order interaction terms involving point charges which vanish for neutral submolecules. Here, we define the point charges of a certain submolecule by the quantity which is equal to the summation of net charges on atoms in the submolecule. However, even if the total point charges are zero, permanent-polarlized subunits have nonzero net charges on nuclei. Such submolecules can exert the electrostatic effect to the ground as well as excited states of other submolecules. In the following section, we wish to show that the static field effect can be brought in the usual polarizability theories by deriving a model Hamiltonian.

For the polymer ground state $|0\rangle$ of the assembly of hypothetically non-interacting chromophores, we may take the product of the ground state wavefunctions of N submolecules, $\xi_0^{(m)}$, such that

$$|0\rangle=|\prod_{m=1}^{N}\xi_0^{(m)}\rangle. \tag{4}$$

The composite excited state $|fm\rangle$ considering only the fth local excitation at site m, $\xi_f^{(m)}$, is then given by

$$|fm\rangle=|\xi_f^{(m)}\prod_{n\neq m}\xi_0^{(n)}\rangle, \tag{5}$$

which may be referred to as one-site excitation state. For simplicity, we shall ignore the additional effect due to the antisymmetrization of those composite states with respect to the exchange of all the electrons between any pair of (sub)molecules. Furthermore, we define a two-site excitation state such as

$$|smtn\rangle=|\xi_s^{(m)}\xi_t^{(n)}\prod_{k\neq m,n}\xi_0^{(k)}\rangle. \tag{6}$$

(A) Polarizability for the Bare Basis Set-Dependent Model Hamiltonian. Let us denote a set of these states defined above as $\{|\psi\rangle\}$, $|0\rangle$ being the polymer ground state. We confine ourselves to weak and intermediate coupling cases, where no reorganization of electrons may occur in the polymer system retaining the identity of submolecules. Even if there exist such interaction terms as $\langle\psi|V|0\rangle$ and $\langle 0|V|\psi\rangle$ that are large but not huge in magnitude, it is convenient not

to take into account the direct mixing of $|0>$ with the rest of $\{|\psi>\}$ in the total wavefunctions of a polymer, $|\text{polymer}(L)>$, but to correct $|0>$ by using the first-order perturbation theory.

We can expand the polymer-state wave function in term of $\{|\psi>\}$ as follows:

$$|\text{polymer}(L)>=\sum_{\psi\neq 0}^{\text{All}}|\psi><\psi|\,\text{polymer}(L)>, \quad L=1,2,3,\cdots \tag{7}$$

with the assumption

$$1=\sum_{\psi\neq 0}^{\text{All}}|\psi><\psi|, \tag{8}$$

where we exclude the ground state $|0>$ for the reason mentioned above.

Now, we expand the primitive Hamiltonian H of Eq. 1 in terms of $\{|\psi>\}$ and put a model Hamiltonian as

$$\begin{aligned}\bar{H}&=\sum_{\psi,\psi'\neq 0}\sum|\psi><\psi|H|\psi'><\psi'|-<0|H|0>\\&=\sum_{\psi,\psi'\neq 0}\sum|\psi>\{<\psi|H|\psi'>-\delta_{\psi,\psi'}<0|H|0>\}<\psi'|\\&=\sum_{\psi'\neq 0}\varepsilon_{\psi,0}|\psi><\psi|+\{\sum_{\psi\neq\psi'}^{\text{intrasite}}\sum|\psi><\psi|V|\psi'><\psi'|\\&\quad+\sum_{\psi'\neq\psi'}^{\text{intersite}}\sum|\psi><\psi|V|\psi'><\psi'|\}\\&=\bar{H}_0+\bar{V}\end{aligned} \tag{9}$$

with

$$\varepsilon_{\psi,0}=<\psi|H|\psi>-<0|H|0>. \tag{10}$$

This model Hamiltonian formally gives the generalized extension of the Fano-DeVoe model. The $\varepsilon_{\psi,0}$ represents the modified excitation energy of a monomer embedded in the hypothetical polymer. By putting solely $|\psi>=|fm>$ in Eq. 9 and neglecting not only the level-shift in the $\varepsilon_{\psi,0}$ of the following Eq. 18 but also the mth intrasite $f\rightarrow$g transition terms such as

$$\begin{aligned}&\sum_{f}\sum_{g}\sum_{m}|fm><fm|V|gm><gm|=\\&\quad\sum_{f}\sum_{g}\sum_{m}\sum_{k}|fm>\mu_{fg}^{(m)}\cdot U_{mk}\cdot\mu_{00}^{(k)}<gm|,\quad (f,g\neq 0)\end{aligned} \tag{11}$$

one can obtain the polarizability tensor for the original Fano-DeVoe model Hamiltonian which was first derived by the present authors.[2)]

For a hypothetically non-interacting copolymer molecule, the crude Green's operator is defined as

$$\begin{aligned}G^{\circ}(E)&=(E-\bar{H}_0+i\eta)^{-1}\\&=(1/E)\{1+[(\bar{H}_0-i\eta)/E]+[(\bar{H}_0-i\eta)/E]^2+\cdots\}\\&=(1/E)\{\sum_{\psi\neq 0}|\psi><\psi|+\sum_{\psi\neq 0}[(\varepsilon_{\psi,0}-i\eta_{\psi})/E]|\psi><\psi|\\&\quad+\sum_{\psi,\psi'\neq 0}\sum[(\varepsilon_{\psi,0}-i\eta_{\psi})/E][(\varepsilon_{\psi',0}-i\eta'_{\psi'})/E]\\&\quad\times|\psi><\psi|\psi'><\psi'|+\cdots\}\\&=\sum_{\psi\neq 0}\frac{|\psi><\psi|}{E-\varepsilon_{\psi,0}+i\eta_{\psi}}.\end{aligned} \tag{12}$$

For a weak coupling case where $\{|\psi>\}$ do not strongly mix with the ground state $|0>$, we define the monomer polarizability tensor $\alpha(E)$ as

$$\alpha(E)=-<0|\mu G^{\circ}(E)\mu|0>=\sum_{\psi\neq 0}\frac{-<0|\mu|\psi><\psi|\mu|0>}{E-\varepsilon_{\psi,0}+i\eta_{\psi}}, \tag{13}$$

with

$$\mu=\sum_{m=1}^{N}\mu_m. \tag{14}$$

For a complete basis set which spans the one- and two-site excitation states, we note that the diagonal Hamiltonian $\bar{H}_0$ and the interaction part $\bar{V}$ in Eq. 9 are written down as

$$\bar{H}_0=\sum_{f}\sum_{m}\varepsilon_{fm,0}|fm><fm|+\sum_{s}\sum_{m}\sum_{t}\sum_{n}\varepsilon_{smtn,0}|smtn><smtn|, \tag{15}$$

$$\begin{aligned}\bar{V}&=\sum_{m>m}\sum\sum_{f}\sum_{g}|fm>\mu_{f0}^{(m)}\cdot U_{mn}\cdot\mu_{0g}^{(m)}<gn|\\&\quad+\sum_{m}\sum_{f}\sum_{g\,(g\neq f)}|fm>\{\sum_{k\neq m}\mu_{fg}^{(m)}\cdot U_{mk}\cdot\mu_{00}^{(k)}\}<gm|\\&\quad+\sum_{m>n}\sum_{s}\sum_{t}\sum\{\sum_{f}[|fm>\mu_{fs}^{(m)}\cdot U_{mn}\cdot\mu_{0t}^{(n)}<smtn|\\&\quad+|fn>\mu_{0s}^{(m)}\cdot U_{mn}\cdot\mu_{ft}^{(n)}<smtn|]\\&\quad+\sum_{g}[|smtn>\mu_{s0}^{(m)}\cdot U_{mn}\cdot\mu_{tg}^{(n)}<gn|\\&\quad+|smtn>\mu_{sg}^{(m)}\cdot U_{mn}\cdot\mu_{t0}^{(n)}<gm|]\}\\&\quad+\sum_{m>n}\sum_{f}\sum_{g}\sum_{s}\sum_{t\,(f,g\neq s,t)}|fmgn>\mu_{fs}^{(m)}\cdot U_{mn}\cdot\mu_{gt}^{(n)}<smtn|.\end{aligned} \tag{16}$$

Here, the first term is the original Fano-DeVoe type of operator. The terms after the first one in Eq. 16 show the interaction operators of the inner excited transition moments $\mu_{fg}^{(\text{site})}$ (involving $0\rightarrow 0$), which are classfied into three types of electric moments such as $\mu_{00}^{(\text{site})}$, $\mu_{0f}^{(\text{site})}$, and $\mu_{fg}^{(\text{site})}$. In particular, the second term is a special version of the transition matrix theory[14,15)] for the static field effect of permanent dipole moments $\mu_{00}^{(\text{site})}$ on all the transition moments $\mu_{fg}^{(\text{site})}$ for a specific site and similar effect for the rest of all the sites.

Thus, the matrix element of the monomer polarizability tensor with respect to sites m and n is given by

$$\begin{aligned}\alpha_{mn}(E)&=-\sum_{f}\sum_{g}<0|\mu|fm><fm|G^{\circ}(E)|gn><gn|\mu|0>\\&\quad-\sum_{s}\sum_{t}\sum_{f}\sum_{g}\sum_{k}\sum_{l}<0|\mu|smtk>\\&\quad\times<smtk|G^{\circ}(E)|flgn><flgn|\mu|0>\\&=\sum_{f}\delta_{mn}\frac{-<0|\mu|fm><fm|\mu|0>}{E-\varepsilon_{fm,0}+i\eta_{fm}}\\&\quad+\sum_{s}\sum_{t}\frac{-<0|\mu|smtn><smtn|\mu|0>}{E-\varepsilon_{smtn,0}+i(\eta_{sm}+\eta_{tn})},\end{aligned} \tag{17}$$

in which $<0|\mu|fm>$ is nothing but $\mu_{0f}^{(m)}$ and where $\varepsilon_{fm,0}$ and $\varepsilon_{smtn,0}$ are calculated to be as follows:

$$\varepsilon_{fm,0}=E_{f0}^{(m)}+\sum_{k\neq m}\mu_{ff}^{(m)}\cdot U_{mk}\cdot\mu_{00}^{(k)}-\sum_{k\neq m}\mu_{00}^{(m)}\cdot U_{mk}\cdot\mu_{00}^{(k)}, \tag{18}$$

$$\varepsilon_{smtn,0}=E_{s0}^{(m)}+E_{t0}^{(n)}+\mu_{ss}^{(m)}\cdot U_{mn}\cdot\mu_{tt}^{(n)}-\mu_{00}^{(m)}\cdot U_{mn}\cdot\mu_{00}^{(n)}. \tag{19}$$

The $E_{f0}^{(m)}=(E_f^{(m)}-E_0^{(m)})$ is the excitation energy of the mth free monomer. The tensor $\alpha_{mn}(E)$ is diagonal, since the second term in Eq. 17 vanishes due to $<0|\mu|smtn>=0$. However, this electric moment comes

to be nonvanishing if we replace the bare ground state $|0\rangle$ with the more exact ground state $|\tilde{0}\rangle$. Actually, we assume the corrected ground state as follows:

$$|\tilde{0}\rangle=|0\rangle-\sum_{k\neq m}\varepsilon_{\psi,0}^{-1}\langle\psi|V|0\rangle|\psi\rangle\equiv|0\rangle-\sum_{\psi\neq m}C_{\psi,0}|\psi\rangle, \tag{20}$$

where $C_{\psi,0}=C_{0,\psi}$. It should be noted that $|0\rangle$ does not mix with one-site excitation states but mix only with two-site excitation states, unless submolecules have permanent dipole moments.

For the true Green's operator

$$\begin{aligned}G(E)&=(E-\bar{H}+i\eta)^{-1}\\&=G^{\circ}(E)+G^{\circ}(E)\bar{V}G^{\circ}(E)+G^{\circ}(E)\bar{V}G^{\circ}(E)\bar{V}G^{\circ}(E)+\cdots,\end{aligned} \tag{21}$$

we can derive the polymer polarizability tensor ${}^{p}\alpha_{mn}(E)$ as follows:

$$\begin{aligned}{}^{p}\alpha_{mn}(E)=&-\sum_{f,g\neq0}\sum\langle0|\mu|fm\rangle\langle fm|G(E)|gn\rangle\langle gn|\mu|0\rangle\\&-\sum_{s,t,f,g\neq0}\sum\sum_{k}\sum_{l}\langle0|\mu|smtk\rangle\\&\times\langle smtk|G(E)|flgn\rangle\langle flgn|\mu|0\rangle.\end{aligned} \tag{22}$$

The second term of Eq. 22 vanishes due to $\langle0|\mu|smtk\rangle=0$ and $\langle flgn|\mu|0\rangle=0$. For the first term of Eq. 22, we only point out that in addition to the original Fano-DeVoe type of matrix elements, various types of matrix elements of one-site part of $G^{\circ}(E)$,

$$\Sigma_f\Sigma_m|fm\rangle\langle fm|G^{\circ}(E)|fm\rangle\langle fm|,$$

mixing with two-site part of $G^{\circ}(E)$,

$$\Sigma_s\Sigma_m\Sigma_t\Sigma_n|smtn\rangle\langle smtn|G^{\circ}(E)|smtn\rangle\langle smtn|,$$

are produced by matching of the bra- and ket-operators for the various types of combinations of the seven interaction operators of Eq. 16. Because of the complexity, we will mention about the matrix elements of Eq. 22 any more. However, it is here interesting to observe that the second term of Eq. 16 leads to the first-order polarizability tensor:

$$\begin{aligned}&-\sum\sum_{f,g\neq0(g\neq f)}\langle0|\mu|fm\rangle\langle fm|G^{\circ}(E)\\&\quad\times[\text{2nd term of }\bar{V}]G^{\circ}(E)|gm\rangle\langle gm|\mu|0\rangle\delta_{mn}\\&=\sum\sum_{f,g\neq0(f\neq g)}\frac{-\mu_{0f}^{(m)}\{\sum_{k\neq m}\mu_{fg}^{(m)}\cdot U_{mk}\cdot\mu_{00}^{(k)}\}\mu_{g0}^{(m)}}{(E-\varepsilon_{fm,0}+i\eta_{fm})(E-\varepsilon_{gm,0}+i\eta_{gm})}\delta_{mn},\end{aligned} \tag{23}$$

which indicates that the static field effect involved is quite large, when $\varepsilon_{fm,0}$ and $\varepsilon_{gm,0}$ are nearly degenerate.

For the intermediate coupling case where there exists a strong mixing of $\{|fm\rangle\}$ with $|0\rangle$, we must evaluate the average value of the correlated ground state $|\tilde{0}\rangle$ instead of the bare ground state $|0\rangle$. Namely, we have a more refined polymer polarizability tensor:

$$\begin{aligned}{}^{rp}\alpha(E)=&-\langle\tilde{0}|\mu G(E)\mu|\tilde{0}\rangle\\=&{}^{p}\alpha(E)+\sum_{\psi\neq0}\langle0|\mu G(E)\mu|\psi\rangle C_{\psi,0}\\&+\sum_{\psi\neq0}C_{0,\psi}\langle\psi|\mu G(E)\mu|0\rangle\\&-\sum_{\psi,\psi'\neq0}\sum C_{0,\psi}\langle\psi|\mu G(E)\mu|\psi'\rangle C_{\psi',0}.\end{aligned} \tag{24}$$

The treatment of Eq. 24 is thus quite analogous to that of the renormalized random-phase approximation for a free molecule. The theoretical procedure outlined above will be more generalized in (B) which contains the calculations of Eqs. 22 and 24.

(B) Polarizability for the Corrected Basis Set-Dependent Model Hamiltonian. Instead of the bare basis set $\{|\psi\rangle\}$ of the excited states, let us make use of a basis set corrected by the first-order perturbation theory, that is,

$$\begin{aligned}|\tilde{\psi}\rangle=&|\psi\rangle+\varepsilon_{\psi,0}^{-1}\langle0|V|\psi\rangle|0\rangle+\sum_{\psi'\neq\psi}\varepsilon_{\psi,\psi'}^{-1}\langle\psi'|V|\psi\rangle|\psi'\rangle\\\equiv&|\psi\rangle+C_{0,\psi}|0\rangle+\sum_{\psi'\neq\psi}C_{\psi',\psi}|\psi'\rangle\\=&|\psi\rangle+C_{\psi,0}|0\rangle+\sum_{\psi'\neq\psi}C_{\psi,\psi'}|\psi'\rangle,\end{aligned} \tag{25}$$

where $\varepsilon_{\psi,\psi'}$ denotes an energy difference $\langle\psi|H|\psi\rangle-\langle\psi'|H|\psi'\rangle$. Again, we must note that the two-site excitation states for ψ always mix with the ground state, while the one-site excitation states can mix with the ground state only if the constituent chromophores have permanent dipole moments $\mu_{00}^{(\text{site})}$. Then, similar to Eq. 7, the wave function for the copolymer system is expanded in terms of the corrected basis set as[19]

$$|\text{polymer}(L)\rangle=\sum_{\psi\neq0}|\tilde{\psi}\rangle\langle\tilde{\psi}|\,\text{polymer}(L)\rangle,\qquad L=1,2,3,\cdots \tag{26}$$

where we assume the completeness for the $\{|\tilde{\psi}\rangle\}$.

The model Hamiltonian is now set to be

$$\begin{aligned}\tilde{H}=&\sum_{\psi,\psi'\neq0}\sum|\tilde{\psi}\rangle\langle\tilde{\psi}|H|\tilde{\psi}'\rangle\langle\tilde{\psi}'|-\langle\tilde{0}|H|\tilde{0}\rangle\\=&\sum_{\psi\neq0}\tilde{\varepsilon}_{\psi,0}|\tilde{\psi}\rangle\langle\tilde{\psi}|+\sum_{\psi\neq\psi}\sum|\tilde{\psi}\rangle\langle\tilde{\psi}|V|\tilde{\psi}'\rangle\langle\tilde{\psi}'|\\=&\sum_{\psi\neq0}\tilde{\varepsilon}_{\psi,0}|\tilde{\psi}\rangle\langle\tilde{\psi}|+\{\overset{\text{intrasite}}{\sum_{\psi\neq\psi'}\sum}|\tilde{\psi}\rangle\langle\tilde{\psi}|V|\tilde{\psi}'\rangle\langle\tilde{\psi}'|\\&+\overset{\text{intersite}}{\sum_{\psi\neq\psi'}\sum}|\tilde{\psi}\rangle\langle\tilde{\psi}|V|\tilde{\psi}'\rangle\langle\tilde{\psi}'|\}\\=&\tilde{H}_0+\tilde{V},\end{aligned} \tag{27}$$

with

$$\tilde{\varepsilon}_{\psi,0}=\langle\tilde{\psi}|H|\tilde{\psi}\rangle-\langle\tilde{0}|H|\tilde{0}\rangle. \tag{28}$$

Equation 27 gives the more generalized Fano-DeVoe model Hamiltonian than that defined by Eq. 9. The modified excitation energy $\tilde{\varepsilon}_{\psi,0}$ is formally corrected up to the order of V^2 by the usual perturbation theory. Also, we define the crude and true Green's operators for $\tilde{H}_0$ and $\tilde{H}$, respectively, as follows:

$$\tilde{G}^{\circ}(E)=(E-\tilde{H}_0+i\tilde{\eta})^{-1}=\sum_{\psi\neq0}\frac{|\tilde{\psi}\rangle\langle\tilde{\psi}|}{E-\tilde{\varepsilon}_{\psi,0}+i\tilde{\eta}_{\psi}}, \tag{29}$$

$$\tilde{G}(E)=(E-\tilde{H}+i\tilde{\eta})^{-1}=\tilde{G}^{\circ}(E)+\tilde{G}^{\circ}(E)\tilde{V}\tilde{G}(E), \tag{30}$$

which may be called a dressed or effective and/or renormalized Green's operator, if we follow the terminology of Mattuck.[23]

The monomer and polymer polarizability tensors for Eqs. 29 and 30 are defined by the average values over the bare ground state $|0>$ as follows:

$$\tilde{\alpha}(E)=-<0|\mu\tilde{G}^{\circ}(E)\mu|0>=\sum_{\psi\neq 0}\frac{-<0|\mu|\tilde{\psi}><\tilde{\psi}|\mu|0>}{E-\tilde{\varepsilon}_{\psi,0}+i\tilde{\eta}_{\psi}}, \tag{31}$$

$$^{p}\tilde{\alpha}(E)=-<0|\mu\tilde{G}(E)\mu|0>$$
$$=-<0|\mu(\tilde{G}^{\circ}(E)+\tilde{G}^{\circ}(E)\tilde{V}\tilde{G}(E)+\cdots)\mu|0>. \tag{32}$$

Unfortunately, it becomes more complicated to calculate the matrix elements for the dressed $^{p}\tilde{\alpha}(E)$ than to do so for the bare $^{p}\alpha(E)$, so that it may be hopeless to linearlize $^{p}\tilde{\alpha}(E)$ by intuitively finding and summing up kinds of modules comprising simple types of polarizabilities and unit interaction factors just like the derivation of the original Fano-DeVoe polarizability.[2]

The most generalized tensor $^{rp}\tilde{\alpha}(E)$ for a copolymer is formally obtained by taking the average over the correlated ground state as follows:

$$^{rp}\tilde{\alpha}(E)=-<\tilde{0}|\mu\tilde{G}(E)\mu|\tilde{0}>$$
$$=^{p}\tilde{\alpha}(E)+\sum_{\psi\neq 0}<0|\mu\tilde{G}(E)\mu|0>C_{\psi,0}$$
$$+\sum_{\psi\neq 0}C_{0,\psi}<\psi|\mu\tilde{G}(E)\mu|0>$$
$$-\sum_{\psi,\psi'\neq 0}\sum C_{0,\psi}<\psi|\mu\tilde{G}(E)\mu|\psi'>C_{\psi',0}, \tag{33}$$

which may be referred to as a self-consistent renormalized RPA, while Eq. 32 is called simply a renormalized RPA.

In what follows, we will mention the procedures described in (A) and (B) in more detail for comparatively simple cases.

(C) Polarizability for the Model Hamiltonian of the bare $\{|fm>\}$. The choice of the bare basis set consisting of one-site excitation states for the total Hamiltonian $\bar{H}(=\bar{H}_{o}+\bar{V})$ leads to the following operators

$$\bar{H}_{0}=\sum_{f}\sum_{m}\varepsilon_{fm,0}|fm><fm|, \tag{34}$$

$$\bar{V}=\sum_{f}\sum_{m}\overset{\text{intersite}}{\sum_{g}\sum_{n}}|fm>\mu_{f0}^{(m)}\cdot U_{mn}\cdot\mu_{0g}^{(n)}<gn|$$
$$+\overset{\text{intrasite}}{\sum_{f}\sum_{m}\sum_{g\neq f}}|fm><fm|V|gm><gm|$$
$$=\bar{V}_{FD}+\bar{V}_{S} \tag{35}$$

where $\bar{V}_{FD}$ denotes the original Fano-DeVoe type of interaction operator. $\bar{V}_{S}$ given by $\sum_{k}\mu_{fg}^{(m)}\cdot U_{mk}\cdot\mu_{00}^{(k)}$ signifies the operator for the Bayley, Nielsen, Schellman type of static field effect[15] to the mth intrasite f→g transitions: i.e., the operator for the intrasite f→g excitation state of the mth subunit which interacts with the ground states of the rest of the kth permanent-polarized subunits. For the off-diagonal static interaction term $<fm|V|gm>$, $\varepsilon_{fm,0}$ contains the diagonal element $<fm|V|fm>$ which is given by the second term of Eq. 18. It may be convenient for the calculations of $^{p}\alpha(E)$ to specify that for example the element $<fm|V|gn>$ represented by $\mu_{0f}^{(m)}\cdot U_{mn}\cdot\mu_{0g}^{(n)}$ implies such a scalar quantity that the operation of $\mu\cdot U\cdot\mu$ has already been performed.

From the calculation of $-<0|\mu G(E)\mu|0>$ with $G(E)=[E-(\bar{H}_{o}+\bar{V})+i\eta]^{-1}$, we can obtain $^{p}\alpha_{mn}(E)$. However, inclusion of $\bar{V}_{S}$ brings about too much complexity, so that we shall collect only several important terms to be linearlized as shown in the following; for the convenience of this purpose, we put

$$^{p}\bar{V}_{FD}(E)=\bar{V}_{FD}+\bar{V}_{FD}G^{\circ}(E)\bar{V}_{FD}+\bar{V}_{FD}G^{\circ}(E)\bar{V}_{FD}G^{\circ}(E)\bar{V}_{FD}+\cdots, \tag{36}$$

$$^{p}\bar{V}_{S}(E)=\bar{V}_{S}+\bar{V}_{S}G^{\circ}(E)\bar{V}_{S}+\bar{V}_{S}G^{\circ}(E)\bar{V}_{S}G^{\circ}(E)\bar{V}_{S}+\cdots. \tag{37}$$

Thus, we have

$$^{p}\alpha_{mn}(E)=-\sum_{f,g\neq 0}\sum<0|\mu|fm><fm|G(E)|gn><gn|\mu|0> \tag{38a}$$

$$\simeq-\sum_{f,g\neq 0}\sum\{\mu_{0f}^{(m)}<fm|G^{\circ}(E)+G^{\circ}(E)^{p}\bar{V}_{FD}(E)G^{\circ}(E)|gn>\mu_{g0}^{(n)}$$
$$+\mu_{0f}^{(m)}<fm|G^{\circ}(E)^{p}\bar{V}_{S}(E)G^{\circ}(E)|gn>\mu_{g0}^{(n)}$$
$$+\mu_{0f}^{(m)}<fm|G^{\circ}(E)^{p}\bar{V}_{S}(E)G^{\circ}(E)^{p}\bar{V}_{FD}(E)G^{\circ}(E)|gn>\mu_{g0}^{(n)}$$
$$+\mu_{0f}^{(m)}<fm|G^{\circ}(E)^{p}\bar{V}_{FD}(E)G^{\circ}(E)^{p}\bar{V}_{S}(E)G^{\circ}(E)|gn>\mu_{g0}^{(n)}$$
$$+\mu_{0f}^{(m)}<fm|G^{\circ}(E)^{p}\bar{V}_{FD}(E)G^{\circ}(E)^{p}\bar{V}_{S}(E)G^{\circ}(E)\times{}^{p}\bar{V}_{FD}(E)G^{\circ}(E)|gn>\mu_{g0}^{(n)}$$
$$+\mu_{0f}^{(m)}<fm|G^{\circ}(E)^{p}\bar{V}_{S}(E)G^{\circ}(E)^{p}\bar{V}_{FD}(E)G^{\circ}(E)\times{}^{p}\bar{V}_{S}(E)G^{\circ}(E)|gn>\mu_{g0}^{(n)}\}$$
$$=\{\mathbf{1}+\alpha(E)\cdot U\}_{mn}^{-1}\cdot\alpha_{nn}(E)-\sum_{f\neq g}\sum\mu_{0f}^{(m)}K_{mm}^{fg}(E)\mu_{g0}^{(m)}\delta_{mn}$$
$$+\sum_{f\neq t}\sum_{k}\sum\mu_{0f}^{(m)}K_{mm}^{ft}(E)\mu_{t0}^{(m)}\cdot\{\mathbf{1}+U\cdot\alpha(E)\}_{mk}^{-1}\cdot U_{kn}\cdot\alpha_{nn}(E)$$
$$+\sum_{k}\sum_{t\neq g}\sum\alpha_{mm}(E)\cdot U_{mk}\cdot\{\mathbf{1}+\alpha(E)\cdot U\}_{kn}^{-1}\cdot\mu_{0t}^{(n)}K_{nn}^{tg}(E)\mu_{g0}^{(n)}$$
$$-\sum_{k}\sum_{l}\sum_{j}\sum_{t\neq g}\sum\alpha_{mm}(E)\cdot U_{mk}\cdot\{\mathbf{1}+\alpha(E)\cdot U\}_{kl}^{-1}\cdot\mu_{0t}^{(l)}K_{ll}^{tg}(E)\mu_{g0}^{(l)}\times\{\mathbf{1}+U\cdot\alpha(E)\}_{lj}^{-1}U_{jn}\cdot\alpha_{nn}(E)$$
$$-\sum_{k}\sum_{f\neq t}\sum_{s\neq g}\sum\mu_{0f}^{(m)}K_{mm}^{ft}(E)\mu_{t0}^{(m)}\cdot\{\mathbf{1}+U\cdot\alpha(E)\}_{mk}^{-1}\cdot U_{kn}\times\mu_{0s}^{(n)}K_{nn}^{sg}(E)\mu_{g0}^{(n)},\ m,\ n=1,2,3,\cdots,\ N \tag{38b}$$

with the relationships

$$\{\mathbf{1}+\alpha(E)\cdot U\}_{mn}^{-1}=\delta_{mn}-\alpha_{mm}(E)\cdot U_{mn}+\sum_{k}\alpha_{mm}(E)\cdot U_{mk}\cdot\alpha_{kk}(E)\cdot U_{kn}-\cdots, \tag{39}$$

$$\{\mathbf{1}+U\cdot\alpha(E)\}_{mn}^{-1}=\delta_{mn}-U_{mn}\cdot\alpha_{nn}(E)+\sum_{k}U_{mk}\cdot\alpha_{kk}(E)\cdot U_{kn}\cdot\alpha_{nn}(E)-\cdots, \tag{40}$$

where we put

$$K_{mm}^{fg}(E)=\left\{\frac{<fm|V|gm>}{E-\varepsilon_{fm,0}+i\eta_{fm}}+\sum_{t\neq f,g}\frac{<fm|V|tm><tm|V|gm>}{(E-\varepsilon_{fm,0}+i\eta_{fm})(E-\varepsilon_{tm,0}+i\eta_{tm})}+\cdots\right\}\Big/(E-\varepsilon_{gm,0}+i\eta_{gm}) \tag{41}$$

In Eq. 38b, the first term gives the pure Fano-DeVoe type of polarizability tensor components,[2] and the second term corresponds to the tensor components involving the static field effect appeared in the transition matrix theory.[15] The remaining four terms show only the simple geometric progressive parts of the tensor components produced from all the crossed terms of $\overline{V}_{FD}$ and $\overline{V}_S$. From the fact that by inspection of Eq. 38b the corrections to the ordinary Fano-DeVoe polarizability tensor are at least the first order in $\langle\psi|V|\psi'\rangle$ for the permanent-polarized system, it is indicated that Eq. 38b gives a significant extension of the Fano-DeVoe model, when the magnitudes of $\boldsymbol{\mu}_{fg}^{(\mathrm{site})}$ and $\boldsymbol{\mu}_{00}^{(\mathrm{site})}$ are large.

Furthermore, for the intermediate coupling case, a higher approximation than that of ${}^{p}\alpha_{mn}(E)$ can be made as follows:

$$
\begin{aligned}
{}^{rp}\alpha_{mn}(E)={}&{}^{p}\alpha_{mn}(E)+\sum_{f}\sum_{g}\langle 0|\boldsymbol{\mu}|fm\rangle\langle fm|G(E)\boldsymbol{\mu}|gn\rangle C_{gn,0}\\
&+\sum_{f}\sum_{s}\sum_{k}\sum_{t}\langle 0|\boldsymbol{\mu}|fm\rangle\langle fm|G(E)\boldsymbol{\mu}|sktn\rangle C_{sktn,0}\\
&+\sum_{f}\sum_{g}C_{0,fm}\langle fm|\boldsymbol{\mu}G(E)|gn\rangle\langle gn|\boldsymbol{\mu}|0\rangle\\
&+\sum_{s}\sum_{t}\sum_{k}\sum_{g}C_{0,smtk}\langle smtk|\boldsymbol{\mu}G(E)|gn\rangle\langle gn|\boldsymbol{\mu}|0\rangle\\
&-\sum_{f}\sum_{g}C_{0,fm}\langle fm|\boldsymbol{\mu}G(E)\boldsymbol{\mu}|gn\rangle C_{gn,0}\\
&-\sum_{f}\sum_{s}\sum_{k}\sum_{t}C_{0,fm}\langle fm|\boldsymbol{\mu}G(E)\boldsymbol{\mu}|sktn\rangle C_{sktn,0}\\
&-\sum_{s}\sum_{t}\sum_{j}\sum_{g}C_{0,smtj}\langle smtj|\boldsymbol{\mu}G(E)\boldsymbol{\mu}|gn\rangle C_{gn,0}\\
&-\sum_{s}\sum_{t}\sum_{j}\sum_{f}\sum_{k}\sum_{g}C_{0,smtj}\langle smtj|\boldsymbol{\mu}G(E)\boldsymbol{\mu}|fkgn\rangle C_{fkgn,0},
\end{aligned}
\tag{42}
$$

which gives the renormalized RPA. The final result of Eq. 42 is not specified for saving space. Actually, the correction terms after the first term in Eq. 42 may be unnecessary to calculate, since the static interactions in Eq. 38b are sufficiently taken into account through $\overline{V}_S$ given by Eqs. 11 and 35. However, for the case where the permanent moments are all zero, the correction terms related with two-site excitations become operative, so that Eq. 42 becomes

$$
\begin{aligned}
{}^{rp}\alpha_{mn}(E)={}&{}^{p}\alpha_{mn}(E)\\
&+\sum_{s}\sum_{k}\sum_{t}\{[\mathbf{1}+\boldsymbol{\alpha}(E)\cdot\boldsymbol{U}]^{-1}_{mk}\cdot\boldsymbol{\mu}_{0s}^{(k)}C_{sktn,0}\boldsymbol{\mu}_{0t}^{(n)}/(E-\varepsilon_{sk,0}+i\eta_{sk})\\
&+[\mathbf{1}+\boldsymbol{\alpha}(E)\cdot\boldsymbol{U}]^{-1}_{mn}\cdot\boldsymbol{\mu}_{0t}^{(n)}C_{sktn,0}\boldsymbol{\mu}_{0s}^{(k)}/(E-\varepsilon_{tn,0}+i\eta_{tn})\\
&+\boldsymbol{\mu}_{t0}^{(k)}C_{0,smtk}\boldsymbol{\mu}_{0s}^{(m)}/(E-\varepsilon_{sm,0}+i\eta_{sm})\cdot[\mathbf{1}+\boldsymbol{U}\cdot\boldsymbol{\alpha}(E)]^{-1}_{mn}\\
&+\boldsymbol{\mu}_{s0}^{(m)}C_{0,smtk}\boldsymbol{\mu}_{0t}^{(k)}/(E-\varepsilon_{tk,0}+i\eta_{tk})\cdot[\mathbf{1}+\boldsymbol{U}\cdot\boldsymbol{\alpha}(E)]^{-1}_{kn}\}\\
&+O(C_{0,smtj}C_{fktn,0}),
\end{aligned}
\tag{43}
$$

which means that in this case the correction of the polymer ground state produced only by the two-site excitations gives the extension of the pure Fano-DeVoe model.

Thus, we can obtain the UV absorption and the CD and ORD bandshape functions either from the calculations[1,2] of $3^{-1}\,Tr\,{}^{p}\alpha_{mn}(E)$ and $12^{-1}\boldsymbol{R}_{mn}\cdot({}^{p}\alpha_{mn}(E):\boldsymbol{\varepsilon})$ for Eq. 38b, or from the calculations of $3^{-1}\,Tr\,{}^{rp}\alpha_{mn}(E)$ and $12^{-1}\boldsymbol{R}_{mn}\cdot({}^{rp}\alpha_{mn}(E):\boldsymbol{\varepsilon})$ for Eq. 42 and/or Eq. 43.

(D) Polarizability for the model Hamiltonian of the Corrected $\{|\tilde{fm}\rangle\}$. The expansion of the primitive Hamiltonian of Eq. 1 in terms of the corrected basis set of the one-site excitation states $\{|\tilde{fm}\rangle\}$ leads to

$$
\begin{aligned}
\tilde{H}=&\sum_{f}\sum_{m}\tilde{\varepsilon}_{fm,0}|\tilde{fm}\rangle\langle\tilde{fm}|\\
&+\{\sum_{g\neq f}\sum_{m}\sum^{\text{intrasite}}|\tilde{fm}\rangle\langle\tilde{fm}|V|\tilde{gm}\rangle\langle\tilde{gm}|\\
&+\sum_{f}\sum_{m}\sum_{g}\sum_{n}\sum^{\text{intersite}}|\tilde{fm}\rangle\langle\tilde{fm}|V|\tilde{gn}\rangle\langle\tilde{gn}|\}\\
=&\tilde{H}_0+\tilde{V}=\tilde{H}_0+\{\tilde{V}_S+\tilde{V}_{FD}\},
\end{aligned}
\tag{44}
$$

with

$$
|\tilde{fm}\rangle=|fm\rangle+C_{0,fm}|0\rangle, \tag{45a}
$$

The corrected ground state is written down as

$$
|\tilde{0}\rangle=|0\rangle-\sum_{g}\sum_{n}C_{gn,0}|gn\rangle-\sum_{s}\sum_{m}\sum_{t}\sum_{n}C_{smtn}|smtn\rangle. \tag{46a}
$$

Since $|0\rangle$ of Eq. 4 can be defined in N different ways by $|0k\rangle$ for $k=1,2,\cdots,N$ and since we wish to represent explicitly the site-dependence of $C_{0,fm}$, $C_{gn,0}$, and $C_{smtn,0}$ so as to show to what extent the transition moments are intermolecularly mixed with which site of the permanent dipole moment in the $|0\rangle$, we write Eqs. 45a and 46a as in the following:

$$
\begin{aligned}
|\tilde{fm}\rangle=&|fm\rangle+\sum_{k}\varepsilon^{-1}_{fm,0}\boldsymbol{\mu}_{00}^{(k)}\cdot\boldsymbol{U}_{km}\cdot\boldsymbol{\mu}_{0f}^{(m)}|0k\rangle\\
=&|fm\rangle+\sum_{k}C_{0,fm}^{(k)}|0k\rangle,
\end{aligned}
\tag{45b}
$$

$$
\begin{aligned}
|\tilde{0j}\rangle=&|0j\rangle-\sum_{g}\sum_{n}C_{gn,0}^{(j)}|gn\rangle\\
&-\sum_{s}\sum_{t}\sum_{n}C_{sjtn,0}^{(jn)}|sjtn\rangle,\quad j=1,2,\cdots,N
\end{aligned}
\tag{46b}
$$

where the two-site excitation coefficients are expressed in terms of $\varepsilon^{-1}_{sjtn,0}\,\boldsymbol{\mu}_{s0}^{(j)}\cdot\boldsymbol{U}_{jn}\cdot\boldsymbol{\mu}_{0t}^{(n)}$. The fth excitation energy of the mth submolecule is obtained as

$$
\begin{aligned}
\tilde{\varepsilon}_{fm,0}=&\langle\tilde{fm}|H|\tilde{fm}\rangle-\langle\tilde{0}|H|\tilde{0}\rangle\\
\simeq&\{1+\sum_{k}2|C_{fm,0}^{(k)}|^2\}\varepsilon_{fm,0}+\sum_{g}\sum_{n}2|C_{gn,0}^{(m)}|^2\varepsilon_{fn,0}\\
&+\sum_{s}\sum_{t}\sum_{n}2|C_{smtn,0}^{(mn)}|^2\varepsilon_{smtn,0}.
\end{aligned}
\tag{47}
$$

Similarly, the transfer integrals over modified interactions come to be of the forms

$$
\begin{aligned}
\langle\tilde{fm}|V|\tilde{gm}\rangle=&\sum_{k}\boldsymbol{\mu}_{fg}^{(m)}\cdot\boldsymbol{U}_{mk}\cdot\boldsymbol{\mu}_{00}^{(k)}+\sum_{l}\boldsymbol{\mu}_{f0}^{(m)}\cdot\boldsymbol{U}_{ml}\cdot\boldsymbol{\mu}_{00}^{(l)}C_{gm,0}^{(l)}\\
&+\sum_{k}C_{0,fm}^{(k)}\boldsymbol{\mu}_{00}^{(k)}\cdot\boldsymbol{U}_{km}\cdot\boldsymbol{\mu}_{g0}^{(m)}+\sum_{k}\sum_{l}C_{0,fm}^{(k)}\boldsymbol{\mu}_{00}^{(k)}\cdot\boldsymbol{U}_{kl}\cdot\boldsymbol{\mu}_{00}^{(l)}C_{gm,0}^{(l)},
\end{aligned}
\tag{48}
$$

$$
\begin{aligned}
\langle\tilde{fm}|V|\tilde{gn}\rangle=&\boldsymbol{\mu}_{f0}^{(m)}\cdot\boldsymbol{U}_{mn}\cdot\boldsymbol{\mu}_{0g}^{(n)}+\sum_{l}\boldsymbol{\mu}_{f0}^{(m)}\cdot\boldsymbol{U}_{ml}\cdot\boldsymbol{\mu}_{00}^{(l)}C_{gn,0}^{(l)}\\
&+\sum_{k}C_{0,fm}^{(k)}\boldsymbol{\mu}_{00}^{(k)}\cdot\boldsymbol{U}_{kn}\cdot\boldsymbol{\mu}_{g0}^{(n)}+\sum_{k}\sum_{l}C_{0,fm}^{(k)}\boldsymbol{\mu}_{00}^{(k)}\cdot\boldsymbol{U}_{kl}\cdot\boldsymbol{\mu}_{00}^{(l)}C_{gn,0}^{(l)}.
\end{aligned}
\tag{49}
$$

In (C), it has been shown that the intrasite interaction $\langle fm|V|gm\rangle$ as well as the renormalization such as $-\langle\tilde{0}|\boldsymbol{\mu}G(E)\boldsymbol{\mu}|\tilde{0}\rangle$ can introduce the static effect in the polarizability theory, while Fano-DeVoe's intersite

interaction term $\langle fm|V|gn\rangle$ does not contain the static effect. However, in (D) we have noted that the Fano-DeVoe type of interaction term $\langle\tilde{f}\tilde{m}|V|\tilde{g}\tilde{n}\rangle$ can involve the electrostatic modification against the bare interaction term $\langle fm|V|gm\rangle$ by using the one-site excitation states mixed with the ground state.

For later convenience, let us define the f,g-matrix elements of the monomer polarizability tensor $\tilde{\alpha}_{mn}(E)$ by

$$\tilde{\alpha}_{fm,gm}(E)=-\langle 0|\mu|\tilde{f}\tilde{m}\rangle\langle\tilde{g}\tilde{n}|\mu|0\rangle/(E-\tilde{\varepsilon}_{gn,0}+i\tilde{\eta}_{gn}), \tag{50}$$

in relation with the diagonal elements

$$\begin{aligned}\tilde{\alpha}_{mm}(E)&=-\sum_f\sum_g\langle 0|\mu|\tilde{f}\tilde{m}\rangle\langle\tilde{f}\tilde{m}|\tilde{G}^{\circ}(E)|\tilde{g}\tilde{n}\rangle\langle\tilde{g}\tilde{n}|\mu|0\rangle\\&=\sum_f\sum_g\tilde{\alpha}_{fm,gn}(E)\delta_{mn}\delta_{fg},\end{aligned} \tag{51}$$

Calculation of the modified transition moment yields

$$\langle 0|\mu|\tilde{f}\tilde{m}\rangle\equiv\tilde{\mu}_{0f}^{(m)}=\mu_{0f}^{(m)}+\sum_k C_{0,fm}^{(k)}\mu_{00}^{(k)}. \tag{52}$$

Then, we introduce the following definitions for the components of $\tilde{\alpha}_{mm}(E)$

$$\tilde{\alpha}_{mm}^{oo}(E)=\sum_{f\neq 0}-\mu_{0f}^{(m)}\mu_{f0}^{(m)}/(E-\tilde{\varepsilon}_{fm,0}+i\tilde{\eta}), \tag{53a}$$

$$\tilde{\alpha}_{mm}^{lo}(E)=\sum_{f\neq 0}-\tilde{\mu}_{0f}^{(m)}\mu_{f0}^{(m)}/(E-\tilde{\varepsilon}_{fm,0}+i\tilde{\eta}), \tag{53b}$$

$$\tilde{\alpha}_{mm}^{ol}(E)=\sum_{f\neq 0}-\mu_{0f}^{(m)}\tilde{\mu}_{f0}^{(m)}/(E-\tilde{\varepsilon}_{fm,0}+i\tilde{\eta}), \tag{53c}$$

While original Fano-DeVoe's polymer polarizability can be linearlized in terms of the monomer polarizability components, the polymer polarizability tensor ${}^p\tilde{\alpha}_{mn}(E)$ cannot be expressed simply in terms of the monomer polarizability tensors $\tilde{\alpha}_{mm}(E)$ and interaction tensors U. We therefore derive ${}^p\tilde{\alpha}_{mn}(E)$ in the following by use of the polarizability components $\tilde{\alpha}_{fm,gn}(E)$ newly defined by Eq. 50. The calculations are performed in the same way as Eq. 38a:

$$\begin{aligned}{}^p\tilde{\alpha}_{mn}(E)&=-\sum_{f,g\neq 0}\sum\langle 0|\mu|\tilde{f}\tilde{m}\rangle\langle\tilde{f}\tilde{m}|\tilde{G}(E)|\tilde{g}\tilde{n}\rangle\langle\tilde{g}\tilde{n}|\mu|0\rangle\\&\simeq-\sum_f\sum_g\tilde{\mu}_{0f}^{(m)}\langle\tilde{f}\tilde{m}|\tilde{G}^{\circ}(E)+\tilde{G}^{\circ}(E)\tilde{V}_{FD}\tilde{G}^{\circ}(E)\\&\qquad+\tilde{G}^{\circ}(E)\tilde{V}_{FD}\tilde{G}^{\circ}(E)\tilde{V}_{FD}\tilde{G}^{\circ}(E)+\cdots|\tilde{g}\tilde{n}\rangle\tilde{\mu}_{g0}^{(n)}\\&\quad-\sum_f\sum_g\tilde{\mu}_{0f}^{(m)}\langle\tilde{f}\tilde{m}|\tilde{G}^{\circ}(E)\tilde{V}_S\tilde{G}(E)\\&\qquad+\tilde{G}^{\circ}(E)\tilde{V}_S\tilde{G}^{\circ}(E)\tilde{V}_S\tilde{G}^{\circ}(E)+\cdots|\tilde{g}\tilde{n}\rangle\tilde{\mu}_{g0}^{(n)}\\&\quad-\sum\sum\{\tilde{\mu}_{0f}^{(m)}\langle fm|\tilde{G}_{FD}^{\circ}(E){}^p\tilde{V}_S(E)\tilde{G}_{FD}^{\circ}(E){}^p\tilde{V}_S(E)\tilde{G}_{FD}^{\circ}(E)|gn\rangle\tilde{\mu}_{g0}^{(n)}\\&\quad+\tilde{\mu}_{0f}^{(m)g}\langle fm|\tilde{G}_{FD}^{\circ}(E){}^p\tilde{V}_{FD}(E)\tilde{G}_{FD}^{\circ}(E){}^p\tilde{V}_S(E)\tilde{G}_{FD}^{\circ}(E)|gn\rangle\tilde{\mu}_{g0}^{(n)}+\\&\quad\tilde{\mu}_{0f}^{(m)}\langle fm|\tilde{G}_{FD}^{\circ}(E){}^p\tilde{V}_{FD}(E)\tilde{G}_{FD}^{\circ}(E)\\&\qquad\times\ {}^p\tilde{V}_S(E)\tilde{G}_{FD}^{\circ}(E){}^p\tilde{V}_{FD}(E)\tilde{G}_{FD}^{\circ}(E)|gn\rangle\tilde{\mu}_{g0}^{(n)}\\&\quad+\tilde{\mu}_{0f}^{(m)}\langle fm|\tilde{G}_{FD}^{\circ}(E){}^p\tilde{V}_S(E)\tilde{G}_{FD}^{\circ}(E){}^p\tilde{V}_{FD}(E)\\&\qquad\times\ \tilde{G}_{FD}^{\circ}(E){}^p\tilde{V}_S(E)\tilde{G}_{FD}^{\circ}(E)|gn\rangle\tilde{\mu}_{g0}^{(n)}\},\end{aligned} \tag{54}$$

except for the third term in which we put merely the pure Fano-DeVoe part as $\tilde{G}_{FD}^{\circ}(E)=\sum_{\psi}(E-\tilde{\varepsilon}_{\psi,0}+i\tilde{\eta}_{\psi})^{-1}|\psi\rangle\langle\psi|$ in the $\tilde{G}^{\circ}(E)$. Also, we make use of the $\langle fm|$ and $|gn\rangle$ instead of the $\langle\tilde{f}\tilde{m}|$ and $|\tilde{g}\tilde{n}\rangle$, and employ only the bare interaction operator $\bar{V}$ instead of the dressed interaction operator $\tilde{V}$. The reason for this last treatment is that the components of the third terms are clearly at least second order in the bare interaction $\langle\psi|V|\psi'\rangle$ and therefore the corrections produced by such truncation of the third term become third order in $\langle\psi|V|\psi'\rangle$.

The working formula for the polymer polarizability tensor is obtained from Eq. 54:

$$\begin{aligned}{}^p\tilde{\alpha}_{mn}(E)&\simeq{}^p\tilde{\alpha}_{mm}^{FD}(E)+{}^p\tilde{\alpha}_{mm}^{S}(E)\delta_{mm}\\&\quad+\sum_{f\neq t}\sum_k\sum\tilde{\mu}_{0f}^{(m)}\tilde{K}_{mm}^{ft}(E)\mu_{t0}^{(m)}\cdot\{\mathbf{1}+\boldsymbol{U}\cdot\tilde{\boldsymbol{\alpha}}^{oo}(E)\}_{mk}^{-1}\cdot\boldsymbol{U}_{kn}\cdot\tilde{\boldsymbol{\alpha}}_{nn}^{ol}(E)\\&\quad+\sum_k\sum_{t\neq g}\sum\tilde{\boldsymbol{\alpha}}_{mm}^{lo}(E)\cdot\boldsymbol{U}_{mk}\cdot\{\mathbf{1}+\tilde{\boldsymbol{\alpha}}^{oo}(E)\cdot\boldsymbol{U}\}_{kn}^{-1}\cdot\boldsymbol{\mu}_{0f}^{(n)}\tilde{K}_{nn}^{tg}(E)\tilde{\boldsymbol{\mu}}_{g0}^{(n)}\\&\quad-\sum_k\sum_l\sum_{t\neq g}\sum\tilde{\boldsymbol{\alpha}}_{mm}^{lo}(E)\cdot\boldsymbol{U}_{mk}\cdot\{\mathbf{1}+\tilde{\boldsymbol{\alpha}}^{oo}(E)\cdot\boldsymbol{U}\}_{kl}^{-1}\cdot\boldsymbol{\mu}_{0f}^{(l)}\tilde{K}_{ll}^{tg}(E)\tilde{\boldsymbol{\mu}}_{g0}^{(l)}\\&\quad\times\{\mathbf{1}+\boldsymbol{U}\cdot\tilde{\boldsymbol{\alpha}}^{oo}(E)\}_{lj}^{-1}\cdot\boldsymbol{U}_{jn}\cdot\tilde{\boldsymbol{\alpha}}_{nn}^{ol}(E)-\sum_{f\neq t}\sum_k\sum_{s\neq g}\sum\tilde{\boldsymbol{\mu}}_{0f}^{(m)}\tilde{K}_{mm}^{ft}(E)\boldsymbol{\mu}_{t0}^{(m)}\\&\quad\times\{\mathbf{1}+\boldsymbol{U}\cdot\tilde{\boldsymbol{\alpha}}^{oo}(E)\}_{mk}^{-1}\cdot\boldsymbol{U}_{kn}\cdot\boldsymbol{\mu}_{0s}^{(n)}\tilde{K}_{ll}^{sg}(E)\tilde{\boldsymbol{\mu}}_{g0}^{(n)}\quad m,n=1,2,3,\cdots,N\end{aligned} \tag{55}$$

with

$$\begin{aligned}K_{mm}^{fg}(E)=\Big\{&\frac{\langle\tilde{f}\tilde{m}|V|\tilde{g}\tilde{m}\rangle}{E-\tilde{\varepsilon}_{fm,0}+i\tilde{\eta}_{fm}}+\sum_{t\neq f,g}\\&\times\frac{\langle\tilde{f}\tilde{m}|V|\tilde{t}\tilde{m}\rangle\langle\tilde{t}\tilde{m}|V|\tilde{g}\tilde{m}\rangle}{(E-\tilde{\varepsilon}_{fm,0}+i\tilde{\eta}_{fm})(E-\tilde{\varepsilon}_{tm,0}+i\tilde{\eta}_{tm})}+\cdots\Big\}/\\&(E-\tilde{\varepsilon}_{gm,0}+i\tilde{\eta}_{gm})\end{aligned} \tag{56}$$

where $\{\mathbf{1}+\boldsymbol{U}\cdot\tilde{\boldsymbol{\alpha}}^{oo}(E)\}_{kn}^{-1}$ and $\{\mathbf{1}+\tilde{\boldsymbol{\alpha}}^{oo}(E)\cdot\boldsymbol{U}\}_{mk}^{-1}$ have similar expressions as Eqs. 39 and 40. Equatition 55 is a renormalized RPA. The first and second terms are put into a single equation:

$$\begin{aligned}{}^p\tilde{\alpha}_{mn}^{FD}(E)+{}^p\tilde{\alpha}_{mn}^{S}(E)\delta_{mm}&=\sum_{f,g\neq 0}\sum\tilde{\alpha}_{fm,gn}(E)\{\delta_{mn}\delta_{fg}\\&+\frac{\langle\tilde{f}\tilde{m}|V|\tilde{f}\tilde{n}\rangle}{E-\tilde{\varepsilon}_{fm,0}+i\tilde{\eta}_{fm}}+\sum_{s\neq f,g}\sum_k\frac{\langle\tilde{f}\tilde{m}|V|\tilde{s}\tilde{k}\rangle\langle\tilde{s}\tilde{k}|V|\tilde{g}\tilde{n}\rangle}{(E-\tilde{\varepsilon}_{fm,0}+i\tilde{\eta}_{fm})(E-\tilde{\varepsilon}_{sk,0}+i\tilde{\eta}_{sk})}\\&+\sum_k\sum_l\sum_{s\neq t,f,g,t\neq g,f,s}\sum\\&\qquad\frac{\langle\tilde{f}\tilde{m}|V|\tilde{s}\tilde{k}\rangle\langle\tilde{s}\tilde{k}|V|\tilde{l}\tilde{l}\rangle\langle\tilde{l}\tilde{l}|V|\tilde{g}\tilde{n}\rangle}{(E-\tilde{\varepsilon}_{fm,0}+i\tilde{\eta}_{fm})(E-\tilde{\varepsilon}_{sk,0}+i\tilde{\eta}_{sk})(E-\tilde{\varepsilon}_{ll,0}+i\tilde{\eta}_{ll})}\\&\equiv\sum_{f,g\neq 0}\sum\tilde{\alpha}_{fm,gn}(E)\,{}^pB_{mn}^{fg}(E),\end{aligned} \tag{57}$$

where we must note that the $n=m$ case corresponds to the Bayley, Nielsen, and Schellman type of polarizability tensor ${}^p\tilde{\alpha}^s(E)$.

The scalar quantity ${}^pB_{mn}^{fg}(E)$ defines the coefficient for the $\tilde{\alpha}_{fm,gn}(E)$. ${}^pB_{mn}^{fg}(E)$ involves the interaction elements $\{\langle\tilde{f}\tilde{m}|V|\tilde{g}\tilde{n}\rangle\}$ up to infinite orders. It goes without saying that ${}^p\tilde{\alpha}(E)$ involves the usual Fano-DeVoe type of term $\{\mathbf{1}+\tilde{\boldsymbol{\alpha}}^{oo}(E)\cdot\boldsymbol{U}\}^{-1}\cdot\tilde{\boldsymbol{\alpha}}^{oo}(E)$. If we resolve all the interaction matrices into the form $\boldsymbol{\mu}\cdot\boldsymbol{U}\cdot\boldsymbol{\mu}$, by use of which if we try to express ${}^p\tilde{\alpha}(E)$ in terms of the average of dyadic products $\boldsymbol{\mu}G^{\circ}(E)\boldsymbol{\mu}$ over the polymer ground state and unit dipole interaction

tensors $\boldsymbol{U}$, we must face with a tremendous variety of complicated matrix elements of ${}^{p}\tilde{\alpha}(E)$, so that it becomes difficult to outline the total image of the theory. However, as shown in Eqs. 55 and 57, it is not difficult to compute ${}^{p}\tilde{\alpha}(E)$ up to higher orders of V without resolving matrix elements into small pieces such as $\boldsymbol{\mu}\cdot\boldsymbol{U}\cdot\boldsymbol{\mu}$. Namely, Eq. 55 gives a simple expression for ${}^{p}\tilde{\alpha}(E)$, in which Eq. 57 is represented in terms of scalar modules such as $\langle\tilde{fm}|V|\tilde{gn}\rangle$. In addition to this merit, ${}^{p}B(E)$ defined by Eq. 57 can easily be linearlized in terms of simple matrix elements such as

$$B^{fg}_{mn}(E)=\langle\tilde{fm}|V|\tilde{gn}\rangle/(E-\tilde{\varepsilon}_{fm,0}+i\tilde{\eta}_{fm}). \tag{58}$$

In the following, we show that ${}^{p}B(E)$ can formally be calculated up to infinite orders of V without resort to such reckless term-by-term calculations as that of Eq. 57.

In relation with Eq. 57, we can put

$$\begin{aligned}{}^{p}B^{fg}_{mn}(E)&=\delta_{mn}\delta_{fg}+B^{fg}_{mn}(E)+\sum_{s}\sum_{k}B^{fs}_{mk}(E)B^{sg}_{kn}(E)\\&\quad+\sum_{s}\sum_{k}\sum_{t}\sum_{l}B^{fs}_{mk}(E)B^{st}_{kl}(E)B^{tg}_{ln}(E)+\cdots\\&=\delta_{mn}\delta_{fg}+\sum_{s}\sum_{k}B^{fs}_{mk}(E)\{\delta_{kn}\delta_{sg}\\&\quad+\sum_{t}\sum_{l}B^{st}_{kl}(E){}^{p}B^{tg}_{ln}(E)\}\\&=\delta_{mn}\delta_{fg}+\sum_{s}\sum_{k}B^{fs}_{mk}(E){}^{p}B^{sg}_{kn}(E)=\{[1-B(E)]^{-1}\}^{fg}_{mn},\end{aligned} \tag{59a}$$

where $B(E)$ is a $(\sum_{m=1}^{N}f_m)\times(\sum_{k=1}^{N}S_k)$ matrix, f_m being the number of the fth oscillators of the mth site. In more detail, if we define the block matrices ${}^{p}B_{mn}(E)$ and $B_{mk}(E)$ with the elements ${}^{p}B^{fg}_{mn}(E)$ and $B^{fs}_{mk}(E)$. Equation 59a yields the relationship of an unknown matrix ${}^{p}B(E)$ with the known matrix $B(E)$ as follows:

$${}^{p}B(E)=1+B(E)\,{}^{p}B(E),\ \text{i.e.,}\ {}^{p}B(E)=\{1-B(E)\}^{-1}, \tag{59b}$$

which gives the involvement of infinite orders of the interaction $\tilde{V}$ in Eq. 57. Actually, it may be sufficient to carry out the calculations of several higher terms in the braces of Eq. 57 without use of Eqs. 59a and 59b.

If we follow the scheme of Eq. 42 which corresponds to the intermediate coupling case, we have

$$\begin{aligned}{}^{rp}\tilde{\alpha}_{mn}(E)&={}^{p}\tilde{\alpha}_{mn}(E)\\&\quad+\sum_{k}\sum_{f}\sum_{g}C^{(k)}_{0,fm}\langle fm|\boldsymbol{\mu}\tilde{G}^{\circ}(E)|\tilde{gn}\rangle\langle\tilde{gn}|\boldsymbol{\mu}|0\rangle\\&\quad+\sum_{k}\sum_{f}\sum_{g}\langle 0|\boldsymbol{\mu}|\tilde{fm}\rangle\langle\tilde{fm}|\tilde{G}^{\circ}(E)\boldsymbol{\mu}|gn\rangle C^{(k)}_{gn,0}\\&\quad+\sum_{k}\sum_{s}\sum_{t}\sum_{g}C^{(m,k)}_{0,smtk}\langle smtk|\boldsymbol{\mu}\tilde{G}^{\circ}(E)|\tilde{gn}\rangle\langle\tilde{gn}|\boldsymbol{\mu}|0\rangle\\&\quad+\sum_{k}\sum_{f}\sum_{s}\sum_{t}\langle 0|\boldsymbol{\mu}|\tilde{fm}\rangle\langle\tilde{fm}|\tilde{G}^{\circ}(E)\boldsymbol{\mu}|sktn\rangle C^{(k,n)}_{sktn,0}\\&\quad+O(|C_{mix}|^{2}),\end{aligned} \tag{60}$$

which is the self-consistent renormalized RPA. The transition moments necessary for the calculations of Eq. 60 are reduced to

$$\langle fm|\boldsymbol{\mu}|\tilde{gn}\rangle=\boldsymbol{\mu}^{(m)}_{fg}\delta_{mn}+\sum_{k}C^{(k)}_{0,gn}\boldsymbol{\mu}^{(m)}_{f0}\delta_{mk}, \tag{61}$$

$$\langle\tilde{fm}|\boldsymbol{\mu}|gn\rangle=\boldsymbol{\mu}^{(m)}_{fg}\delta_{mn}+\sum_{k}C^{(k)}_{0,gn}\boldsymbol{\mu}^{(m)}_{g0}\delta_{nk}, \tag{62}$$

$$\langle smtk|\boldsymbol{\mu}|\tilde{gn}\rangle=\delta_{mn}\delta_{sg}\boldsymbol{\mu}^{(k)}_{t0}+\delta_{kn}\delta_{tg}\boldsymbol{\mu}^{(m)}_{s0}, \tag{63}$$

$$\langle\tilde{fm}|\boldsymbol{\mu}|sktn\rangle=\delta_{mk}\delta_{sf}\boldsymbol{\mu}^{(n)}_{0t}+\delta_{mn}\delta_{ft}\boldsymbol{\mu}^{(k)}_{0s}, \tag{64}$$

As mentioned before regarding to Eq. 43, it may be not necessary to carry out the calculations of the correction terms for Eq. 60. However, for a polymer system of the constituent monomers having no permanent dipole moment, we need to calculate Eq. 60 as follows:

$$\begin{aligned}{}^{rp}\tilde{\boldsymbol{\alpha}}_{mn}(E)&=[\boldsymbol{1}+\tilde{\boldsymbol{\alpha}}^{oo}(E)\cdot\boldsymbol{U}]^{-1}_{mn}\cdot\tilde{\boldsymbol{\alpha}}^{oo}_{nn}(E)\\&\quad+\sum_{s}\sum_{k}\sum_{t}\{[\boldsymbol{1}+\tilde{\boldsymbol{\alpha}}^{oo}(E)\cdot\boldsymbol{U}]^{-1}_{mk}\cdot\boldsymbol{\mu}^{(k)}_{0s}C_{sktn,0}\boldsymbol{\mu}^{(n)}_{0t}/\\&\quad(E-\tilde{\varepsilon}_{sk,0}+i\tilde{\eta}_{sk})\\&\quad+[\boldsymbol{1}+\tilde{\boldsymbol{\alpha}}^{oo}(E)\cdot\boldsymbol{U}]^{-1}_{mn}\cdot\boldsymbol{\mu}^{(n)}_{0t}C_{sktn,0}\boldsymbol{\mu}^{(k)}_{0s}/(E-\tilde{\varepsilon}_{tn,0}+i\tilde{\eta}_{tn})\\&\quad+\boldsymbol{\mu}^{(k)}_{t0}C_{0,smtk}\boldsymbol{\mu}^{(m)}_{0s}/(E-\tilde{\varepsilon}_{sm,0}+i\tilde{\eta}_{sm})\cdot[\boldsymbol{1}+\boldsymbol{U}\cdot\tilde{\boldsymbol{\alpha}}^{oo}(E)]^{-1}_{mn}\\&\quad+\boldsymbol{\mu}^{(m)}_{s0}C_{0,smtk}\boldsymbol{\mu}^{(k)}_{0t}/(E-\tilde{\varepsilon}_{tk,0}+i\tilde{\eta}_{tk})\cdot[\boldsymbol{1}+\boldsymbol{U}\cdot\tilde{\boldsymbol{\alpha}}^{oo}(E)]^{-1}_{kn}\}\\&\quad+O(C_{0,smtj}C_{fkgn,0}),\end{aligned} \tag{65}$$

which is the same as Eq. 43 except for the excitation energies replaced by Eq. 47, where the mixing coefficients of one-site excitation states vanish.

For the dressed polarizability tensors derived above, we can obtain the bandshape functions of the UV absorption, CD, and ORD spectra for the DNA molecules, either from the calculations[1,2] of $3^{-1}\,Tr\,{}^{p}\tilde{\boldsymbol{\alpha}}_{mn}(E)$ and $12^{-1}\,\boldsymbol{R}_{mn}\cdot({}^{p}\tilde{\boldsymbol{\alpha}}_{mn}(E)\colon\boldsymbol{\varepsilon})$ by making use of Eq. 55, or from the calculations of $3^{-1}\,Tr\,{}^{rp}\tilde{\boldsymbol{\alpha}}_{mn}(E)$ and $12^{-1}\,\boldsymbol{R}_{mn}\cdot({}^{rp}\tilde{\boldsymbol{\alpha}}_{mn}(E)\colon\boldsymbol{\varepsilon})$ by making use of Eq. 60 and/or Eq. 65.

Joint Use of Short-Range Monopole and Long-Range Dipole Approximations in All the Interaction Integrals $\langle\psi|V|\psi'\rangle$

The use of the dipole approximation makes it easy to calculate the polarizability tensors, since the transition moments are easily obtainable from the experimental data. However, in order to circumvent the deficiency of the dipole approximation in short distances, it is recommendable to make use of the monopole approximation for the near or nearest neighbors, and to make use of the dipole approximation for the distant monomers, when the data for the monopole densities are easily available. Especially, in very long-chain polymers, such joint use of different approximations will clearly have a lot of practical merits. Consequently, let us show how to introduce the monopole approximation in the present polarizability theory. All the interaction integrals $\langle\psi|V|\psi'\rangle$ as well as the mixing coefficients $C_{0,\psi}$ and $C_{\psi,0}$ are reduced to the forms such as $\boldsymbol{\mu}^{(m)}_{sf}\cdot\boldsymbol{U}_{mn}\cdot\boldsymbol{\mu}^{(n)}_{gt}\equiv V^{(sf,gt)}_{mn}$.

The scalar potential $V^{(sf,gt)}_{mn}$ is expressed by

$$\begin{aligned}V^{(sf,gt)}_{mn}&=\boldsymbol{\mu}^{(m)}_{sf}\cdot\boldsymbol{U}_{mn}\cdot\boldsymbol{\mu}^{(n)}_{gt}\\&=[\boldsymbol{\mu}^{(mx)}_{sf}\ \boldsymbol{\mu}^{(my)}_{sf}\ \boldsymbol{\mu}^{(mz)}_{sf}]\begin{bmatrix}U^{(xx)}_{mn}&U^{(xy)}_{mn}&U^{(xz)}_{mn}\\U^{(yx)}_{mn}&U^{(yy)}_{mn}&U^{(yz)}_{mn}\\U^{(zx)}_{mn}&U^{(zy)}_{mn}&U^{(zz)}_{mn}\end{bmatrix}\begin{bmatrix}\boldsymbol{\mu}^{(nx)}_{gt}\\\boldsymbol{\mu}^{(ny)}_{gt}\\\boldsymbol{\mu}^{(nz)}_{gt}\end{bmatrix}\\&\simeq\sum_{A}^{\text{atoms}}\sum_{B}q^{(m)}_{sf,A}q^{(n)}_{gt,B}/R_{mA,nB},\end{aligned} \tag{66}$$

where the final replacement from the dipole approximation is the so-called transition monopole approximation[9-14,21,22] with the monopole densities separated by the distance $R_{mA,nB}$. Particularly, $q^{(m)}_{0f,A}$ denotes the usual 0→f transition monopole density at atom A in the mth submolecule, and $q^{(m)}_{00,A}$ specifies the permanent monopole density. The knowledge of the transition and permanent monopole densities of a monomer may be obtained by some molecular orbital calculations[9] or by the semiempirical estimates.[10-14,21,22]

The ${}^{p}\alpha(E)$ appeared in Eq. 38b takes the following various forms:

$$\begin{aligned}{}^{p}\alpha(E) &= \{\mathbf{1}+\alpha(E)\cdot U\}^{-1}\cdot\alpha(E)\\ &= \{\alpha^{-1}(E)+U\}^{-1}\\ &= \alpha(E)\cdot\{\alpha(E)+\alpha(E)\cdot U\cdot\alpha(E)\}^{-1}\cdot\alpha(E)\end{aligned} \tag{67}$$

where the second line indicates the equivalence to DeVoe's coupled oscillator theory.[8] The third line is found to be convenient to introduce the transition and permanent monopole approximations for the near neighbor interactions.

It is also convenient for the monopole approximation to rewrite Eqs. 39 and 40 as follows:

$$\{\mathbf{1}+\alpha(E)\cdot U\}^{-1}=\alpha(E)\cdot\{\alpha(E)+\alpha(E)\cdot U\cdot\alpha(E)\}^{-1}, \tag{68}$$

$$\{\mathbf{1}+U\cdot\alpha(E)\}^{-1}=\{\alpha(E)+\alpha(E)\cdot U\cdot\alpha(E)\}^{-1}\cdot\alpha(E). \tag{69}$$

In order to introduce the monopole approximation for the near neighbor submolecules, the matrix elements for $\alpha(E)\cdot U\cdot\alpha(E)$ are calculated as

$$\begin{aligned}&\alpha_{mm}(E)\cdot U_{mn}\cdot\alpha_{nn}(E)\\ &=\sum_f\sum_g (E-\varepsilon_{fm,0}+i\eta_{fm})^{-1}(E-\varepsilon_{gn,0}+i\eta_{gm})^{-1}V^{(f0,0g)}_{mn}\mu^{(m)}_{0f}\mu^{(n)}_{g0},\end{aligned} \tag{70}$$

where the dyadic product $\mu^{(m)}_{0f}\mu^{(n)}_{g0}$ is expressed in terms of the multiplication of the column matrix $\mu^{(m)}_{0f}$ by the row matrix $\mu^{(n)}_{g0}$ and the Coulomb energy $V^{(f0,0g)}_{mn}$ is calculated by Eq. 66.

For non-near neighbors, we can also make use of the monopole approximation, but it is suffcient to make use of the dipole approximation. For the latter case, it may be convenient to calculate the corresponding matrix elements in a way different from Eq. 70 in algolithm as follows:

$$\begin{aligned}&\alpha_{mm}(E)\cdot U_{mn}\cdot\alpha_{mn}(E)\\ &=\sum_f\sum_g (E-\varepsilon_{fm,0}+i\eta_{fm})^{-1}(E-\varepsilon_{gn,0}+i\eta_{gn})^{-1}\times\\ &\quad\{\mu^{(m)}_{0f}\mu^{(m)}_{f0}\}\cdot U_{mn}\cdot\{\mu^{(n)}_{0f}\mu^{(n)}_{f0}\},\end{aligned} \tag{71}$$

where $\mu^{(m)}_{0f}\mu^{(m)}_{f0}$ is a 3×3 matrix.

It is practically important to note that the inverse of the matrix $\{\alpha(E)+\alpha(E)\cdot U\cdot\alpha(E)\}$ concerned should be obtained in units of 10^{-24} cm^3 according to the numerical treatment of the previous paper,[2] whereas the inverse of $\{\mathbf{1}+\alpha(E)\cdot U\}$ can always be calculated to be at most in the vicinity of unity or with much smaller values in its matrix elements.

Summary and Discussion

We have presented a new approach capable of extending the Fano-DeVoe model. Such an approach is inherently based upon the dipole-dipole approximation, which has however a deficiency in the near neighbors of submolecules. In the previous section, we have shown how to bring in the monopole approximation by changing the present forms of polymer polarizability tensors derived. Thus, following Moffitt's idea, it becomes possible to use jointly the short-range-oriented monopole and long-range-oriented dipole approximations in the present theory.

We can first point out that this approach makes it possible to calculate the polarizability tensors by involving the static effect of permanent dipole moments for some DNA molecules and polypeptides,[13-15,17] whereas the ordinary Fano-DeVoe model cannot involve the static field effect in calculations. It should be noted that inclusion of the static effect in the theory is made in the three ways: (i) We can observe the static effect in the level-shift energy of the excitation energy $\varepsilon_{\psi,0}$ given by Eqs. 18 and 19; (ii) The static effect is clearly found to be involved, if we see that the second terms of Eqs. 16 and 35 are expressed by Eq. 11, which corresponds to the static field effect appeared in the transition matrix theory;[15] (iii) The static effect is taken into account by use of the exact basis set $\{|\tilde{\psi}>\}$ as well as by the renormalization of $-<\tilde{0}|\mu G(E)\mu|\tilde{0}>$ of Eqs. 24, 42, and 43 and/or $-<\tilde{0}|\mu\tilde{G}(E)\mu|\tilde{0}>$ of Eqs. 33, 60, and 65. If there is no static effect due to $\mu^{(\text{site})}_{00}=0$, Eq. 38b embodies the original Fano-DeVoe model. Even for this case, as shown in Eq. 43 and also Eq. 65, we can extend the pure Fano-DeVoe model by the renormalization of the polymer ground state through two-site excitation states.

In relation with (ii), we must note that Eq. 38a without truncation is identical to Rabenold's linear response theory.[16,17] His derivation is based upon the transition matrix theory[15] with the use of Green's operator method. Let us take a look at his formulation in terms of our notations. The polymer polarizability tensor is expressed by

$$\begin{aligned}{}^{p}\alpha(E) &= -\sum_{\psi,\psi'\neq 0}\sum <0|\mu|\psi><\psi|(E-\bar{H}+i\eta)^{-1}|\psi'><\psi'|\mu|0>\\ &= -\sum_f\sum_g\sum_m\sum_n \mu^{(m)}_{0f}\{\{[(E\mathbf{1}-\varepsilon+i\eta)\bar{V}_S]-\bar{V}_{FD}\}^{-1}\}^{fg}_{mn}\mu^{(n)}_{g0},\end{aligned} \tag{72}$$

whose matrix elements are

$$\{\bar{V}_S\}^{fg}_{mn}=\delta_{mn}<fm|V|gm>=\delta_{mn}\sum_{k\neq m(f\neq g)}\mu^{(m)}_{fg}\cdot U_{mk}\cdot\mu^{(k)}_{00}, \tag{73}$$

$$\{\bar{V}_{FD}\}^{fg}_{mn}=<fm|V|gm>=\mu^{(m)}_{f0}\cdot U_{mk}\cdot\mu^{(n)}_{g0}, \tag{74}$$

$$\{E\mathbf{1}-\varepsilon+i\eta\}^{fg}_{mn}=(E-\varepsilon_{fm,0}+i\eta_{fm})\delta_{mn}\delta_{fg}. \tag{75}$$

The $[(E\mathbf{1}-\varepsilon+i\eta)-\bar{V}_s]$ in Eq. 72 is an m,m-block diagonal matrix with the off-diagonal f,g,-elements, while

the Fano-DeVoe type interaction $\overline{V}_{FD}$ is an m,n-block off-diagonal matrix. The f,f-diagonal elements $<fm|V|fm>$ of $\overline{V}_S$ for the static field effect are included in the excitation energy $\varepsilon_{fm,0}$. If we follow Rabenold, the equivalence of the two theories can be shown by diagonalizing each m,m-block diagonal matrix of Eq. 72 as follows:

$$\boldsymbol{X}^{+}[(E\mathbf{1}-\varepsilon+i\eta)-\overline{V}_S]\boldsymbol{X}=E\mathbf{1}-\bar{\varepsilon}+i\bar{\eta}, \tag{76}$$

with the eigenvector:

$$\boldsymbol{X}=\mathrm{diag}\{\boldsymbol{X}_1, \boldsymbol{X}_2, \ldots\ldots, \boldsymbol{X}_N\}, \tag{77}$$

by use of which we newly define the dressed interaction matrix for the polymer system

$$\{{}^{px}\overline{V}_{FD}\}_{mn}=\sum_f\sum_j\sum_g\sum_k X^{+}_{m,fj}\{\overline{V}_{FD}\}^{fg}_{jk}X_{gk,n}. \tag{78}$$

In Eq. 72, we can express the secular matrix in terms of the block diagonal matrix of Eq. 77, X, as follows:

$$\boldsymbol{X}^{+}\{[(E\mathbf{1}-\varepsilon+i\eta)-\overline{V}_S]-\overline{V}_{FD}\}X=(E\mathbf{1}-\bar{\varepsilon}+i\bar{\eta})-\boldsymbol{X}^{+}\overline{V}_{FD}\boldsymbol{X}$$
$$\equiv(E\mathbf{1}-\bar{\varepsilon}+i\bar{\eta})-{}^{px}\overline{V}_{FD} \tag{79}$$

where the first term is given by Eq. 76. Equation 79 gives rise to

$$\{[(E\mathbf{1}-\bar{\varepsilon}+i\bar{\eta})-\overline{V}_S]-\overline{V}_{FD}\}^{-1}=\boldsymbol{X}\{(E\mathbf{1}-\bar{\varepsilon}+i\bar{\eta})-{}^{px}\overline{V}_{FD}\}^{-1}\boldsymbol{X}^{+}. \tag{80}$$

Thus, if we make an allowance for

$$\{{}^{px}\overline{V}_{FD}\}^{fg}_{jk}=\sum_m\sum_n X^{+}_{j,fm}<fm|V|gn>X_{gn,k}$$
$$=<\bar{f}\bar{j}|V|\bar{g}\bar{k}>=\bar{\boldsymbol{\mu}}^{(j)}_{f0}\cdot\boldsymbol{U}_{jk}\cdot\bar{\boldsymbol{\mu}}^{(k)}_{0g}, \tag{81}$$

with the relationships

$$|\bar{g}\bar{k}>=\sum_n|gn>X_{gn,k}, \tag{82}$$

$$\{[(E\mathbf{1}-\bar{\varepsilon}+i\bar{\eta})-{}^{px}\overline{V}_{FD}]^{-1}\}^{fg}_{jk}=(E-\bar{\varepsilon}_{fj,0}+\mathrm{i}\,\bar{\eta}_{fj})^{-1}\delta_{jk}\delta_{fg}$$
$$+(E-\bar{\varepsilon}_{fj,0}+i\bar{\eta}_{fj})^{-1}\{{}^{px}\overline{V}_{FD}\}^{fg}_{jk}(E-\bar{\varepsilon}_{gk,0}+i\bar{\eta}_{gk})^{-1}+\ldots, \tag{83}$$

we note that Eq. 72 can be reduced to

$${}^{p}\boldsymbol{\alpha}(E)=-\sum_f\sum_m\sum_g\sum_n\sum_j\sum_k\boldsymbol{\mu}^{(m)}_{0f}X_{fm,j}\{[(E\mathbf{1}-\bar{\varepsilon}+i\bar{\eta})$$
$$-{}^{px}\overline{V}_{FD}]^{-1}\}^{fg}_{jk}X^{+}_{k,gn}\boldsymbol{\mu}^{(n)}_{g0},$$
$$=-\sum_f\sum_j\sum_g\sum_k\bar{\boldsymbol{\mu}}^{(j)}_{0f}\{[(E\mathbf{1}-\bar{\varepsilon}+i\bar{\eta})-{}^{px}\overline{V}_{FD}]^{-1}\}^{fg}_{jk}\bar{\boldsymbol{\mu}}^{(k)}_{g0}$$
$$=-\sum_f\sum_k\{\mathbf{1}+\bar{\boldsymbol{\alpha}}(E)\cdot\boldsymbol{U}\}^{-1}_{jk}\cdot\bar{\boldsymbol{\alpha}}_{kk}(E), \tag{84}$$

where we put

$$\bar{\boldsymbol{\mu}}^{(j)}_{0f}=\sum_m\boldsymbol{\mu}^{(m)}_{0f}X_{fm,j}, \tag{85}$$

$$\bar{\boldsymbol{\alpha}}_{kk}(E)=-\sum_f\bar{\boldsymbol{\mu}}^{(k)}_{0f}\bar{\boldsymbol{\mu}}^{(k)}_{g0}/(E-\bar{\varepsilon}_{fk,0}+i\bar{\eta}_{fk}). \tag{86}$$

Equation 86 defines the kth monomer polarizability tensor corrected by the permanent moments in the rest of monomers. Equation 84 is rather more beautifully linearlized than Eq. 38b. However, Eq. 84 together with Eq. 85 needs the process of the diagonalization for the $\{(E\mathbf{1}-\varepsilon+i\eta)-\overline{V}_s\}$ of each submolecule to obtain X, whereas Eq. 38b requires only to solve the inverse matrix.

In the opening section, we have insisted upon that the theories should be built up so as to be capable of comparing the works made by the ordinary perturbational wavefunction approaches.[19] By doing so, we might find their similarities and clarify the relationships of the present theory with the well-known literature. By applying the present theory to the calculations of quantities such as $<0|\boldsymbol{\mu}G(E)\cdot\boldsymbol{m}|0>$ and $<0|\boldsymbol{\mu}\tilde{G}(E)\cdot\boldsymbol{m}|0>$, $\boldsymbol{m}$ being the magnetic moment operator, we can construct a new polarizability theory capable of discussing the UV absorption, CD, and ORD spectra on the same footing with as that mentioned in Tinoco's review,[19] in which a corrected basis set $\{|\tilde{\psi}>\}$ was introduced. If we confine ourselves to lower-orders approximation in $\overline{V}$ and/or $\tilde{V}$, it will be not so difficult to directly apply the schemes of (A) and (B) for the CD and ORD bandshape calculations without resort to the simplifications of (C) and (D). Such a lower-orders truncation may bring about the theoretical similarity with the results for the ordinary perturbational approaches. However, it is extremely hard to calculate ${}^{p}\boldsymbol{\alpha}(E)$, ${}^{rp}\boldsymbol{\alpha}(E)$, ${}^{p}\tilde{\boldsymbol{\alpha}}(E)$, and ${}^{rp}\tilde{\boldsymbol{\alpha}}(E)$ up to higher orders as mentioned in (A) and (B), so that the simplification is introduced in (C) and (D). Even in the simplified schemes, if we wish to apply the working formula of Eq. 55 to large polymer systems, we must face with the difficulty of solving the inverse matrix extremely larger than the $3N\times3N$ matrix of the working formula of Eq. 38b in (C). The deficiency of DeVoe's coupled oscillator theory also is this case. However, if we wish to allow for the static effect in terms of only the data of $\boldsymbol{\mu}^{(\mathrm{site})}_{00}$ and $\boldsymbol{\mu}^{(\mathrm{site})}_{0f}$ by dropping $\boldsymbol{\mu}^{(\mathrm{site})}_{fg}$ which is not easily available, Eq. 55 is clearly preferred to Eq. 38b. It is again to be pointed out that the renormalized RPA's given by Eqs. 43 and 65 are kind of extensions of the Fano-DeVoe model for the polymer of the constituent chromophores without permanent dipole moments. Applying the theory to the real DNA molecules, the bandshape calculations of UV absorption and CD spectra are now in progress involving the permanent dipole moments.[24-26]

References

1) J. Applequist, *J. Chem. Phys.*, **58**, 421 (1973).
2) H. Ito and Y. J. I'Haya, *J. Chem. Phys.*, **77**, 6270 (1982).
3) W. Rhodes and M. Chase, *Rev. Mod. Phys.*, **39**, 348 (1967).
4) A. Herzenberg and A. Modinos, *Proc. Phys. Soc.*, **87**, 597 (1966).
5) U. Fano, *Phys. Rev.*, **118**, 451 (1960).
6) H. DeVoe, *J. Chem. Phys.*, **41**, 393 (1964).
7) H. DeVoe, *J. Chem. Phys.*, **43**, 3199 (1965).
8) H. DeVoe, *Ann. N. Y. Acad. Sci.*, **158**, 298 (1969).
9) C. L. Cech, W. Hug, and I. Tinoco, Jr., *Biopolymers*, **15**, 131 (1976).
10) C. L. Cech and I. Tinoco, Jr., *Biopolymers*, **16**, 43 (1977).

11) D. S. Moore, *Biopolymers*, **19**, 1017 (1980).
12) A. Williams, Jr. and D. S. Moore, *Biopolymers*, **22**, 755 (1983).
13) R. W. Woody, *J. Chem. Phys.*, **49**, 4797 (1968).
14) E. S. Pysh, *J. Chem. Phys.*, **52**, 4723 (1970).
15) P. M. Bayley, E. B. Nielsen, and J. A. Schellman, *J. Phys. Chem.*, **73**, 228 (1969).
16) D. A. Rabenold, *J. Chem. Phys.*, **73**, 5942 (1980).
17) D. A. Rabenold, *J. Chem. Phys.*, **77**, 4265 (1982).
18) W. Moffitt, *Proc. N. A. Sci.*, **42**, 736 (1956).
19) I. Tinoco. Jr., *Adv. Chem. Phys.*, **4**, 113 (1962).
20) J. A. Schellman, *Acc. Chem. Res.*, **1**, 144 (1968).
21) W. C. Johnson Jr. and I. Tinoco, Jr., *Biopolymers*, **7**, 727 (1969).
22) V. Rizzo and J. A. Schellman, *Biopolymers*, **23**, 435 (1984).
23) R. D. Mattuck, "A Guide to Feynman Daigrams in Many-Body Problem," McGraw-Hill International Book Company (1967).
24) H. DeVoe and I. Tinoco, Jr., *J. Mol. Biol.* **4**, 500 (1962).
25) R. Rein, *Adv. Quantum Chem.*, **7**, 335 (1973).
26) W. Saenger, "Principles of Nucleic Acid Structures," Springer-Verlag, (1984).

 © 1987 The Chemical Society of Japan Bull. Chem. Soc. Jpn., 60, 2803—2807 (1987)

^{63}Cu High Resolution NMR of Cu(I) Halides in Aqueous Solution and Suspension

Kazunaka ENDO,* Kyonosuke YAMAMOTO, Kenzo DEGUCHI,† and Kazuhiro MATSUSHITA†
R & D Laboratories for Photo Materials, Mitsubishi Paper Mills, Ltd., Nagaokakyo, Kyoto 617
†NMR Application Laboratory, Scientific Instrument Division, JEOL Ltd., Akishima, Tokyo 196
(Received March 11, 1987)

In an aqueous solution, ^{63}Cu chemical shielding order ($[CuCl_4]^{3-} \simeq [CuBr_4]^{3-} < [CuI_4]^{3-}$) and line widths (10 to 30 kHz) for CuX-KX systems(where X=Cl, Br, I) have been obtained. The chemical shift(−694 ppm) between $[CuCl_4]^{3-}$ and $[Cu(CN)_4]^{3-}$ is interpreted by the paramagnetic term which depends mainly upon a 3d-hole on a Cu(I) atom by using perturbation theory with an average excitation energy approximation. The line-broadening of Cu(I) halide complexes in aqueous solution is explained dominantly by a Cu(I) nuclear quadrupole interaction with the electric field gradient which arises from a 3d-hole on a Cu atom. For the abnormal increasing metal shielding order of $[MX_4]^{(4-i)-}$($[MCl_4]^{(4-i)-} \leqslant [MBr_4]^{(4-i)-} < [MI_4]^{(4-i)-}$), a possibility of the heavy-atom effect in the metal shielding of $[CuI_4]^{3-}$(649 ppm, using the lowest excitation energy of the diatomic molecule) and $[CdI_4]^{3-}$(1941 ppm using the lowest excitation energy of the diatomic molecule), is evaluated.

It is known that copper(I) halides are photosensitive and semiconductive materials. We think that it is a useful step for determing new materials to study the electronic structure of metal complexes as well as the nature of the chemical bond between metal and ligand. Magnetic properties have long been powerful tools for studies of the electronic structures of transitionmetal complexes. Recently, there have been published a number of papers[1-4] on experimental NMR studies of metal complexes in solid and liquid solution. These studies can be approached from both experimental and theoretical points of view. As one part of a continuing investigation, we have reported ^{109}Ag NMR and MO theoretical studies.[5,6] We now describe a ^{63}Cu high-resolution NMR investigation of nuclear relaxation and chemical shifts for Cu(I) halides in aqueous solution, elucidating correlations with electronic structure in these complexes.

To our knowledge, there were several ^{63}Cu and ^{65}Cu NMR investigations[4a,4b,7,8] dealing with copper(I) halides. Of these studies, Guenther et al.[7] performed a detailed investigation on ^{63}Cu spin-lattice relaxation for solid-state CuX. Lutz et al.[4b] observed that the Cu chemical shift in solid CuX indicates a remarkable increasing shielding order (CuCl≤CuI< CuBr) which does not show a linear dependence on the atomic number of the halide ligand. There have, until now however, been no theoretical study reported for the Cu chemical shift in solid CuX of a repetitive zinc-blende structure. This is because immense time and funds are needed for computer calculations using the ab initio SCFMO method. Thus, first it is necessary to investigate the Cu chemical shift in gaseous and solution-state Cu(I) halides.

Nakatsuji et al.[6] studied the metal chemical shielding constants in Cu, Zn, Ag, and Cd complexes by the ab initio finite perturbation SCF method. For the metal complexes, whose electronic configurations are primarily $d^{10}s^{1-2}p^0$, the metal chemical shifts are due mainly to the paramagnetic term, which depends upon the electrons in the valence np orbital and the holes in the valence (n-1) d orbital. For the Cu complexes(CuCl, $[CuCl_4]^{3-}$, $[Cu(CN)_4]^{3-}$, $[Cu(NH_3)_2]^+$), the d orbital mechanism is predominant. To obtain a physical picture of the Cu shielding of Cu(I) complexes($[CuCl_4]^{3-}$, $[Cu(CN)_4]^{3-}$), a simplified calculation was performed using perturbation theory,[5,9] with an average excitation energy approximation.

This paper presents representative ^{63}Cu NMR spectra obtained from aqueous solutions and suspensions of Cu(I) halides, and provides a theoretical interpretation of the Cu chemical shift and linewidth. We suggest from a qualitative perturbation theory that the Cu chemical shielding is governed by a paramagnetic term, which depends upon a 3d-hole of the Cu(I) atom. For the increasing metal shielding order of $[MX_4]^{(4-i)-}$, we propose the possibility of an effect due to the heavy atom on the metal shielding of $[CuI_4]^{3-}$ and $[CdI_4]^{2-}$. The line-broadening in aqueous solution can be interpreted dominantly by a Cu(I) nuclear quadrupole interaction with the electric field gradient which arises from a 3d-hole in the Cu(I) atom. Lastly, the Cu chemical-shielding difference($[CuCl_4]^{3-} < CuCl \leqslant CuI < [CuI_4]^{3-}$) between a suspension CuX and solution $[CuX_4]^{3-}$ is discussed qualitatively from the standpoint of structure.

Experimental

Materials. $[Cu(CH_3CN)_4]BF_4$ was prepared by a method described in the literature.[10] The compound was checked by elementary analysis and an optical absorption method with the aid of the absorbance at 440 nm of a derived bis(2,2′-bipyridine)copper(I) in acetone(ε_{max}=4800 $M^{-1}cm^{-1}$ (1 M=1 mol dm^{-3})). All chemicals except an NMR reference sample used here were commercially available.

NMR Measurements. All ^{63}Cu spectra were measured at 71.50 MHz with a FX-270 spectrometer. Between 1000 and 10000 transients were accumulated using a 17.5 μs (90°) pulse; 16 K data points were collected over a band width of 50 kHz. These measurements were made at temperature of 30 °C.

Before we measured solutions and suspensions, the samples were bubbled with nitrogen gas for three minutes. The molar ratio of CuX to water for the CuX suspension was 1/28. All ^{63}Cu spectra were externally referenced to liquid

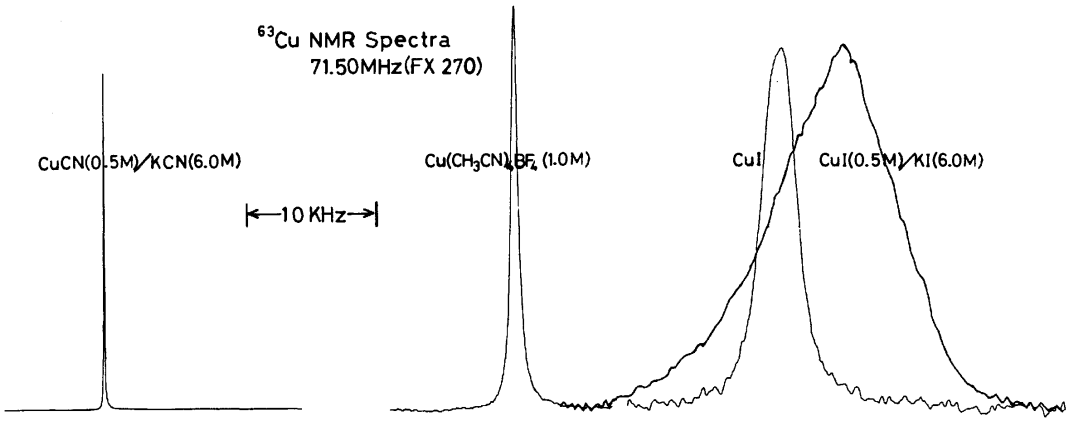

Fig. 1. ^{63}Cu NMR spectra for Cu(I) compounds in aqueous solution and suspension at 71.50 MHz.

Table 1. Chemical Shifts and Linewidths for ^{63}Cu Resonance and Mole Fraction of Cu(I) Complexes for Cu(I) Halides in Aqueous Solution and Suspension at 30°C

Cu(I) salt	Chemical shift[a] (ppm)	linewidth (Hz)	Mole fraction(%) CuX(s)	Cu^+	$[CuX_2]^-$	$[CuX_3]^{2-}$	$[CuX_4]^{3-}$	X^- (M)
CuCl(suspension)	−331	3500	100		0	0	0	
CuCl(0.5M)/KCl(4.0M) (aqueous solution)	−200	28000	0	0	3.4	22.3	74.3	2.7
CuBr(suspension)	−388	3800	100	0	0	0	0	
CuBr(0.5M)/KBr(4.0M) (aqueous solution)	−200	21000	0	0	0	2.0	98.0	2.5
CuI(suspension)	−330	2700	100	0	0	0	0	
CuI(0.5M)/KI(6.0M) (aqueous solution)	−434	12500	0	0	0.3	13.6	86.1	4.6
$[Cu(CH_3CN)_4]BF_4$	0	600						
CuCN(0.5M)/KCN(6.0M) (aqueous solution)	494	70	0	0	0	0.4	99.6	4.5

a) More positive values refer to lower shielding. The reference sample is a 1.0 molar solution of $[Cu(CH_3CN)_4]BF_4$ in CH_3CN.

1.0 M $[Cu(CH_3CN)_4]BF_4$ in CH_3CN. All chemical shifts for ^{63}Cu are defined by

$$\Delta\delta_{sam} = (\nu_{sam} - \nu_{ref})/\nu_{ref},$$

where ν_{sam} is the resonance frequency of a sample and ν_{ref} is the reference frequency. Shifts defined in this manner are positive for lower shielding. The linewidth was evaluated from the widths at half-height. The line shape of the Cu spectra in a suspension and liquid solution is assumed to be Gaussian and Lorentzian, respectively.

Table 2. Solubility Products and Formation Constants of Cu(I) Complexes (30°C)

Cu(I) salt	$-\log K_{sp}$	$\log\beta_1$	$\log\beta_2$	$\log\beta_3$	$\log\beta_4$
CuCl	6.73	*	5.4	5.8	5.9
CuBr[a]	8.28	*	5.16	6.65	7.95
CuI	12.03	*	8.20	9.26	9.40
CuCN	19.5	*	24.0	28.6	30.3

The formation constant has not been obtained. a) The formation constant of $[CuBr_4]^{3-}$ has been obtained by the potential E_{Cu} measurement.[12]

Results and Discussion

Spectra of Solution Cu(I) Complexes. Figure 1 shows a typical ^{63}Cu spectra for Cu(I) complexes in an aqueous solution and suspension; Table 1 gives chemical shift and linewidth data. The total range of chemical shifts is in excess of 900 ppm. Such large variations in shielding are due to a domination of the shielding constant by local paramagnetic contributions.[5,6,9] Note that the shifts and linewidths given in the figure and table represent weighted averages of the shifts and linewidths for various species in equilibrium in the solution. In order to determine the mole fraction of the Cu(I) species in each NMR sample in Table 1, we utilized the solubility products and stability constants[11,12] for Cu(I) salts in Table 2, and performed numerical calculations.

Cu Chemical Shift of Cu(I) Complexes. Table 3

Table 3. The Change in AO Populations of Copper(I) Complexes

Orbital	$[CuCl_4]^{3-}$	$[Cu(CN)_4]^{3-}$
Copper		
$3d_{xx+yy}$	0.000	0.000
$3d_{zz}$	0.000	0.000
$3d_{xy}$	−0.079	−0.164
$3d_{xz}$	−0.079	−0.164
$3d_{yz}$	−0.079	−0.164
4s	0.217	0.292
$4p_x$	0.302	0.357
$4p_y$	0.302	0.357
$4p_z$	0.302	0.357
Ligand		
	Cl^-	CN^-
	(Cl−n=3)	(C−n=2 : N−n=2)
ns	−0.020	−0.494 0.000
np_x	−0.040	−0.119 0.256
np_y	−0.040	−0.119 0.256
np_z	−0.040	−0.119 0.256

In our MO calculation, the AO population of copper(I) ion is given as: AO population of 4s, $4p_x$, $4p_y$, and $4p_z$ was 0.000, that of $2p_x$, $2p_y$, and $2p_z$ in C and N of CN^- was 1.000 (because of $(p\pi)_x$, $(p\pi)_y$, and $(p\pi)_z$ of CN^-) and that of others is 2.000, respectively.

summarizes the change in valence atomic orbital population of the Cu(I) ion and the Cl^- and CN^- ligands due to ligand addition by the ab initio SCF MO method.[5,6] In the table the population increases in the 4s and 4p AOs of Cu(I) atoms and the population decreases in the s and p AOs of ligands indicate an electron transfer from the ligand to copper. Also, a back donation to a ligand produces a hole in the 3d orbitals, coincident with the bonding axes of Cu(I) complexes.

As reported earlier for ^{109}Ag, the chemical shifts of metal complexes for a ligand-metal(Ib and IIb) interaction system can be governed by the paramagnetic term. This will also be explained by the following Eq. 1 for Cu chemical shieldings:

$$\sigma_{para}(Cu(I)) \simeq \frac{-2\alpha^2}{3}\left(\frac{<1/r^3>_p}{E_p}\cdot P_T^e + \frac{<1/r^3>_d}{E_d}\cdot 3D_T^h\right), \quad (1)$$

where P_T^e and D_T^h are the total populations of the p electrons and d holes, respectively.

The paramagnetic term for Cu shielding can be estimated from $E_{p,d}$ and $<1/r^3>_{4p,3d}$ as parameters in the equation. We assume that $E_p=E_d=E$, $<1/r^3>_{4p}=$ 0.59 a.u. and $<1/r^3>_{3d}=5.0$ a.u. (The latter two terms are obtained from the SCF functions by Clementi et al.[13]) The results in Table 4 agree qualitatively with the observed value (Table 1, CuCl/KCl vs. CuCN/KCN). We can also see that the d-orbital contribution is much larger than the p-orbital contribution. This tendency corresponds well to the theoretical result using an ab initio finite-perturbation SCF method.[6]

Possibility of an Effect of a Heavy Atom on Cu Shieldings. In an aqueous solution, we observed an

Table 4. Calculated ^{63}Cu Chemical Shielding Constants of Cu(I) Complexes

	$[CuCl_4]^{3-}$	$[Cu(CN)_4]^{3-}$
d-Contribution $((2\alpha^2/3E_d)$unit)	−3.52	−7.31
p-Contribution $((2\alpha^2/3E_p)$unit)	−0.53	−0.63
Paramagnetic term $((2\alpha^2/3E)$unit)	−4.05	−7.94
$\Delta\sigma$	0	3.89
(E=0.20 a.u.)	0	−690
$\Delta\sigma$(exptl)[a](ppm)	0	−694

a) This value has been obtained from CuCl/KCl vs. CuCn/KCN in Table 1. In this table more negative values refer to lower shielding.

Table 5. Quantities which are Required for the Evaluation of σ_{LS}

	$[CuX_4]^{3-}$	$[AgX_4]^{3-}$	$[CdX_4]^{2-}$
Density[a] of $[MX_4]^{(4-i)-}$			
$3p_{x,y,z}$(Cl)	1.900	1.938	1.960
ns(M)−$3p_{x,y,z}$(Cl)	0.210 (n=4)	0.171 (n=5)	0.702 (n=5)
1st Ionization Potential E[(a.u.)] b)	0.284	0.278	0.330
Excitation Energy[b]	0.0905	0.141	0.135
$\lvert\phi_{s(M)}(0)\rvert^2$(a.u.)[c]	4.37 (^{63}Cu)	8.62 (^{109}Ag)	2.44 (^{111}Cd)

a) The densities were obtained from Ref. 6. b) The values were estimated from the diatomic molecule.[16] c) These values were calculated from the corrected hyperfine splitting constants given by Knight.[17]

anomalous shielding order $[CuI_4]^{3-}$ (for (CuI 0.50M/KI 6.0M))>$[CuBr_4]^{3-}$ (for(CuBr 0.50M/KBr 4.0M))≃ $[CuCl_4]^{3-}$ (CuCl 0.50M/KCl 4.0M)). For other metal(Ag(I), Zn(II), Cd(II)) four coordinate halide complexes, the ^{109}Ag shielding order may be $[AgCl_4]^{3-}$> $[Ag\text{-}Br_4]^{3-}$>$[AgI_4]^{3-}$ (The ^{109}Ag signal for $[AgCl_4]^{3-}$ has not been observed),[5] while the ^{67}Zn and ^{113}Cd shielding order $[ZnI_4]^{2-}$>$[ZnBr_4]^{2-}$>$[ZnCl_4]^{2-}$ and $[CdI_4]^{2-}$ >$[CdBr_4]^{2-}$>$[CdCl_4]^{2-}$ were shown[1a,2] The same shielding order in $[ZnX_4]^{2-}$ and $[CdX_4]^{2-}$ has been observed for ^{13}C in CX_4.[14] Thus, the shielding in $[CuX_4]^{3-}$, $[ZnX_4]^{2-}$, and $[CdX_4]^{2-}$ can be explained in terms of the heavy atom effect (σ_{LS}).[15] On the other hand, the ^{109}Ag shielding may be unaffected by the term but due mainly to the paramagnetic term.

The heavy atom effect has been related to a spin-orbit coupling parameter ζ which is especially large for Br and I in Table 6. The simplified equation for the metal four-coordinate halide complex is

$$\sigma_{LS}^{xx} \simeq -4\pi\zeta\alpha^2|\phi_s(0)|^2\frac{1}{E^2}[\,2P_{yBsA}P_{yBzB}P_{zBsA} - P_{yBsA}^2(P_{zBzB}-1) - P_{zBsA}^2(P_{yByB}-1)], \quad (2)$$

Table 6. Experimental Metal(Ib,IIb) Chemical Shifts and Calculated σ_{LS}(M(I,II)) Shieldings of Metal-Four Coordinate Halide Complexes

X	ξ (a.u.) $\times10^{-2}$	Relative to $[MCl_4]^{(4-i)-}$ $[CuX_4]^{3-}$ (ppm) Obsd	Calcd	$[AgX_4]^{3-}$ (ppm) Obsd	Calcd	$[CdX_4]^{2-}$ (ppm) Obsd	Calcd
Cl	0.266	0	[7.6[c] / 75[d]]	f)	[7.4[c] / 29[d]]	0[b]	[37[c] / 225[d]]
Br	1.11	0	[32[c] / 315[d]]	0[a]	[31[c] / 120[d]]	116[b]	[157[c] / 941[d]]
I	2.29	234	[66[c] / 649[d]]	−115[a]	[64[c] / 248[d]]	424[b]	[325[c] / 1941[d]]

a) The values was obtained from Ref. 5. b) The value was obtained from Ref. 1a. c) The values was calculated from the ionization potential of metal atom. d) The value was estimated from excitation energy of the diatomic molecule. e) In this table more positive values refere to higher shielding. f) The value has not been obtained.

where $P_{\mu\nu}$ is the orbital density: P_{yBsA} denotes the density of the p_y orbital on the B (halogen) atom and an s orbital on the A (metal) atom. Other notations correspond to reference.[15]

In order to estimate the LS shift, σ_{LS}, for $[CuX_4]^{3-}$, $[AgX_4]^{3-}$, and $[CdX_4]^{2-}$, we used the quantities shown in Table 5. There, the densities of the metal four-coordinate halide complexes were approximated by tetrachloride complexes instead of tetrabromide and tetraiodide, which we have not calculated by the ab initio SCFMO method.[6] An inspection of Table 6 shows that the LS shift (using both the 1st ionization potential of the metal atom and the lowest excitation energy of the diatomic molecule) is $[CdX_4]^{2-} > [CuX_4]^{3-} \geqslant [AgX_4]^{3-}$. This tendency corresponds to the observed one. For $[AgX_4]^{3-}$, the observed shift shows the opposite shielding order. This indicates that the Ag paramagnetic term is much larger than the LS term.

Line-Broadening for Cu(I) Halide Complexes. In Table 1, we can see remarkably different line widths for Cu(I) complex species of Cu(I) halides in aqueous solution. The linewidths[18] can be approximated by

$$\Delta\nu_{1/2} \simeq \frac{1}{10}\left(1+\frac{\eta^2}{3}\right)(e^2Qq/\hbar)^2\tau_c\,, \qquad (3)$$

where we can assume the asymmetry parameter, η, is nearly 0 for CuX; the correlation time, τ_c, of the complex $[CuX_4]^{3-}$ is estimated as $2\pi\times10^{-11}$ s in nonviscous water from the Einstein-Stokes relationship, the quadrupole moment of ^{63}Cu, Q, is given as -0.16×10^{-24} cm^2 and the electric field gradient around the Cu nucleus, q, is affected by any change of the p- and d- electron densities. These densities are considered to result from the lone-pair electrons of the ligand. The field gradient will, thus, be the dominant factor for ^{63}Cu linewidths.

An estimation of e^2Qq by Eq. 3 gives 40 and 4 MHz for the different linewidths of 10 and 0.1 kHz in Table 1, respectively. The term e^2Qq can be rewritten as

$$e^2Qq/\hbar = \frac{e^2}{\hbar}\frac{2L(L+1)}{(2L-1)(2L+3)}\langle 1/r^3\rangle Q\,. \qquad (4)$$

We can evaluate e^2Qq for the maximum case where the contribution arises from a single hole or electron on a 3d- or 4p-orbital. The value was estimated to be 110 or 12 MHz for a single 3d-hole or 4p-electron, respectively. It can, therefore, also be seen for the ^{63}Cu observed linewidths (10 to 30 kHz) that the d-contribution (76 kHz) is larger than the p-contribution (0.9 kHz).

When we consider ^{63}Cu linewidths from the sysmmetry of Cu(I) complexes in aqueous solution, the complex with a higher symmetry gives a sharper signal. The sharper signals of $[Cu(CN)_4]^{3-}$ and $[Cu(CH_3CN)_4]BF_4$ in solution are due to their tetrahedral symmetry. However, we observed broader signals for aqueous CuX-KX solution systems. This broadening may be partially attributed to a lower symmetry of $[CuX_3]^{2-}$ and a distortion of $[CuX_4]^{3-}$.

The Difference between ^{63}Cu Chemical Shieldings of Cu(I) Halides in Suspension and in Solution. An inspection of Table 1 indicates that the Cu shift of CuX in suspension is in good accordance with a remarkable increasing shielding order ($CuCl \leqslant CuI < CuBr$) in solid, as reported by Lutz et al.[4b] The ^{63}Cu of $[CuCl_4]^{3-}$ in solution is more deshielded than that of solid CuCl in suspension (the shift between $[CuCl_4]^{3-}$ and CuCl is about 130 ppm), while the $[CuI_4]^{3-}$ in solution is more shielded than the solid CuI in suspension (the shift between $[CuI_4]^{3-}$ and CuI ($\geqslant$CuCl) is about −100 ppm). We can, thus, explain these anomalous shielding orders seen in the Cu(I) halides.

Cu(I) halides, solid CuX in suspension and $[CuX_4]^{3-}$ in solution, have the same tetrahedral four-coordinate symmetry. Their ^{63}Cu nuclei, however, reflect the different chemical shieldings (as mentioned above). The reason can be explained by considering the difference between the lattice repetitive zincblende structure in a solid and a single tetrahedral structure in an aqueous solution (Fig. 2). For a solid, each Cu atom bonds to four halogens, while each halogen atom bonds to four Cu ones for the sake of the repetitive structure of zincblende. On the other hand, in a solution, a copper ion

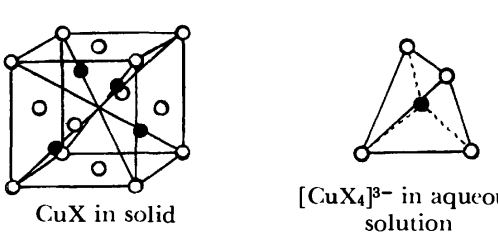

CuX in solid

$[CuX_4]^{3-}$ in aqueous solution

Fig. 2. Zincblende structure of CuX in solid and a tetrahedral structure of $[CuX_4]^{3-}$ in aqueous solution.

has four halogens in a single tetrahedral complex. Then, in a solid, the electron donation from the halogen p orbital to the Cu(I) 4s and 4p orbitals and the back donation from the Cu(I) 3d orbital to the ligand may be much smaller than those in solution.

Here, in order to explain the observed ^{63}Cu shielding order in $[CuX_4]^{3-}$ and CuX, we consider the paramagnetic, σ_{para} (Cu(I)), and LS-shielding, σ_{LS}, terms. For Cu(I) chloride complexes, the shift between $[CuCl_4]^{3-}$ and CuCl is interpreted mainly by the diffrences between the paramagnetic terms in Eq. 1, because the contribution of the LS-shielding is ignored for the chloride complex (Table 6). Now, we assume that ($E_{p,d}$ solution)$\simeq$($E_{p,d}$ in solid) and ($\langle 1/r^3\rangle_{3d,4p}$ in solution) $\simeq$($\langle 1/r^3\rangle_{3d,4p}$ in solid) in Eq. 1. We can also take into account the population orders, P_T ($[CuCl_4]^{3-}$)>P_T (CuCl) and D_T ($[CuCl_4]^{3-}$)>D_T(CuCl), as discussed above. Then, the observed deshielding order, σ($[CuCl_4]^{3-}$)>σ (CuCl), is shown from the paramagnetic shielding order, σ_{para} ($[CuCl_4]^{3-}$)>σ_{para} (CuCl).

In the case of Cu(I) iodide complexes, both σ_{para} (Cu(I)) and σ_{LS} terms must be considered. For the σ_{para} term, we may show the deshielding order, σ_{para} ($[CuI_4]^{3-}$)> σ_{para} (CuI) as well as σ_{para} ($[CuCl_4]^{3-}$)>σ_{para} (CuCl). For σ_{LS}, the difference between σ_{LS} ($[CuI_4]^{3-}$ and σ_{LS} (CuI) depends mainly upon the populations, p_{zBzB} and p_{yAyA} in Eq. 2. The populations in solid CuI are also assumed to be smaller than those in solution, for the sake of the repeat structure in solid. Thus, if ($\sigma_{LS}([CuI_4]^{3-})-\sigma_{LS}(CuI)$)>($\sigma_{para}(CuI)-\sigma_{para}([CuI_4]^{3-})$) is pointed out, we can explain the observed shift between CuI and $[CuI_4]^{3-}$.

Conclusion

In this paper, we presented representative ^{63}Cu NMR spectra obtained from an aqueous solution and a pure solid of Cu(I) halides. Especially, a few tens of kHz of broader ^{63}Cu spectra for CuX-KX systems (where X=Cl, Br, I) were shown. We provided a theoretical interpretation of the ^{63}Cu line width and the chemical shielding. The line width and shielding were found to be due mainly to a 3d-hole in the Cu atom: The broadening is due to a Cu(I) nuclear quadrupole interaction with the electric field gradient, which arises from the 3d-hole. The shielding could be explained by the paramagnetic term which depends dominantly on the 3d-hole. Furthermore, for increasing metal shieldings of $[MX_4]^{(4-i)-}$, we evaluated the possibility of the heavy atom effect on the shielding of $[CuX_4]^{3-}$ and $[CdX_4]^{2-}$.

In a forthcoming paper, we hope to clarify the shielding order of $[CuX_4]^{3-}$ with the ab initio SCF MO method.

We express our appreciation to Prof. G. C. Levy of the N. I. H. Biotechnology Research Resource, Syracuse University who read the manuscript and corrected the English. We wish to thank Dr. Hiroshi Nakatsuji of Kyoto University for his helpful discussion.

References

1) a) J. J. H. Ackerman, V. V. Orr, V. J. Bartsuka, and G. E. Maciel, *J. Am. Chem. Soc.*, **101**, 341 (1979); b) P. G. Mennitt, M. P. Shatlock, V. J. Bartsuka, and G. E. Maciel, *J. Phys. Chem.*, **85**, 2087 (1981); c) A. D. Cardin, P. D. Ellis, J. D. Odom, and J. W. Howard, Jr., *J. Am. Chem. Soc.*, **97**, 1672 (1975).

2) G. E. Maciel, L. Simeral, and J. J. H. Ackerman, *J. Phys. Chem.*, **81**, 263 (1977).

3) a) K. Jacker, W. Sahm and A. Schwenk, *Z. Naturforsch.*, **31A**, 1532 (1976); b) P. M. Henrich, S. Sheard, J. J. H. Ackerman, and G. E. Maciel, *J. Am. Chem. Soc*, **101**, 3222 (1979).

4) a) O. Lutz, H. Oehler, and P. Kroneck, *Z. Physik*, **A288**, 17 (1978); b) O. Lutz, H. Oehler, and P. Kroneck, *Z. Naturforsch.*, **33a**, 1021 (1978); c) T. Yamamoto, H. Haraguchi and S. Fujiwara, *J. Phys. Chem.*, **74**, 4369 (1970).

5) K. Endo, K. Yamamoto, K. Matsushita, K. Deguchi, K. Kanda and H. Nakatsuji, *J. Magn. Reson.*, **65**, 268 (1985); K. Endo, K. Matsushita, K. Deguchi, K. Yamamoto, S. Suzuki, and K. Futaki, *Chem. Lett.*, **1982**, 1497.

6) H. Nakatsuji, K. Kanda, K. Endo, and T. Yonezawa, *J. Am. Chem. Soc.*, **106**, 4653 (1984).

7) B. D. Guenther and R. A. Hultsch, *J. Magn. Reson.*, **1**, 609 (1969).

8) a) R. W. Mebs, G. C. Carter, B. J. Evans and L. H. Bennet, *Solid State Comm.*, **10**, 769 (1972); b) E. R. Andrew, J. L. Carolan, and P. J. Randall, *Chem. Phys. Lett.*, **11**, 298 (1971).

9) C. J. Jameson and H. S. Gutowsky, *J. Chem. Phys.*, **40**, 1714 (1964).

10) D. F. Shriver, "Inorganic Synthesis," Wiley-interscience, New York (1979), Vol. 19.

11) L. G. Sillen and A. E. Martell, *Chem. Soc. Spec. Publ.* No. **25**, (1970).

12) To determine the formation constant β_4 of $[CuBr_4]^{3-}$, an electrode potential (E_{Cu}) measurement has been performed. A homemade solid-state copper electrode was used with a double junction silver chloride reference electrode HS-305DS (TOA Electronics Ltd.). These electrodes were standardized with solubility products of purified CuCl and CuI in 1.0M KNO_3. The measurement cell was bubbled with nitrogen gas during E_{Cu} measurement to prevent oxidation of Cu^+. The potential E_{Cu} value was determined as $E_{Cu}=0.318+0.0261 1n[Cu^+]$, where $[Cu^+]$ denotes molarity. The E_{Cu} value was measured as a function of the free ligand concentration, to obtain the formation constants. The measurements were performed in thermostated vessels at 30±0.1 °C and at an ionic strength of 1.0M KNO_3.

13) E. Clementi, D. L. Raimondi and W. P. Reinhardt, *J. Chem. Phys.*, **47**, 1300 (1967).

14) J. Mason, *J. Chem. Soc., A*, **1971**, 1038.

15) a) I. Morishima, K. Endo and T. Yonezawa, *J. Chem. Phys.*, **59**, 3356 (1973); b) A. A. Cheremisin and P. V. Schastnev, *J. Magn. Reson.*, **40**, 459 (1980).

16) K. P. Huber and G. Herzberg, "Molecular Spectra and Molecular Structure IV. Constants of Diatomic Molecules," Van Nostrand (1979).

17) W. D. Knight, *Solid State Phys.*, **2**, 120 (1956).

18) A. Abragam, "The Principles of Nuclear Magnetism," Clarendon Preaa, Oxford (1961).

Preparation and Time-Resolved in Situ Reflection Spectra of Bilayer Electrodes with Polythiophene Outer Layers

Kenji MURAO* and Kazuhiro SUZUKI
Advanced Research Laboratory, Hitachi, Ltd., Kokubunji, Tokyo 185
(Received March 12, 1987)

Bilayer electrodes, Pt/poly-**1**/polythiophene [**1**: tris(4-vinyl-4′-methyl-2,2′-bipyridine)ruthenium(II) perchlorate], where polythiophene is derived from poly(3-methylthiophene) [poly(3-methyl-2,5-thienylene), abbreviated as PMeT] and poly(2,2′-bithiophene) [poly(2,2′-dithienyl-5,5′-ene), abbreviated as PBT], have been prepared. Electropolymerizations of MeT and BT at Pt/poly-**1** occur at the platinum electrode surface, followed by phase separation of the polymer components which results in the bilayer structure. Significant imbalance, observed between charge densities involved in the cathodic and anodic waves of the cyclic voltammogram for Pt/poly-**1**/PBT, is explained as being due to the positive charge leakage from the PBT layer to the platinum substrate through the 2+/3+ redox level of the intervening poly-**1** during the potential sweep in the negative direction. This charge leakage is ascribed to the consequence of the closely located oxidation potential of PBT to that of the 2+/3+ of poly-**1** ($E^{\circ\prime}$=+0.875 V vs. Ag/Ag^+). Time-resolved in situ reflection spectra taken at Pt/poly-**1**/PMeT immersed in electrolytic solutions give evidence for the mediated redox reactions of PMeT by the poly-**1** layer. The spectral changes strongly suggest the transient occurrence of polarons during the doping process.

Electrically conducting polyheterocycles, e.g., polypyrrole [poly(2,5-pyrrolylene), hereafter abbreviated as PP] and polythiophene [poly(2,5-thienylene), hereafter abbreviated as PT] have attracted increasing interest in the past decade. One of the reasons for this stems from their important situation as examples for non-degenerate ground-state systems. It has been shown that bipolarons are evolved in those polymer chains upon electrochemical dopings (oxidations) as the most stable charged states (Fig. 1).[1-3] Polarons have also been detected in PP.[4,5] Although there has been some controversy,[2] Kaneto et al. and Hattori et al. first obtained the spectroscopic evidence for polarons in very dilutely doped PTs.[6-8] Basically consistent results were subsequently reported for poly(3-methylthiophene) [poly(3-methyl-2,5-thienylene), hereafter abbreviated as PMeT].[9] Thus, the studies of the electrochemically induced changes in PP and PT have provided understanding of the charged states in PP and PT.

It has been recognized that several tens of minutes are required to achieve quasi equilibria in PP[4] and PT[2,8] upon charge injections. The relaxations possibly involve manifold processes in the polymer chains, which apparently has confined the former studies basically to static conditions, except for a transient ESR study of PP.[5] Another aspect of the preceding studies is that they have been based exclusively on the configuration in which the positive and negative charge injections (i.e., doping-undoping reactions) into the conducting polymers are performed at the conducting substrates, simply as a consequence of the electropolymerization of conducting polymers at metallic or semiconducting substrates. In this configuration, the electronic states of the conducting polymers are totally governed by the Fermi level of the substrates, even in the course of relaxations within them. This becomes disadvantageous for studying the relaxation processes taking place in conducting polymers upon charge injections.

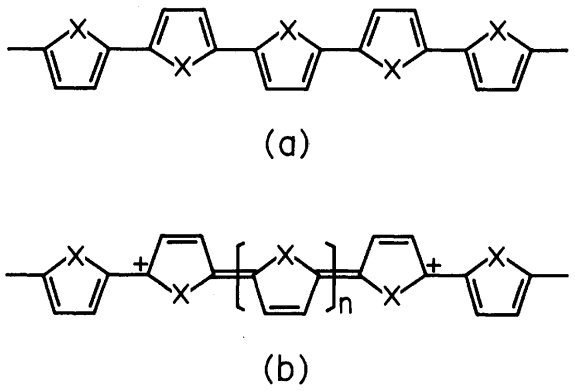

Fig. 1. Structures of polypyrrole (X=NH) and polythiophene (X=S) in neutral (a) and bipolaron (b) states.

In the above context, it would be interesting to realize a configuration in which charge injections into the bulk of conducting polymers are performed via discrete electronic levels of the adjacent layer which is electrochemically active but electrically insulating. In a previous communication,[10] we reported on the first example of PP deposited on the electrically insulating film, poly[tris(4-vinyl-4′-methyl-2,2′-bipyridine)ruthenium(II) perchlorate] (hereafter abbreviated as poly-**1**), to give a bilayer electrode, Pt/poly-**1**/PP. Deposition of PP at the Pt/poly-**1** electrode is initiated at the platinum electrode. The PP film growth occurs within the existing poly-**1** layer and proceeds further outside it. Phase separation of the both polymer components, poly-**1** and PP, is subsequently caused by repeated electrochemical potential sweeps in 0.1 M† TBAP (tetrabutylammonium perchlorate)-acetonitrile, and the above

† 1 M=1 mol dm^{-3}.

bilayer structure is eventually obtained. In this bilayer electrode, oxidation (doping) and reduction (undoping) reactions of the PP layer are mediated by the 2+/1+ and 2+/3+ redox levels of the $[Ru(bpy)_3]^{2+}$ centers (bpy: 2,2′-bipyridine moiety) in the inner layer. Recently,[11] we preliminarily reported on the successful applications of this procedure to PMeT and poly(2,2′-bithiophene) [poly(2,2′-dithienyl-5,5′-ene), hereafter abbreviated as PBT] in preparations of the bilayer electrodes, Pt/poly-**1**/PMeT and Pt/poly-**1**/PBT. Figure 2 depicts the energy diagram for the Pt/poly-**1**/PMeT bilayer electrode. The locations of

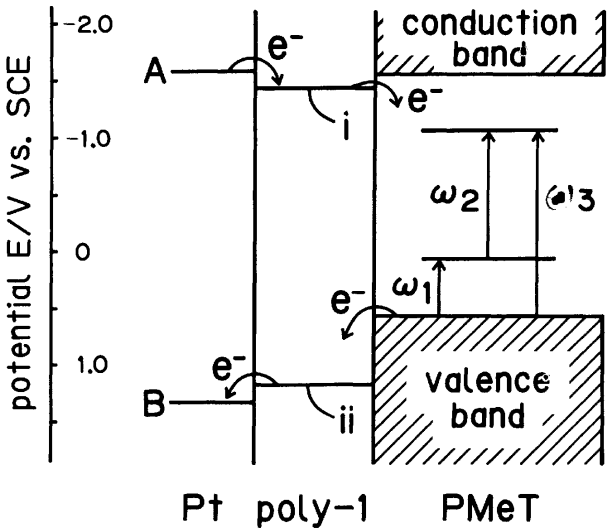

Fig. 2. Energy diagram for the Pt/poly-**1**/PMeT bilayer electrode. i and ii denote 2+/1+ and 2+/3+ redox levels of poly-**1**, respectively. ω_1, ω_2, and ω_3 are the possible optical transitions involving the mid-gap states of PMeT. PMeT: poly(3-methylthiophene). For poly-**1** see text.

the conduction and valence bands are estimated based on optical (band gap energy: 2.1 eV)[6] and electrochemical data,[11] and are consistent to the reported values.[12] The redox potentials of poly-**1** are determined according to the published data.[10,13] The reductive and oxidative charge transfers to the PMeT layer are performed through the electrochemical mediation by 2+/1+ and 2+/3+ redox levels of poly-**1**, respectively. Mid-gap states are evolved upon oxidation of PMeT. In these bilayer systems, it has been found that the quasi equilibria in PMeT and PBT are established within anomalously short periods of time upon electrochemical charge injections. This remarkable feature enabled us to detect transiently occurring polarons in PMeT in the course of achieving equilibria.[14] The above electrochemical procedures might be an important step towards the establishment of molecular technolgy to construct microstructures involving conducting polymers,[15] in view of the generally untractable nature of conducting polymers. This paper describes the preparations, electrochemistry and time-resolved in situ reflection spectra of the bilayer electrodes of PMeT and PBT.

Experimental

Materials. The monomer precursor of poly-**1**, tris(4-vinyl-4′-methyl-2,2′-bipyridine)ruthenium(II) perchlorate (**1**), was synthesized according to a modified method of the reported procedures.[16] Pt/poly-**1** electrodes were prepared using the reported method.[10,13] Commercially obtained TBAP was purified by thermal recrystallization from an EtOH-H_2O 2:3 mixed solvent and was dried in vacuo at 80 °C for 32 h. Commercial acetonitrile was refluxed over P_2O_5 and distilled before use.

Electrochemical Experiments. Platinum disks (4 mm diameter) embedded in glass, and evaporated films of plati-

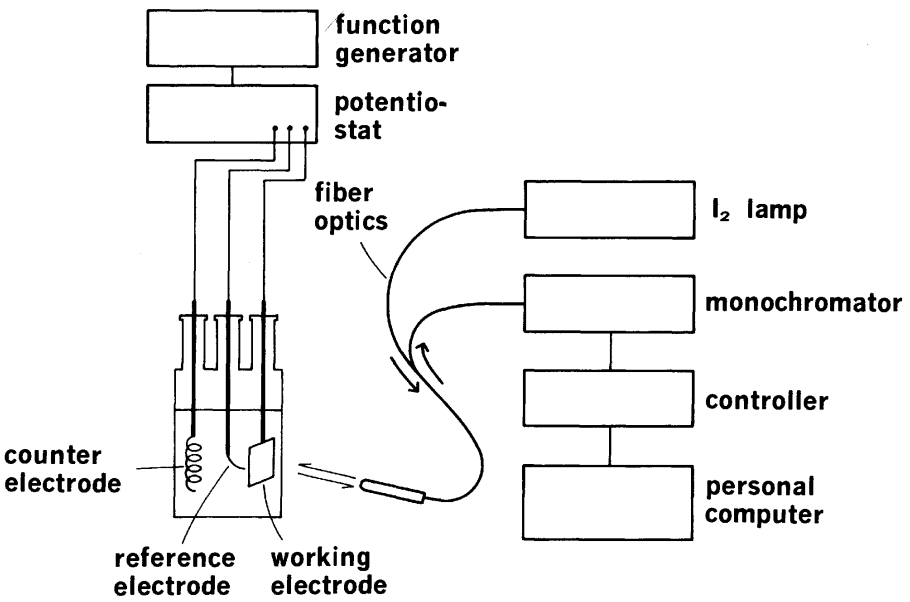

Fig. 3. Schematic representation of the experimental setup for time-resolved in situ reflection spectroscopy during the electrochemical reactions.

num (280 nm thick; active area: 4 mm diameter) on glass substrates (Corning # 7059, 1.2 mm thick) were used as the working substrates. The surfaces of the platinum disks were polished using 1 μm diamond paste. A platinum wire (1 mm diameter) was used as the counter electrode. An Ag/Ag^+ quasi reference electrode was used which showed 290 mV vs. SCE (saturated calomel electrode) in 0.1 M TBAP-acetonitrile. Potentials indicated in the following are all vs. Ag/Ag^+ unless otherwise noted. Preparations and electrochemical measurements were performed by immersing electrodes in electrolytic solutions in one compartment cells. All of the electrochemical experiments were carried out under Argon-purged conditions. The preparations of Pt/poly-**1**/PMeT and Pt/poly-1/PBT electrodes have been outlined in a previous communication.[11] Electrochemical polymerizations of MeT and BT were carried out by both potential sweeps and galvanostatic anodizations. Typically, the galvanostatic polymerizations of MeT and BT were performed at a current density of 275 $\mu A\,cm^{-2}$ at Pt/poly-1 electrodes immersed in anhydrous acetonitrile containing 120 mM monomers and 0.1 M TBAP.

In situ reflection spectra at electrode surfaces were measured with a normally incident light beam led by fiber optics using an MCPD-100 Multi-Channel Photo Detector (Ohtsuka Denshi Co.), as shown in Fig. 3. Each spectrum is based on the accumulated signal obtained by eight repeated wavelength sweeps with a gate time of 12 ms each.

Results and Discussion

Preparations of Pt/Poly-1/PMeT and Pt/Poly-1/PBT. The cyclic voltammograms (CVs) monitored during the electropolymerizations of MeT and BT at Pt/poly-**1** electrodes by potential sweeps are depicted in Fig. 4. The expansion of the waveforms at every cyclic sweep, as indicated by the arrows in Fig. 4(a), is a result of the deposition and the film growth of PMeT at the electrode. When the positive sweeps were limited to potentials lower than +1.1 V, the expansion of the CV waves was not observed and only the redox waves for poly-**1** were repeatedly observed. This means that the electropolymerization of MeT occurs at potentials higher than +1.1 V. This is consistent with the fact that the applied potential upon galvanostatic electropolymerization of MeT (Fig. 5) reached a steady value of +1.17 V. The fact that MeT has a substantially higher oxidation potential than that of 2+/3+ of poly-**1** ($E^{\circ\prime}$=+0.875 V) rules out the possibility of the mediated oxidation of MeT by poly-**1**. The observed potential for MeT oxidation during the galvanostatic anodization is initially lower than the ultimately achieved steady value, +1.17 V. This is understood as being due to the initially predominant oxidation of the poly-**1** layer. The subsequently occurring peak in the V vs. t curve would be representing a crossover from poly-**1** oxidation to MeT oxidation. These observations indicate that the electropolymerization of MeT occurs at the surface of the platinum substrate as a result of the permeation of the monomer molecules through the poly-**1** layer. In fact, the PMeT-as-deposited Pt/poly-**1** electrode showed the CV waves for

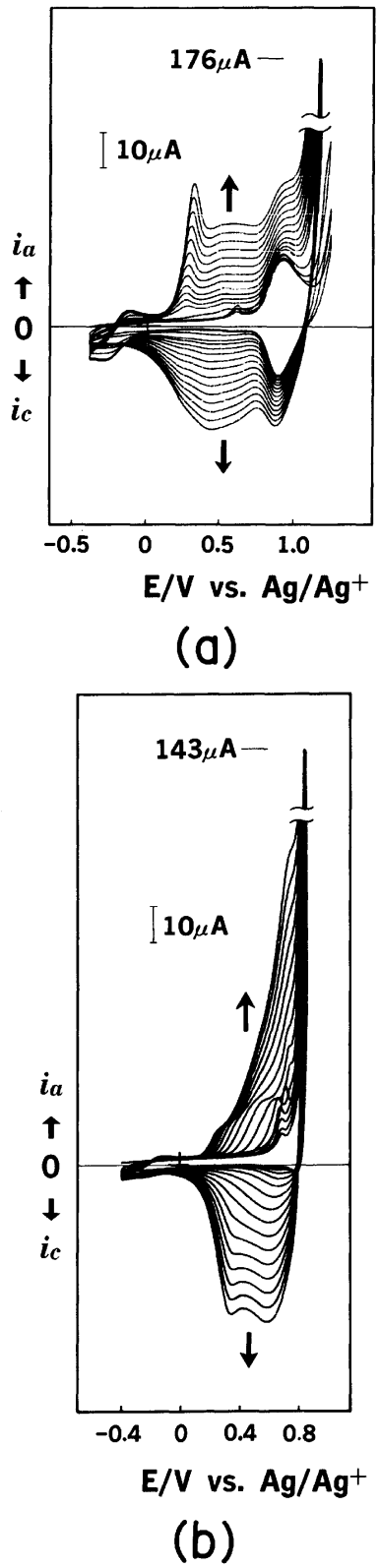

Fig. 4. Cyclic voltammograms monitored on electropolymerizations of 3-methylthiophene (a) and 2,2′-bithiophene (b) at Pt/poly-**1** electrodes immersed in 0.1 M tetrabutylammonium perchlorate-acetonitrile including 30 mM 3-methylthiophene (a) and 2,2′-bithiophene (b), respectively. The employed coverages of poly-**1** layers for (a) and (b) are 1.85×10^{-9} and 3.60×10^{-9} mol cm^{-2}, respectively. Sweep rate: 0.1 $V\,s^{-1}$. For poly-**1** see text.

PMeT and 2+/3+ of poly-**1** independently, essentially as a superimposition of the CV waves for both origins in 0.1 M TBAP-acetonitrile, which means that PMeT was electrochemically accessed directly from the platinum substrate. On the other hand, in the negative potential region, where PMeT is electrochemically inert, the 2+/1+ waves of poly-**1** are totally absent except for a spiky current peak centered at −1.33 V, indicating that PMeT present at the platinum electrode surface is blocking the reduction of the $[Ru(bpy)_3]^{2+}$ centers. The subsequent cyclic potential sweeps between the 2+/1+ and 2+/3+ potentials of poly-**1** caused the CV changes (depicted in Fig. 1 of Ref. 11) as follows; 1) anodic peak shifts of PMeT in the positive direction followed by peak growths as a prewave of the 2+/3+ wave of poly-**1**, 2) gradual loss of the cathodic wave of PMeT, 3) growths of the spiky peak at −1.33 V with a slight shift at every cycle in the negative direction, 4) evolution of the 2+/1+ waves of poly-**1** in the negative potential region. These concurrent changes eventually lead to the final waveform as shown in Fig. 6(a). In Fig. 6(a), the large spiky current peaks (i and iii) are observed only for virgin scans in negative and positive directions after allowing the spiky current peaks of the opposite signs, respectively. When potential sweeps are repeated in the same direction, the second sweeps produce small waves only (ii and iv), which reproduce the CV waves for Pt/poly-**1** before the deposition of PMeT, except for a residual small peak in iv. The CV waves in Fig. 6(a) represent the mediated redox reactions of PMeT by poly-**1**, and are essentially consistent with the electrochemistry of bilayer electrodes.[10,13,17-19]

The electropolymerization of BT at Pt/poly-**1** by potential cyclings occurs at potentials near $E^{\circ\prime}$ of poly-**1** as evidenced by the onsets of large current peaks (Fig. 4(b)). The galvanostatic electropolymerization of BT proceeds at potentials lower than +0.83 V (Fig. 5) which is slightly lower than the $E^{\circ\prime}$ of poly-**1**. This means that oxidation of BT (and hence the deposition of PBT) can be mediated by the poly-**1** layer, which should directly lead to the bilayer structure. However, for both modes of BT oxidations (i.e., by potential cyclings and by galvanostatic anodization) the occurrence of PBT at the platinum substrates was evidenced by the fact that the initial potential sweeps of the PBT-as-deposited electrodes in 0.1 M TBAP-acetonitrile showed the CV waves for PBT that was electrochemically accessed directly from the platinum substrates, in the same way as for the PMeT-deposited poly-**1** electrode described above. These observations, however, do not exclude the possibility that the anodization of BT is partly mediated by $[Ru(bpy)_3]^{2+}$ centers in poly-**1**. The bilayer electrode, Pt/poly-**1**/PBT, was subsequently brought by repeated potential sweeps in 0.1 M

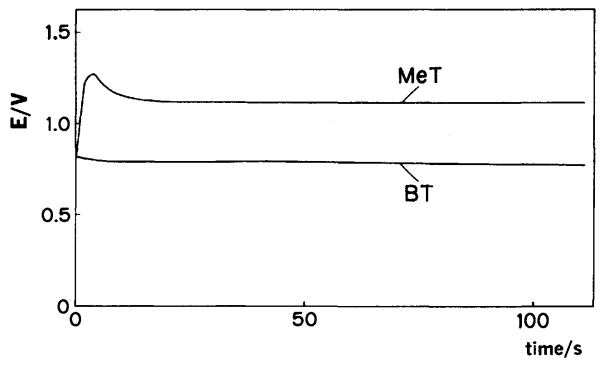

Fig. 5. Potential vs. t curves monitored on galvanostatic polymerizations of 3-methylthiophene (MeT) and 2,2′-bithiophene (BT) at Pt/poly-**1** electrodes immersed in 0.1 M tetrabutylammonium perchlorate-acetonitrile including 120 mM MeT (a) and 120 mM BT (b). Current densities are 275 $\mu A\,cm^{-2}$ for both runs. The employed coverages of poly-**1** layers for (a) and (b) are 1.98×10^{-9} and 2.90×10^{-9} mol cm^{-2}, respectively. For poly-**1** see text.

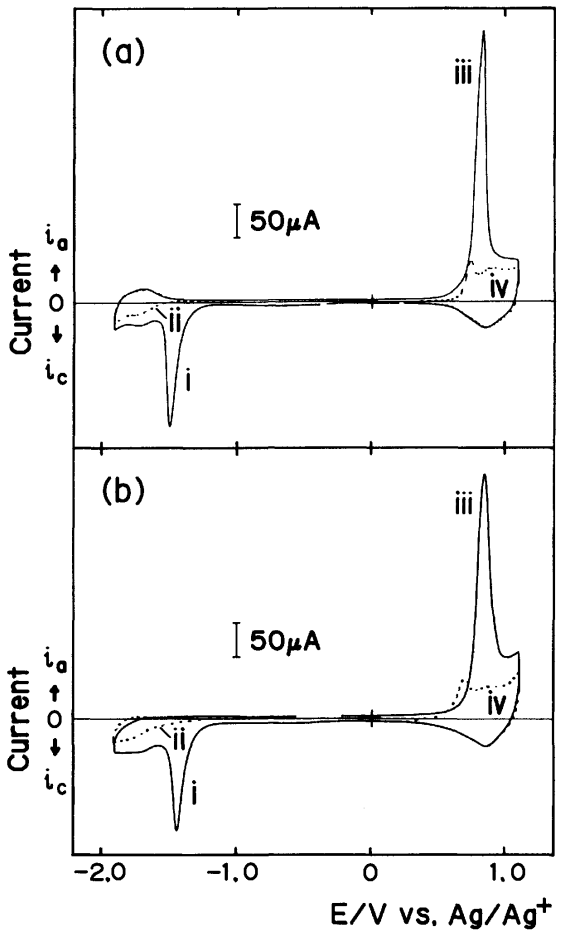

Fig. 6. Cyclic voltammograms for Pt/poly-**1**/poly(3-methylthiophene) (a) and Pt/poly-**1**/poly(2,2′-bithiophene) (b) bilayer electrodes in 0.1 M tetrabutylammonium perchlorate-acetonitrile. Coverages of the inner layer are 2.62×10^{-9} (a) and 2.58×10^{-9} (b) mol cm^{-2}, respectively. Outer layers were deposited by galvanostatic polymerizations at current densities of 275 $\mu A\,cm^{-2}$ and charge densities passed during the depositions of 32.4 mC cm^{-2} for both (a) and (b). For poly-**1** see text.

TBAP-acetonitrile, accompanying CV changes in the same way as for PMeT-deposited poly-**1** electrodes. The above electrochemical scheme in preparing bilayer electrodes — i) permeation of monomeric precursors of the outer layer through the first layer, ii) electropolymerization of the monomer at the surface of the substrate, iii) repeated potential sweeps in 'innocent' electrolytic solutions — is basically the same as that employed for the preparation of the bilayer electrodes with PP as the outer layer,[10] suggesting the extensive applicability of this scheme to other material systems. The above scheme, i—iii), contrasts with other processes employed in obtaining bilayer electrodes,[13,17-19] where the outer layer is deposited directly at the surface of the first layer, i.e., by mediated electropolymerizations of the monomer precursors by the first layer, or droplet evaporation of polymer solutions of the outer layer at the surface of the first layer. In step iii) phase separation occurs between poly-**1** and PMeT or PBT. This phase separation is consistently understood with that of the PP-based bilayer electrode and will be discussed in a separate paper.

Significant imbalance was found to exist between involved charges for anodic (>+0.60 V) and cathodic (<−1.25 V) peaks in the CVs of Pt/poly-**1**/PBT (Fig. 6(b)). The amount of charge involved in the cathodic peak is only 60—70% that of the anodic counterpart. Although precise quantitative arguments regarding the amount of charges are not possible due to the complexities arising from background currents and capacitive components of PBT, such an apparently large imbalance in charges has not been observed for Pt/poly-**1**/PP.[10] It was found from Q (charge densities) vs. V plot that the amount of the negative and positive charges were balanced by adding an amount of cathodic charges collected during the sweeps in the negative direction in the potential region more negative than +0.25 V. This can be reasonably explained by assuming a leakage of positive charges of the outer layer to the platinum substrate through the poly-**1** layer during the sweep in the negative direction. The significant overlapping of the distributions of the electrochemical density of states for PBT oxidation and 2+/3+ oxidation of poly-**1** is likely due to the nearness of their oxidation potentials each other (PBT: E_{pa}=+1.00 V vs. SSCE,[20] 2+/3+ of poly-**1**: $E^{\circ\prime}$=+0.875 V vs. Ag/Ag^+). Actually, substantial optical changes have been detected corresponding to the reduction of the PBT layer, when the applied potential is fixed at 0 V for 20 s after oxidizing the PBT layer by sweeping the potential of the platinum substrate, 0 V → +1.15 V → 0 V,[21] which is indicative of a positive charge leakage from PBT layer to the platinum substrate. Similar leakage behavior has also been observed, though less significantly, for PMeT. In contrast, the corresponding negative charge leakage has not been detected for both PBT and PMeT. This is also consistent with the above explanation. The charge leakage in a polymeric Fe(II) complex bilayer electrode has been similarly explained by Denisevich et al.[17] and Leidner et al.[19]

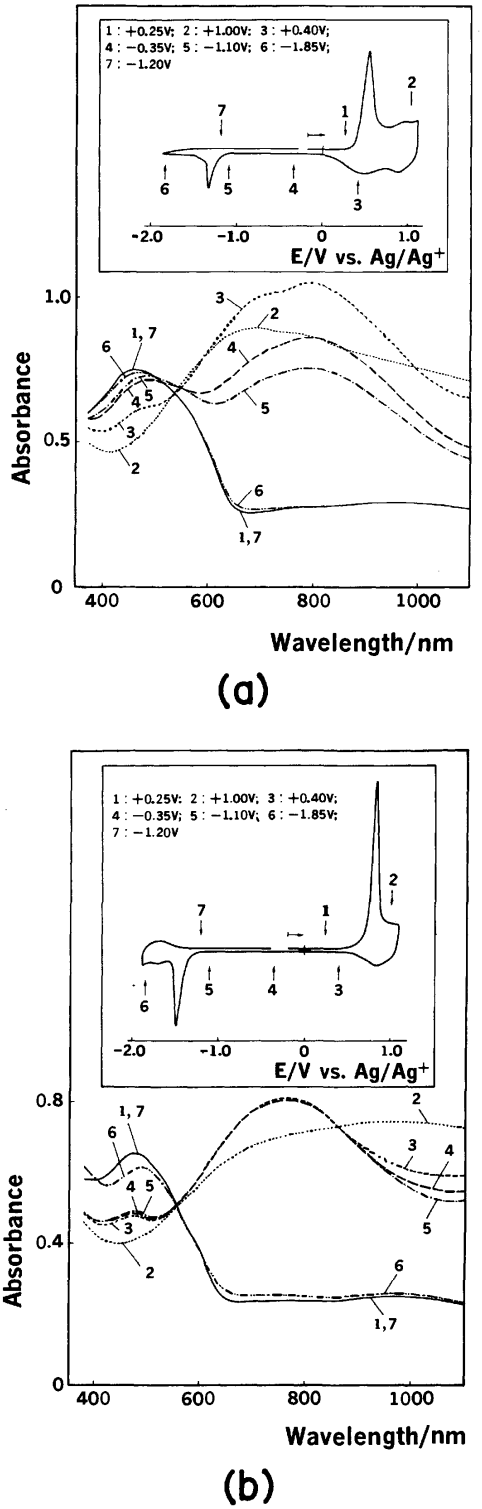

Fig. 7. In situ reflection spectra at Pt/poly-**1**/poly(3-methylthiophene) immersed in 0.1 M tetrabutylammonium perchlorate-acetonitrile during potential sweeps (scan rate: 50 mV s^{-1}, inset), before (a) and after (b) the repeated potential sweeps causing phase separation. The employed coverage of poly-**1** is 2.70×10^{-9} mol cm^{-2}. PMeT was deposited by passing 31.7 mC cm^{-2}. For poly-**1** see text.

Time-Resolved in Situ Reflection Spectra of Pt/Poly-1/PMeT and Pt/Poly-1/PBT. In situ reflection spectra of Pt/poly-**1**/PMeT during the potential sweeps at 50 mV s^{-1} before and after the phase separation are shown in Figs. 7(a) and (b), respectively. Each spectrum is taken within ca. 100 ms. During this period, the potential is swept ca. 5 mV. The absorption band centered at ca. 480 nm in **1** of Fig. 7(a) has been ascribed to the interband transition of PMeT.[2,6] Optical switching occurs on the potential sweep across the sharp oxidation peak of PMeT (**1**→**2**), i.e., loss of the interband absorption and the evolution of bands for 560 nm<λ. However, the sweep **2**→**5** is seen to regenerate the interband absorption with paralleled decrease of the absorption for 560 nm<λ. The subsequent sweep **5**→**6** nearly completes the backward changes. These optical changes imply that a major portion of the PMeT layer is electrochemically accessible directly from the platinum substrate, and that only a small portion of PMeT is electrochemically mediated by poly-**1** before the phase separation. These features are consistent with the concurrent CV (inset).

On the other hand, from the spectra of Fig. 7(b) it is evident that reversible optical switchings occur when the potential is swept across the sharp anodic and cathodic CV waves i.e., **1**→**2** and **5**→**6**. This means that the spectra of Fig. 7(b) give further evidence for the mediated electrochemical doping and undoping reactions of PMeT. The forward (doping) optical change (**1**→**2**) consists of the disappearance of the absorption band for interband transition and the evolution of bands for 560 nm<λ. Small backward increase in absorption below 560 nm is observed for **2**→**3**, while the absorption also increases for 560 nm<λ<870 nm. During the sweep **3**→**5**, absorption below 560 nm changes only slightly, while the absorption intensity decreases for 870 nm<λ. Throughout these changes, the isosbestic point is maintained, which is indicative of quasi-equilibria established in the present system in the time scale of the CV sweep (50 mV s^{-1}); this is surprising, since much longer durations of time have been required for the achievement of the quasi-equilibria in PTs deposited at metallic or other conducting substrates.[2,8]

It should be noted that the essentially consistent optical changes were observed with various modes of positive charge injections, i.e., linear sweep, or potential step with and without subsequent open-circuiting. Figure 8 shows the reflection spectra at Pt/poly-**1**/PMeT taken as follows: Positive charges were first injected by stepping the applied potential of the platinum substrate from 0 to +0.90 V. After the potential was held at +0.90 V for 1 s, the electrode was then opencircuited. The optical change **1**→**2** is due to the doping (oxidation) reaction upon the positive potential step, and the subsequent changes **2**→**3**—**6** occurred during 70 s after the open-circuiting. The observed spectral changes are similar to those for

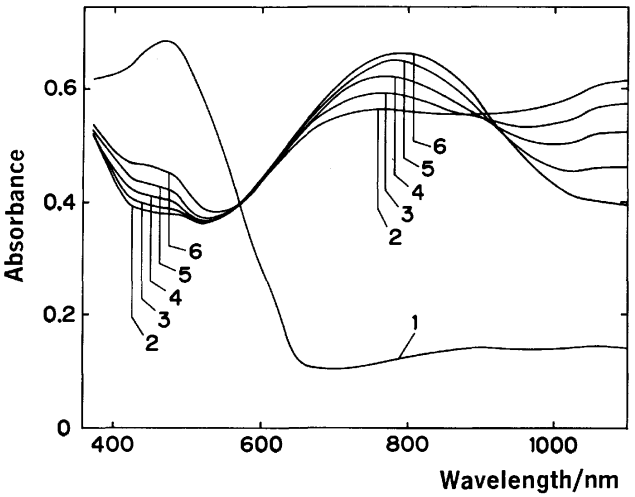

Fig. 8. In situ reflection spectra at a Pt/poly-**1**/poly(3-methylthiophene) bilayer electrode immersed in 0.1 M tetrabutylammonium perchlorate–acetonitrile. Potential was first stepped from 0 V (initial neutral state, spectrum **1**) to +0.90 V vs. Ag/Ag^+. After the potential was held there for 1 s, the electrode was open-circuited. Spectra, 2—6, were taken 1, 5, 13, 33, and 73 s after the open-circuiting, respectively. The coverage of poly-**1** is 2.60×10^{-9} mol cm^{-2}. 27.0 mC cm^{-2} was passed for deposition of PMeT. For poly-**1** see text.

1→**2**→**3** in Fig. 7(b), where the backward increase of the absorption in the interband region is observed here again together with the 'unparalleled' forward increase for 560 nm<λ<870 nm. The optical spectra of a Pt/poly-**1** electrode were measured upon the electrochemical cycle to assess the electrochromic contribution of the inner layer to the observed changes in Figs. 7 and 8, since the potential cycling involves the redox reactions of the inner layer. Figure 9 shows the reflection spectra at Pt/poly-**1** obtained upon potential sweeps. The absorption band centered at 465 nm in Fig. 9(a) is due to the MLCT (metal-to-ligand charge transfer) which is lost upon the positive sweep causing the reaction,

$$[Ru(bpy)_3]^{2+} \xrightarrow{-e^-} [Ru(bpy)_3]^{3+}. \quad (1)$$

The spectral changes indicate that at least for 560 nm<λ, the absorption change caused by the inner layer upon the doping (positive) sweep is negligible, while the Reaction 1 can contribute to the spectral changes in the interband region of PMeT. Therefore, the spectral changes for λ<560 nm in Figs. 7(b) and 8 are the results of i) the Reaction 1, ii) the doping reaction of PMeT driven by $[Ru(bpy)_3]^{3+}$, and iii) the reactions between charged states in PMeT.

Well-defined band maxima centered at 670—680 nm and near 1000 nm are often observed in spectrum **2** in Fig. 7(b) among a number of tested electrodes. The transient occurrence of the bands is also seen in difference spectra upon positive charge injections by a potential step.[14] These characteristic changes are

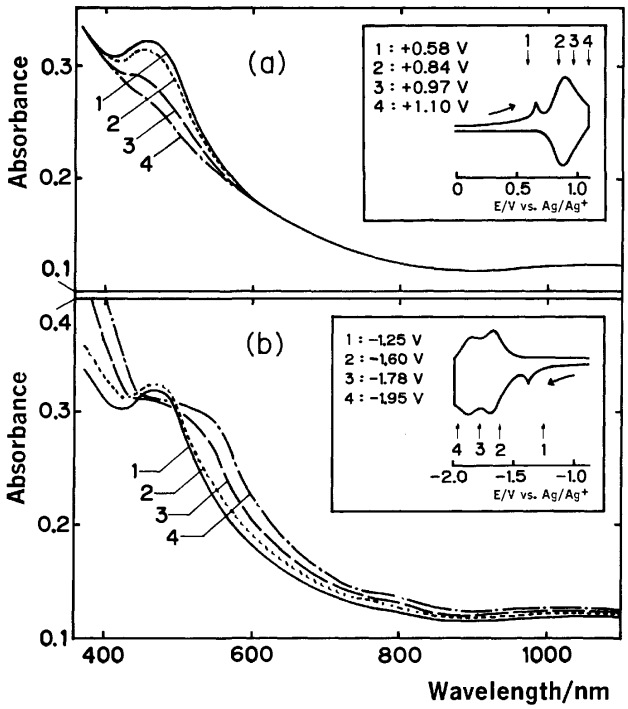

Fig. 9. In situ reflection spectra at Pt/poly-**1** (coverage: 2.90×10^{-9} mol cm^{-2}), immersed in 0.1 M tetrabutylammonium perchlorate–acetonitrile, taken during the potential sweeps (inset). For poly-**1** see text.

strikingly consistent with those reported by Kaneto et al. on very dilutely doped PT under static conditions[8] where the former two bands and the latter band are assigned to polaronic (ω_2 in Fig. 2) and bipolaronic (ω_3 in Fig. 2) transitions, respectively. Harbeke et al.[9] also reported on the similar spectral changes for PMeT at very low doping levels in equilibria, while they did not detect a band corresponding to the band at 670 nm in the present study. Hence, we conclude that the spectral changes of **2**→**3** in Fig. 7(b) and **2**→**3** of Fig. 8 are understood as follows; the polaron states are initially predominant upon doping, but are subsequently transformed to bipolarons due to the self-quenching reaction,

$$P^+ + P^+ \longrightarrow BP^{2+} \quad (2)$$

where P^+ and BP^{2+} represent a polaron and a bipolaron, respectively. Although further experiments are needed to find the origin of the band centered at 670—680 nm, which is higher in energy than the bipolaronic transition, we assume that the band is due to the excitonic transitions which become prominent in the presence of polarons, as a result of strong interactions between excitons and polarons.

In a separate run, backward spectral changes are observed for $\lambda<560$ nm similar to Figs. 7(b) and 8 described above, even when the PMeT in the bilayer configuration is doped by applying a pulse potential, 0 V→+0.90 V for 1 s →0 V vs. Ag/Ag$^+$.[22] The backward spectral relaxations subsequently take place in the time scale similar to Fig. 8. In this mode of potential application, the residual $[Ru(bpy)_3]^{3+}$ centers in the inner layer, after the mediated doping Reaction 3,

$$[Ru(bpy)_3]^{3+} + PMeT^\circ \longrightarrow [Ru(bpy)_3]^{2+} + P^+ \quad (3)$$

where PMeT° denotes a neutral portion in a PMeT chain, are reduced back to the 2+ state at the electrode. Hence, the contribution of $[Ru(bpy)_3]^{3+}$ to the spectral changes for $\lambda<560$ nm is substantially negligible. This means that the mediated doping Reaction 3 is rapid compared to the Reaction 2, and that the backward spectral changes in $\lambda<560$ nm in Fig. 8 should be attributed principally to the Reaction 2. We assume that the backward increase in absorption for $\lambda<560$ nm in Fig. 8, and possibly in Fig. 7(b), is due to the increase in the neutral portion in the PMeT chains as a result of the Reaction 2 and the subsequent reduction of the bipolaron size. The latter effect would occur in the last stage of a series of relaxation processes upon charge injections.

Most of the spectral studies on PTs reported so far have been performed under static conditions based on relatively thick films ($\approx\mu$m). In contrast, the spectral changes for 560 nm$<\lambda$ of Figs. 7(b) and 8 represent dynamic processes in the course of achieving equilibrium within the PMeT layer. This scheme is enabled by the configuration in which a relatively thinner PMeT layer (<100 nm) is isolated from the substrate by the intervention of an electrically insulating but electrochemically active inner layer. Without the intervening layer, i.e., for Pt/PMeT electrodes, no isosbestic behavior was observed even at very low sweep rates (<5 mV s^{-1}) with similar PMeT thickness (<100 nm). Detection of the transient P^+ at Pt/PMeT was not successful with varying doping conditions because the spectral changes under the dynamic conditions were ambiguous and much less systematic, probably reflecting the manifold relaxation processes occurring within the PMeT layer. The charge injections via discrete electronic levels into the conducting polymers would generate charged states which are energetically more confined. These charged states should be able to relax more rapidly through less diversified relaxation pathways, giving rise to the isosbestic behavior in Fig. 7(b). This characteristic feature has allowed the detection of the transiently occurring polarons. Studies of electrochemically induced changes in conducting polymers based on the structure of the present study, i.e., substrate/electrochemically active film/conducting polymer film, would yield further insight into the charged states of the conducting polymers.

References

1) J. C. Scott, P. Pfluger, M. T. Krounbi, and G. B. Street, *Phys. Rev.*, **B28**, 2140 (1983).

2) T.-C. Chung, J. H. Kaufman, A. J. Heeger, and F. Wudl, *Phys. Rev.*, **B30**, 702 (1984).

3) J. C. Scott, J. L. Bredas, K. Yakushi, P. Pfluger, and

G. B. Street, *Synth. Metals*, **9**, 165 (1984).
4) J. H. Kaufman, N. Colaneri, J. C. Scott, and G. B. Street, *Phys. Rev. Lett.*, **53**, 1005 (1984).
5) F. Genoud, M. Guglielmi, M. Nechtschein, E. Genies, and M. Salmon, *Phys. Rev. Lett.*, **55**, 118 (1985).
6) K. Kaneto, Y. Kohno, and K. Yoshino, *Solid State Commun.*, **51**, 267 (1984).
7) T. Hattori, W. Hayes, K. Wong, K. Kaneto, and K. Yoshino, *J. Phys.*, **C17**, L803 (1984).
8) K. Kaneto, S. Hayashi, S. Ura, and K. Yoshino, *J. Phys. Soc. Jpn.*, **54**, 1146 (1985).
9) G. Harbeke, E. Meier, W. Kobel, M. Egli, H. Kiess, and E. Tosatti, *Solid State Commun.*, **55**, 419 (1985).
10) K. Murao and K. Suzuki, *J. Chem. Soc., Chem. Commun.*, **1984**, 238.
11) K. Murao and K. Suzuki, *Chem. Lett.*, **1986**, 2101.
12) S. Glenis, G. Tourillon, and F. Garnier, *Thin Solid Films*, **122**, 9 (1984).
13) H. D. Abruna, P. Denisevich, M. Umana, T. J. Meyer, and R. W. Murray, *J. Am. Chem. Soc.*, **103**, 1 (1981).
14) K. Murao and K. Suzuki, *Solid State Commun.*, **62**, 483 (1987).
15) K. Murao and K. Suzuki, *Appl. Phys. Lett.*, **47**, 724 (1985).
16) M. Furue, K. Sumi, and S. Nozakura, *J. Polym. Sci., Polym. Lett. Ed.*, **20**, 291 (1982).
17) P. Denisevich, K. W. Willman, and R. W. Murray, *J. Am. Chem. Soc.*, **103**, 4727 (1981).
18) K. W. Willman and R. W. Murray, *J. Electroanal. Chem.*, **133**, 211 (1982).
19) C. R. Leidner, P. Denisevich, K. W. Willman, and R. W. Murray, *J. Electroanal. Chem.*, **164**, 63 (1984).
20) R. J. Waltman, J. Bargon, and A. F. Diaz, *J. Phys. Chem.*, **87**, 1459 (1983).
21) K. Murao and K. Suzuki, unpublished results.
22) Doping at lower potentials produces quasi-equilibrated spectral changes as shown in Fig. 2 of Ref. 14.

Use of Propagators in the Hückel Model. VIII. Intermolecular Interaction

Toshiharu KANO, Kiyoshi NISHIKAWA, and Shigeyuki AONO*
Department of Chemistry, Faculty of Science, University of Kanazawa, Marunouchi, Kanazawa, Ishikawa 920
(Received March 18, 1987)

Intermolecular interactions are analyzed by the propagator method, under the tight-binding approximation. The stabilization energy or the change of charge density due to the intermolecular interaction are expressed in terms of propagators, so that the mechanism resulting above effects is satisfactorily realized. As an interesting example, the intermolecular interaction between guanine and benzo[*a*]pyrene (a famous chemical carcinogen) is investigated.

There are various types of intermolecular interactions. If interacting molecules are charged, or have permanent dipoles, the interaction between them is purely classical, due to the static coulomb potentials. If they are neutral, the induced dipole moments are responsible for their combination.[1] The hydrogen-bond is classified as one of the intermolecular interaction, but this would be a rather weak chemical bond. Another one is the charge-transfer complex proposed by Mulliken:[2] Even if the composite molecules are neutral themselves, the charge-transfer state which is energetically higher than the neutral state mixes with the latter to yield the more stable ground state.

Recently a high ability of the computer may enable us to calculate the intermolecular interaction energies on the same footing dealing with simple molecules. If this be done satisfactorily, the effects involving the above mentioned treatments would be wholly taken into account, but the concepts introduced by the respective methods will be lost. In addition, one cannot expect the computer ability to reproduce the experimental details which the common chemists are interested in.

The present analysis which is facilitated by the propagator technique is at most semiquantitaive. The interaction terms responsible for the molecular combination are assumed to have a single-particle character, i.e., are written by the so-called transfer integrals. This mechanism should be interpreted as a mutual charge transfer in Mulliken's sense.[2]

In the followings, we begin with writting the stabilization energy due to the intermolecular interaction in terms of the Green's function up to the second order of the interaction. In the first half of this paper, the first order term plays a central role in searching for the preferable conformations of the composite molecules. In the second half, adopting the unperturbed system of separated molecules, we express the stabilization energy as a second order effect due to the perturbation. This is very easily carried out by the propagator method. Then we advance one more step of approximation procedure called the closure approximation, so that the mechanism yielding the interaction effect is made very much clear. Finally the interaction between guanine and benzo[*a*]pyrene is investigated as a suggestive example for chemical carcinogenesis.

General

As has been shown,[3] in the tight-binding approximation (Hückel approximation in the π-conjugated molecules) the bond order and the total energy are expressed, respectively, in terms of propagators as

$$q_{rs} = \frac{1}{2\pi i}\int_c dz G_{rs}(z), \tag{1}$$

$$E = Tr\frac{1}{2\pi i}\int_c dz z G(z), \tag{2}$$

where r and s are site indices. In the above the propagator G is

$$G(z) = \frac{1}{z-H} \tag{3}$$

with

$$H = \begin{bmatrix} 0 & \beta_{12} & \beta_{13} & \cdot & \cdot \\ \beta_{21} & 0 & \beta_{23} & \cdot & \cdot \\ \cdot & \cdot & \cdot & \cdot & \cdot \end{bmatrix}, \tag{4}$$

where β_{rs} is a transfer integral, which is usually taken into account for the adjacent neighbors. The integration with respect to z is carried out along the Coulson contour, which goes along the circuit enclosing poles referring to the occupied levels. We assume that the integration involves the spin sum. Tr(trace) means the diagonal sum, ensurering the independent character from representations.

If the Hamiltonian is separated as

$$H = H^0 + v, \tag{5}$$

where v is the perturbation, then Eq. 3 is rewritten as

$$\begin{aligned} G(z) &= \frac{1}{z-H} \\ &= \frac{1}{z-H^0} + \frac{1}{z-H^0} v \frac{1}{z-H} \\ &= G^0(z) + G^0(z) v G(z). \end{aligned} \tag{6}$$

In the above, we defined $G^0(z)$ for the unperturbed Hamiltonian.

Expanding $G(z)$ as in Eq. 6 and keeping up to the second order term of v, we can obtain changes of energy and bond order. The energy change due to v is

$$\Delta E = \mathrm{Tr}\frac{1}{2\pi i}\int_c dz z(G-G^0)$$
$$\fallingdotseq \mathrm{Tr}\frac{1}{2\pi i}\int_c dz z(G^0vG^0+G^0vG^0vG^0)$$
$$= \mathrm{Tr}\frac{1}{2\pi i}\int_c dz(G^0v+\frac{1}{2}G^0vG^0v). \quad (7)$$

The last result is obtained by partial integration in the second line. If the perturbation v is independent of z, the first term of Eq 7 is evaluated as

$$\Delta E^{(1)} = 2\sum_{rs} q_{rs}v_{sr} \quad (8)$$

by the use of Eq. 1. The numerical factor 2 is due to the spin sum. If we use the representation diagonalizing the Hamiltonian H^0, $G^0(z)$ is written as

$$G^0(z) = \sum_i \frac{|i><i|}{z-\varepsilon_i}, \quad (H^0|i> = \varepsilon_i|i>). \quad (9)$$

We can evaluate the second term of Eq. 7 as follows:

$$\Delta E^{(2)} = \frac{1}{2\pi i}\int_c dz \frac{1}{2}\sum_{rstu}\sum_{ij}\frac{<r|i><i|s>}{z-\varepsilon_i}v_{st}\frac{<t|j><j|u>}{z-\varepsilon_j}v_{ur}$$
$$= 2\sum_{rstu}\sum_{i}^{occ}\sum_{j}^{un}<r|i><i|s>v_{st}<t|j><j|u>v_{ur}/(\varepsilon_i-\varepsilon_j). \quad (10)$$

This result is also rewritten in terms of polarizabilities.[4]

The similar expression for the bond order is also obtained as well. The above expressions are useful for the case of the interaction v being intramolecular, and in the intermolecular case are replaced by a little more complicated expressions.

Now we advance the approximation procedure (so-called the closure approximation) one more step in Eq. 10. If the denominators are replaced by their average,

$$\Delta\varepsilon \simeq <\varepsilon_j-\varepsilon_i>_{av} (>0), \quad (11)$$

we can carried out the summation with respect to i and j to obtain

$$\Delta E^{(2)} = -\frac{1}{2}\frac{1}{\Delta\varepsilon}\sum_{rstu} q_{rs}v_{st}\hat{q}_{tu}v_{ur}, \quad (12)$$

where

$$q_{rs} = 2\sum_{i}^{occ}<r|i><i|s> \quad (13)$$

is the so-called the bond order, and

$$\hat{q}_{tu} = 2\sum_{i}^{un}<t|i><i|u>$$
$$= 2\delta_{tu} - q_{tu}. \quad (14)$$

The last line is obtained from the completeness relation.

We can understand from Eq. 12 that the additional energy arises from going round a circuit as $r\to s\to t\to u\to r$, which are constructed of bond orders and interaction matrix elements.

As an illustrative example, we ask which is energetically more stable, anthracene or phenanthrene. First we note that the energy difference between them occurs from the second order terms. Observing Fig. 1, we can immediately obtain (noticing that $\Delta\varepsilon>0$), for anthracene

$$\Delta E^{(2)} = -\frac{1}{\Delta\varepsilon}q_{79}v_{9,14}\hat{q}_{14,2}v_{27} = 0, \quad (15)$$

since $q_{79}=\hat{q}_{14,2}=0$, and for phenanthrene

$$\Delta E^{(2)} = -\frac{1}{\Delta\varepsilon}\hat{q}_{69}v_{9,14}q_{14,1}v_{16} < 0, \quad (16)$$

since $q_{14,1}>0$, and $\hat{q}_{69}>0$. Therefore phenanthrene is more stable than anthracene.

Mutual Orientation of Interacting Molecules

Let us imagine that two conjugated ring molecules, A and B approach with each other, and a bond indicated by a solid line in Fig. 2 takes place between them. If molecular planes are mutually parallel, this bond is a σ-type between π-orbitals of A and B molecules. The mutual phases of π atomic orbitals of both molecules are put so that all resonance integrals are attractive. This situation seems appropriate for the beginning of intermolecular reaction. Problem is: Where is the next bond formed (not necessarily restricted only one) to get a firmer combination between? The answer will be provided by Eq. 8. Since we can consider the above molecular compound, A—B as a whole system because

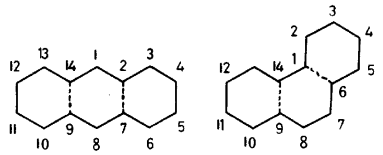

Fig. 1. (a) Anthracene and (b) phenanthrene molecules.

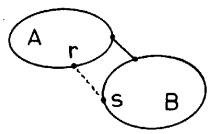

Fig. 2. Schematic diagrame of two interacting molecules.

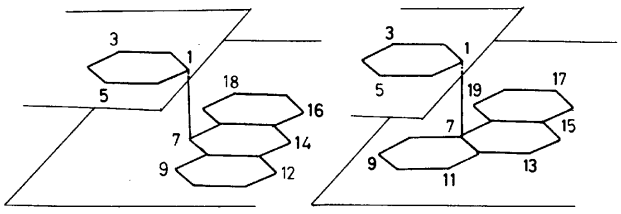

Fig. 3. Schematic diagrames of composite molecule between (a) benzene-anthracene and (b) benzene-phenanthrene.

Table 1. Bond Orders of Benzene–Anthracene Pair

(a)		(b)		(c)		(d)	
Site	q_{rs}	Site	q_{rs}	Site	q_{rs}	Site	q_{rs}
2-8	−0.125	2-7	−0.095	2-7	−0.090	2-8	−0.164
2-14	0.146	2-9	−0.098	2-8	−0.177	2-9	−0.199
4-8	0.097	2-13	−0.082	2-10	−0.091	2-14	0.084
4-14	−0.131	2-14	0.135	2-12	0.066	4-8	0.128
		2-20	−0.119	2-13	−0.083	4-9	0.160
		4-14	−0.122	2-14	0.081		
		4-20	0.093	2-20	−0.076		
				4-7	0.073		
				4-8	0.136		
				4-10	0.067		
				4-13	0.061		
				4-14	−0.070		

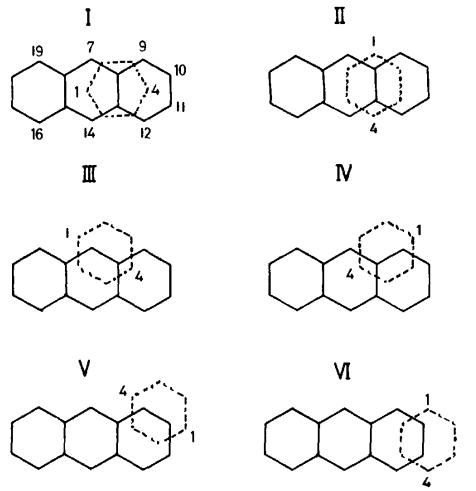

Fig. 4. Various conformations of benzene–anthracene pair.

of the bond described by the solid line, it is expected that the next bond (indicated by the dotted line in Fig. 2) will arise between r and s sites where $\Delta E^{(1)}$ of Eq. 8 is negative and as large as possible in its absolute value. In other words, v_{rs} being negative, q_{rs} should be positive and as large as possible.

We give two examples: Benzene-anthracene pair and benzene-phenanthrene pair. As is shown in Fig. 3(a), benzene and anthracene approach with each other keeping their molecular plane parallel, and make a bond between the *1*-site of benzene and the *7*-site of anthracene. The calculated results of which absolute values are considerably large are shown in Table 1a. Observing the data we can expect new bonds between sites *2* and *14*, or between sites *4* and *8*. If we consider that the new bond is likely under the condition that the original *1-7* bond does not shift so much, it should be concluded that the pair under consideration is stable at the conformation, I or III in Fig. 4.

From the symmetry consideration it is enough to select the anthracene sites *7-10* to make similar treatments. From Table 1b which refers to the *1-8* original bond, we expect again the conformation III. Table 1c corresponding to the *1-9* original bond suggests con-

Table 2. Bond Orders of Benzene–Phenanthrene Pair

Site	q_{rs}	Site	q_{rs}
2-8	−0.122	2-14	0.083
2-10	0.089	4-8	0.093
2-12	−0.1110	4-12	0.085

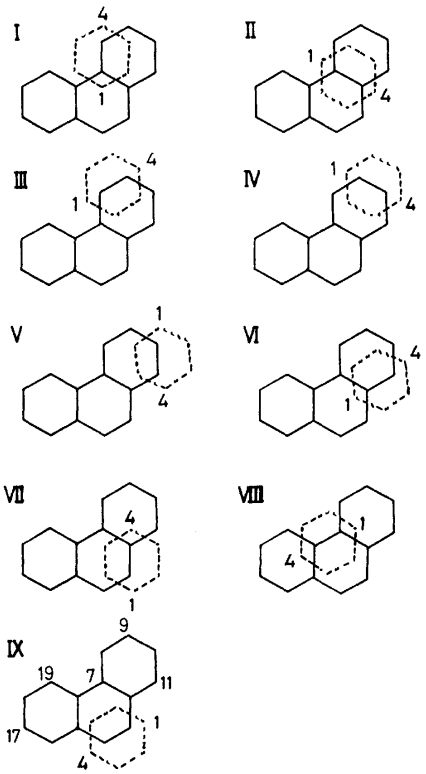

Fig. 5. Various conformations of benzene–phenanthrene pair.

formations II and IV. Finally from Table 1d referring to the original *1-10* bond we can expect the conformation V. Unexpectedly we can not find the conformation VI from Table 1d.

From the preceding considerations we find that, in every compound, benzene rings avoid the face-to-face structure as if the steric effect be satisfactorily taken into account. This fact is already pointed out by one of the present authors.[5]

The entirely same investigation is also applied to the benzene-phenanthrene pair. From the symmetry consideration the phenanthrene sites combining with the benzene *1*-site are selected to be *7—13* in Fig. 3(b). As an example we evaluate bond orders in the case of the pair with the *1-7* original bond. The results are shown in Table 2. From this it is easy to presume that conformations I and II in Fig. 5 are likely. Similar considerations for cases involving sites *8—13* in phenanthrene lead to various conformations III—VII in Fig.5.

Intermolecular Interaction

If we take the separated molecules, A and B as the unperturbed system, the additional energy is of the second order to the perturbation v. We find a little more complicated expression than that of Eq. 7, as

$$\Delta E^{(2)} = Tr \frac{1}{2\pi i}\int_c dz G_A^0 v_{AB} G_B^0 u_{BA} , \tag{17}$$

where the factor 1/2 in the first line of Eq. 7 cancels out with the factor arising in interchanging A and B in the above. Then the straightforward calculation yields:

$$\Delta E^{(2)} = 2\sum_{rs}^{A}\sum_{tu}^{B} \left\{ \sum_{iA}^{occ}\sum_{\mu B}^{un} \frac{1}{\varepsilon_{iA}-\varepsilon_{\mu B}} [<r|i><i|s>]^A v_{st}^{AB} [<t|\mu><\mu|u>]^B v_{ur}^{BA} + \sum_{\mu A}^{un}\sum_{iB}^{occ} \frac{1}{\varepsilon_{iB}-\varepsilon_{\mu A}} [<r|\mu><\mu|s>]^A v_{st}^{AB} [<t|i><i|u>]^B v_{ur}^{BA} \right\} \tag{18}$$

where the numerical factor 2 is due to the spin sum.

Now we want to take the closure approximation. Replacing the energy denominators in the above by suitable averages, for example

$$\Delta\varepsilon_{BA} \simeq <\varepsilon_{\mu B}-\varepsilon_{iA}>_{av},\ \Delta\varepsilon_{AB} \simeq <\varepsilon_{\mu A}-\varepsilon_{iB}>_{av}, \tag{19}$$

we obtain

$$\Delta E^{(2)} = \frac{-1}{2}\sum_{rs}^{A}\sum_{tu}^{B} \left\{ \frac{1}{\Delta\varepsilon_{BA}} q_{rs}^A v_{st}^{AB} q_{tu}^B v_{ur}^{BA} + \frac{1}{\Delta\varepsilon_{AB}} q_{rs}^A v_{st}^{AB} q_{tu}^B v_{ur}^{BA} \right\} \tag{20}$$

where q_{rs}^B is the bond order and (see Eq. 14)

$$\hat{q}_{tu}^B = 2\delta_{tu} - q_{tu}^B . \tag{21}$$

Next we evaluate the change of bond order due to v. To this end we begin with the expansion

$$G_B = G_B^0 + G_B^0 v^{BA} G_A^0 v^{AB} G_B^0 + \cdots \tag{22}$$

and obtain

$$\Delta q_{rs}^B = \frac{1}{2\pi i}\int_c dz (G_B - G_B^0) = \sum_{s's''t't''} \frac{1}{2\pi i}\int_c dz G_{B,rs'}^0 v_{s's''}^{BA} G_{A,s''t'}^0 v_{t't''}^{AB} G_{B,t''s}^0 . \tag{23}$$

Substituting Eq. 9 in the above, and integrating along the Coulson contour, we obtain the result:

$$\begin{aligned}\Delta q_{rs}^B = 2\sum_{s't''}^{A}\sum_{s''t'}^{B} \Bigg\{ & \sum_{iB}^{occ}\sum_{jA}^{occ}\sum_{kB}^{un} \frac{-2}{(\varepsilon_{kB}-\varepsilon_{iB})(\varepsilon_{kB}-\varepsilon_{jA})} \\ & + \sum_{iB}^{coo}\sum_{jA}^{un}\sum_{kB}^{occ} \frac{-1}{(\varepsilon_{jA}-\varepsilon_{iB})(\varepsilon_{jA}-\varepsilon_{kB})} \\ & + \sum_{iB}^{occ}\sum_{jA}^{un}\sum_{kB}^{un} \frac{2}{(\varepsilon_{jA}-\varepsilon_{iB})(\varepsilon_{kB}-\varepsilon_{iB})} \\ & + \sum_{iB}^{un}\sum_{jA}^{occ}\sum_{kB}^{un} \frac{1}{(\varepsilon_{iB}-\varepsilon_{jA})(\varepsilon_{kB}-\varepsilon_{jA})} \Bigg\} \\ & \times <r|i><i|s'>^B v_{s's''}^{BA} <s''|j><j|t'>^A v_{t't''}^{AB} <t''|k><k|s>^B .\end{aligned} \tag{24}$$

Now we employ the closure approximation in the above and obtain

$$\begin{aligned}\Delta q_{rs}^B = \frac{1}{4}\sum_{s't''}^{B}\sum_{s''t'}^{A} \Bigg\{ & \frac{-2}{\Delta\varepsilon_{BB}\Delta\varepsilon_{BA}} q_{rs'}^B v_{s's''}^{BA} q_{s''t'}^A v_{t't''}^{AB} \hat{q}_{t''s}^B \\ & + \frac{-1}{\Delta\varepsilon_{AB}\Delta\varepsilon_{AB}} q_{rs'}^B v_{s's''}^{BA} \hat{q}_{s''t'}^A v_{t't''}^{AB} q_{t''s}^B \\ & + \frac{2}{\Delta\varepsilon_{AB}\Delta\varepsilon_{BB}} q_{rs'}^B v_{s's''}^{BA} \hat{q}_{s''t'}^A v_{t't''}^{AB} \hat{q}_{t''s}^B \\ & + \frac{1}{\Delta\varepsilon_{BA}\Delta\varepsilon_{BA}} \hat{q}_{rs'}^B v_{s's''}^{BA} q_{s''t'}^A v_{t't''}^{AB} \hat{q}_{t''s}^B \Bigg\} .\end{aligned} \tag{25}$$

Here we again stress that the change of bond order does arise from additional contributions of some reaction pathes which are constructed of bond orders and interaction matrix elements. We can get, with a little sacrifice of accuracy in Eq. 24, a very transparent physical insight of the phenomena under consideration.

We present numerical results in the followings. The parameters used here are:

1. The distance of molecular planes (e.g. between benzene and anthrathene planes) is assumed to be 2 in the unit of the benzene bond distance (1.39 Å).

2. The values of v_{rs} are estimated to be reciprocally proportional to the cube of the r-s distance, and are assumed to be zero for cases with distances larger than 8. Then a multicative factor *2* is applied because of the σ-bond character of v_{rs}.

In Table 3, we have shown the calculated results of various conformations of benzene-anthracene pair. The first column presents the types of pairs as displayed in Fig. 4. The energy changes of the second column are given in the unit of $|\beta|$. The minus sign indicates the system to be stable. The values of the first line is obtained by the closure approximarion, Eq. 20, while the second line by the relation without approximation, Eq. 18. Agreements between them are remarkable, though the values themselves are rather qualitative. The following columns present the changes of charge densities at various benzene sites. As to these, the agreements between the first and second lines are not so satisfactory as in the case of energy. This is a

Table 3. Changes of Energy and Charge Densities of Various Types of Benzene-Anthracene Pair

	ΔE	Δq_{rr} of benzene					
		1	2	3	4	5	6
I	−0.0436	0.047	−0.007	−0.043	0.089	−0.043	−0.007
	−0.0591	0.059	−0.017	−0.019	0.049	−0.019	−0.017
II	−0.0584	0.044	−0.016	−0.016	0.044	−0.021	−0.021
	−0.0723	0.030	−0.013	−0.013	0.030	−0.013	−0.013
III	−0.0457	0.023	0.026	0.011	−0.015	−0.008	−0.021
	−0.0629	0.024	0.034	0.008	−0.001	−0.009	−0.006
IV	−0.0714	−0.012	0.003	0.017	0.025	−0.006	−0.009
	−0.0842	−0.000	−0.005	0.028	0.023	0.003	−0.021
V	−0.0122	0.011	0.011	0.010	0.018	−0.006	−0.036
	−0.0074	0.001	0.017	0.022	0.018	−0.016	−0.033
VI	−0.0115	0.021	0.003	0.003	0.021	−0.020	−0.020
	−0.0156	0.011	0.006	0.006	0.011	−0.016	−0.016

Table 4. Changes of Energy and Charge Densities of Various Types of Benzene-Anthracene Pair

	ΔE	Δq_{rr} of benzene					
		1	2	3	4	5	6
I	−0.0447	0.006	−0.014	0.017	0.025	0.001	−0.008
	−0.0436	0.016	−0.014	0.024	0.023	0.010	−0.020
II	−0.0434	0.036	−0.013	−0.014	0.037	−0.003	−0.031
	−0.0451	0.023	−0.013	−0.009	0.027	−0.014	−0.017
III	−0.0524	0.006	0.017	0.008	0.021	−0.006	−0.029
	−0.0635	0.004	0.019	0.018	0.020	−0.016	−0.027
IV	0.0036	0.021	0.005	0.005	0.021	−0.021	−0.020
	0.0045	0.010	0.011	0.011	0.011	−0.020	−0.018
V	−0.0382	0.017	0.009	0.011	0.011	−0.034	−0.006
	−0.0434	0.015	0.019	0.018	0.003	−0.030	−0.016
VI	−0.0593	−0.013	−0.010	−0.007	0.026	0.018	0.005
	−0.0693	−0.002	−0.022	0.001	0.025	0.029	0.001
VII	−0.0325	0.032	−0.005	−0.010	−0.009	0.008	0.021
	−0.0334	0.030	0.013	−0.017	−0.000	0.002	0.031
VIII	−0.0591	−0.005	0.003	0.003	−0.005	0.025	0.025
	−0.0720	0.014	−0.005	−0.005	0.014	0.023	0.023
IX	−0.0261	0.014	0.015	0.015	0.014	−0.021	−0.021
	−0.0279	0.010	0.023	0.023	0.010	−0.022	−0.022

well-known trend in quantum chemistry. We can say, the values of the second lines are more reliable.

We have carried out calculations for the type VI, not acceptable in the previous treatment, and find that this is not so stable, as is type V.

The calculations for the various types of the benzene-phenathrene pair are given in Table 4. The results are almost satisfactory as was seen in the case of benzene-anthracene pair. If we regard phenanthrene as a prototype of benz[*a*]pyrene (a famous chemical carcinogen), we can find stable structures in which the benzene molecule sits on areas extending over the so-called Bay, K, and L regions.

Benzo[*a*]pyrene-Guanine Pair

Benzo[*a*]pyrene is a famous chemical carcinogen, of which activity has been widely discussed connecting with its structure or its derivatives produced by the metabolic reactions.[6] Though recent studies rather stress the metabolic effect, we come back to an old-fashioned view of chemical carcinogenesis, based on the direct combination of carcinogen with nucleotide.

Replacing benzene and phenanthrene in the previous section by guanine and benzo[*a*]pyrene, respectively, we carry out the same treatment as before. However, in this time we have not tried to optimize the mutual orientation of these molecules, but begin with assuming several conformations as described in Fig. 6, which are presumed from the investigation of the benzene-phenanthrene pair. Empirical parameter added to previous ones are

$$\alpha(\ddot{\mathrm{O}})=2.0\beta,\quad \alpha(\ddot{\mathrm{N}})=1.5\beta,\quad \alpha(\dot{\mathrm{N}})=0.5\beta \tag{26}$$

where the dotts represent the number of π electrons given by these atoms.

Strictly speaking, it is inadequate to disregard cytosine bonded with guanine by hydrogen bonds (see Fig. 7). We have to imagine cytosines at the appropriate positions in conformations I—V of Fig. 6. Calculated results are in Table 5. In each row, the numerals of the first line are obtained by the closure approximation (Eqs. 20 and 25), and those of the second line are without this approximation. Therefore the latter is a little

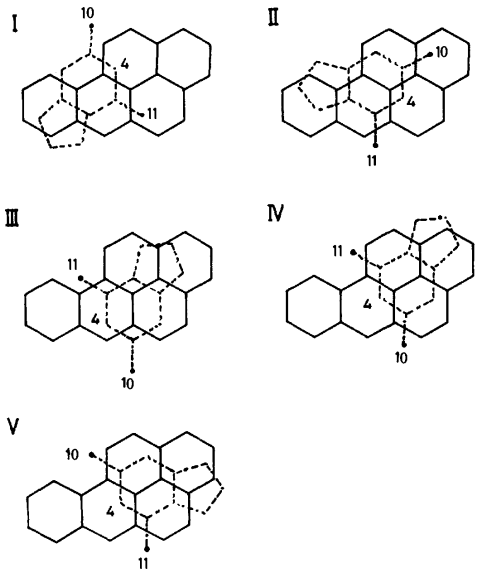

Fig. 6. Various conformations of guanine-benzo[*a*]pyrene pair.

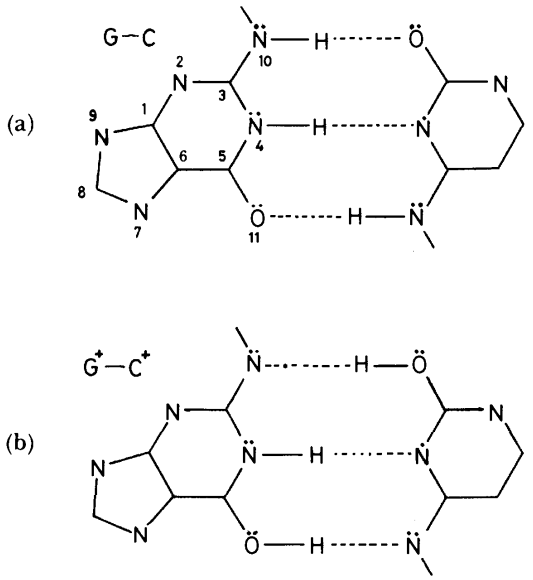

Fig. 7. Conformations of guanine-cytosine pair.

more reliable, even though it is quite crude from the quantitative viewpoints. However we may insist that if we pass from column to column, or from row to row, the trends observed there tell us something true. The types I and II are not energetically stable. The conformation adopted in a current investigation,[7] is an almost face-to-face structure, because of the maximum overlap between π orbitals of the composite molecules being achieved. As mentioned before, this is not necessarily favorable for molecular compounds.

The conformations III—V are stable, where the mutual arrangement of guanine and cytosine is opposite in the direction to that of I and II. In these stable structure we estimated the changes of charge densities at the positions relating to the hydrogen bonds. We proceed discussions based upon the data of the second

Table 5. Changes of Energy and Charge Densitiesof Various Types of Guanine-Benzo[*a*]pyrene Pair.

	ΔE	Δq_π of guanine		
		4·N̈	10-N̈	11-Ö
I	0.0018			
	0.0191			
II	0.0065			
	0.0179			
III	−0.1649	0.122	−0.029	0.046
	−0.0953	0.039	0.004	0.020
IV	−0.1401	0.136	−0.020	0.021
	−0.1235	0.038	0.001	0.013
V	−0.1195	0.153	−0.041	0.023
	−0.0609	0.051	−0.027	0.014

lines in Table 5. In Fig. 7(a), we present the normal guanine-cytosine pair in which three hydrogen bonds are there. We can see that, in Table 5, a considerably large increase of charge arises at the *10*-N̈ (the upper most N̈ in Fig. 7(a)). This shifts the proton of NH group in guanine toward the oxygen of cytosine, and results in shitfing the proton of the NH group in cytosine toward the oxygene of guanine. As a result, we have a new pair denoted G*-C* in Fig. 7(b). It is understood that, in the new pair, the original two hydrogen bonds are lost, and only a weak hydrogen bond remains, and this conformation might be a source of mutation.

One may say the above consideration is old, and seems almost denied. The O- or OH- substituted benzo[*a*]pyrene produced by the metabolic reaction strongly binds the nucleotide, so that the order of nucleotide is confused to arise the mutation. However we may argue the present investigation especially of the mutual orientation between composite molecules is still suggestive in the further investigation to chemical carcinogen.

Concluding Remarks

In the present work, the intermolecular interaction is treated as a perturbation of the sigle-particle character between molecules. We have assumed that the intermolecular distance and other geometrical factors are almost predetermined by other mechanical sources, e.g., the van der Waals interaction and so on. In other words, we consider that two molecules come near to an appropriate position and the charge exchange begins to work between them.

In the usual treatments, the local interactions are taken into account for predominantly determining geometrical structure of the molecular complex, i.e., the maximum overlap between atomic orbitals of composite molecules being achieved. This consideration inevitably leads to the face-to-face structure for the present systems, and then an undesirable feature is avoided by introducing a steric effect of it. Really the structure experimentally observed is not of a face-to-

face type, but is that the benzene ring of one molecule shifts by about a half of width relatively to that of the other moledule. What we have claimed here is follows: This preferable structure is explained energetically, that is to say, the additional energy producing a stable structure is arisen by the product of the transfer integral between sites under consideration and the coresponding long-range bond order. The latter that is hiden before introducing the perturbation is a decisively important factor to determin geometrical structure.

Next, supposing that the geometrical structure of a couple of molecules is given by the previous analysis, we treat the intermolecular interaction as a second order perturbation problem with respect to transfer matrix elements. The propagator technique enable us to obtain the complicated results very easily. The resultant expression is reinterpreted by introducing the closure approximation: The stabilization aises as an effect from a closed path constructed of bond orders and interaction matrix elements. We should like to stress a deep understanding of the bond order of a quantum mechanical and wave-functional character.

As a final example, interaction between guanine and benzo[*a*]pyrene is investigated. This is rather old-fashioned, but might be helpfull in remembering a conformational investigation apt to be missed in the recent studies.

References

1) F. London, *Z. Phys.*, **63**, 245 (1930), *Z. Physik. Chem.*, **11**, 222 (1930).

2) R. S. Mulliken, *J. Am. Chem. Soc.*, **74**, 811 (1952).

3) S. Aono and K. Nishikawa, *Bull. Chem. Soc. Jpn.*, **53**, 3418 (1980); T. Ohmae, K. Nishikawa, K. Deguchi, and S. Aono, *Bull. Chem. Soc. Jpn.*, **54**, 2857 (1981).

4) S. Aono and K. Nishikawa, *Bull. Chem. Soc. Jpn.*, **58**, 288 (1985).

5) S. Aono, *Prog. Thoret. Phys.*, **29**, 133 (1958).

6) J. A. Miller, *Cancer Research*, **30**, 559 (1970); E. C. Miller, *Cancer Research*, **38**, 1479 (1978); D. W. Nebert, *Adv. Canc. Res.*, **25**, 149 (1977); A. Dipple, Polynuclear Aromatic Carcinogens, "Chemical Carcinogens" ACS Monograph 173; Seale, C. F. Ed,; American Chemical Society; Washington D. C. (1976), pp. 245—314. Current references are sited therein.

7) C. Nagata, M. Kodama, Y. Tagashira, and Imamura. *Biopolymers*, **4**, 409 (1966).

 © 1987 The Chemical Society of Japan Bull. Chem. Soc. Jpn., 60, 2825—2831 (1987)

A Study of Inorganic Ion Exchangers. XI. The Hydrothermal Reactions of $ZrOCl_2$ and $M(H_2PO_4)_2$ (M=Mg, Ca, Sr, Ba)

Kiyomi OKABE* and Etsuro KOBAYASHI
National Chemical Laboratory for Industry, Yatabe, Tsukuba, Ibaraki 305
(Received October 22, 1986)

The possibility of the hydrothermal synthesis of layered zirconium phosphates containing various alkaline earth metals (abbreviated as ZrMP; M=Mg, Ca, Sr, Ba) has been studied from $ZrOCl_2$ and $M(HPO_4)_2$, and their characteristics have been investigated. The optimum conditions for the synthesis of a highly crystalline product were as follows; the molar ratio of the starting materials of $Ca(H_2PO_4)_2$ and $ZrOCl_2$ was Ca/Zr=3, and the temperature of the hydrothermal reaction was in the range of 200—270 °C. By the hydrothermal reaction of $ZrOCl_2$ and $Mg(H_2PO_4)_2$, a new compound of $ZrMg_{0.5}H(PO_4)_2 \cdot H_2O$ with a layer-spacing of 11.94 Å was obtained. Layered phosphate (ZrMP) was not obtained by the hydrothermal reaction of $ZrOCl_2$ and $Ba(H_2PO_4)_2$. The temperature range of the inter-layer dehydration of the layered phosphates (ZrMgP, ZrCaP, and ZrSrP) was similar to that of α-zirconium(IV) bis(hydrogenphosphate) (α-ZrP); i.e. the water in the interlayer was lost at 130—240 °C, and dehydro-condensation took place at a higher temperature above 340 °C. Zirconium phosphate containing Mg^{2+} or Ba^{2+} was not obtained by the ion exchange of the protons in α-ZrP with the alkaline earth metal cations (M^{2+}) in MCl_2, while Ca^{2+} and Sr^{2+} were exchanged with the protons. These alkaline earth metal ions except for Ba^{2+} were easily exchanged with H^+ in α-ZrP, when NaOH was added. The layer-spacing of the Mg^{2+}-exchanged zirconium phosphate was 9.6 Å, which was different from that of the hydrothermal product. The layer distances of Ca^{2+}- or Sr^{2+}-exchanged products were similar to those of the hydrothermal products.

Layered tetravalent metal phosphates are widely used as inorganic ion-exchangers of great importance. Much attention has been paid recently for the layered compounds with different molecules and ions as catalysts for various reactions.[1)]

As reported previously,[2)] α-zirconium phosphates containing tertiary amines or aluminum ions between the layers have been synthesized hydrothermally, and used as catalysts for methanol conversion. However, a thermally stable layered phosphate having a wide inter-layer distance was not obtained.

This paper reports whether layered zirconium phosphates containing alkaline earth metal ions (abbreviated as ZrMP; M^{2+}=Mg^{2+}, Ca^{2+}, Sr^{2+}, Ba^{2+}) may be hydrothermally synthesized, and discusses the difference between the hydrothermal products and the layered compounds obtained by ion-exchange of H^+ in α-zirconium(IV) bis(hydrogenphosphate) (abbreviated as α-ZrP) with alkaline earth metal ions.

Experimental

Hydrothermal Reactions of $ZrOCl_2$ and $M(H_2PO_4)_2$ (M=Mg, Ca, Sr, Ba). A glass tube (20 cm^3) was filled with the appropriate amount of $ZrOCl_2 \cdot 8H_2O$, $M(H_2PO_4)_2$, H_2O, and NaCl or $Ca(OH)_2$ as listed in Table 1. After stirring the mixture thoroughly, the tube was sealed, and autoclaved (200—270 °C; 93—106 h). The hydrothermal products were separated from the mother liquor by centrifugation, and were washed with distilled water. The products were dried in a desiccator at 75% relative humidity.

Ion Exchange of H^+ in $Zr(HPO_4)_2$ with M^{2+} in MCl_2 (M=Mg, Ca, Sr, Ba). 100 cm^3 of an aqueous solution of MCl_2 (0.1 mol dm^{-3}) was added to 1.00 g of $\alpha\text{-}Zr(HPO_4)_2 \cdot H_2O$ (α-ZrP) and stirred overnight at room temperature. The precipitate was washed and separated by centrifugation. 50 cm^3 of an aqueous solution of MCl_2 (0.2 mol dm^{-3}) was added to 1.00 g of α-ZrP and stirred. Thirty cm^3 of an aqueous solution of NaOH (0.1 mol dm^{-3}) was slowly added to the mixture with vigorous stirring. The precipitate was washed and separated as described above.

Chemical Analysis. The composition of the products was determined as follows.[3)] The amount of H_2O was determined on the basis of the weight loss of the samples heated up to 800 °C.

The heated product was fused with 2.0 g of flux (Na_2CO_3:K_2CO_3=1:1) at 1000 °C. After cooling, the fused product was dissolved in distilled water at 100 °C, and 6 mol dm^{-3} HCl was added in order to dissolve the solid completely. Zirconium hydroxide was precipitated by adding 6 mol dm^{-3} NH_3 aq to the solution, and separated by filtration. After igniting the precipitate, a gravimetric method was employed for the determination as ZrO_2.

The phosphate ion in the filtrate was determined absorptiometrically, by the JIS K-0102 method.

The alkaline earth metals in the products were determined by atomic absorption after dissolving it.

Instrumental Analysis. The X-ray diffraction (XRD) was performed with Cu $K\alpha$ radiation (30 kV, 20 mA), by using an X-ray diffractometer (Rigaku, Geigerflex RAD). A scanning electron microscope (Shimadzu, ASM-SX) was employed for observation of the surfaces of the hydrothermal products. Surface areas of the products were determined by adsorption of argon at liquid nitrogen temperature using a fully-automatic surface area analyzer (Shimadzu, Micromeritics 2200). A micro-thermal analyzer, with 100 μV of DTA sensitivity and ±20 mg of TG sensitivity was used for the thermal analysis.

Results and Discussion

Hydrothermal Reaction of $ZrOCl_2$ and $Ca(H_2PO_4)_2$. The conditions of the hydrothermal reaction of zirconium(IV) oxychloride and various alkaline earth metal salts of bis(dihydrogenorthophosphate), as well as the analytical data of the products, are listed in Table 1.

Effects of Reaction Temperature. By varying the

Table 1. Hydrothermal Reactions of $ZrOCl_2$ with $M(H_2PO_4)_2$ (M=Mg, Ca, Sr, Ba), and Analysis of the Products

No.	Reaction condition							Reaction product																
	$ZrOCl_2 \cdot 8H_2O$	$M(H_2PO_4)_2$[a]	Additive[b]	H_2O	Zr : M : P : Na (Atomic ratio)	Temp	Time	Mother liquor	Yield	ZrO_2	P_2O_5	MO	H_2O	Na_2O	ZrO_2 : P_2O_5 : MO : H_2O : Na_2O (Molar ratio)								
	g	g	g	cm^3		°C	h	pH	g	%	%	%	%	%									
1	8.05	18.9		30	1 : 3 : 6	200	96	2.5	7.60	41.1	42.7	2.0	13.9		1.1	:	1.0	:	0.1	:	2.6		
2	1.61	3.78		10	1 : 3 : 6	250	106	2.7	1.43	39.7	42.8	1.1	13.1		1.1	:	1.0	:	0.1	:	2.4		
3	16.1	37.8		40	1 : 3 : 6	270	96	2.7	17.0	41.5	41.4	2.7	14.2		1.1	:	1.0	:	0.2	:	2.7		
4	1.61	1.89		10	1 : 1.5 : 3	250	106	2.4	1.36	39.9	42.2	1.5	14.6		1.1	:	1.0	:	0.1	:	2.7		
5	1.61	5.61		10	1 : 4.5 : 9	250	106	2.6	1.68	42.7	42.7	2.9	13.5		1.2	:	1.0	:	0.2	:	2.5		
6	1.61	3.78	0.584	10	1 : 3 : 6 : 2	250	106	2.5	1.35	41.5	43.8	1.3	10.9	0.58	1.1	:	1.0	:	0.1	:	2.0	:	0.03
7	1.61	3.78	0.740	10	1 : 5 : 6	250	93	3.3	3.05	57.9	31.8	6.2	8.0		2.1	:	1.0	:	0.5	:	2.0		
8	8.05	18.75(cm^3)		35	1 : 3 : 6	250	96	1.7	7.60	48.8	34.2	5.1	12.0		1.6	:	1.0	:	0.5	:	2.8		
9	1.61	3.75(cm^3)	0.584	10	1 : 3 : 6 : 2	250	93	1.8	1.18	48.8	33.9	5.4	13.1	0.40	1.7	:	1.0	:	0.6	:	3.1	:	0.03
10	1.61	4.22		10	1 : 3 : 6	250	93	3.4	2.70	32.3	34.3	19.8	13.6		1.1	:	1.0	:	0.8	:	3.1		
11	4.83	12.7	1.75	30	1 : 3 : 6 : 2	250	96	2.6	5.80	44.9	28.2	21.1	5.9	0.07	1.8	:	1.0	:	1.7	:	0.01		
12	1.61	4.97		10	1 : 3 : 6	250	93	3.1	3.47	41.8	28.3	25.1	4.8		1.7	:	1.0	:	0.8	:	1.4		
13	3.22	9.93	1.17	30	1 : 3 : 6 : 2	250	96	3.2	7.00	34.0	37.6	24.8	3.1	0.46	1.0	:	1.0	:	0.6	:	0.03		

a) M=Ca for No. 1—7; M=Mg (4 mol dm^{-3} $Mg(H_2PO_4)_2$) for Nos. 8 and 9; M=Sr for Nos. 10 and 11; M=Ba for Nos. 12 and 13. b) NaCl for Nos. 6, 9, 11, and 13; $Ca(OH)_2$ for No. 7.

reaction temperature, it was found that the products were amorphous below 150 °C, but that highly crystalline products were obtained above 200 °C. The X-ray diffraction intensity of the products increased in the order of No. 1 (200 °C)<No. 2 (250 °C)<No. 3 (270 °C) in Table 1.

The average content of P_2O_5 in these products was about 42% and was almost the same as that of α-zirconium(IV) bis(hydrogenphosphate) (42.09%). About 40% of the ZrO_2 content in the product was a little higher than that of α-zirconium(IV) bis(hydrogenphosphate) (α-Zrp). The CaO content was in the range of 1.1—2.7%, corresponding to about 0.1 mol of P_2O_5. The average H_2O content was 13.7%, which was slightly higher than that (10.68%) of α-ZrP.

Effects of $Ca(H_2PO_4)_2/ZrOCl_2$ Molar Ratio (Ca/Zr). The Ca/Zr molar ratios in the hydrothermal products of Nos. 4, 2, and 5 are listed in Table 1, and the XRD patterns of these samples are shown in Fig. 1. The XRD patterns of the products were almost the same as those of α-ZrP, except for a new peak at 2θ=8.7—8.9°. The new peak suggests the partial expansion of the layer distance of the products by the intercalation of Ca^{2+} between the layers. The crystallinity of the pro-

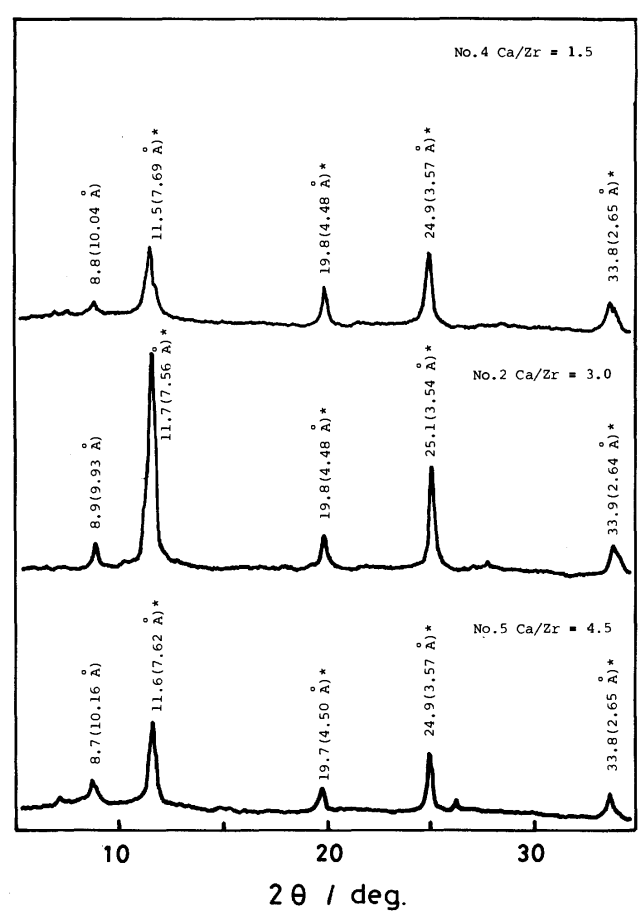

Fig. 1. X-Ray diffraction patterns of reaction products of $ZrOCl_2$ with $Ca(H_2PO_4)_2$ (Influence of molar ratio of $Ca(H_2PO_4)_2/ZrOCl_2$ (Ca/Zr)). Numerals on peaks indicate 2θ/degrees and lattice distances. *: The diffraction peaks of α-ZrP.

duct No. 4 (Ca/Zr=1.5) was low, suggesting an insufficient amount of phosphate in the starting materials. When the Ca/Zr ratio was 4.5 (No. 5), the XRD intensity was low. The crystallization of the product was assumed to be prevented by the excess amount of Ca in the starting materials. Therefore, the molar ratio of Ca/Zr=3.0 (No. 2) was optimal for the crystallization of the hydrothermal product (ZrCaP).

Effects of Additives. On the hydrothermal reaction of $ZrOCl_2$ and $Ca(H_2PO_4)_2$, appropriate amount of NaCl and $Ca(OH)_2$ were added. The XRD patterns of the products are shown in Fig. 2.

It is known that the layer distance is expanded up to 11.8 Å by the ion exchange of H^+ in α-ZrP with Na^+, and then Mg^{2+} is easily introduced between the layers after the expansion.[4,5] Expecting a similur effect, addition of NaCl was carried out in this investigation. The first d-value of the product No. 6 (NaCl addition) was 9.93 Å. The XRD pattern was not changed remarkably by the addition. Additional weak peaks in the XRD pattern were observed at 13.9, 19.5, 23.9, 28.1, and 31.1° by the NaCl addition. These new peaks did not belong to those of α-ZrP in the Na^+ form.

In order to obtain a product having a high content of Ca^{2+}, $Ca(OH)_2$ was added (No. 7). As shown in Table 1, the pH of the mother liquor was a little higher (pH=3.3) than the solution without $Ca(OH)_2$ (pH=2.5—2.7). The reaction product contained higher amounts of ZrO_2 and CaO than the others (Nos. 1—3). It was suspected from this result that the product was a mixture of zirconium(IV) hydroxide, calcium hydrogenphosphate ($CaHPO_4$) and zirconium phosphates.

Hydrothermal Reaction of $ZrOCl_2$ and $Mg(H_2PO_4)_2$. The hydrothermal synthesis of Mg-salts was examined under the optimal conditions similar to the case of Ca (Nos. 2, 6, and 7). The XRD patterns of the products (Nos. 8 and 9 in Table 1) were shown in Fig. 3. The chemical analysis of the samples suggests that the composition of the products corresponded to $ZrMg_{0.5}H(PO_4)_2 \cdot H_2O + 1/2[Zr(OH)_4 \cdot H_2O]$. When NaCl was added (No. 9), the product contained only a slight amount of Na. The XRD pattern was similar to that of No. 8. These results showed that the addition of NaCl had no effect on the crystal form of the product. The first d-value was 11.94 Å, and was larger than that of α-ZrP (7.56 Å). As mentioned below, the XRD pattern showed many additional peaks, suggesting that the product was a mixture of zirconium(IV) hydroxide, magnesium phosphates and layered zirconium(IV)

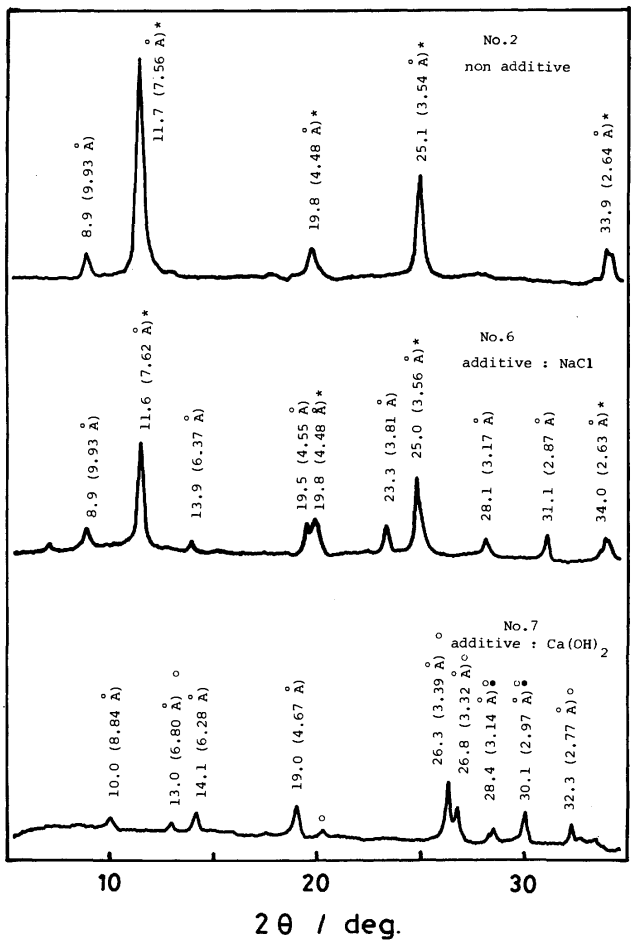

Fig. 2. X-Ray diffraction patterns of reaction products of $ZrOCl_2$ and $Ca(H_2PO_4)_2$ (Influence of additives on the synthesis). Numerals on peaks indicate 2θ/degrees and lattice distances. *: The diffraction peaks of α-ZrP, O: the diffraction peaks of $CaHPO_4$, ●: the diffraction peaks of ZrO_2.

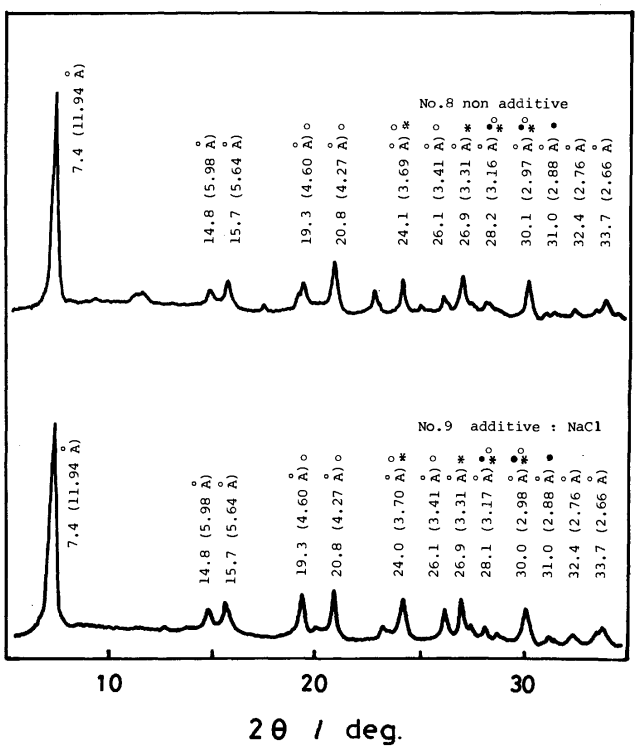

Fig. 3. X-Ray diffraction patterns of reaction products of $ZrOCl_2$ with $Mg(H_2PO_4)_2$. Numerals on peaks indicate 2θ/degrees and lattice distances. *: The diffraction peaks of ZrP_2O_7, O: the diffraction peaks of $Mg_3(PO_4)_2$, $Mg(PO_3)_2$, $Mg_2P_2O_7$, ●: the diffraction peaks of ZrO_2.

phosphate containing Mg^{2+} (ZrMgP).

Hydrothermal Reaction of $ZrOCl_2$ and $Sr(H_2PO_4)_2$. The Sr-containing products are listed in Table 1, and the XRD patterns are shown in Fig. 4. The chemical analysis showed that the ZrO_2 content was lower than α-ZrP by about 10%, and that the SrO content was up to about 20%. The first d-value was 10.39 Å in the XRD pattern, suggesting that the product was a mixture of strontium hydrogenphosphate ($SrHPO_4$) and layered zirconium(IV) phosphate containing Sr^{2+} between the layers (d=10.2 Å).[7] This is supported by the fact that a part of the product was dissolved by treatment with HCl to leave zirconium(IV) bis(hydrogenphosphate). The reaction product No. 11 (NaCl addition) contained larger amount of ZrO_2 than No. 10. The first d-value was 9.02 Å, suggesting a wide layer spacing, but the product was easily dissolved in 1 mol dm^{-3} HCl solution. Therefore, it cannot be layered zirconium phosphate, since zirconium phosphate should be stable in acidic conditions in general.

Hydrothermal Reaction of $ZrOCl_2$ and $Ba(H_2PO_4)_2$. The Ba-salts are listed in Table 1 (Nos. 12 and 13), and the XRD patterns are shown in Fig. 4. The BaO contents of the salts were as high as 25%. The peaks corresponding to α-ZrP were not found in the XRD patterns. The salts were easily dissolved in HCl solution. These results suggest that layered zirconium phosphate did not form in this reaction.

Treatment of Hydrothermal Products with Hydrochloric Acid. As mentioned above, when 1.00 g of the hydrothermal products were treated with 1 mol dm^{-3} HCl solution (100 cm^3), the products containing Mg, Ca, or Sr were partially dissolved and the weight was reduced to 0.76, 0.82, and 0.50 g, respectively. The Ba-salt was completely dissolved by this treatment. The XRD pattern of the Mg-salt treated with HCl is shown in Fig. 5. The XRD pattern of α-ZrP is also shown as the reference. The Mg-salt was turned into α-ZrP by this treatment. The by-products were dissolved in HCl solution, and the alkaline earth cations between the layers of the main products were exchanged with protons by this treatment.

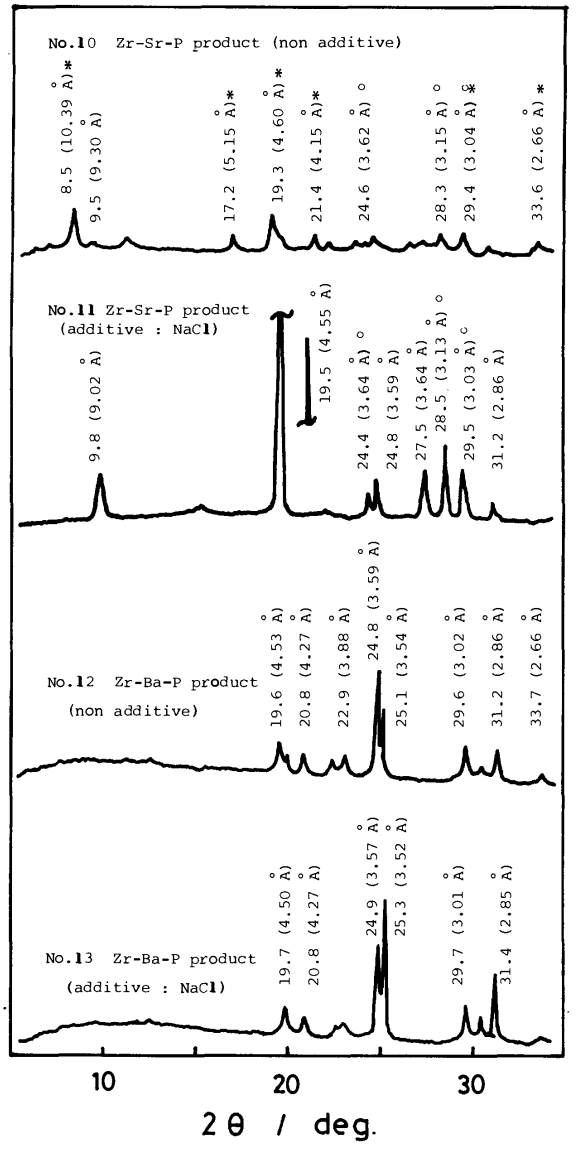

Fig. 4. X-Ray diffraction patterns of reaction products of $ZrOCl_2$ with $Sr(H_2PO_4)_2$ and $ZrOCl_2$ with $Ba(H_2PO_4)_2$. Numerals on peaks indicate 2θ/degrees and lattice distances. *: The diffraction peaks of α-ZrP containing Sr^{2+} between the layers, O: the diffraction peaks of $SrHPO_4$.

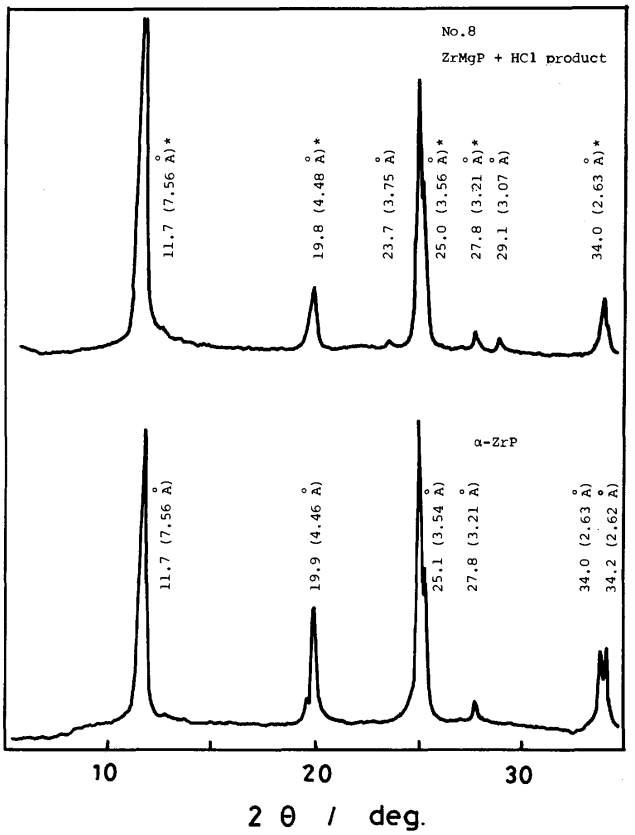

Fig. 5. X-Ray diffraction patterns of HCl-treated products of ZrMgP (No. 8) and α-$Zr(HPO_4)_2 \cdot H_2O$ (α-ZrP). Numerals on peaks indicate 2θ/degrees and lattice distances. *: The diffraction peaks of α-ZrP.

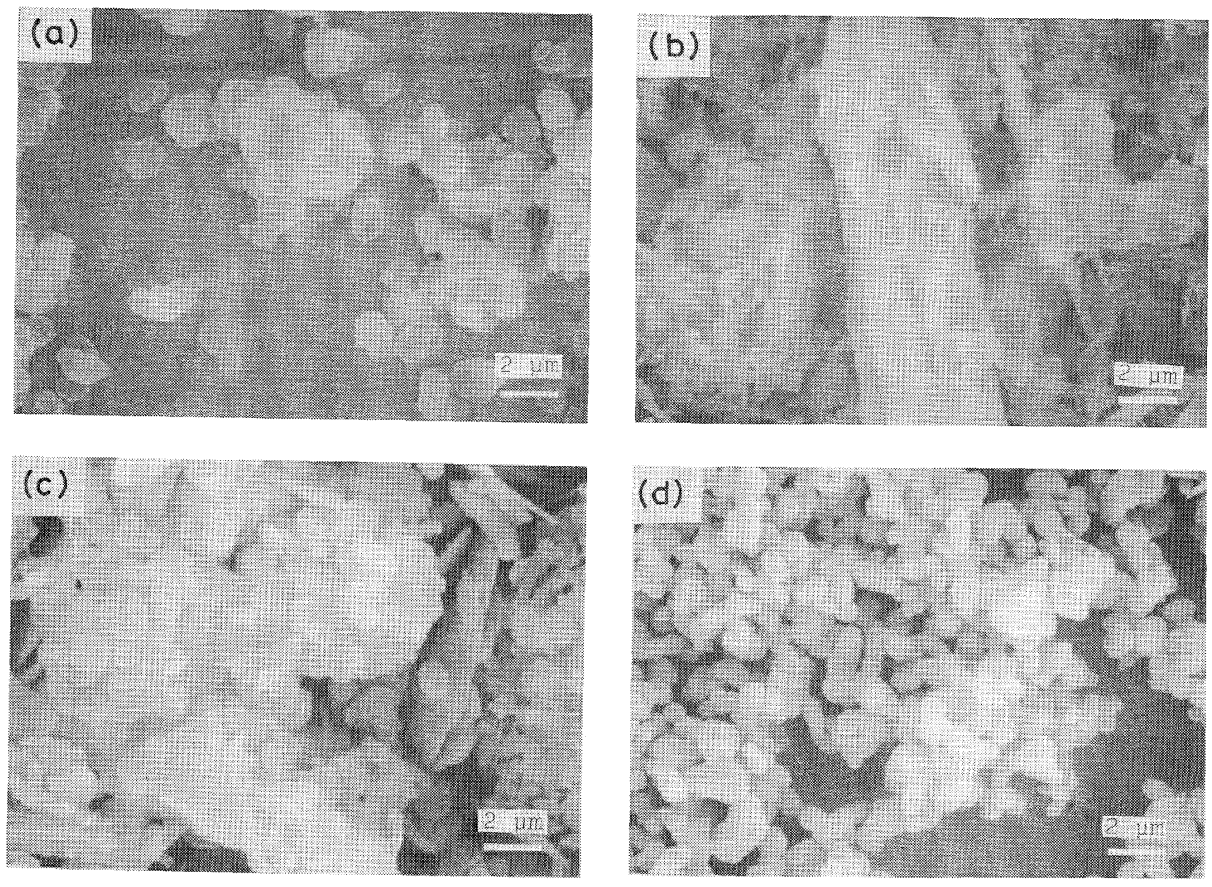

Fig. 6. Scanning electron micrographs of (a) reaction product No. 2, (b) reaction product No. 8, (c) reaction product No. 8 treated with HCl, and (d) α-$Zr(HPO_4)_2 \cdot H_2O$ (α-ZrP).

SEM Results. A few products were observed by a scanning electron microscope (SEM), and are shown in Fig. 6. The scale below right of each picture denotes 2 μm.

The product No. 2 containing Ca (a) had a hexagonal plate shape, with a diameter of about 1 μm. The surface area was estimated by BET method at 9.4 $m^2 g^{-1}$, which was smaller than that of α-ZrP (14 $m^2 g^{-1}$) or γ-ZrP (22 $m^2 g^{-1}$).

The shape of the product No. 8 containing Mg (b) was hexagonal plate. But the crystals seemed to be columns because they were associated and the large crystals were surrounded by small needles. The surface area of the product was estimated at 11 $m^2 g^{-1}$.

After the HCl treatment, the product No. 8 changed into large hexagonal plate crystals (c). The shape resembled that of α-ZrP (d). The crystallinity of the HCl-treated product was high, but the crystals were associated.

Thermal Analyses. The DTA and TG curves of the products are shown in Fig. 7 with those of α-ZrP. The endothermic peaks at 130—245 °C in DTA of the products containing Ca (No. 2) or Mg (No. 8), as well as α-ZrP, corresponded to the desorption of water from the interlayers. The endothermic peak of the Sr-containing product (No. 10) at 100 °C was not due to the dehydration between the layers of zirconium(IV) phosphate containing Sr, but to dehydration of other compounds. The dehydro-condensation between the layers of the phosphates gradually occurred above 340 °C, and the TG curves were similar to that of α-ZrP.

Ion Exchange of H^+ in α-ZrP with M^{2+} ($M=Mg^{2+}$, Ca^{2+}, Sr^{2+}, Ba^{2+}). All of the hydrothermal products obtained by the reaction of $ZrOCl_2$ and $M(H_2PO_4)_2$, except for the case of M=Ba, were turned into α-ZrP by the HCl treatment. Thus, it was investigated whether the same compounds as the hydrothermal products could be obtained by the ion exchange of H^+ in α-ZrP with M^{2+} or not. The ion exchange has already been investigated by Alberti et al.[6] and Clearfield et al.[7] They reported that Na^+ acts as a catalyst for the reactions.[4,5] In this paper, ion exchange of the proton in α-ZrP with M^{2+} was compared (1) in the absence and (2) presence of NaOH. The ion exchange conditions and the analytical data are listed in Table 2. The pH of the reaction solution was acidic in each case. The pH decreased in spite of the addition of NaOH, indicating that the ion exchange was accelerated by the addition. The XRD patterns of the ion-exchanged products are shown in Fig. 8. The XRD profile of (a) was almost the same as that of α-ZrP, indicating that ion exchange did not occur. In the case of (b), the peak corresponding to the basal spacing of α-ZrP at

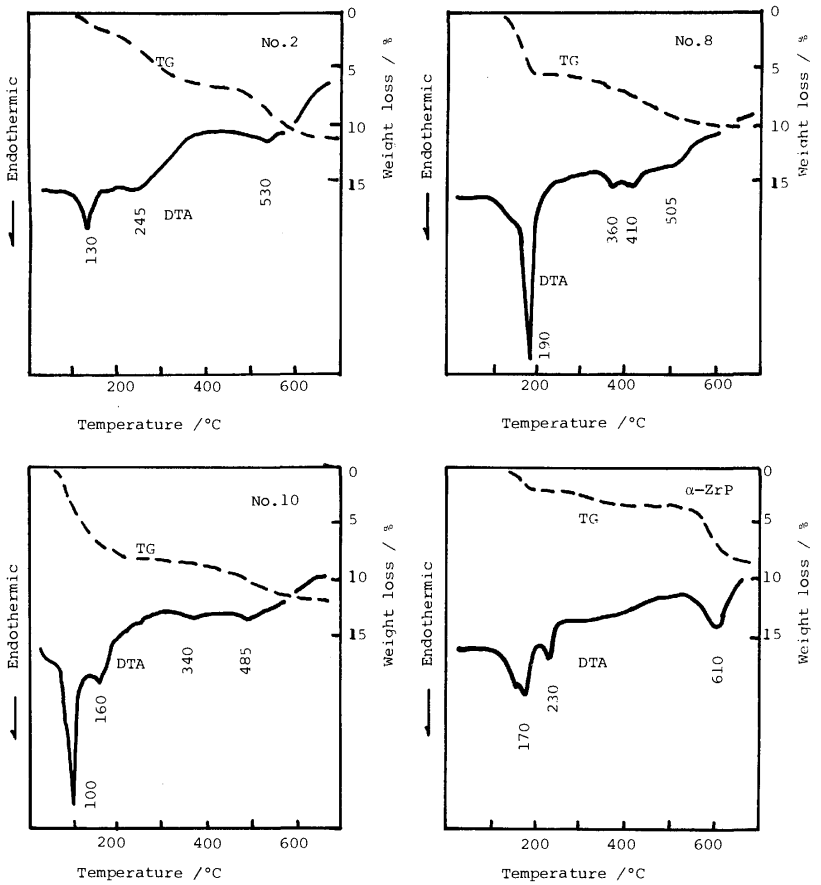

Fig. 7. DTA (——) and TG (----) curves of reaction products of $ZrOCl_2$ and $M(H_2PO)_2$ (M=Mg, Ca, Sr), and α-$Zr(HPO_4)_2 \cdot H_2O$ (α-ZrP). No.2: Reaction product of $ZrOCl_2$ and $Ca(H_2PO_4)_2$, No.8: reaction product of $ZrOCl_2$ and $Mg(H_2PO_4)_2$, No.10: reaction product of $ZrOCl_2$ and $Sr(H_2PO_4)_2$.

Table 2. Ion Exchange of H^+ in α-$Zr(HPO_4)_2$ with M^{2+} (M=Mg, Ca, Sr, Ba), and Analysis of the Products

No.	Ion exchange condition					Reaction product						
	α-ZrP[a]	$MCl_2 \cdot xH_2O$[b]	NaOH[c]	H_2O	Mother liquor	Yield	ZrO_2	P_2O_5	MO	H_2O	Na_2O	ZrO_2 : P_2O_5 : MO : H_2O : Na_2O (molar ratio)
	g	g	cm^3	g	pH	g	%	%	%	%	%	
1	1.00	2.03		100	3.83	0.76	40.5	46.6	0.41	12.5		1.0 : 1.0 : 0.02 : 2.1
2	1.00	2.03	30	70	2.94	0.98	35.2	40.5	4.89	18.5	1.00	1.0 : 1.0 : 0.26 : 3.6 : 0.06
3	1.00	1.47		100	2.36	0.94	38.8	44.7	1.87	14.7		1.0 : 1.0 : 0.18 : 2.6
4	1.00	1.47	30	70	2.53	1.06	34.3	39.6	6.90	19.1	0.07	1.0 : 1.0 : 0.73 : 3.8 : 0.004
5	1.00	2.66		100	2.20	1.01	38.6	44.5	2.89	14.0		1.0 : 1.0 : 0.09 : 2.5
6	1.00	2.66	30	70	2.43	1.25	31.6	36.4	13.1	19.0	0.00	1.0 : 1.0 : 0.49 : 4.1 : 0.00
7	1.00	2.44		100	2.86	0.94	41.0	47.2	0.69	11.2		1.0 : 1.0 : 0.01 : 1.9
8	1.00	2.44	30	70	2.36	1.20	33.5	38.6	16.7	11.1	0.11	1.0 : 1.0 : 0.40 : 2.3 : 0.01

a) α-$Zr(HPO_4)_2 \cdot H_2O$. b) $MgCl_2 \cdot 6H_2O$ for Nos. 1 and 2; $CaCl_2 \cdot 2H_2O$ for Nos. 3 and 4; $SrCl_2 \cdot 6H_2O$ for Nos. 5 and 6; $BaCl_2 \cdot 2H_2O$ for Nos. 7 and 8. c) 0.1 mol dm^{-3}.

2θ=11.7° (7.5 Å) decreased, and a new peak appeared at 2θ=9.2° (9.60 Å). In this reaction, it was considered that the proton in α-ZrP was first exchanged with Na^+ and then with Mg^{2+}. However, the chemical analysis showed that the Na content of the product was negligible. The product was a mixture of α-ZrP and a Mg^{2+}-exchanged compound having the same layer-spacing as $ZrMg_{0.75-1}H_{0.5-0}(PO_4)_2 \cdot H_2O$ (9.64 Å).[7] The layer-spacing was a little smaller than that of reported compounds $ZrMg_{0.5}H(PO_4)_2 \cdot 3H_2O$ (9.9 Å)[8] and $ZrMg_{0.72}H_{0.56}(PO_4)_2 \cdot 4H_2O$ (9.85 Å).[4] The Mg^{2+}-exchanged compound had a different layer-spacing from the hydrothermal product (11.94 Å), as mentioned above.

In the XRD profiles of (c) and (d), the peak intensity corresponding to the basal spacing of α-ZrP (7.56 Å) decreased, and a new peak appeared at 2θ=8.9° (9.93 Å). The intensity of the new peak increased on

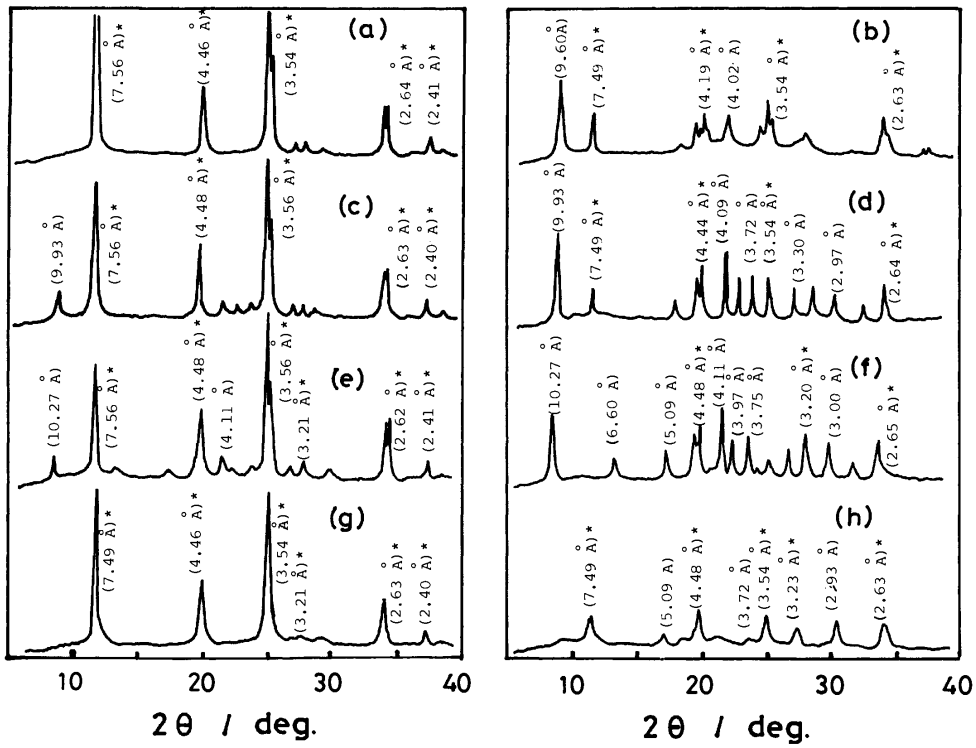

Fig. 8. X-Ray diffraction patterns of ion exchange products of α-ZrP with MCl_2 (M=Mg, Ca, Sr, Ba). Numerals on peaks indicate lattice distances. (a): α-ZrP+$MgCl_2$, (b): α-ZrP+$MgCl_2$+NaOH, (c): α-ZrP+$CaCl_2$, (d): α-ZrP+$CaCl_2$+NaOH, (e): α-ZrP+$SrCl_2$, (f): α-ZrP+$SrCl_2$+NaOH, (g): α-ZrP+$BaCl_2$, (h): α-ZrP+$BaCl_2$+NaOH.

the addition of NaOH (d). This fact clearly implies that the layer distance (9.93 Å) of the ion-exchanged product with Ca^{2+} was similar to that of the corresponding reported compounds, $ZrCa_{0.5\text{-}0.65}H_{1\text{-}1.7}(PO_4)_2 \cdot 3H_2O$ (9.4 Å)[7] or $ZrCa_{0.8\text{-}1.0}H_{0.3\text{-}0}(PO_4)_2 \cdot 4H_2O$ (9.64 Å),[7] and the distance was in accord with that of $ZrCa_{0.63}H_{0.74}(PO_4)_2 \cdot H_2O$ (9.98 Å)[6] within the experimental error, and perfectly agreed with that of the hydrothermal product. The composition of (d) compound (NaOH addition) was determined to be $ZrCa_{0.75}H_{0.5}(PO_4)_2 \cdot 3H_2O$.

The XRD pattern of (e) showed that the proton in α-ZrP was exchaned with Sr^{2+} only slightly. By the addition of NaOH (f), the peak corresponding to the basal spacing of α-ZrP disappeared in the XRD profile, and changed into the peak of the ion-exchanged product (10.27 Å). The value was in good accord with those of the hydrothermal product (10.39 Å) mentioned above and the reported compound $ZrSrH(PO_4)_2 \cdot 3.6H_2O$ (10.2 Å)[8] within the experimental error.

The XRD profile of the reaction product of α-ZrP and $BaCl_2$ (g) was almost the same as that of α-ZrP, suggesting that ion exchange did not occur. In the XRD pattern of (h), the peak intensity decreased and new peaks appeared at 2θ=17.4, 21.4, 23.9, and 30.5°. The peak corresponding to the basal spacing was not clear. As for such a compound, $ZrBa_{0.8\text{-}1}H_{0.4\text{-}1}(PO_4)_2 \cdot 2H_2O$ has been reported.[7]

References

1) G. Alberti and U. Costantino, *J. Mol. Catal.*, **27**, 235 (1984); A. Clearfield, *ibid.*, **27**, 251 (1984); K. Segawa, and M. Kinoshita, *Shokubai*, **27**, 244 (1985).

2) E. Kobayashi, *Bull. Chem. Soc. Jpn.*, **56**, 3756 (1983); E. Kobayashi and S. Shin, *ibid.*, **57**, 465 (1984); E. Kobayashi, *ibid.*, **57**, 3003 (1985).

3) E. Kobayashi, *Bull. Chem. Soc. Jpn.*, **48**, 3114 (1975).

4) G. Alberti, U. Costantino, and J. P. Gupta, *J. Inorg. Nucl. Chem.*, **36**, 2109 (1974).

5) G. Alberti, R. Bertrami, and U. Costantino, *J. Inorg. Nucl. Chem.*, **38**, 1729 (1976).

6) G. Alberti, U. Costantino, and M. Pelliccioni, *J. Inorg. Nucl. Chem.*, **35**, 1327 (1973).

7) A. Clearfield and H. Hagiwara, *J. Inorg. Nucl. Chem.*, **40**, 907 (1978).

8) G. Alberti, R. Bertrami, M. Casciola, U. Costantino, and J. P. Gupta, *J. Inorg. Nucl. Chem.*, **38**, 843 (1976).

 © 1987 The Chemical Society of Japan Bull. Chem. Soc. Jpn., 60, 2833—2837 (1987)

Vapor Phase Fluorination of Silica Surface with Chlorofluoromethanes and CF_4

Susumu OKAZAKI* and Akito KUROSAKI
Department of Industrial Chemistry, Faculty of Engineering, Ibaraki University, Nakanarusawa, Hitachi, Ibaraki 316
(Received November 22, 1986)

For a surface modification, fluorinations of silica samples including a quartz fiber and a commercial glass fiber, were carried out at around 500 °C in a conventional flow reactor. The surface compositions before and after the fluorination were determined by XPS analyses. Among chlorofluoromethanes and CF_4, CCl_3F was the most effective for fluorination. Surface OH groups were completely removed or replaced by the fluorination. Adsorptions of water vapor, hexane, hexafluoropropene, and octafluorocyclobutane showed that the silica surface became more hydro- and lipophobic after the fluorination. On the contrary, the chlorofluoro·methane-treated surface exhibited a higher affinity to the perfluorocarbons compared to the untreated surface.

In general, a SiO_2 surface has been fluorinated in the liquid phase with an aqueous solution of HF,[1] NH_4F,[2] or NH_4HF_2.[3] Recently, it was found that a SiO_2 surface may be more conveniently fluorinated by a vapor phase treatment at high temperatures (e.g., 1500 °C) with volatile fluorine compounds such as CF_4,[4] SF_4,[5] NF_3,[6] and CCl_2F_2.[7] The vapor phase treatment was reported to be especially effective for the removal of surface OH groups which cause a loss of photoactivity when SiO_2 is used as an optical fiber.[8] The treatment process, however, is still undesirable since the fluorine compounds cited above are expensive and/or unstable in moist air except for CCl_2F_2; also, the treatment temperature is too high. Thus, it is preferable to perform a vapor phase treatment or fluorination by using less expensive and more stable fluorides such as chlorofluorocarbons (flon) at lower temperatures.

It was previously found that some chlorofluoromethanes are effective for the vapor-phase fluorination of Al_2O_3 at temperatures lower than 500 °C.[9] In addition, a certain flon, $CClF_3$, was also effective for the surface fluorination of mordenite (SiO_2/Al_2O_3 molar ratio=19) at about 450 °C.[10] Hence, it is possible that some flons are available for the vapor phase fluorination of a SiO_2 surface. However, the reaction conditions must be carefully selected because of the large possibility of SiF_4 formation in such a fluorination of SiO_2.

Thus, in this study the most suitable flon and the optimal treatment conditions to promote the surface fluorination of SiO_2 with flon were sought first. Then, changes in the surface composition and property were examined, since they have only been slightly clarified in previous studies.[4-7] As for surface properties changes in the adsorptive activity for water vapor and hexane are examined to determine the effect of the fluorination on the affinity of a SiO_2 surface to a polar or nonpolar compound. In addition, such perfluoro·compounds as hexafluoropropene and octafluorocyclobutane were selected as adsorbents since they are known to be inert, in general, in interactions with other molecules.

During this study, an emphasis was placed on comparing the effects of a flon-treatment with that of the most widely adopted HF acid-treatment in order to increase the effectiveness of the vapor-phase treatment using flon.

Experimental

Materials. A commercial fine silica powder, Aerosil 200 (Nippon Aerosil Co.) was used as the main silica sample (SA) after heat treatments at temperatures higher than 1000 °C. In addition, a quartz fiber supplied by Gaschro Kogyo Co., and a commercial glass fiber supplied by Nittobo Co. (E Glass, SiO_2 52—56%; Al_2O_3 12—16%; CaO 15—25%; MgO 0—6%; B_2O_3 8—13%; Na_2O+K_2O 0—1%) were used for comparisons of the reactivity with that of SA.

Various chlorofluoromethanes, CF_4, hexafluoropropene, and octafluorocyclobutane, all of which were of purities higher than 99%, supplied by Mitsui-Dupont Fluorochemical Co., were directly used without further purification.

Fluorination Procedure. Fluorinations were carried out in a closed system by circulating gaseous chlorofluoromethane through a sample bed at 450—550 °C. The replacement of OH groups with fluoride ions was also carried out by soaking SA in dilute hydrofluoric acid (0.1 or 1.0 wt%) at room temperature for 30 min.

Structure and Surface Composition. The structure of silica before and after fluorination with flon or diluted hydrofluoric acid was determined from the powder diffraction patterns obtained with a Rigaku Geigerflex X-ray diffractometer by using Cu $K\alpha$ radiation. The structural change was also examined using a scanning electron microanalyzer (SEM).

The compositions in the surface layer were determined by IR and XPS. The XPS was measured with Mg $K\alpha$ radiation. The base pressure of the spectrometer was usually below 10^{-7} Torr (1 Torr=133.322 Pa) during the experiments. The compositions were calculated from the areas of the spectral peaks (i.e., the maximum in the counting rate) on the basis of the photo ionization cross section at 1245 eV in units of the Cls cross section of 22200 barns.[11] The behavior of the surface OH groups was examined by IR spectroscopy using a self-supporting disc.

Determination of Surface Properties. Surface areas were determined by applying the BET equation for the adsorption isotherm of N_2 at −196 °C. The effect of the flon-treatment on the surface properties of silica was examined by the adsorptions of water vapor, hexane, hexafluoropropene, and octafluorocyclobutane at 50 °C.

Table 1. Surface Fluorination of SiO_2

Sample	Treatment condition[a]		Content/atom%		Fls peak position[b]/eV
	Pressure/Toor	Time/min	F	Cl	
SiO_2(1000)-CCl_4	54	30	0	1.2	—
SiO_2(1000)-CCl_3F	54	30	4.2	0	688.7
SiO_2(1000)-CCl_2F_2	54	30	2.5	0	688.5
SiO_2(1000)-$CClF_3$	54	30	0.8	0	688.6
SiO_2(1000)-CF_4	54	30	0	0	—
SiO_2(1000)-CF_4	200	120	2.4	0	688.5
SiO_2(1000)-CHF_3	54	30	0.4	0	688.0
SiO_2(1000)-HF acid[c]	—	30	8.1	0	688.7

a) The treatment temperature was kept constant at 550°C. b) The binding energy values were measured by refering to the Cls value of the contaminant carbon (285 eV). c) The SiO_2 sample was treated with 0.1 wt% HF soln. at room temperature, and then dried at 120°C, followed by evacuation at 500°C for 1 h.

Table 2. Surface Fluorination of SiO_2

Sample	Treatment condition[a]		Content/atom%		Fls peak position[b]/eV
	Pressure/Toor	Time/min	F	Cl	
SiO_2(1000)-CCl_3F	54	30	4.2	0	688.7
SiO_2(1100)-CCl_3F	54	30	3.0	0	688.3
SiO_2(1150)-CCl_3F	54	30	3.2	0	688.8
Quartz fiber-CCl_3F	103	30	5.4	0	689.1
Quartz fiber-CCl_2F_2	105	30	Trace	0	—
E-Glass fiber-CCl_3F	107	30	13.2	0	686.9

a) The treatment temperature was kept constant at 550°C. b) The binding energy values were measured by refering to the Cls value of the contaminant carbon (285 eV).

Results and Discussion

Reactivities of Various Flons and Diluted HF Acid Toward Silica Surface. As shown in Table 1, CCl_3F exhibited the highest fluorination activity among various flons. The order of the fluorination activities of these flons the opposite to that of the C-Cl[12] or C-F[13] bond strength of the flon molecules. Thus, the ease of the C-Cl[12] or C-F[13] bond splitting seems to determine the surface fluorination activities of flon.

Since the CCl_3F having the weakest C-Cl or C-F bond was found to the most active as a fluorinating reagent, it was used for the surface fluorination of SiO_2 in the succeeding study.

Comparison of Reactivities of Various SiO_2 Materials. As shown in Table 2, a quartz fiber sample was fluorinated more readily than SA. A commercial glass fiber sample was fluorinated much more markedly. In this case, however, the Fls peak position (686.9 eV) for the fluorinated sample was remarkably different from that for a simple or pure silica sample, such as the quartz and SA. It rather coincided to that for the CCl_3F-treated Al_2O_3 (686.8 eV). Therefore, the F component introduced by the CCl_3F-treatment was presumed to be bound not to Si, but the Al atom on the treated glass fiber. Evidence suggested that heat treated SiO_2 is less active than Al_2O_3 in the reaction toward the flon. Nevertheless, it is noteworthy that SA was considerably fluorinated with a relatively stable compound CCl_3F, even after heat-treatment at a high temperature, such as 1150°C.

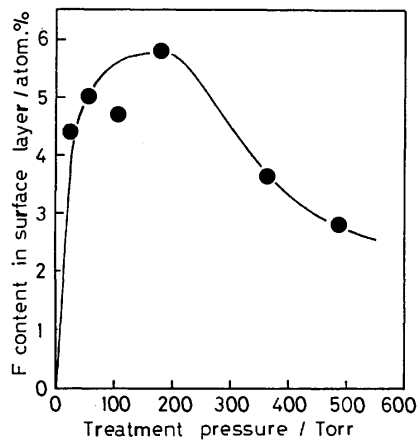

Fig. 1. Effect of the CCl_3F-treatment pressure on the F content in surface layer. Treatment temperature: 550°C; Treatment time: 2 h.

Effect of CCl_3F-Treatment Conditions. As Fig. 1 shows, there was an optimal CCl_3F pressure to increase the F content of the treated silica. The infrared spectra, which were taken for the gaseous components obtained by 54, 200, and 500 Torr treatment, indicated a peak at 1010—1022 cm^{-1} assignable to a Si-F bond[12] only for the product obtained at 500 Torr. This finding suggested that excessive fluorination, or formation of SiF_4, may be avoided when fluorination is gently carried out by using a flon of lower pressure or concentration.

The treatment temperature was more effective on the surface fluorination than the treatment gas pressure. Thus, the F content in the surface layer increased linearly with temperature up to 550 °C (Fig. 2).

Changes of Surface Area and Structure. The specific surface area somewhat decreased with an increase in the F content of the CCl_3F-treated SA. The decrease in the surface area, however, was not so remarkable as in the case of the diluted HF acid treatment (shown in Fig. 3).

The XRD and SEM analyses revealed that SA was still amorphous, even after treatment with the CCl_3F or the diluted HF acid.

Surface Constitution Examined by IR Spectra. The IR spectrum of SA exhibited a sharp and slightly asymmetric peak at 3734 cm^{-1} (Fig. 4). This peak, assignable to the isolated OH groups,[14] was still observed even after heat-treatment at high temperatures, such as 1000 °C. This was also observed for a sample treated with dilute HF acid. On the other hand, this peak due to the isolated OH groups was not found in all for the SA samples which were treated with CCl_3F at 500 °C. The complete removal of surface OH groups is considered to be due to the replacements of the OH groups with F atoms. In fact, a shoulder due to a Si-F bond appeared at 940 cm^{-1},[15] in accordance with the disappearance of the peak due to the OH groups.

Unlike the Si-F bond in SiF_4 molecule, the bond formed on the silica sample was fairly stable towards moisture. Thus, the band due to the Si-F bond of the treated SiO_2 did not disappear after contact with water vapor (10 Torr) at room temperature for 1 h, and even after further contact with that (15 Torr) at 120 °C (Fig. 5). The band attributable to the free silanol groups at 3734 cm^{-1} [15] reformed with difficulty after contact with water vapor (15 Torr) for a long time, such as 15 h.

Changes in Adsorptive Activities for Various Gases. For Water Vapor. As is exhibited in Fig. 6(A), the adsorptive activity of silica for water vapor was remarkably enhanced by a treatment with dilute HF acid. On the other hand, the activity was somewhat decreased by the CCl_3F-treatment at 450 °C. Furthermore, the activity was a entirely removed by a treatment at 500 °C.

Water vapor is considered to be adsorbed on the silica surface through hydrogen bonding,[15] and the amount of physically adsorbed water should be related to the number of the surface OH groups. During a treatment with dilute HF acid, the surface siloxane may be hydrolyzed. The hydrolysis should increase the amount of surface OH groups on silica surface, although a part of the OH groups may be replaced by

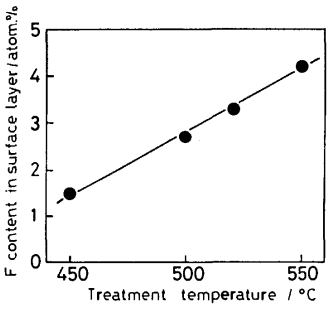

Fig. 2. Effect of the CCl_3F-treatment temperature on the F content in surface layer. Treatment pressure: 54 Torr; treatment time: 0.5 h.

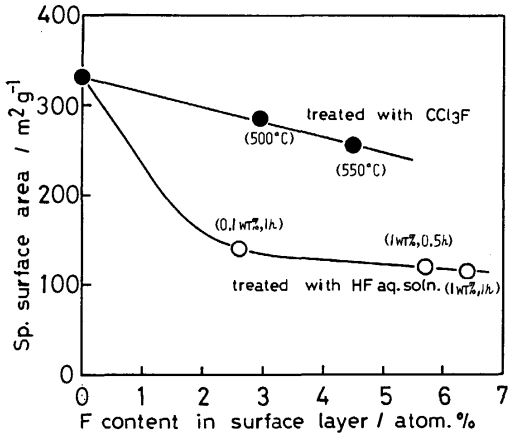

Fig. 3. The variation of specific surface area with F content in surface area. The CCl_3F-treatment was carried out at 54 Torr and 500 or 550 °C. The acid treatment was carried out at room temperature for 0.5 or 1 h with the diluted HF.

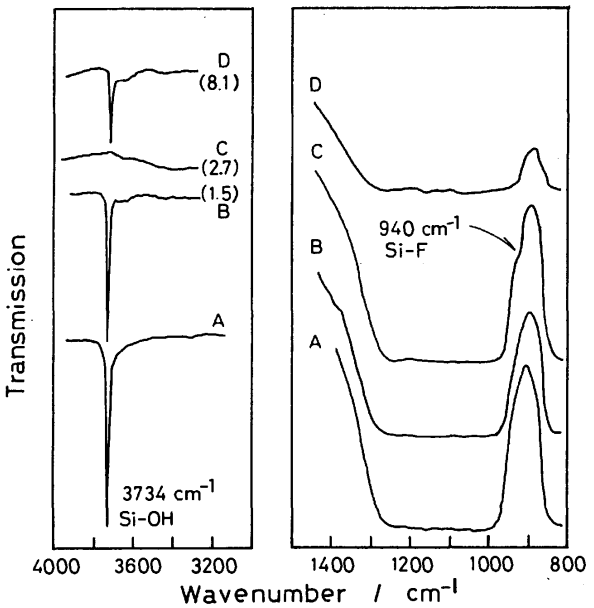

Fig. 4. IR spectra of SiO_2 treated with CCl_3F or diluted HF. A: Background or the untreated sample after evacuation at 500 °C for 2 h; B, C: for the samples treated with CCl_3F (54 Torr) at 450 and 550 °C for 0.5 h, respectively; D: for the sample treated with 0.1 wt% HF solution at room temperature for 0.5 h, and then dried at 120 °C, followed by evacuation at 500 °C for 1 h. The numbers in parentheses indicate the F content of respective samples.

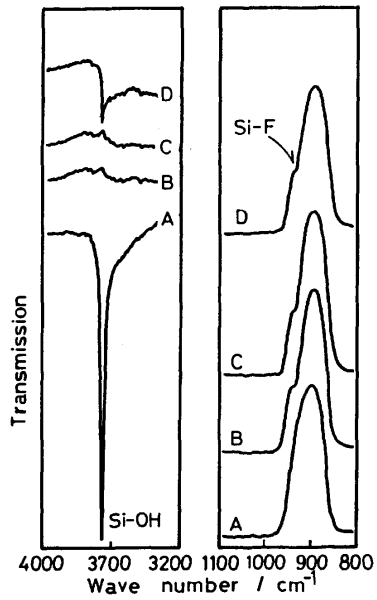

Fig. 5. Effect of contact with water vapor on IR spectra. A: Background or the untreated SiO_2 sample after evacuation at 550 °C for 2 h; B: for the sample treated with CCl_3F (200 Torr) at 550 °C for 0.5 h; C: further contact of B with water vapor (15 Torr) at 120 °C for 1 h; D: further contact of C with water vapor (15 Torr) at room temperature for 15 h.

F^- ion in the acid solution. The net increase in the amount of the surface OH groups should contribute to the enhancement of the adsorptive activity for water vapor.

While, in the case of the CCl_3F-treatment, the amount of the surface OH groups may be reduced in accordance with the progress of the surface fluorination, especially the surface OH group may be fully replaced by a F atom in a treatment at higher temperatures as has been revealed by the IR study for the treated silica (Fig. 4). A silica surface which is sufficiently covered by F atoms may be hydrophobic owing to the low surface energy ascribable to the F atoms. In fact, an SA sample treated with CCl_3F at 550 °C remained floating on water for about 1 week at room temperature; nevertheless, the untreated or the diluted HF acid-treated SA sank into water as soon as it was placed on the water surface.

For Hexane Vapor. As shown in Fig. 6(B), the adsorptive activity of silica for gaseous hexane decreased slightly with a CCl_3F-treatment at 500 °C. It was further decreased by a treatment at a higher temperature, 550 °C. A decrease in the adsorptive activity for hexane was also observed for the dilute HF acid-treated sample in the adsorption at a pressure higher than 20 Torr.

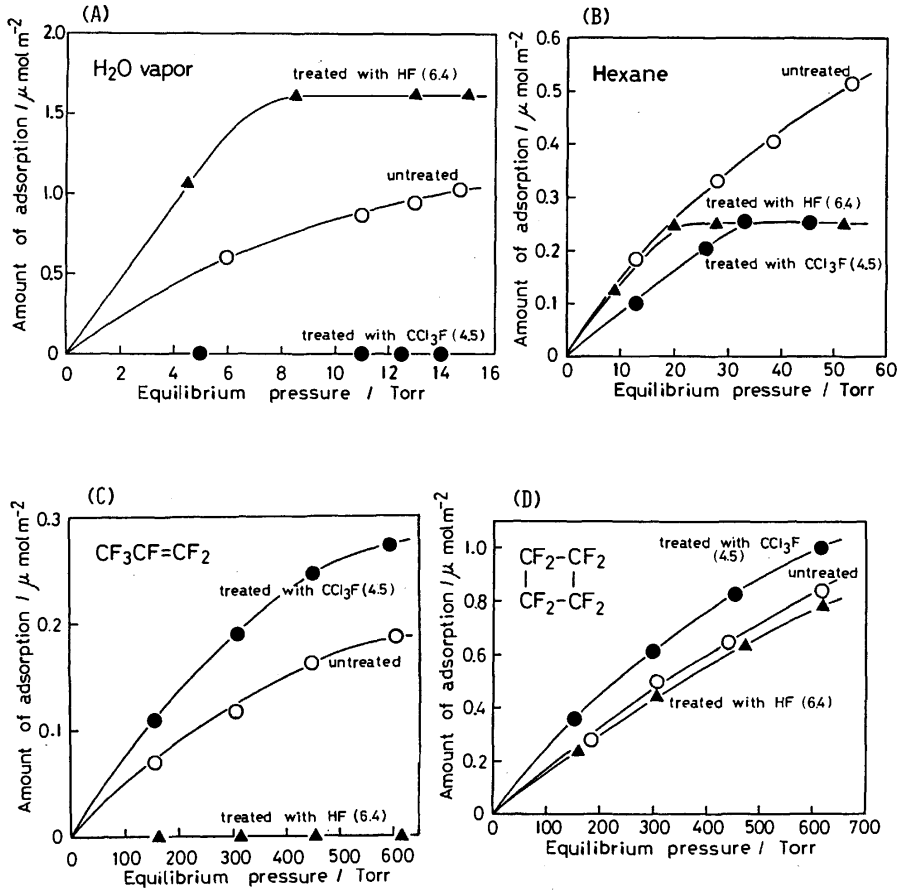

Fig. 6. Effect of the surface fluorination on the adsorptive activities for various compounds. All the adsorptions were carried out at 50 °C, and the numbers in parentheses indicate the F content of respective samples.

The results for the CCl_3F-treated silica seem to be in conflict with the current view that hydrophobic solids should exhibit an affinity for nonpolar or lipophilic compounds. The evidence that the CCl_3F-treated silica is concurrently hydrophobic and lipophobic is considered to be a result of the extremely low surface energy of the solid surface which is well-covered by F atoms. Similar characteristics are also revealed in the oil- and water-repellency of some polyfluoro or perfluoro compounds used as a special fiber treatment agent.[16]

For Perfluorocompounds. Finally, the results of the adsorptions of hexafluoropropene and octafluorocyclobutane are displayed in Figs. 6(C) and (D). In contrast to the adsorptive activities for water and for hexane, those for the perfluorocarbons were fairly increaed by the CCl_3F-treatment. These increases in the adsorptive activities may have resulted from an affinity of the F atoms in the perfluoro-compounds to the atoms of the same kind on the well-fluorinated silica surface. However, the essence and the details of the interaction between the adsorbent and the adsorbates are not clear at the present stage of this study.

In contrast with the CCl_3F-treated surface, a silica surface treated with dilute HF acid was entirely inactive for the adsorption of hexafluoropropene, possibly due to the highly polar character of the acid-treated surface. The decrease in the adsorptive activity of silica was also observed for the adsorption of octafluorocyclobutane (bp −5 °C), which is more condensable than hexafluoropropene (bp −29.4 °C), although the decrease was not so remarkable as that observed for the hexafluoropropene adsorption.

Conclusion

The results of this study are as follows:

(1) Flon-treatments are available for the vapor phase fluorination of a SiO_2 surface at around 500 °C.

(2) Among various chlorofluoromethanes and CF_4, CCl_3F having the weakest C-Cl and/or C-F bonds is especially suitable for the surface fluorination.

(3) Complete removal of surface OH groups on SiO_2 by the CCl_3F-treatment is accomplished at 500 °C. This temperature is much lower than that of another treatment (e.g. 1500 °C) with volatile fluorides (such as Cf_4, SF_4, and NF_3), which was reported to be carried out in order to remove surface OH groups.

(4) The formation of SiF_4 can be suppressed by decreasing the pressure or concentration of CCl_3F in a reactor.

(5) A silica surface becomes more hydro- and lipophobic with the CCl_3F-treatment. On the other hand, the a affinity of a SiO_2 surface to perfluorocompounds is increased by a CCl_3F-treatment.

This work was supported by a Grant-in-Aid for Scientific Research No. 60550562 from the Ministry of Education, Science and Culture.

References

1) S. Okazaki, A. Kurosaki, and S. Suzaki, *Bull. Chem. Soc. Jpn.*, **57**, 1046 (1984); W. N. Webb, *Ind. Eng. Chem.*, **49**, 261 (1957).

2) H. J. Reitsman and C. Boelhower, *J. Catal.*, **33**, 39 (1974). P. O. Sochart, S. A. Selim, J. P. Damon, and P. G. Rouxhet, *J. Colloid Interface Sci.*, **70**, 209 (1979).

3) V. C. F. Holm and A. Clark, *Ind. Eng. Chem., Proc. Res. Dev.*, **2**, 38 (1963).

4) T. Abiru, N. Matsuhiro, T. Ohashi, K. Kosaka, and O. Fukuda, Denkitsushingakkai-sokai, 1984, Abst. 1148, pp. 4—202.

5) M. Robinson, *Mat. Res. Bull*, **15**, 735 (1980).

6) T. Nakai, Y. Mimura, H. Tokiwa, and O. Shinbori, Denkitsushingakkai-sokai, 1985, Abst. 1156, pp. 4—480.

7) H. Kanamori, N. Yoshioka, and G. Tanaka, Denkitsushingakkai-sokai, **1983**, Abst. 1096, pp. 4—182.

8) Y. Sugahara and M. Takeda, *Boeigijutsu*, **1982**, 23.

9) A. Kurosaki and S. Okazaki, *Chem. Lett.*, **1983**, 1741.

10) S. Okazaki and H. Jouhouji, *Bull. Chem. Soc. Jpn.*, **59**, 1931 (1986).

11) J. H. Scofield, *J. Electron Spectros. Relat. Phenomena*, **8**, 129 (1976).

12) R. Foon and K. B. Tait, *J, Chem. Soc., Faraday Trans. 1*, **68**, 104, 1121 (1972).

13) G. Glocker, *J. Phys. Chem,*, **63**, 827 (1959).

14) T. E. Elmer, I. D. Chapman, and M. E. Nordberg, *J. Phys. Chem.*, **1963**, 2219.

15) M. L. Hair, Infrared Spectroscoy in Surface Chemistry, Marcel Dekker Inc., New York (1967), p. 79.

16) N. Ishikawa and Y. Kobayashi, "Fusso no Kagaku," Kodansha, Tokyo (1977), p. 194.

 © 1987 The Chemical Society of Japan Bull. Chem. Soc. Jpn., 60, 2839—2842 (1987)

Preparation and Metal-Adsorption Properties of the Polymer-Coated Silica Gel Having Iminodiacetate Functional Group

Toshishige M. SUZUKI,* Osamu ITABASHI, Tomio GOTO,
Toshiro YOKOYAMA, and Tetsuo KIMURA
Government Industrial Research Institute, Tohoku, 4-2-1 Nigatake, Sendai 983
(Received December 22, 1986)

A new adsorbent containing an iminodiacetate group has been prepared by the surface modification of a polymer-coated silica gel. The obtained beads (SG-IDA) are porous and have a high specific surface area ($\approx 350\,m^2\,g^{-1}$). The adsorption properties of SG-IDA, including the adsorption capacities, equilibrium distribution coefficients (K_d) and adsorption rates, have been examined for divalent metal ions. The selectivity order of SG-IDA is Cu(II) > Pb(II) > Ni(II) > Zn(II) ≫ Ca(II) > Mg(II). The SG-IDA shows appreciably high K_d values and rapid kinetics toward the adsorption of heavy metal ions. The concentration of 10 ppb level of metal ions [Cu(II), Zn(II), and Cd(II)] has been demonstrated using the SG-IDA column.

The application of solid adsorbents for the separation and concentration of trace metal ions has received recent attention owing to their operational conveniences.[1-3] Silica gel is one of the most widely used inorganic supports for a metal adsorbent because of its porous and hydrophilic nature. The nominal shrinking and swelling property is also of great advantage for use in the column stationary phase.[4] So far, numerous kinds of chelating reagents have been immobilized (adsorbed or chemically bound) onto silica-gel surface.[5,6] The use of sililation reagent is one of the most popular approaches for the modification of a silica-gel surface through chemical bonding.[6-11] However, commercially available sililation reagents having a chelating functional group are limited. Furthermore, the cleavage of a Si-O-Si bond formed by a coupling reaction tends to take place upon repeated use, leading to a lowering of the adsorption activity.[6]

We have proposed a convenient procedure for a surface modification which involves the adsorption of vinyl monomers over the surface of porous supports followed by the polymerization of the monomers.[12] The polymer network which covers a silica-gel surface can, subsequently, be functionalized with the desired reagents by the usual synthetic procedures. Preliminary results have been briefly reported.[13] This is a detailed paper in which we describe the preparation of the new adsorbent based on a polystyrene-coated silica gel having iminodiacetic acid (IDA) as the functional group. The adsorption properties of the adsorbent and its application to the column concentration of trace metal ions are reported.

Experimental

Reagents. Silica-gel beads for chromatography shieved to 60—100 mesh were obtained from Nakarai Chemical Co., washed with water and then dried in vacuo. (Chloromethyl)styrene was purified by distillation prior to use. Diethyl iminodiacetate was prepared according to the usual procedure. The commercial chelating resin Dowex A-1 (60—100 mesh) was treated with 2 M (M=mol dm^{-3}) hydrochloric acid, washed thoroughly with water and then dried in vacuo. Other chemicals were reagent grade and used without further purification.

Polymer-Coating of Silica-Gel Beads. Silica-gel beads (100 g) were immersed in a DMF solution (60 cm^3) containing (chloromethyl)styrene (66 g), divinylbenzene (0.7 g) and α,α'-azobisisobutyronitrile (1 g) under cooling below 0 °C and then filtered. The beads were transferred to a glass autoclave and then heated at 80 °C for 5 h under a N_2 atmosphere. The product was washed with benzene in a Soxhlet extractor and dried. The polymer-coated silica-gel beads, thus formed, were functionalized with iminodiacetic acid through a reaction of the surface chloromethyl group with diethyl iminodiacetate in refluxed dioxane (48 h), followed by the hydrolysis of the ester moiety with 6 M hydrochloric acid. The hydrolysis of the ester moiety was monitored by the decrease in the IR intensity of the 1740 cm^{-1} band. The IDA bound silica gel was washed successively with water, ethanol and diethyl ether and then dried in vacuo.

Adsorption Capacity. A batchwise technique was employed to determine the equilibrium adsorption capacity (amount of metal ion adsorbed on one gram of dry beads) with metal ions always being in excess over the ligand capacity.[14]

A 1 g portion of SG-IDA was added to ca. 80 cm^3 of a metal ion solution (0.02 M) of a certain pH; the suspension was stirred at room temperature overnight. Then, the mixture was transferred to a volumetric flask (100 cm^3) and finally diluted to the mark with water. The amount of metal ion that remained in the supernatant solution was determined using an atomic absorption spectrometer. The capacities of the adsorbent were calculated from the change in the observed metal concentration. The beads were then placed into a glass column and thoroughly washed with water. The adsorbed metal ions were liberated from the beads by elution with 2 M hydrochloric acid, and the metal ions in the eluent were analyzed. In most cases, a satisfactory material balance could be observed between the metal ions liberated from the beads and those remaining in the solution.

Distribution Coefficient. The equilibrium distribution coefficients of the metal ions were determined by a batchwise procedure.[14] Typically, dry SG-IDA beads (1 g) were immersed in 100 cm^3 of a 1 mM metal ion solution (I=0.05, $NaClO_4$). The pH from 3.0 to 5.0 was adjusted with an acetate buffer while that below 3.0 was adjusted with hydrochloric acid. After shaking for 3 d, the equilibrium pH was measured and the amount of metal ion remaining in

the supernatant solution were determined. The results are expressed as the distribution coefficient, K_d=(amount of metal adsorbed on 1 g of the beads)/(amount of metal remained in 1 cm^3 of the solution).

Adsorption Rate. The following batchwise procedure was employed: To a buffered metal ion solution (1 mM, 500 cm^3) at pH 4.5 was added 3 g of the SG-IDA beads (H^+ form). Small portions of the metal solution were withdrawn under stirring at appropriate intervals and analyzed with an atomic absorption spectrometer. Similar experiments were carried out by using Dowex A-1 (H^+ form), in which the IDA group is immobilized onto cross-linked polystyrene beads.

Concentration of Metal Ions by the Column of SG-IDA. A 5 dm^3 solution containing 10 ppb each of metal ions [Cu(II), Zn(II), and Cd(II)] at pH 4.5 was continuously passed through a column containing SG-IDA (ϕ 1.2×4 cm, 5 cm^3) at a constant flow rate that could be adjusted with a microtube-type pump. After the whole solution was fed to the column, the bed beads were washed with water in order to eliminate any free metal ions. Then, the adsorbed metal ions were eluted with 20 cm^3 of 2 M hydrochloric acid. The eluate was collected in a volumetric flask (50 cm^3) and finally diluted to the mark with water. The percentage recovery was calculated in terms of the ratio of the amount of metal ion recovered and that in the feed solution.

Measurements. The metal ion concentration was determined with a Shimadzu atomic absorption/flame photometer Model AA-610S. The IR spectra were measured using a KBr method with a Perkin-Elmer Model 599 spectrophotometer. A specific surface area was determined with an Yuasa Ionic MONOSORB; samples were treated for 30 min at 110 °C in the stream of a mixture gas consisting of 32% N_2 and 68% He prior to measurements. The polymer contents of the chemically modified silica gel were determined by a thermal gravimetric analysis using a Rigaku Thermoflex.

Results and Discussion

Preparation and Characterization of SG-IDA. The silica-gel surface was coated with a (chloromethyl)-styrene-divinylbenzene copolymer through the adsorption and subsequent polymerization of the vinyl monomers. Polystyrene chains were partially cross-linked with divinylbenzene in order to avoid leaking of the polymer moiety upon contact with organic solvents. Unreacted monomers and oligomers were eliminated by Soxhlet extraction with benzene. The polymer-coated silica gel, thus formed, could successively be modified with a wide variety of functional groups. In the present study, diethyl iminodiacetate was introduced onto the polymer surface through a reaction of the ligand with the chloromethyl group (Scheme 1). This was confirmed by the characteristic IR bands at

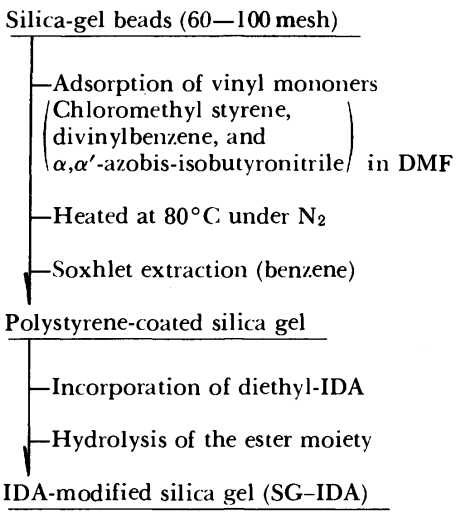

Scheme 1. Procedures for polymer-coating of silica gel beads and subsequent functionalization with iminodiacetic acid.

around 1740 and 1640 cm^{-1} due to (C=O) stretching vibrations of the carboxylic ester group. The band intensity at 1740 cm^{-1} decreases upon the hydrolysis of the ester moiety, whereas that of 1640 cm^{-1} increases. The obtained SG-IDA beads have a sufficient mechanical strength for use in the usual experimental procedures. Different from typical polymer chelating resins, the SG-IDA beads revealed minor volume changes upon adsorption and regeneration cycles. For example, the change in the volume of SG-IDA on interconversion between H^+ and Na^+ forms was only within 10%. However, the Dowex A-1, whose matrix is a gel-type polystyrene, showed an increase in volume by more than 60% with the change in ion forms from H^+ to Na^+. A large volume change must be unfavorable for uniform packing in a column system.

Table 1 shows the analytical data as well as the specific surface area of the functionalized silica gel along with the non-functionalized ones. A nitrogen analysis indicated that SG-IDA contains approximately 0.8 mmol of IDA per gram of the beads. Although SG-IDA is coated with a polymer, the specific surface area remains considerably high, i.e., 350 $m^2 g^{-1}$. This indicates that most of the pores with large diameters are not clogged with polymer, presumably because the inner surfaces of the pores are uniformly covered with a polymer network. The SG-IDA beads form colored complexes with Cu(II), Co(II), and Cr(VI) ions. The colors appeared to be homogeneously distributed over the beads when observed under an optical microscope.

Table 1. Numerical Data of the Chemically Modified Silica Gel

Type of the modified silica	N/%	Polymer content/%[a)]	Specific surface area[b)]/$m^2 g^{-1}$
Silica gel	—	—	440
Coated with poly[(chloromethyl)styrene]	0.1	12.0	357
Functionalized with IDA	1.1	14.0	348

a) Weight percent of polymer determined by thermal gravimetric analysis. b) Obtained by B. E. T. method.

It has been pointed out that the specific surface area is closely related to the amount of polymer coated on silica gel.[15] When the polymer content exceeds about 15%, the specific surface area sharply decreases; in some cases, an aggregation of beads takes place.

The titration curve of SG-IDA with 0.1 M potassium hydroxide gave apparent inflection points at ca. pH 3.8 and 7.7 regions; this can be assigned to a dissociation of protons on the introduced IDA and surface silanol group, respectively, since non-functionalized silica-gel beads gave an inflection point at about pH 7.6.

Equilibrium Adsorption Capacity. The SG-IDA beads adsorb various kind of metal ions in a similar manner to that observed for polymer chelating resins having the IDA groups.[16,17] Profiles of the adsorption capacities vs. pH for several metal ions are given in Fig. 1. The maximum capacity of the SG-IDA lies in the range 0.3—0.4 mmol g^{-1}. The pH dependence of the curves is closely related to the stability of the metal complexes formed with the IDA group. Thus, a metal ion which forms a very stable complex with a functional group is retained to the beads at a much lower pH region. The adsorbed metal ions were released from SG-IDA upon a treatment of the beads with 2 M hydrochloric acid. The adsorption capacities for most of the metal ions examined were reproducible over several adsorption and regeneration cycles, with the exception of Fe(III). The capacity for Cu(II) was reproducible within a ±3% deviation for more than ten repeated cycles of use. Since Fe(III) is strongly retained to the beads, a quantitative recovery is difficult, even by treating with concd hydrochloric acid. In this case, a reduction of Fe(III) to Fe(II) with a 1 M $Na_2S_2O_4$ solution prior to acid leaching gave satisfactory results.

The SG-IDA beads are sufficiently durable in an acidic solution. For example, no obvious change in the Cu(II) capacity has been observed upon treating the beads in refluxed 3 M hydrochloric acid for 3 h. In a strongly alkaline media, on the contrary, a gradual dissolution of silica gel inevitably took place.

Distribution Coefficient. The distribution coefficient (K_d) for several metal ions was examined as a function of the pH; the results are given in Fig. 2. The slopes in the linear plots at a pH lower than 3.0 are approximately 2.0 for the adsorption of Cu(II), Pb(II), Ni(II), and Zn(II). This result indicates that the adsorption of these divalent metal ions at this pH region is accompanied by the release of two protons as given in the following formula, where RH_2 denotes the protonated form of SG-IDA:

$$RH_2 + M^{2+}(aq) \rightleftarrows RM + 2H^+$$

The log K_d vs. pH profile clearly implies that the order of selectivity for SG-IDA is Cu(II)>Pb(II)>Ni(II) >Zn(II)>Cd(II)≫Ca(II)>Mg(II). The behavior of Pb(II) and Ni(II) is somewhat unusual in view of its stability constants of the IDA chelates where log K_{ML} of the Ni(II) chelate is larger than that of the Pb(II) chelate. The shift in the position of the two ions is most likely to be due to the difference in the steric environment between the free and immobilized ligand. A similar change in the selectivity series has also been observed in IDA-type chelating resins with different types of polymer matrix.[16]

Appreciably high K_d values ($\log K_d > 4.0$) were observed for the adsorption of Cu(II), Pb(II), Ni(II), Zn(II), and Cd(II), whereas those for alkaline earth metal ions are relatively low. The K_d values for Mg(II) and Ca(II) are three to four orders of magnitude lower than those for other metal ions. Thus, interference from these alkaline earth metal ions by competed complexation must be less significant.

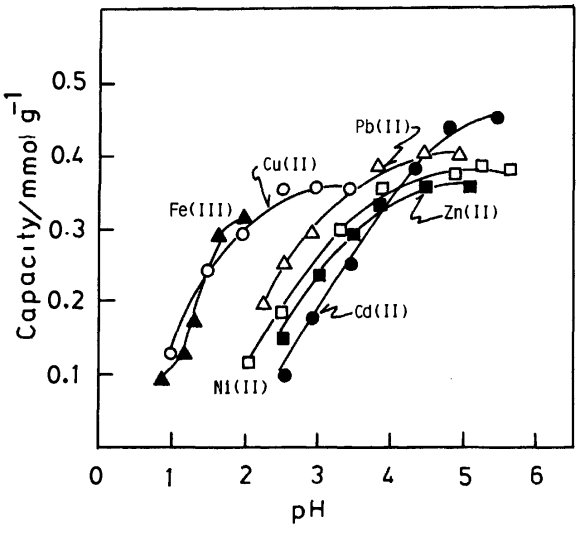

Fig. 1. Equilibrium adsorption capacity of the SG-IDA for Fe(III) (▲), Cu(II) (○), Pb(II) (△), Ni(II) (□), Zn(II) (■), Cd(II) (●).

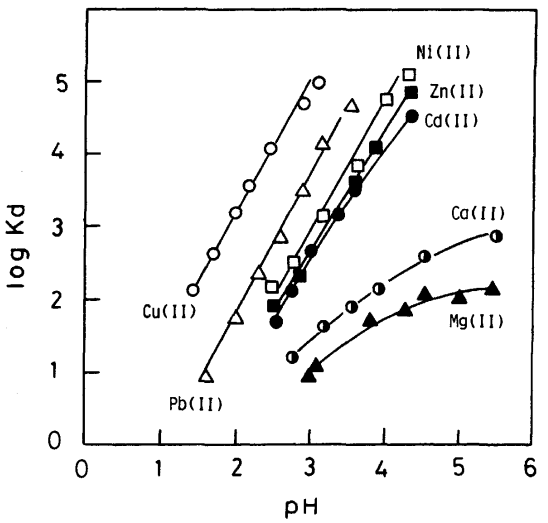

Fig. 2. Distribution coefficients of the SG-IDA for some metal ions as a function of pH. Cu(II) (○), Pb(II) (△), Ni(II) (□), Zn(II) (■), Cd(II) (●), Ca(II) (◑), Mg(II) (▲).

Table 2. Column Concentration of Trace Amount of Metal Ions[a)]

Run	Foreign ion	% Recovered			Flow rate SV/h^{-1}
		Cu(II)	Zn(II)	Cd(II)	
1	—	100	110	102	36
2	—	100	95	70	48
3[b)]	—	107	108	105	50
4	Ca(II), 1000 ppb	100	108	100	36
5	Mg(II), 1000 ppb	100	110	98	36

a) Column bed: 5 cm^3 of SG-IDA feed metal: 10 ppb each (5000 cm^3), pH 4.5. b) The pH of feed solution was 5.5.

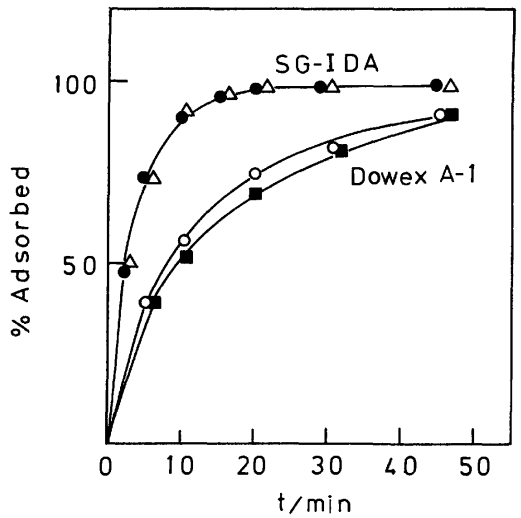

Fig. 3. Time-courses for the adsorption of metal ions with the SG-IDA and Dowex A-1. SG-IDA: Cu(II) (●); Ni(II) (△), Dowex A-1: Cu(II) (○); Ni(II) (■). Conditions: Adsorbent=3 g, $[M]_{feed}$= 1×10^{-3} M (500 cm^3), pH of the feed solution=4.5.

Adsorption Rate. A rapid attainment of adsorption equilibrium is of fundamental importance for the concentration of metal ions from a practical point of view, particularly for the treatment of a large volume of a dilute solution. The time-courses for the adsorption of Cu(II) and Ni(II) were examined by monitoring the change in the metal concentration in the batch systems. Figure 3 shows the rate profiles using the SG-IDA along with those by Dowex A-1 (60—100 mesh). The SG-IDA adsorbed more than 95% of the metal ions within 15 min while the adsorption rate of the Dowex A-1 was relatively slow. The rapid kinetics of SG-IDA can be attributed to the porous structure of the beads which allows a facile diffusion of the metal ions inside the matrix. The hydrophilic nature of the surface due to the unshielded silanol groups may also contribute to the rapid adsorption.

Column Concentration of Metal Ions. Rapid kinetics and sufficiently high K_d values of SG-IDA for the adsorption of heavy metal ions suggest the possibility of a fast concentration of trace metal ions in a column system.

A 5 dm^3 solution containing a 10 ppb level of Cu(II), Zn(II), and Cd(II) was continuously supplied onto the SG-IDA column; finally, the adsorbed metal ions were released from the column by elution with 2 M HCl. The percent recovery was then determined by the metal ratio in the eluate and in the feed solution. Typical results are given in Table 2. When the flow rate was controlled under 3 $cm^3 min^{-1}$, which corresponds to the space velocity (SV) of 36 h^{-1} at the given experimental conditions, all the metal ions of interest were quantitatively recovered in a concentrated form. Copper(II) was quantitatively recovered, even at a higher flow (SV=48 h^{-1}), whereas the recovery of Zn(II) and Cd(II), which form less stable complexes with SG-IDA than Cu(II), decreased at this flow rate. At a much higher pH (=5.5), however, an improved result could be attained.

Interference from alkali and alkaline earth metal ions was not significant when they were present in concentrations of about hundred times that of the metal ions of interest.

References

1) S. K. Sahni and J. Reedijk, *Coord. Chem. Rev.*, **59**, 1 (1984).
2) K. H. Lieser, *Pure Appl. Chem.*, **51**, 1503 (1979).
3) J. A. Smits, J. Nelissen, and J. V. Grieken, *Anal. Chim. Acta*, **111**, 215 (1979).
4) B. R. Willeford and H. Veening, *J. Chromatogr.*, **251**, 61 (1982).
5) K. Terada, K. Matsumoto, and H. Kimura, *Anal. Chim. Acta*, **153**, 237 (1983).
6) R. E. Sturgeon, S. S. Berman, S. N. Willie, and J. A. H. Desaulniers, *Anal. Chem.*, **53**, 2337 (1981).
7) J. M. Hill, *J. Chromatogr.*, **76**, 455 (1973).
8) D. E. Leyden and G. H. Luttrell, *Anal. Chem.*, **47**, 1612 (1975).
9) J. R. Jezorek and H. Freiser, *Anal. Chem.*, **51**, 366 (1979).
10) T. Seshadri and A. Kettrup, *Fresenius' Z. Anal. Chem.*, **296** 247 (1979).
11) R. J. Kvitek, J. F. Evans, and P. W. Carr, *Anal. Chim. Acta*, **144**, 93 (1982).
12) O. Itabashi and T. Goto, *Chem. Ind.(London)*, **1986**, 287.
13) T. M. Suzuki, O. Itabashi, T. Goto, T. Yokoyama, and T. Kimura, *Anal. Sci.*, **2**, 391 (1986).
14) T. M. Suzuki, T. Yokoyama, H. Matsunaga, and T. Kimura, *Bull. Chem. Soc. Jpn*, **59**, 865 (1986).
15) O. Itabashi and T. Goto, unpublished results.
16) R. F. Hirsh, E. Gancher, and F. R. Russo, *Talanta*, **17**, 483 (1970).
17) D. E. Leyden and A. L. Underwood, *J. Phys. Chem.*, **68**, 209 (1964).

 © 1987 The Chemical Society of Japan Bull. Chem. Soc. Jpn., 60, 2843—2847 (1987)

Preparation and Properties of Cobalt(II) Hydroxide-(Sodium Fluoride Tetrasilicic Mica) Intercalation Complexes and of Highly Dispersed Cobalt on Mica

Kunio Ohtsuka,* Johji Koga, Mitsuru Suda, Mikiya Ono, and Minoru Takahashi†
Research & Development Center, Ceramics, Mitsubishi Mining & Cement Co., Ltd.,
2270 Yokoze, Chichibu-gun, Saitama 368
†Department of Applied Physics, Tohoku University, Sendai 980
(Received January 7, 1987)

Cobalt(II) hydroxide-(sodium fluoride tetrasilicic mica) intercalation complexes were prepared by titrating cobalt(II) nitrate solutions in the presence of mica with sodium hydroxide under oxygen-free conditions. These complexes were characterized by chemical analysis, XRD, DTA-TGA, IR, and surface area measurements. These confirmed that the brucite-like cobalt(II) hydroxide sheet developed within the interlayer of the silicate. Cobalt atoms reduced at 400—700 °C by H_2 migrated from the interlayer of the silicate to the external surface of these where highly dispersed cobalt particles were formed. Ultra-fine cobalt metals (50—200 Å) with a hexagonal close-packed form were prepared at 400 °C by H_2. The degree of reduction and the grain diameter of cobalt increased with an increase of the reducing temperature and/or the reducing time.

The preparation and properties of metal hydroxide-expansible layer silicates (montmorillonite, vermiculite, etc.) intercalation complexes are important subjects concerning the research of clay minerals. Much work has been done on this topic: especially, on aluminium hydroxide-,[1] magnesium hydroxide-,[1] and nickel(II) hydroxide-[2,3] expansible layer silicate intercalation complexes in relation to the formation and alternation of clay minerals.

On the other hand, only a few studies have been carried out on the reduction behavior of metal hydroxide interlayers of these complexes.[3,4] We found that highly dispersed nickel particles can be formed on the external surface, not in the interlayer space of the silicates, by the reduction of the nickel hydroxide interlayer of the complex.[3] Therefore, metal (especially transition elements) hydroxide-layer silicate complexes appear to be unique materials as catalysts and magnetic materials etc, since the reduction of these complexes may provide isolated metal atoms on the external surface of the silicates.

Cobalt is a typical transition element that is widely used in catalysts and magnetic materials etc. However, no attempt has been made to study the preparation of cobalt(II) hydroxide-layer silicate complexes. In this work, the preparation of cobalt(II) hydroxide-(sodium fluoride tetrasilicic mica) intercalation complexes, the thermal stability of these complexes, and the reduction behavior with H_2 were investigated. Sodium fluoride tetrasilicic mica, $NaMg_{2.5}Si_4O_{10}F_2$, has very important characteristics: first, it has no acidity at all; second, it has a high thermal stability; and third, it has a sheet-forming capability owing to its flake-like particles.

Experimental

Materials. A 10 wt% sol of sodium fluoride tetrasilicic mica, synthesized silicate material, (supplied by Topy Ind. Co., under the name of Na-TSM) was used. Since this mica sol contains a little α-cristobalite and magnesium fluoride richiterite, $Na_2Mg_6F_2(Si_4O_{11})_2$, as impurities, the sol was diluted with distilled water and most of the impurities were separated by centrifugation. Sodium fluoride tetrasilicic mica was finally dried in air at 100 °C. The characteristics of this mica were described in detail in our previous work.[3] Na^+ ions are located within the interlayer of the silicate and balance the negative layer charge of −1 derived from vacancies in the octahedral sheets. These Na^+ ions are exchangeable in water and the theoretical cation-exchange capacity is 254 meq/100 g · mica.

Preparation and Examination of Intercalation Complexes. Cobalt(II) hydroxide-(sodium fluoride tetrasilicic mica) complexes were prepared by titrating cobalt(II) nitrate solutions in the presence of the mica with sodium hydroxide under oxygen-free conditions. In general, the addition of alkali metal hydroxide to a solution of cobalt(II) salts results in the precipitation of cobalt(II) hydroxide. However, suspensions of cobalt(II) hydroxide are gradually oxidized by air to cobalt(III) oxide hydrate and/or cobalt(III) oxide hydroxide.[5] Therefore, the preparation procedures were operated under a N_2 gas atmosphere. All solutions were prepared using distilled water free of O_2; dissolved oxygen was expelled by keeping N_2 gas bubbling through the boiling water for 2 h.

The preparation procedures were as follows: 1.5 g samples of the mica were dispersed in 150 ml of 0.1 M (1 M=1 mol dm^{-3}) cobalt(II) nitrate solutions to give a 1 mol Co/100 g · mica. After stirring for 1 d, these suspensions were titrated with an appropriate volume of 0.1 M sodium hydroxide solutions to yield OH/Co molar ratios of 0, 0.2, 0.5, 0.8, and 1.0, respectively, at a rate of 5 ml h^{-1} under vigorous stirring, and kept stirring for 3 d. Following these treatment, samples were repeatedly washed in order to remove any electrolyte with the distilled water free of O_2 and dried at 50 °C in a vacuum oven. These samples were stored under nitrogen in a tightly closed desiccator.

Cobalt(II) hydroxide were also prepared by titrating a 2 M cobalt(II) nitrate solution with an equivalent volume of a 2 M sodium hydroxide solution under similar conditions.

† Present address: Tohoku Institute of Technology, Sendai 982.

Table 1. Conditions of Preparation and Chemical Analyses of Sodium Fluoride Tetrasilicic Mica and Cobalt(II) Hydroxide-(Sodium Fluoride Tetrasilicic Mica)

No.	Condition of preparation	Chemical analysis/wt%			Molar ratio (SiO_2=4)		
	OH/Co (1 mol Co/100 g·mica)	SiO_2	Na	Co	SiO_2	Na	Co
a)		57.34	4.36	—	4.00	0.80	—
1	0.0	50.89	0.65	3.37	4.00	0.13	0.27
2	0.2	46.51	0.59	7.45	4.00	0.13	0.65
3	0.5	43.88	0.55	14.41	4.00	0.13	1.34
4	0.8	41.83	0.52	18.57	4.00	0.13	1.81
5	1.0	39.61	0.49	22.36	4.00	0.13	2.30

a) Initial sodium fluoride tetrasilicic mica ($NaMg_{2.5}Si_4O_{10}F_2$). Interlayer charge is +1; interlayer cations are Na^+ and H^+ that replaced the part of Na^+ cations in distilled water.

Table 2. Basal Spacings (Å) of Cobalt(II) Hydroxide-(Sodium Fluoride Tetrasilicic Mica) after Heat Treatment

No.	OH/Co	Heat treatment/°C[a]				
		105	200	250	300	350
Initial mica[b]		9.6	9.6	9.6	9.6	9.6
1	0.0	15.0[c]	9.6	9.6	9.6	9.6
2	0.2	14.5	9.6	9.6	9.6	9.6
3	0.5	14.5	9.6	9.6	9.6	9.6
4	0.8	14.5	14.5	14.5	ML[d]	9.6
5	1.0	14.6	14.5	14.5	ML	9.6

a) Heat treatment for 2 h. b) Basal spacing of sodium fluoride tetrasilicic mica is 9.6 Å (anhydrous form); 12.3 Å (single water layer hydrated form); 15.2 Å (double water layer hydrated form). c) Rehydrated form on exposure to air at room temperature. d) ML=mixed layer (mixtures of 14.5 and 9.6 Å layers).

The resulting precipitate was cobalt(II) hydroxide in pink form (β-$Co(OH)_2$) determined by XRD analysis. The pink cobalt(II) hydroxide has a brucite ($Mg(OH)_2$) structure.

The chemical analyses of the complexes were performed by atomic absorption analyses. Surface areas were measured by the nitrogen-adsorption method with a Carlo Elba Sorptomatic Series 1800. All samples were examined by XRD as thin, oriented films on glass slides. IR spectra were obtained from KBr disks. The thermal stability of the complexes in air and the reduction behavior with H_2 were investigated at 100—700 °C (the mica is stable below 800 °C); the heating rate was 10 °C min^{-1} and slowly cooled after holding for a set time.

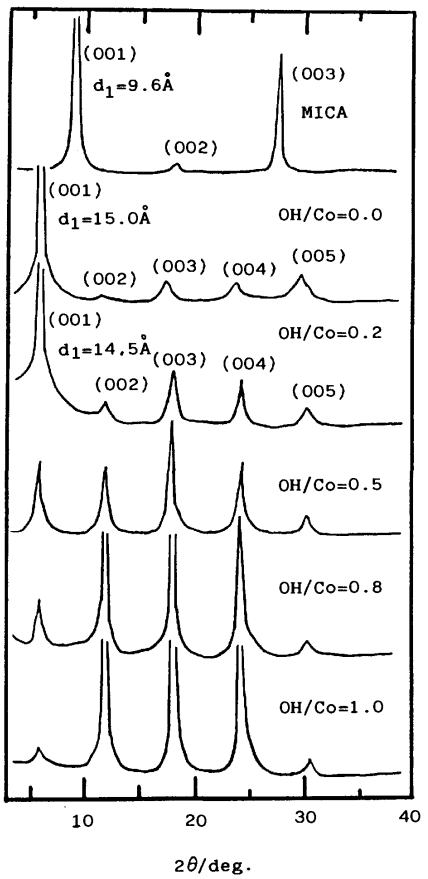

Fig. 1. X-Ray powder diffraction patterns (Cu $K\alpha$ radiation) of cobalt (II) hydroxide-(sodium fluoride tetrasilicic mica). MICA: Anhydrous form.

Results and Discussion

Chemical Analysis and XRD Measurements. Chemical analyses of the mica and its intercalation complexes are listed in Table 1. The amount of Co taken into the mica increased with an increase of the OH/Co ratio. The highest Co yield of about 2.3 mol Co per formula unit of the mica was obtained with a OH/Co ratio of 1.0. As the ion-exchange rate is 87%, this value corresponds to 2.6 mol Co per formula unit of the mica being 100% ion exchanged. In the case a complete cobalt(II) hydroxide developed between the silicate layers, as a nickel(II) hydroxide interlayer,[3] for instance, the limiting composition would be $[Co_3(OH)_5(H_2O)](Mg_{2.5}Si_4O_{10}F_2)$. This composition corresponds to 3 mol Co per formula unit of the mica 100% ion exchanged. Therefore, at a OH/Co ratio of 1.0, the cobalt(II) hydroxide interlayer would be well developed, but not completely.

The basal spacings of these complexes are expanded by about 14.5 Å from the 9.6 Å basal spacing of the mica; these basal spacings are almost constant and independent of the amount of cobalt taken into the mica (Table 2). Moreover, X-ray diffraction analyses did not show any free cobalt(II) hydroxide in these

complexes or cobalt oxide in the heat-treated sample. Therefore, a brucite-like cobalt(II) interlayer must have developed between the silicate layers without free cobalt(II) hydroxide. The X-ray powder diffraction patterns of these complexes are shown in Fig. 1. With an increase in the OH/Co ratio, the (001) first-order reflection decreased in intensity; on the contrary, the (002)—(004) higher-order reflections increased in intensities. These changes of the relative intensities also indicate that a cobalt(II) hydroxide-forming reaction took place in the interlayer of the silicate.[6]

Changes of the basal spacings after heat treatments are shown in Table 2. Basal spacings of the samples with OH/Co=0.8, 1.0 retained 14.5 Å up to 250 °C and reduced to about 9.6 Å with further heating. The XRD patterns of these collapsed samples are almost similar to that of the original mica; the (001) reflection of these collapsed samples increased in intensity. β-Cobalt(II) hydroxide changed to cobalt (II, III) oxide after a heat treatment at 150 °C for 2 h; therefore, well-developed cobalt(II) hydroxide within the interlayer of the silicate has a higher thermal stability than β-cobalt(II) hydroxide.

Thermal Analysis. Figure 2 shows the DTA and TGA curves for the complexes; the heating rate was 10 °C min^{-1}. Sample No. 1 (prepared at OH/Co=0.0) showed a single endothermic peak at about 164 °C with a corresponding weight loss. This dehydration is due to the water of hydration associated with the exchanged cobalt(II) ions within the interlayer of the silicate; this water is much more dissociated than water in the bulk state.[7] Therefore, the composition of these interlayer cobalt(II) ions is $[Co(OH)_\delta(H_2O)_{6-\delta}]^{2-\delta}$.

On the other hand, samples prepared with the addition of sodium hydroxide, OH/Co=0.2—1.0, showed a first endothermic peak at about 140—160 °C and a second one at about 380—400 °C, with corresponding weight losses. With an increase in the OH/Co ratio, the endothermic peak area at about 380—400 °C increased; on the contrary, the endothermic peak area at about 140—160 °C decreased. These correspond to the fact that cobalt(II) hydroxide, to be exact, hydroxocobalt(II) complex $[Co_x(OH)_y(H_2O)_m]^{2x-y}$ developed within the interlayer of the silicate with the progressive hydrolysis and olation of cobalt(II) cations by addition of alkali. Therefore, the first endothermic peak (140—160 °C) corresponds to the loss of absorbed water and coordinated water and the second one (380—400 °C) to the loss of hydroxo. The mechanism of formation of cobalt(II) hydroxide interlayers must be the same as that discussed in the study of the formation of a nickel(II) hydroxide interlayer.[2] The endothermic peaks at about 820 and 884 °C are due to the reactions between cobalt oxide and the mica; cobalt silicate (Co_2SiO_4) was detected by XRD after the measurement of DTA-TGA.

The DTA-TGA curves for β-cobalt(II) hydroxide showed an endothermic peak corresponding to the dehydration of hydroxyl at about 295 °C; this temperature is considerably lower than the dehydration temperature (380—400 °C) of the hydroxo of cobalt(II) hydroxide interlayer. These correspond to the fact that a well developed cobalt(II) hydroxide interlayer has a higher thermal stability than β-cobalt(II) hydroxide; that cobalt(II) hydroxide interlayer is strongly fixed by electrostatic force and hydrogen bond to the silicate layer like as brucite interlayer in chlorite.[8]

Specific Surface Areas. The specific surface areas of the complexes are shown in Fig. 3. With an increase

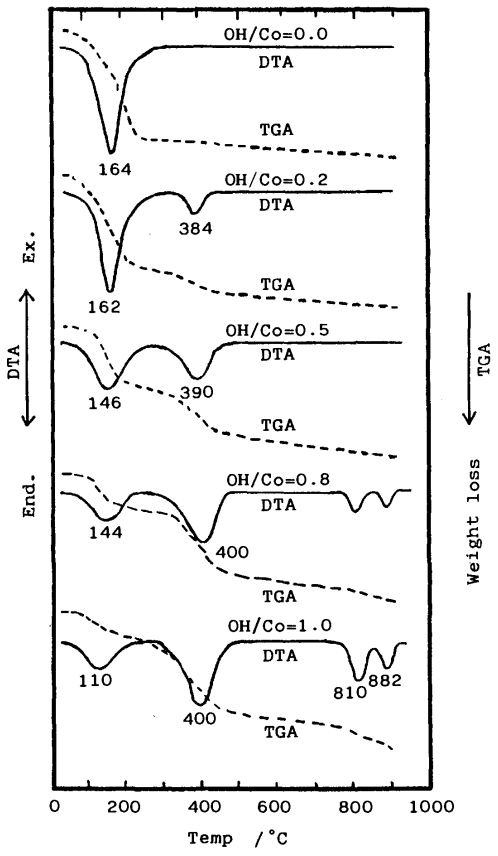

Fig. 2. DTA and TGA curves for cobalt(II) hydroxide-(sodium fluoride tetrasilicic mica).

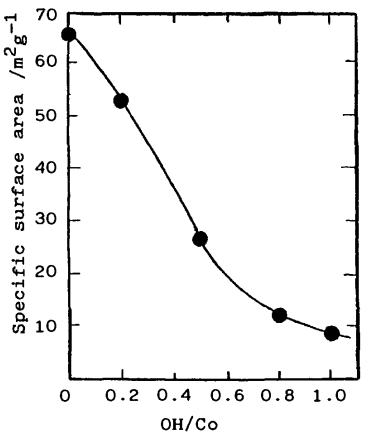

Fig. 3. Specific surface areas of cobalt(II) hydroxide-(sodium fluoride tetrasilicic mica).

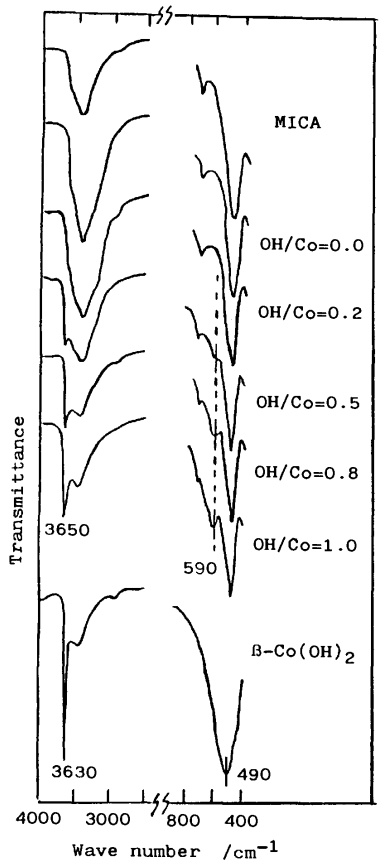

Fig. 4. IR absorption spectra of β-cobalt(II) hydroxide and cobalt(II) hydroxide-(sodium fluoride tetrasilicic mica).

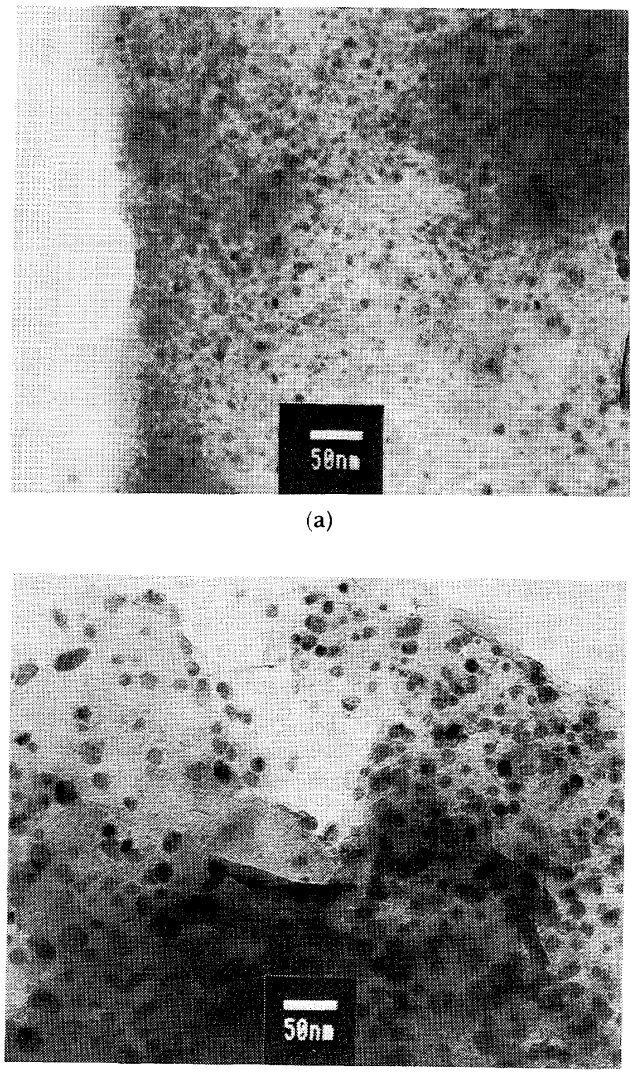

Fig. 5. Transmission electron micrographs of cobalt(II) hydroxide-(sodium fluoride tetrasilicic mica) (OH/Co=1.0) heat treated at 400°C for 24 h (a) and 48h (b) in H_2 flow.

in the OH/Co ratio, the specific surface areas decreased since the interlayer space becomes smaller with the development of a cobalt(II) hydroxide interlayer; finally, the internal surfaces become completely covered.

IR Analysis. The IR absorption spectra of the complexes and β-cobalt(II) hydroxide are shown in Fig. 4. Characteristic absorption bands appeared at about 3650 and 590 cm^{-1} in the complexes with an increase of the OH/Co ratio. The 3650 cm^{-1} band is due to the OH stretching vibration of cobalt(II) hydroxide interlayer. The 590 cm^{-1} band is also from the cobalt(II) hydroxide interlayer and appears to be shifted from 490 cm^{-1} band shown in absorption spectrum of β-cobalt(II) hydroxide.

Reduction Behavior with H_2. Complexes with OH/Co=1.0 were heat treated in flowing H_2 at 400, 500, 600, and 700 °C for 2 h. All samples collapsed to a basal spacing of 9.6 Å and metallic cobalt was detected by XRD above 500 °C. These metallic cobalt structures were mixtures of the face centered cubic and hexagonal close-packing phases. In general, cobalt exists as a h.c.p phase (α-Co) at ordinary temperatures; above 417 °C, it has a f.c.c phase (β-Co). However, mixtures normally coexist because of the very low free energy change associated with the α–β transformation.[9] On the other hand, those complexes with OH/Co=1.0 were also heat treated in flowing H_2 at 400 °C for 2, 4, 6, 24, and 48 h and cobalt with h.c.p form was identified by XRD after over a 4 h heat treatment.

With an increase in the reducing temperature and/or the reducing time, the reflection intensity of cobalt increased and the (001) mica basal reflection peak became sharper. These results indicate that reduced cobalt atoms gradually migrate from the interlayer of the silicates to its external surface. Patel[10] reported that finely divided metal particles (15—100 Å) can be formed in interlayer spaces of clay minerals with an H_2 reduction of transition metal (Ni^{2+}, Cu^{2+}) interlayer cations. However, our results have shown that reduced cobalt metals exist mainly not in the interlayer of the silicates but on the external surface of the silicate, owing to the fact that the basal spacings of the silicate are always 9.6 Å after H_2 reduction. TEM

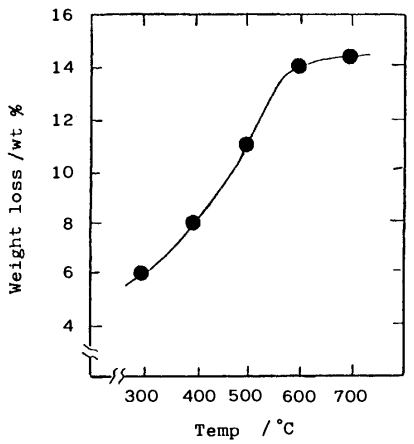

Fig. 6. Weight loss for cobalt(II) hydroxide-(sodium fluoride tetrasilicic mica) after various temperatures of reduction for 2 h.

photographs (heat treated complexes at 400 °C for 24 and 48 h in H_2 flow) show that ultra-fine metallic cobalt particles (50—200 Å) are distributed on the whole surface of the mica and that the grain diameter of this cobalt increases with an increase of the reducing time (Fig. 5). Furthermore, particles with a crystal habit of hexagonal plates can be observed.

Only a few studies have hitherto been made on the reduction behavior of transition metal cations and/or transition metal (=nickel) hydroxide within the interlayer of the expansible layer silicate. However, many studies have been performed on the reduction behavior of metal cations in zeolite. It is generally accepted that the metal ions in a zeolite are reduced to zero valent metal particles by H_2 as follows:[11]

$$Me^{x+}(ZO^-)_x + x/2H_2 \rightarrow M\overset{0}{e} + x(ZOH).$$

Here, $(ZO^-)_x$ represents the zeolite lattice and ZOH represents surface hydroxyl groups. Moreover, a similar reaction mechanism was proposed in the case of metal ions in montmorillonite.[10]

The following reduction mechanism is likely in the case of metal hydroxide-layer silicate complexes as well:

$$[Me_x(OH)_y(H_2O)_m]^{1+} + (O\text{-}MICA)^- + H_2 \rightarrow H^+(O\text{-}MICA)^- + x\overset{0}{Me} + (m+y)\,H_2O, \quad (1)$$

where $[Me_x(OH)_y(H_2O)_m]^{1+}$ represents the metal hydroxide interlayer and $(O\text{-}MICA)^-$ represents a mica layer sheet. The weight loss during H_2 reduction was determined on sample No. 5 (OH/Co=1.0); it was first heat treated at 100 °C for 2 h and then heated in flowing H_2 (i) at 300, 400, 500, 600, and 700 °C for 2 h (Fig. 6), and (ii) at 400 °C for 2, 4, 6, 24, and 48 h. From chemical analyses of sample No. 5, the chemical composition of the complex were evaluated to be

$$\{[Co_{2.64}(OH)_{4.28}(H_2O)]^{+1}\}_{0.87}\,Na_{0.13}\,(Mg_{2.5}Si_4O_{10}F_2) = \{Co_{2.3}(OH)_{3.72}(H_2O)_{0.87}\}Na_{0.13}\,(Mg_{2.5}Si_4O_{10}F_2),$$

assuming that the cobalt(II) hydroxide interlayer has a composition of $[Co_x(OH)_y(H_2O)_m]^{+1}$, $(y+m)/x=2$ with a charge of +1.0 to balance the negative layer charge. The theoretical weight loss of the sample after a complete reduction was calculated to be 13.3 wt% (according to the Eq. 1). As shown in Fig. 6, the cobalt(II) hydroxide interlayer was almost reduced to cobalt metal upon being heat treated at about 600 °C for 2 h; the theoretical and experimental values agreed well. On the other hand, the weight losses after heat treatments at 400 °C for 2, 4, 6, 24, and 48 h were 8.0, 8.8, 9.3, and 10.5 wt%, respectively. Therefore, the reduction reaction was not completed, even after a 48 h treatment.

References

1) G. W. Brindley and Chih-chun Kao, *Clays Clay Miner.*, **28**, 435 (1980).

2) S. Yamanaka and G. W. Brindley, *Clays Clay Miner.*, **26**, 21 (1978).

3) K. Ohtsuka, M. Suda, M. Ono, M. Takahashi, M. Sato, and S. Ishio, *Bull. Chem. Soc. Jpn.*, **60**, 871 (1987).

4) C. Ghesquiere, J. Lemaitre, and A. J. Herbillon, *Clay Miner.*, **17**, 217 (1982).

5) M. Pourbaix, "Atlas of Electrochemical Equilibria in Aqueous Solutions," Pergamon Press, Oxford (1966), p. 325.; D. Nicholls, "Comprehensive Inorganic Chemistry," ed by J. C. Bailar, H. J. Emeleus, Sir Ronald Nyholm, and A. F. Trotman-Dickenson, Pergamon Press, Oxford (1973), Vol. 3, pp. 1071, 1094.

6) C. I. Rich, *Clays Clay Miner.*, **16**, 15 (1968).

7) D. M. C. MacEvan and M. J. Wilson, "Crystal Structures of Clay Minerals and Their X-ray Identification," ed by G. W. Brindley and G. Brown, Mineralogical Society, London (1980), p. 219.

8) S. W. Baily, "Crystal Structures of Clay Minerals and Their X-ray Identification," ed by G. W. Brindley and G. Brown, Mineralogical Society, London (1980), p. 86.

9) D. Nicholls, "Comprehensive Inorganic Chemistry," ed by J. C. Bailar, H. J. Emeleus, Sir Ronald Nyholm, and A. F. Trotman-Dickenson, Pergamon Press, Oxford (1973), Vol. 3, p. 1054.; A. Taylor, *J. Inst. Metals*, **77**, 585 (1950).; M. Hansen and K. Anderko, "Constitution of Binary Alloys 2nd ed," McGraw-Hill, New York (1958), p. 485.

10) M. Patel, *Clays Clay Miner.*, **30**, 397 (1982).; M. Patel, *Trans. Indian Ceram. Soc.*, **42**, 1 (1983).

11) P. A. Jacobs, "Carboniogenic Activity of Zeolite," Elsevier, Amsterdam (1977), p. 183.

 © 1987 The Chemical Society of Japan Bull. Chem. Soc. Jpn., 60, 2849—2852 (1987)

Magnetic Properties of Dimeric Copper(II) Trichloroacetate Adducts with 3-Substituted Pyridines

Yoneichiro MUTO,* Michio NAKASHIMA,† Tadashi TOKII, Michinobu KATO,†† and Ikuo SUZUKI†††
Department of Chemistry, Faculty of Science and Engineering, Saga University, Saga 840
†Research Institute for Diseases of the Chest, Faculty of Medicine, Kyushu University, 3-1-1 Maidashi, Higashi-ku, Fukuoka 812
††Aichi Prefectural University, Mizuho-ku, Nagoya 467
†††Department of Electrical and Computer Engineering, Nagoya Institute of Technology, Showa-ku, Nagoya 466
(Received January 13, 1987)

Dimeric copper(II) trichloroacetate adducts with 3-substituted pyridines, $[Cu(Cl_3CCOO)_2(3\text{-Xpy})]_2$ where X=Cl, Br, H, CN, and CH_3, have been prepared. Magnetic susceptibility and ESR data show that both the singlet-triplet separation ($-2J$) and the zero field splitting (D) decrease in the order: 3-Clpy adduct (193 and 0.397 cm^{-1})≈3-Brpy adduct (191 and 0.399 cm^{-1})>py adduct (188 and 0.385 cm^{-1})>3-CNpy adduct (138 and 0.216 cm^{-1})>3-CH_3py adduct (83 and 0.182 cm^{-1}). Electronic spectra indicate that the adducts with X=Cl, Br, and H have a distorted square-pyramidal copper(II) geometry and that those X=CN and CH_3 have a distorted trigonal-bipyramidal geometry. Form these results, it is concluded that the strength of antiferromagnetic interaction in $[Cu(Cl_3CCOO)_2(3\text{-Xpy})]_2$ complexes decreases as the distortion of copper(II) geometry increases from square-pyramid toward trigonal-bipyramid.

Recent structural studies on dimeric copper(II) carboxylate adducts, $[Cu(RCOO)_2 \cdot L]_2$, have demonstrated that the metal-metal distance becomes longer as either the acidity of the parent carboxylic acid RCOOH[1] or the basicity of the axial ligand L[2] becomes stronger. Then, a longer Cu-Cu distance is usually associated with a greater displacement of the metal ion from the equatorial plane composed of four oxygen atoms. Consequently, the variation of both the group R and the ligand L affects the strength of the Cu-O bonds in the CuO_4 basal plane accompanying a deformation of the bridging framework. For 13 dimeric copper(II) acetate adducts reported up to date, Cu-Cu distances span a narrow range of 2.581—2.671 Å with a variation of 0.09 Å.[2] On the other hand, Cu-Cu distances found for dimeric copper(II) trichloroacetate adducts, $[Cu(Cl_3CCOO)_2 \cdot L]_2$, span a considerably wide range: 2.731 Å for L=benzonitrile (PhCN),[3] 2.776 Å for L=2-chloropyridine (2-Clpy),[1] 2.852 Å for L=caffeine,[4] 3.197 Å for L=2,2,5,5-tetramethyl-1-pyrrolidinyloxyl,[5] and 3.256 Å for L=2,2,6,6-tetramethyl-1-piperidinyloxyl.[5] The coordination environment around each copper(II) ion in the first three adducts is square-pyramidal, whereas that in the last two adducts is trigonal-bipyramidal. These structural data indicate that, for the variation of L, the bridging trichloroacetato ligand coordinates more flexibly than the bridging acetato ligand does. Dimeric copper(II) trichloroacetate adducts may therefore be a suitable choice for the study of structural factors which affect the magnetic properties of copper(II) carboxylate dimers.

This paper reports results of synthetic, magnetic, and spectroscopic studies on five copper(II) trichloroacetate adducts with 3-substituted pyridines, $Cu(Cl_3CCOO)_2(3\text{-Xpy})$, where X=Cl, Br, H, CN, and CH_3.

Table 1. Analytical Data of $Cu(Cl_3CCOO)_2(3\text{-Xpy})$

X	Found (Calcd)/%			
	C	H	N	Cu
Cl	21.85 (21.53)	0.87 (0.87)	2.68 (2.79)	12.58 (12.66)
Br	19.83 (19.78)	0.81 (0.73)	2.35 (2.56)	11.78 (11.63)
H	22.88 (23.13)	1.17 (1.08)	2.87 (3.00)	13.62 (13.60)
CN	24.33 (24.39)	0.82 (0.82)	5.81 (5.69)	12.98 (12.90)
CH_3	24.70 (24.95)	1.53 (1.46)	2.80 (2.91)	13.19 (13.19)

Experimental

Syntheses. $Cu(Cl_3CCOO)_2(3\text{-Xpy})$ (X=Cl, Br, H, CN, and CH_3): $Cu(Cl_3CCOO)_2 \cdot 3H_2O$ (1 mmol) and 3-Xpy (1 mmol) were suspended in a mixture of a solvent (benzene for X=Cl, Br, and CH_3; chloroform for X=H and CN) (30 ml) and 2,2-dimethoxypropane (1 ml). The mixture was warmed gently with stirring and then filtered. After the solution had been concentrated to one-third of its original volume, it was allowed to stand overnight at ca. 5 °C in a refrigerator. The separated green crystals were collected, washed with petroleum ether, and dried in vacuo at room temperature.

The results of the elemental analyses are given in Table 1.

Physical Measurements. The magnetic susceptibility in the temperature range of 80—300 K was determined by the Faraday method. The correction for diamagnetic contribution was made by use of Pascal's constants.[6] The cryomagnetic data were applied to the modified Bleaney-Bowers equation

$$\chi_A = \frac{Ng^2\beta^2}{3kT}\left[1+\frac{1}{3}\exp\left(\frac{-2J}{kT}\right)\right]^{-1}\cdot(1-P) + \frac{Ng_i^2\beta^2}{4kT}\cdot P + N\alpha, \quad (1)$$

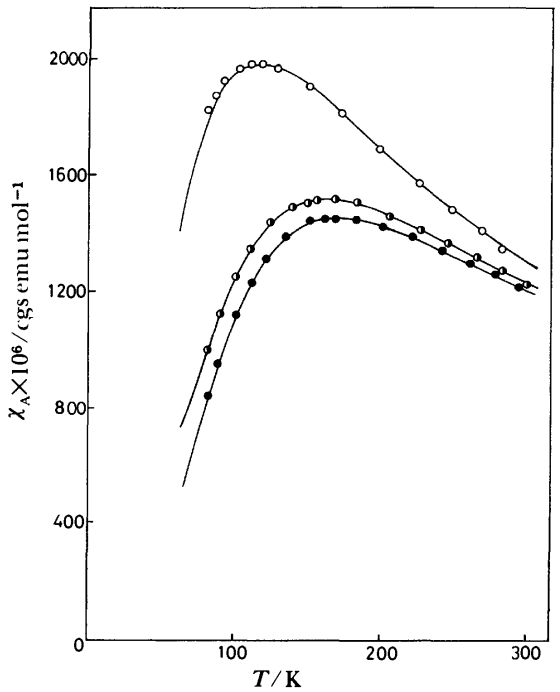

Fig. 1. Variation of magnetic susceptibilities with temperature. (●): $Cu(Cl_3CCOO)_2(3\text{-Brpy})$, (○): $Cu(Cl_3CCOO)_2(py)$, (○): $Cu(Cl_3CCOO)_2(3\text{-CNpy})$. The solid curves were obtained as described in the text.

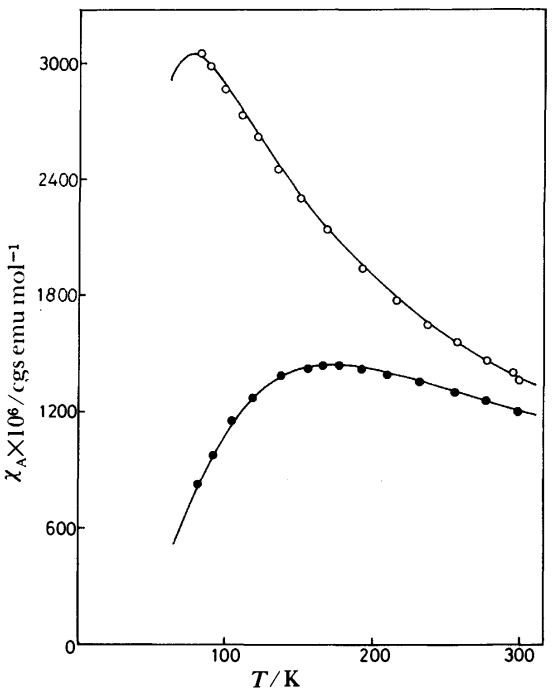

Fig. 2. Variation of magnetic susceptibilities with temperature. (●): $Cu(Cl_3CCOO)_2(3\text{-Clpy})$, (○): $Cu(Cl_3CCOO)_2(3\text{-CH}_3\text{py})$. The solid curves were obtained as described in the text.

where P is the mole fraction of the noncoupled copper(II) impurity and g_i is the average g factor for the impurity. The values of g_i of 2.2 and $N\alpha$ of 60×10^{-6} cgs emu (1 cgs emu=$4\pi\times10^{-6}$ m^3) were used throughout the present study.

Table 2. Magnetic Parameters for $Cu(Cl_3CCOO)_2(3\text{-Xpy})$

X	$-2J$/cm^{-1}	g	$P\times10^2$	$\sigma_{dis}\times10^3$
Cl	193	2.25	1.45	3.28
Br	191	2.24	1.25	3.99
H	188	2.25	4.06	3.72
CN	138	2.20	4.74	5.19
CH_3	83	2.17	0.87	5.45

The best-fit parameters of $-2J$, g, and P were obtained by the non-linear least-squares fitting procedure. The quantity of fit was estimated by means of a discrepancy index

$$\sigma_{dis} = \left[\frac{\sum(\chi_{obsd}-\chi_{calcd})^2}{\sum\chi_{obsd}^2}\right]^{1/2} \quad (2)$$

The thermal magnetic data are shown in Figs. 1 and 2 as plots of χ_A vs. T. The values of $-2J$, g, p, and σ_{dis} are summarized in Table 2.

The IR spectrum of $Cu(Cl_3CCOO)_2(3\text{-CNpy})$ was recorded on a Hitachi 260-10 IR Spectrophotometer with Nujol mulls.

Reflectance spectra were recorded on a Hitachi Recording Spectrophotometer 323. The wave numbers of the ligand-field band maxima in the range 5000—20000 cm^{-1} (so-called Band I) are collected in Table 3 and the spectral curves are shown in Fig. 3. For comparison, the reflectance spectral curve of $[Cu(Cl_3CCOO)_2(2\text{-Clpy})]_2$ is also given in Fig. 3.

Polycrystalline powder ESR X-band spectra were recorded with a Jeolco JES-ME 2 Spectrometer at room temperature. The spectra are shown in Fig. 4 and the ESR parameters are given in Table 4.

Results and Discussion

The magnetic susceptibility data of the complexes, $Cu(Cl_3CCOO)_2(3\text{-Xpy})$, are well represented by Eq. 1, which indicates that these complexes have a carboxylato bridged dimeric structure.[1-3] As shown in Table 2, the $-2J$ values of the 3-substituted pyridine adducts with X=Cl, Br, and H are comparable to those of $[Cu(Cl_3CCOO)_2(2\text{-Clpy})]_2$ (217 cm^{-1})[1] and $[Cu(Cl_3CCOO)_2(PhCN)]_2$ (224 cm^{-1}),[3] whereas those of the adducts with X=CN and CH_3 are considerably small. Such a substituent effect of 3-CN and 3-CH_3 groups will be discussed later. For the 3-cyanopyridine adduct, the CN stretching vibration (2240 cm^{-1}) appears in almost the same region as the free 3-cyanopyridine ligand (2232 cm^{-1}),[7] which suggests that in this adduct the CN group does not coordinate to the metal ion.

The electronic spectra of the adducts with X=Cl, Br, and H are similar to one another and closely resemble that of $[Cu(Cl_3CCOO)_2(2\text{-Clpy})]_2$ (Fig. 3), giving a band maximum at ca. 12500 cm^{-1} and a low-energy shoulder at ca. 8000 cm^{-1}. The separation between these two peaks, $\Delta\tilde{\nu}_{max}$=3890—4930 cm^{-1}, is comparable to those observed for $[Cu(CH_3COO)_2(py)]_2$ (5000 cm^{-1})[8] and $[Cu(Cl_3CCOO)_2(2\text{-Clpy})]_2$ (4900 cm^{-1}). These facts indicate that these three adducts have a

distorted square-pyramidal copper(II) geometry similarly to $[Cu(Cl_3CCOO)_2(2\text{-}Clpy)]_2$.[1] On the other hand, the spectral feature of the adducts with X=CN and CH_3 is quite similar to those of distorted trigonal-bipyramidal copper(II) complexes such as $Cu_4OCl_6(Ph_3PO)_4$ ($\Delta\tilde{\nu}_{max}$=1300 cm^{-1}),[9] $[Cu(bpy)_2Cl]NO_3\cdot 3H_2O$ ($\Delta\tilde{\nu}_{max}$=2000 cm^{-1}),[10] $[Cu(bpy)_2CN]NO_3\cdot 2H_2O$ ($\Delta\tilde{\nu}_{max}$= 2100 cm^{-1}),[11] and $[Cu(Ph_3CCOO)_2(py)]_2\cdot$benzene ($\Delta\tilde{\nu}_{max}$=2510 cm^{-1}).[12] The spectra of the latter two adducts show two peaks of about equal intensity with a separation of ca. 1800—1900 cm^{-1} in the range 10000—15000 cm^{-1} (Fig. 3 and Table 3). These $\Delta\tilde{\nu}_{max}$ values are comparable to those of the distorted trigonal-bipyramidal copper(II) complexes described above. The spectral similarity suggests that these two adducts have a distorted trigonal-bipyramidal copper(II) geometry, which may be produced rather by steric effects of the large CN and CH_3 substituents than by their electronic effects. Such a large size of substituents probably hinders smooth packing of molecules in crystal lattices, resulting in a steric strain in the coordination environment around the metal ion. Harrison et al.[10] demonstrated, in their study of $[Cu(bpy)_2Cl]X$ where X=ClO_4, $NO_3\cdot 3H_2O$, $1/2[(S_5O_6)\cdot 6H_2O]$, Cu^ICl_2, and $Cl\cdot 6H_2O$, that copper(II) complexes with a metal geometry close to the regular trigonal-bipyramid show a single broad peak in their electronic spectra at 12500 cm^{-1} (the $^2E' \leftarrow {}^2A_1'$ transition in the D_{3h} symmetry), whereas those with the square-pyramidally distorted trigonal-bipyramidal CuN_4Cl chromophore show a twin-peaked band in the region of 10000—14500 cm^{-1} with a maximum splitting of 4060 cm^{-1} for the complex whose metal geometry is closest to the regular square-pyramid. This fact suggests that, for five-coordinated copper(II) complexes, the $\Delta\tilde{\nu}_{max}$ value can be taken as a measure of the degree of distortion in metal geometry from square-pyramid to trigonal-bipyramid. As can be seen from Table 3, the $\Delta\tilde{\nu}_{max}$ value observed for the present complexes decreases in the order: 3-Clpy and 3-Brpy adducts>py adduct>3-CNpy adduct>3-CH_3py adduct. This order is just the same as that of the decrease in the $-2J$ values of these complexes (Table 2); there exists a parallel relation between $-2J$ and $\Delta\tilde{\nu}_{max}$ values (smaller $-2J$ with smaller $\Delta\tilde{\nu}_{max}$). This parallelism indicates that the strength of antiferromagnetic interaction in the present complexes decreases as the distortion of copper(II) geometry increases from square-pyramid toward trigonal-bipyramid.

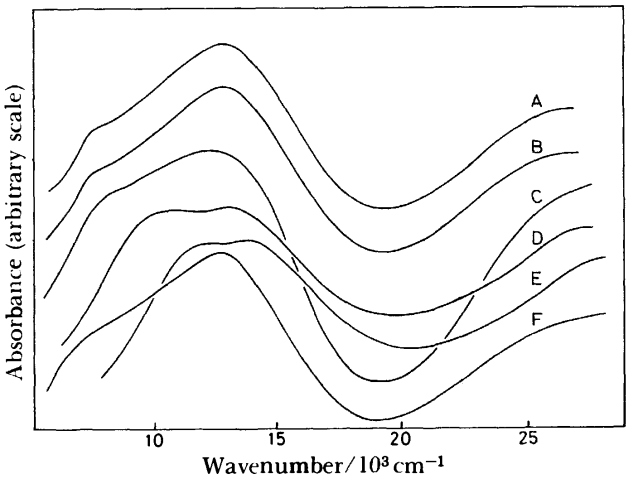

Fig. 3. Reflectance spectra of $Cu(Cl_3CCOO)_2\cdot L$. (A): L=3-Clpy, (B): L=3-Brpy, (C): L=py, (D): L=3-CNpy, (E): L=3-CH_3py, (F): L=2-Clpy.

Table 3. Reflectance Spectral Data of $Cu(Cl_3CCOO)_2(3\text{-}Xpy)$

X	$\tilde{\nu}_{max}\times 10^{-3}$/$cm^{-1}$	$\Delta\tilde{\nu}\times 10^{-3}$/$cm^{-1}$	
Cl	12.50	7.57	4.93
Br	12.50	7.57	4.93
H	12.27	8.40	3.89
CN	12.82	10.86	1.96
CH_3	14.28	12.50	1.78

The ESR spectra of the present complexes show absorption bands arising from the triplet state. The parameters listed in Table 4 were evaluated by a general method for the analysis of powder ESR spectra of dimeric copper(II) complexes.[13] The ESR spectral feature of the adducts with X=Cl, Br, and H is the same as that usually observed for dimeric copper(II) carboxylate adducts, which have a square-pyramidal metal geometry.[13] For these three adducts, the common relation between zero field splitting (D) and resonance magnetic field (H_o), $D>H_o$,[13,14] was observed. On the other hand, the ESR spectra of the adducts with X=CN and CH_3 are quite different from those of the above three adducts (Fig. 4) and fundamentally the same as that of $[Cu(Ph_3CCOO)_2(py)]_2\cdot$benzene ($D$=0.204 cm^{-1}).[12] For the latter two adducts, an uncommon relation, $D<H_o$, was observed; this relation has recently been detected for $[Cu(Ph_3CCOO)_2(py)]_2\cdot$benzene, whose $-2J$ (184 cm^{-1}) is quite small as compared with those of common dimeric copper(II) carboxylates.[12] The order of decrease in the D values of the present complexes is the same as that in the $-2J$ values. Thus, it is concluded that the zero field splitting of $[Cu(Cl_3CCOO)_2(3\text{-}Xpy)]_2$ decreases as the distortion of the metal geometry increases from square-pyramid toward trigonal-bipyramid, just in the same way as the singlet-triplet separation does.

It is noted here that the values of g_{av} obtained from

Table 4. ESR Parameters for $Cu(Cl_3CCOO)_2(3\text{-}Xpy)$

X	D/cm^{-1}	$g_{//}$	$g_\perp$	g_{av}[a]
Cl	0.397	2.536	2.143	2.282
Br	0.399	2.575	2.154	2.304
H	0.385	2.562	2.159	2.301
CN	0.216	2.425	2.155	2.248
CH_3	0.182	2.396	2.183	2.256

a) $g_{av}=[1/3(g_{//}^2+2g_\perp^2)]^{1/2}$.

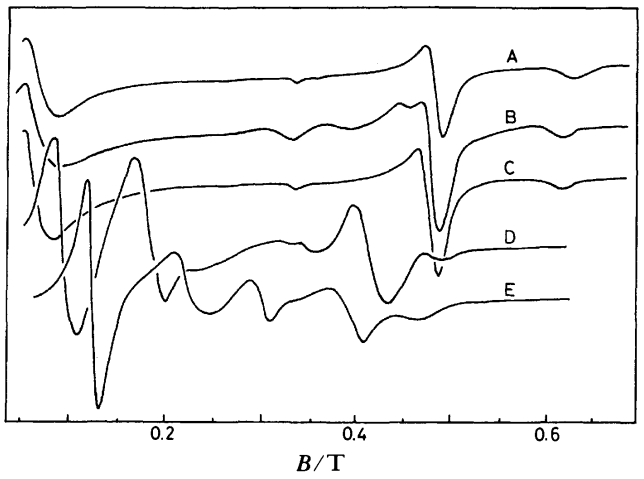

Fig. 4. Room-temperature polycrystalline powder ESR spectra of $Cu(Cl_3CCOO)_2(3\text{-}Xpy)$ at X-band frequency. (A): X=Cl, (B): X=Br, (C): X=H, (D): X=CN, (E): $X=CH_3$.

the present ESR study are smaller than those estimated from the magnetic susceptibility measurements (Tables 2 and 4); this is often observed for dimeric copper(II) carboxylates. The reason for this fact, however, is not clear at present.

References

1) J. A. Moreland and R. J. Doedens, *Inorg. Chem.*, **17**, 674 (1978).

2) V. M. Rao, D. N. Sathyanarayana, and H. Manobar, *J. Chem. Soc., Dalton Trans.*, **1983**, 2168.

3) M. Nakashima, M. Mikuriya, and Y. Muto, *Bull. Chem. Soc. Jpn.*, **58**, 968 (1985).

4) H. Horie, S. Husebye, M. Kato, E. A. Meyers, Y. Muto, I. Suzuki, T. Tokii, and R. A. Zingaro, *Acta Chem. Scand., Ser, A*, **40**, 579 (1986).

5) L. C. Porter, M. H. Dickman, and R. J. Doedens, *Inorg. Chem.*, **25**, 678 (1986).

6) P. W. Selwood, "Magnetochemistry," Interscience Publishers, New York (1956), pp. 78, 91.

7) R. E. Clarke and P. C. Ford, *Inorg. Chem.*, **9**, 495 (1970).

8) M. Kato, Y. Muto, and T. Tokii, 37th Annual Meeting of the Chemical Society of Japan, Tokyo, April 1978, Proceeding I, p. 255; ACS/CSJ Chemical Congress, April 1979, Honolulu, Hawaii, Abstracts I, Inorg. 465.

9) J. A. Bertrand, *Inorg. Chem.*, **6**, 495 (1967).

10) W. D. Harrison, D. M. Kennedy, M. Power, R. Sheahan, and B. J. Hathaway, *J. Chem. Soc., Dalton Trans.*, **1981**, 1556.

11) S. Tyagi and B. J. Hathaway, *J. Chem. Soc., Dalton Trans*, 1983, 199.

12) O. W. Steward, M. Kato, S. C. Chang, M. Sax, C. H. Chang, T. Taura, C. F. Jury, Y. Muto, T. Tokii, J. Pletcher, and C. S. Yoo, Proc, 23rd. Int. Conf. on Coord. Chem., Boulder, CO, USA, July 29, August 3, 1984., Proceedings, p. 247.

13) J. R. Wasson, C. I. Shyr, and C. Trapp, *Inorg. Chem.*, **7**, 469 (1968).

14) J. H. Price, J. R. Pilbrow, K. S. Murray, and T. D. Smith, *J. Chem. Soc., A*, **1970**, 968.

 © 1987 The Chemical Society of Japan Bull. Chem. Soc. Jpn., 60, 2853—2856 (1987)

A New Detection Method of Electromigrating Ions through a Cation-Exchange Membrane

Akihiro KAWAGUCHI,* Shin-ichi MAGAINO, Takashi SUZUKI,† and Yasushi TAKEUCHI††
Industrial Research Institute of Kanagawa Prefecture, 3173 Shouwa, Kanazawa-ku, Yokohama 236
†Department of Applied Chemistry, Yamanashi University, 4 Takeda, Koufu 400
††Department of Industrial Chemistry, Meiji University, 1-1-1 Higashi-mita, Tama-ku, Kawasaki 214
(Received January 20, 1987)

An isotachophoretic analysis and electromigration of ions through a cation-exchange membrane have been investigated. K, Li, Na, and Cu ions were migrated at a constant current. The potential difference between fibrous ion exchanger and cathode reservoir was measured during migration of ion zone. The relative ionic mobility of K^+, Na^+, Li^+, and Cu^{2+} calculated by potential difference was 1, 0.667, 0.420, and 0.218, respectively. The concentration of mobile cations in unit volume of the membrane was calculated by the amount of migration and the migration time of each ion. The concentration of mobile Li^+ in the Li zone was about 10% lower than that of mobile K^+ in the K zone. This difference in concentration is similar to the result by the usual isotachophoresis using a capillary tube. The migration time of each ion zone through detection part was proportional to the amount of migration. K^+ and Li^+ in the concentration range from 0.6×10^{-3} to 0.2 mol dm^{-3} were quantitatively determined by the migration time with reproducible errors less than ±5 %.

The ion-exchange membrane is one of the useful electromigration media for separating ions in isotachophoresis. The ionic mobility in the membrane is different from that in aqueous solution, because ionic mobility is influenced by affinity of the membrane and hydration of the ions. Electromigration using an ion-exchange membrane was reported by Kakihana et al. for separating lithium isotope,[1,2] alkalis,[3] and alkaline earth metals.[4] They described the relationship between electromigration time and electromigration distance at a constant current. For the measurement of migration amount of ions, they used thin membranes and determined ions by means of flame spectrophotometry and mass spectrometry. In a previous paper,[5] the authors have reported a rapid detection method for migrating ions by measuring the potential gradient in the membrane without any sensing electrode on the membrane surface. A more sensitive method, however, is required for the analysis of migrating ions.

In capillary-tube isotachophoresis, platinum electrodes are usually used for potential gradient detectors. Everaerts and Verheggen,[6] and Akiyama and Mizuno[7] reported that bubbles are generated from platinum surface and that the potential gradient fluctuated at high current densities. To prevent these phenomena, they made the electrode surface smooth, and added Triton X-100 or Na_2AsO_4 to electrolyte in the capillary tube.

A redox reaction occurs on platinum surface because of high electronic conductivity. The reaction will be prevented by use of an ionic conductor electrode instead of platinum. The ionic conductivity of ion exchanger has been studied by several workers.[8,9] Although ion exchanger is widely used for electrodialysis,[10,11] fuel cells using solid polymer electrolytes,[12,13] electrolysis,[14] etc., it has not been used for potential gradient measurement in isotachophoresis.

In this study, the authors examined fibrous ion exchanger as a potential gradient detector at high current densities. The fibrous anion exchanger was contacted with cation-exchange membrane as a sensing electrode and the electromigration of K^+, Na^+, Li^+, and Cu^{2+} through membrane was examined. Firstly, the relative ionic mobility was determined in order to detect mobile cation by measuring the potential difference between fibrous anion exchanger and cathode reservoir at a constant current. Secondly, the concentration of mobile cation per unit volume of the membrane was obtained by measuring the amount of migrating ions and the migration time of each ion zone. The relationship between migration time and concentration of sample solution was discussed.

Theoretical

Qualitative Analysis of the Migration Ion. When an ion i migrates in ion-exchange membrane, migration velocity v_{mi}(cm s^{-1}) is the product of potential gradient E_{mi}(V cm^{-1}) and ionic mobility u_{mi} (cm^2 V^{-1} s^{-1}) as

$$v_{mi} = u_{mi}E_{mi}. \quad (1)$$

In isotachophoresis, v_{mi} is a constant. For example, when K^+ and Li^+ are electrically displaced by Cu^{2+} as a terminating ion, we get a formula

$$u_{mK}E_{mK} = u_{mLi}E_{mLi} = u_{mCu}E_{mCu}. \quad (2)$$

When u_{mK} and E_{mK} are defined to be unity, the relative ionic mobility of Li^+ and Cu^{2+} is obtained by the potential gradient

$$u_{mLi} = 1/E_{mLi} \text{ and } u_{mCu} = 1/E_{mCu}. \quad (3)$$

Migration Amount in the Membrane. When ion i migrates from aqueous solution to membrane, the amount of migration A_{mi}(mol) passing through a unit area of interfaces in a unit time is expressed by

$$A_{mi} = v_i c_i/1000, \quad (4)$$

where v_i and c_i are migration velocity in cm s^{-1} and solution concentration in mol dm^{-3}, respectively.

When v_i is proportional to mobility u_i ($cm^2\ V^{-1}\ s^{-1}$) in the solution, the ratio between amounts of migration for Li^+ and K^+ A_{mLi}/A_{mK} is obtained as follows:

$$A_{mLi}/A_{mK} = (u_{Li}/u_K)(c_{Li}/c_K). \quad (5)$$

Concentration of Mobile Cation. From thickness t (cm) and width w (cm) at the detection part of membrane, the concentration of mobile cation c_{mi} (mol dm^{-3}) per unit volume is defined by using migration amount A_{mi} and migration velocity v_m ($cm\ s^{-1}$) by

$$c_{mi} = 1000\,A_{mi}/s_i v_m t w, \quad (6)$$

where s_i (s) is the migration time of i ion zone passed through the center of detection part. The ratio of migration time of K^+ to that of Li^+ is obtained by Eq. 6 as

$$s_{Li}/s_K = (A_{mLi}/A_{mK})/(c_{mLi}/c_{mK}). \quad (7)$$

If A_{mLi}/A_{mK} is unchanged during the migration, s_{Li}/s_K will be constant, because c_{mLi}/c_{mK} is constant in isotachophoresis. Substituting Eq. 5 by Eq. 7, we obtain

$$c_{Li}/c_K = (s_{Li}/s_K)(c_{mLi}/c_{mK})(u_K/u_{Li}). \quad (8)$$

If c_{mLi}/c_{mK} and u_K/u_{Li} remain constant, c_{Li}/c_K will be estimated by measuring s_{Li}/s_K.

Experimental

Electromigration Cell. The symbol c in Fig. 1 indicates the narrowed part of cation-exchange membrane (Selemion CMV). When potential gradient is measured at the narrowed part of membrane, a small amount of migrating ions will be detected. The membrane was washed with 1 mol dm^{-3} NaOH, 1 mol dm^{-3} HCl, and distilled water. The H^+-form membrane was stored in distilled water. Before each run, the membrane was taken out and wiped with filter paper to remove surface water. The membrane was placed on a clean glass plate coated with a small amount of grease. Both ends of the membrane were connected to the bottom edge of each anode and cathode reservoir. A fibrous anion exchanger (Selemion AMV, OH^--form) of 0.02 mm in diameter and 10 mm in length was placed on the membrane at a distance of 1 mm from the cathode reservoir. The membrane was tightly covered with a glass plate coated with grease. The apparatus is shown in Fig. 1.

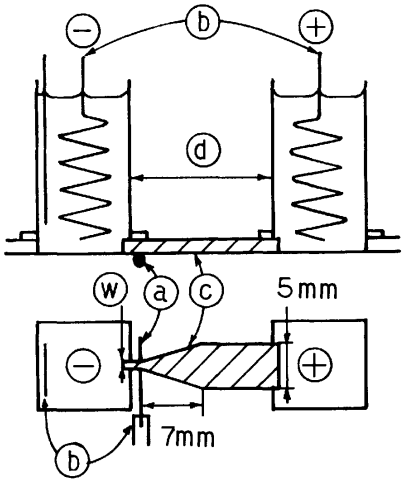

Fig. 1. Cell assemblies.
a; Anion exchange fiber, b; Pt electrode, c; cation-exchange membrane, d; distance of electromigration, w; outlet width (0.60 mm).

Isotachophoretic Separation. Ionic migration was generated by a constant current power source (Toyo PS-1510), which connects to platinum electrodes in cathode and anode reservoirs. The cathode reservoir was filled with 0.5 mol dm^{-3} H_2SO_4 and the anode reservoir with a mixture of KOH and LiOH in the range from 0.6×10^{-3} to 0.2 mol dm^{-3}. In the experiment for separating K^+ and Li^+, the anode reservoir was filled with KOH-LiOH mixture and a constant current of 0.8 mA was applied for 3 min. Then the reservoir solution was replaced by 0.5 mol dm^{-3} $CuSO_4$ to continue the experiment under the same current at room temperature.

Migration Time and Amount of Ion. The fibrous ion exchanger was contacted in series with thin platinum foil and the potential difference between fibrous ion exchanger and cathode reservoir was measured by a high impedance potentiometer (Nichia NP-PM-1). The migration time and potential difference between the fibrous ion exchanger and cathode reservoir were measured. K^+ and Li^+ were allowed to migrate for 3 min under the same current. The membrane was then taken out of the apparatus and K^+ and Li^+ were eluted with 2 mol dm^{-3} HCl. Concentrations of K^+ and Li^+ in HCl were measured by means of flame spectrophotometry.

Results and Discussion

Sensing Electrode. First, a platinum wire of 0.05

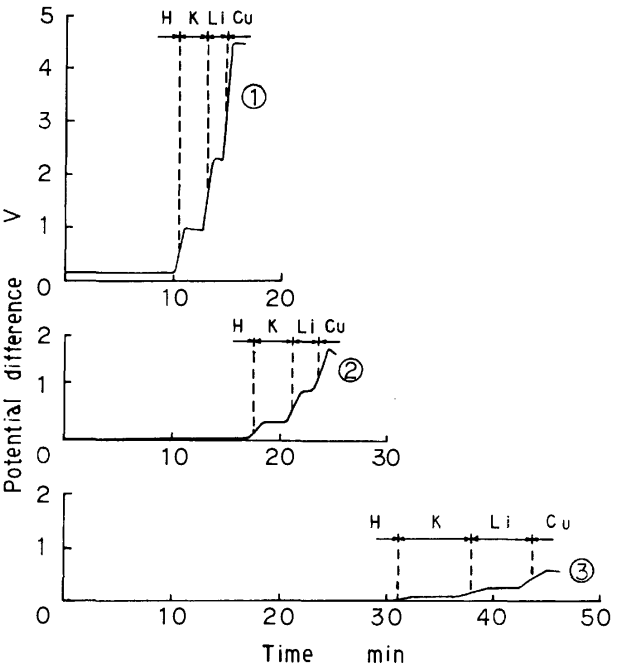

Fig. 2. Electropherograms of K^+ and Li^+. Sample: 0.2 mol dm^{-3} KOH and 0.2 mol dm^{-3} LiOH. Terminal solution: 0.5 mol dm^{-3} $CuSO_4$.

	Current (mA)
①	0.8
②	0.5
③	0.3

Table 1. Relative Mobility of Ions to That of K^+

Ion	K^+	Na^+	Li^+	Cu^{2+}
Ion-exchange membrane[a)]	1.00	0.667	0.420	0.218
Ion-exchange membrane by Hosoe's data[3)]	1.00	0.675	0.431	—
Water soln. infinite dilution[b)]	1.00	0.682	0.526	0.762

a) Obtained in this study. b) From limiting equivalent conductivity at 25 °C.

mm in diameter was used as sensing electrode instead of fibrous anion exchanger. When the potential difference between platinum wire and cathode reservoir was measured, fluctuations were observed in potential curve. Bubbles were simultaneously generated from platinum wire. Moreover, Cu^{2+} passing through the membrane was reduced to black metallic copper on platinum, and black portion grew toward the anode reservoir. This phenomenon shows that a redox reaction occurred on the surface of platinum wire.

On the other hand, when the fibrous anion exchanger was used as a sensing electrode, no redox reaction was observed in the migration. Figure 2 shows typical electropherograms for K^+, Li^+, and Cu^{2+} using fibrous anion exchanger. The first moving boundary between the first zone of H^+ and the second zone of alkali metal ions, the second moving boundary between the second zone of alkali metal ions, and the third zone of Cu^{2+} are sharply recognized during the migration. As shown in Fig. 2, the potential difference between fibrous ion exchanger and cathode reservoir is approximately constant in each zone. When each boundary passed through the detection part, an increase in potential difference was clearly observed. These results are similar to the case of capillary-tube isotachophoresis. It seems that fibrous ion exchanger is a useful medium for detecting potential gradient at high current densities.

Qualitative Analysis. When K^+, Li^+, and Cu^{2+} zones pass through the detection part, the potential difference between fibrous ion exchanger and cathode reservoir is 0.97, 2.31, and 4.44 V, respectively, as shown in① of Fig. 2. The relative value of the potential difference for Na^+, Li^+, and Cu^{2+} to that for K^+ was calculated to be 1.50, 2.38, and 4.58, respectively. Equation 3 indicates that the relative mobility for an ion is the reciprocal of potential value. The calculated relative mobility is given in Table 1. The relative mobility of alkali metals was reported by Hosoe et al.[3)] using a sulfonated cation-exchange membrane. Their values agreed with those obtained in this study within ±3%.

The mobility of Cu^{2+} is considerably lower than that in aqueous solution. It has been mentioned[3,4)] that the ionic mobility in membrane is different from that in aqueous solution, because the mobility is influenced by the affinity of ions with membrane and the hydration of ions. The affinity of membrane with ions increases with the increase in valency of ions.[15)] The relative mobility of Cu^{2+} is, therefore, smaller

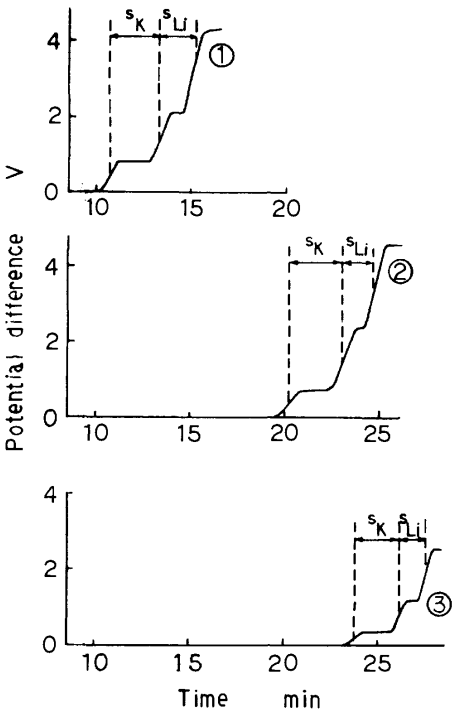

Fig. 3. Effect of the migration distance for the isotachophoretic separation. Sample: 0.2 mol dm^{-3} KOH+0.2 mol dm^{-3} LiOH; 0.8 mA for 3 min. Terminal solution: 0.5 mol dm^{-3} $CuSO_4$; 0.8 mA.

	Migration distance d (mm)
①	10
②	13
③	15

than that of alkali metal ions. It is plausible that migrating ion is identified by the measurement of potential difference in membrane.

Concentration of Mobile Cation. A mixture of each 0.2 mol dm^{-3} KOH and LiOH was put into anode reservoir and a constant current of 0.8 mA was applied, then the solution in reservoir was replaced with 0.5 mol dm^{-3} $CuSO_4$ and migration continued. Figure 3 shows the effect of migration distance for isotachophoretic separation using membranes of 10, 13, and 15 mm in length. The ratio of migration time s_{Li}/s_K was determined to be 0.75, 0.61, and 0.61, respectively. The result indicates that K^+ and Li^+ migrate at a same speed by using membrane longer than 13 mm.

Table 2 gives amounts of migration A_{mK} and A_{mLi} obtained by spectrophotometry when migration current of 0.8 mA was applied for 3 min. The concentration of mobile K^+ and mobile Li^+ in unit volume of membrane was calculated using Eq. 6 and given by c_{mK}

Table 2. A_{mi}, s_i, and c_{mi} for Different Concentration of K^+ and Li^+ at $v_m=6.94\times10^{-3}$ cm s^{-1}, $t=0.0126$ cm, and $w=0.060$ cm

c_K	A_{mK}	s_K	c_{mK}
mol dm^{-3}	μmol	s	mol dm^{-3}
0.06	0.54	105	0.98
0.10	0.92	168	1.04
0.14	1.10	198	1.06
			mean 1.03
c_{Li}	A_{mLi}	s_{Li}	c_{mLi}
mol dm^{-3}	μmol	s	mol dm^{-3}
0.06	0.28	57	0.94
0.10	0.49	102	0.92
0.14	0.70	147	0.91
			mean 0.92

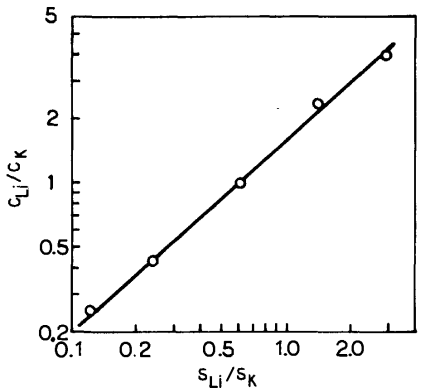

Fig. 4. Relation between c_{Li}/c_K and s_{Li}/s_K. Sample: KOH and LiOH; 0.8 mA for 3 min. Terminal solution; 0.5 mol dm^{-3} $CuSO_4$; 0.8 mA.

and c_{mLi} in Table 2. The mean values of c_{mK} and c_{mLi} were 1.03 and 0.92 mol dm^{-3}, respectively. These values were approximately constant in the range of migration current from 0.3 to 1.0 mA. The concentration of mobile Li^+ in Li^+ zone was about 10% lower than that of mobile K^+ in K^+ zone. This concentration difference is similar to the result in the usual isotachophoresis using a capillary tube.

Quantitative Analysis. Table 3 gives the ratios of A_{mi}, u_i, c_{mi}, and s_i to each value for K^+ for different ratios of concentration c_{Li}/c_K at the same conditions described in Table 2. Using Eq. 5, u_{Li}/u_K was obtained as an approximately constant value of 0.561, independent of A_{mLi}/A_{mK} and c_{Li}/c_K, and it was close to the value of relative ionic mobility in aqueous solution (0.526 at 25 °C). The product of c_{mK}/c_{mLi} multiplied by u_{Li}/u_K is nearly 0.61, then c_{Li}/c_K was obtained from Eq.

Table 3. Relative Values of A_{mi}, u_i, c_{mi}, and s_i for Different c_{Li}/c_K

c_{Li}/c_K	A_{mLi}/A_{mK}	u_{Li}/u_K	c_{mLi}/c_{mK}	s_{Li}/s_K
2.333	1.296	0.556	0.927	1.400
1.000	0.533	0.533	0.880	0.607
0.429	0.255	0.594	0.883	0.288
mean		0.561	0.897	

8 as follows:

$$c_{Li}/c_K=(s_{Li}/s_K)/0.61. \quad (9)$$

Figure 4 shows this relation. The value of c_{Li}/c_K was estimated by use of s_{Li}/s_K in a reproducibility of ±5%. To determine the measurable concentration region of K^+ or Li^+, the migration was investigated in the concentration range of 0.6×10^{-3} to 0.2 mol dm^{-3} KOH and LiOH. In this region, it was confirmed that the concentration of K^+ or Li^+ is estimated by Eq. 9 using s_{Li}/s_K and known concentration of Li^+ or K^+. The limit of detection for K^+ was 0.11 μmol from the electropherogram in this study. The proposed method is more sensitive than the method reported previously.[5]

References

1) H. Kakihana and M. Okamoto, *Nippon Kagaku Zasshi*, **84**, 402 (1963).
2) M. Okamoto and H. Kakihana, *Nippon Kagaku Zasshi*, **88**, 313 (1967).
3) M. Hosoe, H. Kakihana, and C. Tsün, *Nippon Kagaku Kaishi*, **9**, 1421 (1976).
4) M. Hosoe, H. Kashii, and H. Kakihana, *Bunseki Kagaku*, **32**, 530 (1983).
5) A. Kawaguchi, T. Suzuki, and Y. Takeuchi, *Denki Kagaku*, **54**, 366 (1986).
6) F. M. Everaerts and TH. P. E. M. Verheggen, *J. Chromatogr.*, **73**, 193 (1972).
7) J. Akiyama and T. Mizuno, *J. Chromatogr.*, **119**, 605 (1976).
8) J. T. Clarke, J. A. Marinsky, W. Juda, N. W. Rosenberg, and S. Alexander, *J. Phys. Chem.*, **56**, 100 (1952).
9) C. S. Fadley and R. A. Wallace, *J. Electrochem. Soc.*, **115**, 1264 (1968).
10) N. W. Rosenberg and C. E. Tirrell, *Ind. Eng. Chem.*, **49**, 780 (1957).
11) A. Kawaguchi and T. Suzuki, *Denki Kagaku*, **53**, 679 (1985).
12) L. W. Niedrach, *J. Electrochem. Soc.*, **109**, 1092 (1962).
13) R. S. Yeo and J. McBreen, *J. Electrochem. Soc.*, **126**, 1682 (1979).
14) Z. Ogumi, K. Nishio, and S. Yoshizawa, *Denki Kagaku*, **49**, 212 (1981).
15) F. Helfferich, "Ion Exchange," 156 (1962).

 © 1987 The Chemical Society of Japan Bull. Chem. Soc. Jpn., 60, 2857—2860 (1987)

Alkaline Hydrolysis of Inorganic *cyclo*-Polyphosphates

Genichiro KURA
Department of Chemistry, Fukuoka University of Education, Akama, Munakata, Fukuoka 811-41
(Received February 2, 1987)

The hydrolysis rates of inorganic *cyclo*-polyphosphates in alkaline solutions were determined. The rates in a NaOH solution were significantly faster than those in a $(CH_3)_4NOH$ solution. Ion-pair formation between PO^- and Na^+ renders the P atom more positive by reducing the electron density around the atom and more susceptible to the nucleophilic attack by OH^-. In a $(CH_3)_4NOH$ solution, higher-membered *cyclo*-polyphosphates with a larger ring structure became rather stable. Arrhenius' activation energy for each phosphate decreases in the order $HCl>NaOH>(CH_3)_4NOH$.

As the major compounds of the condensed phosphates produced by the dehydration of the oxoacid of phosphorus oxidation number 5, linear phosphates with linear chain structure and *cyclo*-polyphosphates with cyclic structure consisting of middle P-O-P bond have been well-known.[1] In these condensed phosphates, the chemical properties of linear phosphates with shorter chain length, especially those of di- and triphosphate have been extensively investigated in connection with ADP and ATP, both of which are biochemically important.

In the *cyclo*-polyphosphate series, *cyclo*-tri- and *cyclo*-tetraphosphates have been prepared since earlier time, and the chemical properties have extensively been studied.[1] As in the case of linear phosphates with a polymerization degree larger than four, the investigation about *cyclo*-polyphosphates above pentamer with a ten-membered ring structure has been hindered by the difficulty involved in their preparation or isolation. Since the preparation of *cyclo*-hexa- and *cyclo*-octaphosphate were reported by Griffith and Buxton,[2] and by Schülke,[3] respectively, we have investigated various properties of these higher-memberted *cyclo*-polyphosphates.[4-13]

cyclo-Polyphosphates of the general formula $M^I_n(PO_3)_n$ have a high negative charge on their relatively compact molecule and hence they can be utilized as important electrolytes in aqueous solutions since the anion is very weak as a Brønsted base. These *cyclo*-polyphosphates are very stable in a neutral aqueous solution even if they are boiled up to one hour.

However, in strong acidic or basic solutions, they are easily hydrolyzed and their hydrolysis rate is accelerated, especially by hydrogen ions.[13] Their hydrolysis rate in the alkaline solutions has not been elucidated as systematically as in acidic solutions. We predicted that *cyclo*-polyphosphates in alkaline solution would be hydrolyzed more slowly than in strong acidic conditions. Alkaline hydrolysis of *cyclo*-tetraphosphate was employed for the preparation of linear tetraphosphate.[14-17] In this regard, it is important to clarify the alkaline hydrolysis of *cyclo*-hexa- and *cyclo*-octaphosphate. Hydrolysis data on *cyclo*-penta- and *cyclo*-heptaphosphate could not be obtained since the isolation of both phosphates in sufficient quantity is difficult.[4,8]

Experimental

Materials. Sodium salts of *cyclo*-polyphosphates were prepared by the methods described in the literature.[2,3,18,19] Their purities were checked by an analytical system applied to the analysis of the hydrolysis products.[13]

A tetramethylammonium hydroxide solution was prepared by treating the chloride with an anion-exchange resin of the OH^- form.

All other chemicals used were reagent grade and commercially available.

Analytical System. The separation of *cyclo*-polyphosphates to be hydrolyzed from linear phosphates as hydrolysis products was achieved by an anion-exchange chromatography. As an anion exchanger, TSK Gel SAX 10 μm was used; column dimensions were 4 mm in diameter and 250 mm in height. As an eluting agent, 0.4 mol dm^{-3} KCl of pH 10.2 (plus 0.1% EDTA) was used. The phosphates in the effluent were automatically determined by spectrophotometry with the use of a Mo(V)-Mo(VI) reagent.[11]

Futher details on the analytical system are described in the references.[11-13]

Procedure. The initial concentration of each *cyclo*-polyphosphate to be hydrolyzed was adjusted to 1.25×10^{-3} mol dm^{-3} and the hydrolysis reaction was performed in a water bath, the temperature of which was maintained within ±0.1 °C. At measured time intervals, samples were withdrawn and neutralized with the same equivalents of hydrochloric acid, and stored in a refrigerator until taken out for analysis.

Results and Discussion

Hydrolysis rates of four *cyclo*-polyphosphates in 0.25, 0.5, 0.75, and 1 mol dm^{-3} NaOH solutions at 50 °C were determined by the liquid chromatography. If $[P]_0$ and $[P]_t$ denote the concentration of the phosphate at time zero and t, respectively, log $([P]_t/[P]_0)$ versus t plots for *cyclo*-octaphosphate hydrolysis are shown in Fig. 1 and in each case the rates are first order for the phosphate as

$$-\frac{dc}{dt} = k_{obsd}c, \quad (1)$$

where c is the total concentration of the phosphate. Since the hydrolysis rate is also a function of the OH^-

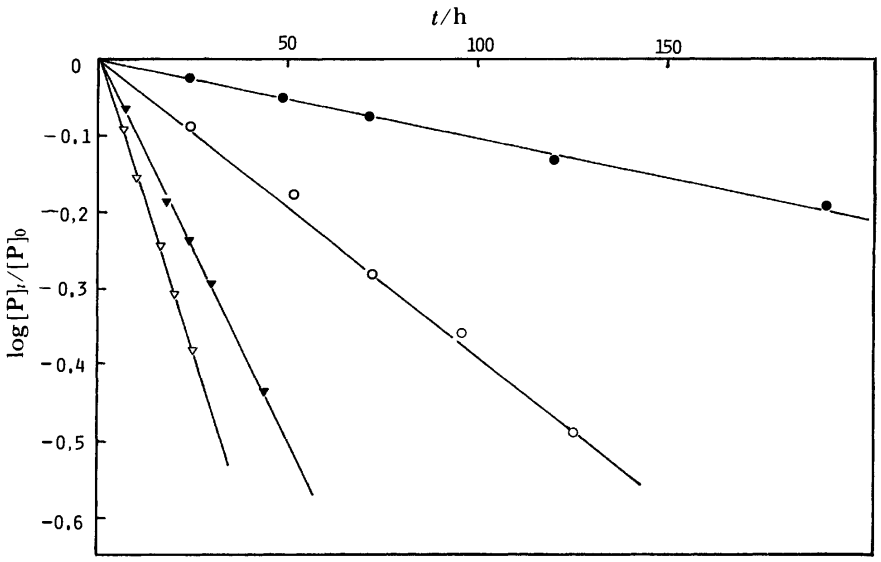

Fig. 1. Hydrolysis rates of *cyclo*-octaphosphate at different NaOH concentrations at 50°C. ●; 0.25 mol dm^{-3}, ○; 0.5 mol dm^{-3}, ▼; 0.75 mol dm^{-3}, ▽; 1 mol dm^{-3}.

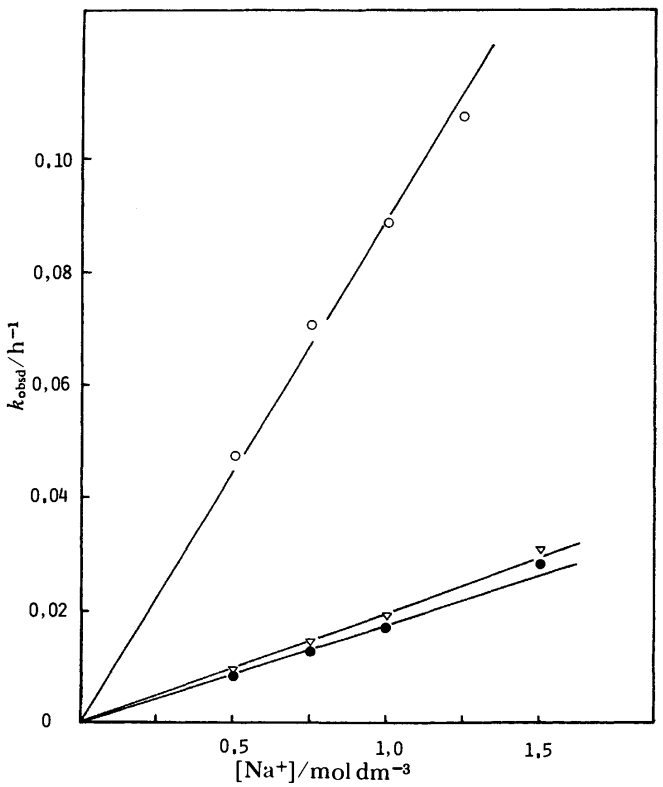

Fig. 2. Plots of the rate constants of *cyclo*-polyphosphates at 50°C against sodium ion concentration ([OH$^-$]≒0.5 mol dm^{-3}). ○; P_{4m}, ●; P_{6m}, ▽; P_{8m}.

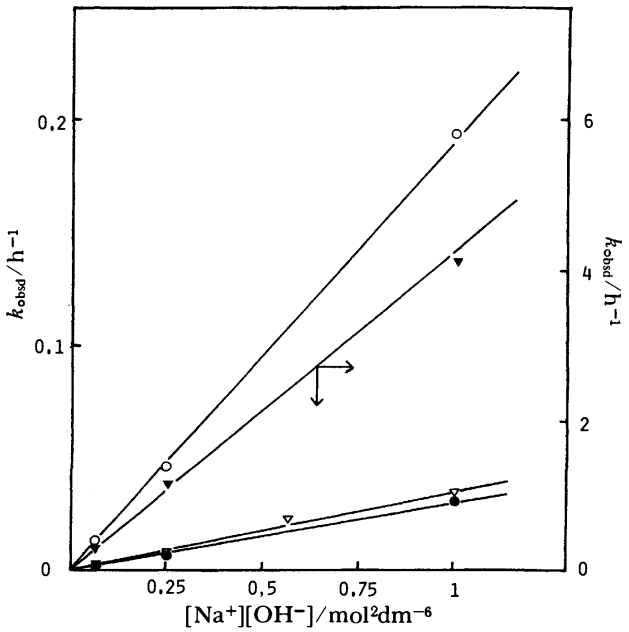

Fig. 3. Plots of the rate constants of *cyclo*-polyphosphates at 50°C against the product of sodium ion and hydroxide ion concentration. ▼; P_{3m}, ○; P_{4m}, ●; P_{6m}, ▽; P_{8m}.

ion concentration, k_{obsd} can be written as $k[OH^-]^n$.

The hydrolysis rate was also measured at a constant hydroxide ion concentration ([OH$^-$]=0.5 mol dm^{-3}) by changing the sodium ion concentration by adding sodium chloride. As shown in Fig. 2, k_{obsd} changed in proportion to [Na$^+$]. From the above fact and the results of the hydrolysis rates at various sodium hydroxide concentration shown in Fig.3, the hydrolysis rate in NaOH solutions can be presented as Eq. 2. Sodium ions directly affect the hydrolysis rate in NaOH solutions.

$$-\frac{dc}{dt} = k[Na^+][OH^-]c \qquad (2)$$

It has been shown[3-5,8] that *cyclo*-polyphosphate anions having such high negative charge form complexes (or ion-pairs) with various cations. The ion-pair formation of PO$^-$ and Na$^+$ renders the phospho-

rus atom more positive by reducing the electron density around the P atom and more susceptible to the nucleophilic attack by OH^- in a similar manner at the acidic conditions.[13]

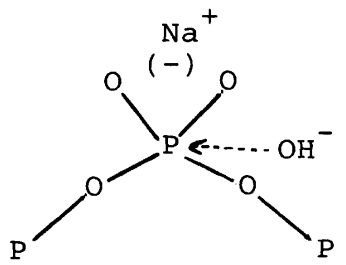

For a comparison with acidic conditions, the activation energy of *cyclo*-octaphosphate hydrolysis in a 0.5 mol dm^{-3} NaOH solution was determined. An Arrhenius' plot is shown in Fig. 4. The activation energy of 82.8±0.3 kJ mol^{-1} is slightly lower than the value of 96.7±0.3 kJ mol^{-1} in a 0.1 mol dm^{-3} HCl solution.[13]

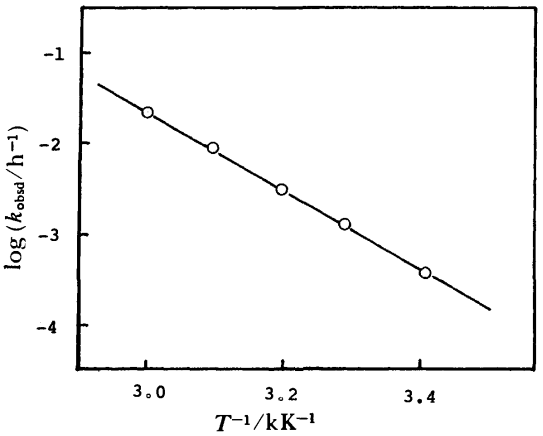

Fig. 4. Arrhenius' plots for *cyclo*-octaphosphate hydrolysis in 0.5 mol dm^{-3} NaOH solution.

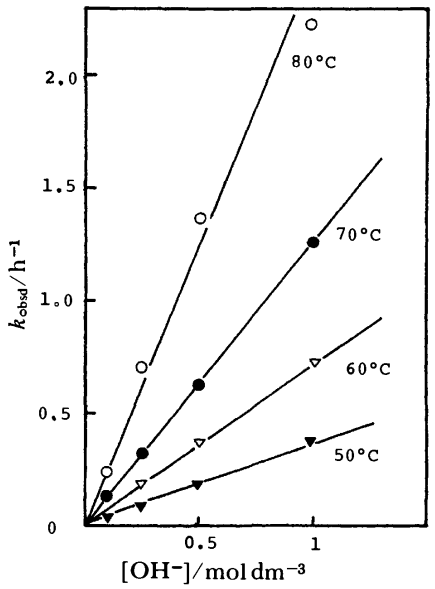

Fig. 5. Plots of the rate constant of *cyclo*-triphosphate at different temperatures and at different tetramethylammonium hydroxide concentrations.

The hydrolysis rates in tetramethylammonium hydroxide solutions were also determined. The hydroxide dose not contain a cation which interacts with *cyclo*-polyphosphate anions. Hydrolysis rates were also first-order for *cyclo*-polyphosphates. Reaction rates of *cyclo*-triphosphate at various hydroxide concentrations and various temperatures are shown in Fig. 5. At each temperature, k_{obsd} varied proportionally with [OH^-]. This suggests that the hydrolysis reaction in alkaline solutions in the absence of any cations which might interact with *cyclo*-polyphosphate anions is caused by the nucleophilic attack of OH^- on P atom in the phosphate tetrahedra. Similar results were obtained for *cyclo*-tetraphosphate hydrolysis. The rate constants in 0.5 and 1.0 mol dm^{-3} $(CH_3)_4NOH$ solutions at various temperatures are shown in Fig. 6. At each temperature, k_{obsd} in a 1.0 mol dm^{-3} $(CH_3)_4NOH$ solution was twice that in a 0.5 mol dm^{-3} $(CH_3)_4NOH$ solution. The activation energy of *cyclo*-tetraphosphate was 75.3±1.8 kJ mol^{-1} regardless of $(CH_3)_4NOH$ concentration. Analogously, that of *cyclo*-triphosphate was 62.8±0.8 kJ mol^{-1}. These values were lower than those in NaOH solutions and a 0.1 mol dm^{-3} HCl solution. However, a large discrepancy between them was not observed.

Since higher-membered *cyclo*-hexa- and *cyclo*-octaphosphates with a larger ring structure were not hydrolyzed very much, even if at higher $(CH_3)_4NOH$ concentrations and at higher temperatures, detailed data on their hydrolysis rate at various conditions were not obtained on the contrary to the case of *cyclo*-tri- and *cyclo*-tetraphosphate hydrolysis.

In Fig. 7, the rate constants of each *cyclo*-polyphosphate in 0.5 mol dm^{-3} $(CH_3)_4NOH$, 0.5 mol dm^{-3} NaOH and 0.1 mol dm^{-3} HCl solutions are shown for comparison. Each *cyclo*-polyphosphate is most rapid-

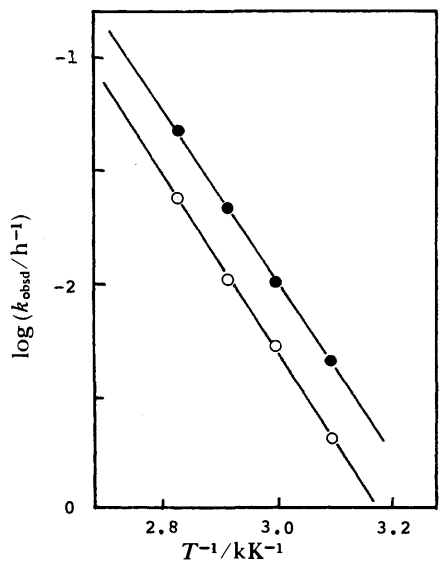

Fig. 6. Arrhenius' plots for *cyclo*-tetraphosphate hydrolysis in 0.5 and 1 mol dm^{-3} $(CH_3)_4NOH$ solution. ●; 1 mol dm^{-3}, ○; 0.5 mol dm^{-3}.

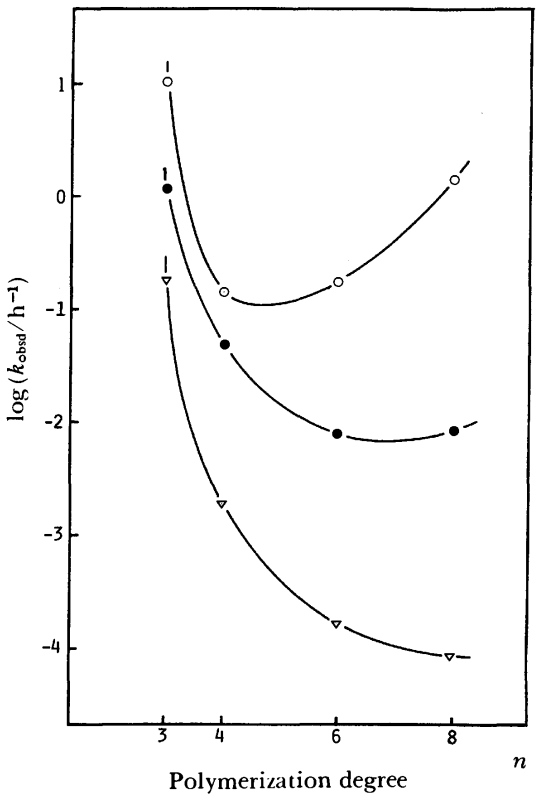

Fig. 7. Variation of the rate constants with the polymerization degree for the *cyclo*-polyphosphates hydrolysis at 50°C. O; 0.1 mol dm^{-3} HCl, ●; 0.5 mol dm^{-3} NaOH, ▽; 0.5 mol dm^{-3} $(CH_3)_4NOH$.

ly hydrolyzed in a 0.1 mol dm^{-3} HCl solution. In a $(CH_3)_4NOH$ solution where there are no cations which might interact with *cyclo*-polyphosphate anions, higher-membered *cyclo*-polyphosphates become extremely stable even at higher OH^- ion concentrations and temperatures.

In NaOH solutions, the interaction of sodium ions with the phosphate anions accelerates the hydrolysis rate. This tendency is more pronounced for *cyclo*-octaphosphate which has the highest flexibility.

The obtained results can be summarized as follows. The hydrolysis rate in alkaline solutions is affected not only by the hydroxide ion concentration but also, more strongly, by the presence of cations. The hydrolysis rates in NaOH solutions were significantly faster than those in $(CH_3)_4NOH$ solutions. This tendency is stronger in the case of higher-membered *cyclo*-polyphosphates. The acceleration of the rate is considered to be due to ion-pair formations between sodium ions and *cyclo*-polyphosphate anions. The activation energy decreases in the order of HCl (0.1 mol dm^{-3})> NaOH>$(CH_3)_4NOH$, but great discrepancies were not observed.

This research was supported in part by a Grant-in-Aid for Scientific Research No. 59540394 from the ministry of Education, Science and Culture.

References

1) J. R. Van Wazer, "Phosphorus and Its Compounds," Interscience, New York (1958).
2) E. J. Griffith and R. L. Buxton, *Inorg. Chem.*, **4**, 549 (1965).
3) U. Schülke, *Z. Anorg. Allg. Chem.*, **360**, 231 (1968).
4) G. Kura and S. Ohashi, *J. Chromatogr.*, **56**, 111 (1971).
5) G. Kura and S. Ohashi, *J. Inorg. Nucl. Chem.*, **34**, 3899 (1972).
6) G. Kura and S. Ohashi, *J. Inorg. Nucl. Chem.*, **36**, 1605 (1974).
7) G. Kura and S. Ohashi, *J. Inorg. Nucl. Chem.*, **38**, 1151 (1976).
8) S. Ohashi, G. Kura, Y. Shimada, and M. Hara, *J. Inorg. Nucl. Chem.*, **39**, 1513 (1977).
9) M. Koganemaru, H. Waki, S. Ohashi, and G. Kura, *J. Inorg. Nucl. Chem.*, **41**, 1457 (1979).
10) G. Kura, *J. Chromatogr.*, **211**, 87 (1981).
11) G. Kura, T. Nakashima, and F. Oshima, *J. Chromatogr.*, **219**, 385 (1981).
12) G. Kura, *J. Chromatogr.*, **246**, 73 (1982).
13) G. Kura, *Bull. Chem. Soc. Jpn.*, **56**, 3769 (1983).
14) E. Thilo and R. Rätz, *Z. Anorg. Allg. Chem.*, **260**, 255 (1949).
15) A. E. R. Westman and A. E. Scott, *Nature (London)*, **168**, 740 (1951).
16) O. T. Quimby, *J. Phys. Chem.*, **58**, 603 (1954).
17) J. I. Watters, P. E. Sturrock, and R. E. Simonaitis, *Inorg. Chem.*, **2**, 765 (1963).
18) R. N. Bell, *Inorg. Syn.*, **3**, 103 (1950).
19) K. R. Andress, W. Gehring, and K. Fisher, *Z. Anorg. Allg. Chem.*, **260**, 331 (1949).

Properties of Alkali-Free Lead Phosphate Glasses as an Ion-Selective Electrode and Their Application to a Potentiometric Detector for Ion Chromatography

Tsuyoshi NOMURA* and Genkichi NAKAGAWA
Department of Materials Science and Engineering, Nagoya Institute of Technology, Gokiso-cho, Showa-ku, Nagoya 466
(Received February 23, 1987)

The properties of alkali-free lead phosphate glasses containing silver oxide as an anion selective electrode were examined, and their application to a potentiometric detector for an ion chromatographic technique were developed. The series of these glasses are characterized by their low softening temperature and are only responsive to anionic substances. The featureless potential response of almost anions tested becomes a rather useful property as a detector for an ion chromatographic analysis of anions. The response characteristics and selectivity coefficients revealed that the glass composition of $10Ag_2O:55P_2O_5:25PbO:10Al_2O_3$ is the most suitable electrode materisl for anion chromatography. With this glass electrode, nonsuppressed anion chromatographic parameters were studied, including a comparison of an eluent composition, the flow rate and the retention time. This detector could be used in a high pH eluent without any interference of the large blank value. In paticular, the detector was highly sensitive to iodide ions. This may be due to the interaction of iodide ions with silver ions which are involved in membrane materials.

Ion-selective electrodes are versatile devices for the continuous monitoring of a wide range of processes and reactions such as titrations, industrial processes, enzyme reaction, flow injection analyses, and high-performance liquid chromatography.

It is well-known that various types of the ion-selective glass electrodes such as alkali silicate glasses,[1] chalcogenide glasses[2] and phosphate glasses[3,4] are available. All alkali-silicate and chalcogenide glasses have been utilized for measurements of cationic substances. On the other hand, it has been suggested that the replacement of aluminium in the sodium alminosilicate glasses by phosphorus can be expected to lead to anion-exchanger properties.[5] Since we had already investigated some phosphate glass membrane as materials of the nitrate ion selective electrode,[6] their alkali-free phosphate glass electrodes were characterized by their anion responsive properties.

Ion chromatography is a very effective method for the analysis of many common anions using an electrochemical detector[7,8] or a UV absorbance detector.[9] Electrochemical detection of inorganic anions by potentiometry, amperometry, or coulometry is generally applied to a restricted number of cases, but can exhibit a greater sensitivity than a conductivity detector. Nonsuppressed ion chromatographic techniques with TSK Gel IC Anion SW as an anion-exchanger column have been successful in a variety of applications.[10]

In this investigation, the physical and chemical characteristics of alkali-free lead phosphate glasses were measured, and a systematic check of the potential response and selectivity coefficients on the glass composition were performed; also, their applicability for an anion selective glass electrodes were examined. Moreover, the potentiometric detector based on the alkali-free lead phosphate glass electrode was constructed and utilized in order to determine various anions by the ion chromstographic technique.

Experimental

Preparation of the Glass Membrane. In order to obtain electrode glasses, the following analytical reagent grades were used: orthophosphoric acid (85%), silver carbonate, lead carbonate, and aluminium hydroxide. The preparation procedures of the phosphate glasses and the glass membranes have been described previously.[11] The chemical compositions of some of the tested glasses are listed in Table 1.

Measurements of physical and chemical properties and membrane potentials have been described previously.[6] The physical and chemical properties of some of the lead phosphate glasses containing Ag_2O and Al_2O_3 are summarized in Table 2.

Reagents and Solutions. Stock solutions were prepared by dissolving the reagent of KF, NaCl, $NaNO_3$, $NaNO_2$, Na_2SO_4, KBr, KI, $Na_2S_2O_3$, Na_2SO_3, $NaClO_4$, $NaBrO_3$, and $NaClO_3$ in twice-distilled water. Sodium tartrate eluents were prepared from the reagent grade tartaric acid in concentration ranging from 2×10^{-4} to 5×10^{-3} mol dm^{-3}; in general the eluents were buffered with sodium hydroxide. Citrate eluents with a pH range of 4.3 to 8.0 were prepared from sodium salt.

Chromatographic Procedure. Figure 1 shows a cross-sectional view of the flow-through type potentiometric detector, which consists of a combination of ion-selective

Table 1. Composition of the Glasses

Glass No.	Ag_2O	P_2O_5	PbO	Al_2O_3
1	—	55	35	10
2	5	48	37	10
3	5	50	35	10
4	5	55	30	10
5	10	48	32	10
6	10	50	30	10
7	10	55	25	10
8	15	48	27	10
9	15	55	20	10

Table 2. Physical and Chemical Properties of the Glasses

Glass No.	Transition temperature T_g/°C	Softening temperature T_s/°C	Thermal expansion $\alpha\times10^7$/cm °C^{-1}	Chemical durability mg mm^{-2}	Membrane resistance MΩ cm^{-1}
1	433	506	102.4	8.96×10^{-4}	37.6
2	426	512	107.3	3.14×10^{-4}	53.8
3	—	—	—	—	21.9
4	447	536	118.1	7.78×10^{-4}	24.4
5	421	485	109.7	1.01×10^{-3}	13.7
6	—	—	—	—	36.7
7	506	567	113.4	1.65×10^{-3}	29.6
8	474	528	136.5	1.05×10^{-3}	32.6
9	493	552	120.6	1.46×10^{-3}	39.2

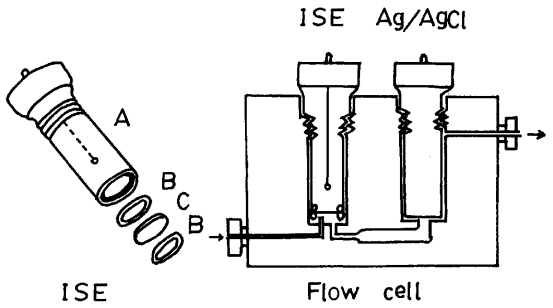

Fig. 1. Structure of ion-selective electrode and a cross section of flow cell. A: Ag/AgCl electrode; B: silicone rubber O-ring; C: glass membrane.

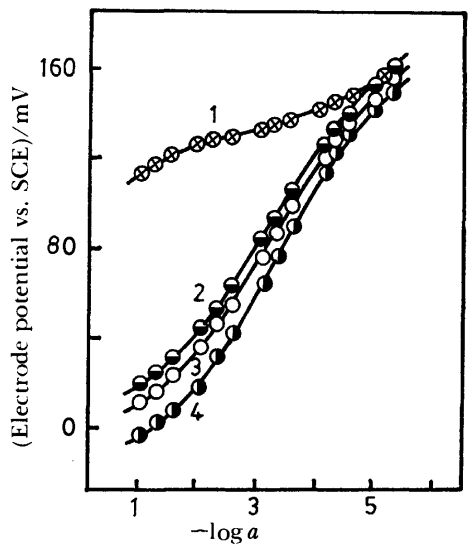

Fig. 2. Electrode response of No. 7 glass membrane electrode as a function of several ion activities. 1: SO_4^{2-}; 2: Cl^-; 3: NO_3^-; 4: I^-.

glass electrodes and an Ag/AgCl reference electrode, both with a direct internal contact.

The ion-selective electrode used consists of a lead phosphate glass working electrode of disks 8.0 mm in diameter and 0.4—0.6 mm thick tightened between a plastic detector body and an Ag/AgCl reference electrode with a silicone rubber O-ring on both sides. The detector cell, which has been developed for flow injection analyses by DKK Co., was used for this purpose with some improvements: a flow path diameter was thinned down by filling in the path way with ID 0.25 mm SUS pipe.

The chromatographic system employed comprised a Toyo Soda Co. HLC-803D pump, a 2 μm pore sintered ceramic filter, a TSK IC-A guard column, a TSK Gel IC Anion PW or SW anion-separator column, a DKK Co. ion-selective flow cell, a DKK COM-20 pH meter, and a Sekonic model SS-250F recorder. Unless otherwise specified, the injector sample loop volume was 100 mm^3, and samples of 1.0 cm^3 were introduced with a Hamilton syringe. The eluent flow rate was 1.0 cm^3 min^{-1}. A 0.1 mol dm^{-3} sodium citrate solution was used for column regeneration before the injection of a sample. The measurement temperature was maintained at 25±1 °C.

Results and Discussion

Physical and Chemical Properties of Glasses. As shown in Table 2, the values of T_g and T_s of the tested glasses were considerably lower than those of the other phosphate glasses.[6] This may be due to the addition of lead oxide instead of magnesium oxide in the glass compositions. Although the membrane resistance increased only slightly, the chemical durability of the tested glasses were better than the magnesium phosphate glasses.

Potential Response of the Lead Phosphate Glasses. The potential response curves of some of the alkali-free lead phosphate glass membranes (No. 7) for various anions are shown in Fig. 2. All the glasses investigated were sensitive to anions, except for sulfate, sulfide and thiosulfate ions. It is apparent that the potential response of the common anions examined were featureless to each others and gave calibration slopes of 45—50 mV per decade, except for iodide ions. It is a rather useful property for the potentiometric detector of ion chromatograph. However, iodide ions show a sensitive electrode response; the slope was at about 58 mV in the concentration range of 5×10^{-2} to 10^{-5} mol dm^{-3} of iodide ion and the analytical range was 10^{-1} to 10^{-6} mol dm^{-3}.

The potential response of several anions for all tested lead phosphate glass electrodes are listed in Table 3.

The response characteristics of the tested glass membranes depended upon its glass composition. In particular, glasses that do not contain Ag_2O show a small electrode response and an unsatisfactory poten-

Table 3. Electrode Function of Several Anions

Glass No.	NO_3^-	Cl^-	I^-	ClO_4^-	SO_4^{2-}
1	30.1	21.8	35.2	28.2	5.5
2	45.9	38.0	46.2	39.3	8.8
3	43.3	—	51.2	36.8	13.9
4	48.3	45.2	52.3	46.6	6.3
5	46.5	35.8	47.6	34.2	7.3
6	44.6	41.7	49.2	44.5	8.2
7	50.2	46.7	58.2	48.9	8.6
8	41.5	40.7	48.2	43.5	6.0
9	47.0	43.5	48.9	42.8	7.8

The numerical value shows a potential response of mV per decade.

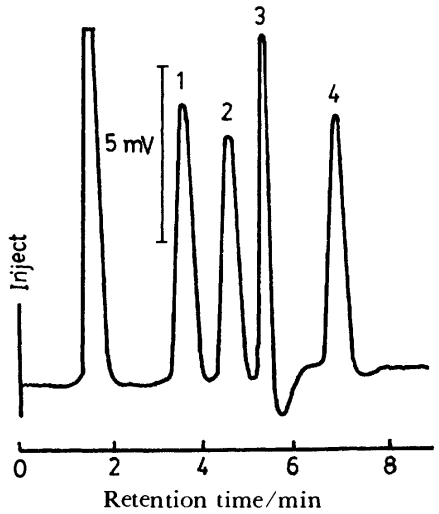

Fig. 3. Ion chromatogram of 4 anions with TSK Gel IC Anion SW column. Eluent: 0.5 mmol dm^{-3} sodium tartrate (pH 6.34), 1: 15 μg mm^{-3} Cl^-; 2: 20 μg mm^{-3} NO_3^-; 3: 2 μg mm^{-3} I^-; 4: 30 μg mm^{-3} ClO_4^-.

tial reproducibility. Moreover, it was observed that the response rate of the glasses with a lower P_2O_5 content (48 mol%) was rather worse than that of the higher P_2O_5 content glasses (55 mol%). This fact suggests that the ultraphosphate glasses corresponding to the branched structure seem to be more structurally useful than the polyphosphate glasses corresponding to the chain structure.

As the results of the potential response of various lead phosphate glass electrodes, the 10 Ag_2O:55 P_2O_5:25 PbO:10 Al_2O_3 glass membrane was concluded to be best in terms of the response speed, reproducibility of potential, and sensitivity of the electrode response for the determination of various anions.

Application of Lead Phosphate Glass Membrane Eectrode for the Potentiometric Detector of Ion Chromatography. The separation of 4 anions with TSK Gel IC Anion SW column using 0.5 mmol dm^{-3} sodium tartrate eluent is shown in Fig. 3.

Peaks of chloride, nitrate, iodide, and perchlorate ion appeared with very good separation. Sulfate, sulfide, and thiosulfate ion produce a small peak, and are unsuitable. The sensitivity of iodide ion is much

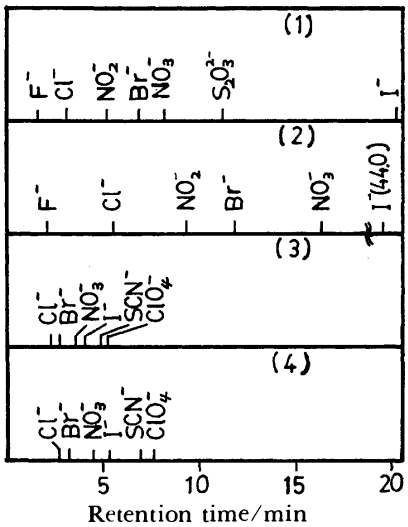

Fig. 4. Comparison of separation column. 1,2: TSK Gel IC Anion PW column; 3,4: TSK Gel IC Anion SW column; 1,3: 0.5 mmol dm^{-3} sodium citrate eluent (pH 6.80); 2,4: 0.5 mmol dm^{-3} sodium tartrate eluent (pH 6.34).

higher than the other anions.

As shown in Fig. 3, a negative dip was observed at the end of the iodide ion peak. It increases with a decrease in the pH of the eluent, and with an increase in the iodide concentration. A negative dip peak signal similar to the present case has been reported when using an iodide selective electrode as the potentiometric detector of ion chromatography.[12] In the present experiment, even if the recorder was operated at much faster chart speed, the elution curve of iodide ion was not splited into its positive and negative parts.

Comparison of the Anion-Exchanger Column. Figure 4 lists the retention times of selected anions using both the TSK Gel IC Anion PW and SW as the separation column, and sodium citrate and sodium tartrate as the eluents. Anions such as chloride, nitrate, nitrite, and bromide show rather small changes in the order of the retention time from one eluent to another. However, iodide shows considerable variations between two columns, changing from a retention time of 5.16 min for SW to 44.0 min for PW wi 0.5 mmol dm^{-3} sodium tartrate eluent. It was considered that a large lag of the retention time of iodide ion with PW column is caused by a characteristics of hydrophobic group anions such as iodide, perchlorate, and thiocyanate.[10]

Effect of Retention Time on the pH and the Concentration of Eluent. The equilibrium reaction for anions exchanging on a strong base anion exchanger is expressed as

$$xA^{-y} + yB\text{-}R_x \rightleftarrows yB^{-x} + xA\text{-}R_y, \quad (1)$$

where R represents the anion exchanger, A and B are competing anions, and y and x are the charge of the anion in the sample solution and the eluent, respectively.

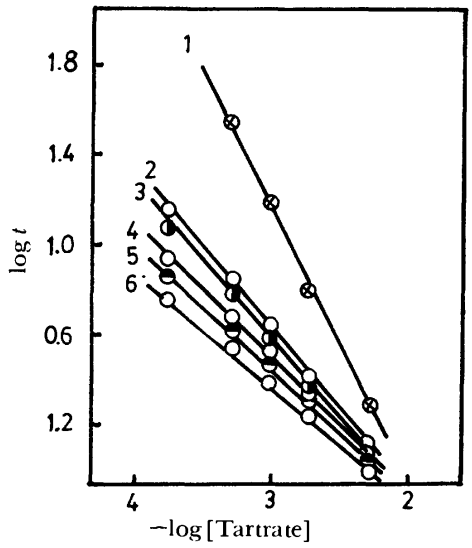

Fig. 5. Effect of eluent concentration on the retention time. TSK Gel IC Anion SW column, sodium tartrate eluent (pH 6.0—6.5), 1: $S_2O_3^{2-}$, 2: ClO_4^-, 3: SCN^-, 4: I^-, 5: NO_3^-, 6: Cl^-.

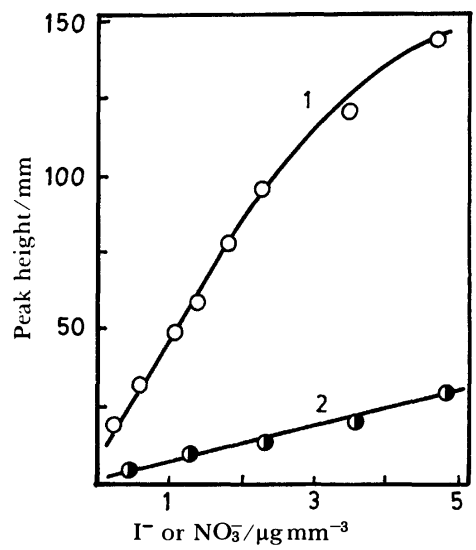

Fig. 6. Calibration curves of nitrate and iodide ion. TSK Gel IC Anion SW column, 0.5 mmol dm^{-3} sodium tartrate eluent (pH 6.34), 1: iodide ion; 2: nitrate ion.

From a consideration of the retention time, t, and the eluent concentration, [eluent], Eq. 2 can be obtained:[13]

$$\log t = \frac{-y}{x} \log [\text{eluent}] - \text{constant.} \quad (2)$$

This shows that a change in the logarithm of the eluent concentration versus the logarithm of the retention time will have the straight line relationship with the slope of $-y/x$, which varies with the charge of the anions involved.

Figure 5 show the relation of the retention time and the concentration of sodium tartrate eluent for the TSK Gel IC Anion SW column. All anions show a straight line. The slopes of the perchlorate and thiocyanate ions are close to the theoretical value of -1, but the slopes of most of the monovalent anions are lower than the predicted values. Sulfate, sulfite, and thiosulfate have a slope of approximately -1.6.

The effect of the pH of the eluent on the retention time, using 0.5 mmol dm^{-3} sodium citrate as the eluent, was examined and revealed that the lower pH of the eluent below about 6.5 caused the larger difference of the retention time. However, the retention time remained almost constant for an eluent with a pH above 6.5.

Sensitivity of Various Anions and the Determination of Iodide Ion. As is shown in Fig. 4, the retention time of anions remains fixed in terms of the species of eluent, the pH of the eluent and the characteristics of anion-exchanger column.

By using the lead phosphate glass membrane as a potentiometric detector and the TSK Gel IC Anion SW as an anion-exchanger column, calibration curves of nitrate and iodide ion were examined; the results are shown in Fig. 6.

With a 100 mm^3 injection loop and 0.5 mmol dm^{-3} sodium tartrate at pH 6.34 as an eluent, calibration curves of the peak hight as a function of these concentration are almost linear at concentrations from 0.5 to 30 μg cm^{-3} for nitrate ion and from 0.1 to 5 μg cm^{-3} for iodide ion. The detection limit for nitrate and iodide are 0.2 and 0.05 μg cm^{-3}, respectively. The detection limit of iodide ions reported here is approximately several times lower than those reported with the use of the conductivity detector.[10]

References

1) H. Freiser, "Ion-selective Electrodes in Analytical Chemistry," Plenum Press, New York (1980), p. 213.

2) Yu. G. Vlasov, E. A. Bychkov, and A. V. Legin, 4th Symposium on Ion-selective Electrodes, Matrafured, 657 (1984).

3) A. H. Truesdell and A. M. Pommer, *Science*, **142**, 1292 (1963).

4) V. S. Bobrov, I. P. Kalmkova, and M. M. Shul'ts, *Zh. Prikl. Khim.*, **40**, 1628 (1967).

5) G. Eisenman, *Biophys. J., Part 2 Suppl.*, **1962**, 259.

6) T. Nomura and G. Nakagawa, *Bull. Chem. Soc. Jpn.*, **57**, 1491 (1984).

7) K. Suzuki, H. Aruga, H. Ishiwada, T. Oshima, H. Inoue, and T. Shirai, *Bunseki Kagaku*, **32**, 585 (1983).

8) P. R. Haddad and A. L. Heckenberg, *J. Chromatogr.*, **300**, 357 (1984).

9) H. Small and T. E. Miller, Jr., *Anal. Chem.*, **54**, 462 (1982).

10) S. Matsushita, Y. Tada, K. Komiya, and A. Ono, *Bunseki Kagaku*, **32**, 562 (1983).

11) T. Nomura and G. Nakagawa, *Bull. Chem. Soc. Jpn.*, **56**, 3632 (1983).

12) E. C. V. Butler and R. M. Gershey, *Anal. Chim. Acta*, **164**, 153 (1984).

13) D. T. Gjerde, G. Schmuckler, and J. S. Fritz, *J. Chromatogr.*, **187**, 35 (1980).

 © 1987 The Chemical Society of Japan Bull. Chem. Soc. Jpn., 60, 2865—2869 (1987)

A Calorimetric Study of Ternary Zinc(II) Complexes with Chloride Ions and 2,2′-Bipyridyl in *N,N*-Dimethylformamide

Shin-ichi Ishiguro,* László Nagy,§ and Hitoshi Ohtaki†
Coordination Chemistry Laboratories, Institute for Molecular Science, Myodaiji, Okazaki 444
†Department of Electronic Chemistry, Tokyo Institute of Technology at Nagatsuta, Nagatsuta, Midori-ku, Yokohama 227
(Received March 5, 1987)

Formation equilibria of ternary zinc(II) complexes with chloride ions and 2,2′-bipyridyl (bpy) have been calorimetrically studied in *N,N*-dimethylformamide (DMF) containing 0.4 mol dm^{-3} $(C_2H_5)_4NClO_4$ as a constant ionic medium at 25 °C. Formation of binary (2,2′-bipyridyl)zinc(II) complexes has also been explored. The calorimetric data were satisfactorily explained in terms of formation of the ternary $[ZnCl(bpy)]^+$ and $[ZnCl_2(bpy)]$ complexes together with the binary $[Zn(bpy)_n]^{2+}$ (n=1—3) ones, and their formation constants and enthalpies were determined. The formation of the ternary $[ZnCl(bpy)]^+$ and $[ZnCl_2(bpy)]$ complexes is not so favorable in DMF. It is suggested that both $[ZnCl(bpy)]^+$ and $[ZnCl_2(bpy)]$ complexes have the four-coordinate tetrahedral structure in DMF.

Complexation of zinc(II) ion with 2,2′-bipyridyl (bpy) has so far been studied in aqueous solution and the formation of mononuclear $[Zn(bpy)_n]^{2+}$ (n=1—3) complexes has been established.[1-6] However, the complexation equilibria in nonaqueous solvents have not been well investigated yet. In fact, the only formation of $[Zn(bpy)]^+$ was kinetically investigated in dimethyl sulfoxide.[7]

Ternary (2,2′-bipyridyl)zinc(II) complexes with various carboxylic acids, amino acids (peptides), and amines have been extensively studied in aqueous solution.[1,8] On the other hand, as to the (2,2′-bipyridyl)zinc(II) complexes with halide ions, their formation equilibria have not been reported in any solvent, although the $[ZnCl_2(bpy)]$ complex was isolated from acetonitrile solution and its crystal structure was determined.[9]

In a previous paper,[10] we reported the formation equilibria of the ternary copper(II) complexes with bromide ions and 2,2′-bipyridyl in DMF. In the present work, in order to shed more light on the formation equilibria of ternary metal(II) complexes with 2,2′-bipyridyl and halide ions in solution, we calorimetrically investigated the formation of the ternary (2,2′-bipyridyl)chlorozinc(II) complexes in DMF. As to the related binary zinc(II)-chloride system, the formation equilibria having been previously explored,[11] the thermodynamic quantities of formation of the $[ZnCl_n]^{(2-n)+}$ (n=1—4) complexes were used as known values in the course of the analysis of calorimetric data obtained in the present study.

Experimental

Reagent. All chemicals used were of reagent grade. *2,2′-Bipyridyl* was used without further purification and dried in vacuum over P_2O_5 in a desiccator. Other chemicals were prepared or purified as described elsewhere.[11]

Measurements. Calorimetric measurements were carried out in a room thermostated at (25.0±0.2) °C. All solutions prepared contained 0.4 mol dm^{-3} $(C_2H_5)_4NClO_4$ as a constant ionic medium. A Dewar vessel was immersed in a thermostated water-bath at (25.0±0.007) °C. 100 cm^3 of a DMF solution with varying concentrations of $Zn(ClO_4)_2$ and $(C_2H_5)_4NCl$ was placed in a Dewar vessel which was filled with dry nitrogen gas and isolated from moisture with a P_2O_5 drying-tube, and then it was titrated with 0.1 mol dm^{-3} 2,2′-bipyridyl DMF solution. The concentration of zinc(II) ion in the initial test solution was varied over the range 3—21 mmol dm^{-3}. Heats of complexation observed at each titration point were ranged 0.3—3 J with a certainty ±0.05 J. The measured heats of complexation were corrected for heats of dilution. Heats of dilution were determined in advance by separate experiments by titrating a 0.4 mol dm^{-3} $(C_2H_5)_4NClO_4$ DMF solution with the 2,2′-bipyridyl solution containing 0.4 mol dm^{-3} $(C_2H_5)_4NClO_4$. The observed heats of dilution were found to be very small. All of the measurements were carried out by using a fully automatic on-line system for calorimetry developed in our laboratory.[12,13] The method of the data treatment was similar to that used in a previous work.[10]

Results and Discussion

Calorimetric titration curves obtained for the binary zinc(II)-2,2′-bipyridyl system are depicted in Fig. 1. In the figure, enthalpies $\Delta H^\circ = -q/(\delta v C_{L,tit})$ are plotted against C_L/C_M, where q, δv, C_L and C_M stand for the heat evolved, the volume of an aliquot of the titrant added and the total concentrations of chloride and zinc(II) ions in solution, respectively, at each titration point, and $C_{L,tit}$ denotes the concentration of 2,2′-bipyridyl in the titrant solution. The observed ΔH° values were all negative, indicating an exothermic formation of zinc(II) 2,2′-bipyridyl complexes. As well as in water,[1] the formation of a series of mononuclear $[Zn(bpy)_n]^{2+}$ (n=1—3) complexes was expected in DMF. The calorimetric data were thus analyzed by assuming the formation of the complexes and their formation constants and enthalpies were optimized, the result being summarized in the column of "Binary" in Table 1. The solid lines in Fig. 1 show the

§Present address: Department of Inorganic and Analytical Chemistry, A. József University, Szeged, Hungary.

titration curves calculated by using the constants in Table 1, which satisfactorily reproduce the experimental points over the whole range of C_L/C_M examined. Therefore, the formation of the $[Zn(bpy)_n]^{2+}$ (n=1—3) complexes was concluded in DMF.

Calorimetric titration curves for the ternary zinc(II)-Cl⁻-2,2′-bipyridyl system are depicted in Fig. 2. In the figure, the titration curves remarkably shift to lower C_L/C_M region as the molar ratio of chloride to metal ions in solution is increased. The titration curves calculated with the only known formation constants and enthalpies of $[ZnCl_n]^{(2-n)+}$ (n=1—4) and those of $[Zn(bpy)_n]^{2+}$ (n=1—3) determined above hardly reproduced the experimental points, and thus the formation of ternary $[ZnCl_p(bpy)_q]^{(2-p)+}$ (denoted as ($1pq$)) complexes must be taken into account. At the first step of approach, a plausible set of the ternary complexes such as (111), (121), and (112) were assumed. Their formation constants and enthalpies were obtained with a satisfactorily small Hamilton R-factor of 0.0437. However, the formation constant of the (112) complex thus obtained was rather small with a relatively large uncertainty, and thus the formation of the complex was ambiguous. The least-squares analysis was then carried out by eliminating the (112) complex from the first set of complexes, the R-factor in this case being 0.0439. In both cases with and without the (112) complex, the R-factor remained practically unchanged, and thus the formation of $[ZnCl(bpy)_2]^+$ may be insignificant in DMF. Subsequent least-squares analyses were performed by assuming the only formation of either (111) or (121) complex, together with the binary chloro and 2,2′-bipyridyl complexes. The Hamilton R-factors in both cases were relatively large, indicating that the formation of both complexes must be taken

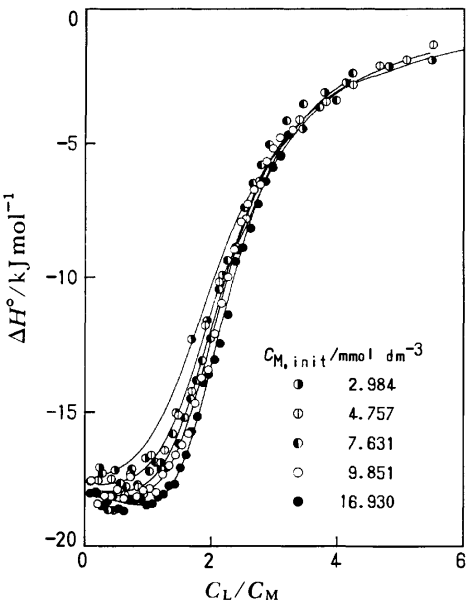

Fig. 1. Calorimetric titration curves of zinc(II) 2,2′-bipyridyl DMF solutions containing 0.4 mol dm^{-3} $(C_2H_5)_4NClO_4$ at 25 °C. Concentrations of zinc(II) ions, $C_{M,init}$/mol dm^{-3}, in the initial test solutions are given in the figure. The solid lines show the curves calculated by using the constants in the column of "Combined" in Table 1.

Table 1. The Least-Squares Refinement of Overall Formation Constants, $\log(\beta_{1pq}/mol^{-(p+q)}dm^{3(p+q)})$, and Enthalpies, $\Delta H^\circ_{\beta 1pq}$/kJ mol^{-1}, of $[ZnCl_p(bpy)_q]^{(2-p)+}$ (bpy=2,2′-bipyridyl) in *N*,*N*-Dimethylformamide Containing 0.4 mol dm^{-3} $(C_2H_5)_4NClO_4$ at 25 °C

	Binary	Ternary	Combined
$\log\beta_{101}$	3.95(0.38)	—	3.88(0.22)
$\log\beta_{102}$	7.07(0.41)	—	6.87(0.23)
$\log\beta_{103}$	8.94(0.50)	—	8.73(0.30)
$\log\beta_{111}$	—	9.31(0.22)	9.24(0.19)
$\log\beta_{121}$	—	14.55(0.10)	14.54(0.08)
$\Delta H^\circ_{\beta 101}$	−18.3(0.3)	—	−18.2(0.3)
$\Delta H^\circ_{\beta 102}$	−38.1(0.8)	—	−39.1(1.0)
$\Delta H^\circ_{\beta 103}$	−56.4(3.0)	—	−55.9(3.2)
$\Delta H^\circ_{\beta 111}$	—	−7.0(3.1)	−7.9(4.3)
$\Delta H^\circ_{\beta 121}$	—	−15.6(1.9)	−16.2(1.5)
$U^{a)}$	0.207	0.490	0.649
$R^{b)}$	0.0251	0.0486	0.0348
$N^{c)}$	135	75	210

Values in parentheses refer to three standard deviations. Values of $\log\beta_{1p0}$ and $\Delta H^\circ_{\beta 1p0}$ of formation of $[ZnCl_p]^{(2-p)+}$ (p=1—4) were fixed. a) Error-square sum. b) The Hamilton R-factor. c) The number of data points.

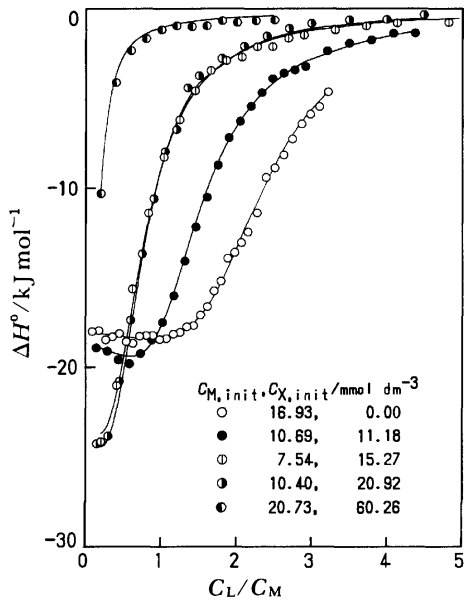

Fig. 2. Calorimetric titration curves of the ternary zinc(II) system obtained by titrating zinc(II) chloride DMF solutions with a 2,2′-bipyridyl DMF solution, each containing 0.4 mol dm^{-3} $(C_2H_5)_4NClO_4$ at 25 °C. Concentrations of zinc(II) and chloride ions, $C_{M,init}$/mol dm^{-3} and $C_{X,init}$/mol dm^{-3}, in the initial test solutions are given in the figure. The solid lines show the curves calculated by using the constants in the column of "Combined" in Table 1.

into account in DMF. The thermodynamic quantities of the (111) and (121) complexes are summarized in the column of "Ternary" in Table 1. Finally the whole calorimetric data obtained for the binary and ternary systems were analyzed altogether to simultaneously optimize the thermodynamic quantities of the binary $[Zn(bpy)_n]^{2+}$ (n=1—3) and ternary $[ZnCl(bpy)]^+$ and $[ZnCl_2(bpy)]$ complexes with the fixed values of the $[ZnCl_n]^{(2-n)+}$ (n=1—4) complexes, the result being listed in the column of "Combined" in Table 1. The values are in satisfactory agreement with the corresponding ones in the columns of "Binary" and "Ternary". As seen in Fig. 2, the solid lines, calculated by using the constants of the binary and ternary zinc(II) complexes in the column of "Combined" in Table 1 and with those of $[ZnCl_n]^{(2-n)+}$ (n=1—4),[11] well reproduce the experimental points over the whole range of C_L/C_M examined.

Distribution of Species. In Fig. 3 the distribution of species in solutions with varying R_c ($=C_X/C_M$) values is shown as a function of $-\log([bpy]/mol\ dm^{-3})$, which was calculated by using the formation constants given in the column of "Combined" in Table 1, together with those of the zinc(II) chloro complexes.[11] In solutions involving chloride ions ($R_c>0$), the ternary (111) and (121) complsxes are formed, the formation of these complexes being strongly suppressed, however. It is indicated that the formation of the ternary complexes is very much unfavorable in solution of $R_c>3$ in which the tri- and tetrachlorozincate(II) complexes are predominated. In Fig. 4 the distribution of species in solutions with varying R_c' ($=C_L/C_M$) values is shown as a function of $-\log([Cl^-]/mol\ dm^{-3})$ for comparison. It is seen in Fig. 4 that the ternary complexes are only formed in a range $-\log([Cl^-]/mol\ dm^{-3})$=3—6 and they disappear in solution of a higher chloride concentration where the $[ZnCl_3]^-$ and $[ZnCl_4]^{2-}$ complexes are mainly yielded.

Binary (2,2'-Bipyridyl)zinc(II) Complexes. The thermodynamic quantities of stepwise formation of the $[Zn(bpy)_n]^{2+}$ (n=1—3) complexes obtained in DMF are listed in Table 2 together with those in water.

The stepwise formation constants of each $[Zn(bpy)_n]^{2+}$ complex in DMF are smaller than those in water, and the smaller values in DMF are mainly due

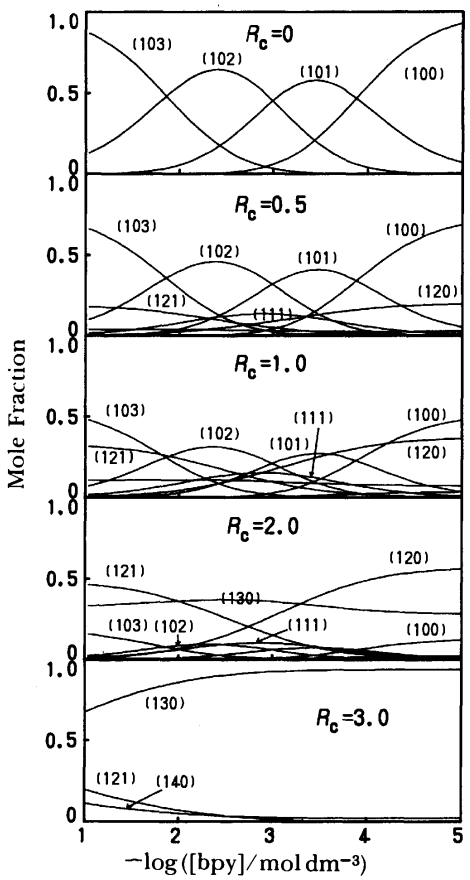

Fig. 3. Distribution of the $[ZnCl_p(bpy)_q]^{(2-p)+}$ (denoted as (l*pq*)) complexes as a function of $-\log([bpy]/mol\ dm^{-3})$ at the total zinc(II) ion concentration of 0.01 mol dm^{-3} in DMF. The R_c value stands for the molar ratio of chloride to zinc(II) ions in solution.

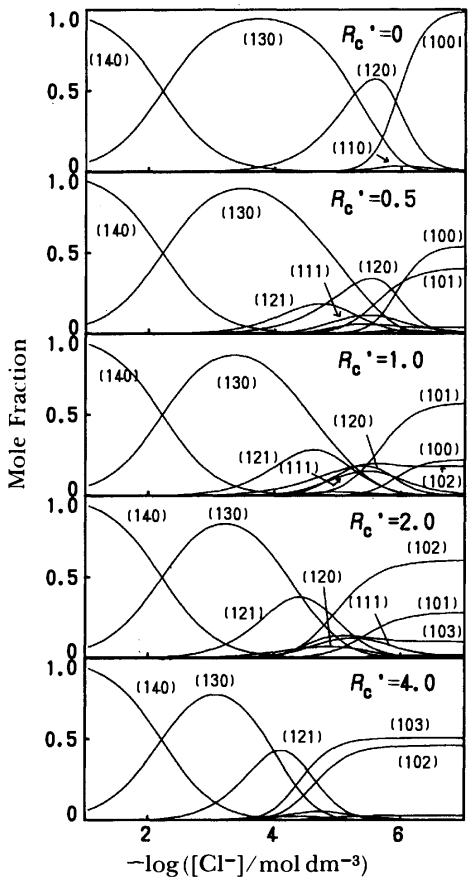

Fig. 4. Distribution of the $[ZnCl_p(bpy)_q]^{(2-p)+}$ (denoted as (l*pq*)) complexes as a function of $-\log([Cl^-]/mol\ dm^{-3})$ at the total zinc(II) ion concentration of 0.01 mol dm^{-3} in DMF. The R_c' value stands for the molar ratio of 2,2'-bipyridyl to zinc(II) ion in solution.

Table 2. Thermodynamic Quantities, $\log(K_n/\text{mol}^{-1}\,\text{dm}^3)$, $\Delta G_n^\circ/\text{kJ mol}^{-1}$, $\Delta H_n^\circ/\text{kJ mol}^{-1}$, and $\Delta S_n^\circ/\text{J K}^{-1}\,\text{mol}^{-1}$, for the Stepwise Formation of $[\text{Zn(bpy)}_n]^{2+}$ ($n=1$—3 and bpy=2,2′-bipyridyl)

	0.4 mol dm^{-3} $(C_2H_5)_4NClO_4$ DMF[d]	0.1 mol dm^{-3} KNO_3[a] Water	0.1 mol dm^{-3} $NaClO_4$[b] Water	1 mol dm^{-3} KNO_3[c] Water
	25 °C	25 °C	20 °C	30 °C
$\log K_1$	3.95	5.16	5.30	5.26
$\log K_2$	3.12	4.44	4.53	4.55
$\log K_3$	1.87	3.74	3.80	3.96
ΔG_1°	−22.5	−29.5	−30.3	−30.0
ΔG_2°	−17.8	−25.3	−25.9	−26.0
ΔG_3°	−10.7	−21.3	−21.7	−22.6
ΔH_1°	−18.3	−29.0	−30.0	−26.2
ΔH_2°	−19.9	−28.4	−22.3	−22.9
ΔH_3°	−18.3	−24.1	−20.9	−17.4
ΔS_1°	14	0	0	15
ΔS_2°	−7	−9	10	11
ΔS_3°	−26	−10	1	18

a) Ref. 2. b) Ref. 4. c) Ref. 5. d) *N,N*-Dimethylformamide.

Table 3. Thermodynamic Quantities, $\Delta G^\circ/\text{kJ mol}^{-1}$, $\Delta H^\circ/\text{kJ mol}^{-1}$, and $\Delta S^\circ/\text{J K}^{-1}\,\text{mol}^{-1}$, of Stepwise Formation of the $[\text{ZnCl}_n(\text{bpy})]^{(2-n)+}$ ($n=0$—2, bpy=2,2′-bipyridyl) Complexes, Together with Those of Stepwise Formation of $[\text{ZnCl}_n]^{(2-n)+}$ ($n=1$—4) in *N,N*-Dimethylformamide at 25 °C

Reaction	ΔG°	ΔH°	ΔS°
$Zn^{2+}+bpy=[Zn(bpy)]^{2+}$	−22.5	−18.3	14
$[ZnCl]^+ + bpy = [ZnCl(bpy)]^+$	−25.7	−21.6	13
$[ZnCl_2] + bpy = [ZnCl_2(bpy)]$	−15.7	−31.7	−54
$[Zn(bpy)]^{2+} + Cl^- = [ZnCl(bpy)]^+$	−30.6	11.4	141
$[ZnCl(bpy)]^+ + Cl^- = [ZnCl_2(bpy)]$	−19.9	−8.6	70
$Zn^{2+} + Cl^- = [ZnCl]^+$	−27.5	14.7	142
$[ZnCl]^+ + Cl^- = [ZnCl_2]$	−39.9	1.4	139
$[ZnCl_2] + Cl^- = [ZnCl_3]^-$	−30.0	−17.6	42
$[ZnCl_3]^- + Cl^- = [ZnCl_4]^{2-}$	−12.7	−7.9	16

to the less negative enthalpy values in the solvent than those in water. Since the donicity of DMF (the donor number D_N=26.6) is stronger than that (D_N=14.8) of water,[14] the less negative enthalpy values of the zinc(II) 2,2′-bipyridyl complexes in DMF than those in water may be mainly ascribed to a stronger solvation of the metal ion in the former solvent than in the latter.

We note that the ΔS_n° ($n=1$—3) values of the zinc(II) 2,2′-bipyridyl complexes are practically the same as those of the nickel(II)-2,2′-bipyridyl ones with octahedral structure in DMF.[15] The stepwise ΔH_n° ($n=1$—3) values are practically kept constant and the corresponding entropy values stepwise decreased by ca. 20 $\text{J K}^{-1}\,\text{mol}^{-1}$ in the zinc(II)-2,2′-bipyridyl system in DMF. Such changes in the stepwise enthalpy and entropy values may hardly be expected provided that the $[\text{Zn(bpy)}_2]^{2+}$ complex has the four-coordinate tetrahedral structure, because the formation of $[\text{Zn(bpy)}_3]^{2+}$ may be very much unfavorable owing to the change from tetrahedral to octahedral structure. Therefore, we suggest an octahedral structure for the bis(2,2′-bipyridyl)zinc(II) complex. It is also suggested that the bis(2,2′-bipyridyl)zinc(II) complex may have the cis-configulation as expressed by $[\text{Zn(bpy)}_2(\text{dmf})_{eq}(\text{dmf})_{ax}]^{2+}$ because the trans-configulation is sterically unfavorable.[16]

Ternary (2,2′-Bipyridyl)chlorozinc(II) Complexes. The thermodynamic quantities of the stepwise formation of the $[\text{ZnCl}_n(\text{bpy})]^{(2-n)+}$ ($n=0$—2) in DMF are summarized in Table 3, which can be calculated from the values in Table 1. The thermodynamic quantities of the stepwise formation of the zinc(II) chloro complexes[11] are also listed in Table 3 for comparison. Comparing the enthalpy and entropy values for the reactions:

$$Zn^{2+} + bpy = [Zn(bpy)]^{2+}, \quad (1)$$

$$[ZnCl]^+ + bpy = [ZnCl(bpy)]^+, \quad (2)$$

$$[ZnCl_2] + bpy = [ZnCl_2(bpy)], \quad (3)$$

in Table 3, we see that the ΔH° and ΔS° values for Reaction 3 are significantly negative compared with those for Reactions 1 and 2, the result suggesting that solvation of the $[ZnCl_2]$ complex is weaker than that of Zn^{2+}, as well as $[ZnCl]^+$ in DMF. As noted in a previous paper,[11] the dichlorozinc(II) complex may have the four-coordinate $[ZnCl_2(dmf)_2]$ structure with weak metal-dmf bonds in DMF, and thus it is plausible that the DMF molecules within the $[ZnCl_2(dmf)_2]$ complex are replaced to 2,2′-bipyridyl and the four-coordinate $[ZnCl_2(bpy)]$ complex is formed in DMF. It has in fact been revealed that the $[ZnCl_2(bpy)]$ complex has the four-coordinate tetrahedral structure in crystal.[9] Similarly, the $[ZnCl_2(phen)]$ (phen=1,10-phenanthroline)[17] and $(ZnX_2(py)_2]$ (X=Cl, Br, and I, and py=pyridine)[18,19] complexes have the tetrahedral

structure in crystal.

We subsequently compare the enthalpy and entropy values for the reactions:

$$[Zn(bpy)]^{2+} + Cl^- \rightleftharpoons [ZnCl(bpy)]^+, \quad (4)$$

$$[ZnCl(bpy)]^+ + Cl^- \rightleftharpoons [ZnCl_2(bpy)]. \quad (5)$$

The $[Zn(bpy)]^{2+}$ complex may have the octahedral structure with four DMF molecules coordinating to the metal ion, and the DMF molecules are stepwise liberated in the course of Reactions 4 and 5. As seen in Table 3, the ΔH° value for Reaction 4 is positive, while that for Reaction 5 is negative. The ΔS° value for Reaction 4 is much more positive than that of Reaction 5. The result suggests that liberation of DMF molecules from the central metal ion takes place relatively extensively in Reaction 4. Therefore, it is plausible that the $[ZnCl(bpy)]^+$ complex has the four-coordinate structure with one DMF molecule within the first coordination sphere of the metal ion.

The present work has been financially supported by the Grant-in-Aid for Special Project Research No. 61134043 from the Ministry of Education, Science and Culture.

References

1) W. A. E. McBryde, "A Critical Review of Equilibrium Data for Proton- and Metal Complexes of 1,10-Phenanthroline, 2,2′-Bipyridyl and Related Compounds," IUPAC Chemical Data Series No. 17, Pergamon Press (1978).
2) S. Cabani and M.Landucci, *J. Chem. Soc.*, **1962**, 278.
3) G. Atkinson and J. E. Bauman, Jr., *Inorg. Chem.*, **1**, 900 (1962).
4) G. Anderegg, *Helv. Chim. Acta*, **46**, 2397 (1963).
5) R. L. Davis and K. W. Dunning, *J. Chem. Soc.*, **1965**, 4168.
6) P. G. Daniele, G. Ostacoli, and V. Zelano, *Ann. Chim. (Rome)*, **65**, 455 (1975).
7) D. M. W. Buck and P. Moore, *J. Chem. Soc., Dalton Trans.*, **1976**, 638.
8) H. Sigel and R. B. Martin, *Chem. Rev.*, **82**, 385 (1982).
9) M. A. Khan and D. G. Tuck, *Acta Crystallogr., Sect. C*, **40**, 60 (1984).
10) S. Ishiguro, L. Nagy, and H. Ohtaki, *Bull. Chem. Soc. Jpn.*, **60**, 2053 (1987).
11) S. Ishiguro, K. Ozutsumi, and H. Ohtaki, *Bull. Chem. Soc. Jpn.*, **60**, 531 (1987).
12) S. Ishiguro, K. Yamamoto, and H. Ohtaki, *Anal. Sci.*, **1**, 263 (1985).
13) S. Ishiguro and H. Ohtaki, *J. Coord. Chem., Sect. B*, **15**, 237 (1987).
14) V. Gutmann, "The Donor-Acceptor Approach to Molecular Interactions," Prenum, New York (1978).
15) S. Ishiguro, L. Nagy, and H. Ohtaki, to be published.
16) E. D. Mckenzie, *Coord. Chem. Rev.*, **6**, 187 (1971).
17) C. W. Reimann, S. Block, and A. Perloff, *Inorg. Chem.*, **5**, 1185 (1966).
18) W. L. Steffen and G. J. Palenik, *Acta Crystallogr., Sect. B*, **32**, 298 (1976).
19) P. T. T. Wong and D. G. Brewer, *Can. J. Chem.*, **47**, 4589 (1969).

 © 1987 The Chemical Society of Japan Bull. Chem. Soc. Jpn., 60, 2871—2874 (1987)

Cis-to-Trans Isomerization of Bis(diamine)bis(isothiocyanato)chromium(III) Thiocyanate in the Solid State

Goutam De, Masatatsu Suzuki, and Akira Uehara*
Department of Chemistry, Faculty of Science, Kanazawa University, Kanazawa 920
(Received March 9, 1987)

Solid-state thermal reactions of *trans*- and *cis*-$[Cr(NCS)_2(AA)_2]SCN$ where AA is 1,2-ethanediamine (en) or 1,3-propanediamine (tn) were studied. Upon heating, both the cis- and trans-complexes lost half mole of diamine to convert into the double complex *trans*-$[Cr(NCS)_2(AA)_2][Cr(NCS)_4(AA)]$. The anion moiety $[Cr(NCS)_4(AA)]^-$ was isolated from the double complex. The thermal reactions are thus useful for easy preparation of $[Cr(NCS)_4(AA)]^-$complex, which has previously been obtained with difficulty from solution reactions.

In 1904, Pfeiffer et al. reported the solid state deamination of the tris(1,2-ethanediamine) complex $[Cr(en)_3]X_3$ ($X=Cl^-$ or NCS^-).[1] The complex, when heated, deaminated to form *cis*-$[CrCl_2(en)_2]Cl$ or *trans*-$[Cr(NCS)_2(en)_2]SCN$. Until recently, the above deamination has been used as the standard procedures for synthesizing a series of *cis*- and *trans*-bis(diamine) complexes.[2] We recently investigated in detail the deamination of a complete series of tris(diamine) complexes: $[Cr(AA)_3]X_3$, $[Cr(AA)_2(BB)]X_3$, and $[Cr(AA)(BB)(CC)]X_3$ where AA, BB, and CC denote different diamines, and X is a halide ion.[3] We noticed that the bis(diamine)complexes obtained by the deamination sometimes undergo subsequent isomerization. Then, we studied the effect of various diamines and anions on the isomerization.[4,5] The solid-state thermal reaction of bis(diamine)bis(isothiocyanato)chromium(III) thiocyanates has never been approached. In this paper, we describe the behavior of the solid *cis*- and *trans*-$[Cr(NCS)_2(AA)_2]SCN$ when heated non-isothermally in open dynamic condition, where AA is 1,2-ethanediamine or 1,3-propanediamine; the former can form a five-membered chelate ring and the latter, a six-membered chelate ring with chromium(III) ion.

Experimental

Preparation of Complexes. *trans*-$[Cr(NCS)_2(en)_2]SCN$ (**1**) was prepared according to the known method.[3] *cis*-$[Cr(NCS)_2(en)_2]SCN$ (**2**), *trans*-$[Cr(NCS)_2(tn)_2]SCN$ (**3**), and *cis*-$[Cr(NCS)_2(tn)_2]SCN\cdot H_2O$ (**4**) were obtained by the metatheses from the corresponding chloro-chloride[6,7] and KSCN as reported previously.[3]

Non-Isothermal Measurements. Thermal reactions of the samples were recorded on SEIKO SSC/580 TG/DTA-30 and SSC/580 DSC/10 thermal analysers in a nitrogen atmosphere (flow rate: 200 $cm^3\ min^{-1}$). All the measurements were carried out at the heating rate of 2 °C min^{-1}. About 15 mg of the samples was used for TG/DTA and about 10 mg, for DSC.

Spectral Measurements. Visible spectra of the samples were measured with a JASCO UVIDEC 505 spectrophotometer. IR spectra were obtained by a KBr method with a JASCO A-3 infrared spectrophotometer.

TLC. The presence of a single species in the deaminated products was confirmed by TLC. The plates used were those of silica gel 60F-254 made by Merck Ltd.

Molar Conductivities. Molar conductivities were measured in acetone at 25 °C to determine the charges of the samples using a Yokogawa Universal Bridge TYPE BU-Z-13A.

Purification of Products Obtained by Deamination. *trans*-$[Cr(NCS)_2(en)_2][Cr(NCS)_4(en)]$(**5**). One gram of finely powdered complex [**1** or **2**] was spread in a thin layer on a watch glass and heated in an air oven [heating conditions: 200—205 °C (2 h) for **1** and 195—200 °C (5 h) for **2**]. The product thus obtained was throughly washed with boiling water (250 cm^3), cold water, ethanol, and ether, and recrystallized from a mixture of acetone-water (4 : 1). Pink flaky crystals thus obtained were collected by filtration and air dried. Yield 80%.

trans-$[Cr(NCS)_2(tn)_2][Cr(NCS)_4(tn)]$ (**6**). The complex was prepared by the same method as that described for **5**. In this case, either the complex **3** or **4** was taken as the starting material [heating conditions: 195—200 °C (5 h) for **3** and 195—200 °C (3 h) for **4**]. This complex appears as red-pink crystals. Yield 80%.

Results

Thermal Reactions under Non-Isothermal Conditions. Figure 1 shows the TGA and DSC curves for the complexes **1** and **2**. As seen from the TG curve of the complex *trans*-$[Cr(NCS)_2(en)_2]SCN\cdot H_2O$ (**1**), it is dehydrated at 38 °C followed by the evolution of half mole of en at 181—254.5 °C and then a clear plateau is obtained. The complex changed in color from yellowish orange to pink due to the formation of the double complex *trans*-$[Cr(NCS)_2(en)_2][Cr(NCS)_4(en)]$. The corresponding DSC curve shows two endothermic peaks for the elimination of diamine. The complex *cis*-$[Cr(NCS)_2(en)_2]SCN$ (**2**) deaminates at 183.5 °C and is transformed to the double complex *trans*-$[Cr(NCS)_2(en)_2][Cr(NCS)_4(en)]$ quantitatively at 250 °C. For this reaction, the DSC curve shows a series of endo- and exothermic peaks (Fig. 1). It is interesting to note that during deamination, the complex undergoes cis-to-trans isomerization. Similar results were observed in case of the 1,3-propanediamine complexes. The complex *trans*-$[Cr(NCS)_2(tn)_2]SCN$ (**3**) undergoes deamination at 170—243 °C and a clear plateau is obtained in the TG curve (Fig. 2). The weight loss corresponds

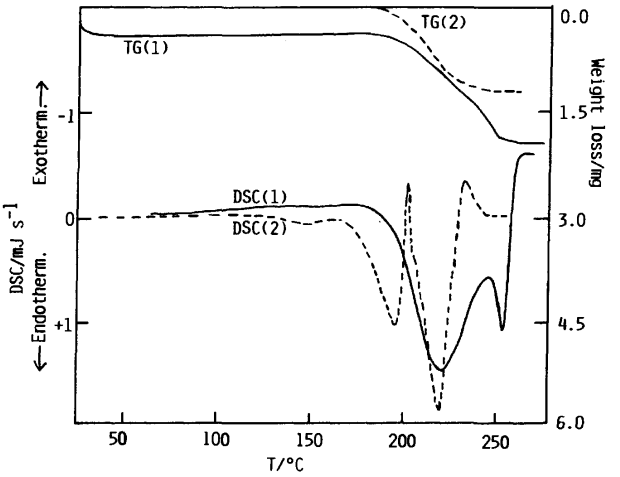

Fig. 1. TG and DSC curves of *trans*-[Cr(NCS)$_2$(en)$_2$]SCN·H$_2$O (**1**) (——) and *cis*-[Cr(NCS)$_2$(en)$_2$]SCN (**2**) (----). Sample weights: for TG, **1**, 18.45 mg, **2**, 13.90 mg; for DSC, **1**, 8.40 mg, **2**, 9.80 mg. (Endothermic DSC peak for the dehydration of **1** is not shown because the compound started dehydration during grinding at ambient temperature).

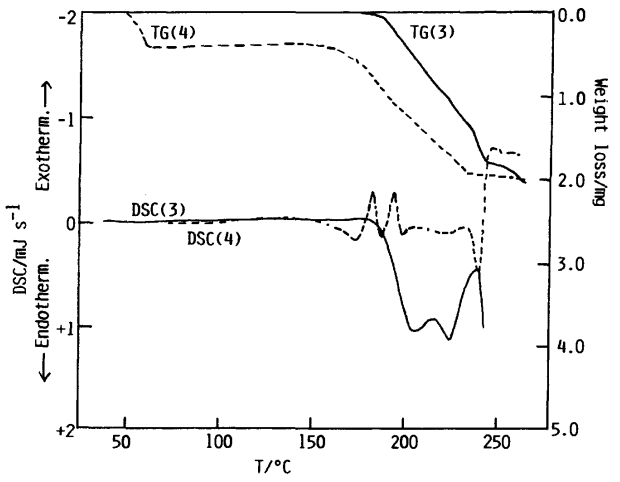

Fig. 2. TG and DSC curves of *trans*-[Cr(NCS)$_2$(tn)$_2$]SCN (**3**) (——) and *cis*-[Cr(NCS)$_2$(tn)$_2$]SCN·H$_2$O (**4**) (----). Sample weights: for TG, **3**, 17.50 mg, **4**, 18.80 mg; for DSC, **3**, 9.70 mg, **4**, 9.58 mg. (Endothermic DSC peak for the dehydration of **4** is not shown because the compound started dehydration during grinding at ambient temperature).

to 0.5 mol of the diamine. The corresponding DSC curve shows two endothermic peaks. In case of *cis*-[Cr(NCS)$_2$(tn)$_2$]SCN·H$_2$O (**4**) (Fig. 2), dehydration starts at 42 °C and anhydrous weight level is attained at 64 °C. As the temperature is raised further, it begins to lose the diamine (146—234 °C) showing a series of endo- and exothermic DSC peaks leaving a stable double complex *trans*-[Cr(NCS)$_2$(tn)$_2$][Cr(NCS)$_4$(tn)]. Like the 1,2-ethanediamine complex, cis-to-trans isomerization also takes place along with deamination. The following schemes summarize the solid state reactions:

$$2\ trans\text{-}[Cr(NCS)_2(AA)_2]SCN \xrightarrow[\Delta]{-(AA)} trans\text{-}[Cr(NCS)_2(AA)_2][Cr(SCN)_4(AA)]$$

$$2\ cis\text{-}[Cr(NCS)_2(AA)_2]SCN \xrightarrow[\Delta]{-(AA)} trans\text{-}[Cr(NCS)_2(AA)_2][Cr(SCN)_4(AA)]$$

Characterization of Complexes 5 and 6. The presence of complex cation and anion in the double complexes **5** and **6** was convincingly demonstrated by the following ion exchange experiments: A concentrated solution of **5** or **6** in acetone-water(3 : 2) mixture [addition of more water causes precipitation of the complex] was passed through a Dowex 1·X8 anion exchanger in Cl$^-$ form (20×1.5 cm) and the cations were eluted with one column volume of acetone-water (3 : 2) mixture. The effluents were orange in color and the upper part of the resins turned red-violet due to the retention of the complex anion. The effluents were quickly concentrated in a rotoevaporator at room temperature and thereto excess NH$_4$SCN was added. Yellowish orange [in case of **5**] and reddish orange [in case of **6**] crystals of *trans*-[Cr(NCS)$_2$(AA)$_2$]SCN separated out on standing. The IR and electronic spectra (350—700 nm) of these products were identical with those of *trans*-[Cr(NCS)$_2$(en)$_2$]SCN·H$_2$O (**1**) and *trans*-[Cr(NCS)$_2$(tn)$_2$]SCN (**3**) respectively. For the isolation of complex anions, similar exchange experiments were performed utilizing the cation exchanger Amberlite IR-120B (Na$^+$ form). In these cases, red-violet effluents were obtained and the resins were turned orange due to the retention of the complex cation. From these effluents the anionic complexes were precipitated out by adding tetraethylammonium bromide (Et$_4$NBr). These products were recrystallized from acetone-water (1 : 1) mixture. [Et$_4$N][Cr(NCS)$_4$·(en)] and [Et$_4$N][Cr(NCS)$_4$(tn)] were obtained as red-violet and red-purple crystals, respectively. All the compounds were characterized by analytical data (Table 1), DSC and TG measurements, electronic and IR data (Table 2), molar conductivities and TLC data (Table 3). Although *cis*- and *trans*-[Cr(NCS)$_2$(AA)$_2$]SCN exhibit similar absorption maxima in their visible electronic spectra, they can be easily distinguished from thier molar absorbances (Table 2). As the trans-complexes are much more symmetrical (D_{4h}) than the cis-complexes (C_{2v}), the former shows much lower molar absorbances than the latter in their visible absorption spectra.

The double complexes obtained from *cis*- and *trans*-[Cr(NCS)$_2$(AA)$_2$]SCN possess exactly similar IR, electronic spectra (350—700 nm), molar conductivities and TLC data. We also separated the cationic and anionic parts by ion exchange chromatography from both the double complexes synthesized from *cis*- and *trans*-[Cr(NCS)$_2$(AA)$_2$]SCN. In both the cases identical prod-

Table 1. Analytical Data for the Complexes Obtained

Complex	H(%)		C(%)		N(%)	
	Found	Calcd	Found	Calcd	Found	Calcd
trans-$[Cr(NCS)_2(en)_2]SCN$[a]	4.67	4.65	24.15	24.26	28.18	28.30
cis-$[Cr(NCS)_2(en)_2]SCN$	4.61	4.65	24.05	24.26	28.14	28.30
trans-$[Cr(NCS)_2(tn)_2]SCN$	5.35	5.38	28.79	28.86	26.26	26.18
cis-$[Cr(NCS)_2(tn)_2]SCN \cdot H_2O$	5.55	5.64	27.57	27.54	25.10	24.98
$[Cr(NCS)_2(en)_2][Cr(NCS)_4(en)]$[b]	3.91	3.82	23.14	22.77	26.26	26.56
$[Cr(NCS)_2(en)_2][Cr(NCS)_4(en)]$[c]	3.98	3.82	22.75	22.77	26.34	26.56
$[Cr(NCS)_2(tn)_2][Cr(NCS)_4(tn)]$[d]	4.55	4.48	26.67	26.69	24.89	24.90
$[Cr(NCS)_2(tn)_2][Cr(NCS)_4(tn)]$[e]	4.48	4.48	26.70	26.69	24.69	24.90
$[Et_4N][Cr(NCS)_4(en)]$	5.88	5.94	35.27	35.42	20.37	20.65
$[Et_4N][Cr(NCS)_4(tn)]$	6.25	6.18	36.76	36.86	19.76	20.06

a) Analyzed in anhydrous form. b) Synthesized from *trans*-$[Cr(NCS)_2(en)_2]SCN$. c) Synthesized from *cis*-$[Cr(NCS)_2(en)_2]SCN$. d) Synthesized from *trans*-$[Cr(NCS)_2(tn)_2]SCN$. e) Synthesized from *cis*-$[Cr(NCS)_2(tn)_2]SCN$.

Table 2. IR and Electronic Spectral Data for the Complexes

No.	Complex	IR data $\tilde{\nu}(CN)$[a]/cm^{-1}	Electronic spectral data nm (ε/$mol^{-1}dm^3cm^{-1}$)
1	*trans*-$[Cr(NCS)_2(en)_2]SCN \cdot H_2O$	2090vs, 2064sh[b]	488(79.5), 364(60.3)[e]
2	*cis*-$[Cr(NCS)_2(en)_2]SCN$	2098vs, 2083vs, 2061s[b]	485(147), 371(88.2)[e]
3	*trans*-$[Cr(NCS)_2(tn)_2]SCN$	2083vs, 2064sh[b]	496(88.9), 370(71.9)[e]
4	*cis*-$[Cr(NCS)_2(tn)_2]SCN \cdot H_2O$	2117vs, 2092vs, 2059vs[b]	488(104.5), 370(72.9)[e]
5	*trans*-$[Cr(NCS)_2(en)_2][Cr(NCS)_4(en)]$[c]	2124sh, 2102sh, 2086vs, 2076sh	510(109.1), 389(84.6)[f]
6	*trans*-$[Cr(NCS)_2(tn)_2][Cr(NCS)_4(tn)]$[d]	2118s, 2088vs, 2074vs, 2060vs	515(103.8), 388(84.3)[f]
7	$[Et_4N][Cr(NCS)_4(en)]$	2017s, 2100sh, 2088vs, 2076sh	525(146.4), 398(109.9)[f]
8	$[Et_4N][Cr(NCS)_4(tn)]$	2123s, 2103sh, 2092vs, 2077vs	525(130.1), 395(114.9)[f]

a) Assignment of ν(CS) and δ(NCS) are difficult due to the presence of ligand bands. b) Due to ionic SCN group. c) The complexes prepared from **1** and **2** showed the same spectral data. d) The complexes prepared from **3** and **4** showed the same spectral data. e) In H_2O. f) In acetone.

ucts were obtained. The molar conductivities of **5** and **6** are slightly lower than that usually found for 1 : 1 electrolyte probably due to the ion pair formation (Table 3).

Discussion

The experimental studies indicate the presence of complex cation (*trans*-$[Cr(NCS)_2(AA)_2]^+$) and anion ($[Cr(NCS)_4(AA)]^-$) in the double complexes which were synthesized pyrolytically from *cis*- and *trans*-$[Cr(NCS)_2(AA)_2]SCN$ according to the following sequence of reactions:

(i) $[Cr(NCS)_2(AA)_2][Cr(NCS)_4(AA)]$ **5** or **6** $\xrightarrow[Cl^- \text{ form}]{\text{Dowex 1-X8}}$

- $[Cr(NCS)_4(AA)]^-$ (retained in column)
- $[Cr(NCS)_2(AA)_2]^+ \xrightarrow{NH_4SCN}$ *trans*-$[Cr(NCS)_2(AA)_2]SCN$ (orange effluent) orange crystal

(ii) $[Cr(NCS)_2(AA)_2][Cr(NCS)_4(AA)]$ **5** or **6** $\xrightarrow[Na^+ \text{ form}]{\text{Amberlite 1R-120B}}$

- $[Cr(NCS)_2(AA)_2]^+$ (retained in column)
- $[Cr(NCS)_4(AA)]^- \xrightarrow{Et_4NBr} [Et_4N][Cr(NCS)_4(AA)]$ (red-violet effluent) red-violet crystal

The interesting feature of these thermal reactions are that the double complexes formed after the deamination of both *cis*- and *trans*-$[Cr(NCS)_2(AA)_2]SCN$ contain *trans*-$[Cr(NCS)_2(AA)_2]^+$ cation. Therefore during the deamination of the cis-complexes, cis-to-trans isomerization occured. In the course of our earlier studies,[4,8,9] we observed trans-to-cis isomerization in the bis(diamine)dihalogeno complexes containing diamine which is capable of forming five-membered chelate ring with chromium(III) ion, whereas cis-to-trans isomerization was found in the complexes containing six-membered diamine chelate ring. However, in this study, only cis-to-trans isomerization is observed irrespective of the ring size of the diamines. From this and previous results,[4,5] we tentatively assume that the anion size also plays a substantial role on the direction of the isomerization. The details are now under investigation.

It is interesting to note that only endothermic DSC peaks are observed for the deamination of trans-complexes (Fig. 2), whereas both endo- and exothermic peaks appeared in case of the cis-complexes. The exothermic peaks appeared during deamination of the cis-complexes is probably responsible for the isomerization because the isomerization of the *cis*-(diamine)-chromium(III) has been found to proceed exothermically.[5]

By utilizing these thermal reactions, the anionic

Table 3. R_f Values Obtained by Thin Layer Chromatography[a] and Molar Conductivities[b] (Λ) of the Complexes

Complex	R_f Value	$\Lambda/\Omega^{-1}\,cm^2\,mol^{-1}$
$[Cr(NCS)_2(en)_2][Cr(NCS)_4(en)]$[c]	0.816	71.0
$[Cr(NCS)_2(en)_2][Cr(NCS)_4(en)]$[d]	0.815	70.4
$[Cr(NCS)_2(tn)_2][Cr(NCS)_4(tn)]$[e]	0.846	70.5
$[Cr(NCS)_2(tn)_2][Cr(NCS)_4(tn)]$[f]	0.850	69.3

a) Acetone was used as eluents. A single plate was employed in each run. b) In acetone. c) Synthesized from *trans*-$[Cr(NCS)_2(en)_2]SCN$. d) Synthesized from *cis*-$[Cr(NCS)_2(en)_2]SCN$. e) Synthesized from *trans*-$[Cr(NCS)_2(tn)_2]SCN$. f) Synthesized from *cis*-$[Cr(NCS)_2(tn)_2]SCN$.

complex $[Cr(NCS)_4(AA)]^-$ can be prepared easily, which has previously been obtained with difficulty from solution reactions.[10] In addition the anionic complex $[Et_4N][Cr(NCS)_4(tn)]$ is newly prepared in the present study. Contrary to the earlier report,[10] we found a little low molar absorptivity (for the transition $^4A_{2g}\rightarrow{}^4T_{2g}$) for the complex $[Et_4N][Cr(NCS)_4(en)]$ in acetone[11] (Table 2).

One of the authors (G. De) thanks the Japan Society for the Promotion of Science (JSPS) for awarding him a Long Term JSPS Research Fellowship for the 1986 fiscal year.

References

1) P. Pfeiffer, P. Koch, G. Land, and A. Treischmann, *Ber. Dtsch. Chem. Ges.*, **37**, 4265; 4269; 4277 (1904).

2) C. L. Rollinson and J. C. Bailar, Jr., *Inorg. Synth.*, **2**, 196 (1946).

3) A. Uehara, Y. Nishiyama, and R. Tsuchiya, *Inorg. Chem.*, **21**, 2422 (1982).

4) S. Mitra, T. Yoshikuni, A. Uehara, and R. Tsuchiya, *Bull. Chem. Soc. Jpn.*, **52**, 2569 (1979).

5) R. Tsuchiya, A. Uehara, and T. Yoshikuni, *Inorg. Chem.*, **21**, 590 (1982).

6) E. Pedersen, *Acta Chem. Scand.*, **24**, 3362 (1970).

7) D. A. House, *Inorg. Nucl. Chem. Lett.*, **6**, 741 (1970).

8) T. Yoshikuni, R. Tsuchiya, A. Uehara, and E. Kyuno, *Bull. Chem. Soc. Jpn.*, **50**, 883 (1977).

9) S. Mitra, A. Uehara, and R. Tsuchiya, *Thermochim. Acta*, **34**, 189 (1979).

10) G. Thomas and V. Holba, *J. Inorg. Nucl. Chem.*, **31**, 1749 (1969).

11) Reference 10 reported absorption bands at 515 (ε_{max}=177 $mol^{-1}\,dm^3\,cm^{-1}$) and 392 nm (ε_{max}=104 $mol^{-1}\,dm^3\,cm^{-1}$) for the complex $Na[Cr(NCS)_4(en)]$ in 10^{-2} mol dm^{-3} $HClO_4$.

 © 1987 The Chemical Society of Japan Bull. Chem. Soc. Jpn., 60, 2875—2879 (1987)

Preparation, Stereochemistry, and CD Spectra of Cobalt(III) Complexes with 1,3-Propanedithiolate and 1,3-Propanedisulfinate. Crystal Structure and Absolute Configuration of $(-)^{CD}_{460}$-(1,3-Propanedisulfinato)(3,6-diazaoctane-1,8-diamine)-cobalt(III) Perchlorate Monohydrate

Ken-ichi Okamoto,* Hideki Umehara, and Jinsai Hidaka
Department of Chemistry, University of Tsukuba, Sakura, Ibaraki 305
(Received March 18, 1987)

The cis-α isomers of the 3,6-diazaoctane-1,8-diamine (trien) cobalt(III) complexes with 1,3-propanedithiolate (pdt) and 1,3-propanedisulfinate (pdsi) were selectively prepared and optically resolved. Of these isomers, the crystal structure and the absolute configuration of $(-)^{CD}_{460}$-[Co(pdsi)(trien)]$ClO_4 \cdot H_2O$ have been determined by X-ray diffraction method. The complex cation takes a Δ-cis-α configuration. The 1,3-propanedisulfinate coordinates to cobalt atom through two sulfur atoms and its chelate ring takes a skew boat form with the λ conformation. The CD spectral behaviors in the d-d transition and the sulfur-to-metal (Co(σ*) ← S(σ)) charge-transfer band regions are discussed in relation to the absolute configurations of the cobalt(III) complexes with sulfinate type sulfur donor atoms and the corresponding thiolate ones.

Cobalt(III) complexes with the 3,6-diazaoctane-1,8-diamine (trien) and its derivatives have been extensively investigated for the relation between their CD spectra in the d-d transition region and the absolute configuration, which arises from the chirality due to the skew pair of the chelate rings.[1-6] Recently, it has been reported that the absolute configuration of the cobalt(III) complexes with two or three thiolate type sulfur donor atoms and the corresponding sulfinate ones can be estimated on the basis of the two CD bands with the opposite signs in the sulfur-to-metal (Co(σ*)←S(σ)) charge-transfer band region, taking the CD spectral pattern in the d-d transition band region into consideration.[7] For the trien cobalt(III) complexes with 1,3-propanedithiolate (pdt; $S(CH_2)_3S^{2-}$) and 1,3-propanedisulfinate (pdsi; $O_2S(CH_2)_3SO_2^{2-}$), which were employed in the present work, however, this empirical estimation based on the CD spectral behaviors in the sulfur-to-metal charge-transfer band region is inconsistent with that in the d-d transition band region.

This paper deals with the preparation and resolution of the trien cobalt(III) complexes with the pdt and pdsi, and with the X-ray crystal structure analysis of $(-)^{CD}_{460}$-[Co(pdsi)(trien)]$ClO_4 \cdot H_2O$. The CD spectra of the pdt and pdsi isomers obtained are discussed in relation to the absolute cofiguration of $(-)^{CD}_{460}$ pdsi isomer, which is determined by the X-ray crystal structure analysis.

Experimental

1) Preparation of Complexes. a) *cis*-α-(1,3-Propanedithiolato)(3,6-diazaoctane-1,8-diamine)cobalt(III) Perchlorate. *cis*-α-[Co(pdt)(trien)]ClO_4. To an ice-cold solution containing 3.1 g (0.01 mol) of *cis*-α-[$Co(Cl)_2$(trien)]Cl in 60 cm^3 of water was added an ice-cold solution containing 1.08 g (0.01 mol) of 1,3-propanedithiol in 40 cm^3 of an 1 mol dm^{-3} NaOH solution of an H_2O-methanol (1 : 1) mixture. The mixture was stirred for 1 h in an ice bath. After removing the precipitate by filtration, about 20 cm^3 of a saturated $NaClO_4$ solution was added to the filtrate and it was kept in a refrigerator for 5 h. The precipitate which appeared was filtered off. The filtrate was concentrated to a half volume and kept in a refrigerator overnight. After this procedure was repeated twice, the desired black complex was collected by filtration. The crude complex was recrystallized from a small amount of water, washed with ethanol and ether, and then dried in a vacuum desiccator. It was found from the absorption and ^{13}C NMR spectral measurements that the complex contained only *cis*-α-[Co(pdt)(trien)]$^+$. Yield: 21%. Found: C, 26.09; H, 5.94; N, 13.52%. Calcd for $C_9H_{24}N_4O_4S_2ClCo \cdot 0.25H_2O$: C, 26.03; H, 5.94; N, 13.49%.

b) *cis*-α-(1,3-Propanedisulfinato)(3,6-diazaoctane-1,8-diamine)cobalt(III) Perchlorate. *cis*-α-[Co(pdsi)(trien)]ClO_4. An excess amount of 8 cm^3 of a 5% H_2O_2 solution was added to a solution containing 0.5 g of *cis*-α-[Co(pdt)(trien)]$ClO_4 \cdot 0.25H_2O$ in 20 cm^3 of water, followed by the addition of 1 cm^3 of a 30% $HClO_4$ solution. The mixture was stirred for 1 h in an ice bath and then kept in a refrigerator overnight. The thiolato complex reacts almost quantitatively with hydrogen peroxide to form the sulfinato complex. The orange crystals which appeared were collected by filtration, washed with ethanol and ether, and then dried in a vacuum desiccator. Orange crystals were obtained more by concentrating the filtrate. Yield: 48%. Found: C, 22.76; H, 5.11; N, 11.82%. Calcd for $C_9H_{24}N_4O_8S_2ClCo$: C, 22.76; H, 5.10; N, 11.80%.

2) Resolution of Complexes. a) *cis*-α-[Co(pdt)(trien)]$^+$. An excess amount (0.5 g) of $Na_2[Sb_2(d\text{-}tart)_2] \cdot 5H_2O$ was added with stirring to a solution containing 0.1 g of *cis*-α-[Co(pdt)(trien)]$ClO_4 \cdot 0.25H_2O$ in 10 cm^3 of water. After the solution was stirred for 3 min, 3 cm^3 of ethanol was added to it and cooled in an ice bath. The precipitate which appeared was filtered. The aqueous solution of the precipitate showed an enantiomeric CD spectrum in the region of 260—650 nm for the filtrate, which contained $(+)^{CD}_{530}$-*cis*-α-[Co(pdt)(trien)]$^+$. This fact seems to indicate that the present complex was partially resolved, because of the small Δε values. However, the complete resolution of this complex was unsuccessful, since the optically active isomer was unstable in the aqueous

solution without the resolving agent.

The partially resolved $(+)^{CD}_{530}$-*cis*-α-[Co(pdt)(trien)]$^+$ isomer could be oxidized by a procedure similar to that used in (1b). This oxidation product showed the identical absorption and CD spectral patterns with $(+)^{CD}_{460}$-*cis*-α-[Co(pdsi)(trien)]$^+$ as in (2b) (vide infra).

b) *cis*-α-[Co(pdsi)(trien)]ClO$_4$. The solution containing 0.4 g of *cis*-α-[Co(pdsi)(trien)]ClO$_4$ in 30 cm^3 of water was poured onto a Dowex 50W-X8 column (Na^+ form, 200—400 mesh, 3.0 cm×20 cm). After sweeping the column with water, the adsorbed band was eluted with a 0.075 mol dm^{-3} aqueous solution of $K_2[Sb_2(d\text{-tart})_2]\cdot H_2O$. Two deep yellow bands were separated completely and then fractionated. It was found from the CD spectral measurements for each of the fractions that the earlier moving band contained $(-)^{CD}_{460}$-*cis*-α-[Co(pdsi)(trien)]$^+$ and the later one contained the $(+)^{CD}_{460}$ isomer. The fractions were combined to two portions and they were concentrated to a small volume with a rotary evaporator below 25 °C. The deposited $K_2[Sb_2(d\text{-tart})_2]$ was filtered off. The filtrate was converted into the perchlorate salt using a QAE-Sephadex A-25 column (ClO_4^- form, 2.5 cm×20 cm) by eluting with water. The eluate was concentrated to a small volume again and kept in a refrigerator overnight. The resulting crystals were collected by filtration. Found: C, 21.82; H, 5.27; N, 11.24%. Calcd for $(-)^{CD}_{460}$-*cis*-α-[Co(pdsi)(trien)]ClO$_4\cdot H_2O$: C, 21.93; H, 5.31; N, 11.36%. A piece of the crystals of the $(-)^{CD}_{460}$ isomer was used for the X-ray crystal structure analysis.

3) General Data. The electronic absorption spectra were recorded on a JASCO UVIDEC-1 or UVIDEC-610 spectrophotometer and the CD spectra on a JASCO J-20 spectropolarimeter. All measurements were carried out in aqueous solution at room temperature. The ^{13}C NMR spectra were recorded in deuterium oxide on a JEOL JNM-FX-100 or-FX-90Q NMR spectrometer at the probe temperature. Sodium 2,2-dimethyl-2-silapentane-5-sulfonate was used as an internal reference. The X-ray analysis calculations were carried out on a Facom M-382 computer in the Science Information Processing Center of the University of Tsukuba.

4) X-Ray Data Collection. Unit cell parameters and intensity data for the single crystal (ca. 0.16×0.20×0.35 mm^3) were measured on a Rigaku-denki four-circle diffractometer (AFC-5) with graphite-monochromatized Mo $K\alpha$ radiation. The unit cell parameters were determined by a least-squares refinement based on 25 reflections. Systematic absences led to the space group $P3_1$ or $P3_2$. The final space group was determined to $P3_1$ by the anomalous scattering technique (vide infra). Crystal Data: $C_9H_{26}N_4O_9S_2ClCo$, M.W.=492.8, trigonal, space group $P3_1$, a=12.350(2), c=10.407(5) Å, V=1374.7(7) Å^3, d_m=1.77 g cm^{-3}, d_x=1.786 g cm^{-3}, Z=3, and μ(Mo $K\alpha$)=1.391 mm^{-1}.

The intensity data were collected by the ω—2θ scan technique up to 2θ=60° with scan rate of 3° min^{-1}. The intensity data were converted to the F_o data in the usual manner. Absorption corrections were not applied. A total of 2453 independent reflections with $|F_o|>3\sigma(|F_o|)$ of the measured 3056 reflections were considered as 'observed' and used for the structure analysis.

5) Determination of the Crystal Structure. The positions of the cobalt atom and the coordinated two sulfur and four nitrogen atoms were determined by the direct method (program MULTAN was used).[8] The difference-Fourier maps based on these atomic positions revealed the other non-hydrogen atoms. The structure was refined by a full-matrix least-squares refinement using the positional parameters, the anisotropic thermal parameters of the non-hydrogen atoms for the complex cation and chloride, and the isotropic thermal parameters for the oxygen atoms of the perchlorate and water molecule (program RFINE[9] was used). Since the positions of the hydrogen atoms of the complex cation were not determined exactly on the difference-Fourier map, we did not add their parameters to the calculation. The neutral atomic scattering factors for all the non-hydrogen atoms were taken from the literatures.[10] The final residual values were R=0.066 and R_w=0.082, respectively.

The absolute configuration was determined by the anomalous scattering technique. When the refinements were carried out by use of a set of the atomic parameters containing the Δ configuration of the complex cation, the residual values converged to R=0.064 and R_w=0.080, respectively. On the contrary, the refinements in the enantiomeric atomic parameters (the Λ configuration) resulted in the residual values of R=0.074 and R_w=0.088, respectively. These facts indicate that the former is probably the correct choice, namely, the complex cation has the Δ configuration (Fig. 1). A similar relationship between the residual values and the absolute configuration was observed for the determination of the crystal structure of cobalt(III) complexes with 2-aminoethaneseleninate.[11,12] The final positional parameters for the Δ-cis-α isomer are listed in Table 1. A list of

Table 1. Positional and Thermal Parameters (with e.s.d.'s)

Atom	x	y	z	B_{eq}/Å^2[a]	Atom	x	y	z	B_{eq}/Å^2[a]
Co	0.1845(1)	0.3320(1)	0.7819[c]	1.54	C3	0.2649(11)	0.4385(11)	0.4881(10)	2.59
S1	0.1346(2)	0.1870(2)	0.6349(3)	1.89	C4	−0.0183(12)	0.3433(10)	0.9095(13)	3.47
S2	0.2183(2)	0.4754(2)	0.6372(3)	1.91	C5	0.0981(12)	0.4669(10)	0.9341(14)	3.40
N1	0.0074(7)	0.2864(7)	0.7945(9)	2.04	C6	0.2429(12)	0.4024(12)	1.0465(11)	3.16
N2	0.2132(9)	0.4510(7)	0.9263(8)	2.37	C7	0.1710(12)	0.2626(11)	1.0503(11)	3.17
N3	0.1732(8)	0.2133(8)	0.9175(9)	2.41	C8	0.2816(11)	0.1910(10)	0.9005(11)	2.62
N4	0.3636(7)	0.3817(8)	0.7733(9)	2.19	C9	0.4005(11)	0.3131(11)	0.8678(13)	3.34
O1	0.0347(8)	0.0652(6)	0.6853(8)	3.05	CL	0.4854(3)	0.2752(3)	0.2376(4)	4.49
O2	0.2457(7)	0.1850(7)	0.5873(8)	2.91	OA1	0.4712(17)	0.1779(19)	0.1485(20)	11.19[b]
O3	0.3259(7)	0.5950(7)	0.6776(8)	3.18	OA2	0.4740(14)	0.3626(14)	0.1718(14)	8.22[b]
O4	0.1053(7)	0.4833(7)	0.6093(7)	2.36	OA3	0.4712(39)	0.2492(38)	0.3525(40)	26.59[b]
C1	0.0665(13)	0.2163(11)	0.4971(12)	3.37	OA4	0.6207(19)	0.3487(17)	0.2658(22)	11.68[b]
C2	0.1615(15)	0.3271(13)	0.4160(14)	4.20	OW	0.8846(16)	0.4390(16)	0.2329(16)	9.69[b]

a) $B_{eq}=8\pi^2(U_{11}+U_{22}+U_{33})/3$. b) Isotropic temperature factor. c) The z coordinate is held constant.

structure factors (Table A), anisotropic thermal parameters (Table B), and bond lengths and angles of the perchlorate ion (Table C) is kept at the Chemical Society of Japan as Document No. 8747.

Results and Discussion

Description of the Structure. A perspective drawing of the complex cation, $(-)^{CD}_{460}$-[Co(pdsi)(trien)]$^+$, is given in Fig. 1,[13] together with a numbering scheme. The bond lengths and angles (with their standard deviations) in the complex cation are summarized in Table 2. The coordination geometry around cobalt atom is approximately octahedral. The trien, which coordinates as a quadridentate ligand, takes the cis-α configuration by coordination.[14] The pdsi ligand coordinates to the cobalt atom through two sulfur atoms to form the six-membered chelate ring. This indicates that the treatment of the thiolato complex with hydrogen peroxide proceeds without the linkage isomerization as in the case of the cobalt(III) complexes with the sulfinate ligands,[15] although the linkage isomerization was observed for the sulfinato complex[16] obtained by the photochemical preparation and the seleninato complex.[11]

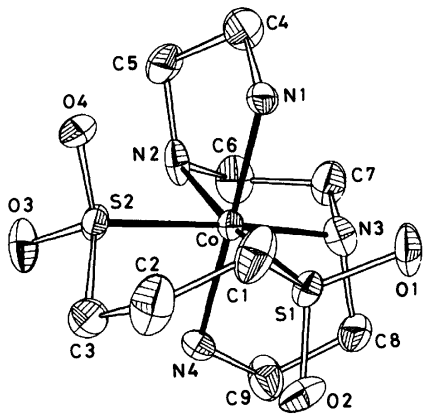

Fig. 1. Perspective view of $(-)^{CD}_{460}$-Δ-*cis*-α-[Co(pdsi)(trien)]$^+$ ion with the numbering scheme.

For *cis*-α-[Co(pdsi)(trien)]$^+$, the optical isomers, Δ and Λ, are possible.[17] The result of the X-ray crystal structure analysis indicates that the absolute configuration of the $(-)^{CD}_{460}$ isomer takes the Δ configuration and the two asymmetric nitrogen atoms in the trien have the absolute configuration S. In the trien ligand, the two outer chelate rings take the unsymmetrical skew form with the λ conformation. The central chelate ring takes nearly symmetrical skew form with the δ conformation. Similar conformational relationship of the chelate rings was also observed for the L-3,8-dimetrien (δλδ conformation) in $(-)_{589}$-*Λ-cis*-α-[$Co(NO_2)_2$(L-3,8-dimetrien)]$^+$,[4,5] where L-3,8-dimetrien denotes (2*S*,7*S*)-2,7-dimethyl-3,6-diazaoctane-1,8-diamine. The pdsi has the symmetrical skew boat form with the λ conformation. Thus, the complex cation of the $(-)^{CD}_{460}$-Δ-cis-α isomer has an approximately two-fold axis.

In $(-)^{CD}_{460}$-*Δ-cis*-α-[Co(pdsi)(trien)]$^+$, the bond lengths and angles around the sulfinato group are almost equal to those in [Co(aesi-*N*,*S*)$(en)_2$]$^{2+}$,[15] except for the angles of Co-S-C (111.2(5) and 110.1(5)° for the pdsi complex and 100.1(2)° for the aesi one) which seem to depend on the difference between the pdsi and aesi chelate rings, where aesi denotes 2-aminoethanesulfinate. The bond lengths and angles for the trien are similar to those for $(-)_{589}$-*cis*-α-[$Co(NO_2)_2$(L-3,8-dimetrien)]ClO_4,[4] except for the Co-N distances. The mean value of the Co-N distance in the pdsi complex, 1.987(9) Å, is significantly longer than the corresponding distance (1.952(7)) Å in $(-)_{589}$-*cis*-α-[$Co(NO_2)_2$(L-3,8-dimetrien)]ClO_4[4] and those (1.95(2) and 1.955(9) Å) in *cis*-β-[Co(*S*-pro)(trien)]$^+$.[18] Lange et al. reported the structural trans effect that the Co-N distance for the group trans to the sulfur atom in the sulfinato group

Table 2. Intermolecular Distances and Bond Angles (with e.s.d.'s)

	(a) Bond distances (*l*/Å)					
Co-S1	2.196(3)	Co-S2	2.200(3)	S2-Co-N4	89.2(3)	N1-Co-N2	85.6(4)
Co-N1	1.971(9)	Co-N2	2.007(9)	N1-Co-N3	94.8(4)	N1-Co-N4	178.3(4)
Co-N3	1.988(10)	Co-N4	1.980(9)	N2-Co-N3	86.0(4)	N2-Co-N4	92.6(4)
S1-O1	1.484(7)	S1-O2	1.471(10)	N3-Co-N4	85.2(4)	Co-S1-O1	109.4(4)
S1-C1	1.788(15)	S2-O3	1.470(7)	Co-S1-O2	111.4(3)	Co-S1-C1	111.2(5)
S2-O4	1.475(10)	S2-C3	1.791(12)	O1-S1-O2	114.3(6)	O1-S1-C1	104.6(5)
N1-C4	1.50(2)	N2-C5	1.53(2)	O2-S1-C1	105.7(6)	Co-S2-O3	109.0(4)
N2-C6	1.51(2)	N3-C7	1.52(2)	Co-S2-O4	112.5(3)	Co-S2-C3	110.1(5)
N3-C8	1.51(2)	N4-C9	1.51(2)	O3-S2-O4	113.6(5)	O3-S2-C3	105.0(5)
C1-C2	1.53(2)	C2-C3	1.53(2)	O4-S2-C3	106.3(6)	Co-N1-C4	112.6(7)
C4-C5	1.51(1)	C6-C7	1.50(2)	Co-N2-C5	107.3(7)	Co-N2-C6	108.5(8)
C8-C9	1.53(1)			C5-N2-C6	115.7(10)	Co-N3-C7	111.1(8)
				Co-N3-C8	108.1(6)	C7-N3-C8	112.1(10)
				Co-N4-C9	113.6(6)	S1-C1-C2	113.2(10)
	(b) Bond angles (φ/°)			C1-C2-C3	117.1(11)	S2-C3-C2	115.1(9)
S1-Co-S2	92.4(1)	S1-Co-N1	89.7(3)	N1-C4-C5	107.0(10)	N2-C5-C4	109.8(11)
S1-Co-N2	173.8(2)	S1-Co-N3	90.3(3)	N2-C6-C7	111.1(9)	N3-C7-C6	108.6(9)
S1-Co-N4	92.1(3)	S2-Co-N1	90.7(3)	N3-C8-C9	110.5(11)	N4-C9-C8	106.7(10)
S2-Co-N2	91.7(3)	S2-Co-N3	173.9(2)				

was longer than the other Co-N distances in [Co(aesi-*N*,*S*)(en)$_2$]$^{2+}$.[15] Therefore, the lengthening of the Co-N distances in the present pdsi complex seems to depend on the trans effect for the two sulfinato groups.

^{13}C NMR Spectra. The ^{13}C NMR spectrum of $(-)^{CD}_{460}$-*Δ-cis-α*-[Co(pdsi)(trien)]$^+$ exhibits five resonance lines (20.37, 46.21, 55.20, 58.08, and 58.35 ppm) due to the nine methylene carbon atoms. This indicates that the $(-)^{CD}_{460}$-Δ-cis-α isomer has C_2 symmetry in an aqueous solution as well as in the crystalline state. The spectrum of [Co(pdt)(trien)]$^+$ exhibits also five resonance lines (24.05, 35.11, 46.43, 57.05, and 57.43 ppm) due to the nine methylene carbon atoms, indicating the C_2 symmetry. Further, [Co(pdt)(trien)]$^+$ reacts with hydrogen peroxide to give selectively *cis-α*-[Co(pdsi)(trien)]$^+$. Similar oxidation reaction has proceeded with retention of the geometrical configuration in the reaction of the thiolato cobalt(III) complexes with hydrogen peroxide.[11,19] These facts indicate that [Co(pdt)-(trien)]$^+$ takes the cis-α configuration.

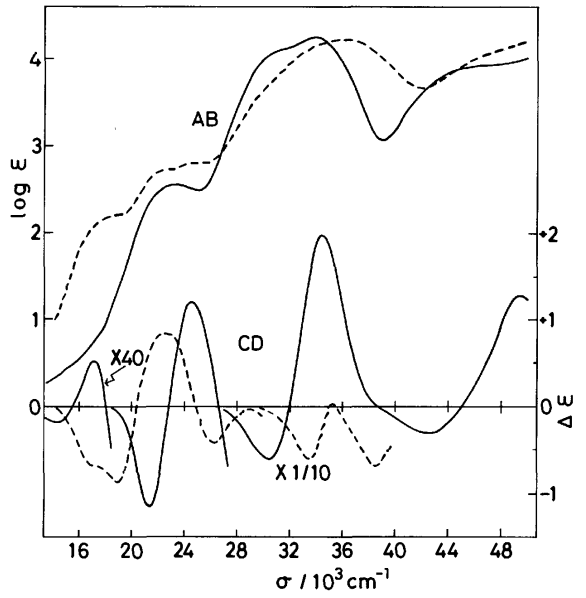

Fig. 2. Absorption and CD spectra of $(-)^{CD}_{460}$-Δ-*cis*-α-[Co(pdsi)(trien)]$^+$ (——) and $(-)^{CD}_{530}$-*cis*-α-[Co(pdt)(trien)]$^+$ (----).

Electronic Absorption and CD Spectra. The electronic absorption and CD spectra of $(-)^{CD}_{460}$-*Δ-cis-α*-[Co(pdsi)(trien)]$^+$ are shown in Fig. 2, together with the corresponding thiolato complex, $(-)^{CD}_{530}$-*cis-α*-[Co(pdt)(trien)]$^+$, and their data are summarized in Table 3. The absorption spectrum of $(-)^{CD}_{460}$-Δ-*cis-α*-[Co(pdsi)(trien)]$^+$ exhibits a broad band at 23.26×10^3 cm^{-1}, similar to those of the cobalt(III) complexes including the sulfinate group.[11] The CD bands of the $(-)^{CD}_{460}$-Δ-cis-α pdsi isomer in this region exhibit a negative and a positive signs from the lower energy (Fig. 2). This CD spectral behavior of the Δ-sulfinato complex is consistent with those of the trien type cobalt(III) complexes.[1-6] which have been successfully assigned to the Δ configuration.

For $(-)^{CD}_{460}$-*Δ-cis-α*-[Co(pdsi)(trien)]$^+$, the intense and broad absorption band in the region of 27—37×10^3 cm^{-1}, which is assigned to the sulfur-to-metal charge-transfer transition,[7,19-21] is composed of two components at ca. 31.50 and 33.94×10^3 cm^{-1} (Fig. 2). This absorption spectral behavior is characteristically observed for the cis(S) geometry of the cobalt(III) complexes with the thiolate and sulfinate ligands.[7,20,21] In this absorption band region, $(-)^{CD}_{460}$-*Δ-cis-α*-[Co(pdsi)-(trien)]$^+$ exhibits the two CD bands with the opposite signs ((−) and (+) from the lower energy). According to the empirical estimation,[7] which a negative and a positive CD bands from the lower energy are favorable

Table 3. Absorption and CD Spectral Data of $(-)^{CD}_{460}$-*cis-α*-[Co(pdsi)(trien)]$^+$ and $(-)^{CD}_{530}$-*cis-α*-[Co(pdt)(trien)]$^+$

Complex	Absorption maxima σ/10^3 cm^{-1}	CD extrema σ/10^3 cm^{-1}
	log ε/mol^{-1} dm^3 cm^{-1}	Δε/mol^{-1} dm^3 cm^{-1}
$(-)^{CD}_{460}$-*cis-α*-[Co(pdsi)(trien)]$^+$	23.26 (2.55)	14.43 (−0.005)
	31.50 (4.12 sh)	17.12 (+0.013)
	33.94 (4.25)	21.36 (−1.154)
	46.51 (3.93 sh)	24.51 (+1.206)
		30.40 (−6.076)
		34.36 (+19.982)
		42.37 (−2.953)
		49.26 (+12.830)
$(-)^{CD}_{530}$-*cis-α*-[Co(pdt)(trien)]$^+$	18.69 (2.19 sh)	17.15 (− sh)
	22.42 (2.72 sh)	18.80 (−)
	25.00 (2.80)	22.47 (+)
	33.33 (4.11 sh)	26.32 (−)
	36.10 (4.22)	33.56 (−)
		35.09 (+)
		38.46 (−)

sh denotes a shoulder.

for the Λ configuration, the present $(-)^{CD}_{460}$-Δ-cis-α pdsi isomer may be assigned to the Λ configuration.

The absorption spectrum of $(-)^{CD}_{530}$-*cis*-α-[Co(pdt)-(trien)]$^+$ coincides with the cis(S) cobalt(III) complexes with L-penicillaminate[20] and the [Co(amine)$_4$-(thiolato)$_2$]-type complexes.[7,21] In the first absorption and sulfur-to-metal charge-transfer band regions, the $(-)^{CD}_{530}$-*cis*-α pdt isomer exhibits a similar CD spectral pattern to $(-)^{CD}_{460}$-*Λ*-*cis*-α-[Co(pdsi)(trien)]$^+$, although the intensities are shown by an arbitrary scale (Fig. 2). Further, the absorption and CD spectra of the oxidation product, which was obtained by the reaction of $(+)^{CD}_{530}$-*cis*-α-[Co(pdt)(trien)]$^+$ with hydrogen peroxide, exhibit the identical patterns with those of the $(+)^{CD}_{460}$-*Λ*-*cis*-α-[Co(pdsi)(trien)]$^+$ (Fig. 2). Accordingly, these facts suggest that $(-)^{CD}_{530}$-*cis*-α-[Co(pdt)(trien)]$^+$ takes the Δ configuration.

The authors wish to express thanks to Miss Yuko Hanada and Mrs. Yoko Koizumi for their aids in the experiment. This work was supported by a Grant-in-Aid for Scientific Research No. 60470043 from the Ministry of Education, Science and Culture.

References

1) A. M. Sargeson and G. H. Searle, *Inorg. Chem.*, **4**, 45 (1965).
2) A. M. Sargeson and G. H. Searle, *Inorg. Chem.*, **6**, 787 (1967).
3) M. Saburi, T. Sawai, and S. Yoshikawa, *Bull. Chem. Soc. Jpn.*, **45**, 1086 (1972).
4) M. Ito, F. Marumo, and Y. Saito, *Acta Crystallogr., Sect. B*, **28**, 457 (1972).
5) Y. Saito, "Inorganic Molecular Dissymmetry," in Inorganic Chemistry Concepts 4, Springer-Verlag, Berlin (1979).
6) M. Shibata. "Modern Syntheses of Cobalt(III) Complexes," in Topics in Current Chemistry, Springer-Verlag, Berlin (1983).
7) K. Yamanari, N. Takeshita, and Y. Shimura, *Bull. Chem. Soc. Jpn.*, **57**, 2852 (1984).
8) G. Germain, P. Main, and M. M. Woolfson, *Acta Crystallogr., Sect. A*, **27**, 368 (1971).
9) L. W. Finger, RFINE-2, Geophysical Lab. Carnegie Institution, Washington, D. C. 1972.
10) "International Tables for X-Ray Crystallography," Kynoch Press, Birmingham (1974), Vol. IV; D. T. Cromer and J. B. Mann, *Acta Crystallogr., Sect. A*, **24**, 321 (1966).
11) K. Okamoto, T. Konno, M. Nomoto, H. Einaga, and J. Hidaka, *Bull. Chem. Soc. Jpn.*, **57**, 1494 (1984).
12) K. Okamoto, T. Yasui, and J. Hidaka, *Chem. Lett.*, **1987**, 551.
13) C. K. Johnson, ORTEP II. Report ORNL-5138. Oak Ridge National Lab., Tennessee (1976).
14) The cis-α isomer corresponds to Refs. 2—6.
15) B. A. Lange, K. Libson, E. Deutsch, and R. C. Elder, *Inorg. Chem.*, **15**, 2985 (1976).
16) H. Macke, V. H. Houlding, and A. W. Adamson. *J. Am. Chem. Soc.*, **102**, 6889 (1980); V. H. Houlding, H. Macke, and A. W. Adamson, *Inorg. Chem.*, **20**, 4279 (1981).
17) *Inorg. Chem.*, **9**, 1 (1970).
18) H. C. Freeman and I. E. Maxwell, *Inorg. Chem.*, **9**, 649 (1970); H. C. Freeman, L. G. Marzilli, and I. E. Maxwell, *Inorg. Chem.*, **9**, 2408 (1970).
19) T. Konno, K. Okamoto, H. Einaga, and J. Hidaka, *Bull. Chem. Soc. Jpn.*, **58**, 1119 (1985), and references sited therein.
20) K. Okamoto, K. Wakayama, H. Einaga, S. Yamada, and J. Hidaka, *Bull. Chem. Soc. Jpn.*, **56**, 165 (1983).
21) K. Yamanari. N. Takeshita, T. Komorita, and Y. Shimura, *Chem. Lett.*, **1981**, 861.

 © 1987 The Chemical Society of Japan Bull. Chem. Soc. Jpn., 60, 2881—2885 (1987)

Control of the Impregnation Profile of Co in an Al_2O_3 Sphere

Masashi Otsuka, Takeshi Fujiyama, Yoshikazu Tsukamoto,
Hideyasu Tsuiki, and Akifumi Ueno*
Department of Materials Science, Toyohashi University of Technology, Tempakucho, Toyohashi, Aichi 440
(Received February 16, 1987)

A radial distribution of cobalt metal particles in an alumina sphere was controlled by impregnation of the spheres with a solution composed of cobalt nitrate dissolved in ethylene glycol, ethyl silicate, and a small amount of nitric acid. The radial position of cobalt narrow band in the sphere was varied with the impregnation time and the cobalt loading was controlled by the concentration of cobalt nitrate in the impregnation solution. It was also found that porous SiO_2 film resulted from the gelling of ethyl silicate covered whole external surface of the sphere.

From the viewpoints of catalyst durability and poison, a control of the impregnation profile of an active component in a support sphere has been desired for catalysts of practical use; especially for steam reforming and automotive catalysts.[1,2] Four kinds of profiles are well-known, designated as uniform, egg shell, egg white, and egg yolk,[3] respectively. The uniform and egg shell types of catalysts are considered to be applied for reactions whose rate determining steps are in the reactions between surface species or in the diffusions of reactant molecules.[4] These profiles are easily achieved by control of the impregnation time[5] or by alteration of the starting materials of the catalyst constituents.[6] While the egg white and egg yolk types of catalysts are often employed to minimize the catalysts poison or the loss of active components during operations.[4] The preparation of catalysts with these profiles requires proper additions to the impregnating solutions. As additives to control the impregnation profiles, citric acid,[7] oxalic acid,[8] urea,[9] and nitric acid[10] have often been employed. These additives are volatile and decomposed when the catalysts are calcined at high temperature.

Besides the technical developments, theoretical approaches to the control of impregnation profiles have been studied by Vincent and Merril[11] with an assumption of one dimensional diffusion of metal ions in micropores of a catalyst support. Komiyama et al.[12] developed the assumption to three-dimensional diffusion of metal ions and showed that this model was consistent with an actual impregnation profile of Ni in an alumina sphere. Despite these advanced techniques and theories, impregnation profiles are not always reproducible, probably because of the heterogeneity of solid surfaces and the lack of knowledge about micropore structure.[13]

In conventional impregnation, free metal ions are formed in the impregnating solution and are ready to penetrate in micropores of support spheres when the spheres are immersed. The size of free metal ions is generally considered to be smaller than those of the micropores in the support spheres. What will happen in the impregnation profile and the metal loading, if macromolecules, larger than the micropores in size, containing metal ions are in the impregnating solution? The present work was done to answer this question using the impregnating solution composed of cobalt nitrate dissolved in ethylene glycol and ethyl silicate. In our earlier paper,[14] the solution consisting of a metal nitrate dissolved in ethylene glycol and ethyl silicate was proved to form macromolecules containing $(-M-O-Si-)_n$ structures, where M represents the metal ion.

Experimental

Impregnation Procedure. $Co(NO_3)_2 \cdot 6H_2O$ (8.9 g) was dissolved in 153 ml of ethylene glycol (EG) at 80 °C and then pored into 30 ml of ethyl silicate at the same temperature with 3 ml of nitric acid. The solution (pH=1) was transparent and colored pale violet. Alumina spheres (5 g) with 3 mm of diameter and 298 m^2g^{-1} of BET surface area were immersed with the solution at room temperature. The impregnation time was varied from 1 min to 30 h. After the impregnation, the spheres were dried at 110 °C in an oven for

Table 1. Procedure for the Preparation of Catalyst with the Controlled Impregnation Profile of Cobalt

$Co(NO_3)_2 \cdot 6H_2O$
EG →
$Si(OC_2H_5)_4$ →
HNO_3 →
↓
Stirring at R.T. for 2 h
↓
Immersing Al_2O_3 beads (3 mmϕ)
↓
Gelling in steam
↓
Dry at 110 °C for 24 h
↓
Calcination in air at 300 °C for 4 h
↓
Reduction in H_2 at 900 °C for 4 h
↓
$Co/SiO_2/Al_2O_3$

24 h and then calcined at 300 °C for 4 h in air, followed by reduction at 900 °C in flowing hydrogen. The impregnation conditions were settled above unless specified. The amount of $Co(NO_3)_2 \cdot 6H_2O$ in EG could be varied, if necessary.

The impregnation procedure employed in this work is summarized in Table 1.

EPMA Measurement. The shperes thus impregnated were mounted in a polyester support and the support was polished with fine alumina powder until the cross section of a sphere appeared. The alumina powder adhered to the support was removed by ultrasonication. In order to avoid charge-up phenomenon, Pt was evaporated over the support surface. The radial distributions of Co and Si in the sphere was measured by electron probed X-ray microanalyser (EPMA, Hitachi model X-650), operated at an accelerating voltage of 20 kV with an energy dispersion detector.

Measurement of Co Loading. The impregnated spheres calcined at 300 °C were ground and then mixed with the appropriate amount of $Na_2B_4O_7$ to be fired at 1000 °C in platinum crucible. In a B_2O_3 disk thus prepared, the catalyst constituents were well dispersed and the disk was subjected to X-ray fluorescence spectrometer (Rigaku Denki, Model 3080), operated at 50 kV with a filament current of 50 mA to generate Rh $K\alpha$ radiation.

Pore Size Measurements. The micropore size distributions of bare alumina spheres and the impregnated spheres reduced at 900 °C were measured with a porosimeter (Carlo Erva, Sorptmatic 1800) using nitrogen as a sorption gas at the liquid nitrogen temperature.

Results

Radial Distribution of Cobalt. Typical photographs of the cross sections of reduced catalysts and the associated EPMA profiles are given in Fig. 1. The position of the narrow cobalt band in the catalyst sphere was proved to shift into the center of sphere with increasing the impregnation time, as shown in Fig. 2. The bars given in Fig. 2 represent the width of the Co metal bands in the impregnated catalysts. The loading of cobalt in the reduced catalyst was found not

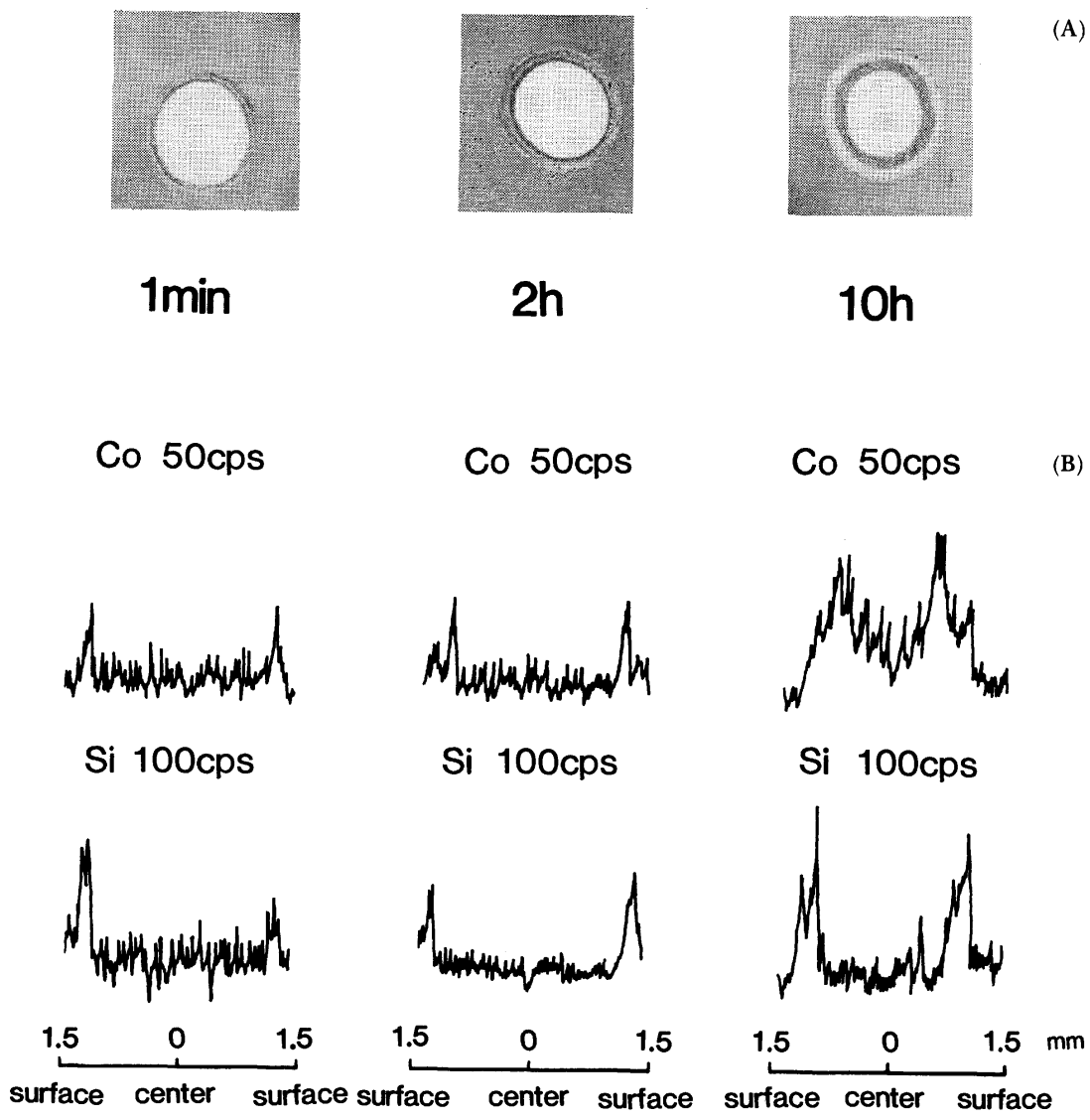

Fig. 1. Typical photographs of the cross sections of impregnated catalysts (A) and the associated EPMA profiles (B) with various impregnation times.

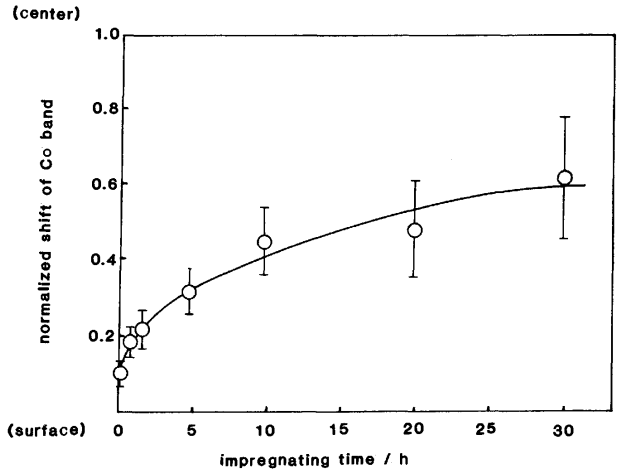

Fig. 2. Shift of the narrow cobalt band in the alumina sphere with the impregnation time; the distance from the center of the sphere was normalized in this Figure.

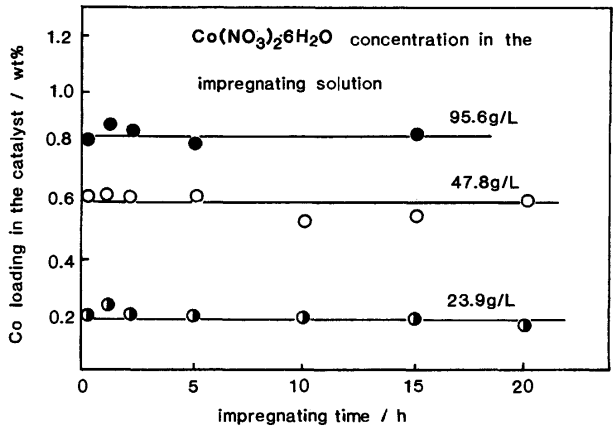

Fig. 3. Change in Co loading with the impregnation time; the concentrations of cobalt nitrate in the impregnation solutions were 23.9, 47.8, and 95.6 g L^{-1}, respectively.

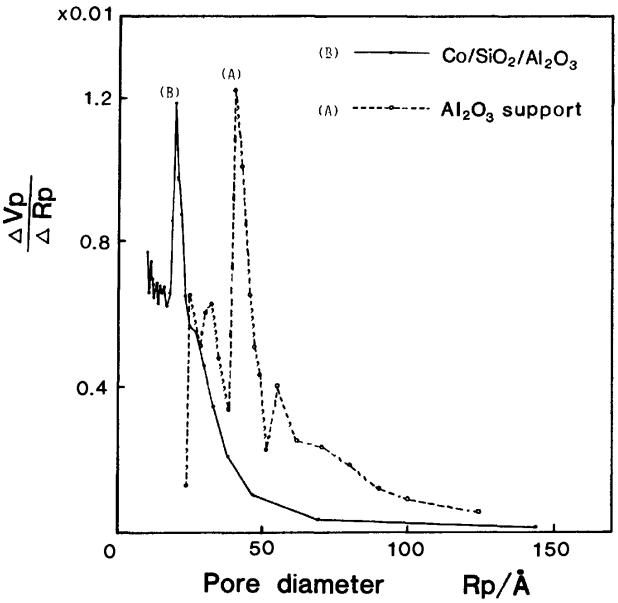

Fig. 4. Pore size distributions of the alumina sphere (A) and the impregnated catalyst (B).

to depend upon the impregnation time but to depend upon the concentration of cobalt nitrate in the impregnating solution (see Fig. 3).

Distribution of Si. On the contrary, Si was observed on the external surface of spheres, forming thin SiO_2 film, revealed by EPMA profiles shown in Fig. 1. The apparent thickness of this SiO_2 film was estimated less than 50 μm from an EPMA result shown in Fig. 4.

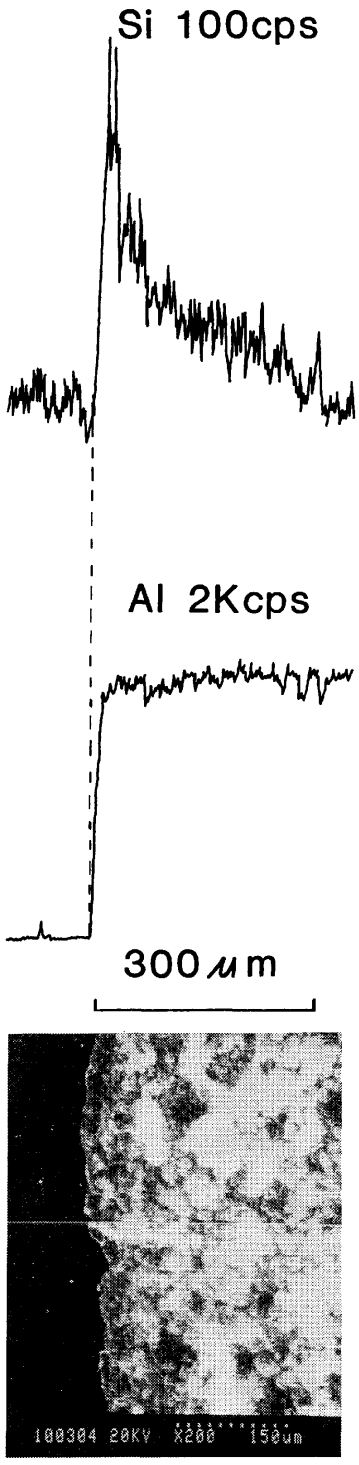

Fig. 5. EPMA profile of the impregnated catalyst at its fringe.

Pore Size Distribution. Pore size distributions of bare alumina spheres and the reduced catalyst are depicted in Fig. 5. The pore size of the bare alumina was sharply distributed at about 45 Å, while that of the reduced catalyst was observed at 20 Å. Thus, the mean pore size of alumina spheres was found to shift to the smaller one when they were immersed with the impregnation solution employed. The pore volume of the reduced catalyst was 0.36 ml g^{-1}, almost the same as that of the bare alumina spheres, 0.33 ml g^{-1}, nevertheless the specific surface area of the reduced catalyst decreased to 256 m^2g^{-1}.

Discussion

As was mentioned previously,[14] metal nitrate dissolved in ethylene glycol forms the metal glycolate as follows;

$$\begin{matrix} H_2C\text{-}OH \\ | \\ H_2C\text{-}OH \end{matrix} + Co(NO_3)_2 \longrightarrow \begin{matrix} H_2C\text{-}O \\ | \quad \diagdown \\ \quad\quad Co \\ | \quad \diagup \\ H_2C\text{-}O \end{matrix} + 2H^+ + 2NO_3^- \qquad (1)$$

The metal glycolate thus produced reacts with tetraethyl silicate to form the species containing -M-O-Si-structure according to the following reaction;

$$\begin{matrix} H_2C\text{-}O \\ | \quad \diagdown \\ \quad\quad Co \\ | \quad \diagup \\ H_2C\text{-}O \end{matrix} + 2Si(OEt)_4 \longrightarrow (EtO)_3Si\text{-}O\text{-}Co\text{-}O\text{-}Si(OEt)_3 + (EtO)\text{-}CH_2\text{-}CH_2\text{-}(OEt). \qquad (2)$$

The reaction between the species containing -M-O-Si- structure results in the three-dimensional expansion of -M-O-Si- structure producing Et-O-Et, diethyl ether. Thus, macromolecules possessing cobalt ions are produced in the impregnating solution employed in this work. If the size of these macromolecules is smaller than that of the micropores on the alumina spheres, the macromolecules may penetrate into the spheres. The EPMA profiles given in Fig. 1 showed that Si ions in the macromolecules are deposited over the external surface of the sphere forming SiO_2 thin film but not inside the sphere. This indicates that the size of the macromolecule is larger than 50 Å, since the micropore size of the alumina spheres is sharply distributed at 50 Å (see Fig. 5). When alumina spheres with micropores sized around 100 Å were immersed with the solution, Si ions were clearly observed inside the spheres by EPMA, suggesting that the macromolecules are sized smaller than 100 Å. Once an appropriate amount of macromolecules adhered over the surface of sphere, no more molecules seem to adsorb on the sphere. This resulted in the constant loading of cobalt ions in the catalyst even when the impregnation time was prolonged (see Fig. 3). By changing the concentration of cobalt nitrate in the impregnating solution, the cobalt concentration in the macromolecules may change, hence the cobalt loading in the catalyst can be controlled by the concentration of cobalt ions in the solution, as also could be seen in Fig. 3.

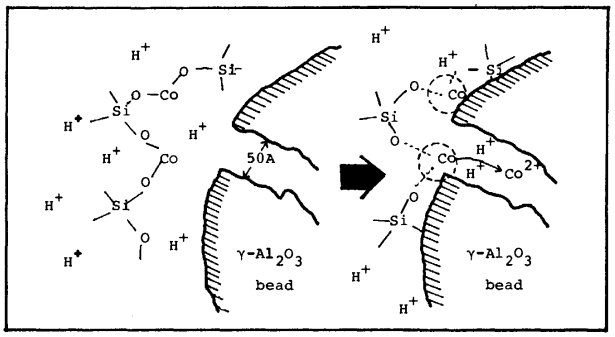

Fig. 6. Model of the mechanism for controlled impregnation profile and formation of SiO_2 thin film.

The impregnation mechanism was imagined as shown in Fig. 6. The $(\text{-M-O-Si-})_n$ structures in adsorbed macromolecules may decompose somehow on the alumina surface and the cobalt ions eliminated diffuse into the spheres,competing with H^+ ions[15] produced by the Reaction 1 and originating from nitric acid added. H^+ ions may adsorb more strongly on alumina than cobalt ions, resulting that the position of cobalt ions adsorbed moved to the center of the sphere with increasing the impregnation time. Thus, the cobalt narrow band is achieved as shown in Fig. 1. The SiO_2 film was not deposited inside the micropores of the reduced catalyst but just over their external surface, since the pore volumes of the bare alumina spheres and the reduced catalyst are almost the same with each other.

It must be mentioned that when the alumina spheres with the pore size of 50 Å were immersed with mere tetraethyl silicate, i.e., monomeric tetraethyl silicate, Si ions were observed not only on the surface but inside the spheres of the reduced catalyst.

Conclusion

The impregnation profile of cobalt in alumina spheres was controlled by the impregnation time of alumina shperes with the micropore sized around 50 Å, the impregnating solution consisting of cobalt nitrate dissolved in ethylene glycol, tetraethyl silicate, and a small amount of nitric acid. The cobalt loading in the catalyst was adjusted by the concentration of cobalt nitrate in the impregnating solution. Thus, by employing an appropriate solution both the impregnation profile and the loading of cobalt in the alumina sphere can be simultaneously controlled. On the external surface of the reduced catalyst thus produced was found to be covered with thin and porous SiO_2 film, the pore size on this SiO_2 film being sharply distributed at 20 Å.

The mechanism and the driving force of the decomposition of macromolecules containing $(-M-O-Si-)_n$ structures over the alumina surface are still unrevealed in the present work.

The authors express their thanks to Dr. Goro Satoh at Shokubai Kasei Company for supplying alumina spheres and to Dr. Akio Furuta at Nikki (JGC) company for measurements of micropore sizes of various catalysts and alumina spheres.

References

1) L. L. Hegedus, T. S. Chou, J. C. Summers, and N. M. Potter, "Preparation of Catalysts II," ed by B. Delmon, P. A. Jacobs, and G. Poncelet, Elsevier Sci. Pub. Co., Amsterdam (1978), p. 171.

2) J. C. Summers and L. L. Hegedus, *J. Catal.*, **51**, 185 (1978).

3) I. Kobiya, "Preparation of Catalysts (Shokubai Chosei)," ed by A. Ozaki, Kodansha Pub. Co., Tokyo (1980), p. 56.

4) E. R. Becker and J. Wei, *J. Catal.*, **48**, 365 (1977).

5) A. W. Adamson, "Physical Chemistry of Surfaces," Interscience Pub. Co., New York (1960), p. 264; Y. Ogino, *Shokubai*, **19**, 334 (1977).

6) M. Kotter and L. Riekert, "Preparation of Catalyst II," ed by B. Delmon, Elsevier Pub. Co., Amsterdam (1979), p. 51.

7) E. R. Becker and T. A. Nuttall, "Preparation of Catalyst II," ed by B. Delmon, Elsevier Pub. Co., Amsterdam (1979), p. 159.

8) E. Michelko, U. S. Patent, 3259454, 3259589 (1966).

9) T. Hori, Jpn. Patent, 54-136589, 149391 (1979).

10) R. W. Maatmann, *Ind. Eng. Chem.*, **51**, 913 (1959).

11) R. C. Vincent and R. P. Merrill, *J. Catal.*, **35**, 209 (1974).

12) M. Komiyama, R. P. Merrill, and H. F. Harnsberger, *J. Catal.*, **63**, 35 (1980).

13) P. M. Tewari and W. J. Lee, *J. Colloid Interface Sci.*, **52**, 77 (1975).

14) A. Ueno, H. Suzuki, and Y. Kotera, *J. Chem. Soc., Faraday Trans. 1*, **79**, 127 (1983); K. Tohji, Y. Udagawa, S. Tanabe, and A. Ueno, *J. Am. Chem. Soc.*, **106**, 612 (1984).

15) I. Kobiya, "Preparation of Catalysts (Shokubai Chosei)," ed by A. Ozaki, Kodansha Pub. Co., Tokyo (1980), p. 59.

 © 1987 The Chemical Society of Japan Bull. Chem. Soc. Jpn., 60, 2887—2889 (1987)

Mössbauer and DTA Studies on the Structure of Semiconducting Sodium Vanadate Glasses

Tetsuaki NISHIDA,* Michiko OGATA, and Yoshimasa TAKASHIMA
Department of Chemistry, Faculty of Science, Kyushu University 33, Hakozaki, Higashiku, Fukuoka 812
(Received March 6, 1987)

Distinct decreases in the quadrupole splitting of the tetrahedral Fe^{3+} ions and the T_g suggest a gradual change from the layer structure composed of the VO_5 tetragonal pyramids to the chain structure composed of the VO_4 tetrahedra. It is also concluded that nonbridging oxygen atoms are present in the VO_4 tetrahedra.

Structural study of the crystalline V_2O_5 has been performed by Byström et al.[1] and Jansen and Sperlich.[2] They revealed that each V^{5+} ion is surrounded by five oxygen atoms making a distorted tetragonal pyramid, which can also be viewed as a distorted trigonal bipyramid, sharing edges and corners to form a layer structure. An IR study of several vanadate glasses performed by Dimitriev et al.[3] revealed that the introduction of alkali or alkaline earth oxides into the V_2O_5 matrix results in a destruction of the layer structure followed by a formation of tetrahedral VO_4 units. Dimitriev et al.[3] also elucidated that only the VO_4 units are present in the skeleton of metavanadate glasses. The same conclusion has been obtained in an NMR study of KVO_3 glass.[4] The crystal structure of the alkali metavanadate crystals including the KVO_3 is known to be composed of chains of VO_4 tetrahedra.[5] Dimitriev et al.[3] also revealed that the introduction of other kind of oxides which play a role of a network former, such as SiO_2, B_2O_3, GeO_2, and TiO_2, affects little structural change on the skeleton of the V_2O_5-based glass originally made of only VO_5 units.[1,2] On the other hand, a neutron diffraction study performed by Wright et al.[6] revealed that the coordination number of the vanadium is always 5 in P_2O_5-V_2O_5, BaO-V_2O_5, and PbO-V_2O_5 glasses irrespective of the glass composition, and that the skeleton of the vanadate glasses is composed of the interconnected and distorted VO_5 tetragonal pyramid. It should be noted that the neutron diffraction study by Wright et al.[6] has not been performed for alkali vanadate glasses. Similar conclusion has been obtained in a simultaneous EXAFS and XANES study of P_2O_5-V_2O_5 glass.[7] Besides the VO_4 and the VO_5 units described above, the presence of octahedral VO_6 units has been proposed based on the ESR measurements of the V^{4+} (VO^{2+}) ions.[8,9] Mössbauer spectroscopy has been utilized for the structural study of potassium vanadate glasses,[10] where the present authors revealed that all the Fe^{3+} ions are tetrahedrally coordinated by oxygen atoms at the substitutional sites of the V^{5+} or V^{4+} ions constituting the VO_4 tetrahedra.

The present Mössbauer study was carried out in order to elucidate the structure of the sodium vanadate glasses. DTA measurements were performed in order to know the structural change through the glass transition temperature (T_g), because the T_g is known to reflect a change in the coordination number of the network-forming atoms and a formation of nonbridging oxygen atoms.[10]

Experimental

Sodium vanadate glasses were prepared by fusing the individual mixtures (1 g) of commercially available Na_2CO_3, V_2O_5, and Fe_2O_3, of guaranteed reagent grade, at 950 °C for 1 h in an electric muffle furnace. After the fusion in the ambient atmosphere, each melt in a platinum crucible was quenched with ice-cold water. The vanadate glasses were tried to prepare in the compositional ranges of 0 mol%$\leqslant$ $Na_2O\leqslant$40 mol%, 50 mol%$\leqslant V_2O_5\leqslant$90 mol%, and 0 mol%$\leqslant$ $Fe_2O_3\leqslant$30 mol%. All the glass samples prepared in the present study are almost black in color. Mössbauer and DTA measurements were performed for the pulverized glasses similarly to the case of the potassium vanadate glasses.[10]

Results and Discussion

The glass-forming region for the ternary Na_2O-V_2O_5-Fe_2O_3 glass system is shown in Fig. 1, where open and closed circles indicate the formations of glass and non-glassy (devitrified) samples, respectively. A Mössbauer spectrum of the sodium vanadate glasses measured at room temperature is shown in Fig. 2, which indicates the presence of paramagnetic Fe^{3+} ions of high spin state.[11,12] The isomer shift and the linewidth of the absorption peaks are located in the ranges of 0.39—0.35 and 0.53—0.47 mm s^{-1}, respectively. As to the coordination number of the iron in glasses, earlier results are reviewed by Kurkjian[13] and Coey.[14] Recent Mössbauer results on the structure of

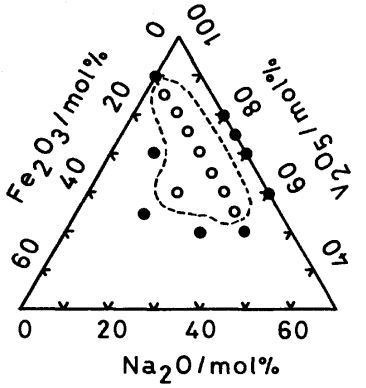

Fig. 1. Glass-forming region of the Na_2O-V_2O_5-Fe_2O_3 system.

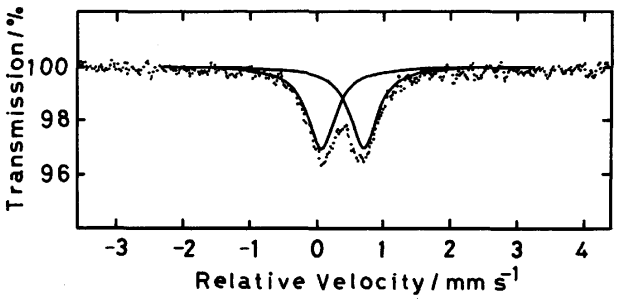

Fig. 2. Mössbauer spectrum of the $25Na_2O \cdot 65V_2O_5 \cdot 10Fe_2O_3$ glass measured at room temperature.

glasses are reviewed by Müller-Warmuth and Eckert.[15] According to Coey, Fe^{3+} ions are reported to be present at the tetrahedral sites in borate and silicate glasses.[14] This is well consistent with the Mössbauer results of borate[16-18] and borosilicate[19-20] glasses, performed by the present authors, where the isomer shift ranges from 0.38 to 0.22 mm s^{-1} with respect to metallic iron. (The experimental error for the isomer shift is usually estimated to be ± 0.01 mm s^{-1}.) Judging from the experimental results shown in those reviews[13-15] and papers,[16-20] the Fe^{3+} ions are concluded to be present at the tetrahedral environments in the sodium vanadate glasses. This conclusion indicates the presence of the tetrahedral VO_4 units, because the Fe^{3+} ions should be present either at the substitutional sites of the V^{5+} or V^{4+} ions constituting the glass matrix or at the interstitial sites of the glass matrix. These results are well consistent with the IR results obtained by Dimitriev et al.[3] and with the Mössbauer results of the potassium vanadate glasses.[10]

The composition dependency of the isomer shift is shown in Fig. 3, which shows a distinct decrease with increasing Na_2O content. Similar composition dependency has been observed in the case of the potassium vanadate glasses,[10] where the decrease in the isomer shift was ascribed to the formation of nonbridging oxygen atoms in the VO_4 tetrahedra. The composition dependency of the isomer shift is well consistent with that of the quadrupole splitting shown in Fig. 4, where the quadrupole splitting shows a distinct decrease with increasing Na_2O content. (The experimental error for the quadrupole splitting is usually estimated to be ± 0.02 mm s^{-1}.) The decrease in the quadrupole splitting of the Fe^{3+} ions is ascribed to the increased symmetry around the Fe^{3+} ions, because the high-spin Fe^{3+} ions have a symmetric electron configuration of $3d^5$ in the outermost orbital. The present results of the isomer shift (Fig. 3) and the quadrupole splitting (Fig. 4) therefore indicate the formation of nonbridging oxygen atoms in the VO_4 tetrahedra constituting the skeleton of the sodium vanadate glasses. The decrease in the quadrupole splitting may be correlated with the decrease in the coordination number of the V^{5+} and V^{4+} ions from 5 to 4, because the electric field gradient (e^2qQ) is considered to be smaller in the

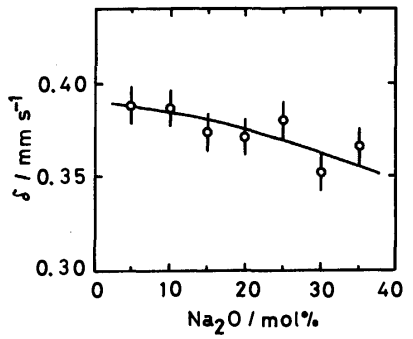

Fig. 3. Composition dependency of the isomer shift (δ) of the Fe^{3+} ions in the Na_2O-V_2O_5 glasses containing 10 mol% Fe_2O_3.

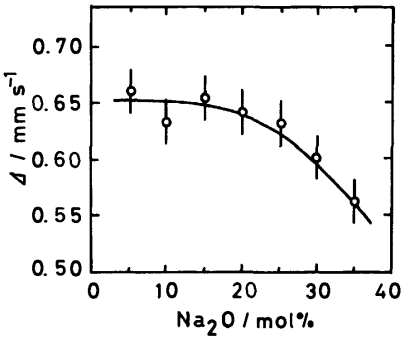

Fig. 4. Composition dependency of the quadrupole splitting (Δ) of the Fe^{3+} ions in the Na_2O-V_2O_5 glasses containing 10 mol% Fe_2O_3.

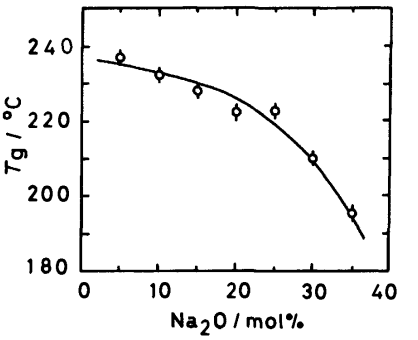

Fig. 5. Composition dependency of the glass transition temperature (T_g) of the Na_2O-V_2O_5 glasses containing 10 mol% Fe_2O_3.

case of the tetrahedral configuration.

Each DTA curve of the sodium vanadate glasses containing 10 mol% Fe_2O_3 consists of an endothermic peak due to glass transition and one or a few exothermic peak(s) due to crytallization. All the glass transition temperatures (T_g) are plotted in Fig. 5, where the T_g values are plotted against the Na_2O content. A Mössbauer and DTA study of potassium vanadate glasses[10] revealed that the T_g shows a distinct decrease when the coordination number of the V^{5+} or V^{4+} ions decreases from 5 to 4 and when the nonbridging oxygen atoms are formed in the VO_4 tetrahedra. The distinct decrease in the T_g from 237 to 195 °C (Fig. 5) is therefore ascribed to the gradual decrease in the coor-

Table 1. Glass Transition and Crystallization Temperatures of the Na_2O–V_2O_5 Glasses Containing 10 mol% Fe_2O_3

Composition	T_g[a)]/°C	T_c[b)]/°C
$5Na_2O \cdot 85V_2O_5 \cdot 10Fe_2O_3$	237	254
$10Na_2O \cdot 80V_2O_5 \cdot 10Fe_2O_3$	232	253
$15Na_2O \cdot 75V_2O_5 \cdot 10Fe_2O_3$	228	247
$20Na_2O \cdot 70V_2O_5 \cdot 10Fe_2O_3$	222	238
$25Na_2O \cdot 65V_2O_5 \cdot 10Fe_2O_3$	223	250
$30Na_2O \cdot 60V_2O_5 \cdot 10Fe_2O_3$	210	239
$35Na_2O \cdot 55V_2O_5 \cdot 10Fe_2O_3$	195	213

a) Glass transition temperature. b) Crystallization temperature.

dination number of the V^{5+} and V^{4+} ions from 5 to 4 and to the formation of the nonbridging oxygen atoms in the VO_4 (and FeO_4) tetrahedra. All the T_g values obtained in the present study are summarized in Table 1, together with the individual crystallization temperatures (T_c). In Table 1, only one crystallization temperature corresponding to the main peak is given for each glass sample.

It is concluded that Fe^{3+} ions are present at the substitutional sites of the V^{5+} or V^{4+} ions constituting the VO_4 tetrahedra. It is also concluded that the introduction of Na_2O into the V_2O_5 matrix results in a gradual change from the layer structure composed of the VO_5 tetragonal pyramids (or trigonal bipyramids) to the chain structure composed of the VO_4 tetrahedra having nonbridging oxygen atoms.

The authors are grateful to Dr. Koji Yamada of Hiroshima University for his useful discussion on the structure of the vanadate glasses. One of the authors (TN) is grateful to the Itoh Science Foundation, Corning Research Grant, and a Grant-in-Aid for Scientific Research No. 61740350 from the Ministry of Education, Science and Culture.

References

1) A. Byström, K. A. Wilhelmi, and O. Brotzen, *Acta Chem. Scand,*. **4**, 1119 (1950).
2) K. Jansen and G. Sperlich, *Phys. Status Solidi B*, **55**, 495 (1973).
3) Y. Dimitriev, V. Dimitrov, M. Arnaudov, and D. Topalov, *J. Non-Cryst. Solids*, **57**, 147 (1983).
4) S. L. Segel and R. B. Creel, *Can. J. Phys.*, **48**, 2673 (1970).
5) H. T. Evans, *Z. Kristallogr.*, **114**, 257 (1960).
6) A. C. Wright, C. A. Yarker, P. A. V. Johnson, and R. N. Sinclair, *J. Non-Cryst. Solids*, **76**, 333 (1985).
7) S. Stizza, I. Davoli, O. Gzowski, L Murawski, M. Tomellini, A. Marcelli, and A. Bianconi, *J. Non-Cryst. Solids*, **80**, 175 (1986).
8) A. K. Bandyopadhyay, M. Ribes, F. Pernot, and J. Zarzycki, *Phys. Chem. Glasses.* **23**, 31 (1982).
9) I. Ardelean, O. Cozar, and Gh. Ironca, *J. Non-Cryst. Solids*, **68**, 33 (1984).
10) T. Nishida and Y. Takashima, *Bull. Chem. Soc. Jpn.*, **60**, 941 (1987).
11) N. N. Greenwood and T. C. Gibb, "Mössbauer Spectroscopy," Chapman and Hall Ltd., London (1971) Chap. 3.
12) R. Ingalls, F. Van der Woude, and G. A. Sawatzky, "Iron and Nickel," in "Mössbauer Isomer Shifts," ed by G. K. Shenoy and F. E. Wagner, North-Holland Pub Co., Amsterdam (1978), Chap. 7.
13) C. R. Kurkjian, *J. Non-Cryst. Solids.* **3**, 157 (1970).
14) J. M. D. Coey, *J. Phys.*, **35**, C6-89 (1974).
15) W. Müller-Warmuth and H. Eckert, *Phys. Rep.*, **88**, 91 (1982).
16) T. Nishida and Y. Takashima, *J. Non-Cryst. Solids*, **37**, 37 (1980).
17) T. Nishida, T. Shiotsuki, and Y. Takashima, *J. Non-Cryst. Solids*, **41**, 161 (1980).
18) T. Nishida, T. Hirai, and Y. Takashima, *J. Non-Cryst. Solids*, **43**, 221 (1981).
19) T. Nishida, T. Hirai, and Y. Takashima, *Phys. Chem. Glasses*, **22**, 94 (1981).
20) T. Nishida, T. Hirai, and Y. Takashima, *Bull. Chem. Soc. Jpn.*, **54**, 3735 (1981).

Photochemical Reactions of Ethoxycarbonyl-Substituted Quinolines

Isao ONO* and Norisuke HATA
Department of Chemistry, College of Science and Engineering, Aoyama Gakuin University, Chitosedai, Setagaya-ku, Tokyo 157
(Received December 20, 1986)

The photochemical reactions of the quinoline derivatives substituted by an ethoxycarbonyl group at the 2-, 3-, and 4-positions of a quinoline nucleus have been investigated in several alcohols and cyclohexane. Irradiation of ethyl 4-quinolinecarboxylate (**1**) yielded ethyl 2-hydroxyalkyl-4-quinolinecarboxylates (**4a—c**) in alcohols and ethyl 2-cyclohexyl-4-quinolinecarboxylate (**4d**) in cyclohexane in a good yield, respectively. The photochemical reactions of ethyl 3-quinolinecarboxylate (**2**) showed remarkable solvent dependency. Irradiation in methanol and cyclohexane afforded a solvent·additive product, ethyl 4-hydroxymethyl-1,4-dihydro-3-quinolinecarboxylate (**5a**) and ethyl 4-cyclohexyl-1,4-dihydro-3-quinolinecarboxylate (**5b**), while such photo-addition of the solvent did not proceed in ethanol and 2-propanol but instead ethyl 1,4-dihydro-3-quinolinecarboxylate (**6**) and dimeric compounds were formed, both of which were unstable and finally reverted to **2** at room temperature in air. In the case of ethyl 2-quinolinecarboxylate two types of the products, ethyl 4-hydroxyalkyl-1,4-dihydro-2-quinolinecarboxylate (**7**) and ethyl 1,4-dihydro-2-quinolinecarboxylate (**8**) were obtained in ethanol and 2-propanol but the yields of those products were poor. On the basis of triplet quenching experiments, the photochemical reactions of those ethyl quinolinecarboxylates are suggested to occur through hydrogen abstraction from the solvents by the ring nitrogen in the S_1 state.

The photochemical reactions of cyano-substituted quinolines have been the subject of a number of investigations.[1] Especially, we have mechanistically investigated in detail the photosubstitution of 2-quinolinecarbonitriles in ethanol and proved that the replacement of a cyano group by a 1-hydroxyethyl one occurred via a hydrogen-bonded radical-pair intermediate formed by hydrogen abstraction by a ring nitrogen from the solvents in the S_1 state.[1b,c] Next, we reported the photochemical reactions of 2-(dimethylcarbamoyl)quinolines, where the ring nitrogen brought about hydrogen abstraction from the dimethylcarbamoyl substituent via the T_1 state to give 2-(methylaminoacetyl)quinolines and cyclized products.[2] In this paper, we report the photochemistry of ethoxycarbonyl quinolines bearing also an electron-withdrawing group such as ethyl 4-quinolinecarboxylate (**1**), ethyl 3-quinolinecarboxylate (**2**), and ethyl 2-quinolinecarboxylate (**3**) in several alcohols and in cyclohexane. Sugimori et al. reported that methyl 2-pyridinecarboxylate underwent methylation at the 5-position in methanol through hydrogen abstraction by the excited carbonyl group from the solvent.[3] In the case of the ethoxycarbonyl quinolines two types of reactions were observed, both of which were initiated by hydrogen abstraction by the ring nitrogen from the solvent. One is a recombination of a radical pair in a solvent cage and another is probably further hydrogen abstraction by a semi-reduced radical from the solvent. We describe the excited state involved in those reactions and reaction mechanism.

Photochemistry of Ethyl 4-Quinolinecarboxylate (1). Irradiation of **1** in several alcohols and cyclohexane under an oxygen atmosphere gave one major photoproduct **4** in good yield as shown in Table 1. Although we attempted irradiation in nitrogen, the yield of **4** decreased about to 20 percent because of an increase in the amount of decomposition products. The NMR spectra of **4** indicated that the ethoxycarbonyl substituent at the 4-position of a quinoline remained and the proton at the 2-position was replaced by a corresponding hydroxyalkyl group derived from the alcohol used as a solvent or a cyclohexyl group when irradiation was carried out in cyclohexane. From the data of MS, IR, or elemental analysis, **4** was assigned to be ethyl 2-hydroxyalkyl-4-quinolinecarboxylate (**4a—c**) or ethyl 2-cyclohexyl-4-quinolinecarboxylate (**4d**), respectively.

Photochemistry of Ethyl 3-Quinolinecarboxylate (2). Irradiation of **2** was carried out in nitrogen atmosphere, because no reaction occurred in oxygen. Any photoproduct obtained in each solvent (MeOH, EtOH, 2-PrOH, or cyclohexane) has a UV spectrum showing its maximum at a wavelength longer than

Table 1. Photochemical Reactions of **1** in Several Solvents

Solvent	Irradiation time/h	Atm	Conversion %		Product yield %
Ethanol	4	O_2	80	**4a**	67
	2.5	N_2	84	**4a**	22
2-Propanol	4	O_2	74	**4b**	50
	2.5	N_2	56	**4b**	21
t-Butyl alcohol	7	O_2	68	**4c**	45
Cyclohexane	4	O_2	64	**4d**	56

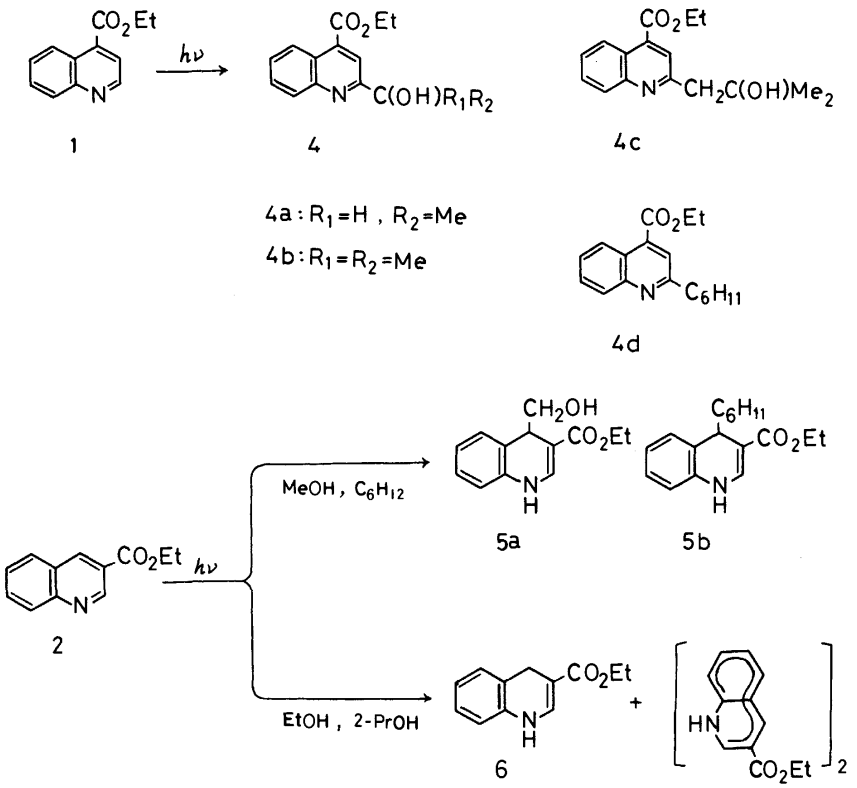

320 nm which remarkably shifts from that of **2** (UV-(MeOH)λ_{max} 286 nm). The types of those products were, however, different depending on the nature of the solvent used. That is, irradiation in methanol and cyclohexane gave the solvent addition products, ethyl 4-hydroxymethyl-1,4-dihydro-3-quinolinecarboxylate (**5a**) and ethyl 4-cyclohexyl-1,4-dihydro-3-quinolinecarboxylate (**5b**) as only one major product, respectively. The structures were determined on the basis of NMR, IR, and MS spectra. NMR proved that the addition of the solvent occurred at the 4-position but not the 2-position. IR showed absorption by NH stretching at about 3340 cm^{-1} and a strong peak due to a CO group at 1650 cm^{-1}. On the other hand, irradiation in both ethanol and 2-propanol did not afford any solvent addition product, but instead lead to two unstable products which finally reverted to the starting material **2**. Both were especially labile in solution, for example, if the solutions after irradiation were allowed to stand 12 h at room temperature in dark, their UV spectra completely reverted to that of **2**. Therefore, the reaction solvent was evaporated under 30 °C immediately after irradiation, and the residue was subjected to separation on plate layer chromatography at 10 °C. As a result, two colorless solid products of mass 203 and 404 were isolated. Although both were unstable at room temperature, especially, the latter more rapidly changed to **2**, they were stable in a sealed tube, indicating that their lability was due to oxygen. The IR spectrum of the former showed absorption by NH stretching at 3340 cm^{-1} and a strong peak due to a CO group at 1640 cm^{-1}. In the NMR spectra taken in

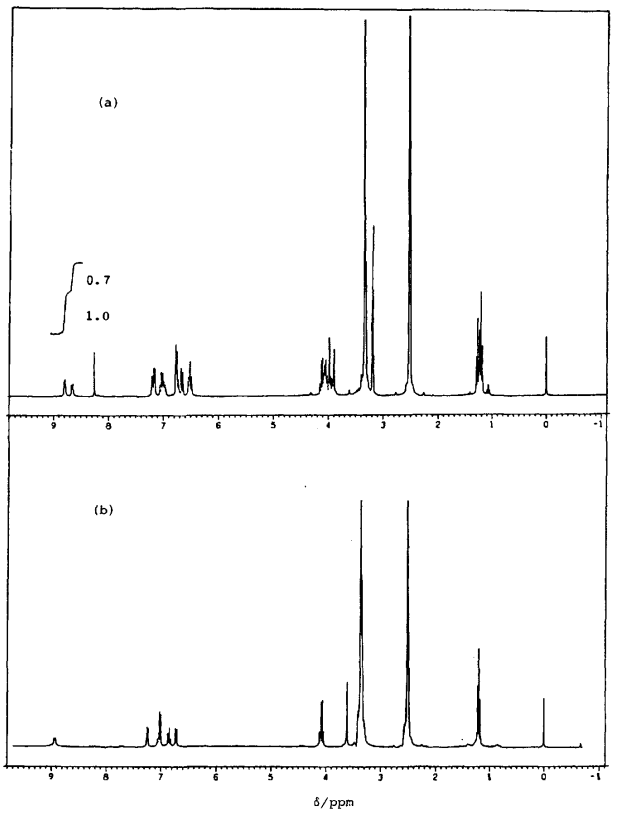

Fig. 1. 270 MHz ^{1}H NMR spectra of (a) dimeric compound and (b) **6** measured in DMSO-d_6 using TMS as a standard.

$CDCl_3$ using TMS as a standard, a broad peak at δ 6.00 due to the NH and a singlet line at δ 3.76 due to two

Table 2. Photochemical Reactions of **2** in Several Solvents in N_2

Solvent	Irradiation time/h	Conversion	Yield of product/%		
		%	**5**	**6**	Dimer
Methanol	5	76	69	—	—
Cyclohexane	5	67	55	—	—
Ethanol	15	72	—	53	33
2-Propanol	10	77	—	24	59
	15	82	—	50	38

protons at the 4-position of the quinoline were observed. Thus, it was determined to be ethyl 1,4-dihydro-3-quinolinecarboxylate (**6**). The treatment of this product with $FeCl_3$ caused quantitative conversion to **2**, giving further proof for this structure. The latter product, which is insoluble in alcohols and chloroform, seems to have the structure akin to the dimeric compound of **6**, considering that its molecular weight was 404 and the IR spectrum was similar to that of **6**. Although the NMR spectrum (in DMSO-d_6) was complicated as shown in Fig. 1a, it seems similar to that of **6** in DMSO (Fig. 1b). Two broad peaks observed at δ 8.65 and 8.79 were confirmed to be due to the protons on the ring nitrogen by decoupling the protons at the 2-position which appeared as two doublets at δ 7.15 and 7.19, respectively. The relative intensity of the signals at δ 8.65 and 8.79 was 0.7 : 1, indicating that this consisted of a mixture of two dimers (0.7 : 1 ratio). The multiplet around δ 1.35 may show the overlap of two triplet signals arising from the methyl groups. A number of peaks around δ 3.9—4.15 corresponding to those of methylene protons are complicated by overlap by the signals of some impurities. At present, the assignment of these dimers was unsuccessful. Separation and purification could not be achieved. On irradiation in *t*-butyl alcohol an unidentified oily product of mass 275 was obtained, but formation of **6** and the dimers was not observed. Table 2 shows the product yields.

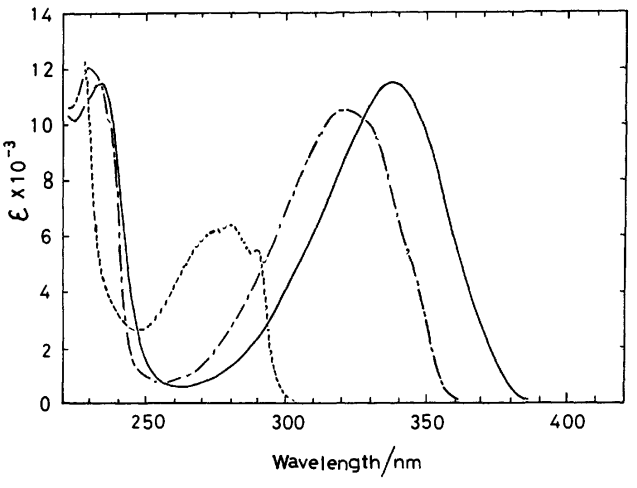

Fig. 2. UV spectra of **6** and **8** in methanol or cyclohexane. (——) **6** in methanol, (-·-·-) **6** in cyclohexane, and (----) **8** in methanol.

It is noteworthy that the UV spectra of the photoproducts arising from the ethyl 3-quinolinecarboxylate shifted to much longer wavelength than that expected from their structures. Figure 2 displayed the absorption spectra of **6** in methanol and cyclohexane together with that of ethyl 1,4-dihydro-2-quinolinecarboxylate (**8**) in methanol. Such a large bathochromic shift can be explained by a resonance contribution from a zwitterion structure. It is supported by the fact that the UV spectrum of **6** shifted to shorter wavelength in cyclohexane. That the IR absorption of the CO group appeared at a considerably lower frequency of 1650 cm^{-1} also supports the possibility of a contribution from an ionic structure.

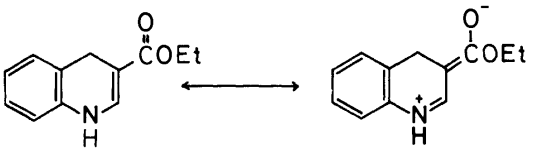

Photochemistry of Ethyl 2-Quinolinecarboxylate (3). The irradiation of **3** in nitrogen lead to two low yield products ethyl 4-hydroxyalkyl-1,4-dihydro-2-quinolinecarboxylate (**7**) and ethyl 1,4-dihydro-2-quinolinecarboxylate (**8**) in ethanol and 2-propanol (Table 3), but the major product in *t*-butyl alcohol or cyclohexane was an intractable tar. The structures of **7** and **8** were determined in a similar manner with to **5** and **6**. The experiments in an atmosphere of oxygen were discontinued, because the reaction in oxygen was hard to achieve.

Triplet Quenching Experiment. In order to identify the reactive excited state of the photochemical reactions of those ethoxycarbonyl quinolines the triplet quenching experiment was carried out for **1** and **2**. The experiment for **3** was excluded because of too low yield of the products. From the phosphorescence spectra measured in ethanol and methylcyclohexane at 77 K the triplet excitation energy (E_T) of **1** was estimated to be 244.1 kJ mol^{-1} in both solutions. E_T for **2** were

Table 3. Photochemical Reactions of **3** in Nitrogen Atmosphere

Solvent	Conversion/%	**7**	**8**
		%	
Ethanol	86	31	9
2-Propanol	65	6	17

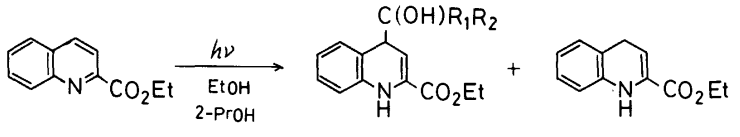

3 7 8

7a: R_1 = H, R_2 = Me
7b: R_1 = R_2 = Me

Table 4. Quantum Yields of Photochemical Reactions of **1** in 2-Propanol and Cyclohexane

Solvent	Atmosphere	Quencher/dm^3 mol^{-1}	Φ_d	Φ_f
2-Propanol	N_2	0	0.064	0.017
	N_2	5.0×10^{-4}	0.071	0.012
	N_2	1.0×10^{-3}	0.056	0.014
	N_2	1.0×10^{-2}	0.067	0.013
	N_2	1.0×10^{-1}	0.054	0.011
	N_2[a)]	0	0.063	<0.004
	O_2	0	0.051	0.024
Cyclohexane	N_2	0	0.048	0.016
	N_2	1.0×10^{-1}	0.042	0.016

a) Nitrogen gas was passed through an aqueous basic solution of pyrogallol.

259.4 kJ mol^{-1} in ethanol and 258.1 kJ mol^{-1} in methylcyclohexane, respectively. As a triplet quencher 1,3-cyclohexadiene (E_T=219 kJ mol^{-1}) could be used for **1** and 1,3-pentadiene (E_T=240.6 kJ mol^{-1}) for **2**. The relatively long phosphorescence lifetimes of 0.9 s for **1** and 0.46 s for **2** in ethanol indicated that the lowest triplet excited states were of π,π^* configuration. The lifetimes could not be estimated in methylcyclohexane because of the very weak phosphorescence intensity. The fluorescence was observed in ethanol for both quinolines but was not clear in methylcyclohexane, suggesting that the singlet n,π^* and π,π^* states lies closely to each other as in the case of 2-quinolinecarbonitrile.[1b)]

Table 4 shows the quantum yields of the disappearance of **1** (Φ_d) and the formation of **4** (Φ_f) on irradiation in 2-propanol or cyclohexane under various conditions. Both the quantum yields Φ_d and Φ_f were independent of the concentration of 1,3-cyclohexadiene, indicating that the S_1 state was responsible for the reaction of **1**. It is noted that Φ_f under an oxygen atmosphere was greater than the value in nitrogen. This means that oxygen plays an important part in the formation of **4b**. In practice, Φ_f was only less than 0.004 in the 2-propanol purged by nitrogen gas from which oxygen was removed more completely through a potassium hydroxide solution of pyrogallol. The quantum yields for the photochemical reaction of **2** were carried out in methanol and cyclohexane using 1,3-pentadiene as a triplet quencher. As shown in Fig. 3, the triplet quencher had no influence on the reaction. We could not take the measurement of the quantum yields in ethanol and 2-propanol because **6** and the dimers obtained in those solution easily changed to the starting material **2** during the isolation procedure.

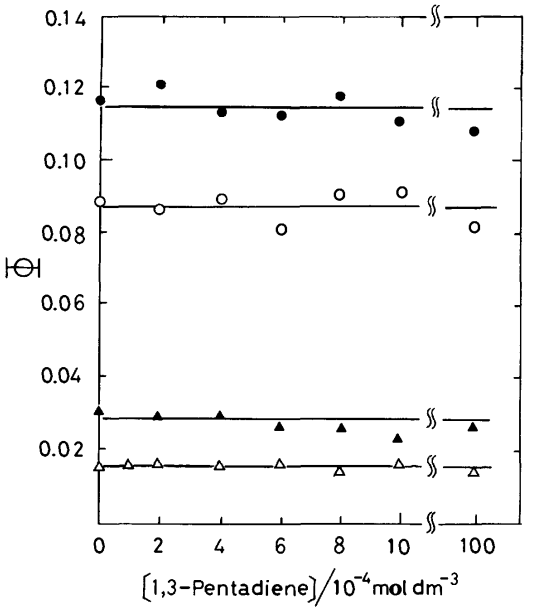

Fig. 3. Effect of triplet quencher on quantum yields of photochemical reactions of **2**. [**2**]=0.002 mol dm^{-3}. —○—: Formation of **5a**, —●—: disappearance of **2** in methanol, —△—: formation of **5b**, —▲—: disappearance of **2** in cyclohexane.

Reaction Mechanism. The photochemistry of **1** could be explained in terms of the mechanism as shown in Scheme 1. Hydrogen abstraction from the solvent by the ring nitrogen in the S_1 state forms a radical pair which combines to give 1,2-dihydroquinoline derivatives expected as a precursor of **4**. Its conversion to **4** may be caused by oxidation but not via disproportionation, considering that Φ_f of **4b** become extremely low in the nitrogen gas including almost no oxygen (Table 4). Although we tried to isolate the precursor from the reaction mixture obtained on irradiation in nitrogen, the attempt failed because of its

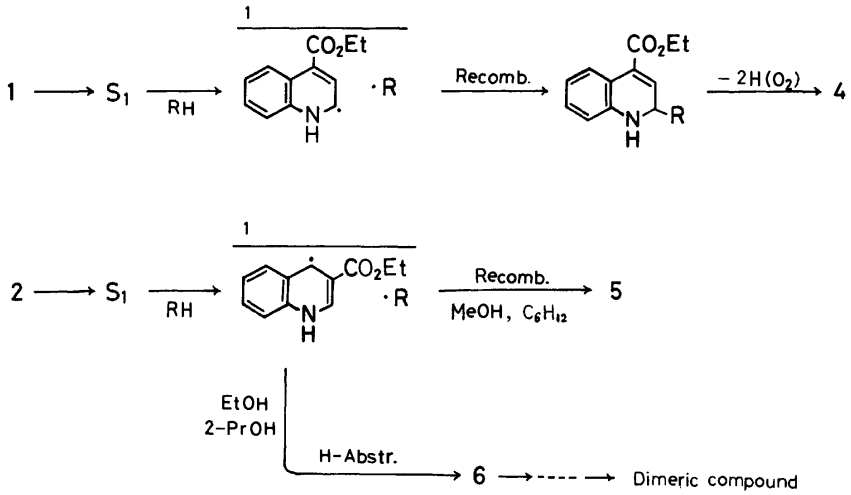

Scheme 1.

lability. Such 1,2-dihydroquinolines are known to be unstable.[4] The initial step of the photochemical reaction of **2** may also be hydrogen abstraction by the ring nitrogen from the solvent in the S_1 state. Considering that this reaction was not affected by 1,3-pentadiene in both high polar methanol and less polar cyclohexane, the photochemical reaction of **2** in ethanol and 2-propanol leading to the formation of **6** is thought to occur also in the S_1 state. Apparently, the solvent dependency of the photoproducts of **2** could be ascribed to the hydrogen-donating efficiency of the solvent used. The reaction mechanism is summarized in Scheme 1. In methanol or cyclohexane the formed radical pair recombines as the case of **1** to give **5**, while in ethanol or 2-propanol being a good hydrogen-donor solvent the semi-reduced radical of **2** may carry out further hydrogen abstraction from the solvent to afford **6** before undertaking recombination. The formation of the dimer types would be expected as follows, considering the results that the yields of **6** and the dimers varied remarkably depending on irradiation time as shown in Table 2, and also that the latter products were not formed in methanol, cyclohexane and *t*-butyl alcohol; **6** (QH_2) excited by light absorption donates a hydrogen atom to **2** (Q) to generate two semi-reduced radicals (2·QH), whose recombination yields the dimeric compounds Q_2H_2.

$$QH_2 \xrightarrow{h\nu} QH_2^*$$

$$QH_2^* + Q \longrightarrow 2\cdot QH$$

$$2\cdot QH \longrightarrow Q_2H_2$$

We tried the irradiation of QH_2 in the ethanol solution in the presence of Q under a nitrogen atmosphere with 366 nm light which could be absorbed only by the former. As a result, QH_2 disappeared rapidly, but the product found in the reaction solution after irradiation was only Q. Perhaps, the formed Q_2H_2 is thought to have reverted to Q by reabsorbing 366 nm light. Actually, the irradiation of Q_2H_2 by 366 nm light in the absence of Q induced its rapid conversion to Q, although the mechanism of the conversion was now ambiguous. Anyway, the photochemical reaction of **2** in ethanol or 2-propanol may shuttle between the starting material **2** and the products.

The photochemical reaction of **3** may be thought to be essentially similar to that of **2**. The simultaneous formation of **7** and **8** shows that the recombination of the radical pair and the hydrogen abstraction by the semi-reduced radical of **3** from the solvent occurs competitively.

Experimental

The NMR spectra were measured on a JEOL GX-270 with TMS as an internal standard. The mass spectra were obtained by a Hitachi RMU-6M, a JEOL JMS-DX303, or a Shimadzu GCMS-9020DF machines. The IR spectra were taken on a JASCO-302. For the measurement of fluorescence and phosphorescence spectra a Hitachi MPF-2A was used, and UV spectra were recorded with a Shimadzu UV-220.

Materials. The solvents used in the irradiation experiments were reagent grade obtained from Wako Pure Chemical Industry. Methanol, ethanol, and *t*-butyl alcohol were used without purification but 2-propanol and cyclohexane were purified by distillation and silica-gel chromatography, respectively. 1,3-Cyclohexadiene and 1,3-pentadiene (Tokyo Kasei Kogyo) were used after distillation. Ethoxycarbonyl quinolines **1**, **2**, and **3** were synthesized by adding trimethylamine and ethanol to the chloroform solution including the corresponding quinolinecarboxylic acids treated with $SOCl_2$.[5] Those carboxylic acids were obtained from the basic hydrolysis of quinolinecarbonitriles. 2-Quinolinecarbonitrile of those was synthesized by a Reisert reaction of quinoline *N*-oxide,[6] but 3-and 4-quinolinecarbonitriles were prepared by heating the corresponding bromoquinoline with copper (I) cyanide.[7] 3-Bromoquinoline was reagent grade from Tokyo Kasei Kogyo and 4-bromoquinoline was synthesized by treatment with phosphorus trichloride of 4-bromoquinoline *N*-oxide obtained by refluxing 4-nitroquinoline *N*-oxide in hydrobromic acid.[8]

Ethyl 4-Quinolinecarboxylate (1). Colorless liquid, bp 120 °C/1 mmHg (1 mmHg=133.32 Pa); IR (neat) 3050, 2990, 2910, 1725 (CO), 1585, 1250, 1150 cm^{-1}; ^1H NMR ($CDCl_3$) δ=1.49 (3H, t, J=7.25 Hz, $CH_2C\underline{H}_3$), 4.53 (2H, q, J=7.25 Hz, $C\underline{H}_2CH_3$), 7.63—7.81 (2H, m, H-6 and 7), 7.90 (1H, d, J=4.43 Hz, H-3), 8.18 (1H, d, J=8.46 Hz), 8.77 (1H, d, J=8.46 Hz), 9.02 (1H, d, J=4.43 Hz, H-2); MS m/z 201 (M^+).

Ethyl 3-Quinolinecarboxylate (2). Mp 68 °C (from hexane-ethanol); IR (KBr) 3050, 2990, 2930, 1710 (CO), 1570, 1240, 1130 cm^{-1}; ^1H NMR($CDCl_3$) δ=1.47 (3H, t, J=7.25 Hz, $CH_2C\underline{H}_3$), 4.49 (2H, q, J=7.25 Hz, $C\underline{H}_2CH_3$), 7.63—7.81 (2H, m, H-6 and 7), 7.94 (1H, d, J=8.24 Hz), 8.17 (1H, d, J=8.25 Hz), 8.85 (1H, s, H-4), 9.46 (1H, s, H-2); MS m/z 201 (M^+).

Ethyl 2-Quinolinecarboxylate (3). Colorless liquid, bp 140 °C/1 mmHg; IR (KBr) 3050, 2980, 2930, 1705 (CO), 1590, 1245, 1140 cm^{-1}; ^1H NMR ($CDCl_3$) δ=1.50 (3H, t, J=7.25 Hz, $CH_2C\underline{H}_3$), 4.57 (2H, q, J=7.25 Hz, $C\underline{H}_2CH_3$), 7.64—7.79 (2H, m, H-6 and 7), 7.88 (1H, d, J=8.25 Hz), 8.19, 8.30 (2H, AB, q, J=8.58 Hz, H-3 and 4), 8.32 (1H, d, J=8.24 Hz); MS m/z 201 (M^+).

Photochemical Reactions of 1 and 3. **1** or **3** (100 mg) dissolved in 70 cm^3 of alcohol (EtOH, 2-propanol, or *t*-BuOH) or cyclohexane was irradiated in a Pyrex vessel with a 100 W high pressure immersion mercury lamp (Riko Kagaku Sangyo Co.) under nitrogen or oxygen. After the evaporation of the reaction solvent, the residue was developed on thin-layer chromatography of Kieselgel (PF_{254}, Merck) with a mixture of chloroform and diethyl ether to isolate the starting material and the products.

Photochemical Reaction of 2. A solution of **2** (50 mg) in 70 cm^3 of alcohol or cyclohexane was irradiated in nitrogen with the same setup. The isolation of the reaction mixture on irradiation in methanol and cyclohexane was carried out by a method similar to the former two cases. However, the photoproducts **6** and dimeric compounds in ethanol and 2-propanol were labile, the latter especially was easily decomposed to the starting material **2**. Therefore, the evaporation of the reaction solvent was done below 30 °C and the development on thin-layerchromatography was undertaken at 10 °C, using chloroform and ethanol (20 : 1 V/V). Still, the dimeric compounds are thought partly to have reverted to **2** during the isolation procedure.

Ethyl 2-(1-Hydroxyethyl)-4-quinolinecarboxylate (4a). Colorless liquid (it gradually decomposed at room temperature); IR (neat) 3400 (OH), 3070, 2990, 2940, 1715 (CO), 1600, 1510, 1240, 1150 cm^{-1}; ^1H NMR ($CDCl_3$) δ=1.51 (3H, t, J=7.25 Hz, $CH_2C\underline{H}_3$), 1.64 (3H, d, J=6.43 Hz, CH (OH)$C\underline{H}_3$), 4.55 (2H, q, J=7.25 Hz, $C\underline{H}_2CH_3$), 4.75 (1H, s, OH), 5.12 (1H, q, J=6.43 Hz, $C\underline{H}$(OH)CH_3), 7.67—7.80 (2H, m, H-6 and 7), 7.88 (1H, s, H-3), 8.16 (1H, d, J=8.91 Hz), 8.75 (1H, d, J=8.91 Hz); Found: m/z 245.1049. Calcd for $C_{14}H_{15}NO_3$: M, 245.1052.

Ethyl 2-(1-Hydroxy-1-methylethyl)-4-quinolinecarboxylate (4b). Mp 72 °C (from hexane); IR (KBr) 3250 (OH), 3050, 2980, 2920, 1720 (CO), 1590, 1505, 1240, 1140 cm^{-1}; ^1H NMR ($CDCl_3$) δ=1.50 (3H, t, J=7.10 Hz, $CH_2C\underline{H}_3$), 1.65 (6H, d, J=5.28 Hz, $(CH_3)_2$), 4.54 (2H, q, J=7.10 Hz, $C\underline{H}_2CH_3$), 5.53 (1H, s, OH), 7.64—7.77 (2H, m, H-6 and 7), 7.95 (1H, s, H-3), 8.14 (2H, d, J=8.57 Hz), 8.70 (1H, d, J=8.24 Hz); MS m/z 259 (M^+); Found: C, 69.41; H, 6.60; N, 5.35%. Calcd for $C_{15}H_{17}NO_3$: C, 69.49; H, 6.61; N, 5.40%.

Ethyl 2-(2-Hydroxy-2-methylpropyl)-4-quinolinecarboxylate (4c). Colorless liquid, picrate 172 °C (decomp); IR (neat) 3380 (OH), 3050, 2990, 2920, 1720 (CO), 1590, 1510, 1240, 1145 cm^{-1}; ^1H NMR ($CDCl_3$) δ=1.31 (6H, s, C(OH)($C\underline{H}_3$)$_2$), 1.48 (3H, t, J=7.23 Hz, $CH_2C\underline{H}_3$), 3.16 (2H, s, C(OH)$C\underline{H}_2$), 4.52 (2H, q, J=7.23 Hz, $C\underline{H}_2CH_3$), 5.71 (1H, s, OH), 7.73—7.79 (3H, m, H-3, 6, and 7), 8.09 (1H, d, J=8.14 Hz), 8.70 (1H, d, J=8.58 Hz); MS m/z 273 (M^+); Found (for picrate): C, 52.51; H, 4.37; N, 11.10%. Calcd for $C_{22}H_{22}N_4O_{10}$: C, 52.59; H, 4.41; N, 11.15%.

Ethyl 2-Cyclohexyl-4-quinolinecarboxylate (4d). Colorless liquid, picrate 156—158 °C; IR (neat) 3070, 2990, 2930, 1720 (CO), 1595, 1240, 1150 cm^{-1}; ^1H NMR δ=1.37—2.07 (10H, m, cyclohexyl), 1.49 (3H, t, J=7.09 Hz, $CH_2C\underline{H}_3$), 2.96 (1H, tt, J=11.9 , 3.5 Hz, H'-1), 4.52 (2H, q, J=7.09 Hz, $C\underline{H}_2CH_3$), 7.54—7.75 (2H, m, H-6 and 7), 7.81 (1H, s, H-3), 8.10 (1H, d, J=8.57 Hz), 8.66 (1H, d, J=8.57 Hz); MS m/z 283 (M^+); Found (for picrate): C, 56.20; H, 4.72; N, 10.87%. Calcd for $C_{24}H_{24}N_4O_9$: C, 56.25; H, 4.72; N, 10.93%.

Ethyl 4-Hydroxymethyl-1,4-dihydro-3-quinolinecarboxylate (5a). Unstable colorless liquid (it easily released H_2O); UV (CH_3OH) λ_{max} 330 nm (ε 11600); IR (neat) 3400 (br, OH and NH), 3110, 2960, 2930, 1680 (CO), 1585, 1490, 1235, 1190 cm^{-1}; ^1H NMR ($CDCl_3$) δ=1.30 (3H, t, J=7.25 Hz, $CH_2C\underline{H}_3$), 3.67 (2H, d, J=5.28 Hz, $C\underline{H}_2OH$), 4.10 (1H, t, J=5.28 Hz, H-4), 4.25 (2H, q, J=7.25 Hz, $C\underline{H}_2CH_3$), 6.32 (1H, s, NH), 6.71—7.21 (4H, m, ArH), 7.55 (1H, d, J=6.72 Hz, H-2); MS m/z 233 (M^+); Found after loss of H_2O(M^+−18): m/z 215.0931. Calcd for $C_{13}H_{11}NO_2$: M, 215.0946.

Ethyl 4-Cyclohexyl-1,4-dihydro-3-quinolinecarboxylate (5b). Mp 149—150 °C (from hexane-ethanol); UV (CH_3OH) λ_{max} 327 nm (ε 11500); IR (KBr) 3290 (NH), 3100, 3030, 2990, 2920, 1650 (CO), 1635, 1585, 1490, 1238, 1160 cm^{-1}; ^1H NMR ($CDCl_3$) δ=0.60—1.60 (11H, m, cyclohexyl), 1.30 (3H, t, J=7.26 Hz, $CH_2C\underline{H}_3$), 3.82 (1H, d, J=4.19 Hz, H-4), 4.15—4.25 (2H, m, $C\underline{H}_2CH_3$), 6.15 (1H, s, NH), 6.68—7.14 (4H, m, ArH), 7.55 (1H, d, J=5.94 Hz, H-2); MS m/z 285 (M^+); Found: C, 75.72; H, 8.13; N, 4.82%. Calcd for $C_{18}H_{23}NO_2$: C, 75.76; H, 8.12; N, 4.91%

Ethyl 1,4-Dihydro-3-quinolinecarboxylate (6). Mp 139 °C (it changed gradually to **2** at room temperature); UV (CH_3OH) λ_{max} 338 nm (ε 11500); IR (KBr) 3280 (NH), 3100, 2980, 2930, 1640 (CO), 1590, 1495, 1250, 1120 cm^{-1}; ^1H NMR ($CDCl_3$) δ=1.29 (3H, t, J=7.04 Hz, $CH_2C\underline{H}_3$), 3.76 (2H, s, H-4), 4.20 (2H, q, J=7.04 Hz, $C\underline{H}_2CH_3$), 6.00 (1H, s, NH), 6.57—7.04 (4H, m, ArH), 7.32 (1H, d, J=5.61 Hz, H-2); Found: m/z 203.0931. Calcd for $C_{13}H_{13}NO_2$: M, 203.0947.

Dimeric Compound. From inspection of the NMR spectrum of Fig. 1a it consisted of two dimers (1 : 0.7 ratio) which melted ranging from 176 to 182 °C, and finally to reverted to **2**. UV (CH_3OH) λ_{max} 336 nm; IR (KBr) 3300 (NH), 3100, 3040, 2990, 2910, 1660 (CO), 1630, 1590, 1495, 1240, 1120 cm^{-1}; MS m/z 404 (M^+).

Ethyl 4-(1-Hydroxyethyl)-1,4-dihydro-2-quinolinecarboxylate (7a). Mp 88.5 °C (from hexane-benzene); IR (KBr) 3450 (NH), 3220 (OH), 3050, 2970, 2920, 1708 (CO), 1620, 1450, 1225, 1165 cm^{-1}; ^1H NMR ($CDCl_3$) δ=1.23 (3H, t, J=7.20 Hz, $CH_2C\underline{H}_3$), 1.55 (3H, d, J=6.92 Hz, CH(OH)$C\underline{H}_3$), 3.80 (1H, s, H-4), 4.16 (2H, q, J=7.20 Hz, $C\underline{H}_2CH_3$), 5.20 (1H, q, J=6.92 Hz, $C\underline{H}$(OH)CH_3), 7.11—7.80 (5H, m, ArH and H-3), 8.79 (1H, s, NH); MS m/z 247 (M^+); Found: C, 67.87; H, 6.89; N, 5.66%. Calcd for $C_{14}H_{17}NO_3$: C, 67.99; H, 6.93, N, 5.66%.

Ethyl 4-(1-Hydroxy-1-methylethyl)-1,4-dihydro-2-quinolinecarboxylate (7b). Colorless liquid, bp 130 °C/1 mmHg; IR (neat) 3500 (br, NH and OH), 3070, 2990, 2940, 1730 (CO),

1610, 1495, 1250, 1160 cm^{-1}; ^1H NMR ($CDCl_3$) δ=1.24 (3H, t, J=7.10 Hz, $CH_2C\underline{H}_3$), 1.29 (6H, d, J=6.26 Hz, $(CH_3)_2$), 3.71 (1H, s, H-4), 4.13 (2H, q, J=7.10 Hz, $C\underline{H}_2CH_3$), 7.07—7.56 (5H, m, ArH and H-3), 8.45 (1H, s, NH); Found: m/z 261.1330. Calcd for $C_{15}H_{19}NO_3$: M, 261.1365.

Ethyl 1,4-Dihydro-2-quinolinecarboxylate (8). Colorless liquid, bp 130 °C/1 mmHg; IR (neat) 3500 (NH), 3070, 2990, 2940, 1730 (CO), 1610, 1495, 1250, 1160 cm^{-1}; ^1H NMR($CDCl_3$) δ=1.26 (3H, q, J=7.12 Hz, $CH_2C\underline{H}_3$), 3.80 (2H, s, H-4), 4.17 (2H, q, J=7.12 Hz, $C\underline{H}_2CH_3$), 7.11—7.25 (3H, m, H-3, 6, and 7), 7.36 (1H, d, J=8.24 Hz), 7.63 (1H, d, J=7.19 Hz), 8.10 (1H, s, NH); Found: m/z 203.0948. Calcd for $C_{12}H_{13}NO_2$: M, 203.0947.

Quantum yields were determined by irradiating a sample solution (2×10^{-3} mol dm^{-3}) in a quartz cylindrical cell (5-cm in diameter and 1-cm in length) with 313 nm-light from a USH-500D lamp. The 313-nm line was isolated by a combination of a $NiSO_4$ solution with a UV-31 filter. The light intensity was determined by means of a potassium trioxalatoferrate(III) actinometer. The amounts of the products and consumed starting material **1** and **2** were spectrometrically measured after the separation on a silica-gel chromatograph using the mixture of chloroform and diethyl ether.

References

1) a) H. Hata, I. Ono, S. Matono, and H. Hirose, *Bull. Chem. Soc. Jpn.*, **46**, 942 (1973); b) N. Hata and T. Saito, *ibid.*, **47**, 942 (1974); c) T. Caronna, S. Morrocchi, and B. M. Vittinberga, *J. Org. Chem.*, **46**, 34 (1981); d) T. Caronna, S. Morrocchi, and P. Traldi, *J. Chem. Soc., Chem. Commun.*, **1979**, 64; e) N. Hata and N. Nishida, *Bull. Chem. Soc. Jpn.*, **58**, 3423 (1985).

2) I. Ono and N. Hata, *Bull. Chem. Soc. Jpn.*, **56**, 3667 (1983).

3) T. Sugimoto, T. Furihata, K. Takagi, M. Sato, S. Akiyama, G. P. Sato, and A. Sugimori, *Bull. Chem. Soc. Jpn.*, **54**, 3785 (1981).

4) a) Y. Ogata, A. Kawanishi, and S. Suyama, *Tetrahedron*, **25**, 1361 (1969); b) R. Noyori, M. Kato, M. Kawanishi, and H. Nozaki, *ibid.*, 1125 (1969).

5) P. Barczynski and M. Szafran, *Rocez. Chem.*, **50**, 353 (1976).

6) E.Ochiai, "Aromatic Amine Oxide," Elsevier, Amsterdam (1967), Chap. 3.

7) H. Gelman and S. M. Spatz, *J. Am. Chem. Soc.*, **63**, 1557 (1941).

8) I. Nakagawa, *Yakugaku Zasshi*, **71**, 1391 (1951).

The Photocycloaddition of *N*-Vinylcarbazole with 3-Cyanostyrene

Akira TSUCHIDA, Masahide YAMAMOTO,* and Yasunori NISHIJIMA
Department of Polymer Chemistry, Faculty of Engineering, Kyoto University, Yoshida, Sakyo-ku, Kyoto 606
(Received January 21, 1987)

The photocycloaddition reaction of *N*-vinylcarbazole (VCZ) as an electron donor, with 3-cyanostyrene as an electron acceptor, was studied. In nonpolar solvents, two cyclobutanes of *cis*-1-(9-carbazolyl)-2-(3-cyanophenyl)-cyclobutane and *trans*-1-(9-carbazolyl)-2-(3-cyanophenyl)cyclobutane (in a ratio of 3 : 1) were obtained from an exciplex intermediate. The structure of cis cyclobutane seemed to originate from a sandwich conformation of the exciplex. In polar solvents, a photodissociation to free ion radicals was observed and *trans*-1,2-di(9-carbazolyl)cyclobutane was produced efficiently by means of a chain mechanism via a cation radical of VCZ. Transient intermediates were measured by means of nanosecond laser photolysis; the results supported the reaction scheme.

Previously, we reported on the photocycloaddition of 4-dimethylaminostyrene (DMASt) with 1-vinylpyrene (VP) and that with styrene (St).[1] In both systems, cyclobutanes were obtained as the main photoproducts in nonpolar solvents, and the stereochemistry of the cyclobutanes produced was explained by the reactivity of the exciplex intermediates. The long lifetime of the exciplex of DMASt with VP or the large pi system of VP allows a wide variety of conformations and leads to a trans-type cyclobutane, whereas in the reaction of DMASt with St, the short lifetime or the overlap of small pi rings limits the conformations of the exciplex and leads to a cis-type cyclobutane.

Here, we will report on the photocycloaddition reactions of *N*-vinylcarbazole (VCZ) with 3-cyanostyrene (CNSt). The photoirradiation of this system in nonpolar solvents gave mainly the cis-type cyclobutane, although an appreciable amount of trans-type cyclobutane formation was found simultaneously. From the results of the solvent effect on the photocycloaddition reaction and from the spectroscopic data, the reaction type of this VCZ-CNSt system is considered to be situated between those of the DMASt-VP and DMASt-St systems.

Experimental

Materials. *N*-Vinylcarbazole (VCZ, Tokyo Kasei Kogyo Co., Ltd.) was purified by recrystallization from ethanol and hexane. 3-Cyanostyrene (CNSt) was prepared from 3-cyanotoluene (Tokyo Kasei Kogyo Co., Ltd.),[2,3] and was purified by distillation under reduced pressure three times. Vinyl methyl terephthalate (VMTP) was synthesized by the ester-exchange reaction of vinyl acetate with the terephthalic acid monomethyl ester.

Benzene, diethyl ether, tetrahydrofuran (THF), methyl ethyl ketone (MEK), and acetone were dried and purified by distillation. *N*,*N*-Dimethylformamide (DMF) was dried and purified by distillation under reduced pressure. 2-Chlorobutane and 2-methyltetrahydrofuran (MTHF) for gamma-ray irradiation were dried by the use of molecular sieves and then distilled prior to use.

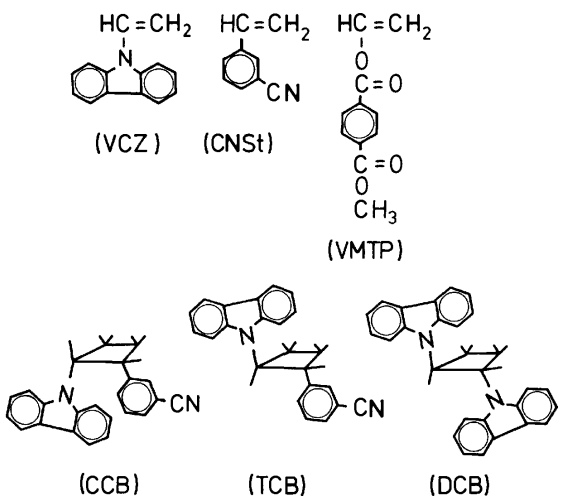

Photoreaction. A solution of VCZ (0.052 mol dm^{-3}) with CNSt (0.19 mol dm^{-3}) in benzene (2 ml) was degassed by repeated freeze-pump-thaw cycles in a Pyrex ampoule. The photoirradiation of the degassed ampoule was done by means of a 300-W high-pressure mercury lamp (Toshiba) fitted with a UV-33 filter (Toshiba) at 298 K: VCZ was selectively photoexcited in this system at 334 nm. After the evaporation of the benzene solvent, the photoproducts were analyzed by means of a gel-permeation chromatograph (Toyo Soda HLC-802UR) fitted with analytical columns eluting with THF. The quantity of products was determined by the use of a refractive index detector, where the refractive index for each compound was calibrated. The effect of thermal side reactions, which produced a small amount of a VCZ dimer or polymer in polar solvents, was corrected by the blank experiment in all cases.

The reaction quantum yield of cycloadducts was determined by using a degassed 1-cm quartz cell where the light intensity at 335 nm was found to be 1.77×10^{-9} E s^{-1} by actinometry.[4,5]

Identification of Cycloadducts. A degassed solution of VCZ (0.4 g) with CNSt (1.0 g) in benzene (40 ml) was photoirradiated for 14 h by means of a 300-W high-pressure mercury lamp fitted with a Pyrex glass filter at 298 K.[1,6] Products were injected into a recycle gel-permeation chromatograph (Toyo Soda HLC-802R) fitted with TSK-GEL-G2000HG6 and TSK-GEL-G2000HG8 columns, with chloroform as the eluent. Recycling for four times gave enough separation of cycloadducts: The cis cycloadduct (CCB) had a larger retention time than the trans cycloadduct (TCB). Recrystallization from hexane gave 79 mg of CCB and 25 mg of TCB. The configuration of the two cycloadducts was determined by NMR (JOEL JNM-FX90Q) on the basis of the chemical shifts.[1,6,7] The positions of the pro-

tons were determined by means of ^1H homonuclear decoupling or selective proton decoupling ^{13}C NMR measurements.

***cis*-1-(9-Carbazolyl)-2-(3-cyanophenyl)cyclobutane (CCB):** Mp 100—101 °C; IR (KBr) 3075w, 2970w, 2290w, 2250s, 1597s, 1487vs, 1448vs, 1409w, 1335vs, 1320m, 1240m, 1224s, 1212m, 1189m, 1160m, 1123m, 1085w, 1031w, 1004w, 925w, 888w, 812s, 802s, 751vs, 722vs, 702w, 620w, 559w, 530w, 515w, and 482w cm^{-1}; ^1H NMR (90 MHz; C_6D_6; Me_4Si) δ=1.68—2.38 (3H, m, $H_{(c)}$ and $H_{(e)}$), 2.74—3.24 (1H, m, $H_{(d)}$), 3.38—3.72 (1H, m, $H_{(b)}$), 4.76—5.12 (1H, m, $H_{(a)}$), 5.92—6.60 (4H, m, aromatic), and 7.00—7.98 (8H, m, aromatic); ^1H NMR (90 MHz; $CDCl_3$; Me_4Si) δ=2.16—3.04 (3H, m, $H_{(c)}$ and $H_{(e)}$), 3.22—3.72 (1H, m, $H_{(d)}$), 3.96—4.36 (1H, m, $H_{(b)}$), 5.34—5.72 (1H, m, $H_{(a)}$), 6.60—7.24 (4H, m, aromatic), and 7.10—8.04 (8H, m, aromatic); MS (70 eV), *m/z* (rel intensity) 322 (10%, M^+), 294 (7, $M^+-C_2H_4$), 193 (100, VCZ^+), and 129 (7, $CNSt^+$).

Found: C, 85.9; H, 5.5; N, 8.5%. Calcd for $C_{23}H_{18}N_2$: C, 85.7; H, 5.6; N, 8.7%.

***trans*-1-(9-Carbazolyl)-2-(3-cyanophenyl)cyclobutane (TCB):** Mp 51—52 °C; IR (KBr) 3140w, 2940w, 2250s, 1628w, 1600s, 1489vs, 1454vs, 1335vs, 1238m, 1224s, 1211m, 1158s, 1124m, 1081w, 1030w, 1005w, 931w, 892w, 842w, 826w, 801m, 751vs, 724vs, 690m, 664m, 620w, 565w, 530w, 504w, and 418w cm^{-1}; ^1H NMR (90 MHz; C_6D_6; Me_4Si) δ=1.38—2.20 (3H, m, $H_{(c)}$ and $H_{(d)}$), 2.46—3.02 (1H, m, $H_{(e)}$) 3.96—4.30 (1H, m, $H_{(b)}$), 4.48—4.84 (1H, m, $H_{(a)}$), 6.40—7.00 (4H, m, aromatic), and 6.96—8.12 (8H, m, aromatic); ^1H NMR (90 MHz; $CDCl_3$; Me_4Si) δ=1.92—2.78 (3H, m, $H_{(c)}$ and $H_{(d)}$), 2.92—3.46 (1H, m, $H_{(e)}$), 4.54—4.92 (1H, m, $H_{(b)}$), 5.00—5.36 (1H, m, $H_{(a)}$), and 7.08—8.22 (12H, m, aromatic); MS (70 eV), *m/z* (rel intensity) 322 (36%, M^+), 294 (1, $M^+-C_2H_4$), 193 (100, VCZ^+), and 129 (8, $CNSt^+$).

Found: C, 85.7; H, 5.7; N, 8.8%. Calcd for $C_{23}H_{18}N_2$: C, 85.7; H, 5.6; N, 8.7%.

Spectroscopic Measurements. All measurements of the absorption and emission spectra and of the lifetime were made on the samples in a degassed 1-cm quartz cell at 298 K. The absorption spectra were measured by means of a UV-200S (Shimadzu) spectrophotometer. The emission spectra were obtained by the use of an RF-501 (Shimadzu) spectrofluorophotometer. The emission quantum yield was determined relative to that of quinine sulfate in sulfuric acid.[8] The lifetime of the emission was measured by the single-photon counting method (PRA, Inc.).

The transient absorption was obtained by the use of a nanosecond ruby laser photolysis apparatus which has been described elsewhere.[9] The exciting 347-nm light pulse had a pulse energy of 10 mJ and a pulse duration of 14 ns.

The reference spectra of VCZ^+ and $CNSt^-$ were measured by means of gamma-ray irradiation at 77 K in 2-chlorobutane and MTHF respectively.[10]

Results and Discussion

Emission Analysis. The fluorescence of VCZ (emission lifetime=10.4 ns in a benzene solvent) was quenched by the addition of CNSt in the degassed solvents. The rate constants of fluorescence quenching (k_q) were determined, by means of the Stern-Volmer plots at 298 K, to be 3.1×10^8 and 2.9×10^9 $M^{-1}s^{-1}$ in nonpolar benzene and polar *N,N*-dimethylformamide (DMF) solvents respectively; the value of k_q in benzene is rather small when it is compared with a diffusion-controlled rate constant (ca. 1×10^{10} $M^{-1}s^{-1}$ in benzene). This fluorescence quenching is considered to occur via an electron-transfer reaction from $^1VCZ^*$ to CNSt; energy-transfer quenching can be excluded by considering their energy levels. In this case, the free energy change of electron-transfer quenching is estimated by Weller's equation[11] to be ca. 5 kcal mol^{-1} exothermic.

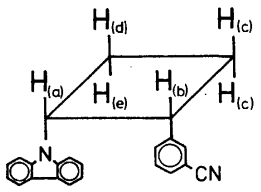

(CCB)

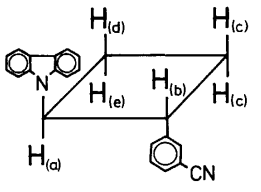

(TCB)

A weak and structureless emission was observed at around 470 nm in a nonpolar benzene solvent when the VCZ fluorescence was quenched by CNSt; the quantum yield of this new emission was ca. 0.01, and the lifetime was 10.7 ns, under these experimental conditions. This new emission is ascribed to the exciplex emission as it disappears in polar solvents, where photodissociation to free-ion radicals competes with exciplex formation from a transient ionic complex.[12]

Photoproduct Formation. The selective photoexcitation (Hg lamp, UV-33 filter) of VCZ (0.052 mol dm^{-3}) in the presence of CNSt (0.19 mol dm^{-3}) in a degassed benzene solvent produced two cyclobutanes: *cis*-1-(9-carbazolyl)-2-(3-cyanophenyl)cyclobutane (CCB) and *trans*-1-(9-carbazolyl)-2-(3-cyanophenyl)cyclobutane (TCB). The quantum yields of the cyclobutane formation were determined by actinometry to be 0.28 and 0.10 for CCB and TCB respectively under the complete quenching of $^1VCZ^*$ by CNSt. In this system, the yield of the cis-type cyclobutane formation was three times larger than that of the trans-type, and the other side reactions gave only a small yield of the by-products. A small amount of a polymer was also produced by photoirradiation, but the initiating species of the polymer was negligible, judging from the estimate based on the molecular weight of the polymer (ca. 10^4). As a control, the following experiments were carried out: the photoirradiation of VCZ (0.052 mol dm^{-3}) in the absence of CNSt in benzene produced the polymer and a very small amount of *trans*-1,2-di(9-carbazolyl)cyclobutane (DCB), while the photoirradiation of CNSt (0.19 mol dm^{-3}), which has no light absorption at 334 nm, in the absence of VCZ produced no photoproduct. The thermal reaction produced only a small amount of a copolymer, the contribution of which was corrected for in all experiments.

Figure 1 shows the time-conversion plots of the photoproducts. Here, the yield of the photoproducts was calculated on the basis of the total amount of VCZ. The formation of CCB and TCB is proportional to the

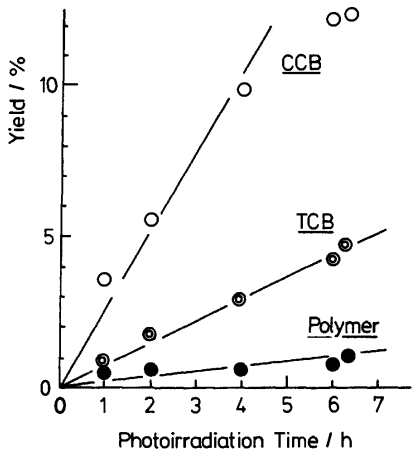

Fig. 1. Time-conversion plots of photoproducts. VCZ (0.052 mol dm^{-3}) was photoirradiated in the presence of CNSt (0.19 mol dm^{-3}) in benzene at 298 K.

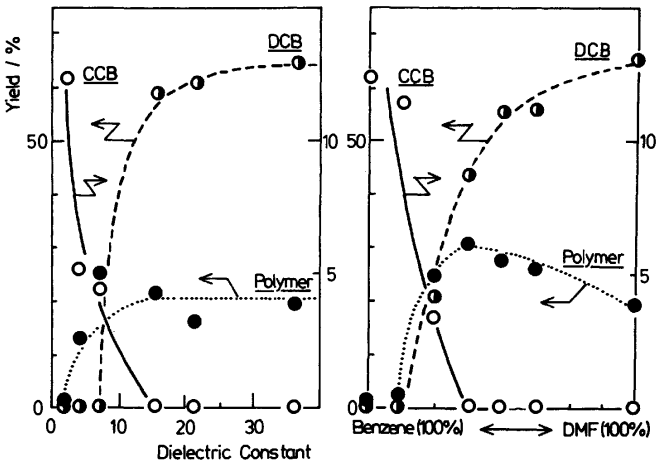

Fig. 2. Effects of solvent polarity on the distribution of photoproducts. Solvents used in the left figure were benzene, diethyl ether, tetrahydrofuran, methyl ethyl ketone, acetone, and *N*,*N*-dimethylformamide. A mixed solvent of benzene and *N*,*N*-dimethylformamide was used in the right figure. VCZ (0.052 mol dm^{-3}) was photoirradiated in the presence of CNSt (0.19 mol dm^{-3}) at 298 K for 320 min. The yield of TCB, which was not plotted in this figure, was ca. 1/3 of CCB in every solvent.

irradiation time, though the yield of CCB reaches the saturation point after a long irradiation time (>4 h). The effect of cis-trans isomerization on the photoproduct distribution is neglected, since the photoisomerization rates from CCB to TCB and from TCB to CCB were slow enough under these experimental conditions.

Solvent Effects. This photocycloaddition reaction of VCZ with CNSt was found to be greatly affected by the solvent polarity. In a polar DMF solvent, no CCB and TCB could be found; a large amount of the VCZ cyclobutane dimer (DCB) was produced instead of these cycloadducts. The photodimerization of VCZ in polar solvents was extensively studied by Ledwith,[13] who found that the dimerization proceeds by means of a chain mechanism via the cation radical of VCZ. In DMF, the participation of the chain mechanism is obvious, as the quantum yield of DCB formation was much larger than unity. The effect of solvent polarity on the photoreaction of VCZ with CNSt is demonstrated in Fig. 2. The left half of Fig. 2 shows the effect of the solvent polarity on the photoreaction in six different solvents, while the right half shows the results in mixed solvents of benzene and DMF. The results of these two experiments are in fairly good agreement. In nonpolar solvents, the cycloadditions are the main reactions, and the dimerization and polymerization are negligible. However, with an increase in the solvent polarity, the yield of the DCB by means of a chain mechanism increases greatly, and the cycloadduct formation is suppressed. This tendency is the same as that we reported previously.[1] In nonpolar solvents, photocycloaddition via an exciplex is dominant, while in polar solvents, the photodissociation of the exciplex to free-ion radicals becomes predominant, and the free-ion radicals so produced lead to product formation. In the photoreaction system of VCZ with CNSt in polar solvents, the dimerization occurs via an ion-radical intermediate, and the reaction is amplified by a chain mechanism.

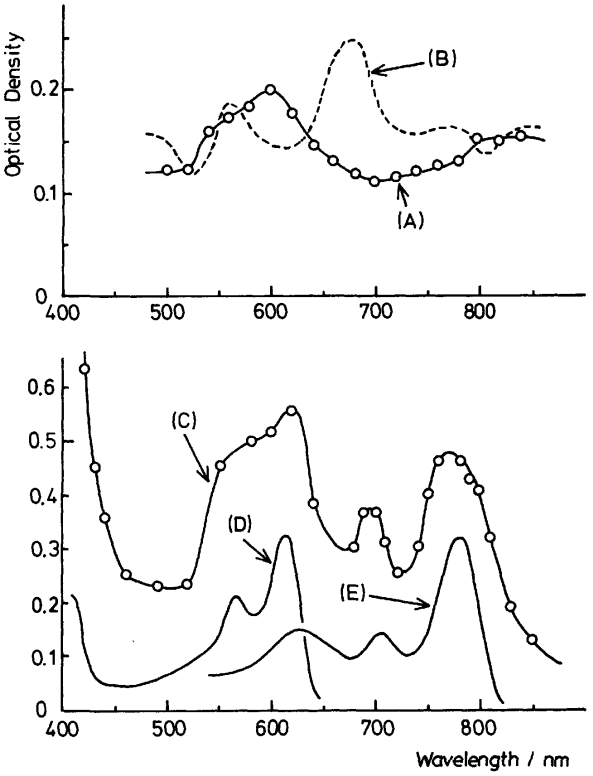

Fig. 3. Transient absorption spectra of VCZ (OD_{347}=1.2) with CNSt (1.1 mol dm^{-3}) measured by ns laser photolysis. Spectra were obtained in benzene at 20 ns (A) or in *N*,*N*-dimethylformamide at 50 ns (C) after excitation. Transient absorption spectrum of VCZ (B) without CNSt was obtained in benzene at 20 ns after excitation as a reference of the spectrum (A). Reference absorption spectra of ion radicals $CNSt^-$ (D) and VCZ^+ (E) were obtained by gamma-ray irradiation in rigid matrices at 77 K.

Transient Spectra. The transient species in this photoreaction were studied by means of ns ruby-laser-photolysis measurements. The upper half of Fig. 3 shows the transient absorption spectra obtained in benzene 20 ns after excitation at 298 K. The photoexcitation of VCZ in the presence of CNSt (1.1 mol dm^{-3}) by means of a laser pulse (347 nm, 14 ns) gave Spectrum (A). This absorption spectrum is different from the S-S absorption of VCZ which was obtained by the reference sample without CNSt and which is shown by Spectrum (B). The lifetime of the transient species of Spectrum (A) agreed well with that of the exciplex emission, and the absorption bands are broad. Therefore, this transient absorption is considered to originate from the exciplex of VCZ with CNSt. No transient absorption which has a longer lifetime could be found except that of ^{3}VCZ*. On the other hand, in DMF, the formation of free-ion radicals was observed, as is shown in the lower half of Fig. 3. Spectrum (C) was obtained by the photoexcitation of VCZ with CNSt in DMF. The transient species found in this spectrum are ascribed to $CNSt^{\cdot-}$ and $VCZ^{\cdot+}$ by reference to the (D) and (E) absorption spectra. The lifetimes of these ion radicals were longer than a micro second, and these ion radicals are considered to be solvated free-ion radicals. The free $VCZ^{\cdot+}$ leads to DCB formation by means of a chain reaction.

The Reaction Mechanism. The scheme summarizes the photochemical reaction mechanism. In nonpolar solvents, two cycloadducts, CCB and TCB, are produced by the photoirradiation of VCZ with CNSt. Three times as much of the cis-type cyclobutane (CCB) is obtained as the trans-type cyclobutane (TCB). In a previous report,[1] we discussed the relationship between the reactivity of the exciplex intermediates and the stereochemistry of the cycloadduct products. The pair of 4-dimethylaminostyrene (DMASt) and 1-vinylpyrene (VP) gave an emissive exciplex whose lifetime was 55 ns in benzene. The long lifetime or the large pi ring of VP allows for a wide variety of exciplex conformations, which in turn leads to a trans-type cyclobutane formation. On the other hand, the photoreaction of DMASt with styrene (St) produces cis-type cyclobutane by means of the short lifetime or the small overlap of pi rings in the exciplex intermediate. Hence, the conformational distribution of the exciplex intermediate was concluded to allow the formation of trans-type cyclobutane. In the present study of the VCZ-CNSt system, the cis-type cyclobutane, which reflects the sandwich structure of the exciplex intermediate, was the main product, but an appreciable amount of the trans-type cyclobutane was also obtained simultaneously. The exciplex lifetime of this system is rather short (10.7 ns), and the pi ring of carbazole is not as large as that of pyrene. The reactivity of this exciplex is considered to be situated between those of the DMASt-VP and DMASt-St systems. On the other hand, in polar solvents, the photodissociation of the exciplex to $VCZ^{\cdot+}$ and $CNSt^{\cdot-}$ becomes a dominant reaction process, and DCB is mainly produced by a chain mechanism of VCZ via $VCZ^{\cdot+}$ as the intermediate; the chain reaction via $VCZ^{\cdot+}$ amplifies the reaction yield. The anion radical of CNSt is considered to be neutralized by the recombination with $VCZ^{\cdot+}$ or $DCB^{\cdot+}$. Hence, the reactivities of the ion radical and exciplex can be clearly distinguished.[14-21]

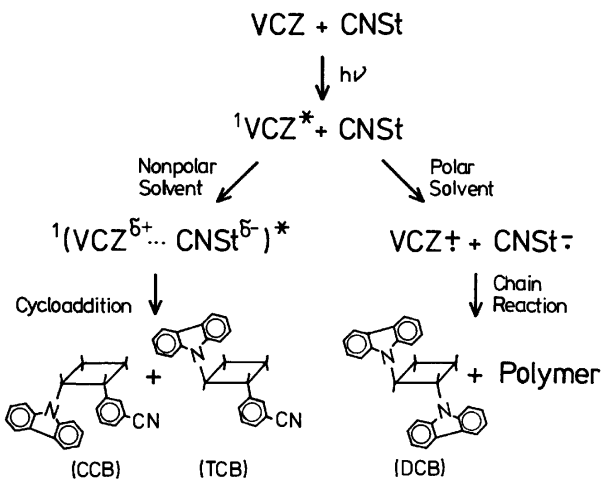

Scheme

To understand the reactivity of the cycloaddition reactions via the exciplex, the VCZ-VMTP system was also examined. The diffusion-controlled quenching of ^{1}VCZ* by VMTP in benzene produced an emissive exciplex (lifetime=49 ns). The free-energy change of the electron transfer from VCZ to VMTP is estimated to be 14-kcal mol^{-1} exothermic by the use of Weller's equation.[11] The photoirradiation of this system, however, produced only a polymer with a very small amount of DCB; no cyclobutane formation between VCZ and VMTP could be detected. It seems that the cyclobutane formation between two vinyl groups of aromatic vinyl monomers requires the pi conjugation of the vinyl group to the aromatic ring in the exciplex state.

Conclusion

The photoexcitation of VCZ with CNSt in nonpolar solvents produced two cycloadducts of CCB and TCB via an exciplex intermediate. In this system, the yield of cis cyclobutane CCB was three times higher than that of the trans-type TCB. The structure of CCB originated from the sandwich conformation of the exciplex. The formation of trans cyclobutane TCB is considered to be due to the looseness of the exciplex conformation. In polar solvents, the photodissociation of the exciplex to free $VCZ^{\cdot+}$ and $CNSt^{\cdot-}$ occurred. The $VCZ^{\cdot+}$ thus produced gave DCB efficiently by means of a chain mechanism, and the products of the exciplex reaction and the ion radical reaction were clearly differentiated.

We wish to thank Professor Hitoshi Yamaoka of the

Research Reactor Institute, Kyoto University, for his help in determining the reference absorption spectra of the ion radicals. This work was partially supported by a Grant-in-Aid for Energy Research (No. 60045061) from the Ministry of Education, Science and Culture.

References

1) A. Tsuchida, M. Yamamoto, and Y. Nishijima, *J. Chem. Soc., Perkin Trans. 2*, **1986**, 239.

2) H. Coleman and G. E. Honeywell, *Org. Synth.*, Coll. Vol. 2, 89 (1943).

3) R. H. Wiley and N. R. Smith, *J. Am. Chem. Soc.*, **70**, 1560 (1948).

4) S. L. Murov, "Handbook of Photochemistry," Marcel Dekker, New York (1973).

5) C. G. Hatchard and C. A. Parker, *Proc. R. Soc. London, Ser A*, **235**, 518 (1956).

6) M. Yamamoto, T. Asanuma, and Y. Nishijima, *J. Chem. Soc., Chem. Commun.*, **1975**, 53; T. Asanuma, M. Yamamoto, and Y. Nishijima, *ibid.*, **1975**, 56; *ibid.*, **1975**, 608.

7) T. Nakano, A. Martin, C. Rivas, and C. Pérez, *J. Heterocycl. Chem.*, **14**, 921 (1977).

8) J. N. Demas and G. A. Crosby, *J. Phys. Chem.*, **75**, 991 (1971).

9) A. Tsuchida, M. Yamamoto, and Y. Nishijima, *J. Phys. Chem.*, **88**, 5062 (1984).

10) W. H. Hamill, "Radical Ions," ed by E. T. Kaiser and L. Kevan, Interscience, New York (1968), Ch. 9.

11) D. Rehm and A. Weller, *Z. Phys. Chem. (Wiesbaden)*, **69**, 183 (1970).

12) H. Masuhara and N. Mataga, *Acc. Chem. Res.*, **14**, 312 (1981).

13) A. Ledwith, *Acc. Chem. Res.*, **5**, 133 (1972).

14) S. L. Mattes and S. Farid, *Acc. Chem. Res.*, **15**, 80 (1982).

15) J. J. McCullough, R. C. Miller, D. Fung, and W.-S. Wu, *J. Am. Chem. Soc.*, **97**, 5942 (1975); J. J. McCullough, R. C. Miller, and W.-S. Wu, *Can. J. Chem.*, **55**, 2909 (1977).

16) F. D. Lewis and R. J. DeVoe, *Tetrahedron*, **38**, 1069 (1982).

17) M. Ohashi, *Kagaku No Ryoiki*, **32**, 703 (1979); *ibid.*, **32**, 830 (1979).

18) H. Sakurai and C. Pac, *Kagaku Sosetsu*, Nos. 33, 37 (1982); *ibid.*, 75 (1982); K. Mizuno, C. Pac, and H. Sakurai, *J. Am. Chem. Soc.*, **96**, 2993 (1974).

19) R. A. Caldwell and D. Creed, *Acc. Chem. Res.*, **13**, 45 (1980).

20) H. Sakuragi, K. Tokumaru, H. Itoh, K. Terakawa, K. Kikuchi, R. A. Caldwell, and C.-C. Hsu, *J. Am. Chem. Soc.*, **104**, 6796 (1982).

21) H. Leismann, J. Mattay, and H.-D. Scharf, *J. Am. Chem. Soc.*, **106**, 3985 (1984); J. Mattay, J. Runsink, T. Rumbach, C. Ly, and J. Gersdorf, *ibid.*, **107**, 2557 (1985).

 © 1987 The Chemical Society of Japan Bull. Chem. Soc. Jpn., 60, 2905—2909 (1987)

Liquid Crystalline Compounds Bearing Pyridine Ring: Azoxy Compounds with Alkyl Substituents

Hiroyoshi KAMOGAWA,* Tsuneharu KASAI, Toshio ANDOH, and Tomoyuki NAKAMURA
Department of Applied Chemistry, Yamanashi University, Kofu 400
(Received February 9, 1987)

Azoxy compounds bearing a 2,5-disubstituted pyridine ring as a principal constituent and at least one alkyl group at a molecular end were synthesized and their mesomorphic (nematic) ranges were examined. As for azoxy compounds containing an alkyl and an alkoxy group at both ends, respectively, mesomorphic ranges appeared with lower alkyl groups than those for azo compounds, their precursors. The ranges were also lower than those with both alkoxy ends. As regards an azoxy compound containing alkyl groups at both ends, no mesomorphic phenomenon appeared within the scope of this study.

Relatively few studies have been reported on liquid crystalline compounds bearing a pyridine ring as a principal constituent. A couple of studies on liquid crystalline Schiff bases[1,2] and phenylpyridines[3] can be found in the literature and we have reported 3-(4-alkoxyphenylazoxy)-6-alkoxypyridines as a novel liquid crystal series.[4] The replacement of the benzene ring by the pyridine, which exerts a sideward dipole moment, appears to profoundly affect the mesomorphic property of a compound.

In this study, we wish to report on the synthesis and the liquid-crystalline properties of azoxypyridines containing at least one terminal alkyl group in comparison with the known compounds containing only benzene rings, as well as the results of the previous study.[4]

Two synthetic sequences (indicated in Schemes 1 and 2) were adopted.

Where R_1=CH_3, C_2H_5; R_2=CH_3, C_2H_5, n-C_6H_{13}; R_3=CH_3, n-C_4H_9.

The mesomorphic behaviors of azoxy compounds **9**, **10**, **10′** and **15**, **16**, **16′** as well as those of azo compounds **7** and **13** were investigated.

Results and Discussion

2-[1,1-Bis(ethoxycarbonyl)alkyl]-5-nitropyridines (**2**) were prepared in a conventional manner by replacing the activated chlorine atom of 2-chloro-5-nitropyridine (**1**) with the carbanion from diethyl alkylmalonate prepared with sodium metal in xylene in 45—70% yields. The hydrolysis and subsequent decarboxylation of **2** with sulfuric acid were carried out according to Champa[2] to give 2-alkyl-5-nitropyridine (**3**) in 40—73% yield. A reduction of nitro to amino groups with cyclohexene in the presence of Pd-C (5%) proceeded quantitatively to afford 2-alkyl-5-amino-pyridines (**4**). A diazotization of **4** followed by coupling with phenol in the conventional manner provided azo compound **6** in high yield (83—91%). Etherification of the phenolic hydroxyl group via phenoxide ion with R_2I in DMF at 20 °C for 48 h afforded crude 3-(*p*-alkoxyphenylazo)-6-alkylpyridine (**7**), which was purified by silica-gel (Wakogel C-300) column chromatography using benzene as the eluting solvent. The oxidative conversion of **7** to azoxy derivatives **8** with hydrogen peroxide in acetic acid took 4 h, until the orange color of the

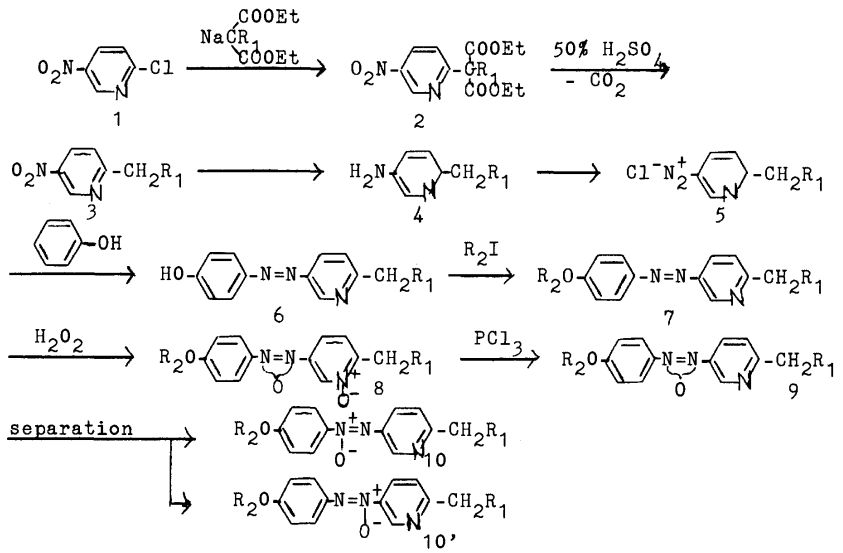

Scheme 1.

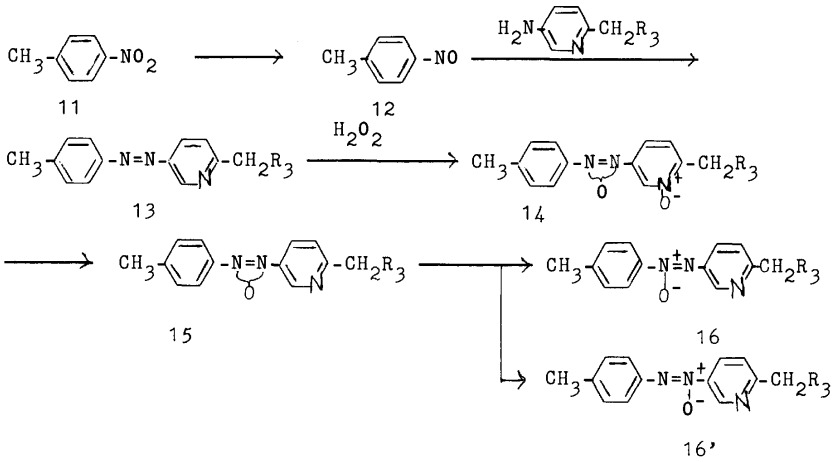

Scheme 2.

solution faded to some extent. IR (1250 cm^{-1}) and mass spectrometry clearly showed that the product was azoxypyridine *N*-oxide (**8**). This took a longer time than in the case of a previous report.[4] *N*-Oxides **8** were converted to the aimed 3-(*p*-alkoxyphenylazoxy)-6-alkylpyridines (**9**) by refluxing in PCl_3-$CHCl_3$ (1 : 4 v/v) followed by the usual work-up and recrystallization from ethanol in reasonable yields. The results of IR, MS, and ^1H NMR studies indicated that **9** was obtained. Since azoxy compounds **9** included two isomers by TLC, silica-gel column chromatography using ether-hexane (1 : 5 v/v) as the eluting solvent was employed in order to separate these isomer mixtures (**10** and **10'**). Identifications of azoxy compounds, thus separated, were satisfactorily made by ^1H NMR signals (δ 9.1—9.2 for **10**; δ 9.4—9.5 for **10'**). The ratioes of **10**/**10'** in **9** (Table 1) were determined from ^1H NMR signals. A remarkable feature is that **10'** is produced exclusively in samples **9b**, **9d**, and **9e**, indicating that the electron-donating effect of R_2O makes the azoxy N-atom more distant from the benzene ring more electrophilic as a result of resonance.

In the 2nd series, *p*-nitrotoluene (**11**) was converted to *p*-nitrosotoluene (**12**) via *p*-tolylhydroxylamine in usual manner.[5] The yield of *p*-nitrosotoluene was 40% on the basis on the starting *p*-nitrotoluene. **12** was reacted with **4** in acetic acid to give the corresponding azo compound **13** in low yield. The oxidation of **13** with hydrogen peroxide took 6 h (this time), and refluxing with PCl_3 afforded crude 3-(*p*-tolylazoxy)-6-alkylpyridine (**15**). A purification of the crude product with column chromatography eluted (hexane-benzene 5 : 1 v/v) the purified product in 21% yield (**15b**; R_3=C_4H_9). The ratio of two isomers in **15**(**16**/**16'**) was also determined from ^1H NMR signals (δ 9.1—9.2 for **16**; δ 9.5—9.6 for **16'**). For **15a**, the separation of two isomers was carried out by centrifugal liquid chromatography using hexane-ether (5 : 1 v/v) as the eluting solvent to afford isomers **16** and **16'**. These azoxy compounds indicated no mesomorphic range, presumably due to the presence of a very short methyl group at the one end.

Tables 1—3 summarize the transition temperatures of **9**, **10**, **10'**, and their precursors **7**, together with the values of the molar absorptivity (ε) in ethanol at the absorption maxima.

It can be recognized from Tables 1 and 2 that the azoxy compounds with relatively short R_2 chains such as Nos. **9a**, **9b**, **10a**, **10'a**, and **10'b** indicate no mesomorphic ranges when R_1=Me; however, the conventional azoxy compounds containing only benzene rings exhibit mesomorphic phases, even in the case of a compound corresponding to **9a**(C37N71I).[6] Therefore, it appears that the introduction of 2,5-

Table 1. Transition Temperature of Azoxy Compound **9** and **15**

No.	R_1	R_2	Yield %	**10**/**10'** Molar ratio	Transition[a] temperature °C	ε $\times 10^4 m^3 cm^{-1} mol^{-1}$
9a	CH_3	CH_3	33	0.8	C43-46I	1.76(352)[c]
9b	CH_3	C_2H_5	47	0	C76-77I	2.43(361)[c]
9c	CH_3	C_6H_{13}	51	0.5	C37N76I	2.30(348)[c]
9d	C_2H_5	C_2H_5	32	0	C68N91I	2.32(361)[c]
9e	C_2H_5	C_6H_{13}	64	0	C51N85I	Undetermined
15a	CH_3[b]	—	36	1.6[d]	C27-28I	2.03(372)[c]
15b	C_4H_9[b]	—	21	0.3[d]	C39-40I	Undetermined

a) C, crystal; N, nematic; I, isotropic. b) R_3. c) Figures in parentheses indicate absorption maxima (EtOH) in nm. d) **16**/**16'**.

Table 2. Transition Temperature of Azoxy Compound **10** and **10′**, **16** and **16′**

No.	R_1	R_2	Transition temperature °C	ε $\times 10^4$ m^3 cm^{-1} mol^{-1}
10a	CH_3	CH_3	C60–62I	2.03(339)
10′a	CH_3	CH_3	C55–56I	2.38(359)
10′b	CH_3	C_2H_5	C76–77I	2.43(361)
10c	CH_3	C_6H_{13}	C56N85I	2.32(241)
10′c	CH_3	C_6H_{13}	C43N85I	2.59(361)
10′d	C_2H_5	C_2H_5	C68N89I	2.32(361)
10′e	C_2H_5	C_6H_{13}	C51N85I	Undetermined
16a	CH_3[a)]	—	C52I	1.26(324)
16′a	CH_3[a)]	—	C22I	3.47(333)

a) R_3. Figures in parentheses indicate absorption maxima (EtOH) in nm.

Table 3. Transition Temperature of Azo Compound **7** and **13**

No.	R_1	R_2	Yield %	Transition temperature °C	ε $\times 10^4$ m^3 cm^{-1} mol^{-1}
7a	CH_3	CH_3	62	C47–48I	2.64(353)
7b	CH_3	C_2H_5	43	C81–83I	2.55(355)
7c	CH_3	C_6H_{13}	31	C58–59I	2.38(355)
7d	C_2H_5	C_2H_5	73	C74N81I	2.53(355)
7e	C_2H_5	C_6H_{13}	59	C57N75I	2.68(355)
13a	CH_3[a)]	—	11	C63I	2.32(327)
13b	C_4H_9[a)]	—	10	C64–65I	Undetermined

a) R_3. Figures in parentheses indicate absorption maxima (EtOH) in nm.

disubstituted pyridine in place of the usual benzene ring in the alkyl-substituted azoxy compounds gives rise to a sideward polar effect on a molecule due to the unshared electron pair present on the 2,5-disubstituted pyridine ring; longer alkyl chains are required than the conventional azoxy compounds[5,7] to exhibit mesomorphism.

The mesomorphic ranges shown in Tables 1 and 2 were comparatively low, even with longer R_2, such as **9e** and **10′e**, as compared with those of the corresponding azoxy compounds with alkoxy groups at both ends.[4] This difference appears to be caused by the fact that alkyl group did not produce any polar effects on the arrays of molecules, as compared with polar alkoxy type. It can also be recognized from Table 3 that azo compounds **7** are inferior to azoxy types in the mesomorphic range formation, since even **7c** with long alkoxy chain does not afford any mesomorphic range. This may be caused by the fact that the polar character of azoxy at the central portion of the molecule would play a role in the appearance of mesomorphism. Generally, ONN isomers had higher CN and CI temperatures than NNO ones, presumably due to the more balanced polarities of the formers (Table 2), where ONN and NNO mean that the nitrogen atom on the benzene ring side and that on the pyridine side were oxidized, respectively. These azo-azoxy series are, more or less, colored; therefore, the values of molar absorptivity (ε) at absorption maxima are shown in Tables 1—3. However, the differences of ε and the absorption maxima are generally small, although visual colors are considerably different due to the difference in the expansion of absorption spectrum.

Experimental

IR, ^{1}H NMR, and mass spectra were recorded on a Hitachi 215 spectrophotometer, a JNM-PMX60 spectrometer, and a Hitachi RMU-6 spectrometer, respectively, under standard conditions. Elemental analyses and centrifugal liquid chromatography were carried out with Perkin-Elmer 250 and Hitachi CLC-5 instruments.

The transition temperatures were determined by means of either a Yamato MP-21 melting-point apparatus or an optical microscope, both equipped with crossed polarizers.

2-[1,1-Bis(ethoxycarbonyl)alkyl]-5-nitropyridine (2). Diethyl alkylmalonate (30 mmol) was stirred with a sand-like suspension of sodium metal(0.7 g, 30 mmol) in xylene (50 ml) at 50 °C until sodium metal completely disappeared (0.5—1 h). The resulting mixture was heated under reflux with 2-chloro-5-nitropyridine (**1**; 4.8 g, 30 mmol) for 4 h. Xylene was distilled off from the reaction mixture and the residue was extracted with ether-water. The organic layer was washed with water, dried over anhydrous sodium sulfate, and concentrated on a rotary evaporator, followed by distillation under reduced pressure (152—210 °C, 0.1 mmHg[†]) to give a fluid. Yield: 68% for R_1=Me, 50% for Et, 45% for C_4H_9. IR ($CHCl_3$) 1740 (C=O), 1350 (NO_2) cm^{-1}. ^{1}H NMR ($CDCl_3$) δ=0.9—2.4 (m, alkyl), 4.3 (q, 4H, $2CH_2O$), 8.0 (d, 1H, pyridine), 8.5 (q, 1H, pyridine), 9.4 (d, 1H, pyridine).

2-Alkyl-5-nitropyridine (3). These compounds were prepared according to a known method.[2] A solution of **2** (30

[†]1 mmHg=133.322 Pa.

mmol) in 50% H_2SO_4 was stirred at 110 °C until the generation of carbon dioxide gas was no longer discernible (2 h). The usual work-up and distillation under reduced pressure (100 °C/0.1 mmHg) gave a pure product. Yield: 61% for R_1=Me, 73% for Et, 40% for C_4H_9.

The results of IR and NMR were satisfactory.

2-Alkyl-5-aminopyridine (4). A solution of **3** (10 mmol) and cyclohexene (5 ml) in absolute ethanol (70 ml) was heated under reflux with the addition of 5% Pd-C (1 g) for 2 h with stirring. The reaction mixture was filtered and the filtrate was concentrated on a rotary evaporator to leave a fluid.

^{1}H NMR ($CDCl_3$) δ=0.9—3.0 (m, alkyl), 3.7 (b, 2H, amine), 6.9 (d, 2H, pyridine), 8.0 (b, 1H, pyridine).

3-(*p*-Hydroxyphenylazo)-6-alkylpyridine (6). To a solution of **4** (10 mmol) in a mixture of hydrochloric acid (4.5 ml) and water (10 ml) was added under ice cooling a solution of sodium nitrite (0.7 g) in water (10 ml), followed by stirring for a while. A solution of phenol (10 mmol) and sodium hydroxide (1.0 g) in water (20 ml) was dropped at 0—5 °C under ice-water cooling. Stirring was continued for one hour; then the solution was neutralized with sodium hydrogencarbonate, and the resulting precipitate was picked up by filtration. Recrystallization was carried out from chloroform-hexane. Yield; 91% for R_1=Me, 83% for Et. Mp 182—183 °C for R_1=Me, 151—151 °C for Et.

R_1	C%	H%	N%	MS(m/z)
CH_3	68.53(68.72)	5.86(5.73)	18.60(18.50)	227(M^+)
C_2H_5	69.57(69.71)	6.25(6.22)	17.28(17.43)	241(M^+)

Figures in parentheses indicate the calcd values.

IR($CHCl_3$) 3600—3150 (OH) cm^{-1}. ^{1}H NMR ($CDCl_3$) δ= 0.9—2.0 (m, alkyl), 2.9 (q, or t, 2H, $ArCH_2$), 6.9—8.1 (m, 6H, ArH+pyridine), 8.9 (d, 1H, pyridine), 10.0 (b, 1H, OH).

3-(4-Alkoxyphenylazo)-6-alkylpyridine (7). **6** (10 mmol) was dissolved in a solution of potassium hydoxide (12 mmol) in methanol (20 ml). Methanol was then removed on a rotary evaporator and the residue was dissolved in anhydrous DMF (20 ml). Alkyl iodide (12 mmol) was dropped and the mixture was stirred at 20 °C for 48 h. A 1 M[††] sodium hydroxide solution was then added and the mixture was extracted with chloroform. The organic layer was first washed with an aqueous sodium hydroxide solution and then with water. It was next dried over anhydrous sodium sulfate and evaporated on a rotary evaporator. Column (SiO_2, Wakogel C-300) chromatography using benzene as the eluting solvent was employed for purification.

No.	R_1	R_2	Yield/%
7a	CH_3	CH_3	62
7b	CH_3	C_2H_5	43
7c	CH_3	C_6H_{13}	31
7d	C_2H_5	C_2H_5	73
7e	C_2H_5	C_6H_{13}	59

No.	C/%	H/%	N/%	MS(m/z)
7a	69.43(69.71)	6.23(6.22)	17.47(17.43)	241(M^+)
7b	71.03(70.59)	7.01(6.67)	16.18(16.47)	255(M^+)
7c	73.20(73.31)	8.08(8.04)	13.42(13.50)	311(M^+)
7d	71.47(71.38)	7.12(7.06)	15.45(15.61)	269(M^+)
7e	73.48(73.85)	8.53(8.31)	12.65(12.92)	325(M^+)

Figures in parentheses indicate calcd values.

[††] 1 M=1 mol dm^{-3}.

^{1}H NMR ($CDCl_3$) δ=0.9—3.0 (m, alkyl), 3.8 for **7a** (s, 3H, CH_3O), 4.0 for others (q or t, 2H, CH_2O), 6.8—8.2 (m, 6h, ArH+pyridine), 9.0 (d, 1H, pyridine).

3-[(4-Alkoxyphenyl)-NON-azoxy]-6-alkylpyridine *N*-Oxide (8). A solution of **7** (5 mmol) and 30% hydrogen peroxide (17 ml) in glacial acetic acid (100 ml) were heated at 65 °C until the color of the solution faded to some extent (4 h). The solution was poured onto ice and the resulting precipitate was picked up by filtration. The precipitate was recrystallized from ethanol-water.

No.	R_1	R_2	Mp(θ_m/°C)	Yield/%
8a	CH_3	CH_3	117—118	32
8b	CH_3	C_2H_5	156—157	12
8c	CH_3	C_6H_{13}	80—82	46
8d	C_2H_5	C_2H_5	123—125	35
8e	C_2H_5	C_6H_{13}	136—137	27

No.	C/%	H/%	N/%	ε / $\times 10^4$ m^3 cm^{-1} mol^{-1}
8a	61.79	5.63	15.29	2.00
	(61.54)	(5.49)	(15.38)	(364)
8b	62.56	5.96	14.48	2.25
	(62.72)	(5.92)	(14.63)	(367)
8c	66.65	7.30	12.25	2.41
	(66.47)	(7.29)	(12.24)	(367)
8d	63.55	6.36	13.79	2.35
	(63.79)	(6.31)	(13.95)	(368)
8e	67.12	7.51	11.69	2.18
	(67.23)	(7.56)	(11.76)	(366)

The figures to the far right of the parentheses indicate the absorption maxima in nm. MS (m/z) of all compounds provided molecular ion peaks. IR (KBr) 1250 (*N*-oxide) cm^{-1}. ^{1}H NMR ($CDCl_3$) δ=0.9—3.0 (m, alkyl), 3.9 for **8a** (s, 3H, CH_3O), 3.8—4.2 for others (q or t, 2H, CH_2O), 6.9—8.5 (m, 6H, ArH+pyridine), 9.3 (d, 1H, pyridine).

3-[(4-Alkoxyphenyl)-NON-azoxy]-6-alkylpyridine (9). A mixture of **8** (0.3 mmol) and phosphorus trichloride (2.5 ml) in chloroform (10 ml) was refluxed for 4 h. To the reaction mixture were added ice and sodium hydroxide in order to make the solution alkaline. The whole was extracted with chloroform. The combined extracts were washed with water, dried over anhydrous sodium sulfate, and evaporated to dryness on a rotary evaporator. Recrystallization from ethanol provided a purified product.

No.	R_1	R_2	Yield/%
9a	CH_3	CH_3	33
9b	CH_3	C_2H_5	47
9c	CH_3	C_6H_{13}	51
9d	C_2H_5	C_2H_5	32
9e	C_2H_5	C_6H_{13}	64

No.	C/%	H/%	N/%
9a	65.00(65.42)	5.85(5.84)	16.18(16.35)
9b	66.35(66.42)	6.29(6.27)	15.43(15.50)
9c	69.86(69.72)	7.76(7.65)	12.85(12.84)
9d	66.91(67.37)	6.59(6.67)	14.92(14.74)
9e	70.22(70.44)	8.04(8.00)	12.26(12.32)

Mass spectra fo all azoxy compounds indicated molecular ion peaks.

^{1}H NMR ($CDCl_3$) δ=0.9—3.0 (m, alkyl), 3.9 for **9a** (s, 3H, CH_3O), 4.1 for others (q or t, 2H, CH_2O), 6.9—8.8 (m, 6H, ArH+pyridine), 9.2, 9.5 (1H, pyridine).

Separation of Isomers. Column (silica gel, Wako C-300) chromatography was applied to **9** using ether-hexane (1 : 5 v/v) as an eluting solvent to afford NNO-azoxy, then ONN-azoxy isomers.

No.	R_1	R_2	ONN-azoxy (**10**) NMR/δ	NNO-azoxy (**10'**) NMR/δ
10(10')a	CH_3	CH_3	9.2(d, 1H, 2-pyridine)	9.5(d, 1H, 2-pyridine)
10'b	CH_3	C_2H_5	—	9.4(d, 1H, 2-pyridine)
10(10')c	CH_3	C_6H_{13}	9.1(d, 1H, 2-pyridine)	9.4(d, 1H, 2-pyridine)
10'd	C_2H_5	C_2H_5	—	9.5(d, 1H, 2-pyridine)
10'e	C_2H_5	C_6H_{13}	—	9.5(d, 1H, 2-pyridine)

MS (m/z) of all isomers indicated molecular ion peaks.

***p*-Nitrosotoluene (12).** *p*-Nitrosotoluene (**12**) was prepared via *p*-tolylhydroxylamine in a conventional manner.[5] Thus, starting with *p*-nitrotoluene (**11**; 13.7 g, 100 mmol), reduction (Zn, NH_4Cl) to the hydroxylamine (yield, 58%), and subsequent oxidation with sodium dichromate and sulfuric acid gave **12** in 40% overall yield. Mp 45 °C. The results of IR and NMR were satisfactory.

3-(4-Methylphenylazo)-6-alkylpyridine (13). To the solution of 2-alkyl-5-aminopyridine (**4**; 0.8 g, 5 mmol) in warm acetic acid (5 ml) was added **12** (0.6 g, 5 mmol) at 20 °C with shaking. The solution was stirred at 50 °C for 24 h. The reaction mixture was made alkaline with a sodium carbonate solution including ice and extracted with chloroform. The organic layer was concentrated on a rotary evaporator. The residue was subjected to SiO_2 column chromatography using hexane-ether (5 : 1 v/v) as the eluting solvent to give a purified product. Yield: 11% for R_3=CH_3; 10% for C_4H_9.

No.	R_3	C/%	H/%	N/%
13a	CH_3	74.17	6.64	18.67
		(74.64)	(6.71)	(18.65)
13b	C_4H_9	76.23	7.75	15.67
		(76.40)	(7.86)	(15.73)

No.	^{1}H NMR
13a	1.4(t, 3H, Me), 2.5(s, 3H, Me), 3.0(q, 2H, CH_2), 7.3—8.4(m, ArH+Rpyridine), 9.3(d, 1H, pyridine)
13b	0.9—2.0(m, 9H, alkyl), 2.4(s, 1H, Me), 2.9(t, 2H, CH_2), 7.0—8.1(m, 6H, ArH+pyridine), 9.0(d, 1H, pyridine)

Mass spectra of these azo compounds indicated molecular ion peaks.

3-(4-Methylphenyl-NON-azoxy)-6-alkylpyridine (15). The same procedure as that for **9** was applied to **13** with the exception that the reaction time was prolonged to 6 h at 65 °C.

No.	R_3	C/%	H/%	N/%
15a	CH_3	66.64	6.26	17.52
		(66.69)	(6.27)	(17.41)
15b	C_4H_9	76.58	7.71	9.90
		(76.60)	(7.80)	(9.93)

No.	MS(m/z)	^{1}H NMR
15a	241(M^+)	9.2, 9.6 (d, 2-pyridine)
15b	283(M^+)	9.1, 9.5 (d, 2-pyridine)

The separation of isomers was tried for the azoxy compound (**15a**; R_3=CH_3) with centrifugal liquid chromatography (CLC) using hexane-ether (5 : 1 v/v) as the eluting solvent. NNO, and then the ONN isomers, were eluted. ^{1}H NMR indicated characteristic peaks at δ 9.2 and 9.6 for ONN (**16a**) and NNO (**16'a**) isomers, respectively.

References

1) C. S. Oh, *Mol. Crys. Liq. Crys.*, **19**, 95 (1972).
2) R. A. Champa, *Mol. Crys. Liq. Crys.*, **19**, 233 (1973).
3) L. A. Karamysheva, E. I. Kovoshev, A. I. Pavluchenko, K. V. Roitman, V. V. Titov, S. I. Irogova, and M. F. Grebenkin, *Mol. Crys. Liq. Crys.*, **67**, 241 (1981).
4) H. Kamogawa and T. Kasai, *Mol. Crys. Liq. Crys.*, **131**, 69 (1985).
5) O. Manabe and T. Ogushi, "Synthetic methods of Organic Compounds, 19," Gihoudo (1969), p. 70.
6) R. Steinsträsser and L. Pohl, *Tetrahedron Lett.*, **1971**, 1921; C, crystal; N, nematic; I, isotropic.
7) J. van der Veen, W. H. de Jeu, A. H. Grobben., and J. Boven, *Mol. Crys. Liq. Crys.*, **17**, 291 (1972).

Synthesis of 5-[(*E*)-1-Alkenyl]-3(2*H*)-furanones by the Stereoselective Dehydration with Me_3SiCl

Takashi SAKAI,* Kazuhiko KOHDA, Sadao TSUBOI, Masanori UTAKA, and Akira TAKEDA
Department of Synthetic Chemistry, School of Engineering, Okayama University, Tsushima, Okayama 700
(Received February 20, 1987)

The stereoselective dehydration of 5-(2-hydroxyalkyl)-3(2*H*)-furanones is accomplished conveniently by the treatment with Me_3SiCl in acetonitrile to give 5-[(*E*)-1-alkenyl]-3(2*H*)-furanones.

5-(1-Alkenyl)-3(2*H*)-furanone is one of the important skeletons observed in natural products, e. g. geiparvarin (**1**)[1] and eremantholide A,[2] and hence much attention has been paid on their stereoselective synthesis. We previously reported a short step synthesis of **1**,[3] in which the (*E*)-olefinic side chain was introduced

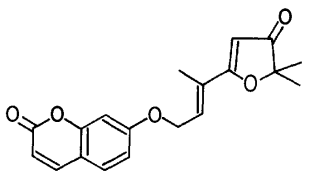

1

by the utilization of tiglic acid. Smith et al.[4] elaborated the olefinic moiety of **1** and the related 3(2*H*)-furanone **4** in a manner as shown in Scheme 1, which involves the aldol reaction of lithium enolate of 5-ethyl-2,2-dimethyl-3(2*H*)-furanone (**2**) with an appropriate aldehyde followed by the DCC-CuCl-catalyzed dehydration of the resulting diastereomeric mixture of 5-(2-hydroxyalkyl)-3(2*H*)-furanone (**3**) in refluxing benzene. However, the E/Z-stereoselectivity of the side chain of **4** is not satisfactory as cited in Table 1 and seems to be still open to further improvement. Recently, Tsuge et al.[5] have reported that the Horner-Emmons olefination of 5-[1-(diethoxyphosphoryl)-ethyl]-3(2*H*)-furanone with aldehydes gives **4a—e** with a considerable E selectivity. In the preceding paper of our laboratory concerning the stereoselective synthesis of polyenoic acids,[6] the Me_3SiCl-NaI reagent was successfully employed for the dehydration of acyclic allylic alcohol to produce a conjugated (E)-olefinic double bond. The fact stimulated us to examine the suitability of the reagent for the dehydration of **3**, and Me_3SiCl itself was found to be remarkably effective on the improvement of the stereoselectivity.

The present reaction merely involves stirring of a mixture of **3a—e** and 2.5 equiv of Me_3SiCl in acetonitrile at room temperature to give the desired product with sufficient purity after washing with aqueous sodium hydrogencarbonate. Addition of NaI to the reaction had no effect on the yield. The reaction time of 10—14 h is required, while the reaction for allylic alcohol **3e** was finished within 1 h. These results are summarized in Table 1. The olefinic side chains of **3a—e** thus obtained have only the E geometry, which was confirmed by the comparison of the ^1H NMR spectral data with those reported.[4b] Furthermore, their ^{13}C NMR spectral data summarized in Table 2 indicate the absence of (Z)-isomer definitely. The yields of the dehydration were also improved generally. The method seems to be more practical as compared with the reported one,[4] because the reagent is inexpensively available and the procedure is quite simple.

A possible mechanism for the present reaction is depicted in Scheme 2, which involves the formation of bis(trimethylsilyl)oxonium chloride intermediate **5**.[7] Subsequent elimination of hexamethyldisiloxane (**6**) from **5** would occur accompanying the abstraction of the reactive allylic proton by a chloride anion. Formation of **6** was confirmed by GLPC analysis.[8] The alcohols **3a—e** used were a diastereomeric mixture. Smith et al.[4] did not describe the detail of the isomeric

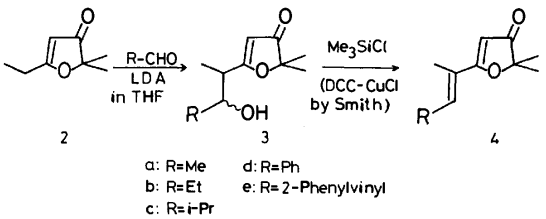

Scheme 1.

Table 1. Yields of 5-[(*E*)-1-Alkenyl]-3(2*H*)-furanones (**4a—e**)

Compd	R	Reach time/h	Yield[a]	Smith's method[b]
			%	Yield/% (E/Z ratio)
4a	Me	14	66	54 (1:1)
4b	Et	12	80	73 (1:2)
4c	*i*-Pr	10	75	—
4d	Ph	10	66	60 (1:2)
4e	2-Phenylvinyl	1	77	55 (3:2)

a) After purification by preparative TLC. b) DCC-CuCl in refluxing benzene. See Ref. 4.

Table 2. ^{13}C NMR Spectral Data of 5-[(*E*)-1-Alkenyl]-3(2*H*)-furanones ($CDCl_3$, ppm)

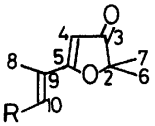

Compd	C-2	C-3	C-4	C-5	C-6,7	C-8	C-9	C-10	R
4a	88.1	207.2	98.5	184.5	23.1	12.7	126.6	133.1	14.2
4b	88.1	207.2	98.7	184.6	23.1	12.9	125.1	139.9	13.2, 21.9
4c	88.2	207.3	98.9	184.9	23.1	13.0	123.6	145.0	22.1, 27.8
4d	88.5	207.2	100.1	184.7	23.2	14.7	126.3	134.7	128.5,[a] 129.8,[a] 135.7
4e	88.2	206.9	99.7	184.0	23.2	13.5	125.1	134.3[b] 123.5[b] 139.4[b]	127.1,[a] 128.8,[a] 136.5
14	88.3	207.1	100.0	184.0	23.1	13.4	126.1	133.0[a,c] 127.0[c] 139.4[c]	14.0, 22.5, 27.3 34.2, 74.7, 128.4,[a] 129.6,[a] 130.3, 165.8
15	88.4	207.1	100.2	183.8	23.2	13.4	126.6[a]	132.5[d] 140.9[d]	13.9, 22.2, 28.6, 38.1, 62.2
17	88.5	207.3	100.3	183.9	23.2	13.2	127.5	125.4[e] 127.5[e] 136.5[e]	14.0, 22.5, 27.1, 71.3, 128.4,[a] 129.6,[a] 130.3, 133.0

a) The signal due to overlapped two carbons with nearly double intensity. b, c, d, e) Assignment of olefinic carbons is interchangeable.

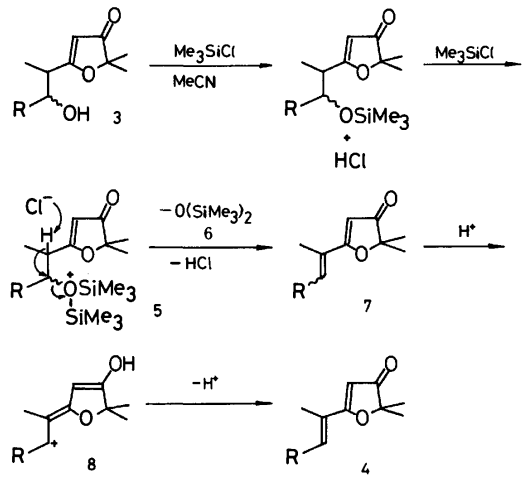

Scheme 2.

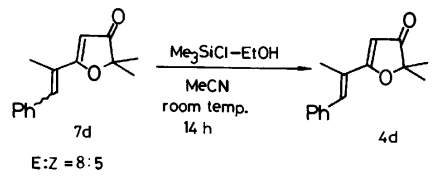

Scheme 3.

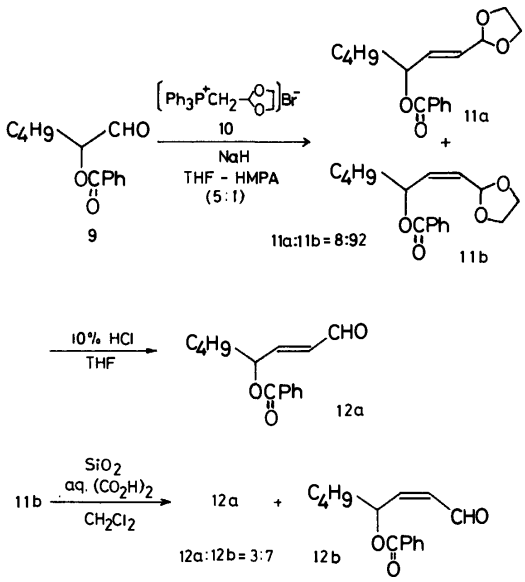

Scheme 4.

ratio of **3a—e** and its participation in the geometry of the resulting **4a—e**. We confirmed that **3d** was ca. 1 : 1 diastereomeric mixture according to the ^{1}H NMR signals due to C-4 proton (δ 5.15 and 5.31), while the isomeric ratios of **3a—c** and **3e** were not clear by ^{1}H NMR analysis. Therefore, the initially formed dehydration product **7** should be a E, Z mixture. The (Z)-isomer of **7** would be converted to a thermodinamically more stable **4** at the acidic conditions[9] via the cationic intermediate **8**. The feasibility of the isomerization was exemplified by using a 8 : 5 E,Z mixture of **7d**,[4] which was readily converted to **4d** by the treatment with Me_3SiCl and EtOH in acetonitrile (Scheme 3).

As a preliminaly experiment for the synthetic study of a related natural product, we wished to confirm the applicability of the above reaction sequence to the stereospecific synthesis of 5-[(1*E*, 3*E*)-5-(benzoyloxy)-1-methyl-1,3-nonadienyl]-2,2-dimethyl-3(2*H*)-furanone (**14**) (Scheme 5) and its (1E, 3Z)-isomer **17** (Scheme 6). For the purpose, a stereoselective synthesis of the starting (*E*)- and (*Z*)-4-(benzoyloxy)-2-octenal (**12a** and **12b**) (Scheme 4) and their transformation to **14** and **17** with retention of the geometry are required.

The Wittig reaction of 2-(benzoyloxy)hexanal (**9**)[10] with (1,3-dioxolan-2-ylmethyl)triphenylphosphonium bromide (**10**)[11] in the presence of NaH in THF-HMPA (5 : 1) gave the (Z)-adduct **11b** stereoselctively (E : Z=8 : 92) in 48% yield (Scheme 4). The yield of **11b** was slightly increased to 52% by carring out the reaction in DMF-HMPA (3 : 1), while the yield of the (E)-isomer **11a** was also raised to 19%.

The treatment of the 8 : 92 mixture of **11a** and **11b** with 10% aqueous HCl-THF (1 : 1) afforded the (*E*)-aldehyde **12a** exclusively in 96% yield as a result of the isomerization Z to E. On the other hand, the hydrolysis of the (*Z*)-acetal **11b**, which was isolated by preparative TLC, with silica gel and 5% aqueous oxalic acid[12] in dichloromethane gave the (*Z*)-aldehyde **12b** (57% yield) together with the (E)-isomer **12a** (23% yield). They were separated chromatographycally. Further attempts to increase the ratio of **12b** by using other hydrolytic conditions such as *p*-TsOH[13] or (±)-10-camphorsulfonic acid monohydrate in acetone·H_2O resulted in unfruitfullness.

The reaction of lithium enolate of **2** with **12a** gave the aldol product **13** (54% yield). The dehydration with Me_3SiCl afforded **14** (61% yield) and its hydrolyzed product **15** (29% yield) under the acidic conditions (Scheme 5). The geometry of newly formed olefinic double bond of **14** and **15** was assigned to be E by the comparison of their ^{13}C NMR spectral data with those of **3a—e** (Table 2).

A similar aldol reaction of **2** with **12b** gave **16** (54% yield) with retention of the Z geometry (Scheme 6). However, at the subsequent dehydration step, the geomerty was partly inverted to give a 53 : 47 mixture of **14** and **17** (57% yield), which were separated by preparative HPLC. The E or Z geometry of the C-3 and C-4 double bond of the side chain is clearly distinguishable by the analysis of the coupling constants in the ^1H NMR spectra [**14**: $J_{3,4}$=14.5 Hz for E; **17**: $J_{3,4}$=12.0 Hz for Z]. Furthermore, in the ^{13}C NMR spectra (Table 2), the allylic carbon bearing a benzoyloxy group of the (Z)-isomer **17** appeared at 71.3 ppm, which was highly shielded as compared with that of the (E)-isomer **14** (74.7 ppm).

As described above, the present reaction offers a convenient and highly stereoselective synthetic method of 5-[1-(*E*)-alkenyl]-3(2*H*)-furanones and would be useful for other related systems.

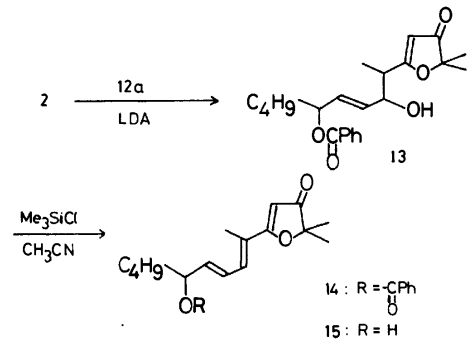

Scheme 5.

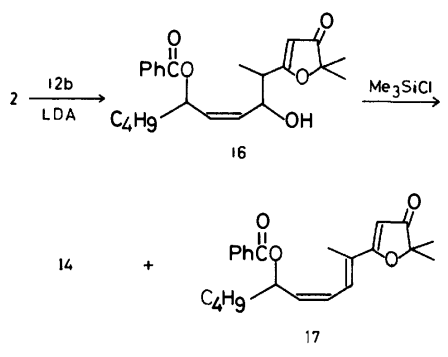

Scheme 6.

Experimental

IR specra were measured with a JASCO A-102 spectrometer. ^1H NMR spectra (60 MHz) were measured with a JEOL JNM PMX 60 SI spectrometer. Both ^1H NMR (100 MHz) and ^{13}C NMR (25 MHz) spectra were taken on a JEOL FX-100 spectrometer using Me_4Si as an internal standard. GLPC analysis was done by using a Hitachi 163 gas chromatograph. HPLC analysis was carried out by using a Yanagimoto L-2000 high-performance liquid chromatograph. Elemental analyses were performed by Eiichiro Amano of our laboratory with a Yanagimoto MT-3 CHN recorder.

Hydroxy 3(2*H*)-furanones **3a—e**, **13**, and **16** were prepared from **2** and appropriate aldehydes by the procedure similar to that reported by Smith et al.[4] Sectral and analytical data of the new compounds **3c**, **13**, and **16** are shown.

5-(1,3-Dimethyl-2-hydroxybutyl)-2,2-dimethyl-3(2*H*)-furanone (3c): 28% yield; mp 113.5—114 °C (CCl_4); IR (KBr) 3400, 1680, 1580 cm^{-1}; ^1H NMR ($CDCl_3$) δ=0.95, 0.98 (each with 3H, d, J=6 Hz), 1.26 (3H, d, J=7 Hz), 1.35 (6H, s), 1.73 (1H, m), 2.30 (1H, br s), 2.79 (1H, m), 3.54 (1H, m), 5.38 (1H, s). Found: C, 67.64; H, 9.42%. Calcd for $C_{12}H_{20}O_3$: C, 67.89; H, 9.50%.

General Procedure for the Dehydration of 5-(2-Hydroxyalkyl)-3(2*H*)-furanone. To a solution of **3** (0.50 mmol) in acetonitrile (1 ml) was added chlorotrimethylsilane (136 mg, 1.25 mmol) through a syringe. The mixture was stirred at room temperature for the time indicated in Table 1. After the reaction was quenched by addition of water, the organic layer was extracted with ether, washed with aqueous sodium hydrogencarbonate and brine, dried ($MgSO_4$), filtered, and then concentrated under reduced pressure. The residual oil was purified by preparative TLC (Merck, Kieselgel PF_{254}, hexane-acetone, 3 : 1) to give **4** in the yield as shown in Table 1. The IR and ^1H NMR spectra of **4a—e** were consistent with those reported.[4,5] The spectral and analytical data of **4c**[5,14] are described below.

5-(1,3-Dimethyl-1-butenyl)-2,2-dimethyl-3(2*H*)-furanone (4c): Mp 68.5—69 °C (hexane); IR (KBr) 1695, 1640, 1560, 1175 cm^{-1}; ^1H NMR ($CDCl_3$) δ=1.06 (6H, d, J=7 Hz), 1.39 (6H, s), 1.89 (3H, d, J=1.3 Hz), 2.70 (1H, m), 5.47 (1H, s), 6.40 (1H, dq, J=9 Hz, and 1.3 Hz). Found: C, 74.36; H, 9.25%. Calcd for $C_{12}H_{18}O_2$: C, 74.19; H, 9.34%.

Isomerization of 7d to 4d. Chlorotrimethylsilane (33 mg, 0.3 mmol) was added to a mixture of **7d** (E: Z=8 : 5)[4] (29 mg,

0.13 mmol), EtOH (14 mg, 0.3 mmol), and acetonitrile (1 ml). After being stirred for 14 h at room temperature, the mixture was diluted with ether, washed with aqueous sodium hydrogencarbonate and water, dried over $MgSO_4$, and filtered. Removal of the solvent left **4d** (28 mg, 97%) with sufficient purity.

(*Z*)-1-Butyl-3-(1,3-dioxolan-2-yl)-2-propenyl Benzoate (11b). To a cooled mixture (0 °C) of NaH (108 mg, 4.5 mmol), THF (7 ml), and HMPA (2 ml), was added **10**[11] (2.02 g, 4.7 mmol) quickly. The mixture was stirred at room temperature for 40 min, and then cooled to −78 °C. A solution of 2-(benzoyloxy)hexanal **9**[10] (560 mg, 2.55 mmol) in THF (3 ml) was introduced through a syringe. The mixture was allowed to warm to room temperature gradually and stirred for 2 d. After the reaction was quenched by addition of water, the organic layer was extracted with hexane-ether (1 : 1), washed with brine, dried ($MgSO_4$), filtered, and then concentrated. The precipitated Ph_3P=O was removed by filtration with suction. The crude product was separated by preparative TLC (hexane-ether, 4 : 1) to give **11a** (R_f 0.22—0.30, 29 mg, 4% yield) and **11b** (R_f 0.30—0.42, 355 mg, 48% yield). **11a**: IR (neat) 1720, 1660, 1600 cm^{-1}. ^1H NMR (CCl_4) δ=0.7—2.0 (9H, m), 3.85 (4H, m), 5.1—6.1 (4H, m), 7.1—8.1 (5H, m); ^{13}C NMR ($CDCl_3$) δ=13.3 (q), 22.5 (t), 27.3 (t), 34.0 (t), 65.0 (t), 73.5 (d), 103.0 (d), 128.0 (d), 128.4 (d), 129.6 (d), 130.4 (s), 132.9 (d), 134.3 (d), 165.7 (s). Found: C, 70.15; H, 7.62%. Calcd for $C_{17}H_{22}O_4$: C, 70.32; H, 7.64%. **11b**: IR (neat) 1720, 1680, 1600 cm^{-1}; ^1H NMR (CCl_4) δ=0.7—2.0 (9H, m), 3.85 (4H, m), 5.2—6.0 (4H, m), 7.1—8.1 (5H, m); ^{13}C NMR ($CDCl_3$) δ=13.9 (q), 22.5 (t), 27.1 (t), 34.5 (t), 65.0 (t), 70.8 (d), 99.2 (d), 128.9 (d), 129.1 (d), 129.6 (d), 130.5 (s), 132.8 (d), 134.3 (d), 165.8 (s). Found: C, 70.11; H, 7.58%. Calcd for $C_{17}H_{22}O_4$: C, 70.32; H, 7.64%.

The reaction in DMF-HMPA was carried out in a similar way.

(*E*)-4-(Benzoyloxy)-2-octenal (12a). An 8 : 92 mixture of **11a** and **11b** (580 mg, 2 mmol), 10% HCl (3 ml), and THF (3 ml) was stirred for 3 h at room temperature. The organic layer was extracted with ether, washed with aqueous sodium hydrogen carbonate and brine, dried ($MgSO_4$), filtered, and then concentrated. The residual oil was purified by column chromatography (Silica gel 60, Katayama Chemical, Co. Ltd., hexane-acetone, 10 : 1) to give **12a** (470 mg, 96% yield): IR (neat) 1720, 1690, 1640, 1600 cm^{-1}; ^1H NMR (CCl_4) δ=0.8—2.1 (9H, m), 5.65 (1H, m), 6.13 (1H, dd, J=15, 8 Hz), 6.70 (1H, dd, J=15, 5 Hz), 7.3—8.1 (5H, m), 9.42 (1H, d, J=8 Hz); ^{13}C NMR ($CDCl_3$) δ=13.9 (q), 22.5 (t), 27.2 (t), 33.5 (t), 72.8 (d), 128.5 (d), 129.7 (d), 131.5 (d), 133.4 (d), 154.1 (d), 165.6 (s), 193.0 (d). Found: C, 73.25; H, 7.43%. Calcd for $C_{15}H_{18}O_3$: C, 73.15; H, 7.57%.

(*Z*)-4-(Benzoyloxy)-2-octenal (12b). A mixture of silica gel (Merck Kieselgel PF_{254}, 5.0 g), 5% aqueous oxalic acid[11] (0.5 ml), and dichloromethane (8 ml) was stirred vigorously. To this was added a solution of **11b** (542 mg, 1.90 mmol) in dichloromethane (2 ml) and the resulting mixture was stirred for 6 h at room temperature. The mixture was neutralized by addtion of aqueous sodium hydrogencarbonate powder, dried ($MgSO_4$), filtered and then concentrated under reduced pressure. The residue was purified by preparative TLC (hexane-ether, 3 : 1) to give **12b** (R_f 0.57—0.67, 261 mg, 57% yield) and **12a** (R_f 0.38—0.54, 108 mg, 23% yield). **12b**: IR (neat) 1720, 1685, 1615, 1600 cm^{-1}; ^1H NMR (CCl_4) δ=0.7—2.1 (9H, m), 5.74—6.63 (3H, m), 7.1—8.2 (5H, m), 10.08 (1H, d, J=7 Hz); ^{13}C NMR ($CDCl_3$) δ=13.8 (q), 22.4 (t), 27.2 (t), 34.4 (t), 70.4 (d), 128.5 (d), 194.6 (d), 130.0 (s), 130.5 (d), 133.2 (d), 147.5 (d), 165.8 (s), 190.6 (d). Fond: C, 73.23; H, 7.57%. Calcd for $C_{15}H_{18}O_3$: C, 73.15; H, 7.37%.

5-[(*E*)-5-(Benzoyloxy)-2-hydroxy-1-methyl-3-nonenyl]-2,2-dimethyl-3(2*H*)-furanone (13). This compound was prepared in a manner similar to Smith's method[4] in 54% yield. **13**: IR (neat) 3450, 1720, 1700, 1660, 1580 cm^{-1}; ^1H NMR (CCl_4) δ=0.7—2.0 (18H, m), 2.78 (1H, m), 3.70 (1H, br s, OH), 4.36 (1H, m), 5.40 (1H, s), 5.4—5.9 (3H, m), 7.2—8.1 (5H, m). Found: C, 71.29; H, 7.91%. Calcd for $C_{23}H_{30}O_5$: C, 71.48; H, 7.82%.

5-[(1*E*,3*E*)-5-(Benzoyloxy)-1-methyl-1,3-nonadienyl]-3(2*H*)-furanone (14). A similar reaction of **13** (77 mg, 0.20 mmol) with Me_3SiCl (55 mg, 0.50 mmol) was done for 4 h at room temperature. The crude product was separated by preparative TLC (hexane-acetone, 3 : 1, developed twice) gave **14** (R_f 0.34—0.41, 45 mg, 61% yield) and **15** (R_f 0.41—0.46, 15 mg, 29% yield). **14**: IR (neat) 1720, 1695, 1635, 1605, 1550 cm^{-1}; ^1H NMR ($CDCl_3$) δ=0.7—2.0 (15H, m), 2.00 (3H, d, J=1.0 Hz), 5.57 (1H, s), 5.60 (1H, m), 6.13 (1H, dd, J=14.5, 6.9 Hz, C-4), 6.68 (1H, dd, J=14.5, 11.3 Hz, C-3), 7.04 (1H, dd, J=11.3 Hz, 1.0 Hz, C-2), 7.3—8.2 (5H, m). Found: C, 74.88; H, 7.79%. Calcd for $C_{23}H_{28}O$: C, 74.79; H, 7.66%. **15**: IR (neat) 3500, 1695, 1630, 1605, 1550 cm^{-1}: ^1H NMR (CCl_4) δ=1.33 (6H, s), 0.8—1.9 (9H, m), 2.01 (3H, s), 4.37 (1H, m), 5.45 (1H, s), 5.8—7.1 (3H, m). Found: C, 72.88; H, 9.32%. Calcd for $C_{16}H_{24}O_3$: C, 72.69; H, 9.15%.

5-[(*Z*)-5-(Benzoyloxy)-2-hydroxy-1-methyl-3-nonenyl]-2,2-dimethyl-3(2*H*)-furanone (16): 54% yield; IR (neat) 3450, 1720, 1700, 1580 cm^{-1}; ^1H NMR ($CDCl_3$) δ=0.7—2.0 (18H, m), 2.84 (1H, m), 3.70 (1H, br s, OH), 4.78 (1H, m), 5.46 (1H, s), 5.4—6.0 (3H, m), 7.2—8.1 (5H, m). Found: C, 71.63; H, 7.90%. Calcd for $C_{23}H_{30}O_5$: C, 71.48; H, 7.82%.

Compounds 14 and 17. The dehydration of **16** (72 mg, 0.19 mmol) with Me_3SiCl (51 mg, 0.47 mmol) was done for 2 h at room temperature in the usual way. The crude product was purified by preparative TLC (hexane-acetone, 3 : 1, developed twice) to give a mixture of **14** and **17** (R_f 0.51—0.56, 39 mg, 57% yield). The product ratio of **14** and **17** was determined to be 53 : 47 based on their weights isolated by using preparative HPLC (Yanagimoto column SA-I; 6 mmϕ×250 mm; hexane-ethyl acetate-ethanol, 100 : 2 : 1; 1.0 ml min^{-1}), which showed two peaks due to **14** (retention time: 29.2 min, 19 mg) and **17** (33.5 min, 17 mg). **17**: IR (neat) 1720, 1700, 1635, 1605, 1555 cm^{-1}; ^1H NMR ($CDCl_3$) δ=0.7—2.0 (15H, m), 2.0 (3H, s), 5.63 (1H, s), 5.95 (2H, m), 6.28 (1H, dd, J=12.0, 10.1 Hz, C-3), 7.3—8.2 (6H, m, phenyl and C-4). Found: C, 74.85; H, 7.71%. Calcd for $C_{23}H_{28}O_4$: C, 74.97, 7.66%.

References

1) F. N. Lahey and J. K. McLeod, *Aust. J. Chem.*, **20**, 1943 (1967).

2) R. F. Raffauf, P. C. Huang, P. W. LeQuensne, S. B. Levery, and T. F. Brennan, *J. Am. Chem. Soc.*, **97**, 6884 (1975).

3) T. Sakai, H. Ito, A. Yamawaki, and A. Takeda, *Tetrahedron Lett.*, **25**, 2987 (1984).

4) a) A. B. Smith, III and P. J. Jerris, *Tetrahedron Lett.*, **1980**, 711; b) P. J. Jerris and A. B. Smith, III, *J. Org. Chem.*, **46**, 577 (1981).

5) O. Tsuge, S. Kanemasa, and H. Suga, *Chem. Lett.*, **1987**, 323.

6) S. Tsuboi, X. H. Wu, S. Maeda, S. Ono, A. Kuroda, K. Kawazu, and A. Takeda, *Bull. Chem. Soc. Jpn.*, **60**, 1103 (1987).

7) An example of the formation of bis(trimethylsilyl)-oxonium ion: M. E. Jung, A. B. Mossman and M. A. Lyster, *J. Org. Chem.*, **43**, 3698 (1978).

8) The GLPC analysis (SE-30 1m, oven temperature 40 °C, N_2 45 ml min^{-1}) of a sample extracted from a reaction mixture of **3b** and Me_3SiCl before the end of the reaction showed a peak of hexamethyldisiloxane at the retention time of 1.2 min, which was identified by comparison with that of an authentic sample.

9) Smith et al.[4] pointed out that the E selectivity in the dehydration to **4** was increased under the acidic media, although they failed to improve the yield. The experimental detail was not described.

10) T. Sakai, K. Seko, A. Tsuji, M. Utaka, and A. Takeda, *J. Org. Chem.*, **47**, 1101 (1982).

11) T. H. Cresp, M. V. Sargent, and P. Vogel, *J. Chem. Soc., Perkin Trans. 1*, **1974**, 37.

12) F. Huet, A. Lechevallier, M. Pellet, and J. M. Conia, *Synthesis*, **1978**, 63.

13) B. Byrne, L. M. L. Lawter, and K. J. Wengenroth, *J. Org. Chem.*, **51**, 2607 (1986).

14) The full details of the spectal and analytical data for **4c** are not given in the literature (Ref. 5).

 © 1987 The Chemical Society of Japan Bull. Chem. Soc. Jpn., 60, 2917—2921 (1987)

A New Method for the Synthesis of 3,5-Disubstituted 2(5*H*)-Furanones. Synthesis of (±)-Acarenoic Acid

Sadao Tsuboi,* Hiroshi Wada, Koichi Muranaka, and Akira Takeda
Department of Synthetic Chemistry, School of Engineering, Okayama University, Tsushima, Okayama 700
(Received February 26, 1987)

Heating of 3,5-disubstituted 4-bromo-3-methoxycarbonyldihydro-2(3*H*)-furanones with NaI in 3-pentanone gave 3,5-disubstituted 2(5*H*)-furanones in 55.8—93.3% isolated yields. A total synthesis of (±)-acarenoic acid was established in 33% overall yield via 4 steps.

The γ-lactone ring system is a common feature in a wide variety of natural products, and a number of methods are available for its construction.[1] Especially, the synthesis of unsaturated γ-lactones has attracted the attention of organic chemists because of their biological activities and versatile utilization in organic synthesis.[2] In connection with our continuous interest in the chemistry of γ-lactones,[3] we reported a convenient synthesis of enolic δ-lactones with a Wittig reaction.[4]

In a previous paper we reported highly stereo- and regioselective alkylation of alkylidenemalonates **1** giving (3*E*)-2-methoxycarbonyl-2-alkyl-3-alkenoate **2**.[5] Recently, we found that the heating of bromolactonization products **3** with sodium iodide in an appropriate solvent affords 3,5-disubstituted 2(5*H*)-furanones **4** in good yields. This paper describes a new synthesis of **4**

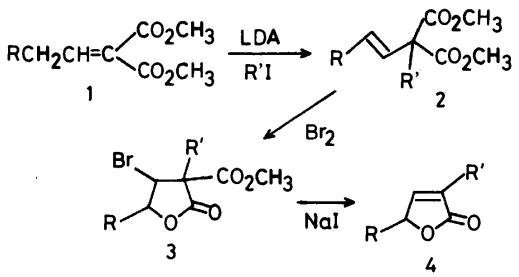

and its application for the synthesis of acarenoic acid **5**.[6]

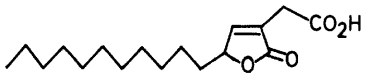

5

Compound **2** was prepared by the reaction of **1** with alkyl iodide in the presence of lithium diisopropylamide (LDA) as reported previously.[5] Bromolactonization of **2**[5] was carried out in chloroform for 2—3 h at 0 °C and the various alkyl-substituted bromolactones **3** were obtained in 42.3—86.6% yields as shown in Table 1. The stereochemistry of **3** was determined by NOE techniques[7] of ^{1}H NMR. For example, when the 3-methyl protons of **3a** were irradiated, a peak enhancement (5%) was observed for the 4-methine proton, while the irradiation on 5-methine proton did not show any effect for signals due to 3-methyl and 4-methine protons.

Conversion of **3** to 2(5*H*)-furanone **4** was extremely facilitated by heating the 3-pentanone solution of **3** with an excess amount of NaI. Various 3,5-disubstituted 2(5*H*)-furanons **4** were prepared from **3** and the results are tabulated in Table 1. The reaction was completed within 3 days and product **4** was obtained in good isolated yields (55.8—93.3%). Furthermore, the effectiveness of other reagents and solvents for the present reaction was investigated. The conversion of (3*R**, 4*R**, 5*S**)-4-bromo-5-butyl-3-ethoxycarbonylmethyl-3-methoxycarbonyldihydro-2(3*H*)-furanone (**3c**) to **4c** was attempted under various con-

Table 1. Syntheses of Malonates **2**, Bromolactones **3**, and 2(5*H*)-Furanones **4**

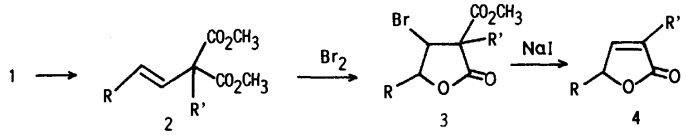

No.	R	R′	Yield[a]/%			Reaction time (d) for **4**
			2	**3**	**4**	
a	C_2H_5	CH_3	63.4	73.7	71.7(89.2)[c]	2
b	C_2H_5	CH_2CO_2Et	98.4	63.6	71.9	2.5
c	$CH_3(CH_2)_3$	CH_2CO_2Et	88.8	53.0	88.5	2
d	$CH_3(CH_2)_5$	CH_3	95[b]	42.3	82.4	3
e	$CH_3(CH_2)_5$	$CH_3(CH_2)_3$	61.1	86.6	55.8(92.6)[c]	2
f	$CH_3(CH_2)_5$	CH_2CO_2Et	86.4	65.1	82.7	2.5
g	$CH_3(CH_2)_{10}$	CH_2CO_2Et	68.8	71.0	93.3	3

a) Isolated yield. b) Previously reported (Ref. 5). c) Yield based on the consumed **3**.

ditions and the results are tabulated in Table 2. Sodium chloride, silica-alumina, silica gel, and alumina were not effective, although KI showed a slight effectiveness. Ethanol, as well as 3-pentanone, was a good solvent for this reaction. Although the reaction in benzene resulted in a recovery of the starting material, that in the presence of 15-crown-5[8] gave **4c** in 50% yield.

The structure of **4** was elucidated by IR and NMR data and elemental analysis. IR, ^{1}H NMR, and analytical data are given in Table 3. IR absorptions of **4** near 1760 and 1660 cm^{-1} are consistent with the structure of α,β-unsaturated γ-lactone.[3b,9] Signals of olefinic protons appeared at δ 6.8—7.4 as a result of a deshielding effect of the α,β-unsaturated carbonyl system. The ^{13}C NMR spectra of the lactone **4** prepared in this work were measured and tentatively assigned as shown in Table 4. These data afford additional support for assigning the structure of 3,5-disubstituted 2(5*H*)-furanone.

Table 2. Attempts in the Synthesis of **4c** with Various Reagents

Reagent[a]	Reaction condition		Yield/%[b]
	Solvent	Time/d	**4**
NaI	3-Pentanone	2	89
NaI	Ethanol	2	80
NaI	Water	2	0[d]
NaI	Benzene	2	0[d]
NaI	Benzene—15-crown-5[c]	2	50
NaI	Xylene	2	0[d]
KI	3-Pentanone	2	21
NaCl	3-Pentanone	4	0[d]
SiO_2-Al_2O_3	3-Pentanone	4	0[d]
SiO_2	3-Pentanone	2	0[d]
Al_2O_3	3-Pentanone	2	0[d]

a) A solution of **3c** in a solvent was heated at the reflux temperature in the presence of an excess amount (5—10 equiv) of the reagent. b) Estimated by ^{1}H NMR analysis. c) An equimolar amount of 15-crown-5 to NaI was used. d) The starting material **3c** was recovered.

This novel reaction of the 2(5*H*)-furanone formation can be explained by the following mechanism. Initially, the reaction would start to give iodo lactone **A** by the substitution of the bromine with NaI.[10] The elimination of methyl iodide from **A** would yield unstable β-lactone **B**, which would release carbon dioxide to afford the 2(5*H*)-furanone **4**.

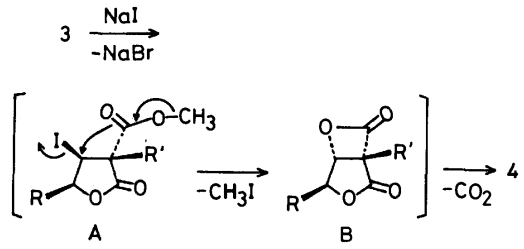

The present reaction was applied for the synthesis of (±)-acarenoic acid **5**, a component of *Acarospora chlorophana*,[6] whose total synthesis has never been reported. Our reaction sequence is shown in Scheme 1. A deconjugative alkylation of dimethyl tridecanylidenemalonate (**1g**) with ethyl iodoacetate afforded, exclusively, ethyl (*E*)-3,3-bis(methoxycarbonyl)-4-

Table 3. Physical and Analytical Data of 2(5*H*)-Furanones **4**

4	IR (neat) cm^{-1}	^{1}H NMR (CCl_4, δ/ppm)	Elemental analysis/% (Calcd)	
			C	H
4a	1755, 1659, 1458	0.98 (3H, t, *J*=6Hz, CH_3), 1.26—2.49 (2H, m, $C\underline{H}_2CH_3$), 1.85 (3H, s, =C-CH_3), 4.60—4.96 (1H, m, CHO-), 6.98—7.14 (1H, m, CH=)	66.42 (66.65)	8.19 (7.99)
4b	1763, 1742, 1663	0.99 (3H, t, *J*=7Hz, CH_3), 1.25 (3H, t, *J*=7Hz, $CO_2CH_2C\underline{H}_3$), 1.45—2.03 (2H, m, $C\underline{H}_2CH_3$), 3.21 (2H, s, CH_2CO_2Et), 4.13 (2H, q, *J*=7Hz, CH_2CO_2Et) 4.71—5.05 (1H, m, CHO-), 7.28—7.42 (1H, m, =CH)	60.87 (60.59)	7.27 (7.12)
4c	1761, 1745, 1665	0.93 (3H, t, *J*=6Hz, CH_3), 1.08—2.01 (6H, m, $3CH_2$), 1.26 (3H, t, *J*=7Hz $CO_2CH_2C\underline{H}_3$), 3.11—3.33 (2H, m, CH_2CO_2Et), 4.12 (2H, q, *J*=7Hz, $CO_2C\underline{H}_2CH_3$), 4.71—5.04 (1H, m, CHO-), 7.24—7.40 (1H, m, =CH)	63.81 (63.70)	8.25 (8.02)
4d	1753, 1659, 1465	0.89 (3H, t, *J*=6Hz, CH_3), 1.10—1.77 (10H, m, $5CH_2$), 1.86 (3H, s, =$CHCH_3$), 4.59—4.93 (1H, m, CHO-), 6.89—7.04 (1H, m, =CH)	72.29 (72.49)	9.76 (9.95)
4e	1755, 1650, 1464	0.66—1.12 (6H, m, $2CH_3$), 1.12—1.94 (14H, m, $7CH_2$), 2.02—2.42 (2H, m, =$CHC\underline{H}_2$), 4.54—4.92 (1H, m, CHO-), 6.83—7.00 (1H, m, =CH)	75.06 (74.95)	10.66 (10.78)
4f	1760, 1740, 1660	0.89 (3H, t, *J*=5Hz, CH_3), 1.29 (3H, t, *J*=7Hz, $CO_2CH_2C\underline{H}_3$), 1.10—1.96 (10H, m, $5CH_2$), 3.21 (2H, s, CH_2CO_2Et), 4.14 (2H, q, *J*=7Hz, $CO_2C\underline{H}_2CH_3$), 4.63—5.08 (1H, m, CHO-), 7.32—7.45 (1H, m, =CH)	66.07 (66.12)	8.73 (8.72)
4g	1760, 1742, 1660	0.88 (3H, t, *J*=5Hz, CH_3), 1.06—1.81 (20H, m, $10CH_2$), 3.15—3.29 (2H, m, $C\underline{H}_2CO_2Et$), 4.13 (2H, q, *J*=7Hz, $CO_2C\underline{H}_2CH_3$), 4.70—5.04 (1H, m, CHO-), 7.17—7.39 (1H, m, =CH)	70.42 (70.33)	9.85 (9.94)

Table 4. ^{13}C NMR Data of 2(5*H*)-Furanones **4**

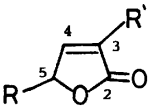

4	C_2(s)	C_3(s)	C_4(d)	C_5(d)	R	R′ (CH_3 or CH_2CO_2Et)
4a	174.4	130.1	148.5	82.1	9.1(q), 26.6(t)	10.6(q)
4b	173.0	127.2	151.3	82.7	8.9(q), 26.1(t)	14.1(q), 33.5(t), 61.2(t), 169.4(s)
4d	174.3	129.7	148.9	81.2	14.0(q), 22.5(t), 25.0(t), 29.0(t), 31.6(t), 30.5(t)	10.5(q)
4f	173.0	126.9	151.6	81.8	14.0(q), 22.5(t), 24.9(t), 29.0(t), 31.6(t), 30.5(t)	14.0(q), 33.3(t), 61.2(t), 169.4(s)
4g	173.0	126.9	151.5	81.8	14.1(q), 22.7(t), 25.0(t), 29.3(t), 29.6(t), 30.5(t), 31.9(t)	14.1(q), 33.3(t), 61.2(t), 169.4(s)

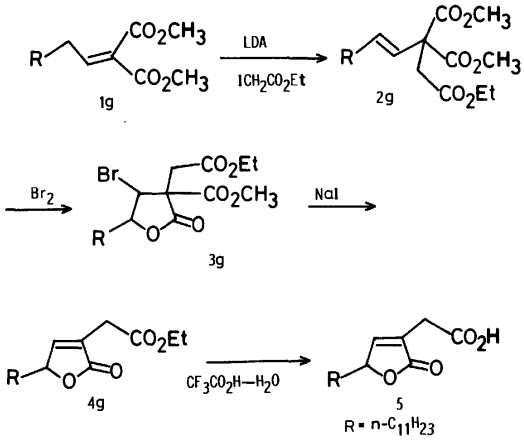

Scheme 1.

hexadecenoate (**2g**) in 68.8% yield; this was subsequently brominated to give (3*R**, 4*R**, 5*S**)-4-bromo-3-ethoxycarbonylmethyl-3-methoxycarbonyl-5-undecyldihydro-2(3*H*)-furanone (**3g**) in 71.0% yield. A treatment of **3g** with 6 equiv of NaI gave (±)-ethyl acarenoate (**4g**) in 93.3% yield and the hydrolysis of **4g** with trifluoroacetic acid-water afforded acarenoic acid **5**[6] in 73% yield.

The present method provides a convenient route to 3,5-disubstituted 2(5*H*)-furanones because of the availability of the starting material, the simplicity of the experiment, and no use of a heavy metal.

Experimental

The melting and boiling points are uncorrected. Infrared (IR) spectra were obtained with a JASCO Model A-102 infrared spectrophotometer. ^1H NMR spectra (60 MHz) were recorded with a JEOL JNM-PMX 60SI apparatus. ^{13}C NMR spectra (25 MHz) were obtained with a JEOL JNM-FX100 apparatus, using $CDCl_3$ as a solvent. NOE experiments were conducted on a deoxygenated sample with a Varian VXR 300 spectrometer. Column chromatography was accomplished with a 100—200 mesh Wakogel C-200. 3-Pentanone was dried over $CaCl_2$ and distilled prior to use. Commercial first-grade aldehydes were distilled prior to use. Ethyl iodoacetate was obtained by a reaction of ethyl bromoacetate with NaI.[10]

Alkylidenemalonates **1** were prepared according to procedures reported in the literature.[11] Compounds, boiling points, and yields are as follows: **1a** (R=C_2H_5), bp 77.5—80 °C/3 Torr (1 Torr=133.322 Pa), **1c** (R=*n*-C_4H_9),[5,11] bp 102 °C/2 Torr, 76%; **1d** (R=*n*-C_6H_{13}), bp 118—120 °C/2 Torr, 80%; **1g** (R=*n*-$C_{11}H_{23}$),[12] 42%.

Compound **2** was prepared according to procedures reported previously.[5] The following exemplifies the synthesis of **2**.

Methyl (*E*)-2-Methoxycarbonyl-2-methyl-3-hexenoate (2a). To a stirred solution of 0.90 ml (6.40 mmol) of diisopropylamine in 6 ml of dry THF was added dropwise 4.1 ml (6.51 mmol) of 1.6 M (1M=1 mol dm^{-3}) butyllithium in hexane at 0 °C. After 20 min, 2.8 ml of HMPA was added, and then the mixture was cooled to −78 °C. Dimethyl butylidenemalonate (1.0 g, 5.38 mmol) was added dropwise and the mixture was stirred for 30 min. After the dropwise addition of methyl iodide (1.43 g, 10.1 mmol), the mixture was allowed to warm up to room temperature for 1 h and was then heated under reflux for 30 min. It was cooled to room temperature, and poured into ice water. The organic material was extracted with ethyl acetate and the combined extracts were washed with dilute HCl and water, and dried over $MgSO_4$. Removal of the solvent gave 0.987 mg of an oil, which was purified by bulb-to-bulb distillation to give 0.682 mg (63.4%) of **2a**: bp 130 °C/7 Torr; IR (neat) 2970 and 1740 cm^{-1}; ^1H NMR (CCl_4) δ=1.02 (3H, t, *J*=7 Hz, $CH_2C\underline{H}_3$), 1.45 (3H, s, CCH_3), 1.87—2.44 (2H, m, $C\underline{H}_2CH_3$), 3.65 (6H, s, $2CO_2CH_3$), 5.40 (1H, dt, *J*=15.5 Hz, $CH_2C\underline{H}$=CH), and 5.81 (1H, d, *J*=16 Hz, CH_2CH=C$\underline{H}$). Found: C, 59.92; H, 7.88%. Calcd for $C_{10}H_{16}O_4$: C, 59.98; H, 8.05%.

Ethyl (*E*)-3,3-Bis(methoxycarbonyl)-4-undecenoate (2f). Dimethyl octylidenemalonate (1.0 g, 4.13 mmol) was treated with LDA and allowed to react with ethyl iodoacetate (1.65 g, 7.77 mmol) as described above. The standard work-up gave 1.57 g of the crude product, which was purified by column chromatography (SiO_2, hexane-ethyl acetate, 30 : 1—5 : 1) to afford 1.17 g (86.4%) of **2f**: TLC (SiO_2; hexane-ethyl acetate, 4 : 1), R_f 0.33; IR (neat) 2950 and 1740 cm^{-1}; ^1H NMR (CCl_4) δ=0.89 (3H, t, *J*=5 Hz), 1.10—1.58 (11H, m, $4CH_2$, $CO_2CH_2C\underline{H}_3$), 1.96—2.36 (2H, m, $C\underline{H}_2CH$=), 3.01 (2H, s, $C\underline{H}_2CO_2Et$), 3.69 (6H, s, $2CO_2CH_3$), 4.04 (2H, q, *J*=8 Hz, $CO_2C\underline{H}_2CH_3$), 5.42 (1H, dt, *J*=15 and 5.5 Hz, $CH_2C\underline{H}$=

and 5.95 (1H, d, J=15 Hz, CH_2CH=C$\underline{H}$).

Other compounds **2** were also prepared by the same procedures as described above.

2b: TLC (SiO_2; hexane-ethyl acetate, 4:1), R_f 0.29; IR (neat) 1740 cm^{-1}. ^1H NMR (CCl_4) δ=1.01 (3H, t, J=7 Hz, C$\underline{H}_3CH_2$), 1.22 (3H, t, J=7 Hz, $CO_2CH_2C\underline{H}_3$), 1.86—2.37 (2H, m, $CH_3C\underline{H}_2$), 3.00 (2H, s, $C\underline{H}_2CO_2Et$), 3.70 (6H, s, $2CO_2CH_3$), 4.05 (2H, q, J=7 Hz, $CO_2C\underline{H}_2CH_3$), 5.47 (1H, dt, J=16 and 6 Hz, $CH_2C\underline{H}$=CH), and 5.95 (1H, d, J=16 Hz, CH_2CH=C$\underline{H}$). Found: C, 57.51; H, 7.40%. Calcd for $C_{13}H_{20}O_6$: C, 57.34; H, 7.40%.

2c: Bp 170 °C/4 Torr (bulb-to-bulb distillation); IR (neat) 2990, 1748, 1735, 1650, and 1438 cm^{-1}; ^1H NMR (CCl_4) δ=0.88 (3H, t, J=6 Hz, $(CH_2)_3C\underline{H}_3$), 1.05—1.53 (4H, m, $2CH_2$), 1.20 (3H, t, J=7 Hz, $CO_2CH_2C\underline{H}_3$), 1.85—2.66 (2H, m, $C\underline{H}_2CH$=), 2.98 (2H, s, $C\underline{H}_2CO_2Et$), 3.66 (6H, s, $2CO_2CH_3$), 4.01 (2H, q, J=7 Hz, $CO_2C\underline{H}_2CH_3$), 5.40 (1H, dt, J=16 and 5.5 Hz, $CH_2C\underline{H}$=CH), and 5.92 (1H, d, J=16 Hz, CH_2CH=C$\underline{H}$).

2e: TLC (SiO_2; hexane-ethyl acetate, 4:1), R_f 0.53; IR (neat) 1742, 1460, 1436, and 1380 cm^{-1}; ^1H NMR (CCl_4) δ=0.89 (3H, t, J=5 Hz, C$\underline{H}_3CH_2$), 1.08—1.70 (12H, m, $6CH_2$), 1.70—2.42 (4H, m, $2CH_2$), 3.65 (6H, s, $2CO_2CH_3$), 5.38 (1H, dt, J=15 and 5.5 Hz, $CH_2C\underline{H}$=CH), and 5.86 (1H, d, J=15 Hz, CH_2CH=C$\underline{H}$). Found: C, 68.14; H, 10.09%. Calcd for $C_{17}H_{30}O_4$: C, 68.42; H, 10.13%.

2g: TLC (SiO_2; hexane-ethyl acetate, 4:1), R_f 0.41; IR (neat) 2950, 1745, 1460, and 1435 cm^{-1}; ^1H NMR (CCl_4) δ=0.88 (3H, t, J=4 Hz, $(CH)_{10}C\underline{H}_3$), 1.03—1.53 (18H, m, $9CH_2$), 1.80—2.25 (2H, m, CH_2), 2.99 (2H, s, $C\underline{H}_2CO_2Et$), 3.68 (6H, s, $2CO_2CH_3$), 4.02 (2H, q, J=7 Hz, $CO_2C\underline{H}_2CH_3$), 5.40 (1H, dt, J=15 and 6 Hz, $CH_2C\underline{H}$=), and 5.92 (1H, d, J=15 Hz, CH_2CH=C$\underline{H}$). Found: C, 66.36; H, 9.57%. Calcd for $C_{22}H_{38}O_6$: C, 66.30; H, 9.61%.

(3*R, 4*R**, 5*S**)-4-Bromo-3-methoxycarbonyl-5-ethyl-3-methyldihydro-2(3*H*)-furanone (3a).** To a solution of **2a** (0.3 g, 1.5 mmol) in chloroform (2.6 ml) was added dropwise bromine (0.264 g, 1.65 mmol) at 0 °C. After the mixture had been stirred for 2.5 h, the solvent was evaporated to give 435 mg of the crude product which crystallized on standing for 1 d. Recrystallization from hexane afforded 0.293 g (73.7%) of **3a**: mp 86.3—87.2 °C; IR (KBr) 2970, 1790, 1742, 1443, and 1428 cm^{-1}; ^1H NMR ($CDCl_3$) δ=1.11 (3H, t, J=7 Hz, $CH_2C\underline{H}_3$), 1.50 (3H, s, CH_3), 1.39—2.30 (2H, m, $C\underline{H}_2CH_3$), 3.78 (3H, s, CO_2CH_3), 3.83 (1H, d, J=8 Hz, CHBr), and 4.46—4.88 (1H, m, CH-O); ^{13}C NMR ($CDCl_3$) δ=9.7 (q, $CH_2\underline{C}H_3$), 18.1 (q, C_3-$\underline{C}H_3$), 25.1 (t, $\underline{C}H_2CH_3$), 51.7 (d, CHBr), 53.1 (q, $CO_2\underline{C}H_3$), 57.0 (s, C_3), 84.7 (d, C_5), 167.2 (s, $\underline{C}O_2CH_3$), and 172.0 (s, C_2). Found: C, 40.75; H, 4.99%. Calcd for $C_9H_{13}BrO_4$: C, 40.78; H, 4.94%.

(3*R, 4*R**, 5*S**)-4-Bromo-3-ethoxycarbonylmethyl-5-ethyl-3-methoxycarbonyldihydro-2(3*H*)-furanone (3b).** To a solution of **2b** (0.509 g, 1.87 mmol) in chloroform (3 ml) was added dropwise bromine (0.33 g, 2.06 mmol) at 0 °C. The mixture was stirred for 3 h and the solvent was removed in vacuo. The crude product (0.688 g) was chromatographed on SiO_2 (hexane-ethyl acetate, 10:1—5:1) to give 0.401 g (63.6%) of **3b**: TLC (SiO_2; hexane-ethyl acetate, 4:1), R_f 0.31; IR (neat) 3000, 1790, 1750, 1730, 1460, and 1435 cm^{-1}; ^1H NMR (CCl_4) δ=1.24 (3H, t, J=6 Hz, $CH_2C\underline{H}_3$), 1.27 (3H, t, J=7 Hz, $CO_2CH_2C\underline{H}_3$), 1.56—2.19 (2H, m, $C\underline{H}_2CH_3$), 2.79 (1H, d, J=18 Hz, CH_2), 3.81 (3H, s, CO_2CH_3), 4.14 (2H, q, J=7 Hz, $CO_2C\underline{H}_2CH_3$), and 4.46—4.80 (2H, m, BrCHCHO-). Found: C, 42.65; H, 5.04%. Calcd for $C_{12}H_{17}BrO_6$: C, 42.75; H, 5.08%.

Other compounds **3** were prepared by the same procedures as those described for **3b**.

3c: IR (neat) 2975, 1792, 1755, 1731, 1435, and 1402 cm^{-1}; ^1H NMR (CCl_4) δ=0.97 (3H, t, J=5 Hz, $CH_2C\underline{H}_3$), 1.13—2.10 (8H, m, $CH_3(C\underline{H}_2)_3$, $C\underline{H}_2CO_2$), 1.27 (3H, t, J=7 Hz, $CO_2CH_2C\underline{H}_3$), 2.77 (1H, d, J=18 Hz, $C\underline{H}_2CO_2Et$), 3.15 (1H, d, J=18 Hz, $C\underline{H}_2CO_2Et$), 3.76 (3H, s, CO_2CH_3), 4.12 (2H, q, J=7 Hz, $CO_2C\underline{H}_2CH_3$), and 4.40—4.84 (2H, m, CHBrCHO). Found: C, 46.17; H, 5.74%. Calcd for $C_{14}H_{21}BrO_6$: C, 46.04; H, 5.80%.

3d: Mp 76.5—78.0 °C (hexane): IR (KBr) 2940, 1910, 1749, 1209, and 1108 cm^{-1}; ^1H NMR ($CDCl_3$) δ=0.89 (3H, t, J=5 Hz, $(CH_2)_5C\underline{H}_3$), 1.10—2.24 (10H, m, $5CH_2$), 1.52 (3H, s, CH_3), 3.69 (3H, s, CO_2CH_3), 3.69 (1H, d, J=10 Hz, CHBr), and 4.42—4.93 (1H, m, CHO-). Found: C, 48.86; H, 6.60%. Calcd for $C_{13}H_{21}BrO_4$: C, 48.61; H, 6.59%.

3e: TLC (SiO_2; hexane-ethyl acetate, 4:1), R_f 0.54; IR (neat) 2950, 1789, 1755, 1460, and 1431 cm^{-1}; ^1H NMR (CCl_4) δ=0.72—1.15 (6H, m, $2CH_3$), 1.15—2.20 (16H, m, $8CH_2$), 3.77 (3H, s, CO_2CH_3), 3.90 (1H, d, J=8 Hz, CHBr), and 4.30—4.75 (1H, m, CHO-). Found: C, 52.89; H, 7.54%. Calcd for $C_{16}H_{27}BrO_4$: C, 52.90; H, 7.49%.

3f: TLC (SiO_2; hexane-ethyl acetate, 4:1), R_f 0.61; IR (neat) 2950, 1788, 1752, 1729, 1460, and 1375 cm^{-1}; ^1H NMR (CCl_4) δ=0.91 (3H, t, J=5 Hz, $(CH_2)_5C\underline{H}_3$), 1.10—2.06 (10H, m, $5CH_2$), 1.27 (3H, t, J=6 Hz, $CO_2CH_2C\underline{H}_3$), 2.79 (1H, d, J=18 Hz, $C\underline{H}_2CO_2Et$), 3.16 (1H, d, J=18 Hz, $C\underline{H}_2CO_2Et$), 3.70 (3H, s, CO_2CH_3), 4.13 (2H, q, J=7 Hz, $CO_2C\underline{H}_2CH_3$), and 4.48—4.70 (2H, m, BrCHCHO-). Found: C, 48.81; H, 6.39%. Calcd for $C_{16}H_{25}BrO_6$: C, 48.87; H, 6.41%.

3g: 71.0% yield; TLC (hexane-ethyl acetate, 4:1), R_f 0.46; IR (neat) 2940, 1781, 1755, and 1735 cm^{-1}; ^1H NMR (CCl_4) δ=0.89 (3H, t, J=5 Hz, CH_3), 1.1—2.0 (25H, m, $(C\underline{H}_2)_{10}CH_3$ and $C\underline{H}_2CO_2Et$), 2.78 (1H, d, J=18 Hz, $C\underline{H}_2CO_2Et$), 3.14 (1H, d, J=18 Hz, $C\underline{H}_2CO_2Et$), 3.78 (3H, s, CO_2CH_3), 4.12 (2H, q, J=7 Hz, $CO_2C\underline{H}_2CH_3$), and 4.46—4.71 (2H, m, CHBrCHO-). Found C, 54.23; H, 7.51%. Calcd for $C_{21}H_{35}BrO_6$: C, 54.43; H, 7.61%.

Some representative syntheses of 2(5*H*)-furanones **4** are shown below.

5-Ethyl-3-methyl-2(5*H*)-furanone (4a). Sodium iodide (275 mg, 1.83 mmol) was charged in a 10 ml two-necked flask and dried in vacuo. A solution of **3a** (81 mg, 0.31 mmol) in 3-pentanone (3 ml) was added and the mixture was heated at the reflux temperature under a nitrogen atmosphere. After 2 d it was poured into ice water and the organic material was extracted with ethyl acetate and the combined extracts were washed with 5% sodium thiosulfate and water, and dried over $MgSO_4$. Removal of the solvent gave 63 mg of the crude product which was chromatographed on SiO_2 (hexane-ethyl acetate, 30:1—5:1). The early fractions gave 15 mg of the starting material **3a**. The later fractions gave 28 mg (72%) (89% based on the consumed **3a**) of **4a**. Spectral and analytical data are shown in Table 3.

3-Ethoxycarbonylmethyl-5-butyl-2(5*H*)-furanone (4c). As shown in **4a**, a stirred mixture of **3c** (200 mg, 0.55 mmol), NaI (495 mg, 3.30 mmol), and 3-pentanone (3 ml) was heated at the reflux temperature under a nitrogen atmosphere for 2.5 d. Column chromatography (SiO_2; hexane-ethyl acetate, 10:1) of the crude product gave 110 mg (88.5%) of **4c**: TLC (SiO_2; hexane-ethyl acetate, 4:1), R_f 0.16. Spectral and analytical data are shown in Table 3.

3-Ethoxycarbonylmethyl-5-undecyl-2(5*H*)-furanone (4g). As shown in **4a**, a mixture of **3g** (200 mg, 0.43 mmol), NaI (387 mg, 2.58 mmol), and 3-pentanone (3 ml) was refluxed with stirring under a nitrogen atmosphere. Column chromatography (SiO_2; hexane-ethyl acetate, 15:1—10:1) gave 130 mg (93.3%) of **4g**: TLC (SiO_2; hexane-ethyl acetate, 4:1), R_f 0.23. Spectral and analytical data are shown in Table 3.

(±)-Acarenoic Acid (5). A mixture of **4g** (45 mg, 0.14 mmol), trifluoroacetic acid (1 ml), and water (2 ml) was stirred for 2 d and then poured into water. The organic material was extracted with dichloromethane, washed with water, and dried over $MgSO_4$. Evaporation of the solvent gave 50 mg of the crude product which was purified by preparative TLC (SiO_2; hexane-ethyl acetate, 4:1). The component of R_f 0.23 gave 12 mg of **4g**. The component of R_f 0—0.13 gave 22 mg (53%) (73% based on the consumed **4g**) of **5**: mp 83.8—84.2 °C (from benzene) (lit,[6] 144—146.5 °C for (−)-**5**); IR (KBr) 2925, 1738, 1708, 1655, 1390, 1298, and 1083 cm^{-1}; ^1H NMR ($CDCl_3$) δ=0.88 (3H, t, J=5 Hz, $(CH_2)_{10}CH_3$), 1.04—1.95 (20H, m, $10CH_2$), 3.38 (2H, s, CH_2CO_2H), 4.80—5.11 (1H, m, CHO-), 7.35 (1H, s, CH=C), and 8.94 (1H, br. s, CO_2H); ^{13}C NMR ($CDCl_3$) δ=14.0 (q), 22.6 (t), 25.0 (t), 29.3 (t), 29.5 (t), 31.7 (t), 31.9 (t), 33.2 (t), 82.1 (d), 126.3 (s), 152.0 (d), 173.1 (s), and 184.2 (s).

We thank Mr. Eiichiro Amano of our laboratory for elemental analyses. We also thank Drs. Kazuhiko Kushida and Hajime Kato of Varian Instrument Ltd. for the NOE experiments.

References

1) F. M. Dean, "Naturally Occurring Oxygen Ring Compounds," Butterworths, London (1963).

2) Some reviews: P. A. Grieco, *Synthesis*, **1975**, 67; Y. S. Rao, *Chem. Rev.* **76**, 625 (1976); M. Yamamoto, *Yuki Gosei Kagaku Kyokai Shi*, **39**, 25 (1981).

3) a) A. Takeda, S. Tsuboi, and Y. Oota, *J. Org. Chem.*, **38**, 4148 (1973); b) A. Takeda, S. Tsuboi, and T. Sakai, *ibid*, **39**, 2601 (1974); c) A. Takeda, S. Tsuboi, and T. Sakai, *Bull. Chem. Soc. Jpn.*, **47**, 2440 (1974).

4) S. Tsuboi, H. Fukumoto, H. Wada, A. Takeda, and K. Fukuyama, *Bull. Chem. Soc. Jpn.*, **60**, 689 (1987).

5) S. Tsuboi, K. Muranaka, T. Sakai, and A. Takeda, *J. Org. Chem.*, **25**, 4944 (1986).

6) J. Santesson, *Acta Chem. Scand.*, **21**, 1993 (1967).

7) J. H. Noggle and R. E. Schirmer, "The Nuclear Overhauser Effect," Academic Press, New York (1985).

8) A reviewer suggested that benzene-crown ether would be effective.

9) A. Takeda, T. Sakai, S. Shinohara, and S. Tsuboi, *Bull. Chem. Soc. Jpn.*, **50**, 1133 (1977).

10) A. H. Ford-Moore, *Org. Synth.*, Coll. Vol., 4, 84 (1963).

11) A. C. Cope, C. M. Hofmann, C. Wyckoff, and E. Hardenbergh, *J. Am. Chem. Soc.*, **63**, 3452 (1941).

12) Purified by column chromatography (SiO_2, hexane-ethyl acetate, 4:1), R_f 0.5.

 © 1987 The Chemical Society of Japan Bull. Chem. Soc. Jpn., 60, 2923—2926 (1987)

Studies on Hydrogenation by Nickel Complexes. 5. The Selective Hydrogenation of 1,4-Cyclohexadienes to Cyclohexenes Catalyzed by a Nickel Complex

Mutsuji SAKAI,* Nobuo HIRANO, Fumiya HARADA, Yasumasa SAKAKIBARA, and Norito UCHINO
Department of Polymer Science and Engineering, Kyoto Institute of Technology, Matsugasaki, Sakyo-ku, Kyoto 606
(Received March 2, 1987)

1,4-Cyclohexadiene was hydrogenated selectively to cyclohexene with a nickel catalyst generated from bis(acetylacetonato)nickel(II), triethyldialuminium trichloride, and triphenylphosphine at 40 °C under an atmospheric pressure of hydrogen. The hydrogenation of eleven kinds of alkyl-substituted 1,4-cyclohexadienes gave the corresponding cyclohexenes in good yields by the nickel catalyst. The structural factors of the alkyl substituent on the diolefin are shown to affect the hydrogenation rate. The homogeneous nickel catalyst system, in which a nickel hydride complex $NiH(PPh_3)(AlCl_4)$ is supposed to be an active species, was effective for the selective hydrogenation of the diolefin to the olefin. A plausible pathway involving π-allylnickel complexes for the hydrogenation is proposed.

Homogeneous hydrogenation has been extensively investigated.[1-3] Concerning nickel catalysts used for selective hydrogenation of diolefins, nickel-based Ziegler catalysts are known to be effective for the hydrogenation of diolefins[4,5] and unsaturated fats.[6,7] The catalyst systems are complicated (homogeneous and/or heterogeneous system) and poorly understood. Phosphine-coordinated nickel catalysts also are active for the hydrogenation of diolefins.[8,9] In many cases, however, less satisfactory results for selective hydrogenation are obtained. We used a homogeneous nickel catalyst generated from $Ni(acac)_2$, $Et_3Al_2Cl_3$, and PPh_3, and found that diolefins were hydrogenated selectively in good yields with the nickel catalyst in a series of studies reported.[10-13]

In this paper, we examine closely the selective hydrogenation of cyclic diolefins by the nickel catalyst under mild conditions and will complete the aspect of the catalytic hydrogenation.

Experimental

Materials. 1,4-Cyclohexadiene and methylcyclohexenes were commercially available. Alkyl-substituted 1,4-cyclohexadienes were prepared from the corresponding alkylbenzenes by Birch reduction.[14-16] Solvents were distilled over sodium. The other reagents were commercially available and used without purification.

General Procedure. Hydrogenation: To a 200 cm^3 flask fitted with a hydrogen buret, a septum inlet, and a magnetic stirring bar were added $Ni(acac)_2$ (0.11 mmol) and PPh_3 (0.55 mmol) in toluene. After the air was replaced with hydrogen the diolefin (11 mmol) in toluene was added. The hydrogenation was started by the addition of $Et_3Al_2Cl_3$ (1.1 mmol) in toluene. The solution was stirred with a magnetic stirrer and kept in a thermostated bath. An aliquot (2 cm^3) of the solution was taken and treated with a methanol-aqueous hydrochloric acid mixture. The organic layer was separated, washed with water, and subjected to GLC analysis.

Competitive Hydrogenation: The mixture of equimolar amounts of two diolefins was hydrogenated by the same procedure. An aliquot of the solution was worked up similarly. The initial rates for disappearance of diolefin were measured and relative rates were calculated, estimating the disappearance rate of 1,4-cyclohexadiene as 1.0.

Isomerization: Under an atmosphere of nitrogen methylcyclohexene was treated with the nickel catalyst under conditions similar to those of hydrogenation. The same work-up was done.

Analysis. The gas chromatographic analyses were made by a Yanaco G-80 apparatus with a TC detector and herium carrier gas using a 3 m column of bis(2-cyanoethyl) ether. ^1H NMR spectra were recorded on a Varian T-60A spectrometer using tetramethylsilane as an internal standard. The composition of methylcyclohexenes was determined by the NMR analyses, in which the relative areas of the characteristic signals for 3- and 4-methylcyclohexene were calculated.

Results and Discussion

Hydrogenation of 1,4-Cyclohexadienes. Under mild conditions 1,4-cyclohexadiene and alkyl-substituted homologs were hydrogenated selectively to cyclohexenes with a nickel catalyst generated from $Ni(acac)_2$, $Et_3Al_2Cl_3$, and PPh_3. The results are shown in Table 1. 1,4-Cyclohexadiene was hydrogenated selectively to produce cyclohexene in a high yield of 81%. Trace amounts of benzene (disproportionation product)[17] were detected. Cyclohexene was hydrogenated very slowly to cyclohexane with the nickel catalyst. In the case of 1,3-cyclohexadiene polymerization predominated over hydrogenation under the same conditions. However, 1,3-cyclohexadiene also was hydrogenated selectively to cyclohexene by adding the 1,3-diene dropwise to the catalyst system.[12] Mono- and dialkyl-substituted 1,4-cyclohexadienes gave the corresponding cyclohexenes in good yields. However, the compositions of alkyl-substituted cyclohexene isomers, except methylcyclohexenes, could not be determined exactly by GLC and NMR analyses because the isomers overlapped each other on the signals.

GLC analysis showed that methylcyclohexenes formed in the hydrogenation of 1-methyl-1,4-cyclohexadiene consisted of 1-methylcyclohexene (yield, 67%) and the mixture (7%) of 3- and 4-methylcyclohexene.

Table 1. The Hydrogenation of 1,4-Cyclohexadienes Catalyzed by a Nickel Complex[a)]

Diolefin	Solvent	Time h	Conv. %	Product (Yield/%)
1,4-Cyclohexadiene[b)]	Toluene	6	100	Cyclohexene (81) Cyclohexane (0)
1-Methyl-1,4-cyclohexadiene[b)]	Toluene	8	100	1-Methylcyclohexene (67) 3- and 4-Methylcyclohexene (7) Methylcyclohexane (2)
1-Ethyl-1,4-cyclohexadiene	Ethylbenzene	8	91	Ethylcyclohexenes (80) Ethylcyclohexane (0)
1,2-Dimethyl-1,4-cyclohexadiene[b)]	Ethylbenzene	22	100	Dimethylcyclohexenes (73) 1,2-Dimethylcyclohexane (0)
1,5-Dimethyl-1,4-cyclohexadiene	Ethylbenzene	22	97	Dimethylcyclohexenes (68) 1,3-Dimethylcyclohexane (0)
1,4-Dimethyl-1,4-cyclohexadiene	Ethylbenzene	28	82	Dimethylcyclohexenes (56) 1,4-Dimethylcyclohexane (6)

a) Reaction conditions: Diolefin 11 mmol; $Ni(acac)_2$ 0.11 mmol; $Ni:Al_2:P=1:10:5$; solvent 100 cm^3; temp 40 °C; H_2 1 atm. b) Data are derived from the Ref. 12.

Table 2. The Hydrogenation of 1-Methyl-1,4-cyclohexadiene Catalyzed by a Nickel Complex[a)]

Time h	Conv. %	Select/%	
		Methylcyclohexene (Composition/%)[b)]	Methylcyclohexane
1	15	77 (59/41)	0
2	34	74 (58/42)	0
4	63	75 (61/39), (61/17/22)[c)]	0
6	87	78 (63/37)	1
8	100	74 (90/10)	2
10	100	72 (90/10)	2

a) Reaction conditions: Diolefin 8 mmol; $Ni(acac)_2$ 0.1 mmol; $Ni:Al_2:P=1:10:5$; toluene 100 cm^3; temp 40 °C; H_2 1 atm. b) The ratio of methylcyclohexene isomers (1-methylcyclohexene/3- and 4-methylcyclohexene) by GLC analysis. c) The ratio of methylcyclohexene isomers (1-methylcyclohexene/3-methylcyclohexene/4-methylcyclohexene) by NMR analysis.

Table 3. The Isomerization of Methylcyclohexenes Catalyzed by a Nickel Complex[a)]

Methylcyclohexene	Time min	Product/mmol (Composition/%)[b)]	
		1-Methylcyclohexene	3- and 4-Methylcyclohexene
1-Methylcyclohexene	0	8.97	Trace
	1	7.91 (90)	0.88 (10)
	150	7.86 (89)	0.94 (11)
4-Methylcyclohexene	0	0.71 (8)	8.11 (92)
	1	7.42 (90)	0.88 (10)
	180	7.41 (90)	0.82 (10)

a) Reaction conditions: $Ni(acac)_2$ 0.2 mmol; $Ni:Al_2:P=1:10:5$; toluene 100 cm^3; temp 40 °C; under N_2. b) The composition of methylcyclohexene/% by GLC analysis.

At the initial stage of hydrogenation primary products were three kinds of methylcyclohexene, 1-, 3-, and 4-methylcyclohexene, in the ratio of 61 : 17 : 22, as shown in Table 2. After the diolefin was consumed the composition of the products was 90% of 1-methylcyclohexene and 10% of 3- and 4-methyl isomer. The above results suggest a subsequent isomerization occurred.

Isomerization. As shown in Table 3, the treatment of methylcyclohexenes with the nickel catalyst under nitrogen atmosphere resulted in the same composition with that of hydrogenation, 90% of 1-methylcyclohexene and 10% of 3- and 4-methyl isomer. It was found that each of methylcyclohexenes isomerized very rapidly by the nickel catalyst and the reaction mixture attained thermodynamically to equilibrium. The nickel catalyst was an excellent catalyst for the isomerization of the olefins.

On the other hand, 1,4-cyclohexadiene and 1-methyl-

Table 4. Relative Rates for the Competitive Hydrogenation of Substituted 1,4-Cyclohexadienes[a)]

Substituent group on 1,4-cyclohexadiene	Reference diolefin[b)]	Solvent[c)]	Relative rate[d)]
1-Methyl	A	E	0.45
1-Ethyl	B	E	0.36
1-Propyl	C	T	0.32
1-Isopropyl	C	E	0.28
1-Butyl	B	E	0.27
1-Isobutyl	A	T	0.19
1-*t*-Butyl	C	T	0.15
1,2-Dimethyl	B	E	0.28
1,5-Dimethyl	B	E	0.085
1,4-Dimethyl	B	E	0.054

a) Reaction conditions: Each diolefin 5 mmol; $Ni(acac)_2$ 0.1 mmol; $Ni:Al_2:P=1:10:5$; solvent 100 cm^3; temp 60°C; H_2 1 atm. b) Reference diolefin: A 1,4-cyclohexadiene; B 1-methyl-1,4-cyclohexadiene; C 1-ethyl-1,4-cyclohexadiene. c) Solvent: E ethylbenzene; T toluene. d) The disappearance rate of 1,4-cyclohexadiene was estimated as 1.0.

1,4-cyclohexadiene hardly isomerized and the 1,3-dienes were detected in trace amounts.

Competitive Hydrogenation. A mixture of equimolar amounts of two diolefins was hydrogenated. The initial rates for disappearance of diolefins were measured and the relative rates were calculated by estimating the disappearance rate of 1,4-cyclohexadiene as 1.0. Table 4 shows that the steric effect of alkyl substituents on the hydrogenation rate. The rate slowed down in the order of the chain length and branching of the alkyl substituent; H(1.0)>Me(0.45)>Et(0.36)>*n*-Pr(0.32)>*n*-Bu(0.27), *n*-Pr(0.32)>*i*-Pr(0.28), and *n*-Bu(0.27)>*i*-Bu(0.19)>*t*-Bu(0.15). Moreover, the number of substituent has a significant influence on the rate, and the order was H(1.0)>1-Me(0.45)>1,2-Me_2(0.28)>1,5-Me_2(0.085)>1,4-Me_2(0.054).

Hydrogenation Pathway. It has been proposed that a nickel hydride complex **1** is the active species for hydrogenation, as represented in the equation.[10,11,18)]

$$Ni(acac)_2 + Et_3Al_2Cl_3 + PPh_3 \longrightarrow \underset{\mathbf{1}}{H(L)Ni(Ph_3P)(Cl\cdot AlCl_3)} \quad (L;\ \text{solvent})$$

Scheme 1 shows a plausible pathway for the selective hydrogenation of 1,4-cyclohexadiene catalyzed by **1**. 1,4-cyclohexadiene coordinates to **1** and an insertion reaction of coordinated diolefin **2** produces a cyclohexenylnickel complex **3**. Its β-hydrogen elimination leads to the isomerization of 1,4-diene to 1,3-diene and then a π-allylnickel complex **5** is formed via an insertion reaction from the complex **4**. These four steps are reversible. The oxidative addition of hydrogen to **5** and the reductive elimination of cyclohexene regenerate **1**, which continues the catalytic cycle.

It has been reported that complexes such as **1** are most probably planar[19,20)] and the fragment of $AlCl_3$ strengthens the protonic character[21,22)] of hydrogen and promotes a ligand exchange.[23,24)] The use of five equimolar amounts of PPh_3 and a large excess of $Et_3Al_2Cl_3$ was favorable for the hydrogenation of 1,4-

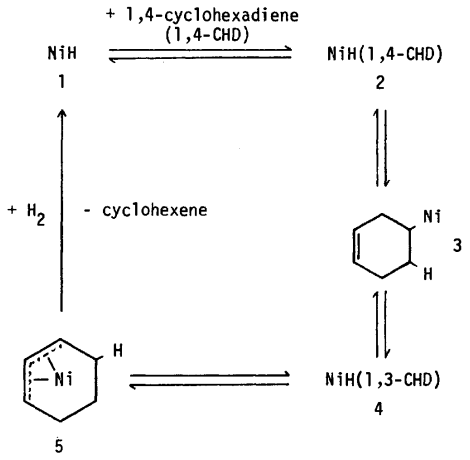

Scheme 1.

cyclohexadiene. It is suggested that appropriate amounts of the phosphine is necessary to form **1** and a second phosphine coordinates to **1** to form NiH-$(PPh_3)_2(AlCl_4)$, an inactive species, in a large excess of the phosphine. The complex **1** would have an excellent catalytic ability for isomerization of olefins and a good catalytic ability for selective hydrogenation of diolefins. Methylcyclohexenes isomerized very rapidly, while, 1,4-cyclohexadiene hardly did. The formation of a π-allylnickel complex[25)] from **4** is suggested by the products in the case of the hydrogenation of 1-methyl-1,4-cyclohexadiene. At the initial stage of the hydrogenation of 1-methyl-1,4-cyclohexadiene primary products were three kinds of cyclohexene,[26)] 1-, 3-, and 4-methylcyclohexene. These cyclohexenes isomerized very rapidly each other in the absence of the diolefin since the strength of coordination of diolefin to **1** is much stronger than that of olefins and the product attained to equilibrium. The formation of three isomers of methylcyclohexene is shown in Scheme 2. 1-Methyl-1,4-cyclohexadiene isomerizes to thermodynamically stable 1,3-isomers. Insertion reactions of coordinated 1,3-diolefin to **1** produce four types of π-allylnickel complex. In these complexes less steric crowding and thermodynamically stable π-allylnickel

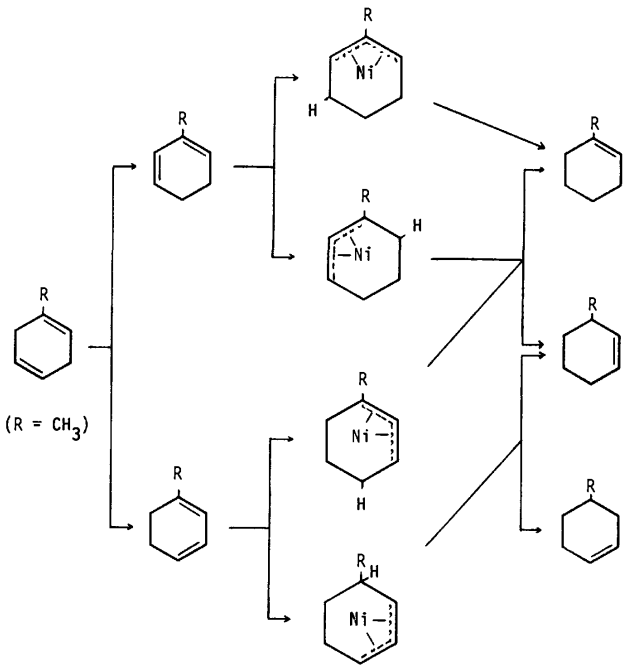

Scheme 2.

complexes appear to be preferred.[25] β-Hydrogen eliminations from the complexes formed by oxidative addition of hydrogen to π-allylnickel complexes yield three kinds of methylcyclohexene, 1-, 3-, and 4-methylcyclohexene. It is reported that β-hydrogen eliminations tend to give internal olefins in the hydrogenation of 1,3-diolefins.[11] Thus, it is expected that 1-methylcyclohexene is a major product in the hydrogenation of 1-methyl-1,4-cyclohexadiene. However, little information on the interconversion between π- and σ-allylnickel complexes, and on the direction of β-hydrogen elimination was obtained from the results.

Although the oxidative addition of hydrogen to **5** may be the slow step in the hydrogenation of diolefins,[11] the steric factors of alkyl-substituted 1,4-cyclohexadienes gave a significant effect on hydrogenation rate. The hydrogenation rate slowed down in proportion to the bulkiness of the substrate coordinated (Table 1). This suggests that the equilibrium shown in Scheme 1 lies so far to the left (coordination side). In the isomerization of linear olefins by the nickel catalyst the insertion of olefin into **1** is assumed to be the slow step.[27]

In conclusion, it is presented that the nickel complex generated from $Ni(acac)_2$, $Et_3Al_2Cl_3$, and PPh_3 is a good catalyst for selective hydrogenation of diolefins and the hydrogenation proceeds via π-allylnickel complexes.

References

1) B. R. James, "Homogeneous Hydrogenation," John Wiley & Sons, New York (1973).
2) G. W. Parshall, "Homogeneous Catalysis. The Application and Chemistry of Catalysis by Soluble Transition Metal Complexes," Wiley-Interscience, New York (1980), Chap. 3.
3) B. R. James, "Comprehensive Organometallic Chemistry," ed by G. Wilkinson, Pergamon Press (1982), Vol. 8, Chap. 51.
4) Y. Tajima and E. Kunioka, *J. Org. Chem.*, **33**, 1689 (1968).
5) S. J. Lapporte, *Ann. N. Y. Acad. Sci.*, **158**, 510 (1969).
6) Y. Tajima and E. Kunioka, *J. Am. Oil Chem. Soc.*, **45**, 478 (1968).
7) A. Misono and Y. Uchida, Jpn. Patent 7021082 (1970); *Chem. Abstr.*, **73**, 87459k (1970).
8) M. Kanai and A. Miyake, Jpn. Patent 7129127 (1971); *Chem. Abstr.*, **75**, 150891d (1971).
9) H. Itatani and J. C. Bailar, Jr., *Ind. Eng. Chem., Prod. Res. Dev.*, **11**, 146 (1972).
10) Y. Sakakibara, H. Hisaki, M. Sakai, and N. Uchino, *Nippon Kagaku Kaishi*, **1976**, 1893.
11) Y. Sakakibara, S. Yagi, M. Sakai, and N. Uchino, *Nippon Kagaku Kaishi*, **1980**, 240.
12) M. Sakai, F. Harada, Y. Sakakibara, and N. Uchino, *Bull. Chem. Soc. Jpn.*, **55**, 343 (1982).
13) M. Sakai, T. Fujii, T. Kishimoto, K. Suzuki, Y. Sakakibara, and N. Uchino, *Nippon Kagaku Kaishi*, **1986**, 126.
14) W. Hückel, B. Graf, and D. Münkner, *Justus Liebigs Ann. Chem.*, **614**, 47 (1958).
15) A. P. Krapcho and A. A. Bothner, *J. Am. Chem. Soc.*, **81**, 3658 (1959).
16) T. Yamaguchi, T. Ono, K. Nagai, and C. C. Sin, *Kogyo Kagaku Zasshi*, **73**, 727 (1970).
17) M. Sakai, T. Kimura, T. Nakaoka, Y. Sakakibara, and N. Uchino, *Bull. Chem. Soc. Jpn.*, **58**, 505 (1985).
18) A. N. Nesmeyanov, L. S. Isaeva, and L. N. Lorens, *J. Organomet. Chem.*, **129**, 421 (1977).
19) M. L. H. Green and T. Saito, *Chem. Commun.*, **1969**, 208.
20) K. Jonas and G. Wilke, *Angew. Chem., Int. Ed. Engl.*, **8**, 519 (1970).
21) O. T. Onsanger, H. Wang, and U. Blindheim, *Helv. Chim. Acta*, **52**, 196 (1969).
22) G. G. Eberhardt and W. P. Griffin, *J. Catal.*, **16**, 245 (1970).
23) J. Chatt and B. L. Shaw, *J. Chem. Soc.*, **1960**, 1718.
24) R. de Haan and J. Dekker, *J. Catal.*, **35**, 202 (1974).
25) C. A. Tolman, *J. Am. Chem. Soc.*, **92**, 6785 (1970).
26) R. R. Schrock and J. A. Osborn, *J. Am. Chem. Soc.*, **98**, 4450 (1976).
27) Y. Sakakibara, M. Mukai, M. Sakai, and N. Uchino, *Nippon Kagaku Kaishi*, **1972**, 1457.

Synthesis of 5,8-Dihydroxy-2-methoxy-1,4-naphthoquinone Derivatives. A Major Naphthoquinone Moiety of Some of Naphthoquinone Antibiotics[1]

Yasuhiro TANOUE, Akira TERADA,* Toshiyuki TSUBOI, Takayuki HAYASHIDA, and Otohiko TSUGE†
Department of Chemistry, Kyushu Institute of Technology, Sensui-cho, Tobata, Kitakyushu 804
†Research Institute of Industrial Science, Kyushu University, Kasugakoen, Kasuga 806
(Received March 16, 1987)

6-Formyl- and 6-hydroxymethyl-5,8-dihydroxy-2-methoxy-1,4-naphthoquinones were, respectively, prepared from 2-formyl- and 2-hydroxymethyl-1,4,5,6,8-pentamethoxynaphthalenes which were synthesized as key intermediates of the new antibiotics containing 2-methoxynaphthazarin structure.

Fusarubin (**1**),[2] Erythrostominone (**2**),[2] Purpuromycin (**3**),[3] and Fredericamycin A (**4**)[4] are new antibiotics of naphthoquinone series, and commonly have a 2-methoxynaphthazarin moiety, that is 5,8-dihydroxy-2-methoxy-1,4-naphthoquinone part (Fig. 1). Although there have been some reports[5] concerning the spiro part construction of **4**, no literature was found regarding the naphthoquinone part.

Recently, we have found an efficient methodology for this 2-methoxynaphthazarin system such as 6-formyl- and 6-hydroxymethyl-5,8-dihydroxy-2-methoxy-1,4-naphthoquinones (**10**) and (**13**) from 2-formyl- and 2-hydroxymethyl-1,4,5,6,8-pentamethoxynaphthalenes (**8**) and (**11**). These compounds have been synthesized in our laboratory as key intermediates for the antibiotics described above. The results prompt us to report at this time.

Results and Discussion

Demethylation of 2-formyl-1,4,5,8-tetramethoxynaphthalene (**5**)[6] with ceric(IV) ammonium nitrate (CAN is used as the abbreviation hereafter) gave 6-formyl-5,8-dimethoxy-1,4-naphthoquinone (**6**) in 85% yield. Only two methoxyl groups of 5- and 8-positions of the original **5** had been cleaved by the oxidation. A treatment of **6** with acetic anhydride in the presence of a catalytic amount of sulfuric acid at room temperature gave 1,2,4-triacetoxy-6-diacetoxymethyl-5,8-dimethoxynaphthalene (**7**) in 98% yield. As shown later in this text, it will be proved that one acetoxyl substituent introduced newly among the five acetoxyl groups, occupied the 2-position in **7**; this conclusion is due to an NMR-structural study of **13** (see later). An alkaline hydrolysis of **7**, and methylation with dimethyl sulfate gave **8** in 67% yield. Demethylation of **8** with CAN afforded 6-formyl-2,5,8-trimethoxy-1,4-naphthoquinone (**9**), where only 5- and 8-positional methoxyl groups were cleaved similarly to the demethylation of **5**. A further demethylation of **9** with aluminum chloride at room temperature gave **10**, and the 2-positional methoxyl group remained unchanged (Scheme 1).

Another target **13** was obtained as follows (Scheme 2). A reduction of the aldehyde **8** with lithium aluminum hydride easily gave the correspoding alcohol **11**. Demethylation of **11** with CAN afforded 6-hydroxymethyl-2,5,8-trimethoxy-1,4-naphthoquinone (**12**), which gave **13** (43%) and 5-hydroxy-6-hydroxymethyl-2,8-dimethoxy-1,4-naphthoquinone (**14**) (38%) by further demethylation with aluminum chloride at room temperature. A prolonged reaction time (20 h), however, resulted in the formation of **13** only in 20% yield, with an unidentified product.

The structure of **13** was established on the basis of an NMR-study,[7] of 5,8-dihydroxy-2-methoxy-1,4-naphthoquinone (**15**). The C_8-OH and C_5-OH protons in **15** absorbed at δ 12.17 and 12.63, respectiviely.[7] It is well-

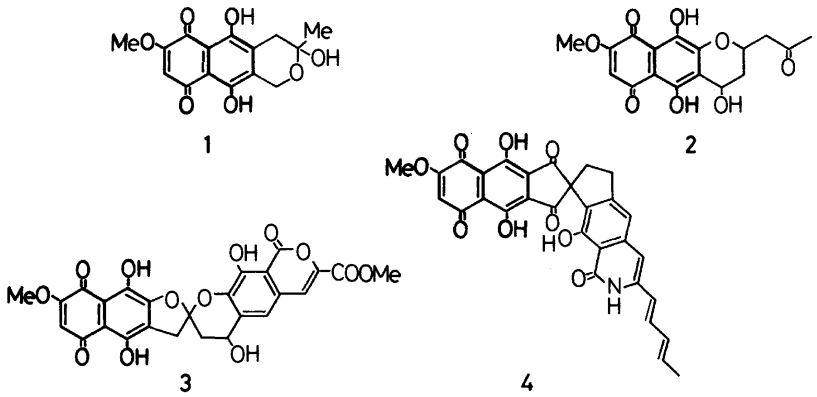

Fig. 1.

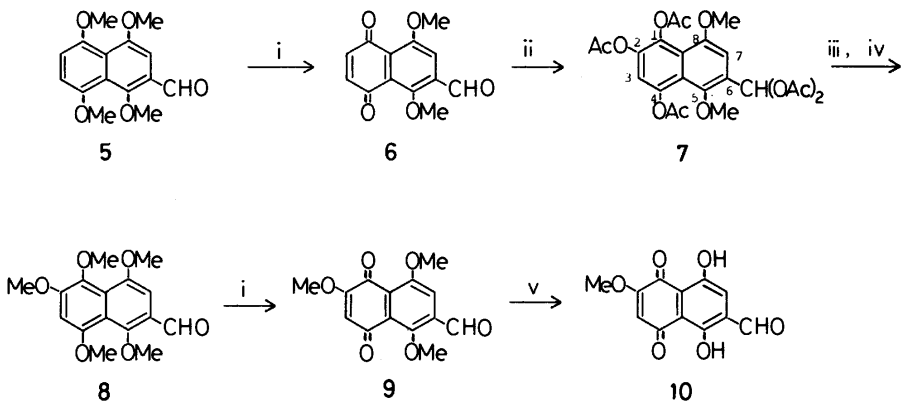

Scheme. 1. i: $(NH_4)_2Ce(NO_3)_6$, H_2O, CH_3CN; ii: Ac_2O, H_2SO_4; iii: OH^-, CH_3OH; iv: OH^-, $(CH_3)_2SO_4$; v: $AlCl_3$, CH_2Cl_2.

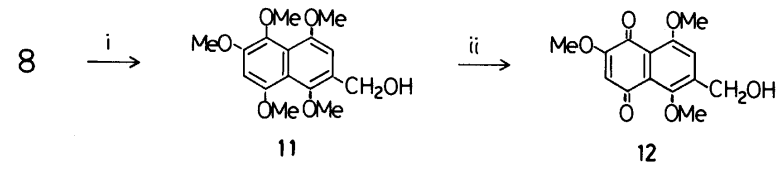

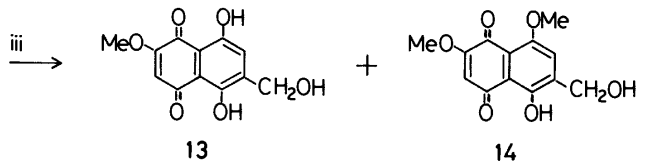

Scheme 2. i: $LiAlH_4$, THF; ii: $(NH_4)_2Ce(NO_3)_6$, H_2O, CH_3CN, $CHCl_3$; iii: $AlCl_3$, CH_2Cl_2.

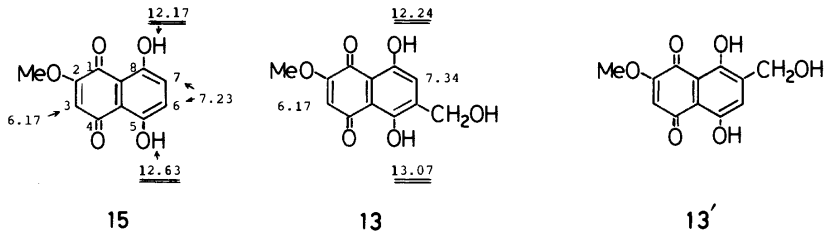

Fig. 2.

known that if **15** has a substituent at either the 6- or 7-position, the chemical shift of the OH proton adjacent to the substituent generally moves in an appreciable extent.[7] In our product **13**, the chemical shift of the C_8-OH proton almost remained unchanged at δ 12.24, whereas that of C_5-OH was found at δ 13.07. As the C_5-OH in our product **13** was observed more downfield than that of **15**, the hydroxymethyl substituent in **13** must be at the 6-position. Therefore, it was concluded that the structure of our product should not be **13'**, but **13**. Then, it could be proved that one of the acetoxyl groups newly introduced by the conversion of **6** to **7**, occupied the 2-position of **7**.

If an aromatic ring has either a formyl or a hydroxymethyl substituent, an ortho-lithiation of the ring is generally possible by the use of butyllithium.[8] Here, the obtained products **8** and **11** have such possibilities to receive new side-chain introductions at their 3-positions; we will be able to apply this to intermediates for syntheses of naphthoquinone antibiotics.

Experimental

^1H NMR spectra were taken on a JEOL JNM-FX60 in $CDCl_3$ and showed in δ values. Mass spectra were obtained with a JEOL DX-300. IR spectra were recorded on a Hitachi 260-30. Column chromatography was carried out on silica gel (Wakogel C-200) with chloroform as an eluent. Melting points were determined with a Yanagimoto micromelting point apparatus and were uncorrected.

6-Formyl-5,8-dimethoxy-1,4-naphthoquinone (6). A solution of CAN (26 g, 47.7 mmol) in water (60 ml) was added to a solution of the aldehyde **5** (5.15 g, 18.7 mmol) in acetonitrile (100 ml) at room temperature, stirred for 30 min, then diluted with water (300 ml). The precipitate was filtered,

washed with water, dried, and gave 3.4 g (74%) of **6** as yellow crystals, mp 175—177 °C. The filtrate was extracted with chloroform. The chloroform solution was washed with brine, dried, and evaporated. Chromatographic purification of the crude product gave 0.51 g (11%) of a sample of **6**. Recrystallization from ligroine-benzene gave an analytical sample, mp 177—178 °C. IR (KBr) 1695 (aldehyde C=O), 1665 (quinone C=O), 1055, and 1020 cm^{-1}; MS *m/z* 246 (M^+), 232, 216, 200, and 189; ^1H NMR δ=4.03 (s, 6H, OCH_3), 6.87 (s, 2H, quinonoid ring H), and 7.77 (s, 1H, benzenoid ring H). Found: C, 63.27; H, 4.06%. Calcd for $C_{13}H_{10}O_5$: C, 63.72; H, 4.09%.

1,2,4-Triacetoxy-6-diacetoxymethyl-5,8-dimethoxynaphthalene (7). A mixture of **6** (8.2 g, 33.4 mmol) in acetic anhydride (50 ml) and concd sulfuric acid (0.5 ml) was allowed to stand at room temperature for 10 d, then poured into ice water and extracted with chloroform. The usual work-up and chromatography gave 16.2 g (98%) of a sample of **7**. Recrystallization from hexane-ethanol gave an analytical sample, mp 174—175 °C. IR (KBr) 1760 (C=O), 1610, 1365, 1200, and 1035 cm^{-1}; MS *m/z* 492 (M^+), 450, 408, 366, and 264; ^1H NMR δ=2.11 (s, 6H, CH_3), 2.32 (s, 3H, CH_3), 2.35 (s, 6H, CH_3), 3.86, 3.93 (each s, 3H, OCH_3), 6.96, 7.08 (each s, 1H, ArH), and 8.15 (s, 1H, CH). Found: C, 56.09; H, 4.94%. Calcd for $C_{23}H_{24}O_{12}$: C, 56.10; H, 4.91%.

2-Formyl-1,4,5,6,8-pentamethoxynaphthalene (8). Sodium hydroxide (12 g, 0.3 mol) dissolved in water (50 ml) was added dropwise to a suspension of **7** (9.93 g, 20 mmol) in methanol (50 ml) under a nitrogen atmosphere and stirred for 1 h. To this was added dimethyl sulfate (76 g, 0.6 mol) and sodium hydroxide (12 g, 0.3 mol) in water (50 ml) alternately and stirred at 40 °C for 5 h. After concentration, the system was extracted with chloroform, worked up as usual, and chromatographed to give 4.14 g (67%) of a sample of **8**. Recrystallization from hexane-ethanol gave yellow crystals, mp 153.5—155.5 °C. IR (KBr) 1660 (C=O), 1595, 1360, 1070, and 1045 cm^{-1}; MS *m/z* 306 (M^+), 291, 276, 263, and 258; ^1H NMR δ=3.81, 3.90, 3.98, 4.01, 4.03 (each s, 3H, OCH_3), 6.78, 7.13 (each s, 1H, ArH), and 10.47 (s, 1H, CHO). Found: C, 62.58; H, 5.92%. Calcd for $C_{16}H_{18}O_6$: C, 62.74; H, 5.92%.

6-Formyl-2,5,8-trimethoxy-1,4-naphthoquinone (9). A solution of CAN (4.0 g, 7.35 mmol) in water (40 ml) was added dropwise to a solution of **8** (0.9 g, 2.94 mmol) in acetonitrile (50 ml), stirred at room temperature for 30 min, then diluted with water and extracted with chloroform. The usual work-up and chromatography gave 0.72 g (89%) of a sample of **9**. Recrystallization from ligroine gave orange crystals, mp 239—241 °C. IR (KBr) 1680 (aldehyde C=O), 1650, 1630 (each quinone C=O), 1585, 1205, 1055, and 1020 cm^{-1}; MS *m/z* 276 (M^+) and 261; ^1H NMR δ=3.88, 3.99, 4.02 (each s, 3H, OCH_3), 6.08 (s, 1H, quinonoid ring H), 7.71 (s, 1H, benzenoid ring H), and 10.50 (s, 1H, CHO). Found: C, 60.83; H, 4.45%. Calcd for $C_{14}H_{14}O_6$: C, 60.87; H, 4.38%.

6-Formyl-5,8-dihydroxy-2-methoxy-1,4-naphthoquinone (10). Anhydrous aluminum chloride (0.48 g, 3.6 mmol) was added to a solution of **9** (0.1 g, 0.36 mmol) in dichloromethane (30 ml), stirred at room temperature for 20 h, decomposed by an addition of 5% aqueous oxalic acid (100 ml), and extracted with chloroform. After the usual work-up, the crude product was chromatographed to give 30 mg (33%) of a sample of **10**, mp 243—244 °C (decomp). IR (KBr) 1690 (aldehyde C=O), 1615 (quinone C=O), 1590, 1560, 1430, 1195, and 1030 cm^{-1}; MS *m/z* 248 (M^+), 220, and 202; ^1H NMR δ=3.98 (s, 3H, OCH_3), 6.25 (s, 1H, quinonoid ring H), 7.75 (s, 1H, benzenoid ring H), 10.55 (s, 1H, CHO), 11.76, and 13.11 (each s, 1H, ArOH). Found: C, 57.70; H, 3.86%. Calcd for $C_{12}H_8O_8$: C, 58.07; H, 3.25%.

2-Hydroxymethyl-1,4,5,6,8-pentamethoxynaphthalene (11). A solution of **8** (0.26 g, 0.86 mmol) in tetrahydrofuran (15 ml) was treated with lithium aluminum hydride (65 mg, 1.7 mmol) under ice cooling, stirred at room temperature for 3 h, then decomposed by an addition of dil hydrochloric acid, and extracted with chloroform. The usual work-up and chromatography gave 0.21 g (78%) of a sample of **11**. Recrystallization from ligroine-benzene gave an analytical sample, mp 138—139 °C. IR (KBr) 3480 (sharp, OH), 1600, 1460, 1370, 1070, and 1050 cm^{-1}; MS *m/z* 308 (M^+), 293 (M^+-CH_3), 265, and 71; ^1H NMR δ=2.33 (s, 1H, OH), 3.77, 3.80, 3.93 (each s, 3H, OCH_3), 3.98 (s, 6H, OCH_3), 4.81 (s, 2H, CH_2), 6.74, and 6.86 (each s, 1H, ArH). Found: C, 62.57; H, 6.59%. Calcd for $C_{16}H_{20}O_6$: C, 62.32; H, 6.54%.

6-Hydroxymethyl-2,5,8-trimethoxy-1,4-naphthoquinone (12). Treatment of **11** (0.57 g, 1.85 mmol) in a mixture of acetonitrile (20 ml) and chloroform (2 ml) with CAN (2.54 g, 4.63 mmol) in water (8 ml) gave a crude product. Chromatography of the crude product gave 0.35 g (68 %) of a sample of **12**. Recrystallization from ethanol gave orange crystals, mp 216.5—217.5 °C. IR (KBr) 3490 (sharp, OH), 1645, 1620 (each C=O), 1585, 1205, 1065, and 1050 cm^{-1}; MS *m/z* 278 (M^+), 248, 234, and 217; ^1H NMR δ=2.21 (t, *J*=5.9 Hz, 1H, OH), 3.84 (s, 6H, OCH_3), 4.00 (s, 3H, OCH_3), 4.85 (d, *J*=5.9 Hz, 2H, CH_2), 6.01 (s, 1H, quinonoid ring H), and 7.43 (s, 1H, benzenoid ring H). Found: C, 60.31; H, 5.18%. Calcd for $C_{14}H_{14}O_6$: C, 60.43; H, 5.07%.

5,8-Dihydroxy-6-hydroxymethyl-2-methoxy-1,4-naphthoquinone (13) and 5-Hydroxy-6-hydroxymethyl-2,8-dimethoxy-1,4-naphthoquinone (14). The reaction of **12** (95 mg, 0.34 mmol) in dichloromethane (30 ml) with anhydrous aluminum chloride (0.46 g, 3.4 mmol) was carried out at room temperature for 2 h. Chromatography of the crude product gave two kinds of crystalline products. One was 37 mg (43%) of a sample of **13**. Recrystallization from ethanol gave reddish brown crystals, mp 218.5—219.5 °C. IR (KBr) 3540 (sharp, OH), 1615 (C=O), 1580, 1430, 1200, and 1080 cm^{-1}; MS *m/z* 250 (M^+), 232, and 221; ^1H NMR δ=2.20 (t, *J*=6.1 Hz, 1H, OH), 3.94 (s, 3H, OCH_3), 4.82 (d, *J*=6.1 Hz, 2H, CH_2), 6.17 (s, 1H, quinonoid ring H), 7.34 (s, 1H, benzenoid ring H), 12.24, and 13.07 (each s, 1H, ArOH). Found: C, 57.96; H, 4.45%. Calcd for $C_{12}H_{10}O_6$: C, 57.61; H, 4.03%.

The other was 34 mg (38%) of a sample of **14**. Recrystallization from ethanol gave reddish orange crystals, mp 222—224 °C. IR (KBr) 3570 (OH), 3470 (OH), 1630 (C=O), 1435, 1215, 1080, and 1050 cm^{-1}; MS *m/z* 264 (M^+), 246, and 203; ^1H NMR δ=2.31 (t, *J*=5.9 Hz, 1H, OH), 3.90, 4.00 (each s, 3H, OCH_3), 4.85 (d, *J*=5.9 Hz, 2H, CH_2), 6.05 (s, 1H, quinonoid ring H), 7.43 (s, 1H, benzenoid ring H), and 13.18 (s, 1H, ArOH). Found: C, 58.68; H, 4.61%. Calcd for $C_{13}H_{12}O_6$: C, 59.09; H, 4.58%.

References

1) Paper IV, on Synthesis of Naphthoquinone Derivatives. Part III, Y. Tanoue, A. Terada, and Y. Sugyō, *J. Org. Chem.*, **52**, 1437 (1987).

2) R. H. Thomson, "Naturally Occurring Quinones," 2nd ed, Academic Press London (1971), pp. 291 and 297.

3) C. Coronelli, H. Pagani, M. R. Bardone, and G. C. Lancini, *J. Antibiot.*, **27**, 161 (1974).

4) R. C. Pandey, M. W. Toussaint, R. M. Stroshane, C. C. Kalita, A. A. Aszalos, A. L. Garretson, T. T. Wei, K. M. Byrne, R. F. Geoghegan, Jr., and R. J. White, *J. Antibiot.*, **34**, 1389 (1981); R. Misra, R. C. Pandey, and J. V. Silverton, *J. Am. Chem. Soc.*, **104**, 4478 (1982).

5) A. V. Rama Rao, D. R. Reddy, and V. H. Deshpande, *J. Chem. Soc., Chem. Commun.*, **1984**, 1119; A. S. Kende, F. H. Ebetino, and T. Ohta, *Tetrahedron Lett.*, **26**, 3063 (1985); K. A. Parker, K. A. Koziski, and G. Breault, *ibid.*, **26**, 2181 (1985); M. Braun and R. Veith, *ibid.*, **27**, 179 (1986).

6) A. Terada, Y. Tanoue, A. Hatada, and H. Sakamoto, *J. Chem. Soc., Chem. Commun.*, **1983**, 987; *idem, Bull. Chem. Soc. Jpn.*, **60**, 205 (1987).

7) R. E. Moore and P. J. Scheuer, *J. Org. Chem.*, **31**, 3272 (1966).

8) For the compounds having formyl group, see: D. L. Comins, J. D. Brown, and N. B. Mantho, *Tetrahedron Lett.*, **23**, 3979 (1982); D. L. Comins and M. O. Killpack, *J. Org. Chem.*, **52**, 104 (1987). For hydroxymethyl group: N. S. Narashimuan and R. S. Mali, *Synthesis*, **1983**, 957.

 © 1987 The Chemical Society of Japan Bull. Chem. Soc. Jpn., 60, 2931—2935 (1987)

Synthesis and Spectroscopic Studies of 1,1′-(1,8-Naphthylene)-di-1*H*-1,2,3-triazoles[1)]

Yoshinobu NAGAWA,* Koichi HONDA, and Hiroshi NAKANISHI
National Chemical Laboratory for Industry, 1-1 Higashi, Yatabe, Tsukuba, Ibaraki 305
(Received March 16, 1987)

The first 1,8-diheteroaromatic naphthalenes, 1,1′-(1,8-naphthylene)di-1*H*-1,2,3-triazoles (**1**), were synthesized by 1,3-dipolar cycloadditions of 1,8-diazidonaphthalene to acetylenic esters. The spectral properties of these compounds were studied and compared with those of the corresponding 1-(1-naphthyl)-1*H*-1,2,3-triazoles (**2**). The two triazole rings at the peri-positions in **1** are in a face-to-face arrangement according to the results of ^{1}H NMR spectra. The UV spectra of **1** are almost identical with each other and show a red shift from those of corresponding **2**. No significant spectral differences between **1** and **2** were observed in the IR spectra. The fragment ion with two azirine groups at the peri-position in the naphthalene ring was observed in the MS spectra of **1**.

Naphthalenes with substituents in the 1 and 8 positions exhibit unique properties in both structure and reactivity, because the substituents exist in close proximity in these compounds.[2)] Recently, 1,8-diarylnaphthalenes have been synthesized and studied extensively in view of their geometry and inherent strain due to steric overcrowding.[3)] However, heteroaromatic analogues with heterocyclic rings in the peri-position have not yet been studied, presumably because of difficulties in synthesizing them.

Thus, we have attempted to synthesize the new 1,8-diheteroaromatic naphthalenes, 1,1′-(1,8-naphthylene)-di-1*H*-1,2,3-triazoles (**1a—k**), by the 1,3-dipolar cycloaddition of 1,8-diazidonaphthalene to several acetylenic esters. This paper deals with their syntheses and spectral properties comparing with corresponding 1-(1-naphthyl)-1*H*-1,2,3-triazoles (**2a—h**).

Results and Discussion

The thermal 1,3-dipolar cycloaddition of azides to alkynes is a well-known route to 1*H*-1,2,3-triazoles, and the reaction of various azides have been investigated.[4)]

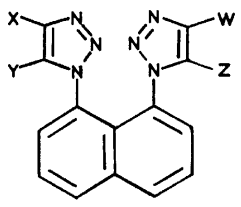

1a: W=X=Y=Z=CO_2Me
1b: W=X=Y=Z=CO_2Et
1c: W=X=Y=Z=CO_2Pr^i
1d: W=X=Y=Z=CO_2Bu^t
1e: W=X=CO_2Et, Y=Z=H
1f; W=X=H, Y=Z=CO_2Et
1g: W=Y=CO_2Et, X=Z=H
1h: W=X=Z=CO_2Et, Y=H
1i: W=Y=Z=CO_2Et, X=H
1j: W=X=COOH, Y=Z=H
1k: W=X=Y=Z=H

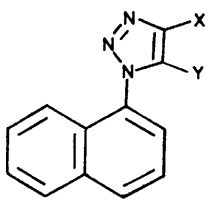

2a: X=Y=CO_2Me
2b: X=Y=CO_2Et
2c: X=Y=CO_2Pr^i
2d: X=Y=CO_2Bu^t
2e: X=CO_2Et, Y=H
2f: X=H, Y=CO_2Et
2g: X=COOH, Y=H
2h: X=Y=H

However, the reactions of 1,8-diazidonaphthalene, as well as 1-azidonaphthalene, have not yet been reported. The reactions of 1,8-diazidonaphthalene with a large excess of acetylenedicarboxylates, RO_2C-C≡CCO_2R (R=Me, Et, Pr^i, and Bu^t), afforded **1a—d** via the formation of dialkyl 1-(8-azido-1-naphthyl)-1*H*-1,2,3-triazole-4,5-dicarboxylate. In order to avoid the decomposition of 1,8-diazidonaphthalene, the reactions were carried out in the dark and at room temperature. The reaction with an unsymmetrical acetylene, ethyl propiolate, gave three isomeric triazoles, **1e—g**. The identification of **1e** and **1f** as shown in the figure was made by comparing the ^{1}H NMR chemical shifts of triazole ring protons in **1e** and **1f** with those in previously reported 1-phenyl-4-methyl-1*H*-1,2,3-triazole and 1-phenyl-5-methyl-1*H*-1,2,3-triazole.[5)] The main product was **1e**, and the most sterically hindered isomer, **1f**, formed very little (**1e**:**1f**:**1g**=26:1:12). The 1:1 addition products of the above reaction, **3a** and **3b**, were employed to synthesize the unsymmetrical triazoles, **1h** and **1i**.

In order to prepare the parent compound, **1k**, following reactions were attempted. Hydrolysis of **1e** in alkaline solution led to carboxylic acid, **1j**. Heating crystals of **1j** up to 180 °C under a nitrogen atmosphere afforded **1k** almost quantitatively. In the similar manner, 1-naphthyltriazoles, **2a—h**, were synthesized from 1-azidonaphthalene.

Spectral properties of **1a—k** and **2a—h** are listed in Tables 1 and 2, respectively. In the ^{1}H NMR spectra of **1k**, the H-4 and H-5 protons appeared at higher field

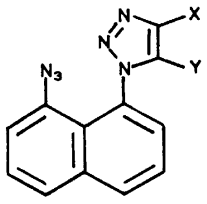

3a: X=CO_2Et, Y=H
3b: X=H, Y=CO_2Et

Table 1. Spectroscopic Data of 1,1′-(1,8-Naphthylene)di-1*H*-1,2,3-triazoles

Product	^{1}H NMR ($CDCl_3$)[a]	IR(KBr)	UV(CH_3OH)	MS
	δ/ppm	ν/cm^{-1}	λ/nm (log ε)	m/z (rel intensity, %)
1a	3.81 (s, 6H, 5-CH_3), 4.01 (s, 6H, 4-CH_3), 7.49 (d, J=7.4Hz, 2H, H-2′), 7.72 (dd, J=8.4, 7.4Hz, 2H, H-3′), 8.27 (d, J=8.4Hz, 2H, H-4′)	1740, 1290, 1245, 1050, 830, 760	288(4.02), 220(4.89)	494(M^+, 67), 379(74), 351(52), 166(52), 152(90), 15(100)
1b	1.09 (t, J=7.2Hz, 6H, 5-CH_3), 1.45 (t, J=7.2Hz, 6H, 4-CH_3), 4.19 (q, J=7.2Hz, 4H, 5-CH_2), 4.45 (q, J=7.2Hz, 4H, 4-CH_2), 7.45 (d, J=7.3Hz, 2H, H-2′), 7.71 (dd, J=8.2, 7.3Hz, 2H, H-3′) 8.25 (d, J=8.2Hz, 2H, H-4′)	1735, 1730, 1285, 1205, 1055, 830	289(4.05), 221(4.94)	550(M^+, 25), 421(10) 274(16), 166(40) 152(48), 29(100)
1c	0.94 (d, J=6.3Hz, 3H, 5-CH_3), 1.01 (d, J=6.3Hz, 3H, 5-CH_3), 1.43 (d, J=6.3Hz, 3H, 4-CH_3), 1.44 (d, J=6.3Hz, 3H, 4-CH_3), 4.96 (m, 2H, 5-CH), 5.30 (m, 2H, 4-CH), 7.43 (d, J=7.3Hz, 2H, H-2′), 7.70 (dd, J=8.4, 7.3Hz, 2H, H-3′), 8.25 (d, J=8.4Hz, 2H, H-4′)	1750, 1735, 1725, 1715, 1290, 1200, 1050, 835	289(3.99), 221(4.87)	606(M^+, 7), 303(12), 276(14), 232(10), 152(15), 43(100)
1d	1.12 (s, 18H, 5-CH_3), 1.63 (s, 18H, 4-CH_3), 7.40 (d, J=7.3Hz, 2H, H-2′), 7.69 (dd, J=8.5, 7.3Hz, 2H, H-3′), 8.23 (d, J=8.5Hz, 2H, H-4′)	1730, 1300, 1245, 1160, 1060, 835	288(3.99), 222(4.88)	662(M^+, 5), 421(18), 366(23), 205(16), 56(48), 41(100)
1e	1.40 (t, J=7.2Hz, 6H, 4-CH_3), 4.38 (q, J=7.2Hz, 4H, 4-CH_2), 7.60 (d, J=7.3Hz, 2H, H-2′), 7.76 (dd, J=8.5, 7.3Hz, 2H, H-3′), 8.07 (s, 2H, H-5), 8.28 (d, J=8.5Hz, 2H, H-4′)	1715, 1270, 1220, 1040, 830	289(4.07) 223(4.91)	406(M^+, 38), 304(59) 277(32), 249(77), 205(100), 29(87)
1f	1.07 (t, J=7.2Hz, 6H, 5-CH_3), 4.15 (q, J=7.2Hz, 4H, 5-CH_2), 7.41 (d, J=7.3Hz, 2H, H-2′), 7.70 (dd, J=8.3, 7.3Hz, H-3′), 7.90 (s, 2H, H-4), 8.24 (d, J=8.3Hz, 2H, H-4′)	1735, 1310, 1285, 1200, 1075, 830	288(3.98), 222(4.91)	406(M^+, 100), 277(20), 249(60), 205(57), 152(32), 29(60)
1g	1.14 (t, J=7.2Hz, 3H, 5″-CH_3), 1.42 (t, J=7.2Hz, 3H, 4-CH_3), 4.17 (q, J=7.2Hz, 2H, 5″-CH_2), 4.42 (q, J=7.2Hz, 2H, 4-CH_2), 7.47—7.50 (m, 2H, H-2′,7″), 7.70—7.73 (m, 2H, H-3′,6′), 7.86 (s, 1H, H-5), 7.88 (s, 1H, H-4″), 8.25 (d, J=8.3Hz, 2H, H-4′,5′)	1740, 1730, 1720, 1250, 1205, 1080, 1030, 830	288(4.02), 223(4.90)	406(M^+, 78), 277(44), 249(100), 205(94) 152(47), 29(92)
1h	1.14 (t, J=7.2Hz, 3H, 5-CH_3), 1.42 (t, J=7.2Hz, 3H, 4″-CH_3), 1.44 (t, J=7.2Hz, 3H, 4-CH_3), 4.22 (q, J=7.2Hz, 2H, 5-CH_2), 4.39—4.46 (m, 4H, 4,4″-CH_2), 7.50—7.54 (m, 2H, H-2′,7′), 7.70—7.75 (m, 2H, H-3′,6′), 8.01 (s, 1H, H-5″), 8.24—8.28 (m, 2H, H-4′,5′)	1740, 1730, 1260, 1205, 1035, 835	288(4.02), 221(4.85)	478(M^+, 63), 349(20), 249(43), 205(38), 152(49), 29(100)
1i	1.02 (t, J=7.2Hz, 3H, 5″-CH_3), 1.12 (t, J=7.2Hz, 3H, 5-CH_3), 1.45 (t, J=7.2Hz, 3H, 4-CH_3), 4.13—4.20 (m, 4H, 5,5″-CH_2), 4.44—4.51 (m, 2H, 4-CH_2), 7.41—7.43 (m, 2H, H-2′,7″), 7.68—7.73 (m, 2H, H-3′,6′), 7.95 (s, 1H, H-4″), 8.23—8.27 (m, 2H, H-4′,5′)	1735, 1290, 1210, 1065, 835	288(3.95), 222(4.86)	478(M^+, 88), 349(27), 249(43), 205(38), 152(58), 29(100)
1j	7.77 (d, J=7.3Hz, 2H, H-2′), 7.87 (dd, J=8.3, 7.3Hz, 2H, H-3′), 8.48 (d J=8.3Hz, 2H, H-4′), 8.68 (s, 2H, H-5), 13.03 (s, 2H, COOH)	2985, 1745, 1730, 1185, 1060, 835	290(3.93), 225(4.75)	262(34), 206(85), 205(100), 166(18), 139(19),44(880)
1k	7.41 (d, J=1.0Hz, 2H, H-5), 7.47 (d, J=1.0Hz, 2H,H-4), 7.55 (d,J=7.3Hz, 2H, H-2′), 7.72 (dd, J=8.4, 7.3Hz, 2H, H-3′), 8.22 (d, J=8.4Hz, 2H, H-4′)	3140, 3120, 1460, 1215, 1025, 830	288(4.01), 224(4.91)	262(M^+, 68), 206(37) 205(100), 166(18), 140(19), 139(20)

a) Since **1j** was insoluble in $CDCl_3$, the ^{1}H NMR spectrum of **1j** was measured in DMSO-d_6.

by ca. 0.5 ppm than the corresponding protons in **2h**. Similar high field shifts of H-5 and H-4 were observed between **1e** and **2e** and between **1f** and **2f**, respectively. These high field shifts of each proton at the triazole ring can be explained by the considerable anisotropic effects of the other triazole ring. This suggests that the two triazole rings in **1** are facing to each other. On the other hand, according to the crystal structure of **1k**, which is determined by an X-ray diffraction study, the two triazole rings take a face-to-face arrangement and a trans conformation to each other.[6] Thus, the results obtained by NMR analyses about the conformation of these triazole rings are in well accordance with that by X-ray analyses. The extent of the high field shifts for these compounds are comparable to that for the facing benzene rings in 1,8-diphenylnaphthalene ($\Delta\delta$=0.53).[3]

Two kinds of ^{1}H NMR signal for methyl groups, which were assigned to 4- and 5- ester groups in the triazole ring, were observed in **1a**, **1b**, and **1d**. However, **1c** gave four kinds of methyl group resonance, each splitted by methine proton. This phenomenon shows that the two methyl moiety of the isopropyl group are not equivalent magnetically. Such nonequivalency is, as well as in the case of 1-phenyl-8-[3-(1-hydroxy-1-methylethyl)phenyl]naphthalene,[7] well explained by asymmetric environment of the molecule. Only two kinds of the methyl signals were observed in the isopropyl groups of **2c** at room temperature. These results indicate that the rotation around the pivot bond between triazole ring and naphthalene ring is restricted in **1c**. Probably, the two triazole rings hinder the rotation each other. On the

Table 2. Spectroscopic Data of 1-(1-Naphthylene)-1*H*-1,2,3-triazoles

Product	^{1}H NMR ($CDCl_3$)[a]	IR(KBr)	UV(CH_3OH)	MS
	δ/ppm	ν/cm^{-1}	λ/nm (log ε)	m/z (rel intensity, %)
2a	3.69 (s, 3H, 5-CH_3), 4.04 (s, 3H, 4-CH_3), 7.27 (d, J=8.4Hz, 1H, H-8′), 7.51—7.62 (m, 4H, arom.), 7.97 (d,J=8.2Hz, 1H, H-5′), 8.08 (d, J=8.2Hz, 1H, H-4′)	1735, 1300, 1215, 1075, 810	281(4.03), 220(4.86)	311(M^+, 58), 283(8), 251(37), 196(33), 193(58), 127(100)
2b	0.90 (t, J=7.2Hz, 3H, 5-CH_3), 1.46 (t, J=7.2Hz, 3H, 4-CH_3), 4.11 (q, J=7.2Hz, 2H, 5-CH_2), 4.52 (q, J=7.2Hz, 2H, 4-CH_2), 7.28 (d, J=8.4Hz, 1H, H-8′), 7.51—7.63 (m, 4H, arom.), 7.97 (d, J=8.2Hz, 1H, H-5′), 8.08 (d, J=8.1Hz, 1H, H-4′)	1740, 1730, 1200, 1070, 800, 770	282(3.96), 220(4.88)	339(M^+, 54), 265(45), 193(100), 169(61), 127(92), 29(85)
2c	0.85 (d, J=6.3Hz, 6H, 5-CH_3), 1.44 (d, J=6.3Hz, 6H, 4-CH_3), 4.91 (m, 1H, 5-CH), 5.39 (m, 1H, 4-CH), 7.29 (d, J=8.4Hz, 1H, H-8′), 7.50—7.60 (m, 4H, arom.), 7.95 (d J=8.2Hz, 1H, H-5′), 8.06 (d, J=8.1Hz, 1H, H-4′)	1740, 1715, 1260, 1235, 1100, 1065, 810	282(3.92), 220(4.91)	367(M^+, 39), 308(7), 211(37), 193(67), 127(42), 43(100)
2d	0.97 (s, 9H, 5-CH_3), 1.65 (s, 9H, 4-CH_3), 7.28 (d, J=8.4Hz, 1H, H-8′), 7.51—7.62 (m, 4H, arom.), 7.96 (d, J=8.2Hz, 1H, H-5′), 8.08 (d, J=8.1Hz, 1H, H-4′)	1745, 1715, 1260, 1120, 1070, 840	282(4.17), 220(5.10)	395(M^+, 12), 266(12), 211(60), 193(31), 127(20), 57(100)
2e	1.47 (t, J=7.2Hz, 3H, 4-CH_3), 4.51 (q, J=7.2Hz, 2H, 4-CH_2), 7.55—7.63 (m, 5H, arom.), 7.99 (d, J=8.2Hz, 1H, H-5′), 8.07 (m, 1H, H-4′), 8.47 (s, 1H, H-5)	1745, 1240, 1205, 1150, 1040, 810	282(3.98), 220(4.91)	267(M^+, 46), 194(42), 193(35), 167(97), 166(98), 127(100)
2f	0.99 (t, J=7.2Hz, 3H, 5-CH_3), 4.09 (q, J=7.2Hz, 2H, 5-CH_2), 7.11 (d, J=8.4Hz, 1H, H-8′), 7.45—7.61 (m, 4H, arom.), 7.95(d, J=8.1Hz, 1H, H-5′), 8.05 (d, J=8.2Hz, 1H, H-4′), 8.41 (s, 1H, H-4)	1730, 1200 1110, 810	281(4.00), 221(5.03)	267(M^+, 93), 194(42), 193(38), 167(87), 166(100), 127(76)
2g	7.46 (d, J=8.3Hz, 1H, H-8′), 7.63—7.82 (m, 4H, arom.), 8.15 (d, J=8.1Hz, 1H, H-5′), 8.24 (d, J=8.3Hz, 1H, H-4′), 9.25 (s, 1H, H-5), 13.24 (s, 1H, COOH)	2910, 1740, 1720, 1185, 1060, 805	282(3.90), 221(4.82)	239(M^+, 6), 195(13), 167(100), 166(42), 140(18), 127(58)
2h	7.92 (d, J=1.0Hz, 1H, H-5), 7.93 (d, J=1.0Hz, 1H, H-4), 7.47—7.57 (m, 5H, arom.), 7.86—7.95 (m, 2H, H-4′,5′),	3150, 1465, 1235, 1020, 800, 770	281(3.95), 221(4.92)	195(M^+, 55), 167(100), 166(58), 140(22), 139(18), 127(83)

a) Since **2g** was insoluble in $CDCl_3$, the ^{1}H NMR spectrum of **2g** was measured in DMSO-d_6.

other hand, the racemization may occur in **2c** because the rotation around the bond is so fast.

The ^{1}H NMR signals for the methyl moiety in the ester group of 5-position at the triazole ring are at higher field than those of 4-position in **1a—i**. As the similar relationships were observed in **2a—f**, it may be explained by the anisotropic effect of the naphthalene ring.

The UV spectra of **1** are almost identical with each other (ca. 221 and 288 nm) and independent of the substituents on the triazole ring, and show a red shift from those of **2**. The extent of the red shift is about 7 nm for the longest wavelength absorption band. Since the absorption band due to the triazole ring exists at ca. 210 nm,[8] the longest wavelength band is assigned to naphthalene ring. The same kind of red shift has been observed between the absorption of 1,8-diphenylnaphthalene and 1-phenylnaphthalene.[9]

In IR spectra, absorptions of C=O (ca. 1700—1750 cm^{-1}) and C-O-C (ca. 1200—1300 cm^{-1}) groups were observed in addition to those of the triazole (ca. 1000—1100 cm^{-1}) and naphthalene rings (ca. 750—850 cm^{-1}) in **1a—j** and **2a—g**. Both **1k** and **2h** show C-H stretching in triazole ring at ca. 3100—3150 cm^{-1}. No significant spectral differences between **1** and **2** were observed in the IR spectra.

In the MS spectra of **1**, molecular ions were observed except for the carboxylic acid, **1j**. The MS spectrum data show that the molecular ion peaks become weaker with the size of the ester groups at the triazole ring become bulkier, as seen in usual carboxyric acid and esters. The fragment ion (m/z=167) of the azirine type, which was generated by the nitrogen elimination from molecular ion, was found in the parent molecules, **2h**. Such fragmentation was reported in the MS spectra of 1-phenyl-1*H*-1,2,3-triazoles.[10] Moreover, the fragment ion (m/z=206) with two azirine groups at peri-position in the naphthalene ring **4** was found in **1k**. The m/z 166 ion, which was produce by the further elimination of one azirine ring from **4**, was also observed in **1k**.

Experimental

Instruments. All melting points were determined on a Mettler FP61 instrument and were uncorrected. ^{1}H NMR spectra were obtained by a JEOL GX-400 spectrometer (399.65 MHz for ^{1}H nuclei) using TMS as an internal standard. IR and UV spectra were measured on a Nicolet 170SX

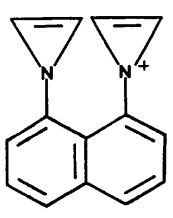

4

and a Shimadzu MPS-2000 spectrometer, respectively. MS spectra were measured with a JEOL JMS-01SG-2 spectrometer at 75 eV of ionization energy. Elemental analyses were performed on a Yanaco MT-3 CHN micro analyzer.

Materials. 1,8-Diazidonaphthalene and 1-azidonaphthalene were prepared from 1,8-diaminonaphthalene and 1-aminonaphthalene as previously reported, respectively.[11,12] Diisopropyl acetylenedicarboxylate was prepared from acetylenedicarboxyric acid and isopropyl alcohol,[13] and di-*t*-butyl acetylenedicarboxylate was synthesized from acetylenedicarboxylic acid and 1-butene according to the synthetic method of di-*t*-butyl malate.[14] Dimethyl acetylenedicarboxylate, diethyl acetylenedicarboxylate, and ethyl propiolate were commercially available.

Reaction of 1,8-Diazidonaphthalene with Acetylene Carboxylates. To a solution of 1,8-diazidonaphthalene (1.0 g, 4.8 mmol) in diethyl ether (10 ml), a large excess of dimethyl acetylenedicarboxylate (5.0 g, 35.2 mmol) was added and the mixture was allowed to react at room temperature in the dark. It took 14 d until the products with two triazole rings were formed. After the completion of the reaction was checked by TLC (silica gel, diethyl ether), the mixture was purified by chromatographic separation on silica gel (Waco gel C-100) with a diethyl ether–dichloromethane mixture to give **1a**.

Tetramethyl 1,1′-(1,8-naphthylene)di-1*H*-1,2,3-triazole-4,5-dicarboxylate(**1a**): Colorless prisms from methanol; mp 222—223 °C, 2.1 g (89%). Found: C, 53.72; H, 3.66; N, 16.86%. Calcd for $C_{22}H_{18}N_6O_8$: C, 53.44; H, 3.67; N, 17.00%.

Similarly, the reactions of 1,8-diazidonaphthalene (1.0 g, 4.8 mmol) with about 8 times as much excess of diethyl, diisopropyl, and di-*t*-butyl acetylenedicarboxylates gave **1b**, **1c**, and **1d**, respectively.

Tetraethyl 1,1′-(1,8-naphthylene)di-1*H*-1,2,3-triazole-4,5-dicarboxylate (**1b**): Colorless prisms from methanol; mp 138—139 °C, 2.2 g (85%). Found: C, 56.81; H, 4.63; N, 15.14%. Calcd for $C_{26}H_{26}N_6O_8$: C, 56.72; H, 4.76; N, 15.27%.

Tetraisopropyl 1,1′-(1,8-naphthylene)di-1*H*-1,2,3-triazole-4,5-dicarboxylate (**1c**): Colorless needles from methanol; mp 107—108 °C, 2.5 g (86%). Found: C, 59.30; H, 5.50; N, 13.71%. Calcd for $C_{30}H_{34}N_6O_8$: C, 59.40; H, 5.65; N, 13.85%.

Tetra-*t*-butyl 1,1′-(1,8-naphthylene)di-1*H*-1,2,3-triazole-4,5-dicarboxylate(**1d**): Colorless needles from methanol; mp 160—161 °C, 2.5 g (80%). Found: C, 61.83; H, 6.62; N, 12.50%. Calcd for $C_{34}H_{42}N_6O_8$: C, 61.62; H, 6.39; N, 12.68%.

In the similar reaction of the 1,8-diazidonaphthalene (1.0 g, 4.8 mmol) with ethyl propiolate (3.5 g, 35.7 mmol) for 14 d, the following three possible products were all isolated by chromatography on silica gel with a diethyl ether–dichloromethane mixture.

Diethyl 1,1′-(1,8-naphthylene)di-1*H*-1,2,3-triazole-4-carboxylate (**1e**): Colorless needles from methanol; mp 173—174 °C, 1.0 g (52%). Found: C, 58.88; H, 4.22; N, 20.59%. Calcd for $C_{20}H_{18}N_6O_4$: C, 59.11; H, 4.46; N, 20.68%.

Diethyl 1,1′-(1,8-naphthylene)di-1*H*-1,2,3-triazole-5-carboxylate (**1f**): Colorless needles from methanol; mp 175—176 °C, 35 mg (2%). Found: C, 58.80; H, 4.46; N, 20.47%. Calcd for $C_{20}H_{18}N_6O_4$: C, 59.11; H, 4.46; N, 20.68%.

Ethyl 1-[8-(5-ethoxycarbonyl-1*H*-1,2,3-triazol-1-yl)-1-naphthyl]-1*H*-1,2,3-triazole-4-carboxylate (**1g**): Colorless needles from methanol; mp 128—129 °C, 460 mg (24%). Found: C, 59.36; H, 4.26; N, 20.57%. Calcd for $C_{20}H_{18}N_{60}O_4$: C, 59.11; H, 4.46; N, 20.47%.

Identical reaction for 24 h gave the intermediate 1 : 1 adducts, **3a** and **3b**, in the maximum yields, and they were isolated by chromatography on silica gel with a hexane–diethyl ether mixture.

Ethyl 1-(8-azido-1-naphthyl)-1*H*-1,2,3-triazole-4-carboxylate (**3a**): Pale yellow needles from methanol; mp 135—136 °C, 700 mg (48%). ^{1}H NMR ($CDCl_3$) δ=1.48 (t, J=7.2 Hz, 3H, CH_3), 4.51 (q, J=7.2 Hz, 2H, CH_2), 7.31 (d, J=7.5 Hz, 1H, H-7′), 7.47 (d, J=7.3 Hz, 1H, H-2′), 7.58 (dd, J=8.1, 7.5 Hz, 1H, H-6′), 7.60 (dd, J=8.3, 7.3 Hz, 1H, H-3′), 7.77 (d, J=8.1 Hz, 1H, H-5′), 8.06 (d, J=8.3 Hz, 1H, H-4′), 8.34 (s, 1H, H-5). IR (KBr) 2130 (N_3), 1730 (C=O) cm^{-1}. MS m/z (rel intensity, %) 308 (10), 280 (9), 208 (96), 180 (35), 126 (100). Found: C, 58.34; H, 3.88; N, 27.03%. Calcd for $C_{15}H_{12}N_6O_2$: C, 58.44; H, 3.92; N, 27.26%.

Ethyl 1-(8-azido-1-naphthyl)-1*H*-1,2,3-triazole-5-carboxylate (**3b**): Pale yellow needles from methanol; mp 109—110 °C, 250 mg (17%). ^{1}H NMR ($CDCl_3$) δ=1.07 (t, J=7.2 Hz, 3H, CH_3), 4.14 (m, 2H, CH_2), 7.27 (d, J=7.4 Hz, 1H, H-7′), 7.42 (d, J=7.3 Hz, 1H, H-2′), 7.55 (dd, J=8.2, 7.4 Hz, 1H, H-6′), 7.60 (dd, J=8.3, 7.3 Hz, 1H, H-3′), 7.77 (d, J=8.2 Hz, 1H, H-5′), 8.05 (d, J=8.3 Hz, 1H, H-4′), 8.34 (s, 1H, H-4). IR (KBr) 2125 (N_3), 1730 (C=O) cm^{-1}. MS m/z (rel intensity, %) 308 (28), 280 (37), 208 (10), 180 (100), 126 (96). Found: C, 58.27; H, 3.86; N, 27.15%. Calcd for $C_{15}H_{12}N_6O_2$: C, 58.44; H, 3.92; N, 27.26%.

The reaction of **3a** (200 mg, 0.65 mmol) and **3b** (200 mg, 0.65 mmol) with 5 times as much excess of diethyl acetylenedicarboxylate for 14 d at room temperature gave **1h** and **1i**, respectively.

Diethyl 1-[8-(4-ethoxycarbonyl-1*H*-1,2,3-triazol-1-yl)-1-naphthyl]-1*H*-1,2,3-triazole-4,5-dicarboxylate(**1h**): Colorless needles from methanol; mp 130—131 °C, 210 mg (68%). Found: C, 57.74; H, 4.66; N, 17.49%. Calcd for $C_{23}H_{22}N_6O_6$: C, 57.74; H, 4.63; N, 17.56%.

Diethyl 1-[8-(5-ethoxycarbonyl-1*H*-1,2,3-triazol-1-yl)-1-naphthyl]-1*H*-1,2,3-triazole-4,5-dicarboxylate(**1i**): Colorless needles from methanol; mp 170—171 °C, 190 mg (61%). Found: C, 57.58; H, 4.45; N, 17.52%. Calcd for $C_{23}H_{22}N_6O_6$: C, 57.74; H, 4.63; N, 17.56%.

Hydrolysis of 1e. A suspension of **1e** (500 mg, 1.2 mmol) in aqueous NaOH (1.0 g, 25 mmol, 40 ml) was refluxed for 12 h. On adjusting the solution to pH 5 with aqueous HCl, a precipitate was formed immediately. The precipitate was collected by filtration and recrystallized from water to give **1j** as colorless needles.

1,1′-(1,8-Naphthylene)di-1*H*-1,2,3-triazole-4-carboxylic acid (**1j**): mp 253—254 °C, 350 mg (81%). Found: C, 54.99; H, 2.94; N, 24.02%. Calcd for $C_{16}H_{10}N_6O_4$: C, 54.86; H, 2.88; N, 23.99%.

Decarboxylation of 1j. The crystals of **1j** (320 mg, 0.91 mmol) were decarboxylated by heating at 180 °C for 3 h under a nitrogen atmosphere. Sublimation of the crude product gave pure **1k** as colorless needles.

1,1′-(1,8-Naphthylene)di-1*H*-1,2,3-triazole(**1k**): mp>300 °C, 235 mg (92%). Found: C, 63.98; H, 3.78; N, 32.05%. Calcd for $C_{14}H_{10}N_6$: C, 64.11; H, 3.84; N, 32.04%.

Preparation of 1-(1-Naphthyl)-1*H*-1,2,3-triazoles. By the reaction of 1-azidonaphthalene (1 g, 5.92 mmol) with 5 times as much excess of acetylenecarboxylates at room temperature for 72 h, **2a—f** were synthesized and purified by silica-gel chromatography with hexane–diethyl ether.

Dimethyl 1-(1-naphthyl)-1*H*-1,2,3-triazole-4,5-dicarboxylate

(**2a**): Colorless needles from hexane-diethyl ether, mp 122—123 °C, 1.5 g (81%). Found: C, 61.54; H, 4.21; N, 13.39%. Calcd for $C_{16}H_{13}N_3O_4$: C, 61.73; H, 4.21; N, 13.50%.

Diethyl 1-(1-naphthyl)-1*H*-1,2,3-triazole-4,5-dicarboxylate (**2b**): Oil, 1.5 g (75%). Found: C, 63.56; H, 5.16; N, 12.52%. Calcd for $C_{18}H_{17}N_3O_4$: C, 63.71; H, 5.05; N, 12.38%.

Diisopropyl 1-(1-naphthyl)-1*H*-1,2,3-triazole-4,5-dicarboxylate (**2c**): Colorless prisms from hexane-diethyl ether, mp 105—106 °C, 1.9 g (87%). Found: C, 65.22; H, 5.73; N, 11.37%. Calcd for $C_{20}H_{21}N_3O_4$: C, 65.38; H, 5.76; N, 11.44%.

Di-*t*-butyl 1-(1-naphthyl)-1*H*-1,2,3-triazole-4,5-dicarboxylate (**2d**): Colorless prisms from hexane-diethyl ether, mp 142—143 °C, 1.9 g (81%). Found: C, 66.75; H, 6.25; N, 10.48%. Calcd for $C_{22}H_{25}N_3O_4$: C, 66.82; H, 6.37; N, 10.63%.

Ethyl 1-(1-naphthyl)-1*H*-1,2,3-triazole-4-carboxylate (**2e**): Colorless needles from hexane-diethyl ether, mp 101—102 °C, 1.1 g (71%). Found: C, 67.31; H, 4.83; N, 15.64%. Calcd for $C_{15}H_{13}N_3O_2$: C, 67.41; H, 4.90; N, 15.72%.

Ethyl 1-(1-naphthyl)-1*H*-1,2,3-triazole-5-carboxylate (**2f**): Colorless needles from hexane-diethyl ether, mp 102—103 °C, 280 mg (18%). Found: C, 67.50; H, 4.72; N, 15.77%. Calcd for $C_{15}H_{13}N_3O_2$: C, 67.41; H, 4.90; N, 15.72%.

Hydrolysis of **2e** (1 g, 3.7 mmol) as in the case of **1e** gave **2g**.

1-(1-Naphthyl)-1*H*-1,2,3-triazole-4-carboxylic acid (**2g**): Colorless needles from water, mp 147—148 °C, 0.8 g (89%). Found: C, 65.23; H, 3.76; N, 17.56%. Calcd for $C_{13}H_9N_3O_2$: C, 65.27; H, 3.79; N, 17.56%.

Decarboxylation of **2g** (0.5 g, 2.1 mmol) was performed in a similar manner to that of **1j**, and pure **2h** was obtained by sublimation as colorless needles.

1-(1-Naphthyl)-1*H*-1,2,3-triazole (**2h**): mp 102—103 °C, 380 mg (93%). Found: C, 73.77; H, 4.51; N, 21.60%. Calcd for $C_{12}H_9N_3$: C, 73.83; H, 4.65; N, 21.52%.

We wish to thank Dr. Nobuhide Wasada, Dr. Sadao Tamura, and Dr. Akira Nomura, in our Laboratory, for their helpful discussions.

References

1) Preliminary communication; K. Honda, H. Nakanishi, Y. Nagawa, and A. Yabe, *J. Chem. Soc., Chem. Commun.*, **1984**, 450.

2) V. Balasubramaniyan, *Chem Rev.*, **1966**, 567.

3) E. Ibuki, S. Ozasa, Y. Fujioka, and H. Mizutani, *Bull. Chem. Soc. Jpn.*, **55**, 845 (1982).

4) H. Wamhoff, "1,2,3-Triazoles and their Benzo Derivatives," in "Comprehensive Heterocyclic Chemistry," ed by A. R. Katritzky and C. W. Rees, Pergamon Press, Oxford (1984), Vol. 5, Part 4a, p. 708.

5) C. E. Olsen, *Acta Chem. Scand.*, **27**, 2983 (1973).

6) Y. Nagawa, M. Goto, K. Honda, and H. Nakanishi, *Acta Crystallogr., Sect. C*, **42**, 478 (1986).

7) H. O. House, W. J. Campbell, and M. Gall, *J. Org. Chem.*, **35**, 1815 (1970).

8) L. W. Hartzel and F. R. Benson, *J. Am. Chem. Soc.*, **76**, 667 (1954).

9) H. O. House, R. W. Magin, and H. W. Thompson, *J. Org. Chem.*, **28**, 2403 (1963).

10) F. Compernolle and M. Dekeirel, *Org. Mass Spectrom.*, **5**, 427 (1971).

11) R. W. Hoffmann, G. Guhn, M. Preiss, and B. Dittrich, *J. Chem. Soc. C*, **1969**, 769.

12) M. O. Forster and H. E. Fierz, *J. Chem. Soc.*, **91**, 1942 (1907).

13) G. H. Jeffery and A. I. Vogel, *J. Chem. Soc.*, **1948**, 674.

14) A. L. McCloskey, G. S. Fonken, R. W. Kluiber, and W. S. Johnson, *Org. Synth.*, Coll. Vol. 4, 261 (1963).

 © 1987 The Chemical Society of Japan Bull. Chem. Soc. Jpn., 60, 2937—2943 (1987)

Mechanistic Approach to the Sensitization Process of Aromatic Ketones in the Isomerization between Norbornadiene and Quadricyclane

Tatsuo Arai,* Takahisa Oguchi, Toshio Wakabayashi, Masahiro Tsuchiya, Yoshinobu Nishimura, Shigero Oishi,†,§ Hirochika Sakuragi, and Katsumi Tokumaru*
Department of Chemistry, University of Tsukuba, Sakura-mura, Ibaraki 305
†Sagami Chemical Research Center, Sagamihara, Kanagawa 229
(Received March 19, 1987)

The quantum yields for norbornadiene(N) → quadricyclane(Q) and Q → N isomerization were determined in acetonitrile using several substituted benzophenones (BPs) as triplet sensitizers. For the N → Q isomerization, BPs with electron-donating substituents exhibited higher quantum efficiency (0.4—0.6) than BPs with electron-accepting substituents. The quantum yields for Q → N isomerization increased with electron-accepting ability of the substituents on BPs, but were lower than 0.1. The rate constants for quenching of triplet BPs by N and Q were also determined in acetonitrile by means of laser flash photolysis. The rate constants for N were not dependent on the triplet energies (E_T) of BPs but dependent on electronic properties of the substituents on BPs. On the contrary, those for Q increased with decreasing E_T of BPs and with increasing Hammett's σ constants of the substituents of BPs. Based on these observations an addition-elimination process is proposed for the N → Q isomerization, and an electron transfer process for the Q → N isomerization.

Recently much attention has been paid to isomerization of norbornadiene (N) to quadricyclane (Q) under solar light irradiation to accomplish molecular storage of energy.[1-3] One of the problems of this system is that N absorbs only light in the UV region. In order to utilize solar irradiation efficiently, two ways of approach have been attempted. The first one using N itself, which is readily supplied as a petrochemical product, employs either sensitizers or reagents capable of forming a complex with N to absorb longer-wavelength light than does N.[1-4] The second is to use substituted norbornadienes exhibiting absorption at much longer wavelengths than N.[5-7]

As for the first approach, benzophenones (BPs) and some other aromatic ketones are known to sensitize N → Q isomerization with light longer than 300 or 350 nm.[8] However, there remain some questions regarding the sensitization mechanism. It is still unclear whether the isomerization of N and Q proceeds through energy transfer from sensitizer or not.

Another problem of this system is consumption of the sensitizer ketones during irradiation due to the formation of addition products. It is desirable to find suitable sensitizers which solely bring about the N → Q isomerization but are not seriously consumed by addition to N or Q.

From these viewpoints we have made a mechanistic approach to the sensitizing ability of substituted BPs for N → Q and Q → N photoisomerization.[9] In this paper we report effects of structural factors of sensitizer ketones on the isomerization efficiency, and propose an addition-elimination mechanism for the BP sensitized N → Q isomerization and an electron-transfer interaction in the quenching of triplet BPs by Q, on the basis of the quantum yields, of the quenching rate constants measured in laser flash photolysis, and of the time profile of the isomerization and adduct formation.

Experimental

Norbornadiene (N) and quadricyclane (Q) were purchased from Aldrich Chemical Co., and purified by distillation. Solvent acetonitrile was Luminasol from Dojin Chemical Co. 4-Cyanobenzophenone was prepared according to the literature.[10] Other substituted benzophenones were purchased from Wako or Nakarai Chemical Co. All the benzophenones were crystallized from methanol, ethanol, hexane, or diethyl ether.

The phosphorescence spectra of some sensitizers were measured on a Hitachi MPF-2A fluorescence spectrophotometer and the triplet energies were determined.

The redox potentials of N, Q, and sensitizers were determined by cyclic voltammetry in acetonitrile with respect to an SCE in the presence of 0.1 mol dm^{-3} tetraethylammonium perchlorate as a supporting electrolyte.

Isomerization quantum yields were determined using potassium tris(oxalato)ferrate(III) actinometry. Benzophenone sensitized N → Q isomerization was carried out in Pyrex tubes with 366 nm light through a UVD-36B glass filter from a 400 W high pressure mercury lamp under nitrogen atmosphere. The conversions were determined by gas chromatography, a Shimadzu GC-4CM PF gas chromatograph equipped with an FID.

Laser flash photolyses were performed as described elsewhere.[11] Sample solutions were deaerated by bubbling with nitrogen for 30 min. The first order decay rate constants (k_{obs}) of triplet benzophenones were measured as a function of N or Q concentration by monitoring their T-T absorptions around 530 nm, and the quenching rate constants (k_q^N and k_q^Q) were obtained from linear plots based on the following equation:

$$k_{obs} = \tau_T^{-1} + k_q^S[S], \quad S = N \text{ or } Q.$$

Results

Quantum Yields for N → Q and Q → N Isomerization. The quantum yields for sensitized isomerization of N (0.1 mol dm^{-3}) and Q (0.1 mol dm^{-3}) were determined at low

§Present address: Radiation Laboratory, University of Notre Dame, Notre Dame, Indiana 46556, U.S.A.

Table 1. Quantum Yields for N→Q Isomerization ($\Phi_{t\to c}$) in Acetonitrile[a)]

Sensitizer	E_T[b)] / kcal mol^{-1}	$\Phi_{N\to Q}$	$\Phi_{Q\to N}$	$\Sigma\sigma$[c)]
4,4′-Dimethoxybenzophenone (**1**)	70.3	0.56	0.05	−0.54
4,4′-Dimethylbenzophenone (**2**)	69.3	0.59		−0.34
4-Methylbenzophenone (**3**)	69.2	0.50		−0.17
Benzophenone (**4**)	69.2	0.45	0.06	0
3-Benzoylpyridine (**5**)	69.0	0.36		
4-Methoxybenzophenone (**6**)	69.0	0.53		−0.27
4-Chlorobenzophenone (**7**)	68.8	0.29		0.23
4,4′-Dichlorobenzophenone (**8**)	68.4[d)]	0.29		0.46
4-Hydroxybenzophenone (**9**)	68.3[d)]	0.42		−0.37
2-Benzoylpyridine (**10**)	67.4	0.35		
4-Benzoylpyridine (**11**)	67.2	0.40		
4-Cyanobenzophenone (**12**)	67.0[d)]	0.33	0.10	0.66
Triphenylene (**13**)	66.5	0.02		
Michler's ketone (**14**)	62	0.04		
4-Phenylbenzophenone (**15**)	60.7	0.23		
Benzil (**16**)	54.3	0.009		

a) Concentration of N, 0.1 mol dm^{-3}. b) Triplet excitation energies of sensitizers taken from Ref. 12, unless otherwise indicated. c) Hammett's sigma constants for substituted benzophenones (O. Exner, "Advances in Linear Free Energy Relationships," ed by N. B. Chapman and J. Shorter, Plenum (1972)). d) Estimated from phosphorescence spectra measured in EPA at 77 K.

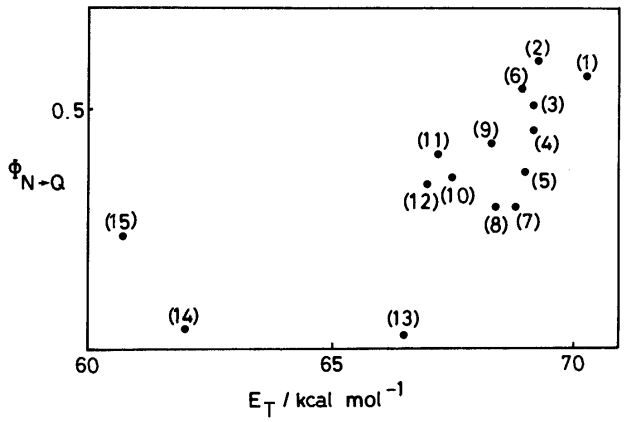

Fig. 1. Plots of isomerization quantum yields ($\Phi_{N\to Q}$) against the triplet energies (E_T) of sensitizers. The numerals refer to the sensitizers in Table 1.

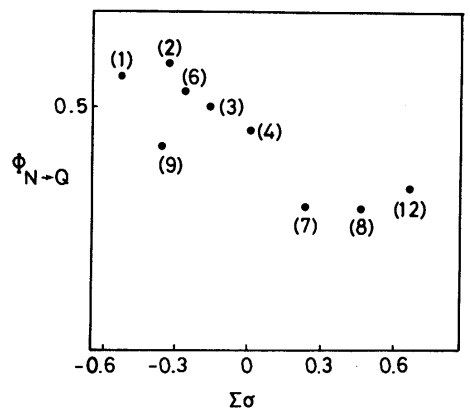

Fig. 2. Plots of isomerization quantum yields ($\Phi_{N\to Q}$) against Hammett's sigma constants. The numerals refer to the sensitizers in Table 1.

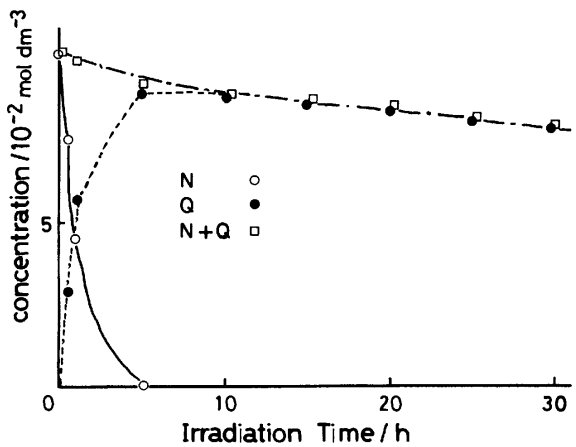

Fig. 3. Irradiation time dependence of concentrations of N, Q, and N+Q in a degassed acetonitrile solution containing 4,4′-dimethoxybenzophenone (0.1 mol dm^{-3}) and N (0.1 mol dm^{-3}).

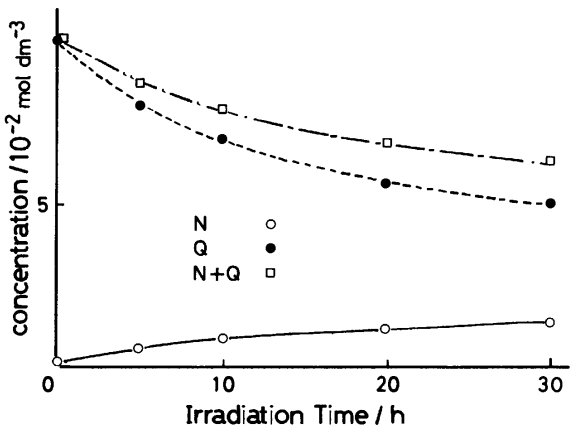

Fig. 4. Irradiation time dependence of concentration of N, Q, and N+Q in a degassed acetonitrile solution containing 4,4′-dichlorobenzophenone (0.1 mol dm^{-3}) and Q (0.1 mol dm^{-3}).

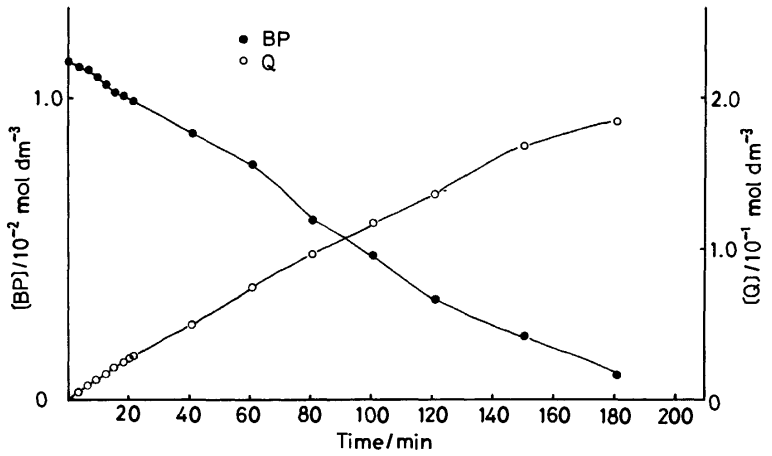

Fig. 5. Time dependence of concentrations of Q and benzophenone in neat N.

Table 2. Quenching Rate Constants of Substituted Benzophenones by Norbornadiene and Quadricyclane

Sensitizer	E_{red}	E_T	$(E_{red}+E_T)$	k_q^N	k_q^Q	$\Delta G_N^{\circ a)}$	$\Delta G_Q^{\circ b)}$
	V vs. SCE	eV	eV	$mol^{-1}dm^3s^{-1}$	$mol^{-1}dm^3s^{-1}$	eV	eV
4,4′-Dimethoxybenzophenone (**1**)	−2.01	3.05	1.04	2.02×10^9	2.04×10^8	0.75	0.01
4,4′-Dimethylbenzophenone (**2**)	−1.96	3.01	1.05	1.62×10^9	6.09×10^8	0.74	0
4-Methoxybenzophenone (**6**)	−1.88	2.99	1.11	2.81×10^9	9.50×10^8	0.68	−0.06
Benzophenone (**4**)	−1.82	3.00	1.18	6.44×10^8	8.78×10^8	0.61	−0.13
4-Chlorobenzophenone (**7**)	−1.73	2.98	1.25	2.35×10^9	3.02×10^9	0.54	−0.20
4,4′-Dichlorobenzophenone (**8**)	−1.67	2.97	1.30	2.35×10^9	3.86×10^9	0.49	−0.25
4-Bromobenzophenone (**17**)	−1.65	2.99	1.34	1.84×10^9	3.43×10^9	0.45	−0.29
4-Benzoylpyridine (**11**)	−1.56	2.91	1.35	1.14×10^9	2.37×10^9	0.46	−0.28
4-Cyanobenzophenone (**12**)	−1.48	2.91	1.43	2.46×10^9	6.53×10^9	0.38	−0.36

a) $\Delta G_N^\circ = E_{ox}(N) - (E_{red}+E_T) - 0.06$. b) $\Delta G_Q^\circ = E_{ox}(Q) - (E_{red}+E_T) - 0.06$.

conversion using several BPs and other triplet sensitizers (0.1 $mol\,dm^{-3}$) in deaerated acetonitrile solutions. The results are summarized in Table 1 together with the triplet excitation energies (E_T) of sensitizers employed and Hammett's σ constants ($\sum\sigma$) of the substituents on BPs. Figure 1 plots the quantum yields against E_T of the sensitizers and Fig. 2 plots the quantum yields against Hammett's σ constants of the substituents on BPs. The quantum yield of N → Q isomerization in neat N was also determined on sensitization with benzophenone ($1.12\times10^{-2} mol\,dm^{-3}$) to be 0.9.

Reaction of Triplet Benzophenones with N and Q. To see the consumption of N and Q clearly, benzophenone (BP), 4,4′-dimethoxybenzophenone [$(MeO)_2BP$], and 4,4′-dichlorobenzophenone (Cl_2BP) were used in extremely high initial concentrations, the same concentration as N or Q (0.1 mol dm^{-3}). Figures 3 and 4 depict typical results starting from N and Q, respectively. BPs examined induced the N → Q isomerization with a rate decreasing in a sequence of $(MeO)_2BP$, BP, and Cl_2BP, which is in parallel to their sensitized N → Q isomerization quantum yields in the initial stage (Table 1). Starting from both Q and N, the total amount of Q+N decreased most remarkably in the presence of Cl_2BP and to a least extent in the presence of $(MeO)_2BP$. On irradiation of BP ($1.12\times10^{-2} mol\,dm^{-3}$) in neat N, particular attention was paid to follow the reaction with frequent intervals in the early stage. Figure 5 shows the results.

Quenching Rate Constants of Triplet Sensitizers by N and Q. The quenching rate constants of the BPs triplets by N and Q measured in acetonitrile by means of laser flash photolysis are summarized in Table 2. All the benzophenones examined here have $n\pi^*$ character in the triplet state.[10b] This table also lists redox potentials measured in acetonitrile, and the change in the Gibbs function (ΔG°) for electron transfer from N or Q to BPs triplets estimated according to Eq. 1.

$$\Delta G^\circ/eV = E_{ox} - E_{red} + z_1z_2e^2/\varepsilon r - E_T \quad (1)$$

The redox potentials E_{ox} and E_{red} refer to E ($N^{+\cdot}/N$) or E ($Q^{+\cdot}/Q$) and E ($BP/BP^{-\cdot}$), respectively, and the term $z_1z_2e^2/\varepsilon r$ represents the Coulombic energy associated with bringing separated radical ions of charges z_1 and z_2 at the encounter

Table 3. Triplet Energies of Sensitizers (S) and Energies of Intermediates over the Ground States of the Sensitizers and N (or Q)[a)]

Sensitizer	E_T[b)]	$E(S^{-\cdot}\cdots Q^{+\cdot})$	$E(S^{-\cdot}\cdots N^{+\cdot})$
1	3.05	3.12	3.86(2.86)
2	3.01	3.07	3.81(2.81)
6	2.99	2.99	3.73(2.73)
4	3.00	2.93	3.67(2.67)
7	2.98	2.84	3.58(2.58)
8	2.97	2.78	3.52(2.52)
17	2.99	2.76	3.50(2.50)
11	2.91	2.67	3.41(2.41)
12	2.91	2.59	3.33(2.33)
Chloranil	2.69[c)]	1.10	1.84(0.84)

a) In eV. In parentheses are indicated those for $S^{-\cdot}$ and $N^{+\cdot}$ based on the energies of the sensitizers and Q. b) See footnote in Table 1. c) From Ref. 28.

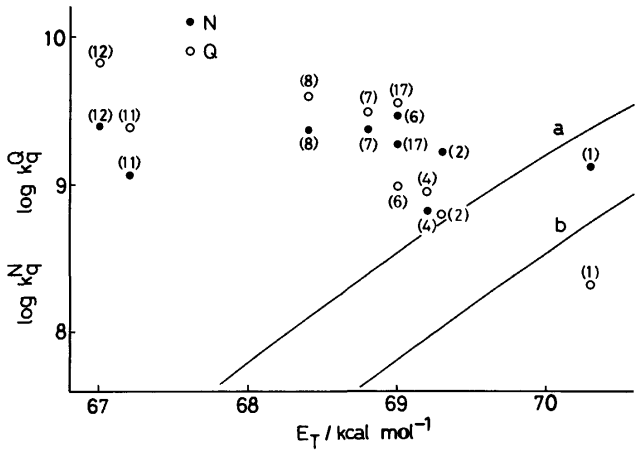

Fig. 6. Plots of quenching rate constants of triplet benzophenones by norbornadiene (k_q^N) and quadricyclane (k_q^Q) vs. triplet energies of benzophenones (E_T). Curves a and b are calculated by Eq. 2 assuming $E_T(N)$=70 and 72 kcal mol^{-1}, respectively.

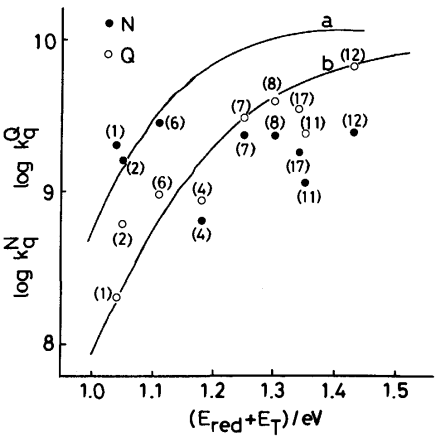

Fig. 8. Plots of quenching rate constants of triplet benzophenones by norbornadiene (k_q^N) and quadricyclane (k_q^Q) vs. $E_{red}+E_T$ of benzophenones. Curves a and b are calculated according to Eq. 3 assuming $\Delta G^{\circ\neq}(0)$=2.4 and 3.5 kcal mol^{-1}, respectively.

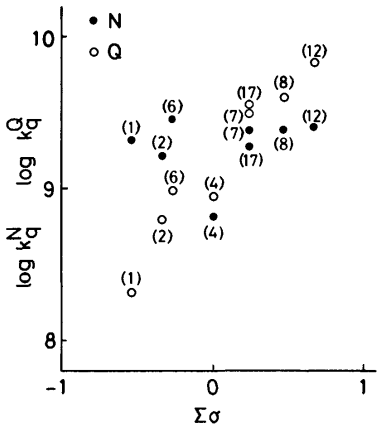

Fig. 7. Plots of quenching rate constants of triplet benzophenones by norbornadiene (k_q^N) and quadricyclane (k_q^Q) vs. Hammett's sigma constants of substituents on benzophenones.

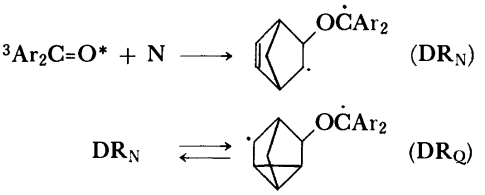

Scheme 1.

distance r in a solvent of dielectric constant ε.[13] The oxidation potentials of Q and N are 1.10 and 1.85 V, respectively, with respect to SCE. The energies of the ion pairs, as calculated as $E_{ox}-E_{red}$ are shown in Table 3. Figures 6 and 7 show logarithmic plots of the quenching rate constants (k_q^N and k_q^Q) against E_T and Hammett's σ constants of BPs, respectively. The plots of log k_q^N and log k_q^Q against the reduction potentials of triplet BPs, as estimated as $E_{red}+E_T$, are illustrated in Fig. 8.

Discussion

Isomerization of N to Q. Three mechanisms are possible for the sensitization of isomerization of N: 1) Triplet energy transfer, 2) electron transfer, and 3) addition-elimination (Scheme 1). As Fig. 1 shows, the efficiency of the N → Q isomerization is not fully governed by the triplet energies of sensitizers. Thus, triphenylene (E_T: 66.5 kcal mol^{-1}, 1 kcal=4.184 kJ) is far less effective than benzophenone (E_T: 69.2 kcal mol^{-1}) and even than 4-phenylbenzophenone with much lower E_T (E_T: 60.7 kcal mol^{-1}). Figure 2 shows that BPs carrying electron-donating substituents act as more effective sensitizers. Accordingly, it is clear that the efficiency of the sensitizer is not fully controlled by its triplet excitation energy, but among BPs some electronic effects of the substituents play an important role in the sensitization.

It is remarkable and consistent with the above results that k_q^N is independent of E_T of the sensitizers and much lower than diffusion controlled limit (Fig. 6). The lack of correlation between k_q^N and E_T suggests that the quenching of triplet BPs by N does not proceed through a simple energy transfer. The curves in Fig. 6 were calculated assuming that the quenching of triplet BPs by N proceeds through energy transfer and obeys Eq. 2,[14] where k_{dif} is the diffusion controlled rate constant, 10^{10} mol^{-1} dm^3 s^{-1}, and ΔE is the triplet energy difference between a BP and N.

$$k_q^N = k_{dif}\exp(-\Delta E/RT)/\{1+\exp(-\Delta E/RT)\} \quad (2)$$

The triplet energy of N was assumed to be 70—72 kcal mol^{-1}.[1,3,15,16] The calculated curves do not fit the plot of the observed rate constants, especially for low energy sensitizers such as 4-cyanobenzophenone, sug-

gesting an important role of quenching processes other than triplet energy transfer.[17]

Electron transfer plays no significant role in the isomerization of N, since the plots of k_q^N against the σ (Fig. 7) and $E_{red}+E_T$ values (Fig. 8) are scattered and seem to have no correlation. From the calculated $\Delta G°$ values in Table 2, the electron transfer from N to triplet BPs is estimated to be more than 0.38 eV endothermic, being in accordance with no correlation in Fig. 6. The rate constant associated with an electron-transfer process usually obeys the Rehm-Weller equation (Eq. 3), where $\Delta G°^{*}(0)$ is the change in the Gibbs function of activation at $\Delta G°=0$ kcal mol^{-1}; $\Delta G°^{*}(0)$ is related to the change in nuclear positions occurring prior to electron transfer, and is 2.4 kcal mol^{-1} for usual electron transfer.[13]

$$k_q = \frac{2\times 10^{10}\ \text{mol}^{-1}\text{dm}^3\text{s}^{-1}}{1+0.25\{\exp(\Delta G°^{*}/RT)+\exp(\Delta G°/RT)\}} \quad (3)$$

$$\Delta G°^{*} = \Delta G°/2+\{(\Delta G°/2)^2+[\Delta G°^{*}(0)]^2\}^{1/2} \quad (4)$$

Because of the large endothermicity (0.38 eV) the rate constant of electron transfer from N to triplet BPs is as low as 2×10^4 mol^{-1} dm^3 s^{-1} according to Eqs. 3 and 4, suggesting less importance of this process.

The addition-elimination mechanism explains reasonably the observed dependence of sensitizing ability of N→Q isomerization on the substituents of BPs[9] and the formation of addition products.[18,19] Comparison of the plot of log k_q^N against E_T with the calculated curve in Fig. 6 suggests that the quenching might proceed mainly through the addition-elimination process for lower energy sensitizers like 4-cyanobenzophenone, while the energy transfer might play a more important role for sensitizers with higher triplet energy like 4,4′-dimethoxybenzophenone.

Shima reported that triplet BP adds to N to give oxetane products.[18] However, later Gorman reported that the formation of the oxetane products is not due to the addition of triplet BP to N but due to the addition to Q resulting from N isomerization.[19] In order to reveal whether the consumption of BP during the irradiation of N is due to its addition to N or to the resulting Q, we carefully reinvestigated irradiation of BP (1.12×10^{-2} mol dm^{-3}) in neat N. Figure 5 clearly shows that the amount of the resulting Q increased linearly with irradiation time and BP decreased even at the very early stage without any induction period.

The present results are in contrast with Gorman's work. Gorman et al. reported that on irradiation of BP in neat N, Q was produced linearly with irradiation time, while the consumption of BP started after an induction period until Q was accumulated in 1.8×10^{-2} mol dm^{-3}.[19] From these results they concluded that the adducts were formed through addition of triplet BP to Q but not to N.[19]

In this concentration of Q, the molar ratio of N (neat: 9.3 mol dm^{-3}) and Q is ca. 520 : 1, and thus by using 6.4×10^8 and 8.8×10^8 mol^{-1} dm^3 s^{-1} as the rate constants for quenching of BP triplets by N and Q, respectively, the fraction of triplet BP to be quenched by Q is estimated to be only 1/380. Inspection of Gorman's data indicates that the relative rate of the Q formation to that of adduct formation is nearly 6—7. This value gives a quantum yield for the adduct formation as strangely high as 49—57 by using 0.9 as the quantum yield for N→Q isomerization determined in the present investigation. Gorman et al. explained their results shortly that the N→Q isomerization must be very inefficient in neat N because of the self quenching of triplet N.[19] However, it is not the case as shown above. The present results are in keeping with the report by Shima which claimed Gorman's arguments and reconfirmed the addition of BP triplets to N.[20]

When the quenching of triplet BPs by N proceeds solely through the addition-elimination mechanism, the observed quenching rate constant (6.4×10^8 mol^{-1} dm^3 s^{-1}) could be supposed to be slightly higher than that expected for the addition of $n\pi^*$ triplet to unsaturated bonds. However, from the analysis of the quantum yields for oxetane formation in the stationary irradiation of benzophenone with furan and for isomerization of *cis*- and *trans*-2-butene induced by benzophenone, the rate constants for the quenching of triplet BP by furan and the cis-alkene mostly by addition are estimated as 4.2×10^7 and 7×10^7 mol^{-1} dm^3 s^{-1}, respectively.[21,22] Also, 4-methoxybenzoyloxyl radical, which has similar electronic configuration to benzophenone triplet carrying an unpaired electron on the oxygen atom, adds to 1,4-cyclohexadiene with a rate constant of ca. 5×10^8 mol^{-1} dm^3 s^{-1} as determined by laser flash photolysis recently.[23] Furthermore, this radical abstracts a hydrogen atom from cyclohexane with ca. 10^6 mol^{-1} dm^3 s^{-1}, nearly the same rate constant for the abstraction of hydrogen atom from 2-propanol by triplet benzophenone.[16] Therefore, it is reasonable to propose that triplet BPs add to N with nearly the same rate constant as that for the addition of 4-methoxybenzoyloxyl radical.

Isomerization of Q to N. As shown in Fig. 6, k_q^Q decreases with increasing E_T of sensitizers. The inverse correlation suggests that E_T of Q is much higher than 58 kcal mol^{-1}, a previously reported value,[15,16] and thus the energy transfer quenching is not important. The fact that the rate constants k_q^Q increases with Hammett's σ of the substituents on BPs indicates that the electron transfer plays an important role in the quenching by Q. The curve a in Fig. 8 was calculated from the Rehm-Weller equation (Eq. 3) using $\Delta G°^{*}(0)=2.4$ kcal mol^{-1} for typical electron transfer.[13] The plot does not fit this curve but fits the curve b calculated by assuming $\Delta G°^{*}(0)=3.5$ kcal mol^{-1}. This means that the electron transfer between BP triplets and Q needs a higher activation energy and thus larger geometrical changes than the usual electron transfer.[24]

The isomerization of Q to N in acetonitrile was not

so efficient as the N→Q isomerization.[8] The quantum yield for Q (0.1 mol dm^{-3})→N isomerization were 0.05, 0.06, and 0.10 in the presence of $(MeO)_2BP$, BP, and 4-cyanobenzophenone, respectively (Table 1). On the other hand, Roth reported that chloranil (CA) sensitized the Q→N isomerization with a high quantum yield, 0.64, and pointed out that the quenching of CA triplets by Q resulted in the production of its radical cations having a geometry close to the transition state of $Q^{+\cdot}\rightarrow N^{+\cdot}$ isomerization.[25] Furthermore, it has been reported that quadricyclane radical cations $Q^{+\cdot}$ generated by γ-irradiation or electrochemical oxidation of Q easily convert into norbornadiene-like radical cations $N^{+\cdot}$ and that the barrier of conversion of $Q^{+\cdot}\rightarrow N^{+\cdot}$ is significantly lower than that for Q→N.[26,27] The low quantum yields observed in the present work could be attributed to the production of N triplets from the radical ion pair consisting of $Q^{+\cdot}$ and $BP^{-\cdot}$. Thus, the isomerization in a radical pair $(BP^{-\cdot}\cdots Q^{+\cdot})\rightarrow(BP^{-\cdot}\cdots N^{+\cdot})$ is exothermic since the ground state of Q is nearly 1 eV higher in energy than that of N.[1] Accordingly, on quenching of triplet BP with Q followed by $Q^{+\cdot}\rightarrow N^{+\cdot}$ isomerization in the pair, the resulting triplet radical pair $^3(BP^{-\cdot}\cdots N^{+\cdot})$ has a higher energy than triplet N (E_T=3.1 eV)[1,3,15,16] as indicated in Table 3, and thus can produce the N triplet effectively. The N triplets deactivate to the ground state to give mainly the starting material Q, therefore leading to low quantum yields of the Q→N isomerization. After the quenching of triplet BP by Q, the resulting radical ion pairs will undergo sequential reactions very quickly since $BP^{-\cdot}$ was not observed after 30 ns of a laser pulse in the nanosecond spectroscopy.

In the case of CA sensitization, however, even if the radical pair $^3(CA^{-\cdot}\cdots N^{+\cdot})$ [triplet energy: 1.84 eV, $E(CA/CA^{-\cdot})$= +0.01 V (SCE)][28] is effectively produced in the quenching of triplet CA by Q, it has a lower energy than has an N triplet (Table 2) and deactivates only to CA+N in the ground state resulting in the higher quantum yield of N.

$$^3BP^* + Q \rightarrow {}^3(BP^{-\cdot}\cdots Q^{+\cdot}) \rightarrow {}^3(BP^{-\cdot}\cdots N^{+\cdot})$$
$$^3(BP^{-\cdot}\cdots N^{+\cdot}) \rightarrow {}^1(BP^{-\cdot}\cdots N^{+\cdot})$$
$$^3(BP^{-\cdot}\cdots N^{+\cdot}) \rightarrow BP + {}^3N^*$$
$$^1(BP^{-\cdot}\cdots N^{+\cdot}) \rightarrow BP + N$$
$$^3N^* \rightarrow Q + N$$

Scheme 2.

In summary, the quenching of triplet BPs by Q proceeds through electron transfer to give norbornadiene-like radical cations, which subsequently recombine with a partner $BP^{-\cdot}$ to generate triplet N reverting to Q finally (Scheme 2). On the other hand, the quenching of triplet BPs by N is proposed to proceed mainly in the addition-elimination fashion which leads finally to effective isomerization to Q (Scheme 1).

The authors thank the Ministry of Education, Science and Culture for the partial support of this work by a Grant-in-Aid for Scientific Research.

References

1) R. R. Hautala, R. B. King, and C. Kutal, "Solar Energy: Chemical Conversion and Storage," ed by R. R. Hautala, R. B. King, and C. Kutal, The Humana Press, Clifton, New Jersey (1979), p. 333.

2) G. Jones II, S. H. Chiang, and P. T. Xuan, *J. Photochem.*, **10**, 1 (1979).

3) P. A. Grutsch and C. Kutal, *J. Am. Chem. Soc.*, **108**, 3108 (1986).

4) C. Kutal, *Adv. Chem. Ser.*, **168**, 158 (1978); D. P. Schwendiman and C. Kutal, *J. Am. Chem. Soc.*, **99**, 5677 (1977); R. R. Hautala, J. L. Little, and E. Sweet, *Solar Energy*, **19**, 503 (1977).

5) Z. Yoshida, *J. Photochem.*, **29**, 27 (1985); K. Hirano, A. Ando, T. Hamada, and O. Yonemitsu, *J. Chem. Soc., Chem. Commun.*, **1984**, 300.

6) K. Maruyama, K. Terada, and Y. Yamamoto, *Chem. Lett.*, **1981**, 839.

7) T. Toda, E. Hasegawa, T. Mukai, H. Tsuruta, T. Hasegawa, and T. Yoshida, *Chem. Lett.*, **1982**, 1551.

8) S. Murov and G. S. Hammond, *J. Phys. Chem.*, **72**, 3797 (1968); G. S. Hammond, P. Wyatt, C. D. Deboer, and N. J. Turro, *J. Am. Chem. Soc.*, **86**, 2532 (1964).

9) For preliminary work, see, T. Arai, T. Wakabayashi, H. Sakuragi, and K. Tokumaru, *Chem. Lett.*, **1985**, 279.

10) a) R. W. R. Humphreys and D. R. Arnold, *Can. J. Chem.*, **55**, 2286 (1977); b) W. J. Leigh, D. R. Arnold, R. W. R. Humphreys, and P. C. Wong, *ibid.*, **58**, 2537 (1980).

11) T. Arai, H. Sakuragi, K. Tokumaru, Y. Sakaguchi, J. Nakamura, and H. Hayashi, *Chem. Phys. Lett.*, **98**, 40 (1983).

12) S. L. Murov, "Handbook of Photochemistry," Marcel Dekker, New York, N. Y. (1973), p. 3.

13) D. Rehm and A. Weller, *Isr. J. Chem.*, **8**, 259 (1970).

14) K. Sandros, *Acta Chem. Scand.*, **18**, 2355 (1964).

15) N. J. Turro, W. R. Cherry, M. F. Mirbach, and M. J. Mirbach, *J. Am. Chem. Soc.*, **99**, 7388 (1977).

16) N. J. Turro, "Modern Molecular Photochemistry," Benjamin/Cummings, Menlo Park, CA, (1978), Chap. 9—11.

17) A. J. B. Barwise, A. A. Gorman, R. L. Leyland, C. T. Parekh, P. G. Smith, and M. A. J. Rodgers, *J. Am. Chem. Soc.*, **100**, 1814 (1978).

18) T. Kubota, K. Shima, and H. Sakurai, *Chem. Lett.*, **1972**, 343.

19) A. A. Gorman and R. L. Leyland, *Tetrahedron Lett.*, **1972**, 5345; A. J. B. Barwise, A. A. Gorman, R. L. Leyland, C. T. Parekh, and P. G. Smith, *Tetrahedron*, **36**, 397 (1980).

20) K. Shima, M. Ikenoue, and K. Kamei, Kokagaku Toronkai (Japan), Tokyo, November, 1979, Abstr. p. 162; *Chem. Abstr.*, **93**, 7263s (1980).

21) H. Sakurai, K. Shima, and S. Toki, *Nippon Kagaku Zasshi*, **89**, 537 (1968).

22) R. A. Caldwell, G. W. Sovocool, and R. P. Gajewski, *J. Am. Chem. Soc.*, **95**, 2549 (1973).

23) J. Chateauneuf, J. Lusztyk, and K. U. Ingold, *J. Am. Chem. Soc.*, **109**, 897 (1987).

24) F. Scandola and V. Balzani, *J. Am. Chem. Soc.*, **100**,

7404 (1978); V. Balzani, F. Bolletta, and F. Scandola, *ibid.*, **102**, 2152 (1980).

25) H. D. Roth, M. L. M. Schilling, and G. Jones II, *J. Am. Chem. Soc.*, **103**, 1246 (1981); H. D. Roth, M. L. M. Schilling, *ibid.*, **103**, 7210 (1981); K. Raghavachari, R. C. Haddon, and H. D. Roth, *ibid.*, **105**, 3110 (1983).

26) E. Haselbach, T. Bailly, Z. Lanyiova, and P. Baertschi, *Helv. Chim. Acta*, **62**, 583 (1979).

27) K. Yasufuku, K. Takahashi, and C Kutal, *Tetrahedron Lett.*, **25**, 4893 (1984).

28) Y. Takahashi, T. Miyashi, and T. Mukai, *J. Am. Chem. Soc.*, **105**, 6511 (1983).

 © 1987 The Chemical Society of Japan Bull. Chem. Soc. Jpn., 60, 2945—2951 (1987)

Unequivalent Chemical Environment of Diene Groups in 1- and 2-Acyl Chains of Polymerizable Lipids Analyzed by Radical Polymerization[1)]

Hiroyuki OHNO, Shinji TAKEOKA, and Eishun TSUCHIDA*
Department of Applied Chemistry, Faculty of Science and Engineering,
Waseda University, Tokyo 160
(Received March 20, 1987)

1,2-Di-*O*-(2,4-octadecadienoyl)-*sn*-glycero-3-phosphorylcholine is polymerized by radical initiators. An azobisisobutyronitrile (AIBN) and an azobis(2-amidinopropane) dihydrochloride (AAPD) are incorporated into hydrophobic membrane region of the lipid liposomes and an aqueous medium, respectively by sonication. The use of either AIBN or AAPD gives polymerization conversion of about 50% at 60 °C. This is not improved by the elongation of polymerization period at 60 °C or the increase of the amount of these radical initiators. The lyophilized lipids thus polymerized by either AIBN or AAPD are soluble in methanol suggesting the formation of linear polymers. Simultaneous polymerization by both AIBN and AAPD provides almost complete polymerization. AIBN and AAPD have been suggested to initiate radical polymerization of diene groups in 1- and 2-acyl chains, respectively. Potassium peroxodisulfate, another water-soluble radical initiator, yields polymerized liposomes with polymerization conversion of more than 80%. This corresponds to the polymerization of diene groups of not only 2- but also 1-acyl chains due to the hydroxyl radicals which are generated by the radial transfer in an aqueous medium. These different initiation reactions are attributed mainly to the unequivalent chemical environment of diene groups in 1- and 2-acyl chains.

Polymerization of assembled molecules is one of potent techniques to construct highly-ordered polymer structure. UV-irradiation is being used frequently to initiate polymerization of the assembled monomers as liposomes or monolayer membranes because of its convenience.[3-9)] This technique was quite effective to polymerize diacetylenic amphiphiles because of their high reactivity,[4-6)] but some problems raised for the polymerization of diene-containing amphiphiles.[2,10-12)] For example, a strong UV-light irradiation provided an average molecular weight of the diene-containing phospholipids around 5000.[12)] Liposomes with relatively lower degree of polymerization were analyzed to be stabilized only a little.[12)] On the other hand, gamma-ray irradiation is one of potent techniques to initiate in situ polymerization of lipids as liposomes.[11)] However this provides excellent stability of the polymerized liposomes than UV-irradiated ones, it is not commonly-usable method because of less availability of the gamma-ray source and careful treatments. Against this, radical initiators are very common reagents, and those have been found to effectively initiate polymerization of diene containing lipids and to improve membrane stability of the liposomes. This method is quite convenient to prepare polymerized liposomes with excellent stability.[13)] We succeeded the selective polymerization of diene groups of polymerizable amphiphiles as liposomes with water-soluble and -insoluble radical initiators.[12)] This finding may lead to finely regulated polymerization of the assembled molecules. It is therefore getting important to summarize the polymerization profile and characteristics of the selectively polymerized diene-containing lipids.

In this paper, relationship between structural characteristics of radical initiators and polymerization profile of diene-containing amphiphiles is discussed as well as physicochemical characteristics of the obtained polymerized liposomes.

Experimental

1,2-Di-*O*-(2,4-octadecadienoyl)-*sn*-glycero-3-phosphorylcholine (DODPC) was purchased from Nippon Oil & Fats Co. Ltd. and was characterized by thin-layer chromatography (Merck, silica-gel plates) with chloroform–methanol–water (65 : 35 : 5, by vol) as solvent before use.[11)] DODPC showing single spot with R_f value of 0.3 on TLC plate was used for further experiments. Azobisisobutyronitrile (AIBN) and azobis(2-amidinopropane) dihydrochloride (AAPD) were purchased from Tokyo Kasei Co. Ltd. Potassium peroxodisulfate ($K_2S_2O_8$) was purchased from Kanto Chem. Co. Ltd. AIBN was purified twice by recrystallization from dehydrated methanol. AAPD and $K_2S_2O_8$ were recrystallized twice from pure water. Crystals of these radical initiators were dried in vacuo. Triton X-100, polyethylene glycol mono-*p*-octylphenyl ether ($HO(CH_2CH_2O)_{10}C_6H_4C_8H_{17}$), was purchased from Tokyo Kasei Co. Ltd. and was used without further purification. Fluorescent grade 5(6)-carboxyfluorescein (CF) was purchased from Kodak Co. CF was used for the experiments without further purification.

Liposome Preparation. The polymerizable lipids (0.20 g) were dissolved in dehydrated chloroform and slowly evaporated in a rotated sample tube to prepare lipid thin film on the inner surface of the tube. Degassed pure water (20 ml) was then added to the tube. This was sonicated (Tomy Seiko, UR-200P) at 60 W for 10 min in water bath (20 °C) under nitrogen atmosphere to prepare single-walled small liposomes with an average radius of 15—25 nm.

Polymerization. The polymerizable lipids (0.20 g) were dissolved with 2.1 mg of AIBN (5.0 mol% to the polymerizable lipids) in chloroform and was slowly evaporated in a rotated sample tube. Degassed pure water (20 ml) was added to the tube. This was co-sonicated at 60 W for 10 min in water bath at 20 °C to prepare liposome suspension. Lipo-

somes containing different amount of AIBN were also prepared by the same method. Small amount of AIBN was decomposed by 10 min sonication at 60 W. Liposomes were incubated at 8 °C for 3 h to minimize the disordered molecular packing. This procedure provided single-walled liposomes with average radius of 40—70 nm. This liposome dispersion was polymerized under nitrogen atmosphere at 60 °C.

Liposome suspension was prepared and incubated by the same method as mentioned above. AAPD or potassium peroxodisulfate with 0.5—10 mol% to the polymerizable lipids, were then added to the suspensions to avoid decomposition of initiators by the sonication. Liposomes thus prepared were considered to have no AAPD molecule in the inner aqueous phase. Some of liposomes thus prepared were resonicated for 10 s to put AAPD molecules into an inner aqueous phase. Liposomes were polymerized at 60 °C for several hrs under nitrogen atmosphere.

A small amount of DODPC liposome suspension was periodically pipetted out from a sealed sample tube during polymerization. Accurately diluted liposome suspension was analyzed by UV spectrometry to quantitatively determine the polymerization conversion. Calculation of the polymerization conversion was based on the changes of molar extinction coefficient at 255 nm which corresponded to diene groups.[11]

Measurements. Polymerized liposome was stained by uranyl acetate and the suspension was dropped on carbon precoated copper grids and dried carefully to confirm their bilayer structure by TEM (JEOL-100CX). Relatively large liposome suspension (aqueous methanol solution) was dropped on copper sample rest. The liposomal structure was directly analyzed with scanning electron microscopy (JEOL-JSM T20). A laser particle analyzer (Coulter N4D, Coulter Electronics) was used to measure average radius of the polymerized liposomes with a theory of quasielastic light scattering and Stokes-Einstein equation. CF was incorporated into an inner aqueous phase of the liposomes by a similar manner as previously reported.[14] Liposomes containing 0.10 M (1 M=1 mol dm^{-3}) CF were isolated by gel permeation chromatography (Sepharose CL-4B). Diluted liposome suspensions were set into quartz cell for fluorescence measurement at settled temperature. The leakage of CF was followed as the increase of fluorescence intensity at 520 nm by fluorescence spectrometer (Hitachi HPF-4) with excitation beam of 330 nm. A 100% CF leakage was carried out as reference by the sonication of the liposome suspension in the presence of a small excess of Triton X-100.[11] Liposome suspension was prepared with D_2O instead of H_2O by the same manner as mentioned above. Polymerized liposome suspension was put into NMR sample tube with diameter of 5 mm. FT-NMR spectroscopy (JEOL FX-90Q) was used to characterize the segmental motion of the polymerized liposomes at different temperature.

Results and Discussion

Radical Polymerization Profile of DODPC as Liposomes. Polymerization of DODPC liposomes cause the decrease of spectral intensity at 255 nm which is attributed to the diene group.[11] This is essentially applicable to estimate the polymerization conversion. Figure 1 shows the polymerization conversion of

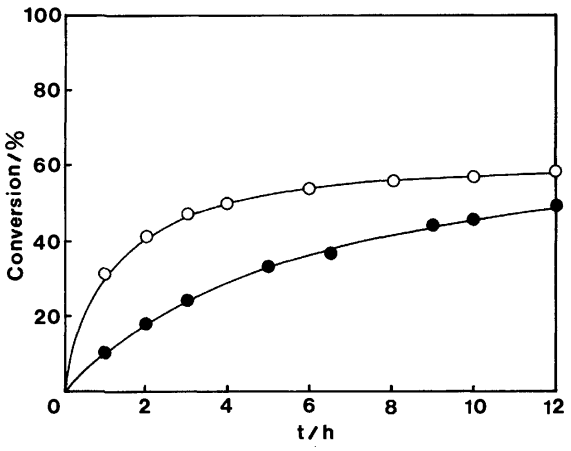

Fig. 1. Polymerization conversion of DODPC as liposomes. DODPC liposomes (10.0 g lipids dm^{-3} H_2O) were polymerized by AIBN (●) or AAPD (○) at 60 °C.

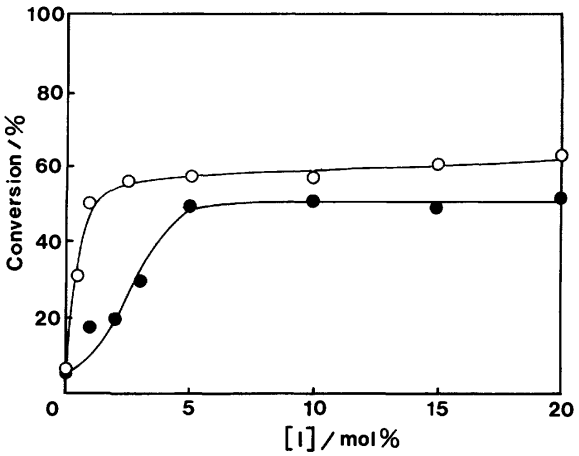

Fig. 2. Relationship between initial concentration of radical initiator and polymerization conversion of DODPC as liposomes (10 h at 60 °C). Liposomes were polymerized by AIBN (●) or AAPD (○).

DODPC lipids initiated by either AIBN or AAPD. The use of either AIBN or AAPD initiated the polymerization with final conversion of about 50% at 60 °C. This conversion was not improved by the elongation of the polymerization time. However certain improvement on the polymerization conversion was observed by further heating, this increase was almost the same as that by thermal polymerization. The increase of the amount of radical initiator did not improve it either as shown in Fig. 2. A thermal polymerization without radical initiator gave about 6—10% polymerization conversion after 12 h heating at 60 °C. AIBN with less than 0.5 mol% to the DODPC lipids was revealed not to participate the initiation of radical polymerization, because such a small amount of AIBN should be decomposed by 10 min sonication at liposome preparation.

The individual radical initiator (AIBN or AAPD) provided only 50% polymerization conversion, which

is important characteristic of DODPC lipids.[12] A 100% polymerization conversion was performed by simultaneous polymerization induced by both of these initiators. This tendency was firstly found by us for the polymerization of DODPC as liposomes.[12] This can be explained by the simple model considering different chemical environment of two diene groups bound to 1- and 2-acyl chains. According to the results of ^{2}D-NMR and X-ray analyses of lipid liposomes or crystals which were reported by Seelig et al.[15,16] and Hitchcock et al.[17] respectively, the glycerol segment was positioned perpendicular to the membrane plane. By applying this result simply to DODPC liposomes, the 2,4-diene group in 2-acyl chain is strongly considered to be faced an aqueous phase.[12] A molecular packing of the polymerizable lipid molecules in the bilayer membrane has already been discussed and the unequivalent characteristics of 1- and 2-acyl chains of the diacetylene-type amphiphiles have already been suggested by O'Brien[18] and Chapman.[19] As in their monomeric lipids, diacetylene groups were located deep in the hydrophobic region, they could not get direct evidence for the unequivalent reactivity of the 1-and 2-acyl chains of monomeric lipid. This unequivalent environment of diene groups was also demonstrated by us with 1-palmitoyl-2-(2,4-octadecadienoyl)-*sn*-glycero-3-phosphorylcholine (POPC).[2] POPC was a model lipid of DODPC and it was easily polymerized as liposomes by water-soluble radical initiator; AAPD, but hardly polymerized by AIBN. Namely, the 2,4-diene group in **2-acyl** chain must be exposed to the aqueous phase. The chemical environment of 2,4-diene groups in 2-acyl chain for POPC should be the same or quite similar to that for DODPC.

The unequivalent chemical environment of the 2,4-diene groups in 1- and 2-acyl chains was also clarified by comparing the polymerization manner with different radical initiators. For example, AAPD could initiate the radical polymerization of the DODPC liposomes which were preliminarily polymerized by AIBN as shown in Fig. 3. This means that the diene groups in 2-acyl chains are not initiated by AIBN radicals but are certainly initiated by AAPD radicals. The simultaneous initiation enabled polymerization with higher conversion than two-step initiation as shown in Fig. 3. This can be explained by the different penetration manner of AAPD through the membranes. The enough amount of AAPD molecules (not radicals) can penetrate the DODPC bilayer to initiate the polymerization of diene groups on 2-acyl chains which were faced the inner surface of the liposome at 60 °C. The penetration of AAPD molecules through bilayer membrane structure was supported by the following results. Some of DODPC liposome solutions containing AAPD in the outer aqueous phase were re-sonicated for 10 s to put AAPD molecules into an inner aqueous phase to compare the polymerization conversion with those for liposomes without re-sonication. There was no difference in the polymerization conversion between systems with and without re-sonication, suggesting that the enough amount of AAPD molecules did penetrate through the membrane at 60 °C. The penetration of radical initiators has already been analyzed to be governed by the temperature and there should be enough penetration to initiate the radical polymerization when temperatures were higher than the phase transition temperature.[12] However, covalent bonds of 1-acyl chains by AIBN-initiated polymerization restricted the permeation of AAPD molecules to cause the initiation less effective.

Similar improvement on the polymerization conversion was found by the addition of other water-soluble radical initiators. Potassium peroxodisulfate also initiated the radical polymerization of DODPC liposomes which were preliminarily polymerized by AIBN

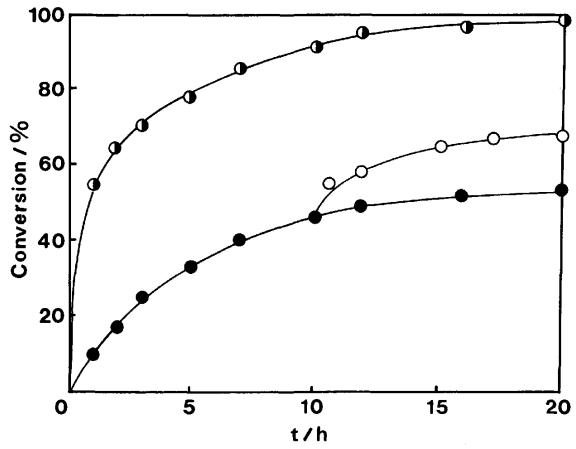

Fig. 3. Polymerization conversion of DODPC as liposomes at 60 °C. DODPC liposomes were polymerized by AIBN and AAPD simultaneously (◑), or by the addition of AAPD (○) to the DODPC liposomes which were pre-polymerized by AIBN (●) at 60 °C.

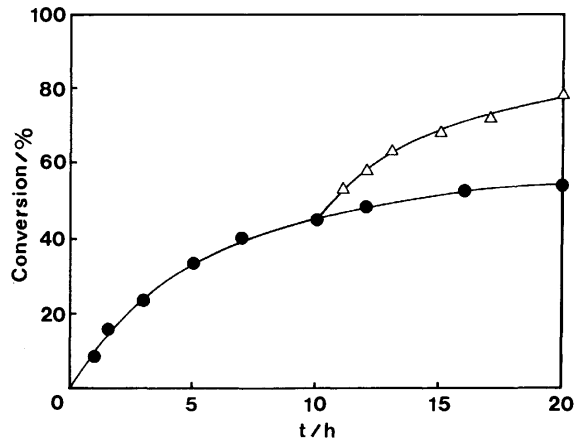

Fig. 4. Polymerization conversion of DODPC as liposomes at 60 °C. Polymerization was newly initiated by the addition of potassium peroxodisulfate (△) to the DODPC liposomes which were pre-polymerized by AIBN (●) at 60 °C.

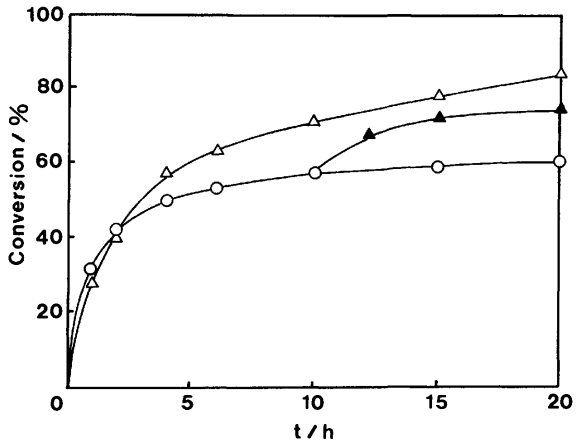

Fig. 5. Polymerization conversion of DODPC as liposomes at 60°C. DODPC liposomes were polymerized by potassium peroxodisulfate (△), or by the addition of potassium peroxodisulfate (▲) to the DODPC liposomes which were prepolymerized by AAPD (○) at 60°C.

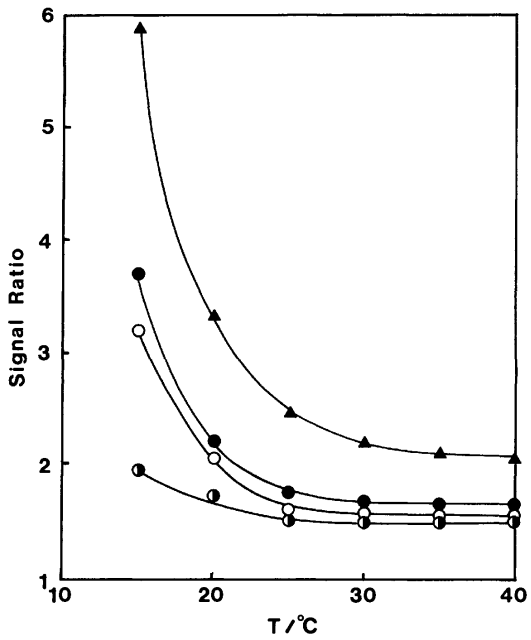

Fig. 6. Effect of temperature on the signal ratio of ^{1}H NMR peak for choline methyl protons to that for terminal methyl protons of polymerized DODPC liposomes. Liposomes were polymerized by; AIBN (●), AAPD (○), or both AIBN and AAPD simultaneously (◑). Data for monomeric DODPC liposomes were also shown as reference (▲).

as shown in Fig. 4. These data suggested that the polymerization reaction of diene groups in 1- and 2-acyl chains were independent with each other and no **intra**molecular polymerization should occur. It should be noted that the polymerization of DODPC liposomes with hydrophilic or hydrophobic radical initiators thus provided direct evidence for the different chemical environment and corresponding selective polymerization of the acyl chains of lipids as liposomes.

A simple addition of potassium peroxodisulfate made the polymerization of DODPC liposomes to reach about 80—90% conversion as shown in Fig. 5. The DODPC liposomes which were prepolymerized by AAPD showed further increase in the polymerization conversion by the addition of potassium peroxodisulfate as also shown in Fig. 5. These results mean that not only diene groups in 2-acyl chains but also those in 1-acyl chains are polymerized by this radical initiator. Potassium peroxodisulfate newly initiated the radical polymerization of DODPC liposomes whereas AAPD did not. The diene groups in 2-acyl chains were considered to be polymerized by AAPD radicals, and no polymerization of other diene groups should be initiated by the further addition of AAPD. The decrease of absorption at 255 nm by the addition of potassium peroxodisulfate should therefore be attributed to the polymerization of diene groups in 1-acyl chains. The possibility for the attack of diene groups in the hydrophobic region could be explained by the size of freshly generated and transferred radicals. Potassium peroxodisulfate radicals were known to generate OH radicals through the radical transfer to water molecules.[20] As OH radicals were much smaller than AAPD radicals, the OH radicals might approach and attack the diene groups in 1-acyl chains.

The different polymerization conversion of DODPC liposomes was certainly observed beyond the experimental error between potassium peroxodisulfate-initiated polymerization (83%) and two-step one (73%) which was polymerized by AAPD first and the initiated by potassium peroxodisulfate as shown in Fig. 5. A simple polymerization of DODPC liposomes which was initiated by the addition of potassium peroxodisulfate made higher polymerization conversion than that for the two-step polymerization. This might be due to the tight covalent bonds on the surface of liposomes provided by the preliminary polymerization of diene groups on 2-acyl chains by AAPD. Some covalent bonds on the surface might restrict the attack of radicals from an aqueous medium to the diene groups in relatively hydrophobic region. A lower segmental motion of hydrophilic region in the DODPC liposomes pre-polymerized by AAPD was actually detected by the ^{1}H NMR measurements as shown in Fig. 6. This data supported the reduction of the radical attack frequency to the hydrophobic region.

A solution polymerization kinetics was applied to the radical polymerization as liposomes. It should be helpful to analyze the polymerization profile of DODPC especially to speculate the polymerization mechanism. Polymerization velocity was calculated from the initial slope of the polymerization conversion profiles as seen in Figs. 1 and 5. Typical polymerization velocity was summarized in Table 1 for each system. A thermal cleavage of AIBN and AAPD to produce radicals has already been analyzed and the

following equations have been empirically presented,[21,22]

$$\text{for AIBN: } k = 1.29 \times 10^{15}\, e^{-30800/RT}, \quad (1)$$

$$\text{for AAPD: } k = 3.77 \times 10^{15}\, e^{-30300/RT} \quad (2)$$

where k, R, and T mean the radical cleavage rate constant (s^{-1}), gas constant and absolute temperature, respectively. A radical cleavage of AAPD is faster than that of AIBN at the same temperature (see Eqs. 1 and 2), but the polymerization in liposome systems can not be compared directly. Because AIBN was dissolved only in the hydrophobic region of the liposomes and the local concentration was about 100 times higher than that for water-soluble one under the present experimental conditions. For example, the local concentration of AIBN in the hydrophobic region of the liposome was calculated to be 5.7×10^{-2} mol dm^{-3} at DODPC concentration of 1.0 wt% and AIBN/DODPC= 1/20 by mol. There was no significant difference in the polymerization velocity for the AIBN-added system at different liposome concentration if DODPC/AIBN mol ratio was set to be constant. The polymerization profile of AIBN-added liposome system was therefore analyzed to be similar to the bulk polymerization. On the other hand, the initial polymerization velocity for the water-soluble radical initiator added system was affected by their initial concentration. The polymerization profile seemed to be analyzable as the emulsion polymerization but these were not the same.

The initial polymerization velocity for AAPD-added system was larger than that for potassium peroxodisulfate-added system as shown in Table 1. This is mainly due to the different radical cleavage rate, and it for AAPD was larger than that for potassium peroxodisulfate. Furthermore peroxodisulfate anions were known to generate radicals and partially transfer them to water molecules to produce hydroxyl radicals.[20] The different polymerization conversion between AAPD- and potassium peroxodisulfate-added system was also explained by the different size of the effective radicals. Namely, small hydroxyl radicals can get in a bilayer membrane structure and initiate polymerization of diene groups in both 1- and 2-acyl chains. This was confirmed by the gamma-ray polymerization of DODPC liposomes.[11] The DODPC lipids provide their diene groups in unequivalent chemical environment due to molecular packing, this strongly suggests possibility of a selective polymerization with the use of suitable radical initiators.

Table 1. Initial Polymerization Velocity of DODPC Liposomes at 60 °C

Initiator	Radical cleavage rate	Polymerization rate
	s^{-1}	mol dm^{-3} s^{-1}
AIBN	8.42×10^{-6}	6.79×10^{-7}
AAPD	5.23×10^{-5}	3.20×10^{-6}
$K_2S_2O_8$	6.89×10^{-6}	1.65×10^{-6}

[DODPC]=1.0 wt%. [Initiator]/[DODPC]=1/20 by mol.

AIBN-initiated polymerization of DODPC was very different from others. One of characteristics of this system is higher local viscosity of the medium, i.e., liquid crystalline state of the hydrophobic region. The AIBN-initiated polymerization of DODPC as liposomes clearly showed the characteristics of the polymerization in viscous liquid-crystalline state. However the radical cleavage rate for AIBN was almost the same as that for potassium peroxodisulfate and local concentration of AIBN was 100 times higher, there was not significant difference in the polymerization velocity as summarized in Table 1. This less efficiency was well explained by the "Cage Effect".[23] The initiation efficiency for AIBN was calculated to be about 0.5—0.7 in ordinary organic solvent where apparent diffusion coefficient of radical pair was around 1×10^{-5} $cm^2 s^{-1}$. In a viscous medium, initiation efficiency of AIBN have already been analyzed by Smets to be getting smaller with increasing viscosity.[24] The liposomal membrane structure provides more viscous matrix, for example the diffusion coefficient of pyrene in dipalmitoylphsophatidylcholine at 60 °C was measured to be 2.0×10^{-7} $cm^2 s^{-1}$ by Sackmann et al.[25] Most of the generated radicals recombined in the matrix and a little radicals could initiate the polymerization of diene groups.

Stability of the Polymerized Liposomes. The leakage of fluorescent probes from an inner aqueous phase of the liposomes has frequently used to evaluate the membrane stability of liposomes. As the carboxyfluorescein (CF) affected the polymerization of DODPC or other monomeric amphiphiles,[26] CF was incorporated into liposomes which had already been polymerized previously.[14] The leakage of CF was extremely suppressed by the DODPC membrane structure which was polymerized by radical initiators as shown in Fig. 7.

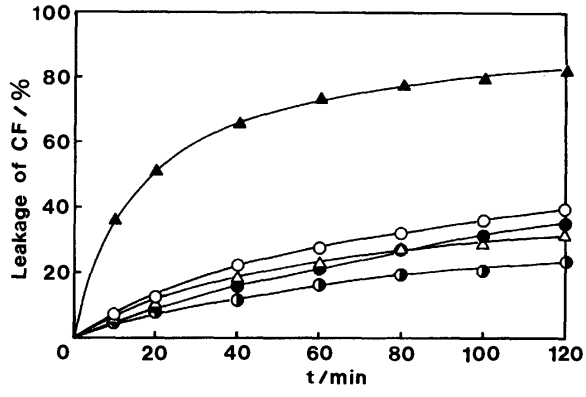

Fig. 7. Leakage of CF from inner aqueous phase of polymerized liposomes at 25 °C. Liposomes were polymerized by; AIBN (●), AAPD (○), potassium peroxodisulfate (△) or both AIBN and AAPD simultaneously (◑). Data for monomeric DODPC liposomes were also shown as reference (▲).

Polymerized liposomes with even 50% polymerization conversion showed excellent membrane stability. The 50% polymerization conversion means the complete polymerization of diene groups in either 1- or 2-acyl chains of lipids as liposome. If certain amount of lipids remained unpolymerized, these liposomes should be in the phase-separated state. For these systems, considerable CF leakage should be observed from the phase boundary.[27] Furthermore, phase separated polymerized liposomes could easily be detected by scanning electron microscopy.[28] These methods might be helpful to analyze the relationship between phase behavior of lipids and membrane stability.

The stability of the liposomes polymerized by both AIBN and AAPD was also examined through the changes of average diameter of the liposomes. The polymerized liposomes were agitated in an aqueous medium at 60 °C, and a small amount of the sample solution was periodically pipetted out and the number-average diameter was determined by a laser particle analyzer. It was confirmed that the polymerized liposomes were actually stable against heat-treating such as 60 °C for over 200 h. The excellent stability should be due to the larger average molecular weight of polymerized DODPC with highly crosslinked state. No diameter change was also found after several temperature cycling between freezing and melting of the polymerized liposomes. The process is well-known as "freeze thaw method" to prepare larger liposomes through liposomal fusion.[29] The polymerized liposomes were revealed to be extremely stable against heating and cooling. Scanning electron microscopy measurements also revealed that the polymerized DODPC liposomes were stable after organic solvent washing. Relatively large DODPC liposomes were polymerized by both AIBN and AAPD, or by potassium peroxodisulfate, and poured into aqueous methanol solution with final methanol content of about 70%. The polymerized liposomes were then characterized by SEM measurements to be stable enough even such a severe conditions. Figure 8 shows stereo-pair of the SEM picture of DODPC liposomes polymerized by potassium peroxodisulfate with polymerization conversion of 80%, and dispersed in an aqueous methanol solution. Spherical liposome structure with no damage was found suggesting that the DODPC liposomes polymerized by radical initiators had excellent membrane stability. Surface of the polymerized DODPC liposomes was smooth but wavy as shown in Fig. 8. For such large polymerized liposomes were generally wavy in surface especially for polymerized DODPC liposomes. This stereo view SEM method is useful to analyze structure for polymerized liposomes especially for the skeletonized ones.[28] The lyophilized DODPC liposomes polymerized by either AIBN or AAPD were stable but soluble in organic solvents such as methanol, ethanol or chloroform under agitation. No liposome structure was seen for these polymeric systems by SEM observation. This fact is the proof of the formation of linear polymers, namely diene groups in 1- and 2-acyl chains can be polymerized selectively.

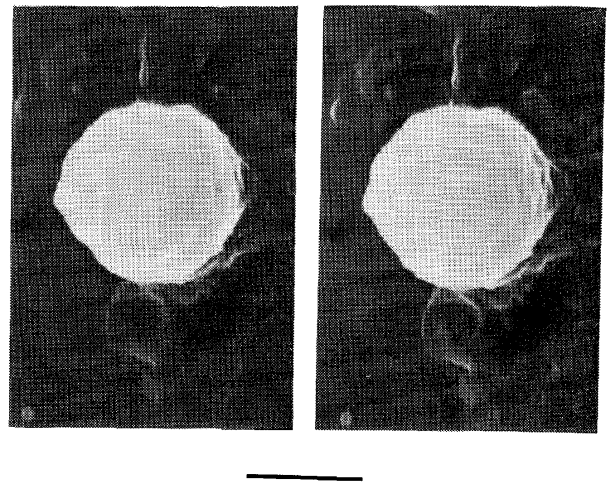

Fig. 8. Stereo pair of scanning electron micrograph of polymerized DODPC liposomes. Space bar indicates 2.0 μm.

It was concluded that radical polymerization behaviors were effectively applied to analyze unequivalent chemical environment of diene groups in both acyl chains. Selective polymerization was also carried out by the suitable selection of the radical initiators.

This work was partially supported by the Grant-in-Aid from the Ministry of Education, Science and Culture (Nos. 61750865 and 62116003).

References

1) This forms part 3 of a series entitled "Polymerization of Diene-containing Lipids as Liposomes by Radical Initiators." Part 2.: Ref. 2.

2) H. Ohno, S. Takeoka, H. Iwai, and E. Tsuchida, *J. Polym. Sci., Polym. Chem. Ed.*, **25**, (1987) in press.

3) S. L. Regen, B. Czech and A. Singh, *J. Am. Chem. Soc.*, **102**, 6638 (1980).

4) D. S. Johnson, S. Sanghera, M. Pons, and D. Chapman, *Biochim. Biophys. Acta*, **602**, 57 (1980).

5) H. H. Hub, B. Hupfer, H. Koch, and H. Ringsdorf, *Angew. Chem., Int. Ed. Engl.*, **19**, 938 (1980).

6) D. F. O'Brien, T. H. Whitesides, and R. T. Klingbiel, *J. Polym. Sci., Polym. Lett. Ed.*, **19**, 95 (1981).

7) L. Gros, H. Ringsdorf, and H. Schupp, *Angew. Chem., Int. Ed. Engl.*, **20**, 305 (1981).

8) B. Hupfer, H. Ringsdorf, and H. Schupp, *Makromol. Chem.*, **182**, 247 (1981).

9) A. Akimoto, K. Dorn, L. Gros, H. Ringsdorf, and H. Schupp, *Angew. Chem., Int. Ed. Engl.*, **20**, 90 (1981).

10) R. Nome, W. Reed, M. Politi, P. Tundo, and J. H. Fendler, *J. Am. Chem. Soc.*, **106**, 8086 (1984).

11) H. Ohno, Y. Ogata, and E. Tsuchida, *J. Polym. Sci., Polym. Chem. Ed.*, **24**, 2959 (1986).

12) H. Ohno, Y. Ogata, and E. Tsuchida, *Macromole-*

cules, **20**, 929 (1987).
13) K. Dorn, R. T. Klingbiel, D. P. Specht, P. N. Tyminski, H. Ringsdorf, and D. F. O'Brien, *J. Am. Chem. Soc.*, **106**, 1627 (1984).
14) H. Ohno, S. Takeoka, N. Hayashi, and E. Tsuchida, *Makromol. Chem., Rapid Commun.*, **8**, 215 (1987).
15) A. Seelig and J. Seelig, *Biochemistry*, **13**, 4839 (1974).
16) A. Seelig and J. Seelig, *Biochim. Biophys. Acta*, **406**, 1 (1975).
17) P. B. Hitchcock, R. Mason, K. M. Thomas, and G. G. Shipley, *Proc. Natl. Acad. Sci., U.S.A.*, **71**, 3036 (1974).
18) E. Lopez, D. F. O'Brien, and T. H. Whitesides, *J. Am. Chem. Soc.*, **104**, 305 (1982); *Biochim. Biophys. Acta*, **693**, 437 (1982).
19) M. Pons, C. Villaverde, and D. Chapman, *Biochim. Biophys. Acta*, **730**, 306 (1983).
20) S. R. Palit, *Makromol. Chem.*, **38**, 96 (1960).
21) J. P. Van Hook and A. V. Tobolsky, *J. Am. Chem. Soc.*, **80**, 779 (1958).
22) J. W. Dreitenbach, K. Kuchner, H. Fritze, and H. Tornowiecki, *Br. Polym. J.*, **2**, 13 (1970).
23) R. M. Noyes, *J. Am. Chem. Soc.*, **77**, 2042 (1955).
24) F. De Schrijver and G. Smets, *J. Polym. Sci., part A-1*, **4**, 2201 (1966).
25) E. Sackmann, *Z. Phys. Chem.*, **101**, 391 (1976).
26) B. Hupfer, H. Ringsdorf, and H. Schupp, *Chem. Phys. Lipids*, **33**, 355 (1983).
27) H. Ohno, K. Ukaji, and E. Tsuchida, *J. Colloid Interf. Sci.*, (1987) in press.
28) H. Ohno, S. Takeoka, and E. Tsuchida, *Polym. Bull.*, **14**, 487 (1985).
29) U. Pick, *Arch. Biochem. Biophys.*, **212**, 186 (1981).

 © 1987 The Chemical Society of Japan Bull. Chem. Soc. Jpn., 60, 2953—2962 (1987)

[2]Metacyclo- and [2]Paracyclo[2](1,3)ferrocenophanes[1)]

Masao HISATOME,* Masamichi YOSHIHASHI, Koji YAMAKAWA, and Yoichi IITAKA†
Faculty of Pharmaceutical Sciences, Science University of Tokyo, Ichigaya-Funagawara, Shinjuku-ku, Tokyo 162
†Faculty of Pharmaceutical Sciences, The University of Tokyo, Hongo, Bunkyo-ku, Tokyo 113
(Received March 26, 1987)

[2]Metacyclo- and [2]paracyclo[2](1,3)ferrocenophanes (**1** and **2**) have been synthesized and characterized by means of X-ray diffraction and spectroscopy. The crystal data of the phanes were determined as follows: **1**, monoclinic, $P2_1$, a=8.851(4), b=15.742(8), c=5.963(3) Å, β=109.76(5)°, Z=2; **2**, orthorhombic, *Pbca*, a=15.308(8), b=24.716(12), c=8.034(4) Å, Z=8. The benzene rings of the both phanes are distorted in a similar manner to [2.2]cyclophanes but the planarities of the cyclopentadienyl (Cp) rings are maintained. The distance between the substituted Cp ring and the iron atom in **1** is considerably extended (1.678(4) Å) in comparison with ferrocene, whereas that of **2** (1.659(3) Å) is not. The 2-hydrogen of the Cp ring and the 9-hydrogen of the benzene ring in **1** are situated right above each other's rings. In the ^{1}H NMR spectrum of 1, the 2- and 9-protons shifted to highfield to a considerable extent (δ 1.18 and 5.34, respectively) due to the diamagnetic anisotropic effects of the benzene and Cp rings. The electronic spectra of both phanes exhibited bathochromic shifts of the d-d absorption band of the iron (**1**, 451 nm, **2**, 447 nm) as compared to [3]metacyclo- and [3]paracyclo[3](1,3)ferrocenophanes (each 442 nm), which were synthesized as reference compounds in this work.

Benzenoid metal π-complexes of cyclophanes have been investigated by many groups in recent years.[2)] On the other hand, there are few reports[3,4)] on intermolecularly bridged (1,3)ferrocenophanes which are ferrocene analogues of the cyclophane π-complexes, although a great number of intramolecular ferrocenophanes and intermolecular (1,1′)ferrocenophanes have been synthesized[5)] since the discovery of ferrocene. One of the reasons why (1,3)ferrocenophanes could not be synthesized until recently would be the difficulty of preparing 1,3-disubstituted ferrocenes, a precursor of the phanes. Since the method obtaining 1,3-disubstituted ferrocene derivatives on a preparative scale was established,[3,4)] it became feasible to synthesize various (1,3)ferrocenophanes by means of conventional methods well-known in preparation of cyclophanes. Incorporation of η^5-C_5H_5 (cyclopentadienyl: Cp) π-complex into [2.2]phane structure is interesting in that it would lead to a more strained system than benzenoid π-complexes. Furthermore, such phanes would enable NMR spectral observation of diamagnetic anisotropy in the upper zone of Cp ring. In this paper we report on the synthesis and characterization of [2]metacyclo- and [2]paracyclo[2](1,3)ferrocenophanes (**1** and **2**),[6,7)]

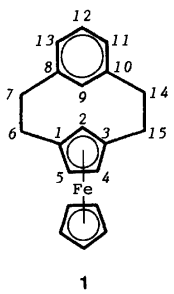

1

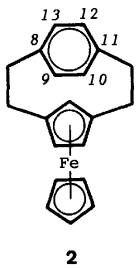

2

which are the first examples of [2.2](1,3)ferrocenophanes. [3]Metacyclo- and [3]paracyclo[3](1,3)ferrocenophanes (**11a** and **11b**) prepared as reference compounds in spectroscopic study are also described.

Results and Discussion

Synthesis. The route via bridge-rearrangement of dithia[3.3]phanes, which is the most convenient method[8-10)] for synthesis of [2.2]phanes, was applied to this work. Dithia[3.3]phanes are generally prepared by coupling of the corresponding mercaptomethyl and bromomethyl derivatives in the presence of base. However, reaction between 1,3-bis(mercaptomethyl)-ferrocene and bis(bromomethyl)benzenes with NaOH or alkali metal/18-crown-6 gave a complex mixture or only a small amount of product. Czeck and Ratajczak[11)] described a coupling reaction between 1,1′-bis-(hydroxymethyl)ferrocene and dimercaptoalkanes with trifluoroacetic acid (TFA) to afford (1,1′)ferrocenophanes. Consequently, the acid catalyzed reaction was applied to the present system. Diol **3** and dithiol **4a** or **4b** were treated with TFA in dichloromethane under

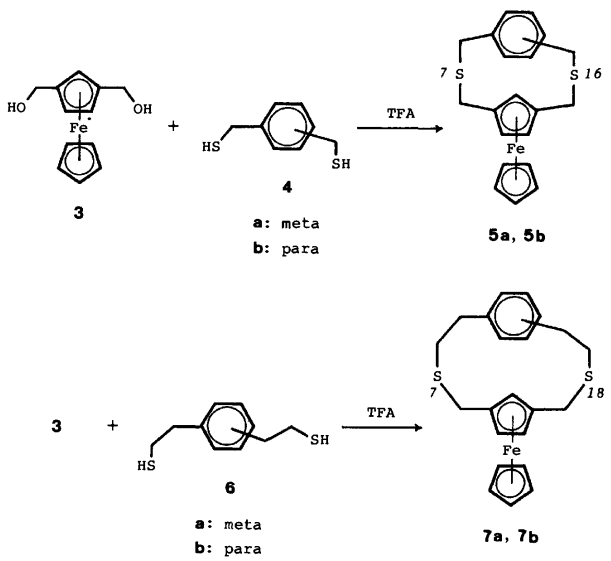

Scheme 1.

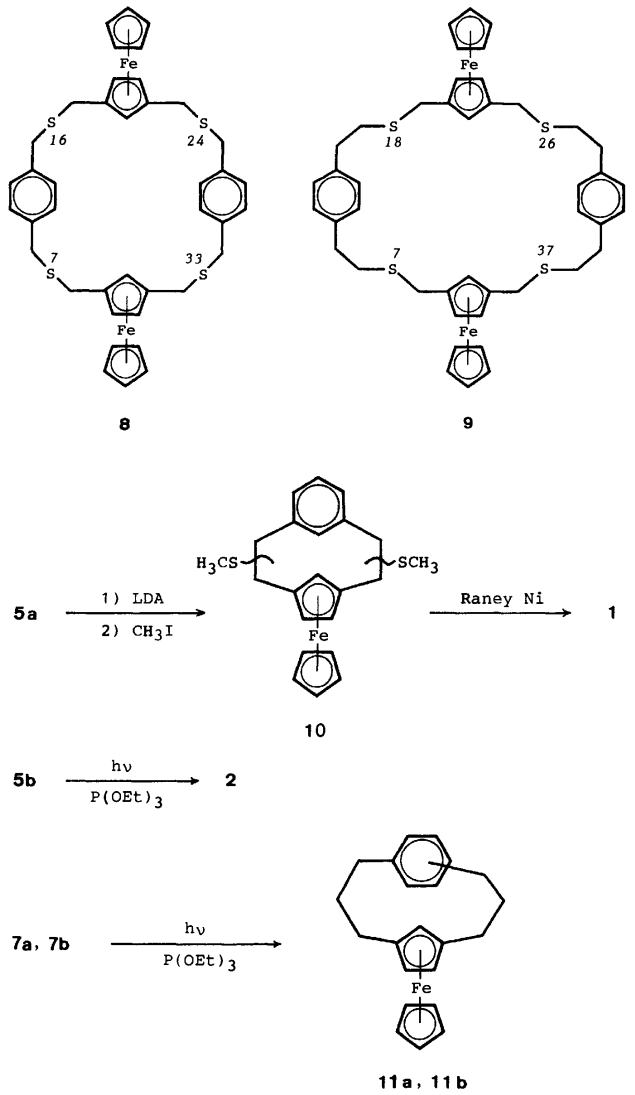

Scheme 2.

high dilution conditions for 15—20 h to give the desired dithia[3.3]ferrocenophanes (**5a**, 55%; **5b**, 21%). In the reaction of **4b** a cyclic dimer **8** containing two benzene rings and two ferrocene moieties was formed in a high yield (67%) besides dithia[3.3]phane **5b**. Macrocyclic dimer **9** was also produced predominantly in the reaction of diol **3** and para-substituted dithiol **6b** (**7b**, 8%, **9**, 62%). The preferential formation of the dimers in the reaction of the para systems is probably due to its thermodynamic stability in comarison with **5b** or **7b**. In fact, treatment of **5b** with TFA gave an equilibrium mixture of **5b** and **8**. The mass spectra of the dimers **8** and **9** by means of the electron impact (EI) ionization showed almost the same spectral patterns as **5b** and **7b**, respectively. The molecular ions of **8** and **9** could be observed only by the field desorption (FD) ionizing technique. The macrocyclic structure of **8** was determined by X-ray crystal analysis.[12]

Methylation of sulfides **5a** and **5b** with Borch reagent[13] to convert these into precursors for Stevens rearrangement[8] afforded only a mixture of unidentifiable products. Wittig rearrangement with lithium diisopropylamide (LDA)/CH_3I was reported by Boekelheide et al.[9] for a convenient synthesis of metacyclophane. An application of the reaction to **5a** gave methylthio[2.2]phane **10** in a good yield (79%). The compound **10** was desulfurized with Raney nickel to give the desired metacyclophane **1**. On the other hand, the Wittig rearrangement of paracycloferrocenophane **5b** afforded only bridge-cleaved compounds in a similar manner as the reaction of paracyclophanes.[9a] Consequently, photochemical extrusion of sulfur bridge[10,14] was attempted. Irradiation of **5b** in triethyl phosphite and benzene with high- or low-pressure

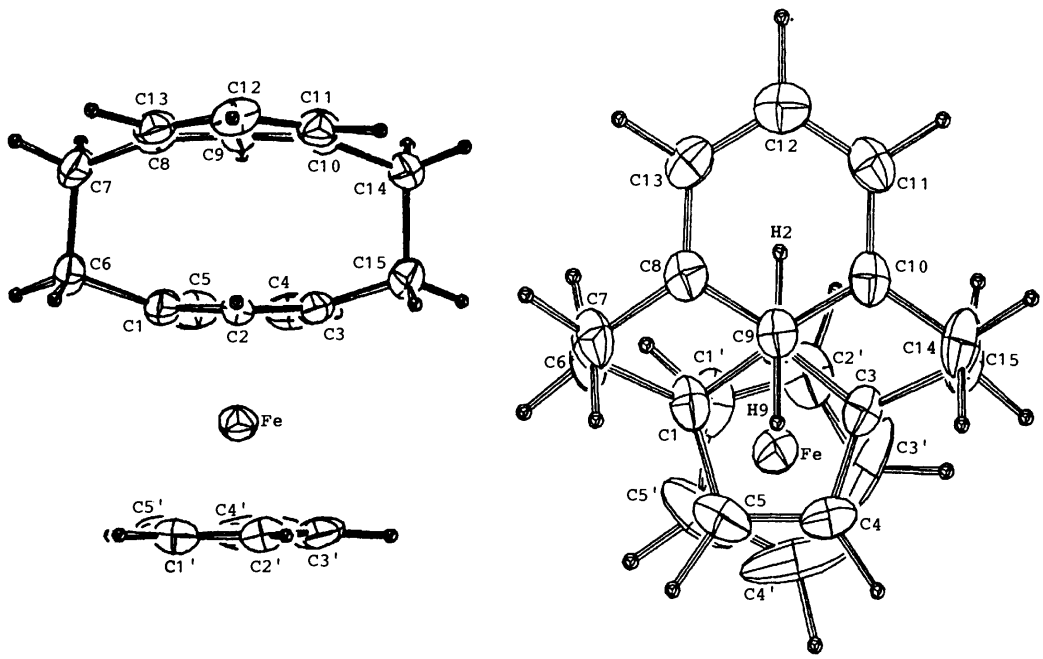

Fig. 1. ORTEP drawings (30% probability thermal ellipsoids) of **1**.

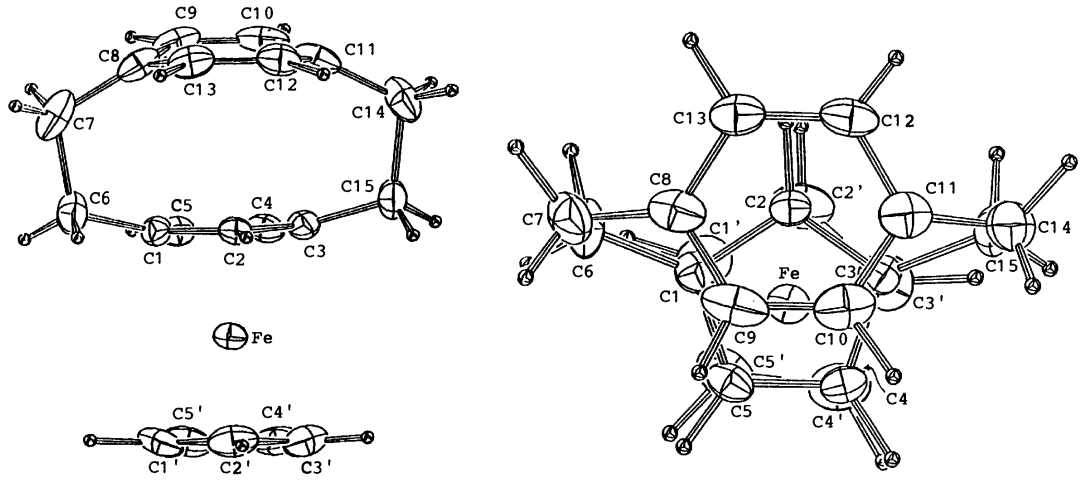

Fig. 2. ORTEP drawings (30% probability thermal ellipsoids) of **2**.

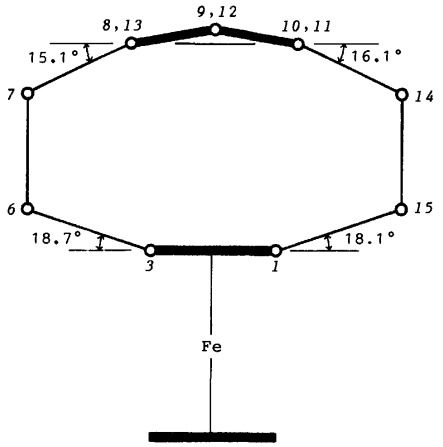

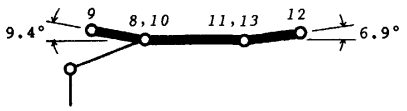

Fig. 3. Selected structural parameters of **1**.

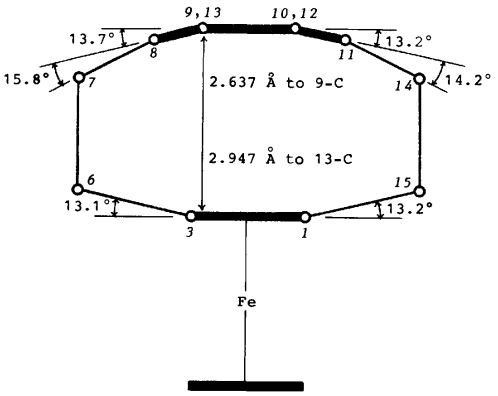

Fig. 4. Selected structural parameters of **2**.

mercury lamp gave [2.2]ferrocenophane **2** in reasonable yields (ca. 50%).

Desulfurization of dithia[4.4]phanes (**7**) was carried out by photochemical method and the corresponding [3.3]phanes **11** were obtained though in low yields.

X-Ray Crystal Structures. The molecular structures and structural parameters of both phanes **1** and **2**

Table 1. Bond Lengths (in Å) of **1** and **2** with Estimated Standard Deviations in Parentheses

Bond	Length		Bond	Length	
	1	**2**		**1**	**2**
Fe-C(1)	2.077(8)	2.086(5)	C(3')-C(4')	1.364(17)	1.408(9)
Fe-C(2)	2.032(7)	2.030(5)	C(4')-C(5')	1.401(23)	1.422(10)
Fe-C(3)	2.091(8)	2.076(5)	C(5')-C(1')	1.424(18)	1.413(9)
Fe-C(4)	2.060(8)	2.042(5)	C(3)-C(6)	1.518(14)	1.513(8)
Fe-C(5)	2.060(8)	2.028(5)	C(6)-C(7)	1.564(12)	1.565(10)
Fe-C(1')	2.018(9)	2.059(6)	C(7)-C(8)	1.509(12)	1.504(10)
Fe-C(2')	2.030(8)	2.037(7)	C(1)-C(15)	1.522(12)	1.498(8)
Fe-C(3')	2.046(10)	2.035(6)	C(14)-C(15)	1.572(12)	1.566(9)
Fe-C(4')	2.000(10)	2.034(6)	C(10)-C(14)	1.518(14)	—
Fe-C(5')	2.024(17)	2.039(7)	C(11)-C(14)	—	1.497(10)
C(1)-C(2)	1.418(13)	1.416(7)	C(8)-C(9)	1.411(13)	1.400(9)
C(2)-C(3)	1.392(10)	1.423(7)	C(9)-C(10)	1.395(10)	1.390(9)
C(3)-C(4)	1.463(15)	1.427(8)	C(10)-C(11)	1.390(13)	1.409(8)
C(4)-C(5)	1.416(13)	1.409(8)	C(11)-C(12)	1.385(15)	1.413(10)
C(5)-C(1)	1.379(12)	1.426(8)	C(12)-C(13)	1.397(13)	1.361(9)
C(1')-C(2')	1.370(18)	1.396(9)	C(13)-C(8)	1.387(13)	1.388(9)
C(2')-C(3')	1.335(13)	1.408(10)			

Table 2. Bond Angles (in Degree) **1** and **2** with Estimated Standard Deviations in Parentheses

Bond	Angle		Bond	Angle	
	1	**2**		**1**	**2**
C(5)-C(1)-C(2)	108.2(7)	105.5(5)	C(2)-C(1)-C(15)	120.3(7)	123.2(5)
C(1)-C(2)-C(3)	109.8(7)	110.2(4)	C(5)-C(1)-C(15)	128.5(8)	129.8(5)
C(2)-C(3)-C(4)	105.7(7)	106.4(4)	C(1)-C(15)-C(14)	108.0(7)	112.0(5)
C(3)-C(4)-C(5)	107.5(8)	108.0(5)	C(15)-C(14)-C(10)	112.2(8)	—
C(4)-C(5)-C(1)	108.7(8)	109.7(5)	C(9)-C(10)-C(14)	118.8(7)	—
C(5′)-C(1′)-C(2′)	107.9(11)	107.7(6)	C(11)-C(10)-C(14)	121.0(8)	—
C(1′)-C(2′)-C(3′)	108.8(9)	108.6(6)	C(15)-C(14)-C(11)	—	110.5(5)
C(2′)-C(3′)-C(4′)	109.9(10)	108.3(6)	C(10)-C(11)-(Cl4)	—	121.4(6)
C(3′)-C(4′)-C(5′)	108.2(11)	107.1(6)	C(12)-C(11)-C(14)	—	121.3(6)
C(4′)-C(5′)-C(1′)	105.1(12)	108.2(6)	C(13)-C(8)-C(9)	118.7(7)	116.4(6)
C(2)-C(3)-C(6)	124.2(8)	122.1(5)	C(8)-C(9)-C(10)	120.8(8)	121.5(6)
C(4)-C(3)-C(6)	126.6(8)	130.0(5)	C(9)-C(10)-C(11)	118.9(8)	120.1(6)
C(3)-C(6)-C(7)	108.1(8)	111.6(5)	C(10)-C(11)C(12)	119.8(8)	115.1(6)
C(6)-C(7)-C(8)	111.6(7)	110.8(6)	C(11)-C(12)-C(13)	121.0(9)	122.4(6)
C(7)-C(8)-C(9)	117.7(7)	121.6(6)	C(12)-C(13)-C(8)	119.4(8)	120.7(6)
C(7)-C(8)-C(13)	122.3(7)	119.4(6)			

Table 3. Deviations of Atoms from Least-Squares Planes[a] through the Cp Rings of **1** and **2** with Estimated Standard Deviations in Parentheses

Atom	Deviation/Å	
	1	**2**
	Bridged ring[b]	Bridged ring[d]
C(1)	−0.020(6)	−0.022(4)
C(2)	0.025(6)	0.025(4)
C(3)	−0.019(6)	−0.018(4)
C(4)	0.007(6)	0.004(4)
C(5)	0.008(7)	0.011(4)
C(6)	−0.507(6)	−0.360(5)
C(15)	−0.494(7)	−0.365(5)
Fe	1.678(4)	1.659(3)
	Unsubstituted ring[c]	Unsubstituted ring[e]
C(1′)	0.000(9)	0.006(5)
C(2′)	−0.011(8)	−0.007(5)
C(3′)	0.018(8)	0.006(5)
C(4′)	−0.017(9)	−0.002(5)
C(5′)	0.010(11)	−0.003(5)
Fe	−1.649(6)	−1.652(4)

a) The least-squares planes are shown in *b*—*e*. b) $0.6411X+0.7012Y+0.3119Z=3.3642$. c) $0.6475X+0.7070Y+0.2844Z=6.6805$. d) $-0.7237X+0.4495Y+0.5237Z=-0.3052$. e) $-0.7402X+0.4272Y+0.5193Z=2.9045$.

are shown in Figs. 1—4 and Tables 1—3. The two aromatic moieties of meta-ferrocenophane **1** are in an anti conformation in analogy with [2.2]metacyclophane.[15] The 2-hydrogen of the Cp ring and the 9-hydrogen of the benzene ring are situated right above each other's rings. The distances between the 9-hydrogen and the Cp ring carbons are 2.60(6)—2.65(6) Å and those between the 2-hydrogen and the benzene carbons are 2.80(6)—3.16(7) Å. The benzene and the bridged Cp ring in para-ferrocenophane **2** are more stacked over each other than those of **1**.

The benzene rings of both phanes **1** and **2** are distorted in a similar manner to [2.2]cyclophanes[15-17] and tricarbonylchromium complex of [2.2]paracyclophane.[18] The deformation of the benzene moiety in **2** is somewhat larger than those of [2.2]paracyclophane.[16] and its metal complex.[18] On the other hand, the Cp carbon atoms of both **1** and **2** deviate only slightly from their least-squares planes (Table 3) and the planarities of the bridged Cp rings are almost maintained in spite of their highly strained structures. However, the deviations of the methylene carbons at 6- and 15-positions from the Cp planes are extremely large. The bond of the Cp ring and 6-carbon (or 15-carbon) in **1** is more bent than that of **2** (Fig. 3). This great bending in **1** indicates that its methylene bridges are more strained than that of **2** due to the rigid meta-substituted benzene ring in comparison with the para-substituted ring.

The distance between the iron atom and the bridged Cp ring plane of **1** is considerably extended (1.678(4) Å) as compared to ferrocene (1.66 Å),[19] whereas that of **2** (1.659(3) Å) is almost similar to ferrocene. The distance of **1** is the largest of ferrocene derivatives previously described. These results in X-ray crystal analysis indicate that **1** is an extremely strained compound in comparison with **2** or other [2.2]cyclophanes.

NMR Spectra. In the ^{1}H NMR spectrum of dithia-[3.3]meta-ferrocenophane **5a**, the signals of the 2- and 4,5-protons on the Cp ring appear at δ 3.97 and 3.65, respectively (ferrocene, δ 4.04). The corresponding Cp ring protons of [3.3]meta-ferrocenophane **11a** resonate at δ 3.85 and 3.27. The upfield shifts of the 4,5-protons in comparison with the 2-protons in **5a** and **11a** indicate that these phanes are in syn conformations. The conformational features of the [3.3]meta-ferrocenophanes are similar to those of [3.3]metacyclophane[20] and [3.3](1,3)ferrocenophane.[4]

In contrast to the [3.3]phanes, the signal of the 2-proton of [2.2]meta-ferrocenophane **1** dramatically

shifted to a high field (δ 1.18), whereas the 4,5-proton signal appeared at δ 3.75. The chemical shift difference ($\Delta\delta$) between the 2-protons of **1** and a reference compound (1,3-diethylferrocene) is 2.82 ppm. The value is larger than those of the corresponding aromatic protons in [2.2]metacyclophanes ($\Delta\delta$=2.62 ppm),[21] [2]metacyclo[2](1,3)azulenophane ($\Delta\delta$=2.34 ppm),[22] and [2]metacyclo[2](5,7)azulenophane ($\Delta\delta$= 2.46 ppm).[23] This extremly high field shift of the 2-proton signal in **1** reflects its molecular structural feature revealed by X-ray crystal analysis; the 2-hydrogen is situated right above the benzene ring plane.

On the other hand, the benzenoid 9-proton of **1** resonates at δ 5.34 and the upfield shift difference ($\Delta\delta$) from the coresponding signal of a reference compound (1,3-diethylbenzene) is 1.58 ppm. Despite unusually close proximity of the 9-proton to the Cp ring plane, the upfield shift value is smaller than that of the 2-proton. This shift behavior of the 9-proton indicates that the shielding effect of the above zone of the Cp ring is smaller than that of benzene ring. Muray and Fox[24] determined the magnetic susceptibilities of ferrocene and found the magnetic anisotropy of the molecule. Turbit and Watts[25] presented a map of the shielding and deshielding zone around ferrocene molecule based on the result of the susceptibilities and discussed on the proton chemical shifts of ferrocene derivatives. However, the shielding shift value of the proton situated right above the Cp ring plane has not been detected until recently. Musso et al.[26] reported on the ^{1}HNMR spectra of 1,1′,3,3′-tetramethyl-2,2′-bis(2,4,6-trialkylphenyl)ferrocenes having "*exo*" alkyl groups which are located on the shielding zone of ferrocene nucleus. The upfield shift difference of the alkyl protons from the reference proton shifts are 0.49—0.74 ppm. The shift difference of the 9-proton (1.58 ppm) of **1** is the largest value in the upfield shifts due to the diamagnetic anisotropy of ferrocene nucleus.

The ^{13}CNMR spectra of **1** and **2** show unusual paramagnetic shifts of the inner aromatic carbon signals at 2- and 9-positions (2- and 9-carbons of **1**, δ 72.90 and 139.07; 2-carbon of **2**, δ 72.32). Such downfield shifts of the inner aromatic carbon resonance are generally observed in [2.2]metacyclophanes,[27] but the chemical shift difference of the benzenoid 9-carbon in **1** ($\Delta\delta$=9.0 ppm) from the corresponding signal of *m*-xylene is larger than that of [2.2]metacyclophane ($\Delta\delta$=6.2 ppm). The shift difference of the 2-carbons in **1** and **2** from that of 1,3-diethylferrocene is 5.7 and 5.1 ppm, respectively. The downfield shifts of those carbons of **1** and **2** seem to reflect the proximity of the carbons to the other aromatic rings. The major origin of the shift is attributable to rehybridization due to excessive strain and direct *p*-orbital compression.[27]

Electronic Spectra. The most remarkable difference in the electronic absorption spectra in ethanol between [2.2]phanes (**1**, **2**) and [3.3]phanes (**11a**, **11b**) is seen in the d-d absorption band near 440 nm. The bands of **1** and **2** appear at 451 and 447 nm (ε=150 and 140), respectively, whereas both **11a** and **11b** exhibit the band at wavelength of 442 nm (ε=130 and 110, respectively) similar to that of 1,3-diethylferrocene (439 nm, ε=110). Pronounced difference in absorption coeficient between [2.2]phanes and [3.3]phanes was not seen in these band. The origin of the bathochromic shifts in **1** and **2** would be mainly attributed to the following factors: (i) Some transannular π-electronic interactions between the two aromatic rings, and (ii) a change of the electronic state in the d-orbital of the iron due to excessive strain.

In the study on intramolecularly bridged ferrocenophanes we found that there was a linear relationship between the wavelengths of the d-d absorption and the Cp-Fe-Cp distances in the X-ray crystal structure.[28] This correlation almost holds for **1** although the wavelength of **2** slightly deviates from the straight line.[28] The elongation of the Cp-Fe distance in **1** should result in a change of the d-electronic configuration of the iron and a shift of the d-d absorption. On the other hand, the large bathochromic shift of the band was observed in [3.3](1,3)ferrocenophane (488 nm)[4] having a strainless molecular structure based on the inspection of a molecular model. Kasahara et al.[4] described that the shift was probably due to a transannular π-electronic interaction between the two ferrocene moieties. Transannular intraction between the Cp and benzene rings should be present in [2.2]ferrocenophanes (**1** and **2**), because the two ring planes approach each other. Therefore, it is likely that the bathochromic shifts of the d-d absoption band in **1** and **2** are caused by the two factors mentioned above, although the degree of their contribution cannot be estimated.

The absorption shoulders in the region near 300 nm in [2.2]phanes **1**, **2** and [3.3]phanes **11a**, **11b** are somewhat swollen in comparison with 1,3-diethylferrocene. The swellings possibly arise from some change of electronic configuration in benzene moieties due to charge-transfer intraction with the Cp ring, because the absorption bands based on the interaction between two benzene rings in cyclophanes are observed in this region.

Experimental

All melting points were uncorrected. NMR spectra were measured on a JEOL JNM-FX100 spectrometer relative to tetramethylsilane as an internal standard. The assignments of the signals were made by homo- (^{1}H{^{1}H}) and selective hetero-nuclear (^{13}C{^{1}H}) decoupling technique. Mass spectra were obtained with a Hitachi RMU-7M or a Hitachi M-80 double focusing mass spectrometer by electron impact (EI) ionizing technique at 70 eV unless otherwise stated. Field desorption (FD) ionization was carried out using a carbon or silicon emitter and the FD mass spectra were measured on

the M-80 spectrometer. Empirical formulae of oily or unstable compounds were determined by means of high-resolution mass spectra, which were analyzed on a Hitachi M-003 data processing system. Electronic absorption spectra were recorded on a Hitachi 323 spectrophotometer in ethanol. 1,3-Bis(hydroxymethyl)ferrocene (**3**) (mp 115—117 °C),[3] 1,3-bis(mercaptoethyl)benzene (**6a**) (oil),[29] and 1,4-bis(mercaptoethyl)benzene (**6b**) (oil)[29] were prepared according to the usual procedures.

General Procedures. Coupling reaction between diol **3** and bis(mercaptoalkyl)benzenes **4**, **6** with trifluoroacetic acid (TFA): Dichloromethane freshly distilled from CaH_2 was used as solvent and oxygen in the solvent was removed as much as possible by ultrasonic vibration followed by bubbling dry nitrogen gas immediately before use. Each solution of 1,3-bis(hydroxymethyl)ferrocene (**3**) and the corresponding bis(mercaptoalkyl)benzene (1 mol equiv to **3**) in dichloromethane was added dropwise to a stirring solution of TFA in dichloromethane under a nitrogen atmosphere. The solvent was used in enough volume to keep a high dilution condition (concn of **3**: ca. 10^{-3} mol dm^{-3}) of the reaction system. The reaction mixture was stirred in the dark at room temperature. Saturated aq $NaHCO_3$ was added and the organic layer was phase-separated, washed with saturated aq NaCl, dried over Na_2SO_4 and evaporated. The residue was column-chromatographed to isolate the coupling products.

Photochemical extrusion of sulfur: A solution of sulfide in benzene and triethyl phosphite was placed in a qualtz tube. A stream of argon gas was bubbled through the solution for 30 min. External irradiation was carried out using a 100 W high pressure mercury lamp (Ushio electric Inc. UM-102 type) or eight of 30 W low pressure mercury lamps (The Southern N.E. Ultraviolet Co., Royal type RS Preparative Photochemical Reactor). The temperature of the reaction mixture was maintained below 30 °C with the aid of a water bath throughout irradiation. After evaporating benzene and triethyl phosphite in vacuo, the residue was column-chromatographed over silica gel.

7,16-Dithia[3]metacyclo[3](1,3)ferrocenophane (5a). Each solution of diol **3** (400 mg, 1.6 mmol) and 1,3-bis(mercaptomethyl)benzene (**4a**) (276 mg, 1.6 mmol) in dichloromethane (each 200 ml) was added to a solution of TFA (1.8 g, 16 mmol) in dichloromethane (1200 ml), and the mixture was stirred for 20 h. The product was column-chromatographed over silica gel, and the first band eluted with hexane-dichloromethane (1 : 1) yielded sulfide **5a** (339 mg, 55%), which was recrystallized from hexane-benzene to give yellow needles; mp 136—137 °C. ^{1}H NMR ($CDCl_3$) δ=3.51 and 3.71 (each 2H, an AB system, J=14.5 Hz, 6, 17-H), 3.53 and 3.69 (each 2H, an AB system, J=11.5 Hz, 8, 15-H), 3.65 (2H, d, J=1.4 Hz, 4, 5-H), 3.93 (5H, s, unsubstd. Cp-H), 3.97 (1H, t, J=1.4 Hz, 2-H), 6.79 (1H, bs, 10-H), 6.90—7.00 (3H, m, 12, 13, 14-H); ^{13}C NMR ($CDCl_3$) δ=33.04 (6, 17-C), 37.13 (8, 15-C), 68.37 (4, 5-C), 68.81 (unsubstd. Cp-C), 72.51 (2-C), 84.60 (1, 3-C), 126.31 (12, 14-C), 127.96 (13-C), 131.57 (10-C), 137.95 (9, 11-C); MS m/z (rel intensity) 380 (100, M$^+$), 315 (50), 222 (21), 193 (23), 135 (33), 121 (56), 91 (93); FD-MS m/z 380 (M$^+$).

Found: C, 64.06; H, 5.39; S, 15.99%; M$^+$, m/z 380.0349. Calcd for $C_{20}H_{20}S_2Fe \cdot 1/6C_6H_6$: C, 64.12; H, 5.38; S, 16.30%; M for $C_{20}H_{20}S_2Fe$, 380.0353.

The second band eluted with hexane-dichloromethane (1 : 2) yielded a yellow powder (218 mg), which was possibly a mixture of oligomer and polymers.

7,16-Dithia[3]paracyclo[3](1,3)ferrocenophane (5b). Each solution of diol **3** (200 mg, 0.81 mmol) and 1,4-bis(mercaptomethyl)benzene **4b** (138 mg, 0.81 mmol) in dichloromethane (each 100 ml) was added to a solution of TFA (0.92 g, 8.1 mmol) in dichloromethane (600 ml), and the mixture was stirred for 15 h. The product was column-chromatograghed over silica gel, and the first band eluted with hexane-dichloromethane (1 : 1) yielded sulfide **5b** (66 mg, 21%), which was recrystallized from benzene-ethyl acetate to give yellow needles; mp 172—173 °C (decomp). ^{1}H NMR ($CDCl_3$) δ=2.89 (1H, t, J=1.4 Hz, 2-H), 3.20 and 3.46 (each 2H, an AB system, J=14.5 Hz, 6, 17-H), 3.79 (4H, s, 8, 15-H), 3.84 (5H, s, unsubstd. Cp-H), 3.91 (2H, d, J=1.4 Hz, 4, 5-H), 6.95 and 7.01 (each 2H, an AA'BB' system, Ph-H); ^{13}C NMR ($CDCl_3$) δ=32.02 (6, 17-C), 38.11 (8, 15-C), 67.59 (4, 5-C), 68.71 (unsubstd. Cp-C), 69.49 (2-C), 86.49 (1, 3-C), 128.11 (10, 11-C), 130.45 (13, 14-C), 137.56 (9, 12-C); MS m/z (rel intensity) 380 (100, M$^+$), 315 (12), 244 (10), 212 (8), 185 (9), 121 (12), 91 (20); FD-MS m/z 380 (M$^+$).

Found: C, 62.96; H, 5.29; S, 16.68%; M$^+$, m/z 380.0364. Calcd for $C_{20}H_{20}S_2Fe$: C, 63.16; H, 5.30; S, 16.86%; M, 380.0353.

The second band eluted with hexane-dichloromethane (1 : 2) yielded 7,16,24,33-tetrathia[3]paracyclo[3](1,3)ferroceno-[3]paracyclo[3](1,3)ferrocenophane (**8**) (206 mg, 67%), which was recrystallized from benzene-ethyl acetate to give orange-yellow needles; mp 172—174 °C (decomp). ^{1}H NMR ($CDCl_3$) δ=3.34 and 3.39 (each 2H, an AB system, J=14.5 Hz, $CpCH_2$-), 3.62 (4H, s, $PhCH_2$-), 3.96 (1H, t, J=1.4 Hz, 2-H), 4.02 (5H, s, unsubstd. Cp-H), 4.13 (2H, d, J=1.4 Hz, 4, 5-H), 7.19 (4H, s, Ph-H); ^{13}C NMR ($CDCl_3$) δ=30.82 ($CpCH_2$-), 35.23 ($PhCH_2$-), 68.69 (4, 5-C), 69.45 (unsubstd. Cp-C), 70.28 (2-C), 84.90 (1, 3-C), 129.05 (unsubstd. C of Ph), 136.91 (substd. C of Ph); MS m/z (rel intensity) 760 (0, M$^+$), 380 (100), 315 (13), 244 (12), 212 (5), 185 (8), 121 (16), 91 (23); FD-MS m/z 760 (M$^+$).

Found: C, 63.10; H, 5.28; S, 16.61%. Calcd for $C_{40}H_{40}S_4Fe_2$: C, 63.16; H, 5.30; S, 16.86%.

7,18-Dithia[4]metacyclo[4](1,3)ferrocenophane (7a). Each solution of diol **3** (400 mg, 1.6 mmol) and 1,3-bis(2-mercaptoethyl)benzene **6a** (320 mg, 1.6 mmol) in dichloromethane (each 200 ml) was added to a solution of TFA (1.9 g, 17 mmol) in the same solvent (1200 ml), and the mixture was stirred for 18 h. The product was column-chromatographed over silica gel, and the first band eluted with hexane-dichloromethane (1 : 1) yielded sulfide **7a** (530 mg, 80%), which was recrystallized from hexane-benzene to give yellow plates; mp 148—149 °C. ^{1}H NMR ($CDCl_3$) δ=2.74 (8H, s, 8, 9, 16, 17-H), 3.49 (4H, s, 6, 19-H), 4.06 (5H, s, unsubstd. Cp-H), 4.11 (1H, t, J=1.4 Hz, 2-H), 4.15 (2H, d, J=1.4 Hz, 4, 5-H), 6.65—7.15 (4H, m, Ph); ^{13}C NMR ($CDCl_3$) δ=30.46, 31.43 and 34.45 (methylene-C), 68.90 (4,5-C), 69.49 (unsubstd Cp-C), 70.80 (2-C), 85.23 (1, 3-C), 126.60 (13, 15-C), 127.14 and 127.67 (11, 14-C), 140.04 (10, 12-C); MS m/z (rel intensity) 408 (100, M$^+$), 343 (29), 252 (23), 251 (35), 218 (14), 206 (20), 121 (33), 91 (56); FD-MS m/z 408 (M$^+$).

Found: C, 65.87; H, 6.47; S, 15.05%; M$^+$, m/z 408.0649. Calcd for $C_{22}H_{24}S_2Fe \cdot 1/6C_6H_6$: C, 65.55; H, 5.98; S, 15.22%; M for $C_{22}H_{24}S_2Fe$, 408.0666.

7,18-Dithia[4]paracyclo[4](1,3)ferrocenophane (7b). Each solution of diol **3** (284 mg, 1.2 mmol) and 1,4-bis(2-mercaptoethyl)benzene **6b** (228 mg, 1.2 mmol) in dichlo-

romethane (each 200 ml) was added to a solution of TFA (13.1 g, 1.2 mmol) in dichloromethane (750 ml), and the mixture was stirred for 2 h. The product was column-chromatographed over silica gel. The first band eluted with hexane-dichloromethane (1 : 1) yielded sulfide **7b** (38 mg, 8%), which was recrystallized from hexane-benzene to give yellow needles; mp 163—164 °C (decomp). ^{1}H NMR ($CDCl_3$) δ=2.40—3.00 (8H, m, 8, 9, 16, 17-H), 3.23 (4H, s, 6, 19-H), 3.60 (1H, t, J=1.4 Hz, 2-H,), 3.78 (2H, d, J=1.4 Hz, 4, 5-H), 3.92 (5H, s, unsubstd. Cp-H), 6.88 and 6.94 (4H, an AA'XX' system, Ph-H); ^{13}C NMR ($CDCl_3$) δ=33.72, 35.23 and 35.43 (methylene-C), 68.71 (4, 5-C), 69.49 (unsubstd. Cp-C), 69.70 (2-C), 85.86 (1, 3-C), 128.50 (unsubstd. C of Ph), 137.37 (substd. C of Ph); MS m/z (rel intensity) 408 (100, M^+), 343 (33), 252 (27), 206 (19), 181 (8), 121 (27), 91 (34); FD-MS m/z 408 (M^+).

Found: C, 65.48; H, 6.43; S, 15.27%; M^+, m/z 408.0676. Calcd for $C_{22}H_{24}S_2Fe \cdot 1/6C_6H_6$: C, 65.55; H, 5.98; S, 15.22%; M for $C_{22}H_{24}S_2Fe$, 408.0666.

The second band eluted with hexane-dichloromethane (1 : 2) yielded 7,18,26,37-tetrathia[4]paracyclo[4](1,3)ferroceno-[4]paracyclo[4](1,3)ferrocenophane (**9**) (292 mg, 62%). Recrystallization of **9** from hexane-benzene gave yellow needles; mp 196—197 °C (decomp). ^{1}H NMR ($CDCl_3$) δ=2.40—2.80 (8H, m, $PhCH_2CH_2$-), 3.49 (4H, s, $CpCH_2$-), 4.08 (5H, s, unsubstd. Cp-H), 3.14 (2H, d, J=1.4 Hz, 4, 5-H), 4.22 (1H, t, J=1.4 Hz, 2-H), 6.86 (4H, s, Ph-H); ^{13}C NMR ($CDCl_3$) δ=31.87, 32.80 and 36.01 (methylene-C), 68.71 (4, 5-C), 69.54 (unsubstd. Cp-C), 69.83 (2-C), 85.71 (1, 3-C), 128.35 (unsubstd. C of Ph), 138.49 (substd. C of Ph); FD-MS m/z 816 (M^+).

Found: C, 64.90; H, 6.24; S, 15.65%. Calcd for $C_{44}H_{48}S_4Fe_2$: C, 64.70; H, 5.92; S, 15.70%.

[2]Metacyclo[2](1,3)ferrocenophane (1). A solution of lithium diisopropyl amide (LDA) in hexane-THF (0.81 ml, 0.65 mmol) was added dropwise to a solution of dithia[3]-metacyclo[3]ferrocenophane (**5a**) (100 mg, 0.26 mmol) in THF (2 ml) under an argon atmosphere at room temperature. After stirring for 3 min, iodomethane (0.08 ml, 1.3 mmol) was added to the brownish yellow solution. The resulting pink solution was stirred for 5 min at room temperature and water was added. The mixture was extracted with dichloromethane, and the organic layer was washed with saturated aq NaCl, dried over $CaCl_2$ and evaporated. The residue was column-chromatograghed over silica gel with hexane-dichloromethane (1 : 1) to yield a mixture of rearrangement products **10** (84 mg, 79%) from the first eluted band. Recrystallization of **10** from hexane-benzene gave orange-yellow crystals; mp 178—181 °C (decomp). ^{1}H NMR ($CDCl_3$, only assignable peaks) δ=1.25 (t, 2-H), 1.95 and 2.09 (each s, SCH_3), 3.98 (s, unsubstd. Cp-H), 5.40 and 5.87 (each bt, 9-H), 6.80—7.50 (m, Ph-H).

Found: M^+, m/z 408.0671. Calcd for $C_{22}H_{24}Fe$: M, 408.0666.

A suspension of methyl sulfide **10** (32 mg, 0.08 mmol) and active Raney nickel(W-7) in ethanol (10 ml) was refluxed for 30 min. The mixture was filtered and evaporation of the filtrate left [2]metacyclo[2](1,3)ferrocenophane (**1**) (24 mg, 98%), which was recrystallized from methanol to give orange-yellow needles; mp 131—132 °C. ^{1}H NMR ($CDCl_3$) δ=1.18 (1H, t, J=1.4 Hz, 2-H), 1.82, 2.22, 2.55, and 2.90 (each 2H, m, methylene-H), 3.75 (2H, d, J=1.4 Hz, 4, 5-H), 3.97 (5H, s, unsubstd. Cp-H), 5.34 (1H, m, 9-H), 6.80—7.15 (3H, m, 11, 12, 13-H). ^{13}C NMR ($CDCl_3$) δ=32.21 (6, 15-C), 39.52 (7, 14-C), 64.71 (4, 5-C), 67.35 (unsubstd. Cp-C), 72.90 (2-C), 89.22 (1, 3-C), 125.38 (11, 12, 13-C), 127.87 (12-C), 139.07 (9-C), 140.15 (8, 10-C); MS m/z (rel intensity) 316 (100, M^+), 246 (13), 222 (9), 191 (6), 190 (6), 189 (6), 165 (6), 121 (17).

Found: C, 75.67; H, 6.59%, M^+, m/z 316.0904. Calcd for $C_{20}H_{20}Fe$: C, 75.96; H, 6.37%, M, 316.0912.

[2]Paracyclo[2](1,3)ferrocenophane (2). A solution of dithia[3]paracyclo[3]ferrocenophane **5b** (30 mg, 0.08 mmol) in benzene (24 ml) and triethyl phosphite (48 ml) was irradiated with a high-pressure mercury lamp for 18 h. On column chromatography of the product over silica gel with hexane-ether (1 : 1), the first band yielded [2]paracyclo-[2](1,3)ferrocenophane (**2**) (13 mg, 53%), which was recrystallized from methanol to give orange-yellow needles; mp 106—107 °C. ^{1}H NMR ($CDCl_3$) δ=2.00—3.15 (8H, m, methylene-H), 2.37 (1H, t, J=1.4 Hz, 2-H), 3.37 (2H, d, J=1.4 Hz, 4, 5-H), 3.87 (5H, s, unsubstd. Cp-H), 6.23 and 6.93 (each 2H, an AA'XX' system, Ph-H); ^{13}C NMR ($CDCl_3$) δ=28.26 (6, 15-C), 35.62 (7, 14-C), 64.76 (4, 5-C), 67.20 (unsubstd. Cp-C), 72.32 (2-C), 90.00 (1, 3-C), 129.82 and 131.77 (unsubstd. C of Ph), 139.95 (substd. C of Ph); MS m/z (rel intensity) 316 (97,

Table 4. Crystal Data and Some Conditions for Data Collections

	1	2
Formula	$C_{20}H_{20}Fe$	$C_{20}H_{20}Fe$
Molecular weight	316.23	316.23
Crystal dimensions/mm	0.015×0.060×0.30	0.17×0.10×0.60
Crystal system	Monoclinic	Orthorhombic
Space group	$P2_1$	*Pbca*
a/Å	8.851(4)	15.308(8)
b/Å	15.742(8)	24.716(12)
c/Å	5.963(3)	8.034(4)
β/°	109.76(5)	—
Z	2	8
V/Å^3	781.9	3039.7
D_x/g cm^{-1}	1.343	1.382
λ/Å	1.5418(Cu $K\alpha$)	0.7107(Mo $K\alpha$)
μ/cm^{-1}	76.5(Cu $K\alpha$)	9.81(Mo $K\alpha$)
Scan speed (2θ min^{-1})	4	6
Independent reflections used [$I_0 > 2\sigma(I_0)$]	1326	1552
2θ range	6°—156°	6°—50°
Final R value	0.053	0.046

Table 5. Atomic Coodinates ($\times10^5$ for Fe; $\times10^4$ for C; $\times10^3$ for H) and Isotropic Equivalent Thermal Parameters (in Å^2 Unit) of **1** with Estimated Standard Deviations in Parentheses

Atom	x	y	z	B_{eq}	Atom	x	y	z	B_{eq}
Fe	82867(13)	0(0)	74706(20)	4.26	H(2)	693(8)	−137(5)	934(12)	
C(1)	8034(9)	−1273(5)	6495(15)	4.22	H(4)	572(8)	21(6)	297(12)	
C(2)	7010(8)	−1040(4)	7778(13)	3.64	H(5)	829(8)	−79(5)	317(12)	
C(3)	5917(9)	−429(5)	6509(17)	4.81	H(6a)	439(9)	−28(4)	873(13)	
C(4)	6366(11)	−232(5)	4419(16)	5.98	H(6b)	377(7)	35(4)	605(11)	
C(5)	7671(11)	−766(6)	4496(14)	5.18	H(7a)	287(9)	−95(5)	353(14)	
C(6)	4298(10)	−271(5)	6786(20)	6.32	H(7b)	199(8)	−99(5)	584(12)	
C(7)	3138(9)	−1003(6)	5484(17)	5.68	H(9)	521(8)	−178(5)	378(12)	
C(8)	3881(8)	−1865(5)	6234(14)	4.32	H(11)	690(9)	−367(5)	922(13)	
C(9)	4981(10)	−2164(5)	5168(15)	4.08	H(12)	477(9)	−323(5)	1085(12)	
C(10)	6125(9)	−2776(5)	6296(15)	4.52	H(13)	273(10)	−217(6)	875(15)	
C(11)	5997(10)	−3195(5)	8275(16)	5.29	H(14a)	736(9)	−277(5)	371(13)	
C(12)	4773(11)	−2983(7)	9130(15)	5.95	H(14b)	820(8)	−348(5)	616(12)	
C(13)	3777(9)	−2286(6)	8220(15)	5.05	H(15a)	936(8)	−227(5)	893(12)	
C(14)	7649(10)	−2832(6)	5674(18)	5.93	H(15b)	994(9)	−213(5)	634(13)	
C(15)	8898(9)	−2125(6)	6956(18)	5.76	H(1′)	1167(8)	−10(6)	896(12)	
C(1′)	10633(10)	301(9)	8931(23)	11.15	H(2′)	1029(8)	−8(6)	1231(12)	
C(2′)	9938(10)	310(6)	10665(16)	6.30	H(3′)	800(10)	103(6)	1116(15)	
C(3′)	8778(11)	895(7)	10107(18)	6.46	H(4′)	783(10)	177(6)	706(14)	
C(4′)	8629(15)	1252(6)	7958(21)	9.59	H(5′)	999(12)	103(6)	545(17)	
C(5′)	9822(19)	910(10)	7169(19)	13.30					

Table 6. Atomic Coodinates ($\times10^5$ for Fe; $\times10^4$ for C; $\times10^3$ for H) and Isotropic Equivalent Thermal Parameters (in Å^2 Unit) of **2** with Estimated Standard Deviations in Parentheses

Atom	x	y	z	B_{eq}	Atom	x	y	z	B_{eq}
Fe	6695(5)	14541(3)	11417(9)	3.09	H(2)	97(3)	164(2)	−218(7)	
C(1)	1859(3)	1583(2)	−64(6)	3.23	H(4)	131(3)	38(2)	162(6)	
C(2)	1205(3)	1389(2)	−1161(6)	2.89	H(5)	232(3)	120(2)	216(6)	
C(3)	916(3)	868(2)	−648(6)	3.07	H(6a)	3(4)	26(2)	−125(7)	
C(4)	1358(4)	752(2)	874(7)	3.45	H(6b)	3(4)	74(2)	−254(8)	
C(5)	1922(3)	1188(2)	1225(7)	3.50	H(7a)	127(4)	−15(2)	−254(8)	
C(6)	414(4)	496(2)	−1799(8)	4.90	H(7b)	68(4)	7(2)	−407(7)	
C(7)	1042(5)	163(3)	−2946(9)	6.15	H(9)	148(4)	91(2)	−507(7)	
C(8)	1887(4)	460(2)	−3213(7)	4.64	H(10)	244(3)	175(2)	−455(6)	
C(9)	1941(4)	908(3)	−4278(7)	4.59	H(12)	350(4)	77(2)	−84(7)	
C(10)	2491(4)	1341(3)	−3933(7)	4.43	H(13)	252(4)	3(3)	−142(8)	
C(11)	3017(4)	1335(3)	−2494(8)	4.65	H(14a)	372(4)	182(2)	−85(7)	
C(12)	3102(4)	824(3)	−1720(7)	5.10	H(14b)	340(4)	220(2)	−240(8)	
C(13)	2557(5)	403(2)	−2062(3)	5.04	H(15a)	266(3)	224(2)	41(7)	
C(14)	3247(4)	1845(3)	−1594(8)	5.53	H(15b)	209(4)	239(3)	−105(9)	
C(15)	2462(5)	2039(3)	−493(8)	5.21	H(1′)	54(3)	253(2)	195(7)	
C(1′)	207(4)	2184(3)	2012(9)	5.31	H(2′)	−61(4)	216(2)	−2(7)	
C(2′)	−399(4)	1941(3)	948(8)	5.41	H(3′)	−106(4)	109(2)	122(8)	
C(3′)	−636(4)	1435(3)	1615(9)	5.50	H(4′)	−18(3)	100(2)	386(7)	
C(4′)	−161(4)	1354(3)	3094(8)	5.29	H(5′)	73(3)	191(2)	433(6)	
C(5′)	365(4)	1822(3)	3339(8)	5.41					

M$^+$), 212 (100), 121 (52), 91 (25).

Found. C, 75.85; H, 6.40%; M$^+$, m/z 316.0887. Calcd for $C_{20}H_{20}Fe$: C, 75.96; H, 6.37%; M, 316.0912.

The second band eluted with hexane-ether (10:1) yielded yellow solid (10 mg) whose ^{1}H NMR and mass spectra showed extrusion of one sulfur bridge. The compound was so unstable that cannot be further purified. The third band yielded the starting material (2 mg, 7%).

Irradiation of **5b** with a low pressure mercury lamp also afforded **2** in a comparable yield (54%).

[3]Metacyclo[3](1,3)ferrocenophane (11a). A solution of dithia[4]metacyclo[4]ferrocenophane **11a** (376 mg, 0.92 mmol) in benzene (10 ml) and triethyl phosphite (75 ml) was irradiated with a low-pressure mercury lamp for 85 h. The resulting residue was column-chromatographed over silica gel with hexane-ether (20:1). The solid yielded from the first band was further chromatographed over thin-layered alumina in a preparative scale with hexane-ether (100:1) to separate into three bands. The first band yielded unknown yellow oil (6 mg), and the yellow crystals (3 mg) yielded from the third band was possibly a partially desulfurized compound. The second band in the thin-layered chromatography afforded [3]metacyclo[3](1,3)ferrocenophane (**11a**) (8 mg, 3%), which was recrystallized from methanol to give yellow needles mp 88—89 °C. ^{1}H NMR ($CDCl_3$) δ=1.60—3.00 (12H, m, methylene-H), 3.27 (2H, d, J=1.4 Hz, 4, 5-H), 3.83 (5H, s, unsubstd. Cp-H), 3.85 (1H, t, J=1.4 Hz, 2-H), 6.50—6.90 (4H, m, Ph); ^{13}C NMR ($CDCl_3$) δ=29.87, 31.92,

and 35.91 (methylene-C), 66.71 (4, 5-C), 68.22 (unsubstd. Cp-C), 69.10 (2-C), 87.08 (1,3-C), 124.41 (12, 14-C), 126.89 (13-C), 134.59 (10-C), 140.78 (9, 11-C); MS *m/z* (rel intensity) 344 (100, M^+), 279 (20), 277 (9), 172 (4), 121 (13), 91 (5).

Found: M^+, *m/z* 344.1212. Calcd for $C_{22}H_{24}Fe$: M^+, 344.1225.

The second band in the first column chromatography yielded the starting material **7a** (40 mg, 11%).

[3]Paracyclo[3](1,3)ferrocenophane (11b). A solution of dithia[4]paracyclo[4]ferrocenophane **7b** (17 mg, 0.042 mmol) in benzene (3 ml) and triethyl phosphite (30 ml) was irradiated with a low pressure mercury lamp for 85 h. The resulting product was column-chromatographed over silica gel with hexane-ether (20:1). The first band yielded [3]paracyclo[3](1,3)ferrocenophane (**11b**) (2 mg, 14%), which was recrystallized from methanol to give yellow needles; mp 115—117 °C. ^{1}H NMR ($CDCl_3$) δ=1.65—3.10 (12H, m, methylene-H), 2.77 (1H, t, J=1.4 Hz, 2-H), 3.59 (2H, d, J=1.4 Hz, 4, 5-H), 3.77 (5H, s, unsubstd. Cp-H), 6.54 and 6.88 (each 2H, an AA'XX' system, Ph-H); ^{13}C NMR ($CDCl_3$) δ=28.90, 32.60, and 35.91 (methylene-C), 65.49 (4, 5-C), 68.32 (unsubstd. Cp-C), 70.46 (2-C), 89.32 (1, 3-H), 128.79 and 128.89 (unsubstd. C of Ph), 139.12 (substd. C of Ph); MS *m/z* (rel intensity) 344 (100, M^+), 279 (19), 277 (13), 213 (4), 172 (6), 121 (23), 117 (15), 91 (10).

Found: M^+, *m/z* 344.1204. Calcd for $C_{22}H_{24}Fe$: M, 344.1225.

Crystallographic Measurements. Both crystals of **1** and **2** (yellow plates) used in the X-ray diffraction were grown from methanol solutions. The lattice parameters and intensity data were measured on a Phillips PW-1100 diffractometer by means of the θ—2θ scan method by using graphite-monochromated radiation. For the crystal of **1**, Cu $K\alpha$ radiation was used due to the small size of the crystal but for **2**, Mo $K\alpha$ radiation was used. Crystal data and some conditions for data collection are given in Table 4. Lorentz and polarization corrections were made but no absorption correction was applied.

The structures were solved by the heavy atom method. Both atomic coordinates of Fe atoms in the two compounds were reduced from the Patterson maps, and all carbon atoms were located in the Fourier maps. The refinements were carried out by block-diagonal-matrix least-squares procedure. The final atomic parameters are given in Tables 5 and 6.††

The authors are indepted to Professor Takeo Akiyama in Sophia University for helpful discussion and suggestion on the photochemical reaction in desulfurization. Thanks are also due to Mr. Tohru Harada for the preparation of compounds **7a** and **7b**.

References

1) A part of this work has been published as a preliminary report: M. Hisatome, M. Yoshihashi, K. Yamakawa, and Y. Iitaka, *Tetrahedron Lett.*, **24**, 5757 (1983).

2) D. J. Cram and D. I. Wilkinson, *J. Am. Chem. Soc.*, **82**, 5721 (1960); Y. Kai, N. Yasuoka, and N. Kasai, *Acta Crystallogr., Sect. B*, **34**, 2840 (1978); C. Elschenbroich, R. Mockel, and U. Zenneck, *Angew. Chem., Int. Ed. Engl.*, **17**, 531 (1978); R. Benn, N. E. Blank, M. W. Haenel, J. Klein, A. R. Koray, K. Weidenhammer, and M. L. Ziegler, *ibid.*, **19**, 44 (1980); E. D. Laganis, R. G. Finke, and V. Boekelheide, *Tetrahedron Lett.*, **21**, 4405 (1980); A. R. Koray, *J. Organomet. Chem.*, **212**, 233 (1981); P. F. T. Schirch and V. Boekelheide, *J. Am. Chem. Soc.*, **103**, 6873 (1981); J. Elzinga and M. Rosenblum, *Tetrahedron Lett.*, **23**, 1535 (1982); W. D. Rohrbach and V. Boekelheide, *J. Org. Chem.*, **48**, 3673 (1983); W. D. Rohrbach, R. Sheley, and V. Boekelheide, *Tetrahedron*, **40**, 4823 (1984); R. H. Mitchell, T. K. Vinod, and G. W. Bushnell, *J. Am. Chem. Soc.*, **107**, 3340 (1985); R. T. Swann, A. W. Hanson, and V. Boekelheide, *ibid.*, **108**, 3324 (1986).

3) M. Hisatome, O. Tachikawa, M. Sasho, and K. Yamakawa, *J. Organomet. Chem.*, **217**, C17 (1981).

4) A. Kasahara, T. Izumi, Y. Yoshida, and I. Shimizu, *Bull. Chem. Soc. Jpn.*, **55**, 1901 (1982).

5) W. E. Watts, *Organomet. Chem. Rev.*, **2**, 231 (1967); A. Kasahara, *Kagaku* (Kyoto), **38**, 859 (1983); U. T. Mueller-Westerhoff, *Angew. Chem., Int. Ed. Engl.*, **25**, 702 (1986).

6) The nomenclature of ferrocenophanes in the present paper is a modification of that presented by Vögtle and Neumann.[7]

7) F. Fögtle and P. Neumann, *Tetrahedron*, **26**, 5847 (1970).

8) R. H. Mitchell and V. Boekelheide, *J. Am. Chem. Soc.*, **92**, 3510 (1970); V. Boekelheide, and R. A. Hollins, *ibid.*, **92**, 3512 (1970); T. Umemoto, T. Otsubo, Y. Sakata, and S. Misumi, *Tetrahedron Lett.*, **1973**, 539; R. H. Mitchell and V. Boekelheide, *J. Am. Chem. Soc.*, **96**, 1547 (1974); R. H. Mitchell, T. K. Vinod, and G. W. Bushnell, *ibid.*, **107**, 3340 (1985).

9) a) R. H. Mitchell, T. Otsubo, and V. Boekelheide, *Tetrahedron Lett.*, **1975**, 219; b) V. Boekelheide and C.-H. Tsai, *Tetrahedron*, **32**, 423 (1976).

10) V. Boekelheide, I. D. Reingold, and M. Tuttle, *J. Chem. Soc., Chem. Commun.*, **1973**, 406; J. Bruhin and W. Jenny, *Tetrahedron Lett.*, **1973**, 1215; T. Umemoto, T. Otsubo, and S. Misumi, *ibid.*, **1974**, 1573; Y. Fukazawa, M. Aoyagi, and S. Ito, *ibid.*, **1978**, 1067.

11) B. Czech and A. Ratajczak, *Polish J. Chem.*, **54**, 767 (1980).

12) M. Hisatome, M. Yoshihashi, K. Yamakawa, and Y. Iitaka, 15th Symposium on Nonbenzenoid Aromatic Compounds, Kyoto, October 1982, Abstr., p. 300; Bull. Chem. Soc. Jpn., in press.

13) R. F. Borch, *J. Org. Chem.*, **34**, 627 (1969).

14) E. J. Corey and E. Block, *J. Org. Chem.*, **34**, 1233 (1969).

15) C. J. Brown, *J. Chem. Soc.*, **1953**, 3278; Y. Kai, N. Yasuoka, and N. Kasai, *Acta Crystallogr., Sect. B*, **33**, 754 (1977).

16) C. J. Brown, *J. Chem. Soc.*, **1953**, 3265; H. Pope, J. Bernstein, and K. N. Trueblood, *Acta Crystallogr., Sect. B*, **28**, 1733 (1972).

17) F. Hama, Y. Kai, N. Yasuoka, and N. Kasai, *Acta Crystallogr., Sect. B*, **33**, 3905 (1977).

18) K. Kai, N. Yasuoka, and N. Kasai, *Acta Crystallogr., Sect. B*, **34**, 2840 (1978).

19) F. Takusagawa and T. F. Koetzle, *Acta Crystallogr., Sect. B*, **35**, 867 (1979).

20) T. Hirakawa, K. Kurosawa, M. Tanaka, T. Shinmyozu,

††Tables of anisotropic temperature factors, and observed and calculated structure factors are deposited as Document No. 8750 at the Office of the Editor of Bull. Chem. Soc. Jpn.

Y. Miyahara, T. Inazu, and T. Yoshino, 33rd Symposium on Structural Organic Chemistry, Kyoto, October 1982, Abstr., p. 120.

21) D. J. Wilson, V. Boekelheide, and R. W. Griffin, *J. Am. Chem. Soc.*, **82**, 6302 (1960).

22) Y. Nesumi, T. Nakazawa, and I. Murata, *Chem. Lett.*, **1979**, 771.

23) Y. Fukazawa, M. Sobukawa, and S. Ito, *Tetrahedron Lett.*, **23**, 2129 (1982).

24) L. N. Mulay and M. E. Fox, *J. Chem. Phys.*, **38**, 760 (1963).

25) T. D. Turbitt and W. E. Watts, *Tetrahedron*, **28**, 1235 (1972).

26) B. Fuchs, R. Fröhlich, and H. Musso, *Chem. Ber.*, **118**, 1968 (1985).

27) T. Takemura and T. Sato, *Can. J. Chem.*, **54**, 3412 (1976); T. Takemura, K. Tokita, S. Kondo, and N. Mori, *Chem. Lett.*, **1977**, 865.

28) M. Hisatome, J. Watanabe, K. Yamakawa, K. Kozawa, and T. Uchida, *Nippon Kagaku Kaishi*, **1985**, 572.

29) T. Otsubo, M. Kitasawa, and S. Misumi, *Bull. Chem. Soc. Jpn.*, **52**, 1515 (1979).

 © 1987 The Chemical Society of Japan Bull. Chem. Soc. Jpn., 60, 2963—2965 (1987)

Synthesis of Opically Active 3-Morpholinecarboxylic Acid and Tetrahydro-2*H*-1,4-thiazine-3-carboxylic Acid

Yuji KOGAMI† and Kenji OKAWA*
Department of Chemistry, Faculty of Science, Kwansei Gakuin University, Nishinomiya 662
(Received March 31, 1987)

A convenient synthesis of optically active 3-morpholinecarboxylic acid and its thio analogue, tetrahydro-2*H*-1,4-thiazine-3-carboxylic acid, has been developed. These intermediates were obtained by reaction of benzyl (*S*)-*N*-benzyloxycarbonyl-2-aziridinecarboxylate and its enantiomer with 2-chloroethanol or 2-chloroethanethiol, respectively.

Many *N*-substituted morpholine analogues have been synthesized and widely used for medical purposes, however, only a few papers have been published on the synthesis of 3-morpholinecarboxylic acid (**3**) and its derivatives. In 1981, racemic *N*-acetyl-3-morpholinecarboxylic acid derivatives were first synthesized by Callens from *N*-acetylmorpholine,[1] but the yield was poor. The thio analogue, tetrahydro-2*H*-1,4-thiazine-3-carboxylic acid (**6**) had been already synthesized in 1964 by Wong as an optically active product from L-cysteine in good yield.[2] However, synthesis of the D-form of **6** remained a problem because optically pure D-cysteine is difficult to obtain.

We report here convenient syntheses of opically active **3** and **6** from benzyl (*S*)-*N*-benzyloxycarbonyl-2-aziridinecarboxylate (L-Z-Azy-OBzl) and its enantiomer (D-Z-Azy-OBzl).

Since several trials to synthesize *O*-(2-chloroethyl)-serine (**2**) from the serine derivative by several methods were unsuccessful, therefore we used Z-Azy-OBzl as the starting material. The synthetic routes via the ring-opening reaction of the aziridine derivatives[3,4] are shown in Scheme 1.

The reaction was carried out between Z-Azy-OBzl (3.0 mmol) and 2-chloroethanol (2 ml) in chloroform containing a catalytic amount of boron trifluoride etherate at room temperature. The expected ring-opening reaction easily occurred, and the intermediate, *N*-benzyloxycarbonyl-*O*-(2-chloroethyl)serine benzyl ester (**1**), of **3** was obtained. The benzyloxycarbonyl and benzyl ester groups were removed by catalytic hydrogenation, followed by cyclization (1.0 mmol in 15 mL of methanol at 64 °C for 7 h) in the presence of triethylamine (0.28 mL) to give **3**. The total yields of **3a** and **3b** from Z-Azy-OBzl were 65.9% and 63.9%, respectively.[5]

The synthesis of **6** is as follows. Z-Azy-OBzl (6.0 mmol) was treated with dichloromethane solution of 2-chloroethanethiol (4.2 g), prepared from thiirane with hydrogen chloride[6] to give **4**. Deprotection was carried out by use of catalytic hydrogenation (H_2/Pd) in the presence of boron trifluoride etherate to give **5** in good yield. This was treated in the same manner as above to give **6**. The total yields of **6a** and **6b** from Z-Azy-OBzl were 27.4 and 9.8%, respectively.

The physical properties of the synthetic products are summarized in Table 1.

Experimental

The melting points are uncorrected. Optical rotations were determined at the D line on a Perkin-Elmer 141 polarimeter. The NMR spectra were obtained with a Hitachi R-20B high-resolution NMR spectrometer, the chemical shifts being obtained using TMS as the internal reference.

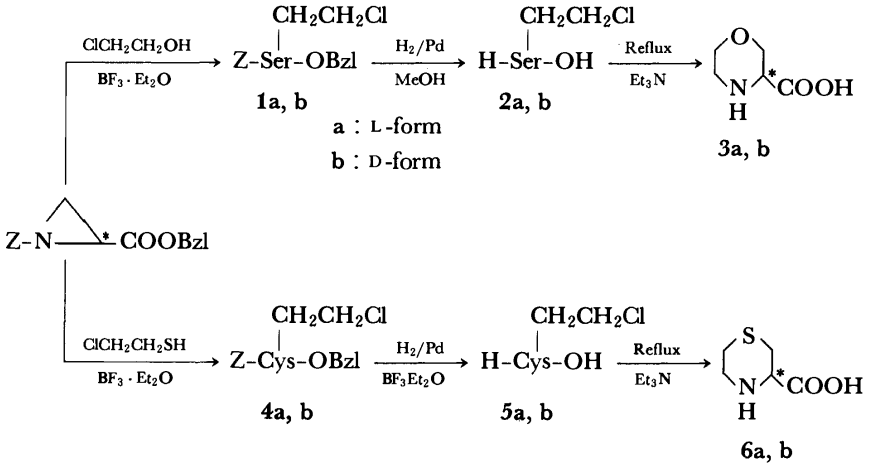

Scheme 1. Synthetic routes of **3a, b** and **6a, b.**

†Present address: Research Center, Toyo jozo Co., Ltd., Ohito, Shizuoka 410-23.

Table 1. Physical Properties of 3-Morpholinecarboxylic Acid (**3a, b**) and Tetrahydro-2*H*-1,4-thiazine-3-carboxylic Acid (**6a, b**)

Characteristic	3a	3b	6a	6b
Melting point θ_m/°C	218(decomp)	216—218(decomp)	251(decomp)	250—251(decomp)
Optical rotation[a] $[\alpha]_D^{25}$/°	−14.4	+13.8	−51.7	+52.0
Solubility (g mL^{-1})[b]	1.26	—	—	—

a) **3a**, **b**: c 2.0, 1 M $HCl_{aq.}$, **6a**, **b**: c 2.0, H_2O. b) Solubility in water at 25 °C; Pro 1.63 g mL^{-1}.

The homogeneity of the products was checked by thin-layer chromatogrphy on silica-gel plates.

L-Z-Ser(OCH_2CH_2Cl)-OBzl (1a). L-Z-Azy-OBzl (0.93 g, 3.0 mmol) was dissolved in $CHCl_3$ (10 mL) and $HOCH_2CH_2Cl$ (2 mL), then $BF_3 \cdot OEt_2$ (2 drops) was added at room temperature. The reaction mixture were stirred for 4 h, then washed with water, dried over Na_2SO_4, and concentrated in vacuo. The residue was subjected to silica-gel column chromatography with elution with ethyl acetate-hexane (1 : 3 v/v). The eluent was concentrated in vacuo and 1.04 g (88.0%) of **1a** was obtained as colorless needles. mp 52.0—52.5 °C, $[\alpha]_D^{25}$ +13.4° (*c* 1.0, MeOH). ^1H NMR ($CDCl_3$): δ=3.52 (4H, m), 3.80 (2H, m, $-CH_2-Cl$), 4.41 (1H, α-proton), 5.08, 5.18 (4H, 2s), 7.26 (10H, s). Found: C, 61.15; H, 5.63; N, 3.60%. Calcd for $C_{20}H_{22}O_5NCl$: C, 61.30; H, 5.66; N, 3.58%.

D-Z-Ser(OCH_2CH_2Cl)-OBzl (1b). D-Z-Azy-OBzl (0.93 g, 3.0 mmol) was dissolved in $CHCl_3$ (10 mL) and $HOCH_2CH_2Cl$ (2 mL), then $BF_3 \cdot OEt_2$ (2 drops) was added at room temperature. The reaction mixture was worked up as described above to give **1b**.

L-H-Ser(OCH_2CH_2Cl)-OH (2a). The solution of **1a** (0.78 g, 2.0 mmol) in methanol (10 mL) was hydrogenated over Pd black. After 30 min, the mixture was filtered and the filtrate was concentrated in vacuo. The residue was crystallized from methanol, 258 mg (77.0%), mp 136.0—137.0 °C, $[\alpha]_D^{25}$ +11.0° (*c* 2.0, 1 M HCl (1 M=1 mol dm^{-3})). Found: C, 35.78; H, 6.04; N, 8.49%. Calcd for $C_5H_{10}O_3NCl$: C, 35.79; H, 6.02; N, 8.36%.

D-H-Ser(OCH_2CH_2Cl)-OH (2b). The solution of **1b** (0.78 g, 2.0 mmol) in methanol was worked up as described above to give **2a**.

L-3-Morpholinecarboxylic Acid (3a). To the solution of **2a** (168 mg, 1.00 mmol) in methanol (15 mL) was added Et_3N (0.28 mL, 2.0 mmol) at room temperature. The reaction mixture was refluxed for 7 h at 64 °C, and concentrated in vacuo. Chloroform was added to the residue and an insoluble material was filtered and recrystallized from water and methanol to give **3a**, 128 mg (97.3%), mp 218 °C (decomp), $[\alpha]_D^{25}$ −14.4° (*c* 2.0, 1 M HCl). NMR (D_2O) δ=3.00 (2H, m, $C-CH_2-N$), 3.50, 3.55 (4H, m, $-CH_2-O-CH_2-$), 3.88 (1H, dd, α-proton). Found: C, 45.42; H, 6.94; N, 10.66%. Calcd for $C_5H_9O_3N$: C, 45.79; H, 6.92; N, 10.70%.

D-3-Morpholinecarboxylic Acid (3b). The reaction mixture in methanol was worked up as described above to give **3b**, mp 216.0—218.0 °C (decomp), $[\alpha]_D^{25}$ +13.8° (*c* 1.0, 1 M HCl). Found: C, 45.78; H, 6.91; N, 10.46%. Calcd for $C_5H_9O_3N$: C, 45.79; H, 6.92; N, 10.70%.

L-Z-Cys(SCH_2CH_2Cl)-OBzl (4a). L-Z-Azy-OBzl (1.86 g, 6.0 mmol) was dissolved in CH_2Cl_2 (20 mL) and $HSCH_2CH_2Cl$ (4.2 g, 43.5 mmol), then $BF_3 \cdot OEt_2$ (5 drops) was added at room temperature. The reaction mixture was stirred for 24 h, then washed with water, dried over Na_2SO_4, and concentrated in vacuo. The residue was purified by silica-gel column chromatography with elution by ethyl acetate-hexane (1 : 3 v/v). The effluent was concentrated in vacuo and 1.89 g (77.0%) of **4a** was obtained as colorless needles. mp 69.5—70.0 °C, $[\alpha]_D^{25}$ −14.3° (*c* 1.0, MeOH). ^1H NMR ($CDCl_3$): δ=2.75 (2H, t, $-S-CH_2-$), 3.01 (2H, d, β-protons), 3.50 (2H, t, $-CH_2-Cl$), 4.63 (1H, br, α-proton), 5.10, 5.17 (4H, 2s), 7.33 (10H, s). Found: C, 58.75; H, 5.38; N, 3.29%. Calcd for $C_{20}H_{22}O_4NSCl$: C, 58.89; H, 5.44; N, 3.43%.

D-Z-Cys(SCH_2CH_2Cl)-OBzl (4b). D-Z-Azy-OBzl (0.93 g, 3.0 mmol) was dissolved in CH_2Cl_2 (10 mL) and pure $HSCH_2CH_2Cl$ (2.1 g, 21.7 mmol), then $BF_3 \cdot OEt_2$ (3 drops) were added at room temperature. The reaction mixture was worked up as described above to give **4b**.

L-H-Cys(SCH_2CH_2Cl)-OH (5a). To the solution of **4a** (410 mg, 1.0 mmol) in abs MeOH were added $BF_3 \cdot OEt_2$ (0.37 mL, 3.0 mmol) and 11.8 M HCl/EtOH (0.16 mL, 2.0 mmol). The mixture solution was hydrogenated over Pd black for **1** h, and filtered. The filtrate was neutralized with Et_3N and concentrated in vacuo. The solid residue was washed with $CHCl_3$ and gave **5a**, 161 mg (88.0%), mp 156.5—157.0 °C, $[\alpha]_D^{25}$ −2.0° (*c* 1.0, 1 M HCl). Found: C, 32.54; H, 5.49; N, 7.54%. Calcd for $C_5H_{10}O_2NSCl$: C, 32.69; H, 5.47; N, 7.56%.

D-H-Cys(SCH_2CH_2Cl)-OH (5b). To the solution of **4b** (410 mg, 1.0 mmol) in abs MeOH (10 mL) were added $BF_3 \cdot OEt_2$ (0.37 mL, 3.0 mmol) and 11.8 M HCl/EtOH (0.16 mL, 2.0 mmol). The mixture solution was worked up as described above to give **5b**.

L-Tetrahydro-2*H*-1,4-thiazine-3-carboxylic Acid (6a). To the solution of **5a** (91.8 mg, 0.5 mmol) in DMF (5 mL) was added Et_3N (0.14 mL, 1.0 mmol) at room temperature. The reaction mixture was refluxed for 2 h at 94 °C and concentrated in vacuo. Chloroform was added to the residue and an insoluble material was filtered and recrystallized from water and methanol to give **6a**, 57.5 mg (78.0%), mp 250.0—251.0 °C, (decomp), $[\alpha]_D^{25}$ −51.7° (*c* 1.0, H_2O) [lit,[7] $[\alpha]_D^{13}$ −52.94° (*c* 2.0, H_2O)]. Found: C, 40.49; H, 6.38; N, 9.37%. Calcd for $C_5H_9O_2NS$: C, 40.79; H, 6.17; N, 9.52%.

D-Tetrahydro-2*H*-1,4-thiazine-3-carboxylic Acid (6b). The reaction mixture in DMF was worked up as described above to give **6b**, mp 248.0—249.0 °C (decomp), $[\alpha]_D^{25}$ +50.6° (*c* 1.0, H_2O). Found: C, 40.46; H, 6.17; N, 9.41%. Calcd for $C_5H_9O_2NS$: C, 40.52; H, 6.12; N, 9.45%.

The authors wish to thank the staff of the research laboratory of Toyo Jozo Co. for the elemental analyses, and Messrs. Tatsuya Inui, Yoshiya Matsuoka, and Shuichi Inaya for their kind assistance. This work was partially supported by a Grant-in-Aid for Scientific Research (No. 59340-034) from the Ministry of Education, Science and Culture.

References

1) V. Asner, C. Becu, M. J. O. Anteunis, and R. Callens, Tetrahedron Lett., **22**, 141 (1981).
2) J. F. Carson and F. F. Wong, *J. Org. Chem.*, **29**, 2203 (1964).
3) K. Nakajima, M. Neya, S. Yamada, and K. Okawa, *Bull. Chem. Soc. Jpn.*, **55**, 3049 (1982).
4) K. Nakajima, H. Oda, and K. Okawa, *Bull. Chem. Soc. Jpn.*, **56**, 520 (1983).
5) Y. Kogami and K. Okawa, "Peptide Chemistry 1985," Protein Research Foundation, Osaka (1986), p 153.
6) E. M. Meade, and F. N. Woodward, *J. Chem. Soc.*, **1948**, 1894.
7) M. Kuriyama, M. Takagi, and K. Murata, *Bull. Fac. Fish., Hokkaido Univ.*, **11**, 58 (1960).

 © 1987 The Chemical Society of Japan Bull. Chem. Soc. Jpn., 60, 2967—2975 (1987)

ESR and FT-IR Studies for Coal Structures. Characteristics of Japanese Coals

Osamu Ito,* Hiroyuki Seki, and Masashi Iino
Chemical Research Institute of Nonaqueous Solutions, Tohoku University, Katahira, Sendai, 980
(Received March 10, 1987)

The ESR parameters (spin concentration, line width, g-value, and spin-lattice relaxation time) of various coals mined in Japan and in many foreign countries have been measured. Low spin concentrations, broad line widths, and long spin-lattice relaxation times have been recognized as characteristics of Japanese bituminous coals (e.g., Akabira, Miike, and Shin-yubari coals) compared with the foreign coals having similar carbon contents. The origins of these differences were interpreted by the aid of the FT-IR spectra. Low fractions of aromatic carbon and rich aliphatic groups of Japanese bituminous coals are closely related to the characteristics in the ESR parameters.

Many spectroscopic methods have been used to obtain chemical information about the structures of organic solids such as coals.[1,2] In addition, the magnetic relaxation measurements give an information about the molecular motions; the nuclear spin-spin relaxation times (T_2) measured with NMR have been successfully applied to polymers and coals.[3,4] The measurements of the electron spin-lattice relaxation times (T_1) of carbonaceous materials including various coals were reported in 1950's.[5-9] Smidt and van Krevelen, however, indicated that the T_1-values were strongly affected by the adsorbed oxygen on coals.[8] Therefore, it has been believed for a long time that information about the dynamic behavior of the molecules in coals is hidden behind the interactions with oxygen. Recently, it was reported that the T_1-values for the polymers including polyacetylenes afford useful information.[10,11] Thus, it may be worth reinvestigating the electron-spin relaxation phenomena for coals. For Japanese coals, Toyoda, Sugawara, and Honda reported the various ESR parameters including T_1-values;[12] they found that the line widths of Japanese coals were broader than foreign ones, which is an only characteristic of Japanese coals; the spin concentrations and T_1-values are similar to those of the foreign coals observed by Smidt and van Krevelen.[8] On the basis of well-known properties of Japanese coals such as rich in hydrogen atom and rich in volatile matters,[13,14] it would be anticipated that Japanese coals have low spin concentrations and that the molecular motions of Japanese bituminous coals are flexible because of their high efficiency in liquefaction[15] and high solubility.[16]

In this study, we chose a wide variety of coals including Japanese and foreign coals having carbon contents from 65 to 93%. In order to help the interpretation of the ESR parameters which give a rather physical information about coals, the FT-IR spectra were measured with the diffuse reflectance method to obtain certain chemical information.

Experimental

Samples: Six kinds of Japanese coals having carbon content from 65 to 86.7% were selected. Foreign coals were selected in a wide range of the carbon contents. The ultimate analytical data were summarized in Table 1 with the abbreviation of coals.

These coal samples (under 60 mesh (<250 μm)) were dried at 80 °C in a vacuum oven. For brown coals (lignites), it is reported that the contact with air affected the ESR signals;[17] especially, coexistence of moisture and oxygen molecule strongly affected the intensities of ESR signals.[18,19] Thus, we dried coals samples in vacuum at lower temperature.

Deashing: In a solution containing 15 ml hydrochloric acid, 5 ml hydrofluoric acid, and 15 ml water, 1 g of original coal was suspended and warmed at 95 °C under nitrogen gas for 3 h; then the residues after filtration were washed with distilled water and dried in a vacuum oven at 80 °C.[20]

Maceral Separation: Some deashed coals were separated into maceral-rich groups with float sink method using a mixed solvent consisting of carbon tetrachloride and cyclohexane.[21]

Alkylation and Acetylation: Alkylation was performed by the reflux of coal (2 mg) in butyl alcohol (150 ml) with coexist of p-toluenesulfonic acid as a catalyst.[22] Deashed coal was acetylated with acetic anhydride in dry pyridine with refluxing under nitrogen gas during 12 h.[23]

ESR Measurements: Pulverized coals (under 100 mesh (<150 μm)) in ESR sample tube of 3 mm outer diameter were measured with a JEOL-FE3X and a Varian E-4 spectrometer (X-band/100 kHz field modulation) at room temperature. The effects of the degassing upon the line shape and saturation phenomena were examined from 4 to 10^{-4} Pa. Spin concentrations were calculated by the integration of the ESR differential signals comparing with standard DPPH. When the ESR signal contained two or more components, each curve was separated with the aid of the computer simulation method using the Lorentzian curve shape which is used for the homogeneous spin system.[24] Spin-lattice relaxation times were evaluated by the continuous wave saturation method with varying the microwave powers.[25,26] When the ESR signals were attributed to the mixture of homogeneous and inhomogeneous, some corrections were necessary according to Castner's method.[27]

FT-IR Measurements: The FT-IR spectra were measured by a JEOL JIR-100 spectrometer equipped with a diffuse reflectance apparatus; 3 mg of pulverized coals (under 200 mesh (<75 μm)) were diluted with 200 mg of KBr powder and the intensities of the IR bands were calculated by Kubelka-Munk function ($f(R_\infty)$) after averaging 200 times scan.[28,29]

Evaluation of f_a: The fraction of aromatic carbon (f_a) were calculated by Brown's method using a constant (0.42)

Table 1. Analytical Data of Coal Samples (daf)

Coal	(Abb.)	Nation	C/%	H/%	N/%	S/%	O/%	f_a
Nakayama	NK	Jpn[a]	69.0	5.3	1.2	0.3	24.1	—[h]
Soyakoishi	SY	Jpn	70.2	5.2	1.8	0.2	22.4	—[h]
Taiheiyo	TY	Jpn	77.0	6.3	1.5	0.3	14.9	0.59
Akabira	AK	Jpn	80.8	6.2	1.9	0.7	10.4	0.65
Miike	MK	Jpn	82.3	6.3	0.8	2.3	8.4	0.71
Shin-yubari	YS	Jpn	86.7	6.2	1.9	0.3	5.2	0.71
Velva	VL	Am[b]	69.1	4.8	1.4	0.6	23.9	—[h]
Peerless	PL	Am	69.9	4.9	0.8	1.6	22.8	—[h]
Noonan	NN	Am	70.8	4.6	1.0	0.6	23.0	—[h]
South Beulah	SB	Am	71.6	4.7	1.4	2.9	19.2	—[h]
Indian Head	IH	Am	72.0	5.0	1.1	1.2	9.5	—[h]
Sufco	SF	Am	73.9	4.9	1.5	0.3	19.3	0.68
Colowyo	CW	Am	74.0	5.7	1.9	0.4	18.6	0.65
King	KN	Am	76.8	5.7	1.8	0.6	15.0	0.67
Illinois No. 6	IL	Am	78.9	5.5	1.8	5.7	8.0	0.66
Indian Ridge	IR	Am	86.5	5.1	1.9	0.9	5.5	0.84
Pittston	PT	Am	86.6	5.3	2.7	0.8	6.2	0.86
Key Stone	KS	Am	89.4	4.4	2.2	0.8	3.1	0.89
Yallourn	YL	Aus[c]	66.1	5.3	0.6	0.3	28.0	—[h]
Morwell	MW	Aus	67.4	5.0	0.5	0.3	26.8	—[h]
Millmerran	MM	Aus	76.9	6.6	0.5	0.6	15.4	0.60
Wandoan	WD	Aus	78.5	5.9	1.0	0.3	14.2	0.60
Hunter Valley	HV	Aus	80.3	5.0	2.0	0.4	12.2	—[h]
Goonyella	GN	Aus	81.7	5.4	2.1	0.7	9.9	0.81
Grose Valley	GV	Aus	81.7	5.1	1.4	0.6	11.4	0.82
Liddell	LD	Aus	83.5	5.4	2.1	0.6	8.3	0.76
Newvale	NV	Aus	84.2	5.0	1.4	0.5	8.9	0.82
Charlestone	CH	Aus	84.7	5.1		0.8	8.1	0.82
Moura	MR	Aus	85.6	5.3		0.5	7.1	0.80
Daido-unnan	DU	Chn[d]	82.7	5.1	1.0	0.7	10.5	0.66
Hai-nan	HN	Chn	84.5	5.2			6.0	0.81
Zao-zhuang	ZZ	Chn	86.9	5.5			5.6	0.80
Sei-kan	ZK	Chn	89.7	4.0	2.5	2.0	1.7	0.81
Rhein Braun	RB	Gem[e]	65.8	5.5	0.8	0.3	27.6	—[h]
Leopold	LP	Gem	79.9	5.8	1.4	1.2	11.7	0.75
Zollverein	ZV	Gem	89.6	4.8	1.7	1.3	2.6	0.73
E.B.V.	EA	Gem	89.6	4.1	1.5	1.1	3.7	0.82
Coal Valley	CV	Can[f]	77.2	4.7		0.2	17.7	0.76
Vicary Creek	VC	Can	87.8	4.7	2.1	0.4	4.9	0.86
Hongay	HG	Viet[g]	93.7	3.3	1.2	0.4	1.3	0.95

a) Japan. b) America (U.S.A.). c) Australia. d) China (P.R.C.). e) Germany (F.R.D.). f) Canada. g) Vietnam. h) The f_a-values could not be estimated, since the aromatic C–H band at 3030 cm^{-1} was weak.

which is the ratio of the extinction coefficient of the aromatic C–H stretching band at 3030 cm^{-1} to that of the aliphatic C–H stretching band at 2940 cm^{-1}. This ratio was estimated by the comparison of ^1H NMR (Hitachi R-600 ^1H FT-NMR) with FT-IR data of the pyridine-soluble parts of some coals.[30] This value is similar to that reported by Painter et al.[28] The f_a-values are summarized in Table 1. The f_a-values thus calculated are compatible with those evaluated by the solid state CP/MAS ^{13}C NMR.[31–33]

Results and Discussion

Hydrogen Contents. Figure 1 shows the ratios of hydrogen atom contents to carbon atom contents (in atomic unit) for all coals listed in Table 1. Dots between 70 and 85 C% show some scatter, but they seem to stud between two lines—upper line and lower line. A tendency that Japanese coals have higher hydrogen contents is confirmed for coal samples adopted in this study. From proximate analysis data, one can also find that Japanese coals contain much volatile matters.[29] These facts have been already pointed out by many investigators as characteristics to Japanese coals;[13,14] The coal samples adopted here also satisfy our purpose in disclosing how such a characteristic appears in the ESR parameters.

Apparent Characteristics of ESR Signals. Figure 2a shows ESR spectra of two kinds of bituminous coals; one is Japanese bituminous coal (Shin-yubari coal 86.7 %C) and another is Canadian bituminous coal (Vicary Creek 87.8 %C). Shin-yubari coal shows a single symmetric signal (line width (ΔH_{pp})=0.74 mT) which is weak and easily saturated with an increase in a microwave power for evacuated sample. On the other hand, the ESR signal of Vicary Creek coal is composed of two components; one is broad line (ΔH_{pp}=0.53 mT) and another is narrow line

(ΔH_{pp}=0.13 mT). The both lines showed the saturation phenomena at high microwave power. Similar phenomena were reported for American coals.[34] The narrow lines are observed in almost all foreign subbituminous and bituminous coals.[1]

As for the origin of the narrow lines, there have been presented some interpretations. Some investigators attributed to one of the macerals such as inertinite (fusinite) group;[34] other researchers to macromolecular component in coals.[24] In general, the spin concentrations originated from the narrow lines are less than 10—20% of the broad ones, when they were compared before saturations.

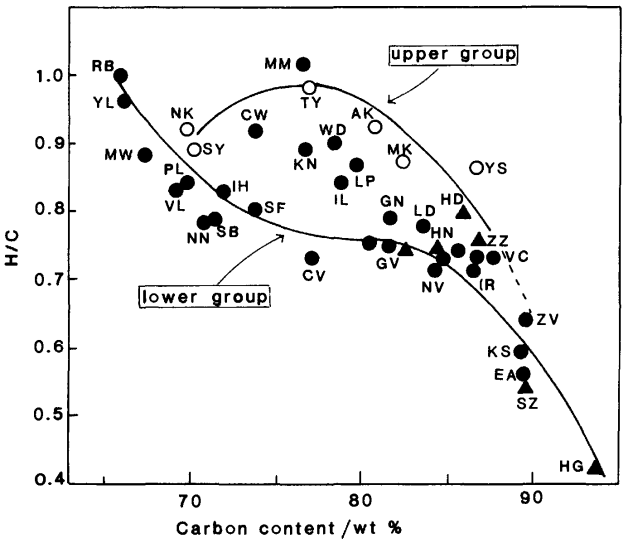

Fig. 1. Hydrogen atom contents (H/C in atomic unit) vs. carbon contents. Abbreviations of coal samples are quoted from Table 1.

Corresponding FT-IR. Figure 2b shows FT-IR spectra of Shin-yubari coal and Vicary Creek coal measured by the diffuse reflectance method. The vibrational band of the aliphatic C-H groups at 2940 cm^{-1} of Shin-yubari coal is stronger than that of Vicary Creek coal. The aromatic C-H groups (at 3030 cm^{-1}) of both coals are approximately equal, but the broad band which increases with wavenumber up to the near-IR region is observed for Vicary Creek. This broad band was not attributed to the scattering of the monitoring light which was frequently observed in the transmittance method using KBr pellet, but to the edge of the real electronic absorption band which is characteristic of the polycondensed aromatic hydrocarbons (the π-π^* transitions) and/or of their layered structures (the intermolecular charge-transfer transitions).[29] Thus, Vicary Creek coal may contain such highly polycondensed aromatic hydrocarbons; the broad band in the near-IR region seems to correspond to the narrow line in the ESR signal. This relation is generalized for other coals.

Spin Concentration. For coal samples showing different saturation phenomena, it is essential to compare the signal intensities before the saturation (at low microwave power). Among the coals investigated in this study, Akabira and Miike coals show the satura-

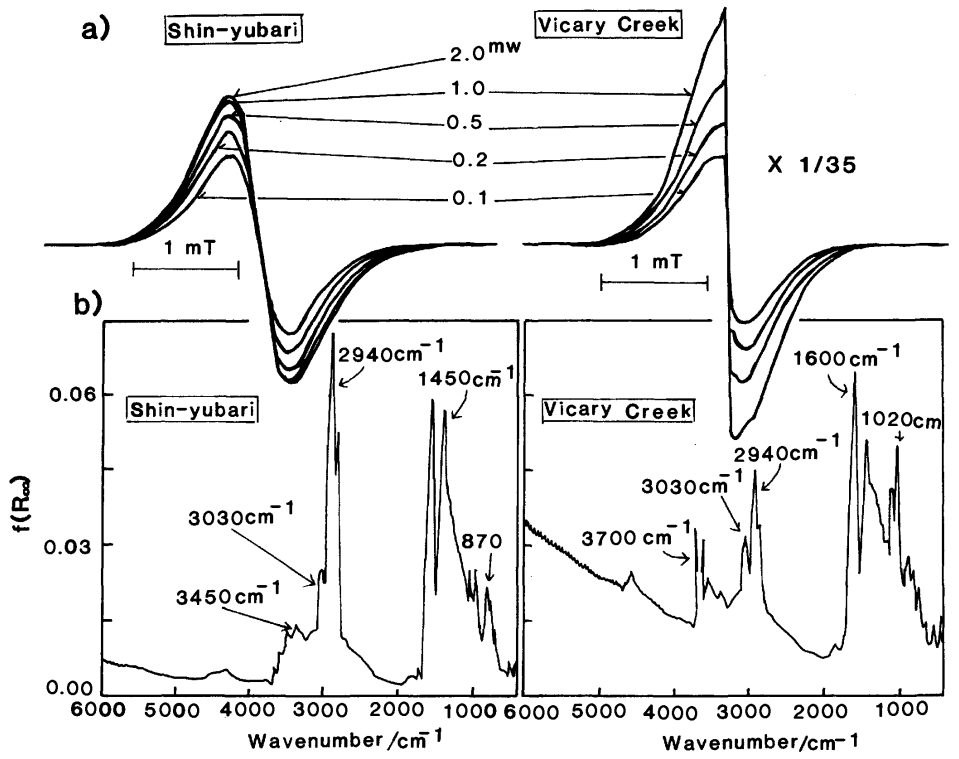

Fig. 2. (a) ESR spectra of Shin-yubari raw coal and Vicary Creek raw coal under vacuum; numbers in figure are microwave powers (JEOL-FE3X). (b) Diffuse reflectance FT-IR spectra of the coals (1 mg sample/150 mg KBr).

Table 2. ESR Parameters for Raw Coals (daf) in Degassed System

Coal	Spin$\times 10^{-19}$/g	ΔH_{pp}/mT	g-Value	T_1/μs
Nakayama	0.13	0.62	2.0035	3
Soyakoishi	0.34	0.70	2.0035	6
Taiheiyo	0.59	0.77	2.0036	9
Akabira	0.69	0.75	2.0030	55
Miike	0.49	0.75	2.0031	59
Shin-yubari	0.71	0.74	2.0028	44
Velva	0.02	0.63	2.0041	8
Peerless	0.11	0.62	2.0039	11
Noonan	1.01	0.65	2.0036	7
South Beulah	0.54	0.70	2.0033	4
Indian Head	0.47	0.63	2.0033	4
Sufco	0.78	0.61	2.0028	—[a]
Colowyo	0.55	0.67	2.0031	4
King	0.50	0.67	2.0030	15
Illinois No. 6	0.94	0.66	2.0026	24
Indian Ridge	2.48	0.54	2.0026	7
Pittston	1.02	0.51	2.0026	—[a]
Key Stone	2.01	0.54	2.0025	7
Yallourn	0.12	0.45	2.0036	8
Morwell	0.09	0.67	2.0036	17
Millmerran	0.50	0.72	2.0031	30
Wandoan	0.87	0.73	2.0033	8
Hunter Valley	0.43	0.55	2.0027	—[a]
Goonyella	1.66	0.60	2.0026	11
Grose Valley	2.29	0.55	2.0027	7
Liddell	0.86	0.68	2.0028	5
Newvale	1.23	0.55	2.0027	—[a]
Charlestone	1.20	0.65	2.0027	5
Moura	1.15	0.65	2.0027	—[a]
Daido-unnan	1.52	0.55	2.0028	—[a]
Hai-nan	0.88	0.50	2.0026	—[a]
Zao-zhuang	0.63	0.60	2.0026	<2
Sei-kan	0.92	0.55	2.0026	—[a]
Rhein Braun	0.24	0.53	2.0038	14
Leopold	0.24	0.50	2.0029	—[a]
Zollverein	1.86	0.56	2.0026	3
E.B.V.	1.70	0.63	2.0026	3
Coal Valley	1.31	0.63	2.0028	3
Vicary Creek	1.62	0.53	2.0027	5
Hongay	2.44	0.38	2.0027	4

a) The T_1-values could not be obtained, since the broad lines could not be completely resolved.

tion at the most low microwave power (1 mW in the cavity of JEOL-FE3X and 5 mW in the cavity of Varian E-4). A strict linear relation holds at lower microwave power than about a half of each maximum value; in the linear range, the spin concentrations were evaluated. They are summarized in Table 2.

In Fig. 3, the spin concentrations thus measured for original coals in evacuated system were plotted against the carbon contents of coal samples. One can see that the spin concentrations increase with an increase in carbon contents; some bituminous coals and anthracite have higher spin concentrations than brown coals and subbituminous coals by a factor of 10—50.[1,2,8,12] This tendency, however, shows a band-type correlation; the spin concentrations of the upper-lying coals are greater than the lower-lying ones by a factor of about 5 times. Around the lower group, we can find Japanese subbituminous and bituminous coals; this is one of characteristics of Japanese coals found in the ESR parameters in this study. The proportionality of the spin concentrations with the f_a-values and the inverse proportionality with the H/C-values (from Table 1) suggest the reasons for the low spin concentrations of Japanese bituminous coals.

For deashed coals, a similar correlation to Fig. 3 was found, although some decreases (1/1.5—1/2) in the spin concentrations by the deashing were observed for some coals. Thus, the band-type correlation shifts toward lower in a small extent. For the reason for the decrease in the spin concentration by deashing, one can consider the instabilization of the spin centers by the protonation of aromatic rings or semiquinone type radicals with the action of mineral acids; another interpretation is the spin-pairing by the removal of inorganic matters.[35]

Similar correlations were found for the aerated sample system; although the narrow ESR lines in foreign coals were broadened by the adsorption of oxygen

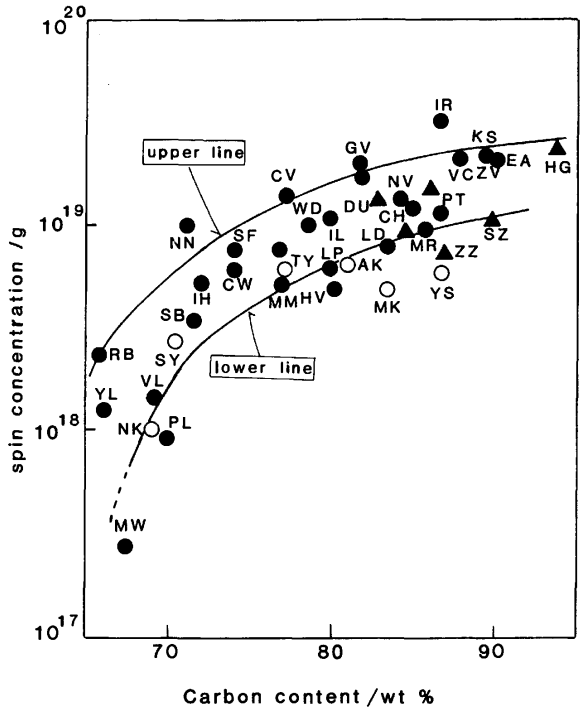

Fig. 3. Dependence of the spin-concentrations for raw coals (measured under vacuum) upon the carbon contents.

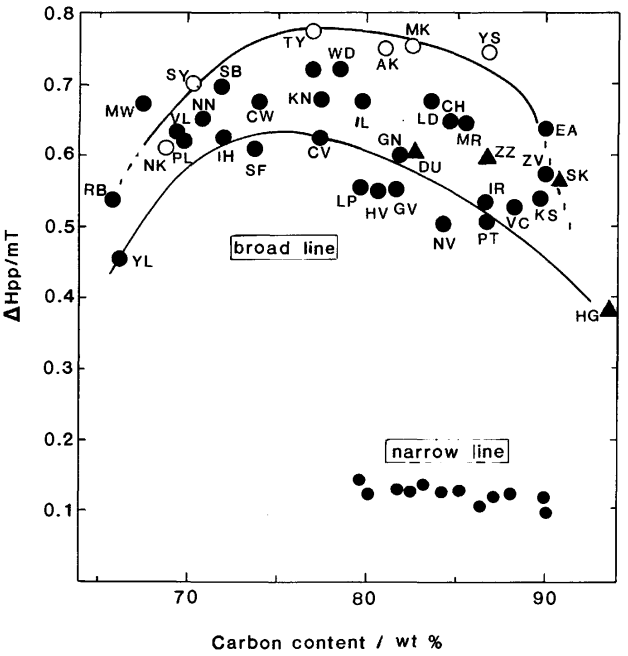

Fig. 4. Line widths (ΔH_{pp}) vs. carbon contents; for coals showing broad and narrow lines, both line widths are shown.

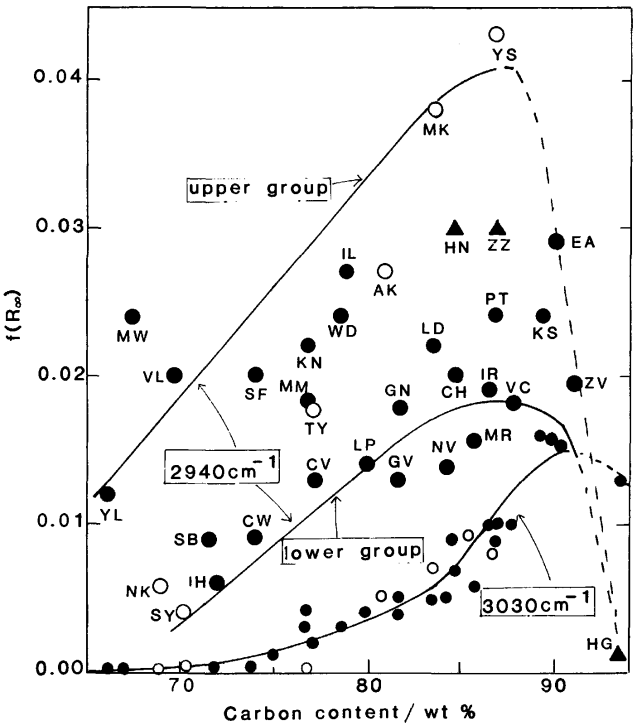

Fig. 5. Intensities ($f(R_\infty)$/1 mg coal) of IR bands at 3030 cm^{-1} (aromatic C-H) and at 2940 cm^{-1} (aliphatic C-H) vs. carbon contents.

molecules, the integrated intensities were not varied in large extent.[36]

Line Widths. In Fig. 4, the line widths of raw coals observed in evacuated system are plotted against the carbon contents; for foreign coals composed of two lines, the both line widths are shown. It can be seen in this figure that the narrow lines appear for the foreign coals having carbon contents greater than about 78% C. Among the broad lines, the lines for Japanese subbituminous and bituminous coals are wider than the foreign ones by about 0.2 mT. This finding was already indicated by Toyoda, Sugawara, and Honda, who suggested on the basis of the H/C-values that the hydrogen atoms around the spin centers broaden the line width by the hyperfine interactions.[12]

The hydrogen atoms can be divided into two groups by the aid of the IR spectra; one is the hydrogen atoms attached directly to the aromatic rings (the bands at 3030 cm^{-1}) and another is aliphatic C-H groups (the band at 2940 cm^{-1}).[28] In the IR spectra of coals having the same carbon content, the intensities of the aromatic C-H bands of the Japanese bituminous coals are similar to those of foreign coals as shown in Fig. 5. On the other hand, a pronounced increase in the intensities of the aliphatic C-H bands is found for Japanese bituminous coals. It is well-known that the hyperfine coupling constants of the hydrogen atoms at the aliphatic groups in the vicinity of the radical center (α- and β-positions) are generally similar to those by the hydrogen atoms attached directly to aromatic rings.[37] Thus, the finding that the line widths of the Japanese bituminous coals are broad is closely related to their rich aliphatic groups. For the narrow ESR lines observed mainly for the foreign coals, one can interpret similarly by the poor aliphatic C-H groups for these components in coals.

g-Values. It is well-known that the g-values of

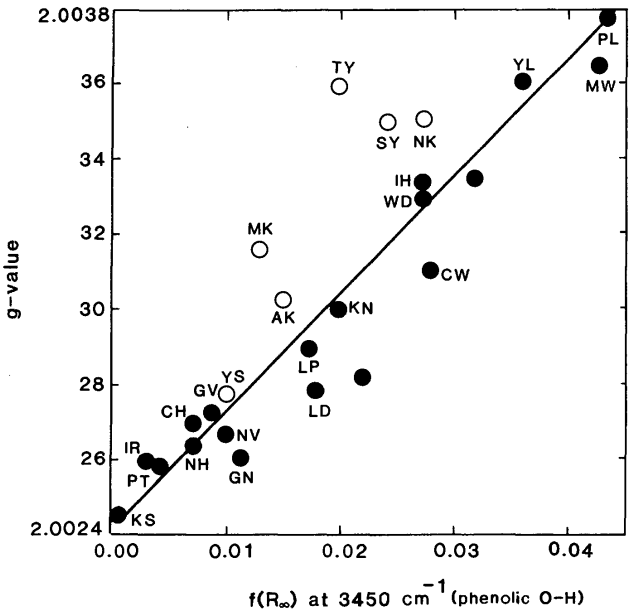

Fig. 6. Plots of g-values vs. $f(R_\infty)/1$ mg coal at 3450 cm^{-1} which is assigned to the phenolic O-H.

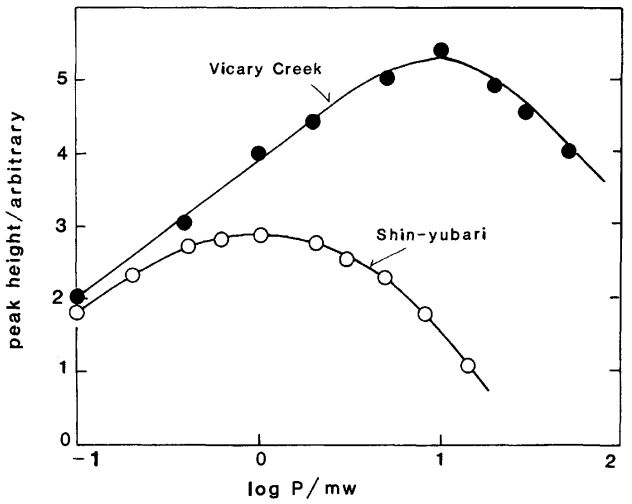

Fig. 7. Dependence of intensities of the ESR signals (peak-peak heights) upon the microwave powers (JEOL-FE3X).

Table 3. Observed T_1-Values for Some Coals and Pitches. Changes with Degree of Vacuum and Densities, and Effects by Alkylation and Acetylation

Sample	Treatment	T_1/μs
Shin-yubari	4.0 Pa	70
	0.67 Pa	69
	0.0001 Pa	67
	In air	4
Zao-zhuang	Raw coal	<2
	Soluble part (33 wt%)	140
Gilsonit pitch	85.4% C (f_a=0.33)	80
Ashiland pitch	92.8% C (f_a=0.43)	490
Taiheiyo	Raw coal	9
	Acetylation	29
	Alkylation	55
Moura	Raw coal	<2
	d=1.28	12
	d=1.30	12
	d=1.33	3
	d=1.38	<2

coals decrease with the degree of coalification; the g-values generally increase with the amount of the hetero atoms such as oxygen, sulfur, and nitrogen atoms,[2,34] in which the oxygen content mainly determines the g-values. It would be anticipated that the oxygen atoms near the spin center are mainly the phenolic oxygen. In order to examine this assumption, we show the correlation between the g-values and the amount of the phenolic O-H which can be easily evaluated from the IR band at ca. 3450 cm^{-1}.[28] In Fig. 6, a good linear proportionality can be seen, suggesting that there are the phenolic O-H groups in the vicinity of the spin center. Although the importance of the nitrogen atom in the exinite groups was recently suggested,[34] their roles are not clear in our study because the nitrogen and sulfur atoms are contained only a small amount in coals (Table 1).

Spin-Lattice Relaxation Times. Spin-lattice relaxation times for various coals could be estimated as relative values by the continuous-wave saturation method.[24] The plots of peak-peak heights of the signals against the microwave powers observed for the samples in vacuum system are shown in Fig. 7. The Japanese bituminous coals such as Shin-yubari coal show the saturation at lower microwave power, whereas the foreign bituminous coals show the saturation at high microwave power.[38] The narrow lines show the saturation at the higher microwave power. When one ESR line is composed of both homogeneous and inhomogeneous components, the upward curvature in Fig. 7 deviated from the symmetric curve with respect to the maximum; in such cases, some corrections are necessary to estimate the maximum microwave power (P_{mx}) according to Castner's method.[27]

The T_1 values can be estimated from the following equation as relative values;

$$T_{1x} = T_{1s}(\Delta H_x/\Delta H_s)(P_{ms}/P_{mx}) \quad (1)$$

where, T_{1x} and T_{1s} refer to the spin-lattice relaxation times for unknown and standard samples, respectively; ΔH refers to the line width.[34] By adopting the T_1 values for Miike coals reported by Toyoda, Sugawara, and Honda (59 μs),[12] the relative values can be converted into the absolute values.

By the comparison of the T_1-values observed in low vacuum (10^{-1} Pa during a few hours) with those in high vacuum (10^{-4} Pa during a week), any appreciable difference in the T_1-values was not observable (Table 3). By the introduction of air into the sample, the T_1-value decreases considerably.[6] These findings indicate that the oxygen effect can be easily eliminated even by low evacuation. The T_1-values summarized in Table 2 were observed for the considerably high

vacuum system (about 10^{-2} Pa).

The T_1-values thus estimated are plotted against the carbon contents as shown in Fig. 8. For the low rank coals from 65%C to about 77%C, a monotonous decrease in the T_1-values with an increase in the carbon contents was observed. In the range of carbon contents greater than 77%C, coals can be divided into two groups; upper group contains Japanese bituminous coals and some foreign coals such as Millmerran coal. In the lower group, some foreign bituminous and subbituminous coals belong.

Duber and Wieckowski estimated the T_1- and T_2-values of the broad lines and narrow lines of Polish coals and observed that the T_1-values of the components showing the broad lines were longer than those of the narrow lines. This was interpreted by them on the basis of the two-phonon Raman process which suggests that the T_1-values become short in a phase with larger regions of crystalline lattice ordering strongly bounded to one another by covalent bonds.[24] Thus, it would be expected that the macromolecules with many cross linkages show shorter T_1-values than the macromolecules with less cross linkages. As shown in Table 3, we observed for Zao-zhuang (Chinese bituminous coal) that the soluble part has longer T_1-values than the corresponding original coal. This finding is compatible with the observation by Kevan et al. that the T_1-value of a SRC (solvent refined coal) is longer than the original coal.[39,40] We observed that the petroleum pitches show the long T_1-values (Table 3); this observation is in agreement with Yen's observation even though they measured in aerated system.[41] From these observations, it can be confirmed that the components strongly connected with cross linkages have short T_1-values than the components with less cross linkages or small molecules. Dependence of the T_1-value upon the degree of polymerization was indicated for polyacetylenes.[11]

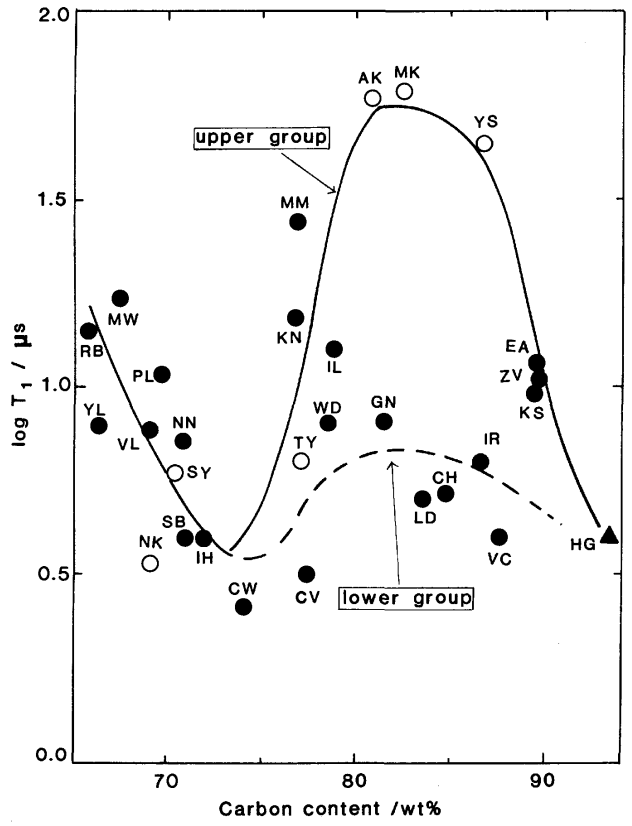

Fig. 8. The T_1-values estimated for raw coals under vacuum vs. carbon contents.

By acetylation of Taiheiyo coal which has rich phenolic O-H groups (Fig. 6), the T_1-values become longer than the original coal (Table 3). This suggests an importance of the interaction via the hydrogen bonds which connect the molecular chains. Alkylation which may occur at the aromatic rings exhibited a strong effect on the T_1-value (Table 3).

It was recently pointed out that the inertinite-rich groups exhibit uneasy saturation.[35] In this connection, we observed the decrease in T_1-values with the increase in the density of Moura coal as shown in Table 3. The inertinite components, in general, have greater f_a-values than the exnite and vitrinite components; thus, an increase in the degree of aromatization tends to decrease the T_1-values.

From these observations, we can interpret Fig. 8; a decrease in the T_1 values from 65 to 77%C may be related to the increase in the cross linkages between the polymer chains with condensation accompanying elimination of small molecules such as water and carbon dioxide as was suggested by van Kreveren's coal band.[42] In the region greater than 77%C, a large splitting was seen; the upper group contains the Japanese coals and some foreign coals which are belonging to the upper group in the H/C-plot (Fig. 1), in the linewidth plot (Fig. 3), and in the aliphatic group-plot (Fig. 5), whereas they are to the lower group in the spin-concentration plot (Fig. 4). In the upper group of Fig. 8, the increase in the T_1-values from 77 to 85%C may be related to the increase in the aliphatic groups, since a similar change was observed in Fig. 5. Decrease in the cross linkages or decrease in the hydrogen bonds would be also expected to occur in this region. Decrease in the T_1-values from 83 to 93%C may be related to the increase in polycondensation of aromatic rings.

As origins of the big difference in the T_1-values between the upper and lower groups, many factors should be taken into the consideration. One is originated from the difference in the f_a-values; the coals belonging to the lower group in Fig. 8 have larger f_a-values than the lower one by a factor of ca. 0.1 (Table 1) which is considerably large difference. A large difference in the amounts of the aliphatic groups may also strongly influence the T_1-values as the result of alkylation suggested.

For deashed coals, a similar figure to raw coals (Fig. 8) was obtained excepting slightly longer T_1-values;

this may suggest that flexibility increase with a loss of the inorganic matters which might connect the coal segments by the coordinations. For the higher degree coals, inorganic matters may hinder the approach of the aromatic rings; i.e., they may destroy the crystalline phase.

It can be pointed out that a similar correlation to the upper group was reported by Yokono and Sanada in the ^1H nuclear spin-lattice relaxation times.[4] The molecular weights between bridges in the crosslinking macromolecules in coals, which were estimated from the swelling measurements in solvents by Sanada and Honda, may also support the longer T_1-values of the coals in the range of 80—86 C%.[43] One of our purposes is to find some relations between the ESR parameters (especially the T_1-value) and the solubility of coals, since it would be anticipated that the coals showing high solubility have less cross linkages or low molecular weights. In pyridine (Soxhlet extraction)[44-46] or in a mixed solvent (pyridine-CS_2 extraction),[47] a tendency that the Japanese bituminous coals are considerably soluble was found. Although such tendency seems to reflect on the T_1-values (Fig. 8), the maximum solubility in the plot against the carbon contents exists at about 86% C; a slight shift from the peak in Fig. 8 was seen. This may be partly attributed to our finding that the T_1-values are influenced not only by the real molecular weights but also by the molecular weights between the cross linkages. Furthermore, physical properties such as maximum fluidity which suggest the high flexibility of Japanese bituminous coals may be related with their observed long T_1-values.[13,14]

Summary

The ESR parameters of various coals were investigated and we found some characteristics of Japanese bituminous coals especially in the electron spin-lattice relaxation times (T_1). These ESR parameters which give a rather physical information were discussed with an aid of the IR data which afford a useful chemical information. In this study, it can be emphasized that the electron spin-lattice relaxation phenomena can be potentially used to estimate the molecular interaction including dynamic behavior of the molecules contained in the carbonized materials. We need further study for the electron spin-relaxation phenomena of the compounds which are appropriate as models for coals.

We thank Professor Masamoto Iwaizumi of Tohoku University for his useful suggestions for the analysis and interpretation of the T_1-values. We are also grateful to Professor Minoru Matsuda of Tohoku University and Dr. Takashi Iwasaki of Tohoku Technical Research Institute for their kindness for the use of ESR spectrometers. Informative discussions with Professors Yoshiyuki Nishiyama, Akira Tomita, and Yasuo Ohtsuka of Tohoku University are gratefully appreciated. Coal samples and their analytical data were kindly presented by Coal Chemistry Laboratory in our Institute.

References

1) H. L. Retcofsky, "Coal Science," ed by M. L. Gorbaty, J. W. Larsen, and I. Wender, Academic Press, New York (1982), Vol. 1, Chap. 3.
2) L. Petrakis and D. W. Grandy, "Free Radicals in Coals and Synthetic Fuels," in "Coal Science and Technology," Elsevier, Amsterdam (1983), Vol. 5.
3) K. Fujimoto, T. Nishi, and R. Kado, *Polym. J.*, **3**, 448 (1972).
4) T. Yokono and Y. Sanada, *Fuel*, **57**, 334 (1978).
5) J. Uebersfeld and E. Erb., *C. R. Acad. Sci., Paris*, **243**, 2043 (1956).
6) N. S. Garf'yanov and B. M. Kozyrev, *Zh. Eksper. Teor. Fis.*, **30**, 1160 (1956).
7) J. Smidt, *Nature*, **181**, 176 (1958).
8) J. Smidt and D. W. van Krevelen, *Fuel*, **38**, 355 (1959).
9) R. C. Pastor and R. H. Hoskins, *J. Chem. Phys.*, **32**, 264 (1959).
10) A. T. Bullock and L. H. Sutcliffe, *Trans. Faraday Soc.*, **60**, 2112 (1964).
11) J. C. W. Chien and M. A. Schen, *Macromolecules*, **19**, 1042 (1986).
12) S. Toyoda, S. Sugawara, and H. Honda, *Nenryo Kyokai Shi*, **45**, 876 (1966).
13) H. Honda, *Nenryo Kyokai Shi*, **37**, 635 (1958).
14) H. Sugimura, Y. Oosawa, M. Hatami, H. Sato, H. Sugawara, and H. Honda, *Nenryo Kyokai Shi*, **45**, 199 (1966).
15) K. Ouchi, S. Ohno, M. Makabe, and H. Itoh, *Fuel*, **64**, 1391 (1985).
16) M. Iino and M. Matsuda, *Fuel*, **62**, 744 (1983).
17) H. Oouchi, S. Shioya, and J. Souma, *Kogyo Kagaku Zasshi*, **71**, 1192 (1968).
18) S. W. Dack, M. D. Hobday, T. D. Smith, and J. R. Pilbrow, *Fuel*, **62**, 1510 (1983).
19) I. B. Goldberg, T. M. Mckinney, K. E. Chung, and R. Galli, *Fuel*, **65**, 241 (1986).
20) A. Oya, T. Fukatsu, S. Otani, and H. Marsh, *Fuel*, **62**, 502 (1983).
21) S. Parkash, D. Carson, and B. Ignasiak, *Fuel*, **62**, 629 (1983).
22) D. K. Sharman, M. K. Srkar, and Z. B. Mirza, *Fuel*, **64**, 449 (1985).
23) K. M. Patel, V. I. Stenberg, R. J. Baltisberger, N. F. Woolsey, and K. J. Klabunde, *Fuel*, **59**, 449 (1980).
24) S. Duber and A. B. Wieckowski, *Fuel*, **61**, 433 (1982).
25) R. S. Aliger, "Electron Paramagnetic Resonance: Techniques and Applications," Interscience, New York (1968), Chap. 2.
26) C. P. Poole, "Relaxation in Magnetic Resonance," Academic Press, New York (1971).
27) T. G. Castner, Jr., *Phys. Rev.* **115**, 1506 (1959).
28) P. Painter, M. Starsinic, and M. Coleman, "Determination of Functional Groups in Coal by Fourier Transform Interferometry," In "Fourier Transform Infrared Spectra; Chemical Application," Academic Press., New York (1985), Vol. 4.

29) O. Ito, H. Seki, and M. Iino, *Fuel*, in press.
30) J. K. Brown, *J. Chem. Soc.*, **1955**, 744.
31) M. J. Sullivan and G. E. Maciel, *Anal. Chem.* **54**, 1606 (1982).
32) M. A. Wilson, R. J. Karas, L. B. Alemany, W. R. Woolfenden, and D. M. Grant, *Anal. Chem.* **56**, 993 (1984).
33) T. Yoshida, K. Tokuhashi, and M. Maekawa, *Fuel*, **64**, 891 (1985).
34) B. G. Silbernagel, L. A. Gebhard, G. R. Dyrkacz, and C. A. A. Bloomquist, *Fuel*, **65**, 558 (1986).
35) G. Srinivasa and M. S. Seehra, *Fuel*, **62**, 792 (1983).
36) L. Petrakis and D. W. Grandy, *Anal. Chem.*, **50**, 303 (1978).
37) J. R. Bolton, "Radical Ions," ed by E. T. Kaiser and L. Kevan, Interscience Publishers, New York (1968), Chap. 1.
38) D. C. Doetschman and D. M. Mustafi, *Fuel*, **65**, 684 (1986).
39) S. Schlick, P. A. Narayana, and L. Kevan, *J. Am. Chem. Soc.*, **100**, 3322 (1978).
40) S. Schlick, M. Narayana, and L. Kevan, *Fuel*, **62**, 1250 (1983).
41) T. F. Yen and J. G. Erdman, *Anal. Chem.*, **34**, 694 (1962).
42) D. W. van Krevelen, "Coal," Elsevier, Amsterdam (1961).
43) Y. Sanada and H. Honda, *Fuel*, **45**, 295 (1966).
44) W. F. K. Wynne-Jones, H. E. B. Blayden, and F. Shaw, *Brennstoff Chem.*, **33**, 201 (1952).
45) H. N. M. Dormans and D. W. van Krevelen, *Fuel*, **39**, 273 (1960).
46) Y. Oosawa, I. Ishiei, T. Kakuta, and M. Fujishiro, *Kogyo Kagaku Zasshi*, **73**, 2212 (1970).
47) M. Iino and M. Matsuda, unpublished data.

 © 1987 The Chemical Society of Japan Bull. Chem. Soc. Jpn., 60, 2977—2981 (1987)

Nucleotide Sequences of DNA and Their Structural Analysis. Categorical Discrimination of 5′-Splice Site Sequences in mRNA Precursors

Yôichi IIDA
Department of Chemistry, Faculty of Science, Hokkaido University, Sapporo 060
(Received February 28, 1987)

The signals which direct excision of introns from mRNA precursors in higher eukaryotes' genes are not well-understood. Although a consensus sequence, $^{C}_{A}$AG/GT$^{A}_{G}$AGT, has been proposed with the 5′-splice site, actual 5′-splice site sequences differ from it to a greater or lesser degree. In the present paper, structural analysis of 5′-splice site sequences was done by using quantification theory (class II). Nucleotide sequences were transformed into categorical data, and categorical discriminant analysis was carried out between 5′-splice site sequences and sequences other than 5′-splice site. Relative importance of each position of nucleotide sequence was then estimated by calculating partial correlation coefficient on each position.

Many eukaryotic genes are interrupted by introns, which are removed from mRNA precursors (pre-mRNAs) by the RNA splicing mechanism.[1-5] The splicing of pre-mRNA includes, as a first step, cleavage of the 5′-splice junction and formation of a lariat involving the 5′-end of the intron joined by a 2′—5′ phosphodiester bond to an A residue upstream of the 3′-splice junction. This is then followed by cleavage at the 3′-splice junction together with ligation of the 5′ and 3′ exons. Although both steps are related to several reactions, the machinery for splicing (macromolecular ribonucleoproteins containing small nuclear RNAs) carries out this process in a concerted manner.[3-5] The compilation of sequences surrounding intron boundaries demonstrates consensus sequences at both the 5′ (donor) and the 3′ (acceptor) splice sites.[1,2] The 5′-splice site consensus sequence is described by 5′-(exon)-$^{C}_{A}$AG/GT$^{A}_{G}$AGT-(intron)-3′, where the stroke (/) indicates boundary between exon and intron. Such a sequence plays an important role in defining the 5′-splice site, because a number of naturally occurring and in vitro derived mutations within the consensus regions result in splice site inactivation.[6,7] However, the consensus sequence has been ambiguous in what degree of matching between observed junction sequences and the consensus sequence is necessary to specify the exact splice site. That is, actual splice site sequences differ from the consensus sequence to a greater or lesser degree. It is also impossible for the consensus sequence to account for relative importances of each of the nucleotides in the sequence. In order to study such situation more quantitatively, Staden used the weight matrix method.[8] On the other hand, we applied previously multivariate statistical analysis to 5′-splice site sequences of pre-mRNAs, and performed categorical discriminant analysis, where nucleotide sequences were transformed into categorical data.[9] In the present paper, discriminating 5′-splice site sequences and sequences other than 5′-splice site, we calculate a value for partial correlation coefficient on each position of the sequence. This approach enables us to know relative importance of each position of nucleotide sequence.

Categorical Discriminant Analysis

Categorical Data. The formulation of categorical data was described in the previous paper.[9] In the following, we summarize the procedure briefly. Our data assume two groups of nucleotide sequences. The first group is composed of 5′-splice site sequences as recognized by the machinery for splicing. They are taken from authentic 5′-splice site sequences in various mammalian genes containing introns, such as globin genes, insulin genes, etc.[10] We take into consideration the consensus sequence, $^{C}_{A}$AG/GT$^{A}_{G}$AGT, for 5′-splice site, and take 9-nucleotide sequence composed of three nucleotides at the 3′-end of exon and six nucleotides at the 5′-end of intron. It is assumed that essential pattern to define 5′-splice site may lie within such 9-nucleotide sequence. In this way, we summarized 155 sequences into the first group. Some of the sequence data are shown in Table 1.

The second group is composed of sequences other than 5′-splice site. They are taken from human β-globin gene in the following way. The β-globin gene sequence is separated into three exons by two introns,

Table 1. Some of the 9-Nucleotide Sequences Belonging to Group 1 and Group 2[a)]

No.	Group	Sequence	Gene
1	1	GAGGTGAGG	Human alpha-Globin
2	1	AAGGTGAGC	
3	1	CAGGTTGGT	Human beta-Globin
4	1	AGGGTGAGT	
:	:	:	
155	1	AGGGTGAGC	Dog Insulin
156	2	ACATTTGCT	Human beta-Globin
157	2	CATTTGCTT	
:	:	:	
1751	2	TTTCATTGC	

a) Group 1 is composed of 5′-splice site sequences, while Group 2, of sequences other than 5′-splice sites. For further details, see text.

and there are two positions of 5′-splice junctions.[11] In this gene, we first take the 9-nucleotide sequence at the 5′-cap site. Next, we progress one nucleotide in the 3′ direction, and take the next 9-nucleotide sequence. In this way, we truncate 9-nucleotide sequence at every position of the whole pre-mRNA. In those sequences, however, there lie two sequences of the authentic 5′-splice sites, belonging to the first group. These two are excluded, and the remaining 1596 sequences are summarized into the second group, as shown in Table 1.

In order to transform sequence data into categorical data, we introduce a dummy variable $x_{i(\alpha)}^{r(\nu)}$ and parameters of r, ν, i, and α. The parameter, r, indicates the groups, where $r=1$ or 2 corresponds to the first or second group, respectively. We denote n_r as sample size of each group, and take $\nu=1, 2, \cdots, n_r$, where $n_1=155$ and $n_2=1596$. Next, we consider item and category. In our case, there are nine items with $i=1, 2, \cdots, 9$. They correspond to the positions of nucleotides in 9-nucleotide sequence, and are defined by the order from the 5′- to 3′-ends of the sequence. Category denotes the kind of nucleotide, where we specify nucleotide A, G, C, or T by $\alpha=1$, 2, 3, or 4 at every item, respectively. Using these parameters, dummy variable of $x_{i(\alpha)}^{r(\nu)}$ is expressed by

$$x_{i(\alpha)}^{r(\nu)} = \begin{cases} 1 : \text{if the sample sequence } (\nu) \text{ of the group } (r) \\ \quad \text{has a nucleotide } (\alpha) \text{ at the position } (i), \\ 0 : \text{otherwise.} \end{cases} \tag{1}$$

In this way, we transformed the sequence data of Table 1 into the categorical data. Here, we note the redundant condition for any sample sequence $r(\nu)$,

$$\sum_{\alpha=1}^{4} x_{i(\alpha)}^{r(\nu)} = 1, \quad (i=1, 2, \cdots, 9). \tag{2}$$

Categorical Discriminant Analysis. It was made according to Hayashi's quantification analysis (class II).[12,13] Quantification of the categorical data leads to the sample score value

$$y^{r(\nu)} = \sum_{i=1}^{9} \sum_{\alpha=1}^{4} x_{i(\alpha)}^{r(\nu)} a_{i(\alpha)}, \tag{3}$$

where $r=1$, 2 and $\nu=1, 2, \cdots, n_r$. Coefficient of $a_{i(\alpha)}$ is the real number and is called category weight. Our analysis estimates the $a_{i(\alpha)}$ and $y^{r(\nu)}$ values in such a way that the two groups of 5′-splice site sequences ($r=1$) and sequences other than 5′-splice site ($r=2$) may be discriminated most distinctly. For this purpose, we calculate the mean value of sample scores within the group r as

$$\bar{y}^r = \frac{1}{n_r} \sum_{\nu=1}^{n_r} y^{r(\nu)} = \sum_{i=1}^{9} \sum_{\alpha=1}^{4} \bar{x}_{i(\alpha)}^{r} a_{i(\alpha)}, \tag{4}$$

where

$$\bar{x}_{i(\alpha)}^{r} = \frac{1}{n_r} \sum_{\nu=1}^{n_r} x_{i(\alpha)}^{r(\nu)}, \quad (r=1, 2). \tag{5}$$

On the other hand, the mean value of the total samples is

$$\bar{y} = \frac{1}{N} \sum_{r=1}^{2} n_r \bar{y}^r, \tag{6}$$

where $N=n_1+n_2=1751$ is the number of total samples. Using these values, variance of the total samples, σ^2, and variance between groups 1 and 2, σ_B^2, are given by

$$\sigma^2 = \frac{1}{N} \sum_{r=1}^{2} \sum_{\nu=1}^{n_r} (y^{r(\nu)} - \bar{y})^2, \tag{7}$$

$$\sigma_B^2 = \frac{1}{N} \sum_{r=1}^{2} n_r (\bar{y}^r - \bar{y})^2. \tag{8}$$

In order to discriminate the groups 1 and 2 most distinctly, we maximize the following η^2 value,

$$\eta^2 = \frac{\sigma_B^2}{\sigma^2}. \tag{9}$$

The procedure to maximize η^2 and to obtain $a_{i(\alpha)}$ values at the optimum condition was briefly summarized in the previous paper.[9]

Partial Correlation Coefficient. Using the optimum values of category weight $\hat{a}_{i(\alpha)}$, ($i=1, 2, \cdots, 9$; $\alpha=1$, 2, 3, 4), we calculate the optimum values of sample scores $\hat{y}^{r(\nu)}$ by Eq 3. Then, we obtain from Eq. 4

$$\hat{y}^r = \frac{1}{n_r} \sum_{\nu=1}^{n_r} \hat{y}^{r(\nu)}, \quad (r=1, 2). \tag{10}$$

We define $x_i^{r(\nu)}$ by

$$x_i^{r(\nu)} = \sum_{\alpha=1}^{4} \hat{a}_{i(\alpha)} x_{i(\alpha)}^{r(\nu)}, \quad (\nu=1, 2, \cdots, n_r;\ i=1, 2, \cdots, 9). \tag{11}$$

Using these parameters, we calculate the following quantities;

$$\sigma_{ij} = \frac{1}{N} \sum_{r=1}^{2} \sum_{\nu=1}^{n_r} (x_i^{r(\nu)} - \bar{x}_i)(x_j^{r(\nu)} - \bar{x}_j), \quad (i, j=1, 2, \cdots, 9), \tag{12}$$

$$\sigma_{iy} = \frac{1}{N} \sum_{r=1}^{2} \sum_{\nu=1}^{n_r} (x_i^{r(\nu)} - \bar{x}_i)(\hat{y}^r - \hat{y}), \quad (i=1, 2, \cdots, 9), \tag{13}$$

$$\sigma_{yy} = \frac{1}{N} \sum_{r=1}^{2} n_r (\hat{y}^r - \hat{y})^2, \tag{14}$$

where

$$\bar{x}_i = \frac{1}{N} \sum_{r=1}^{2} \sum_{\nu=1}^{n_r} x_i^{r(\nu)}, \quad (i=1, 2, \cdots, 9), \tag{15}$$

$$\hat{y} = \frac{1}{N} \sum_{r=1}^{2} n_r \hat{y}^r. \tag{16}$$

Next, we introduce correlation coefficients between

items, r_{ij}, and between item and sample sequence, r_{iy}, by

$$r_{ij} = \frac{\sigma_{ij}}{\sqrt{\sigma_{ii}\sigma_{jj}}}, \quad (i, j = 1, 2, \cdots, 9), \tag{17}$$

$$r_{iy} = \frac{\sigma_{iy}}{\sqrt{\sigma_{ii}\sigma_{yy}}} = r_{yi}, \quad (i = 1, 2, \cdots, 9, y). \tag{18}$$

We construct the 10-dimensional matrix, **R**, composed of those coefficients by

$$\mathbf{R} = \begin{bmatrix} r_{11} & r_{12} & \cdots & r_{19} & r_{1y} \\ r_{21} & r_{22} & \cdots & r_{29} & r_{2y} \\ \vdots & \vdots & & \vdots & \vdots \\ r_{91} & r_{92} & \cdots & r_{99} & r_{9y} \\ r_{y1} & r_{y2} & \cdots & r_{y9} & r_{yy} \end{bmatrix}. \tag{19}$$

This matrix leads to the inverse matrix, $\mathbf{R}^{-1}$, whose matrix elements are

$$\mathbf{R}^{-1} = \begin{bmatrix} r^{11} & r^{12} & \cdots & r^{19} & r^{1y} \\ r^{21} & r^{22} & \cdots & r^{29} & r^{2y} \\ \vdots & \vdots & & \vdots & \vdots \\ r^{91} & r^{92} & \cdots & r^{99} & r^{9y} \\ r^{y1} & r^{y2} & \cdots & r^{y9} & r^{yy} \end{bmatrix}. \tag{20}$$

By the use of these matrix elements, partial correlation coefficient between samples and the i-th item is given by

$$r_{iy \cdot 1,2,\cdots,i-1,i+1,\cdots,9} = \frac{-r^{iy}}{\sqrt{r^{ii}r^{yy}}}, \quad (i = 1, 2, \cdots, 9). \tag{21}$$

where $r_{iy.1,2,\cdots,i-1,i+1,\cdots,9}$ indicates a correlation coefficient between i and y, removing influences of the other items of $1, 2, \cdots, i-1, i+1, \cdots, 9$. The magnitude of this coefficient tells us to what extent the i-th item may contribute to the discrimination of sample sequences between the first and second groups.

Results

We applied the above method to the $N=1751$ sample sequences, and discriminated 5′-splice site sequences ($r=1$) from sequences other than 5′-splice sites ($r=2$) most distinctly. The optimum values for category weights $\hat{a}_{i(\alpha)}$, ($i=1, 2, \cdots, 9$; $\alpha=1, 2, 3, 4$), were estimated as shown in Table 2. Using these values together with Eqs. 10—18, we constructed the **R** matrix. Its matrix elements are symmetrical and the lower half of them is only given in Table 3. After transforming **R** matrix into $\mathbf{R}^{-1}$ matrix, partial correlation coefficients in Eq. 21 are calculated as 0.100, 0.162, 0.264, 0.424, 0.329, 0.175, 0.206, 0.351, and 0.157 for items $i=1, 2, 3, 4, 5, 6, 7, 8$, and 9, respectively.

Discussion

So far, the splice junction signals have been summarized as "consensus" sequences. In the case of 5′-splice site consensus sequence, $^{C}_{A}$AG/GT$^{A}_{G}$AGT has been proposed by Mount.[2] Attempts have been widely made to look for sequences relevant to the consensus sequence in the whole pre-mRNA. However, its technique is rather unsatisfactory, because actual splice site sequences differ from the consensus sequence to a greater or lesser degree. The consensus sequence is also ambiguous in which nucleotides are important to specify the 5′-splice site and which nucleotides are less important. The optimum values of category weight $\hat{a}_{i(\alpha)}$, ($i=1, 2, \cdots, 9$; $\alpha=1, 2, 3, 4$), may answer this problem. In this case, the item, i, corresponds to the position of nucleotide in 9-nucleotide sequence, while the category, α, denotes the kind of nucleotide at the i-th position. Relative importance of the kind of nucleotide at each position was previously discussed in terms of the $\hat{a}_{i(\alpha)}$ value.[9]

Next, we consider relative importance of item (position of nucleotide) in 9-nucleotide sequence. There

Table 2. Optimum Category Weight Values of $\hat{a}_{i(\alpha)}$'s Calculated with Categorical Discriminant Analysis of 5′-Splice Site Sequences[a]

Item No. (i)	Category Name (α)	$\hat{a}_{i(\alpha)}$
1	A-1	0.5300
	G-2	−0.5163
	C-3	1.9291
	T-4	−1.4366
2	A-1	3.1444
	G-2	−1.9297
	C-3	−0.3227
	T-4	−1.3873
3	A-1	−1.9442
	G-2	5.6465
	C-3	0.2679
	T-4	−3.1345
4	A-1	−3.6933
	G-2	9.8117
	C-3	−4.9457
	T-4	−2.9199
5	A-1	−3.1491
	G-2	−4.8216
	C-3	−2.7129
	T-4	5.2915
6	A-1	2.7188
	G-2	1.4351
	C-3	−2.7449
	T-4	−1.8026
7	A-1	4.0432
	G-2	−1.7958
	C-3	−1.1522
	T-4	−1.9755
8	A-1	−3.4019
	G-2	7.9204
	C-3	−3.6093
	T-4	−1.8206
9	A-1	−1.1933
	G-2	−2.8199
	C-3	0.0108
	T-4	2.3215

a) For further details, see the text.

Table 3. The **R** Matrix and Its Matrix Elements r_{ij}, ($i, j=1, 2, \cdots, 9, y$), Shown by Eq. 19 in the Text[a)]

Item No.	1	2	3	4	5	6	7	8	9	10
1	1.000									
2	0.171	1.000								
3	0.120	0.034	1.000							
4	0.103	0.129	0.197	1.000						
5	0.054	0.050	0.093	0.107	1.000					
6	0.036	0.037	0.113	0.140	0.094	1.000				
7	0.055	0.032	0.147	0.166	0.100	0.098	1.000			
8	0.099	0.051	0.123	0.175	0.150	0.133	0.104	1.000		
9	0.018	−0.009	−0.035	0.053	0.104	−0.025	−0.013	−0.026	1.000	
10	0.197	0.206	0.352	0.506	0.377	0.264	0.296	0.416	0.131	1.000

a) The tenth item in this table is read as $i, j=y$. Since $r_{ij}=r_{ji}$, the lower half of the matrix elements is only given.

have been known a few approaches to measure quantitatively contribution of item to the discrimination between two groups of 5′-splice site sequences and sequences other than 5′-splice sites. One approach is to calculate partial correlation coefficient between sample sequences and the i-th item under the optimum condition of discrimination. This was done in the previous sections. Here, the larger the value of such a partial correlation coefficient, the greater the contribution of the i-th item to the discrimination between the two groups. As is shown in Results, the largest value of the partial correlation coefficient was found to be 0.424 at the fourth position. The next largest values range as 0.351 at the eighth position, 0.329 at the fifth position, and 0.264 at the third position, while the smallest values were found to be 0.100 at the first position and 0.157 at the ninth position. Therefore, the fourth, eighth and fifth positions are more important to specify 5′-splice site sequences, whereas the first, ninth and second positions are less important. This prediction is consistent with the experimental results that the GT dinucleotide at the fourth and fifth positions and the G nucleotide at the eighth position are almost invariant in every sequence of 5′-splice junction.[2)] It is also found that nucleotides at the other positions are rather variable, differing from junction to junction. The small values of partial correlation coefficients at the other positions may correspond to this phenomenon.

Another approach to measure relative importance of item (position of nucleotide) is to estimate the range of category weights, R_i, which is defined by

$$R_i = \max_{\alpha}(\hat{a}_{i(\alpha)}) - \min_{\alpha}(\hat{a}_{i(\alpha)}). \quad (22)$$

This parameter implies that the larger the R_i value, the greater the influence of $\hat{a}_{i(\alpha)}$'s at the i-th item on the total sample score $y^{r(\nu)}$. Using the data of $\hat{a}_{i(\alpha)}$ in Table 2, the R_i values are calculated as $R_1=3.3657$, $R_2=5.0741$, $R_3=8.7810$, $R_4=14.7574$, $R_5=10.1131$, $R_6=5.4637$, $R_7=6.0187$, $R_8=11.5297$, and $R_9=5.1414$. These results show that the degree of importance of items aligns in the order of $i=4, 8, 5, 3, 7, 6, 9, 2$, and 1. It appears that this order of importance is in good accordance with that of the previous partial correlation coefficients given in the previous section of Results.

Several other evidences which support our conclusion are provided by experimental results on mutational changes of nucleotides around 5′-splice junctions. One example is the study of Treisman et al.,[6)] who reported three mutants of human β-globin gene. The β-globin gene sequence is separated into three exons by two introns, and there are two positions of 5′-splice junctions.[11)] In the normal gene, the 9-nucleotide sequence at the 5′-splice site of the first intron is ··· CAG/GTTGGT ···. All of the above three mutant genes (i)—(iii) contain single nucleotide changes within the 9-nucleotide sequence, causing β-thalassemia phenotype. The β-thalassemia comprises a group of diseases in which the synthesis of normal β-globin polypeptide is either absent or reduced. In the (i) mutant, a G→A transition took place at the fourth position of the 9-nucleotide sequence, resulting in ··· CAGATTGGT ···. The (ii) mutant underwent a G→C transversion at the eighth position, and has a sequence ··· CAGGTTGCT ···. In the (iii) mutant, a T→C transition took place at the ninth position, resulting in ··· CAGGTTGGC ···. Treisman et al. analyzed the RNA synthesis and expression of the mutant gene after its introduction into cultured mammalian cells on a suitable vector.[6)] In all of the (i)—(iii) genes, the mutational changes inactivated the authentic 5′-splice site signal at the first intron, failing in normal β-globin mRNA synthesis or reducing the synthesis. The mutation at the fourth position completely inactivated the 5′-splice site of the first intron, giving no production of normal β-globin mRNA. On the other hand, the mutation at the eighth position resulted in partial inactivation of the 5′-splice site, while the mutation at the ninth position showed a less dramatic decrease in the production level of normal mRNA. Although the latter two mutations led to β^+-thalassemia, the eighth position mutation caused a more pronounced deficiency of β-globin synthesis than did the ninth position mutation. These experimental results may correspond well to our categorical discriminant analysis. Since the relative importance of items (position of nucleotide) is greatest at the fourth

position, mutation at this position will influence the 5′-splice site signal most strongly. This may be a reason why the G→A change at the fourth position of the (i) mutant inactivated completely the 5′-splice site. According to our discriminant analysis, the next important item corresponds to the eighth position, and the least important item, to the ninth position. In accordance with this view, both of the eighth and ninth position mutations caused partial inactivation of the 5′-splice site, but the deficiency of mRNA synthesis is more severe in the eighth position mutant than in the ninth position mutant.

Another example of mutations which supports our conclusion is the work of Wieringa et al.,[7] who reported mutagenic inactivation of an authentic 5′-splice site of the second intron in rabbit β-globin gene. The 9-nucleotide sequence of the normal gene at this site is ···AGG/GTGAGT···. Six mutant genes were prepared by site-directed mutagenesis involving purine transitions; (i) A→G transition at the first position, (ii) G→A at the second position, (iii) G→A at the third position, (iv) G→A at the fourth position, (v) G→A at the sixth position and (vi) A→G at the seventh position. Expression of these genes in HeLa cells revealed that mutations of (i)—(iii), (v) and (vi) affected neither the quantity nor the structure of correct β-globin mRNA. However, the mutation of (iv) inactivated completely the 5′-splice site, giving no correctly spliced β-globin mRNA. These experimental results seem to be consistent with the previous discriminant analysis, because the 5′-splice site sequence is influenced most strongly by the mutational change at the fourth position, and because the effects of the other positions are much weaker than that of the fourth position.

References

1) M. R. Lerner, J. A. Boyle, S. M. Mount, S. L. Wolin, and J. A. Steitz, *Nature*, **283**, 220 (1980).
2) S. M. Mount, *Nucl. Acids Res.*, **10**, 459 (1982).
3) B. Ruskin, A. R. Krainer, T. Maniatis, and M. R. Green, *Cell*, **38**, 317 (1984).
4) R. Reed and T. Maniatis, *Cell*, **41**, 95 (1985).
5) S. M. Mount, I. Petterson, M. Hinterbergen, A. Karmas, and J. A. Steitz, *Cell*, **33**, 509 (1983).
6) R. Treisman, S. H. Orkin, and T. Maniatis, *Nature*, **302**, 591 (1983).
7) B. Wieringa, F. Meyer, J. Reiser, and C. Weissmann, *Nature*, **301**, 38 (1983).
8) R. Staden, *Nucl. Acids Res.*, **12**, 505 (1984).
9) Y. Iida, *Compt. Appl. Biosci.*, **3**, 93 (1987).
10) GenBank, Genetic Sequence Data Bank, Release 40.0, BBN Laboratories, U. S. A. (1986).
11) R. M. Lawn, A. Efstratiadis, C. O'Connell, and T. Maniatis, *Cell*, **21**, 647 (1980).
12) C. Hayashi, *Ann. Inst. Statist. Math.*, **2**, 35 (1950).
13) C. Hayashi, *Ann. Inst. Statist. Math.*, **3**, 69 (1952).

 © 1987 The Chemical Society of Japan Bull. Chem. Soc. Jpn., 60, 2983—2988 (1987)

Crystal Structure and ^{35}Cl NQR of Copper(II) Trichloroacetate Trihydrate

Hideko KIRIYAMA,† Masao HASHIMOTO,* and Nanami OKUNO
Department of Chemistry, Faculty of Science, Kobe University, Nada, Kobe 657
(Received March 24,1987)

The crystal structure of the title compound has been determined by means of X-ray diffraction. The crystal data and the final R value are: $Cu(CCl_3COO)_2 \cdot 3H_2O$, monoclinic $C2/c$, $a=23.082(3)$, $b=6.253(1)$, $c=9.726(2)$ Å, $\beta=94.67(1)°$, $Z=4$, $R=0.049$. The structure consists of monomeric $Cu(CCl_3COO)_2(H_2O)_3$ molecules, which are linked together by intermolecular O-H···O hydrogen bonds to form a layer parallel to (100). Each Cu(II) atom is coordinated by five oxygen atoms which form nearly a square pyramid; two oxygen atoms of two carboxylate ions and two water molecules form its basal plane and the remaining water molecule occupies the apical position. The mean basal Cu-O length is 1.961 Å and the apical one 2.183 Å. The Cu(II) atom is displaced from the basal plane by 0.110 Å toward the apical oxygen. Thermal analysis (DSC) disclosed two phase transitions at 163 and 207 K, their estimated molar enthalpies being about 0.4 and 0.7 kJ mol^{-1}, respectively. At 77 K, 24 ^{35}Cl NQR signals are observed in the frequency range 38.7—40.3 MHz. The X-ray diffraction photographs for both low-temperature phases indicate the appearance of superstructures with less symmetrical space groups; the b spacing doubles below 207 K, while both b and c spacings double below 163 K.

One of the present authors studied ^{35}Cl nuclear quadrupole resonance (NQR) on a various salts of trichloroacetic acid with a view to obtaining structural informations.[1] Of these, the NQR spectrum of $Cu(CCl_3COO)_2 \cdot nH_2O$ was not consistent with that reported in the literature.[2] In order to solve this question, we investigated the crystal structure of the title compound. In course of this work, it was found that the ^{35}Cl NQR spectrum expected from the crystal structure determined at room temperature is quite different from that observed at 77 K. In fact, thermal analysis confirmed the occurrence of phase transitions at 163 and 207 K. Fortunately, undergoing of both phase transitions did not damage the crystal, and the structural changes could be followed by X-ray diffraction method at low temperatures. To get further information on the transitions the temperature dependence of the ^{35}Cl NQR frequencies were reinvestigated more accurately than in the earlier work.

The present paper deals with the crystal structures of the compound and the nature of the phase transitions newly found. Furthermore, the conformation of CCl_3COO^- group is discussed in detail especially in comparison with that recently found in $CCl_3COONH_4 \cdot 2.5H_2O$.[3]

Experimental

Material. Addition of dicopper carbonate dihydroxide hydrate to an aqueous solution of trichloroacetic acid in a stoichiometric ratio yielded a light blue precipitate at about 40 °C. The trihydrate crystal was obtained by recrystallization of the precipitate from water as a blue, flat plate characterized by perfect cleavage.

X-Ray Structure Determination. The density was measured by pycnometry with petroleum at 18 °C. The lattice parameters and the space group were first determined with a Weissenberg camera (Rigaku Denki Co.); reflection conditions hkl: $h+k=2n$ and $h0l$: $l=2n$ led to monoclinic $C2/c$ or Cc, the former space group being confirmed by successful refinements. A single crystal 0.2×0.3×0.3 mm in size was mounted with [010] coincident with the goniostat axis of an automated Rigaku four-circle diffractometer AFC-4, graphite-monochromated Mo $K\alpha$ radiation ($\lambda=0.7107$ Å), 40 kV-200 mA used. Unit cell parameters were refined by a least-squares method using 25 2θ values ($25° < 2\theta < 34°$). Intensity measurement in ω—2θ scan mode was made up to $2\theta=55°$ ($-30 \leqq h \leqq 30$, $0 \leqq k \leqq 8$, $-12 \leqq l \leqq 12$), three standard reflections (040, 1604, 915) were monitored every 50 reflections throughout the experiment. A total of 3210 reflections were measured. Lorentz-polarization and absorption effects were corrected, empirical absorption correction-factors on F less than 1.19.[4] Equivalent reflections were merged ($R_{av}=\sum||F_o|-<|F_o|>|/\sum|F_o|=0.017$), and of 1608 reflections remained 1441 with $|F_o|>3\sigma(F_o)$ were used for the structure determination.

The positional coordinates of Cu and Cl atoms were obtained by a direct method with MULTAN78[5] and confirmed by a three-dimensional Patterson synthesis. The other non-hydrogen atoms were located by successive Fourier syntheses. The structure was refined by block-diagonal least-squares with anisotropic thermal parameters for non-hydrogen atoms. All hydrogen atoms were located by a difference Fourier synthesis and refined with isotropic thermal parameters. The quantity $\sum w(|F_o|-|F_c|)^2$ with $w=1/[\sigma^2(F_o)+0.13247|F_o|]$ was minimized for 1441 unique reflections and 96 variables. The final refinement including hydrogen atoms gave $R=\sum(||F_o|-|F_c||)/\sum|F_o|=0.049$, $R_w=[\sum w(|F_o|-|F_c|)^2/\sum wF_o^2]^{1/2}=0.073$ and goodness of fit $S=[\sum w(|F_o|-|F_c|)^2/(m-n)]^{1/2}=1.14$, where m is the number of reflections and n the number of refined parameters. The maximum positive and negative electron densities $(\Delta\rho)_{max}$ and $(\Delta\rho)_{min}$ in the final difference Fourier synthesis were +0.9 and −0.9 e Å^{-3}, respectively. The maximum ratio of parameter shift to e.s.d. for non-hydrogen atoms, $(\Delta/\sigma)_{max}$, was 0.017. Neutral atomic scattering factors were used for all atoms and corrections for anomalous dispersion applied.[6] The computer programs used were MULTAN78, ORTEPII and UNICS-OSAKA.[5,7,8] The final atomic parameters are listed in Table 1.[9]

Crystal Data: $[Cu(CCl_3COO)_2(H_2O)_3]$, $M_r=442.34$, $C2/c$, $a=23.082(3)$, $b=6.253(1)$, $c=9.726(2)$ Å, $\beta=94.67(1)°$, $Z=4$,

†Present address: Imajuku 1-12, Ogaki, Gifu 503.

Table 1. Fractional Coordinates and Equivalent or Isotropic Thermal Parameters (Å^2) with Estimated Standard Deviations in Parentheses

$B_{eq}=(4/3)\sum_i\sum_j\beta_{ij}\boldsymbol{a}_i\cdot\boldsymbol{a}_j$

Atom	x	y	z	B_{eq}/B_{iso}*
Cu	0	0.35222(12)	0.25	2.41(1)
Cl(1)	−0.20251(6)	0.30888(32)	0.31465(18)	5.55(3)
Cl(2)	−0.17847(7)	−0.08904(27)	0.44913(21)	5.67(4)
Cl(3)	−0.14626(8)	0.30503(38)	0.58822(16)	6.37(2)
O(1)	−0.0744(2)	0.3477(6)	0.3325(4)	3.89(6)
O(2)	−0.0630(2)	0.0075(7)	0.3807(6)	5.98(11)
O(W1)	0.0420(2)	0.3216(7)	0.4333(4)	4.37(6)
O(W2)	0	0.7014(8)	0.25	4.96(13)
C(1)	−0.0912(2)	0.1710(7)	0.3719(5)	2.71(6)
C(2)	−0.1524(2)	0.1721(7)	0.4285(5)	2.77(6)
H(1)	0.065(3)	0.423(14)	0.490(8)	5(2)*
H(2)	0.050(4)	0.203(14)	0.470(8)	6(2)*
H(3)	−0.019(5)	0.796(17)	0.318(10)	9(3)*

D_m=2.08, D_x=2.10 Mg m^{-3}, μ(Mo $K\alpha$)=2.7 mm^{-1}, F(000)=868, T=291 K.

Thermal Analyses. Thermal gravimetry (TG), differential thermal analysis (DTA) and differential scanning calorimetry (DSC) were carried out with two pieces of Rigaku "thermoflex" apparatus. The temperature ranges studied were 300—450 K for the former two and 100—300 K for the latter one. A relatively large single crystal (3×3×1 mm, about 16 mg) sealed in an aluminium cell under an atmosphere of nitrogen was used for DSC, because the transition enthalpies are too small to be detected with a powdered sample.

^{35}Cl NQR Experiment. The ^{35}Cl NQR frequencies were measured on a polycrystalline sample by use of a superregenerative spectrometer with an accuracy of ±2kHz.[10]

Low-Temperature X-Ray Experiment. Oscillation and Weissenberg photographs were taken with a Cu $K\alpha$ radiation (40 kV, 150 mA) at 183 and 145 K. The specimen was kept at a desired temperature by controlling the flow rate of cold nitrogen gas and the current of a heater wound around an inner tube in which the gas flows. A flow of nitrogen-gas jetted through an outer tube formed a curtain to avoid formation of frost on the crystal during the experiment. A rather large single crystal (0.5 mm on edge) was chosen for the goniometric use at low temperatures.

Results and Discussion

Crystal Structure. A stereo pair of the crystal structure viewed along [010] and the projection along [100] with the atomic numbering scheme are shown in Figs. 1 and 2, respectively. Selected interatomic distances and angles are listed in Table 2. The structure of copper(II) trichloroacetate hydrate consists of discrete monomeric molecules, $[Cu(CCl_3COO)_2(H_2O)_3]$, in agreement with the prediction from the magnetic susceptibility[11] and ESR spectra.[12] The molecule has a crystallographic C_2 axis passing through the Cu and O(W2) atoms. Each copper(II) atom is coordinated by five oxygen atoms (two from monodentate trichloroacetato groups and three from water molecules) in a nearly square pyramidal arrangement. The four donor atoms, O(1), O(W1), O(1^i), O(W1^i), form a slightly distorted square and the water oxygen O(W2)

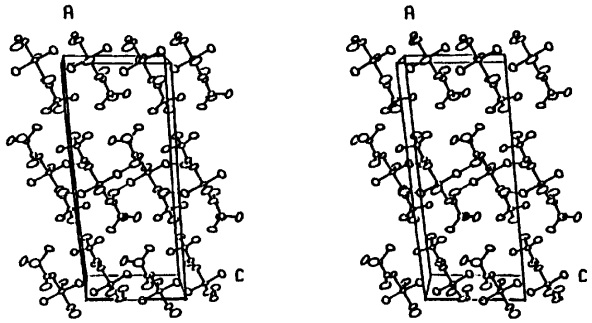

Fig. 1. A stereoscopic view of the crystal structure of $Cu(CCl_3COO)_2\cdot 3H_2O$ along the b axis. Thermal ellipsoids are shown at 50% probability level.

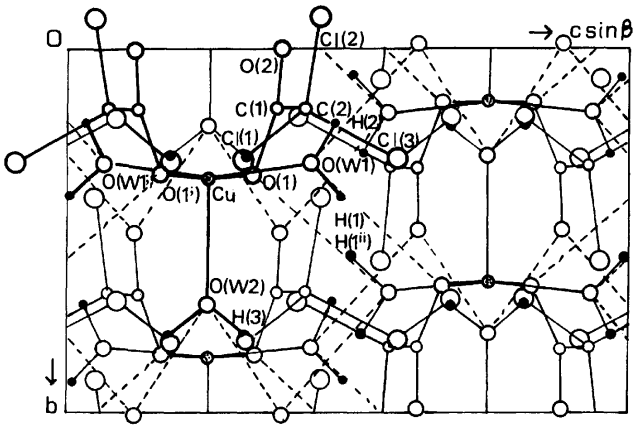

Fig. 2. The projection of crystal structure along the a axis with the atom numbering scheme.

occupies the apical position. The apical Cu-O(W2) distance (R_L=2.183 Å) is significantly longer than the mean basal Cu·O distance (R_s=1.961 Å), the tetragonality T^5(=R_S/R_L) being 0.90.[13] Such lengthening of the apical bond is quite common in copper(II) complexes with coordination numbers of 6 and even 5.[14] The four oxygen atoms in the CuO_5 chromophore is planar within 0.082(6) Å, and the central Cu atom is displaced from this plane by 0.110(2) Å toward O(W2). Although the second oxygen of each carboxylate ion

Table 2. Interatomic Distances (l/Å) and Angles (ϕ/°) with Standard Deviations in Parentheses

(1) CuO_5 chromophor					
Cu-O(1)	1.954(4)	Cu-O(W1)	1.968(4)	Cu-O(W2)	2.183(5)
[Cu-O(2)	2.946(6)]				
O(1)-Cu-O(W1)		90.7(2)	O(1)-Cu-O(W1^{i})		89.2(2)
O(1)-Cu-O(W2)		90.8(2)	O(W1)-Cu-O(W2)		95.6(2)
O(1)-Cu-O(1^{i})		178.3(2)	O(W1)-Cu-O(W1^{i})		168.8(2)
(2) CCl_3COO^- ion					
C(1)-O(1)	1.242(6)	C(1)-O(2)	1.212(8)	C(1)-C(2)	1.557(7)
C(2)-Cl(1)	1.757(5)	C(2)-Cl(2)	1.758(5)	C(2)-Cl(3)	1.758(5)
Cl(1)-C(2)-Cl(2)		108.1(3)	Cl(1)-C(2)-Cl(3)		109.2(3)
Cl(2)-C(2)-Cl(3)		110.0(3)	Cl(1)-C(2)-C(1)		110.4(3)
Cl(2)-C(2)-C(1)		111.4(3)	Cl(3)-C(2)-C(1)		107.7(3)
O(1)-C(1)-O(2)		126.4(5)	O(1)-C(1)-C(2)		114.9(4)
O(2)-C(1)-C(2)		118.4(5)			
O(1)-C(1)-C(2)-Cl(1)		48.1(5)	O(1)-C(1)-C(2)-Cl(2)		168.2(4)
O(1)-C(1)-C(2)-Cl(3)		−71.0(5)	O(2)-C(1)-C(2)-Cl(1)		−137.9(5)
O(2)-C(1)-C(2)-Cl(2)		−17.8(6)	O(2)-C(1)-C(2)-Cl(3)		102.9(5)
(3) Hydrogen bond					
O(W1)···O(1^{ii})		3.122(6)	H(1)-O(W1)-H(2)		105(7)
O(W1)-H(1)		0.97(9)	O(1^{ii})···O(W1)···O(2^{iii})		89.8(2)
H(1)···O(1^{ii})		2.24(8)	O(W1)-H(1)···O(1^{ii})		150(7)
O(W1)···O(2^{iii})		2.757(7)	O(W1)-H(2)···O(2^{iii})		157(8)
O(W1)-H(2)		0.83(9)			
H(2)···O(2^{iii})		1.97(8)			
O(W2)···O(2^{iv})		2.774(8)	H(3)-O(W2)-H(3^{i})		108(9)
O(W2)-H(3)		1.0(1)	O(2^{iv})-O(W2)-O(2^{v})		92.7(3)
H(3)···O(2^{iv})		1.8(1)	O(W2)-H(3)···O(2^{iv})		159(10)

Symmetry code: (i) $-x$, y, $1/2-z$; (ii) $-x$, $1-y$, $1-z$; (iii) $-x$, $-y$, $1-z$; (iv) x, $1+y$, z; (v) $-x$, $1+y$, $1/2-z$.

group is situated at 2.946 Å from the Cu(II) atom, it is not regarded as bonded to Cu(II).

The bond lengths and angles in the trichloroacetato ligand are in agreement with those found in $CCl_3COONH_4 \cdot 2.5H_2O$,[3] except for C-O distances and torsion angles. The lengths of 1.242 Å for C(1)-O(1) and 1.212 Å for C(1)-O(2) are significantly different owing to monodentative coordination of the ligand. More remarkable differences are seen in the torsion angles O-C-C-Cl, which are associated with the conformation of CCl_3COO^- ligand. In the most stable conformation of its free ion, the three torsion angles will be 90, 30, and 150°. In other words, one of the three C-Cl bonds will be perpendicular to the COO plane in the projection along the molecular axis C-C. As given in Table 2, the torsion angles deviate from these ideal values by 12—19° (the mean 15.3°) in contrast to the corresponding values of 0.3—3.0 (the mean 1.4°) for the NH_4 salt.[3] In both compounds, the CCl_3 groups are faced to each other with van der Waals contact and all the carboxylate oxygen atoms are participated in hydrogen bonds as acceptors. However, there exists a serious difference in coordination scheme between the two salts; in the Cu salt, one oxygen atom of the COO group coordinates also to a Cu(II) atom. It was therefore evidenced that the conformation of CCl_3COO moiety is largely affected by the bonding scheme with its surroundings.

As shown in Figs. 1 and 2, the $[Cu(CCl_3COO)_2(H_2O)_3]$ molecules are linked together by intermolecular hydrdogen bonds of O(W1)-H···O(2), O(W1)-H···O(1), and O(W2)-H···O(2), forming a distinct layer parallel to (100). Thus, the terminal CCl_3 groups of trichloroacetato ligands face to each other with van der Waals contact between Cl(1) and Cl(2) (3.659 Å) and between Cl(1) and Cl(3) (3.582 Å) in interlayer space. Such a distinct layer structure is responsible for the perfect cleavage parallel to (100).

Thermal Properties and Phase Transitions. The DTA and TG experiments indicated that the dehydration of $Cu(CCl_3COO)_2 \cdot 3H_2O$ proceeds in two steps; two water molecules were lost at about 338 K and the rest at about 404 K. On the other hand, two faint, but definite endothermic (exothermic) peaks were observed on heating (cooling) runs of DSC, providing a clear evidence for the presence of two phase transitions at 163 and 207 K. The transition enthalpies were estimated to be approximately 0.4 kJ mol^{-1} for the transition at 163 K and 0.7 kJ mol^{-1} for that at 207 K. These values are quite small and suggest very slight structural changes associated with the phase transitions. In fact, the single crystal remained unchanged in appearance after it experienced either phase transition many times. The three phases will be abbreviated as LTP, ITP, and RTP in order of increasing temperature, hereafter.

^{35}Cl NQR in LTP and ITP. The ^{35}Cl NQR frequencies at 77 K (the lowest temperature studied) are

Table 3. ^{35}Cl NQR Frequencies at 77 K and Their Temperature Coefficients at 110 K in $Cu(CCl_3COO)_2 \cdot 3H_2O$

Line No.	Frequency	$(d\nu/dT)$	Line No.	Frequency	$(d\nu/dT)$
	MHz	kHz K^{-1}		MHz	kHz K^{-1}
ν_1	40.289	−6.71	ν_{11}	39.597	−4.19
ν_2	40.156[a]	−3.95	ν_{12}	39.549[a]	−7.92
ν_3	40.062[a]	−3.09	ν_{13}	39.536	−3.88
ν_4	40.005	−3.08	ν_{14}	39.411[a]	−4.72
ν_5	39.861[a]	−4.83	ν_{15}	39.322[a]	−4.94
ν_6	39.851	−3.36	ν_{16}	39.292	−7.12
ν_7	39.813[b]	−5.68	ν_{17}	39.213[a]	−5.89
		−4.18	ν_{18}	39.132[a,b]	−3.11
ν_8	39.807	−3.54			−3.29
ν_9	39.757[a]	−2.27	ν_{19}	39.044[a]	−4.65
ν_{10}	39.697[a,b]	−5.12	ν_{20}	39.041[a]	−4.54
		−6.85	ν_{21}	38.732	−2.87

a) These frequencies coincide with those reported for $Cu(CCl_3COO)_3 \cdot nH_2O$.[2] b) Two ^{35}Cl NQR lines superimpose by accident.

summarized in Table 3. At this temperature, 21 ^{35}Cl NQR lines were apparently observed, but three of them split into two lines at higher temperatures (see below). Therefore, there exist in total 24 NQR lines at 77 K. Twelve of these 24 frequencies coincide well with the 12 frequencies reported for $Cu(CCl_3COO)_2 \cdot nH_2O$.[2] The temperature dependences of the NQR frequencies are shown in Fig. 3. The lines at 39.813, 39.697, and 39.132 MHz at 77 K split into two lines as the temperature was raised. All of the 24 NQR signals faded out in the temperature range 115—170 K. Only a few signals could be observed still above about 160 K, and their frequency vs. T curves showed discontinuities around 163 K, as can be seen in Fig. 3(b). This observation confirms the presence of the phase transition at 163 K found by DSC.

The crystal structure of LTP has not been analyzed, but it is reasonable to expect that the difference in crystal structure between LTP and RTP is very slight. Therefore, one may discuss the ^{35}Cl NQR spectrum of LTP on the basis of the crystal structure of RTP. The ^{35}Cl NQR frequencies of LTP are distributed in a relatively wide frequency range from 38.7 to 40.3 MHz. This frequency splitting (at most 1.6 MHz) is too large to be attributed to mere crystal field effect. The geometry of the CCl_3 group is quite normal: Every C-Cl distance is typical of a single bond length and the angles between the three C-Cl bonds are close to the tetrahedral one. Thus, there seems to be no interaction of intramolecular origin through σ bonds that will be responsible for the frequency splitting. A possibility which could account for the frequency splitting is the rather peculiar configuration of the CCl_3COO group. Because its structure deviates considerably from the ideal one, Cl(2) and O(2) atoms are brought close together (2.863(6) Å) and this contact could contribute to shift the ^{35}Cl NQR frequency of the Cl(2).

Another possibility which could explain the frequency splitting is the interactions between chlorine

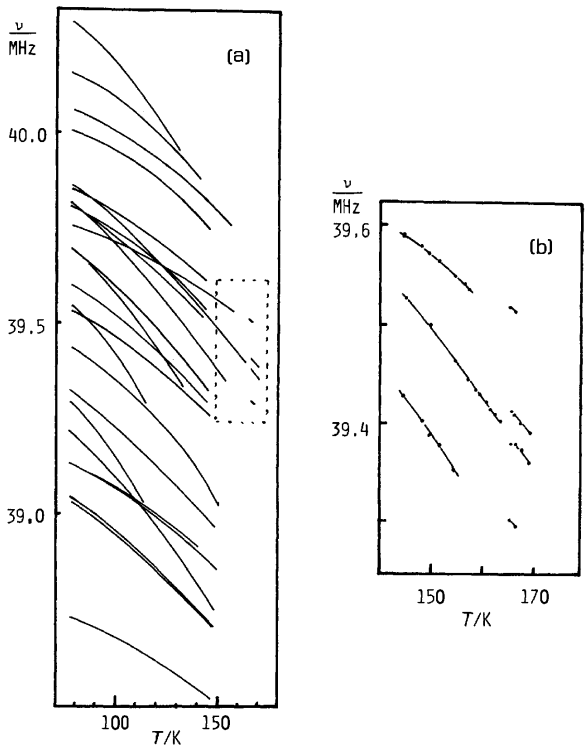

Fig. 3. (a) The temperature dependence of ^{35}Cl NQR frequencies in $Cu(CCl_3COO)_2 \cdot 3H_2O$; (b) enlargement of the region enclosed by dotted line in (a).

and water hydrogen atoms. The Cl(3)···H(1) distance 2.68(8) Å is shorter than the sum of the van der Waals radii (3.0 Å). In addition, H(3) is the second nearest hydrogen atom of the Cl(3) atom (3.6(1) Å), while H(2) and H(1) are the first and second nearest hydrogen atoms of the Cl(2) atom (3.10(8) and 3.36(8) Å). In contrast to these, the Cl(1) atom has no hydrogen neighbor closer than 3.9 Å. In an electrostatic model of hydrdogen bond, it is considered that a net positive charge is produced on the hydrogen atom participated in a hydrogen bond. In the present system, the positive

charge on H(1), H(2), and H(3) can cause excess electric field gradients at the positions of Cl(3) and Cl(2) which could give rise to a shift of ^{35}Cl NQR frequency of about a hundred kHz. Thus, both effects of the hydrogen bonds and the Cl(2)···O(2) contact seem to be responsible for the frequency splitting.

Besides the large frequency splitting mentioned above, the extreme multiplicity is also characteristic of the ^{35}Cl NQR spectrum of LTP. According to the present X-ray analysis, RTP has only one crystallographically independent CCl_3 group in the unit cell. Therefore, the number of the ^{35}Cl NQR lines in RTP, if they were detected, should be three. In contrast, 24 ^{35}Cl NQR lines have been detected for LTP. Because the difference in the crystal structure between RTP and LTP is very slight, one may expect that the 24 NQR lines in LTP can be divided into three frequency groups each of which has 8 lines distributed in a narrow frequency region. However, the 24 lines are distributed almost uniformly and one fails to sort the lines in such a way. This indicates that the change in the crystal structure, though it is very slight, is quite effective to cause the shifts of the NQR frequencies to give a uniform distribution of lines. As shown in Table 3, the values of the temperature coefficients of the NQR frequencies are widely distributed and several of them are extremely large. These facts also suggest that the environment of each chlorine atom in LTP is considerably different from each other.

Structural Changes at Phase Transitions. The X-ray oscillation photographs, and zero- and first-layer Weissenberg photographs around [010] taken at 183 and 145 K provided valuable information on the crystal structures of ITP and LTP. The diffraction patterns of both phases were quite similar to those of RTP, except for extra spots superimposed on them. These additional sets of reflections had the spacings and very weak intensities indicative of the appearance of superstructures. It was therefore evidenced that the structural changes associated with the phase transitions are very slight, but the b spacing in RTP is doubled in ITP and the c spacing is also doubled in LTP. Moreover, the $(h1l)$ Weissenberg photographs for LTP phases suggested the lowering of the crystal symmetry from monoclinic to triclinic with the interaxial angles α' and γ' close to 90°. The observed reflection conditions, hkl: no and $h0l$: $l=2n$, led to monoclinic $P2/c$ or Pc for the superlattice in ITP, while the conditions, hkl: no and $h0l$: no did to triclinic $P\bar{1}$ or $P1$ for the superlattice in LTP.

The crystal data thus obtained are as follows:

$T=183$ K (ITP); $a'(=a)=23.13(5)$, $b'(=2b)=12.42(5)$, $c'(=c)=9.58(2)$ Å, $\beta'=95°$, $P2/c$ or Pc, $Z=8$,

$T=145$ K (LTP); $a'(=a)=23.09(6)$, $b'(=2b)=12.41(9)$, $c'(=2c)=19.04(5)$ Å, $\beta'=95°$, $P\bar{1}$ or $P1$, $Z=16$.

The numbers of ^{35}Cl NQR lines expected from these X-ray results are 12 or 24 for ITP and 48 or 96 for LTP, in contrast with the observations. The fade out of most or all signals in ITP or RTP may be due to rapid reorientation of CCl_3 groups about their threefold axes, in accord with the relatively large thermal parameters of Cl atoms (Table 1). On the other hand, the number of lines observed in LTP is just half of the expected one for more probable space group $P\bar{1}$. The further splitting may be too small to be detected.

In conclusion, the preliminary X-ray studies at low temperatures demonstrated that the positions of the heavy atoms in the three phases are not changed much. However, the appearance of superstructures in both ITP and LTP provided an evidence for some slight changes in geometries of CCl_3COO^- ligand and/or of (4+1) oxygen coordination around the Cu(II) atom, in particular with respect to the arrangements of the light atoms, O, C, and H. Such a mechanism would be supported by the very small enthalpy changes at the phase transitions. If in LTP the torsion angles in CCl_3COO^- groups are modified and consequently the water molecules form several kinds of hydrogen bonds, the interactions between Cl and O atoms and also between Cl and H atoms will be changed and hence the NQR frequencies of these chlorine atoms may shift from those of RTP. As a result, the splitting pattern in LTP will be different from that expected from the crystal structure of RTP.

The authors thank Professor Kazuhide Ogawa, Osaka University for allowing us to use a Weissenberg camera at low temperatures and are grateful also to Dr. Yuriko Yamagata for her help in part of the X-ray work.

References

1) M. Hashimoto, Dr. Science Thesis, Osaka University, Osaka, 1975.

2) H. Chihara and N. Nakamura, *J. Phys. Soc. Jpn.*, **37**, 156 (1974).

3) H. Kiriyama, M. Doi, and Y. Yamagata, *Acta Crystallogr., Sect. C*, **43** in press.

4) A. C. North, D. C. Phillips, and F. S. Mathews, *Acta Crystallogr., Sect. A*, **24**, 351 (1968).

5) P. Main, S. E. Hull, L. Lessinger, G. Germain, J.-P. Declercq, and M. M. Woolfson, Univs. of York, England, and Louvain, Belgium (1978).

6) "International Tables for X-ray Crystallography," Birmingham (1974), Vol. IV, Knoch Press (Present Distributor D. Reidel, Dordrecht).

7) C. K. Johnson, Report ORNL-5138. Oak Ridge National Laboratory, Tennessee (1976).

8) The Universal Crystallographic Computing System Osaka (1979). The Computing Center, Osaka University.

9) The lists of structure factors and anisotropic thermal parameters of non-hydrogen atoms are deposited as Document No. 8761 at the office of the editor of Bull. Chem. Soc. Jpn.

10) M. Hashimoto and Y. Yoshioka, *Ber. Bunsenges. Phys. Chem.*, **87**, 42 (1983).

11) K. S. Patel, J. A. Faniran, and A. Earnshaw, *J. Inorg. Nucl. Chem.*, **38**, 352 (1976).
12) B. B. Adeleke and K. S. Patel, *J. Inorg. Nucl. Chem.*, **42**, 1522 (1980).
13) B. J. Hathaway and P. G. Hodgson, *J. Inorg. Nucl. Chem.*, **35**, 4071 (1973).
14) F. Valach, G. Koreň, P. Sivý, and M. Melník, "Structure and Bonding," Springer-Verlag, Berlin (1983), Vol. 55, p. 101.

 © 1987 The Chemical Society of Japan Bull. Chem. Soc. Jpn., 60, 2989—2992 (1987)

Oscillatory Variation near the C-K Edge in the Photon *W*-Value of Ethylene

Isao H. Suzuki* and Norio Saito
Electrotechnical Laboratory, Sakura-mura, Niihari-gun, Ibaraki 305
(Received April 6, 1987)

The dependence of ethylene *W*-value on photon energy has been precisely measured in the region from 269 to 324 eV by using monochromatized synchrotron radiation. The *W*-value showed an oscillatory variation at the $C_{1s} \rightarrow \pi^*$ excited state as well as the C-K edge. A model has been proposed in which the inner-shell excitation gives rise to a change in the energy of the electron ejected from the molecule having absorbed a photon. It has been found that the model can reproduce the oscillatory variation feature of the *W*-value.

The *W* value of ionizing radiation is a fundamental constant regarding interaction between the radiation and a gas; average energy expended by the radiation to produce an ion pair. A variety of measurements have been carried out on the *W*-values of atoms and molecules for different radiation above several keV.[1] It is well known that the *W*-value is constant for that radiation. Recently some group measured the *W*-value of molecules for electrons in the region below 1 keV.[2-6] Those *W*-values increased with decreasing energy. This phenomenon originates from the fact that the fraction of neutral excitations exceeds that of ionizations in electron-molecule collisions as the electron energy decreases. Srdoč and Obelić measured the *W*-values of methane and propane for photons using characteristic X-rays and filtered bremsstrahlung radiation.[5,6] The measured *W*-values showed a slight increase with decreasing energy. By using line spectra in discharge lamps, Samson and Haddad obtained the *W*-value of Xe for photon in the region of 12 to 90 eV.[7] They found distinct increase of the *W*-value at the ionization threshold of the 4d electron. This increase was ascribed to a decrease of the energy of the electron ejected from the 4d orbital in comparison to that of the O-shell.

Studies on the *W*-value of methane and propane for photons were performed in the ultra-soft X-ray region by the present authors.[8-10] A novel variation near the C-K edge was found in the energy dependence of the *W*-value. This variation was interpreted in connection with the transition of the K-shell electron into the Rydberg orbitals and the ionized state. According to the energy loss spectrum using a high energy electron beam, ethylene shows transitions of the K-shell electron into the $1b_{2g}$ orbital (π^*) at 284.7 eV and into the Rydberg orbitals (3s and 3p) at 287.4 and 287.8 eV.[11] Similar results were found by Eberhardt et al., who obtained an electron yield spectrum using monochromatized synchroton radiation.[12] The transitions of the K-shell electron into the Rydberg orbitals and the ionized state in ethylene probably make the *W*-value oscillate in those energies, as well as methane and propane. However, it remains unsolved how the transition into the π^* orbital affect the *W*-value in ethylene, because methane and propane have no π^* orbital. It is interesting to measure the energy dependence of the *W*-value of ethylele in the region near the excited state $(1s)^{-1}(1b_{2g})^1$.

In the present study, the *W*-value of ethylene for photon has been measured precisely from 269 to 324 eV by using a proportional counter.

Experimental

Synchrotron radiation from the storage ring at the Electrotechnical Laboratory was monochromatized by a plane grating monochromator (resolving power: about 150).[10,13,14] The monochromatized photons entered a gas-flow proportional counter (Manson-04) with a thin Al window (thickness: 1500 Å). Ethylene (purity: 99.9%) was supplied to the counter at 5.3×10^3 Pa. Signals from the counter were amplified and accumulated in a multichannel analyzer (MCA: Canberra-40). The resultant pulse height distributions of the signals were transferred to a micro-computer. Using this computer, the pulse height distributions were analyzed to obtain average pulse height.

The pulse height distribution can be approximately expressed by the following,[10,15]

$$f(z) = \frac{z^{x-1} \cdot \exp(-z/z_a)}{z_a^x \cdot \Gamma(x)} . \quad (1)$$

In the above equation, z indicates the number of electrons amplified by the electric field within the counter, z_a denotes the average gas amplification factor, x is the average number of the electrons initially produced by the radiation effect of a photon, and Γ is the gamma function. The distributions calculated using Eq. 1 were fitted to those obtained by observation.[10] The average pulse height distribution P is given by

$$P(E_p) = \int z \cdot f(z) \cdot dz = z_a \cdot x = \frac{z_a \cdot E_p}{W_p(E_p)} , \quad (2)$$

where E_p indicates the energy of a photon and W_p denotes the *W*-value.[5,6,8-10]

Using Eq. 2, relative *W*-values were obtained for photons with energies from 269 to 324 eV. Any change in P owing to a drift in the gas pressure was cancelled by measuring the P several times at the same photon energy in the course of the experiment. There may be photoabsorption by ethylene in which only neutral fragments are produced but in which no ion pair is formed. This process should alter the *W*-value, although the present technique using a proportional counter cannot count up these types of processes. At present,

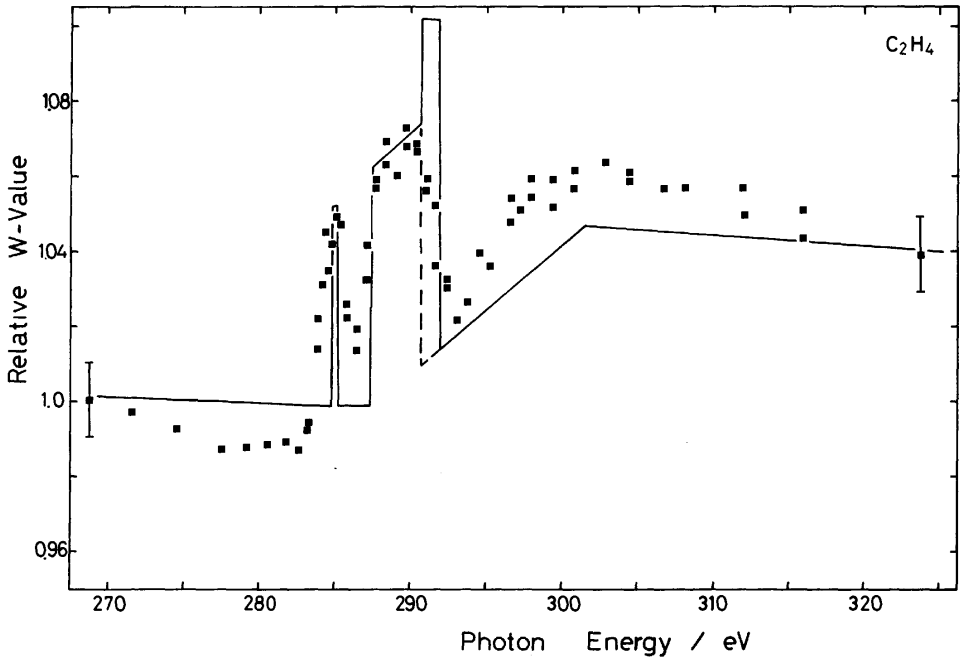

Fig. 1. W-Value of ethylene as a function of photon energy near the C–K edge. Solid squares indicate measured data. Solid curve denotes the calculated profile based on the present model. Bars indicate the error sizes of the measured data. Broken line means the profile when a post-collision interaction does not occur (see text).

Table 1. Energy Values Used in the Calculation of the W-Value (in Units of eV)

W-Value for sufficiently high energy radiation	(W)	25.8
Average energy of subionization electron for an electron with an energy E	(U_1 for $E<30$)	11
	(U_2 for $E>200$)	22
First ionization energy	(E_f)	10.5
Average of ionization energy for valence electron	(E_v)	16.1
Ionization energy of the inner-shell	(E_K)	290.6
Average energy of Auger electron	(E_A)	245.8
Average energy of deexcitation electron from the $(1s)^{-1}(\pi^*)^1$ state	($E_{A\pi}$)	255
Average energy of deexcitation electron from the $(1s)^{-1}(R)^1$ state	(E_{AR})	255
Average energy gain of Auger electron in a post-collision interaction	(a)	E_p-288

π^* and R indicate $1b_{2g}$ and Rydberg orbitals, respectively. E_p denotes photon energy.

these processes are assumed to be negligible, by analogy of the results of ionization yield of methane by Backx and Van der Wiel.[16]

Results and Discussion

The energy dependence of the W-value is shown with solid squares for photon energies from 269 to 324 eV in Fig. 1. The solid curve indicates a calculated profile based on a model described below. The measured W-value gradually decreases from 269 eV to 283 eV as the photon energy increases. The W-value rises to a peak at 285 eV, drops to a sharp valley at 287 eV and again goes up to a broad peak at 290 eV. Above a minimum at 293 eV, the experimental data show a near-linear dependence on the photon energy between 293 and 301 eV. Above the latter energy, the W-value seems to have a slight decreasing trend.

As those of methane and propane, it is important to consider the oscillatory variation of the W-value of ethylene in connection with the excitation transitions of the 1s electron. Hitchcock and Brion observed electron energy loss spectra of ethylene for the 1s electron excitation in the energy resolution of 0.2—0.5 eV.[11] The observed spectra show strongly resonant transitions of the 1s electron to the $1b_{2g}$ orbital at 284.68, 285.04, and 285.50 eV. The transitions into the 3s orbital and the 3p orbital were found to occur at 287.4 and 287.8 eV, respectively. Those to higher Rydberg orbitals and that to the ionized state appeared above 288.3 and 290.6 eV, respectively. They further found shake-up states at 292.6 and 295.2 eV. Eberhardt and coworkers observed an electron yield spectrum of ethylene in the same energy region by use of monochromatized synchrotron radiation.[12] The same transitions were identified although the resolution was lower and the observed energy values deviated slightly (0.3—0.7 eV).

A comparison between the inner-shell excited states and the energy dependence of the W-value gives us a model for interpretation as follows. Table 1 lists

energy values necessary for calculation of the W-value on the basis of the present model. These energies have been estimated from available data in the literature, e.g. Auger electron spectra and photoelectron spectra.

i) Below 284.7 eV: Only a valence electron is ejected by photoabsorption, because the photon cannot excite an inner-shell electron. The average energy of this ejected electron is E_p-E_v, where E_v is the average binding energy of the valence electrons. Ethylene has 6 orbitals for valence electrons, which are $1b_{1u}$, $1b_{1g}$, $1b_{2u}$, $2b_{3u}$, and $2a_g$.[17,18] The value of E_v is assumed to be 16.1 eV. (Adoption of vertical ionization energy is supposed to be appropriate in the present study.) The ejected photoelectrons ionize ambient molecules and produce a number of ion pairs. On the other hand, the W-value of low energy electrons (W_e) can be approximately given by the following equation.[1,19]

$$W_e(E) = \frac{E \cdot W}{E-U} \tag{3}$$

The term W denotes the W-value for radiation with a sufficiently high energy (25.8 eV),[1] U indicates the average energy of sub-ionization electrons, and E is the energy of a primary electron. The sub-ionization electrons mean the electrons which do not contribute to ionization in a system receiving irradiation. In this case, the average number of ion pairs, N_e, is given by

$$N_e = \frac{E}{W_e} = \frac{E-U}{W}. \tag{4}$$

Using Eqs. 3 and 4, the photon W-value is expressed by the following.

$$W_p(E_p) = \frac{E_p}{1+N_e} = \frac{E_p \cdot W}{E_p + W - E_V - U_2}. \tag{5}$$

Where U_2 is assumed to be 22 eV from the data regarding the W-value for low energy electrons.[3] Multiple photoionization of the valence electrons is assumed to occur only at negligibly low probability at present.

ii) Between 284.7 and 285.1 eV: The 1s electrons can be excited to the π^* orbital ($1b_{2g}$) and a hole is formed in the inner-shell. After this excitation, an Auger transition is supposed to occur because fluorescence yield is extremely low in a light element. A variety of Auger transitions have been observed in ethylene.[20,21] The average energy of Auger electrons, E_A, has been estimated to be 245.8 eV, according to the spectrum by Rye et al.[20] However, the average Auger electron energy in the present case is supposed to be somewhat higher than 245.8 eV owing to the existence of that electron in the π^* orbital. This average energy $E_{A\pi}$ is assumed to be 255 eV, by analogy from a resonance-type Auger electron spectrum of CO.[22,23] The W-value is expressed by

$$W_p(E_p) = \frac{E_p}{1+N_e} = \frac{E_p \cdot W}{E_{A\pi} + W - U_2}. \tag{6}$$

When Eq. 6 is compared with Eq. 5, $E_{A\pi}$ (255 eV) is lower than E_p-E_v (e.g., 270.9 eV for the photon with energy of 287 eV). This fact means that the W-value at 287.4 eV becomes higher than that at 287 eV. In the present model, it is assumed that the photoabsorption probability involving the valence electrons can be negligibly low in this photon energy region on account of the spectra of the inner-shell excitation.[11,12] This assumption is also applied for the energy region above 287.4 eV (cases iv) to vii)).

iii) Between 285.1 and 287.4 eV: Photons can excite only valence electrons, because there is no inner-shell excited state in this energy region. Ejected photoelectrons ionize ambient molecules and produce a number of ion pairs. The W_p is expressed by Eq. 5.

iv) Between 287.4 and 290.6 eV: Photons can excite the inner-shell electrons to the Rydberg orbitals and then the formed inner-hole is filled with a valence electron through the subsequent Auger transition. There exists no available report on this type of Auger transition, in which the upper state is a $(1s)^{-1}$ (molecular Rydberg)^1. However, this type of the Auger process is presumed to be very similar to that of the case ii) described above. The average energy of the Auger electrons E_{AR} is assumed to be 255 eV.

v) Between 290.6 and 291.5 eV: The inner-shell electrons can be ejected from the molecule by the photons, but this ejected photoelectron leaves slowly. In the case of CO, the K-shell photoelectron with low energy is retrapped by the molecular ion when a second electron with higher energy is ejected by an Auger transition (post-collision interaction).[24] Since there has been no detailed study in other molecules, the slow photoelectron in the present case is assumed to be retrapped at the instance of the Auger transition. The Auger electron obtains a slightly higher energy owing to the existence of the slow photoelectron than the normal Auger electron. This energy gain of the Auger electron is equal to the energy loss of the trapped electron. The average energy of the Auger electron is here assumed to be $245.8+a$ eV ($a=E_p-288$ eV), because of no available data in molecules. This post-collision interaction is tentatively assumed to occur between 290.6 and 291.5 eV, in consideration of the energy giving a minimum W-value (293 eV) and of the photon energy resolution.

vi) Between 291.5 and 301.1 eV: The inner-shell electrons can be ionized and can promptly escape from the molecular field. This photoelectron ejection is followed by a normal Auger transition. The photoelectron has an energy of $E_p-290.6$ eV. However, this electron can not ionize other ambient molecules because the electron energy is lower than the first ionization energy of the valence electron ($E_f=10.5$ eV). The Auger electron (E_A) has an average energy of 245.8 eV.

vii) Above 301.1 eV: The photoelectron released from the inner-shell has an energy higher than the first ionization energy of ethylene. This electron and the

Auger electron produced subsequently can ionize ambient molecules. The W-value is expressed by the following equation.

$$W_p(E_p) = \frac{E_p}{2+N_{e1}+N_{e2}} = \frac{E_p \cdot W}{E_p+E_A+2W-E_K-U_1-U_2}, \quad (7)$$

where U_1 denotes the average energy of the subionization electrons for the electron with kinetic energy between 11 and 33 eV. The U_1 is assumed to be 11 eV on account of the study by Combecher.[3]

By using the present model, the relative W-value has been calculated and shown with the solid curve in Fig. 1. The resolving power of the monochromator was not included in this calculation. The energy dependence of the calculated W-value is in agreement with the experimental results. Therefore, the present model is essentially correct.

There is a slight discrepancy between the experimental data and the calculated result at a few energies. That at 286 eV is ascribed to the low resolving power of the present monochromator. That between 291 and 293 eV is presumed to originate from the two reasons, except the low resolving power. First, although the energy of the electron may be lowered through a post-collision interaction below 291.5 eV, there is a possibility that some fractions of slow photoelectrons are not retrapped by the molecular ion. If this is the case, the final configuration is that having two holes in the valence orbital. The calculated W-value becomes lower than that shown in Fig. 1 between 290.6 and 291.5 eV. Second, there have been observed slightly distorted pulse height distributions in the proportional counter around 291 eV. The width of the distribution was broader than those in other energies. This phenomenon is supposed to be brought about by a contamination of the used grating, which gave a decrease of output photon intensity near the C-K edge. This should make the effective resolving power lower. From the minimum at 293 eV (not at 290.6 eV), it can be said that the post-collision interaction takes place just above the C-K edge, as well as for methane. However, it is impossible at present to estimate the size of energy region where it occurs. (The broken line between 290.6 eV and 291.5 eV in Fig. 1 shows the calculated result in the case of no occurrence of the post-collision interaction.)

The reason why the experimental data are slightly lower than the calculated curve near 280 eV is not clear at present. The photoabsorption cross section near 280 eV is very low owing to no excitation transition of the inner-shell electrons. The electron cloud induced by photoabsorption is distributed more homogeneously in the proportional counter near 280 eV than other energies. This fact may make a small effect on the average pulse height distribution through a possible change in gas amplification factor.

The shake-up states were reported to exist at 292.6 and 295.2 eV.[11] In contrast to the transition to the π^* orbital, the transition probability to those states was considerably lower than that to the normal continuum state. Thus that transition was not expected to make an appreciable effect on the W-value. The experimental W-value does not show a change at those energies in Fig. 1 within experimental accuracy.

The authors wish to express their sincere thanks to the members of the accelerator group of the Electrotechnical Laboratory for providing synchrotron radiation.

References

1) H. O. Wyckoff, "Average Energy Required to Produce an Ion Pair," *ICRU-Report*, **31**, (1979).
2) E. Weibel and B. Grosswendt, *Nucl. Instr. Meth.*, **211**, 487 (1983).
3) D. Combecher, *Radiat. Res.*, **84**, 189 (1980).
4) B. G. R. Smith and J. Booz, "Proceedings of Sixth Symposium on Microdosimetry," Commission of the European Communities, London (1978) p. 759.
5) D. Srdoč and B. Obelić, "Proceedings of Fifth Symposium on Microdosimetry," Commission of the European Communities, Luxembourg (1976) p. 1007.
6) D.Srdoč, *Nucl. Instr. Meth.*, **108**, 327 (1973).
7) J. A. R. Samson and G. N. Haddad, *Radiat. Res.*, **66**, 1 (1976).
8) I. H. Suzuki and N. Saito, *Radiat. Phys. Chem.*, **26**, 305 (1985).
9) I. H. Suzuki and N. Saito, *Bull. Chem. Soc. Jpn.*, **58**, 3210 (1985).
10) N. Saito and I. H. Suzuki, *Chem. Phys.*, **108**, 327 (1986).
11) A. P. Hitchcock and C. E. Brion, *J. Elect. Spectrosc. Relat. Phenom.*, **10**, 317 (1977).
12) W. Eberhardt, R. P. Haelbach, M. Iwan, E. E. Koch, and C. Kunz, *Chem. Phys. Lett.*, **40**, 180 (1976).
13) T. Tomimasu, T. Noguchi, S. Sugiyama, T. Yamazaki, T. Mikado, and M. Chiwaki, *IEEE Trans. Nucl. Sci.*, NS-**30**, 3133 (1983).
14) N. Saito and I. H. Suzuki, *Bull. Electrotechnical Laboratory*, **49**, 689 (1985).
15) B. Breyer, *Nucl. Instr. Meth.*, **112**, 91 (1973).
16) C. Backx and M. J. Van der Wiel, *J. Phys.*, **B8**, 3020 (1975).
17) K. Kimura, S. Katsumata, Y. Achiba, T. Yamazaki, and S. Iwata, "Handbook of HeI Photoelectron Spectra of Fundamental Organic Molecules," (Jpn. Scient. Soc. Press, Tokyo, 1981).
18) A. J. Dixon, S. T. Hood, and E. Weigold, *J. Elect. Spectrosc. Relat. Phenom.*, **14**, 267 (1978).
19) M. Inokuti, *Radiat. Res.*, **64**, 6 (1975).
20) R. R. Rye, T. E. Madey, J. E. Houston, and P. H. Holloway, *J. Chem. Phys.*, **69**, 1504 (1978).
21) C. M. Liegener, *Chem. Phys.*, **92**, 97 (1985).
22) L. Ungier and T. D. Thomas, *Phys. Rev. Lett.*, **53**, 435 (1984).
23) C. T. Chen, R. A. DiDio, W. K. Ford, E. W. Plummer, and W. Eberhardt, *Phys. Rev.*, **B32**, 8434 (1985).
24) R. B. Key, Ph. E. Van der Leeuw, and M. J. Van der Wiel, *J. Phys.*, **B10**, 2521 (1977).

 © 1987 The Chemical Society of Japan Bull. Chem. Soc. Jpn., 60, 2993—2995 (1987)

Lanthanoid Chirality as a Tool for Assignment of *f*-*f* Transitions. Tb^{3+} and Tm^{3+} Diglycolate

Bhutnath KARMAKAR, Prabir K. CHATTERJEE, Samita BASU, and Mihir CHOWDHURY*
Department of Physical Chemistry, Indian Association for the Cultivation of Science, Jadavpur, Calcutta 700032, India
(Received April 5, 1986)

Although chiral studies have proved to be handy in the assignment of transitions in biological molecules, organic molecules and transition metal complexes, its potentiality for lanthanoid transition needs to be demonstrated. The paper explores the usefulness of CD studies in the assignment of lanthanoid transitions with two specific chiral single crystals-thulium diglycolate (Tm^{3+}-DG) and terbium diglycolate (Tb^{3+}-DG). It has been shown that chirality can distinguish $\Delta J=0, \pm1$ transition from others. The need for studies under higher resolution has been pointed out.

Identification of weak transitions in the presence of a strong one is a challenging problem for spectroscopists. For example, in heterocyclic organic molecules the $^1(n, \pi^*)$ state often remains undetected as this weak band frequently gets masked by the stronger (π, π^*) transitions. The same is the case with many spin-forbidden transitions. Various techniques, such as, measurement of polarized absorption spectra of single crystals or other orienting medium, measurements of polarized luminescence excitation spectrum by photoselection technique, improving the resolution by using supersonic jet-cooled molecules, application of magnetic or electric field, heavy atom or solvent perturbation, circular dichroism spectroscopy, two-photon spectroscopy etc. have been used to locate hidden transitions. We would like to demonstrate here how chiral studies can help in the assignment of the lanthanoid f^N-f^N transitions in situation where a number of J-states crowd together.

Unlike organic molecules or transition metal complexes, most chiral studies of lanthanoid complexes almost invariably involve chiral centers other than the lanthanoid ion. Although such studies can throw light on the interaction between Ln^{3+}-ion and the chiral center, these systems are hardly appropriate for spectra-environment correlation or assignment of Ln^{3+} transitions. Sen, Bera, and Chowdhury[1] was the first to make detailed study of a system where the chirality is derived from the immediate environment of the Ln^{3+} ion. Since then, extensive studies on three interesting chiral single crystal systems Ln^{3+}-DG (hexagonal; site-symmetry-D_3), lanthanoid double nitrate (Ln^{3+}-DN) (cubic; site symmetry-distorted dodecahedron) and lanthanoid pyrogermanate (Ln^{3+}-PG) (tetragonal; site symmetry-distorted pentagonal bipyramid)—have been made.[2-13] In this paper we would like to report the spectra of chiral single crystals of Tb^{3+}- and Tm^{3+}-DG and discuss the extent they can throw light on the asssignment problem. Crowding of different J-states has caused considerable uncertainty and confusion in the identification of $^1I_6$, $^3P_0$, $^3P_1$ states of Tm^{3+} and those states of Tb^{3+} lying above 25000 cm^{-1}; it is therefore worthwhile to explore the potentiality of other types of spectroscopy.[14-16]

A part of the problem in the case of assignment from one-photon forced electric dipole transition arises from the fact that the selection rules,[17] $\Delta J \leqslant 6$, $\Delta L \leqslant 6$, $\Delta S=0$ are not always valid due to J-mixing and breakdown of L-S coupling, and even when they are valid, they are not restrictive enough to be useful in the J-assignment of states.[14,15] A more restrictive J-selection rule ($\Delta J \leqslant 2$), offered by two-photon transition selection rule, has been used by us and others for assignment of Gd^{3+} and other Ln^{3+} transitions.[18-21] Experimental difficulties, however, have stood in the way of carrying out similar studies on Tm^{3+} and Tb^{3+} crystals. We have therefore tried to exploit $\Delta J=0, \pm1$ selection rule for magnetic dipolar transitions. One way of estimating qualitatively the magnitude of magnetic dipolar transition moment is from the CD/OD strength, as pointed out by us in earlier papers.[6-10] It is expected that the transitions to the $^1I_6$ state of Tm^{3+} and $^5G_{5,6}/^5L_{6,7}$ states of Tb^{3+} will be intense in CD spectrum relative to others, leading to their identification.

Experimental

The single crystals were grown from solution by slow evaporation as described earlier.[10] The optic axis was identified by means of a polarizing microscope and the crystals were thinned by grinding and polishing with diamond paste of different grain sizes. In order to minimize the extent of overlap of transitions (which may cause cancellation of rotation) and identify the crystal-field components, the crystals were cooled to 20 K in an Air-product CS202 closed-cycle cryo-cooler. The absorption spectra were taken in a Cary 17D spectrophotometer and the CD spectra in a JASCO 500 spectrophotometer with minimum possible slit. For some of the transitions, the ultimate resolution is limited by the resolving power of the instrument.

Results and Discussion

Figure 1 shows the molecular structure of the Ln^{3+}-diglycolate complex. Each lanthanoid metal is coordinated to nine oxygen atoms, comprising a trigonal prism. The upper and lower triangles were made of

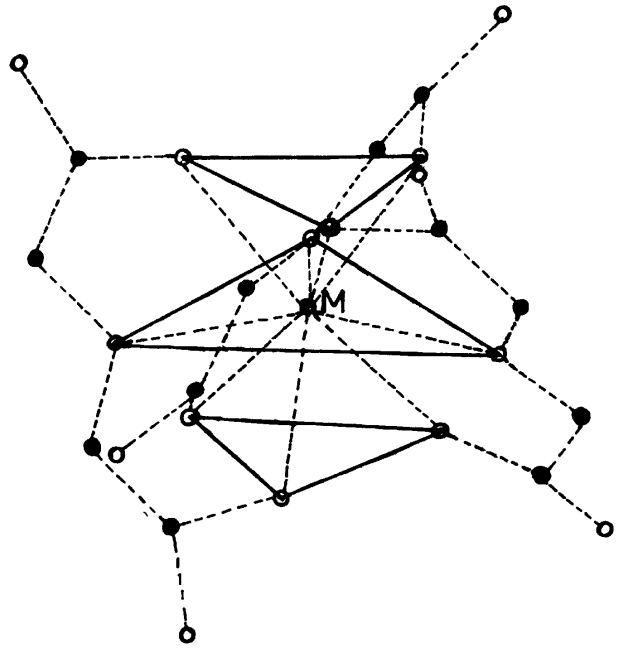

Fig. 1. The molecular structure of $[Ln(OCOCH_2OCH_2OCO)_3]^{3-}$ (Ln^{3+}-DG).

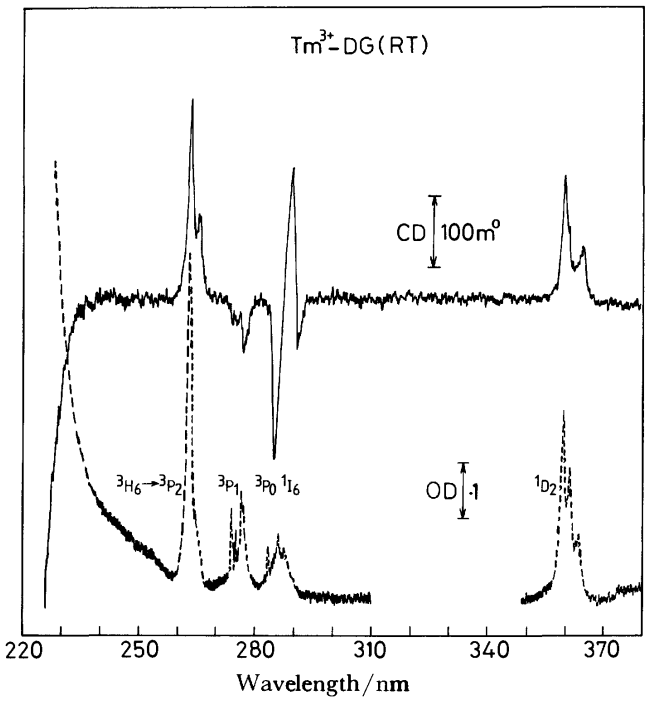

Fig. 2. The low-resolution room temperature absorption (dotted line) and circular dichroism (solid line) spectra of an oriented Tm^{3+}-DG single crystal. Light propagates along the optic axis.

six carboxylate oxygens and they are rotated relative to each other, destroying the plane of symmetry. The middle triangle is formed by the three ethereal oxygens.

Figure 2 shows the CD and absorption spectra of the same single crystal of Tm^{3+}-DG at room temperature. In view of the $\Delta J=0, \pm 1$ selection rule for magnetic dipolar transition, and in view of the fact that circular

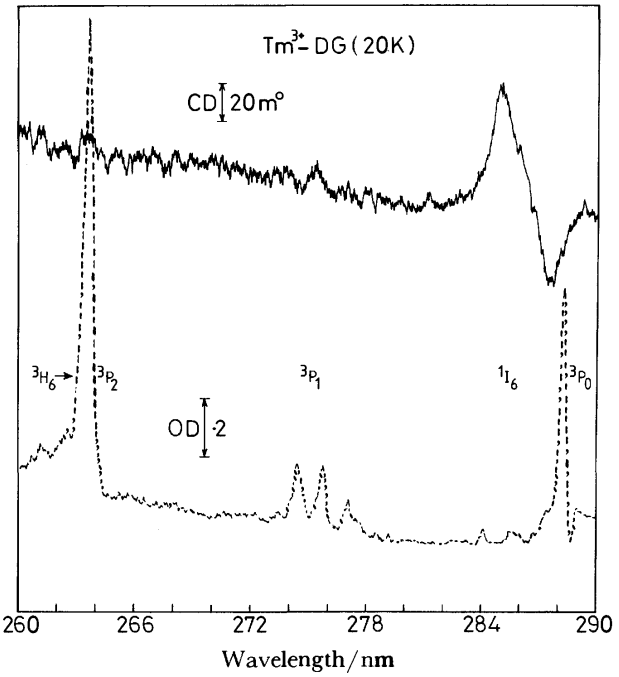

Fig. 3. The resolved absorption (dotted line) and CD (solid line) spectra of Tm^{3+}-DG single crystal at 20 K.

dichroism is a scalar product (imaginary part only) of electric dipolar and magnetic dipolar transition moments while OD depends on the sum of squares (absolute value) of the two moments, the CD/OD ratio is expected to be high for the $^3H_6 \rightarrow {}^1I_6$ transition. The higher CD/OD ratio near 285 nm, the wavelength region for the $^3H_6 \rightarrow {}^1I_6$ transition is apparent from the spectrum. Since the $^3P_0$ state and the components of the $^1I_6$ state overlap, we cooled the crystals to 20 K and carefully scanned the wavelength region 250—300 nm. A phase transition occurs at about 108 K;[7] however, the crystal still remains optically active. In spite of our best effort we have not been able to completely resolve all the components in the commercial CD instruments (Fig. 3). This limitation notwithstanding, the high CD/OD ratio and low OD value leave little doubt that the weak peaks between 283 and 287 nm belong to CF-split components of the $^1I_6$ state. The strong absorption peak at 287.5 nm appears as a weak signal in the slope of the CD band and hence is assigned to the $^3H_6 \rightarrow {}^3P_0$ transition. It is also interesting to note that the $^3P_1$ and $^3P_2$ bands, fairly prominent in absorption spectrum, hardly give any CD signal. Circular dichroism study can therefore be used as a useful tool for identifying the CF components of the spin-forbidden $^3H_6 \rightarrow {}^1I_6$ transition, which are normally masked by spin-allowed $^3H_6 \rightarrow {}^3P_{0,1,2}$ transitions.

In case of Tm^{3+}, neither the crystal field alone nor the spin-orbit coupling alone can cause a mixing, in first order, between the ^3P states and the $^1I_6$ state, although simultaneous application of the two can. It may be expected therefore that $^3P_{0,1,2}$ and $^1I_6$ states will,

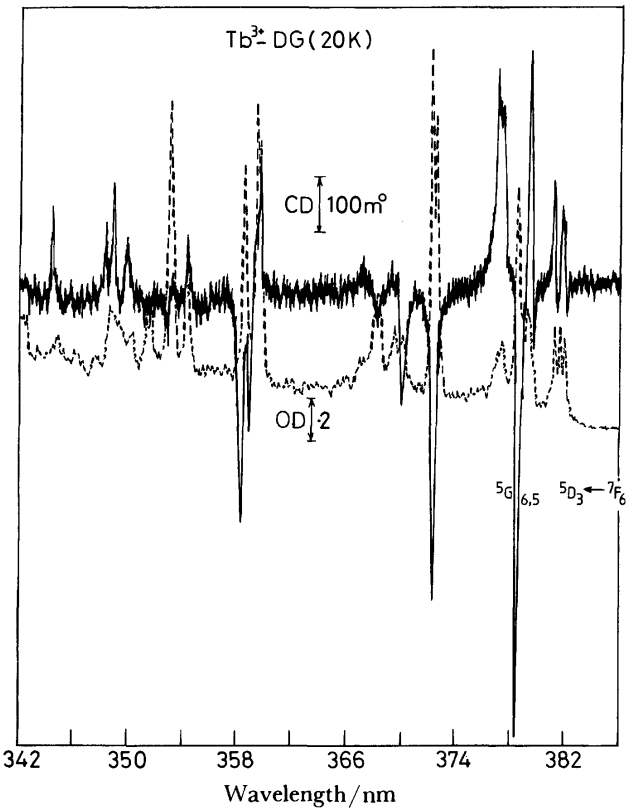

Fig. 4. The absorption (dotted line) and CD (solid line) spectra of a Tb^{3+}-DG single crystal at 20 K.

to a great extent, retain their characteristics regarding magnetic dipolar- or spin-allowedness. The situation is less clear-cut in Tb^{3+}-DG whose spectrum is shown in Fig. 4. In case of Tb^{3+}, the density of levels becomes so high below 348 nm that it becomes virtually impossible to identify the components from the mess of overlapping transitions. However, attempts have been made previously to assign the states in $TbCl_3 \cdot 6H_2O$ and $Tb_2(SO_4)_3 \cdot 6H_2O$. The detailed assignments are given in Dieke's book.[14] In order of increasing energy, the J-states are $^5D_3$, $^5L_{10}$, and $^5G_{5,6}$. In the present case, the first four bands close to 381 nm do not show high CD, although they are more resolved in the CD spectrum than in the normal absorption spectrum. This set of transitions should therefore be ascribed to $^7F_6 \rightarrow {}^5D_3$ transitions. On the other hand, the set of bands between 376 and 381 nm shows very high CD/OD ratio. This agrees with the expected location of the $^5G_{5,6}$ state in this region. However, the resolution of the spectrum is not enough to decide whether only the $^5G_{5,6}$ components appear in the above wavelength region, or there are additional overlapping $^5L_{10}$ components. Other states expected to be CD active are $^5L_{6,7}$. However, they occur at shorter wavelengths where background absorption stands in the way of their identification.

Conclusion

The CD spectrum may be an useful tool for identifying $\Delta J=0, \pm 1$ transitions, specially in situations where J-mixing is expected to be small. However, for unambiguous assignments, all the bands need to be resolved both in absorption and CD spectra. It is also useful for studying the nature of phase transitions.

We thank the National Science Foundation, U.S.A. for supporting the work (Project No. INT 83-19310).

References

1) A. C. Sen, S. C. Bera, and M. Chowdhury, *Chem. Phys. Lett.*, **46**, 594 (1977).
2) A. C. Sen and M. Chowdhury, *Chem. Phys. Lett.*, **79**, 165 (1981).
3) R. W. Schwartz, A. K. Banerjee, A. C. Sen, and M. Chowdhury, *J. Chem. Soc., Faraday Trans. 2*, **76**, 620 (1980).
4) F. S. Richardson, *Inorg. Chem.*, **19**, 2806 (1980).
5) F. S. Richardson and T. R. Faulkner, *J. Chem. Phys.*, **76**, 1595 (1982).
6) A. C. Sen, M. Chowdhury, and R. W. Schwartz, *J. Chem. Soc., Faraday Trans. 2*, **77**, 1293 (1981).
7) R. W. Schwartz, A. K. Banerjee, M. Chowdhury, and R. Kuroda, *J. Chem. Soc., Faraday Trans. 2*, **77**, 557 (1981).
8) P. K. Chatterjee and M. Chowdhury, *J. Chem. Soc., Faraday Trans. 2*, **78**, 429 (1982).
9) P. K. Chatterjee and M. Chowdhury, *Inorg. Chem.*, **21**, 2499 (1982).
10) P. K. Chatterjee, A. Nath, D. Nath, and M. Chowdhury, *Chem. Phys. Lett.*, **110**, 95 (1984).
11) B. Karmakar, P. K. Chatterjee, D. S. Ray, D. Nath, M. Chowdhury, and B. Wanklyn, *Chem. Phys. Lett.*, **107**, 203 (1984).
12) A. Nath, P. K. Chatterjee, and M. Chowdhury, *Chem. Phys. Lett.*, **118**, 427 (1985).
13) B. Karmakar and M. Chowdhury, in Proceedings of the International Conference on Rare Earth Spectroscopy held at Wroclaw, Poland in September, 1984 (World Press publication).
14) G. H. Dieke, "Spectra and Energy Levels of Rare Earth Ions in Crystals," Interscience, New York (1968), and references given therein.
15) B. G. Wybourne, "Spectroscopic Properties of Rare Earth," Wiley Interscience, New York (1965).
16) S. Hufner, "Optical Properties of Transparent Rare Earth Compounds," Academic Press, New York (1978).
17) R. D. Peacock, *Structure and Bonding*, **22**, 83 (1975).
18) B. Karmakar, D. S. Ray, K. Bhattacharyya, A. Samanta, and M. Chowdhury, *Chem. Phys. Lett.*, **97**, 545 (1983).
19) M. Dagenais, M. C. Downer, R. Neumann, and N. Bloembergen, *Phys. Rev. Lett.*, **46**, 561 (1981).
20) M. C. Downer and A. Bivas, *Phys. Rev. B*, **28**, 3677 (1983).
21) C. D. Cordero-Montalvo and N. Bloembergen, *Phys. Rev. B*, **30**, 438 (1984).

 © 1987 The Chemical Society of Japan Bull. Chem. Soc. Jpn., 60, 2997—2999 (1987)

Interaction of Divalent Metal Acids with Pentyl Alcohol and Isopentyl Acetate

Mirza Aijaz Beg* and Mohd. Shakil Kidwai
Department of Chemistry, Aligarh Muslim University, Aligarh 202 001, (U. P.), India
(Received July 29, 1985)

Extraction of monobasic divalent metal bromo acids in pentyl alcohol-benzene and isopentyl acetate-benzene mixtures was studied at room temperature (25 °C). Three molecules of pentyl alcohol ae well as of isopentyl acetate were associated with each metal acid molecule of cobalt and copper in the organic phase. Zinc, cadmium, and mercury acids take up two molecules of pentyl alcohol and one molecule of isopentyl acetate. Metal acids studied here mostly exist as monomer in the organic phase. In pentyl alcohol, however, copper acid is monomeric only at lower concentrations (4×10^{-5} to 2×10^{-4}M) and dimeric at higher concentrations (3.3×10^{-4} to 1.4×10^{-3}M).

It has long been known that aqueous $HClO_4$, $HReO_4$, and HBr are extracted by tributyl phosphate[1] (TBP) in xylene or CCl_4 as $H_3O^+\cdot 3TBP\cdot yH_2O\cdot X^-$, where $O\leqslant y\leqslant 3$, and X^- is the respective anion. A number of mineral and complex metal acids were later extracted in trioctylphosphine oxide[2] (TOPO) in organic solvents.

The extraction studies for metal acids made so far, are mostly limited to species of the type HMX_4. Several polyvalent transition[3] and nontransition[4] metal salts have been extracted with various extractants and solvents. It was thus thought worthwhile to study the extraction of dibasic metal acids,[5-9] $H_2[CoBr_4]$, $H_2[CuBr_4]$, $H_2[ZnBr_4]$, $H_2[CdBr_4]$, and $H_2[HgBr_4]$ which are practically monobasic in pentyl alcohol and isopentyl acetate mixture using benzene as diluent and seek a relation between the acidity of extracted acids and basicity of the solvents.

Experimental

For extraction studies, 3.0 ml aqueous metal acid solution obtained by adding the respective metal bromide in concentrated HBr was shaken with 25.0 ml benzene-pentyl alcohol (1—10%) or isopentyl acetate (8 to 15%) mixture for 1 h and there after allowed to stand for about 10 h. Polymerization studies were, however, made in 10% pentyl alcohol (or 10% isopentyl acetate)-benzene mixture. Metal content in either phase was determined by titrating it against EDTA using indicator (Xylenol Orange for cobalt, PAN for copper, and Erichrome Black T for zinc, cadmium, and mercury). Metal content in the organic phase was determined after evaporating off the solvent completely and digesting the residue in distilled water. Aqueous phase was also evaporated and digested in distilled water before titration.

Extraction Equilibria

In concentrated aqueous HBr, bromides of cobalt, copper, zinc, cadmium, and mercury exist[5-9] as H_2MBr_4, M being surrounded tetrahedrally with Br. As in aqueous phase, the proton is further hydrated through hydrogen bonding[10] and the dissociation constant of $[HMBr_4]^+$ species being negligible, the metal acid species in the aqueous phase may be represented[1,2c] as follows:

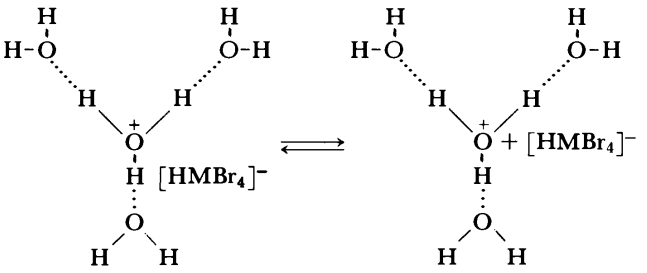

When aqueous metal acid is shaken with the organic phase, some acid passes into the organic phase. In this process, the hydrogen bonded water of the proton is partly or completely replaced by the organic ligand.[2c] Since, pentyl alcohol as well as isopentyl acetate are less basic than water, they do not interact with the second proton, to which even water is inert. In low dielectric constant solvents like benzene (D=2.3) the metal acid anion, $[HMBr_4]^+$ forms the ion pair $H_3O^+\cdot 3AA\cdot[HMBr_4]^-$.

Assuming that metal acid is extracted into the organic phase as one single species, having J metal ion, the extraction equilibrium will be represented by Eq. 1.

$$J[HMBr_4]_w^- + J\,\overset{+}{H_3O}_w + nAA_o \rightleftharpoons nAA.\ J(\overset{+}{H_3O}[HMBr_4]^-)_o \qquad (1)$$

(secondary solvation of proton is not shown)

AA stands for pentyl alcohol and isopentyl acetate, suffix o and w refer to organic and water phases, respectively. The total metal concentration in the organic phase, $[M^{2+}]_o$, is given by Eq. 2 in terms of metal concentration in the aqueous phase and extraction equilibrium constant, K,

$$[M^{2+}]_o = K J[H(MBr_4)^-]_w^J[AA]_o^n[H_3O^+]_w^J, \qquad (2)$$

$$\log[M^{2+}]_o - J\log[M^{2+}]_w = n\log[AA]_o + K', \qquad (3)$$

where $K'=\log K+\log J+J\log[H_3O^+]_w$ and $[H_3O^+]_w$ is invariant. If J equals unity, Eq. 3 rearranges into Eq. 4.

$$\log D = n\log[AA]_o + K'. \qquad (4)$$

D stands for distribution coefficient of metal acid,

between organic and aqueous phases. According to Eq. 3, the plot of log $[M^{2+}]_o$ against log $[M^{2+}]_w$ at a constant concentration of extractant (pentyl alcohol or isopentyl acetate in C_6H_6) should yield a straight line, whose slope would measure, J, the degree of polymerization in the organic phase. For the determination of the number of extractant molecules incorporated with metal acid in the organic phase, a plot of log D versus log $[AA]_o$ was drawn.

Results and Discussion

The log $[M^{2+}]_o$ −log $[M^{2+}]_w$ plot in pentyl alcohol-benzene mixture (Fig. 1) yields straight line, whose slopes show that metal acids are extracted as monomer in the organic phase. The behavior of Cu^{2+} is, however, unique in the sense that it is monomer at lower concentrations (4×10^{-5} to 2×10^{-4} M (1 M=1 mol dm^{-3})) and dimer at higher concentrations (3.3×10^{-4} to 1.4×10^{-3} M).

In isopentyl acetate-benzene system, the plots of log $[M^{2+}]_o$ against log $[M^{2+}]_w$ are straight lines (Fig. 2) with unit slopes, showing that metal acids are present

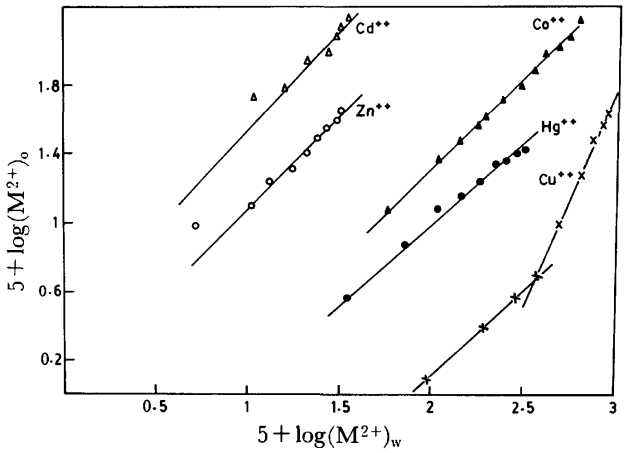

Fig. 1. Log$[M^{2+}]$ versus log$[M^{2+}]_w$ plots, at constant concentration of pentyl alcohol (10% by volume) in benzene at 25°C.

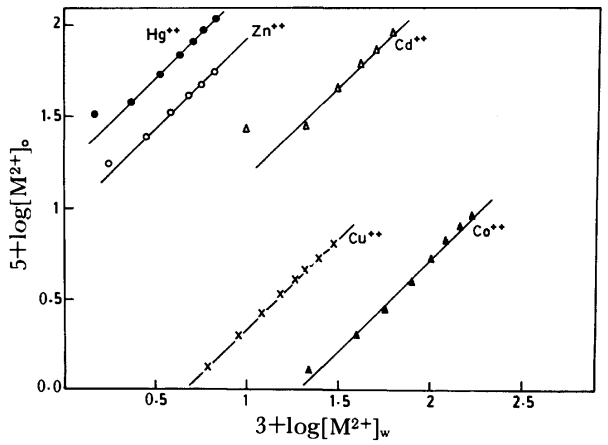

Fig. 2. Log$[M^{2+}]$ versus log$[M^{2+}]_w$ plots, at constant concentration of isopentyl acetate (10% by volume) in benzene at 25°C.

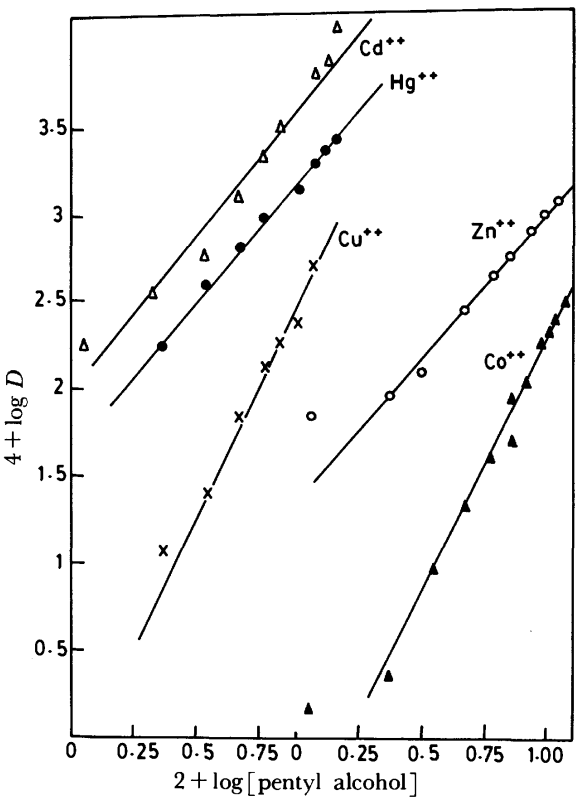

Fig. 3. Log$D$ versus log [pentyl alcohol] plots, for five metal acid. ×: 1.1×10^{-2}, ▲: 1.5×10^{-2}, ○: 5.0×10^{-3}, △: 7.0×10^{-3}, ○: 5.0×10^{-3} mol dm^{-3} at 25°C.

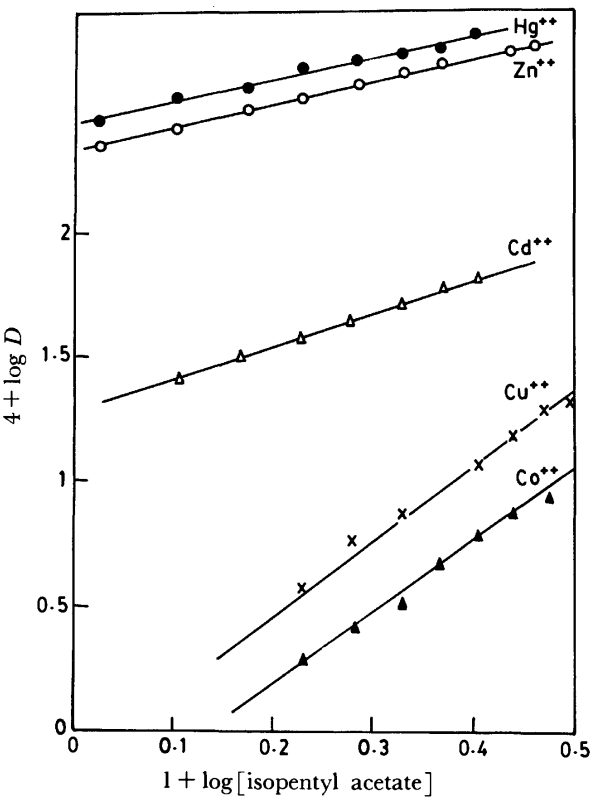

Fig. 4. Log$D$ versus log [isopentyl acetate] plots, for five metal acid. ×: 2.0×10^{-4}, ▲: 3.5×10^{-4}, ○: 1.2×10^{-2}, △: 1.1×10^{-2}, ●: 1.3×10^{-2} mol dm^{-3} at 25°C.

as monomer in the organic phase in this system as well.

Because of proportionately higher transport of HBr from aqueous into the organic phase at lower metal acid concentrations, the slopes (Figs. 1 and 2) become progressively less than unity. As metal acids compete with HBr (present in excess) for coordination with extracts in the organic phase, the extraction of metal acids at their lower metal concentration decreases significantly because excessive flow of HBr into the organic phase reduces the availability of the extracts to metal acids. This becomes distinct in the case of zinc and cadmium. Similar behavior has also been observed[11] in the extraction of tetraalkylammonium hydroxide in different alcohols.

The log plots of distribution coefficient versus concentration of pentyl alcohol in benzene (Fig. 3) at constant metal ion concentration are straight lines for Co^{2+}, Cu^{2+}, Zn^{2+}, Cd^{2+}, and Hg^{2+}, having slopes of 2.8, 2.7, 2.1, 2.3, and 2.3 respectively. Thus, the number of pentyl alcohol molecules, incorporated with metal acids, are assumed to be three for cobalt and copper and two each for the rest.

Again, the log plots of distribution coefficient versus concentration of isopentyl acetate in benzene for the five species of metal ions at constant metal ion concentration are straight lines (Fig. 4) with the slopes showing three incorporated isopentyl acetate molecules each for cobalt and copper and one each for zinc, cadmium, and mercury.

The transition metal (cobalt and copper) acids are comparatively more acidic than those of the zinc family members which have more pronounced covalent character. Hence metal acids of zinc, cadmium, and mercury give more strongly bound ion pairs, whereas those of cobalt and copper give weakly bound ones. Thus in case of cobalt and copper, each cation (hydrated proton) of the ion pair incorporates three extractant molecules (pentyl alcohol or isopentyl acetate) whereas zinc, cadmium, and mercury acid anions being more closely held to the proton accommodate only two pentyl alcohol molecules. Further, due to steric hindrance and crowding, only one isopentyl acetate molecule could be bound with the cation of the ion pair in the zinc family.

References

1) D. C. Whitney and R. M. Diamond, *J. Phys. Chem.*, **67**, 209 (1963); D. C. Whitney and R. M. Diamond, *ibid.*, **67**, 2583 (1963).

2) a) J. C. White and W. J. Ross, *Nat. Acad. Sci. Rept, NAS-NS*, **1961**, 3102; b) R. A. Zingaro and J. C. White, *J. Inorg. Nucl. Chem.*, **12**, 315 (1960); c) B. Martin, D. W. Ockenden, and J. R. Foreman, *ibid.*, **21**, 96 (1961); d) W. J. Ross and J. C. White, *Oak Ridge Natl. Laboratory Rept. ORNL*, **1957**, 2382; e) M. I. Tocher, D. C. Whitney, and R. M. Diamond, *J. Phys. Chem.*, **68**, 368 (1964).

3) Y. Baba, Y. Ikeda, and K. Inoue, *Bull. Chem. Soc. Jpn.*, **58**, 881 (1985).

4) B. S. Sunder, G. V. Rao, E. S. Kumari, and Mangathayaramma, *Indian J. Chem.*, **24A**, 505 (1985).

5) F. A. Cotton, D. M. L. Goodgame, and M. Goodgame, *J. Am. Chem. Soc.*, **83**, 4690 (1961); Dreisch and W. Trommer, *Z. Phys. Chem.*, **B37**, 37—59, 1758 (1937).

6) J. C. Barnes and D. N. Hume, *Inorg. Chem.*, **2**, 444 (1963); P. S. Barterman, *Inorg. Chem.*, **2**, 448 (1963).

7) B. Morosin and E. C. Lingafelter, *Acta Crystallogr.*, **12**, 744 (1959).

8) M. L. Delwaulle, F. Francois, and J. Wiemann, *Comp. Rend. Acad. Sci.*, **208**, 1818 (1939).

9) J. A. Rolfe, D. H. Sheppard, and L. A. Woodward, *Trans. Faraday Soc.*, **50**, 1275 (1951).

10) M. Eigen and L. de Maeyer, "Structure of Electrolytic Solutions," ed by W. J. Hamer, John Wiley and Sons, Inc. New York, N.Y. (1959); E. Wicke, M. Eigen, and T. Ackermann, *Z. Phys. Chem. (Frankfurt)*, **1**, 340 (1954); M. Eigen and L. de Maeyer, *Proc. R. Soc. London, Ser. A*, **247**, 505 (1958); R. Grahn, *Ark. Fys.*, **19**, 18 (1962); H. D. Beckey, *Z. Naturforsch., A*, **14**, 712 (1959).

11) R. M. Diamond and B. R. Aggarwal, *J. Phys. Chem.*, **67**, 2785 (1963).

 © 1987 The Chemical Society of Japan Bull. Chem. Soc. Jpn., 60, 3001—3004 (1987)

Silver-Gelatin Method for the Determination of Trace Amounts of Carbon Monoxide in Air

Tarasankar PAL,* Ashes GANGULY, and Durga S. MAITY
Department of Chemistry, Indian Institute of Technology, Kharagpur 721302, India
(Received April 14, 1986)

The use of silver-gelatin complex was found suitable for the determination of trace amounts of carbon monoxide in air. Silver-gelatin complex is reduced by carbon monoxide to give intensely colored sol. Measurement of the color intensity of the stable silver sol enables the determination of carbon monoxide successful under various environmental conditions. The detection limit is 2—100 ppm. The relative standard deviation for the determination of 10 ppm carbon monoxide is 2.6%.

Carbon monoxide is a man-made pollutant widely distributed in the atmosphere. As the gas is neutral in its character, it is difficult to impinge. It can react with various metals and hence stabilize many low valent metals. Recently with the increased concern about the effects of atmospheric pollution, several methods have been developed for the determination of carbon monoxide in air.

There are many instrumental methods which are often useless for the field evaluation. Though the nondispersive infrared (NDIR) spectroscopy and Robbins[1] photometric methods are suitable for carbon monoxide determination, these methods are of little importance for the routine and continuous determination of carbon monoxide under the environmental conditions. Similarly, gas chromatographic techniques[2,3] are rather sophisticated though the detection limit is about 0.1—1000 ppm. Colorimetric methods for the determination of carbon monoxide date back to more than 50 years but are still gaining ground.[4-8]

The well-known carbon monoxide and iodine pentaoxide reaction can be used for the determination of carbon monoxide by estimating the liberated iodine by various means.[9,10] Gravimetric method[11] converting carbon monoxide into carbon dioxide, color reaction of impregnated silica gel,[12,13] etc. are inexpensive and easy, but the accuracy is not satisfactory. Lambert[14,15] and his coworkers have developed certain reagents for the colorimetric estimation of carbon monoxide, but the sensitivity and instability make the reagents unsuitable for the routine continuous analysis. The use of the less stable silver sol method[16,17] is suitable for the colorimetric estimation of carbon monoxide. The method by Simonescu et al.[16] can be employed in a concentration range of 5—500 ppm and the determination error is less than 3% for carbon monoxide. The last two methods stand on the basis of formation of metallic silver sol from the complex of silver ions with sulfamoyl groups in alkaline medium. Considering the obvious difficulty of impingement of carbon monoxide, West et al.[17] extended the method by Simonescu for the field evaluation just by using a permeation technique.

It was observed that some weak metal-amino acid complexes in alkaline medium were easily reduced by trace amounts of carbon monoxide to form colored metallic sol.[13] But silver sol easily breaks into black precipitates rendering difficulty in color intensity measurements. The present paper describes a simple method for the determination of trace amounts of carbon monoxide using silver-gelatin complex in alkaline medium. The method can be reliably applied to field evaluation without the use of toxic chemicals. Even, no tedious preparation like the recently reported octaethylporphyrinatoruthenium(II)[18] is needed. Moreover, the sol is better stabilized in solution by gelation than by any other previously reported method.

Experimental

Apparatus. A Cary-17D (Varian) spectrophotometer was used to measure all absorbance values.

Impinger. Simple impingers of length 21 cm and internal diameter 2.2 cm were used for gas absorption. The outer wall was covered with black paint to protect the reagent from direct sunlight.

Silver-Gelatin Reagent Solution. The reagent solution was prepared by dissolving 0.5 g gelatin powder (E. Merck) in 100 ml of boiled and warm distilled water with constant stirring. Sixty ml of 10^{-3} M (M=mol dm^{-3}) silver nitrate solution was added. If any turbidity appeared, it was removed by adding a few drops of 2 M sodium hydroxide solution. The solution was heated at 50—60 °C for five minutes. The solution was diluted with 0.5 M sodium hydroxide solution to 250 ml. The reagent solution was stored in an amber-colored bottle and kept in the dark. The solution remained stable for more than 10 weeks.

Reagents. All reagents used were of analytical grade without any further purification.

Results and Discussion

Calibration Curve. Ten ml of silver-gelatin reagent solution was placed in the impinger and exposed to a known concentration of carbon monoxide for a specified period of time, typically 50 ppm for 6 h. Preparation of carbon monoxide-air mixtures was accomplished by successive dilution of a pure carbon monoxide stream with streams of purified air, nitrogen or inert gases; rotameters were used to measure flow rates. Upon completion of the exposure using a flow-rate of 500 ml min^{-1} the solution was kept for 1h and the absorbance was measured at 415 nm against a reagent blank. The concentration of carbon monoxide

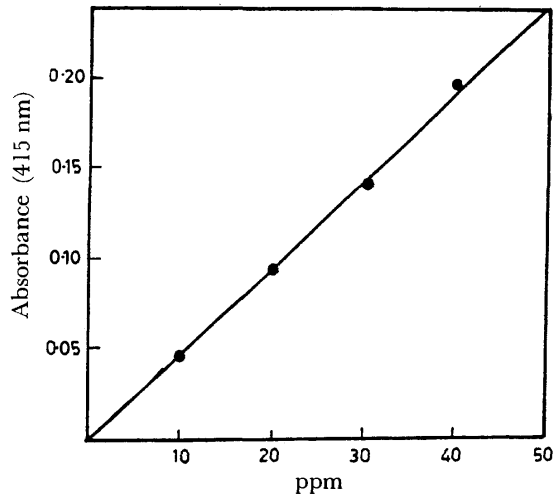

Fig. 1. Calibration curve for CO determination.

was calculated from the equation $A=kCt$; where k is a constant determined experimentally, C is the concentration of carbon monoxide, t is the time of exposure, and A, the absorbance at 415 nm (Fig. 1).

Interferences. The interferents were injected into the carbon monoxide-air stream by using a motor-driven syringe.[19] The accuracy of this syringe technique was checked by controlling the plunger speed by standard methods. Gaseous acetylene, aqueous solutions of formaldehyde (30%), aqueous ammonia (50%), and standard chlorine water were introduced. The results of the interference studies are shown in Table 1.

Data reported for sulfur dioxide, nitrogen dioxide, carbon dioxide, and hydrogen sulfide are based on 24 h exposures to 10 ppm carbon monoxide and interferent species at the level indicated. It was observed that several reducing agents like SO_2 and NO_2 gave unexpected lower absorbance values. This may possibly due to quicker reduction of the silver-gelatin complex and hence aggregation of sol lowers the absorbance values. For maintaining interferent levels of chlorine, ammonia, acetylene, and formaldehyde studies were conducted with 6 h exposures to 40 ppm carbon monoxide and interferent species at four times the level indicated.

The silver-gelatin method has two serious drawbacks. First, the reducing gases like H_2S, SO_2 must be removed by classical means. Secondly, a less serious disadvantage is that the exposed solution is to be taken for the measurement at least after 1 h time.

Numerous techniques for eliminating or reducing interferences were tried without success. It has been reported[19] that potential interferences from hydrogen sulfide for this reagent can be eliminated by passing the air sample through the silver-gelatin complex absorbed on silica gel. The advantage of this method over the conventional methods[16,17] is the stability of the exposed silver sol solution in gelatin.

In conducting the investigations, the concentration levels of possible interferent species were chosen in relation to appropriate Indian standards; the concentration of carbon monoxide chosen was 20 ppm, which corresponds to the typical background level of carbon monoxide found in the laboratory during the study.

Field Evaluation. In order to confirm the usefulness of the proposed method, it was applied to the determination of carbon monoxide in both the laboratory as well as the rural environment. The air sample was sucked after removing the acidic gases like SO_2, CO_2, H_2S using aqueous sodium hydroxide and lead acetate traps. The results are summarized in Table 2, together with the results obtained by the permeation method[17] carried out for comparison.

Precision and Accuracy. The relative standard

Table 2. Determination of Carbon Monoxide in Air Samples

Date	Laboratory air (ppm)		Urban air (ppm)	
	A	B	A	B
3/1/86	40	42	20	20
4/1/86	22	22	18	17
5/1/86	16	15	20	19
6/1/86	42	41	19	19
7/1/86	45	45	25	23
8/1/86	40	39	22	22

A; Present method: B; Permeation method.[17]

Table 1. Determination of Carbon Monoxide (10 ppm) in Synthetic Air Samples Containing Potentially Interfering Gases
Flow rate of the gas 500 ml min^{-1}; time of standing after exposure 1 h

Interferent	Concentration/ppb	Net absorbance (415 nm)	Change/%
None	—	0.074	—
NO_2[a]	200	0.070	−5.4
SO_2[a]	130	0.064	−13.5
H_2S[a]	50	0.088	+18.9
C_2H_2[b]	200	0.076	+2.7
NH_3[b]	50	0.078	+5.4
Cl_2[b]	20 ppm	0.073	−1.3
CH_2O[b]	50	0.080	+8.1
CO_2[b]	200	0.074	Nil

a) Exposure time 24 h. b) Exposure time 6 h and data were obtained using gas concentrations of 4 times the levels indicated.

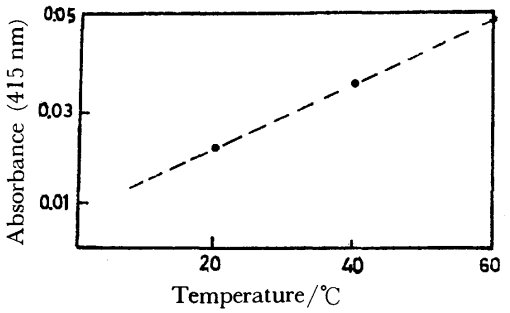

Fig. 2. Temperature effect, flow rate of sample gas 500 ml min^{-1}, standing time after exposure 1 h. CO concentration 8 ppm.

deviation and confidence limits for the determination of carbon monoxide with silver-gelatin complex were calculated and found to be 2.6% and 7.6±0.04 respectively, while the carbon monoxide concentration was 10 ppm and the flow rate of the gas was kept at 500 ml min^{-1}.

Temperature Effect. The reduction of silver-gelatin complex by carbon monoxide is temperature dependent. The effect of temperature was studied by keeping all other factors constant. The same amount of silver-gelatin complex was taken in a different impinger and reduced with the same amount of carbon monoxide at different temperatures. The results are given in Fig. 2, where each point represents an average of six determinations. The data indicate that there may be an error in the determination of carbon monoxide by this method of about 2.3% per degree centigrade, for each degree of temperature difference between the temperature at which a measurement is made and the temperature at which the device was calibrated.

Response of Measurement System. The response of the system as measured by the product Ct (C, Concentration of carbon monoxide; t, time of exposure) must be uniform throughout the useful range of the method. The absorbance value obtained on exposure to 30 ppm for 5 h should be same as that obtained on exposure to 15 ppm for 10 h, for example. It was observed that the absorbance (A) value varies with time (t), and for a sample with a given concentration (C) of carbon monoxide the absorbance is expressed by the equation $A=f(C, S, D, T, t)$, where S stands for gas reagent interface, D for diffusion coefficient, and T for temperature. This observation was made within 1 h time after the disconnection of the gas flow (500 ml min^{-1}) through the absorbing solution (10 ml).

Effect of Light. The diffused sunlight or indoor lighting in the laboratory produces no deterioration in either exposed or unexposed reagent for periods of one week. It was found during the present investigation that placement of exposed and unexposed reagent in direct sunlight results in complete loss of color in about 5 h. As a result of this observed deterioration in the presence of direct sunlight, it was necessary to shield the impinger from light in the shelter used in field evaluations. As a precaution the reagent also was stored in amber-colored bottles and kept in dark place in the Laboratory.

Stability of the Reagent. The present method was developed to determine average concentrations of carbon monoxide over periods of several hours. It was essential, therefore, that the response of the reagent is essentially uniform during the entire exposure period. Any silver sol formed early in the exposure period must be stable during the remainder of the exposure period, and the response of any unexposed reagent must be the same during the last portion of the exposure period as during the early portion.

To determine the stability of both exposed and unexposed reagent, carbon monoxide (400 ppm) was bubbled for 3 h through 50 ml of reagent at a flow rate 500 ml min^{-1}, and the gas flow was then discontinued and sample of exposed and unexposed reagents were placed in constant-temperature baths. The absorbance of each sample was measured at periodic intervals. The results are shown in Table 3. Each absorbance value represents an average of at least three determinations.

The data indicate that the intensity of the color produced by the silver sol is found to decrease with time; the net decrease average is about 1.0% in 6 h and 3.1% in 24 h at 25 °C and the instability increased with temperature.

The blank value at higher temperatures tended to stabilize at an absorbance value of 0.042—0.055 after 48 h. The present method offered the advantage of stabilizing the silver sol over a wide range of concentration of silver and hence silver sol is not precipitated unlike the methods as referenced in literature.

The method developed here is simple, inexpensive and reliable for the determination of average concentrations of carbon monoxide in the ambient atmosphere. The technique requires no electrical or mechanical connections to complex equipment, and

Table 3. Stability of Exposed and Unexposed Silver-Gelatin Reagents

Time/h	Temp 25 °C		Temp 30 °C		Temp 40 °C	
	Blank[a)]	Rgt.[b)]	Blank	Rgt.	Blank	Rgt.
0	0.033	0.193	0.033	0.195	0.033	0.192
6	0.033	0.191	0.035	0.192	0.037	0.189
24	0.034	0.187	0.038	0.189	0.039	0.178

a) Unexposed reagent. b) Reagent exposed to 400 ppm CO.

no tedious sampling technique is required. The method has some limitations, however.

The method is not suitable where high interferent concentrations may be present, nor is it suitable for process stream analysis where very rapid measurement is required and the temperature variation also affect the results.

The reagent is stable at ordinary room temperature up to 10 weeks, and the absorbance value of the blank at 30 °C is less than 0.005; this value varies by less than 0.001.

References

1) R. C. Robbins, K. M. Borg, and E. Robinson, *J. Air Pollut. Contr. Assoc.*, **18**, 106 (1968).
2) K. Porter and D. H. Volman, *Anal. Chem.*, **34**, 748 (1962).
3) F. Bruner, P. Ciccioli, and R. Rastelli, *J. Chromatogr.*, **77**, 125 (1973).
4) "Methods of Air Sampling and Analysis," 2nd ed., American Public Health Association, Inc., Washington, D. C. (1977), p. 345.
5) D. A. Levaggi and M. Feldstein, *Am. Ind. Hyg. Assoc. J.*, **25**, 64 (1964).
6) Z. Burianee and J. Burianova, *Collect. Czech. Chem. Commun.*, **28**, 2895 (1963).
7) G. Ciuhandu and V. Rusu, *Rev. Chim. (Bucharest)*, **16**, 601 (1965).
8) American Industrial Hygiene Association, *Am. Ind. Hyg. Assoc. J.*, **33**, 353 (1972).
9) E. G. Adams and N. T. Simmons, *J. Appl. Chem. (London)*, **1**, (Suppl. 1), 20 (1951).
10) L. Dubois, A. Zdrojewski, and J. R. Monkman, *J. Air Pollut. Contr. Assoc.*, **16**, 135 (1966).
11) A. B. Lamb, W. C. Bray, and J. C. W. Frazer, *J. Ind. Eng. Chem.*, **12**, 213 (1920).
12) M. Shepherd, *Anal. Chem.*, **19**, 77 (1947).
13) T. Pal, *Ind. Chem. Soc., Chem. Conv.*, **Anal 4**, 1980.
14) J. L. Lambert and P. A. Hamlin, *Anal. Lett.*, **4**, 745 (1971).
15) J. L. Lambert and R. E. Wiens, *Anal. Chem.*, **46**, 929 (1974).
16) T. Simonescu and V. Rusu, *Rev. Roum. Chim.*, **22**, 937 (1977).
17) D. R. Bell, K. D. Reiszmer, and P. W. West, *Anal. Chim. Acta*, **77**, 245 (1975).
18) A. Corsini, A. Chan, and H. Mehdi, *Talanta*, **31**, 33 (1984).
19) T. Pal, A. Ganguly, and D. S. Maity, *Analyst*, **111**, 691 (1986).
20) T. Pal, A. Ganguly, and D. S. Maity, *Anal. Chem.*, **58**, 1564 (1986).

 © 1987 The Chemical Society of Japan Bull. Chem. Soc. Jpn., 60, 3005—3009 (1987)

Coordination Chemistry of New Sulfur-Containing Ligands: Transition Metal Complexes of *N*-Ethoxycarbonyl-1-pyrrolecarbothioamide

Veena CHAUHAN and Sheo Kant DIKSHIT*
Department of Chemistry, Indian Institute of Technology, Kanpur 208016, India
(Received July 10, 1986)

Reaction of *N*-ethoxycarbonyl-1-pyrrolecarbothioamide (Hept) with a variety of transition metal ions leads to the formation of $[M^{II}(ept)_2]$ (M=Ni, Cu, Pd, Pt), $[M^{II}(ept)_2(py)]$ (M=Co, Ni), $[Rh^{I}Cl(Hept)(PPh_3)]_2$, and $[M^{III}Cl(ept)_2(H_2O)]$ (M=Ru, Rh). Reaction of Hept with Ag(I), Cu(II), Pb(II), Hg(II), and Cd(II) under refluxing conditions yields the corresponding sulfides and an oxygenated form of the ligand (Hept), which was characterized as 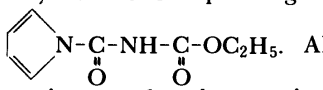 . All metal complexes have been characterized on the basis of analytical, IR and electronic spectral, and magnetic measurement studies.

Over the past five years, we have been interested in the changes in both chemical reactivity and structural properties of thioamide complexes induced by alterations in the peripheral structure of the coordinated ligand.[1-4] Our work recently has centered on thioamide ligands ($R_1CSNHCOR_2$) derived from R_1=2-pyrrolyl, 2-thienyl, or 4-tolyl and R_2=OC_2H_5, NH_2, NHPh. This effort was motivated by an attempt to establish the relative importance of resonance forms (**1**, **2**, and **3**) of the ligand having terminal substituents R_1

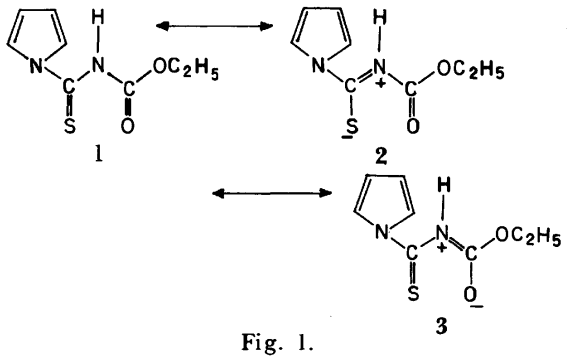

Fig. 1.

and R_2 of wide variety and their contribution to the electronic structure of resulting coordination compounds. With the above objective and as an extension of our work we report here the ligating properties of a new ligand of this class namely *N*-ethoxycarbonyl-1-pyrrolecarbothioamide (Hept). The only report[4] on the complexing behavior of the title ligand is the reaction with $[CuX(MPh_3)_3]$ (M=P or As; X=Cl or Br) in neutral media (benzene solution) resulting in the formation of tetrahedral complexes with the ligand behaving as a monodentate thione-S donor (structure **2**).

Experimental

The chemicals used were either chemically pure or AR grade. The ligand was prepared by the literature method.[5]

Preparation of Complexes. Bis(*N*-ethoxycarbonyl-1-pyrrolecarbothioamidato)copper(II). A cold solution of Hept (0.80 g, 4 mmol) in ethanol (25 ml) was added dropwise to an ice-cold solution of $CuCl_2 \cdot 2H_2O$ (0.34 g, 2 mmol) in water (25 ml). Immediate light brown precipitate results. The precipitate was centrifuged, washed with water, ethanol and ether, and then dried in vacuo.

Bis(*N*-ethoxycarbonyl-1-pyrrolecarbothioamidato)(pyridine)nickel(II). A cold solution of Hept (0.80 g, 4 mmol) in ethanol (10 ml) was added dropwise to an ice-cold solution of $NiCl_2 \cdot 6H_2O$ (0.48 g, 2 mmol) in water (25 ml) containing 10 ml of pyridine, which resulted in the precipitate of green compound. The compound was filtered off, washed with water, and dried in vacuo.

Bis(*N*-ethoxycarbonyl-1-pyrrolecarbothioamidato)nickel(II). This compound was obtained as yellow colored solid by heating the above complex at 90—100 °C.

Bis(*N*-ethoxycarbonyl-1-pyrrolecarbothioamidato)(pyridine)cobalt(II). A cold solution of Hept (0.80 g, 4 mmol) in ethanol (10 ml) was added dropwise to an ice-cold solution of $CoCl_2 \cdot 6H_2O$ (0.48 g, 2 mmol) in water (25 ml) containing 10 ml of pyridine, which resulted in the precipitation of brown compound. The compound was filtered off, washed with water, and dried in vacuo.

(*N*-Ethoxycarbonyl-1-pyrrolecarbothioamidato)silver(I). A solution of Hept (0.40 g, 2 mmol) in ethanol (10 ml) was added to a stirred solution of $AgNO_3$ (0.34 g, 2 mmol) in water (10 ml) at room temperature. The resulted yellow precipitate was filtered off, washed with water, ethanol, ether, and dried in vacuo. This compound decomposes on heating or on standing for more than one day.

Aquachlorobis(*N*-ethoxycarbonyl-1-pyrrolecarboamidato)ruthenium(III). An aqueous solution (25 ml) of hydrated ruthenium trichloride (0.26 g, 1 mmol) was added to an ethanolic solution (25 ml) of Hept (0.40 g, 2 mmol) and the resulting solution refluxed on a water bath for 1—2 h. The black-brown complex which precipitated out was separated by centrifugation, washed successively several times with water, ethanol and ether, and then dried in vacuo.

Aquachlorobis(*N*-ethoxycarbonyl-1-pyrrolecarboamidato)rhodium(III). A solution of Hept (0.40 g, 2 mmol) in ethanol (10 ml) was added to a stirred solution of $RhCl_3 \cdot 3H_2O$ (0.26 g, 1 mmol) in water (50 ml). The resulting orange colloidal solution was digested on a water bath for 2 h and the reddish orange rhodium complex was then filtered off, washed with water, a small quantity of ethanol, and finally with ether, and then dried in vacuo.

Di-μ-chlorobis(*N*-ethoxycarbonyl-1-pyrrolecarboamidato)bis(triphenylphosphine)dirhodium(I). A solution of Hept (0.13 g, 0.6 mmol) in dichloromethane (25 ml) was mixed with a solution of $[RhCl(PPh_3)_3]$ (0.46 g, 0.5 mmol) in dichloromethane (25 ml). The resulting mixture was heated

under reflux for 15 min, the solution was then cooled at room temperature and concentrated to 5 ml at reduced pressure. The addition of petroleum ether (40—60°) to this solution caused precipitation of a yellow complex. It was filtered, washed with petroleum ether, and dried in vacuo.

Bis(*N*-ethoxycarbonyl-1-pyrrolecarbothioamidato)palladium(II). A solution of Hept (0.40 g, 2 mmol) in ethanol (20 ml) was added to a hot solution of $PdCl_2 \cdot 2H_2O$ (0.21 g, 1 mmol) in water (50 ml). Immediately a yellow palladium complex appeared. The precipitate was separated through filtration, washed with water, ethanol and ether, and then dried in vacuo.

Bis(*N*-ethoxycarbonyl-1-pyrrolecarboamidato)platinum(II). A solution of Hept (0.40 g, 2 mmol) in ethanol (25 ml) was added to a solution of H_2PtCl_6 (0.41 g, 1 mmol) in water (25 ml). The mixture was heated under reflux for 1 h. The dark brown precipitate appeared. The precipitate was separated, washed with water, ethanol and ether, and then dried in air.

Sulfur Abstraction from Hept by Soft Metal Ions. An aqueous solution of hydrated metal salts† (ca. 1 mmol) was mixed with an ethanolic solution of Hept (ca. 1.5 mmol). The mixture was heated under reflux for 2—4 h. The respective sulfides Ag_2S (black), CuS (black), PbS (black), Hg_2S (black), and CdS (yellow) were precipitated and characterized after separation. The filtrate obtained was evaporated to dryness and the resulting residue was crystallized from chloroform. The crystals were recrystallized from a mixture of CCl_4 and ethyl acetate (1 : 1 ratio). The resulting crystals were characterized as *N*-ethoxycarbonyl-1-pyrrolecarboamide. Abstraction of sulfur by soft metal ions from similar ligands were also reported from our laboratory.[1,3]

Results and Discussion

All compounds are air stable, insoluble in non-coordinating solvents and soluble in solvents like ethanol, DMF, DMSO, acetone etc. Analytical data (Table 1) are in good agreement with the stoichiometry proposed for the complexes. Metal ions form inner complexes (b—e) rather than simple salts (a). Hept functions both as a mono- and bidentate ligand.

The donor ability of the ligand and the shifts of various IR bands in the spectra of complexes can be best understood in terms of resonance structures (**1**, **2**, and **3**).

The positions of the major bands of interest are shifted in the spectra of complexes. The changes in IR spectra and the inferences drawn regarding site of bonding are summarized below.

The band at 3210 cm^{-1} (ν NH) in the spectrum of ligand disappears in the spectra of the complexes except the Rh(I) complex. This could most probably be explained on the assumption that during the formation of the complexes, the NH group of the ligand is

Table 1. Analytical and Magnetic Data

Compound	Color	Mp[a] θ_m/°C	Yield %	Analysis: Found (Calcd)/% M	S	Cl	C	H	N	μ_{eff}[b] (B.M.)
$[Cu(ept)_2]$	Light Brown	105	50	13.6 (13.8)	13.7 (14.0)	—	42.2 (42.0)	3.8 (4.0)	11.9 (12.2)	DM
$[Ni(ept)_2(py)]$	Green	52	50	11.3 (10.9)	11.8 (12.0)	—	47.2 (47.4)	4.5 (4.3)	13.3 (13.2)	3.14
$[Ni(ept)_2]$	Yellow	56	54	12.6 (12.8)	13.8 (14.2)	—	42.8 (42.4)	3.8 (4.0)	12.2 (12.4)	DM
$[Co(ept)_2(py)]$	Brown	82	52	11.2 (10.9)	11.5 (12.0)	—	47.1 (47.4)	4.7 (4.3)	13.1 (13.2)	2.10
[Ag(ept)]	Yellow	158d	80	35.3 (35.4)	10.2 (10.5)	—	31.4 (31.5)	2.6 (3.0)	9.3 (9.2)	DM
$[RuCl(ept)_2(H_2O)]$	Black Brown	240	56	—	12.0 (11.7)	6.8 (6.5)	35.2 (35.0)	3.2 (3.3)	10.5 (10.2)	1.64
$[RhCl(ept)_2(H_2O)]$	Reddish Brown	238d	60	—	11.7 (11.6)	6.7 (6.4)	34.8 (34.9)	3.6 (3.3)	10.5 (10.2)	DM
$[RhCl(Hept)(PPh_3)]_2$	Yellow	120	70	—	5.1 (5.3)	5.7 (5.9)	52.4 (52.1)	4.5 (4.2)	4.5 (4.7)	DM
$[Pd(ept)_2]$	Yellow	280d	65	20.8 (21.2)	12.5 (12.8)	—	38.7 (38.4)	3.4 (3.6)	10.9 (11.2)	DM
$[Pt(ept)_2]$	Dark Brown	200d	48	32.7 (33.1)	10.6 (10.9)	—	32.9 (32.6)	3.4 (3.0)	9.6 (9.5)	DM

a) Melting points are uncorrected. b) μ_{eff} was taken at room temp.

†$AgNO_3$, $CuCl_2$, $Pb(NO_3)_2$, $HgCl_2$, and $CdSO_4$.

deprotonated with the formation of a metal to nitrogen bond. Two bands at 685 and 630 cm^{-1} assigned to τ(NH) also disappear in the spectra of the complexes, confirming deprotonation of the ligand. In case of $[RhCl(Hept)(PPh_3)]_2$ the band at 3210 cm^{-1} (ν NH) becomes broad, possibly because of hydrogen bonding in the solid state of the compound. The broad bands around 3300—3500 and 1630 cm^{-1} in the spectra of Ru(III) and Rh(III) complexes are tentatively assigned, respectively to stretching (symmetric and asymmetric) and bending modes of water molecule.

For Ni(II), Co(II), Cu(II), and Rh(I) structures **1** and **3** seem to predominate and the band at 1730 cm^{-1} (ν C=O) of Hept shifts towards lower wave numbers (see Table 2). A band at 1125 cm^{-1} of Hept (ν C=S) either remains stationary or goes up and thioamide band IV having major contribution of ν(C=S) (ca. 880 cm^{-1}) undergoes blue shifts in the spectra of complexes. These shifts are indicative of non-involvement of thiocarbonyl sulfur in bond formation, indicating strong interaction of the metal ion with carbonyl oxygen.

For Ag(I), Rh(III), Pt(II), and Pd(II) and Ru(III) complexes structures **1** and **2** of the ligand appear to be operative and the band due to ν(C=O) at 1730 cm^{-1} in the ligand either remains stationary or shifts towards higher wavenumber. This indicates the non-involvement of carbonyl oxygen in the bond formation with the metal ion. The ν(C=S) band of the ligand at 1125 cm^{-1} shifts to lower frequencies whereas in case of $[RuCl(ept)_2(H_2O)]$ the band disappears probably merging with 1095 cm^{-1} band of the ligand. The red shift observed for thioamide band IV further supports the bonding through thiocarbonyl sulfur.

The band at 1500 cm^{-1} in the ligand is assigned to thioamide band I (ν(C-N)+δ(C-H)).[6] In most of the complexes this band shifts to higher wave numbers (see Table 2). Only in the case of $Cu(ept)_2$ the band remains stationary.

A band at 1320 cm^{-1} of Hept assigned to thioamide band II (ν(C=S)+ν(C-N)+δ(C-H)) shifts to lower frequencies (ca. 10—12 cm^{-1}) in the spectra of all the complexes with the exception of $[Rh(Hept)(PPh_3)Cl]_2$ in which Hept is bonded to rhodium(I) through carbonyl oxygen only, as expected, this band shifts to higher wavenumber (1330 cm^{-1}).

Thioamide band III (mainly due to ν(C=S) and ν(C-N) at 1015 cm^{-1} of Hept undergoes red shift on complexation in all the cases.

The new band at 1580 cm^{-1} of $[Cu(ept)_2]$ which has been tentatively assigned to ν(C=N), will have significant contribution of ν(C=O) also as in this complex ν(C=O) of the ligand at 1730 cm^{-1} disappears. Large red shift is indicative of relatively stronger interaction of the Cu(II) ion with carbonyl oxygen. In case of $[Ni(ept)_2(py)]$ band at 1580 cm^{-1} has major contribution of ν(C=N) because there is a band at 1620 cm^{-1} which is assigned as ν(C=O) in the complex. The bands at 1450 and 1490 cm^{-1} for $[Cu(ept)_2]$ and

Table 3. Electronic Spectra of Ligand and Complexes in 95% Ethanol

Compound	Band position λ_{max}/nm
Ligand [Hept]	262
	300
$[Cu(ept)_2]$	285
$[Ni(ept)_2(py)]$	285
	320
$[Ni(ept)_2]$	280
	360
$[Co(ept)_2(py)]$	285
	320
[Ag(ept)]	280
	350
$[RuCl(ept)_2(H_2O)]$	265
	320
	425
$[RhCl(Hept)(PPh_3)]_2$	280
	320
$[RhCl(ept)_2(H_2O)]$	280
	320
$[Pd(ept)_2]$	250
	285
	325
	400
$[Pt(ept)_2]$	295
	450

Table 2. Major IR Bands of Interest. Comparison of IR Spectra of the Complexes with Ligand

Compound	ν(NH)	ν(C=O)	ν(C=S)	Thioamide bands				Possible coordination
				I	II	III	IV	
[Hept]	3210m	1730s	1125s	1500s	1320s	1015s	880s	—
$[Cu(ept)_2]$	—	1580s[a]	1125m	1500s	1320s	990m	880m	N and O
$[Ni(ept)_2(py)]$	—	1620s	1160m	1550s	1310s	980m	900m	N and O
$[Ni(ept)_2]$	—	1610s	1140s	1540s	1310s	980s	900m	N and O
$[Co(ept)_2(py)]$	—	1600s	1160m	1550m	1310	990m	910s	N and O
[Ag(ept)]	—	1750s	1120m	1550s	1300s	980s	850s	N and S
$[RuCl(ept)_2(H_2O)]$	—	1750s	—	1540s	1300s	980s	850s	N and S
$[RhCl(Hept)(PPh_3)]_2$	3300br	1650s	1140m	1540s	1330s	980s	890s	O
$[RhCl(ept)_2(H_2O)]$	—	1750s	1110s	1550s	1300s	990s	850s	N and S
$[Pd(ept)_2]$	—	1760s	1120s	1540s	1300s	980s	860s	N and S
$[Pt(ept)_2]$	—	1765s	1115s	1550s	1300s	985s	860s	N and S

a) This band has significant contribution from both ν(C=N) and ν(C=O).

[Ni(ept)$_2$(py)], respectively have been assigned to ν(N-C=S).[7] The weak broad band at ca. 3500 cm^{-1} in the spectra of [Ni(ept)$_2$(py)] and [Co(ept)$_2$(py)] are characteristic of pyridine, ca. 80 cm^{-1} towards higher frequency (pyridine band ca. 3420 cm^{-1}). In both the complexes bands in free pyridine at 604 cm^{-1} (in plane ring deformation) and 405 cm^{-1} (out-of-plane ring deformation) shift to higher frequencies (ca. 35 cm^{-1}).[8-10]

The appearance of new medium intensity bands in the region 500—300 cm^{-1} is strong evidence of coordination by both nitrogen and oyxgen or sulphur. They have been tentatively assigned to coupled vibrations of ν(M-N), ν(M-O), and ν(M-S). Bands of a few representative compounds in this region are as given below: 330, 345 cm^{-1} [Cu(ept)$_2$]; 335, 360 cm^{-1} [RuCl(ept)$_2$-H$_2$O]; 340, 450, 490 cm^{-1} [Ni(ept)$_2$]; and 300, 390, 440 cm^{-2} [Co(ept)$_2$(py)].

All compounds except Ni(II), Co(II), and Ru(III) complexes were found diamagnetic at room temperature. The magnetic moment of Ni(II) complex corresponds to two unpaired electrons whereas those of Co(II) and Ru(III) indicate the presence of one unpaired electron in each.

The electronic spectrum of Hept in ethanol exhibits two strong transitions at 300 and 262 nm which are assigned to n→π* and π→π* intraligand transitions, respectively. Usually n→π* transitions involving N and S occur at lower energy and are less intense than π→π*.[11,12] The spectra of almost all the compounds show the presence of these two bands with the hypsochromic blue shift. The high intensity of these bands suggest that they should be charge-transfer or intraligand and not d-d transition bands. The absence of band around 300 nm (n→π*) from the spectra of some complexes may be due to stabilization of the energy of the lone pair of electrons on complex formation,[13] and similarly the hypsochromic shift in bands in the spectra of complexes may be explained as that metal ions are bonded through thiocarbonyl sulfur, carbonyl oxygen, and nitrogen.[14] The bond formations lower the energy of non-bonding orbitals as well as π-levels, thus now more energy will be required to promote the electron from the n or π level to π* orbital hence the observed hypsochromic shift (Fig. 2).

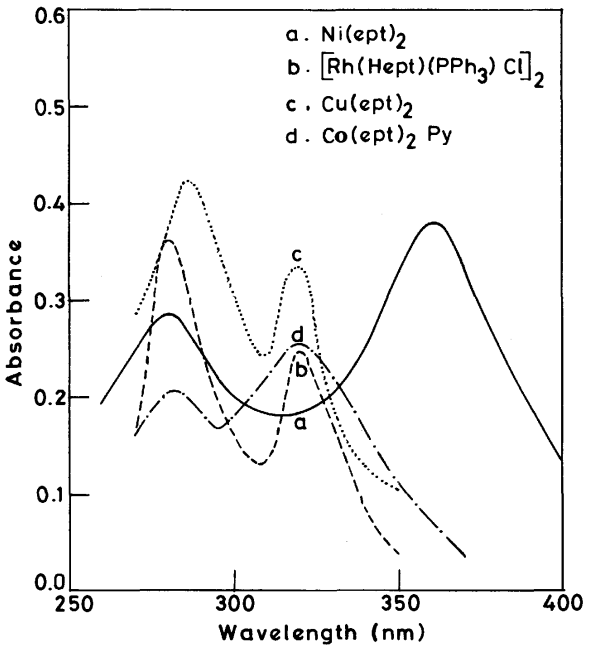

Fig. 2. Electronic spectra.

The IR evidence clearly indicates that the ligand acts as an NO/NS donor in these complexes. Square planar geometry is assigned to Ni(II), Pd(II), Pt(II), Rh(I), and Cu(II) complexes. Ru(III) and Rh(III) complexes are octahedrally coordinated whereas [Ni(ept)$_2$·(py)] and [Co(ept)$_2$(py)] are proposed to have square pyramidal geometry and the Ag(ept) complex is linear one. In case the ligand functions as a bidentate to one metal ion, it will result in a four membered chelate ring (structure b) and this will involve undue strain specially in case when the ligand acts as a NO donor. In view of the above fact and the insolubility of the complexes in most of the non-coordinating solvents the complexes may have open polymeric structures with the nitrogen and oxygen atoms of one ligand being bound to two different metal atoms (structure c).

It is known that OS donor β-thioxoketonates form exclusively cis-complexes with square planar coordinated metal ions and facial complexes with octahedrally coordinated metal ions.[15] Consequently, it is suggested that the Pd(II) and Pt(II) complexes (in which the ligand in NS donor) have the cis square

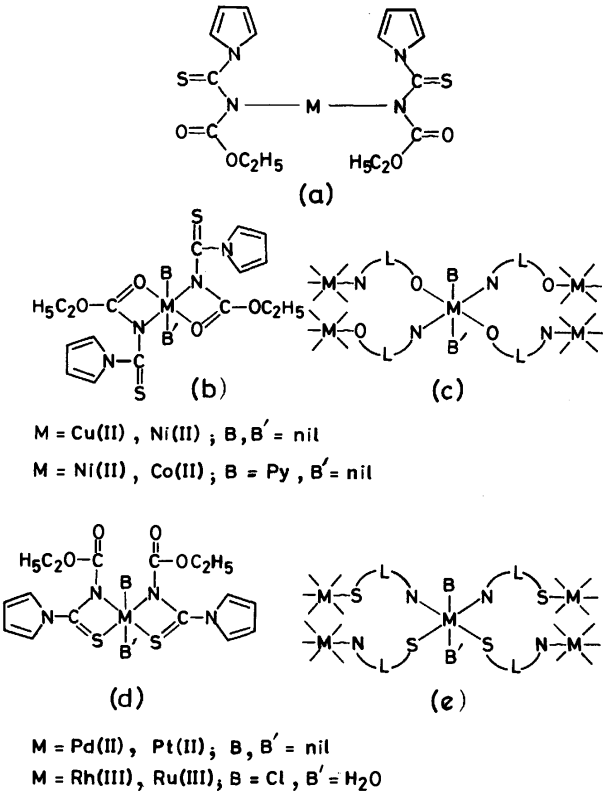

Fig. 3.

planar configuration and those of Ru(III) and Rh(III) are octahedral. Although these structures contain a four membered ring, they do not involve undue strain because of the large size of the sulfur atom. Four membered chelate rings are known with NS ligands.[16] Hence, inspite of insolubility of compounds, in case of NS donor situation, both chelate and open polymeric structures (structures d and e) are equally probable.

References

1) Ray Saheb, U. C. Agarwala, and S. K. Dikshit, *Indian J. Chem.*, **20A**, 1196 (1981); **22A**, 24 (1983); **22A**, 1050 (1983); **23A**, 204 (1984).

2) H. K. Gupta and S. K. Dikshit, *Synth. React. Inorg. Met.- Org. Chem.*, **16**, 931 (1986).

3) Veena Chauhan and S. K. Dikshit, *Transition Met. Chem.*, **11**, 223 (1986).

4) Veena Chauhan and S. K. Dikshit, *Transition Met. Chem.*, **11**, 403 (1986).

5) E. P. Papadopolous, *J. Org. Chem.*, **38**, 667 (1973).

6) E. S. Raper and P. H. Crackett, *Inorg. Chim. Acta*, **50**, 159 (1981).

7) Shukla Banerji, R. E. Byrue, and S. E. Linvingstone, *Transition Met. Chem.*, **7**, 5 (1982).

8) N. S. Gill, R. H. Nuttall, D. E. Scaife, and D. W. A. Sharp, *J. Inorg. Nucl. Chem.*, **18**, 79 (1961).

9) J. R. Durig, B. R. Mitchell, D. W. Sink, J. N. Willis, and A. S. Wilson, *Spectrochim. Acta, Part A*, **23**, 1121 (1967).

10) R. J. H. Clark and C. S. Williams, *Inorg. Chem.*, **4**, 350 (1965).

11) H. Hoso, J. Tanaka, and S. Nagakura, *Bull. Chem. Soc. Jpn.*, **33**, 850 (1960).

12) S. F. Mason, *Quart. Rev.*, **15**, 287 (1961).

13) B. Bosnick, *J. Am. Chem. Soc.*, **90**, 662 (1968).

14) H. H. Jaffe and M. Orchin, "Theory and Application of UV Spectroscopy," John Wiley and Sons, N. Y. (1962), p. 182.

15) M. Das and S. E. Livingstone, *J. Chem. Soc., Dalton Trans.*, **1975**, 452; **1977**, 662.

16) M. Akbar Ali and S. E. Livingstone, *Coord. Chem. Rev.*, **13**, 101 (1974).

 © 1987 The Chemical Society of Japan Bull. Chem. Soc. Jpn., 60, 3011—3016 (1987)

Photochemical Reactions. 21.[1] Sensitized Photooxygenation of *N*-Methylated 4-Aza-5-androsten-3-one and 4-Aza-5-androstene Steroidal Systems[2]

Joan Francesc PINIELLA, Jordi ESTAPÉ, Pilar LUPÓN, Luis MERINO, Mariano PUIG, Juan-Julio BONET,* José Luis BRIANSÓ,† and Gabriel GERMAIN††
Department of Organic Chemistry, Instituto Químico de Sarriá, 08017 Barcelona, Spain
†Departamento de Cristalografía, Universidad Autónoma de Barcelona, Bellaterra, Barcelona, Spain
††Unité de Chimie Physique Moléculaire et de Cristallographie, Université de Louvain, 1, Place Louis Pasteur, B-1348 Louvain-La-Neuve, Belgium
(Received April 8, 1986)

Two steroidal ene lactams, *N*-methyl-4-aza-5-androsten-3,17-dione and *N*-methyl-6-methoxy-4-aza-5-androsten-3,17-dione, and an enamine, *N*-methyl-4-aza-5-androsten-17β-ol, have been synthetized and their sensitized photooxygenations were investigated. The two ene lactams yield fragmentation compounds via the corresponding dioxetanes. Comparison with the previously reported behavior of an analogous *N*-unsubstituted ene lactam, seems to indicate that *N*-substitution is essential for the fragmentation to take place. On the other hand, the enamine yields a ketol. All results are briefly discussed from the mechanistic point of view.

Some years ago we published that the photooxygenation of 17β-acetoxy-4-aza-5-androsten-3-one (**1**) yields, among other products, 17β-acetoxy-5ξ,6ξ-epidioxy-4-azaandrostan-3-one (**2**) and 17β-acetoxy-5ξ-hydroxy-4-azaandrostan-3,6-dione (**3**) (Scheme 1).[3] The dioxetane readily isomerizes to **3**, and was therefore thought to be an intermediate in the transformation **1**→**3**. On the other hand, neither chemiluminescence nor the typical fragmentation to a dicarbonyl compound, were observed when heating **2**. This somewhat anomalous behavior for a 1,2-dioxetane,[4] suggested the necessity of investigating those structural details of the molecule which could be responsible for it. With the purpose of studying their photooxygenation, we decided to synthesize compounds **6**, **9**, and **11** (Scheme 2), which show the following structural modifications:

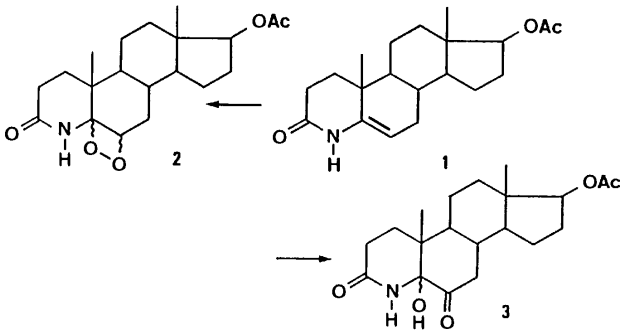

Scheme 1.

(a) *N*-Substitution
(b) Higher electronic density of the double bond (cf. **9**), and
(c) Suppresion of the carbonyl group at C-3, to an enamine (cf. **11**)

Results

Synthesis of the Heterocyclic Steroids. Starting materials for the synthesis of lactams **6** and **9** were, respectively, 4-androsten-3,17-dione (**4**)[5] and 6β-methoxy-4-androsten-3,17-dione (7).[6] Successive von

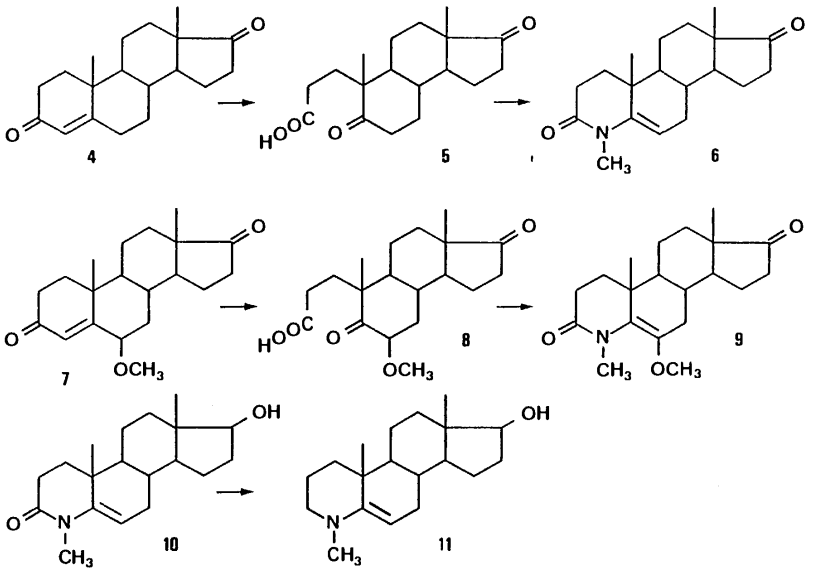

Scheme 2.

Table 1. Atomic Coordinates ($\times 10^4$) and Equivalent Isotropic Thermal Factors ($Å^2$) for **9** (Standard Deviations in Parentheses)

Atom	X/A	Y/B	Z/C	B_{eq}	Atom	X/A	Y/B	Z/C	B_{eq}
C(1)	6570(5)	1421(4)	3608(4)	5.59	C(13)	9530(4)	4889(4)	3449(3)	4.63
C(2)	5460(5)	774(4)	3374(5)	6.14	C(14)	8510(4)	5148(4)	4127(3)	4.30
C(3)	4331(5)	1366(4)	3451(3)	5.13	C(15)	8538(4)	6422(4)	4269(4)	5.51
N(4)	4340(3)	2529(3)	3610(3)	4.81	C(16)	9867(5)	6664(5)	4349(5)	6.21
C(5)	5392(4)	3149(3)	3802(3)	3.88	C(17)	10453(4)	5667(6)	3876(4)	6.09
C(6)	5392(3)	4019(3)	4394(3)	4.13	C(18)	9353(4)	5332(5)	2379(3)	6.10
C(7)	6427(4)	4797(4)	4555(3)	4.70	C(19)	6355(5)	2811(4)	2177(3)	4.92
C(8)	7377(3)	4576(3)	3801(3)	3.74	O(20)	3425(4)	870(3)	3320(3)	7.00
C(9)	7576(4)	3297(3)	3713(3)	4.27	C(21)	3254(5)	3131(5)	3458(4)	6.14
C(10)	6502(4)	2692(3)	3313(3)	4.03	O(22)	4412(3)	4218(3)	4990(2)	5.02
C(11)	8683(4)	2991(5)	3128(5)	6.25	C(23)	3980(4)	5356(4)	5021(4)	5.58
C(12)	9777(4)	3653(5)	3474(5)	6.25	O(24)	11503(3)	5519(4)	3844(5)	8.85

Table 2. Bond Distances (l/Å) for **9** (Standard Deviations in Parentheses)

C(2)-C(1)	1.52(1)	C(10)-C(9)	1.52(1)
C(10)-C(1)	1.56(1)	C(11)-C(9)	1.54(1)
C(3)-C(2)	1.48(1)	C(19)-C(10)	1.56(1)
N(4)-C(3)	1.40(1)	C(12)-C(11)	1.55(1)
O(20)-C(3)	1.21(1)	C(13)-C(12)	1.49(1)
C(5)-N(4)	1.44(1)	C(14)-C(13)	1.52(1)
C(21)-N(4)	1.45(1)	C(17)-C(13)	1.52(1)
C(6)-C(5)	1.31(1)	C(18)-C(13)	1.56(1)
C(10)-C(5)	1.53(1)	C(15)-C(14)	1.52(1)
C(7)-C(6)	1.52(1)	C(16)-C(15)	1.55(1)
O(22)-C(6)	1.40(1)	C(17)-C(16)	1.50(1)
C(8)-C(7)	1.52(1)	O(24)-C(17)	1.22(1)
C(9)-C(8)	1.54(1)	C(23)-O(22)	1.44(1)
C(14)-C(8)	1.53(1)		

Table 3. Bond Angles (θ/°) for **9** (Standard Deviations in Parentheses)

C(10)-C(1)-C(2)	113(1)	C(9)-C(10)-C(1)	109(1)
C(3)-C(2)-C(1)	119(1)	C(9)-C(10)-C(5)	110(1)
N(4)-C(3)-C(2)	118(1)	C(19)-C(10)-C(1)	110(1)
O(20)-C(3)-C(2)	121(1)	C(19)-C(10)-C(5)	108(1)
O(20)-C(3)-N(4)	121(1)	C(19)-C(10)-C(9)	113(1)
C(5)-N(4)-C(3)	123(1)	C(12)-C(11)-C(9)	113(1)
C(21)-N(4)-C(3)	117(1)	C(13)-C(12)-C(11)	110(1)
C(21)-N(4)-C(5)	120(1)	C(14)-C(13)-C(12)	109(1)
C(6)-C(5)-N(4)	121(1)	C(17)-C(13)-C(12)	117(1)
C(10)-C(5)-N(4)	116(1)	C(17)-C(13)-C(14)	101(1)
C(10)-C(5)-C(6)	123(1)	C(18)-C(13)-C(12)	112(1)
C(7)-C(6)-C(5)	125(1)	C(18)-C(13)-C(14)	113(1)
O(22)-C(6)-C(5)	119(1)	C(18)-C(13)-C(17)	104(1)
O(22)-C(6)-C(7)	116(1)	C(13)-C(14)-C(8)	113(1)
C(8)-C(7)-C(6)	111(1)	C(15)-C(14)-C(8)	120(1)
C(9)-C(8)-C(7)	109(1)	C(15)-C(14)-C(13)	105(1)
C(14)-C(8)-C(7)	110(1)	C(16)-C(15)-C(14)	102(1)
C(14)-C(8)-C(9)	109(1)	C(17)-C(16)-C(15)	105(1)
C(10)-C(9)-C(8)	112(1)	C(16)-C(17)-C(13)	109(1)
C(11)-C(9)-C(8)	113(1)	O(24)-C(17)-C(13)	126(1)
C(11)-C(9)-C(10)	112(1)	O(24)-C(17)-C(16)	125(1)
C(5)-C(10)-C(1)	106(1)	C(23)-O(22)-C(6)	117(1)

Rudloff fragmentation[7] to the seco-carboxylic acids **5** and **8**, and condensation with methylamine, yielded the lactams in 40—70% yield (Scheme 2). An X-ray analysis confirmed the structure of **9**. Lithium aluminium hydride reduction of lactam **10**,[8] gave the enamine **11** in 88% yield.

Crystal Data of 9, Structure Solution and Refinement. Suitable crystals of **9** ($C_{20}H_{29}O_3N$) were obtained by slow evaporation of an acetone-petroleum ether solution. The single crystal was mounted on a four-circle diffractometer (Syntex $P2_1$). Unit cell dimensions were as follows: a=11.466(5); b=11.848 (5); c=13.567(6) Å. Space group $P2_12_12_1$ (Z=4). Intensities were collected with Cu K_α radiation (λ=1.54178 Å) monochromatized by a graphite single crystal, using ω-scan technique.

Of 1443 reflections measured, 1382 were considered significant $I \geqslant 2.5\sigma(I)$. After the Lorentz-polarization corrections were applied, the structure was determined by direct methods (MULTAN program[9]). The atomic parameters were refined using SHELX program[10] (full matrix least-squares). The positions of H-atoms were calculated and floated on the adjacent C-atoms assuming C-H=1.08 Å. The final conventional R value was 0.061. Atomic coordinates and equivalent isotropic temperature factors are listed in Table 1, bond distances and angles in Tables 2 and **3** respectively.** Figure 1[11] is a drawing of the molecule with the numbering scheme.

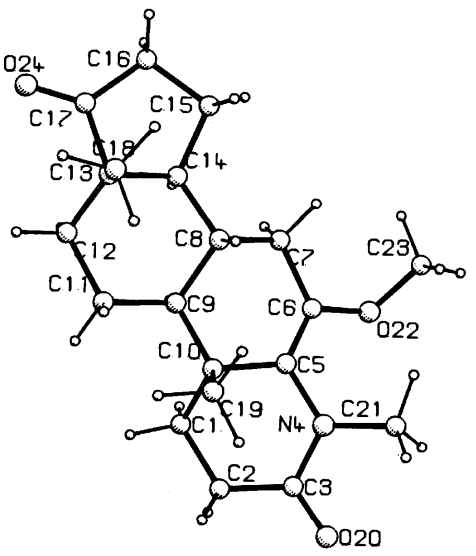

Fig. 1. Perspective view of molecule **9** with numbering scheme.

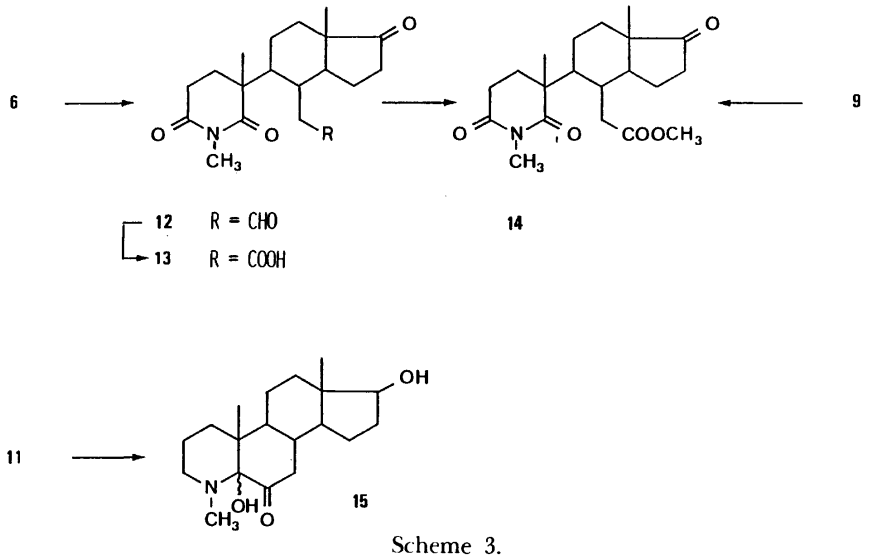

Scheme 3.

Table 4. Atomic Coordinates ($\times 10^4$) and Equivalent Isotropic Thermal Factors (Å^2) for **14** (Standard Deviations in Parentheses)

Atom	X/A	Y/B	Z/C	B_{eq}	Atom	X/A	Y/B	Z/C	B_{eq}
C(1)	4623(8)	5798(6)	9190(1)	4.08	C(14)	5461(7)	2264(5)	8326(1)	3.42
C(2)	4501(10)	6780(6)	9541(1)	5.06	C(15)	4369(11)	2073(6)	7942(1)	4.80
C(3)	5167(11)	5913(7)	9882(2)	5.38	C(16)	4301(12)	323(6)	7908(2)	5.77
N(4)	6883(8)	4920(5)	9830(1)	4.76	C(17)	4343(9)	−263(5)	8306(2)	4.49
C(5)	8028(9)	4748(6)	9495(1)	4.05	C(18)	2065(8)	1312(6)	8684(2)	4.55
C(6)	8230(9)	5140(6)	8080(1)	3.95	C(19)	8432(8)	6400(6)	8958(1)	4.38
C(7)	5949(8)	5065(5)	8238(1)	3.54	O(20)	4336(9)	6112(7)	10188(1)	8.37
C(8)	5423(7)	3811(4)	8517(1)	3.08	C(21)	7805(14)	4139(8)	10161(2)	7.38
C(9)	6832(8)	3710(5)	8878(1)	3.21	O(22)	8513(6)	6434(4)	7900(1)	5.74
C(10)	6893(7)	5177(5)	9126(1)	3.42	C(23)	10602(11)	6675(9)	7734(2)	7.09
C(11)	6076(9)	2352(5)	9126(1)	3.96	O(24)	4235(10)	−1561(4)	8391(1)	7.03
C(12)	5874(8)	869(5)	8921(1)	3.88	O(25)	9819(6)	4196(5)	9500(1)	5.31
C(13)	4463(8)	1044(5)	8574(1)	3.56	O(26)	9584(7)	4179(5)	8093(1)	6.67

Photooxygenation of 6, 9, and 11. The three photooxygenations were carried out in dry benzene solution, with Rose Bengal adsorbed on silica gel as sensitizer[12] (alternatively, polymer-immobilized Rose Bengal, Sensitox,[13] can be used), and a Sylvania 500 watts tungsten-iodine lamp. Lactam **6** yielded one main compound which was identified as the seco-keto aldehyde **12** (46%) (Scheme 3). Jones oxidation of **12** followed by CH_2N_2 treatment, gave the seco-keto ester **14** (**12**→**13**→**14**). This compound was also directly obtained, in 40% yield, by the photosensitized oxygenation of **9**. In this case, a second more polar product was detected by TLC, which with the time evolved towards **14**. The structure of **14** was confirmed by an X-ray analysis.

Crystal Data of 14, Structure Solution and Refinement. A single crystal of **14** was mounted on a Syntex $P2_1$ diffractometer. Cell parameters: a=6.128(2); b=8.929(5); c=35.551(14) Å. Space group $P2_12_12_1$ (Z=4). Intensity data were measured using the same technique as for compound **9**. Of 1576 reflections measured, 1416 ($I \geqslant 2.5\sigma(I)$) were considered reliable and used in the crystal structure analysis. After the Lorentz-polarization corrections were applied the structure was determined by direct methods, (MULTAN program[9]). The atomic parameters were refined by full matrix least-squares calculations (SHELX program[10]). The positions of H-atoms were calculated and floated on the adjacent C-atoms assuming C-H=1.08Å. The final conventional R value was 0.051. Atomic coordinates and equivalent isotropic temperature factors are listed in Table 4, bond distances and angles in Tables 5 and 6 respectively.** Figure 2[11] is a drawing of the molecule with the numbering scheme.

Photooxygenation of **11** yielded the keto alcohol **15** in 22% yield. The structure of **15** is tentatively assigned on the basis of its spectral data: The chemical shift of the 19-methyl group in the ^{1}H NMR spectrum appears at a very high field (δ 0.70) in agreement with the presence of a carbonyl at C(6);[14] on the other hand the IR spectrum exhibits a carbonylic band at 1710 cm^{-1}.

The isolation of the fragmentation compounds **12** and **14** from **6** and **9**, points towards the intermediacy

**The anisotropic thermal parameters of non-hydrogen atoms, the parameters of hydrogen atoms, and the tables of the observed and the calculated structure factors were kept at the Chemical Society of Japan (as Doc. No. 8712).

Table 5. Bond Distances (l/Å) for **14** (Standard Deviations in Parentheses)

C(2)-C(1)	1.52(1)	C(14)-C(8)	1.54(1)
C(10)-C(1)	1.51(1)	C(10)-C(9)	1.58(1)
C(3)-C(2)	1.50(1)	C(11)-C(9)	1.57(1)
N(4)-C(3)	1.39(1)	C(19)-C(10)	1.56(1)
O(20)-C(3)	1.21(1)	C(12)-C(11)	1.52(1)
C(5)-N(4)	1.39(1)	C(13)-C(12)	1.52(1)
C(21)-N(4)	1.48(1)	C(14)-C(13)	1.53(1)
C(10)-C(5)	1.53(1)	C(17)-C(13)	1.51(1)
O(25)-C(5)	1.20(1)	C(18)-C(13)	1.54(1)
C(7)-C(6)	1.51(1)	C(15)-C(14)	1.53(1)
O(22)-C(6)	1.33(1)	C(16)-C(15)	1.57(1)
O(26)-C(6)	1.19(1)	C(17)-C(16)	1.51(1)
C(8)-C(7)	1.53(1)	O(24)-C(17)	1.20(1)
C(9)-C(8)	1.55(1)	C(23)-O(22)	1.43(1)

Table 6. Bond Angles (θ/°) for **14** (Standard Deviations in Parentheses)

C(10)-C(1)-C(2)	112(1)	C(9)-C(10)-C(1)	111(1)
C(3)-C(2)-C(1)	111(1)	C(9)-C(10)-C(5)	106(1)
N(4)-C(3)-C(2)	115(1)	C(19)-C(10)-C(1)	111(1)
O(20)-C(3)-C(2)	123(1)	C(19)-C(10)-C(5)	103(1)
O(20)-C(3)-N(4)	122(1)	C(19)-C(10)-C(9)	112(1)
C(5)-N(4)-C(3)	125(1)	C(12)-C(11)-C(9)	115(1)
C(21)-N(4)-C(3)	119(1)	C(13)-C(12)-C(11)	110(1)
C(21)-N(4)-C(5)	116(1)	C(14)-C(13)-C(12)	108(1)
C(10)-C(5)-N(4)	118(1)	C(17)-C(13)-C(12)	117(1)
O(25)-C(5)-N(4)	120(1)	C(17)-C(13)-C(14)	102(1)
O(25)-C(5)-C(10)	122(1)	C(18)-C(13)-C(12)	111(1)
O(22)-C(6)-C(7)	110(1)	C(18)-C(13)-C(14)	115(1)
O(26)-C(6)-C(7)	127(1)	C(18)-C(13)-C(17)	104(1)
O(26)-C(6)-O(22)	123(1)	C(13)-C(14)-C(8)	112(1)
C(8)-C(7)-C(6)	118(1)	C(15)-C(14)-C(8)	119(1)
C(9)-C(8)-C(7)	117(1)	C(15)-C(14)-C(13)	105(1)
C(14)-C(8)-C(7)	112(1)	C(16)-C(15)-C(14)	101(1)
C(14)-C(8)-C(9)	108(1)	C(17)-C(16)-C(15)	106(1)
C(10)-C(9)-C(8)	115(1)	C(16)-C(17)-C(13)	109(1)
C(11)-C(9)-C(8)	110(1)	O(24)-C(17)-C(13)	126(1)
C(11)-C(9)-C(10)	109(1)	O(24)-C(17)-C(16)	125(1)
C(5)-C(10)-C(1)	112(1)	C(23)-O(22)-C(6)	116(1)

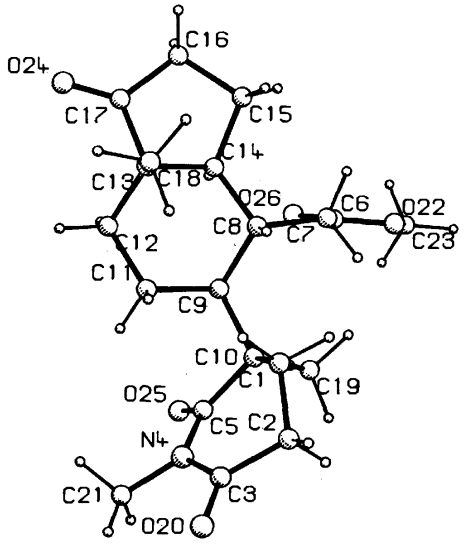

Fig. 2. Perspective view of molecule **14** with numbering scheme.

of the 1,2-dioxetanes **16** and **17**, respectively (Scheme 4). In fact, **16** and **17** have been obtained in quantitative yield in low temperature experiments,[15] and characterized by ^{1}H (300 MHz) and ^{13}C NMR and also by their conversion to the cleavage products **12** and **14** upon heating.[16]

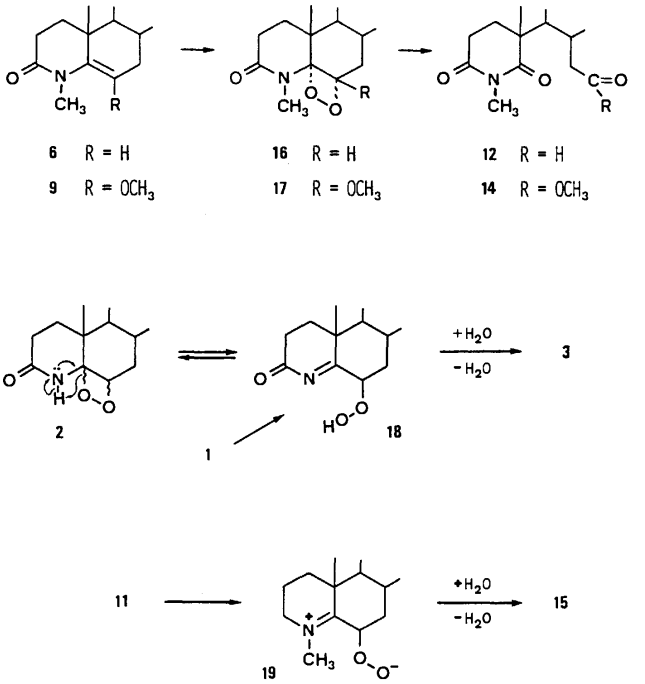

Scheme 4.

Concerning the objectives of our work, the results obtained suggest that in the case of the lactams, the evolution of the dioxetanes towards fragmentation compounds or alternatively towards a ketol derivative, depends on the absence or presence of a hydrogen attached to the nitrogen atom. The anomalous behavior of the dioxetane **2** could be explained assuming a preferential isomerization to the ketol **3**, as shown in Scheme 4 (**2**⇄**18**→**3**), which in the absence of the N-H would not take place (no ketol was detected in the crude photooxygenation mixtures of **6** or **9**). Compound **3** could be also directly formed from **1** via the allylic hydroperoxide **18**.

In the case of the enamine **11**, no fragmentation products have been detected and this result is different from those described in the literature: Usually enamines yield fragmentation compounds via dioxetanes.[17] In the case of **11**, a zwitterionic intermediate of type **19** is proposed,[18] although its formation via dioxetane is not excluded. The difference in behavior between the lactams **6** and **9** and the enamine **11** can be explained by means of the availability of the lone pair electron of amine.

Experimental

General Remarks. By extraction in the usual way is meant: Dilution of the reaction mixture with ethyl acetate, washing of the organic phase with concentrated NaCl solution till neutral, drying on anhydrous Na_2SO_4 and evaporation under reduced pressure with a rotatory evaporator.

Silica gel Merck 0.063—0.2 mm, was used for column

chromatography (ratio to substance, 100:1). Thin-layer chromatography was performed using Merck Silica Gel 60F-254 plates. Spots were detected by direct observation under UV light (253.7 nm) or with 50% sulfuric acid spray followed by heating at 150 °C during 1 min.

Crystallizations were carried out in acetone-petroleum ether (bp 50—70 °C). Melting points were determined in an open capillary (Büchi-Tottoli apparatus) and are uncorrected.

Infrared spectra (KBr) were recorded on a Perkin-Elmer 683 spectrophotometer; absorption is given in ν values (cm^{-1}). The ultraviolet spectra (in Merck Ethanol UVASOL solution) were recorded on a Perkin-Elmer 124 spectrophotometer; absorption is given in λ_{max} (nm) values, followed by the ε value in brackets. Perkin-Elmer R-24 or Varian XL-100 spectrometers were used to obtain the ^1H NMR spectra (in $CDCl_3$ solution, unless otherwise specified). Chemical shifts (δ values) are reported relative to TMS as an internal standard. Coupling constants (J) are given in Hz. Multiplicities are expressed as: singlet (s), doublet (d), triplet (t), quartet (qa), multiplet (m), and broad signal (br). Mass spectra were measured on a Hewlett-Packard 5930A or Varian M-44 spectrometers. EI=Electron Impact, CI=Chemical Ionization, DCI=Desorption Chemical Ionization.

For the photosensitized oxygenations, a Sylvania 500T 3Q/Cl/U 200 V lamp and a typical immersion unit were used.

Synthesis of the Heterocyclic Steroids. *N*-Methyl-4-aza-5-androsten-3,17-dione (6). To a solution of **4** (5.853 g, 20 mmol) in *t*-BuOH (1.5 L), an oxidizing von Rudloff solution (24.8 g $NaIO_4$, 5.96 g K_2CO_3, 0.789 g $KMnO_4$, 1.5 L H_2O) was added, and the mixture was stirred for 2 h at r.t. The *t*-BuOH was evaporated in vacuo, HCl (10%, 60 mL) added and the resulting mixture worked up with EtOAc in the usual way. SiO_2 filtration (benzene-EtOAc 1:1) yielded 5.108 g (81.5%) of 5,17-dioxo-A-nor-3,5-secoandrostan-3-oic acid (**5**). IR (film) 3400—2500 (br), 1745, 1725, 1710. ^1H NMR: 0.95 (s, $H_3C(18)$), 1.16 (s, $H_3C(19)$), 9.68 (br, H-OOC(3), disappears on D_2O addition). MS 306 (M^+).

One hundred mL of a 1.5% solution of Na in EtOH, were added to 1.854 g of methylamine hydrochloride in 22 mL EtOH. After filtration, a solution of **5** (1.119 g, 4 mmol) in EtOH (54 mL) was added and the mixture was heated at 140 °C in a sealed tube, for 15 h. After allowing it to cool to r.t. and evaporation in vacuo, it was worked up with chloroform. SiO_2 chromatography (benzene-EtOAc 1:1) yielded 848 mg (80%) of pure **6**. Mp 162—167.5 °C (d) after three crystallizations. IR: 3040, 1730, 1660, 1635. UV: 235 (13800). ^1H NMR: 0.91 (s, $H_3C(18)$), 1.09 (s, $H_3C(19)$), 3.10 (s, H_3C-N(4)), 5.03 (dd, J_1=4.5, J_2=2, H-C(6)). MS 301 (M^+). Found: C; 75.46, H; 9.05; N 4.57%. Calcd for $C_{19}H_{27}NO_2$ (301.43): C 75.71; H 9.03; N 4.65%.

***N*-Methyl-6-methoxy-4-aza-5-androsten-3,17-dione (9).** To a solution of **7** (0.301 g, 0.8 mmol) in *t*-BuOH (120 mL), an oxidizing von Rudloff solution (2.0 g $NaIO_4$, 0.6 g K_2CO_3, 0.02 g $KMnO_4$, 450 mL H_2O) was added, and the mixture was stirred for 3 h at r.t. The *t*-BuOH was evaporated in vacuo, HCl (2M (1 M=1 mol dm^{-3}), till pH 2) was added and the resulting mixture was worked up with EtOAc to yield 0.251 g (79%) of 6β-methoxy-A-nor-3,5-seco-5,17-dioxoandrostan-3-oic acid (**8**). IR (film) 3600—2500 (br), 1750, 1715, 1100. ^1H NMR 0.93 (s, $H_3C(18)$); 1.26 (s, $H_3C(19)$); 3.30 (s, CH_3-O (6)); 3.58 (t, J_1=J_2=2, H-C(6)); 8.65 (br, H-OOC(3), disappears on D_2O addition).

Liquid methylamine was added in excess to a solution of **8** (0.120 g, 0.3 mmol) in THF (50 mL), and the mixture was heated at 140 °C in a sealed tube for 15 h. After allowing it to cool to r.t., it was worked up with chloroform. SiO_2 chromatography (EtOAc-cyclohexane 2:1) yielded 53 mg (51%) of **9**. IR (film) 2840, 1730, 1670—1645 (br). UV 243 (9900). ^1H NMR 0.96 (s, $H_3C(18)$), 1.05 (s, $H_3C(19)$), 3.15 (s, H_3C-N(4)), 3.53 (s, $CH_3O(6)$). MS 331 (M^+). The compound decomposed during the recrystallization procedure, which prevented its elemental analysis.

***N*-Methyl-4-aza-5-androsten-17β-ol (11).** 1.2 g $LiAlH_4$ in 120 mL dry Et_2O were placed in the round-bottom flask of a Soxhlet apparatus, and 0.400 g (1.3 mmol) of **10** were placed in its cartridge. Reflux of ether slowly added **10** on the reducing agent. After 13 h reflux and 6 h at r.t. with stirring, 6 mL of a saturated Na_2SO_4 solution were added dropwise. After filtration it was worked up with ether to yield 0.353 g (93%) of **11**. Mp 161—164 °C after three crystallizations. IR: 3450, 3075, 1645. UV 218 (5400). MS 289 (M^+). Found: C, 78.79; H, 10.82; N, 4.71%. Calcd for $C_{19}H_{31}NO$ (289.47): C, 78.84; H, 10.79; N, 4.84%.

Photooxygenation Reactions. Photooxygenation of 6. A solution of **6** (680 mg, 2.2 mmol) in dry benzene (15 mL), together with Rose Bengal-SiO_2 (701 mg), was irradiated for 20 min at 5 °C under a current of O_2. After filtration, the solution was concentrated to 10 mL with a N_2 current and immediately SiO_2 chromatographed (benzene-EtOAc 3:2) to yield 316 mg (43%) of *N*-methyl-3,5,17-trioxo-4-aza-5,6-secoandrostan-6-al (**12**), as an oil. IR 2740, 1750, 1725, 1670. UV 214 (9600). ^1H NMR 0.95 (s, $H_3C(18)$), 1.32 (s, $H_3C(19)$), 2.61 (d, J=6, H_2-C(7)), 3.11 (s, H_3C-N(4)), 9.66 (br s, HCO(6)), sharpens when irradiating at 2.61). MS 333 (M^+).

Jones Oxidation of 12. To a solution of **12** (84 mg, 0.25 mmol) in acetone (25 mL), 1.5 mL of Jones reagent were added, till persistence of a red color. MeOH was then added (15 mL) till green coloration and, after evaporation in vacuo, the mixture was worked up with EtOAc, to yield 86 mg (98%) of *N*-methyl-3,5,17-trioxo-4-aza-5,6-secoandrostan-6-oic acid (**13**). IR (film) 3600—2500 (br), 1750—1720 (br), 1670. ^1H NMR 0.89 (s, $H_3C(18)$), 1.30 (s, $H_3C(19)$), 2.60 (d, J=5, H_2-C(7)), 3.10 (s, $H_3CN(4)$), 7.27 (br, H-OOC(6), disappears on D_2O addition). MS 349 (M^+).

Esterification of 13. A solution of 80 mg (0.23 mmol) of **13** in 50 mL ether was treated with an ethereal solution of diazomethane. Solvent elimination in vacuo yielded 77 mg (96%) of methyl *N*-methyl-3,5,17-trioxo-4-aza-5,6-secoandrostan-6-oate (**14**). IR (film) 1745—1720 (br), 1670, 1165. ^1H NMR 0.93 (s, $H_3C(18)$), 1.37 (s, $H_3C(19)$); 2.61 (d, J=5, H_2-C(7)), 3.13 (s, H_3C-N(4)), 3.69 (s, H_3C-OOC(6)). MS 363 (M^+). Decomposition during recrystallization prevented its elemental analysis.

Photooxygenation of 9. A solution of **9** (23 mg, 0.07 mmol) in dry benzene (10 mL), together with Rose Bengal-SiO_2 (25 mg), was irradiated for 1 h under a current of O_2. After filtration, it was left at r.t. for 3 d. SiO_2 chromatography (EtOAc-cyclohexane 1:1) yielded 10 mg (39%) of **14** (mixed TLC, IR, ^1H NMR, and MS).

Photooxygenation of 11. A solution of **11** (260 mg, 0.9 mmol) in dry benzene (100 mL) and Sensitox (200 mg), was irradiated for 50 min at 5 °C and under a current of O_2. Filtration, evaporation with a current of N_2 and SiO_2 chro-

matography yielded mostly decomposition products and 58 mg (20%) of assumed *N*-methyl-5ξ,17ξ-dihydroxy-4-aza-androstan-6-one (**15**), as an oil. IR (film) 3500, 1710. ^{1}H NMR 0.65 (s, H_3C(18)), 0.70 (s, H_3C(19)), 1.92 (s, H_3C-N(4)), 2.2 (br, HO-C(17), simplifies after D_2O addition), 2.3—2.6 (m, H_2-C(3)+H_2-C(7)), 3.80 (m, HO-C(5)+HC(17), simplifies after D_2O addition). MS: EI 321 (M^+), 303(M^+ −18); CI 304 (M^++1−18); DCI 322(M^++1).

We are grateful to Prof. Dr. J. Camps (Instituto de Química Bio-Orgánica, C.S.I.C., Barcelona) for elemental analysis, Prof. Dr. C. Pascual (Instituto de Química Orgánica General, C.S.I.C., Madrid) for 100-MHz ^{1}H NMR spectra, Prof. Dr. E. de Hofmann (Université de Louvain) for MS spectra and to Prof. Dr. A. P. Schaap (Department of Chemistry, Wayne State University, Detroit) for valuable mechanistic discussions.

References

1) Part 20: P. Lupón, F. Grau, and J.-J. Bonet, *Helv. Chim. Acta*, **67**, 332 (1984).

2) Part of the doctoral thesis of J. F. Piniella, IQS, Barcelona, (1982).

3) F. Abelló, J. Boix, J. Gómez, J. Morell, and J.-J. Bonet, *Helv. Chim. Acta*, **58**, 2549 (1975).

4) P. D. Bartlett and M. E. Landis, "Singlet Oxygen," ed by H. H. Wasserman and R. W. Murray, Academic Press, New York (1979), pp. 243—286.

5) L. Ruzicka and A. Wettstein, *Helv. Chim. Acta*, **18**, 986 (1935).

6) P. B. Sollman and R. M. Dodson, *J. Org. Chem.*, **26**, 4180 (1961).

7) a) M. E. Wall and S. Serota, *J. Org. Chem.*, **24**, 741 (1959); b) R. U. Lemieux and E. von Rudloff, *Can. J. Chem.*, **33**, 1701, 1710 (1955); c) E. von Rudloff, *ibid.*, **33**, 1714 (1955); d) E. von Rudloff, *ibid.*, **34**, 1413 (1956).

8) P. Dalmases, G. Cervantes, J. Quintana, J.-J. Bonet, A. Giner-Sorolla, and F. A. Schmid, *Eur. J. Med. Chem.*, **19**, 465 (1984).

9) P. Main, S. J. Fiske, S. E. Hull, L. Lessinger, G. Germain, J. P. Declercq, and M. M. Woolson (1980). MULTAN 80. A system of computer programs for the automatic solution of crystal structures from X-ray diffraction data. Univs. of York, England, and Louvain, Belgium.

10) G. M. Sheldrick (1976). SHELX. Program for crystal structure determination. Univ. of Cambridge, England.

11) S. Motherwell and W. Clegg (1978), PLUTO. University Chemical Laboratory, Cambridge, England.

12) a) R. Nilsson and D. R. Kearns, *Photochem. Photobiol.*, **19**, 181 (1974); b) E. C. Blossey, D. C. Neckers, A. L. Thayer, and A. P. Schaap, *J. Am. Chem. Soc.*, **95**, 5820 (1973).

13) Hydron Laboratories Inc., 783 Jersey Avenue, New Brunswick, N. J. 0892.

14) N. S. Bhacca and D. H. Williams, "Applications of NMR Spectroscopy in Organic Chemistry," Holden-Day, Inc., San Francisco (1964), p. 20.

15) The low temperature experiments, as well as the study of the chemiluminescent decomposition of these dioxetanes, have been carried out by Prof. A. P. Schaap, Dr. L. López, and Dr. S. D. Gagnon (Department or Chemistry, Wayne State University, USA); details will be published elsewhere.

16) J.-J. Bonet, J. Piniella, P. Lupón, J. Estapé, A. P. Schaap, L. López, and S. D. Gagnon, IX IUPAC Symposium on Photochemistry-Pau (July 82), Book of Abstracts p. 36.

17) A. P. Schaap and K. A. Zaklika, "Singlet Oxygen," ed by H. H. Wasserman and R. W. Murray, Academic Press, New York (1979), Chap. 6.

18) H. H. Wasserman and B. H. Lipshutz, "Singlet Oxygen," ed by H. H. Wasserman and R. W. Murray, Academic Press, New York (1979), pp. 477, 479.

 © 1987 The Chemical Society of Japan Bull. Chem. Soc. Jpn., 60, 3017—3024 (1987)

Protein Engineering of Dihydrofolate Reductase. Improved Catalytic Step of Mutant-Enzymes

Kazunari TAIRA,† Jin-Tann CHEN,†† Ruth J. MAYER,††† and Stephen J. BENKOVIC*
Department of Chemistry, The Pennsylvania State University, University Park, Pennsylvania 16802, U.S.A.
†Fermentation Research Institute, Agency of Industrial Science and Technology, Yatabe-machi, Ibaraki 305
††Development Center for Biotechnology, 237, Chien-Kuo S. Rd., Sec. 1, Taipei, Taiwan
†††Smith, Kline and Beckman Laboratories, 1500 Spring Garden St., Philadelphia, PA 19101, U. S. A.
(Received May 6, 1986)

Two site-specific mutations on dihydrofolate reductase from *Escherichia coli* have been carried out at the Phe-31 site. From the crystallographic structure the Phe-31 is located at the dihydrofolate binding site and interacts with both the pteridine ring and the *p*-aminobenzoyl moiety of the substrate. Two mutant enzymes (Phe-31→Tyr and Val) have been purified to homogeneity and characterized by steady-state kinetics. The two mutations are aimed at assessing the hydrophobic interaction between the phenyl ring and the aromatic ring moiety of the substrate. Despite the fact that the first mutation has introduced a polar Tyr-group into a hydrophobic binding site, the Michaelis constant K_{DHF} (K_M with saturating NADPH and varying dihydrofolate) has increased only five-fold. The second mutation (Phe-31→Val-31) results in a 25-fold increase in K_{DHF}. More importantly, the maximum velocity of both mutant enzymes has increased more than 100%, indicating that these are better enzymes under the condition of [substrate]>K_{DHF}. Thus, in both mutant enzymes the decrease in binding has not been translated into a loss of catalytic efficiency.

Site-directed mutagenesis is becoming an increasingly powerful technique for elucidation of the role of specific amino acids in proteins.[1-6] Dihydrofolate reductase (DHFR) catalyzes the reduction of dihydrofolate (H_2-folate) to tetrahydrofolate (H_4-folate) with NADPH as the cofactor. The metabolic importance of

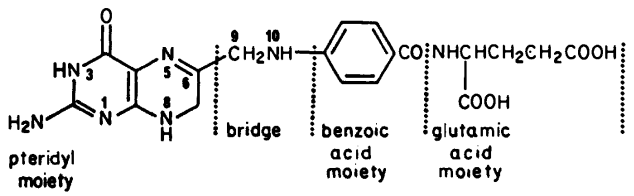

DHF (H_2-folate)

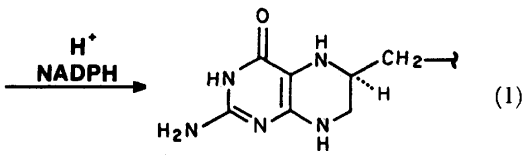

(1)

THF (H_4-folate)

DHFR, which stems from the fact that derivatives of its product, H_4-folate, have coenzyme functions in one-carbon transfer reactions, has inspired extensive research on inhibitors of the enzyme, several of which are widely used as antibacterial or antitumor agents.[7] This enzyme is one of a few proteins whose X-ray crystal structure has been solved to a resolution better than 2 Å.[8,9] It is a single polypeptide chain of 159 amino acids (17800 daltons) and possesses an extensive secondary structure consisting of eight β strands, seven of which are parallel, and four α helices.[8,9] Thus, this richness of structural information enables us to study the relationship between enzyme structure and function in detail by means of site-directed mutagenesis on this enzyme.

The structure of the *E. coli* DHFR-methotrexate binary complex is shown schematically in Fig. 1, with

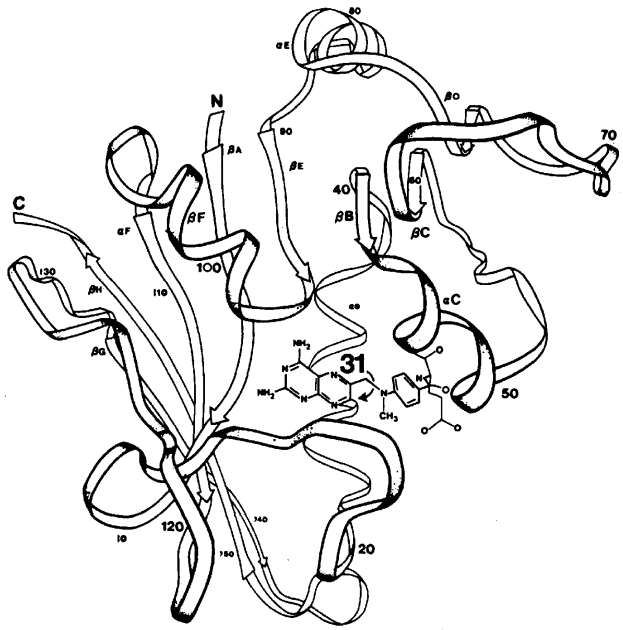

Fig. 1. Backbone ribbon drawing of the *E. coli* DHFR-methotrexate binary complex[8] with the mutation site, Phe-31, indicated by the arrow.

the site of particular interest, Phe-31, indicated by an arrow. This phenylalanine, strictly conserved in all known sequences of DHFR, interacts with both the pteridine ring and the *p*-aminobenzoyl moiety. The *p*-aminobenzoyl moiety is almost perpendicular to the pteridine ring with the Phe-31 being at the corner of the bend providing van der Waals contacts with both aromatic rings. Considering the fact that the hybridization of C6 changes from sp^2 to sp^3 so that C9 swings away from the plane of the pteridine ring upon reduction of the C6=N5 imino bond, it is of interest to inquire whether the interactions with Phe-31 change during product formation.

One might also imagine that the imino double bond

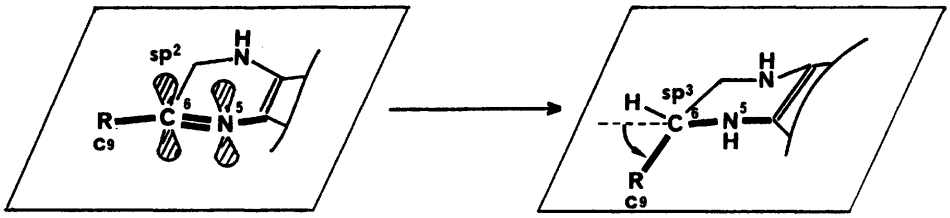

(2)

in H_2-folate may be activated towards reduction through a degree of strain on the imino bond, possibly caused by the bend. By replacing the Phe-31 by a smaller amino acid such as Val, one can assess to what degree reduced substrate-enzyme interactions alter catalysis. In addition we have chosen Tyr for the replacement of Phe-31, which still possesses aromatic character but may be able to facilitate the protonation of N5 prior to reduction since no amino acid exists at the active site that is capable of direct proton transfer.[8]

This approach is made possible through the technique of site-directed mutagenesis. We have successfully created two new proteins (Tyr-31 and Val-31) via site-directed mutagenesis which have been purified to homogeneity and offer significant mechanistic insights which could not be gained merely by studying the wild-type enzyme.

Methods

The method of Dalbadie-McFarland et al. was employed to generate specific mutations using a chemically synthesized oligodeoxynucleotide that directs the mutationl.[1] Figure 2(a) shows the nucleotide sequence of the synthetic 22-mer oligodeoxynucleotide, with asterisks indicating mismatches, together with the corresponding base sequence of the wild-type *E. coli* DHFR. Figure 2(b) illustrates a restriction map of the plasmid DNA, pTY1,[10] in which a 1 Kb fragment containing the DHFR gene (*fol*)[11] is inserted into the *Bam*H I site of a 4.4 Kb pBR322 derivative DNA lacking the *Eco*R I site, as well as the restriction fragments formed upon treatment with *Aha* III and *Bam*H I. The recognition sequence of the *Aha* III is TTTAAA which is found in the wild-type DHFR gene corresponding to Phe-31 and Lys-32 (see Fig. 2(a)). Upon mutation of the Phe-31 the TTT codon is replaced by a corresponding codon for each mutant enzyme, in case of the Tyr-31 mutant, the corresponding codon is TAT. Thus, any successful mutation destroys the *Aha* III recognition site in *fol*, resulting in the resistance of a 1 Kb fragment toward *Aha* III digestion. The isolation of the *Aha* III resistant 1 Kb fragment followed by religation with the 4.4 Kb pBR322

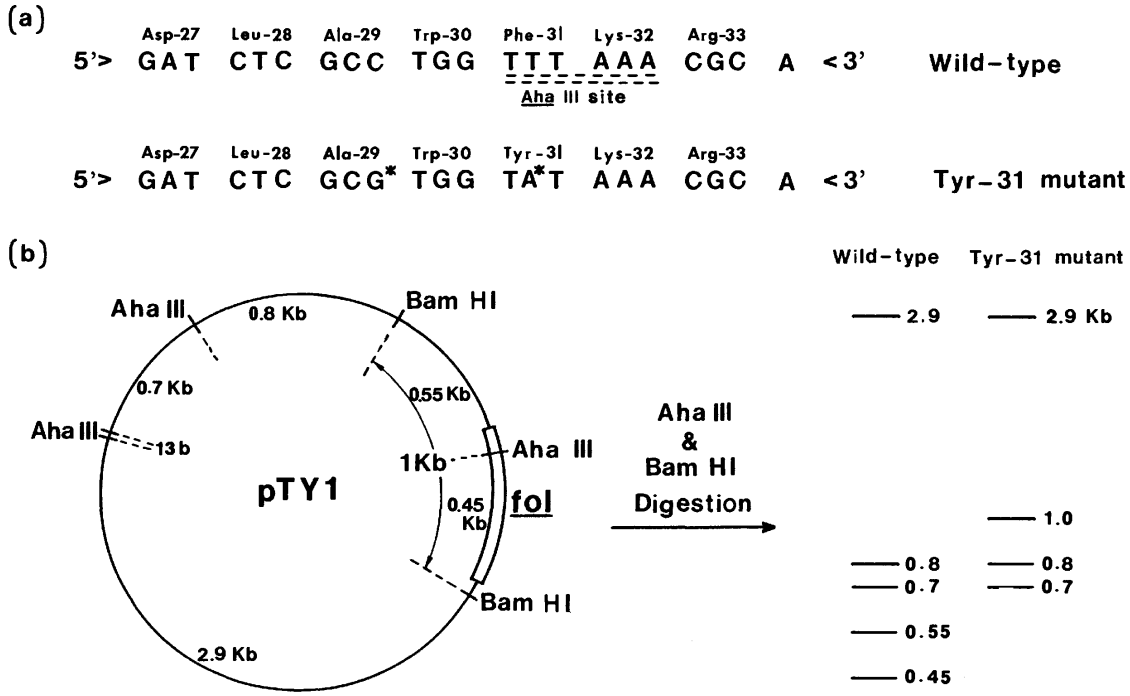

Fig. 2. (a) Nucleotide sequence of the syuthetic oligodeoxynucleotide for Tyr-31 mutant and the corresponding sequence for the wild-type *E. coli* DHFR. The base pair mismatches are indicated by asterisks and the amino acids encoded by both mutant and wild-type sequences are shown. (b) Restriction map of the plasmid DNA, pTY1, showing the location of the DHFR gene (*fol*) by the open box. Gel electrophoresis results of both wild-type and mutant DNAs upon *Aha* III/*Bam*H I digestion are schematically shown.

derivative completes the preparation of mutant plasmid DNA. The exact experimental conditions employed[10-15] are described in the following section.

Experimental

Oligodeoxyribonucleotides. The syntheses of two oligodeoxyribonucleotides were performed on an Applied Biosystems Model 380A DNA synthesizer. Base sequences of the two oligodeoxyribonucleotides were as follows, with asterisks indicating mismatchs.

Tyr (22-mer):
5′>GAT CTC GCG* TGG TA*T AAA CGC A<3′
Val (21-mer):
5′>GAT CTC GCG* TGG G*TT AAA CGC<3′

The oligodeoxyribonucleotides were purified by means of HPLC on a reverse phase μBONDAPAK C18 column employing a 10—30% gradient of CH_3CN in 0.1 M§ triethylammonium acetate (TEAA) pH 7. After detritylation with 3% CH_3COOH at room temperature for 3 min the deblocked oligonucleotides were subject to a second HPLC purification under the above conditions.

Purity of the primers was confirmed by repeating the HPLC procedure as well as running electrophoresis on ^{32}P-end-labelled primers prepared as follows.[12] To an Eppendorf tube were added 4 μl H_2O, 2.5 μl 5X Kinase buffer (0.5 M Tris·HCl, pH 8.0, 0.05 M $MgCl_2$, 0.025 M DTT), 1 μl deoxyribonucleotide (4.0 OD_{260}/ml, ≈12 pmol), 3 μl [γ-^{32}P]-ATP (2500 Ci/mmol, New England Nuclear), and 2 μl T4 Kinase (2 u/μl, New England Biolabs). This solution was incubated at 37 °C for 1 1/4 h, mixed with 10 μl 0.5 M EDTA to stop the reaction, and the solution spin desalted through a G25 fine Sephadex column. The column was washed with 50 μl TE (10 mM Tris·HCl, pH 7.5, 1 mM EDTA). The recovered ^{32}P-end-labelled primer (20×10^3 CPM in 1 μl) was mixed with 9 μl of a sequencing dye and ca. 1 μl of this sample per lane was loaded onto a denaturing 20% polyacrylamide gel calibrated with appropriate standards. This electrophoresis analysis confirmed the purity as well as the length of each primer.

Plasmid pTYl. Two *Hae* III fragments (574 base pairs and 408 base pairs long) containing the DHFR gene were isolated from pCV29 DNA[11] and subcloned by Yaegashi et. al.[10] into the *Bam*H I site of a pBR322 derivative lacking the *Eco*R I site to generate pTYl.

Nicking. Fifty micrograms of supercoiled pTYl DNA and 15 μg of ethidium bromide in 50 μl of 50 mM Tris·HCl, pH 7.5, 50 mM NaCl, 10 mM $MgCl_2$, and 1 mM dithiothreitol (DTT) were treated in the dark at room temperature with 4.0 μl of *Eco*R I (10 units/μl) for 4.5 h.[1] (The reaction was assayed, after stopping the reaction by an addition of 1 μl of 0.5 M EDTA, by electrophoresis on 0.8% agarose gel in 40 mM Tris acetate, pH 8.0, 1 mM EDTA; conditions that separate nicked, linear, and supercoiled DNA molecules.) The solution was extracted once with an equal volume of phenol, which had been equilibrated with TE buffer, once with 1/2 volume of phenol and 1/2 volume of chloroform, twice with equal volumes of chloroform, and then four times with 3—5 times volumes of diethyl ether. The DNA was precipitated by adding 1/10 volume of 3 M sodium acetate, pH 7.1, and 2.5 volumes of absolute ethanol and the mixture maintained at −20 °C for longer than 3 h. After centrifugation, the pellet was washed three times with 70% (vol/vol) ethanol, dried and dissolved in 30 μl of TE, pH 7.5. The concentration of the DNA was calculated to be 1.24 μg/μl, assuming that one OD_{260} equaled 50 μg DNA/ml.

Gapping. Prior to each exonuclease treatment the activity of the enzyme was checked by digesting a linear double-stranded pTYl plasmid and following the formation of two single-stranded fragments by electrophoresis on 0.7% agarose containing 1 μg ethidium bromide per ml. About 5 μg (1.4 pmol) of the nicked DNA was treated for 60 min at room temperature with 100 units of exonuclease III in 50 μl of 66 mM Tris·HCl, pH 8.0, 90 mM NaCl, 5 mM $MgCl_2$, and 10 mM DTT. The reaction was stopped by carrying out phenol extraction followed by ethanol precipitation as described above. This exonuclease III treatment created an approximately 600 bp gap. The gapped DNA was dissolved in 2 μl of TE and stored at −70 °C.

Phosphorylation of Oligonucleotides. Two hundreds pmoles of 5′-OH oligodeoxyribonucleotide (6.7 μM) were treated with 5 units of polynucleotide kinase for 50 min at 37 °C in 30 μl of 100 μM ATP, 100 mM Tris·HCl, pH 8.0, 10 mM $MgCl_2$, and 5 mM DTT.[12] The enzyme was inactivated by heating to 65 °C for 15 min. The final solution was stored at −70 °C.

Annealing of Oligonucleotide, Polymerization, and Ligation. The nicked and exonuclease-treated DNA (1.1 pmol of gapped circular pTY1) was heated to 65 °C for 7 min in the presence of about 44 pmol of the 5′-phosphorylated synthetic oligonucleotide in 40 μl of 40 mM NaCl, 20 mM Tris·HCl, pH 7.5, 10 mM $MgCl_2$, 1 mM DTT, and then the solution was chilled on ice for 4 h.

This oligonucleotide annealed DNA was treated with 7.8 units of Klenow fragment and 2500 units of T4 DNA ligase at 10 °C overnight in 60 μl of 350 μM ATP, 175 μM dATP, 175 μM dCTP, 175 μM dGTP, 175 μM dTTP, 40 mM NaCl, 20 mM Tris·HCl, pH 7.5, 10 mM $MgCl_2$, and 1 mM DTT.[1-5] The resulting heteroduplex containing DNA was isolated as before by phenol extraction followed by ethanol precipitation.

Competent HB101 Cells. Five hundred mls of LB medium (5.0 g of Bacto-trypton, 2.5 g of Bacto-yeast extract, and 5.0 g of NaCl in 500 ml of H_2O) was sterilized and 5.0 ml of this LB medium was transferred to a sterile 16×100 mm Kimble culture tube, inoculated with a single colony of *E. coli* strain HB101, and shaken at 37 °C overnight. Two 250 ml flasks containing 100 ml of LB media with 0.2% glucose were autoclaved, inoculated with 1.0 ml of the overnight culture of HB101, shaken at 250 rpm at 30 °C for 8 h until the OD_{600} had reached 0.65, and then left on ice for 2 h. The intact flask of HB101 (the one not used for the OD measurements) was opened and the cell suspension was centrifuged at 6000 rpm for 5—8 min at 4 °C. After decantation of the supernatant fluid the cells were resuspended in ca. 50 ml of a cold sterile solution of 100 mM $CaCl_2$, 70 mM $MnCl_2$, and 40 mM sodium acetate, pH 5.5, left on ice for 30 min, and centrifuged again at 6000 rpm at 4 °C. The pellet was resuspended in 10 ml of cold 100 mM $CaCl_2$, 70 mM $MnCl_2$, and 40 mM sodium acetate, pH 5.5, and then 1.4 ml of sterile 80% glycerol was added. The competent cells were dispensed as 0.3 ml aliquots into about 34 culture tubes (Kimble, 16×100 mm), and stored at −70 °C.[10,12] These competent cells could

§1 M=1 mol dm^{-3}.

be kept more than 6 months without losing much of the transformation frequency ($\approx 10^5$).

Transformation, Growth of Bacteria, and Amplification of Plasmid. The concentration of the heteroduplex containing circular DNA was adjusted to ca. 0.1 μg DNA per 100 μl TE (pH 7.5). One hundred μl of this solution were incubated with 0.3 ml of competent HB101 cells, kept on ice for 60 min and then heat shocked at 42 °C for 2 min. To this was then added 2.6 ml of LB medium and the solution agitated at 37 °C for 60 min. In order to confirm the transformation, 100 μl of this solution was plated on two agar plates containing 50 μg of ampicillin per ml of medium and the remaining 2.8 ml used to inoculate a one liter LB medium containing the same concentration of ampicillin. The latter was incubated at 37 °C with agitation at 250 rpm until the culture had reached an OD_{650} of 0.5. At this point 4 ml of a solution of chloramphenicol (40 mg/ml in ethanol) was added for amplification of plasmids and the incubation was continued with agitation at 250 rpm at 37 °C for 15 h.[12]

Harvesting, Lysis, and Isolation of Plasmid DNA. Bacterial cells in the one liter culture were harvested, lysed, and the plasmid DNA isolated as in Ref. 12.

***Aha* III and *Bam*H I Digestion of Plasmid DNA and Isolation of Mutant 1 Kb Fragment.** Two hundreds micrograms of the plasmid DNA were digested with both 50 units of *Aha* III and 160 units of *Bam*H I for 16 h at 37 °C in 400 μl of 75 mM NaCl, 10 mM Tris·HCl, pH 8.0, 10 mM $MgCl_2$, and 5 mM DTT. (*Bam*H I digestion produces two fragments: 4.4 Kb fragment of a linear pBR322 derivative lacking the *Eco*R I site and 1 Kb fragment containing the DHFR gene. Of this 1 Kb fragment only a mutated gene at the Phe-31 site is resistant to the *Aha* III digestion because of the destruction of the *Aha* III recognition sequence (see Fig. 2).) The digestion mixture was loaded on a 3.5% polyacrylamide gel and a gel portion containing the 1 Kb fragment was cut out from the gel (the position of the 1 Kb fragment was identified by staining only the control lane containing the 1 Kb fragment with ethidium bromide and the mutant 1 Kb fragment was not exposed to the ethidium bromide). The gel portion containing the mutant 1 Kb fragment was placed in a dialysis bag with 0.1X TBE buffer (5 mM Tris base, 6.6 mM boric acid, 0.1 mM EDTA) and an electroelution[12] was carried out overnight in the same 0.1X TBE buffer at 8 mA at 4 °C. The mutant 1 Kb fragment was absorbed onto 0.1 ml of DE52 which had been prequilibrated in 100 mM NaCl, 50 mM Tris·HCl, pH 7.8, and 1 mM EDTA followed by equilibration with TE, and was eluted from the DE52 by running 300 μl of a high salt solution of 2 M NaCl, 50 mM Tris·HCl, pH 7.8, and 1 mM EDTA. The eluent was dialyzed against 500 ml of 10 mM Tris·HCl, pH 7.5 at 4 °C for 36 h with two changes and concentrated to 250 μl.

Ligation of Mutant 1 Kb Fragment with pBR322 Derivative at *Bam*H I Site. Dephosphorylation of a pBR322 derivative linearized at the *Bam*H I site was carried out, by treating 10 μg of a linear pBR322 derivative with 1.0 unit of alkaline phosphatase for 60 min at 37 °C in 50 μl of 50 mM Tris·HCl, pH 8.0, 1 mM $MgCl_2$, and 0.1 mM $ZnCl_2$, in order to avoid self-ligation and/or polymerization of the linear pBR322 derivative upon ligation with the mutant 1 Kb fragment. The dephosphorylated pBR322 derivative linearized at the *Bam*H I site was purified by phenol extraction followed by ethanol precipitation. One μg of the dephosphorylated 4.4 Kb fragment and 0.2 μg of the mutant 1 Kb fragment were treated with 400 units of T4 DNA ligase at 10 °C for 18 h in 50 μl of 0.5 mM ATP, 50 mM Tris·HCl, pH 7.5, 10 mM $MgCl_2$, and 10 mM DTT. The enzyme was inactivated by phenol extraction and the ligated nicked DNA was purified on a Sephadex G25 fine column. The eluent was used for the second transformation.

Second Transformation and Colony Screening. The second transformation was carried out using the ligated nicked DNA and the same procedure described above. Well-separated single colonies were numbered and seven colonies were arbitrarily chosen. For a rapid isolation of plasmid DNA the transformed HB101 cells were grown on a much smaller scale (15 ml LB medium) without amplification and the isolated DNA was partially purified by a treatment with DNase-free RNase in place of the cesium chloride-ethidium bromide gradients purification. These plasmid DNAs were digested with *Aha* III and *Bam*H I and those 1 Kb DHFR gene fragments which were resistant to the digestion were identified as mutant colonies.

Isolation of Mutant Plasmid DNA and Purification of *Bam*H I 1 Kb Fragment. Five ml of LB medium containing 50 μg of ampicillin per one ml of medium was inoculated with a mutant single bacterial colony. The bacteria were eventually grown in 2 l medium and each mutant plasmid DNA was isolated and purified by the cesium chloride-ethidium bromide gradients as described earlier. The purified mutant plasmid DNA was digested with *Bam*H I and the 1 Kb fragment was isolated as described earlier.

***Dde* I Digestion of 1 Kb Fragment, End-Labelling, and Sequencing.** About 1 μg of the *Bam*H I 1 Kb fragment was treated with 4 units of *Dde* I at 37 °C for 4 h in 20 μl of 100 mM Tris·HCl, pH 7.5, 100 mM NaCl, 5 mM $MgCl_2$, and 6 mM 2-mercaptoethanol. To this were then added 14 μl of H_2O, 4 μl of [α-^{32}P] dTTP (3200 Ci/mmol), and 0.7 μl of reverse transcriptase (16 units/μl), and the solution was kept at room temperature for 6.5 h. The reaction mixture was mixed with a loading dye and two fragments were isolated from a 3.5% polyacrylamide gel (the position of each fragment could be located by an autoradiogram). After both fragments were cut from the gel, they were eluted out (10 mA, 4 °C, overnight), collected on a DE52 column ($\approx$0.05 ml resin). The column was eluted with 400 μl of 2 M NaCl, 50 mM Tris·HCl, PH 7.8, and 1 mM EDTA, the eluent then mixed with 1 μl of *t*-RNA (30 μg/μl), and the DNA fragment precipitated at −20 °C (6 h ethanol precipitation). The pellet was washed with 0.5 ml of cold 70% ethanol three times, dried in a speed vac for 10 min, and dissolved in 50 μl of TE and 5.5 μl of 3 M NaAc, pH 7.1. After an addition of 140 μl of ethanol, the mixture was kept at −20 °C for 1 h and centrifuged. The pellet was washed with 70% ethanol three times, dried in a speed vac, and redissolved in 50 μl of H_2O. The radioactivity of each sample varied from 700 to 3000 cps/5 μl. The DNA sequence of each fragment was determined by the general method[12,13] of Maxam and Gilbert with minor modifications. The DNA sequences were confirmed by autoradiogram.

Isolation of Mutant Enzymes. Five ml of LB medium containing 50 μg of ampicillin per one ml medium were inoculated with a single mutant colony. Cells for each mutant enzyme were grown in 2 l culture containing 50 μg of ampicillin/ml to a final optical density of 1.0 at 650 nm and harvested by centrifugation at 6000 rpm at 4 °C. The cells were suspended in 20 ml of 40 mM Tris·HCl, pH 8.0, 1

mM EDTA and centrifuged at 20000 rpm at 4 °C for 30 min to yield about 6 g of precipitate. All steps for the following cell lysis were conducted at 4 °C. The cells (ca. 6 g) were suspended in 7 ml of buffer (40 mM Tris·HCl, pH 8.0, 1 mM EDTA, 1 mM DTE (dithioerythritol)) with 0.7 μl of PMSF (phenylmethanesulfonyl fluoride) (17.4 mg/ml) and the following additions were made to the suspension: 1) 15 mg of lysozyme in 1 ml of the above buffer and 2.1 ml of EDTA (20 mg/ml in the above buffer) followed by sonication of the mixture for 30 sec then 8 min on ice (this sonication-cooling process was repeated two more times.); 2) 2.1 ml of Brij 58 (5 g/100 ml above buffer) followed by sonication for 30 s then 7 min on ice (this process was repeated two more times.); and 3) 330 μl of $MgCl_2$ (5.1 g/25 ml above buffer) and 500 μl of DNase (6.84 mg/3 ml above buffer) with occasional mixing for 15 min. The suspension was centrifuged at 20000 rpm for 40 min. To the supernatant 1.2 ml of streptomycin sulfate (1 g/10 ml above buffer) was added at 1 min intervals (100 μl/each time) with gentle stirring and the suspension then was centrifuged at 20000 rpm for 40 min. The supernatant (16.5 ml) was made 40% saturated in ammonium sulfate by gradually adding 3.85 g of finely powdered $(NH_4)_2SO_4$ over a period of 15 min with stirring. The stirring was continued for another 15 min. Unwanted protein was removed by centrifugation at 20000 rpm for 1.5 h. The supernatant was then made 90% saturated by gradually adding 5.8 g of $(NH_4)_2SO_4$ over a period of 20 min, and the mixture was gently stirred for additional 15 min and then kept on ice for 1.5 h. Following the centrifugation at 20000 for 30 min, the white pellet was resuspended in 13 ml of 40 mM KH_2PO_4, pH 6.0, 0.2 M KCl, 1 mM EDTA, and 1 mM DTE. To this was then added 2 ml of MTX (methotrexate) resin[14] and the solution gently shook for 20 h. The MTX resin was batch washed each time with 10 ml of 0.2 M KH_2PO_4, pH 6.0, 1 M KCl, 1 mM EDTA, and 1 mM DTE total four times. The MTX resin was transferred to a 10 ml column and washed with the same high salt buffer (0.2 M KH_2PO_4, 1 M KCl, 1 mM EDTA, 1 mM DTE) until the OD_{280} of the eluent was below 0.1. The mutant DHFR was eluted with 0.2 M K_3BO_3, pH 9.0, 1 M KCl, dialyzed against 2 l of 10 mM Tris·HCl, pH 7.4, 1 mM EDTA, and 1 mM DTE for 8 h with two changes, and purified on a column (52×1.1 cm) of DEAE-Sephacel with a linear gradient of 500 ml each of a solution containing 10 mM Tris·HCl, pH 7.4, 1 mM EDTA, 1 mM DTE, and a solution containing 1 M NaCl, 1 mM EDTA, 1 mM DTE. About 1 mg pure mutant DHFR was obtained per 1 g cells. The pure enzyme was made 90% saturated with $(NH_4)_2SO_4$ and stored at −20 °C. Although this DHFR is a Form I (Leu-28) isozyme, it is not necessary to make the eluting buffer 1 mM in folic acid since the mutant enzymes (Tyr-31 and Val-31) bind to the MTX resin less tightly than the wild-type DHFR. This affinity difference for the MTX resin enabled us to separate the mutant DHFR from possible contamination by the wild-type DHFR. The purity of the mutant DHFR was confirmed by the observation of a single band on a 12% polyacrylamide protein gel. There was no contamination by nucleic acids since the OD_{280}/OD_{260} ratio was 1.9 for both mutant enzymes.

Kinetics and Data Analysis. Initial velocities for dihydrofolate reductase were determined at 25 °C following the disappearance of NADPH and DHF at 340 nm (ε=11800 M^{-1} cm^{-1}). The buffer used for the assays contained 50 mM 2-morpholinoethanesulfonic acid (MES), 25 mM tris(hydroxymethyl)aminomethane (Tris), 25 mM 2-aminoethanol, and 100 mM NaCl (MTEN buffer).[15] The concentration of NADPH was maintained constant at 60 μM. The concentrations of DHF and the enzymes are listed in Table 1.

Data obtained at each pH value by varying the concentration of DHF were fitted to Eq. 3 by a nonlinear computer fitting program to yield values for the maximum velocity (V) and the Michaelis constant (K_a) as well as for V/K_a.

$$v = \frac{V[\mathrm{DHF}]}{K_a + [\mathrm{DHF}]} \tag{3}$$

Results

Two mutant plasmid DNAs (Tyr-31 and Val-31) have been constructed by the procedure illustrated in

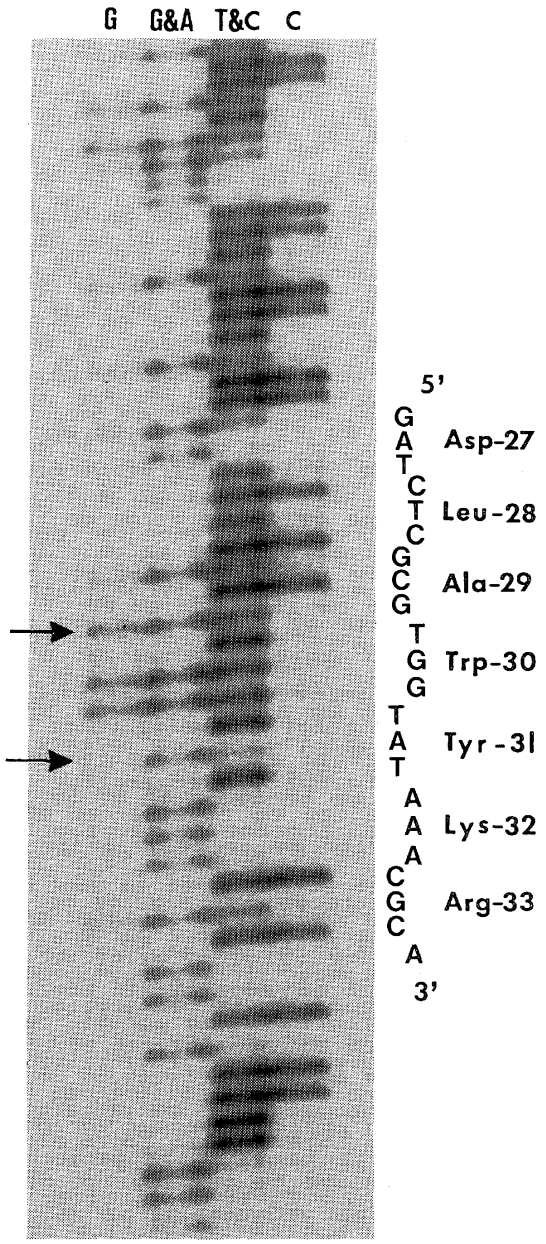

Fig. 3. Maxam-Gilbert sequencing ladder of Tyr-31 plasmid around the mutated *Aha* III site. Two replacements (TA→A and C→G, see Fig. 2(a)) are indicated by arrows.

Table 1. Summary of pH-Independent Values of V, V/K_{DHF}, and K_{DHF}, for Tyr-31 and Val-31[a]

	V/s^{-1}	V/K / $10^{-6}\,M^{-1}\,s^{-1}$	$K_{DHF}/\mu M$
Wild-type	12	11	1.1[b]
Tyr-31	30	5.3	5.7
Val-31	26	0.97	27

a) Conditions: 60 μM NADPH, 3.25—120 μM H_2-folate, 1.1—500 nM (Tyr-31)-DHFR, 6.1—730 nM (Val-31)-DHFR, MTEN buffer, 25 °C, 340 nm. b) Taken from Ref. 15.

Fig. 2. The DHFR coding sequences in these plasmids have been determined by the chemical method of Maxam and Gilbert[12,13] and the sequencing ladder of Tyr-31, as an example, around the mutated *Aha* III site is shown in Fig. 3 with the replacements marked by arrows. The whole structural genes have been completely sequenced and no mutations, other than designed ones, have been detected. The two mutant enzymes were isolated and purified to homogeneity. The purity of the mutant DHFR was confirmed by SDS gel electrophoresis which showed a single band.

Table 1 summarizes the pH independent values of V, V/K, and K_M (see the accompanying paper) determined for the purified mutant enzymes, Tyr-31 and Val-31. The kinetic experiments were performed under conditions similar to those employed by Stone and Morrison.[15] Both of these mutants have V values significantly larger than that of wild-type (wt), while the V/K values are smaller. The Tyr-31 mutant has a 2.5 fold higher V value than that of wt in the pH independent region, indicating that, under saturating DHF conditions, the Tyr-31 mutant is a better catalyst than the wild-type enzyme. The Tyr-31 mutant has a two-fold smaller value for V/K_{DHF} owing to a 5-fold increase in K_{DHF} at low pH. At high pH values, however, the K_{DHF} value increases to 300 μM (pH 9.5), possibly due to the ionization of Tyr, drastically decreasing the hydrophobicity of the side chain. The detailed pH-rate profile will be discussed in the accompanying paper.

The effect of the Val-31 mutation is again a 2.2-fold increase in V and a 25-fold increase in K_{DHF}. This increase in K_{DHF} is probably a reflection of a higher K_D value for H_2-folate, by analogy with a parallel increase in the dissociation constant estimated from its behavior during purification from the methotrexate resin.

Discussion

Site-Directed Mutagenesis. The first controlled modifications of proteins were reported two decades ago using chemical reactions to change the hydroxyl group of a serine residue at the active site of the proteolytic enzyme subtilisin into a mercapto group.[16,17] The problem with chemical modification is that it is harsh and nonspecific. Unless great care is taken, an attempt for example to exchange a serine for a cysteine at the active site may result in exchanging all serines on the surface of the enzyme for cysteines with unpredictable results. Furthermore, many desired changes, as in our Phe-31 → Tyr and Val mutations, cannot be achieved with chemical techniques, beside the fact that many of these residues are in the interior of the enzyme and inaccessible to a reagent. Advances in genetic engineering technology in the last few years, however, have made amino acid substitutions "almost routine."[1-6]

The procedure described in Fig. 2 takes advantage of destroying a restriction site upon successful incorporation of a synthetic oligodeoxynucleotide primer and isolating a new restriction fragment. Even if such a convenient restriction site is not available, the colony hybridization technique,[1,18] with the same oligodeoxynucleotide labeled with ^{32}P as a hybridization probe, allows identification of the desired mutant colony regardless of its phenotype. After the second transformation, the plasmid DNA of each mutant was characterized not only in the region of the mutation but also the entire structural gene and shown to have the desired sequence (see Fig. 3).

DHF Binding Site. Nonpolar interactions between the pteridine ring and the enzyme originate with the side chains of residues Ile-5, Ala-7, Phe-31, and Ile-94 providing most of the van der Waals contacts.[8] Among these residues only Ala-7 and Phe-31 are strictly conserved, although all of them are hydrophobic in all the known sequences. The *p*-aminobenzoyl moiety occupies a hydrophobic pocket formed by the helix αB on one side and by the loop (Gly-51 to Gly-56) connecting αC to βC on the other. In particular, the side chains of Leu-28 and Phe-31 extending from αB interact with the inner face of the *p*-aminobenzoyl group. This Phe-31, but not the Leu-28, is strictly conserved in all known sequences.[8]

A closer examination of the DHF (dihydrofolate) binding site reveals that the *p*-aminobenzoyl moiety is almost perpendicular to the pteridine ring with the Phe-31 at the corner of the bend. We felt that this bend could be important for the catalysis because of the following reasons. The enzyme catalyzes its reaction by having an active site that is complementary in structure to the structure of the transition state of the substrate rather than the substrate itself.[19] During the reduction of H_2-folate to H_4-folate (Eq. 1), the hybridization of C-6 carbon changes from sp^2 to sp^3 accompanying the movement of the C-9 carbon of the side chain from its original in-plane position at sp^2 to the out of plane from the pteridine ring at the sp^3 state (see Eq. 2). If the DHF binding site is designed such that it stabilizes the transition state or product more favorably than the substrate, H_2-folate, some of the intrinsic binding energy is utilized for catalysis.[20] The Phe-31, which is located at the corner of the bend interacting with both the pteridine ring and the *p*-aminobenzoyl moiety, could be a part of an interacting network.[21-25]

Replacement of Phe-31 by a smaller group as in the site-directed mutagenesis experiment of Phe-31 → Val-31, should decrease the affinity of the mutant enzyme for the substrate to some extent depending on the intrinsic binding energy of the mutant enzyme, but the affinity for the transition state would be decreased to a greater extent. This means that the value of K_{DHF} may be increased but the value of k_{cat} will fall. The steady-state kinetic parameters for the Tyr-31 and Val-31 mutants listed in Table 1 are, at first glance, not supportive of the transition state stabilization hypothesis. That the increase in V for the Tyr-31 mutant may result from the facilitated protonation of N5 necessary for reduction is unlikely since a similar increase in V is observed for the Val-31 mutant. However, additional experiments have revealed that the steady-state parameters mask any changes in the hydride transfer step. Pre-steady state stopped-flow measurements convincingly implicate the rate of dissociation of H_4-folate as mainly rate-limiting at this pH.[29] Consequently the increase in V noted in the two mutations arises simply from an increased rate of product dissociation that is reflected in the higher K_D of H_2-folate. Because the hydride transfer step is still not rate-limiting, one cannot readily assess the effect of the mutations in terms of the transition state stabilization hypothesis. The interpretation of the effects of mutations based on steady state parameters is always subject to ambiguities unless one known step in the kinetic sequence is dominant.

Although the mutants we have generated are not necessarily the evolutionary precursors of the present native enzyme, they are possible forms of the enzyme that have been rejected during evolution, since the rate of spontaneous mutation is sufficiently high for them to have arisen and hence been tested. For the sake of the argument, however, let us assume that each of the mutant enzymes, Tyr-31 and Val-31, is an evolutionary precursor of the native Phe-31 enzyme. Various proposals have been made as to how enzymic rate constants should respond to selective pressure in evolution to maximize the overall rate of reaction[30,31] by stabilizing both transition state and substrate-enzyme complexes. This kind of evolutional replacement leads to an increase in rate as long as [S] remains below K_M; other wise ([S]>K_M), stabilization of (ES) and (ES)$^{\neq}$ equally has a neutral effect (no change in rate).[31] Since the concentration of dihydrofolate in vivo is estimated to be below 1 μM, the Tyr-31 and Val-31 mutant enzymes, despite their higher turnover numbers, would be less effective in maintaining H_4-folate levels owing to their greater K_{DHF} values.

In conclusion, the present study has demonstrated that a protein engineering at the level of DNA is a powerful technique for elucidation of the structure-reactivity relationship in an enzyme. Specifically, in both Tyr-31 and Val-31 mutant enzymes the decrease in binding has not been translated into a loss of catalytic efficiency and both the mutant enzymes have generated an improved k_{cat}, most probably by facilitating the product-release step without significantly altering the hydride transfer step.

We thank our colleagues, especially Carol A. Fierke for the helpful discussions and Valerie Mizrahi and Patricia A. Benkovic for their suggestions at various stages of this study.

References

1) G. Dalbadie-McFarland, L. W. Cohen, A. D. Riggs, C. Morin, K. Itakura, and J. H. Richards, *Proc. Natl. Acad. Sci. U.S.A.*, **79**, 6409 (1982).
2) J. E. Villafranca, E. E. Howell, D. H. Voet, M. S. Strobel, R. C. Ogden, J. N. Abelson, and J. Kraut, *Science*, **222**, 782 (1983).
3) A. R. Fersht, J-P. Shi, A. J. Wilkinson, D. M. Blow, P. Carter, M. M. Y. Waye, and G. P. Winter, *Angew. Chem., Int. Ed. Engl.*, **23**, 467 (1984).
4) C. S. Craik, C. Largman, T. Fletcher, S. Roczniak, P. J. Barr, R. Fletterick, and W. J. Rutter, *Science*, **228**, 291 (1985).
5) J.-T. Chen, R. J. Mayer, C. A. Fierke, and S. J. Benkovic, *J. Cell. Biochem.*, **29**, 73 (1985).
6) D. A. Estell, T. P. Graycar, and J. A. Wells, *J. Biol. Chem.*, **260**, 6518 (1985).
7) R. L. Blakley, "Folates and Pterins," ed by R. L. Blakley and S. J. Benkovic, Wiley, New York (1985), p. 191.
8) J. T. Bolin, D. J. Filman, D. A. Matthews, R. C. Hamlin, and J. Kraut, *J. Biol. Chem.*, **257**, 13650 (1982).
9) D. J. Filman, J. T. Bolin, D. A. Matthews, and J. Kraut, *J. Biol. Chem.*, **257**, 13663 (1982).
10) T. Yaegashi and C-P. D. Tu, unpublished results.
11) D. R. Smith and J. M. Calvo, *Nucleic Acids Res.*, **8**, 2255 (1980).
12) T. Maniatis, E. F. Fritsch, and J. Sambrook, "Molecular Cloning, A Laboratory Manual," Cold Spring Harbor Laboratory, New York (1982).
13) A. M. Maxam and W. Gilbert, *Methods Enzymol.*, **65**, 499 (1980).
14) B. T. Kaufman, *Methods Enzymol.*, **34**, 272 (1974).
15) S. R. Stone and J. F. Morrison, *Biochemistry*, **23**, 2753 (1984).
16) K. E. Neet and D. E. Koshland, *Proc. Natl. Acad. Sci. U.S.A.*, **56**, 1606 (1966).
17) L. Polgar and M. L. Bender, *Biochemistry*, **6**, 610 (1967).
18) J. P. Gergen, R. H. Stern, and P. C. Wensink, *Nucleic Acids Res.*, **7**, 2115 (1979).
19) L. Pauling, *Am. Scient.*, **36**, 51 (1948).
20) W. P. Jencks, *Adv. Enzyml.*, **43**, 219 (1975).
21) S. Yamabe, T. Minato, and Y. Kawabata, *Can. J. Chem.*, **62**, 235 (1984).
22) W. L. Mock, *Bioorg. Chem.*, **4**, 270 (1975).
23) P. Deslongchamps, "Stereoelectronic Effects in Organic Chemistry," Pergamon Press, Oxford (1983).
24) A. J. Kirby, "The Anomeric Effect and Related Stereoelectronic Effects at Oxygen," Springer-Verlag, Berlin (1983).
25) K. Taira and D. G. Gorenstein, *J. Am. Chem. Soc.*, **106**, 7825 (1984).

26) Y. Nozaki and C. Tanford, *J. Biol. Chem.*, **246**, 2211 (1971).
27) R. Wolfenden, L. Andersson, P. M. Cullis, and C. C. B. Southgate, *Biochemistry*, **20**, 849 (1981).
28) A. A. Zamyatnin, *Ann. Rev. Biophys. Bioeng.*, **13**, 145 (1984).
29) C. A. Fierke, K. A. Johnson, and S. J. Benkovic, manuscript in preparation.
30) W. J. Albery and J. R. Knowles, *Angew. Chem., Int. Ed. Engl.*, **16**, 285 (1977).
31) A. Fersht, "Enzyme Structure and Mechanism," 2nd ed., Freeman, New York (1985), p. 311.

 © 1987 The Chemical Society of Japan Bull. Chem. Soc. Jpn., 60, 3025—3030 (1987)

Protein Engineering of Dihydrofolate Reductase. pH Dependency of Phe-31 Mutants

Kazunari TAIRA,† Jin-Tann CHEN,†† Carol A. FIERKE, and Stephen J. BENKOVIC*
Department of Chemistry, The Pennsylvania State University, University Park, Pennsylvania 16802, U.S.A.
†Fermentation Research Institute, Agency of Industrial Science and Technology, Yatabe-machi, Ibaraki 305
††Development Center for Biotechnology, 237, Chien-Kuo S. Rd., Sec. 1, Taipei, Taiwan
(Received May 6, 1986)

Site-specific mutations on dihydrofolate reductase from *Escherichia coli* at the Phe-31 site have generated (Try-31)-DHFR and (Val-31)-DHFR mutant enzymes. The pH dependence of log V and log V/K_{DHF} for these enzymes suggests that protonation is important for both the interaction of dihydrofolate and the maximum velocity of the reaction. More importantly, a "hollow" is observed for the Tyr-31 mutant in a log V/K-pH profile, necessitating a modification of the wild-type kinetic scheme. The intrinsic pK_a of 5.8, obtained based on the modified more general kinetic scheme, for the Tyr-31 mutant agrees well with that obtained from inhibition studies by 2,4-diamino-6,7-dimethylpteridine.

During the last two decades the interest and research in enzyme chemistry has expanded so rapidly with applications of physical organic techniques[1] that it now occupies an important position in chemistry as a whole. Moreover, recent recombinant DNA technology has revolutionized our ability to tailor the structure and activity of enzymes by manipulation of their genes.[2-8]

As described in the preceding paper,[8] our interest in the mechanism of dihydrofolate reductase (DHFR), which catalyzes the reduction of dihydrofolate (H_2-folate) to tetrahydrofolate (H_4-folate) with NADPH as the cofactor,[9] has led us to carry out site-specific mutations on this enzyme at the Phe-31 site. From the crystallographic structure[10,11] the Phe-31 is located at the dihydrofolate binding site and interacts with both the pteridine ring and the *p*-aminobenzoyl moiety of the substrate.

The first mutation (Phe-31 → Tyr-31) has resulted in an only five-fold increase in K_{DHF} (K_M with saturating NADPH and varying dihydrofolate), despite the fact that the mutation has introduced a polar Tyr-group into a hydrophobic binding site, and a 2.5-fold increase in the maximum velocity. Similarly, the second mutation (Phe-31 → Val-31) resulted in a 25-fold increase in K_{DHF} with a 2.2-fold increase in the maximum velocity. Thus, in both mutant enzymes the decrease in binding has not been translated into a loss of catalytic efficiency.

We report here the pH dependency of log V and log V/K_{DHF} for these mutant enzymes. Although the pH dependencies of these values for the Val-31 mutant DHFR are clearly half-bell-shaped as they are for the wild-type DHFR,[12] a "hollow"[13] is observed for the Tyr-31 DHFR. The kinetic scheme proposed for the wild-type DHFR[12] is inadequate to explain this "hollow" phenomenon, necessitating a modification of the wild-type kinetic scheme. The modified more general kinetic scheme may also be applicable to explain the wild-type steady-state kinetic data.

Experimental

Mutant Enzymes. Preparation of the mutant enzymes (Tyr-31 and Val-31) has been described.[8]

Kinetics and Data Analysis. Initial velocities for dihydrofolate reductase were determined at 25 °C following the disappearance of NADPH and DHF at 340 nm (ε=11800 M^{-1} cm^{-1} (1 M=1 mol dm^{-3})). The buffer used for the assays contained 50 mM 2-morpholinoethanesulfonic acid (MES), 25 mM tris(hydroxymethyl)aminomethane (Tris), 25 mM 2-aminoethanol, and 100 mM NaCl (MTEN buffer). The concentration of NADPH was maintained constant at 60 μM. The concentrations of DHF and enzymes are listed in Table 1.

Data obtained at each pH value by varying the concentration of DHF were fitted to Eq. 1 by a nonlinear computer fitting program to yield values for the maximum velocity (V) and the Michaelis constant (K_a) as well as for V/K_a.

$$v = \frac{V[\mathrm{DHF}]}{K_a + [\mathrm{DHF}]} \quad (1)$$

The pH-rate profiles were fitted to Eq. 2, and for the special case with a "hollow" phenomenon (Fig. 2(c)) Eq. 3 was used.

Table 1. Summary of pH-Independent Values of V, V/K_{DHF}, K_{DHF}, Apparent p$K_a(V)$, and p$K_a(V/K)$ Values for Tyr-31 and Val-31[a]

	V/s^{-1}	V/K / 10^{-6} M^{-1} s^{-1}	K_{DHF}/μM	pK_a[V]	pK_a[V/K]
Wild-type	12	11	1.1[b]	8.4[b]	8.1[b]
Tyr-31	30	5.3	5.7	7.9	6.8
Val-31	26	0.97	27	7.4	6.9

a) Conditions: 60 μM NADPH, 3.25—120 μM H_2-folate, 1.1—500 nM (Tyr-31)-DHFR, 6.1—730 nM (Val-31)-DHFR, MTEN buffer, 25 °C, 340 nm. b) Taken from Ref. 12.

$$V = \frac{V_{max}}{\left\{1+\frac{K_a}{(H)}\right\}} \quad \text{or} \quad V/K = \frac{(V/K)_{max}}{\left\{1+\frac{K_a}{(H)}\right\}} \tag{2}$$

$$V/K = \frac{C_1\left\{1+\frac{C_2K_1}{(H)}\right\}}{\left\{1+\frac{K_1}{(H)}\right\}\left\{1+\frac{C_3K_1}{(H)}\right\}} \tag{3}$$

Results

Table 1 summarizes the V, V/K, K_M, and pK_a values observed in pH-rate profiles determined for the purified mutant enzymes, Tyr-31 and Val-31. The reported V and V/K terms are pH-independent. The kinetic experiments were performed under conditions similar to those employed by Stone and Morrison.[12] Both of these mutants have V values significantly larger than that of wild-type, while the V/K values are smaller. Also, each mutation results in a pK_a shift to lower pH in both the V and V/K profiles.

The Tyr-31 mutant has a 2.5-times higher V value than that of wild-type in the pH independent region, indicating that, under saturating DHF conditions, the Tyr-31 mutant is a better catalyst than the wild-type enzyme. The increase in V may in one interpretation result from the accelerated product release step which may constitute a significant part of the rate determining step. The Tyr-31 mutant has only a two-fold smaller value for V/K_{DHF} owing to a 5-fold increase in K_{DHF} at low pH. At high pH values, however, the K_{DHF} value increases to 300 μM (pH 9.5), possibly due to the ionization of Tyr, drastically decreasing the hydrophobicity of the side chain.

The effect of the Val-31 mutation is similar; a 25-fold increase in K_{DHF} and a 2.2-fold increase in V. This increase in K_{DHF} is probably a reflection of a higher K_D value for H_2-folate, by analogy with a parallel increase in the dissociation constant for methotrexate resin. The decrease in the apparent pK_a value could be due to the introduction of water in the active site to fill the volume originally occupied by the Phe-31. However, the pK_a value of 8.1 of wild-type in the V/K profile may not reflect the intrinsic pK_a as originally thought.[12] This point will be discussed in more detail in the next section.

In Fig. 1 are shown the pH dependence of log V and log V/K_{DHF} for the reaction catalyzed by the Val-31 mutant DHFR. Values for V and V/K_{DHF} were determined over the pH range 5.0—9.8. The pH dependence of these values suggests that protonation is important for both the interaction of DHF and the maximum velocity of the reaction. The initial velocities, especially at pH values less than 6.0, were corrected for the decomposition of NADPH. Both profiles fit to the theoretical lines calculated from Eq. 2 with the parameters given in Table 1.

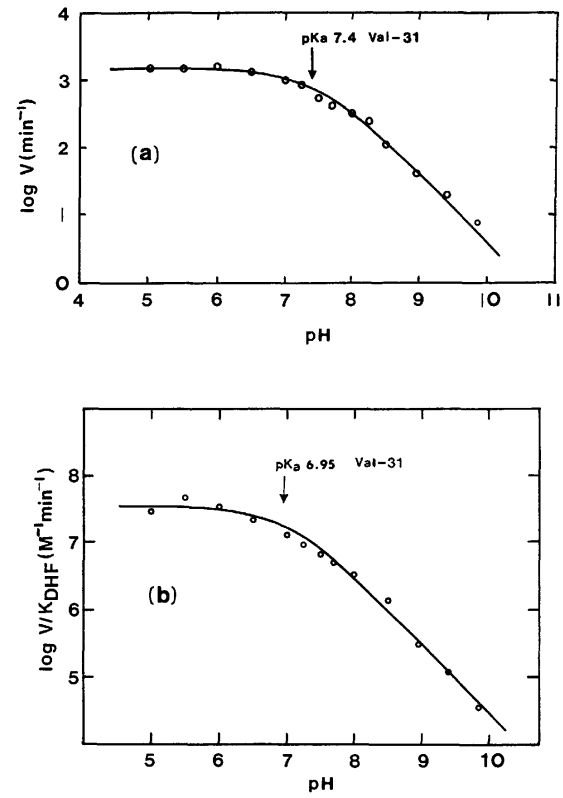

Fig. 1. (a) The pH dependence of log V for the reaction catalyzed by the Val-31 mutant DHFR. (b) The pH dependence of log V/K_{DHF} for the Val-31. The lines represent a best fit to Eq. 2 with the parameters given in Table 1.

Figure 2 illustrates the analogous pH dependence of log V and log V/K_{DHF} for the Tyr-31 mutant. Again, the overall pH dependence of these values indicates that the protonation is important for both the interaction of DHF and the maximum velocity of the reaction. The theoretical lines for Fig. 2(a) and (b) were drawn according to Eq. 2 with the apparent pK_a's shown in the profiles also given in Table 1. Although the theoretical curve in Fig. 2(a) fits the experimental points satisfactorily,that of Fig. 2(b) is inadequate because of the observed "hollow". The use of Eq. 2 for describing the data in Fig. 2(b), was based on the assumption that the kinetic scheme for Tyr-31 is same as that of the wild-type DHFR proposed by Stone and Morrison:[12]

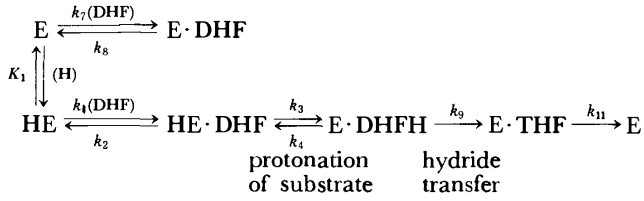

Scheme 1.

where E denotes the enzyme-NADPH binary complex since the kinetic studies were carried out under the saturation with NADPH. The V/K_{DHF} equation for

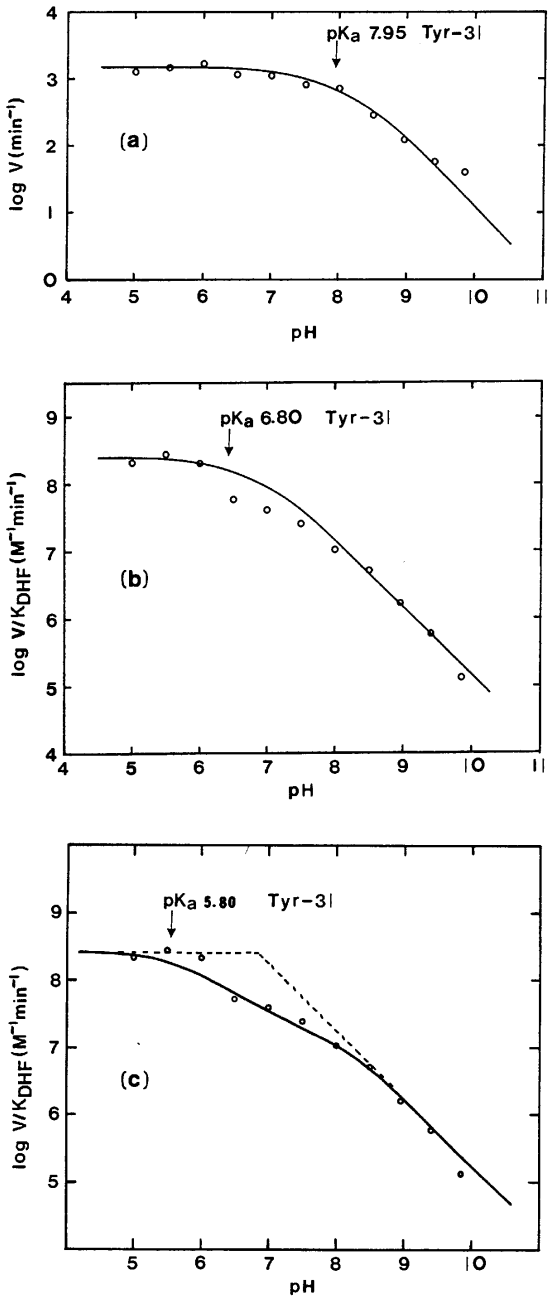

Fig. 2. (a) The pH dependence of $\log V$ for the Tyr-31, where the solid line is the theoretical curve based on Eq. 2. (b) The pH dependence of $\log V/K_{DHF}$ for the Tyr-31, where the theoretical line is based on Eq. 2. (c) The pH dependence of $\log V/K_{DHF}$, same as in (b), for the Tyr-31, where the theoretical line is drawn according to Eq. 7 with the intrinsic pK_a of 5.8 and the conditions of $k_1=10\,k_7$, $k_3=10\,k_6$, $k_6=10\,k_2$, and $k_9=10\,k_4$. The intercept of the dashed line corresponds to the apparent pK_a of 6.8.

the reaction described by Scheme 1 is given by

$$\frac{V}{K}=\frac{k_1k_3k_9\ (E_T)}{(k_2k_4+k_2k_9+k_3k_9)\left\{1+\dfrac{K_1}{(H)}\right\}} \tag{4}$$

which contains only one pH-dependent term yielding a half-bell-shaped curve of the type illustrated in Fig. 1(b).

Since the Eq. 4 derived on the basis of Scheme 1 cannot adequately describe the "hollow" phenomenon[13] of the Tyr-31 mutant shown in Fig. 2(b), the kinetic scheme proposed by Stone and Morrison was expanded to the following more general case:

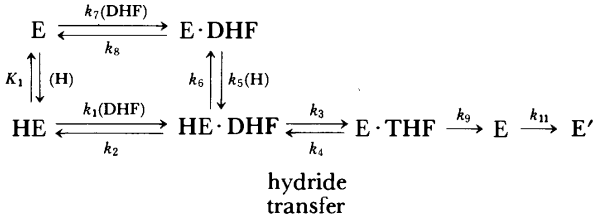

Scheme 2.

where E and E′ denote the enzyme-NADPH complex and free enzyme, respectively. The hydride transfer and protonation of DHF were combined into a single, reversible step (k_3, k_4) with k_9 and k_{11} representing rate coefficients associated with product release. The initial velocity equation for the reaction described by Scheme 2 is given by:

$$v=\frac{k_1k_3k_9(k_8+k_5H+\dfrac{k_5k_7K_1}{k_1})(E_T)(DHF)}{\begin{aligned}&(k_3k_7k_9+k_6k_7k_9+k_4k_6k_7+k_2k_4k_7+k_2k_7k_9+k_5Hk_7k_9+\\&k_4k_5Hk_7+k_3k_5Hk_7+k_3k_5Hk_7k_9/k_{11})\cdot\frac{K_1}{(H)}\\&+k_1(k_4k_6+k_6k_9+k_4k_5H+k_5Hk_9+k_4k_8+k_8k_9+\\&k_3k_5H+k_3k_8+k_3k_5Hk_9/k_{11}+k_3k_8k_9/k_{11})\\(DHF)+&\frac{(k_3k_8k_9+k_6k_8k_9+k_4k_6k_8+k_3k_5Hk_9+k_2k_4k_5H}{+k_2k_5Hk_9+k_2k_4k_8+k_2k_8k_9)\cdot\left\{1+\dfrac{K_1}{(H)}\right\}}\\&\frac{(k_3k_7k_9+k_6k_7k_9+k_4k_6k_7+k_2k_4k_7+k_2k_7k_9}{+k_5Hk_7k_9+k_4k_5Hk_7+k_3k_5Hk_7+}\\&k_3k_5Hk_7k_9/k_{11})\cdot\frac{K_1}{(H)}+k_1(k_4k_6+k_6k_9+k_4k_5H+\\&k_5Hk_9+k_4k_8+k_8k_9+k_3k_5H+k_3k_8+\\&k_3k_5Hk_9/k_{11}+k_3k_8k_9/k_{11})\end{aligned}} \tag{5}$$

The V and V/K_{DHF} relationships for the mechanism given in Scheme 2 are described by Eqs. 6 and 7.

$$V=\frac{\dfrac{k_3k_9k_{11}(E_T)}{k_3k_9+k_3k_{11}+k_4k_{11}+k_9k_{11}}\left\{1+(1+\dfrac{k_2}{k_6})\dfrac{k_7K_1}{k_1(H)}\right\}}{\begin{aligned}&1+\left\{\frac{k_7}{k_1}+(\frac{k_8}{k_6}+\frac{k_4k_{11}+k_9k_{11}}{k_3k_9+k_3k_{11}+k_4k_{11}+k_9k_{11}})\frac{k_2k_7}{k_1k_8}\right\}\frac{K_1}{(H)}\\&+\left\{\frac{k_7k_{11}(k_2k_4+k_2k_9+k_3k_9+k_4k_6+k_6k_9)}{k_1k_5(k_3k_9+k_3k_{11}+k_4k_{11}+k_9k_{11})}\right\}\frac{K_1}{(H)^2}\end{aligned}} \tag{6}$$

$$\frac{V}{K}=\frac{\dfrac{k_1k_3k_9(E_T)}{k_2k_4+k_9(k_2+k_3)}\left\{1+(1+\dfrac{k_2}{k_6})\dfrac{k_7K_1}{k_1(H)}\right\}}{\left\{1+\dfrac{K_1}{(H)}\right\}\left\{1+(1+\dfrac{k_6}{k_2+\dfrac{k_3}{1+\dfrac{k_4}{k_9}}})\cdot\dfrac{k_2k_7K_1}{k_6k_1(H)}\right\}} \quad (7)$$

The Eq. 7, from which the individual rate constants can be combined to form constants C_1, C_2, and C_3 of Eq. 3, has three pH-dependent terms. Thus, depending on the magnitude of C_2 and C_3 in Eq. 3, a fit for the "hollow" in the pH-log V/K profile can be generated. The theoretical curve for the pH-log V/K_{DHF} profile of the Tyr-31 mutant is drawn in Fig. 2(c) according to Eq. 3 with the following parameters: $C_1=5.3\times10^6$ M^{-1} s^{-1} (pH-independent value of V/K_{DHF} in Table 1); $C_2=0.1$, $C_3=0.01$, and the intrinsic pK_a of 5.8 (pK_1 =5.8). Although the individual rate constants in Eq. 7 are not known, the condition of $C_2=0.1$ and $C_3=0.01$ may be met, as one of several possibilities, when $k_6/k_2=k_3/k_6=k_1/k_7=k_9/k_4=10$ in Eq. 7.

Shown in Fig. 3 is the pH dependence of inhibition for the Tyr-31 mutant by a substrate analogue, 2,4-diamino-6,7-dimethylpteridine, which differs from methotrexate (MTX) by the absence of the side chain. Although the pK_a value determined from a V/K profile may be displaced, the analysis of the pH dependence of

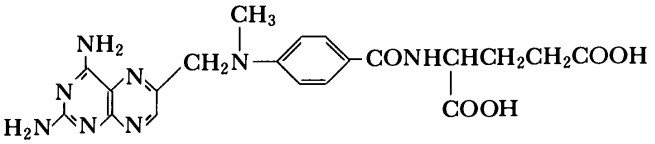

MTX(methotrexate)

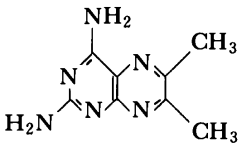

2,4-diamino-6,7-dimethylpteridine

the inhibition caused by a substrate analogue will generally[14] yield the correct[12,13] pK_a value. The variation with pH of the inhibition of the wild-type DHFR by 2,4-diamino-6,7-dimethylpteridine yielded a bell-shaped curve with two pK_a values of 5.9 and 7.9.[12] The lower pK_a value corresponds to the value of 5.75 determined for the protonation of the N-1 nitrogen of the pteridine.[12,15] As can be seen from Fig. 3, however, the mutation Phe-31 → Tyr-31 has shifted the higher pK_a value of the wild-type, Phe-31, to a much lower pH region. The solid line in Fig. 3 is drawn according to Eq. 8 based on Scheme 3.

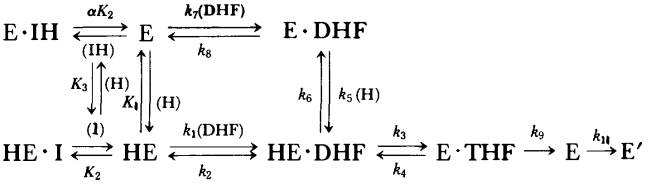

Scheme 3.

In Eq. 8, K_i(app) denotes the apparent inhibition constant which can be obtained by plotting $1/v$ vs. the inhibitor concentration (Dixon plot).[16] K_1, K_2, and K_3 are defined in Scheme 3, of which pK_3, the protonation

$$K_i(\text{app})=\frac{K_2\left\{1+\dfrac{(H)}{K_3}+\dfrac{K_1}{(H)}+\dfrac{K_1}{K_3}\right\}}{1+\dfrac{K_1}{\alpha K_3}}, \quad (8)$$

of the N-1 nitrogen of the pteridine inhibitor, is already reported to be 5.75.[15] Since, at low pH, the inhibition of the Tyr-31 mutant by 2,4-diamino-6,7-dimethylpteridine was comparable to that of the wild-type enzyme, the pH independent value of the inhibition constant, K_2, was assumed to be 13 nM which was the reported value for the wild-type enzyme.[12] Assuming that α equals unity, two theoretical lines are drawn in Fig. 3: The intrinsic pK_a of the enzyme, pK_1, is assumed to be 5.8 for the solid line, and 6.8 for the dashed line. Although the experimental points are limited, the solid line with the intrinsic pK_a of 5.8 better fits to the experimental data. This intrinsic pK_a of 5.8, obtained by the inhibition study, agrees well with the intrinsic pK_a of 5.8 obtained from the "hollow" profile of Fig. 2(c).

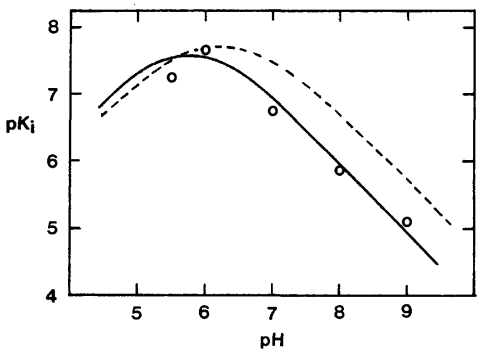

Fig. 3. Variation with pH of the pK_i ($-\log K_i$) value of the Tyr-31 mutant for 2,4-diamino-6,7-dimethylpteridine. The units for K_i are M. The theoretical curves are drawn according to the Eq. 8 with the parameters of pK_3=5.75, K_2=13 nM, α=1, and for the solid curve pK_1=5.80, and for the dashed curve pK_1=6.80.

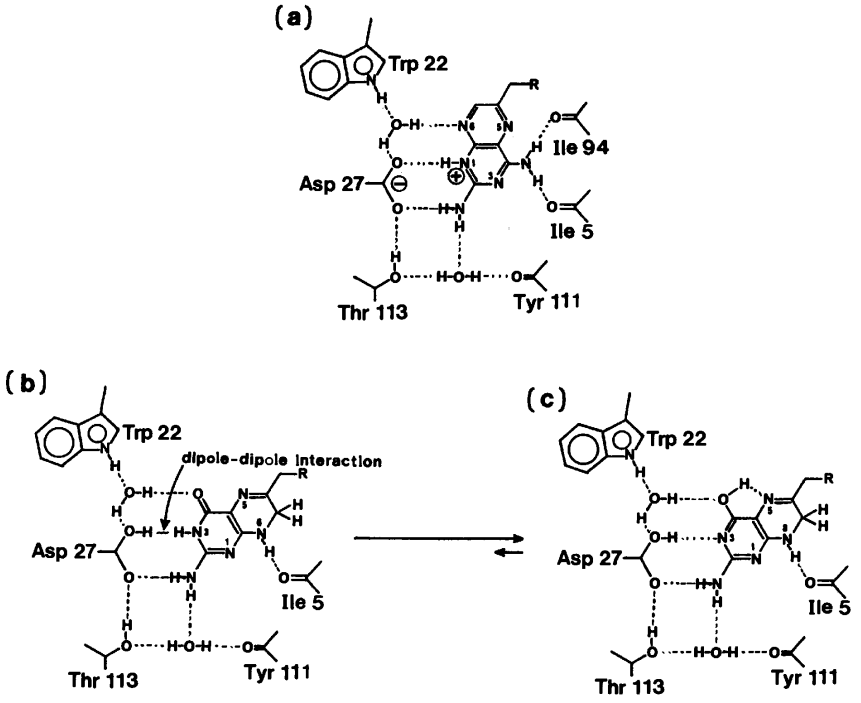

Fig. 4. Schematic representation of hydrogen bonding interaction between dihydrofolate reductase and the pteridine portions of (a) methotrexate and (b), (c) 7,8-dihydrofolate. At neutral pH, the enzyme bound methotrexate is protonated, on the other hand, the enzyme bound dihydrofolate is not protonated.

Discussion

General Kinetic Scheme with Saturating NADPH. From the variation of V and V/K_{DHF} with pH in Figs. 1 and 2, it is apparent that protonation enhances the maximum velocity, V, of the dihydrofolate reductase reaction as well as the flux rate V/K_{DHF}, with the enzyme-NADPH binary complex to yield a productive complex. For the wild-type *E. coli* DHFR, activity is dependent on a group with a pK_{a1} of about 8 that must be protonated, and on another group with a pK_{a2} of about 5 that must be unprotonated.[17] Moreover, it has been suggested that Asp-27 is responsible for the pK_a of 8.[12] In view of the conclusion that DHF is bound to DHFR in an inverted fashion relative to the binding of an inhibitor such as methotrexate and, at neutral pH, productive binding must occur as a result of reaction between unprotonated DHF and protonated enzyme (protonated Asp-27), a modified representation[10] of the hydrogen bonding interaction between DHFR and DHF based on the X-ray crystallographic structure of the methotrexate-DHFR complex is given in Fig. 4(a). One may speculate that tautomerization of the initial complex relieves an unfavorable dipole-dipole interaction and promotes protonation of the N-5 nitrogen, thereby facilitating the following hydride transfer reaction (Figs. 4(b) and (c)).

A general kinetic scheme with saturating NADPH has been proposed[12] as reproduced in Scheme 1. The V/K_{DHF} expression for the reaction described by Scheme 1 is given by Eq. 4. When log V/K_{DHF} is plotted versus pH, the curve described by Eq. 4 is half-bell-shaped with asymptotes given by Eqs. 9 and 10 at low and high pHs, respectively.

$$\log V/K_{DHF} = \log \left(\frac{k_1 k_3 k_9 E_T}{k_2 k_4 + k_2 k_9 + k_3 k_9} \right) \quad (9)$$

$$\log V/K_{DHF} = \log \left(\frac{k_1 k_3 k_9 E_T}{k_2 k_4 + k_2 k_9 + k_3 k_9} \right) - pH + pK_1 \quad (10)$$

It is apparent from these equations that the intersection of the asymptotes with slopes of 0 (Eq. 9) and -1 (Eq. 10) for the plot of log V/K_{DHF} against pH will occur at the point where $pH=pK_1$ and thus yield a true value for the ionizing group on the enzyme. Namely, the pK_a of 8.1 obtained from the log V/K_{DHF}-pH profile of the wild-type enzyme must be the intrinsic pK_a of DHFR.

Although the pK_a of 6.9 for Val-31 mutant obtained from the log V/K_{DHF}-pH profile (Fig. 1(b)) may be considered to be the intrinsic pK_a of the Val-31 mutant presuming that the general kinetic scheme (Scheme 1) still is applicable for this mutant enzyme, the same interpretation cannot be ascribed to the Tyr-31 mutant. In order to accomodate the "hollow" phenome-

nom observed in the log V/K_{DHF}-pH profile for the Tyr-31 mutant, Scheme 1 has been expanded as shown in Scheme 2, where the proton on Asp-27 in the ternary HE-NADPH-DHF complex can now communicate with the solvent. The V/K_{DHF} relationship for the expanded mechanism is described by Eq. 3 or 7. Since there are three pH-dependent terms in these equations, the "hollow" phenomenon can be rationalized. The minimum requirement to observe a hollow in a log V/K_{DHF}-pH profile is that the varied substrate is sticky, that is, the substrate dissociates from the enzyme more slowly than it reacts to yield products ($k_2<k_3$). Otherwise, if $k_2>k_3$, the V/K_{DHF} expression reduces to Eq. 11, with a single dependency on pH.

$$\frac{V}{K} = \frac{k_1k_3k_9(E_T)}{k_2(k_4+k_9)\left\{1+\frac{K_1}{(H)}\right\}} = \frac{C_1'}{\left\{1+\frac{K_1}{(H)}\right\}} \qquad (11)$$

From Eq. 3 the asymptotes of the log V/K_{DHF}-pH profile for the expanded mechanism described by Scheme 2 are calculated to give Eqs. 12 and 13 at low and high pHs, respectively.

$$\log V/K = \log C_1 \qquad (12)$$

$$\log V/K = \log C_1 + \log C_2 - \log C_3 - pH + pK_1 \qquad (13)$$

Thus, a true pK_1 value will not be obtained from the log V/K-pH profile of the expanded mechanism since the intersection will occur at the point where:

$$pH = pK_1 + \log C_2 - \log C_3. \qquad (14)$$

A theoretical line for the hollow of the Tyr-31 mutant is drawn in Fig. 2(c) according to Eq. 3 with the conditions of pK_1=5.8, C_1=5.3×10^6 (M^{-1} s^{-1}), C_2=0.1, and C_3=0.01. This fitting indicates that the apparent pK_a of Tyr-31 is shifted up by one pH unit from its intrinsic pK_1 of 5.8.

In order to confirm this intrinsic pK_a value of 5.8, inhibition studies by 2,4-diamino-6,7-dimethylpteridine were carried out according to Scheme 3. Judging from the two theorectical curves given in Fig. 3, the solid curve with pK_1=5.8 better fits to the experimental points than the dashed curve with pK_1=6.8 which were expected to be the intrinsic pK_a if the original mechanism of Scheme 1 were applicable to the Tyr-31 mutant enzyme. Thus, both the hollow and the inhibition studies are in accord with the intrinsic pK_a of 5.8 for the Tyr-31 mutant.

Conclusion

Examination of the engineered proteins (Tyr-31 DHFR and Val-31 DHFR) has clarified the kinetic sequence for wild-type DHFR. Specifically, the observation of a hollow in the pH-log V/K profile for the Tyr-31 mutant DHFR has necessitated a modification of the wild-type kinetic scheme (Scheme 1) to a more general case (Scheme 2), where the proton on Asp-27 in the ternary complex can now communicate with the solvent. This mechanism can adequately rationalize the kinetic data for both the wild-type and the mutant enzymes. In order to support further our mechanism, more detailed kinetic studies such as deuterium isotope effects and pre-steady state kinetics have been under taken.

We thank our colleagues, especially Ruth J. Mayer for the helpful discussions and Valerie Mizrahi and Patricia A. Benkovic for their suggestions at various stages of this study.

References

1) T. C. Bruice and S. J. Benkovic, "Bioorganic Mechanisms," Vols. 1 and 2, Benjamin, New York (1966).
2) G. Dalbadie-McFarland, L. W. Cohen, A. D. Riggs, C. Morin, K. Itakura, and J. H. Richards, *Proc. Natl. Acad. Sci. U.S.A.*, **79**, 6409 (1982).
3) J. E. Villafranca, E. E. Howell, D. H. Voet, M. S. Strobel, R. C. Ogden, J. N. Abelson, and J. Kraut, *Science*, **222**, 782 (1983).
4) A. R. Fersht, J.-P. Shi, A. J. Wilkinson, D. M. Blow, P. Carter, M. M. Y. Waye, and G. P. Winter, *Angew. Chem., Int. Ed. Engl.*, **23**, 467 (1984).
5) C. S. Craik, C. Largman, T. Fletcher, S. Roczniak, P. J. Barr, R. Fletterick, and W. J. Rutter, *Science*, **228**, 291 (1985).
6) J-T. Chen, R. J. Mayer, C. A. Fierke, and S. J. Benkovic, *J. Cell. Biochem.*, **29**, 73 (1985).
7) D. A. Estell, T. P. Graycar, and J. A. Wells, *J. Biol. Chem.*, **260**, 6518 (1985).
8) K. Taira, J.-T. Chen, R. J. Mayer, and S. J. Benkovic, *Bull. Chem. Soc. Jpn.*, **60**, 3017 (1987).
9) R. L. Blakley, "Folates and Pterins," ed by R. L. Blakley and S. J. Benkovic, Wiley, New York (1985), p. 191.
10) J. T. Bolin, D. J. Filman, D. A. Matthews, R. C. Hamlin, and J. Kraut, *J. Biol. Chem.*, **257**, 13650 (1982).
11) D. J. Filman, J. T. Bolin, D. A. Matthews, and J. Kraut, *J. Biol. Chem.*, **257**, 13663 (1982).
12) S. R. Stone and J. F. Morrison, *Biochemistry*, **23**, 2753 (1984).
13) W. W. Cleland, *Adv. Enzymol. Relat. Areas Mol. Biol.*, **45**, 273 (1977).
14) J. R. Knowles, *CRC Crit. Rev. Biochem., Nov.*, **165** (1976).
15) S. R. Stone and J. F. Morrison, *Biochim. Biophys. Acta*, **745**, 237 (1983).
16) I. H. Segel, "Enzyme Kinetics, Behavior and Analysis of Rapid Equilibrium and Steady-State Enzyme Systems," Wiley, New York (1975), p. 109.
17) E. E. Hoell, J. E. Villafranca, M. S. Warren, S. J. Oatley, and J. Kraut, *Science*, **231**, 1123 (1986).

 © 1987 The Chemical Society of Japan Bull. Chem. Soc. Jpn., 60, 3031—3033 (1987)

In Situ Trapping of NO: Application of *S*-Nitroso Derivatives for Metal Nitrosyls Synthesis

Daya Shankar PANDEY, S. K. SAINI,† and Umesh Chandra AGARWALA*
Chemistry Department, Indian Institute of Technology, Kanpur-208016, India
†Defence Materials & Stores Research & Development Establishment, P. B. No. 320, Kanpur, India
(Received June 26, 1986)

Several known nitrosyl complexes of Ru, Rh, and Co have been synthesized using *S*-nitroso organic compound (*S*-nitrosocysteine). Physicochemical methods such as IR, magnetic measurements, conductance measurements, and elemental analysis were used for characterization of the reaction products.

In situ trapping of NO as a synthetic procedure for metal-nitrosyls using *N*-nitroso derivatives ($\begin{matrix}R'\\R\end{matrix}$>N-NO) has been exploited in our earlier work[1] and an attempt was made there to generalize the method and to reduce multistep process for nitrosyl synthesis to a single-step one. It was also pointed out that the reactivity of a particular *N*-nitroso derivatives is a function of the substituents R and R′.

Because of our continuing interest in finding new procedures for metal nitrosylation, we looked into the possibility of employing recently synthesized *S*-nitroso derivatives[2] as nitrosylating agents which undergo dissociation reaction (2 RS-NO→R-S-S-R+ 2 NO) at varying temperatures depending upon the organic moiety linked to the sulfur. The temperature dependence of *S*-nitroso derivatives has further added an interest in us because for most of the cases the percentage yield of a particular metal nitrosyl using NO as a nitrosylating agent is temperature dependent. (Some metal nitrosyls can not be synthesized even at room temperature[3]). Thus there exists a possibility of choosing a S-nitroso derivative for a particular metal nitrosyl synthesis. The focus of this short note is to study the nitrosyl group transfer in solution from S-nitrosocysteine to metal centers (Ru, Rh, Co) in presence of other coligands.

Experimental

Chemically pure grade chemicals were used throughout. Microanalytical work has been carried out in the Microanalytical Lab. of the Indian Institute of Technology, Kanpur. Infrared spectra have been recorded on a Perkin-Elmer 580 Spectrophotometer in KBr discs. Magnetic measurements were made on a Guoy balance at room temperature. The results are given in Table 1.

Synthetic Reactions. Following are the procedures for the reactions of *S*-nitrosocysteine with the metal ions and their complexes. *S*-Nitrosocysteine was prepared by the literature method[4,5] (Cystine hereafter is referred as cys-cys).

(A) Reaction of $RuCl_3 \cdot xH_2O$ with *S*-Nitrosocysteine in the Presence of Triphenylphosphine. 40 ml of a solution containing 25 ml of ethanolic solution of $RuCl_3 \cdot xH_2O$ (0.5 mmol), triphenylphosphine (2 mmol), 15 ml of *S*-nitrosocysteine (0.48 mmol) in tris solution was heated under reflux for 40—45 min, whereupon shining yellow crystals of [Ru(cys-cys)$_2$Cl(NO)] were separated on cooling the solution. Crystals were filtered, washed with water, ethanol

Table 1.

Compound	Analysis: Calcd (Found)/%				
	C	H	N	X	S
$[RuCl(NO)(cys\text{-}cys)_2]H_2O$	21.6 (21.8)	3.6 (4.1)	10.5 (10.5)	5.4 (4.8)	19.2 (21.5)
$[RuCl_2(NO)(PPh_3)_2(cys\text{-}cys)]$	52.2 (53.9)	4.3 (4.1)	4.3 4.5)	7.1 (7.7)	6.4 (6.5)
$[RuCl_3(NO)(PPh_3)_2]$	56.9 (55.7)	4.1 (3.0)	2.0 (1.9)	14.3 (14.0)	— —
$[RhCl_2(NO)(PPh_3)_2]$	59.3 (58.7)	4.1 (3.8)	1.9 (2.3)	9.7 (10.4)	— —
$[RhCl_2(NO)(cys\text{-}cys)(PPh_3)]$	—	—	—	—	—
$[CoCl(NO)(bpy)_2]ClO_4$	44.8 (44.8)	3.0 (3.1)	13.0 (12.7)	12.8 (11.8)	— —
$[Co(NO)(NO_2)(bpy)_2]ClO_4$	42.7 (42.9)	2.8 (3.1)	14.9 (14.7)	6.2 6.3)	— —

and dried under vacuum.

(B) Reaction of $[RuCl_2(PPh_3)_3]$ with *S*-Nitrosocysteine. 15 ml of an aqueous solution of *S*-nitrosocysteine (0.48 mmol) was added to 10 ml ethanolic solution of $[RuCl_2(PPh_3)_3]$ (0.05 mmol) and the reaction mixture was heated to reflux for 40—45 min whereby a yellowish orange colored compound $[Ru(NO)Cl_2(cys\text{-}cys)(PPh_3)_2]$ was separated. It was filtered and washed as in (A) and dried in vacuum.

(C) Reaction of $[RuCl_2(PPh_3)_3]$ with S-Nitrosocysteine in Presence of $HgCl_2$. The procedure for carrying out the reaction was the same as that given in "B" except that 0.05 g of $HgCl_2$ was added to the reaction mixture. It resulted in the formation of a compound which was analyzed as $[Ru(NO)Cl_3(PPh_3)_2]$.

(D) Reaction of $[RuCl_2(PPh_3)_4]$ with *S*-Nitrosocysteine. 5 ml of an aqueous solution of *S*-nitrosocysteine was allowed to react with 10 ml of an ethanolic solution of $[RuCl_2(PPh_3)_4]$ by the procedure given in "B" whereupon $[Ru(NO)Cl_2(cys\text{-}cys)(PPh_3)]$ was precipitated out.

(E) Reaction of $[RhCl(PPh_3)_3]$ with *S*-Nitrosocysteine. A solution of $[RhCl(PPh_3)_3]$ (0.1 mmol) in 15 ml of ethanol was allowed to react with 15 ml of an aqueous solution of *S*-nitrosocysteine (0.5 mmol), according to the procedure given in "B" whereby $[Rh(NO)Cl_2(PPh_3)]$cys-cys was separated

The same reaction when carried out in presence of $HgCl_2$ yielded $[Rh(NO)Cl_2(PPh_3)_2]$.

(F) Reaction of $CoCl_2\cdot 6H_2O$ with *S*-Nitrosocysteine in Presence of $LiClO_4$ and 2,2′-Bipyridyl. $CoCl_2\cdot 6H_2O$ (0.25 g) and $LiClO_4$ (0.2 g) were dissolved in 20 ml of absolute ethanol and the solution was deaerated by flushing with nitrogen. A solution of 2,2′-bipyridyl (0.37 g) dissolved in hot ethanol (10 ml) was slowly added to the $CoCl_2$ solution under nitrogen, followed by the addition of *S*-nitrosocysteine (0.25 g) in 15 ml water. The resulting solution was stirred at room temperature for 30 minutes, whereby brown microcrystalline compound $[Co(bpy)_2Cl(NO)]ClO_4$ was separated. It was filtered, washed with ethanol, ether and dried under vacuum.

(G) Reaction of $CoCl_2\cdot 6H_2O$ with *S*-Nitrosocysteine in the Presence of $LiClO_4$, $NaNO_2$, and 2,2′-Bipyridyl. 0.15 g 2,2′-bipyridyl, 0.5 g $LiClO_4$, and 0.04 g $NaNO_2$ were mixed in 10 ml of ethanolic solution of $CoCl_2\cdot 6H_2O$ (0.15 g) and deaerated with N_2 gas, followed by the addition of 15 ml of *S*-nitrosocysteine solution in water. The color of the solution turned brown and finally a yellowish brown solid was separated out. It was filtered, washed with ethanol and ether and dried under vacuum. The compound was analyzed for $[Co(bpy)_2(NO)(NO_2)]ClO_4$.

Results and Discussion

The empirical formulae of the compounds resulting by the interaction of *S*-nitrosocysteine with metal ions are enlisted in Table 1. The bright yellow diamagnetic Ru(II) complex $[RuCl(NO)(cys\text{-}cys)_2]$ exhibited in its IR spectrum a band at 1870 cm^{-1} corresponding to ν(NO) besides the characteristic bands of cystine. The positions of all cystine bands (3500, 2900, 2565, 1742, 1577, 1521, 1231, 1216, and 876 cm^{-1}) except one around 1700 cm^{-1} (assigned to ν(CO) of COO^- group) remained constant. The lowering of 1700 cm^{-1} band position suggested bonding of ruthenium through COO^- moiety. Presuming ruthenium in +2 oxidation state with a formal charge of +1 on NO [ν(NO), 1870 cm^{-1}] the charge balance required cystine to be bonded with ruthenium as uninegative ion (Dipositive ruthenium in the complex is also suggested by its diamagnetic nature). It is therefore, assumed that the binding of cystine with ruthenium occurs through COOH group after deprotonation. Further six being the preferred coordination number of Ru(II) in its complexes[6] each cystine anion should provide two bonding sites to the metal center which could be either another oxygen, sulfur or nitrogen atom. Although it is difficult to decide the second donor site, but since the positions of other IR bands assigned to cystine remained practically unaltered, we tentatively assume oxygen atom of the COO^- group to be another bonding site. It is, however, only tentative.

An orange yellow complex having an empirical formula $[RuCl_2(NO)(PPh_3)_2(cys\text{-}cys)]$ has been obtained by the reaction of $[RuCl_2(PPh_3)_3]$ with *S*-nitrosocysteine. The IR spectrum exhibited the characteristic bands of PPh_3 and cystine. The position of ν(CO) of cystine also shifted to lower wave number suggesting the bonding of ruthenium with carboxyl group after deprotonation because of the charge balance as discussed in the preceding paragraph.

It appears that in both Ru(II) complexes sites above cystine formed during the decomposition of *S*-nitrosocysteine also coordinated to ruthenium along with NO group. In order to inhibit the cystine coordination during the reaction, a strategy of removing the cystine from the reaction site formed after decomposition of *S*-nitroso compound was thought. If the reaction is performed in presence of $HgCl_2$, the latter will not only catalyze the decomposition of *S*-nitroso compound[7] but will also pickup preferentially the formed organothio radical leaving NO radical for coordination with the metal ion in accordance with the following reaction:

Thus, the reaction when carried out in the presence of excess $HgCl_2$ yielded pure $[RuCl_3(NO)(PPh_3)_2]$ in our reactions.

Similar to ruthenium complexes the reaction of $[RhCl(PPh_3)_3]$ with *S*-nitrosocysteine yielded a mixture of $[RhCl_2(NO)(PPh_3)(cys\text{-}cys)]$ and $[RhCl_2(NO)(PPh_3)_2]$. However, the same reaction in presence of $HgCl_2$ yielded pure literature known compound $[RhCl_2(NO)(PPh_3)_2]$.

The reaction of Co(II) salts with the *S*-nitroso compound did not yield a complex having bonded cystine even under varying reaction conditions. These reac-

tions, however, yielded pure literature known complexes (Table 1). Possibly Co(II), being 'a' class metal ions may not bind preferentially with sulfur-containing cystine in presence of a better base, viz 2,2′-bipyridyl. The literature known complexes viz. $[RuCl_3(NO)(PPh_3)_2]$,[8] $[RhCl_2(NO)(PPh_3)_2]$,[9] $[CoCl(NO)(bipy)_2]ClO_4$,[10] $[Co(NO_2)(NO)(bpy)_2]ClO_4$[10] were identified by comparing their mp mixed mp spectral (IR, UV, and visible) and magnetic properties with the authenticated samples prepared by the literature methods.

It is evident from the above discussion that there exists a definite possibility of applying successfully *S*-nitrosococysteine, in particular, and *S*-nitroso derivatives, in general, for metal nitrosylation reactions. It is also obvious that the competitive reaction of the generated organothio radical to link with the metal ion (particularly b-class) along with its dimerization can be inhibited by adding excess $HgCl_2$ which not only assists in removing the thio radical from the reaction but also catalyzes the decomposition of S-nitroso compounds. Further work in this direction is in progress where the application of the method will be utilized for the nitrosylation of other metal ions with other *S*-nitroso derivatives, especially those having stability at low temperature. The latter reactions will be carried out with those metal ions where nitrosyls are obtained only at low temperature.

References

1) M. I. Khan and U. C. Agarwal, *Bull. Chem. Soc. Jpn.*, **59**, 1285 (1986).

2) S. Oae and K. Shinhama, *Org. Prep. Proced. Int.*, **15**, 165 (1983).

3) W. P. Griffith, J. Lewis, and G. Wilkinson, *J. Inorg. Nucl. Chem.*, **7**, 38 (1958).

4) L. Field, R. V. Dilts, R. Ravichandran, P. G. Henhert, and C. E. Carrahar, *J. Chem. Soc., Chem. Commun.*, **1978**, 249.

5) L. J. Ignarro, B. K. Barry, D. Y. Gruetter, J. C. Edward, E. H. Ohlstein, C. A. Gruetter, and W. H. Baricos, *Biophys. Res. Commun.*, **94**, 92 (1980).

6) E. A. Seddon and K. R. Seddon, "The Chemistry of Ruthenium," 1st ed., ed by R. J. H. Clark, Elsevier (1984), p. 1135.

7) B. Saville, *Analyst (London)*, **83**, 670 (1958).

8) K. R. Laing and W. R. Ropes, *J. Chem. Soc., A*, **1970**, 2149.

9) S. D. Robinson and M. F. Uttley. *J. Chem. Soc., A*, **1971**, 1254.

10) A. Vleck, Jr. and A. A. Vleck, *Inorg. Chim. Acta*, **9**, 165 (1974).

The Superconductive Compound of the Ba-Y-Cu Oxide

Akira ONO* and Masayuki TSUTSUMI
National Institute for Research in Inorganic Materials, Namiki, Ibaraki 305
(Received March 16, 1987)

Synopsis. Chemical composition of a novel compound in the Ba-Y-Cu-O system is determined. Formulae of the phase is $Ba_4Y_2Cu_7O_{14}$. X-Ray powder pattern can be indexed successfully on the basis of an orthorhombic unit cell. Stability of the phase is preliminary studied by a thermogravimetric method.

Recently, superconductivity of oxide compounds has been reported in the Ba-La-Cu-O and Ba-Y-Cu-O systems.[1-3] In the latter system, the resistivity drop sets in at 95 K, above the stability range of liquid N_2.[3] The phase responsible for the superconductivity is, however, not identified. We have synthesized a novel compound as a nearly pure single phase of which resistivity is zero at 77 K. This paper describes the synthesis, stability, chemical composition, X-ray, and resistivity properties of this novel compound in Ba-Y-Cu-O system.

The compound was prepared by mixing the prescribed amount of powders of Y_2O_3, $BaCO_3$, and CuO followed by reacting the mixture at 900 °C for 10—15 h in air. Re-mixing and re-heating for each run were carried out at least two times during the heat-treatment. The compound prepared was pelletized and sintered at 900—950 °C in air.

The crystalline phases were analyzed on a polished section of the sintered specimen with an electron probe microanalyzer, JXA 5A using standard crystals of a snythetic xenotime (YPO_4), polycrystalline CuO and a synthetic $Ba_{0.75}Al_{11.0}O_{17.25}$.[4] Correction procedure used was the Bence-Albee method.[5] Based on the analytical data of the superconductive material, the mixing ratio of Ba, Y, and Cu of the starting material were determined as 4 : 2 : 7 in the atomic ratio.

The X-ray properties of the material prepared were recorded with a diffractometer JEOL TDX-7F using Cu $K\alpha$ radiation with quartz as internal standard. Thermogravimetric analysis was carried out with an thermogravimetor, ULVAC TA 1500, at a heating rate of 10 K min^{-1}. Surfaces of the powdered specimens were observed with a scanning electron microscope, Akashi, DS 130.

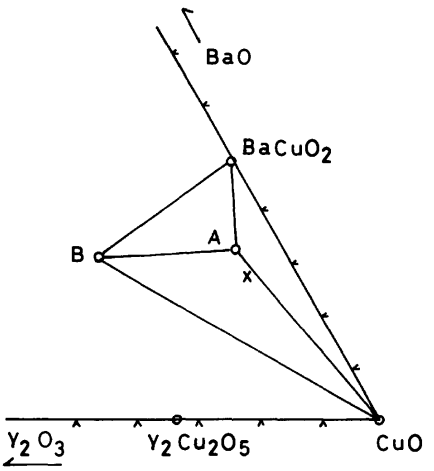

Fig. 1. Phase relations in the BaO-Y_2O_3-CuO system at 900 °C in air. A: $Ba_4Y_2Cu_7O_{14}$. B: $Ba_4Y_8Cu_5O_{21}$.

Figure 1 shows the phase relation in the BaO-Y_2O_3-CuO system at 900 °C in air. Three phases, CuO, $Ba_4Y_2Cu_7O_{14}$, and $BaCuO_2$ exist in the vicinity of the superconduction phase "A". A sintered specimen of the bulk composition X in Fig. 1 consist of CuO, $Ba_4Y_8Cu_5O_{21}$, and the superconductive phase. The chemical compositions of these phases are given in Table 1. These analyses are based on the assumption that the valency of Cu is +2 in these crystals. Y and Ba contents in the crystalline CuO are negligibly small. $Ba_4Y_8Cu_5O_{21}$ has a large and euhedral crystal form. Chemical formula of the superconductive phase may be represented as $Ba_4Y_2Cu_7O_{14}$.

X-Ray powder patterns of the superconductive

Table 1. Chemical Compositions of the Crystalline Phases

	(A)[a]	(B)[b]
Y_2O_3	17.56	47.23
CuO	39.01	20.45
BaO	43.30	32.02
Total	99.87	99.70

a) $Ba_4Y_2Cu_7O_{14}$. b) $Ba_4Y_8Cu_5O_{21}$.

Table 2. X-Ray Powder Diffraction Data for the Superconductive Phase

h k l	2θ	d_{obs} Å	d_{calcd} Å	I_{obs}
0 0 1	7.54	11.72	11.681	2
0 0 2	15.14	5.847	5.841	2
1 0 0	22.84	3.890	3.886	10
0 1 0	23.21	3.829	3.827	3
1 0 2	27.60	3.2291	3.235	5
0 1 2	27.84	3.2018	3.2008	5
1 0 3	32.55	2.7484	2.7504	63
0 1 3	32.81	2.7280	2.7292	100
1 1 2	36.34	2.4700	2.4705	4
1 0 4	38.53	2.3345	2.3345	10
0 1 4	38.74	2.3224	2.3215	7
1 1 3	40.34	2.2339	2.2334	15
2 0 0	46.71	1.9430	1.9429	15
0 2 0	47.50	1.9125	1.9133	8
1 1 5	51.48	1.7736	1.7740	3
2 1 3	58.22	1.5823	1.5827	21
1 2 3	58.72	1.5710	1.5707	10
2 1 4	62.20	1.4912	1.4899	3
2 2 0	68.80	1.3634	1.3633	8

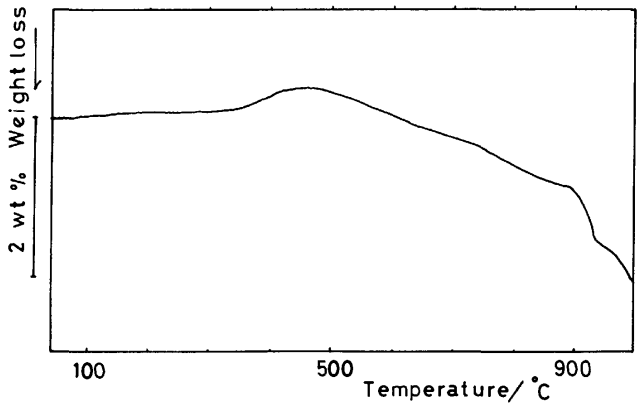

Fig. 2. Thermogravimetric data of the superconductive phase.

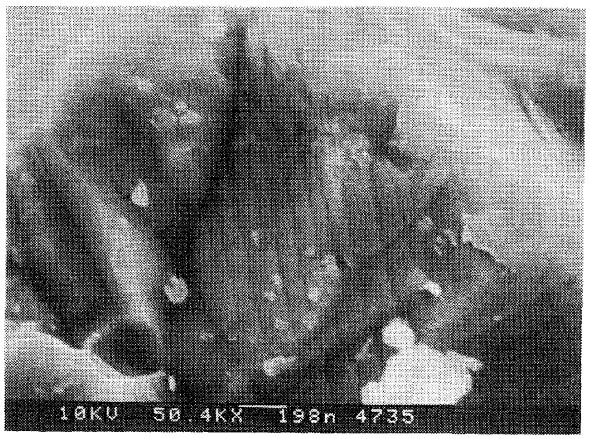

Fig. 3. Scanning electron microscopic image of the superconductive phase. Scale bar: 198 nm.

phase change considerably with heating time. Difference of the lattice parameters a and b become large with increasing heating time. At the same time X-ray peaks of impurity phases decrease its intensities with increasing heating time. An X-ray pattern of well-crystallized material is given in Table 2, which can be indexed on the basis of orthorhombic unit cell with a=3.8857(9) Å, b=3.8267(8) Å, c=11.681(4) Å. Possible space groups are P222, Pmm2, and Pmm. The unit cell dimensions are similar to those of $LaSrVO_4$,[6] and the presence of 001 peak indicates that the crystal symmetry differs from that of La_2CuO_4. The value $c/3$ is similar to those of a and b, so that this crystal is a distorted cubic phase.

Figure 2 illustrates a thermogravimetric curve of powdered superconductive materials synthesized at 900 °C in air. Weight gain takes place near 400 °C with subsequent gradual weight loss. These weight changes may be due to the change of oxygen content in the specimen. However, further study is needed for the confirmation. Considerable weight losses take place in the two different temperature ranges, namely from 900 to 950 and from 950 to 1000 °C. The former loss is due to partial decomposition of the superconductive phase. The latter one may be due to its partial melting.

Our specimens were obtained at 900 °C in air. The heating temperature is slightly above the decomposition temperature of the superconductive phase. This is a reason why small amount of impurity phases (mainly CuO of about 5—10% by volume) were detected in the X-ray diffraction pattern and on the polished section of the sintered material. A study on the compositional change of the superconductive phase as a function of temperature is now in progress.

A scanning electron microscopic image of the fractured surface of the superconductive crystal is shown in Fig. 3. Fine banding structure was observed in most of the crystals. This structure may be transition twin induced during the transformation of high temperature phase with tetragonal or higher symmetry to low temperature orthorhombic phase.

Electrical resistivity of the superconductive phase has been measured from 65 K to room temperature. The methods of the measurements and the results will be described in detail in near future. The resistivity is several m Ω cm at room temperature. Onset temperature of the superconductivity is 103 K, and the final drop is ended at 85 K.

We thanks Dr. Fujio Izumi for re-indexing our initial indexing based on the reduced cell and computing the lattice parameters. Dr. Yoshio Ishizawa was kindly enough to measure electrical resistivity of the specimens.

References

1) J. G. Bendorz and K. A. Muller, *Z. Phys.* B **64**, 189 (1986).
2) S. Uchida, H. Takagi, K. Kitazawa, and S. Tanaka, *Jpn. J. Appl. Phys. Lett.*, **26**, L1 (1987).
3) H. Takagi, S. Uchida, K. Kishio, K. Kitazawa, K. Fueki, and S. Tanaka, *Jpn. J. Appl. Phys.*, **26**, L320 (1987).
4) N. Iyi, S. Takekawa, and S. Kimura, *J. Solid State Chem.*, **59**, 250 (1985).
5) A. E. Bence and A. L. Albee, *J. Geol.* **93**, 500 (1970).
6) J. M. Longo and P. M. Reccah, *J. Solid State Chem.*, **6**, 526 (1973).

Synthetic Photochemistry. XXXVIII.[1] The Photorearrangement of the Tropone Endoperoxide, 6,7-Dioxabicyclo-[3.2.2]nona-3,8-dien-2-one

Akira MORI and Hitoshi TAKESHITA*
Research Institute of Industrial Science, 86, Kyushu University, Kasuga-koen, Kasuga, Fukuoka 816
(Received March 3, 1987)

Synopsis. The photolysis of 6,7-dioxabicyclo[3.2.2]nona-3,8-dien-2-one produced six photolysates, including a cage γ-lactone which belongs to the same type of product as was characterized in each case of the photolysis of the endoperoxides derived from 2-aryl- and 2,7-diaryltropones by Mukai et al. The new products identified were 2,7-dioxabicyclo-[3.2.2]nona-3,8-dien-6-one, a δ-lactone acetal, and 7-exo-formyl-3-oxabicyclo[4.1.0]hept-4-en-2-one, a δ-lactone.

In 1970's, Mukai et al. discovered a photorearrangement of several 1-aryl-, 3-aryl, and 1,3-diaryl-6,7-dioxabicyclo[3.2.2]nona-3,8-dien-2-ones **1a—c**, and the endoperoxides derived from 2-aryl- and 2,7-diaryltropones, to cage γ-lactones **2a—c**.[2] Then, by means of low-temperature IR spectroscopy, they identified a bicyclic ketene as the intermediate leading to the photolysate.[3] On this basis, they proposed a reaction sequence from the endoperoxides **1** to ketene **A** and cage lactones **2**, and explained the mechanism in terms of a transannular interaction of the enone and the isolated double bond[4] in the molecule.

Although, unfortunately, they failed[2] to isolate or characterize any photolysate other than **2**, it is hardly conceivable that the ketene intermediate results selectively in only one type of product. In addition, recently we ourselves have noticed a transannular interaction of the enone part and the dioxa linkage in related compounds.[5] Furthermore, Mukai et al. have stated[2] that no product could be identified in the photolysis mixture of the parent tropone endoperoxide, 6,7-dioxabicyclo[3.2.2]nona-3,8-dien-2-one (**3**).[6] These findings prompted us to carry out a reinvestigation of Mukai's experiments with a synthetically useful parent compound, **3**.[7] The results, identifying six products **4—9**, will be presented briefly.

The irradiation of a benzene solution of the parent peroxide **3** by means of a high-pressure mercury lamp caused a rapid photolysis. The products could be isolated by means of silica-gel chromatography; the structures were deduced mainly from the NMR spectra,[9] which revealed mutually-coupled methine proton systems, allowing for a first-order analysis.

The least polar product **4**, one of the major products, was a bicyclic acetal δ-lactone, showing the carbonyl absorption[9] at 1775 cm^{-1}; an analysis of the whole coupling sequence of protons, four of which were on the sp^2-carbons, by means of an intensive double-irradiation technique,[10] enables us to deduce that **4** was 2,7-dioxabicyclo[3.2.2]nona-3,8-dien-6-one.

Another major product (**5**=**2**; R_1=R_2=H) was shown to be a cyclopropane-containing compound; the characteristic 4-alkoxy-γ-lactone absorption was observed at ν: 1782 cm^{-1}. The well-separated ^1H NMR spectrum of this tricyclic compound, 2,8-dioxatricyclo[4.2.1.$0^{5,9}$]-non-3-en-7-one, showed a close resemblance to those of the reported photolysates **2a—c** from **1a—c**.[2] The third product, an enol δ-lactone aldehyde (**6**) [IR ν: 1760 and 1715 cm^{-1}], was deduced to be 7-exo-formyl-3-oxabicyclo[4.1.0]hept-4-en-2-one on the basis of the spectroscopic data.

The fourth photolysate **7** was an aldehydic enol γ-lactone [IR ν: 1830 and 1807 cm^{-1}]; its structure was deduced by means of detailed ^1H and ^{13}C NMR spectral analyses.

The most polar photolysate **8** was 3-(2-furyl)acrylic acid, as was confirmed by direct comparison with an authentic sample.[11] The remaining photoproduct **9** was obtained in a mixture with the furylacrylic acid **8**. Its ^1H NMR spectral data were compatible with those of 3-(2,5-dihydro-5-oxo-3-furyl)acrylaldehyde.[12]

The present results show a much improved material balance (50% vs. trace to 21%) compared to those of previous studies by Mukai et al.[2] It is now possible to

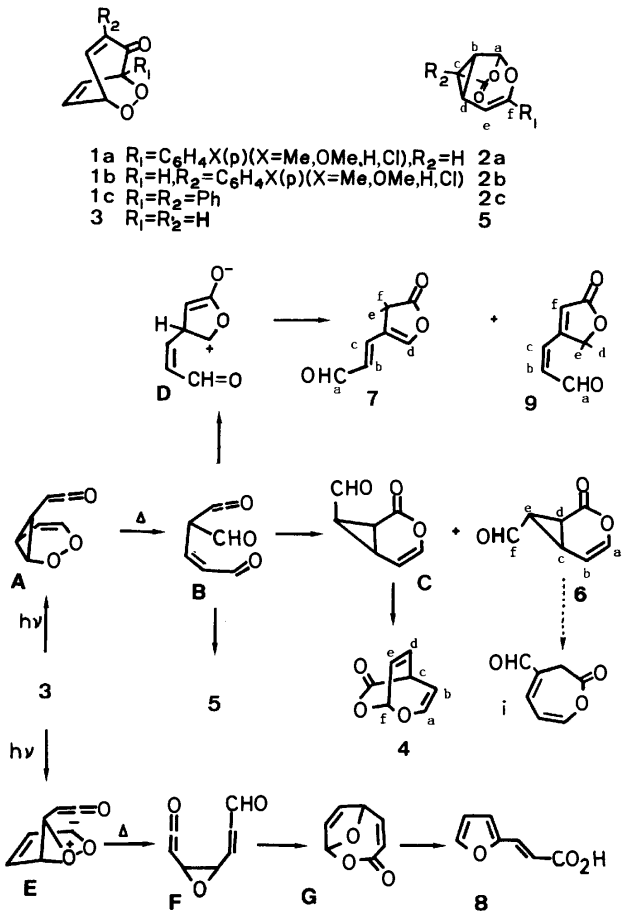

Scheme 1.

discuss the general features of this photorearrangement. There is no photoproduct with a peroxy group, and the absence of an alcoholic function eliminates the heterolytic cleavage of the peroxy linkage. Consequently, the peroxy group might have been transformed via the electrocyclic processes during the irradiation, but it is difficult to explain the formation of all the new photolysates by means of Mukai's mechanism, that is, via a ketene intermediate **A**. These products can thus be classified into two groups according to the *proto*-photolysates, precursor ketenes: i.e., Type I (**4**—**7** and **9**) and Type II (**8**). All the Type I products carry a branched side chain from the α- or β-carbon to the carboxylic carbon, and all could be derived from ketene **A**. Its cycloreversion should give **B**, with which an intramolecular Diels-Alder reaction should form C and its stereoisomer, **6**.[13] Cage lactone acetals, **4** and **5**, could be derived from **C** and **B** respectively, and the furanones, **7** and **9**, should be formed by cyclization at the ketene and aldehyde moieties of **B** to a precursor cyclisate (**D**), followed by two ways of hydrogen transfer. On the other hand, the formation of the remaining compound, **8**, a free carboxylic acid, of Type II, could be explained in terms of another precursor: The ketene E, with a zwitterionic peroxirane group and resulting from a transannular reaction of the α,β-unsaturated keto group and the peroxide linkage, might be isomerized to a neutral epoxy ketene (**F**), which, via a bicyclic ε-lactone (**G**), should afford **8**.

Consequently, the photolysates isolated and characterized from **3** in this study show that the reaction is not so simple as was reported by Mukai et al.; particularly, the formation of **8** must be explained by another precursor, E, with a peroxirane structure.

Experimental

The UV-Light Irradiation of 6,7-Dioxabicyclo[3.2.2]nona-3,8-dien-2-one. A benzene solution (5 cm^3) of **3** (163 mg) was irradiated by means of a 400-W high-pressure mercury lamp through a Pyrex glass filter at 10—20 °C under an N_2 atmosphere for 2 h. The reaction was monitored by the disappearance of the **3** in high-pressure liquid chromatography. The residual mixture obtained by the evaporation of the solvent was then chromatographed on a silica-gel column and eluted with benzene-ethyl acetate to obtain the respective products:

4 [A colorless oil, 27.3 mg; 17%. Found: C, 60.61; H, 4.64%; M. W., 138.0319. Calcd for $C_7H_6O_3$: C, 60.87; H, 4.38%; M. W., 138.0318. ^{1}H NMR δ[10]=3.29 (Hc, ddd, J=8.3, 6.4, 1.5 Hz), 5.06 (Hb, dd, J=8.3, 6.8 Hz), 5.92 (Hf, dd, J=4.4, 2.0 Hz), 5.95 (He, ddd, J=8.3, 4.4, 1.5 Hz), 6.10 (Ha, d, J=6.8 Hz), and 6.70 (Hd, ddd, J=8.3, 6.4, 2.0 Hz). ^{13}C NMR δ=39.3, 95.7, 101.7, 120.8, 136.7, 144.1, and 171.9. IR ν: 1775, 1630 cm^{-1}].

5 [A colorless oil, 30 mg; 18%. Found: C, 60.50; H, 4.37%; M. W., 138.0318. ^{1}H NMR δ=1.86 (Hd, dddt, J=8.5, 7.5, 4.5, 0.5 Hz), 2.28 (Hc, dd, J=8.5, 5.5 Hz), 2.59 (Hb, dddd, J=7.5, 5.5, 5, 0.5 Hz), 5.29 (He, dd, J=6, 4.5 Hz), 6.12 (Ha, d, J=5 Hz), and 6.35 (Hf, dd, J=6, 0.5 Hz). ^{13}C NMR δ=15.1, 15.5, 24.1, 96.3, 100.8, 141.6, and 174.0. IR ν: 1782 cm^{-1}].

6 [A colorless oil, 7.5 mg; 5%. Found: C, 60.67; H, 4.56%; M. W., 138.0302. ^{1}H NMR δ=2.27 (He, td, J=4, 2.5 Hz), 2.42 (Hc, dddd, J=8, 4.5, 4, 1 Hz), 2.78 (Hd, ddd, J=8, 4, 1 Hz), 5.55 (Hb, ddd, J=6, 4.5, 1 Hz), 6.40 (Ha, dd, J=6, 1 Hz), and 9.63 (Hf, d, J=2.5 Hz). ^{13}C NMR δ=24.8, 26.4, 34.2, 104.1, 141.7, 163.7, and 196.1. IR ν: 1760, 1715, and 1657 cm^{-1}].

7 [A colorless oil, 6.5 mg; 4%. Found: M. W., 138.0316. ^{1}H NMR δ=3.37 (He and Hf, dd, J=2, 1 Hz), 6.02 (Hb, dd, J=15.5, 7.5 Hz), 7.16 (Hc, d, J=15.5 Hz), 7.25 (Hd, t, J=2 Hz), and 9.56 (Ha, d, J=7.5 Hz). ^{13}C NMR δ=31.5, 128.5, 129.7, 141.0, 147.7, 173.1, and 192.7. IR ν: 1830, 1807, 1680, and 1630 cm^{-1}].

8 [Colorless crystals, mp 132—133 °C (lit,[11] mp 138 °C), 6.3 mg; 4%. ^{1}H NMR δ=6.28 (1H, d, J=15.5 Hz), 6.45 (1H, dd, J=3.5, 2 Hz), 6.63 (1H, d, J=3.5 Hz), 7.47 (1H, d, J=15.5 Hz), and 7.47 (1H, dm, J=2 Hz). δ(DMSO)=6.13 (1H, d, J=15.5 Hz), 6.60 (1H, dd, J=3.4, 1.7 Hz), 6.90 (1H, d, J=3.4 Hz), 7.36 (1H, d, J=15.5 Hz), and 7.80 (1H, d, J=1.7 Hz)].

9 [A colorless oil, 3.2 mg; 2%. ^{1}H NMR δ=5.02 (Hd and He, dd, J=2, 1 Hz), 6.29 (Hb, t, J=7 Hz), 6.40 (Hf, br s), 6.42 (Hc, d, J=7 Hz), and 9.70 (Ha, d, J=7 Hz)].

We wish to thank Professor Mitsuaki Kodama, of Tokushima Bunri University, for providing us with a valuable 400 MHz NMR spectrum of **4**. We are also grateful to the Ministry of Education, Science, and Culture for its financial support, the Grant-in-Aid for Scientific Research given to A. M. (No. 60470025).

References

1) Part XXXVII: S. Yamasaki, T. Hatsui, and H. Takeshita, *Kyushu Daigaku Seisan Kagaku Kenkyusho Hokoku*, **81**, 7 (1986).

2) T. Tezuka, R. Miyamoto, T. Mukai, C. Kabuto, and Y. Kitahara, *J. Am. Chem. Soc.*, **94**, 9280 (1972).

3) T. Tezuka, R. Miyamoto, M. Nagahama, and T. Mukai, *Tetrahedron Lett.*, **1975**, 327.

4) In fact, the occurrence of this particular type of transannular homoconjugation in various Diels-Alder adducts of tropones has a precedent. See S. Itô, H. Takeshita, Y. Shoji, Y. Toyooka, and T. Nozoe, *Tetrahedron Lett.*, **1969**, 443.

5) H. Takeshita, A. Mori, S. Sugiyama, and T. Tsuda, *Bull. Chem. Soc. Jpn.*, **59**, 3988 (1986). See also T. Sasaki, K. Kanematsu, and K. Hayakawa, *J. Chem. Soc. C*, **1971**, 2142. During the photochemical rearrangement of the Diels-Alder adduct of tropone to 4-phenyl-1,2,4-triazoline-3,5-dione, a similar interaction with unshared electron pairs of the hydrazo group was noticed.

6) M. Oda and Y. Kitahara, *Tetrahedron Lett.*, **1969**, 3295.

7) The usefulness of **3** as a precursor of 2-substituted 4-cyclopentene-1,3-diones has already been shown. See A. Mori and H. Takeshita, *Kyushu Daigaku Sogo Rikogaku Kenkyuka Hokoku*, **3**, 125 (1981).

8) The NMR spectra were measured in $CDCl_3$ solutions, unless otherwise stated, and the chemical shifts were expressed in δ units. The IR spectra were taken as liquid films.

9) The $\nu_{(C=O)}$ of 1,5,5-trimethyl-2,6-dioxabicyclo[2.2.2]-octan-3-one appeared at 1773 cm^{-1}. See I. D. Rae and A. M. Redwood, *Austr. J. Chem.*, **27**, 1143 (1974).

10) This was analyzed by means of the 400-MHz ^{1}H NMR spectrum.

11) B. Capron, C. Paulmier, and P. Pastour, *Bull. Soc. Chim. Fr.*, **1975**, 2575.

12) The carboxylic acid function could not be derived by an auto-oxidation of the aldehydic function; **4**—**7**, and **9** are all on the same oxidation level as **8**.

13) Frequently, an aldehyde **i**, apparently derived from **6**, was identified among the photolysates; its ^{1}H NMR spectrum [δ=3.16 (2H, s), 6.38 (1H, dd, J=12, 6 Hz), 6.98 (1H, d, J=6 Hz), 6.98 (1H, d, J=12 Hz), and 9.48 (1H, s)] indicated the structure depicted.

Fries Rearrangement of 1-Methoxy-4-(4-methyl-2- and -3-pentenoyloxy)benzenes[1)]

Yasuhiro TANOUE and Akira TERADA*
Department of Chemistry, Kyushu Institute of Technology, Tobata, Kitakyushu 804
(Received March 16, 1987)

Synopsis. Not only rearrangement but also cyclization occurred in a Fries rearrangement of 1-methoxy-4-(4-methyl-2- and -3-pentenoyloxy)benzenes and gave 5,8-dihydroxy-4,4-dimethyl-3,4-dihydro-1(2*H*)-naphthalenone. The reduction and oxidation of the dihydronaphthalenone gave 5-hydroxy-8,8-dimethyl-5,6,7,8-tetrahydro-1,4-naphthalenedione and 8,8-dimethyl-7,8-dihydro-1,4,5(6*H*)-naphthalenetrione, respectively.

Naphthoquinone compounds occur widely in nature among plants and fungi.[2)] They have been studied not only with regard to their pigment and structure[3)] but also concerning expectations of physiological activity.[4)] We have recently reported the total synthesis of shikalkin[(±)Shikonin], 5,8-dihydroxy-2-(1-hydroxy-4-methyl-3-pentenyl)-1,4-naphthoquinone.[5)] This paper deals with a result of Fries rearrangements of phenolic esters, 1-methoxy-4-(4-methyl-2- and -3-pentenoyloxy)benzenes, as a model reaction for the introduction of the side chain of shikonin, 1-hydroxy-4-methyl-3-pentenyl moiety, to a phenolic nucleus. The product, 5,8-dihydroxy-4,4-dimethyl-3,4-dihydro-1(2*H*)-naphthalenone(**5**), was derived to 5-hydroxy-8,8-dimethyl-5,6,7,8-tetrahydro-1,4-naphthalenedione(**6**) and 8,8-dimethyl-7,8-dihydro-1,4,5(6*H*)-naphthalenetrione(**7**).

Results and Discussion

Following Caspi's procedure,[6)] a reaction of isobutyraldehyde with malonic acid in pyridine gave *trans*-4-methyl-2-pentenoic acid (**1**). This was then isomerized with alkali to 4-methyl-3-pentenoic acid (**2**). However, this isomerization did not proceed completely and gave an equilibrated isomeric mixture of **1** and **2**. The ^{1}H NMR spectrum of this mixture showed that it contained about 24% acid **1** and 76% of **2**. Since an attempted separation of these isomers was not successful, this acid mixture was used in the next step: treatment with thionyl chloride gave the corresponding acid chlorides, **3a** and **3b**.

p-Methoxyphenol was allowed to react with the acid chlorides to give a mixture of phenolic esters **4a** and **4b** in 68% yield. The ratio of **4a** and **4b** was about 3 : 1 by ^{1}H NMR. The treatment of an ester mixture **4a** and **4b** with a molten mixture of aluminum chloride and sodium chloride prepared at 180 °C, gave a crystalline product in 24% yield. The ^{1}H NMR spectrum showed two signals at δ 12.3 and 8.1 due to the phenolic hydroxyl groups; the former suggested the existence of a strongly hydrogen bonded OH. A single peak at δ 1.5 was due to two methyl groups and the signals of methine groups in the starting materials (**4a**: $-CH=C(CH_3)_2$ and **4b**: $-CH=CHCH(CH_3)_2$) had disappeared. These spectral data could indicate only a cyclic ketone, **5**.

It can be concluded that the Fries rearrangement described here was accompanied with cyclization and demethylation. A Fries rearrangement of pure ester **4b**[7)] also resulted in the formation of cyclic ketone **5** in 16% yield. These results suggested that a rearrangement of the carbon-carbon double bond in the side chain of **4b** had occured. Ketone **5** was also prepared from **4** in 38% yield by using boron trifluoride etherate instead of a molten mixture of $AlCl_3$–NaCl.

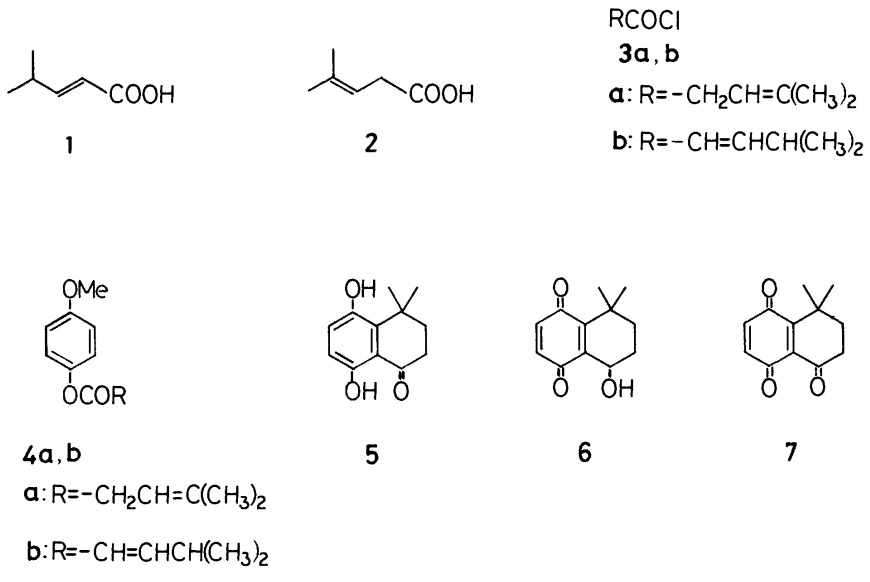

Fig. 1.

A reduction of **5** with lithium aluminum hydride in tetrahydrofuran and subsequent air-oxidation gave **6** in 37% yield.

A oxidation of **5** with ceric (IV) ammonium nitrate gave **7** in 79% yield.

Experimental

^{1}H NMR spectra were taken on a JEOL JNM-FX60 spectrometer using tetramethylsilane as an internal standard; the chemical shifts were reported in δ values. Mass spectral data were obtained with a JEOL DX-300. Infrared spectra were recorded on a Hitachi 260-30 infrared spectrometer and the UV spectra on a Shimadzu recording spectrometer UV-200S. Column chromatography was performed on silica gel (Wakogel C-200). Melting points were determined with a Yanagimoto micromelting point apparatus and were uncorrected.

4-Methyl-3-pentenoyl Chloride (3a) and 4-Methyl-2-pentenoyl Chloride (3b) Mixture. 4-Methyl-3-pentenoic acid **2** (16.8 g, 0.147 mol, containing ca. 24% of **1**) was added dropwise to thionyl chloride (21.0 g, 0.176 mol) under reflux and the mixture was refluxed for another 30 min, then fractionally distilled under reduced pressure to give 14.6 g (75%) of an oil of **3** (**3a**:**3b**=3:1), bp 55—58 °C/22 mmHg (1 mmHg=133.322 Pa). IR (neat) 1795 (C=O), 1755 (C=O), 1625 (C=C), 1030, and 960 cm^{-1}; MS *m/z* 134(M^++2), 132 (M^+), 97, and 69; ^{1}H NMR ($CDCl_3$) **3a**: δ=1.64, 1.74 (6H, $2CH_3$), 3.61 (d, *J*=6.8 Hz, 2H, CH_2), and 5.28 (m, 1H, CH); **3b**: δ=1.04, 1.14 (6H, $2CH_3$), 2.41 (m, 1H, CH), 6.09 (dd, *J*=15.5 and 1.0 Hz, 1H, COCH=CH), and 7.32 (dd, *J*=15.5 and 6.0 Hz, 1H, COCH=CH).

1-Methoxy-4-(4-methyl-3-pentenoyloxy)benzene (4a) and 1-Methoxy-4-(4-methyl-2-pentenoyloxy)benzene (4b) Mixture. A mixture of *p*-methoxyphenol (9.2 g, 74.2 mmol) and the acid chloride mixture **3** (10 g, 75 mmol) was refluxed until the evolution of hydrogen chloride ceased. The reaction product was distilled under reduced pressure to give 11.2 g (68%) of an oil, **4** (**4a**:**4b**=3:1), bp 180—186 °C/20 mmHg. IR (neat) 2850 (OCH_3), 1760 (C=O), 1650 (C=C), 1250, 1196, and 1035 cm^{-1}; MS *m/z* 220 (M^+), 124, and 97; ^{1}H NMR ($CDCl_3$) **4a**: δ=1.69, 1.77 (6H, $2CH_3$), 3.23 (d, *J*=7.3 Hz, 2H, CH_2), 3.74 (s, 3H, OCH_3), 5.39 (m, 1H, CH), and 6.9 (m, 4H, ArH); **4b**: δ=1.03, 1.15 (6H, $2CH_3$), 2.58 (m, 1H, CH), 3.74 (s, 3H, OCH_3), 5.93 (dd, *J*=15.6 and 1.0 Hz, COCH=CH), 6.9 (m, 4H, ArH), and 7.1 (dd, *J*=15.6 and 7.2 Hz, 1H, COCH=CH). Found: C, 70.74; H, 7.45%. Calcd for $C_{13}H_{16}O_3$: C, 70.89; H, 7.32%.

5,8-Dihydroxy-4,4-dimethyl-3,4-dihydro-1(2*H*)-naphthalenone (5). A. 5 from 4 (4a and 4b Mixture) by Using Aluminum Chloride and Sodium Chloride Molten Mixture. A mixture of anhydrous aluminum chloride (30 g) and sodium chloride (10 g) was melted at 180 °C, and to this was added dropwise the ester **4** (7.8 g, 35 mmol) under vigorous stirring. After 10 min, the obtained pasty mass was decomposed by the addition of dil. hydrochloric acid and extracted with ether. The ether solution was washed with water, dried, and evaporated. The crude product was recrystallized from hexane-tetrahydrofuran to give 1.70 g (24%) of **5** as yellow crystals, mp 239—240 °C. IR (KBr) 3300 (OH), 2950, 1623 (C=O), 1475, and 1240 cm^{-1} (OH); MS *m/z* 206 (M^+), 191, and 163; ^{1}H NMR ($(CD_3)_2CO$) δ=1.53 (s, 6H, CH_3), 1.91 (m, 2H, CH_2), 2.71 (m, 2H, CH_2), 6.62 (d, *J*=9.2 Hz, 1H, ArH), 7.08 (d, *J*=9.2 Hz, 1H, ArH), 8.11 (s, 1H, OH), and 12.34 (s, 1H, OH); UV (dioxane) 264 (ε 13800) and 368 nm (ε 7900). Found: C, 69.68; H, 6.78%. Calcd for $C_{12}H_{14}O_3$: C, 69.89; H, 6.84%.

B. 5 from 4b by Using Aluminum Chloride and Sodium Chloride Molten Mixture. The reaction of **4b**[7] (5.18 g, 24 mmol) with a molten mixture of aluminum chloride (15 g) and sodium chloride (1.3 g) was carried out by the procedure described above and gave 0.80 g (16%) of **5**, mp 238—240 °C. All the spectral data agreed with those of **5** prepared from method A.

C. 5 from 4 (4a and 4b Mixture) by Boron Trifluoride Etherate. Boron trifluoride etherate (1.2 ml, 9.6 mmol) was added dropwise to the ester **4** (680 mg, 3.2 mmol) at 140 °C, and after 10 min, was decomposed by addition of dil hydrochloric acid and extracted with chloroform. The usual work-up and chromatography on silica gel with chloroform gave 250 mg (38%) of a sample of **5**. Recrystallization from ligroine-benzene gave an analytical sample, mp 239—241 °C. All the spectral data agreed with those of **5** prepared from method A.

5-Hydroxy-8,8-dimethyl-5,6,7,8-tetrahydro-1,4-naphthalenedione (6). Lithium aluminum hydride (36 mg, 0.97 mmol) was added to a solution of the ketone **5** (100 mg, 0.485 mmol) in tetrahydrofuran (2 ml), stirred at room temperature for 1 h, decomposed with ice water, and extracted with chloroform. The usual work-up and chromatography on silica gel with chloroform gave 37 mg (37%) of a sample of **6** as a semisolid, mp 69—73 °C. IR (KBr) 3410 (OH) and 1645 cm^{-1} (C=O); MS *m/z* 206 (M^+), 188, 173, 151, and 123; HRMS *m/z* calcd for $C_{12}H_{14}O_3$ 206.0943, found 206.0945; ^{1}H NMR ($CDCl_3$) δ=1.29 (s, 3H, CH_3), 1.37 (s, 3H, CH_3), 1.6—2.0 (m, 4H, $2CH_2$), 3.18 (d, *J*=2.6 Hz 1H, OH), 4.72 (m, 1H, CH), and 6.67 (s, 2H, quinonoid ring H).

8,8-Dimethyl-7,8-dihydro-1,4,5(6*H*)-naphthalenetrione (7). A solution of ceric(IV) ammonium nitrate (800 mg, 1.46 mmol) in water (5 ml) was added dropwise to a solution of **5** (100 mg, 0.49 mmol) in tetrahydrofuran (5 ml) at room temperature, stirred for 1 h, diluted with water, and extracted with chloroform. The usual work-up and chromatography on silica gel with chloroform gave 78 mg (79%) of a sample of **7**. Recrystallization from hexane gave an analytical sample, mp 120—121 °C. IR (KBr) 1705 (C=O), 1660 (C=O), 1285, and 855 cm^{-1}; MS *m/z* 204 (M^+), 189, 161, and 149; ^{1}H NMR ($CDCl_3$) δ=1.47 (s, 6H, $2CH_3$), 1.94 (m, 2H, CH_2), 2.67 (m, 2H, CH_2), and 6.71 (s, 2H, quinonoid ring H). Found: C, 70.58; H, 5.92%. Calcd for $C_{12}H_{12}O_3$: C, 69.92; H, 6.18%.

References

1) Paper V, on Synthesis of Naphthoquinone Derivatives. Paper IV, Y. Tanoue, A. Terada, T. Tsuboi, T. Hayashida, and O. Tsuge, *Bull. Chem. Soc. Jpn.*, **60**, 2927 (1987).

2) For example, R. H. Thomson, "Naturally Occurring Quinones," 2nd ed, Academic Press, London (1971).

3) R. E. Moore and P. J. Scheuer, *J. Org. Chem.*, **31**, 3272 (1966); F. Farina, R. M. Utrilla, and M. C. Paredes, *Tetrahedron*, **38**, 1531 (1982).

4) For example, J. S. Driscoll, G. F. Hazard, Jr., H. B. Wood, Jr., and A. Goldin, *Cancer Chemotherapy Reports Part 2*, **4**, 1 (1974). M. Tabata, M. Tsukada, and H. Fukui, *Planta Med.*, **44**, 234 (1982).

5) A. Terada, Y. Tanoue, A. Hatada, and H. Sakamoto, *Bull. Chem. Soc. Jpn.*, **60**, 205 (1987).

6) E. Caspi and K. R. Varma, *J. Org. Chem.*, **33**, 2181 (1968).

7) Treatment of **3b** with *p*-methoxyphenol gave **4b**, bp 176—179 °C/27 mmHg. **3b** was prepared from the reaction of the acid **1** and thionyl chloride.

An Improved Synthesis of 8-Amino-8-demethylriboflavin

Sabu KASAI,* Bernhard J. FRITZ, and Kunio MATSUI
Research Institute for Atomic Energy, Osaka City University, Sugimoto, Sumiyoshi-ku, Osaka 558
(Received March 25, 1987)

Synopsis. 8-Amino-8-demethylriboflavin was synthesized from 3-nitro-4-methylaniline *N*-D-riboside by selective reduction of the *N*-glycoside with sodium borohydride, followed by hydrogenation of the nitro group in the presence of Raney's catalyst. The obtained phenylenediamine was condensed with violuric acid to give the flavin in a high yield.

8-Amino-8-demethylriboflavin (**4**) has been used as a riboflavin (RF) analogue to study reaction mechanisms of flavoenzymes,[2] flavin-protein interactions,[3,4] or antimicrobial action.[1,5] **4** has a low redox potential (about 100 mV lower than RF),[1] and both the conjugation system and the stability of the semiquinone differ from those of RF.[1,2,12] Moreover, **4** is a key compound from which many 8-substituted flavins can be derived via diazotization,[9,10] and 8-substituted flavins such as the naturally occuring 8-hydroxy-8-demethylriboflavin,[6-8] have been used widely. It is noteworthy that most flavins used in biochemical studies carry a ribityl group at 10-position of the isoalloxazine ring, whereas in purely chemical research usually lumiflavin derivatives are used.

4 was already synthesized by Berezovskii et al.,[11] but, using their method, we achieved only low yields of 5 to 10%. In the final step, a dark powder was obtained, making the purification tedious. If the reduction of the riboside is carried out in one step as given by Berezovskii et al., there exists the possibility that the nitro group is reduced first, followed by migration of the ribosyl group. Upon condensation with violuric acid, a product of the lumichrome type would be obtained. We figured this to be the main reason for the low yield of above method, and aimed to reduce first the riboside selectively, thus preventing the migration of the ribosyl group. This was achieved by using excess sodium borohydride in refluxing ethanol. The reaction can also be carried out with sodium cyanotrihydroborate, where smaller amounts of the reductant are sufficient. Samples prepared according to our

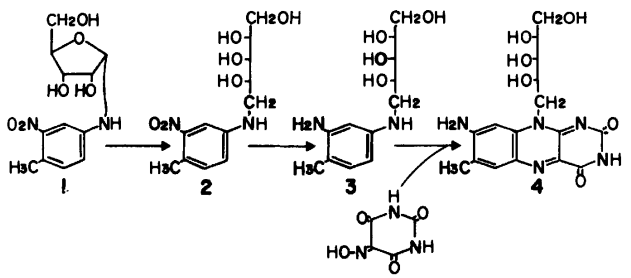

method gave analytical results and absorption spectra identical to samples prepared by us according to Berezovskii et al.

Experimental

Mass spectrum (field desorption) was taken on a JEOL JMS-01SG-2; IR spectrum was recorded on a JASCO model IRA grating infrared spectrophotometer; UV spectra were recorded on a Hitachi 320 recording spectrophotometer; 400 MHz ^{1}H NMR spectra were taken with a JEOL model JMM GX 400. Melting points were measured with a Yanaco MP micro melting point apparatus.

3-Nitro-4-methyl-*N*-ribitylaniline (2). Two grams of 3-nitro-4-methylaniline *N*-D-riboside (**1**)[11] was dissolved in 20 ml ethanol and sodium borohydride (1.5 g) was added. The reaction mixture was refluxed for 1.5 h under stirring, during which the color of the solution changed from orange to red. After cooling to room temperature, the solution was neutralized with 1 M (mol dm^{-3}) hydrochloric acid and evaporated to dryness. A small amount of methanol was added to the residue. Salt precipitated, which was filtered and washed. Filtrates were combined, evaporated, redissolved in a 8:2 mixture of dichloromethane and methanol, charged on a silica-gel column (Wakogel C-200, Wako Pure Chemical Industries, Ltd., 3 cm×20 cm), and developed with the same solvent. Red fractions were collected and evaporated. Attempts to crystallize the syrup from several solvents were unsuccessful. FD-MS: Found *m/z* 286.0. Calcd for $C_{12}H_{18}O_6N_2$: M, 286.28.; IR (Nujol) 1545 and 1350 cm^{-1} (NO_2).

The syrup obtained above was dissolved in 10 ml ethanol and hydrogen chloride gas was introduced into the solution under cooling, upon which the color of the solution changed from red to light brown. 30 ml of diisopropyl ether were added to the solution and 3-nitro-4-methyl-*N*-ribitylaniline hydrochloride (**2'**) separated as syrup, which was crystalized by adding seed crystals. The crystals were filtered off, washed with diisopropyl ether and dried over calcium chloride in vacuo. Yield 2.0 g (88%): mp 138—140 °C; ^{1}H NMR (D_2O) δ=2.61 (3H, s, CH_3), 3.67 (2H, dd, J=12 and 4 Hz, 5'CH_2), 3.79 (4H, m, 1'CH_a, 2'-4'CH), 4.14 (1H, m, 1'CH_b), 7.65 (1H, d, J=8 Hz, 5CH), 7.74 (1H, dd, J=8 and 2 Hz, 6CH), 8.18 (1H, d, J=2 Hz, 2CH). Found: C, 44.63; H, 5.96; N, 8.67%. Calcd for $C_{12}H_{19}N_2O_6Cl$: C, 44.66; H, 5.93; N, 8.68%.

8-Amino-8-demethylriboflavin (4). One gram of **2'** was suspended in 20 ml methanol and 120 mg powdered NaOH was added. Color of the solution was changed from colorless to red and the solution became turbid with crystals of NaCl, which were filtered off and washed with methanol. The combined filtrates were hydrogenated at 50 °C for 30 min under 50 kg cm^{-2} in the presence of Raney's catalyst, which was prepared from 4.0 g of a 50% alloy with 1 M NaOH. The catalyst was filtered from the colorless solution, washed with methanol, and the combined filtrates were evaporated in vacuo. The diamine obtained was easily oxidized, and therefore was used for the next reaction without isolation. The residue, dissolved in 20 ml methanol, was added to a hot solution of 0.6 g violuric acid in 40 ml of a 1 : 3 (v/v) mixture of methanol and water. Soon after addition, the color of the reaction mixture turned dark, fluorescence developed, and fine orange crystals appeared. After reflux for 4 h the reaction mixture was cooled and allowed to stand at room temperature overnight. Crystals (760 mg) were collected by filtration, washed with methanol and dried over $CaCl_2$. Another 210 mg of the crystals were recovered from the mother liquid. Total yield 970 mg (81%). For elemental analysis, the product was recrystallized from hot water.

^{1}H NMR (DMSO-d_6)(*indicates exchangable H) δ=2.48 (3H, s, CH_3), 3.47 (1H, m, 5'CH_a), 3.58 (1H, m, 5'CH_b), 3.67 (2H, m, 3',4'CH), 4.26 (1H, m, 2'CH), 4.32* (1H, t, J=6 Hz, 5'OH), 4.52 (1H, d, J=14 Hz, 1'CH_a), 4.68 (1H, d, J=4 Hz, 1'CH_b), 4.76* (2H, m, OH), 4.90* (1H, d, J=5 Hz, OH), 6.97 (1H, s, ϕ-H), 6.99* (2H, s, NH_2), 7.63 (1H, s, ϕ-H), 10.73* (1H, s, 3NH) (for assignments, see also[13]). UV (0.2M phosphate buffer pH 7.0) 235nm (ε_{mM} 31.7), 296 (8.9), and 476 (43.9); (6M HCl) 246 (36.5), 308 (18.9), 384 (4.6), and 477 (32.3); (0.1M NaOH) 248 (46.9), 292sh (6.3), and 475 (46.9); mp over 300 °C. Found: C, 50.78; H, 4.96; N, 18.41%. Calcd for $C_{16}H_{19}N_5O_6$: C, 50.92; H, 5.08; N, 18.56%. Literature values[10]; mp over 350 °C; UV (water) 252 (49.0), 296 (8.8), and 490 (42.0).

The authors thank Drs. Tetsuo Shiba and Tadashi Teshima of Osaka University for recording the mass spectrum, and Mr. Junichi Goda for the elemental analysis. B.J.F. is grateful for the financial support by the Japanese Ministry of Education, Mombusho.

References

1) S. Kasai, Y. Kubo, S. Yamanaka, T. Hirota, H. Sato, Y. Tsuzukida, and K. Matsui, *J. Nutr. Sci. Vitaminol.*, **24**, 339 (1978).

2) R. C. Stewart and V. Massey, *J. Biol. Chem.*, **260**, 13639 (1985).

3) K. Matsui, K. Sugimoto, and S. Kasai, *J. Biochem.*, **91**, 469 (1982).

4) J.-D. Choi and D. B. McCormick, *Arch. Biochem. Biophys.*, **204**, 41 (1980).

5) E. A. Rudzit, T. A. Zhilina, G. N. Neshchadim, N. S. Kirina, L. S. Tul'chinskaya, Zh. I. Litvak, N. A. Polyakova, and V. M. Berezovskii, *Khim. Farm. Zh.* **12**, 52 (1978).

6) S. Ghisla and S. G. Mayhew, *J. Biol. Chem.*, **248**, 6568 (1973).

7) S. Ghisla and S. G. Mayhew, *Eur. J. Biochem.*, **63**, 373 (1976).

8) S. Kasai, S. Yamanaka, S.-C. Wang, and K. Matsui, *J. Nutr. Sci. Vitaminol.*, **25**, 289 (1979).

9) S. Ghisla and S. G. Mayhew, in "Methods Enzymol.," ed by D. B. McCormick and L. D. Wright, Academic Press, Inc., New York (1980), Vol. 66, pp. 241—253.

10) T. Watanabe, K. Matsui, S. Kasai, and T. Nakamura, *J. Biochem.*, **84**, 1441 (1978).

11) V. M. Berezovskii, L. S. Tul'chinskaya, and N. A. Polyakova, *Zh. Obshch. Khim*, **35**, 673 (1965).

12) C. Walsh, J. Fisher, R. Spencer, D. W. Graham, W. T. Ashton, J. E. Brown, R. D. Brown, and E. F. Rogers, *Biochemistry*, **17**, 1942 (1978).

13) M. Kainosho and Y. Kyogoku, *Biochemistry*, **11**, 741 (1972).

Electrooxidative Functionalizations of Dehydroabietic Acid

Kenji UNEYAMA, Tatsuo KATAYAMA, and Sigeru TORII*
Department of Industrial Chemistry, School of Engineering, Okayama University, Okayama 700
(Received March 26, 1987)

Synopsis. Dehydroabietic acid methyl ester (**1**) was converted into 7-acetoxydehydroabietic acid methyl ester by direct electrooxidation in acetic acid and 7-oxodehydroabietic acid methyl ester by ruthenium dioxide-mediated oxidation. Non-Kolbe type electrodecarboxylation of **1** resulted in the introduction of a double bond into the ring A of **1**.

Dehydroabietic acid[1] (**1a**) is a well-known resin acid of pine tree and usable as a chiral building block for steroid and terpene syntheses.[2] Several oxidative degradations have been attempted to modify the B ring of **1b**,[3] where excess amount of oxidation reagents such as trifluoroperacetic acid, ozone, and hydrogen peroxide have been employed. As one of our research programs on utilization of natural chiral compounds, some of the electrooxidative reactions of **1** have been studied to seek a mild oxidative functionalization of the A and B ring of **1**.

(1) Electro-Acetoxylation on C-7 of 1b. Introduction of acetoxyl group on C-7 of **1b** with cobalt acetate[4] and manganese acetate[5] is unsatisfactory. Meanwhile, electrooxidation of **1b** in an acetic acid-sodium acetate system using carbon electrodes provides **2a** and **2b** in 61 and 13% yields, respectively. The acetate **2a** is a mixture of stereoisomers on C-7 (40:60 by HPLC). To avoid hydrolysis of the acetoxyl group, acetic anhydride was added as a cosolvent, yielding 72% of **2a** along with 3% of **2b**. In contrast to the successful electroacetoxylation using carbon electrodes,[6] the use of platinum electrode was unsuccessful for the present purpose.[7] It is notable that side-chain acetoxylation occurs predominantly on C-7 rather than C-18. A sequence of ECE process, initial one-electron transfer from aromatic ring followed by deprotonation and successive one-electron oxidation leading to a carbenium ion on C-7, would be the most reasonable reaction sequence.[6] Ball-and-stick molecular model reveals that one of the carbon-hydrogen bond orbitals on C-7 overlaps with π-orbital of aromatic ring for the effective deprotonation.

(2) Electrooxidation of Methylene Group on C-7 to Carbonyl Group. Oxidation of methylene group of **1a** and **1b** to carbonyl group has been studied by cobalt acetate-catalyzed oxidation,[3] and chromium trioxide,[8] providing unsatisfactory yield and product-selectivity. Electrooxidation of **1b** in an MeOH-LiClO_4-(C) system (20 mA cm^{-2}, 7 F mol^{-1}) gave **3a** and **3b** in 52 and 27%, respectively along with a trace amount of **2c**. On the other hand, electrolysis at a lower current density (1 mA cm^{-2}) gave 7-methoxy compound **2c** (77:23 mixture of stereoisomers) in 79% yield as a sole product. The predominant formation of **3a** and **3b** reveals that **2c** is further oxidized in the high current density to the corresponding dimethyl acetal which would be converted to **3a** by the electrogenerated acid catalysis. No methoxy compound **1c** was detected, suggesting methylene proton on C-7 is much reactive than methine proton of isopropyl group.

Meanwhile, ruthenium tetraoxide-mediated electrooxidation of **1b** was examined in a CCl_4-H_2O-NaCl-HCl-NaH_2PO_4-(Pt) system, using ruthenium dioxide as an oxidant which could be converted to ruthenium tetraoxide by electrooxidatively generated active chlorine species.[9] This method provides **3a** in 52% yield. No hydroxy compound **2b** was detected suggesting the conversion of hydroxyl group to carbonyl group is facile in this system.

(3) Non-Kolbe Type Electrooxidation of 1a. Pb(IV) acetate is one of the most frequently employed oxidative reagents for decarboxylative olefin synthesis.[10] But the yields of **5** and **6a,b** are unsatisfactory. Pyrolysis of **1a** at 450 °C provided a mixture of **5** and **6a,b**.[11] Non-Kolbe type electrooxidation of carboxylic acid is useful for decarboxylative olefin synthesis.[6] Indeed, electrooxidation of **1a** provided a mixture of **5** and **6a,b**, which would arise from the carbenium ion intermediate **4**. The exo-olefin **5** can be transformed into chiral steroidal compounds by Natsumoto's method.[12]

Experimental

Boiling points are indicated by an air bath temperature and uncorrected. The NMR spectra were obtained with JNM FX-100 spectrometer at 100 MHz in $CDCl_3$ using Me_4Si as an internal standard. Acid **1a** was separated and purified from the resin acid mixture according to the reported method,[1] and its methyl ester **1b** was prepared by esterification with diazomethane.

Electrolysis of 1b in Acetic Acid: A mixture of **1b** (100 mg, 0.32 mmol) and AcONa (150 mg, 1.8 mmol) in AcOH (5 ml) and $(Ac)_2O$ (1 ml) was electrolyzed using carbon plate electrodes (3 cm^2) in an undivided cell. After passing 10 F mol^{-1} (1F=96480C, 20 mA cm^{-2}) of electricity, acetic acid was evaporated under reduced pressure and the residue was dissolved in AcOEt. Usual workup and chromatography (SiO_2, hexane-AcOEt=4:1) gave 86 mg (72%) of **3a**, and 3 mg (3%) of **3b**. The structures of **3a** and **3b** were identified by spectroscopic comparison with those of the authentic samples.[5]

Electrolysis of 1b with RuO_2: Two platinum plates (3 cm^2) were settled in a water layer of the reaction mixture which contains **1b** (100 mg, 0.32 mmol) $RuO_2 \cdot 2H_2O$ (22 mg, 0.13 mmol), saturated NaCl containing 0.1 mol dm^{-3}

Table 1. Non-Kolbe Electrooxidation of **1a**

Run	Solv-electrolyte	Yield/%	5:6a:6b[d]
1	MeOH-MeONa	61[a]	58:25:17
2	H_2O-Hexane-KOH	58[b]	55:31:14
3	H_2O-THF-KOH	74[c]	44:38:18

a) 5 mA cm^{-2}, 4 F mol^{-1}. b) 20 mA cm^{-2}, 15 F mol^{-1}. c) 10—1 mA cm^{-2}, 3 F mol^{-1}. d) HPLC analysis.

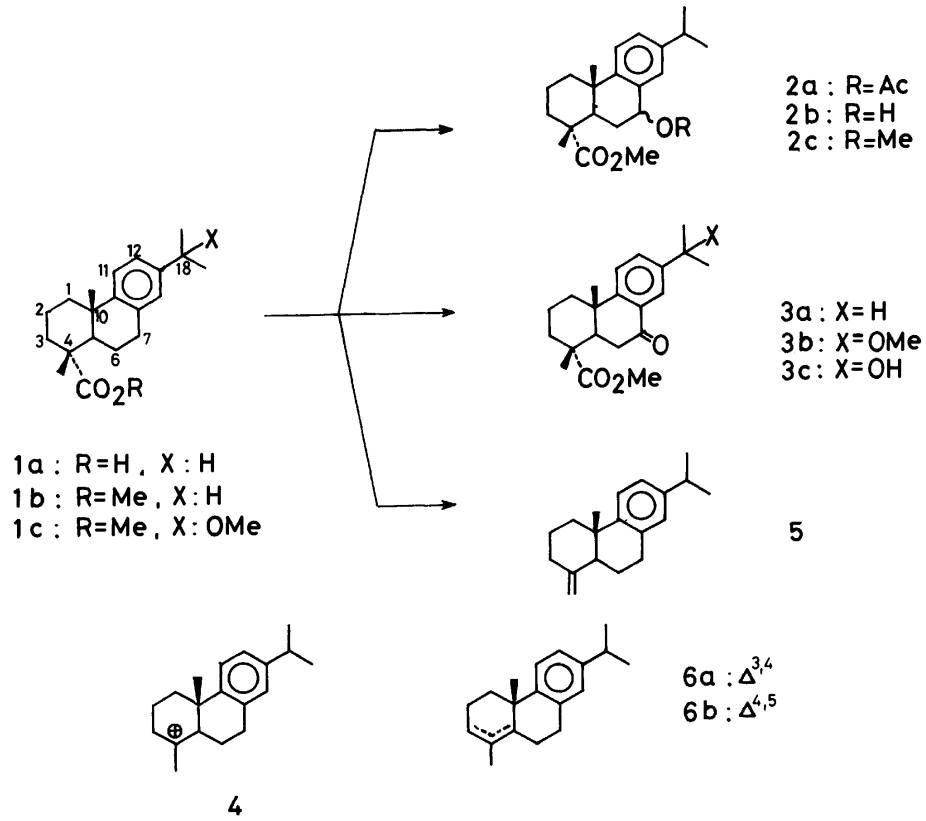

NaH_2PO_4 (4 ml, pH 4), 10% HCl (0.05 ml), and CCl_4 (2 ml). Constant current (20 mA cm^{-2}, 30 F mol^{-1}) was passed at room temperature in an undivided cell. Carbon tetrachloride layer was separated and the water layer was extracted three times with ether. The combined organic extracts were treated as usual, providing **3a**[4] (54 mg, 52%) and **3c**[12] (6 mg, 6%).

Electrolysis of 1b in MeOH: A mixture of **1b** (60 mg, 0.19 mmol), $LiClO_4$ (40 mg, 0.38 mmol), and MeOH (6 ml) was electrolyzed in an undivided cell using two carbon plate electrodes (3 cm^2) [1 mA cm^{-2}, 14 F mol^{-1}]. The usual workup gave **2c** (54 mg, 79%). Methyl 1, 2, 3, 4, 4a, 9, 10, 10a-octahydro-9-methoxy-1, 4a-dimethyl-7-(1-methylethyl)-1-phenanthrenecarboxylate (**2c**). Bp 145 °C [4 Torr(1 Torr= 133.322 Pa)]; IR ($CHCl_3$) 2940, 2844, 2801, 1720, 1459, 1242, 1080, 820 cm^{-1}; ^1H NMR ($CDCl_3$) δ=1.16 (S, 3H, CH_3), 1.23 (d, J=7 Hz, 6H, CH_3), 1.29 (s, 3H, CH_3), 1.6—2.0 (m, 6H, CH_2), 2.04—3.04 (m, 3H, CH, CH_2), 3.38, 3.41 (S, 3H, CH_3), 3.67 (S, 3H, CH_3), 4.22 (t, J=3 Hz, 1H, $CHOCH_3$ for α-OCH_3 isomer), 4.52 (t, J=8 Hz, 1H, $CHOCH_3$ for β-OCH_3 isomer); Found : C, 76.50; H, 9.56%. Calcd for $C_{22}H_{32}O_3$: C, 76.70 ; H, 9.36 %.

Electrolysis of 1a: A mixture of **1a** (120 mg, 0.4 mmol), 1 mol dm^{-3} KOH (0.4 ml), and THF (6 ml) was electrolyzed in an undivided cell using two carbon plate electrodes (3 cm^2) at a constant terminal voltage (40 V) for 6 hr during which current was dropped from 30 to 3 mA. Silica-gel chromatography of the product gave a mixture of **5**, **6a**, and, **6b**, (76 mg, 74%). Separation of **5**, **6a**, and **6b** was performed by HPLC (μ-porasil, hexane) and the structures were identified spectroscopically.[11,13,14]

This work was supported in part by a Grant-in-Aid for Special Project Research (Nos. 60219020 and 61211022) from the Ministry of Education, Science and Culture.

References

1) N. J. Halbrook and R. V. Lawrence, *J. Org. Chem.*, **31**, 4246 (1966).
2) A. Tahara, Y. Harigaya, and M. Onda, *Chem. Pharm. Bull.*, **23**, 1989, 1996 (1975).
3) K. Schaffner, R. Viterbo, D. Arigoni, and O. Jeger, *Helv. Chim. Acta.*, **39**, 174 (1956); Y. Chow and H. Erdtman, *Acta. Chem. Scand.*, **14**, 1852 (1960).
4) A. N. Zhogal'skii, V. A. Azarko, and N. I. Mitskevich, *Vestsi. Akad. Nauvk. BSSR, Ser. Khim. Navuk.*, **5**, 14 (1983). *Chem. Abstr.*, **100**, 68555y (1984).
5) B. F. Malikov, E. N. Shmidt, and N. I. Popova, *Izv. Sib. Otd. Akad. Nauk. SSSR. Ser. Khim. Nauk.*, **1**, 146 (1981). *Chem. Abstr.* **95**, 81259c (1981).
6) S. Torii, "Electroorganic Synthesis" Methods and Applications Part 1, Kodansha-Verlag Chemie (1985).
7) S. Torii, Y. Wake, and T. Inokuchi, Jpn Patent 52-125137 (1977), electroacetoxylation of 4-phenoxytoluene using platinum electrode provides 4-phenoxybenzaldehyde (71%) via 4-phenoxyphenylmethyl acetate.
8) A. Tahara, M. Shimagaki, M. Itoh, Y. Hagiwara, and M. Onda, *Chem. Lett.*, 651 (1974); A. Tahara and H. Mizuno, *Tetrahedron Lett.*, **1974**, 523.
9) S. Torii, T. Inokuchi, and T. Yukawa, *Chem. Lett.*, **1984**, 1063.; S. Torii, T. Inokuchi, and T. Sugiura, *J. Org. Chem.*, **51**, 155 (1986).
10) J. W. Huffman and P. G. Arapakos, *J. Org. Chem.*, **30**, 1604 (1965).
11) R. F. Severson and W. H. Schuller, *Can. J. Chem.*, **51**, 3236 (1973).
12) T. Matsumoto, Y. Imai, Y. Sunaoka, and T. Yoshinari, The 30th Meeting of Perfume, Terpene, and Essential Oil, Hiroshima (1986).
13) T. F. Sanderson, U. S. Patent 2750368 (1956); *Chem. Abstr.* **51**, 1278 (1957).
14) R. F. Severson, W. H. Schuller, and R. V. Lawrence, *Can. J. Chem.*, **49**, 4027 (1971).

Effect of Polymer Matrices on Oxygen-Binding of a Cobalt Porphyrin Complex

Manshi OHYANAGI, Hiroyuki NISHIDE, Koichi SUENAGA, Takehiko NAKAMURA, and Eishun TSUCHIDA*
Department of Polymer Chemistry, Waseda University, Tokyo 160
(Received March 20, 1987)

Synopsis. Oxygen-binding of the (1-methylimidazole)-[α,α′,α″, α‴-5,10,15,20-tetrakis(*o*-pivalamidophenyl)porphinato]cobalt(II) complex fixed in polymer membranes, poly(dimethylsiloxane), poly(butyl methacrylate), and poly(methyl methacrylate), was studied spectroscopically. The apparent oxygen-binding affinity increased with oxygen solubility in the polymer matrix, which was corrected with the solubility coefficient of oxygen in the polymer.

A polymer membrane containing a carrier which interacts specifically and reversibly with oxygen is of great interest as a facilitated transport membrane of oxygen. The authors have recently reported[1] that oxygen transport through a polymeric membrane was augmented by the addition of a (1-methylimidazole)-[α,α′,α″,α‴-5,10,15,20-tetrakis(*o*-pivalamidophenyl)-porphinato]cobalt(II) (CoPIm) complex or a (*N*,*N*′-disalicylideneethylenediamine)cobalt(II) complex, which form oxygen adducts rapidly and reversibly, even in the solid state. One important point in a discussion of the facilitated transport mechanism is to quantitatively elucidate the oxygen-binding property of the carrier, i.e. the cobalt complex, fixed in a membrane.

In this work, the effect of polymer matrices on the oxygen-binding equilibrium of a CoPIm complex was studied spectroscopically by embedding the complex in three polymer membranes with greatly different T_g: poly(dimethylsiloxane) (PDMS), poly(butyl methacrylate) (PBMA), and poly(methyl methacrylate) (PMMA). This situation is discussed in connection with the oxygen solubility in these polymers.

Experimental

Preparation of the Membranes. Toluene solutions of the CoPIm complex and PBMA (Mw=320000) or PMMA (Mw=540000) were mixed, carefully cast on a Teflon plate under an atmosphere free of oxygen, then dried in vacuo to yield a transparent membrane with a thickness of about 60 μm containing 2.5 wt% CoPIm. A PDMS membrane with a thickness of 200 μm was prepared by using a room-temperature vulcanizing silicone rubber (KE-103, Shinetsu Silicone Inc.). The membrane became swollen in a toluene solution containing a large amount of CoPIm; the solvent was carefully evaporated under an atmosphere free of oxygen. The content of the CoPIm, thus prepared, PDMS membrane was also adjusted to 2.5 wt%.

Spectroscopic Measurements. Reversible oxygen-binding to the CoPIm complex fixed in the membranes was observed through the spectral change in the visible absorption using a highly sensitive spectrophotometer Shimazu UV-2000 with a kinetic data processor according to a previously reported method.[1] The spectrophotometer was equipped with a cell having a gas inlet and outlet tube. A membrane sample was attached to the cell wall. A gaseous mixture of oxygen and nitrogen was introduced into the cell through a gas inlet and outlet tube with a standing pressure such that the total pressure in the cell became 1 atm.

Determination of the Solubility Coefficient. The solubility coefficient (k_D) of oxygen in the rubbery PDMS and PBMA membranes and the apparent solubility coefficient of the glassy PMMA membrane were calculated from the results of the following permeation experiment. The oxygen permeation coefficient (P_{O_2}) was measured with a low-vacuum permeation apparatus in a chamber with stable thermostating (Rika Seiki Inc. gas permeation apparatus K-315 N-03). The diffusion coefficient (D) was calculated from time-lag (θ) of the permeation curve ($D=L^2/6\theta$, L; thickness of the membrane), and the division of P_{O_2} by D yields k_D ($P=K_DD$).

Results and Discussion

Oxygen-Binding Equilibrium The visible absorption spectrum of the deoxy CoPIm complex (λ_{max}=528 nm) fixed in the transparent membranes was changed to a spectrum with λ_{max}=545 nm, assigned to the oxy CoPIm complex (O_2/Co=1/1 adduct, Eq 1) immediately after the exposure to oxygen. The oxy-deoxy spectral change was rapid and reversible with isosbestic points at 480, 538, and 667 nm. These visible absorption spectra agreed with those for the corresponding complex in a toluene solution.[2]

$$\text{CoPIm} + O_2 \underset{}{\overset{K}{\rightleftarrows}} \text{CoPIm–}O_2 \qquad (1)$$

Oxygen-binding isotherms of the CoPIm complex fixed in the membranes are shown in Fig. 1; these were drawn by analyzing the spectral changes in response to the exposed oxygen pressure with Drago's equation.[3] The apparent oxygen-binding equilibrium constant (K_{app}) of the CoPIm in the membranes was determined from Fig. 1 and is given in Table 1. The K_{app} value for the CoPIm in the PDMS membrane is larger than those for the CoPIm in the methacrylate polymers. It is considered that a larger amount of oxygen dissolves in the PDMS matrix with a larger k_D (Table 2, mentioned later) and brings about the larger K_{app}.

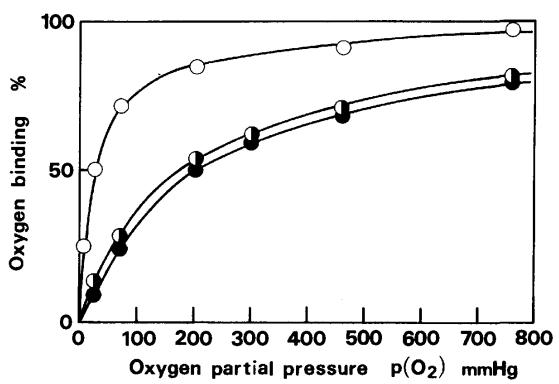

Fig. 1. Oxygen-binding equilibrium curves for the CoPIm membranes at 25 °C. (○; PDMS, ◑; PBMA, ●; PMMA) [CoPIm]=2.5 wt%.

Table 1. The Oxygen-Binding Equilibrium Constants at 25°C and the Thermodynamic Parameters

Membrane	T_g	K_{app}	K	$\Delta H_{app}^{a)}$	$\Delta H^{b)}$	$\Delta S_{app}^{a)}$	$\Delta S^{b)}$
	°C	10^2 cmHg	$cm^3\,10^{-2}$ cm^3(STP)	kcal mol^{-1}	kcal mol^{-1}	e.u.	e.u.
PDMS	−120	37.7	1.0_4	−16.0	−13.1	−54.9	−34.9
PBMA	20	5.6_2	0.51_3	−14.3	−13.1	−53.6	−35.8
PMMA	105	5.1_7	—	−12.9	—	−49.3	—

a) Data for van't Hoff plots (ln K_{app} in $cmHg^{-1}$). b) (ln K in cm^3/cm^3(STP)).

Table 2. The Oxygen Solubility Parameters of the Membranes without a Complex

Membrane	$k^{a)}$ cm^3(STP)	$k_D{}^{b)}$ cm^3(STP)	ΔH_d
	$cm^3\,cmHg$	$cm^3\,cmHg$	kcal mol^{-1}
PDMS	3.8×10^{-5}	3.8×10^{-3}	−2.8
PBMA	1.3×10^{-4}	9.6×10^{-4}	−1.2
PMMA	7.9×10^{-5}	5.9×10^{-4}	−1.2

a) The preexponential factor of Eq. 5. b) At 25°C.

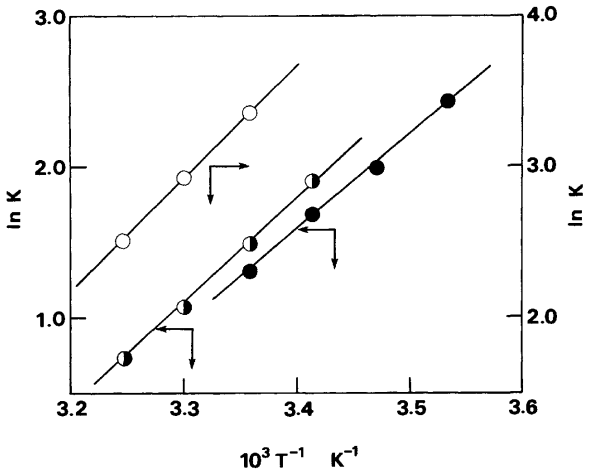

Fig. 2. Van't Hoff plots of the oxygen-binding equilibrium constants for the CoPIm membranes. (○; PDMS, ◑; PBMA, ●; PMMA) [CoPIm]=2.5 wt%.

The apparent thermodynamic parameters for the oxygen-binding were estimated from the temperature dependence of K_{app} (in atm^{-1} in Fig. 2) and are also given in Table 1. The apparent enthalpy change (ΔH_{app}) becomes more negative with a decrease in Tg of the polymer matrix. These apparent thermodynamic parameters for the oxygen-binding equilibrium are corrected with those for oxygen dissolution in the polymer matrix, as follows;

$$K=[\text{CoPIm-O}_2]/[\text{CoPIm}][\text{O}_2] \quad (2)$$

and

$$[\text{O}_2]=k_D p(\text{O}_2), \quad (3)$$

where $[O_2]$ is the oxygen concentration around the CoPIm complex and $p(O_2)$ is atmospheric oxygen pressure to which the membrane is exposed. When $[CoPIm\text{-}O_2]/[CoPIm]$ is 1, K can be written as

$$K=K_{app}/k_D. \quad (4)$$

Accordingly, the thermodynamic parameters from van't Hoff plots of K_{app} ($=k_DK$) are just affected by the k_D values and its heat of dissolution (ΔH_d) as shown in Eq. 7.

$$k_D=ke^{-\Delta H_d/RT} \quad (5)$$

$$\ln K=-\Delta H_{app}/RT+\Delta S_{app}/R \quad (6)$$

$$\Delta H=\Delta H_{app}-\Delta H_d,\ \Delta S/R=\Delta S_{app}/R-\ln k \quad (7)$$

Here, ΔH and ΔS is the thermodynamic parameters in which the effect of the polymer matrix is reduced. ΔH and ΔS are calculated with Eq. 7 by using ΔH_{app}, ΔH_d, and k in Tables 1 and 2 and is shown in Table 2. Both the values of ΔH and ΔS in the PDMS membrane are equal to the ones in the PBMA membrane. Although the apparent equilibrium and thermodynamic parameters of the oxygen-binding reaction of the CoPIm complex fixed in polymer membranes are found to be fairly affected by the oxygen solubility in the polymer matrices, the parameters corresponding to the oxygen-binding reaction to the CoPIm complex are not essentially dependent on the species of the polymer matrix.

This work was partially supported by a Grant-in-Aid for Scientific Research on Priority Area of "Macromolecular Complexes (No. 62612005)" from the Ministry of Education, Science and Culture.

References

1) H. Nishide, M. Ohyanagi, O. Okada, and E. Tsuchida, *Macromolecules*, **19**, 494 (1986): H. Nishide, M. Ohyanagi, O. Okada, and E. Tsuchida, *Macromolecules*, **20**, 417 (1987); E. Tsuchida, H. Nishide, M. Ohyanagi, and H. Kawakami, *Macromolecules* in press. H. Nishide, M. Kuwahara, M. Ohyanagi, Y. Funada, H. Kawakami, and E. Tsuchida, *Chem. Lett.*, **43** (1985); H. Nishide, M. Ohyanagi, H. Kawakami, and E. Tsuchida, *Bull. Chem. Soc., Jpn.*, **59**, 3213 (1986).

2) J. P. Collman, J. I. Brauman, K. M. Doxsee, T. R. Halbert, S. E. Hayes, and K. S. Suslick, *J. Am. Chem. Soc.*, **100**, 2761 (1978).

3) T. Beugelsdijk and R. S. Drago, *J. Am. Chem. Soc.*, **97**, 6466 (1975).

Photochemical Behavior of Aluminum-Ethyl Complex with Tetraaza Macrocyclic Ligand, $Al(C_{22}H_{22}N_4)(C_2H_5)$

Hiroki Oshio,†,* Shozo Tero-Kubota,†,†† and Tasuku Ito†††
†Department of Applied Molecular Science and Coordination Chemistry Laboratories, Institute for Molecular Science, Okazaki National Research Institutes, Okazaki 444
††Chemical Research Institute of Non-Aqueous Solutions, Tohoku University, Katahira, Sendai 980
†††Department of Chemistry, Faculty of Science, Tohoku Univerity, Sendai 980
(Received November 27, 1986)

Synopsis. Homolytic photocleavage of an aluminum carbon bond in ethyl(1,8-dehydro-5,7,12,14-tetramethyldibenzo[*b*,*i*][1,4,8,11]tetraazacyclotetradecinato)aluminum was confirmed by using EPR technique. The photochemistry of this aluminum carbon bond was also studied by NMR and emission spectroscopic experiments.

Photoreactivity of metal-alkyl bonds has been an increasing interest.[1-5] In this note, we report some photochemical behaviors of $Al(C_{22}H_{22}N_4)(C_2H_5)$ (**1**) which has known to be remarkably stable to Al-ethyl dissociation in the dark and resistant to demetallation.[6]

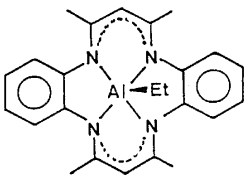

1

Figure 1 shows the electronic spectrum of compound **1**. This compound has a strong absorption band at 358 nm (ε=7.0×10⁴) and a shoulder at about 410 nm ($\varepsilon\simeq10^4$). This spectrum is similar to that of $Ni(C_{22}H_{22}N_4)$,[7] though the bands of **1** lie at shorter wavelengths than those of the Ni complex. Structual study of **1** showed that the in-plane ligand is not planar but take the suddle shape structure.[6] Previous semi-empirical Pariser-Par-Pople MO calculation[8] implied that the visible absorption bands of **1** are predominantly due to the $\pi\pi^*$ transition of deformed macrocyclic ligand.

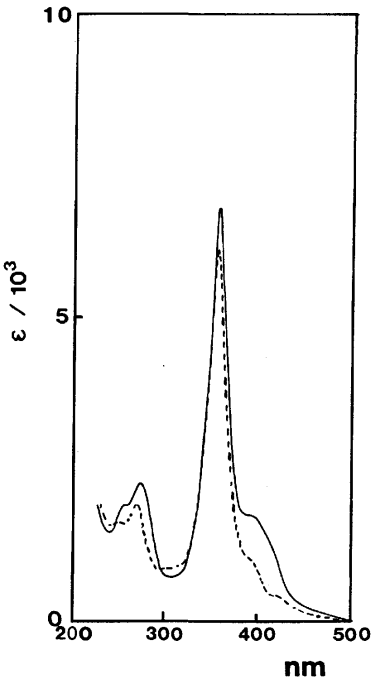

Fig. 1. Electronic spectra of compound **1** (——) and $Al(C_{22}H_{22}N_4)Cl$ (----) in methanol.

Figure 2(A) shows a ^1H NMR spectrum of **1** in $CDCl_3$ at 20 °C. When the solution was irradiated with visible light (λ>450 nm), the spectrum changed with irradiation time (Fig. 2(B—D)). The signal intensities due to the ethyl group at δ 0.18 (t, CH_3) and −0.92 (q, $-CH_2-$) decreased as a new peak of ethane appeared at δ 0.85. Simple spectral change was also observed at lower magnetic field region. Three hours irradiation brought the reaction to completion under the experimental conditions. The main product was identified as $Al(C_{22}H_{22}N_4)Cl$ by means of mass spectrometry of the product (m/z=404). The absorption spectrum of

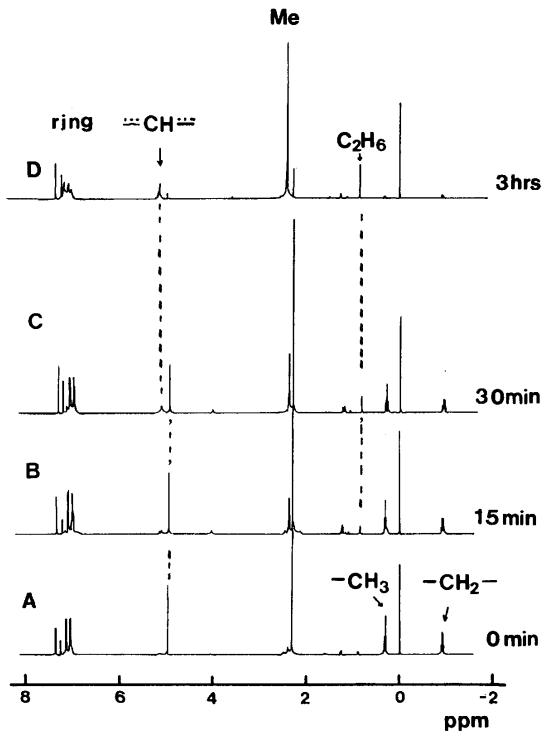

Fig. 2. 400 MHz NMR spectral changes upon photolysis of $CDCl_3$ solution of $Al(C_{22}H_{22}N_4)(C_2H_5)\cdot 1/2C_6H_6$ at 20 °C. A: Before irradiation, B, C, and D: after 15, 30 minutes, and 3 hours irradiations, respectively.

the chloro complex isolated by passing through Al_2O_3 column is also depicted in Fig. 1. The simple spectral change in Fig. 2 indicates that the reaction proceeds rather simply and smoothly at 20 °C. However, prolonged irradiation at room temperature caused the solution dark and turbid, possibly due to the simultaneous side reactions of the radicals arising from the solvent. An attempt to determine the quantum yield of the photo-induced chlorination by the spectrophotometric method[4] was unsuccessful because of the small spectral change during the reaction (see Fig. 1). However, it was roughly estimated to be in the order of 10^{-3} from the initial absorbance change of the reaction at 400 nm. The value was in the same order of magnitude as reported for photolysis of [Al(tpp)Et] in $CHCl_3$.[4]

Figure 3(A) shows an EPR spectrum obtained upon irradiation of a degassed benzene solution of **1** with visible light ($\lambda > 450$ nm) in the presence of ten-fold excess of spin trapping agent, 2,4,6-tri-*t*-butylnitrosobenzene (TBN). Though the spectral pattern is rather complicated, the spectrum can be unequivocally assigned as an overlap of signals due to two spin adducts, **2** and **3** in Eq. 1.

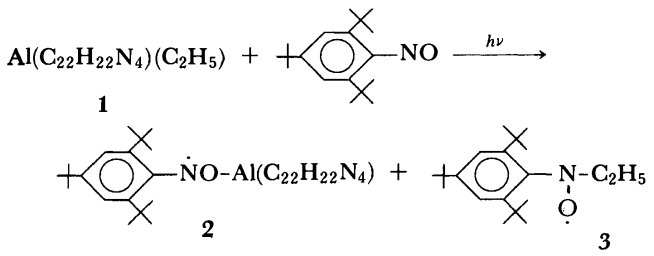

(1)

Figures 3(B) and 3(C) show the simulation spectra of **3** and **2**. EPR parameters obtained were: for **2**, a^N=1.06, a^{Al}=0.14, a_m^H=0.17[9] mT, and g=2.0048; for **3**, a^N=1.34, a^H=1.78, and a_m^H=0.08[9] mT, and g=2.0061. These values are almost identical with those previously reported for TBN spin adducts obtained upon photolysis of [Al(tpp)(Et)].[4] Spin adduct **2** is the anilino radical bonded through O to Al, while **3** is the nitroxyl radical bonded through N to Et. The EPR intensity ratio for spin adducts **3** and **2** was found to be approximately 1 : 1.5. This ratio is likely to depend on trapping rate. In the absence of TBN, no EPR signal was observed under the same conditions. The recombination of radicals may be too fast to detect the EPR signals.

Emission behavior from photoexcited state of **1** and its free ligand $H_2(C_{22}H_{22}N_4)$ has been also studied in 2-methyltetrahydrofuran (MTHF).[10] Complex **1** showed emission with a maximum peak at 580 nm and the lifetime was found to be 50 ms at 77 K. Excitation spectrum was in accord with its absorption. These results indicate that the emitting state is attributable to the excited triplet state of the ligand π-conjugated system. Recently we observed the triplet signal for compound **1** using time resolved EPR technique.[8] It should be noted that the phosphoresence was not observed at 290 K when the oxygenated solution was used, while it was observed at both 77 and 290 K when the solution was degassed. That is, the triplet state was quenched by oxygen at room temperature.

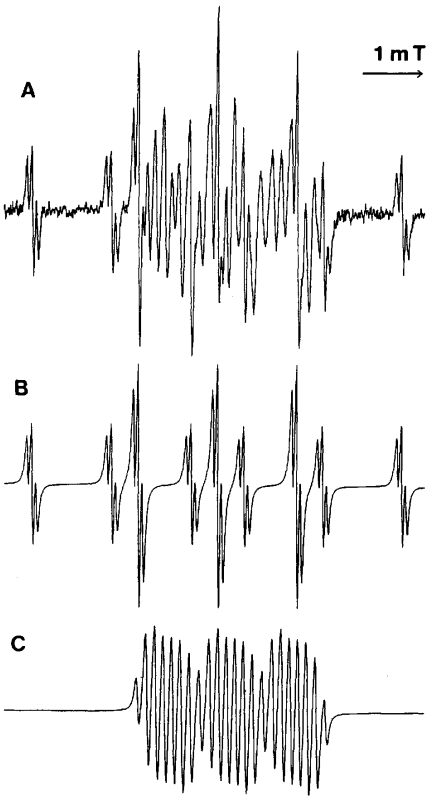

Fig. 3. A: EPR spectrum of a benzene solution of $Al(C_{22}H_{22}N_4)(C_2H_5)$ with TBN upon light irradiation ($\lambda > 450$ nm). B and C: EPR simulation spectra of TBN-C_2H_5 and TBN-$Al(C_{22}H_{22}N_4)$, respectively.

This work clearly indicates that the homolytic cleavage of Al-C bond of the present complex is induced by visible light, that is mainly by the in-plane ligand absorption. However, when the reaction was carried out in non-reactive solvent such as benzene or in the absence of spin traps, neither EPR signal nor NMR spectral change was observed under the irradiation. In order to clarify whether the photochemically reacting species is singlet or triplet, further detailed studies are necessary.

Experimental

Sample Preparation. $Al(C_{22}H_{22}N_4)(C_2H_5)$ was prepared by the method reported in the literature.[6]

NMR Measurement and Visible-Light Irradiation. ^1H NMR spectra were recorded on a JEOL GX-400 spectrometer. An Ushio ultra-high pressure 500 W mercury lamp and Toshiba glass filter ($\lambda > 450$ nm) were used for irradiation of visible light at 20 °C.

EPR Measurement. EPR spectra were recorded on a JEOL FE2XG spectrometer (100 kHz modulation) at room temperature. Visible light irradiation was carried out with the use of the same mercury lamp and glass filter as those in the NMR measurements.

Emission Experiment. Fluoresence and phosphoresence spectra were recorded on a Spex Fluorolog 2 fluorimeter quipped with a Xenon lamp.

References

1) J. F. Endicott and T. L. Netzel, *J. Am. Chem. Soc.*, **101**, 4000 (1979).
2) M. Hoshino, K. Yasufuku, H. Seki, and H. Yamazaki, *J. Phys. Chem.*, **89**, 3080 (1985).
3) S. Inoue, H. Murayama, N. Takeda, and Y. Ohkatsu, *Chem. Lett.*, **1982**, 317.
4) S. Tero-Kubota, N. Hoshino, M. Kato, V. L. Goedken, and T. Ito, *J. Chem. Soc., Chem. Commun.*, **1985**, 99.
5) P. Cocolios, R. Guilard, D. Bayeul, and C. Lecomte, *Inorg. Chem.*, **24**, 2058 (1985).
6) V. L. Goedken, H. Ito, and T. Ito, *J. Chem. Soc., Chem. Commun.*, **1984**, 1453.
7) M. C. Weiss, G. Gordon, and V. L. Goedken, *Inorg. Chem.*, **16**, 305 (1977).
8) S. Tero-Kubota, H. Oshio, T. Ito, V. L. Goedken, and J. Higuchi, *Chem. Phys. Lett.*, **131**, 430 (1986).
9) a_m^H denotes hyperfine coupling constants with benzene ring proton at meta position.
10) The emission from the free ligand was disclosed to be fluoresence. The free ligand showed an emission spectrum with maximum at 560 nm, but its excited state decayed very rapidly after the pulsed excitation. It is suggested that the presence of Al makes the intersystem crossing from S_1 or S_2 to T_1 easier.

The Thermal Decomposition of Lithium Hydrogenphosphoramidate Trihydrate

Choichiro SHIMASAKI,* Hiroki SUZUKI, and Hiroshi TODA
Department of Industrial Chemistry, Faculty of Engineering, Toyama University, Gofuku, Toyama 930
(Received December 17, 1986)

Synopsis. The thermal decomposition of lithium hydrogenphosphoramidate trihydrate $LiHPO_3NH_2 \cdot 3H_2O$ was investigated by means of DTA-TG, X-ray diffraction analysis, IR, ^{31}P NMR, and compositional analysis. The decomposition proceeds via an anhydrous phase, a newly found intermediate phase, and polyphosphates to lithium metaphosphate. The activation energies of the dehydration of the water of crystallization and of the polymerization reaction for the thermal decomposition were estimated to be 96.2 and 105.4 kJ mol^{-1} respectively.

The reaction products[1,2] between urea (or its nitrogen derivatives) and phosphoric acid have been used as a flameproofing and fire-retardant (glow-retardent) agent. The derivatives of phosphoramidates have been investigated systematically for these purposes: The thermal decomposition of ammonium, sodium, and potassium hydrogenphosphoramidate (anhydrous salts) was previously reported by the present authors.[3,4] The decomposition study was been extended to lithium hydrogenphosphoramidate trihydrate $LiHPO_3NH_2 \cdot 3H_2O$ in the present work.

Experimental

Preparation Methods. No anhydrous salt was synthetically obtained. The sample (trihydrated salt, yield; 65—70%) was prepared as follows: Ammonium hydrogenphosphoramidate[5] (4.6 g 0.04 mol) was dissolved in 40 ml of a 2.0 M (1M=1 mol dm^{-3}) lithium hydroxide solution. This solution was then cooled (to 5—10 °C), neutralized (to pH 6) with glacial acetic acid, and precipitated with 300 ml of ethanol. The salt filtered out with suction was recrystallized repeatedly from a water-ethanol solution, washed with ethanol and ether, and air-dreid.

Measurements. The chemical analysis was made by the method reported by Watanabe et al.[6] The DTA-TG (Rigakudenki Co., Ltd., Japan) was performed in air. The dehydrated samples were hygroscopic, so that the X-ray diffraction was measured at high temperatures with nickel-filtered Cu $K\alpha$ radiation with a X-ray diffractometer XD-3A (Shimazu Co., Ltd., Japan). The IR spectra (KBr disc method) of a sample (quenched and preserved in a desiccator) were measured with an IR-810 spectrometer (JASCO, Japan). The ^{31}P NMR spectra of the solutions were measured with a JNM-FX-900FT-NMR spectrometer (JEOL, Japan); the quenched sample (50 mg) was dropped into a 6% EDTA deuterated-water solution and stirred for several minutes.

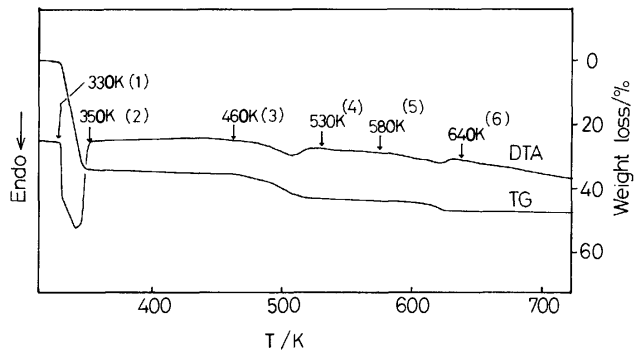

Fig. 1. DTA and TG curves of $LiHPO_3NH_2 \cdot 3H_2O$. Heating rate: 1 K min^{-1}.

Results and Discussion

A typical DTA-TG curve of $LiHPO_3NH_2 \cdot 3H_2O$ is shown in Fig. 1. In this figure, the temperatures for analyzing the samples are indicated; the results of the compositional analysis, the IR spectra, the ^{31}P NMR spectra, and the X-ray diffraction are shown in Table 1, and Figs. 2, 3, and 4 respectively. In Fig. 1, three endothermic peaks and the corresponding weight losses are shown: the first stage (330—350 K), the second stage (slight change, 460—530 K), and the third stage (slight change, 580—640 K).

The first stage of the decomposition is assumed to be the dehydration of the crystalline water as follows:

$$LiHPO_3NH_2 \cdot 3H_2O \rightarrow LiHPO_3NH_2 + 3H_2O. \quad (1)$$

The results of the compositional analysis and the weight loss (Sample No. 2 in Table 1) support this hypothesis. The X-ray diffraction in Fig. 4 has changed from that of $LiHPO_3NH_2 \cdot 3H_2O$ (Sample No. 1) to a new pattern (Sample No. 2) which should be assigned to the anhydrous phase. A splitting of the

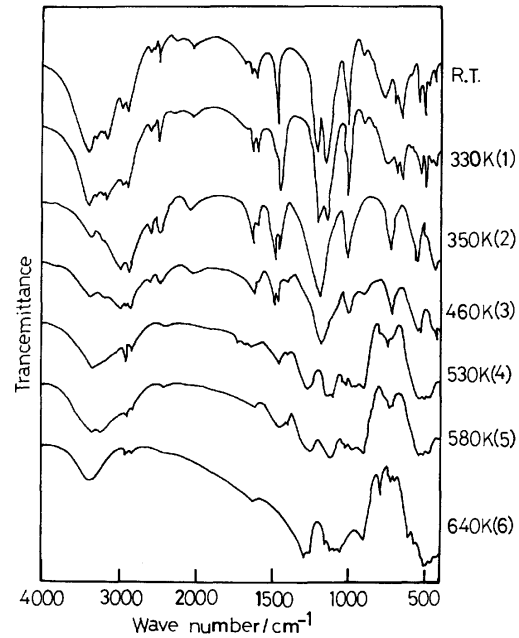

Fig. 2. IR spectra of the thermal decomposition products of $LiHPO_3NH_2 \cdot 3H_2O$.

DTA peak was observed when it was heated rapidly (e.g., 9 or 11 K min^{-1}).

The anhydrous hydrogen phosphoramidate is considered to become zwitterion as follows at 330—350 K, since the IR absorption due to the zwitterion reported by Corbrige et al.[7] were observed at 1460 and 1595 cm^{-1} in Sample Nos. 2 and 3 in Fig. 2. In Fig. 4 (the X-ray diffraction pattern of Sample Nos. 2 and 3), a decrease in the peak intensity of the anhydrous phase and a very weak trace of a different diffraction pattern (detailed analysis impossible) was apparently observed.

Therefore, lithium hydrogen phosphoramidate is considered to become zwitterion when transformed as follows:

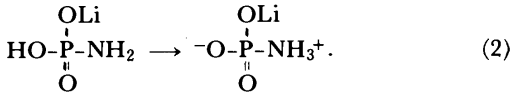

$$HO\text{-}P(=O)(OLi)\text{-}NH_2 \longrightarrow {}^{-}O\text{-}P(=O)(OLi)\text{-}NH_3^{+}. \quad (2)$$

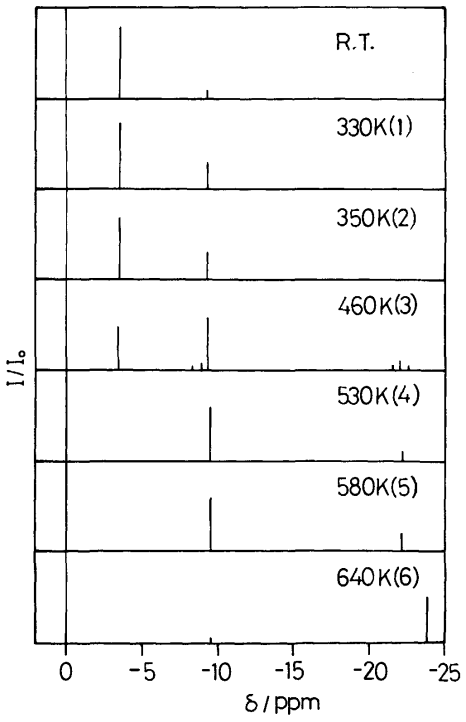

Fig. 3. ^{31}P NMR spectra and of the thermal decomposition products of $LiHPO_3NH_2 \cdot 3H_2O$.

The second stage of the decomposition is assumed to be the following reaction:

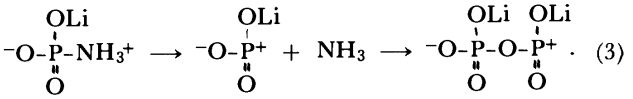

$$HO\text{-}P(=O)(OLi)\text{-}NH_3^{+} \longrightarrow {}^{-}O\text{-}P^{+}(=O)\text{-}OLi + NH_3 \longrightarrow {}^{-}O\text{-}P(=O)(OLi)\text{-}O\text{-}P^{+}(=O)\text{-}OLi \cdot \quad (3)$$

The results of the compositional analysis (Sample No. 4 in Table 1), show the apparent disappearance of the IR absorption, and the X-ray diffraction pattern due to the zwitterion mentioned above (Sample No. 4 in Figs. 2 and 4), and a pungent odor of ammonia.

Concomitantly, the water in Eq. 1 is held by adsorption on the surface of the sample; therefore, the following (dimerization) reaction is assumed to occur simul-

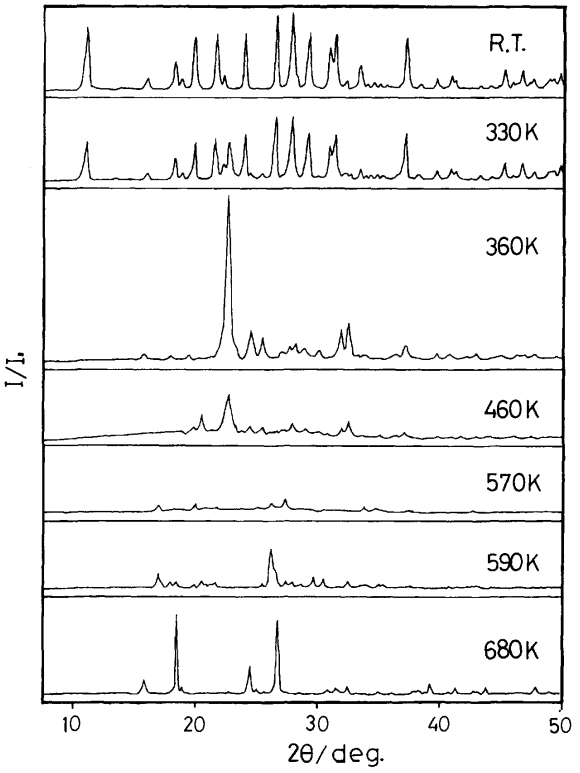

Fig. 4. X-Ray diffraction diagrams of the thermal decomposition products of $LiHPO_3NH_2 \cdot 3H_2O$. Heating rate: 2 K min^{-1}.

Table 1. Weight Loss and Composition of the Thermal Products of $LiHPO_3NH_2 \cdot 3H_2O$

Sample	Wt. loss %	P %	Li %	P/Li[a]	Total N/%	N/% as NH_4^+	H %
R.T.	0.0	20.8 (19.7)[b]	4.8 (4.4)[b]	0.97	9.0 (8.9)[b]	0.0	5.8 (5.8)[b]
1	2.8	20.9	4.5	1.04	9.8	0.0	5.3
2	31.4	30.0	6.4	1.05	13.0	0.0	3.3
3	33.8 (34.4)[c]	30.0 (30.1)[c]	6.5 (6.7)[c]	1.03	12.5 (13.6)[c]	2.9	3.3 (2.9)[c]
4	41.3	33.4	7.2	1.04	3.2	2.5	1.0
5	40.2	33.4	7.4	1.01	4.0	3.0	1.4
6	46.2 (44.6)[d]	36.7 (36.0)[d]	8.2 (8.1)[d]	0.99	0.0	0.0	0.0

a) Mole ratios normalized by Li content. b) Calcd value of $LiHPO_3NH_2 \cdot 3H_2O$. c) Calcd value of $LiHPO_3NH_2$. d) Calcd value of $LiPO_3$.

taneously with the second stage of the decomposition:

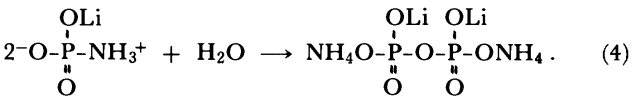

(4)

The ^{31}P NMR spectrum of Sample No. 3 indicated small peaks of middle-PO_4 groups and small peaks of an end-PO_4 group. The product was metastable at room temperature, therefore, the ^{31}P NMR spectrum of the product indicated peaks due to phosphoramidate and an end-PO_4 group, and hardly changed in comparison with Sample No. 2. The IR absorption of a NH_4^+ was observed for Sample No. 3. It may be estimated that any indications of the polymerization reaction could be recognized by means of these results.

The ^{31}P NMR spectrum of Sample No. 6 indicated a small peak of an end-PO_4 group and a peak of a middle-PO_4 group. Sample No. 6 contained no nitrogen and hydrogen. The X-ray diffractions of the resultant thermal product at a given isothermal temperature are shown in Fig. 3. The three strongest lines of $LiPO_3NH_2 \cdot 3H_2O$ disappeared at 360 K, and the three new lines which appeared from 330 K became strong at 360 K. The diffraction lines at 360 K are considered to be those of the anhydrous product. The thermal product at 570 K was found to be amorphous by the use of an X-ray diffractor, while the product at 590 K showed weak, unknown X-ray diffraction peaks. The thermal product at 680 K showed X-ray diffraction peaks of lithium metaphosphate.[8]

The third stage of the decomposition is assumed to be the following reaction:

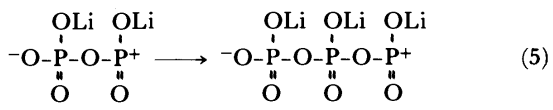

(5)

The activation energies of the first and second stages for the thermal decomposition for $LiHPO_3NH_2 \cdot 3H_2O$ were determined tentatively from the DTA curves (Kissinger method[9]) and the TG curves (Ozawa method[10,11]) with the heating rate of 1, 3, 5, 7, 9, and 11 K min^{-1}: 95.3 and 97.1 kJ mol^{-1} for the first stage (average; 96.2 kJ mol^{-1}) and 103.9 and 106.8 kJ mol^{-1} for the second stage (average; 105.4 kJ mol^{-1}) respectively.

We wish to thank Prof. Ikuya Matsuura for the X-ray diffraction analysis, Mr. Kiyoshi Terayama for the DTA-TG and Mr. Yoshiharu Yoneyama for the NMR spectra.

References

1) R. W. Little, "Flameproofing Textile Fabrics," Reinhold Publishing Corp., New York (1957), p. 410.
2) G. S. Buck, "Encyclopedia of Chemical Technology," ed by R. E. Kirk and D. F. Othmer, Interscience Publishers, New York (1951), Vol. VI, pp. 543—558.
3) C. Shimasaki, Y. Oono, F. Takai, M. Shoji, and M. Yoshizawa, *Nippon Kagaku Kaishi*, **1982**, 376.
4) C. Shimasaki, S. Ookawa, and R. Ishizaka, *Bull. Chem. Soc. Jpn.*, **58**, 592 (1985).
5) F. A. Cotton, "Inorganic Syntheses," McGraw-Hill Book Company, New York (1972), Vol. XIII, p. 23.
6) M. Watanabe, T. Inagaki, and S. Sato, *Bull. Chem. Soc. Jpn.*, **56**, 458 (1983).
7) D. E. C. Corbridge and E. J. Lowe, *J. Chem. Soc.*, **1954**, 493.
8) "Index (inorganic) to the powder diffraction file," American Society for Testing Materials (1968). JCPDS Card 13—438.
9) H. E. Kissinger, *Anal. Chem.*, **29**, 1702 (1957).
10) T. Ozawa, *Bull. Chem. Soc. Jpn.*, **38**, 1881 (1965).
11) T. Ozawa, *J. Therm. Anal.*, **2**, 301 (1970).

Determination of Mercury by Graphite Furnace Atomic Absorption Spectrometry after Ion-Pair Extraction with Zephiramine in Small Scale

Yasuaki OKAMOTO, Takahiro KUMAMARU,* Shigeki HARA,† Hiroshi MATSUO,† and Mitsuo KIBOKU††
Department of Chemistry, Faculty of Science, Hiroshima University, Higashisenda-machi, Naka-ku, Hiroshima 730
†Division of Interdisciplinary Studies of Natural Sciences, Faculty of Integrated Arts and Sciences, Hiroshima University, Higashisenda-machi, Naka-ku, Hiroshima 730
††Department of Applied Chemistry, Faculty of Engineering, Kinki University, Hiro-machi, Kure 737-01
(Received December 24, 1986)

Synopsis. A simple procedure for the determination of mercury(II) by graphite furnace atomic absorption spectrometry is described. Mercury(II) was extracted as tetradecyldimethylbenzylammonium (Zephiramine) thiocyanatomercurate(II) into diisobutyl ketone (DIBK) by using a 10-cm^3 centrifuge tube, and an aliquot of the organic extract was directly pipetted out from the upper layer in the centrifuge tube and injected into the graphite furnace. The heating temperature program by ramp mode and the background correction by means of a 2-channel type atomic absorption spectrometer gave satisfactory results.

In the determination of volatile elements such as mercury by graphite furnace atomic absorption spectrometry (GF-AAS), losses of the analytes may occur during the ashing stage in the thermal cycle. Recently, a number of publications have described matrix modification or stabilization procedures by which analyte losses before atomization stage may be minimized or eliminated.[1-5] For example, the absorbance of mercury can be increased by addition of ammonium sulfide to the sample solution; this effect has been attributed to the formation of stable mercury(II) sulfide at the ashing temperature.[1] Kirkbright et al. have recommended a procedure in which the addition of potassium dichromate to the mercury sample in nitric acid solution allowed the use of ashing temperatures up to 250 °C without significant loss of mercury.[2] Filippelli reported a method for determining low levels of mercury by GF-AAS with preliminary preconcentration using ammonium 1-pyrolidinecarbodithioate (APDC)-chloroform extraction system.[3]

In this paper a method for the determination of mercury by GF-AAS combined with a small scale solvent extraction technique is described; mercury(II) was converted to thiocyanatomercurate and extracted into diisobutyl ketone (DIBK) as the ion-pair with tetradecyldimethylbenzylammonium (Zephiramine), and the extract was injected into graphite tube to measure the atomic absorption of mercury. This method is convenient and rapid, as the extraction is carried out by using a centrifuge tube and an aliquot of the organic phase in the upper layer can be directly pipetted out of the tube. This enables us to use much smaller amounts of samples and reagents compared with those in the conventional extraction, which serves to reduce laboratory-used mercury waste.

Experimental

Apparatus. A Nippon Jarrell-Ash Model AA-8200 two-channel atomic absorption spectrometer equipped with a Model FLA-100 graphite furnace atomizer was used. Background correction was accomplished by using a deuterium lamp. A Rikadenki Model B-381 strip chart recorder was used to monitor both the background-corrected atomic absorption and the background signals. Digital micropipettes of Gilson Model Pipetman P-20, P-200, P-1000, and P-5000 were used. The shaking for the extraction was carried out with a Taiyo Model SR-II shaker, where 10-cm^3 centrifuge tubes with ground stoppers were used instead of separatory funnels.

Reagents. Pure water from an Organo Miniclear Model DC-610 system was used. All chemicals were of analytical-reagent grade and were used without further purification. A 1000 μg cm^{-3} of mercury(II) standard stock solution was prepared by dissolving mercury(II) nitrate in dilute nitric acid. Solutions of suitable concentration were prepared by dilution with 0.1 mol dm^{-3} nitric acid before use. A 5.0×10^{-2} mol dm^{-3} Zephiramine solution was prepared by dissolving 2.02 g of Zephiramine chloride dihydrates (Wako Pure Chemicals) to 100 cm^3 with water. A 2.0 mol dm^{-3} potassium thiocyanate solution was prepared by dissolving 19.4 g of potassium thiocyanate (Wako Pure Chemicals) to 100 cm^3 with water.

Standard Procedure. Transfer an aliquot of the mercury(II) solution containing not more than 80 ng mercury(II) into the centrifuge tube. Add 200 mm^3 of the potassium thiocyanate solution and 80 mm^3 of the Zephiramine solution, and dilute the mixture to 5 cm^3 with water. Then, add 1 cm^3 of DIBK. Shake the centrifuge tube for ca. 5 min by means of the mechanical shaker. After standing for ca. 15 min, inject an aliquot of 20 mm^3 of the upper organic phase into the graphite furnace and measure the atomic absorption peak signal of mercury. The instrument operating conditions are listed in Table 1.

Results and Discussion

Optimization of Instrument Operating Conditions. In order to avoid the loss of mercury before the atomization stage and to separate the atomic absorption peak signal from the background signal, a moderate elevation of temperature throughout the heating cycle was very essential. Experiments were carried out to determine the loss of mercury during the drying and ashing stages of the heating program by recording signals from 20-mm^3 aliquots containing 1.6 ng mercury(II). A setting of 60 °C-50 s for the drying stage was suitable. No appreciable loss of mercury from the furnace was observed at the ashing temperature of up to ca. 300 °C with the ramp mode which avoided abrupt vaporization. The background signal decreased significantly with increase in the ashing temperature. The

Table 1. Instrument Operating Conditions

Atomizer (FLA-100)	
Sample injection	20 mm^3
Drying (Ramp mode)	6 A (60 °C) for 50 s
Ashing (Ramp mode)	25 A (300 °C) for 120 s
Atomization (Maximum ramp mode)	95 A (1300 °C) for 5 s
Clean up	280 A (2900 °C) for 3 s
Purge argon gas flow	2.5 $dm^3 min^{-1}$
Spectrometer (AA-8200)	
Wavelength	
Atomic absorption (HCL)	253.7 nm (Hg I)
Background correction (D_2)	253.0 nm
Damping	1 (0.1 s time constant)
Recorder range	100 mV/full scale

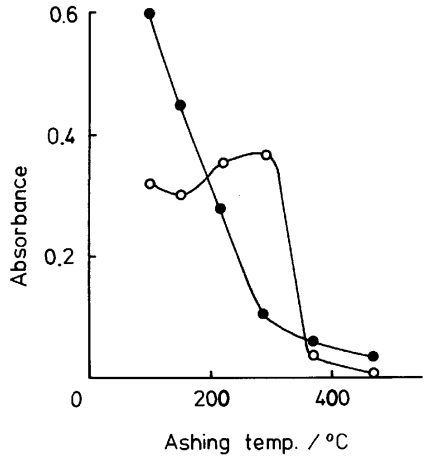

Fig. 1. Effect of ashing temperature on atomic absorption and background peak signals. Mercury(II): 1.6 ng, O: mercury atomic absorption, ●: background. See Table 1 for conditions.

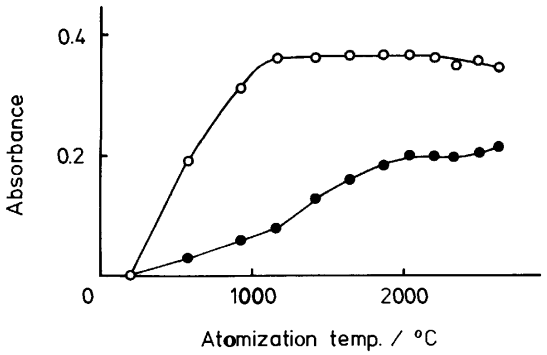

Fig. 2. Effect of atomization temperature on atomic absorption and background peak signals. Mercury(II): 1.6 ng, O: mercury atomic absorption, ●: background. See Table 1 for conditions.

results are shown in Fig. 1. Therefore, the ashing condition of 300 °C-120 s was selected for the standard procedure. The effects of atomization temperature with the maximum ramp mode on the atomic absorption and background peak signals are shown in Fig. 2. The atomic absorption peak signal was maximum and constant over the temperature range of 1200—2200 °C, whereas the background signal increased as the temperature increased. So that, the atomization

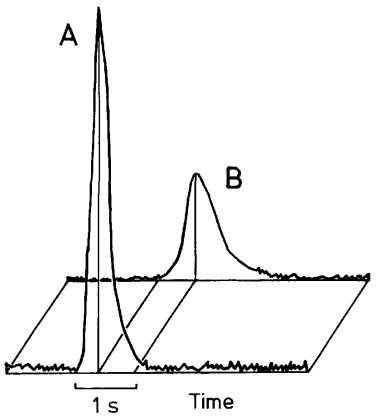

Fig. 3. Signal vs. time profiles. Mercury(II): 1.6 ng. A: Mercury atomic absorption, B: background. See Table 1 for conditions.

temperature of 1300 °C was chosen. Under the conditions, the atomic absorption signal of mercury appeared first, followed by the background peak signal ca. 0.6 s later. The signal vs. time profiles obtained for both the atomic absorption and background are shown in Fig. 3.

Optimization of Conditions of Solvent Extraction. In liquid-liquid extraction, the organic solvent should have a high distribution coefficient for the analyte and be insoluble in water. Moreover, it is preferable for the organic solvent to float on the aqueous phase so that the organic extract can be directly pipetted out of the centrifuge tube without separating the organic layer. DIBK was confirmed to be a favorable solvent in these respects.

The effect of pH on the extraction was investigated by extracting mercury(II) from a series of aqueous solutions containing 400 ng mercury(II) buffered at various pH values, while other variables in the standard procedure were kept constant. The maximum extraction of the ion-pair of Zephiramine thiocyanatomercurate(II) was obtained, when the acidity of the aqueous phase lay within the range of 1 mol dm^{-3} in nitric acid to pH 7.

The effects of the concentration of potassium thiocyanate and Zephiramine in the aqueous phase on the extraction were also examined according to the standard procedure. When the concentration of mercury(II)

Table 2. Analytical Results of Mercury in Several Waste Water Samples

Sample	Mercury found/ng cm^{-3}	
	Calibration curve method	Standard addition method
Raw sewage water A[a)]	1.8±0.2	2.0±0.3
Raw sewage water B[a)]	N.D.[b)]	N.D.[b)]
Raw mercury waste water A	14.3±0.3	14.7±0.3
Raw mercury waste water B	28.6±0.4	28.8±0.3
Raw mercury waste water C	9.8±0.3	12.0±0.2

a) Acid digestion sample.[6] b) N.D.: Not detected.

in the aqueous phase was kept at 80 ng cm^{-3}, it was necessary for the maximum and constant extraction that the concentrations of potassium thiocyanate and Zephiramine were at least 1×10^{-2} and 2×10^{-4} mol dm^{-3}, respectively. In order to minimize the background peak signal which was mainly caused by an excess Zephiramine extracted with the ion-pair, we selected 8×10^{-2} and 8×10^{-4} mol dm^{-3} as the initial concentrations of potassium thiocyanate and Zephiramine in the aqueous phase, respectively.

Extraction Percentage. The extraction efficiency was estimated to be 99% from the results obtained by the successive extraction of mercury(II) in the aqueous phase according to the standard procedure in which the initial concentration of mercury(II) in the aqueous phase was kept at 80 ng cm^{-3}.

Detection Limit and Working Curve. The detection limit was 0.5 ng cm^{-3} on the basis of the above results. The detection limit was defined as the concentration in the aqueous phase required to give a signal three-fold greater than the standard deviation of the base line fluctuation. The calibration curve was linear up to 80 ng cm^{-3} mercury(II) initially present in the aqueous phase. The relative standard deviation for 10 replicate determinations was 1.0% for 40 ng mercury(II). As to the stability of the extract, no appreciable change in the absorbance was observed over the period of 48 h, even when the organic phase was kept standing with the aqueous phase.

Application to Determination of Mercury in Waste Water Samples. Some waste water samples were analyzed for mercury contents by the standard procedure. As a check, the samples were also analyzed by standard addition method. As can be seen from the results given in Table 2, both data are in satisfactory agreement.

References

1) R. D. Ediger, *At. Absorpt. Newsl.*, **14**, 127 (1975).
2) G. F. Kirkbright, H. C. Shan, and R. D. Snook, *At. Spectrosc.*, **1**, 85 (1980).
3) M. Filippelli, *Analyst (London)*, **109**, 515 (1984).
4) R. F. Sanzolone and T. T. Chao, *Analyst (London)*, **108**, 58 (1983).
5) Z. Slovak, *Anal. Chim. Acta*, **115**, 111 (1980).
6) Japanese Industrial Standard, K 0102 (1986).

Synthesis and Characterization of Imidazolate-Bridged Trinuclear (Copper(II)-Manganese(II)-Copper(II)) Complexes

Naohide MATSUMOTO,* Junko KANESAKA, Akira OHYOSHI, Masaaki NAKAMURA,†
Susumu KOHATA,†† and Hisashi ŌKAWA†††
Department of Applied Chemistry, Faculty of Engineering, Kumamoto University, Kurokami 2-39-1, Kumamoto 860
†Department of Chemistry, Faculty of Science, Kumamoto University, Kurokami 2-39-1, Kumamoto 860
††Yatsushiro National College of Technology, Yatsushiro 866
†††Department of Chemistry, Faculty of Science, Kyushu University, Hakozaki, Higashi-ku, Fukuoka 812
(Received February 2, 1987)

Synopsis. Imidazolate-bridged trinuclear(copper(II)-manganese(II)-copper(II)) complexes [CuLMn(tfa)$_2$LCu]-2H$_2$O **1** and [CuLMn(hfa)$_2$LCu]3H$_2$O **2** have been prepared and characterized, where tfa=trifluoroacetylacetonate, hfa=hexafluoroacetylacetonate, H$_2$L=unsymmetrical quadridentate Schiff base derived from the condensation reaction of acetylacetone, ethylenediamine, and 4-formylimidazole with the mole ratio of 1:1:1. The magnetic susceptibility data were represented by a spin-only interaction model(1/2-5/2-1/2) with J_{Mn-Cu} value of -13 cm^{-1} for **1** and -8 cm^{-1} for **2**.

Hetero-polynuclear complexes which contain magnetic centers with different spin-multiplicities are of current interest from the point of view of the development of ferromagnets[1] and models of active sites of some metal enzymes such as bovine erythrocyte superoxide dismutase and cytochrome c oxidase.[2,3] In the previous paper,[4] we reported the synthesis and characterization of imidazolate-bridged binuclear copper(II) complexes in which two coordination spheres of copper(II) ions are not identical. These complexes have been prepared by the reaction of the copper(II) complex with unsymmetrical quadridentate ligand containing an imidazole moiety (a-site component complex) and the copper(Il) complex exhibiting an unsaturated coordination site (b-site component complex) under the presence of one equivalent of alkali. This synthetic method can be easily extended to the synthesis of hetero-metal polynuclear complexes by using another metal complex instead of the copper(II) complex as the b-site complex. In this study, we report the synthesis and characterization of imidazolate-bridged trinuclear copper(II)-manganese(II)-copper(II) complexes **1** and **2** whose schematic structures are shown in the drawing as an example of the complexes containing magnetic centers with different spin-multiplicities.

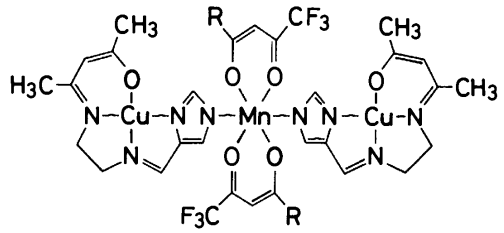

1 (R = CH_3); 2 (R = CF_3)

Experimental

Physical Measurements. Elemental analyses for C, H, and N were performed by Mr. Shinichi Miyazaki at the Technical Service Center of Kumamoto University. Elemental analyses for Mn and Cu were carried out on a Hitachi 508 atomic absorption spectrophotometer. Melting points were measured on a Yanagimoto micro-melting point apparatus and were uncorrected. Electrical conductivity measurements were carried out on a Denki Kagaku Keiki AOC-10 on ca. 10^{-3} mol dm^{-3} solutions in chloroform. Thermogravimetric analyses were carried out on a Shimadzu TGC 20 type microthermobalance at a heating rate of 5 °C min^{-1}, using ca. 10 mg samples for each run. Infrared spectra were recorded on KBr discs with a JASCO A-702 spectrophotometer. Magnetic susceptibilities were obtained by the Faraday method from the temperature of liquid nitrogen to the ambient temperature, according to the procedure reported previously. The susceptibilities were corrected for the diamagnetism of the component atoms by the use of Pascal's constants. The molar effective magnetic moment was calculated by the equation $\mu_{eff}=2.828(\chi_M T)^{1/2}$.

Syntheses. The starting complexes [Mn(tfa)$_2$]2H$_2$O and [Mn(hfa)$_2$]2H$_2$O were prepared by mixing manganese(II) acetate tetrahydrate and each of trifluoroacetylacetone and hexafluoroacetylacetone with the mole ratio of 1:2 in water according to the modified method in the literature.[5] The complex [CuHL](ClO$_4$) was prepared by the method described elsewhere.[6]

Hetero-Metal Trinuclear Complex [CuLMn(tfa)$_2$LCu]2H$_2$O 1. A suspension of [CuHL](ClO$_4$) (382 mg, 1 mmol) and [Mn(tfa)$_2$]2H$_2$O (397 mg, 1 mmol) in 150 cm^3 of chloroform was refluxed for 10 min. To this was slowly added a solution of triethylamine (1 mmol) in 10 cm^3 of chloroform. During the addition of triethylamine, the complex [CuHL](ClO$_4$) was gradually dissolved. After the completion of the addition, the solution was further refluxed for 30 min and then filtered. The filtrate was evaporated to dryness, the residue was dissolved in 50 cm^3 of diethyl ether, and the ether solution was filtered and kept overnight in a refrigerator. During that time, reddish pink microcrystalline materials precipitated. They were collected by suction filtration, washed with a small amount of diethyl ether, and dried in vacuo. Attempts at recrystallization were unsuccessful. Found: C, 39.93; H, 4.46; N, 11.60; Mn, 5.7; Cu, 12.7%. Calcd for $Cu_2MnF_6O_6N_8C_{32}H_{36}\cdot 2H_2O$: C, 39.99; H, 4.17; N, 11.67; Mn, 5.9; Cu, 13.7%. Mp 203—205 °C (decomp), Λ_M 0.4 S mol^{-1} cm^2 (chloroform), TGA: mass loss, 3.2 wt% (95—155 °C); Calcd for 2H$_2$O, 3.7 wt%.

Hetero-Metal Trinuclear Complex [CuLMn(hfa)$_2$LCu]·3H$_2$O 2. This complex was prepared by a similar method except that [Mn(hfa)$_2$]2H$_2$O instead of [Mn(tfa)$_2$]2H$_2$O was used. Attempts at recrystallization were unsuccessful. Found: C, 35.30; H, 3.40; N, 10.29; Mn, 4.7; Cu, 11.6%. Calcd for $Cu_2MnF_{12}O_6N_8C_{32}H_{30}\cdot 3H_2O$: C, 35.37; H, 3.34; N, 10.31; Mn, 5.1; Cu, 11.7%. Mp. 238—241 °C, Λ_M 0.1 S mol^{-1}cm^2 (chloroform), TGA: mass loss, 4.5 wt% (80—140 °C); Calcd for 3H$_2$O, 5.0 wt%.

Results and Discussion

The complexes **1** and **2** assume the chemical formulations [CuLMn(tfa)$_2$LCu]2H$_2$O and [CuLMn(hfa)$_2$-LCu]3H$_2$O, respectively, though the starting materials [CuHL](ClO$_4$) and each of [Mn(tfa)$_2$]2H$_2$O and [Mn-(hfa)$_2$]2H$_2$O were mixed in the mole ratio of 1 : 1 as described in the experimental section. The configuration around the manganese(II) ion in the present complexes **1** and **2** is presumed to be of six-coordination with four oxygen atoms of two β-diketonato ligands and two imidazolate nitrogen atoms of the a-site component complexes. The elemental analyses for Mn and Cu by atomic absorption verified the 1 : 2 ratio of Mn and Cu. The complexes **1** and **2** crystallize as hydrates. The water of crystal was detected by thermogravimetric analyses. The molar electrical conductances measured in chloroform solutions revealed that both complexes **1** and **2** are nonelectrolytes. This suggests that the imidazole-proton of [CuHL]$^+$ is deprotonated and the imidazolate nitrogen of [CuL] thus formed functions as the bridging group to the manganese(II) ion. The deprotonation of the imidazole-proton is supported by infrared spectra: The IR bands due to the imidazole-proton stretching vibration (3350 cm^{-1}) and the perchlorate anion (around 1080 cm^{-1}) of the starting material [CuHL](ClO$_4$] disappear in the spectrum of the complexes **1** and **2**.

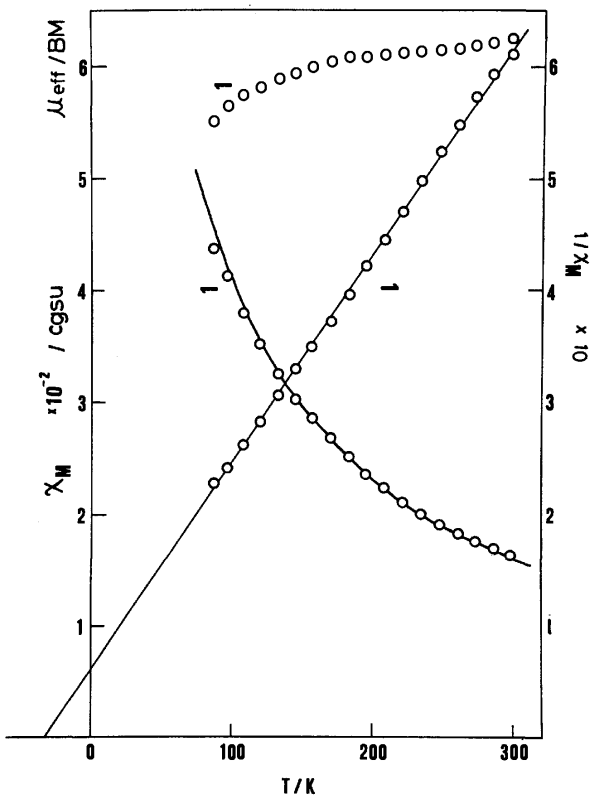

Fig. 1. Plots of the temperature dependence of the molar magnetic susceptibility, of the reciprocal molar magnetic susceptibility, and of the effective magnetic moment for the complex [CuLMn(hfa)$_2$LCu]3H$_2$O, **2**, where the solid curve of χ_M vs. T plot represents the theoretical curve of Eq. 1 with the parameters of g=2.00 and J=−8cm^{-1}.

The complexes **1** and **2** show qualitatively a similar magnetic behavior. Plots of the temperature dependence of the molar magnetic susceptibility, reciprocal molar magnetic susceptibility, and effective magnetic moment for the complex **2** are shown in Fig. 1, where χ_M, $1/\chi_M$, and μ_{eff} is given as the values per trinuclear complex in this text. The $1/\chi_M$ vs. T plots for the complexes **1** and **2** are nearly linear in the temperature range measured (80—300 K) and obey the Curie-Weiss law ($\chi_M=C(T+\theta)$) with the Weiss constants of θ=60 K for **1** and θ=33 K for **2**, where the Weiss constants were obtained by a least-squares method and the maximum deviation of the observed $1/\chi_M$ values from the calculated values is 2.8% for **1** and 3.5% for **2**, respectively. This suggests that there operates intra- or/and intermolecular antiferromagnetic interaction. The molar effective magnetic moment gradually increased from 5.3 BM for **1** and 5.5 BM for **2** at 87 K to 6.2 BM for **1** and 6.2 BM for **2** at 300 K. It is therefore apparent that the manganese(II) ion in the present complexes are high-spin(S=5/2). The temperature dependence of the effective magnetic moments also suggests that there are several spin states derived from Cu(II)-Mn(II)-Cu(II) spin system such as S=7/2, 5/2, and 3/2, where the spin-only values for S=7/2, 5/2, and 3/2 states are 7.94, 5.92, and 3.87 BM, respectively. The magnetic susceptibility data were analyzed on the basis of the spin-only expression for a symmetrical three-spin system (1/2-5/2-1/2). The molar magnetic susceptibility expression is given in Eq. 1.[7]

$$\chi_M = \frac{Ng^2\beta^2}{kT}\left[\frac{5x^{-7}+35(x^{-2}+1)/2+42x^5}{4x^{-7}+6(x^{-2}+1)+8x^5}\right] \quad (1)$$

In Eq. 1, x=exp(J/kT) and the other symbols have their usual meanings, where J is the Cu-Mn coupling constant, the Cu-Cu coupling constant is set to zero, and g is fixed 2.00. The observed susceptibility data for both complexes were closely represented by Eq. 1. For the complex **1**, the best-fit was obtained as J=−13 cm^{-1}. The generalized R factor, $R=[\sum[\chi_M(\text{obsd})-\chi_M(\text{calcd})]^2/\sum\chi_M(\text{obsd})^2]^{1/2}$, using as a convenient statistical indicator of the quality of fit is 0.020. For the complex **2**, the best-fit was obtained as J=−8 cm^{-1} and R=0.022. A theoretical χ_M vs. T curve using the J value obtained above is represented as a solid line in Fig. 1.

The antiferromagnetic parameters of the present complexes are relatively small, in comparison with the J values reported for bis(nitroxyl radical) adducts of bis(hexafluoroacetylacetonato)manganese(II) (J=−79, −105 cm^{-1})[7] and the J values for phenolic oxygen bridged complexes CuFe(fsaR)Cl·nH$_2$O (H$_4$fsaR=*N*,*N*′-bis(3-carboxysalicylidene)alkanediamine) (J=−50 cm^{-1}) which are the largest ones for hetero-metal polynuclear complexes with spin-system (S=5/2-1/2) reported so far.[3] The J values of the present complexes are compatible with that of [Cu(prp)$_2$enMn(hfa)$_2$] ((prp)$_2$en=quadridentate Schiff base ligand derived from 2′-hydroxy-propiophenone and ethylenediamine) (J=−13.2 cm^{-1}).[8]

The present complexes provide a synthetic route for hetero-metal polynuclear complexes with different spin-multiplicities and with unidentical coordination environments which are of current interest because of applications in biological systems. The study of the related hetero-metal binuclear complexes is in progress in our laboratory.

This work was in part supported by a Grant-in-Aid for Scientific Research from the Ministry of Education, Science and Culture.

References

1) Y. Pei, M. Vergauger, and O. Kahn, *J. Am. Chem. Soc.*, **108**, 7428 (1986).

2) J. P. Costes, J. F. Serra, F. Dahan, and J. P. Laurent, *Inorg. Chem.*, **25**, 2790 (1986).

3) H. Ōkawa, W. Kanda, and S. Kida, *Chem. Lett.*, **1980**, 1281.

4) N. Matsumoto, H. Murakami, T. Akui, J. Honbo, H. Ōkawa, and A. Ohyoshi, *Bull. Chem. Soc. Jpn.*, **59**, 1609 (1986).

5) F. A. Cotton and R. H. Holm, *J. Am. Chem. Soc.*, **82**, 2979 (1960).

6) N. Matsumoto, H. Murakami, T. Akui, J. Kanesaka, A. Ohyoshi, and H. Okawa, *J. Chem. Soc., Dalton Trans.*, in press.

7) M. H. Dickman, L. C. Porter, and R. J. Doedens, *Inorg. Chem.*, **25**, 2595 (1986).

8) C. J. O'Connor, D. P. Freyberg, and E. Sinn, *Inorg. Chem.*, **18**, 1077 (1979).

Enantiotropy of 2,4-Diamino-6-[2-(2-methyl-1-imidazolyl)ethyl]-1,3,5-triazine

Kazuo KAMAGATA* and Shuuji YOSHIDA
Research and Development Center, Shikoku Chemicals Corp., 25-1 Miyako, Namegawa, Hiki-gun, Saitama 355
(Received August 28, 1986)

Synopsis. Measurements using elementary analysis, differential thermal analysis, IR spectroscopy, and X-ray diffractometry have revealed that the title triazine assumes two crystalline forms α and β. The conversion from α to β proceeds rapidly at 230 °C, whereas the reversal takes place slowly at 60 °C and 95% RH.

2,4-Diamino-6-[2-(2-methyl-1-imidazolyl)ethyl]-1,3,5-triazine (**1**) is widely used as a curing agent for epoxy resin, because it provides good electric and mechanical properties to cured resin.[1] Compound **1** is synthesized from 2-methylimidazole, acrylonitrile, and dicyanodiamide.[2] It consists of a triazine ring, which is π-defficient, and an imidazole ring, which is π-excessive:[3]

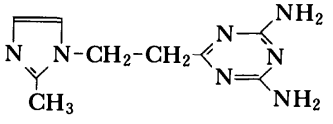

1

Compound **1** is decomposed into 2,4-diamino-6-vinyl-1,3,5-triazine and 2-methylimidazole at elevated temperature.[4] This paper reports of differential thermal analyses (DTA) on **1** and **1** heat-treated at 230 °C for 25 min which detected different curves, their X-ray powder diffractions which also detected entirely different patterns, and DTA examination of chemical reactivities of **1** and heat-treated **1** to diglycidyl ether of bisphenol A (DGEBA).

Experimental

Materials. Compound **1** was purified before use by repeated recrystallization from methanol solution and dried at 60 °C for 8 h under vacuum. Its high-performance liquid chromatogram registered 99.9% purity. Heat treatment on **1** was carried out at 230 °C for 25 min in an oven (heat-treated **1**). Heat-treated **1** was treated under various conditions (samples *a*, *b*, and *c*). Pure DGEBA was kindly supplied from Yuka Shell Epoxy Co., Preliminary mixtures of **1** or heat-treated **1** with DGEBA were prepared at a temperature slightly higher than the melting point of DGEBA (46 °C) and mixed well at room temperature.

Apparatus and Precedures. IR spectra were taken with KBr pellets on a Hitachi 260-10 Spectrophotometer. A Shimadzu Thermal Analyzer DT-20B was used for DTA. In each run of DTA, 5 mg of sample was loaded and the same amount of Al_2O_3 was used as a reference. The temperature was raised from room temperature to 300 °C at a rate of 5 °C min^{-1}. The apparent activation energy of the reaction of **1** or heat-treated **1** with DGEBA was obtained by the Kissinger method[5] using heating rates ranging from 1 to 20 °C min^{-1}. X-Ray powder diffraction was conducted with a Rigaku X-ray powder diffractometer using graphite monochromatized Cu $K\alpha$ radiation (λ=1.5405 Å).

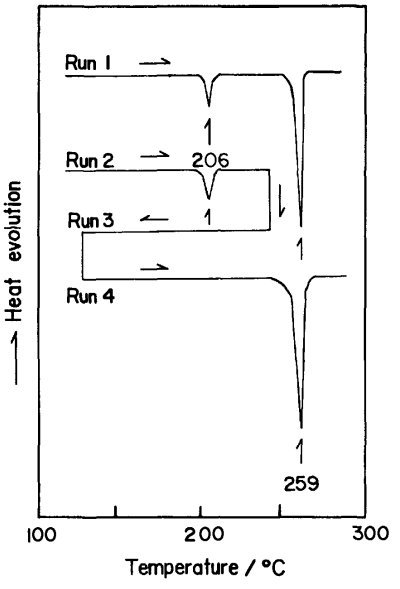

Fig. 1. DTA curves of 2,4-diamino-6-[2-(2-methyl-1-imidazolyl)ethyl]-1,3,5-triazine.

Results and Discussion

Polymorphic Behavior of 1. The DTA curves of **1** are given in Fig. 1. A small endothermic peak appears at 206 °C and a sharp endothermic peak due to fusion

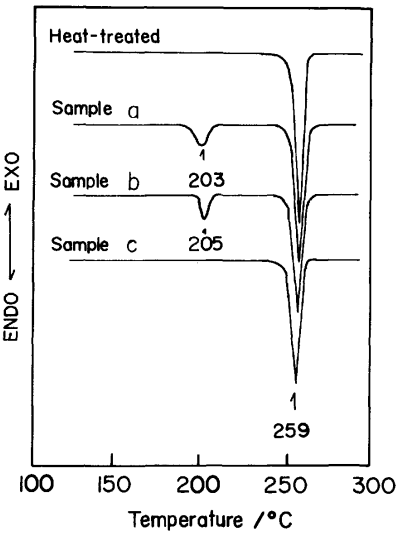

Fig. 2. DTA curves of 2,4-diamino-6-[2-(2-methyl-1-imidazolyl)ethyl]-1,3,5-triazine treated by various conditions after the heat treatment of 230 °C for 25 min. Heat-treated: heat-treated at 230 °C for 25 min.
Sample *a*; Kept at 60 °C, 95% RH for 48 h after the heat treatment. Sample *b*; Recrystallized from a methanol solution after the heat treatment. Sample *c*; Kept at room temperature for 30 d after the heat treatment.

Table 1. Elementary Analysis Data of **1** and Heat-Treated **1**

	C/%	H/%	N/%
Found for **1**	49.21	5.92	44.89
Found for heat-treated **1**	49.25	5.96	45.01
Calcd for $C_9H_{13}N_9$	49.30	5.98	44.72

Table 2. ^{1}H NMR of **1** and Mass Spectral Data of **1** and Heat-Treated **1**

^{1}H NMR (D_2O, 40 °C) (δ/ppm)	MS (75 eV, 140 °C) (m/z)
6.95 (d, H, J=1.5 Hz)	219(M^+), 204, 191
6.82 (d, H, J=1.5 Hz)	177, 149, 138, 125,
4.27 (t, 2H, J=6.8 Hz, -N-CH_2-CH_2-<)	111, 109, 95, 82, 81
2.87 (t, 2H. J=6.8 Hz, -N-CH_2-CH_2-<)	
2.25 (s, 3H, -CH_3)	

appears at 259 °C (run 1). The same heating process as run 1 was applied above the lower endothermic peak (run 2) and was followed by cooling down to room temperature (run 3). Subsequent heating gave no endothermic peak at 206 °C, but reproduced the sharp endothermic peak at 259 °C (run 4).

In order to interpret the above phenomena, **1** was heated at 230 °C for 25 min. The DTA curve (heat-treated **1** in Fig. 2) shows no endothermic peak at about 206 °C. On the other hand, sample *a* (equal to a heat-treated **1** which was kept at 60 °C and 95% RH for 48 h and dried at 60 °C for 8 h under vacuum) and sample *b* (equal to a heat-treated **1** which was dissolved and recrystallized from methanol solution and dried at 60 °C for 8 h under vacuum) gave a small endothermic peak at 203—205 °C in their DTA curves. The IR spectrum of sample *b* is identical with that of **1**. The small endothermic peak was absent in the DTA curve of sample *c* (equal to a heat-treated **1** which was kept at room temperature for 30 d).

The results of elementary analysis of **1** and heat-treated **1** were idential with the calculated value for $C_9H_{13}N_7$ as indicated in Table 1. In Table 2 are given the ^{1}H NMR data of **1** and the mass spectral data of **1** and heat-treated **1**, which are also identical with each other.

Part of the IR spectra of **1** and heat-treated **1** are given in Fig. 3. In Fig. 3, curve **A** represents the spectrum of **1**, which is essentially the same as those of samples *a* and *b*. Curve **B** represents the spectra of heat-treated **1** and sample *c*. The pronounced difference between curves **A** and **B** consists in the absorptions for the NH_2 stretching and bending. The NH_2 stretching bands appear at 3320 and 3100 cm^{-1} (curve **A**) and at 3475, 3320, and 3100 cm^{-1} (curve B). The absorption at 3475 cm^{-1} is possibility due to the stretching of NH_2 in free state.[6] The bending gives rise to the absorption at 1660 cm^{-1} in curve **A** and at 1630 and 1680 cm^{-1} in curve **B**.

Yuki et al. reported[7] an IR spectrum of 2-amino-4-(*N*-methyl-anilino)-6-isopropenyl-1,3,5-triazine (**2**) similar to that of **1** and attributed the difference in

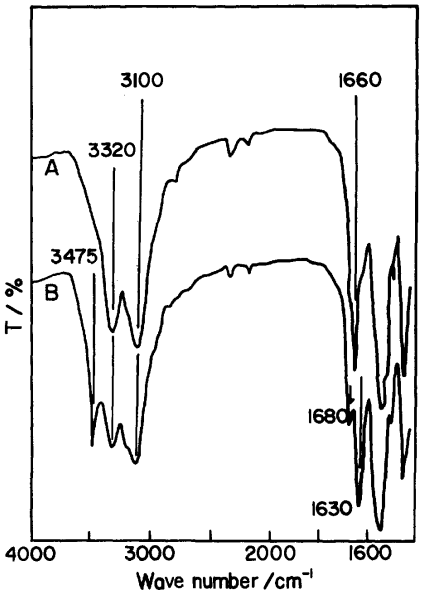

Fig. 3. IR Spectra of 2,4-diamino-6-[2-(2-methyl-1-imidazolyl)ethyl]-1,3,5-triazine (**A**) and heat-treated one at 230 °C for 25 min (**B**).

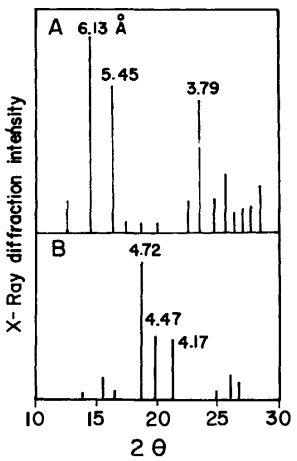

Fig. 4. X-Ray powder diffraction patterns of 2,4-diamino-6-[2-(2-methyl-1-imidazolyl)ethyl]-1,3,5-triazine (**A**) and heat-treated one at 230 °C for 25 min (**B**).

NH_2 absorption to different interactions between the proton of amino group and the π electron of isopropenyl group.

The results so far described are summarized with some inference as follows:

1. Compound **1** and heat-treated **1** give different DTA curves.
2. The measured elementary compositions of **1** and heat-treated **1** are the same as the calculated for $C_9H_{13}N_9$, and the mass spectral data of **1** and heat-treated **1** also are the same with each other.
3. The IR spectra of **1** and heat-treated **1** are different from each other in the absorptions due to NH_2 stretching and bending, suggesting different angles between the imidazole and triazine rings.

In order to investigate the existence of polymorphic forms of **1**, X-ray powder diffraction patterns of **1** and

heat-treated **1** were examined. Both the patterns are entirely different as shown in Fig. 4. A very strong and two strong peaks corresponding to the spacings of 6.13, 5.45, and 3.79 Å, respectively, are observed for **1**, whereas a strong and two medium strong peaks corresponding to the spacings of 4.72, 4.47, and 4.17 Å, respectively, for heat-treated **1**. Samples *a* and *b* gave diffraction patterns similar to **1**, whereas sample *c* gave patterns to similar heat-treated **1**. We refer to the former as the α-form and the latter as the β-form.

Polymorphic phenomenon of triazine compound was previously reported with reference to dimorphic forms of **2** by Yuki et al.[7] Compound **2**, recrystallized from methanol solution, had two different crystalline forms. They referred to the **2** immediately crystallized from methanol solution as the α-form and the **2** slowly crystallized from methanol solution as the β-form. The β-form melts at 104 °C and immediately solidifies into a crystal that melts at 118 °C, while the α-form melts at 118 °C. The X-ray powder diffraction patterns of the α- and β-forms are entirely different. The IR spectrum of **2** that was heated at 115 °C is identical with that of the α-form. From the above results, they concluded that the α-form is a thermodynamically less stable crystal form than the β-form.

The polymorphic phenomena of organic crystals are classified into monotropic and enantiotropic.[8] Compound **2** is polymerized immediately after fusion of its stable form, but **1** is changed gradually from its crystalline form when heated under high humidity as folows:

$$\alpha \underset{60\,^{\circ}C,\ 95\%\ RH,\ 48\ h}{\overset{230\,^{\circ}C,\ 25\ min}{\rightleftharpoons}} \beta$$

The α-form is transformed into the β-form by beeing heated at 230 °C for 25 min, and the β-form into the α-form by beeing kept at 60 °C under 95% RH for 48 h. Since the α- and β-forms gave exactly the same elementary compositions and mass spectra but different DTA curves, IR spectra, and X-ray diffraction patterns, the α- and β-forms may be considered to be conformationally isomeric with respect to the imidazole and triazine rings connected by the ethylene bridge. On the basis of the wavenumber 3475 cm^{-1} at which the absortion due to the stretching of freestate NH_2 appears,[6] the α- and β-forms are taken to be antiperiplaner to each other with different angles θ between the imidazole and triazine rings connected by the ethylene bridge. The conformational isomeric situation is illustrated diagramatically below:

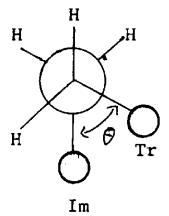

Their conformations are supported by chemical reactivities of **1** and heat-treated **1** to DGEBA described in the following section.

Chemical Reactivity of 1 to DGEBA. Compound **1** is widely used as a curing agent for epoxy resin as mentioned before. The reaction of imidazole compound with epoxy resin consists of two steps.[9] The first step is the addition to epoxide of group NH at the 1-position of the imidazole ring. The second step is the ring opening of epoxide by the catalyst produced in the first step. Since in **1** the hydrogen at the 1-position of the imidazole ring is already substituted, the reaction of **1** or heat-treated **1** with DGEBA essentially starts with the second step. The chemical reactivity of **1** and heat-treated **1** to DGEBA was studied by measuring activation energies of the reaction. Apparent activation energies were obtained by the Kissinger equation:[5]

$$\frac{d(\ln \phi/T_m^2)}{d(1/T_m)} = -\frac{E}{R} \quad (1)$$

where ϕ is the heating rate in °C min^{-1}, T_m is the absolute temperature of the exothermic peak in DTA curves, and R is the gas constant. The exothermic temperature was measured by changing the heating rate from 1 to 20 °C min^{-1}. The activation energies calculated according to Eq. 1 are 38.3 kcal mol^{-1} for the mixture of **1** and DGEBA and 25.3 kcal mol^{-1} for that of heat-treated **1** and DGEBA. It is considered that the difference in activation energy results from the difference in the crystalline forms of **1** and heat-treated **1**.

The authors wish to express their profound thanks to Assistant Professor Yoshio Shibasaki, Saitama University for providing them with the X-ray diffraction patterns and useful discussion. They also wish to express their sincere thanks to Dr. Natsuo Sawa, Excutive Director and Mr. Atsushi Saeki, Shikoku Chemicals Corp. for furnishing them with some of the ^1H NMR and mass spectral data and helpful discussion.

References

1) Shikoku Chemicals Corp., Technical Report, "CUREZOLE," (1977).
2) N. Sawa and S. Okamura, *Nippon Kagaku Kaishi*, **90**, 704 (1969); Shikoku Chemicals Corp., Tokkyo Koho 47-36391 (1972).
3) A. Albert, "Heterocyclic Chemistry," translated into Japanese by K. Nakanishi and H. Yamazaki, Maruzen, Tokyo (1963), pp. 32, 109.
4) K. Kamagata, M. Kinoshita, and S. Yoshida, *Polym. J.*, **18**, 193 (1986).
5) H. E. Kissinger, *Anal. Chem.*, **29**, 1702 (1957).
6) S. Mizushima and T. Shimanouchi, "Sekigaisen Kyushu To Raman Kôka," Kyoritsu Shuppan, Tokyo (1959), p. 43.
7) Y. Yuki, T. Taika, and M. Nagano, *Bull. Chem. Soc. Jpn.*, **45**, 3494 (1972).
8) H. Suga, "Netsubunseki," ed by H. Kambe, Kodansha, Tokyo (1975), p. 216.
9) K. Okahashi, S. Hayashi, and K. Shibayama, *Kobunshi Ronbunshu*, **34**, 497 (1977).

Nonacarbonyldiiron-Induced Reaction of 3-Azido-1,2,3-triphenylcyclopropene and 4,5,6-Triphenyl-1,2,3-triazine

Tomoshige KOBAYASHI, Naoki MURATA, and Makoto NITTA*
Department of Chemistry, School of Science and Engineering, Waseda University, Shinjuku-ku, Tokyo 160
(Received January 6, 1987)

Synopsis. The $[Fe_2(CO)_9]$-induced reaction of 3-azido-1,2,3-triphenylcyclopropene (**1**) undergoes elimination of a nitrogen molecule and C-C bond cleavage to result in the formation of benzonitrile, diphenylacetylene, 2,3-diphenylinden-1-one, and 1,2,3-triphenylpropen-1-one. The similar reaction of 4,5,6-triphenyl-1,2,3-triazine, which is an isomer of **1**, undergoes reductive N-N bond cleavage to give 3,4,5-triphenylpyrazole in good yield.

Previously, we have found that $[Mo(CO)_6]$, $[Fe(CO)_5]$, and $[Fe_2(CO)_9]$ can induce the reductive N-O bond cleavage of isoxazoles in protic media to give β-amino enones in good yields.[1] Application of this method for the synthesis of geiparvarin has been demonstrated.[2] Furthermore, our group[3] and other groups[4-10] have investigated the generation and chemical behaviors of the complexed nitrene intermediates which are derived from the reaction of organic azides with iron carbonyl. A series of these studies then raise the question whether the complexed nitrene intermediate, which is derived from 3-azido-1,2,3-triphenylcyclopropene (**1**) and $[Fe_2(CO)_9]$, undergoes ring expansion to give azete (azacyclobutadiene) or complexed azete derivative or not. Thermal reaction of **1** has been reported to give 4,5,6-triphenyl-1,2,3-triazine (**2**).[11] The photochemical reaction of **2** has also been reported to give benzonitrile, diphenylacetylene, 2,3-diphenylquinoline, and 2,3,5,6,7,8-hexaphenyl-1,4-diazocine via postulated azete intermediate.[11,12] However, up to now, three azete derivatives, tris(dimethylamino)-,[13] tri-*t*-butylazete,[14] and 2-arylbenzazete,[15] have been isolated as the products of the thermal decomposition of the corresponding triazines. We report here the results for the $[Fe_2(CO)_9]$-induced reaction of **1** and **2**.

The reaction of **1** with $[Fe_2(CO)_9]$ at ambient temperature in anhydrous benzene, acetonitrile, and aqueous acetonitrile afforded benzonitrile (**3**), diphenylacetylene (**4**), 2,3-diphenyl-1*H*-inden-1-one (**5**), and 1,2,3-triphenylpropen-1-one (**6**) as shown in Scheme 1. The product **3** was detected by GLC and IR, and the isolation was not carried out. The reaction conditions and the yields of the products except **3** are summarized in Table 1 (Entries 1—3). In contrast, the reaction of **1** and $[Fe_2(CO)_9]$ in methanol gave mainly **6** and the complex **7** in addition to **3**, **4**, and **5** (Table 1, Entry 4).

Table 1. Results of the Reaction of **1** with $[Fe_2(CO)_9]$[a]

Entry	Solvent	Product (yield/%)				
		3	**4**	**5**	**6**	**7**
1	PhH	b)	8	6	8	—
2	MeCN	b)	5	15	9	—
3	MeCN-H_2O[c]	b)	3	4	10	—
4	MeOH	b)	1	1	67	13

a) Reactions were carried out at ambient temperature for 24 h. b) Isolation was not carried out. c) 5.0 Molar equivalent amounts of water was added.

The postulated mechanistic pathways for the reaction are shown in Scheme 2. The reaction of **1** with $[Fe_2(CO)_9]$ initially gives the complexed nitrene intermediate **8**.[3-10] Then, the C-C bond cleavage of **8** seems to occur to give **9**. The direct decomposition of **9** can give **3** and **4**. An alternative route involving an azete intermediate **10**, which can give **3** and **4**, might not be ruled out. However, no evidence has been obtained at this stage.

On the other hand, compound **9** would cyclize to **12**,

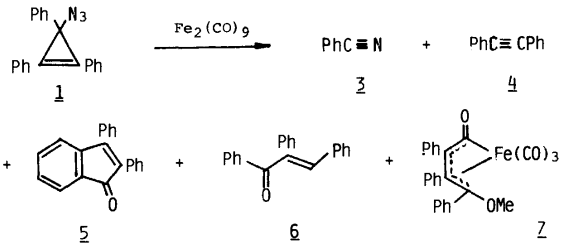

Scheme 1.

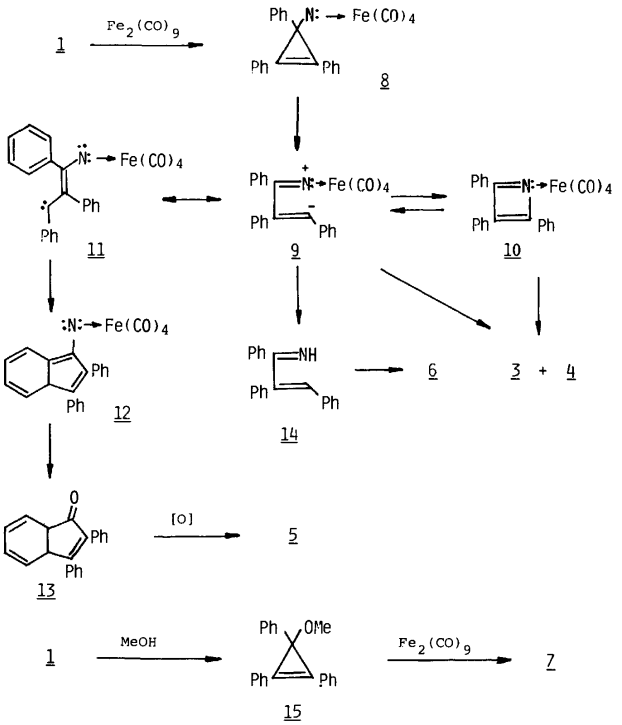

Scheme 2.

probably through intermediarily formed **11**. The reduction of the nitrene moiety of **12** to enamine followed by hydrolysis under workup conditions would give **13**.[1,3] The oxidation of **13** seems to occur easily to give **5**. Furthermore, the protonation and reduction of the nitrogen moiety of **9** giving **14** followed by hydrolysis would give **6**.[16] The compound **6** was obtained even in anhydrous solvents (Table 1, Entries 1 and 2). Even in the reaction in anhydrous solvents, the possibility of stray water can not be ruled out. The compound **6** was obtained in good yield in methanol (Table 1, Entry 4). This fact would be attributable to the effective reduction and protonation of **9** in methanol.[16] The complex **7** has already been isolated in the reaction of iron carbonyls with 3-methoxy-1,2,3-triphenylcyclopropene (**15**).[17] Actually, the reaction of **1** with methanol afforded **15** in a quantitative yield, therefore the formation of **7** would be rationalized. Thus, the complexed cyclopropenylnitrene **8** was demonstrated to undergo easy cleavage of the bent C-C bond. The intervention of the complexed azete **10** is not supported by experimental evidence.

On the other hand, the reaction of **2** with $[Fe_2(CO)_9]$ in methanol or in aqueous acetonitrile under reflux afforded 3,4,5-triphenylpyrazole (**16**) in 80 or 77% yield, respectively.

The reaction is formally explained by the pathways shown in Scheme 3. The initial step should be an n-donor complexation of **2** to the $[Fe(CO)_4]$ species[1] to give **17** [or **18**]. The peroxy acid oxidation of 1,2,3-triazine derivatives gives 1-oxides and/or 2-oxides.[18] No evidence is available to distinguish between the N1 and N2 complexation to give **18** and **17** at the present reaction. The back donation of the d-electron from the iron to the complexed 1,2,3-triazine **17** [or **18**] and subsequent protonation gives **19** [or **20**] and then **21** in protic media. The further complexation of **21** with another $[Fe(CO)_4]$ species giving **22** [or **23**] followed by reductive ring opening gives **24** [or **25**], cyclization of which then affords the pyrazole **16**. The reduction-protonation sequences of **24** [or **25**] seems also possible to give **26** which would give **16**.[11] Although the catalytic hydrogenation of **2** has been known to give **16** in good yield,[11] the present reaction could provide the first example of $[Fe_2(CO)_9]$-induced reductive cleavage of the triazine ring system.

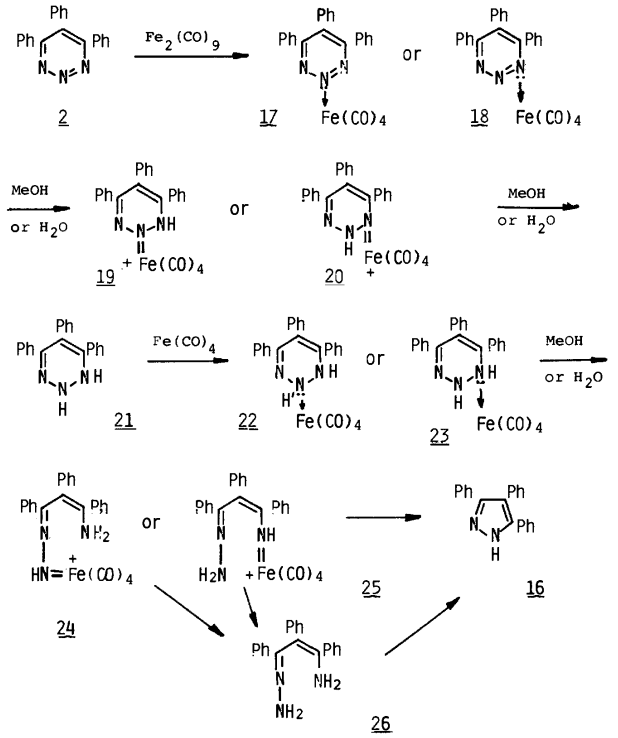

Scheme 3.

Experimental

The IR spectra were recorded on a Shimadzu IR-400 spectrometer. The NMR spectra were recorded on a Hitachi R-24 spectrometer and the chemical shifts are given in ppm (δ) relative to the internal $SiMe_4$ standard. The mass spectral studies were conducted using Shimadzu GCMS QP-1000 spectrometer. $[Fe_2(CO)_9]$ was prepared by the standard method.[19] All of the $[Fe_2(CO)_9]$-induced reactions were carried out under a nitrogen atmosphere. The desired compounds, 3-azido-1,2,3-triphenylcyclopropene (**1**)[11] and 4,5,6-triphenyl-1,2,3-triazine,[20] were prepared according to the literatures. All of the melting points are uncorrected.

General Procedure for the Reaction of 1 with $[Fe_2(CO)_9]$. A solution of **1** (309 mg, 1 mmol) and $[Fe_2(CO)_9]$ (728 mg, 2 mmol) in a solvent (20 cm^3) was stirred for 24 h at ambient temperature. Then, the solution was filtered through Celite to remove insoluble materials, and the filtrate was concentrated in vacuo. The residue contained benzonitrile **3** which was detected by GLC and IR. The residue was separated by column chromatography on silica gel. The fractions eluted with hexane afforded **4**, the mixture of **5** and **6**, and **7**. The mixture was further separated by TLC on silica gel using CCl_4 as a developer to give **5** and **6**. The reaction conditions and the yields of the products are summarized in Table 1. For **5**: mp 145—146 °C (from MeOH) (lit,[21] 149—151 °C); IR ($CHCl_3$) 1709, 1604 cm^{-1}; ^1H NMR ($CDCl_3$) δ=7.19—7.63 (14H, m). For **6**: mp 96—97 °C (from benzene-hexane) (lit,[21] 96.5—97.5 °C). For **7**: mp 131—133 °C (decomp) (from benzene-hexane) (lit,[17] 133—135 °C); IR ($CHCl_3$) 3075, 3033, 2961, 2065, 1998, 1731 cm^{-1}; ^1H NMR ($CDCl_3$) δ=3.79 (3H, s), 6.77—7.36 (15H, m); *m/z* (rel intensity), 466 (M^+−28, 3), 105 (100).

Formation of 15 in Methanol. A solution of **1** (160 mg, 0.5 mmol) in anhydrous methanol (5 cm^3) was stirred for 24 h at ambient temperature. After the methanol was evaporated, the residue was extracted with ether. The organic layer was dried over Na_2SO_4, and evaporated to give 90% of **15**: mp 67—68 °C (lit,[22] 69—70 °C); IR ($CHCl_3$) 1812 cm^{-1}; ^1H NMR ($CDCl_3$) δ=3.40 (3H, s), 7.18—7.59 (10H, m), 7.63—7.89 (5H, m).

General Procedure for the Reaction of 2 with $[Fe_2(CO)_9]$. A solution of **2** (309 mg, 1 mmol) and $[Fe_2(CO)_9]$ (728 mg, 2 mmol) in methanol (20 cm^3) was refluxed for 2 h. The solution was filtered through Celite to remove insoluble materials. The filtrate was concentrated and the residue was purified by column chromatography on Florisil using benzene as the eluant to give **16** in an 80% yield. The reaction carried out in moist acetonitrile containing 5 molar equivalent amounts of water also afforded **16** in a 77% yield. The structure of **16** was confirmed by comparison of the spectral data with those of authentic specimen.[11,23]

References

1) M. Nitta and T. Kobayashi, *J. Chem. Soc., Perkin Trans. 1*, **1985**, 1401.

2) P. G. Beraldi, A. Barco, S. Benetti, M. Guareri, S. Manfredini, G. P. Pollini, and D. Simoni, *Tetrahedron Lett.*, **26**, 5319 (1985); B. H. Lipshutz, *Chem. Rev.*, **86**, 795 (1986).
3) M. Nitta and T. Kobayashi, *Bull. Chem. Soc. Jpn.*, **57**, 1035 (1985).
4) M. Decker and G. R. Knox, *Chem. Commun.*, **1967**, 1243.
5) C. D. Campbell and C. W. Rees, *Chem. Commun.*, **1969**, 537.
6) A. F. M. Iqubal, *Helv. Chim. Acta*, **56**, 655 (1976).
7) T. A. Mannuel, *Inorg. Chem.*, **1**, 1703 (1964).
8) J. A. J. Javis, B. E. Job, B. T. Kilbourn, R. H. B. Mals, P. G. Oweston, and P. F. Todd, *Chem. Commun.*, **1967**, 1149.
9) H. Alper and J. E. Prickett, *Inorg. Chem.*, **16**, 67 (1977).
10) Y. Nakamura, K. Bachmann, H. Heimgartner, and H. Schmid, *Helv. Chim. Acta*, **61**, 589 (1978).
11) E. A. Chandross and G. Smolinsky, *Tetrahedron Lett.*, **1960**, 19.
12) E. M. Burgess and J. P. Sanchez, *J. Org. Chem.*, **38**, 176 (1973).
13) G. Seybold, U. Jersak, and R. Gompper, *Angew. Chem.*, **85**, 918 (1973).
14) U.-J. Vogelbacher, M. Regitz, and R. Mynott, *Angew. Chem., Int. Ed. Engl.*, **25**, 842 (1986).
15) B. M. Adger, M. Keating, C. W. Rees, and R. C. Storr, *J. Chem. Soc., Chem. Commun.*, **1973**, 19.
16) M. Nitta and T. Kobayashi, *J. Chem. Soc., Perkin Trans., 1*, **1984**, 2103; and references cited therein.
17) J. Klimes and E. Weiss, *Chem. Ber.*, **115**, 2606 (1982).
18) A. Ohsawa, H. Arai, H. Ohnishi, and H. Igeta, *J. Chem. Soc., Chem. Commun.*, **1980**, 1182.
19) R. B. King, *Org. Synth.*, Vol. 1, 93 (1965).
20) H. Neunhoeffer, H.-D. Vöter, and H. Ohl, *Chem. Ber.*, **105**, 3695 (1972).
21) J. O. Stoffer and J. T. Bohanon, *J. Chem. Soc., Perkin Trans. 2*, **1978**, 692.
22) R. Breslow and C. Yuan, *J. Am. Chem. Soc.*, **80**, 5991 (1958).
23) P. Yates and E. M. Levi, *J. Org. Chem.*, **40**, 441 (1975).

ESR Spectroscopic Study of Triphenylmethyl-Substituted Thioaminyl Radicals: *N*-(Triphenylmethylthio)alkylaminyls and -arylaminyls[1)]

Yozo Miura,* Mamoru Isogai, and Masayoshi Kinoshita
Department of Applied Chemistry, Faculty of Engineering, Osaka City University, Sumiyoshi-ku, Osaka 558
(Received February 4, 1987)

Synopsis. The title radicals, generated by hydrogen-atom abstraction from the corresponding *N*-(triphenylmethylthio)-alkylamines and -arylamines, have been studied by means of ESR spectroscopy. The alkylaminyls were transient in solution at room temperature, while the arylaminyls persisted for a long period under the same conditions. The ESR parameters are discussed by comparing them with those for structurally related aminyls.

Thioaminyl radicals (RṄSR′) have an interesting structure in which a divalent sulfur atom attaches directly to the radical center. In our ESR studies of a variety of thioaminyl radicals, we have found that, in the radicals, the unpaired electron is delocalized considerably onto the adjacent sulfur and that some thioaminyls can be isolated as hydrazine-like dimers or pure radical crystals.[2,3)] In the present paper we wish to report an ESR spectroscopic study of *N*-(triphenylmethylthio)alkylaminyls and -arylaminyls (**2**), which have never appeared in the literature.[4)]

Results and Discussion

Thioaminyls **2** were generated by the phtolysis of *N*-(triphenylmethylthio)alkylamines or -arylamines (**1**) in benzene in the presence of di-*t*-butyl peroxide. Additionally, the arylaminyls **2d** and **2e** were also generated by treating the corresponding amines with (*t*-BuOOCO-)$_2$. Some typical ESR spectra are illustrated in Figs. 1 and 2, while the ESR parameters are summarized in Table 1.

Although the radical generation was performed at room temperature with a low-power mercury lamp (100 W), all the ESR spectra were relatively strong, as may be found in Fig. 1. However, upon the interruption of UV-irradiation, the ESR signals due to the alkylaminyls **2a—c** disappeared immediately at room temperature. On the other hand, the arylaminyls **2d** and **2e** survived for a long period under the same conditions; in particular, **2e** was quite long-lived; the lifetime shown by a brief kinetic study was more than a week.

In most spectra, an impure radical with a *g* value of 2.003 appeared in the signals of **2**, as is shown in Fig. 1. The low *g* value and its extremely persistent property suggested that the impure radical was the triphenylmethyl radical. This was confirmed by comparing its ESR spectrum with that of an authentic triphenylmethyl radical obtained from a solution of PhN=NCPh$_3$. This impure radical was not observed from the pho-

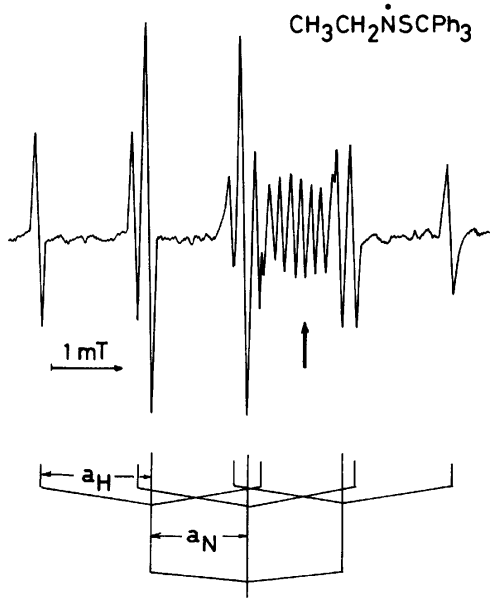

Fig. 1. ESR spectrum of **2b** recorded during photolysis of a solution of **1b** in 1:4 (v/v) di-*t*-butyl peroxide–benzene at 17°C. The impure radical indicated by a bold arrow is the triphenylmethyl radical.

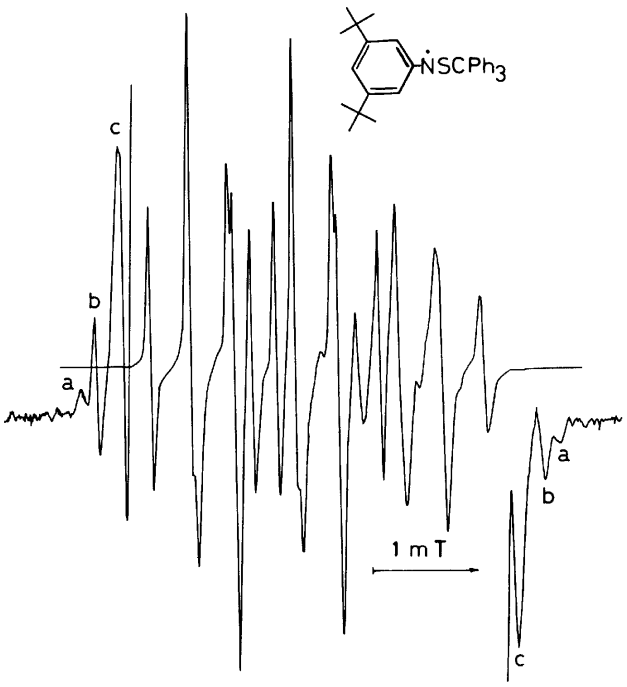

Fig. 2. ESR spectrum of **2e** generated by treating **1e** with (*t*-BuOOCO-)$_2$ in degassed benzene at 17°C. Both wings of the parent signal are shown at high gain (100 times). Assignment of the satellite lines are as follows: a, ^{33}S; b, ^{13}C (1C); c, ^{13}C (3C).

Table 1. ESR Parameters for *N*-(Triphenylmethylthio)alkylaminyls and -arylaminyls[a-c]

Radical	a_N	a_H[d]	g
2a	1.26	1.66 (3)	2.0074
2b	1.25	1.42 (2)	2.0073
2c	1.23	1.48 (2)	2.0073
2d[e]	0.995	0.381 (2),[f] 0.128 (2),[g] 0.426 (1)[h]	2.0062
2e[e,i]	0.988	0.385 (2),[f] 0.443 (1)[h]	2.0062

a) Hyperfine splitting constants are given in mT. b) Solvent: benzene or 1:4 (v/v) di-*t*-butyl peroxide–benzene. c) Temperature: 17±2°C. d) Numbers in parentheses refer to the number of equivalent protons. e) Hyperfine splitting constants have been determined by computer simulation. f) Ortho protons on the anilino benzene ring. g) Meta protons on the anilino benzene ring. h) Para proton on the anilino benzene ring. i) $a_{^{13}C}$=0.55 (3C), 1.03 mT (1C), $a_{^{33}S}$=0.43 mT.

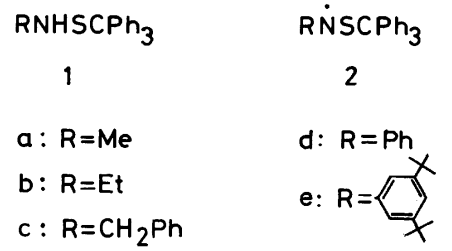

Scheme 1.

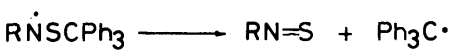

Scheme 2.

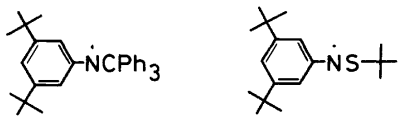

Scheme 3.

tolysis of a solution of **1** alone. Thus, we thought that it was derived from **2**, probably through the homolytic C-S bond cleavage, as is shown in Scheme 2. A similar decomposition reaction of radicals has been reported to occur in aryl triphenylmethyl nitroxide radicals.[5]

Because of its considerably persistent property, the thioaminyl **2e** permitted us to measure some satellite lines due to ^{13}C and ^{33}S atoms at natural abundance (^{13}C 1.11%, ^{33}S 0.76%). As is shown in Fig. 2, three satellite lines were found in each wing of the parent spectrum recorded at a high gain (100 times). From the intensity ratios to the parent spectrum the a peak (<0.2%)[6] was assigned to the satellite lines due to ^{33}S, while the b (0.5%) and c peaks (1.3%) were assigned to those due to one and three magnetically almost equivalent ^{13}C atoms.

Furthermore, *N*-(triphenylmethyl)-3,5-di-*t*-butylphenylaminyl (**3**) was generated, for a comparison of the ESR parameters, by the oxidation of *N*-(triphenylmethyl)-3,5-di-*t*-butylaniline (**4**) with PbO_2. The ESR parameters thus obtained (in benzene at 17 °C) were a_N=0.931, $a_{o\text{-}H}$=0.563 (2H), $a_{p\text{-}H}$=0.727 mT (1H), and g=2.0038. This aminyl was relatively persistent and gave a strong ESR signal.

ESR Parameters. The aminyls **2** give ESR parameters very similar to those for the radicals of the RṄSBu^t[2] and ArṄSBu^t[7] types (R=alkyl, Ar=aryl). For instance, the hyperfine splitting (hfs) constants for **2a** are very close to those for MeṄSBu^t (a_N=1.25, a_β=1.64 mT).[2] Similarly, those for **2e** are very similar to those for **5** (a_N=0.993, $a_{o\text{-}H}$=0.368, $a_{p\text{-}H}$=0.420, $a_{^{33}S}$=0.466 mT).[2,7] Accordingly, we can say that the thioaminyls **2** adopt the same, or almost the same, configuration as the RṄSBu^t or ArṄSBu^t radicals (probably planar around the nitrogen).[2]

In contrast, the ESR parameters are quite different from those of the radicals of the RṄR′ or ArṄR type radicals.[8] A typical example is given by **3**, whose $a_{o\text{-}H}$ and $a_{p\text{-}H}$ values are substantially higher than those for **2e**. The reduction in a_H found in going from **3** to **2e** is obviously a consequence of the conjugative delocalization of the unpaired electron from the nitrogen to the sulfur in **2** (-Ṅ-Ṡ- ↔ -Ṅ⁻-Ṡ⁺-), as is suggested by the relatively high $a_{^{33}S}$ value and the higher g value. Here, the π-orbital spin density (ρ_S^π) on the sulfur in **2e** was estimated from the $a_{^{33}S}$ value by using Equation 1, which had been previously established through an investigation of the ^{33}S hfs constants of a variety of RṄSR′ radicals.[2] The ρ_S^π value thus obtained is 0.18;

$$\rho_S^\pi = a_{^{33}S}/Q_S = a_{^{33}S}/2.3 \text{ mT} \quad (1)$$

this magnitude strongly suggests that the thioaminyls **2** are electronically substantially stabilized by this conjugation. However, because of the relatively weak C-S bonds, the thioaminyls **2** were less persistent than had been anticipated, and no **2** could be isolated as the radical or dimer substance.

Experimental

The melting points and the IR and ^1H NMR spectra were taken as previously reported.[9] Triphenylmethanesulfenyl chloride[10] (Ph_3CSCl), phenylazotriphenylmethane,[11] and 3,5-di-*t*-butylaniline[12] were prepared by the previously reported methods.

The *N*-(triphenylmethylthio)amines (**1**) were prepared by either method, A or B. Method A: a solution of 1.12 g (3.60 mmol) of Ph_3CSCl in 15 ml of CH_2Cl_2 was added dropwise to an aqueous RNH_2 solution (with a large excess of RNH_2) with vigorous stirring at 0 °C. After being stirred for 0.5 h at the same temperature, the organic layer was separated and dried over $MgSO_4$. After filtration, the solvent was evaporated, and the residue was chromatographed on silica gel (Wako gel C-200; column size 4×20 cm) using 1:2 (v/v) benzene–hexane as the eluant and was crystallized from methanol.

Method B: a solution of 1.12 g (3.60 mmol) of Ph_3CSCl in 15 ml of CH_2Cl_2 was added dropwise to a solution of 10 mmol of RNH_2 (or 4.5 mmol of RNH_2 and 7.2 mmol of Et_3N) in 10 ml of CH_2Cl_2 with stirring at 0 °C. After being stirred for 1 h at the same temperature, the reaction mixture was washed with water (30 ml×3), saturated K_2CO_3 (30 ml), and brine (30 ml), and dried over $MgSO_4$. After filtration, the solvent was evaporated, and the residue was chromatographed as above and crystallized from methanol.

N-(Triphenylmethylthio)methylamine (**1a**) [mp 109—111 °C (lit,[13] 119—120 °C)] and *N*-(triphenylmethylthio)ethylamine (**1b**) were obtained by Method A, while *N*-(triphenylmethylthio)benzylamine (**1c**), *N*-(triphenylmethylthio)aniline (**1d**) [mp 96—98 °C (lit,[13] 103 °C)], and *N*-(triphenylmethylthio)-3,5-di-*t*-butylaniline (**1e**) were prepared by Method B.

Thioamine 1b: Colorless prisms; mp 88—90 °C yield 47% (0.54 g, 1.7 mmol); IR (KBr) 3260 cm^{-1} (NH); ^1H NMR ($CDCl_3$) δ=0.82 (t, J=7 Hz, 3H, CH_3), 2.40 (s, 1H, NH), 2.52 (q, J=7 Hz, 2H, CH_2), 7.12—7.42 (m, 15H, aromatic). Found: C, 79.26; H, 6.64; N, 4.44%. Calcd for $C_{21}H_{21}NS$: C, 78.95; H, 6.63; N, 4.38%.

Thioamine 1c: Colorless needles; mp 97—98 °C; yield 61% (0.82 g, 2.2 mmol); IR (KBr) 3300 cm^{-1} (NH); ^1H NMR ($CDCl_3$) δ=2.72 (t, J=5.9 Hz, 1H, NH), 3.62 (d, J=5.9 Hz, 2H, CH_2), 6.92—7.48 (m, 20H, aromatic). Found: C, 81.91; H, 6.13; N, 3.56%. Calcd for $C_{26}H_{23}NS$: C, 81.85; H, 6.08; N, 3.67%.

Thioaniline 1e: Pale yellow prisms; mp 117—119 °C yield 26% (0.45 g, 0.93 mmol); IR (KBr) 3350 cm^{-1} (NH); ^1H NMR ($CDCl_3$) δ=1.19 (s, 18H, *t*-Bu), 4.78 (s, 1H, NH), 6.49—7.42 (m, 18H, aromatic). Found: C, 82.24; H, 7.72; N, 2.82; S, 6.90%. Calcd for $C_{33}H_{37}NS$: C, 82.62; H, 7.77; N, 2.92; S, 6.68%.

***N*-(Triphenylmethyl)-3,5-di-*t*-butylaniline (4).** A mixture of 0.80 g (3.9 mmol) of 3,5-di-*t*-butylaniline, 1.0 g (3.6 mmol) of triphenylmethyl chloride, and 1.5 ml of Et_3N in 50 ml of dry ether was stirred at room temperature for 24 h. After the reaction mixture was filtered and evaporated, the residue was crystallized from methanol to give pale yellow prisms in a 39% yield (0.62 g, 1.4 mmol). Mp 172.5—173.5 °C; IR (KBr) 3410 cm^{-1} (NH); ^1H NMR ($CDCl_3$) δ=1.06 (s, 18H, *t*-Bu), 4.85 (s, 1H, NH), 6.14—7.39 (m, 18H, aromatic). Found: C, 88.81; H, 8.42; N, 2.88%. Calcd for $C_{33}H_{37}N$: C, 88.54; H, 8.33; N, 3.13%.

ESR Measurements. Aminyls **2** were generated by the photolysis or **1** in degassed 1 : 4 di-*t*-butyl peroxide-benzene with a high-pressure mercury lamp. Aminyls **2d** and **2e** were also generated by treating the corresponding **1** with (*t*-BuOOCO-)$_2$ in degassed benzene. Radical **3** was prepared by the oxidation of **4** with PbO_2 in benzene. All the ESR spectra were recorded at 17±2 °C on a JEOL JES-ME-3X spectrometer. The hyperfine splitting constants and g values were determined by comparison with Fremy's salt in a K_2CO_3 aqueous solution (a_N=1.309 mT, g=2.0057).

References

1) ESR studies of nitrogen-centered free radicals, 29. Part 28: Y. Miura, Y. Shibata, and M. Kinoshita, *Bull. Chem. Soc. Jpn.*, **59**, 3291 (1986).

2) Y. Miura, H. Asada, M. Kinoshita, and K. Ohta, *J. Phys. Chem.*, **87**, 3450 (1983).

3) Y. Miura, A. Yamamoto, Y. Katsura, and M. Kinoshita, *J. Org. Chem.*, **45**, 3875 (1980); Y. Miura, A. Yamamoto, Y. Katsura, M. Kinoshita, S. Sato, and C. Tamura, *ibid.*, **47**, 2618 (1982).

4) Y. Miura, M. Isogai, and M. Kinoshita, *Bull. Chem. Soc. Jpn.*, **58**, 751 (1985).

5) O. W. Maender and E. G. Janzen, *J. Org. Chem.*, **34**, 4072 (1969).

6) Since the a peak overlapped partly with the b peak, we could not exactly calculate its intensity ratio to the parent spectrum.

7) Y. Miura, H. Asada, and M. Kinoshita, *Bull. Chem. Soc. Jpn.*, **53**, 720 (1980).

8) W. C. Danen, C. T. West, and T. T. Kensler, *J. Am. Chem. Soc.*, **95**, 5716 (1973); S. F. Nelsen and R. T. Landis, *ibid.*, **95**, 8707 (1973).

9) Y. Miura, Y. Shibata, and M. Kinoshita, *J. Org. Chem.*, **51**, 1239 (1986).

10) B. P. Branchaud, *J. Org. Chem.*, **48**, 3531 (1983).

11) R. G. Kryger, J. P. Lorand, N. R. Stevens, and N. R. Herron, *J. Am. Chem. Soc.*, **99**, 7589 (1977).

12) N. L. Allinger, H. M. Blatter, L. A. Freiberg, and F. M. Karkowski, *J. Am. Chem. Soc.*, **88**, 2999 (1966).

13) D. Vorländer and E. Mittag, *Ber.*, **52**, 413 (1919). (1919).

Ion Selectivity of 14-Crown-4 Derivative Possessing Two Potential Anionic Sites on Extraction of Alkali and Alkaline-Earth Metal Ions

Keiichi KIMURA,* Mutsuo TANAKA, and Toshiyuki SHONO*
Department of Applied Chemistry, Faculty of Engineering, Osaka University, Yamada-Oka, Suita, Osaka 565
(Received March 18, 1987)

Synopsis. A lipophilic 14-crown-4 derivative bearing two dinitrophenol moieties was synthesized and its ion selectivity was elucidated on cation extraction from a basic aqueous phase into an organic phase. The crown ether derivative was found to possess preferences for Ca^{2+} and Sr^{2+} as well as Li^+.

One of the highly selective ligands for Li^+ is 14-crown-4 (1,4,8,11-tetraoxacyclotetradecane) derivatives.[1,2] Such high Li^+ selectivity has also been realized in 14-crown-4 derivatives carrying an proton-dissociable moiety in the side chain, which extract Li^+ selectively from basic aqueous solutions containing alkali and alkaline-earth metal ions by the proton-cation exchange mechanism.[3-6] If a chromogen is included in the proton-dissociable moiety,[6] the ionizable 14-crown-4 derivatives also serve as spectrophotometric reagents after the selective cation extraction.[3,5] In addition, the ionizable 14-crown-4 derivatives carry out proton-driven membrane transport of Li^+ with excellent selectivities.[7] In the Li^+ complexes of 14-crown-4 derivatives bearing a proton-dissociated moiety, the positive charge of the cation is counterbalanced intramolecularly by the monovalent anion. The electroneutrality of the resulted complexes, combined with the fitness of Li^+ into the 14-crown-4 ring, contributes remarkably to the Li^+ selectivity of the crown ethers bearing a potential monovalent anion, especially against multivalent cations like alkaline-earth metal ions. It occurred to us that 14-crown-4 derivatives incorporating two proton-dissociable substituents might exhibit some selectivities for divalent small cations like Mg^{2+} and Ca^{2+} on the cation extraction and the membrane cation transport. This paper reports synthesis of a 14-crown-4 bearing two dinitrophenol moieties and its ion selectivity on the cation extraction.

Experimental

Synthesis of 14-Crown-4 Bis(dinitrophenol) 7 or 6,13-Bis(2-hydroxy-3,5-dinitrobenzyl)-6-dodecyl-1,4,8,11-tetraoxacyclotetradecane The synthetic route is given in Scheme 1. The synthesis of 1,3-propanediol derivatives **1** and **4** has been described elsewhere.[5] The reaction of **1** (77 mmol) with ethyl diazoacetate (230 mmol) in dry dichloromethane (700 cm^3) in the presence of $BF_3 \cdot OEt_2$ (1 cm^3, dropwise addition under a nitrogen atmosphere while cooling in an ice bath) for 1 h at room temperature and then for 2 h at the refluxing temperature gave diethyl 5-(2-methoxybenzyl)-3,7-dioxanonane-1,9-dioate (72%), which (55 mmol) was reduced with $LiAlH_4$ (84 mmol) in diethyl ether (150 cm^3) to yield 5-(2-methoxybenzyl)-3,7-dioxanonane-1,9-diol (**2**, ≈100%). The diol was then converted to corresponding ditosylate **3** in a usual fashion.

The procedures for the cyclization to **5**, demethylation, and nitration are as follows. In a dioxane solution (125 cm^3) of **4** (1.9 mmol), NaH (20 mmol), and $LiClO_4$ (2.5 mmol) were suspended and the mixture refluxed for 0.5 h. To the refluxing suspension was added a dioxane (25 cm^3) solution of **3** (1.9 mmol) dropwise in 1 h. The reflux was continued for 3 d. Preparative reversed-phase liquid chromatography (octadecylsilanized silica(ODS), MeOH-$CHCl_3$(10/1)) afforded colorless liquid of **5** (17%). The demethylation was performed by treating **5** (0.82 mmol) with $LiAlH_4$ (16 mmol) in refluxing octane (100 cm^3) for 8 h to yield colorless liquid of crown bisphenol **6** (50%). The crown bisphenol was nitrated by fuming HNO_3. To a chloroform (200 cm^3) solution of **6** (0.34 mmol) was added fuming HNO_3 (50 cm^3). The mixture was then stirred for 5 min at room temperature. After the reaction, water (200 cm^3) was added to the mixture. The chloroform phase was separated and washed with water. Evaporation of the chloroform gave crude product of **7**, which was purified by the reversed-phase chromatography (MeOH) to yield yellow liquid of **7** (50%): UV-VIS ($ClCH_2CH_2Cl$) 268 (ε 2.64×10^4) and ca. 350 nm (sh, ε 6.14×10^3); IR (neat) 3180 and 1260 (O-H), 1540 (N=O), and 1120 and 1100 cm^{-1} (C-O); ^1H NMR (CCl_4) δ=0.88 (3H, t, J=6 Hz, CH_3), 1.1—1.5 (22H, m, $(CH_2)_{11}CH_3$), 1.9—2.1 (1H, m, $(OCH_2)_2CH$), 2.7—2.9 (4H, m, CH_2Ph), 3.2—3.7 (16H, m, OCH_2), 8.2—9.0 (4H, m, aromatic H), 11.4—11.6 (2H, m, OH). Found: C, 56.83; H, 6.87; N, 7.03%; M^+ 764. Calcd for $C_{36}H_{52}O_{14}N_4$: C, 56.53; H, 6.85; N, 7.33%; M, 764.

Cation Extraction. The metal salts employed here were

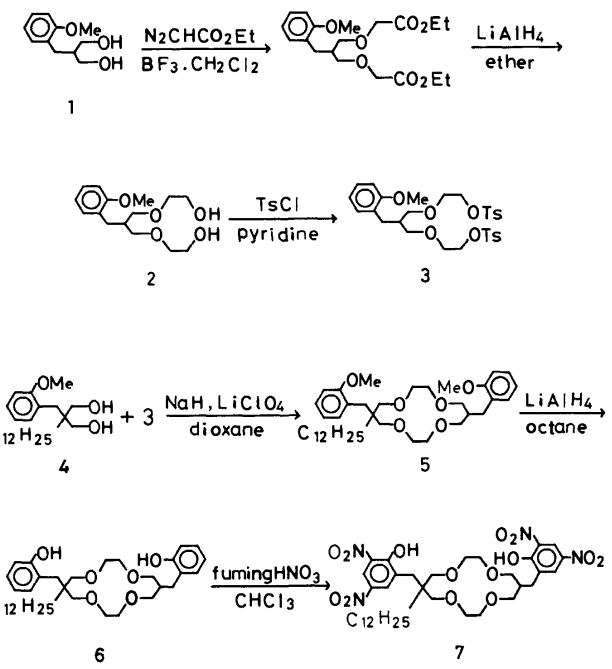

Scheme 1.

of analytical grade. Water and 1,2-dichloroethane were purified by distillation and deionization. The extraction was undertaken at room temperature for the qualitative comparison of cation extractability. Equal volumes (5 cm^3) of a 1,2-dichloroethane solution of 3.5×10^{-5} mol dm^{-3} crown ether and a buffered aqueous solution of 1 mol dm^{-3} metal chloride were placed in a stoppered centrifuge tube (10 cm height×1.5 cm diameter). The pH in the aqueous phase was adjusted to pH 7.23 by using 3-morpholino-1-propanesulfonic acid (MOPS)-tetramethylammonium hydroxide (TMAOH) buffer. The tube was shaken vigorously for 30 s. After the centrifugation, 4 cm^3 of the organic phase solution was taken up for the spectrophotometry.

For the determination of the extraction equilibrium constant, the extraction was carried out at 25 °C by varying the metal ion concentration (0.1—1 mol dm^{-3}) and keeping the crown ether concentration constant (3.5×10^{-5} for Li^+ and Sr^{2+}, 7×10^{-5} for Ca^{2+}, and 1.4×10^{-4} mol dm^{-3} for Ba^{2+}). The pH in the aqueous phase was 7.60 with a MOPS-TMAOH buffer. A stoppered tube connected with 1-cm quartz cell containing the 1,2-dichloroethane and aqueous solutions (3 cm^3 each) was shaken vigorously and was then allowed to stand for 12 h in a thermostated bath of 25 °C. Visible spectra of the organic phase were in situ measured in a cell holder thermostated at the same temperature.

Extraction Equilibrium Constant.[5,6] On the assumption that the crown ether (H_2L) forms only 1:1 cation (M^+)-crown (HL^- or L^{2-}) complexes (MHL or ML), the constants (K_{ex}) are defined as Eq. 1 for monovalent cations and as Eq. 2 for divalent cations, where subscript "a" and "o" denote the aqueous and organic phases, respectively.

$$K_{ex}=([MHL]_o[H^+]_a)/([H_2L]_o[M^+]_a) \quad (1)$$

$$K_{ex}=([ML]_o[H^+]_a^2)/([H_2L]_o[M^{2+}]_a) \quad (2)$$

Since the crown ether is highly lipophilic, its undissociated, proton-dissociated, and complexed species are hardly partitioned to the aqueous phase, i.e., $[H_2L]_a\simeq0$, $[HL^-]_a$ (or $[L^{2-}]_a)\simeq0$, and $[MHL]_a$ (or $[ML]_a)\simeq0$. If the following assumptions are also made, i.e., $[H_2L]_t$ ("t" is "total".)$\simeq$ $[H_2L]_o+[MHL]_o$ (or $[ML]_o$) and $[M^+]_t$ (or $[M^{2+}]_t)\simeq[M^+]_a$ (or $[M^{2+}]_a$), Eqs. 1 and 2 can be transformed to Eqs. 3 and 4, respectively.

$$[H^+]_a/[M^+]_t=(K_{ex}\varepsilon_{MHL}[H_2L]_t/A_o)-K_{ex} \quad (3)$$

$$[H^+]_a^2/[M^{2+}]_t=(K_{ex}\varepsilon_{ML}[H_2L]_t/A_o)-K_{ex} \quad (4)$$

Here, ε_{MHL} (or ε_{ML}) and A_o stand for molar absorptivity and absorbance for MHL (or ML) in the organic phase at a wavelength where H_2L does not absorb at all. Thus the K_{ex} values were determined from the intercepts of the plots of $[H^+]_a/[M^+]_t$ (or $[H^+]_a^2/[M^{2+}]_t$) vs. $1/A_o$.

Results and Discussion

Since 14-crown-4 bearing two dinitrophenol moieties **7** are easily proton-dissociable (the average pK_a: 5.20 in dioxane-water(1/1)), extractions of metal ions that have affinity to the crown ring, based on the H^+-M^+ exchange mechanism, should occur even under mild pH conditions of the aqueous phase, being accompanied by significant spectral changes of the chromogen in the organic phase. Figure 1 depicts typical spectral changes on the cation extraction of alkali and alkaline-earth metal ions. Definitely, increasing absorption in the visible region on the cation extraction is derived from the complex formation between the metal ions and the proton-dissociated species of **7** in the organic phase, inasmuch as any spectral change was not attained without metal ions in the initial aqueous phase under the identical pH conditions. The monovalent metal ion is different from the divalent ones in the wavelength of the visible absorption for the complexes (Table 1). Also, the monovalent cation complex possesses about one half the molar absorptivity for the divalent ones, which in turn is close to that for the ion pair between the dianionic species of **7** and two tetramethylammonium ions (ε 2.68×10^4 at 376 nm). The spectral data suggest that the monovalent and divalent ions (M^+ and M^{2+}) interact with mono- and dianionic species of **7** (HL^- and L^{2-}), respectively, to form electrically-neutral complexes (MHL and ML). In the group of alkali metal ions, Li^+ is extracted most effectively by the crown ether. Slight and practically no extractions were found with Na^+ and the other alkali metal ions, respectively. The high Li^+ selectivity of **7** against other alkali metal ions is quite similar to that of a corresponding 14-crown-4 derivative with only one dinitrophenol moiety, 6-dodecyl-6-(2-hydroxy-3,5-dinitrobenzyl)-1,4,8,11-tetraoxacyclotetradecane.[5] As anticipated from the easy charge compensation for divalent cations, **7** is able to extract alkaline-earth metal ions. This was not the case with the derivative possessing only one dinitrophenol moiety, which hardly extracted any alkaline-earth metal ions under the identical pH conditions.

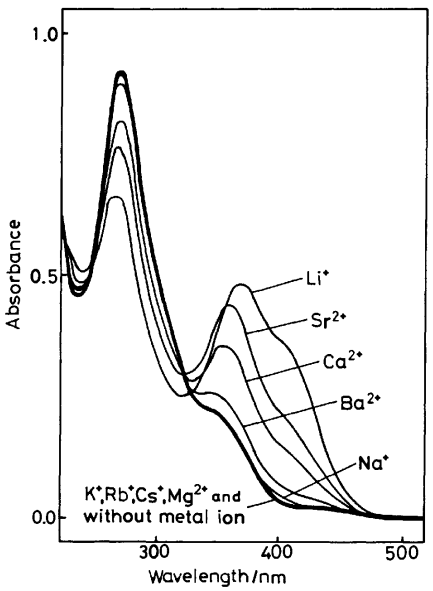

Fig. 1. Spectral change in organic phase on cation extraction with 14-crown-4 bis(dinitrophenol) **7**.

Table 1. Extraction Equilibrium Constants and Spectral Data for Cation Complexes of **7**

Complexed cation	pK_{ex} [a]	ε_{MHL} or ε_{ML} [b] (λ_{max}) [c]
Li^+	7.36	1.62×10^4 (368)
Ca^{2+}	15.61	2.75×10^4 (359)
Sr^{2+}	15.56	2.78×10^4 (359)
Ba^{2+}	16.43	2.92×10^4 (359)

a) In $ClCH_2CH_2Cl$-H_2O system, at 25°C. $pK_{ex}=-\log K_{ex}$. b) In $dm^3\,mol^{-1}\,cm^{-1}$. c) In nm.

Interestingly, **7** exhibited good extractabilities for the medium-size alkaline-earth metal ions, but hardly did any extractability for Mg^{2+} that resembles Li^+ in size. The poor extractability for Ba^{2+} may be ascribable to the fact that the 14-crown-4 ring is too small to form stable complexes with the large cation.

An attempt was made to determine the extraction equilibrium constants of **7** for the electrically-neutral 1 : 1 cation-crown ether complexes. The plots of $[H^+]_a/[M^+]_t$ (for monovalent cations) or $[H^+]_a^2/[M^{2+}]_t$ (for divalent ones) vs. $1/A_o$ gave straight lines with coefficients of correlation of better than 0.999 for Li^+, Ca^{2+}, Sr^{2+}, and Ba^{2+}, thus affording their K_{ex} values (Table 1). The K_{ex} values for the other metal ions could not be obtained because of the poor extractabilities towards them.

In conclusion, the 14-crown-4 derivative bearing two dinitrophenol moieties **7** is still highly Li^+-selective against other alkali metal ions on the cation extraction. In addition, good affinity for some alkaline-earth metal ions, although not very drastic, was attained with the crown ether.

References

1) S. Kitazawa, K. Kimura, H. Yano, and T. Shono, *J. Am. Chem. Soc.*, **106**, 6978 (1984).
2) B. P. Czech, D. A. Babb, B. Son, and R. A. Bartsch, *J. Org. Chem.*, **49**, 4805 (1984).
3) K. Kimura, M. Tanaka, S. Kitazawa, and T. Shono, *Chem. Lett.*, **1985**, 1239.
4) R. A. Bartsch, B. P. Czech, S. I. Kang, L. E. Stewart, W. Walkowiak, W. A. Charewicz, G. S. Heo, and B. Son, *J. Am. Chem. Soc.*, **107**, 4997 (1985).
5) K. Kimura, M. Tanaka, S. Iketani, and T. Shono, *J. Org. Chem.*, **52**, 836 (1987).
6) M. Takagi and K. Ueno, *Top. Curr. Chem.*, **121**, 39 (1984).
7) K. Kimura, H. Sakamoto, S. Kitazawa, and T. Shono, *J. Chem. Soc., Chem. Commun.*, **1985**, 669.

Syntheses and Biological Activities of Neurokinin A Analogs Substituted with Glycine

Tadashi HASHIMOTO,* Katsuro KUROSAWA, and Yoshiki UCHIDA
School of Pharmacy, Hokuriku University, Ho-3, Kanagawa-machi, Kanazawa 920-11
(Received March 28, 1987)

Synopsis. Five neurokinin A (NKA) analogs substituted with glycine at position 3, 4, 5, 6, or 7 were synthesized by Merrifield's solid phase method. The contractile activities of the synthetic analogs were assayed on isolated guinea pig ileum and rat vas deferens. The results suggest that Asp[4], Phe[6], and Val[7] residues of NKA may be essential for the intrinsic activity on guinea pig ileum and on rat vas deferens, respectively.

Neurokinin A (NKA, also called neuromedin L or substance K) and neurokinin B (NKB, also called neuromedin K) are novel neuropeptides isolated from porcine spinal cord. Structure elucidation[1] revealed that NKA and NKB have close structural homologies with tachykinin such as substance P (SP), kassinin and physalaemin (Fig. 1). Decapeptide amides, NKA and NKB, have the same sequence between Phe[6] and Met[10] and are very similar to the mammalian tachykinin SP, particularly in the sequence of C-terminal region.

Our study[3] on the structure activity relationship of NKB provides clear indication on the location of the active site, that is, the replacement of Phe[6] or Val[7] residue with Gly moiety brings drastic decrease of the contractile activities on isolated guinea pig ileum (GPI) and rat vas deferens (RVD), while the substitution of Gly for Phe[5] enhances their activities. In other words, NKB related octapeptide analogs [Gly[6]]-NKB (3-10) and [Gly[7]]-NKB (3-10) have no intrinsic activity on GPI and RVD. Furthermore, it has been revealed that the replacement of Phe[6] in NKB with Gly moiety changes the pharmacological spectrum of NKB from that of an agonist to that of an antagonist.[4] The knowledge has been utilized in the design of NKB analogs, and we have succeeded in the development of several specific antagonists against NKB.[5] Therefore glycine substitution seems to be useful tool for the study of the structure activity relationship of NKA.

In the present investigation, in order to examine the biological effect of the substitution of Gly moiety for Thr[3], Asp[4], Ser[5], Phe[6], and Val[7] residues of NKA and the amino acid residues for recognition of SP-P and SP-E type receptors, we synthesized [Gly[3]]-, [Gly[4]]-, [Gly[5]]-, [Gly[6]]-, and [Gly[7]]-NKA (Fig. 2), and submitted them for biological assay.

Synthesis of NKA analogs used in this study was performed on an automated peptide synthesizer by standard solid phase method[6] starting from *t*-butoxycarbonyl (Boc)-Met benzhydrylamine-resin. Boc protection was used for α-amino function. The side-chain protective groups used were cyclohexyl for Asp, tosyl for His, benzyloxycarbonyl for Lys and benzyl for Ser and Thr. Deprotection and dicyclohexylcarbodiimide (DCC) coupling were programed as given in Table 1.

The second coupling was repeated with additive of one equivalent of 1-hydroxybenzotriazole (HOBt) according to a program without step 1—4. A 2.5 fold excess of amino acid derivatives was used for all couplings. The coupling reaction was monitored by the ninhydrin color test procedure of Kaiser et al.[7] A trace of unreacted amino group was acetylated with acetic anhydride and pyridine. After the completion of the

	1 3 4 5 6 7 10
NKA	H-His-Lys-Thr-Asp-Ser-Phe-Val-Gly-Leu-Met-NH_2
NKB	H-Asp-Met-His-Asp-Phe-Phe-Val-Gly-Leu-Met-NH_2
	1 11
SP	H-Arg-Pro-Lys-Pro-Gln-Gln-Phe-Phe-Gly-Leu-Met-NH_2
Kassinin	H-Asp-Val-Pro-Lys-Ser-Asp-Gln-Phe-Val-Gly-Leu-Met-NH_2
Physalaemin	pGlu-Ala-Asp-Pro-Asn-Lys-Phe-Tyr-Gly-Leu-Met-NH_2

Fig. 1. Amino acid sequences[2] of tachykinin peptides.

1	[Gly[3]]-NKA	H-His-Lys-Gly-Asp-Ser-Phe-Val-Gly-Leu-Met-NH_2
2	[Gly[4]]-NKA	H-His-Lys-Thr-Gly-Ser-Phe-Val-Gly-Leu-Met-NH_2
3	[Gly[5]]-NKA	H-His-Lys-Thr-Asp-Gly-Phe-Val-Gly-Leu-Met-NH_2
4	[Gly[6]]-NKA	H-His-Lys-Thr-Asp-Ser-Gly-Val-Gly-Leu-Met-NH_2
5	[Gly[7]]-NKA	H-His-Lys-Thr-Asp-Ser-Phe-Gly-Gly-Leu-Met-NH_2

Fig. 2. Synthetic NKA analogs.

Table 1. Program for Solid Phase Synthesis

Step	Reagent	Operation	Mix time/min
1	CH_2Cl_2	3×Wash	1.5
2	TFA (25% in CH_2Cl_2)	Prewash	1.5
3	TFA (25% in CH_2Cl_2)	Deprotection	30
4	CH_2Cl_2	3×Wash	1.5
5	CH_2Cl_2	3×Wash	1.5
6	TEA (10% in CH_2Cl_2)	3×Neutralization	1.5
7	CH_2Cl_2	6×Wash	1.5
8	Boc-Amino Acid (in CH_2Cl_2)	Mix	5
9	DCC	Mix	180
10	CH_2Cl_2	6×Wash	1.5

Table 2. Amino Acid Analyses of Synthetic NKA Analogs

Analog	Found (Calcd)										
	Asp	Thr	Ser	Gly	Val	Met	Leu	Phe	His	Lys	NH_3
1	1.04(1)	—	0.89(1)	2.02(2)	1.03(1)	1.00(1)	1.02(1)	1.00(1)	1.01(1)	1.00(1)	1.32(1)
2	—	0.92(1)	0.87(1)	2.04(2)	1.03(1)	0.99(1)	1.03(1)	1.02(1)	1.05(1)	1.04(1)	1.33(1)
3	1.02(1)	0.94(1)	—	1.97(2)	1.01(1)	1.01(1)	1.02(1)	1.01(1)	1.01(1)	1.01(1)	1.37(1)
4	1.02(1)	0.94(1)	0.89(1)	2.00(2)	1.03(1)	1.01(1)	1.04(1)	—	1.03(1)	1.03(1)	1.88(1)
5	1.06(1)	0.96(1)	0.89(1)	2.00(2)	—	1.01(1)	1.04(1)	1.01(1)	1.01(1)	1.02(1)	1.32(1)

Table 3. Physical Properties and Yield of Synthetic NKA Analogs

Analog	$[\alpha]_D^8$/° (*c* 0.2, 50% AcOH)	Retention time[a]/min	R_f^1	R_f^2	Yield/%
1	−20.5	13.3	0.00	0.32	11.0
2	−26.0	12.7	0.00	0.49	9.9
3	−24.5	13.4	0.00	0.43	7.8
4	−32.0	12.7[b]	0.00	0.38	10.9
5	−30.5	10.3	0.00	0.39	6.7

a) Condition of analytical HPLC: column, NOVA-PAK C_{18}; flow rate, 1 ml min^{-1}; Detection, 210 nm; eluent system, linear gradient from 14% [b) 4.2%] to 35% CH_3CN (15 min) in 20 mM phosphate buffer (pH 3.0).

chain elongations, the peptide resin was treated with liquid hydrogen fluoride (HF)[8] in the presence of anisole for 30 min at −20 °C and then 30 min at 0 °C to cleave the peptide from the resin with simultaneous removal of the protecting groups and formation of the carboxyl terminal amide. The excess HF was removed in vacuo, and the resulting material was washed with ethyl acetate prior to extraction of the peptide with aq acetic acid (50%). The crude product was purified by preparative reverse-phase high-performance liquid chromatography (HPLC) using aq trifluoroacetic acid (0.1%) in acetonitrile as eluent. The desired fractions were collected and desalted on a column of Sephadex LH-20 eluted with aq *N*,*N*-dimethylformamide (90%) containing 0.02% 1,2-ethanedithiol, giving pure peptide. The yield was sacrificed for the purity test of the fractions selected. Acid hydrolysates of the peptides contained the constituent amino acids in the ratios predicted by theory (Table 2). Homogeneity of the peptides was demonstrated by analytical HPLC and thin-layer chromatography (TLC) (Table 3). When single peaks and single spots were observed for a peptide in all chromatographic systems, the sample was considered appropriately pure for bioassay.

Biological properties of the synthetic NKA analogs were examined on GPI having SP-P type receptor and RVD having SP-E type receptor. The contractile activities of the analogs were compared with that of our synthetic NKA. The results are shown in Table 4.

On GPI assay, analog **1**, **2**, **3**, and **5** possessed about 25, 10, 20, and 10%, respectively, of the contractile activity of NKA, while analog **4** had little activity. The potency of analog **1** was as high as the intrinsic activity of NKA itself and analog **3** possessed about 80% of the activity on RVD assay, but analogs **2**, **4**, and **5** showed no agonistic activity. Analogs **4** on GPI, and **2**, **4**, and **5** on RVD, were tested for their antagonistic effects against NKA respectively. None of the analogs **2**, **4**, and **5** was found to act as an antagonist of NKA on both assays. These data suggest that the Phe^6 of NKA as well as NKB is essential for binding or stimulation of SP receptors in the two smooth muscle preparations. In contrast to the results obtained in NKB, whereby the substitution of Gly for Phe^6 changes the pharmacological spectrum of NKB from that of an agonist to that of an antagonist, the Gly^6 analog of NKA shows no antagonism to NKA. In comparison with the results that the Gly analogs of NKB provided consistent indications of the active sites, Phe^6 and Val^7, in GPI and RVD,[3] the Gly analogs of NKA indicated the location of the additional active site of Asp^4 in RVD. In other words, Asp^4 moiety as well as Phe^6 and Val^7 in NKA seems to be important for the recognition of SP-E type receptors. The results well agrees with the observation of Osakada et al.,[9] Asp^4 and Val^7 moieties being important for the recognition of SP-E type receptors.

Table 4. Biological Activities of Synthetic NKA Analogs

Analog	GPI		RVD	
	RA[a]	ANT[b]	RA	ANT
1	0.25	NT[c]	1.01	NT
2	0.12	NT	0	—[d]
3	0.20	NT	0.78	NT
4	<0.003	—	0	—
5	0.13	NT	0	—

a) Relative contractile activity to NKA=1. b) Antagonistic activity against NKA. c) Not tested. d) No antagonistic activity.

Experimental

Amino acid derivatives were purchased from Peptide Institute, Inc., Osaka, and benzhydrylamine (BHA) resin (available amine of the resin: 0.6 mmol g^{-1} of support) from Beckman Inc. The solid phase synthesis was carried out using a Beckman System 990C Peptide Synthesizer. Optical rota-

tions were measured in a Nipponbunkoh DIP-4 Polarimeter. Amino acid analyses on samples previously hydrolyzed with 6 M HCl (1 M=1 mol dm^{-3}) (110 °C, 24 h) were performed on a Beckman System 7300 Amino Acid Analyzer. TLC were carried out on silica-gel plates (Merck). The following solvent systems were used and allowed to ascend for 10 cm: R_f^1, *n*-BuOH-AcOH-H_2O (4:1:5, upper phase); R_f^2, *n*-BuOH-pyridine-AcOH-H_2O (30:20:6:24). Analytical HPLC were effected on the following systems: column, NOVA-PAK C_{18} (3.9×150 mm); flow rate, 1 ml min^{-1}, detection, 210 nm; eluent system, linear gradient of CH_3CN in 20 mM phosphate buffer (pH 3.0).

General Procedure for the Preparation of Analog. The first Boc-amino acid was coupled to the BHA-resin (0.60 meq. N g^{-1}) as follows. A half gram of the BHA-resin hydrochloride was neutralized with a solution of 10% (by volume) triethylamine (TEA) in dichloromethane (10 ml). Then the resin was washed with 10 ml of dichloromethane, and was mixed with 2.5 equiv of Boc-Met-OH and DCC in dichloromethane. The quantitation of coupling reaction was carried out by a negative ninhydrin color test. The unreacted amino groups were blocked by acetylation using Ac_2O (5 equiv) and pyridine (1 equiv) in dichloromethane for 20 min. For the coupling reactions after second Boc-amino acids, deprotection and DCC coupling were programed as given in Table 1. For second coupling, a programed without steps 1—4 was used. A 2.5 fold excess of DCC and the amino acid derivative dissolved in dichloromethane were used for all couplings. One equivalent of HOBt was used only for the second DCC-coupling. The protected peptide resin was simultaneously cleaved and deblocked with anhydrous liquid HF containing 10% anisole. Approximately 5 ml of liquid HF was used for 0.25 g resin, and the reaction mixture was kept at −20 °C for 30 min and then 0 °C for 30 min to prevent the succinimide formation in Asp-Gly sequence. After evaporation of HF in vacuo with ice-cooling, the peptide-resin mixture was washed with AcOEt. The peptide was extracted with three portions of 50% AcOH and the extracts combined were lyophilized.

Purification of the Peptides. The crude peptide was subjected to HPLC which is composed of a model 590 pump and an U6K injector (Waters) connecting with a column (20×300 mm) of Chemcosorb ODS (Chemco). The eluates were monitored with an UV detector S-310A model-II (Soma) at 210 nm wavelength. CH_3CN-0.1% TFA solvent system was used as eluent at flow rate 10 ml min^{-1}. Each peptide was emerged at 40—60 min by isocratical elution with 14—20% CH_3CN contents of the solvent system. The desired fraction was desalted on a Sephadex LH-20 column (15×500 mm) eluted with DMF-H_2O (9:1) containing 0.02% 1,2-ethanedithiol and the product was lyophilized. Homogeneity of the peptides was analyzed by analytical HPLC on a column of NOVA-PAK C_{18} (3.9×150 mm) with gradient elution using 20 mM phosphate buffer (pH 3.0)/CH_3CN and by TLC on silica-gel plate. The peptides on silica-gel plate were detected with ninhydrin and chlorine-*o*-tolidine reagents. When single peaks and single spots were observed for a peptide in all chromatographic systems and amino acid composition after hydrolysis of the peptides were consistent with the calculated values, the sample was submitted for bioassay.

Bioassay. The biological activities of NKA analogs were measured on GPI and RVD. Male guinea pig (weighing 200—250 g) and male rat (weighing 250—300 g) were stunned by a blow to the neck and exsanguinated. Ileum and vas deferens were rapidly isolated and kept for dissection in Tyrode's solution (137 mM NaCl, 2.7 mM KCl, 1.8 mM $CaCl_2$, 1.1 mM $MgCl_2$, 0.4 mM NaH_2PO_4, 12 mM $NaHCO_3$, 5.6 mM glucose) at room temperature. Both organs were suspended in a 30 ml organ bath containing Tyrode's solution thermostated at 30 °C and bubbled with 95% O_2 and 5% CO_2 gas for 1 h. The contraction was recorded by means of an isotonic transducer (Nippon Kohden, TD-111T) with load of 2 or 1 g (for ileum and vas deferens respectively) on a Servocorder (Watanabe Instruments, SR6204). Concentration-response curves were obtained using a cumulative dose-assay, the time between two consecutive dose-response curves was longer than 10 min. In the tests for antagonistic activity on GPI and RVD, analog was added 10 min before NKA was added. The cumulative dose-response curve of NKA in the presence or the absence of the analog was obtained. In the presence of analogs at concentration 2×10^{-6} M, the maximal response induced by NKA was almost the same response without analogs.

References

1) S. Kimura, M. Okada, Y. Sugita, I. Kanazawa, and E. Munekata, *Proc. Jpn. Acad.*, **59B**, 101 (1983); H. Kangawa, N. Minamino, A. Fukuda, and H. Matsuo, *Biochem. Biophys. Res. Commun.*, **114**, 533 (1983).

2) Amino acids, peptides and their derivatives mentioned in this paper are of L-configuration. The abbreviations for amino acids and peptides are in accordance with the rules of the IUPAC-IBU Commission on Biochemical Nomenclature in *Eur. J. Biochem.*, **138**, 9 (1984).

3) T. Hashimoto, T. Moro, and Y. Uchida, *Bull. Chem. Soc. Jpn.*, **59**, 4006 (1986).

4) Y. Uchida, K. Okimura, K. Kurosawa, N. Sakura, K. Hirose, and T. Hashimoto, *Bull. Chem. Soc. Jpn.*, **60**, 1561 (1987).

5) T. Hashimoto, Y. Uchida, K. Okimura, and K. Kurosawa, *Chem. Pharm. Bull.*, in press.

6) R. B. Merrifield, *Adv. Enzymol.*, **32**, 221 (1969).

7) E. Kaiser, R. L. Colescott, C. D. Bossinger, and P. I. Cook, *Anal. Biochem.*, **34**, 595 (1970).

8) S. Sakakibara, Y. Shimonishi, Y. Kishida, M. Okada, and H. Sugihara, *Bull. Chem. Soc. Jpn.*, **40**, 2164 (1967).

9) F. Osakada, K. Kubo, K. Goto, I. Kanazawa, and E. Munekata, *Eur. J. Pharmacol.*, **120**, 201 (1986).

Application of the Flow Injection Analysis Based on Iodometry to the Determination of Ozone Decomposition Rate

Yasuo ONARI
Mie Industrial Research Institute, Takajayakomori-cho, Tsu 514
(Received January 20, 1987)

Synopsis. The determination of ozone decomposition rate by flow injection analysis (FIA) was investigated. Under the conditions studied a sampling rate was about 43 samples/h, and the pseudo-first-order kinetic plot of the obtained data showed a good linearity. This FIA method seems to be useful for kinetic measurement of ozone decomposition in water.

Ozone is known as a powerful oxidant, and widely applied to the treatment of drinking water and waste water. In routine water-disinfection application of ozone, residual ozone at 5 minutes after ozone injection is maintained at sub-mg dm^{-3} levels. In order to obtain these residuals, in general, the initial ozone concentration in water is known to be between 0.5 and 4.0 mg dm^{-3}. The decomposition rate of ozone is very important for the achievement of the treatment. The rapid determination of the rate is, therefore, desired.

Ozone in water is commonly determined by iodometry or by photometric detection at 254 nm.[1] The former is a standard analytical method for ozone, but it is disadvantageously time-consuming, and requires a large sample volume. The latter is convenient for continuous measurement of ozone, but the sensitivity is not high enough because of the small molar extinction coefficient of ozone in water, and large interference from coexisting substances in sample solutions is unavoidable. Straka et al.[2] reported the flow injection analysis (FIA) of residual ozone by employing indigo as a reagent. But this method has a disadvantage of evaluating a negative peak caused by ozone decoloration of the dye, and the background absorption level is very high. In ozone measurement, an automated technique based on iodometry is desirable in order to achieve a continuity between the data obtained by a new method and the known data determined by the standard iodometric method. In this paper, the automated iodometric measurement of ozone by FIA and its application to the rapid determination of the ozone decomposition rate were investigated.

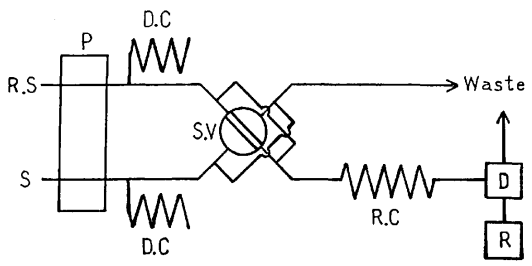

Fig. 1. Schematic flow diagram for ozone analysis. R.S: KI aqueous solution, S: sample solution, P: peristaltic pump (MP-3, Tokyo Rikakikai Co., Ltd.), D.C: damper coil, S.V: sample injection valve (46 μl), R.C: reaction coil (1 mm i.d.), D: detector (Absorbance at 354 nm, UVIDEC-100, Nihon Bunko Co., Ltd.), R: recorder (D2R2M, Ohkura Co., Ltd.).

Experimental

The flow diagram of FIA is shown in Fig. 1. A sample solution was pumped through a flow line by a micro pump. The sample solution(46 μl) was periodically injected into the flow of a reagent solution by rotating a sample injection valve, followed by mixing in a reaction coil, and liberated I_2 was directly measured by photometry at the maximum wavelength 354 nm. The reaction of ozone with I^- is shown as follows: $O_3+2I^-+2H^+ \rightarrow O_2+H_2O+I_2$. The stoichiometry of the ozone-iodide reaction is known to be 1.0 over a wide pH range.[3]

Results and Discussion

Effect of the Reaction Coil Length. The result is presented in Fig. 2. In this case, the peak width of the FIA signal increased with increasing length of the coil, and therefore the sampling rate decreased from 55 samples/h (40 cm coil) to 45 (300). If the coil was shorter than 40 cm, the reproducibility of the FIA signal was not good. Under these experimental conditions, the coil length was shown to be most suitable in the range of about 40—100 cm.

Effect of the KI Concentration of the Reagent Solution. The experimental conditions such as the rea-

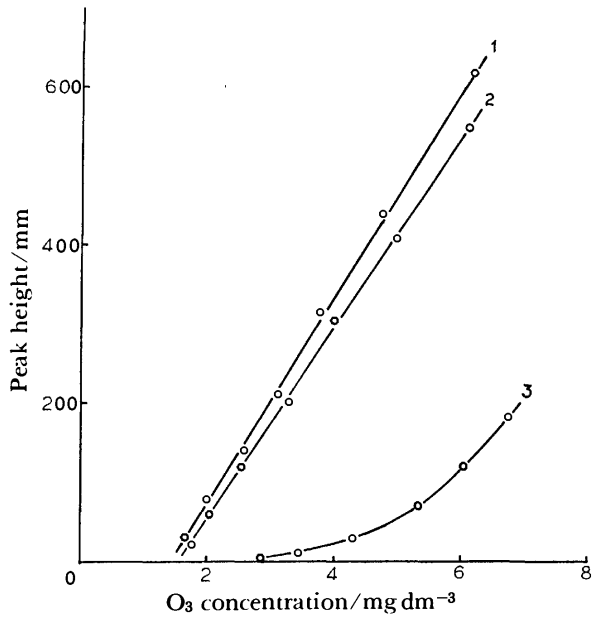

Fig. 2. Effect of reaction coil length on FIA of O_3 at 25 °C. Reagent solution: 5% KI Aqueous solution, reagent flow rate: 1.45 $cm^3 min^{-1}$, 1: 40 cm, 2: 100 cm, 3: 300 cm.

gent flow rate, the temperature of the reagent solution and the reaction coil length were 1.45 $cm^3 min^{-1}$, 25 °C and 100 cm respectively. The detection limit (S/N=2.5) and the sampling rate were as follows: 0.1% KI solution, 0.3 mg dm^{-3} (30 samples/h); 1, 0.7 (43); 5, 1.6 (50); 10, 2.5 (60). A suitable KI concentration should be selected by considering the levels of ozone in sample solutions.

Effect of the Reagent Flow Rate. The effect of the flow rate was investigated in the range 1.70—0.55 $cm^3 min^{-1}$. The experimental conditions such as the reagent solution, its temperature and the reaction coil length were 5% KI, 25 °C and 100 cm, respectively. The peak width increased with decreasing flow rate, and hence the sampling rate decreased from 64 samples/h (1.70 $cm^3 min^{-1}$) to 26 (0.55). A desirable flow rate of the reagent solution was shown to be near 1.45 $cm^3 min^{-1}$ or above.

Conditions of FIA. From experimental results, the conditions of the FIA were decided as follows: Reagent solution, 1% KI; reaction coil, 100 cm; reagent flow rate, 1.45 $cm^3 min^{-1}$; temperature of the reagent solution, 25 °C. Under these conditions, dispersion of sample zone was investigated, and a dispersion coefficient (D) was shown to be 30. The obtained calibration curve was confirmed to be linear up to 11.3 mg dm^{-3} O_3, but the upper limit of the linear range could not be evaluated because of the low power of a ozone generator used. When the sample (2.92 mg dm^{-3} O_3) was injected five times, the precision (C.V.) was 0.67%.

Effect of Coexisting Substances. Tap water (2000 cm^3) was aerated at a constant flow rate of 2.8 $dm^3 min^{-1}$ using a G-2 sintered glass filter for 5 h at 50 °C, and residual chlorine was purged. A sample solution was prepared by using 500 cm^3 of chlorine-free tap water, followed by measurement of dissolved ozone by the standard iodometric method and by this FIA. Typical data are shown in Table 1. Minerals, the levels of which were suitable for drinking water, were shown not to interfere the measurement of O_3 by this FIA. Ozone attacks many organic compounds containing carbon-carbon double bonds to result in oxalic acid as a main final oxidation product.[4] Therefore, in the measurement of residual ozone, the effect of oxalic acid should be examined. Experimental data in Table 1 show that the interference of oxalic acid with the O_3 measurement by this FIA is small.

Application to the Determination of Ozone Decomposition Rate. The decomposition rate of ozone in chlorine-free tap water was measured by this FIA. A sample solution was prepared using 500 cm^3 chlorine-free tap water obtained in the same way as described above. Immediately after the completion of ozone injection, the measurement of ozone by this FIA was started. Typical FIA signals obtained in the experiment are presented in Fig. 3. The pseudo-first-order kinetic plot of the obtained data shows a good linearity (n, 6; γ, −0.994; α, 0.001). Therefore, the decomposition of O_3 in this experiment was shown to be first order with respect to O_3. The kinetic plots are shown in Fig. 4. In these cases, the first half-lives of O_3 were 8.7 and 5.8 min, when the initial concentrations of O_3

Table 1. Determination of Ozone in Water

Sample	FIA/mg dm^{-3}	Iodometry/mg dm^{-3}
Tap water[a]	1.34	1.34
	2.05	2.00
	2.88	2.95
Oxalic acid Solution[b]	3.14	3.00
	4.16	4.19
	5.10	4.90

a) Ozone was injected into chlorine-free tap water. b) Ozone was injected into 361 mg dm^{-3} oxalic acid-water.

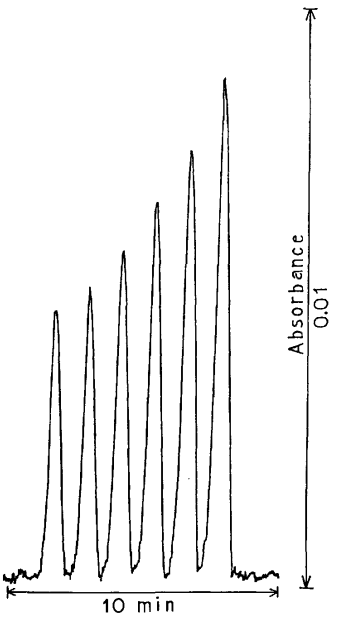

Fig. 3. Typical FIA signals obtained for measurement of O_3 in chlorine-free tap water. Initial concn of O_3: 2.5 mg dm^{-3}, pH of the sample solution: 7.9.

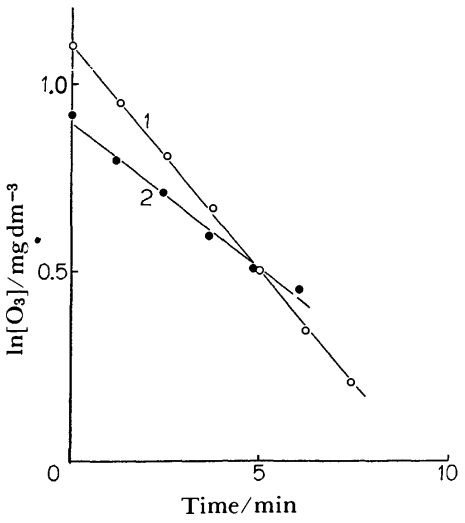

Fig. 4. Pseud-first-order plot for decomposition of ozone in chlorine-free tap water at 25°C. 1, Initial concn of O_3: 3.0 mg dm^{-3}, $\log[O_3]=1.10-0.119 \cdot t$ (n:7, γ:−0.999, α:0.001). 2, Initial concn of O_3: 2.5 mg dm^{-3}, $\log[O_3]=0.895-0.0774 \cdot t$ (n:6, γ:−0.994, α:0.001).

were 2.5 and 3.0 mg dm^{-3}, respectively. Horie and coworkers[5] reported on the half-life of O_3 in water which was processed by coagulation and filtration without chlorine treatment, where the half-lives were 8, 15, and 30 min at 20 °C for the initial concentrations of 2.0, 1.0, and 0.5 mg dm^{-3}, respectively. Half-life measured in this experiment was a reasonable value compared with these results. From these results, this FIA can be applied to the automated measurement of the decomposition rate of O_3 in water. If necessary, the sampling rate and the sensitivity of this FIA can be controlled by slight modifications of the KI concentration and reaction coil.

References

1) R. N. Kinman, "Ozone in Water Disinfection," in Ozone in Water and Wastewater Treatment, ed by Evans, Ann Arbor Sci., Ann Arbor (1972), Chap. VII, P. 131.
2) M. R. Straka, G. E. Pacey, and G. Gordon, *Anal. Chem.*, **56**, 1973 (1984).
3) R. N. Dietz, J. Pruzansky, and J. D. Smith, *Anal. Chem.*, **45**, 402 (1973).
4) Y. Onari, *Bull. Chem. Soc. Jpn.*, **58**, 2526 (1985).
5) M. Horie, K. Shizuno, and H. Takeuchi, *Yosui to Haisui*, **15**, 345 (1973).

Improved Spectrophotometric Determinations of Cobalt(II) and Nickel(II) with Zincon in the Surfactants Micellar

Itsuo MORI,* Yoshikazu FUJITA, Kinuko FUJITA, Takeshi TANAKA, Yukari YANO, and Makiko ASADA
Osaka University of Pharmaceutical Sciences, 2-10-65 Kawai, Matsubara, Osaka 580
(Received December 13, 1986)

Synopsis. Reactions between Zincon and cobalt(II) in the presence of *N*-hexadecylpyridinium chloride (cationic surfactant), and between Zincon and nickel(II) in the presence of poly(vinyl alcohol) (nonionic surfactant) are discussed in terms of the development of simple, sensitive and improved spectrophotometric determinations of cobalt(II) and nickel(II). The calibration graphs were rectilinear in the ranges 0—2.2 μg 10 cm^{-3} cobalt(II) with a Sandell sensitivity of 0.00015 μg cm^{-2} at 550 nm and 0—42.0 μg 10 cm^3 nickel(II) with that of 0.0047 μg cm^{-2} nickel(II) at 470 nm. The proposed methods were relatively sensitive in comparison with the methods in the absence of surfactants with apparent molar extinctions of 4.6×10^5 for cobalt(II) and 2.4×10^4 dm^3 mol^{-1} cm^{-1} for nickel (II). Separative assays of cobalt(II) and various metals (nickel(II), zinc(II), copper(II), and iron(III)) were possible by selections of analytical wavelengths, respectively.

The spectrophotometry of micro amounts of cobalt(II) or nickel(II) has recently attracted much attention regarding heavy metal pollution in enviromental areas. For cobalt(II) or nickel(II), various spectrophotometric determinations using Dithizone,[1] 4-(2-pyridylazo)resorcinol(PAR),[2] nitroso R salt,[3] dimethylglyoxime.[4] Chrome Azurol S,[5] etc., have already been reported. However, most methods are relatively complicated and therefore organic solvent extractions are necessary using a toxic organic solvent such as chloroform. Although determinations of cobalt(II) and nickel(II) using Zincon are comparatively sensitive,[6-9] these methods lack selectivity, stability and reproducibility. On the other hand, we found that the reaction systems between cobalt(II) and Zincon in the presence of a cationic surfactant micellar(such as *N*-hexadecylpyridinium chloride (HPC)) and between nickel(II) and Zincon in the presence of a nonionic surfactant micellar(such as poly(vinyl alcohol) (PVA)) posessed many advantages over these reaction systems (binary complex) in the absence of surfactants: highly sensitive, stability and a wide coloring pH ranges under these experimental conditions.

In this paper, simple, sensitive and improved spectrophotometric determinations of cobalt(II) using Zincon in the presence of HPC, and of nickel (II) using Zincon in the presence of PVA are, respectively, discussed and proposed in water-soluble surfactants micellar media.

Experimental

Reagents and Apparatus. Standard cobalt(II) and nickel(II) solutions, a stock solution containing 1.0×10^{-2} M (1 M≒1 mol dm^{-3}) of cobalt(II) or nickel (II), were prepared by dissolving cobalt nitrate or nickel nitrate in water. The concentrations of these stock solutions were determined by chelatometric titration.[10] A working solution (5.0×10^{-4} M) was prepared by a suitable dilution of this stock solution. A 1.0×10^{-3} M Zincon solution was prepared by dissolving Zincon(Merck Chemical Co., Ltd.) in methanol according to a previous report.[11] A 1.0×10^{-2} M solution of HPC was prepared by dissolving HPC in water. A 1.0% PVA, solution was prepared by dissolving PVA (n≒2000) in water. A Sörensen phosphate buffer solution was used for the pH adjustments.

All the other reagents and materials were of analytical grade and were used without further purification. Twice-distilled water was used throughout this work.

Shimadzu Model UV-200, recording spectrophotometer with 1.0-cm^3 quartz cells was used for the absorption spectra and absorbance measurements. A Hitachi-Horiba Model F-7AD glass electrode pH meter was used for the pH measurements.

Operating Procedure. Determination of Cobalt(II): A standard solution containing up to 2.2 μg of cobalt(II) was placed in a 10-cm^3 volumetric flask; then, 1.0 cm^3 of a 1.0×10^{-2} M HPC solution, 2.0 cm^3 of a Sörensen phosphate buffer solution (pH 8.5), and 2.0 cm^3 of 1.0×10^{-3} M Zincon solution were added. The solution was diluted to the mark with water, mixed well, kept at 60 °C for 30 min, and then cooled in water at room temperature for 10 min. The difference of absorbance at 550 nm between the Zincon-cobalt(II) solution (Solution A) and the Zincon solution (Solution B) was measured against water.

Determination of Nickel(II): A standard solution (0—42.0 μg of nickel (II)) was placed in a 10-cm^3 volumetric flask; 1.0 cm^3 of a 1.0% PVA solution, 2.0 cm^3 of a Sörensen buffer solution (pH7.0), and then 2.0 cm^3 of a 1.0×10^{-3} M Zincon solution were added. The solution was diluted to the mark with water, mixed well (Solution A′), kept at room temperature for 20 min together with Zincon solution (Solution B′). The absorbance difference at 470 nm between Solutions A′ and B′ was measured against water. The concentrations of cobalt(II) or nickel(II) were determined by using a calibration graph.

Results and Discussion

Reaction between Zincon and Cobalt(II) or Nickel(II). The reaction systems between cobalt(II) or nickel(II) and Zincon in the presence or absence of a surfactant (cationic—HPC, anionic—sodium dodecyl sulfate, nonionic—PVA, amphoteric—sodium *N*-lauroylsarcosine) were studied at room temperature or by heating at 60 °C. The reaction systems in the absence were unstable, inconvenient and insensitive in comparison with the reaction systems in the presence of a surfactant. The absorption spectra of Zincon-cobalt(II) and Zincon solutions in the presence of HPC (Solutions A and B), and Zincon-nickel(II) and Zincon solutions in the presence of PVA (Solutions A′ and B′) are shown in Figs. 1 and 2. The Zincon-cobalt(II) solution in the presence of a cationic surfactant such as HPC was more easily decomposed by heating at 60 °C

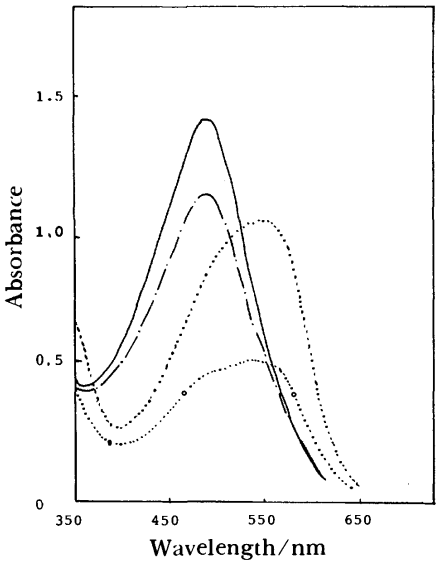

Fig. 1. Absorption spectra of Zincon-cobalt(II) and Zincon solutions in the presence of HPC or in the presence of Tween (0.1%) under the operating procedure. Cobalt(II), 2.0×10^{-6} M; Reference, water. ---o---: Zincon-cobalt(II)-HPC (Solution A); ------: Zincon-HPC solution (Solution B); -·-·-: Zincon-cobalt(II)-Tween 20; ——: Zincon-Tween 20.

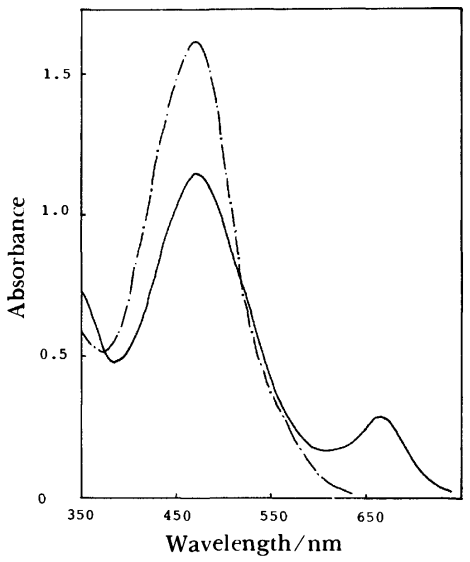

Fig. 2. Absorption spectra of Zincon-nickel(II) and Zincon solutions in the presence of PVA under the operating procedure. Ni(II), 2.5×10^{-5} M; PVA, 0.1%; Reference, water.
——: Zincon-nickel(II) (Solution A'); -·-·-: Zincon (Solution B').

than the Zincon-cobalt(II) solution in the absence of surfactant. There was a large distinct difference of absorbance between Solutions A and B at 550 nm. The difference of absorbances at 470 and 665 nm between Solutions A' and B' in the presence of a nonionic surfactant (such as PVA) at room temperature was stable and abundant in reproducibility compared with reaction systems in the absence of a surfactant. Consequently, the later measurements were carried out by measuring the absorbance of 550 and 470 nm.

A maximum and constant absorbance was obtained in the pH range of 8.0—9.0 for a determination of cobalt(II), and 6.0—8.3 for a determination of nickel(II), by using 2.0 cm^3 of a Sörensen phosphate buffer solution. Later measurements were carried out at pH 8.5 for the assay of cobalt(II) and at pH 7.0 for the assay of nickel(II).

For the determinations of these metal ions, the effects of various surfactants(cationic—HPC, hexadecyltrimethylammonium chloride, zephiramine, benzylhexadecylmethylammonium chloride, nonionic—PVA, poly(oxyethylene) 6-methylheptyl ether, poly(oxyethylene) sorbitan monolaurate(Tween 20), poly(oxyethylene) dodecyl ether, and poly(*N*-vinylpyrrolidone) were studied. The uses of HPC for cobalt(II), and PVA for nickel (II) were best regarding sensitivity and stability. A maximum and constant absorbance could be obtained by the addition of 0.5—2.0 cm^3 of a 1.0×10^{-2} M HPC solution for the determination of cobalt(II), and 0.5—3.0 cm^3 of a 1.0% PVA solution for a determination of nickel(II), at final volume of 10 cm^3.

The effect of the amount of Zincon on the operating procedure was studied while keeping the amounts of cobalt(II) or nickel(II) constant. Though the molar ratio of nickel(II) to Zincon regarding the reaction system was found to be 2:1 by the molar ratio and continuous variation methods, the maximum and almost constant difference of the absorbance was obtained by using 0.5—2.0 cm^3 for the assay of nickel(II), and 1.25—2.5 cm^3 of a 1.0×10^{-3} M Zincon solution for the assay of cobalt(II) in the final 10 cm^3. Although a further investigation is necessary, the molar ratio of Zincon to cobalt(II) could not be explicitly defined.

Effect of Temperature and Time. A study of the influence of temperature on the reaction system was performed at 15—80 °C. The reaction rate (for times between 0 and 60 min) increased with the temperature, and a reproducible absorbance was obtained at 60 °C for 30 min. On the other hand, the reaction system between Zincon and nickel(II) was the best regarding stability and reproducibility at room temperature. From these results, the conditions of 60 °C for 30 min for cobalt(II) and at room temperature for 20 min for nickel(II) were chosen.

Calibration Graphs and Reproducibilities. Calibration graphs for the determinations of cobalt(I) and nickel(II) were obtained by the operating procedure. Beer's laws were followed up to 0—2.2 μg 10 cm^{-3} of cobalt(II), and 0—42.0 μg 10 cm^{-3} of nickel(II). Sandell sensitivities were 0.00015 μg, cm^{-2} cobalt(II) and 0.0047 μg cm^{-2} nickel(II). This proposed method for cobalt(II) was especially about 20 times as sensitive as the method[7] using Zincon alone. Also, the relative standard deviations for cobalt(II) and nickel(II) (n=5) were to be 0.33 and 0.95%, respectively (relatively good values).

Effects of Foreign Ions. Effects of various foreign ions were examined regarding interference. As described in Table 1, the coexistence of such elements as iron(III), copper(II), and zinc(II) showed positive errors owing to the reaction with Zincon. The coexist-

Table 1. Effect of Foreign Ions Under the Operating Procedure

Foreign ion	Added		Difference of absorbance	
	as	μg 10 cm^{-3}	Co(II) at 550 nm	Ni(II) at 470 nm
—	—	—	0.587	0.610
Co(II)	Nitrate	1.5	—	0.615
Ni(II)	Nitrate	0.8	0.615	—
Zn(II)	Nitrate	8.2	0.587	0.615
Cu(II)	Nitrate	7.9	0.592	0.675
Fe(III)	Chloride	0.7	0.590	0.615
Al(III)	Chloride	33.0	0.600	0.608
Pb(II)	Nitrate	10.4	0.569	0.618
Bi(III)	Nitrate	13.1	0.550	0.608
Mg(II)	Nitrate	60.8	0.580	0.609
NO_2^-	Sodium	57.5	0.481	0.609
I^-	Potassium	79.3	0.587	0.610
F^-	Sodium	238.0	0.587	0.610
$S_2O_3^{2-}$	Sodium	14.0	0.405	0.600
Citrate	Sodium	31.0	0.661	0.605
CN^-	Potassium	1.3	0.540	0.605

Ni(II) taken, 14.7 μg 10 cm^{-3}, Co(II) taken 0.9 μg 10 cm^{-3}.

ence of bismuth(III) or tin(IV) up to 2.5×10^{-5}—1.0×10^{-6} M over cobalt(II) or nickel(II) did not interfere. The coexsitence of such anions as sulfate, chloride, iodide, bromide, and nitrate ions did not entirely interfere. The coexistence of cyanide, thiosulfate or nitrite ions, excess over cobalt(II) or nickel(II) 1/2—5 molar ratios gave negative errors. Citrate or oxalate ion gave a positive error for cobalt(II), and a negative error for nickel(II), respectively.

Assay of Cobalt(II) in the Coexistence of Nickel(II) or Some Metal Ions. Although the absorbance at 615 nm of Zincon-cobalt(II) solution was relatively small, its value was not affected by the coexistence of nickel(II). The amounts of cobalt(II) in the coexistence of nickel(II) up to about 25-fold over cobalt(II) could be determined by measuring the absorbance differences at 615 nm between Solution A involving nickel(II) and Solution B prepared according to the operating procedure. On the other hand, the amounts of nickel(II) were calculated using the nickel(II)-calibration graph previously prepared in the coexistence of this assayed cobalt(II) concentrations. Moreover, the separative assay of cobalt(II) in the coexistence of some metal ions(zinc(II), copper(II), iron(III), etc.) was possible by measuring the absorbance on the cobalt(II)-mixed solution involving these each metal ion up to about 10—25-fold over cobalt(II) at proper wavelength; the absorbance difference at 595 nm in the coexsitence of zinc(II), at 580 nm in the coexistence of copper(II) and at 582 nm in the coexistence of iron(III), respectively.

In conclusion, reactions between Zincon and cobalt(II) in the presence of a cationic surfactant, and between Zincon and nickel(II) in the presence of a nonionic surfactant were the best concerning sensitivity and reproducibility. Accordingly, simple, sensitive and improved spectrophotometric determinations of cobalt(II) and nickel(II) were obtained, respectively, by using reaction of Zincon-cobalt(II) in the presence of HPC and Zincon-nickel(II) in the presence of PVA established at basic media. The sensitivity for cobalt(II) was about 20-times larger than that reported method by Gomez et al.[9] Also, the sensitivities on these proposed methods were about 8—10-times larger than the methods using nitrosonaphthol derivatives, etc.[3,8,12] Moreover, the separative assay of cobalt(II) in the coexistence of some metal ions-nickel(II), zinc(II), copper(II), or iron(III), etc. was possible by measuring at indivdual analytical wavelength.

References

1) B. E. McClellan and P. Sabel, *Anal. Chem.*, **41**, 1077 (1969).
2) S. G. Mauliya, I. V. Pyatnitskii, and L. K. Kolements, *Anal. Chem. (Warsaw)*, **35**, 861 (1981).
3) K. J. McNaught, *Analyst (London)*, **67**, 97 (1942).
4) W. A. Forste, *Analyst (London)*, **78**, 560 (1953).
5) V. N. Tikhnova and S. G. Danilova, *Anal. Chem., (Warsaw)* **35**, 828 (1981).
6) A. G. Morris, *Analyst (London)*, **82**, 34 (1957).
7) M. S. Sekheta, G. A. Milosonovic, and T. S. Tanji, *Mikrochim. Acta*, **1978**, 297.
8) E. Kentnwv and H. Zeitlin, *Anal. Chim. Acta*, **49**, 587 (1970).
9) M. A. Dosal Gomez and J. A. Perez-Bustamante, *An. Quim.*, **73**, 968 (1977); *Anal. Abstr.*, **34**, 4B171 (1978).
10) K.Ueno, "Chelatometry," Nankodo Publ. Co., Tokyo (in Japanese), (1972), p. 289.
11) I. Mori, Y. Fujita, K. Fujita, H. Kawabe, Y. Koshiyama, A. Furukawa, and T. Nakamura, *Bunseki Kagaku*, **35**, 408 (1986).
12) M. Tanaka, *Keikinzoku*, **46**, 521 (1961).

Trace Determination of Indium by Electrolytic Preconcentration and Open Circuit Stripping via Localized Galvanic Cells

Sambamoorthy JAYA, Talasila Prasada RAO,† and Gollakota Prabhakara RAO*
Central Electrochemical Research Institute, Karaikudi, India
†Regional Research Laboratory, Industrial Estate P. O., Trivandrum 695019, India
(Received July 10, 1986)

Synopsis. A galvanic stripping analysis procedure is described for the trace determination of indium(III). The determination involves the reoxidation of predeposited indium on the mercury-film-coated glassy carbon electrode in open circuit position (in the absence of external potential or current input or oxidant in solution). The reoxidation of indium was shown to occur due to the formation of localized galvanic cells. The time of reoxidation (stripping) was found to be proportional to the concentration of indium present in the solution (1 to 100 ppb). The details of the development of such a procedure and its possible application to determination of indium in zinc deposits and aluminium alloys are discussed.

Electroanalytical techniques were widely used for the trace determination of indium. These include phase selective[1] and second harmonic[2] a.c. Polarographic, differential pulse polarographic[3] and anodic stripping voltammetric techniques.[4-10] Stripping voltammetric techniques are preferred over polarographic techniques in view of the simplicity, rapidity, and higher sensitivity of these procedures. Most of the researchers utilize halide medium in anodic stripping voltammetric studies as they offer higher sensitivity arising out of the fast reactions of indium in these media. A few of these stripping voltammetric procedures find application in the determination of 1.8 ppm of indium in zinc[6] or 0.2 to 0.7 ppm of indium in aluminium.[7] Recently, we have described a novel electroanalytical technique namely galvanic stripping analysis (GSA) which was successfully utilized for trace determination of cadmium,[11] chromium,[12] and lead.[13] This paper describes the development of galvanic stripping analysis procedure for the determination of traces of indium and its possible application to determination of indium in zinc deposits and aluminium alloys.

Experimental

Reagents. Indium(III) Solution: This solution was prepared by dissolving 0.2212 g of indium(III) chloride in 100 ml of conductivity water (0.01 mol dm^{-3}). A working solution containing 10 ng cm^{-3} of indium was prepared by suitably diluting the stock solution with conductivity water.

Acetate Buffer: This solution was prepared by dissolving 13.608 g of sodium acetate in water and adding 6 ml of glacial acetic acid, adjusting the pH to 3.5 with dilute HCl and diluting the solution to 100 cm^3.

Apparatus: A Wenking potentiostat (Model LB 75 M) coupled with a Wenking scan generator (Model VSG 72) was used for controlling the potential during preconcentration step. A Ricadenki xy/t recorder was used for obtaining galvanic stripping E-t profiles. A conventional three electrode cell consisting of mercury film coated glassy carbon working electrode (MFGCE) prepared as described elsewhere[14] (Tokai & Co., 3 mm dia.), a platinum foil counter and a normal calomel electrode (NCE) as reference was used. All the potentials were expressed with respect to NCE and measurements were made at room temperature.

Porcedure: Transfer a suitable aliquot (upto 40 cm^3) of sample solution containing ≤100 ppb of indium(III) into a 50 cm^3 volumetric flask. Add 5 cm^3 of acetate buffer solution and dilute to volume with conductivity water. Transfer the solution to electrochemical cell and deaerate with N_2 for 15 min. After preconcentrating electrolytically for 4 min at −1.4 V vs. NCE, the galvanic stripping E-t profiles were drawn after keeping the potentiostat in open circuit position (i.e. where the counter electrode is disconnected from the three electrode assembly) and in the absence of any external oxidant or electrical input. The E-t profiles thus obtained represent the variations of the MFGCE working electrode potential with respect to NCE. The time taken for stripping forms the analytical signal of GSA. Prepare a calibration graph for the determination of 1—100 ppb of indium(III) by the above procedure.

Results and Discussion

Figure 1 shows the stripping E-t profiles obtained after preconcentrating 0, 10, 30, and 50 ppb of indium-(III) (curves A, B, C, and D respectively) onto MFGCE at −1.4 V vs. NCE for 4 min. These E-t profiles were drawn by keeping the potentiostat in open circuit mode immediately after preconcentration step and in the absence of any imposed stripping conditions viz. external electrical input (potential or current) or addition of chemical oxidants. On the other hand, when the potentiostat is kept in open circuit position after

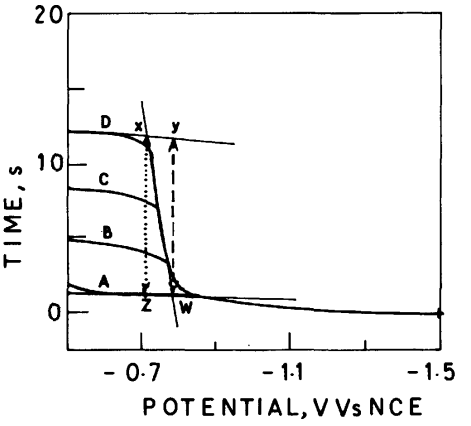

Fig. 1. Galvanic stripping E-t profiles recorded for 0, 10^{-7}, 3×10^{-7}, and 5×10^{-7} M of indium(III) between MFGCE working and normal calomel reference electrode, 0.1 M acetate buffer (pH 3.5); total volume=50 ml; deposition potential (E_d)=−1.4 V vs. NCE; deposition time (t_d)=4 min.

Table 1. Effect of Supporting Electrolyte

Sample No.	Supporting electrolyte (concentration)	Stripping time s
1	KI (0.2 M) or KBr (0.2 M) or NaCl (0.2 M)	Not resolved
2	Chloroacetate buffer (0.1 M)	0.0
3	KNO_3 (0.1 M)	0.60
4	Acetate buffer, pH 3 (0.1 M)	2.00
5	KNO_3 (0.1 M)+Acetate buffer, pH 3 (0.1 M)	0.65
6	Acetate buffer, pH 3 (0.1 M)+KSCN (0.2 M)	0.70
7	Acetate buffer, pH 3 (0.1 M)+KI (0.2 M)	0.60
8	Acetate buffer, pH 3 (0.1 M)+KBr (0.2 M)	1.60
9	Acetate buffer, pH 3 (0.1 M)+NaCl (0.2 M)	2.00

Concentration of indium=10 ppm. Deposition potential (E_d)=−1.4 V vs. NCE. Time of deposition (t_d)=4 min.

depositing for 4 min at −1.4 V vs. NCE, the potential of hanging mercury drop and glassy carbon with respect to NCE drop to −0.8 and 0.1 V vs. NCE respectively. Thus in case of MFGCE, the potential difference between In (Hg) film electrode and uncovered portions of GCE (as mercury film is known to present as fine droplets) is ≈0.9 V. Hence, the stripping profiles of Fig. 1 can be thought of as due to the formation of localized galvanic cells between indium amalgam and uncovered portions of glassy carbon electrode (GCE). Experiments were then carried out to confirm the formation of localized galvanic cells as described elsewhere.[11-13] These include a) observing the flow of current from Pt foil to MFGCE, when Pt foil and MFGCE were connected externally by placing zero resistance ammeter in between (during this experiment potentiostat is kept in open circuit position) b) stability of indium amalgam on hanging mercury drop electrode and c) unaltered GSA stripping profiles with different stirring rates. Further, the time of stripping measured as indicated for curve D in Fig. 1 (xz or yw) is proportional to indium present in solution.

Effect of Supporting Electrolyte. The effect of supporting electrolyte on the galvanic stripping analysis (GSA) signal of 10 ppb of indium using MFGCE was investigated by drawing E-t profiles in open circuit selection mode after preconcentrating for 4 min at −1.4 V vs. NCE. The results obtained are shown in Table 1, from which it is clear that the stripping signal is maximum in acetate or acetate-chloride medium compared to other media.

Effect of pH. The effect of pH in the range 2.5 to 6.0 on the GSA determination of 10 ppb of indium on MFGCE was then studied by employing 0.1 M (1M=1 mol dm^{-3}) acetate buffer as supporting electrolyte. The results obtained are shown in curve A of Fig. 2 from which it is clear that the optimum pH range is 3.0 to 3.8. pH 3.5 acetate buffered medium was chosen in further studies.

Effect of Deposition Potential. In order to ascertain optimum deposition potential, the deposition potential during 4 min preconcentration of 10 ppb of indium was varied in the range −0.8 to −1.5 V vs. NCE in steps of 0.1 V onto MFGCE. Curve B in Fig. 2 shows the time of stripping obtained from E-t profiles drawn during stripping of indium deposited at various deposition potentials. The maximum GSA stripping signal is obtained at potentials more negative to −1.4 V vs. NCE as seen from curve B of Fig. 2.

Effect of Time of Deposition. The effect of deposition time (1 to 16 min) on GSA stripping signal of 10 ppb of indium was next investigated by depositing at −1.4 V vs. NCE onto MFGCE. The results thus obtained revealed that the stripping signal is directly proportional to the time of deposition.

Calibration Graph and Precision. Linear calibration graph passing through the origin was obtained for 1—100 ppb of indium (cf. Fig. 3) with 4 min of deposition time. The relative standard deviation for 5 replicate determinations of 10 ppb of indium(III) was calculated to be 3.8%.

Analysis of Synthetic Samples. The results of the analysis of aluminium and zinc metal samples spiked with known amounts of indium are shown in Table 2. Aluminium do not interfere at all concentrations in the present procedure. But zinc do interfere by codepositing with indium which can be avoided by maintaining deposition potential at −1.05 V vs. NCE. Under these conditions the sensitivity of the procedure decreases by ≈6%. However, the calibration range

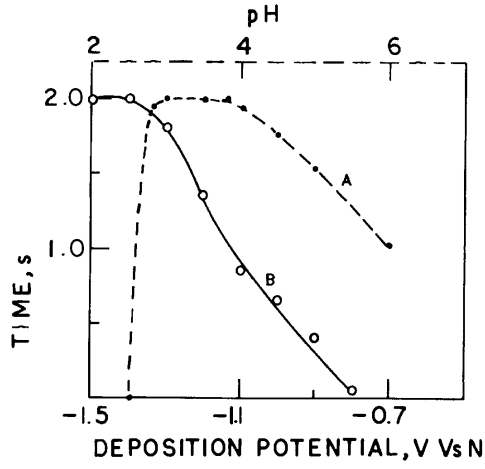

Fig. 2. Effect of pH (curve A) and deposition potential (curve B) on the galvanic stripping signal of 10 ppb of indium; 0.1 M acetate buffer, pH 3.5; t_d=4 min.

Table 2. Analysis of Synthetic Samples

Sample solution	Amount of indium(III) added	Aliquot taken	Indium(III) found	Recovery
	μg/g	ml	μg/g	%
1. Aluminium Metal	—	40	0.0	—
(5 g per 50 ml)	0.5	40	0.49	98.0
	1.0	40	1.01	101.0
2. Zinc metal[a)]	—	40	0.0	—
(5 g per 50 ml)	0.4	40	0.39	97.5
	0.8	40	0.80	100.0
	1.2	25	1.18	98.3

a) By depositing at −1.05 V vs. NCE for 4 min.

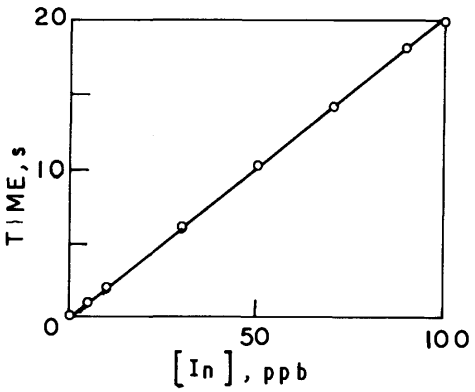

Fig. 3. Calibration graph.

remains unaffected. As the recoveries obtained were quantitative, the developed (cf. Table 3) procedure is expected to find application in ascertaining the concentration of indium in zinc deposits and aluminium alloys.

References

1) T. P. Radhakrishnan and A. K. Sundaram, *B. A. R. C.*, **856**, 17 (1976).
2) M. Ogawa, I. Watanabe, and S. Ikeda, *Anal. Chim. Acta*, **141**, 123 (1982).
3) S. K. Nuar and O. Vitteri, *Anal. Chim. Acta*, **91**, 143 (1979).
4) L. V. Shevehonke, V. P. Portranyi, and V. T. Chuiko, *Gidrokhim. Mater.*, **74**, 88 (1978).
5) T. F. Ryashentseva, A. A. Kaplin, and I. S. Levin, *Izv. Tomak. Politekh. Inst.*, **197**, 51 (1975); *Referat. Zh. Khim.*, **19GO**, 18 (1976); Abstr. No. 18 G 187.
6) E. Ya Neiman, A. A. Nomodruk, and Kh. Z. Brainina, *Zh. Analit. Khim.*, **30**, 1668 (1975).
7) E. Ya Neiman and G. B. Ponomarenka, *Zh. Analit. Khim.*, **28**, 1485 (1973).
8) M. Aihara and S. Tutui, *Saikatau Kagaku*, **13**, 79 (1982).
9) V. V. Slepuskin, N. N. Kuzumina, and M. G. Yartsov, *Zh. Analit. Khim.*, **32**, 535 (1977).
10) L. V. Shovchenko, V. P. Portranyi, and V. T. Chuiko, *Gidrokhim. Mater.*, **74**, 88 (1978); *Referat. Zh. Khim.*, **19GD**, 24 (1978); Abstr. No. 24 G 219.
11) S. Jaya, T. P. Rao, and G. P. Rao, *Anal. Lett.*, **18A**(12), 1441 (1985).
12) S. Jaya, T. P. Rao, and G. P. Rao, *Bull. of Electrochem.*, **2**, 131 (1986).
13) S. Jaya, T. P. Rao, and G. P. Rao, *Talanta*, in press.
14) S. Jaya, T. P. Rao, and G. P. Rao, *Talanta*, **32**, 1861 (1985).

Polymers as Reagents and Catalysts. XI. Stereospecific Iodofluorination of Alkenes in the Presence of Polymer Supported Hydrogen Fluoride[1)]

Ana GREGORČIČ and Marko ZUPAN*
"Jožef Stefan" Institute and Department of Chemistry, "E. Kardelj" University, Ljubljana, Yugoslavia
(Received March 18, 1986)

Synopsis. *N*-Iodosuccinimide reacted with phenyl substituted alkenes in the presence of insoluble polymer supported hydrogen fluoride, which was prepared by reaction of hydrogen fluoride with crosslinked poly(styrene-co-4-vinylpyridine) containing 40—45 mol% of 4-vinylpyridine, thus forming vicinal iodofluorides in high yields. Reactions proceeded with Markovnikov type regioselectivity, and in the case of (*Z*)- and (*E*)-stilbene, (*Z*)- and (*E*)-1-phenylpropene and indene anti stereospecificity was also observed. Iodofluorinations of phenyl substituted acetylenes occurred regio and stereospecifically, forming (*Z*)-1-fluoro-2-iodo-1-phenylalkenes, with lower yields than those observed in the case of alkenes.

Polymeric resins can be chemically transformed so that they can act as reagents or catalyst, and besides offering simpler experimental techniques, the chemical reactivity can also be changed when the reagent is attached to a polymer backbone.[2)] Our continued interest in methods for mild introduction of fluorine into organic molecules stimulated us to search further for new reagents. It is now known that appropriate synthesis of a polymer supported reagent is one of the most important factors influencing its effectiveness. We have already demonstrated that polymer-supported (difluoroiodo) arene could be prepared by reaction of xenon difluoride[3,4)] with polymer supported iodobenzene, while Patrick and coworkers[5)] have shown that a similar reagent cannot be prepared by reaction of HgO-HF with polymer supported (dichloroiodo)-arene. Banks and coworkers[6)] have also very nicely demonstrated how important is the appropriate synthesis of a polymer supported reagent which should be able to convert alcohols into fluorides.

Hydrogen fluoride has been often used for the preparation of fluorine containing molecules, its great disadvantage being its toxicity to living beings and the fact that usually pressure equipment and low temperatures must be used in order to prevent decomposition of some organic molecules. Some of the experimental difficulties can be avoided by use of a mixture of hydrogen fluoride and pyridine which was extensively employed by Olah and coworkers.[7)]

We have found that crosslinked poly(styrene-co-4-vinylpyridine), containing 40—45 mol% of 4-vinylpyridine, reacted with hydrogen fluoride thus forming an easily handled reagent.[8)] We have recently showed that polymer-supported hydrogen fluoride could be used for chloro- and bromofluorination of alkenes at room temperatures, and that reaction proceed with Markovnikov type regioselectivity.[9)]

Results and Discussion

Vicinal iodo fluoro compounds are very unstable compounds and could be prepared with varying degrees of success from a mixture of *N*-iodosuccinimide and hydrogen fluoride. On the other hand, we found that the reactivity of difluoro iodosubstituted compounds strongly depends on the nature of the substituent. Reactions of (difluoroiodo)arenes with olefins usually resulted in rearranged geminal difluorides,[10)] while reactions of (difluoroiodo)methane with various alkenes gave vicinal iodofluorides at room temperature. Reactions follow Markovnikov type regioselectivity and are in most cases stereospecifically anti.[11-15)] Vicinal iodo fluoro compounds are usually accompanied by vicinal difluoro compounds, which are formed by further reaction with fluoride anion or by rearrangement of products. However, this reaction pathway is diminished when (difluoroiodo)methane is used as reagent, but its greatest disadvantage is the high price of xenon difluoride which is used for its room-temperature preparation.

We first studied the reactions of *N*-iodosuccinimide in dichloro methane in the presence of insoluble polymer supported hydrogen fluoride with 1,1-diphenylethene, and found that after 2.5 hours it was quantitatively converted to 1-fluoro-1,1-diphenyl-2-iodoethane. Further, we studied the effect of the structure of the olefin on iodofluorination, and for this reason all the reactions were run for only one hour. Crude reaction mixtures were analyzed by ^{1}H and ^{19}F NMR spectra using octafluoronaphthalene as internal reference.

The effect of the structure of the olefin on iodofluorination is presented in Scheme 1. It is evident that 1,1-diphenylethene is the most reactive olefin, while the introduction of an electron withdrawing group in to the phenyl ring, i.e. 1-(4-chlorophenyl)-1-phenylethene or the introduction of a halogen atom on the double bond, e.g. 2-fluoro-1,1-diphenylethene, diminished the reactivity. All the reactions follow the Markovnikov type regioselectivity and vicinal iodo fluoro compounds were not accompanied by difluorides or rearranged products.

Further, we studied the stereochemistry of iodofluorination of various phenyl substituted alkenes. In all cases, i.e. (*E*)- or (*Z*)-1-phenylpropene, (*E*)- or (*Z*)-stilbene, and indene the formation of only one product was observed. The structures of the products were determined on the basis of their spectroscopic data and their comparison to those of independently synthesized compounds. Iodofluorination of all five olefins followed Markovnikov type regioselectivity and proceeded stereospecifically anti. In order to get information about the effect of the structure of the olefin on the course of the reaction, all the reactions were performed at room temperature for one hour and the

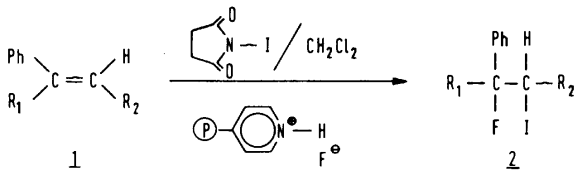

THE EFFECT OF SUBSTITUENTS ON CONVERSION OF ALKENES TO IODO FLUORO COMPOUNDS[a]

1		2(%)	1		2(%)
R_1	R_2		R_1	R_2	
H	H	67	$p\text{-}ClC_6H_4$	H	18
CH_3	H	70	C_6H_5	F	12
H	CH_3	61	C_6H_5	CH_3	62
C_6H_5	H	71			

a) 1h reaction at 20°C

Scheme 1.

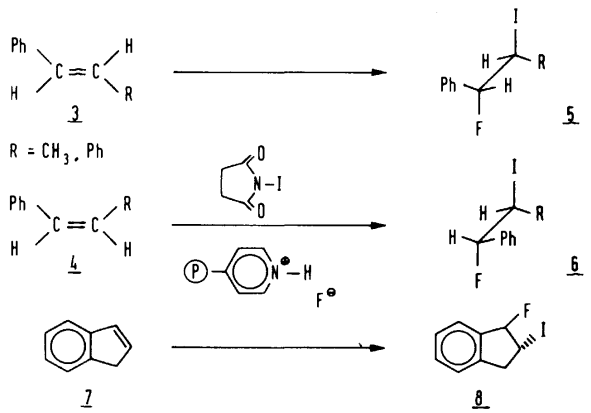

Scheme 2.

amounts of vicinal iodo fluoro compounds determined in the crude reaction mixtures were as follows: 61% from (*E*)-1-phenylpropene, 45% from (*Z*)-1-phenylpropene, 40% from (*E*)-stilbene, 38% from (*Z*)-stilbene, and 56% from indene.

Further, we studied iodofluorination of acetylenes and found that reactions occurred regiospecifically, thus forming (*Z*)-1-fluoro-2-iodo-1-phenylethenes. The substituent R influenced the conversion of acetylene. After a 1.5 h reaction the following amounts of iodo fluoro compounds were determined: 16% from phenylacetylene, 25% 1-phenylpropyne, 31% from 1-phenyl-1-pentyne, while reaction with 1,2-diphenylacetylene failed. Prolongation of the reaction time to 2.5 hours resulted in enhanced reaction and the following amounts were observed: 18, 30, 28, and 5% (data correspond to the same order of substrates as above). However, further prolongation of reaction time did not enlarge the yields of iodofluorides, and after 7 hours even smaller amounts of products than those observed after 2.5 hour reactions were found, which could be explained by decomposition of the products. The structures of the products were determined on the basis of their spectroscopic data and comparison to

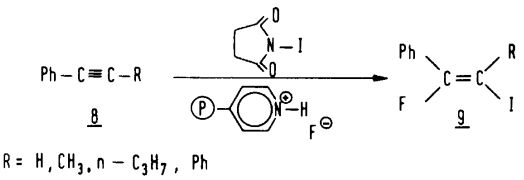

Scheme 3.

those of the independently synthesized ones.[16] It is known that the solvent plays an important role in the transformation of organic molecules with polymer-supported reagents, and for this reason we tried to increase the amount of iodo fluoro compounds from acetylenes by varying the solvent. However it was found that reactions did not occur in tetrahydrofuran and acetonitrile.

The polymer resins could be easily recovered after reaction, and reused several times.

Experimental

IR spectra were recorded using a Perkin Elmer 727 B instrument and ^1H and ^{19}F NMR spectra with a Jeol JNM PS-100 spectrometer with Me_4Si or CCl_3F as internal reference. For determination of the amounts of products formed, octafluoronaphthalene was used as internal standard. Mass spectra and high resolution measurements were taken with a CEC-21-110 spectrometer. GLC was carried out on a Varian Aerograph 1800 instrument and TLC on Merck silica gel F-254. Crosslinked poly(styrene-co-4-vinylpyridine) and polymer supported hydrogen fluoride were prepared according to previously published procedures,[8,17] while *N*-iodosuccinimide of Fluka Purum Quality was used without further purification.

Addition and Isolation Procedures. 0.15 g of polymer supported hydrogen fluoride was mixed with 2 ml of dichloro methane and 1 mmol of *N*-iodosuccinimide was added at 0 °C and stirred until complete dissolution of *N*-iodosuccinimide occured. Further, 0.5 mmol of olefin or acetylene was added and the reaction mixture was stirred for various times (1—7 h), depending on the reactivity of the alkene or acetylene. Polymer beads were filtered off and

washed with 5 ml of dichloro methane, the filtrate was washed with water (10 ml, twice), dried over anhydrous sodium sulfate, and the solvent evaporated in vacuo. The crude reaction mixtures were analyzed by ^{19}F NMR spectroscopy (amounts of products were determined by the use of octafluoronaphthalene in ^{19}F NMR as internal standard). Pure products were isolated as described previously[12-16] and their structures determined by comparison of spectroscopic data to the literature ones. The yields of pure products formed after reactions of olefins and acetylenes were: 1-Fluoro-2-iodo-1-phenylethane (reaction time: 1h, yield of pure product 56%) 2-fluoro-1-iodo-2-phenylpropane (r.t.: 1h, 58%), 1,1-diphenyl-1-fluoro-2-iodoethane (r.t.: 1h, 61%), 1-fluoro-2-iodo-1-phenyl-1-(4'-chlorophenyl)ethane (r.t.: 1h, 16%), 1,2-difluoro-1,1-diphenyl-2-iodoethane (r.t.: 1h, 11%), 1,1-diphenyl-1-fluoro-2-iodopropane (r.t.: 1h, 54%), *erythro*-1-fluoro-2-iodo-1-phenylpropane (r.t.: 1h, 55%), *threo*-1-fluoro-2-iodo-1-phenylpropane (r.t.: 1h, 38%), *erythro*-1,2-diphenyl-1-fluoro-2-iodoethane (r.t.: 1h, 34%), *threo*-1,2-diphenyl-1-fluoro-2-iodoethane (r.t.: 1h, 33%), *trans*-1-fluoro-2-iodoindane (r.t.: 1h, 49%), (*Z*)-1-fluoro-2-iodo-1-phenylethylene (r.t.: 2.5h, 15%), (*Z*)-1-fluoro-2-iodo-1-phenylpropene (r.t.: 2.5h, 26%), (*Z*)-1-fluoro-2-iodo-1-phenyl-1-pentene (r.t.: 2.5h, 24%), (*Z*)-1,2-diphenyl-1-fluoro-2-iodoethylene (r.t.: 2.5h, 4%).

Regenerations of Resins. Beads were washed with methanol, dichloro methane, and chloroform, and dried in air. 5 g of polymer beads were suspended in 5 ml of chloroform and under stirring hydrogen fluoride (1.5 g) was introduced for 0.5 h at 0 °C. The beads were filtered off, washed with chloroform and dried to constant weight at room temperature. Polymer beads can be reused at least ten time for fluorination.

References

1) Part X. B. Šket and M. Zupan, *Tetrahedron*, **40**, 2865 (1984).

2) N. K. Mathur, C. K. Narang, and R. E. Williams, "Polymers as Aids in Organic Chemistry," Academic Press, New York (1980); "Polymer-Supported Reactions in Organic Synthesis," ed by P. Hodge and D. C. Sherrington, John Wiley and Sons, New York (1980).

3) M. Zupan, *Collect. Czech. Chem. Commun.*, **42**, 266 (1977).

4) B. Šket, M. Zupan, and P. Zupet, *Tetrahedron*, **40**, 1603 (1984).

5) T. B. Patrick, J. J. Scheibel, W. E. Hall, and Y. H. Lee, *J. Org. Chem.*, **45**, 4492 (1980).

6) R. E. Banks, A. K. Barrage, and E. Khoshdel, *J. Fluorine Chem.*, **17**, 93 (1981).

7) G. A. Olah, J. T. Welch, Y. D. Vankar, M. Nojina, I. Kerekes, and J. A. Olah, *J. Org. Chem.*, **44**, 3872 (1979).

8) M. Zupan, B. Šket, and Y. Johar, *J. Macromol. Sci., Chem.*, **A 17**, 759 (1982).

9) A. Gregorčič and M. Zupan, *J. Fluorine Chem.*, **24**, 291 (1984).

10) A. Gregorčič and M. Zupan, *Bull. Chem. Soc. Jpn.*, **50**, 517 (1977).

11) M. Zupan and A. Pollak, *Tetrahedron Lett.*, **1957**, 3525.

12) M. Zupan and A. Pollak, *J. Org. Chem.*, **41**, 2179 (1976).

13) M. Zupan and A. Pollak, *J. Chem. Soc., Perkin Trans. 1*, **1976**, 1745.

14) S. Stavber and M. Zupan, *J. Fluorine Chem.*, **12**, 307 (1978).

15) S. Stavber and M. Zupan, *Bull. Chem. Soc. Jpn.*, **52**, 925 (1979).

16) M. Zupan, *Synthesis*, **1976**, 473.

17) Crosslinked copolymer of styrene and 4-vinylpyridine and complexes with halogens are commercially available from AERO, Celje, Yugoslavia.

Bleaching of Bis[1-(4-dimethylaminophenyl)-2-phenylethanedithione]-nickel(0) in Polymer Solution and Polymer Matrix

Koe Enmanji
The Materials Engineering Laboratory of Mitsubishi Electric Co.,
Tsukaguchi-Honmachi, Amagasaki 661
(Received January 23, 1987)

Bis[1-(4-dimethylaminophenyl)-2-phenylethanedithione]nickel(0) (BDN), a Q-switch dye for neodymium lasers, bleached in polymer matrix such as poly(butyl methacrylate). To elucidate the bleaching mechanism, the effect of water-soluble polymer added to dimethyl sulfoxide (DMSO) solution of BDN on the bleaching rate was investigated. BDN was reduced by a water-soluble polymer such as poly(vinyl alcohol) (PVA), starch, and cyclodextrin (CD) in DMSO. BDN bleached in DMSO solution with PVA and bleaching rate depended on the saponification number of PVA. BDN was also bleached by adding CD to DMSO solution. From the concentration dependence of CD on BDN bleaching rate, it was presumed that the vicinity of Ni of BDN is not included in β- and γ-CD, but is included in α-CD. For avoiding reduction of BDN by CD, 2,4,5-tri-*O*-methoxy-β-cyclodextrin (T-β-CD) was examined. BDN was not reduced by an inclusion complex of BDN with T-β-CD. The storage life of Q-switch with matrices of poly(butyl methacrylate) and polystyrene was determined. The Q-switch with polystyrene matrix having transmittance of 70.0% is expected to have transmittance of 70.4% after strage for 10 years at 25 °C.

The toluene solution of bis[1-(4-dimethylaminophenyl)-2-phenylethanedithione]nickel(0) (BDN) in glass cell has been used for a Q-switch of neodymium laser, because BDN has absorption peak at 1060 nm, that is the oscillation wavelength of neodymium laser. A solid state Q-switch is desirable for making it small and its life longer. BDN bleaches so remarkably in vinyl polymers that the solid state Q-switch is impracticable. The bleaching of BDN in solution was studied from various points of view[1-4] and it was found that there are two types of bleaching mechanism of BDN: (1) Oxidative bleaching by attacking of radicals[1-3] and (2) reductive bleaching by coordination of solvent to Ni.[4] The oxidative bleaching could be decreased by removing radicals or by inclusion of BDN with cyclodextrin (CD).[3] The author wishes to elucidate the mechanism of bleaching of BDN in polymer matrix. It seems that reduction of BDN by coordination of oxygen in polymer to Ni of BDN is a cause of the bleaching. In order to confirm this assumption, the correlation between the amount of OH group and the bleaching rate was studied with addition of water-soluble polymers containing plenty oxygen such as poly(vinyl alcohol) (PVA), starch, and CD[3] to a dimethylsulfoxide (DMSO) solution of BDN. The storage time and resistance to oscillation of a solid state Q-switch using polystyrene (PS) matrix will also be reported.

Experimental

Materials. BDN was purchased from Kodak Co. and CD from Tokyo Chemical Co. 2,4,5-Tri-*O*-methoxy-β-cyclodextrin (T-β-CD) was presented by Dr. H. Yamaguchi (Colledge of Technology, Ibaraki University). Low molecular weight PVA samples from Unichika Chemical Co. were used after precipitation three times from methanol solution in toluene. Their saponification number was 81.7 (UMR-20H®), 63.8 (UMR-20M®), and 35.0 (UMR-20L®). Starch 2-hydroxypropyl ether of Matsutani Chemical Co. (Stacodex®) was used as starch which was purified by precipitation three times from toluene–methanol system. Butyl methacrylate (PBMA) polymerized in xylene was purified by precipitation three times from methanol–xylene system. A high impact polystyrene from Denki Kagaku Co. (TPUSH®) was purified by precipitation three times from toluene–methanol system. Benzoin ethyl ether (BEE) was purchased from Nakarai Chemical Co. DMSO and petroleum ether of reagent grade by Nakarai Chemical Co. and toluene of Spectral grade by Wako Junyaku Co. were used.

The inclusion complex of BDN with T-β-CD was prepared by the following procedure: BDN (10 mg) and T-β-CD (100 mg) were dissolved in toluene (100 ml) and the solution was stirred for 10 min at 60 °C. Toluene was evaporated with a rotaryevaporator, and the inclusion complex in residue was dissolved into petroleum ether. The liquid was centrifuged at 1000 g for 10 min to remove excess BDN.

Measurement. UV-visible spectra and IR spectra were measured by Shimadzu MPS-5000 spectrophotometer and Shimadzu 430 infrared spectroscope, respectively. The light source for bleaching experiments was Ushio 500 high-pressure marcury lamp with an output of 150 mW cm^{-2}.

Results and Discussion

The effect of polymer on bleaching rate of BDN in solution. The toluene solution of BDN was not bleached in the experiment for a day. A commercial poly(methyl methacrylate) (PMMA) added to the solution caused bleaching as to decrease the absorption peak at 1100 nm. Because the logarithm optical density (OD) at 1100 nm decreased linearly with time at 25 °C, the bleaching reaction is of the first order BDN. But purified PMMA, which was precipitated

three times from methanol-toluene system, showed no bleaching effect. When 1 ml of aqueous potassium iodide solution (10%) was added to 10 ml of a toluene solution of commercial PMMA (10%), and the mixture was shaken vigorously and made to stand for 30 min, the color of water layer changed to yellow. This phenomenon suggests the existence of peroxide in the commercial PMMA. It was also shown that benzoin peroxide bleached BDN.[3] It is likely that the remaining peroxide in the commercial PMMA used for polymerization bleached BDN. A peroxide must be removed from polymer by reprecipitation when the polymer is used for matrix of Q-switch. On the other hand, BDN was bleached reductively in a DMSO solution and the absorption peak at 1100 nm shifted to 1030 nm. The rate constant of bleaching reaction was 5.24×10^{-4} min^{-1} at 25 °C. The author proposed a previous paper,[4] that two DMSO molecules coordinate to BDN and the coordinated DMSO molecules reduce BDN to an anion radical in the similar manner as *N*,*N*-dimethylformamide (DMF), and that the following equation holds:

$$\mathrm{BDN} + 2(\mathrm{DMSO}) \underset{k_{-1}}{\overset{k_{+1}}{\rightleftharpoons}} \mathrm{BDN(DMSO)_2} \xrightarrow{k_2} \mathrm{BDN}\cdot^{\ominus}. \quad (1)$$

Equation 2 can be obtained from Eq. 1.

$$\frac{d[\mathrm{BDN}]}{dt} = -k_2 \frac{k_{+1}}{k_2+k_{-1}}[\mathrm{BDN}][\mathrm{DMSO}]^2 \quad (2)$$

Addition of commercial PVA to DMSO solution of BDN made the bleaching rate of BDN to increase. The mechanism of this reaction is thought that DMSO coordinating to BDN takes up proton from OH of PVA and reduces BDN with this proton. A similar reaction mechanism was preveously reported for α-tocopherol.[4] The mechanism can be expressed by the following equation.

$$\mathrm{BDN} + 2(\mathrm{DMSO}) \underset{k_{-1}}{\overset{k_{+1}}{\rightleftharpoons}} \mathrm{BDN(DMSO)_2}, \text{ and} \quad (3)$$

$$\mathrm{BDN(DMSO)_2} + \mathrm{PVA} \xrightarrow{k_2} \mathrm{BDN}\cdot^{\ominus}. \quad (4)$$

Equation 5 can be derived from Eqs. 3 and 4.

$$\frac{d[\mathrm{BDN}]}{dt} = -\frac{k_{+1}k_2[\mathrm{PVA}]}{k_{-1}+k_2[\mathrm{PVA}]}[\mathrm{BDN}][\mathrm{DMSO}]^2, \quad (5)$$

where [PVA] is the concentration of monomer unit of PVA. By changing k_{+1}, k_{-1}, and k_2 purposely, the inclination of the plot between [PVA] and bleaching rate varies. For confirming this relation, the experiments were carried out by using PVA with different sapponification numbers. The effect of UMR-20H, -M, and -L in DMSO solution of BDN on the bleaching rate is shown in Fig. 2. Figure 2 shows that the larger the saponification number is, the larger the apparent bleaching rate constant as well as the smaller the slope of plot become. It appears therefore, that the bleaching rate correlates with the number of OH group.

BDN was also reduced by starch. The effect of hydroxypropyl starch (Stacodex®) on the bleaching rate of BDN in DMSO solution is shown in Fig. 3. The hydroxypropyl starch has the following chemical structure.[6]

Starch-O-CH_2-CH(OH)-CH_3.

The inclination of relationship between the concentration of the starch and the bleaching rate of

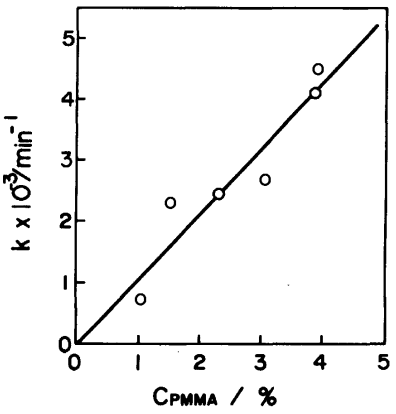

Fig. 1. Dependence of bleaching rate of BDN on the concentration of commercial poly (methyl methacrylate). Concentration od BDN is 5.13×10^{-5} mol dm^{-3}.

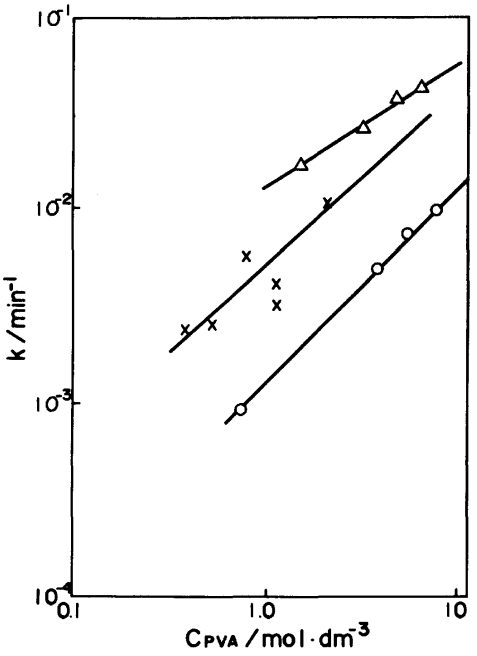

Fig. 2. Dependence of bleaching rate of BDN on the concentration of poly (vinyl alcohol).
—O—: UMR-20L®, —X—: UMR-20M®, —Δ—: UMR-20H®. Concentration of BDN is 5.13×10^{-5} mol dm^{-3}

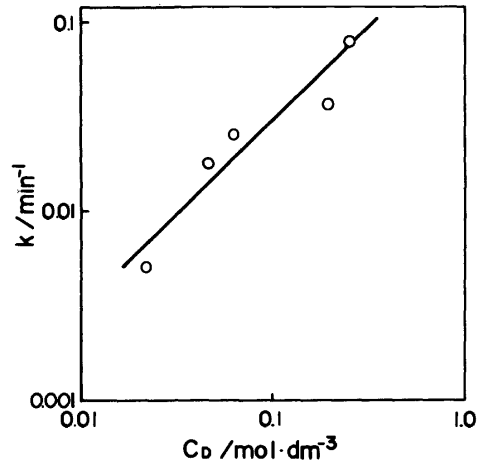

Fig. 3. Dependence of bleaching rate of BDN on the concentration of starch. Concentration of BDN is 5.13×10^{-5} mol dm^{-3}.

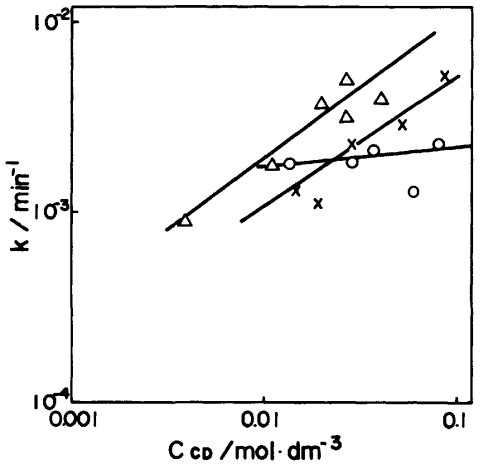

Fig. 4. Dependence of bleaching rate of BDN on the concentration of cyclodextrin.
—O—: α-Cyclodextrin, —X—: β-cyclodextrin, —△—: γ-cyclodextrin. Concentration of BDN is 5.13 $\times10^{-5}$ mol dm^{-3}

BDN is unity from Fig. 3. We was recognized in the previous paper[3] that we must reexamine the behavior of BDN in CD. From the following experiment, it was found that BDN is reduced by CD in DMSO solution. The effect of CD on the reduction rate of BDN is shown in Fig. 4 which shows that the bleaching rate of BDN with γ-CD (glucose number, 8) is larger than that with α-CD (glucose number, 6) and β-CD (glucose number, 7). This result will be due to the fact that γ-CD has more OH groups than α-CD and β-CD. The inclination of the plot between concentration of CD and bleaching rate was 0.6—0.7 for β-CD and γ-CD and that was 0.1 for α-CD. Since the CD concentration exceeds that of BDN, it seems that all BDN molecules are included in CD. The fact that BDN was bleached even by β-CD and γ-CD of

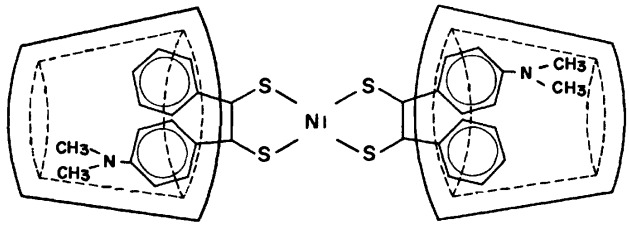

Fig. 5. Assumed structure of the inclusion complex of BDN with β- or γ-cyclodexrin

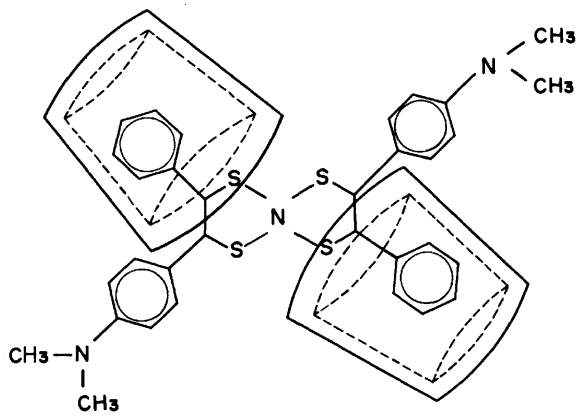

Fig. 6. Assumed structure of the inclusion complex of BDN with α-cyclodextrin.

which have spacious hydrophobic pores indicates that the central Ni of BDN is not included in CD as shown in Fig. 5. Because α-CD has less OH groups than other CD species, it is expected that the slope of plot between concentration of α-CD and bleaching rate must be unity. From the facts that the slope was 0.1, and that α-CD has small hydrophobic pore, a vicinity of Ni of BDN molecule may clog the pore as shown in Fig. 6.

From the above discussion, BDN included in CD seems to be reduced to a product, possibly an anion radical. The material which does not reduce BDN would be considered. T-β-CD with methoxyl instead of OH groups in a toluene solution of BDN did not change the spectrum even after a long time of standing. The optical spectrum of petroleum ether solution of BDN with T-β-CD is shown in Fig. 7. The spectrum differs from that of BDN toluene solution in a point that near-infrared absorption peak at 1100 nm shifts to 960 nm. Because the d-d transition appears at visible region, this compound must not be a reduced product of BDN. A stable inclusion complex was formed, because bleaching rate constant of BDN in petroleum ether with T-β-CD was larger (k=0.151 min^{-1}) than that in toluene solution (k=0.088 min^{-1}), UV light was irradiated after BEE (1%) was added to the solution. IR spectra of BDN included in T-β-CD, BDN, and T-β-CD are compared in Fig. 8. The assignment and absorbance of each peak and the ratios

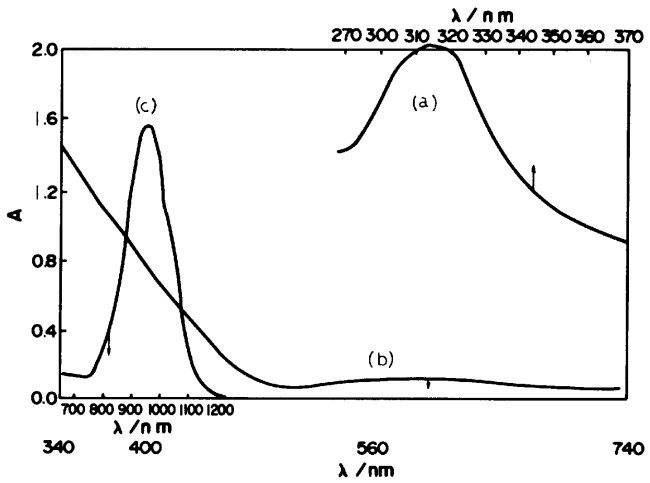

Fig. 7. Optical absorption spectra of inclusion complex of BDN with 2,4,5-tri-*O*-methoxy-β-cyclodextrin. (a) Ultra violet region of spectra, (b) visible region of spectra, (c) near infrared region of spectra. Prepared by the procedure of the Experimental section.

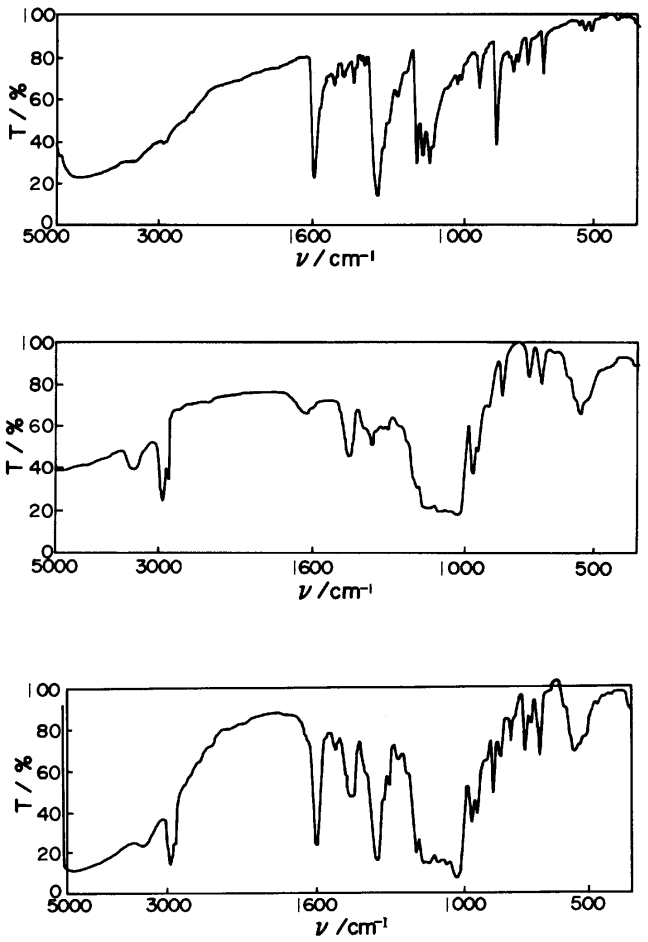

Fig. 8. Infrared spectra of (a) BDN, (b) T-β-CD, (c) inclusion complex of BDN with T-β-CD

Table 1. The Change of Optical Density of Each Infrared Peak of Bis[1-(4-dimethylaminophenyl)-2-phenylethanedithione]nickel(0) by Inclusion to 2,4,5-Trimethoxy-β-cyclodextrin

cm⁻¹	Assignment[9]	BDN		BDN+T-β-CD	
		OD	$OD/OD_{N(CH_3)_2}$	OD	$OD_{N(CH_3)_2}$
1590	$N(CH_3)_2$	0.66	1.0	0.64	1.0
1340	C=C	0.85	1.3	0.80	1.3
875	C–S	0.42	0.64	0.32	0.5

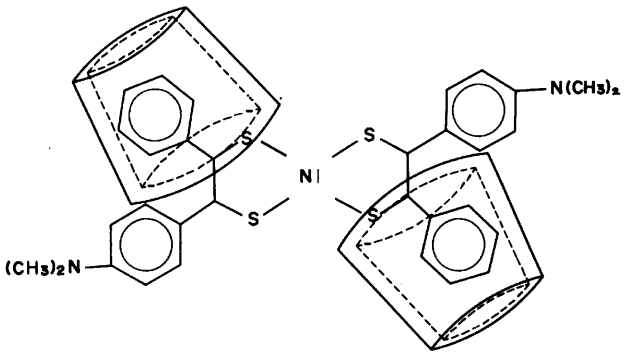

Fig. 9. Assumed structure of the inclusion complex of BDN with T-β-CD.

of optical density for other peaks to that for $\nu(N(CH_3)_2)$ are shown on Table 1. As seen in Table 1, the absorbance of ν(C–S) peak of BDN in T-β-CD decreased by about 20 percent from that of BDN itself. The structure illusteated in Fig. 9 deloneated that $N(CH_3)_2$ group is projected in solvent and benzene ring and C–S are included in CD pores. It will be that BDN is occluded by T-β-CD more shallowly than by α-CD. From this reason, the resistance to attack by radicals of BEE disappears. Storage life of solid state dye Q-switch and resistance to repeating oscillation.

A solid-state dye Q-switch of wich PBMA matrix was prepared. The absorbance was determined with time(days) kept in an electric oven at 69, 83, and 103 °C. Because logarithm absorbance at 1100 nm decreased linearly with the storage time, the rate constant was estimated from tangent of the linear relations. The Arrhenius plot for decay of solid-state dye Q-switch is shown in Fig. 10. Extrapolation of the plot gives the assumed storage life at each temperature (Table 2). The storage time at 30 °C is assumed to be about 2 months. Because PBMA was purified by careful reprecipitation, bleaching of BDN will not occur by residual peroxide, but by reduction with butoxyl group. The Arrhenius plot of bleaching rate of BDN in toluene which contains a small amount of peroxide is also shown in Fig. 10 for comparison.

The author considered that the storage life would be improved by dispersing BDN in a polymer as low-T_g-polystyrene with no N and O atoms, because styrene with lower T_g will decrease damage induced by

Table 2. Estimated Preserved Lifetime of the Q-Switch of Which Dispersion Medium is Buthyl Methacrylate

	Preserved temperature/°C						
	0	10	20	30	40	50	60
k/d^{-1}	3.6×10^{-3}	5.0×10^{-3}	6.7×10^{-3}	8.9×10^{-3}	1.2×10^{-2}	1.5×10^{-2}	1.9×10^{-2}
$T_{70\to75}$/y[a]	0.34	0.25	0.18	0.14	0.10	0.08	0.06

a) The year for increasing transmittance from 70 to 75%.

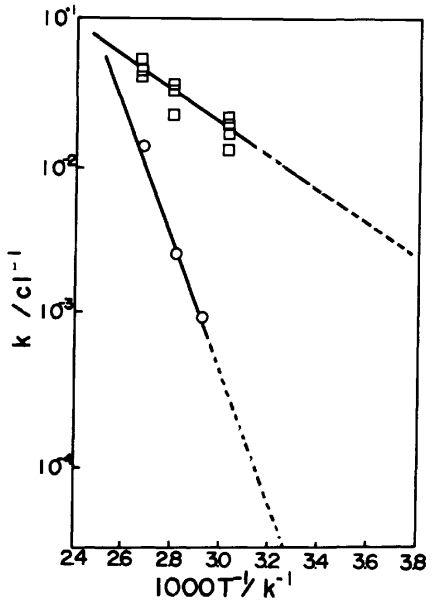

Fig. 10. Arrhenius plot of Q switch which is composed of BDN and poly(*n*-buthyl methacrylate). —□—: Solid state Q switch of which primary transmittance is 70%, —○—: liquid Q switch of which BDN concentration is 5.13×10^{-5} mol dm^{-3}

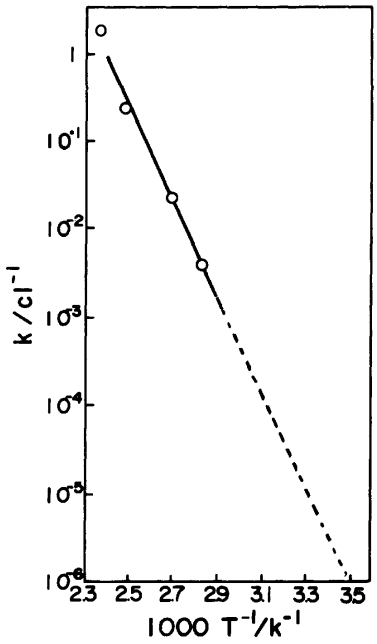

Fig. 11. Arrhenius plot of Q switch which is composed of BDN and polystyrene.

Table 3. Estimated Preserved Lifetime of the Q-Switch of Which Dispersion Medium is Polystyrene

	Preserved temperature/°C					
	0	10	20	30	40	50
k/d^{-1}	8.5×10^{-8}	6.6×10^{-7}	2.3×10^{-6}	1.2×10^{-5}	3.2×10^{-5}	1.4×10^{-4}
$T_{70\to75}$/y[a]	6930	892	256	49	18	4

a) The year for increasing transmittance from 70 to 75%.

laser.[7,8] A mixed solution of BDN and polystyrene in toluene was coated in 10 μm thickness on a PMMA plate of 1 mm thickness and dried at room temperature. The sample was stored in an oven at 88, 100, and 130 °C. Absorbance at 1100 nm plotted against storage time revealed that logalithm OD decreases linearly with storage time. The Arrhenius plot of bleaching rate constant is shown in Fig. 11. The bleaching rate at each temperature and the storage life assumed by rate constant are given in Table 3. The bleaching rate constant k at 25 °C was estimated from Fig. 11 to be 5×10^{-6}d^{-1}. The result indicated that the transmittance of improved solid-state Q-switch of 70.0% will change to 70.4% after 10 years storage.

The resistance to repeating oscillation of the Q-switch was measured. The Q-switch with BDN dispersed in PBMA withstood against oscilation of 20000 times by 200 J YAG laser for one day, while that dispersed in low-T_g-polystyrene withstood 100 times' oscillation by the similar experiment for 2 hours. The solid Q-switch is believed to be useful for practical use.

References

1) K. Enmanji, K. Takahashi, T. Kitagawa, and H. Kusakawa, *Nippon Kagaku Kaishi*, **1978**, 796.

2) K. Enmanji, K. Takahashi, and H. Kusakawa, *Nippon Kagaku Kaishi*, **1983**, 592.

3) K. Enmanji and H. Yamaguchi, *Nippon Kagaku Kaishi*, **1985**, 128.

4) K. Enmanji, *Nippon Kagaku Kaishi*, **1985**, 2094.

5) K. Enmanji, K. Takahashi, and H. Kusakawa, unpublished data.

6) K. Matsuda, "Dempun Kagaku Handbook," ed by J. Nikuni, Asakura Publishers, Tokyo (1977), p. 55.

7) H. Kusakawa, K. Takahashi, and K. Itoh, *J. Appl. Phys.*, **39**, 6116 (1968).
8) H. Kusakawa, K. Takahashi, and K. Itoh, *J. Appl. Phys.*, **40**, 3954 (1969).
9) C. W. Schlapfer and K. Nakamoto, *Inorg. Chem.*, **14**, 1338 (1975).

 © 1987 The Chemical Society of Japan Bull. Chem. Soc. Jpn., 60, 3093—3097 (1987)

Metal Colloids Produced by Means of Gas Evaporation Technique. IV. Size Distribution of Small Mg and In Particles

Keisaku KIMURA
Instrument Center, Institute for Molecular Science, Myodaiji, Okazaki 444
(Received February 4, 1987)

Ultrafine metal particles with different sizes have been obtained by several preparation methods. The smallest Mg particles (the average diameter D_m of about 2 nm) were obtained by the matrix isolation method in He and the largest (D_m, 100 nm) by the conventional gas evaporation method in Ar. By changing the pressure and the kind of gas, particles with an intermediate diameter have been obtained. The size distribution of small In particles was discussed.

There are many reports on the preparation of fine metal particles with the diameter of less than 1 μm by the evaporation of metals in an inert gas.[1-5] However, it is not easy to obtain particles with the diameter of less than 10 nm by the conventional gas evaporation method, because particles become larger by coalescence when they contact with each other on the walls of preparation chamber. To prevent particles from contacting, a liquid is used for intervening between particles. Two approaches have been proposed. Yatsuya et al. reported the VEROS (vacuum evaporation on running oil substrate) method, in which a metal is evaporated in vacuum onto surface of running oil.[6-8] This method yields particles with a size of 3 nm, although there are severe restrictions on the selection of oil. The matrix isolation method combining the gas evaporation technique was also used by several researchers.[9-11] Furthermore, the gas flow-solution trap method and the gas flow-cold trap method were developed in the previous studies by the present author using organic liquids as substrate.[11,12] The particle diameter at the maximum distribution reached the range of 1 nm. Several kinds of well dispersed ultrafine metal particles were obtained such as Ni, Ag, Cu, Au, Sb, and Al by Wada[9] and Ag, Au, Cu, In, Al, Ca, Sn, and Pb by the present author.[11] The reaction of metal particles with liquids and the change in particle diameter due to the reaction were examined in a previous work.[12]

A wide difference of particle diameter between the conventional gas evaporation method (several tens nm) and the liquid substrate method (several nm) suggests difference in particle growth mechanism. The mechanism of nucleation growth from gaseous atoms was studied by analyzing size distribution of the particles produced. As is usually seen in many physical processes, the normal distribution results from a random process. Granqvist[13,14] proposed the log-normal distribution for the metal particles produced by the gas evaporation method. His proposal was confirmed for extremely small particles prepared by the VEROS method[15] irrespective of large difference in particle diameter between two methods. Since no study was performed on the nucleation mechanism of small particles produced by the matrix isolation method, the gas flow-solution trap method, and the gas flow-cold trap method, this paper describes the size distribution by differnt preparation methods in the case of Mg particles in tetrahydrofuran (THF) and In particles in acetone.

Experimental

Small metal particles were prepared by the matrix isolation method, the gas flow-solution trap method, and the gas flow-cold trap method similarly as described in the previous paper.[11] Several kinds of gas atmosphere were examined: He and Ar for the matrix isolation method, and a He/Ar mixture as well for the gas flow method were used. The metals used were 99.999% In, 99.99% Mg, and 99.5% Au. Acetone was purified with CaH_2 and THF was distilled from its Na-benzophenone solution. The size distribution of particles was determined by electron microscopy. A colloidal solution was dropped on a Cu mesh coated with evaporated carbon film of 10 nm in thickness. Hitachi H-500H electron microscope of the Laboratory of Electron Microscopy, the National Institute for Physiological Sciences at Okazaki was used with a 100 kV high resolution mode. The histograms of size distribution were obtained by an Image Analyser, Kontron IBAS-1, of the Center for Analytical Instrument, the National Institute for Basic Biology at Okazaki.

Results and Discussion

Size Distribution of Mg Particles. Figure 1 shows micrographs of Mg particles produced by different methods. The finest particles in Fig. 1a were prepared by the matrix isolation method in He gas atmosphere. Figure 1b shows Mg particles prepared by the same method but in Ar atmosphere. The largest particles in Fig. 1c[16] were obtained by the conventional gas evaporation method in Ar atmosphere, in which hexagonal crystal habit characteristic of hcp structure is seen. The size distributions curves f(d) in Fig. 2 were obtained from Figs. 1a, 1b, and 1c, respectively. It is evident that the average diameter widely varies from 2 to 100 nm with the preparation

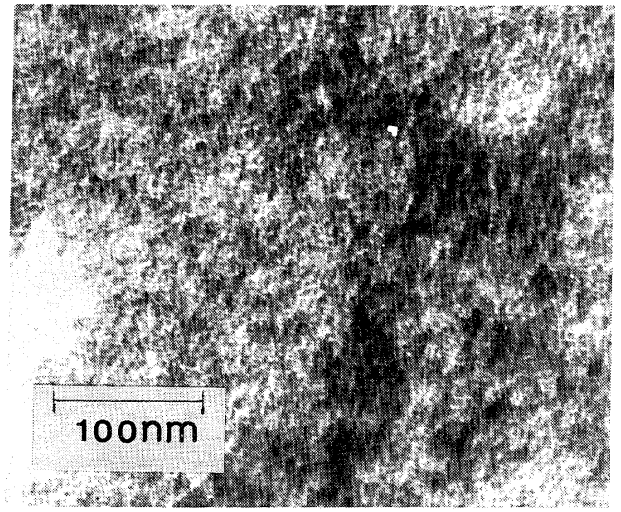

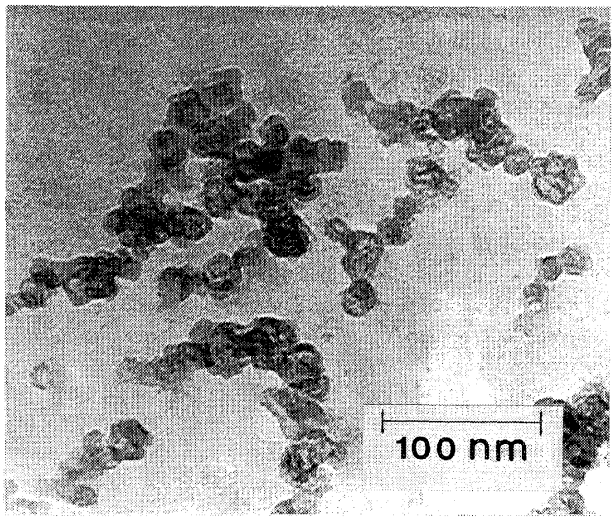

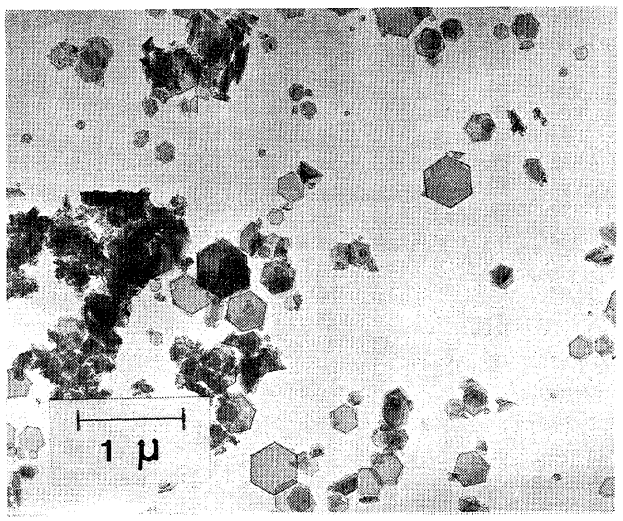

Fig. 1. Electron microscope images of Mg small particles of different sizes.
a) Mg/THF produced by the matrix isolation method in He gas of 1.3 kPa. b) Mg/THF produced by the matrix isolation method in Ar gas of 300 Pa. c) Produced by the conventional gas evaporation method in Ar gas of 4 kPa.[16]

method and conditions. The number of atoms in a single particle accordingly varies from 10^2 to 10^7. This result differs from that of giant clusters produced by the supersonic nozzle beam method, in which the size distribution is a monotonously decreasing function of the size modulated by small cusps at the position of magic numbers.[17,18] It is also noteworthy that the half-value width of distribution is a function of the average diameter. The smaller the particle diameter is, the narrower the width of distribution becomes. This tendency was also reported for Al particles produced in He gas.[19]

The effect of mass and pressure of inert gas on the particle size was reported by Wada on the conventional gas evaporation method.[20] The particle size increases in the order of He, Ar, and Xe. The size also increases with increasing ambient gas pressure. In this experiment, larger particles (Fig. 1b) were obtained in Ar than in He (Fig. 1a). The distribution in Fig. 1b (the diameter at the maximum distribution D_m of 19 nm) is close to that by the gas evaporation method in He (D_m, 21 nm). This shows that the gas evaporation method in a gas with small molecular weight yields the particles of size equivalent to that by the matrix isolation method in a gas with large molecular weight. It seems evident that the matrix isolation method is superior to the gas evaporation technique in order to obtain ultrafine particles when we expect the quantum size effect. For Mg metal, a particle of 2.1 nm (Fig. 1a) is composed of 210 atoms and, therefore, the average electron level spacing near the Fermi level is about 130 K, which is far above the normal cryogenic temperature.[21] Hence, it is easy to observe the quantum size effect for these particles.[22,23]

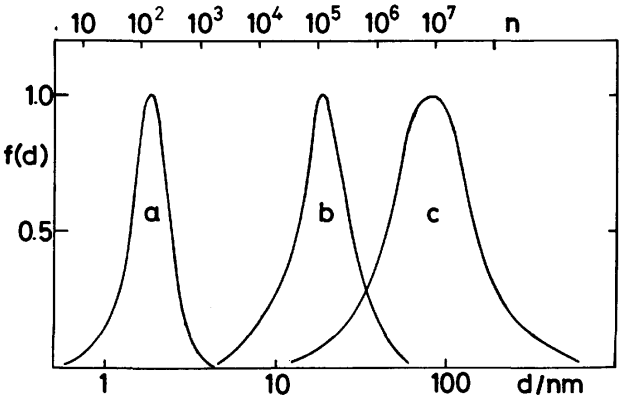

Fig. 2. Size distribution of Mg small particles produced by different method.
Curves, a, b, and c are from those in Fig. 1. The distribution maxima locate at the diameter (D_m) of 2.1 nm for a, 19 nm for b, and 100 nm for c. Numbers in the top abscissa are the number of Mg atoms in a particle whose diameter is designated in the bottom abscissa.

Analysis of Size Distribution of In Particles. Particle size distribution strongly depends on its growth process. Two main processes have been proposed:[24] One is the absorption growth process where particle nuclei grow up with absorption of metal atoms. This gives the normal distribution of particle size. Another is the coalescence growth process where particles grow up by collision of particle nuclei to give a log-normal size distribution. This distribution is derived from the assumption that the change in volume (mass) at each step is a random fraction of the volume after coalescence. The normalized distribution for logarithm of volume is given by

$$f_{LN}(v) = \frac{1}{\sqrt{2\pi}\ln\sigma_v}\exp\left\{-\frac{1}{2}\left[\frac{\ln(v/\bar{v})}{\ln\sigma_v}\right]^2\right\}, \quad (1)$$

where $\bar{v}$ is the mean volume and σ_v is the standard deviation of volume. The number of particles Δn per logarithmic volume interval is, therefore, given by $\Delta n = f_{LN}(v)\Delta(\ln v)\cdot n$. For a sphere particle, one obtains the so-called log-normal distribution function for particle diameter, d, as

$$f_{LN}(d) = \frac{1}{\sqrt{2\pi}\ln\sigma}\exp\left\{-\frac{1}{2}\left[\frac{\ln(d/\bar{d})}{\ln\sigma}\right]^2\right\}. \quad (2)$$

The fraction of the number of particles per diameter interval can be written as $\Delta n/n = f_{LN}(d)\cdot\Delta d/d$.[14] For the log-normal distribution, the mean diameter d is related to the peak diameter D_m as $\bar{d} = D_m\cdot\exp[\ln\sigma]^2$.

Figure 3 shows a typical size histogram of In particles produced by the gas flow-cold trap method in acetone. The best fit with the log-normal distribution is shown by a broken line in Fig. 3. The features of fitting are wholly good. Since it is difficult to achieve the best fit only from the appearance of fitting to the distribution curve, a better technique will be found with reference to graphical "normal-probability" and "log-probability" analyses as stated below. If the size distribution is a linear normal distribution, cumulation of the number of particles of a certain size follows the error function and plotting of the points on normal probability paper will give a straight line. Figure 4a shows the normal-probability plot of the sample shown in Fig. 3. It is clear that the size distribution does not fit with the normal distribution. On the other hand, the log-probability plot of the same sample gives a good straight line as shown in Fig. 4b, indicating that the size distribution of this sample is of a log-normal. The fitting was also checked by the χ^2-test with sample number 250 and the number of classes 29. The best fitting was obtained with σ of 2.13 and $\bar{d}$ of 20 nm and shown in Fig. 3 by a broken line. The significance level is over 75%

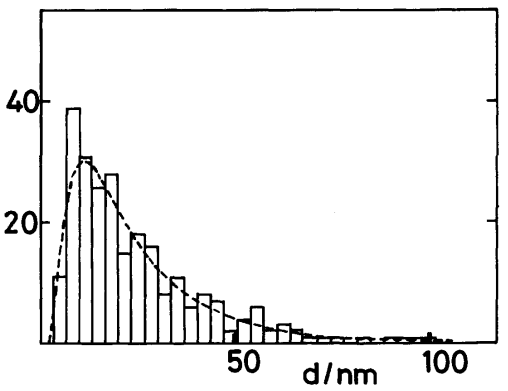

Fig. 3. Size histogram for In samll particles produced by the gas flow-cold trap method in acetone. The pressure of He+Ar mixed gas was 1.3 kPa. Broken line is a calculated curve from the log-normal distribution with fitted parameters σ=2.13 and $\bar{d}$=20 nm. The ordinate represents the number of particles at a given size interval.

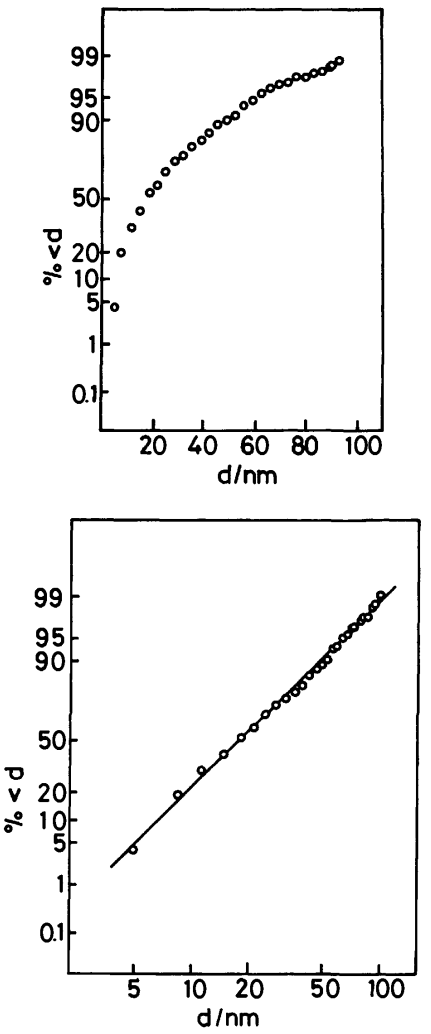

Fig. 4. a) Normal-probability plot and b) log-probability plot for In small particles. The ordinate stands the cumulative percent of particles with diameters smaller than d.

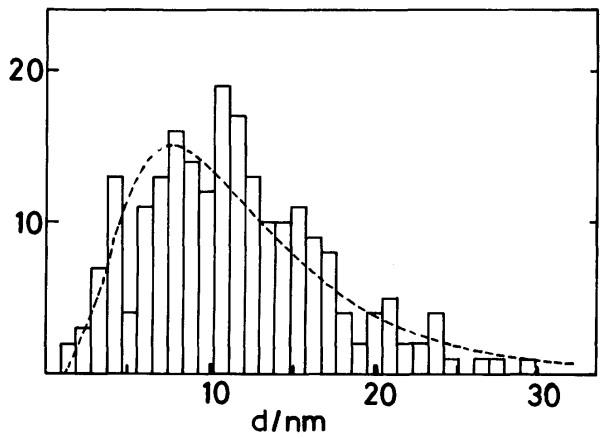

Fig. 5. Size histogram for In small particles produced by the matrix isolation method in acetone. The N_2 gas pressure was 1.3 kPa. Broken line is a calculated curve from the log-normal distribution with fitted parameters σ=1.8 and $\bar{d}$=10.8 nm. The ordinate represents the number of particles at a given size interval.

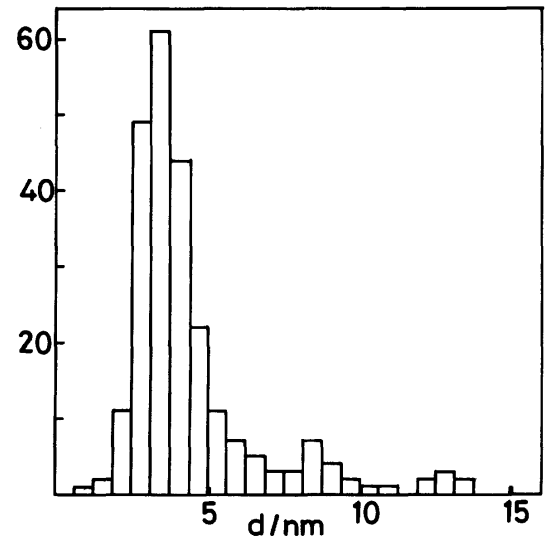

Fig. 6. Size histogram for In small particles produced by the gas flow-solution trap method in acetone.
The He gas pressure was 1.3 kPa. The peak diameter D_m=3 nm. No fitting was obtained for normal-probability and log-probability plots. The ordinate represents the number of particles at a given size interval.

showing the strong reliability of this fit, because the rejection level is normally set at 1 or 5%.

Figure 5 shows the size histogram of In particles produced by the matrix isolation method in acetone under N_2 atmosphere. The fitting of size distribution with the log-normal distribution was also checked by the χ^2-test with a significance level of 30%. This result seems to confirm that the log-normal distribution is applicable to this sample. The technique of the matrix isolation method is similar to that of the conventional gas evaporation method only except for the substrate of low temperature organic matrix.

Figure 6 shows the size histogram of small In particles produced by the gas flow-solution trap method in acetone under He atmosphere. In this preparation, the diameter of maximum distribution is about 3 nm. It was confirmed that the smallest particles are formed in low pressure He as in the case of Mg shown in Fig. 2. The histogram in Fig. 6 fits with neither the normal-distribution nor the log-normal distribution. The size distribution of Au particles in acetone produced by the same method (D_m=1.1 nm) fits with neither of two distribution curves. These distribution functions are derived on the assumption that the system is in thermodynamical equilibrium during particle growth. This is the case for a closed chamber atmosphere such as the conventional gas evaporation method and the matrix isolation method but not for the gas flow method, in which a constant flow of inert gas turbulates the nucleus growth process. The size distribution in Fig. 6, therefore, shows the distribution at the beginning of particle growth. Narrow size distribution of particles supports this assumption. Nevertheless, we need to know why the log-normal distribution is observed in the gas flow-cold trap method as shown in Fig. 3. In this method, the particles co-deposit with organic vapor on the walls of glass reaction vessel and are embedded in the matrix. The volume fraction of metal is so high in the matrix that particles tend to coagulate in the matrix. Large particles of 20 nm produced by the gas flow-cold trap method probably reflect the coagulation process, because the size of particles in a gas stream is believed to be of the order of 3 nm. It will be suggested that the size of small metal particles could be widely and easily changed from 2 to 100 nm in any suitable organic liquid, although only tetrahydrofuran and acetone were examined in the present study.

The author expresses his gratitude to Prof. Sanshiro Sako for presenting the photograph of Mg particles produced by the conventional gas evaporation method.

References

1) L. Harris, D. Jeffries, and B. M. Siegel, *J. Appl. Phys.*, **19**, 791 (1948).
2) K. Kimoto, Y. Kamiya, M. Nonoyama, and R. Uyeda, *Jpn. J. Appl. Phys.*, **2**, 702 (1963).
3) K. Kimoto and I. Nishida, *Jpn. J. Appl. Phys.*, **6**, 1047 (1967).
4) N. Wada, *Jpn. J. Appl. Phys.*, **7**, 1287 (1968).

5) S. Kasukabe, S. Yatsuya, and R. Uyeda, *Jpn. J. Appl. Phys.*, **13**, 1714 (1974).
6) S. Yatsuya, K. Mihama, and R. Uyeda, *Jpn. J. Appl. Phys.*, **13**, 749 (1974).
7) S. Yatsuya, T. Hayashi, H. Akoh, E. Nakamura, and A. Tasaki, *Jpn. J. Appl. Phys.*, **17**, 355 (1978).
8) S. Yatsuya, Y. Tsukasaki, K. Mihama, and R. Uyeda, *J. Cryst. Growth*, **45**, 490 (1978).
9) N. Wada, *J. Phys. (Paris)*, **C2**-219 (1977).
10) H. Abe, W. Schulze, and B. Tesche, *Chem. Phys.*, **47**, 95 (1980).
11) K. Kimura and S. Bandow, *Bull. Chem. Soc. Jpn.*, **56**, 3578 (1983).
12) K. Kimura, *Bull. Chem. Soc. Jpn.*, **57**, 1683 (1984).
13) C. G. Granqvist and R. A. Buhrman, *J. Appl. Phys.*, **47**(5), 2200 (1976).
14) C. G. Granqvist, *J. Phys. (Paris)*, **C2**-147 (1977).
15) K. Koide, S. Yatsuya, and I. Yoshimura, *Jpn. J. Appl. Phys.*, **19**(2), 367 (1980).
16) S. Sako and K. Kimura, *J. Phys. Soc. Jpn.*, **53**(4), 1495 (1984).
17) J. B. Hopkins, P. R. R. Langridge-Smith, M. D. Morse, and R. E. Smalley, *J. Chem. Phys.*, **78**, 1627 (1983).
18) D. M. Cox, D. J. Trevor, R. L. Whetten, E. A. Rohlfing, and A. Kaldor, *J. Chem. Phys.*, **84**, 4651 (1986); *idem*, *Phys. Rev. B.*, **32**, 7290 (1985).
19) S. Yatsuya, S. Kasukabe, and R. Uyeda, *Jpn. J. Appl. Phys.*, **12**, 1675 (1973).
20) N. Wada, *Jpn. J. Appl. Phys.*, **7**, 1287 (1968).
21) W. P. Halperin, *Rev. Mod. Phys.*, **58**(3), 533 (1986).
22) K. Kimura, S. Bandow, and S. Sako, *Surf. Sci.*, **156**, 883 (1985).
23) K. Kimura and S. Bandow, *Phys. Rev. Lett.*, **58**, 1359 (1987).
24) G-Hanne Comsa, *J. Phys. (Paris)*, **C2**-185 (1977).

 © 1987 The Chemical Society of Japan Bull. Chem. Soc. Jpn., 60, 3099—3107 (1987)

The Liquid-Junction Potential at the Contact of Two Immiscible Electrolyte Solutions in the Absence of Supporting Electrolytes Reference Electrodes Reversible to Alkylammonium Ions and Tetraphenylborate Ion in Nitrobenzene

Takashi KAKIUCHI and Mitsugi SENDA*
Department of Agricultural Chemistry, Faculty of Agriculture, Kyoto University, Sakyo-ku, Kyoto 606
(Received March 4, 1987)

The liquid-junction potentials between two immiscible electrolyte solutions have been studied for the interface: $R_4^+TPB^-$(nitrobenzene)/$R_4^+X^-$(water) and $R_4^+TPB^-$ (nitrobenzene)/Li^+TPB^-(water), where R_4^+ is a tetraalkylammonium ion, TPB^- is tetraphenylborate ion, and X^- is a halide ion. These interfaces may be seen as a simplest form of either a liquid ion-exchange membrane ion-selective electrode sensing the activity of the ion in the aqueous phase or a reference electrode of a liquid membrane type reversible to the ion in the nonaqueous phase. The effects of the cationic species(R_4^+), the anionic species(X^-) and the concentration of the electrolytes on the electrical potential difference developed at the interface have been studied. These properties of the interfaces were compared with a simplified theoretical treatment of the liquid-junction potential between the two immiscible solutions. The theory can predict the basic features of the system by knowing the standard ion-transfer potentials and the diffusion coefficients of the relevant ions as well as its concentration. In the concentration range where a significant deviation from the Nernstian response of the liquid-junction potential occurred, the diffusion potential has been demonstrated to contribute significantly to the liquid-junction potential.

In the study of the double layer structure of the interface between two immiscible electrolyte solutions(ITIES) and the electrochemistry of charge transfer at the interface, large hydrophobic ions such as tetrabutylammonium ion(TBA^+) and tetraphenylborate ion(TPB^-) are used for a supporting electrolyte in the nonaqueous phase.[1a,b] In order that the electrical potential difference across the interface be well defined, it is desirable to use a reference electrode which is reversible to one of such organic ions in the nonaqueous phase. For this purpose, an aqueous solution containing the ion which is the same as one of the ions in the nonaqueous phase has been usually employed;[1a,b] the aqueous phase and the nonaqueous phase in contact form a nonpolarized interface through which the common ion works as a potential-determining ion. When all other ions are not transferable across the interface, there exists a so called contact equilibrium[2] between the two phases and there is no net flow of ions through the interface. The potential difference between the two phases is then represented by the Nernst equation with respect to the common ion. When an ion other than the potential determining ion, e.g., a counter ion of the potential-determining ion, is also appreciably transferable between the two phases, a net flow of the ions across the interface generally occurs even at zero-current condition until the final distribution equilibrium is attained.

The potential difference between two immiscible electrolyte solutions has been analyzed in detail by Hung[3] in the case where the distribution equilibrium of the ions between the two phases is established. He derived the equations which predict the distribution potential by knowing the initial concentrations and the standard ion-transfer potentials of the ions as well as the volumes of the two phases. However, in practice, the reference electrodes with ITIES are not always used under the condition of ultimate distribution equilibrium throughout the phases, and the potential difference across the interface is yet quite stable irrespective of the volumes of the two solutions shortly after the initial contact of these solutions. Therefore, it is necessary to study experimentally as well as theoretically the electrical potential difference between two immiscible electrolyte solutions without resorting to the assumption of the distribution equilibrium over the two phases in contact. This is the purpose of this study. We have previously presented the theory of the mixed ion-transfer potential at the ITIES in the presence of the supporting electrolytes in both phases.[4] We report here the theoretical treatment as well as the experimental study of the liquid-junction potential (l.j.p.) of the type: R^+TPB^-(nitrobenzene)/R^+X^-(water) and R^+TPB^-(nitrobenzene)/Li^+TPB^-(water), where R^+ is a tetraalkylammonium ion, TPB^- is tetraphenylborate ion, and X^- is a halide ion. The interfaces of these systems may also be seen as the interface between a liquid membrane and a sample solution in the liquid-membrane ion-selective electrode. Accordingly, this study will also provide us with insight into the basic properities of ion-selective electrodes.

Theoretical

Let us consider the electrical potential difference that develops across a plane interface when we bring into contact a semi-infinite aqueous phase containing 1:1 electrolyte K_1A_1 with a semi-infinite nonaqueous (oil) phase containing 1:1 electrolyte K_1A_2, where K and A denote a cation and an anion, respectively. In most of the cases encountered in practice, the ion transfer of one of these three ionic species can be neglected.[3] In the following, we consider only the case where only two ionic species K_1 and A_1 are transferable across the interface. The K_1 and A_1 may then be considered as a primary ion and an interfering ion, respectively. For the sake of simplicity, we assume the complete dissociations of K_1A_2 in the oil phase and of K_1A_1 in both phases and neglect the activity coefficients of the relevant ions. Let the x-axis be chosen normal to the interface, where $x=0$, and be directed from the oil toward the aqueous phase. The flux of an ion in each phase may be represented by the Nernst-Planck equation:

$$f_i^\alpha = -D_i^\alpha \frac{\partial c_i^\alpha}{\partial x} - \frac{z_i F}{RT} D_i^\alpha c_i^\alpha \frac{\partial \varphi^\alpha}{\partial x}, \tag{1}$$

where f is the flux, D is the diffusion coefficient, c is the concentration of the ion i, φ is the electrical potential(inner potential), x is the distance normal to the plane, z_i is the charge number of ion, and F, R, and T have the usual meanings. The superscript α(α=O or W) denotes the phase, whereas the subscript i(i=K_1, A_1, or A_2) the ionic species. Since there are three ionic species in the oil phase when the ion transfer of the ion A_1 takes place, the diffusion-migration problem in the oil phase is not solved analytically. We treat here the case where the concentration of the interfering ion(A_1) in the oil phase is so small that the migration of A_1 in the oil phase is negligible. This approximation holds as long as the deviation from the Nernstian response is small.

When the condition

$$D_{K1}^O c_{K1}^O + D_{A2}^O c_{A2}^O \gg D_{A1}^O c_{A1}^O \tag{2}$$

is fulfilled, we obtain the following equations for the mass transfer of the ions in the oil phase(See Appendix 1):

$$\frac{\partial c_{K1}^O}{\partial t} = \mathscr{D}_1^O \frac{\partial^2 c_{K1}^O}{\partial x^2} + \mathscr{D}_2^O \frac{\partial^2 c_{A1}^O}{\partial x^2} \tag{3}$$

and

$$\frac{\partial c_{A1}^O}{\partial t} = D_{A1}^O \frac{\partial^2 c_{A1}^O}{\partial x^2} \tag{4}$$

where

$$\mathscr{D}_1^O = \frac{2D_{K1}^O D_{A2}^O}{D_{K1}^O + D_{A2}^O} \tag{5}$$

and

$$\mathscr{D}_2^O = \frac{D_{K1}^O (D_{A1}^O - D_{A2}^O)}{D_{K1}^O + D_{A2}^O} \tag{6}$$

Similarly, for the aqueous phase we may write

$$\frac{\partial c_{K1}^W}{\partial t} = \mathscr{D}^W \frac{\partial^2 c_{K1}^W}{\partial x^2} \tag{7}$$

where

$$\mathscr{D}^W = \frac{2D_{K1}^W D_{A1}^W}{D_{K1}^W + D_{A1}^W} \tag{8}$$

The initial and boundary conditions for the differential Eqs. 3,4, and 7 are:

$$c_{K1}^O = {}^b c_{K1A2}^O \qquad (t=0,\ x<0) \tag{9}$$
$$c_{A1}^O = 0$$

$$c_{K1}^W = {}^b c_{K1A1}^W \qquad (t=0,\ x>0) \tag{10}$$

$$c_{K1}^O = {}^b c_{K1A2}^O \qquad (t>0,\ x=-\infty) \tag{11}$$
$$c_{A1}^O = 0$$

$$c_{K1}^W = {}^b c_{K1A1}^W \qquad (t>0,\ x=+\infty) \tag{12}$$

Here, ${}^b c_{K1A2}^O$ and ${}^b c_{K1A1}^W$ are the bulk concentrations of the electrolyte K_1A_2 in the oil phase and K_1A_1 in the aqueous phase.

The continuity of the flux for K_1 at the interface, $f_{K1}^O|_{x=0} = f_{K1}^W|_{x=0}$, leads to

$$[-D_{A1}^O + t_{A1}^W (D_{K1}^O + D_{A1}^O)] \left.\frac{\partial c_{A1}^O}{\partial x}\right|_{x=0} = -\mathscr{D}^W \left.\frac{\partial c_{A1}^W}{\partial x}\right|_{x=0} + 2t_{A1}^W D_{K1}^O \left.\frac{\partial c_{K1}^O}{\partial x}\right|_{x=0} \tag{13}$$

where

$$t_{A1}^W = \frac{D_{A1}^W}{D_{K1}^W + D_{A1}^W} \tag{14}$$

Furthermore, since the ion-transfer reaction at the oil-water interface is usually a fast process,[5] the surface concentrations of the K_1 in both phases are related through the Nernst equation:

$$p = \frac{c_{K1}^O(0,t)}{c_{K1}^W(0,t)} = \exp\left[\frac{F}{RT}(\Delta_O^W \varphi - \Delta_O^W \varphi_{K1}^0)\right] \tag{15}$$

Similarly, for the anion A_1,

$$q = \frac{c_{A1}^O(0,t)}{c_{A1}^W(0,t)} = \exp\left[-\frac{F}{RT}(\Delta_O^W \varphi - \Delta_O^W \varphi_{A1}^0)\right] \tag{16}$$

In Eqs. 15 and 16, $\Delta_O^W \varphi$ is the inner potential of the aqueous phase with respect to that in the oil phase. It is the quantity usually called the interfacial potential or phase-boundary potential.[4] $\Delta_O^W \varphi_{K1}^0$ and $\Delta_O^W \varphi_{A1}^0$ are the standard ion-transfer potentials for K_1 and A_1.[1]

Solving the Eqs. 3, 4, and 7 under these initial and boundary conditions, Eqs. 9—16, we finally obtain for the interfacial potential at zero current, $\Delta_O^W\varphi_{\text{interfacial},i=0}$ (See Appendix 2):

$$\Delta_O^W\varphi_{\text{interfacial},\,i=0} = \Delta_O^W\varphi_{K1}^W + \frac{RT}{F}\ln\left\{\frac{1}{2}\left[\frac{{}^bc_{K1A2}^O}{{}^bc_{K1A1}^W} + \left\{\left(\frac{{}^bc_{K1A2}^O}{{}^bc_{K1A1}^W}\right)^2 + 4\alpha\xi\right\}^{1/2}\right]\right\} \quad (17)$$

where

$$\alpha = \left(\frac{D_{A1}^O}{\mathscr{D}^W}\right)^{1/2}\frac{{}^bc_{K1A2}^O}{{}^bc_{K1A1}^W} + \frac{1}{2}\left(\frac{\mathscr{D}_1^O}{D_{A1}^O}\right)^{1/2}\left(1+\frac{D_{A1}^O}{D_{K1}^O}\right) + \frac{\mathscr{D}_2^O}{D_{A1}^O+(D_{A1}^O\mathscr{D}_1^O)^{1/2}} \quad (18)$$

and

$$\xi = \exp\left[\frac{F}{RT}(\Delta_O^W\varphi_{A1}^0 - \Delta_O^W\varphi_{K1}^0)\right] \quad (19)$$

The interfacial potential depends on the concentration ratio ${}^bc_{K1A2}^O/{}^bc_{K1A1}^W$, the difference in the values of the standard ion-transfer potentials, and the diffusion coefficients of the relevant ions in both phases, which actually enter into Eq. 17 through the ratio D_{K1}^O/D_{K1}^W, D_{A1}^O/D_{A1}^W, D_{A2}^O/D_{A1}^O, and D_{A1}^O/D_{K1}^O. When the condition

$$\left(\frac{{}^bc_{K1A2}^O}{{}^bc_{K1A1}^W}\right)^2 \gg 4\alpha\xi \quad (20)$$

is fulfilled, Eq. 17 reduces to

$$\Delta_O^W\varphi_{\text{interfacial},i=0} = \Delta_O^W\varphi_{K1}^0 + \frac{F}{RT}\ln\frac{{}^bc_{K1A2}^O}{{}^bc_{K1A1}^W} \quad (21)$$

Namely, as long as the ${}^bc_{K1A1}^W$ is sufficiently small, the ITIES reveals the Nernstian response with respect to the concentraton of the ion K_1, even when ξ is appreciably large, i.e., A_1 is relatively hydrophobic.

Equation 17 has a form similar to the equation derived by Hung(Eq. 34 in Ref. 3) assuming that the distribution equilibrium is established throughout the two phases and the volumes of the two phases are equal. In Hung's equation, α is given by

$$\alpha = 1 + \frac{c_{K1A2}^O}{c_{K1A1}^W} \quad (22)$$

where c_{K1A1}^O and c_{K1A1}^W are the initial concentrations of electrolytes. When all the diffusion constants of the ions are equal in both phases, Eq. 18 reduces to Eq. 22. However, its physical meanings are different from those of Eq. 17. Equation 17 contains the terms involving the diffusion coefficients of the relevant ions, reflecting the importance of the transport processes of the ions. The advantage of Eq. 17 over Hung's equation is that one need not assume any size of the volume for the two solutions nor the establishment of the distribution equilibrium throughout the two phases, which may rarely occur in practical cases.

In addition to the interfacial potential, there exists the diffusion potential on each side of the interface insofar as the system is not at equilibrium. This diffusion potential becomes significant when the transfer of K_1A_1 from the aqueous phase to the oil phase becomes discernable. The diffusion potential in the oil phase, φ_{diff}^O, and that in the aqueous phase, φ_{diff}^W, may be written as (See Appendix 2):

$$\varphi_{\text{diff}}^O = \frac{RT}{F}(1-2t_{K1}^O)\ln\frac{Ap'}{{}^bc_{K1A2}^O} \quad (23)$$

and

$$\varphi_{\text{diff}}^W = \frac{RT}{F}(1-2t_{A1}^W)\ln\frac{A}{{}^bc_{K1A1}^W} \quad (24)$$

where

$$A = \frac{N{}^bc_{K1A2}^O + (\mathscr{D}^W)^{1/2}{}^bc_{K1A1}^W}{Mq'+Np'+(\mathscr{D}^W)^{1/2}} \quad (25)$$

$$M = (D_{A1}^O)^{1/2} - t_{A1}^W\left[\frac{D_{K1}^O+D_{A1}^O}{(D_{A1}^O)^{1/2}} + \frac{2D_{K1}^O\mathscr{D}_2^O}{D_{A1}^O(\mathscr{D}_1^O)^{1/2}+\mathscr{D}_1^O(D_{A1}^O)^{1/2}}\right] \quad (26)$$

$$N = 2t_{A1}^W D_{K1}^O/(\mathscr{D}_1^O)^{1/2} \quad (27)$$

$$t_{K1}^O = D_{K1}^O/(D_{K1}^O+D_{A2}^O)$$

and p' and q' are p and q at zero current. The total potential difference between the two phases at zero current, i.e., the l.j.p. at zero current, $\Delta_O^W\varphi_{i=0}$, is generally given by

$$\Delta_O^W\varphi_{i=0} = \varphi_{\text{diff}}^O + \Delta_O^W\varphi_{\text{interfacial},\,i=0} + \varphi_{\text{diff}}^W \quad (28)$$

It is noted that if we take account of the migration of A_1 ion in the oil phase, the diffusion potential could be much larger than expected from Eq. 23.

Experimental

Reagent-grade nitrobenzene was treated with active alumina and then equilibrated with twice distilled water. Tetraphenylborate salts of tetrahexyl-(THA^+), tetrapentyl-($TPnA^+$), tetrabutyl-, and tetrapropylammonium($TPrA^+$) ions were prepared from sodium tetraphenylborate(Dojin Lab., Japan) and corresponding alkylammonium halides of reagent grade as described previously.[6] Reagent grade tetrabutylammonium chloride and tetrapropylammonium chloride were recrystallized from acetone-ether mixture. The aqueous solutions of these salts were stirred in the presence of AgCl powder to remove a trace amount of bromide and/or iodide ions. Lithium tetraphenylborate (LiTPB) was prepared from sodium tetraphenylborate.[7] The stock solution of 0.0705 mol dm^{-3} LiTPB contained 0.001 mol dm^{-3} lithium hydroxide to prevent the decomposition of LiTPB. The concentration of LiTPB was determined by titration of the solution with zephiramine.[8]

The electromotive force of the cell was measured with a Keithley 616 electrometer. The cell was made in a U-shaped

poly(tetrafluoroethylene) tubing of 9 mm inner diameter and 10 cm tall. About 8 ml of a nitrobenzene solution was first put into the tubing and then a few milliliter of aqueous solution were added onto the nitrobenzene solution in each leg of the cell. Appropriate reference electrodes were then immersed into the aqueous solutions. The liquid-liquid contact in a reference electrode, if necessary, was made via a glass frit when the solvent is water, or a poly(vinyl chloride) gel of nitrobenzene solution when the solvent is nitrobenzene. The cell was immersed in a water bath at 25 ±0.1°C. The emf measurements were started immediately after the contact of the aqueous and nitrobenzene solutions.

Results and Discussion

Nitrobenzene-Water Interface Reversible to Large Tetraalkylammonium Ions. Effect of Cationic Species: The emf response of the interface, RCl(W)/RTPB(NB), to c^{W}_{RCl} was measured at c^{o}_{RTPB}=const. for R=TPrA$^+$, TBA$^+$, TPnA$^+$, and THA$^+$. The following two types of the cell were used;

I	II	III	IV	V	VI	VII
Ag	AgCl	*a* M† RCl (W)	*b* M RTPB (NB)	*c* M RX (W)	AgX	Ag

(I)

and

I	II	III	IV	V	VI	VII	VIII
Ag	AgCl	*a* M LiCl (W)	*a* M LiTBP (W)	*b* M RTPB (NB)	*c* M RCl (W)	AgCl	Ag

(II)

The interface between the phases IV and V in the cell (I) and that between V and VI in the cell (II) are the nonpolarized interfaces at which the l.j.p. we are concerned with resides. The cell (I) was used for R=TPrA$^+$(*a*=1, *b*=1, and *c*=1—500 mmol dm^{-3}) and TBA$^+$(*a*=10, *b*=50, and *c*=0.1—200 mmol dm^{-3}), and the cell(II) for R=TPnA$^+$(a=1, *b*=100, and *c*=0.1—100 mmol dm^{-3}) and THA$^+$(*a*=1, *b*=40, and *c*=0.02—2 mmol dm^{-3}). Since the nitrobenzene phase was thick, the potential between the phases III and IV in the cell (I) and that between IV and V in the cell(II) remain unchanged with the change of c^{W}_{RCl}. The l.j.p. across the phases III and IV in the cell(II) is also constant. The change in the potential difference between phases V and VI in (I) and that between phases VI and VII in the cell(II) with the change of $^{b}c^{W}_{RCl}$ were calculated assuming the Nernstian response of the Ag/AgCl electrodes to the Cl$^-$ ion. The activity coefficients of RCl's were estimated by using the Davies equation.[9] These calculated values were added to the corresponding emf values to obtain the change of the l.j.p. at the interface. The resultant variation of the l.j.p. values was plotted against the logarithm of the concentration ratio, $\log(^{b}c^{W}_{RCl}/^{b}c^{NB}_{RTPB})$. These curves were shifted vertically so that their linear portions were superimposed upon each other, eliminating the difference in the emf values due to the different reference electrode included in each cell. Figure 1 indicates that TPrA$^+$ has the largest concentration range of the Nernstian response. With the increase of the alkyl-chain length, the Nernstian region becomes narrower, as is expected from the theoretical treatment given above, because the increase in the hydrophobicity of the cation gives rise to the increase in ξ in Eq. 17 (see also Eq. 19). The arrows in Fig. 1 indicate the predicted points, where the curves deviate by 1 mV from the Nernstian slope, calculated using Eq. 17 and the values for the diffusion coefficients and the standard ion-transfer potentials given in Table 1. The values of diffusion coefficients for TPnA$^+$ and THA$^+$ are assumed to be the same as that for TBA$^+$. The diffusion coefficient of each ion in the nitrobenzene was taken as a half of the one in aqueous solution.[6]

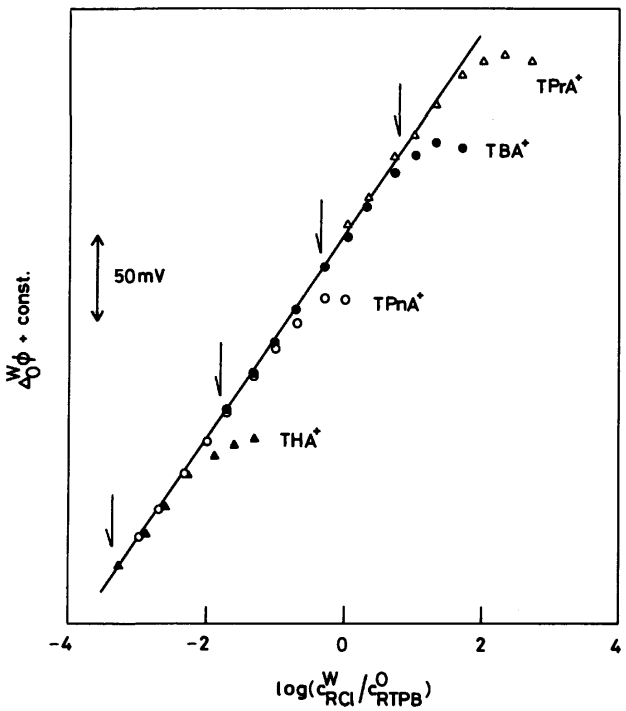

Fig. 1. Change of the liquid junction potentials for the system: RTPB(nitrobenzene)/RCl(water), where R=tetrapropylammonium(TPrA$^+$), tetrabutylammonium(TBA$^+$), tetrapentylammonium(TPnA$^+$), or tetrahexylammonium ion(THA$^+$).

Effect of the Anionic Species: The effect of the counter ionic species was studied for the interface, TBAX(W)/TBATPB(NB) using the cell(I) for X$^-$= Cl$^-$(*a*=1, *b*=50, and *c*=0.1—200 mmol dm^{-3}) and

† 1 M=1 mol dm^{-3}.

Br^-(a=1, b=10, and c=0.01—100 mmol dm^{-3}) and also using the following cell:

I	II	III	IV	V	VI	VII	VIII
Ag	AgCl	1 mM TBACl (W)	0.1 M TBATPB (NB)	0.02—5 mM TBAI (W)	satd. KCl	AgCl	Ag

(III)

for X^-=I^-. The change in l.j.p. values from the measured emf values was obtained as described above for X^-=Cl^- and Br^-, while the l.j.p. at the interface between phases V and VI was neglected in the cell(II). The results were plotted against $\log(c^{W}_{TBAX}/c^{o}_{TBATPB})$ in Fig. 2.

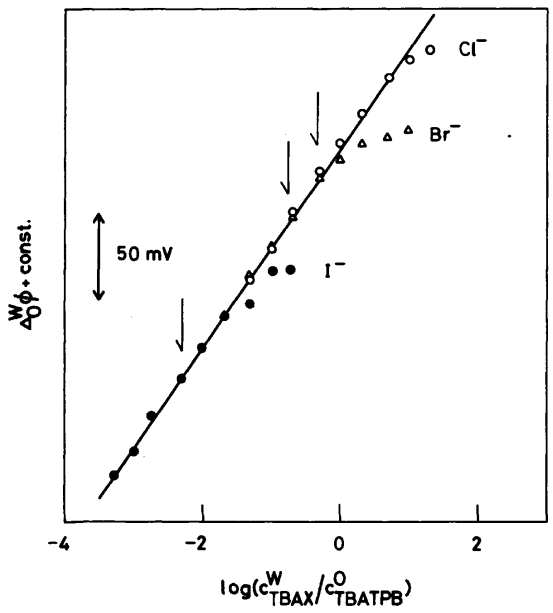

Fig. 2. Change of the liquid-junction potentials for the system: TBATPB(nitrobenzene)/TBAX(water), where R=chloride, bromide, or iodide ion.

Table 1. Standard Ion-Transfer Potentrials of Ion Transfer from Water to Nitrobenzene and Diffusion Coefficients of Ions in Water

Ion	$\Delta^{W}_{NB}\varphi^0$/V[a]	D/cm^2s^{-1}[c]
Li^+	0.395	—
$TPrA^+$	−0.154[b]	6.24×10^{-6}
TBA^+	−0.248	5.21×10^{-6}
$TPnA^+$	−0.343[b]	—
TUA^+	−0.438[b]	—
Cl^-	−0.324	2.0×10^{-5}
Br^-	−0.295	2.1×10^{-5}
I^-	−0.195	2.1×10^{-5}
TBP^-	0.372	—

a) Data in Ref. 3. b) Calculated from the data in Ref. 3. c) Calculated from the limiting equivalent conductances given in Ref. 10.

These curves were shifted vertically to superimpose the linear portions of the curves upon each other. As the radius of the counter ion increases, the curves start to deviate from the Nernstian response at the lower value of the concentration ratio, i.e., the more hydrophobic the counter ion is, the greater is the degree of interference. This is also the behavior expected from Eq. 17. The arrows in Fig. 2 indicate the points where the curves deviate by 1 mV from the Nernstian slope, calculated with Eq. 17 and the values in Table 1.

Effect of the Concentration of the Electrolyte: Equation 17 indicates that when the system K_1A_1(W)/ K_1A_2(O) functions as a liquid-membrane ion-selective electrode at a constant concentration of K_1A_2, the concentration level of K_1A_2 influences the concentration range of K_1A_1 where the system shows Nernstian response. Similarly, when the system works as a reference electrode reversible to the K_1 ion in the oil phase at a constant concentration, the concentration level of K_1A_1 in the aqueous phase limits the range of the Nernstian region. Such a concentration effect has great practical importance to determine the suitable conditions in designing reference electrodes and ion-selective electrodes of a liquid-membrane type.

The change of the l.j.p. for the system TBATPB (NB)/ TBACl(W) was estimated from the emf values of the cell (I) for the various concentrations(a=b/10, b=0.5,1,2,5,10,20,50, and 100, and c=0.1—500 mmol dm^{-3}) of TBATPB and TBACl. Figure 3 shows the response of the system with respect to the concentra-

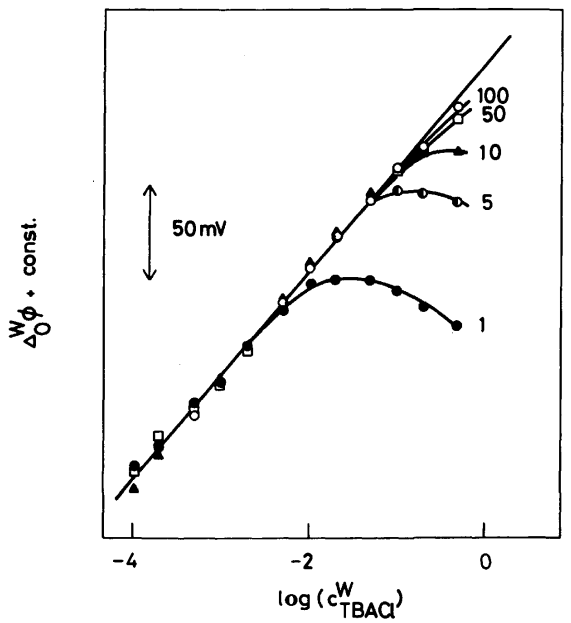

Fig. 3. Effect of the concentration of TBATPB in nitrobenzene on the change of the liquid-junction potential. Labels indicate the concentration of TBATPB in nitrobenzene in mmol dm^{-3}.

tion of TBACl at five different concentrations of TBATPB in the nitrobenzene phase. As the concentrations of TBATPB increases, the Nernstian region becomes wider. In terms of the liquid-membrane ion-selective electrodes, this means that the concentration of the "ion-exchanger"(TPB$^-$ ion in the present system) in the membrane must be high in order to obtain the wider concentration range of the Nernstian response for TBACl. The curve for ${}^{b}c^{O}_{TBATPB}$=1 mmol dm^{-3} in Fig. 3 has a maximum and, in the higher concentration region, the l.j.p. changes in opposite direction with increasing concentration of TBACl. Similar tendency was found also in the curve at ${}^{b}c^{O}_{TBATPB}$=5 mmol dm^{-3}. Such a tendency can be ascribed to the l.j.p. in the nitrobenzene phase caused by the migration of Cl$^-$ ion in the nitrobenzene phase, as will be shown below.

Figure 4 shows the change of the l.j.p. with the mean ionic activity of TBATPB in the nitrobenzene phase, $a^{\pm,NB}_{TBATPB}$, at the three different concentrations of TBACl. The activity instead of the concentration was used in Fig. 4 to check if this system responds thermodynamically to the activity of the TBA$^+$ ion. The activity coefficients of TBA$^+$ and TPB$^-$ ions were calculated by using the Debye-Hückel theory allowing for the finite size of the ions.[11] At ${}^{b}c^{W}_{TBACl}$=1 mmol dm^{-3}, the change of the l.j.p vs. $\log(a^{\pm,NB}_{TBATPB})$

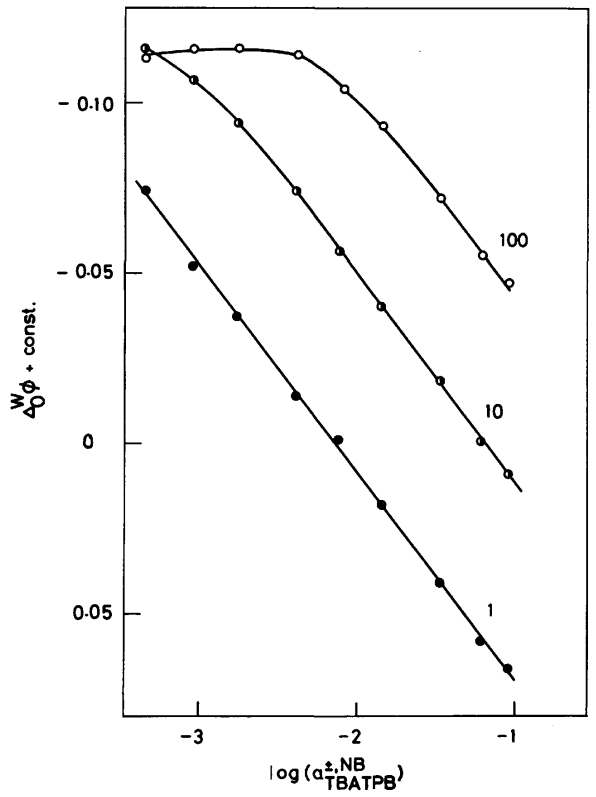

Fig. 4. Effect of the concentration of TBACl in aqueous solution on the change of the liquid-junction potential. Labels indicate the concentration of TBACl in aqueous phase in mmol dm^{-3}.

plot was linear with the slope of 60 mV per decade change of $a^{\pm,NB}_{TBATPB}$ in the whole concentration range studied(0.5—100 mmol dm^{-3}). This indicates that the present system can be employed as a reference electrode reversible to the TBA$^+$ ion in the nitrobenzene phase in this concentration range. At ${}^{b}c^{W}_{TBACl}$=10 mmol dm^{-3} the curve in Fig. 4 deviated from the Nernstian slope in the lower concentration (activity) region of TBA$^+$ ion. The deviation occured at much higher concentration(activity) region when ${}^{b}c^{W}_{TBACl}$=100 mmol dm^{-3}. These results indicate that the concentration of TBACl must be kept as small as possible to obtain a wider range of Nernstian response. This type of the interface has been successfully used at ${}^{b}c^{W}_{TBACl}$=5 mmol dm^{-3} as a reference electrode in studying the specific adsorption of TBA$^+$ and TPB$^-$ ions at the nitrobenzene-water interface by using electrocapillary measurements.[12]

Nitrobenzene-Water Interface Reversible to Tetraphenylborate Ion. It is sometimes convenient to use a reference electrode reversible to an anion instead of a cation dissolved in organic phase. For example, to study thermodynamically the specific adsorption of cations in the nitrobenzene, one must use a reference electrode reversible to the anion in the nitrobenzene phase. In addition, when a cation in the oil phase is very hydrophobic, i.e., in the case $\Delta^{W}_{O}\varphi^{0}_{K1} \leqq \Delta^{W}_{O}\varphi^{0}_{A1}$, one has to keep the ratio ${}^{b}c^{O}_{K1A2}/{}^{b}c^{W}_{K1A1}$ large enough to ensure the Nernstian response of the interface if one uses a cation reversible reference electrode. In such cases, the anion reversible reference electrode is promising. We examined the possibility of the nitrobenzene-water interfaces reversible to the TPB$^-$ ion by measuring the emf of the following cells:

I	II	III	IV	V		
Ag	AgCl	1 mM LiCl (W)	1 mM LiTPB (W)	a M TPnATPB (NB)		
		VI	VII	VIII	IX	
		a/10 M LiTPB (W)	a/10 M LiCl (W)	AgCl	Ag	(IV)

for TPnA$^+$ (a=5—200 mmol dm^{-3}) and

I	II	III	IV	V		
Ag	AgCl	0.5 mM LiCl (W)	0.5 mM LiTPB (W)	a M THATPB (NB)		
		VI	VII	VIII	IX	
		a M TPrATPB (NB)	a M TPrACl (W)	AgCl	Ag	(V)

for THA^+(a=5—40 mmol dm^{-3}).

Since in the cell (IV) the ratio ${}^{b}c^{NB}_{TPnATPB}/{}^{b}c^{W}_{LiTPB}$ was kept constant during the change of ${}^{b}c^{NB}_{TPnATPB}$, the change of the potential difference between the phases V and VI with ${}^{b}c^{NB}_{TPnATPB}$ can be considered negligible. Similarly, the change in the potential difference between the phases VI and VII is also negligible. The changes in the potential falls between phases VII and VIII in the cells (IV) and (V) with ${}^{b}c^{W}_{RCl}$ (R=Li^+ or $TPrA^+$) were allowed for as described above. The changes of the l.j.p.'s which reside between the phases VI and VII in the cell (IV) and between the phases V and VI in the cell (V) were neglected, because the change of the ratio of the equivalent conductances for THATPB and TPrATPB in the nitrobenzene phase with the change of the electrolyte concentration and also that for LiTPB and LiCl in the aqueous phase seem negligibly small. The changes of the l.j.p.'s across the phases IV and V in the cell (IV) and (V) thus estimated are plotted against $\log(a^{\pm,NB}_{RTPB})$ in Fig. 5. Both interfaces respond linearly with the slopw of 58 mV($TPnA^+$) and 60 mV(THA^+) within the concentration range studied. Thus, the system LiTPB (W)/RTPB(NB) can be used as a reference electrode reversible to the TPB^- ion in the nitrobenzene phase. This type of reference electrode has been applied in studying the specific adsorption of cationic surfactants at the nitrobenzene-water interface by using the mixed electrolyte method.[13]

Significance of the Diffusion Potential. Figure 3 shows that the curves at ${}^{b}c^{O}_{TBATPB}$=1 and 5 mmol dm^{-3} have maxima. The approximate theoretical treatment of the l.j.p. described above can predict the concentration at which the l.j.p. starts to deviate from the Nernstian response, but cannot explain the inversion of the slope. In fact, Eq. 17 gives a constant value of $\Delta^{W}_{O}\varphi_{interfacial,i=0}$ when ${}^{b}c^{O}_{K1A2}/{}^{b}c^{W}_{K1A1}\to\infty$. The approximation introduced previously is obviously not adequate in such a high concentration region, since a significant amount of Cl^- ion enters into the nitrobenzene phase, so that its amount is no longer negligible in the vicinity of the interface. The diffusion coefficient of Cl^- ion is probably much larger than those of TBA^+ and TPB^- ions in the nitrobenzene phase (cf. Table 1). Therefore, the positive diffusion potential(the potential is referred to that at the infinity of the nitrobenzene phase), which is opposite in sign to that of the interfacial potential, will develop in the vicinity of the interface.

If this diffusion potential is responsible to the inversion of the potential, the addition of a supporting electrolyte in the nitrobenzene phase should suppress the l.j.p. in that phase, resulting in the disappearance of the maximum. The emf of the following cell was measured with and without 40 mmol dm^{-3} THATPB.

I	II	III		IV	
Ag	AgCl	1 mM TBACl (W)	1 mM TBATPB	+	40 mM THATPB (NB)

V	VI	VII	
a M TBABr (W)	AgBr	Ag	(VI)

The change in the potential drop between the phases V and Vl was allowed for as described above.

Figure 6 shows the change of the l.j.p. vs. $\log({}^{b}c^{W}_{TBABr}/{}^{b}c^{O}_{TBATPB})$ curves. The curve for the cell without THATPB (Curve 1 in Fig. 6) exhibited a maximum at $\log({}^{b}c^{O}_{TBATPB}/{}^{b}c^{W}_{TBABr})\fallingdotseq 1$ and decreased with the further increase of ${}^{b}c^{W}_{TBABr}$. This inverted change of the l.j.p. was almost eliminated by adding 40 mmol dm^{-3} THATPB to the nitrobenzene phase, as is shown in Curve 2 in Fig 6. The slight decrease at the highest concentration is probably due to an insufficient concentration of THATPB to eliminate fully the migration of the Cl^- ion. This experiment clearly indicates the significant contribution of the diffusion potential in the nitrobenzene phase to the inversion of the slope shown in Curve 1 in Fig. 6. To confirm further the effect of the diffusion potential, the diffusion-migration equations were solved numerically using a finite difference method[14] without introducing the assumption given by Eq. 2. The values given in Table 1 were used for the calculation. The result for the system TBABr(W)/TBATPB(NB) is

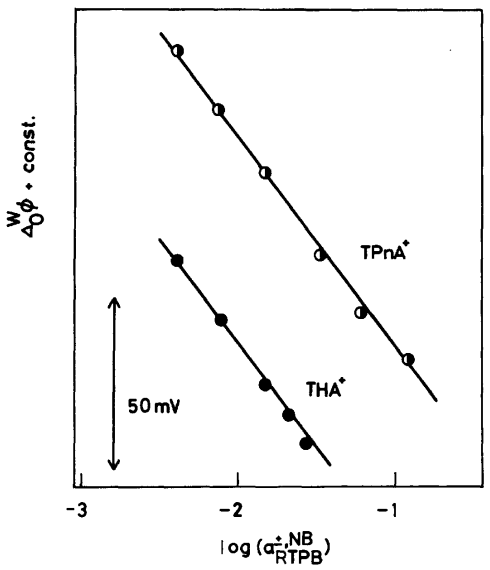

Fig. 5. Change of the liquid-junction potentials for the system: RTPB(nitrobenzene), LiTPB(water), where R=$TPnA^+$ or THA^+ ion.

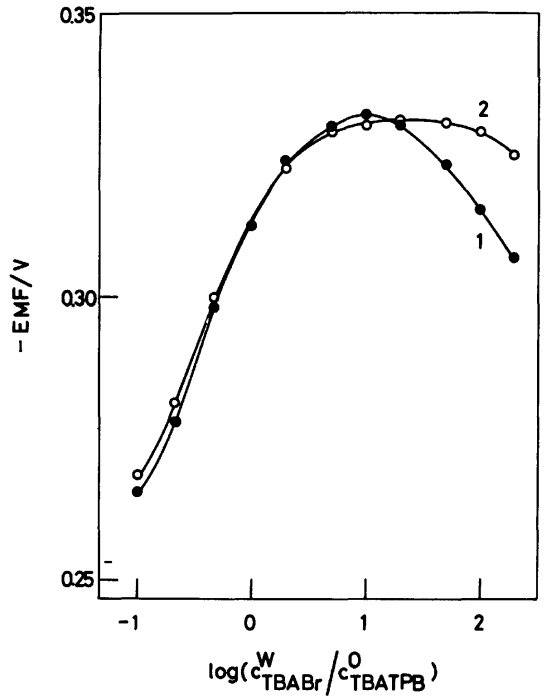

Fig. 6. Change of the liquid-junction potential for the system: TBATPB(nitrobenzene)/TBABr(water), in the presence of (Curve 2) and the absence of (Curve 1) 40 mmol dm^{-3} THATPB in nitrobenzene as a supporting electrolyte.

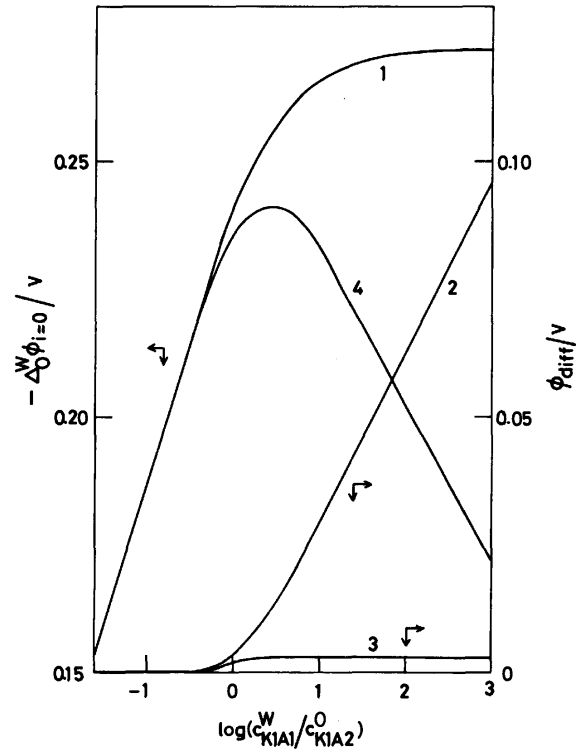

Fig. 7. Calculated values of the interfacial potential(Curve 1), the diffusion potential in nitrobenzene phase(Curve 2), the diffusion potential in aqueous phase(Curve 3), and the total liquid-junction potential(Curve 4) for the system: TBATPB-(nitrobenzene)/TBABr(water).

given in Fig. 7.

In the higher concentration region, the interfacial potential (Curve 1) reached a limiting value. Simultaneously, the diffusion potential in the nitrobenzene phase(Curve 2) increases linearly with the logarithm of the concentration ratio, while the diffusion potential in the aqueous phase(Curve 3) stays at a nominal value. Accordingly, the total liquid-junction potential(Curve 4) possesses a maximum and beyond this point the potential in turn decreases linearly with the concentration. Thus, although the contribution of the diffusion potential seems smaller in the actual system if one compares Fig. 6 with Fig. 7, the numerical calculation essentially reproduces the experimental trend, indicating the importance of the diffusion potential in the concentration range far from the Nernstian response.

Such a contribution of the diffusion potential to the measured emf value may have a practical importance. Liquid-ion exchange membrane ion-selective electrodes have been used to determine the critical micelle concentration of ionic surfactants by making use of the intersection point of the two linear portion of the emf vs. logarithm of the surfactant concentration curve.[15,16] The results in Figs. 6 and 7 indicate that such a method for determining the critical micelle concentration(cmc) may lead to a spurious conclusion. Disagreement has been reported between the cmc value determined from another method and the value from the concentration of the intersection point in the emf vs. the logarithm of the surfactant concentration curve.[17,18]

Appendix 1

From Eq. 1, we may write for the flux of the ions in oil phase

$$f^{o}_{K1} = -D^{o}_{K1}\frac{\partial c^{o}_{K1}}{\partial x} - \frac{F}{RT}D^{o}_{K1}c^{o}_{K1}\frac{\partial \varphi^{o}}{\partial x}, \tag{A1}$$

$$f^{o}_{A1} = -D^{o}_{A1}\frac{\partial c^{o}_{A1}}{\partial x} + \frac{F}{RT}D^{o}_{A1}c^{o}_{A1}\frac{\partial \varphi^{o}}{\partial x}, \tag{A2}$$

$$f^{o}_{A2} = -D^{o}_{A2}\frac{\partial c^{o}_{A2}}{\partial x} + \frac{F}{RT}D^{o}_{A2}c^{o}_{A2}\frac{\partial \varphi^{o}}{\partial x}. \tag{A3}$$

On the other hand, the current density I in oil phase is represented by

$$I = F(f^{o}_{A1}+f^{o}_{A2}-f^{o}_{A1}). \tag{A4}$$

Substituting (A1), (A2), and (A3) into (A4), $\partial\varphi^{o}/\partial_x$ can be represented by

$$\frac{\partial \varphi^{o}}{\partial x} = -\frac{RT}{F}Z, \tag{A5}$$

where

$$Z = (D^{o}_{K1}\frac{\partial c^{o}_{K1}}{\partial x} - D^{o}_{A1}\frac{\partial c^{o}_{A1}}{\partial x} - D^{o}_{A2}\frac{\partial c^{o}_{A2}}{\partial x} + \frac{I}{F})/\beta$$

and

$$\beta = D^{o}_{K1}c^{o}_{K1}+D^{o}_{A1}c^{o}_{A1}+D^{o}_{A2}c^{o}_{A2}.$$

When $D^{o}_{K1}+c^{o}_{K1}+D^{o}_{A2}c^{o}_{A2} \gg D^{o}_{A1}c^{o}_{A1}$, after substituting Eq. A5 into A1, A2, and A3, we obtain

$$f^{o}_{K1} = -\mathscr{D}^{o}_{1}\frac{\partial c^{o}_{K1}}{\partial x} - \mathscr{D}^{o}_{2}\frac{\partial c^{o}_{A1}}{\partial x} + t^{o}_{K1}\frac{I}{F} \tag{A6}$$

and

$$f^{o}_{A1} = -D^{o}_{A1}\frac{\partial c^{o}_{A1}}{\partial x}, \tag{A7}$$

where $\mathscr{D}^{o}_{1}$ and $\mathscr{D}^{o}_{2}$ are given by Eqs. 5 and 6.

Appendix 2

Solving the differential equations, Eqs. 7—9, under the initial and boundary conditions, Eqs. 10—16, we obtain, when $D^{o}_{A1} \neq \mathscr{D}^{o}_{1}$

$$c^{o}_{K1}(x, t) = {}^{b}c^{o}_{K1A2} + \left(pA - \frac{\mathscr{D}^{o}_{2}}{D^{o}_{A1}-\mathscr{D}^{o}_{1}}qA - {}^{b}c^{o}_{K1A2}\right)\mathrm{erfc}\left[-\frac{x}{2(\mathscr{D}^{o}_{1}t)^{1/2}}\right] + \frac{\mathscr{D}^{o}_{2}}{D^{o}_{A1}-\mathscr{D}^{o}_{1}}qA\ \mathrm{erfc}\left[-\frac{x}{2(D^{o}_{A1}t)^{1/2}}\right] \tag{A8a}$$

and

$$c^{o}_{A1}(x, t) = qA\ \mathrm{erfc}\left[-\frac{x}{2(D^{o}_{A1}t)^{1/2}}\right], \tag{A9}$$

where p, q, and A are given by Eqs. 15, 16, and 24, respectively. When $D^{o}_{A1}=\mathscr{D}^{o}_{1}$, instead of Eq. A1, we have

$$c^{o}_{K1}(x, t) = {}^{b}c^{o}_{K1A2} - \frac{\mathscr{D}^{o}_{2}}{2(\mathscr{D}^{o}_{1})^{3/2}}qAx\frac{1}{(\pi t)^{1/2}}\exp\left(-\frac{x^2}{4t\mathscr{D}^{o}_{1}}\right) + (pA-{}^{b}c^{o}_{K1A2})\ \mathrm{erfc}\left[-\frac{x}{2(\mathscr{D}^{o}_{1}t)^{1/2}}\right]. \tag{A8b}$$

On the oher hand, for $c^{w}_{K1}(x, t)$ we have

$$c^{w}_{K1}(x, t) = {}^{b}c^{w}_{K1A1} + A\ \mathrm{erfc}\left[\frac{x}{2(\mathscr{D}^{w}t)^{1/2}}\right]. \tag{A10}$$

From Eqs. A4, A8, A9, and A10, the current-potential relationship can be written as:

$$\frac{I}{F} = -\frac{1}{(\pi t)^{1/2}}\frac{1}{t^{w}_{A1}}A[Np+(M-(D^{o}_{A1})^{1/2})q]-N{}^{b}c^{o}_{K1A2}, \tag{A11}$$

where M and N are given by Eqs. 26 and 27. This equation is valid irrespective of the magnitude of D^{o}_{A1} and $\mathscr{D}^{o}_{1}$. Setting $I=0$ in Eq. A11, we obtain Eq. 17.

Under the conditions of Eq. 2 and at $I=0$ we may write from Eq. 1,

$$\frac{\partial\varphi}{\partial x} = \frac{RT}{F}\frac{D^{o}_{A2}-D^{o}_{K1}}{D^{o}_{K1}+D^{o}_{A2}}\frac{\partial \ln c^{o}_{K1}}{\partial x}. \tag{A12}$$

Integrating this equation from $x=-\infty$ to $x=-0$, we have

$$\varphi(x=0) - \varphi(x=-\infty) = \frac{RT}{F}(1-2t^{o}_{K1})\ln\frac{c^{o}_{K1}(0, t)}{{}^{b}c^{o}_{K1A2}} \tag{A13}$$

Substituting Eq. A8 at $x=-0$, we obtain Eq 23. Eq. 24 can be derived similarly.

This work was supported by Grant-in-Aids for Scientific Research No. 60211017 from the Ministry of Education and Culture.

References

1) a) M.Senda, T. Kakutani, and T. Osakai, *Denki, Kagaku,* **49**, 322 (1981). b) J. Koryta and P. Vanysek, Advances in Electrochemistry and Electrochemical Engineering," ed by H. Gerischer and C. W. Tobias, John Wiley, New York (1981), Vol. 12, p. 113.

2) E. A. Guggenheim, "Thermodynamics," 6th ed, North-Holland, Amsterdam (1977), p. 307.

3) L. Q. Hung, *J, Elecroanal. Chem. Interfacial Electrochem.,* **115**, 159 (1980).

4) T. Kakiuchi and M. Senda, *Bull. Chem. Soc. Jpn.,* **57**, 1801 (1984).

5) T. Osakai, T. Kakutani, and M. Senda, *Bull. Chem. Soc. Jpn.,* **57**, 370 (1984).

6) T. Kakiuchi and M. Senda, *Bull. Chem. Soc. Jpn.,* **56**, 1322 (1983).

7) R. W. Kunze and R. M. Fuss, *J. Phys. Chem.,* **67**, 385 (1963).

8) E. D. Schall, *Anal. Chem.,* **29**, 1044 (1957).

9) C. Davies, "Ion Association," Butterworth, London (1962), p. 39.

10) R. A. Robinson and R. H. Stokes, "Electrolyte Solutions," Butterworth, London(1959), p. 463.

11) H. S. Harned and B. B. Owen, "Physical Chemistry of Electrolyte Solutions,"3rd ed, Reinhold, New York(1958), p. 731.

12) T. Kakiuchi and M. Senda, *Bull. Chem. Soc. Jpn.,* **56**, 1753 (1983).

13) T. Kakiuchi, M. Kobayashi, and M. Senda, *Bull. Chem. Soc. Jpn.,* **60**, 3109 (1987).

14) S. W. Feldberg, "Electroanalytical Chemistry," ed by A. Bard, Marcel Dekker(1969), Vol. 3, p. 199.

15) C. Cavach and C. Bertrand, *Anal. Chim. Acta,* **55**, 385 (1971).

16) N. Ishibashi and H. Ohara, *Bunseki Kagaku,* **21**, 100 (1972).

17) B. J. Birch and D. E. Clarke, *Anal. Chim. Acta,* **61**, 159 (1972).

18) H. Hara, S.Okazaki, and T. Fujinaga, *Nippon Kagaku Kaishi,* **1980**, 1645.

 © 1987 The Chemical Society of Japan Bull. Chem. Soc. Jpn., 60, 3109—3115 (1987)

The Effect of the Electrical Potential Difference on the Adsorption of the Hexadecyltrimethylammonium Ion at the Polarized Nitrobenzene-Water Interface

Takashi KAKIUCHI, Miki KOBAYASHI, and Mitsugi SENDA*
Department of Agricultural Chemistry, Faculty of Agriculture, Kyoto University, Sakyo-ku, Kyoto 606
(Received March 4, 1987)

The adsorption of the hexadecyltrimethylammonium ion(HTMA$^+$) at the polarized nitrobenzene-water interface has been studied using electrocapillary measurements. The adsorption of HTMA$^+$ was found to be markedly dependent on the potential drop across the interface. HTMA$^+$ exhibited no specific adsorption in the potential range where the aqueous phase is positive, whereas a strong adsorption occurred in the potential range where the electric potential in the aqueous phase is negative with respect to that in the nitrobenzene. The adsorption free energy depends linearly on the potential difference across the interface. The specific adsorption of HTMA$^+$ significantly alters the double-layer structure. The outer Helmholtz potential in the nitrobenzene phase was inverted from negative to positive due to the adsorption of HTMA$^+$ ions.

The electrical aspects of the adsorption of molecules and ions at metal-solution interfaces have been studied extensively, and now the double-layer structure and the adsorption mechanism have been elucidated in detail.[1] In contrast, much fewer studies have appeared for oil-water interfaces, and even fewer for air-water interfaces, mainly because of the difficulty of controlling the electrical potential difference between the phases.

Guastalla[1] first reported the change in the interfacial tension with an externally applied potential for the interface between nitrobenzene and water in the presence of the HTMA$^+$ ion. He suggested the "electroadsorption" model for the interpretation of the phenomena. Since then, the adsorption phenomena of ionic surfactants at oil-water interfaces under the influence of an externally applied electric field have been studied by Blank et al.,[3,4] Watanabe et al.,[5,6] Dupeyrat et al.,[7,8] Gavach et al.,[9-11] and Joos et al.[12,13] In the study of the adsorption of various ionic surfactants at the methyl isobutyl ketone-water interface, Watanabe et al. adopted the concept of electrocapillarity,[5] thereby introducing a thermodynamic point of view for the interpretation of electrosorption phenomena at oil-water interfaces. However, in most of the preceding studies of the adsorption phenomena at oil-water interfaces, the electrical state of the interface has not been well-defined, making an unambiguous interpretation of the results difficult. This is partly because of the uncertainty concerning the polarizability of the interfaces employed and partly because of the lack of suitable reference electrodes to define the electrical potential.

It has been shown recently that the polarizability of oil-water interfaces can be characterized in terms of the transfer free energy of ions dissolved in the two neighboring phases,[14] and experimentally[15] we can make the interface virtually ideally polarized by suitably choosing the ions dissolved in the phases. The rigorous thermodynamics of the electrocapillarity of oil-water interfaces[16] and the experimental study of the double layer structure of polarized nitrobenzene-water interfaces[17] have also been presented recently. By using such polarized interfaces, we are now able to study the adsorption of surfactants and ions at the oil-water interfaces in depth as cases of the electrosorption studies at metal-solution interfaces.[1] Only through this polarized type of interface can the electrical aspects of surfactants adsorption in equilibrium be fully explored. The electrocapillarity of nonpolarized oil-water interfaces has also been studied.[18-22] The advantage of an ideal polarized interface over a nonpolarized one in studying the adsorption behavior of surfactants is that it has an additional degree of freedom for the electrical parameter: Electrostatic potential difference or excess surface-charge density. This enables us to estimate the charge due to specifically adsorbed ions separately from the total excess-charge density.[16] The aim of this study is to establish such a new experimental approach for studying the electrochemical aspects of surface phenomena at oil-water interfaces. This paper will report the adsorption properties of the hexadecyltrimethylammonium ion, HTMA$^+$, at the polarized nitrobenzene-water interface, across which the potential difference is regulated externally.

Experimental

The interfacial tension of the nitrobenzene-water interface was measured by means of the drop-time method using a drop-by-drop ascending electrolyte solution electrode.[15] The potential drop across the interface was controlled using a four-electrode potentiostat with a positive feed back circuit for *iR* compensation. The details of the measurements and the conversion of the drop time to interfacial tension have been reported elsewhere.[23] All the measurements were made at 25.00±0.05 °C.

The hexadecyltrimethylammonium tetraphenylborate

(HTMATPB) was prepared from hexadecyltrimethylammonium chloride and sodium tetraphenylborate and was recrystallized twice from acetone. The tetrapentylammonium tetraphenylborate(TPnATPB) and lithium tetraphenylborate were prepared as has been described previously.[24] The nitrobenzene was distilled under reduced pressure, and the middle portion of the distillate was used for preparing the solution. The water was triply distilled.

Results

We used the mixed electrolyte method,[25,26] in which the sum of the concentrations of TPnATPB and HTMATPB in nitrobenzene is held constant at 0.1 mol dm^{-3}, while the concentration of HTMA$^+$ is varied. The TPnA$^+$ ion shows no specific adsorption at the nitrobenzene-water interface.[27] The TPB$^-$ ion is also known to show no specific adsorption.[17] Accordingly, this mixed-electrolyte-solution method allows us to obtain the specifically adsorbed amount of HTMA$^+$ directly from the electrocapillary data.[25,26] An additional advantage of this method here is that it enables us to avoid the undesirable decrease in the conductivity in the nitrobenzene phase in the lower concentration range of HTMATPB.

The electrochemical cell employed in this study may be represented thus;

I	II	III	IV	V	VI	VII	VIII	
Ag	AgCl	1 mM LiCl (W)	1 mM LiTPB (W)	$(0.1-x)$ M TPnATPB + x M HTMATPB (NB)	0.05M LiCl (W)	AgCl	Ag	(I)

where M designates mol dm^{-3} and where x was varied between 0 and 0.1. The nitrobenzene phase V contains TPnATPB and HTMATPB, such that the sum of the concentrations of these salts is 0.1 mol dm^{-3}. The HTMA$^+$ ion was thus dissolved in the nitrobenzene phase as a TPB salt. This is a key point for the study of the adsorption of the HTMA$^+$ ion when the interface is polarized. If we add the HTMA$^+$ ion to the aqueous phase, then the HTMA$^+$ ion will immediately commence transferring across the interface to dissolve into the nitrobenzene phase anywhere in the potential range studied; hence, it will be impossible to achieve the polarization condition of the interface. This is because the standard ion-transfer potential of the HTMA$^+$ ion is greatly negative; i.e., HTMA$^+$ as a whole is a very hydrophobic ion, as will be described below. The aqueous phase VI contains 0.05 mol dm^{-3} LiCl, while Phases III and IV contain 1 mmol dm^{-3} LiCl, and 1 mmol dm^{-3} LiTPB respectively. The interface between Phases V and VI is a polarized interface. The other nitrobenzene-water interface between Phases IV and V is a nonpolarized one, across which the potential drop is determined by the activities of the TPB$^-$ ions in the two adjacent phases,[24] i.e., the interface reversible to the TPB$^-$ ion. The reference electrode reversible to TPB$^-$ ion is essential in detecting the specific adsorption of cations in the nitrobenzene phase.[25,26] Since the concentrations of the TPB$^-$ ion in Phase IV and in Phase V are constant, the potential across the interface between Phases IV and V may be taken as constant, even when the concentration of HTMA$^+$ ion is varied. The liquid junction potential at the interface between Phases III and IV is also unaltered. Consequently, the change in the potential difference between the terminals of Cell (I) is directly related to the change in the potential difference across the polarized nitrobenzene-water interface. We denote the potential of the right-hand side of Cell (I), referred to that of the left, as E_{0-}^{w-}, where the super- and subscripts indicate that the reference electrodes in the aqueous and nitrobenzene phases are both reversible to the anions.

Figure 1 shows the current-potential curves for Cell (I) when the concentration of the HTMA$^+$ ion in Phase V, c, equals 0 (Curve 1) and 0.1 (Curve 2) mol dm^{-3}. The polarized potential range where the current passing through the interface is negligible is between -0.55 and -0.2 V for c=0; i.e., the interface has a potential window of 0.35 V voltage span. The current-potential curve for c=0.1 mol dm^{-3} also has almost the same polarized potential range, demonstrating that the adsorption of HTMA$^+$ as well as the double layer structure of the interface can be studied under a polarized condition. This sugests that

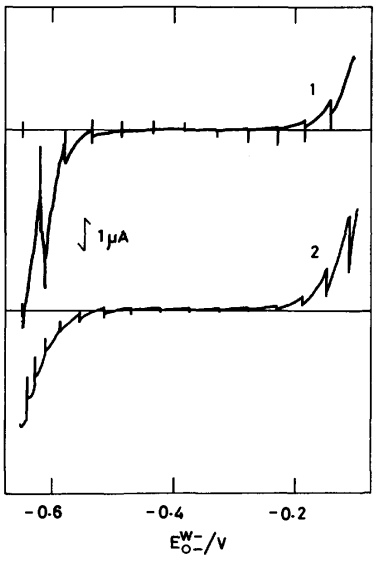

Fig. 1. Current-potential curves recorded using dropwise ascending electrolyte solution electrode for 0.05 mol dm^{-3} LiCl in water and 0.1 mol dm^{-3} TPnATPB(Curve 1) or 0.1 mol dm^{-3} HTMATPB-(Curve 2) in nitrobenzene.

the standard ion-transfer potential of the $HTMA^+$ ion is at least not more positive than those of the Cl^- and $TPnA^+$ ions.

The electrocapillary equation for Cell (I) at a constant temperature and pressure is given by:[16,26]

$$-d\gamma = q^W dE_{o-}^{w-} + \Gamma_{TPnA^+} RT d\ln(1-m) + \Gamma_{HTMA^+} RT d\ln m \quad (1)$$

where γ is the interfacial tension, q^W is the excess surface-charge density in the aqueous phase, E_{o-}^{w-} is the potential of the terminal of the right hand side of Cell (I) with respect to the left, Γ_j is the relative surface excess of the j ion (j=$TPnA^+$ and $HTMA^+$), and $m=x/0.1$. R and the T are the gas constant and the absolute temperature respectively. In deriving Eq. 1, the activity coefficients of the ions in Phase V are assumed to be constant when the composition of this phase is changed. This assumption will not introduce any serious error, because the ionic strength in Phase V is kept constant. If we assume that Γ_{TPnA^+} and the nonspecifically adsorbed portion of Γ_{HTMA^+} follow the Gouy-Chapman diffuse layer theory, Eq. 1 may be rewritten as:[25,26]

$$-d\gamma = q^W dE_{o-}^{w-} + \Gamma^1_{HTMA^+} RT d\ln m + RTm\left[\int_{x_1}^{x_2}\left\{\exp\left(-\frac{F\varphi}{RT}\right)-1\right\}dx\right]d\ln m \quad (2)$$

where $\Gamma^1_{HTMA^+}$ is the specifically adsorbed amount of the $HTMA^+$ ion, φ is the the electrostatic potential, F is the Faraday constant, and x_1 and x_2 are the positions of the outer Helmholtz planes in the nitrobenzene phase for the $HTMA^+$ and $TPnA^+$ ions respectively. The last term in the r.h.s. of Eq. 2 represents the contribution that arises from the difference in the size of the ions. In the following, we will neglect this last term. Therefore, the change in γ due to the change of m may be considered to be a direct measure of the specific adsorption of the $HTMA^+$ ions. (The term *specific adsorption* refers to the part of the adsorption which cannot be explained by the Gouy-Chapman theory.)

Figure 2 shows the electrocapillary cruves for a given cocentration of HTMATPB. The interfacial tension decreases with the increase in the concentration of $HTMA^+$ in the potential range negative to the electrocapillary maximum (ecm), which we will hereafter call "the negative branch," while the interfacial tension remaines unchanged in the potential range positive to the ecm, "the positive branch." Obviously, the $HTMA^+$ ion specifically adsorbs only in the potential range where the potential of the aqueous phase is negative with respect to that of the nitrobenzene phase. At the potential in the neighborhood of the ecm, the change in the interfacial tension with $HTMA^+$ concentration is very small, indicating that the adsorption at the ecm is almost negligible. The specifically adsorbed amount of $HTMA^+$ was calculated from the electrocapillary curves through Eq. 2 by using numerical differentiation with a third-order B-spline function.[28] The results are plotted in electrical units, $q^*=F\Gamma^1_{HTMA^+}$, in Fig. 3 as a function of E_{o-}^{w-}. As is to be expected from the electrocapillary curves, the specific adsorption of the $HTMA^+$ ion in the negative branch increases with the concentration and with the decrease in the potential.

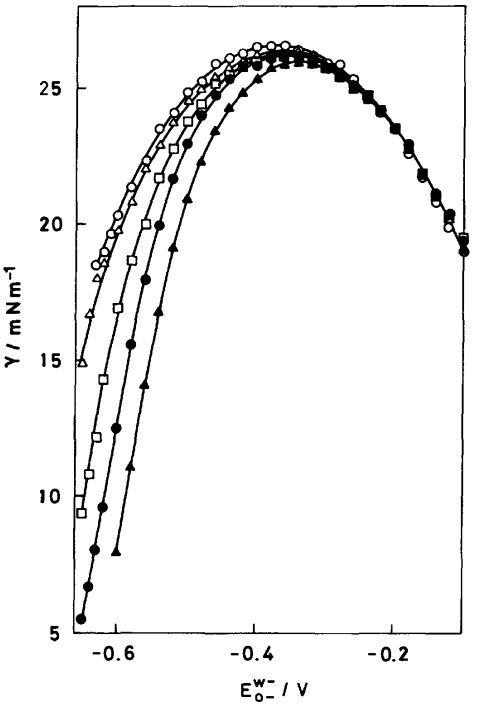

Fig. 2. Electrocapillary curves for the interface between 0.05 mol dm^{-3} LiCl aqueous solution and (0.1−x) mol dm^{-3} TPnATPB+x mol dm^{-3} HTMATPB nitrobenzene solution at 25 °C: x=0(○), 0.005(△), 0.02(□), 0.05(●), and 0.1(▲).

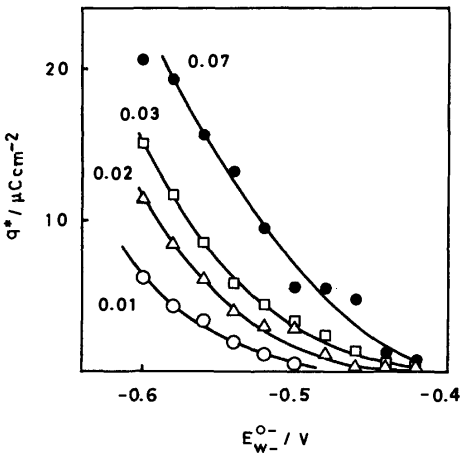

Fig. 3. Specifically absorbed change $q^*=F\Gamma^1_{HTMA^+}$ of $HTMA^+$ for c=0.01(○), 0.02(△), 0.03(□), and 0.07(●) mol dm^{-3}.

Figure 4 shows the adsorption isotherms for $HTMA^+$ for different values of E_{0-}^{W-}. These isotherms were analyzed with a virial isotherm of the form:

$$\ln\left(\frac{c}{q^*}\right)=\frac{\Delta G_a^0}{RT}+2vq^* \quad (3)$$

where ΔG_a° is the adsorption free energy and where v is the second virial coefficient. This isotherm at a given electrode potential was recently proposed by Vorotyntsev;[29,30] it is suitable for describing the adsorption of ions at the metal-solution interface, especially when the discreteness-of-charge effect previals at a lower surface coverage. The $\ln(c/q^*)$ vs. q^* plots at a given value of E_{0-}^{W-} were found to be straight lines (Fig. 5), indicating that Eq. 3 well describes the present experimental isotherms. We also tested the isotherm based on the Grahame-Parsons model of the inner layer at a constant q^W[31,32] and obtained a less satisfactory fitting of the experimental data. In particular, the ΔG_a° value thus obtained increased with the decrease in E_{0-}^{W-}, which seems physically unreasonable.

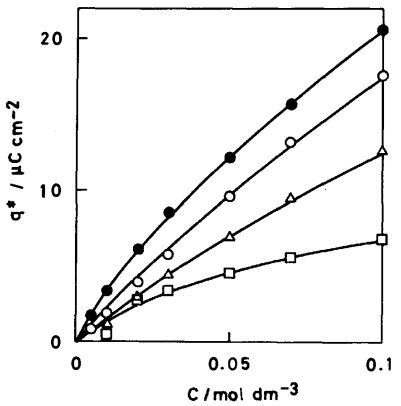

Fig. 4. Adsorption isotherms for specifically adsorbed $HTMA^+$ ions at E_{0-}^{W-}=−0.50(□), −0.52(△), −0.54(○), and −0.56(●)) V.

Discussion

The results clearly indicate that the adsorption of the $HTMA^+$ ion at the nitrobenzene-water interface has a remarkable dependence on E_{0-}^{W-} and, hence, on the potential drop across the interface. This is in marked contrast with the case of the nonionic surfactant adsorption at oil-water interfaces; e.g., Span 60 showed a positive adsorption throughout the polarized potential range at the nitrobenzene-water interface.[33] The fact that the $HTMA^+$ ion does not adsorb in the positive branch means that even a surfactant may not exhibit any surface activity, depending on the electrical potential drop across the interface. In the negative branch, the apparent surface activity of $HTMA^+$ increases with the increase in the potential difference. A similar asymmetric adsorption has previously been reported by Watanabe et al. for various ionic surfactants, but they used less polarized and, hence, electrochemically less characterized, methyl isobutyl ketone-water interfaces.[5]

The adsorption free energy for $HTMA^+$ was evaluated from the intercepts of the plots in Fig. 5. The ΔG_a° value thus obtained refers to the reference states of infinite dilution for both nitrobenzene and adsorption layers and to the standard states of 1 mol dm^{-3} for the nitrobenzene solution and of 1 μC cm^{-2} for the adsorption layer. ΔG_a° values are plotted in Fig. 6 against E_{0-}^{W-} (Curve 1). ΔG_a° was linearly dependent of E_{0-}^{W-}. The slope of this plot gave 5.0×10^4 C mol^{-1}. In general, various factors contribute to the dependence of ΔG_a° on the potential difference across the interface. The change in the applied potential causes not only the change in the inner-layer structure, but also the change in the diffuse-layer structure in the aqueous phase. The effect of the diffuse layer on the aqueous side of the

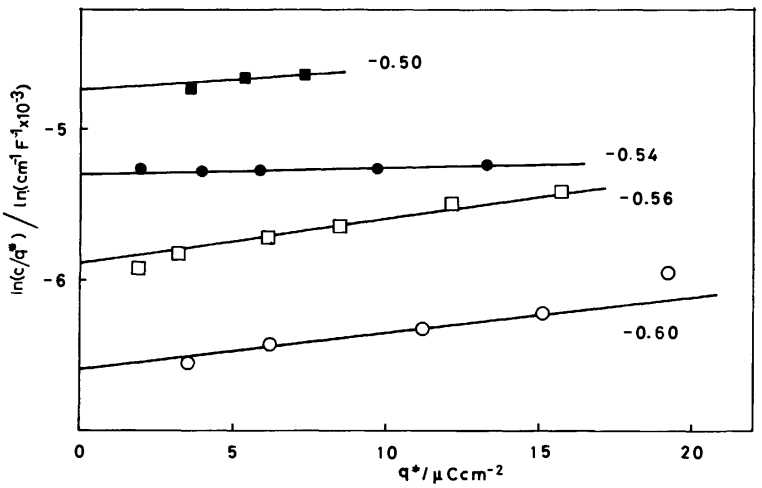

Fig. 5. Plots of $\ln(c/q^*)$ against q^* at E_{0-}^{W-}=−0.50(■), −0.54(●), −0.56(□), and −0.06(○) V.

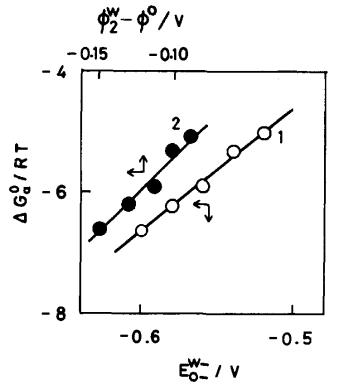

Fig. 6. Absorption free energy of HTMA+, $\Delta G_a°$, as a function of E_{0-}^{W-} (Curve 1) and of φ_2^W-φ^0 (Curve 2).

interface on $\Delta G_a°$ is appreciable, especially when the head group of the HTMA+ ion in its adsorption state is exposed to the aqueous phase. If the head group protrudes into the aqueous phase while leaving the hydrocarbon chain in the aqueous phase,[6] we may expect that the electrical work required to bring the charged head group of a HTMA+ ion from a bulk nitrobenzene phase to a certain point in the aqueous phase, e.g., the outer Helmholtz plane (OHP), constitutes a significant part of $\Delta G_a°$. Then, the change in the potential difference between the bulk of the nitrobenzene phase and the adsorption site caused by the change in E_{0-}^{W-} must contribute greatly to the dependence of $\Delta G_a°$ on E_{0-}^{W-} shown in Fig. 6. If we assume that the head group of an adsorbed HTMA+ ion is located at the OHP in the aqueous phase, then the effective potential difference for the electrical work in the adsorption process will be $\varphi_2^W-\varphi^0$, where φ_2^W and φ^0 are the potentials at the OHP in the aqueous phase and in the bulk of the nitrobenzene phase. $\Delta G_a°$ is replotted in Fig. 6 as a function of $\varphi_2^W-\varphi^0$ on the rational potential scale (Curve 2).[34] The slope was 6.8×10^4 C mol^{-1}. On the other hand, the electrical work for the transfer of 1 mol of monovalent ions across the potential difference of 1 V is 9.6×10^4 J mol^{-1}, and the change in this work with the potential difference is 9.6×10^4 C mol^{-1}. This is of the same order of magnitude as the experimental result, suggesting a large contribution of this electrical work to $\Delta G_a°$. The difference between the two values can be interpreted by assuming that the location of the adsorption site of the head group is on the nitrobenzene side of the OHP in the aqueous phase. In this case, the head group would not be fully exposed to the aqueous phase, and the effective potential difference should be smaller than $\varphi_2^W-\varphi^0$. However, our preliminary findings about the effect of the counterion in the aqueous phase on the adsorption of HTMA+[35] strongly suggest that the head group resides within the aqueous phase. Hence, the numerical difference between these two values seems to indicate the presence of other contributions including those opposing the electrostatic work. One such possible contribution is the work to replace the solvent molecules in the interfacial region with the head group and the hydrocarbon tail of the HTMA+ ion. Since the dielectric constant of the interfacial region is probably higher than that of the hydrocarbon part of the HTMA+ ion, this replacement gives rise to a positive contribution to the adsorption free energy.[36] According to Frumkin's two-parallel-plate condenser model for the adsorption of organic compounds on electrodes, this part of the adsorption free energy depends quadratically on the electrode potential. The range of E_{0-}^{W-} studied is perhaps not enough to detect such a quadratic dependence. It is also probable that there exists another factor which counteracts this quadratic term, leading to an apparent linear dependence. For example, the increase in the concentration of Cl^- at the OHP in the aqueous phase with the negative increase in E_{0-}^{W-} can increase the adsorption of HTMA+ not only by screening the repulsion between the adsorbed HTMA+ ions, but also by enhancing the salting-in effect for the head group of HTMA+.

The change in $\Delta G_a°$ with E_{0-}^{W-} is thermodynamically related to the change in q^W accompanied by the adsorption:[37]

$$\left(\frac{\partial q^W}{\partial \Gamma^1_{HTMA^+}}\right)_{E_{0-}^{W-}} = -\frac{d\Delta G_a^0}{dE_{0-}^{W-}} \quad (4)$$

Thus, the linear variation in $\Delta G_a°$ in Fig. 6 implies that q^W should also vary linearly with $\Gamma^1_{HTMA^+}$. Figure 7 shows the plots of q^W as a function of q^* at different values of E_{0-}^{W-}. All q^W vs. q^* curves gave straight lines whose slopes are very close to each other. The slope at $E_{0-}^{W-}=-0.54$ V was 4.1×10^4 C mol^{-1}, which is very close to the value obtained from Fig. 6. This agreement ensures the internal consistency of the data analysis. It should be noted that the positive value of

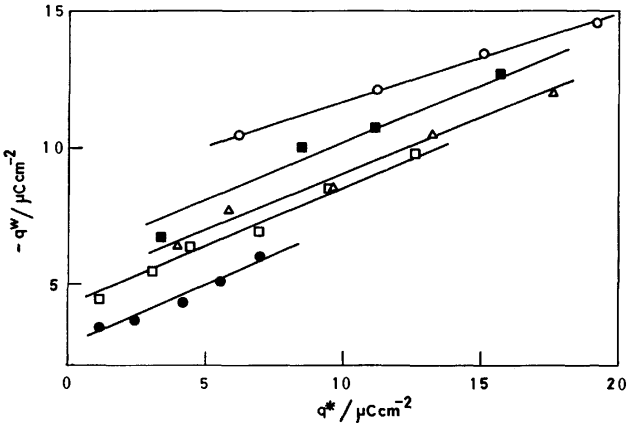

Fig. 7. Change of q^W as a function of q^* at a given value of E_{0-}^{W-}: $E_{0-}^{W-}=-0.48$(●), -0.52(□), -0.54(△), 0.56(●), and -0.60(○) V.

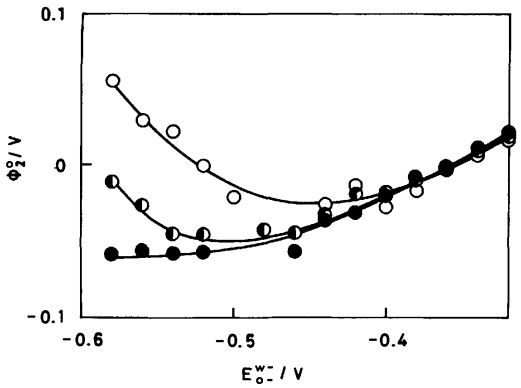

Fig. 8. Change of the potential at the outer Helmholtz plane in the nitrobenzene phase φ_2^0 with the change of E_{0-}^{W-} for the concentrations: c=0.01 (●), 0.02(○), and 0.05(○) mol dm^{-3}.

$(\partial q^W/\partial \Gamma^1_{HTMA^+})E_{0-}^{W-}$ means that the double layer capacity should increase with the adsorption of the $HTMA^+$ ion, because q^W at a constant E_{0-}^{W-} increased with the increase in $\Gamma^1_{HTMA^+}$.

The values of the interaction parameter v obtained from Fig. 5 were in the range from 0.002 to 0.015 cm^2 C^{-1}. These values are considerably lower than those estimated in the adsorption of inorganic ions at a metal-solution interface.[29] Since the intermolecular interaction between the hydrocarbon chains of adsorbed surfactants is usually small at oil-water interfaces,[38] the present results suggest that the repulsive interaction between the charged head groups is very weak.

The double-layer structure of the nitrobenzene-water interface is significantly altered by the adsorption of $HTMA^+$ ions. Figure 8 shows the φ_2^0 potential plotted against E_{0-}^{W-} for a given value of the concentration of the $HTMA^+$ ion. In the negative potential range, the sign of the φ_2^0 potential is inverted from negative to positive, that is, the specifically adsorbed charge q^* exceeds the excess charge density in the aqueous phase, q^W. The double layer structure in the presence of $HTMA^+$ adsorption in the negative branch is illustrated in Fig. 9. Thus, the adsorption of the $HTMA^+$ ion drastically affects the double layer structure especially, resulting in a change in the distribution of the potential across the interface. One important consequence of such an inversion of the φ_2^0 potential is that, by introducing ionic surfactants at the interface, one can modify the electric field sensed by ions participating in ion-transfer reaction through the interface. It may be noted that the φ_2^0 potential thus obtained is of average character and that the *micro potential*[39] could be less affected by the $HTMA^+$ adsorption, since the surface coverage of $HTMA^+$ achieved in the present study was at most 0.4, where the discreteness of the charge is certainly not negligible.

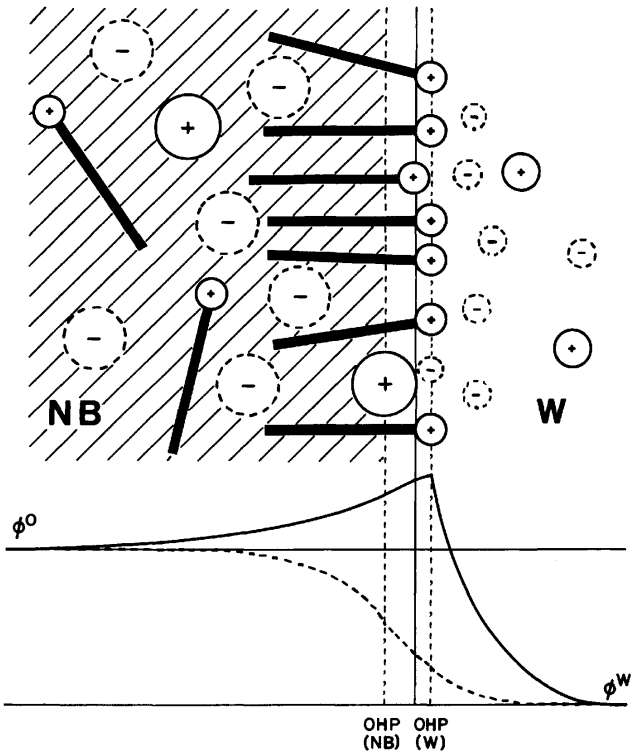

Fig. 9. Schematic representation of the double layer structure of the interface between nitrobenzene and aqueous solutions in the negative branch in the presence of the specific adsorption of $HTMA^+$ ions.

In conclusion, the adsorption of the $HTMA^+$ ion showed marked asymmetry with respect to the electrical potential applied across the interface. Such a dependence of the adsorption on the electrical potential difference is of great importance for the physical chemistry of emulsions, liposomes, micelles, and artificial and biological membranes. This potential dependence provides us with the possibility of regulating the surface activity of surfactants by applying the electrical potential difference across the interface. In the present study, the composition of the aqueous phase was held constant. If we change the composition of the aqueous phase while keeping that of the oil phase constant, then the change in the adsorption characteristics of the ions in the aquous phase due to the presence of surfactant adsorption can be investigated thermodynamically. This approach seems particularly useful in studying counterion effects in surfactant adsorption. Along this line, subsequent papers will deal with the effect of counter-ions in the aqueous phase on the adsorption properties of ionic surfactants.

This work was supported by Grant-in-Aids for Scientific Research No. 60211017 from the Ministry of Education, Science and Culture.

References

1) B. B. Damaskin, O. A. Petrii, and V. V. Batrakov, "Adsorption of Organic Compounds on Electrodes," Plenum Press, New York (1971).

2) J. Guastalla, "Proc. Second International Congress of Surface Activity III," Butterworths, London (1957), p. 112.

3) M. Blank and S. Feig, *Science*, **141**, 1173 (1963).

4) M. Blank, *J. Colloid Interface Sci.*, **22**, 51 (1966).

5) A. Watanabe, M. Matsumoto, H. Tamai, and R. Gotoh, *Kolloid Z. Z. Polym.*, **220**, 152 (1967); **221**, 47 (1967).

6) A. Watanabe and H. Tamai, *Kolloid Z. Z. Polym.*, **246**, 587 (1971).

7) M. Dupeyrat and J. Michel, *J. Colloid Interface Sci.*, **29**, 605 (1969).

8) M. Dupeyrat and E. Nakache, *J. Colloid Interface Sci.*, **73**, 332 (1980).

9) C. Gavach, *Experimentia Suppl.*, **18**, 321 (1971).

10) C. Gavach and B. d'Epenoux, *J. Electroanal. Chem. Interfacial Electrochem.*, **55**, 59 (1974).

11) B. d'Epenoux and C. Gavach, *J. Colloid Interface Sci.*, **56**, 138 (1976).

12) P. Joos and M. Bockstacle, *J. Phys. Chem.*, **80**, 1573 (1976).

13) Y. Verburgh and P. Joos, *J. Colloid Interface Sci.*, **74**, 384 (1980).

14) J. Koryta, P. Vanysek, and M. Brezina, *J. Electroanal. Chem. Interfacial Electrochem.*, **75**, 211 (1977).

15) T. Kakiuchi and M. Senda, *Bull. Chem. Soc. Jpn.*, **56**, 1322 (1983).

16) T. Kakiuchi and M. Senda, *Bull. Chem. Soc. Jpn.*, **56**, 2912 (1983).

17) T. Kakiuchi and M. Senda, *Bull. Chem. Soc. Jpn.*, **56**, 1753 (1983).

18) M. Kahlweit and H. Strehlow, *Z. Elektochem.*, **58**, 658 (1954).

19) H. J. Oel and H. Strehlow, *Z. Elektochem.*, **58**, 665 (1954).

20) C. Gavach, P. Seta, and B. d'Epenoux, *J. Electroanal. Chem. Interfacial Electrochem.*, **83**, 225 (1977).

21) M. Gros, S. Gromb, and C. Gavach, *J. Electroanal. Chem. Interfacial Electrochem.*, **89**, 29 (1978).

22) J. D. Reid, O. R. Melroy, and R. P. Buck, *J. Electroanal. Chem. Interfacial Electrochem.*, **147**, 71 (1983).

23) See. Ref. 15. The Eq. 1 in Ref. 15 for the calculation of the interfacial tension has some typographical errors; the term on the l.h.s. and the first term on the r.h.s. of Eq. 1 should be read as:

$$\frac{vt_d}{3} \text{ and } \sigma^3 \ln\left[\frac{x^0(1-\sigma x)}{x(1-\sigma x_0)}\right]$$

respectively.

24) T. Kakiuchi and M. Senda, *Bull. Chem. Soc. Jpn.*, **60**, 3099 (1987).

25) H. D. Hurwitz, *J. Electroanal. Chem.*, **10**, 35 (1965).

26) E. Dutkiewicz and R. Parsons, *J. Electroanal. Chem.*, **11**, 100 (1966).

27) T. Kakiuchi and M. Senda, unpublished result.

28) FACOM Fortran SSL2 User's Manual, Fujitsu Co., Ltd., (1979).

29) M. A. Vorotyntsev, *J. Res. Inst. Catalysis, Hokkaido Univ.*, **30**, 167 (1982).

30) M. A. Vorotyntsev and V. Yu. Izotov, *Elektrokhimiya.*, **17**, 831 (1983).

31) D. C. Grahame, *J. Am. Chem. Soc.*, **80**, 4201 (1958).

32) D. C. Grahame and R. Parsons, *J. Am. Chem. Soc.*, **83**, 1291 (1961).

33) T. Kakiuchi and M. Senda, to be published.

34) D. C. Grahame, *Chem. Rev.*, **41**, 441 (1947).

35) T. Kakiuchi, M. Kobayashi, M. Nakanishi, and M. Senda, paper presented at the 31st Annual Meeting of the Polarographic Society of Japan, Kyoto, Nov. 1985, Abstract: *Rev. Polarogr. (Kyoto)*, **31**, 84 (1985).

36) A. N. Frumkin and B. B. Damaskin, "Modern Aspects of Electrochemistry," ed by J. O'M. Bockris and B. E. Conway, Butterworths, London (1964), Vol. 3, p. 149.

37) Ref. 1, Chap. 3.

38) D. A. Haydon and F. H. Taylor, *Philos. Trans. R. Soc. London, Ser. A*, **252**, (1960).

39) D. C. Grahame, *Z. Elektrochem.*, **62**, 264 (1958).

 © 1987 The Chemical Society of Japan Bull. Chem. Soc. Jpn., 60, 3117—3124 (1987)

Effect of Molybdenum Codeposition on the Thermal Properties of Electroless Ni-B Alloy Plating Films

Tetsuya OSAKA,* Ichiro KOIWA, Keizo YAMADA, Masao NISHIKAWA, and Masahiko USUDA
Department of Applied Chemistry, School of Science and Engineering, Waseda University, Okubo, Shinjuku-ku, Tokyo 160
(Received March 12, 1987)

Electroless Ni-Mo-B alloy films from a bath using dimethylamine-borane(1/1) (DMAB) as a reducing agent were investigated. Only a small amount of Mo-complex addition to the bath decreased the boron content and increased the molybdenum content drastically. The maximum molybdenum content and maximum resistivity under as-plated conditions were obtained as 22.1 wt% and 322 μΩ cm respectively. Such a high resistivity is characteristic of Ni-Mo-B alloy films. Both crystallized and amorphous states of Ni-Mo-B alloy films, whose Mo contents were above 20 wt% with a small amount of boron, were prepared by controlling the Mo-complex concentration in the bath. The heat change properties of Ni-Mo-B alloy films were quite different from those of the electroless Ni alloy films reported previously. The resistivity of Ni-Mo-B alloy films after heat treatment at 500 or 600 °C became higher than that of those created under as-plated conditions. The structure transformation of Ni-Mo-B alloy films after heat treatment was quite different from that of ordinary electroless Ni alloy films. The Ni-Mo-B alloy film after heat treatment was confirmed by TEM observation to show a mosaic-like structure. Therefore, it was thought that such a high resistivity and such thermal properties of Ni-Mo-B alloy films are caused by such a mosaic-like structure.

In general, electroless nickel deposits contain P or B as impurities from reducing agents, and the properties of electroless alloy films depend strongly on the kind of reducing agent used.[1] It is also well known that a higher impurity content makes a film amorphous.[2-6] Since amorphous alloy films usually possess high resistivity and low temperature coefficient,[7] amorphous electroless Ni alloy films have a high possibility for use as thin film resistors. The amorphous films, however, are unstable because of these easy crystallization upon heat treatment. The high-melting-point element, molybdenum, has been reported to codeposit into electroless Ni films,[8-12] and the codeposition of Mo into the Ni films has the possibility of overcoming the demerit of its less stable thermal property. The present authors have previously attempted the Mo codeposition into Ni-P films on the basis of this point of view and have confirmed that the electroless plated Ni-Mo-P alloy film of a crystallized state has a thermal stability superior to that of amorphous and crystallized Ni-P film.[12]

In this paper, the present authors will report amorphous or crystallized electroless Ni-Mo-B alloy films of a high thermal stability, plated from a bath using dimethylamine-borane(1/1) (DMAB) as the reducing agent.

Experimental

Electroless Ni-Mo-B alloy films were plated from a caustic alkaline bath using dimethylamine-borane(1/1) (DMAB) as the reducing agent. The basic bath compositions and operating conditions are listed in Table 1. Molybdenum was easily codeposited by complexing sodium molybdate with sodium gluconate before constructing the bath by analogy to the method by Mallory.[10] The film thickness was adjusted to 2 μm by controlling the deposition time; however, in the case of transmission electron microscopy (TEM) measurement, the film thickness was adjusted to about 500 Å. Therefore, the initial deposition films were observed by means of TEM. Ninety six wt% alpha-alumina ceramics were used as a plating substrate except for the TEM measurement. For the TEM measurement, polyimide film (25KA, Toray Co. Ltd.) was used as a substrate, and the plated films were separated from the substrate by dipping the specimen in a hydrazine-ethylenediamine solution. The repeated two step process for catalyzation was used (sensitizer:$SnCl_2 \cdot 2H_2O$, 1 g dm^{-3}; 37% HCl, 1.0 ml dm^{-3}; activator:$PdCl_2$, 0.1 g dm^{-3}; 37% HCl, 0.1 ml dm^{-3}).[13] The contents of molybdenum and boron were determined by means of atomic absorption spectroscopy and the use of an inductively coupled argon plasma emission spectrophotometer (ICAP-575 markII, Nippon Jarrell-Ash). For the amorphous Ni-Mo-B alloy film, auger electron spectrometry (15-110A, PHI Co. Ltd.) was used to investigate such impurities as carbon and oxygen. The resistivity of deposits on the alumina substrate was measured by the four-probe method (MODEL K-705RD, Kyowa Riken Co. Ltd.). The structures of the deposits were determined by the use of an X-ray diffractometer (RAD-IIA,

Table 1. Electroless Plating Bath Compositions and Operating Conditions

Chemical	Concentration /mol dm^{-3}
$(CH_3)_2NH \cdot BH_3$	0.06
$C_3H_4(OH)(COONa)_3 \cdot 2H_2O$	0.10
$HOCH_2COOH$	0.20
$NiSO_4 \cdot 7H_2O$	0.05
Mo-complex	0—0.0125

Bath temperature, 90°C; pH adjusted with NaOH 9.0.

Rigaku Denki Co., Ltd.) and TEM measurement (100 kV, HU-12A, Hitachi Seisakusho Co., Ltd.). In the case of the heat treatment of deposits, the samples were heated under 2×10^{-3} Pa from room temperature to the setting temperature at a constant heating rate of 10 °C min^{-1}. The samples were heated for one hour at the setting temperature and were then left to cool spontaneously.

Results and Discussion

Film Composition and Resistivity of Electroless Plated Ni-Mo-B Alloy Films. The film composition and the resistivity as function of the Mo-complex concentration are listed in Table 2. The data of Ni-Mo-P alloy films were quoted from the previous paper[12] so as to compare them with those of Ni-Mo-B alloy films. In the case of Ni-Mo-B alloy films, the maximum Mo content and the highest resistivity value, 22.1 wt% and 322 μΩ cm respectively, were obtained at Mo-complex concentration of 0.0025 mol dm^{-3}. The highest resistivity value is about twice the value of a usual amorphous Ni-P alloy film. Moreover, the Mo content was almost independent of the Mo-complex concentration. This tendency was different from the case of Ni-Mo-P alloy films in the higher Mo-complex concentration region. On the other hand, the boron content was drastically decreased from 6.3 to 0.63 wt% by adding 0.0025 mol dm^{-3} Mo-complex. Moreover, the boron content gradually decreased with an increase in the Mo-complex concentration, and films with a very small 0.10 wt% B content were obtained at the region of a Mo-complex concentration of more than 0.0100 mol dm^{-3}. At the same Mo-complex concentration, the resistivity of Ni-Mo-B alloy film was always higher than that of Ni-Mo-P alloy film.

From the above results, there appears to be a difference between Ni-Mo-P alloy film and Ni-Mo-B alloy film under as-plated conditions. Especially, the Ni-Mo-B alloy film has the characteristics of a higher Mo content and a higher resistivity. In this paper, we mainly discuss the resistivity of Ni-Mo-B alloy film and its heat change properties, in particular, for the film at a Mo-complex concentration of 0.0025 mol dm^{-3}.

Heat Treatment Effect of Electroless Ni-Mo-B Alloy Film on Specific Resistance. Figure 1 demonstrates the effect of heat treatment on the specific resistance of Ni-Mo-B alloy films at Mo-complex concentrations of 0.0025 and 0.0125 mol dm^{-3}. The ρ value of Ni-B alloy film usually decreases with an increase in the heat treatment temperature as just as has been reported previously.[11] This tendency is generally found in Ni-P alloy films.[14]

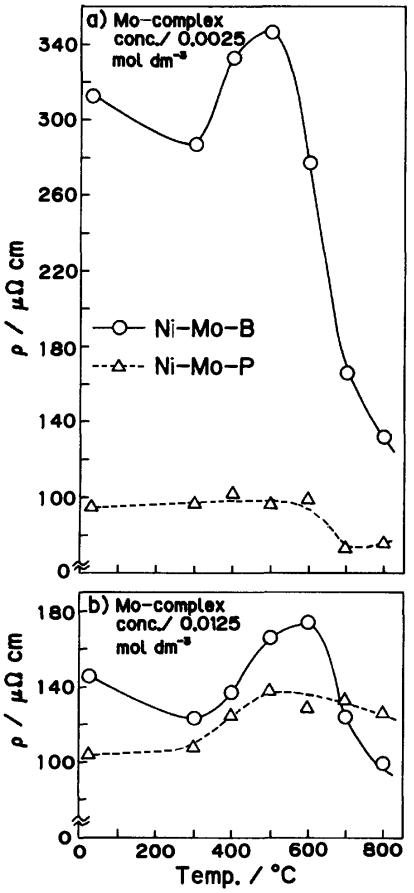

Fig. 1. Effect of heat treatment temperature on specific resistance, ρ. Solid line (circles): Ni-Mo-B. Dashed line (triangle): Ni-Mo-P.[12] a) 0.0025 mol dm^{-3} Mo-complex concentration, b) 0.0125 mol dm^{-3} Mo-complex concentration.

Table 2. Film Composition and Resistivity of Ni-Mo Alloy Films

Mo-complex conc. /mol dm^{-3}	Ni-Mo-B			Ni-Mo-P[12]		
	Mo/wt%	B/wt%	ρ/μΩ cm	Mo/wt%	P/wt%	ρ/μΩ cm
0	0	6.3	120	0	10.2	127
0.0025	22.1	0.63	322	10.0	2.0	95
0.0050	19.8	0.17	138	14.1	1.1	105
0.0075	21.5	0.12	130	14.8	0.98	101
0.0100	22.0	0.10	126	16.5	0.94	99
0.0125	21.1	0.10	146	16.5	0.95	104

The dashed lines are the data of Ni-Mo-P alloy films, quoted from a previous paper[12] for the sake of comparison. The ρ values of Ni-Mo-B alloy film at an Mo-complex concentration of 0.0025 mol dm^{-3} are always higher than those of Ni-Mo-P alloy films at any temperature. In Fig. 1a, the ρ value of Ni-Mo-B alloy film at a Mo-complex concentration of 0.0025 mol dm^{-3} after 300 °C heat treatment becomes a little lower than that of the as-plated conditions. In the heat treatment region from 300 until 500 °C, the ρ value increases with an increase in the heat treatment temperature; the maximum value of 347 $\mu\Omega$ cm was obtained after heat treatment at 500 °C. In the region higher than 500 °C, the ρ value drastically decreases with an increase in the heat treatment temperature. Even after heat treatment at 700 °C, however, the ρ value of Ni-Mo-B alloy film at the Mo-complex concentration of 0.0025 mol dm^{-3} is still higher than the maximum (150 $\mu\Omega$ cm) of electroless binary Ni alloy films. In the case of binary Ni alloy films, the maximum resistivity can be obtained only for the as-plated conditions. Therefore, the amorphous Ni-Mo-B alloy films showed a higher thermal stability of resistivity than did the previously reported binary Ni alloy films.

Moreover, the ρ value tendency of Ni-Mo-B at Mo-complex concentration of 0.0125 mol dm^{-3} is almost the same as that of Ni-Mo-B at the Mo-complex concentration of 0.0025 mol dm^{-3}, as is shown in Fig. 1b. From the above results, the ρ value behavior of amorphous and crystallized Ni-Mo-B alloy films after heat treatment is as follows: i.e., first there appears a little decrease at a low temperature heat treatment; then the ρ value increases in the region of medium-temperature heat treatment before decreasing abruptly at higher heat treatment temperatures.

The characteristics of three typical films are listed in Table 3. In general, a high resistivity film of the electroless plated one is obtained only for the films controlling high impurity. Though the boron contents of both Ni-Mo-B alloy films were very small, $\rho_{\text{as-plated}}$ and ρ_{maximum} values of the Ni-Mo-B alloy film

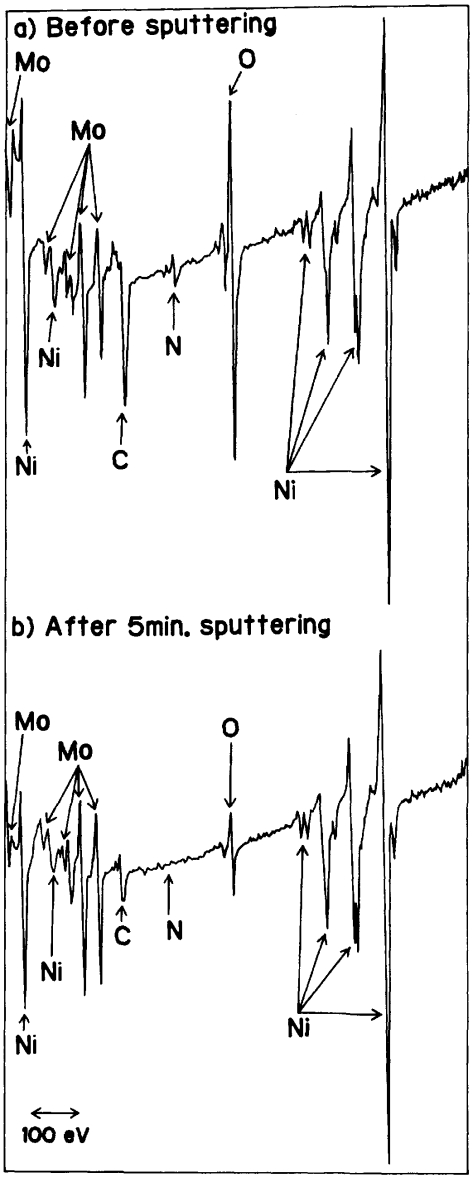

Fig. 2. Auger electron spectroscopy of amorphous Ni-Mo-B alloy films at 0.0025 mol dm^{-3} Mo-complex concentration. a) Before sputtering, b) after 5 min. sputtering.

Table 3. Characteristics of Typical Ni Alloy Films

Mo-complex conc. /mol dm^{-3}	$\rho_{\text{as-plated}}/\mu\Omega$ cm Structure	$\rho_{\text{maximum}}/\mu\Omega$ cm Their condition and structure
0	120 Amorphous	120 Under as-plated conditions Amorphous
0.0025	322 Amorphous	347 After 500°C treatment Almost amorphous
0.0125	146 Crystallized	176 After 600°C treatment Crystallized

are higher than those of the Ni-B alloy film. In particular, the maximum $\rho_{as\text{-}plated}$ value, 322 μΩ cm, is attained at the Mo-complex concentration of 0.0025 mol dm^{-3}. Moreover, the maximum ρ value, 347 μΩ cm, of electroless Ni-Mo-B alloy film was obtained by heat treatment at 500 °C. The heat treatment behavior of the ρ value of Ni-Mo-B alloy films is quite unique and can not be simply explained by the explanation given in the case of binary electroless plated film.[14]

Auger Electron Spectroscopy (AES) Analysis of the Ni-Mo-B Alloy Film. Figure 2 demonstrates the AES spectra of the Ni-Mo-B alloy film at the Mo-complex concentration of 0.0025 mol dm^{-3}. Before sputtering, the peaks corresponding to Ni, Mo, C, N, and O were detected. However, after 5 mins' sputtering, the peaks corresponding to C, N, and O remarkably decreased. The peak intensities of C and O after 5 mins' sputtering are almost the same as those of the other alloy, which means they come from the impurity. Thus, such a highly specific resistance of the Ni-Mo-B alloy film at the Mo-complex concentration of 0.0025 mol dm^{-3} is confirmed not to be the result of its containing an insulator composed of C and O atoms. The origin of such unique characteristics is assumed to come from a structure containing Mo atoms. Below, the structure of electroless Ni-Mo-B alloy films will be discussed.

The Effect of Heat Treatment on the Structure of Electroless Ni-Mo-B Film. Figure 3 demonstrates the X-ray diffraction patterns of Ni alloy films at Mo-complex concentrations of 0, 0.0025 and 0.0125 mol dm^{-3}. Under as-plated conditions, only the two peaks due to the substrate are detected for Ni-B and Ni-Mo-B alloy films at 0.0025 mol dm^{-3}, and they both show an amorphous structure. Amorphous binary alloy films, such as Ni-P and Ni-B alloy films, are usually obtained only in the case of films containing high P or B impurities. In fact, the Ni-B alloy film shows high boron content (6.3 wt%). On the other hand, Ni-Mo-B alloy film at the Mo-complex concentration of 0.0025 mol dm^{-3} shows the same X-ray pattern in spite of its quite low boron content (0.63 wt%). In contrast to the above two alloys, the Ni-Mo-B alloy film at the Mo-complex concentration of 0.0125 mol dm^{-3} shows a highly crystallized structure under as-plated conditions, since the peaks of the Ni matrix were detected, as is shown in Fig. 3c. Moreover, the peaks of the Ni(111) and Ni(200) plane shift to the lower angle side as compared with those of pure Ni; the interplanar spacing of the Ni-Mo-B film was widened by the codeposited Mo atoms. The molybdenum in the deposit may form a solid solution in the nickel matrix. The shift behavior of the Ni(111) plane peak is almost the same as that of Ni-Mo-P alloy film, but the amount of the shift is larger than that of Ni-Mo-P alloy film.[12] This large shift could be caused by the higher Mo content, as is shown in Table 2.

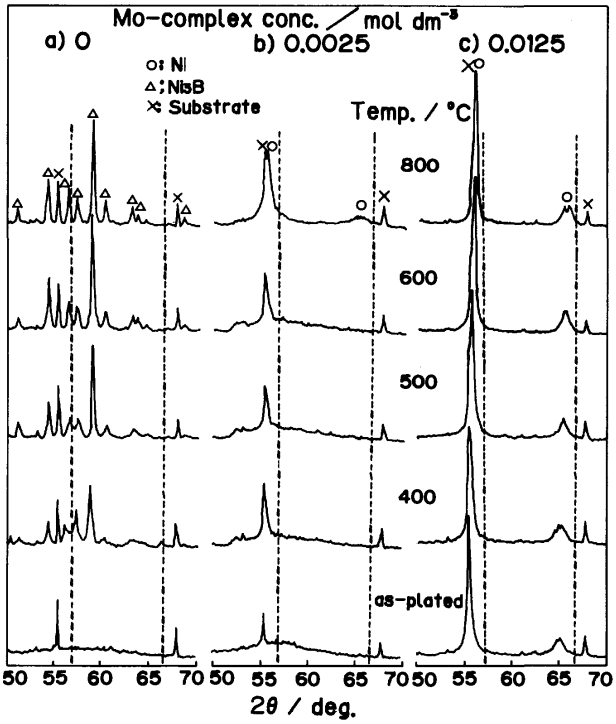

Fig. 3. X-Ray diffraction patterns of Ni-B and Ni-Mo-B alloy films at various annealing temperature using Fe target. The dashed lines represent the peak positions of pure Ni.
a) Ni-B alloy films, b) Ni-Mo-B alloy films plated from 0.0025 mol dm^{-3} Mo-complex concentration bath, c) Ni-Mo-B alloy films plated from 0.0125 mol dm^{-3} Mo-complex concentration bath.

Based upon the above results, we will now discuss the characteristics of electroless Ni-Mo-B alloy films under as-plated conditions in comparison with the results of the previous investigation. First, we will discuss the structures of electroless Ni-Mo-B alloy films. According to our previous investigation of electroless Ni-W-P alloy films, both amorphous and crystallized Ni-W-P alloy films with low P content could be prepared.[15,16] Therefore, the codeposited tungsten causes an amorphous state of the film. Since the boron content of amorphous Ni-Mo-B was extremely small, i.e., 0.63 wt%, the effect of the codeposited Mo atom in the Ni-B film is much greater than that of the codeposited W atom in the Ni-P film. In the case of highly crystallized Ni alloy films under as-plated conditions, the phenomenon of the d value shift, which may mean the formation of the solid solution between the codeposited atom and Ni matrix, can not be observed in the case of Ni-W-P alloy film,[15,16] but it can be observed in the case of Ni-Mo-P alloy film.[12] Therefore, the codeposited molybdenum can form a solid solution.

Next, we will discuss the resistivity of electroless

Ni-Mo-B alloy films. The amorphous Ni-P and Ni-W-P alloy films showed almost the same resistivity, i.e., about 150 μΩ cm, the highly crystallized Ni-P and Ni-W-P alloy films also show almost the same resistivity, i.e., about 50 μΩ cm. Therefore, the resistivities of the Ni-P and Ni-W-P alloy films depend strongly on the film structure. In the case of electroless Ni-Mo-B alloy films, the resistivities are much higher than those of Ni-P and Ni-W-P alloy films under the same structure conditions. Therefore, the resistivity of Ni-Mo-B alloy films can not be explained only by the structure. In general, amorphous alloys between transition metals, such as Zr-Ni[17] and Nb-Ni,[18] show a high resistivity above 200 μΩ cm. Therefore, in the case of amorphous Ni-Mo-B alloy film prepared by the electroless plating method, an effect similar to those of Zr-Ni and Nb-Ni is a possibility.

Based upon the above discussion, the amorphous and crystallized Ni-Mo-B alloy films are considered to be quite different from the amorphous and crystallized Ni-W-P alloy films. Therefore, the codeposited molybdenum is an important factor in determining the structure and resistivity. Moreover, the effect of codeposited molybdenum on film properties is different from that of codeposited tungsten.

In this investigation, three typical alloy films are obtained, i.e., the amorphous Ni-B, the amorphous Ni-Mo-B (plated from a 0.0025 mol dm^{-3} Mo-complex concentration bath), and the crystallized Ni-Mo-B (plated from a 0.0125 mol dm^{-3} Mo-complex concentration bath). These three typical alloy films will now be considered.

In the case of Ni-B alloy, only the peaks due to Ni_3B appear after heat treatment at 400 °C, as is shown in Fig. 3a, where the boron content of this amorphous Ni-B alloy film is almost the same as in the stoichiometric Ni_3B compound (6.3 wt%, i.e., 26.9 at%, see Table 2). The peak intensities gradually increase with an increase in the heat treatment temperature; indicates that the crystallinity of the Ni_3B compound progresses with heat treatment.

On the other hand, for the amorphous Ni-Mo-B alloy film, there is no structure change until 500 °C under heat treatment, as is shown in Fig. 3b, though an obvious structure change is observed after heat

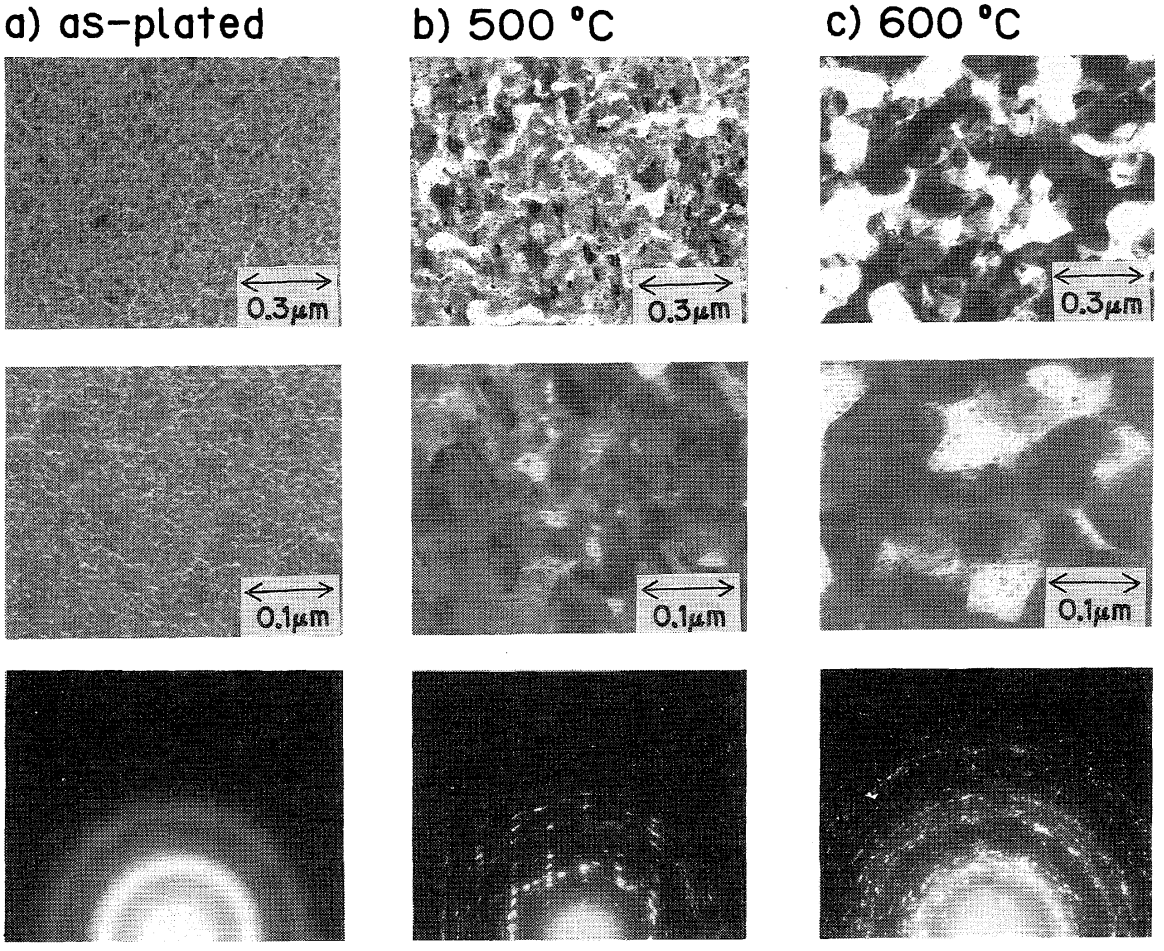

Fig. 4. Transmission electron micrographs (TEM) and transmission high energy electron diffraction (THEED) patterns of Ni-B alloy films. a) As-plated conditions, b) after 500 °C treatment, c) after 600 °C treatment.

treatment at 700 °C. In general, an amorphous alloy is very unstable against heat treatment; however, the thermal stability of this amorphous film has been improved by the codeposition of the Mo atom, much as in the case of Fe-Ni-Mo-B[19,20] and Cr-Mo[21] amorphous alloys. By considering the previous reported facts, such an excellent thermal stability of amorphous Ni-Mo-B alloy film may be assumed to be due to the codeposition of the Mo atom into Ni-B film.

For the crystallized Ni-Mo-B alloy film, the structure shows almost no change until heat treatment at 500 °C as is shown in Fig. 3c. The peak intensities gradually increase with an increase in the heat treatment temperature above 500 °C.

In the cases of both amorphous and crystallized Ni-Mo-B alloy films, the peaks of the Ni(111) and Ni(200) planes are shifted to a lower angle side than those of pure Ni. Thus, there is a stable solid solution between Mo and Ni.

Transmission Electron Microscopy (TEM) and Transmission High Energy Electron Diffraction (THEED) Measurement. Figures 4—6 demonstrate the TEM and THEED patterns for the films at the Mo-complex concentrations of 0, 0.0025, and 0.0125 mol dm^{-3}, respectively. Figure 4a demonstrates the TEM and THEED patterns of Ni-B alloy film under as-plated conditions. The TEM micrographs show an Ni-B alloy film consisting of very small grains, while the THEED pattern gives halo diffraction rings due to the Ni phase. After heat treatment at 500 °C, the film comes to consist of large grains, while the THEED pattern shows the formation of the Ni_3B compound, as is shown in Fig. 4b. After heat treatment at 600 °C, the contrast and the grain size become clearer and larger respectively. These results coincide well with results of the X-ray diffraction measurement. Therefore, a drastic structural transformation is produced by the heat treatment.

Figure 5 demonstrates the TEM and THEED patterns of amorphous Ni-Mo-B alloy film with the same arrangement as is shown in Fig. 4. The results of the TEM and THEED of amorphous Ni-Mo-B alloy film under as-plated conditions are almost the same as those of Ni-B alloy film, as is shown in Fig. 4a. Broad

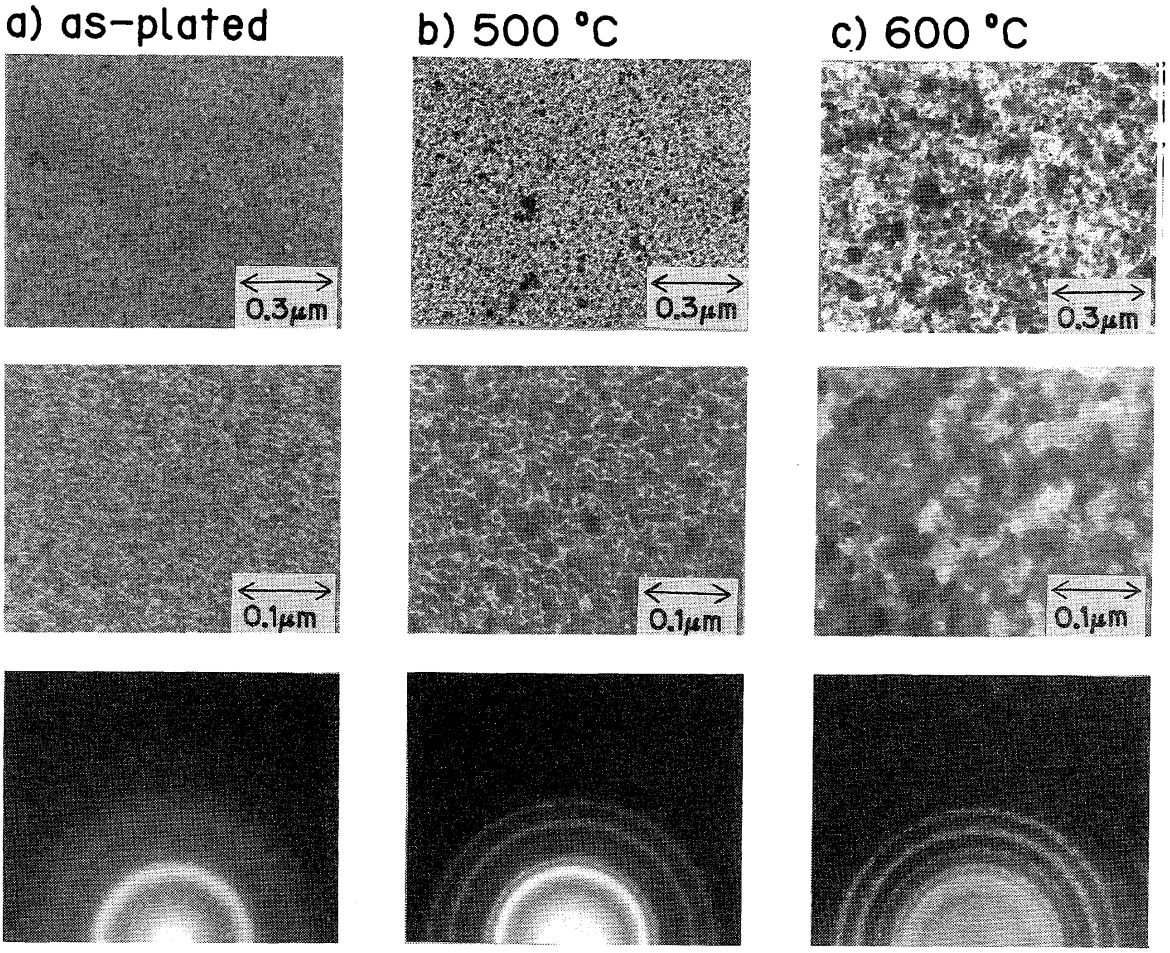

Fig. 5. Transmission electron micrographs (TEM) and transmission high energy electron diffraction (THEED) patterns of Ni-Mo-B alloy films at 0.0025 mol dm^{-3} Mo-complex concentration. a) As-plated conditions, b) after 500 °C treatment, c) after 600 °C treatment.

diffraction rings due to the Ni-Mo alloy are observed under as-plated conditions, and the grain sizes become a little larger after heat treatment at 500 °C treatment. The crystallinity after treatment at 500 °C is not so high, judging from the wider width of the diffraction rings. After heat treatment at 600 °C, the contrast and the grain sizes increase, and there appears a mosaic-like structure; however, the width of the diffraction rings is still wider.

Figure 6 demonstrates the TEM and THEED patterns of crystallized Ni-Mo-B alloy film in the same manner as in Figs. 4 and 5. The same tendency as that in Fig. 5 is observed. As is also seen in the X-ray diffraction measurement results in Fig. 3c, the crystallization proceeds gradually with an increase in the heat treatment temperature. The diffraction rings became sharper after heat treatment at 500 °C. The grain sizes after heat treatment at 600 °C are almost the same as those after heat treatment at 500 °C, only the contrast between 500 and 600 °C becomes clearer.

In general, the crystallized film after heat treatment shows large grown-grains and sharp diffraction rings. In contrast with the usual case, the heat change behavior of electroless Ni-Mo-B alloy films is quite different. Such a mosaic-morphology and broad diffraction rings after heat treatment are characteristic of the Ni-Mo-B alloy film. The usual crystallization process is accompanied by an increase in grain size, and finally the grown-grains combine with each other, thus making possible a free path of electrons.[14] Therefore, the resistivity is usually decreased by the normal crystallization process after heat treatment. In contrast with such a usual crystallized film, the crystallized Ni-Mo-B alloy is crystallized by heat treatment, without any accompanying increase in grain size. The grains are still clearly separated, even after treatment at 600 °C, and such a formation of a grain matrix does not permit a free path for electrons. Thus, the characteristics of such a mosaic-like structure are assumed to be the origin of the high resistivity and high thermal stability. Moreover, in the case of amorphous Ni-Mo-B alloy films, these characteristics are enhanced.

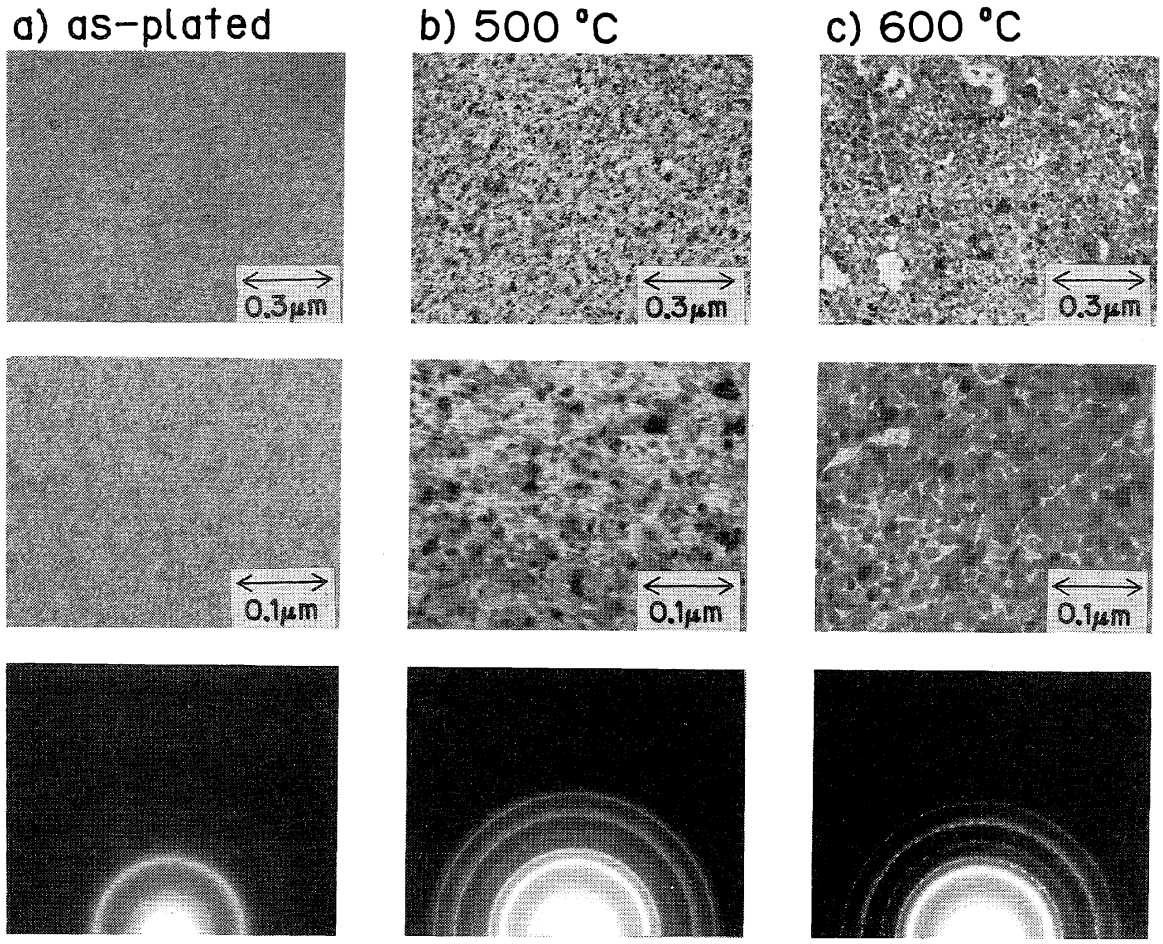

Fig. 6. Transmission electron micrographs (TEM) and transmission high energy electron diffraction (THEED) patterns of Ni-Mo-B alloy films at 0.0125 mol dm^{-3} Mo-complex concentration. a) As-plated conditions, b) after 500 °C treatment, c) after 600 °C treatment.

Conclusion

Electroless Ni-Mo-B alloy films, which had been prepared from a bath using dimethylamine-borane (1/1) (DMAB) as the reducing agent, were studied from the viewpoint of forming thermally stable film. The following results were obtained:

1) Amorphous and crystallized Ni-Mo-B alloy films with Mo contents of more than 20 wt% were obtained from an electroless plating bath.

2) The maximum molybdenum content and the very high resistivity value of Ni-Mo-P film were 22.1 wt% and 322 μΩ cm respectively under as-plated conditions. The origins of such a high resistivity value of Ni-Mo-B alloy film were assumed to be the formation of a solid solution and the unique microstructure.

3) The maximum resistivity of electroless Ni-Mo-B alloy films was obtained after heat treatment. After heat treatment at 500 °C, the maximum resistivity of 347 μΩcm was obtained for the film plated from a 0.0025 mol dm^{-3} Mo-complex concentration bath.

4) The microstructure of Ni-Mo-B alloy film, with a high resistivity, after heat treatments at 500 and 600 °C was due to an unique mosaic-like structure.

The authors are indebted to the financial support of the Asahi Glass Foundation for Industrial Technology.

References

1) E.g., F. Pearlstein, "Electroless Plating," in (F. A. Lowenheim, ed.) Modern Electroplating, 3rd ed., John Wiley & Sons, New York (1974), Chap. 31.

2) A. W. Goldstein, W. Rostoker, F. Schossberger, and G. Gutzeit, *J. Electrochem. Soc.*, **104**, 104 (1957).

3) J. P. Marton and M. Schlesinger, *J. Electrochem. Soc.*, **115**, 16 (1968).

4) K. M. Gorbunova, M. V. Ivanov, and V. P. Moiseev, *J. Electrochem. Soc.*, **120**, 613 (1973).

5) T. Watanabe and Y. Tanabe, *J. Jpn. Inst. Metals*, **39**, 831 (1975).

6) H. Suda, T. Watanabe, and Y. Tanabe, *J. Jpn. Inst. Metals.*, **45**, 5 (1981).

7) E.g., P. T. Cote, *Solid State Communications*, **18**, 1311 (1976).

8) G. O. Mallory, *Plating and Surface Finishing*, **63** (6), 34 (1976).

9) M. Schwartz and G. O. Mallory, *J. Electrochem. Soc.*, **123**, 606 (1976).

10) G. O. Mallory and T. R. Horhn, *Plating and Surface Finishing*, **66** (4), 40 (1979).

11) I. Koiwa, M. Nishikawa, K. Yamada, and T. Osaka, *Denki Kagaku*, **53**, 510 (1985).

12) I. Koiwa, M. Nishikawa, K. Yamada, and T. Osaka, *Bull. Chem. Soc. Jpn.*, **59**, 133 (1986).

13) L. G. Svendsen, T. Osaka, and H. Sawai, *J. Electrochem. Soc.*, **130**, 2252 (1983).

14) E.g., S. T. Pai, J. P. Marton, and J. D. Brown, *J. Appl. Phys.*, **43** (2), 282 (1972).

15) I. Koiwa, T. Osaka, and H. Sawai, *Kinzoku Hyomen Gijutsu*, **34**, 600 (1983).

16) H. Sawai, T. Kanamori, S. Shibata, K. Nihei, T. Osaka, I. Koiwa, and M. Nishikawa, Proc. of 11th Inter. Cong. of Metal Finishing, Israel (Oct. 1984), p. 323.

17) K. H. J. Buschow and N. M. Beekmans, *Phys. Rev.*, **B19**, 3843 (1979).

18) S. R. Nagel, J. Vassilion, P. M. Horn, and B. C. Giessen, *Phys. Rev.*, **B17**, 462 (1978).

19) P. Allia, D. Andreone, R. S. Turtelli, F. Vinai, and G. Riontino, *J. Appl. Phys.*, **53**(12), 8798 (1982).

20) C. Antonione, L. Battezzati, A. Lucci, G. Riontino, M. C. Tabasso, and G. Venturello, *J. de Phys.*, **C8**, 131 (1980).

21) H. Furuya, N. Hasegawa, Y. Misaki, and Y. Tanabe, *Kinzoku Hyomen Gijutsu*, **32**, 637 (1981).

 © 1987 The Chemical Society of Japan Bull. Chem. Soc. Jpn., 60, 3125—3129 (1987)

Silicon-29 NMR Chemical Shifts of Organosilicons as Studied by the FPT CNDO/2 Method

Toshio TAKAYAMA* and Isao ANDO†
Department of Applied Chemistry, Faculty of Technology, Kanagawa University, Rokkakubashi, Kanagawa-ku, Yokohama 221
†Department of Polymer Chemistry, Tokyo Institute of Technology, Ookayama, Meguro-ku, Tokyo 152
(Received March 17, 1987)

The ^{29}Si chemical shifts of silicon hydrides and fluorosilanes were calculated by means of the FPT method within the CNDO/2 framework. It was found that, by a small revision of the formula for the off-diagonal elements of the core Hamiltonian matrix in the CNDO/2 method, the calculated results agree well with the gross trend of the experimental values of the ^{29}Si chemical shifts in the literature. Further, the relationship between the ^{29}Si chemical shift and the electronic structure was discussed.

The widespread interest in ^{13}C NMR has ensured that the chemical shift of this nucleus has received much attention at both the semiempirical MO- and ab initio MO-level approaches, and the comparison of the calculated and experimental ^{13}C chemical shifts has provided useful information on the electronic distribution and molecular structure.[1,2] On the other hand, in spite of the fact that ^{29}Si NMR spectroscopy is widely used for investigating molecular structures and electronic distributions in organosilicon compounds, theoretical investigation has been carried out only by using such a rough approximate theory as the averaged excitation energy (ΔE) method.[3,4] This method has an ambiguity in the estimation of the value of ΔE as parameter in the paramagnetic term by which ^{29}Si chemical shift is predominantly governed. According to our best knowledge, there have been few ^{29}Si chemical-shift calculations using sophisticated methods.

In this work, therefore, we aim to calculate the ^{29}Si chemical shifts of several organic compounds containing a silicon atom by the use of the finite-perturbation theory (FPT)[5] within the CNDO/2 framework, which reproduces well the experimental trend for the ^{13}C chemical-shift values;[6] we will also discuss the relationship between the ^{29}Si chemical shift and the electronic structure through a comparison of the calculated and experimental chemical-shift values.

Theoretical

In the FPT method,[5] the ^{29}Si shielding tensor of a nucleus A, $\sigma_{\alpha\beta}(A)$, is expressed as a sum of the diamagnetic term, $\sigma^{d}_{\alpha\beta}(A)$, and the paramagnetic term, $\sigma^{p}_{\alpha\beta}(A)$ as follows:

$$\sigma_{\alpha\beta}(A) = \sigma^{d}_{\alpha\beta}(A) + \sigma^{p}_{\alpha\beta}(A), \qquad [1]$$

$$\sigma^{d}_{\alpha\beta}(A) = \frac{e^2}{2mc}\sum_{\mu}\sum_{\nu} \boldsymbol{P}_{\mu\nu}(0) < \chi_{\mu} \left| \frac{\delta_{\alpha\beta}\boldsymbol{r}_{\nu}\cdot\boldsymbol{r}_{A} - r_{\nu\alpha}r_{A\beta}}{|\boldsymbol{r}_{A}|^3} \right| \chi_{\nu} >, \qquad [2]$$

$$\sigma^{p}_{\alpha\beta}(A) = -\frac{e\hbar}{mc} i \sum_{\mu}\sum_{\nu} \left(\frac{\partial P_{\mu\nu}(\boldsymbol{H}_{\alpha})}{\partial \boldsymbol{H}_{\alpha}} \right)_{\mathbf{H}=0} < \chi_{\mu} \left| \frac{(\boldsymbol{r}\times\nabla)_{\beta}}{|\boldsymbol{r}_{A}|^3} \right| \chi_{\nu} > \quad (\alpha, \beta = x, y, z), \qquad [3]$$

where the gauge origin of the vector potential is set at the position of the nucleus A. The $\mathbf{r}_{\nu}$ and $\mathbf{r}_{A}$ vectors are the position vectors of an electron considered from the point of view of a nucleus of the atom containing the $\mathbf{AO}_{\chi_{\nu}}$ and from that of nucleus A respectively. $\boldsymbol{P}_{\mu\nu}(\boldsymbol{H}_{\alpha})$ and $\boldsymbol{P}_{\mu\nu}(0)$ are the elements of the density matrix with and without the perturbation due to the magnetic field $\boldsymbol{H}$ respectively; they are obtained by solving the Roothaan equation[7] with the Hartree-Fock matrix, $\boldsymbol{F}_{\mu\nu}(\boldsymbol{H}_{\alpha})$, containing the perturbation terms:

$$\boldsymbol{F}_{\mu\nu}(\boldsymbol{H}_{\alpha}) = \boldsymbol{H}^{\mathrm{core}}_{\mu\nu} + \sum_{\lambda}\sum_{\sigma} \boldsymbol{P}_{\mu\nu}(\boldsymbol{H}_{\alpha})[(\mu\nu|\lambda\sigma) - \frac{1}{2}(\mu\sigma|\lambda\nu)] - i(e\hbar/2mc)\sum_{\alpha} \boldsymbol{H}_{\alpha} < \chi_{\mu}|(\boldsymbol{r}\times\nabla)_{\alpha}|\chi_{\nu} >, \qquad [4]$$

where $\boldsymbol{H}^{\mathrm{core}}_{\mu\nu}$, $(\mu\nu|\lambda\sigma)$, and $(\mu\sigma|\lambda\nu)$ are the unperturbed core Hamiltonian, the Coulomb integral, and the exchange integral respectively; these are estimated by means of the parameters in the INDO method. In the present calculation, we shall adopt Pole's parameters[8] except for the off-diagonal element of the core Hamiltonian, which is estimated from this expression:

$$\boldsymbol{H}^{\mathrm{core}}_{\mu\nu} = (\kappa_{\pi}/2)(\beta^{0}_{\mathrm{A}} + \beta^{0}_{\mathrm{B}})S_{\mu\nu} \qquad (\mu \neq \nu), \qquad [5]$$

in which κ_{π} denotes a correction factor for the π-π interaction. κ_{π}=0.85 was used in this work according to the previous proposal.[5] β^{0}_{A} is the bonding parameter for the atom A, and $S_{\mu\nu}$, the overlap integral. The density matrix is allowed to be complex

to accommodate the purely imagniary nature of the perturbation, while $\mathbf{Im}[\boldsymbol{P}_{\mu\nu}(\boldsymbol{H}_\alpha)]$ represents the imaginary part. The derivative in Eq. 3 is evaluated numerically using the finite-difference technique, in which it is approximated by a single difference:

$$(\partial \boldsymbol{P}_{\mu\nu}(\boldsymbol{H}_\alpha)/\partial \boldsymbol{H}_\alpha)_{\mathbf{H}=0} = \mathbf{Im}[\boldsymbol{P}_{\mu\nu}(\boldsymbol{H}_\alpha)]/\boldsymbol{H}_\alpha. \quad [6]$$

In this calculation, the bond lengths and bond angles used were taken from the X-ray-diffraction data[9] and also from the standard values proposed by Pople and Gordon.[10] All the calculations were carried out by means of a HITAC M-280H computer of the Tokyo Institute of Technology and a S-810 computer at the Computer Center of Tokyo University.

Results and Discussion

Since the ^{29}Si chemical shift is considered to be governed predominantly by the paramagnetic term as well as by the ^{13}C chemical shift, we will evaluate mainly the contribution from this terms using the FPT CNDO/2 method. In such a semiempirical MO calculation, we sometimes encounter the question of whether or not, the CNDO parameters proposed by Pople et al.[11] are appropriate to give a satisfactory agreement between the calculated and experimental chemical shifts. Ando et al.[6] and Ellis et al.[12] showed that the MO parameters proposed by Pople et al. did not give a satisfactory agreement between the calculated and experimental ^{13}C chemical-shift values in hydrocarbons. They therefore altered the bonding parameters for carbon and hydrogen atoms to improve their results. For our experiment, we will use a set of Ando's bonding parameters,[6] β_C=−15 eV and β_H=−13 eV, for the carbond and hydrogen atoms respectively contained in organosilicon compounds; these parameters reproduce reasonably well the gross trends of the observed values of the ^{13}C chemical shifts and the shielding tensor. However, as for the Si atom considered here, the optimized value of the bonding parameter, which reproduces reasonably well the experimental values of the ^{29}Si chemical shifts is not known. Therefore, the optimized value of the β parameter for the silicon atom will be examined.

First, we will consider the ^{29}Si chemical shift of silicon hydride derivatives, which consist of silicon, carbon, and hydrogen atoms. As is shown in Table 1, the experimental ^{29}Si chemical-shift data indicate that, as the degree of hydrogen substitution is increased, the chemical shifts are displaced upfield; the range of the chemical-shift displacement is about 90 ppm. In spite of such a simple structural change, the range of the chemical-shift displacement is quite large. This means that silicon-hydride derivatives are excellent for use in a theoretical study of the ^{29}Si chemical shift.

We will now examine the ^{29}Si chemical-shift behaviour of silicon-hydride derivatives calculated by using a set of Pople's bond parameters[11] (β_H=−9 eV, β_C=−21 eV, and β_{Si}=−13.065 eV) for hydrogen, carbon, and silicon atoms respectively. A plot of the experimental chemical shifts versus the calculated values is shown in Fig. 1a. The dashed line is a theoretical line with the slope of 1. This means that the experimental and calculated values agree with each other exactly. As may be seen from Fig. 1a, the data points greatly deviate from the theoretical line, and the calculated chemical-shift range is quite small compared with the experimental data. This means that the set of Pople's bonding parameters are not appropriate in the ^{29}Si chemical-shift calculation.

As is to be expected from the previous results[6] for the ^{13}C chemical shift, the lowering of the absolute value for β_{Si} leads to a wide expansion of the calculated

Table 1. Calculated ^{29}Si Chemical Shifts of Silicon Hydrides[a]

Compound	d	σ^d	σ^p	σ^T	δ_{calcd} [b]	$\delta_{exp.}$ [c]
1) SiH_4	3.4578	66.78	−321.64	−254.86	−63.87	−92.5
2) SiH_3Me	3.5050	67.43	−336.78	−269.35	−49.38	−65.2
3) SiH_3Ph	3.5236	67.69	−333.55	−265.87	−52.86	−60.0
4) SiH_3Bz	3.5175	67.60	−341.22	−273.62	−45.11	−56.0
5) SiH_2Me_2	3.5376	67.88	−348.38	−280.50	−38.23	−40.0
6) SiH_2MePh	3.5546	68.11	−346.13	−278.02	−40.71	−36.9
7) SiH_2Ph_2	3.5874	68.56	−341.51	−272.95	−45.78	−33.6
8) $SiHMePh_2$	3.6058	68.80	−358.63	−289.82	−28.91	−19.5
9) $SiHPh_3$	3.6286	69.11	−352.99	−283.88	−34.85	−17.8
10) $SiHMe_2Ph$	3.5715	68.34	−367.09	−298.75	−19.98	−17.6
11) $SiHMe_3$	3.5577	68.15	−360.83	−292.67	−26.06	−16.3
12) $SiHPr_3$	3.5918	68.62	−375.43	−306.82	−11.91	−8.5
13) $SiHEt_3$	3.5798	68.45	−372.51	−304.05	−14.68	0.2

a) The bonding parameters used are β_H=−13 eV, β_C=−15 eV, and β_{Si}=−12 eV. b) Values given in ppm. Chemical shifts calculated with respect to TMS. The negative sign means an upfield shift from TMS. c) Data taken from Ref. 14. The negative sign means an upfield shift from TMS.

^{29}Si chemical-shift range. Thus, the value of β_{Si} which yields the best agreement between the experimental and calculated values for all chemical shifts was determined. This examination leads to the selection of the value of −12 eV for β_{Si}. As was mentioned above, a set of Ando's β_C and β_H bonding parameters (β_C=−15 eV and β_H=−13 eV) for carbon and hydrogen atoms was fixedly used. A plot of the experiment chemical shifts versus the calculated ones is shown in Fig. 1b. It may be seen that data points line on the theoretical line. The fit to the least-squares line has a correlation coefficient of 0.933. This means that the calculation reproduces well the experiment.

The diamagnetic, paramagnetic, and total contributions for the ^{29}Si chemical shift calculated using the "new" value of β_{Si}(=−12 eV), together with the experimental values, are listed in Table 1. Note that the calculated chemical shift (σ) is a nuclear shielding constant, and so the negative sign means deshielding.

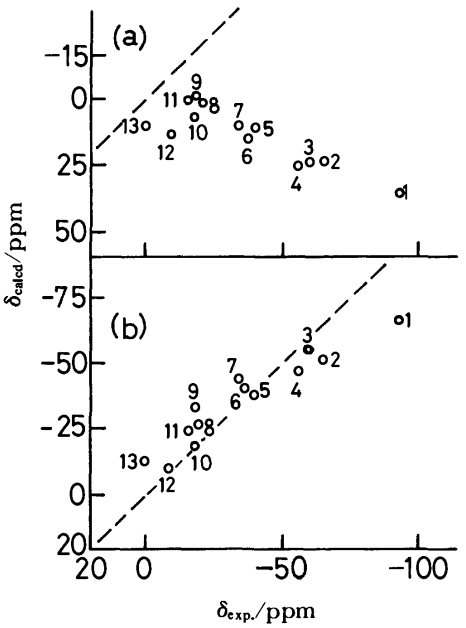

Fig. 1. The plot of the calculated ^{29}Si chemical shifts versus the experimental ones in silicon hydrides.
(a): Pople's β parameters (β_H=−9 eV, β_C=−21 eV, and β_{Si}=−13.065 eV). (b): β parameters proposed in this work (β_H=−13 eV, β_C=−15 eV, and β_{Si}=−12 eV).
The negative sign means upfield shift relative to TMS.
The numbers refer to the following compounds: 1: SiH_4; 2: SiH_3Me; 3: SiH_3Ph; 4: SiH_3Bz; 5: SiH_2Me_2; 6: SiH_2MePh; 7: SiH_2Ph_2; 8: $SiHMePh_2$; 9: $SiHPh_3$; 10: $SiHMe_2Ph$; 11: $SiHMe_3$; 12: $SiHPr_3$; 13: $SiHEt_3$.
The abbreviations used are as follows: Me, methyl; Ph, phenyl; Bz, benzyl; Pr, *n*-propyl; Et, ethyl.
The dashed line is the theoretical one with the slope of 1.0. This means that the experimental and calculated values completely agree with each other.

On the other hand, the negative sign of the experimental chemical shift (δ) means shielding. Therefore, tetramethylsilane was used as the standard reference. As may be seen from Table 1, the diamagnetic term, σ^d, moves upfield by about 2 ppm in going from SiH_4 to $SiHEt_3$. This variation is quite small, and the chemical-shift displacement is in the opposite direction compared with the experimental one. On the other hand, the paramagnetic term, σ^p, moves downfield by about 50—60 ppm. This means that the ^{29}Si chemical shift is predominantly governed by the paramagnetic term.

Next, we will consider the ^{29}Si chemical-shift behavior of organic silicon compounds containing the fluorine atom. The fluorine atom is known to be the most electronegative of all the atoms. This may be attributed to the effect of the higher electron unbalance in the Si-F bond and may lead to a wider range of ^{29}Si chemical shifts compared with the case of silicon-hydride compounds.

In the ^{29}Si chemical-shift calculation, the value of β_{Si} determined above in silicon-hydride compounds was used; also, as the β_F parameter for the fluorine atom, we adopted the value of −20 eV obtained by Ando et al.,[13] by the use of which the ^{19}F chemical-shift calculation reproduces the experiment reasonably well. The diamagnetic, paramagnetic, and total contributions calculated using these β parameters are listed, together with the experimental chemical-shift values, in Table 2. It may be seen that the chemical-shift range is more greatly expanded than in the case of silicon-hydride compounds. It may also be found that the relative chemical shift is

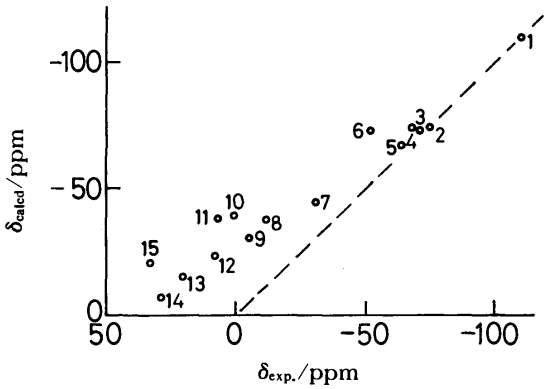

Fig. 2. The plot of the calculated ^{29}Si chemical shifts versus the experimental ones in fluorosilanes.
β bonding parameters (β_H=−13 eV, β_C=−15 eV, β_{Si}=−12 eV, and β_F=−20 eV). The negative sign means upfield shift relative to TMS.
The numbers refer to the following compounds: 1: SiF_4; 2: SiF_3Ph; 3: SiF_3PhMe; 4: SiF_3PhOMe; 5: SiF_3Bz; 6: SiF_3Me; 7: SiF_2Ph_2; 8: SiF_2MePh; 9: $SiFPh_3$; 10: SiF_2Et_2; 11: SiF_2Me_2; 12: $SiFMePh_2$; 13: $SiFMe_2Ph$; 14: $SiFPr_3$; 15: $SiFMe_3$.

Table 2. Calculated ^{29}Si Chemical Shifts of Fluorosilanes[a)]

Compound	d	σ^d	σ^p	σ^T	δ_{calcd} [b)]	$\delta_{exp.}$ [c)]
1) SiF_4	2.1098	45.17	−254.38	−209.20	−109.53	−111.0
2) SiF_3Ph	2.5888	53.50	−296.91	−243.41	−75.32	−73.7
3) SiF_3PhMe	2.5952	53.61	−297.43	−243.83	−74.90	−72.0
4) SiF_3PhOMe	2.5892	53.50	−297.29	−243.78	−74.95	−71.4
5) SiF_3Bz	2.5805	53.36	−303.18	−249.82	−68.91	−64.2
6) SiF_3Me	2.5345	52.59	−296.31	−243.72	−75.01	−51.8
7) SiF_2Ph_2	2.9720	59.64	−331.09	−271.45	−47.28	−30.5
8) SiF_2MePh	2.9314	59.01	−337.96	−278.95	−39.78	−12.4
9) $SiFPh_3$	3.3213	64.85	−351.88	−287.03	−31.70	−4.7
10) SiF_2Et_2	2.9258	58.93	−335.45	−276.52	−42.21	0.5
11) SiF_2Me_2	2.9006	58.53	−336.55	−278.02	−40.71	6.2
12) $SiFMePh_2$	3.2980	64.51	−358.52	−294.01	−24.72	7.7
13) $SiFMe_2Ph$	3.2633	64.01	−367.00	−302.99	−15.74	19.8
14) $SiFPr_3$	3.2819	64.28	−375.19	−310.91	−7.82	28.8
15) $SiFMe_3$	3.2426	63.71	−359.88	−296.17	−22.56	31.9

a) The bonding parameters used are $\beta_H = -13$ eV, $\beta_C = -15$ eV, $\beta_{Si} = -12$ eV, and $\beta_F = -20$ eV. b) Values given in ppm. Chemical shifts calculated with respect to TMS. The negative sign means an upfield shift from TMS. c) Data taken from Ref. 14. The negative sign means an upfield shift from TMS.

predominantly governed by the paramagnetic term, although the diamagnetic term is more greatly varied by the degree of fluorine substitution than in the case of silicon-hydride compounds. A plot of the experimental chemical shifts versus the calculated ones is shown in Fig. 2. It may be seen that data points deviate slightly from the theoretical line with the slope of 1.0, but the overall trend of the experimental data is reproduced by the calculation. In particular, it can be said that it has been established that the ^{29}Si chemical shift in SiR_nF_{4-n} (R means the substitution group, and n, the substitution number) moves upfield as the degree of fluorine substitution is increased. (It is noticeable that the upfield shift with an increase in the degree of fluorine substitution is opposite to the case of the ^{13}C chemical shift in CR_nF_{4-n}.)

Finally, we will consider the relationship between the ^{29}Si chemical shift and the electron density. It has been reported that the ^{13}C chemical shift is closely related to the electron density on the carbon atom. The larger electron density on the carbon leads to the upfield shift. The calculated electron densities on the silicon atoms considered here are listed in Tables 1 and 2. It may be seen that the electron densities on silicon atoms in silicon-hydride compounds decrease as the degree of hydrogen substitution is increased, while those in SiR_nF_{4-n} decrease as the degree of electronegative fluorine substitution is increased. From Tables 1 and 2 it may also be seen that σ^d moves linearly upfield with an increase in the electron density on the silicon atom, as is to be expected from Eq. 2. The direction of such a shift is opposite to that of the experimental chemial shift. On the other hand, σ^p and σ^T move downfield, with a great scatter, with an increase in the electron density. Further, a plot of the experimental chemical shift versus the electron density on the silicon atom is shown in Fig. 3. The experimental chemical shifts move downfield, with a great scatter, with an increase in the electron density. The direction of such a shift is opposite to the general consideration that an increase in the electron density leads to an upfield shift. Therefore, it seems that it is difficult to explain the ^{29}Si chemical shift obtained experimentally only in terms of the electron density.

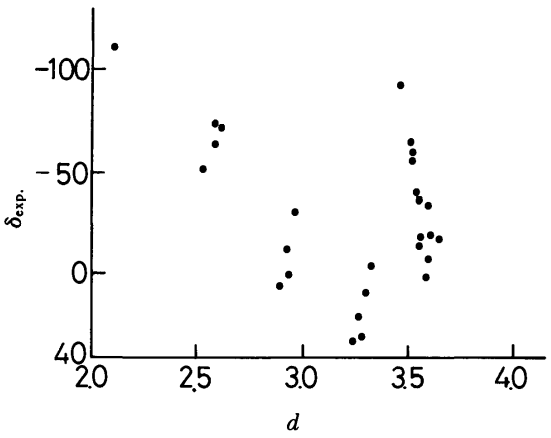

Fig. 3. The plot of the experimental ^{29}Si chemical shift $\delta_{exp.}$ against the calculated electron density d in organosilicon compounds.

From the above-mentioned results, it can be concluded that the experimental overall trend of ^{29}Si chemical shifts in sililcon hydrides and fluorine-containing organic compounds can be fairly reproduced by the FPT CNDO/2 method, with a small improvement of the β-bonding parameter.

References

1) K. A. K. Ebraheem and G. A. Webb, *Prog. NMR in Spectrosc.*, **11**, 149 (1977).

2) I. ANDO and G. A. Webb, "Theory of NMR Parameters," Academic Press, London (1983).

3) F. F. Roelandt, D. F. Van den Vondel, and E. A. Van den Berghe, *J. Organomet. Chem.*, **94**, 377 (1975).

4) R. Wolff and R. Radeglia, *Z. Phys. Chem. (Leipzig)*, **257**, 181 (1976); R. Wolff and R. Radeglia, *Z. Phys. Chem. (Leipzig)*, **258**, 145 (1977); R. Wolff and R. Radeglia, *Org. Magn. Reson.*, **9**, 64 (1977); R. Radeglia, *Z. Phys. Chem. (Leipzig)*, **256**, 453 (1975); R. Radeglia, *Z. Naturforsch*, **32b**, 1091 (1977); R. Wolff and R. Radeglia, *Z. Phys. Chem. (Leipzig)*, **261**, 726 (1980); G. Engelhardt, R. Radeglia, H. Kelling, and R. Stendel, *J. Organomet. Chem.*, **212**, 51 (1981).

5) R. Ditchfield, D. P. Miller, and J. A. Pople, *J. Chem. Phys.*, **54**, 4186 (1971); P. D. Ellis, G. E. Maciel, and J. W. Mciver, Jr., *J. Am. Chem. Soc.*, **94**, 4069 (1972).

6) M. Kondo, I. Ando, R. Chujo, and A. Nishioka, *J. Magn. Reson.*, **24**, 315 (1976).

7) C. J. Roothaan, *Rev. Mod. Phys.*, **23**, 69 (1951).

8) J. A. Pople, D. L. Beveridge, and P. A. Dobosh, *J. Chem. Phys.*, **47**, 2026 (1967).

9) "Tables of Interatomic Distances and Configuration in Molecules and Ions," ed by L. E. Sutton, Chemical Society, London (1958), Spec. Publ., No. 11.

10) J. A. Pople and M. Gordon, *J. Am. Chem. Soc.*, **89**, 4253 (1967).

11) J. A. Pople and G. A. Segal, *J. Chem. Phys.*, **43**, S136 (1965).

12) A. R. Garber, P. D. Ellis, K. Seidman, and K. Schade, *J. Magn. Reson.*, **34**, 1 (1979).

13) I. Ando, T. Yamanobe, N. Akamatsu and T. Komoto, unpublished data.

14) E. A. Williams and J. D. Cargioli, "Annual Reports on NMR Spectroscopy," Academic Press, New York (1979), Vol. 9.

 © 1987 The Chemical Society of Japan Bull. Chem. Soc. Jpn., 60, 3131—3135 (1987)

1,2-Migration of Fluorine Atom in CH_2FCF_2 Radical Produced by the Addition of a Hydrogen Atom to Trifluoroethylene

Tomoyuki KOHIDA, Masahiro KOTAKA, Shin SATO,* Toru ISHIDA,†
Keiji YAMAMOTO,† Takashi YAMAZAKI,†† and Tomoya KITAZUME††
Research Laboratory for Nuclear Reactors, Tokyo Institute of Technology,
Ookayama, Meguro-ku, Tokyo 152
†Department of Chemical Engineering, Tokyo Institute of Technology,
Ookayama, Meguro-ku, Tokyo 152
††Department of Bioengineering, Tokyo Institute of Technology,
Ookayama, Meguro-ku, Tokyo 152
(Received March 18, 1987)

The reaction of hydrogen atoms with trifluoroethylene has been studied at room temperature by using the mercury photosensitized decomposition of hydrogen as the source of hydrogen atoms. Product analyses using gas chromatography and ^1H and ^{19}F NMR spectroscopy confirmed the 1,2-migration of a fluorine atom in the CH_2FCF_2 radical produced by the addition of a hydrogen atom to trifluoroethylene. The rate constant of the migration was estimated to be 2×10^{10} s^{-1} from the pressure dependence of the five kinds of hexafluorobutanes produced. NMR parameters for these fluorinated compounds were determined.

When we consider the addition reaction of a free atom to the olefinic double bond of an organic compound in the gas phase, there arise two naive questions: One is which side of the double bond is attacked by the free atom, and the other is how the radical produced behaves before being thermalized.

In the case of a hydrogen atom-addition reaction to olefinic hydrocarbons, it has been established that a hydrogen atom is added to the less substituted carbon atom in the double bond and that no 1,2-migration of a hydrogen atom occurs in the radical produced.[1,2]

For the last few years, Rowland and his colaborators studied the reactions of radioactive ^{38}Cl atoms with a series of halogenated olefines,[3-5] and found that chlorine and bromine atoms in the produced radical often undergo a 1,2-migration in the radical produced by the addition of a ^{38}Cl atom to the olefin. In fact, the 1,2-migration of chlorine and bromine atoms has been reported even in the liquid phase reaction of complex organic compounds.[6]

In the case of a fluorine atom, however, no 1,2-migration has been reported in liquid phase reactions as far as we are aware. Siefert et al. have recently studied the reactions of recoiled tritium atoms with fluorinated olefins, using $^3He(n,p)T$ as the source of tritium atoms.[7] In a reaction with 1,2-difluoroethylene they found the formation of tritiated 1,1-difluoroethylene as one of the main products and suggested that the 1,2-migration of a fluorine atom occurs in the 1,2-difluoroethyl radical produced by the addition of a tritium atom to 1,2-difluoroethylene. Very recently, our laboratory has also studied the reactions of hot tritium atoms with fluorinated ethylenes ($CFH=CH_2$, $CF_2=CH_2$, and $CF_2=CFH$)[8] and found evidence for the 1,2-migration of a fluorine atom; however, in hot tritium atom reactions so many fragmental products were formed that evidence for the 1,2-migration could not be obtained straightforwardly. We, therefore, looked for a precise method to establish the 1,2-migration of a fluorine atom.

The reaction of hydrogen atoms with hydrocarbon olefins is a prototype subject for chemical kinetics and has been extensively studied.[9] The reaction with fluorinated olefins, however, has not been fully investigated, probably because of the difficulty to identify multi-fluorinated hydrocarbons. Most of these compounds are not commercially available. Scott and Jennings studied the reactions of hydrogen atoms with fluoroethylenes using the mercury photosensitized decomposition of hydrogen as the source of hydrogen atoms.[10] They used gas chromatography and mass spectroscopy for the analysis of products; however, the identification of several fluorinated hydrocarbons was not successful. Consequently, they did not propose a reaction mechanism for the formation of products in the reaction of hydrogen atoms with trifluoroethylene. They derived only the relative rate constants for the addition reactions.

Using this old technique, the mercury photosensitized decomposition of hydrogen as the source of hydrogen atoms, we have reinvestigated the reactions of hydrogen atoms with trifluoroethylene. For an analysis of products, ^1H and ^{19}F NMR spectroscopy were used along with gas chromatography and mass spectroscopy. As a result, we could confirm the 1,2-migration of fluorine atoms in a 1,1,2-trifluoroethyl radical as well as various interesting results.

Experimental

Trifluoroethylene was kindly supplied by Professor Ishikawa of this Institute and was used as received. Other fluorinated compounds used for the identification of products were CH_2FCHF_2 (PCR) and CF_3CH_3 supplied by Central Glass Co. Bottled hydrogen (Showa Denko Co.) and helium (Japan Helium Center), used as a reactant and a carrier gas in a gas chromatograph, respectively, were passed through liquid nitrogen traps before use.

One Torr (133.322 Pa) of trifluoroethylene and about 100 to 750 Torr of hydrogen were introduced into a reaction vessel (359 ml) made of fused quartz, into which a drop of mercury was present, and mixed by means of a glass-covered magnetic fan which could be rotated from outside using a magnet. This reactant mixture was irradiated by a mercury lamp (Sankyo GL6) for a certain time interval. The light intensity absorbed by mercury atoms was found to be 4.8×10^{15} photons/s (estimated by the mercury photosensitized decomposition of N_2O (110 Torr) in the presence of a small amount of butene-1 (5 Torr) on the assumption that the quantum yield of nitrogen is unity).[10] Irradiated samples were slowly pumped out through two long spiral glass traps cooled with liquid nitrogen. Condensed compounds were analyzed with a gas chromatograph equipped with a thermal conductivity detector (Shimadzu GC-6AM) using two columns (one contained dibutyl phthalate (8 m), and the other Porapak-S (4 m)) as well as a temperature-programed operation during chromatography (30 to 80 °C with the dibutyl phthalate column and 70 to 150 °C with Porapak-S column). Reaction products of eleven compounds were found, out of which seven could be identified by using ^1H and ^{19}F NMR spectra obtained with a JEOL FX-90Q spectrometer. Each sample analyzed was the accumulation of 10 to 20 runs of the photochemical reaction.

Results

Identification of Products. The eleven peaks observed with a gas chromatograph of dibutyl phthalate column were named alphabetically from A to K in the order of their retention times (Fig. 1a). When using a Porapak-S column (Fig. 1b), peak A was clearly separated into two peaks; the one named T was a reactant, trifluoroethylene, and the other named A′ was later identified as CF_3CH_3. Since with this column compounds D, F, H, I, J, and K (later identified as mainly fluorinated C_4 compounds with retention times longer than 15 min) were clearly separated from compounds T, A′, B, C, and E (with retention times shorter than 15 min), quantitative gas chromatograms could be obtained by increasing the column temperature from 70 to 150 °C between these two groups of compounds. No authentic samples, except for A′ and E, were available. The relative response of the peak area against the absolute amount was assumed to be 1 to 2 for the C_2 compounds group to the C_4 compounds group, since with this column, the relative sensitivities of C_2—C_4 hydrocarbons for the thermal conductivity detector were found to be proportional to the molecular weight.[11]

Table 1 summarizes the identified products. In the Appendix, their experimental NMR parameters are described. Peaks B and C were too small to be identified. Two compounds corresponding to F and G were also too small and were found to be secondary products (as shown later).

Irradiation Time and Pressure Dependence of Products. Figure 2 shows the irradiation time dependence of the products. The relative yield of 1.0 corresponds to 0.20 μmol. All products, except F and G, were found to be linearly dependent upon the irradiation time. Table 2 summarizes the relative amounts of each product obtained as a function of the hydrogen pressure. The pressure of trifluoroethylene was 1 Torr and the irradiation time was 6 min.

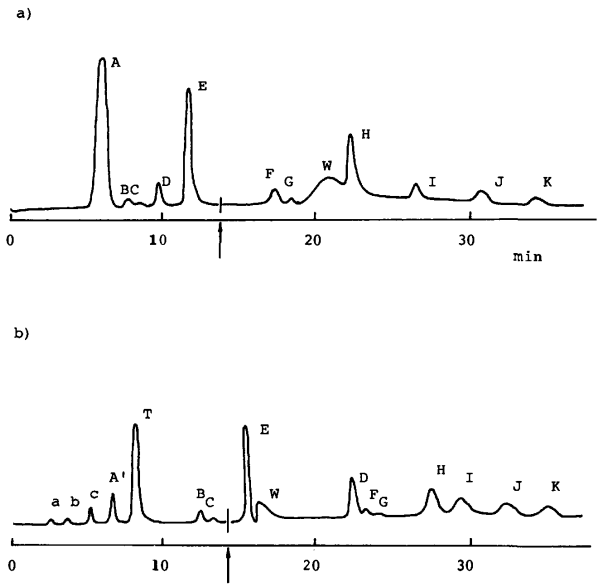

Fig. 1. (a) A typical gas chromatogram obtained with the dibutyl phthalate column. The arrow indicates the start of temperature programed operation from 30 to 80 °C with the rate of 15° min^{-1}. W: Water trapped from the carrier gas. (b) A gas chromatogram obtained with the Porapak S column. The arrow indicates the start of temperature programed operation from 70 to 150 °C with the rate of 5° min^{-1}. a—c were not identified.

Table 1. Identification of Reaction Products

A′	CF_3CH_3
E	CH_2FCHF_2
D	$CF_3CH_2CH_2CF_3$
H	$CF_3CH_2CF_2CH_2F$
I	$CF_3CH_2CHFCHF_2$
J	$CH_2FCF_2CF_2CH_2F$
K	$CH_2FCF_2CHFCHF_2$

Discussion

At very low hydrogen pressures (lower than 50 Torr), the formation of fragmental products such as $CF_2{=}CH_2$ and probably $CF{\equiv}CH$ has been found; however, we ignore them in the present discussion because it is well-known that most of the 253.7-nm resonance line is absorbed within a zone of 1 cm from the window of the reaction vessel and the radicals primarily produced, including hydrogen atoms,

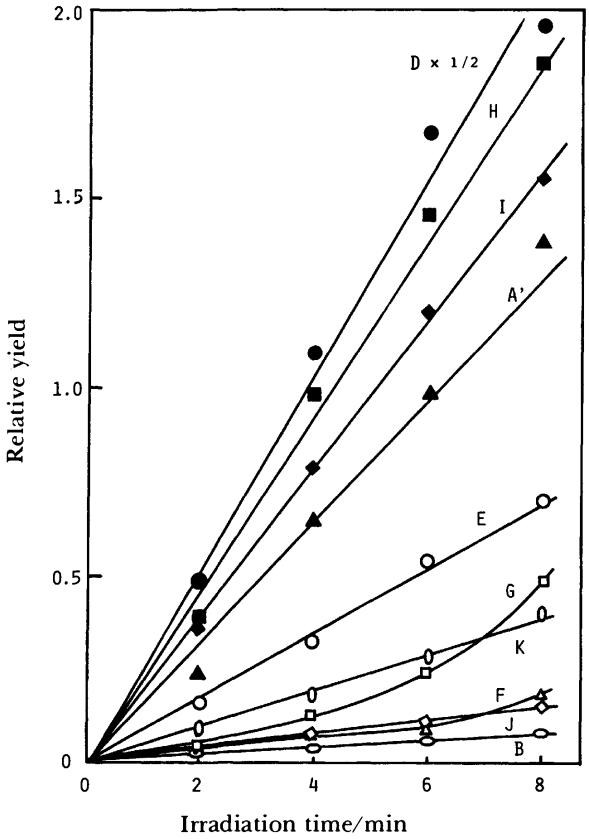

Fig. 2. Irradiation time dependence of the amounts of products. Initial hydrogen pressure is 109.5 Torr and trifluoroethylene is 1 Torr. Relative yield 1.0 corresponds to 0.20 μmol.

Table 2. Hydrogen Pressure Dependence of the Relative Amounts of Products.[a] Trifluoroethylene Pressure is 1 Torr and Irradiation Time is 6 min.

Hydrogen pressure (Torr) Product	19.1	59.1	109.5	516.0	754.9
A′	0.484	0.840	0.976	1.264	1.200
D	2.18	3.23	3.36	1.44	1.14
E	n.d.[b]	0.464	0.524	0.984	1.12
H	1.37	1.59	1.46	1.88	1.98
I	0.808	1.14	1.20	0.624	0.592
J	0.020	0.032	0.113	0.380	0.722
K	0.086	0.130	0.288	0.396	0.596

a) Relative yield 1.0 corresponds to 0.20 μmol. b) Not determined.

diffuse to the quartz surface and react differently from a gas-phase reaction.

Initial reactions may be described as follows:

$$Hg(^1S_0) + h\nu \longrightarrow Hg(^3P_1) \quad (1)$$

$$Hg(^3P_1) + H_2 \longrightarrow Hg(^1S_0) + 2H \quad (2)$$

$$H + CF_2=CFH \longrightarrow \dot{C}F_2CFH_2 \quad \alpha \quad (3)$$

$$\longrightarrow CF_2H\dot{C}FH \quad 1-\alpha. \quad (4)$$

Here, α and $1-\alpha$ denote the fractions of the Markovnikov and anti-Markovnikov additions, respectively. No other reactions such as the formation of HF are considered, since the formation of fragmental products has not been observed at hydrogen pressures higher than 50 Torr.

From two kinds of radicals, $\dot{C}F_2CFH_2$ and $CF_2H\dot{C}FH$, we can expect the formation of following products as the result of radical reactions, if no 1,2-migration of F or H atom is considered.

$$\dot{C}F_2CFH_2 + \dot{C}F_2CFH_2 \longrightarrow CFH_2CF_2CF_2CFH_2 \text{ (J)} \quad (5)$$
$$\longrightarrow CF_2=CFH \text{ (T)} + CF_2HCFH_2 \text{ (E)}$$

$$\dot{C}F_2CFH_2 + CF_2H\dot{C}FH \longrightarrow CFH_2CF_2CFHCF_2H \text{ (K)} \quad (6)$$
$$\longrightarrow CF_2=CFH \text{ (T)} + CF_2HCFH_2 \text{ (E)}$$

$$CF_2H\dot{C}FH + CF_2H\dot{C}FH \longrightarrow CF_2HCFHCFHCF_2H \text{ (L)} \quad (7)$$
$$\longrightarrow CF_2=CFH \text{ (T)} + CF_2HCFH_2 \text{ (E)}$$

Here, the disproportionation reaction accompanied by a fluorine-atom transfer is not taken into consideration, since the expected products have not been observed. Compound L appearing in Reaction 7 has not been observed in the experiments. Judging from the retention times of other products, Compound L probably has a very long retention time and the amount produced may be smaller than other C_4 compounds (discussed later).

Obviously, Reactions 5 to 7 cannot explain the formation of products A′, D, H, and I. We, thus, propose the following 1,2-migration of a fluorine atom in the 1,1,2-trifluoroethyl radical:

$$\underset{1-\beta}{\dot{C}F_2CFH_2} \longrightarrow \underset{\beta}{CF_3\dot{C}H_2}. \quad (8)$$

Here, β denotes the fraction of the radicals which undergo a 1,2-migration and proceed to the following radical reactions:

$$CF_3\dot{C}H_2 + CF_3\dot{C}H_2 \longrightarrow CF_3CH_2CH_2CF_3 \text{ (D)} \quad (9)$$

$$CF_3\dot{C}H_2 + \dot{C}F_2CFH_2 \longrightarrow CF_3CH_2CF_2CFH_2 \text{ (H)} \quad (10)$$
$$\longrightarrow CF_3CH_3\text{(A′)} + CF_2=CFH \text{ (T)}$$

$$CF_3\dot{C}H_2 + CF_2H\dot{C}FH \longrightarrow CF_3CH_2CFHCF_2H \text{ (I)} \quad (11)$$
$$\longrightarrow CF_3CH_3\text{(A′)} + CF_2=CFH \text{ (T)}.$$

In order to estimate α and β, we assume that all radical Reactions 5—7 and 9—11 occur proportionally to the collision number of radicals and let R1, R2, and R3 denote $\dot{C}F_2CFH_2$, $CF_3\dot{C}H_2$ and $CF_2H\dot{C}FH$ radicals, respectively; then, we can obtain the following equations:

$$[R1] : [R2] : [R3] = \alpha(1-\beta) : \alpha\beta : 1-\alpha, \quad \text{(I)}$$

$$a \times [R1] = 2[J] + [H] + [K] + 2N_1[E] + M_1[A'], \quad \text{(II)}$$

$$a \times [R2] = [H] + 2[D] + [I] + [A'], \quad \text{(III)}$$

$$a \times [R3] = [K] + [I] + 2[L] + 2N_2[E] + M_2[A'], \quad \text{(IV)}$$

and $N_1 + N_2 = 1$ and $M_1 + M_2 = 1$.

Here a is a proportional constant. N_1 and N_2 are the relative amounts of product E produced through Reactions 6 and 7, respectively. Similarly, M_1 and M_2 are the relative amounts of product A' produced through Reactions 10 and 11, respectively. These relative values may be expressed as follows:

$$N_1/N_2 = (1-\beta)/(1-\alpha)[\alpha^2(1-\beta) + 4\alpha(1-\alpha)]/[1-\alpha+4(1-\beta)], \text{ and} \quad \text{(V)}$$

$$M_1/M_2 = \alpha(1-\beta)/(1-\alpha). \quad \text{(VI)}$$

When two radicals, X and Y, are recombined at random, the relative amounts of products X_2, XY, and Y_2 can be expressed as $[XY]^2=4[X_2][Y_2]$. The amount of Compound L may be estimated by using the following equation from the amounts of Compounds J and K:

$$[L] = [K]^2/4[J]. \quad \text{(VII)}$$

Figure 3 shows the values of α and β calculated by using Eqs. I to VII as a function of the hydrogen pressure. Obviously, the α value was found to be 0.84, independent of the pressure (as it should be), while the β value was found to be pressure dependent (0.79 at 50 Torr and 0.50 at 750 Torr). This dependence may be explained by the competition between 1,2-fluorine-atom migration in the energy rich radical produced by a hydrogen atom addition reaction and a deactivation of this radical by a collision with a third body, mainly hydrogen molecules in the present system. Reactions 3 and 8 may be rewritten as follows:

$$H + CF_2{=}CFH \longrightarrow \dot{C}F_2CFH_2^*, \quad (3')$$

$$\dot{C}F_2CFH_2^* \underset{k_b}{\overset{k_f}{\rightleftharpoons}} CF_3\dot{C}H_2^*, \quad (8')$$

$$\dot{C}F_2CFH_2^* \xrightarrow{+M} \dot{C}F_2CFH_2, \quad (12)$$

$$\text{and } CF_3\dot{C}H_2^* \xrightarrow{+M} CF_3\dot{C}H_2. \quad (13)$$

Here, k_f and k_b are the rate constants of the forward and reverse isomerization reactions, and M denotes the third body.

A steady state treatment gives

$$(1-\beta)/\beta = k_f/k_b + (z/k_f)[M]. \quad \text{(VIII)}$$

Here, z is the collision number between a radical and a third body; $z=k_{12}=k_{13}$ is assumed. The value of z can be calculated from the collision diameters of the radical and a hydrogen molecule; σ(radical)$\approx\sigma$(ethane)=3.54 A and (H_2)=2.57 A.[12] Figure 4 shows plots of $(1-\beta)/\beta$ as a function of the hydrogen pressure. Although the expected linearity is not so good, we can estimate $k_f=2\times10^{10}$ s^{-1} from the slope and k_b/k_f to be 0.2 from the intercept; this corresponds to the equilibrium constant between two energy rich radicals, $\dot{C}F_2CFH_2^*$ and $CF_3\dot{C}H_2^*$.

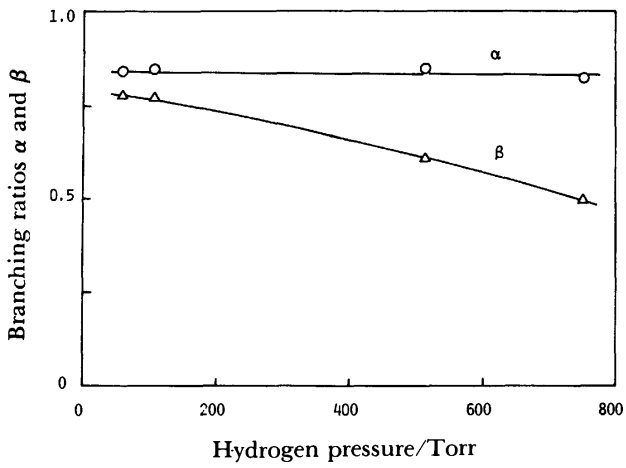

Fig. 3. The branching ratios α and β as functions of hydrogen pressure.

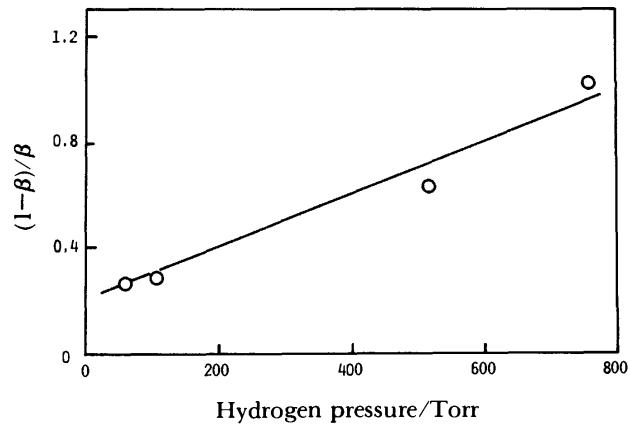

Fig. 4. The plots of $(1-\beta)/\beta$ as a function of hydrogen pressure.

In the above treatment, we ignored the reactions between radicals and the reactant olefin since if R1, R2, and R3 radicals have the same reactivity to the olefin, the above treatment for obtaining the relative ratios, α and β, are not affected by these reactions. Moreover, in this series of experiments, we did not observe the deposition of polymers on the wall of the reaction vessel. This suggests that the reactions leading to the formation of C_6 and/or heavier compounds may be ignored in the present system.

In this report, the 1,2-migration of a fluorine atom in the energy rich trifluoroethyl radical has been phenomenologically proved; however, as described in the Introduction, it is known that the 1,2-migration of a hydrogen atom in an ethyl radical does not occur under similar conditions, in spite of the fact that the binding energy of the C-F bond is usually larger than that of the C-H bond. We, therefore, carried out INDO molecular orbital calculations for these 1,2-migrations. The preliminary results showed that the

fluorine atom migration is much easier than the hydrogen atom migration in partially fluorinated ethyl radicals.[8] More extensive calculations are being undertaken.

Appendix

Molecule	Chemical shift[a] (ppm)	Coupling constant (Hz)
$\overset{1}{C}F_3\overset{2}{C}H_2CH_2CF_3$	(1) −86.7 (2) 2.4	
$\overset{1}{C}F_3\overset{2}{C}H_2\overset{3}{C}F_2\overset{4}{C}H_2\overset{5}{F}$	(1) −91.7 (2) 2.8 (3) −112.5 (4) 4.5 (5) −197.5	(1-2) 9.8 (2-3) 14.3 (1-3A) 8.79 (2-5) 2.1 (1-3B) 8.35 (3-4) 11.8 (1-5) 2.20 (3-5) 15.38 (4-5) 46.1
$\overset{1}{C}F_3\overset{2}{C}H_2\overset{3}{C}\overset{4}{H}F\overset{5}{C}\overset{6}{H}F_2$	(1) −90.2 (2) 2.5 (3) 4.8 (4) −171.8 (5) 5.8 (6A) −136.2 (6B) −130.8	(1A-4) 7.03 (4-6B) 13.2 (1B-4) 6.58 (5-6) 54 (3-4) 55 (6A-6B) 280 (4-6A) 12.3
$\overset{1}{C}H_2\overset{2}{F}\overset{3}{C}F_2CF_2CH_2F$	(1) 4.6 (2) −212 (3) −115.6	(1-2) 46.4 (1-3) 12.1
$\overset{1}{C}H_2\overset{2}{F}\overset{3}{C}F_2\overset{4}{C}\overset{5}{H}F\overset{6}{C}\overset{7}{H}F_2$	(1) 4.5 (2) −194 (3A) −115 (4) 4.7 (3B) −122 (5) −172.9 (6) 6.0 (7) −131.4	(3A-3B) 286 (4-5) 46 (6-7) 54.6

a) Compounds used as standard for ^{19}F and ^{1}H atoms are trifluoroacetic acid and TMS, respectively. The solvent is $CDCl_3$.

References

1) R. J. Cvetanovic, *Adv. Photochem.*, 1, 115 (1963).

2) R. Kh. Friedlina, "Advances in Free Radical Chemistry," ed by G. H. Williams, Academic Press, New York (1965), Vol. 1, p. 211.

3) F. S. C. Lee and F. S. Rowland, *J. Phys. Chem.*, **81**, 1222, 1935 (1977).

4) R. S. Iyer and F. S. Rowland, *Chem. Phys. Lett.*, **103**, 213 (1983), *J. Phys. Chem.*, **89**, 3730 (1985).

5) R. S. Iyer, C.-T. Chen, and F. S. Rowland, *J. Phys. Chem.*, **89**, 2042 (1985).

6) P. S. Skell and K. J. Shea, "Free Radicals," ed by J. K. Kochi, Wiley, New York (1973), Vol. 2, p. 809.

7) E. E. Siefert, D. D. Smith, R. E. Tricca, P. M. Ayoub, and Y.-N. Tang, *J. Am. Chem. Soc.*, **105**, 330 (1983).

8) M. Kotaka and S. Sato, *J. Chem. Soc., Chem. Commun.*, **1986**, 1783.

9) T. Kyogoku, T. Watanabe, S. Tsunashima, and S. Sato, *Bull. Chem. Soc. Jpn.*, **56**, 19 (1983).

10) P. M. Scott and K. R. Jennings, *J. Phys. Chem.*, **73**, 1521 (1969).

11) cf. A. E. Messner, D. M. Rosie, and P. A. Argabright, *Anal. Chem.*, **31**, 230 (1959).

12) J. O. Hirschfelder, C. F. Curtiss, and R. B. Bird, "Molecular Theory of Gases and Liquids," Wiley, New York (1963), p. 552.

 © 1987 The Chemical Society of Japan Bull. Chem. Soc. Jpn., 60, 3137—3142 (1987)

Influence of Br^- Concentration on $(Br)^+$-Mediated Indirect Electrooxidation of Alcohols to the Corresponding Carbonyl Compounds

Tsuyoshi TAKIGUCHI and Tsutomu NONAKA*
Department of Electronic Chemistry, Tokyo Institute of Technology,
4259 Nagatsuta, Midoriku, Yokohama 227
(Received March 19, 1987)

Current efficiency for the $(Br)^+$(positive bromine species)-mediated indirect electrooxidation of alcohols to the corresponding carbonyl compounds decreased with increase in Br^- concentration in dichloromethane and aqueous acidic solutions, while no concentration dependence was observed in an aqueous neutral solution. These facts suggested a general and practical guideline for the indirect electrooxidation, i.e. low Br^- concentration is favorable in an electrolytic solution of low nucleophilicity. It was also found that the kind of $(Br)^+$ species formed anodically in the absence of the alcohols in dichloromethane clearly depended on charge(Q) passed as follows: Br_3^- at $Q \leqslant 2/3$ F mol^{-1} (1F=96480 C), Br_n^- ($n>3$) at $2/3<Q<1$ F mol^{-1}, and Br_2 at $Q=1$ F mol^{-1}. Among these species, Br_3^- and Br_2 seemed to be the weakest and strongest oxidizing agents, respectively. Lower efficiency for the indirect electrooxidation in higher Br^- concentration was rationalized as due to more predominant formation of Br_3^- and/or Br_n^- with smaller n values.

It is well-known that indirect electrolysis using redox couples as mediators for electron transfer between electrodes and substrates is one of very useful methods in electroorganic synthesis.[1,2] Among the redox couples, halide(X^-)/positive halogen species-[$(X)^+$] couples have been often used in the indirect electrooxidation of organic compounds.[2]

Recently an interesting phenomenon has been found in the $(X)^+$-mediated indirect electrooxidation: Increase in X^- concentration results in decrease in current efficiency and/or yield.[3-5] In this work, some additional examples of this kind of phenomenon were also found in the $(Br)^+$-mediated oxidation of alcohols to the corresponding carbonyl compounds. This fact seems to indicate that the phenomenon is considerably universal. Since the $X^-/(X)^+$ mediators can be regarded as electrocatalysts, an apparently paradoxical theorem, the smaller amounts of catalyst used, the more smoothly the reaction proceeds, may be induced from the phenomenon.

Although it has been postulated that the $(X)^+$-mediated oxidation involves X^+, X_3^-, X_2, and/or XO^- as the oxidizing agents, their formation and behavior during electrolysis have not been clarified so far. In this work, the formation and behavior of some kinds of $(Br)^+$ species in dichloromethane were investigated by means of electrochemistry and UV-spectroscopy, and also the above strange phenomenon was rationalized as due to low oxidizing power of Br_3^- species which is formed preferentially in high Br^- concentration or at small amounts of charge passed under indirect electrolysis conditions.

Results and Discussion

Influence of Br^- Concentration on $(Br)^+$-Mediated Indirect Electrooxidation of Alcohols. It is known that benzyl alcohol[6] and 2,3-butanediol[7] can be efficiently oxidized to benzaldehyde and acetoin, respectively, by using a $Br^-/(Br)^+$ redox mediatory system. In this work, first the influence of Br^- concentration on current efficiencies for the products was examined in dichloromethane and aqueous solutions. The current efficiencies were determined by analyzing the anodic solutions in which unreacted $(Br)^+$ species were quenched with $NaHSO_3$ just after the electrolyses finished. As shown in Fig. 1, the current efficiencies decreased with increase in Br^- concentration in the oxidation of either benzyl alcohol or 2,3-butanediol at a platinum anode in n-Bu_4NBr-0.2 M (1 M=1 mol dm^{-3}) n-Bu_4NClO_4/dichloromethane containing 3 equiv 2,6-lutidine. Shorter electrolysis time was required in higher Br^- concentration because of larger electrolytic current. However, no dependence of the electrolysis time on the efficiency was observed when a smaller anode, which

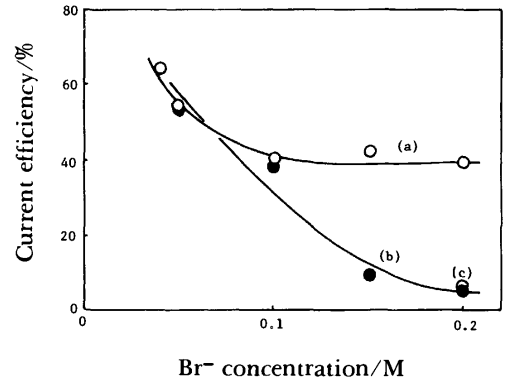

Fig. 1. Influence of Br^- concentration on current efficiency for products in the $(Br)^+$-mediated indirect electrooxidation of alcohols at a platinum anode (5.5 cm^2) in 0.2 M n-Bu_4NClO_4/CH_2Cl_2 containing n-Bu_4NBr and 2,6-lutidine. (a) Oxidation of benzyl alcohol to benzaldehyde at 1.7 F mol^{-1} of charge passed at 1.4 V vs. SCE. (b) Oxidation of 2,3-butanediol to acetoin at 2.0 F mol^{-1} at 1.3 V. (c) Electrolysis similar to (b) using a smaller anode (1.5 cm^2).

required longer electrolysis time, was used (See Fig. 1(c)). This fact indicates that the concentration dependence results directly from concentration effects of Br^- in the anodic solution. A cyclic voltammogram of Br^- gave two oxidation peaks at 0.8 and 1.0 V vs. SCE (See Fig. 3(b)). The oxidation of 2,3-butanediol in a first peak potential region could scarecely proceed even in low Br^- concentration (0.05 M).

A similar concentration dependence was also found in the oxidation of 2,3-butanediol in an acidic aqueous solution (0.2 M H_2SO_4), while no dependence in a neutral solution (0.3 M KH_2PO_4–0.3 M Na_2HPO_4) (See Fig. 2).

The above results may give general guidelines for synthetic use of the $(Br)^+$-mediated indirect electrooxidation: (a) To choose reaction media taking into account their nucleophilicity, (b) to electrolyze at potentials more positive than the second oxidation peak potential of Br^-, and (c) to use auxiliary supporting electrolytes when low Br^- concentration is inevitably required.

An Synthetic Application of the $(Br)^+$-Mediated Indirect Electrooxidation of Benzyl Alcohols with Electron-Withdrawing Groups to the Corresponding Benzaldehydes. Benzaldehydes are very important starting compounds for production of a variety of useful organic chemicals and one of the most common synthetic methods is either chemical or electrochemical oxidation of the corresponding toluenes. However, any practical synthetic method of pentafluorobenzaldehyde, which must be an important compound as a building block for synthesis of useful aromatic fluorine compounds, has not been established, because 2,3,4,5,6-pentafluorotoluene can be prepared only with great difficulty. We have recently reported an efficient conversion method of commercially-available pentafluorobenzoic acid into 2,3,4,5,6-pentafluorobenzyl alcohol.[8] In this work, it was also found that pentafluorobenzyl alcohol could be oxidized by the $(Br)^+$-mediated electrolysis to give pentafluorobenzaldehyde as a sole product without any further oxidation to pentafluorobenzoic acid. These facts suggest a possibility of the conversion of pentafluorobenzoic acid into pentafluorobenzaldehyde via pentafluorobenzyl alcohol.

In addition, a nitro-substituted benzyl alcohol, which is hardly oxidized due to the electron-withdrawing effect of nitro group, could be oxidized in a similar manner.

Electrolytic results obtained are summarized in Table 1.

Cyclic Voltammetric Behavior of Br^- and $(Br)^+$ Species. Anodic behavior of Br^- in organic solvents may be generally characterized by two oxidation waves which indicate the occurrence of the following reactions from wave height ratio:[9,10]

$$3Br^- \longrightarrow Br_3^- + 2e \text{ at the lst wave} \quad (1)$$

$$Br_3^- \longrightarrow \frac{3}{2}Br_2 + e \text{ at the 2nd wave} \quad (2)$$

Figures 3(b) and (c) show cyclic voltammograms of Br^- measured at a platinum electrode in dichloromethane. The above reactions seem to be responsible for two oxidation peaks (P_{a2} and P_{a1}) observed. In the curve(c) which was returned at 1.4 V, a small cathodic peak (P_{c1}) was observed. This may be responsible for the reduction of Br_2 to Br_3^-. When benzyl alcohol was added (See the curve (e)), any change of the two peaks (P_{a2} and P_{a1}) was not observed. In addition, the oxidation peak of benzyl alcohol, which appeared in a potential range more positive than 1.8 V, did not significantly decrease. These facts suggest that the oxidation of the alcohol by $(Br)^+$ species formed at P_{a2} is not fast.

Br_3^- may be formed by the reaction of Br^- with Br_2 generated at an anode.[10]

$$Br_2 + Br^- \rightleftharpoons Br_3^- \quad (3)$$

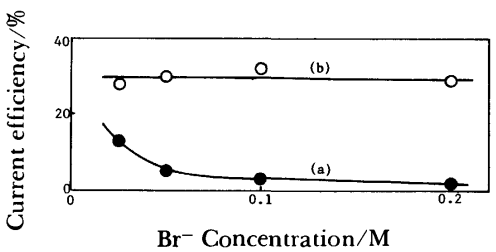

Fig. 2. Influence of Br^- concentration on current efficiency for acetoin in the $(Br)^+$-mediated indirect electrooxidation of 2,3-butanediol at a graphite anode (5.5 cm^2) in aqueous solutions. (a) Electrolysis at 1.5 F mol^{-1} of charge passed at 1.4 V vs. SCE in 0.2 M H_2SO_4. (b) Electrolysis at 2.0 F mol^{-1} at 1.2 V in 0.3 M KH_2PO_4–0.3 M Na_2HPO_4.

Table 1. The $(Br)^+$-Mediated Indirect Electrooxidation of Benzyl Alcohols to the Corresponding Benzaldehydes

Benzyl alcohol	Anode potential[a] V vs. SCE	Conversion %	Yield[b] of benzaldehyde %	Current efficiency %
Benzyl alcohol	1.4	89	83	46
p-Nitro-benzyl alcohol	2.0	79	65	31
Penta-fluoro-benzyl alcohol	2.0	57	67	22

a) 3.3 F mol^{-1} of charge were passed at potentials less positive than those for oxidation of the starting benzyl alcohols themselves in the presence of Br^- (0.05 M). b) Based on benzyl alcohols consumed.

It is well-known that Br_3^- is much less active than Br_2 as a oxidizing agent.[11-13] Therefore, lower current efficiency for the $(Br)^+$-mediated indirect electrooxidation in higher Br^- concentration (See Fig. 1) can be rationalized as due to more smooth formation of Br_3^-. In the neutral aqueous solution which has a higher nucleophilicity than the acidic aqueous and dichloromethane solutions, no dependence of Br^- concentration was observed as shown in Fig. 2(b). This may be rationalized as due to the formation of another active $(Br)^+$ species as shown below:[11]

$$Br_2 + H_2O \longrightarrow HBrO + HBr \quad (4)$$

At the next stage of investigation, cyclic voltammetric behavior of Br_2 was examined in dichloromethane. As shown in Figs. 4(a)—(c), Br_2 showed many reduction and oxidation peaks, among which P_{c1}, P_{c2}, P_{a2}, and P_{a1} seemed to be responsible for the following reactions:

$$Br_2 + \frac{2}{3}e \underset{P_{a1}}{\overset{P_{c1}}{\rightleftharpoons}} \frac{2}{3}Br_3^- \quad (5)$$

$$\frac{2}{3}Br_3^- + \frac{4}{3}e \underset{P_{a2}}{\overset{P_{c2}}{\rightleftharpoons}} 2Br^- \quad (6)$$

However, any reactions responsible for the other peaks (P_{c3}, P_{a4}, and P_{a3}) could not be reasonably thought out.

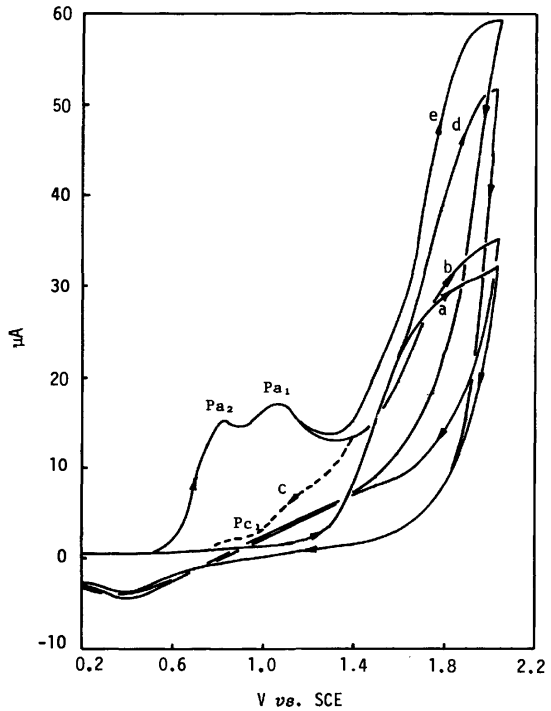

Fig. 3. Cyclic voltammograms of Br^- at a platinum electrode (1.3 mm^2) in the presence of benzyl alcohol. (a) Background solution, 0.1 M n-Bu_4NClO_4/CH_2Cl_2. (b) 5 mM n-Bu_4NBr. (c) 5 mM n-Bu_4NBr (returned at 1.4 V vs. SCE). (d) 10 mM benzyl alcohol. (e) 5 mM n-Bu_4NBr-10 mM benzyl alcohol. Scan rate: 0.1 V s^{-1}.

As shown in Fig. 4(d), the addition of 1 equiv Br^- resulted in a decrease of P_{c1} and increases of P_{a2} and P_{a1}. However, P_{c2} disappeared unexpectedly, while a new peak (P_{c4}) appeared in a negative potential range around −1.8 V but a reaction responsible for this peak also could not be thought out.

UV-Spectroscopic Study of $(Br)^+$ Species Formed Chemically and Electrochemically. Considerable ambiguity has been ramained in the above analysis of the cyclic voltammetric behavior of Br^- and Br_2. Therefore, next it was attempted to identify $(Br)^+$ species by UV-spectroscopy.

Figures 5(a) and (b) show the spectra of Br_2(λ_{max} 230 nm) and Br^-(λ_{max} 231 nm), respectively. A mixture of 2 mM Br_2 and 0.03 mM Br^- gave the spectrum(c) consisting of an absorption peak for Br_2 with an almost equal height to that in the spectrum(a) and a new peak at λ_{max} 271 nm. The height of this new peak increased in proportion to Br^- concentration (See spectra(c)—(e)), while the Br_2 peak decreased gradually (spectra(c), (d)) and disappeared in the concentration equivalent to Br_2(spectrum(e)). As shown in the spectrum(f), the presence of excess Br^- resulted in no change in height of the new peak and in appearance of the Br^- peak as a shoulder. Formation constants of Br_3^- on the basis of Eq. 3 are as extremely large as 10^7—10^9 in aprotic solvents.[14] Gabes and Stufkens[15] reported the λ_{max} and ε_{max} of Br_3^-

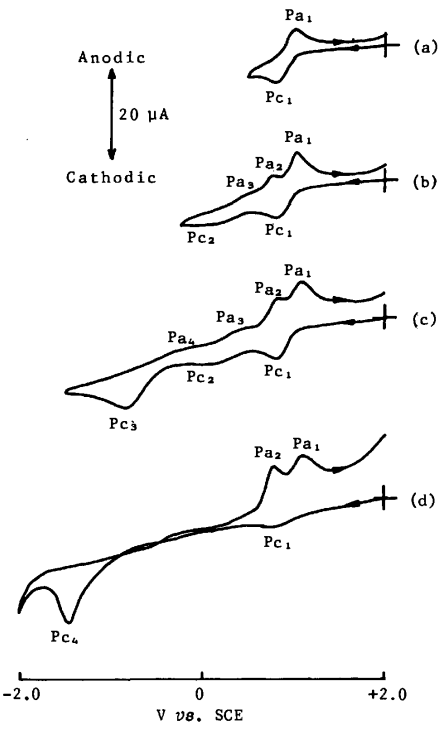

Fig. 4. Cyclic voltammograms of Br_2 at a platinum electrode (1.3 mm^2) in 0.1 M n-Bu_4NClO_4/CH_2Cl_2. (a)—(c) 2 mM Br_2. (d) 2 mM Br_2+2 mM n-Bu_4NBr. Scan rate: 0.1 v s^{-1}.

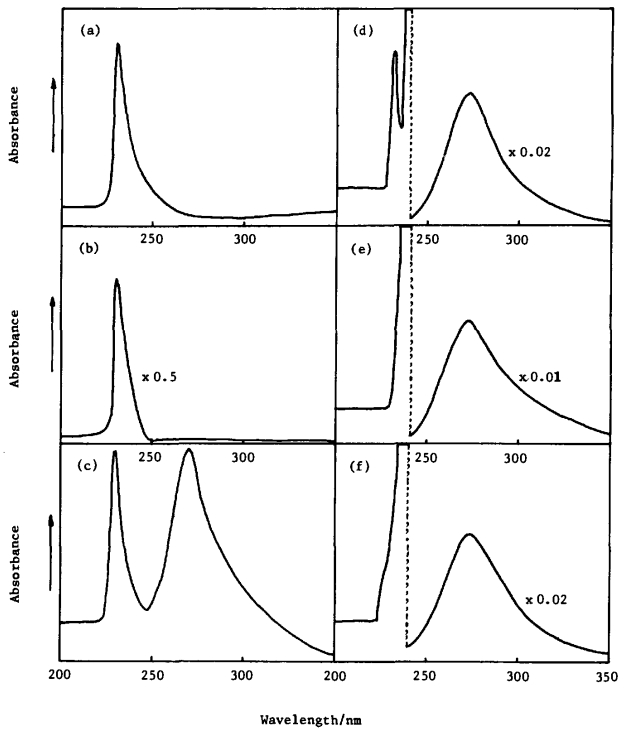

Fig. 5. UV-Spectra of bromine species prepared by mixing Br_2 and n-Bu_4NBr in CH_2Cl_2.
(a) 2 mM Br_2. (b) 2 mM n-Bu_4NBr. (c) 2 mM Br_2+0.03 mM n-Bu_4NBr. (d) 1 mM Br_2+2 mM n-Bu_4NBr. (e) 2 mM Br_2+2 mM n-Bu_4NBr. (f) 2 mM Br_2+1 mM n-Bu_4NBr.

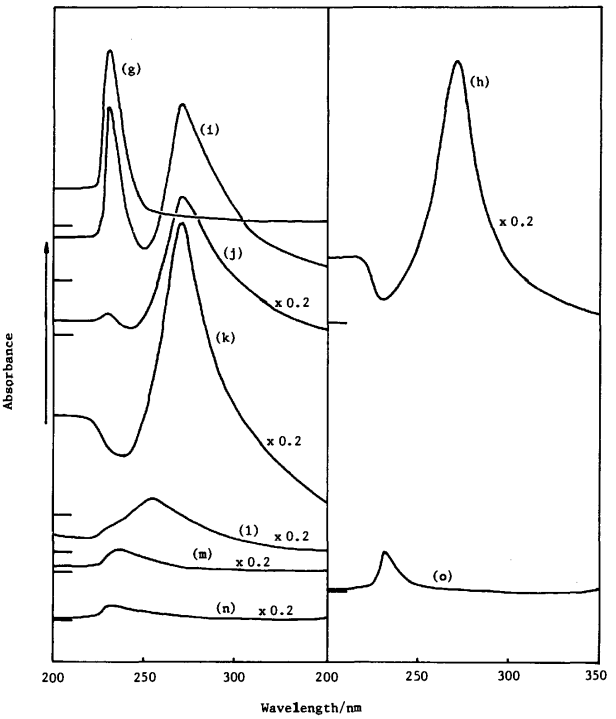

Fig. 6. Changes in UV-spectra of 50 mM n-Bu_4NBr/CH_2Cl_2 with increase in charge passed at a platinum anode (5.5 cm^2). The spectra were measured after diluted fifty times. (g) 50 mM n-Bu_4NBr. (h) 0.70 F mol^{-1} at 1.0 V vs. SCE. (i) 0.06 F mol^{-1} at 1.7 V. (j) 0.28 F mol^{-1} at 1.7 V. (k) 0.67 F mol^{-1} at 1.7 V. (l) 1.00 F mol^{-1} at 1.7 V. (m) 1.10 F mol^{-1} at 1.7 V. (n) 1.13 F mol^{-1} at 1.7 V. (o) 1.10 F mol^{-1} at 2.0 V.

in dichloromethane to be 272 nm and 46600, respectively. Based on these facts observed in this work and reported in the literatures, the new peak was assigned to Br_3^- and its ε_{max} was estimated to be ca. 47000. It is hereby confirmed that Br_3^- is formed almost quantitatively through the reaction shown in Eq. 3 and any $(Br)^+$ species can not be formed in dichloromethane even if excess Br_2 were used.

Figure 6 shows spectra of anodic solutions (50 mM n-Bu_4NBr/CH_2Cl_2) which were electrolyzed by passing various amounts of charge at various potentials using a platinum anode in a divided cell. The spectrum(g) was measured before the electrolysis. When the solution was electrolyzed coulometrically at 1.0 V, the electrolytic current diminished to a residual current level at 0.70 F mol^{-1} (1 F=96480C) of charge passed. Spectrum(h) of the solution after the electrolysis showed a Br_3^- peak, of which height corresponded to 15 mM of Br_3^- concentration, and no Br^- peak. This fact indicates the almost complete occurrence of the reaction shown in Eq, 1, if the reaction mechanism is left out of consideration, since the theoretical Br_3^- concentration is calculated to be 17 mM.

Larger amounts of charge could be passed at more positive potentials. Figures 6(i)—(n) are spectra of the solutions electrolyzed at 1.7 V. When 0.06—0.67 F mol^{-1} were passed, the concentrations of Br_3^- and Br^- were estimated from their peak heights (spectra(i)—(k)) as follows: 1.9 mM Br_3^- (theoretical, 1.5 mM) and 49 mM Br^-(theoretical, 46 mM) at 0.06 F mol^{-1}; 8 mM Br_3^-(theoretical, 7 mM) and 31 mM Br^-(theoretical, 29 mM) at 0.28 F mol^{-1}; 17 mM Br_3^-(theoretical, 17 mM) and 0 mM Br^-(theoretical, 0 mM) at 0.67 F mol^{-1}. These aqreements of found values of the concentrations with the theoretical ones indicate the predominant occurrence of the reaction shown in Eq. 1. However, a strange phenomenon was observed at charge more than 0.67 F mol^{-1} which is the theoretical amount based on Eq. 1.

As shown in Fig. 6(l) and (m), a new peak appeared, while the Br_3^- peak disappeared. Moreover, the λ_{max} and height of this new peak shifted to shorter wavelengths and decreased, respectively, though the Br_3^- and Br_2 peak heights should decrease and increase, respectively, with increase in charge passed if the Eq. 2 reaction occurred following Eq. 1.[9,10] A small Br_2 peak could be observed only as a shoulder in the spectrum(l). When a slightly larger amount of

charge than 1 F mol^{-1}, which is the theoretical amount based on the combination of Eqs. 1 and 2, was passed, the electrolytic current diminished to the residual current level and the new peak apparently overlapped the Br_2 peak. However, Br_2 concentration calculated from the overlapped peak was as much higher as 60 mM than the theoretical value (25 mM). This fact means the peak contains a contribution of another component which has a larger ε_{max} than that of Br_2. The electrolysis at a more positive potential such as 2.0 V resulted in the formation of Br_2(found, 23 mM; theoretical, 25 mM) (See spectrum(o)).

It was also confirmed by iodometry using $Na_2S_2O_3$ that the anodic solutions always had oxidizing capacities equivalent to amounts of charge passed at all the potentials used.

From the results obtained above, it is likely that the peaks observed in the spectra(l)—(n) are assigned to polybromides(Br_n^-, $n>3$) of which the possible preparation as the corresponding quaternary ammonium salts (n=5, 7, 8, 9, 11, and 33) by the direct reaction of bromide salts with liquid or gaseous Br_2 has been reported,[16-18] though only an uncertain evidence for the formation of Br_5^- in solutions has been reported.[19] It is noticeable that a possibility for the formation of Br_n^- ($n>3$) by the anodic oxidation of Br^- in solutions was suggested in this work.

Conclusion

(a) The formation of Br_3^- depends not on potential(E) as indicated by Eqs. 1 and 2 but on charge(Q) passed as shown below.

$$Q \leqslant \frac{2}{3}\text{F mol}^{-1};\ E\text{, independent:}$$

$$2Br^- \xrightarrow{-2e} [Br_2] \xrightarrow{Br^-} Br_3^- \qquad (7)$$

(b) The formation of Br_n^- ($n>3$) occurs by a cascade type of reactions shown below. The reactions depend on both E and Q, in other words n is a function of E and Q.

$$\frac{2}{3}<Q<1\ \text{F mol}^{-1};\ 1<E<2\ \text{V vs. SCE:}$$

$$Br_3^- \longrightarrow \frac{3}{4}Br_4^- + \frac{1}{4}e$$

$$Br_4^- \longrightarrow \frac{4}{5}Br_5^- + \frac{1}{5}e$$

$$\cdots\cdots\cdots\cdots\cdots\cdots$$

$$Br_{n-1}^- \longrightarrow \frac{n-1}{n}Br_n^- + \frac{1}{n}e \qquad (8)$$

Remarkably sensitive changes observed in the spectra of Br_n^- with increase in Q can be reasonably rationalized as due to the occurrence of this type of reactions.

(c) The formation of Br_2 as a final product occurs when 1 F mol^{-1} is completely passed at potentials more positive than 2 V. $\lim_{n\to\infty} Br_n^-$ actually corresponds to Br_2.

(d) The order of oxidizing powers of $(Br)^+$ species is speculated as below.

$$Br_3^- < Br_4^- < \cdots\cdots < Br_n^- < \cdots\cdots < Br_2$$

(e) Low current efficiency for the $(Br)^+$-mediated indirect electrooxidation in high Br^- concentration is explained on the basis of the above items(a)—(d). Therefore, it is recommended for efficient $(Br)^+$-mediated indirect electrooxidation to use low Br^- concentration and positive potential as possible: It is undesirable to make bromide salts serve a double purpose for the mediator and supporting electrolyte, since their concentration must be so high that electroconductivity of the electrolytic solutions is high enough. It is also recommended to use large amounts of other salts, which can play a role as the supporting electrolytes, in addition to small amounts of bromides, in order to perform the electrolysis at a satisfactorily low cell voltage.

Experimental

Materials. All the chemicals were commercially supplied and were used, if necessary, after purification by common methods. Platinum electrodes, which were used as the working electrodes, were polished with alumina powder and washed with acetone before used. Graphite electrodes were also polished with an emery paper (No. 1200), washed with water, polished again with the emery paper, and then washed with acetone. Platinum counter electrodes were used after treatment with diluted nitric acid.

Controlled-Potential Electrolysis. All the macro electrolyses of the alcohols were carried out using 40 cm^3 of anodic solutions in a divided cell at room temperature. The electrolyses of Br^- were also carried out in a similar manner.

Product Analysis. Anodic solutions were subjected to gas chromatography (on PEG 20 M column at 120—160 °C) for analysis of products of electrolyses of the alcohols after quenched with aqueous $NaHSO_3$.

Cyclic Voltammetry. All the measurements were carried out at room temperature in an ordinary procedure.

UV-Spectroscopic Measurement. All the spectra were measured in a 1 cm cell, if necessary after dilution of the sample solutions, using a spectrometer (Hitachi Degital Spectrophotometer Model 624).

References

1) J. Simonet, "Electrogenerated Bases," in "Organic Electrochemistry," 2nd ed, ed by M. M. Baizer and H. Lund, Marcel Dekker, New York (1983), Chap. 26.

2) S. Torii, "Electroorganic Synthesis," Kodansha·VCH, Tokyo·New York (1985), Part 1, Chap. 11.

3) D. Cipris and I. L. Mador, *J. Electrochem. Soc.*, **125**, 1954 (1978).

4) T. Shono, Y. Matsumura, and K. Inoue, *J. Org. Chem.*,

51, 549 (1986).
5) S. Torii, H. Tanaka, Y. Tsutsui, T. Ohshima, and S. Yamashita, *Chem. Lett.*, **1986**, 1535.
6) D. Pletcher and N. Tomov, *J. Appl. Electrochem.*, **7**, 501 (1977).
7) M. M. Baizer, T. Nonaka, K. Park, Y. Saito, and K. Nobe, *J. Appl. Electrochem.*, **14**,197 (1984).
8) T. Iwasaki, T. T. Fuchigami, T. Nonaka, and M. Sasaki, '86 Fall Meeting of the Electrochemical Society of Japan, Tokyo, September 1986, Abstr. No. B114.
9) F. Magno, G.-A. Mazzocchin, and G. Bontempelli, *Electroanol. Chem.*, **47**, 461 (1973).
10) M. Mastragostino, S. Valcher, and P. Lazzari, *J. Electroanal. Chem.*, **126**, 189 (1981).
11) A. E. Bradfield, G. I. Davis, and E. Long, *J. Chem. Soc.*, **1949**, 1389.
12) W. J. Wilson and F. G. Sopec, *J. Chem. Soc.*, **1949**, 3376.
13) J. E. Dubois and X. O. Huynh, *Tetrahedron Lett.*, **1971**, 3369.
14) I. V. Nelson and R. T. Iwamoto, *J. Electroanal. Chem.*, **7**, 218 (1964).
15) W. Gabes and D. J. Stufkens, *Spectrochim. Acta*, **30A**, 1835 (1974).
16) R. Bloch, L. Farkas, J. Schnerb, and F. Winogron, *J. Phys. Colloid Chem.*, **53**, 117 (1949).
17) P. L. Mercier and C. A. Kraus, *Proc. Natl. Acad. Sci. U.S.A.*, **42**, 65 (1956).
18) F. Rallo and P. Silvestroni, *J. Electrochem. Soc.*, **119**, 1471 (1972).
19) J. C. Evans and G. Y.-S. Lo, *Inorg. Chem.*, **6**, 1483 (1967).

 © 1987 The Chemical Society of Japan Bull. Chem. Soc. Jpn., 60, 3143—3147 (1987)

Photochemical Stability of Polycyclic Aromatic Hydrocarbons in the Interstellar Medium

Jun-ichi AIHARA
Department of Chemistry, Faculty of Science, Shizuoka University, Oya, Shizuoka 422
(Received March 20, 1987)

The astronomical IR spectra of molecular origin have been attributed to compact polycyclic aromatic hydrocarbons. This interpretation can be rationalized in terms of the percent resonance energies of the excited-state species. In general, large compact polycyclic aromatic hydrocarbons are not only thermodynamically stable but also photochemically stable. These hydrocarbons have large percent resonance energies in the excited state, and are expected to survive the rough conditions in space. In contrast, relatively small aromatic hydrocarbons are greatly destabilized when they are excited electronically or deprived of two π electrons.

The infrared astronomical satellite (IRAS) launched in 1983 initiated a new era of interstellar chemistry.[1] Surprisingly, the IRAS satellite found that a series of discrete infrared (IR) bands are emitted from the interstellar medium (ISM). The emission maxima are located at 3.3, 6.2, 7.7, 8.6, and 11.3 μm, all of which are always observed as a set.[1] They are observed in a wide variety of astronomical objects: reflection nebulae, bipolar nebulae, planetary nebulae, and the whole regions of active galaxies.[1] The five IR bands are obviously of molecular origin. Fundamental molecular vibrations must be responsible for these bands.

It was in 1984 that Léger and Puget reported that a similar set of bands appears in the IR absorption spectrum of coronene (**8**).[2,3] They proposed that a mixture of various polycyclic aromatic hydrocarbons (PAHs) is responsible for the astronomical IR spectra. Allamandola et al. supported this view by showing the good agreement between the wavelengths of the astronomical IR bands and the Raman spectrum of automobile soot (a mixture of PAHs and small carbon particles).[4-6]

The five discrete IR bands can really be assigned to fundamental vibrations of PAHs.[1-8] The 3.3 μm band is assignable to an aromatic C–H stretch. The 6.2 μm band is assignable to a C=C stretch in an aromatic ring. The 7.7 μm band is not found in benzene (**1**) and naphthalene (**3**), and may be specific to large PAHs such as coronene.[3,8] The 8.6 μm band is assignable to an in-plane aromatic C–H bend. Finally, the 11.3 μm band is assignable to an out-of-plane aromatic C–H bend.

The wavelength position of the out-of-plane C–H bending mode is very sensitive to the number of adjacent hydrogen atoms on a ring.[3,5,6] The more hydrogens which are adjacent on the same ring, the longer the wavelength of this bending mode becomes. The predominance of the 11.3 μm emission in the 11—13 μm region implies that most interstellar PAHs have many solo hydrogens (see Fig. 1).[3] The emission observed in the 11.5—13 μm region might indicate the presence of PAHs with duo and trio hydrogens (see Fig. 1).

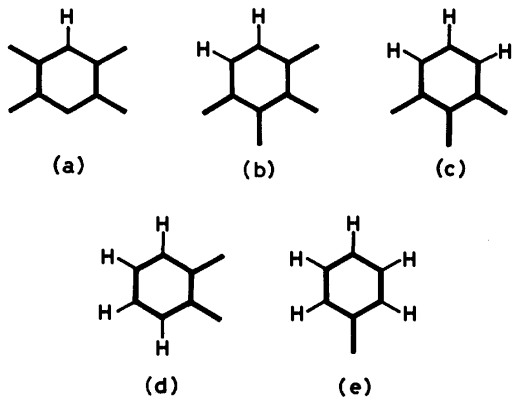

Fig. 1. Classification of hydrogens in PAHs: (a) solo hydrogen, (b) duo hydrogens, (c) trio hydrogens, (d) quartet hydrogens, and (e) quintet hydrogens.

These observations imply that rather compact PAHs with many solo hydrogens dominate the interstellar PAH mixture.[1-6] Typical compact PAHs have only solo and duo hydrogens. Léger and d'Hendecourt then found that the astronomical IR spectra resemble the IR spectra of compact PAHs very closely.[3] The fit with the IR spectra of non-compact PAHs is very poor. PAHs with quartet or quintet hydrogens (see Fig. 1) can be excluded because the emission bands concerned are very weak in the astronomical IR spectra.

Léger et al. further noticed that the extinction coefficient per solo hydrogen is much larger than that per duo hydrogen in the two measured PAHs ovalene (**28**) and dicoronene,[9] which have both solo and duo hydrogens.[3] The large extinction coefficient of a solo hydrogen is commonly found in many smaller PAHs.[8] Therefore, it is reasonable to assume that PAHs in the ISM can have some duo or trio hydrogens in addition to not a few solo hydrogens. This feature is consistent with the molecular structure of large compact PAHs, in which there must be some duo and/or trio hydrogens.

It is now fairly clear that interstellar PAHs, if any, must be limited to a large compact type. If so, we must seek for the reason why such PAHs are dominant

in space. Are these PAHs really stable enough to survive the rough conditions in the ISM? In order to find a clue to this problem, our graph theory of aromaticity[10-13] was applied to a variety of PAHs including those which have so far been the candidates for explaining astronomical IR data.

Results and Discussion

We have developed the graph theory of aromaticity since 1975.[10-13] We defined a new type of resonance energy in graph-theoretical terms. The percent resonance energy (%RE) of a given molecule is then defined as 100 times the resonance energy, divided by the total π-electron energy of its olefinic reference structure.[11,12] The %RE has been recognized as an excellent index for determining the degree of thermodynamic stability of a cyclic conjugated molecule. The %RE is approximately proportional to the resonance energy per π electron.[14,15] A PAH with a large %RE is considered to be thermodynamically stable and typically aromatic in nature.[11,12]

We calculated the %REs of a variety of PAHs (**1—46**) to test the above interpretation of the astronomical IR spectra. The obtained %REs are listed in Table 1. The %REs of relatively small PAHs have already been published.[11,12] As shown by the %REs, most PAHs are stable in our chemical sense. Here, we tentatively assume that a PAH with a %RE larger than 2.15 is very stable. This means that PAHs which are thermo-

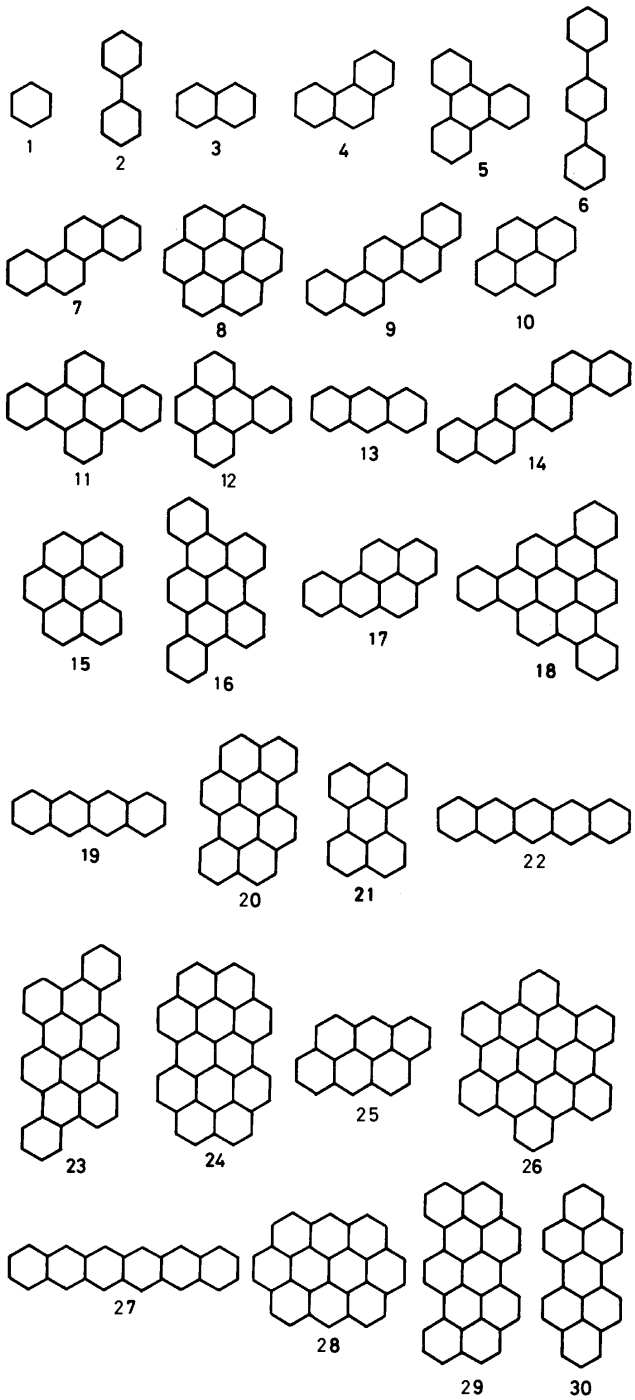

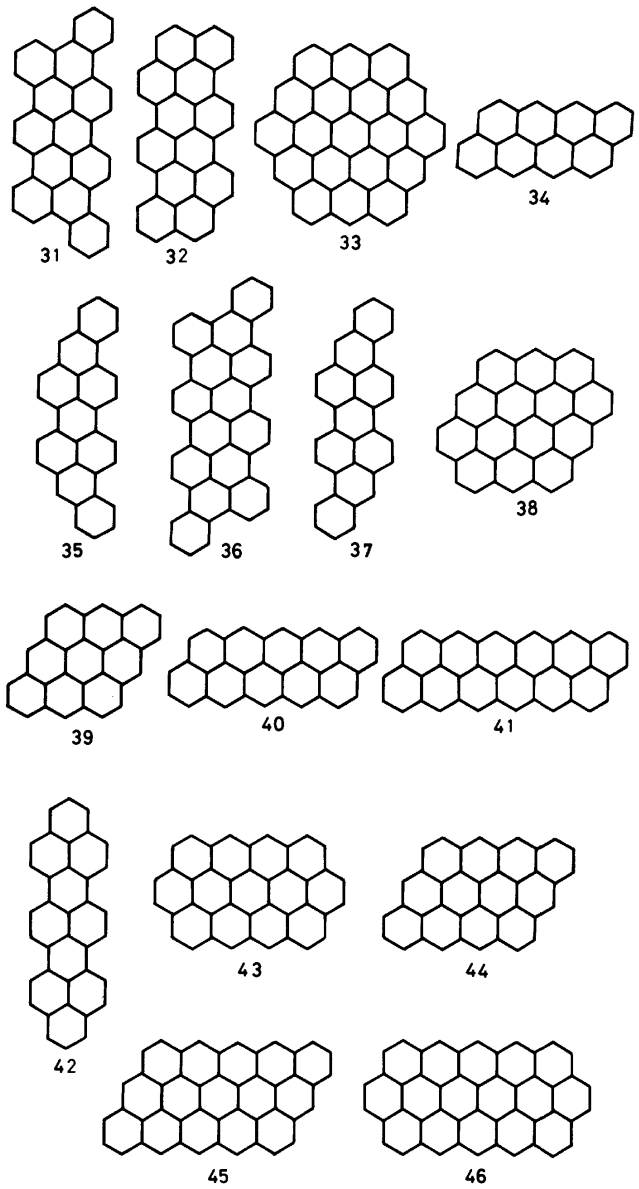

dynamically more stable than pentacene (**22**) must be very stable.

First of all, there are a group of very stable PAHs called fully benzenoid hydrocarbons (or fully benzenoid PAHs).[16-18] They are PAHs whose Clar structures consist of aromatic sextets alone.[16] PAHs **1**, **5**, **11**, **16**, **18**, **23**, **26**, **31**, and **36** are such PAHs. Since double bond character is scarcely localized anywhere in each of these PAHs, they provide the ultimate in stability which synthetic chemistry can offer.[15] The energy of the highest occupied molecular orbital (HOMO) in these PAHs is very low in energy, indicating that the HOMO contributes much to the thermodynamic stability of the entire molecule.[11,15] The %REs are all larger than 2.80.

Table 1. Percent Resonance Energies of PAHs

Species	%RE	
	Ground state	Excited state
1	3.528	−10.342
2	3.159	−1.175
3	2.924	−1.113
4	2.888	−0.453
5	3.012	−0.453
6	3.022	0.541
7	2.809	0.599
8	2.817	0.729
9	2.773	0.929
10	2.729	0.930
11	2.963	0.931
12	2.872	0.946
13	2.519	0.947
14	2.743	1.257
15	2.792	1.261
16	2.933	1.420
17	2.635	1.468
18	2.922	1.510
19	2.269	1.573
20	2.791	1.693
21	2.689	1.735
22	2.105	1.780
23	2.914	1.783
24	2.816	1.808
25	2.512	1.818
26	2.917	1.828
27	1.992	1.842
28	2.703	1.870
29	2.798	1.882
30	2.607	1.944
31	2.818	1.957
32	2.801	2.048
33	2.696	2.070
34	2.369	2.108
35	2.543	2.128
36	2.889	2.145
37	2.534	2.147
38	2.668	2.156
39	2.414	2.172
40	2.278	2.194
41	2.217	2.209
42	2.564	2.225
43	2.593	2.252
44	2.348	2.287
45	2.309	2.316
46	2.515	2.383

Accordingly, it is quite natural that Schmidt et al. regarded such fully benzenoid PAHs as attractive candidates to account for the astrophysical IR data.[16,17] The PAHs chosen by them are highly symmetric hexa-*peri*-benzocoronene (**26**) and tribenzocoronene (**18**). However, there is one serious difficulty with these PAHs. They have no solo hydrogens. Compact fully benzenoid PAHs have only duo and quartet hydrogens, and exhibit no 11.3 μm emission line. Therefore, they are not a major molecular component of the ISM although they are thermodynamically very stable. Benzene (**1**) is the most stable PAH with the largest %RE conceivable. However, there is no evidence for the existence of this molecule in the ISM. These facts strongly suggest that the ground-state stability is not a sufficient condition of the interstellar PAHs.

In this context, it may be worth noting that all IR-emitting PAHs must be placed in the strong radiation field since they must first be excited electronically to emit IR lines.[1-6] In other words, we can observe only PAHs in the emission zone. If a given PAH is fragile in the excited state, it cannot survive the severe radiation field in the ISM. Therefore, the stability of the excited-state species or the photochemical stability must be the most important factor in the present interstellar chemistry. In order to see the photochemical stability, we then calculated the %REs of all PAHs in the first excited state.[19] They are listed in Table 1.

Furthermore, it is very probable that the radiation field in the emission zone is intense enough to ionize many of the PAHs.[3,5,21] The PAHs were estimated to exist in cationic forms to more than 50% in extent.[4,20] The importance of double ionization was stressed by Leach.[22] d'Hendecourt pointed out in Ref. 23 that the radiation field in reflection nebulae is so high that most of the PAHs are probably ionized. From this point of view, the stability of the dications, as well as that of the excited-state species, must be taken into account when the type of interstellar PAHs is sought.

All PAHs are alternant hydrocarbons. Therefore, the energy of the lowest unoccupied molecular orbital (LUMO) is equal to the negative of the energy of the HOMO. Then, the %RE of the dianion of any PAH is equal to that of the dication. The %RE of a given PAH in the first excited state is also equal to that of the dication. Accordingly, we do not need to calculate

the %REs of the dications. The %REs of the excited-state species in Table 1 automatically represent the %REs of the dications. The %RE of the monocation or the monanion can readily be obtained by averaging the %REs of the ground-state species and the dication.

As can be seen from Table 1, fully benzenoid hydrocarbons are unable to form stable dications. The %REs of tribenzocoronene (**18**) and hexa-*peri*-benzocoronene (**26**) decrease much when they are excited electronically or doubly ionized. The same is fairly true for other fully benzenoid hydrocarbons. This is possibly the primary reason why such fully benzenoid PAHs do not contribute appreciably to the astronomical IR spectra. Polyphenyls, such as biphenyl (**2**) and terphenyl (**6**), are a kind of fully benzenoid PAHs. They are also supposed to be photochemically unstable.

There are many solo hydrogens in large linear polyacenes. However, none of them are thermodynamically very stable in the ground state.[11,15] Pentacene (**22**) and hexacene (**27**) must be handled under nitrogen since they are very oxidizable.[16] Higher members of this series are not isolable. Angulated polyacenes, such as phenanthrene (**4**), chrysene (**7**), picene (**9**), and fulminene (**14**), are very stable in the ground state. However, both linear and angulated polyacenes are unstable in the excited state. Therefore, they are not qualified for the PAHs in the ISM. All polyacenes have quartet hydrogens, the presence of which are also inconsistent with the astronomical IR spectra. Angulated polyacene do not have solo hydrogens.

Léger and Puget[2] and Allamandola et al.[5] estimated the carbon content of the interstellar PAHs to lie in the range of 20—50 carbon atoms. PAHs having less than 20 carbons must be much less abundant in the ISM. As shown in Table 1, this suggestion corresponds to the fact that dications derived from relatively small PAHs are not stable. For small PAHs the contribution of the HOMO to the RE is very large. Therefore, they become fairly unstable by losing two π electrons in the HOMO. Among the PAHs in Table 1 those having 30 or less carbon atoms behave in this manner. Dications of PAHs **1**—**5** are antiaromatic with negative %REs. Many of small PAHs do not have solo hydrogens.

Finally, large compact PAHs with solo hydrogens constitute the group of PAHs which have large %REs both in the ground and excited states. They are best exemplified by circumnaphthacene (**46**), dibenzocircumanthracene (**45**), dibenzovalene (**44**), circumanthracene (**43**), and circumpyrene (**38**). The %REs of these PAHs are all larger than 2.15 both in the ground state and in the excited or doubly ionized states. Accordingly, they must be fairly stable not only at high temperature but also in the strong radiation field. Since these PAHs have not a few solo hydrogens, they presumably match the pattern of the astronomical IR spectra. The large compact PAHs can be considered as the best candidates for the interstellar PAHs. The abundance of large compact PAHs has thus been explained satisfactorily.

It should be noted that large compact PAHs are not always qualified for the interstellar PAHs. Only those having large %REs in the excited state are eligible for them. Many compact PAHs do not have solo hydrogens, and their dications have small %REs. PAHs **8**, **20**, **24**, and **28** are all large and compact in shape. However, they are greatly destabilized in the excited state. As stated above, all fully benzenoid PAHs are not stable in the excited or doubly ionized states. Although hexa-*peri*-benzocoronene (**26**) is a large compact PAH, it is not an exception. All fully benzenoid PAHs investigated have no solo hydrogens.

Tielens et al. inferred that hexagonally symmetric PAHs, such as coronene (**8**) and circumcoronene (**33**), might dominate the interstellar PAH mixture.[24] This type of PAHs have doubly degenerate HOMOs. Benzene (**1**) also belongs to this type of PAHs. Dianions of such PAHs necessarily have much smaller %REs than those of other PAHs of similar size. Therefore, the compact PAHs responsible for the astronomical IR spectra must be less symmetric than coronene and circumcoronene. Coronene forms one of the most unstable dications among the PAHs investigated.

PAHs in Table 1 are numbered in such a manner that the excited-state species are arranged in order of increasing %RE. It is evident that rather large compact PAHs come later. Many PAHs with large %REs have not a few solo hydrogens. Circumnaphthacene (**46**) and circumanthracene (**43**) appear to be excellent candidates conceivable at present. These two PAHs are thermodynamically very stable as indicated by the large %REs of the ground-state species. They are also photochemically very stable as indicated by the large %REs of the dianions or the excited-state species.

As shown in Table 1, there are some non-compact PAHs which are photochemically as stable as large compact ones. PAHs **40**—**42** are examples of this kind. PAH **42** does not have solo hydrogens. If there are synthetic routes to these PAHs in the ISM, they must also contribute more or less to the interstellar IR emission.

Concluding Remarks

In general, benzene and fully benzenoid hydrocarbons constitute the most stable group of PAHs. The absence of this group in the ISM suggests that there must be another criterion for determining the type of interstellar PAHs. Fully benzenoid hydrocarbons and most of relatively small PAHs were found to be photochemically unstable. Considering that the IR-emission zone are situated in the strong radiation

field, these photochemically unstable PAHs can be excluded. Then, large compact PAHs remained.

Fortunately, large compact PAHs have many solo hydrogens, and can be considered as excellent candidates for explaining the astronomical IR spectra taken by the IRAS satellite. Thus, it is photochemical stability that determines the type of PAHs in the ISM. The ground-state stability is of course important. However, almost all PAHs satisfy this condition. We believe that the existence of large compact PAHs in the interstellar IR-emission zone[1] has thus been rationalized.

Helpful discussions with Professor Kunio Fukushima are gratefully acknowledged.

References

1) "Polycyclic Aromatic Hydrocarbons and Astrophysics," ed by A. Léger, L. d'Hendecourt, and N. Boccara, D. Reidel, Dordrecht, The Netherlands (1987).
2) A. Léger and J. Puget, *Astron. Astrophys.*, **137**, L5 (1984).
3) A. Léger and L. d'Hendecourt in Ref. 1, pp. 223—254.
4) L. J. Allamandola, A. G. G. M. Tielens, and J. R. Barker, *Astrophys. J.*, **290**, L25 (1985).
5) L. J. Allamandola, A. G. G. M. Tielens, and J. R. Barker in Ref. 1, pp. 255—271.
6) A. G. G. M. Tielens, L. J. Allamadola, and J. R. Barker, and M. Cohen in Ref. 1, pp. 273—286.
7) L. J. Bellamy, "The Infrared Spectra of Complex Organic Molecules," 2nd ed, Wiley, New York (1966).
8) C. J. Pouchert, "The Aldrich Library of Infrared Spectra," 2nd ed, Aldrich Chemical, Milwaukee, Wisconsin (1975).
9) H. J. Lempka, S. Obenland, and W. Schmidt, *Chem. Phys.*, **96**, 349 (1985).
10) J. Aihara, *J. Am. Chem. Soc.*, **98**, 2750 (1976); *Netsu Sokutei*, **12**, 61 (1985).
11) J. Aihara, *J. Am. Chem. Soc.*, **99**, 2048 (1977).
12) J. Aihara, *Pure Appl. Chem.*, **54**, 1115 (1982).
13) I. Gutman, M. Milun, and N. Trinajstić, *J. Am. Chem. Soc.*, **99**, 1692 (1977); N. Trinajstić, "Chemical Graph Theory," CRC Press, Boca Raton, Florida (1983), Vol. II, Chap. 1.
14) B. A. Hess, Jr. and L. J. Schaad, *J. Am. Chem. Soc.*, **93**, 305 (1971).
15) B. A. Hess, Jr. and L. J. Schaad, *J. Am. Chem. Soc.*, **93**, 2413 (1971).
16) E. Clar, "The Aromatic Sextet," Wiley, London (1972).
17) W. Hendel, Z. H. Khan, and W. Schmidt, *Tetrahedron*, **42**, 1127 (1986).
18) S. Obenland and W. Schmidt in Ref. 1, pp. 165—172.
19) J. Aihara, *Bull. Chem. Soc. Jpn.*, **51**, 1788 (1978).
20) A. Léger and L. d'Hendcourt, *Astron. Astrophys.*, **146**, 81 (1985).
21) A. Omont, *Astron. Astrophys.*, **164**, 159 (1986).
22) S. Leach, *J. Electron Spectrosc. Relat. Phenom.*, **41**, 427 (1986); Ref. 1, pp. 99—127.
23) M. Jura in Ref. 1, pp. 367—370.
24) A. G. G. M. Tielens, L. J. Allamandola, J. R. Barker, and M. Cohen in Ref. 1, pp. 273—286.

 © 1987 The Chemical Society of Japan Bull. Chem. Soc. Jpn., 60, 3149—3155 (1987)

A New Type of Tetradentate Square-Planar N_2O_2 Ligands. Copper(II) Complexes of 6,6′-Bis(acylamino)-2,2′-bipyridines

Masaki YAMADA, Koji ARAKI,* and Shinsaku SHIRAISHI*
Institute of Industrial Science, The University of Tokyo, 7-22-1 Roppongi, Minato-ku, Tokyo 106
(Received March 20, 1987)

A new type of N_2O_2 tetradentate ligands, 6,6′-bis(acylamino)-2,2′-bipyridines, was synthesized and their complex formations with copper(II) were investigated. They form two types of 1:1 complexes; one is the non-deprotonated type having external counter anions and the other is the deprotonated type having no external counter anions. They serve as square planar N_2O_2 tetradentate ligands in either case and the structures of the complexes are very similar to salen complexes. The structures and properties of these complexes were investigated and discussed.

The complexes of tetradentate square-planar N_2O_2 ligands, *N,N′*-di(salicylidene)ethylenediamine (salen) and its derivatives, have been the subject of intense studies because of their ability to activate various molecules, especially, molecular oxygen coordinated to the axial positions of the complexes.[1] Property-control (tuning) by modification of diimine moiety and/or ring substitution of salen is limited in versatility, and exploitation of the complexes of analogous structure has been demanded.

We have been investigating chemistry of 6,6′-diamino-2,2′-bipyridine (dabp).[2,3] The amino groups of dabp are easily modifiable, and, in previous papers, we reported alkylation of the amino groups of dabp and application of these alkyl-substituted derivatives to metal-ion transport.[3] Here, we wish to report another type of derivatives, 6,6′-bis(acylamino)-2,2′-bipyridines, obtained by acylation of the amino groups of dabp, which are found to serve as a new type of N_2O_2 ligands.

The coordination sites in these ligands are expected to be ring-nitrogens and amide-oxygens serving as N_2O_2 tetradentate planar ligands. Dissociation of amide protons upon complex formation may afford the complexes analogous to the salen complexes. Furthermore, the complexes are expected to be more stable than the salen complexes, especially in an acidic solution, because the easily hydrolyzable Schiff base moieties of the salen complexes are replaced by the bipyridine moiety. Two ligands, 6,6′-bis(benzoylamino)-2,2′-bipyridine ($babpH_2$) and 6,6′-bis(hexanoylamino)-2,2′-bipyridine ($habpH_2$) were prepared, and their complexations with copper(II) were investigated. The results were discussed in comparison with the coordination chemistry of salen and its derivatives, and also with that of analogous ligands, 2-(benzoylamino)pyridine (bapH) and 2-(acetylamino)-pyridine (aapH) reported by Nonoyama et al.[4-7]

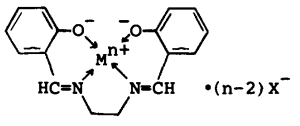

Salen Complex

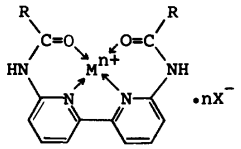

Non-Deprotonated Complex

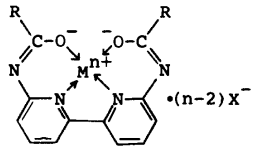

Deprotonated Complex

Complexes of 6,6'-Bis(acylamino)-2,2'-bipyridine

Results

Syntheses. 6,6′-Bis(acylamino)-2,2′-bipyridines ($babpH_2$ and $habpH_2$) were prepared by acylation of amino groups of dabp with the corresponding acyl chlorides (Scheme 1). 2,9-Bis(benzoylamino)-1,10-phenanthroline ($baptH_2$) was also prepared from 2,9-diamino-1,10-phenanthroline.[8] Elemental analyses agreed well with the calculated values within a permitted experimental error (<±0.3%, Table 1). Chemical shifts in ^{13}C and ^1H NMR spectra of the ligands in dimethyl-d_6 sulfoxide (DMSO-d_6) (Tables 2 and 3, respectively) confirmed their structures, most of which were quite similar to those of corresponding 2-(acylamino)pyridines.[9]

Complexation of $babpH_2$ with copper(II) nitrate and acetate gave different types of complexes, i.e., the non-deprotonated complex **1a** and the deprotonated one **2a** respectively (Table 1). A blue complex $Cu(babpH_2)(H_2O)_2(NO_3)_2$, **1a** was obtained by complexation with copper(II) nitrate in methanol (Scheme 1). The IR spectrum of complex **1a** showed the presence of amide carbonyl and N-H stretching bands (Table 4). The change in IR spectrum upon complexation was quite similar to those of 2-(acylamino)-pyridines.[4-6] On the other hand, a green complex [Cu(babp)], **2a** was obtained by complexation with copper(II) acetate (Scheme 1). This showed neither amide carbonyl nor N-H stretching bands in its IR spectrum (Table 4), indicating the deprotonation of both of the two amide protons. The characteristic IR

Table 1. Analytical and Physical Data of Ligands and Their Copper(II) Complexes

Material[a]	Appearance	Mp(θ_m/°C)	Elemental analysis/% (Calcd)
$babpH_2$	White flake	289—291	C, 72.94; H, 4.54; N, 14.04 ($C_{24}H_{18}N_4O_2$: C, 73.08; H, 4.60; N, 14.20)
$habpH_2$	White flake	220—223	C, 69.00; H, 7.89; N, 14.67 ($C_{22}H_{30}N_4O_2$: C, 69.08; H, 7.91; N, 14.65)
$baptH_2$	Pale yellow needle	250—253	C, 74.39; H, 4.27; N, 13.73 ($C_{26}H_{18}N_4O_2$: C, 74.63; H, 4.34; N, 13.79)
$Cu(babpH_2)(H_2O)_2(NO_3)_2$ (**1a**)	Light blue plate	ca. 250[c]	C, 46.70; H, 3.42; N, 13.50 ($C_{24}H_{22}CuN_6O_{10}$: C, 46.64; H, 3.59; N, 13.60)
[Cu(babp)][b] (**2a**)	Green needle	>300	C, 63.10; H, 3.32; N, 12.36 ($C_{24}H_{16}CuN_4O_2$: C, 63.22; H, 3.54; N, 12.29)
$Cu(habpH_2)(H_2O)(NO_3)_2$ (**1b**)	Blue plate	ca. 250[c]	C, 45.22; H, 5.38; N, 14.11 ($C_{22}H_{32}CuN_6O_9$: C, 44.93; H, 5.48; N, 14.29)

a) $BabpH_2$, 6,6′-bis(benzoylamino)-2,2′-bipyridine; $habpH_2$, 6,6′-bis(hexanoylamino)-2,2′-bipyridine; $baptH_2$, 2,9-bis(benzoylamino)-1,10-phenanthroline. b) Babp, the deprotonated form of $babpH_2$ (both of amide protons). Similar abbreviations are used for other deprotonated ligands. c) Decomposition.

Table 2. Chemical Shifts in ^{13}C NMR Spectra of Metal-Free Ligands

Material[a]	Chemical shift/ppm (from TMS)										
	C=O	Heteroaromatic ring (Position)						Others			
$aapH$[b]	169.30	—	147.82 (6)	119.13 (5)	137.92 (4)	113.53 (3)	152.25 (2)	23.60 (Methyl Group)			
$bapH$[b]	169.98	—	147.81 (6)	119.73 (5)	138.05 (4)	114.77 (3)	152.18 (2)	127.94 (Benzene Ring)	128.32	130.85	
$babpH_2$	166.15	—	151.60 (2)	116.52 (3)	139.03 (4)	115.18 (5)	153.50 (6)	128.00 (Benzene Ring)	128.34	131.99	134.10
$habpH_2$	172.36	—	151.60 (2)	115.67 (3)	138.95 (4)	113.73 (5)	153.40 (6)	13.81 36.05 (Alkyl Chain)	21.85	24.59	30.83
$baptH_2$	166.02	124.81 (5, 6)	143.46 (10a, b)	126.44 (4a, 6a)	138.24 (4, 7)	116.97 (3, 8)	151.21 (2, 9)	127.95 (Benzene Ring)	128.38	132.07	133.70

a) AapH, 2-(acetylamino)pyridine; bapH, 2-(benzoylamino)pyridine. Other abbreviations, see Table 1. b) Ref. 9a.

Table 3. Chemical Shifts in ^1H NMR Spectra of Metal-Free Ligands

Material	Chemical shift/ppm (from TMS)						
	N-H	Heteroaromatic ring (Position)					Others
$aapH$[a]	10.48	—	8.31 (6)	7.08 (5)	7.76 (4)	8.08 (3)	2.10 (Methyl Group)
$bapH$[a]	10.81	—	8.40 (6)	7.18 (5)	7.86 (4)	8.21 (3)	8.05, 7.60, 7.52 (Benzene Ring)
$babpH_2$	10.75	—	—	8.20 (3)	8.02 (4)	8.23 (5)	8.07, 7.60, 7.55 (Benzene Ring)
$habpH_2$	10.43	—	—	7.99 (3)	7.90 (4)	8.13 (5)	2.42, 1.60, 1.30, 0.87 (Alkyl Chain)
$baptH_2$	10.98	7.94 (5, 6)	—	—	8.49 (4, 7)	8.56 (3, 8)	8.15, 7.64, 7.56 (Benzene Ring)

a) Ref. 9a.

bands of **2a** at 1555 and 1366 cm^{-1} were quite similar to those of the palladium complex of 2-(acetylamino)-pyridine [Pd(aap)] (1568 and 1393 cm^{-1}).[4] The ligand $habpH_2$ also gave a blue complex **1b** of similar structure to **1a** by complexation with copper(II) nitrate (Tables 1 and 4). Furthermore, $habpH_2$ gave a green complex **2b** with copper(II) acetate which showed a similar IR bands to **2a** (1554 and 1380 cm^{-1}), suggesting the formation of the deprotonated complex. However, the complex **2b** could not be isolated in a pure form (from elemental analysis).

The ESR spectra of the complexes obtained were also measured (Fig. 1). The spectrum of **1b** was quite similar to that of **1a** (Fig. 1-A).

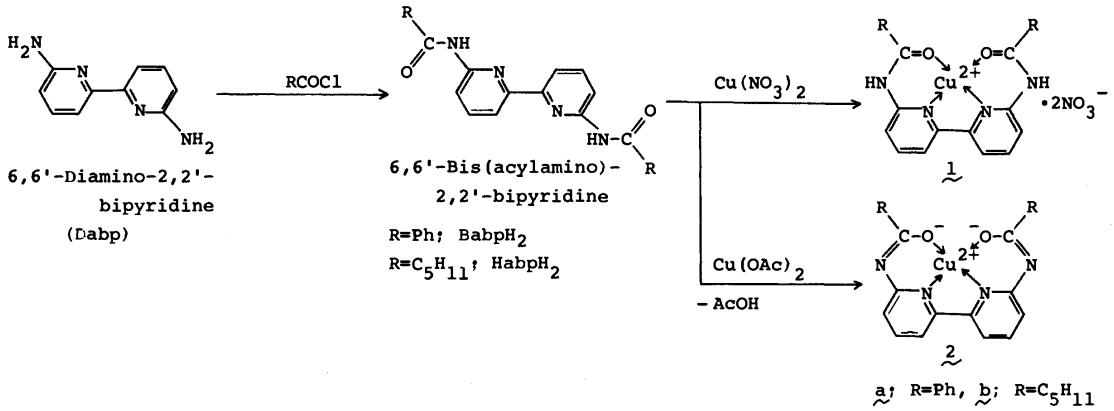

Scheme 1.

Table 4. Characteristic IR Bands of Ligands and Complexes in KBr Disks

Material	IR Band/cm^{-1}				
	$\nu_{(N-H)}$	Amide band			$\nu_{(N-O)}$ [a]
		I	II	III	
aapH [b]	3183	1693	1531	1242	—
bapH [c]	3200	1675	1580	1245	—
$babpH_2$	3310	1651	1521	1245	—
$habpH_2$	3242	1655	1519	1247	—
$baptH_2$	3410	1673	1509	1243	—
$[Cu(aapH)_2]Cl_2$ [b]	2872	1645	1537	1346	—
$[Cu(bapH)_2][NO_3]_2$ [c]	3230	1660sh [d]	1570	1331	1280
1a	3430	1615	1535	1323	1381
1b	3380	1635	1527	1317	1373
$[Pd(aap)_2][H_2O]_4$ [b]	—	(1568)	(1393)	—	—
2a	—	(1555)	(1366)	—	—

a) Nitrate anion, b) Ref. 4, c) Ref. 6, d) shoulder.

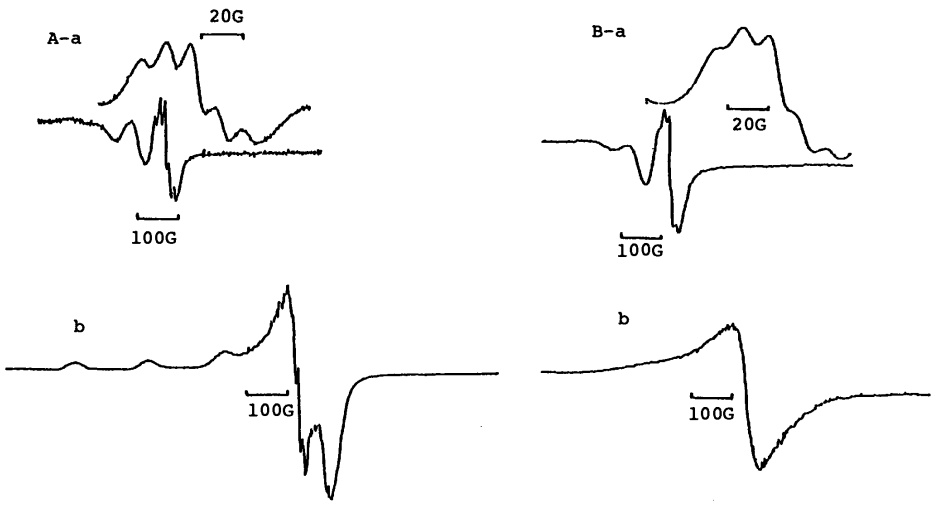

Fig. 1. ESR spectra of copper(II) complexes (1×10^{-3} mol dm^{-3}). A: **1a** in methanol (a) at room temperature (g=2.15) and (b) at 77 K ($g_{//}$=2.26, $g_{\perp}$=2.10), B: **2a** in DMSO (a) at room temperature (g=2.12) and (b) at 77 K (g=2.07).

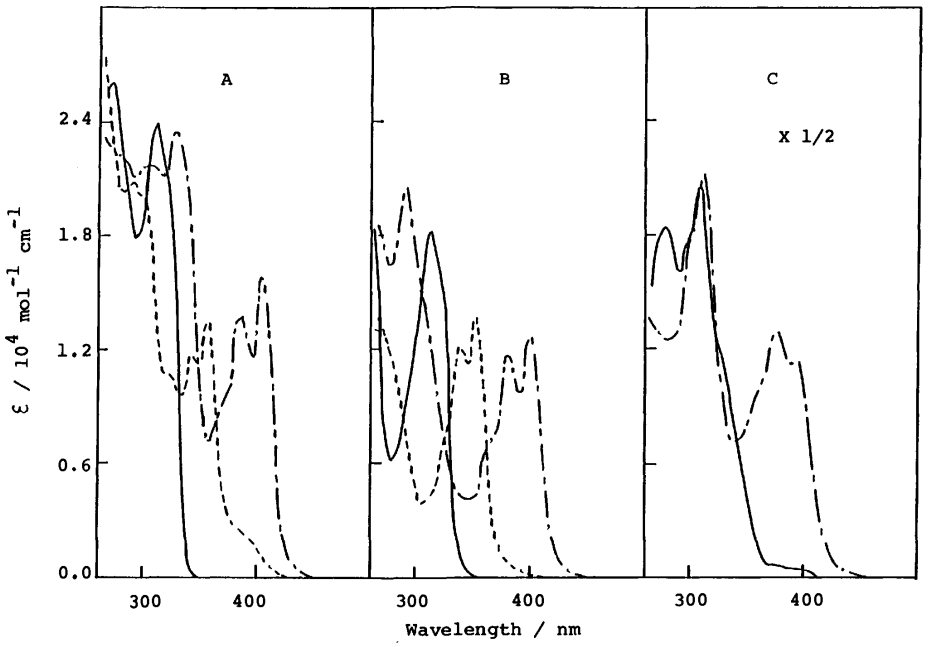

Fig. 2. The electronic spectra of (A) babpH$_2$, (B) habpH$_2$, and (C) baptH$_2$ and their copper(II) complexes in DMSO (6.67×10^{-5} mol dm^{-3}) at 20 °C; (——): metal-free ligands, (------): non-deprotonated complexes in the presence of HNO_3, and (—·—): fully-deprotonated complexes. The spectra of the fully-deprotonated complexes for habpH$_2$ (B) and baptH$_2$ (C) are those of the 1:1 mixture of Cu(OAc)$_2$ with corresponding ligands.

Properties. The electronic spectra of metal-free ligands and their copper(II) complexes are shown in Fig. 2. The spectral changes of the metal-free ligands in DMSO (6.67×10^{-5}mol dm^{-3}) by addition of various amounts of copper(II) acetate indicated the quantitative formation of the 1:1 complexes. The spectra of the equimolar solutions of the ligands and copper(II) acetate in DMSO were quite similar to that of **2a**, indicating the formation of deprotonated complexes, [Cu(babp)], [Cu(habp)], and [Cu(bapt)], in a DMSO solution. The spectra of the equimolar solutions of the ligands and copper(II) nitrate with an excess amount of HNO_3 in DMSO were also almost the same as those of the complexes **1a** and **1b**. The apparent complex-formation constants were too large to measure by the Rose-Drago's method[10] (concentration of ligads; ca. 10^{-5} mol dm^{-3}), and the complexations proceeded completely in the presence of an excess amount of HNO_3 (non-deprotonated complexes) and in the presence of acetic acid produced upon deprotonation (deprotonated complexes) (Scheme 1).

The spectra at 260—500 nm region of the copper(II) complexes of babpH$_2$ and habpH$_2$ in DMSO were sensitive to their concentrations or presence of an acid or a base (Fig. 3). The spectral changes indicated that the two types of the complexes **1** and **2** were in equilibrium. In the course of transformation between the two types of the complexes, two different set of isosbestic points appeared successively, i.e., one is the

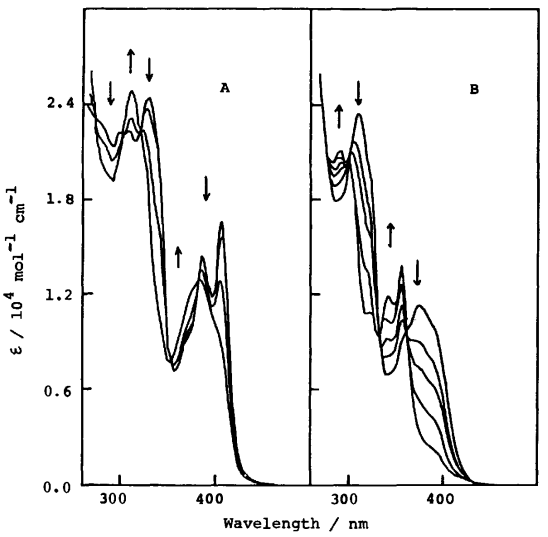

Fig. 3. The changes of electronic spectra of the copper(II) complex **2a** by addition of HNO_3 in DMSO. Concentration of complex **2a**: 6.67×10^{-5} mol dm^{-3}, molar ratio of added nitric acid were as follows; A: 0.0, 0.4, 0.8, and 1.2, and B: 2.0, 4.0, 6.0, 10.0, and 22.0.

set at 382, 352, 322, and 303 nm (Fig. 3-A) and the other at 363, 332, and 300 nm (Fig. 3-B). This indicates the intervention of monodeprotonated species, i.e., one of the amide protons dissociated (Scheme 2). The spectral changes due to the interconversion of the three types of the complexes were also observed in an aqueous medium, though the

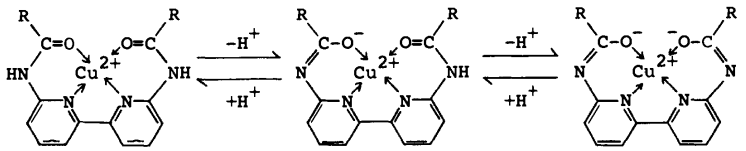

Scheme 2.

fully-deprotonated complex precipitated out in this case. The equilibrium was dependent on the pH of the solution. As the result of the spectrometric titration with concd HNO_3 or KOH (6.67×10^{-5} mol dm^{-3} of the complex), first dissociation of the amide proton in **1b** occured at pH 6.7, and second at pH 9.5. While, the complex **1a** dissociated both of the amide protons almost simultaneously at pH 5.1 in aqueous medium. The complexes themselves were stable during such treatment and neither decomplexation of metal ion nor hydrolysis of the ligands occured even in the presence of an acid or a base.

The copper(II) complexes showed additional bands due to d-d transition in their electronic spectra. The absorption maxima of **1a** and **1b** were 640 nm either in DMSO (ε=110) or in methanol (ε=121). On the other hand, a large solvent effect was observed for **2a**, the absorption maximum of which was 595 nm in DMSO (ε=167), 550 nm in chloroform (ε=227), 585 nm in tetrahydrofuran (ε=180), and 605 nm in pyridine (ε=173).

Discussion

Conformation of the Metal-Free Ligands. The conformation of the metal-free ligands was confirmed to have planar structure by the ^1H NMR spectrometry (Table 3). Chemical shifts of 3,3′-protons are sensitive to the conformation of the two pyridine rings of bipyridine.[11] The large lower-field shift (ca. 0.8-1 ppm) of 3,3′-protons of the bipyridine moiety compared with that of 5-proton of 2-(acylamino)pyridines (bapH and aapH) indicates that the two pyridine rings of the bipyridine moiety are in the plane in "*transoid*" conformation.[11] The chemical shifts of the other ring-protons of $babpH_2$ and $habpH_2$ were almost the same as those of the corresponding protons of 2-(acylamino)pyridines. The large lower-field shift of 5,5′-protons (ca. 1.8 ppm) of 6,6′-bis(acylamino)-2,2′-bipyridines compared with those of dabp[2] is due to the strong deshielding effect by the amide oxygen, suggesting that the amide groups and the pyridine rings are in the plane in "*trans-cis*" conformation as reported for 2-(acylamino)pyridines.[9] Thus, it was concluded that the metal-free ligands have a planar structure as shown below.

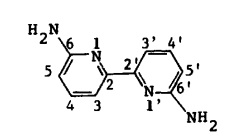

"*transoid*" Conformation of Dabp

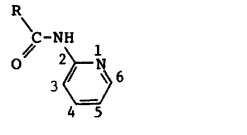

"*trans·cis*" Conformation of 2-(Acylamino)pyridine

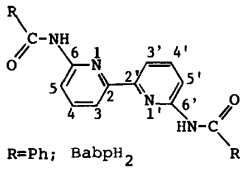

R=Ph; $BabpH_2$
R=C_5H_{11}; $HabpH_2$

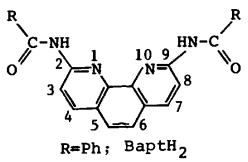

R=Ph; $BaptH_2$

Complex Formation with Copper(II). 2-(Acetylamino)pyridine (aapH) has been reported to form two types of complexes with palladium(II), i.e., $[Pd(aapH)_2]_2^+$ gave deprotonated one, $[Pd(aap)_2]$[4] in alkaline condition. However, $[Cu(aapH)_2]^{2+}$ was decomposed in alkaline solution to give $Cu(OH)_2$ instead of $[Cu(aap)_2]$.[4] In the present case, $babpH_2$ and $habpH_2$ formed both types of copper(II) complexes as described in the previous section.

Structure of the Copper(II) Complexes. 2-(Acylamino)pyridines has been shown unambiguously to coordinate to metal ions as planar NO bidentate ligands from their spectral data[4-7] and X-ray crystal structure analysis.[7] Aap (deprotonated aapH) also serves as a planar NO bidentate ligand.[4,7] Usually deprotonated amide group is known to coordinate at its nitrogen atom,[12] but in the cases of (2-acylamino)pyridine derivatives described here the oxygen is shown to act as the coordination site to form more stable 6-membered ring structure. The shifts of the amide bands of $babpH_2$ and $habpH_2$ in IR spectra upon formation of the complexes **1** (Table 4) are similar to those of the corresponding 2-(acylamino)-pyridines, suggesting the coordination at the amide oxygens[12] (i.e., amide I; red shift, amide II and III; blue shift). The characteristic IR bands of **2** are also similar to those of the deprotonated complex of 2-(acylamino)pyridine, $[Pd(aap)_2]$.[4] Thus, the similarities of IR bands of copper(II) complexes **1a**, **1b**, and **2a** to the corresponding complexes of 2-(acylamino)-pyridines indicate that 6,6′-bis(acylamino)-2,2′-bipyridines act as the square-planar N_2O_2 tetradentate ligands.

The ESR spectra of **1a** and **2a** at room temperature (Fig. 1) were quite similar to each other. They showed the usual four-line pattern due to coupling of electron to the spin 3/2 copper nucleus, and showed five

superhyperfine splitting due to the two nitrogens in the copper coordination sphere. These pattern were almost the same as that of salen derivatives.[13] The ESR spectra at 77 K (Fig. 1), however, were quite different from each other. The complex **2a** showed no fine structure probably due to an intermolecular interaction between copper(II) ions under the measured conditions. The complex **1a** and **1b** showed a typical axial-type spectrum, confirming the structure of a square-planar symmetry. The electronic spectrum of **2a** in 260—500 nm region was similar to that of [Cu(bapt)] (Fig. 2). The ligand baptH$_2$ is regarded as a babpH$_2$ analogue and the conformation of the bipyridine moiety in baptH$_2$ is rigidly fixed in plane. The spectral similarities of the two complexes support the planar structures of the complex **2a**. The complexes **1a**, **1b**, and **2a** have the absorption maxima due to d-d transition appeared at 550—640 nm, similar to that observed in a variety of square-planar copper(II) complexes hitherto reported. The absorption maximum of **2a** in chloroform (550 nm) is similar to that of d-d transition band of copper(II) complex of *N,N'*-bis(1-methyl-3-oxobutylidene)ethylenediamine rather than that of salen (570 nm),[14] suggesting the presence of strong square-planar ligand field around copper(II) ion in the deprotonated complexes. Therefore, these spectral data indicate the square-planar structure of the complexes of 6,6'-bis(acylamino)-2,2'-bipyridine.

The absorption maximum of *d-d* transition band of **2a** in DMSO (Fig. 3) was markedly red-shifted (45 nm) compared with that in chloroform, while that of copper(II) complex of salen or acen showed only a small solvent effect (max. 20 nm).[14] This larger solvent effect may be interpreted in terms of coordination of the solvent molecules at the axial positions of **2a**.

In conclusion, 6,6'-bis(acylamino)-2,2'-bipyridines have been shown to form two different types of 1:1 complexes with copper(II) salt depending on the counter anions of the salts. The deprotonated complexes are similar to salen complexes in their N_2O_2 tetradentate coordination sites, square-planar structure, and the anionic sites on oxygens. Furthermore, in the ligands obtained here, the Schiff base moieties in salen complexes are replaced by bipyridine moieties which have higher chemical stability.

Experimental

Materials 6,6'-Diamino-2,2'-bipyridine was prepared from 2,6-dibromopyridine according to the method previously reported.[3] 2,9-Diamino-1,10-phenanthroline was prepared from 1,10-phenanthroline by the literature method.[8] Other chemicals were obtained commercially, and some of them were purified by conventional methods prior to use.

Spectral Measurements. ^{1}H and ^{13}C NMR spectra were measured with a JEOL JNM-GX270 Spectrometer at 27 °C. ESR spectra were measured with a JEOL JES-FE3X spectrometer operated at X band. Electronic and IR spectra were recorded on a JASCO UVIDEC-505 spectrophotometer at 20 °C and a IRA-1 spectrophotometer, respectively.

6,6'-Bis(benzoylamino)-2,2'-bipyridine (babpH$_2$): Into a solution of dabp (186 mg, 1 mmol) in 10 cm^3 of dry pyridine was added dropwise a solution of benzoyl chloride (1.41 g, 10 mmol) in 10 cm^3 of dry pyridine at 0 °C with stirring. The mixture was stirred for another 15 min at the temperature. Then 100 cm^3 of methanol was added to the mixture in order to precipitate a white solid, which was collected by filtration, washed successively with diluted hydroohloric acid, acetone, diluted aqueous ammonia, and methanol. Recrystallization from benzene yielded 294 mg (75%).

6,6'-Bis(hexanoylamino)-2,2'-bipyridine (habpH$_2$): This was prepared from 186 mg (1 mmol) of dabp and 1.34 g (10 mmol) of hexanoyl chloride in a similar manner to that of babpH$_2$. Yield 298 mg (78%).

2,9-Bis(benzoylamino)-1,10-phenanthroline (baptH$_2$): Into a solution of 2,9-diamino-1,10-phenanthroline (100 mg, 0.47 mmol) in 5 cm^3 of dry pyridine was added dropwise a solution of benzoyl chloride (0.66 g, 4.7 mmol) in 5 cm^3 of dry pyridine at 0 °C with stirring and the mixture was stirred for 15 min at the temperature. Then, 100 cm^3 of ether was added to the mixture to precipitate pale yellow solid, which was collected by filtration and subjected to column chromatography (Wakogel C-200–chloroform). The fraction obtained was washed with diluted aqueous ammonia. Evaporation of chloroform and recrystallization from methanol gave pale yellow needles which was dried at 80 °C under reduced pressure. Yield 84 mg (39%).

Copper(II) Complex 1a: A mixture of babpH$_2$ (78 mg, 0.2 mmol) and Cu(NO$_3$)$_2$·3H$_2$O (48 mg, 0.2 mmol) in 10 cm^3 of methanol was stirred at room temperature until the mixture became a homogeneous blue solution. Then methanol was removed by evaporation. The residual blue solid was recrystallized from water to give light blue plates of Cu(babpH$_2$)(H$_2$O)$_2$(NO$_3$)$_2$, yield 71 mg (58%).

Copper(II) Complex 2a: A mixture of babpH$_2$ (78 mg, 0.2 mmol) and Cu(OAc)$_2$·H$_2$O (40 mg, 0.2 mmol) in 100 cm^3 of chloroform was stirred at room temperature until the mixture became a homogeneous purple solution. Then chloroform was removed by evaporation. The residual green solid was washed by methanol containing KOH, and recrystallized from benzene, yielding 70 mg (76%) of [Cu(babp)].

Copper(II) Complex 1b: This was obtained from 76 mg (0.2 mmol) of habpH$_2$ and 48 mg (0.2 mmol) of Cu(NO$_3$)$_2$·3H$_2$O in a similar manner to the preparation of **1a**. Recrystallization from water gave blue plate of Cu(habpH$_2$)(H$_2$O)(NO$_3$)$_2$, yield 26 mg (18%).

References

1) J. Csaszar, *Acta Phys. Chem.*, **28**, 45 (1982); A. Nishinaga and H. Tomita, *J. Mol. Catal.*, **7**, 179, (1980); R. D. Jones, D. A. Summerville, and F. Basolo, *Chem. Rev.*, **79**, 139 (1979); E. C. Niederhoffer, J. H. Timmons, and A. E. Martell, *ibid*, **84**, 137 (1984).

2) N. Kishii, K. Araki, and S. Shiraishi, *Bull. Chem. Soc. Jpn*, **57**, 2121 (1984).

3) N. Kishii, K. Araki, and S. Shiraishi, *J. Chem. Soc.*,

Chem. Commu., **1984**, 103; N. Kishii, K. Araki, and S. Shiraishi, *J. Chem. Soc., Dalton Trans.*, **1985**, 373.

4) M. Nonoyama, S. Tomita, and K. Yamasaki, *Inorg. Chim. Acta*, **12**, 33 (1975).

5) J. Bould and B.J. Brisdon, *Inorg. Chim. Acta*, **19**, 159 (1976).

6) M. F. El-Shazly, A. El-Dissowky, T. Salem, and M. Osman, *Inorg. Chim. Acta.*, **40**, 1 (1980).

7) V. Sheller-Krattiger, K. H. Scheller, E. Sinn, and R. B. Martin, *Inorg. Chim. Acta*, **60**, 45 (1982).

8) S. Ogawa, T. Yamaguchi, and N. Gotoh, *J. Chem. Soc., Perkin Trans 1.*, **1974**, 976.

9) L. V. Sudha and D. N. Sathyanarayana, *J. Coord. Chem.*, **13**, 207 (1984); R. F. C. Brown, L. Random, S. Sternhell, and I. D. Rae, *Can. J. Chem.*, **46**, 2577 (1968).

10) N. J. Rose and R. S. Drago, *J. Am. Chem. Soc.*, **81**, 6138 (1959).

11) I. C. Calder, T. McL. Spotswood, and C. I. Tanzer, *Aust. J. Chem.*, **20**, 1195, (1967); T. McL. Spotswood and C. I. Tanzer, *ibid.*, **20**, 1213 (1967); T. McL. Spotswood and C. I. Tanzer, *ibid.*, **20**, 1227 (1967).

12) M. B. Robin, F. A. Bovey, and H. Basch, "The Chemistry of Amide," ed by J. Zabicky, Interscience, London (1970), p. 1; M. Nonoyama and K. Nonoyama, *Kagaku No Ryoiki*, **31**, 136 (1977); H. Sigel and R. B. Martin, *Chem. Rev.*, **82**, 385 (1982).

13) D. L. DuBois, G. R. Eaton, and S. S. Eaton, *J. Am. Chem. Soc.*, **101**, 2624 (1979); *ibid*, **100**, 2686 (1978).

14) L. Belford and W. A. Yeranos, *Mol. Phys.*, **6**, 121 (1963).

 © 1987 The Chemical Society of Japan Bull. Chem. Soc. Jpn., 60, 3157—3161 (1987)

Mixed Alcohol Synthesis from CO-H_2 by Use of KCl-Promoted Mo/SiO_2 Catalysts

Atsushi MURAMATSU, Takashi TATSUMI,* and Hiro-o TOMINAGA
Department of Synthetic Chemistry, Faculty of Engineering, The University of Tokyo, Hongo, Bunkyo-ku, Tokyo 113
(Received March 23, 1987)

Highly active Mo catalysts for mixed alcohol synthesis were prepared using Fuji Davison ID silica gel as a carrier. KCl promoted the selectivity to alcohols but reduced CO conversions in particular to hydrocarbons. Productivity of alcohols was largely affected by the reaction conditions. High pressure and short contact time enhanced space-time yield of alcohols, i.e. 420 g (kg-catalyst)$^{-1}$ h^{-1} at 5.0 MPa, 573 K, and W/F≈ 1.4 g-catalyst h mol^{-1}. The presence of K effectively prevented the complete reduction of Mo to metal, resulting in the increase in the production of alcohols. The study on addition of ethene and ethanol to synthesis gas revealed that the other roles of K are to retard dehydration of alcohols to alkenes and their hydrogenation to alkanes.

The development of a selective catalyst for co-production of methanol and C_2+ higher alcohols remains as one of the main goals of C_1 chemistry. The principal use of the alcohol mixtures is for blending in automotive fuel to meet the octane requirement raised by the global trend to lead phase-down. Blending methanol with gasoline requires the addition of cosolvent to mitigate the problems due to phase separation and high volatility. The C_2+ higher alcohols have proved effective as cosolvent.

It is well-known that appropriate modifications of the methanol synthesis catalyst and also of the reaction conditions result in the production of higher alcohols together with methanol.[1,2] The conventional Fischer-Tropsch catalysts based on iron, ruthenium, and cobalt have been also reported to give long chain alcohols. Institut Francias du Petrole patented catalysts for the synthesis of mixed alcohols, consisting of methanol synthesis catalysts (Cu) and Fischer-Tropsch catalysts (Co).[3]

Molybdenum catalysts have long been recognized as being effective for the Fischer-Tropsch synthesis of light hydrocarbons.[4,5] In our previous study, however, the supported molybdenum catalysts were found to be active in the synthesis of mixed alcohols, which was significantly influenced by support and additive.[6] Moreover, the successive impregnation method, in which addition of K to silica gel was followed by impregnation with molybdenum solution, was found to give higher activity and selectivity for alcohol formation.[7] Dow and Union Carbide have claimed a number of patents of the catalysts based on MoS_2, promoted by CoS and alkali metal salts for higher alcohol synthesis.[8-10]

Here we report the improved design of catalyst and reaction conditions for the production of mixed alcohols. High activity and selectivity for alcohols were attained on the KCl-promoted, ID silica-gel-supported Mo catalyst at high pressure and short contact time; alcohol yield exceeded 420 g (kg-catalyst)$^{-1}$ h^{-1} with 68 C-atom% selectivity.

Experimental

Catalysts were prepared by impregnating various silica gels (Fuji Davison ID, RD, and B) with an aqueous solution of KCl first, followed by air calcination at 673 K for 1 h and impregnation with $(NH_4)_6Mo_7O_{24}$ solution. The Mo metal loading was 10 and 20 wt% and the K/Mo ratio was varied in the range of 0—0.4. The impregnates were dried overnight at 393 K and treated in the He stream at 673 K for 1 h and then reduced by H_2 773 K for 12 h.

The synthesis reaction was carried out in a flow reactor made of stainless steel tube with 0.6 cm inside diameter, containing 1.0 g catalyst. The synthesis gas (H_2/CO=1) was supplied to the reactor through the stainless-steel tube heated at 473 K for decomposition of carbonyl impurities. Hydrogen was purified to remove oxygen by passage through a DEOXO unit (Engelhard), followed by a molecular sieve trap. Activity and selectivity of the catalyst were observed over a reaction period of 50—130 h until their steady states were attained. Products were analyzed by gas chromatographs. Concentrations of CO, CO_2, and CH_4 in the off-gas were determined by a TCD gas chromatograph with an active carbon separation column at 323 K using H_2 as a carrier gas. The organic compounds were analyzed by an FID gas chromatograph with the following separation column using N_2 as a carrier gas; 2 m Porapak Q for C_1—C_5 hydrocarbons, 2 m polyethylene glycol 1500 for oxygenates, 2 m Silicone SE-30 for C_6+ hydrocarbons, and 8 m VZ-7 for isomers of C_3, C_4, and C_5.

The catalytic surface areas of reduced Mo catalysts were measured by O_2 adsorption at 195 K. X-Ray powder diffraction measurements were performed using a Rigaku Denki diffractometer RU-200A with Cu $K\alpha$ radiation.

Results and Discussion

As previously reported, excellent activity for alcohol synthesis activity was obtained by the use of KCl as a promoter in preparing silica-supported Mo catalysts. Three kinds of silica gel were investigated as a carrier for Mo-KCl catalyst and the results are summarized in Table 1. With all of the catalysts, both alcohol selectivity and CO conversion gradually increased with time on stream and therefore the data were

obtained after 50—130 h on stream when the catalytic activity reached the nearly steady state. As is expected from the shift activity of the molybdenum catalysts,[4,5] these catalysts yielded CO_2, instead of water, almost exclusively. Hence the product selectivities (carbon atom%) in this work are given on a CO_2-free basis. Alcohol synthesis activity is represented by space-time yield of alcohols, STY, which stands for the total weight of alcohols produced per unit weight of catalyst per unit time on stream.

The alcohol formation activity over the KCl-promoted silica-supported Mo catalysts increased in the following order; B<RD<ID. Apparent average oxidation number, estimated from O_2 consumption from 195 to 773 K, increased in the order; B<RD<ID. This sequence conforms to the order of alcohol formation activity. This suggests that Mo species with a relatively high oxidation state participates in the key step of alcohol formation.

Alcohols/hydrocarbons ratio in space-time yield increased in the order; RD<B<ID. This order is in accordance with the sequence of pore diameter of support. The silica-supported Mo catalysts have moderate activity for alcohol dehydration as described below. Therefore, if the pores are smaller, product alcohols would have more chance to be readsorbed and dehydrated to hydrocarbons before leaving the catalysts. RD-silica-supported catalyst gave the highest C_2+ alcohol/methanol ratio. The C_2+ hydrocarbons/methane ratio was in the same order but less dependent on the kind of silica gel than C_2+ alcohols/methanol ratio.

Total activities increased in the order; B<ID<RD. This order is not consistent with the order of O_2 uptake.[11] Na_2O impurity (0.25 wt%) in B-silica gel might have the effect of poison on CO hydrogenation activity.[1] ID-silica-supported Mo catalysts were employed for further investigation.

Table 2 shows the influence of Mo loading on the activity for alcohol synthesis, with the K/Mo ratio kept constant at 0.4. The selectivity for alcohols increased with increasing Mo loading. The C_2+ alcohols/methanol ratio and the olefin content also increased. Total activities, however, increased in the order: 5% Mo<20% Mo<10% Mo. In view of the effect of K content on catalyst performance as is described below, this change in activity and selectivity could be accounted for by the K content proportional to the Mo content.

The influence of K content on activities of 20 wt% Mo catalysts is shown in Fig. 1. The addition of KCl reduced CO conversion and also hydrocarbon yield in particular. The selectivity for alcohols increased with KCl content and reached 70 C-atom% at K/Mo=0.4. The yield of alcohols, however, reached a maximum at K/Mo=0.2. With the increase in K/Mo ratio the C_2+ alcohols/methanol ratio largely increased. It

Table 1. Effect of Silica Gel on Performance of Mo(10 wt%)+KCl(K=1.63 wt%)/SiO_2 Catalysts[a]

Silica gel	ID	B	RD
CO conversion/%	5.5	4.6	6.8
CO_2 yield/%	2.3	2.0	3.1
Carbon atom selectivity/%			
CH_4	19.2	27.1	24.4
C_2H_4	3.3	2.3	3.7
C_2H_6	9.9	14.3	12.3
C_3H_6	5.7	5.3	7.0
C_3H_8	2.1	4.4	3.0
C_4+HC	9.2	9.7	11.1
MeOH	17.3	14.6	9.4
EtOH	20.5	15.2	19.2
n-PrOH	7.1	4.4	5.9
C_4+alcohol	4.3	1.4	2.2
Other oxygenate	1.5	1.5	1.8
Space-time yield/g kg·catalyst^{-1} h^{-1}			
Hydrocarbon	12	11	16
Alcohol	21	11	15
Net O_2 uptake following reduction/μmol g^{-1}[b]	122	131	50
Apparent oxidation number of Mo following reduction[c]	2.1	1.4	1.8
Surface area of support/m^2 g^{-1}	270	450	720
Average pore diameter of support/Å	140	70	22

a) Reaction conditions; 573 K, 1.6 MPa, W/F=10 g-catalyst h mol^{-1}. b) Measured at 195 K. c) Estimated from O_2 consumption from 195 to 773 K.

Table 2. Effect of Mo Loading on Alcohol Synthesis over Mo+KCl(K/Mo=0.4)/SiO_2(ID)[a]

Mo loading	5%	10%	20%
CO conversion/%	3.3	5.5	3.4
CO_2 yield/%	1.4	2.3	1.4
Carbon atom selectivity/%			
CH_4	24.7	19.2	14.9
C_2H_4	3.7	3.3	4.2
C_2H_6	12.8	9.9	7.2
C_3H_6	5.8	5.7	5.2
C_3H_8	2.6	2.1	1.6
C_4+HC	9.6	9.2	9.4
MeOH	17.9	17.3	15.5
EtOH	15.5	20.5	24.2
n-PrOH	4.8	7.1	8.3
C_4+alcohol	1.2	4.3	8.2
Other oxygenate	1.4	1.5	1.4
Space·time yield/g kg·catalyst^{-1} h^{-1}			
Hydrocarbon	9.1	12	6.1
Alcohol	11	21	13

a) Reaction conditions; 573 K, 1.6 MPa, W/F=10 g-catalyst h mol^{-1}.

should be noted that C_2+ hydrocarbons/methane ratio remained almost unchanged.

Table 3 represents the O_2 uptakes for the 20 wt% Mo catalysts. Without KCl addition, O_2 uptake for the fresh (reduced) Mo catalyst amounted to 532 μmol g^{-1}. O_2 uptake was significantly reduced by addition of KCl and was at virtually constant level beyond K/Mo $\geqslant$0.2. The decrease in CO conversion by addition of K should be partly due to the decrease in O_2 uptake. Concha and Bartholomew reported a linear correlation between CO hydrogenation activity and O_2 uptake for unsupported MoS_2.[11]

Figure 2 shows X-ray diffractograms of reduced Mo (20 wt%) catalysts with K/Mo ratio changed. Lines corresponding to metallic Mo and MoO_2 appeared on all the catalyst. With increase in K/Mo ratio, the intensity of MoO_2 lines increased at the expense of metallic Mo.[12] The productivity of alcohols is supposed to depend significantly upon the oxidation state of Mo; MoO_2-like species are responsible for alcohol synthesis while metallic Mo is associated with carbon chain growth and hydrocarbon formation.[13] Thus the presence of K could retard the reduction of Mo, resulting in increase in the production of alcohols.

The influence of the time factor (W/F) on CO conversion, the yields of alcohols and hydrocarbons, the selectivity to alcohols and C_2+ alcohols/methanol ratio over Mo(20 wt%)+KCl(K=1.63 wt%)/SiO_2(ID) at 573 K and 1.6 MPa are illustrated in Figs. 3 and 4.

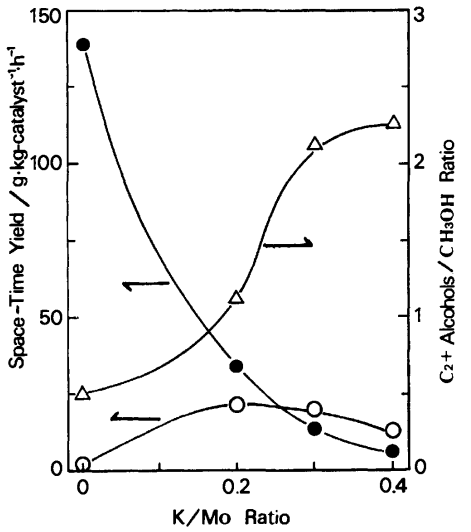

Fig. 1. Effect of K content (K/Mo ratio) on space-time yields of alcohols (O) and hydrocarbons (●), and C_2+OH/CH_3OH ratio (△) over Mo(20 wt%)+KCl/SiO_2(ID) at W/F=10 g-catalyst h mol^{-1}, 573 K, and 1.6 MPa.

Table 3. O_2 Uptake of Mo(20 wt%)+KCl/SiO_2(ID) Catalysts

K/Mo molar ratio	CO conv. %	CO_2 yield %	Net O_2 uptake before use μmol g^{-1}
0	38.3	18.2	532
0.2	10.7	4.8	144
0.3	5.8	2.5	163
0.4	3.4	1.4	126

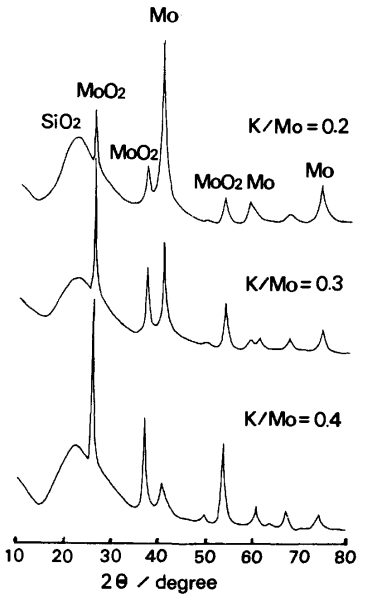

Fig. 2. X-Ray diffractograms of reduced Mo catalysts with K/Mo ratio changed.

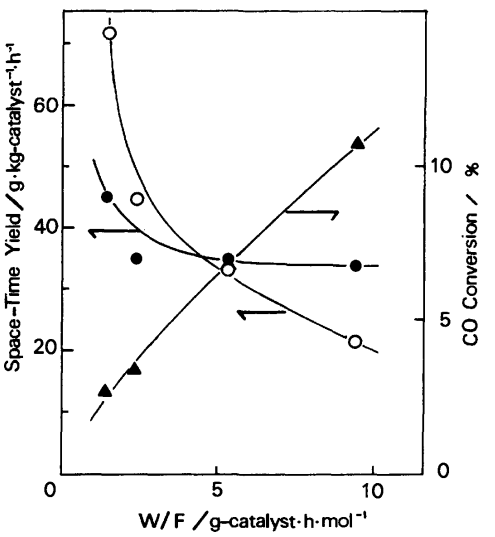

Fig. 3. Effect of time factor on CO conversion (▲) and space-time yields of alcohols (O) and hydrocarbons (●) over Mo(20 wt%)+KCl(K=1.63 wt%)/SiO_2(ID) catalyst at 573 K and 1.6 MPa.

Short contact time enhanced the selectivity for alcohols. The CO conversion vs. W/F plot displayed a convex curvature, which might suggest that the rate of intrinsic surface reaction is not the rate controlling step. At short contact time, the selectivity for alcohols was markedly improved. C_2+ alcohols/methanol ratio was independent of the time factor, ruling out the significant contribution of alcohol homologation, e.g., methanol conversion to ethanol. The alcohol yield tended to be more influenced by W/F with lower K/Mo ratios, indicating that there is a route from alcohols to hydrocarbons promoted by acid sites of the catalysts.

The influence of the addition of ethanol and ethene to CO-H_2 feedstock was investigated on unpromoted and KCl-promoted Mo catalysts. Pertinent data are given in Table 4. Over the unpromoted catalyst, added ethanol momentarily converted to ethene and ethane. This alcohol dehydration activity of Mo/SiO_2 indicates that Mo/SiO_2 has significant acidity, in agreement with the observation by Maruyama et al.[14]

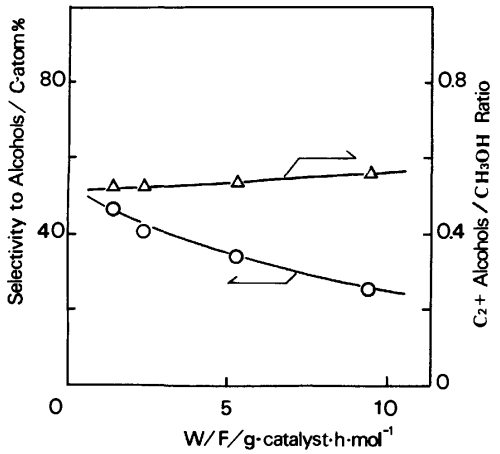

Fig. 4. Effect of time factor on alcohol selectivity (O) and C_2+alcohols/methanol ratio (△) over Mo(20 wt%)+KCl(K=1.63 wt%)/SiO_2(ID) catalyst at 573 K and 1.6 MPa.

Table 4. Addition of Ethanol and Ethene to CO-H_2 over Mo(20 wt%) + KCl/SiO_2(ID)[a]

KCl content	Ethanol conversion rate to ethene and ethane[b]	Ethene conversion rate to ethane[c]
wt%	mmol (kg-catalyst)$^{-1}$ h^{-1}	
0	352	410
1.63	12	105

a) Increase in ethene and/or ethane on addition of ethanol and ethene to synthesis gas. b) Reaction conditions; 523 K, 1.6 MPa, W/F= 10 g·catalyst h mol^{-1} C_2H_5OH= 1.0 mol(kg·catalyst)$^{-1}$h^{-1}. c) Reaction conditions; 473 K, 1.6 MPa, W/F= 10 g·catalyst h mol^{-1}, C_2H_4= 1.3 mol(kg-catalyst)$^{-1}$ h^{-1}.

The addition of KCl led to the considerable decrease in ethene and ethane. This is supposed to be due to the K-induced decrease in acidity. It can be seen in Table 4 that addition of KCl to Mo/SiO_2(ID) remarkably suppressed the ethene conversion rate to ethane. Thus the additional role of K in improving alcohol selectivity is to retard dehydration of alcohol to alkenes and to slow hydrogenation of the alkenes to alkanes.

The yield of alcohols was considerably influenced by raising the total pressure. The effect of total pressure on the product distribution over Mo(20 wt%)+KCl(K=1.63 wt%)/SiO_2(ID) at 573 K and W/F= 1.4 g-catalyst h mol^{-1} was indicated in Fig. 5 and Table 5. Raising the pressure, the yield of alcohols was greatly improved. The C_2+/C_1 ratios of hydrocarbons and alcohols were independent of the pressure. It should be noted that at 5.0 MPa STY of alcohols as large as 420 g (kg-catalyst)$^{-1}$ h^{-1} was obtained in 68 C-atom% selectivity. This STY is comparable with those reported so far with Cu-Co based catalyst[15] and MoS_2-Co-K_2CO_3 catalyst.[11] At 6.5 MPa the selectivity for alcohol formation was deteriorated, while the yield of hydrocarbons was greatly increased. This would also result from the successive reaction of alcohols to hydrocarbons owing to the increase in the contact time under the high pressure. Xie et al. recently claimed that alcohol

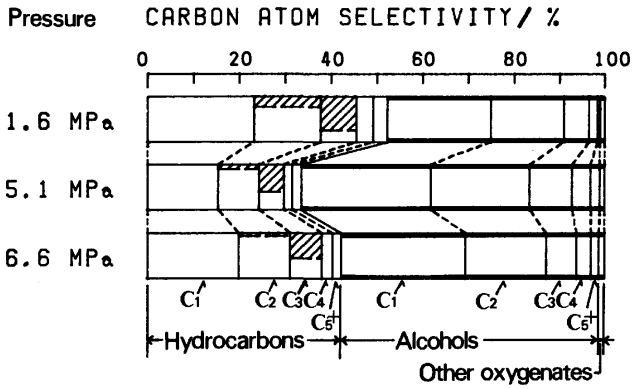

Fig. 5. Effect of total pressure on product distribution over Mo(20 wt%)+KCl(K=1.63 wt%)/SiO_2(ID) catalyst at W/F=1.4 g-catalyst h mol^{-1} and 573 K.

Table 5. Effect of Total Pressure on Activity over Mo(20 wt%) + KCl(K= 1.63 wt%)/SiO_2(ID) Catalyst[a]

Total pressure	CO conversion	CO_2 yield	Space-time yield Hydrocarbon	Alcohol
MPa	%	%	g(kg-catalyst)$^{-1}$ h^{-1}	
1.6	2.7	1.1	45	72
5.0	10	3.1	124	420
6.5	13	4.5	181	428

a) Reaction conditions; see footnote in Fig. 5.

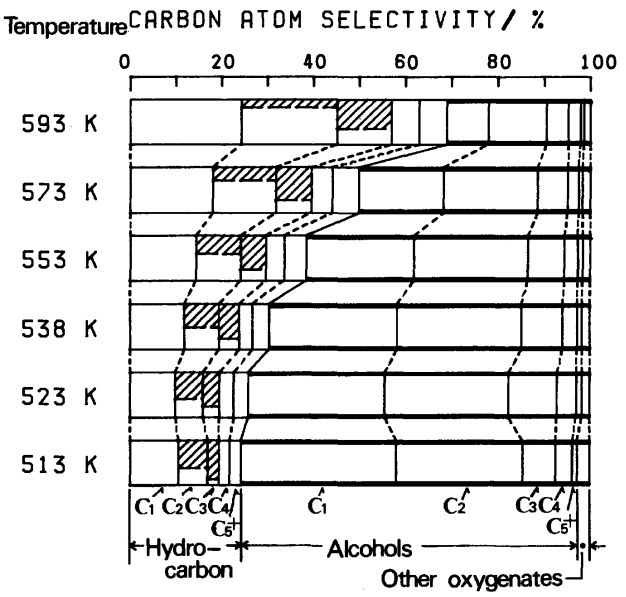

Fig. 6. Effect of temperature on product distribution over Mo(10 wt%)+KCl(K=1.63 wt%)/SiO_2(ID) catalyst at W/F=10 g-catalyst h mol^{-1} and 1.6 MPa.

Table 6. Effect of Temperature on Activity over Mo(10 wt%)+KCl(K=1.63 wt%)/SiO_2(ID) Catalyst[a)]

Temperature	CO conversion	CO_2 yield	Space-time yield Hydrocarbon	Alcohol
K	%	%	g(kg·catalyst)$^{-1}$ h^{-1}	
593	7.3	3.2	22	16
573	5.5	2.3	12	21
553	2.0	0.67	4.0	11
538	1.0	0.33	1.7	6.7
523	0.52	0.15	0.74	3.6
513	0.32	0.10	0.41	2.2

a) Reaction conditions; see footnote in Fig. 6.

yields were very sensitive to total pressure over MoS_2 based catalysts.[16)]

Figure 6 and Table 6 show the effect of reaction temperature on the product distribution over Mo(10 wt%)+KCl(K=1.63 wt%)/SiO_2(ID) at 1.6 MPa and W/F=10 g-catalyst h mol^{-1}. With the decrease in temperature, the selectivity to alcohols was greatly improved. At 513 K, 76 C-atom% of the alcohol selectivity was obtained. A maximum yield of alcohols was attained at 573 K. At temperatures above 573 K, the yield of alcohols was decreased while that of hydrocarbons was strongly promoted. C_2+ alcohols/methanol ratio gradually increased with the increase in temperature.

In the Mo catalyst system, water, the primary product, is rapidly converted to CO_2. This makes the alcohol separation simple and less energy consuming as there is no problem due to azeotrope formation.[17)] Moreover, it is feasible to utilize a synthesis gas with a low H_2/CO ratio produced from coal gasifiers without a separate shift converter.[18)]

References

1) G. Natta, U. Colombo, and I. Pasquon, "Catalysis," ed by P. H. Emmett, Reinhold, New York (1957), Vol. V, p. 131.

2) K. Klier, "Catalysis of Organic Reactions," ed by W. R. Moser, Dekker, New York (1981), p. 195.

3) A. Sugier and E. Freund, U. S. Patent 4122110 (1978).

4) J. F. Schultz, F. S. Karn, and R. B. Anderson, U. S. Bureau of Mines Report, 1967, 6974.

5) C. B. Murchison and D. A. Murdick, *Hydrocarbon Process.*, **60**, 159 (1981).

6) T. Tatsumi, A. Muramatsu, and H. Tominaga, *Chem. Lett.*, **1984**, 685.

7) T. Tatsumi, A. Muramatsu, and H. Tominaga, *J. Catal.*, **101**, 553 (1986).

8) G. J. Quarderer, EPO-0119609 (1984).

9) N. E. Kinkade, EPO-0149255; EPO-0149256 (1985).

10) R. R. Stevens, EPO-0172431 (1986).

11) B. E. Concha and C. H. Bartholomew, *J. Catal.*, **79**, 327 (1983).

12) M. Kantschewa, F. Delannay, H. Jeziorowski, E. Delgado, S. Eder, G. Ertl, and H. Knozinger, *J. Catal.*, **87**, 482 (1984).

13) T. Tatsumi, A. Muramatsu, and H. Tominaga, *Shokubai*, **28**, 481 (1986).

14) K. Maruyama, H. Hattori, and K. Tanabe, *Bull. Chem. Soc. Jpn.*, **50**, 86 (1977).

15) A. Sugier, J. F. La Page, P. Courty, and A. Forestiere, French Patent 2533554 (1982).

16) Y. C. Xie, B. M. Naasz, and G. A. Somorjai, *Appl. Catal.*, **27**, 233 (1986).

17) N. J. Chen and H. M. Feder, "Catalysis of Organic Reactions," ed by W. R. Moser, Dekker, New York (1981), p. 273.

18) B. Cornils, J. H. Hibhel, P. Ruprecht, R. Durrfeld, and J. W. Rathke, *Hydrocarbon Process.*, **60**, 149 (1981).

 © 1987 The Chemical Society of Japan Bull. Chem. Soc. Jpn., 60, 3163—3167 (1987)

Electrical Conductivities of Tetrakis(alkylthio)tetrathiafulvalene (TTC_n-TTF) and Tetrakis(alkyltelluro)-tetrathiafulvalene ($TTeC_n$-TTF)

Kenichi Imaeda,* Toshiaki Enoki, Zurong Shi,† Peiji Wu,† Naoko Okada,††
Hideki Yamochi,†† Gunzi Saito,†† and Hiroo Inokuchi
Institute for Molecular Science, Okazaki 444
††The Institute for Solid State Physics, The University of Tokyo,
Roppongi, Minato-ku, Tokyo 106
(Received April 10, 1987)

Electrical conductivities have been measured for TTC_n-TTF and $TTeC_n$-TTF. In the case of TTC_n-TTF, the compounds with short alkyl chains (n=1—3) show the high resistivities above 10^{10} Ω cm, while the resistivities of the compounds with long alkyl chains ($n\geq4$) decrease to 10^5—10^7 Ω cm. The relatively low resistivities of the compounds with long alkyl chains are attributed to the considerable reduction in intermolecular distance between adjacent TTF skeletons caused by intermolecular interactions through alkyl chain groups taking into account the results of their crystal structures, thermal properties and densities. As for $TTeC_n$-TTF compounds, the carbon number dependence of resistivity is almost similar to that of TTC_n-TTF in the range of large n ($n\geq8$). Exceptionally, $TTeC_1$-TTF exhibits noticeably low resistivity of 6.9×10^4 Ω cm. X-Ray diffraction study confirms that the high conductivity of $TTeC_1$-TTF is caused by the formation of zigzag Te chains due to the presence of strong intermolecular Te-Te atomic contacts.

Since the discovery of a metallic conductivity in TTF-TCNQ, many interests have been devoted to organic conductors with TTF derivative donors. A large number of organic metals are found in charge-transfer complexes with TTF derivative donors such as TMTTF (tetramethyl-TTF), HMTTF (hexamethylene-TTF), and BEDT-TTF (bis(ethylenedithio)-TTF)) complexes. Tetrakis(alkylthio)tetrathiafulvalene (abbreviated as TTC_n-TTF) used in this work is one of these derivatives, which is obtained by the introduction of four alkylthio substitutional groups to a TTF skeleton, as shown in Fig. 1. Some of charge-transfer complexes with TTC_1-TTF have been investigated[1] and an iodine complex with a composition of $(TTC_1\text{-TTF})(I_3)_{0.823}$ shows a metallic conductivity.[2,3] Besides the studies related to CT complexes, TTC_n-TTF attracts interests in anomalous electrical property as a single component organic solid which does not belong to charge-transfer complexes, because of its good electrical conduction.[4] TTC_n-TTF consists of a conjugated part of tetrathio-TTF (C_6S_8) moiety and an aliphatic part of four alkyl chain groups. It is interesting to investigate systematically how the conjugated and the aliphatic parts affect the physical properties of TTC_n-TTF's by changing the carbon number of alkyl group. Moreover, it is easy to extend our system by replacing sulfur atoms with other chalcogen atoms such as selenium or tellurium having bigger van der Waals radius. This strategy will enable to increase the magnitudes of intermolecular interactions and enhance the conductivity. We have reported the novel crystal structure, high electrical conductivity and low ionization energy of TTC_9-TTF compound,[4,5] which are supposed to be associated with the reduction in intermolecular distance between TTF skeletons caused by the function of intermolecular interactions between alkyl chains. In this work, we present the experimental results of electrical conductivities of TTC_n-TTF and tetrakis(alkyltelluro)tetrathiafulvalene (abbreviated as $TTeC_n$-TTF). The origins of relatively low resistivities for the compounds with long alkyl chains are discussed in connection with crystal structures and the other physical properties such as thermal properties, densities, and ionization energies. Furthermore, the differences of electrical properties between TTC_n-TTF and $TTeC_n$-TTF are also discussed according to intermolecular interactions.

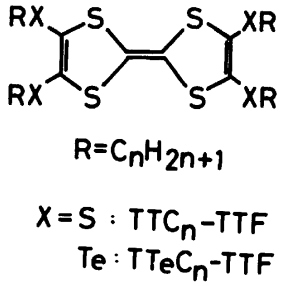

Fig. 1. The molecular structure of TTC_n-TTF and $TTeC_n$-TTF.

Experimental

The synthetic procedures of TTC_n-TTF and $TTeC_n$-TTF compounds (n=1—18) were reported in the previous papers.[1,6] The purification of these compounds was performed by column chromatography with silica gel and recrystallization. The purity was checked by thin-layer chromatography. Single crystals of TTC_n-TTF with n=1—11 were prepared by recrystallization in a mixed solution of hexane and methanol or acetone and methanol. Crystals of

† Permanent address: Institute of Chemistry, Academia Sinica, Beijing, China.

Table 1. Resistivities and Activation Energies of TTC_n-TTF

Compound	ρ_{RT}[a)]/Ω cm	E_a/eV
TTC_1-TTF	2.9×10^{10}	0.38
TTC_2-TTF	1.2×10^{10}	0.29
TTC_3-TTF	9.6×10^{9}	0.52
TTC_4-TTF	6.2×10^{6}	0.22
TTC_5-TTF	6.4×10^{7}	0.29
TTC_6-TTF	3.0×10^{7}	0.28
TTC_7-TTF	3.8×10^{7}	0.26
TTC_8-TTF	7.0×10^{7}	0.21
TTC_9-TTF	5.0×10^{7}	0.21
TTC_{10}-TTF	3.7×10^{5}	0.13
TTC_{11}-TTF	5.6×10^{5}	0.17
TTC_{12}-TTF	5.3×10^{7}	0.25
TTC_{13}-TTF	2.3×10^{6}	0.24
TTC_{14}-TTF	7.8×10^{7}	0.33
TTC_{15}-TTF	2.9×10^{6}	0.24
TTC_{16}-TTF	9.9×10^{6}	0.28
TTC_{17}-TTF	1.6×10^{7}	0.26
TTC_{18}-TTF	6.8×10^{9}	0.48

a) Single crystals for the compounds with $n=1$—11 and compaction pellets for the compounds with $n=12$—18. The measurements for the crystals were performed along the long axis of the crystal.

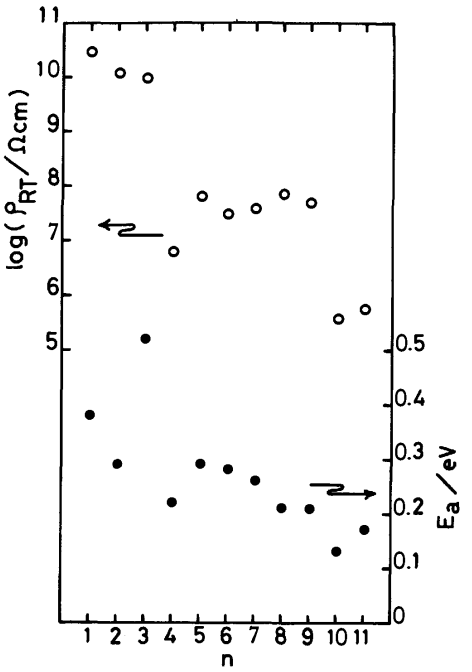

Fig. 2. The correlation between the carbon number n of alkyl group and $\log\rho_{RT}$ or E_a for the single crystals of TTC_n-TTF (n=1—11).

TTC_n-TTF were mainly grown as needle-like crystals except thick plates of n=1, 2, and 9. The colors of the samples were yellow for n=1, 3, and 18 and orange for the other compounds. Single crystals of $TTeC_n$-TTF with n=1, 2, 8, and 9 were obtained as needle-like crystals with dark orange color. Electrical conductivity was measured by a two-probe method between room temperature and a temperature just above a melting point under a vacuum of $\approx10^{-4}$ Pa to avoid an oxidation effect. In the case of the compounds with n=12—18 for TTC_n-TTF and the compounds with n=13—18 for $TTeC_n$-TTF which are difficult to be crystallized as single crystals, conductivity was measured with compaction pellets.

Results and Discussion

TTC_n-TTF. The results of resistivities at room temperature ρ_{RT} and activation energies E_a for semiconductive TTC_n-TTF compounds are summarized in Table 1. Figure 2 shows the correlation between the carbon number n of alkyl group and $\log\rho_{RT}$ or E_a for the single crystal samples with n=1—11. The resistivities of the compounds with n=1—3 are very high (above 10^{10} Ω cm), while those of the compounds with $n\geq4$ decrease to 10^5—10^7 Ω cm except n=18 with $\approx10^{10}$ Ω cm. Especially, the resistivity values of 3.7×10^5 and 5.6×10^5 Ω cm for TTC_{10}-TTF and TTC_{11}-TTF, respectively, are remarkably low among single component organic solids ever observed (TTT (tetrathiotetracene) single crystal was reported to have the lowest resistivity 1.5×10^5 Ω cm among the organic solids including sulfur atoms though there have been arguments against the result because of the possibility of extrinsic features associated with the complex formation with oxygen[7]). The n dependence of the activation energies is correlated to that of room temperature resistivities as seen in Fig. 2, where TTC_{10}-TTF with a minimum resistivity corresponds to a minimum activation energy E_a=0.13 eV.

Up to now the crystal structures are presented for the compounds with n=1, 2, 4, 5, 9, and 10.[8,9] The central C_6S_8 moieties of n=1 and 2 are nonplanar and the molecular structure has a boat form. The intermolecular interactions between adjacent C_6S_8 moieties are weak and can be described in terms of the van der Waals interactions because of the absence of discernible intermolecular overlaps between adjacent π systems. Therefore, the high resistivities of n=1 and 2 can be understood taking account of this fact. On the contrary, C_6S_8 moieties of n=4, 5, 9, and 10 are planar and the molecular structure has a chair form. The intermolecular overlaps between adjacent π systems are effectively large because there exists columnar stacking structures consisting of the conjugated π systems which are not found in TTC_1-TTF and TTC_2-TTF. Thus the compounds with $n\geq4$ show the relatively low resistivities due to the crystal structures which are favorable for electron transport. The remarkable enhancement of the conductivity with increasing n can be explained by the fact that TTC_9-TTF and TTC_{10}-TTF have the short interplanar distance of 3.49 Å between adjacent C_6S_8

Table 2. Anisotropies of Resistivities of TTC_n-TTF

Compound	ρ_x[a]/Ω cm	ρ_y[b]/Ω cm	ρ_z[c]/Ω cm
TTC_1-TTF	2.9×10^{10}	1.7×10^{11}	2.7×10^{12}
TTC_2-TTF	1.2×10^{10}	1.2×10^{10}	1.4×10^{14}
TTC_9-TTF	5.0×10^{7} [d]	1.2×10^{8} [d]	2.9×10^{13} [d]

a) Parallel to the long axis of the crystal. b) Perpendicular to the x-direction in the broad face of the crystal. c) Perpendicular to the x-direction and to the broad face of the crystal. d) The directions x, y, and z correspond to the c-, a-, and b-axes, respectively, in the crystal data.

Table 3. Resistivities and Activation Energies of $TTeC_n$-TTF

Compound	ρ_{RT}[a]/Ω cm	E_a/eV
$TTeC_1$-TTF	6.9×10^{4}	0.25
$TTeC_2$-TTF	2.3×10^{9}	0.47
$TTeC_8$-TTF	1.7×10^{6}	0.24
$TTeC_9$-TTF	2.0×10^{6}	0.21
$TTeC_{13}$-TTF	1.1×10^{8}	0.41
$TTeC_{14}$-TTF	2.6×10^{8}	0.48
$TTeC_{15}$-TTF	1.7×10^{8}	0.43
$TTeC_{16}$-TTF	1.2×10^{8}	0.49
$TTeC_{17}$-TTF	1.4×10^{8}	0.43
$TTeC_{18}$-TTF	3.5×10^{8}	0.47

a) Single crystals for the compounds with $n=1$—9 and compaction pellets for the compounds with $n=13$—18. The measurements for the crystals were performed along the long axis of the crystal.

moieties which is considerably reduced in comparison with 3.73 Å in TTC_5-TTF (The difference in the observed resistivities between TTC_9-TTF and TTC_{10}-TTF with the same interplanar distance of 3.49 Å is considered to be caused by the difference in the magnitude of the transfer integrals between adjacent molecules which are easily changed by subtle difference in crystal structures.) These facts concerning crystal structures confirm that the remarkably low resistivities in the compounds with long alkyl chains are accomplished by strong intermolecular interactions due to the reduction in the intermolecular distance between adjacent C_6S_8 moieties.

The anisotropies of resistivities at room temperature for the compounds with n=1, 2, and 9 are summarized in Table 2. According to the structure analysis, TTC_9-TTF shows a large anisotropy $\rho_b/\rho_c\approx10^6$ as shown in Table 2 and the easy axis for electrical conduction (ρ_c) corresponds to the stacking direction of C_6S_8 moiety parallel to the c-axis, while the hard axis corresponds to the b-axis, in which direction adjacent TTC_9-TTF molecules face to each other through long alkyl chains elongated parallel to the b-axis. Along the a-axis, there exist strong S-S contacts which give rise to about the same magnitude of ρ_a to ρ_c. The investigation of resistivity just above the melting point (T_m=57 °C) shows that ρ_c increases to $\approx10^{12}$ Ω cm which is nearly equal to ρ_b in the crystal around T_m. This fact gives evidence that the regular stacks of the conjugated π systems parallel to the c-axis favorable to the good conduction is destroyed in liquid state. These results suggest the presence of the electrical conduction path associated with the large intermolecular overlaps and the short S-S contacts between adjacent π systems. On the other hand, TTC_1-TTF and TTC_2-TTF show a relatively small anisotropy (10^2—10^4) because of the absence of a special direction for easy electrical conduction.

Ultraviolet photoelectron spectroscopic studies presented that the compounds with long alkyl chains showed extraordinarily low ionization energies of 4.7—4.85 eV.[5] Such low values can be explained by the enhancement of polarization energy through large intermolecular interactions due to the small intermolecular distance. The studies of the thermal property suggest that intermolecular interactions are dominated mainly by the van der Waals interaction of C_6S_8 moieties in the range of small n ($n\leqslant7$), while they are dominated mainly by alkyl chain groups in the range of large n.[10] Taking into consideration of the results of crystal structures, the short interplanar distance for the compounds with large n is caused by these intermolecular interactions between alkyl chain groups, which is consistent with the following result of the density. The density measurements showed that the ratio of effective volumes of C_6S_8 moieties to those of alkyl chain groups for the compounds with $n\geqslant8$ decreased obviously as compared with the ratio of the compounds with $n<8$.[10] This fact means that effective volumes of C_6S_8 moieties for the compounds with $n\geqslant8$ are effectively depressed by intermolecular interactions caused by long alkyl chains. These results suggest that intermolecular interactions through alkyl chain groups work to reduce the interplanar distance between adjacent C_6S_8 moieties, which leads to remarkably high conductivities of the compounds with long alkyl chains.

$TTeC_n$-TTF. $TTeC_n$-TTF compounds also have semiconductive characters and the results of their electrical resistivities at room temperature ρ_{RT} and activation energies E_a are summarized in Table 3. Single crystals were employed only in n=1, 2, 8, and 9 for the present resistivity measurement. The magnitude of the resistivity of 6.9×10^4 Ω cm for $TTeC_1$-TTF, which is the lowest in the series of $TTeC_n$-TTF, is lower than the minimum resistivity in the TTC_n-TTF system. Crystal structure analysis gives the knowledge to understand noticeably low resistivity of this compound.[11] The central $C_6S_4Te_4$ moiety of $TTeC_1$-TTF is planar unlike TTC_1-TTF. $TTeC_1$-TTF molecules are stacked to form a column

structure with the interplanar distance of 3.76 Å. Tellurium atoms between neighbouring columns form zigzag chains along the stacking axis of $TTeC_1$-TTF molecules. The shortest Te-Te distance between neighbouring columns is 3.64 Å, which is significantly smaller than the van der Waals distance 4.12 Å of Te atom. The network of the zigzag Te chains in this material is reminiscent of the crystal structure of inorganic pristine Te where strong interatomic interactions associated with a short Te-Te distance (2.84 Å) bring about high conductivity (1 Ω cm). Therefore, the strong Te-Te interactions of $TTeC_1$-TTF compound is considered to give noticeably high conductivity. The short Te-Te contact has been observed also in the crystal of HMTTeF (bis(trimethylene)tetratellurafulvalene),[12] where HMTTeF molecules form columns stacked alternately with Te-Te distances of 3.583 and 3.743 Å. The dimerization effect of HMTTeF may be unfavorable to realize good electrical conduction.[13] On the contrary, for $TTeC_1$-TTF, the uniform zigzag Te interchains network can contribute to accomplish noticeably high conductivity. $TTeC_1$-TTF reveals the well-conductive character even just above melting point (T_m=170 °C) with the resistivity of $\approx 10^7$ Ω cm. This fact means that the short range ordering of molecular stacking associated with intermolecular interactions still remain in the molten state because of strong interatomic interactions between tellurium atoms. $TTeC_2$-TTF is found to have higher resistivity than $TTeC_1$-TTF. The high resistivity of $TTeC_2$-TTF can be easily understood by crystal structure analysis,[11] which suggests that the shortest Te-Te distance 3.99 Å in $TTeC_2$-TTF is considerably large as compared with 3.64 Å in $TTeC_1$-TTF and the interplanar distance between $C_6S_4Te_4$ moieties is very large (4.2 Å). For the compounds with $n \geq 8$, the resistivity is in the similar range to that for TTC_n-TTF with $n \geq 8$. According to the results of thermal properties, the series of $TTeC_n$-TTF is divided into two subgroups depending on the length of alkyl chain, which are different from the series of TTC_n-TTF.[14] For the compounds with long alkyl chains ($n \geq 7$), similar to TTC_n-TTF, intermolecular interactions associated with long alkyl chains predominate molecular packing, leading to the reduction in the distance between the $C_6S_4Te_4$ π systems which can act to enhance electrical conduction. The behavior of the resistivity for the compounds with $n \geq 7$ can be explained along this line. For the compounds with $n < 7$, which belong to the other subgroup, competition among three kinds of intermolecular interactions originating from alkyl chains, tellurium atoms and TTF π systems gives peculiar crystal structures depending on n. In the case of $TTeC_1$-TTF which has the shortest alkyl chains, strong intermolecular interaction between tellurium atoms plays an important role to determine a crystal structure and works to realize good electrical conduction as well as pristine tellurium.

Summary

The solid state properties of TTC_n-TTF and $TTeC_n$-TTF have been investigated by electrical conductivity measurement. In the case of TTC_n-TTF, the compounds with small n (n=1—3) show the high resistivities of above 10^{10} Ω cm, while those with large n ($n \geq 4$) show relatively low resistivities of 10^5—10^7 Ω cm. Especially, TTC_{10}-TTF and TTC_{11}-TTF show the remarkably low resistivities of 3.7×10^5 and 5.6×10^5 Ω cm, respectively. These values are exceptionally low among organic conductors which do not belong to charge-transfer complexes. The fairly good conductivities of the compounds with long alkyl chains are caused by the reduction in the distance between π systems of adjacent C_6S_8 moieties parallel to the stacking axis, which is accomplished by intermolecular van der Waals interactions through alkyl chain groups. The function of long alkyl chains for the reduction in the distance between the adjacent π systems can be called as "a molecular fastener effect". The optical band gaps are ≈2 eV for TTC_n-TTF compounds.[15] Thus the small activation energies of 0.1—0.3 eV from conductivity cannot be explained by a simple band picture for semiconducting materials. Electrical properties of $TTeC_n$-TTF are qualitatively same to those of TTC_n-TTF for the long alkyl chain compounds ($n \geq 8$). $TTeC_1$-TTF shows the lowest resistivity of 6.9×10^4 Ω cm among a series of TXC_n-TTF (X=S and Te). The noticeably high conductivity of this compound is considered to be caused by strong intermolecular interactions due to the presence of uniform zigzag Te chains similar to inorganic pristine Te.

The authors wish to thank Prof. Tadaoki Mitani of Institute for Molecular Science for his helpful discussion. This work was supported by a Grant-in-Aid for Scientific Research No. 61133008 from the Ministry of Education, Science and Culture.

References

1) P. Wu, G. Saito, K. Imaeda, Z. Shi, T. Mori, T. Enoki, and H. Inokuchi, *Chem. Lett.*, **1986**, 441.

2) P. Wu, T. Mori, T. Enoki, K. Imaeda, G. Saito, and H. Inokuchi, *Bull. Chem. Soc. Jpn.*, **59**, 127 (1986).

3) K. Imaeda, T. Enoki, T. Mori, P. Wu, M. Kobayashi, G. Saito, and H. Inokuchi, *Synthetic Metals*, **19**, 721 (1987).

4) H. Inokuchi, G. Saito, P. Wu, K. Seki, T. B. Tang, T. Mori, K. Imaeda, T. Enoki, Y. Higuchi, K. Inaka, and N. Yasuoka, *Chem. Lett.*, **1986**, 1263.

5) K. Seki, T. B. Tang, T. Mori, P. Wu, G. Saito, and H. Inokuchi, *J. Chem. Soc., Faraday Trans. 2*, **82**, 1067 (1986).

6) N. Okada, H. Yamochi, F. Shinozaki, K. Oshima, and G. Saito, *Chem. Lett.*, **1986**, 1861.

7) Y. Matsunaga, *J. Chem. Phys.*, **42**, 2248 (1965); H.

Inokuchi, M. Kochi, and Y. Harada, *Bull. Chem. Soc. Jpn.*, **40**, 2695 (1967); I. F. Shchegolev and E. B. Yagubskii, "Extended Linear Chain Compounds Vol. 2," ed by J. S. Miller, Plenum, New York (1982), Chap. 9, pp. 386—392.

8) C. Katayama, M. Honda, H. Kumagai, J. Tanaka, G. Saito, and H. Inokuchi, *Bull. Chem. Soc. Jpn.*, **58**, 2272 (1985).

9) Y. Higuchi, K. Inaka, and N. Yasuoka, private communication, n=2, monoclinic, $P2_1/c$, a=10.220(2), b=8.759(2), c=22.950(4) Å, β=96.69(1)°; n=5, triclinic, $P\bar{1}$, a=9.031(3), b=17.604(3), c=5.367(4) Å, α=90.26(2), β=105.90(4), γ=90.85(2)°; n=9, monoclinic, $P2_1/a$, a=8.707(2), b=55.498(8), c=5.171(2) Å, β=103.45(2)° (The definition of the lattice parameters a and c in the previous paper (Ref. 4) is revised by exchanging between a and c.); n=10, triclinic, $P\bar{1}$, a=7.850(3), b=32.960(9), c=5.115(4) Å, α=92.46(3), β=101.16(3), γ=88.18(3)°.

10) Z. Shi, T. Enoki, K. Imaeda, K. Seki, P. Wu, G. Saito, and H. Inokuchi, *Bull. Chem. Soc. Jpn.*, to be published.

11) Y. Higuchi and N. Yasuoka, private communication, n=1, monoclinic, $P2_1/n$, a=13.769(3), b=5.480(3), c=12.245-(2) Å, β=90.49(1)°; n=2, monoclinic, $P2_1/a$, a=14.017(4), b=9.021(2), c=9.239(5) Å, β=104.34(3)°.

12) P. J. Carroll, M. V. Lakshmikantham, M. P. Cava, F. Wudl, E. Aharon-Shalom, and S. D. Cox, *J. Chem. Soc., Chem. Commun.*, **1982**, 1316.

13) I. Shirotani and G. Saito, unpublished result.

14) J. K. Jeszka, T. Enoki, Z. Shi, K. Imaeda, H. Inokuchi, N. Okada, H. Yamochi, and G. Saito, private communication.

15) T. Mitani, private communication.

 © 1987 The Chemical Society of Japan Bull. Chem. Soc. Jpn., 60, 3169—3173 (1987)

Photo-Excitable Membranes. Photoinduced Potential Changes across Poly(vinyl chloride)/Spirobenzopyran Membranes Doped with Valinomycin and Nonactin

Jun-ichi Anzai, Yasushi Hasebe, Akihiko Ueno, and Tetsuo Osa*
Pharmaceutical Institute, Tohoku University, Aobayama, Sendai 980
(Received April 27, 1987)

Poly(vinyl chloride)/spirobenzopyran membranes doped with valinomycin or nonactin were prepared to study the photoresponse of the membrane potential in the presence of K^+ or NH_4^+ ion. Ultraviolet (UV) light irradiation induced more than 100 mV of potential change across the membrane doped with valinomycin in the presence of 10^{-8}—10^{-6} M† KCl, whereas the potential change was extremely suppressed in the presence of higher KCl concentration (>10^{-3} M). The photoresponse of the membrane potential depended upon the direction from which the membrane was irradiated. The nonactin-doped membranes showed a similar tendency in photoresponse in the presence of NH_4Cl to that observed for the valinomycin-doped membrane in the presence of KCl. The results were explained in terms of surface potential changes at the irradiated surface of the membrane, associated with the photochemical reaction of spirobenzopyran and the specific adsorption of cations to the surface of the membrane.

Several reports have described efforts to photochemically regulate the membrane potential across the polymer membranes doped with spiropyran derivatives. Suzuki et al. have reported that 20—30 mV of membrane potential can be induced by photoirradiating a cellulose/phosphatidylcholine composite membrane doped with 1′,3′,3′-trimethyl-6-nitrospiro-[2*H*-1-benzopyran-2,2′-indoline].[1,2] The results have been explained in terms of photochemically-induced changes in the fixed charge density in the membrane arising from the photochemical reaction of the spiropyran derivative. They have also prepared asymmetric membrane which contains spiropyran derivative at the surface of one side of the membrane.[3] Bellobono et al. have prepared cellulose membranes incorporating five kinds of spiropyran compounds to examine their photoresponse in membrane potential, with the intention of applying the membrane in constructing photoresponsive devices used in the field of optical data storage.[4,5] Synthetic polymers which contain spiropyran side chains have also been used to study photoresponse of the membrane. Irie et al. have prepared polymer membranes composed of poly(methacrylate) having spiropyran pendant groups and measured membrane potential under irradiation.[6] They have suggested the importance of the conformational changes of the polymer chains as well as the charge density in the membrane.

In all cases cited above, the magnitude of photoinduced potential was 20—30 mV and the response was somewhat slow. We have succeeded in highly improving the photoresponse in membrane potential across the spiropyran-contaning membrane, by the use of plasticized poly(vinyl chloride) (PVC) as a membrane matrix.[7-14] In the course of our study on the PVC/spiropyran membranes, the followings were found; (1) UV irradiation induces membrane potential changes of more than 100 mV with a response time of 1—2 min, (2) the photoinduced potential changes arise from the change in charge density on the membrane surface (i.e., surface potential change), which, in turn, stems from the photo-generated open form of spiropyran, (3) the content of open form of spiropyran is higher on the UV-irradiated surface than that on the nonirradiated surface (i.e., formation of asymmetric membrane). The present paper describes the photoresponse in membrane potential across the PVC/1′-hexadecyl-3′,3′-dimethyl-6-nitrospiro[2*H*-1-benzopyran-2,2′-indoline] (**1**) membranes doped with nonactin and valinomycin. These systems are useful for studying the effects of specific adsorption of ions on the membrane surface upon the photoresponse of the membrane, because valinomycin and nonactin are ionophores which bind K^+ and NH_4^+ ions, respectively.

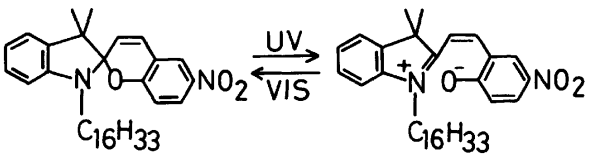

Closed-(1) Open-(1)

Experimental

Materials. PVC (molecular weight of ca. 70000) was purchased from Wako Chemical Co. and used without further purification. Dibutyl phthalate (DBP), tetrahydrofuran (THF), ammonium chloride (NH_4Cl), potassium chloride (KCl), nonactin, and valinomycin are of extra pure reagent grade. The synthetic procedure and analytical data of **1** were reported elsewhere.[12]

Membrane Preparation. PVC/**1**/nonactin membrane was prepared by pouring the mixture of 250 mg of PVC, 0.5 ml of DBP, 30 mg of 1, 5 mg of nonactin, and 20 ml of THF onto a flat Petri dish (8.5 cm diameter), and allowing the solvent to evaporate at room temperature. PVC/**1**/valinomycin membrane was prepared in the same manner

† 1 M=1 mol dm^{-3}.

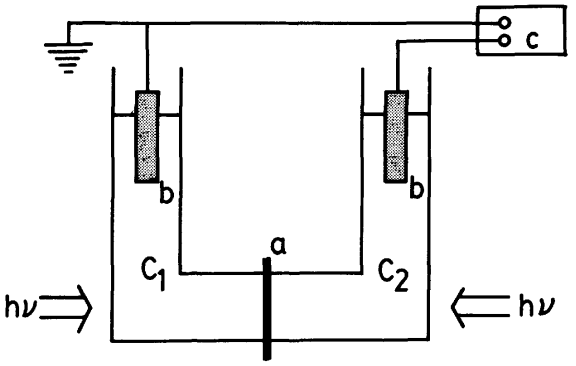

Fig. 1. Schematic representation of the cell for measuring membrane potential.
a; Membrane, b; Ag/AgCl electrode, c; potentiometer.

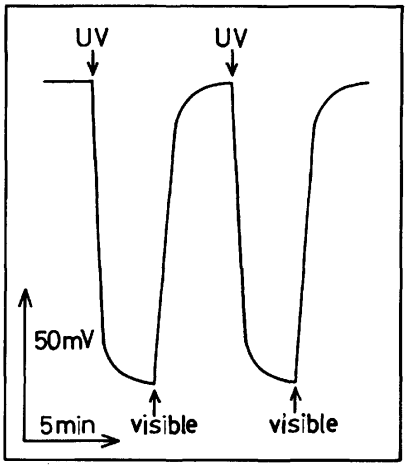

Fig. 2. Typical photoresponse of the membrane potential across the PVC/**1**/valinomycin membrane.
c_1 side; pure water, c_2 side; 10^{-4} M KCl.

using 5 mg of valinomycin in place of nonactin. The thickness of the membranes thus prepared was ca. 0.15 mm.

Measurements. Membrane potential measurements were conducted at 25 °C using a U-shaped glass cell illustrated in Fig. 1. The composition of the electrochemical cell for the membrane potential measurements was as follows; Ag/AgCl |0.1 M $(CH_3)_4NCl$|electrolyte solution (c_1)|PVC/**1**/nonactin or PVC/**1**/valinomycin membrane|electrolyte solution (c_2) |0.1 M $(CH_3)_4NCl$|Ag/AgCl. The electrode in the c_1 compartment was earthed. Photoirradiation was carried out from the c_1 or c_2 side with a 500 W xenon lamp using cut-off filters Toshiba UVD-35S and O-55 to isolate UV (320 nm$<\lambda<$400 nm) and visible ($\lambda>$490 nm) light, respectively. Noise level in the potential was within 1 mV under the present experimental conditions. Absorption spectra of the membrane were recorded on a Shimadzu UV-visible spectrophotometer (Type UV-250).

Results and Discussion

We have already reported that the membrane potential across the PVC/**1** membrane changes upon photoirradiation, associated with the photochemical interconversion of **1** between closed form and open form.[7-14] The photoinduced membrane potential was ascribed to changes in charge density at the UV-irradiated surface of the membrane, arising from the photochemically-generated open form of **1**.

Figure 2 depicts a typical photoresponse of the membrane potential across the PVC/**1**/valinomycin membrane. When the membrane was exposed to UV light from c_2 side, the membrane potential shifted in the negative direction and, subsequently, the membrane potential was restored to the original value upon visible light irradiation. The photoresponsive behavior of the PVC/**1**/valinomycin membrane was essentially comparable to those previously observed for valinomycin-free PVC/**1** membrane.[12] This was also the case for photoresponse of the PVC/**1**/nonactin membrane. These results suggest that valinomycin and nonactin have scarcely any influence on the photochemical reaction of **1** in the membrane.

PVC/1/Valinomycin Membrane. In general, the potential difference across a charged membrane (membrane potential, $\Delta\phi$) is given as an algebraic sum of the diffusion potential in the membrane and the surface potential difference at membrane-solution interfaces.[15-18] In the case of plasticized PVC membranes, the contribution from the diffusion potential is considered small due to the depressed ionic permeability in the highly hydrophobic membrane interior, as was discussed for PVC/crown ether membranes in the previous paper.[19] For the PVC/**1**/valinomycin membrane, it is reasonable to assume that the surface potentials at the membrane-solution interfaces depend on the density of the ions which are adsorbed to the membrane surface by forming complexes with valinomycin, as well as on the content of open-**1**.

We therefore measured the membrane potential across the PVC/**1**/valinomycin membrane under visible and UV light in the presence of 10^{-8}—10^{-1} M KCl in the c_2 side solution (Fig. 3). In the dark or under visible light, where **1** assumes wholly closed form (noncharged form), the $\Delta\phi$ values increased linearly with increasing concentration of K^+ ion over the range of 10^{-5}—10^{-1} M. This should be caused by adsorption of K^+ ions on the membrane surface as a result of complexation between K^+ ions and valinomycin. This means that the charge density on the membrane surface reflects the concentration of K^+ ion in the aqueous solution adjacent to the membrane surface. The $\Delta\phi$ values measured under UV light irradiation from c_1 or c_2 side were also affected by the concentration of K^+ ion. UV irradiation from the c_1 side induced positive shift of the membrane potential, while the potential shifted in the negative direction upon UV irradiation from c_2 side. The polarity of the potential shift was reasonably explained based on the

asymmetric membrane formation under UV light irradiation.[12]

Figure 4 shows the $\Delta(\Delta\phi)$ values, the difference between the $\Delta\phi$ value under UV light irradiation and that in the dark or under visible light, observed upon UV irradiation from c_1 or c_2 side. When the membrane was irradiated from c_2 side, an approximately linear relationship existed between the $\Delta(\Delta\phi)$ values and the concentration of K^+ ion over the range of 10^{-6}—10^{-3} M. The magnitude of $\Delta(\Delta\phi)$ value was enhanced in the lower concentration region of K^+ ion, whereas, over 10^{-2} M KCl, the photoresponse was suppressed, being 5 mV or less. On the contrary, the $\Delta(\Delta\phi)$ values were always about 100 mV when the membrane surface facing the c_1 solution, where K^+ ion was absent, was exposed to UV light. These observations imply that the higher charge density on the irradiated surface of the membrane is not favorable for the enhanced photoresponse.

Figure 5 shows the $\Delta\phi$ values across the membrane under the conditions that KCl concentrations in both sides are equal with each other. The membrane potential was always near to zero under visible light or in the dark. UV light irradiation from c_1 or c_2 side induced shifts in membrane potential in the positive or negative direction, respectively, in spite of the conditions of $c_1=c_2$. This can be ascribed to asymmetric membrane formation under UV light irradiation,[20-22] i.e., the photochemical reaction of **1** from closed form to open form proceeds more efficiently on the irradiated surface of the membrane than on the opposite surface. Therefore, the content of open-**1** on the irradiated surface is higher than that on the nonirradiated surface. This is the reason why photoinduced potential changes were observed even for $c_1=c_2$. The $\Delta(\Delta\phi)$ values were dependent on the KCl concentration, in both cases when irradiated from c_1 and c_2 sides. These results can be also explained based on the idea that the higher charge density on the irradiated surface of the membrane suppresses the photoresponse in membrane potential.

We also checked the photoresponse of PVC/**1** membrane without valinomycin in the presence of KCl, and found that the $\Delta(\Delta\phi)$ values were always about 100 mV irrespective of KCl concentration. This means that valinomycin is essentially required for binding K^+ ions to regulate the charge density on the membrane surface.

In previous papers,[7-14] we have explained the photoresponse of **1**-doped PVC membranes in terms of the formation of asymmetric membrane under UV irradiation. To obtain a further evidence for this, we

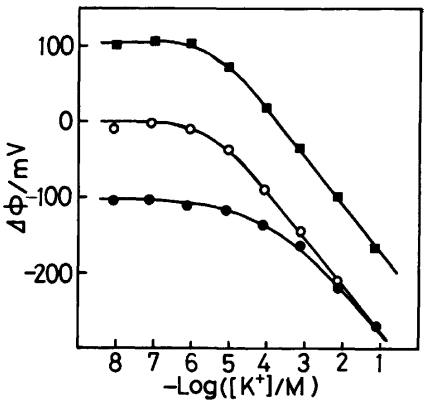

Fig. 3. The membrane potential across the PVC/1/valinomycin membrane under UV light irradiation from c_1 side (—■—) and c_2 side (—●—) and visible light (—○—) from c_2 side as a function of KCl in the c_2 solution. The concentration of KCl in the c_1 side solution was zero.

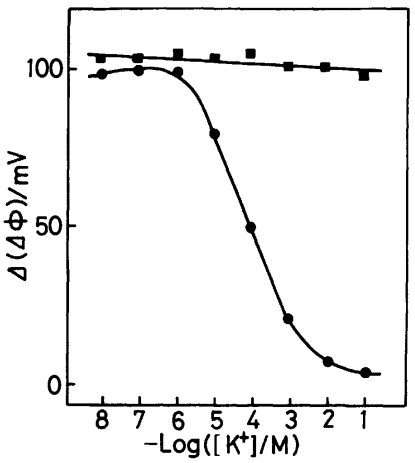

Fig. 4. The effects of KCl concentration on the $\Delta(\Delta\phi)$ value. The membrane was irradiated from c_1 side (—■—) and c_2 side (—●—). The concentration of KCl in the c_1 side solution was zero.

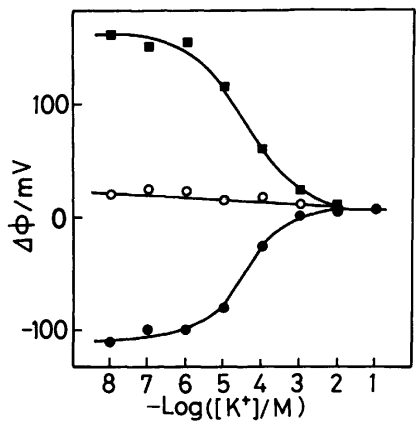

Fig. 5. The asymmetric membrane potential across the PVC/1/valinomycin membrane in the presence of KCl under UV light irradiation from c_1 side (—■—) and c_2 side (—●—) and under visible light from c_2 side (—○—). The concentration of KCl in both solutions was equal with each other.

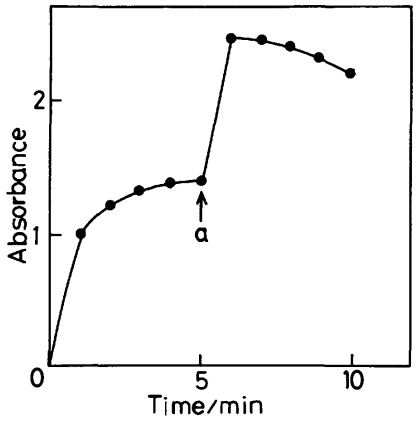

Fig. 6. Change of absorbance of the membrane at 565 nm under UV light irradiation. After 5 min-irradiation from one side of the membrane, the opposite surface of the membrane was exposed to UV light at (a).

measured absorption spectra of the membrane. As depicted in Fig. 6, the absorbance of the membrane at 565 nm, which is absorption maximum of open-**1**, increased rapidly at the initial stage of UV irradiation and declined to reach a steady-state value after about 5 min. The absorbance no longer increased even after prolonged irradiation from the same direction. When the membrane, after the steady-state value of absorbance had been attained by UV irradiation from one side of the membrane, was exposed to UV light, in turn, from the opposite direction, a further increase of the absorbance was observed. This is a clear evidence for the formation of asymmetric membrane under UV light irradiation.

PVC/1/Nonactin Membrane. Photoresponse of PVC/**1**/nonactin membrane was also examined in the presence of NH_4^+ ions. We have already reported some results concerning photoresponse of the PVC/**1**/nonactin membrane.[14] Figure 7 shows the dependence of $\Delta\phi$ values on the NH_4Cl concentration in the aqueous solution. The basic profiles of the membrane potentials under visible and UV light were essentially the same as those observed for PVC/**1**/valinomycin membrane in the presence of KCl.

The $\Delta(\Delta\phi)$ values were shown in Fig. 8. When the membrane surface facing c_1 solution was exposed to UV light, the $\Delta(\Delta\phi)$ values measured 180—190 mV irrespective of the concentration of NH_4Cl in c_2 solution. The $\Delta(\Delta\phi)$ values, in contrast, depended remarkably on the NH_4Cl concentration when irradiated from c_2 side. This behavior can be explained based on the same idea which explicated the photoresponse of PVC/**1**/valinomycin membrane in the presence of KCl. Namely, the specific adsorption of NH_4^+ ions on the membrane surface facing c_2 solution affected the magnitude of the $\Delta(\Delta\phi)$ values.

Figure 9 shows the $\Delta\phi$ values across the PVC/**1**/

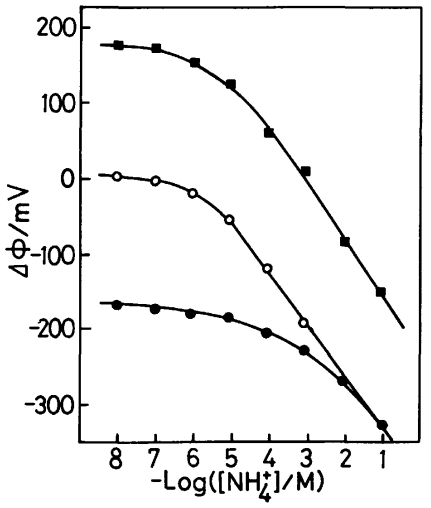

Fig. 7. The membrane potential across the PVC/**1**/nonactin membrane in the presence of NH_4Cl under UV light irradiation from c_1 side (—■—) and c_2 side (—●—) and under visible light from c_2 side (—○—). The concentration of NH_4Cl in the c_1 side solution was zero.

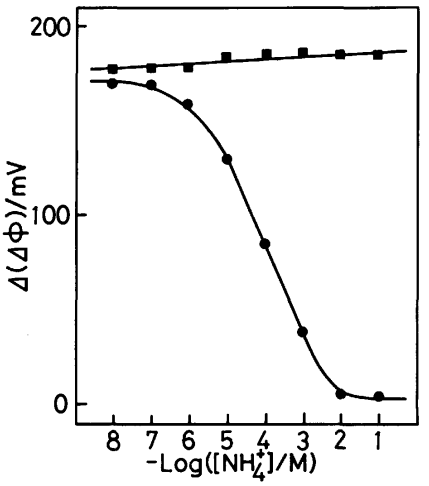

Fig. 8. The effects of NH_4Cl concentration on the $\Delta(\Delta\phi)$ value. The membrane was irradiated from c_1 side (—■—) and c_2 side (—●—). The concentration of NH_4Cl in the c_1 side solution was zero.

nonactin membrane under the conditions that the concentrations of NH_4Cl in c_1 and c_2 solutions are equal with each other. The membrane potentials under visible light or in the dark were always near to zero. UV irradiation from c_1 or c_2 side induced positive or negative shift of the membrane potential, respectively. The $\Delta\phi$ values observed under UV light irradiation drastically depended on the NH_4Cl concentration in the aqueous phase.

We elucidated the effects of nonactin concentration in the membrane on the magnitude of $\Delta(\Delta\phi)$ values in the presence of 10^{-4} M NH_4Cl (Fig. 10). When the nonactin-free membrane was irradiated, more than

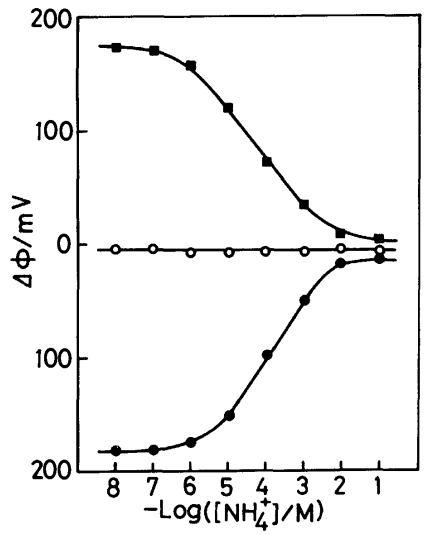

Fig. 9. The asymmetric membrane potential across the PVC/1/nonactin membrane in the presence of NH_4Cl under UV light irradiation from c_1 side (—■—) and c_2 side (—●—) and under visible light (—○—). The concentration of NH_4Cl in both side solutions was equal with each other.

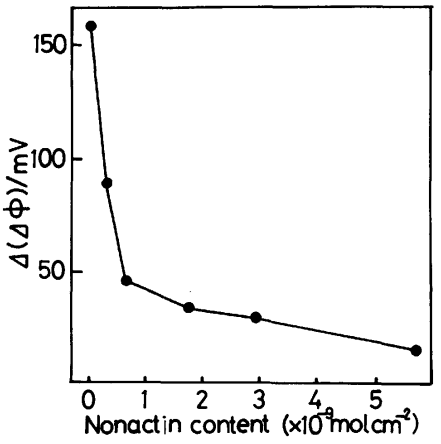

Fig. 10. Effects of nonactin content in the membrane on the photoresponse of the PVC/**1**/nonactin membrane. The concentration of NH_4Cl in both side solutions was 10^{-4} M.

150 mV of photoinduced potential was observed. On the other hand, the $\Delta(\Delta\phi)$ values lowered to 50 mV or less in the presence of 1×10^{-9}—5×10^{-9} mol cm^{-2} of nonactin in the membrane. This clearly indicates that the formation of nonactin/NH_4^+ ion complexes on the membrane surface has a serious influence on the $\Delta(\Delta\phi)$ values.

In conclusion, the photoresponse in membrane potential across the PVC/**1** membranes doped with valinomycin and nonactin drastically depended on the concentration of K^+ and NH_4^+ ions, respectively, in the aqueous solution adjacent to the UV-irradiated surface of the membrane. These membranes may be applicable to the sensitive layer of a novel class of ion sensors which change the $\Delta(\Delta\phi)$ value in response to the concentration of ions such as K^+ and NH_4^+ in the solution.

The authors are grateful to the Ministry of Education, Science and Culture for support of this work through a Grant-in-Aid for Special Project Research (No. 61127003).

References

1) S. Kato, M. Aizawa, and S. Suzuki, *J. Membr. Sci.*, **1**, 289 (1976).
2) S. Kato, M. Aizawa, and S. Suzuki, *Kobunshi Ronbunshu*, **34**, 793 (1977).
3) S. Kato, M. Aizawa, and S. Suzuki, *J. Membr. Sci.*, **2**, 39 (1977).
4) I. R. Bellobono, S. Giovanardi, B. Marcandalli, S. Calgari, and D. Nasari, *Polym. Photochem.*, **4**, 59 (1984).
5) I. R. Bellobono, B. Marcandalli, E. Selli, and S. Calgari, *Photogr. Sci. Eng.*, **28**, 162 (1984).
6) M. Irie, A. Menju, and K. Hayashi, *Nippon Kagaku Kaishi*, **1984**, 227.
7) J. Anzai, A. Ueno, and T. Osa, *J. Chem. Soc., Chem. Commun.*, **1984**, 688.
8) J. Anzai, H. Sasaki, A. Ueno, and T. Osa, *Chem. Lett.*, **1985**, 1443.
9) J. Anzai, H. Sasaki, A. Ueno, and T. Osa, *Chem. Pharm. Bull.*, **33**, 5589 (1985).
10) J. Anzai, H. Sasaki, A. Ueno, and T. Osa, *Makromol. Chem., Rapid Commun.*, **7**, 133 (1986).
11) J. Anzai, A. Ueno, and T. Osa, *Makromol. Chem., Rapid Commun.*, **7**, 433 (1986).
12) J. Anzai, Y. Hasebe, A. Ueno, and T. Osa, *Kobunshi Ronbunshu*, **43**, 683 (1986).
13) J. Anzai, Y. Hasebe, M. Shimada, A. Ueno, and T. Osa, *Maku (Membrane)*, **12**, 165 (1987).
14) J. Anzai, Y. Hasebe, A. Ueno, and T. Osa, *Bull. Chem. Soc. Jpn.*, **60**, 1515 (1987).
15) T. Teorell, *Proc. Soc. Exp. Biol.*, **33**, 282 (1935).
16) K. H. Mayer and J. F. Sievers, *Helv. Chim. Acta*, **19**, 649 (1936).
17) R. Schlogl and F. Helfferich, *Z. Electrochem.*, **65**, 644 (1952).
18) M. Nakagaki and K. Miyake, *Yakugaku Zasshi*, **93**, 1105 (1973).
19) J. Anzai, H. Sasaki, A. Ueno, and T. Osa, *J. Chem. Soc., Perkin Trans. 2*, **1985**, 903.
20) A. M. Liquili and C. J. Botre, *J. Phys. Chem.*, **71**, 3765 (1967).
21) S. Ohki, *J. Colloid Interface Sci.*, **37**, 318 (1971).
22) M. Nakagaki and R. Takeda, *Chem. Pharm. Bull.*, **32**, 3812 (1984).

 © 1987 The Chemical Society of Japan Bull. Chem. Soc. Jpn., 60, 3175—3181 (1987)

Multi-Ionic Potential and Membrane Permeability Matrix. II. Na^+-Ca^{2+} Bi-Ionic System with a Cation-Exchange Membrane and Effects of Cl^- on Cation Transport

Kozue KAIBARA,* Hiroyoshi INOUE, and Hideo KIMIZUKA
Department of Chemistry, Faculty of Science, Kyushu University,
Hakozaki, Higashi-ku, Fukuoka 812
(Received April 18, 1987)

Transport characteristics of Na^+-Ca^{2+} bi-ionic system with a highly selective cation-exchange membrane were investigated on the basis of nonequilibrium thermodynamic theory. As a principal transport parameter, the membrane permeability matrix or membrane conductance matrix can be estimated from the membrane potential, conductance, and ion flux data. Significances of diffusional and electroconductive processes of ion transport across membrane were systematically discussed in terms of these matrix elements. Partial contributions of inter-cationic (Na^+-Na^+, Na^+-Ca^{2+}, and Ca^{2+}-Ca^{2+}) correlations to the membrane transport process of ions were examined by means of comparing the estimated values of corresponding matrix elements. It was suggested that Ca^{2+} ions, of which membrane concentrations are kept at high level independently of the Na^+/Ca^{2+} concentration ratio of external aqueous solutions, play a critical role in the membrane transport phenomena. Participations of Cl^- transport in the cation-exchange processes were also discussed on the basis of membrane conductance matrix theory.

Characterization of the ion-transport processes across membrane is a fundamental and important subject in wide varieties of artificial and biological systems, such as ion exchange membranes, lipid bilayers, and biological cellular membranes. Phenomenological analyses on the membrane-transport processes are performed generally utilizing linear formulations relating the thermodynamic driving forces with fluxes across membrane based on the nonequilibrium thermodynamics.[1,2] An appropriate set of the linear phenomenological equations formulating the coupling of driving forces and fluxes can be derived for various transport phenomena arising across membranes.[3]

In case of the ionic membrane transport processes, detailed descriptions of the electrochemical properties, by means of estimating the appropriate phenomenological coefficient as a membrane transport parameter of permselectivity index, are essential procedures to characterize the membrane systems. In this context, the membrane permeability matrix and the membrane conductance matrix were introduced as a principal membrane transport parameter in an earlier paper to describe membrane permselectivities to ions based on the electrochemical and ion flux measurements.[4] By utilizing these membrane permeability parameters in a matrix form, the membrane transport processes of ions can be characterized in terms of the correlations between permeating ions. Furthermore, fundamental aspects of the diffusional and electroconductive movements of ions within membrane phase can be discussed based on these transport parameters.[5,6]

The present investigations were designed to systematically analyze the ion permselectivities and electrochemical properties of $NaCl$-$CaCl_2$ aqueous systems with a cation-exchange membrane on the basis of nonequilibrium thermodynamics. Effects of Ca^{2+} as a bivalent cation on the ion transport across cation-exchange membrane and effects of Cl^- on the cation transport were examined and compared with the results obtained in the NaCl-CsCl systems reported in the preceding paper.[6] Detailed analyses on the correlations between ion fluxes across charged membranes would contribute toward an improvement of efficiencies in the membrane process operations. Recently, it was clarified that a part of K^+ flux across excitable cell membrane, Ca^{2+}-dependent K^+ flux, is strongly affected and triggered by the entry of Ca^{2+} into the cell.[7] Quantitative descriptions of the coupling between permeating ions are also important in biological systems, since the Ca^{2+}-dependent K^+ movement has become established and important physiological concept and Ca^{2+}, which plays a crucial role in many biological reactions, is considered to be a mediator for the ion transport across cellular membranes.

Experimental

Experimental systems consisted of a "CK-1, 1.0t" cation-exchange membrane (Asahi Chemical Industry, Co., Ltd.)[6] with aqueous solution phases I and II separated by the membrane, one of which contains NaCl and the other, $CaCl_2$. Transport numbers of the CK-1, 1.0t membrane to Na^+ and Ca^{2+} were estimated at 0.97—0.99 and 0.95—0.98 from the membrane potential measurements on concentration cell systems with electrolyte concentration ranges of 10^{-1}—10^{-3} mol dm^{-3}. In this study, electrochemical and ion flux measurements were carried out on the systems where concentrations of NaCl or $CaCl_2$ in phase I were varied from 10^{-1} to 10^{-3} mol dm^{-3} and those of the other electrolyte in phase II were kept constant at 10^{-1}, 10^{-2}, or 10^{-3} mol dm^{-3}. Electrolyte solutions were prepared from extra pure salts with conductivity water.

Experimental arrangements for the membrane potential

and conductance measurements were the same as reported earlier.[6] Cation fluxes were measured by the tracer flux method. ^{22}Na and ^{45}Ca in chloride form as a radioactive tracer were purchased from the Japan Radioisotope Association. Radioactive NaCl or $CaCl_2$ aqueous solution with an appropriate specific activity was set in the solution chamber on one side of the membrane, then, the time courses of increases in radioactivity of solution on the other side were detected by the γ-ray scintillation counter or liquid scintillation counter to estimate the steady cation fluxes across membrane. Cl^- fluxes were estimated from Na^+ and Ca^{2+} flux data under the experimental conditions where the total electric membrane currents were zero. Cl^- flux was also checked in some systems by measuring the tracer flux using ^{36}Cl as a tracer ion.

All the measurements were carried out at regulated room temperature, 25 ± 1 °C.

Results and Discussion

General Formulations. A set of the phenomenological equations characterizes well the ion transport processes by formulating the relationships of ion fluxes across membrane with coupled thermodynamic forces, gradients of electrochemical potentials of ions. For the present system studied, the linear phenomenological equations can be written as:[4,6]

$$\begin{bmatrix} J_{Na} \\ J_{Ca} \\ J_{Cl} \end{bmatrix} = -\begin{bmatrix} P_{Na\cdot Na} & P_{Na\cdot Ca} & P_{Na\cdot Cl} \\ P_{Ca\cdot Na} & P_{Ca\cdot Ca} & P_{Ca\cdot Cl} \\ P_{Cl\cdot Na} & P_{Cl\cdot Ca} & P_{Cl\cdot Cl} \end{bmatrix} \times \begin{bmatrix} a^{II}_{Na}\exp(FV/2RT) - a^{I}_{Na}\exp(-FV/2RT) \\ a^{II}_{Ca}\exp(FV/RT) - a^{I}_{Ca}\exp(-FV/RT) \\ a^{II}_{Cl}\exp(-FV/2RT) - a^{I}_{Cl}\exp(FV/2RT) \end{bmatrix} \quad (1)$$

or

$$\begin{bmatrix} i_{Na} \\ i_{Ca} \\ i_{Cl} \end{bmatrix} = -\begin{bmatrix} g_{Na\cdot Na} & g_{Na\cdot Ca} & g_{Na\cdot Cl} \\ g_{Ca\cdot Na} & g_{Ca\cdot Ca} & g_{Ca\cdot Cl} \\ g_{Cl\cdot Na} & g_{Cl\cdot Ca} & g_{Cl\cdot Cl} \end{bmatrix} \begin{bmatrix} V-V_{Na} \\ V-V_{Ca} \\ V-V_{Cl} \end{bmatrix} \quad (2)$$

In these formulations, solvent fluxes are neglected, since the effects of solvent transport across membrane on the interactions of permeant ions are fairly small in the highly charged membrane system.[8] Here, J is the ion flux across membrane, a is the activity, V is the membrane potential, and i is the ionic membrane current; the subscripts Na, Ca, and Cl identify permeant ions; the superscripts I and II refer to the solution phases I and II separated by the membrane; F, R, and T are the Faraday constant, gas constant, and absolute temperature, respectively. V_{Na}, V_{Ca}, and V_{Cl} are the equilibrium membrane potentials to Na^+, Ca^{2+}, and Cl^- calculated by the Nernst equations for the respective ions. The 3×3 matrices in Eqs. 1 and 2 are the membrane permeability matrix and membrane conductance matrix, respectively. Elements of these matrices correspond to modified phenomenological coefficients indicating the participations of interactions between permeant ions specified by the subscript indices to the membrane transport processes. Only the membrane conductance elements satisfy the reciprocal relations, since, in Eq. 1, the permeability matrix element is recognized as a phenomenological coefficient relating the ion flux with electrochemical activity difference between solution phases I and II as a substituted conjugated thermodynamic force.[4,6] The conductance matrix element is defined as a coefficient describing the ohmic relation between ionic membrane current with effective membrane potential difference.

The membrane permeability parameters, which indicate the permselectivities to ions by means of referring the permeating speed of ions across membrane, are expressed as a function of the permeability matrix elements:[4]

$$\begin{aligned} P_{Na} &= P_{Na\cdot Na} + 2P_{Ca\cdot Na} - P_{Cl\cdot Na} \\ P_{Ca} &= \tfrac{1}{2}P_{Na\cdot Ca} + P_{Ca\cdot Ca} - \tfrac{1}{2}P_{Cl\cdot Ca} \\ P_{Cl} &= -P_{Na\cdot Cl} - 2P_{Ca\cdot Cl} + P_{Cl\cdot Cl} \end{aligned} \quad (3)$$

where P_{Na}, P_{Ca}, and P_{Cl} are the electroconductive permeabilities to Na^+, Ca^{2+}, and Cl^-, respectively. Similarly, the membrane conductance, G_m, and ionic membrane conductances, g_{Na}, g_{Ca}, and g_{Cl}, are expressed as a function of the conductance matrix elements:

$$\begin{aligned} G_m &= g_{Na} + g_{Ca} + g_{Cl} \\ &= (g_{Na\cdot Na} + g_{Ca\cdot Na} + g_{Cl\cdot Na}) \\ &\quad + (g_{Na\cdot Ca} + g_{Ca\cdot Ca} + g_{Cl\cdot Ca}) \\ &\quad + (g_{Na\cdot Cl} + g_{Ca\cdot Cl} + g_{Cl\cdot Cl}) \end{aligned} \quad (4)$$

Therefore, the ohmic relations for the total membrane electric current, I, are expressed as:

$$\begin{aligned} I &= -F\{P_{Na}[a^{II}_{Na}\exp(FV/2RT) - a^{I}_{Na}\exp(-FV/2RT)] \\ &\quad + 2P_{Ca}[a^{II}_{Ca}\exp(FV/RT) - a^{I}_{Ca}\exp(-FV/RT) \\ &\quad - P_{Cl}[a^{II}_{Cl}\exp(-FV/2RT) - a^{I}_{Cl}\exp(FV/2RT)]\} \\ &= -g_{Na}(V-V_{Na}) - g_{Ca}(V-V_{Ca}) - g_{Cl}(V-V_{Cl}) \\ &= -G_m(V-V_0) \end{aligned} \quad (5)$$

where V_0 is the membrane potential in the absence of membrane electric current and the following relation is satisfied:

$$\begin{aligned} &2P_{Ca}a^{II}_{Ca}\exp(2FV_0/RT) + (P_{Na}a^{II}_{Na} + P_{Cl}a^{I}_{Cl})\exp(3FV_0/2RT) \\ &\quad - (P_{Na}a^{I}_{Na} + P_{Cl}a^{II}_{Cl})\exp(FV_0/2RT) - 2P_{Ca}a^{I}_{Ca} = 0 \end{aligned} \quad (6)$$

Electrochemical and Flux Data. Figure 1 summarizes the membrane potential, membrane conductance, and cationic flux data. The NaCl-$CaCl_2$ bi-ionic systems with a highly selective cation-exchange membrane studied here can be classified into two large groups: the systems in which Cl^- fluxes are negligible order and the membrane processes are characterized only by Na^+ and Ca^{2+} transports, and the systems in

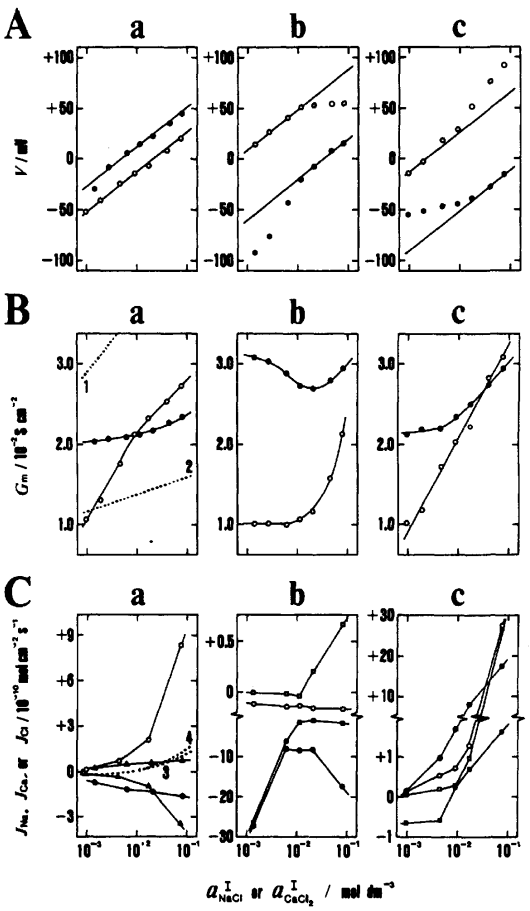

Fig. 1. Membrane potential (A), membrane conductance (B), and ionic flux (C) data as a function of mean electrolyte activity of phase I. Closed and open symbols refer to: a, $CaCl_2$(I)-10^{-2} mol dm^{-3} NaCl(II) and NaCl(I)-10^{-2} mol dm^{-3} $CaCl_2$(II); b, $CaCl_2$(I)-10^{-1} mol dm^{-3}NaCl(II) and $CaCl_2$(I)-10^{-3} mol dm^{-3} NaCl(II); c, NaCl(I)-10^{-1} mol dm^{-3} $CaCl_2$-(II) and NaCl(I)-10^{-3} mol dm^{-3} $CaCl_2$(II). In A, the solid lines refer to the ideal Na^+-Ca^{2+} bi-ionic potential responses estimated by Eq. 7 with a constant P_{Na}/P_{Ca} assumption. In C, ●, ○: J_{Na}; ▲, △: J_{Ca}; ■, □: J_{Cl}. The broken lines 1 and 3 refer to membrane conductance data and J_{Na} data in NaCl(I)-10^{-2} mol dm^{-3} NaCl(II) system; the broken lines 2 and 4 refer to membrane conductance data and J_{Ca} data in $CaCl_2$(I)-10^{-2} mol dm^{-3} $CaCl_2$ (II) systems.

which Cl^- fluxes comparable to cationic fluxes are observed and, accordingly, the cation transport is affected considerably by Cl^- transport.

As illustrated in Fig. 1-C-a, Cl^- fluxes are negligible order as compared with Na^+ and Ca^{2+} fluxes in the $CaCl_2$(I)-10^{-2} mol dm^{-3} NaCl(II) and NaCl(I)-10^{-2} mol dm^{-3} $CaCl_2$(II) systems. When the membrane processes in these systems are characterized only by the cation transport, the next equation can be derived from Eq. 6:

$$V_0 = -(2RT/3F)\ln(P_{Na}a_{Na}^{II}/2P_{Ca}a_{Ca}^{I}) \text{ or } -(2RT/3F)\ln(2P_{Ca}a_{Ca}^{II}/P_{Na}a_{Na}^{I}) = V_{Na\text{-}Ca} \quad (7)$$

The membrane potential expressed by Eq. 7 can be recognized as a cationic equilibrium potential for bi-ionic system being equivalent to the Nernst potential in concentration cell systems. In the present cases, observed membrane potentials correspond to the equilibrium potentials for Na^+ and Ca^{2+}, $V_{Na\text{-}Ca}$. Equation 7 deduces that the constant Na^+/Ca^{2+} permeability ratio is realized for the system in which the linear membrane potential responses of 39.44 mV/(logarithmic electrolyte activity of phase I) at 25 °C are observed.[9-11] Figure 1-A-a indicates that the 10^{-2}mol dm^{-3} NaCl(II) and 10^{-2}mol dm^{-3} $CaCl_2$ (II) systems realize these situations.

On the contrary, non-linear potential responses were observed in the systems where the NaCl or $CaCl_2$ concentrations in phase II were fixed at 10^{-1} or 10^{-3}mol dm^{-3} as can be seen in Figs. 1-A-b and A-c. The ideal slope of the Na^+-Ca^{2+} bi-ionic membrane potential plots mentioned above, 39.44 mV/logarithmic activity of phase I, shifted to increase as relative NaCl concentrations increased and to decrease as relative $CaCl_2$ concentrations increased. In these systems, definite amounts of Cl^- are transported simultaneously with two cations as shown in Figs. 1-C-b and C-c, and it is expected that the Na^+/Ca^{2+} permeability ratio is no longer constant with the external electrolyte concentration changes.

Membrane conductances of the present systems changed within the limits of the conductance values lower than those of NaCl concentration cell system and higher than those of $CaCl_2$ concentration cell system. Accordingly, it is suggested to occur a competitive sharing of available ion-exchange sites by Na^+ and Ca^{2+}.

In the following part of this section, membrane transport characteristics of the present systems are discussed firstly for the case in which only cations, Na^+ and Ca^{2+}, are permeable with a constant membrane permselectivity ratio, and secondly for the case in which the transport of Cl^- has significant effects on the membrane selectivity to these cations.

System with a Constant Na^+/Ca^{2+} Permeability Ratio. The membrane processes in the 10^{-2} mol dm^{-3} NaCl(II) or 10^{-2} mol dm^{-3} $CaCl_2$(II) systems are characterized by the cation transport alone and, consequently, by four membrane permeability matrix elements, $P_{Na\cdot Na}$, $P_{Ca\cdot Na}$, $P_{Na\cdot Ca}$, and $P_{Ca\cdot Ca}$. Including these matrix elements, all the membrane transport parameters can be evaluated from the available experimental data, the membrane potential, conductance, and ion flux, by the same manner as reported earlier based on the following relationships, Eqs. 8—11, with Eqs. 3, 5, and 7.[4,6] The membrane conduct-

ance is expressed as:

$$G_m = (F^2/RT)[P_{Na}a^I_{Na}\exp(-FV_0/2RT) + 2P_{Ca}a^I_{Ca}\exp(-FV_0/RT)] = (F^2/RT)[P_{Na}a^{II}_{Na}\exp(FV_0/2RT) + 2P_{Ca}a^{II}_{Ca}\exp(FV_0/RT)] \quad (8)$$

When the membrane electric current is absent, Na^+ and Ca^{2+} fluxes are characterized by diffusional membrane permeabilities, P^0_{Na} and P^0_{Ca}:

$$J_{Na} = -P^0_{Na}[a^{II}_{Na}\exp(FV_0/2RT) - a^I_{Na}\exp(-FV_0/2RT)] = 2P^0_{Ca}[a^{II}_{Ca}\exp(FV_0/RT) - a^I_{Ca}\exp(-FV_0/RT)] = -2J_{Ca} \quad (9)$$

The diffusional permeability to electroconductive permeability ratio is expressed as:

$$P^0_{Na}/P_{Na} = P^0_{Ca}/P_{Ca} = 1-(2P_{Ca\cdot Na}/P_{Na}) - (P_{Na\cdot Ca}/2P_{Ca}) \quad (10)$$

The cross coefficients of membrane permeability matrix, $P_{Na\cdot Ca}$ and $P_{Ca\cdot Na}$, are related each other as:

$$\frac{P_{Na\cdot Ca}}{P_{Ca\cdot Na}} = \frac{(a^I_{Na}a^{II}_{Na})^{1/2}}{(a^I_{Ca}a^{II}_{Ca})^{1/2}} \times \frac{\sinh[F(V_O-V_{Na})/2RT]/[F(V_O-V_{Na})/2RT]}{\sinh[F(V_O-V_{Ca})/RT]/[F(V_O-V_{Ca})/RT]} \quad (11)$$

The diffusional membrane permeabilities to Na^+ and to Ca^{2+}, P^0_{Na} and P^0_{Ca}, are expressed as a function of the permeability matrix elements.

$$P^0_{Na} = (P_{Na\cdot Na}P_{Ca\cdot Ca} - P_{Na\cdot Ca}P_{Ca\cdot Na})/P_{Ca}$$
$$P^0_{Ca} = (P_{Na\cdot Na}P_{Ca\cdot Ca} - P_{Na\cdot Ca}P_{Ca\cdot Na})/P_{Na} \quad (12)$$

The diffusional permeabilities, P^0_{Na} and P^0_{Ca}, which should be discriminated from the electroconductive permeabilities, P_{Na} and P_{Ca}, satisfy the following phenomenological equation in the absence of membrane electric current:

$$\begin{bmatrix} J_{Na} \\ J_{Ca} \end{bmatrix}_{I=0} = -\begin{bmatrix} P^0_{Na} & 0 \\ 0 & P^0_{Ca} \end{bmatrix} \times \begin{bmatrix} a^{II}_{Na}\exp(FV_0/2RT) - a^I_{Na}\exp(-FV_0/2RT) \\ a^{II}_{Ca}\exp(FV_0/RT) - a^I_{Ca}\exp(-FV_0/RT) \end{bmatrix} \quad (13)$$

The electroconductive permeability represents conductive process of ions across membrane, while the diffusional permeability represents diffusion process of ions, and accordingly, the former is related to the mobility of permeant ion and the latter, to the diffusion coefficient.[5,6]

Evaluated membrane transport parameters are summarized in Fig. 2. As illustrated in Figs. 2-A-a and A-b, the CK-1, 1.0t membrane is more permselective to Ca^{2+} than to Na^+ in these systems. Since the CK-1, 1.0t membrane is developed so as to be more permeable to

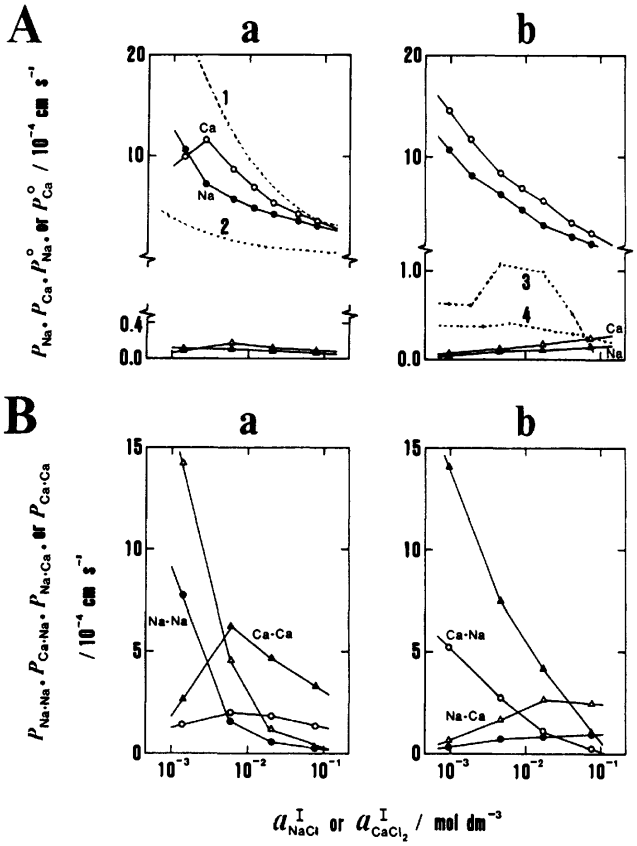

Fig. 2. Electroconductive and diffusional membrane permeabilities (A) and permeability matrix elements (B) as a function of mean electrolyte activity of phase I. a: $CaCl_2$(I)-10^{-2} mol dm^{-3} NaCl(II). b: NaCl(I)-10^{-2} mol dm^{-3} $CaCl_2$(II). In A, ●: P_{Na}; ○: P_{Ca}; ▲: P^0_{Na}; △: P^0_{Ca}. The broken lines 1 and 3 refer to P_{Na} and P^0_{Na} in NaCl(I)-10^{-2} mol dm^{-3} NaCl(II) system; the broken lines 2 and 4 refer to P_{Ca} and P^0_{Ca} in $CaCl_2$(II)-10^{-2} mol dm^{-3} $CaCl_2$(II) systems. In B, ●: $P_{Na\cdot Na}$; ○: $P_{Ca\cdot Na}$; △: $P_{Na\cdot Ca}$; ▲: $P_{Ca\cdot Ca}$.

univalent cations than to bivalent cations for the desalination process applications, the membrane permeability to Na^+ in concentration cell system is almost 10 times larger than that to Ca^{2+}. Furthermore, Figs. 2-B-a and B-b indicate that the calculated values of the membrane permeability matrix element conjugated with an electrochemical activity difference of Ca^{2+} between phases I and II are larger than those conjugated with an electrochemical activity difference of Na^+, namely, $P_{Ca\cdot Na} > P_{Na\cdot Na}$ and $P_{Ca\cdot Ca} > P_{Na\cdot Ca}$. These influential contributions of Ca^{2+} to the membrane transport processes seem to be due to the fact that membrane concentrations of Ca^{2+} relative to those of Na^+ are kept at high level within a wide range of external Na^+/Ca^{2+} concentration ratio. In the present 10^{-2} mol dm^{-3} NaCl(II) and 10^{-2} mol dm^{-3} $CaCl_2$(II) systems, measurements of the cation concentrations in the CK-1, 1.0t membrane phase indicated that 90—99% of cations in the membrane

phase are site-bound and that more than 80% of cations are Ca^{2+} in the membrane (unpublished observations). In general both the membrane/solution partition of ions and the migration speed of ions across membrane are dominant factors to control the membrane permselectivity to ions. The Ca^{2+} controlled membrane processes in the present systems are due to the facts that the greater part of fixed cation-exchange sites are occupied by Ca^{2+} and the Donnan adsorption of electrolyte is suppressed at quite low level.

Figure 3 shows Na^+/Ca^{2+} membrane permeability ratios and diffusional/electroconductive membrane permeability ratios, as well as comparisons with these ratios evaluated in concentration cell systems. The P_{Na}/P_{Ca} values in the present bi-ionic systems changed drastically from those in the concentration cell systems so as to reverse the cationic permselectivity sequences. As expected from the linear membrane potential responses and Eq. 7, almost constant P_{Na}/P_{Ca} vslues were obtained. P^0_{Na}/P_{Na} $(=P^0_{Ca}/P_{Ca})$ values less than 0.1 indicate that electroconductive movements of cations progress much more efficiently than diffusion of cations. These situations were more remarkable in the bi-ionic systems than in the concentration cell systems. Furthermore as indicated by Eq. 10, deviations of the diffusional/conductive permeability ratio from unity denote the order of participations of the correlative or cooperative effects between different permeant ions, namely the Na^+-Ca^{2+} correlations in the present bi-ionic systems and Na^+-Cl^- or Ca^{2+}-Cl^- correlations in the respective concentration cell systems, to the membrane processes.[5]

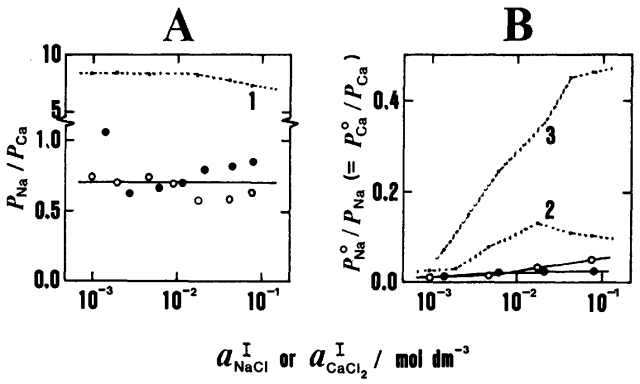

Fig. 3. Cationic membrane permeability ratio ($P_{Na}/P_{Ca}=P^0_{Na}/P^0_{Ca}$) (A) and diffusional/electroconductive permeability ratio ($P^0_{Na}/P_{Na}=P^0_{Ca}/P_{Ca}$) (B) as a function of mean electrolyte activity of phase I. Closed and open circles indicate $CaCl_2$(I)-10^{-2} mol dm^{-3} NaCl(II) and NaCl(I)-10^{-2} mol dm^{-3} $CaCl_2$(II) systems, respectively. The broken lines 1, 2, and 3 refer to P_{Na}/P_{Ca}, P^0_{Na}/P_{Na}, and P^0_{Ca}/P_{Ca} values estimated in NaCl(I)-10^{-2} mol dm^{-3}NaCl(II) and $CaCl_2$(I)-10^{-2} mol dm^{-3} $CaCl_2$(II) systems.

System with a Varying Na^+/Ca^{2+} Permeability Ratio and Effect of Cl^- Permeation. Estimations for the transport parameters relating Cl^- are required for the systems where NaCl or $CaCl_2$ concentrations of phase II are fixed constant at 10^{-1} or 10^{-3} mol dm^{-3}, since definite amounts of Cl^- are transported across the membrane as can be seen in Figs. 1-C-b and C-c. Within the limits of approximately 10-fold concentration difference between the external NaCl and $CaCl_2$ solutions, almost all the Cl^- fluxes were suppressed and only Na^+ and Ca^{2+} permeated across the membrane holding the relationship, $J_{Na}=-2J_{Ca}$. However, as the external NaCl concentrations increased, Na^+-Ca^{2+} bi-cationic transport processes shifted gradually to NaCl transport processes ($J_{Na}=J_{Cl}$) and, as the $CaCl_2$ concentrations increased, to $CaCl_2$ transport processes ($J_{Ca}=1/2J_{Cl}$). These experimental facts seem to indicate redistribution processes of Na^+ and Ca^{2+} within membrane, in which the one cation species tend to occupy entirely the negatively charged fixed sites and simultaneously to exclude the other cation species from the membrane phase depending upon the external cation concentrations.

Equation 5 can be modified to the following form in which the membrane electric current is expressed as the sum of two terms describing currents carried by cations, Na^+ and Ca^{2+}, and Cl^-:

$$\begin{aligned} I &= -2FP_{Na\text{-}Ca}a_{Na\text{-}Ca}\sinh[3F(V-V_{Na\text{-}Ca})/4RT] \\ &\quad -2FP_{Cl}(a^I_{Cl}a^{II}_{Cl})^{1/2}\sinh[F(V-V_{Cl})/2RT] \\ &= -g_{Na\text{-}Ca}(V-V_{Na\text{-}Ca})-g_{Cl}(V-V_{Cl}) \end{aligned} \quad (14)$$

where $P_{Na\text{-}Ca}$ is the membrane permeability to whole cations refer to P_{Cl} defined as:

$$P_{Na\text{-}Ca} = (2P_{Na}P_{Ca})^{1/2}\exp(\pm FV/4RT) \quad (15)$$

The signs in the exponential term in Eq. 15 refer to + for NaCl (I)-$CaCl_2$(II) system and to − for $CaCl_2$(I)-NaCl(II) system. $a_{Na\text{-}Ca}$ $(=(a^I_{Na}a^{II}_{Ca})^{1/2}$ or $(a^I_{Ca}a^{II}_{Na})^{1/2})$ is the averaged concentration of external cations. $g_{Na\text{-}Ca}$ is the cationic membrane conductance dependent upon Na^+ and Ca^{2+} refer to g_{Cl}:

$$\begin{aligned} g_{Na\text{-}Cl} &= \frac{3F^2}{2RT}P_{Na\text{-}Ca}a_{Na\text{-}Ca}\frac{\sinh[3F(V-V_{Na\text{-}Ca})/4RT]}{3F(V-V_{Na\text{-}Ca})/4RT} \\ g_{Cl} &= \frac{F^2}{2RT}P_{Cl}(a^I_{Cl}a^{II}_{Cl})^{1/2}\frac{\sinh[-F(V-V_{Cl})/2RT]}{-F(V-V_{Cl})/2RT} \end{aligned} \quad (16)$$

The membrane conductance, G_m, and potential, V_0 for these systems are expressed as:

$$\begin{aligned} G_m &= g_{Na\text{-}Ca} + g_{Cl} \\ &= (F^2/RT)\exp(-FV_0/2RT) \\ &\quad \times[P_{Na}a^I_{Na}+2P_{Ca}a^I_{Ca}\exp(-FV_0/2RT)+P_{Cl}a^{II}_{Cl}] \\ &= (F^2/RT)\exp(FV_0/2RT) \\ &\quad \times[P_{Na}a^{II}_{Na}+2P_{Ca}a^{II}_{Ca}\exp(FV_0/2RT)+P_{Cl}a^I_{Cl}] \end{aligned} \quad (17)$$

$$V_0 = (g_{Na-Ca}/G_m)V_{Na-Ca} + (g_{Cl}/G_m)V_{Cl} = t_{Na-Ca}V_{Na-Ca} + t_{Cl}V_{Cl} \quad (18)$$

where t_{Na-Ca} and t_{Cl} are the transport number to whole cations and to Cl^-, respectiely.

On the basis of assumptions where permeability ratios are constant within the limits of narrow concentration range of the external electrolyte solution, P_{Na}/P_{Ca} values can be evaluated by utilizing Eq. 6 to a pair of membrane potential values. Then, at given electrolyte concentrations, V_{Na-Ca} values are determined by Eq. 7, and consequently, P_{Na}, P_{Ca}, and P_{Cl} values can be calculated using the above equations and electrochemical data. Figure 4 shows t_{Na-Ca} values with P_{Na}/P_{Ca} and P_{Cl}/P_{Na} ratios; the plotted membrane permeability ratios were calculated from the respective permeability values to Na^+, Ca^{2+}, and Cl^- estimated as described above. Furthermore, in this figure, the P_{Na}/P_{Ca} values were compared with those calculated by Eq. 7 assuming that Cl^- permeations can be ignored, namely, that the relation, $V_0=V_{Na-Ca}$, is satisfied. For the case where relative NaCl concentrations are high (see Fig. 4-a: 10^{-1} mol dm^{-3} NaCl(II) system and Fig. 4-d: 10^{-3} mol dm^{-3} $CaCl_2$(II) system), P_{Na}/P_{Ca} values increase rapidly as relative Na^+ concentration increases, while P_{Cl}/P_{Na} and t_{Cl} values are kept at almost constant and low levels. On the contrary, when relative $CaCl_2$ concentrations are high (see Fig. 4-b: 10^{-3} mol dm^{-3} NaCl(II) system and Fig. 4-c: 10^{-1} mol dm^{-3} $CaCl_2$(II) system), t_{Na-Ca} values decrease gradually as relative Ca^{2+} concentrations increase, while P_{Na}/P_{Ca} values are kept at almost constant levels similarly to those in the system with a negligible Cl^- permeation discussed in earlier parts of this section. So it is suggested that the positive deviations from the linear relationships of ideal Na^+-Ca^{2+} bi-ionic potential responses are due to a rise in the Na^+ permeation and that the negative deviations are due to a rise in the Cl^- permeatins.

When three ionic species, Na^+, Ca^{2+}, and Cl^-, are involved in the transport processes, the membrane system is characterized by the 3×3 permeability matrix or conductance matrix as shown in Eqs. 1 and 2. Accordingly, detailed phenomenological analyses on membrane permselectivity are required to estimate nine elements of the permeability matrix or six elements of the conductance matrix from available experimental data. However, estimations of the complete sets of these phenomenological coefficients are required to carry out complicated measurements with extreme cares under various experimental conditions. In the present study, only the effects of Cl^- permeation on the entire cation transport are discussed according to the following simplified formulations based on the potential, conductance, and flux data:

$$\begin{bmatrix} i_{Na-Ca} \\ i_{Cl} \end{bmatrix} = -\begin{bmatrix} g_{Na-Ca\cdot Na-Ca} & g_{Na-Ca\cdot Cl} \\ g_{Cl\cdot Na-Ca} & g_{Cl\cdot Cl} \end{bmatrix} \begin{bmatrix} V-V_{Na-Ca} \\ V-V_{Cl} \end{bmatrix} \quad (19)$$

where i_{Na-Ca} ($=i_{Na}+i_{Ca}$) is the cationic membrane current. By means of evaluating three matrix elements, such as $g_{Na-Ca\cdot Na-Ca}$ depending only upon cations, $g_{Na-Ca\cdot Cl}$ ($=g_{Cl\cdot Na-Ca}$) describing the correlations between whole cation and Cl^-, and $g_{Cl\cdot Cl}$, the effects of Cl^- permeations on the permselectivities to cations are characterized quantitatively on the basis of nonequilibrium thermodynamics. Results are given in Fig. 5. It can be seen in these figures that the changes in $g_{Na-Ca\cdot Na-Ca}$ and $g_{Na-Ca\cdot Cl}$ with external electrolyte concentration are relatively small, whereas $g_{Cl\cdot Cl}$ increases rapidly as the concentration differences between NaCl and $CaCl_2$ solutions separated by the

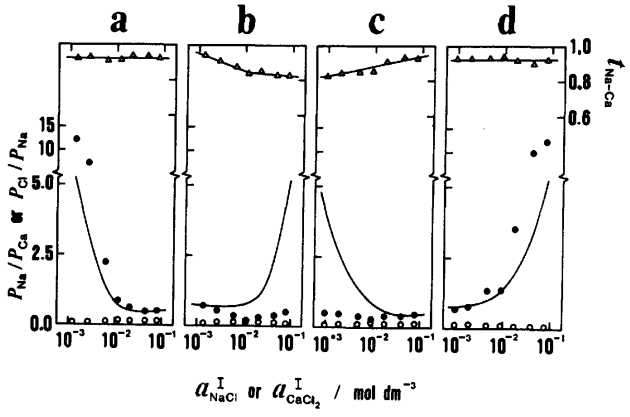

Fig. 4. Transport number to whole cations, t_{Na-Ca} (△), and permeability ratios, P_{Na}/P_{Ca}(●) and P_{Cl}/P_{Na} (○), as a function of mean electrolyte activity of phase I. a: $CaCl_2$(I)-10^{-1} mol dm^{-3} NaCl(II). b: $CaCl_2$(I)-10^{-3} mol dm^{-3} NaCl(II). c: NaCl(I)-10^{-1} mol dm^{-3} $CaCl_2$(II). d: NaCl(I)-10^{-3} mol dm^{-3} $CaCl_2$(II). The solid lines refer to P_{Na}/P_{Ca} values calculated by Eq. 7 from membrane potential data assuming $P_{Cl}=0$.

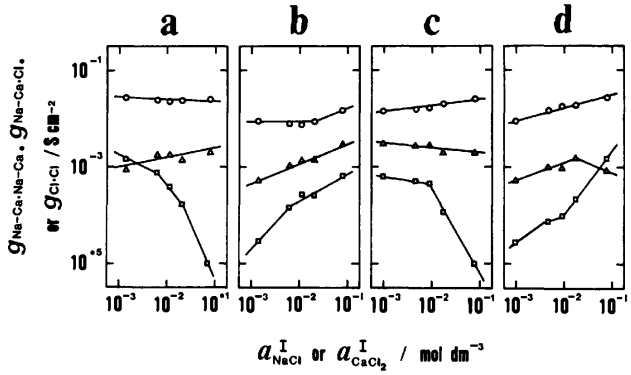

Fig. 5. Membrane conductance matrix elements, $g_{Na-Ca\cdot Na-Ca}$(○), $g_{Na-Ca\cdot Cl}$($=g_{Cl\cdot Na-Ca}$)(△), and $g_{Cl\cdot Cl}$(□), as a function of mean electrolyte activity of phase I. a, b, c, and d denote the same systems as in Fig. 4.

membrane increase. By referring Fig. 5 with Figs. 1-A-b, A-c, and 4, it is seen that the conductance matrix element as a linear phenomenological coefficient in Eq. 19 can describe well the deviation from ideal Na^+-Ca^{2+} bi-ionic potential response and the mode of ionic permselectivity in the CK-1, 1.0t membrane sytem.

Na^+-Cs^+ and Na^+-Ca^{2+} Bi-Ionic Systems. As reported earlier for the NaCl-CsCl system,[6] Na^+ and Cs^+ contributed equally to the transport processes across highly selective cation-exchange membrane, CK-1, 1.0t. The extents of participations of Na^+ and Cs^+ to the membrane processes depended simply on the rates of external concentrations of respective cations, which should be parallel to the rates of membrane concentrations of cations. In case of the Na^+-Cs^+ bi-ionic systems, effects of Cl^- permeations were almost perfectly excluded within the limits of wide ranges of external electrolyte concentrations.

On the contrary in the present NaCl-$CaCl_2$ system, Ca^{2+} contributions to the membrane processes are dominant and the permselectivity to Ca^{2+} is improved to reverse the sequences to Na^+ compared with those in the respective concentration cell systems. These Ca^{2+} effects originate in the high membrane concentrations of Ca^{2+}. Cation-exchange membranes developed for the applications in desalination processes are usually performed the membrane surface treatments to prevent from penetrations of multivalent cations, especially Ca^{2+}, into the membrane phase. However, Ca^{2+}, once penetrating into the membrane due to the high external $CaCl_2$ concentrations, plays a dominant role in the membrane transport processes according to the high concentrations and tight interactions with negatively charged sites within the membrane phase. It was also suggested that increases in Cl^- permeations are closely related to the increase in external Ca^{2+} concentrations. The present studies served as a quantitative representations of these cooperative interactions between permeating ions and of Ca^{2+} effects on the basis of nonequilibrium thermodynamic theory.

The authors wish to thank the Ministry of Education, Science and Culture for a Grant-in-Aid for Scientific Research (No. 61540332) and the Asahi Chemical Industry Co. Ltd. for providing the ion exchange membranes used in this work. One of the authors (K. K) is also grateful to the Kurata Foundation for supporting the research grant.

References

1) A. Katchalsky and P. F. Curran, "Nonequilibrium Thermodynamics in Biophysics," Harvard University Press, Cambridge, Mass. (1965).

2) S. R. De Groot and P. Mazur, "Nonequilibrium Thermodynamics," North-Holland Publishing Co., Amsterdam (1969).

3) N. Lakshminarayanaiah, "Transport Phenomena in Membranes," Academic Press, New York (1969).

4) H. Kimizuka and K. Kaibara, *J. Colloid Interface Sci.*, **52**, 516 (1975).

5) H. Kimizuka, K. Kaibara, E. Kumamoto, and M. Shirozu, *J. Membr. Sci.*, **4**, 81 (1978).

6) K. Kaibara and H. Kimizuka, *Bull. Chem. Soc. Jpn.*, **55**, 1743 (1982).

7) P. R. Adams, A. Constanti, D. A. Brown, and R. B. Clark, *Nature (London)*, **296**, 746 (1982).

8) H. Kimizuka, Y. Nagata, and K. Kaibara, *Bull. Chem. Soc. Jpn.*, **56**, 2371 (1983).

9) H. Kimizuka and K. Koketsu, *J. Theoret. Biol.*, **6**, 290 (1964).

10) A. Yamauchi and H. Kimizuka, *J. Theoret. Biol.*, **30**, 285 (1971).

11) K. Kaibara, J. Nakajima, Y. Nagata, and H. Kimizuka, *Mem. Fac. Sci., Kyushu Univ. Ser. C*, **14**, 239 (1984).

 © 1987 The Chemical Society of Japan Bull. Chem. Soc. Jpn., 60, 3183—3188 (1987)

Clogging and Gel-Layer Formation during Membrane Filtration and Its Effect on Analytical Data

Manabu IGAWA,* Takeshi YOSHIDA, Chiaki OHTAKE, and Takashi HAYASHITA
Department of Applied Chemistry, Faculty of Engineering, Kanagawa University, Rokkakubashi, Kanagawa-ku, Yokohama 221
(Received September 25, 1986)

Clogging and gel-layer formation during membrane filtration affect the concentration of ions in the filtrate as well as the concentration of suspended solids. The flow rate analysis and the observation of the filter surface with a scanning electron microscope show that a gel-layer is formed subsequently after the clogging. Humic acids, fulvic acids, metal hydroxides, and soft particles dispersed in natural waters cause the clogging and hence the gel-layer formation. Cross-flow filtration decreases the rate of the clogging and the gel-layer formation and gives little rise to the filtration effects on analytical results.

Membrane filters have been commonly used to separate suspended solids from natural waters.[1,2] However, it is known that the filtration by membrane filters seriously affect the analytical results in the following ways; contamination from and/or adsorption on a membrane filter; sieve effect, that is, partial permeation of the solute depending on the ratio of the pore diameter to the particle diameter; clogging and gel-layer formation on the filter.

The amounts of impurities in membrane filters,[3-5] variation of impurity levels[6] and elutions of total organic carbon(TOC), chemical oxygen demand (COD), NO_3^- from membrane filters[7] have been studied in detail. Furthermore the physical and physicochemical properties of the membrane, such as the sieve effect and the gel-layer formation on the filter, are important in relevance to filtration,[8,9] ultrafiltration,[10] and reverse osmosis.[11] However, little attention has been paid to the latter problems until now.

Seldon has reported on the size separation of marine seston by membrane filters.[12] Danielsson has studied the influence of filtration on the determined values of the colloid contents in a natural sample as a function of the sample volumes treated,[13] and Laxen et al. have reported that screen filters provide accurate size fractionation, as long as the filter is not allowed to clog.[14] Errede et al. have studied the effect of the surface modification on the flow rate of water.[15]

In this paper, the mechanism of the clogging and the gel-layer formation were studied on filtration of natural waters by various membrane filters. The possible materials which may cause the clogging and then form the gel-layer are also discussed. Cross-flow filtration was tried to minimize the influence of the membrane filtration on the analytical results.

Experimental

General Procedure for Filtration. The filters used in this study were Nuclepore 47 mm diameter filters of 0.10, 0.40, and 1.0 μm pore size (N010CPR04700, N040CPR04700, and N100CPR04700, respectively, Nuclepore Corp.) and Millipore 47 mm diameter filters of 0.45 μm pore size (HAWP04700, Millipore Corp.). A membrane filter set in a holder (FH047PL001101, Nuclepore Corp.) was washed with 200 cm^3 of deionized water and then a certain volume of sample solution was filtered under a reduced pressure of 60 cm Hg (1 cm Hg=1333.22 Pa) using a handy aspirator (WP-45, Yamato Sci., Corp.). An apparatus used for cross-flow filtration is shown in Fig. 1. It was handmade using acrylic resin boards and 3 mm-thick silicone rubber sheets. For trace analysis, Teflon sheets should be used instead of the silicone rubber sheets. The sample solution was circulated and flowed on the membrane filter with a pump at a rate of 15 $dm^3\ min^{-1}$.

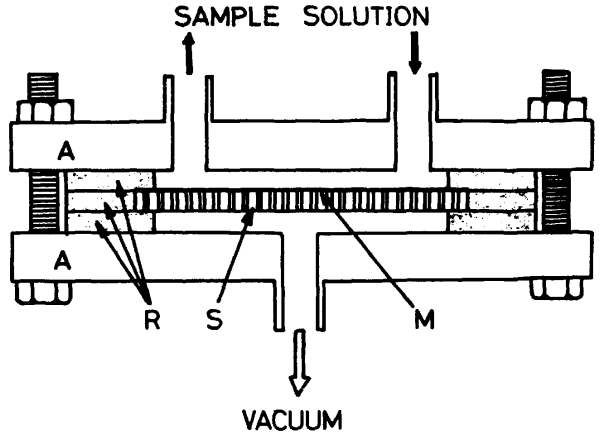

Fig. 1. Apparatus of cross-flow filtration: A, acrylic resin frame; M, membrane filter; R, silicone rubber sheet; S, membrane filter support.

Samples. The sample solutions used in this filtration experiment were river waters, a carbon black dispersion, a humic acid solution, a fulvic acid solution, and a sulfuric acid extract from a river sediment.

The river waters were sampled in 1984 and 1985 at the Kawamukoh bridge on the Tsurumi river† in Yokohama.

The carbon black used was Thermax (Thermatomic Carbon Company), whose particle size ranges from 0.1 to 1.0 μm and the maximum was between 0.4 to 0.5 μm. The

† The Tsurumi river flows through urban regions of both Yokohama city and Kawasaki city; the total length of the river is 42.3 km, and much domestic sewage discharges into it.

surface of the carbon black particles was oxidized by H_2O_2 and a definite amount was dispersed in water by shaking in a ultrasonic bath just before the filtration.

The sediment was collected at the same sampling location. It was dried in an oven 110 °C and milled to pass through a 40 mesh screen. A 14 g sample of the dried sediment was boiled with 600 cm^3 of 0.5% NaOH solution for 30 min and centrifuged at 2000 min^{-1} for 20 min. To a 500 cm^3 portion of the supernatant, 5.0 cm^3 of concentrated H_2SO_4 was added. The solution was stirred vigorously and filtered through a Whatman glass filter GC/D. The filtrate was diluted 2-fold with pure water and used as a fulvic acid solution.[16] The precipitate on the filter was dissolved throughly with 500 cm^3 of 0.1% NaOH and the filtrate diluted 2-fold and used as a humic acid solution.[16] Another 14 g of the dried sediment was dispersed in 600 cm^3 of 0.5 mol dm^{-3} H_2SO_4 and boiled for 30 min. When cooled, the sample was centrifuged at 2000 min^{-1} for 20 min. The supernatant was diluted 2-fold and used as a sulfuric acid extract, containing much metal ions, for example, ca. 100 ppm of iron.

Detemination of Metal Ion Concentrations and Suspended Solids Contents. The metal ions in the filtrate were determined by a flame and/or flameless atomic absorption spectrophotometer (Varian AA-1275). The contents of suspended solids were determined from the difference of the weights of the membrane filter dried at 60 °C for 2 h before and after the filtration.

Observation of Membrane Surface. The surface were observed by a scanning electron microscope (JSM-35C SEM, Japan Electron Optics Laboratory Corp.) before and after the filtration. The samples were imaged with gold in vacuo.

Results and Discussion

Effect of Filtration on Analytical Results. The concentrations of metal ions in the river water sample were measured by varying the sample volume treated on one filter. It was reported by Danielsson[13] that the concentrations of heavy metal ions such as iron decreased with the increase of the volume. While, the concentrations of alkaline and alkaline earth metal ions such as sodium and calcium did not change with the increase of the volume.

By using the sample solutions, the concentration of suspended solids was examined similarly, and it was found that the amount of solids trapped on the filter varied depending on the properties of the suspended solids. Figure 2 shows the change of the suspended solids concentration against the sample volume treated. The concentrations of suspended solids in a river water sample apparently increase with the volume, but that of a carbon black dispersion in pure water remains constant as would normally be expected. The values determined by Millipore filters were different from those determined by Nuclepore filters because of the difference of the filter structures between Millipore and Nuclepore filters.[14]

Variation of Rate of Filtration. The membrane filtration influences the values of metal ions and

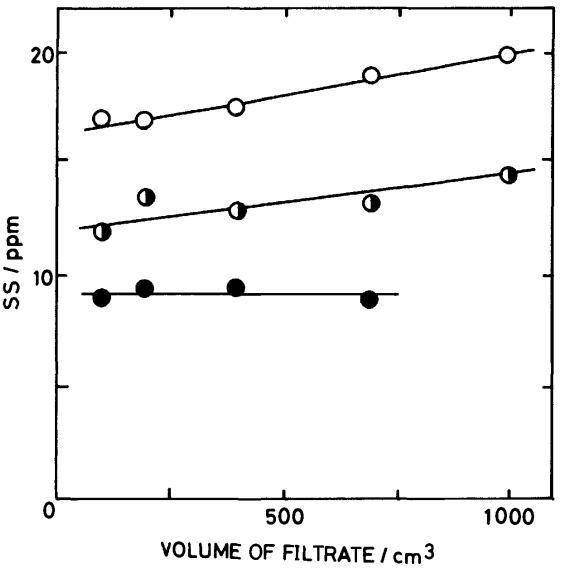

Fig. 2. Effect of volume of filtrate on measured value of suspended solids concentration: membrane filter, Nuclepore filter (0.40 μm, ●, ◑) and Millipore filter (0.45 μm, ○); sample, river water (◑, ○) and carbon black dispersion (●).

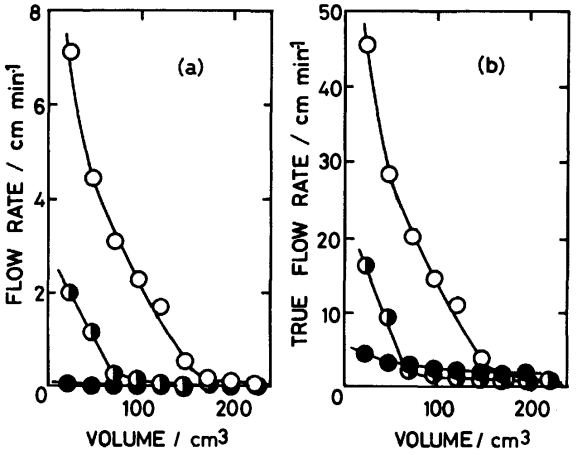

Fig. 3. (a) Flow rate vs. volume of filtrate and (b) true flow rate vs. volume of filtrate: membrane filter, Nuclepore filter; ○, 1.0 μm pore size; ◑, 0.40 μm pore size; ●, 0.10 μm pore size; sample, river water.

suspended solids determines because of clogging and gel-layer formation. To clarify the mechanism of the clogging and the gel-layer formation, the following experiments were carried out: The filtration rates were measured on various types of membrane filters, the electron microscopic images of the membrane surface were compared before and after the filtration, and the permeation properties of natural waters through the filters were compared with those of the synthesized solutions containing certain components of natural waters.

A flow rate through a filter decreases on increasing the volume of the filtrate as is shown in Figs. 3(a) and

3(b). "Flow rates" here are defined as the volumes of filtrate obtained in unit time through unit filter area, and "true flow rates" are those obtained in unit time through unit pore area on the filter. Based on the pore density of the filter:[17] 2×10^7, 1×10^8, and 3×10^8 cm^{-2} for 1.0, 0.4, and 0.1 μm pore size filter, respectively, the ratios of the pore area to the filter area are calculated to be 16, 13, and 2.4%, respectively. In the initial period, "true flow rates" through the larger pores were faster than those through the smaller pores and this was parallel with the case of the "flow rates." As the volume of the filtrate increased, the former rate became slower than the latter. That is, at an early stage of filtration the total area of the filter pores controlled the rate, but later, the pore area remaining unclogged or unshielded by the gel-layer began to control the rate. This can be described quantitatively as follows.

It has been known that in the cake filtration process a linear relationship exists between the ratio of the filtration time to the volume of filtrate, t/V, and the volume, V.

In the standard blocking process a linear relationship also holds between t/V and the filtration time, t.[18-19] These relations can be expressed in Eqs. 1 and 2 for a given constant pressure,

$$t/V = K_c/2 \times V + 1/Q_c \quad (1)$$

$$t/V = K_s/2 \times t + 1/Q_s \quad (2)$$

where K_c, K_s, Q_c, and Q_s are constants dependent on the filter structure and the solution properties. In Fig. 4, the plots of t/V vs. V and t/V vs. t are shown for membrane filters having different pore sizes. It can be seen from the Figure that there are two processes in the filtration. The one, cooresponding to the linear relation of t/V–t, is observed in the early stage of filtration and is due to the development of clogging. The other corresponding to the linear relation of t/V–V, is due to a gel-layer formation on the surface of the membrane filter, which occurs subsequently after the clogging. As shown by curves in Fig. 4, the smaller the pore size, the earlier the gel-layer formation begins. Comparing this result with that of the filtration effect on determined values, the filtration does not have much affect on the values during the clogging process.

SEM Images of Filter Surface. The clogging and the formation of gel-layer can be visualized by the SEM technique. Figure 5(a) shows the surface of a Nuclepore filter (0.4 μm) washed with pure water running through it at 25 cm min^{-1}, and Fig. 5(b) shows the surface of the same membrane filter but filtrated with 20 cm^3 river water. The flow rate of the river water was calculated as 2.5 cm min^{-1}, the clogging of pores is clearly observed but not the gel-layer. Figure 5(c) is the surface of the membrane filter

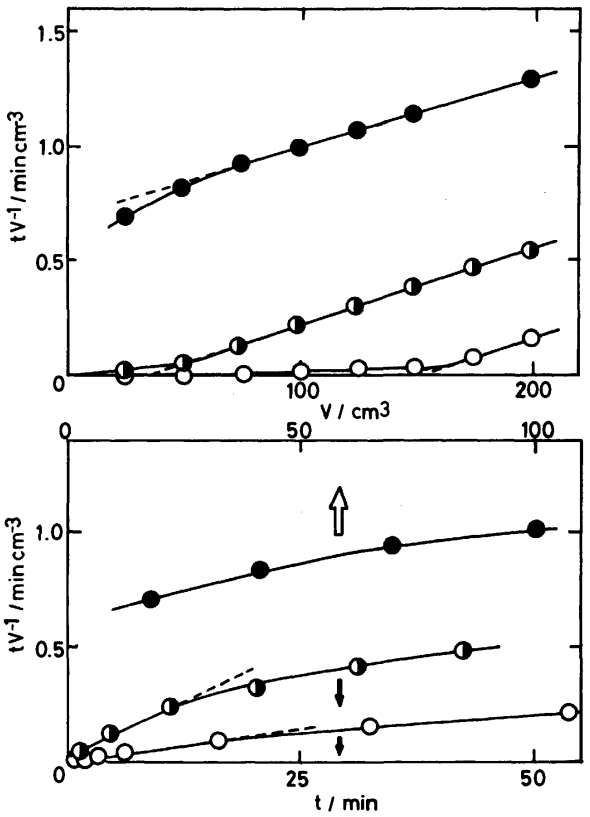

Fig. 4. t/V vs. volume of filtrate, V and t/V vs. filtration time, t: membrane filter, Nuclepore filter; ○, 1.0 μm pore size; ◑, 0.40 μm pore size; ●, 0.10 μm pore size; sample, river water.

after the filtration of 40 cm^3 river water with the rate of 0.41 cm min^{-1}, the whole surface of the filter is seen to be covered with a gel-layer, and no pores are observed.

Comparison of Permeabilities of Some Components in Natural Waters. In river waters, there are many kinds of colloids and particles which may cause clogging and gel-layer formation, such as humic acids, fulvic acids, metal hydroxides, bacteria suspended sediments, and so on. For the investigation of the materials which caused the clogging and the gel-layer on filters, the river water samples and the solutions of some major components of river waters, a fulvic acid, a humic acid, and surfuric acid extract were filterd at various pH and their filtration rates and suspended solids contents were compared. The pH of the samples was adjusted with HNO_3 and NaOH, and 100 cm^3 aliquots were filtered. The mean flow rates and the concentrations of suspended solids are shown in Fig. 6.

In the case of the river water, the flow rate was high when the pH was over 10 or under 2 and minimum in the range of pH 2 to 3. On the other hand, the suspended solids concentration was high when the pH was over 10 and low when the pH was under 2. The pH dependence of flow rate and the suspended solids

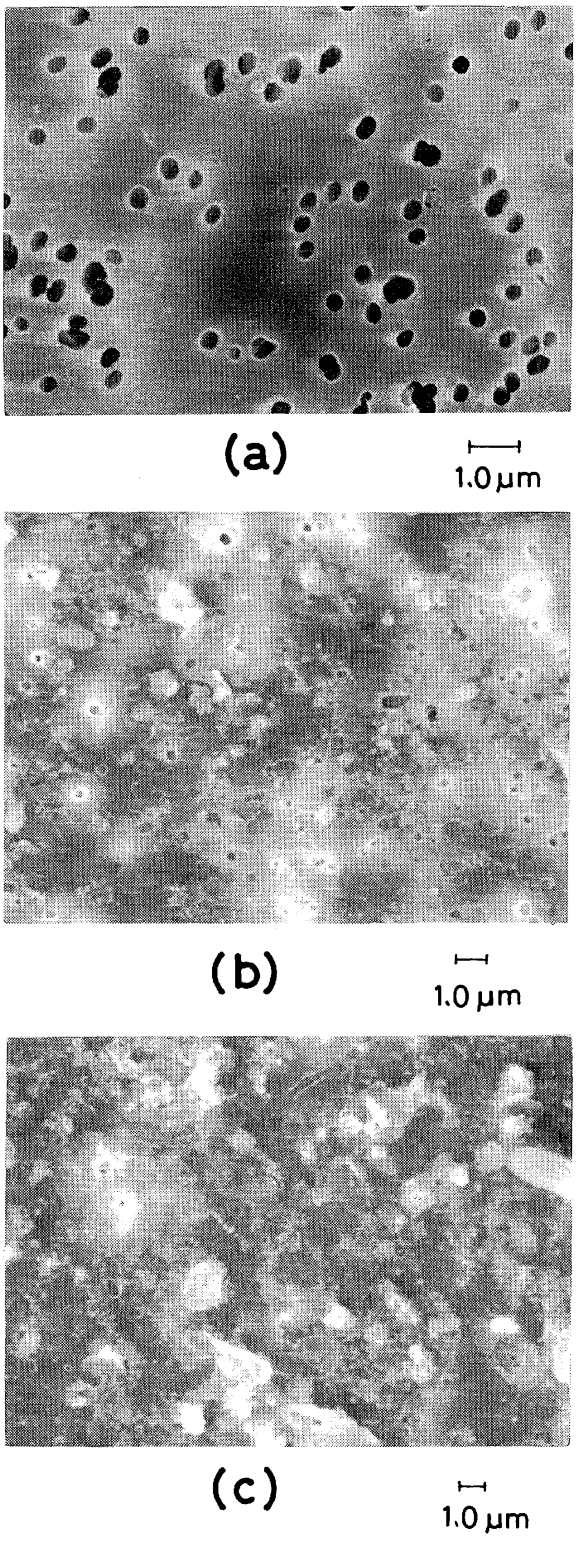

Fig. 5. Observation by scanning electron microscope on surface of Nuclepore filter. (a) Before filtration. (b) After filtration of 20 cm^3 river water. (c) After filtration of 40 cm^3 river water: membrane filter, Nuclepore filter (0.4 μm).

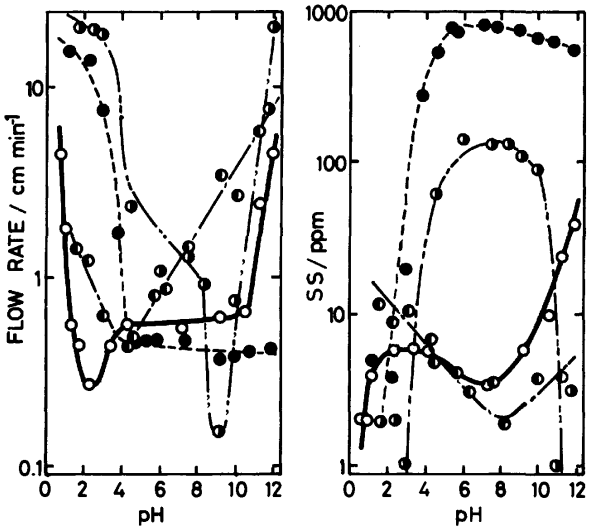

Fig. 6. Flow rate and suspended solids concentration, SS vs. pH: membrane filter, Nuclepore filter (0.40 μm); ○, river water; ◐, humic acid solution; ◑, fulvic acid solution; ●, acid extracted solution; volume of each solution, 100 cm^3.

concentration of the river water were not the same as those of the solutions of the fulvic acid, the humic acid, and the sulfuric acid extract. However some points were commonly observed in them; the minimum flow rate and minimum suspended solids concentration in intermediated pH range for the humic acid; the high flow late and the low suspended solids concentration in low pH range for the fulvic acid and the sulfuric acid extract.

These pH dependences are due to the change of the surface charge of the colloids in the solutions.[20] In a high pH range, they are negatively charged, whereas they are positively charged in a low pH range. The filtration rates are high at low or high pH, because the causing materials in the river water are highly charged and repel each other at the pH and a gel-layer with loose structure is formed on the filter. The high concentration of suspended solids at high pH is due to the precipitation of metal hydroxide. In the intermediate pH range, the charge on the colloids became low and they coagulate at their isoelectric points. Then, a layer with high density was formed on the filter as a result of van der Waals forces of attraction and the filtration rate was low.[21] The flow rate was constant in a wide pH range, because there are many kinds of materials causing the clogging and the gel-layer and their isoelectric points vary widely. It is also reported that humic acids and fulvic acids are coagulated with polyvalent metal ions in a neutral pH range,[22] while iron by itself is coagulated mostly at pH 6.5.[11]

Consequently, in the filtration of river waters, humic acids, fulvic acids, and metal ions or

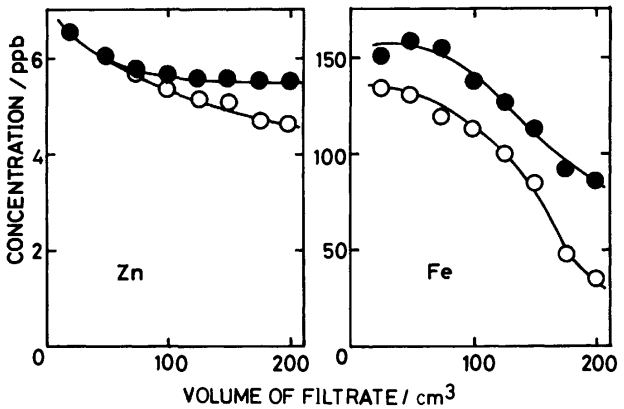

Fig. 7. Concentration change with volume of filtrate: Membrane filter, Nuclepore filter (0.40 μm); ○, usual filtration; ●, cross-flow filtration; sample, river water.

hydroxides cause the clogging and the gel-layer formation independently or in combination with each other. Furthermore, as it is known that soft particles readily plug the pores of the membrane filter,[23] soft and fine particles dispersed in river waters such as bacteria also cause clogging and gel-layer formation. The pH range of 2 to 3 where the flow rate of the river water was minimum may be related to the isoelectric points of most of the bacteria and colloidal silica particles (pH 2 to 3 and pH 2, respectively[20]) which are also major components of river waters.

The effect of the ionic strength on the filtration behavior was also studied by adding NaCl to river waters. The flow rate decreased and the suspended solids concentration increased gradually with NaCl concentration.

Cross-Flow Filtration. Cross-flow filtration is commonly applied to prevent gel-layer formation in reverse osmosis and ultrafiltration. For the improvement of the filtration behaviors, the cross-flow filtration was developed. The apparent changes of solute concentration with the volume of filtrate was observed on cross-flow filtration, and the results were compared with those of the usual filtration. As shown in Fig. 7, the decrease of the concentrations in the cross-flow filtration was less significant than in the usual filtration.

Figure 8 shows the plots of t/V vs. t and V observed in the cross-flow filtration. As is obvious from the comparison with those of the usual filtration, the filtration is much facilitated in the cross-flow filtration because the clogging and the gel-layer formation grows much more slowly. By cross-flow filtration, a large quantity of sample solution can be treated without a significant decrease of the filtration rate and a large deposition of metal hydroxides on the filter. To further improve filtration, more filter material is necessary to weaken the interaction between the colloidal particles and the filter matrix.

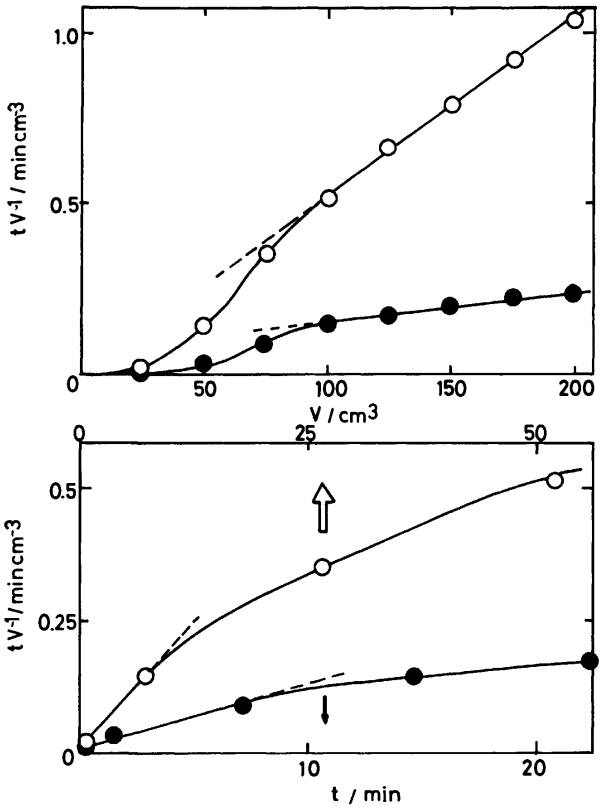

Fig. 8. Relationships between t/V and V, and t/V and t in usual filtration and in cross-flow filtration: Membrane filter, Nuclepore filter (0.40 μm); ○, usual filtration; ●, cross-flow filtration; sample, river water.

The authors thank Mr. Shigeyoshi Hagiwara for helpful suggestion on carbon black, Mr. Yūki Abe for taking the scanning electron microscope photographs, and Miss Tomoko Hiyori and Mr. Tsuyoshi Ohashi for conducting parts of the experiment.

References

1) R. D. Vanous, P. E. Larson, and C. C. Hach, "Water Analysis I," ed by R. A. Minear and L. H. Keith, Academic Press, New York (1982), p. 227.
2) D. P. H. Laxen and R. M. Harrison, *Water Res.*, **15**, 1053 (1981).
3) W. H. Zoller and G. E. Gordon, *Anal. Chem.*, **42**, 257 (1970).
4) R. Dams, K. A. Rahn, and J. W. Winchester, *Environ. Sci. Technol.*, **6**, 441 (1972).
5) P. C. Jay, *Anal. Chem.*, **57**, 780 (1985).
6) C. McDonald and H. J. Duncan, *Anal. Chimica Acta*, **102**, 241 (1978).
7) C. P. Hwang, T. H. Lackie, and R. R. Munch, *Environ. Sci. Technol.*, **13**, 871 (1979).
8) B. F. Ruth, G. H. Montillon, and R. E. Montonna, *Ind. Eng. Chem.*, **25**, 153 (1933).
9) B. F. Ruth, *Ind. Eng. Chem.*, **27**, 708 (1935).
10) J. D. Ferry, *Chem. Rev.*, **18**, 373 (1936).

11) J. M. Jackson and D. Landolt, *Desalination,* **12**, 361 (1973).
12) R. W. Sheldon, *Limnol. Oceanogr.*, **17**, 494 (1972).
13) L. G. Danielsson, *Water Res.*, **16**, 179 (1982).
14) D. P. H. Laxen and I. M. Chandler, *Anal. Chem.*, **54**, 1350 (1982).
15) L. A. Errede and P. D. Martinucci, *Ind. Eng. Chem. Prod. Res. Dev.*, **9**, 573 (1980).
16) The Japan Society for Analytical Chemistry, "Bunseki Kagaku Binran," 2nd ed, Maruzen, Tokyo (1971), p. 1471.
17) "1984 Nuclepore Catalogue and Purchasing Guide," Nuclepore Corporation, Pleasanton, California (1984), p. 39.
18) H. P. Grace, *AIChE J.*, **2**, 307 (1956).
19) P. H. Hermans and H. L. Bredée, *J. Soc. Chem. Ind.*, **55**, 1T (1936).
20) S. E. Manahan, "Environmental Chemistry," 4th ed, Willard Grant Press, Boston (1983), p. 126.
21) V. K. L. Mer and T. W. Healy, *J. Phys. Chem.*, **67**, 2417 (1963).
22) E. M. Thurman, "Organic Geochemistry of Natural Waters," Martinus Nijhoff/Dr W. Junk Publishers, Dordrecht (1985), p. 420.
23) P. J. V. Duin, J. W. V. Heuven, J. Muetgeert, and H. G. J. Overmars, "Proceedings of the Fifth International Symposium on Fresh Water from the Sea," ed by A. Delyannis and E. Delyannis. Athens (1976), Vol. 4, p. 201.

 © 1987 The Chemical Society of Japan Bull. Chem. Soc. Jpn., 60, 3189—3193 (1987)

Preparation and Characterization of $U_2O_2F_7$

Kameo ASADA,† Keiko EMA,* and Takashi IWAI††
Radiation Laboratory, Department of Nuclear Engineering, Kyoto University,
Uji, Kyoto 611
(Received January 22, 1987)

Reaction of UO_2F_2 with UF_5 at 400 °C under UF_6-pressure of 3 atm followed by evaporation of excess UF_5 has yielded a greenish white residue. Its X-ray diffraction pattern and infrared spectrum are sufficiently unique to establish that this material is a true compound. Its chemical formula has been shown to be $U_2O_2F_7$, on the grounds of chemical analysis and thermal decomposition. The oxygen content was determined directly by means of ^{18}O isotopic dilution method based on the combustion of the samples with BrF_5.

In our article on the studies of the physical properties of liquid UF_5,[1] a brief mention was made of our encounter with a possibly new fluoride oxide of uranium which was definitely lower than hexavalent. This article describes the results of the closer investigation into this compound.

Preparation and Isolation

(1) Encounter with the New Compound.[1] UF_5 melts at 348 °C.[2] Physical properties of liquid UF_5 were measured with an alumina tube of high purity (>99.5%) as the container. Sufficient pressure of UF_6 (e.g., 3 atm at 400 °C) was maintained over the melt, to prevent the disproportionation of UF_5.[3]

Examination of the solidified UF_5 after measurements revealed that the bottom part of the sample was occasionally very hard and whitish in color, in contrast with the upper main mass which was easy to be raked out and saphire-blue in color. X-Ray diffraction pattern of this whitish material contained a series of characteristic reflections (Table 1) together with those assigned to α-UF_5.[3] The substance identifiable with these reflections as the fingerprint will be named tentatively the phase *X*.

The phase *X* is presumably insoluble in liquid UF_5. And its density is between that of liquid UF_5 (4.50 g cm^{-3} [1]) and U_2F_9 (7.60 g cm^{-3}, at room temperature[3]), because they were found in this order in the alumina container when they coexisted.

Volatility of UF_5 (vapor pressure: 65 mmHg (1 mmHg=133.322 Pa) at 400 °C[2]) gives a means to purify UF_5. An impure sample of UF_5 contained in an alumina tube was put into a bigger alumina tube and heated to 400 °C under UF_6-pressure of 3 atm. Evaporated UF_5 condensed on the upper (cooler) wall of the outer tube in the form of ice-blue needles. The residue in the inner tube was white with a tinge of green and its X-ray diffraction pattern contained no reflection other than those assigned to the phase *X*. Chemical analysis made on a small sample gave a value, 5.39, for the mean valence of uranium in that material.

Table 1. Comparsion of X-Ray Diffraction Patterns of the Phase *X* (This Article) and the Phase ϕ[11]

Phase *X*		Phase ϕ	
d/Å	Intensity/%	*d*/Å	Intensity/%
4.92	100	4.87	s
4.33	w	4.26	ww
3.97	w	3.91	ms
3.86	w	3.82	mw
3.80	15	3.73	ms
3.62	10	3.57	m
3.34	10	3.30	w
3.06	10	3.04	w
2.77	w	2.77	ww
2.70	10	2.69	w
2.612	10	2.60	w
2.520	w	2.50	w
2.473	30	2.46	m
2.102	20	2.09	s
2.088	20	2.02	mw
		1.99	mw
1.951	w	1.95	m
1.928	w		
1.916	w		
1.854	w		
1.809	w		
1.685	w		
1.652	10		
1.483	w		
1.448	w		

(2) Preparation. Since UF_5 is very hygroscopic, it was natural to assume that the phase *X* had its origin in the hydrolysis of UF_5, though the latter was handled always in a dry box. On exposure to moist air, α-UF_5 changed rapidly into a yellow-green mouldy mass, which proved to be amorphous by X-ray diffraction. A mixture of this intentionally hydrolyzed UF_5 and ordinary UF_5 was subjected to the isolation process described in the above, and the solid residue showed again the X-ray diffraction pattern characteristic of the phase *X*.

Though the above-stated procedure certainly gives a synthetic route to the phase *X*, it is impossible to incorporate oxygen in a quantitative manner. This

† Present address: Japan Storage Battery Co.

†† Present address: Japan Atomic Energy Research Institute.

difficulty has been overcome by replacement of hydrolyzed UF_5 with well-crystallized UO_2F_2. (The latter was prepared as follows. UF_6 was hydrolyzed by water in a Kel-F tube. The pasty product was dried under vacuum at 180 °C, transferred into an alumina tube and heated at 600 °C in an equimolar mixture of HF and O_2 at about 1 atm.[4] To our surprise, alumina was inert to this atmosphere.) A typical synthetic result was as follows; treatment of 1.0 g of UO_2F_2 and 1.6 g of α-UF_5 at 370 °C for 16 h yielded about 2 g of product free from α-UF_5 and UO_2F_2.

The phase *X* was very hygroscopic, too.

Identification

(1) X-Ray Powder Diffraction. All the uranium compounds appearing in this article are more or less sensitive to moisture, so we have designed an air-tight sample holder which can be handled in a dry box and mounted on the goniometer of an X-ray diffractometer. The windows of the holder are equipped with aluminum foils 30 μm in thickness; a pair of these foils reduces the intensity of Cu $K\alpha$ X-ray to about one half.

Diffraction patterns of more than ten samples from different preparations are put in order as shown in the left column of Table 1. The values of *d* have been corrected with those of α-UF_5 as the internal standard. This pattern is unique; definitely different from those of UO_2F_2,[5] $U_3O_5F_8$,[6] α-UOF_4,[7] and β-UOF_4[8] and also dissimilar to those of Pa_2OF_8[9] and $NpOF_3$.[10]

A comparison of diffraction patterns (Table 1) shows a close similarity between the phase *X* and the phase ϕ reported by Rude et al.[11] Their work will be referred to later in the Discussion section.

(2) Infrared Spectrum. Infrared spectra of good quality were recorded by Jacob and his coworkers in their studies on some hygroscopic compounds of uranium.[7,12] They resorted to the Nujol method with CsI disks as the windows, using a vacuum kneader. Instead, we added CaH_2 powder into Nujol to prevent hydrolysis of samples[13] and could thus obtain spectra comparable to theirs.

The infrared spectrum of the phase *X* is shown in Fig. 1. It is definitely different from those of UO_2F_2,[14] α- and β-UF_5,[12] and UOF_4,[7] and could be used for identification purposes.

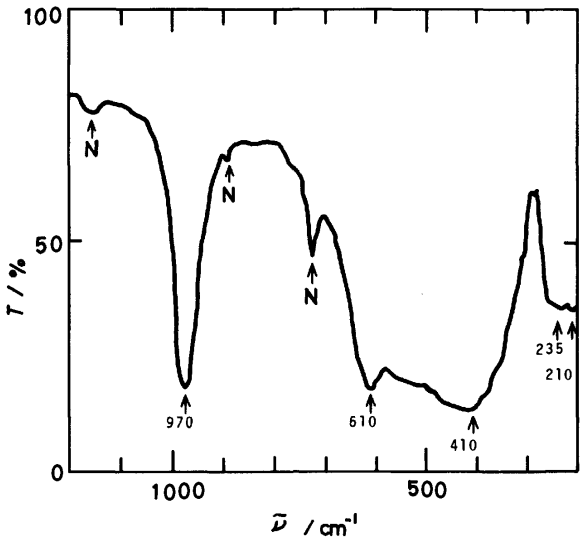

Fig. 1. Infrared spectrum of the phase *X*. (Absorption bands denoted by N are those due to Nujol.)

Determination of Oxygen

In the determination of chemical formula of uranium oxyfluorides, it has been a common practice that the uranium and fluorine content are obtained by actual analyses and the oxygen content by difference. Since the weight fraction of oxygen in those fluoride oxides is generally small (10% or less) the accuracy of the oxygen content thus obtained is open to question, though measured values of the valence of uranium serve as a check.

Jacob et al.[7] determined the oxygen content in UOF_4 by reacting the samples with carbon at 2000 °C and analyzing CO by infrared spectroscopy. On the other hand, Otey et al.[6] burned their sample of $U_3O_5F_8$ with ClF_3, put the gaseous product to gas chromatography and obtained the O/U ratio from the peaks of O_2, ClO_2F, and UF_6. At first we followed Otey's method, with BrF_5 replacing ClF_3. This modification was made, first because BrO_2F is far less stable than ClO_2F[15,16] and hence no oxygen-containing compound other than elemental oxygen would be formed; and secondly because a Br-compound has generally longer retention time than the corresponding Cl-compound, leading to better separation. This approach was, however, abandoned because the retention time of BrF_3, a by-product, was found nearly equal to that of UF_6. Thereupon, we made a shift to an ^{18}O isotopic dilution method, as described below.

An unknown sample and ^{18}O-labelled U_3O_8 (spike), each containing 5—10 mg of oxygen, were weighed in turn into a nickel crucible. The crucible was put into a monel reaction tube and the valve on the latter was closed. The reaction tube was taken out of the dry box and connected to a vacuum manifold. After evacuation, BrF_5 (pre-purified by distillation) was collected into the tube with liquid nitrogen to Br/U ratio of about 5. (By the way, IF_7 was found inadequate as the fluorinating agent; it seemed not to decompose water completely into elemental oxygen at room temperature. IF_7 was tried, because it was known to clean apparatus contaminated with uranium-bearing deposits at 20 °C or above.[17]) The tube was then held at 300 °C for about 1 h, to convert the sample and the spike together completely into a gaseous product.

With the tube immersed in liquid nitrogen, part of the elemental oxygen liberated was expanded into a pair of glass samplers through a liquid nitrogen trap, and subsequently analyzed for ^{18}O atom-fraction by mass spectrometry (Atlas, model CH 4). The ^{18}O atom-fraction in the spike (U_3O_8) was obtained in the same manner. Thus, oxygen content of the unknown sample was estimated by the conventional isotope dilution method.

The chemical form U_3O_8 was chosen as that of the spike, because it is a weighing form in gravimetry of uranium, in spite of the existence of some solid solution ranges.[3] Ammonium diuranate formed on introduction of UF_6 into aqueous ammonia (about 28 wt%) was filtered, dried at 130 °C and ignited at 800—900 °C in open atmosphere to constant weight. Next, a portion of thus prepared U_3O_8 was brought to contact with ^{18}O-enriched oxygen (0.2 atm) at 700 °C, with the gaseous phase renewed every 10—15 h. (The enriched oxygen used (The British Oxygen Co.) was found to be a synthetic mixture of nearly pure $^{18}O_2$ and $^{16}O_2$ in the ratio of 1:4. Since the ^{17}O atom-fraction of this gas was as small as 0.045 atom% and the natural abundance of ^{17}O is 0.0374 atom%, no correction was required for the contribution of $^{17}O_2$ to the MS peak, m/z=34.) The ^{18}O atom-fraction of the spike measured repeatedly over a period extending for a few months ranged at random between 13.86 to 14.06 atom% with the mean value at 14.01±0.03 atom%. This seemed to form a strong evidence for the absence of any exchange reaction between U_3O_8 and atmospheric oxygen at room temperature, as well as the absence of water adsorbed within the reaction system which should have interfered the analysis.

The accuracy of this analytical method was tested with the U_3O_8 sample of isotopically natural composition, which had been prepared as described in the foregoing paragraph. The mean value of six determinations of the oxygen content was 15.24±0.11 wt% (theor.: 15.20 wt%) and the O/U ratio was calculated to be 2.68±0.02 (theor.: 2.67) on the assumption that the sample contained no element other than uranium and oxygen.

It may be worthwhile to refer to the isotopic equilibrium in the oxygen gas evolved on combustion of U_3O_8. Equilibrium was always attained in the case of the spike only, but not in the case of the mixture of the spike and natural U_3O_8. The ratio of MS peaks, m/z=32, 34, and 36, was away from the binominal distribution, but closer to it than in the hypothetical case that oxygen was liberated separately from the enriched and natural U_3O_8 and then mixed together. Since no isotopic exchange was observed between $^{18}O_2$ and $^{16}O_2$ at 300 °C, it is safely presumed that some oxygen-bearing compound, such as U_3O_8, some fluoride oxide or OF_2, should have taken part in the exchange.

The analytical method was tested further with the crystallized UO_2F_2 mentioned before. Satisfactory results were obtained again, with the mean value of two determinations being 10.39±0.13 wt% (theor.: 10.39 wt%).

In the following a brief mention is to be made of some articles related to the analytical method developed in the present work. Trace of oxygen in metals was determined by ^{18}O isotopic dilution, with the oxygen extracted as CO and CO_2.[18] Oxygen contents in metal oxides were determined gasometrically, by burning the oxides with either BrF_3 or $KBrF_4$ and collecting elemental oxygen with a Toepler pump.[19,20]

Determination of Chemical Formula

(1) Chemical Analysis. Determination of U(IV) was made by oxidation with $K_2Cr_2O_7$ followed by back titration with Fe(II). The total uranium content was obtained as follows; the sample was dissolved in an alkaline H_2O_2 solution, evaporated to dryness as sulfate, passed through a Jones Reductor and after addition of $K_2Cr_2O_7$ back-titrated with Fe(II).

Fluorine was determined by the method of Combs and Grove.[21] The sample was brought to solution as in the total uranium analysis. Fluorine was precipitated by $SmCl_3$ at pH 3.0—3.5 and the excess Sm(III) was titrated with EDTA. Under carefully controlled conditions, no interference by uranium was observed; for example, a weighed sample of UF_6 was hydrolyzed in a NaOH solution and after neutralization with H_2SO_4 six aliquots were subjected to analysis, with the result of 32.53±0.09 wt% (theor.: 32.38 wt%).

Results of analysis of the phase *X* are summarized in Table 2. Main conclusions deduced from this table are as follows.

a) The mean valence of uranium calculated from data of U(IV) and Total U is 5.51±0.02, while that from data of Total U, O, and F is 5.47±0.07. These values are very close to $5\,1/2$.

b) The O/U ratio calculated from the data of Total U and O is equal to 1.04±0.02, a value very close to unity. The simplest formula in agreement with these two findings is $U_2O_2F_7$.

Table 2. Composition of the Phase *X* (wt%)

	Phase *X*	$U_2O_2F_7$ (Theoretical)
U (IV)	17.82±0.04 (2) [a]	18.57
Total U	72.15±0.87 (2) [a]	74.27
O	5.05±0.06 (5) [a]	4.99
F	19.55±0.22 (6) [a]	20.74
Total	96.75±0.90	100

a) Number of determinations.

(2) Thermal Decomposition. Composition of the fluoride oxide can be estimated by the weight loss on thermal decomposition, referring to the method reported by Wilson.[22,23] That is, the following experimental results can be explained by assuming the decomposition reaction:

$$2U_2O_2F_7=2UO_2F_2+UF_4+UF_6\uparrow$$

In a dry box, about 200 mg of the sample was weighed into a platinum crucible equipped with a lid and the crucible was put into a monel reaction tube. The tube was connected to a vacuum manifold and was heated for 24 h at 300 °C under continuous evacuation through a liquid nitrogen trap. The residue was whitish green and was composed of UO_2F_2 and UF_4 by X-ray analysis. The O/U and F/U ratio of the original sample calculated from the weight loss (30.3%) and the mean valence of uranium in the original sample (5.51) were 0.96 and 3.60, respectively, while those calculated from the weight loss and the valence in the residue (5.45) were 1.05 and 3.50, respectively. Though the relative errors of these ratios might be as large as 5%, this decomposition experiment was regarded as a corroboration of our conclusion based on chemical analyses.

$U_2O_2F_7$ does not decompose at 400 °C under UF_6 pressure of 3 atm, though it decomposes at 300 °C in vacuum, as detailed in the earlier section. It would be of value to measure its dissociation pressure at different temperatures, as in the work of Agron on intermediate fluorides of uranium.[3]

Discussion

The chemical formula $U_2O_2F_7$ can be found in the report by Rude et al. published in 1971.[11] They reacted UF_4 with ClO_3F or OF_2 at 200—300 °C, to produce UF_6. The solid residue was diversified in color, ranging from white to green. Its X-ray diffraction pattern contained a series of reflections, together with those of UO_2F_2 and/or UF_4. They named the substance identified with these reflections the phase ϕ. As shown in Table 1, there is certainly a close similarity between *their* phase ϕ and *our* phase X, though the synthetic routes are entirely different from each other.

They assigned the chemical formula $U_2O_2F_7$ to this phase ϕ; but without well-grounded evidence, as summarized in the following. First, their samples were more or less contaminated with UO_2F_2 and/or UF_4, because they had no means to isolate their phase ϕ. Secondly, their analytical data were too much scattered to allow any quantitative deduction (for example, their data for U(IV) content on seven preparations ranged from 9.7 to 28 wt%). So, we claim this work as the first confirmation of the compound, $U_2O_2F_7$.

Appendix

In conjunction with the present work, some other attempts to prepare fluoride oxides of uranium in lower oxidation states were made, but were terminated without great success, as described below.

(1) Reaction of UF_4 with Oxygen. This reaction has attracted much attention as a method for the production of UF_6 without the use of elemental fluorine.[3,24,25] The work of Kirslis et al.[26] has a distinctive feature, in that the reaction was carried out with alternating oxygen pressure and vacuum. A cloud of white particles was blown out of the reactor into a filter chamber. The chemical formula, U_2OF_8, was assigned to this white material, on the ground of chemical analysis (wt% Found U, 72±2; U(IV), 36±1; F, 21±2). Assignment of this formula is, however, not convincing, since straightforward calculation from their analytical data (mean valence of U: 5.00±0.04 and F/U: 3.65±0.36) gives a value, 0.67±0.18, for the O/U ratio. They claimed that thermal decomposition of the material at 300 °C yielded UF_6, UO_2F_2 and UF_4 in the proportion 1:1:2 in agreement with the formula, U_2OF_8, but no analytical data were shown. Its X-ray diffraction pattern was reported to be similar to that of U_4F_{17}.[3]

Our experimental procedure was nearly identical with Kirslis's. A platinum boat containing UF_4 was placed in a monel tubular reactor lined with a platinum plate. After evacuation and introduction of HF to about 0.5 atm, the reactor was heated to 500 °C. Then HF was replaced by oxygen at 1 atm, and the temperature was raised to, typically, 685 °C. As observed by Kirslis, the lower the temperature and the shorter the period of alternating evacuation and pressurization with O_2, the greater was the yield of the white material collected on a sintered nickel filter placed 30 cm downstream of the reactor. Out best result was as follows. Starting with 1.3$_5$ g of UF_4, the reaction was carried out for 150 min, with the cycle of 0.5 min for evacuation and 0.5 min for pressurization. The residue on the boat weighed 0.7 g and was composed mainly of UO_2F_2, together with some unreacted UF_4 (X-ray analysis). (A few thin leaves, transparent and amber-colored, were found attached to the rim of the boat. The X-ray diffraction pattern of this material had reflections *only* at d=5.20, 2.60, and 1.74 Å. These reflections correspond to those of UO_2F_2 with the hexagonal Miller indices, $h=k=0$ and $l=3n$ (n=1, 2, ···).[5]) Over the downstream half of the platinum plate was found about 0.2 g of UF_4. A cold trap at the farmost downstream collected 0.11 g of UF_6. About 0.1 g of the white material had deposited on the filter.

The X-ray diffraction pattern of the white material revealed that it was amorphous, excepting a trace of UO_2F_2 and/or UF_4. Its infrared spectrum as shown in Fig. 2 is unique. Values of the mean valence of uranium determined for three preparations were 5.1$_4$, 5.1$_3$, and 4.9$_5$. We have thus reconfirmed the main features of the experiments by Kirslis et al. And it was established that *our* $U_2O_2F_7$ is different from *their* U_2OF_8.

(2) Hot Filament Reduction of UF_6. In 1970 Schröder and Grewe[27] claimed the first synthesis of WF_5, by reducing WF_6 with a hot tungsten filament and collecting WF_5 on the wall of a cooled glass container. Later, Falconer et al.[28] synthesized some metal fluorides by use of a less

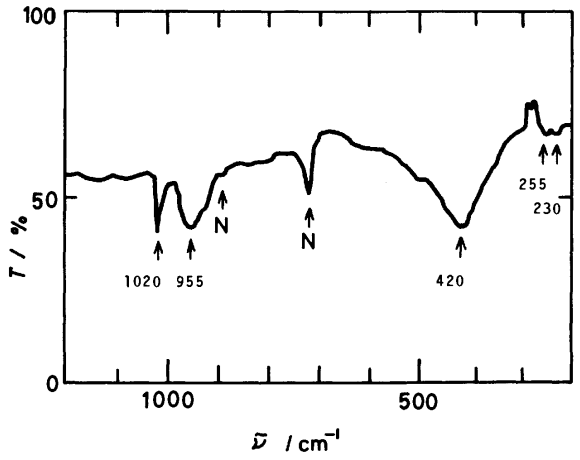

Fig. 2. Infrared spectrum of the white material deposited on the filter. (Absorption bands denoted by N are those due to Nujol.)

sophisticated apparatus.

After successfully reproducing the results of Falconer's on MoF_5, we tried reduction of UF_6 with a nickel filament. Three nickel wires, 0.5ϕ×1200 mm, were coiled to the length of 300 mm, connected in parallel, rinsed with HNO_3 and suspended in a Pyrex tube, 31ID×370 mm. After evacuation, UF_6 was introduced and purified until its vapor pressure was reduced to 25 mmHg or less at 0 °C. (The pressure was measured by a bellows gauge.[29]) With the tube immersed in ice water to the neck, the filaments were heated electrically to dull red (800 °C). The inner wall of the tube was gradually covered with a white material. After 3 h of lighting, 0.15 g of the white material was recovered, which proved to be β-UF_5 by X-ray analysis and determination of mean valence of uranium. No contamination with nickel fluoride was detected.

Next, we repeated the experiment with 80 mmHg of elemental oxygen added into the system, with the intention of preparing some fluoride oxide. But the product was again β-UF_5. Experiments with the nickel filaments covered with platinum black could not alter the result.

The authors thank Mr. Keiichi Hayashi, now with Sumitomo Atomic Industries, who took charge of the earlier stages of the determination of the oxygen content.

References

1) K. Asada, K. Ema, K. Tanaka, and K. Hayashi, *J. Inorg. Nucl. Chem.*, **43**, 2049 (1981).
2) A. S. Wolf, J. C. Posey, and K. E. Rapp, *Inorg. Chem.*, **4**, 751 (1965).
3) J. J. Katz and E. Rabinowitch, "The Chemistry of Uranium," McGraw Hill, New York (1951).
4) E. H. P. Cordfunke and W. Ouweltjes, *J. Chem. Thermodyn.*, **9**, 71 (1977).
5) W. H. Zachariasen, *Acta Crystallogr.*, **1**, 277 (1948).
6) M. G. Otey and R. A. LeDoux, *J. Inorg. Nucl. Chem.*, **29**, 2249 (1967).
7) E. Jacob and W. Polligkeit, *Z. Naturforsch., B*, **28**, 120 (1973).
8) J. C. Taylor and P. W. Wilson, *J. Chem. Soc., Chem. Commun.*, **1974**, 232.
9) L. Stein, *Inorg. Chem.*, **3**, 995 (1964).
10) K. W. Bagnall, D. Brown, and J. F. Easey, *J. Chem. Soc. A*, **1968**, 2223.
11) H. Rude, R. Benoit, et O. Hartmanshenn, *CEA-R-4205* (1971).
12) E. Jacob, *Z. Anorg. Allg. Chem.*, **400**, 45 (1973).
13) D. F. Shriver, "The Manipulation of Air Sensitive Compounds," McGraw Hill, New York (1969), p. 193.
14) H. R. Hoekstra, *Inorg. Chem.*, **2**, 492 (1963).
15) M. Schmeisser and E. Pammer, *Angew. Chem.*, **69**, 781 (1957).
16) M. J. Heras, P. J. Aymonino, und H. J. Schumacher, *Z. Phys. Chem., neue Folge*, **22**, 161 (1959).
17) E. Jacob, *Chem. Abstr.*, **85**, 132580d (1976).
18) A. D. Kirshenbaum and A. V. Grosse, *Trans. Am. Soc. Metals*, **45**, 758 (1953).
19) H. R. Hoekstra and J. J. Katz, *Anal. Chem.*, **25**, 1608 (1953).
20) G. Goldberg, A. S. Meyer, Jr., and J. C. White, *Anal. Chem.*, **32**, 314 (1960).
21) H. F. Combs and E. L. Grove, *Talanta*, **17**, 599 (1970).
22) P. W. Wilson, *J. Inorg. Nucl. Chem.*, **36**, 303 (1974).
23) P. W. Wilson, *J. Inorg. Nucl. Chem.*, **36**, 1783 (1974).
24) L. M. Ferris, *J. Am. Chem. Soc.*, **79**, 5419 (1957); *Ind. Eng. Chem.*, **51**, 200 (1959).
25) C. J. Mandleberg and D. Davies, *J. Inorg. Nucl. Chem.*, **20**, 58 (1961).
26) S. S. Kirslis, T. S. McMillan, and H. A. Bernhardt, *K-567* (1950).
27) J. Schröder und F. J. Grewe, *Chem. Ber.*, **103**, 1536 (1970).
28) W. E. Falconer, G. R. Jones, W. A. Sunder, I. Haigh, and R. D. Peacock, *J. Inorg. Nucl. Chem.*, **35**, 751 (1973).
29) S. Tsujimura, A. Takahashi, G. Fujisawa, and K. Suzuki, *JAERI-1064* (1964).

 © 1987 The Chemical Society of Japan Bull. Chem. Soc. Jpn., 60, 3195—3198 (1987)

The Iodine Content of Atmospheric Aerosols as Determined by the Use of a Fluoropore Filter® for Collection

Hirofumi TSUKADA,*,† Hiroshi HARA, Kiyoshi IWASHIMA, and Noboru YAMAGATA†
Institute of Public Health, 4-6-1 Shirokanedai, Minato-ku, Tokyo 108
(Received February 7, 1987)

Atmospheric aerosols were collected onto a Fluoropore filter in order to determine the iodine by means of instrumental neutron activation analysis. The collection filter was found to be the best material among the nine filters examined, for it has the lowest blank values for iodine as well as for other halogens and sodium. The iodine concentrations in Tokyo were found to be 1.7—12.7 ng m^{-3}. Of the soluble iodine, 10% or less was in the form of IO_3^-.

Among the radionuclides released from nuclear fuel reprocessing plants, radioiodine is of special concern because of its high fission yield, its volatility, and its accumulation in the human thyroid. An extraordinary long half-life of ^{129}I (1.6×10^7 y) necessitates the knowledge of the geochemical cycle of stable iodine in order to assess the behavior of ^{129}I in the environment and to estimate internal exposure through food ingestion.

The concentrations of aerosol iodine have been reported to be from several to several tens ng m^{-3}.[1-8] However, in most of the reported cases, the filter blank of iodine was not sufficiently low as compared with the amount of iodine collected on the filter, suggesting the potential inaccuracy of the reported values of the iodine concentration. This paper deals with the choice of an appropriate collection filter and the determination of stable iodine in atmospheric aerosols.

The present study examined nine filters for the blank iodine by means of instrumental neutron activation analysis; it demonstrated that the Fluoropore AF07P filter had the lowest iodine blank values. This filter was employed as the collection material for atmospheric aerosol in Tokyo. The aerosol was analyzed for iodine and some other elements, such as bromine, sodium, and aluminum, in order to obtain information regarding the environmental behavior of iodine.

Experimental

Three kinds of filters were analyzed by means of the instrumental neutron activation method: (a) filters prepared for standards, (b) filters for blank contents, and (c) filters with collected aerosols on them.

Standard Samples. Standard solutions of iodine, bromine, and chlorine were prepared by dissolving the respective potassium salts in twice-distilled water. For the iodine solution, the pH was adjusted to 8 with lithium hydroxide so as to prevent any iodine from being lost from the solution. Each of the solutions was impregnated uniformly onto a cellulose filter (Toyo 7) of the same size and shape as the other samples. For the standard of sodium and aluminum, powder of Standard Rock JG-1 (Porphyrite biotite granodiorite: Na, 2.51; Al, 7.53%), prepared by the Geological Survey of Japan, was caused to adhere onto a cellulose filter (Toyo 7) in the way described above.

Table 1. Filter Blanks Determined by Instrumental Neutron Activation Analysis

Filter	Element				
	I	Br	Cl	Na	Al
	ng cm^{-2}				
Sumitomo Fluoropore AF07P	0.044±0.021[a]	<0.08[b]	7.5± 0.6	1.2± 0.4	1.9± 0.1
Whatman 41	0.14 ±0.07	2.3±0.2	509 ±11	130 ± 6	22 ± 1
Toyo 7	0.21 ±0.05	4.8±0.2	322 ± 8	87 ± 4	5.2± 0.5
Toyo 51A	0.21 ±0.06	4.1±0.2	474 ±11	53 ± 4	3.1± 0.5
Gelman	<0.46	<1.4	216 ±16	183 ±11	—
Millipore HA	<0.54	2.5±0.6	1190 ±50	352 ±16	—
Sartorius SM	0.50 ±0.21	2.1±0.7	382 ±24	290 ±15	—
Nuclepore	2.4 ±0.5	503 ±7	34 ± 5	11 ± 3	2.5± 1.2
Palflex 2500QST	<1.7	<6.4	457 ±38	3890 ±60	32400 ±500

a) The ± values indicate the counting errors. b) Lower limit of detection.

† Present address: Japan Chemical Analysis Center, 295-3, Sanno-cho, Chiba-shi, Chiba 281.

Filter Blanks. Table 1 covers the analyzed nine filters. The filters were subjected to the analysis without any particular treatment.

Filters with Collected Aerosols on Them. A Fluoropore AF07P filter (Sumitomo Electric Industries, 22.8×17.7 cm) was employed as the aerosol-collection material (aerosol collection efficiency: 99.9%).[9] Atmospheric aerosol was collected for from three to ten hours by means of a high-volume air sampler set on the rooftop of the Institute of Public Health, Tokyo (about 15 m above the ground).

Instrumental Neutron Activation Analysis. The filters were sealed in polyethylene bags previously washed with nitric acid. A number of bags were put into a polyethylene capsule and irradiated in the Rikkyo University TRIGA II Reactor at a flux rate of 1.5×10^{12} n cm^{-2} s^{-1} for 10 minutes. The samples were cooled for five minutes after irradiation and then counted by means of a Ge(Li) detector (volume: 55 cm^3) for five minutes.

Results and Discussion

Concentrations of Blank Filters. The blank contents of iodine and the other elements are listed in Table 1, which shows that Fluoropore AF07P (polytetrafluoroethylene) has the lowest blank iodine, 0.04 ng cm^{-2}, one or two orders of magnitude lower than any other filters analyzed. The same thing goes for the other determined elements. In addition, this filter is designed for air filtration and so it designed to have a small pressure drop (0.69 Pa s m^{-1}), as small as that of the commonly used quartz-fiber filter. All of these findings establish the appropriateness of this filter for collecting aerosol iodine.

S/N Ratio of Iodine Concentrations. The accuracy of the observed iodine concentrations is directly affected by the blank value of iodine for the filter employed. The accuracy is quantified as the S/N ratio, where signal and noise correspond to the iodine content per unit of area of the filter with collected aerosol on it and to the blank value of iodine for the filter itself. This ratio was applied to the present results and the previously reported data. When the blank value was not reported by the original authors, it was replaced in this work by the corresponding blank values.

The S/N ratios are listed in Table 2. The present work is characterized by a high S/N ratio, around 100, whereas most of the other works have had smaller ratios, 1—10. It follows that our measured iodine concentrations are exceedingly reliable.

Evaluation of Iodine Volatilization in the Neutron Irradiation Process. Iodine loss by means of volatilization might be suspected in the process of neutron irradiation. In order to examine this problem, the iodine content was compared between two pieces of filters with collected aerosol. A filter with collected aerosol was cut into two pieces of equal size. One piece was impregnated with a lithium hydroxide solution before irradiation to prevent the iodine from volatalizing, while the other was not treated thus. Two samples, S2 and S3, were thus compared. The respective iodine contents for the treated and not-treated filter pieces were as follows: S2: 7.4±0.4 and 6.6±0.4; S3: 11.5±0.5 and 11.9±0.5 ng cm^{-2}. No significant difference between the treated and untreated pieces was noted, indicating that no such treatment was necessary to apply the samples in this study.

Table 2. Values of Iodine in Aerosols vs. in Blank Filter (S/N ratio)

Filter	Blank / ng cm^{-2}	S/N ratio	Authors
Sumitomo	0.044[a]	97	This work S 1
Fluoropore		150	S 2
AF07P		51	S 3
		33	S 4
		160	S 5
		110	S 6
		240	S 7
Whatman 41	0.14[a]	≈100	W. John et al.[4]
		≈16	R. Dams et al.[10]
Delbag polystyren	<0.5	>30	N. K. Aras et al.[7]
Whatman 541	0.65	6.9	W. Maenhaut and W. H. Zoller[11]
Nuclepore	0.94	14.6	W. Maenhaut and W. H. Zoller[11]
	2.4[a]	≈5	K. A. Rahn et al.[6]
Millipore EA	1	≈1	R. A. Duce et al.[3]
Millipore AA	14	≈1	T. Kato et al.[12]

a) Determined by this work.

Atmospheric Concentration of Iodine in Aerosols. Table 3 shows the atmospheric concentrations of iodine in the aerosol collected in Tokyo. The iodine concentrations ranged between 1.7 and 12.7 ng m^{-3}. For the other elements, the factors of air to air fluctuation were one order, about the same as that of iodine. In the present work, samples were analyzed for several tens of cubic meters.

The obtained iodine concentrations are in the range of reported values not only for Tokyo but also for various sites in the world (ng m^{-3}): 3.2—15.4 (Tokyo),[8] 1.32—>24.6 (Hawaii),[1] 1.5—5.2 (Hawaii),[2] 0.3—9.4 (Alaska),[3] 4.7—10 (San Francisco),[4] 2—10 (Massachusetts),[5] and 2.2—5.1 (New York).[6]

Different Mechanisms of Iodine and Chloride in Aerosols. The principal source of iodine in the atmosphere has been reported to be marine.[13,14] However, soil-derived iodine and surface soil particles in air are collected together with airborne particles. For that reason, their iodine content can be calculated on the basis of the aluminum concentrations listed in Table 3, which range from 56 to 338 ng m^{-3}, assuming that the average contents of aluminum and iodine in

Table 3. Atmospheric Concentrations of I, Br, Cl, Na, and Al in Aerosols

Sample No.	Air volume	Date	Element				
			I	Br	Cl	Na	Al
	m^3		$ng\ m^{-3}$				
S1	230	14/7/83	7.5±1.1[a]	20.6±4.6	2510±120	2810±80	—
S2	525	29/10/83	5.0±0.3	14.6±1.3	789± 21	892±20	338±6
S2·T[b]			5.7±0.3	14.6±1.3	699± 20	827±19	335±6
S3	375	1/11/83	12.7±0.5	26.8±2.1	2160± 40	1970±40	265±6
S3·T[b]			12.4±0.5	24.0±2.1	2020± 40	1920±40	270±5
S4[c]	14.9	13/11/83	1.7±0.3	4.0±1.0	402± 19	187±14	56±3
S5	1230	12-13/3/84	4.6±0.5	—	—	—	—
S6	1345	21-22/3/84	3.0±0.3	—	—	—	—
S7	1172	23-24/3/84	7.3±0.6	—	—	—	—

a) The ± values indicate the counting errors. b) Treated with a LiOH solution before irradiation.
c) Collected by means of a low-volume air sampler.

Table 4. Water-soluble-I and IO_3^--I in Aerosols

Sample No.	Total (T_I)	Water-soluble(S_I) (in IO_3^- form: S_{IO_3})	Residue(R_I)	Recovery(S_I+R_I)
	$ng\ m^{-3}$			
S5	4.6±0.5[a]	2.0 ±0.1 (0.19±0.03)	1.2±0.2	3.3±0.2
S6	3.0±0.3	1.4 ±0.1 (0.15±0.02)	1.4±0.3	2.8±0.3
S7	7.3±0.6	3.3 ±0.1 (0.10±0.03)	4.3±0.4	7.5±0.4

a) The ± values indicate the counting errors.

soil are 71 g kg^{-1} and 5 mg kg^{-1} respectively.[15] The calculated values are 0.024 (S2), 0.019 (S3), and 0.004 (S4) ng m^{-3} respectively. Thus, the contribution of soil particles to the total iodine content of aerosols is negligibly small. Most of the iodine in aerosols may thus be of marine origin.

The principal source of chloride in the atmosphere has been also considered to be marine, but recently there was appeared an anthropogenic supply of chloride, formed from the hydrogen chloride emitted from incinerating plants. At the same site over a period from June, 1979, to July, 1982, one of the present authors determined the particle-size distributions for chloride and other components in order to ascertain the seasonal variation of the chloride distribution.[16] On a monthly averaged basis, the chloride in the coarse-particle region was 78, 61, and 27% of the total chloride for July, October, and November respectively. On the basis of these values, the chloride concentration in aerosols of marine origin can be postulated. The calculated values of I/Cl (by weight) in marine-origin aerosols are $0.38—2.2\times10^{-2}$, but the I/Cl (by weight) in sea water is 3.2×10^{-6}.

If the behavior of iodine through transport is the same as that of chloride, the same order of magnitude of I/Cl in aerosols should be expected as in sea water, but the result indicates an extraordinarily high ratio (by a factor of about 10^3). This is in accord with similar observations of the total I/Cl ratios in aerosols and precipitation reported by many researchers[1,3,5,13] and strongly suggests a different behavior of iodine through transport from that of chloride.

A Simple Fractionation of Iodine Species. Atmospheric aerosol probably contains various sorts of iodine compounds. Aerosol iodine was tentatively fractionated into water-soluble and insoluble residues, and iodate was collected so as to be determined for the former fraction.

Two equivalent pieces were cut out of a sample filter in the manner described before. One piece was analyzed for total iodine (T_I). The other was subjected to ultrasonic extraction with water: iodine was determined for the water extract (S_I) and for the insoluble residue (R_I). This measurement was applied to three samples.

The extraction was satisfactory because no appreciable chlorine, all of which could be regarded water-soluble, was observed for the insoluble residue. The water-soluble fraction was further passed over the

anion-exchange resin (Dowex 2-X8) to separate the iodate fraction (S_{IO_3}), which was them analyzed for iodate.[17,18]

Table 4 indicates that the recovery was almost satisfactory, that only 42—73% of the iodine was water-soluble, and that 10% or less of the soluble iodine was iodate, IO_3^-.

The existence of the IO_3^- form in aerosols was established in the present work, although there could be various kinds of iodine compounds in the atmosphere.

We are grateful to Mr. Hiroyuki Takagi for his help in the Gamma-ray measurements.

References

1) R. A. Duce, J. W. Winchester, and T. W. VanHahl, *J. Geophys. Res.*, **70**, 1775 (1965).

2) J. L. Moyers and R. A. Duce, *J. Geophys. Res.*, **77**, 5229 (1972).

3) R. A. Duce, J. W. Winchester, and T. W. VanHahl, *Tellus*, **18**, 238 (1966).

4) W. John, R. Kaifer, K. Rahn, and J. J. Wesolowski, *Atmos. Environ.*, **7**, 107 (1973).

5) R. L. Lininger, R. A. Duce, J. W. Winchester, and W. R. Matson, *J. Geophys. Res.*, **71**, 2457 (1966).

6) K. A. Rahn, R. D. Borys, E. L. Butler, and R. A. Duce, *Ann. N. Y. Acad. Sci.*, **322**, 143 (1979).

7) N. K. Aras, W. H. Zoller, G. E. Gordon, and G. J. Lutz, *Anal. Chem.*, **45**, 1481 (1973).

8) K. Kametani, T. Matsumura, and M. Sakurai, *Bunseki Kagaku*, **35**, 622 (1986).

9) Technical Report of Sumitomo Electric Industries, No. 75106 (1975).

10) R. Dams, J. Billiet, C. Block, M. Demuynck, and M. Janssens, *Atmos. Environ.*, **9**, 1099 (1975).

11) W. Maenhaut and W. H. Zoller, *J. Radioanal. Chem.*, **37**, 637 (1977).

12) T. Kato, N. Sato, and N. Suzuki, *Talanta*, **23**, 517 (1976).

13) Y. Miyake and S. Tsunogai, *J. Geophys. Res.*, **68**, 3989 (1963).

14) V. D. Korzh, *Atmos. Environ.*, **18**, 2707 (1984).

15) H. J. M. Bowen, "Environmental Chemistry of the Elements," Academic Press (1979), p. 60.

16) H. Hara, K. Honda, K. Nagara, and A. Goto, *Nippon Kagaku Kaishi*, **1983**, 1221.

17) K. Takiura and Y. Takino, *Bunseki Kagaku*, **10**, 483 (1961).

18) J. B. Luten, J. R. W. Woittiez, H. A. Das, and C. L. DeLingny, *J. Radioanal. Chem.*, **43**, 175 (1978).

 © 1987 The Chemical Society of Japan Bull. Chem. Soc. Jpn., 60, 3199—3205 (1987)

Chromatographic Study of Optical Resolution. XIV.[1] Optical Resolution of Amine Complex Cations of the Type $[Co(N)_6]^{3+}$ by Reversed-Phase Ion-Pair Chromatography Using Bis(μ-*d*-tartrato)diantimonate(III) and Arsenic Analog as an Ion-Pairing Reagent

Shinji Izumoto,† Katsuhiko Miyoshi, and Hayami Yoneda*
Department of Chemistry, Faculty of Science, Hiroshima University,
Higashi-senda-machi, Naka-ku, Hiroshima 730
(Received February 24, 1987)

Reversed-phase ion-pair chromatography (RPIPC) was applied to the optical resolution of amine complex cations of the type $[Co(N)_6]^{3+}$ using either bis(μ-*d*-tartrato)diantimonate(III) ion, $[Sb_2(d\text{-tart})_2]^{2-}$ or its arsenic analog, $[As_2(d\text{-tart})_2]^{2-}$ as an ion-pairing reagent. With either reagent, efficient optical resolution was attained for $[Co(en)_3]^{3+}$, $[Co(tn)_3]^{3+}$, [Co(sen)]$^{3+}$, [Co(sep)]$^{3+}$, and [Co(diNOsar)]$^{3+}$ (en=ethylenediamine, tn=trimethylenediamine, sen=1,1,1-tris[[(2-aminoethyl)amino]methyl]ethane, sep=1,3,6,8,10,13,16,19-octaazabicyclo[6.6.6]icosane, and diNOsar=1,8-dinitro-3,6,10,13,16,19-hexaazabicyclo[6.6.6]icosane). Dependence of retention volumes and separation factors of these complexes on the concentration and the counterion of the ion-pairing reagents was examined with Na^+, Me_4N^+, and Et_4N^+ employed as counterions. Experimental results were discussed with reference to those obtained by means of normal-phase ion-exchange chromatography (NPIEC) using the same eluents. It was concluded that $[As_2(d\text{-tart})_2]^{2-}$ serves as a more effective eluent in both RPIPC and NPIEC than $[Sb_2(d\text{-tart})_2]^{2-}$, and that RPIPC is a much more useful tool for the optical resolution of the $[Co(N)_6]^{3+}$-type complex cations than NPIEC.

In a previous work,[2] optical resolution of some *cis*(N)-$[Co(O)_4(N)_2]^-$-type complex anions was accomplished by means of reversed-phase ion-pair chromatography (abbreviated as RPIPC hereafter) using cinchona alkaloid cations as an ion-pairing reagent. In the present study, optical resolution of some amine complex cations of the type $[Co(N)_6]^{3+}$ was attempted by the same technique. The key factor here is to find out a suitable chiral anion capable of functioning as an ion-pairing reagent. The two chiral anions, *d*-tartrate (*d*-tart^{2-}) and bis(μ-*d*-tartrato)diantimonate(III) ($[Sb_2(d\text{-tart})_2]^{2-}$) ions have been successfully utilized as a chiral eluent to resolve a variety of complex cations by normal-phase ion-exchange chromatography[3] (abbreviated as NPIEC). The former anion is found to be too hydrophilic to be distributed to the stationary phase composed of linear-chain alkyl moieties in RPIPC. The latter anion, $[Sb_2(d\text{-tart})_2]^{2-}$ does not contain any alkyl chains nor aromatic rings and it carries a high electric charge compared with commonly used ion-pairing reagents such as tetraalkylammonium and alkanesulfonate ions. However, it is regarded as rather hydrophobic, since its charged groups are all coordinated to Sb(III) ions and it is fairly large in size. Therefore, this chiral anion is expected to serve as a potential ion-pairing reagent in RPIPC.[4a] $[As_2(d\text{-tart})_2]^{2-}$ ion, an As analog of $[Sb_2(d\text{-tart})_2]^{2-}$, has seen limited use as a chiral eluent, since it is not commercially available. Thus, it seems attractive to compare the two anions with respect to their ability as an eluent in chromatography.

In RPIPC, structural characteristics of ion-pairing reagents have been examined in detail, since they have a profound influence on the retention volumes as well as on the separation factors.[4] By contrast, the functions of the counterions M^+ of the ion-pairing reagents have been hardly taken into consideration. In the present study, however, the electric charge of the tervalent complex cation is not completely neutralized in the 1 : 1 association with $[Sb_2(d\text{-tart})_2]^{2-}$, and thus the complex cation is distributed to the stationary phase probably in the form of $M[Co(N)_6]][Sb_2(d\text{-tart})_2]_2$ rather than $[Co(N)_6]_2[Sb_2(d\text{-tart})_2]_3$ if the counterion M^+ is more hydrophobic than $[Sb_2(d\text{-tart})_2]^{2-}$. Consequently, a hydrophobic counterion M^+ is expected to promote cooperatively the retention of the complex cation to a considerable extent, since $[Sb_2(d\text{-tart})_2]^{2-}$ is less hydrophobic than usual ion-pairing reagents.

Experimental

Materials. The $[Co(N)_6]^{3+}$-type complexes used were $[Co(en)_3]^{3+}$,[5] $[Co(tn)_3]^{3+}$,[6] [Co(sen)]$^{3+}$,[7] [Co(sep)]$^{3+}$,[8] *lel*$_3$-$[Co(chxn)_3]^{3+}$,[9] and [Co(diNOsar)]$^{3+}$[10] (en=ethylenediamine, tn=trimethylenediamine, sen=1,1,1-tris[[(2-aminoethyl)amino]methyl]ethane, sep=1,3,6,8,10,13,16,19-octaazabicyclo[6.6.6]icosane, chxn=*trans*-1,2-cyclohexanediamine, and diNOsar=1,8-dinitro-3,6,10,13,16,19-hexaazabicyclo[6.6.6]icosane). For comparison, $[Co(gly)(en)_2]^{2+}$[11] was also used (gly=glycinate anion). Figure 1 illustrates schematic structures of some of these complexes, which were prepared as chloride salts by the literature methods. Absolute configurations have been already assigned to all of them.

† Present address: Daicel Chemical Industries, Ltd., Research Center, Shinzaike, Aboshi-ku, Himeji 761-12.

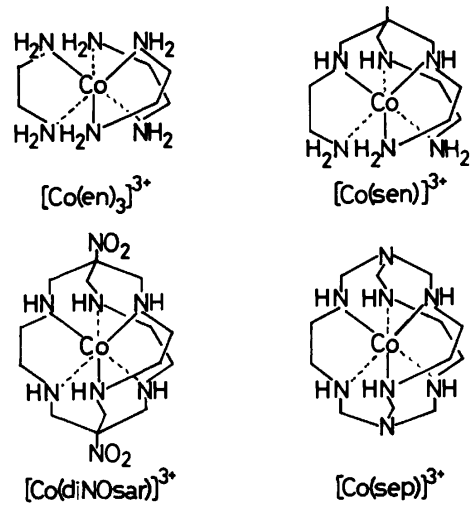

Fig. 1. Structures of Δ-enantiomers of the $[Co(N)_6]^{3+}$-type complexes investigated in the present study.

$K[Co(edta)]\cdot 2H_2O$ (edta=ethylenediaminetetraacetate anion), used as a marker for the void volume measurement, was prepared by a well-established method.[12]

Following salts of $[Sb_2(d\text{-tart})_2]^{2-}$ or $[As_2(d\text{-tart})_2]^{2-}$ were used as ion-pairing reagents; $Na_2[Sb_2(d\text{-tart})_2]\cdot 5H_2O$, $K_2[Sb_2(d\text{-tart})_2]\cdot 3H_2O$, $(NH_4)_2[Sb_2(d\text{-tart})_2]\cdot 3H_2O$, $(Me_4N)_2[Sb_2(d\text{-tart})_2]\cdot 3.5H_2O$, $(Et_4N)_2[Sb_2(d\text{-tart})_2]\cdot 1.5H_2O$, and $Na_2[As_2(d\text{-tart})_2]\cdot 5H_2O$. The potassium salt was obtained commercially and was used without purification. The sodium salt was prepared by the literature method.[3b] The ammonium salt was similarly prepared using ammonium hydrogen *d*-tartrate in place of sodium hydrogen *d*-tartrate. Found: C, 15.43; H, 2.94; N, 4.40%. Calcd for $C_8H_{12}N_2O_{12}Sb_2\cdot 3H_2O$: C, 15.35; H, 2.91; N, 4.48%. The tetramethylammonium and tetraethylammonium salts were prepared in a following way. An equivalent amount of antimony(III) oxide was added to an aqueous solution of *d*-tartaric acid. After heating just to the boiling point, an equivalent amount of aqueous MOH ($M^+=Me_4N^+$ or Et_4N^+) was carefully added dropwise with stirring. The suspension was concentrated and undissolved substances were filtered off. The filtrate was evaporated to dryness to obtain a glassy material. Its purity was checked by elemental analysis. Found: C, 25.69; H, 4.71; N, 3.70%. Calcd for $C_{16}H_{28}N_2O_{12}Sb_2\cdot 3.5H_2O$: C, 25.72; H, 4.73; N, 3.75%. Found: C, 34.89; H, 5.65; N, 3.37%. Calcd for $C_{24}H_{44}N_2O_{12}Sb_2\cdot 1.5H_2O$: C, 35.01; H, 5.77; N, 3.40%. $Na_2[As_2(d\text{-tart})_2]\cdot 5H_2O$ was easily prepared according to well-established procedures[13] followed by recrystallization from water. Found: C, 16.47; H, 2.42%. Calcd for $C_8H_4As_2Na_2O_{12}\cdot 5H_2O$: C, 16.62; H, 2.45%.

The column packings used in the present study were TSK gel ODS-120A (Toyo Soda Manufacturing Co., Ltd.), which carries linear-chain alkyl moieties (octadecyl groups) covalently bonded to the surface of silica gel (for RPIPC), and TSK gel SP-2SW (Toyo Soda Manufacturing Co., Ltd.), which carries sulfopropyl groups covalently bonded to the surface of silica gel (for NPIEC).

Chromatographic Experiments. A stainless steel column (4×300 mm) packed with TSK gel ODS-120A or a similar column (7.5×75 mm) packed with TSK gel SP-2SW was equilibrated with an aqueous eluent solution. A mixture of 20 μl of an aqueous solution of a racemic complex (0.1 mol dm^{-3}) with 10 μl of an aqueous solution of a marker (0.01 mol dm^{-3}), was injected by a syringe on the top of the column and was eluted at an elution rate of 0.25 $cm^3\ min^{-1}$. The effluents were fractionally collected and their absorption and circular dichroism (CD) spectra were measured to obtain elution curves and to determine elution orders. The chromatographic apparatus used here consisted of a JASCO BIP-1 pump for HPLC, a JASCO variable loop injector VL-613, and a Shimadzu UV-140 double beam spectrophotometer. The CD spectra were recorded on a JASCO J-40CS recording spectropolarimeter.

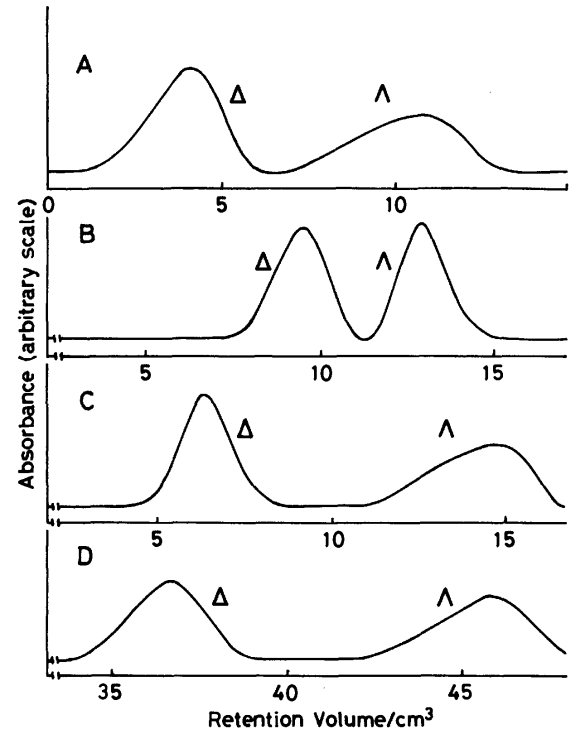

Fig. 2. Elution curves of $[Co(en)_3]^{3+}$ (A), $[Co(tn)_3]^{3+}$ (B), $[Co(sen)]^{3+}$ (C), and $[Co(sep)]^{3+}$ (D) obtained by RPIPC. Eluent: aqueous $K_2[Sb_2(d\text{-tart})_2]$ (0.1 mol dm^{-3}).

Results and Discussion

Reversed-Phase Ion-Pair Chromatography (RPIPC). Typical elution curves obtained for the $[Co(N)_6]^{3+}$-type complexes with $K_2[Sb_2(d\text{-tart})_2]$ employed as an eluent in RPIPC are shown in Fig. 2. Though the curves are rather broad, base-line resolution is assured for each complex. It is noteworthy that complete resolution is accomplished easily even for $[Co(tn)_3]^{3+}$, complete resolution of which has been barely attained with resort to time-consuming recycling chromatography.[14] Experimental data obtained with $M_2[Sb_2(d\text{-tart})_2]$ ($M^+=Na^+$, K^+, NH_4^+, Me_4N^+, and Et_4N^+) used

Table 1. Effect of Counterion M^+ on Retention Volume V_R and Separation Factor α Obtained by RPIPC with Aqueous M_2 $[Sb_2(d\text{-tart})_2]$ (0.1 mol dm^{-3})

	$M^+=Na^+$		K^+		NH_4^+		Me_4N^+		Et_4N^+	
	V_R[a)]/cm^3	α	V_R[a)]/cm^3	α	V_R[a)]/cm^3	α	V_R[a)]/cm^3	α	V_R[a)]/cm^3	α
$[Co(en)_3]^{3+}$	10.95	2.03	11.05	2.63	12.63	2.99	23.18	3.84	12.15	4.76
$[Co(tn)_3]^{3+}$	7.15	1.32	12.73	1.33	10.75	1.34	13.38	1.39	4.98	1.52
$[Co(sen)]^{3+}$	11.60	2.04	15.03	2.39	13.70	2.95	21.40	3.43	12.03	4.25
$[Co(sep)]^{3+}$	28.00	1.27	46.03	1.25	37.40	1.25	48.53	1.29	14.55	1.36

a) Retention volume of the later-eluted Λ-enantiomer.

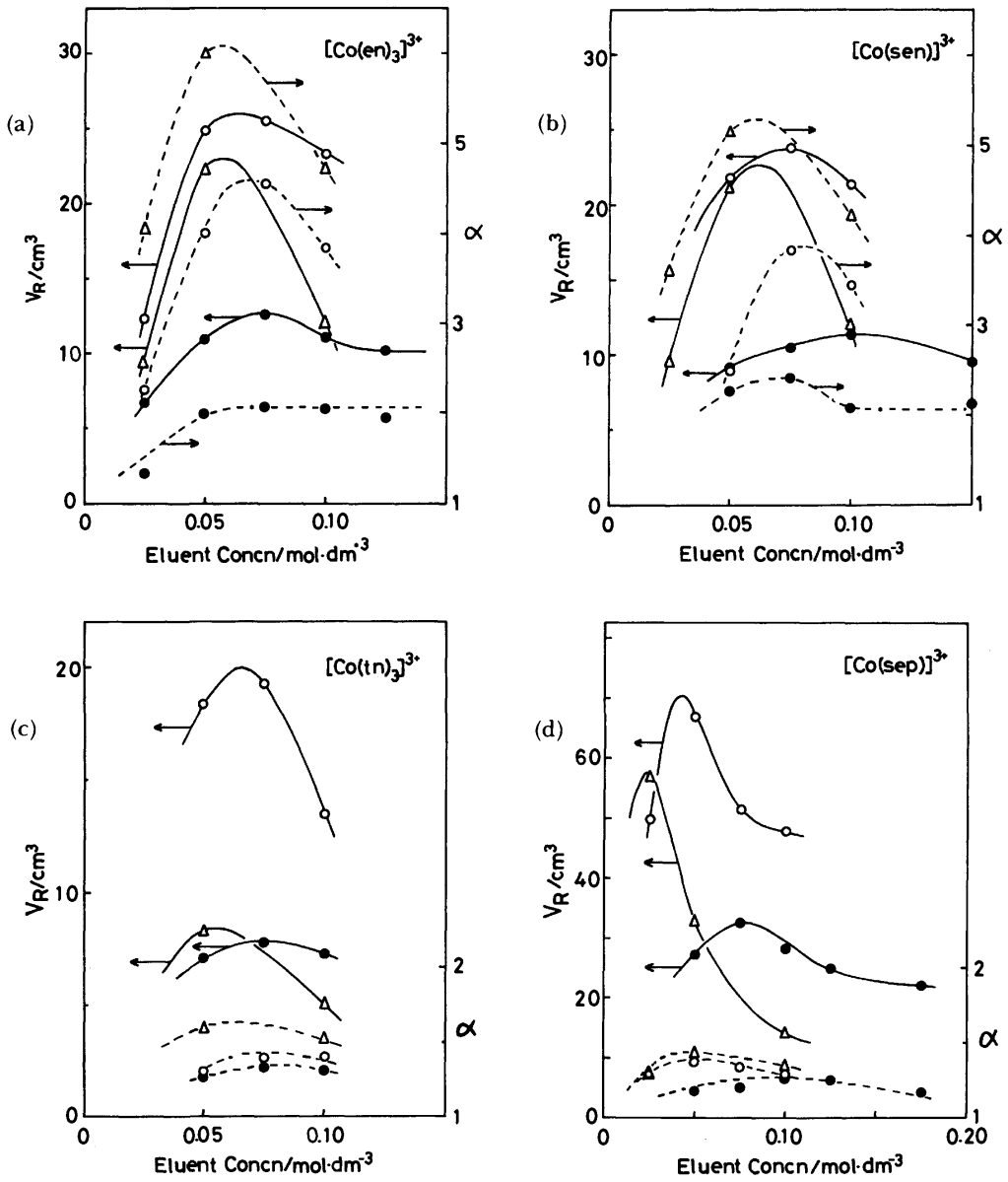

Fig. 3. Plots of retention volumes V_R (——) of the later-eluted enantiomer and of separation factors α (------) obtained by RPIPC against the eluent concentration. Eluent: $Na_2[Sb_2(d\text{-tart})_2]$ (●), $(Me_4N)_2[Sb_2(d\text{-tart})_2]$ (○), and $(Et_4N)_2[Sb_2(d\text{-tart})_2]$ (Δ).

as an ion-pairing reagent are summarized in Table 1.[15] For all the complexes, the Λ-enantiomers are eluted later. This means that $[Sb_2(d\text{-tart})_2]^{2-}$ gets associated more readily with the Λ- than with the Δ-enantiomer, in keeping with the association constants estimated for these complex cations with $[Sb_2(d\text{-tart})_2]^{2-}$ in aqueous solution.[16] Furthermore, this observation does not contradict with the elution orders predicted from the chiral discrimination mechanism established earlier between $[Sb_2(d\text{-tart})_2]^{2-}$ and $[Co(N)_6]^{3+}$-type complexes.[17] One different elution order is noted between RPIPC and NPIEC. The complex cation, $[Co(tn)_3]^{3+}$, when eluted from either an SP-Sephadex C-25 or Dowex 50W-X2 cation-exchange column with aqueous $Na_2[Sb_2(d\text{-tart})_2]$, was partially resolved with the Δ-enantiomer eluted slightly faster unlike other $[Co(N)_6]^{3+}$-type complexes.[18] This suggests that $[Sb_2(d\text{-tart})_2]^{2-}$ favors the Δ- over the Λ-enantiomer for $[Co(tn)_3]^{3+}$ in NPIEC. In RPIPC, on the contrary, $[Sb_2(d\text{-tart})_2]^{2-}$ always exhibits a greater affinity toward the Λ-enantiomer for all the complexes including $[Co(tn)_3]^{3+}$. The anomalous behavior of $[Co(tn)_3]^{3+}$ will be discussed later.

Data in Table 1 reveal that different counterions M^+ of $[Sb_2(d\text{-tart})_2]^{2-}$ give different retention volumes V_R and separation factors α for each $[Co(N)_6]^{3+}$-type complex. In general, the larger the size of M^+, i.e., the more hydrophobic nature M^+ bears, the greater the retention volume of each complex. However, when M^+ is as large as Et_4N^+, the retention volume starts to decrease. Then, in Figs. 3-a to 3-d are plotted the V_R and α values of $[Co(en)_3]^{3+}$, $[Co(sen)]^{3+}$, $[Co(tn)_3]^{3+}$, and $[Co(sep)]^{3+}$, in this order, as a function of the concentration of ion-pairing reagents with $M^+=Na^+$, Me_4N^+, and Et_4N^+. For each complex, V_R shows a clear maximum with $M^+=Me_4N^+$ and Et_4N^+, the latter exhibiting it at lower eluent concentrations and the former giving a higher maximum at least in the concentration range covered. On the contrary, the V_R curve with $M^+=Na^+$ shows a less clear maximum. Appearance of such maxima in V_R may be explained as follows. Since Me_4N^+ and Et_4N^+ are much more hydrophobic than Na^+, they are more easily distributed together with $[Sb_2(d\text{-tart})_2]^{2-}$ to the stationary phase composed of linear-chain alkyl moieties,[19] generating more cation-exchange sites on the stationary phase.[4b] This will lead to remarkably increased retention volumes. On the other hand, the effect of expelling the complex cation already distributed to the stationary phase by the counterion M^+ present in the moving phase, viz., the exclusion effect of M^+, becomes more and more dominant with increasing concentration of the eluent and with increasing hydrophobic nature of M^+. Thus, a maximum in V_R appears at a lower eluent concentration for $M^+=Et_4N^+$ than for $M^+=Me_4N^+$, since the former counterion is more hydrophobic and thus has a greater exclusion effect. A lower maximum in V_R observed for the former is similarly interpreted, and the absence of a clear V_R maximum for $M^+=Na^+$ may be due to its hydrophilic nature which leads to a small retention volume and to a weak exclusion effect. These interpretations are indirectly supported by the observation that $[Co(sep)]^{3+}$, regarded as the most hydrophobic of the four complexes, exhibits the V_R maxima at the lowest eluent concentrations, and that it always gives greater retention volumes than $[Co(en)_3]^{3+}$ regardless of the kind of M^+.[20]

Let us next look into the separation factors α obtained by RPIPC. It is seen in Table 1 and Fig. 2 that fairly high separation factors are obtained to such an extent that complete resolution is attained with ease for each complex. In a previous study, for example, optical resolution of $[Co(en)_3]^{3+}$ resulted in a separation factor of 1.45[21] on an SP-Sephadex C-25 column with an aqueous $K_2[Sb_2(d\text{-tart})_2]$ solution (0.1 mol dm^{-3}) employed as an eluent. The α value of 2.63 obtained in the present RPIPC under a similar set of conditions (Table 1) demonstrates a remarkable improvement in the resolution efficiency. As noted above, $[Co(tn)_3]^{3+}$ can also be resolved completely with a separation factor of 1.33 under the same conditions as above, though NPIEC gives a separation factor of 1.00 for this complex, as seen later in Table 3.

It is noticeable in Fig. 3 that surprisingly high α values are obtained for $[Co(en)_3]^{3+}$, $[Co(sen)]^{3+}$, and $[Co(tn)_3]^{3+}$,[22] particularly when their retention volumes are increased with Me_4N^+ or Et_4N^+. On the contrary, $[Co(sep)]^{3+}$ gives an almost constant separation factor even if its retention volume is increased appreciably. Structural characteristics of these complexes (Fig. 1) indicate that the former three complexes allow the hydrogen-bonding association of $[Sb_2(d\text{-tart})_2]^{2-}$ from the direction of the C_3 axis (C_3 association) or the C_2 axis (C_2 association), while only the C_2 association is allowed for $[Co(sep)]^{3+}$ because it has alkyl caps along the C_3 axis. These characteristics seem to be responsible for the chromatographic behavior mentioned above, which will be discussed more closely in the last section.

Now, a comparison is made between $[Sb_2(d\text{-tart})_2]^{2-}$ and its As analog, $[As_2(d\text{-tart})_2]^{2-}$ with respect to their ability as an ion-pairing reagent in RPIEC. Table 2 compares the experimental data obtained with the two ion-pairing reagents. It is evident that first, $[As_2(d\text{-tart})_2]^{2-}$ gives much greater retention volumes than $[Sb_2(d\text{-tart})_2]^{2-}$ for all the complexes, second, the former gives correspondingly somewhat higher separation factors, and finally, the Λ-enantiomers are eluted later with either of the two eluents. These results lead us to conclude that $[As_2(d\text{-tart})_2]^{2-}$ interacts more strongly with these amine complex cations of the type $[Co(N)_6]^{3+}$ than does $[Sb_2(d\text{-tart})_2]^{2-}$ and thus can be

Table 2. Comparison of Retention Volumes V_R and Separation Factors α Obtained by RPIPC with $Na_2[As_2(d\text{-tart})_2]$ and with $Na_2[Sb_2(d\text{-tart})_2]$ (0.1 mol dm^{-3})

	$[As_2(d\text{-tart})_2]^{2-}$		$[Sb_2(d\text{-tart})_2]^{2-}$	
	V_R[a]/cm^3	α	V_R[a]/cm^3	α
$[Co(en)_3]^{3+}$	61.25	3.33	10.95	2.03
$[Co(tn)_3]^{3+}$	61.35	1.30	7.15	1.32
[Co(sen)]$^{3+}$	60.75	3.25	11.60	2.04
[Co(sep)]$^{3+}$	101.43	1.37	28.00	1.27
[Co(diNOsar)]$^{3+}$	52.30	1.84	14.33	1.70

a) Retention volumes of the later-eluted Λ-enantiomer.

Table 3. Comparison of Retention Volumes V_R and Separation Factors α Obtained by NPIEC with $Na_2[As_2(d\text{-tart})_2]$ and with $Na_2[Sb_2(d\text{-tart})_2]$ (0.075 mol dm^{-3})

	$[As_2(d\text{-tart})_2]^{2-}$		$[Sb_2(d\text{-tart})_2]^{2-}$	
	V_R[a]/cm^3	α	V_R[a]/cm^3	α
$[Co(en)_3]^{3+}$	41.4	1.23	62.0	1.32[d]
$[Co(tn)_3]^{3+}$	56.6	1.00[b]	104.0[c]	1.00[b]
[Co(sen)]$^{3+}$	46.2	1.28	60.0	1.39[d]
[Co(sep)]$^{3+}$	27.6	1.41	65.2	1.31[d]
[Co(diNOsar)]$^{3+}$	...	...	40.2	1.83[d]

a) Retention volumes of the faster-eluted Λ-enantiomer. b) Single elution curve observed. c) The Δ-enantiomer is eluted faster. d) Data taken from Ref. 17b.

used more preferably as an ion-pairing reagent for the optical resolution of these complex cations in RPIPC, and that the chiral discrimination mechanisms are essentially the same for the two ion-pairing reagents.

[Co(diNOsar)]$^{3+}$ behaves somewhat anomalously in that it gives smaller V_R values and considerably greater α values than the analogous cage complex, [Co(sep)]$^{3+}$ with either ion-pairing reagent (Table 2). Highly efficient optical resolution attained for [Co(diNOsar)]$^{3+}$ has been already interpreted in terms of the severe steric repulsion expected stereoselectively between the nitro group of the Δ-enantiomer and the distal carboxylato group of $[Sb_2(d\text{-tart})_2]^{2-}$.[17b] The smaller retention volumes obtained for this complex may be attributed to the presence of the polar nitro groups which render this complex less hydrophobic than the parent complex [Co(sep)]$^{3+}$.[23]

Normal-Phase Ion-Exchange Chromatography (NPIEC). For the purpose of elucidating why $[As_2(d\text{-tart})_2]^{2-}$ gives greater V_R values than $[Sb_2(d\text{-tart})_2]^{2-}$ in RPIPC, NPIEC was applied to the optical resolution of the $[Co(N)_6]^{3+}$-type complexes with the two chiral anions employed as an eluent. The results are listed in Table 3. For each of these complexes, $[As_2(d\text{-tart})_2]^{2-}$ and $[Sb_2(d\text{-tart})_2]^{2-}$ give comparable separation factors, but the former gives smaller retention volumes, indicative of the stronger affinity of the former anion for these complexes. This is in complete conformity with the results obtained by RPIPC. In other words, $[As_2(d\text{-tart})_2]^{2-}$ has inherently a stronger association tendency toward these complexes than $[Sb_2(d\text{-tart})_2]^{2-}$.

An X-ray crystallographic analysis has revealed that $[As_2(d\text{-tart})_2]^{2-}$ is somewhat smaller in size than $[Sb_2(d\text{-tart})_2]^{2-}$. If the two oxygen atoms coordinated to the same Sb or As atom, i.e., the alcoholic oxygen atom of one *d*-tartrate moiety and the carboxylic oxygen atom of the other *d*-tartrate moiety are used for the double hydrogen bonding to the two axial NH protons of the complex directed along either the C_3 or the C_2 axis, as assumed before,[17] the matching of the O-O and H-H distances is of prime importance to the interaction. The O-O distance actually estimated is 2.561 Å[24] for $[As_2(d\text{-tart})_2]^{2-}$ and 2.692 Å[25] for $[Sb_2(d\text{-tart})_2]^{2-}$. The H-H distance of $[Co(en)_3]^{3+}$ is 2.283 and 2.270 Å for the C_3 and C_2 axial protons, respectively.[26] It will then follow that $[As_2(d\text{-tart})_2]^{2-}$ is more susceptible to intimate hydrogen bonds to $[Co(en)_3]^{3+}$ and other related complexes than $[Sb_2(d\text{-tart})_2]^{2-}$ is. In this way, smaller and greater V_R values obtained with $[As_2(d\text{-tart})_2]^{2-}$ in NPIEC and RPIPC, respectively, are interpreted reasonably within the framework of the C_3 and C_2 association modes proposed previously.[17]

Comparison between RPIPC and NPIEC. A comparison of the experimental results obtained between RPIPC and NPIEC (Tables 2 and 3) reveals very interesting facts as follows. For such complexes as $[Co(en)_3]^{3+}$, [Co(sen)]$^{3+}$, and $[Co(tn)_3]^{3+}$ for which both of the C_3 and C_2 association modes are possible, the application of RPIPC leads to a remarkable improvement in the separation factor. For example, $[Co(tn)_3]^{3+}$ gives a single elution curve in NPIEC, while base-line resolution is attained for this complex in RPIPC. By contrast, no such drastic improvement is detected for [Co(sep)]$^{3+}$, [Co(diNOsar)]$^{3+}$, and *lel*$_3$-$[Co(chxn)_3]^{3+}$ (chxn=*trans*-1,2-cyclohexanediamine) (Table 4)[27] for which only the C_2 or the C_3 association mode is possible owing to the presence of alkyl caps along the C_3 axis or bulky substituents along the C_2 axis (Fig. 1).

Several reasons are conceivable why RPIPC offers highly improved resolution efficiency for the former three complexes. The sample retention in NPIEC depends on the sample-ion-exchange resin interaction which is not related to chiral discrimination as well as on the sample-resolving reagent interaction, and the contribution of the former is unfortunately dominant generally in NPIEC. For example, for *lel*$_3$-$[Co(chxn)_3]^{3+}$ having presumably a very strong affinity for the resin, the α value is as high as 1.09 (Table 4). In other words, NPIEC appears unable to take full advantage of the chiral discrimination ability of the resolving reagent. On the other hand, the sample

Table 4. Comparison of Retention Volumes V_R and Separation Factors α Obtained with $Na_2[Sb_2(d\text{-tart})_2]$ by NPIEC and by RPIPC

	NPIEC			RPIPC		
	Eluent concn / mol dm^{-3}	V_R[a] / cm^3	α	Eluent concn / mol dm^{-3}	V_R[b] / cm^3	α
$[Co(en)_3]^{3+}$	0.1	10.2	1.35	0.175	9.98	2.09
$[Co(en)_3]^{3+}$	0.075	62.0	1.32	0.075	12.63	2.06
lel$_3$-$[Co(chxn)_3]^{3+}$	0.1	55.4	1.09	0.175	82.5	1.31
$[Co(gly)(en)_2]^{2+}$	0.075	10.6	1.21	0.075	1.85	1.42

a) Retention volume of the faster-eluted Λ-enantiomer. b) Retention volume of the later-eluted Λ-enantiomer.

retention in RPIPC is governed mainly by the sample-resolving reagent interaction which is directly associated with chiral discrimination. Consequently, RPIPC has a general possibility to afford a higher separation factor than NPIEC for a particular sample. However, it is hard to accept that the improvement in α detected in the present study has been brought about simply by the above-mentioned reason, because α is greatly improved only for those complexes which adopt both the C_3 and the C_2 modes.

The chiral discrimination mechanism of $[Sb_2(d\text{-tart})_2]^{2-}$ proposed previously can be summarized as follows.[17] $[Sb_2(d\text{-tart})_2]^{2-}$ comes into interaction with the complex cation from the direction of either the C_3 or the C_2 axis to form hydrogen bonds to the axial NH protons directed along the C_3 or the C_2 axis, respectively. When the C_3 association mode is adopted, the chiral anion favors the Λ- over the Δ-enantiomer, whereas the Δ-enantiomer is favored in the C_2 association mode.[28] As a result, the chiral discrimination efficiency is in general low for those complexes which can adopt both association modes. A typical example is provided by $[Co(tn)_3]^{3+}$ for which so low resolution is attained in NPIEC that its elution order is reversed even when the eluent employed is changed from $[Sb_2(d\text{-tart})_2]^{2-}$ to $[As_2(d\text{-tart})_2]^{2-}$ (Table 3). This means that the elution order of $[Co(tn)_3]^{3+}$ is determined by a delicate balance of the two comparable association modes prevailing in NPIEC. However, in the stationary phase of RPIPC where the effective dielectric constant is probably very low, the second-step association forming an ion triplet $[Co(N)_6][Sb_2(d\text{-tart})_2]_2^-$, the electric charge of which is finally neutralized by the counterion M^+,[19] will take place, because the tervalent charge of the complex cation is not completely neutralized in the ion pair $[Co(N)_6][Sb_2(d\text{-tart})_2]^+$ formed in the first-step association. In the ion triplet where the electrostatic repulsion is inevitable between the two anions, the C_3 association mode should be much more favored than in the ion pair, since the electrostatic repulsion is the least when the two anions approach the complex cation along the C_3 axis from the opposite side. Consequently, the relative fraction of the C_3 mode will be increased and thus the discrimination efficiency will be greatly improved, when RPIPC is applied to the tervalent complex cations for which both of the C_3 and C_2 modes are possible. In fact, the α value of the divalent complex $[Co(gly)(en)_2]^{2+}$ for which the two modes are similarly possible, is not appreciably improved in RPIPC (Table 4). This is because the electric charge of $[Co(gly)(en)_2]^{2+}$ has been completely neutralized in the first-step association and thus the ion triplet is not formed even in RPIPC.

It should be noted here that the α value of $[Co(sen)]^{3+}$ is greatly improved in RPIPC, though both of the two ion-pairing anions cannot adopt the C_3 mode in the ion triplet $[Co(sen)][Sb_2(d\text{-tart})_2]_2^-$ owing to the steric demand of $[Co(sen)]^{3+}$ (Fig. 1). It is certain that the C_3 mode favors the Λ-enantiomer, while the C_2 mode favors the Δ-enantiomer for $[Co(sen)]^{3+}$ like for $[Co(en)_3]^{3+}$, as far as the first-step association is concerned.[17] In the ion triplet of $[Co(sen)]^{3+}$, however, both the C_3 and the C_2 modes favor the Λ-enantiomer, since the chiral ion-pairing anion adopting the C_2 mode is disposed so as to escape the electrostatic repulsion from the other ion-pairing anion adopting the C_3 mode, imposing a severe steric repulsion stereoselectively on the alkyl cap of the Δ-enantiomer.[17b] As a result, an improved α value is also expected for $[Co(sen)]^{3+}$ in RPIPC, though one chiral anion adopts the C_3 mode and the other anion adopts the C_2 mode in the ion triplet $[Co(sen)][Sb_2(d\text{-tart})_2]_2^-$.

For those complexes which adopt either the C_3 or the C_2 mode only, on the other hand, no appreciable improvement in α is expected,[27] since the relative fraction of the C_3 or the C_2 mode adopted by them is always unity even if the ion triplet is formed in RPIPC. The above interpretations are highly speculative, but they seem quite attractive.

References

1) Part XIII of this series: H. Yoneda, T. Yukimoto, Y. Kushi, and H. Nakazawa, *J. Liq. Chromatogr.*, **9**, 573 (1986).

2) S. Izumoto, U. Sakaguchi, and H. Yoneda, *Bull. Chem. Soc. Jpn.*, **56**, 1646 (1983).

3) a) H. Yoneda, *J. Chromatogr.*, **313**, 59 (1984); b) Y.

Yoshikawa and K. Yamasaki, *Coord. Chem. Rev.*, **28**, 205 (1979).

4) For example, D. A. Buckingham, C. R. Clark, M. M. Deva, and R. F. Tasker, *Inorg. Chem.*, **22**, 2754 (1984); C. Horvath, W. Melander, I. Molnar, and P. Molnar, *Anal. Chem.*, **49**, 2295 (1977).

5) J. B. Work, *Inorg. Synth.*, **2**, 221 (1946).

6) J. C. Bailar, Jr. and J. B. Work, *J. Am. Chem. Soc.*, **68**, 232 (1946).

7) J. E. Sarneski and F. L. Urbach, *J. Am. Chem. Soc.*, **93**, 884 (1971); K. Tomioka, U. Sakaguchi, and H. Yoneda, *Inorg. Chem.*, **23**, 2865 (1984).

8) J. MacB. Harrowfield, A. J. Herlt, and A. M. Sargeson, *Inorg. Synth.*, **20**, 85 (1980); I. I. Creaser, R. J. Geue, J. MacB. Harrowfield, A. J. Herlt, A. M. Sargeson, M. R. Snow, and J. Springborg, *J. Am. Chem. Soc.*, **104**, 6016 (1982).

9) S. E. Harnung, B. S. Sørensen, I. I. Creaser, H. Maegaard, U. Pfenninger, and C. E. Schäffer, *Inorg. Chem.*, **15**, 2123 (1976).

10) R. J. Geue, T. W. Hambley, J. M. Harrowfield, A. M. Sargeson, and M. R. Snow, *J. Am. Chem. Soc.*, **106**, 5478 (1984).

11) C. T. Liu and B. E. Douglas, *Inorg. Chem.*, **3**, 1356 (1964).

12) F. P. Dwyer, E. Gyarfas, and D. Mellor, *J. Phys. Chem.*, **59**, 296 (1955).

13) G. Schlessinger, *Inorg. Synth.*, **12**, 267 (1970).

14) M. Fujita, Y. Yoshikawa, and H. Yamatera, *J. Chem. Soc., Chem. Commun.*, **1975**, 941; *idem, Chem. Lett.*, **1982**, 437.

15) Somewhat large differences between previously reported[3a] and present results are unfortunately due to excessive contamination of diverse salts in the ion-pairing reagents used previously, and partly due to different experimental conditions chosen.

16) U. Sakaguchi, A. Tsuge, and H. Yoneda, *Inorg. Chem.*, **22**, 3745 (1983).

17) a) K. Miyoshi, S. Izumoto, and H. Yoneda, *Bull. Chem. Soc. Jpn.*, **59**, 3475 (1986); b) K. Miyoshi, S. Izumoto, K. Nakai, and H. Yoneda, *Inorg. Chem.*, **25**, 4654 (1986).

18) H. Nakazawa, C. E. Oh, K. Miyoshi, and H. Yoneda, *Bull. Chem. Soc. Jpn.*, **53**, 273 (1980).

19) In other words, these tervalent complex cations are distributed to the stationary phase in the form of $M[Co(N)_6][Sb_2(d\text{-tart})_2]_2$ which carries no net electric charge. Therefore, the retention of the complex cation $[Co(N)_6]^{3+}$ should be directly affected by the nature of the counter ion M^+, as is actually the case.

20) Greater retention volumes obtained for $[Co(sep)]^{3+}$ than for $[Co(en)_3]^{3+}$ are attributed not only to the greater hydrophobic nature of the former complex, but also to its greater hydrogen-bonding ability to the ion-pairing reagent. See, Refs. 16 and 23.

21) H. Nakazawa and H. Yoneda, *J. Chromatogr.*, **160**, 89 (1978).

22) A glance of Fig. 3-c might indicate that the α value is not appreciably increased for $[Co(tn)_3]^{3+}$ with $M^+=Me_4N^+$ or Et_4N^+. However, the optical resolution efficiency of this complex is actually improved to a considerable extent in RPIPC, since NPIEC gives a separation factor of 1.00 for this complex. See, Table 3.

23) U. Sakaguchi, S. Tamaki, K. Tomioka, and H. Yoneda, *Inorg. Chem.*, **24**, 1624 (1985).

24) K. Matsumoto, H. Kawaguchi, H. Kuroya, and S. Kawaguchi, *Bull. Chem. Soc. Jpn.*, **46**, 2424 (1973).

25) For example, Y. Nakayama, K. Matsumoto, S. Ooi, and H. Kuroya, *Bull. Chem. Soc. Jpn.*, **50**, 2304 (1977); K. Matsumoto, S. Ooi, H. Kuroya, M. Nakano, and S. Kawaguchi, *ibid.*, **55**, 1840 (1982); Y. Kushi, M. Kuramoto, S. Utsuno, and H. Yoneda, *ibid.*, **56**, 2742 (1983).

26) S. Izumoto, Y. Kushi, and H. Yoneda, 35th Symposium on Coordination Chemistry, Hiroshima, October 1985, Abstr. No. 2PB05.

27) For *lel*$_3$-$[Co(chxn)_4]^{3+}$ which adopts the C_3 mode only, a somewhat higher α is obtained in RPIPC than in NPIEC. This is what is expected, because the two C_3 modes in the ion triplet contribute additively to the chiral discrimination with some inevitable electrostatic repulsion between them in RPIPC, while only one C_3 mode contributes in NPIEC. Similar additive contribution of the two association modes is expected more or less for other $[Co(N)_6]^{3+}$-type complexes in RPIPC.

28) Why the C_2 association mode favors the Λ-enantiomer but not the Δ-enantiomer for the cage complexes, has been discussed in detail in Ref. 17b.

Synthesis, and Crystal and Molecular Structure of Bis[2-(2-benzoxazolyl)-phenolato]nitratoiron(III), $Fe(C_{13}H_8O_2N)_2(NO_3)$

Akiko FURUHASHI,* Tomoko INAYOSHI, and Akira OUCHI†
Department of Chemistry, Aoyama Gakuin University, Morinosato-Aoyama, Atsugi, Kanagawa 243-01
†Department of Chemistry, College of Arts and Sciences, The University of Tokyo, Komaba, Meguro-ku, Tokyo 153
(Received March 17, 1987)

The title complex was newly synthesized and its crystal and molecular structure was determined by the single-crystal X-ray diffraction technique. The crystal is monoclinic, space group $C2/c$, a=16.005(4), b=10.520(2), c=15.338(4) Å, β=114.68(2)°, and Z=4. In the complex, the central metal atom is hexa-coordinated being in a deformed octahedral geometry: Two 2-(2-benzoxazolyl)phenolato ligands form six-membered chelate rings being coordinated with their oxazolyl nitrogen and phenolato oxygen atoms, while the nitrate ion acts as a bidentate with its two oxygen atoms. As the benzoxazolyl ring is parallel and overlapped with that of the neighboring complex along the c-axis, where the interplane distance is 3.557 Å, some interaction between the rings is expected. As this complex in solid state is deep violet, almost black, in color, some charge-transfer bands are expected to exist in its electronic spectra. The bis[2-(2-benzothiazolyl)phenolato]-nitratoiron(III) was found to be isomorphous to the title complex.

The 2-(2-benzoxazolyl)phenol (Hbxp) is known as a chelating reagent for many bivalent metals. Analyses of zinc(II), cadmium(II), palladium(II), and copper(II) using Hbxp as the colorimetric reagent, have been reported in several literatures.[1-4] The crystal structures of copper(II) and cadmium(II) salts of Hbxp ($M(bxp)_2$, M=Cu, Cd) were already determined by the single-crystal X-ray diffraction method.[5] The 2-(2-benzothiazolyl)phenol (Hbtp) is also a good analytical reagent which forms stable complexes with bivalent metals. An analytical chemistry study of its metal complexes had been presented by Charles and Freiser[6] and the authors have investigated the solvent-extraction of some metals using Hbtp.[7]

However, there have been yet very few studies about the tervalent metal complexes of bxp and btp, nor any reports of their structure.

This time, we could obtain the iron(III) salts of both Hbxp and Hbtp, $Fe(bxp)_2(NO_3)$ (**1**) and $Fe(btp)_2(NO_3)$ (**2**), though the FeL_3 type complex was not obtained. Both salts resemble each other in color (deep violet, almost black), in their solubilities in various solvents, as well as in their crystal forms. As **1** and **2** were found to be isomorphous, the crystal and molecular structure of **1** was determined by the single-crystal X-ray diffraction technique.

Experimental

Synthesis of Bis[2-(2-benzoxazolyl)phenolato]nitratoiron-(III) (1). The solutions of iron(III) nitrate enneahydrate (0.81 g, 2.0 mmol in 30 cm^3 of ethanol), and of Hbxp (1.69 g, 8 mmol in 200 cm^3 of ethanol) were mixed and stirred. After left standing the mixed solution overnight, the precipitate was filtered off, washed with a small portion of ethanol, and dried in vacuo over silica gel. Yield, 0.54 g (50%). Found; Fe, 10.44; C, 58.09; H, 2.99; N, 7.78%. Calcd for ($FeC_{26}H_{16}O_7N_3$); Fe, 10.38; C, 58.02; H, 3.00; N, 7.81%.

Synthesis of Bis[2-(2-benzothiazolyl)phenolato]nitratoiron-(III) (2). The solutions of iron(III) nitrate enneahydrate (0.81 g, 2.0 mmol in 30 cm^3 of ethanol), and of Hbtp (1.82 g, 8 mmol in 300 cm^3 of hot ethanol) were mixed and stirred. The product began to precipitate soon, and the reaction was completed in several hours. The product was filtered off, washed with ethanol, and dried in vacuo over silica gel. Yield, 0.65 g (57%). Found; Fe, 9.63; C, 54.75; H, 2.87; N, 7.40; S, 11.22%. Calcd for ($FeC_{26}H_{16}O_5N_3S_2$); Fe, 9.79; C, 54.75; H, 2.83; N, 7.37; S, 11.24%.

The recrystallization of the products have been unsuccessful so far. From the solution of the complex in the solvents such as chloroform, ethanol, and others, only decomposition products were obtained when a part of the solvent was evaporated off.

Single-Crystal X-Ray Analysis. A crystal of **1** used for the X-ray analysis was chosen from the synthesized product. The crystallographic data and some experimental conditions used to obtain the intensity data are tabulated in Table 1. The reflections were collected on a Rigaku AFC-6A automated four-circle X-ray diffractometer with graphite monochromated Mo $K\alpha$ radiation (λ=0.71073 Å) (scan speed: 4° $min^{-1}(\theta)$) using the ω—2θ scan technique.

Structure Determination. The structure of the complex

Table 1. Crystallographic Data and Some Experimental Conditions

Chemical Formula:	$FeC_{26}H_{16}O_7N_3$	F. W. 538.28	
Monoclinic		Space group:	$C2/c$
a(l/Å)	16.005(4)	(ϕ/°)	114.68(2)
b(l/Å)	10.520(2)	U(v/Å^3)	2346.6(11)
c(l/Å)	15.338(4)	Z	4
D_m(d/Mg m^{-3})	1.50(3)	D_x(d/Mg m^{-3})	1.52
μ(Mo $K\alpha$)(n/mm^{-1})	0.718	Final R value	0.070
Reflections measured		2208	
Reflections used for calculation[a]		1038	
Used crystal (v/mm^3)		0.22×0.27×0.15	
Scan width (θ/°)		1.04+0.5 tan θ	
Scanned range (2θ/°)		3—50	

a) Reflections with $|F_o|>3\sigma(|F_o|)$ were used.

was solved by the heavy-atom method. The positions of the iron and some nitrogen and oxygen atoms were deduced from a three dimensional Patterson map, and the other non-hydrogen atoms were successively located by the repeated Fourier syntheses. Their positional, isotropic and then anisotropic thermal parameters were refined by a block-diagonal least-squares method. At the final cycle of the refinement with anisotropic temperature factors for all non-hydrogen atoms, all the parameter shifts were less than one-third of the corresponding standard deviations.

All the calculations were carried out on a HITAC-680H at the Computer Center of the University of Tokyo, using a local version of the UNICS program.[8] The atomic scattering factors were taken from Ref. 9.

Other Measurements. The X-ray powder patterns of the complexes were obtained by a diffractometer of Model DX-GO-F JEOL, using Cu $K\alpha$ radiation in the range of 4° to 35° in 2θ. Infrared spectra were measured with a JASCO IRA-1 type infrared spectrophotometer using KBr disk technique. The electronic spectra in chloroform solutions (immediately after dissolving the complexes) were obtained with a Shimadzu UV-240 spectrophotometer. Magnetic moments of the complexes were measured using a Gouy balance at ambient temperature.

Results and Discussion

The final atomic parameters and their equivalent thermal parameters of the complex are listed in Table 2, while the bond lengths and bond angles are tabulated in Table 3.[10] A perspective drawing of the complex around the metal atom including the overlapping benzoxazole ring of the neighboring complex are shown in Fig. 1, while the projection of a unit cell to the ac-plane in Fig. 2.

The central metal atom, as well as the N(N) and

Table 2. Final Atomic Coordinates ($\times 10^4$) with Estimated Standard Deviations in Parentheses, and Their Equivalent Isotropic Temperature Factors (B_{eq}/Å^2)

Atom	x	y	z	B_{eq}/Å^2 b)
Fe	5000	6450.8(19)	2500	4.2$_8$
N(N)	5000	8898(11)	2500	6.5$_8$
O(N1)	5000	10038(10)	2500	10.8$_4$
O(N2)	4323(4)	8231(6)	2465(4)	6.1$_2$
N(1)	5438(4)	6417(7)	3984(4)	4.0$_7$
O(1)	6416(4)	6277(5)	5515(3)	5.2$_6$
O(2)	6070(3)	5530(5)	2709(4)	5.0$_7$
C(1)	4958(5)	6686(8)	4545(5)	4.6$_9$
C(2)	5573(6)	6619(8)	5487(6)	5.3$_0$
C(3)	5350(7)	6805(8)	6270(6)	7.7$_1$
C(4)	4434(7)	7145(10)	6000(7)	8.5$_0$
C(5)	3778(7)	7193(9)	5033(7)	7.5$_4$
C(6)	4033(6)	6993(8)	4284(7)	6.5$_0$
C(7)	6286(5)	6182(7)	4589(5)	4.3$_4$
C(8)	7051(5)	5838(7)	4372(5)	3.9$_4$
C(9)	6919(5)	5542(8)	3441(5)	4.7$_3$
C(10)	7652(5)	5224(9)	3209(7)	6.0$_1$
C(11)	8535(6)	5218(9)	3968(7)	6.4$_0$
C(12)	8678(6)	5482(8)	4915(7)	6.0$_5$
C(13)	7936(5)	5803(8)	5144(6)	5.1$_3$

b) The equivalent isotropic temperature factors were computed using the following equation:

$B_{eq}=4/3(B_{11}a^2+B_{22}b^2+B_{33}c^2+B_{13}ac\cos\beta)$.

The B_{ij}'s are defined by:

$T=\exp[-(h^2B_{11}+k^2B_{22}+l^2B_{33}+2klB_{23}+2hlB_{13}+2hkB_{12})]$.

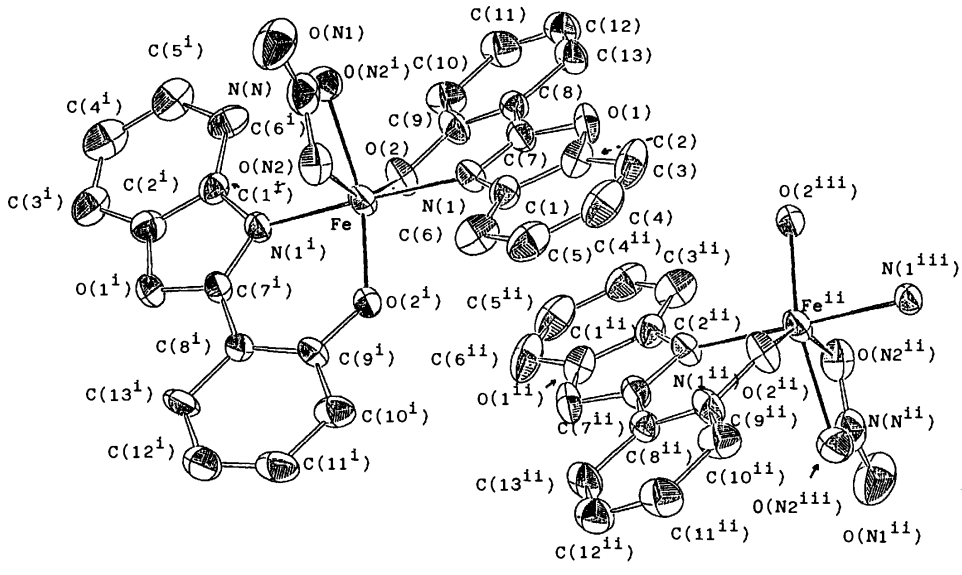

Fig. 1. A perspective drawing of a complex molecule together with the overlapping benzoxazole ring of the neighboring complex; the numbering scheme of the atoms is also shown.[11]

Table 3. Bond Lengths and Bond Angles of the Complex

Bond length	(l/Å)	Bond length	(l/Å)
Fe-O(N2)	2.154(7)	Fe-N(1)	2.084(12)
Fe-O(2)	1.875(6)	N(N)-O(N1)	1.199(15)
N(N)-O(N2)	1.273(11)	N(1)-C(1)	1.402(18)
O(2)-C(9)	1.354(10)	N(1)-C(7)	1.308(9)
O(1)-C(2)	1.379(13)	O(1)-C(7)	1.351(17)
C(1)-C(2)	1.369(16)	C(2)-C(3)	1.40(2)
C(3)-C(4)	1.392(16)	C(4)-C(5)	1.42(2)
C(5)-C(6)	1.39(2)	C(1)-C(6)	1.400(13)
C(7)-C(8)	1.441(16)	C(8)-C(9)	1.39(2)
C(9)-C(10)	1.401(18)	C(10)-C(11)	1.406(13)
C(11)-C(12)	1.40(2)	C(12)-C(13)	1.414(18)
C(13)-C(8)	1.417(11)		
Bond angle	**(ϕ/°)**	**Bond angle**	**(ϕ/°)**
N(1)-Fe-N(1^i)	178.1(5)	N(1)-Fe-O(N2)	88.8(4)
N(1)-Fe-O($N2^i$)	92.9(4)	N(1)-Fe-O(2)	86.4(4)
N(1)-Fe-O(2^i)	92.6(4)	O(N2)-Fe-O(2)	150.2(3)
O(N2)-Fe-O($N2^i$)	59.1(2)	O(N2)-Fe-O(2^i)	91.8(2)
O(2)-Fe-O(2^i)	117.8(3)	Fe-O(N2)-N(N)	93.9(5)
O(N2)-N(N)-O($N2^i$)	113.2(9)	O(N2)-N(N)-O(N1)	123.4(8)
Fe-N(1)-C(1)	130.3(7)	Fe-N(1)-C(7)	123.7(8)
N(1)-C(7)-O(1)	113.0(10)	C(2)-O(1)-C(7)	105.5(8)
O(1)-C(2)-C(1)	108.1(12)	N(1)-C(1)-C(2)	107.5(9)
N(1)-C(1)-C(6)	131.0(11)	O(1)-C(2)-C(3)	127.2(11)
N(1)-C(7)-C(8)	127.8(12)	C(6)-C(1)-C(2)	121.5(12)
C(1)-C(2)-C(3)	124.6(11)	C(2)-C(3)-C(4)	113.3(12)
C(3)-C(4)-C(5)	123.4(16)	C(4)-C(5)-C(6)	121.1(12)
C(5)-C(6-)C(1)	116.1(12)	O(1)-C(7)-C(8)	119.2(8)
C(7)-C(8)-C(9)	121.0(9)	C(7)-C(8)-C(13)	117.6(11)
C(13)-C(8)-C(9)	121.5(10)	C(8)-C(9)-C(10)	122.1(10)
C(9)-C(10)-C(11)	116.8(13)	C(10)-C(11)-C(12)	112.0(12)
C(11)-C(12)-C(13)	121.0(11)	C(12)-C(13)-C(8)	116.7(12)
Fe-O(2)-C(9)	131.7(7)	O(2)-C(9)-C(8)	121.6(10)
O(2)-C(9)-C(10)	116.4(12)		

Key to the symmetry operations: i, $1-x$, y, $0.5-z$.

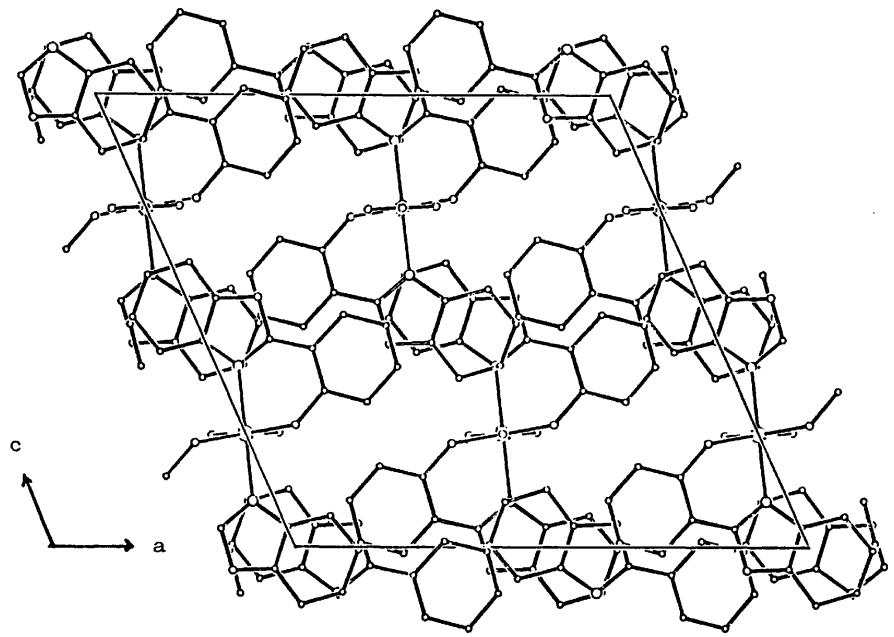

Fig. 2. A projection of the unit cell to the ac-plane.

O(N1) atoms of the nitrate ion are at the respective special positions: 0.5, y, 0.25. The metal atom is 2*N*4*O*-hexa-coordinated being in a deformed octahedral geometry. From both ends of an axis, two oxazole nitrogen atoms of the respective ligands, N(1) and N(1^{i})[11] are ligated. On the equatorial plane, two oxygen atoms of the phenolato groups of the ligands, O(2) and O(2^{i})[11], as well as two nitrato oxygen atoms of an ion O(N2) and O(N2^{i})[11] are coordinated to the metal atom. The oxazolyl oxygen atom, O(1), is not ligated to the metal atom. Thus the bxp anion forms a six-membered chelate ring, while the nitrate ion makes a four-membered ring.

The least-squares plane of O(2), O(2^{i}), O(N2), O(N2^{i}), and Fe atoms[12] (average of the positional deviations of the atoms from the plane is 0.070 Å) is approximately perpendicular to Fe–N(1) (88.4°), and the angle N(1)–Fe–N(1^{i}) is 178.1(5)°. However, on the equatorial plane, the angles O(2)–Fe–O(2^{i}) and O(N2)–Fe–O(N2^{i}) are 117.8(2), and 59.1(2)°, respectively: They deviate greatly from the right angle. The bond lengths Fe–N(1) and Fe–O(2) are 2.084(12) and 1.875 Å, respectively. As the sum of Shannon's ionic radii[13] are Fe–N, 2.11 and Fe–O, 2.00 Å, both of the observed values are shorter than the expected values. On the other hand, as Fe–O(N2) was found to be 2.154(7) Å, which is much longer than the sum of the ionic radii, the bond is thought to be weak. The two such weakly bonding oxygen atoms, O(N2) and O(N2^{i}), are regarded as cooperating with each other and occupying one equatorial position of the trigonal-bipyramidal penta-coordination geometry.

The benzoxazole ring (A), the phenyl ring of the phenolato group (B), and the six-membered chelate ring (C) are about on the respective planes. The average deviations of the atoms from the respective ring planes are: (A) 0.011; (B) 0.011; and (C) 0.113 Å. The dihedral angles between the planes are: (A–B) 9.22; (A–C) 7.45; (B–C) 10.79°. As shown in Table 3, all the bond lengths of C–C, C–N, and C–O in the ligand bxp, including C(9)–O(2), are intermediate of the single and double bonding ones (according to Pauling's presentation; the single bonding and double bonding C–C, C–N, and C–O are: 1.544 and 1.334; 1.47 and 1.29; and 1.51 and 1.29° Å respectively[14]). Almost all C–C–C bond angles of the phenylene and phenyl rings of the ligand are about 120°. The angles of C(1)–C(6)–C(5) and C(2)–C(3)–C(4) are a little smaller, but these deviations were also found in those of the free ligand.[15] Consequently, the conjugated double bond system is likely extended all over the bxp ligand, probably including the chelate ring, too. The N(N)–O(N1) and N(N)–O(N2) lengths of the nitrate ion are 1.199(15) and 1.273(11) Å, respectively. Therefore, the N=O double bonding is a little localized in the former bond, although both of them are shorter than the single bonding N–O expected from the sum of the covalent bonding radii.[14]

As shown in Fig. 2, the benzoxazole ring of the ligand is parallel and overlapped with the ring of the complex molecule next to the c-axis direction, although its phenylene ring side of the overlapping ligand is above the oxazole side of the original ligand ring, and vice versa. The interplane distance of both ring planes is 3.557 Å. As the thickness of an aromatic ring is about 3.5 Å, these rings are likely in contact with each other. Therefore, some interaction, such as charge transfer, is expected to occur between them. Although there are no coordination bridgings between the complexes, they are thought to be connected in this way, and they are laid in the c-axis direction. As shown in Fig. 2, there is no overlapping of the ligands in the part of the phenolato group as well as the chelate ring; the interatomic distances between the carbon atoms of these parts and of the neighboring ligand are more than 3.5 Å. The central matl parts are lined along the a-axis, although no ligand bridgings exist between them. The barrier of the nonpolar ligand skeleton part is intercalated between the lines of the metal part; thus in the crystal, the polar part and nonpolar part (both of them are parallel to the ab plane) appear alternately.

As shown in Table 2, the equivalent isotropic temperature factor of O(N1) is relatively large. This is probably due to the fact that no atoms approach near to the atom in the crystal: There is a vacancy near the atom, and the atom is not tightly fixed.

As there was no good crystal of the btp complex, **2** to use for X-ray analysis, the single-crystal study has not yet been completed on **2**. But as the powder X-ray pattern of **1** and **2** closely resemble each other, a similar type of structure is expected for the complex **2**.

In their IR spectra, the peaks observed at 1634 cm^{-1} for Hbxp and 1625 cm^{-1} for Hbtp are lowered on chelation to 1612 and 1598 cm^{-1}, respectively. These bands are assigned to the C=N stretching vibration primarily.[16-17] These facts indicate that the coordination takes place through the unsaturated nitrogen atom on the oxazole or thiazole ring. The peaks at 1532, 1318, and 1015 cm^{-1} in the bxp complex and at 1522, 1300, and 1010 cm^{-1} in the btp complex are regarded as the bands of the bidentate nitrate ion. In general, the separation of the two highest frequency bands for the bidentate nitrato complex appears in the range 350—200 cm^{-1},[18] and the separations in **1** and **2** spectra are found to be 214 and 222 cm^{-1} respectively.

The maximum wavenumberes of electronic absorption spectra together with the absorption coefficients (in log ε) of their chloroform solutions are shown in Table 4.

The strong violet color may be caused by a charge-transfer band at 18600 cm^{-1} for the bxp complex and at 18200 cm^{-1} for the btp complex which may occur between very closely overlapped aromatic or pseudo-

Table 4. The Maximum Peak Wavenumbers ($\bar{\nu}$/cm^{-1}) of the Complexes and of the Ligands; Their Absorption Coefficients, log ε, in Parentheses (ε/dm^3 cm^{-1} mol^{-1})

Hbxp	42000 (2.90)	38200 (sh) (3.06)	36600 (3.12)		34100 (3.30)	31300 (3.25)	30100 (3.20)			
$Fe(bxp)_2NO_3$	41300 (4.38)		36400 (4.43)	35000 (4.54)	34100 (4.56)		30100 (4.39)	27800 (sh) (4.13)	23300 (sh) (3.46)	18600 (3.59)
Hbtp	41700 (4.03)	38600 (3.89)		34720 (4.18)	33300 (sh) (4.08)		29900 (4.26)	28900 (sh) (4.21)		
$Fe(btp)_2NO_3$		38800 (4.30)	36000 (sh) (4.45)	34800 (4.50)	33300 (sh) (4.42)		30000 (4.54)	29000 (sh) (4.50)		18200 (3.31)

sh: shoulder.

aromatic rings.[19] Such strong CT bands are also recognized in the salts of tetrahalogenoferate(III) with 3,5-dialkyl-1,2-dithiolium cation.[20,21]

When the violet color solutions of both bxp and btp complexes were left standing for several hours, the color faded away gradually and a brown precipitate was formed.

Magnetic moments were 6.11 BM for the bxp complex and 6.10 BM for the btp complex. Although these values are a little higher than those of the common Fe(III) complexes, there are some other complexes with such high values.[22]

References

1) Y. Horiuchi and T. Kawamoto, *Bunseki Kagaku*, **18**, 329 (1969).

2) J. L. Walter and H. Freiser, *Anal. Chem.*, **24**, 984 (1952).

3) R. F. Wilson and L. J. Baye, *Z. Anal. Chem.*, **166**, 359 (1959).

4) E. E. Byrn and J. H. Robertson, *Anal. Chem.*, **26**, 1605 (1954).

5) P. Stenson, *Acta Chem. Scand.*, **23**, 1514 (1969).

6) R. G. Charles and H. Freiser, *Anal. Chim. Acta*, **11**, 1 (1954).

7) K. Shimizu and A. Furuhashi, *Bull. Chem. Soc. Jpn.*, **57**, 3593 (1984).

8) "Universal Crystallographic Computation Program System (UNICS)," ed by T. Sakurai, Crystallographic Society of Japan, Tokyo (1967).

9) "International Tables for X-Ray Crystallography," Kynoch Press, Birmingham (1974), Vol. IV, pp. 72, 150.

10) The final anisotropic thermal parameters, and the F_o-F_c table are deposited as Document No. 8753 at the Office of the Editor of Bull. Chem. Soc. Jpn.

11) Key to the symmetry operations: i, 1−x, y, 0.5−z; ii, 1−x, 1−y, 1−x; iii, x, 1−y, 0.5+z.

12) The least-squares plane at the deviation of atoms (l/Å) are as follows.

$$0.1310X - 0.0089Y - 0.9913Z + 2.6808 = 0$$

O(2), 0.0956; O(2^i), −0.0678; O(N2), 0.0795; O(N2^i), −0.1022; Fe, 0.0053,

where

$$\begin{pmatrix} X \\ Y \\ Z \end{pmatrix} = \begin{pmatrix} a & b\cos\gamma & c\cos\beta \\ 0 & b\sin\gamma & -c\cos\alpha^*\sin\beta \\ 0 & 0 & c\cos\alpha^*\sin\beta \end{pmatrix} \begin{pmatrix} x \\ y \\ z \end{pmatrix}.$$

Key to symmetry operation: i, 1−x, y, 0.5−z.

13) R. D. Shannon, *Acta Crystallogr., Sect. A*, **32**, 751 (1976). (Fe(High spin, Coordination Number(CN)=6, Valence=3+), 0.645; N(CN=4, Valence=3−), 1.46; O(CN=2, Valence=2−), 1.35 Å)

14) L. Pauling, "The Nature of the Chemical Bonds," 3rd ed, Cornell Univ. Press, N. Y. (1960), pp. 246, 247.

15) P. Stenson, *Acta Chem. Scand.*, **24**, 3729 (1970).

16) T. J. Lane, I. Nakagawa, J. L. Walter, and A. J. Kandathil, *Inorg. Chem.*, **1**, 267 (1962).

17) M. M. Cordes and J. L. Walter, *Spectrochim. Acta, Part A*, **24**, 1421 (1968).

18) C. C. Addison, N. Logan, and S. C. Wallwork, *Quart. Rev., Chem. Soc.*, **25**, 289 (1971).

19) R. L. Martin and A. H. White, *Inorg. Chem.*, **3**, 1368 (1964).

20) A. Furuhashi, K. Watanuki, and A. Ouchi, *Bull. Chem. Soc. Jpn.*, **41**, 110 (1968).

21) A. Furuhashi, K. Watanuki, and A. Ouchi, *Bull. Chem. Soc. Jpn.*, **45**, 2942 (1972).

22) "Landolt-Börnstein," New Series, II/2, ed by K. H. Hellwege and A. M. Hellewege, Springer-Verlag, Berlin, Heidelberg, N. Y. (1966), pp. 121, 129.

 © 1987 The Chemical Society of Japan Bull. Chem. Soc. Jpn., 60, 3213—3217 (1987)

Optical and ESR Spectra for High-Spin Tetrahedral Complexes of Co(III) and Co(II) in Keggin-Structure Heteropolytungstate

Kazuo KOJIMA, Jiro MATSUDA,* Norimichi KOJIMA,† Toshiro BAN,† and Ikuji TSUJIKAWA†
Department of Chemistry, Faculty of Science and Engineering, Ritsumeikan University, Kita-ku, Kyoto 603
†Department of Chemistry, Faculty of Science, Kyoto University, Sakyo-ku, Kyoto 606
(Received March 17, 1987)

The ligand-field spectra for the cobalt complexes in the single crystals of $K_3H_2[Co^{III}W_{12}O_{40}]\cdot 16H_2O$ and $K_4H_2[(Co^{II}, Zn^{II})W_{12}O_{40}]\cdot nH_2O$ have been observed at several temperatures above 1.4 K and assigned under D_2 site symmetry. In the spectrum of the elongated $Co^{III}O_4$ complex, two absorption bands of 8250 and 8953 cm^{-1} strengthen with increasing temperature by vibronic mechanism. The X-band ESR spectra of both complexes have also been measured at 77 K. The signal from the Co(III) complex is not observed. The signal of the high-spin Co(II) complex of tetrahedral symmetry is unequivocally observed even at relatively high temperature of 77 K. From the analysis of the ESR spectrum, it is concluded that the $Co^{II}O_4$ tetrahedron of D_2 symmetry is flattened and deviated slightly from axial symmetry.

The tetrahedral high-spin complexes of both Co(III) and Co(II) are known to exist in the heteropolyanions of Keggin type as $[Co^{III}W_{12}O_{40}]^{5-}$ and $[Co^{II}W_{12}O_{40}]^{6-}$, respectively. The high-spin complex of Co(III) ($3d^6$, $S=2$) is very few. Another example is found only in Co(III)-doped garnets.[1,2] The high-spin Co(II) complex ($3d^7$, $S=3/2$) is also interesting especially from the viewpoint of ESR study because ESR data of high-spin complexes are relatively few compared with those of low-spin complexes.[3-6] It would be of great interest, therefore, to study these Co(III) and Co(II) complexes by means of the optical and ESR spectra.

Concerning the low-temperature properties of these complexes, there have been some reports on the magnetic susceptibility of powder samples[7,8] and the brief report on the ESR frozen spectrum of the Co(II) complex.[9] In the previous paper,[10] we have first reported the single-crystal absorption spectra of the pure Co(III) and Co(II) complexes at 77 K.

Yanonni[11] has reported that the crystal of Co(III) complex belongs to hexagonal system ($P6_222$, $Z=3$) at room temperature and the tetrahedron of $Co^{III}O_4$ is elongated, having three pairs of oxygen-oxygen distance of 2.69, 3.20, and 3.31 Å. From these data, Simmons[7] has concluded that the symmetry of this tetrahedron is D_2 which is nearly S_4. Unfortunately, the exact orientation of the tetrahedron with respect to the crystal axes has not been shown in the reports.[11,12] The crystals of both complexes of Co(III) and Co(II) are known to be isomorphous, but the exact symmetry of the $Co^{II}O_4$ tetrahedron is unknown.

In this report, we will discuss the single-crystal optical spectra at various temperatures above 1.4 K and the ESR spectra at 77 K both of the pure Co(III) complex and of the pure and diluted Co(II) complexes in the potassium salts of the Keggin-structure heteropolyanions.

Experimental

The potassium salts were prepared and crystallized by the method in the literature.[10,13] For comparison, $(K,H)_5[Ga^{III}W_{12}O_{40}]\cdot mH_2O$[14] and $K_2\{(C_4H_9)_4N\}_4[Co^{II}W_{12}O_{40}]\cdot lCH_3CN$[15] were also crystallized from aqueous and CH_3CN solutions, respectively. Mixed crystal of Co(III) with Ga(III) could not be obtained.

For the spectroscopic measurements, a JASCO CT-100 grating spectrometer was used with a HTV-R376 photomultiplier for the visible range or with a HTV-P819 PbS detector in the near-infrared range. Photoelectric signals were amplified and converted into logarithmic scale. A Glan-Taylor prism served as a polarizer. The samples were immersed in liquid helium for measurements at 1.4 and 4.2 K. For measurements at higher temperatures, the method in the literature[16] was used. That is, the samples were placed in a glass vessel immersed in liquid helium, and cooled by exchange helium gas inserted into the vessel or heated with an electric heater on the copper sample holder. The temperatures were measured with a Ge resistor and a thermocouple of Chromel vs. Au-Fe.

X-Band ESR spectra were recorded on a JEOL-FE2XG spectrometer equipped with a liquid-nitrogen-insertion Dewar. DPPH served as a magnetic field calibrant.

Results and Discussion

Co(III) Complex. The spectra of the Co(III) complex are shown in Figs. 1—3 and listed in Table 1. The relative intensities among the Figures are not shown, but the spectra in Fig. 3 are very weak compared with those in Figs. 1 and 2, as reported in the previous paper.[10] In Fig. 1, the D-band is assigned, as described previously,[10] to the spin-forbidden transition of $^5A \rightarrow {}^3T_1$. This transition may gain intensity by mixing of the $^3T_1$ state with the nearby $^5T_2$ state. The actual intensity of the A-band is larger for $E//c$ than for $E\perp c$, but the reverse of that is found for the B- and C-bands. The B- and C-bands

Table 1. Observed Energies for $K_3H_2[Co^{III}W_{12}O_{40}]\cdot 16H_2O$ (in cm^{-1})

$E\perp c$	$E//c$
Visible (1.4 K)	
17753[a]	
17191	≈17600
15586	
	≈15300
14635	
	≈14200
14085	
Near-infrared (4.2 K)	
≈10000[a]	≈10000
≈9000[a]	
≈8250	8249.9
6579	6587.0
6371.0[a]	
	6361.9
(200 K)	
8953[b]	
6959[b]	

a) Shoulder. b) Unpolarized.

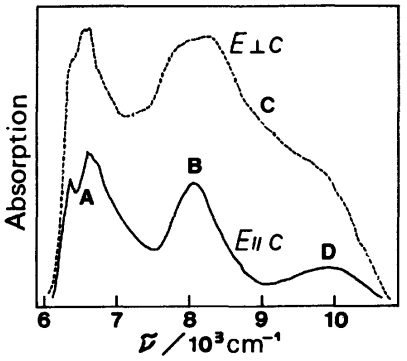

Fig. 1. Absorption spectra of the $^5E\rightarrow{}^5T_2$ transition of $K_3H_2[Co^{III}W_{12}O_{40}]\cdot 16H_2O$ at 4.2 K. E denotes the electric vector of the incident light. c denotes the crystal c-axis.

extremely strengthen with increasing temperature; the spectrum at 200 K becomes comparable to that of the complex soluted in CH_3CN (Fig. 2).

To interpret these spectra, the energy levels for Co(III) in the complex of D_2 site symmetry are considered (Fig. 4). The energy-level order in the ligand field of an elongated tetrahedron of S_4 symmetry ($^5E>{}^5B>{}^5A>{}^5B$) has been determined for yttrium iron garnet[17] and adopted for the interpretation of the spectrum of Co(III) in yttrium gallium garnet.[2] Simmons[7] has discussed the order of the magnitude for these energy levels in the ligand field of S_4 or D_2 symmetry. Defining the elongated axis of the $Co^{III}O_4$ tetrahedron as the z-axis and taking the z-axis parallel to the c-axis of the crystal, then, for electric

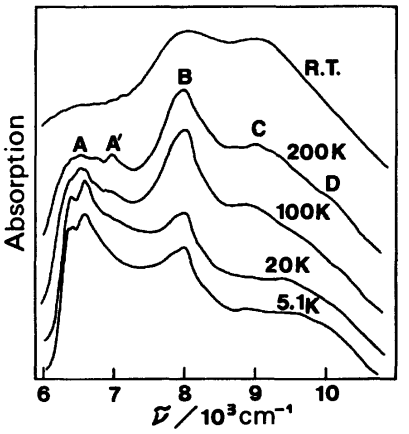

Fig. 2. Temperature dependence of the $^5E\rightarrow{}^5T_2$ transition of $K_3H_2[Co^{III}W_{12}O_{40}]\cdot 16H_2O$ (unpolarized). For comparison, the spectrum of $[Co^{III}W_{12}O_{40}]^{5-}$ in CH_3CN solution at room temperature is also shown uppermost. In aqueous solution, the spectrum is almost unchanged.

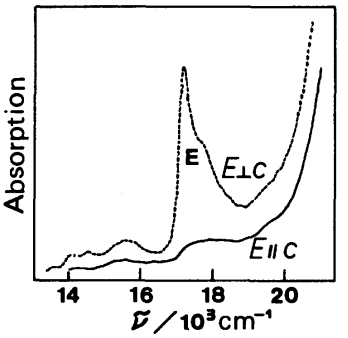

Fig. 3. Absorption spectra of the spin-forbidden transitions of $K_3H_2[Co^{III}W_{12}O_{40}]\cdot 16H_2O$ at 1.4 K. Note that the ordinate is enlarged compared with that in Fig. 1.

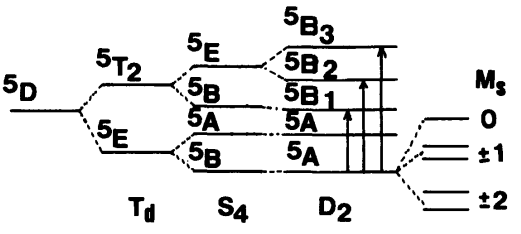

Fig. 4. Schematic energy levels of the ^5D state.

dipole radiation, the $^5A\rightarrow{}^5B_1$ transition is expected to be allowed in z-polarization ($E//c$) and the transitions of $^5A\rightarrow{}^5B_2$ and $^5A\rightarrow{}^5B_3$ allowed in y- and in x-polarization ($E\perp c$), respectively. Moreover, considering the contribution of a internal vibration of B_1-type either to the ground state or to each excited state, then the $^5A\rightarrow{}^5B_2$ and $^5A\rightarrow{}^5B_3$ transitions are allowed

vibronically also in x- and in y-polarization, respectively. Some vibrations of the $Co^{III}O_4$ tetrahedron have been reported.[18]

From these results, it seems most reasonable that the A-, B-, and C-bands are assigned as the $^5A \rightarrow {}^5B_1$, $^5A \rightarrow {}^5B_2$, and $^5A \rightarrow {}^5B_3$ transitions, respectively. The B-and C-bands may strengthen by the vibronic mechanism at higher temperatures. Note that the alternate interpretation of the $^5B_2$ and $^5B_3$ levels is possible in the present study.

The A-band is composed of the two peaks (6361.9, 6587.0 cm^{-1}) in the $E//c$ spectrum. There are two possibilities of the assignment of these peaks. One is that the lower-energy peak is the zero-phonon line of the $^5A \rightarrow {}^5B_1$ transition and the higher-energy peak is the one-phonon line, and the other is that the peaks are derived from the splitting of the $^5B_1$ state by the spin-orbit interaction

The A'-band which strengthens with increasing temperature may be a phonon band associated with the A-band.

The E-band in Fig. 3 which is very weak compared with the A- and B-bands as described in the previous paper[10] is allowed in the $E \perp c$ spectrum. The spectra at 4.2 K are almost the same as those at 1.4 K (not shown). This band has been assigned to the transitions to the $^3A_2$, $^3A_1$, and ^1E states only on the basis of the energy-level fitting in T_d symmetry.[10] However, the intensities of the spin-forbidden transitions to the $^3T_1$ and $^3T_2$ states will be larger than those to the $^3A_2$, $^3A_1$, and ^1E states because of the strong spin-orbit interaction between the $^5T_2$ state and the $^3T_1$ and $^3T_2$ states. Moreover, the positions of the $^3T_1$ and $^3T_2$ states can not be determined only from the energy-level fitting in T_d symmetry because of the splitting of these states in D_2 symmetry as observed in the $^5T_2$ state. Therefore, the E-band seems to be ascribed to the splitting components of the higher excited levels of $^3T_1$ and $^3T_2$ in T_d symmetry.

From the results described above, it is concluded that the spectra of the Co(III) complex are explained in the ligand field of the elongated tetrahedron of D_2 symmetry.

ESR signal from Co(III) is not observed at 77 K. The preliminary measurement at 5.5 K shows also no signal. Sturge et al.[2] have suggested that the ^5B ground state in S_4 symmetry would have the $M_s=\pm 2$ states the lowest. This holds also in D_2 symmetry (Fig. 4). In the Co(III)-doped garnets, Sturge et al.[2] have observed the forbidden transition of $\Delta M_s=4$ between the two states of $M_s=\pm 2$ using 24 GHz (K-band) and 56 GHz frequencies, but Chiba et al.[4] have not observed using $\approx$9.5 GHz (X-band). Therefore, the possible explanation for no signal observed from Co(III) in the present study is that the energy separation between the two states of $M_s=\pm 2$ is too large for X-band frequencies.

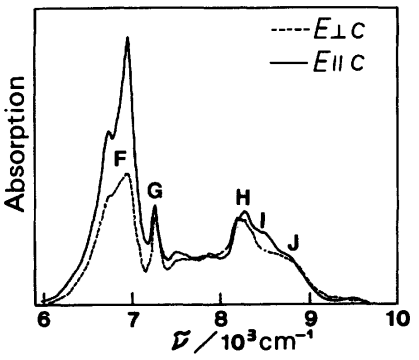

Fig. 5. Absorption spectra of the $^4A_2 \rightarrow {}^4T_1(F)$ transition of $K_4H_2[(Co^{II}, Zn^{II})W_{12}O_{40}]\cdot nH_2O$ at 4.2 K.

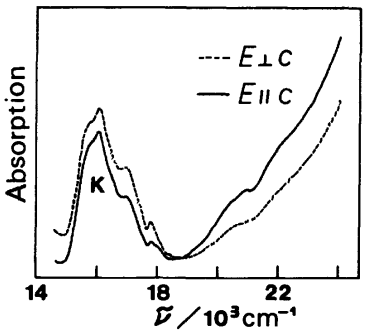

Fig. 6. Absorption spectra of the $^4A_2 \rightarrow {}^4T_1(P)$ transition of $K_4H_2[(Co^{II}, Zn^{II})W_{12}O_{40}]\cdot nH_2O$ at 1.4 K. Note that the ordinate is shortened compared with that in Fig. 5.

Co(II) Complex. The spectra are shown in Figs. 5 and 6 and listed in Table 2. The ESR spectra are shown in Fig. 7. The F-band in Fig. 5 is attributed to the vibrational band of the water of crystallization, because the corresponding band is also observed for $(K,H)_5[Ga^{III}W_{12}O_{40}]\cdot mH_2O$ but not observed for $K_2\{(C_4H_9)_4N\}_4[Co^{II}W_{12}O_{40}]\cdot lCH_3CN$.

As is found in Figs. 5 and 6, the crystal of Co(II) diluted with Zn(II) shows hardly any poralization anisotropy. Its ESR spectrum shows nonaxial symmetry with three effective g-values (a in Fig 7). The angular dependence is hardly found for $H//c$ or for $H \perp c$ (not shown). That is, ESR spectrum similar to a in Fig. 7 is always observed independent of the direction of magnetic field. Contrary to the mixed crystal, the significant angular dependence is observed in the preliminary ESR measurement for the single crystal of pure Co(II) complex. From these observations, the $Co^{II}O_4$ tetrahedron may have nonaxial symmetry and oriented fairly irregurally in the crystals doped with Zn(II).

By assuming D_2 symmetry as nonaxial symmetry of the $Co^{II}O_4$ tetrahedron, the splitting of energy levels could be shown in Fig. 8. On the basis of these energy

Table 2. Observed Energies for $K_4H_2[(Co^{II}, Zn^{II})W_{12}O_{40}]\cdot nH_2O$ (in cm^{-1})

	$E\perp c$	$E//c$
Visible (1.4 K)		
	22276	22222
		21692
	21645	
		20846
	20530	
		20358
	19720	
	19209[a]	
	18447	
	18278[a]	
		18041[a]
	17771	17784
	17473[a]	
	17229[a]	
	16938	16900
	16041	16021
	15788	15765[a]
	15596[a]	15535[a]
	15373[a]	15363[a]
	15216[a]	15207[a]
Near-infrared (4.2 K)		
	8809.8	8802.8
	8597.7	
		8503.4
	8280.9	8280.2
	8165.9	8165.3[a]
	7258.5	7250.6

a) Shoulder.

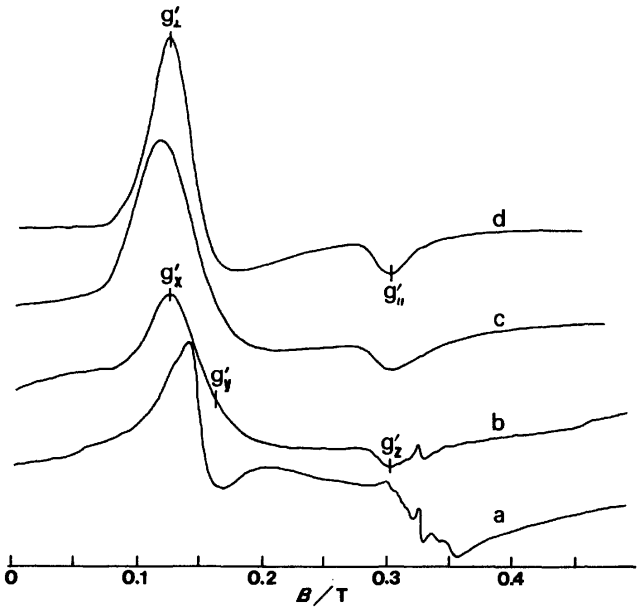

Fig. 7. ESR spectra of Co(II) complexes at 77 K. a: $K_4H_2[(Co^{II},Zn^{II})W_{12}O_{40}]\cdot nH_2O$ (single crystal), b: powder pattern of a, c: $K_4H_2[Co^{II}W_{12}O_{40}]\cdot 17H_2O$ (powder), d: $K_2\{(C_4H_9)_4N\}_4[Co^{II}W_{12}O_{40}]\cdot lCH_3CN$ (powder).

levels, the absorption bands in the $^4A_2\rightarrow{}^4T_1(F)$ region shown in Fig. 5 may be assigned to the transitions all of which are allowed for electric dipole radiation as follows: The G-band is due to the $^4B_1\rightarrow{}^4A$ transition, and the H-band is assigned to the lower branch splitted from the ^4E state in S_4 symmetry ($^4B_2$ or $^4B_3$) and the I- or J-shoulder to the upper branch ($^4B_2$ or $^4B_3$).

In Fig. 6, the spectral shape of the K-band which is mainly due to the $^4A_2\rightarrow{}^4T_1(P)$ transition is very similar to that of the solution spectrum.[10] In this visible region there may be many spin-forbidden transitions which gain intensity by interaction with spin-allowed bands, therefore, it is not possible to discuss the details of the K-band in the present study.

The ESR spectrum of the Zn-doped complex, $K_4H_2[(Co^{II},Zn^{II})W_{12}O_{40}]\cdot nH_2O$, shows a nonaxial pattern with $g'_x=5.20$, $g'_y=4.02$, and $g'_z=2.15$ (**b** in Fig. 7). On the other hand, the tetrabutylammonium salt of the pure Co(II) complex, $K_2\{(C_4H_9)_4N\}_4[Co^{II}W_{12}O_{40}]\cdot lCH_3CN$, shows an axial pattern with $g'_\perp=5.09$ and $g'_{//}=2.17$ (**d** in Fig 7). Similar spectrum with $g'_\perp=5.02$ and $g'_{//}=2.14$ is observed in the preliminary experiment at 5.5 K (not shown). It is interesting that the ESR spectrum of the high-spin Co(II) complex is unequivocally observed even at relatively high temperature of 77 K. It seems that the spin-lattice relaxation time of Co(II) in this complex is rather long. The powder pattern of the pure Co(II) complex in $K_4H_2[Co^{II}W_{12}O_{40}]\cdot 17H_2O$ crystallized from aqueous solution is intermediate between **b** and **d** (**c** in Fig. 7).

In the same manner as the halo complexes,[3,5] the resonances in Fig. 7 can be assigned as the transition between the lowest $M_s=\pm 1/2$ states (Fig. 8). By the method of Drulis et al.[5] using the g'_x, g'_y, and g'_z values observed, the parameters can be calculated in the spin Hamiltonian, $H=D\{S_z^2-1/3S(S+1)\}+E(S_x^2-S_y^2)+\beta(g_xS_xH_x+g_yS_yH_y+g_zS_zH_z)$, for the Zn-doped Co(II) complex (**b** in Fig. 7). On the assumption of $g_x=g_y=g_\perp$ and $g_z=g_{//}$, the parameters can be estimatd as follows: $g_\perp=2.32$, $g_{//}=2.20$, and $E/D=0.0858$. Similar result is obtained from the equations of Fukui et al.[6]

From the facts that $g_\perp$ is larger than $g_{//}$ and that the $M_s=\pm 1/2$ states may be the lowest, the $Co^{II}O_4$

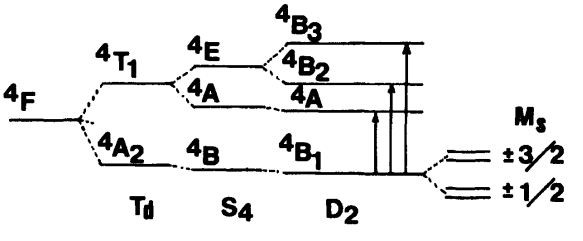

Fig. 8. Schematic energy levels of the ^4F state.

tetrahedron may be flattened.[5,19] This is in contrast with the $Co^{III}O_4$ tetrahedron described above. The nonaxiality parameter (E/D) of 0.0858 is one of the smallest among the reported values.[5,6] Therefore, the $Co^{II}O_4$ tetrahedron in the Zn-doped complex may be only slightly deviated from axial symmetry.

The $g_\perp$ and $g_{//}$ values give g_{eff}=2.28 and μ_{eff}=4.41. Simmons[7] has obtained the values of g_{eff}=2.20 and μ_{eff}=4.27—4.28 from the magnetic susceptibility.

From the equation of $g_{eff}=2.001-(8\lambda)/10D_q$, where D_q=460 cm^{-1},[10] the spin-orbit coupling constant λ is estimated to be $-160\ cm^{-1}$. The fact that the $|\lambda|$ value is smaller than the free-ion value of $178cm^{-1}$ is consistent with the result that the Racah parameter B of $650cm^{-1}$ for the Co(II) complex[10] is smaller than the free-ion value B_0 of $971cm^{-1}$. Considering the magnitude of $|\lambda|$, there is also possibility that the absorption bands ranging from the H-band to the J-shouder in Fig. 5 are accounted for the spin-orbit splitting of the ^4E state in nearly S_4 symmetry.

For comparison, the values of $g_\perp$=2.55, $g_{//}$=2.17, g_{eff}=2.43, and μ_{eff}=4.71 are obtained for $K_2\{(C_4H_9)_4N\}_4[Co^{II}W_{12}O_{40}]\cdot 1CH_3CN$ (**d** in Fig. 7).

Comparison between Co(III) and Co(II) Complexes. By lowering of symmetry from T_d to S_4, the $^5T_2$ state for Co(III) complex and the $^4T_1$(F) state for Co(II) complex are estimated to split by ≈2100 and $\approx 1300cm^{-1}$, respectively.[20] This larger splitting for Co(III) complex may be due to the Jahn-Teller effect in the ^5E ground state or in the $^5T_2$ excited state. As described above, the $Co^{III}O_4$ tetrahedron is elongated and shows D_2 symmetry, but the $Co^{II}O_4$ tetrahedron is probably flattened and shows D_2 symmetry which is nearly S_4.

Thanks are due to Professor Hiroaki Ohya of Kyoto University for helpful discussions of the ESR spectra and to Dr. Masahiro Khono of JEOL Ltd. for measurements of the ESR spectra at 5.5 K. This work was partially supported by a Grant-in-Aid for Scientific Research No. 61740356 from the Ministry of Education, Science and Culture.

References

1) D. L. Wood and J. P. Remeika, *J. Chem. Phys.*, **46**, 3595 (1967).
2) M. D. Sturge, F. R. Merritt, J. C. Hensel, and J. P. Remeika, *Phys. Rev.*, **180**, 402 (1969).
3) A. Bencini, C. Benelli, D. Gatteschi, and C. Zanchini, *Inorg. Chem.*, **18**, 2137 (1979).
4) Y. Chiba, T. Yoshida, and M. Date, *J. Phys. Soc. Jpn.*, **50**, 3925 (1981).
5) H. Drulis, K. Dyrek, K. P. Hoffmann, S. K. Hoffmann, and A. Weselucha-Birczyńska, *Inorg. Chem.*, **24**, 4009 (1985).
6) K. Fukui, H. Ohya, N. Hirota, H. Ogoshi, and K. Aoyagi, 25th ESR Conference of Japan, Sapporo, December 1986, Abstr. No. 15A04.
7) V. E. Simmons, Ph. D. Thesis, Boston University, 1963.
8) L. C. W. Baker, V. E. S. Baker, S. H. Wasfi, G. A. Candela, and S. H. Kahn, *J. Chem. Phys.*, **56**, 4917 (1972).
9) G. M Varga, Jr., E. Papaconstantinou, and M. T. Pope, *Inorg. Chem.*, **9**, 662 (1970).
10) K. Kojima and J. Matsuda, *Bull. Chem. Soc. Jpn.*, **58**, 821 (1985).
11) N. F. Yanonni, Ph. D. Thesis, Boston University, 1961.
12) H. So and M. T. Pope, *J. Chem. Phys.*, **55**, 2786 (1971).
13) L. C. W. Baker and T. P McCutcheon, *J. Am. Chem. Soc.*, **78**, 4503 (1956).
14) O. W. Rollins, *Inorg. Chem.*, **11**, 3114 (1972).
15) K. Nomiya, M. Miwa, R Kobayashi, and M. Aiso, *Bull. Chem. Soc. Jpn.*, **54**, 2983 (1981).
16) N. Kojima, T. Ban, and I. Tsujikawa, *J. Phys. Soc. Jpn.*, **44**, 919 (1978); N. Kojima, Doctor Thesis, Kyoto University, 1978.
17) R. Pappalardo, *Nuovo Cimento*, **26**, 748 (1962).
18) K. Nomiya, R. Kobayashi, and M. Miwa, *Bull. Chem Soc. Jpn.*, **56**, 2272 (1983).
19) W. D. Horrocks, Jr. and D. A. Burlone, *J. Am. Chem. Soc.*, **98**, 6512 (1976).
20) The value of $\approx 2100\ cm^{-1}$ is the energy separation between the A-band and the center of the B- and C-bands (Fig. 1), and the value of $\approx 1300\ cm^{-1}$ is that between the G-band and the center of the H-, I-, and J-bands (Fig. 5).

 © 1987 The Chemical Society of Japan Bull. Chem. Soc. Jpn., 60, 3219—3223 (1987)

Fluorescence Reactions of "Crowned" Benzothiazolylphenols with Alkali and Alkaline Earth Metal Ions and Their Analytical Applications

Kenichiro NAKASHIMA, Yukari NAGAOKA, Shin'ichi NAKATSUJI, Takahiro KANEDA,† Isamu TANIGAWA,† Keiji HIROSE,† Soichi MISUMI,† and Shuzo AKIYAMA*

Faculty of Pharmaceutical Sciences, Nagasaki University, 1-14 Bunkyo-machi, Nagasaki 852
†The Institute of Scientific and Industrial Research, Osaka University, Mihogaoka, Ibaraki 567

(Received April 2, 1987)

The fluorescence behavior by a complexation of "crowned" benzothiazolylphenols (CBTP and CBBTP) with alkali and alkaline earth metal ions in the presence of triethylamine was examined in various organic solvents. The fluorescence spectra of these CBTP- and CBBTP-metal ion complexes were measured in order to compare mutually both their excitation and emission maxima together with the relative fluorescence intensities (RFI). Both the Li-CBTP and Li-CBBTP complexes showed considerably higher RFI than the other metal complexes. The stability of the fluorescence intensity and various conditions for the determination of Li^+ or Ca^{2+} were fully examined. On the basis of these experiments, fluorometric methods were developed for a sensitive determination of trace amounts of Li or Ca by using the crown compounds (CBTP and/or CBBTP). Moreover, a thin-layer chromatographic method for the separation of Li from other metal ions was examined in order to selectively determine Li by using CBBTP.

New applications of crown compounds as reagents for chemical analyses are becoming of interest in analytical chemistry.[1] A great many improvements and further applications in this field have been extensively carried out. For example, several crown compounds have been studied for their usefulness as neutral carriers of Li^+-selective electrodes.[2] However, it seems that their sensitivity is as yet quite unsatisfactory for applications to the determination of lithium, as compared with atomic and light absorption spectrometry. Recently, a new method has been proposed[3] for the spectrophotometric determination of Li^+ in the concentration range of 25—250 ng ml^{-1} with a "crowned" dinitrophenylazophenol (CDPA) in chloroform–dimethyl sulfoxide–triethylamine (TEA). This was the first example of a colorimetric determination of Li^+ with a crown ether. Succeedingly, a complexation of CDPA with alkali and alkaline earth metal ions in chloroform–MeOH–TEA was studied by means of their absorption spectra; two kinds of linear relationships were found between the ionic radii of these ions, both with the wavenumbers of the absorption maxima and with the molar absorption coefficients of the resulting complexes except for Be^{2+}.[4,5] Moreover, a new sensitive and simple method for the spectrophotometric determination of alkylamine with a CDPA–Ba^{2+} complex in MeOH was developed.[6]

The incorporation of a fluorescent moiety in the place of the dinitrophenylazo group of CDPA should greatly improve the sensitivity in the determination of Li^+. The new fluorescent "crowned" benzothiazolylphenols (CBTP and its bis-type compound, CBBTP) have now been synthesized and show characteristic fluorescence with alkali and alkaline earth metal ions.[7] In this paper, we report the fluorescence reactions of CBTP and CBBTP with alkali and alkaline earth metal ions, and a highly sensitive fluorometric determination of Li^+ or Ca^{2+}. This is based on a complex formation with CBTP and/or CBBTP, followed by a measurement of the fluorescence of the phenolate of the complex obtained by a treatment with TEA. Attempts to improve the selectivity for lithium were made and then fluorometry of Li^+ combined with a thin-layer silica-gel chromatography (TLC) was proposed.

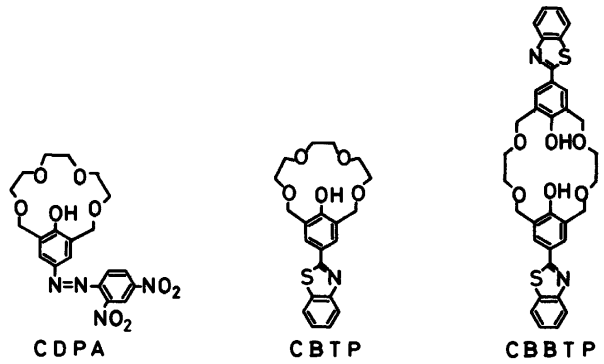

Experimental

Reagents. Metal chlorides and TEA were of analytical grade. Organic solvents (MeOH, EtOH, benzene, and CH_2Cl_2) were used after distillation. Commercially available silica-gel plates (Kieselgel 60, Merck) were used.

Apparatus. The fluorescence spectra and intensities were measured with a Shimadzu RF-540 spectrofluorometer in 10×10 mm quartz cells.

General Procedures. a)[8] Determination of Li^+ by CBTP: To a 50-μl portion of a LiCl solution in MeOH in a 10-ml standard volumetric flask, 5.0 ml of 10^{-4} M (1 M=1 mol dm^{-3}) CBTP in benzene were added and mixed. After the addition of TEA (50 μl) the mixture was diluted to the mark with benzene and mixed well; then the relative fluorescence intensity (RFI) was measured at 410 nm

(emission, λ_{em}) with excitation (λ_{ex}) at 375 nm (cf. Fig. 2).

b) Determination of Li^+ by CBBTP: To a 50-μl portion of LiCl solution in MeOH, 5 ml of CH_2Cl_2 and a solution of CBBTP in CH_2Cl_2 (2×10^{-4} M, 100 μl) were added successively and mixed. Then TEA (20 μl) was added and the whole was finally adjusted to 10 ml with CH_2Cl_2 and mixed well. RFI was measured at 410 nm (λ_{em}) with λ_{ex} at 360 nm.

c) Determination of Ca^{2+} by CBBTP: For a 100-μl portion of a $CaCl_2$ solution in MeOH, the same operation as b) was carried out and then RFI was measured at 400 nm with λ_{ex} at 360 nm.

TLC Method. a) Procedure: A 1 wt% aq solution (10 μl) of metal ion (Li, Na, K, Rb, Cs, Be, Mg, Ca, Sr, or Ba) was spotted on a TLC plate. The plate spotted was developed up to 12 cm by using EtOH–acetic acid (100:1), and dried at room temperature. After being sprayed with violuric acid (1.5 wt%, in EtOH), the plate was dried for 20 min at 110 °C. b) Li^+-determination: The spot for Li^+ developed according to the above procedure was thoroughly scratched and transferred into a 10-ml glass-stoppered tube, to which MeOH (2 ml) was added, vortexed for 2 min, and then centrifuged at 2000 g for 10 min. The supernatant (100 μl) was taken into a 10-ml volumetric flask; to this, CH_2Cl_2 (5 ml) and a solution of CBBTP in CH_2Cl_2 (10.8×10^{-4} M, 250 μl), and then TEA (20 μl) were added successively. The mixture was diluted to the mark with CH_2Cl_2 and mixed well; the RFI was measured at λ_{ex} and λ_{em}. For the blank, the methanol eluate of the part of the corresponding Li-spot on the TLC, which was free from Li salt, was used.

Results and Discussion

Fluorescence Reactions of CBTP and CBBTP with Alkali and Alkaline Earth Metal Ions. The crown rings of CBTP and CBBTP easily form complexes with alkali and alkaline earth metal ions in various solvents such as benzene, chloroform, and dichloromethane. Their fluorescence spectra have been shown to be almost identical with those of the corresponding ligands. By an addition of TEA, the spectra exhibited red shifts as well as the enhanced relative fluorescence intensities (RFI) due to the formation of phenolates. It has been demonstrated that neither CBTP nor CBBTP dissociates in the aprotic solvents, even in the presence of excess TEA.[7] In the present experiments, since MeOH, even in small amounts, should be used for the preparation of a standard solution (homogeneous) of metal salts, a dissociation of the phenols is, more or less, unavoidable. However, the spectra of the phenolates complexed with metal ions have been clearly shown to be different from those derived from the corresponding ligands themselves (Table 1 and cf. Figs. 2 and 3). Thus, it was interestingly observed on the complexes that both excitation and emission maxima were shifted to the longer wavelengths with

Table 1. Fluorescence Spectral Data for the Complexes of CBTP and CBBTP with Alkali and Alkaline Earth Metal Ions

Metal ion	Ligand	
	CBTP	CBBTP
	λ_{em}(λ_{ex}: 375 nm)	λ_{em}(λ_{ex}: 345 nm)
Li^+	410 nm	411 nm
Na^+	414	411
K^+	419	379
Rb^+	421	378
Cs^+	424	380
Be^{2+}	408	381
Mg^{2+}	410	408
Ca^{2+}	412	410
Sr^{2+}	411	413
Ba^{2+}	414	379

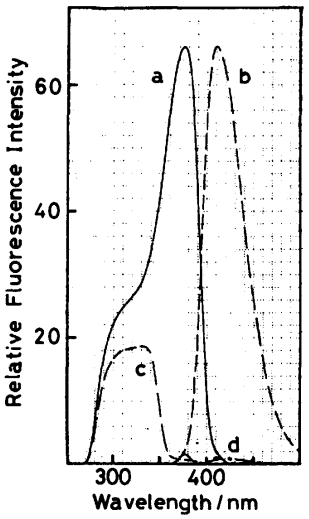

Fig. 1. Fluorescence spectra of the CBTP-Li^+ complex in benzene (Li^+: 1×10^{-6}M).
Excitation spectra: a, the complex; c, CBTP. Emission spectra: b, the complex; d, CBTP (λ_{ex}: 330 nm).

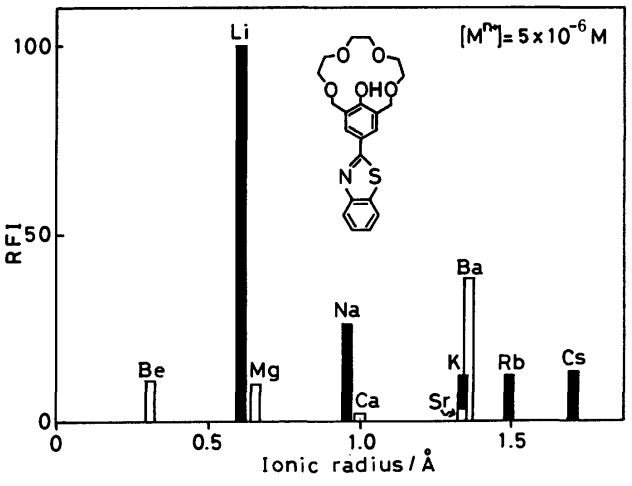

Fig. 2. RFI of the CBTP complexes vs. ionic radius.

an accompanying increase of RFI.

a) CBTP. The fluorescence reaction of CBTP with alkali and alkaline earth metal ions was examined in benzene. The fluorescence of the Li^+-complex is fairly unstable in the light, even though it is the most stable among all the complexes examined in the dark. The fluorescence spectral data are listed in Table 1. Figure 1 shows the excitation spectra of the CBTP-Li^+ complex (a) and a reagent blank (c) and the emission spectra of the complex (b) and the reagent blank (d) excited at 375 nm. The excitation maximum for the reagent blank is at 330 nm, and the emission intensity of the reagent blank is negligible compared with that of the complex when an excitation wavelength (λ_{ex}) of 375 nm is used. The emission maximum of the blank is at 382 nm if λ_{ex} is 330 nm. This choice of λ_{ex} in the above measurement is important for a determination of Li^+ stated later. The relation of the CBTP-M^{n+} complex (M^{n+}=alkali or alkaline earth metal ion) between RFI and ionic radius is shown in Fig. 2 (RFI=100 to the CBTP-Li^+ complex). The order of decreasing RFI is as follows:

$Li^+ > Ba^{2+} > (Na^+, Sr^{2+}) \gg (K^+, Rb^+, Cs^+, Be^{2+}, Mg^{2+}, Ca^{2+})$.

In this series the intensity of Li^+ was extremely high and its ratios of Li^+ to Ba^{2+}, Na^+, and K^+ were about 2, 4, and 10, respectively. It is interesting to note that the RFI of the Na^+, Be^{2+}, Ba^{2+}, and Sr^{2+} complexes, which would interfere in the determination of Li^+, decrease remarkably within 30 min, even in the dark. In the experiment carried out on the Ba^{2+}-complex, it was observed that the RFI decreased promptly and then recovered temporarily, upon adding the standard Ba^{2+} methanolic solution. However, the addition of barium chloride powder into the resulting solution caused an increased RFI which persisted even in the light. We have no idea yet of how to account for this anomalous behavior, which seems to be related to changes in the composition of the host to the guest ion in the complexes yielded in the presence of trace amounts of metal ions.

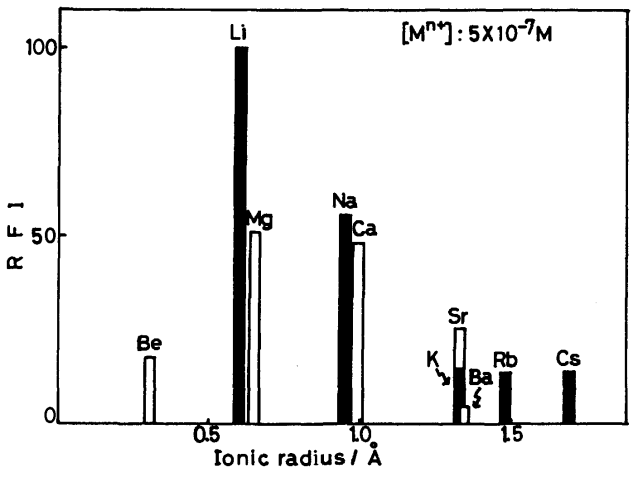

Fig. 3. RFI of the CBBTP complexes vs. ionic radius.

b) CBBTP. In the case of the fluorescence reaction of CBBTP with the metal ions, dichloromethane was particularly chosen as a solvent in order to obtain optimum conditions (Table 1). It is noted that the fluorescence resulting from complexation in the presence of TEA is quite stable relative to the CBTP-complexes, even in the light. In a correlation with the

Table 2. The Mole Ratio of Metal Ion to CBBTP[a)]

Ion	Mole ratio
Li^+	2 : 1
Na^+	2 : 1
K^+	2 : 1
Rb^+	2 : 1
Cs^+	2 : 1
Be^{2+}	4 : 1
Mg^{2+}	2 : 1
Ca^{2+}	1 : 1
Sr^{2+}	1 : 1
Ba^{2+}	1 : 1

a) RFI was measured at λ_{em} described in Table 1, and ([CBBTP]+[M^{n+}])/mol dm^{-3} in which square blankets denote amount-of-substance concentration, corresponds to (1—2)$\times 10^{-6}$ M.

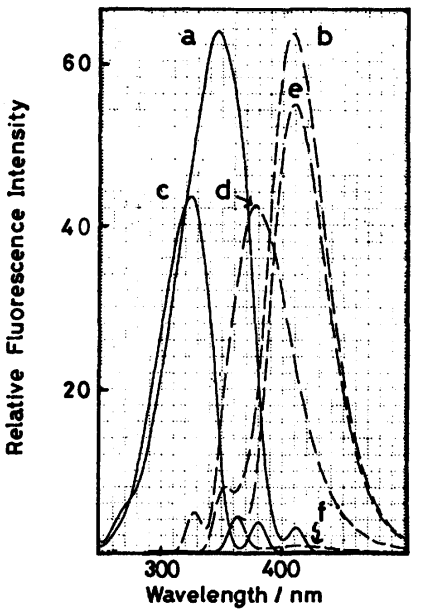

Fig. 4. Fluorescence spectra of the CBBTP-Li^+ complex in CH_2Cl_2 (Li^+: 5X10^{-7}M).
Excitation spectra: a, the complex; c, CBBTP.
Emission spectra: b, the complex at λ_{ex} 345 nm; d, CBBTP; e, the complex at λ_{ex} 360 nm; f, CBBTP at λ_{ex} 360 nm.

ionic radii of the metals, Fig. 3 shows the RFI (the Li^+-complex, 100) of the CBBTP complexes, with a decreasing order of:

$$Li^+ \gg Na^+ > (Mg^{2+}, Ca^{2+}) \gg Sr^{2+} > (Be^{2+}, K^+, Rb^+, Cs^+) \gg Ba^{2+}.$$

In this connection, it is interesting to examine the composition ratios of the complexes. The mole ratio of metal to CBBTP were examined spectrofluorometrically by the continuous variation method (Table 2). The anomalous behavior of Be^{2+} seems to be largely caused by its extremely small ionic size. As typical representative spectra, the case of the CBBTP-Li^+ complex is shown with the blank (CBBTP free from Li^+) in Fig. 4, in which the selection of 360 nm as the λ_{ex} can minimize the influence of the blank. This selection is very important for a highly sensitive determination of Li^+.

Determination of Li^+ or Ca^{2+}. Before establishing a procedure for the determination of Li^+ using CBTP, the CBTP, TEA, and MeOH concentrations were examined. It was shown that at least a 10-fold molar excess of reagent was necessary in the final concentration. The maximal RFI of the complex was obtained with final concentrations of 0.5—1.1 vol% TEA and 0.3—0.5 vol% MeOH. The fluorescence developed immediately and its RFI was constant for at least 120 min or more when the solution was kept in the dark. The calibration curve obtained by the standard method passed through the origin and was linear from 0.39 to 39 ng ml^{-1}. The relative standard deviation (RSD) for five replicates at the 24-ng ml^{-1} was 2.2%. The use of CBBTP instead of CBTP resulted in about a three-fold increase in the sensitivity for Li. The calibration graph obtained by the established standard procedure was linear from 0.14—7.0 ng ml^{-1} [RSD, 2.7% at 2.1-ng ml^{-1} (n=8)].

Moreover, in connection with an assay of Ca^{2+} in biological products, CBBTP was examined and was found to be useful for a sensitive determination of trace amounts of Ca^{2+}. After examining the fluorometric conditions, the maximal FRI of the Ca-complex was obtained with a final concentration of 0.2 vol% TEA and 2×10^{-6} M CBBTP. The calibration curve for Ca^{2+} was obtained in the concentration range 0.8—20.0 ng ml^{-1} [RSD, 3.8% at 22-ng ml^{-1} (n=4)].

Separation and Determination of Lithium by TLC. Lithium-selective reagents should be very important for monitoring the Li^+ activity in biological systems. The realization of a simple and sensitive Li^+-determination method is expected for the therapy of maniacal psychosis.[9] In our present studies, it has become apparent that an improvement in the selectivity is inevitable for a Li^+-determination. We preliminarily examined the separation and determination of Li^+ by a TLC method.[10] According to the chromatographic conditions described in Experimental, the spots due to metal salts can first be clearly visualized by drying at 110 °C after spraying a solution of violuric acid in EtOH as a potential color-producing reagent:[11] Li^+, reddish pink; Na^+, reddish orange; K^+, bluish violet; Rb^+, reddish violet; Cs^+, blue; Be^{2+}, pale blue; Mg^{2+}, yellowish orange; Ca^{2+}, orange; Sr^{2+}, reddish violet; Ba^{2+}, reddish violet. Li^+, Be^{2+}, and Mg^{2+} showed their R_f-values at 0.35, 0.17, and 0.15 respectively, and other metal spots stayed at the origins. For a determination the Li^+-spot colored was completely scratched and eluted with MeOH. The eluate was treated according to b) in Experimental. The fluorometric measurements of the Li^+-CBBTP complex showed that the calibration graph was linear from 3.3 to 16.5 μg/10 ml. The lower limit of the determination was 0.82 μg/10 ml (S/N>2). Aoyama reported that the range of the effective content of Li in normal human blood is generally 0.6—1.2 mEq l^{-1}.[12] Since 0.6 mEq of Li corresponds to 0.1 μg/0.1 ml blood, the TLC method examined here cannot be applicable to the determination of Li in normal blood. This TLC method, which has preliminarily been carried out, may prove to be useful in both its simplicity and selectivity. However, regarding sensitivity, the development of stronger color-producing reagents than violuric acid for trace amounts of Li should intensively be carried out next.

References

1) W. T. Smith, Jr. and J. M. Patterson, *Anal. Chem.*, **105**, 102R (1986); J. A. Howell and L. G. Hargis, *ibid.*, **105**, 108R (1986); E. Blasius and K.-P. Janzen, "Analytical Applications of Crown Compounds and Cryptands," in "Host Guest Complex Chemistry I," in "Topics in Current Chemistry," ed by F. Vögtle, Springer-Verlag (1981), pp. 163—197; E. Weber, Kontakte (Darmstadt), 1984 (1) 26 and references cited therein.

2) K. M. Aalmo and J. Krane, *Acta Chem. Scand., Ser. A*, **36**, 227 (1982); U. Olsher, *J. Am. Chem. Soc.*, **104**, 4006 (1982); K. Kimura, S. Kitazawa, and Shono, *Chem. Lett.*, **1984**, 639; S. Kitazawa, K. Kimura, H. Yano, and T. Shono, *J. Am. Chem. Soc.*, **106**, 6978 (1984).

3) K. Nakashima, S. Nakatsuji, S. Akiyama, T. Kaneda, and S. Misumi, *Chem. Lett.*, **1982**, 1781.

4) K. Nakashima, Y. Yamawaki, S. Nakatsuji, S. Akiyama, T. Kaneda, and S. Misumi, *Chem. Lett.*, **1983**, 1415.

5) K. Nakashima, S. Nakatsuji, S. Akiyama, T. Kaneda, and S. Misumi, *Chem. Pharm. Bull.*, **34**, 168 (1986).

6) K. Nakashima, N. Mochizuki, S. Nakatsuji, S. Akiyama, T. Kaneda, and S. Misumi, *Chem. Pharm. Bull.*, **32**, 2468 (1984).

7) I. Tanigawa, K. Tsuemoto, T. Kaneda, and S. Misumi, *Tetrahedron Lett.*, **25**, 5327 (1984).

8) Cf., K. Nakashima, S. Nakatsuji, S. Akiyama, I. Tanigawa, T. Kaneda, and S. Misumi, *Talanta*, **31**, 749 (1984).

9) D. Samuel and Z. Gottesfeld, *Endeavour*, **32**, 122 (1973); A. Amdisen, *Dan. Medic. Bull.*, **22**, 277 (1975); M. Canessa, N. Adragna, H. S. Solomon, T. M. Connolly, and D. C. Tosteson, *New England J. Medic.*, **302**, 772 (1980).
10) Cf., H. Seiler and W. Rothweiler, *Helv. Chim. Acta*, **44**, 941 (1961).
11) The structures of these complexes are now under study.
12) T. Aoyama, *Nippon Rinsho*, **40**, 1064 (1982).

 © 1987 The Chemical Society of Japan Bull. Chem. Soc. Jpn., 60, 3225—3231 (1987)

Synthesis and Chromogenic Properties of Some Phthalazinylhydrazones and Extractive Spectrophotometric and Analogue-Derivative Spectrophotometric Determination of Trace Amounts of Nickel with Di-2-pyridylmethanone 1-Phthalazinylhydrazone

Tsugikatsu ODASHIMA, Minoru YAMADA, Naoki YONEMORI, and Hajime ISHII*
Chemical Research Institute of Non-Aqueous Solutions, Tohoku University, Katahira, Sendai, Miyagi 980
(Received April 3, 1987)

Four kinds of 1-phthalazinylhydrazones have been synthesized and their chromogenic properties and reactivities with metal ions investigated. Of the synthesized hydrazones, di-2-pyridylmethanone 1-phthalazinylhydrazone (DPPhH) proved to be the best chromogenic reagent for nickel. It reacts with nickel(II) at pH above 2.5 to form a 1:2 (nickel-ligand) complex extractable into various organic solvents. The extracted species into benzene has an absorption maximum at 500 nm and gives a maximum and constant absorbance in the pH range 4.3—10.7. Beer's law is obeyed over the range 0.1—1.0 μg cm^{-3} of nickel. The molar absorptivity (ε) and the sensitivity for an absorbance of 0.001 are 5.4×10^4 dm^3 mol^{-1} cm^{-1} and 1.08 ng cm^{-2} at 500 nm, respectively. A sensitive and selective extraction-spectrophotometric method for the determination of nickel at μg cm^{-3} levels is proposed and has been applied successfully to the analysis of iron and steel samples. The proposed method can be made more sensitive by the introduction of an analogue-derivative spectrophotometric technique.

Since Lions et al.[1,2] first reported the preparation of hydrazones derived from 2-pyridylhydrazine and the properties of their metal complexes, a lot of nitrogen-containing heterocyclic hydrazones[3-6] have been synthesized and proposed as analytical reagents. On the other hand, we have prepared, over the period of more than 10 years, a series of hydrazones derived mainly from 2-benzothiazolylhydrazine[7-10] and proposed them as sensitive and useful reagents for metals. As for the phthalazinylhydrazone, however, only a few compounds[11,12] were prepared to date, since furfural 1-phthalazinylhydrazone and its analogue[13] were first synthesized and proposed as sensitive chromogenic reagents by us.

In the work presented here, 4 new hydrazones derived from 1-phthalazinylhydrazine, 2-pyridinecarbaldehyde 1-phthalazinylhydrazone (PAPhH), 1-(2-pyridyl)ethanone 1-phthalazinylhydrazone (MPPhH), phenyl(2-pyridyl)methanone 1-phthalazinylhydrazone (PPPhH), and di-2-pyridylmethanone 1-phthalazinylhydrazone (DPPhH) were synthesized and their chromogenic properties and reactivities with metal ions investigated and compared, as part of our continuing studies on the analytical application of hydrazones. Of the synthesized hydrazones, DPPhH was superior to the others as a spectrophotometric reagent for nickel(II) in terms of both sensitivity and selectivity. A sensitive and practical extraction-spectrophotometric method for the determination of trace amounts of nickel with DPPhH has been developed and successfully applied to the analysis of iron and steel samples. Further sensitization of the method by employing an analogue-derivative technique was feasible.

Experimental

Synthesis of Hydrazones. In 40 cm^3 of 5% hydrochloric acid dissolve 0.01 mol of 1-phthalazinylhydrazine, then add 20 cm^3 of ethanol solution containing 0.01 mol of the corresponding aldehyde or ketone. Heat the solution under reflux for 3 h. After cooling to room temperature, neutralize the solution with dilute aqueous ammonia. Filter off the resultant crystalline product with suction, recrystallize twice from ethanol and dry in vacuo.

Reagents. All reagents were of analytical-reagent grade and all solutions were prepared with distilled, deionized water, unless stated otherwise.

Hydrazone solutions, 2.5×10^{-3} M (1 M=1 mol dm^{-3}). Prepared by dissolving the required mass of each synthesized hydrazone in ethanol. These solutions were stable for at least several months when stored in an amber bottle.

Standard nickel(II) solution. Prepared by dissolving 2.5 g of nickel nitrate [$Ni(NO_3)_2\cdot6H_2O$] in about 100 cm^3 of water, adding 10 cm^3 of nitric acid (1+1) and diluting to 500 cm^3 with water. This solution was standardized by EDTA titration with copper 1-(2-pyridylazo)-2-naphtholate (Cu-PAN) as an indicator. Working solutions were prepared by diluting this solution with water.

Buffer solutions. Buffers consisting of 1 M chloroacetic acid–1 M sodium chloroacetate, 1 M acetic acid–1 M sodium acetate, M/15 potassium dihydrogenphosphate–M/15 disodium hydrogenphosphate, (0.2 M boric acid+0.05 M sodium chloride)–0.05 M sodium borate, and 1 M aqueous ammonia–1 M ammonium chloride systems were used according to the pH values required.

Apparatus. For measurements of the absorbance and the absorption spectrum, a Hitachi 139 and a Hitachi 200-10 spectrophotometer, respectively, were used. To obtain the derivative spectrum, a modified Hitachi 200-0576 derivative unit composed of two analogue differentiation circuits (each having six different time constants from 0.07 to 2.0 s) was

connected in series between the output of a Hitachi 556 dual-wavelength spectrophotometer and the input of a Hitachi 057 X-Y recorder, the former being used as an ordinary double-beam spectrophotometer. The details of this apparatus and the principle and characteristics of analogue-derivative spectrophotometry have already been described.[14,15]

Procedures. Ordinary Spectrophotometry: Place a sample or standard solution containing up to 10 μg of nickel(II) in a 50-cm³ separating funnel and add suitable masking agents if necessary, 2 cm³ of 2.5×10^{-3} M DPPhH solution, followed by 2 cm³ of 1 M acetate buffer (pH 5.0) and dilute to approximately 20 cm³ with water. Extract the nickel complex into 10 cm³ of benzene by shaking mechanically for a few minutes. Allow the phases to separate and transfer the organic phase into a flask containing about 1 g of anhydrous sodium sulfate in order to dehydrate it. Measure the absorbance of the extract at 500 nm against a reagent blank prepared under the same conditions using 1-cm cells.

Second-Derivative Spectrophotometry: When the nickel content of the extract prepared by the procedure described above is too low to give a measurable absorbance, record the second-derivative spectrum from 550 to 380 nm against a reagent blank by using a combination of both first- and second-order differentiation circuits of No. 6 and a scan speed of 150 nm min^{-1} and measure the second-derivative value (the vertical distance from a peak to a trough or that from the base line to a trough of the peak).

Dissolution and Pretreatment of Iron and Steel Samples: Prepare 100 cm³ of the sample solution by decomposing about 0.1 g of the sample with aqua regia and perchloric acid and then removing iron by extraction with 4-methyl-2-pentanone, by the same way as described earlier.[13] Use 2 cm³ or other appropriate aliquot of the resultant solution for the determination.

Results and Discussion

Identification of the Hydrazones. The infrared spectra of the synthesized hydrazones, PAPhH, MPPhH, PPPhH, and DPPhH, were measured with potassium bromide tablets in order to confirm their structures. The spectra had absorption peaks assigned to the stretching vibration of an azomethine bond (-N=C<) around 1600 cm^{-1}.[16] On the basis of these results and those of the elemental analysis shown in Table 1, the synthesized hydrazones are presumed to have the structures shown in Table 1.

Table 1. Structures and Physical Properties of Hydrazones

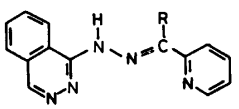

R: —H (PAPhH)
—CH_3 (MPPhH)
— (PPPhH)
— (DPPhH)

	Mp(θ_m/°C)	$\nu_{C=N}$/cm^{-1}	Elemental analysis/%[a] C	H	N
PAPhH	181	1610	67.2	4.3	28.0
			(67.5)	(4.5)	(28.1)
MPPhH	191	1590	68.2	5.0	26.6
			(68.4)	(5.0)	(26.6)
PPPhH	176	1585	73.7	4.6	21.0
			(73.8)	(4.7)	(21.5)
DPPhH	235	1600	69.9	4.3	25.8
			(69.9)	(4.3)	(25.8)

a) Results in parentheses indicate calculated values.

Properties and Characteristics of the Hydrazones. PAPhH, MPPhH, PPPhH, and DPPhH are insoluble in water but soluble in organic solvents such as benzene, chloroform, and 4-methyl-2-pentanone.

As is evident from the structures of these hydrazones, at least 4 species, H_3L^{2+}, H_2L^+, HL, and L^-, are involved in their acid dissociation equilibria, depending on the pH:

$$H_3L^{2+} \overset{K_{a3}}{\rightleftharpoons} H_2L^+ \overset{K_{a2}}{\rightleftharpoons} HL \overset{K_{a1}}{\rightleftharpoons} L^-$$

Where L denotes the undissociable part of the hydrazone and K_{a1}, K_{a2}, and K_{a3} are the acid dissociation constants. The pK_a values were determined by extraporating the linear ethanol concentration (10—40%) versus apparent pK_a plot to the intercept. The apparent pK_a values were determined spectrophoto-

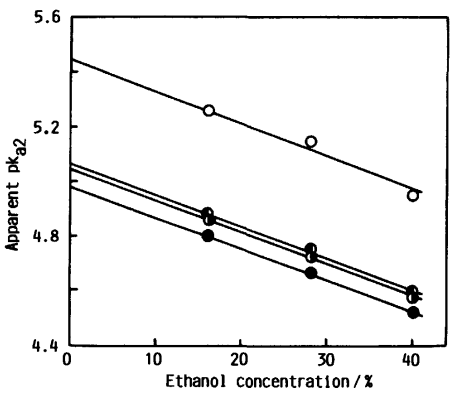

Fig. 1. Plots of apparent pK_{a2} vs. ethanol concentration. Hydrazone: 2.5×10^{-4} M, ionic strength: 0.2. temperature: 25±0.1 °C. —○—: MPPhH, —◐—: PPPhH, —◑—: DPPhH, —●—: PAPhH.

Table 2. Acid Dissociation Constants of the Hydrazones. Ionic Strength = 0.2; and Temperature = 25±0.1 °C

Hydrazone	pK_{a_1}[a] (Imino group)	pK_{a_2} (Pyridine nitrogen)	pK_{a_3} (Phthalazino nitrogen)
MPPhH	14.6_6	5.4_4	2.4_9
PAPhH	14.6_0	4.9_8	2.5_4
PPPhH	14.6_1	5.0_6	2.4_1
DPPhH	14.4_5	5.0_5	1.8_7

a) Ionic strength = 3.0, calculated by simplex method with a personal computer.

metrically at an ionic strength of 0.2, at 25±0.1 °C and at various ethanol concentrations. As an example, typical plots of apparent pK_{a2} of the 4 synthesized hydrazones versus ethanol concentration are shown in Fig. 1. The pK_a values of all the hydrazones thus obtained are summarized in Table 2. The pK_{a1} corresponds to the deprotonation of the secondary amino group, whereas the pK_{a2} and pK_{a3} correspond to that of the protonated pyridine-nitrogen and phthalazine-nitrogen, respectively.

Reactivities of the Hydrazones with Metal Ions. The reactivities of the synthesized hydrazones with metal ions and the extractabilities of the resultant complexes into benzene from aqueous media of pH 4,

Table 3. Extractability of Metal-PAPhH Complexes

Complex	pH 4		pH 7		pH 10	
	λ_{max}/nm	ε/M^{-1} cm^{-1}	λ_{max}/nm	ε/M^{-1} cm^{-1}	λ_{max}/nm	ε/M^{-1} cm^{-1}
Ag(I)	—	—	—	—	—	—
Al(III)	—	—	—	—	—	—
Ca(II)	—	—	—	—	—	—
Cd(II)	—	—	—	—	478	37000
Co(II)	—	—	—	—	—	—
Cr(III)	—	—	—	—	—	—
Cr(VI)	—	—	—	—	—	—
Cu(II)	—	—	455	9800	455	34000
Fe(II)	464 638	31000 8000	464 638	33000 8000	464 638	33000 8000
Hg(II)	—	—	466	17000	—	—
Mg(II)	—	—	—	—	—	—
Mn(II)	—	—	—	—	—	—
Ni(II)	—	—	470	52000	470	54000
Pb(II)	—	—	—	—	—	—
Pd(II)	538	9000	—	—	—	—
Ti(IV)	—	—	—	—	—	—
V(IV)	—	—	—	—	—	—
V(V)	—	—	—	—	—	—
Zn(II)	—	—	—	—	473	43000

Table 4. Extractability of Metal-MPPhH Complexes

Complex	pH 4		pH 7		pH 10	
	λ_{max}/nm	ε/M^{-1} cm^{-1}	λ_{max}/nm	ε/M^{-1} cm^{-1}	λ_{max}/nm	ε/M^{-1} cm^{-1}
Ag(I)	—	—	—	—	—	—
Al(III)	—	—	—	—	—	—
Ca(II)	—	—	—	—	—	—
Cd(II)	—	—	—	—	476	59000
Co(II)	—	—	—	—	—	—
Cr(III)	—	—	—	—	—	—
Cr(VI)	—	—	—	—	—	—
Cu(II)	—	—	—	—	468	24000
Fe(II)	442 653	19000 10000	460 653	24000 11000	460 653	28000 11000
Hg(II)	—	—	466	31000	466	18000
Mg(II)	—	—	—	—	—	—
Mn(II)	—	—	—	—	483	34000
Ni(II)	—	—	487	48000	487	52000
Pb(II)	—	—	—	—	—	—
Pd(II)	532	6000	532	6000	—	—
Ti(IV)	—	—	—	—	—	—
V(IV)	—	—	—	—	—	—
V(V)	517	8000	517	6000	—	—
Zn(II)	—	—	474	46000	474	66000

7, and 10 were investigated. The results are summarized in Table 3—6. Every hydrazone is found to react with cadmium(II), copper(II), iron(II), nickel(II), zinc(II), etc. to give colored complexes having large molar absorptivities. Of these, the reaction of DPPhH with nickel(II) proceeds over the wide pH region from weakly acidic to alkaline media to give a complex having large molar absorptivity (ε) and in addition, one can expect not only high sensitivity but also high selectivity when this complexation reaction in the weakly acidic medium is utilized to the determination of nickel, so the conditions for this complexation were examined in detail in subsequent experiments.

Table 5. Extractability of Metal-PPPhH Complexes

Complex	pH 4		pH 7		pH 10	
	λ_{max}/nm	ε/M^{-1} cm^{-1}	λ_{max}/nm	ε/M^{-1} cm^{-1}	λ_{max}/nm	ε/M^{-1} cm^{-1}
Ag(I)	—	—	—	—	—	—
Al(III)	—	—	—	—	—	—
Ca(II)	—	—	—	—	—	—
Cd(II)	—	—	486	55000	486	68000
Co(II)	493	16000	493	12000	488	19000
Cr(III)	—	—	—	—	—	—
Cr(VI)	—	—	—	—	—	—
Cu(II)	503	16000	482	41000	482	52000
Fe(II)	475 657	32000 13000	475 657	32000 13000	475 657	32000 13000
Hg(II)	—	—	477	31000	477	28000
Mg(II)	—	—	—	—	—	—
Mn(II)	—	—	—	—	495	45000
Ni(II)	484	53000	484	53000	484	57000
Pb(II)	—	—	—	—	—	—
Pd(II)	545	6000	545	8000	—	—
Ti(IV)	—	—	—	—	—	—
V(IV)	535	8000	535	12000	—	—
V(V)	535	21000	535	12000	—	—
Zn(II)	—	—	486	37000	486	57000

Table 6. Extractability of Metal-DPPhH Complexes

Complex	pH 4		pH 7		pH 10	
	λ_{max}/nm	ε/M^{-1} cm^{-1}	λ_{max}/nm	ε/M^{-1} cm^{-1}	λ_{max}/nm	ε/M^{-1} cm^{-1}
Ag(I)	—	—	—	—	—	—
Al(III)	—	—	—	—	—	—
Ca(II)	—	—	—	—	—	—
Cd(II)	—	—	485	27000	485	76000
Co(II)	—	—	—	—	—	—
Cr(III)	—	—	—	—	—	—
Cr(VI)	—	—	—	—	—	—
Cu(II)	500	7000	480	41000	480	54000
Fe(II)	474 653	32000 18000	474 653	32000 18000	474 653	32000 18000
Hg(II)	475	9000	475	29000	475	41000
Mg(II)	—	—	—	—	—	—
Mn(II)	—	—	—	—	496	64000
Ni(II)	500	54000	500	54000	500	54000
Pb(II)	—	—	—	—	—	—
Pd(II)	—	—	—	—	—	—
Ti(IV)	—	—	—	—	—	—
V(IV)	—	—	—	—	—	—
V(V)	533	14000	—	—	—	—
Zn(II)	—	—	485	71000	485	74000

Spectrophotometric Studies for the Determination of Nickel with DPPhH. Extraction Solvent, Effect of pH and Absorption Spectra: Nickel(II) reacts rapidly with DPPhH to form a red complex in weakly acidic to alkaline media. The complex is insoluble in water but soluble in organic solvents such as benzene, chloroform, 4-methyl-2-pentanone, and 1,2-dichloroethane. Of these, benzene was the most preferred extraction solvent, because the benzene extract gave the highest molar absorptivity. As shown in Fig. 2, the complex gave a constant, maximum absorbance when extracted from aqueous media of pH 4.3—10.7. Thus a pH of 5.0 is recommended. Figure 3 illustrates the absorption spectra of DPPhH and its nickel complex in benzene, together with the corresponding second-derivative spectrum. The complex has an absorption maximum at 500 nm, whereas the absorption of DPPhH at this wavelength is almost negligible.

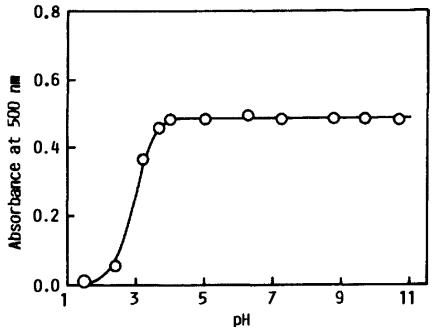

Fig. 2. Effect of pH. Ni(II): 5.1 μg/10 cm³, DPPhH: 2.5×10^{-4} M, reference: reagent blank.

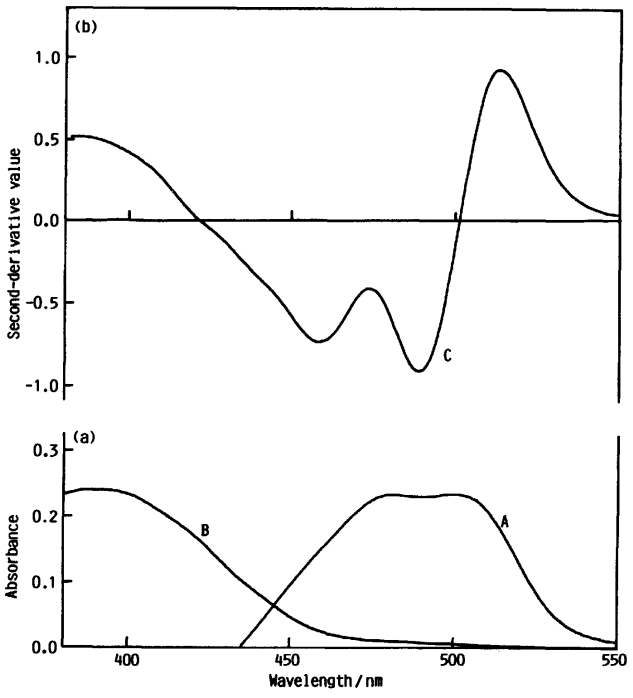

Fig. 3. (a) Absorption spectra of DPPhH and its nickel complex and (b) second-derivative spectrum of nickel-DPPhH complex in benzene. Ni(II): 2.53 μg/10 cm³, DPPhH: 1.25×10^{-5} M, pH: 5.0, A, C: complex against reagent blank, B: reagent blank against benzene. Second-derivative spectrum was measured with scan speed 150 nm min^{-1} and circuits all No. 6.

Effects of DPPhH Concentration and Shaking Time: A 3-fold molar excess of DPPhH was the minimum required for obtaining constant absorbance, and excess of DPPhH did not interfere. Shaking for a few minutes was sufficient for quantitative extraction of the complex.

Effect of Other Variations in Extraction: Variations in temperature from 15 to 30 °C, the ethanol concentration up to 15% in aqueous phase and the organic to aqueous phase ratio from 1:1 to 1:5 did not affect the absorbance. The absorbance of the extract remained constant even after several hours, which suggests that the extracted complex is very stable.

Composition of the Complex: The composition of the extracted complex was determined by the continuous variation method. The result, which is shown in Fig. 4, revealed that the metal to ligand ratio of the complex was 1:2. So DPPhH is considered to act presumably as a tridentate ligand, but no further detailed experiments to confirm this were carried out.

Calibration Graph, Sensitivity, and Precision: The calibration graph obtained by the recommended procedure was linear over the range 1—10 μg of nickel and passed through the origin. The equation for the line obtained by least-squares treatment was

$$\mathrm{Ni}(\mu g) = 10.8A \qquad (1)$$

where A is the absorbance. The molar absorptivity and the sensitivity for an absorbance of 0.001 calculated from Eq. 1 were 5.4×10^{4} dm³ mol^{-1} cm^{-1}

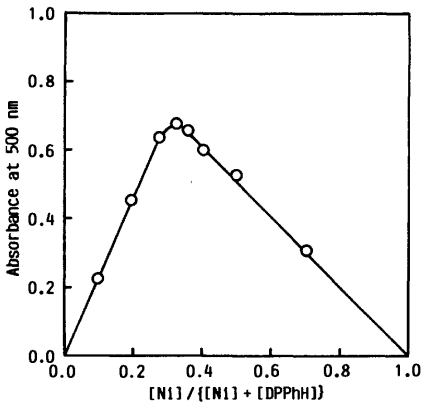

Fig. 4. Continuous variation graph for the nickel-DPPhH system. [Ni]+[DPPhH]=1.72×10^{-4} M, pH: 5.0.

and 1.08 ng cm^{-2}, respectively. These values indicate that the proposed method is extremely superior in sensitivity to that with 5-methylfurfural 1-phthalazinylhydrazone reported previously by us.[13] The relative standard deviation for 5.1 μg of nickel was 0.7%.

Effect of Diverse Ions: In order to study the effect of other ions on the determination of nickel, a fixed amount (5.1 μg) of nickel(II) was taken with various amounts of foreign ions and the recommended procedure was followed. An error of ±3% in the absorbance reading was considered tolerable. Tolerances for various foreign ions are shown in Table 7. Copper(II), iron(II,III), mercury(II), vanadium(IV,V), and zinc(II) interfere when no masking agent is added, whereas the other ions do not interfere. These interferences except that by iron(II) can be removed by the addition of masking agents noted in Table 7. Interference from iron(II) can be eliminated by masking with fluoride after oxidizing it to iron(III). Interference from a large amount of iron(III) can easily be removed by extracting it with 4-methyl-2-pentanone prior to the nickel determination, as mentioned already. On the other hand, most anions do not interfere, although the tolerance limit for iodide is somewhat low in comparison with those for other anions. The proposed method, therefore, may be regarded as very selective as well as sensitive for nickel.

Application to Actual Samples: In order to confirm the usefulness of the proposed method, it was applied to the determination of nickel in standard iron and steel samples. The results, shown in Table 8, are in good agreement with certified values.

Sensitization by Employing Analogue-Derivative Spectrophotometry. As described in earlier papers[14,15] the determination limit of ordinary spectrophotometry can remarkably be lowered by the introduction of a derivative spectrophotometric technique using the analogue differentiation circuit. As an example of sensitization, the second-derivative spectrophotomet-

Table 7. Tolerance Limits for Other Ions

Ion	Tolerance limit
Al(III), Ca(II), Mg(II)	1000 μg[a]
Ag(I), Cd(II), Co(II), Cr(III), Cu(II)[b], Fe(III)[c], Hg(II)[d], Pb(II), Ti(IV), V(IV)[e], V(V)[f], Zn(II)[b]	100 μg
Fe(II)	below 5 μg
Br^-, Cl^-, ClO_4^-, NO_3^-, $H_2PO_4^-$, SCN^-, SO_4^{2-}, Tartrate, Citrate	0.04 M[a]
I^-	0.02 M

Nickel(II) taken: 5.1μg a) Maximum tested. b) One cm^3 of 10% mercaptoacetic acid was added. c) One cm^3 of 1 M sodium fluoride was added. d) One cm^3 of 1 M sodium thiosulfate was added. e) One cm^3 of 0.1 M oxalic acid was added. f) One cm^3 of 1% ascorbic acid and 1 cm^3 of 0.1 M oxalic acid were added.

Table 8. Determination of Nickel in Standard Iron and Steel Samples

Sample	Sample taken / g		Nickel content/% Proposed method	Certified value
Carbon steel[a] (JSS-162)	0.1013		0.31_1	0.31
	0.1013		0.31_2	
	0.2103		0.30_0	
	0.2103		0.30_1	
		Average	0.30_6	
Carbon steel[a] (JSS-163)	0.1017		0.10_8	0.11
	0.1017		0.11_4	
	0.1998		0.11_5	
	0.1998		0.11_4	
		Average	0.11_3	

a) JSS: Japan Standard Sample of Iron and Steel.

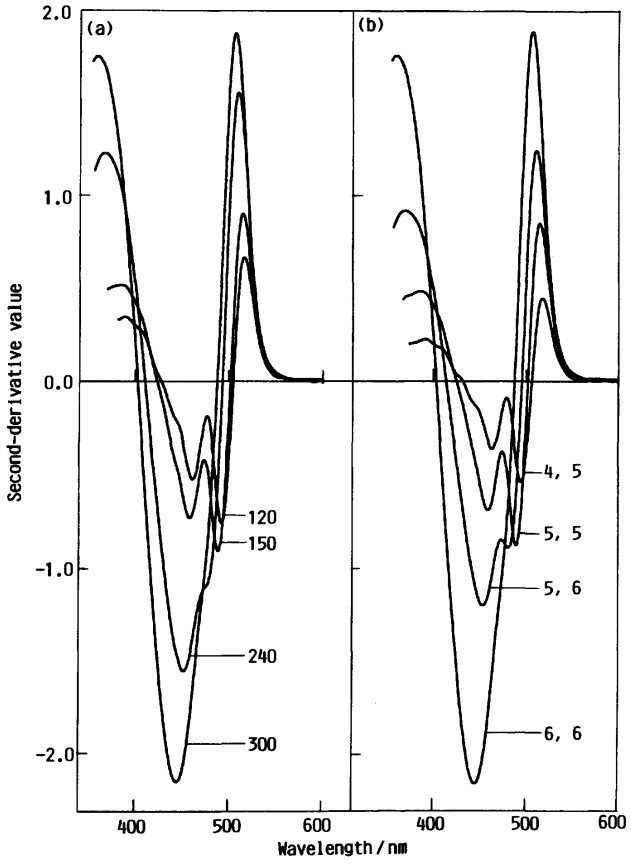

Fig. 5. Influence of (a) scan speed (with circuits all No. 6) and (b) circuit number (with scan speed 300 nm min^{-1}) on second-derivative spectra of the complex in benzene. Ni(II): 2.53 μg/10 cm^3, DPPhH: 1.25×10^{-5} M. pH: 5.0, slit width: 1 nm; recorder sensitivity: ×1/4, reference: reagent blank. Numerical values indicate scan speeds in (a) and first- and second-differentiation circuits in (b).

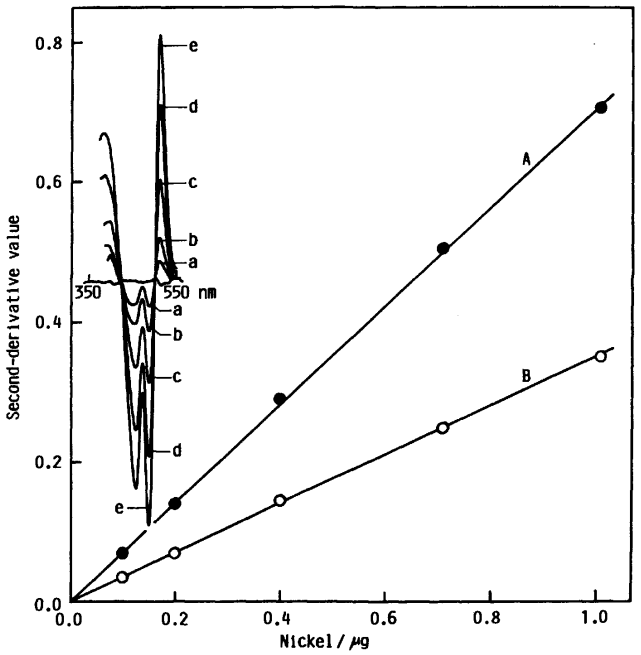

Fig. 6. Calibration graph for nickel in second-derivative spectrophotometry. Circuits: All No. 6, Scan speed: 150 nm min^{-1}, slit width: 1 nm, recorder sensitivity: ×1, reference: reagent blank. A: Peak-to-trough values are plotted, B: base line-to-trough values are plotted. Nickel (μg)—a: 0.10, b: 0.20, c: 0.40, d: 0.71, e: 1.01.

ric determination of nickel is described here.

Selection of Conditions for Merasurements: As the second-derivative value (the vertical distance from a peak to trough or that from the base line to a trough of the spectrum) depends on both the time constant of the analogue differentiation circuit and the scan speed of the spectrophotometer in second-derivative spectrophotometry, these need to be optimized to give a well resolved large peak (to give good selectivity and higher sensitivity). Figure 5 shows the second-derivative spectra of the nickel-DPPhH complex solution measured with varying circuit number or scan speed. A combination of circuit No. 6 (which has the largest time constant, 2.0 s, the time constant increasing with increasing circuit number in our apparatus) and a scan speed of 300 nm min^{-1} gives the highest sensitivity, but the resolution (i.e., selectivity) is poor in this combination. Taking both the sensitivity and selectivity into consideration, a combination of circuit No. 6 and a scan speed of 150 nm min^{-1} or that of No. 5 and 300 nm min^{-1} is recommended for the nickel determination.

Calibration Graph, Sensitivity, and Precision: The calibration graph prepared by plotting the second-derivative value versus the nickel concentration, an example of which is shown in Fig. 6, is linear and passes through the origin when either the peak-to-trough values or the base line-to-trough values were plotted. The equation for each line measured with a combination of circuit No. 6 and a scan speed of 150 nm min^{-1} was

$$\text{Ni}(\mu\text{g}) = 1.42\,D \quad (2)$$

$$\text{Ni}(\mu\text{g}) = 2.86\,D \quad (3)$$

respectively, where D is the second-derivative value represented by the conversion of the value into absorbance. It will be seen that as little at 100 ng or less of nickel can easily be determined in this way. Twelve standard solutions containing 400 ng of nickel(II) were analyzed. The results gave a relative standard deviation of 1.3%.

References

1) F. Lions and K. Martin, *J. Am. Chem. Soc.*, **80**, 3858 (1958).
2) J. F. Geldard and F. Lions, *J. Am. Chem. Soc.*, **84**, 2262 (1962).
3) R. E. Jensen, N. C. Bergman, and R. J. Helvig, *Anal. Chem.*, **40**, 624 (1968).
4) J. E. Going and R. T. Pflaum, *Anal. Chem.*, **42**, 1098 (1970).
5) R. T. Pflaum and E. S. Tucker, *Anal. Chem.*, **43**, 458 (1971).
6) M. Otomo and R. B. Singh, *Anal. Sci.*, **1**, 165 (1985).
7) T. Odashima and H. Ishii, *Nippon Kagaku Kaishi*, **1973**, 729.
8) T. Odashima and H. Ishii, *Anal. Chim. Acta*, **74**, 61 (1975).
9) H. Ishii, R. B. Singh, and T. Odashima, *Mikrochim. Acta*, **1983**, III, 149.
10) T. Odashima, R. B. Singh, and H. Ishii, *Microchem. J.*, **33**, 138 (1986).
11) M. Otomo and I. Nakayama, *Microchem. J.*, **25**, 75 (1981).
12) M. C. Mochon, M. C. Gallego, and A. G. Perez, *Talanta*, **33**, 631 (1986).
13) H. Ishii, T. Odashima, and T. Imamura, *Analyst*, **107**, 885 (1982).
14) H. Ishii and H. Koh, *Nippon Kagaku Kaishi*, **1980**, 203.
15) H. Ishii and K. Satoh *Fresenius' Z. Anal. Chem.*, **312**, 114 (1982).
16) R. M. Silverstein and G. C. Bassler, "Spectrometric identification of organic compounds," 2nd ed, John Wiley, New York (1967) [translated by S. Araki and Y. Mashiko, Tokyo Kagaku Dojin, Tokyo (1969)], p. 102.

 © 1987 The Chemical Society of Japan Bull. Chem. Soc. Jpn., 60, 3233—3239 (1987)

Estimation of Salt and Temperature Effects on Ion Product of Water in Aqueous Solution

Masunobu MAEDA,* Osamu HISADA, Yoshiaki KINJO,† and Kaname ITO
Department of Applied Chemistry, Nagoya Institute of Technology,
Gokiso-cho, Showa-ku, Nagoya 466
†Chemical Laboratory, College of Education, University of the Ryukyus, Okinawa 903-01
(Received April 13, 1987)

The ion product of water at 298.15 K was evaluated according to the Pitzer ionic interaction theory in LiCl, NaCl, KCl, KNO_3, $LiClO_4$, and $NaClO_4$ media of different concentrations (0.1—5 mol kg^{-1}) and in artificial seawaters at different salinities (20—44‰). The Pitzer approach was also applied to the estimation of the ion products of water in NaCl media at temperatures (288—373 K) different from 298.15 K. The theoretically evaluated values showed reasonable agreement with experimental ones.

In studying ionic equilibria over an alkaline range in an aqueous solution, a knowledge of the ion product of water in that solution is indispensable. By inspection of the ion products of water available (see Tables 1—9),[1-3] it is apparent that they are influenced in diverse manners by the type and concentration of the electrolyte as well as by the temperature. Thus, the theoretical evaluation of the ion product of water in an aqueous electrolyte solution at a desired composition and temperature, where the experimental information is absent or difficult to be obtained, is of crucial importance.

In a previous paper[4] the enthalpy changes for ionization of water were determined at 298.15 K in

Table 1. Comparison between Observed and Estimated Ion Products of Water in LiCl Media at 298.15 K (pK_w Values in Molal Units)[a]

Ionic strength/mol kg^{-1}	Obsd[15]	Est		
		Without[b]	With[c]	With[d]
0.110	13.759(1)	13.769	13.766	13.766
0.200	13.705(1)	13.725	13.719	13.718
0.500	13.636(1)	13.665	13.650	13.648
1.010	13.599(1)	13.649	13.618	13.610
2.010	13.609(1)	13.708	13.647	13.614
3.000	13.670(1)	13.819	13.728	13.654

a) The numbers in parentheses are uncertainties of the last decimal place. b) Without θ's and Ψ's, c) with θ_{HLi}, θ_{OHCl}, and Ψ_{HLiCl} available in the literature, d) with all the needed θ's and Ψ's (θ_{HLi}, θ_{OHCl}, and Ψ_{HLiCl} available and Ψ_{OHCLi} determined from observed pK_w values).

Table 2. Comparison between Observed and Estimated Ion Products of Water in NaCl Media at 298.15 K (pK_w Values in Molal Units)[a]

Ionic strength/mol kg^{-1}	Obsd[15]	Est	
		Without[b]	With[c]
0.110	13.780(1)	13.784	13.782
0.210	13.742(1)	13.747	13.744
0.510	13.708(1)	13.719	13.712
1.010	13.725(1)	13.746	13.730
2.010	13.839(1)	13·879	13.837
3.000	13.980(1)	14.056	13.981

a) The numbers in parentheses are uncertainties of the last decimal place. b) Without θ's and Ψ's, c) with all the needed θ's and Ψ's.

Table 3. Comparison between Observed and Estimated Ion Products of Water in KCl Media at 298.15 K (pK_w Values in Molal Units)[a]

Ionic strength/mol kg^{-1}	Obsd[15]	Est	
		Without[b]	With[c]
0.110	13.788(1)	13.793	13.788
0.210	13.756(1)	13.763	13.755
0.510	13.724(1)	13.754	13.733
1.010	13.769(1)	13.808	13.762
2.010	13.893(1)	13.984	13.879
3.000	14.020(1)	14.196	14.020

a) The numbers in parentheses are uncertainties of the last decimal place. b) Without θ's and Ψ's, c) with all the needed θ's and Ψ's.

Table 4. Comparison between Observed and Estimated Ion Products of Water in KNO_3 Media at 298.15 K (pK_w Values in Molal Units)[a]

Ionic strength/mol kg^{-1}	Obsd[3]	Est		
		Without[b]	With[c]	With[d]
0.060	13.809(2)	13.823	13.823	13.818
0.105	13.778(2)	13.791	13.792	13.784
0.140	13.753(2)	13.775	13.776	13.765
0.182	13.749(2)	13.762	13.763	13.749
0.262	13.730(2)	13.746	13.747	13.727
1.056	13.730(2)	13.770	13.775	13.711
2.187	13.880(2)	13.924	13.933	13.853

a) The numbers in parentheses are uncertainties of the last decimal place. b) Without θ's and Ψ's, c) with θ_{HK} available in the literature, d) with all the needed θ's and Ψ's (θ_{HK} available and θ_{OHNO_3}, Ψ_{HKNO_3}, and Ψ_{OHNO_3K} determined from observed pK_w values).

concentrated aqueous single electrolyte solutions of several kinds, and compared with those predicted in terms of the Pitzer ionic interaction model.[5,6] The observed and estimated values agreed fairly well. It was also found that the free energy and enthalpy changes for dissociation of ammonium ion determined at 298.15 K in concentrated single electrolyte solutions and in artificial seawaters[7-9] showed good agreement with those estimated via the Pitzer approach.

In the present work, the free energy changes for ionization of water (ion products of water) at 298.15 K were evaluated according to the Pitzer approach in LiCl, NaCl, KCl, KNO_3, $LiClO_4$, and $NaClO_4$ media with different concentrations (0.1—5 mol kg^{-1}) and in artificial seawaters at various salinities (20—44‰). The Pitzer approach was also applied to the estimation of the ion products of water in NaCl media at temperatures (288—373 K) different from 298.15 K. The theoretical values thus evaluated were compared with the experimental ones available in the literature.

The experimental values of the ion products, which are subjected to the comparison with the predicted values, are given in Tables 1—9. The ion products of water at 298.15 K in $LiClO_4$ media, which have not been reported, were experimentally determined in a usual way by acid-base titrations with hydrogen

Table 5. Comparison between Observed and Estimated Ion Products of Water in $LiClO_4$ Media at 298.15 K (pK_w Values in Molal Units)[a]

Ionic strength/mol kg^{-1}	Obsd[b]	Est		
		Without[c]	With[d]	With[e]
0.512	13.66(1)	13.656	13.663	13.66
1.049	13.64(1)	13.636	13.649	13.64
2.202	13.66(1)	13.711	13.737	13.67
3.481	13.74(1)	13.879	13.915	13.74

a) The numbers in parentheses are uncertainties of the last decimal place. b) Experimentally obtained in the present work, c) without θ's and Ψ's, d) with θ_{HLi} and Ψ_{HLiClO_4} available in the literature, e) with all the needed θ's and Ψ's (θ_{HLi} and Ψ_{HLiClO_4} available and θ_{OHClO_4} and Ψ_{OHClO_4Li} determined from observed pK_w values).

Table 6. Comparison between Observed and Estimated Ion Products of Water in $NaClO_4$ Media at 298.15 K (pK_w Values in Molal Units)[a]

Ionic strength/mol kg^{-1}	Obsd[15]	Est		
		Without[b]	With[c]	With[d]
0.100	13.77(1)	13.789	13.792	13.79
0.510	13.72(1)	13.717	13.732	13.72
1.050	13.76(1)	13.748	13.773	13.75
2.210	13.88(1)	13.913	13.948	13.88
3.000	14.03(1)	14.061	14.092	14.00
3.500	14.07(1)	14.165	14.189	14.07
4.660	14.24(1)	14.429	14.424	14.25

a) The numbers in parentheses are uncertainties of the last decimal place. b) Without θ's and Ψ's, c) with θ_{HNa} and Ψ_{HNaClO_4} available in the literature, d) with all the needed θ's and Ψ's (θ_{HNa} and Ψ_{HNaClO_4} available and θ_{OHClO_4} and Ψ_{OHClO_4Na} determined from observed pK_w values).

Table 8. Comparison between Observed and Estimated Ion Products of Water in 1.019 mol kg^{-1} NaCl Medium at Temperatures Higher than 298.15 K (pK_w Values in Molal Units)[a]

Temperature/K	Obsd[20]	Est
303.15	13.535(5)	13.583
313.15	13.234(5)	13.288
323.15	12.955(5)	13.012
333.15	12.698(5)	12.745
343.15	12.461(5)	12.486
353.15	12.243(5)	12.238
363.15	12.038(5)	12.026
373.15	11.854(5)	11.879

a) The numbers in parentheses are uncertainties of the last decimal place.

Table 7. Comparison between Observed and Estimated Ion Products of Water in Artificial Seawaters of Different Salinities at 298.15 K (pK_w Values in Molal Units)

Salinity/‰		19.90		26.87		34.82		44.00	
		Obsd[19]	Est	Obsd[19]	Est	Obsd[19]	Est	Obsd[19]	Est
pK_w		13.31	13.26	13.23	13.14	13.17	13.03	13.09	12.92
Composition[a] /mol kg^{-1}	Na^+	0.2768		0.3793		0.4960		0.6319	
	Mg^{2+}	0.0302		0.0416		0.0546		0.0695	
	Ca^{2+}	0.00598		0.00820		0.01073		0.01365	
	Cl^-	0.3168		0.4345		0.5690		0.7242	
	SO_4^{2-}	0.0162		0.0222		0.0288		0.0370	
Ionic strength[b] /mol kg^{-1}		0.4016		0.5509		0.7208		0.9184	

a) Estimated in the present work, b) calculated with neglect of ion-pairing.

Table 9. Comparison between Observed and Estimated Ion Products of Water in NaCl Media at 308.15 and 288.15 K (pK_w Values in Molal Units)[a)]

Ionic strength/mol kg^{-1}	308.15 K			288.15 K	
	Obsd[3)]	Est[b)]	Est[c)]	Obsd[3)]	Est
0.500	13.37(1)	13.402	13.395	14.07(1)	14.074
1.02	13.38(1)	13.434	13.421	14.06(1)	14.103
2.08	13.46(1)	13.588	13.559	14.15(1)	14.247

a) The numbers in parentheses are uncertainties of the last decimal place. b) Estimated with parameter values in Table 13, c) estimated with parameter values in Table 14.

Table 10. Ion Products of Water at Ionic Strength=0 and Different Temperatures[3)]

Temperature/K	pK_w
288.15	14.345(1)
298.15	13.997(1)
303.15	13.834(1)
308.15	13.680(1)
313.15	13.535(1)
323.15	13.263(1)
333.15	13.016(1)
343.15	12.800(1)
353.15	12.598(1)
363.15	12.422(1)
373.15	12.266(1)

The numbers in parentheses are uncertainties of the last decimal place.

electrodes.[10)] The pK_w values originally expressed in molar concentration units were converted to the values with the molality scale by the use of the densities of the salt solutions. The densities of electrolyte solutions, when not available in the literature, were measured pycnometrically.

Procedures for Theoretical Estimation of Ion Product. The autoprotolytic reaction of water is denoted by Eq. 1,

$$H_2O = H^+ + OH^-. \quad (1)$$

The relation of the ion product, $K_w(I,T)$, with the activity coefficients of the relevant ionic species, γ, and the water activity, a_{H_2O}, in solution at ionic strength I mol kg^{-1} and temperature T K is represented by Eq. 2,

$$pK_w(I,T) = pK_w(0,T) + (\ln \gamma_H + \ln \gamma_{OH} - \ln a_{H_2O})/\ln 10, \quad (2)$$

where $pK_w(0,T)$ denotes the ion product in a salt-free solution. Since the $pK_w(0,T)$ value is usually available in the literature, the present problem is reduced to estimating the γ values of H^+ and OH^- ions and the a_{H_2O} in the solution at ionic strength I and temperature T. The accepted $pK_w(0,T)$ values at temperatures of interest are given in Table 10.[3)]

According to Pitzer's approach,[11)] the trace activity coefficients of the ionic components of unit charge, H^+ and OH^-, and the water activity in the solution containing cations c's and anions a's of ionic strength I can be determined from Eqs. 3, 4, and 5, respectively.

$$\ln \gamma_H = F + \sum_{a=1}^{N_a} m_a(2B_{Ha} + ZC_{Ha}) + \sum_{c=1}^{N_c} m_c(2\theta_{Hc} + \sum_{a=1}^{N_a} m_a\Psi_{Hca}) + \sum_{a=1}^{N_a-1}\sum_{a'=a-1}^{N_a} m_a m_{a'}\Psi_{aa'H} + \sum_{c=1}^{N_c}\sum_{a=1}^{N_a} m_c m_a C_{ca}, \quad (3)$$

$$\ln \gamma_{OH} = F + \sum_{a=1}^{N_c} m_c(2B_{cOH} + ZC_{cOH}) + \sum_{a=1}^{N_a} m_a(2\theta_{OHa} + \sum_{c=1}^{N_c} m_c\Psi_{OHac}) + \sum_{c=1}^{N_c-1}\sum_{c'=c-1}^{N_c} m_c m_{c'}\Psi_{cc'OH} + \sum_{c=1}^{N_c}\sum_{a=1}^{N_a} m_c m_a C_{ca}, \quad (4)$$

$$\ln a_{H_2O} = -0.0180\phi \sum_i m_i. \quad (5)$$

For use in Eqs. 3—5 the following terms are defined.

$$F = -A^\phi[I^{1/2}/(1+1.2I^{1/2}) + (2/1.2)\ln(1+1.2I^{1/2})] + \sum_{c=1}^{N_c}\sum_{a=1}^{N_a} m_c m_a B'_{ca} + \sum_{c=1}^{N_c-1}\sum_{c'=c+1}^{N_c-1} m_c m_{c'}\theta'_{cc'} + \sum_{a=1}^{N_a-1}\sum_{a'=a+1}^{N_a} m_a m_{a'}\theta'_{aa'}, \quad (6)$$

$$C_{ca} = C^\phi_{ca}/2|z_c z_a|1/2 \quad (7)$$

$$Z = \sum_i z_i m_i \quad (8)$$

$$\sum_i m_i(\phi - 1) = 2(-A^\phi I^{3/2}/(1+1.2I^{1/2}) + \sum_{c=1}^{N_c}\sum_{a=1}^{N_a} m_c m_a(B^\phi_{ca} + ZC_{ca}) + \sum_{c=1}^{N_c-1}\sum_{c'=c+1}^{N_c} m_c m_{c'}(\theta^\phi_{cc'} + \sum_{a=1}^{N_a} m_a\Psi_{cc'a}) + \sum_{a=1}^{N_a-1}\sum_{a'=a+1}^{N_a} m_a m_{a'}(\theta^\phi_{aa'} + \sum_{c=1}^{N_c} m_c\Psi_{aa'c}) \quad (9)$$

In Eq. 3 m_c is the molality of cation c, and N_c the total number of cations. Similar definitions apply for anions a's. A^ϕ in Eqs. 6 and 9 is the Pitzer-Debye-Hückel limiting slope given by Eq. 10,

$$A^\phi = (1/3)(2\pi N_0 d_w/1000)^{1/2}(e^2/DkT)^{3/2}, \quad (10)$$

where N_0 is Avogadro's number, d_w and D are the density and dielectric constant of water, respectively. The second virial coefficients B in Eqs. 3, 4, 6, and 9 are given by the following ionic strength dependence.

$$B^{\phi}_{ca} = \beta^{(0)}_{ca} + \beta^{(1)}_{ca} \exp(-\alpha_{ca} I^{1/2}) + \beta^{(2)}_{ca} \exp(-12 I^{1/2}) \quad (11)$$
$$B_{ca} = \beta^{(0)}_{ca} + \beta^{(1)}_{ca} g(\alpha_{ca} I^{1/2}) + \beta^{(2)}_{ca} g(12 I^{1/2}) \quad (12)$$
$$B'_{ca} = \beta^{(1)}_{ca} g'(\alpha_{ca} I^{1/2})/I + \beta^{(2)}_{ca} g'(12 I^{1/2})/I \quad (13)$$

The functions, g and g', are defined by the equations.

$$g(x) = 2(1-(1+x)\exp(-x))/x^2 \quad (14)$$
$$g'(x) = -2(1-(1+x+x^2/2)\exp(-x))/x^2 \quad (15)$$

with $x=\alpha_{ca}/I^{1/2}$ or $12I^{1/2}$. When either cation c or anion a is univalent, $\alpha_{ca}=2$. For 2:2 or higher valence pairs $\alpha_{ca}=1.4$. The second virial coefficients θ, which depend on the ionic strength, are given in the following form.

$$\theta^{\phi}_{ij} = \theta_{ij} + {}^{E}\theta_{ij}(I) + I\,{}^{E}\theta'_{ij}(I) \quad (16)$$
$$\theta_{ij} = \theta_{ij} + {}^{E}\theta_{ij}(I) \quad (17)$$
$$\theta'_{ij} = {}^{E}\theta_{ij}(I) \quad (18)$$

When the ions i and j are of the same charge, ${}^{E}\theta_{ij}(I)$ and ${}^{E}\theta'_{ij}(I)$ are set equal to zero. The third virial coefficients, C^{ϕ}_{ca} and ψ_{ijk} are assumed to be independent of the ionic strength.[6] Usually, the contributions of the higher order terms θ and ψ are small, and significant only at high ionic strength.

The values for $\beta^{(0)}$, $\beta^{(1)}$, $\beta^{(2)}$, and C^{ϕ} at 298.15 K have been calculated from the activity coefficient and osmotic coefficient data of single electrolytes, and the values for θ and ψ at 298.15 K from the data of mixed electrolytes.[12-14] The relevant parameter values used in the calculations by means of Eqs. 3—5 are collected in Tables 11 and 12.

Since the parameter values for the Mg^{2+}-OH^- interactions, which are needed for the theoretical calculations in artificial seawaters, are not available, they were estimated on the basis of hydrolysis data for Mg^{2+} and Ca^{2+} ions. The equilibrium constant for the reaction $M^{2+}(M=Mg \text{ or } Ca)+OH^-=MOH^+$ has been reported to be ca. 360 for Mg^{2+} and 14 for Ca^{2+} at 298.15 K in a salt-free solution,[15] while no data for their enthalpy changes having been reported. Thus, the $\beta^{(0)}$, $\beta^{(1)}$, $\beta^{(2)}$, and C^{ϕ} for the Mg^{2+}-OH^- interactions were estimated simply on the assumption that they were 360/14 times the corresponding values for the Ca^{2+}-OH^- interactions. These parameter values are given in Table 11.

The parameter values $\beta^{(0)}$, $\beta^{(1)}$, and C^{ϕ} for HCl,

Table 11. Single Electrolyte Parameters in Pitzer's Equations at 298.15 K

Catioa	Anion	$\beta^{(0)}$	$\beta^{(1)}$	$\beta^{(2)}$	C^{ϕ}
H	Cl	0.1775	0.2945		0.0008
H	NO_3	0.1119	0.3206		0.0010
H	ClO_4	0.1747	0.2931		0.00819
H	SO_4	0.0298			0.0438
Li	OH	0.015	0.14		
Na	OH	0.0864	0.253		0.0044
K	OH	0.1298	0.320		0.0041
Mg	OH	−4.49[a]	−5.92[a]	−147[a]	
Ca	OH	−0.1747	−0.2303	−5.72	
Li	Cl	0.1494	0.3074		0.00359
Na	Cl	0.07650	0.2664		0.00127
K	Cl	0.04835	0.2122		−0.00084
Mg	Cl	0.35235	1.6815		0.00519
Ca	Cl	0.31590	1.6140		−0.00034
Li	NO_3	0.1420	0.2780		−0.0051
Na	NO_3	0.0068	0.1783		−0.00072
K	NO_3	−0.0816	0.0494		0.00660
Li	ClO_4	0.1973	0.3996		0.0008
Na	ClO_4	0.0554	0.2755		−0.00118
Na	SO_4	0.01958	1.1130		0.00497
Mg	SO_4	0.22100	3.3430	−37.25	0.025
Ca	SO_4	0.20000	2.650	−57.70	

a) Estimated by multiplying 360/14.0 the corresponding values for the Ca^{2+}-OH^- interactions.

Table 12. Common-Ion Two Electrolyte Parameters in Pitzer's Equations at 298.15 K

Cation (c)	Cation (c')	$\theta_{cc'}$	$\Psi_{cc'Cl}$	$\Psi_{cc'NO_3}$	$\Psi_{cc'ClO_4}$
H	Li	0.015	0.000		−0.001$_7$
H	Na	0.036	−0.004		−0.016
H	K	0.005	−0.007	−0.015[a]	
H	Mg	0.10	−0.011		
H	Ca	0.092	−0.015		

Anion (a)	Anion (a')	$\theta_{aa'}$	$\Psi_{aa'Li}$	$\Psi_{aa'Na}$	$\Psi_{aa'K}$	$\Psi_{aa'Ca}$
OH	Cl	−0.050	−0.019[a]	−0.006	−0.008	−0.025
OH	NO_3	−0.094[a]			0.062[a]	
OH	ClO_4	0.0013[a]	−0.037[a]	−0.008[a]		
OH	SO_4	−0.013		−0.009		

a) Estimated from observed pK_w values.

NaCl, and NaOH required to predict the pK_w values in NaCl media at temperatures higher than 298.15 K were estimated in the following.

Recently, Pitzer and coauthors[16,17] have estimated the ion-interaction parameters $\beta^{(0)}$, $\beta^{(1)}$, and C^ϕ for several 1:1 electrolytes including HCl and NaCl as a function of temperature on the basis of the apparent molar heat capacities above 298.15 K, and represented the temperature dependence of the parameter values by simple empirical equations. The parameter values for $\beta^{(0)}$, $\beta^{(1)}$, and C at T K and 1.01×10^5 Pa are expressed by the following equations,

$$\begin{aligned}\beta^{(0)} = {} & A^c_\beta(T/2+298^2/2T-298) \\ & + B^c_\beta(T^2/6+298^3/3T-298^2/2) \\ & + C^c_\beta(T^3/12+298^4/4T-298^3/3) \\ & + (298-298^2/T)(\partial\beta^{(0)}(298)/\partial T) \\ & + \beta^{(0)}(298), \end{aligned} \quad (19)$$

$$\beta^{(1)} = (298-298^2/T)(\partial\beta^{(1)}(298)/\partial T) + \beta^{(1)}(298), \quad (20)$$

$$C = (298-298^2/T)(\partial C(298)/\partial T) + C(298), \quad (21)$$

where A^c_β, B^c_β, and C^c_β are the fitting parameters independent of temperature. The temperature derivatives of the parameter values at 298.15 K have been obtained from the heat of dilution data for the electrolytes.[6] The parameter values $\beta^{(0)}$, $\beta^{(1)}$, and C^ϕ for HCl at temperatures of interest were calculated with the values for A^c_β, B^c_β, and C^c_β and those for the temperature derivatives of $\beta^{(0)}$, $\beta^{(1)}$, and C. The values for NaCl were taken from Ref. 16. They are collected in Table 13. Since the three A^c_β, B^c_β, and C^c_β values for NaOH are not available, they were estimated on the basis of the observed pK_w data at three temperatures; i.e., Eqs. 19—21 were introduced into Eqs. 3—5, and the rearranged Eqs. 3—5 into Eq. 2. The observed pK_w values in 1.019 mol kg^{-1} NaCl medium at 353, 363, and 373 K in Table 8 and the $pK_w(0,T)$ values at the corresponding temperatures in Table 10 were then introduced into Eq. 2 to solve the three resultant equations for the A^c_β, B^c_β, and C^c_β values. In these calculations was made no introduction of the higher order terms θ and ψ, because their contributions are expected to be small at this level of concentration. The A^c_β, B^c_β, and C^c_β values for NaOH were estimated to be 21.6, −0.132, and 2.01×10^{-4}, respectively. In Table 13 are also shown the parameter values $\beta^{(0)}$, $\beta^{(1)}$, and C^ϕ for NaOH at temperatures in question calculated according to Eqs. 19—21 with the relevant parameter values.

The ion-interaction parameter values $\beta^{(0)}$, $\beta^{(1)}$, and C^ϕ for HCl, NaOH, and NaCl at 308.15 K were calculated according to Eq. 22[6] on the basis of their activity coefficients at that temperature available in the literature.[18]

$$\ln\gamma_{ca} = f^\gamma + m_{ca}B^\gamma_{ca} + m^2_{ca}C^\gamma_{ca}, \quad (22)$$

where

$$\begin{aligned} f^\gamma = {} & -A^\phi[I^{1/2}/(1+1.2I^{1/2}) \\ & + (2/1.2)\ln(1+1.2I^{1/2})], \end{aligned} \quad (23)$$

$$\begin{aligned} B^\gamma_{ca} = {} & 2\beta^{(0)} + (\beta^{(1)}_{ca}/2I)[1 \\ & - \exp(-2I^{1/2})(1+2I^{1/2}-2I)], \end{aligned} \quad (24)$$

$$C^\gamma_{ca} = (3/2)C^\phi_{ca}. \quad (25)$$

The calculated ion-interaction parameter values at

Table 13. Single Electrolyte Parameters in Pitzer's Equations at Temperatures above 298.15 K

	$\beta^{(0)}$			$\beta^{(1)}$			$C^\phi\times10^3$		
Temperature/K	HCl	NaOH	NaCl	HCl	NaOH	NaCl	HCl	NaOH	NaCl
303.15	0.1782	0.0907	0.0788	0.2952	0.254	0.2814	1.1	3.4	0.88
308.15	0.1788	0.101	0.0817	0.2959	0.254	0.2833	1.4	2.6	0.40
313.15	0.1791	0.110	0.0846	0.2965	0.255	0.2893	1.6	1.7	−0.04
323.15	0.1793	0.120	0.0892	0.2977	0.256	0.2967	2.2	0.0	−0.80
333.15	0.1788	0.114	0.0927	0.2989	0.257	0.3038	2.7	−1.5	−1.46
343.15	0.1777	0.0848	0.0956	0.3000	0.258	0.3109	3.2	−3.0	−2.04
353.15	0.1767	0.0521	0.0977	0.3010	0.259	0.3180	3.6	−4.3	−2.52
363.15	0.1764	0.0326	0.0992	0.3020	0.260	0.3253	4.1	−5.7	−2.94
373.15	0.1778	0.0621	0.1002	0.3030	0.261	0.3326	4.5	−6.9	−3.30

Table 14. Single Electrolyte Parameters in Pitzer's Equations at 288.15 and 308.15 K

	$\beta^{(0)}$			$\beta^{(1)}$			$C^\phi\times10^3$		
Temperature/K	HCl	NaOH	NaCl	HCl	NaOH	NaCl	HCl	NaOH	NaCl
288.15	0.1782	0.0833	0.0675	0.2940	0.2434	0.2615	2.2	3.8	3.1
308.15	0.1746	0.0971	0.0790	0.2913	0.2507	0.2882	−0.6	0.1	1.7

308.15 K are given in Table 14. The observed pK_w values in NaCl media at 308.15 K (Table 9) were compared with both of the values predicted with the parameter values in Table 13 and with those in Table 14.

The parameter values for HCl, NaOH, and NaCl given in Table 13, which have been estimated by the use of the heat capacities at temperatures above 298 K, are not applicable to the prediction of pK_w values at temperatures below 298 K. Thus, for the prediction of pK_w values in NaCl media at 288.15 K (observed pK_w values in Table 9) the ion-interaction parameter values for HCl, NaOH, and NaCl were calculated in the same manner as for the case at 308.15 K according to Eq. 22 by using their activity coefficients at 288.15 K available in the literature.[18] The calculated parameter values are given in Table 14.

Results and Discussion

Evaluation of pK_w Values in Single Electrolyte Solutions at 298.15 K. In Tables 1—6 there are quantitative comparisons between the observed and predicted pK_w values in single electrolyte solutions at 298.15 K. The calculations were made with and without the higher order terms θ and ψ so that the need for considering the terms was examined. All the θ and ψ values required for the calculations are known only in NaCl and KCl media. As for the NaCl and KCl media it is apparent from Tables 2 and 3 that the values calculated with the higher order terms in Table 12 are in agreement with the observed ones within the experimental uncertainties, while the differences are fairly large, especially at high molalities in the calculations without them. These results point out the need to use θ and ψ values at high ionic strengths when they are available. The agreement between the values observed and those predicted with the higher order terms in the NaCl and KCl media demonstrates the validity of the Pitzer approach, and thus, suggests that unknown θ and ψ values are determinable from the observed pK_w values. With the other electrolyte solutions (Tables 1, 4—6), where all the higher order terms are not always available, it is seen that rather large discrepancies between the values observed and those calculated without the higher order terms occur at higher ionic strengths. The introduction of a partial set of the higher order terms leads to worse agreement between the observed and predicted values (an exception being the LiCl system). The higher order terms should be included when a full set of them are known. However, the omission of unknown θ and ψ values is unlikely to have a serious effect at low ionic strengths. Unknown θ and ψ values were estimated according to Eqs. 2—5 on the basis of the observed pK_w values in Tables 1 and 4—6. In Table 12 are also given the θ and ψ values thus estimated, which may be employed for the theoretical calculations of equilibrium constants in other systems where H^+ and/or OH^- ions participate.

Evaluation of pK_w Values in Artificial Seawaters at 298.15 K. The values observed and predicted with the parameter values in Tables 11 and 12 are compared each other in Table 7. Although the deviations are seen to exceed the experimental uncertainties, the agreement may be reasonable in view of the fact that the parameter values for the Mg^{2+}–OH^- interactions were estimated with the simple assumption (360/14 times the parameter values for the Ca^{2+}–OH^- interactions) and that the composition for each seawater, which was not given in Ref. 19, was deduced on the basis of the description about its preparation procedures. From a comparison of the pK_w values in Tables 2 and 7 it is apparent that the pK_w values in the seawaters are much smaller than the values in the NaCl solutions at the corresponding ionic strengths. An attempt was made to calculate the pK_w values in the seawaters on the assumption that the parameter values for the Mg^{2+}–OH^- interactions were the same as those for the Ca^{2+}–OH^- interactions. It was found that the calculated pK_w values were around 13.7-(19.90‰)—13.5(44‰), which are much higher by 0.4 than the observed values. This result indicates that the main difference between the pK_w values in the seawaters and those in the NaCl media results from the Mg^{2+}–OH^- interactions in the seawaters.

Evaluation of pK_w Values in NaCl Media at Temperatures Different from 298.15 K. a) pK_w Values in 1.019 mol kg^{-1} NaCl Medium at Temperatures above 298.15 K. It is seen from Table 8 that the observed values are in reasonable agreement with the predicted ones in consideration of the fact that the activity coefficients of NaOH have been estimated by using the A_β, B_β, and C_β values calculated from a limited number of pK_w values for lack of the apparent heat capacity data for NaOH.

b) pK_w Values at 308.15 K. The observed values are compared in Table 9 with both the values estimated with the parameter values in Table 13 and with those in Table 14. The observed values yield better agreement with the values estimated with the data in Table 14, which is reasonable, if one considers some uncertainties introduced in the calculations of the parameter values for NaOH in Table 13. The rather large discrepancy at 2.08 mol kg^{-1} may be due to the neglect of the higher order terms which are not available.

c) pK_w Values at 288.15 K. The observed and calculated values in Table 9 are seen to show good agreement each other.

In the light of the above results, it may be said that although the deviations between the observed and estimated values exceed in some cases by far the experimental uncertainties probably due to approximations made in the calculations and the unavail-

ableness of higher order terms, the present results demonstrate the reliability of the ionic interaction model by Pitzer and co-workers to estimate free energy changes in concentrated salt solutions over a wide range of temperature. It is necessary to determine higher order terms by e.g., isopiestic measurements in mixed electrolyte solutions so that free energy changes at high ionic strengths should be predicted more accurately.

The work was supported in part by a Grant-in-Aid for Scientific Research from the Ministry of Education, Science and Culture (No. 61540444).

References

1) L. G. Sillén and A. E. Martell, "Stability Constants," The Chemical Society, London (1964) and "Stability Constants," Supplement No. 1, The Chemical Society, London (1970).

2) E. Högfeldt, "Stability Constants of Metal-Ion Complexes," Part A, Pergamon Press, Oxford (1979).

3) J. J. Christensen, L. D. Hansen, and R. M. Izatt, "Handbook of Proton Ionization Heats and Related Thermodynamic Quantities," John Wiley & Sons, New York (1976).

4) M. Maeda, *J. Phys. Chem.*, **90**, 1134 (1986).

5) K. S. Pitzer, *J. Phys. Chem.*, **77**, 268 (1973).

6) K. S. Pitzer, "Activity Coefficients in Electrolyte Solutions," ed by R. M. Pytkowicz, CRC Press, Boca Raton, Florida (1979), Vol. 1, Chap. 7 and references cited therein.

7) M. Maeda, G. Nakagawa, and G. Biedermann, *J. Phys. Chem.*, **87**, 121 (1983).

8) M. Maeda, *Denki Kagaku*, **55**, 61 (1987).

9) M. Maeda, M. Hayashi, S. Ikeda, Y. Kinjo, and K. Ito, *Bull. Chem. Soc. Jpn.*, **60**, 2047 (1987).

10) F. J. C. Rossotti and H. Rossotti, "The Determination of Stability Constants and Other Equilibrium Constants in Solution," McGraw-Hill, New York (1961). Chap. 7.

11) C. E. Harvie and J. H. Weare, *Geochim. Cosmochim. Acta*, **44**, 981 (1980).

12) K. S. Pitzer and J. J. Kim, *J. Am. Chem. Soc.*, **96**, 5701 (1974).

13) K. S. Pitzer and G. Mayorga, *J. Phys. Chem.*, **77**, 2300 (1973).

14) C. E. Harvie, N. Møller, and J. H. Weare, *Geochim. Cosmochim. Acta*, **48**, 723 (1984).

15) C. G. Baes, Jr. and R. E. Mesmer, "The Hydrolysis of Cations," John Wiley & Sons, New York (1976).

16) K. S. Pitzer, J. C. Peiper, and R. H. Busey, *J. Phys. Chem. Ref. Data*, **13**, 1 (1984).

17) P. P. Salu, K. S. Pitzer, and R. C. Phutela, *Can. J. Chem.*, **64**, 1328 (1986).

18) H. S. Harned and B. B. Owen, "The Physical Chemistry of Electrolytic Solutions," Reinhold, New York (1950).

19) C. H. Culberson and R. M. Pytkowicz, *Mar. Chem.*, **1**, 309 (1973).

20) P. Becker and B. A. Bilal, *J. Solution Chem.*, **14**, 367 (1985).

 © 1987 The Chemical Society of Japan Bull. Chem. Soc. Jpn., 60, 3241—3246 (1987)

Mössbauer Study of Iron Oxide Surface Layers Formed on Fine Iron Particles

Yonezo MAEDA,* Masaaki ARAMAKI, Yoshimasa TAKASHIMA, Michiharu OOGAI,† and Takeshi GOTO†
Department of Chemistry, Faculty of Science, Kyushu University 33, Hakozaki, Higashi-ku, Fukuoka 812
†Toyo Soda Manufacturing Co., Tonda, Shinnanyo, Yamaguchi 746
(Received February 19, 1987)

Mössbauer studies of iron oxides formed on the surface of fine iron particles (acicular type about 15 nm in diameter and 100 nm long) and of an oxidation process in air have been done in the temperature range from 4.2 to 298 K. The Mössbauer spectra indicate that the main component of the oxide layers 2.1—5.6 nm thick, except for a few oxide layers from the iron surface, is composed of fine particles of γ-Fe_2O_3, and that fine iron oxide particles are produced freshly during the oxidation process at 110 °C in air with the growth of iron oxide particles. It is concluded that an oxide layer 2.1 nm thick is formed on the iron surface if a fresh iron surface is exposed to air at room temperature.

The oxidation or corrosion behavior of iron has yielded a number of interesting results concerning the magnetic properties[1-5] and the corrosion process and products,[6-12] and it has been studied by a number of investigators because iron is an important material in our daily life. However, our knowledge about the corrosion process is far from being sufficient, and the chemical species of the corrosion products formed on the iron surface have not been fully elucidated because the amount of products directly in contact with the metal surface is less that of the corrosion products of relatively thick oxide layers. Sewell and Cohen[13] and van Diepen et al.[14] indicated that the oxides formed up to 175 °C on the surface of iron are cubic Fe_3O_4 and γ-Fe_2O_3. Haneda and Morrish[15] indicated that the oxide layer is a mixture of Fe_3O_4 and γ-Fe_2O_3. Shinjo et al.[16] suggested that the oxide layer is γ-Fe_2O_3. Various methods of preparation (by the evaporation of iron, electrochemical deposition, and chemical reduction from α-FeOOH) for metallic iron were used in these studies, each method produced characteristic result regarding particle size, shape, and micropores in the metal. Furthermore, the corrosive conditions were different, and there has been disagreement as to which part of the oxide layer is actually detected.

Conversion electron Mössbauer spectroscopy (CEMS) is known to be suitable for the study of a surface. However, CEMS gives information of the surface range at a depth 60 nm from the particle surface. Therefore, the information obtained by CEMS is not related to the products directly in contact with the metal surface.[17] Fine samples with a large surface area are needed for a study of the oxide formed on iron. In the present study, corrosion products with a thickness of the order of 2—5 nm on the iron surface have been examined using fine particles of metallic iron.

Experimental

Iron powder was prepared by the reduction of α-FeOOH (doped with aluminium of 1.8 wt%) and stocked in a toluene solution until use because fine particles of iron are very easily oxidized in air at room temperature and are strongly pyrophoric because of their high surface area. The average particle dimensions of the acicular iron powder used here were determined, by means of an analytical electron microscope JEM-2000FX of HVEM Laboratory, Kyushu University, to be 15 nm in diameter and 100 nm in length. The specific surface area was determined by the BET nitrogen adsorption method to be 46.5 $m^2 g^{-1}$. This value is slightly larger than that of 39.2 $m^2 g^{-1}$ estimated on the base

Fig. 1. Electron micrograph of the original iron powder (×15000).

of the geometrical values. An electron micrograph for original iron powder is shown in Fig. 1. The particle size is estimated to be uniformly distributed in diameter, but to vary widely in length. The particle forms a single crystal of metallic iron covered with fine oxides, and no micropore was observed in the iron particles. The electron-diffraction patterns for these samples indicated that the sample was composed of metallic α-iron and iron oxide with a spinel structure.

X-Ray diffraction patterns were taken using Cu $K\alpha$ radiations. The data indicate that the iron powder contains a spinel iron oxide phase besides an iron phase. Line broadening for the spinel lines was observed because of the ultrafine particles of iron oxide formed on the surface of the iron particles.

Mössbauer spectroscopy was effected by using a constant-acceleration spectrometer described elsewhere.[18] The spectra were corrected for the curvature of the baseline due to the geometry of the measurement system and then fitted to the Lorentzian line shape, by using a least-squares method, at the Computer Center, Kyushu University. Isomer shifts are reported with respect to the centroid of the spectrum of an iron foil enriched with ^{57}Fe.

Results and Discussion

Oxidation/annealing of the iron powder was done at 110 °C in an air bath. The Mössbauer spectra of samples which has been oxidized/annealed at 110 °C in air for 2, 8, 26, 76, and 220 h were taken at 298 and 78 K; some of them are shown in Figs. 2 and 3. The Mössbauer parameters estimated for the samples are listed in Table 1. The spectrum of the original iron powder at 298 K consists of a superposition of a sextet with a magnetic hyperfine structure of metallic iron and a paramagnetic doublet of iron oxide. Broad lines are added in the spectra for the annealed samples, and the intensities of the broad lines and paramagnetic lines increase at the expense of that for metallic iron with an increase in the annealing time. The full width at a half maximum (fwhm) for metallic iron is narrow, and the hyperfine field coincides with the standard α-Fe value.

The Mössbauer spectra for the samples at 78 K consist of a superposition of the sextets with a magnetic hyperfine structure of both metallic iron and iron oxide. The fwhm for the iron oxide having a larger hyperfine field is wider than that of bulk γ-Fe_2O_3 or Fe_3O_4. A large value of fwhm for iron oxide is usually observed in the case of fine particles.[15] The average hyperfine fields for the iron oxide part were estimated to be 488—492 kOe at 78 K. These values are

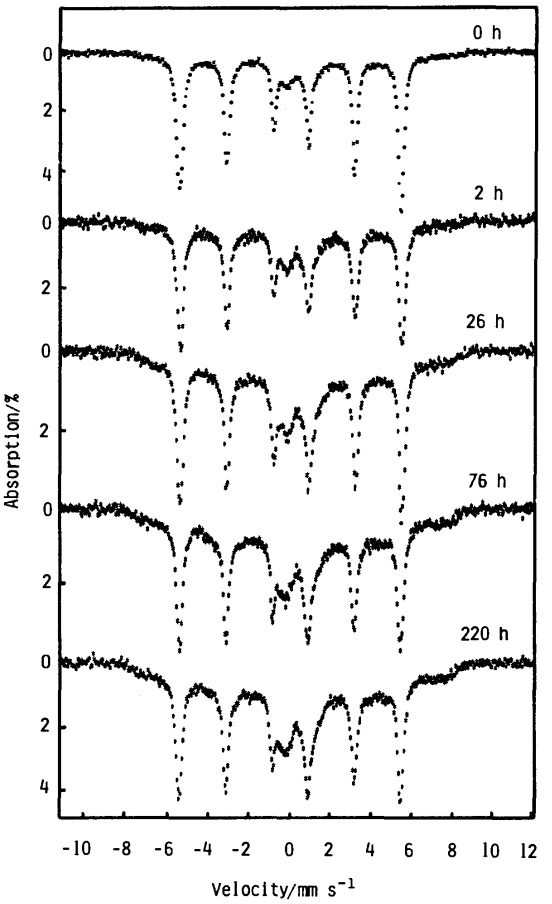

Fig. 2. Mössbauer spectra for the representative samples at 298 K.

Table 1. Mössbauer Data for the Samples at 78 K and the Diameter of the Metallic Iron Part

Sample (annealing time)/h	Metallic iron				Iron oxide					
	δ / mm s^{-1}	H / kOe	Γ_1[a] / mm s^{-1}	δ / mm s^{-1}	ΔE / mm s^{-1}	H / kOe	Γ_1[a] / mm s^{-1}	Γ_6[b] / mm s^{-1}	F[c] / %	d[d] / nm
0 (original)	0.168	345	0.405	0.549	−0.275	492	0.657	0.919	29	12.2
2	0.170	345	0.388	0.585	−0.336	487	1.398	1.222	44	10.6
8	0.163	345	0.440	0.575	−0.245	490	1.199	1.331	51	9.8
26	0.163	345	0.412	0.562	−0.280	489	1.208	1.250	57	9.2
76	0.171	346	0.469	0.487	−0.009	488	1.231	1.315	63	8.4
220	0.170	346	0.542	0.463	+0.079	488	1.315	1.389	61	8.8

a) Fwhm for the lowest energy line. b) Fwhm for the highest energy line. c) The ratio of absorption area for the oxide species to the total absorption area. d) The diameter of the metallic iron part remaining in the sample.

close to 494 kOe (the average of those for A and B sites at room temperature) for bulk γ-Fe_2O_3[19] and less than the value of 527 kOe (78 K) for 18 nm α-Fe_2O_3.[20] That for bulk Fe_3O_4 is known to be 492 kOe for Site A (tetra) and 461 kOe for Site B (octa) above the Verwey temperature (T_v=119 K for bulk).[21] The fields for Fe_3O_4 below the Verwey temperature are reported to be 511 and 499 kOe(at 4.2 K);[22] the line positions of their spectra approach each other, and it becomes difficult to distinguish clearly between γ-Fe_2O_3 and Fe_3O_4 except for a small shoulder in the lowest energy line. The Verwey temperature is reported to lie between 101 and 87 K for 10 nm Fe_3O_4.[23] The spectra show the existence of no Verwey transition above 78 K and no existence of absorption due to iron in the B sites. These facts support the idea that the iron oxides are not Fe_3O_4.

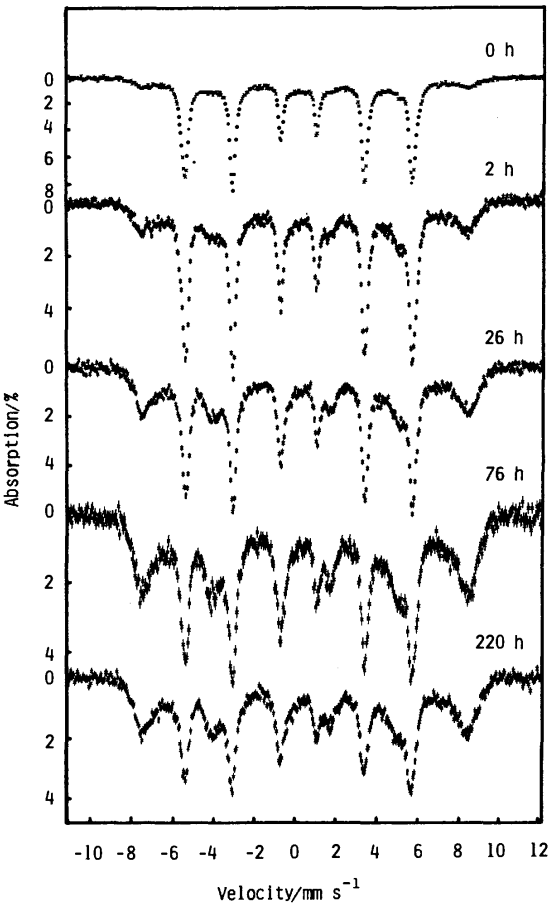

Fig. 3. Mössbauer spectra for the representative samples at 78 K.

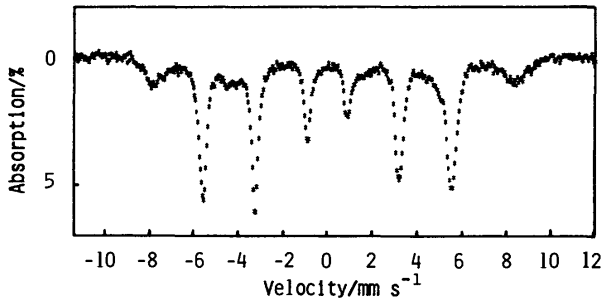

Fig. 4. Mössbauer spectrum for the original iron powder at 4.2 K.

A Mössbauer spectrum for the original sample was measured at 4.2 K; the spectrum is shown in Fig. 4. The spectrum consisted of two simple sextet patterns due to iron oxide and metallic iron, and the hyperfine field for the oxide was estimated to be 498 kOe, close to the value of 500 kOe (at 4.2 K) reported for 0.4 nm thick iron film (actually, this sample was oxidized) by Shinjo et al.[16] The lowest energy line does not split into a doublet, as is observed in the spectra of Fe_3O_4. Our spectra(δ=0.451 mm s^{-1}, ΔE=0.0 mm s^{-1} for the oxide) are in accord with those for γ-Fe_2O_3 and do not resemble the superparamagnetic behavior for Fe_3O_4 observed by Aharoni and Litt,[24] who reported larger isomer-shift values (δ=0.59 mm s^{-1} at 77 K and δ= 0.89 mm s^{-1} at 4.2 K).

The Mössbauer spectra for iron oxides in the original sample are similar to those for the annealed samples. Therefore the chemical structure of iron oxides in the original sample seems to be the same as that for the annealed sample. It is assumed that a minor component (less than 10—20% of the total absorption area in the spectra) can not be detected/resolved because the line positions for γ-Fe_2O_3 are close to those for Fe_3O_4 at 78 K or below. On the other hand, the surface of Fe_3O_4 undergoes a transformation from Fe_3O_4 to γ-Fe_2O_3 which is prominent on fine particles.[25] The thickness of the oxide layer for the original sample is estimated to be 5 monolayers, as will be described later. Therefore, the pattern observed supports the conclusion that the oxide consists of γ-Fe_2O_3. However, it is not possible to reach even a tentative conclusion concerning the mean 1—2 layers from the iron surface, which occupy 10—20% of the total ^{57}Fe in the original sample.

The intensity ratio of the six line patterns at 298 K for metallic iron is close to 3 : 2 : 1 : 1 : 2 : 3, which indicates that the magnetization is orientated at random. The intensity ratio for the spectra at 78 K is different from this ratio. The reason for this is derived from the facts that the samples prepared for low-temperature measurement were pressed to make a disk and that the shape anisotropy of the samples prefers to orientate.

The six lines for the metallic species are clearly observed, and the metallic absorption can be drawn unambiguously. The spectra of Fig. 5 were obtained by the subtraction of the metallic iron peaks from the spectra at 298 K shown in Fig. 2. These spectra show the characteristics of relaxation due to fine iron oxide particles; the superparamagnetic relaxation should

also be taken into account. The spectra are symmetric, and the FeO or Fe^{2+} absorptions observed in the spectra of ultrathin Fe_3O_4 film by Terashima and Bando[26] were not visible. A spectrum of the finest iron oxide particle is shown in Fig. 5(a), while a sextet of the magnetic hyperfine structure of iron oxide begins to appear in Figs. 5(c)—(f). However, a strong doublet in the center of the spectra is observed, even in Fig. 5(f), the sample of which was annealed at 110 °C for 220 h.

Interesting variations are found for the line positions. If the lines of the magnetic hyperfine pattern are denoted from low to high energy by the indices from $p1$ to $p6$, the parameter;

$$\Delta E' = p6 - p5 - (p2 - p1),$$

relates to the quadrupole interaction by means of this relationship;

$$\Delta E' = \frac{e^2qQ}{2} \times \frac{3\cos^2\theta - 1}{2}.$$

The parameter $\Delta E'$ for the iron oxide is approximately zero at 78 K. However, the quadrupole splitting ($\Delta E = e^2qQ/2$) for the paramagnetic components at 298 K is about 1.10 mm s^{-1}. The difference between $\Delta E'$ and ΔE is caused by the angle θ, which specifies the orientation of the V_{zz} axis with respect to the direction of the magnetic hyperfine field. It has been established that the spin structure is canted at temperatures below 300 K in the surface layer and/or in particles smaller than about 10 nm.[15,20,23]

Figure 6 shows a spectrum simulated for Fig. 5(e) using the motional narrowing formula derived by Wickman et al.[27] although fitting a theoretical curve is quite difficult and it is impossible to get a unique solution. The relaxation time of $3\tau_L$ (τ_L is the Larmor precession time 2×10^{-8} s) was obtained, the other parameters (positions, intensity ratio, and fwhm of the sextet of the magnetic hyperfine structure) used for the fitting were determined with reference to the spectra at 78 K. The fit is not good because of the reasons described above and because of the distribution of the particle size of the iron oxide. It should be noted that the paramagnetic components are observed in the spectra of samples annealed for a long time and that their intensities do not decrease with the annealing time, although the absorption lines with the magnetic hyperfine structure due to larger particles of the iron oxides do increase in intensity. These facts imply that very fine particles are always produced newly on iron surface during the annealing process. The oxide of the first monolayer on the iron surface is different from that of other layers, and an increase in the mole volume upon further chemical transformation leads to a disruption of the next first oxide layer into fine particles which grow over the iron surface. The following simple model of corrosion is considered (Fig. 7): I. In a first step, oxygen is adsorbed on the metal surface. The metal is now covered by one or two monolayers (these layers are considered to consist of Fe^{2+} and O^{2-}, but there has not yet been experimental proof of this.) II. Further oxidation leads to the formation of layers of γ-Fe_2O_3 up to about 5 nm. New fine iron oxides are formed on iron during the progress of the corrosion.

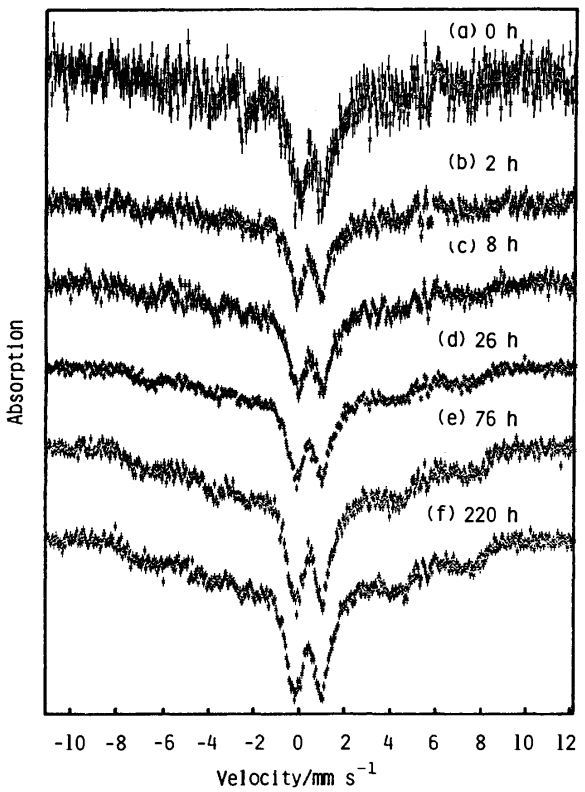

Fig. 5. Mössbauer spectra subtracted metallic iron peaks from the spectra at 298 K.

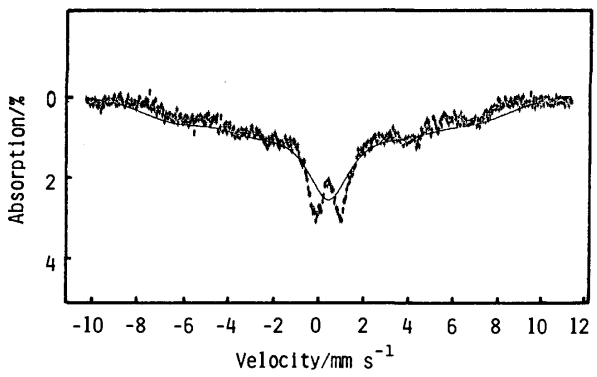

Fig. 6. Mössbauer spectrum for oxide species in the sample annealed at 110 °C for 220 h. The experimental spectrum is compared with a theoretical curve calculated on the basis of a simple model discussed in the text.

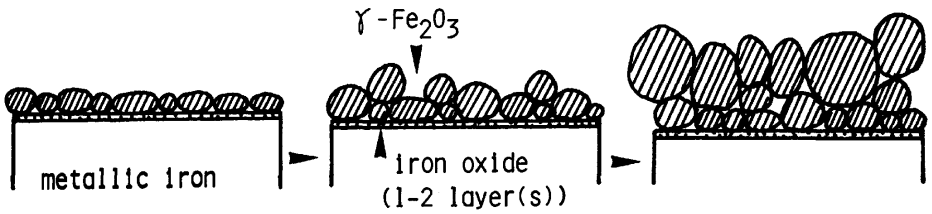

Fig. 7. A model proposed for corrosion of iron.

The recoilless fraction (f) of fine particles is of great interest. The Mössbauer spectrum of the original iron powder was measured at 4.2K in order to evaluate the fraction of metallic iron or iron oxide in the sample, for the recoilless fraction of iron oxide can be supposed to be equal to that of metallic iron at 4.2K. The metallic iron components in the original sample were estimated to be 86% of the total ^{57}Fe. From the relation of this value to the absorption area for individual chemical species at 78K, the ratios of residual metallic iron part to the total ^{57}Fe were evaluated for all the samples; they are shown in Table 1. The recoilless fraction of our sample is not very small; the f(78 K)/f(4.2 K) ratio for iron oxide was 0.78. It has been reported that f(300 K)/f(4.2 K) is 0.43 for very fine oxide (corresponding to 0.4 nm thick iron) and 0.78 for the oxide on 2.0 nm thick iron film.[16] Our datum supports the idea that recoilless fraction for very fine oxides is not so small as was suggested by Belozerskii et al.[28]

Taking a model that iron is oxidized uniformly from the surface of metallic iron and that metallic iron forms a continuous solid without micropores, the thickness of the metallic iron is estimated to be as listed in Table 1. The thickness of the oxide layer for the original sample is evaluated to be 2.1 nm. This thickness corresponds to the case formed if 1.4 nm of an iron layer (corresponding to 5 monolayers) is oxidized. Haneda and Morrish[15] have reported, from the line-broadening observed in the X-ray diffraction pattern using the Scherrer relation, that the average size of oxide is 2.7 nm. However, the Mössbauer spectrum reported by Haneda is similar to that for the sample annealed at 110 °C for 76 h in our experiment. Shinjo et al.[16] have reported that the oxide part is 59% of the total ^{57}Fe in 2.0 nm-thick iron film (corresponding to the thickness of 1.2 nm of metallic iron for a very thin layer of iron). From the kinetic study of oxygen absorption into iron metal, Quinn and Roberts[29] reported that oxidation to 6 layers occurs at 78 K. Fromm[30] and Fromm and Mayer[31] investigated the kinetics of oxygen absorption on evaporated metal film and reported that sorption-layer formation plus molecular chemisorption take place in the O_2/Fe system, that the initial sticking probability is not dependent on the temperature, and that layer formation is thermally activated at a higher coverage sorption. Although the sample treatment was not described in detail in these papers, our value (2.1 nm of iron oxide) is in accordance with the values they reported. This layer may be the thinnest one necessary to prepare metallic iron without severe autoxidation at room temperature in air.

References

1) L. N. Liebermann, D. R. Fredkin, and H. B. Shore, *Phys. Rev. Lett.*, **22**, 539 (1969).
2) W. Schnitker and H. Rau, *IEEE Trans. Magn.*, **16**, 14 (1980).
3) T. Shinjo, T. Matsuzawa, T. Mitutani, and T. Takada, *Jpn. J. Appl. Phys.*, **13**, Suppl. 2, Pt. 2, 729 (1974).
4) J. Lauer, W. Keune, and T. Shinjo, *Physica*, **86—88B**, 1409 (1977).
5) K. Levin, A. Liebsch, and K. H. Bennemann, *Phys. Rev.*, **B7**, 3066 (1973).
6) A. M. Pritchard and C. M. Dobson, *Nature*, **224**, 1295 (1969).
7) H. Onodera, H. Yamamoto, H. Watanabe, and H. Ebiko, *Jpn. J. Appl. Phys.*, **11**, 1380 (1972).
8) V. Ramshesh and K. Ravichandran, *Radiochem. Radioanal. Lett.*, **29**, 87 (1977).
9) N. Hosoito, T. Shinjo, and T. Takada, *J. Phys. Soc. Jpn.*, **50**, 1903 (1981).
10) K. Nomura and Y. Ujihira, "Applications of the Mössbauer Effect," ed by Yu. M. Kagan and I. S. Lyubutin, Gordon and Breach Sci. Pub., New York (1983), Vol. 3, p. 1185.
11) S. Asada, *Nippon Kagaku Kaishi*, **1984**, 1372.
12) W. Meisel, *J. Phys.*, **41**, Cl-63 (1980).
13) P. B. Sewell and M. Cohen, *J. Electrochem. Soc.*, **111**, 501 (1964).
14) A. M. van Diepen, H. J. Vledder, and C. Langereis, *Appl. Phys.*, **15**, 163 (1977).
15) K. Haneda and A. H. Morrish, *Surf. Sci.*, **77**, 584 (1978).
16) T. Shinjo, T. Iwasaki, T. Shigematsu, and T. Takada, *Jpn. J. Appl. Phys.*, **23**, 283 (1984).
17) G. W. Simmons, E. Kellerman, and H. Leidheiser, Jr., *Corrosion*, **29**, 227 (1973).
18) Y. Maeda, H. Oshio, Y. Takashima, M. Mikuriya, and M. Hidaka, *Inorg. Chem.*, **25**, 2958 (1986).
19) R. J. Armstrong, A. H. Morrish, and G. A. Sawatzky, *Phys. Lett.*, **23**, 414 (1966).
20) W. Kündig and H. Bömmel, *Phys. Rev.*, **142**, 327 (1966).

21) W. Kündig and R. S. Hargrove, *Solid State Commun.*, **7**, 223 (1969).
22) T. K. McNab, R. A. Fox, and A. J. F. Boyle, *J. Appl. Phys.*, **39**, 5703 (1968).
23) H. Topsøe and S. Mørup, "Proc. Intern. Conf. in Mössbauer Spectroscopy," Cracow, Vol. 1, 321 (1975).
24) S. M. Aharoni and M. H. Litt, *J. Appl. Phys.*, **42**, 352 (1971).
25) K. Haneda and A. H. Morrish, *J. Phys.*, **38**, Cl-321 (1977).
26) T. Terashima and Y. Bando, *J. Phys. Soc. Jpn.*, **54**, 3920 (1985).
27) H. H. Wickman, M. P. Klein, and D. A. Shirley, *Phys. Rev.*, **152**, 345 (1966).
28) G. Belozerskii, C. Bohm, T. Ekdahl, and D. Liljequist, *Nucl. Instrum. Methods*, **192**, 539 (1982).
29) C. M. Quinn and M. W. Roberts, *Trans. Faraday Soc.*, **60**, 899 (1964).
30) E. Fromm, *Surf. Sci.*, **52**, 401 (1975).
31) E. Fromm and O. Mayer, *Surf. Sci.*, **74**, 259 (1978).

 © 1987 The Chemical Society of Japan Bull. Chem. Soc. Jpn., 60, 3247—3254 (1987)

Chemical Behavior of an Oxygen Ligand in the Reaction between Oxo Complex of Ru^{IV} and Alcohols to Give Both Hydroxo and Alkoxo Complexes of Ru^{III}

Hirotaka NAGAO, Kimitake AOYAGI, Yasuhiko YUKAWA,† F. Scott HOWELL, Masao MUKAIDA,* and Hidetake KAKIHANA
Department of Chemistry, Faculty of Science and Technology, Sophia University, 7-1 Kioi-cho, Chiyoda-ku, Tokyo 102
(Received March 9, 1987)

Under mild conditions, *trans*-$[RuCl(O)(py)_4]^+$ in alcohols changes to an alkoxo complex, *trans*-$[RuCl(OR)(py)_4]^+$, The hydroxo complex, *trans*-$[RuCl(OH)(py)_4]^+$, which retains the reactive oxygen of the oxo complex, was found to exist as a precursor in the formation of the alkoxo complex. The reaction progress was traced by spectrometrical and ^{18}O-labelling experiments.

There has been growing interest in high-valence ruthenium complexes with a reactive oxygen ligand ($Ru^{IV}=O^{2-}$). This interest centers mainly on the chemical and electrochemical generation of the oxo ligand,[1-5] on structural and spectrochemical characterization of the moiety,[6-8] and on its reactivity, in particular as an oxygen-transfer agent.[9-13] We have reported a new synthetic route for an oxo complex of Ru^{IV}, *trans*-$[RuCl(O)(py)_4]^+$, which was prepared by the oxidation of a nitrosyl complex of Ru^{II}.[5,6] As an extension of this study, the chemical behavior of the ($Ru^{IV}=O^{2-}$) unit in the oxo complex toward alcohols (MeOH, EtOH, and *n*- and *i*-PrOH) was investigated. Such a study has not yet been reported, although Meyer et al. investigated a reaction of *cis*-$[Ru(O)(bpy)(trpy)]^{2+}$ (trpy: 2,2′:6′,2″-terpyridine) with *i*-PrOH containing large amounts of water from kinetic and mechanistic viewpoints.[10] They concluded that the reaction is initiated by a formation of the corresponding hydroxo complex of Ru^{III}, as an intermediate, which is the one-electron reduced species of the oxo complex of Ru^{IV}. Here, we report on synthetic evidence which proves the existence of the hydroxo complex of Ru^{III} as a precursor in the reaction of the oxo complex of Ru^{IV} with alcohols. Also reported is evidence that the reactivity of the ($Ru^{IV}=O^{2-}$) unit, as an oxidant toward alcohols, depends on the property of the oxo complex used for the reaction. Five new complexes were isolated as the reaction products between *trans*-$[RuCl(O)(py)_4]^+$ and the alcohols. Among the alkoxo complexes obtained here, the methoxo complex of Ru^{III} has already been reported in part.[5]

Experimental

Instruments and Reagents. IR spectra were measured on a Hitachi EPI G2 spectrometer. UV-vis spectra were recorded on a Hitachi 200-20 spectrometer. Magnetic moments were measured by the Gouy method. Elemental analyses were performed by the Sophia University Analytical Facility. Cyclic voltammetry and normal pulse voltammetry were carried out by using a Fuso Polarograph Model 321 with a stationary platinum disk electrode. $RuCl_3 \cdot nH_2O$ was purchased from Nippon Engelhardt. MeOH(Spectrosol), used for both synthetic and spectrometric studies was purchased from Wako Chemical Co. The CH_3CN, used for the electrochemical experiment, was purified by a procedure described in the literature.[5] All other chemicals were obtained as reagent grade and used without further purification. $H_2{}^{18}O$ (99.0%) was purchased from the Japan Radioisotope Association. Oxo complexes, *trans*-$[RuX(O)(py)_4]Y$ (X=Cl, Br; Y=ClO_4, PF_6), were prepared as starting materials of the present reactions by procedures described elsewhere.[5,13]

Isolation of Reaction Products. Chloro(hydroxo)tetrakis(pyridine)ruthenium(III) Hexafluorophosphate, [RuCl(OH)(py)$_4$]PF$_6$ (1A): $[RuCl(O)(py)_4]PF_6$ (100 mg) was dissolved in the mixed solution of MeOH–H_2O (15–15 cm^3). It was refluxed for 15 min., until the color changed from green to yellow. The solution was kept standing for 1—2 d at room temperature. The yellow crystals which appeared were collected, washed with ether, and dried in vacuo. Yield 70%. Found: C, 38.8; N, 9.0; H, 3.4%. Calcd for $C_{20}H_{21}ON_4ClPF_6Ru$: C, 39.1; N, 9.1; H, 3.4%.

Chloro(hydroxo)tetrakis(pyridine)ruthenium(III) Perchlorate, [RuCl(OH)(py)$_4$]ClO$_4$ (1B): This was prepared by the same procedure, using the corresponding oxo complex of perchlorate salt. Yield 60%. Found: C, 42.1; N, 9.8; H, 3.7%. Calcd for $C_{20}H_{21}N_4O_5Cl_2Ru$: C, 42.2; N, 9.8; H, 3.7%.

Chloro(methoxo)tetrakis(pyridine)ruthenium(III) Hexafluorophosphate, [RuCl(OMe)(py)$_4$]PF$_6$ (2A): Oxo complex (PF_6 salt 50 mg) was dissolved in methanol (25 cm^3), using a Erlenmeyer flask, and kept at room temperature for 2 d in the dark, until the solution color changed to greenish yellow. The volume of the solution was reduced to 5 cm^3 using a rotary evaporator to produce a red crystalline material. The product was filtered out, washed with acetone and then ether, and dried in vacuo. Yield 60%. Found: C, 40.0; H, 3.6; N, 8.8%. Calcd for $C_{21}H_{23}N_4OClPF_6Ru$: C, 40.1; H, 3.7; N, 8.9%.

Chloro(methoxo)tetrakis(pyridine)ruthenium(III) Perchlorate [RuCl(OMe)(py)$_4$]ClO$_4$ (2B): This was prepared by almost the same procedure as in **2A**, using the corresponding perchlorate salt of the oxo complex. Found: C, 43.4; H,

† Present address: Division of Chemistry, General Education Department, Niigata University, 8050 Ikarashi, Ninocho, Niigata 950-21.

4.0; N, 9.6%. Calcd for $C_{21}H_{23}N_4O_5ClRu$: C, 43.4; H, 4.0; N, 9.6%. The corresponding bromo complex, $[RuBr(OMe)(py)_4]PF_6$, was obtained by the same procedure, using the bromo complex as a starting material. Found: C, 40.1; H, 3.6; N, 8.9%. Calcd for $C_{21}H_{23}N_4OBrPF_6Ru$: C, 40.2; H, 3.7; N, 8.9%.

Chloro(ethoxo)tetrakis(pyridine)ruthenium(III) Hexafluorophosphate $[RuCl(OEt)(py)_4]PF_6$ (3A): Oxo complex (PF_6 salt, 80 mg) was dissolved in EtOH (100 cm^3), using a Erlenmeyer flask, and kept at room temperature for 5—6 d in the dark. When the solution color changed from green to pale yellow, the volume of the solution was quickly reduced using a rotary evaporator. A small amount of red crystals deposited. Excess ether was added to the solution (total volume 80—100 cm^3); this was then kept in a refrigerator overnight. The product was filtered out, washed with a mixed solvent (EtOH–ether) and then ether, and dried in vacuo. Yield 50%. Found: C, 40.8; H, 3.9; N, 8.5%. Calcd for $C_{22}H_{25}N_4OPF_6ClRu$: C, 41.1; H, 3.9; N, 8.7%. The corresponding bromo complex, $[RuBr(OEt)(py)_4]PF_6$, was obtained by the procedure described above, using $[RuBr(O)(py)_4]PF_6$. Found: C, 38.3; H, 3.7; N, 8.2%. Calcd for $C_{22}H_{25}ON_4BrPF_6Ru$: C, 38.4; H, 3.7; N, 8.2%.

Chloro(propoxo)tetrakis(pyridine)ruthenium(III) Hexafluorophosphate, $[RuCl(OPr^n)(py)_4]PF_6$ (4): Oxo complex (PF_6 salt, 35 mg) was suspended in *n*-PrOH (50 cm^3) using a Erlenmeyer flask (50 cm^3). The suspension was stirred for one week at room temperature in the dark, until a homogeneous pale yellow solution was obtained. After the solution was filtered out, the filtrate was concentrated using a rotary evaporator. When a small amount of red crystals deposited, ether was added to the solution (total volume 50 cm^3); this was then kept in a refrigerator overnight. The red crystals were collected, washed with ether–EtOH and then ether, and dried in vacuo. Found: C, 42.4; H, 4.3; N, 8.3%. Calcd for $C_{23}H_{27}ON_4ClPF_6Ru$: C, 42.0; H, 4.1; N, 8.5%. Yield 40%. The corresponding bromo complex, $[RuBr(OPr^n)(py)_4]PF_6$, could be obtained by the same procedure, using the PF_6 salt of the bromo oxo complex. Found: C, 39.2; H, 4.0; N, 7.9%. Calcd for $C_{23}H_{27}ON_4BrPF_6Ru$: C, 39.4; H, 3.9; N, 8.0%.

Chloro(isopropoxo)tetrakis(pyridine)ruthenium(III) Hexafluorophosphate, $[RuCl(OPr^i)(py)_4]PF_6$ (5): The complex was prepared by almost the same procedure as that for **4**. Yield 40%. Found: C, 41.8; H, 4.1; N, 8.3%. Calcd for $C_{23}H_{27}ON_4ClPF_6Ru$: C, 42.0; H, 4.1; N, 8.5%. All the alkoxo complexes were stored under argon to avoid hydrolysis (described later).

^{18}O Labelling. Complex **4** (8 mg) was dissolved in $H_2{}^{18}O$ (1 cm^3) containing a small amount of HPF_6; the solution was heated until a pale green solid ($[RuCl(^{18}OH)(py)_4]PF_6$) deposited. After removal of the solid, $(NH_4)_2Ce(NO_3)_6$ was added to the mother liquor, and the solution was gently warmed until its color changed to green (2—3 min), and then cooled down to room temperature. NH_4PF_6 (6 mg) was added until a green product ($[RuCl(^{18}O)(py)_4]PF_6$) appeared. Both products were collected by sintered-glass filters and washed by a mixed solvent of EtOH and ether and then by ether. The ^{18}O incorporation was found to be achieved almost completely, based on the relative intensity of the $\nu(^{18}OH)$ and $\nu(^{16}OH)$ in the hydroxo complex.

X-Ray Data Collection. Crystals (**1A** and **2B**) were used for the measurements without shaping. Crystal data are as follows. For **1A**: tetragonal, with space group $P4/ncc$, a=25.937(4) Å, c=14.469(1) Å, V=9733(2) Å^3, μ(Mo $K\alpha$)=8.78 cm^{-1}, F.W.=614.9, Z=16, D_m=1.67 g cm^{-3}, D_x=1.68 g cm^{-3}. For **2B**: monoclinic, $P2_1/n$, a=22.311(3) Å, b=13.546(2) Å, c=8.091(1) Å, β=95.89°, V=2432.4(6) Å^3, μ=8.91 cm^{-1}, F.W.=583.4, Z=4, D_m=1.58 g cm^{-3}, D_x=1.59 g cm^{-3}. The reflections were collected by ω-scan technique ($2\theta<55°$ for **1A**, $2\theta<50°$ for **2B**) on a Rigaku AFC-6A automated four-circle diffractometer, with graphite monochromated Mo $K\alpha$ radiation (0.7107 Å). The 3123 (for **1A**) and 6154 (for **2B**) independent reflections with $|F_o|>3\sigma(|F_o|)$ were used for a structure refinement. The intensities were corrected for Lorentz and polarization factors, but no correction was made for the absorption. All the calculations were carried out in a HITAC M-200H computer at the Computer Center of the University of Tokyo, using a local version of UNICS.[14] The atomic scattering factors were taken from the Tables.[15]

Structure Determination. The structures were solved by a heavy-atom method. The positions of Ru and Cl atoms were obtained from a three-dimensional Patterson function, while the positions of all the non-hydrogen atoms were successively located by Fourier syntheses. In case of **2B**, all hydrogen atoms of both pyridine and methoxyl groups were found at reasonable positions on the final difference Fourier map; they were then included in the calculation, while those of **1A** were calculated and fixed, since only a few positions of hydrogen atoms were obtained.

Positions and thermal parameters of all other atoms were refined by a repeated block-diagonal least-squares method. The weighting scheme was $W=1/[\{\sigma(|F_o|)\}^2+(0.02\times|F_o|)^2]$. In the last cycle of the refinement with anisotropic temperature factors for all non-hydrogen atoms, all the parameter shifts were less than one-third of the corresponding standard deviations. The final R values ($R=\Sigma||F_o|-|F_c||/\Sigma|F_o|$) were 0.083 for **1A** and 0.040 for **2B**. The F_o-F_c data and the anisotropic temperature parameters are deposited as Document No. 8752 at the Office of the Editor of the Bulletin of the Chemicai Society of Japan.

Results and Discussion

Spectral Change Observed for *trans*-$[RuCl(O)(py)_4]^+$ in MeOH. A green methanol solution of *trans*-$[RuCl(O)(py)_4]PF_6$ changes gradually to yellow-orange while standing at room temperature. The reaction which gave the hydroxo complex of Ru^{III} was monitored by spectrophotometry; its progress can be conveniently divided into three steps (in Fig. 1). A freshly prepared methanol solution of the oxo complex exhibits a strong absorption band at 265 nm and a weak band at 690 nm. In the first stage of the reaction ([A] in Fig. 1), the intensity of the band at 265 nm slowly decreased as a new band appeared at 285 nm. The intensity of this new band developed as it moved to 296 nm (this took about 50 h). The weak band at 690 nm also decreased in intensity and was replaced by a weak band at 640 nm, which remained without remarkable changes in either wave length or intensity until the solution color changed to yellow.

In the second stage ([B]), the band at 296 nm shifted slightly to 300 nm, while its intensity decreased (60—70 h). Later (dotted line in [B]), two new bands appeared near 245 and 375 nm, with further decreasing of the intensity of the two bands at 265 and 300 nm. The presence of an isosbestic point could not be observed in any stage. When the experiment was attempted in a preparative scale, using the PF_6 salt of the oxo complex, the solution obtained in the first stage of the reaction gave a yellow product when the solution volume is reduced, while that of the second step gives red crystals. The yellow crystalline product could be isolated when the intensities of the two absorption bands at 265 and 296 nm became almost the same.

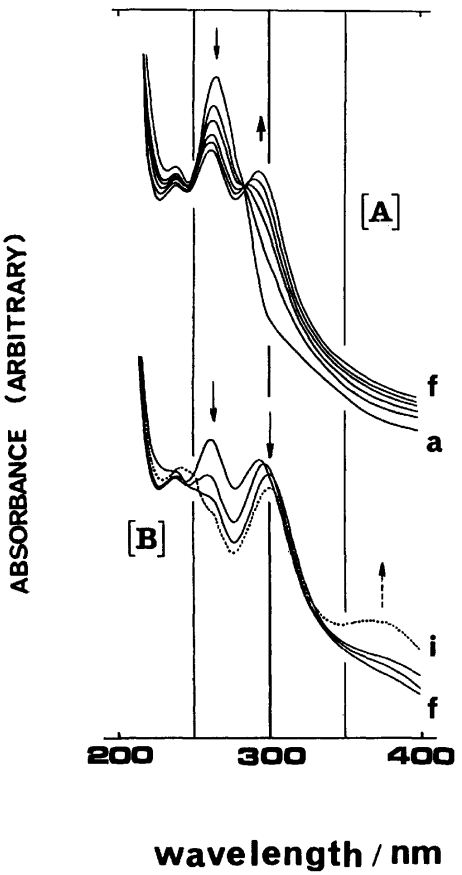

Fig. 1. UV spectral Change of $[RuCl(O)(py)_4]PF_6$ (6.5×10^{-5} mol dm^{-3}) in MeOH at room temperature (22 °C).
[A]: 1st step of the reaction, (a) immediately after, (b) 10 h, (c) 25 h, (d) 37 h, (e) 45 h, (f) 51 h. [B]: 2nd and 3rd (dotted line) steps, (f) 51 h, (g) 61 h, (h) 68 h, (i) 75 h. Arrows illustrate the direction of change of the peaks on subsequent scans.

The experimental conditions for the isolation of the yellow crystals are rigid, since it appears to be short-lived relative to the red one. The experimental data (analyses, CV, UV-vis, and IR) observed for both yellow and red crystals are the same as those of **1A** and **2A** prepared as authentic samples. The spectrometric experiment showed that the addition of a small amount of water (1—3 cm^3) to the methanol solution served to slow down the progress of the reaction, where the same products can be observed to form. No spectral evidence which suggested the formation of the aqua complex of Ru^{II}, $[RuCl(H_2O)(py)_4]^+$, as the two-electron reduced species of the original oxo complex, could be observed. The aqua complex of Ru^{II} could only be formed when the oxo complex was reduced in an acidic aqueous solution by a strong reductant such as Zn-Hg amalgam.[16]

Characterization of Reaction Products between the Oxo Complex and Alcohols. The reaction products were formulated as the hydroxo and alkoxo complex of Ru^{III}, **1** and **2—5** (Table 1), based on analyses, magnetic measurements, cyclic voltammetry, IR spectra, and X-ray structure determination (for **1A** and **2B**). The effective magnetic moments for **1A** and **2B** were found to be 2.05 and 2.15 B.M., respectively. These values are almost the same as that observed for $[RuCl_2(py)_4]PF_6$ and are close to spin-only values for one-unpaired spin.[17]

The cyclic voltammograms of all these complexes in CH_3CN exhibit reversible reduction waves at −0.7——0.8 V (vs. $Ag|AgClO_4$ (0.1 mol dm^{-3} in CH_3CN) at 25 °C), which is a reasonable potential

Table 1. Products and Their Properties

Complex		μ_{eff}/μ_B[a]	$E_{1/2}$/V[b]	$E_{pc(ox)}$/V	$\lambda(\varepsilon)$[c]
$[RuCl(OH)(py)_4]PF_6$	**1A**	2.05	−0.68	≈1.4	297 (1.2×10^4) 262 (1.0×10^4)
$[RuCl(MeO)(py)_4]ClO_4$	**2B**	2.15	−0.74	1.0, ≈1.4	427 (2.3×10^3) 301 (1.2×10^4)
$[RuCl(EtO)(py)_4]PF_6$	**3A**		−0.77	1.0, ≈1.4	434 (2.2×10^3) 302 (1.1×10^4)
$[RuCl(n\text{-}PrO)(py)_4]PF_6$	**4**		−0.78	1.0, ≈1.4	437 (2.1×10^3) 302 (1.0×10^4)
$[RuCl(i\text{-}PrO)(py)_4]PF_6$	**5**		−0.79	1.0	433 (2.2×10^3) 300 (1.0×10^4)

a) 22 °C. b) Ru^{II}/Ru^{III} couple (vs. $Ag|AgClO_4$ (0.1 mol dm^{-3} in CH_3CN)) at 25 °C. c) nm(ε/dm^3 mol^{-1} cm^{-1}) in CH_3CN.

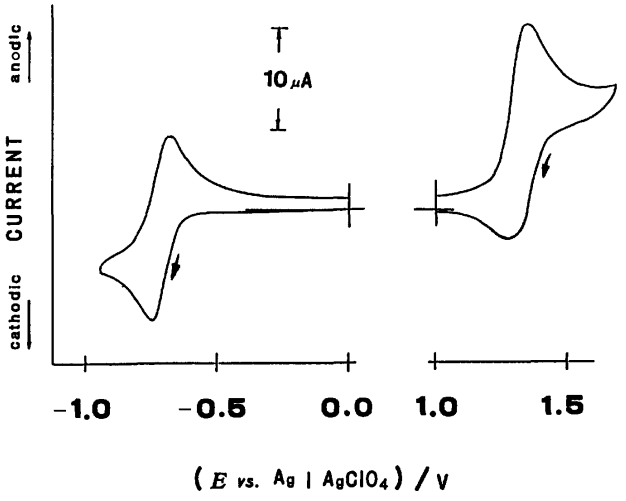

Fig. 2. Cyclic voltammograms of $[RuCl(OH)(py)_4]^+$ **1A** at a stationary platinum electrode in 0.1 mol dm^{-3} TEAP-CH_3CN at 25 °C (scan rate 200 mV s^{-1}).

region for $Ru^{III/II}$ reduction. A typical cyclic voltammogram of **1A** is shown in Fig. 2. The results are summarized in Table 1. The current heights, observed by the normal pulse voltammetry at the same experimental conditions, of the reduction waves of these complexes were almost the same as that of $[RuCl_2(py)_4]PF_6$, which has been well characterized in our laboratory.[17] At the oxidative scan the cyclic voltammogram of **1A** exhibits an irreversible one-electron oxidation wave at 1.39 V. The oxidation potential of **1A** appeared at almost the same potential region as that of $[RuCl_2(py)_4]PF_6$, which indicates a

Table 2. Infrared Spectra of **1A** and the Labelled (^2H and ^{18}O) Complexes

1A	^2H-**1A**[a]	^{18}O-**1A**[b]		Assignment
3544	2620	3530	s,sharp	ν(OH)
938	c)	936	m	δ(RuOH)
599	580	570	s	ν(RuO)

a) $[RuCl(OD)(py)_4]PF_6$. b) $[RuCl(^{18}OH)(py)_4]PF_6$. c) Overlapped with a band due to py ligand.

Table 3. Final Positional Parameters ($\times 10^4$ for Non-Hydrogen Atoms Except for the Atoms of PF_6 Anion; $\times 10^3$ for Hydrogen Atoms and for PF_6 Anion) and Equivalent Isotropic Temperature Factors (B_{eq}/Å^2) for $[RuCl(OH)(py)_4]^+$ **1A**

Atom	*X*	*Y*	*Z*	B_{eq}/Å^2	Atom	*X*	*Y*	*Z*	B_{iso}/Å^2
Ru	52.5(3)	1827.5(3)	1333.0(6)	2.79	P (7)	−250	250	500	4.30(1)
Cl	5(1)	2429(1)	96(2)	3.98	F (51)	−71(1)	448(1)	188(1)	15.00
O	113(3)	1370(3)	2404(5)	4.31	F (52)	−22(1)	496(1)	153(1)	15.00
N (1)	587(3)	1377(3)	597(7)	3.63	F (53)	12(1)	435(1)	221(1)	15.00
N (2)	643(4)	2256(3)	1930(6)	3.20	F (61)	250	250	367(1)	5.13(3)
N (3)	−491(3)	2253(3)	2070(7)	3.35	F (62)	250	250	587(1)	5.15(3)
N (4)	−527(3)	1378(3)	752(6)	3.29	F (63)	206(0)	208(0)	473(1)	9.54(3)
C (11)	975(5)	1151(5)	1024(10)	4.76	F (71)	−250	250	389(2)	16.66(7)
C (12)	1317(5)	837(6)	548(13)	6.82	F (72)	−311(0)	246(0)	494(1)	8.31(2)
C (13)	1263(6)	774(6)	−370(12)	6.69	H (11)	102	121	176	7.00
C (14)	871(6)	1009(5)	−817(11)	6.37	H (12)	163	64	94	7.00
C (15)	537(5)	1309(5)	−330(9)	4.29	H (13)	153	53	−75	7.00
C (21)	641(5)	2343(5)	2851(8)	4.12	H (14)	82	96	−158	7.00
C (22)	1032(5)	2629(5)	3299(9)	4.41	H (15)	21	151	−70	7.00
C (23)	1418(5)	2806(5)	2785(8)	4.50	H (21)	33	218	326	7.00
C (24)	1427(4)	2724(5)	1884(10)	4.78	H (22)	101	271	405	7.00
C (25)	1048(4)	2439(4)	1451(8)	3.69	H (23)	173	302	312	7.00
C (31)	−875(5)	2015(5)	2538(9)	4.77	H (24)	174	289	147	7.00
C (32)	−1240(5)	2269(6)	3020(10)	6.17	H (25)	106	236	70	7.00
C (33)	−1236(6)	2826(5)	2998(11)	5.90	H (31)	−89	159	252	7.00
C (34)	−871(6)	3054(5)	2525(11)	5.74	H (32)	−154	205	342	7.00
C (35)	−488(5)	2775(4)	2090(9)	4.14	H (33)	−153	305	337	7.00
C (41)	−490(5)	870(4)	769(10)	4.60	H (34)	−87	348	247	7.00
C (42)	−878(5)	537(5)	457(12)	6.10	H (35)	−17	298	174	7.00
C (43)	−1313(6)	742(6)	100(13)	6.88	H (41)	−13	70	104	7.00
C (44)	−1351(5)	1264(6)	64(11)	5.70	H (42)	−83	11	52	7.00
C (45)	−958(5)	1581(5)	417(9)	4.49	H (43)	−163	50	−17	7.00
				B_{iso}/Å^2	H (44)	−170	145	−24	7.00
P (5)	−30(0)	470	250	6.61(1)	H (45)	−101	201	40	7.00
P (6)	250	250	474(0)	4.10(1)					

reversible couple of $Ru^{III/IV}$.[17] The smallness of the cathodic response in **1A** indicates that the facile deprotonation occurs in (Ru^{III}-OH^{-}) group to give ($Ru^{IV}=O^{2-}$).[5] In the methoxo complex **2B**, two irreversible oxidation waves were observed at 1.0 and 1.4 V regions. A ligand oxidation reaction in MeO ligand is expected to occur in these potential regions.

The IR spectra of **1A** are essentially the same as those of $[RuCl_2(py)_4]PF_6$, except for the absorption bands observed at 3544, 938, and 599 cm^{-1}, which are assignable to ν(OH), δ(RuOH), and ν(RuO) respectively, as are shown in Table 2. ^2H- and ^{18}O- labelling experiments using $[RuCl(OD)(py)_4]^+$ and $[RuCl(^{18}OH)(py)_4]^+$ support these assignments. The IR spectra of **2** could also be reasonably assigned by a comparison with those for its deuterated complex, $[RuCl(OCD_3)(py)_4]^+$. Several IR studies on the assignment of the methoxyl ligand have been reported.[18] Upon the deuteration, the methoxyl CH stretching vibration bands at 2860 and 2786 cm^{-1} shifted to 2172 and 2040 cm^{-1}, respectively. The methoxyl CH bending vibration band at 1422 cm^{-1} disappeared; it is thought to have shifted over to near the 1100 cm^{-1} region, where a strong absorption band due to ClO_4^- was observed. The band at 1035 cm^{-1} which is believed to be due to methoxyl CO stretching vibration, shifted to 1004 cm^{-1}. The Ru-O stretching vibration at 549 cm^{-1} shifted to 526 cm^{-1} in its deuterated complex. These shifts found in C-O and Ru-O stretching vibrations are regarded as being reasonable for the deuteration of a methoxyl group coordinated to metals.[18]

The structure of both **1A** and **2B** were determined to confirm the above characterization. The final atomic parameters are listed in Tables 3 and 4. The perspective drawings of **1A** and **2B**, and the numbering schemes of the atoms are given in Figs. 3 and 4. Selected interatomic distances and angles are given in Tables 5 and 6. The cations are a hydroxo complex ion and a methoxo complex ion of Ru^{III}. They have the expected trans octahedral geometry, with pyridine nitrogen atoms approximately in a plane containing the ruthenium atom. As can be seen in Figs. 3 and 4, **1A** and **2B** have a propeller-like structure similar to those of both oxo and nitrosyl complexes,[5,19] used as starting material for the present reaction. No remarkable difference between the

Table 4. Final Positional Parameters ($\times 10^4$ for Non-Hydrogen Atoms; $\times 10^3$ for Hydrogen Atoms) and Equivalent Isotropic Temperature Factors (B_{eq}/Å^2) for $[RuCl(OMe)(py)_4]^+$ **2B**

Atom	X	Y	Z	B_{eq}/Å^2	Atom	X	Y	Z	B_{eq}/Å^2
Ru	1145.1(1)	−1781.4(2)	88.5(4)	2.40	O(51)	3856(3)	−90(3)	1911(6)	9.63
Cl(1)	527.2(5)	−813.7(8)	−1855.6(16)	3.72	O(52)	3451(3)	−1465(4)	474(6)	9.24
O(1)	1685(1)	−2597(2)	1529(4)	3.49	O(53)	3451(2)	−1392(4)	3271(6)	7.86
N(1)	1439(2)	−502(3)	1360(5)	2.95	O(54)	4327(2)	−1610(4)	2044(9)	10.39
N(2)	1855(2)	−1649(3)	−1388(5)	3.40					B_{iso}/Å^2
N(3)	892(2)	−3082(2)	−1213(5)	2.91	H(11)	228(2)	−94(3)	167(6)	3.58(10)
N(4)	399(2)	−1901(2)	1474(5)	2.81	H(12)	264(2)	47(3)	293(5)	3.11(9)
C(11)	1066(2)	240(3)	1638(6)	3.45	H(13)	207(2)	168(4)	349(7)	6.97(14)
C(12)	1265(2)	1096(4)	2419(7)	4.46	H(14)	97(3)	144(5)	263(7)	7.44(15)
C(13)	1870(3)	1201(4)	2956(7)	4.78	H(15)	62(2)	16(4)	134(6)	4.78(12)
C(14)	2254(2)	445(4)	2681(7)	4.26	H(21)	171(2)	−20(3)	−197(6)	4.61(10)
C(15)	2030(2)	−391(3)	1895(6)	3.37	H(22)	245(3)	−3(5)	−374(8)	8.81(18)
C(21)	1968(2)	−800(4)	−2142(7)	4.96	H(23)	302(3)	−125(6)	−399(10)	11.06(25)
C(22)	2426(3)	−720(6)	−3162(8)	6.62	H(24)	295(2)	−275(4)	−285(7)	7.22(15)
C(23)	2765(3)	−1521(7)	−3463(8)	7.35	H(25)	215(2)	−302(3)	−98(5)	3.18(9)
C(24)	2648(3)	−2408(6)	−2673(8)	6.48	H(31)	86(2)	−255(4)	−352(6)	5.11(12)
C(25)	2197(2)	−2438(4)	−1646(7)	4.40	H(32)	73(3)	−408(5)	−483(8)	9.33(19)
C(31)	820(2)	−3108(3)	−2884(6)	3.61	H(33)	43(3)	−523(5)	−334(7)	8.02(16)
C(32)	699(3)	−3971(4)	−3752(7)	4.68	H(34)	72(2)	−536(4)	−58(6)	5.27(13)
C(33)	654(3)	−4830(4)	−2916(7)	5.23	H(35)	93(2)	−386(3)	73(6)	4.13(10)
C(34)	713(3)	−4816(4)	−1206(7)	5.10	H(41)	−9(2)	−239(3)	−34(6)	4.11(11)
C(35)	840(2)	−3927(3)	−404(6)	3.74	H(42)	−99(2)	−267(4)	91(7)	6.35(14)
C(41)	−119(2)	−2262(4)	732(6)	3.55	H(43)	−94(3)	−217(4)	363(7)	6.06(15)
C(42)	−632(2)	−2355(4)	1520(7)	4.33	H(44)	−2(2)	−147(4)	493(7)	6.02(12)
C(43)	−622(2)	−2072(5)	3151(7)	5.07	H(45)	76(2)	−130(3)	360(6)	4.01(10)
C(44)	−100(2)	−1677(4)	3921(7)	4.61	H(61)	195(2)	−305(3)	365(6)	5.39(12)
C(45)	399(2)	−1600(4)	3057(6)	3.47	H(62)	152(3)	−270(5)	361(7)	9.39(16)
C(Me)	1738(3)	−2625(4)	3224(7)	5.01	H(63)	163(2)	−188(4)	379(7)	6.14(14)
Cl(50)	3762(1)	−1110(1)	1923(2)	3.71					

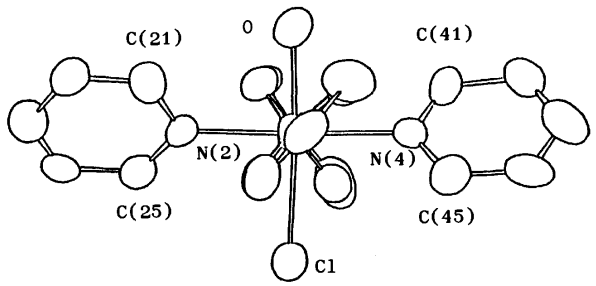

Fig. 3. Perspective drawing of $[RuCl(OH)(py)_4]^+$ **1A** and the numbering scheme.

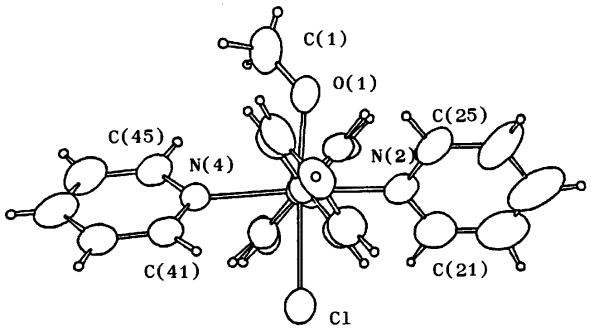

Fig. 4. Perspective drawing of $[RuCl(OMe)(py)_4]^+$ **2B** and the numbering scheme.

Table 5. Selected Interatomic Distances and Bond Angles for $[RuCl(OH)(py)_4]^+$ **1A**

	l/Å		*l*/Å
Ru-Cl	2.377(3)	N(1)-C(11)	1.32(2)
Ru-O	1.957(9)	C(11)-C(12)	1.38(2)
Ru-N(1)	2.100(10)	C(12)-C(13)	1.35(3)
Ru-N(2)	2.086(9)	C(13)-C(14)	1.35(2)
Ru-N(3)	2.081(9)	C(14)-C(15)	1.37(2)
Ru-N(4)	2.086(9)	C(15)-N(1)	1.36(2)
	φ/°		*φ*/°
Cl-Ru-O	176.0(3)	N(1)-Ru-N(3)	178.1(4)
Cl-Ru-N(1)	91.0(3)	N(2)-Ru-N(4)	178.2(4)
Cl-Ru-N(2)	90.0(3)		
Cl-Ru-N(3)	90.2(3)		
Cl-Ru-N(4)	91.5(3)		

Table 6. Selected Interatomic Distances and Bond Angles for $[RuCl(OMe)(py)_4]^+$ **2B**

	l/Å		*l*/Å
Ru-Cl	2.376(1)	O(1)-C(1)	1.365(5)
Ru-O(1)	1.937(2)	N(1)-C(11)	1.353(5)
Ru-N(1)	2.086(2)	C(11)-C(12)	1.375(5)
Ru-N(2)	2.087(3)	C(12)-C(13)	1.357(5)
Ru-N(3)	2.099(2)	C(13)-C(14)	1.368(5)
Ru-N(4)	2.104(2)	C(14)-C(15)	1.368(5)
		C(15)-N(1)	1.337(4)
	φ/°		*φ*/°
Cl-Ru-O	175.45(6)	Ru-O(1)-C(1)	127.1(2)
Cl-Ru-N(1)	89.93(7)	N(1)-Ru-N(3)	177.27(9)
Cl-Ru-N(2)	89.80(8)	N(2)-Ru-N(3)	177.17(10)
Cl-Ru-N(3)	91.33(6)		
Cl-Ru-N(4)	87.65(7)		

structures of **1A** and of **2B** could be observed, except that the CH_3 group of the methoxyl ligand was directed to bisect the N(1)-Ru-N(4) angle, with Ru-O-C angle of 127.1.(2)°. A similar structure of the CH_3O moiety has been found in $[Mn^{IV}(TPP)(OCH_3)_2]$.[18] The hydroxyl or the methoxyl oxygen and the chlorine atoms are almost on the line including the Ru atom: 175°. The Ru-O bond distances, 1.957(9) Å (for **1A**) and 1.937(2) Å (for **2B**) are shorter than the sum of the single bond radii for Ru^{III}-O^{2-} 2.03 Å),[20] but they are significantly longer than the value of 1.862(8) Å observed for the oxo complex, the starting material. Its bond length is consistent with the bond order of two. The Ru-Cl distances, trans to the oxygen atom, are 2.377(3) Å (for **1A**) and 2.376(1) Å (for **2B**). These distances are comparable to the values reported for various Ru^{III} complexes, and they are considerably longer than those of the original nitrosyl or the oxo complexes, where the shortening of the Ru-Cl distance trans to NO^+ or O^{2-} has been expected due to their ability to act as strong acceptor ligands.[2,21] The Ru-N distances vary from 2.081(9) Å to 2.104(2) Å. These values are almost the same as those of the original oxo complex, though less shortening was observed than in the cases of $[RuCl(NO)(py)_4]^{2+}$ or $[Ru(py)_6]^{2+}$.[19,22] The crystal data of **1A**, as well as its crystal packing, are almost the same as those of the original oxo complex.[5,23] The existence of the hydrogen atom in the OH moiety appears to be an unimportant factor in determining their crystal structures.

Reactivity of (Ru^{IV}=O^{2-}) Unit. Under mild conditions, *trans*-$[RuCl(O)(py)_4]^+$ in neat MeOH gave two complexes: The hydroxo and the methoxo complex. A formulation of the latter as a complex which involves a methanol molecule as a ligand or a solvent of crystallization can be ruled out. The spectral and synthetic investigations mentioned earlier proved that the hydroxo complex was a precursor in the formation of the methoxo complex. This appears to be the first example to be synthetically confirmed. It had also become apparent that the reactivity of the (Ru^{IV}=O^{2-}) unit depends on the oxo complex used for the reaction. As described above, the hydroxo complex of Ru^{III}, *trans*-$[RuCl(OH)(py)_4]^+$, and the methoxo complex of Ru^{III}, *trans*-$[RuCl(OMe)(py)_4]^+$, were confirmed to be the first and the

second products obtained. Although the first product of the present reaction was the same as that reported by Meyer et al. in the mechanistic study of *cis*-$[Ru(O)(bpy)(trpy)]^{2+}$ in 2-propanol containing water,[10] the second product was different; the second product in their work was an aqua complex of Ru^{II}, while that found in the present work was the alkoxo complex of Ru^{III}. Their reaction progress where 2-propanol is oxidized to acetone has been reported as follows (Eqs. 1—4):[10]

$$2(Ru^{IV}=O^{2-})^{2+} + (CH_3)_2CHOH \longrightarrow 2(Ru^{III}-OH^{-})^{2+} + (CH_3)_2CO\cdot \quad (1)$$

This reaction (Eq. 1) has been believed to occur via the following reactions (Eqs. 2 and 3):

$$(Ru^{IV}=O^{2-})^{2+} + (CH_3)_2CHOH \longrightarrow (Ru^{II}-OH_2)^{2+} + (CH_3)_2CO \quad (2)$$

$$(Ru^{IV}=O^{2-})^{2+} + (Ru^{II}-OH_2)^{2+} \longrightarrow 2(Ru^{III}-OH^{-})^{2+}. \quad (3)$$

In the final step, the hydroxo complex produced in Eq. 1 undergoes a further reduction to an aqua complex of Ru^{II}:

$$2(Ru^{III}-OH^{-})^{2+} + (CH_3)_2CHOH \longrightarrow 2(Ru^{II}-OH_2)^{2+} + (CH_3)_2CO\cdot \quad (4)$$

It should be emphasized that, under our experimental conditions, no evidence indicating any formation of the aqua complex of Ru^{II}($[RuCl(OH_2)(Py)_4]^+$), which corresponds to the final product in Eq. 4, could be observed by spectral monitoring.

The origin of the hydroxyl hydrogen atom in **1** could no be clarified. Meyer et al., have stated that the reduction of *cis*-$[Ru(O)(bpy)(trpy)]^{2+}$ to the corresponding hydroxo complex (Eq. 1) is initiated by a hydride transfer from the α-C-H bond of the 2-propanol to ($Ru^{IV}=O^{2-}$) unit.[10] A direct application of their mechanism to the present reaction appears to be difficult, owing to a disagreement in the spectral observations. They found isosbestic points due to the formation of first the hydroxo complex of Ru^{III} (Eq. 1) and then the aqua complex of Ru^{II} (Eq. 4), whereas the present reaction does not exhibit those points. Although a hydride-transfer mechanism can be acceptable if the aqua complex of Ru^{II} is confirmed to exist before the hydroxo complex formation occurs (Eq. 2), such an aqua complex as the intermediate species is not detectable, because it appears that the intermediate species is not built up to appreciable concentrations or is too short-lived to be seen spectrophotometrically.[10]

The alkoxo complex **3**—**5** undergo a facile hydrolysis to give the hydroxo complex, while the hydrolysis of **2** is extremely slow. Treatment of the hydrolysis solution with Ce^{4+}, used as an oxidant in acidic conditions, gave the original oxo complex quantitatively. By the same procedure using $H_2{}^{18}O$ (99%) $[RuCl(^{18}O)(py)_4]PF_6$ could be obtained from the alkoxo complex **4**. Upon ^{18}O substitution, the IR absorption band due to ν(RuO), observed at 804 cm^{-1} for the original oxo complex, disappeared. This finding suggests the existence of an ^{18}O atom in the product, although the IR absorption band ($\nu(Ru^{18}O)$) could not be confirmed, since the region where this would be expected (780—760 cm^{-1}) was hidden by the strong absorption band from the pyridine moiety. $[RuCl(^{18}OH)(py)_4]PF_6$ could also be isolated in this stage before the formation of the ^{18}O-labelled oxo complex occurs, without addition of any oxidant. The labelling experiment can be illustrated by the following scheme:

$$[Ru^{III}Cl(OR)(py)_4]^+ + H\text{-}\overset{*}{O}\text{-}H \longrightarrow [Ru^{III}Cl(\overset{*}{O}H)(py)_4]^+ + ROH \quad (5)$$

$$[Ru^{III}Cl(\overset{*}{O}H)(py)_4]^+ \longrightarrow [Ru^{IV}Cl(\overset{*}{O})(py)_4]^+ + e^- + H^+. \quad (6)$$

If we assume that the alkoxo complex formation occurs by a water-condensation reaction between alcohol and the hydroxo complex, the reverse reaction of the schemes (Eqs. 5 and 6) may be indicative of the behavior of the ($Ru^{IV}=O^{2-}$) unit in *trans*-$[RuCl(O)(py)_4]^+$ toward alcohols; the alkoxo complex does not retain the oxygen atom in the ($Ru^{IV}=O^{2-}$) unit, whereas the hydroxo complex can be considered to retain it.

At room temperature, *trans*-$[RuCl(OMe)(py)_4]^+$ **2B** dissolved in methanol changed from yellow-orange to red after long standing. The absorption spectra of the solution was scanned repeatedly between 230—500 nm for 20 d. As shown in the dotted line of [B] (Fig. 1), decreasing of intensities of the bands at 265 and 300 nm and developing of the bands at 245 and 375 nm were observed, with isosbestic points forming at 237, 255, and 327 nm. A methoxo complex of Ru^{II}, $[RuCl(OMe)(py)_4]$, appears to from at this stage of the reaction. The electrochemical experiment described above showed that the methoxo complex **2** underwent a reversible one-electron reduction. Attempts to isolate the species were unsuccesful. In place of the methoxo complex of Ru^{II}, small amounts of red crystals, which could easily be identified as $[RuCl_2(py)_4]$,[25] deposited after further standing of the solution.

The authors wish to express their thanks to Professor Akira Ouchi, the University of Tokyo, and Associate Professor Mamoru Shimoi, Tohoku University, for the X-ray diffraction measurements and for their helpful discussions. Thanks are also due to Mariko Ogura and Akito Kuwayama for their technical assistance. The present work was partially supported by Grant-in-Aid for Science Research No. 61540454 from the Ministry of Education, Science and Culture.

References

1) B. A. Moyer and T. J. Meyer, *J. Am. Chem. Soc.*, **100**, 3601 (1978).

2) B. A. Moyer and T. J. Meyer, *Inorg. Chem.*, **20**, 436 (1981).

3) S. Goswami, A. R. Chakravarty, and A. Chakravorty, *J. Chem. Soc., Chem. Commun.*, **1982**, 1288.

4) C.-M. Che, T.-W Tang, and C.-K. Poon, *J. Chem. Soc., Chem. Commun.*, **1984**, 641.

5) K. Aoyagi, Y. Yukawa, K. Shimizu, M. Mukaida, T. Takeuchi, and H. Kakihana, *Bull. Chem. Soc. Jpn.*, **59**, 1493 (1986).

6) Y. Yukawa, K. Aoyagi, M. Kurihara, K. Shirai, K. Shimizu, M. Mukaida, T. Takeuchi, and H. Kakihana, *Chem. Lett.*, **1985**, 283.

7) C.-M. Che K.-Yin, and T. C. W. Mark, *J. Chem. Soc., Chem. Commun.*, **1985**, 546.

8) C.-M. Che, K.-Yin, and C.-K. Poon, *Inorg. Chem.*, **24**, 1794 (1985).

9) B. A. Moyer, B. K. Sipe, and T. J. Meyer, *Inorg. Chem.*, **20**, 1475 (1981).

10) M. S. Thompson and T. J. Meyer, *J. Am. Chem. Soc.*, **104**, 4106 (1982)

11) L. Roeker and T. J. Meyer, *J. Am. Chem. Soc.*, **108**, 4066 (1986).

12) M. S. Thompson, W. F. Giovani, B. A. Moyer, and T. J. Meyer, *J. Org. Chem.*, **49**, 4972 (1984).

13) A. Endo, *Bull. Chem. Soc. Jpn.*, **56**, 2733 (1985).

14) "The Universal Crystallographic Computation Program System (UNICS)," ed by T. Sakurai, Crystallographic Society of Japan, Tokyo (1967).

15) "International Tables for X-Ray Crystallography," Kynoch Press, Birmingham, U. K. (1974), Vol. IV.

16) The chloroaquatetrakis(pyridine)ruthenium(II) complex has not been reported yet. The complex could reasonably be formulated as $[RuCl(H_2O)(py)_4]PF_6 \cdot H_2O$ based on the following results. Found: C, 37.3; N, 8.7; H, 4.0%. Calcd for $C_{20}H_{24}N_4O_2PF_6ClRu$: C, 37.9; N, 8.8; H, 3.8%. Diamagnetic. The cyclic voltammogram in CH_3CN exhibits a reversible one-electron oxidation wave at $E_{1/2}$=0.50 V, which indicates the oxidation of Ru^{II}. The result will be published separately.

17) μ_B=2.10 B.M. (25 °C). $E_{1/2}$., 0.14 V ($Ru^{II/III}$), E_{pc}= 1.46 V ($Ru^{III/IV}$).

18) M. J. Camenzind, F. J. Hollander, and C. L. Hill, *Inorg. Chem.*, **21**, 4301 (1982).

19) T. Kimura, T. Sakurai, M. Shima, T. Togano, M. Mukaida, and T. Nomura, *Inorg. Chim. Acta*, **69**, 135 (1883).

20) J. E. Huhggy, "Inorganic Chemistry," 2nd ed, Harper and Row, New York (1978), p. 71.

21) F. Bottomley, *Coord. Chem. Rev.*, **26**, 7 (1978).

22) J. L. Templeton, *J. Am. Chem. Soc.*, **101**, 4906 (1979).

23) $RuC_{20}H_{20}N_4O_5Cl_2$: F.W., 568.4, tetragonal, *P4/ncc*, Z=16, a=25.781(5) Å, c=14.130(4) Å, V=9391(4) Å^3, D_x=1.61, D_m=1.59 g cm^{-3}, μ(Mo $K\alpha$)=9.21 cm^{-1}.

24) F. Bottomley and M. Mukaida, *J. Chem. Soc., Dalton Trans.*, **1982**, 283.

 © 1987 The Chemical Society of Japan Bull. Chem. Soc. Jpn., 60, 3255—3259 (1987)

Infrared Absorption Study of Human Hemoglobin α-Chain (123-136) Fragments in Dichloromethane[1)]

Mitsuaki NARITA,* Masamitsu DOI, and Takao NAKAI
Department of Industrial Chemistry, Faculty of Technology,
Tokyo University of Agriculture and Technology, Koganei 184
(Received February 3, 1987)

In connection with the relationship between the conformation and solubility of peptide intermediates having polar side chains, IR spectroscopic conformational analysis of peptide fragments of human hemoglobin α-chain (123-136) was performed in dichloromethane. In dichloromethane, the conformational behavior of the peptide fragments was, in essence, dependent on their amino acid sequences, and Boc-Ser(Bzl)-Thr(Bzl)-Val-Leu-OPac through Boc-Ala-Ser(Bzl)-Val-Ser(Bzl)-Thr(Bzl)-Val-Leu-OPac had predominantly unordered structures including some intramolecular hydrogen bonds, while Boc-Ala-Ser(Bzl)-Leu-Asp(OBzl)-Lys(Z)-Phe-Leu-OPac had successive intramolecular hydrogen bonds, probably corresponding to an α-helical structure. On the other hand, in carbon tetrachloride, the conformation of Boc-Val-Ser(Bzl)-Thr(Bzl)-Val-Leu-OPac and Boc-Ser(Bzl)-Val-Ser(Bzl)-Thr(Bzl)-Val-Leu-OPac had a typical β-sheet structure. These results are discussed on the basis of the amino acid sequences of the peptide fragments.

One of the serious problems in protein synthesis by the classical solution method is the low yields of the fragment condensation reactions, along with the decrease in the solubility of peptide intermediates with the increase in peptide chain length. In fact, Hofmann and coworkers[2)] reported that the azide condensation of tetraeicosapeptide with heptapentacontapeptide gave ribonuclease T_1 (24-104) only in 5% yield. The extreme decline in coupling yields with increasing peptide chain length was presumed to be caused by conformational factors. The reactive ends of the peptides may become sterically hindered because of folding into the peptide chain. Since conformational stability can be expected to increase with increasing chain length, conformation may become the overriding factor influencing the coupling yields. In synthetic studies of peptides and proteins, however, conformational analysis in solution has seldom been performed,[3-5)] since the role of the polar amino acid residues in the conformational behavior of peptide fragments is complicated. This is in contrast with the fact that conformational analyses of homo- and sequential peptides have been widely carried out.[6-8)]

In relation to the problem of the extreme decrease in the solubility and reactivity of peptide intermediates with increasing peptide chain length, we have developed the solubility-improvement[9,10)] and solubility-prediction methods[11)] and proposed the design method of the synthetic route for peptides and proteins based on the solubility prediction method.[12)] In connection with the relationship between the conformation and solubility of peptide intermediates having polar side chains, we here report IR spectroscopic conformational analysis of peptide fragments of human hemoglobin α-chain (123-136) in dichloromethane, which is most commonly used in solid phase peptide synthesis and is the best solvent for coupling reactions when peptide intermediates are soluble. Our concern in this paper is to elucidate the role of polar amino acid residues in the conformational behavior of peptide fragments.

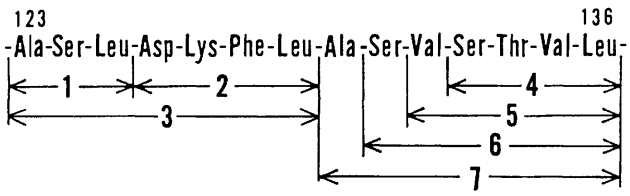

1 Boc-Ala-Ser(Bzl)-Leu-OPac
2 Boc-Asp(OBzl)-Lys(Z)-Phe-Leu-OPac
3 Boc-Ala-Ser(Bzl)-Leu-Asp(OBzl)-Lys(Z)-Phe-Leu-OPac
4 Boc-Ser(Bzl)-Thr(Bzl)-Val-Leu-OBzl
5 Boc-Val-Ser(Bzl)-Thr(Bzl)-Val-Leu-OBzl
6 Boc-Ser(Bzl)-Val-Ser(Bzl)-Thr(Bzl)-Val-Leu-OBzl
7 Boc-Ala-Ser(Bzl)-Val-Ser(Bzl)-Thr(Bzl)-Val-Leu-OBzl

Fig. 1. The amino acid sequence of human hemoglobin α-chain (123-136) and the peptides **1**—**7** used in this study.

The amino acid sequence of human hemoglobin α-chain (123-136) corresponds to the partial sequence of the helical H region (Fig. 1).[13,14] Figure 1 also illustrates the protected peptide fragments **1—7** used in this study.

Experimental

Materials. The preparation of the samples of human hemoglobin α-chain (123-136) fragments will be reported elsewhere. The purity of the peptides was confirmed by amino acid and elemental analyses. The peptides also gave a single peak on HPLC.

IR Measurements. The IR absorption spectra of the samples in dichloromethane were recorded at room temperature with a JEOL Model JIR-100 FT-IR spectrometer by employing 0.5 mm- and 5 mm-path length cells with potassium bromide windows.

Results

IR Absorption Spectra of the Tripeptide 1, the Tetrapeptides 2 and 4, and the Pentapeptide 5 in Dichloromethane. The peptides **1**, **2**, **4**, and **5** are easily soluble in dichloromethane, and their IR absorption spectra were obtained over a wide range of concentration (0.10—10 mM (1 M=1 mol dm^{-3})). In Fig. 2, we show the N-H stretching bands of the peptides **1**, **2**, **4**, and **5** in dichloromethane and clearly see two distinct bands around 3425 and 3360 cm^{-1} over the entire concentration range. The 3425-cm^{-1} band is clearly due to the free N-H stretching vibration, while the 3360-cm^{-1} band is due to a hydrogen-bonded species.[3,4,6-8,15] Since the intensities of these two bands show little dependence on concentrations, the 3360-cm^{-1} band is mainly attributed to the intramolecular hydrogen-bonded species. The band around 3440 cm^{-1} of the peptide **2** is assigned to the free N-H stretching band of the side chain urethane group of the Lys residue. The IR absorption spectra in the amide I region of the peptides **1**, **2**, **4**, and **5** are also illustrated in Fig. 3. Their IR spectra measured over the wide range of concentration show the bands around 1755—1740, 1711—1707, and 1678—1670 cm^{-1}, corresponding to the Pac and Bzl ester carbonyl, Boc urethane carbonyl, and amide carbonyl groups, respectively. The absorption band around 1690 cm^{-1} of the peptide **1** may be attributed to the Pac ketone carbonyl group. The band around 1718 cm^{-1} of the peptide **2** is also assigned to Z urethane carbonyl group free from hydrogen bonding. The amide carbonyl bands of the peptides **1**, **2**, **4**, and **5** also showed little dependence on concentration (0.10—10 mM).

IR Absorption Study of the Hexapeptide 6 in Dichloromethane. The IR absorption spectra in the N-H stretching region of the peptide **6** in dichloromethane (0.10—10 mM) are shown in Fig. 4A. Those in the amide I region are also shown in Fig. 4B. At lower concentrations, the spectral patterns of the peptide **6** are essentially the same as those of the

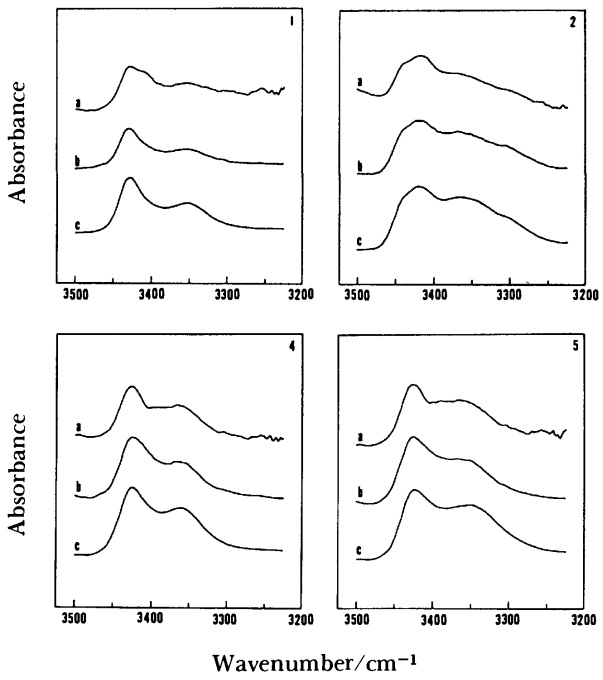

Fig. 2. IR absorption spectra in the amide A region of the tripeptide **1**, the tetrapeptides **2** and **4**, and the pentapeptide **5** in dichloromethane over the wide range of concentrations (0.10—10 mM). **a**: 0.10 mM, **b**: 1.0 mM, **c**: 10 mM.

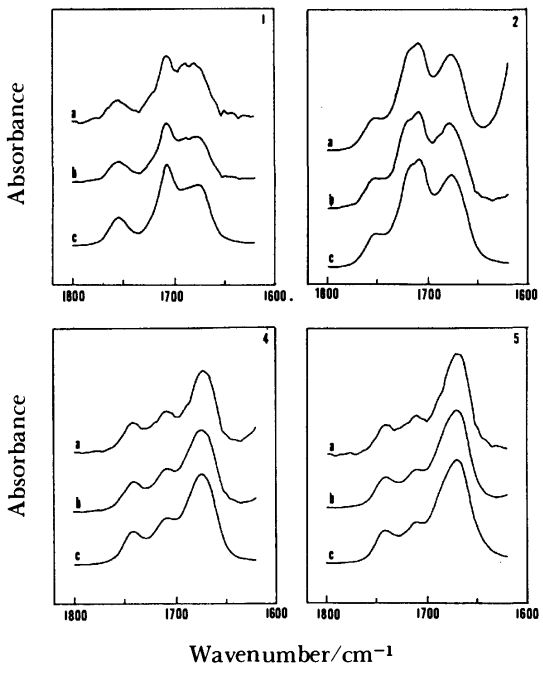

Fig. 3. IR absorption spectra in the amide I region of the tripeptide **1**, the tetrapeptides **2** and **4**, and the pentapeptide **5** in dichloromethane over the wide range of concentrations (0.10—10 mM). **a**: 0.10 mM, **b**: 1.0 mM, **c**: 10 mM.

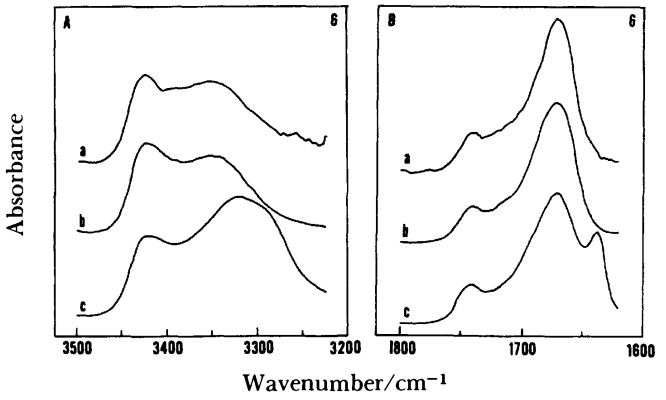

Fig. 4. IR absorption spectra of the hexapeptide **6** in dichloromethane over the wide range of concentrations (0.10—10 mM). A: The amide A region, B: the amide I region. **a**: 0.10 mM, **b**: 1.0 mM, **c**: 10 mM.

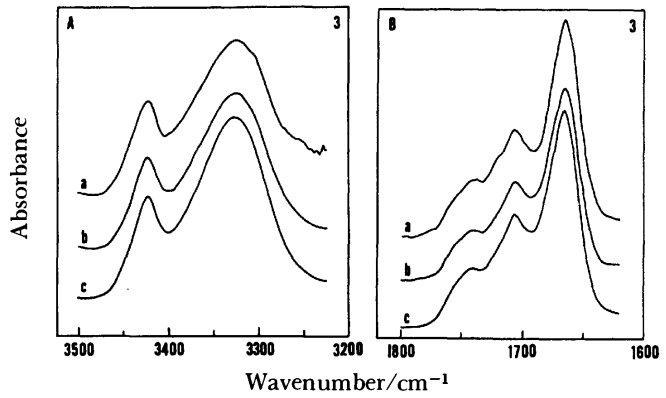

Fig. 5. IR absorption spectra of the heptapeptide **3** in dichloromethane over the wide range of concentrations (0.10—10 mM). A: The amide A region, B: the amide I region. **a**: 0.10 mM, **b**: 1.0 mM, **c**: 10 mM.

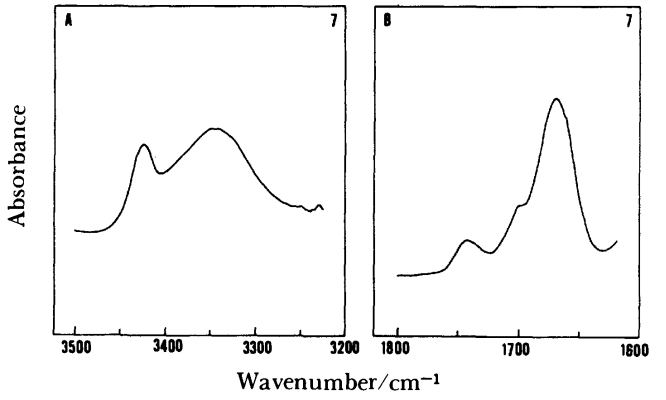

Fig. 6. IR absorption spectra of the heptapeptide **7** in dichloromethane (below 0.1 mM, saturated concentration). A: The amide A region, B: the amide I region.

peptides **4** and **5**, while at the high concentration, the concentration-depending absorption bands appear around 3300 cm^{-1} and at 1637 cm^{-1}, suggesting the onset of a β-sheet structure.[3,4,6-8,15] In fact, the IR absorption spectra of the peptides **5** and **6** in carbon tetrachloride (**5**: 2 mM, **6**: ca. 0.1 mM, saturated concentration) have the bands at 3280—3278, 1695, and 1635—1631 cm^{-1}, indicating an antiparallel β-sheet structure.[3,4,6-8,15,16]

IR Absorption Spectra of the Heptapeptides 3 and 7 in Dichloromethane. The IR absorption spectra in the N-H stretching region of the peptide **3** in dichloromethane (0.10—10 mM) are shown in Fig. 5A. We also see two distinct bands at 3425 cm^{-1} and around 3325 cm^{-1} over the entire concentration range. Again, the 3425-cm^{-1} band is due to the free N-H stretching vibration, while the band around 3325 cm^{-1} is due to a hydrogen-bonded species. The intensity of the hydrogen-bonded band (Fig. 5A) is little dependent on concentration, indicating it is nearly free from intermolecular hydrogen bonding. The positions and intensity ratios of the carbonyl bands (Fig. 5B) are also independent of concentration (0.10—10 mM). Assignment of each band at 1743, 1707, and 1666 cm^{-1} is essentially the same as that of the peptides **1**, **2**, **4**, and **5**. Figures 6A and 6B show the IR absorption spectra in the amide A and amide I regions of the peptide **7** in dichloromethane (below 0.1 mM, saturated concentration), respectively. The free N-H stretching band also appears at 3425 cm^{-1}, while the hydrogen-bonded band of the peptide **7** shifts to a higher frequency (3344 cm^{-1}) than that of the peptide **3** (3325 cm^{-1}). The absorption bands in the amide I region appear at 1743, 1701, and 1670 cm^{-1}.

Discussion

With respect to conformational analysis of Boc-Leu_4-OBzl and Boc-Leu_5-OBzl in dichloromethane, in a previous paper,[17] we showed that the positions and intensity ratios of the bands at 3430—3420 and 3350—3320 cm^{-1} are nearly independent of concentration and that the absorptions of the three free N-H groups in Boc-Leu_4-OBzl and Boc-Leu_5-OBzl are almost clearly comparable with similar absorption in Boc-Leu_3-OBzl. On the basis of these results, we suggested the occurrence of successive intramolecular hydrogen bonds like incipient α-helical structures in Boc-Leu_4-OBzl and Boc-Leu_5-OBzl. In Fig. 2, the positions and intensity ratios of the bands around 3425 and 3360 cm^{-1} are also nearly independent of concentrations, and the 3360-cm^{-1} band is thus to be attributed to intramolecular hydrogen-bonded species. Compared to the intensity ratios of the hydrogen-bonded N-H absorption to the free N-H absorption (A_H/A_F) for Boc-Leu_4-OBzl and Boc-Leu_5-OBzl, however, those for the peptides **2**, **4**, and **5** are relatively small, indicating that the hydrogen-bonded

species of the latter are different from those of the former. The same conformational behavior is also observed in the hexapeptide **6** at lower concentrations (Fig. 4A), being in contrast to the fact that Boc-Leu-Pro-Leu$_4$-OBzl develops successive intramolecular hydrogen bonds in dichloromethane.[17] This different conformational behavior is clearly attributed to the low potential of the peptides **2** and **4**—**6** for the formation of an α-helical structure. The helical structure of the peptides **5** and **6** in dichloromethane may be unstable due to repulsion among C^{β}-branched Val and Thr(Bzl) residues, although the sequence of -Ser-Val-Ser-Thr-Val-Leu- is included in the helical H region of human hemoglobin α-chain.[14] Furthermore, interactions among protected polar side chains and peptide bonds disturb the formation of an α-helix or β-sheet structure, leading to an unordered structure. Thus, the conformations of the peptides **1**, **2**, and **4**—**6** are inferred to be unordered structures including intramolecular hydrogen bonds among protected polar side chains and peptide bonds. At the high concentration (10 mM), the peptide **6** in dichloromethane indicates the onset of a β-sheet structure, and the conformations of the peptides **5** and **6** in carbon tetrachloride of low polar solvent are indeed typical β-sheet structures. The results in carbon tetrachloride exhibit that the structures of the peptides **5** and **6** in carbon tetrachloride are the same as those in the solid state.[18] Further development of interpeptide-chain interactions through hydrogen bonds with increase in peptide chain length gives rise to the severe insolubility of peptides in carbon tetrachloride.

On the other hand, the conformational behavior of the heptapeptide **3** in dichloromethane is in contrast to that of the hexapeptide **6** and the heptapeptide **7**. Over the entire range of concentrations, the positions and spectral patterns of the N-H and C=O absorption bands are independent of concentrations and resemble those of Boc-Leu$_2$-Pro-Leu$_4$-OBzl in dichloromethane,[17] which is inferred to have a large contribution of α-helical structure. For the purpose of elucidating the intramolecularly hydrogen-bonded species, the IR difference spectra between the peptides **3** and **1** and between the peptides **3** and **2** were examined in the amide A and amide I regions (Figs. 7A and 7B). In the difference spectrum between the peptides **3** and **1**, the shoulder band around 3440 cm^{-1} is also assigned to the free N-H stretching band of the side chain urethane group of the Lys residue, and the band around 1720 cm^{-1} to the corresponding urethane carbonyl group. On the other hand, the IR difference spectrum between the peptides **3** and **2** shows a negative band at 1720 cm^{-1}, indicating that the Z urethane carbonyl group of the peptide **3** is subjected to hydrogen bonding more than that of the peptide **2**. Although both IR difference spectra in the amide A region still show the existence of a small amount of the free N-H stretching vibration, the bands at 3323—3321 and 1664—1662 cm^{-1} strongly suggest a large contribution of successive intramolecular hydrogen bonds similar to an α-helical structure.[17] With respect to the conformational behavior of the peptide **7**, the spectrum in the amide A region indicates an increase of hydrogen-bonded species, compared to the peptides **5** and **6**. Since the spectrum in the amide I region shows no band around 1635 cm^{-1}, the increase in the band at 3344 cm^{-1} probably corresponds to the increase in the intramolecular hydrogen-bonded species, suggesting the onset of an α-helical structure around N-terminal portions. The conformational behavior of the peptides **3** and **5**—**7**, which are equal

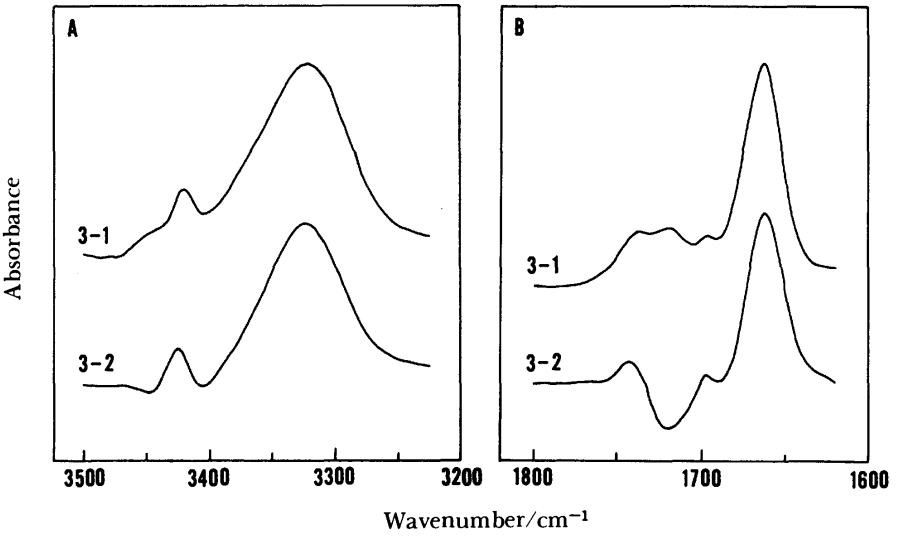

Fig. 7. IR difference spectra between the peptides **3** and **1** and between the peptides **3** and **2** (1.0 mM). A: The amide A region, B: the amide I region.

to or larger than a pentapeptide, clearly reflects their potential for the formation of an α-helical structure and are estimated using the average helix conformation $\langle P_\alpha \rangle$ values[19] of each peptide as discussed for the effect of shear stress on conformational behaviors of the peptides **3** and **5—7** in the solid state.[18]

The present work was partially supported by a Grant-in-Aid for Scientific Research (No. 61540393) from the Ministry of Education, Science and Culture.

References

1) This paper forms Part VII of "Design of the Synthetic Route for Peptides and Proteins Based on the Solubility Prediction Method" series. For part VI of this series, see M. Narita, M. Doi, and H. Takegahara, *Bull. Chem. Soc. Jpn.*, **60**, 2445 (1987). The abbreviations for amino acids are those recommended by the IUPAC-IUB Commission on Biochemical Nomenclature, *J. Biol. Chem.*, **247**, 977 (1972). Amino acid symbols denote the L-configuration. Additional abbreviations used are the following: IR, infrared; Boc, *t*-butoxycarbonyl; Bzl, benzyl; Pac, phenacyl; Z, benzyloxycarbonyl.

2) H. Romovacek, S. R. Dowd, K. Kawasaki, N. Nishi, and K. Hofmann, *J. Am. Chem. Soc.*, **101**, 6081 (1979).

3) M. Narita, Y. Tomotake, S. Isokawa, T. Matsuzawa, and T. Miyauchi, *Macromolecules*, **17**, 1903 (1984).

4) M. Narita, T. Ogura, K. Sato, and S. Honda, *Bull. Chem. Soc. Jpn.*, **59**, 2445 (1986).

5) C.-I. Niu, Q.-L. Shi, S.-Z. Yang, Y.-N. Chen, T.-J, Huang, and Z.-X. Lu, *Biopolymers*, **25**, S157 (1986).

6) R. Katakai, *Biopolymers*, **25**, 1 (1986) and references cited therein.

7) U. Narayanan, T. A. Keiderling, G. M. Bonora, and C. Toniolo, *J. Am. Chem. Soc.*, **108**, 2431 (1986) and references cited therein.

8) K.-H. Altmann, A. Florsheimer, and M. Mutter, *Int. J. Peptide Protein Res.*, **27**, 314 (1986), and references cited therein.

9) M. Narita, T. Fukunaga, A. Wakabayashi, K. Ishikawa, and H. Nakano, *Int. J. Peptide Protein Res.*, **23**, 306 (1984).

10) M Narita, M. Doi, H. Sugasawa, and K. Ishikawa, *Bull. Chem. Soc. Jpn.*, **58**, 1473 (1985).

11) M. Narita, K. Ishikawa, J.-Y. Chen, and Y. Kim, *Int. J. Peptide Protein Res.*, **24**, 580 (1984).

12) M. Narita, T. Ogura, K. Sato, and S. Honda, *Bull. Chem. Soc. Jpn.*, **59**, 2433, 2439, 2445 (1986).

13) G. Braunitzer, R. Gehring-Muller, N. Hilschmann, K. Hilsen, G. Hobom, V. Rudloff, and B. Wittmann-Liebold, *Z. Physiol. Chem.*, **325**, 283 (1961).

14) M. F. Perutz, M. G. Rossmann, A. F. Cullis, H. Muirhead, G. Will, and A. C. T. North, *Nature (London)*, **185**, 416 (1960); E. J. Heidner, R. C. Ladner, and M. F. Perutz, *J. Mol. Biol.*, **104**, 707 (1976).

15) M. Narita, S. Isokawa, Y. Tomotake, and S. Nagasawa, *Polymer J.*, **15**, 25 (1983), and references cited therein.

16) T. Miyazawa and E. J. Blout, *J. Am. Chem. Soc.*, **83**, 712 (1961); Yu. N. Chirgadze and N. A. Nevskaya, *Biopolymers*, **15**, 627 (1976).

17) M. Narita, S. Isokawa, M. Doi, and R. Wakita, *Bull. Chem. Soc. Jpn.*, **59**, 3547 (1986).

18) M. Narita, M. Doi, and H. Takegahara, *Bull. Chem. Soc. Jpn.*, **60**, 2445 (1987).

19) P. Y. Chou and G. D. Fasman, *Biochemistry*, **13**, 211 (1974).

 © 1987 The Chemical Society of Japan Bull. Chem. Soc. Jpn., 60, 3261—3267 (1987)

Regio- and Stereoselective Introduction of Functional Groups into 1-Isoindolinone and 1(2*H*)-Isoquinolone Systems[1)]

Michihiko NOGUCHI,* Manabu YOSHIOKA, Shinji KAKIMOTO, and Shoji KAJIGAESHI
Department of Industrial Chemistry, Faculty of Engineering, Yamaguchi University, Tokiwadai, Ube 755
(Received February 4, 1987)

The oxidation of 3*a*,4-dihydro-1-isoindolinone derivatives with MCPBA was carried out regio- and stereoselectively to afford the 5,6-epoxide products **2**. The ring opening reaction of **2** with amines, alcohols, and sodium azide gave homoallyl alcohol type of products, derived from the ring opening at C-5 of **2**. Lithium (cyano-*C*)methylcuprate reacted with **2** to give homoallyl and/or allyl alcohol, which is due to the conjugate addition to the C-7a position. This approach for selective introduction of functional groups into the heterocycles was extended for 3,4,4*a*,5-tetrahydro-1(2*H*)-isoquinolone system.

Recently, we reported the preparation of 3*a*,4-dihydro-1-isoindolinone and 3,4,4*a*,5-tetrahydro-1(2*H*)-isoquinolone derivatives, **1** and **17**, via an intramolecular "diene-regenerable" Diels-Alder reaction of 2-pyrone-6-carboxamides.[1b)] Compounds **1** and **17** were regarded as cyclo-1,3-diene systems fused by lactam rings, and the lactam rings seemed to control the stereochemistry of the succeeding intermolecular Diels-Alder reaction.[1b)]

A stereoselective formation of oxiranes[2)] and successive ring-opening reactions[3)] with various nucleophiles are recognized as a promising pathway for selective functionalization in molecules.

If the stereochemistry of the epoxidation of **1** and **17** is also controlled by their lactam moieties and the selective ring-opening reaction of the resulting oxiranes is possible, the selective introduction of functional groups into the above heterocyclic systems would be achieved. Thus, we investigated the epoxidation of **1** and **17** followed by ring opening reaction with several nucleophiles. The sequence of these two reactions proceeded regio- and stereoselectively and revealed to be suitable for our purpose. The regiochemistry for the ring opening reactions is also discussed.

Results and Discussion

Regio- and Stereoselective Oxidation of 3*a*,4-Dihydro-1-isoindolinones 1. The oxidation of 2-phenyl- (**1a**), 2-benzyl-4-methyl- (**1b**), and 2-benzyl-4-phenyl-3*a*,4-dihydro-1-isoindolinone (**1c**) with *m*-chloroperbenzoic acid (MCPBA) in dichloromethane-water at room temperature resulted in epoxidation of the 5,6-double bond of **1a—c**, and the oxiranes **2a—c** were isolated in almost quantitative yields as single isomers (Scheme 1). The configuration between the oxirane and lactam rings of **2** was assigned to be syn on the basis of the values of the coupling constants among the protons and the 3a-, 4-, 5-, and 6-positions of **2a—c** (Table 1). For **2a** the vicinal coupling constants J_{3a-4} (7.5 and 11.7 Hz) between methine (3a-position) and methylene (4-position) were assignable as cis and trans[1b)] and J_{4-5} (2.8 and ca. 0 Hz) to be also cis and trans,[4)] respectively. The values of J_{3a-4} (ca. 10.5 Hz) and J_{4-5} (less than 1 Hz) for **2b** or **2c** are deduced to be trans and trans configurations among the three protons.

Therefore, the oxygen is introduced to the C–C double bond on the same side as the lactam ring with high stereoselectivity regardless of the kind of substituent at the 4-position. The syn-directing effect of allylic hydroxyl[5)] or allylic amido group[6)] is well-known in the stereoselective epoxidation of the cyclohexene system by peracids. Interestingly, the lactam ring of **1** causes an excellent syn-directing effect, nevertheless it is located far from the oxidized double bond in this case.

Ring Opening Reaction of Oxiranes 2 with Nucleophiles. The oxiranes **2a—c** have four reaction sites for nucleophiles as demonstrated in Fig. 1. In order to establish the regioselectivity of the nucleophilic attack, we examined for the first time the reaction with hard bases[7)] such as heteroatomic

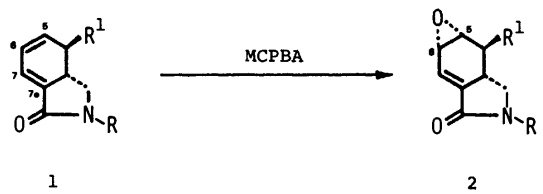

1 2

a: R=Ph, R^1=H; b: R=CH_2Ph, R^1=CH_3; c: R=CH_2Ph, R^1=Ph

Scheme 1.

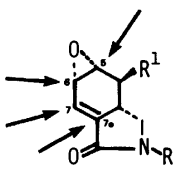

Fig. 1. Reaction sites of oxiranes **2** for nucleophiles.

nucleophiles. Recently, Posner et al. reported that the ring opening of oxiranes with nucleophiles proceeded smoothly in the presence of commercially available neutral alumina.[8]

In a similar manner to Posner's method, **2a—c** were allowed to react with benzylamine (**3**) and pyrrolidine (**4**) to afford homoallyl alcohols, **5a—c** and **6a—c**, derived from the ring opening at the C-5 of **2**. No products derived from that of C-6 were observed. The structural assignment for the homoallyl alcohols was accomplished on the basis of their spectral data. Especially, in their mass spectra the fragment ion peaks due to the elimination of aldehydes from the molecular ion, $M^+-R^1CH_2CHO$, were observed. The stereochemical relationships between the functional groups carrying oxygen and nitrogen atoms could not be determined only from the coupling constants because of the complexity of the signal patterns. However, these were tentatively assigned to be trans according to the reaction pathway[9] reported heretofore.

The analogous reaction of **2b** with methanol (**7**) and 1-pentanol (**8**) gave the same type of adducts **9** and **10** together with diol **11**, respectively. Under similar conditions the ring opening of **2b** with water afforded **11** in only 19% yield with the recovery of **2b** (64%). Therefore, the formation of **11** in the reaction with alcohol would be attributable to the secondary reaction via **9** or **10**.

The ring opening of **2** using azide ion as a softer base was examined. The reaction of **2a—c** with sodium azide (**12**) in aqueous THF gave homoallyl alcohols **13a—c** in good yields.

These results are shown in Schemes 2 and 3. The regio- and stereochemistries of these adducts were confirmed on the basis of the similarities of the spectral data to those of the adducts with amines.

The introduction of an alkyl group into the 1-oxoisoindoline system was finally investigated. The reaction of **2** with Grignard reagents or alkyllithiums afforded only disappointing results. So, the reaction

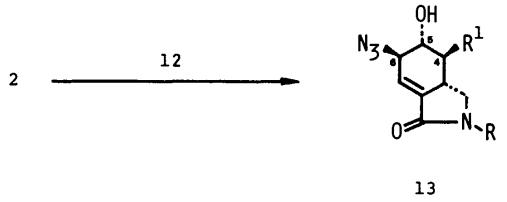

13

Scheme 3.

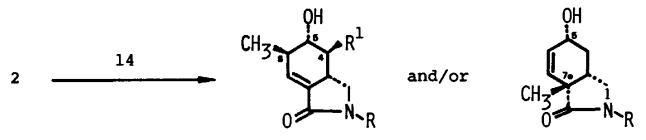

15 16a

Products	(Yield/%)
15a (32)	16a (9)
15b (60)	——
15c (44)	——

Scheme 4.

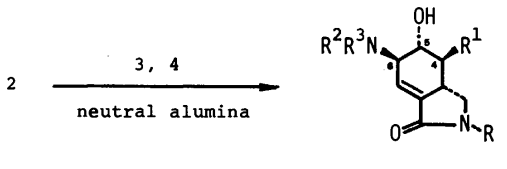

	R^2	R^3
5	H	CH_2Ph
6	$-(CH_2)_4-$	

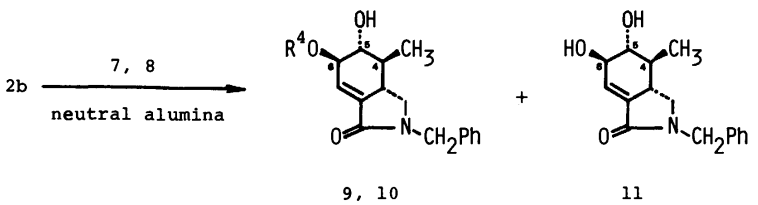

9, 10 11

R^4	Products	(Yield/%)
CH_3	9 (68)	11 (12)
$n-C_5H_{11}$	10 (27)	11 (53)

Scheme 2.

of **2** with lithium (cyano-*C*)methylcuprate (**14**) was examined, which is widely used as an effective reagent for opening oxiranes.[10] Oxirane **2a** reacted with **14** in THF at −30 °C to give homoallyl alcohol **15a** and allyl alcohol **16a**, which was derived from the conjugate addition of methyl anion onto the C-7a. However, in a similar reaction of **2b** or **2c** with **14**, only homoallyl alcohol **15b** or **15c** was obtained (Scheme 4).

The structure of **16a** was elucidated on the basis of its spectral data. In its ^{1}H NMR spectrum, two olefinic proton signals at δ=6.44(doublet) and 5.72 (double doublet) were observed. Its mass spectrum showed a fragment ion peak due to (M^+-CH_3), but the peak characteristic of a homoallyl alcohol type of product, M^+-CH_3CHO, was not observed.

The relationship between the methyl group at the 7a-position and the hydroxyl at the 5-position is tentatively assigned to be trans because the conjugate addition of lithium alkyl(cyano-*C*)cuprates to 1,3-diene monooxides have been shown to proceed in a highly selective manner.[11] This assignment is also supported by the findings that the conjugate addition of **14** only occurs at the reaction with **2a**, which bears the least hindered substituent (R^1=H) at the 4-position among oxiranes **2**.

The hard and soft acid–base concept[7] appears to be useful in considering the regioselectivities of these ring-opening reactions. According to the concept, the 5- and 6-positions are hard and the 7- and 7a-position are soft reaction sites,[12] respectively. The reaction with hard nucleophiles as well as with azide ion occurred exclusively at the 6-position, which is more reactive than the 5-position owing to it being an allylic position. Methyl anion prefers to react with the softer acid site, e.g., C-7a position. However, the regiochemistry of the addition was eventually determined on the balance between the affinity and the steric hinderance, which becomes serious for attack at the 7a-position when the substituent at the 4-position is bulky.

Regio- and Stereoselective Oxirane Formation of 3,4,4*a*,5-Tetrahydro-1(2*H*)-isoquinolone System and Its Ring Opening Reaction. The regio- and stereoselective oxidation of **1** to **2** followed by the regioselective ring opening allowed to the introduction of functional groups into the 3*a*,4-dihydro-1-isoindolinone system. Accordingly, we investigated the oxidation of 2-benzyl-3,4,4*a*,5-tetrahydro-1(2*H*)-isoquinolone (**17**), a higher homolog of **1**, and the successive introduction of functional groups into the 1(2*H*)-isoquinolone system.

The oxidation of **17** with MCPBA in dichloromethane–water below 0 °C[13] and treatment by column chromatography on silica gel gave an oxirane **18**, resulting in oxidizing of the 6,7-double bond of **17**, in 84% yield (Scheme 5).

The structure of **18** was confirmed on the basis of spectral data and, especially, the configuration between the oxirane and lactam rings was also syn. Therefore, the fused lactam moiety in **17** as well as **1** caused the directing effect in the oxidation with MCPBA.

The ring opening reaction of **18** with pyrrolidine (**4**) and sodium azide (**12**) gave homoallyl alcohol type of products **19** and **20**. On one hand, oxirane **18** reacted with lithium (cyano-*C*)methylcuprate (**14**) to afford homoallyl alcohol **21** and allyl alcohol **22** in 60 and 21% yields, respectively (Scheme 6).

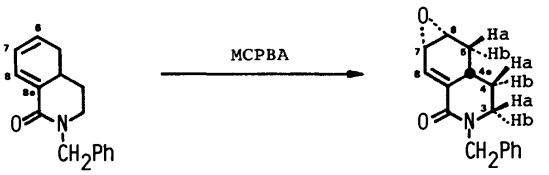

17 18

Scheme 5.

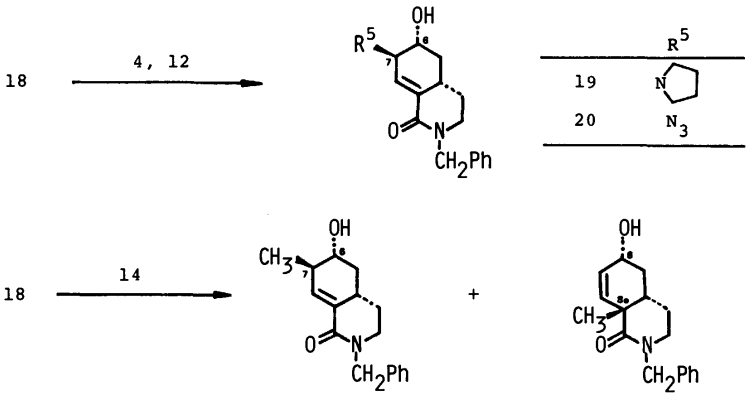

21 22

Scheme 6.

Experimental

General. All melting points are uncorrected. The IR spectra were measured on a JASCO IRA-1 spectrometer. The ^{1}H NMR spectra were obtained on JEOL FX-200, FX-100, and/or JMN-MH-100 spectrometers. The chemical shifts are expressed in parts per million downfield from internal tetramethylsilane. Splitting patterns are indicated as s, singlet; d, doublet; t, triplet; q, quartet; m, multiplet; ov, overlapped with each other. The mass spectra were determined with a JEOL JMS-012G-2 or JMS-D spectrometer and at an ionization energy of 75 eV. The elemental analyses were performed on a Hitachi 026 CHN analyzer. The progress of most reactions was monitored by thin-layer chromatography (Silica gel 60F-254, Merck). The visualization was made with ultraviolet light (254 and 365 nm). Wakogel C-200 and C-300 were used for the preparative chromatography. As catalysts for the ring opening of the oxiranes, Woelm-200 neutral alumina (activity grade I) was used.

Epoxidation of 3*a*,4-Dihydro-1-isoindolinones 1 with MCPBA. Typical Procedure: A mixture of 0.50 g (2.4 mmol) of **1a** and 0.57 g (3.3 mmol) of MCPBA in dichloromethane–water (60—20 mL) was stirred for 12 h at room temperature. After destroying the excess MCPBA with sodium hydrogensulfite, the organic layer was collected and evaporated to dryness. The residue was subjected to a short column chromatography on silica gel (chloroform) to afford 0.51 g (96%) of oxirane **2a**.

2a: Colorless plates (benzene); mp 168—169 °C; IR (KBr) cm^{-1}: 1670 (CO); MS *m/z* (rel intensity) 227 (M^+, base peak) and 77 (77).

Found: C, 73.97; H. 5.76; N, 6.26%. Calcd for $C_{14}H_{13}NO_2$: C, 73.99; H, 5.77; N, 6.16%.

2b: Yield 100%; colorless plates (benzene); mp 139—140 °C; IR (KBr) cm^{-1}: 1660 (CO); MS *m/z* (rel intensity) 255 (M^+, 40) and 91 ($C_7H_7^+$, base peak).

Found: C, 75.25; H, 6.66; N, 5.60%. Calcd for $C_{16}H_{17}NO_2$: C, 75.27; H, 6.71; N, 5.49%.

2c: Yield 99%; colorless prisms (benzene); mp 139—140 °C; IR (KBr) cm^{-1}: 1660 (CO); MS *m/z* (rel intensity) 317 (M^+, 48) and 91 ($C_7H_7^+$, base peak).

Found: C, 79.44; H, 6.05; N, 4.55%. Calcd for $C_{21}H_{19}NO_2$: C, 79.47; H, 6.03; N, 4.41%.

The ^{1}H NMR spectral data for **2** are demonstrated in Table 1.

Reaction of Oxiranes 2 with Amines. Typical Procedure: A mixture of 300 mg (1.32 mmol) of **2a** and 710 mg (6.64 mmol) of benzylamine (**3**) in dry THF (10 mL) was stirred in the presence of 10 g of the neutral alumina for 6 h at room temperature. The alumina was filtered off and washed with methanol. The filtrate was collected and evaporated to dryness. The residue was subjected to column chromatography on silica gel (chloroform) to give 280 mg (63%) of **5a**.

5a: Colorless needles (ethanol); mp 186—188 °C; IR (KBr) cm^{-1}: 3320 (OH), 3280 (NH), and 1650 (CO); ^{1}H NMR ($CDCl_3$) δ=1.56 (1H, m, 4-Hb), 2.16 (1H, m, 3a-H), 2.4—3.2 (3H, ov, 4-Ha, OH, and NH), 3.24 (1H, m, 6-H), 3.45 (1H, t, 3-Hb, $J_{gem}=J_{3-3a}$=9.5 Hz), 3.84 (1H, m, 3-Ha), 3.92 (2H, s, $-CH_2-$Ph), 4.05 (1H, m, 5-H), 6.55 (1H, br s, 7-H), and 7.0—7.8 (10H, m, phenyl); MS *m/z* (rel intensity) 334 (M^+, 6), 290 (M^+-CH_3CHO, base peak), 199 (290—CH_2Ph, 46), and 77 (92).

Found: 75.61; H, 6.70; N, 8.37%. Calcd for $C_{21}H_{22}N_2O_2$: C, 75.42; H, 6.63; N, 8.38%.

5b: Yield 73%; colorless needles (ethanol); mp 197—199 °C; IR (KBr) cm^{-1}: 3320 (OH), 3270 (NH), and 1640 (CO); ^{1}H NMR ($CDCl_3$) δ=1.04 (3H, d, CH_3, J=8.5 Hz), 1.54 (1H, m, 4-H), 2.4—2.9 (3H, ov, 3a-H, NH, and OH), 2.90

Table 1. ^{1}H NMR Spectral Data for Oxiranes **2** in $CDCl_3$: δ

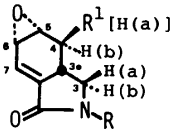

Compd	3-H(a)	3-H(b)	3a-H	4-H(a)	4-H(b)	5-H	6-H	7-H	Others
2a	4.03	3.5—3.6	3.03	2.73	1.47	3.65	3.5—3.6	6.89	7.1—7.7 (Phenyl)
	t	a)	m	ddd	dd	dd	a)	t	
	J (Hz): 3(a)-3(b)=3(a)-3a=9.6, 3a-4(a)=7.2, 3a-4(b)=11.7, 3a-7=4.6, 4(a)-4(b)=14.2, 4(a)-5=2.8, 4(b)-5=0, 5-6=3.4, 6-7=4.6								
2b	3.47	2.91	2.53		1.58	3.35	3.54	6.75	1.25 (CH_3)
	t	dd	m		dq	d	t	t	4.45, 4.62 ($-CH_2$-Ph)
	J (Hz): 3(a)-3(b)=3(a)-3a=10.2, 3(b)-3a=7.2, 3a-4=10.5, 3a-7=4.5, 4-5=0, 5-6=4.5, 6-7=4.5								7.2—7.4 (Phenyl)
2c	3.17	2.9	2.9		2.62	3.57	3.54	6.87	4.48, 4.63 ($-CH_2$-Ph)
	t	a)	a)		d	d	t	t	
	J (Hz): 3(a)-3(b)=12.0, 3a-4=10.3, 3a-7=3.9, 4-5=0, 5-6=3.9, 6-7=3.9								7.2—7.4 (Phenyl)

a) Overlapped with each other.

(1H, t, 3-Hb, $J_{gem}=J_{3-3a}=9.5$ Hz), 3.32 (1H, m, 6-H), 3.42 (1H, t, 3-Ha, $J_{gem}=J_{3-3a}=9.5$ Hz), 3.80 (1H, br, s, 5-H), 3.93 (2H, s, $-CH_2-Ph$), 4.41, 4.63 (1H each, 2d, $-CH_2-Ph$, $J_{gem}=16.2$ Hz), 6.50 (1H, br s, 7-H), and 7.1—7.6 (10H, m, phenyl); MS *m/z* (rel intensity) 362 (M^+, 10), 304 ($M^+-CH_3CH_2CHO$, 57), 213 (304—CH_2Ph, 37), and 91 ($C_7H_7^+$, base peak).

Found: C, 75.96; H, 7.22; N, 7.57%. Calcd for $C_{23}H_{26}N_2O_2$: C, 76.21; H, 7.23; N, 7.73%.

5c: Yield 53%; colorless needles (ethanol); mp 139—141 °C; IR (KBr) cm^{-1}: 3250 (OH), 3000 (NH), and 1670 (CO); ^1H NMR ($CDCl_3$) δ=1.9 (2H, br s, OH and NH), 2.6—2.9 (2H, ov, 3-Hb and 4-H), 3.28 (1H, t, 3-Ha, $J_{gem}=J_{3-3a}=9.5$ Hz), 3.3—3.6 (2H, ov, 3a-H and 6-H), 3.90 (3H, ov, 5-H and CH_2-Ph), 4.41 (2H, s, $-CH_2-Ph$), 6.50 (1H, br s, 7-H), and 7.0—7.4 (15H, m, phenyl); MS *m/z* (rel intensity) 424 (M^+, 8), 406 (M^+-H_2O, 4), 304 (M^+-PhCH_2CHO, 35), 213 (304—CH_2Ph, 21), and 91 ($C_7H_7^+$, base peak).

Found: C, 79.09; H, 6.85; N, 6.67%. Calcd for $C_{28}H_{28}N_2O_2$: C, 79.21; H, 6.65; N, 6.60%.

6a: Yield 74%; colorless needles (ethanol); mp 182—184 °C; IR (KBr) cm^{-1}: 3050 (OH) and 1660 (CO); ^1H NMR ($CDCl_3$) δ=1.62 (1H, m, 4-Hb), 1.77 (4H, m, pyrrolidinyl), 2.15 (1H, m, 3a-H), 2.70 (4H, m, pyrrolidinyl), 3.0—3.4 (3H, ov, 4-Ha, 6-H, and OH), 3.52, 3.98 (1H each, 2t, 3-Hb and 3-Ha, $J_{gem}=J_{3-3a}=9.2$ Hz), 4.15 (1H, m, 5-H), 6.68 (1H, br s, 7-H), and 7.0—7.8 (5H, m, phenyl); MS *m/z* (rel intensity) 298 (M^+, 8), 254 (M^+-CH_3CHO, base peak), and 77 (17).

Found: C, 72.37; H, 7.56; N, 9.23%. Calcd for $C_{18}H_{22}N_2O_2$: C, 72.45; H, 7.43; N, 9.39%.

6b: Yield 89%; colorless needles (ethanol); mp 141—143 °C; IR (KBr) cm^{-1}: 3120 (OH) and 1670 (CO); ^1H NMR ($CDCl_3$) δ=1.05 (3H, d, CH_3, J=7.7 Hz), 1.5 (1H, m, 4-H), 1.8 (4H, m, pyrrolidinyl), 2.65 (1H, m, 3a-H), 2.75 (4H, m, pyrrolidinyl), 2.95, 3.44 (1H each, 2t, 3-Hb and 3-Ha, $J_{gem}=J_{3-3a}=9.4$ Hz), 3.24 (1H, br s, 6-H), 4.00 (1H, br s, 5-H), 4.32 (1H, br s, OH), 4.35, 4.70 (1H each, 2d, $-CH_2-Ph$, $J_{gem}=16.3$ Hz), 6.55 (1H, br s, 7-H), and 7.1—7.5 (5H, m, phenyl); MS *m/z* (rel intensity) 326 (M^+, 2), 268 ($M^+-CH_3CH_2CHO$, base peak), 177 (268—CH_2Ph, 62), and 91 ($C_7H_7^+$, 73).

Found: C, 73.79; H, 8.10; N, 8.74%. Calcd for $C_{20}H_{26}N_2O_2$: C, 73.59; H, 8.03; N, 8.58%.

6c: Yield 71%; colorless needles (ethanol); mp 212—215 °C; IR (KBr) cm^{-1}: 3050 (NH) and 1660 (CO); ^1H NMR ($CDCl_3$) δ=1.78, 2.68 (4H each, 2m, pyrrolidinyl), 2.75—3.05 (3H, ov, 3-Hb, 3a-H, and 4-H), 3.15—3.7 (3H, ov, 3-Ha, 6-H, and OH), 4.12 (1H, m, 5-H), 4.39, 4.61 (1H each, 2d, $-CH_2-Ph$, $J_{gem}=15.8$ Hz), 6.62 (1H, br s, 7-H), and 7.1—7.5 (10H, m, phenyl); MS *m/z* (rel intensity) 388 (M^+, 2), 268 (M^+-PhCH_2CHO, base peak), 177 (268–CH_2Ph, 91), and 91 ($C_7H_7^+$, 63).

Found: C, 77.35; H, 7,34; N, 7.25%. Calcd for $C_{25}H_{28}N_2O_2$: C, 77.29; H, 7.27; N, 7.21%.

The reaction of **2** with alcohols was performed in a similar manner to that with amines.

9: Colorless oil; IR (Neat) cm^{-1}: 3390 (OH) and 1660 (CO); ^1H NMR ($CDCl_3$) δ=1.01 (3H, d, CH_3, J=7.4 Hz), 1.53 (1H, m, 4-H), 2.5—3.3 (2H, ov, 3-Hb and 3a-H), 3.3—3.4 (1H, m, 3-Ha), 3.38 (3H, s, OCH_3), 3.76 (1H, br s, OH), 3.82 (1H, br s, 5-H), 4.08 (1H, m, 6-H), 4.35, 4.52 (1H each, 2d, $-CH_2-Ph$, $J_{gem}=15.7$ Hz), 6.43 (1H, br s, 7-H), and 7.0—7.4 (5H, m, phenyl); MS *m/z* (rel intensity) 287 (M^+, 10), 229 ($M^+-CH_3CH_2CHO$, 28), 138 (229—CH_2Ph, 13), and 91 ($C_7H_7^+$, base peak).

Found: *m/z* 287.1528. Calcd for $C_{17}H_{21}NO_3$: M, 287.1520.

10: Colorless oil; IR (Neat) cm^{-1}: 3380 (OH) and 1660 (CO); ^1H NMR ($CDCl_3$) δ=0.7—1.8 (10H, m, ov, 4-H and butyl), 1.05 (3H, d, CH_3, J=7.7 Hz), 2.90 (1H, m, 3a-H), 2.93 (1H, t, 3-Hb, $J_{gem}=J_{3-3a}=8.6$ Hz), 3.2—3.7 (4H, ov, 3-Ha, $-CH_2-O$, and OH), 3.90 (2H, ov, 5- and 6-H), 4.45, 4.62 (1H each, 2d, $-CH_2-Ph$, $J_{gem}=16.0$ Hz), 6.52 (1H, br s, 7-H), and 7.1—7.4 (5H, m, phenyl); MS *m/z* (rel intensity) 343 (M^+, 2), 285 ($M^+-CH_3CH_2CHO$, 12), and 91 ($C_7H_7^+$, base peak).

Found: *m/z* 343.2147. Calcd for $C_{21}H_{29}NO_3$: M, 343.2146.

11: Colorless plates (ethanol); mp 180—182 °C; IR (KBr) cm^{-1}: 3380—3320 (OH) and 1660 (CO); ^1H NMR ($CDCl_3$) δ=1.06 (3H, d, CH_3, J=7.1 Hz), 1.70 (1H, m, 4-H), 2.6—3.1 (2H, ov, 3a-H and OH), 2.97, 3.49 (1H each, 2t, 3-Hb and -Ha, $J_{gem}=J_{3-3a}=7.7$ Hz), 3.8 (1H, m, 5-H), 4.14 (1H, br d, OH, J=4.9 Hz), 4.24 (1H, m, 6-H), 4.58 (2H, s, $-CH_2-Ph$), 6.52 (1H, br s, 7-H), and 7.35 (5H, m, phenyl); MS *m/z* (rel intensity) 273 (M^+, 23), 215 ($M^+-CH_3CH_2CHO$, 23), 124 (215—CH_2Ph, 11), and 91 ($C_7H_7^+$, base peak).

Found: C, 70.50; H, 7.08; N, 5.20%. Calcd for $C_{16}H_{19}NO_3$: C, 70.31; H, 7.01; N, 5.13%.

Reaction of 2 with Sodium Azide (12). Typical Procedure: A mixture of 500 mg (2.20 mmol) of **2a** and 160 mg (2.46 mmol) of **12** in aqueous THF (20 mL) was stirred for 5 h at room temperature. The reaction mixture was extracted with chloroform (20 mL×3) and the organic layer was evaporated to dryness. The residue was subjected to column chromatography on silica gel with chloroform–ethyl acetate (3/1) elution to give 400 mg (67%) of **13a**.

13a: Colorless prisms (chloroform); mp 132—133 °C; IR (KBr) cm^{-1}: 3370 (OH), 2080 (N_3), and 1660 (CO); ^1H NMR ($CDCl_3$) δ=1.5 (1H, m, 4-Hb), 2.12 (1H, m, 3a-H), 3.1—3.6 (2H, ov, 4-Ha and OH), 3.63, 4.08 (1H each, 2t, 3-Hb and -Ha, $J_{gem}=J_{3-3a}=8.3$ Hz), 4.03 (1H, br s, 5-H), 4.28 (1H, br s, 6-H), 6.65 (1H, br s, 7-H), and 7.2—7.9 (5H, m, phenyl); MS *m/z* (rel intensity) 270 (M^+, 69), 229 (31), 228 (M^+-N_3, 28), and 77 (base peak).

Found: C, 62.00; H, 5.28; N, 20.68%. Calcd for $C_{14}H_{14}N_4O_2$: C, 62.21; H, 5.22; N; 20.73%.

13b: Yield 74%; colorless prisms (ethanol); mp 74—76 °C; IR (KBr) cm^{-1}: 3230 (NH), 2050 (N_3), and 1640 (CO); ^1H NMR ($CDCl_3$) δ=1.08 (3H, d, CH_3, J=9.0 Hz), 1.56 (1H, br dq, 4-H, $J_{3a-4}=11.8$ and $J_{4-Me}=9.0$ Hz), 2.89 (1H, m, 3a-H), 2.96, 3.49 (1H each, 2t, 3-Hb and -Ha, $J_{gem}=J_{3-3a}=10.7$ Hz), 3.07 (1H, br s, OH), 3.89 (1H, br s, 5-H), 4.07 (1H, br s, 6-H), 4.47, 4.70 (1H each, 2d, $-CH_2-Ph$, $J_{gem}=16.9$ Hz), 6.50 (1H, br s, 7-H), and 7.2—7.5 (5H, m, phenyl); MS *m/z* (rel intensity) 298 (M^+, 21), 256 (M^+-N_3, 98), and 91 ($C_7H_7^+$, base peak).

Found: C, 64.51; H, 6.08; N, 18.85%. Calcd for $C_{16}H_{18}N_4O_2$: C, 64.41; H, 6.08; N, 18.78%.

13c: Yield 65%; colorless prisms (ethanol); mp 160—162 °C; IR (KBr) cm^{-1}: 3290 (OH), 2090 (N_3), and 1660 (CO); ^1H NMR ($CDCl_3$) δ=2.70 (1H, m, 4-H), 2.90, 3.40 (1H each, 2t, 3-Hb and -Ha, $J_{gem}=J_{3-3a}=9.2$ Hz), 3.0—3.8 (2H, ov, 3a-H and OH), 4.10 (1H, br s, 5-H), 4.24 (1H, br s, 6-H), 4.45, 4.68 (1H each, 2d, $-CH_2-Ph$, $J_{gem}=16.0$ Hz), 6.62 (1H, br s, 7-H), and 7.2—7.6 (10H, m, phenyl); MS *m/z* (rel intensity) 360 (M^+, 18), 318 (M^+-N_3, 89) and 91 ($C_7H_7^+$, base peak).

Found: C, 69.81; H, 5.66; N, 15.68%. Calcd for $C_{21}H_{20}N_4O_2$: C, 69.98; H, 5.59; N, 15.55%.

Reaction of 2 with Lithium (Cyano-*C*)methylcuprate (14). Typical Procedure: To a mixture of 580 mg (6.5 mmol) of cuprous cyanide and 10 mL of THF, 6.4 mmol of methyllithium was added under nitrogen atmosphere at −78 °C. The temperature was slowly raised to −30 °C, and 500 mg (2.2 mmol) of **2a** in THF (2 mL) was injected into the reaction mixture. The mixture was stirred at the same temperature for an additional one hour, then warmed up to 0 °C and kept at that temperature for 6 h. The mixture was made acidic with conc. hydrochloric acid and extracted with dichloromethane (20 mL×3). The organic layer was collected and evaporated to dryness. The residue was subjected to column chromatography on silica gel (chloroform–ethyl acetate: 4/1) to give 180 mg (32%) of **15a** and 50 mg (9%) of **16a**.

15a: Colorless needles (ethanol); mp 163—164 °C; IR (KBr) cm^{-1}: 3400 (OH) and 1670 (CO); ^1H NMR ($CDCl_3$) δ=1.05 (3H, d, CH_3, J=8.0 Hz), 1.40 (1H, ddd, 4-Hb, J_{gem}=12.6, J_{3a-4}=11.2, and J_{4-5}=2.0 Hz), 2.16 (1H, ddd, 4-Ha, J_{gem}=12.6, J_{3a-4}=5.7, and J_{4-5}=4.8 Hz), 2.45 (1H, m, 6-H), 2.67 (1H, br d, OH, J=4.0 Hz), 3.18 (1H, m, 3a-H), 3.49, 3.95 (1H each, 2t, 3-Hb, and -Ha, J_{gem}=J_{3-3a}=8.8 Hz), 3.98 (1H, m, 5-H), 6.49 (1H, t, 7-H, J_{3a-7}=J_{6-7}=2.8 Hz), and 7.1—7.5 (5H, m, phenyl); MS *m/z* (rel intensty) 243 (M^+, base peak), 200 (24), 199 (M^+−CH_3CHO, 71), and 77 (52).

Found: C, 73.88; H, 7.16; N, 5.86%. Calcd for $C_{15}H_{17}NO_2$: C, 74.05; H, 7.04; N, 5.76%.

16a: Colorless oil; IR (Neat) cm^{-1}: 3380 (OH) and 1680 (CO); ^1H NMR ($CDCl_3$) δ=1.10 (3H, s, CH_3), 2.02 (1H, m, 4-Hb), 2.13 (1H, dd, 4-Ha, J_{gem}=15.7 and J_{3a-4}=7.0 Hz), 2.2—2.7 (2H, ov, 3a-H and OH), 3.5—3.6 (2H, ov, 3-Ha and -Hb), 4.36 (1H, br s, 5-H), 5.72 (1H, dd, 6-H, J_{5-6}=5.0 and J_{6-7}=11.7 Hz), 6.44 (1H, d, 7-H, J_{6-7}=11.7 Hz), and 7.0—7.7 (5H, m, phenyl); MS *m/z* (rel intensity) 243 (M^+, base peak), 228 (M^+−CH_3, 7), 106 (62), and 77 (44).

Found: *m/z* 243.1254. Calcd for $C_{15}H_{17}NO_2$: M, 243.1258.

15b: Colorless oil; IR (Neat) cm^{-1}: 3400 (OH) and 1660 (CO); ^1H NMR ($CDCl_3$) δ=1.06 (3H, d, CH_3, J=7.1 Hz), 1.39 (1H, m, 4-H), 2.4—3.1 (4H, ov, 3-Hb and -Ha, 3a-H, and 6-H), 3.50 (1H, br s, OH), 3.66 (1H, m, 5-H), 4.44, 4.74 (1H each, 2d, $-CH_2$-Ph, J_{gem}=15.4 Hz), 6.47 (1H, br s, 7-H), and 7.2—7.6 (5H, m, phenyl); MS *m/z* (rel intensity) 271 (M^+, 84), 214 (57), 213 (M^+−CH_3CH_2CHO, 25), 122 (11), and 91 ($C_7H_7^+$, base peak).

Found: *m/z* 271.1573. Calcd for $C_{17}H_{21}NO_2$: M, 271.1571.

15c: Colorless prisms (ethanol); mp 176—177 °C; IR (KBr) cm^{-1}: 3310 (OH) and 1660 (CO); ^1H NMR ($CDCl_3$) δ=1.19 (3H, d, CH_3, J=7.7 Hz), 2.23 (1H, m, 4-H), 2.5—2.8 (2H, ov, 6-H and 3a-H), 2.83, 3.38 (1H each, 2t, 3-Hb and -Ha, J_{gem}=J_{3-3a}=9.2 Hz), 3.58 (1H, br s, OH), 3.83 (1H, m, 5-H), 4.45, 4.67 (1H each, 2d, $-CH_2$-Ph, J_{gem}=15.7 Hz), 6.58 (1H, t, J_{3a-7}=J_{6-7}=3.0 Hz), and 7.2—7.5 (10H, m, phenyl); MS *m/z* (rel intensity) 333 (M^+, 47), 214 (73), 213 (M^+−$PhCH_2CHO$, 10), and 91 ($C_7H_7^+$, base peak).

Found: C, 79.45; H, 6.98; H, 4.51%. Calcd for $C_{22}H_{23}NO_2$: C, 79.25; H, 6.95; N, 4.20%.

Formation of Oxirane 18 and Its Ring Opening Reaction with Nucleophiles 4, 12, and 14. The oxidation of **17** with MCPBA was performed in a similar manner to that of **1** with the exception of reaction temperature (below 0 °C).[13]

18: Colorless oil; IR (Neat) cm^{-1}: 1600 (CO); ^1H NMR ($CDCl_3$) δ=1.42 (1H, m, 5-Hb), 1.55 (1H, m, 4-Hb), 1.86 (1H, m, 4-Ha), 2.40 (1H, ddd, 5-Ha, J_{gem}=14.2, J_{4-5}=8.4, and J_{5-6}=3.3 Hz), 2.55 (1H, m, 4a-H), 3.21 (1H, ddd, 3-Hb, J_{gem}=13.9, J_{3-4}=5.7, and J_{3-4}=3.2 Hz), 3.33 (1H, ddd, 3-Ha, J_{gem}=13.9. J_{3-4}=12.6, and J_{3-4}=3.7 Hz), 3.48 (1H, t, 7-H, J_{6-7}=J_{7-8}=4.5 Hz), 3.59 (1H, dd, 6-H, J_{5-6}=3.3 and J_{6-7}=4.5 Hz), 4.55, 4.76 (1H each, 2d, $-CH_2$-Ph, J_{gem}=16.2 Hz), and 7.2—7.4 (6H, ov, 8-H and phenyl); MS *m/z* (rel intensity) 255 (M^+, 45), 164 (M^+−CH_2Ph, 8), and 91 ($C_7H_7^+$, base peak).

Found: *m/z* 255.1264. Calcd for $C_{16}H_{17}NO_2$: M, 255.1258.

The ring opening reactions of **18** with **4**, **12**, and **14** were performed in similar manners to those of the corresponding reactions of oxirane **2**.

19: Colorless prisms (ethanol); mp 156—158 °C; IR (KBr) cm^{-1}: 3390 (OH) and 1610 (CO); ^1H NMR ($CDCl_3$) δ=1.25 (1H, m, 5-Hb), 1.5—2.1 (7H, ov, 4-Ha and -Hb, 5-Ha, and pyrrolidinyl), 2.5—2.9 (5H, ov, 4a-H and pyrrolidinyl), 3.18 (1H, m, 3-Hb), 3.2—3.6 (3H, ov, 3-Ha, 7-H, and OH), 4.02 (1H, m, 6-H), 4.76 (2H, s, $-CH_2$-Ph), 7.15 (1H, br s, 8-H), and 7.3—7.6 (5H, m, phenyl); MS *m/z* (rel intensity) 326 (M^+, 41), 282 (M^+−CH_3CHO, base peak), 191 (282−CH_2Ph, 76), and 91 ($C_7H_7^+$, 89).

Found: C, 73.49; H, 8.21; N, 8.30%. Calcd for $C_{20}H_{26}N_2O_2$: C, 73.59; H, 8.03; N, 8.58%.

20: Colorless prisms (ethanol); mp 117—118 °C; IR (KBr) cm^{-1}: 3400 (OH), 2100 (N_3), and 1610 (CO); ^1H NMR ($CDCl_3$) δ=1.2—1.8 (2H, ov, 4-Ha and 5-Hb), 1.7—2.2 (2H, ov, 4-Ha and 5-Ha), 2.76 (1H, m, 4a-H), 3.3—3.6 (2H, ov, 3-Ha and -Hb), 3.88 (3H, ov, 6-H, 7-H, and OH), 4.65, 4.89 (1H each, 2d, $-CH_2$-Ph, J_{gem}=16.0 Hz), 7.05 (1H, m, 8-H), and 7.3—7.6 (5H, m, phenyl); MS *m/z* (rel intensity) 298 (M^+, 12), 256 (M^+−N_3, 40), 91 ($C_7H_7^+$, 51), and 42 (base peak).

Found: C, 64.59; H, 6.17; N, 18.82%. Calcd for $C_{16}H_{18}N_4O_2$: C, 64.41; H, 6.08; N, 18.78%.

21: Colorless needles (ethanol); mp 170—171 °C; IR (KBr) cm^{-1}: 3400 (OH) and 1600 (CO); ^1H NMR ($CDCl_3$) δ=1.05 (3H, d, CH_3, J=8.6 Hz), 1.2—1.7 (2H, ov, 4-Hb and 5-Hb), 1.6—2.1 (2H, ov, 4-Ha and 5-Ha), 2.2—2.9 (2H, ov, 4a-H and 7-H), 3.1—3.6 (3H, ov, 3-Ha and -Hb, and OH), 3.91 (1H, br s, 6-H), 4.64, 4.89 (1H each, 2d, $-CH_2$-Ph, J_{gem}=16.0 Hz), 7.08 (1H, br s, 8-H), and 7.4 (5H, m, phenyl); MS *m/z* (rel intensity) 271 (M^+, 78), 227 (M^+−CH_3CHO, 23), 136 (227−CH_2Ph, 9), and 91 ($C_7H_7^+$, base peak).

Found: C, 75.07; H, 7.84; N, 5.27%. Calcd for $C_{17}H_{21}NO_2$: C, 75.24; H, 7.80; N, 5.16%.

22: Colorless needles (benzene-hexane); mp 143—145 °C; IR (KBr) cm^{-1}: 3310 (OH) and 1615 (CO); ^1H NMR ($CDCl_3$) δ=1.18 (3H, s, CH_3), 1.6—2.0 (4H, ov, 4-Ha and -Hb and 5-Ha and -Hb), 2.24 (1H, m, 4a-H), 2.76 (1H, br s, OH), 3.0—3.5 (2H, ov, 3-Ha and -Hb), 4.26 (1H, br s, 6-H), 4.41, 4.89 (1H each, 2d, $-CH_2$-Ph, J_{gem}=16.2 Hz), 5.90 (1H, dd, J_{6-7}=5.4 and J_{7-8}=11.7 Hz), 6.79 (1H, d, 8-H, J_{7-8}=11.7 Hz), and 7.4 (5H, m, phenyl); MS *m/z* (rel intensity) 271 (M^+, 76), 256 (M^+−CH_3, 17), 180 (M^+−CH_2Ph, 10), 148 (24), and 91 ($C_7H_7^+$, base peak).

Found: C, 75.20; H, 7.98; N, 5.33%. Calcd for $C_{17}H_{21}NO_2$: C, 75.24; H, 7.80; N, 5.27%.

We wish to thank Professor Masashi Tashiro, Research Institute of Industrial Science, Kyushu

University, for the measurement of high mass spectra and the elemental analyses.

References

1) a) Cycloaddition Reactions of 2-Pyrones and Related Compounds. Part V; b) For part IV of this series: M. Noguchi, S. Kakimoto, H. Kawakami, and S. Kajigaeshi, *Bull. Chem. Soc. Jpn.*, **59**, 1355 (1986).

2) For recent reviews: G. Berti, "Topics in Stereochemistry," John Wiley & Sons, New York (1973), Vol. 2; K. B. Sharpless, *Aldrichimica Acta*, **12**, 63 (1979); P. A. Bartlett, *Tetrahedron*, **36**, 2 (1980).

3) For recent reviews: S. Patai, "The Chemistry of the Ether Linkage," John Wiley & Sons, New York (1967); T. J. Mason, *Heterocyclic Chem.*, **3**, 1 (1982); J. G. Smith, *Synthesis*, **1984**, 629.

4) K. Tori, T. Komeno, and T. Nakagawa, *J. Org. Chem.*, **29**, 1136 (1964).

5) T. Itoh, K. Kaneda, and S. Teranishi, *J. Chem. Soc., Chem. Comm.*, **1976**, 421; T. Itoh, K. Jitsukawa, K. Kaneda, and S. Teranishi, *Tetrahedron Lett.*, **1976**, 3157; *Idem, J. Am. Chem. Soc.*, **101**, 159 (1979).

6) J.-E. Bäckvall, K. Oshima, R. E. Palermo, and K. B. Sharpless, *J. Org. Chem.*, **44**, 1953 (1979).

7) T.-S. Ho, "Hard and Soft Acids and Bases Principle in Organic Chemistry," Academic Press, New York (1977).

8) G. H. Posner, D. Z. Rogers, C. M. Kinzing, and G. M. Gurria, *Tetrahedron Lett.*, **1975**, 3597; G. H. Posner and D. Z. Rogers, *J. Am. Chem. Soc.*, **99**, 8208 (1977); G. H. Posner, S. Moon, and P. E. Peterson, *Synth. Commun.*, **11**, 737 (1981).

9) A. Rosowsky, "Heterocyclic Compounds with Three- and Four-Membered Rings," ed by A. Weissberger, Interscience Pub. Inc., New York (1964) and also (see Ref. 4).

10) R.-D. Acker, *Tetrahedron Lett.*, **1977**, 3407 and **1978**, 2399.

11) J. P. Marino and N. Hatanaka, *J. Org. Chem.*, **44**, 4467 (1979); J. P. Marino and H. Abe, *Synthesis*, **1980**, 872; *idem, J. Am. Chem. Soc.*, **103**, 2907 (1981).

12) C. R. Johnson, R. W. Herr, and D. M. Wieland, *J. Org. Chem.*, **38**, 4263 (1973).

13) The reaction at room temperature gave undesirable results; lowering the yield of **18** and producing side reaction products including dioxiranes.

 © 1987 The Chemical Society of Japan Bull. Chem. Soc. Jpn., 60, 3269—3275 (1987)

Photochromic Behavior of Pyridoxal-α-Amino Acid-Zn(II) Complexes in Methanol

Kazuya OHGA* and Yoshiaki KURAUCHI
Department of Environmental Chemistry and Engineering, Oita University,
Dannoharu, Oita 870-11
(Received March 13, 1987)

Zn(II) complexes of pyridoxal-α-amino acid Schiff bases showed photochromic behavior in methanol. Spectral studies revealed that intramolecular nucleophilic attack of 5′-hydroxyl group on imine linkage forms cyclic α-amino ether intermediates which thermally return to the original complexes. The photochromism was characteristic of complexes having a 1:1 ligand-metal ratio. Analogous photochromism was also observed with the Cd(II) complex of *N*-pyridoxylidenevaline having a fully occupied d-orbital like the Zn(II) complexes, whereas no photochromism was observed with other transition metal complexes such as Ni(II), Cu(II), Mn(II), and Co(II) complexes.

We have previously reported that Zn(II) complexes of Schiff bases derived from pyridoxal-5′-phosphate and α-amino acids exhibit photochromism in an aqueous solution.[1] The photochromism is caused by photoinduced hydrolysis of the Schiff base ligands, as delineated in Scheme 1. This nucleophilic attack of water on imine carbon made us presume that an intramolecular nucleophilic attack will occur in 5′-hydroxyl group of pyridoxal-α-amino acid-Zn(II) complexes (Scheme 2).

The best-known cyclic ether analogous to the cyclization product **5** is the hemiacetal form of pyridoxal (PL) which is in equilibrium with the aldehyde form in solution and predominant in acidic and neutral methanol solutions.[2] Most metal complexes of PL-α-amino acid Schiff bases, on the other hand, exist exclusively in the imine form.[3] Cyclic isomer **5** is assumed to be thermally unstable so as to return to the original isomer **4**. This report describes spectral examination to confirm the photochromic mechanism. We will further discuss the difference in photochemical behavior between 1:1 (ligand-metal ratio) and 2:1 complexes. The effect of acid on the photochromism will also be examined.

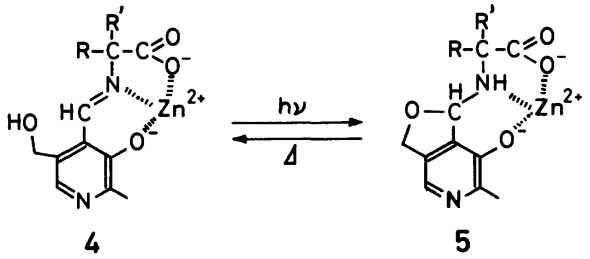

Scheme 2.

Experimental

PL hydrochloride (Sigma Chem. Co.) was converted to free base in the same manner as described by Christensen.[4] Bis(*N*-pyridoxylidenevalinato)zinc(II) (bis[*N*-(3-hydroxy-5-hydroxymethyl-2-methyl-4-pyridylmethylene)valinato]zinc-(II)) was prepared according to the procedure of Christensen[4] except for the use of zinc perchlorate and KOH instead of chloride and NaOH. 5′-Deoxypyridoxal (3-hydroxy-2,5-dimethyl-4-pyridinecarbaldehyde; 5′-DPL) was prepared by a five-step synthesis[5] starting from pyridoxine hydrochloride (3-hydroxy-4,5-dihydroxymethyl-2-methylpyridine hydrochloride) and was purified by sublimation at 80 °C (mp 108—109 °C). α-Amino acids (Wako Pure Chem. Co.)[6] and metal perchlorates (Kishida Chem. Co.) of the reagent grade or better were used without further purification. Acetonitrile and methanol (Dojin Chem. Co.) of the spectral grade were used as received. UV absorption and fluorescence spectra were recorded on a Shimadzu UV 202 or a JASCO UVIDEC-610A spectrophotometer and a Shimadzu RF-510 spectrometer, respectively. ^{1}H NMR spectra were obtained by a Hitachi R-24B spectrometer with tetramethylsilane as an internal standard. IR spectra were obtained by a Hitachi 285S spectrophotometer using KBr disk method.

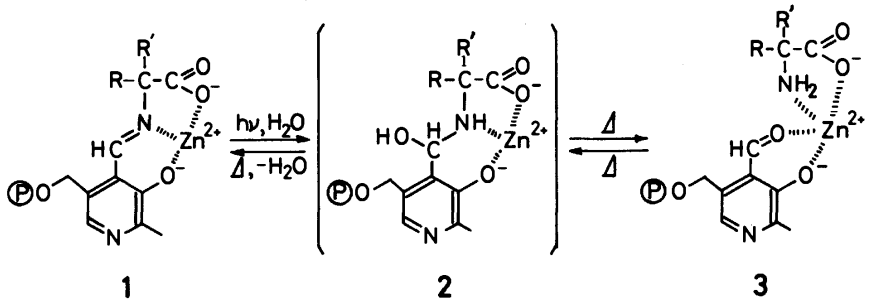

Scheme 1.

UV Spectral Studies. Metal complexes of PL-α-amino acid Schiff bases for UV studies were prepared in situ unless otherwise noted. A methanolic solution of the PL free base was mixed with α-amino acids dissolved in methanol with an equimolar KOH. After 1 h, a solution of a given metal perchlorate in methanol was added to the yellow Schiff base solution. The concentration of amino acids and metal perchlorates was 5 and 10 times as high as that of PL (1.0×10^{-4} M (1 M=1 mol dm^{-3})), respectively. The use of excess amino acids and metal ions was required to complete the complex formation promptly. Methanolic solutions of the Zn(II) complexes of 5'-DPL-α-amino acid Schiff bases were also prepared in situ in the similar manner. The solutions showed almost the same UV spectra as those of the PL complexes.

The metal complex solutions thus obtained were deaerated by repeated evacuation and flushing with argon three or more times, placed in a 1-cm quartz spectrophotometric cell, and then irradiated with a 500-W super high-pressure mercury lamp (Ushio USH-500D) at room temperature through a filter system composed of a glass filter (Toshiba UV-39) and water in a 5-cm cylindrical cell with quartz windows. After the irradiation, the UV absorption spectra were recorded at appropriate time intervals.

Desired acid or base species of the Zn(II) complexes, when necessary, were obtained by adding standard methanolic solutions of $HClO_4$ or KOH.

^{1}H NMR Spectral Studies of PL-Valine-Zn(II) System. A weighed amount of $Zn(ClO_4)_2\cdot6H_2O$ was dissolved in D_2O and the D_2O solution was evaporated to dryness. After this procedure was repeated several times, the residue was dissolved in CD_3OD. CD_3OD solution of zinc perchlorate thus obtained (1.0 M, 0.1 cm^3) was added to a suspension of 63 mg of bis(*N*-pyridoxylidenevalinato)zinc(II) in 0.5 cm^3 CD_3OD, and the complex was dissolved completely. The complete dissolution of 2:1 complex by the addition of Zn^{2+} implies that 1:1 complex is more soluble in methanol than 2:1 complex. To the clear solution was added 0.08 cm^3 of a CD_3OD solution of KOD (1.0 M) in order to slow down a thermal back reaction; the retardation will be mentioned later. At this time, a small amount of pale yellow precipitate was separated out.[7] After standing for 30 min, the precipitate was filtered out. The resulting clear solution was devided into two parts, and each part was transferred to a Pyrex tube (18 mm diameter) and deaerated by the method described above. The tubes were then dipped in water (20.0±0.5 °C) and irradiated separately with the same Hg lamp as used in the UV studies without any glass filters. In order to ensure efficient mixing, the sample tubes were slanted and rotated while being irradiated. After the irradiation, the photolysates were transferred quickly to NMR sample tubes and NMR spectra were taken at ambient temperature at appropriate time intervals. The spectral changes of two samples in lower and higher magnetic fields were examined. This procedure was required to obtain more unambiguous signals of a photochemically produced intermediate and to follow their momentary changes.

Isolation of Intermediate. When the above sample for the NMR measurement was not efficiently agitated during the irradiation, a small amount of precipitate was deposited on the inner wall of Pyrex tube. The precipitate, which is an intermediate formed in the photochromic change as will be described later, disappeared within 10 min on standing at room temperature. In order to isolate it, an analogous CH_3OH solution of the Zn(II) complex was irradiated without agitation at a low temperature (ca. 0 °C) and the photolysate was quickly centrifuged. The precipitate clinging to the bottom of the centrifuge glass tube was dried in vacuo and used for IR measurement in that condition. No attempt to isolate the intermediate was successful.

Determination of Quantum Yield. The quantum yield for the disappearance of the starting complex **4** determined by means of an optical-bench system equipped with Ushio USH-500D lamp at 25±1 °C. A beam of 365 nm band isolated with a monochromator (Shimadzu, Baush & Lomb, Grating 1350 grooves/mm) was devided into two beams by a beam splitter, one of which was used to monitor the intensity of incident light. Another beam was used to irradiate the same sample solutions as UV studies in a cylindrical quartz cell of 20×10 mm. The number of photons (2.2×10^{15} quanta s^{-1}) absorbed by the sample solutions was evaluated by subtracting the intensity of transmitted light from that of incident light. The light intensity was determined by the trioxalatoferrate(III) actinometry using 0.006 M potassium trioxalatoferrate(III).[8] The thermal recovery of absorbance at λ_{max} (382—384 nm) obeyed the first-order kinetics. The amount of **4** regenerated during the irradiation was ignored, because it was less than 5% of the amount of **4** reduced by the irradiation.

Relative Fluorescence Intensity. The relative fluorescence intensity at 465 nm of the Zn(II) complex of *N*-pyridoxylidenevaline ([PL]=1.0×10^{-4} M) was measured at 25±1 °C with an excitation wavelength of 385 nm.

Results and Discussion

UV Spectral Studies. Irradiation of a methanolic solution of the Zn(II) complex of *N*-pyridoxylidenevaline with light of wavelengths longer than 390 nm led to an immediate decrease in intensity of absorption bands at 384 and 271 nm and a new absorption band with the maximum wavelength at 314 nm appeared (Fig. 1). When the photolysate was kept in the dark, the UV spectrum returned more than 98% of its initial figure within 60 min at room temperature and showed two isosbestic points at 287 and 333 nm. Almost the same spectral changes were observed with other α-amino acids. The spectral data are summarized in Table 1 together with the quantum yield for photoinduced disappearance of the starting complexes.[9] It is noted that glycine, phenylalanine, homoserine, and serine, in common, gave a weak but discernible shoulder at about 250 nm. In the cases of alanine, valine, α-aminoisobutyric acid, and methionine, this absorption band seems to be buried in an intense band at a shorter wavelength of about 230 nm.

The divalent metal complexes of Schiff bases derived from PL and α-amino acids usually have two characteristic absorption bands in UV region; the longer wavelength band at about 390 nm has been

called the π_1 band and the shorter one at about 270 nm the π_2 band.[2a] These bands are assigned as π-π^* transitions of the extended conjugated system formed from pyridine ring, phenolic oxygen and imine linkage. The lack of the conjugated imine linkage, on the other hand, causes shift of these absorption bands to a shorter wavelength. For example, the π_1 and π_2 bands of the Zn(II) complex of pyridoxamine (4-aminomethyl-3-hydroxy-5-hydroxymethyl-2-methylpyridine) appear at 301 and 240 nm, respectively;[2a] those of the Zn(II) complex of an α-hydroxy amine derived from PL and *N*-methylglycine appear at 316 and 248 nm, respectively.[3c] Thus, the appearance of new absorption bands at about 315 and 250 nm suggests the transformation of imine linkage to a saturated C-N bond. This result seems to agree with the prediction outlined in Scheme 2; however, the formation of an α-amino ether **6** by nucleophilic addition of solvent molecule to imine carbon can also be envisaged.

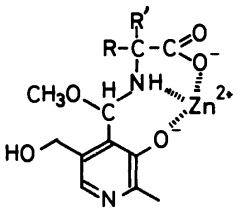

6

Table 1. Photochromism of the Zn(II) Complexes of PL-α-Amino Acid Schiff Bases **4** in Methanol[a]

α-Amino acid	λ_{max}/nm		Isosbestic points/nm	Quantum yield[b]
	Before irradiation	Just after irradiation		
Glycine	384, 270	316, ca. 250[c]	336, 287	0.22
Alanine	383, 269	314	334, 285	0.17
Valine	384, 271	314	333, 287	0.19
Phenylalanine	384, 273	316, ca. 250[c]	337, 290	0.23
AIB[d]	382, 270	310	332, 284	0.18
Methionine	383, 278	315	335, 290	0.05
Homoserine	382, 281	316, ca. 250[c]	335, 290	0.17
Serine	382, 279	315, ca. 250[c]	336, 292	0.20

a) The initial concentrations of PL, α-amino acids, Zn^{2+}, and KOH were 1.0×10^{-4}, 5.0×10^{-4}, 1.0×10^{-3}, and 5.0×10^{-4} M, respectively. b) Quantum yield for the disappearance of **4**.[9] c) Shoulder. d) α-Amino-isobutyric acid.

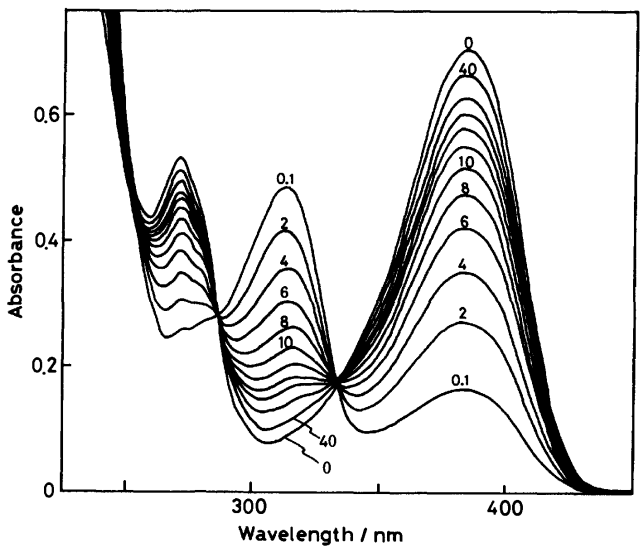

Fig. 1. UV spectral changes of the Zn(II) complex of *N*-pyridoxylidenevaline in methanol. The numeral 0 gives the spectrum before irradiation, and other numerals give the time in minutes after 1-min irradiation at the start of each scan.

IR Spectral Studies. A small amount of precipitate was obtained by irradiating more concentrated solution of the Zn(II) complex of *N*-pyridoxylidenevaline at a low temperature (see Experimental section). When the precipitate was dissolved in methanol again, almost the same thermal UV spectral changes as those in Fig. 1 were observed. This fact suggests that the precipitate is an intermediate of the photochromism.

As shown in Fig. 2(a), the IR spectrum of the intermediate showed a band at 1085 cm^{-1} which can be assigned to the C-O-C stretching vibration. In addition, the intensity of the bands due to the

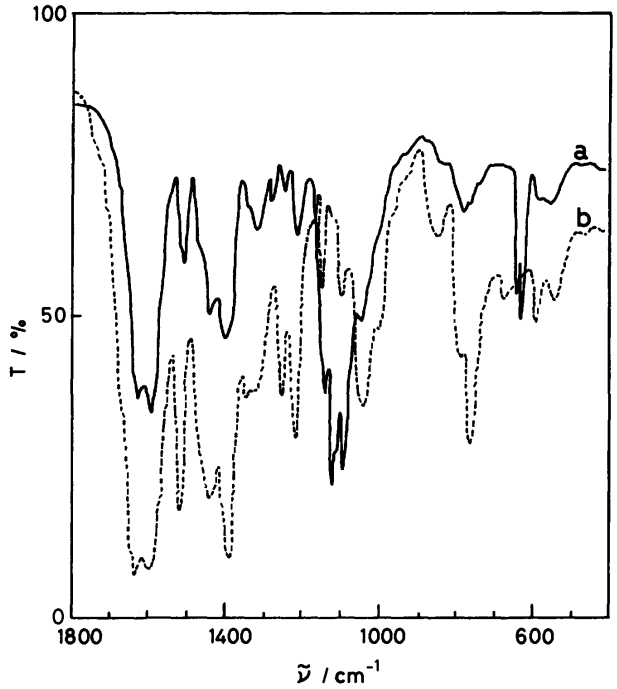

Fig. 2. Comparison of the infrared spectrum of a precipitate obtained through irradiation (a) with that of bis(*N*-pyridoxylidenevalinato)zinc(II) (b).

alcoholic 5′-OH group of bis(*N*-pyridoxylidenevalinato)zinc(II) at 1248, 1045, and 760 cm^{-1} (Fig. 2(b)) decreased remarkably.[10] These facts suggest that the formation of **5** by the intramolecular addition of 5′-OH is predominant over the formation of solvent adduct **6**. This is also supported by the following two facts from UV spectral studies: (1) The Zn(II) complexes of 5′-DPL-α-amino acid Schiff bases without 5′-OH group showed an irreversible slow photoreaction instead of photochromism; (2) almost the same photochromic spectral changes were observed in acetonitrile with low nucleophilicity.[11]

^{1}H NMR Spectral Studies. The ^{1}H NMR spectrum of the Zn(II) complex of *N*-pyridoxylidenevaline in slightly alkaline CD_3OD showed five prominent signals (Fig. 3, 0: before irradiation), which were readily assigned on the basis of data reported for several Schiff base metal complexes:[3b,7b,12] δ 8.80 (1H, s, HC=N-), 7.50 (1H, s, 6-H), 3.82 (1H, d, α-H of valine moiety), 2.55 (3H, s, 2-CH_3), and 1.08 and 0.99 (6H, d and d, CH_3 of isopropyl group). The signal of methylene proton of 5-hydroxymethyl group is probably obscured by the solvent absorption.

Figure 3 also shows that new signals appeared on irradiation and then disappeared within 10 min at ambient temperature. The UV spectral changes simultaneously observed were almost the same as those in Fig. 1.

NMR spectra by imine proton showed a marked shift with irradiation from δ 8.80 to a higher magnetic field at δ 5.85. It has been reported[13] that the imine proton resonance of *N*-pyridoxylidenehistidine at δ 8.33 shifts to a higher magnetic field at δ 5.81 by cyclization forming a tetrahydropyridine derivative. Moreover, the 4-CH signal of an α-hydroxy amine formed from PL and *N*-methylglycine appears at δ 6.09,[14] and the signals of methine protons at 2 position of various 2-phenyloxazolidine compounds appear at about δ 5.8.[15] Thus, the photocyclization to **5** described above was further confirmed by the singlet signal induced at δ 5.85 as well as by other newly-induced signals which can be readily assigned to pyridine ring proton (δ 7.62, s), the valine moiety α-proton (δ 3.48, d), the 2-methyl protons (δ 2.53, s), and the methyl protons of the isopropyl group (δ 1.12—0.94, m) of **5**.

Effects of Acid and Base on Photochromism. UV spectra of the metal complexes of PL-α-amino acid Schiff bases have two characteristic bands, i.e., the π_1 and π_2 bands described above. These bands were affected by the addition of $HClO_4$ or KOH. For example, the π_1 band (382 nm) of the Zn(II) complex of *N*-pyridoxylidenevaline in an acidic solution shifted to a longer wavelength (385 nm) with a decrease in absorbance by the addition of KOH,

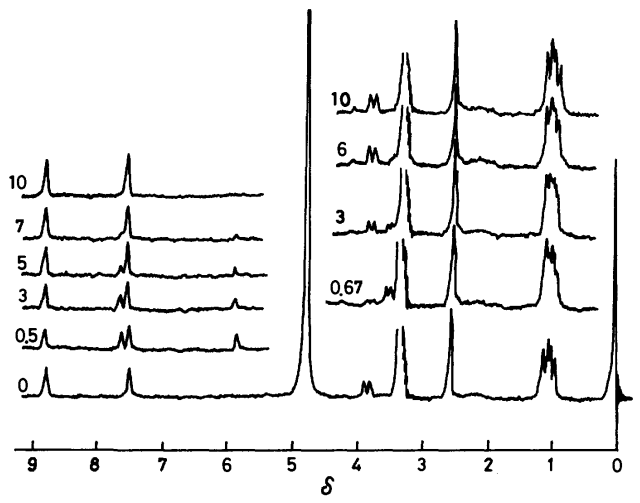

Fig. 3. ^{1}H NMR spectra of a CD_3OD solution of the Zn(II) complex of *N*-pyridoxylidenevaline. The numeral 0 gives the spectrum before irradiation and other numerals give the time in minutes after irradiation at the start of each scan. The spectra in lower and higher magnetic fields were separately taken using two samples.

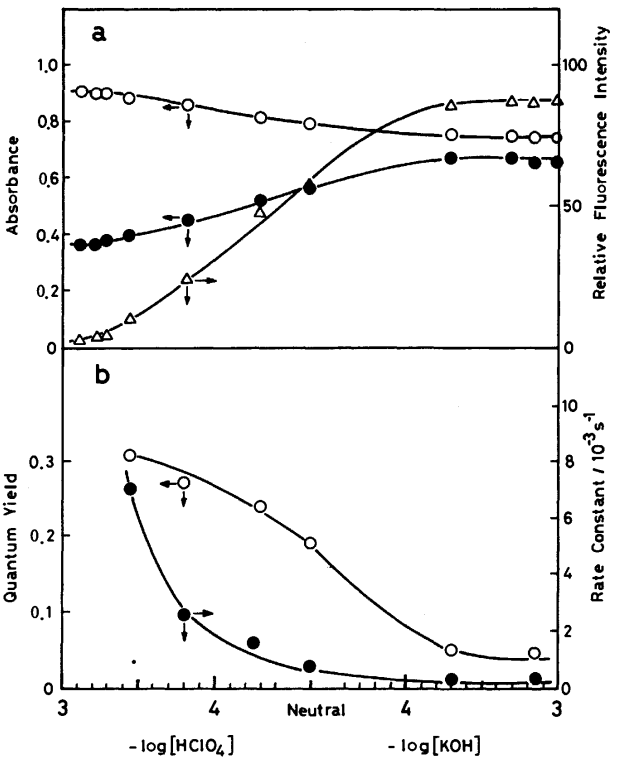

Fig. 4. (a) UV absorbance changes at 385 nm (○) and 272 nm (●) and fluorescence intensity changes (△) of the Zn(II) complex of *N*-pyridoxylidenevaline as a function of $HClO_4$ or KOH concentration in methanol. (b) Quantum yields for the disappearance of the Zn(II) complex of *N*-pyridoxylidenevaline (○) and rates of the thermal back reaction (●) as a function of $HClO_4$ or KOH concentration.

whereas the π_2 band at 280 nm shifted to a shorter wavelength (272 nm) with an increase in absorbance. Plots of the absorbances at 272 and 385 nm vs. the negative common logarithm of concentration of the added $HClO_4$ or KOH (Fig. 4(a)) gave titration curves similar to those in H_2O,[16] and can be well explained by the proton equilibrium on pyridine nitrogen. The relative fluorescence intensity also varied with adding $HClO_4$ or KOH and the resulting titration curve had an inflection point similar to that of UV absorbance (Fig. 4(a)).[17] This fact indicates that the pK value for the proton equilibrium of pyridine nitrogen in the excited singlet state is nearly equal to that in the ground state.

All solutions used for preparing the titration curves in Fig. 4(a) showed photochromic spectral changes, and the π_1 band of the intermediate occurred at 300 nm in a slightly alkaline solution (the concentration of KOH added, 5.0×10^{-5} M), whereas the band in solutions acidified with $HClO_4$ occurred at 314 nm. This difference can also be explained by the proton equilibrium on pyridine ring of the intermediate. A similar proton equilibrium has been reported for the Cu(II) complex of *N*-(3-hydroxy-5-hydroxymethyl-2-methyl-4-pyridylmethyl)valine:[18] The deprotonation of the complex causes a blue shift of the absorption maximum from 315 to 300 nm.

The quantum yield for disappearance of the Zn(II) complex of *N*-pyridoxylidenevaline became greater with an increase in the concentration of $HClO_4$ and the titration curve (Fig. 4(b)) showed an inflection point similar to those observed in UV and fluorescence spectral studies. The photocyclization seems, therefore, to be accelerated by protonation of pyridine nitrogen in the excited singlet state or in the ground state. The rate of thermal back reaction increased with an increase in the amount of $HClO_4$ added, and inversely decreased as the amount of KOH added increased (Fig. 4(b)). The rate change can be interpreted in terms of proton catalysis in a ring cleavage reaction of **5**.

Difference in Photochemical Behavior between 2:1 and 1:1 Complex. Addition of much larger amount of KOH (e.g., 1.05×10^{-2} M) caused the disappearance of photochromism, and instead, a slow irreversible spectral change took place to give a band of product with λ_{max} at 322 nm. The irreversible change was also observed in systems containing less than equimolar amount of Zn^{2+}: for example, in a system containing Zn^{2+} of 0.6×10^{-4} M and PL, valine, and KOH of 1.0×10^{-4} M.

The Zn(II) complexes of PL-α-amino acid Schiff bases exist as 2:1 form in solid state.[4,7b,15b] Gansow and Holm,[7b] on the other hand, showed by NMR analyses that 2:1 and 1:1 species co-exist in an aqueous PL-alanine-Zn(II) system and that the extent of formation of 2:1 species increases with an increase in pH. The 2:1 species is also formed in aqueous solutions containing appreciably smaller amounts of Zn^{2+} (0.016—0.05 M) than those of PL and alanine (0.1 M). These facts made us infer that the irreversible change is induced by excitation of 2:1 species, whereas the photochromism is induced by excitation of 1:1 species.

In order to ascertain this idea, the influence of Zn^{2+} on ^1H NMR spectra of the Zn(II) complex of *N*-pyridoxylidenevaline was investigated and the results are depicted in Fig. 5. A saturated solution of the Zn(II) complex in alkaline CD_3OD (0.12 M KOD) prepared by dissolving 2:1 complex showed, as a whole, upfield-shifted signals compared to those of solutions containing extraneous Zn^{2+}, indicating that the signals of 2:1 species appear in higher magnetic fields than 1:1 species. It seems important that the solution without extraneous Zn^{2+} failed to show the photochromic spectral changes as observed in a solution containing excess Zn^{2+} (Fig. 3). These results support the idea that the presence of 1:1 species is a prerequisite for the photochromism.

Irradiation of Other Metal Complexes. Photochemical behavior of *N*-pyridoxylidenevaline complexes with other divalent metal ions such as Cu^{2+}, Ni^{2+}, Co^{2+}, Mn^{2+}, and Cd^{2+} was investigated in

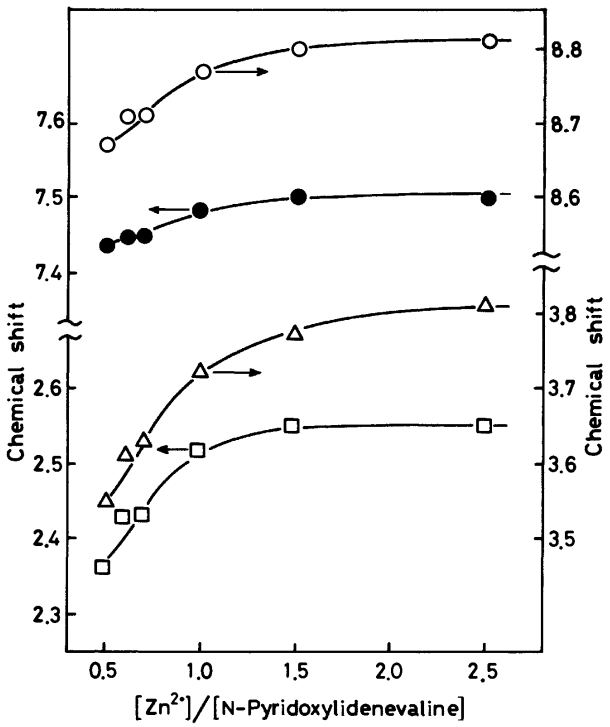

Fig. 5. ^1H NMR chemical shifts as a function of the concentration of Zn^{2+} in a methanolic solution of the Zn(II) complex of *N*-pyridoxylidenevaline ([*N*-pyridoxylidenevaline]=4.0×10^{-2} M, [KOH]=0.12 M): ○; -CH=N-, ●; ArH, △; α-H of valine moiety, □; Ar-CH_3.

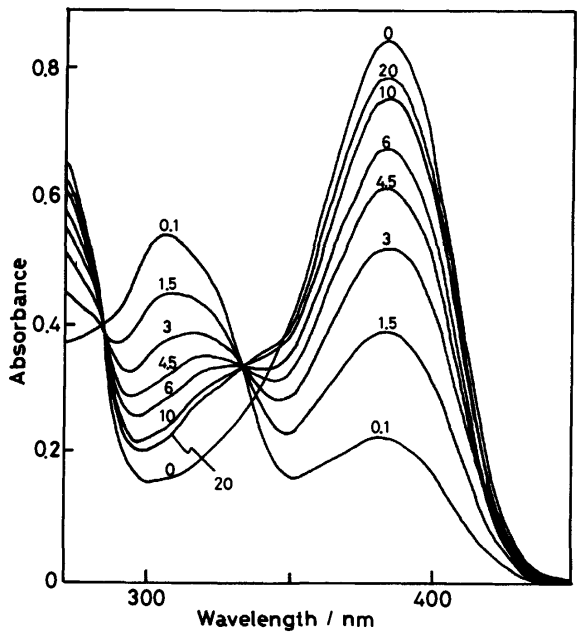

Fig. 6. UV spectral changes of the Cd(II) complex of *N*-pyridoxylidenevaline in methanol. The numeral 0 gives the spectrum before irradiation, and other numerals give the time in minutes after 3-min irradiation at the start of each scan.

methanol containing excess metal ions. The Cd(II) complex having the d^{10} electronic structure like the Zn(II) complexes showed photochromism (Fig. 6), whereas the Cu(II) and Ni(II) complexes were exceedingly photostable. For the Co(II) and Mn(II) complexes, only a slight irreversible decrease was observed in the absorbance of intraligand π–π^* bands at about 385 nm: less than 5% decrease after irradiation for 3 min. In addition, fluorescence intensity of the complexes showing no photochromism was negligibly weak in comparison with those of the photochromic Zn(II) and Cd(II) complexes. Thus, lack of photochromism in the transition-metal complexes with unfilled d-shells appears to be attributed to the presence of nonradiative processes from the intraligand π–π^* singlet state to d-d or charge-transfer excited state, although it is not yet clear whether the singlet state is photoreactive or not in the cases of the Zn(II) and Cd(II) complexes.

References

1) Y. Kurauchi, K. Ohga, A. Yokoyama, and S. Morita, *Bull. Chem. Soc. Jpn.*, **56**, 357 (1983).

2) a) Y. Matsushima and A. E. Martell, *J. Am. Chem. Soc.*, **89**, 1322 (1967); b) R. J. Johnson and D. E. Metzler, "Methods in Enzymology," ed by D. B. McCormick and L. D. Wright, Academic Press, New York (1970), Vol. XVIII, part A, p. 479.

3) a) It is well-known that alternative cyclization takes place thermally in the cases of Schiff bases or their metal complexes having highly nucleophilic functional groups at β or γ position of the amino acid moieties.[3b–e] For example, the Schiff base of cysteine gives a thiazolidine derivative.[3b] Such cyclization products are not formed with any one of amino acids employed in the present study (listed in Table 1); b) E. H. Abbot and A. E. Martell, *J. Am. Chem. Soc.*, **92**, 1754 (1970); c) D. Heyl, S. A. Harris, and K. Folkers, *J. Am. Chem. Soc.*, **70**, 3429 (1948); d) Y. Matsushima, *Chem. Pharm. Bull.*, **16**, 2046 (1968); e) *ibid.*, **16**, 2143 (1968).

4) H. N. Christensen, *J. Am. Chem. Soc.*, **79**, 4073 (1957).

5) R. J. Johnson and D. E. Metzler, "Methods in Enzymology," ed by D. B. McCormick and L. D. Wright, Academic Press, New York (1970), Vol. XVIII, Part A, p. 558; D. Heyl, S. A. Harris, and K. Folkers, *J. Am. Chem. Soc.*, **75**, 653 (1953).

6) Optically-active amino acids were of L-configuration.

7) a) The precipitate appears to be a mixture of 2:1 complex, $Zn(OD)_2$, and $KClO_4$, because the IR spectrum of the precipitate was similar to that of 2:1 complex and because the addition of KOD possibly leads to deposition of $Zn(OD)_2$ and $KClO_4$. The precipitation of the complex is in harmony with the formation of a 2:1 complex at high pH in an aqueous PL–alanine–Zn(II) system,[7b] as will be discussed later in detail; b) O. A. Gansow and R. H. Holm, *J. Am. Chem. Soc.*, **90**, 5629 (1968); *ibid.*, **91**, 573 (1969).

8) C. G. Hatchard and C. A. Parker, *Proc. R. Soc. London, Ser. A*, **235**, 518 (1956).

9) As will be described later, the Zn(II) complex of *N*-pyridoxylidenevaline existed as the 1:1 form rather than 2:1 form when the concentration of Zn^{2+} was 1.5 times or above as high as that of the Schiff base ligand (see Fig. 5). Since the solutions used here contained excess Zn^{2+} ($[Zn^{2+}]/[\text{ligand}]=10$, see Experimental section), all the starting complexes probably exist as 1:1 forms.

10) Careful inspection of IR spectrum of the precipitate (Fig. 2(a)) revealed that the intermediate was contaminated with a small amount of starting complex and $Zn(ClO_4)_2$. A new band at 1110 cm^{-1} is attributed to the stretching vibration of a perchlorate anion which was added to the sample solution as zinc perchlorate.

11) a) Acetonitrile solution was prepared by mixing the crystalline 2:1 complex and zinc perchlorate at a 1:5 molar ratio. At this time, the addition of a small amount of water (2%) was required to dissolve two components. The direct participation of water in the photochromism, if any, would give an α-hydroxy amine analogous to **2** which has a UV spectrum similar to those of the cyclic ethers **5**. However, this type of α-hydroxy amine has not yet been detected,[11b] and thus is expected to be readily transformed into a mixed complex analogous to **3**.[1] Careful inspection of the spectrum just after the irradiation revealed the absence of the mixed complex which probably has a similar spectrum to that of PL, dismissing the possibility of the photohydrolysis; b) D. Hopgood and D. L. Leussing, *J. Am. Chem. Soc.*, **91**, 3740 (1969); D. L. Leussing and C. K. Stanfield, *J. Am. Chem. Soc.*, **88**, 5726 (1966).

12) E. H. Abbot, *J. Inorg. Nucl. Chem.*, **33**, 567 (1971); E. H. Abbot and A. E. Martell, *J. Am. Chem. Soc.*, **92**, 5845 (1970).

13) L. Casella and M. Gullotti, *J. Am. Chem. Soc.*, **103**, 6338 (1981).

14) Y. Matsushima and T. Hino, *Chem. Pharm. Bull.*, **16**, 2277 (1968).

15) H. Aoyama, M. Sakamoto, K. Kuwabara, K. Yoshida, and Y. Omote, *J. Am. Chem. Soc.*, **105**, 1958 (1983).

16) a) Davis et al.[16b] reported an increase in the absorbance of the π_1 band and a decrease in the π_2 band in H_2O by lowering pH, and obtained the pK_a value of 6.5 for the proton dissociation on the pyridine nitrogen. b) L. Davis, F. Roddy, and D. E. Metzler, *J. Am. Chem. Soc.*, **83**, 127 (1961).

17) Although the absorbances at the excitation wavelength (385 nm) decreased with a decrease in the $HClO_4$ concentration and an increase in the KOH concentration (Fig. 4(a)), the fluorescence intensity inversely increased. Thus the acid and base effects on the fluorescence intensity are somewhat underestimated.

18) H. N. Christensen, *J. Am. Chem. Soc.*, **81**, 6495 (1959).

 © 1987 The Chemical Society of Japan Bull. Chem. Soc. Jpn., 60, 3277—3283 (1987)

Optical Resolution by Preferential Crystallization of DL-Thiazolidine-4-carboxylic Acid

Tadashi SHIRAIWA,* Yujin SADO, Masamitsu KOMURE, and Hidemoto KUROKAWA
Faculty of Engineering, Kansai University, Yamate-cho, Suita, Osaka 564
(Received March 19, 1987)

Infrared spectrum, solubility, and ternary solubility diagram indicated that DL-thiazolidine-4-carboxylic acid (DL-THC) is a conglomerate at room temperature. The free energy of critical nucleation in supersaturated solutions for the crystallization of D- and L-THC was examined to resolve DL-THC efficiently by preferential crystallization. Successive preferential crystallization of DL-THC was experimented at 20 °C for an aqueous racemic solution with a supersaturation of 150%, and D- and L-THC with optical purity of 96—100% were obtained in the range of resolution of 58—76%. The optical resolution was more successfully done in 1 mol dm^{-3} aqueous glycine to give D- and L-THC with optical purity of 93—99% in the degree of resolution of 77—87%. Recrystallization of D- and L-THC obtained with a succeeding treatment with hydroxylamine hydrochloride gave D- and L-cysteine with 100% optical purity.

L-Cysteine (abbreviated as L-Cys) as a useful material for medicines, food additives, and cosmetics has been obtained mainly from hair. Although D-Cys was also noted, recently, as a pharmaceutical material,[1] it is difficult to find D-Cys in natural products. An efficient synthesis of DL-Cys has been known,[2] and DL-Cys can be optically resolved by the diastereomeric procedure.[3,4] The optical resolution by a preferential crystallization seems to be more useful for an industrial purpose than the diastereomeric procedure. However, the optical resolution by preferential crystallization of DL-Cys was tried only for DL-cysteine hydrochloride monohydrate.[1] This paper describes an attempt to obtain D- and L-Cys efficiently by the preferential crystallization.

DL-Thiazolidine-4-carboxylic acid (DL-THC) was easily obtained by the reaction of DL-cysteine hydrochloride monohydrate with formaldehyde.[5] By infrared spectrum, solubility, and ternary solubility diagram, DL-THC seemed to be a conglomerate. DL-THC was subjected to optical resolution in water at 20 °C. The free energy of critical nucleation in supersaturated solutions of D- and L-THC was examined to find the appropriate conditions for optical resolution by preferential crystallization of DL-THC.[6-8] The optical resolution in 1 mol dm^{-3} aqueous glycine was also examined to obtain D- and L-THC more efficiently than in water.

Experimental

Materials. DL- and L-Cysteine hydrochloride monohydrate were purchased from Sigma Chemicals Co. and Wako Pure Chemicals Ind., respectively, and formaldehyde, hydroxylamine hydrochloride, and triethylamine from Wako Pure Chemicals Ind.

Synthesis of Thiazolidine-4-carboxylic Acid. DL- and L-Thiazolidine-4-carboxylic acid were prepared by the reaction of each cysteine hydrochloride monohydrate with formaldehyde.[5] DL-THC: Mp 195—198 °C (decomp) (lit,[9] mp 183—184 °C, 195 °C (decomp)). L-THC: Mp 202—204 °C (decomp) (lit,[9] mp 196—197 °C, 205—209 °C (decomp)); $[\alpha]_D^{20}$ −141° (*c* 1.00, water) (lit,[9] $[\alpha]_D^{20}$ −141° (water)).

D-THC of 37.5% optical purity was obtained from the mother liquor in optical resolution of DL-THC. After dissolving 26.64 g of D-THC in 280 cm^3 of water at an elevated temperature, and the solution was stirred for 1 h at 20 °C. The precipitated D-THC was collected by filtration, washed with a small amount of cold water and ethanol successively, and dried to give 9.88 g of optically pure D-THC; mp 202—204 °C (decomp); $[\alpha]_D^{20}$ +141° (*c* 1.00, water).

Optical Resolution. Preferential Crystallization: DL-THC was dissolved in 50 cm^3 of water at 40 °C to give racemic solutions with different degrees of supersaturation from 120 to 170% (20 °C) as shown in Table 1. The solution was slowly cooled to 20 °C and seeded with 0.050 g of L-THC. After stirring the mixture at 100 rpm and 20 °C, the precipitated L-THC was collected by filtration, washed with a small amount of ethanol, and dried. The optical purity, yield of optically pure modification (YOPM/g), degree of resolution of L-THC, and amounts of crystallization of D- and L-THC (W_D and W_L/g) were determined by

$$\text{Optical purity}/\% = (\text{Specific rotation of obtained THC}/^\circ \times 100)/(-141), \quad (1)$$

$$\text{YOPM/g} = (\text{Yield/g} \times \text{Optical purity}/\%)/100 - 0.050, \quad (2)$$

Table 1. Preparation of Supersaturated Solution in Water[a]

Degree of supersaturation[b]/%	Amount of DL-THC[c]/g
120	3.586
130	3.885
140	4.184
145	4.333
150	4.483
155	4.632
160	4.782
170	5.080

a) Water: 50 cm^3. b) Temperature: 20 °C. c) DL-THC: DL-Thiazolidine-4-carboxylic acid.

$$\text{Degree of resolution}/\% = (\text{YOPM/g} \times 100)/(1/2)(\text{Amount of consumed DL-THC/g} - 2.989), \quad (3)$$

$$W_D/\text{g} = (1/2)(\text{Yield/g} - \text{YOPM/g} - 0.050), \quad (4)$$

$$W_L/\text{g} = \text{YOPM/g} + W_D/\text{g}. \quad (5)$$

Successive Preferential Crystallization: DL-THC was dissolved in 50 cm^3 of water or 1 mol dm^{-3} aqueous glycine at 40 °C; 4.483 g in water (150% supersaturation) and 4.710 g in 1 mol dm^{-3} aqueous glycine (155% supersaturation). The solution was cooled to 20 °C and seeded with 0.050 g of L-THC. After stirring the mixture at 100 rpm and 20 °C, the precipitated L-THC was collected by filtration. DL-THC was dissolved in the filtrate at 40 °C; the amount was equal to that of crystallized THC. After seeding the solution with 0.050 g of D-THC at 20 °C, the mixture was treated similarly as above. The degree of resolution of D- and L-THC was calculated by

$$\text{Degree of resolution}/\% = (\text{YOPM/g} \times 100)/(\text{Operation amount of D- or L-THC/g} - M), \quad (6)$$

where M is 1.494 g in water, and 1.520 g in 1 mol dm^{-3} aqueous glycine.

The optical resolution was also performed for a solution containing 26.892 g of DL-THC in 300 cm^3 of water using 0.300 g of D- or L-THC as seed crystals; the supersaturation of the initial solution was 150%.

Preparation of Optically Active Cysteine. A mixture of D- or L-THC recrystallized from water (1.332 g, 0.010 mol) and 0.732 g (0.010 mol) of hydroxylamine hydrochloride in 50 cm^3 of methanol was refluxed for 60 min. After adding 0.366 g (0.005 mol) of hydroxylamine hydrochloride to the mixture and refluxing for 60 min, the solution was stirred in an ice bath for 60 min. The formed formaldehyde oxime was removed by filtration, and pH of the filtrate was adjusted to 5—6 with triethylamine. Precipitated crude Cys (0.02 g) was filtered out; $[\alpha]_D^{20}$ +18.7 or −18.0° (water). After drying the filtrate under reduced pressure at 30 °C, the residue was added to 50 cm^3 of methanol. The mixture was stirred for 1 h at 40 °C and insoluble Cys was filtered, washed with methanol, and dried. D-Cys: Yield 0.989 g; $[\alpha]_D^{20}$ +16.5° (*c* 2.00, water). L-Cys: Yield 0.995 g; $[\alpha]_D^{20}$ −16.5° (*c* 2.00, water) (lit,[10] $[\alpha]_D$ −16.5° (water)).

Measurements. The specific rotation was measured by a Union Giken PM-101 digital polarimeter with a quartz cell of 0.5 dm path length. The infrared spectra were obtained in the range 4000—400 cm^{-1} by a JASCO A-102 infrared spectrophotometer using the KBr disk method.

Results and Discussion

Racemic Structure. DL-THC shows identical infrared spectrum with that of L-THC and is more soluble than L-THC as described in Table 2. The ternary solubility diagram is shown in Fig. 1.

The above results infer that DL-THC is a conglomerate at room temperature.[11]

Preferential Crystallization. Since DL-THC was optically resolved by preferential crystallization in 50 cm^3 of water at 20 °C in the presence of 0.050 g of L-THC seed crystals, as shown in Table 3, DL-THC was confirmed to be a conglomerate at room temperature. Relationships between the amounts of crystallization of D- and L-THC and the resolution

Table 2. Solubility of DL- and L-Thiazolidine-4-carboxylic Acid[a]

Solvent	Solubility/g/(100 cm^3 solvent)	
	DL-THC	L-THC
Water	5.977	3.193
Gly[b]	6.078	3.314

a) Temperature: 20 °C. b) Gly: 1 mol dm^{-3} aqueous glycine.

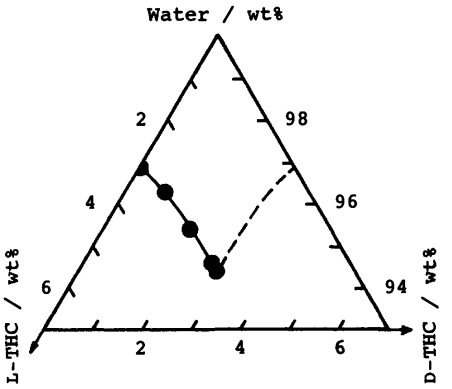

Fig. 1. Ternary solubility diagram of thiazolidine-4-calboxylic acid.
Temperature: 20 °C. Solvent: Water.

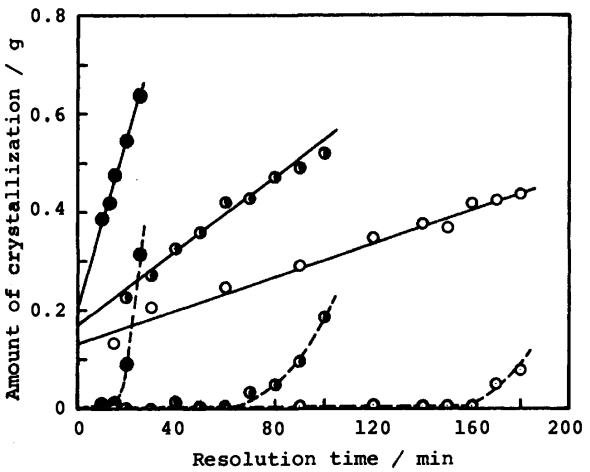

Fig. 2. Relationship between amounts of crystallization and resolution time.
Solvent: 50 cm^3 of water. Seed crystals: 0.050 g of L-THC. Temperature: 20 °C. ——: L-THC. — —: D-THC. ○: 130% degree of supersaturation. ◑: 140% degree of supersaturation. ●: 160% degree of supersaturation.

time are shown in Fig. 2 for the solutions of supersaturation of 130, 140, and 160%, where the solvent is 50 cm^3 of water.

After a rapid crystallization in extremely short time, L-THC appears to crystallize at a constant speed with respect to the increase in resolution time. The speed of crystallization of L-THC (R_L/g min^{-1}) and the amount of crystallization extrapolated to zero resolution time (W_0/g) were calculated from linear plots in Fig. 2 for different degrees of supersaturation; the correlation coefficient of the linear relationships ranges from 0.989 to 0.997. The retardation time for crystallization of D-THC (Θ_D/min), defined as the resolution time until D-THC begins to crystallize rapidly, was estimated from Fig. 2. Although Fig. 2 indicates that D-THC co-exists in L-THC crystallized in shorter resolution time than Θ_D, DL-THC adhered on precipitates should have been considered in the estimation. These factors on crystallization of D- and L-THC are given in Table 4.

Optical Resolution by Preferential Crystallization. Relationship between Factors Controlling Crystallization and Free Energy of Critical Nucleation: In our previous paper,[8] it was reported that the

Table 3. Preferential Crystallization of DL-Thiazolidine-4-carboxylic Acid in Water[a]

Degree of supersaturation	Resolution time	Yield	Optical purity	YOPM[b]	Degree of resolution	Amount of crystallization/g	
%	min	g	%	g	%	L-THC	D-THC
120	360	0.284	100	0.234	78.4	0.234	0
	490	0.319	94.7	0.252	84.3	0.261	0.009
130	15	0.182	100	0.132	29.5	0.132	0
	30	0.253	100	0.203	45.3	0.203	0
	60	0.293	100	0.243	54.2	0.243	0
	90	0.346	97.1	0.286	63.8	0.291	0.005
	120	0.405	96.4	0.340	75.9	0.348	0.008
	140	0.426	98.7	0.370	82.6	0.373	0.003
	150	0.424	97.5	0.363	81.0	0.369	0.006
	160	0.470	99.0	0.415	92.6	0.418	0.003
	170	0.524	80.9	0.374	83.5	0.424	0.050
	180	0.567	71.8	0.357	79.7	0.437	0.080
140	20	0.274	100	0.224	37.5	0.224	0
	30	0.321	100	0.271	45.3	0.271	0
	40	0.387	93.9	0.313	52.3	0.325	0.012
	50	0.408	100	0.358	59.9	0.358	0
	60	0.474	98.1	0.415	69.4	0.420	0.005
	70	0.509	87.8	0.397	66.4	0.428	0.031
	80	0.572	82.5	0.422	70.6	0.472	0.050
	90	0.633	70.6	0.397	66.4	0.490	0.093
	100	0.758	50.7	0.334	55.9	0.521	0.187
145	40	0.500	97.4	0.437	65.0	0.444	0.007
	50	0.598	82.9	0.446	66.4	0.497	0.051
150	20	0.419	98.3	0.362	48.5	0.366	0.004
	30	0.527	96.3	0.458	61.3	0.468	0.010
	40	0.617	81.8	0.455	60.9	0.511	0.056
	50	0.912	54.2	0.444	59.4	0.653	0.209
155	20	0.510	96.7	0.443	53.9	0.452	0.009
	30	0.711	74.5	0.480	58.4	0.571	0.091
160	10	0.442	96.3	0.376	42.0	0.384	0.008
	13	0.476	97.1	0.412	46.0	0.419	0.007
	15	0.534	96.4	0.465	51.9	0.475	0.010
	20	0.687	73.9	0.458	51.1	0.548	0.090
	25	0.998	37.1	0.320	35.7	0.634	0.314
170	6	0.461	91.5	0.372	35.6	0.392	0.020
	15	0.959	46.1	0.392	37.5	0.651	0.259

a) Water: 50 cm^3. Seed crystals: 0.050 g of L-THC. Temperature: 20 °C. b) YOPM: Yield of optically pure modification.

Table 4. Factors on Preferential Crystallization in Water[a)]

Degree of supersaturation	R_L[b)]/$\times 10^{-3}$ g min^{-1}		W_0[c)]/g		θ_D[d)]/min		$W_{(-5)}$[e)]/g	
%	Found	Calcd[f)]	Found	Calcd[g)]	Found	Calcd[h)]	Found	Calcd[i)]
130	1.716	1.593	0.132	0.135	165	174.1	0.418	0.404
140	3.682	4.186	0.169	0.164	65	68.4	0.420	0.430
145	—	6.197	—	0.177	45	46.8	0.444	0.436
150	9.040	8.787	0.183	0.190	35	33.4	0.468	0.444
155	—	12.033	—	0.204	25	24.7	0.452	0.439
160	16.898	16.015	0.212	0.214	18	18.7	0.419	0.434
170	—	26.492	—	0.237	11	11.5	0.392	0.409

a) Water: 50 cm^3. Seed crystals: 0.050 g of L-THC. Temperature: 20 °C. b) R_L: Speed of crystallization of L-THC. c) W_0: Amount of crystallization of L-THC extrapolated to zero resolution time. d) θ_D: Retardation time for crystallization of D-THC. f) The value was calculated by Eq. 7. g) The value was calculated by Eq. 9. h) The value was calculated by Eq. 8. i) The value was calculated by Eq. 10.

Table 5. Properties of Critical Nucleus in Supersaturated Solution[a)]

Degree of supersaturation	r_{cr}[b)]	σ_{cr}[c)]	Δg_{max}[d)]
%	$\times 10^{-9}$ m	$\times 10^{-2}$ J m^{-2}	$\times 10^{-18}$ J nucleus^{-1}
120	15.978	4.466	47.758
130	10.911	4.388	21.883
140	8.368	4.317	12.663
145	7.518	4.283	10.140
150	6.837	4.250	8.321
155	6.278	4.218	6.964
160	5.811	4.187	5.924
170	5.075	4.129	4.455

a) Solvent: Water. Temperature: 20 °C. b) r_{cr}: Radius of critical nucleus. c) σ_{cr}: Interfacial energy of critical nucleus. d) Δg_{max}: Free energy of critical nucleation.

appropriate conditions for the optical resolution by preferential crystallization is predictable by the free energy of critical nucleation (Δg_{max}/J nucleus^{-1}) in supersaturated solutions. The values of Δg_{max} were calculated for aqueous solutions of DL-THC with various degrees of supersaturation,[6-8,12)] and given in Table 5. The relationship between R_L and Δg_{max} for different degrees of supersaturation of 130, 140, and 160% and that between Θ_D and Δg_{max} were obtained by Eqs. 7 and 8,[8)] respectively,

$$\ln R_L = -1.766 \ln \Delta g_{max} - 74.19, \quad (7)$$

$$\ln \theta_D = 1.707 \ln \Delta g_{max} + 70.64, \quad (8)$$

where the correlation coefficients for Eqs. 7 and 8 were 0.995 and 0.997, respectively. The relationship between W_0 and Δg_{max} is expressed by Eq. 9

$$\ln W_0 = -0.3543 \ln \Delta g_{max} - 15.59, \quad (9)$$

where the correlation coefficient was 0.993. The amount of crystallization of L-THC at Θ_D can be estimated by Eqs. 7—9 for various degrees of supersaturation.

The values of R_L, W_0, and Θ_D for an aqueous solution with 120% supersaturation were calculated to be 4.01×10^{-4} g min^{-1}, 0.102 g, and 660 min, respectively; the solvent was 50 cm^3 of water. The value of Θ_D suggests that D-THC does not crystallize rapidly within 660 min. The optical resolution at 360 min gave L-THC with 100% optical purity in 0.284 g yield as shown in Table 3. The amount of crystallized L-THC was 0.234 g and agreed well with the calculated value at 360 min by Eqs. 7 and 9 (0.247 g). The calculated values of R_L and W_0 suggest that the theoretical amount of L-THC (0.299 g) crystallizes after 490 min. The optical resolution at 490 min gave L-THC with 94.7% optical purity in 0.319 g yield; the amount of crystallization of L-THC was 0.261 g. The relatively large difference between the experimental result and calculated value suggests that the crystallization of L-THC is inhibited after a long resolution time, because the supersaturation of L-THC in the solution decreases considerably with crystallization of L-THC. However, for the solutions with supersaturation of 130—160%, L-THC seems to crystallize at a rate proportional to the resolution time until at least Θ_D min as demonstrated in Fig. 2 and indicated by Eq. 7.

Appropriate Conditions of Optical Resolution: Although the optical resolution at Θ_D will give the maximum yield of L-THC with high optical purity, the optical resolution at Θ_D—5 min seems to be more suitable to stable operation than that at Θ_D, because D-THC begins to crystallize rapidly after Θ_D. The amount of L-THC produced at Θ_D—5 min ($W_{(-5)}$/g) is expressed by Eq. 10

$$W_{(-5)} = R_L(\theta_D - 5) + W_0. \quad (10)$$

The values of R_L, W_0, Θ_D, and $W_{(-5)}$ for various degrees of supersaturation were calculated by Eqs. 7—10. The relationship between $W_{(-5)}$ and the degree of

supersaturation is shown in Fig. 3.

The calculated $W_{(-5)}$ values showed an identical tendency with that of experimental data in supersaturation between 130 and 170%. Figure 3 suggests that the optical resolution at 150% supersaturation gives the muximum amount of L-THC. This optical resolution was performed at resolution time in the range 20—50 min as given in Table 3, because Θ_D is 33.4 min calculated by Eq. 8. The experimental amounts of crystallization of L-THC are compared with those calculated by Eqs. 7 and 9 in Fig. 4.

The value of Θ_D is 35 min in Fig. 4 and agrees well with the calculated value of 33.4 min. The optical resolution at 30 min, namely at Θ_D−5 min, gave L-THC with 96.3% optical purity of 61.3% degree of resolution. The amount of crystallization of L-THC is 0.468 g; the amount calculated is 0.440 g at 28.4 min by

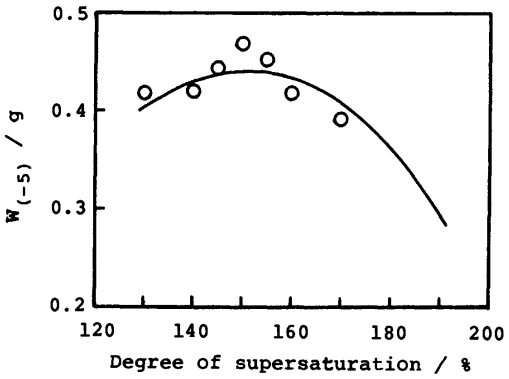

Fig. 3. Relationship between amount of crystallization of L-thiazolidine-4-carboxylic acid at θ_D−5 min and degree of supersaturation.
Conditions: Solvent 50 cm³ of water; seed crystals 0.050 g of L-THC; temperature 20 °C. $W_{(-5)}$: Amount of crystallization of L-THC at θ_D−5 min; —— calculated amount by Eq. 10; O found. θ_D: Retardation time for crystallization of D-THC.

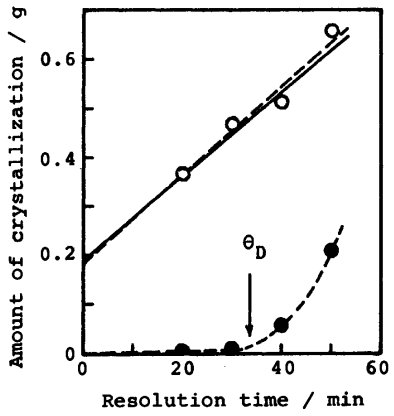

Fig. 4. Preferential crystallization from aqueous solution with 150% degree of supersaturation.
Solvent: 50 cm³ of water. Seed crystals: 0.050 g of L-THC. Temperature: 20 °C. ——: Calculated amount of crystallization of L-THC. Found: O L-THC; ● D-THC. θ_D: Calculated retardation time for crystallization of D-THC (33.4 min).

Table 6. Successive Preferential Crystallization in Water[a)]

Run	Added amount of DL-THC	Operation amount[b)]/g		Resolution time	THC obtained			
					Yield	Optical purity	YOPM[c)]	Degree of resolution
	g	D-THC	L-THC	min	g	%	g	%
1[d)]	4.482	2.241	2.241	30	L 0.527	96.3	0.458	61.3
2	0.477	2.469	2.011	20	D 0.624	100	0.574	58.9
3	0.574	2.182	2.298	30	L 0.685	97.2	0.619	77.0
4	0.635	2.491	1.988	30	D 0.668	98.8	0.610	61.2
1[e)]	26.892	13.446	13.446	30	L 3.024	80.1	2.122	47.3
2	2.724	14.507	12.385	25	D 3.785	100	3.485	62.9
3	3.485	12.765	14.128	30	L 3.713	100	3.413	66.1
4	3.413	14.472	12.422	30	D 4.168	96.6	3.726	67.6
5	3.865	12.609	14.285	30	L 4.300	98.1	3.918	73.6
6	4.000	14.568	12.326	30	D 4.439	96.8	3.997	71.3
7	4.139	12.570	14.325	30	L 4.509	99.4	4.182	78.0
8	4.209	14.661	12.234	30	D 4.668	98.0	4.275	75.0
9	4.368	12.523	14.371	30	L 4.564	98.0	4.172	77.2
10	4.264	14.609	12.284	30	D 4.839	92.0	4.152	73.6
11	4.539	12.533	14.360	30	L 4.711	96.5	4.246	78.7

a) Temperature: 20 °C. Degree of supersaturation of initial solution: 150%. b) The operation amounts of D- and L-THC in Runs 2—4 or 2—11 were calculated on the basis of the analyses of the obtained THC in Runs 1—3 or 1—10. c) YOPM: See note b) in Table 3. d) Water: 50 cm³. Seed crystals: 0.050 g of D- or L-THC. e) Water: 300 cm³. Seed crystals: 0.300 g of D- or L-THC.

Table 7. Successive Preferential Crystallization in Aqueous Glycine[a)]

Run	Added amount of DL-THC	Operation amount[b)]/g		Resolution time	THC obtained			
		D-THC	L-THC		Yield	Optical purity	YOPM[c)]	Degree of resolution
	g			min	g	%	g	%
1	4.710	2.355	2.355	60	L 0.740	93.6	0.643	77.0
2	0.690	2.676	2.033	50	D 1.024	97.9	0.952	82.4
3	0.974	2.200	2.509	50	L 0.927	98.6	0.864	87.4
4	0.877	2.632	2.077	50	D 1.031	95.0	0.929	83.5

a) Solvent: 50 cm^3 of 1 mol dm^{-3} aqueous glycine. Seed crystals: 0.050 g of D- or L-THC. Temperature: 20 °C. Degree of supersaturation of initial solution: 155%. b) The operation amounts of D- and L-THC in Runs 2—4 were calculated on the basis of the analyses of the obtained THC in Runs 1—3. c) YOPM: See note b) in Table 3.

Eqs. 7 and 9. The maximum yield of optically pure modification (YOPM/g) in Table 3 appears at θ_D−5 min for each degree of supersaturation (cf. also Table 4). The optical resolution at 30 min with 150% supersaturation is most favorable to obtain efficiently L-THC with high optical purity.

These results revealed that appropriate conditions can be estimated by Δg_{max} in the optical resolution by preferential crystallization.

Successive Preferential Crystallization: Based on the above results, the successive preferential crystallization was carried out in 50 cm^3 of water at 20 °C for 30 min using a solution with 150% initial supersaturation, as listed in Table 6. The procedure gave D- and L-THC with optical purity of 96—100% and resolution of 58—77%.

The optical resolution under the same conditions was scaled up 6 times as described in Table 6. The optical purity of L-THC fell to 80.1%, and hence the degree of resolution was 47.3%. This low optical purity will be due to a change of stirring condition by the scale up. However, the optical resolution in runs 2—11 was satisfactory for producing D- and L-THC with optical purity of 92—100% and resolution of 62—79%.

Optical Resolution in Aqueous Glycine Solution. D- and L-THC with high optical purity were efficiently obtained by the successive preferential crystallization in water under appropriate conditions estimated by Δg_{max}, but the values of YOPM were only 10—14% of the amount of DL-THC dissolved in the initial solution; YOPM denotes the theoretical amount of optically pure THC obtained by recrystallization.

Since the solubility of DL- and L-THC is slightly higher in 1 mol dm^{-3} aqueous glycine than in water, as shown in Table 2, an attractive interaction may exist between glycine and THC molecules. This suggests that the value of θ_D is larger in the glycine solution than in water, because the growth of critical nuclei of THC is inhibited by glycine molecules.[7] Since the crystallization of L-THC will also be inhibited by glycine, the successive preferential crystallization was attempted in 1 mol dm^{-3} aqueous glycine for a solution with 155% supersaturation. This result was listed in Table 7.

L-THC with 93.6% optical purity was obtained in degree of resolution of 77.0% by the procedure for 60 min; YOPM was 13.7% of the amount of DL-THC dissolved in the initial solution. THC in aqueous glycine may crystallize as a molecular compound with glycine,[13] but the elemental analyses show that only L-THC crystallizes.[14] This result is supported by the fact that D-THC does not crystallize for at least 60 min.

The D- and L-THC with optical purity of 95—99% were obtained in degree of resolution of 82—87% in runs 2—4, and YOPM were approxymately 20% of the amount of DL-THC dissolved in the initial solution.

The recrystallization of obtained D- and L-THC from water, followed by treatment with hydroxylamine hydrochloride, gave optically pure D- and L-Cys in 82% yield.

References

1) C. Inoue, Y. Kurima, and S. Moriguchi, Jpn. Patent, 70859 (1982); *Chem. Abstr.*, **97**, 163490 (1982).
2) J. Martens, H. Offermans, and P. Scherberich, *Angew. Chem., Int. Ed. Engl.*, **20**, 668 (1981).
3) J. L. Wood and V. du Vigneaud, *J. Biol. Chem.*, **130**, 109 (1939).
4) H. Nohira, Jpn. Patent, 51239 (1984); *Chem. Abstr.*, **101**, 131104 p (1984).
5) S. Ratner and T. Clarke, *J. Am. Chem. Soc.*, **59**, 200 (1937).
6) T. Nakai, *Bull. Chem. Soc. Jpn.*, **42**, 2143 (1969).
7) T. Nakai, "Shoseki Kogaku," Baifukan, Tokyo (1986), Section 2.
8) T. Shiraiwa, H. Miyazaki, T. Imai, M. Sunami, and H. Kurokawa, *Bull. Chem. Soc. Jpn.*, **60**, 661 (1987).
9) J. S. Davies, "Amino Acids and Peptides," Chapman and Hall, London, New York (1985), p. 302.
10) Ref. 9, p. 130.
11) H. Nohira, "Shizen Bunsho no Joken to Jitsuyo Rei," in "Fusei Gosei to Kogaku Bunkatsu no Shinpo," ed by S. Ohtsuka and T. Mukaiyama, Kagaku Dojin, Kyoto

(1982), p. 165.

12) In order to calculate Δg_{max}, the molecular volume of THC (1.320×10^{-28} m^3) was measured in water at 20 °C. The molecular radius was calculated to be 3.159×10^{-10} m on the assumption of spherical molecule. The average values of the radius (4.027×10^{-10} m) and interfacial energy (1.807 J m^{-2}) of embryo in the saturated aqueous solution at 20 °C were calculated on the basis of the solubility of DL-THC according to the procedure reported in Ref. 6; the average number of THC molecule forming the embryo in the solution was 2.072.

13) T. Shiraiwa, A. Ikawa, K. Sakaguchi, and H. Kurokawa, *Bull. Chem. Soc. Jpn.*, **57**, 2234 (1984).

14) Elemental analyses of the L-THC crystallized from 1 mol dm^{-3} aqueous glycine: Found C, 36.18; H, 5.30; N, 10.52% (Calcd for $C_4H_7NO_2S$: C, 36.08; H, 5.30; N, 10.52%).

 © 1987 The Chemical Society of Japan Bull. Chem. Soc. Jpn., 60, 3285—3290 (1987)

Palladium-Promoted Transformation of β-Amino Ketones to Enaminones

Shun-Ichi Murahashi,* Yo Mitsue, and Tatsuo Tsumiyama
Department of Chemistry, Faculty of Engineering Science, Osaka University,
Machikaneyama, Toyonaka, Osaka 560
(Received March 18, 1987)

The reaction of β-amino ketones with bis(acetonitrile)dichloropalladium(II) in the presence of triethylamine gives the corresponding enaminones regioselectively. The cyclic β-amino ketones can be converted into the corresponding exocyclic enaminones. The enaminones thus obtained are versatile synthetic intermediates. The reaction of (E)-enaminones with organocuprates gave the corresponding (E)-α,β-unsaturated ketones.

Transition metals insert into the carbon–hydrogen bond α to the nitrogen of tertiary amines to give iminium ion hydride complexes.[1] In relation to the study of these intermediates, we have found that palladium-promoted transformation of β-amino ketones **1** to enaminones **2** proceeds efficiently as depicted in Eq. 1.

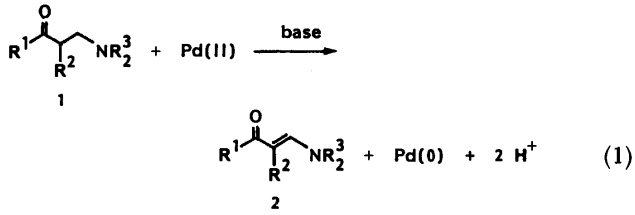

(1)

Enaminones are versatile synthetic intermediates because of their regioselective reactions with either nucleophiles or electrophiles[2] Nucleophiles attack at the carbonyl carbon and the β-carbon of carbonyl groups,[3] while electrophiles attack at the carbonyl oxygen[4] and the α-carbon of carbonyl groups. In the presence of bases, electrophiles attack at the α′ and γ-carbons of carbonyl groups selectively.[5] Enaminones have been prepared by the limited methods,

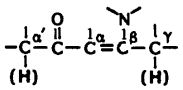

which include condensation of 1,3-diketones with amines,[6] reaction of enamines with ketenes,[7] addition of amines to ethynyl ketones,[8] oxidative amination of α,β-unsaturated ketones,[9] reaction of ketones with formamide acetals,[10] and condensation of silyl enol ethers with oxime mesylates.[11] The present palladium-induced reaction of β-amino ketones provides a new strategy, since the starting substrates, β-amino ketones are readily available by Mannich reaction of carbonyl compounds[12] as depicted in Eq. 2.

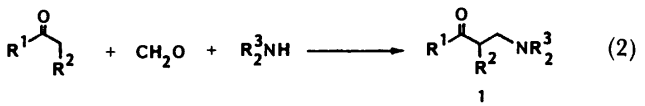

(2)

Described herein are the preparation of enaminones, mechanistic aspects, and synthetic applications.[13]

Results and Discussion

Treatment of 4-diethylamino-2-butanone (**1a**) with $PdCl_2(MeCN)_2$ in the presence of two equivalents of triethylamine in acetonitrile gave (*E*)-4-diethylamino-3-buten-2-one (**2a**) in 95% yield. The HCl salt of β-amino ketone can be also utilized as substrates by adding three equivalents of bases. Generally, the reaction is strongly affected by the solvent used as shown in Table 1.

Although a polar aprotic solvent, such as acetonitrile gives enaminones in high yields, using a nonpolar solvent, such as benzene, the reaction rates become slow. Ethanol is a poor solvent because the reduction of the Pd(II) complex with ethanol proceeds fast. The reaction of β-amino ketones (R^2=H) with $PdCl_2(MeCN)_2$ in the absence of bases gave 1,3,5-triacylbenzenes and none of enaminones was detected. The reaction can be rationalized by assuming the reaction pathway shown in Eq. 3.[14] Apparently, the

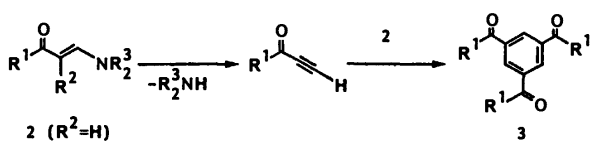

(3)

enaminones derived from β-amino ketones are the precursor. Deamination of enaminones gives acetylenic ketones, which undergo acid catalyzed condensation, with **2** to give 1,3,5-triacylbenzenes **3**. Indeed, the treatment of (*E*)-3-dimethylamino-1-phenyl-2-

Table 1. The Solvent Effect on the Pd(II)-Induced Transformation of 4-Diethylamino-2-butanone (**1a**) to (*E*)-4-Diethylamino-3-buten-2-one (**2a**)[a]

Entry	Solvent	(ε[b])	Yield[c]/%
1	MeCN	(37.5)	95
2	Acetone	(20.7)	47
3	THF	(7.58)	37
4	Benzene	(2.28)	26
5	EtOH	(24.6)	15

a) All reactions were carried out using 1 molar equivalent of $PdCl_2(MeCN)_2$ and 2 molar equivalents of Et_3N in a solvent at reflux for 0.5 h. b) Dielectric constant at 20 °C, and at 25 °C for MeCN. c) Determined by GLC.

propen-1-one (**2b**) with hydrochloric acid in acetonitrile gave 1,3,5-tribenzoylbenzene (**3b**) in 95% yield. This reaction is highly efficient for the preparation of 1,3,5-triacylbenzenes.

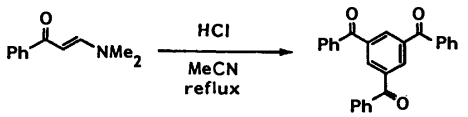

2b 3b

The formation of enaminones is strongly affected by the bases added as shown in Table 2. When a weaker base such as Na_2CO_3 was used for the palladium-promoted reaction of **1b**, both enaminones and triacylbenzenes were obtained. For these reactions $Pd(OAc)_2$ is more reactive than $PdCl_2(MeCN)_2$, although the yields with $Pd(OAc)_2$ are lower. The conversion of 1-dimethylamino-4,4-dimethyl-3-pentanone (**1c**) is low because of the steric effect of *t*-butyl group. Therefore, we examined the effect of bases on the $Pd(OAc)_2$-promoted reaction of **1c**. As shown in Table 3 the conversion of **1c** in the presence of

Table 2. The Effect of Bases on the Pd(II)-Induced Reaction of β-Amino Ketones[a]

Entry	β-Amino ketone	Base	Time/h	Product/%[b]	
1	**1a**	Et_3N	0.5	**2a** (95[c])	**3a** (Trace)
2	**1a**	Na_2CO_3	0.5	**2a** (28[c])	**3a** (Trace)
3	**1a**	None	5	**2a** (0)	**3a** (32)
4	**1b**[d]	Et_3N	12	**2b** (81)	**3b** (0)
5	**1b**[d]	Et_3N[e]	4	**2b** (73)	**3b** (0)
6	**1b**[d]	Na_2CO_3	12	**2b** (36)	**3b** (35)
7	**1b**[d]	None	6	**2b** (0)	**3b** (35)
8	**1c**[d]	Et_3N	4.5	**2c** (53)	**3c** (0)

a) All reactions were carried out using 1 molar equivalent of $PdCl_2(MeCN)_2$ and 2 molar equivalents of base in MeCN at reflux unless otherwise noted. b) Isolated yield. c) Determined by GLC. d) β-Amino ketone hydrochloride and 3 molar equivalents of base were used. e) $Pd(OAc)_2$ was used.

Table 3. The Effect of Bases on the Pd(II)-Induced Transformation of 1-Dimethylamino-4, 4-dimethyl-3-pentanone (**1c**) to (*E*)-1-Dimethylamino-4, 4-dimethyl-1-penten-3-one (**2c**)[a]

Entry	Base	Conv.[b]/%	Yield[c]/%
1	Et_3N	50	38
2	Et_3N[d]	50	38
3	DABCO[e]	85	24
4	DBN[f]	53	42
5	4-Methylmorpholine	79	46
6	Na_2CO_3	88	92 (74)

a) All reactions were carried out using **1c** hydrochloride (0.5 mmol), $Pd(OAc)_2$ (0.5 mmol), and base (1.5 mmol) in MeCN at reflux for 0.5 h unless otherwise noted. b) Determined by GLC. c) GLC yield and isolated yield in parentheses. d) 2 h. e) 1,4-Diazabicyclo[2.2.2]octane. f) 1,5-Diazabicyclo[4.3.0]non-5-ene.

Table 4. Pd(II)-Induced Transformation of β-Amino Ketones to Enaminones[a]

Entry	β-Amino ketone		Time/h	Product		Yield[b]/%
1	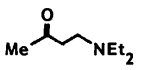	(**1a**)	0.5	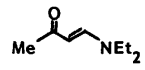	(**2a**)	70 (95)
2	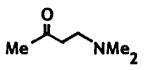	(**1e**)	0.5	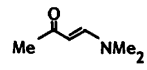	(**2e**)	75
3	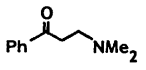	(**1b**)[c]	12	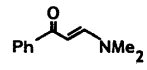	(**2b**)	81
4	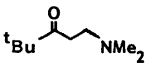	(**1c**)[c]	0.5[d]	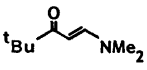	(**2c**)	74 (18)
5	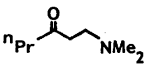	(**1d**)	0.5	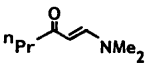	(**2d**)	71
6	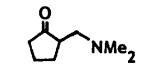	(**1f**)	0.5	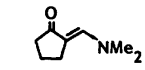	(**2f**)	47
7	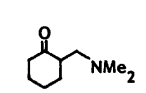	(**1g**)	0.5	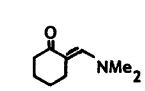	(**2g**)	43
8	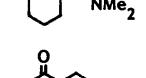	(**1h**)	0.25	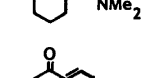	(**2h**)	95

a) All reactions were carried out using β-amino ketone (0.8 mmol) and $PdCl_2(MeCN)_2$ (0.8 mmol) in the presence of Et_3N (1.6 mmol) in MeCN (10 mL) at reflux unless otherwise noted. b) Isolated yields and GLC yields in the parentheses. c) β-Amino ketone hydrochloride was used. d) $Pd(OAc)_2$ and Na_2CO_3 were used.

triethylamine is 50% and the yield of **2c** is quite low. However, Na_2CO_3 was found to be an excellent base for the conversion of **1c**.

The present reaction is generally applicable for the conversion of various β-amino ketones as shown in Table 4. Various enaminones are obtained in moderate to very good yields. The structures of the enaminones were established by IR, NMR, and mass spectral data and elemental analyses. The stereochemistry was established to be trans by the NMR spectra.[15] The cyclic β-amino ketones can be converted into the corresponding exocyclic enaminones, which are important synthetic intermediates, such as dihydrojasmones and others.[16] Cyclic amino ketones such as **1i** and **1j** do not undergo dehydrogenation.

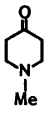

1i

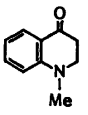

1j

Low-valent palladiums such as Pd black and $Pd(PPh_3)_4$, which are excellent catalysts for the activation of amines to give iminium ion complexes,[1] are almost inert to the present reaction.

Ketones generally undergo dehydrogenation by either direct[17] or indirect methods[18] to give α,β-unsaturated ketones. In these reactions, β-carbonyl palladium intermediates or oxo(π-allyl)palladium complexes have been postulated. The present reaction proceeds similarly as shown in Scheme 1.

The coordination of Pd(II) complex to the enol of β-amino ketones gives π-complex **4** which undergoes insertion to give HX and β-carbonyl palladium complex **5**.[19] Further elimination of $PdHXL_n$ gives enaminone **2**. The stable conformer of **5**, where the carbonyl group may occupy the trans position to the amino group, undergoes cis-elimination of PdH species to give (E)-enaminones **2**. The present reaction shows different reactivity in comparison with the direct palladium-promoted transformation of ketones to α,β-unsaturated ketones. In contrast to the poor regioselectivity of the direct palladium-induced dehydrogenation, the present reaction gives enaminones regioselectively. Further the direct dehydrogenation of α-alkylated cyclic ketones can be converted into endocyclic olefins, while the present reaction gives exocyclic ketones. The regioselectivity seems to be determined at the stage of the coordination of palladium to the nitrogen of β-amino ketones. Actually, cyclic keto amines such as **1i** and **1j** do not undergo dehydrogenation, because the coordination of palladium to the nitrogen and the enol of cyclic amino ketones at the same time is difficult.

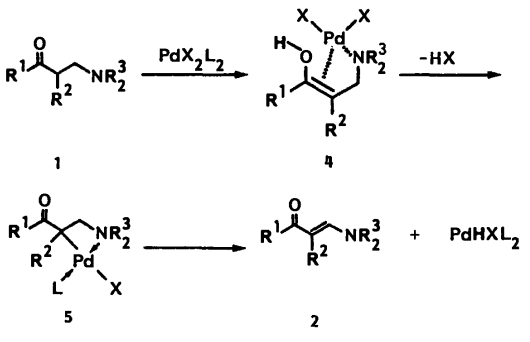

Scheme 1.

Although various synthetic application of enaminones have been demonstrated,[2-5,20] the nucleophilic reactions of enaminones with organocuprates provide a new strategy for the stereoselective synthesis of α,β-unsaturated ketones. Combining Eq. 2, ketones can be converted into (E)-substituted α,β-unsaturated ketones via enaminones by the substitution of the dialkylamino group with the alkyl group of organocuprates. Thus, the treatment of (*E*)-3-dimethylamino-1-phenyl-2-propen-1-one (**2b**) with dimethylcuprate gave (*E*)-1-phenyl-2-buten-1-one (**6**) stereoselectively in 86% yield. Further the reaction of methyl 4-(1-oxo-3-dimethylamino-2-propenyl)benzoate with excess amounts of cyanodimethylcuprate gave (*E*)-1-[4-(1-hydroxy-1-methylethyl)phenyl]-2-buten-1-one (**7**) in 66% yield. Again, the alkylation of dimethylamino group of enaminones proceeds selectively. These reactions are compatible to the stereo-selective synthesis of α,β-unsaturated ketones by the reaction of organocuprates with β-alkylthio α,β-enones.[21]

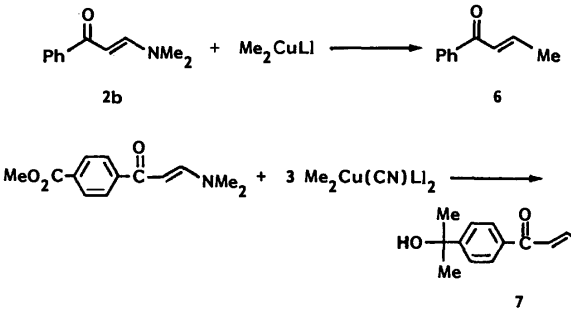

This study describes the palladium(II)-promoted, regioselective transformation of β-amino ketones to enaminones, which are versatile synthetic intermediates.

Experimental

General. ^1H NMR spectra were run as $CDCl_3$ and CCl_4 solutions on a 60 MHz JNM-PMX-60 SI (JEOL) and a 100 MHz JNM-FX-100 (JEOL) spectrometer; chemical shifts (δ) were expressed in parts per million downfield from Me_4Si. IR spectra were taken in a NaCl cell on a Hitachi 215

spectrometer. Analytical GLC evaluations of product mixtures were performed on a JEOL JGC-20-KFP or Shimadzu GC-8A gas chromatograph equipped with a flame ionization detector, while preparative GLC was performed on a JEOL JGC-20KT equipped with a thermal conductive detector. Mass spectra were obtained on a Hitachi RMS-4 mass spectrometer. Elemental analyses were obtained on a Yanagimoto MT-2 CHN recorder.

Materials. Bis(acetonitrile)dichloropalladium(II) was prepared by stirring $PdCl_2$ in acetonitrile at room temperature overnight followed by recrystallization from acetonitrile. Palladium(II) acetate was prepared according to the reported method.[22] Triethylamine was distilled over calcium hydride under nitrogen. Acetonitrile was dried over phosphorus pentoxide and distilled over calcium hydride under nitrogen. Methyl-4-piperidinone (**1i**) was purchased from Tokyo Kasei Co. 4-Diethylamino-2-butanone (**1a**),[23] 3-dimethylamino-1-phenyl-1-propanone (**1b**) hydrochloride,[24] 1-dimethylamino-4,4-dimethyl-3-pentanone (**1c**) hydrochloride,[25] and 2,3-dihydro-1-methyl-4(1*H*)-quinolinone (**1j**)[26] were prepared according to the reported procedures. 1-Dimethylamino-3-hexanone (**1d**),[24] 4-dimethylamino-2-butanone (**1e**),[23] 2-(dimethylaminomethyl)cyclopentanone (**1f**),[27] 2-(dimethylaminomethyl)cyclohexanone (**1g**),[27] and 5,5-dimethyl-2-(dimethylaminomethyl)cyclohexanone (**1h**)[27] were prepared by modification of the reported procedures.

Palladium-Induced Dehydrogenation of β-Amino Ketones to Enaminones: The following procedure for the preparation of (*E*)-4-diethylamino-3-buten-2-one (**2a**) is typical. To a suspension of $PdCl_2(MeCN)_2$ (0.208 g, 0.80 mmol) in acetonitrile (10 mL) were added 4-diethylamino-2-butanone (**1a**, 0.114 g, 0.80 mmol) and triethylamine (0.162 g, 1.6 mmol). The mixture was heated at reflux for 0.5 h under nitrogen. The palladium metal precipitated was filtered off. The filtrate was concentrated in vacuo, poured into water (10 mL), and extracted with ether (10 mL×3). The combined extracts were dried over Na_2SO_4. After the solvent was removed in vacuo, Kugelrohr distillation gave **2a** (0.078 g, 70%): bp 101—110 °C/1.6 mmHg (1 mmHg=133.3 Pa); IR (neat) 2990, 2950, 2892, 1654 (C=O), 1563, 1367, 1257, 1203, 1128, 986, 771 cm^{-1}; ^1H NMR ($CDCl_3$) δ=1.20 (6H, t, J=7.2 Hz, $-CH_3$), 2.07 (3H, s, $CO-CH_3$), 3.22 (4H, q, J=7.2 Hz, $-CH_2-$), 5.07 (1H, d, J=13.0 Hz, CO-CH=C), 7.41 (1H, d, J=13.0 Hz, N-CH=C). Found: C, 67.73; H, 10.58; N, 9.48%. Calcd for $C_8H_{15}NO$: C, 68.04; H, 10.71; N, 9.92%.

Enaminones **2b**, **2d**—**2h** were prepared in a similar manner that used for **2a** and the purification was achieved by Kugelrohr distillation, preparative TLC (SiO_2), or chromatographic separation (Al_2O_3) as indicated respectively. The IR and ^1H NMR spectra of these products were identical with those of the authentic materials prepared by the reported procedure.[10]

(*E*)-3-Dimethylamino-1-phenyl-2-propen-1-one (2b): Preparative TLC (SiO_2, THF–hexane=95/5, R_f=0.65); mp 95—100 °C; IR ($CHCl_3$) 3010, 1646 (C=O), 1588, 1551, 1435, 1423, 1364, 1248, 1121, 1056, 903 cm^{-1}; ^1H NMR ($CDCl_3$) δ=3.01 (6H, s, $N(CH_3)_2$), 5.73 (1H, d, J=12.2 Hz, CO-CH=C), 7.34—8.05 (6H, m, ArH, N-CH=C). Found: C, 75.10; H, 7.37; N, 8.05%. Calcd for $C_{11}H_{13}NO$: C, 75.40; H, 7.48; N, 7.89%.

(*E*)-1-Dimethylamino-1-hexen-3-one (2d): Chromatographic separation (Al_2O_3, eluent=benzene–ether); IR (neat) 2963, 1658 (C=O), 1569, 1437, 1362, 1283, 1112, 1054, 767 cm^{-1}; ^1H NMR ($CDCl_3$) δ=0.96 (3H, t, J=6.8 Hz, $-CH_3$), 1.65 (2H, tq, J=7.0 Hz and 6.8 Hz, $-CH_2-$), 2.33 (2H, t, J=7.0 Hz, $CO-CH_2-$), 2.92 (6H, s, $N(CH_3)_2$), 5.04 (1H, d, J=12.8 Hz, CO-CH=C), 7.49 (1H, d, J=12.8 Hz, N-CH=C). Found: C, 67.56; H, 10.48; N, 9.79%. Calcd for $C_8H_{15}NO$: C, 68.04; H, 10.71; N, 9.92%.

(*E*)-4-Dimethylamino-3-buten-2-one (2e): Kugelrohr distillation; bp 123—128 °C/6.0 mmHg; IR (neat) 2920, 1655 (C=O), 1568, 1430, 1356, 1261, 1192, 1110, 958, 847, 798, 760 cm^{-1}; ^1H NMR ($CDCl_3$) δ=2.08 (3H, s, $C-CH_3$), 2.92 (6H, s, $N(CH_3)_2$), 5.01 (1H, d, J=12.6 Hz, CO-CH=C), 7.40 (1H, d, J=12.6 Hz, N-CH=C). Found: C, 63.49; H, 9.66; N, 12.36%. Calcd for $C_6H_{11}NO$: C, 63.68; H, 9.80; N, 12.38%.

(*E*)-2-(Dimethylaminomethylene)cyclopentanone (2f): Preparative TLC (SiO_2, THF, R_f=0.49); mp 40—42.5 °C; IR (neat) 2950, 1677 (C=O), 1573, 1437, 1380, 1307, 1273, 1208, 1116, 1002, 849, 787 cm^{-1}; ^1H NMR (CCl_4) δ=1.39—2.98 (6H, m, $-CH_2-$), 3.06 (6H, s, $N(CH_3)_2$), 6.90—7.01 (1H, m, N-CH=C).

(*E*)-2-(Dimethylaminomethylene)cyclohexanone (2g): Kugelrohr distillation; bp 99—104 °C/0.7 mmHg; IR (neat) 2942, 1648 (C=O), 1547, 1428, 1326, 1299, 1158, 1130, 1037, 926, 827 cm^{-1}; ^1H NMR ($CDCl_3$) δ=1.54—2.87 (8H, m, $-CH_2-$), 3.07 (6H, s, $N(CH_3)_2$), 7.44—7.59 (1H, m, -CH=C).

(*E*)-5,5-Dimethyl-2-(dimethylaminomethylene)cyclohexanone (2h): Kugelrohr distillation; bp 110—115 °C/1.4 mmHg; mp 75.5—76.0 °C; IR (KBr) 2912, 1635 (C=O), 1428, 1299, 1223, 1122, 1058, 960 cm^{-1}; ^1H NMR ($CDCl_3$) δ=0.96 (6H, s, $C(CH_3)_2$), 1.49 (2H, t, J=6.6 Hz, $-CH_2-$), 2.12 (2H, s, $CO-CH_2-$), 2.71 (2H, t, J=6.6 Hz, $CH_2C=C$), 3.08 (6H, s, $N(CH_3)_2$), 7.48 (1H, br, N-CH=C). Found: C, 72.22; H, 10.36; N, 7.68%. Calcd for $C_{11}H_{19}NO$: C, 72.88; H, 10.57; N, 7.73%.

(*E*)-4,4-Dimethyl-1-dimethylamino-1-penten-3-one (2c): A suspension of $Pd(OAc)_2$ (0.225 g, 1.0 mmol), Na_2CO_3 0.319 g, 3.0 mmol), and 4,4-dimethyl-1-dimethylamino-3-pentanone (**1c**) hydrochloride (0.194 g, 1.0 mmol) in acetonitrile (10 mL) was heated at reflux for 0.5 h under nitrogen. The reaction mixture was worked up as described above. Kugelrohr distillation gave **2c** (0.115 g, 74%) as a colourless solid: bp 96—101 °C/3.2 mmHg; mp 37.4—37.8 °C; IR (KBr) 2957, 1650 (C=O), 1554, 1429, 1356, 1288, 1085, 1014, 917, 767 cm^{-1}; ^1H NMR ($CDCl_3$) δ=1.13 (9H, s, $C(CH_3)_3$), 2.91 (6H, s, $N(CH_3)_2$), 5.21 (1H, d, J=12.4 Hz, CO-CH=C), 7.56 (1H, d, J=12.4 Hz, N-CH=C). Found: C, 69.27; H, 10.10; N, 8.96%. Calcd for $C_9H_{17}NO$: C, 69.63; H, 11.04; N, 9.04%

1,3,5-Triacetylbenzene (3): A mixture of 4-diethylamino-2-butanone (**1a**, 0.217 g, 1.5 mmol), $PdCl_2(MeCN)_2$ (0.395 g, 1.5 mmol), and acetonitrile (5 mL) was heated at reflux for 5 h. The reaction mixture was worked up as described above. Preparative TLC (SiO_2, THF–hexane=4/6, R_f=0.48) gave 1,3,5-triacetylbenzene (**3a**, 0.033 g, 32%): mp 159—162 °C; IR ($CHCl_3$) 2965, 2933, 1695 (C=O), 1365, 1233, 785 cm^{-1}; ^1H NMR ($CDCl_3$) δ=2.78 (9H, s, $-CH_3$), 8.95 (3H, s, ArH). The IR and ^1H NMR spectra of the product were identical with those of the authentic sample.

In a similar manner, 1,3,5-tribenzoylbenzene (**3b**) was obtained in 35% yield by the reaction of 3-dimethylamino-1-phenyl-1-propanone (**1b**) and $PdCl_2(MeCN)_2$: Preparative TLC (SiO_2, ether–hexane=4/5, R_f=0.36); mp 119—121 °C;

IR ($CHCl_3$) 3019, 1655 (C=O), 1599, 1451, 1318, 1255, 1180, 1130, 1005, 907 cm^{-1}; ^1H NMR ($CDCl_3$) δ=7.58—8.01 (15H, m, $-C_6H_5$), 8.55 (3H, s); MS *m/z* (rel intensity) 390 (M^+, 100), 313 (66), 285 (42). Found: C, 82.92; H, 4.60%. Calcd for $C_{27}H_{18}O_3$: C, 83.06; H, 4.65%.

Conversion of Enaminone 2b to Triacylbenzene 3b: To a solution of enaminone **2b** (0.300 g, 1.71 mmol) in acetonitrile (5 mL) was added a mixture of H_2O (0.300 g, 16.7 mmol) and three drops of concentrated HCl solution. After heating at reflux for 4 h, the reaction mixture was extracted with CH_2Cl_2 (30 mL) The extract was washed with water (10 mL×3) and dried over $MgSO_4$. Evaporation of the solvent gave **3b** (0.210 g, 95%).

Reaction of (*E*)-3-Dimethylamino-1-phenyl-2-propen-1-one (2b) with Dimethylcuprate: To a suspension of CuI (0.419 g, 2.20 mmol) in dry ether (5 mL) was added a solution of 1.32 M (1M=1 mol dm^{-3}) of methyllithium (3.3 mL, 4.40 mmol) in ether at 0 °C. The mixture was stirred at room temperature for 15 min. The $LiCuMe_2$ solution in ether was added to a solution of (*E*)-3-dimethylamino-1-phenyl-2-propen-1-one (**2b**, 0.351g, 2.00 mmol) in dry ether (8 mL) with stirring at room temperature. The reaction mixture was allowed to stand overnight and quenched with water (5 mL) and extracted with ether. The organic layer was washed and dried over Na_2SO_4. Evaporation of the solvent gave the residue, which was subjected to column chromatography (Al_2O_3). Elution with benzene–ether (9:1) gave (*E*)-1-phenyl-2-buten-1-one (**6**, 0.253g, 86%): IR (neat) 1672, 1626, 1452, 1298, 1226cm^{-1}; ^1HNMR ($CDCl_3$) δ=1.98 (3H, d, *J*=5.0Hz, CH_3), 6.60—7.13 (2H, m, CH=CH), 7.30—7.57 (3H, m, ArH), 7.80—8.13 (2H, m, ArH); MS *m/z* 146 (M^+). The structure was established by comparing the spectral data with those of the authentic sample.

Reaction of Methyl 4-(1-Oxo-3-dimethylamino-2-propenyl)benzoate with Cyanodimethylcuprate: To a slurry of CuCN (0.806 g 9.0 mmol) in ether (10 mL) was added a solution of 1.32 M methyllithium (18 mmol) in ether with stirring at −78°C under argon, and the mixture was stirred at 0°C. To a suspension of methyl 4-(1-oxo-3-dimethylamino-2-propenyl)benzoate (0.467 g, 2.0 mmol) which was prepared from ethyl 4-acetylbenzoate and *N,N*-dimethylformamide dimethyl acetal, mp 177 °C; ^1H NMR ($CDCl_3$) δ=3.01 (6H, s, $N(CH_3)_2$), 3.88 (3H, s, OCH_3), 5.67 (1H, d, *J*=6.2 Hz, COCHC=), 7.75 (1H, d, *J*=6.2 Hz, COCH=CH), 7.75—8.15 (4H, m, ArH), in ether (5.0 mL), was added the above $Li_2CuCN(Me)_2$ solution with stirring at −78 °C for 5 min. After stirring at room temperature for 6 h, the mixture was quenched with water and extracted with ether (10 mL×5). The ether extracts were dried over Na_2SO_4 and concentrated. Chromatography on silica gel gave pure (*E*)-1-[4-(1-hydroxy-1-methlethyl)phenyl]-2-buten-1-one (**7**) (0.272 g, 66%): IR (neat) 3430, 2980, 1670, 1620, 1302, 1232 cm^{-1}, ^1H NMR ($CDCl_3$) δ=1.58 (6H, s, CH_3), 1.96 (3H, d, *J*=5.0 Hz, CH_3), 2.43 (1H, br, OH), 6.65—7.09 (2H, m, CH=CH), 7.42—7.97 (4H, m, ArH). Found: C, 76.24; H, 7.86%. Calcd for $C_{13}H_{16}O_2$: C, 76.44; H, 7.90%.

We wish to thank Mr. Kazuo Ike for the experimental assistance.

References

1) S.-I. Murahashi and T. Watanabe, *J. Am. Chem. Soc.*, **101**, 7429 (1979); S.-I. Murahashi, N. Yoshimura, T. Tsumiyama, and T. Kojima, *ibid.*, **105**, 5002 (1983).

2) Review, T. Nishio, C. Kashima, and Y. Omote, *Yuki Gosei Kagaku Kyokai Shi*, **34**, 526 (1976); J. V. Greenhill, *Chem. Soc. Rev.*, **6**, 277 (1977).

3) A. I. Meyers and S. Singh, *Tetrahdron Lett.*, **1967**, 5319; R. F. Abdulla and K. H. Fuhr, *J. Org. Chem.*, **43**, 4248 (1978).

4) A. I. Meyers, A. H. Reine, and R. Gault, *J. Org. Chem.*, **34**, 698 (1969).

5) M. Yoshimoto, N. Ishida, and T. Hiraoka, *Tetrahedron Lett.*, **1973**, 39; T. A. Bryson and R. B. Gammill, *ibid.*, **1974**, 3963; J. E. Telschow and W. Reusch, *J. Org. Chem.*, **40**, 862 (1975).

6) P. G. Baraldi, D. Simoni, and S. Manfredini, *Synthesis*, **1983**, 902, and references cited therein.

7) R. H. Hasek and J. C. Martin, *J. Org. Chem.*, **28**, 1468 (1963).

8) R. Mestres, *J. Chem. Soc., Perkin Trans. 1*, **1972**, 805.

9) J. J. Bozell and L. S. Hegedus, *J. Org. Chem.*, **46**, 2561 (1981).

10) R. F. Abdulla and R. S. Brinkmeyer, *Tetrahedron*, **35**, 1675 (1979); P. F. Schuda, C. B. Ebner, and T. M. Morgan, *Tetrahedron Lett.*, **27**, 2567 (1986).

11) Y. Matsuyama, J. Fujiwara, K. Maruoka, and H. Yamamoto, *J. Am. Chem. Soc.*, **105**, 6312 (1983).

12) M. Tramontini, *Synthesis*, **1973**, 763.

13) Preliminary communication, S.-I. Murahashi, T. Tsumiyama, and Y. Mitsue, *Chem. Lett.*, **1984**, 1419.

14) K. K. Balasubramanian, S. Selvaraj, and P. S. Venkataramani, *Synthesis*, **1980**, 29.

15) C. Kashima, H. Aoyama, Y. Yamamoto, and T. Nishio, *J. Chem. Soc., Perkin Trans. 2*, **1975**, 665.

16) J. C. Sircar and A. I. Meyers, *J. Org. Chem.*, **32**, 1248 (1967); H. Dugas, R. A. Ellison, Z. Valenta, K. Wiesner, and C. M. Wong, *Tetrahedron Lett.*, **1965**, 1279.

17) B. Bierling, K. Kirschke, H. Oberender, and M. Schulz, *J. Pract. Chem.*, **314**, 170 (1972); R. J. Theissen, *J. Org. Chem.*, **36**, 752 (1971); J. Muzart and J. P. Pete, *J. Mol. Cat.*, **15**, 373 (1982).

18) Silyl enol ethers, Y. Ito, T. Hirao, and T. Saegusa, *J. Org. Chem.*, **43**, 1011 (1978); Y. Ito, H. Aoyama, and T. Saegusa, *J. Am. Chem. Soc.*, **102**, 4519 (1980); T. Mukaiyama, M. Oshima, and T. Nakatsuka, *Chem. Lett.*, **1983**, 1207.

19) N. Yoshimura, S.-I. Murahashi, and I. Moritani, *J. Organomet. Chem.*, **52**, C58 (1973).

20) Review, I. Ninomiya and T. Naito, *Yuki Gosei Kagaku Kyokai Shi*, **42**, 225 (1984); H. Iida, Y. Yuasa, and C. Kibayashi, *J. Am. Chem. Soc.*, **100**, 3598 (1978); T. Nagasaka, H. Inoue, M. Ichimura, and F. Hamaguchi, *Synthesis*, **1982**, 848; T. Oishi, M. Nagai, T. Onuma, H. Ninomiya, K. Tsutae, M. Ochiai, and Y. Ban, *Chem. Pharm. Bull.*, **17**, 2230 (1969).

21) R. K. Dieter and L. A. Silks, III, *J. Org Chem.*, **51**, 4687 (1986).

22) T. A. Stephenson, S. M. Morehouse, A. R. Powell, J. P. Heffer, and G. Wilkinson, *J. Chem. Soc.*, **1965**, 3632.

23) A. L. Wilds, R. M. Nowak, and K. E. McCaleb, *Org. Synth.*, Coll. Vol. 4, 281 (1963).

24) C. E. Maxwell, *Org. Synth.*, Coll. Vol. 3, 305 (1955).

25) C. G. Overberger and A. M. Schiller, *J. Polym. Sci., C*, **1963**, 325.
26) J. A. C. Allison, J. T. Braunholtz, and F. G. Mann, *J. Chem. Soc.*, **1954**, 403.
27) H. O. House and B. M. Trost, *J. Org. Chem.*, **29**, 1339 (1964).

 © 1987 The Chemical Society of Japan Bull. Chem. Soc. Jpn., 60, 3291—3297 (1987)

Silicon Polonovski Reaction. Formation and Synthetic Application of α-Siloxy Amines

Norihiro Tokitoh† and Renji Okazaki*
Department of Chemistry, Faculty of Science, The University of Tokyo,
Hongo, Bunkyo-ku, Tokyo 113
(Received March 20, 1987)

A new and versatile synthetic intermediate, α-siloxy amine was prepared in situ by the base-promoted rearrangement of a siloxyammonium salt obtained by treatment of a tertiary amine *N*-oxide with trialkylsilyl trifluoromethanesulfonate. The best combination of the base and silylating reagent was found to be methyllithium and *t*-butyldimethylsilyl trifluoromethanesulfonate. The reactions of α-siloxy amines with acyl halides and haloformates gave the corresponding amides and carbamates in moderate to good yields, respectively. Treatment of α-siloxy amines with acetic acid resulted in a direct dealkylation to free secondary amines. Fluoride induced alkylation of α-siloxy amines using alkyl halides as electrophiles leading to tertiary amines was also examined and demonstrated to be a new transalkylation method of amines.

Amine *N*-oxides are readily available compounds by oxidation of tertiary amines and the functionalization of the amines taking advantage of the oxidation state of the nitrogen atom seems potentially useful. Actually, the reaction of tertiary amine *N*-oxides with some acid anhydrides is well-known as the Polonovski reaction[1] and is used as a useful dealkylation method for tertiary amines to afford the corresponding amides. The Polonovski reaction is considered to proceed via α-acetoxyamine intermediate **3** which reacts again with the anhydride to give the dealkylated product **5** via ammonium salt **4** (Scheme 1). The use of acid anhydrides necessarily results in the formation of amide **5** as a final product although, in some limited cases, the formation of enamines or Mannich bases have been reported.[2] It occurred to us that the use of siloxyammonium ions **6** instead of acyloxyammonium ions **2** would lead to α-siloxy amine **7** by an appropriate base (Scheme 2). Since **7** can be expected

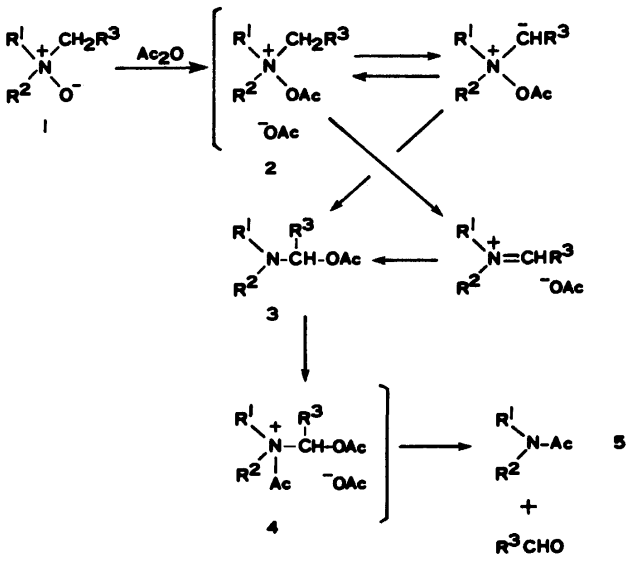

Scheme 1.

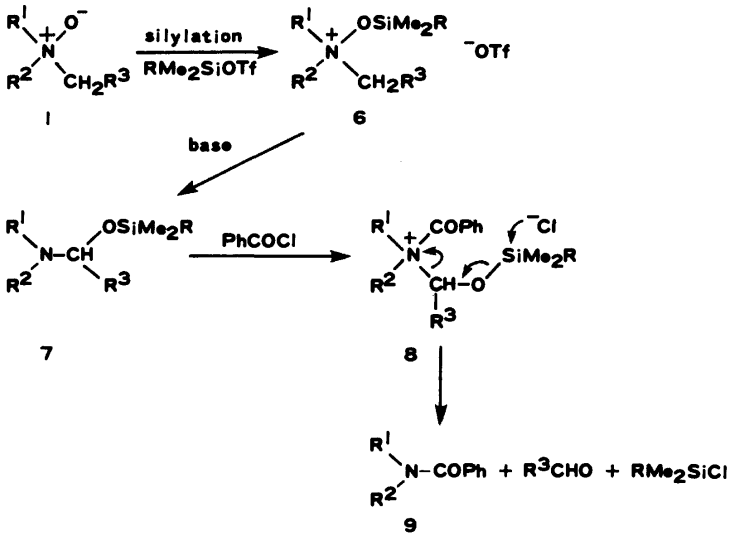

Scheme 2.

† Present address: Department of Chemistry, University of Tsukuba, Sakura-mura, Niihari-gun, Ibaraki 305.

to react with various electrophiles, it would become a useful intermediate in functionalization of tertiary amines. In this article we report that this expectation was indeed fulfilled and tertiary amines could be converted into various types of secondary amine derivatives by this methodology.[3]

Results and Discussion

Rearrangement of Siloxyammonium Salts; Formation of α-Siloxy Amines. Siloxyammonium salts were prepared from the tertiary amine *N*-oxides and trialkylsilyl trifluoromethanesulfonate and subjected to a base-promoted rearrangement leading to α-siloxy amines (Scheme 2). The formation of the siloxy amines was confirmed by trapping with acyl halides to give the corresponding amides. For example, *N*-methylpiperidine *N*-oxide (**1a**) was allowed to react with *t*-butyldimethylsilyl trifluoromethanesulfonate (TBDMSOTf) in dichloromethane at 0 °C to give the corresponding siloxyammonium salt **6a**, the quantitative formation of which was confirmed by NMR spectroscopy.[4] After replacement of the solvent by tetrahydrofuran (THF), **6a** was treated with methyllithium at 0 °C and then with benzoyl chloride at room temperature to afford the expected amide **9a** in 76% yield (Eq. 1). The effects of silylating agents and

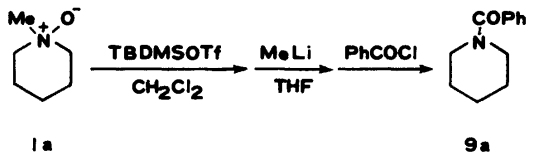

(1)

1a 9a

bases on the yields were studied by using the reaction of Eq. 1 and the results are shown in Table 1.[5]

Although alkyllithiums, lithium amides, lithium phenoxide, and potassium *t*-butoxide were effective as a base, methyllithium gave the best result. Tertiary amines such as triethylamine, *N*,*N*-diisopropylethylamine (Hünig base), and 1,8-diazabicyclo[5.4.0]-undec-7-ene (DBU), which were often used as a base in the Polonovski reaction, were of no use in the present case probably because their basicity is not high enough to cause rearrangement because of low leaving ability of the siloxyl group. As for a silylating reagent, TBDMSOTf was more effective than TMSOTf.[6] This is most likely due to the steric protection of the silicon atom by the *t*-butyl group which makes the expected deprotonation preferable to the undesirable nucleophilic attack to the silicon atom by the base. Since the best combination of the reagents was found to be TBDMSOTf and methyllithium, this combination is used in the following reactions.

Table 1. Yields of *N*-Benzoylpiperidine (**9a**)

Base	Me_3SiOTf	*t*-$BuMe_2SiOTf$
n-BuLi	50	70
s-BuLi	c)	66
t-BuLi	65	73
MeLi	66	76
$(Me_2CH)_2NLi$[a]	48	c)
$(Me_3Si)_2NLi$[a]	49	45
ArOLi[a,b]	c)	36
t-BuOK[a]	c)	12

a) These bases were prepared and used as a THF solution. b) Ar = 2,6-di-*t*-butyl-4-methylphenyl. c) These combinations were not examined.

Table 2. Amide Formation from Tertiary Amine *N*-Oxides[a]

Entry	*N*-Oxide **1**		Amide **9**		Yield/%[b]
a	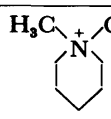	**1a**	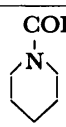	**9a**	76
b	$(PhCH_2)_3N^+-O^-$	**1b**	$(PhCH_2)_2PCOPh$	**9b**	88[c]
c	$PhMe_2N^+-O^-$	**1c**	PhMeNCOPh	**9c**	51
d	$Et_3N^+O^-$	**1d**	Et_2NCOPh	**9d**	57
e	$(PhCH_2)Me_2N^+-O^-$	**1e**	R^1R^2NCOPh	**9e**, **9e'**	81[d]
f	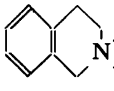	**1f**	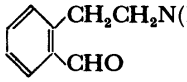	**9f**	67
g	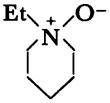	**1g**		**9a**	33
h	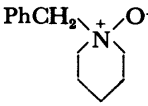	**1h**		**9a**	45

a) Used reagents were TBDMSOTf, methyllithium, and benzoyl chloride. b) Isolated yield. c) Benzaldehyde (56%) was also obtained. d) $R^1=R^2=Me$ **9e** 52%; $R^1=Me$, $R^2=PhCH_2$ **9e'** 29%.

Dealkylation of Tertiary Amines. a) Amide Formation. The conversion of several amine *N*-oxides into the corresponding benzamide with TBDMSOTf and methyllithium was carried out, and the results are summarized in Table 2. Since tertiary amines can be oxidized to the corresponding *N*-oxides almost quantitatively, this reaction provides a new general method for the dealkylation of tertiary amines to secondary amine derivatives. Although, as mentioned above, a similar conversion of tertiary amine *N*-oxides into amides of secondary amines can be achieved by the Polonovski reaction using acid anhydrides, the present method has the advantage of affording a dealkylated product selectively in some cases, since the Polonovski reaction of aromatic amine *N*-oxides such as *N*,*N*-dimethylaniline oxide (**1c**) is reported to give a rearranged product, *o*-acetoxy-*N*,*N*-dimethylaniline (**10**), as a main product (Eq. 2).[8] In the case of

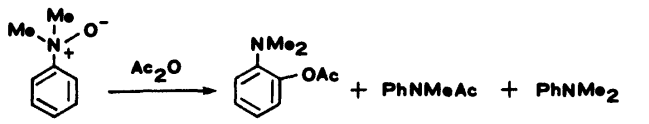

1c 10 (2)

tribenzylamine oxide (**1b**), benzaldehyde, an expected product, was isolated in 56% yield in addition to amide **9b**. The formation of the aldehyde was also confirmed by the isolation of its 2,4-dinitrophenylhydrazone in 56% yield. Furthermore, it is also noteworthy that the product was a benzaldehyde derivative **9f** in the case of 2-methyl-1,2,3,4-tetrahydroisoquinoline *N*-oxide (**1f**), since it suggests that the rearrangement took place regioselectively at the benzyl position.

The results listed in Table 2 suggest that the regioselectivity of this dealkylation is controlled by the acidity of α-hydrogen in the siloxyammonium salts **6** to be deprotonated by the base, and in the cases of **1a** and **1f** the dealkylation proceeded regioselectively to give the amides **9a** and **9f**, respectively.

b) Carbamate Formation. When phenyl chloroformate was used as an electrophile in the reaction with α-siloxy amines, the final product was the corresponding carbamate **11**. The results obtained for the reactions of several tertiary amine *N*-oxides are given in Table 3.

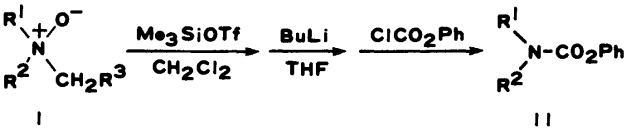

I II

Since the combination of TBDMSOTf and methyllithium was not used in these reactions, the yields of the carbamates have not been optimized.

c) Direct Dealkylation into Secondary Amines. We next examined the direct dealkylation of tertiary amines via α-siloxy amines. If an appropriate protic acid is used as an electrophile, α-siloxy amine **7** is expected to be converted into the corresponding secondary amine (Scheme 3).

As expected, sequential treatment of tribenzylamine oxide (**1b**) with TBDMSOTf, methyllithium, and acetic acid afforded dibenzylamine in 67% yield.

Furthermore, when treatment with acetic acid was carried out in the presence of isopentyl nitrite, *N*-nitrosodibenzylamine was obtained in 85% yield. A similar result was obtained in the case of *N*-methylpiperidine *N*-oxide (**1a**) to give *N*-nitrosopiperidine in 41% yield.

Transalkylation of Tertiary Amines. Although transalkylation reactions (i.e., the replacement of a substituent on the nitrogen atom by other groups) are useful for the introduction of a new functional group

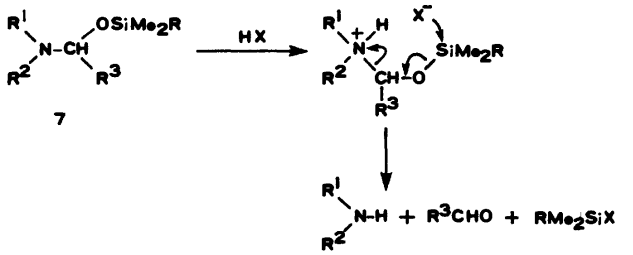

Scheme 3.

Table 3. Carbamate Formation via α-Siloxy Amine[a]

Entry	*N*-Oxide **1**		Carbamate **11**		Yield/%
1		**1a**	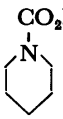	**11a**	65
2	$PhMe_2N^+$-O^-	**1c**	$PhMeNCO_2Ph$	**11c**	40
3	Et_3N^+-O^-	**1d**	Et_2NCO_2Ph	**11d**	41
4	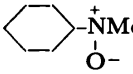	**1i**	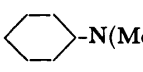	**11i**	23

a) TMSOTf, butyllithium, and phenyl chloroformate were used.

into amines, there have been very few reports on direct transalkylation[9] and the conventional methods involve some steps, i.e., dealkylation to free secondary amines and their realkylation.[10] We have found that the use of alkyl halides as an electrophile in the reaction of α-siloxy amines in the presence of fluoride ion results in transalkylation of tertiary amines (Scheme 4). Thus, treatment of α-siloxy amines **7** (obtained in situ from amine *N*-oxides **1**) with alkyl halides followed by desilylation with fluoride ion (*n*-$Bu_4N^+F^-$/THF) in a sealed tube at 110 °C afforded the corresponding transalkylation products **12** in moderate yields.[11] Results obtained from the reactions of *N*-methylpiperidine *N*-oxide (**1a**) and triethylamine oxide (**1d**) with several alkyl halides are summarized in Table 4. In contrast to the dealkylation reaction by acyl halide or haloformate, this transalkylation proceeds only in the presence of fluoride ion and with heating perhaps due to poor reactivity of alkyl halides in quaternization and to low activating facility of the alkyl group in desilylation step. Of particular note among these results is the introduction of carbonyl functionality into new alkyl groups (entries 4, 5, and 8), which provides a route not only for the prolongation of alkyl chains but for the modification of *N*-alkyl groups, i.e., the formal functionalization of α-position of tertiary amines.

In summary, we have established a new method for a facile formation of α-siloxy amines by "silicon Polonovski reaction," and some successful applications of this versatile synthetic intermediate to the functionalization of amines by the reactions with electrophiles. Although dealkylation of tertiary amines to secondary amine derivatives can be achieved by several methods such as the Polonovski reaction[2] and the von Braun reaction,[12] the present method has the following advantages. (1) Various derivatives of secondary amines including free amines can be obtained directly using appropriate electrophiles. (2) Facile transalkylation reactions of tertiary amines are feasible using fluoride induced desilylation of α-siloxy amines. In view of ready availability of tertiary amine *N*-oxides and a variety of electrophiles and of the achievement of the direct dealkylation and transalkylation of tertiary amines, we believe that the "silicon Polonovski reaction" described here will provide a new convenient synthetic method for nitrogen containing compounds including natural products.

Experimental

All the melting points and boiling points were not corrected. ^1H NMR spectra were measured with Hitachi R-

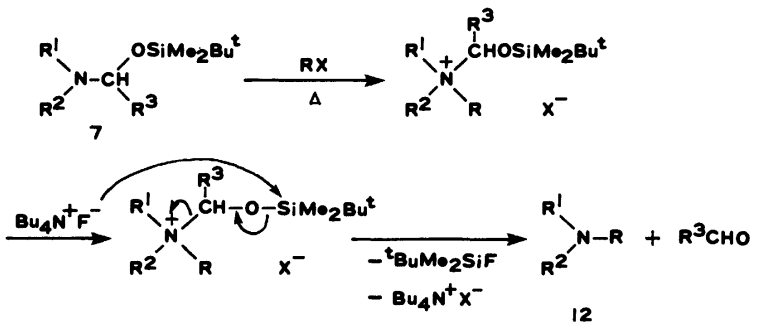

Scheme 4

Table 4. Transalkylation of Tertiary Amines via Their *N*-Oxides

Entry	*N*-Oxide **1**		RX	Time/h	Product **12**	Yield/%
1	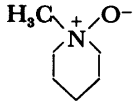	**1a**	$PhCH_2Cl$	10	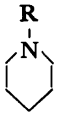 **12a**; R=CH_2Ph	58
2		**1a**	*n*-AmBr[a]	10	**12a**; R=*n*-Am	45
3		**1a**	*n*-OcBr[b]	6	**12a**; R=*n*-Oc	47
4		**1a**	$BrCH_2CO_2Et$	5	**12a**; R=CH_2CO_2Et	38
5		**1a**	$BrCH_2COPh$	10	**12a**; R=CH_2COPh	33
6	Et_3N^+–O^-	**1d**	$PhCH_2Cl$	10	Et_2N-CH_2Ph (**12d**)	65
7		**1d**	*n*-OcBr	10	Et_2N-*n*-Oc (**12d**)	51
8		**1d**	$BrCH_2CO_2Et$	10	Et_2N-CH_2CO_2Et (**12d**)	31

a) *n*-Am=$(CH_2)_4CH_3$. b) *n*-Oc=$(CH_2)_7CH_3$.

24B, Hitachi R-20B (60 MHz), and JEOL JNM-FX90Q (90 MHz) spectrometers using tetramethylsilane as an internal standard. ^{13}C NMR spectra were measured with JEOL JNM-FX90Q. The NMR spectra were measured in deuteriochloroform at room temperature unless otherwise noted. MS spectra were measured with JEOL JMS-D300 mass spectrometer. All the experiments were carried out in argon or nitrogen atmosphere.

Materials. Amine *N*-oxides were prepared by oxidation of the corresponding amines by either 30% hydrogen peroxide or *m*-chloroperbenzoic acid. 2-Methyl-1,2,3,4-tetrahydroisoquinoline[13] and *N*-benzylpiperidine[14] were prepared by the reported method. The other amines used were commercial products.

Formation of Amides. The procedure with *N*-methylpiperidine *N*-oxide (**1a**) is typical.

General Procedure. Transformation of *N*-Methylpiperidine *N*-Oxide (1a) into *N*-Benzoylpiperidine (9a). To a solution of *N*-methylpiperidine *N*-oxide (**1a**) (140.4 mg, 1.22 mmol) in 10 ml of dichloromethane was added *t*-butyldimethylsilyl trifluoromethanesulfonate (TBDMSOTf) (355 mg, 1.1 equiv) at 0 °C and the mixture was stirred for 30 min at this temperature. After the replacement of the solvent into 10 ml of THF, to this solution was added methyllithium (1.59 mmol, 1.3 equiv) at 0 °C, during which time an evolution of gas was observed. After stirring for 1 h, to this solution was added 0.21 ml (1.81 mmol, 1.5 equiv) of benzoyl chloride at 0 °C, and the mixture was stirred overnight at room temperature. The solvent was evaporated and the resulting oil was submitted to chromatography (Al_2O_3, hexane–ether 3:1) to afford *N*-benzoylpiperidine (**9a**) (175.3 mg, 76%, oil). The structure of the product was confirmed by the following spectral data and by comparison with an authentic sample. **9a**: ^1H NMR δ=1.6 (brs, 6H), 3.5 (brs, 4H), and 7.35 (s, 5H); MS *m/z* (rel, intensity) 189 (M^+, 16%), 188 (34), 122 (29), 105 (100), and 77 (86).

The amide formation from other *N*-oxides listed in Table 2 were carried out in a similar way. The spectral data of the products were as follows. **9b—e** were identified by comparison of these spectral data with those of anthentic samples prepared by benzoylation of the amines. **9b**: White solid; ^1H NMR δ=4.5 (brs, 4H) and 6.7—7.6 (m, 15H); MS *m/z* 301 (M^+, 3%), 211 (18), 210 (34), 149 (12), 105 (100), 98 (8), 91 (19), 84 (30), and 77 (36). **9c**: Pale yellow oil; ^1H NMR δ=3.48 (s, 3H) and 6.7—7.6 (m, 10H); MS *m/z* 211 (M^+, 21%), 122 (22), 105 (100), and 77 (92). **9d**: Colorless oil; ^1H NMR δ=1.1 (brt, *J*=7 Hz, 6H), 3.0—3.7 (m, 4H), and 7.3 (s, 5H); MS *m/z* 177 (M^+, 18), 176 (25), 105 (100), and 77 (42). **9e**: Colorless oil; ^1H NMR δ=2.93 (s, 6H) and 7.25 (s, 5H). **9e'**: Pale yellow oil; ^1H NMR δ=2.87 (s, 3H), 4.53 (brs, 2H), and 7.27 (s, 5H). **9f**: White paste; ^1H NMR δ=1.9—4.1 (m, 7H), 6.9—7.6 (m, 9H), and 9.81, 10.24 (brd, 1H); ^{13}C NMR (−50 °C) δ=193.75, 193.40, 172.03, 171.13, 140.80, 139.33, 135.84, 135.73, 135.49, 134.49, 133.86, 133.37, 133.21, 131.94, 129.50, 129.01, 128.23, 128.07, 127.36, 126.77, 126.01, 51.46, 48.67, 38.17, 33.15, 31.96, and 30.45; MS *m/z* 267 (M^+, 1%), 161 (22), 149 (11), 148 (29), 136 (12), 132 (5), 119 (5), 118 (39), 106 (9), 105 (100), 91 (6), 90 (16), 77 (31), and 57 (10); High-MS, Found: *m/z* 267.1258. Calcd for $C_{17}H_{17}NO_2$: M, 267.1258.

Trapping of Benzaldehyde. To a solution of tribenzylamine oxide (147.5 mg, 0.49 mmol) in dichloromethane (10 ml) was added TBDMSOTf (142.3 mg, 1.1 equiv). After the solvent exchange into 5 ml of THF, MeLi (0.59 mmol, 1.2 equiv) was added at 0 °C and the mixture was stirred for 30 min. To this yellow solution was added an excess of acidic solution of 2,4-dinitrophenylhydrazine (0.25 g, 1.25 mmol/concd H_2SO_4 1.9 ml/EtOH 19 ml/H_2O 65 ml) and the mixture was stirred vigorously. The red brown precipitates were collected by filtration and dried to give benzaldehyde hydrazone (77.6 mg, 56%), mp 237 °C.[15]

Formation of Carbamates. As a typical example, the procedure with *N*-methylpiperidine *N*-oxide (**1a**) is described.

Transformation of 1a to 11a. To a solution of **1a** (226 mg, 1.97 mmol) in 12 ml of dichloromethane was added TMSOTf (656 mg, 1.5 equiv) and after the replacement of the solvent into THF (15 ml) was added *n*-BuLi (2.96 mmol, 1.5 equiv). To this solution was added 0.37 ml of phenyl chloroformate (462 mg, 1.5 equiv) at 0 °C and the mixture was stirred overnight at room temperature. After the removal of the solvent the residual oil was subjected to chromatography (Al_2O_3, hexane–ether 3:1) to afford the corresponding carbamate **11a** (264.3 mg, 65%) as a white solid.[16] **11a**: ^1H NMR δ=1.5—1.8 (m, 6H), 3.2—3.8 (m, 4H), and 6.8—7.5 (m, 5H); ^{13}C NMR δ=153.68, 151.67, 129.11, 124.97, 121.72, 45.30, 25.74, and 24.30; MS *m/z* 205 (M^+, 10%), 112 (100), 94 (45), 77 (16), and 72 (29).

Other *N*-oxides listed in Table 3 (**1c**, **1d**, and **1i**) were converted into the corresponding carbamates **11c**, **11d**, and **11i** in a similar way to **1a** in 40, 41, and 23% yields, respectively.[17] **11c**: Colorless oil; ^1H NMR δ=3.33 (s, 3H) and 6.5—7.4 (m, 10H); MS *m/z* 227 (M^+, 20%), 134 (100), 106 (34), 94 (42), and 77 (45). **11d**: Pale yellow oil; ^1H NMR δ=1.20 (t, *J*=7.5 Hz, 6H), 4.63 (q, *J*=7.5 Hz, 4H), and 6.8—7.5 (m, 5H); MS *m/z* 193 (M^+, 9%), 100 (100), 98 (15), 94 (12), 77 (7), and 72 (64). **11i**: Colorless oil; ^1H NMR δ=0.9—2.1 (m, 10H), 2.90 (s, 3H), 4.0 (brs, 1H), and 6.7—7.6 (m, 5H); MS *m/z* 233 (M^+, 7%), 140 (50), 94 (100), 83 (73), and 77 (10).

Dealkylation of Tribenzylamine via Its *N*-Oxide. To a solution of tribenzylamine oxide (**1b**) (172 mg, 0.57 mmol) in 10 ml of dichloromethane was added TBDMSOTf (180.6 mg, 1.2 equiv) and after the solvent exchange into THF (10 ml) was added MeLi (0.74 mmol, 1.3 equiv) at 0 °C. After stirring for 1 h at room temperature 0.32 ml (5.6 mmol, 9.8 equiv) of acetic acid was added to the reaction mixture at room temperature and then the mixture was refluxed for 2 h. After removal of the solvent the mixture was shaken with 30 ml of dichloromethane and 5% aq. NaOH solution. The aqueous layer was extracted with dichloromethane (20 ml×2) and the extracts were combined with the organic layer, dried over $MgSO_4$, and concentrated. The resulting oil was subjected to chromatography on alumina (hexane–ether) to give dibenzylamine (75.0 mg, 67%). The ^1H NMR spectrum of the product was consistent with that of an authentic sample.

***N*-Nitrosation Reactions. a) Dibenzylamine.** To a solution of tribenzylamine oxide (**1b**) (213 mg, 0.7 mmol) in 7.5 ml of dichloromethane was added TBDMSOTf (240 mg, 1.3 equiv) and MeLi (0.91 mmol, 1.3 equiv) as described above and after the addition of acetic acid (0.4 ml, 10 equiv) the mixture was refluxed for 1 h. To this mixture was added isopentyl nitrite (0.47 ml, 5 equiv) at room temperature and

then the mixture was refluxed for 1 h. After evaporation of the solvent the residual oil was treated with 50 ml of 5% aq. NaOH solution and 50 ml of dichloromethane. The aqueous layer was extracted with dichloromethane (30 ml×3), and the extracts were combined with the organic layer, dried over $MgSO_4$, and concentrated. The residual oil was submitted to chromatography (Al_2O_3, hexane-CH_2Cl_2 6:1) to give *N*-nitrosodibenzylamine (135.3 mg, 85%) as a white solid; ^{1}H NMR δ=4.61 (s, 2H), 5.14 (s, 2H), and 6.7—7.8 (m, 10H); ^{13}C NMR δ=135.46, 134.81, 129.78, 129.56, 129.26, 129.11, 128.61, 55.76, and 45.85; MS *m/z* 226 (M^+, 11%), 181 (5), 149 (3), 118 (3), 105 (4), 92 (11), 91 (100), and 65 (13); white solid mp 57—8 °C (lit,[18] mp 58 °C).

b) Piperidine. To a solution of **1a** (192.7 mg, 1.68 mmol) in 10 ml of dichloromethane was added TBDMSOTf (532 mg, 1.2 equiv) at 0 °C, and after the solvent exchange into THF (15 ml) was added MeLi (2.1 mmol, 1.25 equiv). To this mixture was added 1 ml (10 equiv) of acetic acid and subsequently 15% ethanol solution of ethyl nitrite (2.5 ml, 3 equiv) and then the mixture was refluxed overnight. The solvent was evaporated and chromatography (Al_2O_3, hexane–ether 3:1) of the residual oil gave *N*-nitrosopiperidine (78.9 mg, 41%); colorless oil; ^{1}H NMR δ=1.2—1.9 (m, 6H), 3.6—3.9 (m, 2H), and 4.1—4.3 (m, 2H); ^{13}C NMR δ=50.84, 39.84, 26.49, 24.78, and 24.22. The properties of the product were identical with those of an authentic sample.[19]

Transalkylation. The procedure with **1a** and benzyl chloride is typical.

a) Transformation of 1a into *N*-Benzylpiperidine. To a solution of **1a** (115.0 mg, 1 mmol) in 10 ml of dichloromethane was added TBDMSOTf (290 mg, 1.1 equiv) and after the solvent exchange into THF (15 ml) was added MeLi (1.2 mmol, 1.2 equiv) at 0 °C. After stirring for 1 h at room temperature, to this solution was added benzyl chloride (0.17 ml, 189 mg, 1.5 equiv) and tetrabutylammonium fluoride (n-$Bu_4N^+F^-$) (THF solution, 1.1 mmol, 1.1 equiv) at room temperature. The mixture was then heated in a sealed tube at 110 °C for 10 h. After the evaporation of the solvent the resulting oil was subjected to chromatography (Al_2O_3, hexane–ether 3:1) to afford *N*-benzylpiperidine (**12a**; R=CH_2Ph) (101.7 mg, 58%). **12a** (R=CH_2Ph):[20] Colorless oil; ^{1}H NMR δ=1.1—1.8 (m, 6H), 2.1—2.5 (m, 4H), 3.5 (s, 2H), and 7.3 (s, 5H); MS *m/z* 175 (M^+, 46%), 174 (49), 98 (53), 92 (16), 91 (100), and 84 (56).

The other transalkylation reactions listed in Table 4 were carried out silimarly. In the case of benzoylmethylation, solid phenacyl bromide was added in one portion. **12a** (R=$(CH_2)_4CH_3$):[21] colorless oil; ^{1}H NMR δ=0.8—1.8 (m, 14H) and 1.9—2.5 (m, 6H); MS *m/z* 155 (M^+, 5%), 100 (8), 99 (9), 98 (100), 70 (6), and 57 (11). **12a**: (R=$(CH_2)_7CH_3$):[22] Colorless oil; ^{1}H NMR δ=0.6—1.8 (m, 21H), and 2.0—2.6 (m, 6H). **12a** (R=$CH_2CO_2CH_2CH_3$):[23] Pale yellow oil; ^{1}H NMR δ=1.27 (t, J=8 Hz, 3H), 1.2—2.0 (m, 6H), 2.4—2.7 (m, 4H), 3.21 (s, 2H), and 4.24 (q, J=8 Hz, 2H); MS *m/z* 171 (M^+, 5%), 157 (2), 127 (2), 114 (3), 99 (12), 98 (100), 86 (21), 84 (34), 71 (16), and 57 (21). **12a** (R=CH_2COPh):[24] Pale yellow oil; ^{1}H NMR δ=1.1—1.9 (m, 6H), 2.2—2.6 (m, 4H), 3.70 (s, 2H), 7.2—7.7 (m, 3H), and 7.9—8.3 (m, 2H). **12d** (R=CH_2Ph):[25] Pale yellow oil; ^{1}H NMR δ=1.00 (t, J=8 Hz, 6H), 2.53 (q, J=8 Hz, 4H), 3.64 (s, 2H), and 7.53 (s, 5H); MS *m/z* 163 (M^+, 5%), 162 (4), 148 (23), 142 (3), 105 (3), 92 (16), 91 (100), 86 (5), 77 (3), and 65 (8). **12d** (R=$(CH_2)_7CH_3$):[26] Colorless oil; ^{1}H NMR δ=0.7—1.9 (m, 15H), 0.89 (t, J=7.5 Hz, 6H), 2.0—2.5 (m, 2H), and 2.40 (q, J=7.5 Hz, 4H); MS *m/z* 185 (M^+, 15%), 170 (4), 142 (42), 100 (15), 91 (100), 58 (10), and 57 (15). **12d** (R=$CH_2CO_2CH_2CH_3$):[27] Pale yellow oil; ^{1}H NMR δ=1.00 (t, J=7.5 Hz, 3H), 1.16 (t, J=7.5 Hz, 6H), 2.57 (q, J=7.5 Hz, 4H), 3.54 (s, 2H), and 4.10 (q, J=7.5 Hz, 2H); MS *m/z* 159 (M^+, 5%), 145 (8), 144 (91), 130 (4), 116 (18), 88 (12), 86 (100), 72 (20), and 58 (25).

The authors are grateful to Shin-etsu Chemical Co. Ltd. for the generous gift of chlorosilanes.

References

1) M. Polonovski and M. Polonovski, *Bull. Soc. Chim. Fr.*, **41**, 1190 (1972). For reviews, see G. A. Russell, and J. G. Mikol, "Mechanism of Molecular Migrations," ed by B. S. Thagarajan, Interscience, New York (1968), Vol. 1, p. 176; A. R. Katritzky and J. N. Lagowski, "Chemistry of Heterocyclic N-Oxides," Academic Press, New York (1971), pp. 279 and 362; M. Ikeda and Y. Tamura, *Yuki Gosei Kagaku Kyokai Shi*, **38**, 10 (1980).

2) a) Atta-ur-Rahman, A. Basha, and M. Ghazala, *Tetrahedron Lett.*, **1976**, 351. b) P. Mangeney, R. Z. Andriamialisoa, N. Langlois, Y. Langlois, and P. Potier, *J. Am. Chem. Soc.*, **101**, 2244 (1979). c) N. Langlois, F. Guéritte, Y. Langlois, and P. Potier, *J. Am. Chem. Soc.*, **98**, 7017 (1976).

3) Part of this work has been reported as preliminary communications: R. Okazaki and N. Tokitoh, *J. Chem. Soc., Chem. Commun.*, **1984**, 192; N. Tokitoh and R. Okazaki, *Chem. Lett.*, **1984**, 1937.

4) The quantitative formation of siloxyammonium salts **6** was confirmed by the following experiment. To a deuteriochloroform solution (0.5 ml) of **1a** (40 mg, 0.35 mmol) was added TMSOTf (93 mg, 1.2 equiv) under argon at 0 °C in an NMR sample tube. In the ^{1}H NMR spectrum of the mixture a singlet at δ 3.67 due to the *N*-methyl protons of siloxyammonium salts **6a** appeared at the expense of a singlet at δ 3.19 due to the *N*-methyl protons of **1a**. Furthermore, the *N*-α protons of the piperidine ring of **6a** appeared as a multiplet at about δ 3.6, while those of **1a** were observed as a multiplet at about δ 3.2, and the protons of trimethylsilyl group of **6a** were observed at δ 0.48 as a singlet peak. The low-field shift of the *N*-methyl and *N*-α protons suggested the formation of siloxyammonium salt **6a** and the absence of the *N*-methyl signal of **1a** at δ 3.19 showed the almost quantitative conversion into **6a**.

5) Any change in reaction time, temperature, stoichiometry of reactants, and additives did not improve the yield of the amide.

6) Trimethylsilyl chloride can also be used as a silylating agent, but much less effectively as expected from its low silylation ability.[7] The reaction using **1a**, trimethylsilyl chloride, butyllithium and phenyl chloroformate gave the corresponding carbamate in 24%, while the use of TMSOTf under otherwise identical conditions resulted in the yield of 65% (see Table 3).

7) H. Emde, D. Domsch, H. Feger, U. Frick, A. Gots, H. H. Hergott, K. Hofmann, W. Kober, K. Krageloh, T. Oesterle, W. West, and G. Simchen, *Synthesis*, **1982**, 1.

8) R. Huisgen, F. Bayerlein, and W. Heydkamp, *Chem. Ber.*, **92**, 3233 (1959).
9) T. S. Manoharan, K. M. Madyastha, B. B. Singh, S. P. Bhatnagar, and U. Weiss, *Synthesis*, **1983**, 809.
10) R. A. Olofson, R. C. Schnur, L. Bunes, and J. P. Pepe, *Tetrahedron Lett.*, **1977**, 1567 and references cited therein.
11) Without the use of a sealed tube, it took a few days to get a similar yield of **12a** from the reaction of **7a** with benzyl chloride and tetrabutylammonium fluoride in refluxing tetrahydrofuran.
12) H. A. Hageman, *Organic Reactions*, **7**, 198 (1953).
13) N. J. Leonard and G. W. Leubner, *J. Am. Chem. Soc.*, **71**, 3408 (1949).
14) H. B. Ponahoe, S. I. Trotz, and K. K. Kimura, *J. Org. Chem.*, **25**, 1059 (1960).
15) "Handbook of Tables for Organic Compound Identification," Complied by Z. Rappoport, The Chemical Rubber Co., Cleaveland, 3rd ed p. 147.
16) T. Hassel and D. Seebach, *Helv. Chim. Acta*, **61**, 2237 (1978).
17) "Dictionary of Organic Compounds," ed by I. M. Heilbron et al., Oxford University Press, London (1965), p. 2295; H. Schmidt, O. Hollitzer, A. Seewald, and W. Steiglich, *Chem. Ber.*, **112**, 727 (1979).
18) P. A. S. Smith and R. N. Loeppley, *J. Am. Chem. Soc.*, **89**, 1147 (1967).
19) Y. L. Chow, *Can. J. Chem.*, **43**, 2711 (1965).
20) I. Scriabline, *Bull. Soc. Chim. Fr.*, **1947**, 454.
21) C. Glacet, *Bull. Soc. Chim. Fr.*, **1953**, 1056.
22) H. W. Magnusson and E. R. Schierz, *Univ. Wyoming Pub.*, **7**, 1—11 (1940); *Chem. Abstr.*, **34**, 6867 (1940).
23) H. Adkins and H. R. Billica, *J. Am. Chem. Soc.*, **70**, 3121 (1948).
24) F. Minisci and R. Galli, *Tetrahedron Lett.*, **1964**, 3197.
25) R. Hazard, E. Corteggiani, and S. H. Renard, *Compt. Rend.*, **227**, 95 (1948); *Chem. Abstr.*, **42**, 8329f (1948).
26) H. J. Schneider, H. Adkins, and S. M. EcElvain, *J. Am. Chem. Soc.*, **74**, 4287 (1952).
27) V. Franzen and H. Kuntze, *Justus Liebigs Ann. Chem.*, **627**, 15 (1959).

 © 1987 The Chemical Society of Japan Bull. Chem. Soc. Jpn., 60, 3299—3306 (1987)

Reactions of Trialkylstannane Anions R_3Sn^- with Arylstannanes $ArSnR'_3$

Kunio MOCHIDA
Department of Chemistry, Faculty of Sciences, Gakushuin University,
1-5-1 Mejiro, Tokyo 171
(Received March 24, 1987)

The reactions of trialkylstannane anions R_3Sn^- with arylstannanes $ArSnR'_3$ have been investigated; trialkylstannane anions with arylstannanes at 50 °C gave substitution products $ArSnR_3$ in good yields. Most of these substitution products are diverted to reduction products ArH when *t*-butylamine for trapping free anionoids is present in the reaction mixture. These results are consistent with an initial tin-alkali metal exchange or an electron-transfer forming aryl anions and distannanes which subsequently react to the substitution products. Aryl radical intermediates by an electron-transfer process are also important in the reactions of trialkylstannane anions with electron-withdrawing groups-substituted arylstannanes, 1-naphthylstannanes, diphenylstannanes, and triphenylmethylstannane as good electron acceptor substrates.

The displacement of halides and other groups from alkyl and aryl substrates by alkali metal derivatives of organometal anions represents one of the most important methods for the formation of carbon–metal σ bonds.[1] This approach to the formation of carbon–metal σ bonds has been particularly useful in group 4B chemistry.

Arylstannanes can be synthesized by the reactions of triorganostannane anions with aryl halides.[2-12] This formal nucleophilic aromatic substitution by triorganostannane anions is of considerable interest both in synthetic chemistry and regarding reaction mechanisms. Recently, Kuivila and co-workers,[11] and Pereyre and co-workers[12] have reported on the reactions of trialkylstannane anions with aryl halides and discussed on the mechanism involving alkali metal exchange, electron-transfer, and benzyne process in detail. However, a study of nucleophilic aromatic substitution by triorganostannane anions has been limited to aryl halides as substrates.

In this paper, we describe other nucleophilic aromatic substitutions by trialkylstannane anions: that is, reactions of trialkylstannane anions with arylstannanes.

Results

Reactions of Trimethylstannane Anions with Phenyltrialkylsilane, -germane, and -stannane. Reactions of sodium, lithium, and potassium trimethylstannate, prepared from chlorotrimethylstannane or hexamethyldistannane and alkali metals with phenyltrialkylsilane, -germane, and -stannane were examined under various conditions. These results are

Table 1. Reactions of Trimethylstannane Anions with Phenyltrialkylsilane, -germane, and -stannane under Various Conditions

No.	Reactant/mmol		Condition[a]	Product, yield/%[b]				
	$PhMR_3$	Me_3SnM'		PhH	$PhSnMe_3$	$(Me_3Sn)_2$	$(R_3M)_2$	Me_3SnMR_3
1	$PhSiMe_3$ (1.74)	Li/THF (1.67)	A, B	0	0	50	0	0
2	$PhGeMe_3$ (1.22)	Li/THF (1.12)	A, B	0	0	49	0	0
3	$PhSnEt_3$ (1.22)	Li/THF (1.67)	A	0	0	49	0	1
4	$PhSnEt_3$ (1.12)	Li/THF (1.67)	B	<1	24	16	<1	18
5	$PhSnEt_3$ (1.12)	Li/DME (1.33)	B	<1	10	25	0	13
6	$PhSnEt_3$ (1.12)	Li/TG (1.42)	B	<1	8	43	0	7
7	$PhSnEt_3$ (1.12)	Li/HMPA (0.36)	A	0	22	11	—[c]	8
8	$PhSnEt_3$ (1.22)	Na/THF (1.08)	B	<1	26	13	4	18
9	$PhSnEt_3$ (1.22)	K/THF (1.78)	B	<1	24	22	2	25

a) A: at 24 °C for 1 h; B: at 50 °C for 30 min. b) Based on the concentration of Me_3SnM'. c) Yields of products could not be determined by GLC.

summarized in Table 1.

The reaction of lithium trimethylstannate with phenyltriethylstannane in tetrahydrofuran (THF) at 24 °C for 1 h gave no substitution products. Hexamethyldistannane was formed quantitatively and phenyltriethylstannane was nearly recovered. Lithium trimethylstannate reacted with phenyltriethylstanane at 50 °C for 30 min to give phenyltrimethylstannane, hexamethyldistannane, and trimethylstannane (No. 4). The reaction time and temperature effected the yields of products. At a constant temperature of 50 °C, the yield of phenyltrimethylstannane reached a maximum (ca. 30%) in 40—50 min and, then, gradually decreased. On the other hand, the yield of the product rose to ca. 40% as the temperature was increased to 60 °C for 30 min. However, it is known that lithium trimethylstannate reacts with THF to give ring-opening products at high temperatures and for a long reaction time.[13] Under the reaction conditions (50 °C and 30 min) employed here, the yield of phenyltrimethylstannane is better and side reactions occur only slightly.

The stability of lithium trimethylstannate was stable at 50 °C for 30 min (Fig. 1). A part of lithium trimethylstannate changed to hexamethyldistannane.

As shown in Table 1, a substitution product was also produced in the reactions of lithium trimethylstannate with phenyltriethylstannane in 1,2-dimethoxyethane (DME), tetraglyme (TG), and hexamethylphosphoric triamide (HMPA) (Nos. 5—7). The product was produced even at 24 °C in HMPA. The yield of a substitution product by lithium trimethylstannate in various solvents (Table 1) was variable and depended upon the polarity of the solvents employed.

Sodium and potassium trimethylstannate in THF also reacted with phenyltriethylstannane at 50 °C (Nos. 8 and 9). The yields of the substitution products were almost constant with experimental errors, despite counter ions.

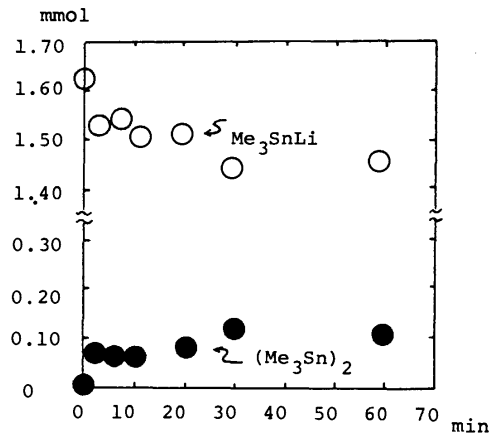

Fig. 1. The stability of lithium trimethylstannate (1.63 mmol) at 50 °C.

Through reactions of lithium trimethylstannate with phenyltrimethylsilane and -germane, the corresponding substitution products were not produced. Only hexamethyldistannane was formed (Nos. 1 and 2).

Reactions of Lithium Trimethylstannate with Arylstannanes. Reactions of lithium trimethylstannate with various arylstannanes in THF were examined. The results are summarized in Table 2.

Table 2 shows the effects of substituents of aryl groups on the yields of the substitution and reduction products in the reactions of lithium trimethylstannate and aryltriethylstannanes. The yields of substitution and reduction products increased as the substituents of aryl groups became electron-withdrawing: *m*-CF_3≫*H*>*p*-CH_3≳*p*-OCH_3 (Nos. 4, 10, 11, and 12). With [*m*-(trifluoromethyl)phenyl]triethylstannane, α,α,α-trifluorotoluene was produced in 9% yield. Furthermore, the color of the solution of [*m*-(trifluoromethyl)phenyl]triethylstannane and lithium trimethylstannate changed to red, unlike other solutions. These facts probably suggest that the reaction of lithium trimethylstannate with [*m*-(trifluoromethyl)-phenyl]triethylstannane involves an electron transfer

Table 2. Reactions of Lithium Trimethylstannate with Arylstannanes

No.	Reactant/mmol		Condition[a]	Product, yield/%[b]	
	Ar_nSnR_{4-n}	Me_3SnLi		ArH	$ArSnMe_3$
10	MeO-C$_6$H$_4$-$SnEt_3$ (1.22)	Me_3SnLi (1.21)	B	<1	9
11	Me-C$_6$H$_4$-$SnEt_3$ (1.21)	Me_3SnLi (1.21)	B	<1	10
12	CF_3-C$_6$H$_4$-$SnEt_3$ (1.26)	Me_3SnLi (1.21)	B	9	64
13	$PhSnPr_3$ (1.23)	Me_3SnLi (1.98)	B	0	4
14	$PhSnBu_3$ (1.09)	Me_3SnLi (1.98)	B	0	4
15	Ph_2SnBu_2 (1.03)	Me_3SnLi (1.98)	A	0	4
16	Ph_2SnBu_2 (1.03)	Me_3SnLi (1.98)	B	4	32
17	Ph_3SnMe (0.83)	Me_3SnLi (1.98)	A	—[c]	4
18	Ph_3SnMe (0.83)	Me_3SnLi (1.98)	B	—[c]	99
19	1-NpSnEt$_3$ (1.17)	Me_3SnLi (1.67)	A	2	7
20	1-NpSnEt$_3$ (1.17)	Me_3SnLi (1.67)	B	4	31

a) A: at 24 °C for 1 h; B: at 50 °C for 30 min. b) Based on the concentration of Me_3SnLi. c) Yields of products could not be determined by GLC.

followed by a free radical process, rather than a simple bimolecular nucleophilic reaction.

Table 2 also shows the effects of aryl groups on the yields of substitution and reduction products in the reactions of lithium trimethylstannate with arylstannanes. Lithium trimethylstannate reacted with phenyltripropylstannane and phenyltributylstannane with difficulty to produce phenyltrimethylstannane, (Nos. 13 and 14, respectively). However, with diphenyldibutylstannane, triphenylmethylstannane, and 1-naphthyltriethylstannane, lithium trimethylstannate reacted at 24 °C to give substitution products, although the yields of the products were very low. Especially, triphenylmethylstannane was very reactive toward lithium trimethylstannate and the substitution product by the reaction of lithium trimethylstannate with triphenylmethylstannane at 50 °C was formed quantitatively (No. 18).

The formation of reduction products was fairly well observed in the reactions of lithium trimethylstannate with [*m*-(trifluoromethyl)phenyl]triethylstannane, diphenyldibutylstannane, and 1-naphthyltriethylstannane. These arylstannanes are known to be good electron acceptor substrates.

Reactions of Lithium Trialkylstannates with Phenyltrimethylstannane. The effect of modest changes in the steric bulk at the tin atom were estimated by examining the reactions of lithium triethylstannate, tripropylstannate, and tributylstannate with respect to the yields of substitution products. These results are summarized in Table 3. The reaction of lithium triethylstannate with phenyltrimethylstannane occurred with great facility to give a substitution product, phenyltriethylstannane, in high yield. Benzene was formed in low yield (No. 21). However, lithium tripropylstannate or tributylstannate did not react with phenyltrimethylstannane. Hexaalkyldistannanes were detected in both reactions. It is clear that the difference of reactivities of lithium trialkylstannates may be due to either the steric bulk at the tin atom or the degree of associations of lithium trialkylstannates.

By taking the results in Tables 1 and 3 into consideration, the reaction of lithium trimethylstannate with phenyltriethylstannane at 50 °C is reversible. Equilibrium of this reaction leans to the reverse direction.

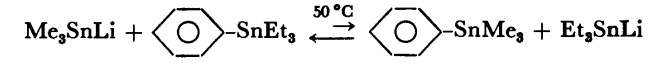

On the other hand, the reactions of lithium trimethylstannate with phenyltripropylstannane and phenyltributylstannane are irreversible.

Reactions of Lithium Trimethylstannate with Aryltriethylstannanes in the Presence of Trapping Reagents. Recently, Kuivila and co-workers have reported that *t*-butylamine is a very effective trapping reagent for free anionoids.[14] In order to obtain further information on the mechanism of the reactions of trialkylstannane anions with arylstannanes, the reactions of lithium trimethylstannate with phenyltriethylstannane, [*m*-(trifluoromethyl)phenyl]triethylstannane, and 1-naphthyltriethylstannane in the presence of *t*-butylamine for aryl anions and cumene

Table 3. Reactions of Lithium Trialkylstannates with Phenyltrimethylstannane at 50 °C for 30 min

No.	Reactant/mmol		Product, yield/%[a]	
	$PhSnMe_3$	R_3SnLi	PhH	$PhSnR_3$
21	$PhSnMe_3$ (1.74)	Et_3SnLi (1.32)	2	82
22	$PhSnMe_3$ (1.74)	*n*-Pr_3SnLi (1.55)	0	0
23	$PhSnMe_3$ (1.74)	*n*-Bu_3SnLi (1.17)	0	0

a) Based on the concentrations of R_3SnLi.

Table 4. Reactions of Lithium Trimethylstannate wtih Aryltriethylstannanes in the Presence of Trapping Reagents at 50 °C for 30 min

No.	Reactants/mmol			PhH	Product, yield/%[a]			
	$ArSnEt_3$	Me_3SnLi	Trap		$PhSnMe_3$	$(Me_3Sn)_2$	$Me_3SnSnEt_3$	$(Et_3Sn)_2$
24	Ph (1.12)	Me_3SnLi (1.28)	TBA[b] (1.43)	10	2	44	19	0
25	Ph (1.12)	Me_3SnLi (1.28)	Cumene (1.44)	0	12	42	11	0
26	*m*-$CF_3C_6H_4$ (1.26)	Me_3SnLi (1.36)	TBA (1.43)	54	17	25	62	11
27	*m*-$CF_3C_6H_4$ (1.26)	Me_3SnLi (1.36)	Cumene (2.16)	3	45	9	33	8
28	1-Np (1.17)	Me_3SnLi (1.97)	TBA (1.90)	19	14	31	26	—[c]
29	1-Np (1.17)	Me_3SnLi (1.36)	Cumene (2.16)	1	10	15	14	—[c]

a) Based on the concentration of Me_3SnLi. b) *t*-Butylamine. c) Yields of products could not be determined by GLC.

for free aryl radicals were examined. These results are summarized in Table 4.

t-Butylamine reacted more rapidly with the carbanion intermediates to give the corresponding alkanes than with lithium trimethylstannate under these conditions. The stability of lithium trimethylstannate in the presence of *t*-butylamine was examined at 50 °C. Lithium trimethylstannate is susceptible to form hexamethyldistannane. However, the concentration of lithium trimethylstannate is sufficiently large to react with aryltriethylstannanes under these conditions (Fig 2).

Lithium trimethylstannate reacted with phenyltriethylstannane in THF at 50 °C to produce <1% benzene, 24% phenyltrimethylstannane, 16% hexamethyldistannane, and 17% 1,1,1-trimethyl-2,2,2-triethyldistannane (No. 4). When *t*-butylamine was present in the initial reaction mixture, the yields of benzene, hexamethyldistannane, and 1,1,1-trimethyl-2,2,2-triethyldistannane increased upon increasing the concentration of *t*-butylamine, and that of phenyltrimethylstannane deccreased correspondingly (Fig. 3). Lithium trimethylstannate reacted with phenyltriethylstannane at higher *t*-butylamine concentrations to give 10% benzene, 2% phenyltrimethylstannane, 44% hexamethyldistannane, and 19% 1,1,1-trimethyl-2,2,2-triethyldistannane. Similarly, the effects of the *t*-butylamine concentration on the yields of products in the reactions of lithium trimethylstannate with [*m*-(trifluoromethyl)phenyl]triethylstannane and 1-naphthyltriethylstannane were examined. The yields of reduction products, hexamethyldistannane, and 1,1,1-trimethyl-2,2,2-triethyldistannane increased with the concentration of *t*-butylamine, and the substitution products decreased correspondingly. The yields of substitution products at the higher *t*-butylamine concentrations decreased in order: [*m*-(trifluoromethyl)phenyl]triethylstannane>1-naphthyltriethylstannane>phenyltriethylstannane. In contrast with the results of [*m*-(trifluoromethyl)phenyl]triethylstannane (Nos. 12 and 26) and 1-naphthyltriethylstannane (Nos. 20 and 28), a total amount of increased reduction product and decreased substitution product in the reaction of lithium trimethylstannate with phenyltriethylstannane in the presence of *t*-butylamine is not consistent with that of reduction and substitution products in the initial reaction (Nos. 4 and 24). This inconsistency may be explained by the fact that lithium trimethylstannate in part changes to hexamethyldistannane before a nucleophilic reaction by trimethylstannane anion in the presence of *t*-butylamine; then, the concentration of lithium trimethylstannate decreases.

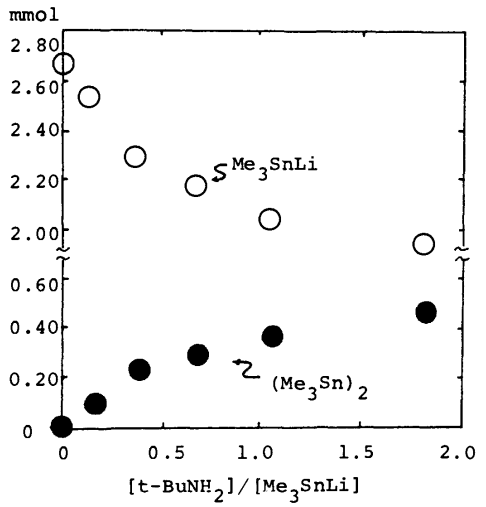

Fig. 2. The stability of lithium trimethylstannate (2.66 mmol) in the presence of *t*-butylamine at 50 °C for 30 min.

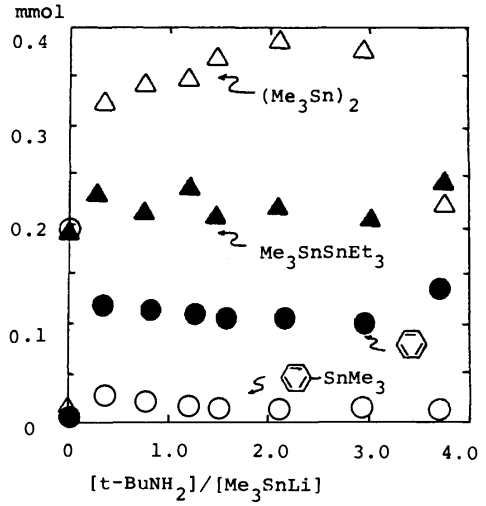

Fig. 3. Effects of TBA concentration on yields of products in the reaction of lithium trimethylstannate (1.28 mmol) with phenyltrimethylstannane (1.12 mmol) at 50 °C for 30 min.

Cumene is known to be an effective reagent for trapping free aryl radicals. Lithium trimethylstannate reacted with phenyltriethylstannane in the presence of cumene to produce <1% benzene, 12% phenyltrimethylstannane, 42% hexamethyldistannane, and 1,1,1-trimethyl-2,2,2-triethyldistannane (No. 25). Similarly, the effects of cumene on the yields of products in the reactions of lithium trimethylstannate with [*m*-(trifluoromethyl)phenyl]triethylstannane and 1-naphthyltriethylstannane were also examined. The yields of the reduction products, substitution products, 1,1,1-trimethyl-2,2,2-triethyldistannane, and hexaethyldistannane decreased, and hexamethyldistannane increased in both reactions in the presence of cumene (Nos. 27 and 29). By taking into consideration that lithium trimethylstannate is susceptible to form hexamethyldistannane in the presence of cumene at 50 °C, the decreased yields of products,

except for hexamethyldistannane, may be due to the low concentration of lithium trimethylstannate. Thus, cumene may not be an effective trapping reagent for free aryl radical intermediates under these reaction conditions. The results of reactions of lithium trimethylstannate with arylstannanes in the presence of trapping reagents are summarized in Table 4.

ESR Studies. In addition to the chemical evidence, ESR studies on the reactions of lithium trimethylstannate with phenyltriethylstannane and [*m*-(trifluoromethyl)phenyl]triethylstannane were examined. No ESR signals in the reaction of lithium trimethylstannate with phenyltriethylstannane in THF were observed. On the other hand, a very complexed ESR spectra attributed to carbon centered radicals (judging from the *g* factor) were observed in the case of [*m*-(trifluoromethyl)phenyl]triethylstannane. However, the ESR spectra could not be analyzed.

Discussion

The results summarized in Tables 1—3 demonstrate that trimethylstannane and triethylstannane anions react with arylstannanes to give substitution products, aryltrimethylstannane and aryltriethylstannane, respectively. The reactions of trialkylstannane anions with aryltriethylstannanes are endothermic. The yields of reduction and substitution products are highly variable, depending on the arylstannanes employed. In general, the yields of reduction products increased in the reactions of trialkylstannane anions with electron-withdrawing groups-substituted aryltriethylstannanes, 1-naphthyltriethylstannane, diphenyldibutylstannane, and triphenylmethylstannane as good electron acceptor substrates.

Recently, Kuivila and co-workers have demonstrated that *t*-butylamine is an effective reagent for trapping free anionoids.[14] The results in Table 4 show that the yields of reduction products increase in the presence of *t*-butylamine. These facts strongly imply that aryl anions are imporatnt intermediates in these reactions by trialkylstannyl anions. The formation of aryl anions can be explained by tin–alkali metal exchange or electron-transfer process. By the results of tin–alkali metal exchange in the reactions of trialkylstannyl anions with arylstannanes, aryl anions and distannanes are formed in the cage. Continuously, aryl anions react with distannanes to form substitution products (arylstannanes) and the corresponding stannane anions. Furthermore, the reactions of stannane anions, thus prepared, with the substitution products (arylstannanes) occur if circumstance requires. When *t*-butylamine is present in the reaction mixture, escaped aryl anions from the cage are trapped to give reduction products. As a result, the yields of reduction products and unattacked distannanes by aryl anions increase and those of substitution products decrease.

On the other hand, in light of trialkylstannane anions to act as one electron reducing reagents toward suitable substrates, the formation of aryl anions may also be explained by an electron-transfer process.[15] The first step is an electron-transfer from trialkylstannane anions to arylstannanes that leads to arylstannane anion radicals and trialkylstannane radicals in a cage. Subsequently, aryl anions and stannane radicals are formed from unstable arylstannane anion radicals. Distannanes are formed by a cage combination of stannane radicals from unstable arylstannane anion radicals and trialkylstannane radicals. The property of the formation of aryl anions by electron-transfer is discussed later. The attack on either tin atoms of the formed distannanes by aryl anions depends on the nature of the aryl anions and the stannane compounds. The mechansim for aryl anion intermediates in the reactions of trialkylstannane anions with arylstannanes is proposed in the following (Scheme 1).

The reaction of lithium trimethylstannate with phenyltriethylstannane at 50 °C is reversible. Equilibrium of this reaction shifts to the reverse direction. This shift may be due to either the difference of nucleophilicity or the degree of association of trimethylstannane and triethylstannane anions. On the other hand, the reactions of lithium trimethylstannate with phenyltripropylstannane and phenyltributylstannane at 50 °C are irreversible, respectively. This irreversibility of the reaction may result from either the steric hindrance or degree of association of tributylstannane and tripropylstannane anions.

However, by judging from the results of the formation of reduction products at the higher *t*-butylamine concentrations, aryl radical intermediates are also formed in the reactions of trialkylstannane anions with arylstannanes. The formation of aryl radicals may be explained by an electron-transfer process. The first step is an electron-transfer from trialkylstannane anions to arylstannanes that leads to

$$R_3Sn^-M^+ + ArSnR_3' \longrightarrow \begin{cases} \overline{Ar^-M^+\ R_3SnSnR_3'} \\ \text{or} \\ \overline{R_3Sn\cdot\ M^+\ [ArSnR_3']^{\pm}} \longrightarrow \overline{Ar^-M^+\ R_3Sn\cdot\ \cdot SnR_3'} \end{cases} \longrightarrow \text{products}$$

Scheme 1. The mechanism for aryl anion intermediates.

$$R_3Sn\text{-}M^+ + ArSnR_3' \longrightarrow \overline{R_3Sn\cdot\ M^+\ [ArSnR_3']^{\pm}}$$
$$\longrightarrow \overline{R_3Sn\cdot\ \cdot Ar\ M^+SnR_3'^-}$$
$$\longrightarrow \text{products}$$

Scheme 2. The mechanism for aryl radical intermediates.

arylstannane anion radicals and trialkylstannane radicals in the cage. Subsequent dissociation of aryl radicals produced from unstable arylstannane anion radicals followed by cage combination with trialkylstannane radicals and by proton abstraction from solvents employed would provide substitution products, aryltrialkylstannanes, and reduction products, respectively. According to this scheme, the formations of reduction and substitution products can be observed despite of *t*-butylamine (Scheme 2).

In fact, the formation of reduction products in the absence of *t*-butylamine and substitution products at the higher *t*-butylamine concentrations were observed in the reactions of trialkylstannane anions with [*m*-(trifluoromethyl)phenyl]triethylstannane, 1-napthyltriethylstannane, diphenyldibutylstannane, and triphenylmethylstannane. These facts imply that aryl radical intermediates are also involved in the reactions of trialkylstannane anions with good electron acceptors such as the above arylstannanes.

A pattern of cleavage of the aryl–tin bond for arylstannane anion radicals may be shown in the following.

$$[ArSnR_3]^{\pm} \begin{cases} \longrightarrow Ar^- + \cdot SnR_3 \\ \longrightarrow Ar\cdot + {}^-SnR_3 \end{cases}$$

A pattern of cleavage of the aryl–tin bond for arylstannane anion radicals may depend on the nature of the aryl group (Ar) and the alkyl group (R).

In conclusion, the reactions of trialkylstannane anions with arylstannanes proceed via two different key intermediates: aryl anions and aryl radicals. Aryl anion intermediates formed by tin–alkali metal exchange or electron-transfer are most important in the reactions of trialkylstannane anions with arylstannanes. However, aryl radical intermediates formed by an electron-transfer is also important in the reactions of trialkylstannane anions with [*m*-(trifluoromethyl)phenyl]triethylstannene, 1-naphthyltriethylstannane, diphenyldibutylstannane, and triphenylmethylstannane as good electron acceptor substrates.

Experimental

^{1}H NMR spectra were recorded on a Varian FT 80A, with tetramethylsilane as internal standard. GC-Mass spectra were obtained with JEOL JMS-DX 303 mass spectrometer. Infrared spectra were recorded on a Hitachi 260-10 spectrometer. Gas chromatography was performed on a Shimadzu GC-6A and -8A with 2 m 20% SE-30 and 2 m 30% Apiezon L columns.

Materials. *t*-$BuNH_2$ and cumene are commercially available and purified prior to use. Me_3SnCl, bp 152—154 °C,[16] Et_3SnCl, bp 109—110 °C/20 mmHg†,[17] Pr_3SnCl, bp 123 °C/13 mmHg,[18] Bu_3SnCl, bp 145—147 °C/5 mmHg,[19] $Me_3SnSnMe_3$, bp 182 °C,[20] $Et_3SnSnEt_3$, bp 160 °C/23 mmHg,[20] $Pr_3SnSnPr_3$, bp 142 °C/15 mmHg,[21] $Bu_3SnSnBu_3$, bp 156—160 °C/0.03 mmHg,[20] $Me_3SnSnEt_3$, bp 105 °C/6 mmHg,[20] Me_3SnH, bp 59 °C,[22] Et_3SnH, bp 79—81 °C/92 mmHg,[23] $PhSiMe_3$, bp 72 °C/27 mmHg,[24] $PhGeMe_3$, bp 80 °C/27 mmHg,[25] $PhSnMe_3$, bp 91 °C/30 mmHg,[27] *p*-$MeC_6H_4SnMe_3$, bp 105 °C/3 mmHg,[27] *p*-$MeOC_6H_4SnMe_3$, bp 115 °C/3 mmHg,[28] *m*-$CF_3C_6H_4SnMe_3$, bp 78—81 °C/14 mmHg,[28] 1-$NpSnMe_3$, bp 120 °C/1 mmHg,[27] $PhSnEt_3$, bp 113—114 °C/6 mmHg,[29] *p*-$MeC_6H_4SnEt_3$, bp 91 °C/1 mmHg,[29] *p*-$MeOC_6H_4SnEt_3$, bp 138 °C/5 mmHg,[29] *m*-$CF_3C_6H_4SnEt_3$, bp 105 °C/3 mmHg,[30] $PhSnPr_3$, bp 150 °C/15 mmHg,[31] $PhSnBu_3$, bp 139 °C/0.6 mmHg,[31] Ph_2SnBu_2, bp 137 °C/0.2 mmHg,[31] and Ph_3SnMe, mp 61 °C were prepared as cited literatures.

Preparation of 1-Naphthyltriethylstannane. A Grignard reagent was prepared from 1-bromonaphthalene (11.0 g, 0.05 mol) and magnesium (1.2 g, 0.05 g atom) in a mixture solvent of THF (50 cm^3), benzene (30 cm^3), and ether (20 cm^3). To this Grignard reagent was added chlorotriethylstannane (12.0 g, 0.05 mol) in a mixture solvent of THF (20 cm^3), benzene (10 cm^3), and ether (5 cm^3). The reaction mixture was stirred with reflux for 5 h. After hydrolysis with water, the organic layer was extracted with ether and dried over sodium sulfate. The solvent was removed and then fractional distillation gave 1-naphthyltriethylstannane (10 g, 0.03 mol, 60% yield), bp 142—145 °C/3 mmHg; ^{1}H NMR ($CDCl_3$) δ=1.30 (s, 15H), 7.25—8.00 (m, 7H); n^{20} 1.5957. Found: C, 57.48; H, 6.72%. Calcd for $C_{16}H_{22}Sn$: C, 57.70; H, 6.66%.

Preparation of Lithium Trimethylstannate. Lithium trimethylstannate was prepared from hexamethyldistannane or chlorotrimethylstannane and lithium metal in THF, DME, TG, or HMPA in an atmosphere of nitrogen for 4—5 h. Yields were determined by treatment with bromobenzene or *p*-tolyl bromide and the amounts of phenyltrimethylstannane or *p*-tolyltrimethylstannane produced, respectively, by GLC with an internal standard method. Yields were 80—85%.

Preparation of Sodium Trimethylstannate. Sodium trimethylstannate was prepared from hexamethyldistannane and sodium metal as described above for lithium trimethylstannate. Yields were 80—90%.

Preparation of Potassium Trimethylstannate. Potassium trimethylstannate was prepared as described above lithium trimethylstannate. Yields were 85—90%.

Preparation of Lithium Triethylstannate, Tripropylstannate, and Tributylstannate. Lithium triethylstannate, tripropylstannate, and tributylstannate were prepared from the corresponding chlorides and lithium metal in THF in an atmosphere of nitrogen for 4—5 h. Yields were determined by treatment with an excess of bromobenzene or *p*-tolyl bromide and by the amounts of the corresponding tin compounds formed.

Stability of Lithium Trimethylstannate at 50 °C. Li-

† 1 mmHg=133.322 Pa.

thium trimethylstannate in THF was heated at 50 °C. Yields of lithium trimethylstannate were determined by the reaction of excess of bromobenzene or *p*-tolyl bromide at constant time and the amounts of phenyltrimethylstannane or *p*-tolyltrimethylstannane, respectively, and hexamethyldistannane produced.

Stability of Lithium Trimethylstannate in the Presence of *t*-Butylamine at 50 °C. A mixture of lithium trimethylstannate and *t*-butylamine in THF was heated at 50 °C. Yields of lithium trimethylstannate were determined as described above for the stability of lithium trimethylstannate at 50 °C.

Stability of Lithium Trimethylstannate in the Presence of Cumene. A mixture of lithium trimethylstannate and cumene in THF was heated at 50 °C. Yields of lithium trimethylstannate were determined as described above of the stability of lithium trimethylstannate at 50 °C.

Reaction of Lithium Trimethylstannate with Phenyltrimethylsilane. Lithium trimethylstannate (1.67 mmol) was added to phenyltrimethylsilane (1.74 mol) in THF (2 cm^3) and stirred at 24 °C for 1 h or 50 °C for 30 min. After hydrolysis with water, the organic layer was extracted with ether. The ether solution was dried over sodium sulfate. Phenyltrimethylsilane (1.74 mmol) and hexamethyldistannane (0.86 mmol) were determined by an internal standard method by GLC. Each product was isolated by preparative GLC and structures were verified by comparing their GC-Mass, IR, and NMR retention times on GLC of authentic samples.

Reaction of Lithium Trimethylstannate with Phenyltrimethylgermane. Lithium trimethylstannate (1.12 mmol) was added to phenyltrimethylgermane (1.22 mmol) in THF (2 cm^3) and stirred at 24 °C for 1 h or at 50 °C for 30 min. After hydrolysis with water, the organic layer was extracted with ether. The ether solution was dried over sodium sulfate. Phenyltrimethylgermane (1.20 mmol) was recovered and hexamethyldistannane (0.53 mmol) was produced. Each product was isolated by preparative GLC and the structures were identified by comparing their GC-Mass, IR, and NMR spectra, and retention times on GLC with those of authentic samples.

Reaction of Lithium Trimethylstannate with Phenyltriethylstannane at 24 °C. Lithium trimethylstannate (1.67 mmol) was added to phenyltriethylstannane (1.2 mmol) in THF (2 cm^3) and stirred at 24 °C for 1 h. After hydrolysis with water, the organic layer was dried over sodium sulfate. Phenyltriethylstannane (1.18 mmol) was recovered and hexamethyldistannane (0.61 mmol), and 1,1,1-trimethyl-2,2,2-triethyldistannane (0.01 mmol) were formed. Each product was isolated by preparative GLC and the structures were identified by comparing their GC-Mass, IR, NMR, and retention times on GLC with those of authentic samples.

Reaction of Lithium Trimethylstannate with Phenyltriethylstannane at 50 °C. Lithium trimethylstannate (1.67 mmol) was added to phenyltriethylstannane (1.12 mmol) in THF (2 cm^3) and stirred at 50 °C for 30 min. After hydrolysis with water, the solution was extracted with ether. The organic layer was dried over sodium sulfate. Yields of benzene (trace), phenyltrimethylstannane (0.40 mmol), phenyltriethylstannane (0.68 mmol), hexamethyldistannane (0.27 mmol), 1,1,1-trimethyl-2,2,2-triethyldistannane (0.30 mmol), and hexaethyldistannane (trace) were determined by an internal standard method by GLC.

Reactions of Trialkylstannane Anions with Arylstannanes. Reactions of trialkylstannane anions with arylstannanes were carried out as described above for the reaction of lithium trimethylstannate with phenyltriethylstannane. Yields of the reaction products were determined in the same manner as those of the reaction of lithium trimethylstannate with phenyltriethylstannane.

Reaction of Lithium Trimethylstannate with Aryltriethylstannanes in the Presence of *t*-Butylamine. A typical example for the reactions of lithium trimethylstannate with aryltriethylstannanes in the presence of *t*-butylamine is described. Lithium trimethylstannate (1.28 mmol) was added to a mixture of phenyltriethylstannane (1.12 mmol) and *t*-butylamine (1.43 mmol) in THF (2 cm^3) and stirred at 50 °C for 30 min. After hydrolysis with water, the solution was extracted with ether. The organic layer was dried over sodium sulfate. Yields of benzene (0.12 mmol), phenyltrimethylstannane (0.03 mmol), hexamethyldistannane (0.56 mmol), and 1,1,1-trimethyl-2,2,2-triethyldistannane (0.24 mmol) were formed.

Reactions of Lithium Trimethylstannate with Aryltriethylstannanes in the Presence of Cumene. A typical example for the reactions of lithium trimethylstannate with aryltriethylstannanes in the presence of cumene is described. Lithium trimethylstannate (1.28 mmol) was added to a mixture of phenyltriethylstannane (1.12 mmol) and cumene (1.44 mmol) in THF (2 cm^3) and stirred at 50 °C for 30 min. After hydrolysis with water, the solution was extracted with ether. The organic layer was dried over sodium sulfate. Yields of phenyltrimethylstannane (0.15 mmol), hexamethyldistannane (0.53 mmol), and 1,1,1-trimethyl-2,2,2-triethyldistannane (0.14 mmol) were formed.

ESR Studies on the Reactions of Lithium Trimethylstannate with Aryltriethylstannanes. In a typical example, a solution of lithium trimethylstannate in THF was added using a hypodermic syringe to a small amount of phenyltriethylstannane contained THF in a glass tube constructed with a 6×60 mm upper portion and 2×80 mm lower portion. The tube was then sealed off after freeze-pump-thaw cycles on a vacuum line.

References

1) For examples: D. D. Davies, *Organomet. Chem. Rev., Sect. A*, **6**, 283 (1970); W. P. Neuman, "The Organic Chemistry of Tin," Wiley, New York (1970); J. G. A. Luijten and G. J. M. van der Kerk, "The Bond to Carbon," ed by A. G. MacDiamid, Marcel Dekker, New York (1968), Chapt. 4; G. E. Coates, M. L. H. Green, and K. Wade, "Organometalic Compounds," Methuen, London (1967), Vol. 1.

2) C. A. Kraus and W. Sessions, *J. Am. Chem. Soc.*, **47**, 2361 (1925).

3) R. H. Bullard and W. B. Robinson, *J. Am. Chem. Soc.*, **49**, 1368 (1927).

4) H. Gilman and S. D. Rosenburg, *J. Am. Chem. Soc.*, **74**, 531 (1952).

5) H. Gilman and S. D. Rosenburg, *J. Org. Chem.*, **18**, 680 (1953).

6) C. Tambrski, F. E. Ford, and E. J. Sokolski, *J. Org. Chem.*, **28**, 181 (1963),

7) H. Stegman and K. Scheffler, *Tetrahedron Lett.*, **1964**,

3387.
8) H. G. Kuvila and K. R. Wursthorn, *Tetrahedron Lett.*, **1975**, 4357.
9) H. G. Kuivila and K. R. Wursthorn, *J. Organomet. Chem.*, **105**, C6 (1976).
10) K. R. Wursthorn and H. G. Kuivila, *J. Organomet. Chem.*, **140**, 29 (1977).
11) K. R. Wursthorn, H. G. Kuivila, and G. F. Smith, *J. Am. Chem. Soc.*, **100**, 2779 (1978).
12) J.-P. Quintard, S. H-Frey, and M. Pereyre, *J. Organomet. Chem.*, **159**, 147 (1978).
13) "Shin Jikken Kagaku Koza," ed by Nippon Kagaku Kai, Maruzen, Tokyo (1976), Vol. 12.
14) G. F. Smith, H. G. Kuivila, R. Simon, and L. Sultan, *J. Am. Chem. Soc.*, **103**, 833 (1981).
15) For example; J. S. Filippo, Jr., J. Silbermann, and P. J. Fagan, *J. Am. Chem. Soc.*, **100**, 4834 (1978), J. S. Filippo, Jr., and J. Silbermann, *ibid.*, **104**, 2831 (1982), W. Kitching, H. Olszowy, and J. Waugh, *J. Org. Chem.*, **43**, 898 (1978), W. Kitching, H. A. Olszowy, and K. Harvey, *J. Org. Chem.*, **47**, 1893 (1982).
16) S. Pappetti and H. W. Post, *J. Org. Chem.*, **22**, 526 (1957).
17) K. A. Kozeschkow, *Ber.*, **66**, 1661 (1933).
18) J. Chatt and A. A. Williams, *J. Chem. Soc.*, **1954**, 4403.
19) G. J. M. van der Kerk and J. G. A. Luijten, *J. Appl. Chem.*, **4**, 301 (1954).
20) W. P. Neuman, B. Schneider, and R. Sommer, *Justus Liebigs Ann. Chem.*, **692**, 1 (1966).
21) G. Gruttner, *Ber.*, **50**, 1808 (1917).
22) A. E. Finholt, A. C. Bond, Jr., K. E. Wilzbach, and H. I. Schlesinger, *J. Am. Chem. Soc.*, **69**, 2692 (1947).
23) G. J. M. van der Kerk, J. G. Noltes, and J. G. A. Luijten, *J. Appl. Chem.*, **7**, 366 (1957).
24) H. Freiser, M. V. Eagle, and J. L. Speier, *J. Am. Chem. Soc.*, **75**, 2821 (1953).
25) H. Bauer and K. Burschkies, *Ber.*, **66**, 1156 (1933).
26) J. Nagy, J. Reffy, A. Kuszmann-Borbely, and K. Pallossy-Becker, *J. Organomet. Chem.*, **7**, 393 (1967).
27) O. Buchman, M. Grosjeanm, and J. Nasielski, *Bull. Soc. Chim. Belges.*, **71**, 467 (1962).
28) C. Eaborn, H. L. Hornfeld, and D. R. M. Walton, *J. Chem. Soc., B*, **1967**, 1036.
29) H. Hashimoto and Y. Marimoto, *J. Organomet. Chem.*, **8**, 271 (1967).
30) C. Eaborn, H. L. Hornfeld, and D. R. M. Walton, *J. Organomet. Chem.*, **10**, 529 (1967).
31) R. W. Weiss, "Organometallic Compounds-Methods of Synthesis, Physical Constants and Chemical Reactions," ed by M. Dub, Springer-Verlag, New York (1967), Vol. II.
32) M. R. Kula, E. Amberger, and K. K. Mayor, *Chem. Ber.*, **98**, 634 (1965).

 © 1987 The Chemical Society of Japan Bull. Chem. Soc. Jpn., 60, 3307—3313 (1987)

Synthesis, Properties, and Reactivity of (1*H*,1*H*-Perfluoroalkyl)- and (1*H*-Perfluoro-1-alkenyl)aryliodonium Triflates and Their Analogs

Teruo UMEMOTO* and Yoshihiko GOTOH
Sagami Chemical Research Center, Nishi-Ohnuma 4-4-1, Sagamihara, Kanagawa 229
(Received March 26, 1987)

(1*H*,1*H*-Perfluoroalkyl)phenyl- and -(*p*-fluorophenyl)iodonium triflates, fluorosulfate, sulfate (**3**)—(**7**) were synthesized in good yields by the oxidation of 1-iodo-1*H*,1*H*-perfluoroalkanes ($RfCH_2I$) with trifluoroperacetic acid followed by treatment with triflic acid and benzene or fluorobenzene. (1*H*,1*H*,5*H*,5*H*-Perfluoropentane-1,5-diyl)bisphenylbisiodonium triflate was synthesized similarly. (*trans*-1*H*-Perfluoro-1-alkenyl)phenyliodonium triflates (**11**) were synthesized by dehydrofluorination of **3** with a base in good yields. Thermolysis of **3** produced 1*H*,1*H*-perfluoroalkyl triflate and iodobenzene, while **11** gave (*Z*)-1-iodo-1*H*-perfluoro-1-alkene and phenyl triflate. The thermolysis experiment, including (perfluoroalkyl)phenyliodonium triflate (**17**), demonstrated that the C–I bond strength of the trivalent iodine compounds increased in the order of $RfCH_2$–I, Rf–I<Ph–I<RfCF=CH–I. The ionic mechanism containing $RfCH_2^+$, Ph^+, and Rf^+ for the thermal decomposition of **3**, **11**, and **17**, respectively, was proposed. The reactivities of **3** and **11** to such nucleophiles as phenoxide, alkoxide, and alkanethiolate anions were studied and compared with that of **17**. Remarkable changes in the reactivity were found depending on the nature of the fluoro-alkyl and -alkenyl groups. The reaction of **11** with the oxide anions yielded (2-phenoxy- and -alkoxy-1*H*-perfluoro-1-alkenyl)phenyliodonium triflates.

Hypervalent iodine compounds have been of increasing importance from the viewpoint of the consideration of their bonding and structures, or of the organic synthesis as useful reagents or reactive intermediates.[1] Many kinds of hypervalent iodine compounds were synthesized and their properties or reactivities were studied.[1] The hypervalent iodines carrying fluoro-alkyl or -alkenyl groups have been expected to have interesting properties because of the high electronegativity of the fluoro groups.[2]

We have already synthesized a series of (perfluoroalkyl)aryliodonium triflates and their analogs, and have demonstrated that they act as reactive electrophilic perfluoroalkylating agents.[3] In this connection, it is of great interest to study the syntheses and reactivities of (1*H*,1*H*-perfluoroalkyl)- and (polyfluoroalkenyl)-aryliodonium salts where the trivalent iodine atom is separated from the electronegative perfluoroalkyl group by a methylene and a vinyl unit, respectively. It was reported that (1*H*,1*H*,ω*H*-perfluoropentyl or heptyl)-*p*-tolyliodonium halides and (1*H*,1*H*,6*H*,6*H*-perfluorohaxane-1,6-diyl)bis(*p*-tolyl)bisiodonium halides were unstable and only the bromides could be isolated in pure form in low yields.[4] The hypervalent iodines possessing fluorinated alkenyl groups have never been synthesized.

This paper describes the syntheses, properties, and reactivities of a series of (1*H*,1*H*-perfluoroalkyl)- and (1*H*-perfluoro-1-alkenyl)aryliodonium triflates and their analogs.

Results and Discussion

1-[Bis(trifluoroacetoxy)iodo]-1*H*,1*H*-perfluoroalkanes **2** were prepared almost quantitatively by treating 1-iodo-1*H*,1*H*-perfluoroalkanes **1** with trifluoroperacetic acid by the modified Yagupol'skii's procedure.[4] **2a—e** were allowed to react with benzene and triflic acid in 1,1,2-trichloro-1,2,2-trifluoroethane at 0 °C for 1 day to give (1*H*,1*H*-perfluoroalkyl)phenyliodonium triflates **3a—e** with different carbon numbers of the perfluoroalkyl (Rf) groups in good yields. ^1H NMR spectra of **3** exhibited the characteristic peaks of methylene groups which appeared at δ ca. 4.8 downfield compared to that of **1** (δ ca. 3.7), as triplets or quartets due to coupling with the vicinal fluorine atoms.

$$\underset{\textbf{1a—e}}{RfCH_2I} \xrightarrow{[O]} \underset{\textbf{2a—e}}{RfCH_2I(OCOCF_3)_2} \xrightarrow{PhH,\ TfOH} RfCH_2\text{-}\underset{\underset{Ph}{|}}{I}\text{-}OTf^{5)} \quad (1)$$

3a (Rf=CF_3, 88%)
3b (Rf=C_2F_5, 72%)
3c (Rf=*n*-C_3F_7, 70%)
3d (Rf=*i*-C_3F_7, 77%)
3e (Rf=*n*-C_7F_{15}, 89%)

The use of fluorobenzene instead of benzene gave *p*-fluorophenyl isomer **4** exclusively. Fluorosulfuric acid and sulfuric acid, instead of triflic acid, gave fluorosulfate **5** and sulfate **6**, respectively. Similarly, 1-iodo-1*H*,1*H*, ω*H*-perfluorododecane gave **7**.

$$2 \xrightarrow{ArH,\ RSO_3H} RfCH_2\text{-}\underset{\underset{Ar}{|}}{I}\text{-}OSO_2R \quad (2)$$

4 (Ar=*p*-FC_6H_4, R=CF_3, Rf=CF_3, 72%)
5 (Ar=Ph, R=F, Rf=*n*-C_7F_{15}, 95%)
6 (Ar=Ph, R=OH, Rf=*n*-C_7F_{15}, 49%)
7 (Ar=Ph, R=CF_3, Rf=$(CF_2)_{10}H$, 85%)

Bis(iodonium) triflate **9** was similarly synthesized from diiodide **8** in high yield.

$$\underset{\mathbf{8}}{ICH_2(CF_2)_3CH_2I} \xrightarrow[2,\ PhH,\ TfOH]{1,\ [O]} \underset{\mathbf{9}\quad 96\%}{TfO\text{-}I(Ph)\text{-}CH_2(CF_2)_3CH_2\text{-}I(Ph)\text{-}OTf} \qquad (3)$$

We found that triflates **3b**, **3c**, and **3e** underwent easy dehydrofluorination by treatment with sodium hydride in acetonitrile at 0 °C to give (*trans*-1*H*-perfluoro-1-alkenyl)phenyliodonium triflates **11b**, **11c**, and **11e** in good yields. The treatment of **3e** with a

$$\mathbf{3b,\ c,\ e} \xrightarrow{NaH} \underset{F}{\overset{Rf'}{\diagdown\!=\!\diagup}}\!\!\underset{Ph}{I\text{-}OTf} \qquad (4)$$

11b ($Rf' = CF_3$, 80%)
11c ($Rf' = C_2F_5$, 86%)
11e ($Rf' = n\text{-}C_6F_{13}$, 87%)

$$\left[\ Rf'CF_2\bar{C}H\text{-}\overset{+}{I}(Ph)\ \right]$$

10

weak base, 2,4,6-collidine, at room temperature gave **11e** in a 40% yield. This indicates that the methylene protons of **3** are considerably acidic. **11** were assigned as trans isomers from the coupling constant (33 Hz) between the olefinic proton and the fluorine atom. The NMR resonance (δ ca. 8.2) of the olefinic protons of **11** appeared at a very low magnetic field. The corresponding proton of iodide **15** appeared at δ 6.63. On the other hand, it is interesting that **3a** and **3d** did not afford the expected (2,2-difluorovinyl)- and (2-trifluoromethyl-3,3,3-trifluoro-1-propenyl)-phenyliodonium triflates, **11a** and **11d**, respectively, by

$$\mathbf{3a,\ d} \xrightarrow{//} \underset{Rf_2}{\overset{Rf_1}{\diagdown\!=\!\diagup}}\!\!\underset{Ph}{I\text{-}OTf} \qquad (5)$$

11a ($Rf_1 = Rf_2 = F$)
11d ($Rf_1 = Rf_2 = CF_3$)

the same procedure, but, rather, the decomposition of **3a** and **3d** occurred. We isolated sodium triflate in the latter case. This might be due to the instability or high reactivity of **11a** and **11d** compared to **11b**, **11c**, or **11e**. It is known that the 2,2-difluorovinyl moiety is sensitive to a nucleophilic attack at the C–F carbon site, while the 2,2-bis(trifluormethyl)vinyl moiety is sensitive at the C-1 site.[6]

We failed in synthesizing the fluoroalkynyl analogs **12** from **11** by the action of sodium hydride in acetonitrile. The decomposition of **11** occurred and sodium triflate was isolated.

$$\mathbf{11} \xrightarrow{NaH} Rf'\text{-}C{\equiv}C\text{-}\underset{Ph}{I}\text{-}OTf \qquad (6)$$

12

The dehydrofluorination of **3** should occur via interesting halogen ylides **10**. An attempt to react the intermediate **10e** with such an electrophile as benzaldehyde was unsuccessful.

Salts **3** are apparently nonhygroscopic, stable crystals; the stability increases as the chain of a Rf group is lengthened. In general, they are soluble in acetonitrile and almost insoluble in diethyl ether, tetrahydrofuran, or haloalkanes such as dichloromethane. **3e** is satisfactorily stable, but **3a** decomposed very slowly and almost completely in about 3 weeks at room temperature (ca. 25—31 °C). **3a** is stable enough to be handled at room temperature and can be stored for long time in a refrigerator or a freezer. *p*-Fluorophenyl analog **4** is more stable than **3a**, judging from their decomposition points. **4** decomposed completely in 2—3 days in a moist acetonitrile-d_3 solution at room temperature.

Fluoroalkenyl analogs **11** are apparently nonhygroscopic crystals and have a high stability compared to **3**. While **3** decomposed at their melting points, **11** melted without decomposition near the decomposition points of **3**.

Salts **3** appeared to us to be less stable than (perfluoroalkyl)phenyliodonium triflates **17**. This suggests that the stability of the trivalent iodine compounds decreases as the electronegativity of the alkyl groups decreases, and makes it very clear to us that nobody can succeed in the isolation of the hydrocarbon analogs,[1a,7] alkyl(aryl)iodonium salts, because of the instability arising from the low electronegativity of the hydrocarbon alkyl group.

The I···O bonds of **3—7**, **9**, and **11** appear to be highly ionic, but not completely polarized, on the

$$R\text{-}\overset{\delta+}{I}(Ph)\cdots\overset{\delta-}{O}SO_2R'$$

(R = Rf, $RfCH_2$, RfCF=CH)

basis of the fact that the ^{19}F NMR analysis of analogous iodine compounds **17** and their derivatives has demonstrated that the I···OSO_2R' bonds are not completely polarized and that the degree of polarization varies depending on the electronegativity of R'.[3a] Therefore, we can express the bonds as $>I\text{-}OSO_2R'$, but not as $>I^+\ ^-OSO_2R'$.

The thermolysis of **3** and **11** gave very interesting results: **3e** decomposed at 140—145 °C to produce 1*H*,1*H*-perfluroalkyl triflate **13** and iodobenzene **14** in good yields, while **11e** remained intact at 140 °C and decomposed at 200 °C to give (*Z*)-1-iodo-1*H*-perfluoro-1-alkene **15** and phenyl triflate **16** in good yields. As reported previously, the thermolysis of **17a**

$$\mathbf{3e}\ (Rf=n\text{-}C_7F_{15}) \xrightarrow{140-145\,^\circ C} RfCH_2OTf + PhI \quad (7)$$
$$\mathbf{13}\ (90\%) \quad \mathbf{14}\ (89\%)$$

$$\mathbf{11e}\ (Rf=n\text{-}C_8F_{13}) \xrightarrow{200\,^\circ C} \begin{matrix} Rf \\ F \end{matrix}\!\!\diagdown\!\!\diagup\!\!\begin{matrix} \\ I \end{matrix} + PhOTf \quad (8)$$
$$\mathbf{15}\ (79\%) \quad \mathbf{16}\ (76\%)$$

$$Rf\text{-}I(Ph)\text{-}OTf \xrightarrow{145-151\,^\circ C} RfOTf + \mathbf{14} + I\text{-}C_6H_4\text{-}Rf \quad (9)$$
$$\mathbf{17a}\ (Rf=n\text{-}C_8F_{17}) \quad \mathbf{18}\ (73\%) \quad (63\%) \quad \mathbf{19}\ (25\%)$$

at 145—151 °C produced perfluorooctyl triflate **18**, **14**, and (perfluorooctyl)iodobenzene **19**.[3a] It is worth noting that the cleavage of CH_2–I and Rf–I bonds occurred in **3** and **17**, while the Ph–I bond was broken in **11**. **11** and **3** or **17** differ much from each other regarding the fission pattern. The above results clearly demonstrate that the C–I bond strength increases in the order of $RfCH_2$–I, Rf–I<Ph–I<RfCF=CH–I. It is noticeable that the C–I bond of RCF=CH–I is much stronger than that of Ph–I. Furthermore, the thermolysis of **11** is in sharp contrast to that of a hydrocarbon analog, vinyl(phenyl)iodonium bromide, which revealed that the bond fission between the vinyl carbon and the iodine atom occurred exclusively.[1b,8] The vinyl(phenyl)iodonium salts have been shown to be useful vinylating agents.[1b,9] They are based on a weak bonding between the vinyl carbon and the iodine atom compared to the Ph–I bond. The strong bonding between the fluorinated vinyl carbon and the iodine atom of **11** would be due to the high electronegativity of a Rf group and a fluorine atom binding to the vinyl moiety.

The cleavage of the bond between the sp^3 carbon and the iodine of **3** probably proceeds by an ionic mechanism, which is in agreement with the fact that **3** acts as a very useful source of a $RfCH_2$ cation.[10] **15** and **16** should also be formed from **11e** by the ionic mechanism, since the free-radical mechanism containing the homolytic cleavage of the C–I bond should require the improbable formation of the extremely high-energy trifluoromethanesulfonyloxyl radical for the production of **16**. The following two routes for **15** and **16** can be thought as the possible ionic mechanism: (1) The addition of TfO^- to a phenyl nucleus followed by the elimination of the positive iodine atom, and (2) the combination of a phenyl cation generated and TfO^-. Since TfO^- is one of the strongest leaving groups, the nucleophilicity is extremely low.[11] Furthermore, if the mechanism of (1) is real, why doesn't process B that gives **20** and **14** occur rather than A which gives **15** and **16**? The reason is because a Rf group has a strong stabilizing effect on the intermediate anion at the α-position. Neither **20** nor **14** was produced. Accordingly, we

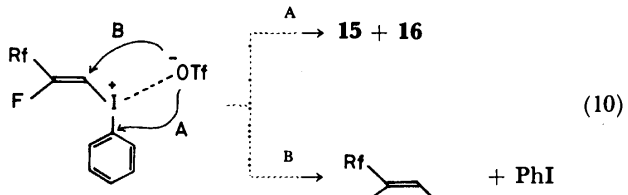

(10)

$$\mathbf{11} \longrightarrow \underset{\mathbf{15}}{RfCF{=}CHI} + \underbrace{[Ph^+] + {}^-OTf}_{\downarrow\ PhOTf\ \ \mathbf{16}} \quad (11)$$

propose the phenyl cation mechanism (2) (Eq. 11). The relatively easy formation of a phenyl cation compared to the fluorinated vinyl cation is surprising in view of the fact that a phenyl cation is much less stable than a nonfluorinated vinyl cation.[12] It would reflect the strong electronegative effect of a Rf group and a fluorine atom bonding to the vinyl moiety.

18 and **14** would also be formed from **17** by an ionic mechanism containing a Rf cation. However, it is unclear by which mechanism **19** was formed, ionic or free radical. Since such a compound as **19** was not produced in the case of **3**, the formation of **19** from **17** appears to be closely related to the difference in the electronegativity between Rf and $RfCH_2$ or in the easiness in the formation between their cations, Rf^+ and $RfCH_2^+$. Rf is more electronegative than $RfCH_2$[2] and, thus, Rf^+ is more difficult to generate than $RfCH_2^+$.

The mass spectra of **3** and **11** well reflected the strength of the bonds around the trivalent iodine atoms. All of **3** showed neither peaks corresponding to $[RfCH_2(Ph)I]^+$ nor ones corresponding to $[RfCH_2I]^+$, but base peaks or strong peaks of $[PhI]^+$. The peaks of $[RfCH_2OTf]^+$ were not observed in **3** and **7**. **5** and **6** showed small peaks of $[RfCH_2I]^+$ in addition to the base peak of $[PhI]^+$. On the other hand, all of **11** showed the strong peaks of $[RfCF{=}CHI]^+$ and $[PhOTf]^+$, and **11c** and **11e** exhibited the small peaks of $[RfCF{=}CHI(Ph)]^+$. The mass spectrum of **17** ($Rf=n\text{-}C_3F_7$) showed a strong peak of $[PhI]^+$ and a small peak of $[RfI(Ph)]^+$, but no peak of $[RfI]^+$. In this way, the fission pattern of the iodonium salts in the mass spectra is closely related to the bond strength order mentioned before. Since the mass spectra were measured at 100 °C, the spectrum of **3a** with a decomposition point of less than 100 °C may almost or partly consist of the decomposition products.

As expected from the thermolysis experiment, **3**, **11**, and **17** are very different from each other regarding reactivity. As reported, **3** reacted with phenoxide, alkoxide, and alkanethiolate anions to give *1H,1H*-perfluoroalkyl phenyl ether **21a**, alkyl ether **21b**, and alkyl sulfide **21c** in good yields, respectively,[10]

indicating an easy heterolytic fission of the C–I bonds of **3**. However, the treatment of **11b** with phenoxide and 2-phenylethoxide anions gave [[2-phenoxy- and 2-phenylethoxy-2-trifluoromethyl]vinyl]phenyliodonium triflates, **22** and **23**, in 42 and 32% yields, respectively. This should be due to a strong C–I bonding around the iodine atom of **11**. **22** was one

$$\mathbf{3} \xrightarrow{RX^-} RXCH_2Rf \qquad (12)$$

21a (X=O, R=Ph)
21b (X=O, R=CH_2CH_2Ph)
21c (X=S, R=n-$C_{12}H_{25}$)

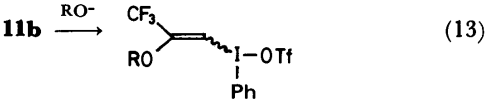

(13)

22 (42%, R=Ph)
23 (32%, R=CH_2CH_2Ph)

isomer and **23** was a 12:88 mixture of two isomers. The structures could not be determined. On the other hand, it is interesting that **11b** reacted with an arenethiolate anion to afford monosulfide **24** and disulfide **25** in 16 and 32% yields, respectively, as a

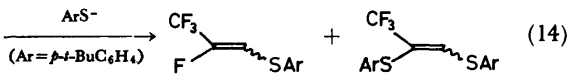

(14)

24(16%, E/Z=1/4) **25**(32%, E/Z or Z/E=1/6)

mixture of each two structural isomers. Although the detailed reaction mechanism is unclear, the difference between the oxide and the thiolate anions may be attributed to the high nucleophilicity of the thiolate anion since **11** has a double bond activated with two leaving groups, a fluorine atom and the polarized iodine atom.

3 are quite different from **17** in their reactivities. The treatment of **17** with an alkoxide produced no perfluoroalkyl ether, but a decomposition of **17** occurred.[3b] However, **17** reacted with arenethiols and alkanethiols in the presence of a base in dichloromethane to give perfluoroalkyl aryl and alkyl sulfides in good yields.[3b,13] **17** smoothly reacted with phenol in the presence of a base to afford a mixture of *o*-, *m*-, and *p*-Rf-phenyls **25** in a 55% yield with a ratio of 4.1:1:4.6, but not an ether, RfOPh[3b,14] (Eq. 15). With phenols having bulky substituents, **17** gave the

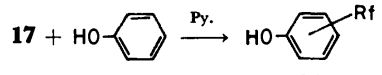

(15)

25

perfluoroalkyl ethers along with the *C*-perfluoroalkylated phenols.[15] As mentioned above, **3** reacted only at the oxygen site of the phenoxide anion, but **3** reacted with the anion of phenol having an electron-donating substituent to give a small amount of *C*-$RfCH_2$-phenol in addition to *O*-$RfCH_2$-phenol.[16] Whereas **3** reacted with aniline derivatives at the nitrogen sites to give *N*-$RfCH_2$-anilines or *N*-$RfCH_2$-anilinium triflates,[10] **17** underwent a displacement at the aromatic ring to give a mixture of *o*- and *p*-Rf-aniline derivatives.[3b,14] **17** showed a higher reactivity than **3** as follows: **3** did not react with alkenes such as styrene and butadiene, while **17** reacted smoothly with them to give Rf-alkenes in good yields, and **17** reacted much more smoothly with aromatic compounds than **3**.[3b,10,14]

As a whole, the reaction pattern of **3**, **11**, and **17** agrees with the bond strength order mentioned before. Namely, $RfCH_2$–I and Rf–I bonds of **3** and **17** are easily broken and the cleavage of the corresponding bonds of **11** is difficult. The above results also reveal that the pattern depends not only on the nature of the iodine compounds but also on the reactants. The remarkable difference between **3** and **17** might finally be attributed to the easy formation of $RfCH_2^+$ compared to Rf^+ cations, or to the high electron deficiency at the iodine sites of **17** due to the high electronegativity of the Rf groups, compared to that of **3**.

The predominant fluoroalkylation of **3** at the O- and N-sites of phenols and anilines and the preferential reaction of **17** at the C-sites may suggest that, while **3** could be directly attacked by nucleophiles at highly positively polarized CH_2 carbon sites, the reactions of **17** might be initiated preferably by a one-electron transfer[17] from the nucleophiles to the iodine sites, resulting in the homolytic fission of Rf–I bonds, because of the difficulty in the formation of Rf^+ species.

In conclusion, the presented results show that the properties and reactivity of the trivalent iodine compounds vary to a remarkable degree depending on the static or dynamic properties of the fluoro-alkyl or -alkenyl groups bonding to the iodine atoms.

Experimental

General. Melting points were uncorrected. ^1H NMR spectra were recorded with a Varian XL-100 NMR spectrometer, a Varian EM 390 NMR spectrometer, or a Bruker AM-400 NMR spectrometer with tetramethylsilane as an internal standard. ^{19}F NMR spectra were measured with a Varian XL-100 NMR spectrometer or a Hitachi R-20B NMR spectrometer. ^{19}F NMR chemical shifts were reported in ppm upfield from trichlorofluoromethane as an internal standard. IR spectra were measured on a Jasco A-202 diffraction grating infrared spectrometer. Mass spectra were recorded on a Hitachi RMU-6MG spectrometer at 70 eV and 100 °C.

Materials. 1,1,1-Trifluoro-2-iodoethane is commercially available. Other 1-iodo-1*H*,1*H*-perfluoroalkanes and 1-iodo-1*H*,1*H*,ωH-perfluorododecane were prepared from 1*H*,1*H*- and 1*H*,1*H*,ωH-perfluoro-1-alkanols, respectively, according to the reported method.[18] Diiodide **8** was

similarly prepared from the corresponding diol. 2,3,3,3-Tetrafluoro-2-trifluoromethyl-1-propanol was prepared by the reduction with lithium aluminium hydride from perfluoroisobutyric acid which was prepared from 2-iodoperfluoropropane according to the reported method.[19]

(Polyfluoroalkyl)aryliodonium salts 3, 4, 5, 6, and 7. General Procedure; Into a mixture of 82 ml of trifluoroacetic anhydride and 0.7 ml of trifluoroacetic acid was dropwise added 6.45 ml of 60% aq hydrogen peroxide with stirring under cooling on an ice bath. After stirring for additional 10 min, 1-iodopolyfluoroalkane (143 mmol) was added into the mixture. The reaction mixture was stirred for 1 day at 0 °C to room temperature, and evaporated up to dryness to give almost quantitatively 1-[bis(trifluoroacetoxy)iodo]polyfluoroalkane **2** as a white solid. An arene (189 mmol) and a sulfonic acid (122 mmol) were added into a mixture of 122 mmol of **2** in 150 ml of 1,1,2-trichloro-1,2,2-trifluoroethane at 0 °C and it was stirred for 1 day at 0 °C. The reaction mixture was evaporated up to dryness and the resulting solid was washed with chloroform to give pure crystals of an iodonium salt. For further purification the crystals were recrystallized from acetonitrile or acetonitrile–ether at room temperature. **3a**: 88% yield; mp 88—89 °C (decomp); ^{1}H NMR (CD_3CN) δ=4.80 (2H, q, J=10 Hz, CH_2), 7.40—7.90 (3H, m, ArH), 8.00—8.30 (2H, m, ArH); ^{19}F NMR (CD_3CN) 61.5 (3F, t, J=10 Hz, CF_3), 77.9 (3F, s, CF_3S); IR (KBr), 3060, 3040, 2970, 1565, 1470, 1440, 1400, 1280, 1240, 1195, 1170, 1120, 1040, 985, 840, 760, 730, 680, 650, 620 cm^{-1}; MS m/z 204 (PhI^+, 100%). Found: C, 25.03; H, 1.51%. Calcd for $C_9H_7F_6IO_3S$: C, 24.79; H, 1.62%. **3b**: 72% yield; mp 130 °C (decomp); ^{1}H NMR (acetone-d_6) δ=5.20 (2H, t, J=18 Hz, CH_2), 7.46—7.96 (3H, m, ArH), 8.26—8.50 (2H, m, ArH); ^{19}F NMR (acetone-d_6) 77.3 (3F, s, CF_3S), 82.7 (3F, m, CF_3), 106.5 (2F, t, J=18 Hz, CF_2); IR (KBr), 3040, 2980, 1570, 1480, 1445, 1410, 1340, 1220, 1180, 1050, 1015, 995, 920, 790, 735, 710, 680, 650, 630, 575, 520 cm^{-1}; MS m/z 204 (PhI^+, 100%). Found: C, 24.78; H, 1.19%. Calcd for $C_{10}H_7F_8IO_3S$: C, 24.70; H, 1.45%. **3c**: 70% yield; mp 133 °C (decomp); ^{1}H NMR (CD_3CN) δ=4.80 (2H, t, J=18 Hz, CH_2), 7.60—7.95 (3H, m, ArH), 8.10—8.30 (2H, m, ArH); ^{19}F NMR (CD_3CN) 80.8 (3F, s, CF_3S), 82.6 (3F, t, J=15 Hz, CF_3), 107.2 (2F, m, CF_2), 128.1 (2F, m, CF_2); IR (KBr) 3070, 3050, 1570, 1480, 1440, 1410, 1350, 1250, 1180, 1110, 1030, 960, 930, 770, 740, 680, 650, 580, 510 cm^{-1}; MS m/z 204 (PhI^+, 100%). Found: C, 24.39; H, 1.24%. Calcd for $C_{11}H_7F_{10}IO_3S$: C, 24.64; H, 1.32%. **3d**: 77% yield; mp 151 °C (decomp); ^{1}H NMR (CD_3CN) δ=4.88 (2H, d, J=18 Hz, CH_2), 7.46—7.94 (3H, m, ArH), 8.06—8.30 (2H, m, ArH); ^{19}F NMR (CD_3CN) 74.3 (6F, d, J=8.5 Hz, CF_3), 77.6 (3F, s, CF_3S), 167.3 (1F, m, F); IR (KBr) 3100, 3080, 3040, 2980, 1580, 1570, 1475, 1440, 1410, 1330, 1300, 1280, 1240, 1170, 1140, 1020, 990, 965, 915, 800, 770, 730, 720, 675, 650, 630, 570, 540, 515 cm^{-1}. Found: C, 24.67; H, 1.43%. Calcd for $C_{11}H_7F_{10}IO_3S$: C, 24.54; H, 1.32%. **3e**: 89% yield; mp 142—143 °C (decomp); ^{1}H NMR (CD_3CN) δ=4.83 (2H, t, J=18 Hz, CH_2), 7.40—7.80 (3H, m, ArH), 8.05—8.25 (2H, m, ArH); ^{19}F NMR (CD_3CN) 78.0 (3F, s, CF_3S), 80.6 (3F, t, J=10 Hz, CF_3), 102.8 (2F, m, CF_2), 120.8 (8F, m, CF_2), 124.9 (2F, m, CF_2); IR (KBr) 3070, 3000, 1480, 1450, 1410, 1370, 1250, 1100, 1060, 1030, 1010, 890, 770, 750, 710, 640, 520 cm^{-1}; MS m/z 204 (PhI^+, 40%), 69 (CF_3^+, 100%). Found: C, 24.38; H, 0.85%. Calcd for $C_{15}H_7F_{18}IO_3S$: C, 24.48; H, 0.96%. **4**: 72% yield; mp 103—104 °C (decomp); ^{1}H NMR (CD_3CN) δ=4.77 (2H, q, J=10 Hz, CH_2), 7.33 (2H, dd, J=9, 9 Hz, ArH), 8.20 (2H, dd, J=9, 4.5 Hz, ArH); ^{19}F NMR (CD_3CN) 61.1 (3F, t, J=10 Hz, CF_3), 77.5 (3F, s, CF_3S), 102.8 (1F, bs, ArF); IR (KBr) 3050, 2980, 1583, 1490, 1261, 1180, 1035, 825, 650, 645, 578, 525 cm^{-1}. Found: C, 23.68; H, 1.16%. Calcd for $C_9H_6F_7IO_3S$: C, 23.81; H, 1.33%. **5**: 95% yield; mp 107 °C (decomp); ^{1}H NMR (CD_3CN) δ=4.83 (2H, t, J=18 Hz, CH_2), 7.40—7.90 (3H, m, ArH), 8.10—8.30 (2H, m, ArH); ^{19}F NMR (CD_3CN) −38.5 (1F, s, FSO_2), 80.3 (3F, t, J=10 Hz, CF_3), 103.2 (2F, m, CF_2), 120.8 (6F, m, CF_2), 122.0 (2F, m, CF_2), 125.5 (2F, m, CF_2); IR (KBr) 3070, 3000, 1480, 1440, 1400, 1370, 1280, 1220, 1140, 1100, 1070, 1010, 990, 740, 710, 670, 590 cm^{-1}; MS m/z 510 ($C_7F_{15}CH_2I^+$, 1.3%), 204 (PhI^+, 100%). Found: C, 24.24; H, 0.96%. Calcd for $C_{14}H_7F_{16}IO_3S$: C, 24.51; H, 1.03%. **6**: 49% yield; mp 90—91 °C (decomp); ^{1}H NMR (acetone-d_6) δ=5.16 (2H, t, J=18 Hz, CH_2), 5.30 (broad peak, OH), 7.40—7.80 (3H, m, ArH), 8.20—8.40 (2H, m, ArH); ^{19}F NMR (DMSO-d_6) 80.0 (3F, t, J=10 Hz, CF_3), 120.5 (2F, m, CF_2), 121.6 (4F, m, CF_2), 122.2 (2F, m, CF_2), 122.8 (2F, m, CF_2), 125.6 (2F, m, CF_2); IR (KBr) 3450, 3080, 3050, 2970, 1580, 1480, 1460, 1410, 1370, 1320, 1210, 1150, 1100, 1050, 1010, 890, 730, 710, 660, 590, 530 cm^{-1}; MS m/z 510 ($C_7F_{15}CH_2I^+$, 25%), 204 (PhI^+, 100%). Found: C, 23.73; H, 1.25%. Calcd for $C_{14}H_{10}F_{15}IO_5S$ (as monohydrate): C, 23.95; H, 1.44%. **7**: 85% yield; mp 157—158 °C; ^{1}H NMR (CD_3CN) δ=4.92 (2H, t, J=18 Hz, CH_2), 6.52 (1H, dd, J=51.0, 4.8 Hz, CF_2H), 7.5—8.32 (5H, m, ArH); ^{19}F NMR (CD_3CN) 78.1 (3F, s, CF_3), 103.1 (2F, m, CF_2) 120.2—123.1 (14F, m, CF_2), 128.7 (2F, m, CF_2), 137.8 (2F, d, J=51 Hz, CF_2H); MS m/z 204 (PhI^+, 36%), 69 (CF_3^+, 100%). Found: C, 24.80; H, 0.89%. Calcd for $C_{18}H_8F_{23}IO_3S$: C, 24.90; H, 0.93%.

The NMR data of the intermediate bis(trifluoroacetates) **2** are as follows. **2a**: ^{1}H NMR ($CDCl_3$) δ=4.92 (q, J=9 Hz, CH_2); ^{19}F NMR ($CDCl_3$) 62.9 (3F, t, J=9 Hz, CF_3CH_2), 73.4 (6F, s, CF_3). **2b**: ^{1}H NMR ($CDCl_3$) δ=4.93 (t, J=15 Hz, CH_2); ^{19}F NMR ($CDCl_3$) 74.1 (6F, s, CF_3CO), 83.8 (3F, s, CF_3), 109.8 (2F, t, J=15 Hz, CF_2). **2c**: ^{1}H NMR (CD_3CN) δ=5.03 (t, J=16.5 Hz, CH_2); ^{19}F NMR (CD_3CN) 74.3 (6F, s, CF_3CO), 80.3 (3F, s, CF_3), 105.4 (2F, s, CF_2), 125.3 (2F, s, CF_2). **2d**: ^{1}H NMR (CD_3CN) δ=5.25 (d, J=16.5 Hz, CH_2); ^{19}F NMR (CD_3CN) 72.8 (6F, s, CF_3CO), 75.0 (6F, d, J=8.5 Hz, CF_3), 169.5 (1F, m, F). **2e**: ^{1}H NMR (CD_3CN) δ=5.13 (t, J=18 Hz, CH_2); ^{19}F NMR (CD_3CN) 74.3 (6F, s, CF_3CO), 81.0 (3F, s, CF_3), 104.3 (2F, m, CF_2), 120.8 (8F, m, CF_2), 124.5 (2F, m, CF_2).

(1*H*,1*H*,5*H*,5*H*-Perfluoropentane-1,5-diyl)bisphenylbisiodonium Triflate 9. The procedure was the same as for **3—7** except for the use of double the quantity of trifluoroperacetic acid, benzene, and triflic acid. **9**: 96% yield; mp 113—114 °C (decomp); ^{1}H NMR (CD_3CN) δ=4.80 (4H, t, J=18 Hz, CH_2), 7.40—7.90 (6H, m, ArH), 8.00—8.20 (4H, m, ArH); ^{19}F NMR (CD_3CN) 78.0 (6F, s, CF_3), 102.6 (4F, m, CF_2CH_2), 120.9 (2F, s, CF_2); IR (KBr) 3080, 1580, 1480, 1440, 1430, 1410, 1260, 1180, 1040, 890, 740, 660, 640, 530 cm^{-1}; MS m/z 432 [$ICH_2(CF_2)_3CH_2I^+$, 1.4%], 204 (PhI^+, 100%). Found: C, 25.63; H, 1.60%. Calcd for $C_{19}H_{14}F_{12}I_2O_6S_2$: C, 25.81; H, 1.60%.

Dehydrofluorination of 3b, 3c, and 3e. General Procedure; Into a solution of 1 mmol of **3** in 7 ml of acetonitrile was added 1 mmol of sodium hydride (50% in oil) at 0 °C with stirring under argon atmosphere. The reaction mixture was stirred for 30 min, filtered with celite, and

evaporated up to dryness. The resulting solid was recrystallized from 1,2-dichloroethane. **11b**: 80% yield; mp 127—128 °C; ^{1}H NMR (acetone-d_6) δ=7.50—7.90 (3H, m, ArH), 8.20—8.50 (2H, m, ArH), 8.20 (1H, d, J=33 Hz, vinyl proton); ^{19}F NMR (acetone-d_6) 71.3 (3F, d, J=10 Hz, CF_3), 77.6 (3F, s, CF_3S), 99.8 (1F, dq, J=33, 10 Hz, vinyl F); IR (KBr) 3100, 1680, 1475, 1455, 1340, 1270, 1250, 1220, 1170, 1160, 1040, 1020, 990, 820, 740, 720, 675, 650, 630 cm^{-1}; MS m/z 240 (CF_3CF=CHI^+, 100%), 226 ($PhOTf^+$, 40%), 204 (PhI^+, 19%). Found: C, 25.49; H, 1.10%. Calcd for $C_{10}H_6F_7IO_3S$: C, 25.77; H, 1.30%. **11c**: 86% yield; mp 144 °C; ^{1}H NMR (acetone-d_6) δ=7.33—8.10 (3H, m, ArH), 8.20—8.70 (2H, m, ArH), 8.26 (1H, d, J=33 Hz, vinyl proton); ^{19}F NMR (acetone-d_6) 78.0 (3F, s, CF_3S), 83.1 (3F, dt, J=6, 2 Hz, CF_3), 96.2 (1F, dtq, J=33, 14.5, 6 Hz, vinyl F), 120.1 (2F, dq, J=14.5, 2 Hz, CF_2); IR (KBr) 3070, 3040, 1680, 1570, 1475, 1445, 1325, 1315, 1275, 1250, 1230, 1180, 1090, 1040, 1020, 995, 730, 670, 650, 630 cm^{-1}; MS m/z 367 (C_2F_5CF=$CHIPh^+$, 1.4%), 290 (C_2F_5CF=CHI^+, 100%), 226 ($PhOTf^+$, 52%), 204 (PhI^+, 25%). Found: C, 25.15; H, 1.10%. Calcd for $C_{11}H_6F_9IO_3S$: C, 25.60; H, 1.17%. **11e**: 87% yield; mp 128—130 °C; ^{1}H NMR (acetone-d_6) δ=7.50—7.96 (3H, m, ArH), 8.32 (1H, d, J=33 Hz, vinyl proton), 8.30—8.50 (2H, m, ArH); ^{19}F NMR (acetone-d_6) 78.0 (3F, s, CF_3S), 80.5 (3F, m, CF_3), 95.0 (1F, m, vinyl F), 116.0 (2F, m, CF_2), 121.3 (2F, m, CF_2), 122.1 (4F, m, CF_2), 125.6 (2F, m, CF_2); IR (neat) 3130, 3080, 1670, 1590, 1570, 1475, 1450, 1370, 1250, 1200, 1180, 1145, 1090, 1030, 990, 950, 920, 850, 800, 790, 760, 740, 720, 680, 650, 640 cm^{-1}; MS m/z 567 ($C_6F_{13}CF$=$CHIPh^+$, 10%), 490 ($C_6F_{13}CF$=CHI^+, 32%), 226 ($PhOTf^+$, 100%), 204 (PhI^+, 40%). Found: C, 24.97; H, 0.75%. Calcd for $C_{15}H_6F_{17}IO_3S$: C, 25.16; H, 0.84%.

Thermolysis of 3e. The crystals of **3e** was heated at 140—145 °C for 10 min under atmospheric pressure. The decomposition products were separated by column chromatography on silica gel with pentane as an eluent. The structural assignment of the products **13** and **14** was carried out by the comparison with authentic samples.

Thermolysis of 11e. The crystals of **11e** was heated at 200 °C under pressure of 180 mmHg (1 mmHg=133.322 Pa) by using a glass tube oven. The decomposition products **15** and **16** condensed at the cooled part of the glass tube and their yields were determined by ^{19}F NMR technique. Each of the products was isolated by the usual method. **15**: 79% yield, oil, ^{1}H NMR ($CDCl_3$) δ=6.63 (1H, J=31 Hz, vinyl proton); ^{19}F NMR ($CDCl_3$) 81.6 (3F, s, CF_3), 103.3 (1F, m, CF), 116.7 (2F, m, CF_2), 122.7 (2F, m, CF_2), 123.4 (4F, m, CF_2), 126.9 (2F, m, CF_2); IR (neat) 3120, 1670, 1370, 1320, 1300, 1240, 1200, 1150, 1125, 1090, 1040, 1020, 840, 795, 735, 710, 655 cm^{-1}; MS m/z 490 (M^+). **16**: 76% yield, oil, ^{1}H NMR ($CDCl_3$) δ=7.10—7.70 (5H, m); ^{19}F NMR ($CDCl_3$) 73.1 (s, CF_3); IR (neat) 3080, 1605, 1590, 1490, 1420, 1250, 1210, 1140, 1070, 1020, 910, 880, 780, 760, 730, 680, 620, 600 cm^{-1}; MS m/z 226 (M^+).

Reaction of 11b with Sodium Phenoxide. Under argon atmosphere, 0.667 mmol of sodium hydride (50% in oil) was added into a solution of 0.667 mmol of phenol in 2 ml of dichloromethane and the mixture was stirred for 5 min. **11b** (0.606 mmol) was added and the mixture was stirred for 30 min at 0 °C. Then the reaction mixture was filtered with celite and evaporated up to dryness. The resulting solid was recrystallized from dichloromethane–diethyl ether–pentane to give **22** in a 42% yield. **22**: mp 86—87 °C; ^{1}H NMR (400 MHz, $CDCl_3$) δ=6.94—7.00 (2H, m, ArH), 7.20—7.63 (6H, m, ArH), 7.43 (1H, s, vinyl proton), 7.90—7.96 (2H, m, ArH); ^{19}F NMR ($CDCl_3$) 66.8 (3F, s, CF_3), 78.8 (3F, s, CF_3S); IR (KBr) 3100, 1640, 1590, 1490, 1440, 1320, 1280, 1250, 1210, 1160, 1060, 1030, 990, 860, 790, 730, 635 cm^{-1}; MS m/z 314 [$CF_3(PhO)C$=CHI^+]. Found: C, 35.35; H, 1.95%. Calcd for $C_{16}H_{11}F_6IO_4S$: C, 35.58; H, 2.05%.

Reaction of 11b with Sodium 2-Phenylethoxide. The procedure was similar to the above case. The crude product was recrystallized from ethyl acetate–pentane to give **23** as a mixture of E- and Z-isomers in a 32% yield. **23**: mp 62—63 °C (a 88:12 or 12:88 mixture of E- and Z-isomers); ^{1}H NMR (400 MHz, $CDCl_3$) A:B component=88:12, A component; δ=3.07 (2H, t, J=6.7 Hz, benzyl protons), 4.44 (2H, td, J=6.8, 0.7 Hz, allyl protons), 6.91 (1H, s, vinyl proton), 7.74—7.80 (2H, m, ArH), B component; δ=3.06 (2H, t, J=6.4 Hz, benzyl protons), 4.23 (2H, t, J=6.5 Hz, allyl protons), 6.74 (1H, s, vinyl proton), 7.98—8.02 (2H, m, ArH), A+B component; δ=7.15—7.62 (m, ArH); ^{19}F NMR ($CDCl_3$) A:B component=88:12, A component; 66.0 (3F, s, CF_3), 78.8 (3F, s, CF_3S), B component; 65.2 (3F, s, CF_3), 78.8 (3F, s, CF_3S); IR (KBr) 3080, 1620, 1560, 1500, 1470, 1440, 1325, 1270, 1250, 1190, 1160, 1090, 1050, 1030, 990, 730, 700, 660, 630 cm^{-1}. Found: C, 37.93; H, 2.65%. Calcd for $C_{18}H_{15}F_6IO_4S$: C, 38.04; H, 2.66%.

Reaction of 11b with Sodium *p*-*t*-Butylbenzenethiolate. In analogy with that described above, **11b** was treated with sodium *p*-*t*-butylbenzenethiolate in dichloromethane at 0 °C for 1 h, which was prepared in situ from *p*-*t*-butylbenzenethiol and sodium hydride. The usual post-treatment and then thin-layer chromatography gave **24** and **25** in 16 and 32% yields, respectively. **24**: A 78:22 mixture of Z- and E-isomers; oil, ^{1}H NMR ($CDCl_3$) Z-isomer; δ=1.40 (9H, s, *t*-Bu), 6.38 (1H, d, J=31.5 Hz, vinyl proton), 6.85—7.30 (3H, m, ArH), 7.56—7.75 (2H, m, ArH), E-isomer; δ=1.40 (9H, s. *t*-Bu), 6.48 (1H, d, J=19.5 Hz, vinyl proton), 6.85—7.35 (3H, m, ArH), 7.56—7.75 (2H, m, ArH); ^{19}F NMR ($CDCl_3$) Z-isomer; 72.1 (3F, d, J=13 Hz, CF_3), 131.6 (1F, dq, J=31.5, 13 Hz, vinyl F), E-isomer; 68.7 (3F, d, J=10 Hz, CF_3), 128.2 (1F, dq, J=19.5, 10 Hz, vinyl F); IR (KBr) 3090, 2980, 2880, 1500, 1350, 1240, 1190, 1140, 1060, 1010, 840 cm^{-1}; MS m/z 278 (M^+). Found: C, 56.01; H, 5.15%. Calcd for $C_{13}H_{14}F_4S$: C, 56.10; H, 5.07%. **25**: A 86:14 mixture of two isomers A and B; bp 230 °C/5 mmHg (using a glass tube oven); ^{1}H NMR ($CDCl_3$) δ=1.31 (18H, s, *t*-Bu), 7.20—7.50 (8H, m, ArH), 7.78 (1H, bs, vinyl proton); ^{19}F NMR ($CDCl_3$) A isomer; 64.1 (s, CF_3), B isomer; 56.6 (s, CF_3); IR (KBr) 3100, 2980, 2920, 2890, 1570, 1495, 1460, 1400, 1365, 1270, 1250, 1200, 1160, 1130, 1010, 960, 840, 825, 710, 650 cm^{-1}; MS m/z 424 (M^+). Found: C, 66.00; H, 6.78%. Calcd for $C_{23}H_{27}F_3S_2$: C, 65.05; H, 6.41%.

References

1) a) G. F. Koser, "The Chemistry of Functional Groups, Supplement D: The Chemistry of Halides, Pseudo-halides, and azides," ed by S. Patai and Z. Rappoport, John Willey & Sons, Chichester, (1983), Part 1, Chap. 18; b) *idem, ibid.*, Part 2, Chap. 25; c) A. Varvoglis, *Synthesis*, **1984**, 709; d) *idem, Chem. Soc. Rev.*, **1981**, 337; e) D. F. Banks, *Chem. Rev.*, **66**, 243 (1966); f) Recent papers; R. M. Moriarty, R. Penmasta, and I. Prakash, *Tetrahedron Lett.*, **28**, 877 (1987); W. B.

Farnham and J. C. Calabrese, *J. Am. Chem. Soc.*, **108**, 2449 (1986); H. J. Reich, N. H. Phillips, and I. L. Reich, *ibid.*, **107**, 4101 (1985) and references cited therein.

2) J. E. Huheey, *J. Phy. Chem.*, **69**, 3284 (1965).

3) a) T. Umemoto, Y. Kuriu, H. Shuyama, O. Miyano, and S. Nakayama, *J. Fluorine Chem.*, **31**, 37 (1986) and references cited therein. b) T. Umemoto, *Yuki Gosei Kagaku Kyokai Shi*, **41**, 251 (1983).

4) V. V. Lyalin, V. V. Orda, L. A. Alekseeva, and L. M. Yagupol'skii, *J. Org. Chem. USSR*, **8**, 1027 (1972).

5) Although iodonium salts are generally expressed as $>I^+X^-$, we represent our fluoroalkyl- and -alkenyliodonium sulfonates as $>I-OSO_2R'$ according to our consideration stated late in this paper.

6) N. Ishikawa, and M. Maruta, *Yuki Gosei Kagaku Kyokai Shi*, **39**, 51 (1985).

7) J. B. Dence and J. D. Roberts, *J. Org. Chem.*, **33**, 1251 (1968).

8) P. E. Peterson, P. R. Clifford, and F. J. Slama, *J. Am. Chem. Soc.*, **92**, 2840 (1970).

9) M. Ochiai, K. Sumi, Y. Nagao, and E. Fujita, *Tetrahedron Lett.*, **26**, 2351 (1985).

10) T. Umemoto and Y. Gotoh, *J. Fluorine Chem.*, **31**, 231 (1986).

11) P. J. Stang, M. Hanack, and L. R. Subramanian, *Synthesis*, **1982**, 85.

12) Y. Apeloig and D. Arad, *J. Am. Chem. Soc.*, **107**, 5285 (1985).

13) T. Umemoto and Y. Kuriu, *Chem. Lett.*, **1982**, 65.

14) T. Umemoto, Y. Kuriu, and H. Shuyama, *Chem. Lett.*, **1981**, 1663.

15) T. Umemoto and O. Miyano, *Bull. Chem. Soc. Jpn.*, **57**, 3361 (1984).

16) T. Umemoto and Y. Gotoh, in preparation.

17) T. Umemoto, Y. Kuriu, and S. Nakayama, *Tetrahedron Lett.*, **23**, 1169 (1982).

18) K. L. Paciorek, B. A. Merkl, and C. T. Lenk, *J. Org. Chem.*, **27**, 266 (1962); A. Meller, M. Wechsberg, and V. Gutman, *Monatsh. Chem.*, **96**, 388 (1965) and references cited therein.

19) N. Ishikawa, M. Takahashi, T. Sato, and T. Kitazume, *J. Fluorine Chem.*, **22**, 585 (1983).

 © 1987 The Chemical Society of Japan Bull. Chem. Soc. Jpn., 60, 3315—3320 (1987)

Electrochemical Synthesis of Poly(amino acid)s, Poly(amino acid)-Urethane Copolymers, and Electroconductive Poly(amino acid)-Polypyrrole Complex Films

Tetsuo KOMORI, Tsutomu NONAKA,* Toshio FUCHIGAMI, and Kunmao ZHANG†
Department of Electronic Chemistry, Tokyo Institute of Technology,
4259 Nagatsuta, Midoriku, Yokohama 227
†Department of Chemistry, Shanxi University,
Taiyuan City, People's Republic of China
(Received March 28, 1987)

When amino acid *N*-carboxy anhydrides (NCA's) were polymerized with various electrogenerated base (EGB) catalysts, the yield of poly(amino acid)s remarkably increased and the reaction time was extremely shortened compared with the conventional method using triethylamine catalyst. This novel polymerization method was successfully applied to the copolymerization of different kinds of NCA's and to the preparation of poly(amino acid)-urethane copolymers. NCA's were also polymerized with the EGB's in the matrix of polypyrrole simultaneously formed by the anodic polymerization of pyrrole to provide electroconductive poly(amino acid)-polypyrrole complex films which were stable in the air and flexible.

Poly(amino acid)s and their related polymers are widely used as synthetic leathers, medicines, medical materials, fibers, surfactants, and piezodevices. Poly(amino acid)s are commercially produced by the *N*-carboxy anhydride(NCA) method,[1] in which NCA's are polymerized with base catalysts such as primary and tertiary amines. It is well-known that the yield and quality of poly(amino acid)s are greatly affected by impurities in NCA's and kind of the base catalysts.[2] Since NCA's are usually prepared from amino acids and phosgene or trichloromethyl chloroformate(phosgene dimer), enormous efforts must be made to remove chlorine-contaminants from the NCA's, especially in the case of amino acid such as L-valine which is polymerized with difficulty.[2]

Recently, cathodically-generated anionic species, so-called electrogenerated bases(EGB's), have been widely used as reducing reagents, nucleophiles, and bases.[3] In our previous work,[4] it was found that the EGB catalysts polymerized valine NCA's much more efficiently than conventional catalyst such as triethylamine, though both catalysts would induce the polymerization in similar of reaction mechanism in which an initiation step is the abstraction of amido hydrogen of NCA's.[2] In this work, this cathodic polymerization was successfully extended to the preparation of a variety of homopoly (amino acid)s, copoly(amino acid)s, poly(amino acid)-urethane copolymers, and electroconductive poly(amino acid)-polypyrrole complex films.

Results and Discussion

EGB's are generated by the one-electron reduction of acidic hydrogen compounds (PB's) such as amides, carboxylic acids, phenols, alcohols, and carbon acids in general as shown below.[3].

$$\mathrm{XH} \xrightarrow[\mathrm{M^+Y^-}]{\mathrm{e}} \mathrm{X^-M^+} + \frac{1}{2}\mathrm{H_2} + \mathrm{Y^-}$$

(PB) (Supporting electrolyte) (EGB)
(X: N, O, C)

The reactivity of the EGB's thus formed is affected by their counter cations (M^+) coming from supporting electrolytes (M^+Y^-) used.[5,6] In this work, two methods for the polymerization of amino acid NCA's with EGB's were employed. In the first method (Method A), amides such as α-pyrrolidone,[7] ε-caprolactam, acetanilide and *N*-methylacetamide and a phenol such as 2,6-di-*t*-butyl-*p*-cresol[10] were cathodically reduced in dry THF solutions and then EGB solutions thus prepared were added to THF solutions of NCA's. In Method B, NCA's, themselves were used as probases (PB's) without any other PB's, since they have molecular structures of amides. No contamination of poly(amino acid)s by the catalysts used was expected in this case where the self-catalyzed polymerization should proceed. The polymerization seemed to proceed not only on the surface of cathode but also in the whole cathodic solution (divided cell). In addition to these methods,a conventional one was examined by using triethylamine as the catalyst under the similar conditions (Method C). In all these methods, 0.05 mol/mol-NCA of the EGB and amine catalysts were used. Amounts of EGB's used were controlled by the amounts of charge passed.

Electrochemical and Chemical Syntheses of Homopoly(amino acid)s. As shown in Fig. 1, L-valine NCA was reduced in a potential range less negative than the background solution. Therefore, the EGB catalyst in Method B seemed to be anion (**1**) generated by the reduction of the NCA itself rather than the supporting electrolyte.

Results of the polymerization of L-valine NCA using EGB catalysts generated from various PB's in

Method A are shown in Table 1. Among the PB's used, α-pyrrolidone gave the best result in either reaction time or yield, optical rotating power([α]D)

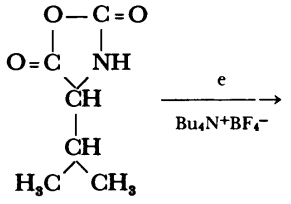

L-Valine NCA

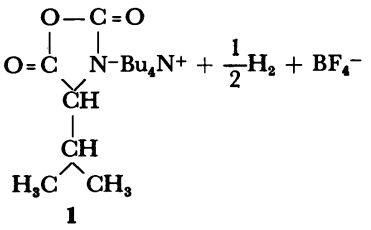

1

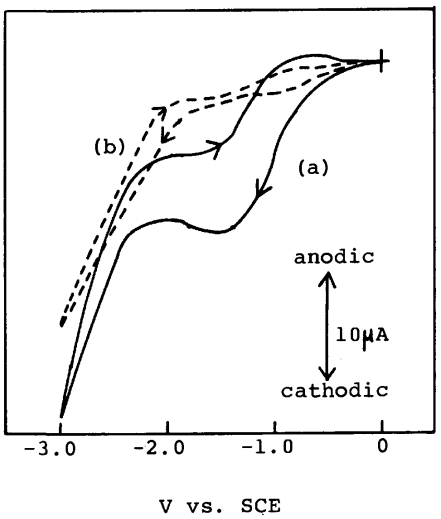

Fig. 1. Cyclic voltammogram of L-valine NCA at a platinum electrode (0.013 cm^2) in 0.1 mol dm^{-3} *n*-Bu_4NBF_4/THF. Scan rate, 0.1 V s^{-1}.
(a) 3.8 mmol dm^{-3} L-valine NCA. (b) Background.

and molecular weight (kinematic viscosity) of poly(L-valine) obtained. The largest value of $[\alpha]_D^{20}$ is 155° (in CF_3COOH).[11] The molecular weight could not be directly measured because of insolubility of poly(L-valine) in solvents other than CF_3COOH. A standard sample of poly(L-valine) (MW, 7200) which was commercially supplied from Sigma Chemical Co. showed 0.616×10^{-6} m^2 s^{-1} of kinematic viscosity in 0.5 w/v% CF_3COOH solution at 25°C. However, estimation of the molecular weight from the viscosity could not be performed for lack of a standard sample with a different MW. The secondary structure of poly(L-valine) obtained was confirmed to be β-coil form from IR-spectrum (an amido carbonyl band observed at 1630 cm^{-1}).[12]

As shown in Table 2, the EGB catalysts with Na^+ as their counter cations did not induced the polymerization of L-valine NCA. This fact is rationalized as due to low basicity of the EGB's with hard counter cations such as Na^+ of high Lewis acidity.[5] Inferior results obtained with the catalysts with *n*-Oct_4N^+ counter cation to those with *n*-Bu_4N^+ may be due to steric hindrance effect.

Results of the polymerization of various NCA's by the electrochemical (Methods A and B using α-pyrrolidone as PB and *n*-Bu_4N^+ as counter cation) and

Tabld 1. Polymerization of L-Valine NCA Using EGB Catalysts[a] Generated from Various PB's (Method A)

PB	Reaction time/h	Poly(L-valine)		
		Yield/%	$[\alpha]_D^{20}$/°	Kinematic viscocity /10^{-6} m^2 s^{-1}
α-Pyrrolidone[b]	0.02	98	−110	0.708
ε-Caprolactam	2	58	−95	0.676
N-Methylacetamide	2	26	−96	0.598
Acetanilide	2	16	−80	0.640
2,6-Di-*t*-butyl-*p*-cresol	2	19	−87	0.657

a) With Bu_4N^+ counter cation. b) Charge required to generate 0.02 mol/mol-NCA of EGB was passed.

Table 2. Influence of Counter Cations of EGB Catalysts on the Polymerization of L-Valine NCA by Methods A and B

Method	PB	Counter cation	Reaction time/h	Poly(L-valine)		
				Yield/%	$[\alpha]_D^{20}$/°	Kinematic viscosity /10^{-6} m^2 s^{-1}
A	α-Pyrrolidone	Na^+	2	7	−82	—[a]
A[b]	α-Pyrrolidone	*n*-Bu_4N^+	0.02	98	−110	0.708
A	α-Pyrrolidone	*n*-Oct_4N^+	2	50	−95	0.681
B	L-Valine NCA	Na^+	2	4	−101	—[a]
B	L-Valine NCA	*n*-Bu_4N^+	2	59	−120	0.670
B	L-Valine NCA	*n*-Oct_4N^+	2	55	−100	0.639

a) Not measured. b) Charge required to generate 0.02 mol/mol-NCA of EGB was passed.

chemical (Method C using triethylamine as base catalyst) methods are summarized in Table 3 for comparison. The Methods A and B were clearly superior to Method C in terms of reaction time and yield, while Method C gave poly(L-valine) and poly(L-leucine) with somewhat larger values of $[\alpha]_D^{20}$ than other methods. It is noticeable that *N*-methylglycine NCA without any acidic amido hydrogen atom could be polymerized by Method B. This NCA can not be polymerized with tertiary amine catalysts.[2] These facts may suggest possible cathodic formation of unknown effective catalyst other than *n*-Bu_3N which can be generated by electroreductive decomposition of *n*-Bu_4N^+. Therefore, polymerization mechanism in this case would be quite different from that in cases of other amino acid NCA's.

The molecular weight($\bar{M}n$) of poly(γ-benzyl L-glutamate) soluble in THF was estimated to be 1730

Table 3. Electrochemical and Chemical Polymerization of Amino Acid NCA's with EGB and Triethylamine Catalysts, Respectively

Amino acid	Method	Reaction time/h	Poly(amino acid)		
			Yield/%	$[\alpha]_D^{25}$/°	Kinematic viscosity /10^{-6} m^2 s^{-1}
L-Valine	A[a,b]	0.02	98	−110	0.708
L-Valine	B	2	59	−120	0.670
L-Valine	C	96	17	−145	0.654
D-Valine	A[a]	0.25	45	+94	0.699
D-Valine	B	2	93	+115	0.748
D-Valine	C	96	84	+100	0.711
DL-Valine	B	2	70	—	0.631
L-Leucine	A[a,c]	2	74	−109	0.711
L-Leucine	C	96	38	−124	—[d]
γ-Benzyl L-glutamate	B[b]	0.63	78	+22	—[d]
L-Tryptophan	B	2	36	—[e]	—[e]
L-Tryptophan	C	96	34	—[e]	—[e]
DL-Phenylalanine	A[f]	1.3	90	—	0.625
DL-Phenylalanine	B[f]	1.3	65	—	0.607
DL-Methionine	A	0.4	49	—	0.622
DL-Methionine	B	0.4	30	—	0.596
N-Methylglycine	B[g]	0.5	65	—	—[d]

a) α-Pyrrolidone was used as a PB. b) 0.01 mol/mol-NCA of catalyst was used. c) 0.02 mol/mol-NCA of catalyst was used. d) Not measured. e) Could not be measured because of insolubility. f) 0.1 mol dm^{-3} Et_4NOTs/DMF was used as an electrolytic solution. g) 0.08 mol/mol-NCA of catalyst was used.

Table 4. Electrochemical and Chemical Copolymerization of Amino Acid NCA's with EGB and Triethylamine Catalyst, Respectively

NCA		Method[a]	Copoly(amino acid)	
a+b	Mol. ratio a : b		Yield[b] /wt%	Mol. ratio[c] a : b
L-Leucine+γ-Benzyl L-glutamate	4 : 1	A	82	3 : 1
L-Leucine+γ-Benzyl L-glutamate	4 : 1	B	87	3 : 1
L-Leucine+γ-Benzyl L-glutamate	2 : 1	B	85	2 : 1
L-Leucine+γ-Benzyl L-glutamate	1 : 4	B	36	1 : 5
L-Leucine+γ-Benzyl L-glutamate	4 : 1	C	50	4 : 1
L-Valine+γ-Benzyl L-glutamate	1 : 1	A	57	1 : 2
L-Valine+γ-Benzyl L-glutamate	1 : 4	B	35	1 : 2
L-Valine+γ-Benzyl L-glutamate	1 : 1	C	38	1 : 2
DL-Valine+DL-Alanine	1 : 1	A	20	—[d]
DL-Valine+DL-Alanine	1 : 1	B	30	—[d]
DL-Valine+DL-Alanine	1 : 1	C	20	—[d]

a) Reaction time, 2 h. b) {[(a+b)(wt.) in copoly(amino acid)]/[(a+b)(wt.) in starting NCA's]}×100(%). c) Approximately estimated from ^{1}H-NMR. d) Not determined.

(polystyrene standard) by GPC. The secondary structures of poly(D-valine), poly(L-leucine) and poly(L-tryptophan) were confirmed to be β-, α helix- and α-forms, respectively, from IR spectra.[12]

Electrochemical and Chemical Syntheses of Copoly (amino acid)s. The coplymerization of mixtures of amino acid NCA's was carried out in a manner similar to the homopolymerization in Table 3. As shown in Table 4, Methods A an B gave higher yields of copoly(amino acid)s than Method C. Properties of copoly(amino acid)s can be varied by changing either the combination or composition ratio, or both amino acid components. The composition ratio in copoly(amino acid)s formed was approximately equal to those of the starting mixtures of NCA's. It was confirmed that the copoly(amino acid)s with γ-benzyl L-glutamate could be cast from their benzene solutions to provide flexible transparent films, though their molecular weights and secondary structures were not determined. It has been also remained unknown whether the copoly(amino acid)s are homogeneous or block copolymers.

Electrochemical and Chemical Syntheses of Poly(amino acid)–Urethane Block Copolymers. Improvement of properties of poly(amino acid)s can also be achieved by the block copolymerization of amino acid NCA's with urethane prepolymers (**2**).[2,13] The copolymerization was carried out in the presence of **2**(n, ca. 28) in a manner similar to the homopolymerization in Table 3 and the corresponding poly(amino acid)-urethane block copolymers(**3**) were obtained.

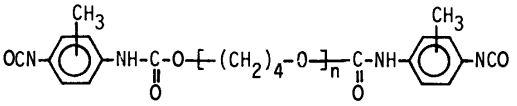

Urethane prepolymer (**2**)

As shown in Table 5, Methods A and/or B gave higher yields of the block copolymers than Method C. Molar ratios of amino acid components to the urethane prepolymer in the block copolymers thus obtained were almost equal to those in the starting mixtures in all the methods. The copolymers with γ-benzyl L-glutamate were able to cast from their THF solutions to provide flexible films. The molecular weight of a poly(γ-benzyl L-glutamate)–urethane copolymer with 17 of molar ratio of γ-benzyl L-glutamate to the urethane prepolymer was determined to be $\bar{M}$n 7900 and $\bar{M}$w 21100 (polystyrene standard) by GPC.

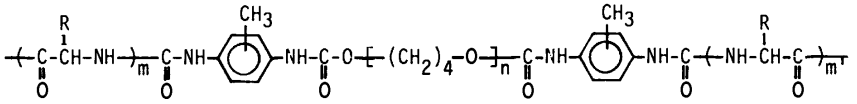

Poly(amino acid)-urethane block copolymer (**3**)

Table 5. Electrochemical and Chemical Block Copolymerization of Amino Acid NCA's with an Urethane Prepolymer (2; n, ca. 28) with EGB and Triethylamine Catalysts, Respectively

NCA		Method[a]	Poly(amino acid)-urethane block copolymer	
Amino acid	Mol. ratio to urethane prepolymer		Yield/%[b]	Mol. ratio of amino acid to urethane prepolymer[c]
L-Leucine	16	A	65	17
L-Leucine	8	A	67	9
L-Leucine	16	B	59	18
L-Leucine	8	B	74	7
L-Leucine	16	C	35	17
L-Valine	8	B	70	7
L-Valine	16	C	35	18
DL-Valine	16	A	53	18
DL-Valine	16	B	59	16
DL-Valine	8	B	74	8
γ-Benzyl L-glutamate	18	A	63	17
γ-Benzyl L-glutamate	9	A	61	8
γ-Benzyl L-glutamate	18	B	69	17
γ-Benzyl L-glutamate	9	B	70	8
γ-Benzyl L-glutamate	4	B	67	3
γ-Benzyl L-glutamate	9	C	40	10

a) Reaction time, 2 h. b) For amino acid component in block copolymer formed. c) Approximately estimated from ^{1}H NMR.

Table 6. Electrochemical Preparation of Flexiable Conductive Poly(amino acid)-Polypyrrole complex Films

Poly(amino acid) component	Thickness /mm	Polypyrrole content /wt%	Conductivity/Ω^{-1} cm^{-1}	
			Surface side	Back side
Poly(L-leucine)	0.4	48	15	35
Poly(γ-benzyl L-glutamate)	0.5	43	4	5
Poly(γ-benzyl L-glutamate)-urethane block copolymer	1.2	35	0.04	1

Electrochemical Preparation of Flexible Electroconductive Poly(amino acid)-Polypyrrole Complex Films. It is well-known that the anodic oxidative polymerization of pyrrole forms electroconductive polypyrrole coatings on anodes but they are not so flexible to be peeled off as films from the anodes.[14] It may be the way to get the electroconductive polypyrrole films to make blend polymers with other flexible polymers, but it is not so easy because of insolubility of polypyrrole in most solvents.

Efforts have been made to prepare flexible polypyrrole films. It has recently been reported that flexible polypyrrole films can be prepared by anodically polymerizing pyrrole using electrodes coated with a variety of nonconductive polymers such as poly(vinyl chloride), polystyrene, and poly(methyl methacrylate).[14-17] The films thus prepared show good thermal and mechanical properties.[14]

In this work, poly(amino acid)-polypyrrole complex films were prepared by anodically polymerizing pyrrole on platinum anode in the presence of amino acid NCA's in an undivided cell. It is noted that the polymerization of NCA's proceeds in the whole area of the cell, as described previously. Therefore, poly(amino acid)s formed in the vicinity of the anode during the electrolysis might be incorporated into polypyrrole films deposited on the anode surface. The films were easily peeled off from the anode. As shown in Table 6, there were not any great differences in conductivity between the surface and back sides. The films are also expected to have hydrophilic nature and affinity for biomaterials: This may suggest possibility of their in vivo use.

Experimental

Materials. Amino acid NCA's were prepared from amino acid and trichloromethyl chloroformate (phosgene dimer).[18] The urethane prepolymer(**2**) was kindly supplied by Mitsubishi Kasei Co. All the other chemicals were commercially available.

Syntheses of Homopoly(amino acid)s, Copoly(amino acid)s, and Poly(amino acid)-Polyurethane Copolymers. In Method A, PB's (0.7 mmol) were electrolyzed at a platinum cathode (12 cm^2) in 60 cm^3 of dry THF containing n-Bu_4NBF_4 (0.1 mol dm^{-3}). The electrolysis was carried out by passing 0.05 F/mol-NCA of charge under galvanostatic conditions (at 0.08 A dm^{-2} of current dencity) in a divided cell and then the resulting cathodic solution was added to an NCA solution. Electrolysis in Method B was also carried similarly in the absence of PB's.

After the electrolysis, precipitating poly(amino acid) was filtered and washed with THF. IR and ^{1}H NMR spectra were measured in KBr and CF_3COOH, respectively. Kinematic viscosity of poly(amino acid) (0.5 w/v% in CF_3COOH) was also measured using an Ubbelohde's viscometer at room temperature.

Preparation of Poly(amino acid)-Polypyrrole Complex Films. Amino acid NCA (1 g) was electrolyzed using platinum electrodes (12 cm^2) in 0.1 mol dm^{-3} n-Bu_4NBF_4/CH_3CN(200 cm^3) containing pyrrole (0.01 mol) for 1 h under galvanostatic conditions(20 mA) in an undivided cell. After the electrolysis, the film deposited on the anode surface was peeled off and its conductivity was measured under dry conditions by the two probe method. Poly(amino acid) content in the films was determined from UV-spectra of solutions which were prepared by extracting the films with CF_3COOH or benzene under ultrasonic irradiation.

References

1) R. Katakai and Y. Iizuka, *J. Org. Chem.*, **50**, 715 (1985)

2) Y. Fujimoto, "Pori-Amino-San," ed by Y. Fujimoto, Kodansha, Tokyo (1974), Chap. 3.

3) M. M. Baizer, *Tetrahedron*, **40**, 935 (1984).

4) T. Komori, T. Nonaka, T. Fuchigami, *Chem. Lett.*, **1986**, 11.

5) M. Minato, T. Nonaka, and T. Fuchigami, *Chem. Lett.*, **1986**, 1071.

6) T. Fuchigami, T. Awata, T. Nonaka, and M. M. Baizer, *Bull. Chem. Soc. Jpn.*, **59**, 2873 (1986).

7) Shono et al. reported that the EGB derived from α-pyrrolidone was useful for some organic syntheses as a proton-abstracting reagent and a base catalyst.[8,9]

8) T. Shono, S. Kashimura, K. Ishizawa, and O. Ishige, *Chem. Lett.*, **1983**, 1311.

9) T. Shono, S. Kashimura, and H. Nogusa, *J. Org. Chem.*, **49**, 2043 (1984)

10) We have reported the electrogenerated hindered phenolate anion-promoted aldol condensation of acetophenone with benzaldehyde.[6]

11) T. Akaike, Y. Aogaki, and S. Inoue, *Biopolymers*, **14**, 2577 (1975).

12) E. R. Blout, C. de Loze, S. M. Bloom, and G. D. Fasman, *J. Am. Chem. Soc.*, **82**, 3787 (1960).

13) Y. Kobayashi and S. Uchida, Japan Kokai (Patent) 58-57420 (1983).

14) M.-A. De Paoli, R. J. Waltman, A. F. Diez, and J. Bargon, *J. Polym. Sci., Polym. Chem.*, **23**, 1687 (1985).
15) O. Niwa and T. Tamamura, *J. Chem. Soc., Chem. Commun.*, **1984**, 871.
16) M.-A. De Paoli, R. J. Waltman, A. F. Diez, and J. Bargon, *J. Chem. Soc., Chem. Commun.*, **1984**, 1051.
17) T. T. Wang, S. Tasaka, R. S. Hutton, and P. Y. Lu, *J. Chem. Soc., Chem. Commun.*, **1985**, 1343.
18) Y. Koiwa, K. Tatsukawa, A. Miike, M. Teranishi, and Y. Fujimoto, *Yuki Gosei Kagaku Kyokai Shi*, **33**, 628 (1975).

 © 1987 The Chemical Society of Japan Bull. Chem. Soc. Jpn., 60, 3321—3330 (1987)

Decay Reactions of Aryldiazenyl Radicals in Solution

Tadashi SUEHIRO,* Seiichi MASUDA, Ryuichi NAKAUSA, Masamichi TAGUCHI, Atsushi MORI, Akemi KOIKE, and Munehiro DATE†

Department of Chemistry, Faculty of Science, Gakushuin University, Mejiro, Toshimaku, Tokyo 171

†The Institute of Physical and Chemical Research, Wako, Saitama 351

(Received March 30, 1987)

The decay processes of aryldiazenyl radicals were studied by using a time-resolved ESR method. The first order rate constants of decomposition were determined at −117—−48 °C in cyclopropane solutions in the presence or absence of olefins. Aryldiazenyl radicals were relatively persistent and the k_1 of phenyldiazenyl-d_5 at −96 °C in cyclopropane was 34 s^{-1}. The k_1 of 20 aryldiazenyl radicals at −96 °C afforded a ρ value of +1.53 (r=0.91) in a Hammett plot. Activation energies ranged from 46.2 to 25.2 kJ mol^{-1} and the frequency factors, log A, from 13.2 to 8.2 s^{-1}. The second-order decay rates were measured at the initial period of the decay process at lower temperatures, in a batch system (cyclopropane) and in a flow system (isohexane). The rate constant of phenyldiazenyl-d_5 in cyclopropane was $9.2 \cdot 10^5$ M^{-1} s^{-1} at −93 °C and the Arrhenius parameters were E_a=23.5 kJ mol^{-1} and log A=12.77 M^{-1} s^{-1}, respectively.

Aryldiazenyl radicals have been studied as transient radicals in organic syntheses such as the Gomberg-Bachmann reaction,[1] and from theoretical interests in thermolysis of acylarylnitrosamines[2] and of aryl(triphenylmethyl)diazenes.[3] Informations concerning the lifetime of the radicals were reported in a trapping experiment of the radicals by using triphenylmethyl radicals[4] and in CIDNP experiment using diazenes or nitrosamine.[4-6] These investigations suggested a very rapid decay nature of aryldiazenyl radicals. Another estimation of a rather slow decay rate of phenyldiazenyl radicals was reported from a study of activation free energy of azo compounds.[7] We could observe aryldiazenyl radicals in solutions by an ESR technique and this fact supported a rather persistent nature of the radicals.[8] We will here report the rate constants of decomposition of aryldiazenyl radicals in solutions, obtained in a time-resolved ESR study.

Experimental

(1) Time-Resolved ESR Spectroscopy a) Apparatus. The measurement of the decay rates of aryldiazenyl radicals was carried out on a Varian E-109E spectrometer with 100 kHz modulation for the first order decay rate, after insertion of a 100 kOhm resistance in the receiver to attain a faster responce of about 0.3 ms. For determination of second order rate constant, we constructed a 1 MHz modulation amplifier and a coherent receiver by the method of Smith and coworkers,[9] thereby a pair of hair-pin type modulation coil was set around the Dewar tube in the cavity.

To follow the decay of aryldiazenyl radicals, we measured one line of the ESR spectrum of aryldiazenyl radical at a specified resonance magnetic field under a rather high modulation amplitude. The signal intensities were transferred via a transient memory, Biomation 805, into a microcomputer, Multi-16, accumulating up to 2^{16} transients. The microcomputer output decay curves, signal intensity-time plots for the first and second order rate analyses, and the calculated rate constants.

For flash photolysis we used a 1 kW Xe lamp with a rotating sector (flash duration 30 to 50 ms) for k_1 measurements and a Nitrogen Laser, Molectron UV-14 for k_2 measurements. The block diagram of the system was shown in Fig. 1.

b) Reaction Cell. For determination of k_1 and k_2 using a higher concentration of aryl(arylthio)diazenes, $\geqslant 2 \cdot 10^{-2}$ M††, we used a sample tube as that used in a previous study.[8] (We call this a batch method.) For measurements of k_2 using a solution of low concentration, $4 \cdot 10^{-4}$ M, we adopted a flow method, using a sample tube (quartz, ϕ 4 mm), closed by a screw cap, through which a concentric inlet tube (Pyrex, ϕ 2 mm), a teflon outlet tube (ϕ 2 mm), and a copper-constantan thermocouple were introduced.

In the flow system an air-free sample solution under Ar, 300—500 ml, cooled in Dry Ice-methanol bath, was forced to flow into the sample tube by Ar pressure, via a cold thermostat (ca. −130 °C) and a cold path (teflon, ca. −100 °C),

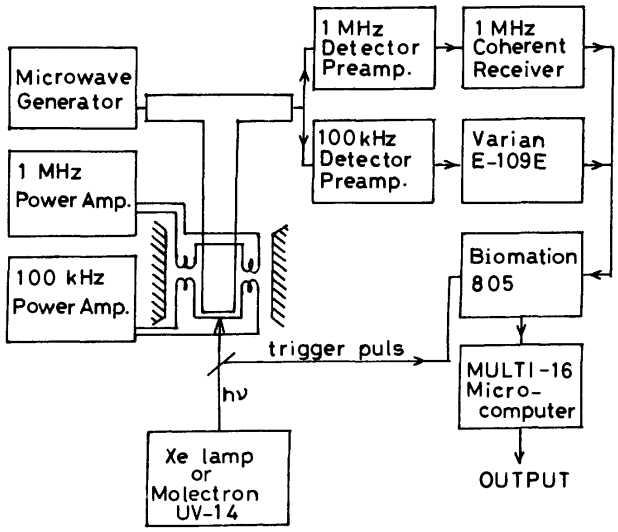

Fig. 1. Block diagram of time-resolved ESR spectrometer.

†† 1 M=1 mol dm^{-3}.

both regulated by cold nitrogen tream and monitored by copper-constantan thermocouple. About 10 m teflon tube in the thermostat was sufficient to attain a desired low temperature. The sample tube was placed in the Dewar tube in the ESR cavity. (Ref. Fig. 6 and the description on it.)

(2) Materials. a) Aryl(arylthio)diazenes. Aryl(arylthio)-diazenes were prepared as described in a previous paper.[8] Additional diazenes used in this kinetic study were listed in Table 1.

For the measurement of second order rate constants we used perdeuteriophenyl-, 4-methoxy-3,5-dideuteriophenyl-, and 4-chloro-3,5-dideuteriophenyldiazenyl radicals to eliminate the hfs of ESR spectrum due to 3,5-hydrogens. The preparation of 4-substituted 3,5-dideuterioanilines was performed as follows: 1) 4-nitrophenol was deuterated by heating with D_2O–D_2SO_4, then methylated by diazomethane and then reduced by $SnCl_2$–HCl, ii) 4-nitroaniline was deutetrated by heating with D_2O–DCl, and then transformed into 4-chloro-3,5-dideuterionitrobenzene by the Sandmeyer reaction and then reduced to aniline.

The deuterium exchange was monitored by ^1H NMR method.

b) Solvents. Cyclopropane, methylcyclopentane, toluene, 1-butene, *cis*-2-butene, ethoxyethene, propene, bromoethene, 1-chloropropene, were used after they have been degassed by repeated freeze and thaw in vacuum and distilled from bulb into sample tube. Isohexane for the flow method was purified by wasing with concd. H_2SO_4, boiled over sodium wire, followed by distillation over lithium tetrahydridoaluminate under Ar. The purity of isohexane was monitored by determining peroxyl radical during photolysis by ESR measurement.

(3) Kinetic Analysis. a) First Order Reaction Rate. Decay curves obtained by using time-resolved ESR technique were examined by plotting, 1) $1/(R\cdot)_t$ against time for second order decay reaction, and 2) $\ln[(R\cdot)_0/(R\cdot)_t]$ against time for first order reaction, here $(R\cdot)_0$ and $(R\cdot)_t$ stand for the concentrations of aryldiazenyl radicals at time 0 and t, respectively (Figs. 2 and 3).

b) Second Order Reaction Rate. In a batch method we

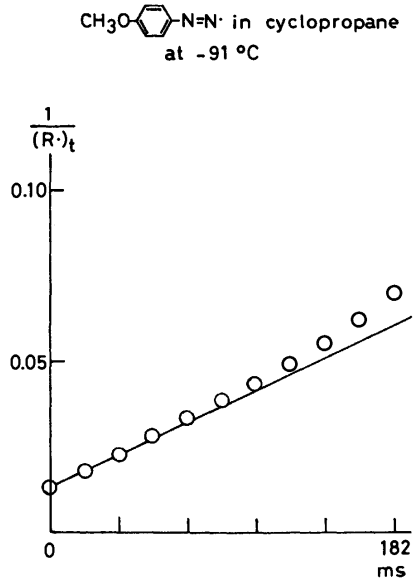

Fig. 2. Polt of $1/(R\cdot)_t$ against time.

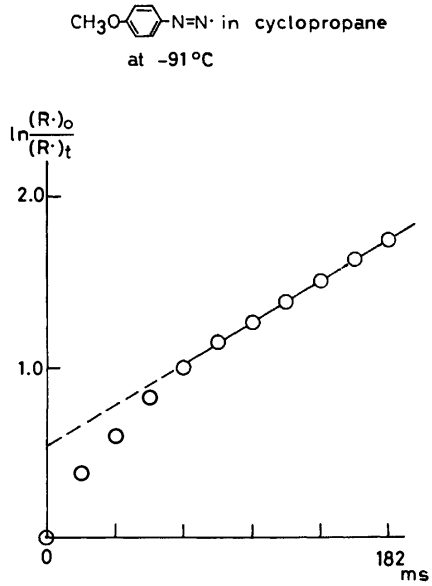

Fig. 3. Plot of $\ln[(R\cdot)_0/(R\cdot)_t]$ against time.

Table 1. Aryl(4-*t*-butylphenylthio)diazenes

Subst. in Aryl	Mp (θ_m/°C)	ESR spectra					Remarks elemental		anal.
		g-Value	Hfs. constant						
			a_N1	a_N2	$a_{3,5\text{-H}}$	*n*-H	C/%	H/%	N/%
3-CN	60—62, d	2.0003	9.30	23.7	1.00	1H	f. 68.91 c. 69.12 for $C_{17}H_{17}N_3S$	5.83 5.80	14.13 14.22
4-CN	83.5—84·5, d	2.0004	9.42	23.6	1.10	2H	f. 69.15	5.79	14.12
3-CH_3CO	66.3—69.2, d	2.0004	9.35	24.5	1.10	1H	f. 69.39 c. 69.20 for $C_{18}H_{20}N_2OS$	6.60 6.45	9.39 8.97
4-CH_3CO	61—63, d	2.0003	9.50	22.9	1.15	2H	f. 68.94	6.66	9.18
4-CH_3O-3,5-d_2	61—62, d	2.0004	9.25	22.3	none	0	3,5-d%: 90% in 4-CH_3O-3,5-d_2-$C_6H_2NO_2$		
4-Cl-3,5-d_2	29—31, d	2.0004	9.35	23.2	0.50 $a_{2\text{-H}}$?	1H?	3,5-d%: 92% in 4-Cl-3,5-d_2-$C_6H_2NH_2$		

used solutions of aryl(arylthio)diazenes of a higher concentration, $2.0 \cdot 10^{-2}$ M. In this case the light introduced in the solution was completely absorbed and the radicals formed in the solution were not distributed homogenously in the solution but the radical concentration decreased exponentially from the front surface of the sample tube into the inner part of solution. On this problem H. Fischer and his coworkers have discussed and estimated the accuracy of the experimental values of k_2.[10] We have analyzed the decay curves by taking account of this exponential distribution of the radicals in the following way.

In our experiments we assumed a front area of the light path to be half of the surface of the sample tube of inner diameter 0.253 cm, multiplied by 1.20 cm height, and devided by 2 because of the lattice of the cavity window.

The distibution of aryldiazenyl radicals in solution at time 0 was assumed to be the exponential curve A as depicted in Fig. 4.

The bimolecular decay reaction of aryldiazenyl radicals proceeds in a small volume section at l_i of the solution, thereby we assumed no diffusion of the radicals out of or into the section l_i.[11]

For the second order reaction in section l_i we can apply the equations

$$-d(R\cdot_i)/dt = 2\cdot k_2\cdot(R\cdot_i)^2 \quad (1)$$

and

$$1/(R\cdot_i)_t - 1/(R\cdot_i)_0 = 2\cdot k_2\cdot t, \quad (2)$$

where $(R\cdot_i)_0$ and $(R\cdot_i)_t$ stand for radical concentrations in the section l_i at time 0 and t, respectively.

On summation of $(R\cdot_i)$ over all sections at l_i, we get total radical concentration $(R\cdot)_0$ and $(R\cdot)_t$ at time 0 and t, respectively, i.e.,

$$(R\cdot)_0 = \sum_{l_i} (R\cdot_i)_0$$

and

$$(R\cdot)_t = \sum_{l_i} (R\cdot_i)_t \quad (3)$$

We observed experimentally the decay process of $(R\cdot)_0$ from time 0 to ∞, as illustrated in Fig. 5.

The initial radical distribution, $(R\cdot_i)_0$, can be expressed by Eq. 4, assuming that the aryldiazenyl radicals were produced from diazene by photolysis:

$$(R\cdot_i)_0 = (R\cdot_0)_0\cdot\exp(-2.30\cdot\varepsilon\cdot c\cdot l_i), \quad (4)$$

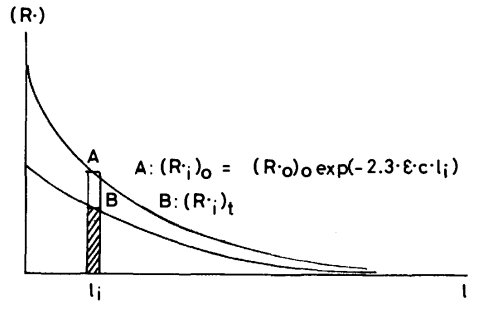

Fig. 4. Exponential distribution of concentration of aryldiazenyl radicals in solution.

where $(R\cdot_0)_0$ denotes the initial radical concentration at time 0 in the section at l_0, ε the molar absortion coefficient of the starting compound aryl(arylthio)diazene at wavelength 337 nm, $6.5 \cdot 10^3$ M cm^{-1} for (4-*t*-butylphenylthio)-phenyldiazene, and c the concentration of the diazene.

The radical concentration at time t, $(R\cdot)_t$, can be expressed in terms of $(R\cdot_i)_0$, by using Eqs. 2 and 3 as follows:

$$(R\cdot)_t = \sum_{l_i} (R\cdot_i)_t = \sum_{l_i} [1/\{1/(R\cdot_i)_0 + 2\cdot k_2\cdot t\}]. \quad (5)$$

Equation 5 was transformed by integration into Eq. 6,

$$(R\cdot)_t = \frac{\ln\{1+2\cdot(R\cdot_0)_0\cdot k_2\cdot t\}}{2\cdot 30\cdot 2\cdot\varepsilon\cdot c\cdot k_2\cdot t}, \quad (6)$$

which was changed by approximation using the first 3 terms of the Maclaurin Expansion into

$$(R\cdot)_t = \frac{(R\cdot_0)_0}{2.30\cdot\varepsilon\cdot c\cdot\{1+(R\cdot_0)_0\cdot k_2\cdot t\}}, \quad (7)$$

or into Eq. 8,

$$1/(R\cdot)_t = 2.30\cdot\varepsilon\cdot c/(R\cdot_0)_0 + 2.30\cdot\varepsilon\cdot c\cdot k_2\cdot t, \quad (8)$$

when $1 \gg 2\cdot(R\cdot_0)_0\cdot k_2\cdot t$.[12] On plotting $1/(R\cdot)_t$ against time, we can obtain k_2.

In the flow method using a $4 \cdot 10^{-4}$ M solution of diazene we assumed a homogenous distribution of radicals throughout the irradiated solution and the volume of the solution was taken as one half of the outer sphere in the sample tube (Fig. 6).

The rate constants were calculated by using Eq. 9 of the second order decay reaction.

$$1/(R\cdot)_t - 1/(R\cdot)_0 = 2\cdot k_2\cdot t \quad (9)$$

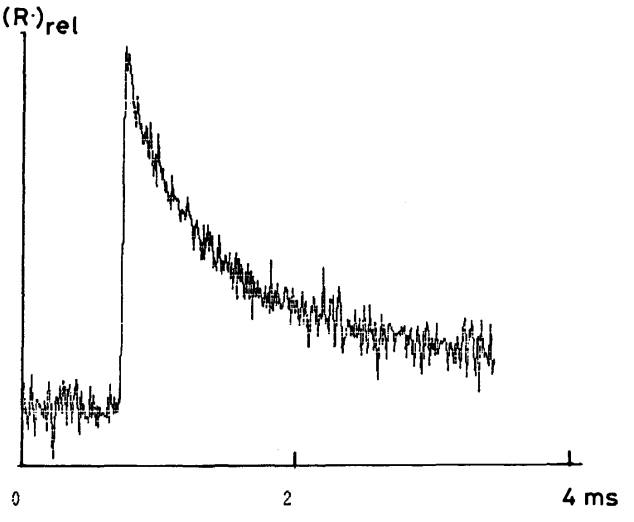

Fig. 5. Second-order decay curve of phenyldiazenyl-d_5 radicals, at −102 °C in $2 \cdot 10^{-2}$ molar diazene in cyclopropane. Batch method.

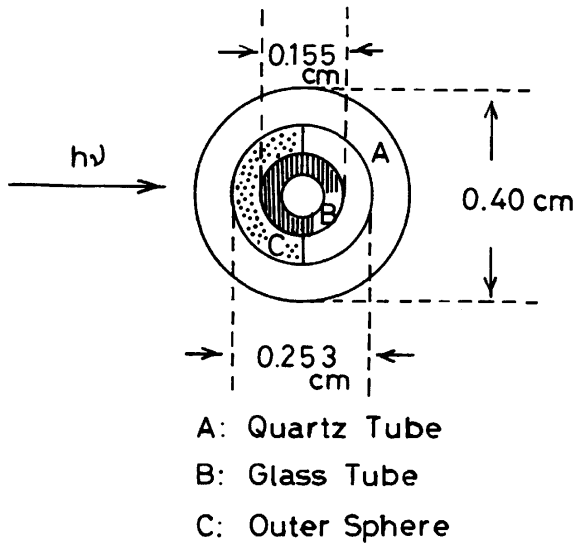

Fig. 6. Aryldiazenyl radicals formed in the outer sphere of sample tube.

It was determined that the effect of k_1 was negligible in the calculation of k_2.

c) Calibration Curve for Determination of the Radical Concentration. As a standard solution of known concentration of free radicals we used solutions of pure nitrosodisulfonate in slightly ammoniacal aq. solution. It was thereby assumed that the line shape of the ESR spectrum of aryldiazenyl radicals was the same as that of nitrosodisulfonate and that the sensitivity of the ESR apparatus was kept constant for free radicals even though the solvent for the radicals was changed from water (nitrosodisulfonate) to a variant of organic solvent (aryldiazenyls).

One line of the triplet of ESR spectrum of nitrosodisulfonate of $0.4\cdot10^{-9}$ to $1.6\cdot10^{-9}$ mol was determined by averaging 20 runs at 25 °C and then double-integrated digitally. A linear correlation of the spectrum peak height to the integrated value was obtained. The conditions of ESR spectrometer for the measurement of calibration curve were set to those for the time-resolved ESR experiment in microwave power, modulation amplitude, and receiver gain.

The kinetic studies were performed at low temperatures and so it was necessary to correct the signal intensity. The increase in intensity was assumed to be proportional to $1/T$ and the signal heights were corrected by multiplying $T/298$.

Results and Discussion

To understand the decay kinetics of aryldiazenyl radicals, it is plausible to describe the following Scheme 1: Aryl(arylthio)diazene was decomposed photochemically to yield aryldiazenyl–arylthiyl radical pair, and then proceeded two reactions, k_{comb} and k_{diff}, in competition. Thereafter occured bimolecular and unimolecular reactions in the solution.

$$\text{Ar-N=N-S-Ar}' \xrightarrow{h\nu} \overline{\text{Ar-N=N}\cdot\ \cdot\text{S-Ar}'} \quad (10)$$

$$\overline{\text{Ar-N=N}\cdot\ \cdot\text{S-Ar}'} \xrightarrow{k_{comb}} \text{Ar-N=N-S-Ar}' \quad (11)$$

$$\text{or Ar-S-Ar}' + \text{N}_2 \quad (12)$$

$$\xrightarrow{k_{diff}} \text{Ar-N=N}\cdot + \cdot\text{S-Ar}' \quad (13)$$

$$2\ \text{A-N=N}\cdot \xrightarrow{k_2} \text{Ar-N=N-Ar} + \text{N}_2$$

$$\text{or Ar-Ar} + 2\text{N}_2 \quad (14)$$

$$\text{Ar-N=N}\cdot + \cdot\text{S-Ar}' \xrightarrow{k_{term}^1} \text{Ar-S-Ar}' + \text{N}_2 \quad (15)$$

$$2\ \text{Ar}'\text{-S}\cdot \xrightarrow{k_{term}^2} \text{Ar}'\text{-S-S-Ar}' \quad (16)$$

$$\text{Ar-N=N}\cdot \xrightarrow{k_1} \text{Ar}\cdot + \text{N}_2 \quad (17)$$

Scheme 1.

Aryl radicals formed in Reaction 17 react with solvent molecules, affording stable products and secondary radicals.

The bimolecular reactions of aryldiazenyl radicals, Reactions 14 and 15, became measurable at the initial period of decay process, when the radical concentrations were high enough or on occasions of slow unimolecular decay of aryldiazenyl radicals by lowering the reaction temperature.

Arylthiyl radicals formed photochemically in 10^{-2} molar diazene solution disappeared in a half-life of several microseconds at −100 °C, which we could follow by measuring the transient UV absorption around 450 to 550 nm of arylthiyl radicals.[13] We can therefore neglect Reaction 15 in calculation of the second order reaction rate of aryldiazenyl radicals. In dilute solutions of 10^{-4} molar aryldiazenes the reaction 15 may cause an effect in k_2 measurements.

(1) First Order Reaction Rate. a) Rate Constant of Phenyldiazenyl-d_5 Radicals. The first order decay rates of aryldiazenyl radicals were obtained by using a 100 kHz modulation ESR spectrometer. The decay curves were analyzed by plotting $\ln\{(\text{R}\cdot)_0/(\text{R}\cdot)_t\}$–time and $1/(\text{R}\cdot)_t$–time to separate the first order reaction from the second-order decay process. The first order rate constants so obtained are listed in Table 2 and Arrhenius Plot of k_1 of some aryldiazenyl radicals is reproduced in Fig. 7.

Aryldiazenyl radicals are relatively persistent and the first order rate constant of phenyldiazenyl-d_5 radical was $34\ \text{s}^{-1}$ at −96 °C. Porter and his coworkers[4] have estimated the rate of decomposition of the order of 10^7 to $10^9\ \text{s}^{-1}$ at 40 °C for phenyldiazenyl radical from the analysis of CIDNP experiment of phenyl(1-methyl-1-phenylethyl)diazene. Another estimation from CIDNP of the half-life of phenyldiazenyl was reported by Kasukhin and colaborators[5] as $t_{1/2}=10^{-7}$ s ($k_1\fallingdotseq 7\cdot10^6\ \text{s}^{-1}$) at 60 °C.

Our rate constant of phenyldiazenyl-d_5 was extrapolated to +60°C to afford $k_1 = 4.8 \cdot 10^5\ s^{-1}$. This value was by far lower than the values estimated from CIDNP experiments.

At lower temperatures when the unimolecular decay became slower, bimolecular decay reactions proceeded at the initial period of the decay: The bimolecular reactions were observed at −87 °C for 4-methoxyphenyldiazenyl radicals, at −96 °C for 4-methylphenyldiazenyl radicals, and even at −73 °C for 4-dimethylaminophenyldiazenyl radicals, which were the most persistent radicals among those we studied.

b) Substituent Effect on the First Order Reaction Rate of Aryldiazenyl Radicals. The first order rate constants of 20 aryldiazenyl radicals at −96 °C were plotted against the Hammett sigma constants for 3- and 4-substituted phenyldiazenyl radicals and against the values equivalent to sigma value for 2-substituted phenyldiazenyl radicals. The latter "ortho sigma values" were derived from the acid dissociation constants of 2-substituted benzoic acid[14] based on the definition of the Hammett sigma constant.

For 2-methylthio substituent, the "sigma value" was calculated from σ_p by means of Eq. 18, presented by

Table 2. First Order Rate Constants of Aryldiazenyl Radicals in Cyclopropane, k_1/s^{-1}

Temp/°C	4-Me_2N	4-MeO	4-Me	3,5-Me_2	3-Me	d_5	2,4,6-Me_3	4-Cl	4-Br	4-I
−48	390									
−56	193									
−65	91									
−70		86			530					
−73	16					540	290			
−78		26	100							
−80						140				
−82							154			295
−87		8.7	44	160	80	90			195	
−91							74			104
−96			11	58	21	34		61	48	
−99										41
−104				19		17		30		
−108										
−113								9		
−117										
E_a/kJ mol^{-1}	46.0	42.3	35.6	33.1	38.5	29.7	23.4	26.8		32.2
$\frac{\log A}{s^{-1}}$	13.21	12.77	11.54	11.49	12.65	10.31	8.55	9.76		11.30
σ-Value	−0.88	−0.28	−0.18	−0.14	−0.07	0.00	0.24	0.23	0.23	0.18

Temp/°C	2-Me	2-MeO	2-MeS	3-MeO	4-CN	3-CH_3CO	3-CN	2-F	2-Cl	2-Br
−48										
−56										
−65										
−70										
−73										
−80										
−82	140									
−87										
−91	84	215	80							
−96				70	114	260	352			
−99	36	77	30		84		250	300	700	1200
−104		21		33				101	220	370
−108	14									
−113				8.8						
−117								29	60	93
E_a/kJ mol^{-1}	22.2	34.3		29.3				29.7	31.0	32.2
$\frac{\log A}{s^{-1}}$	8.26	12.20		10.44				11.31	12.17	12.79
σ-Value	0.68	0.23	0.40	0.12	0.66	0.38	0.56	0.92	1.12	1.16

Yoshida and Hojo[15]

$$\sigma_o = 0.72 + 1.91 \cdot \sigma_p \quad (18)$$

The rate constants of aryldiazenyl radicals correlated linearly to sigma values with ρ=+1.53 (r=0.91). We did not find any evidence for the extra stabilization effect of 2- and 4-substituents nor extra acceleration effect by the 2-substituents on the decomposition reaction. The fairly linear nature of the Hammett plot is a characteristic feature of aryldiazenyl radicals and stands in a clear contradictory to those of aryldiazonium ions.[16] In the diazonium ions the mesomeric effect of substituents at 2-and 4-positions of the benzene ring, regardless of electron-releasing and electron-withdrawing natures, retarded the decompositions.

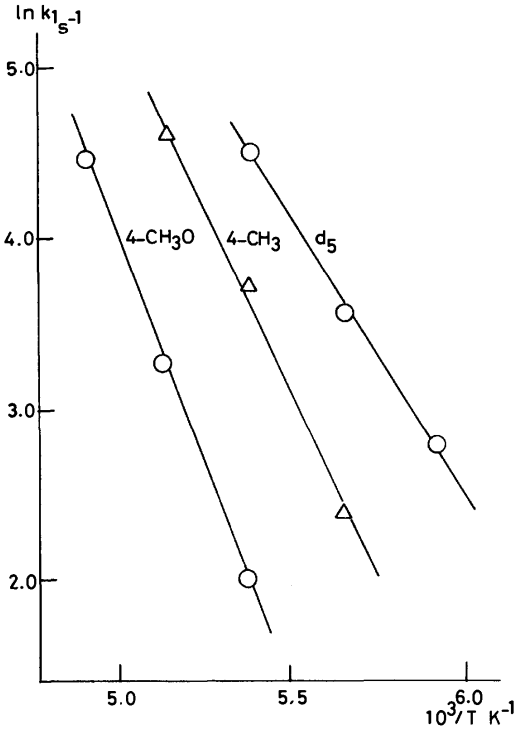

Fig. 7. Arrhenius plot of k_1 for substituted phenyldiazenyl radicals in cyclopropane.

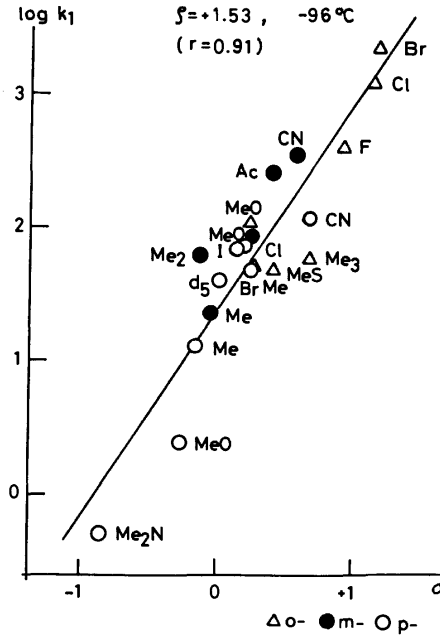

Fig. 8. Hammett plot of k_1 for substituted phenyldiazenyl radicals at −96 °C in cyclopropane.

The positive reaction constant, +1.53, implies a stabilization effect of electron-releasing substituent groups of aryldiazenyl radicals, polarizing thereby negatively at the -N=N group. The INDO calculation[8] suggested also a polar nature of the radicals with a dipole moment of ca. 2.8.

The negatively polarized -N=N group evokes an electrophilic property of aryldiazenyl radicals in their unimolecular decomposition in a variant of solvents. This became true in the determination of rate constants in olefinic solvents.

c) Solvent Effect on the First Order Reaction Rate. The effect of solvent on the rate of the unimolecular decomposition of 4-methoxyphenyldiazenyl radical was studied at −87 °C by using, i) inert hydrocarbon solvents, and ii) olefinic solvents, both in neat or in a 1 : 1 (volume) mixture of cyclopropane.

i) Inert Hydrocarbon Solvent. In inert hydrocarbon of higher molecular weight, such as 2,2,4-trimethylpentane, methylcyclopentane, and toluene in a 1 : 1 mixture of cyclopropane, the unimolecular decay rate of 4-methoxyphenyldiazenyl radical increased by a factor of 2 to 3, independent of the aliphatic or aromatic nature of the solvents. The increase in rate, effected by 2,2,4-trimethylpentane, must be due to viscosity of the solvent, and the effect caused by the trimethylpentane exceeded that of

Table 3. First Order Rate Constant of 4-Methoxyphenyldiazenyl Radical in 1 : 1 Mixture with Cyclopropane at −87 °C

Solvent added	k_1/s^{-1}	E_a/kJ mol^{-1}	$\log A$ / s^{-1}
None	8.7	42.3	12.77
2,2,4-Trimethylpentane	23	—	—
Methylcyclopentane	12	—	—
Toluene	9.3	—	—
1-Butene	73	—	—
cis-2-Butene	62	34.7	12.69
Ethoxyethene	60	39.7	12.86
Propene	42	—	—
Bromoethene	35	—	—
1-Chloropropene	26	—	—

toluene, i.e., hydrogen abstraction reaction by 4-methoxyphenyldiazenyl radical from the methyl group of toluene was probably not important at these low temperatures.

ii) Olefinic Solvents. Olefinic solvents on the other hand accelerated the decay rate of 4-methoxyphenyldiazenyl radicals remarkably. An effect other than that of viscosity must be important. The rate constants in olefinic solvents are listed together with those in hydrocarbon solvents in Table 3.

In 1-butene or *cis*-2-butene neat, we could observe the same ESR spectrum of 4-methoxyphenyldiazenyl radical as that in cyclopropane solution (Fig. 9). This result supports strongly that we are studying the primary radicals formed by photolysis of aryl(arylthio)diazenes and not the radical derived secondarily by some addition reaction of a radical to the starting diazenes.

The increase in rate effected by olefinic solvents is probably caused by a reaction between aryldiazenyl radical and the olefin molecule in a manner such as π-complexing, but not by addition reaction of aryldiazenyl radicals to olefinic double bond.

The minor roll of this addition reaction was deduced from a product study of photolysis of (4-*t*-butylphenylthio)(4-methoxyphenyl)diazene in propene at −78 °C. The reaction products were analyzed by using GC, HPLC, TLC, and NMR techniques, and identified as **a**: anisole (15%), **b**: 4-methoxyphenylpropane (6%), **c**: 4-*t*-butylphenyl 4-methoxyphenyl sulfide (in a small yield), **d**: 4,4′-di-t-butyldiphenyl disulfide (in an appreciable yield), and **e**: probably 2-(4-*t*-butylphenylthio)-1-(4-methoxyphenyl)propane (in a high yield). The compounds **d** and **e** decomposed seriously under the GC conditions. Aryldiazenyl radicals were transformed into dediazoniated products in the main routes of the reactions and this suggested that the dediazoniation was the first step of the reaction of aryldiazenyl radicals.

The mechanism of dediazoniation of aryldiazenyl radicals in olefinic solvents resembles the molecular mechanism of perbenzoic acid in methyl methacrylate[17] and proceeds probably through a formation of complex between aryldiazenyl radical and olefinic linkage under charge transfer from olefinic double bond to diazenyl nitrogen, followed by dediazoniation. The Hammett correlation of the decay rate of 4-methoxyphenyldiazenyl radical to the substituent constants of olefins, $\rho \fallingdotseq -1.0$, although of a poor linearity, and the decrease in activation energy in olefinic solvents, both support a mechanism of dediazoniation accelerated by charge transfer, and this is parallel to the substituent effect in the unimolecular rate constant of aryldiazenyl radicals in cyclopropane: Aryldiazenyl radicals are the more labile, the more neutral the −N=N groups in the radicals are (Fig. 10).

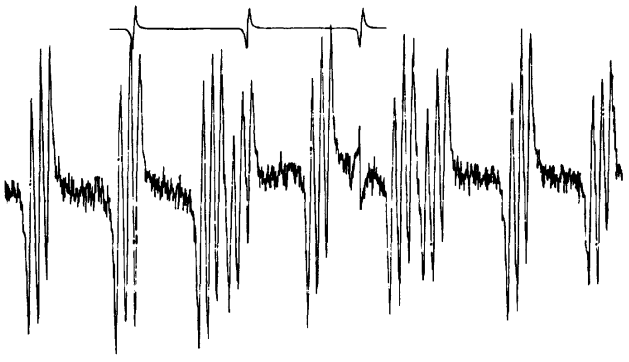

Fig. 9. ESR spectrum of 4-methoxyphenyldiazenyl radicals in 1-butene neat.

d) Possible Reaction Sequence of Unimolecuar Decomposition of Aryldiazenyl Radicals. The characteristic feature of k_1 of aryldiazenyl radicals is the very low frequency factor and the low activation energy, log A=12.8 to 8.3 s^{-1} and E_a=46 to 25 kJ mol^{-1}, respectively. The nature of this is not clear as yet, but can be probably explained by collision activation: aryldiazenyl radicals are activated by collision in a specific configuration, followed by decomposition. The sequence of the processes may be expressed as Eq. 19,

$$\mathrm{d} + \mathrm{m} \underset{k_r}{\overset{k_f}{\rightleftharpoons}} \mathrm{a} + \mathrm{m} \xrightarrow{k_{\text{spontan.}}} \text{products} \qquad (19)$$

where a denotes aryldiazenyl radicals in activated state and d those in the ground state. The symbol m stands for the second molecule of collision, usually solvent molecule. When k_f is rate-determining, then k_1 can be expressed as

$$k_1 = k_f \cdot (\mathrm{m})$$

and the rate should be of low frequency factor and dependent on solvent properties. Depolarization of aryldiazenyl radical would be the key step in the decomposition of the radical.

(2) Second Order Reaction Rate. a) Second Order Rate Constant of Phenyldiazenyl-d_5 by Batch Method. In the batch method a cyclopropane solution (2 ml) of $2 \cdot 10^{-2}$ M of aryl(arylthio)diazene was sealed in sample tube in vacuum. After 300 pulse irradiations the irradiated solution in the quartz cell-tube was refreshed by mixing with that of the reservoir, keeping

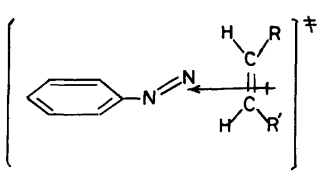

Fig. 10. Charge transfer in the dediazoniation step.

thus the concentration of solution at that of the initial one during the experiment. The rate constants were calculated by using Eq. 8.

The second order decay rates were determined by using 1 MHz modulation technique. A typical decay curve of phenyldiazenyl-d_5 in cyclopropane at $-102\,^{\circ}C$ is reproduced in Fig. 5. The rate constants, k_2, and the Arrhenius parameters are listed in Table 4 and plotted in Fig. 11, respectively.

b) Second Order Rate Constants by Flow Method. In order to examine the rate constants obtained by the batch method using Eq. 8, we measured the rate constant by using more dilute solutions of aryl-(arylthio)diazenes $4\cdot10^{-4}$ M in a flow system. In this experiment we used isohexane as solvent instead of cyclopropane because of the low boiling point of cyclopropane and of the low melting point of isohexane.

The concentration of the diazene of $4\cdot10^{-4}$ M, and the depth of the cell solution, 0.048 cm gave an estimation that about 70% of the light intensity irradiated into the solution would pass through unabsorbed and the aryldiazenyl radicals formed were assumed to be homogeneously distributed in the solution. In the calculation of the rate constant we used Eq. 9. The rate constants k_2 of phenyldiazenyl-d_5 in isohexane are listed in Table 5.

The rate constants obtained by the flow method in isohexane were ca. 30 times as high as those obtained by the batch method in cyclopropane, showing the same activation energy. The reason for this difference can be devided in two: 1) the difference of the properties of solvents used, and 2) the conditions for determination of rate constants.

The manuals in the flow method were established as was confirmed by the same rate data by the batch method using isohexane as solvent for $2\cdot10^{-2}$ molar diazene solution as those obtained by the flow method using the isohexane solution of $2\cdot10^{-2}$ M, calculating the rate constant by Eq. 8 for both. The results are shown in Table 6 and in Fig. 11.

The about 3 times higher rate constants by the flow method in isohexane of Table 5 than those by the batch and flow methods in isohexane of Table 6 may arise from the unknown bimolecular side reactions occurring in the more dilute solutions. We believe that the true rate constants are those of the Table 6, judging from 3 points:

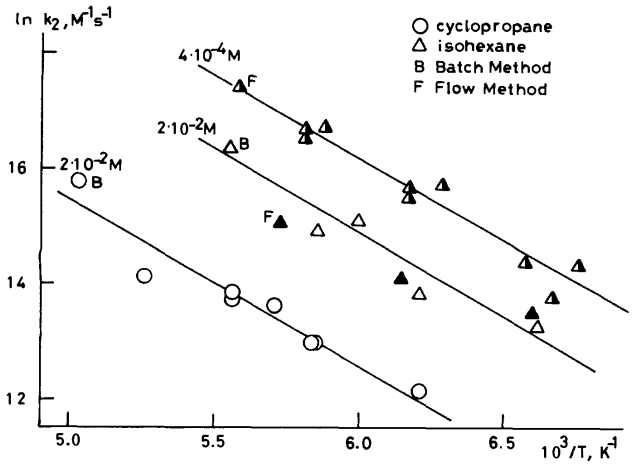

Fig. 11. Arrhenius plots of k_2 for phenyldiazenyl-d_5 radicals. O: Cyclopropane; Δ: isohexane; B: batch method; F: flow method.

Table 4. Second Order Rate Constants, k_2, and Arrhenius Parameters of Phenyldiazenyl-d_5 Radical in Cyclopropane, Batch Method, $2\cdot10^{-2}$ M

Temp/°C	k_2/M^{-1}s^{-1}	E_a/kJ mol^{-1}	log A/M^{-1}s^{-1}
−74	$7.3\cdot10^6$	23.4	12.77
−83	$1.4\cdot10^6$		
−93	$9.2\cdot10^5$		
−93	$1.0\cdot10^6$		
−98	$8.2\cdot10^5$		
−102	$4.3\cdot10^5$		
−102	$4.3\cdot10^5$		
−112	$1.9\cdot10^5$		

Table 5. Second Order Rate Constants, k_2, of Phenyldiazenyl-d_5 Radical in Isohexane, Flow Method, $4\cdot10^{-4}$ M

Temp/°C	k_2/M^{-1}s^{-1}	E_a/kJ mol^{-1}	log A/M^{-1}s^{-1}
−94	$3.7\cdot10^7$	24.3	14.58
−101	$1.8\cdot10^7$		
−101	$1.5\cdot10^7$		
−103	$1.9\cdot10^7$		
−111	$6.5\cdot10^6$		
−111	$5.5\cdot10^6$		
−114	$7.1\cdot10^6$		
−121	$1.8\cdot10^6$		
−123	$9.6\cdot10^5$		
−126	$1.7\cdot10^6$		

Table 6. Second Order Rate Constants, k_2, of Phenyldiazenyl-d_5 Radical in Isohexane, Batch and Flow Methods, $2\cdot10^{-2}$ M

Method	Temp/°C	k_2/M^{-1}s^{-1}	E_a/kJ mol^{-1}	log A/M^{-1}s^{-1}
Batch	−93	$1.3\cdot10^7$	24.3	14.02
	−103	$3.1\cdot10^6$		
	−107	$3.5\cdot10^6$		
	−112	$9.9\cdot10^5$		
	−122	$5.9\cdot10^5$		
Flow	−99	$3.4\cdot10^6$		
	−111	$1.3\cdot10^6$		
	−122	$7.4\cdot10^5$		

1) the approximation Eq. 8 of the batch method gives a correct rate constant when the condition, $1 \gg 2 \cdot (R\cdot_o)_o \cdot k_2 \cdot t$, is satisfied.[12] If not, the equation could give a rate constant about 50% lower than the correct one, and the condition was fulfilled in our experiments. The neglect of the fourth term in the derivation of Eq. 7 can cause only ca. 10% lowering of the rate constant.

2) The estimation of the surface and the volume of the reaction cell in the batch and the flow methods would be too high, may be ca. 2 times. This could give an overestimation of k_2 of ca. 2 times for the both cases.

3) In the flow method using a more dilute radical solution, the apparent rate constant could become higher owing to concurrent radical reactions of aryldiazenyl radicals with other radicals such as arylthiyl radicals, Reaction 15, and with alkylperoxyl radicals formed from peroxide of the solvent molecule when the exclusion of air from the diazene solution was not perfect. We have eliminated the rate data when we have observed traces of peroxyl radicals in the ESR spectrum of aryldiazenyls in the flow method. The accurate amount of the contribution of these concurrent reactions was not clear.

The rate constants in isohexane were about 10 times higher than those in cyclopropane. The accelerating effect of hydrocarbon solvents of higher molecular weight in k_1 is shown in Table 3. We measured k_2 of phenyldiazenyl-d_5 radicals in propane solution at $-102\,^\circ C$ to be $9.71 \cdot 10^5\ M^{-1}\,s^{-1}$ by the batch method. This value was ca. twice as high as that in cyclopropane, $4.3 \cdot 10^5\ M^{-1}\,s^{-1}$ at the same temperature. Viscosity of the solvent could affect the bimolecular decay rate of aryldiazenyl radicals. The exact nature of the accelerating effect of propane and isohexane was not clear.

The extrapolation of k_2 in cyclopropane by the batch method to $60\,^\circ C$ afforded a value $1.1 \cdot 10^9\ M^{-1}\,s^{-1}$ which was rather high. We are not in the position to discuss on it now.

c) Substituent Effect in the Second-Order Rate Constants of Phenyldiazenyl Radicals. The second-order rate constants of 4-methoxy-3,5-dideuteriophenyldiazenyl and 4-chloro-3,5-dideuteriophenyldiazenyl radicals were measured by the flow method in isohexane and the results are listed in Table 7.

We found a little increase in activation energy from 21.3 (4-methoxy-3,5-dideuteriophenyldiazenyl) to 24.3 (perdeuteriophenyldiazenyl) to 25.9 (4-chloro-3,5-dideuteriophenyldiazenyl) kJ mol^{-1} but the effect of increase in frequency factors was dominant. The increase in the frequency factor log A, from 13.23 to 14.58 to 15.83 $M^{-1}\,s^{-1}$ was supposed to be due to the increase in the degree of freedom in the activation collision, because the aryldiazenyl radicals are more and more neutral in the -N=N group in the order 4-methoxy- to hydrogen to 4-chloro-substituted phenyldiazenyls and the interaction leading to dediazoniation would be possible from a longer distance in this order.

Table 7. Substituent Effect in the Second-Order Rate Constants of Substituted Phenyldiazenyl Radicals, Flow Method, $4 \cdot 10^{-4}$ M

Substit. in phenyldiazenyl	Temp °C	k_2 $M^{-1}\,s^{-1}$	E_a kJ mol^{-1}	log A $M^{-1}\,s^{-1}$
4-CH_3O-3,5-d_2	−86	$1.9 \cdot 10^7$	21.3	13.23
	−97	$8.6 \cdot 10^6$		
	−107	$3.0 \cdot 10^6$		
	−117	$1.3 \cdot 10^6$		
4-Cl-3,5-d_2	−100	$1.1 \cdot 10^8$	25.9	15.83
	−113	$2.0 \cdot 10^7$		
	−113	$2.2 \cdot 10^7$		
	−124	$5.4 \cdot 10^6$		

For the chemical processes we propose reactions of Eq. 14 for the bimolecular reaction of aryldiazenyl radicals. In accordance with this an emission signal of azoarene was reported in the CIDNP studies of azo compounds.[18]

We are very greateful to Prof. Masahiro Kotani of Gakushuin University for his kind advices and suggestions for our research work.

References

1) W. E. Bachmann and R. A. Hoffman, *Organic React.*, Vol. 2, 224 (1944).

2) R. Ito, T. Migita, N. Morikawa, and O. Simamura, *Tetrahedron*, **21**, 955 (1965); J.I. G. Cadogan, "Advances in Free Radical Chemistry," ed by G. H. Williams, Heyden & Son Ltd., London, Philadelphia, Rheine (1980), Vol. 6, p. 185.

3) W. A. Pryor and K. Smith, *J. Am. Chem. Soc.*, **89**, 1741 (1967); **92**, 5403 (1970); N. A. Porter, M. E. Landis, and L. J. Marnett, *J. Am. Chem. Soc.*, **93**, 795 (1971); R. C. Neuman, Jr., G. D. Lockyer, Jr., and M. J. Amrich, *Tetrahedron Lett.*, **1972** 1221; N. A. Porter, L. J. Matnett, C. H. Lockmüller, G. L. Closs, and M. Shobataki, *J. Am. Chem. Soc.*, **94**, 3664 (1972); N. A. Porter and J. G. Green, *Tetrahedron Lett.*, **1975** 2667.

4) N. A. Porter, G. R. Dubay, and J. G. Green, *J. Am. Chem. Soc.*, **100**, 920 (1978).

5) L. F. Kasukhin, M. P. Ponomarchuk, and A. L. Buchachenko, *Chem. Phys.*, **3**, 136 (1974).

6) E-L. Dreher, P. Niederer, A. Rieker, W. Schwarz, and H. Zollinger, *Helv. Chim. Acta*, **64**, 488 (1981).

7) P. S. Engel and D. B. Gerth, *J. Am. Chem. Soc.*, **105**, 6849 (1983).

8) T. Suehiro, S. Masuda, T. Tashiro, R. Nakausa, M. Taguchi, A. Koike, and A. Rieker, *Bull. Chem. Soc. Jpn.* **59**,

1877 (1986): Preliminary report, T. Suehiro, T. Tashiro, and R. Nakausa, *Chem. Lett.*, **1980**, 1339.

9) G. E. Smith, R. E. Blankenship, and M. P. Klein, *Rev. Sci. Instr.*, **48**, 282 (1977).

10) H. Fischer, H. Paul, K. Münger, and T. Dschen, *J. Chem. Soc., Perkin Trans. 2*, **1985**, 213.

11) The diffusion distance of free radical, D_R., during the decay period of 1 ms was estimated to be ca. 10^{-2} times as small as the thickness of the radical solution of $1/2.3 \cdot \varepsilon \cdot c = 3.34 \cdot 10^{-3}$ cm. The coefficient of disffusion D of CCl_4, for example, at infinite dilution was reported to be $\approx 10^{-5}$ cm^2 s^{-1} in cyclohexane at 25 °C, and D decreases by a factor of 40 by lowering the temperature from 25 to −100 °C, as expressed by an experimental equation: $D = 2.386 \cdot 10^{-3} \cdot \exp(-3076\ \text{cal}/RT)$ cm^2 s^{-1} (1 cal=4.184 J), reported by A. F. Collings and R. Mills, *Trans. Faraday Soc.*, **66**, 2761 (1970).

$$\bar{D}_R = (2D \cdot t)^{1/2} = (5 \cdot 10^{-7} \cdot 10^{-3})^{1/2} \fallingdotseq 2 \cdot 10^{-5}\ \text{cm}.$$

12) The condition was satisfied when $t \fallingdotseq 10^{-3}$ s, $k_2 = 10^6$—10^7 M^{-1} s^{-1}, and $(R\cdot_o)_o = 10^{-4}$—10^{-5} M, as those found in our experiments, affording $2 \cdot (R\cdot_o)_o \cdot k_2 \cdot t = 10^{-1}$—$10^{-2}$.

13) The UV absorption spectra of transient free radicals formed by photolysis of aryl(arylthio)diazenes using 307 nm were the same as those from diary disulfides. Ref. T. Miyashita, M. Iino, and M. Matsuda, *Bull. Chem. Soc. Jpn.*, **50**, 317 (1977); F. C. Thyrion, *J. Phys. Chem.*, **77**, 1478 (1973). For these experiments we thank Dr. S. Ishizaka of Gakushuin University very much.

14) Landolt-Börnstein "Zahlenwerte und Funktionen aus Physik, Chemie, Astronomie, Geophysik, Technik," II Band, 7. Teil, p. 865.

15) Z. Yoshida and M. Hojo, Baifukan Monograph Series on Basic Principles of Organic Chemistry, No. 12, "Ortho Effect" (1968), p. 72.

16) M. L. Crossley, R. H. Kienle, and C. H. Benbrook, *J. Am. Chem. Soc.*, **62**, 1400 (1940).

17) H. Terada, *Yuki Gosei Kagaku Kyokai Shi*, **19**, 721 (1961); **20**, 74, 158 (1962): An induced free radical decomposition of perbenzoic acid was shown there by the reaction with methyl methacrylate. Nitrons induce also free radical decomposition of free radical initiators, ref., A. R. Forrester and S. P. Hepburn, *J. Chem. Soc. C*, **1971**, 701.

18) M. Yoshida, N. Furuta, and M. Kobayashi, *Bull. Chem. Soc. Jpn.*, **54**, 2356 (1981).

 © 1987 The Chemical Society of Japan Bull. Chem. Soc. Jpn., 60, 3331—3336 (1987)

Photochemical Reactions of Contact Charge-Transfer Pairs of 1-Arylcyclohexenes and Oxygen

Masanobu KOJIMA,* Hirochika SAKURAGI,† and Katsumi TOKUMARU†,*
Department of Chemistry, Faculty of Liberal Arts, Shinshu University, Asahi, Matsumoto 390
†Department of Chemistry, University of Tsukuba, Sakura-mura, Ibaraki 305
(Received April 7, 1987)

Photoexcitation of contact charge-transfer (CCT) pairs of 1-arylcyclohexenes **1** (aryl: phenyl, 4-methylphenyl, and 4-methoxyphenyl) and oxygen in acetonitrile and benzene gave 1,2-epoxy-1-arylcyclohexanes **2** as major products together with 2-aryl-2-cyclohexen-1-ols and acetophenones **4**. Similar irradiation of the CCT pairs in methanol/acetonitrile afforded mainly 2-aryl-2-methoxycyclohexanols instead of **2** and small amounts of 1-aryl-1-methoxycyclohexanes, 2-aryl-2-cyclohexen-1-ones, and **4**. The formation of these products can be explained by photoinduced electron transfer in the excited CCT pairs generating radical cations of **1** and superoxide anions.

Dye-sensitized oxygenation of organic substrates has been extensively investigated.[1,2] However, photochemistry of contact charge-transfer (CCT) pairs of the organic substrates and oxygen has not been so well investigated,[3-5] though spectral evidence for the CCT pairs has been documented.[6-8] Recently, we have reported selective photoexcitation of the CCT pairs of some organic compounds and molecular oxygen leading to specific reactions, in which their radical cations and superoxide anions play important roles. These reactive intermediates, after generation through electron transfer in the excited CCT pairs, can produce other reactive intermediates, for example, a) neutral free radicals through deprotonation of the radical cations, b) carbocations through electron transfer of the free radicals, and c) singlet oxygen through back electron transfer between the radical cations and superoxide anions.[9-12] The CCT pairs of olefins, such as 4-methoxy- and 4-methylstyrene, and oxygen in acetonitrile afforded, on excitation, their dimers accompanied by small amounts of their oxygenated products.[10,12] The reaction proceeds through their radical cations, which undergo addition to the ground-state olefin to give dimeric radical cations followed by electron transfer probably from superoxide anions. We now report structure dependence of the reaction course of excited CCT pairs of aromatic olefins and oxygen; 1-arylcyclohexenes (aryl: phenyl, 4-methylphenyl, and 4-methoxyphenyl) give mainly the corresponding epoxides or their derivatives in contrast to the above styrene derivatives.

Experimental

^{13}C NMR spectra were recorded on a JEOL FX-90Q spectrometer with TMS as an internal standard. Infrared and UV spectra were measured on a Hitachi 260-10 and a Shimadzu UV-300 spectrophotometer, respectively. Mass spectra were determined on a Shimadzu QP-1000 mass spectrometer.

Materials. 1-Phenylcyclohexene (**1a**),[13] 1-(4-methylphenyl)cyclohexene (**1b**),[13] and 1-(4-methoxyphenyl)cyclohexene (**1c**)[14] were prepared by the reaction of cyclohexanone with the corresponding 4-substituted phenylmagnesium bromide followed by treatment with 4-methylbenzenesulfonic acid in benzene.

1,2-Epoxy-1-phenylcyclohexane (**2a**)[15] was prepared from 2-bromo-1-phenylcyclohexanol by treatment with an aqueous potassium hydroxide solution;[16] bp 94 °C/5 Torr (1 Torr=133.322 Pa).

1-Methoxy-1-phenylcyclohexane (**6a**)[17] and 2-phenyl-2-cyclohexen-1-one (**7a**)[18] were prepared as previously described.

Acetonitrile, methanol, and benzene (guaranteed reagents) were purchased from Wako Pure Chemical Industries, and distilled before use.

Absorption Spectra of CCT Pairs. Samples of **1** (neat or 1 mol dm^{-3} in benzene) were placed in a sample cell and a reference cell, and a stream of oxygen was passed for several minutes through the sample in the sample cell, and a stream of argon through the sample in the reference cell. Immediately after a spectrum was measured, argon was passed through the sample cell and a spectrum was again recorded. The band observed under oxygen atmosphere disappeared completely by argon bubbling.

Measurements of Oxidation Potentials. Oxidation potentials of olefins **1**'s were determined by cyclic voltammetry using a three-electrode cell with a Nikko Keisoku NPG-501 potentiogalvanostat and a Nikko Keisoku NFG-3 function generator. The working electrode was a platinum wire (diameter, 1 mm) sealed into glass and a counter electrode was a platinum gauze. A saturated caromel electrode (SCE) was used as a reference electrode and tetraethylammonium perchlorate (0.1 mol dm^{-3}) as a supporting electrolyte. The current-potential curves were recorded directly from the output of the potentiogalvanostat on a Watanabe WX-1000 X-Y recorder. The oxidation potentials were 1.59, 1.51, and 1.28 V (vs. SCE) for **1a**, **1b**, and **1c**, respectively.

Irradiations. Photochemical reactions were carried out with a 400 W high-pressure mercury lamp (Riko UVL-400HA) and a 160 W low-pressure mercury lamp (Riko UVL-160LA). The irradiation mixtures were analyzed on a Shimadzu GC-8A gas chromatograph equipped with a flame ionization detector using 3.2 mm×2 m glass columns

packed with Silicone OV-17 (2%, Chromosorb W AW-DCMS, 60—80 mesh) and FON (10%, Chromosorb W AW-DCMS, 80—100 mesh). An internal standard (1,2-diphenylethane) was used to determine composition of the reaction mixtures.

Irradiation of 1-Arylcyclohexenes (1). In Acetonitrile: A solution (3 cm^3) of **1a** (0.1 mol dm^{-3}) in acetonitrile was irradiated under oxygen atmosphere for 9 h at 20 °C in a Pyrex tube with a 400 W high-pressure mercury lamp. GLPC analysis of the sample revealed the formation of 1,2-epoxy-1-phenylcyclohexane (**2a**, 22%), 2-phenyl-2-cyclohexen-1-ol (**3a**, 6%), and acetophenone (**4a**, 4%) at 68% consumption of **1a**.

Cyclohexene **1a** (3.16 g, 20 mmol) was irradiated in acetonitrile (200 cm^3) under oxygen with the high-pressure mercury lamp for 3.5 h. The reaction mixture was concentrated and chromatographed on silica gel under pressure. Epoxide **2a** was isolated and the structure was determined by comparing its ^{13}C NMR spectra with those of an authentic sample.

In Benzene: A solution (3 cm^3) of **1a** (0.1 mol dm^{-3}) in benzene was irradiated for 9 h in a similar way to that in acetonitrile. The yields of **2a** (22%), **3a** (8%), and **4a** (3%) were determined by GLPC.

In Methanol/Acetonitrile: A solution (3 cm^3) of **1a** (0.1 mol dm^{-3}) in a mixture of methanol and acetonitrile (1:2 by volume) in a Pyrex tube was irradiated under oxygen atmosphere with a 400 W high-pressure mercury lamp for 20 h at 20 °C. GLPC analysis of the reaction mixture showed almost complete consumption of **1a** and the formation of **4a** (9%), 2-methoxy-2-phenylcyclohexanol (**5a**, 30%), 1-methoxy-1-phenylcyclohexane (**6a**, 2%), and 2-phenyl-2-cyclohexen-1-one (**7a**, 5%).

A solution of **1a** (0.1 mol dm^{-3}) was similarly irradiated in the mixed solvent under argon atmosphere. No reaction products were detected in the irradiation mixture by GLPC analysis.

Cyclohexene **1a** (3.96 g, 25 mmol) was irradiated under oxygen in a 1:2 methanol–acetonitrile mixture (250 cm^3) with the high-pressure mercury lamp for 21 h. The reaction mixture was concentrated and chromatographed on silica gel under pressure. Cyclohexanol **5a** was isolated together with **4a**, **6a**, and **7a**. GLPC and ^{13}C NMR spectra showed that **5a** consisted of two stereoisomers.

2-Methoxy-2-phenylcyclohexanol (**5a**).[19] Isomer **5a**-A: ^{13}C NMR($CDCl_3$) δ=141.0 (s), 127.3 (d), 126.5 (d), 126.3 (d), 79.6 (s), 74.8 (d), 48.9 (q), 29.6 (t), 23.0 (t), and 20.6 (t); MS (70 eV) *m/z* (rel intensity) 206 (M^+, 34), 147 (100), 121 (75), 105 (44), 91 (49), and 77 (40); isomer **5a**-B: ^{13}C NMR($CDCl_3$) δ=142.6 (s), 128.0 (d), 127.2 (d), 127.0 (d), 79.5 (s), 73.2 (d), 49.0 (q), 28.1 (t), 24.0 (t), 20.5 (t), and 18.9 (t); MS (70 eV) *m/z* (rel intensity) 206 (M^+, 29), 147 (100), 121 (51), 105 (40), 91 (37), and 77 (32).

A solution (3 cm^3) of epoxide **2a** (0.069 mol dm^{-3}) in a 1:2 methanol–acetonitrile mixture was irradiated in a Pyrex tube with a 400 W high-pressure mercury lamp for 9 h. GLPC analysis showed that **5a** was produced in 65% yield at 24% conversion of **2a**.

Cyclohexene **1b** (3.5 g, 20 mmol) was irradiated in a 1:2 methanol–acetonitrile mixture (200 cm^3) under oxygen with a 400 W high-pressure mercury lamp for 16 h. The reaction mixture was concentrated and chromatographed on silica gel under pressure. 2-Methoxy-2-(4-methylphenyl)cyclohexanol (**5b**), 1-methoxy-1-(4-methylphenyl)cyclohexane (**6b**), and 2-(4-methylphenyl)-2-cyclohexen-1-one (**7b**) were isolated (Table 1).

Similarly, when **1c** (0.1 mol dm^{-3}) was irradiated in a 2:3 methanol–acetonitrile mixture (50 cm^3) under oxygen in a uranium glass tube with a 400 W high-pressure mercury lamp for 39 h. 2-Methoxy-2-(4-methoxyphenyl)cyclohexanol (**5c**) and 1-methoxy-1-(4-methoxyphenyl)cyclohexane (**6c**) were isolated from the irradiation mixture (Table 1).

2-Methoxy-2-(4-methylphenyl)cyclohexanol (**5b**). Isomer **5b**-A: ^{13}C NMR ($CDCl_3$) δ=138.0 (s), 135.9 (s), 128.2 (d), 126.6 (d), 79.6 (s), 74.9 (d), 48.9 (q), 29.6 (t), 23.1 (t), 20.9 (t), and 20.3 (q); MS (70 eV) *m/z* (rel intensity) 220 (M^+, 30), 161 (100), 135 (74), 105 (43), and 91 (36); isomer **5b**-B: ^{13}C NMR($CDCl_3$) δ=139.6 (s), 136.4 (s), 128.6 (d), 126.8 (d), 79.2 (s), 72.9 (d), 48.7 (q), 28.0 (t), 23.8 (t), 20.4 (t and q), and 18.8 (t); MS (70 eV) *m/z* (rel intensity) 220 (M^+, 28), 161 (100), 159 (43), 135 (74), 105 (72), and 91 (49). Found (for mixture of the isomers): C, 76.09; H, 8.85%. Calcd for $C_{14}H_{20}O_2$: C, 76.33; H, 9.15%.

1-Methoxy-1-(4-methylphenyl)cyclohexane (**6b**): bp 102—103 °C/5 Torr; ^{13}C NMR($CDCl_3$) δ=142.8 (s), 136.0 (s), 128.7 (d), 125.9 (d), 76.9 (s), 49.1 (q), 35.4 (t), 25.6 (t), 21.9 (t), and 20.8 (q); MS (70 eV) *m/z* (rel intensity) 204 (M^+, 33), 161 (100), 129 (17), and 105 (27). Found: C, 82.57; H, 10.06%. Calcd for $C_{14}H_{20}O$: C, 82.30, H, 9.87%.

2-(4-Methylphenyl)-2-cyclohexen-1-one (**7b**):[20] ^{13}C NMR ($CDCl_3$) δ=197.9 (s), 147.2 (d), 140.1 (s), 137.0 (s), 133.5 (s), 128.5 (d), 128.3 (d), 38.9 (t), 26.4 (t), 22.8 (t), and 20.9 (q); MS (70 eV) *m/z* (rel intensity) 186 (M^+, 100), 130 (51), 129 (43), and 115 (49).

2-Methoxy-2-(4-methoxyphenyl)cyclohexanol (**5c**). Isomer **5c**-A: ^{13}C NMR ($CDCl_3$) δ=158.6 (s), 133.3 (s), 128.2 (d), 113.5 (d), 79.7 (s), 75.4 (d), 55.1 (q), 49.4 (q), 30.0 (t), 23.3 (t), and 21.4 (t); MS (70 eV) *m/z* (rel intensity) 236 (M^+, 39), 177 (100), 151 (90), and 121 (30); isomer **5c**-B: ^{13}C NMR($CDCl_3$) δ=159.2 (s), 134.6 (s), 128.6 (d), 114.0 (d), 79.5 (s), 73.7 (d), 55.3 (q), 49.3 (q), 28.2 (t), 24.4 (t), 20.9 (t), and 19.3 (t); MS (70 eV) *m/z* (rel intensity) 236 (M^+, 36), 177 (100), 151 (84), and 121 (30). Found (for mixture of the isomers): C, 70.89; H, 8.73%. Calcd for $C_{14}H_{20}O_3$: C, 71.16; H, 8.53%.

1-Methoxy-1-(4-methoxyphenyl)cyclohexane (**6c**): bp 123 °C/6 Torr; ^{13}C NMR ($CDCl_3$) δ=158.5 (s), 137.9 (s), 127.3 (d), 113.6 (d), 55.1 (q), 49.3 (q), 35.5 (t), 25.7 (t), and 22.1 (t); MS (70 eV) *m/z* (rel intensity) 220 (M^+, 72), 189 (62), 177 (100), and 121 (73). Found: C, 76.53; H, 9.30%. Calcd for $C_{14}H_{20}O_2$: C, 76.33; H, 9.15%.

Dye-Sensitized Oxygenation of 1a. A solution (50 cm^3) of **1a** (1g, 6.32 mmol) in a 1:2 methanol–acetonitrile mixture containing Methylene Blue (50 mg, 0.134 mmol) was put in five uranium glass tubes (10 cm^3 each), and irradiated for 40 h under oxygen atmosphere through a filter solution of K_2CrO_4 (0.27 g dm^{-3}) and Na_2CO_3 (1 g dm^{-3}). The combined reaction mixture was evaporated in vacuo and 2-phenyl-2-cyclohexenyl hydroperoxide was isolated from the residue by flash-column chromatography[21] using a 1:3 hexane–benzene as an eluent. This compound was decomposed into cyclohexenol **3a** and cyclohexenone **7a** (**3a**/**7a**=1/1) in the GLPC column (240 °C). Reduction of the hydroperoxide by $NaBH_4$ gave cyclohexenol **3a** as a sole product. The yield of the peroxide was determined by

GLPC analysis after treatment with $NaBH_4$.

2-Phenyl-2-cyclohexenyl hydroperoxide (**8a**):[22] ^{13}C NMR ($CDCl_3$) δ=140.3 (s), 133.5 (s), 132.3 (d), 127.9 (d), 126.5 (d), 125.4 (d), 78.6 (d), 25.9 (t), 25.8 (t), and 16.2 (t).

2-Phenyl-2-cyclohexen-1-ol (**3a**):[23] ^{13}C NMR($CDCl_3$) δ=140.3 (s), 139.1 (s), 128.2 (d), 126.8 (d), 125.9 (d), 65.2 (d), 31.6 (t), 26.0 (t), and 17.2 (t); MS (70 eV) *m/z* (rel intensity) 174 (M^+, 68), 117 (53), 115 (56), and 91 (100).

Photooxidation of 1a in the Presence of 2,3-Dimethyl-2-butene (TME) and 1,4-Diazabicyclo[2.2.2]octane (DABCO). A solution (3 cm^3) of **1a** (0.1 mol dm^{-3}) in a 1:2 methanol–acetonitrile mixture containing TME (0.1 mol dm^{-3}) in a Pyrex tube was irradiated under oxygen atmosphere with a 400 W high-pressure mercury lamp for 20 h at 20 °C. GLPC analysis of the irradiation mixture showed that the yields and distribution of the products are quite similar to those in the photooxidation of **1a** in the absence of TME. The results are shown in Table 2.

Under similar conditions, **1a** (0.1 mol dm^{-3}) was irradiated with DABCO (0.1 mol dm^{-3}) for 20 h. The olefin was recovered almost quantitatively and trace amounts of **2a** and **4a** were detected by GLPC analysis.

Autoxidation of 1a. A solution (10 cm^3) of **1a** (0.1 mol dm^{-3}) in a 1:2 methanol–acetonitrile mixture containing AIBN (30 mg, 0.22 mmol) was heated at 65 °C for 20 h in an oxygen stream in the dark. The yields of the products, **2a**, **3a**, and **5a**, were determined by GLPC, and are shown in Table 1. **4a** and **6a** were not detected at all.

Results and Discussion

Absorption Spectra of the CCT Pairs of 1-Arylcyclohexenes and Oxygen. Under oxygen atmosphere, 1-phenylcyclohexene (**1a**) (neat or in benzene solution) exhibited a new weak absorption in the range of 320—400 nm. 1-(4-Methylphenyl)- (**1b**) and 1-(4-methoxyphenyl)cyclohexene (**1c**) also showed new absorptions at 320—410 and 325—450 nm, respectively, under similar conditions. These bands disappeared reversibly on introduction of argon to their solutions to exclude oxygen. These bands can be reasonably assigned to the CCT pairs of **1** and oxygen.[10,12]

Irradiation of the CCT Pairs of 1-Arylcyclohexenes and Oxygen. Selective irradiation into the CCT band of **1a** and oxygen in acetonitrile (effective wavelength of light: 313 nm) afforded 1,2-epoxy-1-phenylcyclohexane (**2a**, 22% based on **1a** consumed) together with 2-phenyl-2-cyclohexen-1-ol (**3a**, 6%), and acetophenone (**4a**, 4%). Similar irradiation of **1a** in benzene gave nearly the same distribution of the products (Table 1). However, in a mixture of methanol and acetonitrile (1:2 by volume) 2-methoxy-2-phenylcyclohexanol (**5a**, 30%) instead of epoxide **2a** was a main product, accompanying 1-methoxy-1-phenylcyclohexane (**6a**, 2%), 2-phenyl-2-cyclohexen-1-one (**7a**, 5%), and **4a** (9%). The formation of **5a** is assumed to be due to (photochemical) methanolysis of **2a** as a primary product since, in a control experiment, irradiation of **2a** with 313 nm light gave **5a** (a mixture of the cis- and trans-isomers) in a methanol–acetonitrile mixture.

However, on irradiation of **1a** under argon with 313 nm light in a methanol–acetonitrile mixture, no reaction products were detected by GLPC analyses. Also, on direct excitation of **1a** with 254 nm light, no products were obtained and the starting **1a** was recovered quantitatively both under argon and under oxygen. From these results it is reasonably concluded that all the products result from a sequence of reaction of the excited CCT pairs.

Table 1. Yields of Products on Irradiation and Autoxidation of 1-Arylcyclohexenes **1** under Oxygen in Solvents

Substrate	Additive	Solvent	Atmosphere	Irrad. wavelength /nm[b]	React. time /h	Conv. /%	Yield[a]/%				
							2	**3**[c]	**4**	**5**	**6**
1a	—	MeCN	O_2	313	9	68	22	6	4	—	—
	—	PhH	O_2	313	9	38	22	8	3	—	—
	—	PhH	O_2	313	20	66	28	6	4	—	—
	—	MeOH/MeCN	O_2	254	15	0	—	—	—	—	—
	—	MeOH/MeCN	Ar	254	15	0	—	—	—	—	—
	—	MeOH/MeCN	O_2	313	20	95	Trace	6	9	30	2
	—	MeOH/MeCN	Ar	313	20	0	—	—	—	—	—
	AIBN/65 °C[d]	MeOH/MeCN	O_2	—	20	53	8	4	—	46	—
	AIBN/65 °C	PhH	O_2	—	20	60	43	6	—	—	—
1b	—	MeOH/MeCN	O_2	313	15	96	—	3[e]	2	23	8
	—	MeOH/MeCN	Ar	313	15	0	—	—	—	—	—
1c	—	MeOH/MeCN	O_2	366	20	98	—	—	Trace	59	13
	—	MeOH/MeCN	Ar	366	20	6	—	—	—	—	Trace

a) Yields of products: [(moles of products)/(moles of **1** consumed)] × 100. The conversions of olefins **1** and the yields of the products were determined by GLPC analyses. b) Effective excitation wavelength. c) The sum of cyclohexenol **3** and cyclohexenone **7**. d) AIBN: azobisisobutyronitrile. e) The yield of cyclohexenone **7b**.

Irradiation into the CCT bands of 1-(4-methylphenyl)- (**1b**) and 1-(4-methoxyphenyl)cyclohexene (**1c**) under oxygen in a methanol–acetonitrile mixture led to similar results to the case of **1a** as shown in Table 1; **1b** afforded 2-methoxy-2-(4-methylphenyl)cyclohexanol (**5b**), 1-methoxy-1-(4-methylphenyl)cyclohexane (**6b**), 2-(4-methylphenyl)-2-cyclohexen-1-one (**7b**), and 1-(4-methylphenyl)ethanone (**4b**), and **1c** gave 2-methoxy-2-(4-methoxyphenyl)cyclohexanol (**5c**), 1-methoxy-1-(4-methoxyphenyl)cyclohexane (**6c**), and 1-(4-methoxyphenyl)ethanone (**4c**).

Some control experiments were carried out to examine oxygen species involved in the present oxygenation. In Methylene Blue(MB)-sensitized photooxygenation of **1a**, 2-phenyl-2-cyclohexenyl hydroperoxide (**8a**), which is known as a product in singlet oxygen oxygenation of **1a**,[22] was solely isolated (45%), but none of the products obtained from the CCT pair excitation was detected. Accordingly, it can be concluded that singlet oxygen is not associated with the reactions induced by CCT pair excitation of **1**.[10,11]

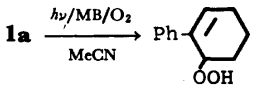

8a

Furthermore, addition of 2,3-dimethyl-2-butene (TME), a highly reactive singlet oxygen trap, brought about no effects on the product distribution in the CCT pair excitation of **1a** in a methanol–acetonitrile mixture (Table 2).

When **1a** was irradiated under oxygen in a methanol–acetonitrile mixture in the presence of 1,4-diazabicyclo[2.2.2]octane (DABCO), only trace amounts of **2a** and **6a** were formed (Table 2). DABCO works not only as a singlet oxygen quencher but also

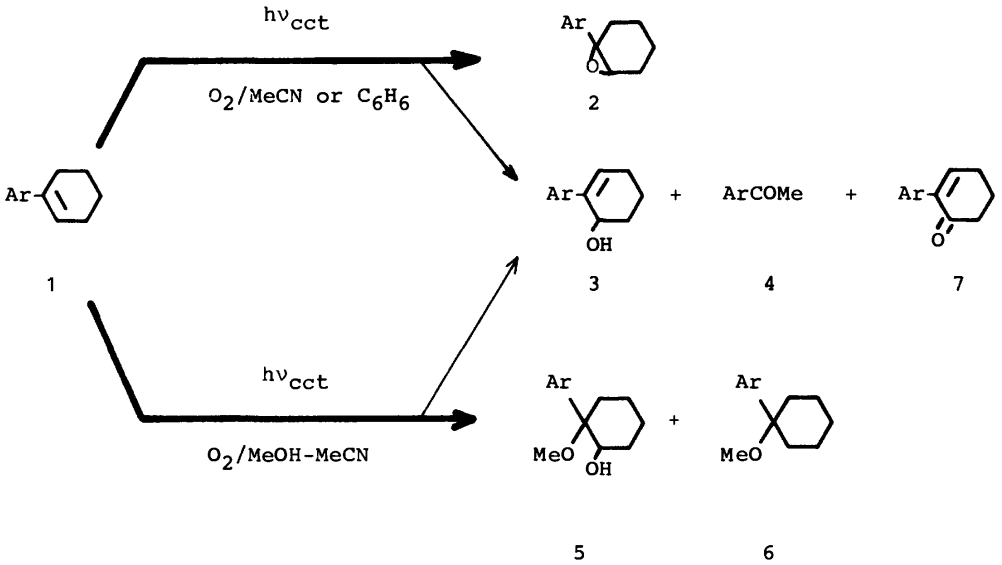

Scheme 1. **1a**: Ar=Ph; **1b**: Ar=4-MeC$_6$H$_4$; **1c**: Ar=4-MeOC$_6$H$_4$.

Table 2. Effects of 2,3-Dimethyl-2-butene (TME) and 1,4-Diazabicyclo[2.2.2]octane (DABCO) on Irradiation of 1-Arylcyclohexenes (**1**) under Oxygen in MeOH/MeCN

Substrate	Additive	Irrad. wavelength /nm[b]	Conversion /%	Yield[a]/%				
				2	**3**[c]	**4**	**5**	**6**
1a	—	313	95	Trace	6	9	30	2
	TME	313	83	Trace	5	9	34	4
	DABCO	313	12	Trace	—	—	—	—
	MB[d]	>400	97	—	45[e]	—	—	—
1c	—	366	98	—	—	Trace	59	13
	TME	366	94	—	—	Trace	62	25
	DABCO	366	8	—	—	—	—	—

a) Yields of products: [(moles of products)/(moles of **1** consumed)] × 100. b) Effective excitation wavelength. c) The sum of cyclohexenol **3** and cyclohexenone **7**. d) Methylene Blue(MB)-sensitized oxygenation. e) The yield of hydroperoxide **8a**, which was determined by GLPC analysis after treatment with sodium borohydride.

as an electron-donating quencher. Since the oxidation potential of DABCO (E_{ox}: 0.68 V vs. SCE) is by ca. 0.9 V lower than that of **1a** (1.59 V) and, as mentioned above, TME does not affect the photoreaction of the CCT pairs of **1a**, it is reasonably supposed that **1a** radical cations generated from the excited CCT pairs were reduced by DABCO, thus recovering **1a**.

Reaction Course of Excited CCT Pairs. The above product study shows that the photochemical reactions take place only when the CCT pairs of **1** and oxygen were excited. The main product is epoxide **2** in acetonitrile and benzene; however, in the presence of methanol **2** is converted into methoxyalcohol **5**.

Azobisisobutyronitrile(AIBN)-initiated autoxidation of **1a** also gave **2a** as a main product (Table 1). As already reported, β-alkoxystyrenes give, on excitation of their CCT pairs with oxygen, the corresponding epoxides through an olefin–oxygen copolymerization process together with carbonyl compounds resulting from oxidative cleavage of the double bond.[24,25] Therefore, similar processes may be operative in the present oxygenation of **1** (Scheme 2).

More remarkable is the formation of 1-methoxy-1-arylcyclohexanes **6**, Markownikoff adducts of methanol to **1**. It is well-known that *trans*-cyclohexenes react with methanol to give addition products such as **6a**.[26–31] The adducts **6** were formed on excitation of the CCT pairs with oxygen, but not on direct excitation of the olefins under argon. Therefore, it is probable that excitation of the CCT pair leads to the formation of the triplet state of **1** [triplet energy (E_T) of **1a**: 56±3 kcal mol^{-1}],[32,33] which is deactivated from its twisted geometry to the *trans*-cyclohexene in the ground state. The cyclohexene triplets may be generated by back electron transfer between the olefin radical cations and superoxide anions, the energy of these pairs being 57 kcal mol^{-1} over the ground state as estimated from their electrochemical potentials.[34] The yields of ethers **6** were increased by introduction of an electron-donating group on the aromatic ring of **1a** (**6a**, 2%; **6b**, 8%; **6c**, 13%), probably because of increase in electron density on the double bond of *trans*-arylcyclohexene with increasing electron-donating ability of the substituent.[36]

Another possibility for **6** formation might be a reaction of the **1** radical cation with methanol followed by electron transfer and protonation. However, this possibility can be ruled out since addition of methanol to the **1** radical cation is assumed to take place at the 2-position of **1** on the basis of cyanoaromatics-sensitized addition of methanol to **1a**.[37] The present results indicate that the **1** radical

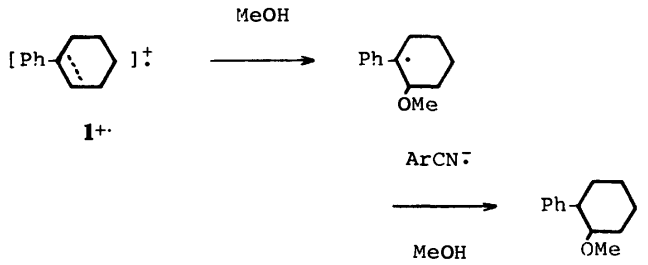

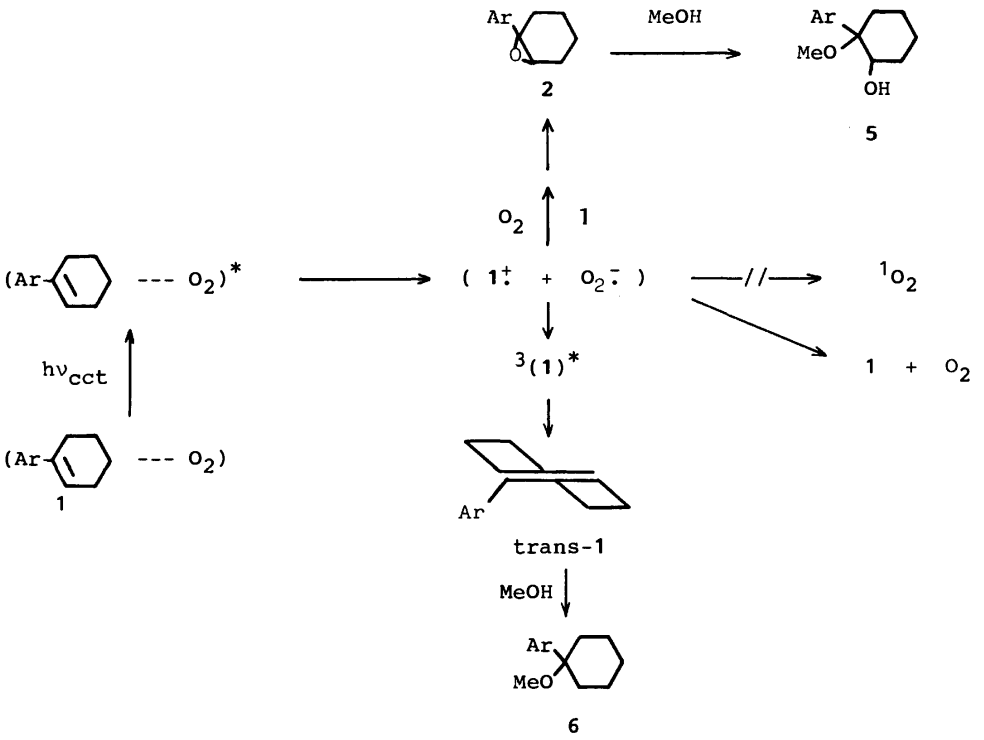

Scheme 2.

cations react probably with superoxide anions to give either some radical intermediates initiating autoxidation of **1** affording the epoxides or the triplet **1** decaying to *trans*-**1** (Scheme 2).

Photochemical behavior of CCT pairs of arylcyclohexenes **1** is in contrast with that of 4-methoxystyrene which gives a dimeric product as reported previously.[10,12] The difference in the reaction course between these CCT pairs may be associated with reactivity of the olefins towards their radical cations. Generally, trisubstituted and 1,2-disubstituted olefins are less reactive than monosubstituted olefins in free radical addition reactions,[38] whereas **1a** undergoes photodimerization in the excited state.[31,39] Therefore, it is reasonably supposed that arylcyclohexenes **1** are not so reactive with their radical cations as 4-methoxystyrene with its radical cation. As a result, the radical cations of **1** react with superoxide anion or oxygen rather than with **1**.

The authors thank the Ministry of Education, Science and Culture for partial support of this work by Grant-in-Aid for Scientific Research to M. K. (Nos. 60740269 and 61740286). The authors are also grateful to Dr. Hiroaki Misawa, University of Tsukuba, for helpful discussions.

References

1) "Singlet Oxygen," ed by H. H. Wasserman and R. W. Murry, Academic Press, New York, N. Y. (1979).
2) A. A. Frimer, *Chem. Rev.*, **79**, 359 (1979).
3) K. S. Wei and A. H. Adelman, *Tetrahedron Lett.*, **38**, 3297 (1969).
4) V. I. Stenberg, R. D. Olson, C. T. Wang, and N. Kulevsky, *J. Org. Chem.*, **32**, 3227 (1967); V. I. Stenberg, C. H. Wang, and N. Kulevsky, *J. Org. Chem.*, **35**, 1774 (1970).
5) R. C. Petterson, *Angew. Chem., Int. Ed. Engl.*, **9**, 644 (1970).
6) D. F. Evans, *J. Chem. Soc.*, **1953**, 345; D. F. Evans, *ibid.*, **1957**, 1351.
7) H. Tsubomura and R. S. Mulliken, *J. Am. Chem. Soc.*, **82**, 5966 (1960).
8) M. Tamres and R. L. Strong, "Molecular Association," ed by R. Foster, Academic Press, London (1979), Vol. 2, p. 331.
9) K. Onodera, H. Sakuragi, and K. Tokumaru, *Tetrahedron Lett.*, **21**, 2831 (1980).
10) M. Kojima, H. Sakuragi, and K. Tokumaru, *Tetrahedron Lett.*, **22**, 2889 (1981).
11) H. Sakuragi, G. Furusawa, K. Ueno, and K. Tokumaru, *Chem. Lett.*, **1982**, 1213.
12) K. Onodera, G. Furusawa, M. Kojima, M. Tsuchiya, S. Aihara, R. Akaba, H. Sakuragi, and K. Tokumaru, *Tetrahedron*, **41**, 2215 (1985).
13) E. J. Garbisch, Jr., *J. Org. Chem.*, **26**, 4165 (1961).
14) S. Murahashi and I. Moritani, *Bull. Chem. Soc. Jpn.*, **41**, 1884 (1968).
15) G. Berti, F. Bottari, B. Macchia, and F. Macchia, *Tetrahedron*, **21**, 3277 (1965).
16) B. A. Marples and C. G. Saint, *Synth. Commun.*, **12**, 545 (1982).
17) H. M. Rosenberg and M. P. Serve, *J. Org. Chem.*, **37**, 141 (1972).
18) W. E. Bachmann and L. B. Wick, *J. Am. Chem. Soc.*, **72**, 3388 (1950).
19) C. Battistini, P. Crotti, D. Damiani, and F. Macchia, *J. Org. Chem.*, **44**, 1643 (1979).
20) Elphimoff-Felkin and P. Sarda, *Tetrahedron*, **31**, 2781 (1975).
21) W. C. Still, M. Kahn, and A. Mitra, *J. Org. Chem.*, **43**, 2923 (1978).
22) C. W. Jefford and C. G. Rimbault, *Tetrahedron Lett.*, **1976**, 2479.
23) D. Ginsburg and R. Pappo, *J. Chem. Soc.*, **1951**, 516.
24) T. Kanno, M. Hisaoka, H. Sakuragi, and K. Tokumaru, *Bull. Chem. Soc. Jpn.*, **54**, 2330 (1981).
25) F. R. Mayo, *Acc. Chem. Res.*, **1**, 193 (1968), and references therein.
26) P. J. Kropp, *J. Am. Chem. Soc.*, **91**, 5783 (1969).
27) S. Fujita, Y. Hayashi, T. Nomi, and H. Nozaki, *Tetrahedron*, **27**, 1607 (1971).
28) M. Tada and H. Shinozaki, *Bull. Chem. Soc. Jpn.*, **43**, 1270 (1970).
29) R. Bonneau, J. Joussot-Dubien, L. Salem, and A. J. Yarwood, *J. Am. Chem. Soc.*, **98**, 4329 (1976).
30) W. G. Dauben, H. C. H. A. van Riel, C. Hauw, F. Leroy, J. Joussot-Dubien, and R. Bonneau, *J. Am. Chem. Soc.*, **101**, 1901 (1979).
31) W. G. Dauben, H. C. H. A. van Riel, J. D. Robbins, and G. J. Wagner, *J. Am. Chem. Soc.*, **101**, 6383 (1979).
32) P. M. Crosby, J. M. Dyke, J. Metcalfe, A. J. Rest, K. Salisbury, and J. R. Sodeau, *J. Chem. Soc., Perkin Trans. 2*, **1977**, 182.
33) J. L. Goodman, K. S. Peters, H. Misawa, and R. A. Caldwell, *J. Am. Chem. Soc.*, **108**, 6802 (1986).
34) Estimated as $E(D^{+\cdot}/D)-E(O_2/O_2^{-\cdot})$ where $E(D^{+\cdot}/D)=1.59$ V and $E(O_2/O_2^{-\cdot})=-0.87$ V vs. SCE.[35]
35) D. T. Sawyer, G. Chiericato, Jr., C. T. Angelis, E. J. Nanni, Jr., and T. Tsuchiya, *Anal. Chem.*, **54**, 1720 (1982).
36) H. Misawa and R. A. Caldwell, private communication.
37) Y. Shigemitsu and D. R. Arnold, *J. Chem. Soc., Chem. Commun.*, **1975**, 407.
38) C. Walling, "Free Radicals in Solution," John Wiley and Sons, New York (1957), Chapters 6 and 7.
39) R. S. Davidson and T. D. Whalen, *J. Chem. Soc., Chem. Commun.*, **1977**, 361.

 © 1987 The Chemical Society of Japan Bull. Chem. Soc. Jpn., 60, 3337—3340 (1987)

Nitrone Cycloaddition Route to the 1β-Methylcarbapenem Key Intermediate[1,2]

Yoshio Ito, Yoshikazu Kimura, and Shiro Terashima*
Sagami Chemical Research Center, Nishi-Ohnuma, Sagamihara, Kanagawa 229
(Received April 11, 1987)

The 1β-methylcarbapenem key intermediate, (3*S*,4*S*)-3-[(*R*)-1-(*t*-butyldimethylsilyloxy)ethyl]-4-[(*R*)-1-carboxyethyl]-2-azetidinone, was prepared from (*S*)-methyl 3-hydroxy-2-methylpropionate by employing 1,3-dipolar cycloaddition of the chiral nitrone with benzyl crotonate as a key reaction.

Since its development first by Kametani[3,4] and later by Stevens,[5] the nitrone cycloaddition route has been recognized as one of the most reliable methods of preparing several structural types of carbapenem key intermediates.[4] The preparation of optically active carbapenem key intermediates has been also accomplished by the same methodology which utilizes the chiral nitrones derived from (*R*)-(+)-*N*-(α-phenylethyl)hydroxylamine[6] or (−)-menthyl glyoxylate hydrate.[7]

Based on these successful results so far reported,[3-7] we examined to explore the nitrone cycloaddition route for preparing the optically active 1β-methylcarbapenem key intermediate (**1**). The novel nitrone (**2**) obtainable from commercially available (*S*)-methyl 3-hydroxy-2-methylpropionate (**3**), was employed as a dipole by expecting that the chiral center involved in **2** may control the steric course of addition reaction in a

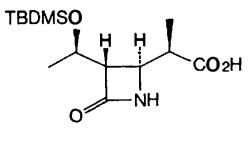

1

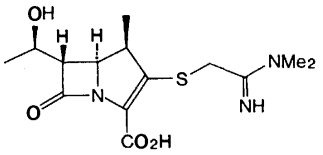

4

desired sence. The 1β-methylcarbapenem such as **4** is currently well-known as the synthetic carbapenem antibiotic showing excellent antibacterial activity, chemical stability, and insensitivity to renal dipeptidase-I.[8] We wish to report here that, while the control of steric course of cycloaddition reaction is not realized contrary to our expectation, the synthetic scheme can really produce optically pure **1** starting from **3**.

As shown in Scheme 1, sequential silylation of **3** and reduction of the methyl ester (**5**) gave the chiral aldehyde (**6**) in a good combined yield. Treatment of **6** with benzylhydroxylamine[9] produced a 64% yield of the optically active nitrone (**2**). The cycloaddition of **2** with benzyl crotonate was effected by heating 80 °C in toluene, producing the adduct (**7**) in 80% yield. Disappointingly, the 400 MHz NMR spectrum of **7** clearly disclosed that it consisted of almost the same amounts of four possible diastereomers (**7a—d**) in a ratio of 21:29:23:27. This represents that the endo- and exo-additions occur in an almost equal probability and the chiral center of **2** originating from **3** can not control the steric course of addition reaction. The diastereoselectivity could not be improved in favor of the desired diastereomer (**7a**) even by employing various crotonic acid esters and amides and

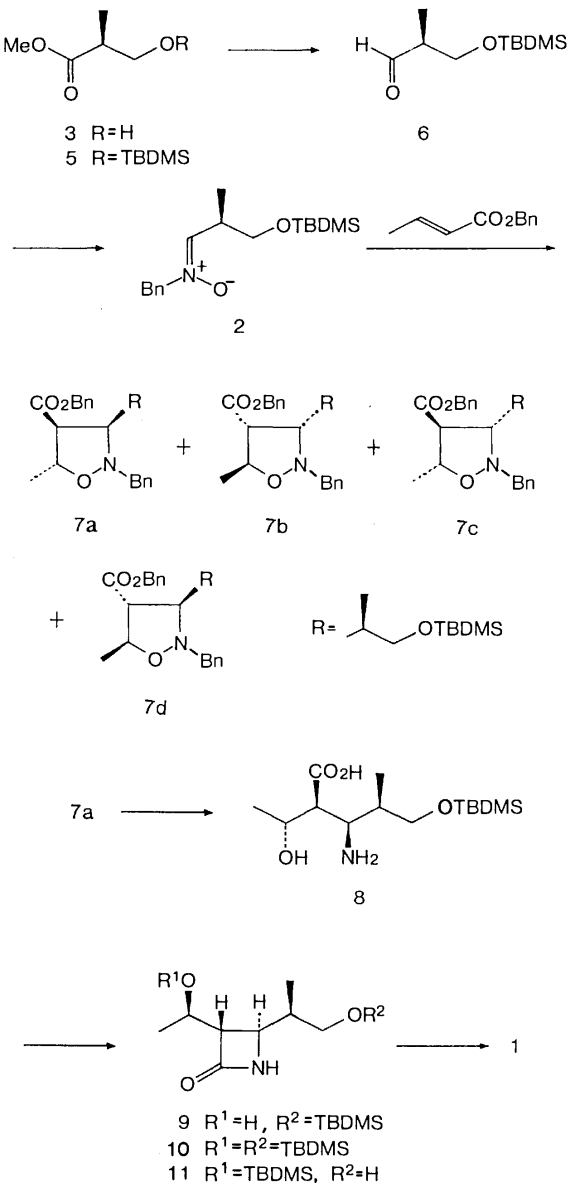

several solvent systems. Accordingly, the selective hydrolysis of **7a—d** was next examined by expecting that the ester groups of the useless $C_{3,4}$-trans adducts (**7c,d**) should be more rapidly saponified than those of the sterically congested $C_{3,4}$-cis isomers (**7a,b**). As expected, when the mixture of **7a—d** was treated with aq barium hydroxide in tetrahydrofuran[10] and the ester mixture (**7a—d**) obtained in 55% recovery was analyzed by 400 MHz NMR spectrum, the ratio of **7a—d** was found to be improved to 34:20:5:41. These results definitely suggest that the orginal reaction product (**7a—d**) contains the $C_{3,4}$-cis- and the $C_{3,4}$-trans-isomers (**7a,b** and **7c,d**) in a ratio of 48(21+27):52(29+23) and the partial saponification increases the ratio of **7a,b** to **7c,d** to 75(34+41):25(20+5).

Since the separation of **7a—d** turned out to be fruitless, the preparation of the optically active β-amino acid (**8**) was attempted by using the ester mixture in which the fraction of **7a** had been enriched. Treatment of **7a—d** under hydrogenolysis conditions followed by careful separation with column chromatography gave **8** from the major fraction in 21% yield,[11] mp 178—179 °C (decomp) and $[\alpha]_D^{20}$ −2.0° (methanol). Although it was quite ambiguous whether the isolated β-amino acid involves the desired stereochemistry, **8** was rigorously verified by obtaining the alcohol (**11**) from this compound.

The optically active β-amino acid (**8**) was lactamized by the Mukaiyama-Ohno method,[12] giving the lactam (**9**) in a quantitative yield, mp 105—106 °C and $[\alpha]_D^{20}$ −8.6° (chloroform). Studies on the ^{1}H NMR spectrum measured in the presence of the chiral shift reagent (Eu(hfc)$_3$) clearly disclosed that each synthetic step to the stage of **9** can proceed without substantial racemization (see Experimental.) Introduction of a *t*-butyldimethylsilyl group into the secondary alcohol of **9**, followed by selective acidic removal of the *t*-butyldimethylsilyl group which protects the primary alcohol of **10**, produced the optically pure alcohol (**11**) in 79% overall yield, mp 89—90 °C and $[\alpha]_D^{20}$ −20.9° (chloroform). This was identified with the authentic sample[13] by spectral comparisons. It has already been established that oxidation of **11** with pyridinium dichromate can produce **1** in 91% yield.[13]

As described above, we have succeeded in developing the new synthetic route to optically pure **1** by featuring the nitrone cycloaddition as a key reaction. The overall scheme may have a practical value if the diastereoselectivity of the addition reaction could be much more improved.

Experimental

General. All melting points were determined with a Yamato MP-21 melting point apparatus and were uncorrected. IR spectral measurements were carried out with a JASCO A-202 diffraction grating infrared spectrometer. ^{1}H NMR spectra were recorded with a Hitachi R-90H spectrometer (90 MHz) and a Bruker AM-400 spectrometer (400 MHz). All signals were expressed as ppm downfield from TMS used as an internal standard (δ value). Mass spectra were taken with a Hitachi RMU-6MG mass spectrometer. Measurements of optical rotations were performed with a Horiba SEPA-200 automatic digital polarimeter. Wakogel C-200 was used as an adsorbent for column chromatography.

(*S*)-(+)-Methyl 3-(*t*-Butyldimethylsilyloxy)-2-methylpropionate (5). *t*-Butyldimethylchlorosilane (1.30 g, 8.6 mmol) was added to a solution of commercially available **3** (1.00 g, 8.5 mmol) and imidazole (1.15 g, 17 mmol) in DMF (10 mL) at rt and the mixture was stirred there for 1.5 h. After H_2O (10 mL) and hexane (20 mL) were added to the reaction mixture, the organic layer was separated and the aqueous layer was extracted with hexane. The combined organic layers were washed with water and dried over anhyd $MgSO_4$. Filtration and concentration in vacuo gave **5** as a colorless oil (1.91 g, 97%). Bulb-to-bulb distillation (120 °C, 14 mmHg†) afforded an analytical sample of **5**. $[\alpha]_D^{20}$ +18.9° (*c* 1.00, $CHCl_3$). IR (neat) 2950, 2860, 1740, 1460, 1255, 1196, 1173, 1096, 833, 775 cm^{-1}. ^{1}H NMR ($CDCl_3$) δ=0.03 (6H, s, Me_2Si), 0.87 (9H, s, Me_3CSi), 1.13 (3H, d, *J*=7.0 Hz, MeCH), 2.64 (1H, m, MeCH), 3.66 (3H, s, COOMe), 3.60—3.80 (2H, m, CH_2O). MS *m/z* 217 $[M-Me]^+$, 201 $[M-MeO]^+$, 175 $[M-t\text{-}Bu]^+$.

(*S*)-(+)-3-(*t*-Butyldimethylsilyloxy)-2-methylpropanal (6). A one mol dm^{-3} solution (8.4 mL) of diisobutylaluminium hydride in hexane was added to a stirred solution of **5** (1.31 g, 5.6 mmol) in Et_2O (18.5 mL) over 5 min at −78 °C. After the stirring was continued at the same temperature for 30 min, the reaction mixture was diluted successively with MeOH (0.09 mL) and H_2O (0.84 mL). The resulting gelatinous mixture was filtered and washed with Et_2O. The filtrate was dried over anhyd $MgSO_4$, concentrated in vacuo, then purified with column chromatography (SiO_2: hexane–EtOAc 9:1), giving **6** as a colorless oil (0.890 g, 78%). Bulb-to-bulb distillation (110 °C, 14 mmHg) gave an analytical sample of **6**. $[\alpha]_D^{20}$ +37.8° (*c* 1.20, $CHCl_3$). IR (neat) 2950, 2860, 1735, 1470, 1256, 1100, 1029, 835, 777 cm^{-1}. ^{1}H NMR ($CDCl_3$) δ=0.00 (6H, s, Me_2Si), 0.82 (9H, s, Me_3CSi), 1.04 (3H, d, *J*=7.0 Hz, MeCH), 2.50 (1H, m, MeCH), 3.78 (2H, d, *J*=5.9 Hz, CH_2O), 9.74 (1H, d, *J*=1.5 Hz, CHO).

(*R*)-(−)-*N*-(3-*t*-Butyldimethylsilyloxy-2-methylpropylidene)benzylamine *N*-Oxide (2). The aldehyde (**6**) (0.600 g, 3.0 mmol) was added dropwise to a mixture of *N*-benzylhydroxylamine[9] (0.368 g, 3.0 mmol) and $CaCl_2$ (0.330 g, 3.0 mmol) in Et_2O (30 mL) at 0 °C. The stirring was continued there for 1 h and at rt for 2 h. After being filtered, the reaction mixture was concentrated in vacuo. The concentration residue was purified with column chromatography (SiO_2: hexane–EtOAc 1:1—0:1) to give **2** as a colorless oil (0.658 g, 64%). $[\alpha]_D^{20}$ −37.7° (*c* 0.89, $CHCl_3$). IR (neat) 2950, 2870, 1595, 1460, 1256, 1098, 840, 780, 702 cm^{-1}. ^{1}H NMR ($CDCl_3$) δ=−0.02, 0.00 (6H, two s, Me_2Si), 0.84 (9H, s, Me_3CSi), 1.10 (3H, d, *J*=6.8 Hz, MeCH), 3.10—3.40 (1H, m, MeCH), 3.63 (2H, m, CH_2O), 4.87 (2H, s, $PhCH_2$), 6.59 (1H, d, *J*=7.0 Hz, CH=N), 7.37 (5H, s, C_6H_5). MS *m/z* 307 $[M]^+$, 292 $[M-Me]^+$, 290 $[M-OH]^+$, 250 $[M-t\text{-}Bu]^+$. Found:

† 1 mmHg=133.322 Pa.

C, 65.86; H, 9.25; N, 4.46%. Calcd for $C_{17}H_{29}NO_2Si$: C, 66.40; H, 9.51; N, 4.55%.

Cycloaddition of (*R*)-(−)-*N*-(3-*t*-Butyldimethylsilyloxy-2-methylpropylidene)benzylamine *N*-Oxide (6) with Benzyl Crotonate. Preparation of a Mixture of the Four Diastereomers of 2-benzyl-4-benzyloxycarbonyl-3-[(*R*)-2-*t*-butyldimethylsilyloxy-1-methylethyl]-5-methylisoxazolidine (**7a**—d). Benzyl crotonate (0.89 g, 5.6 mmol) was added to a solution of **5** (0.86 g, 2.8 mmol) in anhyd toluene (2.8 mL) and the mixture was stirred at 80 °C for 24 h. After toluene and excess benzyl crotonate were distilled off at 110 °C in vacuo, the oily residue was purified with column chromatography (SiO_2: hexane–EtOAc 19:1), giving a mixture of **7a**—d as a colorless oil (1.03 g, 80%). IR (neat) 2950, 2880, 1738, 1454, 1255, 1178, 1090, 837, 777, 698 cm^{-1}. ^1H NMR ($CDCl_3$, 400 MHz) δ=−0.053, −0.046, −0.036, −0.029, −0.021, 0.005, 0.014 (6H, seven s, Me_2Si, intensity ratio: 12:23:14:12:14:14:11), 0.836, 0.839, 0.873 (9H, three s, Me_3CSi intensity ratio: 22:52:26), 1.33, 1.34, 1.35, 1.36 (3H, four d, *J*=6.07, 5.86, 5.81, and 6.03 Hz, MeCHCH$_2$O intensity ratio: 21:29:23:27), 1.65—2.05 (1H, m, MeCH CH$_2$O), 2.70—4.42 (6H, other protons) 4.40—4.66 (1H, m, MeCHO), 5.10—5.50 (2H, m, PhCH$_2$O), 7.20—7.42 (10H, m, aromatic protons). Based on the NMR spectrum, the formation ratio of **7a**—d could be estimated as 21:29:23:27. Since several attempts to separate **7a**—d turned out to be fruitless, the assignment of NMR signals and the determination of chemical yield for each diastereomer could not be achieved. However, comparison of the NMR spectra of the mixture of **7a**—d before and after saponification rigorously uncovered the formation ratio of the $C_{3,4}$-cis isomers (**7a,b**) to the $C_{3,4}$-trans ones (**7c,d**) as 48(21+27):52-(29+23). MS *m/z* 483 $[M]^+$, 468 $[M-Me]^+$, 426 $[M-t\text{-}Bu]^+$.

Selective Saponification of the Mixture of the Four Diastereomers of 2-Benzyl-4-benzyloxycarbonyl-3-[(*R*)-2-*t*-butyldimethylsilyloxy-1-methylethyl]-5-methylisoxazolidine (7a—d). Satd aq $Ba(OH)_2$ (50 mL) was added to a solution of the four diastereomers mixture of **7** (5.50 g) in THF (50 mL) and the mixture was stirred vigorously at the same temperature for 24 h. After an insoluble material was removed by filtration, the filtrate was diluted with hexane (150 mL). The upper organic layer was separated, washed successively with satd aq $NaHCO_3$, satd NaCl, then dried over anhyd $MgSO_4$. Filtration and concentration in vacuo gave an oily residue which was purified with column chromatography (SiO_2, hexane–EtOAc 1:0→19:1) to give a mixture of **7a**—d (3.00 g, 55% recovery). ^1H NMR ($CDCl_3$, 400 MHz) δ=−0.053, −0.046, −0.036, −0.029, −0.021, 0.005, 0.014 (6H, seven s, Me_2Si, intensity ratio: 17:11:20:4:8:23:17), 1.33, 1.34, 1.35, 1.36 (3H, four d, *J*=6.07, 5.86, 5.81, and 6.03 Hz, intensity ratio: 34:20:5:41). Since the $C_{3,4}$-trans isomers (**7c,d**) was expected to be saponified more preferencially than the $C_{3,4}$-cis ones (**7a,b**), this selective saponification could improve the ratio of the latter isomers to the former ones (**7a,b**:**7c,d**) from 48:52 to 75:25.

(2*S*,3*R*,4*R*)-3-Amino-5-*t*-butyldimethylsilyloxy-2-[(*R*)-1-hydroxyethyl]-4-methylpentanoic Acid (8). 10% Palladium on carbon (1.00 g) was added to a methanolic solution (50 mL) containing **7a—d** (10.0 g, 20.7 mmol) directly obtained by the above selective saponification, and the whole mixture was stirred under a hydrogen atmosphere (5 atm) for 7 h. The catalyst was filtered off and the filtrate was concentrated in vacuo. The concentration residue was purified by column chromatography (SiO_2: $CHCl_3$–MeOH 10:1→8:1) to give **8** as a colorless solid (1.30 g, 21%)[11] from the major fraction. Recrystallization of **8** from EtOH–H_2O (1:2) gave an analytical sample of **8** as colorless needles, mp 178—179 °C (decomp.) and $[\alpha]_D^{20}$ −2.0° (*c* 1.18, MeOH). IR (KBr) 3500, 2900, 2120, 1640, 1540, 1480, 1405, 1340, 1284, 1258, 1198, 1126, 1100, 1080, 1055, 1005, 960, 840, 813, 782, 728, 680, 620, 594, 557, 474 cm^{-1}. ^1H NMR ($CDCl_3$) δ=0.06 (6H, s, Me_2Si), 0.89 (9H, s, Me_3CSi), 1.12 (3H, d, *J*=7.0 Hz, MeCHCH$_2$O), 1.23 (3H, d, *J*=6.4 Hz, MeCHO), 1.95 (1H, m, MeCHCH$_2$O), 2.51 (1H, m, CHCOOH), 3.69 (3H, m, MeCHCH$_2$ and CHNH$_2$), 4.21 (1H, m, MeCHO). MS *m/z* 290 $[M-Me]^+$, 260 $[M-COOH]^+$, 248 $[M-t\text{-}Bu]^+$. Found: C, 54.81; H, 10.26; N, 4.48%. Calcd for $C_{14}H_{31}NO_4Si$: C, 55.04; H, 10.23; N, 4.59%.

(3*S*,4*R*)-4-[(*R*)-1-(*t*-Butyldimethylsilyloxymethyl)ethyl]-3-[(*R*)-1-hydroxyethyl]-2-azetidinone (9). A solution of triphenylphosphine (1.01 g, 3.9 mmol) in acetonitrile (62 mL) was added dropwise to a solution of recrystallized **8** (0.980 g, 3.2 mmol) and di-2-pyridyl disulfide (0.850 g, 3.9 mmol) in acetonitrile (300 mL) under reflux. After the heating at reflux was continued for 3 h, the mixture was concentrated in vacuo and the residue was dissolved in ether (40 mL). The ethereal solution was washed successively with 1 mol dm^{-3} NaOH and satd NaCl, then dried over anhyd Na_2SO_4. After filtration and concentration in vacuo, the residue was dissolved in EtOAc (3.7 mL). The ethyl acetate solution was diluted with hexane (8.9 mL) to crystallize triphenylphosphine oxide. After filtration, the filtrate was concentrated in vacuo to give almost pure **9** as a colorless solid (0.970 g, quantitative yield). A part of the residue was purified with TLC (SiO_2: hexane–EtOAc 3:7) and recrystallized from benzene, affording an analytical sample as colorless crystals, mp 105—106 °C and $[\alpha]_D^{20}$ −8.6° (*c* 1.08, $CHCl_3$). IR (KBr) 3370, 3230, 2950, 2870, 1722, 1475, 1363, 1314, 1255, 1154, 1089, 997, 840, 777, 708, 684 cm^{-1}. ^1H NMR ($CDCl_3$) δ=0.09 (6H, s, Me_2Si), 0.91 (9H, s, Me_3CSi), 0.96 (3H, d, *J*=6.8 Hz, MeCHO), 1.34 (3H, d, *J*=6.4 Hz, MeCHCH$_2$O), 1.77 (1H, m), 2.73 (1H, d, *J*=4.6 Hz, MeCHOH), 3.01 (1H, dd, *J*=7.8, 2.0 Hz, CHNH), 3.51 (1H, dd, *J*=7.8, 2.0 Hz, CHCO), 3.62 (2H, m, MeCHCH$_2$O), 4.14 (1H, m, MeCHO), 5.95 (1H, bs, NH). MS *m/z* 272 $[M-Me]^+$, 270 $[M-OH]^+$, 259 $[M-Me-OH]^+$, 230 $[M-t\text{-}Bu]^+$. Found: C, 58.71; H, 10.00; N, 4.87%. Calcd for $C_{14}H_{29}NO_3Si$: C, 58.49; H, 10.17; N, 4.87%. In order to examine an extent of racemization to the stage of **9** in the synthetic scheme, another lot of **9** (21.0 mg, 20%) was prepared from the mixture of **7a—d** (175 mg, 0.36 mmol) without any recrystallizations according to the reaction steps described above. Measurement of the ^1H NMR spectrum carried out with this sample in the presence of the chiral shift reagent [Eu(hfc)$_3$] clearly showed the methyl group of MeCHCH$_2$O moiety in an intensity ratio of 97.5:2.5 as two doublets at 1.82 and 1.79 ppm. Since the racemic β-lactam (*dl*-**9**)[14] exhibited the same methyl group as two sets of doublets of equal intensity at 1.79 and 1.82 ppm, the optical purity of **9** was estimated 95%ee. Accordingly, it became evident that each synthetic step to the stage of **9** could proceed without substantial racemization.

(3*S*,4*R*)-4-[(*R*)-1-(*t*-Butyldimethylsilyloxymethyl)ethyl]-3-[(*R*)-1-(*t*-butyldimethylsilyloxy)ethyl]-2-azetidinone (10). *t*-

Butyldimethylchlorosilane (35.0 mg, 0.23 mmol) was added to a solution of **9** (22.4 mg, 0.078 mmol) and imidazole (32.0 mg, 0.47 mmol) in DMF (0.5 mL) and the mixture was stirred at rt for 1.5 h. After the reaction was quenched by adding H_2O (0.5 mL), the mixture was extracted with EtOAc. The combined extracts were washed with H_2O, dried over anhyd $MgSO_4$, filtered, then concentrated in vacuo. The residue was purified with column chromatography (SiO_2: hexane–EtOAc 9:1→17:3) to give **10** as colorless crystals (31.1 mg, 99%). Recrystallization from MeOH–H_2O gave an analytical sample of **10** as colorless crystals, mp 97—99 °C and $[\alpha]_D^{20}$ −6.7° (*c* 0.95, $CHCl_3$). IR (KBr) 3470, 3180, 3120, 2950, 2880, 1760, 1717, 1480, 1258, 1140, 1101, 968, 840, 780 cm^{-1}. ^1H NMR ($CDCl_3$) δ=0.04, 0.07 (12H, two s, Me_2Six2), 0.87, 0.89 (18H, two s, Me_3CSix2), 0.96 (3H, d, *J*=6.8 Hz, MeCHCH$_2$O) 1.22 (3H, d, *J*=6.4 Hz, MeCHO), 1.79 (1H, m, MeCHCH$_2$), 2.88 (1H, m, CHNH), 3.55 (2H, d, *J*=4.8 Hz, MeCHCH$_2$), 3.70 (1H, dd, *J*=5.4, 2.3 Hz, CHCO), 4.17 (1H, dq, *J*=6.4, 5.4 Hz, MeCHO), 5.74 (1H, bs, NH). MS *m/z* 386 $[M-Me]^+$, 344 $[M-t\text{-}Bu]^+$. Found: C, 59.84; H, 10.71; N, 3.41%. Calcd for $C_{20}H_{43}NO_3Si_2$: C, 59.80; H, 10.79; N, 3.49%.

(3*S*,4*R*)-3-[(*R*)-1-(*t*-Butyldimethylsilyloxy)ethyl]-4-[(*R*)-1-(hydroxymethyl)ethyl]-2-azetidinone (11). One mol dm^{-3} hydrochloric acid (4.0 μL) was added to a solution of **10** (10.7 mg, 0.027 mmol) in MeOH (1.0 mL) and H_2O (0.2 mL) at 0 °C and the mixture was stirred there for 2 d. After satd aq $NaHCO_3$ (0.5 mL) and satd NaCl (1.0 mL) were added, the mixture was extracted with EtOAc. The combined organic extracts were washed with satd NaCl, dried over anhyd $MgSO_4$, filtered, then concentrated in vacuo. The residual solid was purified with column chromatography (SiO_2: hexane–EtOAc 1:1) to give **11** (6.1 mg, 80%) as colorless crystals, mp 89—90 °C and $[\alpha]_D^{20}$ −20.9° (*c* 0.37, $CHCl_3$) (lit.,[11] mp 90—91 °C and $[\alpha]_D^{20}$ −21.7° (*c* 0.46, $CHCl_3$)). IR (KBr) 3450, 3180, 3100, 2950, 1755, 1713, 1373, 1255, 1140, 1098, 1062, 1050, 1027, 984, 963, 838, 810, 780 cm^{-1}. ^1H NMR ($CDCl_3$) δ=0.13 (6H, s, Me_2Si), 0.90 (3H, d, *J*=6.8 Hz, MeCHCH$_2$O), 0.92 (9H, s, Me_3CSi), 1.35 (3H, d, *J*=6.0 Hz, MeCHO), 1.86 (1H, m, MeCHCH$_2$O), 2.96 (1H, dd, *J*=8.3, 4.9 Hz, OH), 3.15 (1H, ddd, *J*=9.0, 2.2, 1.0 Hz, CHN), 3.30 (1H, dd, *J*=8.8, 2.2 Hz, CHCO), 3.53 (2H, m, CH$_2$OH), 4.13 (1H, dq, *J*=8.8, 6.0 Hz, MeCHO), 5.99 (1H, bs, NH). MS *m/z* 272 $[M-Me]^+$, 230 $[M-t\text{-}Bu]^+$. These spectral properties were identical with those of the authentic sample independently prepared by our hands.[13] Found: C, 58.30; H, 10.15; N, 4.75%. Calcd for $C_{14}H_{29}NO_3Si$: C, 58.49; H, 10.17; N, 4.87%.

The authors are indebted to Dr. M. Sunagawa, Research Laboratories, Research and Development Division, Sumitomo Pharmaceuticals Co. Ltd., for valuable suggestions.

References

1) A part of this work has been published in a form of the patent. S. Terashima, Y. Kimura, Y. Ito, K. Sakai, and T. Hiyama, Japan Kokai Tokkyo Koho JP 62-29577 (1987).

2) After completion of this work, the same synthetic scheme to **1** as that reported herein has been reported by Kametani et al. They have also disclosed that the isoxazolidine derivative of desired stereochemistry can be obtained as a sole product by the intramolecular version of the cycloaddition reaction. The 107th Annual Meeting of the Pharmaceutical Society of Japan, Kyoto, April, 1987. Abstract Paper, p. 271.

3) T. Kametani, S-P. Huang, A. Nakayama, and T. Honda, *J. Org. Chem.*, **47**, 2328 (1982).

4) T. Kametani and M. Ihara, *Yuki Gosei Kagaku Kyokai Shi*, **38**, 1025 (1980). T. Nagahara and T. Kametani, *Heterocycles*, **25**, 729 (1987).

5) R. V. Stevens and K. Albizati, *J. Chem. Soc., Chem. Commun.*, **1982**, 104.

6) T. Kametani, T. Nagahara, and T. Honda, *J. Org. Chem.*, **50**, 2327 (1985).

7) T. Kametani, S-D. Chu, and T. Honda, *Heterocycles*, **25**, 241 (1987).

8) D. H. Shih, F. Baker, L. Cama, and B. G. Christensen, *Heterocycles*, **21**, 29 (1984).

9) M. Kawase and Y. Kikugawa, *J. Chem. Soc., Perkin Trans. 1*, **1979**, 643.

10) When aq sodium hydroxide or aq potassium hydroxide solution was employed in place of aq barium hydroxide solution and alcoholic solvents were used as the reaction medium, significant epimerization of the C_4 esters of the $C_{3,4}$-cis-adducts (**7a,b**) was observed.

11) In another hydrogenolysis carried out in a small scale, we have succeeded in obtaining the other two diastereomers of **8** in pure states by TLC separation (SiO_2, $CHCl_3$–MeOH 6:1) although their yields could not be specified. When being treated under the Mukaiyama–Ohno conditions,[12] these two compounds were found to produce the *trans*- and the *cis*-β-lactams whose stereochemistry could be definitely determined by NMR analyses. Accordingly, the diastereomers of **7** which gave the *trans*-β-lactam was identified as **7b** and the other producing the *cis*-β-lactam as **7c** or d (Y. Ito, Y. Kimura, and S. Terashima, unpublished results).

12) M. Ohno, S. Kobayashi, T. Iimori, Y.-F. Wang, and T. Izawa, *J. Am. Chem. Soc.*, **103**, 2405 (1981).

13) T. Kawabata, Y. Kimura, Y. Ito, S. Terashima, A. Sasaki, and M. Sunagawa, *Tetrahedron Lett.*, **27**, 6241 (1986).

14) The racemic β-lactam (*dl*-**9**) was prepared from racemic 3-(*t*-butyldimethylsilyloxy)-2-methylpropanal according to the same synthetic route as that reported for optically active **9** (Y. Ito, Y. Kimura, and S. Terashima, unpublished results).

 © 1987 The Chemical Society of Japan Bull. Chem. Soc. Jpn., 60, 3341—3345 (1987)

Optically Active Polyamides Having (−)-Anti Head-to-Head Coumarin Dimer Component. 3. Chiral Recognition Ability

Yun CHEN, Kazuhiko SAIGO,* Noriyuki YONEZAWA, Kouzou TACHIBANA, and Masaki HASEGAWA
Department of Synthetic Chemistry, Faculty of Engineering, The University of Tokyo, Bunkyo-ku, Tokyo 113
(Received April 21, 1987)

Optically active polyamides (**3a—f**) and *O*-methylated polyamides (**5a,d,e**), derived from (−)-anti head-to-head coumarin dimer [(−)-**1**], were absorbed on macroporous silica gel particles and used as chiral stationary phases for direct resolution of racemates (**6—13**) having aromatic moiety by high-performance liquid chromatography. Polyamide **3a** and **3e** could resolve **6—10** and **9—13**, respectively (separation factor $\alpha>1.03$), and **3d** showed especially high selective recognition ability to **7** ($\alpha=1.63$). However, **3c,f** and **5a** showed no resolution ability to all of the racemates. The high recognition ability of **3a** is attributed mainly to the difference in stability between the diastereomeric complexes formed by the simultaneous interaction of **3a** with the racemates. The recognition ability of polyamides derived from piperazine (**3d**, **5d**) and 1,4-phenylenediamine (**3e**, **5e**) seems to be attributed not only to the simultaneous interaction but also to their ordered conformations in the film state.

A variety of optically active polymers have been synthesized,[1] but only a few of them have been found to be applicable as chiral packing materials in high-performance liquid chromatography (HPLC).[2-5] In most polymeric chiral stationary phases such as isotactic (+)-poly(triphenylmethyl methacrylate),[6-10] poly(amino acid)s,[11,12] microcrystalline cellulose triacetate,[13,14] and phenylcarbamates of polysaccharides,[15] high chiral recognition ability depends strongly on their secondary or higher ordered structures. The chiral recognition by crosslinked polyacrylamides with chiral pendant group is known to be due to the contribution of hydrogen-bonding.[2,16] For low-molecular-weight chiral stationary phases, chiral recognition requires at least three simultaneous interactions between the chiral stationary phase and one of the enantiomer of racemate.[17-23]

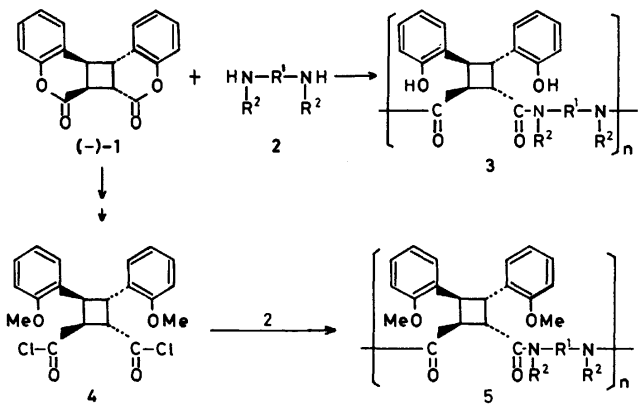

Polyamide	R^1	R^2	η_{inh}
3a	$-(CH_2)_6-$	H	0.88
3b	$-(CH_2)_6-$	CH_3	0.35
3c	$-CH_2-C_6H_4-CH_2-$	H	0.63
3d	$-N\langle\rangle N-$		0.51
3e	$-C_6H_4-$	H	0.36
3f	$-C_6H_4-O-C_6H_4-$	H	0.31
5a	$-(CH_2)_6-$	H	1.01
5d	$-N\langle\rangle N-$		1.00
5e	$-C_6H_4-$	H	0.50

Previously, we reported the synthesis of a series of optically active polyamides (**3a—f**), composed of (−)-anti head-to-head coumarin dimer component [(−)-**1**] subunit, and showed that by varying the rigidity of diamine component the ordered conformations of these polyamides in solutions can also be controlled to some extent.[24,25] Moreover, we reported briefly that some of polyamide **3a—f**, depending on the structure of diamine component, are applicable as chiral packing materials for direct HPLC resolution of racemates.[26] But the different chiral recognition behavior of **3a—f** could not be explained merely by the simultaneous interactions between the racemates and the interaction sites in the polyamides, i.e. phenolic hydroxyl group, aromatic group, and amide linkage, and/or the ordered conformation in solutions. In order to elucidate the recognition mechanism, we also synthesized *O*-methylated polyamides **5** and investigated the chiroptical properties of **3** and **5** in the film state,[27] which is considered to be analogous to the coated state for recognition process. Similar to the results obtained in solutions,[25] the conformations in the film state also depended strongly on the structure of diamine components. Polyamides derived from piperazine (**3d**, **5d**) and aromatic diamines (**3e,f** and **5e**) formed ordered conformation, while other polyamides existed in random conformation in the film state. In this paper we wish to report in detail the chiral recognition ability of **3** and **5**, and possible correlation between the chiral recognition ability and the simultaneous interaction or ordered conformation in the film state.

Experimental

General. Synthesis, characterization, and chiroptical properties of optically active polyamides **3** and **5**, derived from (−)-anti head-to-head coumarin dimer, were described in previous papers.[25,26] Racemates **6**—**13** and diphenylsilane coupler were of commercial origins.

Chromatographic Resolution of Racemates. Direct chromatographic separation of racemates was accomplished on a Shimadzu LC-5A HPLC system equipped with a Toyo Soda UV-8-II detector and, in some cases, a Jasco DIP-181 polarimeter detector at room temperature. The eluent was a mixture of hexane and 2-propanol, but in some cases methanol or ethanol only was used. The flow rate was 0.5 ml min^{-1}.

Macroporous silica gel particles (4.0 g) (Merck LiChrospher SI 1000),[28] pretreated with diphenylsilane coupler, were coated with about 25 wt% of polyamides in DMAc solution (ca. 0.85 g/8 ml) and then dried in vacuo at 60 °C for 5 h. The polyamide-coated silica gel thus obtained was packed in a stainless steel column [25×0.46 (i.d.) cm] by the slurry method. Theoretical plate number of the columns bearing **3a**—**f** for benzene were 2600, 2800, 4200, 2100, and 2200, respectively. Theoretical plate number of the columns bearing *O*-methylated polyamide **5a**, **5d**, and **5e** were 1600, 2200, and 1150, respectively. The void volume was estimated to be about 3.0 ml with a trace amount of water in methanol.

Results and Discussion

It is well-known that one of the driving forces for chiral recognition is a simultaneous interaction between the functional groups in a stationary phase and a solute.[3] Optically active polyamides **3** and **5** possess possible interaction sites for chiral recognition, i.e. phenolic hydroxyl (methoxyl) group, aromatic group, and amide linkage. Then, we expected that racemates **6**—**13**, having an aromatic group and a site for hydrogen-bonding, would be resolved by these polyamide-coated silica gel columns.

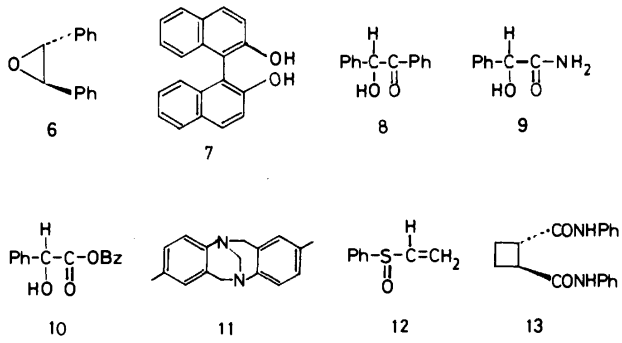

Figure 1 shows the chromatograms of 2,2′-dihydroxy-1,1′-binaphthyl (**7**), benzoin (**8**), and *trans*-1,2-cyclobutanedicarboxanilide (**13**) on the columns bearing **3d**, **3a**, and **3e**, respectively. The chromatographic parameters for the resolution of **6**—**13** using the polyamide-coated silica gel columns are summarized in Table 1.

Contrary to the expectation, it was shown clearly that the chiral recognition by these chiral stationary phases was diverse and strongly depended on the structure of diamine component in the main chain.

Polyamide **3a** resolved **6**—**10** efficiently (α is larger than 1.10), which all contain an aromatic group and a site for hydrogen-bonding. This suggests that the chiral discrimination of **3a** would involve the simultaneous interactions of aromatic stacking and hydrogen-bonding with the racemates. The separation factor of **3a** has tendency to decrease as the inherent viscosity increases (Table 2). More importantly, **3a** with higher theoretical plate number for benzene (η_{inh} 0.68 and 0.98 dl g^{-1}) showed smaller separation factors than those with lower theoretical plate number (η_{inh} 0.43 and 0.53 dl g^{-1}). This phenomenon would be explained as follow; with

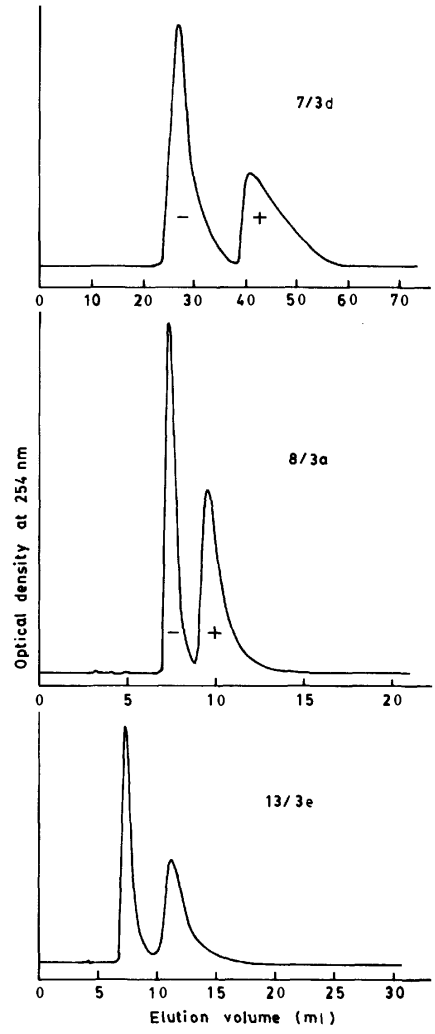

Fig. 1. Chromatograms of **7**, **8**, and **13** on the columns bearing 3d, **3a**, and **3e**, respectively. Columns, 25×0.46 (i.d.) cm; eluent, hexane/2-propanol (v/v=9/1); flow rate, 0.50 ml min^{-1} at room temperature.

Table 1. Chromatographic Resolution of Racemates **6**—**13** by Polyamide-Coated Silica Gel Columns[a,b]

Racemates	Column bearing **3a**			Column bearing **3d**			Column bearing **5d**			Column bearing **3e**			Column bearing **5e**		
	k_1'	α	Rs	k_1'	α	Rs	k_1'	α	Rs	k_1'	α	Rs	k_1'	α	Rs
6	0.40	1.42	0.92	0.64(−)	1	PR[c]	0.88	1.11	0.4	0.41	1	NR[d]	0.62	1	NR
7	4.36(−)	1.17	0.60	9.91(−)	1.63	1.19	5.06	1	NR	2.19	1	NR	18.67	1	NR
8	1.91	1.46	1.45	4.17(+)	1	NR	8.24	1	NR	2.16	1	NR	5.20	1.15	0.50
9	5.59(−)	1.29	0.88	—	—	—	11.06	1	NR	8.04(+)	1.03	0.50	14.25	1.22	0.52
10	1.60	1.10	0.60	3.12(−)	1.04	0.50	8.70	1	NR	1.68(−)	1.05	0.50	5.00	1.20	0.4
11	0.57	1	NR	1.15(−)	1	PR	0.58	1	NR	0.89	1.12	0.60	0.83	1	NR
12	2.12(+)	1	PR	5.80	1	NR	1.64	1	NR	5.64	1.04	0·50	6.92	1	NR
13	1.40	1	NR	3.30	1	NR	7.85	1	NR	2.00	1.81	1.73	11.20	1	NR

a) Eluent, hexane-2-propanol (v/v=9/1); flow rate, 0.50 ml min^{-1}. k_1' (capacity factor for less retained racemate) = (retention volume − void volume)/void volume. α(separation factor) = (capacity factor for more retained racemate)/k_1'. Rs(resolution factor) = 2 × (distance of the two peak position)/(sum of band-widths of the two peaks). The sign in the parentheses are those of optical rotations at 365 nm. b) Polyamide **3c**, **3f**, and **5a** showed no resolution ability to all of these racemates (α=1), polyamide **3b** resolved **13** only (α=1.38). c) PR: Partial resolution which could be detected only by a polarimeter. d) NR: No resolution.

Table 2. Chromatographic Resolution of Racemates **6**—**10** by **3a**-Coated Silica Gel Columns[a]

η_{inh}[b]	Theoretical plate number[c]	Separation factor/α				
		6	**7**	**8**	**9**	**10**
0.43	1430	1.64	1.46	1.64	1.25	1.10
0.53	1200	2.51	1.34	1.65	1.29	1.11
0.68	4000	1.31	1	1.45	1	1
0.88	2600	1.42	1.17	1.46	1.29	1.10
0.98	2900	1.37	1.18	1.38	1.17	1.09

a) Resolution conditions are the same as those in Table 1. b) 0.30 g dl^{-1} in DMAc at 30 °C. c) For benzene.

increasing π–π interaction ability of **3a**, which contributes to the theoretical plate number of the column, the π–π interaction between phenyl groups in **3a** and the racemates surpasses the polar interaction and the difference in stability between diasteriomeric complexes decreases. Moreover, **3b** and **5a** having no amide hydrogen or phenolic hydrogen showed no resolution ability to racemates **6**—**13**. These results indicate that hydrogen-bonding plays more important role than π–π interaction in the chiral recognition process by **3a**.

On the other hand, **3c** shows no resolving ability to all of the racemates, although it also possess the same interaction sites as **3a**. This can be caused by the interference of aromatic moiety in diamine residue during recognition process.

The influence of the eluent with different amount of 2-propanol was also investigated. As shown in Table 3, the racemates resolved by polyamide **3a** can be divided into two groups. Racemates **8**—**10** can form an intramolecular hydrogen-bonding, and the other racemates **6**, **7**, and **13** don't possess this possibility due to the lack of hydrogen-bonding pair for **6** or the trans orientation of the possible interaction sites for **7** and **13**. With increasing the content of protic solvent in the eluent from 10% 2-propanol (IPA) to ethanol only, the separation factor (α) of **8**—**10** all increased at first and then decreased. This phenomena would be caused by the equilibrium between the inter- and intramolecular hydrogen-bonding, which changes depending on the content of protic solvent in the eluent. At low content of protic solvent, the chiral recognition is lower due to the dominance of intramolecular hydrogen-bonding within the racemate, which is disadvantageous to the chiral discrimination. With increasing the ratio of 2-propanol, the racemate would be solvated and the interaction between the racemate and polyamide **3a** surpasses the intramolecular interaction within the racemate, resulting in better recognition. However, at very high content of protic solvent the interaction between the racemate and the eluent becomes major, and the interaction between the racemate and polyamide **3a** is diminished, resulting in low separation factor. For racemates **6**, **7**, and **13**, separation factor decreased harmoniously with increasing the content of protic solvent in the eluent. This would arise from the decrease of the interaction between the racemates and polyamide **3a** by solvation. These results also support the simultaneous interaction mechanism of chiral recognition by **3a**.

Polyamide **3e** resolved **9**—**13**, which is partially different from those resolved by **3a**. Especially, **13** with propeller-like phenyl groups was resolved with a high separation factor (α=1.81). Moreover, contrary to **5a**, *O*-methylated polyamide **5e** still showed resolution ability to **8**—**10** although it has no phenolic hydroxyl group, which exists in polyamide **3e**. From these results, it seems that the driving force for chiral recognition by **3e** is different from that by **3a**. Since

Table 3. Chromatographic Resolution of Racemates **6**—**13** by **3a** or **3e**-Coated Silica Gel Column Using Different Eluents[a)]

Racemates	Parameter[c)]	Column bearing **3a**				Column bearing **3e**[b)]	
		10% IPA[c)]	20% IPA	30% IPA	EtOH	10% IPA	30% IPA
6	k_1'	0.35	0.30	0.23	0.15	0.41	0.18
	α	2.51	2.27	2.29	15.1	1	1
7	k_1^1	7.22	3.17	2.50	0.33	2.19	0.83
	α	1.34	1.25	1	1	1	1
8	k_1'	2.53	1.50	1.03	0.13	2.16	1.11
	α	1.65	1.79	1.75	1.45	1	1
9	k_1'	9.33	2.70	1.57	0.20	8.04	1.43
	α	1.29	1.40	1.43	1	1.03	1
10	k_1'	2.13	1.13	0.74	0.11	1.68	0.72
	α	1.11	1.15	1.16	1	1.05	1
11	k_1'	0.71	0.47	0.37	0.29	0.89	0.47
	α	1	1	1	1	1.12	1
12	k_1'	2.12	1.40	0.87	0.13	5.64	2.17
	α	1	1	1	1	1.04	1
13	k_1'	1.41	0.63	0.48	0.12	2.00	0.60
	α	1.28	1.24	1	1	1.81	1.59

a) The resolution conditions and the definition of parameters are the same as those in Table 1; polyamide **3a** with $\eta_{inh}=0.53$ dl g^{-1} was used. b) It showed no resolution ability to all of the recemates when methanol was used as an eluent. c) Eluent used is a mixture of hexane and 2-propanol (IPA).

both **3e** and **5e** form an ordered conformation of macromolecular asymmetry in the film state,[27] it is reasonable to say that this ordered conformation plays an important role in chiral recognition process. As shown in Table 3, with increasing the content of 2-propanol in eluent from 10 to 30%, **3e** showed no recognition to the racemates except for **13** (α=1.59). This is also quite different from the observed for **3a** which showed no resolution ability to **13** when an eluent containing 30% 2-propanol is used. From these facts, the chiral discrimination ability of **3e** can be attributed to its ordered conformation in the film state. The ordered conformation makes the difference in stability between diasteriomeric complexes large, which arises from the interaction of hydroxyphenyl groups of **3e** with aromatic groups of the racemates.

However, **3f** showed no resolution ability to all of the racemates, although it possesses polymer main chain structure with mesomeric aromatic residue similar to **3e**. This can be ascribed to its incompleteness of the ordered conformation[27] or to longer and more flexible diphenyl ether linkage in comparison with 1,4-phenylene linkage in **3e**.

Polyamide **3d** resolved atropisomeric compound **7** with a high separation factor (α=1.63). *O*-methylated polyamide **5d** resolved **6** with trans phenyl groups. This high selective resolution ability of **3c** to **7** and **5d** to **6** would be attributed to their rigid and fixed structure,[25,27] which makes the aromatic packing with racemates more stable for one of the enantiomer than the other.

The present results show that optically active polyamides **3** and **5**, derived from (−)-anti head-to-head coumarin dimer, are useful as chiral stationary phases for direct resolution of racemates having aromatic groups by HPLC. Polyamide **3a** derived from 1,6-hexanediamine shows the best results, and its recognition ability is mainly attributed to the simultaneous interactions with the solutes. The chiral discrimination ability of polyamides **3e** and **5e**, derived from 1,4-phenylenediamine, may be attributed to their ordered conformation in the film state as well as the simultaneous interaction with the racemates. The selective recognition ability of **3d** to **7** and **5d** to **6** seems due to their rigid and fixed conformation in the film state. The ordered conformation of the polyamides derived from piperazine and 1,4-phenylenediamine are less effective for chiral recognition than the simultaneous interaction with polar groups in **3a** unless the ordered conformation is fully-developed.[6-10]

References

1) E. Selegny, "Optically Active Polymers," D. Reidel, Dordrecht (1979).

2) G. Blaschke, *Angew. Chem., Int. Ed. Engl.*, **19**, 13 (1980).

3) W. H. Pirkle and J. Finn, "Asymmetric Synthesis," ed by J. D. Morrison, Academic Press, New York (1983), Vol. 1, p. 87.

4) D. W. Armstrong, *J. Liq. Chromatogr.*, **7**(s-2), 353 (1984).

5) *J. Liq. Chromatogr.*, **9**(2/3) (1986). "Special Issue On Optical Resolution By Liquid Chromatography," ed by S. Hara and J. Cases.
6) H. Yuki, Y. Okamoto, and I. Okamoto, *J. Am. Chem. Soc.*, **102**, 6356 (1980).
7) Y. Okamoto, I. Okamoto, and H. Yuki, *Chem. Lett.*, **1981**, 835.
8) Y. Okamoto, I. Okamoto, and H. Yuki, *J. Polym. Sci., Polym. Lett. Ed.*, **19**, 451 (1981).
9) Y. Okamoto, S. Honda, I. Okamoto, and H. Yuki, *J. Am. Chem. Soc.*, **103**, 6971 (1981).
10) Y. Okamoto, S. Honda, E. Yashima, and H. Yuki, *Chem. Lett.*, **1983**, 1221.
11) S. Allenmark and B. Bomgren, *J. Chromatogr.*, **264**, 63 (1983).
12) J. Hermansson, *J. Chromatogr.*, **269**, 71 (1983).
13) G. Hesse and R. Hagel, *Chromatographia*, **6**, 277 (1973).
14) G. Hesse and R. Hagel, *Chromatographia*, **9**, 62 (1976).
15) Y. Okamoto, M. Kawashima, and K. Hatada, *J. Am. Chem. Soc.*, **106**, 5357 (1984).
16) G. Blaschke, H.-P. Kraft, and H. Markgraf, *Chem. Ber.*, **113**, 2318 (1980).
17) R. Baczuk, G. Landram, R. Dubois, and H. Dehm, *J. Chromatogr.*, **60**, 351 (1971).
18) W. H. Pirkle and D. W. House, *J. Org. Chem.*, **44**, 1957 (1979).
19) W. H. Pirkle and J. M. Finn, *J. Am. Chem. Soc.*, **103**, 2964 (1981).
20) W. H. Pirkle and J. M. Finn, *J. Org. Chem.*, **46**, 2935 (1981).
21) W. H. Pirkle and J. L. Schreiner, *J. Org. Chem.*, **46**, 4988 (1981).
22) W. H. Pirkle, C. J. Welch, and M. H. Hyun, *J. Org. Chem.*, **48**, 5022 (1983).
23) W. H. Pirkle and M. H. Hyun, *J. Org. Chem.*, **49**, 3043 (1984).
24) N. Yonezawa, T. Kanoe, K. Saigo, Y. Chen, K. Tachibana, and M. Hasegawa, *J. Polym. Sci., Polym. Lett. Ed.*, **23**, 617 (1985).
25) K. Saigo, Y. Chen, N. Yonezawa, T. Kanoe, K. Tachibana, and M. Hasegawa, *Macromolecules*, **19**, 1552 (1986).
26) K. Saigo, Y. Chen, N. Yonezawa, K. Tachibana, T. Kanoe, and M. Hasegawa, *Chem. Lett.*, **1985**, 1891.
27) Y. Chen, K. Saigo, N. Yonezawa, M. Hasegawa, *Bull. Chem. Soc. Jpn.*, **60**, 1895 (1987).
28) Macroporous spherical silica gel has 10 μm of mean particle size with 100 nm of mean pore diameter and 20000 $m^2 kg^{-1}$ of specific surface area.

 © 1987 The Chemical Society of Japan Bull. Chem. Soc. Jpn., 60, 3347—3358 (1987)

Michael Addition and Alkylation of 2-Azaallyl Anions Derived from *N*-(1-Cyanoalkyl)imines, and Stereoselective Cyclization of Imine Esters or Ketones Leading to 1-Pyrrolines

Otohiko Tsuge,* Kazunori Ueno, Shuji Kanemasa, and Kiyotaka Yorozu
Institute of Advanced Material Study, and Department of Molecular Science and Technology, Interdisciplinary Graduate School of Engineering Sciences, Kyushu University, Kasugakoen, Kasuga 816
(Received April 30, 1987)

The 2-azaallyl anions derived from *N*-(1-cyanoalkyl)imines and DBU undergo Michael addition or alkylation to produce *N*-(1-alkylated 1-cyanoalkyl)imines. The Michael addition of some aryl-substituted imines are highly diastereoselective. The alkylated Michael adducts are converted into lactams through a hydrolysis and recyclization sequence. Base-induced cyclization furnishes 1-pyrrolines through a cyclization and HCN elimination sequence. In the latter reaction, 4,5-*cis*-1-pyrrolines are selectively produced when the adducts are treated with LDA in the presence of lithium iodide.

Deprotonation of imines adjacent to the nitrogen generates 2-azaallyl anions, while prior *N*-protonation or *N*-alkylation leads to azomethine ylides. These two anionic species are conplementary in organic synthesis: 2-Azaallyl anions undergo either nucleophilic addition to electrophilic multiple bonds or cycloaddition with nonactivated olefins,[1] while azomethine ylides react only with electron-poor activated olefins affording cycloadducts.[2] Recently both azomethine ylide and 2-azaallyl anion species have been generated by a separated procedure using a common precursor and their reactions with electron-poor olefins showed reverse regioselectivity, synthetic value of the precursor being increased.[3]

Deprotonation of the imines of 2-amino esters occurs readily to generate ester-stabilized 2-azaallyl anions. Reaction of the anions with Michael acceptors or alkylating agents followed by hydrolysis is one of the most important preparation method of 2-alkylated 2-amino acids.[4] Compared to the broad applications of the imines of 2-amino esters, synthetic utilization of the imines of 2-amino nitriles is quite limited.[5]

We have continued to study on the synthetic utility of the imines of 2-amino nitriles. The most important reaction on these imines must be its thermal tautomerization generating *N*-protonated azomethine ylides of cyano-stabilized types.[6] These ylides are found to be useful synthetic equivalents of non-stabilized nitrile ylides through a cycloaddition and HCN elimination sequence.

The present article deals with the chemistry of 2-azaallyl anions which can be generated by deprotonation of *N*-(1-cyanoalkyl)imines. Michael additions as well as alkylation reactions using these anions are investigated. Cyclization reactions of the Michael adducts and alkylated products lead to a variety of nitrogen heterocycles. Some of these conversions can be carried out in a stereoselective fashion.

Results and Discussion

Michael Addition and Alkylation of *N*-(1-Cyanoalkyl)imines. *N*-(1-Cyanoalkyl)imines **1** are available by condensation of 2-amino nitriles with carbonyl compounds (Scheme 1). Among these imines **1a** is most easily accessible from aminoacetonitrile and benzaldehyde. Treating **1a** with LDA in THF at −78 °C forms the anion **A** and it can be smoothly alkylated with methyl iodide, benzyl bromide, or isopropyl bromide all in excellent yields. Accordingly the alkylation of **1a** is the most easy access to the alkylated derivatives **1b—1d**. Other imines **1e—1i** were prepared by the reactions of α-aminophenylacetonitrile or α-amino-(1-naphthyl)acetonitrile with the corresponding aldehydes.

N-(1-Cyanoalkyl)imines **1a—1i** generate the corresponding 2-azaallyl anions **B** when treated with DBU in THF at −78 °C and undergo Michael additions to a variety of electron-deficient olefins such

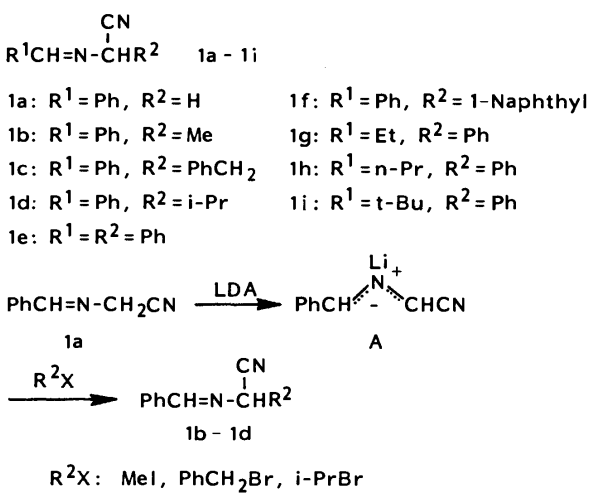

Scheme 1.

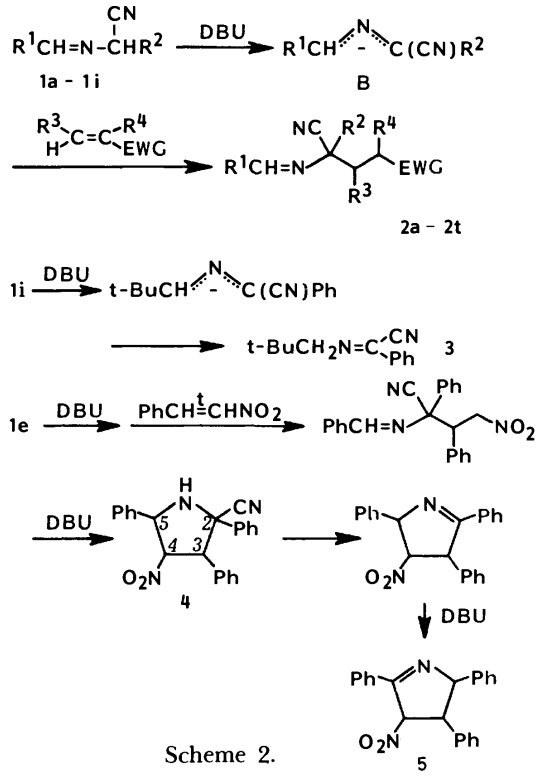

Scheme 2.

as methyl and *t*-butyl acrylates, 3-buten-2-one, acrylonitrile, methyl crotonate, and methyl α-silylacrylate, and (*E*)-β-nitrostyrene (Scheme 2 and Table 1). Acrylates, 3-buten-2-one, and acrylonitrile which carry a sterically less hindered β-carbon smoothly reacted with the anions **B** (R^1=Ph, R^2=$PhCH_2$ or *i*-Pr) derived from imines **1c** and **1d** bearing a bulky alkyl moiety on the carbon. However, these anions showed only decreased reactivity toward methyl crotonate even under harder conditions probably due to a steric hindrance.

The anion **B** (R^1=Ph, R^2=H) from **1a** is very reactive to methyl acrylate to furnish a Michael adduct. This adduct can be again deprotonated to form the anion **B** (R^2=CH_2CH_2COOMe) which can react with the second molecule of the acrylate, frequently yielding a mixture of 1:1 and 1:2 Michael adducts.

Though 2-azaallyl anions **B** have two nucleophilic sites, all the Michael additions took place regioselectively at the carbon substituted by CN. These high selectivity presumably resulted from the anion-stabilizing ability of sterically small CN group.

The anion **B** (R^1=*t*-Bu, R^2=Ph) from **1i** was found

Table 1. Michael Addition of *N*-(1-Cyanoalkyl)imines **1a**—**1i** to Electron-Deficient Olefins Leading to **2a**—**2t** and **3**—**5**[a]

Acceptor	Donor	DBU (equiv)	Time/h (−78 °C→rt)	Product	R^1	R^2	R^3	R^4	EWG	Yield/%[b]	Isomer ratio[c]
CH_2=CHCOOMe	**1b**	0.5	0.5→1	**2a**	Ph	Me	H	H	COOMe	100	—
	1c	0.5	0.5→15	**2b**	Ph	$PhCH_2$	H	H	COOMe	71	—
	1d	0.5	0.5→17	**2c**	Ph	*i*-Pr	H	H	COOMe	74	—
	1e	0.5	0.5→1	**2d**	Ph	Ph	H	H	COOMe	92	—
	1g	1.1	0.2→0.5	**2e**	Et	Ph	H	H	COOMe	100	—
CH_2=CHCOOBu^t	**1b**	1.1	0.2→3	**2f**	Ph	Me	H	H	COOBu^t	95	—
CH_2=CHCOMe	**1c**	0.5	0.5→15	**2g**	Ph	$PhCH_2$	H	H	COMe	88	—
	1e	0.5	0.5→1	**2h**	Ph	Ph	H	H	COMe	90	—
	1g	1.1	0.2→0.7	**2i**	Et	Ph	H	H	COMe	100	—
CH_2=CHCN	**1e**	0.5	0.5→1	**2j**	Ph	Ph	H	H	CN	73	—
	1g	1.1	1→3	**2k**	Et	Ph	H	H	CN	95	—
MeCH=CHCOOMe	**1a**	0.5	0.5→22	**2l**	Ph	H	Me	H	COOMe	78	1:1
	1b	0.5	2→0	**2m**	Ph	Me	Me	H	COOMe	95	3:2
	1b	1.1	1→14	**2m**						82	3:1
	1c	0.5	0.5→15	No reaction[d]							
	1c	0.5	8 (reflux)	**2n**	Ph	$PhCH_2$	Me	H	COOMe	92	1:1
	1d	0.5	10 (reflux)	No reaction[d]							
	1e	0.5	1→8	**2o**	Ph	Ph	Me	H	COOMe	81	single
	1f	0.5	1→8	**2p**	Ph	1-Nph	Me	H	COOMe	81	single
	1g	0.5	2.5→0	**2q**	Et	Ph	Me	H	COOMe	95	single
	1h	0.8	2.5→0	**2r**	*n*-Pr	Ph	Me	H	COOMe	91	single
	1i	0.5	2.5→0	**3**						100	—
CH_2=C(TMS)COOMe	**1e**	0.1	0.5→1	**2s**	Ph	Ph	H	TMS	COOMe	97	single
	1g	0.1	1→1.5	**2t**	Et	Ph	H	TMS	COOMe	100	mixture
PhCH=CHNO$_2$	**1e**	1.0	0→3	**4**+**5**						**4**:11	
										5:83	

a) All reactions were carried out in THF by using each one equivalent amount of **1** and an olefin. b) Yield of isolated products. c) Isomer ratio was determined by ^{1}H NMR spectrum. d) The starting imine was recovered intact.

inactive. It was quenched to form quantitatively a double bond-migrated imine **3** (Scheme 2). Cyclization products **4** and **5** of the Michael adducts were produced (**4**: 11%, **5**: 83%), both as single stereoisomers, in the reaction of the anion **B** (R^1=R^2=Ph) derived from **1e** with (*E*)-β-nitrostyrene. Elimination of HCN and subsequent double bond migration of pyrrolidine **4** would be a route leading to 1-pyrroline **5**. Strong electron-withdrawing property of the nitro group should be responsible for the instability of the Michael adduct.

It was surprising that the anions **B** bearing an aryl group as R^2 underwent stereoselective Michael additions to methyl crotonate to produce single diastereomers **2o—2r**, while reactions of other anions bearing an aliphatic R^2 are nonregioselective (Table 1).

These stereoselective adducts **2o**, **2q**, and **2r** were converted into the same 2-pyrrolidinone **6** as a single stereoisomer through hydrolytic cyclization (Scheme 3). This compound **6** was assigned to be an isomer in which 4-Me and 5-Ph are cis to each other on the basis of spectral data. For instance irradiation at the 4-Me (δ=1.24) resulted in a 13% of NOE enhancement of the 5-Ph. A similar hydrolytic cyclocondensation of **2p** produced **7** also as a single isomer.

On the other hand diastereomeric mixtures **21** (1:1) and **2m** (3:1) gave stereoisomeric mixtures of 2-pyrrolines **8** (1:1) and **9** (2.8:1), respectively. The major isomer of **9** was assigned to be cis, and minor one trans, on the basis of the ^{1}H chemical shifts of 4-Me and 5-Me (cis: δ=1.13 and 1.51; trans: 1.30 and 1.63) as well as the ^{13}C chemical shifts of 4-Me, 5-Me, 4-C, 5-C, and CN (cis: δ=14.30q, 21.24q, 38.94d, 55.89s, and 121.54s; trans: 15.00q, 24.76q, 41.36d, 59.06s, and 119.36s).

Stereoselectivity in the Michael addition of 2-azaallyl anions **B** is most likely to depend upon the electronic nature of R^2 substituent; Steric effect of R^2 is not important. We believe that there exists an attractive interaction between the aryl of 2-azaallyl anions **B** and the ester of methyl crotonate in the transition state.[7] As shown in Fig. 1, there are two possible approaches **C** and **C′** in which the ester is effectively overlapping with the aryl plane. The approach **C′** is more crowded between the methyl and the imine part so that the approach **C** leading to **2o—2r** becomes more favored. When R^2 is alkyl group no such attractive interaction exists. Neither of the two

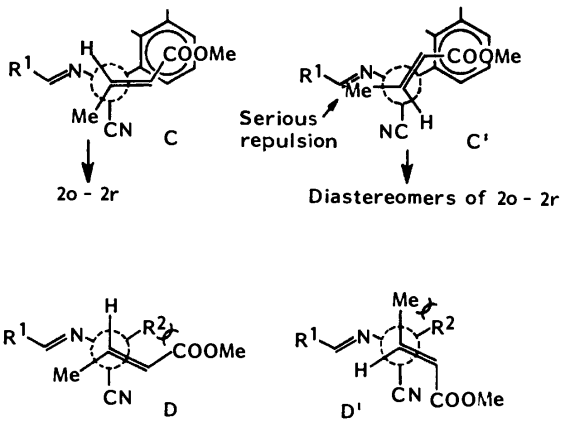

Fig. 1. Stereoselective Michael additions of aryl-substituted imines **1e—1g** with methyl crotonate.

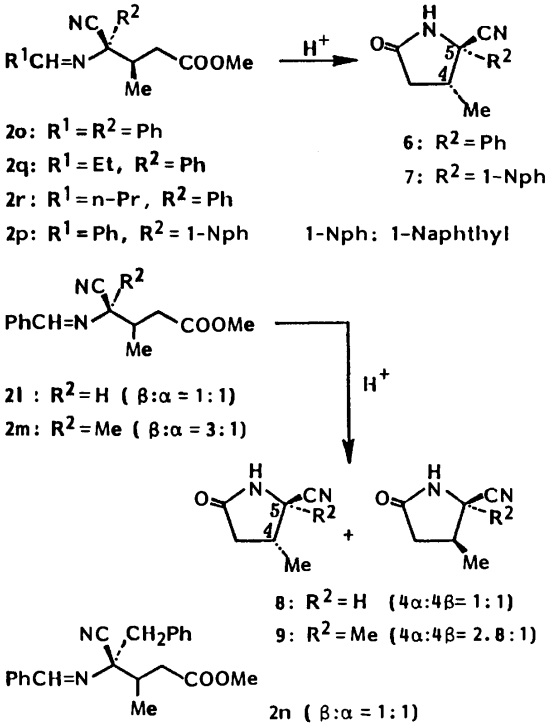

Scheme 3.

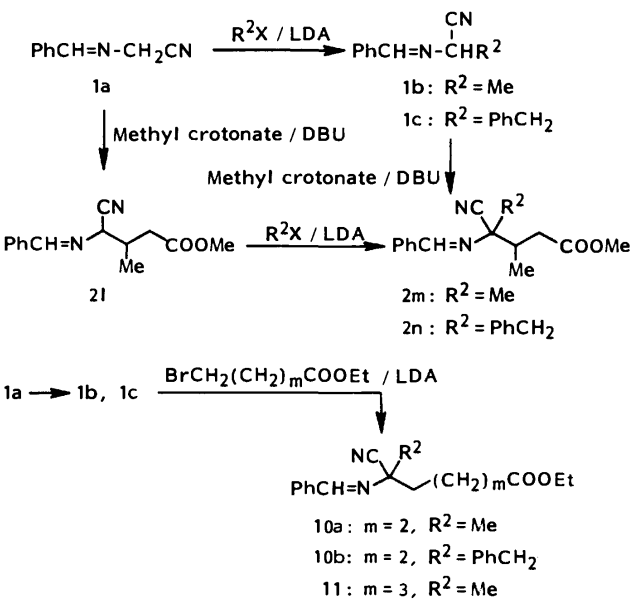

Scheme 4.

most likely approaches **D** and **D'** can find sterical predominance over the other. Accordingly the Michael additions become non-stereoselective, two diastereomers of Michael adducts being formed.

As described above two alkyl substituents can be introduced to α-(benzylideneamino)acetonitrile (**1a**) by two sequential alkylations using an alkyl halide/LDA and then a Michael acceptor/DBU (Scheme 4, **1a**, **1b**, **1c**, **2m**, **2n**). On the other hand the Michael addition of **1a** can be followed by the alkylation with an alkyl halide. For example **1a** was first allowed to react with methyl crotonate to afford a Michael adduct **21** which was then alkylated with methyl iodide or benzyl bromide to give the same dialkylated products **2m** and **2n** (Table 2).

Alkylation of **1** by the Michael addition route using α,β-unsaturated esters leads to 4-amino esters **2**. 6-Amino as well as 5-amino esters are also available when imines **1** are alkylated with ω-halo esters as alkylating agents (Scheme 4). Thus **1a** was first methylated or benzylated into **1b** or **1c**, and then alkylated with ethyl 4-bromobutanoate or 5-bromopentanoate to produce **10a**, **10b**, or **11**.

A quantitative conversion of the Michael adducts **21**—**2m** into γ-lactams **6**—**9** through a hydrolytic cyclization process was above mentioned in Scheme 3. The imine **10** bearing a longer framework by one carbon could undergo a similar hydrolytic cyclization to produce δ-lactams, 2-piperidinones **12a** and **12b** (Scheme 5). However the hydrolysis of **11** under comparable conditions gave methyl 6-aminoheptanoate **13**, no further cyclization being observed.

Base-Induced Cyclization of 2-(Alkylideneamino) Esters Leading to 1-Pyrrolines. Grigg and his coworkers have demonstrated the base-induced Michael additions between the imines of 2-amino esters and α,β-unsaturated esters.[8] These Michael adducts were converted into pyrrolidines by treatment with potassium *t*-butoxide or benzyltrimethylammonium methoxide in benzene. Stereoselectivity of these cyclizations was not high.

We first employed his cyclization procedure to *N*-(1-cyanoalkyl)imines **2** (Scheme 6 and Table 3). The cyclization of imines **2** was exclusively accompanied by a spontaneous elimination of CN group giving 1-pyrrolines **14** and/or **14'**. As shown with Entries 1, 6, 8, 13, 14, 24 (KOBu-*t*) and Entries 11 and 23 (BTAM) in Table 3, the cyclization of **2** under these conditions

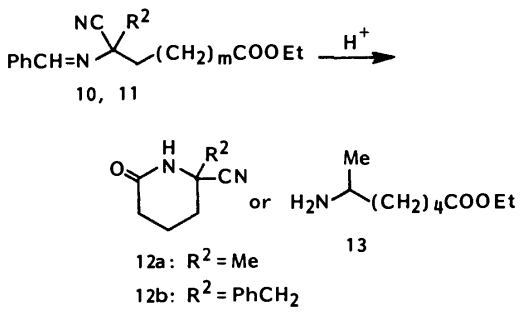

Scheme 5.

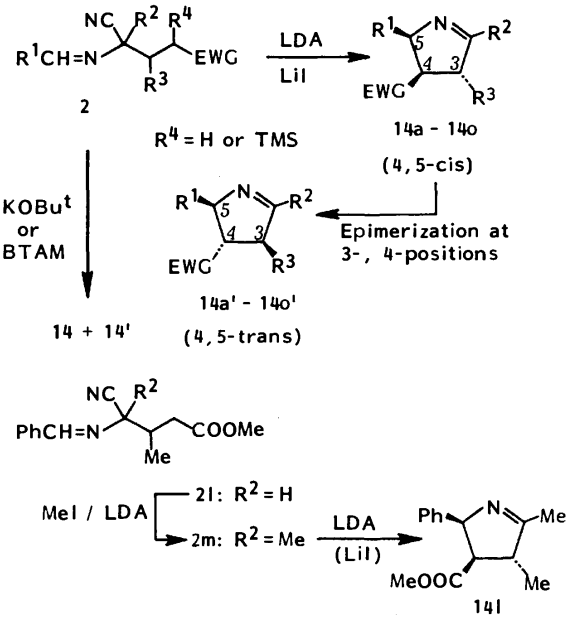

Scheme 6.

Table 2. Consecutive Alkylation of α-(Benzylideneamino)acetonitrine (**1a**)

Reaction sequence	1st Alkylation[a]				2nd Alkylation[a]				Total yield
	Alkylating agent	Temp	Time	Yield[b]	Alkylating agent	Temp	Time	Yield[b]	
1a→**1b**→**2m**	MeI/LDA	−78 °C	0.5 h	85%	$MeCH{=}^{t}CHCOOMe$/DBU	c)		95%	**2m**: 81%
1a→**1c**→**2n**	$PhCH_2Br$/LDA	−78 °C	0.5 h	88%	$MeCH{=}^{t}CHCOOMe$/DBU	c)		92%	**2n** : 81%
1a→**21**→**2m**	$MeCH{=}^{t}CHCOOMe$/DBU	c)		78%	MeI/LDA	−78 °C	1 h	100%	**2m**: 78%[d]
1a→**21**→**2n**	$MeCH{=}^{t}CHCOOMe$/DBU	c)		78%	$PhCH_2Br$/LDA	−78 °C	1 h	82%	**2n** : 64%[e]
1a→**1b**→**10a**	MeI/LDA	f)		85%	$Br(CH_2)_3COOEt$/LDA	rt	2 h	96%	**10a** : 82%
1a→**1c**→**10b**	$PhCH_2Br$/LDA	f)		88%	$Br(CH_2)_3COOEt$/LDA	rt	1.5 h	63%	**10b** : 55%
1a→**1b**→**11**	MeI/LDA	f)		85%	$Br(CH_2)_4COOEt$/LDA	rt	2 h	67%	**11** : 57%

a) Carried out in THF in the presence of LDA or DBU (1 equiv). b) Yield of isolated products. c) The reaction conditions are listed in Table 1. d) Isomer ratio : 4:1 (^{1}H NMR). e) Isomer ratio : 1.5:1 (^{1}H NMR).

is very poor in stereoselectivity. Either mixtures of two 4,5-stereoisomers **14**+**14′** were obtained or the only isomers were 4,5-*trans*-1-pyrrolines **14′** when the cyclization was stereoselective (Entries 11 and 13). Stereochemistry at the 3-position is not important since this position is known to isomerize into a thermodynamically more stable 3,4-trans configuration through an imine/enamine tautomerization.[9]

To our great surprise methylation of the Michael adduct **2l** with LDA and methyl iodide provided 4,5-*cis*-1-pyrroline **14l** as a single isomer (Scheme 6 and Entry 17 in Table 3). Although it was easily understood that **2l** was first methylated leading to **2m**, why the cyclization of **2m** under the methylation conditions was so fast and cis-selective? Both **2l** and **2m** were completely recovered intact on treatment with LDA at −78 °C (Entries 16 and 18), but a 1:1 stereoisometric mixture of cyclized products **14l**+**14l′** was obtained at an elevated temperature (Entry 19). In the presence of methyl iodide the cyclization was again cis-selective to give **14l** as a single product (Entry 20). In the end we noticed that lithium iodide would play an important role in the cis-selective cyclization reactions. Actually only cis isomer **14l** was given in an excellent yield in the reaction of **2m** with LDA in the presence of lithium iodide (Entry 21).

Thus cyclizations of other imines **2** were carried out under the cyclization conditions using LDA and lithium iodide, and 4,5-*cis*-1-pyrrolines **14** were the only products in most cases (Table 3). Lithium iodide probably worked as a Lewis acid to activate the C=N bond of imines **2** so that the intramolecular cyclization was considerablly facilitated. The high stereoselectivity would be discussed later.

Cyclization of imines **2g**—**2i** which bear an acetyl moiety as EWG was found also stereoselective but 4,5-*trans*-1-pyrrolines **14′** were the only or major products (Entries 10—13). As 4,5-*cis*-1-pyrroline **14i** readily epimerizes into 4,5-trans isomer **14i′** under the cyclization conditions, the predominant formation of **14g′**—**14i′** would be a result of facile epimerization at the carbon which is substituted with EWG (Scheme 6).

Table 3. Base-Induced Cyclization of Alkylated Imines **2**

Entry	Imine	Condition[a]	Time/h −78 °C	Time/h rt	Product	R^1	R^2	R^3	EWG	Yield/%[b]	Isomer ratio
1	**2a**	A	0.5	18	No reaction (recovered **2a**:96%)					0	
2	**2a**	B	6	0	**14a**	Ph	Me	H	COOMe	65	
3	**2a**	C	2	1	**14a**					82	
4	**2b**	C	0.5	2	**14b**	Ph	$PhCH_2$	H	COOMe	80	
5	**2c**	C	0.5	1.5	**14c**+**14c′**	Ph	*i*-Pr	H	COOMe	61[c]	**14c**:**14c′**=2:1[d]
6	**2d**	A	0.5	15	**14d**+**14d′**	Ph	Ph	H	COOMe	65[e]	**14d**:**14d′**=1:1[d]
7	**2e**	C	0.7	1.5	**14e**	Et	Ph	H	COOMe	57	
8	**2e**	A	0.5	19	**14e**+**14e′**					82	**14e**:**14e′**=4:1[d]
9	**2f**	B	6	0	**14f**+**14f′**	Ph	Me	H	$COOBu^t$	60	**14f**:**14f′**=3:2[d]
10	**2g**	C	0.5	1.5	**14g′**	Ph	$PhCH_2$	H	COMe	82	
11	**2h**	D	0	22	**14h′**	Ph	Ph	H	COMe	84	
12	**2i**	C	0.8	0.5	**14i**+**14i′**	Et	Ph	H	COMe	81	**14i**:**14i′**=1:2[d]
13	**2i**	A	1	20	**14i′**					93	
14	**2k**	A	1	19	**14j**+**14j′**	Et	Ph	H	CN	80	**14j**:**14j′**=10:1[d]
15	**2l**	C	0.5	1.5	**14k**	Ph	H	Me	COOMe	25	
16	**2l**	B	9	0	No reaction (recovered **2l**:100%)					0	
17	**2l**	B (MeI)	0.5	1	**14l**	Ph	Me	Me	COOMe	77	
18	**2m**	B	7	0	No reaction (recovered **2m**:95%)					0	
19	**2m**	B	0.5	2	**14l**+**14l′**					70	**14l**:**14l′**=1:1[d]
20	**2m**	B (MeI)	0.5	1	**14l**					66	
21	**2m**	C	0.5	2	**14l**					84	
22	**2n**	C	0.2	3	**14m**	Ph	$PhCH_2$	Me	COOMe	81	
23	**2o**	D	0	16	**14n**+**14n′**	Ph	Ph	Me	COOMe	60[f]	**14n**:**14n′**=1:3[d]
24	**2q**	A	1	27	**14o**+**14o′**	Et	Ph	Me	COOMe	80	**14o**:**14o′**=3:2[d]
25	**2t**	E	1	17	**14e**+**14e′**					40[g]	h)
26	**2t**	F	1 (0° C)	2	**14e**+**14e′**					71	h)

a) A: $KOBu^t$ (1.1 equiv) in THF. B: LDA (1 equiv) in THF. B (MeI): LDA (2 equiv) and then MeI (1.1 equiv) in THF. C: LDA + LiI (each 1 equiv) in THF. D: Benzyltrimethylammonium methoxide in THF. E: TBAF (0.1 equiv) in THF. F: TBAF (0.1 equiv) in HMPA. b) Yield of isolated products. c) Recovered **2c**: 31%. d) Inseparable mixture. Isomer ratio was determined by ^1H NMR or ^{13}C NMR spectrum. e) Recovered **2d**: 14%. f) Recovered **2o**: 11%. g) Yield determined by ^1H NMR spectrum (recovered **2t**: 60%). h) Isomer ratio is uncertain.

When 4-H of 4,5-cis isomers **14** is highly acidic, this position epimerizes presumably via an enol intermediate to lead to thermodynamically more stable 4,5-trans relationship. Quick isomerization at the 3-position is followed through an imine/enamine tautomerization to give **14'**.[9]

In other base-induced cyclizations of imines **2**, 4,5-*cis*-1-pyrrolines **14** would be formed exclusively or predominantly as the initial products. They undergo a similar epimerization both at the 3- and 4-positions leading to 4,5-*trans*-1-pyrrolines **14'**. It is apparent that isomer ratios **14**:**14'** depend upon the cyclization conditions (base, temperature, time etc.). As LDA/LiI-induced cyclization occurs more rapidly than the other cyclizations, one can conduct this reaction at a low temperature in a short period. As a result the subsequent epimerization is suppressed.

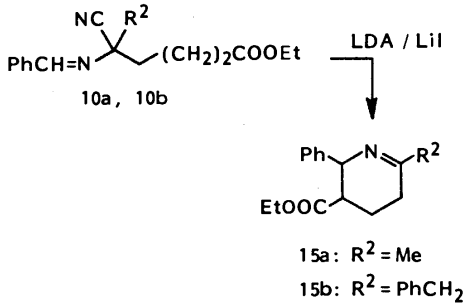

Scheme 7.

The alkylated imines **10a** and **10b** with one more carbon also underwent a similar cyclization under the influence of LDA and lithium iodide to give tetrahydropyridines **15a** and **15b** both as mixtures of two stereoisomers, respectively (Scheme 7). Contrary to this the cyclization of **11** under comparable conditions was entirely unsuccessful, **11** being quantitatively recovered.

The above 4,5-*cis*-selective cyclizations of Michael adducts **2** is explained with an example of cyclization of **2m** (Fig. 2). One possible transition model is called Cyclic Model which implies a seven-menbered ring of lithium chelate **F** and **F'** The other one called Open Chain Model involves a chair-like enolate geometry **G** and **G'**. The LDA/LiI-induced cyclization of **2m** which is a 1:1 mixture of two diastereomers (*ul*-**2m** and *lk*-**2m**) at −78 °C allowed the selective consumption of one isomer *ul*-**2m** forming **14** l. The other isomer *lk*-**2m** was recovered intact. In the both models the enolate intermediates **F** and **G** derived from *ul*-**2m** are sterically more favored than their isomeric intermediates **F'** and **G'** making possible the kinetical separation.

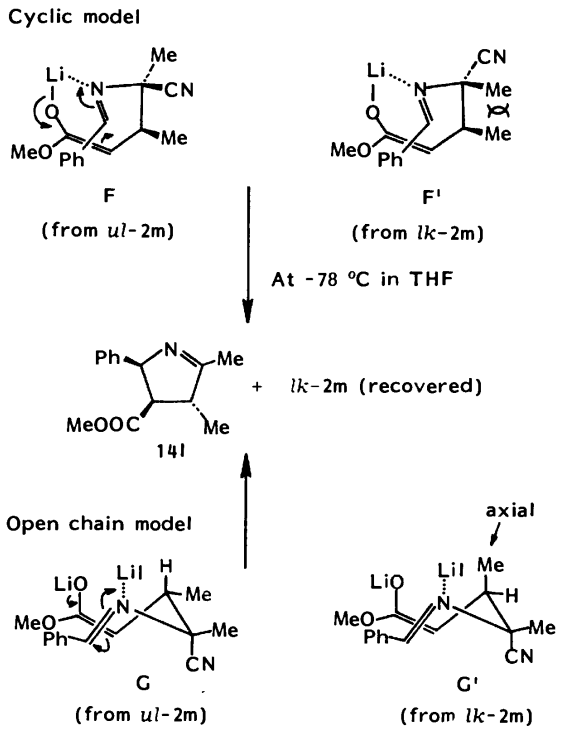

Fig. 2. Two possible transition models for the stereoselective cyclization of **2m** leading to **14**l.

Experimental

General. Melting points were determined on a Yanagimoto melting point apparatus and are uncorrected. IR spectra were taken with a JASCO IRA-1 or a JASCO A-702 spectrometer. ^{1}H NMR spectra were recorded on a Hitachi R-40 (90 MHz) or a JEOL FX-100 instrument (100 MHz) and ^{13}C NMR on a JEOL FX-100 spectrometer at 25.05 MHz. Chemical shifts are expressed in parts per million downfield from tetramethylsilane as an internal standard. Mass spectra as well as high resolution mass spectra were measured with a JEOL-01SG-2 spectrometer at 70 eV of ionization energy. Elemental analyses were performed on a Hitachi 026 CHN analyzer. Thin-layer chromatography (TLC) was accomplished on 0.2 mm precoated plates of silica gel 60 F-254 (Merck). For preparative column chromatography Wakogel C-200, C-300 (Wako), and Silicagel 60 (Merck) were employed. Flash chromatography was carried out on an EYELA EF-10 apparatus using a column (20×180 mm) packed with Silicagel 60 (Merck, size: 0.04—0.063 mm). Micro vacuum distillation was made on a Sibata GTO-250R Kugelrohr distilling apparatus. Solvents were evaporated with a Tokyo Rikakikai rotary evaporator type-V.

General Procedure for Preparation of *N*-(1-Cyanoalkyl)-imines 1a—1i. Imines **1a** and **1e—1i** were prepared by the condensation of 2-aminoalkanenitriles with carbonyl compounds: Equimolar mixture of a 2-aminoalkanenitrile and a carbonyl compound was heated under reflux in the solvent described below (2—5 ml for 1 mmol of the substrate). The solution was dried over anhydrous magnesium sulfate and evaporated in vacuo to give imines **1** in an almost quantitative yield. Imines **1a**, **1e**, and **1g** are known.[6d] The reaction solvent and time are as follows: **1f**: In benzene for 1 h; **1h**: in chloroform for 2 h; **1i**: in benzene for 2 h. Imines **1b—1d** were prepared by the alkylations of **1a**: To a solution

of LDA (3 mmol in THF (3 ml)) freshly prepared from butyllithium and diisopropylamine was added imine **1a** (0.43 g, 3 mmol in THF (5 ml)) at −78 °C. After 5 min an alkylating agent (methyl iodide, benzyl bromide, or isopropyl bromide, each 3.3 mmol in THF (2—3 ml)) was added. The mixture was stirred under the following conditions: **1b**: at −78 °C for 2 h; **1c** and **1d**: at −78 °C for 1 h and then at room temperature for 1 h. The reaction was quenched by treating with ice water and the products were extracted with diethyl ether (30 ml×2). The combined extracts were dried over magnesium sulfate and evaporated in vacuo. The residue was chromatographed over silica gel by using chloroform to give **1b** (0.4 g, 85%), **1c** (0.614 g, 88%), or **1d** (0.48 g, 52%).

1b: Pale yellow liquid; bp 150 °C (133 Pa, bulb-to-bulb); IR (neat) 2225 and 1640 cm^{-1}; ^1H NMR ($CDCl_3$) δ=1.63 (3H, d, J=6.0 Hz, Me), 4.64 (1H, dq, J=6.0 and 2.0 Hz, CH), 7.2—7.6 (3H, m, Ph), 7.7—7.9 (2H, m, Ph), and 8.42 (1H, d, J=2.0 Hz, CH=N); ^{13}C NMR ($CDCl_3$) δ=21.06 (q, Me), 53.24 (d, CH), 118.89 (s, CN), 128.89, 131.83 (each d), 135.07 (s), and 162.66 (d, CH=N); MS m/z (rel intensity, %) 158 (M^+, 62), 143 (64), 131 (19), 130 (14), 117 (base peak), 105 (26), 104 (49), 103 (17), 90 (16), 89 (33), and 77 (88). HRMS Found: m/z 158.0840. Calcd for $C_{10}H_{10}N_2$: M, 158.0839.

1c: Pale yellow liquid; IR (neat) 2250, 1740, and 1645 cm^{-1}; ^1H NMR ($CDCl_3$) δ=3.17, 3.22 (each 1H, dd, J=13.0 and 8.0 Hz, CH_2Ph), 4.77 (1H, dt, J=8.0 and 2.0 Hz, NCH), 7.2—7.9 (10H, m, Ph), and 8.20 (1H, d, J=2.0 Hz, CH=N); MS m/z (rel intensity, %) 234 (M^+, 37), 143 (54), 118 (17), 117 (18), 116 (29), 107 (43), 91 (base peak), and 77 (30). HRMS Found: m/z 234.1165. Calcd for $C_{16}H_{14}N_2$: M, 234.1157.

1d: Pale yellow liquid; IR (neat) 2240 and 1640 cm^{-1}; ^1H NMR ($CDCl_3$) δ=1.05, 1.13 (3H, d, J=8.0 Hz, *i*-Pr), 2.23 (1H, m, *i*-Pr), 4.44 (1H, dd, J=6.0 and 2.0 Hz, NCH), 7.3—7.5 (3H, m, Ph), 7.70 (2H, m Ph), and 8.35 (1H, d, J=2.0 Hz, CH=N); ^{13}C NMR ($CDCl_3$) δ=17.94, 19.18 (each q, *i*-Pr), 32.88 (d, *i*-Pr), 65.06 (d, NCH), 117.24 (s, CN), 128.95, 129.19, 131.83, 134.66, and 163.00 (d, CH=N); MS m/z (rel intensity, %) 186 (M^+, 11), 144 (50), 143 (68), 116 (base peak), 104 (16), 91 (12), 90 (36), and 89 (54). HRMS Found: m/z 186.1158. Calcd for $C_{12}H_{14}N_2$: M, 186.1157.

1f: Yellow liquid; IR (neat) 2240 and 1640 cm^{-1}; ^1H NMR ($CDCl_3$) δ=6.33 (1H, d, J=2.0 Hz, CH), 7.2—8.2 (12H, m, Ar), and 8.52 (1H, d, J=2.0 Hz, CH=N); MS m/z (rel intensity, %) 270 (M^+, 45), 166 (base peak), 140 (11), and 127 (4). HRMS Found: m/z 270.1168. Calcd for $C_{19}H_{14}N_2$: M, 270.1168.

1h: Pale yellow liquid; bp 150 °C (133 Pa, bulb-to-bulb); IR (neat) 2430 and 1660 cm^{-1}; ^1H NMR ($CDCl_3$) δ=0.95 (3H, t, J=7.0 Hz, *n*-Pr), 1.60 (2H, m, *n*-Pr), 2.34 (2H, m, *n*-Pr), 5.46 (1H, s, CH), 7.36 (5H, s, Ph), and 8.00 (1H, t, CH=N); ^{13}C NMR ($CDCl_3$) δ=13.69 (t, *n*-Pr), 19.01, 37.79 (each t, *n*-Pr), 61.90 (d, CH), 117.20 (s, CN), 127.30, 129.00, 129.12 (each d), 134.97 (s), and 168.55 (d, CH=N); MS m/z (rel intensity, %) 186 (M^+, 8), 181 (16), 158 (39), 157 (18), 132 (22), 118 (22), 116 (base peak), 89 (21), and 58 (11). HRMS Found: m/z 186.1160. Calcd for $C_{12}H_{14}N_2$: M, 186.1157.

1i: Pale yellow liquid; bp 130 °C (133 Pa, bulb-to-bulb); IR (neat) 2250 and 1660 cm^{-1}; ^1H NMR ($CDCl_3$) δ=1.10 (9H, s, *t*-Bu), 5.46 (1H, d, J=2.0 Hz, CH), 7.30 (5H, s, Ph), and 7.85 (1H, d, J=2.0 Hz, CH=N); ^{13}C NMR ($CDCl_3$) δ=26.65 (q, *t*-Bu), 36.94 (s, *t*-Bu), 61.36 (d, CH), 117.30 (s, CN), 127.24, 128.48, 129.01 (each d), 135.19 (s), and 175.19 (d, CH=N); MS m/z (rel intensity, %) 200 (M^+, 26), 185 (33), 117 (39), 116 (base peak), 89 (18), and 58 (39). HRMS Found: m/z 200.1310. Calcd for $C_{13}H_{16}N_2$: M, 200.1991.

General Procedure for Michael Additions of *N*-(1-Cyanoalkyl)imines 1a—1i to Olefins Leading to 2a—2t. To a solution of imine **1** (1 mmol) in dry THF (5 ml) was added at −78 °C DBU (0.167 to 0.015 g, 1.1 to 0.1 mmol in 1 ml of THF). After 5 min, an olefin (1.1 mmol in 1 ml of THF) was added to the resulting red solution. This mixture was allowed to react under the conditions listed in Table 1 in an atmosphere of nitrogen, poured into ice water, and then extracted with diethyl ether (25 ml×2). The combined extracts were dried over anhydrous magnesium sulfate and evaporated in vacuo. The residue was chromatographed through a short column packed with silica gel by using chloroform as an eluent. The results are listed in Table 1.

2a: Pale yellow liquid; IR (neat) 2225, 1740, and 1640 cm^{-1}; ^1H NMR ($CDCl_3$) δ=1.62 (3H, s, Me), 2.2—2.4 (4H, m, 2×CH_2), 3.56 (3H, s, COOMe), 7.2—7.6 (3H, m, Ph), 7.7—7.9 (2H, m, Ph), and 8.46 (1H, s, CH=N); ^{13}C NMR ($CDCl_3$) δ=27.65 (q, Me), 29.41, 36.18 (each t, CH_2), 51.59 (q, COOMe), 62.59 (s, q-C), 119.36 (s, CN), 128.83, 131.77 (each d), 135.07 (s), 160.36 (d, CH=N), and 172.42 (s, COOMe); MS m/z (rel intensity, %) 244 (M^+, 2), 213 (38), 158 (39), 157 (base peak), 141 (82), and 104 (34). HRMS Found: m/z 244.1209. Calcd for $C_{14}H_{16}N_2O_2$: M, 244.1209.

2b: Pale yellow liquid; IR (neat) 2240, 1740, and 1645 cm^{-1}; ^1H NMR ($CDCl_3$) δ=2.37 (4H, m, 2×CH_2), 3.12 (2H, s, CH_2Ph), 3.52 (3H, s, COOMe), 7.1—7.4 (8H, s and m, Ph), 7.60 (2H, m, Ph), and 7.97 (1H, s, CH=N); ^{13}C NMR ($CDCl_3$) δ=29.47, 35.12, 46.18 (each t, CH_2), 51.65 (q, COOMe), 68.06 (s, q-C), 118.07 (s, CN), 127.60, 128.30, 128.83, 131.00, 131.77, 134.07, 134.83, 161.66 (d, CH=N), and 172.65 (s, COOMe); MS m/z (rel intensity, %) 320 (M^+, 15), 230 (16), 229 (base peak), 197 (12), 169 (56), and 104 (17). HRMS Found: m/z 320.1546. Calcd for $C_{20}H_{20}N_2O_2$: M, 320.1567.

2c: Pale yellow liquid; IR (neat) 2250, 1740, and 1640 cm^{-1}; ^1H NMR ($CDCl_3$) δ=0.95, 1.15 (each 3H, d, J=7.0 Hz, *i*-Pr), 2.0—2.4 (4H, m, CH_2), 3.55 (3H, s, COOMe), 7.3—7.5 (3H, m, Ph), 7.78 (2H, m, Ph), and 8.42 (1H, s, CH=N); ^{13}C NMR ($CDCl_3$) δ=17.53, 17.71 (each q, *i*-Pr), 29.53, 32.59 (each t, CH_2), 36.65 (d, *i*-Pr), 51.77 (q, COOMe), 61.06 (s, q-C), 117.89 (s, CN), 128.95, 131.80 (each d), 135.00 (s), 160.89 (d, CH=N), and 173.07 (s, COOMe); MS m/z (rel intensity, %) 272 (M^+, 14), 241 (26), 230 (32), 229 (93), 186 (32), 185 (36), 144 (67), and 143 (base peak). HRMS Found: m/z 272.1533. Calcd for $C_{16}H_{20}N_2O_2$: M, 272.1541.

2d: Colorless liquid; IR (neat) 2220, 1715, and 1640 cm^{-1}; ^1H NMR ($CDCl_3$) δ=2.3—2.7 (4H, m, CH_2), 3.50 (3H, s, COOMe), 7.2—7.8 (10H, m, Ph), and 8.50 (1H, s, CH=N); MS m/z (rel intensity, %), 306 (M^+, 26), 220 (22), 219 (base peak), 142 (60), and 115 (39). HRMS Found: m/z 306.1363. Calcd for $C_{19}H_{18}N_2O_2$: M, 306.1360.

2e: Pale yellow liquid; IR (neat) 2220, 1740, and 1665 cm^{-1}; ^1H NMR ($CDCl_3$) δ=1.15 (3H, t, J=7.0 Hz, Et), 1.7—2.0 (2H, m, Et), 2.2—2.6 (4H, m, CH_2), 3.60 (3H, s, COOMe), 7.2—7.7 (5H, m, Ph), and 8.07 (1H, t, J=5.0 Hz, CH=N); ^{13}C NMR ($CDCl_3$) δ=9.59 (q, Et), 29.12, 29.41 (each t, Et and CH_2), 38.77 (t, CH_2), 51.65 (q, COOMe), 70.01 (s,

q-C), 118.36 (s, CN), 126.07, 128.83, 129.01 (each d), 139.66 (s), 166.66 (d, CH=N), and 172.42 (s, COOMe); MS *m/z* (rel intensity, %) 258 (M^+, 4), 203 (16), 171 (24), 143 (23), 142 (base peak), 116 (39), 115 (57), 104 (36), 91 (29), 77 (32), and 41 (31). HRMS Found: *m/z* 258.1361. Calcd for $C_{15}H_{18}N_2O_2$: M, 258.1367.

2f: Yellow liquid; IR (neat) 2240, 1725, and 1645 cm^{-1}; ^1H NMR ($CDCl_3$) δ=1.40 (9H, s, *t*-Bu), 1.63 (3H, s, Me), 2.1—2.5 (4H, m, CH_2), 7.3—7.5 (3H, m, Ph), 7.6—7.8 (2H, m, Ph), and 8.41 (1H, s, CH=N); ^{13}C NMR ($CDCl_3$) δ=27.77 (q, Me), 28.00 (q, *t*-Bu), 30.77, 36.24 (each t, CH_2), 62.65 (s, *t*-Bu), 80.48 (s, q-C), 119.36 (s, CN), 128.83, 128.95, 131.77 (each d), 135.07 (s), 160.18 (d, CH=N), and 171.24 (s, COOBu-*t*); MS *m/z* (rel intensity, %) 286 (M^+, 1), 230 (15), 213 (98), 203 (28), 183 (34), 158 (42), 127 (65), 104 (52), and 57 (base peak). HRMS Found: *m/z* 286.1680. Calcd for $C_{17}H_{22}N_2O_2$: M, 286.1680.

2g: Pale yellow liquid; IR (neat) 2200, 1720, and 1645 cm^{-1}; ^1H NMR ($CDCl_3$) δ=2.04 (3H, s, COMe), 2.2—2.6 (4H, m, CH_2), 3.10 (2H, s, CH_2Ph), 7.07 (5H, s, Ph), 7.20 (3H, m, Ph), 7.60 (2H, m, Ph), and 7.93 (1H, s, CH=N); ^{13}C NMR ($CDCl_3$) δ=25.94 (q, COMe), 30.06, 34.06, 38.77 (each t, CH_2), 68.12 (s, q-C) 118.12 (s, CN), 127.66, 128.36, 128.89, 131.13, 131.89, 134.13, 134.89, 161.66 (d, CH=N), and 206.72 (s, COMe); MS *m/z* (rel intensity, %) 304 (M^+, 19), 213 (58), 198 (16), 171 (23), 105 (27), 91 (base peak), and 77 (28). HRMS Found: *m/z* 304.1596. Calcd for $C_{20}H_{20}N_2O$: M, 304.1616.

2h: Colorless liquid; IR (neat) 2220, 1715, and 1640 cm^{-1}; ^1H NMR ($CDCl_3$) δ=2.03 (3H, s, COMe), 2.50 (4H, m, CH_2), 7.2—7.9 (10H, m, Ph), and 8.49 (1H, s, CH=N); MS *m/z* (rel intensity, %) 290 (M^+, 46), 220 (25), 219 (base peak), 186 (25), 116 (16), and 89 (16). HRMS Found: *m/z* 290.1417. Calcd for $C_{19}H_{18}N_2O_2$: M, 290.1417.

2i: Pale yellow liquid; IR (neat) 2220, 1715, and 1665 cm^{-1}; ^1H NMR ($CDCl_3$) δ=1.15 (3H, t, *J*=7.0 Hz, Et), 1.7—1.9 (2H, m, Et), 2.10 (3H, s, COMe), 2.2—2.6 (4H, m, CH_2), 7.2—7.7 (5H, m, Ph), and 8.08 (1H, t, *J*=5.0 Hz, CH=N); ^{13}C NMR ($CDCl_3$) δ=9.65 (q, Et), 29.06 (t, Et), 29.88 (q, COMe), 37.53, 38.47 (each t, CH_2), 69.83 (s, q-C), 118.54 (s, CN), 126.01, 128.72, 128.95 (each d), 139.71 (s), 166.37 (d, CH=N), and 206.30 (s, COMe); MS *m/z* (rel intensity, %) 242 (M^+, 36), 187 (24), 186 (98), 171 (50), 168 (30), 144 (69), 115 (30), and 43 (base peak). HRMS Found: *m/z* 242.1424. Calcd for $C_{15}H_{18}N_2O$: M, 242.1418.

2j: Colorless liquid; IR (neat) 2450, 2390, and 1640 cm^{-1}; ^1H NMR ($CDCl_3$) δ=2.3—2.7 (4H, m, CH_2), 7.3—7.6 (8H, m, Ph), 7.85 (2H, m, Ph), and 8.60 (1H, s, CH=N); MS *m/z* (rel intensity, %) 273 (M^+, 2), 219 (17), 169 (12), 142 (26), 129 (34), 116 (25), 115 (33), 105 (36), and 77 (base peak). HRMS Found: *m/z* 273.1266. Calcd for $C_{18}H_{15}N_3$: M, 273.1266.

2k: Colorless liquid; IR (neat) 2240, 2190, and 1670 cm^{-1}; ^1H NMR ($CDCl_3$) δ=1.14 (3H, t, *J*=7.0 Hz, Et), 1.6—2.1 (2H, m, Et), 2.2—2.5 (4H, m, CH_2), 7.2—7.6 (5H, m, Ph), and 8.07 (1H, t, *J*=5.0 Hz, CH=N); MS *m/z* (rel intensity, %) 225 (M^+, 1), 210 (3), 198 (59), 172 (28), 169 (69), 145 (93), 144 (36), 143 (41), 132 (27), 131 (48), 130 (base peak), 116 (44), 104 (66), 103 (23), 96 (24), 91 (28), 77 (37), and 52 (21). HRMS Found: *m/z* 225.1263. Calcd for $C_{14}H_{15}N_3$: M, 225.1263.

2l (a 1:1 mixture of diastereomers): Yellow liquid; IR (neat) 2240, 2200, 1740, and 1645 cm^{-1}; ^1H NMR ($CDCl_3$) δ=1.15 (3H, d, J=7.0 Hz, Me), 2.2—2.8 (3H, m, CH_2 and CH), 3.63, 3.66 (each 1/2×3H, s, COOMe), 4.72 (1H, m, CHN), 7.2—7.5 (3H, m, Ph), 7.6—7.8 (2H, m, Ph), and 8.40 (1H, d, *J*=2.0 Hz, CH=N); ^{13}C NMR ($CDCl_3$) δ=16.06, 16.30 (each q, Me), 34.59, 34.88 (each d, CH), 36.77, 37.71 (each t, CH_2), 51.77 (q, COOMe), 62.36, 62.95 (each d, CHN), 116.95 (s, CN), 129.01, 132.01 (each d), 135.07 (s), 163.65, 163.89 (each d, CH=N), 172.36, and 172.60 (each s, COOMe); MS *m/z* (rel intensity, %) 244 (M^+, 37), 213 (25), 171 (base peak), 144 (20), 143 (36), 117 (16), 116 (41), 89 (20), and 76 (15). HRMS Found: *m/z* 244.1204. Calcd for $C_{14}H_{16}N_2O_2$: M, 244.1209.

2m (a 3:2 mixture of diastereomers): Pale yellow liquid; IR (neat) 2225, 1735, and 1645 cm^{-1}; ^1H NMR ($CDCl_3$) δ=1.0—1.3 (3H, m, Me), 1.60 (3H, s, Me), 2.0—2.8 (3H, m, CH_2 and CH), 3.53 (2/5×3H, s, COOMe), 3.62 (3/5×3H, s, COOMe), 7.2—7.6 (3H, m, Ph), 7.7—7.9 (2H, m, Ph), and 8.48 (1H, s, CH=N); ^{13}C NMR ($CDCl_3$) δ=15.30, 15.71 (each q, Me), 24.77, 26.24 (each q, Me), 36.77 (t, CH_2), 39.53 (d, CH), 51.71, 51.83 (each q, COOMe), 67.00, 67.59 (each s, q-C), 118.89, 119.42 (each s, CN), 125.66, 128.95, 129.95, 131.83 (each d), 135.24 (s), 160.13, 160.54 (each d, CH=N), and 172.72 (s, COOMe); MS *m/z* (rel intensity, %) 258 (M^+, 2), 158 (77), 157 (base peak), 155 (26), 143 (48), 131 (23), 121 (23), 116 (49), 105 (37), 104 (36), 77 (52), and 52 (28). HRMS Found: *m/z* 258.1368. Calcd for $C_{15}H_{18}N_2O_2$: M, 258.1368.

2n (a 1:1 mixture of diastereomers): Pale yellow liquid; IR (neat) 2210, 1730, and 1640 cm^{-1}; ^1H NMR ($CDCl_3$) δ=1.18, 1.27 (each 1/2×3H, d, *J*=7.0 Hz, Me), 2.2—3.0 (3H, m, CH_2 and CH), 3.12 (2H, s, CH_2Ph), 3.52, 3.62 (each 1/2×3H, s, COOMe), 7.04 (5H, s, Ph), 7.30 (3H, m, Ph), 7.55 (2H, m, Ph), 7.76, and 7.79 (each 1/2H, s, CH=N); ^{13}C NMR ($CDCl_3$) δ=15.30, 16.00 (each q, Me), 37.18, 39.06 (each t, CH_2), 39.24 (d, CH), 42.53, 43.77 (each t, CH_2Ph), 51.65, 51.89 (each q, COOMe), 72.36, 72.95 (each s, q-C), 117.42, 117.95 (each s, CN), 127.54, 128.18, 128.83, 131.24, 131.71, 134.30, 134.95 135.07, 141.83, 161.48 (d, CH=N), 161.89 (d, CH=N), 172.65, and 172.78 (each s, COOMe); MS *m/z* (rel intensity, %) 334 (M^+, 9), 244 (10), 243 (61), 183 (base peak), 116 (18), 104 (24), and 91 (86). HRMS Found: *m/z* 334.1983. Calcd for $C_{21}H_{22}N_2O_2$: M, 334.1683.

2o: Colorless liquid; IR (neat) 2220, 1740, and 1645 cm^{-1}; ^1H NMR ($CDCl_3$) δ=1.02 (3H, d, *J*=7.0 Hz, Me), 2.23 (1H, dd, *J*=15.0 and 9.0 Hz, one of CH_2), 2.55 (1H, dd, *J*=15.0 and 5.0 Hz, the other of CH_2), 3.00 (1H, m, CH), 3.50 (3H, s, COOMe), 7.2—7.8 (10H, m, Ph), and 8.54 (1H, s, CH=N); MS *m/z* (rel intensity, %) 320 (M^+, 6), 219 (base peak), 115 (55), 91 (26), 90 (22), 89 (54), and 77 (46). HRMS Found: *m/z* 320.1516. Calcd for $C_{20}H_{20}N_2O_2$: M, 320.1510.

2p: Pale yellow liquid; IR (neat) 2235, 1740, and 1640 cm^{-1}; ^1H NMR ($CDCl_3$) δ=1.00 (3H, d, *J*=7.0 Hz, Me), 2.36 (1H, dd, *J*=16.0 and 9.0 Hz, one of CH_2), 2.75 (1H, dd, *J*=16.0 and 6.0 Hz, the other of CH_2), 3.46 (3H, s, COOMe), 3.76 (1H, ddq, *J*=9.0, 6.0, and 7.0 Hz, CH), 7.2—7.9 (11H, m, Ar), 8.55 (1H, s, CH=N), and 8.82 (1H, d, ArH); ^{13}C NMR ($CDCl_3$) δ=16.47 (q, Me), 37.30 (t, CH_2), 38.53 (d, CH), 51.53 (q, COOMe), 77.47 (s, q-C), 117.77 (s, CN), 124.72, 126.13, 126.24 126.48, 126.60, 126.89, 128.13, 128.95, 129.19, 129.42, 129.60, 130.53, 132.07, 134.18, 135.19, 162.71 (d, CH=N), and 172.83 (s, COOMe); MS *m/z* (rel intensity, %) 370 (M^+, 20), 270 (25), 269 (base peak), 192 (10), and 191 (18). HRMS Found: *m/z* 370.1684. Calcd for $C_{24}H_{22}N_2O_2$: M, 370.1684.

2q: Pale yellow liquid; IR (neat) 2230, 1740, and

1670 cm^{-1}; ^{1}H NMR ($CDCl_3$) δ=0.9—1.3 (6H, m, Et and Me), 1.6—2.0 (2H, m, Et), 2.1—3.0 (3H, m, CH_2 and CH), 3.56 (3H, s, COOMe), 7.2—7.6 (5H, m, Ph), and 7.96 (1H, t, J=5.0 Hz, CH=N); ^{13}C NMR ($CDCl_3$) δ=9.18 (q, Et), 15.00 (q, Me), 28.77 (t, Et), 35.88 (t, CH_2), 41.00 (d, CH), 51.18 (q, COOMe), 74.71 (s), 117.19 (CN), 126.13, 128.48 (each d), 138.89 (s), 166.66 (d, CH=N), and 172.18 (COOMe). MS m/z (rel intensity, %) 272 (M^+, 11), 172 (59), 171 (base peak), 144 (50), 143 (87), 104 (36), 91 (49), 77 (22), 59 (20), 41 (31), and 39 (23). HRMS Found: m/z 272.1525. Calcd for $C_{16}H_{20}N_2O_2$: M, 272.1525.

2r: Colorless liquid; IR (neat) 2230, 1740, and 1665 cm^{-1}; ^{1}H NMR ($CDCl_3$) δ=0.8—1.0 (6H, m, Me and n-Pr), 1.3—1.7 (2H, m, n-Pr), 2.0—2.6 (4H, m, CH_2 and n-Pr), 2.80 (1H, m, CH), 3.60 (3H, s, COOMe), 7.2—7.6 (5H, m, Ph), and 8.00 (1H, t, J=5.0 Hz, CH=N); ^{13}C NMR ($CDCl_3$) δ=13.82, 15.47 (each q, Me and n-Pr), 18.94 (t, n-Pr), 36.36, 37.82 (each t, CH_2 and n-Pr), 41.36 (d, CH), 51.71 (q, COOMe), 75.24 (s, q-C), 117.71 (s, CN), 126.60, 128.83, 129.53 (each d), 139.24 (s), 166.60 (d, CH=N), and 172.83 (s, COOMe); MS m/z (rel intensity, %) 286 (M^+, 1), 258 (16), 255 (7), 186 (30), 185 (58), 158 (22), 144 (23), 143 (63), 116 (51), 104 (55), 103 (31), 91 (base peak), and 76 (41). Elemental analysis by HRMS could not be achieved because of the weak parent ion peak.

2s: Colorless liquid; IR (neat) 2200, 1740, 1645, 1250, and 845 cm^{-1}; ^{1}H NMR ($CDCl_3$) δ=0.85 (9H, s, Me_3Si), 1.92 (1H, d, J=12.0 Hz, one of CH_2), 2.08 (1H, d, J=15.0 Hz, the other of CH_2), 2.81 (1H, dd, J=15.0 and 12.0 Hz, CH), 3.31 (3H, s, COOMe), 7.1—7.7 (10H, m, Ph), and 8.43 (1H, s, CH=N); ^{13}C NMR ($CDCl_3$) δ=−3.12 (q, Me_3Si), 32.94 (d, CH), 41.83 (t, CH_2), 51.24 (q, COOMe), 71.06 (s, q-C), 118.65 (s, CN), 126.48, 128.83, 128.95, 129.19, 131.95, 135.24, 139.54, 160.95 (d, CH=N), and 174.71 (s, COOMe); MS m/z (rel intensity, %) 378 (M^+, 12), 363 (3), 306 (26), 219 (base peak), and 159 (40). HRMS Found: m/z 378.1779. Calcd for $C_{22}H_{26}N_2O_2Si$: M, 378.1795.

2t (mixture of two diastereomers): Pale yellow liquid; IR (neat) 2220, 1715, 1250, and 840 cm^{-1}; ^{1}H NMR ($CDCl_3$) δ=0.00 (9H, s, Me_3Si), 1.15 (3H, t, J=7.0 Hz, Et), 1.7—3.0 (5H, m, Et, CH_2, and CH), 3.50 (3H, s, COOMe), 7.2—7.6 (5H, m, Ph), and 8.08 (1H, t, J=5.0 Hz, CH=N); ^{13}C NMR ($CDCl_3$) δ=0.00 (q, Me_3Si), 9.47 (q, Et), 29.12 (t, Et), 32.77 (d, CH), 41.41 (t, CH_2), 51.06, 51.65 (each q, COOMe), 70.89 (s, q-C), 118.30, 118.54 (each s, CN), 125.95, 126.13, 126.36, 127.36, 128.65, 128.89 (each d), 139.24, 139.54 (each s), 165.30, 166.42 (each d, CH=N), and 174.60 (s, COOMe); MS m/z (rel intensity, %) 330 (M^+, 1), 115 (42), 104 (33), 89 (33), 73 (base peak), 59 (29), 55 (40), and 44 (32). Elemental analysis based on HRMS was unsuccessful because of the parent ion peak with a low intensity.

3: Pale yellow liquid; IR (neat) 2250 and 1660 cm^{-1}; ^{1}H NMR ($CDCl_3$) δ=1.00 (9H, s, t-Bu), 3.65 (2H, s, CH_2), 7.39 (3H, m, Ph), and 7.90 (2H, m, Ph); ^{13}C NMR ($CDCl_3$) δ=27.88 (q, t-Bu), 33.30 (s, t-Bu), 70.53 (t, CH_2), 109.71 (s, CN), 127.60, 128.95 (each d), 132.07 (s). The imine carbon can not be observed.

4: Pale yellow needles (chloroform–hexane); mp 190—192 °C; IR (KBr) 3340, 2430, and 1550 cm^{-1}; ^{1}H NMR ($CDCl_3$) δ=2.96 (1H, br, NH), 4.40 (1H, d, J=8.0 Hz, 3-H), 5.36 (1H, d, J=8.0 Hz, 5-H), 5.78 (1H, t, J=8.0 Hz, 4-H), and 7.0—7.7 (15H, m, Ph); MS m/z (rel intensity, %) 369 (M^+, 1), 296 (2), 220 (8), 193 (base peak), 178 (18), 116 (17), and 115 (79). Found: C, 74.69; H, 5.27; N, 11.36%. Calcd for $C_{23}H_{19}N_3O_2$: C, 74.78; H, 5.18; N, 11.38%.

5: Yellow liquid; IR (neat) 1620 cm^{-1}; ^{1}H NMR ($CDCl_3$) δ=3.95 (1H, t, J=8.0 Hz, 4-H), 5.37 (1H, dd, J=8.0 and 2.0 Hz, 5-H), 6.22 (1H, dd, J=8.0 and 2.0 Hz, 3-H), 7.0—7.5 (8H, m, Ph), and 7.85 (2H, m, Ph); ^{13}C NMR ($CDCl_3$) δ=61.06 (d, 4-C), 78.42 (d, 5-C), 99.36 (d, 3-C), 126.89, 127.54, 127.83, 128.06, 128.30, 128.48, 128.95, 129.19, 129.54, 131.30, 131.54, 132.07, 138.42, 141.01, and 164.89 (s, 2-C); MS m/z (rel intensity, %) 296 (M^+−46, 2), 218 (10), 165 (19), 115 (26), 105 (12), 104 (66), and 77 (base peak). Elemental analysis based on HRMS failed because of the absence of the parent ion peak.

General Procedure for Hydrolytic Cyclization of Michael Adducts 2 Leading to 2-Pyrrolidinones 6—9. A solution of the Michael adduct **2** in MeOH (5 ml for 1 mmol of **2**) was heated under reflux in the presence of p-toluenesulfonic acid (PTSA, 30 mg) or concentrated hydrochloric acid (HCl, a few drops). The mixture was poured into ice water and extracted with dichloromethane (25 ml×2). The combined extracts were dried over magnesium sulfate and evaporated in vacuo. The residue was chromatographed over silica gel by using chloroform to give **6—9**.

6: Obtained in 96% from **2o**, 79% from **2q**, and 95% from **2r** in the reactions with PTSA for 2h each as a single isomer: Colorless prisms (chloroform–hexane); mp 126—127 °C; IR (KBr) 3380, 2250, 1755 and 1720 cm^{-1}; ^{1}H NMR ($CDCl_3$) δ=1.24 (3H, d, J=7.0 Hz, 4-Me), 2.3—2.7 (3H, m, 3- and 4-H), 6.84 (1H, s, NH), and 7.3—7.6 (6H, m, Ph and NH); ^{13}C NMR ($CDCl_3$) δ=14.18 (q, 4-Me), 37.77 (t, 3-C), 45.54 (d, 4-C), 66.77 (s, 5-C), 117.95 (s, CN), 125.24, 129.48, 129.77 (each d), 136.54 (s), and 176.89 (s, 2-C). Found: C, 72.04; H, 6.08; N, 13.84%. Calcd for $C_{12}H_{12}N_2O$: C, 71.98; H, 6.04; N, 13.99%.

7: Obtained as a single isomer in 89% yield in the reaction with HCl for 3 h: Colorless prisms (chloroform–hexane); mp 205—206 °C; IR (KBr) 3200—2800, 2240, and 1700 cm^{-1}; ^{1}H NMR ($CDCl_3$) δ=1.42 (3H, d, J=7.0 Hz, 4-Me), 2.05 (1H, dd, J=17.0 and 6.0 Hz, one of 3-H), 2.46 (1H, dd, J=17.0 and 8.0 Hz, the other of 3-H), 3.00 (1H, ddq, J=8.0, 6.0, 3×7.0 Hz, 4-H), 7.4—8.2 (7H, m, Ar), and 9.40 (1H, s, NH); ^{13}C NMR ($CDCl_3$+DMSO-d_6) δ=17.59 (q, 4-Me), 36.65 (t, 3-C), 39.83 (d, 4-C), 65.18 (s, 5-C), 118.89 (s, CN), 123.83, 124.42 125.00, 126.24, 126.89, 129.00, 129.91, 130.65, 132.13, 134.66, and 175.42 (s, 2-C); Found: C, 76.63; H, 5.59; N, 10.97%. Calcd for $C_{16}H_{14}N_2O$: C, 76.78; H, 5.64; N, 11.19%.

8: Obtained in 79% yield as a 1:1 mixture of 4,5-trans and 4,5-cis isomers (^{1}H NMR) in the reaction with PTSA for 2 h. These isomers were separated from each other through column chromatography over silica gel by using chloroform (4,5-trans: 36%, 4,5-cis: 32%). 4,5-trans-**8:** Pale yellow liquid; IR (neat) 3200, 2250, and 1700 cm^{-1}; ^{1}H NMR ($CDCl_3$) δ=1.26 (3H, d, J=7.0 Hz, 4-Me), 1.9—3.0 (3H, m, 3- and 4-H), 3.98 (1H, d, J=5.0 Hz, 5-H), and 7.35 (1H, br, NH); ^{13}C NMR ($CDCl_3$) δ=18.94 (q, 4-Me), 35.59 (d, 4-C), 37.12 (t, 3-C), 50.42 (d, 5-C), 118.48 (s, CN), and 177.50 (s, 2-C); MS m/z (rel intensity, %) 124 (M^+, 50), 70 (12), 55 (26), and 42 (base peak). HRMS Found: m/z 124.0629. Calcd for $C_6H_8N_2O$: M, 124.0624. 4,5-cis-**8:** Colorless prisms (diethyl ether–hexane); mp 92—94 °C; IR (KBr) 3200, 2440, and 1660 cm^{-1}; ^{1}H NMR ($CDCl_3$) δ=1.25 (3H, d, J=7.0Hz, 4-Me),

2.14 (1H, dd, J=16.0 and 10.0 Hz, one of 3-H), 2.20 (1H, dd, J=16.0 and 8.0 Hz, the other of 3-H), 2.80 (1H, m, 4-H), 4.44 (1H, d, J=8.0 Hz, 5-H), and 6.80 (1H, br, NH). Found: C, 58.19; H, 6.54; N, 22.47%. Calcd for $C_6H_8N_2O$: C, 58.05; H, 6.50; N, 22.57%.

9: Obtained in 95% yield as an inseparable mixture of 4,5-cis and 4,5-trans isomers (2.8:1) in the reaction with PTSA for 2 h: Colorless solid; IR (KBr) 2250 and 1670 cm^{-1}, ^1H NMR ($CDCl_3$) 4,5-cis: δ=1.13 (3H, d, J=7.0 Hz, 4-Me), 1.51 (3H, s, 5-Me), 2.0—3.0 (3H, m, 3- and 4-H), and 7.75 (1H, br, NH); 4,5-trans: δ=1.30 (3H, d, J=7.0 Hz, 4-Me), 1.63 (3H, s, 5-Me), 2.0—3.0 (3H, m, 3- and 4-H), and 7.75 (1H, br, NH); ^{13}C NMR ($CDCl_3$) 4,5-cis: δ=14.30 (q, 4-Me), 21.24 (q, 5-Me), 37.30 (t, 3-C), 38.94 (d, 4-C), 55.89 (s, 5-C), 121.54 (s, CN), and 176.85 (s, 2-C); 4,5-trans: δ=15.00 (q, 4-Me), 24.76 (q, 5-Me), 38.00 (t, 3-C), 41.36 (d, 4-C), 59.06 (s, 5-C), 119.36 (s, CN), and 177.01 (s, 2-C). Found: C, 60.70; H, 7.27; N, 20.00%. Calcd for $C_7H_{10}N_2O$: C, 60.85; H, 7.30; N, 20.28%.

General Procedure for Alkylation of 2 l Leading to 2m—2n and of 1b—1c Leading to 10 and 11. An imine **2 l**, **1b**, or **1c** (1 mmol in THF (1 ml)) was added to a solution of LDA (1.1 mmol in THF (2 ml)) at −78 °C. After 5 min, methyl iodide or benzyl bromide (1 mmol) was added and the mixture was allowed to stir under the conditions listed in Table 2. The mixture was poured into ice water and extracted with diethyl ether (20 ml×2). The combined extracts were dried over magnesium sulfate and evaporated in vacuo. The residue was chromatographed over silica gel by using chloroform as an eluent. The results are summarized in Table 2.

10a: Colorless liquid; bp 180 °C (133 Pa, bulb-to-bulb); IR (neat) 2200, 1730 and 1640 cm^{-1}; ^1H NMR ($CDCl_3$) δ=1.25 (3H, t, J=7.0 Hz, Et), 1.5—2.5 (6H, m, CH_2), 1.64 (3H, s, Me), 4.07 (2H, q. J=7.0 Hz, Et), 7.3—7.4 (3H, m, Ph), 7.7 (2H, m, Ph), and 8.40 (1H, s, CH=N); ^{13}C NMR ($CDCl_3$) δ=14.24 (q, Et), 20.18 (q, Me), 27.94, 33.71, 40.59 (each t, CH_2), 60.42 (t, Et), 63.36 (s, q-C), 119.83 (s, CN), 128.89, 131.71 (each d), 135.24 (s), 159.94 (d, CH=N), and 172.95 (s, COOEt); MS m/z (rel intensity, %) 272 (M^+, 21), 227 (54), 169 (90), 158 (83), 157 (base peak), 123 (36), and 104 (26). HRMS Found: m/z 272.1522. Calcd for $C_{16}H_{20}N_2O_2$: M, 272.1522.

10b: Colorless liquid; IR (neat) 2240, 1725, and 1640 cm^{-1}; ^1H NMR ($CDCl_3$) δ=1.20 (3H, t, J=7.0 Hz, Et), 1.5—2.4 (6H, m, CH_2), 3.12 (2H, s, CH_2Ph), 4.05 (2H, q, J=7.0 Hz, Et), 7.1—7.6 (10H, m, Ph), and 7.97 (1H, s, CH=N); ^{13}C NMR ($CDCl_3$) δ=14.30 (q, Et), 20.18, 33.88, 39.53, 46.47 (each t, CH_2), 60.53 (t, Et), 68.83 (s, q-C), 118.65 (s, CN), 127.66, 128.36, 128.95, 131.19, 131.71 (each d), 134.42, 135.19 (each s), 161.30 (d, CH=N), and 173.07 (s, COOEt); MS m/z (rel intensity, %) 254 (M^+−94, 11), 253 (62), 233 (50), 143 (68), 116 (30), 91 (base peak), 88 (17), 85 (30), 83 (43), and 77 (16). Elemental analysis based on HRMS could not be performed because of the absence of the parent ion peak.

11: Colorless liquid; IR (neat) 2260, 1735, and 1645 cm^{-1}; ^1H NMR ($CDCl_3$) δ=1.20 (3H, t, J=7.0 Hz, Et), 1.3—2.3 (8H, m, CH_2), 1.60 (3H, s, Me), 4.03 (2H, q, J=7.0 Hz, Et), 7.2—7.4 (3H, m, Ph), 7.30 (2H, m, Ph), and 8.40 (1H, s, CH=N); MS m/z (rel intensity, %) 286 (M^+, 6), 172 (17), 158 (59), 157 (base peak), 143 (57), 130 (29), 116 (70), and 77 (88). HRMS Found: m/z 286.1686. Calcd for $C_{17}H_{22}N_2O_2$: M, 286.1681.

General Procedure for Hydrolytic Cyclization of 10 Leading to 12 and Hydrolysis of 11 into 13. A solution of **10a**, **10b**, or **11** (1 mmol) in methanol (3 ml) was heated under reflux in the presence of a catalytic amount of concentrated hydrochloric acid. The mixture was poured into water and extracted with dichloromethane (15 ml×2). The combined extracts were washed with water, dried over magnesium sulfate, and evaporated in vacuo. Evaporation of the solvent gave solid of **12** which was purified by crystallization. The residue containing **13** was purified by column chromatography over silica gel by using chloroform as an eluent. The reaction time and yield were as follows: **12a**: 7.5 h, 78%; **12b**: 6 h, 58%; **13**: 6 h, 78%.

12a: Colorless prisms (chloroform–hexane); mp 175—176 °C; IR (KBr) 3220, 2460, and 1660 cm^{-1}; ^1H NMR ($CDCl_3$) δ=1.66 (3H, s, Me), 1.8—2.6 (6H, m, CH_2), and 7.65 (1H, br, NH); MS m/z (rel intensity, %) 138 (M^+, 42), 123 (89), 82 (10), 70 (35), 55 (base peak), and 43 (74). Found: C, 60.95; H, 7.32; N, 20.08%. Calcd for $C_7H_{10}N_2O$: C, 60.85; H, 7.30; N, 20.28%.

12b: Colorless prisms (chloroform–hexane); mp 215—216 °C; IR (KBr) 3200 2430, and 1665 cm^{-1}; ^1H NMR ($CDCl_3$) δ=1.8—2.5 (6H, m, CH_2), 2.95, 3.15 (each 1H, d, J=15.0 Hz, CH_2Ph), 6.40 (1H, br, NH), and 7.25 (5H, s, Ph); ^{13}C NMR ($CDCl_3$) δ=18.30, 30.88, 33.24, 46.77 (each t, CH_2), 56.30 (s, q-C), 120.36 (s, CN), 128.60, 129.30, 130.65 (each d), 132.18 (s), and 171.36 (s, CO); MS m/z (rel intensity, %) 214 (M^+, 12), 123 (28), 91 (base peak), 65 (46), 55 (43), and 43 (26). Found: C, 72.69; H, 6.49; N, 12.79%. Calcd for $C_{13}H_{14}N_2O$: C, 72.87; H, 6.59; N, 13.08%.

13: Colorless liquid; IR (neat) 3500, 3400, 3200, 2250, and 1725 cm^{-1}; ^1H NMR ($CDCl_3$) δ=1.22 (3H, t, J=7.0 Hz, Et), 1.5—1.7 (4H, m, CH_2), 2.10 (3H, s, Me), 2.2—2.5 (4H, m, CH_2), 4.05 (2H, q, J=7.0 Hz, Et), and 7.35 (2H, br, NH_2); MS m/z (rel intensity, %) 172 (M^+−26, 17), 127 (31), 126 (17), 116 (27), 112 (11), 101 (22), 87 (11), 84 (14), 81 (23), 73 (14), and 43 (base peak). Elemental analysis by HRMS was not available because of the absence of the parent ion.

General Procedure for Base-Induced Cyclization of Alkylated Imines 2 Leading to 14. To a solution of appropriate base was added an imine **2** (1 mmol) at −78 °C: Method A: Imine **2** (in 2 ml of THF) was added to t-BuOK (1.1 mmol in THF (2 ml)); Method B: Imine **2** (in 2 ml of THF) was added to LDA (1 mmol) freshly prepared in THF (3 ml); Method B (MeI): Imine **2** (in 4 ml of THF) and then MeI (1.1 mmol in THF (0.6 ml)) were added to LDA (1.5 mmol in 7 ml); Method C: Lithium iodide (1 mmol) and then imine **2** (in 2 ml of THF) was added to LDA (1 mmol in THF (3 ml)); Method D: Imine **2** (in 5 ml of THF) was added to benzyltrimethylammonium methoxide (BTAM, 1 mmol in THF (1 ml)); Method E: Tetrabutylammonium fluoride (TBAF, 1M† solution in THF, 0.1 ml, 0.1 mmol) was added to imine **2** (in 5 ml of THF); Method F: TBAF (0.1 ml, 0.1 mmol) was added at 0 °C to imine **2** (in 5 ml of HMPA). The resulting mixture was stirred under the conditions listed in Table 3 and poured into ice water. The products were collected in dichloromethane (15 ml×2). The combined extracts were dried over magnesium sulfate and evaporated in vacuo. The residue was chromatographed over silica gel by using chloroform or chloroform–diethyl

† 1 M=1 mol dm^{-3}.

ether as an eluent to give **14**. Pyrrolines **14a**, **14d**, **14d'**, **14e**, **14k**, **14l**, **14n**, and **14o** are all known.[10]

14b: Pale yellow liquid; IR (neat) 1735 and 1640 cm^{-1}; ^1H NMR ($CDCl_3$) δ=2.55 (1H, dd, J=18.0 and 9.0 Hz, one of 3-H), 3.03 (3H, s, COOMe), 3.3—3.7 (2H, m, 4-H and the other of 3-H), 3.80 (2H, s, CH_2Ph), 5.43 (1H, d, J=9.0 Hz, 5-H), and 6.9—7.3 (10H, m, Ph); ^{13}C NMR ($CDCl_3$) δ=39.23, 40.65 (each t, 3-C and CH_2Ph), 48.18 (d, 4-C), 51.18 (q, COOMe), 78.24 (d, 5-C), 127.07, 127.65, 128.13, 128.95, 129.30 (each d), 136.54, 138.77 (each s), 172.59 (s, 2-C), and 177.48 (s, COOMe); MS m/z (rel intensity, %) 293 (M^+, 51), 234 (57), 207 (36), 206 (22), 115 (18), 105 (23), and 91 (base peak). HRMS Found: m/z 293.1391. Calcd for $C_{19}H_{19}NO$: M, 293.1413.

14c+14c' (a 2:1 mixture): Yellow liquid; IR (neat) 1730 and 1640 cm^{-1}; ^1H NMR ($CDCl_3$) δ=1.20 (1/3×6H, d, J=7.0 Hz, *i*-Pr), 1.25 (2/3×6H, d, J=7.0 Hz, *i*-Pr), 2.5—3.0 (3H, m, *i*-Pr and 3-H), 3.07 (2/3×3H, s, COOMe), 3.2—3.6 (1H, m, 4-H), 3.66 (1/3×3H, s, COOMe), 5.22 (1/3H, t, J=3.0 Hz, 5-H), 5.40 (2/3H, d, J=9.0 Hz, 5-H), and 6.9—7.4 (5H, m, Ph); ^{13}C NMR ($CDCl_3$) δ=20.24 (q, *i*-Pr), 32.65 (d, *i*-Pr), 38.01, 39.30 (each t, 2:1, 3-C), 48.06, 50.94 (each d, 2:1, 4-C), 51.24, 52.18 (each q, 2:1, COOMe), 77.82, 78.95 (each d, 2:1, 5-C), 126.48, 127.54, 128.07, 128.65 (each d), 138.89, 143.31 (each s), 172.83, 174.89 (each s, 2:1, COOMe), 181.95, and 183.60 (each s, 1:2, 2-C); MS m/z (rel intensity, %) 245 (M^+, 63), 214 (15), 186 (57), 159 (base peak), 117 (79), 91 (19), and 90 (34). HRMS Found: m/z 245.1368. Calcd for $C_{15}H_{19}NO_2$: M, 245.1413.

14e+14e' (a 4:1 mixture): Pale yellow liquid; IR (neat) 1735 and 1620 cm^{-1}; ^1H NMR ($CDCl_3$) δ=1.10 (3H, m, Et), 1.4—1.9 (2H, m, Et), 2.5—3.7 (3H, m, 3- and 4-H), 3.70 (3H, s, COOMe), 4.45 (1H, m, 5-H), 7.2—7.6 (3H, m, Ph), and 7.7—7.9 (2H, m, Ph); ^{13}C NMR ($CDCl_3$) **14e**: δ=11.59 (q, Et), 25.41 (t, Et), 38.06 (t, 3-C), 45.83 (d, 4-C), 51.65 (q, COOMe), 75.65 (d, 5-C), 127.89, 128.60, 130.77 (each d), 134.30 (s), 171.01 (s, 2-C), and 173.72 (s, COOMe); **14e'**: δ=10.41 (q, Et), 25.41 (t, Et), 38.06 (t, 3-C), 45.83 (d, 4-C), 51.65 (q, COOMe), 75.95 (d, 5-C), 127.89, 128.60, 130.77 (each d), 134.30 (s), 171.01 (s, 2-C), and 173.72 (s, COOMe); MS m/z (rel intensity, %) 231 (M^+, 33), 216 (24), 202 (36), 172 (72), 145 (42), 144 (42), 143 (38), 130 (base peak), 117 (24), 115 (41), 104 (70), and 77 (45). HRMS Found: m/z 231.1262. Calcd for $C_{14}H_{17}NO_2$: M, 231.1258.

14f+14f' (a 3:2 mixture): Pale yellow liquid; IR (neat) 1725 and 1650 cm^{-1}; ^1H NMR ($CDCl_3$) δ=1.00 (3/5×9H, s *t*-BuOOC), 1.46 (2/5×9H, s, *t*-BuOOC), 2.17 (6H, d, J=2.0 Hz, Me), 2.5—3.7 (3H, m, 3- and 4-H), 5.25 (2/5H, br s, 5-H), 5.45 (3/5H, d, J=10.0 Hz, 5-H), and 7.1—7.4 (5H, m, Ph); ^{13}C NMR ($CDCl_3$) δ=19.60 (q, *t*-Bu), 27.44, 28.08 (each q, 2-Me), 42.36, 42.94 (each t, 3-C), 49.73, 52.36 (each d, 4-C), 78.34 (s, *t*-Bu), 79.62, 80.44 (each d, 5-C), 126.37, 127.13, 128.00, 128.47 (each d), 139.12, 143.27 (each s), 171.18, 173.23, 173.93, and 174.98 (each s, 2-C and COOBu-*t*); MS m/z (rel intensity, %) 259 (M^+, 7), 227 (15), 222 (18), 204 (22), 203 (base peak), 201 (53), 158 (53), and 157 (40). HRMS Found: m/z 259.0771. Calcd for $C_{21}H_{16}NO_2$: M, 259.0774.

14g': Colorless liquid; IR (neat) 1710 and 1640 cm^{-1}: ^1H NMR ($CDCl_3$) δ=2.10 (3H, s, COMe), 2.6—3.3 (3H, m, 3- and 4-H), 3.80 (2H, br s, $PhCH_2$), 5.25 (1H, br d, J=6.0 Hz, 5-H), and 7.2—7.4 (10H, m, Ph); MS m/z (rel intensity, %) 277 (M^+, 1), 249 (5), 248 (22), 234 (26), 186 (32), and 105 (base peak). Elemental analysis by HRMS could not be achieved because of the weak parent ion peak.

14h': Yellow liquid; IR (neat) 1710 and 1620 cm^{-1}; ^1H NMR ($CDCl_3$) δ=2.10 (3H, s, COMe), 3.28 (3H, m, 3- and 4-H), 5.33 (1H, ddd, J=5.0, 3.2, and 2.0 Hz, 5-H), 7.1—7.5 (8H, m, Ph), and 7.85 (2H, m, Ph); MS m/z (rel intensity, %) 263 (M^+, 14), 221 (17), 220 (base peak), 193 (41), 117 (11), and 115 (16). HRMS Found: m/z 263.1303. Calcd for $C_{18}H_{17}NO$: M, 263.1308.

14i': Pale yellow liquid; IR (neat) 1710 and 1620 cm^{-1}; ^1H NMR ($CDCl_3$) δ=1.04 (3H, t, J=7.0 Hz, Et), 1.5—2.0 (2H, m, Et), 2.16 (3H, s, COMe), 2.9—3.4 (3H, m, 3- and 4-H), 4.29 (1H, m, 5-H), 7.2—7.6 (3H, m Ph), and 7.7—7.9 (2H, m, Ph); ^{13}C NMR ($CDCl_3$) δ=10.35 (q, Et), 28.65 (q, COMe), 29.47 (t, Et), 37.30 (t, 3-C), 54.42 (d, 4-C), 77.30 (d, 5-C), 127.71, 128.42, 130.60 (each d), 133.95 (s), 170.19 (s, 2-C), and 207.89 (s, COMe); MS m/z (rel intensity, %) 215 (M^+, 4), 172 (22), 144 (43), 143 (61), 130 (42), 117 (24), 116 (33), 115 (base peak), 104 (73), 103 (41), 89 (24), 77 (50), 76 (24), 63 (22), and 55 (32). HRMS Found: m/z 215.1331. Calcd for $C_{14}H_{17}NO$: M, 215.1309.

14i+14i': This mixture (1:2) was identified on the basis of ^1H NMR in $CDCl_3$: δ=1.04 (3H, J=7.0 Hz, Et), 1.60 (1/3×2H, q, J=7.0 Hz, Et), 1.80 (2/3×2H, q, J=7.0 Hz, Et), 2.10 (3H, s, MeCO), 2.8—3.6 (3H, m, 3- and 4-H), 4.30 (2/3H, m, 5-H), 4.56 (1/3H, m, 5-H), 7.3—7.4 (3H, m, Ph), and 7.8—7.9 (2H, m, Ph). The signal at 4.30 ppm (5-H of **14i'**) showed a 15% of NOE enhancement when the acetyl signal at 2.10 ppm was irradiated, confirming the 4,5-trans structure of **14i'**.

14j+14j' (a 10:1 mixture): Pale yellow liquid; IR (neat) 2240 and 1620 cm^{-1}; ^1H NMR ($CDCl_3$) δ=1.13 (3H, t, J=7.0 Hz, Et), 1.7—2.2 (2H, m, Et), 2.6—2.9 (2H, m, 3-H), 3.40 (1H, m, 4-H), 4.30 (1H, m, 5-H), 7.3—7.6 (3H, m, Ph), and 7.7—7.9 (2H, m, Ph); ^{13}C NMR ($CDCl_3$) δ=11.29 (q, Et), 26.71 (t, Et), 31.00 (d, 4-C), 40.30 (t, 3-C), 74.77 (d, 5-C), 116.77 (s, CN), 127.95, 128.89, 129.07, 129.42 (each d), 131.42, 133.36 (each s), and 169.77 (s, 2-C); MS m/z (rel intensity, %) 198 (M^+, 3), 130 (60), 115 (25), 105 (26), 104 (58), 103 (44), 77 (base peak), 76 (30), and 63 (24). HRMS Found: m/z 198.1161. Calcd for $C_{13}H_{14}N_2$: M, 198.1159.

14l+14l': All data of **14l** were presented in Ref. 10. Formation of **14l'** was deduced on the basis of ^1H NMR ($CDCl_3$) of the mixture with **14l**: δ=1.30 (3H, d, J=7.0 Hz, 3-Me), 2.05 (3H, d, J=2.0 Hz, 2-Me), 3.65 (3H, s, COOMe) and 5.10 (1H, m, 5-H). The other signals are overlapping with those of **14l**.

14m: Pale yellow liquid; IR (neat) 1735 and 1640 cm^{-1}; ^1H NMR ($CDCl_3$) δ=1.16 (3H, d, J=7.0 Hz, Me), 3.0—4.0 (4H, m, CH_2Ph, 3-H, and 4-H), 3.07 (3H, s, COOMe), 5.45 (1H, d, J=9.0 Hz, 5-H), and 7.0—7.4 (10H, m, Ph); ^{13}C NMR ($CDCl_3$) δ=16.53 (q, Me), 38.36 (t, CH_2Ph), 46.27 (d, 3-C), 51.18 (q, COOMe), 57.04 (d, 4-C), 75.71 (d, 5-C), 126.60, 128.13, 128.65, 128.89, 129.36, 131.30 (each d), 136.36, 138.21 (each s), 172.18 (s, COOMe), and 180.60 (s, 2-C); MS m/z (rel intensity, %) 307 (M^+, 15), 248 (20), 207 (29), 206 (19), 131 (19), 130 (16), 115 (14), 105 (32), 91 (base peak), and 76 (31). HRMS Found: m/z 307.1569. Calcd for $C_{20}H_{21}NO_2$: M, 307.1570.

14n+14n' (a 1:3 mixture): All data of **14n** were presented in Ref. 10. ^1H NMR ($CDCl_3$) of **14n'** was abstracted from that of the mixture with **14n**: δ=1.30 (3H, d, J=7.0 Hz, Me),

2.80 (1H, t, J=6.2 Hz, 4-H), 3.76 (3H, s, COOMe), 3.85 (1H, m, 3-H), 5.53 (1H, dd, J=6.2 and 1.5 Hz, 5-H), 7.2—7.5 (8H, m, Ph), and 7.85 (2H, m, Ph).

14o+14o′ (a 3:2 mixture): Pale yellow liquid; IR (neat) 1730 and 1620 cm^{-1}; ^1H NMR ($CDCl_3$) δ=0.9—1.4 (6H, m, Et and Me), 1.5—2.0 (2H, m, Et), 2.50 (2/5H, t, J=6.0 Hz, 4-H), 2.96 (3/5H, dd, J=8.0 and 4.2 Hz, 4-H), 3.63 (2/5×3H, s, COOMe), 3.68 (3/5×3H, s, COOMe), 3.6—4.0 (1H, m, 3-H), 4.27 (1H, m, 5-H), 7.2—7.6 (3H, m, Ph), and 7.7—7.9 (2H, m, Ph); ^{13}C NMR ($CDCl_3$) δ=10.71, 11.88 (each q, 2:3, Et), 17.53, 19.71 (each q, 3:2, Me), 25.41, 29.94 (each t, 3:2, Et), 45.89, 47.06 (each d, 2:3, 3-C), 51.59, 52.12 (each q, 3:2 COOMe), 54.89, 55.89 (each d, 3:2, 4-C), 74.12, 76.77 (each d, 2:3 5-C), 128.25, 128.65, 130.48 (each d), 133.71, 133.95 (each s), 173.83, 174.60, and 175.66 (each s, 2-C and COOMe); MS m/z (rel intensity, %) 245 (M^+, 77), 216 (22), 186 (94), 158 (21), 145 (base peak), 131 (24), 130 (95), 127 (24), and 104 (41). HRMS Found: m/z 245.1414. Calcd for $C_{15}H_{19}NO_2$: M, 245.1415.

General Procedure for LDA-Induced Cyclization of 10 Leading to 15. To a solution of LDA (in THF 3 ml) freshly prepared from butyllithium and diisopropylamine (each 1 mmol) was added at −78 °C **10a** or **10b** (1 mmol) in THF (2 ml). After 30 min at −78 °C the mixture was stirred under nitrogen at room temperature for 6 h. The reaction was quenched with saturated aqueous ammonium chloride and extracted with diethyl ether (20 ml×2). The combined extracts were dried over anhydrous magnesium sulfate and evaporated in vacuo. The residue was chromatographed over silica gel to give **15a** or **15b** (**15a**: 37%; **15b**: 25%).

15a (a 2:1 mixture of stereoisomers): Yellow liquid; IR (neat) 1730, 1660, and 1640 cm^{-1}; ^1H NMR ($CDCl_3$) δ=1.04 (3H, t, J=7.0 Hz, Et), 1.5—3.0 (5H, m, CH_2 and 5-H), 2.02 (1/3×3H, d, J=2.0 Hz, Me), 2.06 (2/3×3H, d, J=2.0 Hz, Me), 3.90 (2H, m, Et), 4.67 (1/3H, br d, J=9.0 Hz, 6-H), 5.10 (2/3H, br d, J=5.0 Hz, 6-H), and 6.9—7.5 (5H, m, Ph); MS m/z (rel intensity, %) 245 (M^+, 96), 172 (60), 145 (40), 144 (28), and 104 (base peak). HRMS Found: m/z 245.1406. Calcd for $C_{15}H_{19}NO_2$: M, 245.1413.

15b Yellow liquid; IR (neat) 1725 and 1650 cm^{-1}; ^1H NMR ($CDCl_3$) δ=1.03 (3H, t, J=7.0 Hz, Et), 1.6—3.0 (5H, m, CH_2 and 5-H), 3.60 (2H, br s, CH_2Ph), 4.80 (1H, br d, J=10.0 Hz, 6-H), and 7.25 (10H, m, Ph); ^{13}C NMR ($CDCl_3$) δ=14.00 (q, Et), 22.29 (d, 4-C), 27.12 (d, CH_2Ph), 46.89 (t, 3-C), 48.06 (d, 5-C), 60.53 (t, Et), 64.06 (d, 6-C), 126.95, 127.36, 127.60, 128.30, 128.60, 128.89, 129.24, 131.13, 137.71, 143.07, 170.30 (s, 2-C), and 174.42 (s, COOEt); MS m/z (rel intensity, %) 321 (M^+, 46), 248 (56), 220 (19), 130 (35), 116 (29), 91 (base peak), and 77 (32). HRMS Found: m/z 321.1724. Calcd for $C_{21}H_{23}NO_2$: M, 321.1727.

References

1) T. Kauffmann, *Angew. Chem.*, **86**, 715 (1974) and *Angew. Chem., Int. Ed. Engl.*, **13**, 627 (1974).

2) J. W. Lown, "Azomethine Ylides," in "1,3-Dipolar Cycloaddition Chemistry," ed by A. Padwa, John Wiley and Sons, New York, Chichester, Brisbane, Toronto, Singapore (1984), Vol. 1, Chap. 3, pp. 653—732.

3) O. Tsuge, S. Kanemasa, A. Hatada, and K. Matsuda, *Bull. Chem. Soc. Jpn.*, **59**, 2537 (1986); O. Tsuge, S. Kanemasa, T. Yamada, and K. Matsuda, *J. Org. Chem.* **52**, 2523 (1987).

4) S. Yamada, T. Oguri, and T. Shioiri, *J. Chem. Soc., Chem. Commun.*, **1976**, 136; G. Stork, A. Y. W. Leong, and A. M. Touzin, *J. Org. Chem.*, **41**, 3491 (1976); P. Bey and J. P. Vevert, *Tetrahedron Lett.*, **1977**, 1455; T. Oguri, T. Shioiri, and S. Yamada, *Chem. Pharm. Bull.*, **25**, 2287 (1977); J. J. Fitt and H. W. Gschwend, *J. Org. Chem.*, **42**, 2639 (1977); M. J. O'Donell, J. M. Boniece, and S. E. Earp, *Tetrahedron Lett.*, **1978**, 2641; D. Hoppe and L. Beckmann, *Liebigs Ann. Chem.*, **1979**, 2066 and *ibid.*, **1980**, 1751; P. Bey and J. P. Vevert, *J. Org. Chem.*, **45**, 3249 (1980); N. Imai, H. Tokiwa, Y. Akahori, and K. Achiwa, *Chem. Lett.*, **1986**, 1113.

5) M. J. O'Donell and T. M. Eckrich, *Tetrahedron Lett.*, **1978**, 4625.

6) a) O. Tsuge and K. Ueno, *Heterocycles*, **19**, 1411 (1982); b) O. Tsuge and K. Ueno, *ibid.*, **20**, 2133 (1983); c) O. Tsuge, S. Kanamasa, K. Yorozu, and K. Ueno, *Chem. Lett.*, **1985**, 1601; d) O. Tsuge, K. Ueno, S. Kanemasa, and K. Yorozu, *Bull. Chem. Soc. Jpn.*, **59**, 1809 (1986).

7) Such interaction is well-known in the field of cycloaddition: O. Tsuge, S. Kanemasa, and S. Takenaka, *Bull. Chem. Soc. Jpn.*, **58**, 3137 and 3320 (1985).

8) R. Grigg, J. Kemp, G. Scheldrick, and J. Trotter, *J. Chem. Soc., Chem. Commun.*, **1978**, 109; R. Grigg, J. Kemp, J. Malone, and A. Tangthongkum, *ibid.*, **1980**, 648.

9) The imine/enamine tautomerism of 1-(or 2-)pyrroline systems have been already discussed by us (Ref. 6d). See also O. Tsuge, S. Kanemasa and K. Matsuda, *Chem. Lett.*, **1985**, 1411; O. Tsuge, S. Kanemasa, T. Yamada, and K. Matsuda, *Heterocycles*, **23**, 2489 (1985); O. Tsuge, S. Kanemasa, and K. Matsuda, *J. Org. Chem.*, **51**, 1997 (1986).

10) O. Tsuge, S. Kanemasa, K. Yorozu, and K. Ueno, the following article in this bulletin.

 © 1987 The Chemical Society of Japan Bull. Chem. Soc. Jpn., 60, 3359—3366 (1987)

Metallic Base-Induced Cycloadditions of *N*-(1-Cyanoalkyl)imines via *N*-Metalated Azomethine Ylides: Enhanced Reactivity and High Regio- and Stereoselectivity

Otohiko Tsuge,* Shuji Kanemasa, Kiyotaka Yorozu, and Kazunori Ueno
Institute of Advanced Material Study, and Department of Molecular Science and Technology, Interdisciplinary Graduate School of Engineering Sciences, Kyushu University, Kasugakoen, Kasuga 816
(Received April 30, 1987)

Lithiation of *N*-(1-cyanoalkyl)imines with LDA generates new *N*-lithiated azomethine ylide 1,3-dipoles which show enhanced reactivity toward dipolarophiles. They undergo exclusively regio- and stereoselective 3+2 cycloaddition reaction with α,β-unsaturated esters to give 1-pyrrolines after the elimination of LiCN. Metallic bases other than LDA can be also effective. Such high regio- and stereoselectivity is explained by the involvement of *N*-metalated azomethine ylides.

A 1,3-anionic cycloaddition of 2-azaallyl anions leading to five-membered nitrogen heterocycles was pioneered by Kauffmann.[1] Though this reaction with olefins looked promising as a method for the preparation of pyrrolidine skeletons, the difficulty of structural modification of 2-azaallyl anions[2] and the serious limitation of anionophiles employable[3,4] have discouraged its wide applications to heterocyclic synthesis. If an anion-stabilizing substituent is attached on the 1- and/or 3-carbon of 2-azaallyl anionic system, the anion generation by deprotonation of imines becomes easy.[5] However, such highly stabilized 2-azaallyl anions are known to undergo Michael addition rather than cycloaddition.[6,7]

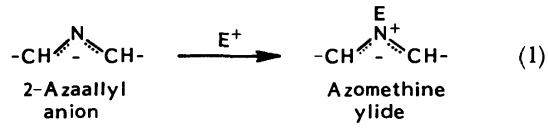

(1)

Though complementary in a synthetic use, 2-azaallyl anions and azomethine ylides are isoelectronic, both carrying 4 pai conjugation along a carbon–nitrogen–carbon framework. The only difference is the presence of a pair of nonbonding electrons on the nitrogen of the anions. Accordingly, 2-azaallyl anions as hard nucleophiles can be converted into azomethine ylides as soft species if this electron pair is utilized to make a bond with an electrophile (E^+).

In the previous articles we have presented some

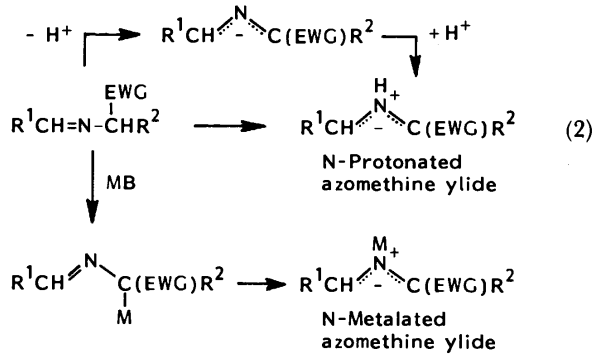

(2)

examples in which both an azomethine ylide and a 2-azaallyl anion species can be generated from the common precursor.[8,9] Reactions of these anionic species with electron-deficient olefins frequently show reverse regioselectivity.

Imines of 2-amino esters[10] and 2-amino nitriles[9,11] are known to undergo a ready thermal tautomerization into rare *N*-protonated azomethine ylides. This tautomerization formally involves the deprotonation forming 2-azaallyl anions and the reprotonation at the imine nitrogen. Accordingly, metalation of imines with a metallic base (MB) would offer a new and general route to *N*-metalated azomethine ylides because the metal countercation (M^+) in the resulting 2-azaallyl anions is most likely to sit on the nitrogen rather than to stay on the carbon.[12]

The present article describes the first successful example for the generation of *N*-lithiated azomethine ylides by reaction of imines with LDA and their highly regio- and stereoselective cycloaddition with electron-deficient olefins. Use of metallic bases other than LDA is also discussed.

Results and Discussion

α-(Benzylideneamino)acetonitrile (**1a**) was treated with LDA (1 equiv) in dry THF at −78 °C turning bright red. This color faded away as immediately as dimethyl maleate was added. After 6 h at −78 °C the reaction was quenched with aqueous ammonium chloride to give dimethyl *cis*-5-phenyl-2-pyrroline-3,4-dicarboxylate (**2a**) in 71% yield as a single isomer (Scheme 1 and Table 1). As will be discussed later, this reaction involves the initial generation of *N*-lithiated azomethine ylide **Aa**, its stereoselective cycloaddition to dimethyl maleate forming cycloadduct **B**, and the quick elimination of LiCN leading to dimethyl *c*-5-phenyl-1-pyrroline-*r*-3,*c*-4-dicarboxylate (**C**). Ready double bond migration through an imine–enamine tautomerization[13] produced the isolated 2-pyrroline **2a**.

The same 2-pyrroline-3,4-dicarboxylate **2a** is also

available in 66% yield by a stereoselective cycloaddition of *N*-protonated azomethine ylide **Da** which can be generated more simply through a thermal tautomerization of **1a** (Scheme 1).[14] The advantage is that this LDA-induced cycloaddition can be performed at a low temperature (−78 °C), indicating the enhanced reactivity of *N*-lithiated azomethine ylide **Aa** compared to **Da**. We already know that only highly activated olefins such as maleimides, maleates, and fumarates are reactive with the *N*-protonated azomethine ylide **D**. The reaction with an acrylate does proceed, but only under harsh conditions and with a poor stereoselectivity.[14] Therefore it must be interesting to test the reactivity of *N*-lithiated azomethine ylide **Aa** toward such olefin esters as crotonates, cinnamates, and methacrylates which are known to be all inactive toward *N*-protonated ylide **Da**.

The ylide **Aa** was found to show an enhanced reactivity toward methyl acrylate, crotonate, cinnamate, and methacrylate (Scheme 2 and Table 1). The products isolated in high yields were either 1-pyrrolines **2b—2d** or pyrrolidines **3a** and **3b**. They are apparently the results from highly regio- and stereoselective cycloadditions of **Aa** with these olefins: 1-Pyrrolines **2b—2d** were produced by the elimination of LiCN and pyrrolidines **3a**, **3b** were derived by the protonation, both from the initial cycloadducts **E** in which 5-phenyl and 4-methoxycarbonyl are cis. High stereoselectivity with respect to the 2-position of **3a** as

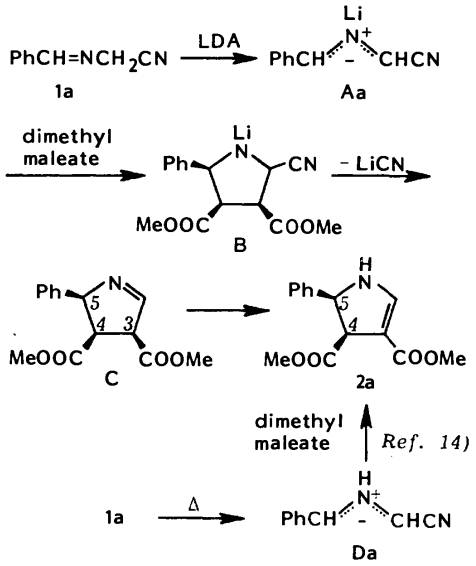

Scheme 1.

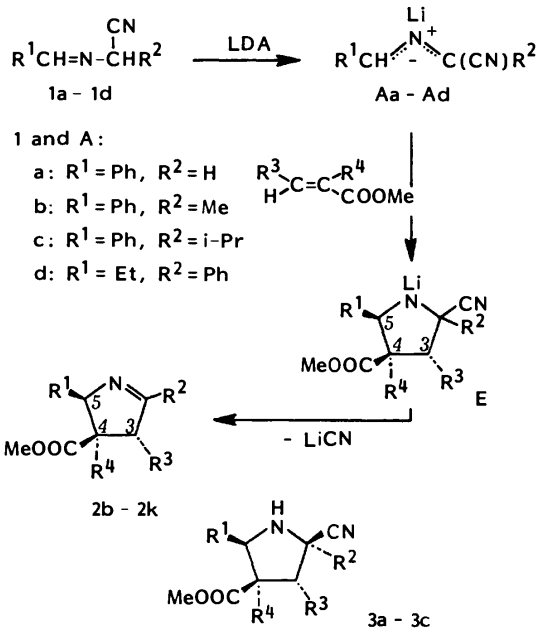

Scheme 2.

Table 1. LDA-Induced Cycladdition of *N*-(1-Cyanoalkyl)imines **1a—1d**

N-(1-Cyanoalkyl)imine		Dipolarophile	Time/h[a]	Product(yield/%)[b]		R^1	R^2	R^3	R^4
PhCH=NCH$_2$CN	**1a**	MeOOCCH≡CHCOOMe	6	**2a** (71)	**2a**	Ph	H	COOMe	H
		CH$_2$=CHCOOMe	4	**2b** (71)	**2b**	Ph	H	H	H
		MeCH≡CHCOOMe	6	**2c** (43) + **3a** (45)	**2c**	Ph	H	Me	H
					3a	Ph	H	Me	H
		PhCH≡CHCOOMe	6	**2d** (90)	**2d**	Ph	H	Ph	H
CN		CH$_2$=C(Me)COOMe	6	**3b** (100)	**3b**	Ph	H	H	Me
PhCH=NCHMe	**1b**	CH$_2$=CHCOOMe	8	**2e** (71)	**2e**	Ph	Me	H	H
		MeCH≡CHCOOMe	7	**2f** (68)	**2f**	Ph	Me	Me	H
CN		CH$_2$=C(Me)COOMe	6	**2g** (100)	**2g**	Ph	Me	H	Me
PhCH=NCHPr-*i*	**1c**	MeCH≡CHCOOMe	6	**2h** (20) + **3c** (52)[c]	**2h**	Ph	*i*-Pr	Me	H
CN					**3c**	Ph	*i*-Pr	Me	H
EtCH=NCHPh	**1d**	CH$_2$=CHCOOMe	6	**2i** (83)	**2i**	Et	Ph	H	H
		MeCH≡CHCOOMe	6	**2j** (84)	**2j**	Et	Ph	Me	H
		CH$_2$=C(Me)COOMe	6	**2k** (83)	**2k**	Et	Ph	H	Me

a) At −78 °C in THF in the presence of LDA (1 equiv). b) Yield of isolated products. c) Cycloadduct **3c** eliminates HCN leading to **2h** when chromatographed over silica gel.

well as **3b** is surprising. This indicates the exclusive participation of one of two possible ylide isomers.[15]

Such high reactivity as well as excellent selectivity was maintained when alkylated imines, *N*-(1-cyanoethyl)imine **1b** and *N*-(1-cyano-2-methylpropyl)imine **1c**, were employed instead of **1a** (Scheme 2 and Table 1). The successful LDA-induced cycloaddition of **1c** indicates that even a bulky alkyl group may be introduced at the 2-position of 1-pyrrolines or pyrrolidines. Alkylated imines can be readily accessible from **1a** and alkyl halides in the presence of LDA.[9b]

Although α-(propylideneamino)phenylacetonitrile (**1d**) bears highly acidic α-hydrogens of imine ($MeC\underline{H}_2CH{=}N-$), its lithiation with LDA took place smoothly at the carbon substituted by a cyano moiety to generate *N*-lithiated azomethine ylide **Ad**, indicating that the stability of *N*-lithiated azomethine ylide may be higher than that of *N*-lithio enamine. Similar cycloadditions of **Ad** with olefins produced **2i**—**2k** in excellent yields (Scheme 2 and Table 1).

The advantages of LDA-induced cycloaddition of *N*-(1-cyanoalkyl)imines **1** are summarized below (Scheme 3).

1) *N*-Lithiated azomethine ylide **Aa** is highly reactive to the olefin esters which can not react with *N*-protonated azomethine ylides **D**.

2) Alkylated ylides **Ab** and **Ac** are similarly reactive, while *N*-protonated counterparts **Db** and **Dc** are absolutely inactive even to maleimides as the most reactive dipolarophiles.

3) Smooth generation of ylide **Ad** is also possible.

4) Cycloaddition of **A** takes place in a highly regio- and stereoselective manner.

5) In cycloadditions with methyl acrylate, both *N*-lithiated **Ad** and *N*-protonated azomethine ylides **Dd** show high regioselectivity, but their regiochemistry is opposite. Ylide **Ad** gave 4,5-disubstituted 1-pyrroline **2i** whose regiochemistry was assigned by an alternative synthesis from **5**,[9b] while 3,5-disubstituted 1-pyrroline **4** was obtained in the reaction of **Dd**.

On the other hand, these LDA-induced cycloaddition route involves a disadvantage that the reaction has to be carried out under strongly basic conditions. The reactions of **Aa** with such olefins as maleimides, acrylonitrile, 3-buten-2-one, and phenyl vinyl sulfone led to the formation of polymeric products of olefins, warning that the olefinic dipolarophiles which are susceptible to bases may not be employed.

Metalation of *N*-(1-cyanoalkyl)imines **1** can be accomplished with other metallic bases. For example the reaction of **1a** with ethylmagnesium bromide generated *N*-magnesio azomethine ylide **F** (M=MgBr) which underwent cycloaddition with methyl acrylate or crotonate (Scheme 4 and Table 2). The products isolated as single isomers were pyrrolidines **3a′** and **3b′**, stereoisomers at the 2-position of **3**. The exclusive formation of **3′** indicates the selective participation of the anti form of ylide **F**. This makes a striking contrast with the exclusive participation of the syn form of *N*-lithio azomethine ylide **Aa** (see Scheme 2 and Table 1). Structures of **3a** and **3a′** were based upon the ^{13}C chemical shifts of 2-, 3-C, 2-CN, 3-Me as well as no NOE enhancement between 3-Me and 2-H of **3a′**.[16]

Treatment of ethylmagnesium bromide with an

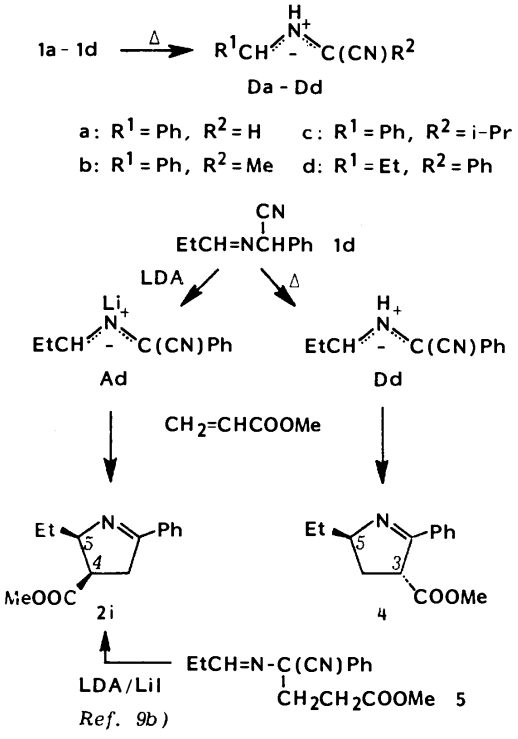

Scheme 3.

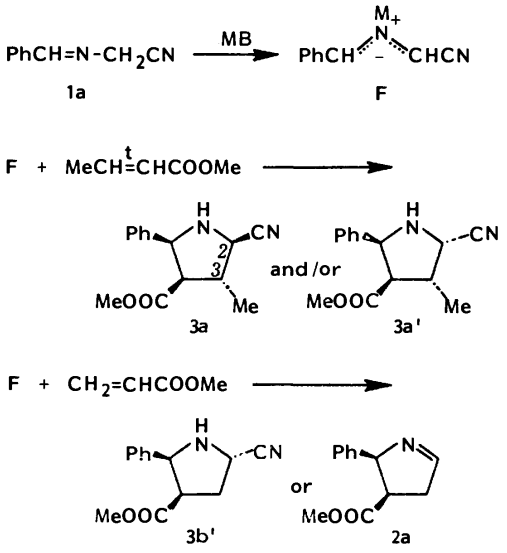

Scheme 4.

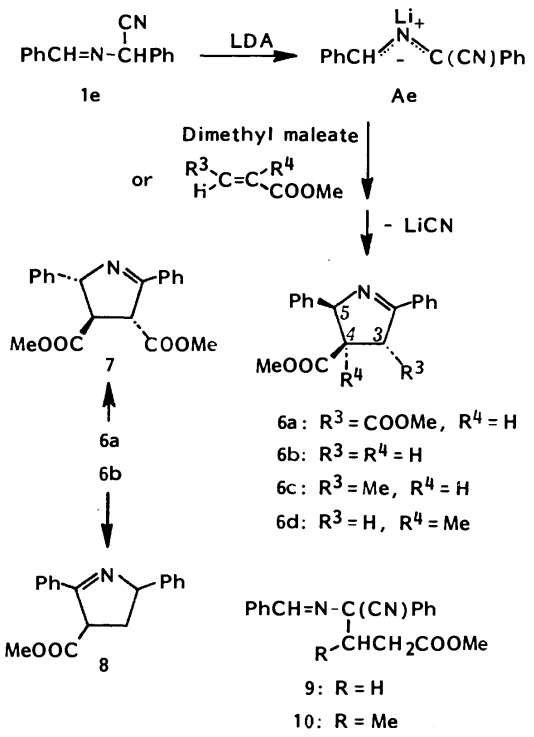

Scheme 5.

equimolar amount of diisopropylamine forms magnesium bromide diisopropylamide.[17] This magnesium amide was also effective as a metallic base. *N*-Metalated azomethine ylide **F** (M=MgBr·HN(*i*-Pr)$_2$) was generated from **1a** and reacted with methyl acrylate to give 1-pyrroline **2a**. It is likely that the presence of diisopropylamine facilitated the elimination of MCN as observed in this case and also in the reactions of **A**. Accordingly generation of diisopropylamine-free *N*-lithiated azomethine ylides **F** (M=Li) was next examined.

Thus **1a** was first treated with butyllithium and then with methyl crotonate to produce a mixture of two stereoisomeric pyrrolidines **3a** and **3a'**. Further such other bases as *n*-BuLi/LiI, *n*-BuLi/NEt$_3$, and *n*-BuLi/Ti(OPr^i)$_4$ were employed. Isomer ratio **3a** : **3a'** depends upon the nature and amount of additives, and the highest selectivity for **3a'** was obtained (**3a**:**3a'**= 8 : 92) when triethylamine was used as an additive (Table 2).

N-Lithiated azomethine ylide **Ae** was generated from imine **1e** which bears two phenyl groups. Subsequent cycloadditions with dimethyl maleate, methyl acrylate, crotonate, and methacrylate produced 4,5-*cis*-1-pyrrolines **6a**—**6d** as the initial or isolated products (Scheme 5 and Table 3). The 5-H of 1-pyrrolines **6** is highly acidic because both the 2- and 5-positions are substituted by anion-stabilizing

Table 2. Reaction of α-(Benzylideneamino)acetonitrile (**1a**) with Metallic Bases Other than LDA

Base	Additive (equiv)	*N*-Metalated azomethine ylide **C**	Dipolarophile	Time/h[a]	Product (yield/%)[b]
EtMgBr	—	M=MgBr	MeCH=CHCOOMe	7	**3a'** (95)
	—	M=MgBr	CH_2=CHCOOMe	6	**3b'** (45)[c]
	HN(*i*-Pr)$_2$ (1)	M=MgBr·HN(*i*-Pr)$_2$	CH_2=CHCOOMe	6	**2a** (61)
n-BuLi	—	M=Li	MeCH=CHCOOMe	6	**3a** (45) + **3a'** (55)
	LiI (1)	M=Li·LiI	MeCH=CHCOOMe	6	**3a** + **3a'** (quant., 20:80)[d]
	LiI (1.5)	M=Li·LiI	MeCH=CHCOOMe	6	**3a** + **3a'** (quant., 11:89)[d]
	NEt$_3$ (1.1)	M=Li·NEt$_3$	MeCH=CHCOOMe	6	**3a** + **3a'** (quant., 8:92)[d]
	Ti(OPr^i)$_4$ (1)	e)	MeCH=CHCOOMe	6	**3a** + **3a'** (quant., 60:40)[d]

a) All reactions were carried out in dry THF at − 78 °C with each one equivalent amount of **1a**, an olefin, and a base. b) Yield of isolated products. c) Fifty five percent of **1a** was recovered. d) Isomer ratio was determined by ^{1}H NMR spectrum. e) The reacting species is not certain.

Table 3. LDA-Induced Cycloaddition of **1e**

Dipolarophile	Condition[a]	Product (yield/%)[b]
MeOOCCH=CHCOOMe	− 78 °C, 0.5 h	**6a** + **7** (80, 1 : 6)[c]
	− 78 °C, 4 h	**7** (89)
CH_2=CHCOOMe	− 78 °C, 4 h	**6b** (41) + **8** (13) + **9** (36)
	− 78 °C, 0.5 h then rt, 1 h	**6b** (59) + **8** (39)
MeCH=CHCOOMe	− 78 °C, 3 h	**6c** (46) + **10** (23)
CH_2=C(Me)COOMe	− 78 °C, 3 h	**6d** (61)

a) All reactions were performed in THF by using LDA (1 equiv). b) Yield of isolated products. c) Inseparable mixture. The product ratio was determined by ^{1}H NMR spectrum.

phenyl groups. Therefore **6a** experienced a ready epimerization at the 5-position into 4,5-*trans*-1-pyrroline **7** in the presence of LDA, presumably via a 2-azaallyl anion intermediate. Formation of **8**, a regioisomer of **6b**, as a side product in the reaction between **Ae** and methyl acrylate may have arisen from a similar 2-azaallyl anion intermediate. Some cycloadditions were accompanied by Michael adducts, for instance **9** and **10**.

It is clear that *N*-lithiated anionic species are involved in these LDA-induced cycloaddition reactions. These species should be refered to as *N*-lithiated azomethine ylides **A** because the nonbonding electron pair on the imine nitrogen has been utilized to make a nitrogen-lithium bond. The involvement of *N*-lithiated azomethine ylide **A** is confirmed on the ground of the following facts: a) High regio- and stereoselectivity can be well-interpreted by a chelation between the lithium metal on the imine nitrogen and the carbonyl oxygen; b) DBU-Induced Michael addition of **la** with methyl acrylate gives not only the 1:1 adduct but also 1:2 adduct;[9b] c) DBU-Induced Michael addition of imine **1b** with methyl crotonate is poor in stereoselectivity, and of imine **1b** is sterically too hindered;[18] d) Michael adduct of **1b** to methyl crotonae does not cyclize leading to **2f** on treatment with LDA at −78 °C.[19]

Thus it is concluded that the LDA-induced cycloadditions of *N*-(1-cyanoalkyl)imines **1** proceed through a chelated transition state (Fig. 1). There are two possible paths, but we can not so far discriminate the following two routes: Path a: A concerted endo cycloaddition promoted by an attractive interaction between the ester carbonyl of the crotonate and the lithium metal of **A** (**G**→**J**); Path b: A sequence of Michael addition and intramolecular imine addition where the lithium metal migrates from the imine nitrogen to the ester oxygen so that high stereoselectivity may result (**H**→**I**→**J**). These two paths are virtually identical since the synchronousness of bond formations is only slightly different. The discrimination seems to be trivial.

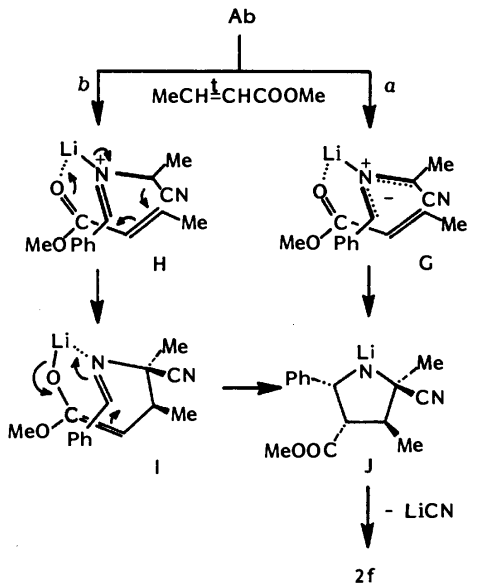

Fig. 1. Two possible mechanisms for the LDA-induced cycloaddition of **1b** to methyl crotonate.

Experimental

General. Melting points were determined on a Yanagimoto melting point apparatus and are uncorrected. IR spectra were taken with a JASCO IRA-1 or a JASCO A-702 spectrometer. ^{1}H NMR spectra were recorded on a Hitachi R-40 (90 Hz) or a JEOL FX-100 instrument (100 MHz) and ^{13}C NMR on a JEOL FX-100 spectrometer at 25.05 MHz. Chemical shifts are expressed in parts per million downfield from tetramethylsilane as an internal standard. Mass spectra were measured with a JEOL-01SG-2 spectrometer at 70 eV of ionization energy. High resolution mass spectra were obtained on the same instrument. Elemental analyses were performed on a Hitachi 026 CHN analyzer. Thin-layer chromatography (TLC) was accomplished on 0.2 mm precoated plates of silica gel 60 F-254 (Merck). Visualization was made with ultraviolet light (254 and 365 nm), iodine, molybdophosphoric acid (5% in ethanol), or *p*-anisaldehyde (5% in ethanol containing 5% of sulfuric acid). For preparative column chromatography, Wakogel C-200, C-300 (Wako), and Silicagel 60 (Merck) were employed. Solvents were evaporated with a Tokyo Rikakikai rotary evaporator type-V at about 50 °C unless otherwise stated.

Imine **1a** or **1d** was prepared from the reaction of aminoacetonitrile or α-aminophenylacetonitrile with the corresponding aldehyde;[9a] **1b** and **1c** were available by alkylation of **1a**.[9b] Tetrahydrofuran (THF) was dried over sodium and distilled on sodium wire immediately before use.

General Procedure for LDA-Induced Cycloaddition of *N*-(1-Cyanoalkyl)imines 1a—1d with Electron-Deficient Olefins Leading to 2b—2k and/or 3a—3c. The reaction of α-(benzylideneamino)acetonitrile **1a** with dimethyl maleate is described as a typical example: To a solution of lithium diisopropylamide (LDA, 2.2 mmol) freshly prepared from butyllithium and diisopropylamine in dry THF (10 ml) was added slowly imine **1a** (0.29 g, 2.01 mmol in THF (2 ml)) at −78 °C. After 5 min at the same temperature, dimethyl maleate (0.316 g, 2.19 mmol in THF (0.5 ml)) was added. The mixture was allowed to stir at −78 °C under nitrogen for 6 h, poured into saturated ammonium chloride, and extracted with diethyl ether (30 ml×3). The combined extracts were dried over anhydrous mgnesium sulfate and evaporated in vacuo. The residue (0.433 g) was chromatographed over silica gel by using chloroform–diethyl ether (5 : 1) to give 2-pyrroline **2a** (0.372 g, 71%).

Other LDA-induced cycloadditions of **1a—1d** with olefins were carried out under the reaction conditions listed in Table 1 in which the results are also summarized.

2a: Colorless prisms (benzene–hexane); mp 120—122 °C; IR (KBr) 3300, 1720, and 1670 cm^{-1}; ^{1}H NMR ($CDCl_3$)

δ=3.08 (3H, s, 4-COOMe), 3.61 (3H, s, 3-COOMe), 4.12 (1H, dd, J=12.3 and 1.0 Hz, 4-H), 4.84 (1H, br, NH), 5.30 (1H, dd, J=12.3 and 1.6 Hz, 5-H), 7.2—7.4 (5H, m, Ph), and 7.46 (1H, dd, J=3.0 and 1.0 Hz, 2-H); ^{13}C NMR ($CDCl_3$) δ=50.48, 51.12 (each q, COOMe), 52.14 (d, 4-C), 66.08 (d, 5-C), 100.29 (s, 3-C), 127.14, 127.96 (each d), 137.66 (s), 150.62 (d, 2-C), 166.07, and 171.24 (each s, COOMe); MS m/z (rel intensity, %) 261 (M^+, 35), 202 (base peak), 170 (45), 143 (50), 117 (21), and 115 (34). Found: C, 64.38; H, 5.84; N, 5.57%. Calcd for $C_{14}H_{15}NO_4$: C, 64.36; H, 5.79; N, 5.36%.

2b: Pale yellow liquid; IR (neat) 1730 and 1625 cm^{-1}; ^{1}H NMR ($CDCl_3$) δ=2.80 (2H, m, 3-H), 3.08 (3H, s, COOMe), 3.50 (1H, ddd, J=9.6, 9.2, and 6.0 Hz, 4-H), 5.52 (1H, ddd, J=9.2, 4.0, and 2.0 Hz, 5-H), 7.0—7.4 (5H, m, Ph), and 7.80 (1H, dt, J=2.0, 1.0, and 1.0 Hz, 2-H); ^{13}C NMR ($CDCl_3$) δ=40.24 (t, 3-C), 46.30 (d, 4-C), 51.36 (q, COOMe), 78.83 (d, 5-C), 127.66, 128.13 (each d), 138.07 (s), 167.24 (d, 2-C), and 172.65 (s, COOMe); MS m/z (rel intensity, %) 203 (M^+, 15), 144 (34), 143 (20), 117 (42), 90 (23), and 43 (base peak). HRMS Found: m/z 203.0932. Calcd for $C_{12}H_{13}NO_2$: M, 203.0945.

2c: Pale yellow liquid; IR (neat) 1740 and 1625 cm^{-1}; ^{1}H NMR ($CDCl_3$) δ=1.22 (3H, d, J=7.1 Hz, Me), 3.06 (1H, dd, J=9.5 and 7.0 Hz, 4-H), 3.15 (3H, s, COOMe), 3.4—3.7 (1H, m, 3-H), 5.60 (1H, dt, J=9.5, 2.0, and 2.0 Hz, 5-H), 7.0—7.4 (5H, m, Ph), and 7.66 (1H, br s, 2-H); ^{13}C NMR ($CDCl_3$) δ=16.06 (q, Me), 46.77 (d, 3-C), 51.24 (q, COOMe), 55.24 (d, 4-C), 78.42 (d, 5-C), 127.54, 127.71, 128.13 (each d), 137.60 (s), and 172.01 (d and s, 2-C and COOMe); MS m/z (rel intensity, %) 217 (M^+, 11), 158 (44), 157 (21), 130 (20), 129 (23), 128 (25), 117 (91), 116 (40), 115 (46), 104 (29), 103 (23), 91 (54), 90 (base peak), 89 (78), 77 (51), 69 (78), 63 (44), 59 (58), 54 (26), 52 (48), 42 (55), and 40 (56). HRMS Found: m/z 217.1097. Calcd for $C_{13}H_{15}NO_2$: M, 217.1100.

2d: Pale yellow liquid; IR (neat) 1740 and 1620 cm^{-1}; ^{1}H NMR ($CDCl_3$) δ=3.14 (3H, s, COOMe), 3.44 (1H, dd, J=9.5 and 7.8 Hz, 4-H), 4.67 (1H, ddd, J=7.8, 3.0, and 2.0 Hz, 3-H), 5.75 (1H, dt, J=9.5, 2.0, and 2.0 Hz, 5-H), 6.9—7.6 (10H, m, Ph), and 7.76 (1H, dd, J=3.0 and 2.0 Hz, 2-H); ^{13}C NMR ($CDCl_3$) δ=51.36 (q, COOMe), 56.83 (d, 4-C), 57.71 (d, 3-C), 78.83 (d, 5-C), 127.54, 127.66, 127.77, 128.18, 128.83, 129.19 (each d), 136.95, 138.77 (each s), 169.19 (d, 2-C), and 171.48 (s, COOMe); MS m/z (rel intensity, %) 279 (M^+, 13), 220 (23), 163 (25), 158 (22), 131 (29), 117 (83), 115 (30), 105 (53), 90 (31), 85 (67), 83 (base peak), 77 (41), and 47 (25). Stability of this compound was not enough for the molecular weight measurement by HRMS.

2e: Pale yellow liquid; IR (neat) 1730 and 1650 cm^{-1}; ^{1}H NMR ($CDCl_3$) δ=2.19 (3H, d, J=2.0 Hz, Me), 2.68 (1H, dd, J=17.5 and 9.5 Hz, one of 3-H), 3.0—3.3 (1H, m, the other of 3-H), 3.08 (3H, s, COOMe), 3.56 (1H, dt, J=9.5 and 6.0 Hz, 4-H), 5.44 (1H, dd, J=9.5 and 2.0 Hz, 5-H), and 7.0—7.4 (5H, m, Ph); ^{13}C NMR ($CDCl_3$) δ=19.47 (q, Me), 41.94 (t, 3-C), 48.36 (d, 4-C), 51.24 (q, COOMe), 78.30 (d, 5-C), 127.54, 128.07 (each d), 138.77 (s), 172.76 (s, COOMe), and 175.83 (s, 2-C); MS m/z (rel intensity, %) 217 (M^+, 11), 158 (38), 157 (29), 131 (61), 130 (67), 116 (29), 115 (61), 104 (36), 103 (24), 91 (31), 90 (base peak), 89 (85), 77 (40), 63 (40), 59 (20), 55 (81), 51 (44), and 38 (46). HRMS Found: m/z 217.1068. Calcd for $C_{13}H_{15}NO_2$: M, 217.1084.

2f: Pale yellow liquid; IR (neat) 1735 and 1645 cm^{-1}; ^{1}H NMR ($CDCl_3$) δ=1.18 (3H, d, J=7.0 Hz, 3-Me), 2.30 (3H, s, 2-Me), 3.13 (3H, s, COOMe), 3.1—3.5 (1H, m, 4-H), 3.6—3.7 (1H, m, 3-H), 5.36 (1H, d, J=9.5 Hz, 5-H), and 7.0—7.4 (5H, m, Ph); ^{13}C NMR ($CDCl_3$) δ=16.53, 17.59 (each q, Me), 30.94 (d, 4-C), 47.89 (d, 3-C), 51.36 (q, COOMe), 57.00 (d, 5-C), 127.54, 127.71, 128.18 (each d), 138.48 (s), 172.42 (s, COOMe), and 179.42 (s, 2-C); MS m/z (rel intensity, %) 231 (M^+, 45), 172 (13), 131 (base peak), 130 (39), and 90 (26). HRMS Found: m/z 231.1255. Calcd for $C_{14}H_{17}NO_2$: M, 231.1257.

2g: Pale yellow liquid; IR (neat) 1730 and 1650 cm^{-1}; ^{1}H NMR ($CDCl_3$) δ=1.48 (3H, s, 4-Me), 2.17 (3H, d, J=1.8 Hz, 2-Me), 2.19 (1H, d, J=17.8 Hz, one of 3-H), 3.04 (3H, s, COOMe), 3.42 (1H, dd, J=17.8 and 1.1 Hz, the other of 3-H), 4.95 (1H, br s, 5-H), and 7.0—7.4 (5H, m, Ph); ^{13}C NMR ($CDCl_3$) δ=19.30 (q, 3-Me), 24.65 (q, 2-Me), 49.65 (t, 3-C), 50.89 (q, COOMe), 54.65 (s, 4-C), 85.89 (d, 5-C), 126.89, 127.19, 127.54 (each d), 138.54 (s), 174.01, and 174.89 (each s, 2-C and COOMe); MS m/z (rel intensity, %) 231 (M^+, 12), 131 (base peak), 130 (46), 90 (50), 89 (33), and 41 (22). HRMS Found: m/z 231.1265. Calcd for $C_{14}H_{17}NO_2$: M, 231.1270.

2h: Yellow liquid; IR (neat) 1740 and 1640 cm^{-1}; ^{1}H NMR ($CDCl_3$) δ=1.2—1.3 (9H, m, Me and *i*-Pr), 2.6—2.9 (1H, m, *i*-Pr), 3.12 (1H, dd, J=9.5 and 7.2 Hz, 4-H), 3.16 (3H, s, COOMe), 3.3—3.7 (1H, d, J=9.5 Hz, 5-H), and 7.0—7.5 (5H, m, Ph); MS m/z (rel intensity, %) 259 (M^+, 58), 159 (base peak), 131 (28) 117 (70), 91 (21), and 90 (21). HRMS Found: m/z 259.1609. Calcd for $C_{16}H_{21}NO_2$: M, 259.1645.

2i: Pale yellow liquid; IR (neat) 1735 and 1625 cm^{-1}; ^{1}H NMR ($CDCl_3$) δ=1.12 (3H, q, J=7.0 Hz, Et), 1.4—1.8 (2H, m, Et), 3.0—3.6 (3H, m, 3- and 4-H), 3.68 (3H, s, COOMe), 4.3—4.4 (1H, m, 5-H), 7.3—7.5 (3H, m, Ph), and 7.7—7.9 (2H, m, Ph); ^{13}C NMR ($CDCl_3$) δ=11.65 (q, Et), 25.41 (t, Et), 38.12 (t, 3-C), 45.83 (d, 4-C), 51.65 (q, COOMe), 75.95 (d, 5-C), 127.95, 128.65, 130.83 (each d), 134.30 (s), 171.13, and 173.77 (each s, 2-C and COOMe); MS m/z (rel intensity, %) 231 (M^+, 4), 172 (24), 144 (27), 143 (47), 130 (base peak), 117 (24), 116 (33), 115 (92), 104 (97), 77 (62), and 51 (37). HRMS Found: m/z 231.1250. Calcd for $C_{14}H_{17}NO_2$: M, 231.1244.

2j: Pale yellow liquid; IR (neat) 1735 and 1620 cm^{-1}; ^{1}HNMR ($CDCl_3$) δ=1.14 (3H, q, J=7.0 Hz, Et), 1.22 (3H, d, J=7.0 Hz, Me), 1.4—1.8 (2H, m, Et), 3.00 (1H, dd, J=8.0 and 4.2 Hz, 4-H), 3.6—4.0 (1H, m, 3-H), 3.64 (3H, s, COOMe), 4.32 (1H, q, J=8.0 Hz, 5-H), 7.2—7.5 (3H, m, Ph), and 7.6—7.9 (2H, m, Ph); ^{13}C NMR($CDCl_3$) δ=11.82 (q, Et), 17.41 (q, Me), 25.35 (t, Et), 45.83 (d, 4-C), 51.47 (q, COOMe), 54.77 (d, 3-C), 74.01 (d, 5-C), 128.18, 128.60, 130.42 (each d), 133.60 (s), 173.72, and 175.66 (each s, 2-C and COOMe); MS m/z (rel intensity, %) 245 (M^+, 8), 156 (31), 145 (23), 130 (79), 115 (30), 104 (base peak), 103 (30), 91 (36), 77 (64), 51 (46), and 41 (55). HRMS Found: m/z 245.1413. Calcd for $C_{15}H_{19}NO_2$: M, 245.1143.

2k: Pale yellow liquid; IR (neat) 1730 and 1625 cm^{-1}; ^{1}HNMR ($CDCl_3$) δ=1.10 (3H, q, J=7.5 Hz, Et), 1.38 (3H, s, Me), 1.3—1.8 (2H, m, Et), 2.76 (1H, d, J=17.0 Hz, one of 3-H), 3.64 (1H, dd, J=17.0 and 2.0 Hz, the other of 3-H), 3.66 (3H, s COOMe), 3.8—4.1 (1H, m, 5-H), 7.3—7.5 (3H, m, Ph), and 7.7—7.9 (2H, m, Ph); ^{13}C NMR ($CDCl_3$) δ=11.77 (q, Et), 25.12 (t, Et), 25.59 (q, Me), 46.00 (t, 3-C), 52.00 (q, COOMe), 83.77 (d, 5-C), 127.83, 128.60, 130.72 (each d), 134.54 (s), 170.84 (s, COOMe), and 175.66 (s, 2-C); MS m/z (rel intensity, %) 245 (M^+, 9), 186 (20), 157 (23), 156 (32), 130 (base peak), 104 (95), 77 (60), and 41 (49). HRMS Found: m/z

245.1422. Calcd for $C_{15}H_{19}NO_2$: M, 245.1428.

3a: Pale yellow liquid; IR (neat) 3360, 2230, and 1735 cm^{-1}; ^1H NMR ($CDCl_3$) δ=1.22 (3H, d, J=7.0 Hz, Me), 2.0—2.4 (1H, br, NH), 2.94 (1H, ddd, J=9.0, 7.0, and 5.5 Hz, 3-H), 3.10 (1H, dd, J=8.7 and 5.5 Hz, 4-H), 3.21 (3H, s, COOMe), 3.66 (1H, d, J=9.0 Hz, 2-H), 4.63 (1H, d, J=8.7 Hz, 5-H), and 7.1—7.4 (5H, m, Ph); ^{13}C NMR ($CDCl_3$) δ=15.94 (q, Me), 40.89 (d, 3-C), 51.47 (q, COOMe), 54.24 (d, 4-C), 56.59 (d, 2-C), 63.24 (d, 5-C), 120.24 (s, CN), 127.36, 127.89, 128.18 (each d), 140.18 (s), and 171.13 (s, COOMe); MS m/z (rel intensity, %) 244 (M^+, 5), 144 (56), 143 (76), 117 (32), 116 (36), 115 (32), 104 (29), 91 (45), 90 (26), 89 (35), 78 (24), 77 (50), 69 (base peak), 59 (53), 58 (24), 56 (20), 52 (33), 44 (25), 42 (77), and 40 (49). HRMS Found: m/z 244.1212. Calcd for $C_{14}H_{16}N_2O_2$: M, 244.1212.

3b: Colorless liquid; IR (neat) 3350, 2240, and 1725 cm^{-1}; ^1H NMR ($CDCl_3$) δ=1.45 (3H, s, Me), 2.02 (1H, dd, J=13.4 and 4.5 Hz, one of 3-H), 2.54 (1H, br s, NH), 3.04 (1H, dd, J=13.4 and 8.5 Hz, the other of 3-H), 3.17 (3H, s, COOMe), 4.22 (1H, s, 5-H), 4.45 (1H, dd, J=8.5 and 4.5 Hz, 2-H), and 7.0—7.4 (5H, m, Ph); ^{13}C NMR ($CDCl_3$) δ=21.94 (q, Me), 41.41 (t, 3-C), 45.94 (d, 2-C), 51.06 (q, COOMe), 53.83 (s, 4-C), 72.12 (d, 5-C), 121.66 (s, CN), 126.54, 127.83 (each d), 137.48 (s), and 173.90 (s, COOMe); MS m/z (rel intensity, %) 244 (M^+, 7), 144 (base peak), 143(86), 117 (26), and 116 (24). HRMS Found: m/z 244.1200. Calcd for $C_{14}H_{16}N_2O_2$: M, 244.1190.

3c: Formation of this compound **3c** was only observed in the ^1H NMR spectrum of crude reaction mixture obtained from **1c** and methyl crotonate. When chromatographed over silica gel by using chloroform-diethyl ether (10 : 1 vol/vol), ready elimination of HCN took place and 72% yield of **2h** was isolated. The ratio between **2h** and **3c** was determined by the ^1H NMR of the crude mixture. ^1HNMR ($CDCl_3$) δ=3.03 (s, COOMe) and 4.65 (dd, J=10.0 and 5.5 Hz, 5-H).

Cycloaddition of 1a Induced by Metallic Bases Other than LDA. Preparation procedure for the *N*-metalated species from **1a** is as follows. All the procedures were conducted under dry nitrogen at −78 °C:

EtMgBr: To EtMgBr (2.2 mmol) freshly prepared in THF (7 ml) was added **1a** (0.295 g, 2.05 mmol in THF (2 ml)). An olefin (2.2 mmol) was added after 15 min.

EtMgBr/HN(*i*-Pr)$_2$: To EtMgBr (2.2 mmol in THF (8 ml)) was added diisopropylamine (2.2 mmol in THF (10 ml)) and then **1a** (0.29 g, 2.01 mmol in THF (2 ml)). After 14 min, methyl acrylate (0.19 g, 2.21 mmol) was added.

***n*-BuLi**: To *n*-BuLi (1 M† solution in hexane, 2.2 ml, 2.2 mmol) in THF (5 ml) was added **1a** (0.151 g, 1.05 mmol). After 5 min, methyl crotonate (0.123 g, 1.23 mmol in THF (1 ml)) was added.

***n*-BuLi/LiI, *n*-BuLi/NEt$_3$, or *n*-BuLi/Ti(OPr^i)$_4$**: To LiI (1 mmol or 1.5 mmol), NEt_3 (1.11 mmol), or $Ti(OPr^i)_4$ (1 mmol) in THF (5 ml) was added *n*-BuLi (1.1 mmol). Imine **1a** (0.147 g, 1.02 mmol) was added after 10 min and then the mixture was stirred for an additional 10 min before methyl crotonate (0.115 g, 1.15 mmol) was introduced.

Subsequent cycloadditions were conducted under the conditions listed in Table 2 and the results are shown in the same table. The data for **2a** and **3a** were already presented above.

3a′: Colorless prisms (benzene-hexane); mp 96—97 °C; IR (KBr) 3350, 2230, and 1725 cm^{-1}; ^1H NMR ($CDCl_3$) δ=1.26 (3H, d, J=6.5 Hz, Me), 2.40 (br s, NH), 2.9—3.2 (2H, m, 3-and 4-H), 3.10 (3H, s, COOMe), 4.36 (1H, d, J=6.0 Hz, 2-H), 4.81 (1H, d, J=9.1 Hz, 5-H), and 7.1—7.3 (5H, m, Ph); ^{13}C NMR ($CDCl_3$) δ=15.18 (q, Me), 38.30 (d, 3-C), 51.47 (q, COOMe), 54.18 (d, 4-C), 55.24 (d, 2-C), 62.77 (d, 5-C), 119.30 (s, CN), 127.71, 128.18 (each d), 139.83 (s), and 171.78 (s, COOMe); MS m/z (rel intensity, %) 244 (M^+, 16), 163 (39), 145 (base peak), and 144 (77). Found: C, 68.99; H, 6.72; N, 11.42%. Calcd for $C_{14}H_{16}N_2O_2$: C, 68.83; H, 6.60; N, 11.47%.

3b′: Colorless needles (diethyl ether-hexane); mp 78.5—79 °C; IR (KBr) 3330, 2230, and 1730 cm^{-1}; ^1H NMR ($CDCl_3$) δ=2.00 (1H, br s, NH), 2.32 (1H, ddd, J=13.0, 8.5, and 3.0 Hz, one of 3-H), 2.72 (1H, ddd, J=13.0, 8.0, and 7.0 Hz, the other of 3-H), 3.13 (3H, s, COOMe), 3.41 (1H, dt, J=8.5, 8.5, and 7.0 Hz, 4-H), 4.44 (1H, dd, J=8.0 and 3.0 Hz, 2-H), 4.72 (1H, d, J=8.5 Hz, 5-H), and 7.23 (5H, s, Ph); MS m/z (rel intensity, %) 230 (M^+, 2), 144 (88), 143 (base peak), 142 (23), 117 (61), 116 (51), 115 (63), 104 (49), 91 (33), 90 (45), 89 (66), 78 (22), 77 (68), 66 (24), 65 (25), 63 (27), 55 (67), 51 (51), 50 (20), and 38 (44). Found: C, 67.72; H, 6.13; N, 12.05%. Calcd for $C_{13}H_{14}N_2O_2$: C, 67.81; H, 6.13; N, 12.17%.

General Procedure for LDA-Induced Cycloddition of 1e Leading to 6—10. To a solution of LDA freshly prepared from butyllithium (1.5 mmol) and diisopropylamine in THF (3 ml) was added imine **1e** (0.33 g, 1.5 mmol) at −78 °C in a period of 2 min. After 5 min, an olefin (1.6 mmol) was added to this red solution and the mixture was stirred under the conditions shown in Table 3. The reaction mixture was poured into ice water and extracted with diethyl ether (25 ml×2). The combined extracts were dried over magnesium sulfate and evaporated in vacuo. The residue was chromatographed over silica gel. All the results are listed in Table 3. Products **6a**, **6b**, **7**, and **8** have been already prepared from the reactions of *N*-protonated azomethine ylide derived from **1e**,[9a] and Michael adducts **9** and **10** are also known.[9b]

6c: Colorless prisms (hexane); mp 152—153 °C; IR (KBr) 1730 and 1620 cm^{-1}; ^1H NMR ($CDCl_3$) δ=1.26 (3H, d, J=7.0 Hz, Me), 3.06 (3H, s, COOMe), 3.25 (1H, dd, J=9.0 and 4.0 Hz, 4-H), 4.00 (1H, ddd, J=7.0, 4.0, and 2.0 Hz, 3-H), 5.56 (1H, dd, J=9.0 and 2.0 Hz, 5-H), 7.0—7.4 (8H, m, Ph), and 7.7—7.9 (2H, m, Ph); MS m/z (rel intensity, %) 293 (M^+, 28), 234 (41), 193 (base peak), 115 (26), 91 (43), and 77 (27). Found: C, 77.78; H, 6.54; N, 5.01%. Calcd for $C_{19}H_{19}NO_2$: C, 77.79; H, 6.53; N, 4.77%.

6d: Colorless liquid; IR (neat) 1730 and 1620 cm^{-1}; ^1H NMR ($CDCl_3$) δ=1.60 (3H, s, Me), 2.80 (1H, d, J=18.0 Hz, one of 3-H), 3.13 (3H, s, COOMe), 3.90 (1H, dd, J=18.0 and 2.0 Hz, the other of 3-H), 5.23 (1H, d, J=2.0 Hz, 5-H), 7.0—7.5 (8H, m, Ph), and 7.95 (2H, m, Ph); ^{13}C NMR ($CDCl_3$) δ=25.59 (q, Me), 46.18 (t, 3-C), 51.47 (q, COOMe), 54.71 (s, 4-C), 86.59 (d, 5-C), 127.54, 127.83, 128.13, 128.77, 131.24 (each d), 134.07, 138.72 (each s), 173.72, and 174.54 (each s, 2-C and COOMe); MS m/z (rel intensity, %) 293 (M^+, 21), 234 (26), 193 (base peak), 165 (21), 103 (29), 90 (49), and 89 (57). HRMS Found: m/z 293.1415. Calcd for $C_{19}H_{19}NO_2$: M, 293.1425.

† 1M=1 mol dm^{-3}.

References

1) a) T. Kauffmann, H. Berg, and E. Koppelmann, *Angew. Chem.*, **82**, 396 (1970); b) A review: T. Kauffmann, *Angew. Chem., Int. Ed. Engl.*, **13**, 627 (1974).

2) Only anions bearing two or more aryl groups can be generated by the deprotonation of imines.

3) As described in the review (Ref. 1b) azo compounds, imines, heterocumulenes, and nitriles as well as aryl-substituted olefins have been employed. References published thereafter are as follows: T. Kauffmann, K. Habersaat, and E. Koppelmann, *Chem. Ber.*, **110**, 638 (1977); L. V.-Quang and Y. V.-Quang, *Tetrahedron Lett.*, **1978**, 4679; K. Kamata and M. Terashima, *Heterocycles*, **14**, 205 (1980); D. J. Bower and E. H. Howden, *J. Chem. Soc., Perkin Trans. 1*, **1980**, 672; L. V.-Quang, H. Gaessler, and Y. V.-Quang, *Angew. Chem., Int. Ed. Engl.*, **20**, 880 (1981); L. V.-Quang, Y. V.-Quang, M. J. Pouet, and M. P. Simonnin, *Tetrahedron*, **37**, 4343 (1981); L. V.-Quang and Y. V.-Quang, *J. Heterocycl. Chem.*, **19**, 145 (1982).

4) Although quite limited, electron-deficient olefins have been also used: T. Kauffmann, H. Ahlers, A. Hamsen, H. Schulz, H.-J. Tilhard, and A. Vahrenhorst, *Angew. Chem.*, **89**, 107 (1977); S. Sinbandhit and J. Hamelin, *J. Chem. Soc., Chem. Commun.*, **1977**, 768; V. Dryanska, K. P. -Yambolieva, and C. Ivanoz, *Tetrahedron Lett.*, **1979**, 443; V. Dryanska, K. Popandova, and C. Ivanov, *Syn. Commun.*, **12**, 343 (1982); T. Kauffmann, H. Ahlers, K.-J. Echsler, H. Schulz, and H.-J. Tilhard, *Chem. Ber.*, **118**, 4496 (1985).

5) T. Oguri, T. Shioiri and S. Yamada, *Chem. Pharm. Bull.*, **25**, 2287 (1977); M. J. O'Donell, J. M. Boniece, and S. E. Earp, *Tetrahedron Lett.*, **1978**, 2641; M. J. O'Donell and T. M. Eckrich, *ibid.*, **1978**, 4625; D. Hoppe and L. Beckmann, *Liebigs Ann. Chem.*, **1979**, 2066; E. Cawkill and N. G. Clark, *J. Chem. Soc., Perkin Trans. 1*, **1980**, 244; P. Bey and P. Vevert, *J. Org. Chem.*, **45**, 3249 (1980).

6) G. Stork, A. Y. W. Leong, and A. M. Touzin, *J. Org. Chem.*, **41**, 3491 (1976); P. Bey and J. P. Vevert, *Tetrahedron Lett.*, **1977**, 1455; J. J. Fitt and H. W. Gschwend, *J. Org. Chem.*, **42**, 2639 (1977).

7) Formation of both Michael adducts and cycloadducts was reported: R. Grigg, J. Kemp, J. Malone, and A. Tangthongkum, *J. Chem. Soc., Chem., Commun.*, **1980**, 648.

8) a) O. Tsuge, S. Kanemasa, A. Hatada, and K. Matsuda, *Bull. Chem. Soc. Jpn.*, **59**, 2537 (1986); b) O. Tsuge, S. Kanemasa, T. Yamada, and K. Matsuda, *J. Org. Chem.*, **52**, 2523 (1987).

9) a) O. Tsuge, K. Ueno, S. Kanemasa, and K. Yorozu, *Bull. Chem. Soc. Jpn.*, **59**, 1809 (1986); b) O. Tsuge, K. Ueno, S. Kanemasa, and K. Yorozu, *ibid.*, **60**, 3347 (1987).

10) R. Grigg and J. Kemp, *J. Chem. Soc., Chem. Commun.*, **1978**, 109; M. Joucla and J. Hamelin, *Tetrahedron Lett.*, **1978**, 2885; O. Tsuge, K. Ueno, and K. Oe, *Chem. Lett.*, **1979**, 1407; R. Grigg, *Bull. Soc. Chim. Belg.*, **93**, 593 (1984) and references cited therein.

11) a) O. Tsuge and K. Ueno, *Heterocycles*, **19**, 1411 (1982); b) O. Tsuge, S. Kanemasa, K. Yorozu, and K. Ueno, *Chem. Lett.*, **1985**, 1601.

12) Some related examples of *N*-metalated azomethine ylides have been recently reported: L. Casella, M. Gullotti, and E. Melani, *J. Chem. Soc., Perkin Trans. 1*, **1982**, 1827; R. Grigg and J. Devlin, *J. Chem. Soc., Chem. Commun.*, **1986**, 631; R. Grigg, V. Sridharan, and S. Thianpatanagul, *J. Chem. Soc., Perkin Trans. 1*, **1986**, 1669.

13) As double bond migration of 1-pyrrolines through an imine-enamine tautomerization: O. Tsuge, S. Kanemasa, and K. Matsuda, *Chem. Lett.*, **1985**, 1411; O. Tsuge, S. Kanemasa, T. Yamada, and K. Matsuda, *Heterocycles*, **23**, 2489 (1985); Refs. 9a and 11b.

14) Refs. 9a and 11b.

15) Each one isomer of the anti and syn forms of *N*-lithiated azomethine ylides **Aa** may join in cycloadditions (see Ref. 9a). The exclusive participation of the anti isomer of **Aa** took place in these cases.

16) Similar structural assignment based upon ^{13}C chemical shifts and NOE enhancement has been discussed in the preceding article (Ref. 9b).

17) T. Hiyama and K. Kobayashi, *Tetrahedron Lett.*, **23**, 1567 (1982).

18) DBU-Induced Michael addition of **1c** to methyl crotonate never takes place even when the reaction mixture was heated under reflux in THF for 10 h. The Michael adduct of **1b** is a mixture of two diastereomers (Ref. 9b).

19) Only one stereoisomer of the Michael adduct of **1b** to methyl crotonate smoothly cyclizes into **2f** only in the presence of lithium iodide at −78 °C. The other isomer is recovered intact (Ref. 9b).

 © 1987 The Chemical Society of Japan Bull. Chem. Soc. Jpn., 60, 3367—3372 (1987)

Electrochemical Redox Intercalation of Copper(I) Cation for $Cu_xMo_6S_8$ Superconductor Accompanied with a Reversible Structure Change

Tooru INOUE* and Toshihiro YAMASE
Research Laboratory of Resources Utilization, Tokyo Institute of Technology,
4259 Nagatsuta-cho, Midori-ku, Yokohama 227
(Received November 18, 1986)

Ternary compounds (Chevrel phase compounds) of molybdenum $Cu_xMo_6S_8$ were prepared by sintering mixed powders of MoS_2, Mo, and CuS and employed as electrodes in aqueous solutions. Electrochemical polarization of the electrodes gives rise to intercalation and deintercalation processes of Cu^+, resulting in deformative change in crystal structure of the compounds. The lattice constants of rhombohedral unit cells of the compounds are a_r=6.66 Å, α_r=96°, and V_r=290 Å^3 for the intercalated compound $Cu_4Mo_6S_{7.8}$, and a_r= 6.43 Å, α_r=91.2°, and V_r=267 Å^3 for the fully deintercalated $Mo_6S_{7.8}$. Both the copper(I) composition and the crystal structure of $Cu_xMo_6S_{7.8}$ can be controlled by the electric quantity in electrochemical redox treatment. Structure deformation results from change in electronic distribution of crystal, as well as in charge density of a Mo octahedral cluster, due to electrolysis.

Ternary compounds of molybdenum designated by $M'_xMo_6S_8$ (M′ is a metal such as Cu, Pb, Sn, or Fe) have been known as one group of atractive superconducting materials since Chevrel reported relevantly the synthetic methods and basic structures of compounds of this group.[1-5] With respect to critical temperature (T_c) and critical magnetic field (H_c) as characteristic properties of superconductors, $PbMo_6S_8$ possesses the highest T_c (16 K) and H_c (600 kG) values of the members of this group, although Mo_6S_8 which has no metal M′ does not show any superconducting property. The T_c value of $Cu_xMo_6S_8$ (x=0—4) changes from 0 to 11 K with increasing value of x. Recent studies have been carried out with their focus on phase digrams, effects of variation in components, and developments of applications such as the construction of secondary batteries and the fabrication of superconducting wires. The crystal structure of the compounds of this group is rhombohedral with a sulfur quasi-cubic cell containing an octahedral molybdenum Mo_6 cluster and metal intercalants. Critical superconducting properties of various Chevrel phase compounds have been reported.[8-10]

Chemical and electrochemical intercalations have been reported for transition metal dichalcogenides (MX_2 where M=Mo, W, Ti, Ta; X=S, Se, Te). Molecules and ions can enter interlayer spaces of these compounds, and it is expected that their electrical conductivities, especially superconductivity, can be enhanced by anisotropic change in electronic charge distribution and crystal structure.[11,12] Chevrel phase compounds may also contain metallic intercalants along the channel space, i.e., a kind of tunnel, of crystal. It is suggested that composition shift of intercalants can affect the superconductive property of compounds. Therefore, study on the relationship between crystal structure and intercalation processes has significance from the standpoint of physical and chemical characterizations and development of applications.

In a previous report, we have described that the redox behavior of $Cu_xMo_6S_{7.8}$ is reversible with respect to both intercalation process and crystal structure change.[13] In this study, redox processes of various copper Chevrel compounds are investigated with particular reference to the deformation of crystal structure in course of redox charge transfer. Anodic and cathodic polarizations of electrode materials lead to reversible redox processes, that is, intercalation and deintercalation of copper(I) cation Cu^+ and result in reversible change in crystal structure. It will be shown that the intercalant composition of $Cu_xMo_6S_{7.8}$ can be controlled by electrolytic charges.

Experimental

Stoichiometric mixtures of powders of CuS, MoS_2, and Mo were ground in acetone. The powder sample was put in a quartz tube, evacuated and dried at ca. 200 °C. The evacuated tube was sealed and set in an electric furnance, and then heated so gradually to 500 °C as to avoid explosion of the tube due to rapid vaporization of the sulfur. The temperature was raised up to 1000 °C, and held there for as long as 100 h for complete equilibration. The sample was then quickly quenched in cold water. A dark gray powder was obtained as a Chevrel phase material. If the sample contained unreacted powder as revealed by powder X-ray diffraction analysis, the above heating procedure was repeated on the sample. The host compound $Mo_6S_{7.8}$, without Cu, was obtained by shaking a 5 M (1 M= 1 mol dm^{-3}) HCl solution with suspended $Cu_2Mo_6S_{7.8}$ in an ultrasonic bath for 1 week. The number of Cu^+ ions which were dissolved into the solution from 1 g of sample powder was ca. 1.25×10^{21} as estimated by a polarographic analysis on the suspended HCl solution. The copper(I) compositions (x) of the other sample compounds were determined, within 3% error, similarly by polarographic analysis on HCl solutions with suspended $Cu_xMo_6S_{7.8}$ powders after shaking. In order to prepare electrodes, the sample powder of 0.3 g was pressed at 300 kg cm^{-2} into a disk with a diameter of

1 cm and a thickness of 1 mm. One face of the disk was connected to a Cu lead wire with conductive silver epoxy resin and covered with insulative epoxy resin.

For electrochemical measurement, three electrodes, i.e., a sample electrode, a Pt counter electrode, and a saturated colomel electrode (SCE), were set in a flask-type glass cell and controlled by a potentiogalvanostat (HD-301, Hokuto Denko Co.). The supporting electrolyte was 0.1 M KNO_3 or 1 M KCl. The intercalant was supplied in the form of CuCl or $Cu(NO_3)_2$. Prior to running electrolyses the aqueous solution was deaerated by N_2 bubbling. In order to detect deintercalated species, the rotating ring-disk electrode (RRDE) method was adopted which used a sample disk of 5 mm diameter and a Pt ring of 7 mm inner 9 mm outer diameter. The measuring technique was described elsewhere.[14,15]

The crystal structures of the samples before and after electrolysis were determined with a powder X-ray diffrometer from Rigaku Denki Co. using Cu $K\alpha$.

Results and Discussion

The behavior of sample electrodes was first investigated in course of redox electrolysis in 0.1 M KNO_3 solutions. Figure 1 shows four cyclic voltammograms of $Cu_xMo_6S_{7.8}$ (x=0, 2, 3, and 4). The oxidation and reduction currents were obtained under anodic and cathodic polarizations. Broad redox waves appear in the potential range [A] between −1.0—0.3 V vs. SCE. These waves have high current densities (>ca. 10 mA cm^{-2} at 0 V vs. SCE) and show good reversibility. The magnitude of redox currents decreases with decrease in the copper composition (x), that is, these currents depend on the composition (x). In the potential range [B] above 0.3 V vs. SCE, another oxidation wave also appears with a remarkably large curent density. When an oxidation current appears at a sample electrode under anodic polarization, a part of solution near the sample electrode turns greenish yellow, with evolution of gas (probably hydrogen) and deposition of Cu on the Pt counter electrode. Although no exact processes occurring on the sample electrode can be determined only from the above potential cycling experiments, it may be estimated that copper cation participates in the redox processes of $Cu_xMo_6S_{7.8}$.

In order to clarify the redox processes for $Cu_xMo_6S_{7.8}$, the rotating ring disk electrode technique was used with application of a $Cu_xMo_6S_{7.8}$ disk and a Pt ring electrode. Figure 2 shows the analytical current–potential curves for the $Cu^{+/2+}$ couple on the Pt ring electrode when oxidation occurs on the $Cu_4Mo_6S_{7.8}$ disk electrode. When oxidation proceeds on the disk at a potential of −0.2 V vs. SCE in the range [A], a large oxidation current from Cu^+ to Cu^{2+} is observed above 0.2 V at the Pt ring electrode. This phenomenon indicates that dissolution of Cu^+ occurs on the sample disk electrode. Then, when an oxidation current appears on the disk at a potential of 0.35 V in the range [B], the oxidation current from Cu^+ to Cu^{2+} decreases and the reduction current from Cu^{2+} to Cu^+ increases on the Pt ring. This phenomenon means that production of Cu^{2+} instead of Cu^+ increases on the disk electrode in this potential

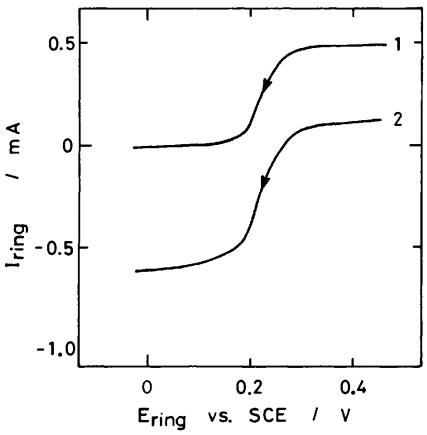

Fig. 2. Current-potential curves at a Pt ring electrode in the course of $Cu_4Mo_6S_{7.8}$ oxidation at a disk at 1000 rpm in 1 M KCl solution. Potentail scan rate is 30 s V^{-1}.
(1) E_{disk}=−0.2 V, I_{disk}=2.5 mA, (2) E_{disk}=0.35 V, I_{disk}=5.2 mA.

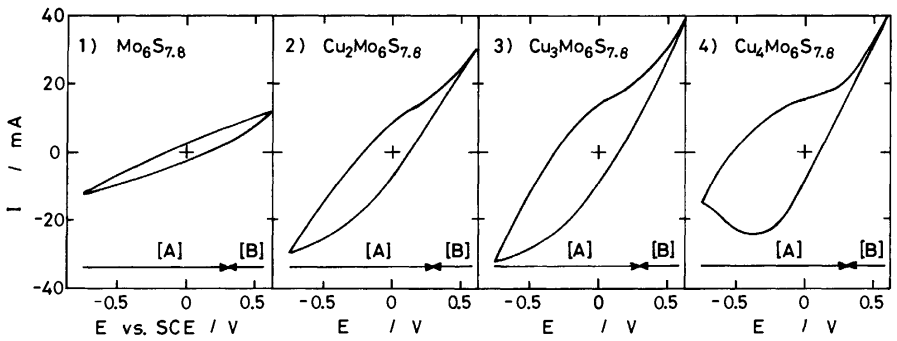

Fig. 1. Cyclic voltammograms of $Cu_xMo_6S_{7.8}$ (x=0, 2, 3, and 4) in 0.1 M KNO_3 solution. Potential scan rate is 30 s V^{-1}.

range, where Cu^{2+} is stabler than Cu^{+} because the standard redox potential of $Cu^{+/2+}$ is ca. 0.3 V vs. SCE in aqueous chloride solution.[14] From these results it is derived that products due to oxidation on $Cu_4Mo_6S_{7.8}$ are Cu^{+} in the potential range [A] and Cu^{2+} in the potential range [B]. The same products were obtained from redox electrolyses on $Cu_2Mo_6S_{7.8}$ and $Cu_3Mo_6S_{7.8}$. For the reduction processes on the $Cu_xMo_6S_{7.8}$ electrodes, similar RRDE techniques were employed on solutions saturated with CuCl. From the RRDE measurements it is derived that the reduction process on $Cu_xMo_6S_{7.8}$ is a consumption process of Cu^{+} in solution. However, no deposition of metallic copper on $Cu_xMo_6S_{7.8}$ disk surface was observed. When we employed Cu^{2+} instead of Cu^{+} in solution for reductive electrolysis, it was recognized through an X-ray diffraction analysis, as mentioned later, that intercalation with Cu^{2+} also occurred on $Cu_xMo_6S_{7.8}$, on the basis of the result of identification that the intercalated sample had the same crystal structure as in the case of Cu^{+}. Therefore, a reduction process of $Cu_xMo_6S_{7.8}$ leads to intercalation of copper(I) cation. From these results, the redox processes can be formulated as;

for oxidation below 0.3 V

$$Cu_xMo_6S_{7.8} \longrightarrow Cu_{x-1}Mo_6S_{7.8} + Cu^{+} + e^{-}, \quad (1)$$

for oxidation above 0.3 V

$$Cu_xMo_6S_{7.8} \longrightarrow Cu_{x-1}Mo_6S_{7.8} + Cu^{2+} + 2e^{-}, \quad (2)$$

for reduction in a solution with Cu^{+}

$$Cu_{x-1}Mo_6S_{7.8} + Cu^{+} + e^{-} \longrightarrow Cu_xMo_6S_{7.8}, \quad (3)$$

and for reduction in a solution with Cu^{2+}

$$Cu_{x-1}Mo_6S_{7.8} + Cu^{2+} + 2e^{-} \longrightarrow Cu_xMo_6S_{7.8}. \quad (4)$$

The redox waves in Fig. 1 correspond to the above reversible intercalations of copper to $Cu_xMo_6S_{7.8}$.

Figure 3 shows a chronopotentiogram of $Cu_3Mo_6S_{7.8}$ under galvanostatic conditions with an oxidation current I=1 mA. This chronopotentiogram shows a positive shift of potential due to deintercalation of Cu^{+}. The Cu composition (x) of the compound decreases with increase in electric quantity (Q) due to oxidative deintercalation. The rest potential of the electrode varies from −0.1 to 0.3 V vs. SCE with oxidation. This electrode potential change which results from stoichiometric variation of $Cu_xMo_6S_{7.8}$ means a shift of the Fermi energy of the compound, which is reflected by variation in electronic distribution within a crystal due to composition change.

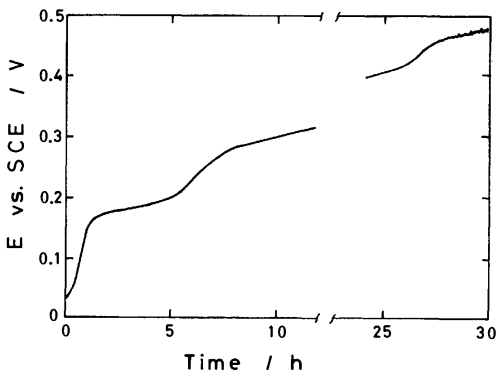

Fig. 3. Chronopotentiogram of a potential of $Cu_3Mo_6S_{7.8}$ under a galvanostatic oxidation with 1 mA in a 0.1 M KNO_3 solution.

It is reported that group compounds with a rhombohedral Chevrel phase contain a variety of metal cation intercalants and that their widely varying superconducting properties depend on both their stoichiometry and crystal structure.[9,10] From the results shown in Figs. 1 and 2, the conformation change of Chevrel phase compounds is expected to be associated with the composition change resulting from the copper cation transfer across the electrode-solution interface. The electric quantity (Q) which is consumed in the course of electrochemical intercalation and deintercalation can affect the stoichiometry of compounds. The relationship between crystal structure of compounds and redox electrolysis was investigated. Powder X-ray diffraction analyses were carried out for compounds $Cu_xMo_6S_{7.8}$ after redox treatment under in galvanostatic conditions with +/− 5 mA. Figure 4 shows the powder X-ray diffraction patterns which were obtained for $Cu_2Mo_6S_{7.8}$ after oxidations with Q=0, 6, and 12 C. The phenomenon that the diffraction patterns change with the degree of oxidation indicates conformation change in crystal. These patterns were analyzed by the Hull-Davey method. Lattice constants for hexagonal unit cell were calculated and converted into those for rhom-

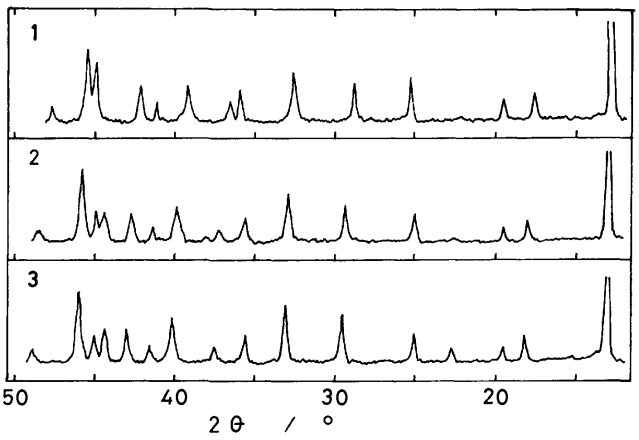

Fig. 4. X-Ray diffraction patterns with Cu $K\alpha$ in the course of an oxidation of $Cu_2Mo_6S_{7.8}$ (0.3 g).
(1) Initial $Cu_2Mo_6S_{7.8}$ (2) oxidized with 6 C, (3) oxidized with 12 C.

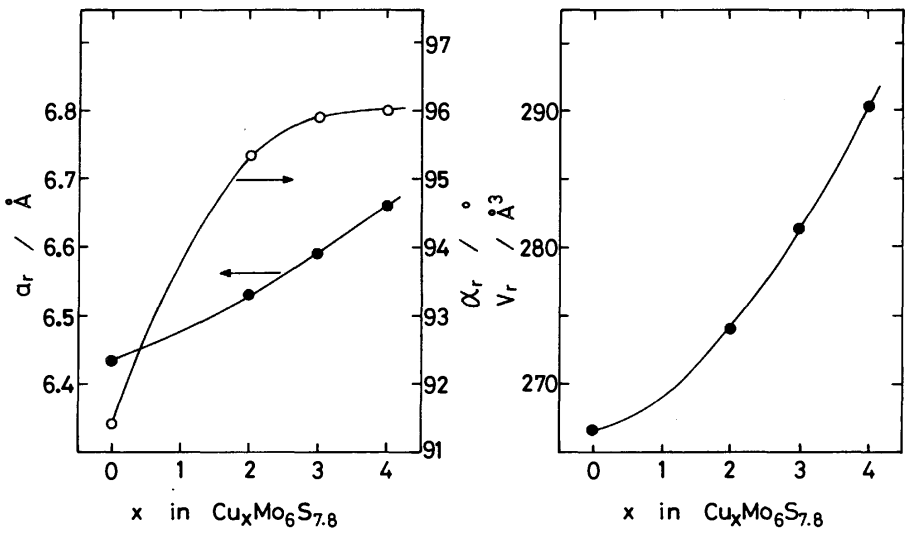

Fig. 5. Lattice constants of $Cu_xMo_6S_{7.8}$ compounds as a function of Cu composition (x).

bohedral unit cell.[16] The rhombohedral crystal structure of $Cu_2Mo_6S_{7.8}$ changes with the electric quantity in oxidation processes.

For the Chevrel phase compounds $Cu_xMo_6S_{7.8}$ (x=0, 2, 3, and 4) which were synthesized with stoichiometric ratios, their rhombohedral structures were also analyzed before redox electrolysis. Figure 5 shows the rhombohedral lattice constants (a_r and α_r) and unit cell volumes (V_r) as a function of Cu composition (x) as determined by the quantitative analysis of dissolved Cu^+ described in the experimental section. This relationship shows a clear dependence of the Chevrel phase structure on Cu composition (x), as described in detail elsewhere.[17] The compounds with various Cu compositions are employed for redox electrolysis, and their structure changes are analyzed as a function of the electric quantity (Q) consumed during the electrolysis.

Figure 6 shows the relationship between rhombohedral lattice constants (a_r, α_r) and oxidative electric quantity (Q_{ox}) for $Cu_4Mo_6S_{7.8}$. Before oxidation, the sample has a rhombohedral structure with a_r=6.65 Å, α_r=96.5°, and V_r=287.5 Å^3. In the course of oxidation, the lattice constants drastically decrease in proportion to the oxidative Q_{ox} to a_r=6.5 Å, α_r=94°, and V_r=273 Å.[3] For $Cu_3Mo_6S_{7.8}$ and $Cu_2Mo_6S_{7.8}$, phenomena similar to that of $Cu_4Mo_6S_{7.8}$ were observed with respect to the relationship between oxidative Q_{ox} and lattice constants, as shown in Figs. 7 and 8. Both a_r and α_r decrease with the degree of oxidation. Especially, the change in lattice angle α_r is characteristic of distorted contraction of crystal. The volume difference (ΔV_r) between $Cu_4Mo_6S_{7.8}$ and $Mo_6S_{7.8}$ is ca. 25 Å^3, which is ca. 10% of the unit cell volume and larger than the ionic volume (14.8 Å^3) as calculated for 4 Cu^+ by using the Cu^+ ionic radius of 0.96 Å.[18] These anisotropic changes in lattice

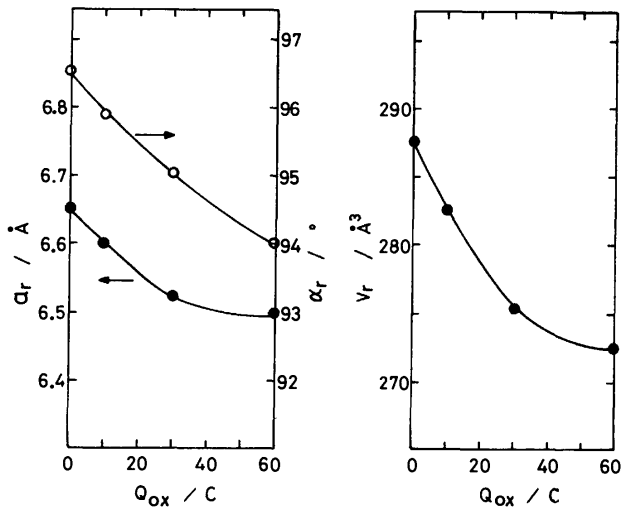

Fig. 6. Dependence of lattice constants on Q_{ox} for an oxidative deintercalation of $Cu_4Mo_6S_{7.8}$.

constants as a function of Q_{ox} claim that the deintercalation process gives rise to a series of changes from $Cu_4Mo_6S_{7.8}$ through $Cu_3Mo_6S_{7.8}$ and $Cu_2Mo_6S_{7.8}$ to the copper-free $Mo_6S_{7.8}$. As seen from a comparison of the crystal parameters in Figs. 6—8 with that in Fig. 5, the copper composition (x) decreases by 1 for each Q_{ox}=ca. 27 C for these compounds:

$$Cu_4Mo_6S_{7.8} \xrightarrow[-e^-]{-Cu^+} Cu_3Mo_6S_{7.8} \xrightarrow[-e^-]{-Cu^+} Cu_2Mo_6S_{7.8} \xrightarrow[-e^-]{-Cu^+} CuMo_6S_{7.8} \xrightarrow[-e^-]{-Cu^+} Mo_6S_{7.8}. \quad (5)$$

When the compound was oxidized at a potential (>0.35 V) in the rane [B], a change in crystal structure similar to that occurring in the range [A] was observed. However, a constant change in lattice

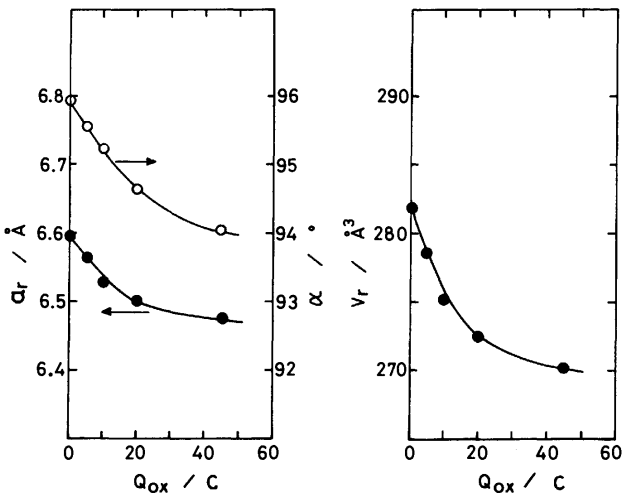

Fig. 7. Dependence of lattice constants on Q_{ox} for an oxidative deintercalation of $Cu_3Mo_6S_{7.8}$.

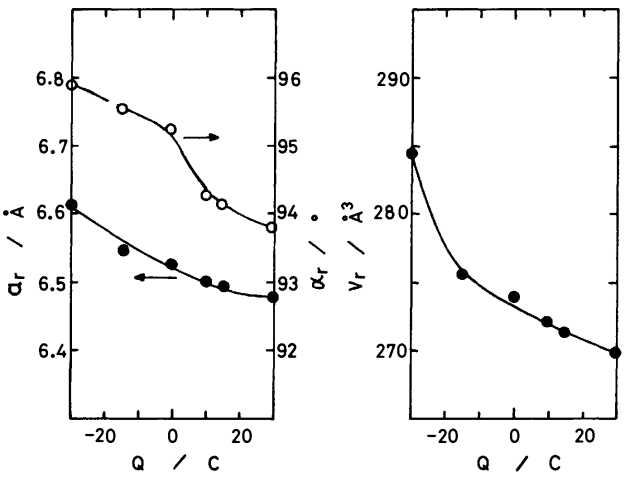

Fig. 8. Dependence of lattice constants on Q for redox intercalation and deintercalation of $Cu_2Mo_6S_{7.8}$.

constant required nearly twice Q_{ox} for the case in the potential range [A]. This means that the deintercalation process according to Eq. 2 involves an oxidation process from Cu^+ to Cu^{2+} at the surface of electrode.

On the other hand, when the sample is reduced, that is, intercalated with Cu^+, it is expected that reverse change in crystal structure will occur in proportion to the reductive electric quantity (Q_{red}), because the cyclic voltammogram of the compound is reversible as shown in Fig. 1. When $Cu_2Mo_6S_{7.8}$ is reduced in a saturated CuCl solution, the crystal structure changes as shown in Fig. 8. In the range of negative Q, the lattice constants increase as intercalation proceeds. Figure 9 shows the relationship between lattice constant and reductive Q_{red} in the course of intercalation for $Mo_6S_{7.8}$. Cu^+ intercalation into a host compound results in increase in the lattice

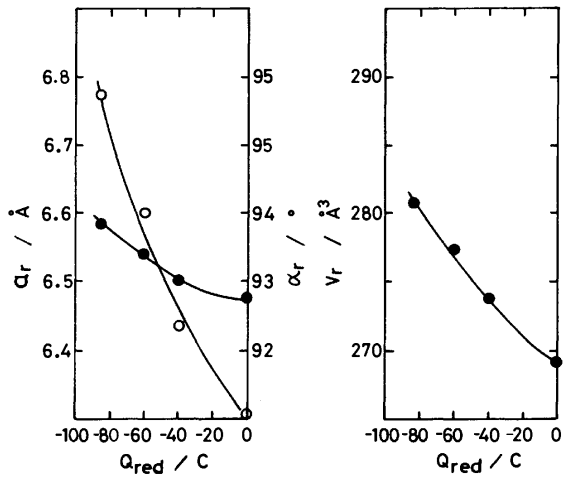

Fig. 9. Dependence of lattice constants on Q_{red} for a reductive intercalation of $Mo_6S_{7.8}$ in a saturated CuCl solution.

constants, that is, expansion of the crystal unit cell.

When an $Mo_6S_{7.8}$ electrolde was reduced in a solution with 0.1 M Cu^{2+}, similar increases in the lattice constants were observed. However, a certain constant degree of intercalation required nearly twice the Q_{red} for the case with Cu^+, that is, the crystal structure at Q_{red}=40 °C with Cu^+ was almost the same as that at Q_{red}=80 °C with Cu^{2+}. This phenomenon suggests that the intercalation reaction according to Eq. 4 involves a reduction process of Cu^{2+} to Cu^+. This result is consistent with the state of copper(I) cation in crystal disclosed by a crystallographic analysis.[9] Therefore, the intercalation and deintercalation of the compound are transfer processes of copper(I) cation across the compound-solution interface.

As seen from the results of Figs. 6—9, the structures of the rhombohedral crystals undergo reversible and continuous change during the redox intercalation and deintercalation processes of Cu^+. The unit cell of the compound expands due to intercalation and contracts due to deintercalation of Cu^+, accompanying structure distortions due to change in lattice angle.

Figure 10 shows the schematic view of a basic rhombohedral Chevrel phase compound. The copper which is surrounded by the S quasi cubics can be deintercalated by oxidation and intercalated reduction. The crystal deformation results from the effect that the Cu^+ intercalation gives rise to change in the relative distances among the S quasi cubics as well as among the Mo_6 octahedra. Moreover, in the course of the redox processes, if the ionic condition is kept as Cu(+1) and S(2−) in $Cu_xMo_6S_{7.8}$ crystal, the valency Z of Mo shifts from 2.6 to 1.93 due to intercalation. That is, the electron density of a Mo_6 cluster also increases due to intercalation. As electronic structure is generally correlated to crystal structure, the electronic

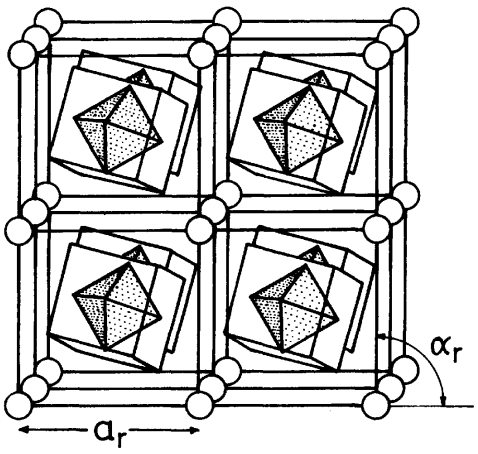

Fig. 10. Schematic illustration of a rhombohedral Chevrel phase compound. Circles denote the Cu Sites. A sulfur cubic contains an octahedral molybdenum Mo_6 cluster.

distribution as well as the density of states of the compound should be affected by the metal cation intercalation and deintercalation. This can explain the observation that the deintercalation of a Cu^+ intercalant from the compound results in a shift of electrode potential which is equivalent to a Fermi energy level, as discussed in connection with the result shown in Fig. 3. The phenomenon that critical temperature T_c of $Cu_xMo_6S_8$ associated with superconducting phenomena varies with Cu composition,[9,10] is evidence for the intercalation effect which leads to change in both the d-electron density of Mo and the crystal structure. Therefore, electrochemical intercalation is useful for studies on superconducting properties of these compounds.

References

1) R. Chevrel, M. S. Sergent, and J. Prigent, *J. Solid State Chem.*, **3**, 515 (1971).
2) J. Hauk, *Mat. Res. Bull.*, **12**, 1015 (1977).
3) R. Flukiger, R. Baillif, and E. Walker, *Mat. Res. Bull.*, **13**, 7443 (1978).
4) S. Yamamoto, K. Matsui, M. Wakihara, and M. Taniguchi, *Mat. Res. Bull.*, **18**, 1311 (1983).
5) R. Chevrel and M. S. Sergent, in "Topics in Current Physics," ed by O. Fischer and M. B. Maple, Springer-Verlag, Berlin (1982), Vol. 32, pp. 25—86.
6) Y. Takeda, R. Kanno, M. Noda, and O. Yamamoto, *Mat. Res. Bull.*, **20**, 771 (1985).
7) R. Chevrel, M. Hirrien, and M. Sergent, *Polyhedron*, **5**, 87 (1986).
8) O. Fischer, *Appl. Phys.*, **16**, 1 (1978).
9) K. Yvon, in "Current Topics in Materials Science," ed by E. Kaldis, Elsevier, Amsterdam (1979), Vol. 3, pp. 53—130.
10) R. Flukiger and R. Baillif, in "Topics in Current Physics," ed by O. Fischer and M. B. Maple, Spriner-Verlag, Berlin (1982), Vol. 32, pp. 113—142.
11) "Physics and Chemistry of Materials with Layered Structures," ed by F. A. Levy, Reide, Dortrecht, (1979), Vol. 6.
12) M. Ikebe and Y. Muto, *Kotai Butsuri*, **16**, 428 (1981).
13) T. Inoue and T. Yamase, *Denki Kagaku*, **54**, 812 (1986).
14) A. Fujishima, M. Aizawa, and T. Inoue, "Denkikagaku Sokuteiho," Gihodo, Tokyo (1984).
15) T. Inoue, T. Watanabe, A. Fujishima, K. Honda, and K. Kohayakawa, *J. Electrochem. Soc.*, **124**, 719 (1977).
16) B. D. Cullity, "Elements of X-Ray Diffraction," Addison-Wesley Pub. Co. Inc., Massachusetts (1956).
17) R. Flukier, R. Baillif, J. Muller, and K. Yvon, *J. Less-Common Met.*, **72**, 193 (1980).
18) "Lange's Handbook of Chemistry," ed by J. A. Dean, McGraw-Hill, New York (1973).

 © 1987 The Chemical Society of Japan Bull. Chem. Soc. Jpn., 60, 3373—3378 (1987)

An Efficient Regeneration of Singlet Oxygen from 2,5-Diphenylfuran Endoperoxide Produced by a Dye-Sensitized Oxygenation

Yoshiharu Usui,* Hiroshi Koike, and Yoshimi Kurimura
Department of Chemistry, Faculty of Science, Ibaraki University, Mito 310
(Received March 4, 1987)

The maximum quantum yield of 4.5 was evaluated from the kinetic analysis for the Methylene Blue-sensitized oxygenation of 2,5-diphenylfuran, and the contribution of a chain process to produce the furan endoperoxide was suggested. After the photoreaction, the thermolysis of the endoperoxide occurred to regenerate 2,5-diphenylfuran and singlet oxygen and to produce *cis*-1,2-dibenzoylethylene simultaneously. The activation energy of singlet oxygen recovery was estimated to be 18.5 kcal mol^{-1}. The reversible conversion of singlet oxygen took place efficiently with thiazine and xanthene dyes. A concerted dissociation of singlet oxygen from the endoperoxide was supposed from the negative value of activation enthropy (−9.8 e.u.) for the reaction.

Singlet oxygen($^1O_2$) is one of the active oxygen species which are utilized for synthetic chemistry with oxidative reactions and which affect the photodynamic action in the field of photobiology and photomedecine.[1] Since these active species of $^1O_2$, $O_2^-\cdot$, $OH\cdot$, H_2O_2, etc., are of a high-energy compound thermodynamically and are interconvertible with each other through the respective oxidation and reduction processes, the photochemical formation of $^1O_2$ is significant in the performance on various reactions of the up-hill type upon free energy change.

Provided that the $^1O_2$ formed with a photosensitized reaction is once trapped and stored, and is then regenerated in the dark, such a phenomena of $^1O_2$ formation will show a fascinating feature of the reversible conversion with light energy; visible light can be efficiently used for $^1O_2$ formation by means of an energy transfer from the triplet organic dyes without the decomposition of sensitizers. Choosing 2,5-diphenylfuran (DPF) as an efficient acceptor for the $^1O_2$ formed photochemically, we found the quantum yields on the DPF oxygenation which exceeded the intersystem crossing probability of the triplet sensitizers.

In the present paper, the reaction mechanism of the efficient oxygenation of DPF has been discussed. Then, the decomposition of the product of DPF endoperoxide, resulting in the regeneration of $^1O_2$ has been kinetically investigated.

Experimental

Materials. All the organic dyes (G.R. grade) of Methylene Blue ($C_{16}H_{18}N_3SCl$; MB), Thionine ($C_{12}H_{20}N_3SCl$; Th), Eosine Y ($C_{20}H_6O_5Br_4Na_2$; EY), Erythrosine B ($C_{20}H_6O_5I_4Na_2$; Ery), and Rose Bengal ($C_{20}H_2O_5I_4Cl_4Na_2$; RB) were recrystallized twice from ethanol. The 2,5-diphenylfuran(Tokyo Kasei Co., G.R.) and 1,3-diphenylisobenzofuran(Aldrich Co., G.R; DPBF) and all the solvents (Kanto Kagaku Co., G.R.) of acetonitrile, methanol, chloroform, 1,1,2,2-tetrachloroethane, etc. were used as received.

Procedures. An iodometry reported for the similar compounds was used to determine the amount of DPF-peroxide.[2,3] The extinction coefficient of I_3^- in acetonitrile was 2.55×10^4 M^{-1} cm^{-1} (1 M=1 mol dm^{-3}) at the peak of 363 nm. The sensitized oxidation of DPF and DPBF was monitored with an usual cross-illumination apparatus, as has been reported previously.[4] After the irradiation within a few minutes, the recovery of DPF was also monitored by means of the same apparatus for several tens of minutes in the dark. The photobleaching of MB in an air-saturated aqueous solution was used as a chemical actinometer (the quantum yield: 4.5×10^{-5}) to obtain the light intensity from a 300W tungsten lamp and to estimate the quantum yield of DPF oxidation (Φ).[5] For the spectral and kinetical analyses of the reactions, a system composed of a spectrophotometer (Hitachi, 200-10), a microcomputer(NEC, PC8801), and a digitizer(Mitablet) was used.

In the kinetical analysis of the present photochemical reaction, the rapid irradiation with a higher intensity has to be performed at low temperatures in order to avoid the influence of the thermal decomposition during irradiation.

Results and Discussion

DPF Concentration Effect on the Quantum Yield, Φ. The singlet oxygen($^1O_2$) which is produced by the energy transfer from the triplet sensitizer(^{3}Sens) decays to the ground state molecule($^3O_2$) in a solution or reacts with the added DPF to produce the endoperoxide($DPFO_2$) competetively. The scheme for such reactions has already been reported to be as follows:[4,6-10]

$$^3\text{Sens} \longrightarrow {}^1\text{Sens} \quad (1)$$

$$^3\text{Sens} + {}^3O_2 \longrightarrow {}^1\text{Sens} + {}^1O_2 \quad (2)$$

$$^1O_2 \longrightarrow {}^3O_2 \quad k_d \quad (3)$$

$$^1O_2 + \text{DPF} \longrightarrow DPFO_2 \quad k_q \quad (4)$$

Scheme 1.

According to the above essential scheme, the initial quantum yield of DPF oxygenation(Φ) is expressed as Eq. 5:

$$\Phi = \Phi_{so}\frac{[DPF]}{\beta_{DPF}+[DPF]} \quad (5)$$

where Φ_{so} and β_{DPF} stand for the $^1O_2$ formation yield from ^{3}Sens and the rate parameter of k_d/k_q respectively. From the linear relationship between $1/\Phi$ and 1/[DPF], the reactivity index, β_{DPF}, can be estimated.[4,6] The experimental results for the DPF concentration effect on Φ is shown in Fig. 1. Although the Φ_{so} value for the sensitizer of MB is 0.52, the Φ value at higher concentrations of DPF exceeds Φ_{so}, and its limitation goes up to about eight times of the Φ_{so} value.[11] The amounts of peroxide produced photochemically were determined by means of iodometry; they are listed in Table 1. Although the thermal decomposition of the unstable endoperoxide occurred during irradiation, and thus the amounts of the peroxide decreased at higher temperatures (>25 °C), it was shown that the added DPF changed completely to the peroxide, as is shown in Fig. 1. These results suggest that Eq. 5 cannot be adopted and that DPF might be oxygenated through a chain-reaction process. Since the effect of temperature (0—55 °C) on Φ values was not observed under the present experimental conditions, it seems that the chain cycles for DPF oxygenation proceed rapidly without an activation energy and that the thermal decomposition of the product can also be neglected at the initial stage of irradiation.

Thus we can tentatively introduce a mechanism in which the thermically activated state or intermediate ($DPFO_2$*) reacts with DPF, competing with its own deactivation. The activated state, DPF*, is oxygenated by dissolved oxygen via Eqs. 7—9. This chain mechanism is shown as Scheme 2:

$$^3\text{Sens} \longrightarrow {}^1\text{Sens} \quad (1)$$
$$^3\text{Sens} + {}^3O_2 \longrightarrow {}^1\text{Sens} + {}^1O_2 \quad \Phi_{so} \quad (2)$$
$$^1O_2 \longrightarrow {}^3O_2 \quad k_d \quad (3)$$
$$^1O_2 + \text{DPF} \longrightarrow DPFO_2^* \quad k_q \quad (4)$$
$$DPFO_2^* \longrightarrow DPFO_2 \quad k_1 \quad (6)$$
$$DPFO_2^* + \text{DPF} \longrightarrow DPFO_2' + \text{DPF}^* \quad k_2 \quad (7)$$
$$\text{DPF}^* \longrightarrow \text{DPF} \quad k_3 \quad (8)$$
$$\text{DPF}^* + {}^3O_2 \longrightarrow DPFO_2^* \quad k_4 \quad (9)$$

Scheme 2.

The activated intermediates of $DPFO_2$* and DPF* act as chain carriers, and the chain cycle is involved by means of Eqs. 7 and 9 as long as sufficient DPF exists. $DPFO_2$* produces the endoperoxide($DPFO_2$), competing with the reverse reaction of Eq. 4. $DPFO_2'$ is tentatively assumed to be the peroxide which produces *cis*-1,2-dibenzoylethylene(DBE) via a thermal decomposition as will be described below. In the studies of the reactivity of $^1O_2$ for endoperoxide formation, the existence of such intermediates as an addition complex or a π complex between $^1O_2$ and an acceptor was frequently assumed.[6,12,13] These complexes can be assigned to the $DPFO_2$* and $DPFO_2'$ in Scheme 2. Although $DPFO_2$ regenerated $^1O_2$ and DPF thermically after the irradiation, the degree of DBE formation against the thermal recovery of DPF became small, after irradiation when the initial concentration of DPF was low ([DPF]<20 μM). When the irradiation procedures after the thermal recovery of DPF from $DPFO_2$ were repeated, the added DPF changed to DBE quantitatively. These results are consistent with Scheme 2.

Table 1. Temperature Effect on the Amounts of DPF-Peroxide

Temperature °C	Concentration(/10^{-4} M) of	
	reacted DPF	produced $DPFO_2$
55	1.18	0.344
35	1.18	0.639
25	1.06	0.831
15	1.18	1.01
5	1.18	1.05
−2	1.06	0.92
−7	1.06	1.03
−11	1.06	1.03

[MB]=10 μM, $[DPF]_0$=120 μM, in CH_3CN.

The quantum yield of DPF disappearance, Φ_C, which is derived by applying the stationary-state method to ^{3}Sens, $^1O_2$, and these activated intermediates in Scheme 2, can be expressed as in Eq. 10:

$$\Phi_C = \Phi_{so}\frac{[DPF]}{\beta_{DPF}+[DPF]}\left(1+(1-r)\frac{k_2[DPF]}{k_1+rk_2[DPF]}\right) \quad (10)$$

where $r=k_3/(k_3+k_4[O_2])$; i.e., r means the degree of DPF* deactivation of Eq. 8 in competition with the process of Eq. 9. Under the conditions of $k_1/k_2 \gg$[DPF], the expression of Φ_C coincides with Eq. 5, which is the equation of Φ without the chain process. Further, the rate of the photochemical oxygenation of DPF was analyzed as a first-order reaction under the approximate condition of $\beta_{DPF} \gg$[DPF], and the rate constant was found to be inversely proportional to β_{DPF}. In the case of the DPBF oxygenation, β_{BF} in acetonitrile, which stands for the rate parameter of k_d/k_q' for the reactions, was similarly obtained as 1.26×10^{-5} M at 20 °C. From the comparison of the rate constants for the DPF and DPBF oxygenations, the β_{DPF} value for DPF in acetonitrile (8.3×10^{-5} M) can be estimated.[4] By substituting the k_d value ($=3\times10^4$ s^{-1} in acetonitrile) into the β_{DPF}, k_q was obtained as 3.7×10^8 M^{-1} s^{-1}.[4,6,9,14]

On the other hand, at the higher concentration of DPF ([DPF]$\gg k_1/k_2$), Φ_C can be approximately written as in the following equation:

$$\Phi_C = \Phi_{so}\frac{[DPF]}{\beta_{DPF}+[DPF]}\frac{1}{r}$$
$$= \Phi_{so}\frac{1}{r} = \Phi_{max} \quad (\beta_{DPF} \ll [DPF]) \qquad (11)$$

Therefore, a linear relationship between $1/\Phi$ and 1/[DPBF] was derived from Eq. 11 over the DPF concentration of 20 μM, as is shown in Fig. 1: i.e, the reciprocal plot holds approximately with Eq. 11, but with Eq. 5. From the interception in Fig. 1 a maximum value of $\Phi_C(\Phi_{max})$ was obtained as 4.5. The β_{DPF} value of 6.9×10^{-5} M was obtained from the interception and the slope. By substituting the Φ_{max} value into Eq. 11, the r value of 0.116 is obtained. This suggests that DPF* reacts with $^3O_2$ as an efficient chain carrier in Eq. 9.

Incidentally, the following numerical equation is shown as a dotted line in Fig. 1:

$$\Phi_C(calcd) = \frac{0.52[DPF]}{6.9\times10^{-5}+[DPF]} \times\left(1+\frac{0.884[DPF]}{1.7\times10^{-6}+0.116[DPF]}\right) \qquad (12)$$

From this equation, which is drawn to coincide with the experimental data, the ratio of the rate constants ($k_1/k_2=1.67\times10^{-6}$ M^{-1}) was obtaind using the r value of 0.116. Thus, at the higher concentrations of DPF$\gg k_1/k_2(=1.67\times10^{-6}$ M), it seems that $DPFO_2$* reacts with DPF predominantly and that the chain reaction occurs efficiently.

Recovery Process of DPF from the Endoperoxide. It has been reported that the endoperoxides are unstable and that the thermal decomposition occurs easily.[2,15,16] In order to clarify the reaction mechanism of the decomposition from the point of view of $^1O_2$ regeneration, a kinetic investigation was carried out. By measuring the UV-spectral change of the sample immediately after irradiation, it was confirmed that the regeneration of DPF occurred by means of the $DPFO_2$ decomposition in the dark. Simultaneously, *cis*-1,2-dibenzoylethylene(DBE) with the absorption maximum at 265 nm was produced as is shown in Fig. 2.[2] After irradiation at a higher concentration of DPF (10—300 μM) and at a lower temperature (0—20 °C), the percentage recoveries of DPF and DBE to the added DPF concentration were 55 and 40% in acetonitrile respectively. At lower concentrations of DPF(<10 μM), the percentage recovery of DPF increased, but that of DBE decreased to some extent.

The rate of DPF recovery could be apparently analyzed as first-order with the peroxide concentration, which was estimated as the value of $[DPF]_{max}-[DPF]$ from the maximal recovery of DPF, ($[DPF]_{max}$):

$$\ln([DPF]_{max}-[DPF]) = \ln[DPF]_{max}-k_r t \qquad (13)$$

Similarly, the DBE formation was also analyzed as a first-order reaction. The rate constants were $7.0(\pm0.2)\times10^{-4}$ s^{-1} for DPF (k_r) and $6.9(\pm0.2)\times10^{-4}$ s^{-1} for DBE respectively at 25 °C. The initial rates for the recovery were not influenced by the DPF concentration. Provided that the back reaction of Eq. 14 occurred, the kinetic treatment on DPF should deviate from the first order analysis of Eq. 13:

$$DPFO_2 \longrightarrow DPF + {}^1O_2 \qquad k_r \qquad (14)$$
$$^1O_2 \longrightarrow {}^3O_2 \qquad (15)$$

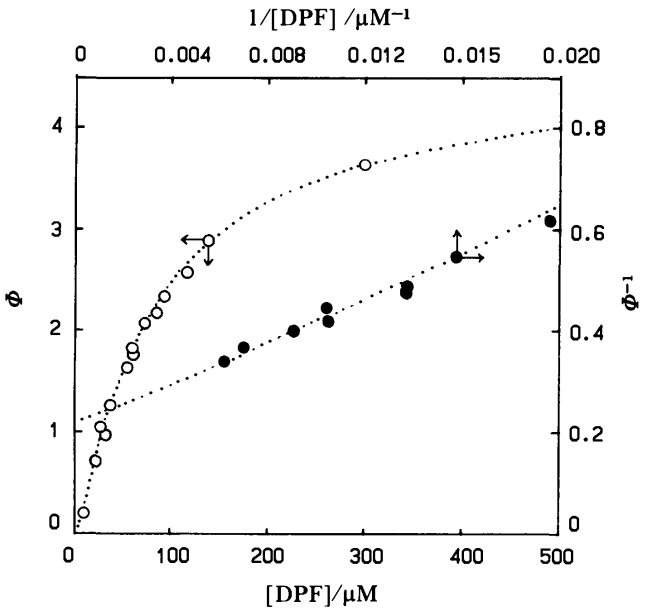

Fig. 1. DPF concentration effect on the oxidation yield, Φ in acetonitrile. (Dotted line: Eq. 12 in text) [MB]: 5 μM; 5 °C.

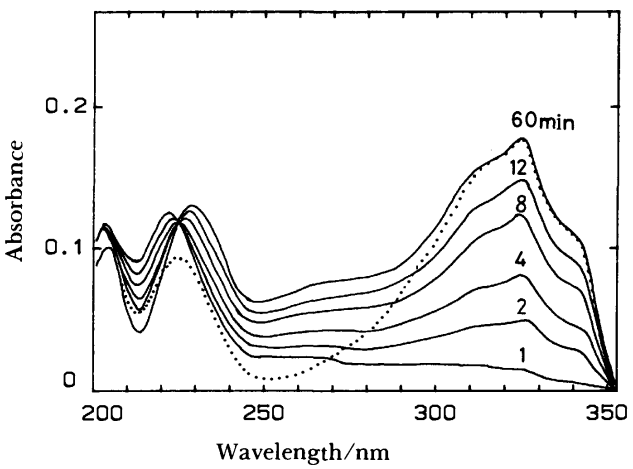

Fig. 2. UV-spectral change for DPF-recovery and DBE formation processes after irradiation in acetonitrile. (Dotted line: Spectrum of DPF in which the absorption was normalized at a peak after 60 min-recovery) [MB]: 5 μM; [DPF]: 10 μM; 50 °C.

However, when the stationary concentration of $^1O_2$ is low (about 30% for the $DPFO_2$ concentration), Eq. 13 approximately holds in a computer simulation for the concentration change in each component, even if both the equilibrium for Eq. 14 and the competitive reactions of Eq. 15 are involved. Since $^1O_2$ is deactivated by acetonitrile, it seems that a first order reaction of Eq. 13 was practically observed under the present conditions.

From the temperature effect on the rate constants of DPF recovery and DBE formation, the apparent activation energies (E_A) were obtained as 18.5± 0.5 kcal mol^{-1}(DPF) and 17.0±0.5 kcal mol^{-1}(DBE) respectively. These values are smaller than those in the cases of the endoperoxides of anthracene derivatives(for example; 9,10-diphenylanthracene endoperoxide: 27.8 kcal mol^{-1}, rubrene endoperoxide: 32.6 kcal mol^{-1}).[17-19] By reference to the behavior of the endoperoxide of 3-(4-methyl-1-naphthyl)propionic acid, which has been reported to have the E_A value of 17 kcal mol^{-1}, DPF recovery was actually observed even at room temperature.[20]

It has been reported that the decomposition mechanism of the furan endoperoxides was dependent on the solvent.[16] In alcohol, the addition of a solvent to $DPFO_2$ produces the hydroperoxide. Hardly no DPF recovery was observed in methanol, ethanol, and 1-propanol, etc. In the mixture of acetonitrile and heptane or ethyl acetate, a good DPF recovery was observed, since the reaction of Eq. 14 occurs successively as a result of the rapid deactivation of $^1O_2$ in these solvents. However, in the solvent mixture of acetonitrile and 1,1,2,2-tetrachloroethane, though the rate of DPF recovery was increased to some extent, the amount of recovery was decreased, as is shown in Table 2. This means that the back reaction in Eq. 14 was not neglected during the recovery, since the lifetime of $^1O_2$ is longer in 1,1,2,2-tetrachloroethane or carbon tetrachloride.[8,21-23]

Regeneration of Singlet Oxygen. DPBF reacts rapidly and specifically with $^1O_2$, without being complicated by any side reactions. In order to check experimentally whether or not $^1O_2$ was produced in the DPF recovery process, DPBF was added to the sample immediately after the irradiation. For the kinetical treatment to $^1O_2$ and the DPBF reaction, the following scheme can be introduced:

$$DPFO_2 \longrightarrow DPF + {}^1O_2 \qquad k_r \qquad (14)$$

$$^1O_2 \longrightarrow {}^3O_2 \text{ (in } CH_3CN) \qquad k_d \qquad (15)$$

$$^1O_2 + DPBF \longrightarrow DPBFO_2 \qquad k_q' \qquad (16)$$

Scheme 3.

Since $^1O_2$ is easily deactivated in acetonitrile, and also since DPBF traps $^1O_2$ in competition with the deactivation, the reaction rate of DPBF in Scheme 3 can be analyzed as in Eqs. 17 and 18 under the assumption of the stationary state method for $[^1O_2]$, using the relation of $[DPFO_2]=[DPFO_2]_0\exp(-k_rt)$. The reaction probability between DPBF and $^1O_2$ was assumed to be unity.[8,9] The β_{BF} value($=k_d/k'_q$) and the k_r value for the DPF recovery reaction in acetonitrile were used in Eq. 18, which was the integrated equation to Eq. 17:

$$-\frac{d[DPBF]}{dt} = k'_q[^1O_2][DPBF] \qquad (17)$$

$$\beta_{BF}\ln[DPBF] + [DPBF] = \beta_{BF}\ln[DPBF]_0 + [DPBF]_0 - [DPFO_2]_0(1-\exp(-k_rt)) \qquad (18)$$

The linear relationship in Eq. 18 is shown in Fig. 3. Since the slope in Fig. 3 was equal to $[DPFO_2]_0$, the initial concentration of $DPFO_2$ which produced $^1O_2$ was calculated to be 60 μM under the present conditions; the amount was approximately equal to the recovered DPF concentration. Accordingly, it can be suggested that the $^1O_2$ regenerated in Eq. 14 was

Table 2. Solvent Effect on the Recovery Rate and Amounts of DPF (25°C)[a]

Solvent χ_{TeCE}[b]	$k_r/10^{-4}$ s^{-1}	Recovered [DPF]/μM (percent recovery)
0	7.01	15.3 (54.9)
0.048	6.5	13.7 (49.0)
0.13	10.1	10.6 (37.1)
0.20	10.4	10.0 (36.0)
0.30	12.0	7.6 (27.1)

a) [MB]=5 μM, [DPF]=27.9 μM. b) Molar fraction of 1,1,2,2-tetrachloroethane.

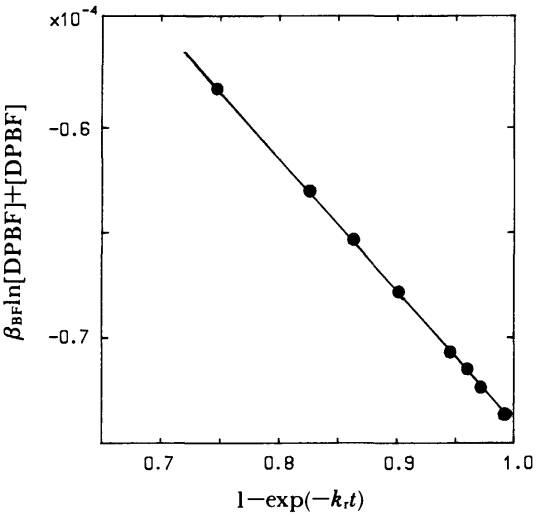

Fig. 3. Kinetic treatment for oxygenation of DPBF with $^1O_2$ regenerated by the thermal decomposition of $DPFO_2$ at 45 °C. (The values for k_r of 1.59×10^{-2} and for β_{BF} of 1.99×10^{-5} are used in Eq. 18.) [MB]: 5 μM; [DPF]: 68 μM; [DPBF]: 49 μM.

reacted with DPBF as is shown in Scheme 3. Provided that DPF and DBE were simultaneously produced from $DPFO_2$, the k_r value in Eq. 18 must be a sum of the rate constants of the formations of DPF and DBE. Putting the sum value into k_r, the plot in Fig. 3 is not expressed as a linear relationship. Thus, as is shown in Scheme 2, it may be supposed that the peroxide which leads to DPF and $^1O_2$ regeneration is not the same as that in the DBE formation.

The possibility of the direct reaction of DPBF with $DPFO_2$ might be considered instead of Eqs. 14—16:

$$DPFO_2 + DPBF \longrightarrow DPF + DPBFO_2 \quad (19)$$

However, the above reaction was obviated by the facts that the DPF recovery rate was not analyzed as exemplifying the second order kinetics in the case of DPBF addition, and that the reaction rate of DPBF becomes faster in the solvents mixed with the 1,1,2,2-tetrachloroethane or carbon tetrachloride, where the lifetime of $^1O_2$ is longer and where the reaction of Eq. 16 predominates.

Confirming that $^1O_2$ was regenerated as an equivalent molar with DPF, the molar ratio of the reacted DPBF against the recovered DPF was calculated under a higher concentration of DPBF (260 μM). The ratio was 0.65 at 20 °C, but became 0.99 at a temperature higher than 50 °C, where an equimolar production of DPF and $^1O_2$ was confirmed, as is shown in Scheme 3.

A detailed mechanism for the release of $^1O_2$ by the thermal decomposition of the endoperoxides of anthracene derivatives was discussed by Turro et al. They checked the temperature effect on the first-order rate constants, k_r for the recoveries of anthracence derivatives. From the analysis of the Eyring plots for the reaction rate, the activation enthropy, ΔS^*, and the activation enthalpy, ΔH^*, were calculated (k: Boltzmann's constant; h: Planck's constant):[24]

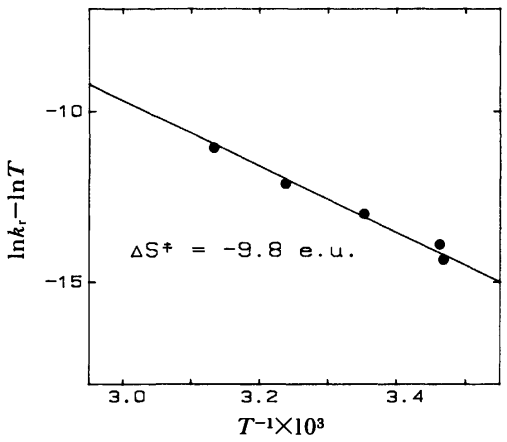

Fig. 4. Estimation of activation entropy for $^1O_2$ formation from $DPFO_2$ in acetonitrile. (Eyring plots) [MB]: 5 μM; [DPF]: 28 μM.

$$\ln k_r - \ln T = \ln(k/h) + (\Delta S^*/R) + (\Delta H^*/RT) \quad (20)$$

Since the ΔS^* values obtained for the endoperoxides of 1,4-dimethyl-9,10-diphenylanthracene and of 1,4-dimethoxy-9,10-diphenylanthracene were comparatively small(i.e., zero or negative), they reported that the $^1O_2$ production from these endoperoxide occurs in the manner of the concerted dissociation of the coupled C–O bonds. For such anthracene endoperoxides as 9,10-diphenylanthracene, which provided the positive values of ΔS^*, C–O bonds dissociate in a step-by-step fashion, and the peroxide radicals are produced. If the parallel spin-state is involved in the process of the positive ΔS^*, $^3O_2$ will be produced, and then the yield of $^1O_2$ will decrease.

In the present case of DPF formation, the kinetical results were similar to these for anthracene endoperoxides with a negative ΔS^*. The ΔS^* and ΔH^* values from the Eyring plots for the reaction were −9.8 e.u. and 18.9 kcal mol^{-1} respectively, as is shown in Fig. 4. According to Turro's model, it may be considered that the following concerted dissociation on $DPFO_2$ operates for the $^1O_2$ formation:

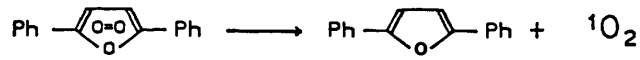

Quantum Efficiency for Single Oxygen Conversion. At higher concentrations of DPF, about 55 percent of the DPF was recovered and an equimolar amount of $^1O_2$ was regenerated at 50 °C in the dark. If significant reactions with regenerated $^1O_2$ occur successively, the recovery reaction can be utilized as a chemical storage of $^1O_2$ from the sensitization by the use of solar-light energy, since $DPFO_2$ is stable at a lower temperature-(<0 °C). In order to increase the efficiency of $^1O_2$-trapping and the conversion of light energy, the following conditions are required practically: (1) The initital concentration of DPF must be larger than the β value in order to trap the $^1O_2$ completely at the photochemical stage. (2) The sensitized reaction should be performed at a lower temperature (<0 °C) and with a higher light intensity to avoid the decomposition of the $DPFO_2$ produced during irradiation.

The conversion efficiency, γ, of $^1O_2$ reproduced in the dark can be defined as the ratio of the total amount of the $^1O_2$ reproduced, $[^1O_2]_\infty$, estimated by means of the amount of recovered DPF, to the total light quantities absorbed in the sample($I_{ab}t$), i.e., $\gamma=[^1O_2]_\infty/I_{ab}t$. In Table 3, the γ values which were obtained by the use of various sensitizers are listed at a constant DPF concentration (150 μM). Higher values were obtained for the sensitizers of MB and Th, which did not bleach durring the irradiation and which were usefully utilized at longer wavelengths. The lower values for xanthene dyes were obtained in spite of the large intersystem crossing probability. Although

Table 3. Quantum Efficiency, γ for the Conversion to $^1O_2$[a]

Sensitizer	λ_{max}/nm[b]	Φ_{so}[c]	γ/%[d]
Methylene blue	655	0.52	61.5
Thionine	592	0.58	88.9
Eosine Y	538	0.57	11.6
Erythrosine	543	0.68	43.1
Rose Bengal	559	0.83	45.0

a) [DPF]=150 μM. b) Absorption maximum of sensitizer. c) Quantum yield for $^1O_2$ formation. d) $\gamma=[^1O_2]/I_{ab}t$.

these results might be due to the quenching of the dye triplet by DPF, the detailed reason will be investigated in further works.

This work was supported by a Grant-in-Aid for Scientific Research (No. 61040003) from the Mimistry of Education, Science and Culture.

References

1) H. H. Wasserman and W. Murray, "Singlet Oxygen," Academic Press, London (1979); B. Rånby and J. F. Rabek, "Singlet Oxygen-Reaction with Organic Compounds and Polymers," John Wiley, London (1978); A. Singh and A. Petkau, "Singlet Oxygen and Related Species in Chemistry and Biology," Vol. 28 (4/5), Pergamon Press, New York (1978).

2) C. Dufraisse, G. Rio, and A. Ranjon, *C. R. Hebd. Seances Acad. Sci. Ser. C*, **264**, 516 (1967). After DPF had changed to DBE quantitatively by repeated irradiations and subsequent recovery in the present experiment, the DBE was identified by a comparison of the UV, NMR, and IR spectra with the respective data.

3) J. Martel, *Comptes rendus*, **244**, 626 (1957).

4) Y. Usui, M. Tsukada, and H. Nakamura, *Bull. Chem. Soc. Jpn.*, **51**, 379 (1978).

5) H. Obata, K. Kogasaka, and M. Koizumi, *Bull. Chem. Soc. Jpn.*, **32**, 125 (1959).

6) Y. Usui and M. Koizumi, *Mol. Photochem.*, **4**, 57 (1972); M. Koizumi, S. Kato, N. Mataga, T. Matsuura, and Y. Usui, "Photosensitized Reactions," Kagaku-Dohjin, Kyoto (1977), Chap. 8.

7) C. S. Foote, *Acc. Chem. Res.*, **1**, 104 (1968).

8) D. R. Kearns, *Chem. Rev.*, **71**, 395 (1959).

9) R. H. Young, D. Brewer, and R. A. Keller, *J. Am. Chem. Soc.*, **95**, 375 (1973).

10) Y. Usui and K. Kamogawa, *Photochem. Photobiol.*, **19**, 245 (1974).

11) Y. Usui, *Chem. Lett.*, **1973**, 743.

12) O. Chalvet, R. Daudel, and G. H. Schmid, *Tetrahedron*, **26**, 365 (1970).

13) D. R. Kearns, *J. Am. Chem. Soc.*, **91**, 6554 (1969).

14) A. A. Gorman, G. Lovering, and M. A. J. Rodgers, *J. Am. Chem. Soc.*, **101**, 3050 (1979).

15) A. M. Trozzolo and S. R. Fahrenholtz, *Ann. N.Y. Acad. Sci.*, **171**, 61, (1970).

16) W. Adams and A. Rodriguez, *J. Am. Chem. Soc.*, **102**, 404 (1980).

17) H. H. Wasserman and J. R. Scheffer, *J. Am. Chem. Soc.*, **89**, 3074 (1967).

18) H. H. Wasserman, J. R. Scheffer, and J. L. Cooper, *J. Am. Chem. Soc.*, **94**, 4991 (1972).

19) B. Stevens and R. D. Small, Jr., *J. Am. Chem. Soc.*, **81**, 1605 (1977).

20) I. Saito, K. Inoue, and T. Matsuura, *J. Am. Chem. Soc.*, **97**, 2018 (1975).

21) C. A. Long and D. R. Kearns, *J. Am. Chem. Soc.*, **97**, 2018 (1975).

22) B. Stevens and K. L. Marsh, *J. Phys. Chem.*, **86**, 4473 (1982).

23) B. Stevens, K. L. Marsh, and A. Sylvia, *J. Phys. Chem.*, **88**, 669 (1984).

24) N. J. Turro, M.-F. Chow, and J. Rigandy, *J. Am. Chem. Soc.*, **103**, 7218 (1981) and the references cited therein.

 © 1987 The Chemical Society of Japan Bull. Chem. Soc. Jpn., 60, 3379—3383 (1987)

The Interaction of Pigment with Polystyrene Latex Particles Prepared Using an Amino-Acid-Type Amphoteric Emulsifier

Kazufumi KATO, Kouichiro KANDA, Harumi KONDO, Kunio ESUMI,* and Kenjiro MEGURO

Department of Applied Chemistry and Institute of Colloid and Interface Science, Science University of Tokyo, Kagurazaka, Shinjuku-ku, Tokyo 162

(Received March 24, 1987)

An emulsion polymerization of styrene in the presence of an amino-acid type amphoteric emulsifier (N^{ε}-lauroyl-N^{α},N^{α}-dimethyllysine (DMLL)) was carried out at pH 7.0. The stability of mixed dispersions containing the latex particles prepared with DMLL and titanium dioxide (TiO_2) was then discussed as a function of the pH in a mixed dispersed solution. The zeta-potential of the synthesized latex particles was significantly dependent on the pH and showed the existence of an isoelectric point (IEP) at pH 4.5. On the other hand, TiO_2 particles had their IEP at pH 8.5. Below pH 4.5 and above pH 8.5, the mixed dispersions of the synthesized latex particles and TiO_2 particles were well-dispersed because of their electric repulsion. In the range of pH 4.5—8.5, where the latices were negatively charged, while the TiO_2 were positively charged, at low concentrations of the latex particles the mixed suspension was dispersed, but with an increase in the number of latex they heterocoagulated and were then redispersed at high concentrations of the latex particles. The mechanisms of these processes are discussed.

Latices are added to various pigments in order to achieve many industrial objectives, for example, increases in weatherability, storage stability, and pigment compatibility, and good resistance against alkaline reagents and water. Further, latices play two important roles as film formers and binders. Therefore, it has become a very important problem to study the interaction of pigments with latices.

There have been many reports on mixed dispersion systems containing latices and inorganic pigments by measuring the turbidity, the sedimentation velocity, the sedimentation volume, the viscosity, the particle size, and the surface potential.[1-7] In general, the surface charge of the latex particles prepared using a conventional anionic emulsifier is hardly dependent at all on the pH of their suspended solution, and they have a negative charge everywhere over the pH. On the other hand, normal pigments which are used for coating or painting are almost all dependent on the pH, since H^+ or OH^- acts as a potential determining ion. The pigment particles have a positive charge below the isoelectric point (IEP) and have a negative charge above the IEP. Therefore, in the pH range below the IEP, the mixed aqueous suspension of the latex particles and pigment particles is composed of a loose three-dimensional network structure with an electric force of attraction between the positively charged inorganic pigment and the negatively charged latex particles.

We have previously reported the surface properties of styrene latex prepared by emulsion polymerization in the presence of N^{ε}-lauroyl-N^{α},N^{α}-dimethyllysine (DMLL) as an amphoteric emulsifier, and have found that the latex particles exhibit characteristic properties: they change their surface potential with their pH, and they have an isoelectric point, since the ionic form of the DMLL molecules adsorbed onto the latex surfaces alters with the pH.[8] However, there have been only a few reports relating to the interaction of inorganic pigments with latices prepared by using amphoteric surfactants.

In this work, the effect of the addition of latex particles prepared with DMLL to inorganic pigments on mixed dispersion systems was investigated in respect with the pH of their suspended solutions.

Experimental

Materials. $C_{11}H_{23}CONH(CH_2)_4CH[N(CH_3)_2]COOH$ (DMLL) supplied by the Ajinomoto Co., Ltd., was purified by repeated recrystallization from mixture of hexane and 2-propanol (7:3) and then carefully dried in vacuo before use. The purity of the sample was confirmed by the absence of a minimum in its surface tension vs. concentration curve.

The styrene monomer (Wako Pure Industries, Ltd.) was distilled under a nitrogen atmosphere and was stored in a refrigerator under nitrogen. The potassium peroxodisulfate ($K_2S_2O_8$) used as an initiator was of an analytical grade, supplied by Wako Pure Industries, Ltd.

Titanium dioxide (TiO_2 (rutile)), with a surface treated by Al_2O_3 and supplied by Teikoku Kako Co., Ltd., was used. The characteristics of this pigment are indicated in Table 1. The specific surface area of the pigments was measured using a Shimadzu GAS CHROMATOGRAPH GC-7A connected with a Shimadzu SORPTOGRAPH ADS-1B and was determined by applying the BET theory to the nitrogen adsorption at the temperature of liquid nitrogen.

Table 1. Characteristics of TiO_2 Particles

Pigment	Density / g cm^{-3}	Particle size / nm	Specific surface area / m^2 g^{-1}
TiO_2 (rutile)	4.2	326.8	19.1

Procedure. An isoelectric region of the DMLL solution has been determined using the method described in a previous paper.[8]

Preparation of Latex Particles. The emulsion polymerization was performed in a one-liter glass reactor, fitted with a metal screw and a thermometer. The emulsion polymerization recipe is shown in Table 2. First, water and emulsifier (DMLL) were added to the reactor at room temperature, and then styrene monomer was added to them. The reaction flask was immersed in a constant-temperature bath adjusted to 60±1 °C under a nitrogen atmosphere, and the mixture was stirred at 250 rpm. After the temperature had risen to 60 °C, an aqueous solution of $K_2S_2O_8$ (0.1 g/50 cm^3) was added to the contents of the reactor, resulting in the final initiator concentration (0.1 g/300 g of the mixture). The polymerization time was taken as 3 h. The particle diameter of the synthesized latex particles was determined by means of Transmission Electron Microscopy and by the use of a particle sizer. The molecular weight distribution of polystyrene in the latices was determined by use of a GPC. The number of latex particles per cubic decimeter of the aqueous solution (N) was calculated by means of the particle size and the conversion, which was estimated by means of the (polystyrene latex/styrene monomer) ratio.

Interaction of Pigment with the Latex. The mixed systems of polystyrene latex and TiO_2 were prepared by the following method: First, a known weight of TiO_2 was put into 27 cm^3 of a 10^{-3} mol dm^{-3} sodium chloride aqueous solution in a sedimentation tube. This suspension was dispersed by the use of supersonic waves for an hour, and then 3 cm^3 of a styrene latex suspension was added to it. The mixed suspensions were adjusted to various pH values. After 48 h of standing, the turbidity of the suspension collected from the top portion of the sedimentation tube was measured with a turbidimeter (SEP-PT 501, Nippon Precision Optical Instrument Co., Ltd.).

The zeta-potentials (Zp) of the latex particles and TiO_2 were measured at 25 °C by means of an electrophoresis apparatus [Laser Zee TM Model-500 (PEN-KEM, Inc.)]. The amounts of latex particles adsorbed onto the surface of the TiO_2 particles were determined by means of the difference between the weight of the latices before and after the adsorption.

All of the suspensions for measuring the particle size, the electrophoresis, and the turbidity were prepared with a 10^{-3} mol dm^{-3} sodium chloride aqueous solution in order to keep the ionic strength as constant as possible. The pH of the suspension was adjusted by the addition of sodium hydroxide or hydrochloric acid.

Table 2. Emulsion Polymerization Recipe

Ingredient	Gram
Styrene	50
Water	250
Potassium peroxodisulfate	0.2
N^{ϵ}-Lauroyl-N^{α},N^{α}-dimethyllysine(DMLL)	6.0

Results and Discussion

Characterization of DMLL. DMLL has both acidic and basic groups in the same molecule, and can change its ionic form depending on the pH value of its aqueous solution. DMLL aqueous solutions have a wide isoelectric region ranging from pH 4 to 9: the cationic structure predominates below pH 4, and the zwitterionic one occurs in the range of pH 4—9, whereas the anionic one exists mainly above pH 9.[8-11]

Characterization of the Latex. In the emulsion polymerization of styrene in the presence of DMLL at pH 7.0, it was confirmed that the final latices were stable. The number-average particle diameter (D_n) and its polydispersity (D_w/D_n), as measured by Transmission Electron Microscopy, the z-average particle diameter (D_z) and its polydispersity (Q fac.), as measured by a particle sizer, and the weight-average molecular weight (M_w) and the distribution of the synthesized latex (M_w/M_n) are summarized in Table 3. From the two polydispersities, which give an indication of the breadth of the particle size distributions, it can be seen that the particle size of latex formed with DMLL has a relatively narrow distribution and that the latex consists of rather monodispersed microspheres.

Zeta-Potentials of the Latex and TiO_2. The

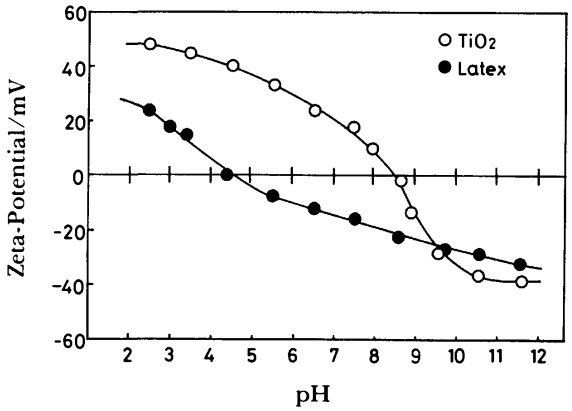

Fig. 1 The change in zeta-potentials of latex particles synthesized with DMLL and TiO_2 particles.

Table 3. Characteristics of the Latex Particles Prepared in a DMLL Solution

Particle size			
Dn/nm	Dw/Dn	Dz/nm	Q.f
48.4	1.07	59.9	0.05
Molecular weight			
$Mw(\times 10^6)$		Mw/Mn	
1.94		5.24	

change in the zeta-potentials of the latex particles and TiO_2 as a function of the pH is shown in Fig. 1. All the curves had an extended S shape, and the zeta-potentials were largely dependent on the pH.

The latex particles had an isoelectric point (IEP) at pH 4.5. They were positively charged below IEP, while they were negatively charged above it. This variation in the zeta-potential of the latex particles with the change in the pH of the solution is attributable to DMLL molecules adsorbing onto the surface of the latex particles.

TiO_2 had a positive charge below pH 8.5, and its zeta-potential became negative with an increase in the pH. TiO_2 had an isoelectric point at pH 8.5.[12]

The Mixed System of Polystyrene Latex and TiO_2. The change in the turbidity of the mixed suspension with the particle number (N) of the latices at a constant pH (3.0, 5.0, 11.0) is shown in Fig. 2. Here, the amount of TiO_2 added was 10.0 mg. In this figure, a high turbidity means a good titania dispersion and a low one for flocculation. On the measurement of the turbidity, TiO_2 particles were clearly detected, but hardly any latex particles were detected.

At pH 3.0, the turbidity even slightly increased upon the addition of a number of the latex particles, indicating that the mixture of TiO_2 and the latex particles is well-dispersed throughout the range of the number of latex particles (N). At pH 11.0, since the turbidity was constant throughout the range of N values, the mixed suspension was also well-dispersed.

Figure 3 shows the zeta-potentials of TiO_2 particles in the mixed suspension as a function of the N. At pH 2.5 and 3.0, Zp was constantly positive. At pH 10.0 and 11.0, Zp was constantly negative. Since the latex particles and TiO_2 particles are both positively charged below pH 4.5, the good dispersion of their mixed suspension occurs by means of the positive mutual electric repulsion between hetero particles.[13-15] Similarly, above pH 8.5 it is understood that the mixtures are well-dispersed as a result of the mutual electric repulsion between these negatively charged particles.

At pH 5.0, as may be found from Fig. 2, at a low concentration of the latex particles the mixed suspensions are in the dispersed state, but with an increase in the number of latices they are heterocoagulated until they redisperse at a high concentration of the latex particles. At this pH, the polystyrene latex particles have a negative charge, while TiO_2 particles are positively charged.

In order to evaluate in more detail the interaction between the latex and TiO_2 with a different charge, the changes in the turbidity of the mixed suspension with N were measured at the constant pH values of 5.0, 6.0, and 7.0: These results are also shown in Fig. 2. At these pH values (pH 5.0, 6.0, and 7.0), the flocculation and the redispersion of the mixed suspensions were also observed. In the pH range of 4.5—8.5, the mixed aqueous suspensions of the latex particles and pigment particles were composed of a loose three-dimensional network structure. It may be found from Fig. 3 that the particle number of the latex at which the flocculation occurs shifts toward lower numbers of latex particles (N) with an increase in the pH.

The changes in the zeta-potential of the mixed suspension at a constant pH (5.0, 6.0, 7.0) with log N are shown in Fig. 4. The zeta-potential of TiO_2 altered from positive to negative with the increase in N and showed a zero point of charge. The particle number of the latex (N) at the zero point of the charge shifted toward a lower N with an increase in the pH. It was confirmed that the particle number of the latex at the zero point of charge was in good agreement with that at the flocculation of the mixed suspension.

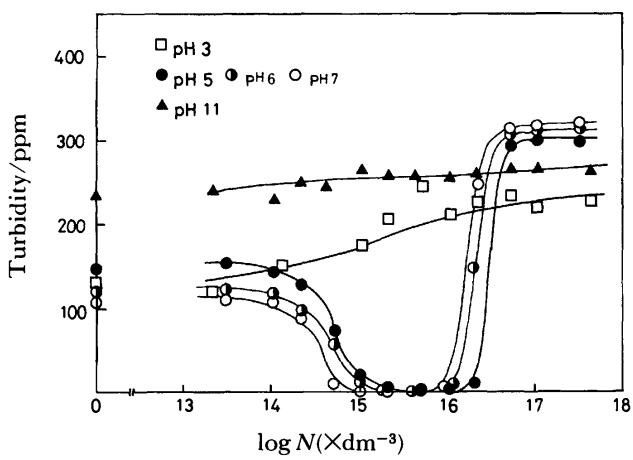

Fig. 2. The change in turbidities of mixed suspensions of latex particles and TiO_2 particles with number of latex particles added at various pH.

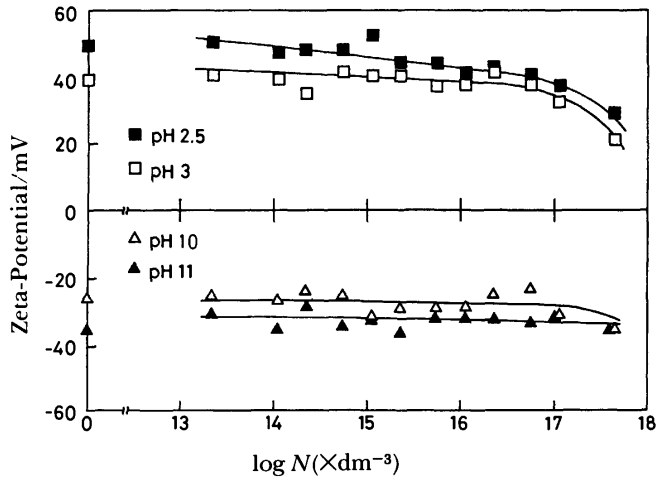

Fig. 3 The change in zeta-potentials of mixed suspension with number of latex particles added at pH 2.5, 3.0, 10.0, 11.0.

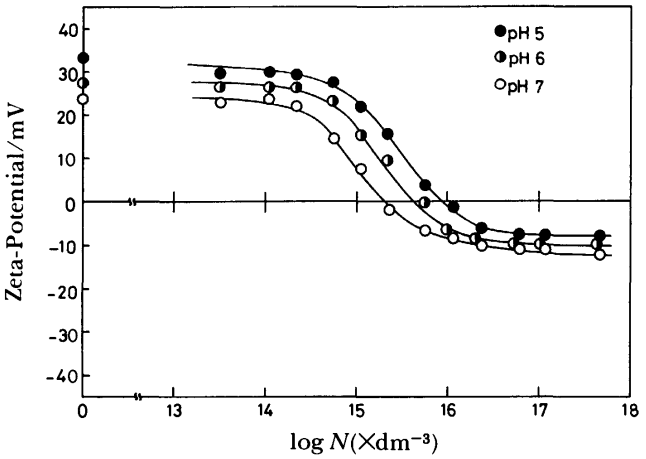

Fig. 4. The change in zeta-potentials of mixed suspensions with number of latex particles added at pH 5.0, 6.0, 7.0.

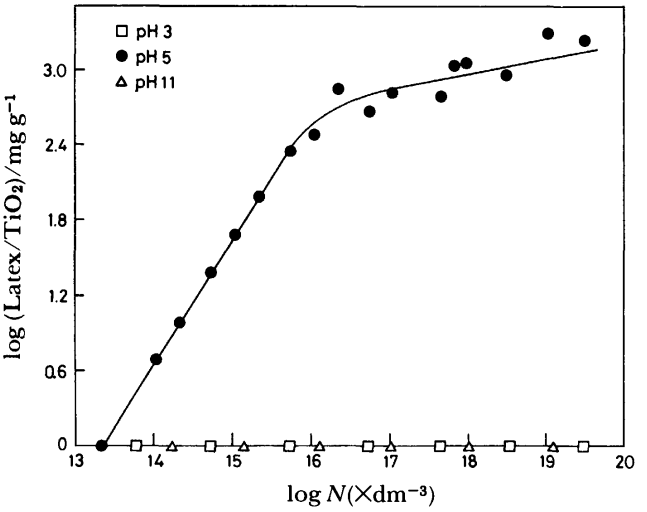

Fig. 5. The amount of latices adsorbed on surface of TiO_2 particles at various pH of suspended solution at 25 °C.

Figure 5 shows the amount of latices adsorbed onto the surface of TiO_2 particles. At pH 3 and 11 of the mixed suspended solutions, hardly any latex particles adsorbed onto TiO_2. This was because of the electric repulsion between the latex particles and the TiO_2 particles. On the other hand, at pH 5 the amounts of latices adsorbed increased in proportion to the number of latex particles added until they were approximately constant. These results indicate that the latex particles surely adsorb onto the surface of TiO_2 particles in the range of the opposite charge between these particles.

Accordingly, the flocculation and the redispersion phenomena in the mixed suspension can be explained by the adsorption of the latex particles onto the TiO_2 particles. A model for the mechanism of these phenomena is shown in Fig. 6:

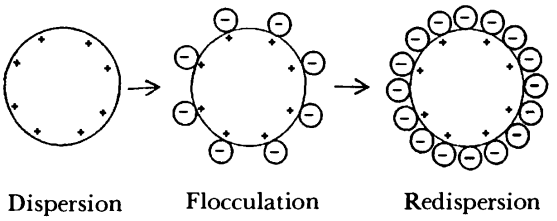

Fig. 6. A model for mechanism of flocculation and redispersion.

(a) At the initial state, without the addition of any latex, TiO_2 particles disperse in the aqueous solution because of the electric repulsion of their own surface's negative charge.

(b) With an increase in the number of the latex particles which have a negative charge, the latex particles are adsorbing on the TiO_2 particles which have a positive charge, and the zeta-potential of the TiO_2 particles covered with latex particles alters from positive to zero. As a result, the flocculation of the mixed suspension occurs at a point of zero charge of the mixed suspension, a result mainly of the electric force of attraction. The results are also supported by the good agreement between the number of latex particles (N) at flocculation (shown in Fig. 2) and that at the point of zero charge of the mixed suspension (shown in Fig. 4).

(c) At a high concentration of the latex particles, as more of the latex particles adsorb on TiO_2, the mixed suspension redisperses, a result of the electric repulsion among latices which have a negative charge. As a result, the TiO_2 particles have a negative charge in the redispersed state. These results are supported by the agreement between the values of the zeta-potential of the single latex and that of the zeta-potential of TiO_2 in the redispersed state (pH 5.0, 6.0, and 7.0).

Furthermore, with an increase in the pH from 5 to 7, since the negative charge of the latex particles increases and the positive charge of TiO_2 particles decreases, the particle number of the latex (N) required for the flocculation of the TiO_2 particles is shifted to a low concentration with the pH.

References

1) H. J. Leugering, *J. Oil Col. Chem. Assoc.*, **47**, 208 (1968).

2) A. Bleier and E. Matijević, *J. Colloid Interface Sci.*, **55**, 510 (1976).

3) H. Sasaki, E. Matijević, and E. Barouch, *J. Colloid Interface Sci.*, **76**, 319 (1980).

4) F. K. Hansen and E. Matijević, *J. Chem. Soc., Faraday Trans. 1*, **76**, 1240 (1980).

5) H. Tamai, Y. Nagai, and T. Suzawa, *J. Colloid Interface Sci.*, **91**, 464 (1983).

6) Serge N. Timasheff, *J. Colloid Interface Sci.*, **21**, 489

(1966).
7) E. Matijević and Y. Kitazawa, *Colloid Polymer Sci.*, **261**, 527 (1983).
8) K. Kato, H. Kondo, K. Yokota, K. Esumi, and K. Meguro, *J. Appl. Polym. Sci.*, in press.
9) K. Tsujii, *Yukagaku*, **29**, 562 (1980).
10) K. Tori and T. Nakagawa, *Kolloid-Z, Z. Polymere*, **187**, 44 (1963).
11) H. Hidaka, Y. Kawajiri, and S. Noro, *Yukagaku*, **28**, 190 (1979).
12) P. Somasundaran and D. W. Fuerstenau, *J. Phys. Chem.*, **70**, 90 (1965).
13) R. Derek Harding, *J. Colloid Interface Sci.*, **40**, 165 (1971).
14) G. R. Wiese and T. W. Healy, *J. Colloid Interface Sci.*, **52**, 458 (1975).
15) G. R. Wiese and T. W. Healy, *J. Colloid Interface Sci.*, **51**, 428 (1975).

 © 1987 The Chemical Society of Japan Bull. Chem. Soc. Jpn., 60, 3385—3390 (1987)

A Stopped-Flow Kinetic Study on the Binding of Phenylbutazone to Human Serum Albumin Using Absorption and Circular Dichroism Techniques

Kiyofumi MURAKAMI, Yasuo FUJISAKI, and Takayuki SANO*,†
Department of Chemistry, Faculty of Science, Yamaguchi University, Yoshida 1677-1, Yamaguchi 753
†Department of Materials Science, Faculty of Science, Hiroshima University, Higashisenda-Machi, Hiroshima 730
(Received April 3, 1987)

The mechanism of the binding of phenylbutazone(4-butyl-1,2-diphenyl-3,5-pyrazolidinedione) to human serum albumin has been investigated by kinetic experiments using both optical absorption and circular dichroism (CD) stopped-flow methods. Three distinct processes were found to exist by the absorption technique; one of these was within the dead time of the apparatus and other two slow processes were at around 10^{-2} and 1 s, of which the relaxation times were determined. On the other hand, only two processes, which correspond in time range to the first and third processes seen by optical absorption, were found using CD technique. By examining the concentration dependence of the reciprocal relaxation time of each process and by taking account of the binding isotherm, a binding mechanism has been proposed. According to the elucidated reaction scheme, successive binding of two molecules of phenylbutazone is followed by a conformational change which destabilizes one of the bound species. The detailed nature is discussed in the light of the circular dichroism change of each process.

The anti-inflammatry agent phenylbutazone has a high affinity for albumin, and is present predominantly in the bound state in serum.[1] Therefore, the binding of phenylbutazone to albumin plays an important role in the activity, metabolism and excretion of this agent in the body. In connection with these physiological significances, the binding characteristics have been investigated by many static methods such as equilibrium dialysis,[2] spectrophotometric titration,[3] fluorescence titration,[3,4] circular dichroism (CD) titration,[2,5] and spin labeling.[6] From these studies, it has been suggested that hydrophobic interactions play an important role in the binding of phenylbutazone to albumin. Furthermore, from the view point of pharmacology, competitive or cooperative binding of phenylbutazone, fatty acids and other drugs with albumin have also been studied.[7-9]

In contrast to the large amount of static information available, there has been no kinetic study on phenylbutazone binding to albumin, which is necessary in order to gain a profound understanding of these interesting phenomena.

In the present study, the binding mechanism between phenylbutazone and human serum albumin was investigated by the stopped-flow method using absorption as well as CD detection in order to obtain a detailed picture of the binding mechanism from different optical properties.

Experimental

Materials. Human serum albumin (HSA, essentially fatty acid free: less than 0.005%) was purchased from Sigma Chemical Company, and used without further purification. The molar concentration of the protein was determined by spectrophotometrically[10] Phenylbutazone(4-butyl-1,2-diphenyl-3,5-pyrazolidinedione) was also purchased from Sigma Chemical Company. A stock solution was prepared by dissolving the agent in a small quantity of 0.1 M†† NaOH solution, and then mixing with a 0.1 M phosphate buffer of pH=7.4. The concentration of phenylbutazone was determined using the molar extinction coefficient $\varepsilon_{267}=2.0\times10^4\ \mathrm{cm^{-1}\,M^{-1}}$.[3] The concentration of HSA was 3×10^{-5} M for all measurements. (In the stopped flow experiments, this concentration corresponds to the final one).

Equilibrium Dialysis. An Oxford type dialysis cell made of acryl resin was used. The volume of each compartment was 4.5 ml and it was separated by a semipermeable cellulose membrane, purchased from Visking Company. The contact area was 9.6 $\mathrm{cm^2}$. One compartment was filled with HSA solution, and the other with phenylbutazone solution. The cell was continuously rotated at 15 rpm in thermostated water at 20 °C. After 36 h, the concentration of the phenylbutazone solution was measured spectrophotometrically.

Apparatus. The absorption and CD spectra were measured with a spectrophotometer (Union Giken SM 401) and a dichrograph (Jobin-Yvon Mark III-J), respectively. The kinetic measurements were carried out using a stopped-flow apparatus (Union Giken RA 401 and RA 1100) of which dead time is 3 ms. The CD detection in the stopped experiments has been performed by combining the stopped flow apparatus with the CD spectrometer.[11] All the measurements were carried out at 20±1.2 °C.

Results and Discussion

Kinetic Data. The binding of phenylbutazone to HSA generates positive change in absorbance and CD around 285 nm;[2,5] which are, respectively, considered to be due to hydrophobic environment around phenyl

†† 1 M=1 mol $\mathrm{dm^{-3}}$.

rings of phenylbutazone at the binding site[2] and perturbation of the carbonyl chromophore of the drug by an asymmetrical locus at the site.[2,5] The present measurements were performed at 285 nm and results were similar to those in literature.[2,5]

Two distinct reaction processes were observed by optical absorption detection; typical time courses of them are shown in Fig. 1. By comparing the magnitude of the corresponding absorbance change after the dead time with that found under static conditions, another very rapid process was found to be exist within the dead time of the apparatus. In all, three phases of the kinetic processes were accompanied by a decrease in transmittance. These processes were named, in increasing order of relaxation time (τ), as the first (unobserved one within the dead time; $\tau_1<3$ ms), the second ($\tau_2\approx10$ ms) and the third ($\tau_3\approx1$ s) process. In the case of CD detection, however, only one process with a negative CD change was observed (Fig. 2). This process corresponds in time to the third one observed by absorption detection. But no relaxation corresponding to the second process was observed even by accumulating 1000 sets of data. Instead, another very rapid process with a "large positive" CD change was found to exist also within the dead time by the similar method as in the absorption detection experiments. From these observations, it can be seen that in the absorbtion detection, three kinetic processes comparably contribute to the static absorption change, but in the CD detection the unobservable first process within the dead time of apparatus dominates the static CD

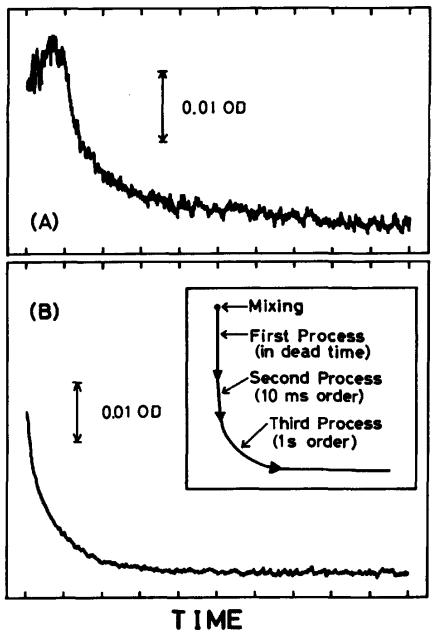

Fig. 1. Typical traces of the transmittance change at 285 nm after the mixing of phenylbutazone (1.5×10^{-5} M) and HSA (6×10^{-5} M). (A) 40 ms/div., (B) 4 s/div. The insert shows a schematic illustration of the relative scale of the transmittance change due to each process.

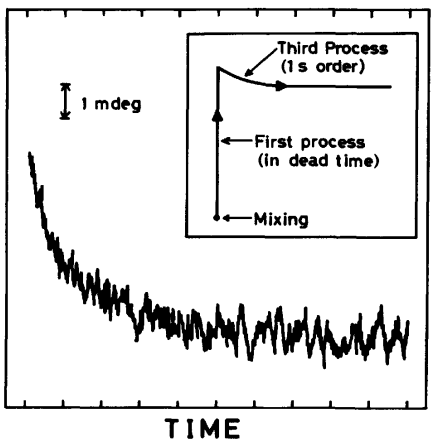

Fig. 2. A typical trace of the CD change at 285 nm after the mixing of phenylbutazone (1.5×10^{-5} M) and HSA (6×10^{-5} M). The horizontal scale is 4 s/div. The data was obtained by averaging over 40 experiments. The insert represents a schematic illustration of the relative CD change due to each process.

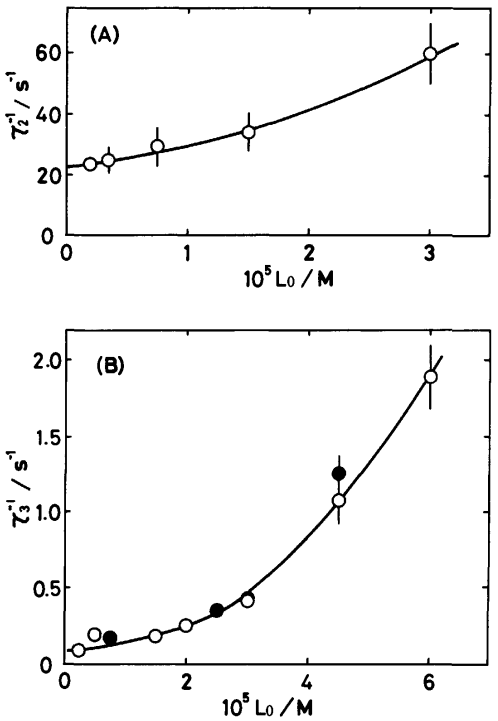

Fig. 3. The total ligand concentration (L_0) dependence of the reciprocal relaxation times of the second and third processes. (A) The second process, and (B) the third processes. (○): Determined from the change in transmittance, (●): determined from the change in CD. The solid lines are drawn to emphasize the tendencies.

change. The inserts in Figs. 1 and 2 show schematic illustrations of the relative size of the transmittance and CD changes due to these processes. The ligand concentration dependence of τ for the second and third processes is shown in Fig. 3. As can be seen in Fig. 3(B), the relaxation times of the third process obtained by the absorption and CD measurements agree well with each other.

The Binding Isotherm. A plot of $\nu/[L]$ versus ν, according to the conventional Scatchard equation; $\nu/[L]=K(n-\nu)$ where ν is the moles of ligand bound per mole of macromolecule, [L] the concentration of free ligand, K the binding constant and n the number of binding site, provides information about binding ability of the macromolecules.[12] A Scatchard plot for the present system was curved (Fig. 4), indicating that there are at least two kinds of binding site. On the conventional assumption that these binding sites are independent of each other and have an integral number of binding sites, a least squares fit analysis according to next equation; $\nu/[L]=\sum K_i(n_i-\nu_i)$ yields the binding parameters: $n_1=1$, $K_1=1.7\times10^6\ M^{-1}$, $n_2=3$, and $K_2=2.0\times10^4\ M^{-1}$, where the subscripts 1 and 2 refer to the primary and secondary binding sites. The values of the binding parameters given in the literature[2-4] differ from each other depending on the method and conditions used to obtain them. The present results are compatible with those obtained by Chignell and Starkweather[2] except for a somewhat larger value of K_1 for the present case, which is probably due to a difference in temperature and/or fatty acid content of the sample.

Analyses of the Kinetic Data. (i) The First and Second Processes: In the analyses of the stopped flow data, each kinetic process must be analyzed in increasing order of time range of the observed process because the law of mass conservation is hold at each step. Here, the second process will be analyzed taking into consideration the unobserved first process in the dead time of apparatus. For the present analysis, considering the existence of at least two kinds of binding site as suggested from the Scatchard plot, analyses were limited to models which involve more than one binding step. The following three models were examined,

$$\text{Model 1:}\quad \mathrm{L + P} \underset{\text{first}}{\overset{K_1}{\rightleftharpoons}} \mathrm{C_1} \underset{k_{-2}\ \text{second}}{\overset{K_2\ k_2}{\rightleftharpoons}} \mathrm{C_2} \qquad (1)$$

$$\mathrm{L + P'} \underset{\text{first}}{\overset{K_1'}{\rightleftharpoons}} \mathrm{C_1'}$$

where L, P, and $C_i(i=1,2)$ denote free ligand, free primary binding site and complex species, respectively, and K_i, k_i and k_{-i} are the equilibrium constant, the forward and backward rate constant of the i-th step, respectively, and superscript "′" denotes the reaction on the secondary binding site of HSA. This mechanism implies the fast competitive binding of phenylbutazone to the primary and secondary sites as the first process within the dead time of apparatus and the conformational change of the complex on the primary site as the second process. Further, this model satisfies the independency of binding sites adopted in the conventional analysis of binding isotherm.

$$\text{Model 2:}\quad \mathrm{L + P} \underset{\text{first}}{\overset{K_1}{\rightleftharpoons}} \mathrm{C_1} \underset{k_{-2}\ \text{second}}{\overset{K_2\ k_2}{\rightleftharpoons}} \mathrm{C_2} \overset{\mathrm{L}\ K_3}{\longrightarrow}_{\text{very fast}} \mathrm{C_3} \qquad (2)$$

This is a cooperative binding mechanism in which a conformational change of the first complex induces a new binding site for phenylbutazone. The third step of above scheme is not observable because of the very fast establishment of its equilibrium.

$$\text{Model 3:}\quad \mathrm{L + P} \underset{\text{first}}{\overset{K_1}{\rightleftharpoons}} \mathrm{C_1} \overset{\mathrm{L}\ K_2\ k_2}{\rightleftharpoons}_{k_{-2}\ \text{second}} \mathrm{C_2} \qquad (3)$$

This is also a cooperative binding mechanism, but without any step of conformational change. In each of Eqs. 1—3, the second step is regarded as the observed second process. Of these models, the former two models (Model 1 and Model 2) gave the minus value for the rate constant k_{-2}, and only Model 3 was found to give acceptable results. Under the condition of rapid formation of C_1, reciprocal relaxation time of the second step in Eq. 3 can be expressed by

$$\tau_2^{-1} = k_2\frac{K_1[L]([L]+4[P]+K_1[L][P])}{1+K_1([L]+[P])} + k_{-2} \qquad (4)$$

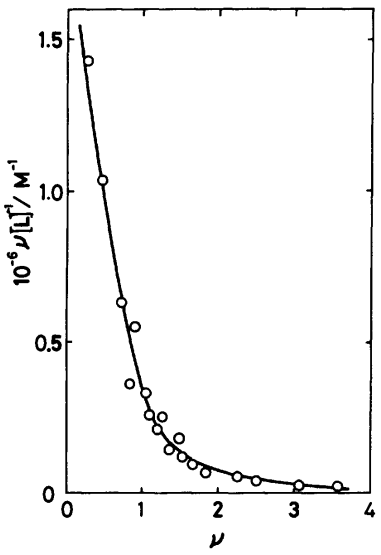

Fig. 4. The binding isotherm obtained from the equilibrium dialysis(O) and its comparison with that reconstructed from the values of the parameters associated with Model 7 (——) (see text).

where [L] and [P] are the concentration of free ligand and free binding site, respectively. This equation shows linear dependence of τ_2^{-1} on $\{K_1[L]([L]+4[P]+K_1[L][P])\}/\{1+K_1([L]+[P])\}$. [L] and [P] can be calculated by assuming values for K_1 and K_2. The plot of τ_2^{-1} versus the concentration term in Eq. 4 provides k_2 and k_{-2} as the slope and the intercept, respectively. With the guidance of linearity of the plot and self-consistent relation between parameters, the model was examined for many different values of K_1 and K_2. Figure 5 shows the plot for $K_1=(1.2\pm0.4)\times10^6\ M^{-1}$, and $K_2=(1.8\pm0.6)\times10^5\ M^{-1}$. The rate constants were determined as $k_2=(4.3\pm1.1)\times10^6\ M^{-1}$ and $k_{-2}=(23\pm6)\ s^{-1}$. The high degree of linearity suggests that Model 3 may be applied to the first and second processes. The fact that Model 1 could not satisfied the kinetic data, gives rise to question on the conventional assumption of independency of binding site which has been adopted in the binding isotherm analysis.

(ii) The Third Process: For the third process, the following models incorporated with the above Model 3 satisfing the first and second processes were examined.

Model 4:

$$L + P \underset{}{\overset{K_1}{\rightleftharpoons}} C_1 \overset{L,\ K_2}{\rightleftharpoons} C_2 \underset{k_{-3}}{\overset{K_3,\ k_3}{\rightleftharpoons}} C_3 \quad (5)$$

first second third

Model 5:

$$L + P \underset{}{\overset{K_1}{\rightleftharpoons}} C_1 \overset{L,\ K_2}{\rightleftharpoons} C_2 \overset{L,\ K_3}{\underset{k_{-3}}{\rightleftharpoons}} C_3 \quad (6)$$

first second third

Model 6:

$$L + P \overset{K_1}{\rightleftharpoons} C_1 \overset{L,\ K_2}{\rightleftharpoons} C_2 \underset{k_{-3}}{\overset{K_3,\ k_3}{\rightleftharpoons}} C_3 \overset{L,\ K_4}{\rightleftharpoons} C_4 \quad (7)$$

first second third very fast

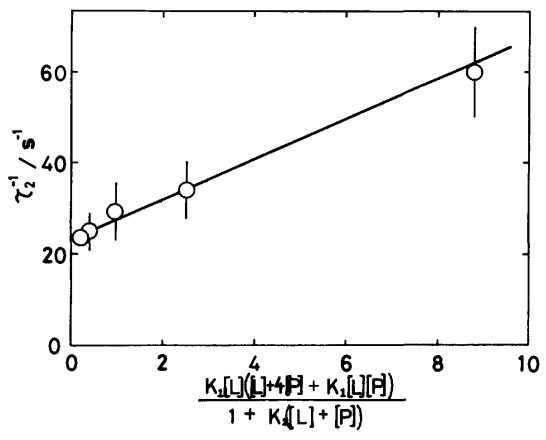

Fig. 5. Plot of τ_2^{-1} versus $K_1[L]([L]+4[P]+K_1[L][P])/(1+K_1([L]+[P]))$ for Model 3. The values on the horizontal axis were calculated using the values of the parameters cited in the text.

Model 7:

$$L + P \overset{K_1}{\rightleftharpoons} C_1 \overset{L,\ K_2}{\rightleftharpoons} C_2 \overset{K_3,\ k_3}{\underset{k_{-3}}{\rightleftharpoons}} C_3 \overset{L,\ K_4}{\rightleftharpoons} C_4 \quad (8)$$

first second third very fast

In these models, the each of third steps implies i) a conformational change of the second complex C_2 (Model 4), ii) further ligand binding to the complex C_2 (Model 5), iii) a conformational change of the complex C_2 which induces further ligand binding (Model 6), and iv) a conformational change of C_2 by which a ligand is released from the complex (Model 7). Using the values of K_1 and K_2 determined from the analysis of the second process, for each model, the concentration dependence of the reciprocal relaxation time of the third process τ_3^{-1} was examined using many sets of values of K_3 and K_4. Of these models, the first three failed from the view points of (i) the linear relationship between the observed τ_3^{-1} and the concentration dependent factor in its theoretical expression and (ii) the self-consistent relationship between the parameters. Finally, it was found that Model 7 is the only possible model for the present system. If the forth binding process in the model is very rapid, the reciprocal relaxation time for the third step in Model 7 can be expressed as

$$\tau_3^{-1} = k_3E + k_{-3}F = k_{-3}(K_3E+F) \quad (9)$$

where

$$E = (K_1K_2[L](1+K_4[L](1+K_4[L](2+K_1[L]))([L]+4[P]+K_1[L][P])+K_1K_2[L]^2(1+K_1([L]+[P])+K_1K_2K_3[L][P](2+K_1[L]))/((1+K_1[L])((1+K_4([L]+[P])+K_1K_2[L]([L]+4[P]+K_1[L][P]))+K_1K_2K_3[L][P](1+K_1[L]+K_1K_2[L]^2)),$$

$$F = (K_4[L](1+K_1([L]+[P])+K_1K_2[L]([L]+4[P]+K_1[L][P]))+K_1K_2K_3[L][P](K_1K_2[L]^2-1))/((1+K_4[L])(1+K_4[L])(1+K_1+K_1([L]+[P])+K_1K_2[L]([L]+4[P]+K_1[L][P]))+K_1K_2K_3[L][P](1+K_1[L]+K_1K_2[L]^2)).$$

Here, K_4 is defined as the association constant: $K_4=[C_3]/[L]\cdot[C_4]$. Equation 9 shows that a plot of τ_3^{-1} versus K_3E+F must be a straight line which goes through the origin, the slope of which provides the value of k_{-3}.[13] Since the linear dependency has been satisfied for some set of K_3 and K_4, all the parameters are determined so as to satisfy both the kinetic and static experimental data. The results are shown in Figs. 4 and 6. These figures demonstrate that Model 7 is full expression applicable to the present system from a kinetic and static point of view. The values of the parameters were evaluated as $K_3=(1.3\pm0.4)$, $k_3=(4.3\pm1.3)\ s^{-1}$, $k_{-3}=(14\pm4)\ s^{-1}$, and $K_4=(1.0\pm0.3)\times10^5\ M^{-1}$. These values and those associated with the

Table 1. Equilibrium and Rate Constants for Model 7

K_1 / $10^6\ M^{-1}$	K_2 / $10^5\ M^{-1}$	k_2 / $10^6\ M^{-1}\ s^{-1}$	k_{-2} / s^{-1}	K_3	k_3 / s^{-1}	k_{-3} / s^{-1}	K_4 / $10^5\ M^{-1}$
1.2±0.4	1.8±0.5	4.3±1.3	23±6	0.3±0.1	4.3±1.3	14±4	1.0±0.3

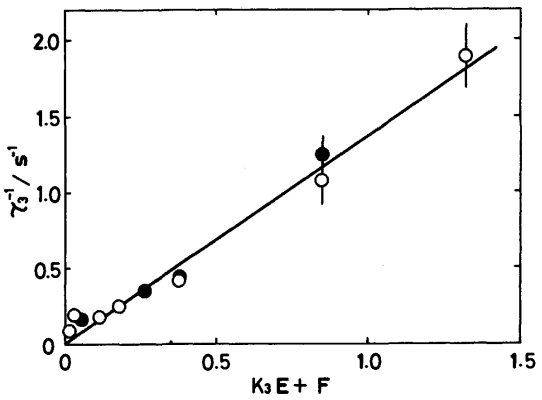

Fig. 6. Plot of τ_3^{-1} versus K_3E+F in Eq. 9 calculated using the values of the prameters cited in the text.

faster processes are summarized in Table 1. From the persent analysis of the kinetic data as well as the static one, it was clarified that the binding of phenylbutazone to HSA is cooperative binding but not the isolated binding which has been reported so far on the basis of only the static experiments.

The Binding Mechanism. From the location of the ellipticity band (287 nm), the CD change for the present system has been interpreted by asymmetrically perturbed carbonyl chromophore of phenylbutazone at the binding site.[2,5] The large positive CD change associated with the first process suggests that phenylbutazone in C_1 is already in highly asymmetrical enviroment. The binding of the secondary ligand to C_1 without any distinct conformational change suggests that the primarily bound phenylbutazone together with its environment may form a site advantageous for the secondary binding. The failure to detect any CD change associated with the second process seems to show that the secondarily bound phenylbutazone exists in a symmetrical environment. The complex C_2 thus formed, then, is converted into C_3 by rearranging of the bound ligands showing small negative CD change and thereby destabilizing one of the two bound states.

In general, and extrinsic Cotton effect reflects the state of an asymmetrically perturbed chromophore. Particularly, a close and rigid contact with an asymmetric center, which exerts an electrostatic force on the chromophore, is effective.[2,14] For the present system, the complex, C_1, which has a predominant contribution to the static CD change, may be formed by such an electrostatic interaction as well as a hydrophobic interaction.[2,3] The relatively large value of K_1 ($1.2\times10^6\ M^{-1}$) could be realized by such a dual nature of interaction.

In recent years, the extrinsic Cotton effect has frequently been used in studies of ligand binding properties of albumin.[16-22] Sometimes, a binding isotherm constructed from the CD data has been compared with that obtained from other methods.[20,21] In some cases, a relatively good agreement has been obtained through the crude assumption that all bound species give the same Cotton effect. At other times, drug interactions with albumin molecule have also been investigated using the extrinsic Cotton effect.[17,21] However, as shown by the present study as well as the kinetic studies which have been performed previously[15,23-27], the mechanism of binding between albumin and ligand is not simple but complicated involving several conformational changes. Hence, it should be noted that a deep understanding of the mechanism of complex phenomena such as drug interactions with albumin is difficult without intensive works. In this connection, kinetic studies like the present one may provide important information. Especially, the use of CD may be informative about the bound states of ligands.

The authors wish to express their thanks to Professor Tatsuya Yasunaga of Kinki University for his helpful discussions. This work was partly supported by Grant-in-Aid for Science Research (No. 6078029) from the Ministry of Education, Science and Culture.

References

1) E. M. Sellers and J. Koch-Weser, "Clinical Implication of Drug-Alubumin Interaction," in "Albumin Structure Function and Uses," ed by V. M. Rosenoer, M. Oratz, and M. A. Rothshild, Pergamon Press, New York (1977), pp. 159—182.

2) C. F. Chignell, *Mol. Pharmacol.*, **5**, 244 (1969); C. F. Chignell and D. K. Starkweather, *Pharmacology*, **5**, 235 (1971).

3) V. Maes, J. Hoebeke, A. Vercreuysse, and L. Kanarek, *Mol. Pharmacol.*, **16**, 147 (1979).

4) J. C. Galleyrand, M. Vie, and R. Margnan, *Trav. Soc. Pharm. Montpellier*, **38**, 357 (1978).

5) A. Rosen, *Biochem. Pharmacol.*, **19**, 2075 (1970).

6) J. Blanchard, T. N. Tozer, D. L. Sorby, and L. Dallastuck, *J. Pharm. Sci.*, **62**, 1545 (1973).

7) H. M. Solomon, J. J. Schrogie, and D. Williams, *Biochem. Pharmacol.*, **17**, 143 (1968).

8) E. G. Rippie, *Biochem. Pharmacol.*, **30**, 1169 (1981).
9) B. W. Madesen and G. M. Ellis, *Biochem. Pharmacol.*, **30**, 1169 (1981).
10) P. Clark, M. R. Rachinsky, and L. F. Foster, *J. Biol. Chem.*, **237**, 2509 (1962); F. B. Edwards, R. B. Rombauer, and B. J. Campbell, *Biochem. Biophys. Acta.*, **194**, 234 (1969).
11) K. Murakami, T. Sano, N. Kure, K. Ishii, and T. Yasunaga, *Biopolymers*, **22**, 2035 (1983).
12) G. Scatchard, *Ann. N. Y. Acad. Sci.*, **51**, 660 (1949).
13) The derivation of Eqs. 4 and 9 can be referred to monographs on the fast reaction kinetics. e.g.; F. C. Bernasconi, "Relaxation Kinetics," Academic Press, New York (1976).
14) J. A. Schellman, *J. Chem. Phys.*, **44**, 55 (1966).
15) N. Riethrock and A. Lassman, *Naunyn-Schmiedeberg's Arch. Pharmacol.*, **313**, 269 (1980).
16) J. H. Perrin, *J. Pharmacol.*, **25**, 208 (1973).
17) R. Brodersen, *J. Biol. Chem.*, **252**, 5067 (1977).
18) Y. Y. Thomas Su and B. Jirgensons, *Biochem, Pharmacol.*, **27**, 1043 (1978).
19) W. Mueller and U. Wollert, *Naunyn-Schmiedeberg's Arch. Pharmacol.*, **278**, 301 (1973).
20) W. Mueller and U. Wollert, *Naunyn-Schmiedeberg's Arch. Pharmacol.*, **283**, 67 (1974).
21) W. Mueller and U. Wollert, *Biochem. Pharmacol.*, **25**, 147 (1976).
22) T. Sjoedin, N. Rooddorp, and I. Sjoehokm, *Biochem. Pharmacol.*, **25**, 2131 (1976).
23) W. Scheider, *Proc. Natl. Acad. Sci. USA*, **76**, 2283 (1979).
24) P. A. Adams and M. C. Berman, *Biochem. J.*, **191**, 95 (1980).
25) T. Faerch and J. Jacobsen, *Arch. Biochem. Biophys.*, **184**, 282 (1977).
26) K. Murakami, T. Sano, and T. Yasunaga, *Bull. Chem. Soc. Jpn.*, **54**, 862 (1981).
27) K. Murakami, T. Sano, A. Tsuchie, and T. Yasunaga, *Biophys. Chem.*, **21**, 127 (1985).

 © 1987 The Chemical Society of Japan Bull. Chem. Soc. Jpn., 60, 3391—3395 (1987)

Peroxy Acid Oxidations. I. A Kinetic and Mechanistic Study of Oxidation of Acetylacetone by Peroxomonophosphoric Acid and Hydrogen Peroxide in Alkaline Medium

Chakrapani P. PATNAIK, Surendra Nath MOHAPATRO, Akhil Krishna PANIGRAHI, and Radhasyam S. PANDA*
Department of Chemistry, Khallikote College, Berhampur 760 001, Orissa, India
(Received December 17, 1985)

The kinetics of oxidation of acetylacetone by peroxomonophosphoric acid and hydrogen peroxide have been investigated in the pH range 8—13.7. The oxidations by peroxomonophosphoric acid at 308 K and I= 0.6 mol dm^{-3} follow the rate expressions,

$$\text{(i)}\quad -\frac{d[PMPA]_T}{dt} = \{k_1[A]+k_2[A^-]\}[HPO_5^{2-}]$$

in the pH range 8—10.63, where k_1=1.96 dm^3 mol^{-1} s^{-1} and k_2=0.177 dm^3 mol^{-1} s^{-1}, and

$$\text{(ii)}\quad -\frac{d[PMPA]_T}{dt} = \{k_3[A]+k_4[A^-]\}[HPO_5^{2-}]+\{k_5[A]+k_6[A^-]\}[PO_5^{3-}]$$

in the pH range 11.5—13.7, where k_3=30.4 dm^3 mol^{-1} s^{-1} and $k_6\approx 0$. The rate law for hydrogen peroxide oxidations in the pH range 9.2—13 at 308 K and I=0.1 mol dm^{-3} is given by,

$$-\frac{d[\text{Hydrogen peroxide}]_T}{dt} = \{k_7[A]+k_8[A^-]\}[H_2O_2]+\{k_9[A]+k_{10}[A^-]\}[HO_2^-]$$

the k_7 and k_{10} values being 0.393 dm^3 mol^{-1} s^{-1} and 0.143×10^{-2} dm^3 mol^{-1} s^{-1} respectively. A and A$^-$ represent the diketo and enol form of acetylacetone respectively. The kinetic data and activation parameters are consistent with nucleophilic attack by peroxo species on both diketo and enol form of acetylacetone followed by oxygen-oxygen bond fission.

Studies[1-4] on oxidation of β-diketones by various peroxy compounds, e.g. peroxy acetic acid, peroxy benzoic acid and diperoxy phthalic acid have shown that enolizable β-dicarbonyl compound first reacted with the peroxy acid forming α-hydroxy diketone which on further reaction with peroxy acid or on hydrolytic cleavage afforded the observed products. Epoxidation of the enol form of the diketone was considered to be the reasonable path for the formation of hydroxy ketone.

Payne examined[5] oxidation of a series of β-diketones with hydrogen peroxide in t-butyl alcohol in presence of a mineral acid catalyst and reported that the reaction involved the formation of an intermediate cyclic peroxide which underwent acid-catalyzed decomposition to yield products.

The oxidation of β-diketones ($R^1CO\cdot CR^2R^3COR^4$) with alkaline hydrogen peroxide[6] afforded two types of carboxylic acids depending upon the nature of R^2 and R^3. The unsubstituted β-diketone (in which both R^2 and R^3 are H) suffered an oxidative cleavage producing formic acid (from the central carbon atom) and the acid corresponding to the acyl group involved. The 2-monosubstituted 1,3-diketones underwent two types of reactions (i) an oxidative rearrangement involving migration of R^1 or R^4 from C_1 or C_3 to C_2, yielding the corresponding carboxylic acids, and (ii) an oxidative cleavage similar to that suffered by the unsubstituted β-diketones. The 2,2-disubstituted 1,3-diketones underwent only oxidative rearrangement. The oxidation mechanisms have been discussed on the basis of product studies.

The present study concerns with the kinetics and mechanism of oxidation of acetylacetone by peroxomonophosphoric acid (PMPA) and by hydrogen peroxide in aqueous alkaline medium. The oxidations have been studied in the pH range 8—14 and the reactivities of various peroxo species are discussed.

Experimental

All the chemicals used were of reagent grade or of certified purity. Doubly distilled water was used in preparing solutions. Acetylacetone was distilled just before use and the fractions distilling at 139—140 °C were collected rejecting the large head and tail portions. Peroxomonophosphoric acid was prepared[7-10] by the acid hydrolysis of potassium peroxodiphosphate. For each experiment, PMPA was prepared afresh with care so that further hydrolysis of PMPA to hydrogen peroxide was suppressed. Perchloric acid (Baker analyzed, 70%), used for hydrolysis, was neutralized by addition of requisite amount of carbonate-free sodium hydroxide. The ionic strength of the medium was maintained with sodium perchlorate which was prepared in situ in the oxidation flask by neutralizing $HClO_4$ with NaOH. The pH of the solution, adjusted with standard buffers or carbonate-free NaOH, was determined using a Systronics digital pH meter Model 335. Reactions were followed by measuring the rate of disappearance of PMPA which was estimated by iodometry at pH 4—5 with a drop of ammonium molybdate solution. In case of hydrogen peroxide oxidations, the kinetics was followed by

measuring the rate of disappearance of H_2O_2 by the usual iodometric procedure.[11] Due allowance was given to the self decomposition of peroxide while computing the oxidation rates. In case of H_2O_2 the reaction could not be followed at pH>13 in view of slowness of the reaction and high decomposition of the oxidant. The agreement between replicate runs was within ±5%.

Results and Discussion

The kinetics of oxidation of acetylacetone (diketone) by peroxomonophosphoric acid and by hydrogen peroxide have been investigated in aqueous alkaline medium at 308 K.

Plots of log titer versus time are linear for well over three half-lives showing the first order nature of the oxidation with respect to the peroxo compound. The first order disappearance of peroxide is further supported by the fact that the pseudo first order rate constant (k_1') does not change with the variation of initial peroxide concentration.

The oxidation (by both PMPA and H_2O_2) also exhibits a first order dependence on [diketone], as shown by the constancy of the second order rate constants $k_2'(=k_1'/[\text{diketone}])$ for varying initial diketone concentrations (Tables 1 and 4).

Ionic strength (I) of the medium was varied with $NaClO_4$. For PMPA oxidations, I was varied in the range 0.2—0.8 mol dm^{-3}, and for H_2O_2 oxidations in the range 0.1—0.4 mol dm^{-3}. The rate increased with increase of ionic strength (Tables 1 and 4).

Table 1. Oxidation of Acetylacetone by Peroxomonophosphoric Acid[a]

[diketone]×10^2 / mol dm^{-3}	[PMPA]×10^4 / mol dm^{-3}	k_2'×10^3 / dm^3 mol^{-1} s^{-1} [b]
1.02	2.61	76.4
1.01	3.91	70.8
1.04	4.82	68.3
1.01	5.2	75.7
1.06	8.38	84.2
0.31	6.2	85.0
0.51	5.11	82.8
2.14	5.35	80.2
1.03	4.76	55.5[c]
1.03	5.11	90.0[d]
1.03	5.45	108[e]
1.06	5.65	75.8[f]
1.04	5.56	82.6[g]
1.01	5.93	38.2[h]
1.08	5.42	53.0[i]
1.06	4.98	99.5[j]

a) [OH$^-$]=0.1 mol dm^{-3}, I=0.4 mol dm^{-3}, aqueous medium, 308 K. b) Observed second order rate constant. c) I=0.2 mol dm^{-3}. d) I=0.6 mol dm^{-3}. e) I=0.8 mol dm^{-3}. f) [Acrylamide]=5×10^{-3} mol dm^{-3}. g) [EDTA]=5×10^{-4} mol dm^{-3}. h) At 298 K. i) At 303 K. j) At 313 K.

The oxidation rate is insensitive to the addition of acrylamide indicating absence of radicals in the reaction system. Addition of EDTA also does not affect the oxidation rate (Table 1).

For both the oxidations, the second order rate constants at four different temperatures are recorded in Tables 1 and 4. Activation parameters have been determined from the linear Arrhenius plots of log k_2' vs. T^{-1}, and are recorded in Table 3.

The energy of activation (E_a), for both the oxidations, lie in the range 46—71 kJ mol^{-1}. Homolytic cleavage of the peroxide bond requires[12] an energy of activation of ≈138 kJ mol^{-1}. Further, (a) bimolecular kinetics (b) negative entropy of activation and (c) insensitivity to radical trapping agents, show that both PMPA and H_2O_2 oxidations involve polar mechanisms.[13]

The study of effect of pH on oxidation rate constitutes a significant part of the oxidation studies. The kinetics of the PMPA oxidation were explored over the pH range 8.3—13.7 (Table 2), and that of H_2O_2 oxidation over the pH range 9.25—13.0 (Table 4). Plots of pH versus log k_2' for both the oxidations are shown in Fig. 1. The sigmoid nature of the plot for PMPA oxidation suggests the participation of various species of PMPA, arising out of the following equilibria (Eqs. 1—3), in the oxidation. In case of H_2O_2, the plot of pH versus log k_2' is a straight line

Table 2. Oxidation of Acetylacetone by Peroxomonophosphoric Acid: Effect of pH[a]

pH	k_2'×10^3 / dm^3 mol^{-1} s^{-1}	$k_{2(\text{calcd})}'$×10^3 / dm^3 mol^{-1} s^{-1}
13.69	25.1	26.1
13.32	51.4	53.6
13.0	90.0	89.5
12.51	160	157
11.82	245	245
11.54	291	291
11.49	305	302
10.63	288	214
10.0	354	325
9.34	618	694
9.19	852	830
8.34	1646	1639

a) [PMPA]=(3.2—5.5)×10^{-4} mol dm^{-3}, [diketone]=(2.02—10.3)×10^{-3} mol dm^{-3}, I=0.6 mol dm^{-3}, 308 K, Aqueous medium.

Table 3. Thermodynamic Parameters at 313 K

Peroxy acid	E_a / kJ mol^{-1}	ΔH^* / kJ mol^{-1}	ΔS^* / J mol^{-1} K^{-1}
PMPA[a]	49.8	47.3	−113
H_2O_2[b]	68.2	65.8	−69

a) I=0.4 mol dm^{-3}, [OH$^-$]=1.0×10^{-1} mol dm^{-3}. b) I=0.1 mol dm^{-3}, [OH$^-$]=4.6×10^{-2} mol dm^{-3}.

Table 4. Oxidation of Acetylacetone by Alkaline Hydrogen Peroxide[a)]

[diketone]×10³ / mol dm⁻³	[H_2O_2]×10³ / mol dm⁻³	pH	I / mol dm⁻³	k_2'×10³ / dm³ mol⁻¹ s⁻¹	$k_{2(calcd)}'$×10³ / dm³ mol⁻¹ s⁻¹
50.0	2.3	13.0	0.4	11.6	
50.0	17.5	13.0	0.4	14.6	
1.27	2.21	12.65	0.1	11.9	
2.5	2.21	12.65	0.1	11.0	
5.06	2.19	12.65	0.1	10.6	
10.2	2.2	12.65	0.1	12.6	
5.06	2.7	12.69	0.2	12.6	
5.06	2.2	12.69	0.4	15.4	
5.03	2.2	12.65	0.1	17.2[b)]	
5.03	2.4	12.65	0.1	30.2[c)]	
5.03	2.2	12.65	0.1	38.0[d)]	
5.1	2.65	12.94	0.15	6.7	6.7
5.1	2.2	12.66	0.1	10.6	11.1
6.2	2.6	11.52	0.1	28.6	64.6
5.1	2.6	10.83	0.1	48.2	99.5
5.1	3.4	10.16	0.1	106	123
5.1	1.7	9.66	0.1	147	155
5.03	2.1	9.26	0.1	203	203

a) Aqueous medium, 308 K. b) At 313 K. c) At 318 K. d) At 323 K.

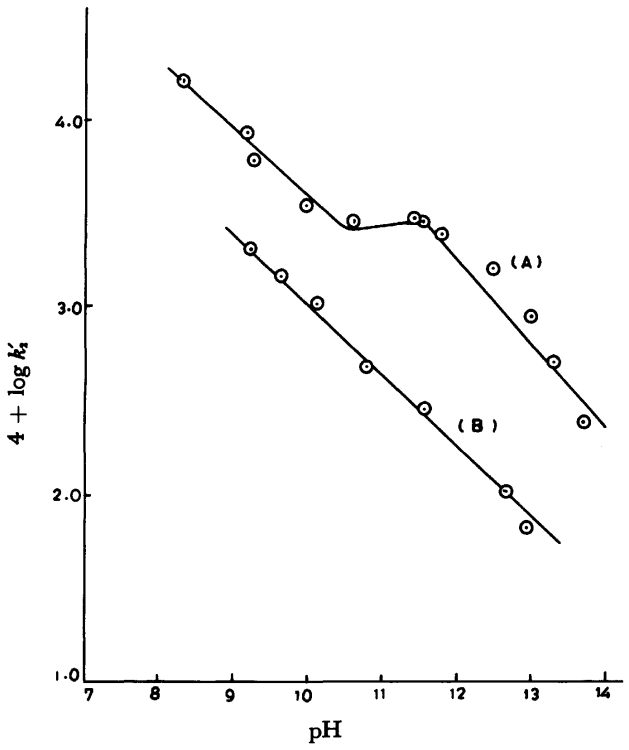

Fig. 1. Plots of log k_2' vs. pH.
A: PMPA-acetylacetone, B: Hydrogen peroxide-acetylacetone.

(r=0.998).

Various equilibria[7)] involving PMPA, in aqueous solution, are

$$H_3PO_5 \overset{K_1}{\rightleftharpoons} H_2PO_5^- + H^+, \quad (1)$$

$$H_2PO_5^- \overset{K_2}{\rightleftharpoons} HPO_5^{2-} + H^+, \quad (2)$$

$$HPO_5^{2-} \overset{K_3}{\rightleftharpoons} PO_5^{3-} + H^+, \quad (3)$$

where K_1=8.0×10⁻², K_2=4.2×10⁻⁶, and K_3=1.6×10⁻¹³, at 298 K and I=0.2 mol dm⁻³.

The dissociation equilibrium[14)] for acetylacetone in aqueous solution is

$$CH_3COCH_2COCH_3 \overset{K_a}{\rightleftharpoons} CH_3\bar{C}OCHCOCH_3 + H^+, \quad (4)$$

where $K_a = 1 \times 10^{-9}$.

In the pH region of 8.3—13.7 PMPA exists[7,15)] mainly as HPO_5^{2-} and PO_5^{3-}. As the pK_a of acetylacetone[16)] is 8.95, in this pH region it is present both as a neutral diketone and as an anion.

$$CH_3COCH_2COCH_3 + OH^- \overset{K_4}{\rightleftharpoons}$$

(A)

$$(CH_3\bar{C}OCHCOCH_3 \leftrightarrow CH_3COCH{=}\overset{O^-}{\overset{|}{C}}CH_3) + H_2O \quad (5)$$

(A⁻)

A and A⁻ represent the diketo form and the enol form of acetylacetone.

In the alkaline hydrolysis of β-diketones, it was the neutral diketone which cleaved rather than the carbanion or the enol form. The reaction was initiated by the attack of OH^- at the carbonyl carbon; k_{obsd} was reported to be 0.573×10⁻³ min⁻¹ at 308 K and [$Ba(OH)_2$]=0.355 mol dm⁻³.

The reaction of β-diketones with alkaline hydrogen peroxide has been shown[6)] to occur by the attack of

hydrogen peroxide ion on carbonyl group. The oxidative cleavage was routed through the formation of an enol epoxide resulting in the formation of acidic products.

The reactions of enol ethers[18] and enol esters[19] with peroxy acid have been shown to form epoxides as well. Kinetic studies relating to epoxidation using alkaline hydrogen peroxide was reported to involve a nucleophilic attack by hydrogen peroxide ion on the alkene double bond.[20]

It can thus be assumed that in the oxidation of acetylacetone by PMPA and hydrogen peroxide both diketo form and enol form of the diketone are reactive.

In the pH range 8—10.6, PMPA exists[7,13] only as HPO_5^{2-}. The reaction steps in this pH range can, therefore, be presented as

$$HPO_5^{2-} + A \xrightarrow{k_1} \text{Products}, \quad (6)$$

$$HPO_5^{2-} + A^- \xrightarrow{k_2} \text{Products}. \quad (7)$$

The rate law is,

$$\text{Rate} = -\frac{d[PMPA]_T}{dt} = k_1[HPO_5^{2-}][A] + k_2[HPO_5^{2-}][A^-]. \quad (8)$$

$$\text{But} \quad [PMPA]_T = [HPO_5^{2-}] \quad (9)$$

$$\text{and} \quad [\text{diketone}]_T = [A] + [A^-] \quad (10)$$

$[PMPA]_T$ and $[\text{diketone}]_T$ represent the total stoichiometric concentration of PMPA and acetylacetone respectively.

From Eqs. 5 and 10,

$$[A] = \frac{K_h[\text{diketone}]_T}{K_h + [OH^-]} \quad (11)$$

$$\text{and} \quad [A^-] = \frac{[\text{diketone}]_T[OH^-]}{K_h + [OH^-]}, \quad (12)$$

$$\text{where} \quad K_h = \frac{[H_2O]}{K_4} \quad (13)$$

Eq. 8, therefore, takes the form,

$$-\frac{d[PMPA]_T}{dt} = \left\{\frac{k_1K_h + k_2[OH^-]}{K_h + [OH^-]}\right\}[PMPA]_T[\text{diketone}]_T \quad (14)$$

$$\text{where} \quad k_2' = \frac{k_1K_h + k_2[OH^-]}{K_h + [OH^-]}. \quad (15)$$

Plot of $k_2'(K_h+[OH^-])$ versus $[OH^-]$ (using $K_h=K_w/K_a$), in the pH range 8—10.6, is found to be linear (r=1.00). From the intercept and slope of this plot the values of k_1 and k_2 are calculated to be 1.96 $dm^3\ mol^{-1}\ s^{-1}$ and 0.177 $dm^3\ mol^{-1}\ s^{-1}$ respectively, indicating the diketo form of acetylacetone is more reactive than the enol form. The second order rate constants k_2'(calcd), calculated from Eq. 15 using these kinetically estimated values of k_1 and k_2, are collected in Table 2.

In the pH range 11.5—13.7, the major oxidant species[7] are HPO_5^{2-} and PO_5^{3-}; the concentration of PO_5^{3-} increasing with increase of pH.

The steps of the oxidation in pH region 11.5—13.7 can be written as,

$$HPO_5^{2-} + OH^- \overset{K_5}{\rightleftharpoons} PO_5^{3-} + H_2O, \quad (16)$$

$$HPO_5^{2-} + A \xrightarrow{k_3} \text{Products}, \quad (17)$$

$$HPO_5^{2-} + A^- \xrightarrow{k_4} \text{Products}, \quad (18)$$

$$PO_5^{3-} + A \xrightarrow{k_5} \text{Products}, \quad (19)$$

$$PO_5^{3-} + A^- \xrightarrow{k_6} \text{Products}. \quad (20)$$

The reaction sequence leads to the rate expression,

$$-\frac{d[PMPA]_T}{dt} = k_3[HPO_5^{2-}][A] + k_4[HPO_5^{2-}][A^-] + k_5[PO_5^{3-}][A] + k_6[PO_5^{3-}][A^-] \quad (21)$$

From Eq. 16, we have

$$[HPO_5^{2-}] = \frac{[PMPA]_TK_h'}{K_h' + [OH^-]}, \quad (22)$$

$$\text{and} \quad [PO_5^{3-}] = \frac{[PMPA]_T[OH^-]}{K_h' + [OH^-]}, \quad (23)$$

$$\text{where} \quad [PMPA]_T = [HPO_5^{2-}] + [PO_5^{3-}] \quad (24)$$

$$\text{and} \quad K_h' = \frac{[H_2O]}{K_5} \quad (25)$$

Now using Eqs. 11, 12, 22, and 23 in Eq. 21, we get,

$$-\frac{d[PMPA]_T}{dt} = \left\{\frac{k_3K_h'K_h + (k_5K_h + k_4K_h')[OH^-] + k_6[OH^-]^2}{(K_h' + [OH^-])(K_h + [OH^-])}\right\} \times [PMPA]_T[\text{diketone}]_T \quad (26)$$

$$\text{or} \quad k_2' = \frac{k_3K_h'K_h + (k_5K_h + k_4K_h')[OH^-] + k_6[OH^-]^2}{(K_h' + [OH^-])(K_h + [OH^-])}. \quad (27)$$

A least-squares analysis of Eq. 27 was done (using $K_h'=K_w/K_3$) and the values of k_3, $(k_5K_h/K_h'+k_4)$ and k_6 were obtained as 30.4 $dm^3\ mol^{-1}\ s^{-1}$, 0.0144 and $\approx$0 respectively. These values were used to obtain k_2' (calcd) which showed excellent agreement with observed k_2' (Table 2).

Oxidation of acetylacetone by alkaline PMPA resulted in the formation of formic acid and acetic acid. Formic acid could be detected[6] from its reaction with ammoniacal silver nitrate. Acetic acid in presence of formic acid was detected[21] by the color reaction with a solution of sodium nitroprusside containing morpholine. In the reaction of unsubstituted β-diketones with alkaline hydrogen peroxide Cocker and Grayson too have reported[6] the formation of formic acid and acetic acid as oxidation products.

In the present study the formation of formic acid,

even under kinetic experimental conditions, suggests that the α-hydroxy-β-diketone produced undergoes hydrolysis and further reaction with the peroxy acid in a fast step forming the products. The formation of hydroxy diketone is presumed to occur by the intermediate formation of epoxy alcohol. The epoxy alcohol supposedly results from the rate-limiting nucleophilic attack of the peroxo species on carbonyl carbon of the diketo form or alkene double bond of the enol form of acetylacetone followed by the oxygen-oxygen bond fission.

The kinetics of oxidation of acetylacetone by hydrogen peroxide have been studied over the pH range 9.2—13.

In dilute aqueous solution hydrogen peroxide is more acidic than water.[22]

$$H_2O_2 \overset{K_6}{\rightleftharpoons} H^+ + HO_2^- \quad (K_6 = 2.24\times10^{-12},\ 25\ ^\circ C). \tag{28}$$

In the pH region under study since hydrogen peroxide exists as H_2O_2 and HO_2^-, the reaction in this pH range would involve the interaction of these species with both the diketo form and enol form of acetylacetone.

$$H_2O_2 + OH^- \overset{K_7}{\rightleftharpoons} HO_2^- + H_2O, \tag{29}$$

$$H_2O_2 + A \xrightarrow{k_7} \text{Products}, \tag{30}$$

$$H_2O_2 + A^- \xrightarrow{k_8} \text{Products}, \tag{31}$$

$$HO_2^- + A \xrightarrow{k_9} \text{Products}, \tag{32}$$

$$HO_2^- + A^- \xrightarrow{k_{10}} \text{Products}. \tag{33}$$

The above reaction steps would lead to the rate law (Eq. 34)

$$-\frac{d[\text{Hydrogen peroxide}]_T}{dt} = k_7[H_2O_2][A] + k_8[H_2O_2][A^-] + k_9[HO_2^-][A] + k_{10}[HO_2^-][A^-]. \tag{34}$$

$$\text{But } [\text{Hydrogen peroxide}]_T = [H_2O_2] + [HO_2^-] \tag{35}$$

From Eqs. 29 and 35,

$$[H_2O_2] = \frac{[\text{Peroxide}]_T K_h''}{K_h'' + [OH^-]} \tag{36}$$

$$\text{and } [HO_2^-] = \frac{[\text{Peroxide}]_T [OH^-]}{K_h'' + [OH^-]}, \tag{37}$$

$$\text{where } K_h'' = \frac{[H_2O]}{K_7} \tag{38}$$

Using Eqs. 11, 12, 36, and 37 in Eq. 34, we get,

$$-\frac{d[\text{Peroxide}]_T}{dt} = \left\{\frac{k_7K_h''K_h + (k_9K_h + k_8K_h'')[OH^-] + k_{10}[OH^-]^2}{(K_h'' + [OH^-])(K_h + [OH^-])}\right\} \times [\text{Peroxide}]_T[\text{Diketone}]_T, \tag{39}$$

$$\text{where } k_2' = \frac{k_7K_h''K_h + (k_9K_h + k_8K_h'')[OH^-] + k_{10}[OH^-]^2}{(K_h'' + [OH^-])(K_h + [OH^-])}. \tag{40}$$

The values of k_7, k_{10}, and $(k_9K_h/K_h'' + k_8)$ were obtained by least-squares analysis of Eq. 40, and were found to be 0.393 $dm^3\,mol^{-1}\,s^{-1}$, 0.143×10^{-2} $dm^3\,mol^{-1}\,s^{-1}$ and 0.494×10^{-3} respectively. Using these values second order rate constants calculated (k_2' calcd) from Eq. 40 are collected in Table 4.

The authors are thankful to Professor G. P. Panigrahi, Department of Chemistry, Berhampur University for helpful discussions and encouragement.

References

1) J. Boeseken and J. Jacob, *Recl. Trav. Chim. Pays-Bas*, **55**, 804 (1936).
2) P. Karrer, J. Kebrle, and R. M. Thakkar, *Helv. Chim. Acta*, **33**, 1711 (1950).
3) P. Karrer, J. Kebrle, and U. Albers-Schonberg, *Helv. Chim. Acta*, **34**, 1014 (1951); **35**, 1498 (1952).
4) H. O. House and W. F. Gannon, *J. Org. Chem.*, **23**, 879 (1958).
5) G. B. Payne, *J. Org. Chem.*, **26**, 4793 (1961).
6) W. Cocker and D. H. Grayson, *J. Chem. Soc., Perkin Trans. 1*, **1975**, 1347.
7) C. J. Battaglia and J. O. Edwards, *Inorg. Chem.*, **4**, 552 (1965).
8) G. P. Panigrahi and R. S. Panda, *Bull. Chem. Soc. Jpn.*, **52**, 3084 (1979).
9) G. P. Panigrahi and R. S. Panda, *Int. J. Chem. Kinet.*, **12**, 491 (1980).
10) G. P. Panigrahi and R. S. Panda, *Bull. Chem. Soc. Jpn.*, **53**, 2366 (1980).
11) A. I. Vogel, "A Textbook of Quantitative Inorganic Analysis," London (1961), p. 363.
12) L. Pauling, "The Nature of Chemical Bond and the Structure of Molecules and Crystals," Cornell University Press, Ithaca, New York (1960), p. 85.
13) E. J. Behrman and J. O. Edwards, "Progress in Physical Organic Chemistry," ed by A. Streitwieser and R. W. Taft, Interscience, New York (1967), Vol. 4, p. 95.
14) E. S. Gould, "Mechanism and Structure in Organic Chemistry," Holt, Rinehart and Winston, New York (1959), p. 367.
15) R. S. Panda, Ph. D. Thesis, Berhampur University, 1980.
16) "Lange's Handbook of Chemistry," 11th ed, ed by J. A. Dean, McGraw-Hill, New York (1973), pp. 5—16.
17) R. G. Pearson and E. A. Mayerle, *J. Am. Chem. Soc.*, **73**, 926 (1951).
18) C. L. Stevens and J. Tazuma, *J. Am. Chem. Soc.*, **76**, 715 (1954).
19) P. D. Gardner, *J. Am. Chem. Soc.*, **78**, 3421 (1956).
20) C. H. Bunton and G. J. Minkoff, *J. Chem. Soc.*, **1949**, 665.
21) F. Feigl, "Spot Tests in Organic Analysis," Elsevier, New York (1960), p. 515.
22) Ref. 14, pp. 5—14.

Kinetics of Oxidation of Amino Acids by Chloramine-T. A Reinvestigation on the Oxidation of Alanine, 2-Aminobutyric Acid, Valine, Serine, and Threonine

M. Shanmugam RAMACHANDRAN* and T. Subburamiyer VIVEKANANDAM
School of Chemistry, Madurai Kamaraj University, Madurai-625 021, India
(Received January 16, 1986)

The kinetics of oxidation of amino acids in aqueous medium were reinvestigated. The rate of oxidation follows second order with respect to chloramine-T (CAT) and an inverse dependence on [*p*-toluenesulfonamide] (RNH_2). At constant [RNH_2] the rate of the reaction can be represented as (in the absence of chloride ion)

$$\frac{-d[CAT]}{dt} = k_a[CAT]^2 + k_b\frac{[\text{Amino Acid}][CAT]^2}{[H^+]} + k_c\frac{[\text{Amino Acid}]^2[CAT]^2}{[H^+]^2}.$$

A linear relationship exists between pK_1 and the rate constants. This shows the electrophilic attack of the oxidant at the carboxylato group of the amino acid. The effect of chloride ion on k_{obsd} is catalytic. The mechanisms of the reactions are discussed in terms of the kinetic results.

The kinetics of oxidations of amino acids by sodium *N*-chloro-*p*-toluenesulfonamidate, generally known as chloramine-T (CAT) have been studied extensively.[1] The mechanism proposed by the earlier workers could not explain some of the observed facts and this leads us to reinvestigate the kinetics of oxidation of amino acids by CAT in acid medium. The results on the oxidation of threonine by CAT were reported in our earlier paper[2] wherein we observed that the active species of the oxidant (CAT) is the dichloramine-T and not the acid chloramine-T as observed by the earlier workers. The main object in this report is to extend the reinvestigation to other amino acids and to elucidate suitable mechanisms and put forward rate laws consistent with the experimental data with a view to shedding more light on the mechanisms of oxidation. CAT was considered once as a quantitative decarboxylating agent for the measurement of amino acid concentration[3] but this expectation fell shortly into disrepute because of reports reflecting on its reliability.[4] Therefore a careful study on the mechanism may give some idea about the analytical use of this reaction. With these views, we discuss here the results obtained on the oxidation of alanine, 2-aminobutyric acid (butryne), valine, and serine by CAT in aqueous perchloric acid medium. The results seem to be different from the oxidation of threonine by CAT reported earlier and hence a careful reexamination on the oxidation of threonine is also made and the results are included.

Experimental

The materials used and experimental methods were discussed in detail in our previous report.[2]

Different ratios of [amino acid] to [CAT], always with [CAT]>[amino acid], were mixed in the absence of acid† at room temperature. Estimation of unreacted [CAT] after 48 h showed that one mole of amino acid consumed more than two moles of CAT as in the following equations.

Alanine + 2.6 CAT ⟶ Products
Butryne + 2.8 CAT ⟶ Products
Valine + 2.7 CAT ⟶ Products
Threonine + 2.8 CAT ⟶ Products
Serine + 2.8 CAT ⟶ Products

The products were identified as a mixture of nitrile, aldehyde and traces of ammonia. Nitrile was identified by the color reaction with hydroxylamine and iron(III) chloride as suggested by Soloway and Lipschietz.[5] Presence of aldehyde was also confirmed by Schiff's reagent. Ammonia was detected by Nessler's reagent. The consumption of more than two moles of CAT per mole of amino acid may be due to the reaction of ammonia with CAT as observed by the earlier workers[6] and may also be due to the further oxidation of aldehyde.

Results and Discussion

The kinetics of oxidations by CAT were followed by observing the disappearance of [CAT] at different time intervals and from the rate of disappearance of [CAT], pseudo first-order rate constants, k_{obsd}, were calculated. All the kinetic runs were carried out with the concentrations of amino acids always, at least five times, in excess of [CAT]. All the reactions were studied in the presence of known amount of *p*-toluenesulfonamide, one of the reaction product obtained from CAT, denoted as RNH_2 where R=*p*-$MeC_6H_4SO_2$-.

Careful analysis of the results, as shown in Fig. 1, indicates that the disappearance of [CAT] does not obey either the integrated first order plot or the integrated second order plot. The plots of log V_t versus time, where V_t is the volume of thiosulfate consumed at time (t), as well as 1/[CAT] versus time show a curvature/deviation in the latter part of the

† At this [CAT] (0.072 M) precipitation occurs in the presence of H^+ and the product analysis were carried out in the absence of H^+ and RNH_2.

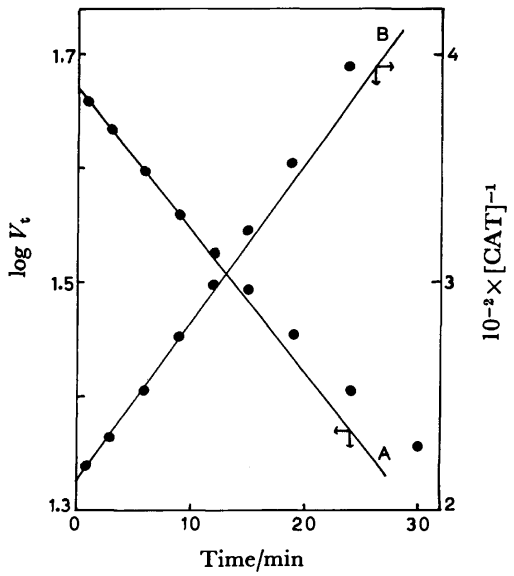

Fig. 1. Rate of disappearance of [CAT] at 30 °C.
A : First order plot, B : Second order plot. [Alanine]= 0.05 M; [RNH_2]=0.01 M; [H^+]=0.10 M; [CAT]= 4.6×10^{-3} M; μ=0.15. 1 M=1 mol dm^{-3}.

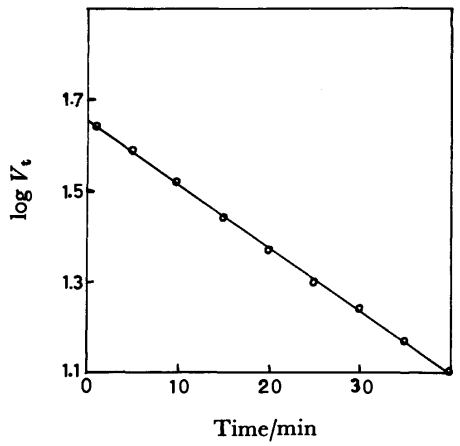

Fig. 2. Rate of disappearance of [CAT] in presence of Cl^- ion at 30 °C.
[Serine]=0.05 M; [RNH_2]=0.01 M; [H^+]=0.2 M; [CAT]=4.42×10^{-3} M; [Cl^-]=0.025 M; μ=0.2.

reaction (Fig. 1). This behavior is observed even in the presence of chloride ion also when [Cl^-]<[CAT]. But when [Cl^-]>[CAT], the reaction is a perfect first order even up to 70% conversion of [CAT] (Fig. 2). Therefore in all the kinetics the rates were followed only up to 25% conversion of [CAT] and the rate constants thus calculated (k_{obsd}) were only the initial rate constants. Examination of k_{obsd} values reveals that the increase in the concentration of CAT causes a proportional increase in the rate constant k_{obsd}. A plot of k_{obsd} versus [CAT] is a straight line passing through the origin (Fig. 3). This clearly proves that the rates of oxidations follow second order with respect to [CAT]. In the presence of chloride ion (0.025 M) (1 M=1 mol dm^{-3}) the plot of k_{obsd} versus [CAT] result in a definite

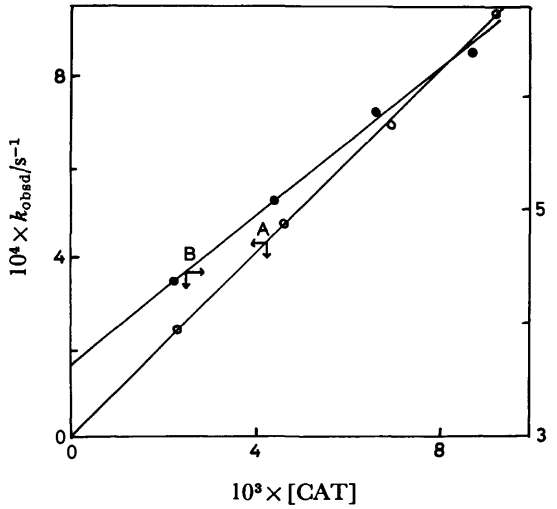

Fig. 3. Plot of k_{obsd} versus [CAT] at 30 °C.
A: [Alanine]=0.05 M; [RNH_2]=0.01 M; [H^+]= 0.1; μ=0.1. B: [Serine]=0.05 M; [RNH_2]=0.01; [H^+]=0.2 M; μ=0.2; [Cl^-]=0.025 M.

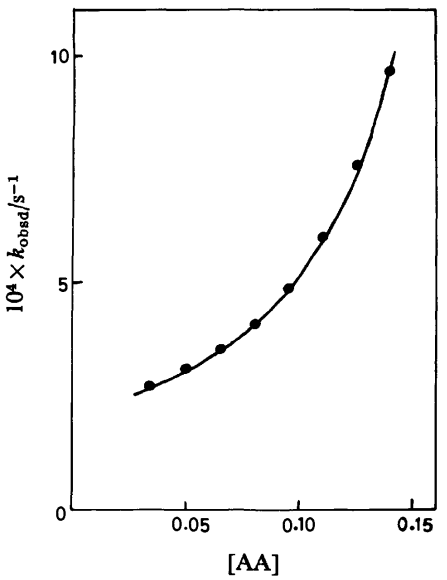

Fig. 4. Plot of k_{obsd} versus [Amino Acid] at 30 °C.
Butryne: [CAT]=4.6×10^{-3} M; [RNH_2]=0.01 M; [H^+]=0.15 M; μ=0.15.

positive intercept (Fig. 3).

The effect of [amino acids] (AA) on the rates of oxidation was studied at constant [H^+] and [RNH_2]. The plots of k_{obsd} versus [amino acids] are parabolic curves with positive intercept ($k_{intercept}$)†† (Fig. 4) and subsequently the plots of k_{obsd}'/[amino acid] versus [amino acid], where k_{obsd}' denotes ($k_{obsd}-k_{intercept}$), are linear at higher concentrations of amino acids (Fig. 5). The initial part of the above plots are parallel to the abscissa. This clearly shows that at lower concentrations of amino acids the reaction follows only first order with respect to [amino acid] whereas at higher

†† Intercept was obtained by linear extrapolation.

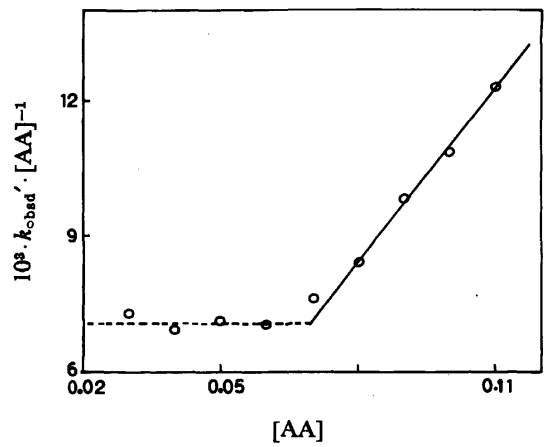

Fig. 5. Plot of k_{obsd}'[Amino Acid]$^{-1}$ versus [Amino Acid] at 30 °C.
Alanine: [CAT]$=4.6\times10^{-3}$ M; [RNH_2]$=0.01$ M; [H^+]$=0.10$ M; $\mu=0.15$.

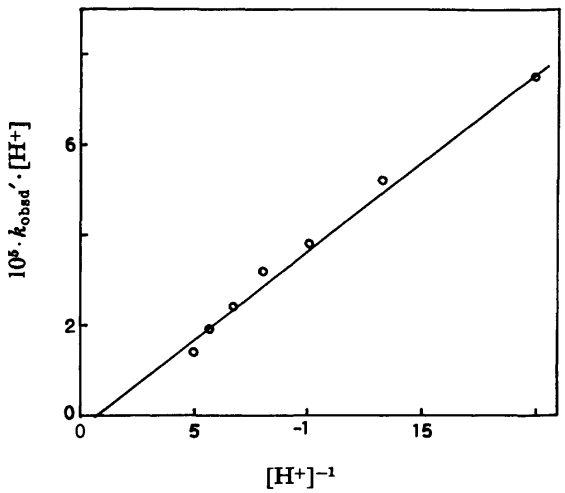

Fig. 6. Plot of k_{obsd}'[H^+] versus $[H^+]^{-1}$ at 30 °C.
[Butryne]$=0.05$ M; [CAT]$=4.6\times10^{-3}$ M; [RNH_2]$=0.01$ M; $\mu=0.25$.

concentration the oxidation obeys second order too.

The values of k_{obsd} decrease with increase in H^+ concentration at constant [amino acid], [CAT], and [RNH_2]. The plots of k_{obsd}' versus $1/[H^+]$ are curves whereas $k_{obsd}'[H^+]$ versus $1/[H^+]$ are straight lines (Fig. 6) with a small negative intercepts in alanine and butryne which can be considered as zero within the experimental error. In all other cases (a small) positive intercept is obtained.

The values of k_{obsd} decrease with increase in [RNH_2] at constant [amino acid], [CAT], and [H^+]. The effect of [Cl^-] on the rate of oxidations is a catalytic one. The influence of ionic strength on the reaction is negligible. The reactions were studied, without Cl^- ion, at four different temperatures (30—45 °C) and from the temperature dependence of k_{obsd} the values of $\Delta H^{\neq}$ for the overall reactions are calculated and tabulated in Table 1.

The oxidation reactions involving CAT are very complex because various species derived/formed from the oxidant are more reactive than CAT itself.

Chloramine-T (RNNaCl where R=*p*-$MeC_6H_4SO_2$-) behaves like a strong electrolyte[7] in aqueous solution as

$$RNNaCl \rightleftharpoons RNCl^- + Na^+.$$

The anion reacts with a proton in acid solution to give free acid monochloramine-T, RNHCl.[8]

$$RNCl^- + H^+ \rightleftharpoons RNHCl \quad K=3.5\times10^4 \text{ at } 25\,^\circ C$$

The formation of free acid RNHCl in acid solution is confirmed by experimental evidence.[7] The free acid RNHCl disproportionates giving rise to *p*-toluenesulfonamide (RNH_2) and dichloramine-T ($RNCl_2$).[9]

$$2RNHCl \overset{K_d}{\rightleftharpoons} RNH_2 + RNCl_2 \quad K_d=6.1\times10^{-2} \text{ at } 25\,^\circ C$$

The free acid RNHCl and dichloramine-T hydrolyze[10] as

Table 1. Kinetic Parameters of Oxidation of Amino Acids by CAT at 30 °C

Amino acid	pK_1[a]	$10^3\times k_1'$ / s^{-1}	k_2 / $dm^3\,mol^{-1}\,s^{-1}$	$10^{-3}\times k_3$ / $dm^6\,mol^{-2}\,s^{-1}$	K_2 / $dm^3\,mol^{-1}$	$10^4\times k_4$ / s^{-1}	$\Delta H^{\neq}$ / kJ mol^{-1}
Alanine	2.35	4.7[b]	6.4	2.4 (3.1)	75	3.6	56.9
Butryne[e]	2.29	5.9[c]	3.8	1.9 (2.4)	56	5.0	62.4
Valine	2.29	4.9[c]	4.0	1.6 (1.8)	32	7.1	59.4
Serine	2.19	5.2[d]	1.8	0.3 (0.9)	35	8.3	62.1
Threonine	2.09	5.0[c]	1.3	0.2 (0.4)	58	5.0	61.7

a) Ref. 14. b) [H^+]$=0.1$ M. c) [H^+]$=0.15$ M. d) [H^+]$=0.20$ M. Values of k_3 given in the parentheses are calculated from [H^+] variation. e) 2-Aminobutyric acid.

$$RNCl_2 + H_2O \overset{K_h}{\rightleftharpoons} RNHCl + HOCl$$
$$K_h = 8.0 \times 10^{-7} \text{ at } 25\,^\circ C,$$
$$RNHCl + H_2O \overset{K_h'}{\rightleftharpoons} RNH_2 + HOCl$$
$$K_h' = 4.88 \times 10^{-8} \text{ at } 25\,^\circ C.$$

Free chlorine has also been detected by Rao et al.[11] in acid medium in the presence of Cl^- ion. Therefore the possible oxidizing species in acidified CAT solution are RNHCl, $RNCl_2$, HOCl, Cl_2, and probably H_2OCl^+.

Bishop and Jennings[7] have calculated the order of the concentration of the various species at different pH. First approximation calculations by Bishop and Jennings on 0.1 M solution of CAT have shown that the concentrations of RNHCl and HOCl are ca. 10^{-2} M and 10^{-7} M respectively at pH ca. 0—3. Soper et al.[10,12,13] have stated that the direct interaction of RNHCl with the substrate could be slow while HOCl formed by the hydrolysis of RNHCl and $RNCl_2$ would attack at a faster rate. This has been recently disproved by Swain and Crist[14] who have shown that HOCl is relatively unreactive and Cl_2, H_2OCl^+, and possibly Cl^+ formed from HOCl are relatively more reactive species. So, under our experimental conditions, the interaction of HOCl with amino acids can be eliminated.

Bishop and Jennings[7] have also shown that an acidified solution of 0.05 M CAT contains 9.6×10^{-5} M of $RNCl^-$, 4.01×10^{-2} M of RNHCl and 9.9×10^{-3} M of $RNCl_2$ in the pH<1.5 or $[H^+]>0.03$ M and the concentration of these species were insensitive to increase in $[H^+]$, generally greater than 0.03 M. Ruff and Kucksman[15] have shown that the reactivities of various species due to CAT in acid solution are in the order $RNCl_2 > RNHCl > OCl^- > RNNaCl$. So under these experimental conditions it is quite likely that $RNCl_2$ and RNHCl would be the reactive species. The observed experimental facts namely the second order dependence of CAT and inhibitory effect of $[RNH_2]$ suggest that $RNCl_2$ would be the more probable active species. Since the concentrations of RNHCl and $RNCl_2$ are constant and independent of $[H^+]$ when $[H^+]>0.03$ M, the present kinetics were studied with $[H^+]=0.1$ M or >0.1 M (even in the $[H^+]$ variation the lowest concentration we used was 0.05 M). Therefore observed inverse hydrogen ion effect would have come from the substrate side.

It is interesting to note that the rate constants for all the five amino acids are almost of the same order of magnitude. This is not surprising as all amino acids have almost same pK_1 values.[16] This shows that the active species is the same for all the amino acids studied. Amino acids exist as dipolar ions (zwitter ions) in aqueous solution as

$$R'\text{-}\underset{\underset{NH_2}{|}}{CH}\text{-}COOH \rightleftharpoons R'\text{-}\underset{\underset{+NH_3}{|}}{CH}\text{-}COO^-.$$

The dissociation of the amino acids depends on the pH of the medium. In acid solutions, amino acids exist as the mixture of cationic and zwitterionic forms

$$R'\text{-}\underset{\underset{+NH_3}{|}}{CH}\text{-}COO^- + H^+ \overset{K_1}{\rightleftharpoons} R'\text{-}\underset{\underset{+NH_3}{|}}{CH}\text{-}COOH.$$

The observed inverse hydrogen ion effect and the experimental conditions employed suggest that the amino acids in the zwitterionic form would be the more probable reactive species.

Based on the experimental conditions, the more probable mechanistic pathway will be (in the absence of Cl^- ion)

$$RNCl^- + H^+ \overset{k}{\rightleftharpoons} RNHCl, \quad (1)$$
$$2RNHCl \overset{K_d}{\rightleftharpoons} RNCl_2 + RNH_2, \quad (2)$$
$$RNCl_2 + H_2O \overset{k_1}{\longrightarrow} RNCl^- + H_2OCl^+, \quad (3)$$
$$R'\text{-}CH(\overset{+}{N}H_3)COO^- + H^+ \overset{K_1}{\rightleftharpoons} R'\text{-}CH(\overset{+}{N}H_3)COOH, \quad (4)$$
$$R'\text{-}CH(\overset{+}{N}H_3)COO^- + RNCl_2 \overset{k_2}{\longrightarrow} \text{Products}, \quad (5)$$
$$2R'\text{-}CH(\overset{+}{N}H_3)COO^- + RNCl_2 \overset{k_3}{\longrightarrow} \text{Products}, \quad (6)$$
$$R'\text{-}CH(\overset{+}{N}H_3)COO^- + H_2OCl^+ \overset{fast}{\longrightarrow} \text{Products}. \quad (7)$$

In the presence of Cl^- ion, in addition to the reaction steps 1—7, the following reactions may also occur

$$RNHCl + Cl^- \overset{K_2}{\rightleftharpoons} \text{Complex}, \quad (8)$$
$$\text{Complex} \overset{k_4}{\longrightarrow} Cl_2 + RNH_2, \quad (9)$$
$$R'\text{-}CH(\overset{+}{N}H_3)COO^- + Cl_2 \overset{fast}{\longrightarrow} \text{Products}. \quad (10)$$

Dakin[3] employed chloramine-T as the oxidizing agent for a variety of amino acids and the products formed were found to be aldehyde, NH_3, and CO_2. In the presence of excess of [CAT] the corresponding nitrile was formed at the expense of aldehyde and ammonia.[3] This observed fact clearly shows that two different reactions are taking place to give the entirely different products, namely nitrile and aldehyde. The present experimental observations, namely the plots k_{obsd}'/[amino acid] versus [amino acid] and $k_{obsd}'[H^+]$ versus $1/[H^+]$, show that both first order and second order reactions with respect to amino acid concentrations as shown in Eqs. 5 and 6, are equally probable and this may be the reason for getting two different products. The final products obtained in our study, namely nitrile and aldehyde, also give evidence for the above fact.

Since the value of the equilibrium constant K is very high[8] (3.6×10^4 at 25 °C), under the experimental conditions all the [CAT] will be in the protonated form, [RNHCl]. Using this approximation and based on the above reaction schemes the rate equation can be written as

$$\frac{-d[CAT]}{dt} = k_1[RNCl_2][H_2O] + k_2[RNCl_2][R'\text{-}CH(\overset{+}{N}H_3)COO^-] + k_3[RNCl_2][R'\text{-}CH(\overset{+}{N}H_3)COO^-]^2. \quad (11)$$

In the presence of Cl^- ion Eq. 11 becomes

$$\frac{-d[CAT]}{dt} = k_1[RNCl_2][H_2O] + k_2[RNCl_2][R'\text{-}CH(\overset{+}{N}H_2)COO^-] + k_3[RNCl_2][R'\text{-}CH(\overset{+}{N}H_3)COO^-]^2 + k_4[\text{complex}]. \quad (12)$$

Substituting the concentrations of $RNCl_2$, $R'\text{-}CH(NH_3)\text{-}COO^-$ and complex from Eqs. 2, 4, and 8 we get

$$\frac{-d[CAT]}{dt} = \frac{K_d[RNHCl]^2}{4K_d[RNHCl]+[RNH_2]}\left\{k_1[H_2O] + \frac{k_2[\text{amino acid}]}{K_1[H^+]} + \frac{k_3[\text{amino acid}]^2}{K_1^2[H^+]^2}\right\} + \frac{k_4K_2[RNHCl][Cl^-]}{1+K_2[RNHCl]+K_2[Cl^-]}, \quad (13)$$

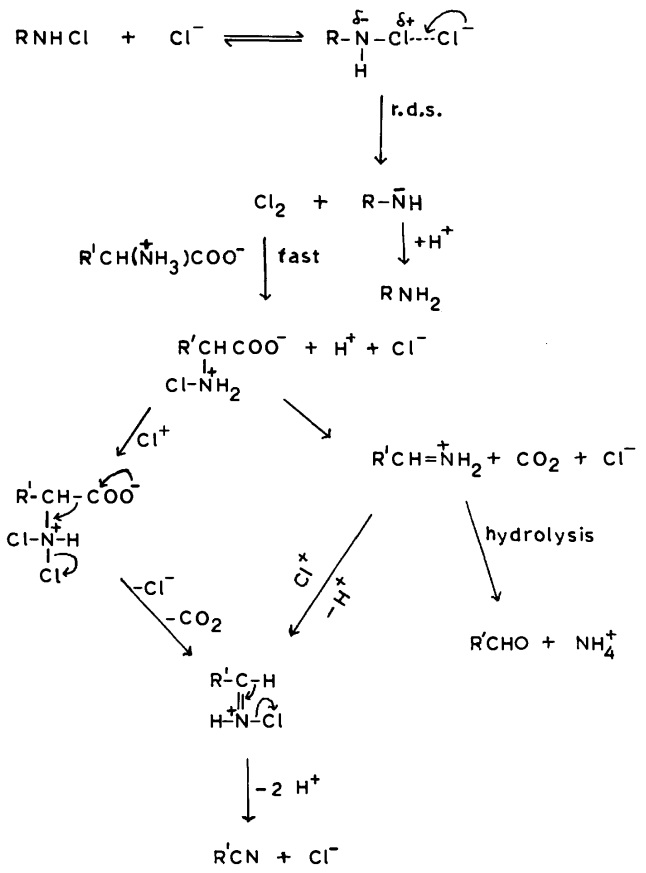

Scheme 1. The catalytic cycle of the reaction in the presence of chloride ion.

$$k_{obsd} = \frac{K_d[RNHCl]}{4K_d[RNHCl]+[RNH_2]}\left\{k_1' + \frac{k_2[\text{amino acid}]}{K_1[H^+]} + \frac{k_3[\text{amino acid}]^2}{K_1^2[H^+]^2}\right\} + \frac{k_4K_2[Cl^-]}{1+K_2[RNHCl]+K_2[Cl^-]} \quad (14)$$

where $k_1' = k_1[H_2O]$.

In the absence of Cl^- ion the last term in Eq. 14 is neglected and k_{obsd} becomes

$$k_{obsd} = \frac{K_d[RNHCl]}{4K_d[RNHCl]+[RNH_2]} \times \left\{k_1' + \frac{k_2[\text{amino acid}]}{K_1[H^+]} + \frac{k_3[\text{amino acid}]^2}{K_1^2[H^+]^2}\right\}. \quad (15)$$

This Eq. 15 explains all the observed experimental facts. At $[CAT]=4.6\times10^{-3}$ M, $[RNH_2]=1.0\times10^{-2}$ M, and $K_d=6.1\times10^{-2}$ the value of the term $4K_d[RNHCl]=0.11\times10^{-2}$ which is only 10% of the magnitude of $[RNH_2]$. Therefore over the range of CAT varied, the term $4K_d[RNHCl]+[RNH_2]$ will be more or less constant and hence a plot of k_{obsd} versus [CAT] will be a straight line passing through the origin.

According to the reaction mechanism if the hydrolysis of $RNCl_2$ to give H_2OCl^+ is the rate-limiting step, then the values of k_1' obtained from the different substrate and at different $[H^+]$ should be identical in magnitude. The value of k_1' can be calculated from the intercept obtained in the plot of k_{obsd} versus [amino acid] where

$$k_{intercept} = \frac{K_d[RNHCl]k_1'}{4K_d[RNHCl]+[RNH_2]}.$$

Using the literature value of K_d as 6.1×10^{-2}, the values obtained for k_1' at different conditions are tabulated in Table 1. The agreement between these values proves our assumption.

The Eq. 15 can be rearranged as

$$k_{obsd} - k_{intercept} = k_{obsd}' = \frac{K_d[RNHCl]}{4K_d[RNHCl]+[RNH_2]}\left\{\frac{k_2[\text{amino acid}]}{K_1[H^+]} + \frac{k_3[\text{amino acid}]^2}{K_1^2[H^+]^2}\right\}, \quad (16)$$

and this Eq. 16 explains the effect of [amino acid] and $[H^+]$ on k_{obsd}. At low concentration of amino acid the second term in the bracket can be neglected so that k_{obsd}' is directly proportional to [amino acid]. Hence the plots k_{obsd}'/[amino acid] versus [amino acid] are parallel to the abscissa at lower concentration. At higher concentration of amino acids, the contribution from the second term is also appreciable and hence k_{obsd}'/[amino acid] versus [amino acid] are straight lines. Similarly at high $[H^+]$, k_{obsd}' may become proportional to $1/[H^+]$ and probably this may be the reason for getting a small negative intercepts in the plots $k_{obsd}'[H^+]$ versus $1/[H^+]$. The values of k_1', k_2, and k_3 are tabulated in Table 1.

Alexander and Gough[17] reported that the oxida-

tions of amino acids, with the exception of glycine, by chlorine are rapid at pH 2 and 10. Results from this laboratory also show that chloride ion shows no effect on the oxidation of glycine by CAT in acid medium[18] whereas with all other amino acids the effect of chloride ion is found to be a catalytic one. This catalytic effect of Cl^- ion shows that CAT may react with Cl^- ion in the rate-determining step to give Cl_2 which reacts rapidly with amino acids as shown in Eqs. 8—10. Free chlorine, in acidified CAT solution in the presence of Cl^-, has been detected.[11] Jayaraman and Mayanna[19] have proved that, in the oxidation of pyridoxine by *N*-chlorobenzenesulfonamidate in HCl medium, the active species is Cl_2.

The plots of k_{obsd} versus [CAT] in the presence of Cl^- ion which result in a positive intercept clearly shows that the reaction proceeds through two independent steps: (i) second order and (ii) first order with respect to [CAT]. At these reaction conditions almost 75% of [CAT] remains as monochloramine-T (RNHCl).[7] This fact together with the assumption, namely the complex formation between RNHCl and Cl^-, will explain why the reaction follows a perfect first order even up to 70% conversion when $[Cl^-] \gg [CAT]$.

The above discussion clearly shows that Cl^- forms complex only with RNHCl. Similar observations were also made in the oxidation reactions by *N*-chlorobenzenesulfonamidate.[20] The formation constant K_2 for the complex (Eq. 8) can be calculated by considering the effect of Cl^- ion on k_{obsd}. The first term in Eq. 14 represents the value of k_{obsd} in the absence of Cl^- ion and this can be represented as k_a. A plot of $(k_{obsd}-k_a)^{-1}$ i.e. $k_{obsd}''^{-1}$ versus $1/[Cl^-]$ should be a straight line with $1/K_2k_4+[RNHCl]/k_4$ as slope and $1/k_4$ as intercept (Fig. 7). The values for k_4 and K_2 are also given in Table 1 and these values also bring out the fact that the values of k_4 and K_2 are independent of the amino acids used.

We can consider the structure of the complex formed between CAT and Cl^- as, similar to that reported by Jayaraman et al.[20] in *N*-chlorobenzenesulfonamidate-Cl^- system,

$$\text{R-N(H)-Cl} + Cl^- \underset{}{\overset{K_2}{\rightleftharpoons}} \text{R-N(H)-Cl}^{\delta-} \cdots\cdots Cl^-.$$

Apart from the difference in the substituents of the phenyl group, both CAT (*N*-chloro-*p*-toluenesulfonamidate) and CAB (*N*-chlorobenzenesulfonamidate) are structurally similar. Hence the difference in the magnitude of K_2 of CAB-Cl^- and CAT-Cl^- should depend on the electron-releasing/withdrawing nature of the substituent in the phenyl ring. Since the interaction of RNHCl with Cl^- is electrophilic in nature, one would expect a positive value of ρ (susceptibility constant). Therefore the ratio of K_2s, $K_{2(CAT)}/K_{2(CAB)}$, should be less than unity since Hammett substituent constants,[21] σ, for $CH_3=-0.17$ and $H=0.0$. Using the literature value[20] of $K_{2(CAB)}$ as 1.2×10^2 the value obtained for $K_{2(CAT)}/K_{2(CAB)}$ is $\simeq 0.45$. This shows that the values of K_2 obtained for CAT-Cl^- system are of the right order of magnitude.

According to Eq. 14 the values of k_{obsd} should be approximately proportional to CAT as, after neglecting the second part, $k_{obsd}=k[RNHCl]$. Therefore, as the reaction proceeds the concentration of RNHCl depletes. Hence the initial value of k_{obsd} will be entirely different from the values at the latter part of

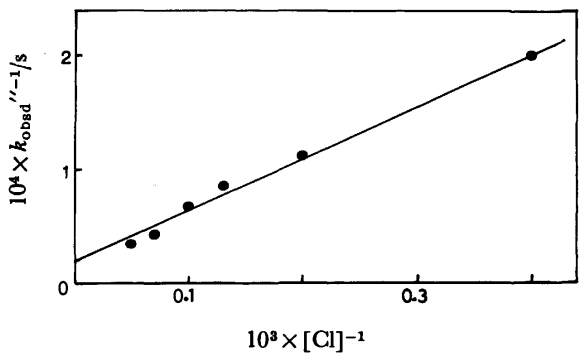

Fig. 7. Plot of $1/k_{obsd}''$ versus $1/[Cl^-]$ at 30 °C. [Butryne]=0.05 M; [CAT]=4.6×10^{-3} M; [NH_2]=0.01 M; [H^+]=0.15 M; μ=0.15.

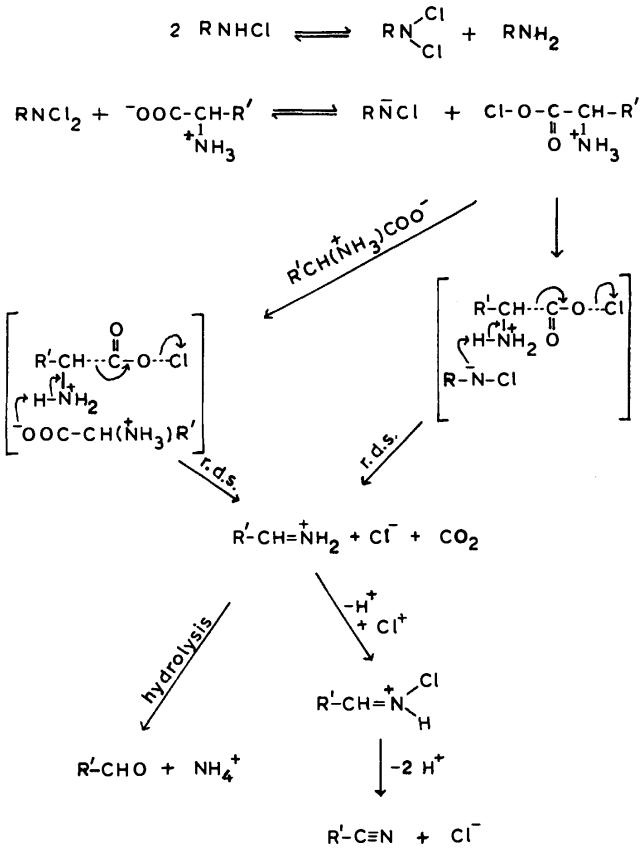

Scheme 2. Reaction scheme.

the reaction. This may be the reason for the curvature in the first order plots.

The accuracy of k_1', k_2, k_3, k_4, and K_2 can be verified by calculating the k_{obsd} using the Eqs. 15 and 16. The results are given only for serine–CAT system. k_{obsd} are calculated using the two independent values of k_3 derived from substrate and [H+] variation. The results are given in Table 2. Perusal of the values shows that the k_{calcd} values calculated using the k_3 derived from the [H+] variation is always higher than k_{obsd}. This is because that k_3 value from the [H+] effect on k_{obsd} is always greater than the k_3 value from [substrate] variation (Table 1). Since the [H+] term occur in the denominator, even a small change in [H+] will show a large effect on k_{obsd}. Moreover, at low [H+] some other side reactions may also occur so that k_{obsd} obtained would be greater than what would be its actual value if no such side reactions. That is why we get a straight line almost passing through origin when we plot k_{obsd}'[H+] versus 1/[H+], but according to Eq. 16 we should get a definite positive intercept.

Based on the experimental results we can propose the following mechanism (Scheme 2) for the reaction of CAT with amino acids.

If the electrophilic substitution takes place at the COO^- group, then the observed reactivity should depend upon the nucleophilicity of the carboxylato group. Any change in the structure of R′ group in the amino acid R′-CH(NH_2)COOH will change the nucleophilicity of the COO^- group which will be reflected on the magnitude of pK_a. According to the pK_1's of the amino acids (Table 1) the order of nucleophilicity should be as alanine>butryne= valine>serine>threonine. Therefore we can expect that the values of k_2 and k_3 should also be in the same order and this expectation is found to be true from the values of k_2 and k_3 (Table 1). A plot of log k_2 or log k_3 with pK_1 of the amino acids is a straight line with positive slope. This clearly proves that the reactions proceed through the electrophilic substitution of CAT at the COO^- group of the amino acid.

This reaction scheme also explains why Dakin observed that in the presence of excess of chloramine-T, the corresponding nitrile was formed at the expense of aldehyde. At higher concentration of CAT, oxidation of imine R′-CH=$\overset{+}{N}H_2$ to give R′CN may also compete with the hydrolysis of R′-CH=$\overset{+}{N}H_2$ to R′CHO.

Reports on the action of chlorine and hypochlorite on amino acids has been reported.[17,22,23] However no adequate explanation has been given for the reactions of these compounds with chlorine. Cl_2 is an effective

Table 2. Comparison of k_{calcd} and k_{obsd} at 30 °C

[Serine] M	$10^3\times$[CAT] M	[H+] M	[RNH_2] M	[Cl−]a) M	$10^4\times k_{obs}$ s^{-1}	$10^4\times k_{calcd}$b)/s^{-1}	
						k_I	k_{II}
0.03	4.42	0.2	0.01	—	1.69	1.90	1.78
0.05	4.42	0.2	0.01	—	1.93	2.56	2.19
0.07	4.42	0.2	0.01	—	2.26	3.40	2.67
0.09	4.42	0.2	0.01	—	2.58	4.43	3.23
0.11	4.42	0.2	0.01	—	2.90	5.64	3.86
0.13	4.42	0.2	0.01	—	3.45	7.05	4.56
0.15	4.42	0.2	0.01	—	4.15	8.64	5.32
0.05	4.42	0.05	0.01	—	10.8	7.51	13.32
0.05	4.42	0.075	0.01	—	6.0	7.30	4.68
0.05	4.42	0.10	0.01	—	3.92	5.02	3.54
0.05	4.42	0.125	0.01	—	3.13	3.89	2.95
0.05	4.42	0.150	0.01	—	2.53	3.25	2.60
0.05	4.42	0.175	0.01	—	2.32	2.84	2.36
0.05	6.61	0.2	0.01	—	2.79	3.17	2.65
0.05	8.84	0.2	0.01	—	3.84	3.82	3.19
0.05	4.42	0.2	0.006	—	2.40	3.48	2.90
0.05	4.42	0.2	0.01	0.0025	0.42	0.52	
0.05	4.42	0.2	0.01	0.005	0.93	0.97	
0.05	4.42	0.2	0.01	0.0075	1.31	1.38	
0.05	4.42	0.2	0.01	0.01	1.65	1.74	
0.05	4.42	0.2	0.01	0.015	2.25	2.37	
0.05	4.42	0.2	0.01	0.02	2.68	2.88	
0.05	4.42	0.2	0.01	0.025	3.40	3.32	

a) Values of k_{obsd} and k_{calcd} given for [Cl−] variation corresponds to $(k_{obsd}-k_a)=k_{obsd}''$ as given in Fig. 7. b) k_I corresponds to the values calculated using k_3 obtained from [H+] variation and k_{II} corresponds to the values calculated using k_3 from [AA] variation.

chlorinating agent.[24] It attacks the substrate in a fast step as shown in the catalytic cycle of the reaction in the presence of Cl^- ion. Had the reaction between substrate and Cl_2 been via the formation of $R'\text{-}CH(\overset{+}{N}H_3)COOCl$ as in the case of CAT, the rate constant for the Cl^- catalysed reaction (k_4) would have a dependence upon the structure of substrate. The results given in Table 1 clearly shows that the rate is almost independent of the structure of the substrate. This clearly shows that the reaction proceeds through the *N*-chloro derivative as shown in the Scheme. Many investigators have observed or proposed the formation of *N*-chloro derivatives as intermediates. Kantouch and Abdel-Fattah[23] have observed the formation of such chloro derivatives as intermediates on the oxidation of amino acids with sodium hypochlorite at pH 2 or 8. By investigating the role of the free amino group in the reaction with chlorine they showed that only substitution of the hydrogen atoms of the amino group takes place. Haberfield and Paul[25] have shown the existence of *N*-chloro intermediate in the chlorination of anilines. *N*-chloro derivatives were proposed as the intermediates to explain the mechanism of chlorination of anilines and related compounds.[26]

In our previous report[2] on the oxidation of threonine by CAT, we have observed

$$\frac{-d[CAT]}{dt} = (\text{const})\frac{[\text{amino acid}][CAT]^2}{[H^+]},$$

in the absence of Cl^- ion and at constant RNH_2. This observation is due to a slip in the experimental set up and hence this erroneous observation of $k_{obsd.}$ However a careful study on the oxidation of threonine by CAT shows that this system also behaves similar to the other amino acids.

The encouragement and laboratory facilities from Professor Dr. N. R. Subbaratnam is gratefully acknowledged with pleasure. M.S.R. acknowledges the financial assistance from the U.G.C., New Delhi, India (Code No. 277). The authors also acknowledge the referees for their constructive criticisms and invaluable suggestions.

References

1) B. T. Gowda and D. S. Mahadevappa, *J. Chem. Soc., Perkin Trans. 2*, **1983**, 323 and references therein.
2) M. S. Ramachandran, T. S. Vivekanandam, and R. Nithyanandham, *J. Chem. Soc., Perkin Trans. 2*, **1985**, 1507.
3) H. D. Dakin, *Biochem. J.*, **10**, 319 (1916); **11**, 79 (1917).
4) P. P. Cohen, *J. Biol. Chem.*, **136**, 565 (1940).
5) S. Soloway and A. Lipschietz, *Anal. Chem.*, **24**, 898 (1952).
6) A. R. Kemble and H. A. MacPherson, *Biochem. J.*, **56**, 548 (1954).
7) E. Bishop and V. J. Jennings, *Talanta*, **1**, 197 (1958) and references therein.
8) J. C. Morris, J. A. Satazer, and M. A. Wineman, *J. Am. Chem. Soc.*, **70**, 2036 (1948).
9) T. Higuchi, K. Ikeda, and A. Hussain, *J. Chem. Soc. B*, **1967**, 546; **1968**, 1031.
10) F. G. Soper, *J. Chem. Soc.*, **1924**, 1899.
11) V. R. S. Rao, D. Venkappayya, and G. Aravamudan, *Talanta*, **17**, 770 (1970).
12) D. R. Pryde and F. G. Soper, *J. Chem. Soc.*, **1931**, 1514.
13) F. G. Soper and G. F. Smith, *J. Chem. Soc.*, **1956**, 1582.
14) G. G. Swain and D. R. Crist, *J. Am. Chem. Soc.*, **94**, 3195 (1972) and references therein.
15) F. Ruff and A. Kucksmann, *J. Chem. Soc., Perkin Trans. 2*, **1975**, 509.
16) "Lange's Handbook of Chemistry," 11th ed, ed by J. A. Dean, McGraw-Hill, New York (1973), Chaps. 5—15.
17) P. Alexander and G. Gough, *Biochem. J.*, **48**, 504 (1951).
18) Unpublished results from this laboratory.
19) B. Jayaraman and S. M. Mayanna, *Bull. Chem. Soc. Jpn.*, **57**, 1439 (1984).
20) B. Jayaraman and S. M. Mayanna, *Tetrahedron*, **39**, 2271 (1983).
21) L. P. Hammett, *Chem. Rev.*, **17**, 125 (1935).
22) L. Stankovic and J. Vasatko, *Chem. Zvesti*, **14**, 434 (1960) and references therein.
23) A. Kantouch and S. H. Abdel-Fattah, *Chem. Zvesti*, **25**, 222 (1971).
24) M. Wayman and E. W. C. W. Thomm, *Can. J. Chem.*, **47**, 2561 (1969) and references therein.
25) P. Haberfield and D. Paul, *J. Am. Chem. Soc.*, **87**, 5502 (1965).
26) P. G. Gassman and G. A. Campbell, *J. Am. Chem. Soc.*, **93**, 2567 (1971).

Acyclic *C*-Nucleoside Analogs of the Type of 5-*C*-Polyhydroxyalkyl-1,3,4-thiadiazoles[1)]

Elsayed S. H. El Ashry,* Mahmoud A. Nassr, Yeldez El Kilany, and Ahmed Mousaad
Chemistry Department, Faculty of Science, Alexandria University, Alexandria, Egypt
(Received March 10, 1986)

The synthesis of some acyclic *C*-nucleoside analogs possessing thiadiazole rings was achieved by the heterocyclization of the 4-arylthiosemicarbazones of D-galactose, D-glucose, D-mannose, D-arabinose, and lactose, Acetylation of the thiadiazoles afforded the corresponding 2-(*N*-acetylarylamino)-5-polyacetoxyalkyl-1,3,4-thiadiazoles and periodate oxidation gave the corresponding 5-(arylamino)-1,3,4-thiadiazole-2-carbaldehyde.

As a consequence of the biological significance of the naturally occurring *C*-nucleosides, various approaches have been explored for their synthesis. One of the main goals in this laboratory is the synthesis of the acylic *C*-nucleoside analogs,[2)] particularly via the heterocyclization of the nitrogen derivatives of sugars.

Thiadiazoles are interesting targets due to their chemotherapeutic value.[3-5)] Consequently, we report in this paper the synthesis of some corresponding acyclic *C*-nucleosides as a continuation of our interest[2,6)] in this work.

Results and Discussion

Acetylation of sugar hydrazones was found to be dependent upon the structure of the hydrazone residue as well as the acylating agent.[7-13)] Saccharide arylhydrazones gave *O*-acetylated derivatives upon reaction with acetic anhydride in pyridine, whereas boiling acetic anhydride caused further acetylation of the hydrazone residue to give *O*,*N*-acetylated derivatives.[7-9)] On the other hand, sugar aroylhydrazones showed a similar behavior to the arylhydrazones upon reaction with acetic anhydride in pyridine under mild conditions whereas boiling acetic anhydride caused cyclization of the aroylhydrazones residue to the corresponding 1,3,4-oxadiazoline derivatives.[10-12)] Reaction of D-galactose thiosemicarbazone (**1**) with hot acetic anhydride in pyridine gave 5-acetylamino-3-acetyl-2-(D-*galacto*-1,2,3,4,5-pentaacetoxypentyl)-2,3-dihydro-1,3,4-thiadiazole (**2**).[13)]

When the thiadiazole **4** was acetylated, a product **5** was obtained whose ^{1}H NMR spectrum showed a singlet at δ 13.2 indicating the presence of only one NH. This as well as the presence of six singlets corresponding to six acetyl groups confirmed the acetylation of the amino group in addition to the hydroxyl groups. The spectrum did not show a

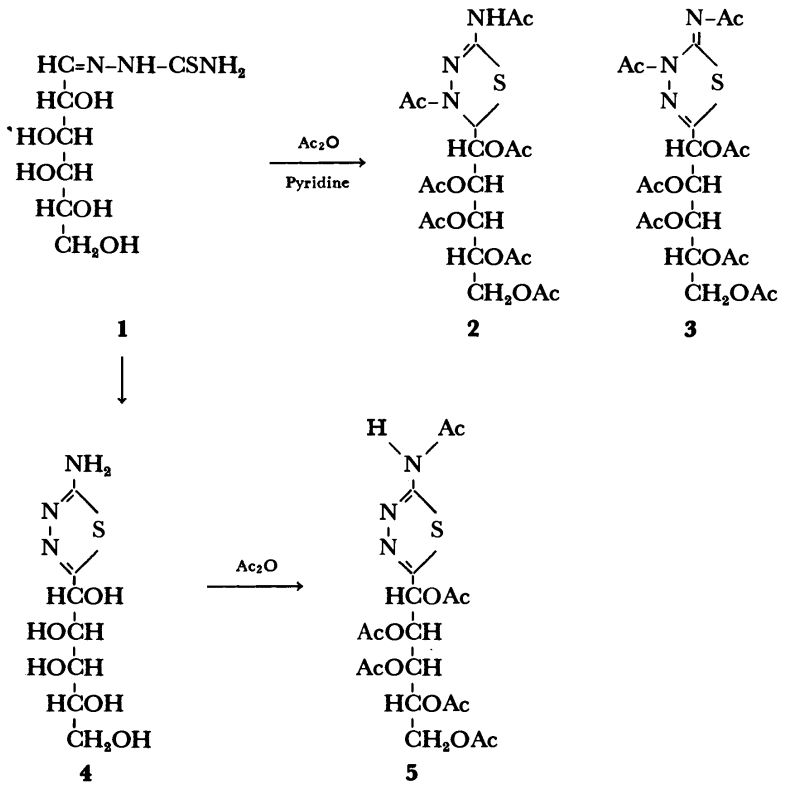

Scheme 1.

doublet at δ 5.83 which appeared in the ^{1}H NMR spectrum of the dihydrothiadiazole derivative (**2**) and attributed to the H-2 of the heterocyclic ring. Moreover, the spectrum showed a doubled at δ 6.37 due to H-1 of the polyacetoxyalkyl side chain. The pronounced downfield shift of H-1 of **5** compared with that of **2** can be attributed to the difference in hybridization of the heterocyclic carbon attached to C-1 of the acetoxyalkyl side chain. These data agreed with structure **5** rather than **2** or **3**.

To explore the scope of heterocyclization of thiosemicarbazones, the 4-substituted thiosemicarbazones were prepared by the condensation of equimolar equivalents of the sugars with 4-substituted thiosemicarbazides. Two variants have been changed; the substituents on the 4-position of the thiosemicarbazide as well as the saccharides, whereby monosaccharides such as D-galactose, D-glucose, D-mannose, and D-arabinose as well as the oligosaccharide lactose were used. Thus the saccharide 4-arylthiosemicarbazones (**6**—**21**) were prepared, and most of them are crystalline compounds (see Table 1). The infrared (IR) spectra of the sugar 4-arylthiosemicarbazones (**6**—**21**) showed NH absorption at 3120—3210 cm^{-1} in addition to the OH band at 3300—3450 cm^{-1}.

Reaction of D-galactose 4-phenylthiosemicarbazone (**6**) with iron(III) chloride, in a similar manner to that reported[14] for thiosemicarbazones and thiobenzoylhydrazones, gave the colorless crystalline product **22**, whose elemental analysis agreed with the structure, 2-anilino-5-(D-*galacto*-1,2,3,4,5-pentahydroxypentyl)-1, 3,4-thiadiazole (**22**), indicating the loss of two hydrogen atoms. This oxidative cyclization could be extended to the whole series of the prepared thiosemicarbazones to give the corresponding thiadiazoles **22**—**34**. As the nitrogen heterocycles derived

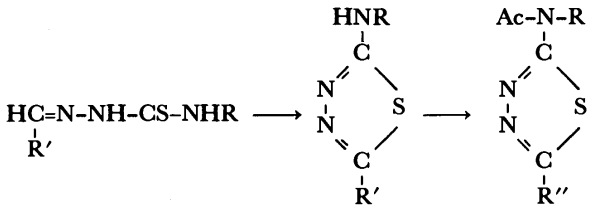

6	R=C_6H_5,	R′= a	⟶ **22**	⟶ **37**	R″= f
7	R=C_6H_4Me-*p*,	R′= a	⟶ **23**	⟶ **38**	R″= f
8	R=C_6H_4Me-*m*,	R′= a	⟶ **24**	⟶ **39**	R″= f
9	R=C_6H_4OMe-*p*,	R′= a	⟶ **25**	⟶ **40**	R″= f
10	R=C_6H_4Cl-*m*,	R′= a	⟶ **26**	⟶ **41**	R″= f
11	R=C_6H_4Br-*p*,	R′= a	⟶ **27**	⟶ **42**	R″= f
12	R=1-Naphthyl,	R′= a	⟶ **28**		
13	R=2-Naphthyl,	R′= a	⟶ **29**		
14	R=C_6H_4Cl-*p*	R′= b			
15	R=C_6H_4Me-*p*,	R′= c	⟶ **30**	⟶ **43**	R″= g
16	R=C_6H_4OMe-*p*,	R′= c	⟶ **31**	⟶ **44**	R″= g
17	R=C_6H_4Cl-*p*,	R′= c	⟶ **32**	⟶ **45**	R″= g
18	R=C_6H_4Me-*p*,	R′= d	⟶ **33**	⟶ **46**	R″= h
19	R=C_6H_4Cl-*p*,	R′= d	⟶ **34**	⟶ **47**	R″= h
20	R=C_6H_4Me-*p*,	R′= e	⟶ **35**		
21	R=C_6H_4Cl-*p*,	R′= e	⟶ **36**		

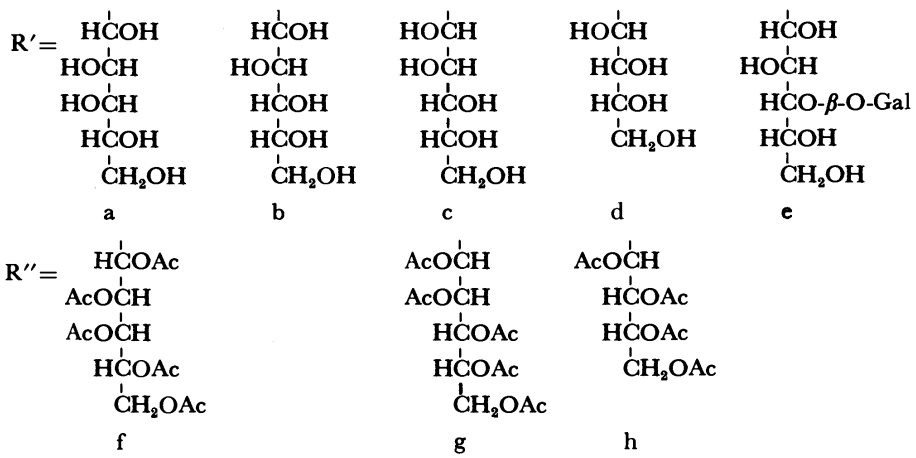

Scheme 2.

from oligosaccharides may have the tendency to be more soluble than the corresponding monosaccharides, a behavior of great advantage in preparing a chemotherapeutic agent, the thiadiazoles **35** and **36** were prepared from the corresponding thiosemicarbazones of lactose.

Acetylation of the thiadiazoles **22—27** and **30—36** gave **37—47**, whose elemental analysis agreed with the molecular formulas having six acetyl groups, indicating that acetylation of the amino groups has occurred in addition to the per-*O*-acetylation of the hydroxyl groups. The IR spectra of the acetates showed the absorptions due to the *O*-Ac groups at 1755—1780 cm^{-1} and the *N*-Ac groups at 1670—1695 cm^{-1}.

Periodate oxidation of the 2-(substituted anilino)-5-(D-*galacto*-1,2,3,4,5-pentahydroxypentyl)-1,3,4-thiadiazoles, afforded the anticipated aldehydes 5-(substituted anilino)-1,3,4-thiadiazole-2-carbaldehyde **48—50**, whose IR spectra showed bands due to the formyl group (1685 cm^{-1}) and the NH group (3200 cm^{-1})

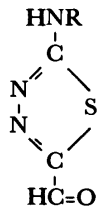

48 R = C_6H_4Me-*p*
49 R = C_6H_4OMe-*p*
50 R = C_6H_4Cl-*m*

Experimental

General. Melting points were determined with a Kofler block apparatus and are uncorrected. Infrared spectra were recorded in Nujol film, with a Pye Unicam SP-1025 spectrophotometer. ^1H NMR spectra were carried out, in deuteriochloroform solutions containing tetramethylsilane as the internal standard, with a Jeol-100 spectrometer. Chemical shifts are given on the δ scale. Microanalyses were performed in the Chemistry Department, Faculty of Science, Cairo University, Cairo, Egypt.

5-Acetylamino-3-acetyl-2-(D-*galacto*-1,2,3,4,5,-pentaacetoxypentyl)-1,2-dihydro-1,3,4-thiadiazole (2). Acetic anhydride (7 ml) was added to a suspension of D-galactose thiosemicarbazone (**1**) (1 g) in dry pyridine (10 ml). This mixture was heated under reflux at 110 °C for 1.5 h, cooled, and then poured onto crushed ice, and the separated solid was collected by filtration, washed with water, and dried, mp 215 °C (lit,[13] mp 217 °C).

2-Acetylamino-5-(D-*galacto*-1,2,3,4,5-pentaacetoxypentyl)-1,3,4-thiadiazole (5). A solution of **4**[14] (2 g) in pyridine (10 ml) was treated with acetic anhydride (15 ml) and the mixture was kept overnight at room temperature. The reaction mixture was poured onto crushed ice, and the product that separated out was filtered off, washed repeatedly with water and sodium hydrogencarbonate solution, and dried. It was crystallized from ethanol in colorless needles, (yield: 60%), mp 165 °C; ν_{max}^{Nujol} 1750 (OAc) and 1670 cm^{-1} (NCO); ^1H NMR ($CDCl_3$) δ=2.00, 2.03, 2.04, 2.13, 2.17, 2.43 (6s, 18H, 6Ac), 3.09 (q, 1H, $J_{5,5'}$=12.0, $J_{4,5'}$=6.0 Hz, H-5'), 4.30 (q, 1H, $J_{5,5'}$=12.0, $J_{4,5}$=5.0 Hz, H-5), 5.30 and 5.38 (2 m, 3H, H-2, -3, -4), 6.37 (d, 1H, $J_{1,2}$=2.0 Hz, H-1), and 13.2 (s, 1H, NH).

Found: C, 45.6; H, 5.3: N, 7.9%. Calcd for $C_{19}H_{25}N_3O_{11}S$: C, 45.3; H, 5.0; N, 8.3%.

Saccharide 4-Arylthiosemicarbazones (6—21). A solution of the sugar (0.01 mol) in water (5 ml) was treated with a solution of 4-substituted thiosemicarbazide (0.01 mole) in ethanol (50 ml) and the mixture was heated under reflux for 1 h. The resulting solution was concentrated, and the product that separated out upon cooling, was filtered off, washed with ethanol, and dried. It was crystallized from ethanol, giving colorless needles. The noncrystalline thiosemicarbazones were directly transformed into the corresponding thiadiazoles, (yield ≈75%). (see Table 1).

2-Arylamino-5-polyhydroxyalkyl-1,3,4-thiadiazoles (22—36). A 2 M iron(III) chloride solution in ethanol (5 ml) was

Table 1. Elemental Analyses and IR Spectral Data of Saccharide 4-Arylthiosemicarbazones (**7**, **12**, **14—19**)

Compound	Mp θ_m/°C	Molecular formula		Analysis/% C	H	N	S	X	ν_{max}^{Nujol}/cm^{-1} OH	NH
7	190	$C_{14}H_{21}N_3O_5S$	Calcd	49.0	6.1	12.2	9.3	—	3450	3210
			Found	49.1	5.8	12.3	9.4			
12	165	$C_{17}H_{21}N_3O_5S$	Calcd	53.8	5.6	11.1	8.5	—	3450	3210
			Found	53.7	5.4	10.8	8.6			
14	188	$C_{13}H_{18}ClN_3O_5S$	Calcd	42.9	5.0	11.6	8.6	9.7	3390	3200
			Found	43.1	4.8	11.8	8.8	10.1		
15	187	$C_{14}H_{21}N_3O_5S$	Calcd	49.0	6.1	12.2	9.3	—	3450	3200
			Found	49.3	5.8	11.9	9.1			
16	177°	$C_{14}H_{21}N_3O_6S$	Calcd	46.8	5.9	11.7	8.9	—	3410	3170
			Found	46.8	5.7	11.5	8.6			
17	180	$C_{13}H_{18}ClN_3O_5S$	Calcd	42.9	5.0	11.6	8.8	9.7	3400	3150
			Found	43.1	4.6	11.2	8.9	9.6		
18	220	$C_{13}H_{19}N_3O_4S$	Calcd	49.8	6.1	13.4	10.2	—	3395	3210
			Found	50.1	5.8	13.2	10.1			
19	205	$C_{12}H_{16}ClN_3O_4S$	Calcd	43.2	4.8	12.6	9.6	10.6	3400	3150
			Found	43.4	4.9	12.4	9.6	10.7		

Table 2. Elemental Analyses and IR Spectral Data of 2-Arylamino-5-polyhydroxyalkyl-1,3,4-thiadiazoles (**4**, **22**—**36**)

Compound	Mp θ_m/°C	Molecular formula		Analysis/% C	H	N	S	X	IR ν_{max}^{Nujol}/cm^{-1} OH	NH	C=N
4	203	$C_7H_{13}N_3O_5S$	Calcd	33.5	5.2	16.7	12.8	—	3400	3150	1620
			Found	33.8	4.9	16.4	12.4				
22	240	$C_{13}H_{17}N_3O_5S$	Calcd	47.7	5.2	12.8	9.8	—	3390	3210	1610
			Found	48.1	5.3	12.4	9.9				
23	234	$C_{14}H_{19}N_3O_5S$	Calcd	49.3	5.6	12.3	9.4	—	3350	3100	1610
			Found	49.1	5.8	12.2	9.4				
24	230	$C_{14}H_{19}N_3O_5S$	Calcd	49.3	5.6	12.3	9.4	—	3500	3250	1610
			Found	48.8	5.5	11.9	9.4				
25	248	$C_{14}H_{19}N_3O_6S$	Calcd	47.1	5.4	11.8	9.0	—	3400	3220	1605
			Found	46.7	5.1	11.6	9.3				
26	240	$C_{13}H_{16}ClO_5N_3S$	Calcd	43.2	4.5	11.6	8.9	9.8	3400	3150	1605
			Found	42.9	4.4	11.4	8.7	9.8			
27	230	$C_{13}H_{16}BrN_3O_5S$	Calcd	38.4	4.0	10.3	7.9	19.7	3380	3215	1620
			Found	38.7	3.8	10.6	8.2	20.0			
28	262	$C_{17}H_{19}N_3O_5S$	Calcd	54.1	5.1	11.1	8.5	—	3250	3100	1605
			Found	54.1	5.4	11.5	8.7				
29	250	$C_{17}H_{19}N_3O_5S$	Calcd	54.1	5.1	11.1	8.5	—	3350	3150	1610
			Found	54.1	4.9	11.3	8.5				
30	214	$C_{14}H_{19}N_3O_5S$	Calcd	49.3	5.6	12.3	9.4	—	3330	3100	1605
			Found	49.5	5.7	12.1	9.5				
31	220	$C_{14}H_{19}N_3O_6S$	Calcd	47.1	5.4	11.8	9.0	—	3400	3200	1610
			Found	46.7	5.1	11.6	8.9				
32	222	$C_{13}H_{16}ClN_3O_5S$	Calcd	43.2	4.5	11.6	8.8	9.8	3400	3200	1605
			Found	43.5	4.4	11.7	8.9	9.9			
33	226	$C_{13}H_{17}N_3O_4S$	Calcd	50.1	5.5	13.5	10.3	—	3350	3100	1610
			Found	50.1	5.4	13.2	10.5				
34	220	$C_{12}H_{14}ClN_3O_4S$	Calcd	43.4	4.3	12.7	9.7	10.7	3450	3300	1605
			Found	43.6	4.4	12.5	9.7	11.0			
35	195	$C_{20}H_{29}N_3O_{10}S$	Calcd	47.7	5.8	8.3	6.4	—	3400	3200	1620
			Found	47.3	5.5	8.1	6.4				
36	205	$C_{19}H_{26}ClN_3O_{10}S$	Calcd	34.6	5.0	8.0	6.1	6.8	3420	3100	1610
			Found	43.1	4.7	7.7	6.2	6.9			

Table 3. Elemental Analyses and IR Spectral Data of 2-(*N*-Acetylarylamine)-5-polyacetoxyalkyl-1,3,4-thiadiazoles (**37**—**47**)

Compound	Mp θ_m/°C	Molecular formula		Analysis/% C	N	H	S	X	ν_{max}^{Nujol}/cm^{-1} OAc	NAc
37	210	$C_{25}H_{29}N_3O_{11}S$	Calcd	51.8	5.0	7.3	5.5	—	1770	1695
			Found	51.8	5.0	7.2	5.9			
38	201	$C_{26}H_{31}N_3O_{11}S$	Calcd	52.6	5.3	7.1	5.4	—	1755	1690
			Found	52.3	5.3	7.2	5.8			
39	201	$C_{26}H_{31}N_3O_{11}S$	Calcd	52.6	5.3	7.1	5.4	—	1775	1690
			Found	52.3	5.3	7.2	5.6			
40	162	$C_{26}H_{31}N_3O_{12}S$	Calcd	51.2	5.1	6.9	5.3	—	1775	1690
			Found	51.5	5.2	7.1	5.8			
41	226	$C_{25}H_{28}ClN_3O_{11}S$	Calcd	48.9	4.6	6.8	5.2	5.8	1770	1690
			Found	49.2	4.7	7.0	5.6	5.9		
42	204	$C_{25}H_{28}BrN_3O_{11}S$	Calcd	45.6	4.3	6.4	4.9	12.1	1780	1690
			Found	46.0	4.1	6.3	5.3	12.2		
43	134	$C_{26}H_{31}N_3O_{11}S$	Calcd	52.6	5.3	7.1	5.4	—	1780	1690
			Found	53.0	5.3	7.0	5.6			
44	162	$C_{26}H_{31}N_3O_{12}S$	Calcd	51.2	5.1	6.9	5.3	—	1780	1690
			Found	51.5	5.2	6.6	5.7			
45	148	$C_{25}H_{28}ClN_3O_{11}S$	Calcd	48.9	4.6	6.8	5.2	5.8	1780	1680
			Found	49.1	4.8	6.9	5.2	6.0		
46	115	$C_{23}H_{27}N_3O_9S$	Calcd	53.0	5.2	8.1	6.2	—	1760	1670
			Found	53.2	5.5	7.8	5.9			
47	143	$C_{22}H_{24}ClN_3O_9S$	Calcd	48.8	4.5	7.8	5.9	6.5	1780	1690
			Found	49.1	4.6	7.5	5.8	6.6		

Table 4. Elemental Analyses and IR Spectral Data of 5-(Substituted Anilino)-1,3,4-thiadiazole-2-carbaldehydes (**48—50**)

Compound	Mp θ_m/°C	Molecular formula	Analysis/%					IR ν_{max}^{Nujol}/cm^{-1}		
				C	H	N	S	X	NH	HC=O	C=N
48	211	$C_{10}H_9N_3OS$	Calcd	54.8	4.1	19.2	14.6	—	3100	1682	1620
			Found	54.7	4.2	19.5	14.5				
49	186	$C_{10}H_9N_3O_2S$	Calcd	51.1	3.9	17.9	13.6	—	3200	1685	1615
			Found	51.3	4.0	17.5	13.8				
50	207	$C_9H_6ClN_3OS$	Calcd	45.1	2.5	17.5	13.4	—	3150	1675	1610
			Found	45.4	2.8	17.2	13.6				

added dropwise to a boiling solution of the saccharide 4-substituted thiosemicarbazone (1 g) in ethanol (100 ml). Boiling was continued for further 10 min, and the mixture was then concentrated. The product which separated out on cooling, was filtered off, washed with ethanol, dried and crystallized from ethenol in colorless needles, (yield ≈80%), (see Table 2).

2-(*N*-Acetylarylamino)-5-polyacetoxyalkyl-1,3,4-thiadiazoles (37—47). A solution of saccharide 4-arylthiosemicarbazone (1 g) in a mixture of *N*,*N*-dimethylformamide (10 ml) and dry pyridine (7 ml) was treated with acetic anhydride (10 ml) and the mixture was kept overnight at room temperature. The reaction mixture was poured onto crushed ice, and the product that separated out was filtered off, washed repeatedly with water, and sodium hydrogencarbonate solution and dried. The product was recrystallized from ethanol in colorless needles, (yield ≈ 60%), (see Table 3).

5-(Substituted Anilino)-1,3,4-thiadiazole-2-carbaldehyde (48—50). A suspension of compounds **7,9,10** (0.01 mol) in water (100 ml) was treated with a solution of sodium periodate (0.05 mol) in water (50 ml). The mixture was stirred at room temperature for 2 h, and kept overnight in the dark. The product was filtered off, washed with water, dried and crystallized from ethanol in yellow needles, (yield ≈70%), (see Table 4).

References

1) Heterocycles from Carbohydrate Precursors, Part 35; A Part in the series Scope of the Reactions of Hydrazines and Hydrazones Part 18.

2) E. S. H. El Ashry, *Adv. Chem. Ser. Am. Chem. Soc.*, **200**, 179 (1982).

3) E. Regel and P. E. Frohberger, German Patent, 2712630 (1978); *Chem. Abstr.*, **90**, 6401 (1979).

4) D. A. Berges, German Patent, 2742726 (1978); *Chem. Abstr.*, **89**, 24335 (1978).

5) H. Hagen and H. Fleig, German Patent 2329653 (1975); *Chem. Abstr.*, **86**, 189963 (1977).

6) E. S. H. El Ashry, M. Nassr, Y. El Kilany, and A. Mousaad, *J. Prakt. Chem.*, **328**, 1 (1986).

7) M. L. Wolfrom, G. Fraenkel, D. R. Lineback, and F. Komitsky, *J. Org. Chem.*, **29**, 457 (1964).

8) H. El Khadem, Z. M. El Shafei, and M. M. Mohamed-Ali, *J. Org. Chem.*, **29**, 1565 (1964).

9) Z. M. El Shafei and E. S. H. El Ashry, *Carbohydr., Res.*, **3**, 184 (1966).

10) L. Somogyi, *Carbohydr. Res.*, **54**, C14 (1977).

11) L. Somogyi, *Carbohydr. Res.*, **64**, 289 (1978).

12) E. S. H. El Ashry, Y. El Kilany, A. A. Abdallah, and K. Makawy, *Carbohydr. Res.*, **113**, 273 (1983).

13) L. Somogyi, *Carbohydr. Res.*, **75**, 325 (1979).

14) B. Holmberg, *Arkiv Kemi*, **7**, 517, 529 (1954).

Reaction of Nitrosyl Chloride Gas with Unsaturated Steroids

Shafiullah,* Ansari M. Rafiuddin, and Shakir Husain
Department of Chemistry, Aligarh Muslim University, Aligarh-202001, U.P. India
(Received April 14, 1986)

Reaction of nitrosyl chloride gas at 0 °C with 3,5-cholestadiene (**1**) provided 3,6β-dinitro-5-chloro-5α-cholest-3-ene (**4**) and with 3α,5-cyclo-5α-cholestan-6-one (**2**) afforded 3β-chloro-5-nitro-5α-cholestan-6-one (**7**) and 3β-chloro-6-nitrato-5-cholestene (**8**). Similar reaction with 6-hydroxylimino 3α,5-cyclo-5α-cholestane (**3**) gave 3β,6-dichloro-5-cholestene (**10**), 3β-chloro-6-nitratoimino-5α-cholestane (**11**) and 3β,5-dichloro-6-nitroimino-5β-cholestane (**12**). Compound **12** upon hydrolysis furnished 3β,5-dichloro-5β-cholestan-6-one (**14**). The structures of these compounds were established on the basis of their spectral properties, and some pertinent chemical transformations. Mechanisms for the formation of some unusual products are discussed.

One of the remarkable features of nitrosyl chloride gas is that with the help of it nitro and chloro groups can simultaneously be introduced with ease at unsaturated regions of an organic molecule. Taking advantage of this ability of nitrosyl chloride, nitro and chloro groups were successfully incorporated on adjacent carbon atoms in steroidal olefins.[1-4] For this purpose we have selected, 3,5-cholestadiene (**1**), 3α,5-cyclo-5α-cholestan-6-one (**2**) and its oxime (**3**) to study the chemical behavior of nitrosyl chloride on the unsaturated functionalities in steroids. Interesting results were envisaged because nitrosyl chloride has been used, exiguously in the advancements of steroid chemistry.

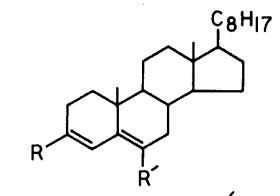

	R	R′
1,	H	H
5,	NO_2	NO_2

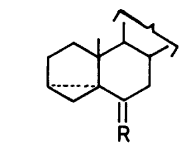

	R
2,	O
3,	N-OH

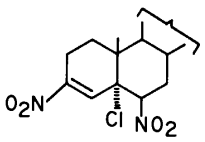

4

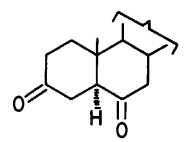

6

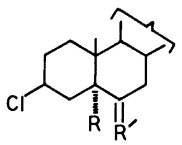

	R	R′
7,	NO_2	O
9,	H	O
11,	H	N-ONO_2
13,	H	N-OH

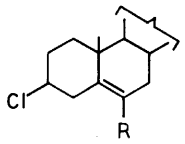

	R
8,	-O-NO_2
10,	-Cl

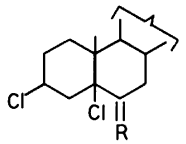

	R
12,	N-NO_2
14,	O
15,	N-OH

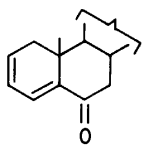

16

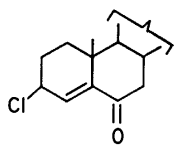

17

Chart 1.

Results and Discussion

Reaction of nitrosyl chloride with **1** in CCl_4 at 0 °C afforded a crystalline product **4** which in its IR spectrum showed an absorption band at 1640 for (C=C), two sets of strong bands at 1570, 1385 and at 1530, 1355 cm^{-1}, clearly indicated the presence of two nitro groups, former being a saturated and latter the unsaturated one.[5] Its proton NMR spectrum displayed a singlet at δ 6.35 for C-4 vinylic proton and a triplet at δ 4.80 (J=3 Hz) for C6-αH (equatorial).[6] Compound (**4**) gave 3,6-dinitro-3,5-cholestadiene (**5**) on heating in pyridine and on reducing with Zn-acetic acid, it gave 5α-cholestane-3,6-dione (**6**). These observations helped in concluding that the compound **4** is 5-chloro-3,6β-dinitro-5α-cholest-3-ene: The formation of which follows the same mechanism as given earlier.[4]

Compound **2** when treated with nitrosyl chloride in the similar fashion afforded 3β-chloro-5-nitro-5α-cholestan-6-one (**7**) and 3β-chloro-6-nitrato-5-cholestene (**8**). The position of nitro group at C-5 in **7** was established by the fact that the signal of the methine proton (>C<u>H</u>-NO_2) was absent in its proton NMR

spectrum and the presence of the absorption bands at 1578 and 1380 cm^{-1} in its IR spectrum supported the saturated and tertiary nature of the nitro group.[5]

The IR spectrum of **8** exhibited characteristic absorption bands for nitrato group[5,7] at 1645, 1285, 875, and 770 cm^{-1} and a weak band at 1630 cm^{-1} for (C=C). Moreover, Zn–acetic acid reduction is known to convert the nitrato group into hydroxyl group.[8] When **8** was subjected to this reduction it gave 3β-chloro-5α-cholestan-6-one (**9**): Presumably the enol formed in the reaction tautomerized to **9** owing to the acidic conditions of the reaction medium. Mechanism for the formation of **8** is given in Scheme 1.

Treatment of **3** with nitrosyl chloride as described earlier provided 3β,6-dichloro-5-cholestene (**10**), 3β-chloro-6-nitratoimino-5α-cholestane (**11**) and 3β,5-dichloro-6-nitroimino-5β-cholestane (**12**).

Formation of *gem*-chloronitroso derivatives from the reaction of nitrosyl chloride and oximes is known.[9] Further nitrosation of *gem*-chloronitro derivative may lead to the elimination of N_2O_2 from the molecule. In view of this aspect the mechanism for the formation of **10** is proposed as in Scheme 2.

The compound **11** showed four intense bands at 1630, 1275, 875, and 770 cm^{-1} for nitrate function besides a medium band at 1650 cm^{-1} for (C=N) in its IR spectrum. The notching observed in the band at 875 was perhaps due to the N–O–N bonding, hence accounts for the presence of *N*-nitrate grouping. Zn–acetic acid reduction of **11** provided the ketone **9**

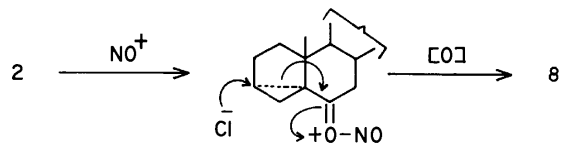

Scheme 1.

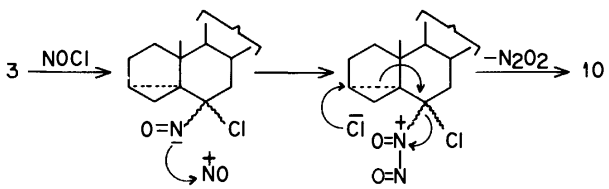

Scheme 2.

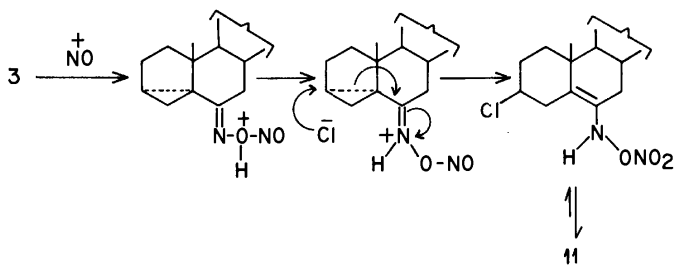

Scheme 3.

and its oxime **13**. The formation of **11** involves enamine–imine tautomerism which is depicted in Scheme 3.

As far as the formation of **12** is concerned, it is assumed that the cyclopropane ring is opened by the attack of chlorine generated as a result of the dissociation of nitrosyl chloride gas. The conversion of hydroxylimino group into nitroimino group by nitrosyl chloride[10,11] involves the formation of *N*-nitrosonitrone species as intermediate which spontaneously rearranges to nitroimine.[12]

In the proton NMR spectrum of **12** the C-3 proton resonated at relatively downfield and showed half band width (≈6.5 Hz) indicating its equatorial nature and cis geometry of A/B ring junction.[6] Chemical justification for this fact was obtained by the hydrolysis of nitroimine **12** to obtain 3β,5-dichloro-5β-cholestan-6-one (**14**) which was found different from its 5α-epimer.[13] The ketone **14** was converted into its oxime **15** which in turn gave the parent nitroimine **12** when treated with nitrosyl chloride. Dehydrochlorination of **14** provided 2,4-cholestadien-6-one (**16**) and 3β-chloro-4-cholesten-6-one (**17**).

Experimental

Melting points were determined on a Koffler hot stage apparatus and are uncorrected. Infrared spectra were recorded on a Pye-Unicam SP3-100 spectrophotometer. Proton nuclear magnetic resonance spectra were taken on a Varian A 60 instrument with $(CH_3)_4Si$ as internal reference, and mass spectra were recorded on a JEOL JMS-D 300 spectrometer. Elemental analyses were performed by Instrumentation Centre at our University. Compounds **1**,[14] **2**,[15] and **3**[16] were prepared according to the literature. Nitrosyl chloride gas was prepared according to Morton and Wilcox's method.[17]

Reaction of 1 with NOCl. The solution of **1** (2 g) in CCl_4 (100 mL) was cooled to 0 °C and dried NOCl was bubbled into it for 2 h. The reaction mixture was kept overnight at 0 °C and the solvent was evaporated under reduced pressure and the residue was taken in ether, washed with water, and dried (Na_2SO_4). After removal of the solvent, the oily residue was subjected to the column chromatography over silica gel (40 g). Elution with light petroleum (bp 60—80 °C):ether (25:1) gave **4**, recrystallized from methanol (1.4 g, 70%); mp 156 °C (positive Beilstein test); IR (KBr) 1640, 1570, 1530, 1385, 1355, 690 cm^{-1}; ^1H NMR ($CDCl_3$) δ=0.72 (3H, s, 18-CH_3), 1.05 (3H, s, 19-CH_3), 4.80 (1H, t, J=3 Hz, 6α-H), 6.35 (1H, s, 4-H); MS, *m/z* (relative intensity) 496/494 (0.20/0.60, M^+), 413 (5), 396 (12), 383 (6), 382 (14), 107 (25), 105 (25). Found: C, 65.56; H, 8.67; N, 5.60%. Calcd for $C_{27}H_{43}N_2O_4Cl$: C, 65.52; H, 8.69; N, 5.66%.

Dehydrochlorination of 4. In pyridine (200 mL), **4** (500 mg) was refluxed for 2 h. The reaction mixture was diluted with water and organic mass was extracted with ether and ethereal layer was washed with dil HCl (5%), $NaHCO_3$ solution (5%) and water and dried (Na_2SO_4). Removal of the solvent gave **5** as an oil, crystallized from methanol (400 mg, 80%); mp 113 °C (lit,[4] 113 °C) (negative Beilstein test); IR (KBr) 1651, 1515, 1380 cm^{-1}; ^1H NMR

($CDCl_3$) δ=0.71 (3H, s, 18-CH_3), 1.10 (3H, s, 19-CH_3), 7.7 (1H, s, 4-H).

Zinc-Acetic Acid Reduction of 4. In 50 mL of warm acetic acid, **4** (500 mg) was dissolved and zinc dust (2 g) was added gradually over a period of 10 min. The mixture was heated under reflux for 4 h, water (5 mL) was added with regular intervals. It was diluted with water and organic mass was extracted with ether. The ethereal layer was worked up, dried (Na_2SO_4) and the solvent was evaporated to get **6** as an oil, crystallized from acetone (300 mg, 60%); mp 167 °C (lit,[18] mp 169 °C) (negative Beilstein test); IR (nujol) 1710 cm^{-1}.

Reaction of 2 with NOCl. The reaction of **2** (5 g) in CCl_4 (250 mL) with NOCl was performed as earlier. After usual work up an oily mass was obtained which was chromatographed over a column of silica gel (80 g). Elution with light petroleum (bp 60—80 °C) afforded **7**, recrystallized from methanol (1.8 g, 36%): mp 92 °C (positive Beilstein test), IR (nujol) 1718, 1578, 1390, 740 cm^{-1}; ^1H NMR (CCl_4) δ=0.75 (3H, s, 18-CH_3), 1.18 (3H, s, 19-CH_3), 1.7 (2H, d, 4-H_2), 3.4 (1H, m, $W_{1/2}$=16 Hz, 3α-H, A/B ring junction trans;[6] MS, *m/z* (relative intensity) 421/419 (2/6, M-NO_2), 418 (20), 416 (61), 318 (45), 306 (3), 304 (9), 270 (35). Found: C, 69.61; H, 9.49; H, 3.02%. Calcd for $C_{27}H_{44}NO_3Cl$; C, 69.60; H, 9.45; N, 3.01%. Further elution with light petroleum (bp 60—80 °C):ether (25:1) afforded **8**, recrystallized from methanol (2.5 g, 50%); mp 124 °C (positive Beilstein test); IR (KBr) 1645, 1630, 1285, 875, 770, 725 cm^{-1}; ^1H NMR (CCl_4) δ=0.77 (3H, s, 18-CH_3), 1.20 (3H, s, 19-CH_3), 3.80 (1H, m, $W_{1/2}$=17 Hz, 3α-H); MS, *m/z* (relative intensity) 467/465 (0.50/1.50 M^+), 416 (1), 414 (2), 398 (45), 370 (15).

Zinc-Acetic Acid Reduction of 8. In warm acetic acid (100 mL), **8** (1 g) was dissolved and zinc dust (5 g) was added portionwise during 15 min. The mixture was stirred for 1 h at 30 °C. It was concentrated to half volume and diluted with saturated brine (300 mL) and filtered, and then worked up as usual to obtaine crude **9**, crystallized from methanol (600 mg, 60%); mp 127 °C (lit,[19] 128—129 °C); IR (nujol) 1705, 740 cm^{-1}.

Reaction of 3 with NOCl. Reaction of NOCl with **3** (5 g) in CCl_4 (250 mL) was carried out worked up in the similar fashion. An orange-colored oily mass thus obtained was chromatographed over a column of silica gel (80 g). Elution with light petroleum (bp 60—80 °C) furnished **10**, recrystallized from light petroleum (bp 40—60 °C) (1.1 g, 22%); mp 95 °C (positive Beilstein test); IR (nujol) 1650, 770, 760 cm^{-1}; ^1H NMR ($CDCl_3$) δ=0.65 (3H, s, 18-CH_3), 1.28 (3H, s, 19-CH_3), 3.68 (1H, m, $W_{1/2}$=17 Hz, 3α-H); MS, *m/z* (rel intensity) 440/438 (2/6, M^+), 437 (3), 435 (9), 424 (6), 422 (17), 405 (16), 403 (47). Found: C, 73.88; H, 10.00%. Calcd for $C_{27}H_{44}Cl_2$: C, 73.80; H, 10.02%. Further elution with light petroleum (bp 60—80 °C):ether (85:1) afforded **11**, recrystallized from acetone (2.3 g, 46%); mp 114 °C (positive Beilstein test); IR (KBr) 1650, 1630, 1275, 865, 770, 760 cm^{-1}; ^1H NMR ($CDCl_3$) δ=0.72 (3H, s, 18-CH_3), 1.19 (3H, s, 19-CH_3), 4.7 (1H, m, $W_{1/2}$=18 Hz, 3α-H, A/B ring junction trans);[6] MS, *m/z* (rel intensity) 467/465 (1/3, M-CH_3), 440 (12), 438 (35), 405 (4), 403 (3), 403 (7). Found: C, 67.47; H, 9.31; N, 5.85%. Calcd for $C_{27}H_{45}N_2O_3Cl$: C, 67.43; H, 9.37; N, 5.83%. Continued elution with light petroleum (bp 60—80 °C):ether (80:1) provided **12**, recrystallized from methanol (1.3 g, 26%); mp 124—126 °C (positive Beilstein test); IR (KBr) 1638, 1557, 1362, 760, 680 cm^{-1}; ^1H NMR ($CDCl_3$) δ=0.72 (3H, s, 18-CH_3), 1.12 (3H, s, 19-CH_3), 2.8 (2H, d, J=4.5 Hz, 4-Hz), 4.82 (1H, m, $W_{1/2}$=6.5 Hz, 3β-H, A/B ring junction cis);[6] MS, *m/z* (rel intensity) 464/462 (3/9, M-HCl), 431 (5), 404 (13), 402 (40), 386 (4), 384 (12). Found: C, 65.00; H, 8.86; N, 5.58%. Calcd for $C_{27}H_{44}N_2O_2Cl_2$: C, 64.93; H, 8.82; N, 5.61%.

Zinc-Acetic Acid Reduction of 11. In warm acetic acid (100 ml), **11** (1 g) was dissolved and zinc dust (10 g) was added portionwise in 15 min. The mixture was stirred for 30 min at 30 °C. Acetic acid was evaporated to its half volume and saturated brine (300 mL) was added. After working up in usual fashion and oil was obtained which was chromatographed over silica gel (40 g) column. Elution with light petroleum (bp 60—80 °C): ether (40:1) gave **9** (500 mg, 50%). Further elution with light petroleum (bp 60—80 °C): ether (10:1) furnished **13**, recrystallized from methanol (100 mg, 10%); mp 172 °C (lit,[20] mp 175 °C); IR (nujol) 1653, 730 cm^{-1}.

Hydrolysis of 12. A mixture of **12** (2 g), methanol (250 mL) and HCl (10 mL) was heated under reflux for 1 h and was diluted with excess of water, and worked up in usual fashion which fetched **14** as yellowish sticky semisolid (1.7 g, 85%), (positive Beilstein test); IR (nujol) 1720, 760, 675 cm^{-1}; ^1H NMR ($CDCl_3$) δ=0.80 (3H, s, 18-CH_3), 1.15 (3H, s, 19-CH_3), 1.9 (2H, d, J=4 Hz, 4-Hz), 4.0 (1H, m, $W_{1/2}$= 8 Hz, 3β-H, A/B ring junction cis);[6] MS *m/z* (rel intensity) 456/454 (5/15, M^+), 452 (26), 418 (20), 416 (62), 398 (4), 382 (10), 353 (13). Found: C, 71.29; H, 9.62%. Calcd for $C_{27}H_{44}OCl_2$: C, 71.21; H, 9.67%.

Oximation of 14. A mixture of **14** (500 mg), hydroxylamine hydrochloride (1 g) and sodium acetate trihydrate (1.5 g) in ethanol (60 mL) was heated under reflux for 1.5 h. The excess of ethanol was evaporated and cold water was poured in. The crude oxime was filtered, washed with water and air dried. Recrystallization from ethanol yielded **15** (350 mg, 70%); mp 153 ° (lit,[21] mp 155 °C): IR (KBr) 3450, 1668, 750, 695 cm^{-1}; ^1H NMR (CCl_4) δ=0.65 (3H, s, 18-CH_3), 1.18 (3H, s, 19-CH_3), 4.50 (1H, m, $W_{1/2}$=8 Hz, 3β-H, A/B ring junction cis),[6] 7.90 (1H, s, 6=N-OH).

Reaction of 15 with NOCl. In CCl_4 (20 mL), 15 (250 mg) was dissolved and cooled to 0 °C. NOCl gas was passed through the solution for 1 h. The solvent was evaporated and taken in ether and worked as usual. Removal of the solvent gave crude **12**, crystallized from methanol (150 mg, 60%); mp 123—126 °C.

Dehydrochlorination of 14. **14** (1 g) was refluxed in pyridine (20 mL) for 2 h. The reaction mixture after work up provided an oil which was chromatographed over silica gel (25 g). Elution with light petroleum (bp 60—80 °C): ether (20:1) afforded **16**, recrystallized from acetone (200 mg, 20%); mp 127—128 °C (lit,[22] mp 128 °C) (negative Beilstein test); IR (KBr) 1673, 1625 cm^{-1} continued elution with light petroleum (bp 60—80 °C):ether (15:1) furnished **17**, recrystallized from light petroleum (bp 40—60 °C) (350 mg, 35%); mp 165 °C (lit,[21] mp 165 °C) (positive Beilstein test); IR (KBr) 1685, 1620, 740 cm^{-1}.

We are grateful to Professor M. S. Ahmad for provision of facilities and useful discussion.

References

1) K. Tanabe and R. Hayashi, *Chem. Pharm. Bull. (Tokyo)*, **10**, 1177 (1962).
2) A. Terada and A. Hassner, *Bull. Chem. Soc. Jpn.*, **40**, 1937 (1967).
3) Shafiullah and M. R. Ansari, *J. Indian. Chem. Soc.*, in press.
4) Shafiullah and S. Husain, *J. Chem. Res. (S)*, **1983**, 255.
5) R. M. Silverstein, G. C. Basster, and T. C. Morill, "Spectrometric Identification of Organic Compounds," Wiley, San-Fransisco (1981).
6) N. S. Bhacca and D. H. Williams, "Application of NMR Spectroscopy in Organic Chemistry," Holden-Day, San-Fransisco (1964).
7) N. B. Colthup, L. H. Daly, and S. S. Wiberley, "Introduction to Infrared and Raman Spectroscopy," Academic Press, New York (1975).
8) F. Hodoson, I. Jude, N. Serben, and A. Balogh, *Chem. Ber.*, **95**, 1094 (1962).
9) H. Rheinboldt and M. Dewald, *Liebigs. Ann. Chem.*, **451**; 273 (1927); **455**; 300 (1927); **460**: 305 (1928).
10) M. J. Hair and G. A. Boswell, Jr., *J. Org. Chem.*, **42**, 4251 (1977).
11) Y. Komeichi, S. Tomioka, T. Iwasaki, and K. Watanabe, *Tetrahedron Lett.*, **1970**, 4677.
12) J. A. Boswell, *J. Org. Chem.*, **33**, 3699 (1968).
13) B. Rezabora, J. Hora, V. Landa, Cerny, and F. Sorm, *Steroids*, **11**, 475 (1968).
14) F. Jarreau, M. B. Tchouber, and R. Gouteral, *Bull. Soc. Chim. Fr.*, **1962**, 887.
15) I. M. Heilbron, J. Hodges, and F. S. Spring, *J. Chem. Soc.*, **1938**, 759.
16) M. S. Ahmad, Shafiullah, and M. Mushfiq, *Tetrahedron Lett.*, **1970**, 2739.
17) J. R. Morton and H. W. Wilcox, *Inorg. Synth.*, **4**, 48 (1953).
18) I. M. Heilbron, E. R. H. Jones, and F. S. Spring, *J. Chem. Soc.*, **1937**, 801.
19) A. Windans and O. Dalmer, *Chem. Ber.*, **52**, 162 (1919).
20) E. G. Ford, P. Chakravorty, and E. S. Wallis, *J. Am. Chem. Soc.*, **60**, 413 (1938).
21) M. Hussain and N. H. Khan, *Synth. Commun.*, **11**, 185 (1981).
22) H. Reich, F. E. Walker, and R. W. Collins, *J. Org. Chem.*, **16**, 1753 (1951); M. S. Ahmad and N. K. Pillai, *Aust. J. Chem.*, **26**, 603 (1973).

Hydrogenation of Aromatic Nitro Compounds with A Pt/SiO_2-$AlPO_4$ Catalyst

M. Angeles Aramendía Lopidana, Victoriano Borau Bolos, Cesar Jiménez Sanchídrían, J. María Marinas Rubio,* and Francisco Rodero Luque
Department of Organic Chemistry, Faculty of Sciences, Córdoba University, Córdoba, Spain
(Received April 28, 1986)

In this work we have carried out the reduction of aromatic nitro compounds bearing different substituents with gaseous hydrogen, over a Pt catalyst (3% by weight) supported on a SiO_2-$AlPO_4$ system. The catalyst was obtained by impregnation, the impregnating metal salt being reduced with α-phellandrene. The kinetic data found allow us to describe the reduction of nitrobenzene as a Langmuir-Hinslwood kinetic. The sequence of reaction rates for the different nitro compounds assayed conforms to the Hammett-Taft equation, which allows relating the electron density of the aromatic ring to the reduction rate of the nitro group. Finally, we propose mechanism for the process, characterized by the absence of intermediates with net charges.

The reduction of nitro compounds has been comprehensively studied by many authors with the aid of the metal-acid system,[1] using gaseous hydrogen,[2,3] or by hydrogen transfer[4-6] over Fe, Ni, or Pd catalysts supported on silica or alumina,[7,8] as well as in homogeneous phase.[9,10] In spite of being a well-known process, its remarkable industrial applications are responsible for the interest which it still arises among researchers. The solids most frequently used as supports are silica, alumina, carbon, and zeolites.

Aluminum orthophosphates, either pure or mixed with SiO_2 or Al_2O_3, are stable solids whose texture properties and acidity may be controlled in the synthetic procedure[11,12] and which have proved to be excellent as supports for Pd and Pt catalysts in some reduction processes.[13,14] These systems have also been used as supports for nickel (both by our team[15-17] and by Marcelin et al.[18,19]) and rhodium.[20,21] Recently, some authors have begun to prepare catalysts prereduced under reflux with olefinic[22] or hydroaromatic compounds or even other substances which decompose to simple products.[23]

The mechanism through which the reduction of nitro compounds takes place is quite well understood when the reduction is carried out with the metal-acid system; this process begins with the attack of a hydrogen atom:

$$C_6H_5NO_2 \xrightarrow[\text{slow}]{H\cdot} C_6H_5\text{-}\overset{\oplus\cdot}{N}\begin{matrix}\diagup O\text{-}H \\ \\ \diagdown \ddot{O}:^{\ominus}\end{matrix} \rightarrow \rightarrow \rightarrow C_6H_5NH_2 \quad (1)$$

(fast)

However, when the reduction is performed with supported metals, the nature of the support may result in the formation of protons and hydride ions on the metal surface, these species becoming the actors of the reduction process.

On the other hand, in the hydrogenation of nitro compounds with supported palladium catalysts, Carturan et al.[24] found that the rate-determining step in the reduction of a nitro compound with a metal catalyst may be the hydrogenation of the metal surface oxidized by the sorbed nitro compound.

In this work we have carried out the reduction of aromatic nitro compounds with different substituents over Pt catalysts supported on SiO_2-$AlPO_4$. The results obtained seem to indicate that the reduction of the nitro group is not an isolated process of the molecular rest, and that the electron density of the neighboring aromatic ring influences the reduction rate.

Experimental

Support. We have used a support made of SiO_2-$AlPO_4$ (80:20% by weight) named F72, the synthesis and properties of which were described elsewhere.[11,12] Summarized, its texture properties are described as follows: S_{BET}=247 m^2g^{-1}; average pore radius=32 Å; cumulative pore volume= 0.59 mLg^{-1}.

Catalyst. We have used a Pt catalyst (3% by weight) deposited on support F72. It was prepared by impregnation from an aqueous solution of K_2PtCl_6.

The supported metal salt was reduced by keeping the solid under reflux with α-phellandrene at 453 K for 2 h. The resulting catalyst was washed several times with methanol and vacuum-dried prior to use.

The catalyst nomenclature includes the symbol of the metal deposited, the percent loading and the name of the support (F72 in this case).

Apparatus. The reduction of nitrobenzene with gaseous hydrogen was accomplished in a low pressure Gerhardt reactor fitted with a pressure gauge which measured the evolution of the hydrogen pressure in the reaction vessel. All reactions were carried out at 300 K, using methanol as solvent (V_{total}= 20 mL) and 3×10^{-3} g of metal. The reaction temperature was controlled by means of a thermostatic bath.

The reaction rate was calculated from the slope of the straight line obtained by plotting the consumption (in moles of hydrogen) as a function of time.

All reagents used were high-purity commercial chemicals.

Product Analysis. The reaction products were analyzed by gas chromatography, using high-purity standards in their characterization. Their presence was confirmed by mass spectrometry using GC-MS systems.

The products obtained were the corresponding anilines; no by-products or reaction intermediates were detected in

any case. *m*-Dinitrobenzene was reduced selectively to *m*-nitroaniline.

Determination of Metal Particle Size. The metal particle size was determined by X-ray diffraction. The X-ray diffractogram was recorded on a Philips 1130/00/60 apparatus, using the Co $K\alpha$ radiation, with λ=1.7889 Å. The half-peak width was measured graphically at an angle 2θ=46.52° corresponding to plane (1 1 1) of Pt, assuming a value of 0.89 for the Debye-Scherrer constant.

The metal surface, $S(m^2g_{Pt}^{-1})$ was obtained from the mean particle diameter, D (Å), using the relation: $S=6\times10^{-4}/\rho D$, where ρ is the density of platinum (g cm^{-3}).

The metal surface was determined by assuming the spherical particle model. The mean diameter of the metal cristallites was 55 Å and the metal surface 51 $m^2g_{Pt}^{-1}$ for the synthesized catalyst.

Results and Discussion

Influence of the Solvent. Table 1 shows the results obtained in the hydrogenation of nitrobenzene in various solvents. As can be observed, methanol provided the best results and was therefore chosen for all subsequents experiments.

Reaction Kinetic. We have carried out blank test at 300 K in order to confirm the absence of phenomena extraneous to the catalytic process. Neither the support nor any other part of the reactor was found to be active in the nitro compound reduction. Neither did we observe any diffusion phenomena when shaking the reaction mixture at 200 shakes min^{-1} nor intraparticular diffusion in the catalyst studied.

We have checked that the transfer hydrogen from the gas phase to the reaction medium is not the rate-limiting step of the process. Figure 1 shows the straight line obtained by plotting the reciprocal of the reaction rate (in mol of nitrobenzene s^{-1}) obtained at 300 K as a function of the reciprocal of the amount of catalyst used.

The rate of transfer of hydrogen from the gas phase to the catalyst, calculated from the intercept, is much higher than any of the reaction rates found in our experiments. Thus, we can state that the process is not governed by the diffusion of hydrogen to the catalyst surface through the liquid phase.

Hydrogen pressures in the range 3.1—6.2 bar and nitrobenzene concentrations between 0.1—1.0 M (1 M=1 mol dm^{-3}) were used in the determination of the kinetic parameters. The reaction kinetic was studied using methanol as solvent.

We have observed that, under the reaction conditions used, the reaction order with respect to nitrobenzene changes in the manner illustrated in Fig. 2. This order which has a value of 0.48 for nitrobenzene concentrations between 0.1—0.25 M, begins to decrease above this range until eventually becoming zero at a concentration of 0.4 M. The dependence of the reaction order on the concentration may be attributed to the sensitivity of adsorption equilibria to changes in the concentration of a liquid phase reactant.[25,26]

In the range wherein the order in nitrobenzene is zero, the reaction order with respect to hydrogen is 0.92. Under these conditions, the kinetic rate law found was:

$$V = K|P_{H_2}|^{0.92}, \quad (2)$$

where K is the pseudo rate constant.

Table 1. Influence of the Solvent on the Reduction of Nitrobenzene with Gaseous Hydrogen Catalyst Pt 3 F72

Solvent	V_0/mol s^{-1} $m_{Pt}^{-2}\times10^6$	ε
Methanol	48.4	32.6
Tetrahydrofuran	15.7	
N,*N*-Dimethylformamide	14.4	38.0
Dioxane	11.1	2.2
Chloroform	3.6	4.8

* Hydrogen pressure: 5.06 bar; nitrobenzene concentration: 0.5 M; total volume: 20 mL; reaction temperature: 300 K. ε: dielectric constant at 298 K.

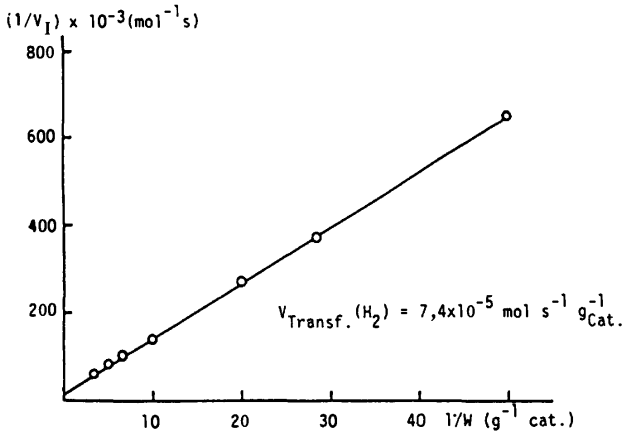

Fig. 1. Plot of $1/V_1$ vs. $1/W$ for the reduction of nitrobenzene with H_2 gaseous.

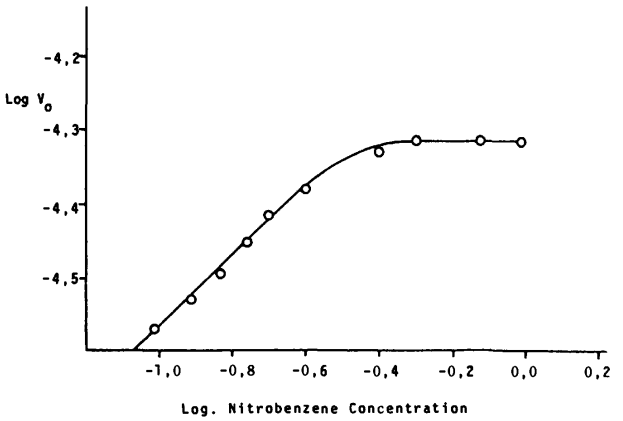

Fig. 2. Logarithmic plot of V_0 as a Function of the nitrobenzene concentration.

The results found are consistent with a Langmuir-Hinselwood type mechanism for which several expressions may be formulated.[27] Our experimental results comform the expression:

$$r_1 = K_0 \frac{KP_{H_2}}{1+KP_{H_2}}, \quad (3)$$

with a correlation coefficient better than 0.99 and with a positive intercept for all temperatures studied. These results are in favor of a noncompetitive adsorption Langmuir-Hinselwood mechanism.

Hydrogenation of Various Nitro Compounds. Table 1 lists the rates of nitrobenzene reduction obtained by using different solvents. There is no correlation between the dielectric constant of the solvent and the reaction rate obtained, which indicates that no net charges (which would result in the formation of carbonium ions or carbanions) develop along the process. Similar results were obtained by using Pd catalysts supported on the same solid in the reaction of nitro compounds with dihydrogen.[28] However, the process is essentially different when the nitro compound reduction is carried out by hydrogen transfer.[29] In that case, the solvent polarity has a strong influence on the reduction rate of the nitro compound, and the determining step of the process may be assumed to involve the attack of a hydride ion or a proton, depending on the electron-withdrawing or electron-releasing nature of the substituent borne by the aromatic ring.[30,31]

Figure 3 illustrates how the results obtained in the reduction of various nitrocompounds in different solvents conform to the Hammett equation in the form: Log $V_1/V_{1o}=\sigma\rho$, where V_1 and V_{1o} are the reduction rate of the substitued nitrobenzene and nitrobenzene respectively.

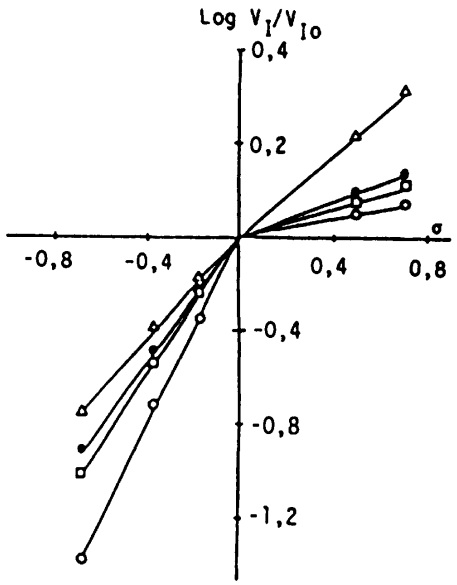

Fig. 3. Correlation between $\log(V_1/V_{10})$ and for various nitro compounds.

○ Methanol; □ DMF; ● THF; △ $CHCl_3$.

The straight line obtained show a different behavior of the nitro compounds according to whether the substituent is an electron-releasing of electron-withdrawing one. The substituents present only seem to participate through their electric effects. A worse fitting of the experimental results is observed by plotting the corresponding σ^+ or σ^- of the substituents, assuming the involvement of mesomeric effects which would stabilize charged intermediates. The electric effect of the substituent is transmitted through the aromatic ring, either increasing or decreasing the electron density on the nitro group to be reduced. The value of ρ (specific reaction constant), calculated from the slope of the straight lines shown in Fig. 3, provides information on the mechanism through which the process takes place. The value of ρ depends on the particular solvent used, as well as on the electron-releasing or electron-withdrawing nature of the substituents.

As can be observed, the slope changes at the origin, which is indicative of a change either in the mechanism proper or in the sensitivity of the process to the electron-releasing or electron-withdrawing effect of the substituents. The small absolute values of ρ show the slow step of the process to involve a transfer of charge or electron density rather than an appreciable mass transfer.

The results obtained can be accounted for in two ways:

a) According to the following scheme:

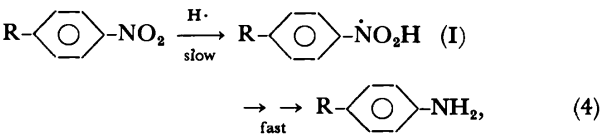

(4)

in which the stability of intermediate I is affected by the electron-releasing or electron-withdrawing nature of group R. The mechanism involved in the reduction of nitro compounds is basically the same as that described for the reduction with metal-acid systems,[1] and differs from the one proposed for the reduction of aromatic nitro compounds by hydrogen transfer using Pd supported catalysts in that the rate-determining step of these is supposed to be the transfer of a hydride ion.[28] Other authors have proposed mechanism for the reduction of nitro compounds with metal hydrides[32] or by transfer[9] in which the process starts with the attack of a hydride ion. Recently, it has been observed that the attack of the hydride species can be regarded as the result of three successive stages; an electron, a proton and a new electron.[33] Our results do not seem to indicate the presence of species with net charges in the rate-determining step. The nature of substituent may facilitate or hinder the adsorption of the nitro compound, since it modifies the electron

density on the aromatic ring. Taft et al.[34-36] have studied the variation of the electron density on the carbon atom to which the nitro group is linked as a function of the substituent borne by the ring in different aromatic nitro compounds. Such electron density varies in much the same way as the reaction rates found in this work and in several others.[28,32] For electron-withdrawing substituents, the slope of the straight line obtained is 0.1, whereas for electron-releasing groups, the slope is 2.0, the line corresponding to the reference compound (nitrobenzene) showing an inflection point. Therefore, the aromatic ring seems to inequivocally cooperate in the reduction of the nitro group. Electron withdrawing substituents favor the adsorption of the nitro compound and contribute to stabilize the intermediate generated, which bears unpaired electrons.

In view of the results obtained, the catalyst must have a metal surface with a high electron density which favors the adsorption of the nitro compound. By assuming the possible interaction between the aromatic ring and the metal surface, the ease of adsorption of the nitro compound will increase with decreasing electron density on the aromatic ring as a result of the electron withdrawing effect of the substituent. Table 2 shows the initial rates of hydrogenation of various nitro compounds. The electron configuration of platinum, $5d^9\ 6s^1$, suggests the possibility of an electron flux from the support to the metal, which would result in the filling of the vacant upper levels and hence in increased surface electron density.

b) On the other hand, the mechanism of the process may involve nitrenes according to the scheme proposed by Carturan et al.[24] for the hydrogenation of aliphatic and aromatic nitro compounds by use of supported palladium catalysts:

$$ArNO_2 + \text{metal} \xrightarrow[(1')]{} \text{oxidized metal surface} + ArN\text{:}\ (ads)$$

$$\xrightarrow[(2')]{ArNO_2} R\text{-}\overset{|}{N}\text{-}O\text{-}\ (\text{dimeric or oligomeric intermediates})$$

$$\xrightarrow{H_2} R\text{-}NH_2 + \text{metal} + H_2O\,. \qquad (5)$$

Table 2. Initial Rates of Hydrogenation of Various Nitro Compounds. Catalyst: Pt 3 F72

Nitro compound	σ	V_I/mol s^{-1} $m_{Pt}^{-3} \times 10^6$
p-Aminonitrobenzene	−0.66	2.0
p-Nitrophenol	−0.37	9.0
p-Nitrotoluene	−0.17	21.6
Nitrobenzene	0.00	48.4
p-Nitroacetophenone	0.50	54.3
m-Dinitrobenzene	0.71	56.8

* Hydrogen pressure: 5.06 bar; nitro compound concentration: 0.5 M; Total volume: 20 mL; reaction temperature: 300 K; solvent: methanol.

By analogy with the mechanism proposed by these authors, we may think that the presence of electron releasing groups would slow down stage (1') and hence inhibit the formation of the nitrene, thus giving rise to lower conversion than nitrobenzene. Conversely, the presence of electron withdrawing substituents would stabilize the intermediate nitrene and speed up stage (2') with respect to nitrobenzene.

According to Carturan et al.,[24] the tentative formulation of dimeric or oligomeric R-N-O- intermediates is consistent with nitrene reactivity. On the other hand, the deoxygenation of nitro groups by metal catalysts via intermediate nitrenes is similar to the process described by Cadogan, who uses homogeneous phosphine catalysts.[37] The occurrence of nitrenes has also been proposed by Watanabe et al.[38] as intermediates in the reduction of nitroarenes to aminoarenes with carbon monoxide and water.

This study has been carried out with a grant from the "Consejería de Educación y Ciencia de la Junta de Andalucía".

References

1) J. March, "Advanced Organic Chemistry. Reactions, Mechanisms and Structure," 3rd ed, John Wiley, New York (1985), p. 1103.

2) P. Rylander, "Catalytic Hydrogenation over Platinum Metals," Academic Press Inc., New York (1967), p. 168.

3) T. Cole, R. Ramage, C. Cann, and R. Pettit, *J. Am. Chem. Soc.*, **102**, 6182 (1980).

4) A. Bar-Ilan and J. Manassen, Procc, Vth International Congress on Catalysis, ed by Elsevier., New York (1973), Vol. II, p. 1149.

5) N. A. Cortesse and R. F. Heck, *J. Org. Chem.*, **42**, 3491 (1977).

6) D. C. Dittmer and J. M. Koyler, *J. Org. Chem.*, **27**, 56 (1962).

7) E. A. Braude, R. P. Linstead, and P. W. D. Mitchell, *J. Chem. Soc.*, **1954**, 3578.

8) G. Brieger, T. J. Nestrick, and T. H. Fu, *J. Org. Chem.*, **44**, 1876 (1979).

9) A. Ohno, H. Yamamoto, and S. Oka, *Tetrahedron Lett.*, **42**, 406 (1979).

10) K. Cann, T. Cole, W. Slegeir, and R. Pettit, *J. Am. Chem. Soc.*, **100**, 3969 (1978).

11) C. Jimenez, J. M. Marinas, R. Perez-Ossorio, and J. V. Sinisterra, *An. Quim.*, **73**, 1164 (1976).

12) J. M. Marinas, C. Jimenez, J. M. Campelo, M. A. Aramendía, V. Borau, and D. Luna, Vth Symp. Iber-Amer. on Catal., La Plata (Argentina) (1980), Vol. I, p. 79.

13) M. A. Aramendía, V. Borau, C. Jimenez, and J. M. Marinas, *Bull. Soc. Chim. Belg.*, **91**, 743 (1982).

14) M. A. Aramendía, V. Borau, C. Jimenez, J. M. Marinas, and J. A. Pajares, *J. Catal.*, **78**, 188 (1982).

15) J. M. Campelo, A. García, J. M. Gutierrez, D. Luna, and J. M. Marinas, *Appl. Catal.*, **7**, 307 (1985).

16) J. M. Campelo, A. García, D. Luna, and J. M. Marinas, *Bull. Soc. Chim. Belg.*, **92**, 851 (1983).

17) J. M. Campelo, A. García, D. Luna, and J. M. Marinas, *J. Catal.*, **97**, 108 (1986).
18) G. Marcelin, R. F. Vogel, and H. E. Swift, *J. Catal.*, **83**, 47 (1983).
19) G. Marcelin and J. E. Lester, *J. Catal.*, **93**, 270 (1985).
20) J. M. Campelo, A. García, D. Luna, and J. M. Marinas, *Colloids Surfaces*, **5**, 227 (1982).
21) J. A. Cabello, J. M. Campelo, A. García, D. Luna, and J. M. Marinas, *J. Catal.*, **94**, 1 (1985).
22) R. Gorevit and M. Tsutsui, *Adv. Catal.*, **27**, 227 (1978).
23) L. Cerveny, J. Mojzisova, and V. Cuzicka, *Appl. Catal.*, **12**, 35 (1984).
24) G. Carturan, G. Facchin, G. Cocco, G. Navazio, and C, Gubitosa, *J. Catal.*, **82**, 56 (1983).
25) J. W. E. Coenen, R. Z. C. Van Meerten, and H. Rijnten, Vth International Congress on Catalysis, ed by J. W. Hightower, Miami Beach (1972), Vol. I, p. 671.
26) M. A. Aramendía, C. Jimenez, V. Borau, and J. M. Marinas, *Acta Cientifica Venezolana*, in press.
27) K. J. Laidler, "Chemical Kinetics," ed by McGraw-Hill, New York (1965), p. 273.
28) M. A. Aramendía, V. Borau, J. Gomez, C. Jimenez, and J. M. Marinas, *Appl. Catal.*, **10**, 347 (1984).
29) M. A. Aramendía, M. S. Climent, C. Jimenez, and J. M. Marinas, *React. Kinet. Catal. Lett.*, **14**, 489 (1980).
30) D. Beaupere, P. Bauer, and R. Uzan, *Can. J. Chem.*, **57**, 218 (1979).
31) J. P. Seguin, D. Beaupere, P. Bauer, and R. Uzan, *Bull. Soc. Chim. Fr.*, **1-2**, 168 (1978).
32) M. G. Swanwich, and W. A. Waters, *J. Chem. Soc., D*, **1970**, 63.
33) M. I. Kalinkin, G. D. Kolomnikova, Z. N. Parnes, and D. N. Kursanov, *Russ. Chem. Rev.*, **48**, 332 (1979).
34) J. Bromilow, R. Y. Brownlee, D. J. Craik, M. Sadek, and R. W. Taft, *J. Org. Chem.*, **45**, 2429 (1980).
35) J. Bromilow, R. T. Brownlee, V. O. Lopez, and R. W. Taft, *J. Org. Chem.*, **44**, 4766 (1979).
36) R. T. Brownlee, D. G. Cameron, A. R. Katritzky, and A. F. Pozharsky, *J. Chem. Soc., Perkin Trans. 2*, **1974**, 247.
37) J. J. G. Cadogan, *Q. Rev. Chem. Soc.*, **22**, 222 (1968).
38) Y. Watanabe, Y. Tsuji, T. Ohsumi, and R. Takeuchi, *Bull. Chem. Soc. Jpn.*, **57**, 2867 (1984).

t-BuCl-NaI as a Reagent for the Selective Reduction of Olefinic Double Bond of β-Phenyl α,β-Unsaturated Carbonyl Compounds

Takashi SAKAI,* Kazuyoshi MIYATA, Kazuomi HONDO, Masanori UTAKA, and Akira TAKEDA

Department of Synthetic Chemistry, School of Engineering, Okayama University, Tsushima, Okayama 700

(Received March 24, 1987)

Synopsis. β-Phenyl α,β-unsaturated carbonyl compounds were conveniently reduced to the corresponding saturated aromatic compounds by heating with t-BuCl-NaI in acetonitrile.

We recently disclosed that the Me_3SiCl-NaI-ROH reagent was useful for the selective reduction of olefinic double bond of β-phenyl α,β-unsaturated carbonyl compounds and that the reduction was explained by the 1,4-addition of HI and subsequent attack of an iodide anion to the resulting β-iodo carbonyl intermediate.[1] In this paper, we report that t-BuCl-NaI was found to be effective for a similar reduction (Scheme 1). The applicability of the reaction was examined by using the same substrates **1a-f** as those employed in the preceeding paper.[1] The present method has advantages that the reagent is readily available and can be handled without a special care to moisture. Yields of the reduction products **2a—f** shown in Table 1 were comparable with those observed for the reaction with Me_3SiCl-NaI-ROH reagent.[1]

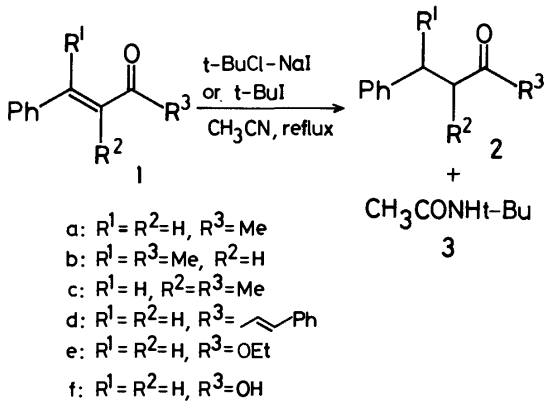

Scheme 1.

The reaction simply involves heating of the substrates **1a—f** with a six-molar excess of the reagent in acetonitrile for 24 h, giving **2a—f** together with a small amount of *N*-*t*-butylacetamide[2] (**3**) in every case. The reaction mixture was colored dark purple gradually due to liberation of iodine. In a typical reduction with **1a**, shortening of the reaction time to 5 h decreased the yield of **2a** and the starting **1a** was recovered in a considerable amount. Unfortunately, the present reaction is not suitable for aliphatic conjugated enones. For example, mesityl oxide was recovered unchanged.

Table 1. Reduction of β-Phenyl α,β-Unsaturated Carbonyl Compounds with t-BuCl-NaI Reagent[a]

	Substrate 1			Method[b]	Product 2
	R^1	R^2	R^3		Yield/%[c]
1a	H	H	Me	A	74[d]
				A	34[e]
				B	80[f]
1b	Me	H	Me	A	74
				B	49
1c	H	Me	Me	A	46
1d	H	H	-CH=CHPh	A	51
1e	H	H	OEt	A	86[g]
1f	H	H	OH	A	72
				B	59[f]

a) The reaction was usually done for 24 h under refluxing unless otherwise noted. b) A: t-BuCl-NaI in CH_3CN; B: t-BuI in CH_3CN. c) Yield after purification by preparative TLC. d) Reaction time of 12 h. e) Reaction time of 5 h. Thirtytwo per cent of **1a** was recovered. f) Reaction time of 7 h. g) A 65:35 mixture of the ester **2e** and its acid.

The present reduction would be caused by the in situ generated HI in a manner similar to that described previously.[1] The handling of gaseous HI is not easy, because it readily decompose to iodine and hydrogen molecules.[3] The t-BuCl-NaI reagent is suitable for generation of HI in a reaction vessel. The liberation of isobutene[4] was detected by GLPC analysis.[5] The minor by-product **3** may be formed by the reaction of acetonitrile either with isobutene[2a] or t-BuCl.[2b] Furthermore, the applicability of t-BuI to the reaction was ascertained, although it is far more expensive than t-BuCl.

The present reaction is the first example utilizing t-BuCl-NaI as a reagent for the selective reduction of conjugated olefin of β-phenyl α,β-unsaturated carbonyl compounds.

Experimental

General. IR spectra were taken on a JASCO A-102 spectrometer. ^1H NMR spectra (60 MHz) were measured with a JEOL JNM-60 SI spectrometer using Me_4Si as an internal standard. GLPC analysis was done with a Hitachi 163 gas chromatograph.

General Procedure for the Reduction of 1a—f. Sodium iodide (1.80 g, 12 mmol) was placed in a reaction vessel and the atmosphere is replaced by nitrogen. To this was added a

solution of the substrate **1** (2 mmol) and *t*-butyl chloride (1.11 g, 12 mmol) in acetonitrile (2 ml). The mixture was stirred for the time indicated in Table 1 under refluxing. After addition of water, the ether extract was washed with aqueous sodium thiosulfate to remove liberated iodine and then with water, dried ($MgSO_4$), and concentrated. The residual oil was purified by preparative TLC (Merck, Kieselgel 60, PF_{254}, hexane–ether, 3:1) to give the reduction product **2** and *N*-*t*-butylacetamide[2] (60—70 mg).

Reduction of 1a with *t*-BuI. A mixture of **1a** (73 mg, 0.5 mmol), *t*-BuI (0.35 ml, 3.0 mmol), and acetonitrile (1 ml) was heated under reflux for 7 h. The reaction mixture was treated in a similar manner. The yield of **2a** by GLPC analysis of the crude product was 80%.

References

1) T. Sakai, K. Miyata, M. Utaka, and A. Takeda, *Bull. Chem. Soc. Jpn.*, **60**, 1063 (1987).

2) a) K. Ya. Alieva, D. Z. Samedova, S. S. Avanesova, Kh. M. Gadzhieva, and T.. N. Shalchtakhtinskii, *Dokl. Akad. Nauk Az. SSR.*, **32**, 18 (1976), *Chem. Abstr.*, **86**, 43157z; b) R. D. Bach, J. W. Holubka, and T. A. Taaffee, *J. Org. Chem.*, **44**, 1739 (1979).

3) E. R. Caley and M. G. Burford "Inorganic Syntheses," Vol. 1, p. 159.

4) E. D. Hughes, C. K. Ingold, and J. D. Mackie, *J. Chem. Soc.*, **1955**, 3173.

5) The retention time was compared with that of a commercially available sample (3.0 min, liquid phase thermon-1000, type FFS, 0.25 mm×30 m, oven temperature 70 °C, N_2 180 ml min^{-1}).

Selective 1,2-Reduction of α,β-Unsaturated Carbonyl Compounds with $LnCpCl_2(THF)_3/NaBH_4$

Sanshiro KOMIYA* and Osamu TSUTSUMI
Department of Applied Chemistry for Resources, Tokyo University of Agriculture and Technology, 2-24-16 Nakamachi, Koganei, Tokyo 184
(Received March 27, 1987)

Synopsis. Highly selective 1,2-reduction of conjugated α,β-unsaturated carbonyl compounds such as enones and unsaturated aldehydes has been achieved by $NaBH_4$/$LnCpCl_2(THF)_3$ (Ln=Sm and Er) in MeOH under ambient conditions.

Utilization of organolanthanoid reagents to organic reactions has been recently attracting growing attention.[1] Although lanthanoid compounds are now available in large quantities and in very pure form, their chemical uses are still very limited. Luche et al. reported lanthanoid ion-promoted reduction of enones to allylic alcohol with $NaBH_4$,[2] which is of interest, since the regio- and chemoselectivity is in sharp contrast to the reduction promoted by $NaBH_4$ in the presence of late transition metal complexes as well as to the reduction with $NaBH_4$ in pyridine.[2,3] We now report the highly chemo- and regioselective 1,2-reduction of conjugated unsaturated carbonyl compounds with $NaBH_4$ assisted by organolanthanide complexes, $LnCpCl_2(THF)_3$ (Ln=Sm and Er)[4] in methanol.

Table 1 summarizes the results of selective reduction of α,β-unsaturated carbonyl compounds with $NaBH_4/LnCpCl_2(THF)_3$. When a half-molar amount of $NaBH_4$ per substrate was added into a 4:1 mixture of crotonaldehyde and $SmCpCl_2(THF)_3$ (**1**) in methanol at room temperature, crotyl alcohol was selectively obtained in an almost quantitative yield. Cinnamaldehyde was also reduced cleanly to cinnamyl alcohol. Only slight amounts of saturated alcohols and 1,4-reduction products were formed in these reactions. The present selective reduction is also applicable to various alicyclic and cyclic enones such as methyl vinyl ketone, cyclopentenone and cyclohexenone, to give corresponding allylic alcohols in

Table 1. Reduction of α,β-Unsaturated Ketones and Aldehydes with $NaBH_4/LnCpCl_2(THF)_3$[a]

Substrate	Complex	Yield/%[b]	Product ratio/%[c]		
			A	B	C
	1	97.7	100	0	0
	2	95.6	100	0	0
	1	90.2	92.4	0	7.6
	2	95.2	96.6	0	3.4
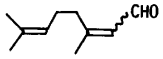	**1**	91.9	100	0	0
	2	93.3	99.9	0	0.1
	1	97.3	100	0	0
	2	97.3	99.5	0	0.5
	1	95.3	98.8	0	1.2
	2	82.7	100	0	0
	1	98.8	97.9	0	2.1
	2	98.8	97.8	0	2.2
	1	No reaction			
	2	No reaction			
	1	87.0	90.7	1.3	8.0
	1	75.1	73.0	0	27.0

a) In methanol (1.0 cm^3) at room temperature for 6 h. The ratio of substrate, $NaBH_4$, and $LnCpCl_2(THF)_3$ used was 4.4:2.2:1. b) Yields are based on the starting substrates by GLC. c) A: Allylic alcohol, B: saturated ketone, C: saturated alcohol.

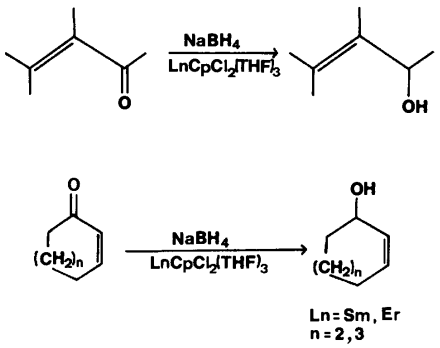

high yields as well as in high selectivity.

Although the reaction products were determined after 6 h, the reduction was actually completed after 5 min. On the other hand, reduction of 2,3,4,5-tetramethylcyclopentenone failed. Selectivity and the yields of 1,2-reduction products decrease when methyl and methoxycarbonyl substituents are placed on the cyclic enone ring. Steric effect may be important in these reduction process. Similar selective 1,2-reduction of α,β-unsaturated carbonyl compounds was also performed by using $ErCpCl_2(THF)_3$ (**2**).

Limitation of the present reduction to other organic substances was determined. Reductions of allyl phenyl ether, cyclohexene oxide, cyclohexene, allyl bromide, methyl acrylate, and crotonic acid have failed. The results demonstrate the high chemoselectivity of the reaction. Thus, the reduction of citral (neral:geranial=37:63) with **1** or **2** gave quantitative yields of a mixture of nerol and geraniol in 37:63 ratio.

Table 2 shows the reduction of 2-cyclohexen-1-one in various solvents. Polar and protonic solvent such as methanol seems to be the best for the reduction. A considerable amount of dimethoxymethane (31.2 mol%/Sm) was detected in the reduction of crotonaldehyde, suggesting participation of methanol during the reduction. An analogous mechanism proposed by Luche[2] involving solvent assisted intermediate seems to be operative.

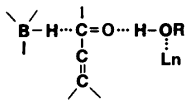

Present results are considered to be complement to the Luche's selective reduction of enones with lanthanoid metal salts.[2]

Table 2. Solvent Effect on the Reduction of 2-Cyclohexen-1-one with $NaBH_4/SmCpCl_2(THF)_3$[a]

Solvent	Yield/%	Product ratio/%[b]		
		A	B	C
Hexane	0.1	0	100	0
Benzene	0.1	0	100	0
CH_2Cl_2	0.1	0	100	0
Et_2O	1.9	84.2	15.8	0
THF	24.8	93.5	0.5	6.0
DMSO	78.2	92.9	2.8	4.3
MeOH	98.8	97.8	0	2.2
EtOH	66.9	81.6	0.8	17.6
i-PrOH	98.2	88.3	0	11.7

a) Solvent=1.0 cm^3. At room temperature for 6 h. Yields are based on 2-cyclohexen-1-one. The ratio of substrate, $NaBH_4$, and **1** was 4.4:2.2:1. b) A: 2-Cyclohexen-1-ol, B: cyclohexanone, C: cyclohexanol.

Experimental

General. All the reactions were carried out under nitrogen. Solvents were dried by usual procedure, distilled, and stored under nitrogen. Enones and unsaturated aldehydes were used after distillation of commercially available materials. $SmCpCl_2(THF)_3$ were prepared according to the literature methods.[4]

Reduction of α,β-Unsaturated Carbonyl Compounds. Typical procedure of the reduction is described below: To a homogeneous solution of a mixture of 2-cyclohexen-1-one (0.240 mmol) and $SmCpCl_2(THF)_3$ (0.057 mmol) in methanol(1.0 cm^3), $NaBH_4$ (0.120 mmol) was added at room temperature. After 6 h a quantitative yield of 2-cyclohexenol (0.232 mmol) was detected by GLC analysis. A small amount of 2-cyclohexan-1-ol (0.005 mmol) was also formed. Other experiments were carried out similarly and the results are listed in Tables 1 and 2.

References

1) T. J. Marks and I. L. Fragala, "Fundamental and Technological Aspects of Organo-f-Element Chemistry," Reidel Publishing Company, Dordrecht (1984) and references cited therein.

2) J.-L. Luche, *J. Am. Chem. Soc.*, **100**, 2226 (1978); J.-L. Luche and A. L. Gemal, *ibid.*, **101**, 5848 (1979); **103**, 5454 (1981).

3) A. Hajos, "Complex Hydrides," Elsevier Scientific Publishing Company, Amsterdam (1979), p.46.

4) S. Manastyrskyj, R. E. Maginn, and M. Dubeck, *Inorg. Chem.*, **2**, 904 (1963).

Preparation of 2-Nitromethyl-2-cycloalkenol and 2-Nitromethyl-2-cycloalkenone

Tohru SAKAKIBARA, Mangala devi MANANDHAR,*,† Noriaki OHKITA, and Yoshiharu ISHIDO*
Department of Chemistry, Yokohama City University, Seto, Kanazawa-ku, Yokohama 236
*Department of Chemistry, Faculty of Science, Tokyo Institute of Technology, Ookayama, Meguro-ku, Tokyo 152
(Received April 11, 1987)

Synopsis. Oxidation of 1-nitromethylcycloalkenes with *m*-chloroperbenzoic acid afforded the corresponding 2-nitromethyl-2-cycloalkenols, which were further converted into 2-nitromethyl-2-cycloalkenones.

We found that the double bond of α-nitro alkene **1** migrated to give the β-nitro alkene **2** on treatment with triethylamine.[1] In order to clarify if such a facile double bond migration is caused by the conjugation of the double bond formed with the ring oxygen atom, we performed the epoxidation of 1-nitromethylcycloalkenes[2] and subsequent ring opening, anticipating that an exo double bond formed should migrate to the corresponding endo isomer.

Epoxidation of 1-nitromethylcyclohexene (**3a**) with *m*-chloroperbenzoic acid (MCPBA) afforded the epoxide **4a** in 96% yield. As suggested by Takamoto et al. in oxidation of α,β-epoxy ketone oximes,[3] the epoxide ring readily opened by treatment with sodium carbonate to give a mixture of the exo **5a** and endo isomers **6a**. Although complete purification of **5a** was not accomplished, its IR [3500 (OH), 1635 and 1505 cm^{-1} (C=C-NO_2)] and ^1H NMR spectra (olefinic proton at δ=7.17) made us possible to assign the exo structure. In the case of cycloheptene derivative **4b**, the exo isomer **5b** was isolated. Treatment of **4a** with triethylamine afforded **6a** in 83% yield, indicating that, among the hydrogen atoms activated by the nitro alkene moiety, H-1 which attached to the carbon atom having the hydroxyl group is less acidic than the alternative one (H-3). This may be partly attributable to the formation of alkoxide, which should deactivate H-1 and suppress an approach of a base by electrostatic repulsion. Compound **6a** thus formed has potential utility for synthetic purposes, since nitromethyl group thus introduced should be convertible into formyl,[4] nitrile,[5] nitrile oxide,[6] and the nitro group into arylthio,[7] arylsulfonyl groups,[7] and active methylene compounds.[8] Oxidation of **6a** with pyridinium chlorochromate (PCC) afforded the ketone **7a** in 58% yield.

Similar epoxidation of the cycloheptene **3b** gave the epoxide **4b** in 84% yield, of which ring opening with sodium carbonate and triethylamine gave **5b** and **6b** in 60 and 78% yield, respectively. Oxidation of **6b** with PCC afforded the ketone **7b** in 67% yield.

Contrary to the cases of other cycloalkanones, nitromethane condensation of cyclopentanone according to the method described by Eckstein et al.[9] gave a mixture of the exo **8** and endo isomers **3c**. The mixture, without separation, was oxidized with MCPBA to afford the epoxide **4c** and unchanged exo isomer **8**. Epoxide ring opening with triethylamine gave the alcohol **6c** (60%), of which oxidation with PCC gave the ketone **7c** in 41% yield.

Unfortunately, stereoselectivity of epoxidation was low; oxidation of 1-nitromethyl-4-*t*-butylcyclohexene (**9**) with MCPBA afforded a 3:1 mixture of the epoxides **10** (based on ^1H NMR spectroscopy) in 90% yield. Without separation of the mixture, it was treated with triethylamine to afford the allyl alcohol **11** in 97% yield and subsequent oxidation gave the ketone **12** (53% overall yield from **9**).

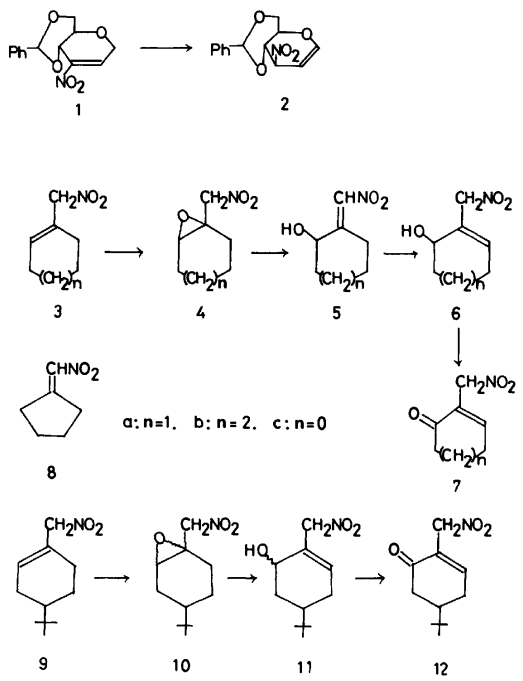

Experimental

IR spectra were recorded with a Hitachi 285 Infrared Spectrophotometer on sodium chloride plate. ^1H NMR spectra were determined in chloroform-*d* with tetramethylsilane as an internal standard with a Varian EM360A NMR Spectrometer. Column chromatography was carried out on silica gel (Wakogel, C-300). Analytical samples except for **12** were prepared by bulb to bulb distillation at the oven temperature as described.

General Procedure for the Epoxidation of 1-Nitromethylcycloalkene. To a solution of **3b** (1.55 g, 10 mmol) in dichloromethane (20 ml) was added MCPBA (1.9 g, 11 mmol), and the mixture was stirred until the starting material **3b** had disappeared in TLC (ca. 1 h) and then

† UNESCO Student, 1981—1982.

diluted with water. The aqueous layer was extracted with dichloromethane and the combined organic layers were successively washed with saturated aqueous sodium hydrogen carbonate, aqueous sodium hypochlorite, and saturated aqueous sodium chloride, dried, and evaporated to a syrup. It was purified by flash column chromatography with 3:1 (v/v) cyclohexane-benzene to give 1.44 g (84%) of 1-nitromethylcycloheptene oxide (**4b**): bp 117 °C (0.35 Torr, 1 Torr=133.322 Pa); IR 1540 cm^{-1} (NO_2); ^1H NMR δ=4.38 (2H, s, CH_2NO_2), 3.07 (1H, t, $J_{2,3}=J_{2,3'}=4.5$ Hz, H-2); Found: C, 55.76; H, 7.40; N, 7.81%. Calcd for $C_8H_{13}NO_3$: C, 56.12; H, 7.65; N, 8.18%.

1-Nitromethylcyclohexene Oxide (4a): Yield 96%, bp 78—80 °C (0.2 Torr); IR 1545 cm^{-1} (NO_2); ^1H NMR δ=4.38 (2H, s, CH_2NO_2), 3.13 (1H, t, $J_{2,3}=J_{2,3'}=2.0$ Hz, H-2); Anal. ($C_7H_{11}NO_3$) C, H, N.

1-Nitromethylcyclopentene Oxide (4c). Similar treatment of cyclopentenone (1 mmol) with nitromethane (1.5 mmol) and piperidine (0.2 ml) for 10 h gave a mixture of exo- and endo-products in the ratio of 1:2. Epoxidation of the crude product, followed by column chromatography with 9:1 (v/v) cyclohexane-benzene, gave successively the unreacted exo isomer (900 mg) and 1.05 g (72% yield, based on the starting endo isomer) of **4c**. Compound **4c**: bp 100 °C (0.35 Torr); IR 1550 cm^{-1} (NO_2); ^1H NMR δ=5.08, 4.61, 4.58, 4.11 (2H, AB type, CH_2NO_2), 3.40 (br. s, 1H, H-2); Anal. ($C_6H_9NO_3$) C, H, N.

2-Nitromethylene-1-cycloheptanol (5b). A mixture of **3b** (325.5 mg, 2.1 mmol), MCPBA (725 mg, 4.2 mmol), and dichloromethane (20 ml) was stirred for 1 h. To the mixture was added saturated aqueous sodium carbonate (20 ml) and the mixture was stirred for 8 h. Conventional work up gave a syrup, which was chromatographed with 3:1 (v/v) benzene-cyclohexane to give **6b** (8%) and **5b** (60%) in turn. Compound **5b**: bp 122 °C (0.35 Torr); IR 3450 (broad OH), 1635 and 1515 cm^{-1} (C=C-NO_2); ^1H NMR δ=7.29 (1H, s, $CHNO_2$), ca. 4.45 (1H, m, H-1); Anal. ($C_8H_{13}NO_3$) C, H, N.

General Procedure for Preparation of 2-Nitromethyl-2-cycloalkenol (6b). A solution of the epoxide **4b** (1.52 g, 8.9 mmol) in chloroform (10 ml) in the presence of triethylamine (0.1 ml) was kept at room temperature for 0.5 h. Conventional work up afforded a syrup. It was chromatographed with 3:1 (v/v) benzene-cyclohexane to give 1.19 g (78%) of the alcohol (**6b**), which was pure as judged from TLC and ^1H NMR spectroscopy: bp 125 °C (0.35 Torr); IR 3450 (broad OH), 1540 cm^{-1} (NO_2); ^1H NMR δ=6.05 (1H, br. t, $J_{3,4}=J_{3,4'}=6.5$ Hz, H-3), 4.99 (2H, s, CH_2NO_2), 4.55 (1H, m, H-1), 2.97 (1H, s, OH); Anal. ($C_8H_{13}NO_3$) C, H, N.

2-Nitromethyl-2-cyclohexenol (6a): Yield 83%, bp 125 °C (0.35 Torr); IR 3350 (OH), 1550 cm^{-1} (NO_2); ^1H NMR δ=6.03 (1H, br. t, $J_{3,4}=J_{3,4'}=3.3$ Hz, H-3), 5.16 (1H, d, J=14 Hz, $CHNO_2$), 4.76 (1H, d, $CHNO_2$), 4.25 (1H, br. t, $J_{1,6}=J_{1,6'}=4.0$ Hz, H-1), 3.20 (1H, br. s, OH); Anal. ($C_7H_{11}NO_3$) C, H, N.

2-Nitromethyl-2-cyclopentenol (6c): Yield 60%, bp 115 °C (0.35 Torr); IR 3370 (OH), 1550 cm^{-1} (NO_2); ^1H NMR δ=6.05 (1H, br. s, H-3), 5.04 (2H, s, CH_2NO_2), 4.81 (1H, m, H-1), 2.80 (1H, s, OH); Anal. ($C_6H_9NO_3$) C, H, N.

General Procedure for Preparation of 2-Nitromethyl-2-cycloalkenone (7b). To an ice-cooled solution of PCC (500 mg, 2.3 mmol) in dichloromethane (20 ml) was added dropwise a solution of the alcohol **6b** (164 mg, 0.96 mmol) in dichloromethane (2 ml) under a nitrogen atmosphere and the mixture was stirred for additional 3 h at ambient temperature and diluted with diethyl ether. After removal of a solid material by filtration, the filtrate was evaporated and the residue was chromatographed with 9:1 (v/v) benzene-ethyl acetate to give 109 mg (67%) of the ketone **7b**, which was pure as judged from TLC and ^1H NMR spectroscopy: bp 120 °C (0.35 Torr); IR 1670 (CO), 1550 cm^{-1} (NO_2); ^1H NMR δ=6.77 (t, 1H, $J_{3,4}=J_{3,4'}=6.0$ Hz, H-3), 5.03 (s, 2H, CH_2NO_2); Anal. ($C_8H_{11}NO_3$) C, H, N.

2-Nitromethyl-2-cyclohexenone (7a): Yield 58%, bp 120 °C (0.35 Torr); IR 1680 (CO), 1550 cm^{-1} (NO_2); ^1H NMR δ=7.09 (1H, t, $J_{3,4}=J_{3,4'}=4.0$ Hz, H-3), 4.95 (2H, s, CH_2NO_2); Anal. ($C_7H_9NO_3$) C, H, N.

2-Nitromethyl-2-cylopentenone (7c): Yield 41%, bp 95 °C (0.35 Torr); IR 1705 (CO), 1550 cm^{-1} (NO_2); ^1H NMR δ=7.81 (1H, br. s, H-3), 5.06 (2H, s, CH_2NO_2); Anal. ($C_6H_7NO_3$) C, H, N.

5-*t*-Butyl-2-nitromethyl-2-cyclohexenone (12): According to the method described by Eckstein et al.[9] **9** was obtained in 60% yield from 4-*t*-butylcyclohexanone; bp 115 °C (0.45 Torr); IR 1550 cm^{-1} (NO_2); ^1H NMR δ=5.89 (1H, br.s, H-2) and 4.77 (2H, s, CH_2NO_2); Anal. ($C_{11}H_{19}NO_2$) C, H, N.

Similar epoxidation of **9** afforded a 3:1 mixture of **10** as judged from its ^1H NMR spectrum, the epoxide ring of which was opened by treatment with triethylamine, followed by oxidation with PCC, to give **12** in 53% overall yield (from **9**); syrup, purified by column chromatography without distillation; IR 1675 (CO), 1550 cm^{-1} (NO_2); ^1H NMR δ=7.1 (1H, m, H-3), 4.98 (2H, s, CH_2NO_2); Found: C, 62.82; H, 8.08; N, 6.28%. Calcd for $C_{11}H_{17}NO_3$: C, 62.54; H, 8.11; N, 6.63%.

References

1) T. Sakakibara, Y. Nomura, and R. Sudoh, *Bull Chem. Soc. Jpn*, **53**, 1642 (1980).

2) Very recently Tamura and co-workers have reported the selective synthesis of β-nitro alkenes from ketones and nitroalkanes in the presence of *N,N*-dimethylethylenediamine; R. Tamura, M. Sato, and D. Oda, *J. Org. Chem.*, **51**, 4368 (1986).

3) T. Takamoto, Y. Ikeda, Y. Tachimori, A. Seta, and R. Sudoh, *J. Chem. Soc., Chem. Commun.*, **1978**, 350.

4) N. Kornblum, A. S. Erickson, W. J. Kelly, and B. Henggeler, *J. Org. Chem.*, **47**, 4534 (1982), and the references cited therein.

5) For example; J. N. Denis and A. Krief, *Tetrahedron Lett.*, **1979**, 3995.

6) C. Grundman and P. Grunanger, "The Nitrile Oxides," Spring-Verlag, New York (1971), p. 351.

7) N. Ono, I. Hamamoto, T. Yanai, and A. Kaji, *J. Chem. Soc., Chem. Commun.*, **1985**, 523.

8) R. Tamura and L. S. Hegedus, *J. Am. Chem. Soc.*, **104**, 3727 (1982).

9) Z. Eckstein, A. Sacha, and T. Urbanski, *Bull. Acad. Polon. Sci., Classe III*, **5**, 213 (1957) [cf. *Chem. Abstr.*, **51**, 16318 (1957)].

Tin-Promoted Electrochemical Hydrodimerization of Ionones

Kenji UNEYAMA, Takumi TOKUNAGA, and Sigeru TORII*
Department of Industrial Chemistry, School of Engineering, Okayama University, Okayama 700
(Received April 23, 1987)

Synopsis. Electrochemical hydrodimerization of α and β-ionones in the presence of metal tin provides the corresponding hydrodimers in 77 and 60% yields, respectively.

Reductive hydrodimerization of carbonyl compounds is important for the carbon-carbon bond formation. Especially, hydrodimerization of polyenyl carbonyl compounds is useful for the carotenoid synthesis. The electrochemical hydrodimerization would be usable for the purpose. In fact, the electroreductive hydrodimerization is successfully employed for the saturated carbonyl compounds.[1] On the other hand, the hydrodimerization of α, β-unsaturated carbonyl compounds has not been studied in details. 3-Methyl-2-butenal,[2] citral,[3] ionone,[4] and retinal[4] have been electrochemically hydrodimerized by the use of a mercury electrode, but the isolated yields are unsatisfactory. Moreover, the electrolysis has been mostly conducted by the use of a mercury electrode and very few electrodes have been examined for the purpose. On these backgrounds and in connection with our recent study on the electrochemical generation and recycle of the reactive tin reagent,[5] this paper describes a tin-promoted electroreductive hydrodimerization of ionones by the use of platinum electrodes.

Results and Discussion

The electrolysis of α-ionone **1a** was conducted in a methanol-acetic acid-water-1 M (1.M=1 mol dm^{-3}) sulfuric acid solution containing metal tin. Constant current was supplied using two platinum foils as electrodes in a beaker type undivided cell. The result is summarized in Table 1. The reaction at around 40 °C gave the hydrodimer **2a**[6] in more than 70% yield. The reaction at the lower temperature resulted in the increase of the recovered **1** (**2a**; 46% and **1a**; 33%).

Table 1. Electrochemical Hydrodimerization of Ionones

Substrate	Sn/mol%	F mol^{-1}	**2a** or (**2b**)/%
1a[a]	5	8.6	69
	10	7.5	73
	50	6.6	74
	100	5.8	77
	0	2.5	46
1b[b]	20	3.0	(60)

a) **1a** (1 mmol), MeOH (1.5 cm^3), AcOH (0.5 cm^3), H_2O (0.5 cm^3), 1 M H_2SO_4 (0.03 cm^3). b) **1b** (1 mmol), MeOH (2.0 cm^3), H_2O (1.0 cm^3), Et_4NOTs (0.1 mmol).

The increase of metal tin amount led to a slight increase of the yield of **2a**. On the other hand, only 46% of **2a** was obtained in the absence of metal tin after 2.5 F mol^{-1} (1F=96480 C) of current passage. The prolonged electrolysis in the absence of metal tin lost the product **2a** since **2a** was in part converted into the pinacolone **3a**[6] via the pinacol-pinacolone rearrangement in the electrolysis conditions.

The action of metal tin in the same electrolysis solution under no current passage did not induce the hydrodimerization, clearly suggesting that the metal tin is not a reducing agent. Presumably, di- or tetravalent tin generated in situ would chelate the 1,2-diol to suppress the rearrangement. Another role of tin ion would associate the reductively generated anion radical from **1a** as proposed for chromium(III)[7] to promote an effective dimerization of the metal-associated anion radical **4**. In fact, **2a**(54%) and **3a**(36%) were obtained by the electrolysis in the presence of tin(II) sulfate ($SnSO_4$). The electrolysis of **1b** in a methanol-acetic acid-water-1 M sulfuric acid solution containing metal tin as employed for **1a** provided a trace of **2b**.[4] The pinacol **2b** is so acid-sensitive that it smoothly undergoes the pinacol-pinacolone rearrangement. The electrolysis at −7 °C gave **2b** in 46% yield. Therefore, the electrolysis was conducted in a neutral solution such as in an MeOH-H_2O-Et_4NOTs system, affording **2b** in 60% yield.

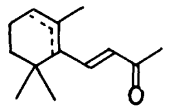

1a α-isomer
b β-isomer

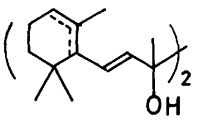

2a α-isomer
b β-isomer

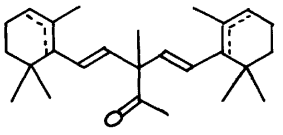

3a α-isomer
b β-isomer

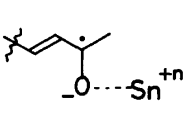

4

Experimental

Electrolysis of 1a. A mixture of **1a** (1.0 mmol) and tin powder (0.1 mmol) dissolved in methanol (1.5 cm^3), water (0.5 cm^3), acetic acid (0.5 cm^3), and 1 M sulfuric acid (0.03 cm^3) was electrolyzed in an undivided beaker type cell at 40 °C using platinum foil electrodes (1×1.5 cm^2) under a constant current (20 mA for 10.5 h, 7.5 F mol^{-1}, Metronix

543B DC power supply). After neutralization with saturated sodium hydrogencarbonate, methanol was removed under reduced pressure. Then, the mixture was extracted with ethyl acetate several times. The combined extracts were washed with brine, dried over sodium sulfate, and concentrated in vacuo. The residue was chromatographed on silica gel (hexane–AcOEt) to give **2a**[6] in 73% yield (141 mg).

This work was supported in part by a Grant-in-Aid (No. 61550640) from the Ministry of Education, Science and Culture.

References

1) E. K. Miller and T. J. Mahachi, *J. Org. Chem.*, **51**, 1041 (1986); M. D. Bhatti and O. R. Brown, *J. Chem. Soc., Faraday Trans. 1.*, **71**, 106 (1975); H. Kita, S. Ishikura, and A. Katayama, *Electrochim. Acta*, **20**, 441 (1975).

2) D. Miller, L. Mandell, and R. A. Day, Jr., *J. Org. Chem.*, **36**, 1683 (1971).

3) J. C. Johnston, J. D. Faulkner, L. Mandell, and R. A. Day Jr., *J. Org. Chem.*, **41**, 2611 (1976)

4) R. E. Shioda, B. Terem, J. H. P. Utley, and B. C. L. Weedon, *J. Chem. Soc., Perkin Trans. 1*, **1976**, 561; L. A. Powell and R. M. Winghtman, *J. Am. Chem. Soc.*, **101**, 4412 (1979); D. W. Sopher and J. H. P. Utley, *J. Chem. Soc., Chem. Commun.*, **1970**, 1087.

5) K. Uneyama, H. Matsuda, and S. Torii, *Tetrahedron Lett.*, **25**, 6017 (1984)

6) A. Ishida and T. Mukaiyama, *Chem. Lett.*, **1976**, 1127

7) D. W. Sopher and J. H. P. Utley, *J. Chem. Soc., Perkin Trans. 2*, **1984**, 1361.

The Reaction of Calcium Atoms with Group 4B Catenates, Me_3E-E'Me_2R (E, E'=Si, Ge, Sn; R=Me, Cl)

Kunio MOCHIDA* and Takayuki YAMANISHI
Department of Chemistry, Faculty of Sciences, Gakushuin University,
1-5-1 Mejiro, Tokyo 171
(Received March 20, 1987)

Synopsis. Calcium atoms are thought to be inserted into E-E' bonds of group 4B catenates, Me_3E-E'Me_2R (E, E'=Si, Ge, Sn; R=Me, Cl) to give the corresponding Me_3E-Ca-E'Me_2R compounds.

The activation of metal-metal bonds of group 4B catenates by metals and metal complexes has received considerable attention in a variety of synthetic organic procedures and catalytic processes.[1-7] In this activation, the oxidation addition of metals or metal complexes into metal-metal bonds of group 4B catenates is generally thought to be the most important process. However, there has been no definite report on insertion reactions of the metal-metal bonds of group 4B catenates by metals.

On the other hand, the study of metal-vapor reactions is of considerable interest in organometallic chemistry since by these methods it is possible to synthesize organometallic compounds which would be difficult, if not impossible, to prepare by other methods, and to study their reactive intermediates.[8]

In this report, we first describe the insertion reactions of metal-metal bonds of group 4B catenates by calcium atoms.

Results and Discussion

Calcium atoms were generated by evaporation from a tungsten filament using essentially the same apparatus and conditions as have been described in the literature (ca. 900 °C and 5×10^{-3} Torr, 1 Torr=133.322 Pa).[9-11] Calcium metal was evaporated at a rate of ca. 20 mg min^{-1}, while an excess of the group 4B catenate compound was co-condensed on the walls of a quartz reaction flask containing a crucible and a perforated inlet tube through which the group 4B catenate compound was admitted. The reaction flask was immersed in liquid nitrogen during calcium evaporation. The color of the co-condensation product of calcium atoms-group 4B catenate compound vapor at 77 K is deep blue, probably due to a weak σ complex.[12] After the calcium evaporation and admission of the group 4B catenate was completed, the reaction flask was warmed to room temperature. The co-condensation product of calcium atoms-group 4B catenate compound vapor turns black. Then, an excess of the organic substrate was admitted as vapor and the reaction flask was left to stand for 1 h. After removing the reaction flask from the vacuum line, the reaction mixture was slowly hydrolyzed with water. The organic layer was extracted with ether.

All products were identified by comparing their GC-MASS and retention times on GLC with those of authentic samples. The results are summarized in Table 1.

Group 4B element-centered anions react with organic halides to give the corresponding substitution products; unreacted anions are converted to the hydrides by hydrolysis.[13]

As shown in Tbale 1, the reaction products of calcium atoms/hexamethyldisilane ($Me_3SiSiMe_3$) and pentamethylchlorodisilane ($Me_3SiSiMe_2Cl$) vapors when treated with phenyl bromide or hydrolyzed gave hexamethylsiloxane. Blank experiments of $Me_3SiSiMe_3$ and $Me_3SiSiMe_2Cl$ in the absence of calcium metal were carried out under identical conditions to give no hexamethylsiloxane ($M_3SiOSiMe_3$). The compound $Me_3SiOSiMe_3$ is probably formed by the insertion of Si-Si bonds by calcium atoms to give Si-Ca-Si followed by hydrolysis in a basic medium.[14] Silylcalcium compounds, thus formed,may be inactive toward phenyl bromide under these conditions.[10]

The reaction products of calcium atoms/(trimethylgermyl)trimethylsilane vapor when treated with phenyl bromide gave phenyltrimethylgermane ($PhGeMe_3$), as expected, besides $Me_3SiOSiMe_3$.

The reaction products of calcium atoms/hexamethyldigermane vapor with phenyl bromide afforded trimethylgermane (Me_3GeH) and $PhGeMe_3$ (Table 1). The formations of $PhGeMe_3$ and Me_3GeH provide strong evidence of the insertion of a Ge-Ge bond of $Me_3GeGeMe_3$ by calcium atoms.

Table 1. Reactions of Calcium Atoms/Group 4B Catenate Compound Vapors with Substrates[a]

Compound	Substrate	Product (Yield/%)[b]
$Me_3SiSiMe_3$	H_2O or PhBr/H_2O	$Me_3SiOSiMe_3$ (5.0)
$Me_3SiSiMe_2Cl$	H_2O	$Me_3SiOSiMe_3$ (15.0)
$Me_3SiGeMe_3$	PhBr/H_2O	$Me_3SiOSiMe_3$ (1.0)
		$PhGeMe_3$ (trace)
$Me_3GeGeMe_3$	PhBr/H_2O	$PhGeMe_3$ (6.0)
		Me_3GeH (0.5)
$Me_3SiSnMe_3$	PhBr/H_2O	$Me_3SiOSiMe_3$ (36.0)
		$PhSnMe_3$ (2.0)
		Me_3SnH (42.0)
		$Me_3SnSnMe_3$ (8.0)
		Me_3SnOH (10.0)

a) Reactions were performed at room temperature for 1 h. b) Yields of products were based on the calcium metals consumed.

The reaction products of calcium atoms/(trimethylsilyl)trimethylstannane vapor when treated with phenyl bromide afforded $Me_3SiOSiMe_3$, phenyltrimethylstannane ($PhSnMe_3$), trimethylstannane (Me_3SnH), hexamethyldistannane ($Me_3SnSnMe_3$), and trimethylstannol (Me_3SnOH) shown in Table 1. A blank experiment of $Me_3SiSnMe_3$ in the absence of calcium metal was carried out under identical conditions. $Me_3SiOSiMe_3$, $Me_3SnSnMe_3$, and Me_3SnOH were produced in the ratio of 1:1:2. Taking the experimental results into consideration, most of the $Me_3SiOSiMe_3$, $PhSnMe_3$, and Me_3SnH may be derived from the insertion of a Si–Sn bond by a calcium atom.

The degree of insertion of metal–metal bonds of group 4B catenates by calcium atoms increased in the order Si–Si<Ge–Ge<Si–Sn in accord with the metal–metal bond dissociation energy.

The yields of the products shown in Table 1 are very low. The yields of these products were determined on the basis of the amount of calcium metal consumed on the assumption that all of the vaporized calcium metal completely reacted with the substrate.

Experimental

GLC analyses were performed on a Shimazu GC-6A and 8A gas chromatograph with 2 m 20% SE-30 and 2 m 30% Apiezon L columns. GC-MASS spectra were obtained with a JEOL JMS-DX 303 mass spectrometer. NMR spectra were obtained with a Varian FT-80A spectrometer using $CDCl_3$ as the solvent and TMS as the internal standard.

Materials. Calcium metal (granule, 99% pure, Wako chemicals) was commercially available. $Me_3SiGeMe_3$,[15] $Me_3GeGeMe_3$,[16] $Me_3SiSnMe_3$,[17] $PhGeMe_3$,[18] Me_3GeH,[19] $PhSnMe_3$,[20] Me_3SnH,[21] $Me_3SnSnMe_3$,[22] and Me_3SnOH[23] were prepared as described in the cited references.

Reactions of Calcium Atoms/Group 4B Catenate Compound Vapors with Substrate. As a typical example, the reaction of calcium atoms/hexamethyldigermane vapor with phenyl bromide is described. Calcium metal (500 mg, 12.5 mmol) was vaporized at a temperature of ca. 900 °C using a filament of tungsten in vacuo (ca. 5×10^{-3} Torr), at a rate of ca. 20 mg min^{-1}. During the vaporization of calcium metal, digermane (12 g, 51.3 mmol) was introduced into the quartz reaction flask as vapor. Calcium atoms/digermane vapor condensed on the walls of the reaction vessel, which was cooled to 77 K with liquid nitrogen. The initial product at 77 K was a deep blue. The reaction vessel was warmed to room temperature and an excess of phenyl bromide was then admitted as vapor. The reaction vessel was left to stand for 1 h. After removing the reaction vessel from a vacuum line, the reaction mixture was slowly hydrolyzed with water. The organic layer was extracted with ether. The products were identified by comparing their GC-MASS and retention times on GLC with those of authentic samples. The yields of the products were determined by an internal-standard method.

The authors thank Professor Hideki Sakurai and Dr. Kenkichi Sakamoto of Tohoku University for a gift of organosilyl compounds. Partial financial support of this research by the Saneyoshi Scholarship Foundation is greatly acknowledged (1984).

References

1) H. Sakurai, *J. Organomet. Chem.*, **200**, 261 (1980) and reference cited therein.
2) H. Matsumoto, K. Shono, A. Wada, I. Matsubara, H. Watanabe, and Y. Nagai, *J. Organomet. Chem.*, **199**, 185 (1980) and reference cited therein.
3) K. Tamao, T. Hayashi, and M. Kumada, *J. Organomet. Chem.*, **114**, C19 (1976).
4) M. Ishikawa, T. Fuchigami, and M. Kumada, *J. Am. Chem. Soc.*, **99**, 245 (1977).
5) K. Tamao, S. Okazaki, and M. Kumada, *J. Organomet. Chem.*, **146**, 87 (1981).
6) A. Azizian, C. Eaborn, and A. Pidcock, *J. Organomet. Chem.*, **215**, 49 (1981).
7) M. Kosugi, T. Ohya, and T. Migita, *Bull. Chem. Soc. Jpn.*, **56**, 3855 (1983).
8) For examples; J. R. Blackborow, "Metal Vapor Synthesis in Organometallic Chemistry," Springer-Verlag, New York (1979); K. J. Klabunde, "Chemistry of Free Atoms and Particles," Academic Press, New York (1980); K. J. Klabunde, "Reactive Intermediates," ed by R. A. Abramovitch, Plenum Press, New York (1980).
9) K. Mochida and H. Ogawa, *J. Organomet. Chem.*, **243**, 131 (1983).
10) K. Mochida and M. Manishi, *Chem. Lett.*, **1984**, 1077.
11) K. Mochida, H. Takeuchi, Y. Hiraga, and H. Ogawa, *Chem. Lett.*, **1984**, 1989.
12) K. J. Klabunde, H. F. Efner, T. O. Murdock, and R. Ropple, *J. Am. Chem. Soc.*, **98**, 1021 (1976).
13) D. D. Davies, *Organomet. Chem. Rev., Sect. A*, **6**, 283 (1970).
14) R. L. Merker and M. J. Scott, *J. Am. Chem. Soc.*, **81**, 975 (1959).
15) C. Show, F. III; Allred, and L. Albert, *J. Organomet. Chem.*, **28**, 53 (1971).
16) M. P. Brown and G. W. A. Fowles, *J. Chem. Soc.*, **1958**, 2811.
17) H. Schumann and S. Ronecker, *Z. Naturforsch.*, **B22**, 452 (1967).
18) H. Bauer and K. Burschkies, *Chem. Ber.*, **66**, 1156 (1933).
19) R. H. Fish and M. G. Kuivila, *J. Org. Chem.*, **31**, 2445 (1966).
20) J. Nagy, J. Reffy, A. Kuszmann-Borbely, and K. Pallossy-Becker, *J. Organomet. Chem.*, **7**, 393 (1967).
21) A. E. Finholt, A. C. Bond, Jr., K. E. Wilzbach, and H. I. Schlesinger, *J. Am. Chem. Soc.*, **69**, 2692 (1947).
22) W. P. Neuman, B. Schneider, and R. Sommer, *Justus Liebigs Ann. Chem.*, **692**, 1 (1966).
23) D. A. Kochkin, L. U. Luk'yanova, and E. B. Reznikova, *Zh. Obshch. Khim.*, **33**, 1945 (1963).

Titanium Oxide-Supported Carbonylmolybdenum Catalyst in Liquid Phase: Application to Allylic Alkylation of Methyl *p*-Tolylsulfonylacetate

Yoshiro MASUYAMA,* Yutaka MITSUNAGA, Yasuhiko KURUSU, and Koh-ichi SEGAWA
Department of Chemistry, Faculty of Science and Technology, Sophia University,
7-1 Kioicho, Chiyoda-Ku, Tokyo 102
(Received March 26, 1987)

Synopsis Titanium oxide-supported carbonylmolybdenum catalyst was applied to selective monoallylation of methyl *p*-tolylsulfonylacetate using allylic acetates or carbonates in refluxing dioxane. This reaction required both 2,2′-bipyridyl as a ligand and sodium hydride as a base for preparation of the salt of methyl *p*-tolylsulfonylacetate.

We have applied metal oxide-supported carbonylmolybdenum [$Mo(CO)_3$–metal oxide] catalyst to allylic alkylation of carbon nucleophiles using allylic acetates.[1] The $Mo(CO)_3$–TiO_2 catalytic system is superior to others, and exhibits desirable characteristics as regards 1) long life and easy separation of the catalyst and 2) regio- and stereochemistry. Application of sulfones which stabilize an adjacent carbanion as carbon nucleophiles, instead of diethyl malonate or ethyl 2-oxocyclopentanecarboxylate, should further enhance the desirability of the $Mo(CO)_3$–TiO_2 catalyst in the allylic alkylation.[2] Homogeneous $Mo(CO)_6$ catalyst did not catalyze any reactions of allylic acetates with sulfones, whereas allylic carbonates did serve as allylating agents.[3] Here, we report the selective monoallylation of methyl *p*-tolylsulfonylacetate with several allylic acetates or carbonates by means of the $Mo(CO)_3$–TiO_2 catalytic system.

The reactions of 2-butenyl acetate (**1a**) or 2-butenyl methyl carbonate (**2b**) with the salt **3**, derived from methyl *p*-tolylsulfonylacetate and sodium hydride, were investigated under various conditions. The reaction proceeded in the presence of both the $Mo(CO)_3$–TiO_2 catalyst and 2,2′-bipyridyl (bpy) in refluxing dioxane. Some examples are shown in the Table 1. Neither **1a** nor **2b** reacted with **3** in refluxing toluene, which is a common solvent.[1,4] Allylic acetates could be utilized in this reaction, which was not the case with the homogeneous $Mo(CO)_6$ system (Entries 1—3).[3] However, the reactivity of the allylic acetates was less than that of the corresponding allylic carbonates. Monoallylation occurred selectively without diallylation. *p*-Tolylsulfonylacetonitrile, which was a good nucleophile in the homogeneous system, did not react under these conditions.[3]

The reaction of **3** with **9**, containing both an allylic acetate moiety and an allylic carbonate moiety, occurred chemoselectively at the carbonate moiety and regioselectively at the less substituted end of the allyl unit (Eq. 1).

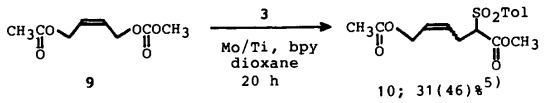

(1)

In order to extend this allylic alkylation to a cyclization, several intramolecular reactions were investigated under the same conditions.[6] The sodium salts of carbonates **11a** and **11b** reacted regioselectively to afford five- and six-membered ring compounds **14a** and **14b** respectively. No cyclizations occurred in the case of sodium salts of acetates **12** and **13** under the same conditions (Scheme 1).

Table 1. Allylic Alkylation of **3**

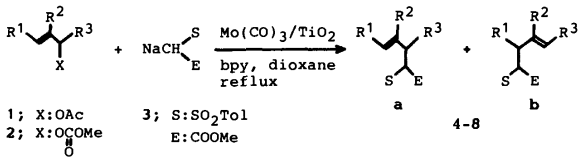

Entry	Allylic compd.		Time / h	Product R¹	R²	R³		Yield[a] / %	Ratio[b] a : b
1	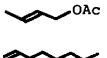	**1a**	15	CH_3	H	H	**4**	33	42 : 58
2	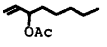	**1b**	31	H	H	n-C_5H_{11}	**5**	36	11 : 89
3		**1c**	24	H	-$(CH_2)_4$-		**6**	40	81 : 19
4	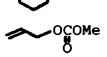	**2a**	19	H	H	H	**7**	67	—
5		**2b**	17	CH_3	H	H	**4**	72	40 : 60
6	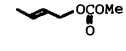	**2c**	15	Ph	H	H	**8**	76	33 : 67

a) Isolated yields. b) The ratio was determined by ^1H NMR. Diastereomer ratios: **4a** (60/40), **5a** (60/40), **6a** (71/29), and **8b** (58/42).

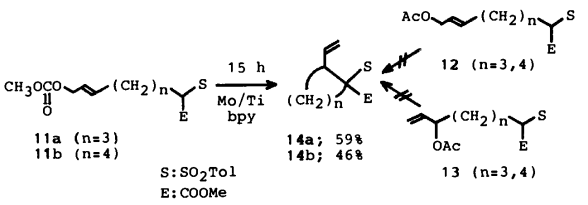

Scheme 1.

As mentioned above, the heterogeneous $Mo(CO)_3$–TiO_2 catalyst enabled us to use allylic acetates as allylating agents, and was found to show higher selectivity of monoallylation of **3** than that for homogeneous $Mo(CO)_6$ catalyst and higher chemoselectivity to allylic carbonates than acetates.

Experimental

Reaction of Allylic Acetates 1 or Carbonates 2 with Methyl *p*-Tolylsulfonylacetate. 4: To a solution of salt **3** derived from methyl *p*-tolylsulfonylacetate (0.23 g, 1.0 mmol) with sodium hydride (27 mg, 1.1 mmol) in dioxane (10 ml) were added 2-butenyl acetate (**1a**) (0.11 g, 1.0 mmol) and bpy (8.0 mg, 0.05 mmol) under argon atmosphere. The solution was added to a vessel, in which $Mo(CO)_3$–TiO_2 catalyst, prepared from TiO_2 (0.50 g) and $Mo(CO)_6$ (13 mg, 0.05 mmol),[1] had been placed. This mixture was refluxed for 15 h under argon atmosphere. The reaction mixture was diluted with ether (50 ml) and the catalyst was removed by filtration. Evaporation of solvents followed by purification of the residue by column chromatography (silica gel, hexane-ethyl acetate=3/1) gave the monoallylated product **4** as colorless oil in 33% yield (93 mg). The structure was confirmed by IR and ^1H NMR spectral comparison with an authentic sample.[3]

5: IR (neat) 1735 (C=O), 1320 and 1140 cm^{-1} (SO_2); ^1H NMR ($CDCl_3$) δ=0.85 (t, J=7.0 Hz, 3H), 1.12—1.36 (m, 6.2H), 1.87—2.00 (m, 1.8H), 2.46 (s, 3H), 2.50—2.77 (m, 1.8H), 2.80—2.94 (m, 0.1H), 3.51 (s, 0.12H), 3.64 (s, 0.18H), 3.66 (s, 2.7H), 3.96 (dd, J=4.0, 11.4 Hz, 0.9H), 3.98, 4.01 (2d, J=2.6 Hz, 0.1H), 5.02—5.10 (m, 0.2H), 5.12—5.31 (m, 0.9H), 5.44—5.57 (m, 0.9H), 5.58—5.66 (m, 0.1H), 7.30—7.40 (m, 2H), and 7.71—7.81 (m, 2H); MS (70 ev) m/z (rel intensity) 338 (M^+, 1), 183 (100), 182 (39), 123 (34), 111 (30), 91 (46), 81 (39), and 67 (33). Found: m/z 338.1546. Calcd for $C_{18}H_{26}O_4S$: M, 338.1550.

6: IR (neat) 1735 (C=O), 1320 and 1140 cm^{-1} (SO_2); ^1H NMR ($CDCl_3$) δ=1.34—1.97 (m, 5.6H), 2.02—2.17 (m, 1.8H), 2.23—2.35 (m, 0.6H), 2.44(s, 3H), 2.60 (br, 0.4H), 3.06—3.17 (m, 0.8H), 3.43 (s, 1.7H), 3.63 (s, 0.7H), 3.65 (s, 0.6H), 4.11 (dd, J=4.6, 10.8 Hz, 0.2H), 4.43 (d, J=11.7 Hz, 0.56H), 4.49 (d, J=9.8 Hz, 0.24H), 4.61 (s, 0.56H), 4.68 (s, 0.56H), 4.82 (s, 0.24H), 4.84 (s, 0.24H), 5.41 (br, 0.2H), 7.29—7.40 (m, 2H), and 7.72—7.82 (m, 2H); MS (70 ev) m/z (rel intensity) 322 (M^+, 0.7), 167 (82), 166 (100), 138 (26), 135 (50), 107 (46), 94 (40), 91 (58), and 79 (35). Found: m/z 322.1229. Calcd for $C_{17}H_{22}O_4S$: M, 322.1238.

7: The structure was confirmed by IR and ^1H NMR spectral comparison with an authentic sample.[3]

8: IR (neat) 1735 (C=O), 1320 and 1140 cm^{-1} (SO_2); ^1H NMR ($CDCl_3$) δ=2.41 (s, 3H), 2.75—2.98 (m, 0.66H), 3.62 (s, 1H), 3.68 (s, 0.8H), 3.70 (s, 1.2H), 4.07 (dd, J=8.5, 12.1 Hz, 0.4H), 4.08 (dd, J=4.3, 10.7 Hz,0.33H), 4.18 (dd, J=8.5, 10.1 Hz, 0.27H), 4.50 (d, J=8.5 Hz, 0.4H), 4.54 (d, J=8.5 Hz, 0.27H), 4.99—5.20 (m, 1.34H), 5.80—6.04 (m, 0.67H), 6.23 (dt, J=6.9, 15.9 Hz, 0.33H), 6.47 (d, J=15.9 Hz, 0.33H), 7.02—7.36 (m, 7H), and 7.71—7.82 (m, 2H); MS (70 eV) m/z (rel intensity) 344 (M^+, 0.3), 189 (100), 188 (33), 157 (38), 130 (35), 129 (99), 128 (32), 117 (42), and 91 (41). Found: m/z 344.1080. Calcd for $C_{19}H_{20}O_4S$: M, 344.1081.

10: IR (neat) 1740 (C=O), 1320 and 1140 cm^{-1} (SO_2); ^1H NMR (CCl_4) δ=1.93 (s, 3H), 2.40 (s, 3H), 2.58—2.82 (m, 2H), 3.56 (s, 3H), 3, 88 (dd, J=7,9 Hz,1H), 4.38—4.60 (m, 2H), 5.22—5.71 (m, 2H), 7.29 (d, J=7.5 Hz, 2H), and 7.67 (d, J=7.5 Hz, 2H); MS (70 eV) m/z (rel intensity) 340 (M^+, 0.3), 185 (72), 184 (100), 141 (36), 125 (22), and 91 (23). Found: m/z 340.0976. Calcd for $C_{16}H_{20}O_6S$: M, 340.0979.

Intramolecular Cyclization of 11. 14a: A solution of **11a** (0.19 g, 0.5 mmol) in dioxane (5 ml) was added to the suspension of sodium hydride (17 mg, 0.7 mmol) in dioxane (5 ml) at room temperature under argon atmosphere. The solution followed by bpy (8.0 mg, 0.05 mmol) were added to a vessel, in which $Mo(CO)_3$–TiO_2 catalyst, prepared from TiO_2 (0.50 g) and Mo $(CO)_6$ (13 mg, 0.05 mmol),[1] had been placed. After refluxing for 15 h under argon atmosphere, the mixture was diluted with ether (50 ml) and the catalyst was removed by filtration. Evaporation of solvents followed by purification of the residue by column chromatography (silica gel, hexane-ethyl acetate=2:1) gave the cyclic product **14a** as colorless oil in 59% yield (91 mg). IR (neat) 1735 (C=O), 1310, and 1140 cm^{-1} (SO_2); ^1H NMR (CCl_4) δ=1.44—2.73 (m, 6H), 2.41 (s, 3H), 3.09—3.44 (m, 1H), 3.51 (s, >2.85H), 3.59 (s, <0.15H), 4.84 (d, J=10 Hz, 1H), 4.87 (d, J=16 Hz, 1H), 5.53 (ddd, J=7,10, 16 Hz, 1H), 7.21 (d, J=8 Hz, 2H), and 7.71 (d, J=8 Hz, 2H); MS (70 ev) m/z (rel intensity) 308 (M^+, 0.3), 153 (57), 152 (50), 121 (31), 93 (100), and 91 (39). Found: m/z 308.1082. Calcd for $C_{16}H_{20}O_4S$: M, 308.1081.

14b: IR (neat) 1735 (C=O), 1320, and 1140 cm^{-1} (SO_2); ^1H NMR (CCl_4) δ=0.91—2.36 (m, 8H), 2.40 (s, 3H), 2.60—2.93 (m, 0.6H), 3.04—3.31 (m, 0.4H), 3.51 (s, 1.2H), 3.62 (s, 1.8H), 4.84—5.20 (m, 2H), 6.02—6.51 (m, 1H), 7.07—7.28 (m, 2H), and 7.42—7.64 (m, 2H); MS (70 ev) m/z (rel intensity) 322 (M^+, 0.3), 167 (58), 121 (32), 119 (97), 117 (100), 107 (78), and 91 (23). Found: m/z 322.1236. Calcd for $C_{17}H_{22}O_4S$: M, 322.1237.

References

1) Y, Masuyama, Y. Kurusu, and K. Segawa, *J. Mol. Catal.*, **40**, 183 (1987).

2) B. M. Trost and T. R. Verhoeven, "Comprehensive Organometallic Chemistry," ed by G. Wilkinson, Pergamon Press, Oxford (1982), Vol. 8, p. 825; L. S. Hegedus, "Comprehensive Carbanion Chemistry," ed by E. Buncel and T. Durst, Elsevier, Amsterdam (1984), p. 30; R. F. Heck, "Palladium Reagents in Organic Syntheses," Academic Press, London (1985), p. 130.

3) Y. Masuyama, H. Hirai, Y. Kurusu, and K. Segawa, *Bull. Chem. Soc. Jpn.*, **60**, 1525 (1987).

4) B. M. Trost and M. Lautens, *J. Am. Chem. Soc.*, **104**, 5543 (1982); **105**, 3343 (1983).

5) The figure in parentheses is the yield based on the consumed starting material **9**. The ratio of stereoisomers (E/Z) was not determined by ^1H NMR.

6) Preparation of **11** was carried out in the following manner:

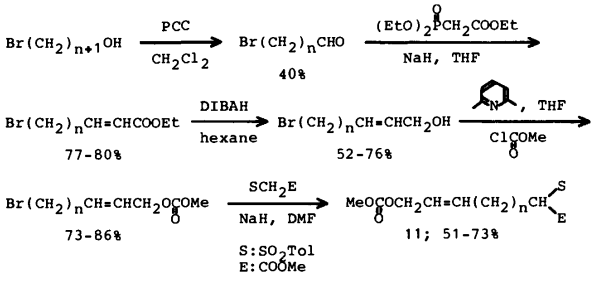

Ordering of Cations in $Ba(Mg_{1/3}Nb_{2/3})O_3$ and $Ba(Zn_{1/3}Nb_{2/3})O_3$

Hideki YOSHIOKA
Industrial Research Institute of Hyogo Prefecture, Yukihira-cho 3-1-12, Suma-ku, Kobe 654
(Received March 16, 1987)

Synopsis. The ordering of B-site cations in $Ba(Mg_{1/3}Nb_{2/3})O_3$ (BMN) and $Ba(Zn_{1/3}Nb_{2/3})O_3$ (BZN) was studied from superlattice reflections in X-ray diffraction patterns. The degree of ordering in BMN increases with increasing sintering temperature. While in BZN an ordered structure was observed up to 1673 K, and an order-disorder phase transition was found below 1773 K.

The ordering of B-site cations has been studied by Galasso et al.[1] for a number of $A(B'B'')O_3$ type complex perovskite oxides. $Ba(Mg_{1/3}Nb_{2/3})O_3$ (BMN) and $Ba(Zn_{1/3}Nb_{2/3})O_3$ (BZN) were also synthesized by Galasso et al.[2] and their ordering properties were investigated by X-ray powder diffraction analysis. They reported that Mg^{2+} and Nb^{5+} in BMN are hexagonally ordered, while BZN has a disordered structure in terms of its B-site Zn^{2+} and Nb^{5+} cations.

It was considered that the ordering of B-site cations depends upon the defferences in their ionic charges and ionic radii.[2] Since the differences in the ionic charges are equal for BMN and BZN, their ordering properties may depend upon the differences in the ionic radii of B-site cations. As the ionic radii of Mg^{2+}, Zn^{2+}, and Nb^{5+} are 0.066, 0.074, and 0.069 nm, respectively,[3] the differences are 0.003 nm for BMN and 0.005 nm for BZN, which are also very close. Therefore, it is considered that the ordering properties of these compounds are located near the boundary of stability between order and disorder, and that the possibility of changing the degree of ordering by a heat treatment exists for these compounds. In this study the ordering of B-site cations for BMN and BZN under various heat treatments was investigated using superlattice reflections in the X-ray powder diffraction patterns.

BMN and BZN were prepared by solid state reactions. The mixtures of stoichiometric proportions of $BaCO_3$, MgO or ZnO, and Nb_2O_5 (purity>99.99%) were calcined at 1273 K for 8 h. The obtained powders gave X-ray patterns of a cubic perovskite structure. After pressing into pellets, these were sintered under various conditions, as shown in Table 1. The ordering of B-site cations produces superlattice reflections such as (1/3 1/3 1/3) and (2/3 1/3 1/3) with an original perovskite unit cell in the X-ray powder diffraction patterns. If B-site cations are completely ordered, the unit cell can be described as a hexagonal lattice and the superlattice reflections, (1/3 1/3 1/3) and (2/3 1/3 1/3), can be indexed as (001) and (100), respectively, with this hexagonal unit cell.

Table 1. Sintering Conditions of BMN and BZN

BMN	T/K	t/h	BZN	T/K	t/h
1	1473	16	1	1473	16
2	1573	4	2	1573	16
3	1673	4	3	1573	4
4	1773	4	4	1673	4
5	1833	4	5	1773	4

X-Ray diffraction patterns of the superlattice reflections (001) and (100) in BMN with Cu $K\alpha$ radiation are shown in Fig. 1. In all samples, (100) reflections are about twice as large in peak heights as the (001) reflections. The lattice spacings of (001) and (100) obtained from the diffraction angles are 0.71 and 0.50 nm, respectively; these are constant among samples under various sintering conditions. However, with increasing sintering temperature, the increase in peak heights and the sharpening of peaks are evident in Fig. 1. The degree of ordering can be represented by the intensity of the superlattice peak, while the ordered domain size can be calculated from the broadening of the peak. To estimate the degree of ordering in samples, the intensity ratio of the (100) reflection, which is the strongest superlattice reflection, to (110) and (102) reflections, which are overlapped and the strongest of all reflections, was calculated. The ordered domain sizes were obtained from the half widths of the superlattice reflections. The results are listed in Table 2. An increase in the degree of ordering was observed for a sample sintered at more than 1773 K; this is attributed to an enhancement of the rate of ordering with increasing temperature. Since the intensity ratio in a sample sintered at 1833 K is comparable with the theoretical value calculated from the completely ordered arrangement, the ordering of Mg^{2+} and Nb^{5+} in BMN is almost achieved by sintering at 1883 K for 4 h. The

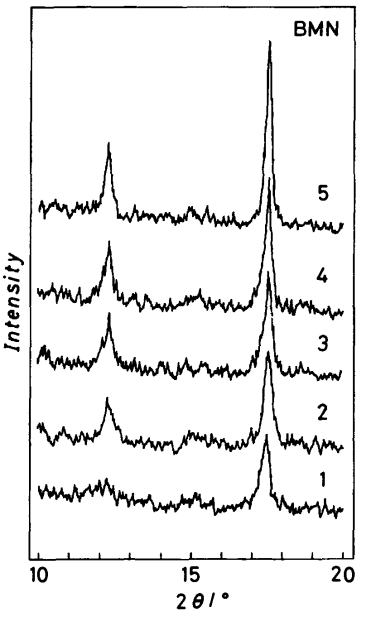

Fig. 1. X-Ray diffraction patterns of superlattice reflections for BMN.

Table 2. Intensity Ratio of Superlattice Peak and Size of Ordered Domains for BMN

	$(I_{100}/I_{110,102}) \times 100$	L/nm
1	2.18	62
2	2.38	73
3	2.28	75
4	2.78	>100
5	3.27	>100

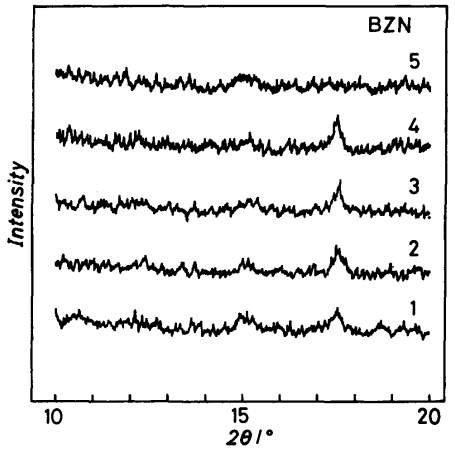

Fig. 2. X-Ray diffraction patterns of superlattice reflections for BZN.

ordered domain sizes increase steadily with increasing sintering temperature, reaching more than 100 nm at 1773 K.

Superlattice peaks of (100) reflections were detected for BZN sintered at less than 1673 K (Fig. 2), corresponding to the cation ordering, although Galasso et al.[2] reported that BZN was a disordered perovskite. Scattering factors of Zn^{2+} and Nb^{5+} are so close that the (100) reflections are much smaller than those in BMN and that the (001) reflections, which are considered to be about half as much as the (100) reflections in intensities like in BMN, are invisible. Since no significant difference with sintering time was observed between the diffraction patterns of samples 2 and 3 in Fig. 3, it seems that sintering for 4 h is sufficient for investigating the ordering property of BZN. One characteristic is the fact that the peak intensities increase with increasing sintering temperature for a sample sintered at less than 1673 K, and that no superlattice reflection could be observed for a sample sintered at 1773 K. This indicates that below 1673 K the ordered arrangement is stable, but above 1773 K the disordered arrangement is stable for BZN. This could be confirmed by X-ray diffraction patterns of the samples subjected to two-step heat treatments. In Fig. 3, the diffraction pattern of a sample sintered at 1573 K for 4 h (labeled as 3) in which the (100) reflection can be clearly observed. After sintering this sample again at 1773 K for 4 h (represented by 3 R in Fig. 3), the (100) reflection could no longer be detected. Though the sample first sintered at 1773 K for 4 h showed no superlattice reflection (labeled as 5 in Fig. 3), a weak superlattice reflection was detected

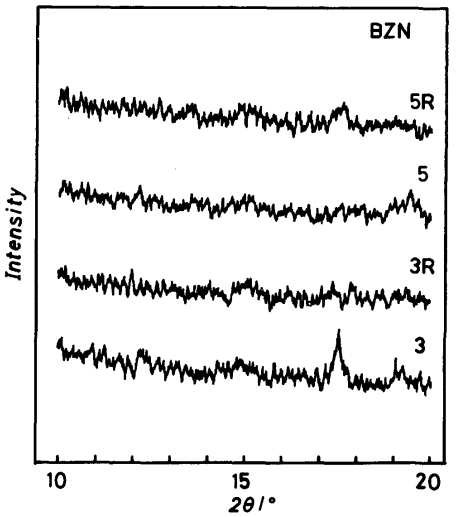

Fig. 3. Superlattice reflections of BZN subjected to two-step heat treatments.

when reheated to 1573 K for 4 h (5 R in Fig. 3). This result clearly indicates that the ordered structure is stable up to 1573 K, but that the disordered structure is stable above 1773 K. Also, there is a reversible phase transition between the ordered and disordered structures in the temperature range from 1573 to 1773 K.

Few of the complex perovskite oxides, which show an order-disorder phase transition like BZN, are known except for $Pb(Sc_{1/2}Ta_{1/2})O_3$ (PST) studied by N. Setter et al.[4] They found that the degree of Sc^{3+} and Ta^{5+} ordering in PST sintered at 1833 K increases from 0.37 to more than 0.80 after annealing at 1273 K for 4 h; this strongly suggests that there is an order-disorder phase transition between 1273 and 1833 K.

The appearance of the order-disorder phase transition can be explained in terms of an increase in the entropy contribution to the free energy at high temperatures. The free energy of the ordered structure in BMN is lower than that of the disorderd structure (up to 1833 K); however, in BZN that of the disordered structure is lower than that of the ordered structure in 1773 K. The free energies of these materials mainly consist of the Madelung energy, due to an electrostatical interaction, and the entopy contribution which increases at high temperatures. Both are very close between BMN and BZN at the same temperature. Thus, it is noted that as G. Patrat et al.[5] pointed out for $Sr(Fe_{1/2}Ta_{1/2})O_3$, that the polarization energy and the displacement energy, which are caused by the size and the polarizability of the constituent ions, must be included in calculations of their free energies.

References

1) F. Galasso and J. Pint, *Nature (London)*, **207**, 70 (1965).
2) F. Galasso and J. Pyle, *J. Phys. Chem.*, **67**, 1561 (1963).
3) L. H. Ahrens, *Geochim. Cosmochim. Acta*, **2**, 155 (1952).
4) N. Setter and L. E. Cross, *J. Appl. Phys.*, **51**, 4356 (1980).
5) G. Patrat, M. Brunel, and F. de Bergevin, *J. Phys. Chem. Solids*, **37**, 285 (1976).

Infrared Study of Structural and Compositional Changes in Orthorhombic Hydrogen Molybdenum Bronze, $H_{0.3}MoO_3$, by Heating in Vacuo

Takashi OHNO, Hisashi MIYATA,† Fumikazu HATAYAMA,* and Noriyuki SOTANI††
School of Allied Medical Sciences, Kobe University,
Tomogaoka, Suma, Kobe 654-01
†Department of Applied Chemistry, University of Osaka Prefecture,
Mozu-umemachi, Sakai, Osaka 591
††College of Liberal Arts, Kobe University, Tsurukabuto, Nada, Kobe 657
(Received March 30, 1987)

Synopsis. Hydrogen molybdenum bronze, $H_{0.3}MoO_3$, heated in vacuo was studied by FT-IR spectroscopy. The spectrum near 1000 cm^{-1} analyzed by a microcomputer system was confirmed to be composed of three bands. Among them, bands at 1005 and 990 cm^{-1} correspond to the Mo=O bonds of orthorhombic bronze and rhombic MoO_3, respectively.

It is well-known that by insertion of atomic hydrogen into MoO_3, the rhombic MoO_3 structure turns to the orthorhombic bronze structure.[1] This structural change is expected to effect strongly on the Mo=O stretching vibration. It is confirmed by thermogravimetry[2] and TPD method[3] that orthorhombic hydrogen molybdenum bronze, $H_{0.3}MoO_3$, is decomposed into $MoO_{2.86}$, a nonstoichiometric compound with the rhombic MoO_3 structure, by heating in vacuo with evolution of H_2O. The change in IR spectra has also been studied on samples heated in vacuo, but no quantitative analysis has been made for the bands in the region 1000—800 cm^{-1} which can be assigned to the Mo=O or Mo–O stretching vibration in molybdenum oxide.[4,5] Because of low infrared transmittance of the samples, IR spectra obtained by a conventional grating IR spectrophotometer were not able to be analyzed quantitatively. In the present work, the authors have studied the dehydrogenation process of hydrogen molybdenum bronzes by using a Fourier transform infrared spectrophotometer directly connected with a microcomputer systems and analyzed in detail how dehydrogenation influenced on changes in the structure and composition. This paper mainly deals with the behavior of the bands near 1000 cm^{-1} assigned to the Mo=O stretching vibration of the samples heated in vacuo.

Experimental

The preparation and identification of orthorhombic hydrogen molybdenum bronze, $H_{0.3}MoO_3$, were described previously.[2,3,6] Samples having various hydrogen contents (formulated as H_xMoO_y) were prepared by heating the bronze at various temperatures in vacuo and in air. The composition was determined by thermogravimetry[2] and by Choain and Marion's method.[7] The samples after heating were pressed into disks (ca. 0.5 wt% in KBr). All spectra were recorded in dry air by a Fourier transform infrared spectrophotometer (SHIMADZU, FTIR-4000: with 2 cm^{-1} resolution) directly connected with the microcomputer system (NEC, PC-9801 F2).

Results and Discussion

The hydrogen molybdenum bronze, $H_{0.3}MoO_3$, with the orthorhombic structure was decomposed to a nonstoichiometric compound with the rhombic MoO_3 structure as follows;[6]

$$H_{0.30}MoO_3 \rightarrow H_{0.21}MoO_{2.95} \rightarrow H_{0.06}MoO_{2.88} \rightarrow MoO_{2.85}.$$

This was confirmed to the dehydration process by mass spectrometry. Atomic hydrogens in samples reacted with lattice oxygens and the water was liberated. At the same time, vacancies were produced.

Figure 1 shows the FT-IR spectra of the samples heated in vacuo. The bands at 999, 650, 590, and 430 cm^{-1} of orthorhombic bronze, $H_{0.30}MoO_3$, are almost the same as those reported by Schroder and Weizel.[8] The intensities of the bands at 999, 650, and 430 cm^{-1} gradually reduced with the decrease in hydrogen content of the samples. On the other hand, new bands appeared in the region 900—800 cm^{-1} and the band at 590 cm^{-1} was intensified as dehydration process proceeded. Figure 1 also shows that the band at 999 cm^{-1} was split into two bands at 1004 and 990 cm^{-1} in the case of the samples with lower hydrogen contents than the lowest limit (x=0.21) of

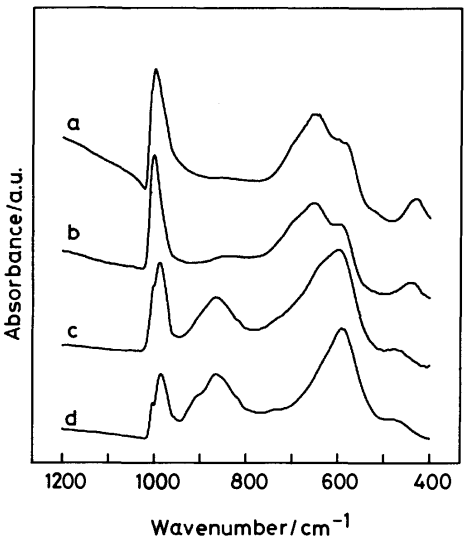

Fig. 1. FT-IR spectra of the samples, H_xMoO_y. a, $H_{0.30}MoO_3$; b, $H_{0.21}MoO_{2.95}$; c, $H_{0.080}MoO_{2.89}$; d, $MoO_{2.85}$.

the orthorhombic structure. This behavior could not be observed clearly by using the grating IR spectrophotometer. It is well-known that the bands near 1000 cm^{-1} can be assigned to the Mo=O stretching vibration in molybdenum oxide.[4,5] The results suggest that samples with lower hydrogen contents than x=0.21 give at least two kinds of the Mo=O stretching vibration. While in the case of the bronze heated in air, only the bands due to MoO_3 appeared at 993, 878, and 820 cm^{-1}, though a small amount of hydrogen remained. By thermogravimetry and mass spectrometry, atomic hydrogens inserted in the sample were removed easily as hydrogen molecules in this case. The samples gave immediately the rhombic MoO_3 structure. Therefore, the bands also appeared at the same frequencies with those of MoO_3.

In the previous work,[6] the authors observed the band at 1004 cm^{-1} due to the Mo=O stretching vibration of the orthorhombic bronze and the one at 998 cm^{-1} for the rhombic MoO_3. This suggests that the band shifts of Mo=O stretching vibration was caused by a structural change. As shown in Fig. 1, the band near 1000 cm^{-1} was at least composed of two peaks. Therefore, the band shape analysis has been carried out to obtain further information of the Mo=O bonds by a microcomputer system using the same techniques described previously.[9,10] Although there exists no theoretical justification for IR bands of solid to fit any specific functional form, the Gaussian form was applied.[9] One of the results in the region 1050—950 cm^{-1} is shown in Fig. 2. The band was confirmed to be overlapped by three bands with peaks at 1005, 990, and 972 cm^{-1}, although the original band has two peak maxima. The convoluted curve of these separated bands fits in well with the original spectrum. Thus all spectra of the samples gave three bands with the peaks at nearly the same frequencies in the region 1050—950 cm^{-1}. These results led to the conclusion that the band near 1000 cm^{-1} of each sample is composed of three kinds of Mo=O stretching vibration which shows the peaks at 1005, 990, and 972 cm^{-1}, respectively.

The intensity of each band calculated for unit weight of the samples in disks is plotted against the hydrogen content of the sample as shown in Fig. 3. From this result the intensity ratio of each band to the sum of three bands is calculated at the same hydrogen content as shown in Fig. 4. The value of 1005 cm^{-1} band decreases monotonously, while that of 990 cm^{-1} increases, as hydrogen content decreases. The intensity ratio of the band at 1005 cm^{-1} to that of the

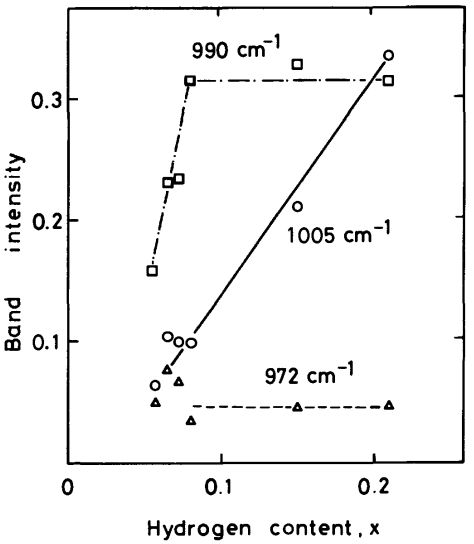

Fig. 3. Relationship between intensity of each band and hydrogen content, x, of the samples; 1005 cm^{-1} (○), 990 cm^{-1} (□), 972 cm^{-1} (△).

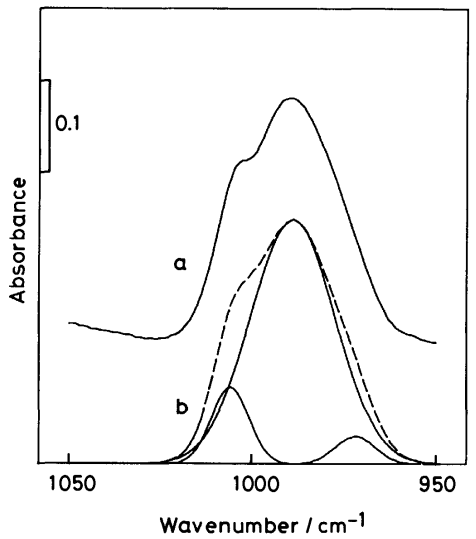

Fig. 2. An example of band shape analysis in the region 1050—950 cm^{-1} (sample: $H_{0.080}MoO_{2.89}$). a, original spectrum; b, separating peaks (——) and convoluted curve (----).

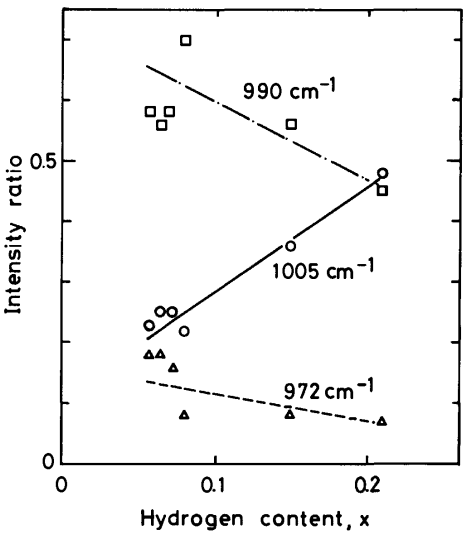

Fig. 4. Relationship between intensity ratio of each band to the sum of three bands and hydrogen content, x, of the samples; 1005 cm^{-1} (○), 990 cm^{-1} (□), 972 cm^{-1} (△).

band at 990 cm^{-1} is calculated from the values in Fig. 4. The ratio is 0.48/0.45=0.52/0.48 at x=0.21, 0.36/0.56=0.39/0.61 at x=0.15, and 0.22/0.70=0.24/0.76 at x=0.08, respectively. These values are in close agreement with the ratios of the orthorhombic to rhombic components obtained from the X-ray and thermogravimetric data.[6] Thus, it is concluded that the band at 1005 cm^{-1} is assigned to the Mo=O stretching vibration of the orthorhombic bronze formed by the insertion of hydrogen atom and that at 990 cm^{-1} is assigned to that of the oxide with rhombic MoO_3 structure. It is clear that existence of the atomic hydrogen induced the change of crystal structure which is strongly correlated with the mode of Mo=O bond as described previously (see Fig. 3 in Ref. 6). On the other hand, the ratio of band at 972 cm^{-1} is small in the whole region and gradually increased as the hydrogen content decreased. It is not sure that this band can be assigned to another kind of Mo=O stretching vibration of polymolybdate such as Mo_4O_{11}, Mo_9O_{26}, and so forth.

References

1) O. Glemser and G. Lutz, *Z. Anorg. Allg. Chem.* **264**, 17 (1951).
2) N. Sotani, Y. Kawamoto, and M. Inui, *Mat. Res. Bull.*, **18**, 797 (1983).
3) N. Sotani, N. Yoshida, Y. Kawamoto, S. Kishimoto, and M. Hasegawa, *Bull. Chem. Soc. Jpn.*, **57**, 3032 (1984).
4) K. Nakamoto, "Infrared Spectra of Inorganic and Coordination Compound," John Willey and Sons, New York (1970), p. 166.
5) J. R. Feraro, "Low Frequency Vibration of Inorganic and Coordination Compounds," Plenum Press, New York (1971), p. 75.
6) N. Sotani, N. Yoshida, Y. Yoshioka, and S. Kishimoto, *Bull. Chem. Soc. Jpn.*, **58**, 1626 (1985).
7) C. Choain and F. Marion, *Bull. Soc. Chim. Fr.*, **1963**, 212.
8) F. A. Schroder and H. Weitzel, *Z. Anorg. Allg. Chem.*, **435**, 247 (1977).
9) H. Miyata, K. Fujii, S. Inui, and Y. Kubokawa, *Appl. Spectrosc.*, **40**, 1177 (1986).
10) H. Miyata, K. Fujii, T. Ono, Y. Kubokawa, T. Ohno, and F. Hatayama, *J. Chem. Soc., Faraday Trans. 1*, **83**, 675 (1987).

Irreversible Nature of the Stacked β-Pleated Sheets of a Model Polypeptide

Hiroshi MAEDA
Department of Chemistry, Faculty of Science, Nagoya University,
Chikusa-ku, Nagoya 464
(Received April 15, 1987)

Synopsis. A mode of association of β-sheets, most probably the stacking of the pleated sheets, has been studied by circular dichroism and light scattering on the 5×10^{-2} mol dm^{-3} NaCl solutions of poly(*S*-carboxymethyl-L-cysteine). It was found that the association is highly irreversible with respect to concentration change at constant pH. Relevance of the study of synthetic polypeptides is discussed in relation to the association mode found in proteins.

It has been frequently reported that aggregation of polypeptide chains takes place when the β-structure is formed.[1-10] Association of extended chains, observed on short chains,[2,11-14] couples with the formation of the β-structure. In this case, the β-content from circular dichroism (CD) parallels the aggregation number. In low ionic strength media, dissociation of β-aggregates occurs very slowly.[11,12,14] On addition of a salt, however, reversible association-dissociation takes place depending on the concentration of the salt.[12,13] Another well-defined association process was found recently,[15] in which the extent of aggregation incerases with concentration accompanied by a negligible change of the β-content, as indicated by a nearly constant residue ellipticity. An edge-to-edge association of the folded-chain-pleated sheets was suggested for this process,[15] mediated by hydrogen bonds between peptide groups of different chains. This edge-to-edge association of β-sheets has been proposed for the monomer-monomer interface within a dimer of concanavalin A.[16]

There are many facts concerning the aggregation of the β-structure of synthetic polypeptides which cannot be understood consistently in terms of these two types of association and their mixtures. Different lines of evidence have been accumulated for different polypeptides that a face-to-face association, or stacking, of the pleated sheets also occurs in addition to the above edge-to-edge association of pleated sheets. Various diagnostic means have been used for the detection of the stacking, including fluorescence (hydrophobic probe),[3,17-19] hydrodynamic properties,[6,7] potentiometric titration,[7,20,21] counterion activity,[20] and isodichroic point associated with the β-coil conversion.[10] Recently, it was indicated that increase of aggregation number is enormous when stacking occurs and hence this could be used as another diagnostic tool for the detection of the stacking.[15]

In the present study, circular dichroism (CD) and aggregation number by light scattering were measured on 5×10^{-2} M (mol dm^{-3}) NaCl solutions of different concentrations of poly(*S*-carboxymethyl-L-cysteine)-(poly[Cys(CH_2COOH)]) at a constant pH of 4.86±0.02 with special reference to the reversibility of the association. The aggregation is expected of face-to-face type according to the results from the above mentioned diagnostic means.

Experimental

The weight average molecular weight ($\bar{M}_w$) and degree of polymerization (DP_w) of the sample were 5.8×10^4 and 360, respectively. Light scattering was measured on a Chromatix low-angle light scattering photometer KMX-6 at room tmperature (24±2 °C). A value of 0.220 was used for the refractive index increment,[15] since it could not be measured at the pH used (4.86±0.02) due to the low solubility of the polypeptide in the β-structure. Apparent aggregation number m was evaluated at each concentration, assuming nonideal contribution to be negligible. CD spectra were taken on a Jasco J-40A Circular Dichrograph at 25±0.1 °C using cells of 0.5, 1, 2, 5, 10, and 20 mm light paths. Four to eight scans were accumulated. Measurements were made on the solutions about 24 hours after their preparation.

Results and Discussion

In Fig. 1, the concentration dependence of the apparent aggregation number m is shown on a double logarithmic plot. At the lowest polypeptide concentration C_p of about 1×10^{-4} residue M, aggregation already occurs for the chain of DP_w=360, which is consistent with the previous result on the

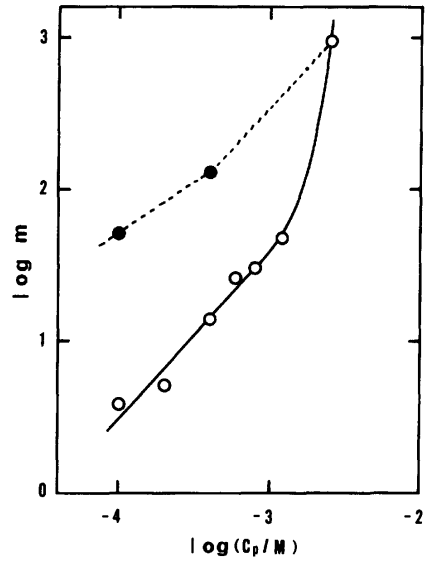

Fig. 1. Concentration dependence of apparent aggregation number m. Filled circles refer to solutions prepared by diluting the solution of the highest concentration.

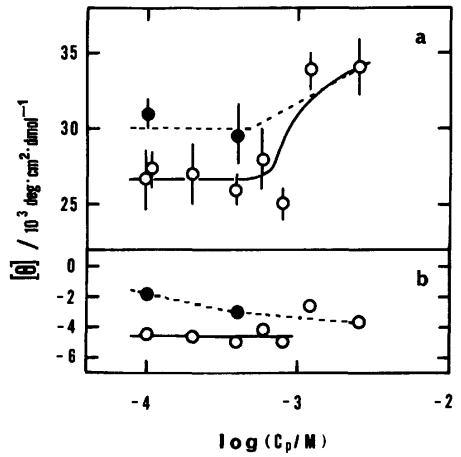

Fig. 2. Concentration dependence of residue ellipticities at 200 nm (a) and 218 nm (b). Filled circles refer to the solutions prepared by diluting the solution of the highest concentration.

same sample[15] but is in contrast with the previous result on a sample of DP_w=630 that approximately unassociated folded-chain β-structure exists at this concentration.[15] Upon increasing the concentration, the aggregation increases steadily. At C_p=2.48×10^{-3} M, however, the aggregation number increases enormously, suggesting that the stacking of pleated sheets occurs. Each solution corresponding to an open circle was prepared from each solution of the same concentration at neutral pH by the addition of HCl. At neutral pH, polypeptides were molecularly dispersed as random coils irrespective of the concentration.

In Fig. 2(a), the concentration dependence of the residue ellipticity at 200 nm, $[\theta]_{200}$, is given as a measure of the β-content. In a concentration range below about 1×10^{-3} M, $[\theta]_{200}$ remains nearly unchanged in spite of the increase of the aggregation number m. It is likely that edge-to-edge association of pleated sheets occurs in this concentration range, consistent with previous result.[15] When C_p exceeds about 1×10^{-3} M, $[\theta]_{200}$ increases sharply, which seems to correspond to the stacking process, although the correspondence between m and $[\theta]_{200}$ is not complete enough.

It has been shown that an isodichroic point around 218 nm, associated with the β-coil conversion of poly[Cys(CH_2COOH)], disappeared when the stacking of pleated sheets was expected to occur.[10] In Fig. 2(b), values of $[\theta]_{218}$ are plotted against log C_p. The presence of an isodichroic point around 218 nm is suggested in the concentration range lower than about 1×10^{-3} M. Disappearance of the isodichroic point is clear at C_p=1.2×10^{-3} M.

Two solutions were prepared by diluting the solution at C_p=2.48×10^{-3} M. The results on these two solutions are indicated by filled circles in Figs. 1 and 2. In Fig. 1, aggregation numbers found on these solutions are greater by nearly an order of magnitude than those found on the corresponding solutions of the same concentration prepared by the addition of HCl to the solution of neutral pH. On dilution, values of $[\theta]_{200}$ decrease but remain significantly greater than those of the solutions containing negligible amount of stacked aggregates. The observed slight decrease of $[\theta]_{200}$ may indicate the dissociation of either a small amount of stacked aggregates or unstacked portion of aggregates. A clearer indication of irreversible change at $[\theta]_{200}$ than shown here was reported previously. (Figure 5 of Ref. 11). Disappearance of the isodichroic point is clearly indicated for the solutions prepared by dilution. Therefore, dissociation of stacked aggregates by dilution is largely inhibited even in the presence of excess salt in the present case.

It is to be stated that essentially identical behavior to that is shown in Figs. 1 and 2 was obtained in three independent sets of experiments. However, all these results could not be put together into a single figure, since residue ellipticities differed appreciably for different sets due to slight differences in pH (smaller than 0.04) among them.

In conclusion, a mode of association which most likely corresponds to face-to-face association, or stacking, of pleated sheets is shown to be irreversible in the present study. It is to be noted that the (assumed) stacked aggregates can be easily dissociated by charging the side chains, i.e., by raising pH in the present case.

It is pertinent to ask whether this face-to-face association of β-sheets occurs in proteins. A good counterpart is found in the dimer of Streptomyces subtilisin inhibitor (SSI), which has been indicated to be formed by the stacking of two β-sheets belonging to each subunit.[22] Consistent with the present result, dimeric SSI does not dissociate into monomer on dilution, showing strong adhesive interaction.[23] The dissociation rate constant was obtained recently by clever means.[24]

The auther thank Mr. Kohei Kadono for his help in some CD measurements.

References

1) B. Davidson and G. D. Fasman, *Biochemistry*, **6**, 1616 (1967).
2) S.-Y. C. Wooley and G. Holzwarth, *Biochemistry*, **9**, 3604 (1970).
3) R. Hartman, R. C. Schwaner, and J. Hermans, Jr., *J. Mol. Biol.*, **90**, 415 (1974).
4) E. Patrone, G. Conio, and S. Brighetti, *Biopolymers*, **9**, 897 (1970).
5) M. B. Senior, S. L. H. Gorell, and E. Hamori, *Biopolymers*, **10**, 2387 (1971).
6) E. Patton and H. E. Auer, *Biopolymers*, **14**, 849 (1975).
7) H. E. Auer and R. P. McKnight, *Biochemistry*, **17**, 2798 (1978).
8) S. Ikeda, *Biopolymers*, **5**, 359 (1967).
9) S. Ikeda and G. D. Fasman, *J. Mol. Biol.*, **30**, 419 (1967).
10) H. Maeda and K. Ooi, *Biopolymers*, **20**, 1549 (1981).
11) H. Maeda, K. Kadono, and S. Ikeda, *Macromolecules*, **15**, 822 (1982).

12) K. Saito, H. Maeda, and S. Ikeda, *Biophys. Chem.*, **16**, 67 (1982).
13) H. Maeda, K. Saito, and S. Ikeda, *Bull. Chem. Soc. Jpn.*, **56**, 602 (1983).
14) H. Maeda, T. Iwase, and S. Ikeda, *Polymer J.*, **16**, 471 (1984).
15) H. Maeda, Y. Gatto, and S. Ikeda, *Macromolecules*, **17**, 2031 (1984).
16) G. N. Reeke, Jr., J. W. Becker, and G. M. Edelman, *J. Biol. Chem.*, **250**, 1525 (1975).
17) J. Lynn and G. D. Fasman, *Biochem. Biophys. Res. Commun.*, **33**, 327 (1968).
18) G. Witz and B. L. van Duuren, *J. Phys. Chem.*, **77**, 648 (1973).
19) Y. Sato and R. W. Woody, *Biopolymers*, **19**, 2021 (1980).
20) K. Ooi, H. Maeda, and S. Ikeda, *Biopolymers*, **19**, 1743 (1980).
21) R. P. McKnight and H. E. Auer, *Macromolecules*, **9**, 939 (1976).
22) Y. Mitsui, Y. Satow, Y. Watanabe, and Y. Iitaka, *J. Mol. Biol.*, **131**, 697 (1979).
23) K. Inouye, B. Tonomura, K. Hiromi, T. Kotaka, H. Inagaki, S. Sato, and S. Murao, *J. Biochem. (Tokyo)*, **84**, 843 (1978).
24) K. Akasaka, S. Fujii, F. Hayashi, S. Rokushika, and H. Hatano, *Biochemistry International*, **5**, 637 (1982).

The Crystal and Molecular Structures of the Scandium(III) and Yttrium(III) Chloroacetates, $[Sc(ClCH_2CO_2)_3]_n$ and $[Y_3(ClCH_2CO_2)_9(H_2O)_4]_n \cdot nH_2O$

Yoshihiko SUGITA, Yoshiyuki OHKI,† Yasuo SUZUKI,† and Akira OUCHI*
Department of Chemistry, College of Arts and Sciences, The University of Tokyo, Komaba, Meguro-ku, Tokyo 153
†Department of Industrial Chemistry, Faculty of Engineering, Meiji University, Higashi-Mita, Tama-ku, Kawasaki, Kanagawa 214
(Received January 7, 1987)

Synopsis. The crystal and molecular structures of the titled scandium(III) (**1**) and yttrium(III) chloroacetates (**2**) were determined by the single-crystal X-ray diffraction method. **1** is monoclinic, with the space group $P2_1/n$, a=12.148(4), b=8.860(5), c=11.028(4) Å, and β=103.31(3)°. In **1**, the metal atom has the hexa-coordinated octahedral geometry, and any pair of the neighboring metal atoms are bridged by three bidentate carboxylate ions, forming an infinite chain. **2** is isomorphous with the heavy lanthanoid salts, $[Ln_3(ClCH_2CO_2)_9(H_2O)_4]_n \cdot nH_2O$ (Ln=Gd—Yb), and its crystal structure closely resembles that of the erbium(III) complex.

We have previously reported on the complicated structures of the series of light and heavy lanthanoid-(III) chloroacetates.[1,2] Although it is well-known that the properties of the scandium(III) and yttrium(III) complexes resemble those of the lanthanoids(III)[3,4] there are not much structural data about their carboxylates; moreover, the data regarding complexes synthesized under the same conditions as those for the corresponding lanthanoid complexes are rare.

The structural data of scandium(III) formate is the sole example;[5] its metal atoms are in the hexa-coordinated octahedral geometry, and are bridged by the anions forming a two-dimensional polymeric form. Therefore, it is desirable to obtain more structural data concerning the scandium complexes in order to clarify whether their coordination numbers are always six or not, and to determine its polymeric form.

The yttrium(III) formate dihydrate[6,7] and yttrium-(III) acetate tetrahydrate[8] are known to be isomorphous with the corresponding heavy lanthanoid salts.[6,9,10,11] If the yttrium and heavy lanthanoids always give complexes isomorphous with each other, the high coordination number and the complicated bridging found in the lanthanoid complexes should not be due to the 4f-orbitals of the latters.

Therefore, we have synthesized the scandium(III) and yttrium(III) chloroacetates, $Sc(ClCH_2CO_2)_3$ (**1**) and $[Y_3(ClCH_2CO_2)_3(H_2O)_4]_n \cdot nH_2O$ (**2**), under synthetic conditions almost the same as that for the lanthanoid salts.

Experimental

Syntheses of the Scandium(III) and Yttrium(III) Chloroacetates. Scandium(III) hydroxide (obtained from 0.193 g (1.0 mmol) of Sc_2O_3) was dissolved into an aqueous solution of chloroacetic acid (0.59 g (6.2 mmol) into 10 cm^3 of water). The solution was filtered off, left standing in a silica-gel desiccator for several days until 2/3 of the water was evaporated off; crystals of **1** were deposited. Yield: 0.33 g (51%). The yttrium salt, **2**, was obtained almost in the same way starting from 0.229 g (1.0 mmol) of Y_2O_3 and chloroacetic acid (0.59 g, 6.2 mmol). Yield, 0.61 g (75%). Found; Sc, 13.77; C, 22.11; H, 1.58%; Calcd for $ScC_6H_6O_6Cl_3$, Sc, 13.81; C, 22.15; H, 1.86%. Found; Y, 22.15; C, 17.50; H, 2.31%; Calcd for $Y_3C_{18}H_{28}O_{23}Cl_9$; Y, 22.26; C, 18.04; H, 2.36%.

X-Ray Structure Analysis. Crystallographic data and some experimental conditions for obtaining their intensities are tabulated in Table 1. The intensities were collected on a Rigaku AFC-6A automated 4-circle X-ray diffractometer with graphite monochromated Mo $K\alpha$ radiation, a ω—2θ scan technique being employed (the scan speed was 4° min^{-1} (θ)).

The structure of the scandium complex was solved by the heavy-atom method. In the case of the yttrium salt, the structure was solved starting with the final parameters of the erbium complex, $[Er_3(ClCH_2CO_2)_9(H_2O)_4]_n \cdot nH_2O$,[2] and were refined as usual.

In both cases, all the hydrogen atoms were fixed at the calculated positions (C-H=1.08 Å), B_{iso}=8.00 $Å^2$ being given.

All the calculations were carried out on a HITAC M-682H

Table 1. Crystallographic Data and Various Experimental Conditions to Obtain the Reflection Intensities

Complex	**1**	**2**
F.W. (n=1)	325.42	1198.20
Crystal system	monoclinic	triclinic
Space group	$P2_1/n$	$P\bar{1}$
a(l/Å)	12.148(4)	13.349(12)
b(l/Å)	8.860(5)	13.691(10)
c(l/Å)	11.028(4)	12.126(8)
α(ϕ/°)	90	96.62(6)
β(ϕ/°)	103.31(3)	100.64(7)
γ(ϕ/°)	90	67.35(6)
U(v/Å^3)	1155.1(9)	2008(3)
Z	4	6
D_m(d/Mg m^{-3})	1.86(3)	1.95(3)
D_x(d/Mg cm^{-3})	1.87	1.98
μ(Mo $K\alpha$) (n/mm^{-1})	1.34	5.13
N_m[a]	3292	7173
N_c[b]	1400	4481
R[c]	0.069	0.072
V_c[d]	0.3×0.15×0.10	0.3×0.2×0.14
S_W[e]	1.12+0.5 tanθ	1.08+0.5 tanθ
S_R[f]	3—55	3—50

a) Number of reflections measured. b) Reflections used for the calculation (reflections of $|F_o| > 3\sigma(|F_o|)$). c) $R=\Sigma||F_o|-|F_c||/\Sigma|F_o|$. d) Size of crystals ($v$/mm^3). e) Scan width ($\theta$/°). f) Scan range ($2\theta$/°).

apparatus at the Computer Center of The University of Tokyo using a local version of the UNICS program.[12] The atomic scattering factors were taken from Ref. 13.

Infrared Spectrum Measurements. Their infrared spectra were obtained by means of a JASCO 202A grating infrared spectrophotometer using liquid paraffin and hexachloro-1,3-butadiene mull.

Results and Discussion

The final parameters and their equivalent thermal parameters of **1** are listed in Table 2.[14]

In **1**, the metal atom has an octahedral coordination by six oxygen atoms of six different anions (Fig. 1); the octahedral geometry is not much deformed.[15] The mean Sc–O distance is 2.075 Å (Table 3), not far from the sum of the Shannon's ionic radii of Sc and O, 2.10 Å.[16] The metal atoms are laid along the b-axis in a zig-zag way, and any pair of side-by-side metal atoms are bridged by three carboxylate ions, where all carboxylate ions act as *Z,Z*-type bidentate (Fig. 2).[17] Such a type of the triple carboxylate ion bridging is rarely found, even in any other metal complexes. The three oxygen atoms (O(**11**), O(**21**), and O(31)) of the respective three carboxylate ions bridging to the one side next metal atom are in an *fac*-configuration (Fig. 1). The carboxylato carbon and oxygen atoms (C(**n1**), O(**n1**), and O(**n2**)) of each carboxylato bridge, together with the metal atoms Sc and Sc^{ii},[18] are approximately on each plane. The average deviations of the atoms from the respective planes are: **11**, 0.065; **21**, 0.131; and **31**, 0.027 Å. The dihedral angles between them are: **11**—**21**, 114.2; **11**—**31**, 56.7; **21**—**31**, 57.5°.[19] Although all of the bridging ions are approximately the *Z,Z*-type, angles C(**11**)-O(12)-Sc^{ii} (164.1(5)°) and C(31)-O(31)-Sc (171.6(7)°) are larger than, and C(**11**)-O(**11**)-Sc (133.8(5)°) and C(31)-O(32)-Sc^{ii} (131.8(6)°) are smaller than the standard value (145—150°) of the type of bridge[14,17] On the other hand, although ion **21** has almost a normal C–O–Sc angle, the planarity of the Sc-O-C-O-Sc^{ii} plane is not good. Relatively short Sc-O(12^{i}) and Sc-O(31) bonds are found where

Table 2. Final Atomic Coordinates ($\times 10^4$) and Equivalent Isotropic Temperature Factors (B_{eq}/Å^2) of Non-Hydrogen Atoms of the Scandium Complex with Estimated Standard Deviations in Parentheses

Atom	*x*	*y*	*z*	B_{eq}/Å^2 a)
Sc	2769.5(12)	1573.8(14)	2379.3(13)	1.9_6
O(11)	4219(4)	2914(5)	2853(5)	2.5_3
O(12)	3629(4)	5236(5)	3112(5)	3.0_6
O(21)	2207(5)	2908(5)	803(5)	3.0_5
O(22)	1591(4)	5233(5)	1057(4)	2.7_3
O(31)	1920(4)	2889(5)	3390(5)	2.9_7
O(32)	1387(4)	5222(5)	3682(5)	3.1_7
C(11)	4387(6)	4281(8)	3113(6)	2.2_5
C(12)	5612(6)	4756(8)	3444(7)	2.7_0
C(21)	1811(6)	4158(8)	423(7)	2.1_6
C(22)	1502(8)	4452(9)	−979(7)	3.6_2
C(31)	1401(6)	3818(7)	3874(7)	2.2_1
C(32)	753(8)	3332(9)	4809(9)	4.6_8
Cl(11)	5822(2)	6642(2)	3938(2)	4.2_7
Cl(21)	2333(2)	3426(3)	−1799(2)	5.0_7
Cl(31)	836(3)	1395(3)	5111(3)	6.0_4

a) The equivalent isotropic temperature factors were computed using the following expression: $B_{eq}=4/3(B_{11}a^2+B_{22}b^2+B_{33}c^2+B_{13}ac\cos\beta)$. The B_{ij}'s are defined by: $T=\exp[-(h^2B_{11}+k^2B_{22}+l^2B_{33}+2hkB_{12}+2hlB_{13}+2klB_{23})]$.

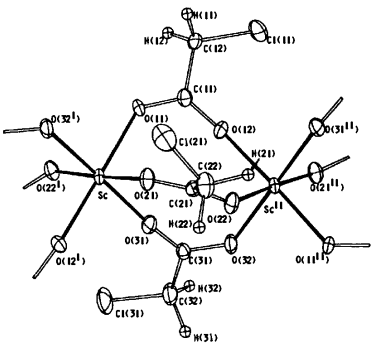

Fig. 1. A perspective drawing of the scandium(III) complex showing the metal atoms and the bridging carboxylate ions.

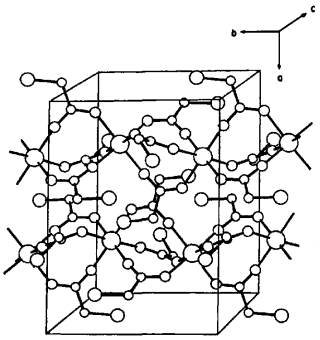

Fig. 2. Crystal packing diagram of the scandium(III) complex.

Table 3. Bond Lengths and Bond Angles of the Scandium Complex with the Standard Deviations in Parentheses[18]

Bond length	(*l*/Å)	Bond length	(*l*/Å)	Bond length	(*l*/Å)
Sc-O(11)	2.088(5)	Sc-O(21)	2.083(7)	Sc-O(31)	2.048(7)
Sc-O(12^{i})	2.040(5)	Sc(22^{i})	2.091(7)	Sc-O(32^{i})	2.099(7)
O(11)-C(11)	1.251(8)	O(12)-C(11)	1.250(9)	O(21)-C(21)	1.241(9)
O(22)-C(21)	1.246(11)	O(31)-C(31)	1.230(11)	O(32)-C(31)	1.262(8)
Sc···Sc^{ii}	4.495(4)				
Bond angle	**(*φ*/°)**	**Bond angle**	**(*φ*/°)**	**Bond angle**	**(*φ*/°)**
O(11)-Sc-O(21)	89.0(2)	O(11)-Sc-O(31)	92.4(2)	O(11)-Sc-O(12^{i})	178.7(2)
O(11)-Sc-O(22^{i})	89.1(2)	O(11)-Sc-O(32^{i})	88.4(2)	O(21)-Sc-O(31)	91.2(3)
O(21)-Sc-O(22^{i})	177.3(3)	O(31)-Sc-O(12^{i})	88.9(2)	O(31)-Sc-O(32^{i})	178.9(3)

Table 4. Selected Bond Lengths of the Yttrium Complex with the Standard Deviations in Parentheses

Bond length	(l/Å)	Bond length	(l/Å)	Bond length	(l/Å)
Y(1)-O(11)	2.388(10)	Y(1)-O(12)	2.455(9)	Y(1)-O(13)	2.391(9)
Y(1)-O(14)	2.551(9)	Y(1)-O(15)	2.233(8)	Y(1)-O(23)	2.219(12)
Y(1)-O(W1)	2.288(10)	Y(1)-O(14^{i})	2.322(10)	Y(2)-O(12)	2.354(9)
Y(2)-O(16)	2.383(7)	Y(2)-O(21)	2.300(12)	Y(2)-O(24)	2.305(12)
Y(2)-O(25)	2.310(8)	Y(2)-O(31)	2.270(9)	Y(2)-O(W2)	2.401(9)
Y(2)-O(W5)	2.511(10)	Y(3)-O(22)	2.241(11)	Y(3)-O(33)	2.281(9)
Y(3)-O(26)	2.238(8)	Y(3)-O(31)	2.764(10)	Y(3)-O(32)	2.401(9)
Y(3)-O(33^{ii})	2.845(10)	Y(3)-O(34^{ii})	2.402(11)	Y(3)-O(35)	2.334(13)
Y(3)-O(W4)	2.420(8)	Y(1^{i})···Y(1)	4.057(3)	Y(1)-Y(2)	4.246(4)
Y(2)···Y(3)	4.326(4)	Y(3)···Y(3^{ii})	4.309(4)		

Key to the symmetry operations: i, $-x$, $-y$, $-z$; ii, $1-x$, $1-y$, $1-z$.

the C-O-Sc angles of the oxygen atoms are large.[18,19] Therefore, in the case of the chloroacetate, scandium makes a polymeric complex like the heavier IIIA elements; however, its coordination number is six, not so high as yttrium and the lanthanoids. This fact is probably due to its small ionic radius.

The structure of **2** is isomorphous with heavy lanthanoid salts, $[Ln_3(ClCH_2CO_2)_9(H_2O)_4]_n \cdot nH_2O$, (Ln=Gd—Yb).[2] The Shannon's ionic radius of the yttrium ion resemble those of holmium and erbium.[16] The bond lengths and angles of the yttrium salt (Table 4) are not so much different from the corresponding values of the latter salts.[2] The average of the 25 Y-O bond lengths of **2** is 0.012 Å longer than that of the Er-O bonds of the erbium complex,[2] reflecting a longer ionic radius, Y(1.019 Å), than that of Er(1.004 Å) (where the valence of the metal atoms is 3+, and the coordination number is 8).[16]

Therefore, we deduce from these results that both yttrium and the lanthanoids form the same complicated polimeric-type carboxylate complexes; 4f electrons are not greatly related with the characteristic structures.

In the infrared spectrum of **1**, the ν_{as}(COO) and ν_s(COO) bands appear as singlets at 1565 and 1442 cm^{-1}, and do not split as those of the lanthanoid salts. These peaks probably correspond with bands of the *Z,Z*-type bridging carboxylate ion.[17] The general feature as well as the wavenumbers of the ν_{as}(COO) and ν_s(COO) bands of **2**(which appear at 1662, 1627, 1595, 1572 (strongest); and 1442 and 1399 cm^{-1}, respectively) are approximately similar to those of the erbium salt.[2]

The authors wish to thank the Shin-Etsu Chemical Ind. Co., Ltd., for presenting us with the highly pure lanthanoid oxides.

References

1) T. Imai, M. Shimoi, and A. Ouchi, *Bull. Chem. Soc. Jpn.*, **60**, 159 (1987).
2) Y. Sugita and A. Ouchi, *Bull. Chem. Soc. Jpn.*, **60**, 171 (1987).
3) R. C. Vickery, "Comprehensive Inorganic Chemistry," Vol. 3, Pergamon Press, Oxford, U. K. (1973), p. 329.
4) E. R. Birnbaum, "Gmelin Handbook of Inorganic Chemistry," 8th ed, System No. 39, Part D5 (1984), pp. 1—111.
5) M. K. Gusejnova, A. S. Antsyshkina, and M. A. Porai-Koshits, *Zh. Strukt. Khim.*, **9**, **1040** (1968).
6) H. R. Wenk, *Z. Krist.*, **154**, 137 (1981).
7) A. S. Antsyshkina, M. A. Porai-Koshits, I. V. Arkhangel'ski, and L. A. Butman, *Koord. Khim.*, **2**, 565 (1976).
8) A. S. Antsyshkina, M. A. Porai-Koshits, I. V. Arkhangel'ski, V. N. Ostrikova, and A. Amanov, *Izv. Akad. Nauk. Az. SSSR*, **34**, 22 (1978).
9) N. G. Furmanova, L. V. Soboleva, N. V. Belov, and L. M. Belyaev, *Kristallografiya*, **26**, 1315 (1981).
10) J. A. Bats, P. Kalus, H. Fuess, *Acta Crystallogr., Sect. B*, **35**, 1225 (1979).
11) L. A. Aslanov, Z. K. Abdul'minev, M. A. Porai-Koshits, and V. I. Ivanov, *Dokl. Akad. Nauk. SSSR*, **205**, 343 (1972).
12) "Universal Crystallographic Computation Program System (UNICS)," ed by T. Sakurai, Crystallographic Society of Japan, Tokyo (1967).
13) "International Tables for X-Ray Crystallography," Kynoch Press, Birmingham, U. K. (1974), Vol. IV, pp. 72, 150.
14) "Final thermal parameters of the non-hydrogen atoms, the positional parameters of **2** and those of the hydrogen atoms of **1**, final F_o-F_c tables of **1** and **2**, and some of their additional data for the bond lengths and angles are deposited as Document No. 8748 at the office of the Editor of the Bull. Chem. Soc. Jpn.
15) Average of the six edge lengths of two triangles is 2.950 (2.922—2.985) Å, and the average of their six angles is 60.16 (58.95—61.08)°. The dihedral angle between the O(11), O(21), O(31), and the O(12^{i}), O(22^{i}), O(32^{i}) planes is 0.19°.
16) R. D. Shannon, *Acta Crystallogr., Sect. A*, **32**, 751 (1976). The proposed ionic radii are as follows (where CN means coordination number; the valence of the metal atoms is 3+, and that of oxygen is 2−): Sc(CN=6), 0.745; Y(CN=8), 1.019, (CN=9), 1.075; Er(CN=8), 1.004, (CN=9), 1.062; Ho(CN=8), 1.015, (CN=9), 1.072; O(CN=2), 1.35 Å.
17) H. Sawase, Y. Koizumi, Y. Suzuki, M. Shimoi, and A. Ouchi, *Bull. Chem. Soc. Jpn.*, **57**, 2730 (1984).
18) Key to the symmetry operations of the scandium complex: i, $0.5-x$, $-0.5+y$, $0.5-z$; ii, $0.5-x$, $0.5+y$, $0.5-z$.
19) From now on, each carboxylate ion of **1** is numbered by the number of each carboxylate carbon atom in it: **11**, **21**, and **31**.

Solid-Phase Thermal Reactions of Chromium(III) and Copper(II) Complexes Containing Pentadentate Ethylenediaminetetraacetate and 1,2-Propanediaminetetraacetate Ions

Goutam De, Masatatsu Suzuki, and Akira Uehara*
Department of Chemistry, Faculty of Science, Kanazawa University, Kanazawa 920
(Received March 5, 1987)

Synopsis. Thermal reactions of the solid complexes [Cr{Hedta or (*RS*)-Hpdta}(H_2O)] and [Cu{H_2edta or (*RS*)-H_2pdta(H_2O)] were investigated under quasi-isothermal and -isobaric conditions (Q-conditions) and under open dynamic conditions (D-conditions), where Hedta and H_2edta, and Hpdta and H_2pdta denote mono- and diprotonated ethylenediaminetetraacetate and 1,2-propanediaminetetraacetate ions, respectively.

We previously reported the thermal deaquation of the chromium(III) complex [Cr{Hedta or (*RS*)-Hpdta}(H_2O)][1] and thermal dehydrohalogenation of the cobalt(III) complex Na[CoX{Hedta or (*RS*)-Hpdta}] (X=Cl or Br) under D-conditions, where Hedta and Hpdta are monoprotonated ethylenediaminetetraacetate and 1,2-propanediaminetetraacetate ions, respectively.[2] In the latter case, pentadentate edta or pdta changed to hexadentate ligand after dehydrohalogenation, but in the former case we failed to isolate hexadentate edta and pdta chromium(III) complexes by deaquation because the reaction was accompanied by a subsequent decomposition. Quasi-isothermal and -isobaric conditions (Q-conditions) are fundamentally different from D-conditions.[3] The present study was therefore undertaken to investigate the thermal reactions of [Cr{Hedta or (*RS*)-Hpdta}-(H_2O)]·nH_2O (n is 0 for the Hedta and 1 for the Hpdta complexes) under Q-conditions. Thermal reactions of [Cu{(*RS*)-H_2pdta}(H_2O)]·1/2H_2O and their optical antipodes are not yet known. The optical pairs $(+)_D$- and $(-)_D$-[Cu{(*S*)- and (*R*)-H_2pdta}]·1/2H_2O were newly prepared in this study, of which thermal reactions were also investigated.

Experimental

Preparation of Complexes. [Cr(Hedta)(H_2O)] (**1**),[4] [Cr{(*RS*)-Hpdta}(H_2O)]·H_2O (**2**),[4] [Cu(H_2edta)(H_2O)] (**3**),[5] and [Cu(*RS*)-H_2pdta(H_2O)]·1/2H_2O (**4**)[6] were prepared according to the respective methods of literatures.

$(+)_D$-[Cu{(*S*)-H_2pdta}]·1/2H_2O (**5**) was prepared from $(-)_D$-Ba[Cu{(*S*)-pdta}(H_2O)]·2H_2O.[6] The barium salt (2.78 g) in hot water (45 cm^3) was treated with exactly one equivalent of sulfuric acid (10 cm^3, 0.5 mol dm^{-3}), and the mixture was heated to boiling. The $BaSO_4$ thus formed was removed by filtration, the filtrate was evaporated to 10 cm^3 and cooled in refrigerator. The light blue colored compound was collected by filtration and washed with ethanol and then ether. Found: C, 34.94; H, 4.53; N, 7.60%. Calcd for $C_{11}H_{17}N_2O_{8.5}Cu$: C, 35.05; H, 4.51; N, 7.43%.

$(-)_D$-[Cu{(*R*)-H_2pdta}]·1/2H_2O (**6**) was prepared by the same method as that described for complex **5** except that $(+)_D$-Ba[Cu{(*R*)-pdta}(H_2O)]·2H_2O was used as the starting material. Found: C, 34.86; H, 4.40; N, 7.10%. Calcd for $C_{11}H_{17}N_2O_{8.5}Cu$: C, 35.05; H, 4.51; N, 7.43%.

Thermal Measurements. The thermal reactions of the complexes were carried out under Q-conditions and D-conditions by using Q-derivatograph[3,7] and a Seiko SSC/580 TG/DTA-30 thermal analyzer, respectively. The measurements under D-conditions were carried out under a constant flow of nitrogen at the heating rate of 2 °C min^{-1}.

Spectral Measurements. The electronic spectra of the samples in aqueous solution were monitored on a Jasco UVIDEC-505 UV/VIS recording digital spectrophotometer, and those in powder state on a Hitachi EPU-2A spectrophotometer equipped with a standard Hitachi reflection attachment (Type R-3). IR spectra of the samples were measured by a KBr-disk method with a Jasco A-3 infrared spectrophotometer.

Specific Rotation Measurement. All rotations were measured in 1 dm tube in aqueous solution at 15 °C by a Jasco DIP—181 digital polarimeter. An 18.0 mg sample in 10 cm^3 of water was used for each measurement.

Results and Discussion

Figure 1 shows the TG curves of complexes **1** and **2** measured under Q-conditions. The TG curve of [Cr(Hedta)(H_2O)] (**1**) is essentially similar to that of D-derivatogram reported earlier[1] except that the deaquation temperature under Q-conditions is higher (302 °C) than that under D-conditions (280 °C), and it suggests a slim possibility of synthesizing the deaquated hexadentate complex H[Cr(edta)]. Thermal behavior of [Cr{(*RS*)-Hpdta}(H_2O)]·H_2O (**2**) under Q-conditions is different from that under D-conditions. Under Q-conditions, the complex starts to lose water molecule slowly at 171 °C, then a sharp mass loss can be seen at 235—247 °C and a clear plateau is obtained. The weight loss (9.0%) is close to that (9.2%) calculated for 2 mol of water. The product isolated at 250 °C under Q-conditions is pure H[Cr{(*RS*)-pdta}], where pdta functions as hexadent-

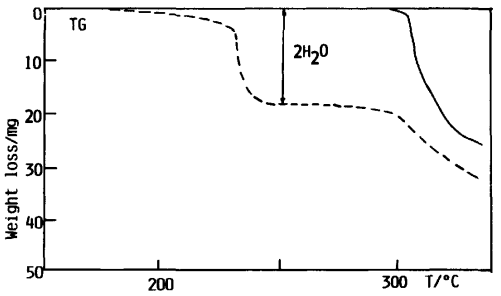

Fig. 1. Q-Derivatoggrams of [Cr(Hedta)(H_2O)] (**1**) (——) and [Cr{(*RS*)-Hpdta}(H_2O)]·H_2O (**2**) (----). Sample weight: **1**, 205 mg; **2**, 210 mg.

ate ligand. It is interesting to note that the lattice and coordinated waters are evolved simultaneously. The complex before heating shows two IR bands at 1738 and 1610 cm^{-1} which are due to free -COOH and coordinated $-COO^-$ groups, respectively. The product, however, does not give the band due to free -COOH group. It is thus clear that the non-coordinated -COOH group comes into coordination toward chromium(III) ion after the elimination of the coordinated water molecule.

The crystal structure of $[Cu(H_2edta)(H_2O)]$ (**3**) is known.[8] The potentially hexadentate edta ligand acts as pentadentate with a water molecule taking up the sixth position, giving rise to a six-coordinated environment about copper(II) ion. The IR (in the carbonyl region) and electronic reflectance spectra of complex **3** and $[Cu\{(RS)\text{-}H_2pdta\}(H_2O)]\cdot 1/2H_2O$ (**4**) are essentially similar to each other. These results suggest that the stereochemistry around the copper(II) ion in complex **4** must be the same as that of complex **3**.

Figure 2 shows the TG and DTA curves (D-conditions) and TG curve of complex **4** under Q-conditions. Under D-conditions, the complex loses its lattice water (Found: 2.23%, Calcd: 2.28%) and coordinated water (Found: 4.57%; Calcd: 4.56%) in the temperature range of 75—90 °C and 150—175 °C respectively, and then a clear plateau is obtained. The corresponding DTA curve shows initially an endothermic peak due to the elimination of lattice water then two overlapping endothermic peaks for the evolution of coordinated water molecule. The elimination of the coordinated water takes place in two steps, but details thereof are still unknown.

$$\underset{\text{light blue}}{[Cu\{(RS)\text{-}H_2pdta\}(H_2O)]\cdot 1/2H_2O} \xrightarrow[\Delta]{-1/2H_2O}$$

$$\underset{\text{light greenish blue}}{[Cu\{(RS)\text{-}H_2pdta\}(H_2O)]} \xrightarrow[\Delta]{-H_2O} \underset{\text{deep blue}}{[Cu\{(RS)\text{-}H_2pdta\}]}$$

The IR spectrum of complex **4** shows a medium strong band at 1740 cm^{-1} due to free -COOH group and a very strong broad peak at 1590 cm^{-1} due to coordinated COO^- group. As the dehydrated complex has a tendency to absorb water molecule, the IR spectrum of **4** has been recorded at 125 and 190 °C in nitrogen atmosphere. The peak due to free -COOH group was always observed. This suggests that the non-coordinated -COOH group remains free even after the elimination of the coordinated water molecule, and pdta still functions as pentadentate ligand. Consequently, Cu^{II} ion is penta-coordinated in the dehydrated complex. The solid state reflectance spectra (350—850 nm) of complex **4** and its dehydrated form show bands at about 740 and about 710 nm. The shifting of the absorption band toward the shorter wavelength region also suggests the formation of penta-coordinated Cu^{II} complex.[9] The dehydrated complex may be either trigonal bipyramidal or square pyramidal in structure, but the decision could not be made.

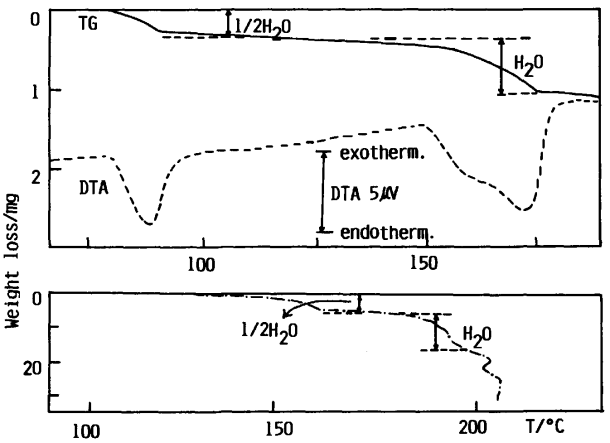

Fig. 2. TG (——) and DTA (----) curves (D-conditions), and TG (—·—) curve (Q-conditions) of $[Cu\{(RS)\text{-}H_2pdta\}(H_2O)]\cdot 1/2H_2O$ (**4**). Sample weight: for TG-DTA (D-conditions), 15.6 mg; for TG (Q-conditions), 199 mg.

Under Q-conditions, the thermal reaction of complex **4** is unusual. The complex evolves its lattice water in the temperature range of 124—163 °C, and above 163 °C evolution of coordinated water molecule takes place upto 195 °C. The product isolated in this stage is violet in color. The product shows a broad absorption band at 561 nm and its analytical composition nicely fits with $[Cu(H_2pdta)]$ (Found: C, 35.10; H, 4.39; N, 7.46%. Calcd for $C_{11}H_{16}N_2O_8Cu$: C, 35.19; H, 4.35; N, 7.61%). The IR spectrum of the product shows two peaks of comparable intensity at 1733 and 1718 cm^{-1} due to free -COOH group and a broad peak at 1610 cm^{-1} due to coordinated carboxylato groups. The two peaks at 1733 and 1718 cm^{-1} indicate the presence of two free -COOH groups in the product.[10] From the spectral and analytical data, it is conceivable that pdta functions as tetradentate ligand toward Cu^{II} ion.

We attempted to get a pair of optical antipodes of complex **4** from $(-)_D$-$Ba[Cu\{(S)\text{-pdta}\}(H_2O)]\cdot 2H_2O$ ($[\alpha]_D$: −126°) and $(+)_D$-$Ba[Cu\{(R)\text{-pdta}\}(H_2O)]\cdot 2H_2O$ ($[\alpha]_D$: +128°)[6]. However, complexes **5** and **6** were always isolated which do not contain any coordinated water molecule. The specific rotations of complexes **5** and **6** are $[\alpha]_D$=+136.4° and −133.7°, respectively. It is interesting to note that pure complexes **5** and **6** can be obtained from the respective barium complexes. Appearance of a medium strong band at 1738 cm^{-1} in the IR spectra of complexes **5** and **6** does not support the full coordination of pdta. Therefore, Cu^{II} ion is probably pentacoordinated in the isomers. The electronic spectra of complex **6** in water and in the solid state (reflectance) were not identical, suggesting that the structure in water is different from that in the solid state. The electronic spectra of the racemic complex **4** and optical pairs **5** and **6** in water were identical. Thus, in water the optical pairs possess similar structure to that of the racemic complex **4**.

TGA runs of the optical isomers (under both Q- and D-conditions) show that dehydration occurs soom

after heating is begun (30—35 °C). Anhydrous weight levels are attained at 140—190 °C (amounting to 2.4% of the total weight). As the temperature is raised further, there is a slow loss of weight resulting from the decomposition of the complexes. The dehydrated complexes **5** and **6** show $[\alpha]_D$=+138.3° and −137.3°, respectively. The increase of rotations are due to the loss of molecular weight resulting from the elimination of lattice water.

One (G. De) of the authors is indebted to the Japan Society for the Promotion of Science (JSPS) for awarding him a Long Term JSPS Research Fellowship for the 1986 fiscal year.

References

1) R. Tsuchiya, A. Uehara, and E. Kyuno, *Bull. Chem. Soc. Jpn.*, **42**, 1886 (1969).
2) R. Tsuchiya, K. Manzaki, S. Sekiya, A. Uehara, and E. Kyuno, *Bull. Chem. Soc. Jpn.*, **48**, 2805 (1975).
3) R. Tsuchiya, A. Uehara, and K. Kobayashi, *Bull. Chem. Soc. Jpn.*, **53**, 921 (1980).
4) R. E. Hamm, *J. Am. Chem. Soc.*, **75**, 5670 (1953).
5) G. S. Smith and J. L. Hoard, *J. Am. Chem. Soc.*, **81**, 556 (1959).
6) F. P. Dwyer and F. L. Garvan, *J. Am. Chem. Soc.*, **83**, 2610 (1961).
7) A. Uehara, M. Kitayama, M. Suzuki, and R. Tsuchiya, *Inorg. Chem.*, **24**, 2184 (1985).
8) F. S. Stephens, *J. Chem. Soc. A*, **1969**, 1723.
9) R. J. Dudley and B. J. Hathaway, *J. Chem. Soc. A*, **1970**, 2794.
10) F. P. Dwyer and F. L. Garvan, *J. Am. Chem. Soc.*, **82**, 4823 (1960).

Syntheses of New Multi-Sulfur 1,2-Dithiolene Complexes. Ni- and Pd-Complexes of 1,4-Dithiin-2,3-dithiolate

Tadashi NAKAMURA, Takashi NOGAMI,* and Yasuhiko SHIROTA
Department of Applied Chemistry, Faculty of Engineering, Osaka University, Yamadaoka, Suita, Osaka 565
(Received March 13, 1987)

Synopsis. The title dithiolene complexes possessing eight sulfur atoms were synthesized. They are expected to give highly conductive organic salts. The improved synthesis of 4,5-(vinylenedithio)-1,3-dithiole-2-thione is also reported.

Studies on highly conductive organic materials have progressed greatly since the discovery of the low-dimensional metallic behavior of TTF·TCNQ.[1] The one-dimensional metallic system is susceptible to a metal-insulator transition due to Peierls distortion. Therefore, increase in the dimensionality was pursued. One of the most successful results along this line was achieved for BEDT-TTF salts,[2] which have a sulfur-sulfur network in the solid and exhibit two-dimensional electrical properties. BEDT-TTF salts possessing trihalide anions were found to be organic superconductors without applying pressure.[3] TTF-[Ni(dmit)$_2$]$_2$ was found to be a new type of organic superconductor last year.[4] Cassoux et al. postulated that this material has a three-dimensional property due to the sulfur-sulfur network in the solid.[4] Multi-sulfur 1,2-dithiolene complexes like M(dmit)$_2$ salts[5] have been postulated as promising candidates for highly conductive organic materials.[6] However, reports on the syntheses of such complexes are surprisingly few, and have appeared in recent years.[7] We have synthesized a new type of multi-sulfur dithiolene complexes (Ni- and Pd-complexes of 1,4-dithiin-2,3-dithiolate), which are also expected to give highly conductive organic complexes. The improved synthesis of 4,5-(vinylenedithio)-1,3-dithiole-2-thione, which is a starting material for the above new complexes, is also reported.

Results and Discussion

Improved Synthesis of 4,5-(Vinylenedithio)-1,3-dithiole-2-thione. 4,5-(Vinylenedithio)-1,3-dithiole-2-thione (**3**) was synthesized as a precursor to bis(vinylenedithio)tetrathiafulvalene (VT).[8] We have now found an improved synthetic method for **3**, and it is shown in Scheme 1. $(Et_4N)_2[Zn(dmit)_2]$ (**1**) was reacted with 1,2-dibromoethyl ethyl ether in acetone at room temperature, and 4,5-(ethoxyethylenedithio)-1,3-dithiole-2-thione (**2**) was obtained. Elimination of ethanol from **2** was achieved by heating the chlorobenzene solution of **2** with anhydrous *p*-toluenesulfonic acid (TsOH) to afford **3**. The currently accepted method[8] has the following drawbacks; (1) it requires expensive 1,2-dichloroethyl ethyl ether in the first step of the reaction; (2) 4,5-(phenylethylenedithio)-1,3-dithiole-2-thione (**4**) was found as a by-product in the second step of the reaction. It was produced by an electrophilic attack of the intermediate carbenium ion (resulting from the elimination of ethanol from **2**) to benzene (solvent).[9] The first drawback was overcome by using 1,2-dibromoethyl ethyl ether which can easily be synthesized on a large scale.[10] The reaction time was shortened from 24 h for the previous method to 10 h for the present method. Moreover, the reaction can be conducted at room temperature, whereas the previous method requires refluxing conditions. The second drawback was overcome by using chlorobenzene as a solvent. The reaction time was also shortened from 24 h for the previous method to 1.5 h for the present method, and the yield of **3** was improved from 23.7% to 32% owing to the absence of the side reaction. This is because the electrophilic attack of the carbenium ion[9] on chlorobenzene is suppressed as a result of the presence of the electron-withdrawing chloride group. Purification of **2** and **3** in the present method was simpler than that of the previous method. Thus, the method shown in Scheme 1 should also be used for the synthesis of VT.

Syntheses of Ni- and Pd-Complexes of 1,4-Dithiin-2,3-dithiolate. The synthetic route of Ni- and Pd-complexes of 1,4-dithiin-2,3-dithiolate is shown in Scheme 2. 4,5-(Vinylenedithio)-1,3-dithiole-2-thione (**3**) was reacted with KOH in ethanol to give a potassium salt (**5**) The salt was then reacted with $NiCl_2 \cdot 6H_2O$ or $Na_2PdCl_4 \cdot 3H_2O$; the product was oxidized by air, and subsequently reacted with

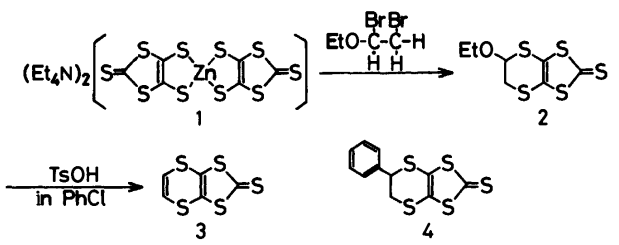

Scheme 1.

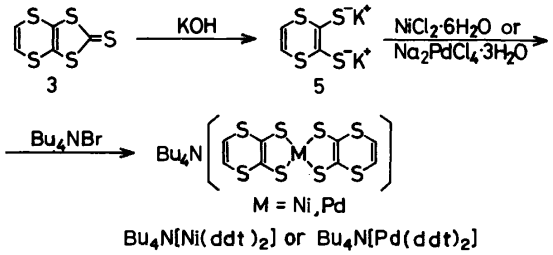

Scheme 2.

Table 1. Electrochemical Data for $Bu_4N[Ni(ddt)_2]$ and $Bu_4N[Pd(ddt)_2]$, Together with Those of the 1,2-Dithiolene Complexes Reported

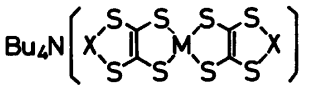

Complex	M	X	E_1 V vs. SCE	E_2 V vs. SCE	$\Delta E(E_1-E_2)$ V
$Ni(ddt)_2$	Ni	-CH=CH-	0.06	−0.51	0.57
$Pd(ddt)_2$	Pd	-CH=CH-	0.11	−0.37	0.43
a	Ni	$-CH_2CH_2-$	0.06	−0.69	0.75
b	Ni	$-CH_2CH_2CH_2-$	0.16	−0.71	0.87
c	Ni	$-CH_2SCH_2-$	0.28	−0.59	0.87
$Ni(dmit)_2$	Ni	C=S	0.22	−0.13	0.35
$Pt(dmit)_2$	Pt	C=S	0.19	−0.13	0.32

tetrabutylammonium bromide to give the new multi-sulfur dithiolene complexes ($Bu_4N[Ni(ddt)_2]$, $Bu_4N[Pd(ddt)_2]$). Here, the ligand portion (1,4-dithiin-2,3-dithiolate) is abbreviated as ddt as shown in Scheme 2. The synthetic approach to $Bu_4N[Pt(ddt)_2]$ by using K_2PtCl_4[7] was unsuccessful. The redox potentials of the dithiolene complexes obtained by the cyclic voltammograms vs. SCE in acetonitrile are shown in Table 1, together with those of the other multi-sulfur 1,2-dithiolene complexes reported[7] for the sake of comparison. The redox waves in the negative potential range were reversible. However, those in the positive potential range were irreversible. In spite of this, E_1 and E_2 of the present complexes were defined as the middle points between the redox peak potentials. The $\Delta E(=E_1-E_2)$ values of the present complexes are 0.43—0.57 V, while those for **a**—**c**, and $M(dmit)_2$ complexes in Table 1 are 0.75—0.87 V and 0.32—0.35 V respectively. This suggests that in the case of the present complexes the intermolecular Coulomb repulsion energy in the conducting state lies between that of $M(dmit)_2$ complexes and other 1,2-dithiolene complexes **a**—**c**.[11]

Experimental

4,5-(Ethoxyethylenedithio)-1,3-dithiole-2-thione (2). To the acetone solution (1.8 L) of $(Et_4N)_2[Zn(dmit)_2]$ (**1**) (25 g) was added dropwise an acetone solution (200 cm³) of 1,2-dibromoethyl ethyl ether (17 g) for a 6-h period with stirring at room temperature, and the mixture was stirred for another 4 h. The orange powder was filtered off, and the solvent removed to obtain an orange solid. It was extracted with benzene, washed with aqueous sodium hydrogencarbonate, and then with water. After drying over Na_2SO_4, the benzene was evaporated, and the residue recrystallized from a mixed solvent of hexane and chloroform (1 : 1) to give **2** (51% yield based on **1**). Its ^1H NMR, mass spectrum, and melting point were identical to those reported previously.[8] Elemental analyses gave satisfactory results.

4,5-(Vinylenedithio)-1,3-dithiole-2-thione (3). The reaction was conducted under nitrogen atmosphere. *p*-Toluenesulfonic acid monohydrate ($TsOH\cdot H_2O$, 7.09 g) was added to a mixed solvent of chlorobenzene (100 cm³) and benzene (100 cm³). Water in the solution was eliminated by azeotropic distillation of benzene. The above solution was heated to 120 °C and chlorobenzene solution (200 cm³) of **2** (5 g) was added. The mixture was stirred for 1.5 h at 110 °C. After filtering off TsOH, the filtrate was washed with aqueous sodium hydrogencarbonate, and then with water. After drying over Na_2SO_4, the solvent was distilled under vacuum. The black solid was chromatographed on silica gel using hexane and chloroform (4:1) as eluent, and the first reddish yellow fraction gave **3** (32% yield). Its ^1HNMR, mass spectrum, and melting point were identical to those reported previously.[8] Elemental analyses gave satisfactory results.

Preparation of Complexes. $Bu_4N[Ni(ddt)_2]$. An ethanol solution (20 cm³) of **3** (1 g) and KOH (2 g) was stirred at 40—45 °C for 2 h under nitrogen atmosphere. The potassium salt **5** precipitated was collected in a hurry, washed with ethanol under nitrogen atmosphere, and dried in vacuum. It was then dissolved in methanol (10 cm³), and a methanol solution (20 cm³) of $NiCl_2\cdot 6H_2O$ (0.4 g) was added. The solution was stirred for 2 h at room temperature under a nitrogen atmosphere. After air-bubbling for 15 min, tetrabutylammonium bromide (2 g) was added to the solution. The dark purple precipitate was collected, washed with methanol, dissolved into acetone (65 cm³), and the solution filtered. To the filtrate was added isopropyl alcohol (65 cm³), the solution was concentrated by rotary evaporator, and $Bu_4N[Ni(ddt)_2]$ was crystallized out. It was collected, washed with methanol and diethyl ether, and dried in vacuum (0.45 g, 73% yield). 135 °C (decomp). Found: C, 43.42; H, 6.08; N, 2.02; S, 38.92%. Calcd for $C_{24}H_{40}NNiS_8$: C, 43.82; H, 6.13; N, 2.13; S, 38.99%. $\lambda_{max}^{CH_3CN}$ ($\log\varepsilon$): 252 nm (4.42); 316 nm (4.40); 564 nm (3.11).

$Bu_4N[Pd(ddt)_2]$. Using $Na_2PdCl_4\cdot 3H_2O$ (0.6 g) instead of $NiCl_2\cdot 6H_2O$ in the above reaction, $Bu_4N[Pd(ddt)_2]$ was obtained as black needles (32% yield). 133 °C (decomp). Found: C, 40.30; H, 5.72; N, 1.86; S, 35.88%. Calcd for $C_{24}H_{40}NPdS_8$: C, 40.86; H, 5.72; N, 1.99; S, 36.33%. $\lambda_{max}^{CH_3CN}$ ($\log\varepsilon$): 258 nm (4.57); 289 nm (4.55); 549 nm (3.16).

References

1) L. B. Coleman, M. J. Cohen, D. J. Sandman, F. G. Yamagishi, A. F. Garito, and A. J. Heeger, *Solid State Commun.*, **12**, 1125 (1973).

2) G. Saito, T. Enoki, K. Toriumi, and H. Inokuchi, *Solid State Commun.*, **42**, 557 (1982).

3) W. -H. Whangbo, J. M. Williams, A. J. Schultz, T. J. Emge, and M. A. Beno, *J. Am. Chem. Soc.*, **109**, 90 (1987), and papers cited therein.

4) M. Bousseau, L. Valade, J. Legros, P. Cassoux, M.

Garbauskas, and L. V. Interrante, *J. Am. Chem. Soc.*, **108**, 1908 (1986).

5) dmit=4,5-dimercapto-1,3-dithiole-2-thione.

6) A. E. Underhill and M. M. Ahmad, *J. Chem. Soc., Chem. Commun.*, **1981**, 67; L. Valade, J. Bouseau, A. Gleizes, and P. Cassoux, *ibid.*, **1983**, 110; H. Kobayashi, R. Kato, A. Kobayashi, and Y. Sasaki, *Chem. Lett.*, **1985**, 535.

7) G. Steimecke, H. Sieler, R. Kirmse, and E. Hoyer, *Phosphorus and Sulfur*, **7**, 49 (1979); G. Steimecke, H. Sieler, R. Kirmse, W. Dietzsch, and E. Hoyer, *ibid.*, **12**, 237 (1982); H. T. Vance, R. D. Bereman, J. Bordner, W. E. Hatfield, and J. H. Helms, *Inorg. Chem.*, **24**, 2905 (1985); R. Kato, H. Kobayashi, A. Kobayashi, and Y. Sasaki, *Bull. Chem. Soc. Jpn.*, **59**, 627 (1986); For a review of 1,2-dithiolene complexes of transition metals, see, R. P. Burns and C. A. McAuliffe, *Adv. Inorg. Chem. Radiochem.*, **22**, 303 (1979).

8) T. Nakamura, S. Iwasaka, H. Nakano, K. Inoue, T. Nogami, and H. Mikawa, *Bull. Chem. Soc. Jpn.*, **60**, 365 (1987).

9) T. Nogami, K. Inoue, T. Nakamura, S. Iwasaka, H. Nakano, and H. Mikawa, *Synth. Metals*, **19**, 539 (1987).

10) H. Morii, S. Fujishige, K. Matsuzaki, and T. Uryu, *Macromol. Chem.*, **183**, 1445 (1982).

11) A. W. Addison, J. P. Barnier, V. Gujval, Y. Hoyano, S. Huizinga, and L. Weiler, "Molecular Metals," ed by W. E. Hatfield, Plenum Press. New York (1979), p. 15.

Asymmetric Synthesis Using Chiral Piperazine. I. Asymmetric Synthesis of 2-Substituted Alcohol and Carboxylic Acid by Diastereoselective Alkylation of Chiral Diamides Derived from Piperazines

Kenso Soai,* Hiroshi Hayashi, Akihiro Shinozaki, Hideaki Umebayashi, and Yasuyuki Yamada
Department of Applied Chemistry, Faculty of Science, Science University of Tokyo, Shinjuku, Tokyo 162
(Received February 17, 1987)

Synopsis. The diastereoselective alkylation of chiral diamides derived from chiral piperazines afforded optically active alcohols and acids in moderate enantiomeric excesses (up to 68% e.e.).

The diastereoselective alkylation of enolates derived from chiral amides is an important method for the synthesis of chiral acids.[1] However, in these reactions one mole is the maximum quantity of the product that can be obtained from one mole of the chiral auxiliary.

In this paper, we report a diastereoselective alkylation of chiral diamides derived from chiral piperazines. In the present system, one mole of chiral diamide affords (in principle) two moles of the product. Chiral 2,5-disubstituted piperazines(**2a,b**)[2] were synthesized by a reduction of the corresponding 2,5-piperazinediones(**1a,b**)[3] with sodium borohydride-titanium tetrachloride[4] (Scheme 1). Chiral diamides(**3a—c**) were obtained in good yields from **2a,b** by the *N*-acylation using the corresponding acid chloride and triethylamine.

The diamides(**3a—c**) were deprotonated and treated with various alkyl halides. The reduction of the alkylated diamides(**4a—c**) with lithium hydrotriethylborate($LiBHEt_3$) removed the chiral auxiliary to afford the corresponding optically active 2-substituted alcohols(**5a,b**). Results are shown in Table 1.

Lithium enolate was formed from **3a** by lithium diisopropylamide (LDA), and was alkylated with methyl iodide. The reductive removal of the chiral auxiliary afforded (*S*)-2-methyl-3-phenyl-1-propanol (**5a**, S:R=71:29) (Entry 1). In diastereoselective alkylation, additives to the enolates had a considerable effect on the degree of diastereoselectivity and the sense of the asymmetric induction. Diastereoselectivities increased in the presence of hexamethylphosphoric triamide(HMPA). Thus, (*S*)-**5a** (S:R=81:19) was obtained from the methylation of lithium enolate of **3a** in the presence of HMPA (LDA:HMPA=1:1) (Entry 3). Butylation under the same conditions showed better diastereoselectivity, and (*S*)-2-benzylhexanoic acid(**6**, S:R=84:16, 68% e.e., Entry 9) was obtained after the oxidation of alcohol(**5b**) (Eq. 1). Meanwhile, the benzylation of **3b** using LDA without any additive afforded (*R*)-**5a**. However, (*S*)-**5a** was obtained from the reaction in the presence of HMPA or *N,N,N′,N′*-tetramethylethylenediamine (TMEDA). This shows that the sense of the asymmetric induction in benzylation was reversed by these additives. Crown ethers as additives showed

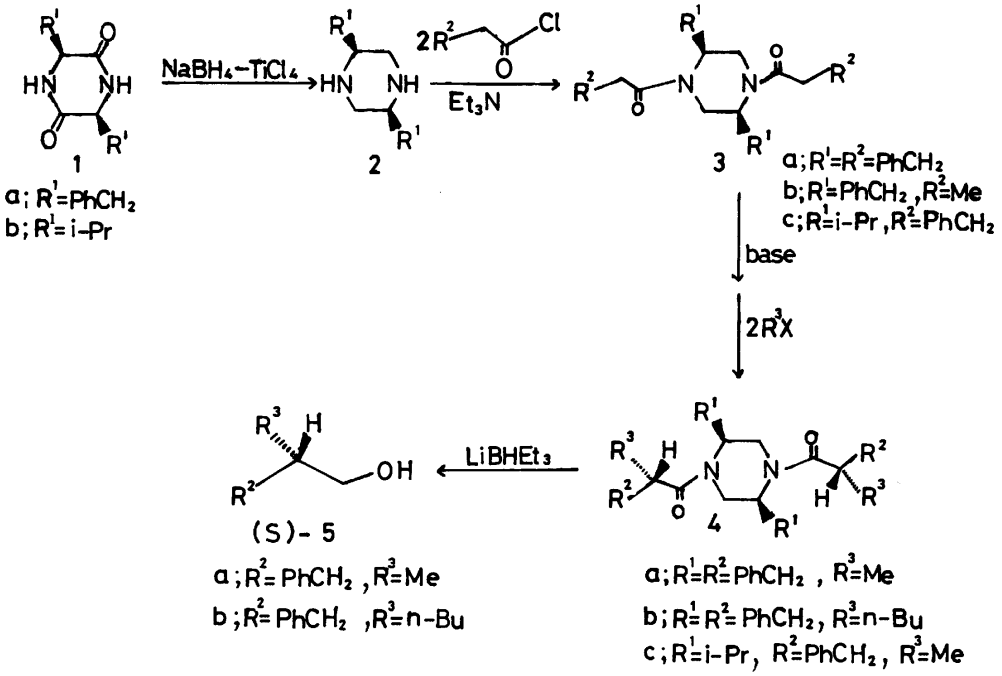

Scheme 1.

Table 1. Diastereoselective Alkylation of Diamide **3** via Metal Enolates

Entry	3	R^3X	Base	Yield of 4/%	Yield of 5/%		Ratio of 5 S:R[a]
1	**3a**	MeI	LDA	53	**5a**	33	71:29
2	**3a**	MeI	LDA:HMPA=1:2	66	**5a**	38	73:27
3	**3a**	MeI	LDA:HMPA=1:1	65	**5a**	64	81:19[b]
4	**3a**	MeI	LDA:HMPA=1:0.5	81	**5a**	59	74:26
5	**3a**	MeI	LDA:TMEDA=1:0.5	80	**5a**	66	76:24
6	**3a**	MeI	LDA:TMEDA=1:0.25	67	**5a**	27	72:28
7	**3a**	MeI	LDA:12-Crown-4=1:1	42	**5a**	59	70:30
8	**3a**	*n*-BuI	LDA	80	**5b**	38	74:26[c]
9	**3a**	*n*-BuI	LDA:HMPA=1:1	64	**5b**	32	84:16[c,d]
10	**3a**	*n*-BuI	LDA:TMEDA=1:0.5	72	**5b**	45	64:36[c]
11	**3b**	$PhCH_2Br$	LDA	81	**5a**	48	45:55
12	**3b**	$PhCH_2Br$	LDA:TMEDA=1:1	52	**5a**	45	50:50
13	**3b**	$PhCH_2Br$	LDA:TMEDA=1:0.5	41	**5a**	59	59:41
14	**3b**	$PhCH_2Br$	LDA:HMPA=1:1	58	**5a**	49	63:37
15	**3c**	MeI	LDA	72	**5a**	19	59:41
16	**3c**	MeI	LDA:HMPA=1:2	90	**5a**	14	68:32
17	**3c**	MeI	LDA:HMPA=1:1	76	**5a**	14	63:37
18	**3c**	*n*-BuI	LDA:HMPA=1:1	76	**5b**	14	82:18[c]
19	**3a**	MeI	$NaN(SiMe_3)_2$	69	**5a**	37	65:35
20	**3a**	MeI	$NaN(SiMe_3)_2$: 18-Crown-6=1:1	82	**5a**	41	70:30[e]

a) Determined by the measurement of the optical rotation. Literature value of **5a**; $[\alpha]_{578}^{22}$ −11.5° (*c* 0.5, C_6H_6). M. M. Leclercq, J. Billed, and J. Jacques, *Mol. Cryst. Liq. Cryst.*, **8**, 367 (1969). b) Observed $[\alpha]_{577}^{28}$ −7.07° (*c* 0.99, C_6H_6). c) Alcohol **5b** was oxidized to the acid **6**, and the optical rotation of **6** was measured. Lit value; $[\alpha]_D^{20}$ −22.8° (*c* 2.06, C_6H_6), M. B. Atson and G. W. Youngson, *J. Chem. Soc. C*, **1968**, 258. d) Observed $[\alpha]_D^{23}$ +15.5° (*c* 0.69, C_6H_6). e) Observed $[\alpha]_{577}^{24}$ −4.58° (*c* 1.02, C_6H_6); $[\alpha]_D^{22}$ −4.29° (*c* 0.63, C_6H_6), 39% e.e. based on lit value for 74% e.e., $[\alpha]_D^{24}$ −8.2° (*c* 4.63, C_6H_6), S. Terashima and S. Yamada, *Chem. Pharm. Bull.*, **16**, 1953 (1968).

relatively little effect. The addition of 12-crown-4 (1 molar equiv) to lithium enolate of **3a** gave **5a** (S:R=70:30, Entry 7).

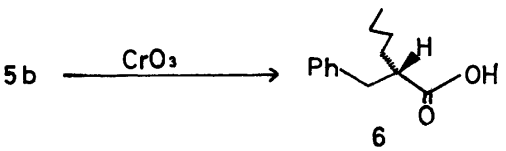

6 (1)

Lithium enolate was more effective than sodium and zirconium enolates. Sodium enolate was formed using sodium disilazane, and was alkylated by methyl iodide at room temperature to give **5a** (S:R=65:35, Entry 19). The addition of 18-crown-6 (1 molar equiv) to sodium enolate gave **5a** (S:R=70:30, Entry 20). The desired product was not obtained in an attempted methylation of zirconium enolate, which had been prepared from lithium enolate using dicyclopentadienylzirconium dichloride.[1a]

Experimental

(2*S*,5*S*)-2,5-Dibenzylpiperazine (2a) was synthesized by the reduction of *cyclo*-L-Phe-L-Phe (**1a**) with sodium borohydride–titanium tetrachloride ($NaBH_4$–$TiCl_4$) according to a previously reported procedure.[2]

(2*S*,5*S*)-2,5-Diisopropylpiperazine (2b): Compound **2b** was synthesized from *cyclo*-L-Val-L-Val (**1b**) by the same procedure as above (64% yield); mp as dihydrochloride, 265.5—267.0 °C (decomp), $[\alpha]_D^{25}$ −21.1° (*c* 1, H_2O). ^1H NMR (CCl_4) δ=0.90 (dd, 12H), 1.30 (s, 2H), 2.09 (m, 4H), 2.65 (s, H, NH), 2.72 (m, 2H); IR (neat) 3000, 1540, 920 cm^{-1}; Found: *m/z* 170.1779. Calcd for $C_{10}H_{22}N_2$: M, 170.1785.

(2*S*,5*S*)-2,5-Dibenzyl-1,4-bis(3-phenylpropanoyl)piperazine (3a): To a solution of **2a** (1.697g, 5mmol) in 20ml of CH_2Cl_2 in ice-cooling bath, triethylamine (Et_3N, 1.012g, 10mmol) was added. Then, 3-phenylpropanoyl chloride (2.023g, 12mmol) in 10ml of CH_2Cl_2 and Et_3N (1.214g 12mmol) were added successively. The mixture was stirred for 1h. The cooling bath was removed and the mixture was stirred for 12h. The mixture was filtered, and the filtrate was evaporated under reduced pressure. The residue was dissolved in ethyl acetate and was washed successively with 1 M† HCl, H_2O, satd. aq $NaHCO_3$. Purification by silica-gel column chromatography (eluent EtOAc–hexane=1:2) gave **3a** as an oil in 82% yield; ^1H NMR (CCl_4) δ=2.3—2.7 (m, 14H), 4.1 (broad, 4H), 7.0 (m, 20H); IR (neat) 3050, 1640, 1420, 740 cm^{-1}; Found: *m/z* 530.2906. Calcd for $C_{36}H_{38}N_2O_2$: M, 530.2935; $[\alpha]_D^{22}$ +55.0° (*c* 1.073, EtOH).

(2*S*,5*S*)-2,5-Dibenzyl-1,4-dipropanoylpiperazine (3b): Compound **3b** was prepared by the same procedure as described above in 62% yield as an oil; ^1H NMR (CCl_4) δ=1.0 (t, 6H), 1.95 (m, 4H), 2.7 (m, 6H), 4.2 (m, 4H), 7.05 (s, 10H);

† 1 M=1 mol dm^{-3}.

IR (neat) 3000, 1640, 1430 cm^{-1}; Found: *m/z* 378.2278. Calcd for $C_{24}H_{30}N_2O_2$: M, 378.2309; $[\alpha]_D^{27}$ +64.0° (*c*1.00, EtOH).

(2*S*,5*S*)-2,5-Diisopropyl-1,4-bis(3-phenylpropanoyl)piperazine (3c): Compound **3c** was prepared by the same procedure as described for **3a** in 95% yield; ^1H NMR (CCl_4) δ=0.90 (dd, 12H), 1.68 (m, 2H), 2.45—2.83 (m, 10H), 4.05 (m, 4H), 7.05 (s, 10H); IR (neat) 2950, 1640, 1420 cm^{-1}; MS (70 eV) *m/z* 434(M^+), 391, 259, 127, 91; $[\alpha]_D^{22}$ +100.3° (*c* 1.00, EtOH).

Diastereoselective Alkylation of the Lithium Enolate Derived from 3a in the Presence of HMPA. Typical Procedure: A THF solution of lithium diisopropylamide-(LDA)[5] (0.50 M, 2.3 mmol) was added slowly to diamide (**3a**, 0.512 g, 0.96 mmol) dissolved in THF (6 ml) at −78 °C under an argon atmosphere; the mixture was stirred for 30 min at −30 °C and HMPA (0.412 g, 2.3 mmol) was added. Then, the mixture was cooled again to −78 °C. Methyl iodide (0.545 g, 3.84 mmol) was added and the mixture was stirred for 3 h, quenched with phosphoric acid buffer (pH 7), and 1 M HCl was added. The mixture was extracted with $CHCl_3$, dried over anhydrous sodium sulfate, and concentrated under reduced pressure. The purification by silica-gel TLC (developing solvent EtOAc–hexane=1 : 2) gave dialkylated diamide **4a** in 65% yield as an oil; ^1H NMR (CCl_4) δ=1.00 (s, 6H), 2.40—2.67 (m, 12H), 4.02(broad, 4H), 7.05 (s, 20H); IR (neat) 3000, 1640, 1420 cm^{-1}.

Diastereoselective Methylation of Sodium Enolate of 3a in the Presence of 18-Crown-6 (Table 1, Entry 20): A solution of sodium disilazane (1.0 M, 2.0 mmol) was slowly added to the mixture of diamide **3a** (0.264 g, 0.5 mmol) and 18-crown-6(0.529 g 2.0 mmol) dissolved in THF (3.0 ml) at room temperature under an argon atmosphere; the mixture was stirred for 30 min at room temperature. Methyl iodide (0.426 g, 3.0 mmol) was added and the mixture was then stirred over night at room temperature and worked up in the same manner as described above. Compound **4a** was obtained in 82% yield.

Preparation of Optically Active Alcohols 5a, b by the Reductive Cleavage of the Alkylated Diamide 4a—c with Lithium Hydrotriethylborate: $LiBHEt_3$ (1.0 M solution in THF, 5 ml) was added to **4** and stirred for 24 h at 35 °C; it and was then quenched with a careful addition of H_2O. The mixture was made acid with 1 M HCl. The mixture was extracted with $CHCl_3$, evaporated under reduced pressure. The residue was purified on silica gel TLC (developing solvent $CHCl_3$) followed by bulb-to-bulb distillation to afford 2-methyl-3-phenyl-1-propanol (**5a**) or 2-benzyl-1-hexanol (**5b**), respectively. The enantiomeric excess of **5a** was determined by the optical rotation of the sample. The enantiomeric excess of **5b** was determined by optical rotation after **5b** was oxidized to **6**.

(*S*)-2-Benzylhexanoic Acid (6): Chromium(VI) oxide[6] (2.32 g) in sulfuric acid (4M, 5 ml) was added to an acetone solution (2.0 ml) of **5b** in an ice cooled bath. After the mixture was stirred for 1 h, sodium sulfite (4.0 ml of 10% aq solution) was added; extraction was performed using ether. The extract was dried over anhydrous sodium sulfate, evaporated under reduced pressure. The residue was purified on silica-gel TLC (developing solvent EtOAc–hexane=1 : 1). (*S*)-**6** was obtained in 64% yield.

References

1) a) D. A. Evans, "Asymmetric Synthesis," ed by J. D. Morrison, Academic Press, New York (1984), Vol. 3, p. 11; b) W. Oppolzer, P. Dudfield, T. Stevenson, and T. Godel, *Helv. Chim. Acta*, **68**, 212 (1985).

2) K. Soai, H. Hayashi, and H. Hasegawa, *Heterocycles*, **24**, 1287 (1986).

3) T. Ueda, M. Saito, T. Kato, and N. Izumiya, *Bull. Chem. Soc. Jpn.*, **56**, 568 (1983).

4) S. Kano, Y. Tanaka, E. Sugino, and S. Hibino, *Synthesis*, **1980**, 695.

5) E. Vedejs, D. A. Engler, and J. E. Telschow, *J. Org. Chem.*, **43**, 188 (1978).

6) K. Bowden, I. M. Heilbron, and E. R. H. Jones, *J. Chem. Soc.* **1946**, 39.

The Novel Syntheses of Photoreversible Cyclobutanocrown Ethers by the Intramolecular Photoaddition of α,ω-Dicinnamoyl Polyethylene Glycol Derivatives

Sadatoshi Akabori,* Yoichi Habata, Misako Nakazawa, Yoko Yamada, Yoichi Shindo, Tokuko Sugimura, and Sadao Sato†

Department of Chemistry, Faculty of Science, Toho University, Funabashi, Chiba 274
†Analytical and Metabolic Research Laboratories, Sankyo Co. Ltd., Hiromachi, Shinagawaku, Tokyo 140

(Received March 24, 1987)

Synopsis. Irradiation of a solution of dicinnamates of *o*-bis(3-hydroxy-1-oxapropyl)benzene and *o*-bis(6-hydroxy-1,4-dioxahexyl)benzene in methanol by Pyrex-filtered UV light gave the corresponding intramolecular pseudophotodimerized crown ethers, and irradiation of the crown ethers in methanol by 220 nm UV light gave the open chain starting dicinnamates in reverse. The structures of the isolated crown ethers were confirmed to be δ-form by the ^{1}H NMR spectra and X-ray analysis.

It is well-known[1] that crown ethers can be complexed with alkali, alkaline earth, and other metal cations, despite the poor complexing abilities of the corresponding open chain polyethers. Recently, several kinds of photoresponsive crown ethers have been reported by Shinkai et al.[2] and Osa et al.[3] For example, the alkali cation-binding abilities of benzocrown ethers containing azo group were enhanced by photoirradiation.[2] There are many reports on the photodimerization of cinnamic acid and its derivatives.[4] Furthermore, intramolecular photocycloaddition has received attention from the synthetic viewpoints of crown ethers. For example, Mizuno et al.[5] obtained cyclobutanocrown ethers (cyclobutane-fused crown ethers) by intramolecular photocycloaddition of the bis(vinyloxy) compounds using a sensitizer. Recently, Egerton et al.[6] have suggested that photodimerization of the ethyl cinnamate in solution gives a cyclodimer in high yield. It was further reported that, on irradiation of 210 nm UV light, the cyclodimer regenerated the starting monomer. In connection with the above results, the preparation of polymers having both crown ether moiety as a cation binding site and a cinnamic acid ester moiety as a photodimerizable pendant group has been recently reported by Shirai et al.[7] They showed that, in 310 nm UV light, the cinnamoyl groups of these polymers caused dimerization in a dilute solution and the cation extraction abilities of the photoreacted polymers were higher than those of the original polymers. Also, Kimura et al.[8] and Hiratani et al.[9] reported the preparation of the cyclobutanocrown ethers by photoirradiation of the dicinnamates of the polyethylene glycol derivatives. These findings suggest that dicinnamates of polyethylene glycol and their homologs in solution could be cyclized by intramolecular additions in 310 nm light; then, in 210 nm UV light, the cyclized crown ethers could possibly give the corresponding open chain dicinnamates in reverse. Therefore, the extraction abilities of the crown ether could be controlled by photoaddition. However, these authors did not describe the reversible photocleavage of the cyclobutanocrown ethers. We therefore in this paper report on the syntheses of cyclobutanocrown ethers by intramolecular photocycloaddition of the polyethylene glycol derivatives and their photoreversible reaction.

Catechol (**1a**) reacted with cinnamoyl chloride in the presence of pyridine in benzene to give **2a** in 57.3% yield. Also, the dicinnamates **2b** and **2c** were obtained in 61% yields, respectively by the reaction of cinnamic acid with **1b** and **1c** in the presence of a catalytic amount of *p*-toluenesulfonic acid in benzene.

Irradation of methanol solutions (1 dm^3) of **2b** and **2c** (4×10^{-4} mol) with a 450W high-pressure mercury lamp through a Pyrex filter gave **3b** and **3c** in 27 and 41% yields, respectively. However, **3a** could not be isolated from the photoirradiated products. The thin-layer chromatography of the reaction mixture of **2a** or **2c** showed the presence of several products. However, in both cases, the products, which may be isomers of **3a** or **3c**, could not be separated because of their negligible amounts.

Template-typed photoreaction was also determined, however the yields of **3** were not improved. In the ^{1}H NMR spectra of **3b** and **3c**, the aromatic protons caused by the phenyl moieties shifted upfield (ca. 0.11 ppm), compared with those of the starting materials. Kuzuya et al.[10] reported that the signals of the phenyl protons in the δ-truxinate of polymethylene dicinnamates were shifted upfield about 0.13 and 0.35 ppm, compared with those of the starting dicinnamates, respectively. Therefore, there was an upfield shift of ca. 0.11 ppm of the signal of the phenyl moieties when going from the dicinnamates

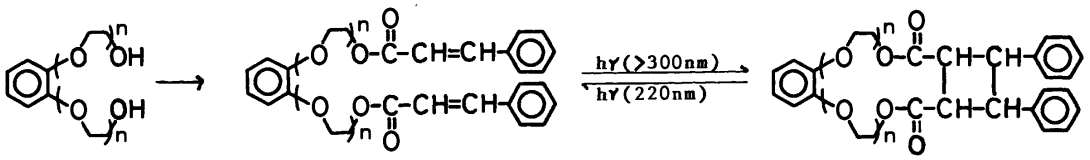

1a: n=0 **2a**: n=0 **3a**: n=0
1b: n=1 **2b**: n=1 **3b**: n=1
1c: n=2 **2c**: n=2 **3c**: n=2

(**2b** and **2c**) to the crown ethers (**3b** and **3c**). Furthermore, the discovery of the coupling constant (ca. 5.7 Hz) between the Ha and Hb in the cyclobutane ring of **3b** and **3c** is also supported by the above results. Also, the hydrolysis of **3b** and **3c** with dil hydrochloric acid gave δ-truxinic acid quantitatively.[8] In addition, irradiation of **3b** and **3c** with 220 nm UV light gave the starting dicinnamates quantitatively.

In order to investigate in more detail, photocycloaddition was carried out at a concentration of 4×10^{-5} mol dm^{-3} of **2a—c** in methanol. These results showed the relationship between the lengths of oxyethylene units and formation rates of photocycloaddition. In specific results, the rate of the decrease of the absorption at 275 nm of the dicinnamates was in the following order (min): **2b**(98.7)>**2c**(105.9)>**2a** (590.7). This finding is explicable when the length of the oxyethylene units in the dicinnamates is considered, because the overlapping of two cinnamoyl groups in **2b** could easily occur due to their suitable bond lengths compared with the longer and shorter chain units of **2c** and **2a**, respectively, although other influences cannot be ruled out.

Photocleavage of **3b** and **3c** was carried out in acetonitrile under irradiation at 220nm UV light using a grating monochromator with a 500W xenon lamp. The solution was measured by UV-VS spectra at appropriate intervals. The absorption band at 275 nm increased with UV irradiation of the solution and a steady state was attained within 7 h. The photoreversible cleavage of **3b** and **3c** proceeded to give **2b** and **2c** in 40 and 60% yields, respectively.

Measurement of the extraction ability was carried out by the method described in a previous paper.[11] The extraction abilities of the compounds **2a—c**, **3b**, and **3c** toward alkali metal cations were very low or negligible in values. Also, the differences in the extraction abilities between the **2** and **3** could not be observed in all cases. The low extraction ability of the dicinnamates **2** is explicable by the large steric repulsion between the two terminal cinnamoyl groups when a guest cation is surrounded by the oxygen atoms of the host molecule. Also, the distortion of the structure of the macrocyclic moiety as well as the presence of the ester moiety in **3** seems to be the reason for their low extraction abilities. Therefore, **3b** was further characterized by X-ray crystallographic study.

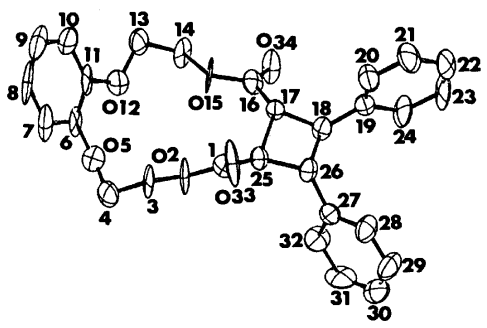

Fig. 1. ORTEP drowing of the molecular structure of **3b**.

The conformation of **3b** is illustrated in Fig. 1, which also shows the atom labels used. The result confirmed the δ-configuration of the toluxinate moiety in **3b**, indicating that the cyclobutane structure bearing two ester groups largely distorts the macrocyclic structure as shown in Fig. 1. The distances between O(5)-O(15), O(2)-O(15), and O(2)-O(12) are 3.819(5), 3.515(4) and 4.379(4) Å, respectively, although the distances between O(2)-O(5) (2.844(5) Å), O(12)-O(15) (2.740(4) Å) are better located to form the complex. The conformation and the long distances (3.819, 3.515, and 4.379 Å) between those oxgen atoms of the macrocyclic moiety are disadvantageous for forming the complex with a guest cation.

In conclusion, the complexing abilities of the cyclobutanocrown ether **3b** with alkali metal cation were decreased by the two factors of long distances between the oxygen atoms of the ether linkage and the presence of the ester moieties in the macrocyclic polyether part. However, the photoreversible reaction between **2** and **3** suggests the possibility of its use as photoresponsive crown ether.

Experimental

The melting points are uncorrected. The ^{1}H NMR spectra were obtained on Hitachi R-90 and GEOL GX400 spectrometers, with TMS as an internal standard. The UV spectra were obtained on a Hitachi 330 Spectrometer. The IR spectra were measured on a JASCO IRA-2 Diffraction Grating Infrared Spectrometer. For irradiation of **2** on a preparative scale, a solution charged in a vessel fitted with a Pyrex cooling jacket was purged with dry nitrogen for 10 min and internally irradiated with an Ushio High-pressure mercury lamp (HPL) (UM-452). Also, photocleavage of **3** to **2** was carried out by means of a 220 nm UV light using a grating monochromater (Model JASCO CT-10) with a 500 W xenon lamp(JASCO PS-X500) and 0.5 nm band width.

2a. Dry pyridine (40 cm^3) was added dropwise to a solution of chatechol (1.65 g, 15 mmol) and cinnamoyl chloride (5.0 g, 30 mmol) in benzene (100 cm^3) and the mixture was stirred for 3 h at room temperature. Water (100 cm^3) was then added dropwise to the mixture, and an aqueous layer was separated. The organic layer was then washed with dil hydrochloric acid, water, 10% aq sodium hydrogencarbonate solution and water, and then dried over anhyd. sodium sulfate. After evaporation of the solvent under reduced pressure, the residue was recrystallized from ethanol to give **2a** as colorless crystals in 57.3% yield. Mp 123.5—124.5 °C. Found: C, 77.80, H, 4.99%. Calcd for $C_{24}H_{18}O_4$: C, 77.82, H, 4.90%. MS (70 eV) *m/z* 370 (M^+). IR(KBr) 1720 cm^{-1} (C=O). UV (in MeOH) 275 nm (ε 9000). ^{1}H NMR ($CDCl_3$) δ=6.58 (d, *J*=16.0 Hz, 2H, C_α-H), 7.86(d, *J*=16.0 Hz, 2H, C_β-H), 7.58—7.31 (m, 10H, aromatic H), and 7.31(s, 4H, aromatic H).

2b. A solution of **1b** (0.68 g, 3.5 mmol), cinnamic acid (2.1 g, 14 mmol), and a trace of *p*-toluenesulfonic acid in toluene (80 cm^3) was refluxed for 26 h. The reaction mixture was cooled to room temperature and washed with a 0.01% aq sodium hydroxide solution and water, and then evaporated. The residual solid was recrystallized from hexane to give **2b** as colorless needles in 61% yield. Mp 59.0—59.5 °C. Found: C, 73.03, H, 5.86%. Calcd for $C_{28}H_{26}O_6$: C, 73.35, H, 5.72%. MS (70 eV) *m/z* 458 (M^+). UV (in MeOH) 277 (ε 49000). IR (KBr) 1720 cm^{-1} (C=O). ^{1}H NMR ($CDCl_3$) δ=4.64—4.25 (m, 8H, CH_2), 6.45 (d, *J*=16.0 Hz, 2H, C_α-H), 7.69 (d, *J*=16.0 Hz,

2H, C_β-H), 7.48—7.32 (m, 10H, aromatic H), 6.98 (s, 4H, aromatic H).

2c. A solution of lc (1.03 g, 3.64 mmol), cinnamic acid (2.16 g, 15 mmol) and a trace of *p*-toluenesulfonic acid in toluene (80 cm^3) was refluxed for 44 h. The reaction mixture was cooled, evaporated in vacuo and the residue was dissolved in chloroform. The solution was washed with a 10% aq sodium hydrogencarbonate solution and water, and evaporated. The residue was chromatographed on silica gel using a benzene-acetone (12:1) solution as an eluent. The evaporation of the second fraction gave **2c** as pale yellow viscous oil in 61.0% yield. Found: C, 70.12, H, 6.33%. Calcd for $C_{32}H_{34}O_8$: C, 70.31, H, 6.27%. MS (70 eV) *m/z* 546 (M^+). IR (KBr) 1720 cm^{-1} (C=O). UV (in MeOH) 277 nm (ε 49000). ^{1}H NMR ($CDCl_3$) δ=4.45—4.10 (m, 8H, CH_2), 3.95—3.72 (m, 8H, CH_2), 6.45 (d, *J*=16.0 Hz, 2H, C_α-H), 7.70 (d, *J*=16.0 Hz, 2H, C_β-H), 7.52—7.32 (m, 10H, aromatic H), 6.92(s, 4H, aromatic H).

Irradiation of 2b. Dicinnamate **2b** (0.137 g, 0.3 mmol) dissolved in methanol (1 dm^3) was irradiated internally with HPL (450 W) through a Pyrex filter at running water temperature for 5 h. The solvent was evaporated and the residue was recrystallized from methanol resulting in **3b** as colorless crystals. Yield 20%, Mp 142.0—143.0 °C. Found: C, 73.05, H, 5.68%. Calcd for $C_{28}H_{26}O_6$: C, 73.33, H, 5.72%. MS (70 eV) *m/z* 458(M^+). UV (in MeOH) 275 nm (ε 2300); ^{1}H NMR ($CDCl_3$) δ=7.29 (s, 10H), 6.97 (s, 4H), 4.92—4.50(m, 2H), 4.50—4.03 (m, 6H), 4.00—3.80 (m, 2H), 3.50—3.31 (m, 2H).

Irradiation of 2c. Dicinnamate **2c** (0.109 g, 0.2 mmol) dissolved in methanol (1 dm^3) was irradiated as described above. After irradiation, the solvent was evaporated. An oily residue was chromatographed on silica gel. Elution with benzene-ethyl acetate (4:1) gave pure **3c** as an oily product. Yield 24%. Found: C, 69.93, H, 6.40%. Calcd for $C_{32}H_{34}O_8$; C, 70.30, H, 6.28%. MS (70 eV) *m/z* 546 (M^+). UV (in MeOH) 275 nm (ε 2400), ^{1}H NMR($CDCl_3$) δ=7.28 (s, 10H), 6.91 (s, 4H), 4.57—4.01 (m, 8H), 4.01—3.58 (m, 10H), 3.53—3.36 (m, 2H).

Irradiation of 3b and 3c. An acetonitrile solution of **3** (ca. 2.0×10^{-5} mol dm^{-3}) was placed in a quartz cell (1×1×4 cm) and was irradiated at room temperature with a 220 nm UV light for 6—7 h. The UV spectra during irradiation were recorded with a Hitachi 330 spectrometer. The photoreversible yields of **2b** and **2c** were calculated from the intensity of the absorption band at 275 nm in the stead state. After irradiation, the solvent was evaporated in vacuo and the residue was chromatographed on silica-gel TLC using chloroform as an eluent. The main fraction was extracted with chloroform and the solution was then evaporated in vacuo to give **2c** or **2b**. The structures of **2b** and **2c** were confirmed by comparison with R_f values of TLC, the melting point (for **2b**) and spectral data of the authentic samples.

Hydrolysis of 3b and 3c. A solution of **3b** (0.107 g, 0.23 mmol) in methanol (20 cm^3) containing dil hydrochloric acid (10 cm^3) was refluxed for 4.5 h. After the solution has been cooled to room temperature, aq sodium hydroxide solution was added. The resulting alkaline solution was extracted with chloroform. To the aqueous solution was added dil hydrochloric acid until it became acidic and then the solution was extracted with chloroform. The extract was dried over anhyd. sodium sulfate and concentrated. To the residue was added an ether solution (50 cm^3) of diazomethane. Evaporation of the solvent gave dimethyl δ-toluxinate in 33% yield. Mp 78.0—79.5 °C(lit,[12] 77 °C). ^{1}H NMR (in $CDCl_3$) δ=7.24 (s, 10H), 3.94—3.29 (m, A_2B_2 pattern, 4H), 3.82 (s, 6H).

δ-Toluxinate was also obtained from **3c** by the same method.

X-Ray Crystallography. Crystal of dimensions 0.4×0.2×0.1 mm was used for the X-ray crystallography. Crystal data are as follows: $C_{28}H_{26}O_6$, Mw=450.5. Monoclinic, $P2_1/n$, a=19.325(5), b=5.323(1), c=22.838(5)Å, β=95.14(2)°, U=2339.9 $Å^3$, Z=4, Dx=1.30 g cm^{-3}, ν(Cu Kα)=7.6 cm^{-1}. Intensity data for $2\theta\leqslant128°$ were recorded on a Rigaku AFC-5R with graphite monochromatized CuKα radiation. A total of 3898 independent reflections were corrected for Lorentz and polarization factors but not for absorption. The structure was solved by direct methods using MULTAN84,[13] and refined by block diagonal least-squares methods. The positions of the hydrogen atoms were estimated using standard geometry. The final refinements with anisotropic temperature factors for the non-hydrogen atoms and isotropic temperature factors for the hydrogen atoms were lowered R values 0.079 (R_w=0.050, $w=1/\sigma^2(F_o)$, 2646 observed reflections with $F_o\geqslant2\sigma(F_o)$). Parameters for bond lengths, angles and structure factors (observed and calculated) are kept at the Chemical Society of Japan (Document No.8751).

The present work was partially supported by a Grant-in-Aid for Scientific Research (No. 6154038) from the Ministry of Education, Science and Culture.

References

1) F. de Jong and D. N. Reinhoudt, "Stability and Reactivity of Crown-ether Complexes," Academic Press, New York (1981).

2) S. Shinkai, T. Minami, Y. Kusano, and O. Manabe, *J. Am. Chem. Soc.*, **104**, 1967 (1982); S. Shinkai, T. Nakaji, T. Ogawa, K. Shigematsu, and O. Manabe, *J. Am. Chem. Soc.* **103**, 111 (1981).

3) H. Sasaki, A. Ueno, J. Anzai, and T. Osa, *Bull. Chem. Soc. Jpn.*, **59**, 1953 (1986).

4) Y. Shindo, K. Horie, and I. Mita, *J. Photochem.*, **26**, 165 (1984), *Chem. Lett.*, **1983**, 639; T. Ishigami, T. Murata, and T. Endo, *Bull. Chem. Soc. Jpn.*, **49**, 3578 (1976).

5) K. Mizuno, T. Hashizume, and Y. Otsuji, *J. Chem. Soc., Chem. Commun.*, **1983**, 977.

6) P. L. Egerton, E. Pitts, and A. Reiser, *Macromolecules*, **14**, 95 (1981); P. L. Egerton, E. M. Hyde, J. Trigg, A. Payne, P. Begnon, M. V. Mijovic, and A. Reiser, *J. Am. Chem. Soc.*, **103**, 3895 (1981).

7) M. Shirai, A. Ueda, and M. Tanaka, *Makromol. Chem.*, **186**, 493 (1985); M. Shirai, J. Orikata, and M. Tanaka, *Makromol. Chem., Rapid Commun.*,**4**, 65 (1983), *J. Polym. Sci., Polymer Chem. Ed.*, **23**, 463 (1985).

8) M. Kimura, M. Kishimoto, and S. Morosawa, 48th National Meeting of the Chemical Society of Japan, April 1983, Kyoto, Abstr., No. 1E32.

9) K. Hiratani and S. Aiba, *Bull. Chem. Soc. Jpn.*,**57**, 2657 (1984).

10) M. Kuzuya, M. Tanaka, M. Hosoda, A. Noguchi, and T. Okuda, *Nippon Kagaku Kaishi*, **1984**, 22; M. Kuzuya, M. Tanaka, and T. Okuda, *Tetrahedron Lett.*, **24**, 4237 (1983).

11) S. Akabori, Y. Habata, Y. Sakamoto, M. Sato, and S. Ebine, *Bull. Chem. Soc. Jpn.*, **56**, 537 (1983).

12) "Kagaku Daijiten," Kyouritsu Shutsupan, Tokyo (1963), Vol. 6, p. 551.

13) P. Main, G. Germain, and M. M. Woolfson, "MULTAN84: A System of Computer Programs for the Automatic Solution of Crystal Structures from X-Ray Diffraction Data," Universities of York, England, and Louvain, Belgium (1984).

Ruthenium Complex-Catalyzed N-Heterocyclization. Syntheses of *N*-Substituted Pyrroles and Pyrrolidines from 1,4-Diols and Primary Amines

Yasushi TSUJI, Yasuharu YOKOYAMA, Keun-Tae HUH, and Yoshihisa WATANABE*
Department of Hydrocarbon Chemistry, Faculty of Engineering, Kyoto University, Sakyo-ku, Kyoto 606
(Received March 26, 1987)

Synopsis. 2-Butyne-1,4-diol reacts with aliphatic amines in the presence of a catalytic amount of [$RuCl_2(PPh_3)_3$] at 150 °C to give *N*-alkylpyrroles in good yields. 1,4-Butanediol reacts with aromatic or aliphatic amines to give *N*-substituted pyrrolidines in excellent yields; [$RuCl_2(PPh_3)_3$] and [$RuCl_3 \cdot nH_2O$-3PBu_3] are the best catalysts for aromatic and aliphatic amines, respectively. The reaction of 2-butene-1,4-diol with alkyl amines gives a 1:1 mixture of *N*-substituted pyrroles and pyrrolidines in high yield.

Pyrroles and pyrrolidines, well-known and very important compounds in organic syntheses and in many other fields, are prepared by various methods[1] including inter- and intramolecular cyclization of tetramethylene dibromides,[2] 4-halo-1-butanamines,[3] α-amino ketones,[4] α-halo ketones,[5] and 1,4-diketones.[6] Recently, transition metal-catalyzed synthetic methods of pyrrole derivatives have been developed.[7,8] In the course of our studies on the ruthenium complex-catalyzed *N*-heterocyclization using alcohols[9] we found a novel synthetic method of *N*-substituted pyrroles and pyrrolidines from readily availabe 1,4-diols and primary amines.

Experimental

General Reaction Procedure. All boiling points and melting points were uncorrected. The ^1H and ^{13}C NMR spectra were recorded in $CDCl_3$ at 100 and 25.05 MHz, respectively, with a JEOL JNM FX-100 spectrometer. Elemental analyses were performed at the Microanalytical Center of Kyoto University. The GLC analyses were made using Shimadzu GC-4CM with a column (3 mm×3 m) packed with Apiezon Grease L (10%) on Neopack 1A, 60—80 mesh. Gel-permeation chromatograms (GPC) were recorded on a Waters ALC/GPC 244 system equipped with a Shodex GPC H-2002 column. Typical reaction conditions were as follows. A stainless-steel reactor (50 ml Taiatsu Glass Industry, TVS-1 type) containing a glass liner was used. Under an argon stream, dioxane (5 ml), amine (2 mmol), 2-butyne-1,4-diol (3 mmol), and [$RuCl_2(PPh_3)_3$] (0.02 mmol, 1 mol% based on the amines used) were added into the glass liner. After the reactor was flushed with argon (10 atm) four times, the reactor was held at 150 °C for 5 h. The products were isolated by vacuum distillation or medium-pressure column chromatography (hexane or benzene–aluminum oxide 90, Merck, No. 1076). Spectral data of unreported compounds are as follows.

(±)-1-(2-Ethylhexyl)pyrrole: Colorless oil; Kugelrohr pot temp. 60 °C (0.04 mmHg†); ^1H NMR δ=0.80—0.93 (6H, m, $2CH_3$), 1.14—1.34 (8H, m, $4CH_2$), 1.48—1.86 (1H, m, CH), 3.71 (2H, d, CH_2), 6.09 (2H, t), 6.60 (2H, t); ^{13}C NMR δ=10.6 (q, CH_3), 14.0 (q, CH_3), 23.0 (m, CH_2), 23.8 (m, CH_2), 28.7 (m, CH_2), 30.6 (m, CH_2), 41.3 (d, CH), 53.1 (t, CH_2), 107.6 (d), 120.9 (d). Found:C, 80.13; H, 11.93; N, 7.63%. Calcd for $C_{14}H_{21}N$: C, 80.38; H, 11.80; N, 7.63%.

1-(5-Indanyl)pyrrolidine: White crystals; mp 42—44 °C; bp 112—118 °C (0.60 mmHg); ^1H NMR δ=1.86—2.16 (6H, m, $3CH_2$), 2.73—2.92 (4H, m, $2CH_2$), 3.15—3.28 (4H, m, 2N-CH_2), 6.36 (1H, dd, J=7.6 and 2.6 Hz, Ph), 6.46 (1H, s, Ph), 7.05 (1H, d, Ph); ^{13}C NMR δ=25.4 (t, $2CH_2$), 25.8 (t, CH_2), 31.9 (t, CH_2), 33.3 (t, CH_2), 48.0 (t, 2N-CH_2), 107.8 (d), 110.0 (d), 124.6 (d), 130.9 (s), 145.1 (s), 147.1 (s). Found: C, 83.16; H, 9.26; N, 7.21%. Calcd for $C_{13}H_{17}N$: 83.37; H, 9.15; N, 7.48%.

1-(3-Trifluoromethylphenyl)pyrrolidine: Colorless oil; bp 60—62 °C (0.27 mmHg); ^1H NMR δ=1.65—1.78 (4H, m, $2CH_2$), 2.90—3.03 (4H, m, 2N-CH_2), 6.31—7.14 (5H, m, Ph); ^{13}C NMR δ=25.5 (m, $2CH_2$), 47.6 (t, 2N-CH_2), 107.9 (d; $J_{F\text{-}C\text{-}C\text{-}C}$=3.66 Hz), 111.5 (d; $J_{F\text{-}C\text{-}C\text{-}C}$=4.88 Hz), 114.6 (d), 124.7 (q, CF_3; $J_{F\text{-}C}$=272.3 Hz), 129.4 (d), 131.4 (q, $J_{F\text{-}C\text{-}C}$=31.7 Hz), 147.9 (s). Found: C, 61.59; H, 5.61; N, 6.55; F, 26.20%. Calcd for $C_{11}H_{12}NF_3$: C, 61.39; H, 5.62; N, 6.51; F, 26.48%.

1-(3,4-Methylenedioxyphenyl)pyrrolidine: White crystals; mp 70 °C; bp 110 °C (0.30 mmHg); ^1H NMR δ=1.91—2.04 (4H, m, $2CH_2$), 3.15—3.28 (m, 4H, 2N—CH_2), 5.84 (s, 2H, O-CH_2-O), 5.98 (dd, 1H, J=8.8 and 2.6 Hz, Ph), 6.23 (1H, d, J=2.6 Hz, Ph), 6.71 (1H, d, J=8.8 Hz, Ph); ^{13}C NMR δ=25.3 (t, $2CH_2$), 48.3 (t, 2N-CH_2), 94.4 (d), 100.3 (t, O-CH_2-O), 103.0 (d), 108.6 (d), 138.1 (s), 144.4 (s), 148.2 (s). Found: C, 68.79; H, 6.87; N, 7.17; O, 16.82%. Calcd for $C_{11}H_{13}NO_2$: C, 69.09; H, 6.85; N, 7.32; O, 16.73%.

Results and Discussion

Synthesis of *N*-Substituted Pyrroles from 2-Butyne-1,4-diol and Amines. The reaction between 2-butyne-1,4-diol (**1**) and aliphatic primary amines **4** at 150 °C in dioxane in the presence of catalytic amounts of a ruthenium complex afforded *N*-substituted pyrroles **5** (Eq. 1, Table 1). When [$RuCl_2(PPh_3)_3$] was

$$\underset{\mathbf{1}}{HOCH_2C{\equiv}CCH_2OH} + \underset{\mathbf{4}}{RNH_2} \xrightarrow[-2H_2O]{RuL_n} \underset{\mathbf{5}}{R\text{-}N\!\!\begin{array}{l}\diagup\!=\\ \diagdown\!=\end{array}} \qquad (1)$$

used as a catalyst, the reaction of octylamine with 2-butyne-1,4-diol gave 1-octylpyrrole in 63% yield. The catalytic activity was little affected by the phosphorus ligands; [$RuCl_2(PPh_3)_3$], [$RuCl_3 \cdot nH_2O$-3PBu_3], and [$RuCl_3 \cdot nH_2O$] showed high catalytic activity (63, 52, and 57% yield of **5**, respectively) and other ruthenium complexes such as [$RuHCl(CO)(PPh_3)_3$] and [$RuBr_2(PPh_3)_3$] were also effective (58 and 53% yield of **5**, respectively). Addition of bis(diphenylphosphino)-ethane (dppe) as a bidentate phosphorus ligand or a bulky PCy_3 suppressed the catalytic activity considerably (4 and 1% yield, respectively). No satisfactory results were obtained in case of aromatic amines. When 2-butyne-1,4-diol (**1**) was treated with a

† 1 mmHg=133.322 Pa.

Table 1. *N*-Substituted Pyrrole Synthesis[a)]

Run	Amine	1,4-Diol	Product	Yield[c)]/%
1	$n\text{-}C_8H_{17}NH_2$	$HOCH_2C{\equiv}CCH_2OH$	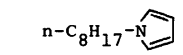	63 (59)
2	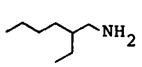	$HOCH_2C{\equiv}CCH_2OH$	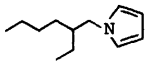	(49)
3	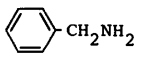	$HOCH_2C{\equiv}CCH_2OH$	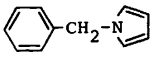	49 (24)
4	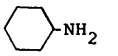	$HOCH_2C{\equiv}CCH_2OH$	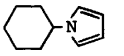	(27)
5[b)]	$n\text{-}C_8H_{17}NH_2$	$HO(CH_3)CHC{\equiv}CCH(CH_3)OH$	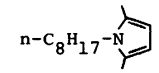	(47)

a) Amine (2.0 mmol), 1,4-diol (3.0 mmol), $RuCl_2(PPh_3)_3$ (0.02 mmol), dioxane (5 mL), at 150 °C for 5 h. b) Amine (10 mmol), 1,4-diol (15 mmol), $RuCl_2(PPh_3)_3$ (0.10 mmol). c) Determined by GLC based on the amine and figures in the parentheses are isolated yields.

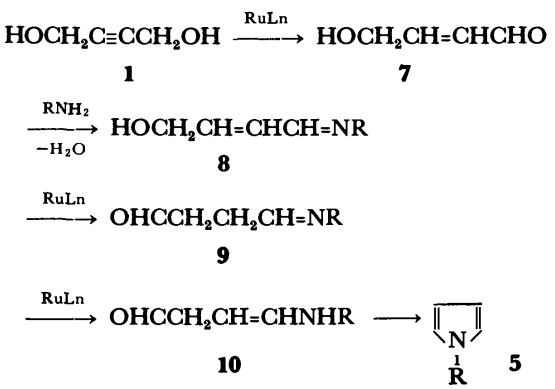

Scheme 1.

catalytic amount of $[RuCl_2(PPh_3)_3]$ in dioxane at 150 °C, the diol was converted into an oligomeric intractable mixture (conversion 100%, molecular weight 200—1000 by GPC). The ruthenium complexes are well-known catalysts for the isomerization of olefins[10] and of allyl alcohol to aldehyde.[11] Therefore, we postulate a reaction route (shown in Scheme 1) including the isomerization of 2-butyne-1,4-diol (**1**) to γ-hydroxy-α,β-unsaturated aldehyde (**7**),[12] which reacts with amines **3** to give imine intermediates **8**. An allylic alcohol moiety of **8** isomerizes again to an imino aldehyde species **9**, which subsequently gives **10** via imine-enamine isomerization.[13] *N*-Substituted pyrroles **5** would be produced by intramolecular cyclization of **10**.

The N-heterocyclization to the pyrroles seems to compete with the oligomerization of **7**, since α,β-unsaturated aldehydes are reported to be easy to oligomerize.[14] When more basic aliphatic amines are employed as the substrate, most of **7** is trapped with them to give **8**. On the other hand, with less basic aromatic amines, a considerable amount of **7** is consumed by the oligomerization.

Synthesis of *N*-Substituted Pyrrolidines from 1,4-Butanediol and Amines. The reaction of 1,4-butanediol (**2**) with primary amines **4** in the presence of a catalytic amount of a ruthenium complex to give *N*-substituted pyrrolidines **6** in excellent yields (Eq. 2,

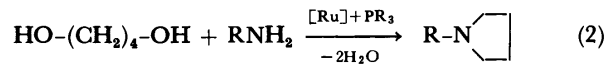

(2)

Table 2). The reaction is drastically affected by the nature of the phosphorus ligand employed, and the most suitable phosphorus ligand depends on the basicity of the amine.[15]

Dichlorotris(triphenylphosphine)ruthenium ($[RuCl_2(PPh_3)_3]$) was the most effective catalyst for less basic amines (Runs 6—11), while $[RuCl_3 \cdot nH_2O\text{–}3PBu_3]$ was highly effective for the amines with high basicity (Runs 12—15). Methoxy, chloro, trifluoromethyl, and methylenedioxy groups did not affect the catalysis appreciably (Runs 7, 9—11). Amines containing an *N*-hetero ring such as 3-picolylamine and tryptamine also afforded the desired *N*-substituted pyrrolidines in good yields (Runs 14 and 15).

The reaction would proceed via a route analogous to that proposed in the previous paper.[9]

The Reaction of *cis*-2-Butene-1,4-diol with Amines. *cis*-2-Butene-1,4-diol (**3**) reacted with octylamine in the presence of 1.0 mol% of $[RuCl_3 \cdot nH_2O\text{–}3PBu_3]$ to afford a mixture of 1-octylpyrrole (**5**; R=n-C_8H_{17}) and 1-octylpyrrolidine (**6**; R=n-$C_{18}H_{17}$) in 1:1 molar ratio (Eq. 3). Their combined yields were 69% at 150 °C and

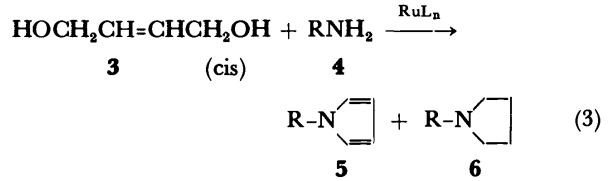

(3)

73% at 180°C. On the other hand, aniline reacted with cis-2-butene-1,4-diol (**3**) to afford 1-phenylpyrrole (**5**; R=Ph) and 1-phenylpyrrolidine (**6**; R=Ph) in only 4—9% yields (**5**:**6**=1:9).

Table 2. *N*-Substituted Pyrrolidine Synthesis[a)]

Run	Amine	Catalyst[c)]	Temp/°C	Time/h	Product	Yield[d)]/%
6	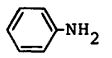	A	140	5	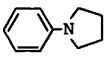	85 (80)
7	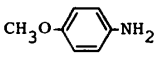	A	140	5	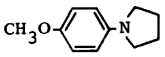	(73)
8	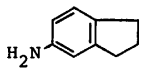	A	140	5	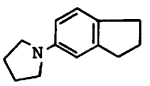	(72)
9	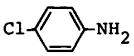	A	160	20	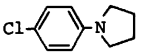	(78)
10	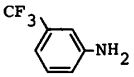	A	180	10	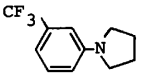	(81)
11[b)]	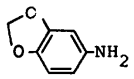	A	180	20	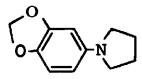	(45)
12	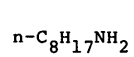	B	180	5	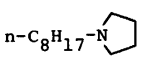	91 (91)
13	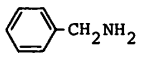	B	180	5	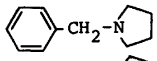	(91)
14[b)]	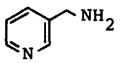	B	180	20	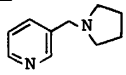	(61)
15[b)]	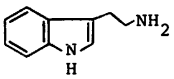	B	180	24	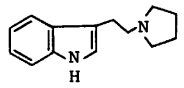	(59)

a) Amine (10 mmol), 1,4-butanediol (15 mmol), catalyst (1.0 mol% based on the amine), dioxane (5 mL). b) Dioxane (15 mL). c) A: $RuCl_2(PPh_3)_3$; B: $RuCl_3 \cdot nH_2O + 3PBu_3$. d) Determined by GLC based on the amine and figures in the parentheses are isolated yields.

In this case, a mixture of **10** and 4-aminobutanal would be formed by the intermolecular hydrogen transfer followed by cyclization to give pyrroles and pyrrolidines, respectively.

References

1) a) A. H. Jackson, "Comprehensive Organic Chemistry," ed by P. G. Sammes, Pergamon, Oxford (1979), Vol. 4, p. 275. b) A. R. Katritzky, "Handbook of Heterocyclic Chemistry," Pergamon, Oxford (1985), p. 391.

2) Ref. 1a, p. 294.

3) Ref. 1b, p. 393.

4) H. Fischer, *Org. Synth.*, **15**, 17 (1935). *Org. Synth.*, **17**, 96 (1937).

5) M. W. Roomi and S. F. MacDonald, *Can. J. Chem.*, **48**, 1689 (1970).

6) A. Gossauer, "Die Chemie der Pyrrole," Springer-Verlag, Berlin (1974), p. 240.

7) S.-I. Murahashi, T. Shimamura, and I. Moritani, *J. Chem. Soc., Chem. Commun.*, **1974**, 931.

8) B. M. Trost and E. Keinan, *J. Org. Chem.*, **45**, 2741 (1980).

9) Y. Tsuji, K.-T. Huh, Y. Ohsugi, and Y. Watanabe, *J. Org. Chem.*, **50**, 1365 (1985).

10) M. Takahashi, H. Suzuki, Y. Moro-oka, and T. Ikawa, *Chem. Lett.*, **1981**, 1435, and references cited therein.

11) Y. Watanabe, Y. Tsuji, Y. Ohsugi , and J. Shida, *Bull. Chem. Soc. Jpn.*, **56**, 2452 (1983) and references cited therein.

12) Moro-oka et al. reported that acetylenic silyl ethers were converted catalytically to the corresponding conjugated dienyl silyl ethers by ruthenium hydride complexes; K. Hirai, H. Suzuki, Y. Moro-oka, and T, Ikawa, *Tetrahedron Lett.*, **21**, 3413 (1980).

13) G. Optiz, H. Hellmann, and H. W. Schubert, *Justus Liebigs Ann. Chem.*, **623**, 117 (1959).

14) H. W. Post, *J. Org. Chem.*, **5**, 244 (1940)

15) The effect of the catalyst precursors on the synthesis of *N*-substituted pyrrolidines was similar to that on the synthesis of *N*—substituted piperidines, morpholines, and piperazines described in Ref. 9.

An Anion Radical Salt of a Quinone Fused with 1,3-Dithiole Units. Crystal and Molecular Structure of a Tetraethylammonium Salt of 2,6-Dithioxobenzo[1,2-*d*:4,5-*d'*]-bis[1,3]dithiole-4,8-dione

Takanori SUZUKI, Chizuko KABUTO,†,* Yoshiro YAMASHITA, and Tsutomu MIYASHI
Department of Chemistry, Faculty of Science, Tohoku University, Aramaki, Sendai 980
†Instrumental Analysis for Chemistry, Faculty of Science, Tohoku University, Aramaki, Sendai 980
(Received April 7, 1987)

Synopsis. Crystal structure of the title salt was determined by the X-ray analysis. Segregated columnar stacks of anion radicals are formed along the c axis, in which quinone molecules are not spaced equally but forming dyads with short contacts between sulfur atoms.

We have recently found that the quinones fused with sulfur heterocycles such as 1,3-dithiole rings possess strong electron affinities to give highly conductive CT complexes with tetrathianaphthacene (TTN) or tetrathiafulvalene (TTF) derivatives.[1] For example, quinone **1** formed CT complexes with TTN and tetramethyltetraselenafulvalene (TMTSF) whose electrical resistivities measured on compaction samples at room temperature are 9.9 Ω cm and 2.4 Ω cm, respectively. It is expected in these highly conductive complexes that the quinone molecules may form segregated columnar stacks with some interheteroatom interactions which can stabilize the metallic state by forming two-dimensional networks. However, unfortunately the crystallization of these complexes have still been unsuccessful. On the other hand, the anion radicals of quinone **1** have been isolated as stable salts.[1] To investigate the possible interheteroatom interactions in the negatively charged quinone molecules, we carried out the X-ray structural analysis of the title salt which was obtained as suitable single crystals. The role of the 1,3-dithiole rings which enhance the electron affinity of the quinone skeleton is discussed from the view point of the molecular structure.

Experimental

Material. Quinone **1** was prepared according to the literature.[2] The title 1:1 anion radical salt was prepared by the reaction of quinone **1** (64 mg) with tetraethylammonium iodide (514 mg, 10 equivalents) in hot dry acetonitrile (40 ml). Black needles of the salt thus obtained (85 mg, decomp. 240—241 °C) show the following analytical values, Calcd for $C_{16}H_{20}NS_6O_2$: C, 42.64; H, 4.47; N, 3.11%. Found: C, 42.43; H, 4.43; N, 3.11%. Its electrical resistivity (ρ_{RT}) measured on a compaction sample at room temperature was 1.2×10^7 Ω cm. Single crystals were obtained when the hot acetonitrile solution was cooled slowly. When four equivalents of the iodide were used, green-black needles (mp > 400 °C) were obtained whose molar ratio was determined to be 1:2 on the basis of the elemental analysis. Calcd for $C_{24}H_{20}NS_{12}O_4$: C, 37.38; H, 2.61; N, 1.82%. Found: C, 37.30; H, 2.54; N, 1.93%. The resistivity (ρ_{RT}) of the 1:2 salt was 8.7×10^3 Ω cm.

Table 1. Fractional Atomic Coordinates ($\times10^4$) and Equivalent Temperature Factors (Å²)

Atom	*X*	*Y*	*Z*	B_{eqv}[a]
S 1	8676(1)	531(2)	3282(3)	4.2
S 2	1370(1)	590(2)	1066(3)	4.0
S 3	7675(1)	2034(1)	2206(2)	3.1
S 4	2439(1)	−820(1)	1998(2)	2.9
S 5	6163(1)	−882(1)	3279(2)	3.0
S 6	3930(1)	2093(1)	917(2)	3.0
O 1	6472(3)	3370(3)	1033(6)	3.5
O 2	3704(3)	−2072(3)	2777(6)	3.7
C 1	7574(5)	569(5)	2938(8)	3.0
C 2	2525(4)	634(5)	1297(8)	2.8
C 3	6248(4)	1315(5)	2000(8)	2.4
C 4	3917(4)	−32(4)	1903(7)	2.4
C 5	5540(4)	−67(4)	2481(7)	2.4
C 6	4618(4)	1339(4)	1417(7)	2.3
C 7	4337(4)	−834(5)	2408(8)	2.7
C 8	5841(4)	2121(4)	1422(7)	2.4
N	1976(4)	4051(4)	5543(6)	2.7
C11	1071(5)	3330(5)	7670(9)	3.4
C12	1020(6)	4251(7)	8322(11)	5.1
C21	3241(5)	5099(6)	5473(9)	3.8
C22	3676(6)	4530(8)	7022(12)	5.5
C31	1842(6)	2920(6)	5178(9)	4.1
C32	2661(8)	3423(8)	3135(12)	6.6
C41	1734(5)	4853(5)	3842(8)	3.3
C42	487(6)	4029(7)	3741(11)	4.7

a) $B_{eqv}=(4/3)\sum_{ij}\beta_{ij}(a_i\cdot a_j)$.

Structural Analysis. A needle-like crystal with the dimensions of 0.15×0.15×0.25 mm³ was used for the data collection on a Rigaku AFC-5R automated four-circle diffractometer. A total of 4366 reflections within $2\theta=52°$ was collected using graphite monochromated Mo $K\alpha$ radiation ($\lambda=0.71069$ Å). Crystal data are as follows: MF $C_{16}H_{20}NS_6O_2$, MW 450.72, triclinic, $P\bar{1}$, $a=14.300(1)$, $b=13.243(1)$, $c=7.251(1)$ Å, $\alpha=69.58(1)$, $\beta=86.73(1)$, $\gamma=124.56(1)°$, $V=1000.2(3)$ Å³, $Z=2$, $D_{calcd}=1.50$ g cm⁻³. The structure was solved by the direct method using RANTAN 81[3] with some modification whereby only quinone molecule appeared in the Fourier map. After the block-diagonal least-squares refinement for these atoms, the remaining atoms of the ammonium ion were located in the difference Fourier map. After the refinement with anisotropic temperature factors, all the hydrogen atoms were successively picked up from the difference Fourier

map. The final R value is 4.36% for the 2636 reflections with $|F_o|>3\sigma|F_o|$. The final atomic coordinates are given in Table 1.

The atomic scattering factors from the International Tables for X-Ray Crystallography[4] were used. All the computation were carried out by an ACOS 1000 computer at Tohoku University using the applied library programs of UNICS III system.[5]

Results and Discussion

The crystal structure viewed along the b axis and the c axis are shown in Figs. 1 and 2. The quinone molecules form segregated columnar stacks along the c axis. These columns are linearly arranged to the a axis and separated by the ammonium ions along the b axis. In the column, the anion radicals are not equally spaced but pairing to form dyads. So there are two different modes of overlapping, and the quinone molecules are stacked parallel to each other in both overlapping. In the dyad, the overlapping is a well-known "ring-double bond" type[6] of a high symmetry with the short interplanar distance of 3.21 Å. There exist some short contacts such as C(7)-C(7) (3.13 Å) and O(2)-C(8) (3.11 Å) in this dyad, and particularly the S(4)-S(5) contact (3.42 Å) is quite shorter than the sum of van der Waals radii (3.70 Å)[7], indicating the strong interactions between sulfur atoms which may contribute to the dyad formation with "ring-double bond" type overlapping. Although the quinone molecule is nearly planar, slight deviations of atoms from the molecular plane are observed. These deviations afford the dihedral angles of 4.5° for the planes containing S(1)-S(3)-S(5) and C(3)-S(3)-S(5)-C(5), 2.5° for the planes containing C(3)-C(5)-C(4)-C(6) and O(2)-C(4)-C(5), and 2.3° for the planes containing C(4)-C(6)-(8)-C(7) and C(3)-C(5)-C(7)-C(8). Since molecules bow in the opposite direction in the dyad, this slight molecular defomation is considered to be accompanied by the short interplanar distance in the dyad which is formed in the crystal. Between the dyads, the interplanar distance (molecule C and D in Fig. 1) is 3.65 Å which is much longer than that in the dyad (molecule A and B), and the distances among the inner sulfur atoms are also long [S(3)-S(4) 3.90 Å, S(5)-S(6) 3.91 Å]. This type of segregated stack accompanied by the dyad formation is also observed in

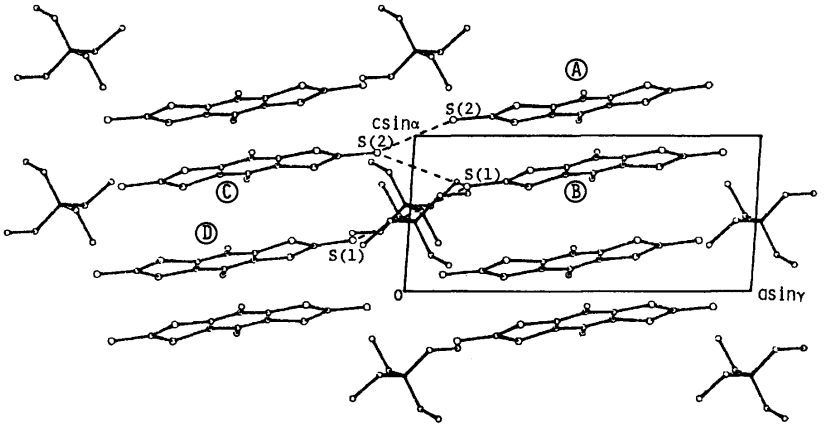

Fig. 1. Crystal structure viewed along the b axis. Molecules A—D are related by the following symmetry operations: A (x, y, z), B ($1-x$, $-y$, $-z$), C ($-x$, $-y$, $-z$), D ($-1+x$, y, $-1+z$). Intercolumn S-S contacts are indicated by broken line: 3.95 Å for molecule A and C, 4.04 Å for molecule B and C, 5.21 Å for molecule B and D.

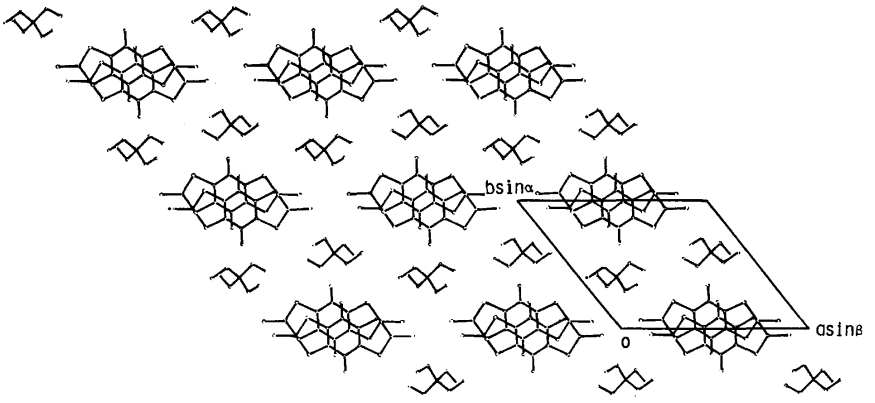

Fig. 2. Crystal structure viewed along the stacking c axis. Nitrogen atom of the ammonium ion is located on the same plane of the quinone molecule.

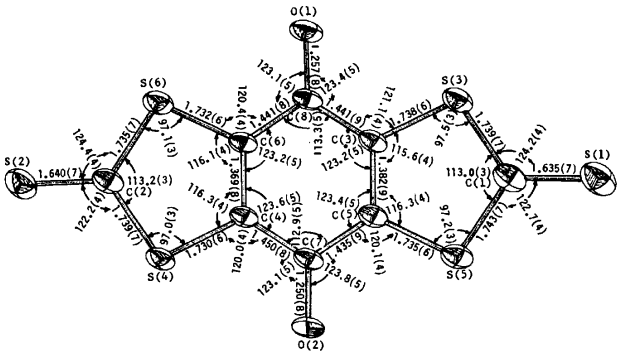

Fig. 3. Molecular geometry of quinone anion radical with bond lengths and angles.

the Et_4N^+ $(BTDA\text{-}TCNQ)_2^-$ anion radical salt which shows low electrical conductivity.[8] Therefore, the low conductivity of the present salt is accounted for by this dyad formation. However, it is noted that the segregated columnar stacks are formed with "ring-double bond" type overlapping, and this stacking motif is facilitated by the interaction between the sulfur atoms. This finding suggests that the highly conductive CT complexes of quinone **1** may have the segregated columnar stacks[9] which are facilitated by the S-S contacts observed here. Although the intercolumn interactions were also expected by the contacts between the terminal sulfur atoms, the distances among S(1) and S(2) are too long (3.95—5.21 Å, Fig. 1) to undergo such interactions.

The molecular geometry of the quinone anion radical is shown in Fig. 3. It is apparent that the C(8)=O(1) (1.257 Å) and C(7)=O(2) (1.250 Å) bonds are elongated than the corresponding bonds of ordinary neutral quinones (ca. 1.22 Å)[10] although those for the quinone **1** are not available. This means that the negative charge is largely localized on the carbonyl moieties, indicating that the anion radical mainly exists as the semiquinone form **2a**. The possibility of **2c** was excluded by considering the molecular overlapping in the dyad and the location of counter cation which may reflect the charge density of the anion radical species. However, the six-membered ring of **1** takes a quinoid structure and the bond lengths of S(1)=C(1) (1.635 Å) and S(2)=C(2) (1.640 Å) are longer than those of ordinary thiocarbonyl bonds (1.61 Å). This fact can be attributed to the contribution of the structure **2b**, in which aromatic 1,3-dithiolium cations are formed. This result leads to the conclusion that the electron affinity of the quinone **1** fused with 1,3-dithiole units is enhanced inductively by the contribution of the polarized form in the 1,3-dithiol-2-ylidene moieties.

Tables of observed and calculated structure factors, atomic positional parameters, anisotropic temperature factors, and bond lengths and angles are kept at the Chemical Society of Japan, Document No. 8755.

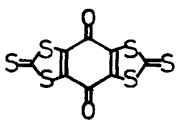

1

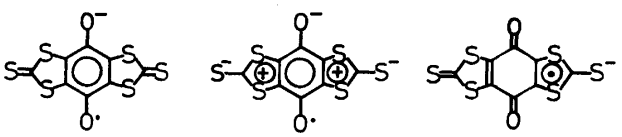

2a 2b 2c

References

1) Y. Yamashita, T. Suzuki, G. Saito, and T. Mukai, *J. Chem. Soc., Chem. Commun.*, **1986**, 1489.

2) N. G. Demetriadis, S. J. Huang, and E. T. Samulski, *Tetrahedron Lett.*, **1977**, 2223.

3) Y. Jia-xing, *Acta Crystallogr., Sect. A*, **37**, 642 (1981); Y. Jia-xing, *ibid.*, **39**, 35 (1983).

4) "International Tables for X-Ray Crystallography," Kynoch Press, Birmingham (1962), Vol. 3, p. 202.

5) T. Sakurai and K. Kobayashi, *Rikagaku Kenkyusho Hokoku*, **55**, 69 (1979).

6) C. J. Fritchie, Jr., *Acta Crystallogr.*, **20**, 892 (1966).

7) L. Pauling, "The Nature of the Chemical Bond," 3rd ed., Cornell University Press, Ithaca, N. Y. (1960), p. 260, Tables 7—20.

8) BTDA-TCNQ: bis[1,2,5]thiadiazolotetracyanoquinodimethan. T. Suzuki, C. Kabuto, Y. Yamashita, T. Mukai, T. Miyashi, and G. Saito, submitted for publication.

9) Generally, CT complexes of quinones tend to form mixed stacks with alternated overlapping of donors and acceptors which leads to low electrical conductivity.

10) The C=O bond lengths of quinones are as follows: 1.218 Å for benzoquinone (J. Trotter, *Acta Crystallogr.*, **13**, 86 (1960); 1.21 and 1.22 Å for naphthoquinone (J. Gaultier and C. Hauw, *Acta Crystallogr.*, **18**, 604 (1965)); 1.213 Å for anthraquinone (A. Prakash, *Acta Crystallogr.*, **22**, 439 (1967)).

Preparation and Some Properties of Acyltin Compounds

Masanori KOSUGI,* Hiroyuki NAKA, Hiroshi SANO, and Toshihiko MIGITA*
Department of Chemistry, Faculty of Technology, Gunma University,
Kiryu, Gunma 376
(Received April 14, 1987)

Synopsis. According to Quintard's method, acyltin compounds were prepared by the reaction of tributylstannylmagnesium chloride with an excess of aldehyde, and their physical data were described. These compounds were sensitive to oxygen air to give the corresponding tributyltin carboxylates. Free radical chain mechanism was suggested.

For lack of a suitable synthetic method, acyltin compounds have been virtually unkown and are believed to be very labile compounds.[1,2] Recently, the acyltins have been reported by Quintard et al. to form through the reaction of tributylstannylmagnesium chloride prepared in situ from isopropylmagnesium chloride and tributyltin hydride, with an excess of aldehyde.[3]

$$Bu_3SnMgCl+2\ RCHO \rightarrow Bu_3SnCOR+RCH_2OMgCl$$

However, physical data of the acyltins thus formed were not fully provided.[3] In this note, several trials of the syntheses of acyltins, and some of their physical data were described.

The reaction presented by Quintard et al. is interesting and thought to be a kind of Cannizzaro reaction of aldehyde involving Grignard reagent instead of a base. In 1925, the reaction of Grignard reagent with benzaldehyde giving benzyl alcohol was reported.[4] We re-examined the reaction of some ordinary Grignard reagents with excess of aldehydes,

$$RMgBr + 2PhCHO \rightarrow \rightarrow PhCOR + PhCH_2OH$$

R=Et, Ph: Et; 77%, Et; 83%; Ph; 60%, Ph; 61%

$$EtMgCl + 2PhCH_2CH_2CHO \rightarrow \rightarrow EtCOCH_2CH_2Ph + PhCH_2CH_2CH_2OH$$

44% 49%

and found that Cannizzaro type reactions between the Grignard reagent and an excess of aldehyde actually occurred to give the corresponding ketones and alcohols in moderate to good yields, even with aldehydes bearing α-hydrogen atoms.[5]

Based on the above results, the reactions of various tributylstannylmetal compounds (Bu_3Sn–M) with an excess of propanal were carried out, expecting to give the propanoyltributyltin. Tributylstannylmagnesium chloride was the best reagent which reacted with an excess of aldehyde to give the acyltins in 84% yield. The reaction with diethyl(tributylstannyl)aluminum also gave the acyltins, although the yields were low (18%). The reaction with other reagents, Bu_3Sn–M (M: Li, ZnCl, $ZnSnBu_3$, $SiMe_3$, $SnBu_3$ etc.) did not give the acyltins.

The following two coupling reactions were also carried out for the purpose of preparation of acyltins.

$$Bu_3SnLi + EtCOBr \longrightarrow Bu_3SnCOEt + LiBr$$

$$Bu_3SnSnBu_3 + EtCOCl \xrightarrow{[Pd]} Bu_3SnCOEt + Bu_3SnCl$$

These two reactions gave the propanoyltributyltin, although the yields (12 and 15% yields, respectively) were not satisfactory.[6] At present, Quintard's method was found to be the best for the preparation of acyltins.

Table 1 shows the physical properties of acyltins thus obtained. Propanoyl- and 2-methylpropanoyltributyltin were greenish yellow liquid with the absorption at ca. 380nm and could be distilled under reduced pressure. Their GC–MS(CI) showed the parent peak with the reasonable isotopic patterns. ^1H NMR, ^{13}C NMR, and IR spectrum were also reasonable. On the other hand, benzoyltributyltin was thermally unstable and decomposed to give the white solid on distillation under reduced pressure. Its GC–MS showed the pattern quite different from that of GLC and benzil was detected, showing that the

Table 1. Physical Data of Acyltins

	$Bu_3SnCOCH_2CH_3$	$Bu_3SnCOCH(CH_3)_2$	$Bu_3SnCOPh$
^1H NMR(CCl_4) δ:	0.70—1.80(m, Bu, CH_3)	0.65—1.85(m, Bu, CH_3)	0.63—1.80(m, Bu)
	2.66(q, J=7 Hz, CH_2)	2.35(h, J=6 Hz, CH)	7.26—8.26(m, Ph)
^{13}C NMR($CDCl_3$) δ:	13.6, 27.2, 29.1,	13.6, 27.4, 29.3,	13.6, 27.3, 29.2,
	10.5 (Bu)	11.0 (Bu)	11.5 (Bu)
	250.1 (CO)	249.8 (CO)	241.3 (CO)
	48.9 (CH_2)	50.7 (CH)	142.9, 127.6, 128.6,
	6.2 (CH_3)	15.8 (CH_3)	132.4 (Ph)
UV(hexane)	385, 370 nm	390, 375 nm	440 nm
IR(neat)	1640 (CO) cm^{-1}	1640 (CO) cm^{-1}	1610 (CO) cm^{-1}
Bp[a]	107 °C/0.5 mmHg	119 °C/0.8 mmHg	Decomposed
GC-MS(CI) m/z, M^+:	345, 346, 347, 349	359, 361, 362, 363[b]	Decomposed[c]

a) 1 mmHg=133.322 Pa. b) Peak at 360 was not detected. c) Decomposition was occurred in the MS chamber and benzil was detected.

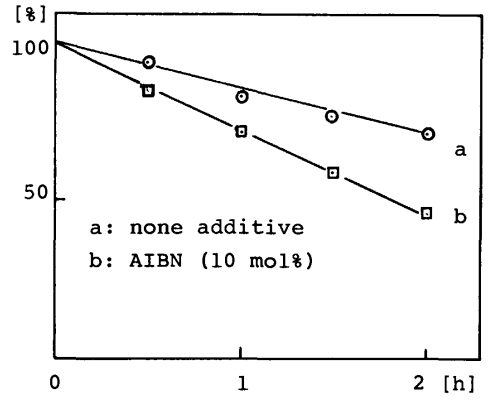

Fig. 1. Effect of AIBN on the disappearance of $Bu_3SnCOEt$ at 60 °C.

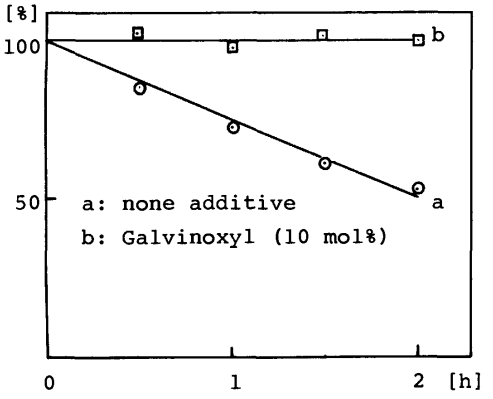

Fig. 2. Effect of Galvinoxyl on the disappearance of $Bu_3SnCOEt$ at room temperature.

benzoyltin decomposed in the GC-MS chamber. However, the product before distillation showed the reasonable spectroscopic data.

The acyltins were fairly stable under dark and inert atmosphere, being capable to be kept more than a month. One of the most characteristic reactions of acyltin was oxidation by molecular oxygen, giving the corresponding tributyltin carboxylates quantitatively. As Figs. 1 and 2 show, the autoxidation was completely inhibited in the presence of galvinoxyl (10 mol%) and was slightly accelerated by addition of AIBN (azobisisobutyronitrile). Based on these observations, free radical chain mechanism involving attack of acylperoxyl radical to a tin atom, followed by Baeyer-Villiger type oxidation, may be suggested.

$$Bu_3SnCOR \longrightarrow Bu_3Sn\cdot + R\dot{C}O$$

$$R\dot{C}O + O_2 \longrightarrow RCOOO\cdot$$

$$RCOOO\cdot + Bu_3SnCOR \longrightarrow RCOOOSnBu_3 + R\dot{C}O$$

$$RCOOOSnBu_3 + Bu_3SnCOR \longrightarrow 2RCOOSnBu_3$$

Moreover, propanoyltributyltin was found to reduce Tollens reagent. Thus, acyltin shows chemical behavior quite similar to aldehyde.

Experimental

Infrared spectra were recorded on a JASCO Model A-100 infrared spectrometer. ^1H NMR spectra (in carbon tetrachloride with tetramethylsilane internal standard) were run on a Varian Associates Model EM-360 spectrometer. ^{13}C NMR spectra (in deuteriochloroform with tetramethylsilane internal standard) were taken on a Hitach Model R-90H spectrometer. GC-MS spectra (Chemical Ionization) were recorded on a Shimadzu Model QP-1000 spectrometer. UV spectra (in hexane) were taken on a Hitachi Model 200-10 spectrophotometer. GLC analyses (10% of SF-96 on Celite 545) were performed by Ohkura Model 202 instrument.

Materials. Ethyl- and phenylmagnesium bromide were prepared by a standard method. Benzaldehyde, propanal, 2-methylpropanal, 3-phenyl-1-propanal, propanoyl chloride and bromide, propiophenone, benzophenone, benzyl alcohol, 1-phenyl-3-pentanone, 3-phenylpropanol, galvinoxyl, and AIBN were commercially available and used without further purification. Bu_3SnLi,[7] $Bu_3SnZnCl$,[8] $Bu_3SnZnBr$,[8] $(Bu_3Sn)_2Zn$,[8] $Bu_3SnSiMe_3$,[7] $Bu_3SnSnBu_3$,[7] $Bu_3SnAlEt_2$,[8] $Bu_3SnMgCl$,[4] $Bu_3SnOCOEt$,[9] $Bu_3SnOCOCHMe_2$,[9] and $Bu_3SnOCOPh$[9] were prepared from the method described in the literatures.

Cannizzaro Type Reaction of Aldehyde with Grignard and Stannylmetal Reagents. After dropwise addition of benzaldehyde into an ethereal solution of ethyl Grignard reagent, the solution was refluxed for 2 h. The resulting reaction mixture was hydrolyzed with aqueous saturated ammonium chloride, and extracted with ether. The extracts were analyzed by GLC and ethyl phenyl ketone and benzyl alcohol were detected as products. Other reactions with Grignard reagents and the reactions of propanal with various stannylmetals were also carried out similarly.

Preparation of Acyltributyltins. Tributyltin hydride (45 g, 0.15mmol) was added to a solution of the Grignard reagent prepared from 14.1 g of isopropyl chloride (0.18 mol) and 4.4 g of magnesium (0.18 mol). The solution was then refluxed for an hour. The flask was cooled with an ice bath and 26.1 g of propanal (0.45 mol) was added into the solution dropwisely, which was further refluxing for an hour. Subsequent treatment of the resulting reaction mixture with aqueous ammonium chloride was carried out. Distillation under reduced pressure gave 32 g of propanoyltributyltin (62% yield). 2-Methylpropanoyltin (59%) and crude benzoyltin (64% yield) were obtained similarly. However, the latter was decomposed on heating under reduced pressure. Physical data of acyltins are shown in Table 1.

Reaction of Propanoyltributyltin with Oxygen. The disappearance of propanoyltributyltin in the presence of Galvinoxyl or AIBN was followed by GLC. The results are shown in Figs. 1 and 2.

The gift of tributyltin oxide by Hokkoh Kagaku Kogyo Co. Ltd. is gratefully acknowledged. The present work was partially supported by a Grant-in-Aid for Special Project Research No. 61225002 from the Ministry of Education, Science and Culture.

References

1) J. A. Soderquist and A. Hassner, *J. Am. Chem. Soc*, **102**, 1577 (1980); J. A. Soderquist and G. J. Hsu, *Organometallics*, **1**, 830 (1982).

2) K. J. H. Kruithof, R. F. Schmitz, and G. W. Klumpp, *J. Chem. Soc., Chem. Commun.*, **1983**, 239.
3) J-P. Quintard, B. Elissondo, and D. Mouko-Mpegna, *J. Organomet. Chem.*, **251**, 175 (1983).
4) J Meisenheimer, *Justus Liebigs Ann. Chem.*, **442**, 180 (1925).
5) After submitted this work, we found similar trials published. B. Byrne and M. Karras, *Tetrahedron Lett.*, **28**, 769 (1987).
6) N. A. Bumagin, Y. V. Gulevich, and I. P. Beletskaya, *J. Organomet. Chem.*, **282**, 421 (1985).
7) C. Tamborski, F. E. Ford, and E. J. Soloski, *J. Org. Chem.*, **28**, 237 (1963).
8) J. Hibino, S. Matsubara, Y. Morisawa, K. Oshima, and H. Nozaki, *Tetrahedron Lett.*, **25**, 2151 (1984).
9) G. J. M. van der Kerk and J. G. A. Luijten, *J. Appl. Chem.*, **6**, 49 (1956).

Synthesis of α-Methylene-γ-butyrolactones via Addition of Tin Hydride to Enynes Induced by Triethylborane

Kyoko NOZAKI, Koichiro OSHIMA,* and Kiitiro UTIMOTO
Department of Industrial Chemistry, Faculty of Engineering, Kyoto University, Yoshida, Kyoto 606
(Received April 25, 1987)

Synopsis. Et_3B induced addition of Ph_3SnH to suitably constituted enynes provides (triphenylstannylmethylene) oxolanes stereoselectively in one pot. Destannylation followed by oxidation affords α-methylene-γ-butyrolactones in fair yields.

We have recently shown[1] that triphenyltin hydride adds easily to acetylenes regioselectively in the presence of Et_3B under mild conditions. The reaction has been found to be effective for vinyl-radical cyclization[2] of suitably constituted acetylenic olefins.[1,3] Here we wish to report the applicaton of this new method to the stereoselective synthesis of α-methylene-γ-butyrolactones, which represent a major class of known natural products and possess wide-ranging biological activities.[4]

A hexane solution of Et_3B was added to a solution of Ph_3SnH and enyne, 1,3-dimethyl-2-butenyl propargyl ether (**1a**) in toluene at 25 °C under an argon atmosphere. The mixture was stirred for 3 h at 25 °C and workup followed by preparative tlc purification gave cyclized product **2a** in 84% yield.

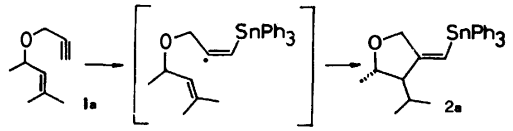

The results are summarized in Table 1. The yields of cyclized products depend on the concentration of the substrate and Ph_3SnH. High dilution favors the formation of the desired cyclized product **2**. On the other hand, without solvent or high concentration provided uncyclized product along with **2**.[5] It is worth noting that the cyclized products, **2a—d**, consist of only (Z)-trans-isomer independently of the stereochemistry of the double bond in the starting enynes (**1c** and **1d**). In contrast, treatment of **1e** with Ph_3SnH gave cis-fused oxolane **2e** exclusively which is thermodynamically more stable than trans-isomer.

Table 1. Synthesis of α-Methylene-γ-butyrolactone

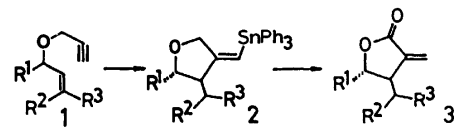

1	R^1	R^2	R^3	Yield/%	
				2	3[a]
a	Me	Me	Me	84	57
b	Ph	Me	Me	70	39
c	*n*-Bu	H	*n*-Pr	83	41
d	Me	*n*-Bu	H	75	59
e	$-(CH_2)_4-$		H	71[b]	31

a) Overall yield from **2**. b) Cis product was obtained. See experimental part.

Destannylation[6] (*n*-BuLi/THF and H_2O) followed by oxidation[7] with $CrO_3 \cdot 2py$ gave the desired α-methylene-γ-butyrolactones.[8]

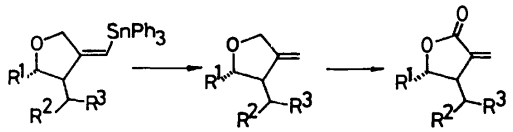

Experimental

The IR spectra were determined on a JASCO IR-810 spectrometer, the mass spectra on a Hitachi M-80 machine, the ^1H NMR spectra were recorded on a Varian EM-390H and XL-200 spectrometers, and the ^{119}Sn NMR spectra on a JEOL JNM-FX 90Q spectrometer. The chemical shifts of the proton NMR are given in δ with TMS as an internal standard, and those of the ^{119}Sn NMR are given in δ with Me_4Sn as an internal standard. The analyses were performed at the Elemental Analyses Center of Kyoto University. Tetrahydrofuran was dried in benzophenone ketyl and distilled. All the experiments were carried out under an argon atmosphere.

Preparation of Alkenyl Propargyl Ether. Generation of (*E*)-1-butyl-2-hexenyl propargyl ether (**1c**) is representative. A hexane solution of butyllithium (1.5 M, 1 M=1 mol dm^{-3}, 13.3 ml, 20.0 mmol) was added to a solution of (*E*)-2-hexenal (1.96 g, 20.0 mmol) in THF (30 ml) at 0 °C. After stirring for 15 min, HMPA (5 ml) and propargyl bromide (1.87 ml, 21.0 mmol) was added. The resulting mixture was stirred at 0 °C for 15 min, then at 25 °C for 3 h. Workup (AcOEt, 1 M HCl) followed by purification by silica-gel column chromatography and distillation gave **1c** (2.6 g, 67% yield) as a colorless oil: Bp 120 °C (20 Torr, 1 Torr=133.322 Pa); IR (neat) 3308, 2956, 2928, 2860, 1655, 1638, 1459, 1076 cm^{-1}; ^1H NMR ($CDCl_3$) δ=0.84—0.97 (m, 6H), 1.27—1.70 (m, 8H), 2.00—2.12 (m, 2H), 2.37 (dd, *J*=2.0, 2.0 Hz, 1H), 3.75—3.87 (m, 1H), 4.01 (dd, *J*=16.0, 2.0 Hz, 1H), 4.18 (dd, *J*=16.0, 2.0 Hz, 1H), 5.25 (dd, *J*=15.5, 9.0 Hz, 1H), 5.65 (dt, *J*=15.5, 6.5 Hz, 1H); ^{13}C NMR ($CDCl_3$) δ=13.6, 14.0, 22.3, 22.6, 27.6, 34.2, 35.2, 54.6, 73.4, 79.8, 80.5, 129.9, 135.1. Found: C, 80.34; H, 11.64%. Calcd for $C_{13}H_{22}O$: C, 80.35; H, 11.41%.

1,3-Dimethyl-2-butenyl Propargyl Ether (1a): Bp 120 °C (760 Torr); IR (neat) 3300, 2972, 2928, 1671, 1445, 1376, 1265, 1208, 1150, 1104, 1077, 1037, 844 cm^{-1}; ^1H NMR ($CDCl_3$) δ=1.20 (d, *J*=7.0 Hz, 3H), 1.69 (s, 3H), 1.72 (s, 3H), 2.38 (bs, 1H), 4.02 (d, *J*=15.0 Hz, 1H), 4.13 (d, *J*=15.0 Hz, 1H), 4.40 (dq, *J*=10.0, 7.0 Hz, 1H), 5.02 (d, *J*=10.0 Hz, 1H); ^{13}C NMR ($CDCl_3$) δ=18.0, 21.2, 25.27, 54.4, 70.5, 73.3, 80.6, 126.2, 136.3.

1-Phenyl-3-methyl-2-butenyl Propargyl Ether (1b): Bp

160 °C (20 Torr); IR (neat) 3290, 2968, 2916, 2852, 1451, 1376, 1066, 1027, 755, 698 cm^{-1}; ^{1}H NMR ($CDCl_3$) δ=1.76 (s, 3H), 1.83 (s, 3H), 2.42 (dd, J=2.4, 2.4 Hz, 1H), 4.07 (dd, J=17.0, 2.4 Hz, 1H), 4.20 (dd, J=17.0, 2.4 Hz, 1H), 5.33 (s, 2H PhCH-OCH_2+Me_2C=CH), 7.35 (m, 5H), ^{13}C NMR ($CDCl_3$) δ 18.4, 26.0, 54.8, 74.0, 76.5, 80.4, 125.2, 126.8, 127.6, 128.5, 137.1, 142.1. Found: C, 83.88; H, 8.07%. Calcd for $C_{14}H_{16}O$: C, 83.96; H, 8.05%.

(*Z*)-1-Methyl-2-heptenyl Propargyl Ether (1d): Bp 130 °C (20 Torr); IR (neat) 3306, 2956, 2926, 2858, 1460, 1440, 1371, 1132, 1087, 1071, 1042, 913, 734 cm^{-1}; ^{1}H NMR ($CDCl_3$) δ= 0.91 (t, J=10.0 Hz, 3H), 1.24 (d, J=6.3 Hz, 3H), 1.25—1.50 (m, 4H), 2.05—2.25 (m, 2H), 2.39 (dd, J=2.4, 2.4 Hz, 1H), 4.04 (dd, J=15.7, 2.4 Hz, 1H), 4.14 (dd, J=15.7, 2.4 Hz, 1H), 4.49 (dq, J=9.2, 6.3 Hz, 1H), 5.22 (dd, J=9.2, 11.0 Hz, 1H), 5.60 (dt, J=11.0, 7.5 Hz, 1H): ^{13}C NMR ($CDCl_3$) δ=13.8, 21.4, 22.3, 27.3, 31.9, 54.7, 69.5, 73.5, 80.1, 130.6, 133.9. Found: C, 79.25; H, 11.11%. Calcd for $C_{11}H_{18}O$: C, 79.46; H, 10.91%.

2-Cyclohexenyl Propargyl Ether (1e): Bp 140 °C (760 Torr); IR (neat) 3296, 3024, 2930, 2854, 1438, 1263, 1081, 1020, 725 cm^{-1}; ^{1}H NMR ($CDCl_3$) δ=1.43—2.20 (m, 8H), 2.42 (dd, J=2.4, 2.4 Hz, 1H), 4.05—4.17 (m, 1H), 4.20 (d, J=2.4 Hz, 1H), 4.22 (d, J=2.4 Hz, 1H), 5.81 (d, J=10.0 Hz, 1H), 5.92 (dt, J=10.0, 3.8 Hz, 1H); ^{13}C NMR ($CDCl_3$) δ=19.0, 25.1, 28.0, 55.2, 71.7, 73.8, 81.4, 127.0, 131.4. Found: m/z 136.0742, 135.0768. Calcd for $C_9H_{12}O$: M, 136.0887, M−1, 135.0808.

General Procedure for the Enyne Cyclization Mediated by Et_3B. A hexane solution of Et_3B (1.0 M, 0.2 ml, 0.2 mmol) was added to a solution of Ph_3SnH (0.42 g, 1.2 mmol) and enyne **1a** (0.14 g, 1.0 mmol) in toluene (100 ml) at 25 °C. After stirring for 3 h at 25 °C, the reaction mixture was poured into water and extracted with ethyl acetate. Purification by preparative tlc gave (*Z*)-*trans*-3-isopropyl-2-methyl-4-(triphenylstannylmethylene)oxolane (**2a**) as a colorless oil (0.41 g, 84% yield): Bp 170 °C (bath temp, 0.1 Torr); ^{13}C NMR ($CDCl_3$) δ=18.9, 20.7, 21.6, 30.4, 59.9, 72.3, 77.5, 112.8, 128.6, 136.2, 138.3, 165.0. Found: C, 66.43; H, 6.29%. Calcd for $C_{27}H_{30}OSn$: C, 66.29; H, 6.18%. IR, ^{1}H NMR, and ^{119}Sn NMR data are shown in Ref. 1.

(*Z*)-*trans*-3-Isopropyl-2-phenyl-4-(triphenylstannylmethylene)oxolane (2b): Bp 220 °C (bath temp, 0.2 Torr); IR (neat) 3060, 2956, 2924, 1429, 1075, 1059, 1023, 908, 727, 697 cm^{-1}; ^{1}H NMR ($CDCl_3$) δ=1.01 (d, J=7.0 Hz, 3H), 1.11 (d, J=7.0 Hz, 3H), 2.73 (m, 1H), 4.22 (d, J=14.0 Hz, 1H), 4.35 (d, J=14.0 Hz, 1H), 4.97 (d, J=5.0 Hz, 1H), 6.12 (s, 1H), 7.28—7.70 (m, 20H); ^{13}CNMR ($CDCl_3$) δ=19.5, 20.5, 30.8, 61.7, 73.2, 83.5, 114.1, 125.9, 127.3, 128.3, 128.4, 128.6, 136.8, 137.2, 138.1 164.3; ^{119}Sn NMR ($CDCl_3$) δ=−145.99. Found: C, 69.87; H, 5.81%. Calcd for $C_{32}H_{32}OSn$: C, 69.72; H, 5.85%.

(*Z*)-*trans*-2,3-Dibutyl-4-(triphenylstannylmethylene)-oxolane (2c): Bp 200 °C (bath temp, 20 Torr); IR (neat) 3060, 3010, 2952, 2926, 2854, 1466, 1458, 1429, 1075, 726, 697 cm^{-1}; ^{1}H NMR ($CDCl_3$) δ=0.85—0.99 (m, 6H), 1.25—1.68 (m, 12H), 2.33—2.43 (m, 1H), 3.62—3.75 (m, 1H), 4.06 (dd, J=16.0, 2.2 Hz, 1H), 4.18 (dd, J=16.0, 2.2 Hz, 1H), 6.06 (dd, J=2.2, 2.2 Hz, 1H), 7.34—7.79 (m, 15H); ^{13}C NMR ($CDCl_3$) δ=14.0, 22.7, 23.0, 28.2, 29.3, 32.1, 35.1, 51.9, 72.0, 84.5, 111.2, 128.6, 129.0, 136.8, 138.3, 166.5; ^{119}Sn NMR ($CDCl_3$) δ=−143.98. Found: C, 68.36; H, 6.89%. Calcd for $C_{31}H_{38}OSn$: C, 68.28; H, 7.02%.

(*Z*)-*trans*-2-Methyl-3-pentyl-4-(triphenylstannylmethylene)-oxolane (2d): Bp 190 °C (bath temp, 0.1 Torr); IR (neat) 3060, 3046, 3012, 2954, 2926, 2854, 1740, 1619, 1480, 1459, 1429, 1380, 1240, 1111, 1075, 1048, 1023, 997 cm^{-1}; ^{1}H NMR ($CDCl_3$) δ=0.91 (t, J=6.8Hz, 3H), 1.27 (d, J=6.0Hz, 3H), 1.15—1.65 (m, 8H), 2.15—2.30 (m, 1H), 3.68—3.78 (m, 1H), 3.92 (d, J=14.0 Hz, 1H), 4.10 (d, J=14.0 Hz, 1H), 6.03 (s, 1H), 7.23—7.68 (m, 15H); ^{13}C NMR ($CDCl_3$) δ=14.1, 22.6, 24.2, 26.7, 31.6, 32.2, 53.4, 72.1, 80.7, 111.0, 128.6, 129.0, 136.8, 138.3, 166.5; ^{119}Sn NMR ($CDCl_3$) δ=−144.96. Found: C, 67.36; H, 6.52%. Calcd for $C_{29}H_{34}OSn$: C, 67.34; H, 6.63%.

(*Z*)-*cis*-Hexahydro-3-(triphenylstannylmethylene)benzofuran (2e): Mp 85 °C (hexane); IR (neat, before crystallization) 3060, 2928, 2825, 1623, 1480, 1428, 1074, 1052, 727, 697 cm^{-1}; ^{1}H NMR ($CDCl_3$) δ=1.20—1.83 (m, 8H), 2.63—2.77 (m, 1H), 4.00—4.33 (m, 3H), 6.06 (s, 1H), 7.35—7.80 (m, 15H); ^{13}C NMR ($CDCl_3$) δ=21.4, 23.0, 27.2, 27.8, 46.8, 71.3, 78.0, 110.3, 128.6, 129.0, 136.8, 138.2, 166.4; ^{119}Sn NMR ($CDCl_3$) δ=−143.01. Found: C, 66.36; H, 5.77%. Calcd for $C_{27}H_{28}OSn$: C, 66.56; H, 5.79%.

Typical Procedure for Destannylation. Butyllithium (1.5 M hexane solution, 2.7 ml, 4.0 mmol) was added to a soluton of (triphenylstannylmethylene)oxolane (**2a**) (0.49 g, 1.0 mmol) in THF (5 ml) at −78 °C. After stirring for 15 min, MeOH (1.0 ml) was added and the resulting mixture was allowed to warm to 25 °C. The mixture was poured into 1 M HCl solution and extracted with ethyl acetate. The organic extracts were washed with brine, dried (Na_2SO_4), and concentrated. The crude product was purified by preparative TLC (silica gel, hexane-ethyl acetate=20:1) to give (*Z*)-*trans*-3-isopropyl-2-methyl-4-methyleneoxolane (IR (neat) 3064, 2956, 2924, 2872, 1659, 1459, 1371, 1090, 1048 cm^{-1}; ^{1}H NMR ($CDCl_3$) δ=0.94 (d, J=6.8 Hz, 3H), 0.96 (d, J=6.9 Hz, 3H), 1.24 (d, J=6.2 Hz, 3H), 1.68—1.97 (m, 1H), 2.08—2.20 (m, 1H), 3.98—4.17 (m, 1H), 4.24 (d, J=12.5 Hz, 1H), 4.36 (d, J=12.5 Hz, 1H), 4.96 (bs, 1H), 5.01 (bs, 1H)) which was contaminated by unidentified compounds and converted into α-methylene-γ-butyrolactone without further purification.

Transformation of Methyleneoxolane to α-Methylene-γ-butyrolactone. According to the procedure described in the literature,[7] methyleneoxolane derived from **2a** was oxidized with Collins reagent to give *trans*-4,5-dihydro-4-isopropyl-5-methyl-3-methylene-2(3*H*)-furanone (**3a**, 88 mg, 57% yield): Bp 90 °C (bath temp, 20 Torr); IR (neat) 2962, 2928, 2874, 1762, 1654, 1459, 1275, 1126, 1099, 1033 cm^{-1}; ^{1}H NMR ($CDCl_3$) δ=0.94 (d J=6.7 Hz, 3H), 0.95 (d, J=6.9 Hz, 3H), 1.37 (d, J=6.4 Hz, 3H), 1.84—2.05 (m, 1H), 2.52—2.61 (m, 1H), 4.47 (dq, J=3.3, 6.4 Hz, 1H), 5.62 (d, J=2.1 Hz, 1H), 6.35 (d, J=2.1 Hz, 1H); ^{13}C NMR ($CDCl_3$) δ=18.2, 19.0, 22.7, 31.4, 52.1, 76.8, 123.5, 137.6, 170.7. Found: m/z 154.0831, 139.0744. Calcd for $C_9H_{14}O_2$: M, 154.0992, M−CH_3, 139.0758.

***trans*-4,5-Dihydro-4-isopropyl-3-methylene-5-phenyl-2(3*H*)-furanone (3b)**: Bp 120 °C (bath temp, 20 Torr); IR (neat) 2960, 2872, 1765, 1656 1458, 1401, 1390, 1270, 1126, 1021, 1001, 964 cm^{-1}; ^{1}H NMR ($CDCl_3$) δ=1.01 (d, J=5.7 Hz, 3H), 1.05 (d, J=5.6 Hz, 3H), 1.95—2.13 (m, 1H), 2.85—2.93 (m, 1H), 5.31 (d, J=2.9 Hz, 1H), 5.65 (d, J=2.2 Hz, 1H), 6.41 (d, J=2.2 Hz, 1H), 7.49—7.70 (m, 5H); ^{13}C NMR ($CDCl_3$) δ=18.5, 18.9, 32.2, 53.6, 81.1, 123.9, 125.3, 128.3, 128.8, 136.8, 140.6, 170.6. Found: C, 77.47; H, 7.65%. Calcd for $C_{14}H_{16}O_2$: C, 77.75; H, 7.46%.

***trans*-4,5-Dibutyl-4,5-dihydro-3-methylene-2(3*H*)-furanone (3c)**:[9] Bp 155 °C (bath temp, 20 Torr); IR (neat) 2954, 2928, 2860, 1763, 1467, 1459, 1268, 1151, 1110 cm^{-1}; ^{1}H NMR ($CDCl_3$) δ=0.90—1.01 (m, 6H), 1.33—1.76 (m, 12H), 2.60—2.75 (m, 1H), 4.22 (dt, J=4.1, 6.2 Hz, 1H), 5.59 (d, J=2.4 Hz, 1H), 6.26 (d, J=2.4 Hz, 1H); ^{13}C NMR ($CDCl_3$) δ=13.9, 22.4, 22.6, 27.2, 28.5, 33.9, 35.9, 44.5, 83.5, 122.0, 139.5, 170.3.

***trans*-4,5-Dihydro-5-methyl-4-pentyl-3-methylene-2(3*H*)-furanone (3d)**: Bp 150 °C (bath temp, 20 Torr); IR (neat) 2956, 2928, 2856, 1764, 1664, 1459, 1402, 1382, 1271, 1162, 1126, 1102, 1053, 948, 815 cm^{-1}; ^{1}H NMR ($CDCl_3$) δ=0.90 (t, J=5.0 Hz, 3H), 1.33—1.74 (m, 9H), 1.41 (d, J=6.3 Hz, 3H), 2.56—2.70 (m, 1H), 4.37 (dq, J=4.8, 6.3 Hz, 1H), 5.59 (d, J=2.6 Hz, 1H), 6.26 (d, J=2.6 Hz, 1H); ^{13}C NMR ($CDCl_3$)

δ=13.9, 21.7, 22.4, 26.1, 31.7, 33.5, 46.3, 79.8, 121.9, 139.6, 170.3. Found: C, 72.55; H, 10.24%. Calcd for $C_{11}H_{18}O_2$: C, 72.49; H, 9.95%.

***cis*-Hexahydro-3-methylene-2(3*H*)-benzofuranone (3e)**: The compound was obtained from **1e** in similar fashion described for the conversion of **1a** into **3a**. The physical deta of **3e** were identical with those in the literature.[10]

Financial support by the Ministry of Education, Science, and Culture, (Grant-in-Aid for Special Project Research No. 61211016) is acknowledged.

References

1) K. Nozaki, K. Oshima, and K. Utimoto, *J. Am. Chem. Soc.*, **109**, 2547 (1987).

2) G. Stork and N. H. Baine, *J. Am. Chem. Soc.*, **104**, 2321 (1982); G. Stork, and R. Mook, Jr., *ibid.*, **105**, 3720 (1983); N. A. Porter, D. R. Magnin, and B. T. Wright, *ibid.*, **108**, 2787 (1986); D. P. Curran, M.-H. Chen, and D. Kim, *ibid.*, **108**, 2489 (1986).

3) G. Stork and R. Mook, Jr., *Tetrahedron Lett.*, **27**, 4529 (1986); A. L. J. Beckwith and D. M. O'Shea, *ibid.*, **27**, 4525 (1986); C. A. Broka and D. E. C. Reichert, *ibid.*, **28**, 1503 (1987); G. Stork and R. Mook, Jr., *J. Am. Chem. Soc.*, **109**, 2829 (1987).

4) H. M. R. Hoffmann and J. Rabe, *Angew. Chem., Int. Ed. Engl.*, **24**, 94 (1985) and references cited theren.

5) High dilution favors the intramolecular radical cyclization. Y. Ueno, K. Chino, and M. Okawara, *Tetrahedron Lett.*, **23**, 2575 (1982) For instance, the enyne, Me_2C=$CHCH_2CH_2C(OH)MeC{\equiv}CH$ gave cyclized product, 3-isopropyl-1-methyl-2-(triphenylstannylmethylene)cyclopentanol exclusively at 0.012 M concentration of Ph_3SnH. Meanwhile, the reaction at 80 °C without solvent gave a complex mixture consisting of (*E*)- and (*Z*)-vinylstannanes (Me_2C=$CHCH_2CH_2C(OH)MeCH$=$CHSnPh_3$, 46%), regioisomer (Me_2C=$CHCH_2CH_2C(OH)MeC(SnPh_3)$=$CH_2$, 9%), and the desired cyclized product (38%).

6) Triphenylstannylalkenes were easily transformed into alkenyllithium upon treatment with *n*-BuLi as tributylstannylalkenes. E. J. Corey, P. Ulrich, and J. M. Fitzpatrick, *J. Am. Chem. Soc.*, **98**, 222 (1976).

7) M. Okabe, M. Abe, and M. Tada, *J. Org. Chem.*, **47**, 1775 (1982).

8) An addition of galvinoxyl (0.1 mmol) to a reaction mixture of 1-dodecyne (1.0 mmol), Ph_3SnH (1.1 mmol), and Et_3B (0.1 mmol) resulted in a recovery of the acetylene (85%). The organoboranes are known to be excellent sources of free radicals in the presence of oxygen (H. C. Brown and M. M. Midland, *Angew. Chem., Int. Ed. Engl.*, **11**, 692 (1972); A. Suzuki, S. Nozawa, M. Itoh, H. C. Brown, G. W. Kabalka, and G. W. Holland, *J. Am. Chem. Soc.*, **92**, 3503 (1970)). Thus, we are tempted to assume a radical chain mechanism for the reaction. A trace of oxygen could be in a reaction mixture and initiate the free-radical reaction, although the reactions have been achieved under an argon atmosphere.

9) *cis*-Dibutyl-4,5-dihydro-3-methylene-2(3*H*)-furanone[10d] was obtained as minor product (trans:cis=96:4). ^1H NMR ($CDCl_3$) δ=4.56 (m, 1H), 5.52 d, J=2.4 Hz, 1H), 6.21 (d, J=2.4 Hz, 1H).

10) a) H. Saimoto, K. Nishio, H. Yamamoto, M. Shinoda, T. Hiyama, and H. Nozaki, *Bull. Chem. Soc. Jpn.*, **56**, 3093 (1983); b) J. A. Marshall and N. Cohen, *J. Org. Chem.*, **30**, 3475 (1965); c) L.-C. Yu and P. Helquist, *ibid.*, **46**, 4536 (1981); d) Y. Okuda, S. Nakatsukasa, K. Oshima, and H. Nozaki, *Chem. Lett.*, **1985**, 481; e) S. E. Drewes and R. F. A. Hoole, *Syn. Commun.*, **15**, 1067 (1985).

Palladium Catalyzed Hydrostannylation and Hydrogermylation of Acetylenes

Yoshifumi ICHINOSE, Hiroji ODA, Koichiro OSHIMA,* and Kiitiro UTIMOTO
Department of Industrial Chemistry, Faculty of Engineering, Kyoto University, Yoshida, Kyoto 606
(Received April 27, 1987)

Synopsis. Treatment of acetylenes with Ph_3SnH or Ph_3GeH in the presence of a catalytic amount of $Pd(PPh_3)_4$ provides the corresponding alkenyltriphenylstannanes or alkenyltriphenylgermanes in good yields.

Transition-metal-catalyzed hydrosilylation reaction has been extensively developed.[1] On the other hand, hydrostannylation[2] and hydrogermylation[3] have not been well-established. Here we wish to disclose the hydrostannylation and hydrogermylation of acetylenic compounds in the presence of a palladium catalyst to give the corresponding alkenyltriphenylstannanes and alkenyltriphenylgermanes.

The hydrostannylation or hydrogermylation of acetylenes takes place readily in the presence of a catalytic amount of free radical initiator such as azobisisobutyronitrile (AIBN) to give the corresponding alkenylstannanes or alkenylgermanes in good yields.[4] The reaction is regioselective but nonstereoselective. Thus, terminal acetylenes give 1-stannyl-1-alkenes or 1-germyl-1-alkenes as stereoisomeric mixtures (E and Z) upon treatment with R_3SnH or R_3GeH.

On the other hand, triphenylstannane adds to acetylenes in the presence of a catalytic amount of $Pd(PPh_3)_4$ to give a mixture of three isomeric alkenyltriphenylstannanes. The representative results are summarized in Table 1. (E)-Isomer **2** (cis addition products) predominates and (Z)-isomers **3** and its regio isomers **1** are obtained as minor products. Solvents (CH_2Cl_2, THF, and benzene) did not affect the isomeric ratios of the products. Palladium complexes such as $PdCl_2(PPh_3)_2$, $PdCl_2(CH_3CN)_2$, and $Pd(OAc)_2$ are equally effective as $Pd(PPh_3)_4$. Distribution of the isomeric products depends on the ligand on palladium. For instance, the reaction of 1-dodecyne with Ph_3SnH in the presence of $PdCl_2(n\text{-}Bu_3P)_2$ or $Pd(OAc)_2$-$(p\text{-}MeOC_6H_4)_3P$ combination[5] provided a mixture of **1a**, **2a**, and **3a** (**1a**:**2a**:**3a**=10:80:10) as $Pd(PPh_3)_4$. Meanwhile, $PdCl_2[P(o\text{-}MeC_6H_4)_3]_2$-catalyzed reaction gave (*E*)-1-triphenylstannyl-2-dodecene (**4a**) in 42% yield along with **1a** (3%), **2a** (24%), and **3a** (2%).[6] Catalysts such as $Pd(OAc)_2$ and $PdCl_2(CH_3CN)_2$ without phosphine compounds were also effective for the addition of Ph_3SnH to acetylenes to give allylic stannane as a major product. For instance, 1-dodecyne gave a mixture of **4a** and **2a** (**4a**:**2a**=7:3, combined yield 65—75%) upon treatment with Ph_3SnH in the presence of these palladium salts.

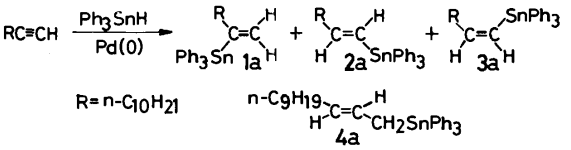

Hydrogermylation reaction could also be catalyzed by $Pd(PPh_3)_4$. The use of $Pd(PPh_3)_4$ was essential for the successful reaction. Triphenylgermane is less reactive hydrogen donor than Ph_3SnH and can not

Table 1. $Pd(PPh_3)_4$-Catalyzed Hydrostannation and Hydrogermylation of Acetylenes

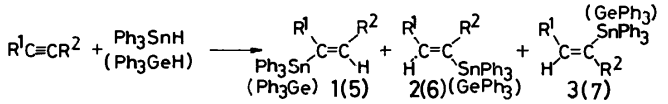

Run		Acetylene R¹	Acetylene R²	Ph_3SnH (Ph_3GeH)	Yield %	Ratio of **1(5)**:**2(6)**:**3(7)**
1	**a**	$C_{10}H_{21}$	H	Ph_3SnH	77	11:82:7
2	**b**	Ph	H	Ph_3SnH	61	12:71:17
3	**c**	$PhCH_2OCH_2CH_2$	H	Ph_3SnH	82	25:65:10
4	**d**	Me_3Si	H	Ph_3SnH	69	0:100:0
5	**e**	C_5H_{11}	C_5H_{11}	Ph_3SnH	53	0:100:0
6	**a**	$C_{10}H_{21}$	H	Ph_3GeH	97	14:86:0
7	**a**	$C_{10}H_{21}$	H	nPr_3GeH	83	20:80:0
8	**b**	Ph	H	Ph_3GeH	89	9:91:0
9	**c**	$PhCH_2OCH_2CH_2$	H	Ph_3GeH	52	7:91:<2
10	**f**	$HOCH_2CH_2$	H	Ph_3GeH	57	0:100:0
11	**d**	Me_3Si	H	Ph_3GeH	98	0:100:0
12	**e**	C_5H_{11}	C_5H_{11}	Ph_3GeH	80	a)

a) (*E*)-6-Triphenylgermyl-6-dodecene (**5a**) and (*E*)-7-triphenylgermyl-5-dodecene (**8**) were obtained (**5a**:**8**=1:2).

reduce $PdCl_2(PPh_3)_2$, $PdCl_2(CH_3CN)_2$, and $Pd(OAc)_2$ to zerovalent palladium which is an active catalyst for the reaction. Thus, these palladium complexes were not effective for the hydrogermylation. In contrast to hydrostannylation, the reaction of terminal acetylenes proceeds stereoselectively[7] and no (Z)-isomers are formed (Table 1). 6-Dodecyne gave a mixture of alkenylgermane **5e** and allylic germane, (*E*)-7-triphenylgermyl-5-dodecene (**8**).

We are tempted to assume following reaction mechanism: (1) Oxidative addition of Ph_3SnH (Ph_3GeH) to Pd(0), (2) stannylpalladation (cis addition),

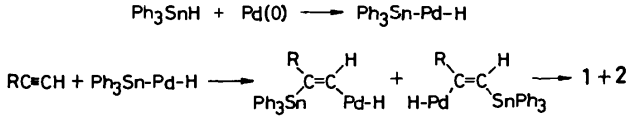

and (3) reductive elimination to produce alkenylstannanes (alkenylgermanes) and regenerate the palladium(0) complex. The formation of allylic stannane **4a** and allylic germane **8** presumably is explained by elimination of a palladium hydride from vinylpalladium species **A** and subsequent readdition in the opposite end of the 1,2-diene system followed by reductive elimination (path (a) in Scheme 1). The path (b) in Scheme 1 (readdition followed by reductive elimination) may explain the formation of (Z)-isomer **3**.[8]

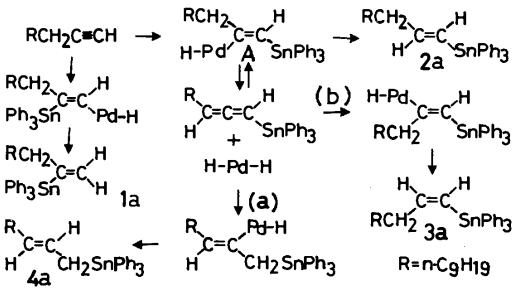

Scheme 1.

Experimental

General Procedure for the Reaction of Acetylenic Compounds with Triphenylstannane in the Presence of $Pd(PPh_3)_4$. The reaction of 1-dodecyne with Ph_3SnH is representative. $Pd(PPh_3)_4$ (58 mg, 0.05 mmol) was added to a solution of 1-dodecyne (0.17 g, 1.0 mmol) and Ph_3SnH (0.43 g, 1.2 mmol) in CH_2Cl_2 (10 ml) under an argon atmosphere. The reaction mixture was stirred at 25 °C for 5 h, then poured into water, and extracted with 3 portions of ethyl acetate. The organic extracts were dried (Na_2SO_4) and evaporated. Purification by preparative TLC on silica gel provided a mixture of 2-triphenylstannyl-1-dodecene (**1a**), (*E*)-1-triphenylstannyl-1-dodecene (**2a**), and (Z)-isomer **3a** in 77% combined yield (**1a**:**2a**:**3a**=11:82:7, the isomeric ratio was determined by its ^1H NMR spectrum). The spectral data were identical with those reported in the literature.[9] Phenylacetylene and 4-benzyloxy-1-butyne were treated with Ph_3SnH under the same reaction conditions to give the corresponding mixture of alkenylstannanes whose IR, ^1H NMR, and ^{119}Sn NMR spectra were identical with those reported.[9]

(*E*)-1-Trimethylsilyl-2-triphenylstannylethane: Mp 74 °C (hexane); IR (Nujol) 2950, 1482, 1428, 1246, 1160, 1077, 1016, 861, 838, 724, 696 cm^{-1}; ^1H NMR ($CDCl_3$) δ=0.01 (s, 9H), 6.91 (d, J=22.5 Hz, 1H), 7.14 (d, J=22.5 Hz, 1H), 7.30—7.50 (m, 9H), 7.50—7.81 (m, 6H); ^{119}Sn NMR ($CDCl_3$) δ=−147.0. Found: C, 61.09; H, 5.75%. Calcd for $C_{23}H_{26}SiSn$: C, 61.49; H, 5.83%.

(*E*)-6-Triphenylstannyl-6-dodecene: Bp 170 °C (bath temp, 0.3 Torr, 1 Torr=133.322 Pa); IR (neat) 3060, 3012, 2953, 2922, 2852, 1480, 1465, 1458, 1428, 1074, 725, 697 cm^{-1}; ^1H NMR ($CDCl_3$) δ=0.72—0.84 (m, 6H), 0.85—1.55 (m, 12H), 2.01 (dt, J=7.2, 7.2 Hz, 2H), 2.28 (t, J=7.1 Hz, 2H), 6.32 (t, J=7.2 Hz, 1H), 7.3—7.8 (m, 15H); ^{119}Sn NMR ($CDCl_3$) δ=−139.4. Found: C, 69.66; H, 7.51%. Calcd for $C_{30}H_{38}Sn$: C, 69.65; H, 7.40%.

General Procedure for the Hydrogermylation of Acetylenes. 1-Dodecyne (0.17 g, 1.0 mmol) and Ph_3GeH (0.36 g, 1.2 mmol) were combined in THF (10 ml). $Pd(PPh_3)_4$ (58 mg, 0.05 mmol) was added to the solution and the resulting mixture was stirred at 25 °C for 5 h under an argon atmosphere. Workup (AcOEt, brine) followed by silica-gel TLC purification gave alkenyltriphenylgermane (0.46 g, 97% combined yield) as a 14:86 (**5a**:**6a**) mixture of regioisomers as determined by the integrations of the olefinic protons in the ^1H NMR spectrum: Bp 120 °C (bath temp, 0.1 Torr); IR (neat) 2880, 2820, 1425, 1085, 730, 695 cm^{-1}; ^1H NMR ($CDCl_3$) δ=0.8—0.98 (m, 3H), 1.04—1.51 (bm, 16H), 2.18—2.35 (m, 2H), 5.39 (m, 0.14H), 5.90 (m, 0.14H), 6.12—6.23 (m, 1.72H), 7.32—7.65 (m, 15H). Found: C, 76.23; H, 8.15%. Calcd for $C_{30}H_{38}Ge$: C, 76.47; H, 8.13%.

2-Tripropylgermyl-1-dodecene (5c′) and (*E*)-1-Tripropylgermyl-1-dodecene (6c′) (5c′:6c′=20:80): Bp 88 °C (bath temp, 0.08 Torr); IR (neat) 2890, 2820, 1455, 1065, 690 cm^{-1}; ^1H NMR ($CDCl_3$) δ=0.67—1.02 (m, 24H), 1.17—1.51 (bm, 16H), 2.03—2.19 (m, 2H), 5.12 (m, 0.2H), 5.54 (m, 0.2H), 5.68 Found: C, 68.46; H, 11.94%. Calcd for $C_{21}H_{44}Ge$: C, 68.32; H, 12.01%.

1-Phenyl-1-triphenylgermylethene (5b) and (*E*)-1-Phenyl-2-triphenylgermylethene (6b) (5b:6b=9:91): Mp 144—146 °C (benzene-hexane(1:1)); IR (CCl_4) 3020, 1480, 1425, 1085, 985, 710, 695 cm^{-1}; ^1H NMR ($CDCl_3$) δ=5.61 (d, J=2.3 Hz, 0.09 H), 6.30 (d, J=2.3 Hz, 0.09 H), 6.95 (d, J=18.9 Hz, 0.91H), 7.05 (d, J=18.9 Hz, 0.91H), 7.25—7.63 (m, 20H). Found; C, 76.55; H, 5.39%. Calcd for $C_{26}H_{22}Ge$: C, 76.72; H, 5.45%.

2-Triphenylgermyl-4-benzyloxy-1-butene (5c) and (*E*)-1-Triphenylgermyl-4-benzyloxy-1-butene (6c) (5c:6c:7c=7:91:<2): Bp 129 °C (bath temp, 0.08 Torr); IR (neat) 1425, 1090, 735, 695 cm^{-1}; ^1H NMR ($CDCl_3$) δ=2.57 (dt, J=6.7, 6.0 Hz, 2H), 3.59 (t, J=6.7 Hz, 2H), 4.52 (s, 2H), 5.50 (bs, 0.07H), 6.01 (bs, 0.07H), 6.14 (dt, J=18.2, 6.0 Hz, 0.91H), 6.31 (d, J=18.2 Hz, 0.91H), 7.28—7.62 (m, 20H). Found: C, 74.40; H, 6.15%. Calcd for $C_{29}H_{28}OGe$: C, 74.89; H, 6.07%.

(*E*)-2-Triphenylgermyl-1-buten-4-ol (6f): Mp 111—113 °C (hexane-CH_2Cl_2); IR (KBr) 3318, 1638, 1484, 1430, 1091, 1039, 999, 983, 735, 698 cm^{-1}; ^1H NMR ($CDCl_3$) δ=1.55 (s, 1H), 2.49 (dt, J=6.3, 6.4 Hz, 2H), 3.69 (dt, J=6.4 Hz, 2H), 6.09 (dt, J=18.3, 6.3 Hz, 1H), 6.35 (d, J=18.3 Hz, 1H), 7.44—7.62 (m, 9H), 7.62—7.87 (m, 6H); ^{13}C NMR ($CDCl_3$) δ=39.9, 61.4, 127.3, 128.1, 128.9, 134.9, 136.4, 146.1. Found: C, 70.35; H, 5.82%. Calcd for $C_{22}H_{22}OGe$: C, 70.46; H, 5.81%.

(*E*)-1-Trimethylsilyl-2-triphenylgermylethene (6d): Mp 92—94 °C (hexane); IR (KBr) 1430, 1245, 1092, 870, 834, 735, 694 cm^{-1}; ^1H NMR ($CDCl_3$) δ=0.14 (s, 9H), 6.78 (d, J=21.8 Hz, 1H), 7.14 (d, J=21.8 Hz, 1H), 7.32—7.47 (m, 9H), 7.47—7.67 (m, 6H); ^{13}C NMR ($CDCl_3$) δ=−1.5, 128.2, 128.9, 135.4, 136.5, 143.1, 155.2. Found: C, 68.41; H, 6.51%. Calcd for $C_{23}H_{26}SiGe$: C, 68.52; H, 6.50%.

(*E*)-6-Triphenylgermyl-6-dodecene (6d) and (*E*)-7-Tri-

phenylgermyl-5-dodecene (8): Bp 165 °C (bath temp, 0.2 Torr); IR (neat) 3048, 2922, 2852, 1430, 1090, 733, 697 cm^{-1}; ^1H NMR ($CDCl_3$) δ=0.69—1.01 (m, 6H), 1.01—1.51 (m, 10H), 1.89—2.10 (m, 2H), 2.15—2.37 (m, 2H), 2.58—2.73 (m, 1.33H), 5.24—5.50 (m, 1.33H), 5.80 (t, J=7.0 Hz, 0.33H), 7.05—7.23 (m, 9H), 7.23—7.42 (m, 6H). Found: C, 76.31; H, 8.14%. Calcd for $C_{30}H_{38}Ge$: C, 76.46; H, 8.13%.

Reaction of 1-Dodecyne with Ph_3SnH in the Presence of $PdCl_2[P(o\text{-}MeC_6H_4)_3]_2$. A catalytic amount of $PdCl_2[P(o\text{-}MeC_6H_4)_3]_2$ (35 mg, 0.05 mmol) was added to a solution of 1-dodecyne (0.17 g, 1.0 mmol) and Ph_3SnH (0.42 g, 1.2 mmol) at 25 °C under an argon atmosphere. The resulting mixture was stirred at 25 °C for 6 h. The mixture was poured into water and extracted with ethyl acetate. The organic layers were dried (Na_2SO_4) and concentrated. The residual oil was submitted to preparative TLC (hexane as eluant) gave a mixture of **1a** (15 mg, 3%), **2a** (0.12 g, 24%), **3a**, (10 mg, 2%), and (*E*)-1-triphenylstannyl-2-dodecene (**4a**) (0.22 g, 42%). **4a**: ^1H NMR ($CDCl_3$) δ=2.38 (d, J=6.0 Hz, 2H), 5.40 (dt, J=15.0, 8.0 Hz, 1H), 5.51 (dt, J=15.0, 7.0 Hz, 1H).

References

1) K. Tamao, T. Nakajima, R. Sumiya, H. Arai, N. Higuchi, and Y. Ito, *J. Am. Chem. Soc.*, **108**, 6090 (1986); K. Tamao, J. Yoshida, H. Yamamoto, T. Kakui, H. Matsumoto, M. Takahashi, A. Kurita, H. Murata, and M. Kumada, *Organometallics*, **1**, 355 (1982).

2) Transition-metal-catalyzed hydrostannation: K. Kikukawa, H. Umekawa, T. Idemoto, and T. Matsuda, 33rd Symposium on Organometallic Chemistry, Japan (1986), Abstract A223.

3) Rhodium and platinum complexes catalyzed hydrogermylation: R. J. P. Corriu and J. J. E. Moreau, *J. Organomet. Chem.*, **40**, 73 (1972).

4) E. J. Corey, P. Ulrich, and J. M. Fitzpatrick, *J. Am. Chem. Soc.*, **98**, 222 (1976); H. Sano, Y. Miyazaki, M. Okawara, and Y. Ueno, *Synthesis*, **1986**, 776; K. Nozaki, K. Oshima, and K. Utimoto, *J. Am. Chem. Soc.*, **109**, 2547 (1987); Y. Ichinose, K. Nozaki, K. Wakamatsu, K. Oshima, and K. Utimoto, *Tetrahedron Lett.*, **28**, 3709 (1987).

5) $Pd(OAc)_2$ (0.02 mmol) and (p-$MeOC_6H_4)_3P$ (0.1 mmol) were combined in CH_2Cl_2 and the resulting mixture was stirred for 30 min before the addition of 1-dodecyne (0.5 mmol) and Ph_3SnH (0.6 mmol).

6) (*E*)- or (*Z*)-1-Triphenylstannyl-1-dodecene (**2a** or **3a**) was revovered unchanged, respectively, without isomerization into (*E*)-1-triphenylstannyl-2-dodecene (**4a**) on treatment with Ph_3SnH–$PdCl_2[P(o\text{-}MeC_6H_4)_3]_2$.

7) Benzyl ether of 3-butyn-1-ol gave trace of (*Z*)-alkenyltriphenylgermane **7c** (<2%).

8) The formation of (*Z*)-1-phenyl-2-triphenylstannylethene can not be explained by the above mechanism. Thus, an initial trans-addition of Ph_3Sn–Pd to acetylenic bond can not be excluded.

9) T. Nonaka, Y. Okuda, S. Matsubara, K. Oshima, K. Utimoto, and H. Nozaki, *J. Org. Chem.*, **51**, 4716 (1986).

Stereoselective Synthesis of Conjugated Dienones via the Palladium-Catalyzed Cross-Coupling Reaction of 1-Alkenylboronates with 3-Halo-2-alken-1-ones

Naoyuki SATOH, Tatsuo ISHIYAMA, Norio MIYAURA, and Akira SUZUKI*
Department of Applied Chemistry, Faculty of Engineering, Hokkaido University, Sapporo 060
(Received April 27, 1987)

Synopsis. The synthesis of conjugated dienones by means of palladium-catalyzed cross-coupling reaction between (*E*)-1-alkenyl-1,3,2-benzodioxaboroles or diisopropyl (*Z*)-1-hexenylboronate with 3-halo-2-alken-1-ones is described.

In our recent papers,[1-3] we reported a stereoselective synthesis of (*E,E*)-, (*E,Z*)-, (*Z,E*)-, and (*Z,Z*)-alkadienes and trienes by the palladium-catalyzed cross-coupling reaction of (*E*)- or (*Z*)-1-alkenylboronates and (*E*)- or (*Z*)-1-halo-1-alkenes. In this paper, we describe the development of reaction for the synthesis of conjugated dienones **5** as shown in Eqs. 1 and 2.

Since 1-alkenylboronates are quite inert toward many functional groups including carbonyl, the coupling reaction can be carried out without any protection of these groups. On the other hand, the reaction proceeds in the presence of bases such as sodium alkoxides and hydroxide. Consequently, vinylic halides with functional groups sensitive to base, such as halo enones **4** may cause difficulties.

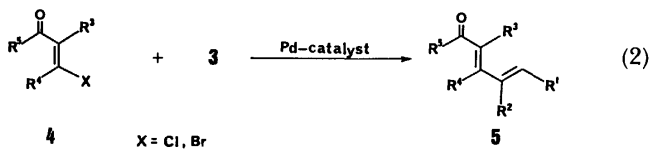

(*E*)-1-Hexenyl-1,3,2-benzodioxaborole (**3**, R^1=*n*-Bu, R^2=H) was initially chosen, and its reaction with 3-bromo-5,5-dimethyl-2-cyclohexen-1-one (**4**, R^3=H, R^4, R^5=CH_2–CMe_2–CH_2) was investigated under various different conditions as shown in Table 1.

Unlike our earlier palladium-catalyzed reactions,[1-3] relatively weak bases such as sodium acetate and triethylamine are effective in obtaining high yields of the coupling product **6**. The solvent also appears to play a critical role in determining the yield of **6**. Comparison of THF, DMF, and MeOH as solvents under various conditions demonstrates that the higher yields of dienone **6** are obtained in a methanol solution. When THF and DMF are employed as solvents, a substantial amount of the head-to-tail coupling product **7**[4] was prepared as a by-product. The solvent effect seems to be concerned with the mechanism of cross-coupling. We previously proposed a mechanism[1] which involves the intermediacy of alkoxopalladium(II) complexes for the cross-coupling reaction of 1-alkenylboronates with 1-halo-1-alkenes. The present reaction should also involve a methoxopalladium(II) **9**, prior to the transmetalation with 1-alkenylboronates. Such an exchange reaction of ligand in **8** can be accelerated by the trans effect[5] of electron-withdrowing carbonyl group, which may be a major reason to explain the difference between the present and former results.[1-3] All of the palladium complexes studied were proved to be used in catalytic amounts. Both palladium(II) acetate and dichlorobis(triphenylphosphine)palladium(II) appear to be more effective than tetrakis(triphenylphosphine)palladium(0). Thus, we used $PdCl_2(PPh_3)_2$ and sodium acetate in refluxing methanol as a general procedure for the reaction. Under these conditions, the coupling with 1-alkenylboronates is fortunately faster than the nucleophilic displacement of halogen in **4** with sodium acetate or other side reactions such as aldol condensation. The full scope of this cross-coupling reaction has been investigated by using a variety of 1-alkenylboronates **3** and halo enones **4**. The results are summarized in Table 2.

Table 1. Effects of Reaction Conditions for Cross-Coupling of (*E*)-1-Hexenyl-1,3,2-benzodioxaborole with 3-Bromo-5,5-dimethyl-2-cyclohexen-1-one[a]

Catalyst	Base	Solvent	Yield/%[b]	(**6**:**7**)
$Pd(OAc)_2$	NaOAc	MeOH	91	(100: 0)
$Pd(OAc)_2$	NaOAc	DMF	65	(41:59)
$Pd(OAc)_2$	Et_3N	DMF	37	(37:63)
$Pd(OAc)_2$	Et_3N	THF	23	(60:40)
$Pd(OAc)_2$	Et_3N	MeOH	97	(100: 0)
$Cl_2Pd(PPh_3)_2$	NaOAc	MeOH	98	(100: 0)
$Pd(PPh_3)_4$	NaOAc	MeOH	33	(100: 0)

a) Reactions were carried out under conditions described in the text. b) Yields are based on the haloenone used.

Diisopropyl (*Z*)-1-hexenylboronate **10a**[13] prepared by the hydroboration of 1-bromo-1-hexyne with dibromoborane, followed by the reaction with 2-propanol and potassium hydrotriisopropoxyborate also gave the dienone **11a** preserving the stereochemistry of (Z)-double bond, Z>96% (Eq. 3). The reaction of diisopropyl (*E*)-(1-methyl-1-hexenyl)boronate (**10b**) with 3-chloro-5,5-dimethyl-2-cyclohexen-1-

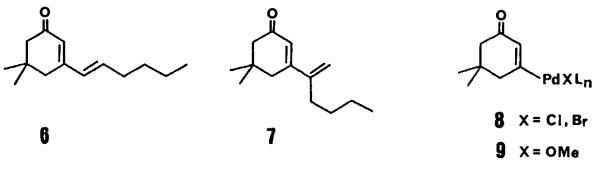

Table 2. Synthesis of Dienones and Trienones **5**

Run	1-Alkenylboronate		Haloenone				Product	No.	Yield/%[a]
	R^1=	R^2=	R^3=	R^4=	R^3=	X=			
1	*t*-Bu	H	H	$-CH_2CMe_2CH_2-$		Cl	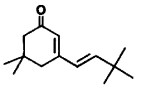	**5a**	—(87)
2	Et	Et	H	$-CH_2CMe_2CH_2-$		Cl	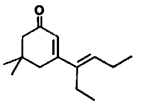	**5b**	96
3		H	H	$-CH_2CH_2CH_2-$		Cl	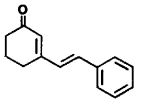	**5c**	98
4		H	H	$-CH_2CH_2CH_2-$		Cl	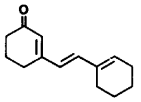	**5d**	84
5	*n*-Bu	H	Me	$-CH_2CMe_2CH_2-$		Br	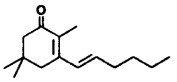	**5e**	98
6	*n*-Bu	H	Me	$-CH_2CH_2-$		Br	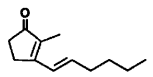	**5f**	97
7	*t*-Bu	H					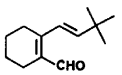	**5g**	—(85)

a) GLC yields based on haloenones and the isolated yields are shown in parenthesis.

one was reported elsewhere.[3]

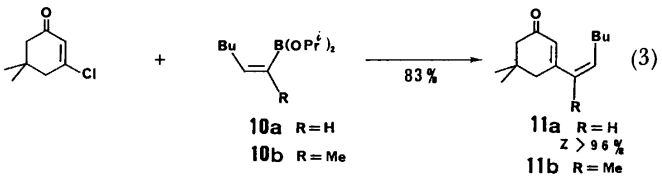

(3)

Conjugated dienones and polyenones are promising versatile intermediates for the synthesis of naturally occurring compounds. Most recently, we reported a stereoselective synthesis of a fungal prohormone (±)trisporol B[6] by means of such a crosscoupling reaction of 1-alkenylboronates. The present reaction affords an alternative and general procedure of obtaining stereodefined conjugated dienones and trienones.

Experimental

All reactions were carried out under nitrogen atmosphere. 1-Hexyne, 3,3-dimethyl-1-butyne, phenylethyne, and 3-hexyne are commercial products and purified by distillation before use. 1-Cyclohexenylethyne was prepared according to the method reported by Brandsma.[7] 3-Halo-2-cycloalkene-1-ones[8,9] were prepared from the corresponding 1,3-cycloalkadienones.

The IR spectra were recorded on a Hitachi-Perkin Elmer Model 125 spectrometer. The ^{1}H NMR spectra were taken on a Hitachi R-22 spectrometer (90 MHz, TMS as the internal reference). The measurement of mass spectra was carried out on a JEOL JMS-D 300 spectrometer (70 eV).

Palladium Complexes. Palladium(II) acetate was commercial. Dichlorobis(triphenyphosphine)palladium(II)[10] and tetrakis(triphenylphosphine)palladium(0)[11] were prepared according to the reported procedures.

1-Alkenylboronate 3. 1-Alkenyl-1,3,2-benzodioxaboroles were prepared by the Brown's method[1,12] from 1,3,2-benzodioxaborole (catecholborane) and 1-alkynes, and they were purified by distillation before use; **3a** (R^1=*n*-Bu, R^2=H): Bp 86—87 °C/ 0.3 mmHg (1 mmHg=133.322 Pa) (lit,[12] 82 °C/0.25 mmHg); **3b** (R^1=*t*-Bu, R^2=H): Bp 128 °C/ 12 mmHg; **3c** (R^1=Et, R^2=Et): Bp 63 °C/0.1 mmHg (lit,[12] 81 °C/0.2 mmHg); **3d** (R^1=phenyl, R^2=H): Mp 78 °C (lit,[12] 78—78.5 °C); **3e** (R^1=cyclohexenyl, R^2=H): Bp 135—149 °C/0.1 mmHg, Mp 76—79 °C. 1-Alkenylboronates except **3e** are stable toward air and can be handled by the usual method.

Reaction Conditions (Table 1). The best conditions for the formation of conjugated dienone **6** were determined by the following general procedure. The palladium complex (0.03 mmol), an appropriate solvent (3.5 ml of MeOH, DMF, or THF), base (1.5 mmol of NaOAc or Et_3N), and 3-bromo-5,5-dimethyl-2-cyclohexen-1-one (1.0 mmol) were placed in a 25 ml-flask, and flushed with nitrogen. (*E*)-1-Hexenyl-1,3,2-benzodioxaborole (1.1 mmol) was then added by means of a hypodermic syringe through the septum inlet, and the resultant mixture was heated under reflux for 3 h. In the case of DMF, the reaction temperature was controlled at 80 °C for 3 h. After the completion of reaction, the mixture was cooled to room temperature and the residual organoborane was oxidized with an aqueous solution (3 M (1 M=1 mol dm^{-3}), 0.2 ml) of NaOH-H_2O_2 (30% solution, 0.2 ml) for 1 h. The product was extracted with benzene, washed with brine, dried over $MgSO_4$, and analyzed directly by GLC (15% SE-30 on Uniport B, 2 m). The product was isolated by column chromatography over silica gel with hexane/ether. **6**: Bp 90—93 °C/0.1 mmHg; n^{22}=1.5149; IR

(film) 3040, 1670, 1635, 1595, and 975 cm^{-1}; ^1H NMR (CCl_4) δ=0.93 (t, 3H, J=6.5 Hz), 1.08 (s, 6H), 1.2—1.7 (m, 4H), 2.0—2.3 (m, 6H), 5.78 (broad s, 1H), 6.0 (dt, 1H, J=6.5 and 16 Hz) and 6.26 (d, 1H, J=16 Hz); Found:C 81.27; H, 10.55%. Calcd for $C_{14}H_{22}O$: C, 81.50; H, 10.75%.

Standard Procedure for the Synthesis of Dienone 5c (Table 2). In a dry 100 ml-flask equipped with a septum inlet and a magnetic stirring bar were placed $PdCl_2(PPh_3)_2$ (0.21 g, 0.3 mmol) and NaOAc (1.23g, 15 mmol). The flask was flushed with nitrogen and charged with 15 ml anhydrous methanol, 3-halo-2-alken-1-one (10 mmol), and 1-alkenyl-1,3,2-benzodioxaborole (11 mmol). The reaction mixture was then refluxed for 3 h. After completion of the reaction, aqueous NaOH (0.5 ml of a 3 M solution) and 30%-H_2O_2 (0.5 ml) were added at room temperature in order to oxidize the unreacted borane. The product was extracted with benzene, washed with brine and dried over $MgSO_4$. The extracts thus obtained were analyzed by GLC (15% SE-30 on Uniport B, 2 m, or fused silica capillary colum, 20 m). Analytically pure samples were obtained by chromatography over silica gel with hexane-ether or distillation under reduced pressure.

The dienones prepared by the above procedure are as follows.

5a: Mp 54 °C; IR (film) 3040, 1670, 1635, 1595, and 975 cm^{-1}; ^1H NMR ($CDCl_3$) δ=1.07 (s, 6H), 1.09 (s, 9H), 2.26 (s, 2H), 2.32 (broad s, 2H), 5.91 (t, 1H, J=1.3 Hz), 6.24 (d, 1H, J=16 Hz), and 6.26 (d, 1H, J=16 Hz); MS m/z (rel intensity) 107 (100), 191 (83) and 206 (47); Found: m/z 206.16711. Calcd for $C_{14}H_{22}O$: M, 206.16711.

5b: Bp 68—69 °C/0.05 mmHg; n^{21}=1.5217; IR (film) 3040, 1660, 1615, and 1580 cm^{-1}; ^1H NMR (CCl_4) δ=0.9—1.2 (m, 6H), 1.07 (s, 6H), 2.12 (s, 2H), 2.3 (s, 2H), 2.0—2.5 (m, 4H), 5.85 (t, 1H, J=7 Hz), and 5.96 (s, 1H); Found: C, 81.30; H, 10.55%. Calcd for $C_{14}H_{22}O$: C, 81.50; H, 10.75%.

5c: Bp 139—140 °C/0.15 mmHg; Mp 49 °C; IR (film) 3030, 1665, 1615, and 1580 cm^{-1}; ^1H NMR (CCl_4) δ=2.0—2.25 (m, 2H), 2.25—2.50 (m, 2H), 2.60 (t, 2H, J=6 Hz), 5.99 (s, 1H), 6.90 (s, 2H), and 7.2—7.6 (m, 5H); Found: C, 84.97; H, 7.07%. Calcd for $C_{14}H_{14}O$: C, 84.81; H, 7.12%.

5d: Bp 123—125 °C/1.5 mmHg; Mp 55 °C; IR (film) 3040, 1725, 1670, 1605, 965, and 865 cm^{-1}; ^1H NMR (CCl_4) δ=1.5—1.8 (m, 4H), 1.9—2.6 (m, 10H), 5.87 (s, 1H), 5.96 (broad s, 1H), 6.18 (d, 1H, J=16 Hz), and 6.58 (d, 1H, J=16 Hz); Found: C, 82.90; H, 9.12%. Calcd for $C_{14}H_{18}O$: C, 83.12; H, 8.97%.

5e: Bp 93—94 °C/0.3 mmHg; n^{21}=1.5192; IR (film) 3040, 1660, 1630, 1585, and 965 cm^{-1}; ^1H NMR (CCl_4) δ=0.905 (t, 3H, J=6.5 Hz), 1.02 (s, 6H), 1.2—1.6 (m, 4H), 1.34 (s, 3H), 2.19 (s, 2H), 2.29 (s, 2H), 2.0—2.4 (m, 4H), 6.06 (dt, 1H, J=6 and 16 Hz), and 6.60 (d, 1H, J=16 Hz); Found: C, 81.52; H, 10.73%. Calcd for $C_{15}H_{24}O$: C, 81.76; H, 10.98%.

5f: Bp 84—86 °C/0.3 mmHg; n^{20}=1.5350; IR (film) 3025, 1690, 1640, 1600, and 965 cm^{-1}; ^1H NMR (CCl_4) δ=0.90 (t, 3H, J=6.5 Hz), 1.1—1.6 (m, 4H), 1.67 (s, 3H), 2.1—2.4 (m, 2H), 2.4—2.7 (m, 2H), 6.14 (dt, 1H, J=6 and 16 Hz), and 6.57 (d, 1H, J=16 Hz); Found: C, 80.60; H, 10.13%. Calcd for $C_{12}H_{18}O$: C, 80.85; H, 10.18%.

5g: n^{20}=1.5272; IR (film) 1700, 1670, 1630, 1595, 1145, and 963 cm^{-1}; ^1H NMR (CCl_4) δ=1.09 (s, 9H), 1.45—1.90 (m, 4H), 2.15—2.6 (m, 4H), 6.0 (d, 1H, J=16 Hz), 6.83 (d, 1H, J=16 Hz), and 10.27 (s, 1H); MS m/z (rel intensity) 135 (100), 136 (14), 149 (4), 177 (0.6), and 192 (0.2); Found: m/z 192.15097; Calcd for $C_{13}H_{20}O$: M, 192.15093.

Synthesis of (*Z*)-1-Hexenylboronate 10a and Its Reaction with Halo Enone (Eq. 3). To a solution of diisopropyl (*Z*)-(1-bromo-1-hexenyl)boronate[12,13] (1.1 mmol) in ether (2 ml) was added a solution of potassium hydrotriisopropoxyborate in THF (1 M solution, 1.2 mmol) at 0 °C. The mixture was stirred for 15 min at 0 °C. The cooling bath was removed, and stirring was continued for 30 min at room temperature. The solvent was evaporated under reduced pressure (0.01 mmHg) and then diisopropyl (*Z*)-1-hexenylboronate **10a** thus obtained was dissolved in methanol (4 ml). Sodium acetate (1.5 mmol), $PdCl_2(PPh_3)_2$ (0.03 mmol), and 3-chloro-5,5-dimethyl-2-cyclohexen-1-one (1.0 mmol) were added, and the mixture was refluxed for 5 h. The reaction mixture was diluted with benzene-hexane(1/1) (30 ml), washed with water, and dried over $MgSO_4$. Chromatography over silica gel with hexane-ether gave **11a** (0.17 g, 83%). Analysis by GLC (fused silica capillary column, OV-101, 20 m) indicated that E/Z is 4/96. **11a:** IR (film) 3020, 1670, and 1630 cm^{-1}; ^1H NMR (CCl_4) δ=0.90 (t, 3H, J=6.5 Hz), 1.07 (s, 6H), 1.2—1.5 (m, 4H), 2.1—2.4 (m, 6H), 5.7 (dt, 1H, J=6.5 and 12 Hz), 5.9 (d, 1H, J=12 Hz), and 5.93 (broad s, 1H); MS m/z (rel intensity) 206 (76), 191 (10), 177 (15), 163 (15), 149 (30), 121 (39), and 108 (100); Found: C, 81.27; H, 10.55%. Calcd for $C_{14}H_{22}O$: C, 81.50; H, 10.75%.

References

1) N. Miyaura, K. Yamada, H. Suginome, and A. Suzuki, *J. Am. Chem. Soc.*, **107**, 972 (1985).

2) N. Miyaura, M, Satoh, and A Suzuki, *Tetrahedron Lett.*, **27**, 3745 (1986).

3) M. Satoh, N. Miyaura, and A. Suzuki, *Chem. Lett.*, **1986**, 1329.

4) N. Miyaura and A. Suzuki, *J. Organomet. Chem.*, **213**, C53 (1981).

5) R. F. Heck, "Organotransition Metal Chemistry," Academic Press, New York (1974), p. 16; P. M. Maitlis, "The Organic Chemistry of Palladium," Academic Press, New York (1971), Vol. 1, p. 119.

6) N. Miyaura, Y. Satoh, S. Hara, and A. Suzuki, *Bull. Chem. Soc. Jpn.*, **59**, 2029 (1986).

7) L. Brandsma, "Preparative Acetylenic Chemistry," Elsevier Pub. Co., New York (1971), p. 137.

8) R. D. Clark and C. H. Heathcock, *J. Org. Chem.*, **41**, 636 (1976).

9) R. D. Clark, J. E. Ellis, and C. H. Heathcock, *Synth. Commun.*, **5**, 193 (1975).

10) J. Chatt and F. G. Mann, *J. Chem. Soc.*, **1939**, 1631.

11) D. R. Coulson, *Inorg. Synth.*, **13**, 121 (1972).

12) H. C. Brown and S. K. Gupta, *J. Am. Chem. Soc.*, **94**, 4370 (1972); H. C. Brown, "Organic Synthesis via Boranes," John Wiely & Sons, New York (1975), p. 64.

13) H. C. Brown and T. Imai, *Organometallics*, **3**, 1392 (1984).

X-Ray Crystal Structure of 7,16,24,33-Tetrathia[3]paracyclo[3](1,3)-ferroceno[3]paracyclo[3](1,3)ferrocenophane[1)]

Masao HISATOME,* Masamichi YOSHIHASHI, Koji YAMAKAWA, and Yoichi IITAKA†
Faculty of Pharmaceutical Sciences, Science University of Tokyo,
12 Ichigaya-Funagawara, Shinjuku-ku, Tokyo 162
†Faculty of Pharmaceutical Sciences, The University of Tokyo,
Hongo, Bunkyo-ku, Tokyo 113
(Received May 2, 1987)

Synopsis. The crystal structure of the title compound, a macrocyclic thioether containing two 1,3-ferrocene and two 1,4-benzene moieties, has been determined by X-ray diffraction. The compound is in a chair-like conformation in the crystal and solvated with one molecule of benzene which was used for crystallization.

Czech and Ratajczak[2)] reported on the synthesis of ferrocene polythioethers by coupling reaction of 1,1′-bis(hydroxyalkyl)ferrocenes and alkanedithiols with trifluoroacetic acid (TFA) in dichloromethane. We applied the reaction to the synthesis of dithia[3]-benzeno[3]ferrocenophanes, which were used as synthetic intermediates of [2]benzeno[2]ferrocenophanes.[3,4)] In these reactions of 1,3-bis(hydroxymethyl)ferrocene with TFA, an oligomeric compound **1** was the main product in coupling with 1,4-bis(mercaptomethyl)benzene, whereas reaction with 1,3-bis(mercaptomethyl)benzene gave mononuclear coupling product, 7,14-dithia[3]metacyclo[3](1,3)ferrocenophane (**3**),[5,6)] in a good yield. The yield of **1** was always higher than that of mononuclear coupling product, 7,14-dithia[3]paracyclo[3](1,3)ferrocenophane (**2**), even though in high dilution conditions (10^{-3} mol dm^{-3}).

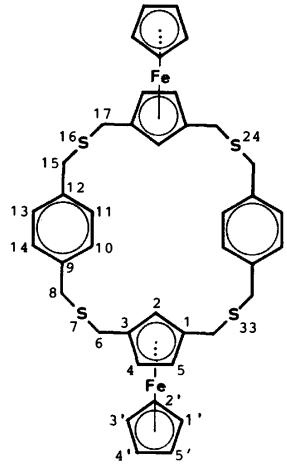

1

The molecular structure of **1** could not unequivocally confirmed by spectroscopy. The mass spectrum by means of electron impact ionization showed the same spectral pattern as that of **2**. The peak corresponding to the molecular weight of binuclear coupling product (*m/z* 760) was detected by field desorption (FD) ionizing technique. Furthemore, treatment of **1** or **2** with TFA in dichloromethane gave an equilibrium mixture of **1** and **2** (formation ratio, 3:1). These facts suggest that formation of **1** and **2** is thermodynamically controlled. Accordingly, it was not certain whether the peak observed in the FD mass spectrum indicates the exact molecular weight of **1**. On the other hand, there is no paper on the X-ray crystal structure of macrocyclic thioether containing metallocenes except for 1,1′-substituted metallocenes.[7,8)] Therefore, determination of the crystal structure of **1** was carried out by X-ray diffraction.

Experimental

Material: Coupling reaction of 1,3-bis(hydroxymethyl)-ferrocene and 1,4-di(mercaptomethyl)ferrocene with trifluoroacetic acid gave **1** (67%) and **2** (21%). The reaction conditions and the procedure were previously described.[4)]

Table 1. Atomic Coordinates ($\times 10^5$ for Fe; $\times 10^4$ for C and S) and Isotropic Equivalent Thermal Parameters (in Å^2 Unit) of **1** with Estimated Standard Deviations in Parentheses

Atom	*x*	*y*	*z*	B_{eq}
Fe	18358 (10)	25292 (8)	54649 (8)	3.93
C(1)	1372 (7)	3071 (6)	3636 (6)	4.37
C(2)	1838 (7)	1967 (6)	3483 (5)	4.32
C(3)	3347 (7)	2191 (5)	4249 (6)	4.09
C(4)	3834 (7)	3419 (6)	4888 (6)	4.76
C(5)	2618 (7)	3974 (6)	4508 (7)	5.08
C(6)	4222 (8)	1250 (6)	4428 (6)	5.19
S(7)	5882 (2)	1432 (2)	3560 (2)	5.38
C(8)	5043 (8)	1302 (6)	1800 (6)	5.46
C(9)	3757 (7)	174 (6)	1254 (6)	4.50
C(10)	2574 (8)	274 (6)	253 (6)	5.29
C(11)	1352 (8)	−713 (6)	−272 (7)	5.46
C(12)	1227 (7)	−1827 (6)	164 (6)	4.77
C(13)	2430 (8)	−1940 (6)	1134 (6)	4.81
C(14)	3690 (8)	−949 (6)	1663 (6)	5.02
C(15)	−180 (8)	−2862 (7)	−338 (7)	5.66
S(16)	93 (2)	−4018 (2)	−1575 (2)	5.28
C(17)	162 (7)	−3253 (6)	−3064 (6)	5.10
C(1′)	−32 (9)	2538 (8)	6388 (7)	6.59
C(2′)	110 (9)	1352 (7)	6139 (7)	6.55
C(3′)	1593 (9)	1314 (7)	6819 (7)	6.24
C(4′)	2340 (9)	2526 (7)	7506 (6)	6.58
C(5′)	1344 (10)	3260 (7)	7227 (7)	6.59
C(S1)	5451 (10)	5508 (7)	−1110 (9)	7.61
C(S2)	4197 (9)	5731 (7)	−614 (10)	7.93
C(S3)	3749 (9)	5224 (7)	491 (10)	7.66

Crystals of **1** were grown in a benzene–ethyl acetate solution as orange yellow plates of irregular shape.

X-Ray Crystallography: A crystal of approximate dimensions 0.1×0.2×0.3 mm was chosen for X-ray diffraction work. The cell dimensions and intensity data were collected on a Philips PW 1100 diffractometer using Mo $K\alpha$ radiation monochromated by a graphite plate. A total of 2588 reflections out of 3560 theoretically possible ones were measured as above the $2\sigma(I)$ level in a 2θ range of 6—50°. Intensities were corrected for Lorentz and polarization factors but not for absorption.

(Crystal Data): 7,16,24,33-Tetrathia[3]paracyclo[3](1,3)ferroceno[3]paracyclo[3](1,3)ferrocenophane (**1**) benzene solvate; $C_{40}H_{40}S_4Fe_2 \cdot C_6H_6$; FW=838.8; triclinic; space group $P\bar{1}$; a=9.123(5), b=11.598(6), c=10.109(5) Å, α=96.10(5), β=97.95(5), γ=104.42(5)°; U=1014.9 Å^3; D_{calc}=1.372 g cm^{-3}; Z=1.

The molecule posseses a center of symmetry which lies on a crystallographic symmetry center. The presence of one molecule of benzene in a unit cell laying on another symmetry center was noticed during the refinement. The structure was solved by the heavy atom method and refined by the method of block-diagonal least-squares. The present R factor is 0.06 for 2588 reflections including anisotropic temperature factors for all atoms but hydrogen atoms are not included.

The atomic coordinates are listed in Table 1.[9]

Results and Discussion

The perspective ORTEP drawings are shown in Fig. 1. The compound **1** is a macrocyclic thioether containing two ferrocene and two benzene moieties, as expected by FD mass spectrometry. The thioether **1** is the first example of macrocyclic 1,3-substituted ferrocenophane of which the structure was established by X-ray crystal analysis.

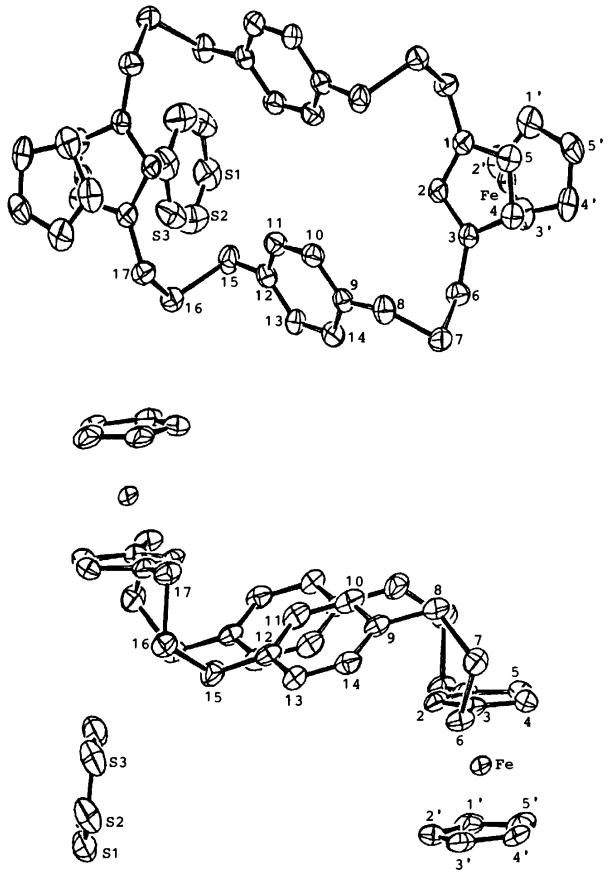

Fig. 1. ORTEP drawings (30% probability thermal ellipsoids) of **1**.

All bond lengths and angles[9] are in almost normal ranges; the C–C distances of the cyclopentadienyl (Cp) rings, 1.413(12)—1.452(10) Å; the C–C distances of the benzene ring, 1.381(9)—1.410(9) Å; the C–S bond lengths, 1.812(7)—1.832(8) Å. The average distance of the substituted Cp ring carbons from the iron (2.046 Å) is almost similar to that of the unsubstituted ring carbons (2.054 Å). These results indicate that the macrocyclic ring is strain-free. On the other hand, inspection of mononuclear coupling product **2** with a Dreiding molecular model reveals its strained molecular structure, because the distance between the benzene and Cp ring planes in the most stable conformation is 2.5—2.7 Å, which would be enough space to cause mutual repulsion between the two rings. Therefore, the macrocyclic compound **1** is more thermodynamically stable than **2**. The experimental result that the macrocyclic compound **1** was formed in preference to [3.3]phane **2** in the synthetic reaction and under an equilibrium condition with TFA, as mentioned above, can be reasonably explained on the basis of the stabilities of their structures.

The conformation of **1** is in an interesting chair-like shape as a whole. The size of the macrocyclic cavity is about 3×6 Å. The planes of the two benzene rings of the phane are faced each other with a little inclination. The two ferrocene nucleus take an "anti" direction parallel to one another about the Cp–Fe–Cp axes. The rotational conformation about the Cp–Fe–Cp axis of each ferrocene moiety is almost eclipsed.

One molecule of benzene is packed in a unit cell as a solvent of crystallization. Attempted preparations of single crystals with other some solvents were unsuccessful. Accordingly, the benzene molecule would play an important role to the packing of the macrocyclic ring in crystallization.

References

1) This work has been presented as a preliminary report: M. Hisatome, M. Yoshihashi, K. Yamakawa, and Y. Iitaka, 15th Symposium on Nonbenzenoid Aromatic Compounds, Kyoto, Nov. 1982, Abstr. No. C2-27.

2) B. Czech and A. Ratajczak, *Polish J. Chem.*, **54**, 767 (1980).

3) M. Hisatome, M. Yoshihashi, K. Masuzoe, K. Yamakawa, and Y. Iitaka, *Organometallics*, **6**, 1498 (1987).

4) M. Hisatome, M. Yoshihashi, K. Yamakawa, and Y. Iitaka, *Tetrahedron Lett.*, **24**, 5757 (1983); *Bull. Chem. Soc. Jpn.*, **60**, 2953 (1987).

5) The nomenclature of ferrocenophanes in the present paper is a modification[3,4] of that presented by Vögtle and Neumann.[6]

6) F. Vögtle and P. Neumann, *Tetrahedron*, **26**, 5847 (1970).

7) S. Akabori, Y. Habata, S. Sato, K. Kawazoe, C. Tamura, and M. Sato, *Acta Crystallogr.*, **C42**, 682 (1986).

8) S. Akabori, S. Sato, T. Tokuda, Y. Habata, K. Kawazoe, C. Tamura, and M. Sato, *Bull. Chem. Soc. Jpn.*, **59**, 3189 (1986).

9) The anisotropic thermal parameters, the bond lengths and angles, and the structure factors are deposited at the office of the Chemical Society of Japan (Document No. 8754).

 © 1987 The Chemical Society of Japan Bull. Chem. Soc. Jpn., 60, 3477—3483 (1987)

Studies of Collectors. IX. The Flotation of a Trace Amount of Uranium by Using 2-(Alkylamino)propionohydroxamic Acid and Cotelomer-Type Surfactants Bearing Hydroxyaminocarbonyl and Pyridyl Groups

Yoshifumi KOIDE,* Masazumi UCHINO, and Kimiho YAMADA
Department of Applied Chemistry, Faculty of Engineering, Kumamoto University, Kurokami, Kumamoto 860
(Received February 23, 1987)

Chelating surfactants bearing hydroxyaminocarbonyl and amino groups (R_nAHx) and cotelomer-type surfactants bearing hydroxyaminocarbonyl and pyridyl groups (Ls-VP-Q-Hx) were prepared and applied as flotation collectors for a trace amount of uranium. The uranium in an aqueous solution of pH 4—8 and in seawater was floated more effectively by ion flotation using R_nAHx or by foam fractionation using Ls-VP-Q-Hx, compared with alkylhydroxamic acid (R_nHx) and telomers bearing hydroxyaminocarbonyl groups (Lo-Hx). The effective flotation was concluded to be due to the chelate effects between the two groups on the complex formation and to the HLB of the resulting complex. Furthermore, the uranium recoveries were examined by using a hydroxamic acid polymer (62Hx), a *N*-methylhydroxamic acid telomer (Ls5.6MHx), and its cotelomer (Ls3.2VP4.5MHx).

Hydroxyaminocarbonyl group (hydroxamic acid),[1] N^2-hydroxyamidino group (amidoxime),[2] and the pyridyl group[3] are known as affinity groups for uranium ions, and chelating resins bearing such selective functional groups were applied to uranium recovery from seawater. On the other hand, uranium flotation has been studied by using decanedioic acid,[4] hexadecyltrimethylammonium chloride,[4] and sodium dodecyl sulfate-sodium 9-octadecenate in the presence of Fe^{3+} and Al^{3+}.[5] However, there are few reports on a flotation for a trace amount of uranium by using a surfactant bearing selective functional groups. Amidoxime-type surfactants were, though, applied as uranium-floating collectors in a previous paper.[6] Furthermore, surfactants bearing hydroxyaminocarbonyl and amino groups can be expected to be excellent ion-flotation and foam-fractionation collectors for uranium, because surfactants bearing the two groups are considered to exert chelate effects on the complex formation of uranium. This paper will describe the examinations of 2-(alkylamino)propionohydroxamic acid (R_nAHx n= 10, 12, 16) and of cotelomer-type surfactants bearing hydroxyaminocarbonyl and pyridyl groups (Ls-VP-Q-Hx) as flotation collectors for uranium, compared with the hydroxamic acid derivatives (alkanehydroxamic acid: R_nHx n=10, 12, 14, telomer-type surfactants bearing hydroxyaminocarbonyl groups: Lo-Hx, and polymer: 62Hx). No study of an uranium flotation using R_nAHx and Ls-VP-Q-Hx has yet been reported as far as the present authors are aware.

Experimental

Synthesis of Surfactants. Decanehydroxamic acid ($R_{10}Hx$), Dodecanehydroxamic acid ($R_{12}Hx$), and tetradecanehydroxamic acid ($R_{14}Hx$) were prepared by the reaction of equimolar amounts of corresponding alkanoyl chloride and hydroxylamine,[7] and then 2-(decylamino)propionohydroxamic acid ($R_{10}AHx$), 2-(dodecylamino)propionohydroxamic acid ($R_{12}AHx$), and 2-(hexadecylamino)propionohydroxamic acid ($R_{16}AHx$) were prepared by the reaction of the synthesized methyl 2-(alkylamino)propionate with hydroxylamine, which had themselves been prepared by the esterification of the corresponding 2-(alkylamino)propionic acid[8] with methanol. The yields were $R_{10}Hx$ 53%, $R_{12}Hx$ 48%, $R_{14}Hx$ 45%, $R_{10}AHx$ 54%, $R_{12}AHx$ 38%, and $R_{16}AHx$ 44%. The structures were confirmed by means of their IR spectra (Shimadzu IR-408), NMR spectra (JEOL JMN-MH-100), and elementary analyses (Yanako CHN Corder MT-3). Mp: $R_{10}Hx$ 86.2—88.8 °C, $R_{12}Hx$ 97.0—98.6 °C, $R_{14}Hx$ 93—95 °C, $R_{10}AHx$ 158.5—160.4 °C, $R_{12}AHx$ 155.9—157.2 °C, $R_{16}AHx$ 143—145 °C. IR (KBr): ν_{N-H} 3220 cm^{-1}, ν_{C-H} 2890, 2820 cm^{-1}, $\nu_{C=O}$ 1630—1650 cm^{-1}, δ_{N-H} 1610 cm^{-1}. ^1H NMR (CF_3COOH): δ=0.9 (3H, t, CH_3CC-), 1.3—1.4 (methylene in alkane), 1.8 {3H, t, -CNC(CH_3)CO-}, 2.7 (2H, t, -CCH_2CO-), 3.3 (2H, t, -CCH_2NC<), 4.2 {1H, -CNCH(Me)CO-}, 7.4 {1H, -CNHC(Me)CO-}. $R_{10}Hx$ Found: C, 63.37; H, 11.30; N, 7.38%; Calcd for $C_{10}H_{21}O_2N$: C, 64.13; H, 11.30; N, 7.48%. $R_{12}Hx$ Found: C, 66.15; H, 11.47; N, 6.20%; Calcd for $C_{12}H_{25}O_2N$: C, 66.95; H, 11.70; N, 6.51%. $R_{14}Hx$ Found: C, 68.44; H, 11.83; N, 5.80%; Calcd for $C_{14}H_{29}O_2N$: C, 69.08; H, 12.00; N, 5.75%. $R_{10}AHx$ Found: C, 64.07; H, 11.66; N, 11.41%; Calcd for $C_{13}H_{28}O_2N_2$: C, 63.89; H, 11.55; N, 11.46%. $R_{12}AHx$ Found: C, 65.92; H, 11.89; N, 10.50%; Calcd for $C_{15}H_{32}O_2N_2$: C, 66.13; H, 11.84; N, 10.28%. $R_{16}AHx$ Found: C, 68.73; H, 12.24; N, 8.50%; Calcd for $C_{19}H_{40}O_2N_2$: C, 69.46; H, 12.27; N, 8.52%.

The cotelomer-type surfactants used in this study were obtained as described in a previous paper:[9] The mixed monomers of 4-vinylpyridine and methyl acrylate were polymerized by using 2,2′-azobisisobutyronitrile as an initiator in a 1-dodecanethiol solvent of a chain-transfer agent, and the products were treated with benzyl chloride in order to quaternize them. The degree of polymerization and the composition were determined by means of the elementary analyses, the molecular weight (Corona 114 vapor-pressure osmometer), and the ^1H NMR spectra. In order to obtain the *N*-methylhydroxamic acid derivative, the more reactive *p*-nitrophenyl acrylate was also introduced to the cotelomer instead of the methyl acrylate;[10] it had been prepared by the reaction of acrylic chloride with *p*-nitrophenol. Then, the methyl and *p*-nitrophenyl esters were converted into hydroxamic acid or *N*-methylhydroxamic acid by treatment with a 5-fold amount of hydroxylamine or *N*-methylhydroxylamine.

The formation of the hydroxamic acid derivatives was confirmed by the strong broad absorption of hydroxamic acid at $\nu_{C=O}$ 1660 cm^{-1} in the IR spectrum and by that of the hydroxamate anion (pH 12) at 285 nm in the UV spectrum, but the conversion of the esters into the hydroxamic acid was incomplete; the resulting compounds exhibited the weak absorption of carboxylic acid, $\nu_{C=O}$ 1730—1750 cm^{-1}, in the IR spectrum. The ratios of the hydroxyaminocarbonyl and *N*-methylhydroxyaminocarbonyl groups were calculated from the absorbance to be about 80% of the methyl ester groups in the starting cotelomer and about 70% of the *p*-nitrophenyl ester groups.

Benzohydroxamic acid (BHx), *o*-aminobenzohydroxamic acid (BAHx), and the telomer (Lo-Hx), were prepared according to the methods described in the literature.[6,11,12] The chemical formulas and the abbreviations are shown in Fig. 1.

Apparatus and Procedures. The flotation apparatus was the same as that previously reported.[6] A uranium solution was prepared by dissolving $UO_2(NO_3)_2$ in an aqueous solution, while seawater was taken at the seacoast of Akase, Utogun, Kumamoto, in January 1983. The surfactant was added to 500 cm^3 of the uranium solution or the seawater in the flotation vessel, and air was introduced into the solution through the sintered-glass disk (No. 4) at the bottom of the vessel at the rate of 30—40 $cm^3 min^{-1}$ for 20 min. The amount of uranium in the aqueous solution or the seawater was determined from the absorbance of the uranium-arsenazo III complex (660 nm).[13] The floatabilities of uranium in ion flotation and foam fractionation were calculated using this formula:

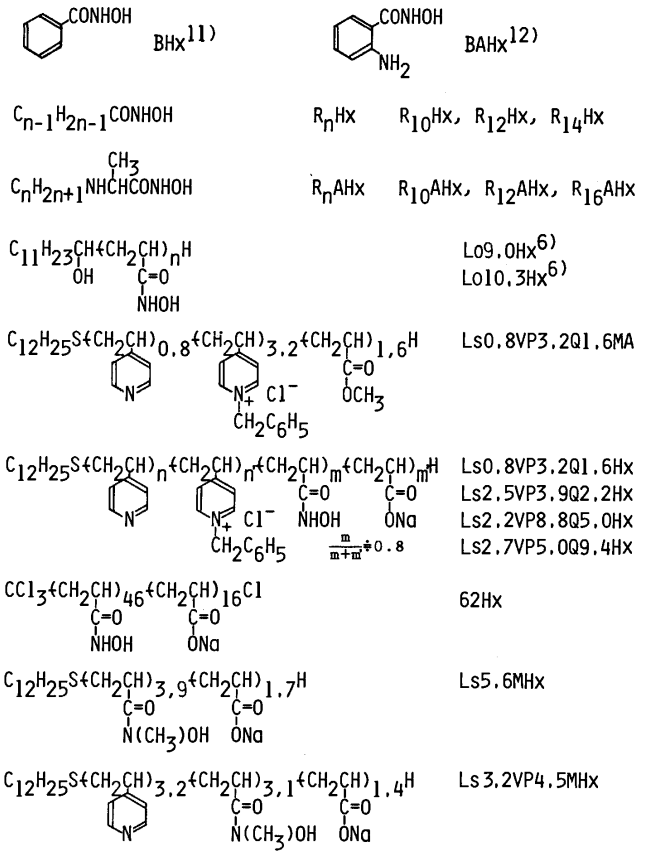

Fig. 1. Chemical formulas and abbreviations.

$$F(\%)=\frac{a_0-a_1}{a_0}\times 100$$

where a_0 and a_1 denote the initial and the final uranium concentrations.

Results and Discussion

Surface Activity. Chelating surfactants used as ion-flotation and foam-fractionation collectors should be surface-active, as was mentioned in a previous paper.[6] The surface tensions of these surfactant solutions were measured by means of a Du Noüy surface-tension balance. The values at their critical micellar concentration (cmc) are 53 dyn cm^{-1} (1 dyn=1×10^{-5} N) for 5×10^{-4} M (1M=1 mol dm^{-3}) $R_{10}Hx$ (pH 10), 61 dyn cm^{-1} for 1.5×10^{-4} M $R_{12}Hx$ (pH 10), 48 dyn cm^{-1} for 8×10^{-5} M $R_{10}AHx$ (pH 10), 62 dyn cm^{-1} for 5×10^{-5} M $R_{12}AHx$ (pH 10), 34 dyn cm^{-1} for 10^{-2} M $R_{10}AHx$ (pH 4), 40 dyn cm^{-1} for 10^{-2} M $R_{12}AHx$ (pH 4), 37 dyn cm^{-1} for 0.4 wt% Ls5.6MHx (pH 8.0), and 47 dyn cm^{-1} for 0.2wt% Ls3.2VP4.5MHx (pH 8.0). The cmc of R_nAHx at pH 10 was lower than that at pH 4, and a milky turbidity appeared at pH 4—11.5. The acid dissociations were pk_a 9.29 for BAHx,[14] and pk_{a_1} 3.52, pk_{a_2} 6.33, pk_{a_3} 8.00, and pk_{a_4} 9.07 for *N,N'*-ethylenediaminediacetic-*N,N'*-diacethydroxamic acid.[15] Therefore, the acid dissociations of R_nAHx may be assumed to be pk_{a_1} about 6 and pk_{a_2} 9.1—9.3, while R_nAHx at pH 10 would still have weakly nonionic properties because of its free amine and undissociated hydroxamic acid. The surface tensions of the Lo9.0Hx and Lo10.3Hx solutions were 38—40 dyn cm^{-1} in pH 7—10, as was mentioned in a previous paper.[16] Therefore, these surfactants were used as ion-flotation and foam-fractionation collectors because they have surface-active properties.

Flotation Using R_nAHx. Ion flotation for a 10 ppb

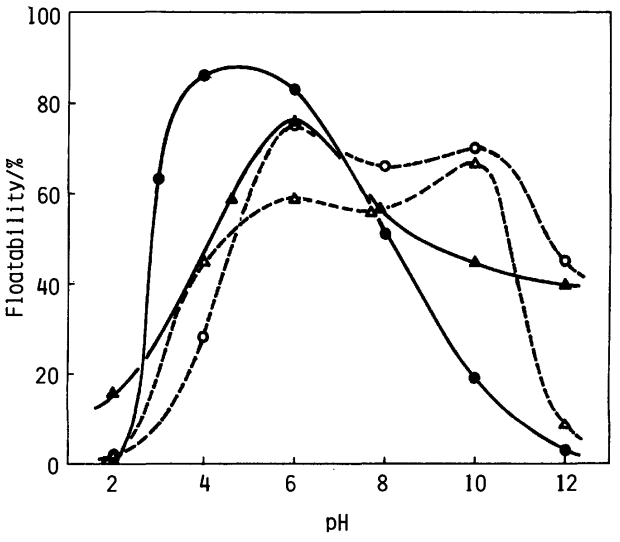

Fig. 2. PH dependence of U-floatability.
U: 10 ppb. R_nHx, R_nAHx: 10 mg.
△: $R_{10}Hx$, ○: $R_{12}Hx$, ▲: $R_{10}AHx$, ●: $R_{12}AHx$.

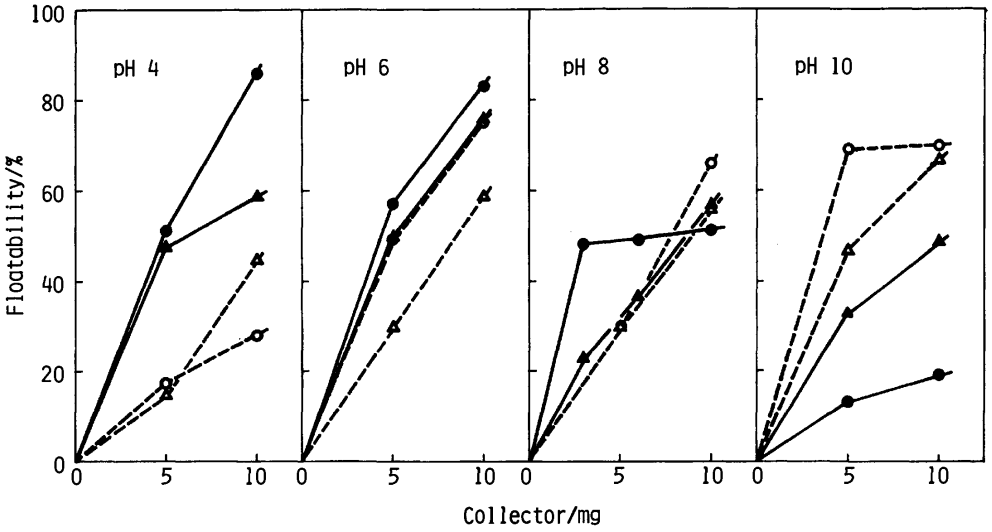

Fig. 3. Effect of collector-concn.
U: 10 ppb. △: $R_{10}Hx$, ○: $R_{12}Hx$, ▲: $R_{10}AHx$, ●: $R_{12}AHx$.

Table 1. Distribution of Uranium Complexes with Various pH Values

Species	Distribution[a]/%				
	pH 4	pH 6	pH 8	pH 10	pH 12
UO_2^{2+}	42	0	0	0	0
$UO_2(OH)^+$	4	0	0	0	0
$UO_2(OH)_2$	0	0	0	0	0
$UO_2(OH)_3^-$	0	0	7(18)[b]	24(99)[b]	100
UO_2BHx^+	33	2	0	0	0
$UO_2(BHx)_2$	20	97	30(81)[b]	0	0
UO_2Cl^+	1	0	0	0	0
$UO_2(CO_3)_2^{2-}$	0	0	0.4	0	0
$UO_2(CO_3)_3^{4-}$	0	0	62	76	0

a) The distributions of the uranium ion species in the 0.72 M NaCl-2.3×10^{-3} M $NaHCO_3$ solution, which were calculated from the acid-dissociation and stability constants:[17,18] $\log K_{UO_2Cl^+}=-0.1$, $\log K_{UO_2Cl_2}=-0.81$, $\log K_{UO_2Cl_3^-}=-1.69$, H_2CO_3 pk_{a_1} 6.35, pk_{a_2} 10.33, $\log K_{UO_2CO_3}=9.11$, $\log K_{UO_2(CO_3)_2^{2-}}=6.46$, $\log K_{UO_2(CO_3)_3^{4-}}=7.23$, BHx($4.65\times10^{-5}$ M) pk_{a_1} 8.8,[14] $\log K_{UO_2BHx^+}=9.03$, $\log K_{UO_2(BHx)_2}=8.91$.
b) The distribution of uranium complexes in the absence of CO_3^{2-}.

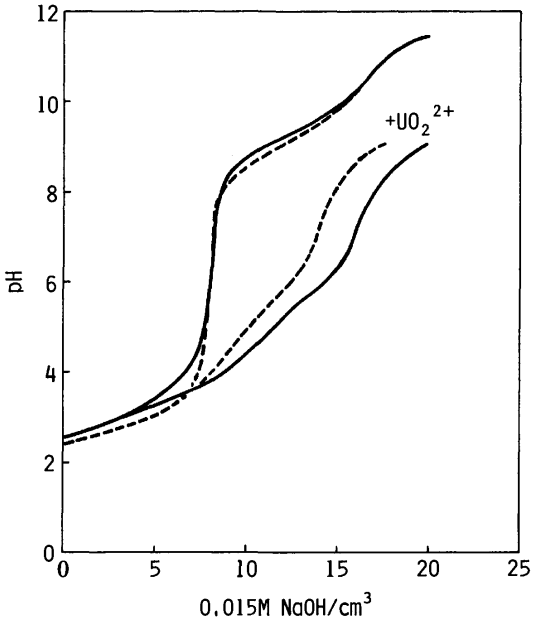

Fig. 4. PH titration curves of BHx and BAHx with UO_2^{2+}.
BHx, BAHx: 1.1×10^{-4} mol in 11 cm^3 ($=10^{-2}$ M).
UO_2^{2+}: 3.63×10^{-5} mol in 11 cm^3 ($=3.3\times10^{-3}$ M).
----: BHx, ——: BAHx.

uranium solution was examined by using R_nHx and R_nAHx. Figure 2 shows the pH-dependent floatabilities. R_nHx were effective in pH 4—10, while R_nAHx were effective in pH 4—8. The most effective collectors among them were $R_{12}AHx$ in pH 4—6 and $R_{12}Hx$ in pH 8—12. The floatabilities were naturally affected by the concentration of the collector, as is shown in Fig. 3. R_nAHx were clearly more effective than R_nHx at pH 4 and slightly more so in pH 6—8. However, the floatabilities at pH 10 achieved by using R_nAHx were less effective than those achieved by using R_nHx.

The uranium ions in an aqueous solution exist in the forms of free cation and hydroxo complexes, and the species changes with the pH. The stability constants of the BHx and hydroxouranium complexes are $\log K_{MBHx}$ 9.03, $\log K_{M(BHx)_2}$ 8.91,[17] $\log K_{MOH}$ 9.0, $\log K_{M(OH)_2}$ 7.8, and $\log K_{M(OH)_3}$ 8.1.[18] The ratios of the hydroxo-, BHx-, chloro-, and carbonato species calculated under the same conditions as seawater are shown in Table 1. The formation of the R_nHx-uranium complex could be explained by assuming its stability constant to be close to that of BHx. Most of the complexes in the 10-ppb uranium solution were BHx species in pH 4—8 and hydroxo species in pH 10—12. The long-alkylated R_nHx would form the floatable uranium complexes more in pH 4—8 because the surfactant was concentrated at the gas-liquid interface of the bubble, and then the R_nHx would make the colloidal hydroxo species float in pH 10—12. Ligand-

Table 2. Uranium Flotation from a 10-ppb Uranium Solution of pH 8

Condition of flotation[a]		Uranium-floated	
Collector	mg	Floatability %	Amount mg/g-collector
$R_{10}Hx$	5	30	0.30
$R_{12}Hx$	5	30	0.30
$R_{10}AHx$	3	23	0.38
$R_{12}AHx$	3	49	0.82
R_8Hx	3+N[b]	50	0.19
Lo9.0Hx	3+N[b]	64	0.24
Ls2.2VP8.8Q5.0Hx	30	93	0.16

a) 500 cm³ of a 10-ppb uranium solution (pH 8.0). R_8Hx, Lo9.0Hx, Ls2.2VP8.8Q5.0Hx: foam fractionation. b) 10 mg of a nonionic surfactant (Nissan nonion O-6).

bearing hydroxyaminocarbonyl and amino groups may be expected to exhibit a higher stability. However, the stability constants for the UO_2^{2+} complex of *o*-hydroxybenzohydroxamic acid (BHHx), a ligand-bearing hydroxyaminocarbonyl and hydroxyl group, is not higher than those for the UO_2^{2+}-BHx complex: log $K_{M\cdot BHHx}$ 7.71, log $K_{M(BHHx)_2}$ 6.80.[17] In order to examine the chelate effect of R_nAHx between hydroxyaminocarbonyl and amino groups, pH titrations for the BAHx-UO_2^{2+} and BHx-UO_2^{2+} complexes were carried out because of the low solubilities of R_nHx and R_nAHx. It can be seen from Fig. 4 that the BAHx complex is more stable than the BHx complex. The long-alkylated R_nAHx is also considered to be more stable than the R_nHx. Therefore, the enhancement when R_nAHx was used in pH 4—6 was considered to be due to the chelate effect between hydroxyaminocarbonyl and amino groups on the uranium-complex formation. Therefore, the HLB values of the floatable metal complexes should be in the range of 4—14, as was mentioned in a previous paper.[6] The six alkyl chains in the R_nAHx and R_nHx series were used in order to examine the hydrophobic variation in HLB; they were all surface-active collectors. The HLB values of the uranium complexes (2 : 1) were calculated according to the Oda equation:[19] $R_{10}Hx$ 6 (collector 15), $R_{12}Hx$ 5 (13), $R_{14}Hx$ 4 (11), $R_{10}AHx$ 6 (14), $R_{12}AHx$ 5 (12), and $R_{16}AHx$ 4 (10). Therefore, R_nAHx-UO_2-$(R_nAHx)_2$ and R_nHx-$UO_2(R_nHx)_2$ would float simultaneously, and the collectors would make the colloidal $UO_2(OH)_3^-$ species float.

Uranium Flotation from Seawater. Seawater is pH 8.0, and the concentration of uranium is 3 ppb. The flotation for a 10-ppb uranium solution of pH 8.0 is shown in Table 2. Among those collectors, $R_{12}AHx$ was the most effective; the floated amount of the uranium was 0.82 mg/g-$R_{12}AHx$. $R_{16}AHx$ was useful as an ion-flotation collector, but was only slightly soluble in water. R_8Hx and the telomer, Lo9.0Hx, were not useful because of their rich solubilities, whereas the foamy sublate was formed by the addition of a nonionic surfactant. Therefore, the uranium recoveries using the latter collectors were carried out by means of foam fractionation. The apparatus and the procedures in the foam fractionation were the same as those in the ion flotation, except for the continuous removal of the resulting foam.[6] The floatabilities became 50% by using the R_8Hx-nonionic surfactant and 64% by using the LoHx-nonionic surfactant. The cotelomer-type surfactant, Ls2.2VP8.8Q5.0Hx, exhibited an excellent foaming ability and the floatabilities by using Ls2.2VP8.8Q5.0Hx became more effective. A cationic surfactant, hexadecyltrimethylammonium bromide(HTABr), made the uranium float highly:[4] There was a 99%-floatability with 20 mg of HTABr, which is not indicated in Table 2. It was considered that the uranium could be floated because of the electrostatic force of attraction between the cationic HTABr and the anionic $[UO_2(OH)_3]^-$. However, HTABr did not make the uranium float from seawater: There was only a 3% floatability with 20 mg of HTABr. Many salts are highly dissolved in seawater, so that recovery from seawater is usually difficult. Figure 5 shows the ion flotation using R_nAHx and R_nHx for the uranium in seawater. The uranium floatabilties in pH 4—6 were similar to those for the 10-ppb uranium solution, whereas the floatabilities in pH 8—10

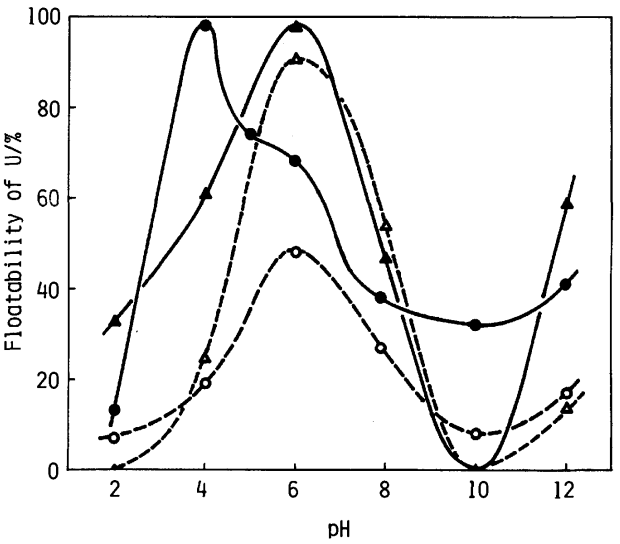

Fig. 5. Relation between pH and flotation for U. Sample: 500 cm³ of seawater. R_nHx, R_nAHx: 20 mg. △: $R_{10}Hx$, ○: $R_{12}Hx$, ▲: $R_{10}AHx$, ●: $R_{12}AHx$.

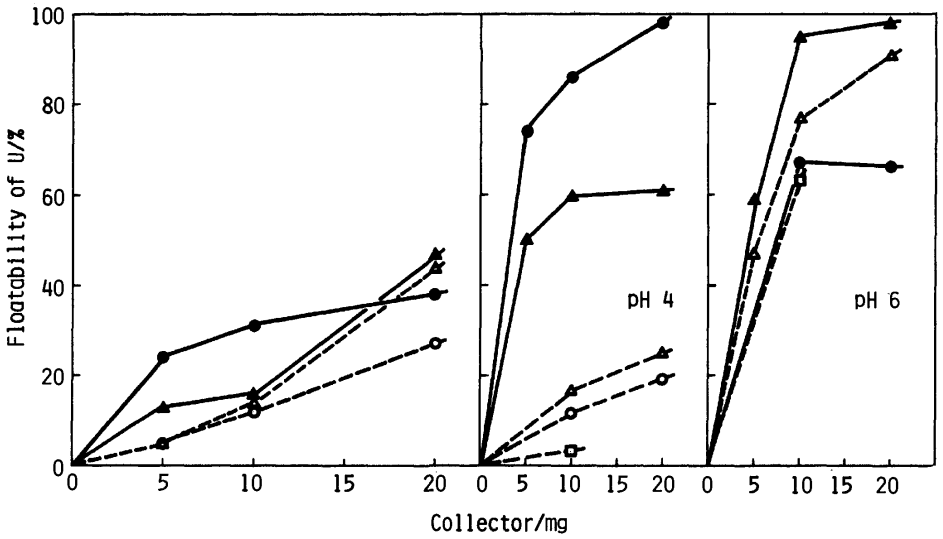

Fig. 6. Recovery of U from seawater.
Sample: 500 cm³ of seawater, and seawater adjusted to pH 4 and 6.
△: $R_{10}Hx$, ○: $R_{12}Hx$, □: $R_{14}Hx$, ▲: $R_{10}AHx$, ●: $R_{12}AHx$.

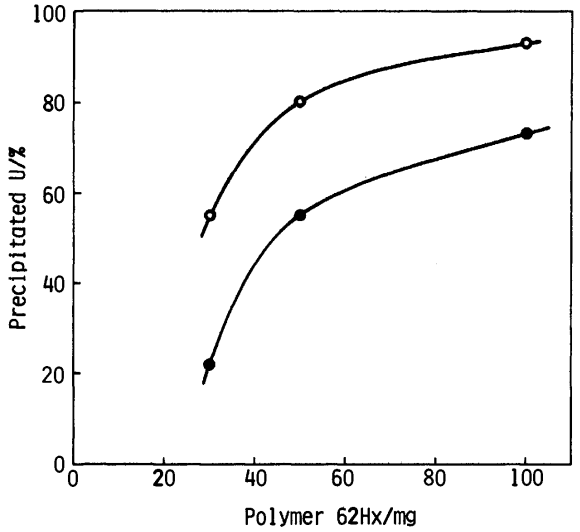

Fig. 7. Precipitated U with polymer 62Hx.
Seawater: 500 cm³. Precipitated U: Ratios of precipitated U to initial amount. Precipitated U was calcd from the differences between the initial and the final concns after the filtration of the resulting ppt(U-62Hx); ○: Dissolved the polymer 62Hx in a 50 cm³ of seawater on heating and then the hot seawater was added to a 450 cm³ of seawater with stirring: ●: Dispersed the fine particles of the polymer 62Hx into a 500 cm³ of seawater for 2 h with stirring.

differed considerably from these. The distribution of uranium complexes in Table 1 shows that most of them are carbonato species in pH 8—10. Therefore, the low floatability at pH 10 is probably due to the difficulty of the complex formation with the collectors. Therefore, the uranium flotation from natural seawater and seawater adjusted to pH 4 or 6 with HNO_3 was examined. The floatabilities depended on the R_nAHx and R_nHx concentrations, as is shown in Fig. 6. The flotation from natural seawater was not so effective, but the floatabilities in pH 4—6 were high. R_nAHx was far more effective than R_nHx was at pH 4, while it was only a little effective at pH 6. $R_{12}AHx$ became most effective because of its excellent chelating ability and the lower HLB value ($R_{16}AHx$ was slightly soluble in seawater).

Foam Fractionation Using Cotelomer-Type Surfactants. The uranium in an aqueous solution was floated by foam fractionation using the telomer (Lo9.0Hx)-nonionic surfactant.[6] In this section, the recoveries of uranium from seawater will be examined by depositing uranium ions with a polymer-bearing hydroxamic acid, 62Hx, and by foam fractionation using the cotelomer, Ls-VP-Q-Hx.

The polymer 62Hx was dissolved in 50 cm³ of seawater on heating, and the hot seawater was stirred into 450 cm³ of seawater. The other polymer, 62Hx, was dispersed in 500 cm³ of seawater for 2 h with stirring so that the uranium could be adsorbed to the 62Hx particles. After the filtration of the resulting 62Hx-uranium precipitate, the concentration of the uranium in the seawater was determined. The results are shown in Fig. 7. The affinity of the hydroxyaminocarbonyl group for uranium was evident. The recovery by the dissolution method using 62Hx was more effective than that by the dispersion method. However, the polymer precipitant was still difficult to keep in contact with the bulk solution and to collect from the solution.

Then, the foam fractionation of uranium from seawater was carried out by using Ls-VP-Q-Hx; the results are shown in Table 3, together with those obtained by using Lo-Hx, R_nAHx(ion flotation: the largest amounts of uranium floated was at 0.07 mg/g-$R_{12}AHx$), and R_nHx(ion flotation). The uranium in seawater was floated a little by foam fractionation

Table 3. Uranium Recovery from Seawater

Condition of flotation[a] Collector	mg	Uranium-floated Floatability %	Amount mg/g-collector
$R_{10}Hx$	5	5	0.02
$R_{12}Hx$	3	6	0.03
$R_{12}Hx$	5	5	0.02
$R_{12}Hx$	20	17	0.01
$R_{12}Hx$	30	34	0.02
$R_{14}Hx$	5	6	0.02
$R_{10}AHx$	5	13	0.04
$R_{12}AHx$	5	24	0.07
$R_{16}AHx$	5	10	0.03
$R_{10}Hx$	3+N[b]	5	0.01
Lo9.0Hx	3+N[b]	15	0.02
Lo10.3Hx	3+N[b]	9	0.01
Ls1.4VP7.2Hx	30	29	0.01
Ls0.8VP3.2Q1.6MA	30	0	0
Ls0.8VP3.2Q1.6Hx	20	62	0.05
Ls0.8VP3.2Q1.6Hx	30	81	0.04
Ls0.8VP3.2Q1.6Hx	40	64	0.02
Ls2.5VP3.9Q2.2Hx	20	30	0.02
Ls2.5VP3.9Q2.2Hx	30	63	0.03
Ls2.5VP3.9Q2.2Hx	40	45	0.02
Ls2.2VP8.8Q5.0Hx	30	73	0.04
Ls2.7VP5.0Q9.4Hx	30	80	0.04

a) 500 cm^3 of seawater. R_nHx, R_nAHx: Ion flotation. Lo-Hx, Ls-VP-Hx, Lo-VP-Q-Hx: Foam fractionation.
b) 10 mg of a nonionic surfactant (Nissan nonion O-6).

using the Lo9.0Hx and a nonionic surfactant. The cationic Ls-VP-Q-MA, quarternized for dissolving it into seawater, was expected to be useful as a foam-fractionation collector for the anionic uranyl carbonate. However, Ls0.8VP3.2Q1.6MA (unsubstituted by hydroxamic acid) was ineffective for the foam-fractionation of uranium. The hydroxamic acid derivatives (Ls-VP-Q-Hx) from the cationic Ls-VP-Q-MA made the uranium float highly; e.g., the floatabilities were 81% with 30 mg of Ls0.8VP3.2Q-1.6Hx and 80% with 30 mg of Ls2.7VP5.0Q9.4Hx. The HLB values of the cotelomer-type surfactants were calculated to be Lo9.0Hx 36, Lo10.3Hx 37, Ls1.4VP7.2Hx 23 (Hx/VP=1.4: the ratio of hydroxyaminocarbonyl groups to pyridyl groups), Ls0.8VP3.2Q1.6MA 11 (0), Ls0.8VP3.2Q1.6Hx 14 (1.6), Ls2.5VP3.9Q2.2Hx 14 (0.7), Ls2.2VP8.8Q5.0Hx 16 (1.8), and Ls2.7VP5.0Q-9.4Hx 19 (2.8). The HLB values for the effective Ls-VP-Q-Hx in foam fractionation were 14—19; these values were near to those in a previously reported foam-fractionation (HLB 21).[20] The ratio of hydroxyaminocarbonyl groups to pyridyl groups was also a cause of the variation in the floatability. The most useful ratios were 1—2.8, so that the complex formation based on the chelate effects between the two groups were considered. In addition to the chelate effects, the cationic Ls-VP-Q-Hx would be more favorable for the attraction of the anionic uranyl carbonate.

N-Methylhydroxamic Acid Derivatives. The hydroxamic acid derivatives are apt upon *N*-deprotonation on heating, to decompose to isocyanates or to amines in an aqueous solution.[21] Therefore, *N*-methylhydroxamic acid derivatives were prepared, and their resistance to decomposition was periodically examined in acidic and alkaline solutions. *N*-Methylhydroxamic acid derivatives, Ls5.6MHx and Ls3.2VP4.5MHx, were stable for a week at pH 1 and 12, whereas Ls-VP-Q-Hx in an alkaline solution of pH 12 decomposed within 20 h, as is shown in Fig. 8. Therefore, the foam fractionation of uranium was examined by using

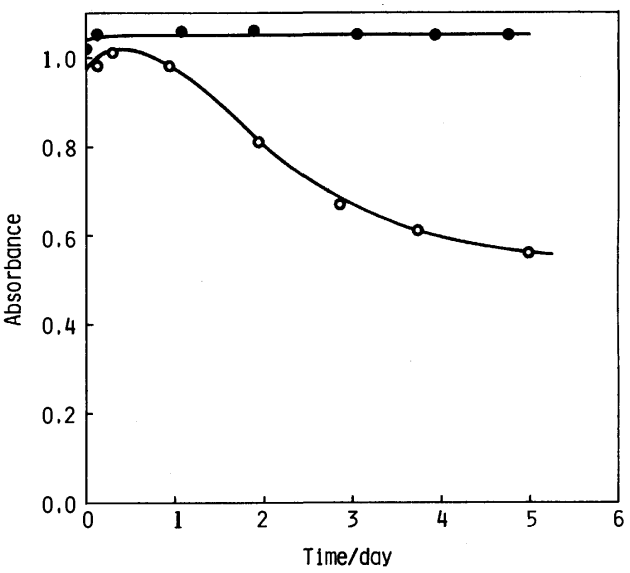

Fig. 8. Stability of hydroxamic acid derivatives at pH 12.
●: Ls3.2VP4.5MHx, ○: Ls2.5VP3.9Q2.2Hx.

Table 4. Foam Fractionation of Uranium by Using Ls-VP-MHx

Condition of flotation[a]		Uranium-floated	
Collector	mg	Floatability	Amount
		%	mg/g-collector
Ls5.6MHx	10	16	0.02
Ls5.6MHx	40	41	0.02
Ls3.2VP4.5MHx	10	27	0.04
Ls3.2VP4.5MHx	40	56	0.02

a) 500 cm^3 of seawater.

Ls5.6MHx and Ls3.2VP4.5MHx. The uranium floatabilities from seawater are shown in Table 4. Ls5.6MHx and Ls3.2VP4.5MHx showed the foam-fractionation effects on the uranium in seawater, the Ls3.2VP4.5MHx being more effective than the Ls5.6MHx. The high floatability is considered to be due to the chelate effects between the *N*-methylhydroxyaminocarbonyl and pyridyl groups and to the surface activities (HLB: Ls5.6MHx 21, Ls3.2VP4.5MHx 14).

Thus, the effects of the chelating surfactants bearing hydroxyaminocarbonyl and amino groups or hydroxyaminocarbonyl and pyridyl groups on uranium flo tation have been established as a result of one investigation.

The present authors are indebted to Mr. Kuniaki Jinnai for his help in the foam fractionation using cotelomer-type surfactants.

References

1) W. Kern and R. C. Schulz, *Angew. Chem.*, **69**, 153 (1957).

2) C. A. Fetscher, U. S. Patent, 3088798 (1963), 3088799 (1963); *Chem. Abstr.*, **59**, P 3642e (1963); H. Tani, H. Hakayama, and F. Sakamoto, Jpn. Patent, 134911 (1975); *Chem. Abstr.*, **84**, 93286v (1976); H. Egawa, H. Harada, and T. Shuto, *Nippon Kagaku Kaishi*, **1980**, 1773.

3) S. Hirono, M. Takesute, and T. Miyamatsu, Jpn. Patent, 7987622 (1979); *Chem. Abstr.*, **91**, P 178926y (1979).

4) J. Shibata, S. Nishimura, and S. Mukai, *Fusen*, **55**, 2 (1975).

5) T. Nozaki and H. Yamashita, *Nippon Kaisui Gakkaishi*, **40**, 95 (1986).

6) Y. Koide, H. Takamoto, K. Matsukawa, and K. Yamada, *Bull. Chem. Soc. Jpn.*, **56**, 3364 (1983).

7) C. D. Hurd and H. J. Brownstein, *J. Am. Chem. Soc.*, **47**, 176 (1925).

8) Y. Koide, K. Izumi, K. Okuzono, and K. Yamada, *Nippon Kagaku Kaishi*, **1980**, 742.

9) Y. Koide, Y. Eda, and K. Yamada, *Bull. Chem. Soc. Jpn.*, **59**, 2963 (1986).

10) M. Narita, T. Teramoto, and M. Okawara, *Bull. Chem. Soc. Jpn.*, **45**, 3149 (1972).

11) A. H. Blatt, *Org. Synth.*, Coll. Vol. II, 67 (1943).

12) A. W. Scott and B. L. Wood, *J. Org. Chem.*, **7**, 508 (1942).

13) K. Motojima, T. Yamamoto, and Y. Kato, *Bunseki Kagaku*, **18**, 208 (1969).

14) S. A. Abbasi and J. Ahmed, *Bull. Chem. Soc. Jpn.*, **49**, 2013 (1976).

15) R. J. Motekaitis, I. Murase, and A. E. Martell, *J. Coord. Chem.*, **1**, 77 (1971).

16) K. Yamada, T. Kihara, H. Yamaguchi, and T. D. Chie, *Yukagaku*, **25**, 347 (1976).

17) N. K. Dutt and T. Seshadri, *J. Inorg. Nucl. Chem.*, **31**, 2153 (1969).

18) N. Ogata, N. Inoue, and H. Kakihara, *J. At. Energy Soc. Jpn.*, **13**, 560 (1971); H. Yamashita, Y. Ozawa, and F. Nakajima, *Bull. Chem. Soc. Jpn.*, **53**, 1 (1980).

19) R. Oda and K. Teramura, "Kaimen-kasseizai No Gosei To Sonooyo," Makishoten, Tokyo (1962), p. 501.

20) Y. Koide, S. Sato, and K. Yamada, *Bull. Chem. Soc. Jpn.*, **59**, 715 (1986).

21) R. Alexander, "Principles of Ionic Organic Reactions," John Wiley & Sons, New York and London (1950), p. 77.

 © 1987 The Chemical Society of Japan Bull. Chem. Soc. Jpn., 60, 3485—3489 (1987)

An NMR Study of Phenyl- and Diphenylphosphine Alkali Metal Salts

Yukihiro YOKOYAMA and Kensuke TAKAHASHI*
Department of Applied Chemistry, Nagoya Institute of Technology,
Gokiso-cho, Showa-ku, Nagoya 466
(Received February 25, 1987)

The ^{1}H, ^{13}C, and ^{31}P NMR spectra were observed for the title salts in several solvents. The formation of the salts by the deprotonation of the neutral precursors causes significant changes in their NMR parameters. First, the delocalization of the excess charges into the phenyl ring of the salts was confirmed from the ^{1}H and ^{13}C chemical-shift data. Second, the parameters concerned with the center of the anions are dependent on the circumstances of the center atom, phosphorus, such as the hybridization. The results are discussed in terms of the effects of the counter cations and the solvents. Third, a strong polar solvent, HMPA, exerts significant effects on the chemical shifts and the one-bond ^{13}C-^{31}P coupling constants. These parameter changes are explained in terms of an equilibrium between two kinds of ion-pairs (contact ion-pairs and solvent-separated ion-pairs). The parameters obtained in this solvent, HMPA, correspond to those of the solvent-separated ion-pairs or the free anions.

The NMR technique is a useful and efficient technique for investigating many aspects of the anionic species of organic compounds in solutions. Among such species, the carbanions are the most investigated species; they have a carbon atom as an anionic center.[1,2] Recently, there have appeared several articles concerned with the anionic species with heteroatoms as anionic centers.[3,4] However, there has not yet been sufficient discussion on the accumulation of enough data about the problems of these anions, such as their structures, electron distributions, bondings, and counter cations.

In this article we wish to report our measurements of the ^{1}H, ^{13}C, and ^{31}P chemical shifts for the anionic species produced from phenyl- and diphenylphosphines, whose sodium salts were reported previously.[3a] The results are discussed in terms of the structures of the anions, solvents, and counter cations, and the temperature.

Experimental

The phenylphosphine and chlorodiphenylphosphine used as starting materials were commercially available and were used without further purification. These starting materials were dried and distilled over calcium hydride, and then degassed and stored in sealed vessels with a break seal.

The tetrahydrofuran (THF), 1,2-dimethoxyethane (DME), and 2-methyltetrahydrofuran (2MTHF) were refluxed and distilled over sodium metal and then stored over sodium-potassium alloy. The hexamethylphosphoric triamide (HMPA) and tetrahydrofuran-d_8 (THF-d_8) were dried and distilled over calcium hydride, and then degassed and stored in sealed vessels with a break seal.

The phenylphosphine was allowed to react with butyllithium in hexane under a vacuum. Then, after all volatile materials had been distilled off in a vacuum, the residue was dissolved in a solvent (THF, DME, 2MTHF, HMPA, or THF-d_8). The solution of the resulting lithium salt was filtered into an NMR tube, which was then sealed under a vacuum.

Diphenylphosphine alkali metal salts were generated from chlorodiphenylphosphine by means of a halogen-metal exchange reaction. The reaction was carried out so that the starting material was in contact with lithium, sodium, or potassium metal flakes in a solvent at room temperature in a reaction vessel under a vacuum. The solution was kept in the vessel with stirring for a day for the reaction to be completed. Then, the resulting solution was filtered into an NMR tube, which was then sealed under a vacuum. All the NMR samples were prepared as approximately 1M solutions sealed in 5- or 10-mm o.d. tubes.

All the NMR spectra were measured on a Varian XL-200 Fourier transform spectrometer at the ambient temperature (ca. 25 °C). The ^{1}H and ^{13}C chemical shifts were referred to the more (or most) shielded peaks of the solvents, and then converted to the values from TMS by taking 1.79 and 26.40 (or 1.75 and 25.40) for δ_H and δ_C of THF(or THF-d_8), and 21.20, 37.00, and 58.80 for δ_C of 2MTHF, HMPA, and DME respectively. The ^{31}P chemical shifts were measured externally relative to a 1 wt% H_3PO_4 solution dissolved in D_2O.

Results and Discussion

^{1}H Chemical Shifts. The ^{1}H chemical-shift data for the compounds measured in THF-d_8 are summarized in Table 1, together with the citation numbers of the compounds. The ^{1}H chemical shifts of the anionic

Table 1. ^{1}H Chemical Shifts of Phenyl- and Diphenylphosphines and Their Anions in ppm[a)]

No.	Compound	P-H	H-2	H-3	H-4
1	$PhPH_2$	3.97	7.51	7.28[b)]	7.28[b)]
1a	PhPHLi	2.13	7.09	6.56	6.27
1b	PhPHNa[c)]	2.23	7.16	6.58	6.29
2	Ph_2PH	5.24	7.51	7.31[b)]	7.31[b)]
2a	Ph_2PLi	—	7.46	6.79	6.50
2b	Ph_2PNa	—	7.53	6.84	6.57
2c	Ph_2PK	—	7.48	6.80	6.48

a) Chemical shifts are measured for ca. 1M (1M=1 mol dm^{-3}) solutions in THF-d_8 relative to the more shielded residual solvent peak, which is taken as 1.75 ppm from TMS. b) The values are not determined precisely because of the signal overlapping. c) The values are cited from Ref. 3a.

compounds from **1a** to **2c** are more shielded than those of the corresponding neutral molecules, **1** and **2**, except that the ortho-proton shifts of the diphenylphosphine alkali metal salts are slightly deshielded. The shift changes of the P-H protons from phenylphosphines to their anionic molecules are ca. 1.7 ppm because of an increased shielding caused by the negative charge on the phosphorus atom. There is a small but significant downfield shift of the P-H proton on going from **1a** to **1b** (0.10 ppm), in accord with a greater charge density in this position in the former species.

The changes in the ^{1}H chemical shifts of the phenyl-ring protons are in the ranges from −0.42 to 0.02, from −0.72 to −0.47, and from −1.01 to −0.83 ppm for the ortho, meta, and para protons respectively. The ring-proton shifts are influenced by various factors. The ortho-proton shift is affected by inductive, resonance, magnetic anisotropy, and electric-field effects from the phosphorus atom as an anionic center. These effects, however, are much smaller for the meta-proton shift, and probably only the resonance effect is important for the para proton shift.[5] This is why the upfield shifts of the para-protons are regarded as a rough estimation of the charge delocalization.

The reason that the ortho-proton shifts have smaller changes than those expected from the resonance effect of the substituent is presumably attributable to some electronic effects caused by the excess charge and the lone-pair electrons on the phosphorus atom.

^{13}C Chemical Shifts. The ^{13}C chemical-shift data for the compounds studied in several solvents are presented in Table 2. The general trends that are apparent in the table are as follows: The formation of the anion species from the corresponding neutral molecules causes the ipso carbon to be significantly deshielded (21 to 42 ppm) and the para carbon to be shielded (9 to 18 ppm), while the ortho and meta carbons show small upfield shifts (2 to 7 ppm).

Table 2. ^{13}C Chemical Shifts of Phenyl- and Diphenylphosphines and Their Alkali Metal Salts in ppm[a]

No.	Compound	Solvent	C-1	C-2	C-3	C-4
1	$PhPH_2$	THF	129.21	135.33	129.15	128.79
		HMPA	128.34	135.01	129.22	128.82
1a	PhPHLi	2MTHF	158.05	130.27	126.57	117.70
		DME	161.05	130.06	126.87	116.74
		THF	161.63	129.91	126.80	116.53
		HMPA	170.31	127.84	125.50	110.58
1b	PhPHNa[b]	THF	159.98	130.18	127.15	117.28
2	Ph_2PH	THF-d_8	135.96	134.77	129.28	129.45
		HMPA	135.05	134.27	129.20	129.37
2a	Ph_2PLi	2MTHF	153.92	130.98	127.04	120.11
		THF	157.03	130.55	127.27	119.24
		HMPA	161.45	128.31	126.37	115.70
2b	Ph_2PNa	2MTHF	153.96	130.68	127.44	120.32
		DME	158.29	129.55	127.10	118.21
		THF	156.15	130.55	127.61	119.75
		HMPA	161.71	128.46	126.25	115.53
2c	Ph_2PK	2MTHF	155.02	130.14	127.53	119.78
		DME	159.20	129.02	127.31	117.76
		THF	158.40	129.49	127.76	118.63
		HMPA	161.70	128.50	126.37	115.64

a) Chemical shifts are measured for ca. 1M solutions relative to the more or most shielded peak of the solvent used. See text. b) The values are cited from Ref. 3a.

The ipso-carbon resonances shift clearly towards the downfield direction, contrary to what would be expected from the excess charge delocalization into the phenyl rings, corresponding to a decrease in the electron density at that position. However, such downfield shifts are observed as a general trend for monosubstituted benzenes, in which the substituent is an anionic center, like phenylmethyl carbanions and so on.[3,4,6,7]

The ortho-carbon shifts are affected by various factors because their position is near, second only to the ipso position, to the substituent. However, the ortho- and meta-carbon shifts are indeed of similar magnitudes. This is also a characteristic feature of these anions.[3,4]

It has been considered that para-carbon chemical shifts provide a good measure of charge delocalization, just as para-proton shifts do. It is found that the changes in the para-carbon shifts in the anions produced from **1** and **2** are slightly smaller than those of the phenylmethyl carbanions,[7] but there are significant upfield shifts. Therefore, these upfield shifts show that the degree of charge delocalization into the phenyl ring is relatively large.

^{31}P Chemical Shifts. The ^{31}P NMR data for the compounds studied in several solvents are summarized in Table 3. The trends of the ^{31}P chemical shifts are in agreement with the previously published data.[3a] It is known that the formation of the anions from PH_3 causes the phosphorus atoms to be shielded (16 to 58 ppm).[3a] This is in agreement with the general tendency for the increase in the electron density to result in more shielding on an atom. However, the ^{31}P chemical-shift changes of the anions in Table 3 are in the direction opposite to that expected from the increasing electron density on the phosphorus atoms (5 to 36 ppm downfield shifts).

Batchlor and Birchall have mentioned that the downfield shifts of the phenyl- and diphenylphosphines upon deprotonation might be attributed to a $p\pi$-$p\pi$ interaction between the phenyl ring and the phosphorus atom.[3a] However, such downfield shifts have been observed for the carbons in some carbanions due to the rehybridization of the α-carbon atom.[7] Considering the changes in the ^{31}P-^{13}C coupling constants that will be mentioned later, it seems that the effects of rehybridization (resulting in downfield shifts) and electron density (resulting in upfield shifts) play significant roles in the ^{31}P shifts.

It is found that the solvents with a stronger polarity result in more downfield ^{31}P chemical shifts of the anions as well as more ^{13}C chemical shifts of the

Table 3. ^{31}P Chemical Shifts(ppm) and Coupling Constants(Hz) of Phenyl- and Diphenylphosphines and Their Anions

No.	Compound	Solvent	δ_P	$^1J_{PC}$	$^2J_{PC}$	$^3J_{PC}$	$^1J_{PH}$
1	$PhPH_2$	THF	−125.7	10	15	6	199
		HMPA	−124.1	7	15	6	200
1a	PhPHLi	2MTHF	−114.3	37	14	5	172
		DME	−111.9	44	16	5	162
		THF	−112.6	43	16	4	163
		HMPA	−74.9	59	18	5	144
1b	PhPHNa[a]	THF	−120.9	44	16	6	162
2	Ph_2PH	THF-d_8	−41.1	11	17	5	216
		HMPA	−40.9	10	17	5	218
2a	Ph_2PLi	2MTHF	−26.2	34	17	6	—
		THF	−20.2	44	18	6	—
		HMPA	5.0	60	20	4	—
2b	Ph_2PNa	2MTHF	−29.2	40	17	6	—
		DME	−12.5	50	20	—	—
		THF	−23.2	45	18	5	—
		HMPA	5.3	63	20	5	—
2c	Ph_2PK	2MTHF	−23.0	44	18	5	—
		DME	−7.6	55	19	5	—
		THF	−10.0	55	18	4	—
		HMPA	5.0	60	20	5	—

a) The values are cited from Ref. 3a.

anions. The ^{31}P chemical shifts of the anions in HMPA are ca.30 to 40 ppm more deshielded than those of the same anions in 2MTHF, whereas the neutral molecules have similar chemical shifts in several solvents.

^{31}P-^{13}C and ^{31}P-^1H Coupling Constants. The phosphorus-carbon and phosphorus-proton coupling constants are summarized in Table 3. It may be pointed out that the values of $^1J_{PC}$ of the anions (34—63 Hz) are significantly larger than those of the neutral molecules (7—12 Hz) and that the solvents with a stronger polarity result in larger values in the $^1J_{PC}$ of the anions. It has been known that the $^1J_{PC}$ are very sensitive to the hybridization of the phosphorus atom and the substituents attached to the atom.[8] The change in the $^1J_{PC}$ of the anions, therefore, may be attributed to the rehybridization of the phosphorus atom in the anions.

On the other hand, the values of $^2J_{PC}$ and $^3J_{PC}$ of the anions are almost like the values of the neutral molecules. The effects of both the counter cations and the solvents scarcely influence the two- and three-bond phosphorus-carbon coupling constants.

The trend of the change in the one-bond phosphorus-proton coupling constants is in agreement with the previously reported values for sodium salts.[3a] That is, it is found that the magnitude of $^1J_{PH}$ of the anions (144—172 Hz) is significantly smaller than that of the neutral molecule (ca. 200 Hz). If the signs of the $^1J_{PH}$ are considered to be positive, as has been reported for other systems,[8] the reduction of the $^1J_{PH}$ in the salts corresponds to a decrease in the s character of the hybridized orbital directed to the hydrogen from the phosphorus atom in the salts as compared with that in **1** or **2**. Further, the increase in the magnitude of the $^1J_{PC}$ in the salts corresponds to the greater conjugation between the p-π orbitals of the two atoms forming the P-C bond as compared with those of the phenylphosphines, **1** and **2**. Additionally, the signs of the $^1J_{PC}$ of several alkylphosphines were noted to be the opposite of those of their phosphonium salts.[8] Therefore, studies along this line are in progress for several related phosphines and their salts.

It is of interest to point out that the solvents with a stronger polarity result in smaller values of the $^1J_{PH}$ of the anions. The changes in $^1J_{PH}$ are clearly towards the direction opposite to those of $^1J_{PC}$; therefore, the sum of the $^1J_{PH}$ and $^1J_{PC}$ is approximately constant in each species, although the reasons for this are not well understood.

Counter-Cation and Solvent Effects on NMR Parameters. The ^1H chemical shifts of P-H and ortho protons for the phenylphosphine alkali metal salts are slightly affected by the counter cation, but the ring-proton shifts of the anions produced from diphenylphosphines are scarcely affected by the cation, except for the shifts of the sodium salt, which behave differently from the lithium and potassium salts. The counter-cation effects on the carbon and phosphorus chemical shifts are illustrated schematically in Figs. 1 and 2 respectively. According to the variation in the cations from lithium to potassium, the resonance lines of the ipso-carbon and phosphorus atoms move downfield, while the lines of the para-carbons move upfield. However, the ortho and meta carbons scarcely shift at all. These trends can be explained by the fact that carbon and phosphorus chemical shifts show differences, accompanied by changes in the cation size, that reflect the electron-distribution changes in the ion-pairs, like those observed for phenylmethyl carban-

ions.[6,7] However, the chemical shifts of the ipso carbon and phosphorus atoms of the sodium salts behave curiously, unlike the general expected trend, as is shown in Figs. 1 and 2. For example, the ^{31}P chemical shifts of the sodium salts **2b** are the most shielded among the three salts, **2a**—**c**. Especially, the characteristic feature of the sodium salts is significant in moderately polar solvents, such as 2MTHF and THF. Therefore, it seems that this phenomenon is connected with an equilibrium between contact ion-pairs and solvent-separated ion-pairs in the anionic solutions. In more polar solvents such as HMPA, therefore, the counter cations do not affect the chemical shifts, because in such solvents the ion-pairs exist only a form of solvent-separated ion-pairs or free ions. It must be noted that the chemical shifts measured in HMPA are quite different from those measured in THF, which is mostly used in carbanion chemistry.[6] Therefore, it is recommended to use HMPA as a solvent for obtaining the chemical-shift values for the solvent-separated ion-pairs in the ion-pair equilibrium. Further, such solvent effects are not observed in the chemical shifts of the neutral molecules, **1** and **2**.

One of the molecular theoretical parameters that gives the degree of solvation consists of Gutmann's donor and acceptor numbers (DN and AN).[9] In view of the concepts of DN and AN, the different behavior of the sodium salts can be explained by saying that, in solvents with a medium DN (20) value, such as 2MTHF and THF, the sodium ion is solvated less than the lithium one because of its smaller AN. Therefore, the sodium salts have an equilibrium with more contact ion-pairs in the ion-pair equilibrium. Therefore, the negative charge is localized more on the anionic-center atom. Therefore, the ^{31}P chemical shifts of **2b** tend to shift towards a more shielded direction than those of the other salts, **2a** and **2c**. Further, the slightly smaller changes in the C_i and C_p chemical shifts of **2b** show that the delocalization of the excess charges into the phenyl ring is less than those of **2a** and **2c**. The solvent effects on the ^{13}C chemical shifts of **1a** are given in Fig. 3. The solvent effects for the shifts of these salts are larger than their counter cation effects. The former effects increase in the order of 2MTHF,DME,THF, and HMPA. As may be seen in Tables 2 and 3, however, the effects for the salts from **2a** to **2c** increase in a slightly different order. The order of DME≳THF>2MTHF is consistent with that found for the alkali

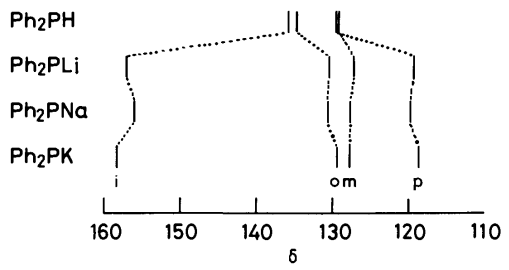

Fig. 1. Schematic diagram of phenyl-^{13}C chemical shifts: Ph=phenyl; i=ipso; o=ortho; m=meta; p=para.

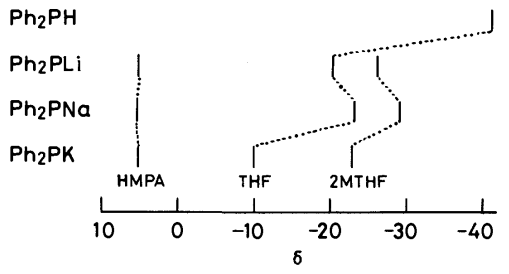

Fig. 2. Schematic diagram of ^{31}P chemical shifts in different solvents and counter cations.

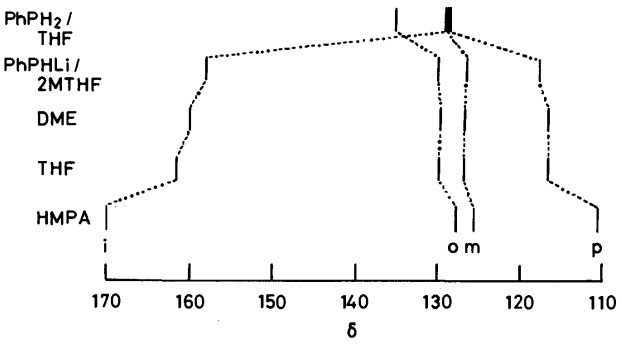

Fig. 3. Schematic diagram of phenyl-^{13}C chemical shifts of **1** and **1a** in four different solvents.

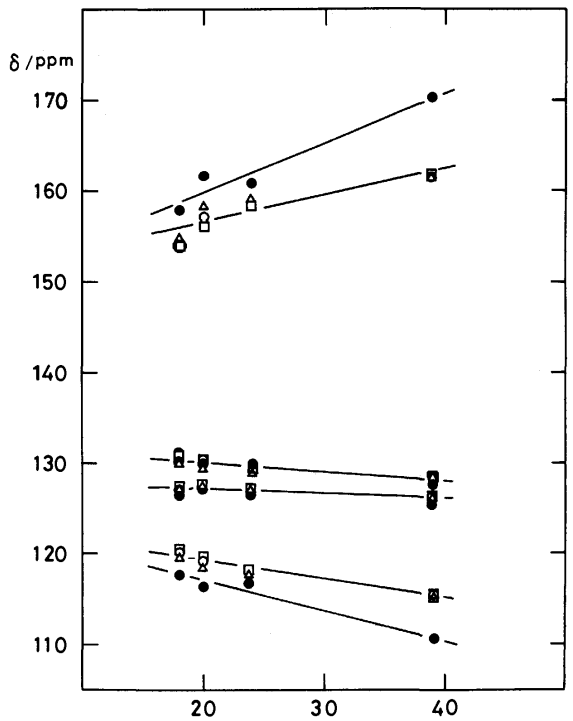

Fig. 4. Plot of phenyl-^{13}C chemical shifts in ppm (ordinate) vs. the DN values of the solvents, which are 18, 20, 24, and 39 for 2MTHF, THF, DME, and HMPA respectively (Ref. 9) (abscissa): **1a**; ●, **2a**; ○, **2b**; □, **2c**; △.

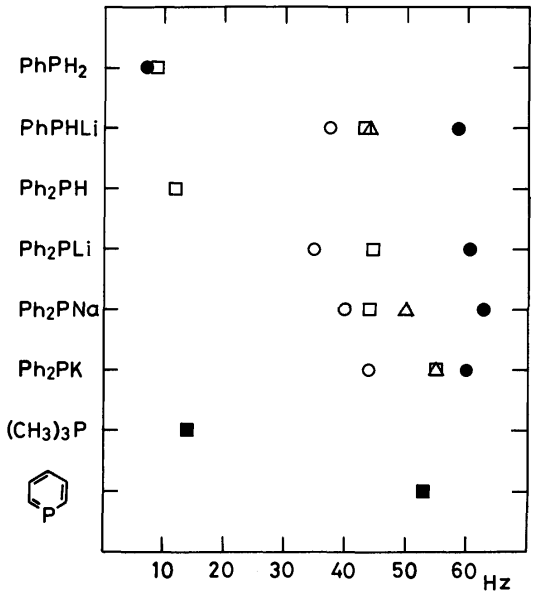

Fig. 5. Schematic diagram of one-bond carbon-phosphorus coupling constants in Hz observed in different solvents: 2MTHF; ○, THF; □, DME; △, HMPA; ●, neat; ■.

metal salts of diphenylmethane.[6] O'Brien et al. stated several reasons for the solvent effects. Their explanation is essentially the same as the concepts of DN and AN. The correlation between such DN and the ^{13}C chemical shifts in several solvents is shown in Fig .4. This shows that the ^{13}C chemical shifts largely reflect the equilibrium between two kinds of ion-pairs. On the other hand, the ^{31}P chemical shifts are not correlated with such DN. This may be because the ^{31}P chemical shifts are not affected by only ion-pair equilibrium, but also by polarization as an anionic center and by rehybridization.

The solvent and counter-cation effects for the $^1J(^{13}C-^{31}P)$ are given in Fig. 5. In the cases of **1** and **2** the coupling constants have a magnitude of about 10 Hz, similar to that of trimethylphosphine. On the other hand, for the alkali metal salts the values tend to increase to a magnitude of about 50 Hz, although their signs were not determined. These values are similar to that of phospharine.[10] The changes in the values are the largest for **2a** (34 to 60) and the least for **2c** (44 to 60 Hz). Further, the effect of the counter cations appears with the largest range in 2MTHF and the least in HMPA. Perhaps the value of 60 Hz is characteristic of the anionic species of **2**. The change in the $^1J_{PC}$ values is affected by the equilibrium between the contact ion-pairs and solvent-separated ion-pairs. The hybridization of the phosphorus atom as an anionic center is similar to that of phospharine.

Recently, two research groups have reported that **2a** exists in a dimeric state in ether at a lower temperature or in a polymeric state in the solid crystal with a covalent bonding between the phosphorus atom and the counter cation.[11,12]

No splitting of the ^7Li NMR signal of **2a** was observed in a THF solution in the temperature range from 25 to −110 °C, although the signal moved slightly upfield (0.4 ppm). This may be considered to indicate that the nature of the bonding between phosphorus and lithium atoms of **2a** is essentially ionic or that there exists some other mechanism of signal narrowing in **2a**.

References

1) R. N. Young, *Progr. Nucl. Magn. Reson. Spectrosc.*, **12**, 261 (1979).

2) D. H. O'Brien, "Comprehensive Carbanion Chemistry," ed by E. Buncel and T. Durst, Elsevier, New York (1980), pp. 271—322.

3) a) R. Batchlor and T. Birchall, *J. Am. Chem. Soc.*, **104**, 674 (1982); b) *ibid*, **105**, 3848 (1983).

4) E. Buncel, T. K. Venkatachalam, B. Eliasson, and U. Edlund, *J. Am. Chem. Soc.*, **107**, 303 (1985).

5) H. Spiesecke and W. G. Schneider, *J. Chem. Phys.*, **35**, 731 (1961).

6) D. H. O'Brien, C. R. Russell, and A. J. Hart, *J. Am. Chem. Soc.*, **98**, 7427 (1976); *ibid.*, **101**, 633 (1979).

7) K. Takahashi, Y. Kondo, R. Asami, and Y. Inoue, *Org. Magn. Reson.*, **6**, 580 (1974); K. Takahashi, Y. Kondo, and R. Asami, *J. Chem. Soc., Perkin Trans. 2*, **1978**, 577.

8) G. Mavel, "Annual Reports on NMR Spectrscopy," ed by E. F. Mooney, Academic Press, London (1973), Vol.5B, p. 68.

9) V. Gutmann, "The Donor-Acceptor Approach to Molecular Interactions," Plenum Press, New York (1978).

10) A. J. Ashe, III, R. R. Sharp, and J. W. Tolan, *J. Am. Chem. Soc.*, **98**, 5451 (1976).

11) I. J. Colquhoun, H. Christina, E. McFarlane, and W. McFarlane, *J. Chem. Soc., Chem. Commun.*, **1982**, 220.

12) R. A. Bartlett, M. M. Olmstead, and P. P. Power, *Inorg. Chem.*, **25**, 1243 (1986).

 © 1987 The Chemical Society of Japan Bull. Chem. Soc. Jpn., 60, 3491—3497 (1987)

An Ab Initio Molecular Orbital Study on Infrared Absorption Spectrum of ν_1 Vibration in Chloroform Vapor

Tomoaki HAYANO,* Hisao TAKEUCHI,† and Tomoo MIYAZAKI
Department of Applied Chemistry, Faculty of Science and Engineering, Waseda University, Ohkubo Shinjuku-ku, Tokyo 160
†Mitsubishi Chemical Industry, Kamoshida-cho Midori-ku, Yokohama-shi 227
(Received February 25, 1987)

The infrared absorption frequency and intensity of the ν_1 vibration, referring to the C-H stretching of chloroform vapor, have been calculated from the theoretical potential energy and dipole-moment functions determined by an ab initio molecular orbital calculation. The selection effect of a Gaussian basis set in the ab initio MO method on the calculated frequency and intensity has been studied. It has been pointed out that the theoretical dipole-moment function is sensitive to a slight displacement of the chlorine in the ν_1 vibrational mode.

In two earlier papers,[1,2] the abnormal absorption intensity of the ν_1 vibration band in chloroform vapor was discussed on the basis of results calculated by the semi-empirical molecular orbital (MO) method (CNDO/2).[3] From the result it was confirmed that the abnormal absorption intensity of the C-H stretching vibration band in chloroform vapor arises from the electrical properties of a vibrating bond and that the 3d orbitals on chlorine play an important role in determining the molecular properties by the CNDO/2 method.

In the previous study we assumed that the normal mode of ν_1 vibration is approximately equivalent to the pure C-H stretching mode. Since the mass of chlorine is much heavier than those of other atoms, it seemed reasonable to assume that a slight displacement of the chlorine in the ν_1 vibration is negligible. From the results of a recent preliminary investigation, however, it was found that the theoretical infrared absorption intensity is affected by a slight displacement of the chlorine in the ν_1 vibration. Then, by employing an ab initio MO calculation, the effects of this approximation for the ν_1 vibrational mode on the theoretical potential energy and dipole-moment functions are discussed in detail. Also, the infrared absorption frequencies and intensities of the fundamental and first overtone of the ν_1 vibration, calculated on the basis of these functions, are compared with the experimental values. In an effort to determine the selection effect of the basis set in the ab initio MO method on the theoretical frequency and intensity, the results calculated from five kinds of Gaussian basis sets are compared with one another.

Computational Procedure

All ab initio MO calculations were performed by employing the Gaussian 80 program provided by the QCPE, and HITAC M-680H system of the Computer Center in the University of Tokyo.

The theoretical equilibrium geometry of chloroform has been determined by the use of an energy gradient method. The basis sets employed in this work are the 4-31G, 4-31G*, 6-31G*,[4] 6-31G**[4] and Dunning contraction to [6s4p/4s2p/2s] basis[5,6] from the Huzinaga (11s7p/9s5p/4s) primitive set,[7,8] augmented by a set of d-type polarization functions on carbon and chlorine. For the exponent of the polarization function, the values recorded in the Gaussian 80 program were adopted, except for the cases described below. The exponent values of chlorine in 4-31G* (0.47) and the Huzinaga-Dunning (0.65) basis sets were evaluated on the condition of minimizing the total energy at the equilibrium structure, determined without the polarization function in question, the exponent of carbon in the latter case following the value (0.75) adopted by Kato.[11] For the exponent of the chlorine polarization function in 6-31G* and 6-31G**, the value (0.70) selected by Pople et al. was employed.[9,10]

The quadratic force constants with respect to the internal symmetry coordinates were evaluated by a numerical second differentiation of the potential energy of chloroform. By using these force constants, a normal coordinate analysis could be carried out with the Wilson's GF matrix method.[12] In the next step, the derivatives of the detailed potential energy function, $V(Q)$, with respect to the normal coordinate Q_1 were determined from the increment of total energy of the molecule distorted along the normal mode in question. The derivatives of another potential energy function, $V'(Q)$, were obtained in the same way, except that the molecule was distorted under a local-mode approximation: the normal mode ν_1 is equal to the C-H stretching mode. These two types of potential energy functions, $V(Q)$ and $V'(Q)$, have been determined by calculations with five kinds of basis sets.

From the same treatment, the derivatives of the dipole-moment functions, $\mu^z(Q)$ and $\mu^{z\prime}(Q)$, with respect to the normal coordinate Q_1 were determined from the variation of the dipole moment calculated under the two types of vibrational modes, i.e. the normal mode and the local mode. In determining these potential energy and dipole-moment functions, the cross terms between normal coordinates were neglected. By the use of these potential energy functions, the variation method has been adopted in order to obtain the vibrational energy levels in view of the mechanical anhar-

monicity of the vibration.[13] The wave functions, ψ_i, of the molecular vibration were described as a linear combination of the harmonic oscillator wave functions, ϕ_k. By employing the vibrational wave function, ψ_i, and the dipole-moment function, $\mu^z(Q)$, the infrared absorption intensities of the fundamental and first overtone with respect to the ν_1 vibration have been determined in view of the mechanical and electrical

Table 1. Equilibrium Geometries, Dipole Moments, and Total Energies of Chloroform with Various Basis Sets

Property	Basis set					Ref.[b]	Obsd	
	4-31G	4-31G*	6-31G*	6-31G**	Huz-Dun[a]			
Geometric Parameter								
r_{CH}/Å[c]	1.06561	1.06809	1.07124	1.07247	1.07124	1.069	1.073[d]	1.100[e]
r_{CCl}/Å	1.83256	1.78324	1.76205	1.76185	1.76420	1.788	1.762	1.758
θ_{HCCl}/°	108.240	107.995	107.732	107.766	107.648	108.0	108.5	107.5
Dipole moment /Debye[f]	1.734	1.330	1.303	1.313	1.282		1.01[g]	1.20[h]
Total energy[i]/au[j]	−0.322	−0.421	−0.502	−0.503	−1.852			

a) Dunning contractions to the [6s4p/4s2p/2s] basis from Huzinaga's (11s7p/9s5p/4s) primitive set augmented with a set of d-polarization functions on both carbon and chlorine atoms. b) From Ref. 11. c) 1 Å=10^{-10} m. d) From Ref. 14. e) From Ref. 19. f) 1 Debye=3.335641×10^{-30} Cm. g) From Ref. 20. h) From Ref. 21. i) 1415 au was added to all total energies. j) 1 au=4.359814×10^{-18} J.

Table 2. Force Constants for Internal Symmetry Coordinates Calculated by Various Basis Sets

Force constant[b]	Basis set			Ref.[a]
	6-31G*	6-31G**	Huz-Dun	
F_{11}/mdyn Å^{-1}	6.6940	6.2358	6.4447	5.0335
F_{12}/mdyn Å^{-1}	−0.0036	0.1220	0.1027	0.1301
F_{13}/mdyn	0.1327	0.0008	−0.0132	0.0067
F_{22}/mdyn Å^{-1}	4.8734	4.9044	4.9469	4.3249
F_{23}/mdyn	−0.3196	−0.2758	−0.3174	0.2651
F_{33}/mdyn Å	1.3538	1.2692	1.3991	1.1245

a) From Ref. 15. b) 1 mdyn Å^{-1}=10^2 N m^{-1}, 1 mdyn=10^{-8} N, 1 mdyn Å=10^{-18} N m. F_{11} is the force constant for the C-H stretching, F_{22} for the symmetric C-Cl stretching and F_{33} for the symmetric H-C-Cl bending.

Table 3. Displacements of Atoms per Unit of Normal Coordinate, Q_1, referring to the C-H Stretching Mode (ΔR/Å, Q/amu$^{1/2}$Å)[b]

Atom		4-31G	6-31G*	6-31G**	Huz-Dun	Ref.[c]
C	Δx	0.0	0.0	0.0	0.0	0.0
	Δy	0.0	0.0	0.0	0.0	0.0
	Δz	−0.082456	−0.080994	−0.082563	−0.082821	−0.083342
H	Δx	0.0	0.0	0.0	0.0	0.0
	Δy	0.0	0.0	0.0	0.0	0.0
	Δz	0.954496	0.955982	0.954388	0.954134	0.953590
Cl_1	Δx	0.000125	−0.000225	0.000032	−0.000045	−0.000086
	Δy	−0.000215	−0.000087	−0.000019	−0.000077	−0.000149
	Δz	0.000266	0.000390	0.000276	0.000311	0.000374
Cl_2	Δx	0.000125	−0.000225	0.000032	−0.000045	−0.000086
	Δy	0.000215	0.000087	0.000019	0.000077	0.000149
	Δz	0.000266	0.000390	0.000276	0.000311	0.000374
Cl_3	Δx	−0.000250	0.000450	−0.000064	0.000089	0.000172
	Δy	0.0	0.0	0.0	0.0	0.0
	Δz	0.000266	0.000390	0.000276	0.000311	0.000374

a) The C-H bond is placed along the Z axis. b) 1 amu=1.660565×10^{-27} kg. c) The normal coordinates analysis was carried out using the force constant set in Ref. 15 at the experimental geometry in Ref. 14.

Table 4. Derivatives of Potential Energy Function[a)]
$V(Q)=1/2\lambda Q^2+gQ^3+hQ^4+iQ^5$, ($V$/g cm^2 s^{-2}, Q/g$^{1/2}$ cm)

Derivative	4-31G	4-31G*	6-31G*	6-31G**	Huz-Dun
$1/2\lambda/10^{29}$	2.09771	2.03375	2.04217	2.00619	2.08426
	(2.09482)	(2.06325)	(2.03701)	(2.00478)	(2.08345)
$g/10^{49}$	−3.34090	−3.25388	−3.20363	−3.11932	−3.22587
	(−3.41561)	(−3.27515)	(−3.17872)	(−3.10523)	(−3.20956)
$h/10^{69}$	3.54013	3.52320	3.55615	3.48373	3.44164
	(3.57343)	(3.59960)	(3.54312)	(3.45947)	(3.35905)
$i/10^{89}$	−2.75444	−3.09752	−3.24533	−3.22683	−3.29353
	(−0.44835)	(−2.91560)	(−3.22850)	(−3.19301)	(−3.29023)

a) Values in parentheses were calculated under the local mode approximation.

anharmonicities of the vibrating bond. Details of above the treatments were reported in a previous paper.[13)]

Another series of calculations have been performed in order to consider this problem on the basis of a variation of the dipole moment in the vicinity of the experimental equilibrium geometry.[14)] The treatment in this calculation is the same as that described above except for the calculation of the force constants. We adopted the force constants[15)] determined from the experimental absorption frequencies since there is a difference between the experimental and theoretical geometries, the latter being determined by minimizing the total energy.

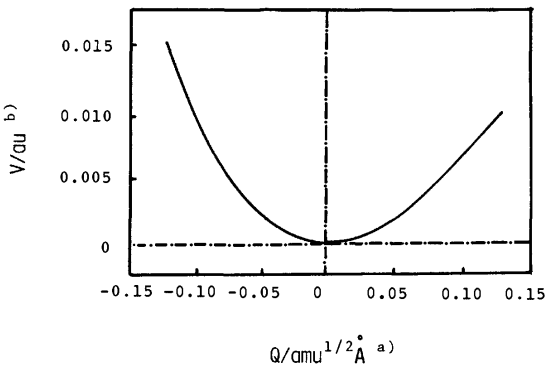

Fig. 1. Potential energy (V) vs. normal coordinate (Q). a) 1 amu=1.660565×10^{-27} kg. b) 1 au=4.359814×10^{-18} J.

Results and Discussion

The theoretical equilibrium geometries, dipole moments and total energies calculated by each basis set are shown in Table 1. These values are generally in good agreement with the experimental values; in detail, the results calculated by the high-level basis set are more improved than those by other basis sets.

Table 2 indicates the force constants with respect to the internal symmetry coordinates, which are used in Wilson's GF matrix method.[12)] These theoretical force constants, F_{ii}, are slightly overestimated. This is the general tendency in the result of a Hartree-Fock level calculation.

The displacements of atoms for a unit of normal coordinate, referring to the C-H stretching mode, are summarized in Table 3. It can be seen from the table that the displacements of chlorine in the normal mode are quite small in comparison with those of other atoms. Therefore, it seems reasonable to assume that the ν_1 normal mode of chloroform can be replaced by the pure C-H stretching mode. Practically, the derivatives of $V(Q)$ and $V'(Q)$, calculated from any basis set, are in almost good agreement with each other (Table 4). As indicated in Fig. 1, the profiles of the respective potential energy functions obtained by different basis set are drawn as a thick curve together, since there has a close resemblance regarding their shapes.

The fundamental and first-overtone frequencies calculated by the variation method are indicated in Table 5. These results make clear the delicate differences between the potential energy functions. In the table, the values in parentheses are the results obtained under a local-mode approximation. The absolute deviations of the theoretical frequencies from their mean value are within 1.8%, and the frequencies calculated under the local-mode approximation coincide with those calculated under the normal-mode treatment without an approximation. This fact shows that the potential energy function with respect to the ν_1 vibration is little affected by the motion of chlorine in the normal mode and the selection of the basis set in the ab initio MO calculation.

The agreement between the theoretical and experimental frequencies is generally unsatisfactory and a calculation with a high-level basis set does not always produce a better result. However, by the variation method, the frequencies are improved by 3—4% in comparison with the harmonic results which are given in italics in Table 5. These results indicate the effect of the mechanical anharmonicity on the fundamental and first-overtone frequencies of the ν_1 vibration. Table 6 indicates an example of the energy levels and wave functions of the ν_1 vibration calculated by the

variation method. From these results, the high anharmonicity of the C-H stretching mode can be obviously recognized. In this calculation, the cross terms between ν_1 and other vibrational modes in the potential energy function have been neglected.

In a previous paper, the CNDO/2 method was adopted for the molecular orbital calculation. Also, the calculated potential energy function was scaled in order to obtain the appropriate energy levels, since the force constants of stretching vibration calculated by

Table 5. Frequencies of ν_1 Vibrational Mode in view of Mechanical Anharmonicity[a] (Unit: cm^{-1})[b]

Frequency	Basis set					Obsd
	4-31G	4-31G*	6-31G*	6-31G**	Huz-Dun	
Fundamental	3309.78 (3330.06)	3252.98 (3287.95)	3280.41 (3278.77)	3254.54 (3254.53)	3312.83 (3311.29)	3032.9[c]
1st Overtone	6476.94 (6598.68)	6346.19 (6439.42)	6448.58 (6448.17)	6401.41 (6402.99)	6509.58 (6506.97)	5941.4[c]
Harmonic frequency	*3438.64* (*3436.27*)	*3385.81* (*3410.28*)	*3392.82* (*3388.53*)	*3362.80* (*3361.61*)	*3427.61* (*3426.94*)	(3462)[d]

a) Values in parentheses were calculated under the local mode approximation. b) $1\ cm^{-1}=1.986481\times10^{-23}$ J. c) From Ref. 18. d) Theoretical value in Ref. 11.

Table 6. Coefficients of Vibrational Wave Functions, ψ, developped as a Linear Combination of Harmonic Wave Functions, ϕ[a]

$$\psi_i(Q)=\sum_k c_{i,k}\phi_k(Q)$$

	ψ_0	ψ_1	ψ_2	ψ_3
Eigen value/10^{-20} J	*3.31707*	*9.76258*	*15.92195*	*21.64411*
Coefficient				
$c_{i,0}$	**0.99385**	−0.10603	0.00746	0.02072
$c_{i,1}$	0.10594	**0.94638**	−0.29044	−0.05767
$c_{i,2}$	0.00953	0.28896	**0.79302**	0.48191
$c_{i,3}$	0.02974	0.06092	0.47799	**−0.47065**
$c_{i,4}$	0.00697	0.06845	0.16834	−0.56723
$c_{i,5}$	0.00112	0.03171	0.13630	−0.30716
$c_{i,6}$	0.00223	0.01068	0.08840	−0.24089
$c_{i,7}$	0.00081	0.00861	0.04401	−0.19144
$c_{i,8}$	0.00023	0.00497	0.02996	−0.12611
$c_{i,9}$	0.00027	0.00231	0.02049	−0.09031
$c_{i,10}$	0.00014	0.00164	0.01230	−0.06643
$c_{i,11}$	0.00005	0.00104	0.00809	−0.04497
$c_{i,12}$	0.00005	0.00058	0.00551	−0.03098
$c_{i,13}$	0.00002	0.00030	0.00271	−0.01627

a) These results were obtained by the variation method employing the potential energy function calculated with the 6-31G** basis set under the normal mode treatment.

Table 7-1. Derivatives of Dipole-Moment Function Calculated at Theoretical Geometry[a] $\mu^z(Q)=\mu_0^z+M_1^zQ+M_2^zQ^2+M_3^zQ^3$,[b] ($\mu^z$/esu cm, $Q/g^{1/2}$ cm)[c]

Derivative	4-31G	4-31G*	6-31G*	6-31G**	Huz-Dun	Ref.
$\mu_0^z/10^{-18}$	1.734	1.330	1.303	1.313	1.282	
$M_1^z/10$	1.060 (2.428)	−0.019 (1.861)	−1.633 (−0.252)	−1.469 (−0.256)	−2.398 (−1.169)	−0.60,[d] 0.0[e]
$M_2^z/10^{21}$	−7.962 (−7.115)	−8.469 (−7.081)	−10.033 (−9.022)	−9.164 (−8.462)	−7.572 (−6.753)	−5.60,[d] ±5.60[e]
$M_3^z/10^{41}$	−2.159 (−1.441)	−2.655 (−1.951)	−1.090 (−0.070)	−1.874 (−1.163)	1.317 (1.914)	±1.93[e]

a) Values in parentheses were calculated under the local-mode approximation. b) The dipole-moment function has only a Z component, since the Z axis is the rotational (C_{3v}) axis and the normal mode in question is symmetric. c) 1 esu cm = 3.33561×10^{-12} Cm. d) Values were calculated on the basis of results in Ref. 16. e) Values were calculated on the basis of experimental intensities in Ref. 17.

Table 7-2. Derivatives of Dipole-Moment Function Calculated at Experimental Geometry[a)]

Derivative	4-31G	4-31G*	6-31G*	6-31G**	Huz-Dun
$\mu_0^z/10^{-18}$	1.656	1.311	1.399	1.348	1.317
$M_1^z/10$	−0.204 (1.203)	−0.530 (0.549)	−1.407 (−0.159)	−1.395 (−0.145)	−2.318 (−1.048)
$M_2^z/10^{21}$	−8.964 (−8.272)	−8.795 (−8.200)	−9.440 (−8.711)	−8.926 (−8.179)	−7.458 (−6.560)
$M_3^z/10^{41}$	−1.623 (−4.196)	−3.245 (−3.409)	−1.623 (−1.479)	−1.623 (−1.690)	1.623 (1.479)

a) Values in parentheses were calculated under the local-mode approximation.

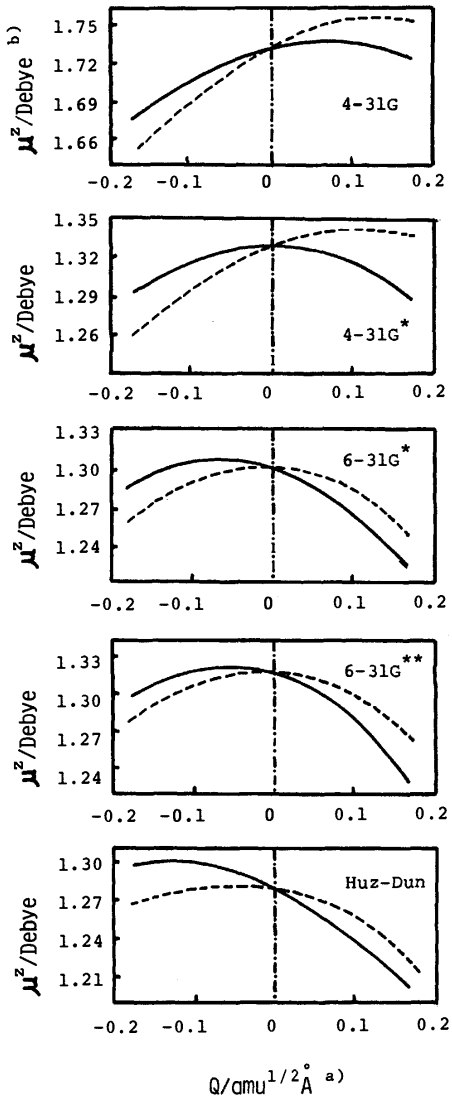

Fig. 2. Dipole moments (μ^z) vs. normal coordinate (Q). (——) normal-mode treatment, (------) local-mode treatment. a) 1 amu=1.660565×10^{-27} kg. b) 1 Debye=3.335641×10^{-30} C m.

the CNDO/2 method is much larger than those generally found. In this work, however, such a treatment has not been performed since the results from the ab initio MO calculation are much more favourable than those from the CNDO/2 calculation.

Table 7-1 records the derivatives of the dipole-moment functions calculated by each basis set with regard to a normal-mode treatment and a local-mode approximation. In the relation between $\mu^z(Q)$ and $\mu^{z\prime}(Q)$, a different tendency can be found in comparison with the case of the potential energy functions, $V(Q)$ and $V'(Q)$. The corresponding derivatives of $\mu^z(Q)$ and $\mu^{z\prime}(Q)$ are different from each other, except for the μ_0^z values.

Especially, the M_1^z values are sensitive to the type of vibrational mode as well as the basis set in the MO calculation, although they are generally small. The $\mu^z(Q)$ and $\mu^{z\prime}(Q)$ calculated from each basis set are displayed in Fig. 2. By the use of the high-level basis set, the extremum of $\mu^z(Q)$ is generally shifted to the direction of short interatomic distance. The values of M_1^z in all cases are close to zero; in other words, the dipole-moment function has an extremum in the vicinity of the equilibrium structure of chloroform.

As generally pointed out, the absorption intensities of the fundamental and first overtone mainly depend on the magnitude of the absolute values of M_1^z and M_2^z, respectively. It is noteworthy, however, that the absorption intensities are affected by the mechanical and electrical anharmonicities of vibration. Especially, these effect in the case of the ν_1 vibration cannot be neglected since the C-H stretching mode is considerably anharmonic, as shown in Table 6.

The fundamental and first-overtone intensities calculated in view of the mechanical and electrical anharmonicities are listed in Table 8-1. Also, the intensities calculated under the harmonic approximation are summarized in Table 8-2. By a comparison between the results in Table 8-1 and those in Table 8-2, the effects of the mechanical and electrical anharmonicities on the infrared absorption intensities can be easily estimated as follows: the fundamental intensity is increased and the first-overtone intensity decreased.

The infrared absorption intensities calculated by using the 6-31G* and 6-31G** basis sets under the local-mode approximation are in agreement with the experimental results. However, from a comparison between these results and those from the normal-mode

Table 8-1. Infrared Absorption Intensities in view of Mechanical and Electrical Anharmonicities[a]
(Unit: 10^{-10} cm^2 s^{-1} mol^{-1})

Intensitiy (at 300 K)	Basis set					Obsd
	4-31G	4-31G*	6-31G*	6-31G**	Huz-Dun	
Fundamental	7.59 (127.75)	15.53 (61.02)	184.18 (24.09)	153.39 (23.82)	279.59 (83.08)	7.9,[b] 15[c]
1st Overtone	80.65 (83.92)	74.84 (77.21)	76.50 (76.65)	65.68 (68.79)	30.99 (32.43)	51.2,[b] 80[c]

a) Values in parentheses were calculated under the local-mode approximation. b) from Ref. 18. c) From Ref. 22.

Table 8-2. Infrared Absorption Intensities under Harmonic Approximation at Theoretical Equilibrium Geometries[a]
(Unit: 10^{-10} cm^2 s^{-1} mol^{-1})

Intensitiy (at 300 K)	Basis set					Ref.[b]
	4-31G	4-31G*	6-31G*	6-31G**	Huz-Dun	
Fundamental	39.25 (205.04)	0.01 (121.03)	93.20 (2.21)	75.35 (2.29)	200.88 (47.71)	12.7
1st Overtone	72.11 (57.61)	82.84 (57.50)	116.04 (93.95)	97.68 (83.32)	65.43 (52.04)	40.4

a) Values in parentheses were calculated under the local-mode approximation. b) Values were derived from the data in Ref. 16. The harmonic functions used here were obtained on the basis of experimental results in Refs. 14 and 15.

Table 8-3. Infrared Absorption Intensities under Harmonic Approximation at Experimental Equilibrium Geometries[a]
(Unit: 10^{-10} cm^2 s^{-1} mol^{-1})

Intensity (at 300K)	Basi set				
	4-31G	4-31G*	6-31G*	6-31G**	Huz-Dun
Fundamental	2.17 (41.30)	13.40 (7.22)	73.67 (1.40)	72.41 (1.28)	180.42 (35.40)
1st Overtone	103.58 (88.19)	99.71 (86.66)	114.87 (97.80)	102.69 (86.22)	71.71 (55.46)

a) Values in parentheses were calculated under the local-mode approximation.

treatment, in which a slight displacement of chlorine in the normal mode is considered, it is found that the treatment under the local-mode approximation requires circumspection in determining the dipole-moment function.

In the present work, we did not obtain satisfactory results by employing the high-level basis set under the normal-mode treatment. However, reasonable results would be obtained if we introduced the following treatments: a configuration interaction treatment in the MO calculation, an appropriate exponent for polarization functions, and cross terms between ν_1 and other vibrational modes in the potential energy function. These are subjects for future studies.

The theoretical dipole moment is affected by the charge distribution and equilibrium geometry of a molecule. In order to investigate the effect of the charge distribution calculated by different basis sets, the dipole-moment functions have been determined by each basis set under the same equilibrium geometry. In this treatment, the experimental geometry[14] has been adopted and the force constants determined on the basis of the experimental data[15] have been employed. The normal coordinates of the ν_1 vibration can be determined by the use of these force constants, however, the potential energy function $V(Q)$ cannot be obtained since the experimental equilibrium geometry is not generally in agreement with the theoretical equilibrium geometry, which are determined by minimizing the total energy.

Table 7-2 indicates the derivatives of the dipole-moment functions calculated by using the experimental equilibrium geometry. These results are similar to those displayed in Fig. 2, in which the results were obtained by using the theoretical equilibrium geometry. Therefore, the graphical representation of Table 7-2 have not been provided. The fundamental and first-overtone intensities calculated from these dipole-

moment functions and harmonic wave functions are listed in Table 8-3, the harmonic wave function being determined on the basis of the experimental results. These results from high-level basis sets are similar to those in Table 8-2 which are derived from the harmonic approximation at the theoretical equilibrium geometry.

The results of an ab initio MO calculation at the 6-31G* level for the dipole-moment function, referring to the ν_1 vibration of chloroform, were published by Tamagake et al.[16,17] It was reported in their papers that the first- and second-order coefficients of a dipole-moment function $\mu(R)$ were -0.08 and -1.0, respectively. For convenience, these values have been transformed to the coefficients of a function $\mu^z(Q)$. The values are -0.60 and -5.60, respectively, while the corresponding values obtained in this work are -0.252 and -9.022. They also reported that the dipole-moment function has an extremum at a distance smaller (-0.04 Å) than the theoretical equilibrium structure. Our corresponding result is -0.0109 Å. The cause of these differences between Tamagake's results and ours for the coefficients and extremum of the dipole-moment function cannot be discussed here since their report does not mention details regarding the following points: the equilibrium geometry and the exponent value of the polarization function on chlorine.

The absorption intensities based on Tamagake's results can be calculated only in the case of the harmonic approximation; however, a detailed treatment cannot be performed since a potential energy function is not published in their paper. The calculated intensities reproduce the experimental results as indicated in Table 8-2. However, if the mechanical anharmonicity is considered, it is expected that the fundamental intensity will be increased and the first-overtone intensity decreased in a similar manner (as our results indicated in Table 8-1).

Conclusion

The infrared absorption frequencies of the chloroform ν_1 vibration calculated by the ab initio MO method under the Hartree-Fock level treatment were larger than the experimental values (by about 10%). The potential energy function was insensitive to a slight displacement of the chlorine in the normal mode ν_1. Also, the selection effect of a Gaussian basis set in the ab initio MO method for the potential energy function was smaller than we have expected.

The theoretical infrared absorption intensities calculated by the 6-31G* and 6-31G** basis sets under the local-mode approximation reproduced the experimental results for the ν_1 vibration. However, satisfactory results could not be obtained by the high-level basis sets, including 6-31G* and 6-31G**, under the normal-mode treatment, which is faithful to the theoretical vibrational mode. The dipole-moment function was sensitive to a displacement of the chlorine in the normal mode ν_1 and to the selection of a Gaussian basis set in the ab initio MO method. It has been found that the local-mode treatment for ν_1 vibration requires circumspection in determining the dipole-moment function.

References

1) T. Miyazaki, T. Shigetani, and H. Yamamoto, *Bull. Chem. Soc. Jpn.*, **45**, 678 (1972)
2) T. Miyazaki and H. Yamamoto, *Bull. Chem. Soc. Jpn.*, **45**, 1669 (1972).
3) J. A. Pople and D. L. Beveridge, "Approximate Molecular Orbital Theory," McGraw-Hill, New York (1970).
4) The inner-shell functions of a chlorine atom are represented by four gaussian primitives.
5) T. H. Dunning, *Chem. Phys. Lett.*, **7**, 423 (1970).
6) T. H. Dunning, *J. Chem. Phys.*, **53**, 2823 (1970).
7) S. Huzinaga, *J. Chem. Phys.*, **42**, 1293 (1965).
8) S. Huzinaga and Y. Sakai, *J. Chem. Phys.*, **50**, 1371 (1969).
9) P. C. Hariharan and J. A. Pople, *Theor. Chim. Acta*, **28**, 218 (1973).
10) J. D. Binkley, M. S. Gordon, D. J. DeFrees, and J. A. Pople, *J. Chem. Phys.*, **77**, 3654 (1981).
11) S. Kato, *J. Chem. Phys.*, **83**, 1085 (1985).
12) E. B. Wilson, Jr., J. C. Decius, and P. C. Cross, "Molecular Vibrations," McGraw-Hill, New York (1955).
13) T. Miyazaki, M. Ikeda, and M. Shibata, *Bull. Chem. Soc. Jpn.*, **48**, 1138 (1975).
14) P. N. Wolfe, *J. Chem. Phys.*, **29**, 976 (1956).
15) K. Ramaswamy and S. Karunanithi, *Acta Chim. Acad. Sci. Hung.*, **98**, 167 (1978).
16) K. Tamagake, S. Hyodo and T. Fujiyama, *Bull. Chem. Soc. Jpn.*, **55**, 1267 (1982).
17) S. Hyodo, K. Tamagake and T. Fujiyama, *Bull. Chem. Soc. Jpn.*, **55**, 1272 (1982).
18) I. Rossi, Ngnyen-van-Than, and C. Haeusler, *Can. J. Chem.*, **47**, 3319 (1969).
19) M. Jen and D. R. Lide., Jr., *J. Chem. Phys.*, **36**, 2525 (1962).
20) "Handbook of Chemistry and Physics," 57th ed, ed by R. C. Weast. Chemical Rubber Company, Cleveland, 63—64, 1976—1977.
21) C. H. Townes and A. L. Shawlow, "Microwave Spectoscopy," McGraw-Hill, New York, London, and Toronto, (1955).
22) C. C. Robinson, S. T. Tare, and H. W. Thompson, *Proc. R. Soc. London, Ser. A*, **269**, 492 (1962).

The Phase Transitions of 1-Alkyl-1-azoniabicyclo[2.2.2]octane Bromides, C_n-ABCO-Br ($10 \leqq n \leqq 22$)

Kengo IMAMURA, Takashi NOGAMI,* and Yasuhiko SHIROTA
Department of Applied Chemistry, Faculty of Engineering, Osaka University, Yamadaoka, Suita, Osaka 565
(Received March 25, 1987)

The phase transitions of a series of 1-alkyl-1-azoniabicyclo[2.2.2]octane bromides were studied on the basis of DSC, the measurements of the ionic conductivities of the bromide anion, and Raman spectroscopy. Most of the materials exhibited three endothermic signals at T_{c1}, T_{c2}, and T_{c3} ($T_{c1}<T_{c2}<T_{c3}$) when they were heated. The temperature dependence of the ionic conductivities of the bromide anion showed conductivity jumps by a factor of 2—4 at around T_{c3}. In order to clarify the phase transition, the temperature dependences of the Raman spectra were measured. It was found that the phase transition at T_{c1} is caused by the molecular rearrangement in the solid, while the transitions at T_{c2} and T_{c3} are caused by both the conformational change in the alkyl chain and the rotational motion of the ABCO portion.

In a series of papers,[1-6] the phase transitions of bis(quaternary alkyl halides) of 1,4-diazabicyclo[2.2.2]octane (DABCO) and mono(quaternary alkyl bromides) of DABCO were studied on the basis of DSC, the measurements of the ionic conductivities of the halide anion, and IR and Raman spectroscopy. All of the symmetric bis(quaternary salts) of DABCO exhibited one transition, which was accompanied by abrupt increases in the ionic conductivities of the halide anion by two to three orders of magnitude.[1,2] The temperature dependence of the IR spectra showed abrupt disappearance of the band progressions at the transition temperature. This fact shows that the motion of the alkyl chain involving conformational change is excited above the transition temperature. On the other hand, unsymmetric bis(quaternary alkyl bromide salts) of DABCO exhibited somewhat different phenomena.[3-5] Although they also showed abrupt increases in the ionic conductivities of the halide anion at the transition temperatures, they were converted to the metastable state after they had been heated above the transition temperature and then cooled to room temperature. The thermodynamic properties of the unsymmetric DABCO salts could be explained on the basis of the free energy-temperature relation. Interesting correlations were found between the difference in the two alkyl-chain lengths of the unsymmetric DABCO salts and the phase transitions, the thermodynamic properties, and the ionic conductivities of the bromide anion.

As an extension of the above studies, we have now studied the phase transitions of a series of 1-alkyl-1-azoniabicyclo[2.2.2]octane bromides, which have only one nitrogen. We have found that most of the salts exhibited three transitions, and that the conductivity jumps of the bromide anion occurred at the highest transition temperature of the three. The phase transition could be analysed on the basis of the temperature dependence of the Raman spectra. In this paper, 1-azabicyclo[2.2.2]octane is abbreviated as ABCO. The materials studied are abbreviated by the numbers of the alkyl-carbons attached to ABCO nitrogen, shown in Fig. 1. For example, 1-decyl-1-azoniabicyclo[2.2.2]octane bromide is abbreviated as C_{10}-ABCO-Br. Thus, the materials in Fig. 1 are generally abbreviated as C_n-ABCO-Br ($10 \leqq n \leqq 22$).

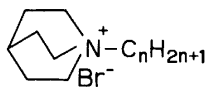

C_n-ABCO-Br
(n = 10, 11, 12, 13, 14
15, 16, 17, 18, 22)

Fig. 1. Quaternary alkyl bromide salts of ABCO.

Experimental

Syntheses of C_n-ABCO-Br. Equimolar amounts (5 mmol) of ABCO and alkyl bromide were dissolved into methanol (20 ml), and the solution was refluxed for 10 h. In the cases of C_n-ABCO-Br (n=10, 11, 12, 13, 15, 17, 22), the methanol was evaporated to dryness, and the white residue was recrystallized three times from a mixed solvent of ethyl acetate and ethanol. In the cases of C_n-ABCO-Br (n=14, 16, 18), the methanol solution of the reaction was poured directly into diethyl ether (300—400 ml), the white precipitate was collected and recrystallized three times from the mixed solvent of ethyl acetate and ethanol. All the products were somewhat hygroscopic, and they were dried under a vacuum after recrystallization. They gave good analytical agreement; the residual solvent and moisture were negligible.

Measurements. A portion of 3—5 mg of the sample, dried beforehand under vacuum, was used for the measurement of the DSC. The details of the DSC and the measurements of the ionic conductivities of the bromide anion were described previously.[1,2] The Raman spectra were measured for the powdered sample by a method which will be reported elsewhere.[6]

Results and Discussion

DSC Measurements. The DSC measurements were

Table 1. Materials, Transition Temperatures, Transition Enthalpies, Transition Entropies, and Conductivity Ratios of the Bromide Anion before and after Transition

Material	T_{c1}	T_{c2}	T_{c3}	ΔH_1	ΔH_2	ΔH_3	ΔS_1	ΔS_2	ΔS_3	σ_h/σ_l
	°C			kJ mol^{-1}			J mol^{-1} K^{-1}			
C_{10}-ABCO-Br[a)]										2.4
C_{11}-ABCO-Br	48	b)	89	16.3	b)	16.4	45	b)	51	4.1
C_{12}-ABCO-Br	61	b)	91	19.9	b)	17.4	48	b)	60	2.5
C_{13}-ABCO-Br	44	72	94	7.1	8.6	17.9	22	25	49	3.0
C_{14}-ABCO-Br	56	63	96	11.9	6.4	23.3	36	19	63	3.0
C_{15}-ABCO-Br	43	83	100	9.8	10.0	24.5	31	28	66	2.6
C_{16}-ABCO-Br	42	66	102	5.6	7.5	26.6	18	22	71	2.6
C_{17}-ABCO-Br	34	87	98	8.5	10.3	25.8	28	29	70	3.4
C_{18}-ABCO-Br	39	75	104	2.7	10.3	34.6	9	30	92	2.4
C_{22}-ABCO-Br	16, 73	83	110	2.2, 3.2	8.7	48.3	9, 24	126	8	2.5

a) Transition temperatures (°C), 13, 54, 71, 131; the corresponding transition enthapies (kJ mol^{-1}), 3.4, 16.8, 2.3, 2.2; the corresponding transition entropies (J mol^{-1} K^{-1}), 12, 51, 7, 5. b) The corresponding endothermic signal was not observed.

made in order to gain insight into the phase transition. Since all samples decomposed above 200 °C, their DSC measurements were made from room temperature to just above the highest transition temperature. Part of Table 1 shows the materials, the transition temperatures, the transition enthalpies, and the transition entropies. The transition temperature was obtained by the onset of the DSC signal. C_n-ABCO-Br (n=13, 14, 15, 16, 17, 18) showed three transitions. C_n-ABCO-Br (n=11, 12) and C_n-ABCO-Br (n=10, 22) showed two and four transitions respectively. Figure 2 shows the DSC thermogram of C_{13}-ABCO-Br as a typical example. When the sample was heated from room temperature, three endothermic signals were observed at T_{c1}, T_{c2}, and T_{c3} ($T_{c1} < T_{c2} < T_{c3}$). The corresponding exothermic signals were observed in the temperature region lower than T_{c1}, T_{c2}, and T_{c3} when the samples were cooled after they had been heated above T_{c3}; the hysteresis between the endothermic and exothermic signals was especially large for the transitions at T_{c1} and T_{c2}. In the second heating cycle, all of the materials showed endothermic signals identical to those of the first cycle. The transition temperatures of C_n-ABCO-Br ($11 \leqq n \leqq 22$) were classified into T_{c1}, T_{c2}, and T_{c3} in Table 1 for the following reasons. Almost iden-

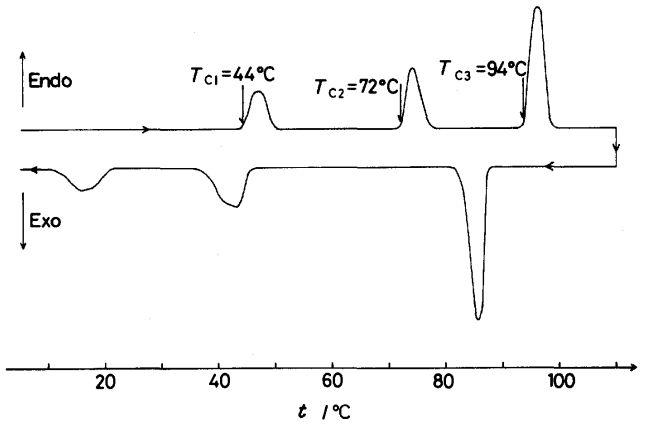

Fig. 2. DSC thermogram of C_{13}-ABCO-Br. Scan speed=5 °C min^{-1}.

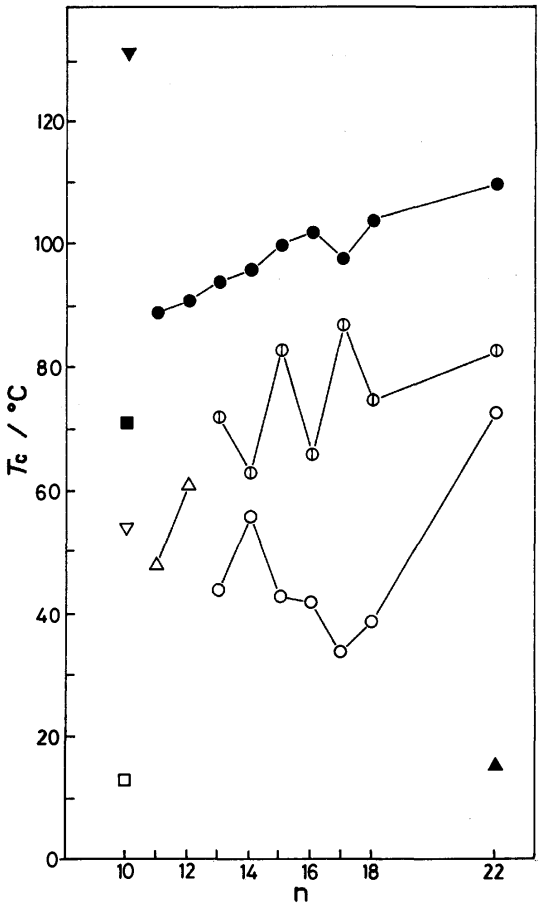

Fig. 3. The plot of the transition temperatures against carbon numbers of alkyl groups in C_n-ABCO-Br.
○ T_{c1}; ⦶ T_{c2}; ● T_{c3}; □▽■▼ transition temperatures of C_{10}-ABCO-Br; △ T_{c1} of C_n-ABCO-Br (n=11, 12); ▲ the lowest transition temperature of C_{22}-ABCO-Br.

tical structural changes seem to occur at T_{c1}, as will be discussed later in connection with the Raman spectroscopy. Regarding the transitions at T_{c2}, another type of structural change, which was also clarified by Raman spectroscopy, occurs for these materials. Since the conductivity jumps of the bromide anion occur at the highest transition temperatures (T_{c3}) for C_n-ABCO-Br ($n \geqq 11$), as will be described later, these transitions seem to be caused by the common structural change in the solid. On the other hand, the transitions of C_{10}-ABCO-Br seem to be different from those of the other ABCO salts.[7] Thus, its thermodynamic data are shown in the footnote of Table 1. The first transition of C_n-ABCO-Br (n=11, 12) is tentatively assigned to T_{c1}, for it has two transition temperatures, in contrast to the three transition temperatures of most of the other salts.

Figure 3 plots the transition temperatures (T_{c1}, T_{c2}, and T_{c3}) of C_n-ABCO-Br ($n \geqq 11$) and the four transition temperatures of C_{10}-ABCO-Br against the carbon numbers of the alkyl group attached to ABCO-nitrogen. Although T_{c1} showed a complex behavior, a distinct even-odd number effect of the alkyl carbons was observed for T_{c2}. T_{c3} increased gradually with the increase in the alkyl-chain lengths except for C_{17}-ABCO-Br. Figure 4 plots the transition enthalpies (ΔH_1, ΔH_2, ΔH_3) against the carbon numbers of the alkyl groups attached to ABCO nitrogen. Here, ΔH_1, ΔH_2, and ΔH_3 correspond to the values of the endothermic heats at T_{c1}, T_{c2}, and T_{c3} respectively. The values of ΔH_1 and ΔH_2 are not so different, being about 10 kJ mol^{-1} or less. An even-odd number effect of the alkyl carbons was observed for ΔH_2 (C_n-ABCO-Br, $n \geqq 13$). On the other hand, ΔH_3 increased with the increase in the alkyl-chain lengths. The transition temperatures (T_{c1} and T_{c2}) for C_n-ABCO-Br ($n \geqq 13$) seem to coalesce to a single transition temperature (T_{c1}) for C_n-ABCO-Br (n=11, 12), because the sum of ΔH_1 and ΔH_2 for the former salts gives values similar to those of ΔH_1 for the latter salts (see Fig. 4). This point will be discussed later in connection with the Raman spectroscopy. The above characteristics of the transition enthalpies were also applicable to the cases of transition entropies ($\Delta S_1 = \Delta H_1/T_{c1}$, $\Delta S_2 = \Delta H_2/T_{c2}$, $\Delta S_3 = \Delta H_3/T_{c3}$).

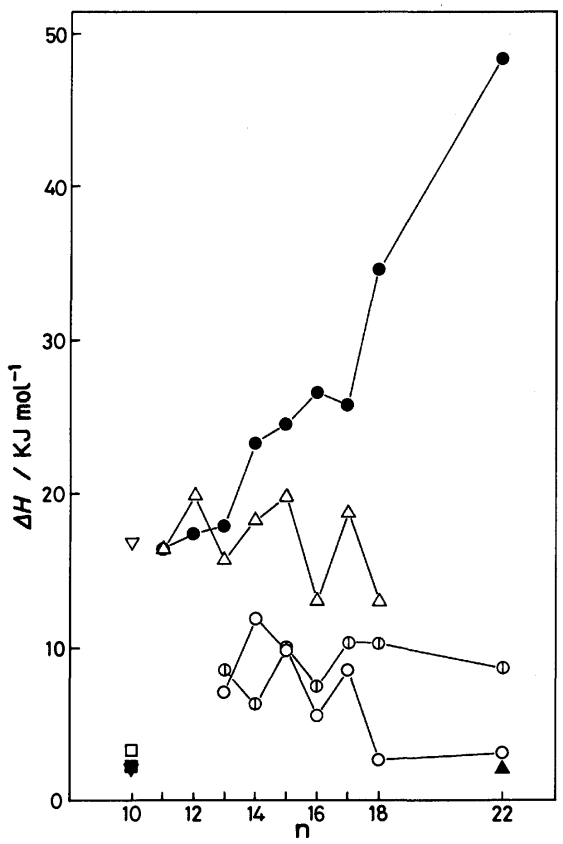

Fig. 4. The plot of the transition enthalpies against carbon numbers of alkyl groups in C_n-ABCO-Br. ○ ΔH_1; ⊕ ΔH_2; ● ΔH_3; △ $\Delta H_1+\Delta H_2$ and ΔH_1's of C_n-ABCO-Br (n=11, 12); □▽■▼ ΔH of C_{10}-ABCO-Br, corresponding to Fig. 3; ▲ ΔH for the transition of C_{22}-ABCO-Br at 16°C.

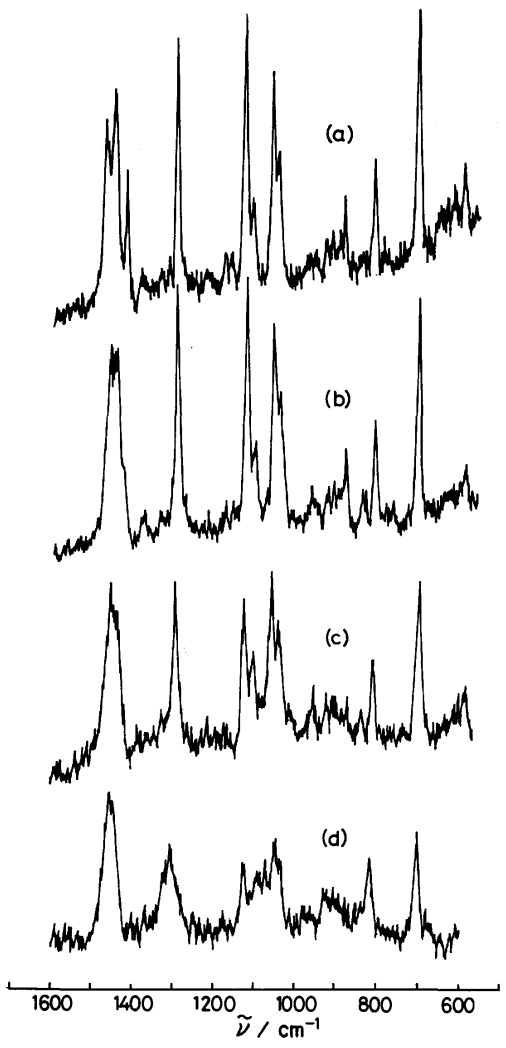

Fig. 5. Temperature dependence of the Raman spectra of C_{18}-ABCO-Br. (a) 17°C, (b) 50°C, (c) 80°C, (d) 110°C.

Raman Spectroscopy. In order to clarify the phase transitions at T_{c1}, T_{c2}, and T_{c3} in more detail, the temperature dependence of the Raman spectra was measured. Figure 5 shows the result observed for C_{18}-ABCO-Br as a typical example. Below T_{c1} (39 °C), crystal-field splitting[8] was observed at 1419 and 1450 cm^{-1} (see the spectrum at 17 °C). This fact shows that the zigzag planes of the nearest neighboring alkyl chains are packed nearly perpendicular to each other.[8] The crystal-field splitting disappeared above T_{c1} (see the spectrum at 50 °C). In view of the small value of ΔH_1 (2.7 kJ mol^{-1}), the transition at T_{c1} seems not to be caused by the onset of a rotator phase.[9] The lack of the crystal-field splitting above T_{c1} shows that a reorientation of the molecules takes place in the solid. No appreciable decreases in the Raman intensities were observed for the C-C skeletal vibration (1061, 1130 cm^{-1}) and the CH_2 twisting mode (1297 cm^{-1}) in the temperature range of $T_{c1} < T < T_{c2}$. In this context, Kobayashi et al. investigated the correlation between the Raman intensities and the length of the *trans*-zigzag structure in polyethylene.[10] They found that the Raman intensities decreased with the decrease in the length of the *trans*-zigzag portion, and that the Raman bands were broadened by the onset of vigorous reorientational motion of the molecule. Taking these results into account, the present findings suggest that no conformational change of the alkyl group occurs between T_{c1} and T_{c2}.[10] Above T_{c2} (75 °C), the intensities of these vibrational modes decreased significantly (see the spectrum at 80 °C). This fact shows that the conformational change in the alkyl group occurs above T_{c2}. Since the Raman intensities of the NC_4 symmetric stretching mode (706 cm^{-1}) also decreased to some extent above T_{c2}, the rotational motion of ABCO seems to be excited.[10] All of the Raman signals decreased in their intensities and were considerably broadened above T_{c3} (see the spectrum at 110 °C). This fact shows that the alkyl chain seems to be "melt" from the dynamical point of view and that a vigorous rotational motion of ABCO occurs in this temperature range. The coalescence of T_{c1} and T_{c2} observed for C_n-ABCO-Br ($n \geqq 13$) into T_{c1} for C_n-ABCO-Br ($n=11$, 12) was clearly demonstrated by the fact that both the disappearance of the crystal-field splitting and the decrease in the Raman intensities at 1064, 1130, and 1297 cm^{-1} were simultaneously observed above T_{c1} for the latter materials; the former observation corresponds to the rearrangement of the molecule in the solid, and the latter, to the conformational change in the alkyl group. Thus, the structural changes observed at T_{c1} and T_{c2} for C_n-ABCO-Br ($n \geqq 13$) occurred simultaneously at T_{c1} for C_n-ABCO-Br ($n=11$, 12).

Ionic Conductivities of the Bromide Anion. The temperature dependences of the ionic conductivities of the bromide anion were measured for the compressed pellet samples by an AC impedance method.[1,2] Figure

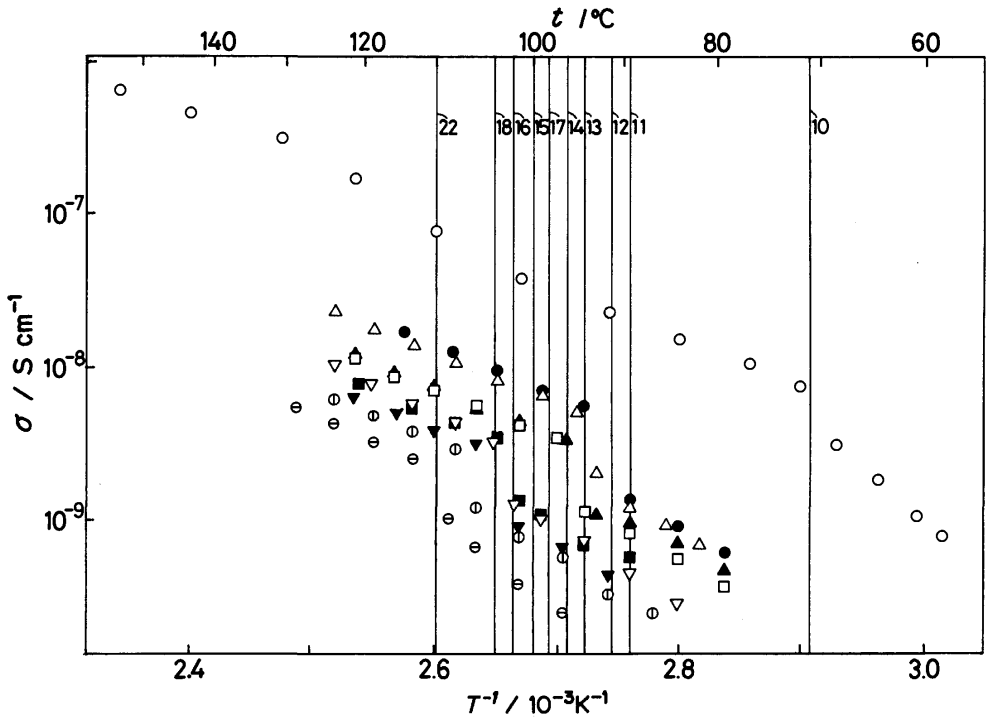

Fig. 6. Temperature dependence of the ionic conductivities of bromide anion of C_n-ABCO-Br. ○ $n=10$; ● $n=11$; △ $n=12$; ▲ $n=13$; □ $n=14$; ■ $n=15$; ▽ $n=16$; ▼ $n=17$; ⦶ $n=18$; ⊖ $n=22$. The vertical solid lines and the numbers nearby represent T_{c3} and n respectively.

6 shows the observed results. All of the materials exhibited conductivity jumps, and the ratios of the ionic conductivities of the bromide anion before (σ_l) and after (σ_h) the transitions were found to be in the range of 2—4 (see Table 1). These values are much smaller than those of the bis(quaternary alkyl bromide salts) of DABCO,[1-5] but are almost identical with those of the mono(quaternary alkyl bromide salts) of DABCO.[6] In order to correlate the conductivity jumps with the transition temperatures, T_{c3}'s are also shown as vertical solid lines in this figure. The numbers near these lines represent the numbers of the alkyl carbons attached to ABCO nitrogen. From Fig. 6, the following characteristics can be seen: (1) The conductivity jump occurs at around T_{c3} by a factor of 2—4. (2) The shorter the alkyl-chain lengths, the higher the ionic conductivities of the bromide anion. (3) The activation energies of the conduction above T_{c3} are lower than those below T_{c3}.

The first characteristic shows that no appreciable conductivity jump occurs at T_{c1}, where molecular rearrangement takes place, or at T_{c2}, where the conformational motion of the alkyl chain and the rotational motion of ABCO are excited to some extent. Only at T_{c3} where vigorous molecular motion sets in, does the conductivity jump take place. The values of the conductivity jump seem to be related with the degree of the molecular motion for the following reason. The temperature dependence of the Raman spectra of the symmetric bis(quaternary alkyl bromides) of DABCO exhibited an almost complete disappearance of the C-C skeletal modes above the transition temperature.[11] This fact shows that the molecular motion of the alkyl group is too vigorous to be regarded as if it were "liquid." As a result, the conductivity jumps of these materials were large. On the other hand, the molecular motion of the present materials are retarded to some extent, in view of the presence of the C-C skeletal mode even above T_{c3} (see Fig. 6); this gives rise to the small conductivity jump. The second characteristic above can be explained by the fact that the distance between the hopping sites of the bromide anion becomes shorter as the alkyl-chain lengths decrease. The third characteristic above can be explained by the fact that the bromide anion can move more easily in the high-temperature range ($T > T_{c3}$) than in the low temperature range ($T < T_{c3}$) because of the presence of a large number of voids which are produced by the vigorous motion of the alkyl group and the ABCO portion.

Summary. The phase transitions of C_n-ABCO-Br ($10 \leqq n \leqq 22$) were studied on the basis of the DSC, the Raman spectroscopy, and the measurements of the ionic conductivities of the bromide anion. Concluding a series of the studies,[1-6] three characteristic points (the numbers of the transitions, the existence of a metastable state, and the conductivity ratios of the bromide anion before and after the transition) were compared: The results are summarized in Table 2. Here, C_n-DABCO-C_n-Br_2,[1,2] C_n-DABCO-C_m-Br_2,[3-5] and C_n-DABCO-Br[6] denote symmetric bis(quaternary alkyl bromides) of DABCO, unsymmetric bis(quaternary alkyl bromides) of DABCO, and mono(quaternary alkyl bromides) of DABCO respectively; n and m denote the numbers of alkyl carbons. As to the numbers of the transitions, C_n-DABCO-C_n-Br_2, C_n-DABCO-C_m-Br_2, C_n-DABCO-Br, and C_n-ABCO-Br exhibited one, one, two, and three transitions respectively. Regarding the thermodynamic properties, no metastable state was observed for C_n-DABCO-C_n-Br_2, C_n-DABCO-Br, or C_n-ABCO-Br. In the case of the unsymmetric bis(quaternary alkyl bromide salts) of DABCO (C_n-DABCO-C_m-Br_2), however, the low-temperature phase was converted to the metastable state after they had been heated above the transition temperature and then cooled. All of the quaternary salts studied up to now showed conductivity jumps of the bromide anion. The conductivity jumps (the σ_h/σ_l values) are found to be in the range of 100—6000 for the bis(quaternary alkyl bromides) of DABCO. On the other hand, they are small (2—10) for the mono(quaternary alkyl bromides) of DABCO and of ABCO. In the cases of C_n-DABCO-C_n-Cl_2 and C_n-DABCO-C_n-I_2, the conductivity jumps of the chloride anion and iodide anion by a factor of 150—190 and 140—350 respectively were also observed.[2]

We are grateful to Professor Masamichi Kobayashi and Dr. Tsutomu Ishioka, Faculty of Science, Osaka University, for their fruitful discussions with regard to the analysis of the Raman spectra. We are also grateful to Professor Shigekazu Kusabayashi and Dr. Shunsuke

Table 2. Comparison of the Phase Transitions of Quaternary Alkyl Bromides of DABCO and of ABCO

	C_n-DABCO-C_n-Br_2	C_n-DABCO-C_m-Br_2	C_n-DABCO-Br	C_n-ABCO-Br
Number of transition	1	1	2	3
Metastable state	Absent	Present	Absent	Absent
Conductivity jumps of the bromide anion	630—3600[a]	700—3070 ($m=n+2$)[b] 100— 770 ($n=10$)[c] 1500—6000 ($m=n+1$)[d]	2—10[e]	2—4

a) The conductivity jumps of C_n-DABCO-C_n-Cl_2 and C_n-DABCO-C_n-I_2 were found to be in the range of 150—190 and 140—350 respectively (see Ref. 2). b) Ref. 3. c) Ref. 4. d) Ref. 5. e) Ref. 6.

Takenaka, Faculty of Engineering, Osaka University, for the use of the DSC apparatus.

References

1) J. Shimizu, T. Nogami, and H. Mikawa, *Solid State Commun.*, **54**, 1009 (1985).

2) J. Shimizu, K. Imamura, T. Nogami, and H. Mikawa, *Bull. Chem. Soc. Jpn.*, **59**, 1443 (1986).

3) K. Imamura, J. Shimizu, and T. Nogami, *Bull. Chem. Soc. Jpn.*, **59**, 2699 (1986).

4) J. Shimizu, K. Imamura, T. Nogami, and H. Mikawa, *Bull. Chem. Soc. Jpn.*, **59**, 3367 (1986).

5) K. Imamura, T. Nogami, and Y. Shirota, *Bull. Chem. Soc. Jpn.*, **60**, 111 (1987).

6) K. Imamura, T. Nogami, Y. Shirota, T. Ishioka, and M. Kobayashi, *Bull. Chem. Soc. Jpn.*, in press.

7) C_n-ABCO-Br ($n \geqq 11$) were found to be converted to the isotropic phase above T_{c3} by observing their crystals with a polarization microscope under a crossed Nicols condition. On the other hand, C_{10}-ABCO-Br exhibited unusual phenomena; with an elevation of the temperature, the birefringence once disappeared at 62 °C, appeared again at 80 °C, and then disappeared again at 145 °C. Furthermore, the conductivity jump of the bromide anion was observed at around the third transition temperature (71 °C) of the four.

8) R. S. Stein, *J. Chem. Phys.*, **23**, 734 (1955); F. J. Boerio and J. L. Koenig, *ibid.*, **52**, 3425 (1970).

9) The transition enthalpies of *n*-alkanes (C_nH_{2n+2}, $11 \leqq n \leqq 22$) from a low-temperature phase to a rotator phase were found to be in the range of 7—30 kJ mol^{-1}; see M. G. Broadhurst, *J. Res. National Bureau Standards*, **66A**, 241 (1962).

10) Y. Cho, M. Kobayashi, and H. Tadokoro, *Macromolecules*, in press.

11) Unpublished data.

 © 1987 The Chemical Society of Japan Bull. Chem. Soc. Jpn., 60, 3505—3508 (1987)

Fluorescence Quenching of *N*-Phenyl-1-naphthylamine by Nitriles, Esters, and Amines

Sanyo HAMAI
Department of Physics, Miyazaki Medical College, Kiyotake, Miyazaki 889-16
(Received April 2, 1987)

The equilibrium constants for the hydrogen bonding between *N*-phenyl-1-naphthylamine (NPNA) and proton acceptors (1,4-dioxane, nitriles, esters, and amines) in cyclohexane and the corresponding thermodynamic parameters have been determined. The fluorescence of NPNA is quenched by nitriles, esters, and amines. In the cases of nitriles and esters, the quenching is caused by compounds in which a cyano or carboxyl group is conjugated with a double bond. The rate constants for quenching of the NPNA fluorescence by methyl tiglate, methyl 3,4,5-trimethoxybenzoate, and 2,4,6-trimethylpyridine are 81, 73, and 69% of those by methyl acrylate, methyl benzoate, and pyridine, respectively. These findings can be interpreted in terms of the charge-transfer interaction through the hydrogen bond between NPNA (an electron donor) and the proton acceptors (electron acceptors) except for the amines, for which a mechanism different from the charge-transfer mechanism may be important in explaining the fluorescence quenching.

It is well-known that 1- or 2-naphthylamine is hydrogen-bonded to pyridine etc.[1-3] It has been shown that when two conjugated π-electronic systems are directly combined by the hydrogen-bonding interaction, the fluorescence of 1- or 2-naphthylamine is quenched.[1-4] As the quenching mechanism in these cases, a charge-transfer interaction between a proton donor and a proton acceptor through the hydrogen bond has been suggested.[1-5]

Derivatives of *N*-phenyl-1-naphthylamine (NPNA), 1,8-ANS (8-anilino-1-naphthalenesulfonate) etc., are frequently used as fluorescent probes in the areas of biochemistry and biology.[6,7] However, the hydrogen-bonding interaction between a fluorescent probe and substrates has not been noted, although these probes may be hydrogen bonded to substrates. Thus, we studied the quenching behavior of the fluorescence of NPNA in cyclohexane by using additives forming a hydrogen bond with NPNA.

Experimental

N-Phenyl-1-naphthylamine (NPNA) was recrystallized from cyclohexane three times. Ethers, nitriles, esters, and amines were distilled under atmospheric or reduced pressure except for methyl 3,4,5-trimethoxybenzoate and 1,4-diazabicyclo[2.2.2]octane (DABCO) which were recrystallized twice from ethanol and hexane, respectively. Cyclohexane was purified by percolation through a silica-gel column. Absorption spectra were recorded with a Shimadzu UV-260 spectrophotometer. Fluorescence spectra were taken with a Shimadzu RF-501 spectrofluorometer. Fluorescence spectra were corrected for the spectral response of the spectrofluorometer.[8] The fluorescence lifetime of NPNA was measured with an Ortec 9200 nanosecond decay time fluorimeter equipped with a Horiba NFL-111A ns lamp. Fluorescence quantum yields were determined relative to a quantum yield of 0.90 of 9,10-diphenylanthracene in nitrogenated cyclohexane.[9] The concentrations of NPNA for the measurement of absorption and fluorescence were 10^{-4} and 3×10^{-5} mol dm^{-3}, respectively. Sample solutions for the fluorescence measurement were nitrogen bubbled. Unless otherwise stated, all the measurements were made at 25±0.1 °C.

Results and Discussion

Figure 1 shows the absorption spectra of NPNA in cyclohexane in the absence and presence of 1,4-dioxane. The absorption maximum of NPNA is shifted to the red with isosbestic points at 284 and 332 nm. These spectral changes indicate a hydrogen bonding between NPNA and 1,4-dioxane. In the hydrogen-bonding complex with 1,4-dioxane, a proton donor is NPNA and a proton acceptor 1,4-dioxane. From the spectral changes of NPNA in Fig. 1, an equilibrium constant (K_g) for the hydrogen bonding in the ground state could be evaluated, and its value is shown in Table 1 together with the enthalpy change (ΔH) and the entropy change (ΔS) of K_g which were determined from the temperature dependence of K_g.[10] For nitriles, esters, and amines, similar changes to those for 1,4-dioxane in the absorption spectra of NPNA were observed, indicating a hydrogen bonding with NPNA.

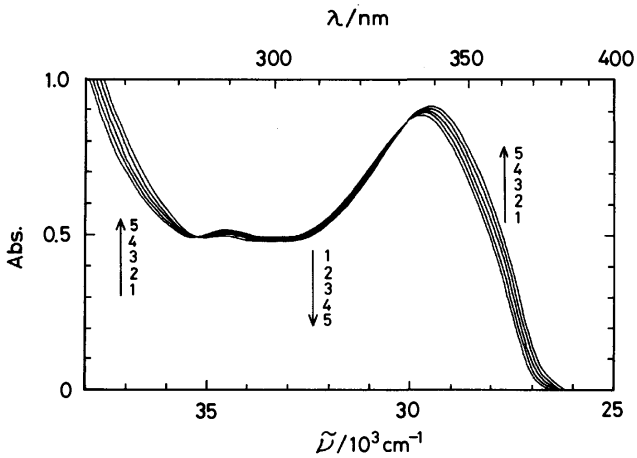

Fig. 1. Absorption spectra of NPNA (10^{-4} mol dm^{-3}) in cyclohexane in the presence of 1,4-dioxane. Concentration of 1,4-dioxane: (1) 0 mol dm^{-3}; (2) 0.117 mol dm^{-3}; (3) 0.234 mol dm^{-3}; (4) 0.585 mol dm^{-3}; (5) 1.17 mol dm^{-3}.

Table 1. Equilibrium Constants for Hydrogen Bonding of NPNA in the Ground State at 25 °C (K_g), Enthalpy Changes (ΔH), and Entropy Changes (ΔS)

	K_g/mol^{-1} dm^3	ΔH/kJ mol^{-1}	ΔS/J K^{-1} mol^{-1}
1,4-Dioxane	1.8	−26	−84
Propionitrile	2.5	−10	−27
Acrylonitrile	1.6	−12	−38
Benzonitrile	2.0	−12	−33
Ethyl acetate	1.8	−17	−50
Methyl acrylate	1.2	−18	−58
Methyl tiglate	1.4	−22	−72
Dibutyl oxalate	2.5	−21	−63
Dibutyl maleate	4.1	−21	−60
Methyl benzoate	1.4	−20	−63
Methyl 3,4,5-trimethoxybenzoate	6.3	−17	−42
Pyridine	3.2	−8.8	−20
2,4,6-Trimethylpyridine	5	—	—
Triethylamine	0.3	−35	−130
DABCO	2	−42	−130

The compounds are proton acceptors like 1,4-dioxane for NPNA. The values of K_g, ΔH, and ΔS for these esters, nitriles, and amines are also given in Table 1. As can be seen from Table 1, similar values of K_g are obtained for each group of proton acceptors except for dibutyl oxalate, dibutyl maleate, methyl 3,4,5-trimethoxybenzoate, and triethylamine. About twofold larger values of K_g for dibutyl oxalate and dibutyl maleate than those for monocarboxylates (ethyl acetate, etc.) can be explained by the fact that two carboxyl groups are involved in one molecule. The large difference in K_g between triethylamine and DABCO may be partly due to the difference of the number of the amino nitrogen. The larger value of K_g for methyl 3,4,5-trimethoxybenzoate or 2,4,6-trimethylpyridine than that for methyl benzoate or pyridine can be interpreted in terms of an increase of the electron density on a carboxyl oxygen atom or a nitrogen atom caused by an electron-donating substituent (methoxy or methyl group). The values for ΔH and ΔS are not too different within the same groups of acceptors.

The fluorescence spectra of NPNA in cyclohexane in the presence of 1,4-dioxane are shown in Fig. 2. When 1,4-dioxane is added to an NPNA solution, the fluorescence maximum of NPNA is shifted to longer wavelengths with an isoemissive point at 388 nm. An enhancement of the integrated fluorescence intensity is also observed. These spectral changes can be ascribed to the hydrogen bonding between NPNA and 1,4-dioxane. The enhancement of the NPNA fluorescence indicates that the fluorescence quantum yield (ϕ_f) is larger in a hydrogen-bonding form of NPNA than in a free form.

We examined the solvent dependence of ϕ_f and the fluorescence maximum position of NPNA. The values of ϕ_f in cyclohexane (ε=2.02), 1,4-dioxane (ε=2.21), ethyl acetate (ε=6.02), propionitrile (ε=27.2),

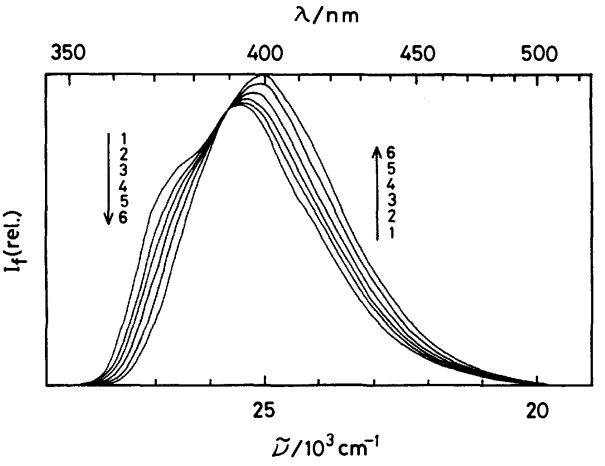

Fig. 2. Fluorescence spectra of NPNA (3×10^{-5} mol dm^{-3}) in cyclohexane in the presence of 1,4-dioxane. Concentration of 1,4-dioxane: (1) 0 mol dm^{-3}; (2) 0.059 mol dm^{-3}; (3) 0.117 mol dm^{-3}; (4) 0.234 mol dm^{-3}; (5) 0.585 mol dm^{-3}; (6) 1.17 mol dm^{-3}. λ(exc.)=332 nm.

and water (ε=78.5) were 0.68, 0.72, 0.63, 0.54, and 0.029, respectively. The larger the dielectric constant of the solvent, the smaller ϕ_f of NPNA except for 1,4-dioxane. The dielectric constant of 1,4-dioxane (2.21) is very close to that of cyclohexane (2.02). In the case of 1,4-dioxane, therefore, the effect of the hydrogen bonding, which enhances the fluorescence intensity, prevails over the effect of the solvent polarity. The fluorescence maximum in cyclohexane, 1,4-dioxane, ethyl acetate, propionitrile, and water are at 393, 413, 420, and 485 nm, respectively. The maximum position is red-shifted as the solvent polarity is increased. Such characteristics of both ϕ_f and the fluorescence peak have been reported for other naphthylamine derivatives.[11,12]

Figure 3 shows the fluorescence spectra of NPNA solutions containing varying concentrations of propionitrile. Below ≈0.07 mol dm^{-3} of propionitrile, the spectral change, with an isoemissive point at 389 nm, is similar to that for 1,4-dioxane (Fig. 2). Although the dielectric constant of propionitrile (27.2) is very large compared with that of cyclohexane (2.02), the polarity of the cyclohexane solution containing such a low concentration of propionitrile is not too different from that of neat cyclohexane. Above ≈0.14 mol dm^{-3} of propionitrile, the fluorescence intensity is reduced, accompanied by a red shift of the fluorescence maximum; also, the isoemissive point at 389 nm disappears. In the high-concentration range of propionitrile, the solvent polarity becomes fairly high. Thus, the effect of solvent polarity which decreases the fluorescence intensity overcomes the effect of the hydrogen bonding to decrease the fluorescence intensity.

In Table 2 are summarized the proton acceptors by which the fluorescence quenching of NPNA is caused (O) or not caused (X). The ethers examined in this study show no fluorescence quenching. In the nitrile series, acrylonitrile and benzonitrile quench the NPNA fluorescence, while acetonitrile and propionitrile do not quench. Acrylonitrile and benzonitrile have a double bond which is conjugated with a cyano group although in benzonitrile a conjugated double bond belongs to a benzene ring. For the fluorescence quenching of naphthylamines, quenchers forming a hydrogen bond are pyridine and quinoline whose conjugated double bond is present as a part of an aromatic ring.[1-3] In the case of acrylonitrile, however, a cyano group is conjugated with a nonaromatic double bond. In the ester series, ethyl acetate and vinyl acetate do not quench the NPNA fluorescence. However, the

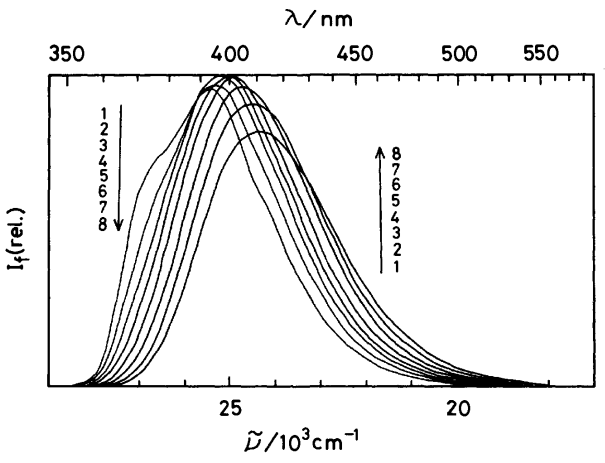

Fig. 3. Fluorescence spectra of NPNA (3×10^{-5} mol dm^{-3}) in cyclohexane in the presence of propionitrile. Concentration of propionitrile: (1) 0 mol dm^{-3}; (2) 0.028 mol dm^{-3}; (3) 0.071 mol dm^{-3}; (4) 0.142 mol dm^{-3}; (5) 0.284 mol dm^{-3}; (6) 0.710 mol dm^{-3}; (7) 1.42 mol dm^{-3}; (8) 2.84 mol dm^{-3}. λ(exc.)=326 nm.

Table 2. Proton Acceptors Which Exhibit Quenching (O) or No Quenching (X) for the NPNA Fluorescence

Proton acceptor	Result
1,4-Dioxane	X
Ethyl vinyl ether	X
Furan	X
Acetonitrile	X
Propionitrile	X
Acrylonitrile	O
Benzonitrile	O
Ethyl acetate	X
Vinyl acetate	X
Methyl acrylate	O
Methyl tiglate	O
Dibutyl oxalate	O
Dibutyl maleate	O
Methyl benzoate	O
Methyl 3,4,5-trimethoxybenzoate	O
Pyridine	O
2,4,6-Trimethylpyridine	O
Triethylamine	O
DABCO	O

fluorescence quenching takes place by methyl acrylate, methyl tiglate, dibutyl oxalate, dibutyl maleate, methyl benzoate, and methyl 3,4,5-trimethoxybenzoate. These esters also possess a double bond which is conjugated with a carboxyl group. For methyl acrylate, methyl tiglate, dibutyl oxalate, and dibutyl maleate, the double bonds are nonaromatic ones. In the case of amines, pyridine and 2,4,6-trimethylpyridine are effective quenchers for the NPNA fluorescence. Besides pyridine and 2,4,6-trimethylpyridine, aliphatic amines (triethylamine and DABCO) were found to quench the fluorescence.

All the quenchers shown in Table 2 are hydrogen bonded to NPNA in the ground state. Because the K_g values for these quenchers are not so large (1.2—6.3 mol^{-1} dm^3), the concentration of a hydrogen-bonding complex can be neglected in the low-concentration range of the quencher. Thus, the fluorescence quenching by these proton acceptors was analyzed according to the Stern-Volmer plot. From the Stern-Volmer quenching constants and the fluorescence lifetime of NPNA (3.9 ns), the rate constants for fluorescence quenching could be determined and are listed in Table 3.[13] These values in Table 3 represent the rate constants for the dynamic quenching in the excited state of NPNA. Almost diffusion-controlled rate constants are obtained for the nitriles. Although the quenchers shown in Table 3 can be hydrogen bonded to excited NPNA, the nonfluorescent exciplex formation may be possible for benzonitrile, methyl benzoate, and methyl 3,4,5-trimethoxybenzoate. Thus, we investigated the fluorescence quenching of *N*,*N*-dimethyl-1-naphthyl-

Table 3. Rate Constants for Fluorescence Quenching of NPNA (k_q)

Proton acceptor	$k_q/10^{10}$ mol^{-1} dm^3 s^{-1}
Acrylonitrile	1.60
Benzonitrile	1.53
Methyl acrylate	1.17
Methyl tiglate	0.95
Dibutyl oxalate	1.08
Dibutyl maleate	1.42
Methyl benzoate	1.14
Methyl 3,4,5-trimethoxybenzoate	0.83
Pyridine	1.19
2,4,6-Trimethylpyridine	0.82
Triethylamine	0.28
DABCO	1.00

amine (DMNA) by these proton acceptors. Its oxidation potential (0.46 V), estimated from the fluorescence maximum position of the perylene exciplexes with DMNA, *N*,*N*-diethylaniline, and *N*-ethylcarbazole, is much smaller than that of NPNA estimated in a similar fashion (0.89 V).[14,15] In addition, DMNA cannot be hydrogen bonded to proton acceptors in contrast to NPNA. It was found that no fluorescence quenching of DMNA took place by the above proton acceptors which quenched the NPNA fluorescence. From this finding, it is clearly evident that NPNA does not form a nonfluorescent exciplex with the above proton acceptors. Therefore, the hydrogen bonding in the excited state of NPNA is responsible for the fluorescence quenching. As shown in Table 3, the quenching constants of methyl tiglate, methyl 3,4,5-trimethoxybenzoate, and 2,4,6-trimethylpyridine are about 81, 73, and 69% of those for methyl acrylate, methyl benzoate, and pyridine, respectively, indicating a reduction of the quenching constant by the substitution of an electron-donating group (methyl or methoxy group) in a proton acceptor. Therefore, the quenching is caused by the charge-transfer interaction between NPNA and proton acceptors through the hydrogen bond. In these cases, NPNA is an electron donor and the proton acceptors electron acceptors.

For a 2-naphthylamine-pyridine system, Ikeda et al. has successfully detected a transient absorption of a charge-transfer state from excited 2-naphthylamine to hydrogen-bonded pyridine.[5] Our results that the fluorescence of NPNA is quenched only by the proton acceptors possessing a double bond which is conjugated with a functional group and that NPNA acts as an electron donor in the fluorescence quenching are consistent with the observations for the 2-naphthylamine-pyridine system. The findings that ethers, nonconjugated nitriles and esters do not quench the NPNA fluorescence can also be interpreted in terms of the charge-transfer interaction through a hydrogen bond.

Since the aliphatic amines (triethylamine and DABCO) were found to quench the perylene fluorescence to a smaller extent than NPNA does, they seem to be weaker electron donors than NPNA. If so, it is difficult to attribute the fluorescence quenching of NPNA by these amines to their electron donating nature. Other mechanisms, such as a proton transfer or a hydrogen atom transfer, may be responsible for the fluorescence quenching by the aliphatic amines.

The author wishes to thank Professor Fumio Hirayama for his valuable discussion.

References

1) N. Mataga, *Bull. Chem. Soc. Jpn.*, **31**, 481 (1958).
2) N. Mataga, Y. Torihashi, and Y. Kaifu, *Z. Phys. Chem. N. F.*, **34**, 379 (1962).
3) T. Miwa and M. Koizumi, *Bull. Chem. Soc. Jpn.*, **36**, 1619 (1963).
4) M. M. Martin and W. R. Ware, *J. Phys. Chem.*, **82**, 2770 (1978).
5) N. Ikeda, T. Okada, and N. Mataga, *Bull. Chem. Soc. Jpn.*, **54**, 1025 (1981).
6) G. K. Radda and J. Vanderkooi, *Biochim. Biophys. Acta*, **265**, 509 (1972).
7) L. Brand and J. R. Gohlke, *Ann. Rev. Biochem.*, **41**, 843 (1972).
8) S. Hamai, *Bull. Chem. Soc. Jpn.*, **57**, 2700 (1984).
9) S. Hamai and F. Hirayama, *J. Phys. Chem.*, **87**, 83 (1983).
10) N. Mataga and S. Tsuno, *Bull. Chem. Soc. Jpn.*, **30**, 368 (1957).
11) S. K. Chakrabarti and W. R. Ware, *J. Chem. Phys.*, **55**, 5494 (1971).
12) J. Drew, P. Thistlethwaite, and G. Woolfe, *Chem. Phys. Lett.*, **96**, 296 (1983).
13) The fluorescence lifetime of 4.10 ns for NPNA in cyclohexane has been reported by P. J. Sadkowski and G. R. Fleming (*Chem. Phys. Lett.*, **54**, 79 (1980)).
14) D. Rehm, *Z. Naturforsch.*, **25A**, 1442 (1970).
15) D. Rehm and A. Weller, *Z. Phys. Chem. N. F.*, **69**, 183 (1970).

 © 1987 The Chemical Society of Japan Bull. Chem. Soc. Jpn., 60, 3509—3513 (1987)

Photocatalytic Oxidative Dehydrogenation of 2-Propanol with Niobium Oxide Supported on Porous Vycor Glass

Yuji WADA* and Akira MORIKAWA
Department of Chemical Engineering, Tokyo Institute of Technology, O-okayama, Meguro-ku, Tokyo 152
(Received April 22, 1987)

2-Propanol was catalytically converted to acetone on niobium oxide supported on porous Vycor glass in the presence of oxygen or nitrogen monoxide under UV irradiation. The light of wavelength shorter than 300 nm was effective for the reaction. The VIS-UV absorption measurements showed that niobium oxide was reduced by 2-propanol under the irradiation and Nb^{4+} formed by the photoreduction was reoxidized by oxygen. The kinetics of the reoxidation was investigated by means of spectroscopic measurements. The redox mechanism is proposed for the photocatalytic oxidation of 2-propanol.

In the periodic table, niobium belongs to 5A group and is located closely to Ti, Mo, and V. The catalytic activity of these oxides effective for chemical processes assisted by visible or ultraviolet irradiation has been well-investigated.[1] Similarity of niobium oxide in chemical and physical properties, such as crystal structure[2] and a semiconducting property,[3] to the oxides of the elements mentioned above suggests that the oxide can be a candidate of a catalyst for photoassisted chemical processes.

Photoactivation of niobium oxide catalyst has been reported.[4] Niobium oxide, which is catalytically inactive for ethylene dimerization, becomes active for the reaction by irradiation with ultraviolet light in the presence of ethylene. The catalyst once activated by the irradiation maintains its activity after the irradiation is ceased. This phenomenon has been attributed to the formation of Nb^{4+} ions, which are active sites for the reaction, by the reduction of Nb^{5+} ions with ethylene under the irradiation. If Nb^{4+} ions are readily oxidized by a proper oxidant, this photo-system can be designed as a photo-redox cycle.

The authors have found that 2-propanol is continuously converted to acetone in the presence of oxygen gas on niobium oxide supported on porous Vycor glass under irradiation with ultraviolet light. This paper deals with kinetic and spectroscopic investigations of this photocatalysis system to clarify the role of the niobium species in the photo-redox cycle.

Experimental

Materials. Porous Vycor glass was purchased from Corning Glass Works. Niobium pentachloride was kindly supplied from Professor M. Nangyo at Tohoku University. Its purity of 99.96% has been guaranteed. 2-Propanol purchased from Wako Chemical Co. was dried with molecular sieve 5A and thoroughly degassed before use.

Preparation of Catalyst. Porous Vycor glass of ca. 1 mm thickness was calcined at 550 °C in oxygen gas and then soaked at room temperature into a solution of niobium pentachloride in concentrated hydrochloric acid (0.5 mol-Nb l-HCl_{aq}^{-1}). After 12 h, the glass was washed with deionized water and stored in the water for 12 h to ensure hydrolysis of niobium chloride in the pore system of the Vycor glass. The amount of supported Nb, determined by radioactivation analysis, was 3 wt%-Nb_2O_5. The weights of the catalyst used were 0.356 and 0.482 g for the reaction experiments and the spectroscopic measurements, respectively. The catalyst is denoted by Nb_2O_5/PVG hereafter.

Apparatus. The reaction was carried out in a conventional gas-circulating system with a reaction volume of 149 ml, connected to a vacuum system. A reactor (Fig. 1-a) was made of quartz glass whose bottom was a flat, transparent quartz plate. The catalyst was laid on the bottom, through which the catalyst was irradiated by the light of a medium-pressure mercury lamp. The reaction temperature was controlled by an electric furnace whose bottom was open for the irradiation.

For measurements of visible and ultraviolet absorption spectra, a quartz-made rectangular cell was used, where the catalyst could be treated in the same way as in the reaction experiments. A small room is attached at the top of the cell for admitting oxygen gas onto the catalyst during the measurements. The catalyst was placed as shown in Fig. 1-b. A spectrometer, Shimadzu UV-200, was employed for light absorption measurements.

Procedures. The catalyst, Nb_2O_5/PVG, was treated with oxygen in the reactor at 500 °C for 1 h and degassed at the same temperature for 1 h before the reaction. The reaction was initiated by the irradiation after 2-propanol and oxygen gas were introduced into the reaction system. A portion of a

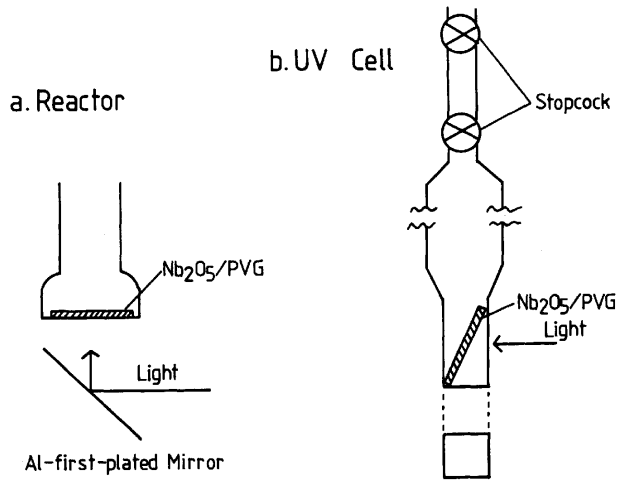

Fig. 1. Reactor and container of catalysts for VIS-UV absorption measurements.

reaction mixture was taken at appropriate time interval and analyzed by gas chromatography. A column (2 m) with packing, PEG 20M on Chromosorb W/AW, was used at 80 °C for the chromatography.

Results

It has been found that acetone was produced from the mixture of 2-propanol and oxygen gas on niobium oxide supported on porous Vycor glass under the irradiation at room temperature. No acetone was detected without the irradiation even at 100 °C. Propene, acetaldehyde, and CO_2 were observed beside acetone. They were less than 1% in yield even after the reaction was performed for 3 h. Figure 2 shows the formation of acetone along the irradiation time on Nb_2O_5/PVG, at room temperature (23—26 °C). Acetone was produced proportionally to the duration of the irradiation.

When no oxygen was present in the reaction system, the formation of only a small amount of acetone was observed within 60 min of the reaction time and its amount was not increased further (see Fig. 2). The acetone formation started again by the addition of oxygen and its rate was the same as that in the presence of oxygen gas. The catalyst was turned to black in color with a bluish cast after the reaction without oxygen gas, suggesting that niobium ion (IV) was produced during the reaction. The catalyst returned to transparent immediately by the addition of oxygen gas.

Figure 3 is a dependence of the rate of the acetone formation on a pressure of oxygen gas. A curve fits to the Langmuir-Hinshelwood type rate equation where the rate follows the first order of the amount of adsorbed oxygen (Eq. 1).

$$r = \mathrm{d(acetone)}/\mathrm{d}t = kKP(O_2)/\{1 + KP(O_2)\} \quad (1)$$

where k and K are constants and $P(O_2)$ denotes a pressure of oxygen gas.

The effect of the reaction temperature was examined in the range of the temperature, 75—150 °C. Rather large amount of propene was produced at these temperatures. This type of dehydration of 2-propanol took place in a dark in the same rate as in the irradiation. Figure 4 shows an Arrhenius type plot of the acetone formation rate. The apparent activation energy of 23 kJ mol^{-1} was estimated from the linear line of the plot.

In order to reveal an effective region of the wavelength to the dehydrogenation, light filters were inserted in between the reactor and the light source. Figure 5 shows that the light of wavelength shorter than 300 nm was effective for the reaction.

Oxidants other than oxygen, such as NO and N_2O, were tested. NO acted as an oxidant, but, the reaction rate was slower by a factor of 3 than when oxygen gas was used. When N_2O was used, the amount of acetone and its change along the irradiation time were the same as those observed in the absence of any oxidant as mentioned above.

UV-Absorption Analysis. As described in the previous section, the color of the catalyst turned to black

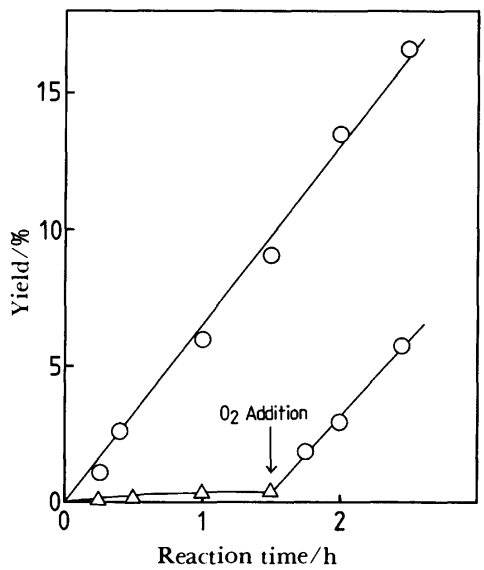

Fig. 2. Acetone formation along the irradiation time. Reaction temperature, 25 °C. 2-Propanol, 3.1×10^{-4} mol. Pressure of oxygen, 40 Torr (1 Torr= 1.33×10^2 Pa). (○) In the presence of O_2, and (△) in the absence of O_2.

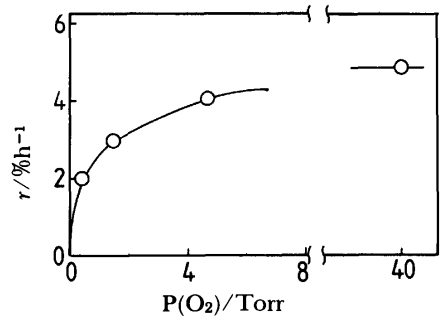

Fig. 3. Dependence of the reaction rate on oxygen pressure. Reaction temperature, 25 °C. 2-Propanol, 3.1×10^{-4} mol.

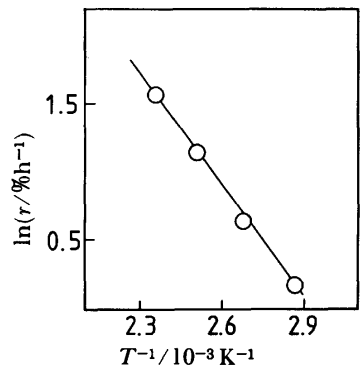

Fig. 4. Dependence of the rate of acetone formation on the reaction temperature. 2-Propanol, 3.4×10^{-4} mol. Pressure of oxygen, 40 Torr.

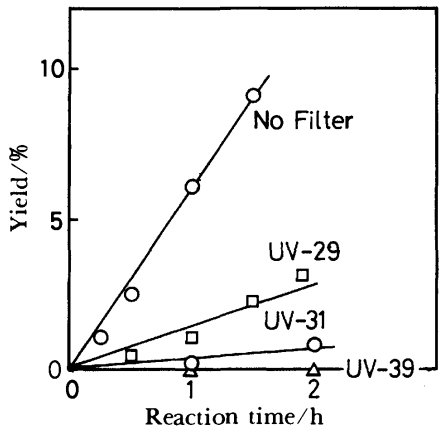

Fig. 5. Effect of the light filters on the reaction. Reaction temperature, 25°C. 2-Propanol, 3.4×10^{-4} mol. Pressure of oxygen, 40 Torr. The notation of the filters is after Toshiba Co. The number of filter denotes one tenth of the wavelength at 50% reduction of light intensity transmitted.

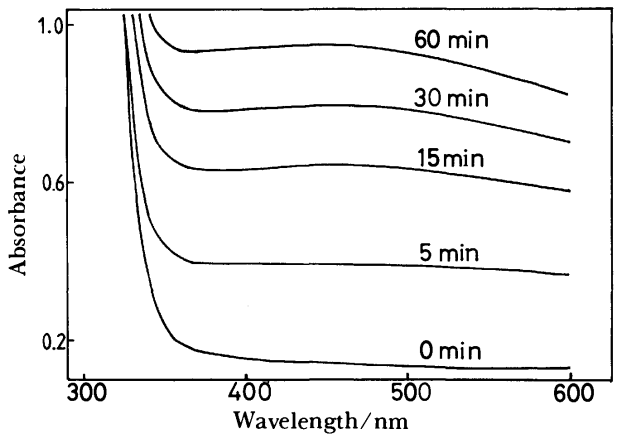

Fig. 6. VIS-UV absorption spectra of Nb_2O_5/PVG photoreduced by 2-propanol. The numbers shown are the irradiation times.

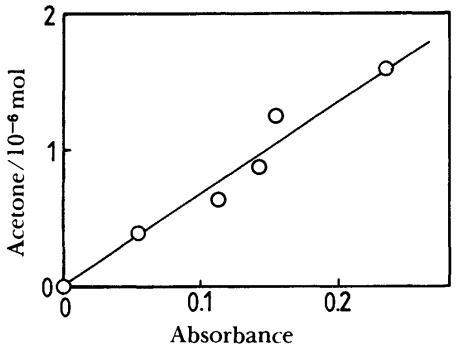

Fig. 7. Relation between the absorbance at 450 nm of the photoreduced Nb_2O_5/PVG and the amount of acetone formed.

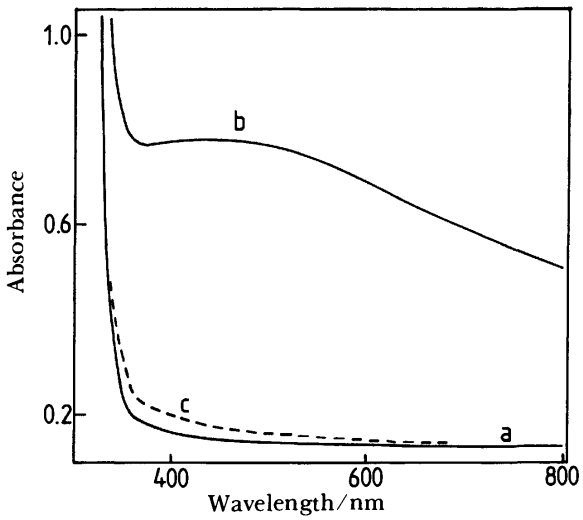

Fig. 8. Change in the VIS-UV absorption spectrum of photoreduced Nb_2O_5/PVG by the admission of oxygen. (a) Before the photoreduction, (b) photoreduced, (c) after O_2 admission to the sample of (b).

with bluish cast by UV irradiation in the presence of 2-propanol alone. This change in color suggests the formation of Nb^{4+} ion.

Figure 6 shows VIS-UV absorption spectra of the catalyst observed before and after the irradiation. The sample strongly absorbed UV light of wavelength shorter than 300 nm. After the irradiation in the presence of only 2-propanol, a broad absorption band appeared in the region from UV to visible light, corresponding to the color change of the catalyst observed when the reaction was carried out without oxygen gas.

An absorption maximum is distinguished at 450 nm in the spectra shown in Fig. 6. It has been reported that Nb^{4+} in an aqueous oxalic-acid solution has an absorption maximum at around 450 nm.[5] Compared to the latter absorption spectrum, the absorption band observed for the oxide supported on the glass was very broad. The broadening of absorption bands observed for a condensed phase is rather general phenomenon in the observation of electronic spectra. Therefore, the absorption band of the Nb_2O_5/PVG observed after the irradiation in the presence of only 2-propanol is attributed to Nb^{4+} ion which is situated on the surface of the porous glass in its rather strong interaction with either the silica network of the glass or the niobia framework supported on the glass. It is suggested that the Nb^{4+} ion must be produced through reduction of Nb_2O_5 by 2-propanol, being converted to acetone at the same time. Figure 7 represents a relation between the amount of acetone formed during the various irradiation times and the absorbance at 450 nm of the catalyst measured after the irradiation. Acetone was collected by degassing the catalyst after a certain irradiation time of the catalyst with UV light in the presence of only 2-propanol. A proportional relationship between the two values rationalized the above suggestion for the path of the Nb^{4+} ion production.

Transient Analysis of Reoxidation of Catalyst. Figure 8 shows a change in the spectrum of the photoreduced catalyst by its exposure to oxygen gas. The

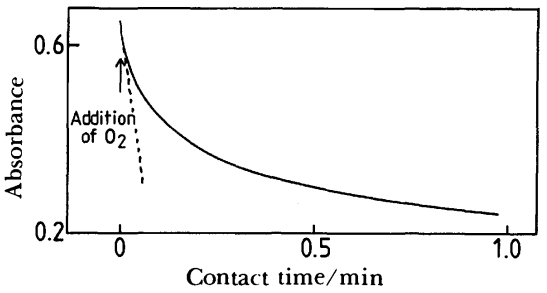

Fig. 9. Decrease of the absorbance at 450 nm by the admission of oxygen.

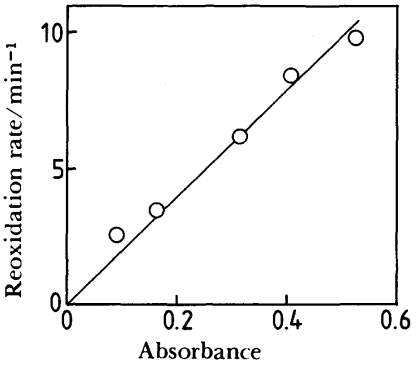

Fig. 10. Dependence of the Nb^{4+} reoxidation rate on the absorbance at 450 nm.

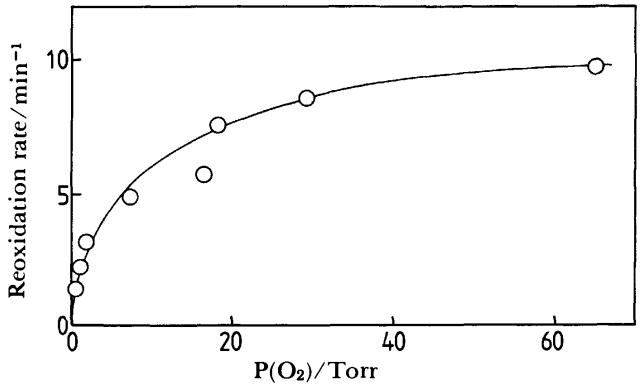

Fig. 11. Dependence of the Nb^{4+} reoxidation rate on the pressure of oxygen.

absorption band disappeared immediately by the exposure, indicating that Nb^{4+} was reoxidized easily by oxygen gas. The spectrum measured after the exposure was almost coincident with that observed before the reduction. The change of the absorbance at 450 nm could be recorded continuously by admitting oxygen gas onto the photoreduced catalyst (Fig. 9). Since the absorbance corresponds to the concentration of Nb^{4+} species, the result in Fig. 9 shows that the rate of the oxidation of the Nb^{4+} species decreases with increasing the exposure time, but the oxidation completed 80% within 1 min. This method allowed kinetic investigation of the reoxidation of the catalyst. The initial rate of the oxidation was evaluated from the slope of the dotted line drawn in Fig. 9 at the contact time, 0 min. Figures 10 and 11 show the dependencies of the initial rate on the initial absorbance of Nb^{4+} species and on the pressure of oxygen admitted on the catalyst showing a constant, initial absorbance of Nb^{4+} species, respectively. It is concluded from the two figures that the oxidation rate follows the first order kinetics on the concentration of Nb^{4+} on the surface and depends upon the concentration of oxygen molecules in a Langmuir-Hinshelwood type of equation as follows.

$$r = k[Nb^{4+}]KP(O_2)/\{1 + KP(O_2)\} \quad (2)$$

Discussion

Photoreduction. The present spectroscopic investigation has shown that the irradiation causes photoreduction of Nb^{5+} in the oxide to Nb^{4+} in the presence of 2-propanol. Visible and ultraviolet absorption spectrum of thin film of niobium oxide has shown the light absorption below 400 nm,[6] which overlaps to the same region (<300 nm) effective for the reaction of 2-propanol photooxidation. The linear relationship between the amount of formed acetone and the absorbance of Nb^{4+} on the catalyst (Fig. 7) shows that alcohol reacts with Nb^{5+} to produce acetone and Nb^{4+} according to the stoichiometry described in the Reaction i.

$$Nb^{5+}\text{-}O^{2-}\text{-}Nb^{5+} + CH_3CH(OH)CH_3 \rightarrow 2Nb^{4+} + CH_3COCH_3 + H_2O \quad (i)$$

As far as the homogeneous character of Nb^{4+} species formed in the Reaction i is supposed, its absorption coefficient at 450 nm was evaluated to be 1.5×10^6 mol^{-1} g-cat. cm^{-1} from the slope of the line in Fig. 7 and the thickness of the catalyst, 1 mm. Nb^{4+} formed by photoreduction must be present only on the surface and cannot migrate into the bulk of the niobium oxide, since the reduction occurs at room temperature. The amount of Nb^{4+} estimated from the stoichiometry of the Reaction i is 3.4×10^{-6} mol g-cat.$^{-1}$ for the catalyst photoreduced for 15 min. This amount corresponds to 1.3% of the total Nb^{5+} ions supported on the glass.

When titanium oxide was irradiated in the presence of alcohol, the color of the oxide turned to purple, showing that the photoreduction occurred.[7] This is essentially the same phenomenon as was observed for the present Nb_2O_5/PVG system.

Photoactivation of niobium oxide observed for the dimerization of ethylene has been explained by the photoreduction of the niobium oxide, which results in the formation of Nb^{4+} species by the photoreduction, which acts as an active site for ethylene dimerization.[4] Thus the niobium oxide is generally photoreduced in the presence of an organic reductant such as alcohols or olefins to give Nb^{4+} species.

Reoxidation. Nb^{4+} formed by the photoreduction is readily reoxidized by oxygen gas at room tempera-

ture as shown in Fig. 8. The oxidation curve in Fig. 9 fits to Elovich equation, suggesting that Nb^{4+} ions are heterogeneous in their reactivity for oxygen.

The rate equation for the reoxidation, obtained as shown by Eq. 2, indicates that Nb^{4+} species disappears through a reaction of adsorbed molecular oxygen, $O_2(a)$, with Nb^{4+}, as follows.

$$O_2 \rightleftarrows O_2(a) \quad \text{(ii)}$$

$$Nb^{4+} + O_2(a) \rightarrow Nb^{5+} - O_2^- \quad \text{(iii)}$$

It is plausible that O_2^- oxygen species must be formed at the first step of the reoxidation as shown in the Reaction iii. This is supported by the ESR observation that O_2^- is formed by oxygen admission on the silica-niobia which has been preliminarily reduced by hydrogen gas.[8] The O_2^- must be successively oxidized and finally converted to lattice oxygen (O^{2-}).

Catalytic Oxidation of 2-Propanol. The photooxidation of 2-propanol on Nb_2O_5/PVG proceeds via a redox mechanism of the oxide. The whole reaction steps are in the following.

$$Nb^{5+}\text{-}O^{2-}\text{-}Nb^{5+} + h\nu \rightarrow (Nb^{4+}\ O^-\text{-}Nb^{5+})^* \quad \text{(iv)}$$

$$(Nb^{4+}\ O^-\text{-}Nb^{5+})^* + \text{2-PrOH} \rightarrow 2Nb^{4+} + CH_3COCH_3 + H_2O \quad \text{(v)}$$

$$2Nb^{4+} + O_2 \rightarrow (Nb^{5+}\text{-}O_2^-\ Nb^{4+}) \quad \text{(vi)}$$

$$(Nb^{5+}\text{-}O_2^-\ Nb^{4+}) + 2Nb^{4+} \rightarrow 2(Nb^{5+}\text{-}O^{2-}\text{-}Nb^{5+}) \quad \text{(vii)}$$

This redox mechanism contains the photoreduction and the reoxidation discussed in the previous sections.

Yoshida et al. have proposed a redox mechanism for the photooxidation of CO and propene on V_2O_5 supported on silica.[9,10] The lattice oxygen of the oxide is responsible for the oxidation reaction in this mechanism.

Formenti et al. have proposed a mechanism of photooxidation of paraffin on TiO_2, where alcohols are formed from paraffins at first, and then the alcohols are converted to olefins, which are oxidized to ketones finally.[11] Since a small amount of propene was detected for the Nb_2O_5/PVG system, olefin can be an intermediate in the Reaction v.

A similarity of the rate equations of the acetone formation, Eq. 1, and of the reoxidation of the catalyst, Eq. 2, leads us to assume that the reoxidation, either of the reactions, vi or vii, is rate determining. In the mechanism of photodehydrogenation of alcohol on metal-supported titania proposed by Pichat et al.[7] and Herrmann et al.,[12] the abstraction of α-hydrogen from alcohol is rate determining. However the abstraction of hydrogen does not seem to be rate determining for the Nb_2O_5 system, because no isotope effect was observed when $CD_3CD(OD)CD_3$ was used as a reactant.

To get a general idea of 2-propanol photooxidation on metal oxides, literature data were compared as follows. The rate of the acetone formation in the present system was 4.0×10^{-7} mol s^{-1} for 1g of Nb_2O_5 at room temperature. Cunningham et al. have reported that the rates of the same reaction on irradiated TiO_2 and ZnO were 3×10^{-8} and 8×10^{-9} mol s^{-1} g^{-1}, respectively.[13] The rate calculated from the data for TiO_2 in the report by Bickley et al. was 1.2×10^{-10} mol s^{-1} g^{-1}.[14] The formation of acetaldehyde on TiO_2 has been 10 times slower than that of acetone.[13] On ZnO the two products were formed almost at the same rate.[13] The amount of acetaldehyde formed during the reaction on niobium oxide supported on porous Vycor glass was less than 1/50 of acetone. Although comparison in experimental procedures and conditions, i.e., a shape of a reactor, intensity and energy distribution of light, and a form of a catalyst, must be taken into account among these photocatalytic systems, the difference between the photocatalytic performances of TiO_2 or ZnO and that of niobium oxide is so large that it can be mentioned that niobium oxide is more active than TiO_2 and ZnO in the photooxidation of 2-propanol and far more selective for the formation of acetone.

The present research was supported by a Grant of the Asahi Glass Foundation for Industrial Technology.

References

1) Ti: P. Pichat "Photoelectrochemistry, Photocatalysis, and Photoreactors," ed by M. Schiavello, D. Reidel Publishing Company, 1985, p. 425. S. J. Teichner and M. Formenti, in the same book, p. 457. Mo: M. Anpo, I. Tanahashi, and Y. Kubokawa, *J. Chem. Soc., Faraday Trans. 1*, **78**, 2121 (1982). V: M. Anpo, I. Tanahashi, and Y. Kubokawa, *J. Phys. Chem.*, **84**, 3440 (1980). S. Yoshida, Y. Matsumura, S. Noda, and T. Funabiki, *J. Chem. Soc., Faraday Trans. 1*, **77**, 2237 (1981).

2) H. Shaefer, R. Gruehn, and F. Shule, *Angew. Chem.*, **78**, 28 (1966).

3) P. Clechet, J. R. Martin, R. Olier, and C. Vollny, *C. R. Acad. Sci. Paris*, **282C**, 887 (1976).

4) A. Morikawa, T. Nakajima, I. Nishiyama, and K. Otsuka, *Nippon Kagaku Kaishi*, **1984**, 239; A. Morikawa, T. Nakajima, I. Nishiyama, and K. Otsuka, Proc. 8th Intern. Congr. Catal., **4**, 815 (1984).

5) R. E. Elson, *J. Phys. Chem.*, **75**, 4193 (1953).

6) D. C. Conlon and W. P. Doyle, *J. Chem. Phys.*, **35**, 752 (1961).

7) P. Pichat, J.-M. Herrmann, J. Disdier, H. Courbon, and M.-N. Mozzanega, *Nouv. J. Chim.*, **5**, 627 (1981).

8) Unpublished data.

9) S. Yoshida, Y. Matsumura, S. Noda, and T. Funabiki, *J. Chem. Soc., Faraday Trans. 1*, **77**, 2237 (1981).

10) S. Yoshida, T. Tanaka, M. Okada, and T. Funabiki, *J. Chem. Soc., Faraday Trans. 1*, **80**, 119 (1984).

11) M. Formenti, F. Juillet, and S. J. Teichner, *Bull. Soc. Chim. France*, **1976**, 1031, 1315.

12) J. M. Herrmann and P. Pichat, "Spillover of adsorbed species," Studies in Sur. Sci. Catal., **17**, ed by G. M. Pajonk, S. J. Teichner, and J. E. Germain, Elsevier (1983), pp. 77—87.

13) J. Cunningham and B. K. Hodnett, *J. Chem. Soc., Faraday Trans. 1*, **77**, 2777 (1981).

14) R. I. Bickley, G. Munuera, and F. S. Stone, *J. Catal.*, **31**, 398 (1973).

 © 1987 The Chemical Society of Japan Bull. Chem. Soc. Jpn., 60, 3515—3518 (1987)

New Discogenic Compounds: *N,N'*-Dialkanoyl-2,3,5,6-tetrakis-(alkanoyloxy)-1,4-benzenediamines

Yukio KOBAYASHI and Yoshio MATSUNAGA*
Department of Chemistry, Faculty of Science, Hokkaido University, Sapporo 060
(Received April 18, 1987)

A series of *N,N'*-dialkanoyl-2,3,5,6-tetrakis(alkanoyloxy)-1,4-benzenediamines has been prepared and found to be mesogenic over a wide temperature range. The transformation into an isotropic liquid at a temperature between 189 and 209 °C is followed by thermal decomposition. The X-ray diffraction pattern of unoriented specimens in the mesophase consists of two sharp inner peaks and a broad outer one assignable to 100, 110, and 001 reflections respectively, indicating that the phase is hexagonal columnar.

A number of single compounds composed not only of elongated molecules but also of disk-like molecules are known to form stable or metastable thermotropic liquid crystals.[1,2] The first series of the latter group was discovered by Chandrasekhar et al. in 1977.[3,4] The compounds examined by them were hexakis(alkanoyloxy)benzenes (**1**), which were synthesized forty years earlier by Backer and van der Baan.[5] The discotic mesophase is observable only when n=6, 7, and 8. The temperature ranges are 5.8 and 3.6 °C in the first and the second members respectively. The mesophase appearing in the last member is metastable. In these mesophases, the disk-like molecules are stacked one on top of the other in columns forming a hexagonal arrangement but the spacing between the molecules in each column is irregular. As the substituent $NHCOC_nH_{2n+1}$ is efficient to promote the thermal stability of nematic and smectic phases,[6,7] the partial replacement of $OCOC_nH_{2n+1}$ groups in the above-mentioned hexasubstituted benzenes by $NHCOC_nH_{2n+1}$ groups might also stabilize discotic phases. Therefore, we have undertaken a study of *N,N'*-dialkanoyl-2,3,5,6-tetrakis(alkanoyloxy)-1,4-benzenediamines (**2**). A discotic mesophase was found over temperature ranges as wide as 140 °C when n=4 to 15.

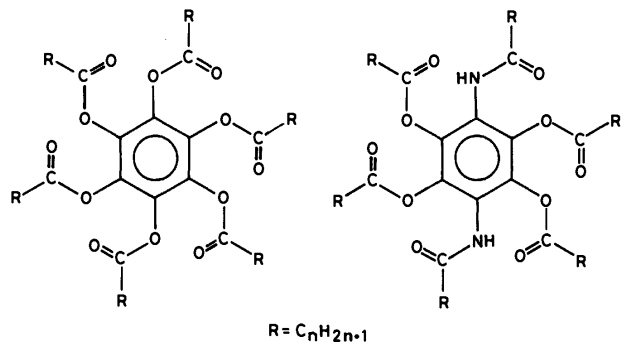

1 **2**

Experimental

Materials. The sodium salt of 2,5-dihydroxy-3,6-dinitro-*p*-benzoquinone prepared by starting from *p*-chloranil was reduced to 3,6-diamino-1,2,4,5-benzenetetrol according to Nietzki and Benckiser.[8] The acylation was carried out employing acyl chloride in the presence of pyridine. For example, Found: C, 68.09; H, 9.61; N, 3,31%. Calcd for $C_6(NHCOC_6H_{13})_2(OCOC_6H_{13})_4$: C, 68.21; H, 9.54; N, 3.31%. Found: C, 73.90; H, 11.24; N, 2.33%. Calcd for $C_6(NHCOC_{11}H_{23})_2(OCOC_{11}H_{23})_4$: C, 74.00; H, 11.15; N, 2.21%. Hexakis(heptanoyloxy)benzene to be used as a reference discogen was prepared by the reaction between heptanoic anhydride and benzenehexol.[5] The latter compound was derived from the diaminobenzenetetrol.[8]

Measurements. Calorimetric curves up to the transition to isotropic liquids were recorded on a Rigaku Thermoflex differential scanning calorimeter at a heating rate of 5 K min^{-1}. The enthalpy changes were estimated by comparing the peak areas with that due to the melting of indium, 3.26 kJ mol^{-1}. The phase diagram was determined by the calorimetric curves of mixtures at every ten mol%. X-Ray diffractions were measured with a Rigaku auto-diffractometer, model RAD IVB, using filtered copper radiation. Proton NMR spectra were recorded as the first derivatives at 40 MHz, using a JEOL model JES-ME-3X spectrometer with a broad-line NMR attachment, model JES-BE-1, which employs a crossed-coil system.

Results and Discussion

The thermal properties of *N,N'*-dialkanoyl-2,3,5,6-tetrakis(alkanoyloxy)-1,4-benzenediamines are summarized in Table 1. Here, K, D, and I stand for crystalline, discotic, and isotropic phases respectively. No solid-solid transition is observed above room temperature for any member. The valeryl derivative (n=4)

Table 1. Transition Temperatures (°C) and Enthalpy Changes (kJ mol^{-1}) of Compounds **2**[a]

n[b]	K		D		I
3	.		219 (53)		.
4	.	134 (26)	.	208 (45)	.
5	.	71 (18)	.	209 (45)	.
6	.	64 (28)	.	208 (40)	.
7	.	75 (39)	.	205 (37)	.
8	.	77 (50)	.	200 (36)	.
9	.	77 (62)	.	199 (33)	.
10	.	81 (65)	.	198 (31)	.
11	.	89 (82)	.	197 (28)	.
13	.	92 (103)	.	189 (22)	.
15	.	94 (115)	.	190 (18)	.

a) The latter quantities are in parentheses. b) The number of carbon atoms in the alkyl group.

forms a viscous birefringent fluid upon the transition located at 134 °C. All the higher homologous members melt below 100 °C. It is noted that the melting (K-D transition) points of the heptanoyl, octanoyl, and nonanoyl derivatives (n=6, 7, and 8) are not far from those of the compounds **1** with the same alkyl groups, 81, 80, and 80 °C respectively. On the other hand, the clearing (D-I transition) point is at a temperature higher than 200 °C in the case of the valeryl to nonanoyl derivatives and gradually lowers as the series is ascended. Thus, the temperature range of the mesophase is so expanded upwards by the replacement that the D-I transition of compound **2** is followed by thermal decomposition. The enthalpy of the D-I transition decreases with the increase of the alkyl chain length as is known for discotic hexasubstituted triphenylenes by the work of Destrade et al.[9] The same tendency may be noted also for the short series of compounds **1**. However, the value in the present compound is larger almost by a factor of two than that of the corresponding member in the series **1**. For example, 40 kJ mol^{-1} versus 22.2 kJ mol^{-1} when n=6.

The X-ray diffraction patterns of unoriented liquid crystals were measured at temperatures 10 to 15 °C below the clearing point. The major feature resembles that known for smectic A or C phase. The innermost peak is sharp and strong and is often accompanied by the second order reflection. An additional weak sharp peak is found in all the diffraction patterns. The spacing given by the former peak increases linearly within the limits of our experimental errors from 1.36 nm of the valeryl derivative to 2.37 nm of the hexadecanoyl derivative (n=15) and that given by the latter from 0.79 to 1.37 nm (see Fig. 1). These two spacings are in a ratio of about $1/\sqrt{3}$ characteristic of a hexagonal lattice. Therefore, the strong inner peak may be assigned to 100 reflection and the weak one to 110 reflection. This observation is interpreted by the presence of lamellar order with hexagonal symmetry in two dimensions in agreement with that reported for compounds **1**.[3,4] The diffuseness of the outer peak assignable to the 001 reflection must be evidence of the liquid-like disorder in the third dimension. The mean intermolecular spacing calculated using the formula $2d_{001}=\lambda/\sin\theta$ is 0.47 nm throughout the series **2** and essentially agrees with the values reported for compounds **1**, namely, 0.46 nm.

The identification of the mesophase is supported by an uninterrupted miscibility between the phases of compounds **1** and **2**. Figure 2 presents the diagram of the binary system composed of *N*,*N*′-dinonanoyl-2,3,5,6-tetrakis(nonanoyloxy)-1,4-benzenediamine (n=8) and hexakis(heptanoyloxy)benzene (n=6) as the reference discogenic compound. The open and shaded circles on the reference compound-rich side (the right-hand side) show the transitions recorded on the calorimetric curves during the processes of heating and cooling respectively, while recording during cooling on the other side was not made because of the thermal instability of compound **2** at high temperatures. The D-I transition does not occur sharply and the curve exhibits a minimum around 72.5 °C and 60 mol% of the reference compound. The destabilization of the mesophase by mixing may account for the differences in the geometrical, chemical, and mechanical properties of the component molecules. The estimated ratio of spacings is about 1.3. Such a value is known to be large

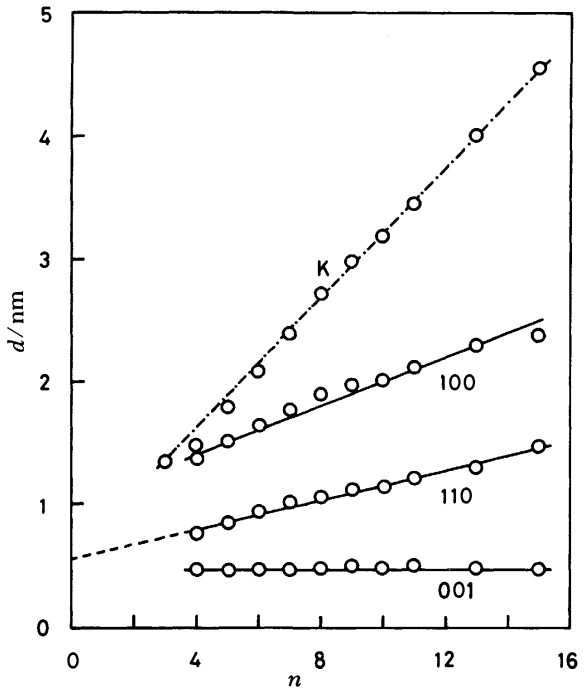

Fig. 1. Plot of spacings against the number of carbon atoms in the alkyl group for compounds **2**.

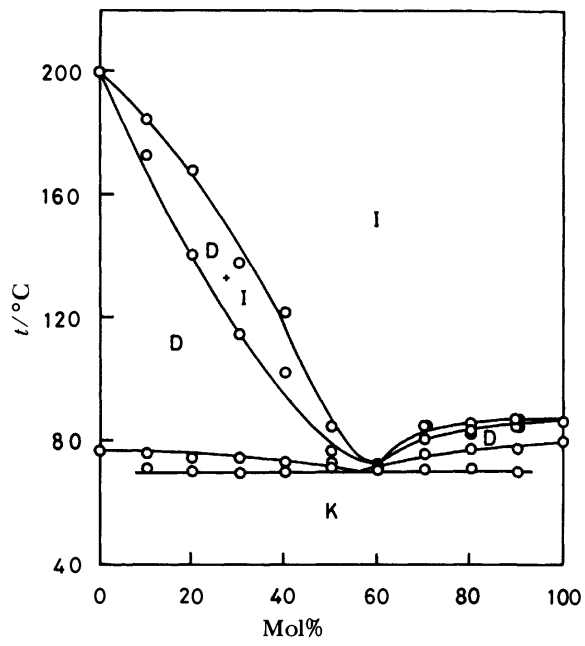

Fig. 2. Phase diagram of the compound **2** (n=8)–compound **1** (n=6) system. The former compound is located on the left-hand side.

enough to produce a marked deviation from a straight line even when the monomolecular smectic A phases of two homologous members are mixed.[10] Although this minimum lies close to the eutectic point, these two are readily distinguished from each other in the process of cooling because the I-D transition is never delayed but the discotic phase is markedly supercooled.

The spacing d_{100} in the mesophase of compound **1** reported by Chandrasekhar et al. is 1.50 nm for the octanoyl derivative and 1.59 nm for the nonanoyl derivative. The corresponding values for compounds **2** are appreciably longer; that is, 1.77 and 1.89 nm. The paraffinic chains in the present compounds are apparently more stretched and conformationally less disordered than those in compounds **1**. Such a dissimilarity is well indicated by the much larger enthalpy and entropy changes at the clearing point shown by compounds **2**. As is seen in Fig. 1, a linear relationship is found between n and the longest spacing in the crystalline phase, suggesting that the crystal structure is similar throughout this homologous series. The spacing shrinks only slightly upon melting when n=4 but by a factor of more than two when n=15. This behavior is not contradictory to the thermal data since the enthalpy change at the melting point increases remarkably with the increase of the alkyl chain length; for example 18 kJ mol^{-1} in the hexanoyl derivative and 115 kJ mol^{-1} in the hexadecanoyl derivative.

It may be added that the d_{110} value obtained by the extrapolation to n=0, 0.55 nm, is in good agreement with the radius estimated for the core structure, $C_6(NHCHO)_2(OCHO)_4$. Although rotation of the whole molecule about the normal to the molecular plane and the fluctuations of this axis around the preferred aromatic director are conceivable in the discotic phase,[11] the coincidence may be considered as an indication that the disk planes are, on an average, perpendicular to the columns in which the molecules are stacked.

The increment of spacing d_{110} per methylene group in the mesophase is merely 0.05 nm and is much shorter than that expected for the all-trans configuration of alkyl chains, 0.128 nm. Therefore, the longer the alkyl groups the faster on the NMR time scale, conformational changes of the alkyl groups are more extensive, resulting in more significant softening of the paraffinic crown. This proposition is in accordance with the considerable decrease of enthalpy change upon the D-I transition as the series is ascended. The change in the extent of liquid-like characteristic in the mesophase by the alkyl chain length is also manifested by the following proton second moments (the mean-square widths of the resonance lines), $\langle \Delta H^2 \rangle$, above the melting point; 0.3 G^2 (G=10^{-4} T) in the case of the octanoyl derivative and 0.03 G^2 in the case of the hexadecanoyl derivative. As is shown in Fig. 3, the moment measured at room temperature is as large as

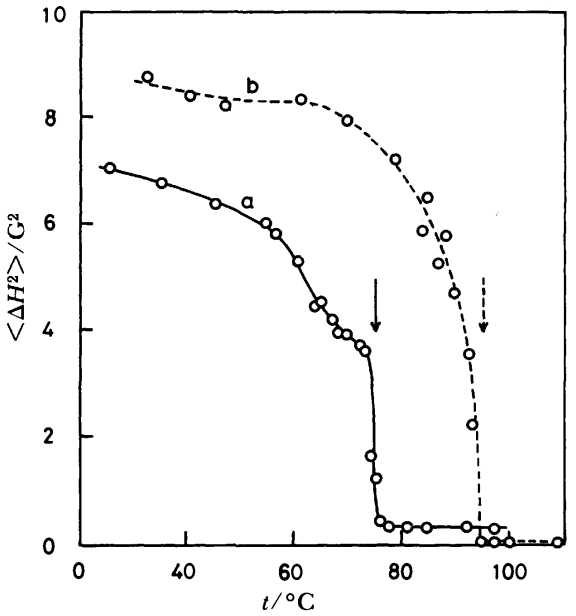

Fig. 3. Second moments of the broad-line proton NMR spectrum of compound **2**, (a) n=7 and (b) n=15. The vertical arrow indicates the melting point determined by calorimetry.

about 7 G^2 for the former compound and about 9 G^2 for the latter. It decreases gradually as the temperature is raised and then sharply near the transition temperature. The vertical arrows in this figure indicate the transition points determined by calorimetry.

In conclusion, the substituent $NHCOC_nH_{2n+1}$ is an efficient group to promote the thermal stability of hexagonal columnar mesophase. As noted by Gray in his reasoning why the nematic and smectic efficiencies of $NHCOCH_3$ group are high,[12] the polarizable substituent employed by us has a strong dipole and can form hydrogen bonds. The dipole-dipole interaction and intermolecular hydrogen bonding operating across the molecular plane appear to contribute greatly to the enhancement of thermal stability of the discotic mesophase.

This work was supported by a Grant-in-Aid for Scientific Research No. 60470001 from the Ministry of Education, Science and Culture.

References

1) J. Billard, "Liquid Crystals of One- and Two-Dimensional Order," ed by W. Helfrich and G. Heppke, Springer-Verlag, Berlin (1980), pp. 385—395.

2) S. Chandrasekhar, "Advances in Liquid Crystals, Vol. 5," ed by G. H. Brown, Academic Press, New York (1982), pp. 47—78.

3) S. Chandrasekhar, B. K. Sadashiva, and K. A. Suresh, *Pramana*, **9**, 471 (1977).

4) S. Chandrasekhar, B. K. Sadashiva, K. A. Suresh, N. V. Madhusudana, S. Kumar, R. Shashidhar, and G. Venkatesh, *J. Phys. (Paris)*, **40**, C3-120 (1979).

5) H. J. Backer and S. van der Baan, *Rec. Trav. Chim.*, **56**, 1161 (1937).
6) E. Chino, Y. Matsunaga, and M. Suzuki, *Bull. Chem. Soc. Jpn.*, **57**, 2371 (1984).
7) Y. Matsunaga and M. Terada, *Mol. Cryst. Liq. Cryst.*, **141**, 321 (1986).
8) R. Nietzki and T. Benckiser, *Ber.*, **18**, 499 (1885).
9) C. Destrade, M. C. Mondon, and J. Malthete, *J. Phys. (Paris)*, **40**, C3-17 (1979).
10) R. Dabrowski, B. Wazynska, and B. Sosnowska, *Liq. Cryst.*, **1**, 415 (1986).
11) V. Ruter, R. Blinc, M. Vilfan, A. Zann, and J. C. Dubois, *J. Phys. (Paris)*, **43**, 761 (1982).
12) G. W. Gray, "Liquid Crystals and Plastic Crystals, Vol. 1," ed by G. W. Gray and P. A. Winsor, Ellis Horwood, Chichester (1974), p. 125.

 © 1987 The Chemical Society of Japan Bull. Chem. Soc. Jpn., 60, 3519—3523 (1987)

Unimolecular Decomposition of Silane in Shock Waves

Hitoshi TANAKA, Mitsuo KOSHI,* and Hiroyuki MATSUI
Department of Reaction Chemistry, University of Tokyo, Hongo, Bunkyo-ku, Tokyo 113
(Received May 2, 1987)

Thermal decomposition of silane highly diluted in argon was studied behind incident shock waves at the temperatures ranging from 1250 to 1600 K. The decomposition course was followed by monitoring the infrared emission of silane at 4.4 μm. It was confirmed that the effects of consecutive reactions on the decay rate of silane were negligible under our experimental conditions. The unimolecular rate constants obtained directly from the decay curve of silane were found to be smaller than previous experimental values but consistent with the result of the recent trajectory-RRK calculation. It was also found that the addition of molecular hydrogen or nitrogen monoxide to the reactant mixtures had no effect on the decomposition rate of silane.

The homogeneous gas-phase decomposition of silane has already been investigated by several groups of workers. Various methods including static pyrolysis,[1-4] single pulse shock tube technique[5,6] and IR laser powered homogeneous pyrolysis[7,8] have been used to investigate the mechanistic detail of silane pyrolysis. Although some ambiguities on the role of the inhomogeneous production of hydrogen atoms are still remained,[9,10] the primary step of the homogeneous gas-phase decomposition has been now well established. At low temperature this step is the elimination of molecular hydrogen to form silylene.

$$SiH_4 \rightarrow SiH_2 + H_2 \qquad (1)$$

The homolytic cleavage of one SiH bond only becomes important at internal silane energies in excess of about 106 kcal mol^{-1} [11] (1 cal=4.184J). The conclusion has been supported by a consideration of symmetry of the reaction,[12] a calculation of the potential energy surface[13] and a trajectory-RRK calculation.[11]

Rate constants for the unimolecular decomposition of the Reaction 1 have already been measured by several investigators[1,2,5,6] and it was found that the reaction was in its pressure fall-off region at the atmospheric pressure and below. Purnell and Walsh[1] found that the rate constant of Reaction 1 was proportional to the square root of the total pressure. White et al.[3] observed the same pressure dependence in the similar pressure and temperature range and this pressure dependence was well explained by their RRKM calculations. However, the mechanism of the consecutive reactions of silylene is rather complex. Rate inhibition of the silane decay by molecular hydrogen which was attributed to the reverse process of the Reaction 1 was observed.[3] Also the reaction of silylene with silane would play a significant role on the silane loss rate.

It should be noted that all of these previous studies were based on the products analysis. If the decomposition process of silane has the induction period, as suggested by Newman et al.,[6] it might be difficult to get precise rate constant for the initiation reaction by the products analysis only. Time resolved measurement of silane concentration is desirable to investigate the mechanism of silane decomposition in details. Moreover, the published experimental works have been done for relatively high concentrations of silane, which made the roles of the consecutive reactions unclear, and the temperatures covered in these works have been limited to a relatively low range.

In the present study, we derived the unimolecular rate constant for the Reaction 1 directly from the time history of silane highly diluted in argon by monitoring infrared emission. The present study was performed for high temperatures up to 1600 K. The results were compared with those of the previous experimental and theoretical studies.

Experimental

A diaphragmless stainless-steel shock tube of 5 cm diameter was used. The driven section was 4 m in length and was evacuated to less than 2×10^{-6} Torr (1 Torr=133.322Pa) before charging it with a sample gas. The shock tube window (CaF_2) was located at 3.0 m downstream from the driver section. Highly diluted mixtures of silane (500 ppm) in argon were heated behind incident shock waves. The temperature, pressure and density of shocked gas were calculated from the shock velocity measured by piezo electric pressure gauges. The temperature and pressure of the reaction zone varied from 1250 to 1600 K and from 0.25 to 1.3 atm, respectively.

The intensity of the infrared emission at 4.4 μm, which could be attributed to the ν_3 fundamental band of silane, was monitored by an interference band pass filter (0.19 μm FWHM) and an InSb detector. The time response of the detection system was estimated to be less than 8 μs.

The gas mixtures were prepared manometrically with a calibrated diaphragm-type pressure gauge. Commercially available ultra-high purity gases (SiH_4: 99.9999%, Ar: 99.9995%, H_2: 99.9999%, and NO: 99.8%) were used without further purification.

Results and Discussion

An example of the time profile of 4.4 μm emission intensity is shown in Fig. 1. The intensity decreases exponentially behind the shock front and increases slowly near the contact surface of the shock wave. According to the recent ab initio calculation on the Si-containing species,[14] many of Si_2H_x and Si_3H_x

molecules have fundamental vibration-rotation bands in 4.5—4.7 μm region. For example, SiH_4, Si_2H_4, Si_2H_6, and Si_3H_8 have the fundamental bands at 4.56, 4.5, 4.63—4.66, and 4.63—4.69 μm respectively. Therefore it is possible that the observed emission is caused by not only SiH_4 but also other species like Si_2H_4. However, for the IR emission at initial decay this possibility is rejected by the following observations. 1) The decay of the emission intensity is described by a single exponential function as shown in Fig. 1. This implies that any product species which increase with time may not have significant contributions to the emission intensity, since the intensity goes down to the ground line before it shows gradual increase near the contact surface. 2) The solution of the simultaneous kinetic equations, which is discussed later in detail, predicts that the main reaction intermediates or products during the course of the silane decomposition under our experimental conditions are H_2, Si_2, Si, Si_2H_2, Si_3, and SiH_2. These species do not emit at 4.4 μm. 3) We also observed the emission at 4.87 μm with an interference band pass filter. The time profile of 4.87 μm emission intensity was the same as that of 4.4 μm intensity. No emission was observed at 5.22 μm. Therefore there is no significant contribution of the emission from SiH (4.88 μm), SiH_3 (5.0 μm), and SiH_2 (4.95 μm) to the emission at 4.4 μm.

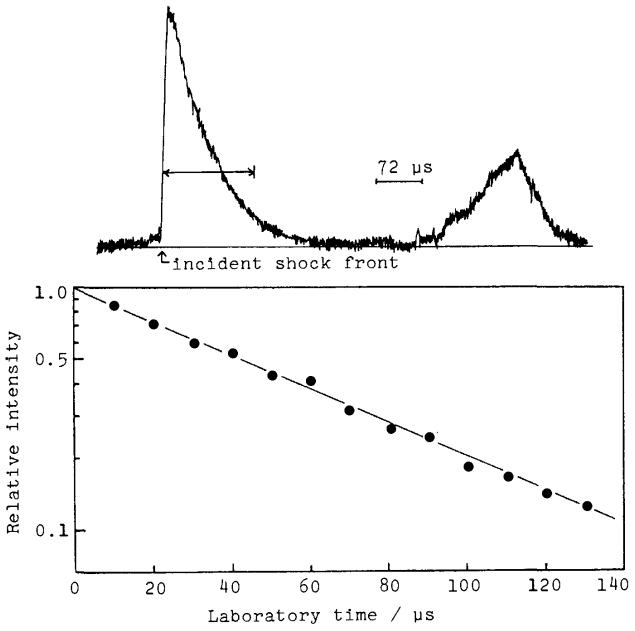

Fig. 1. Time history of the emission intensity at 4.4 μm. Upper panel: An example of the oscillogram trace. Lower panel: A log plot of the normarized intensity. T=1380 K, P=0.28 atm, 500 ppm SiH_4 in Ar. The region indicated by an arrow in the upper panel is plotted in the lower panel.

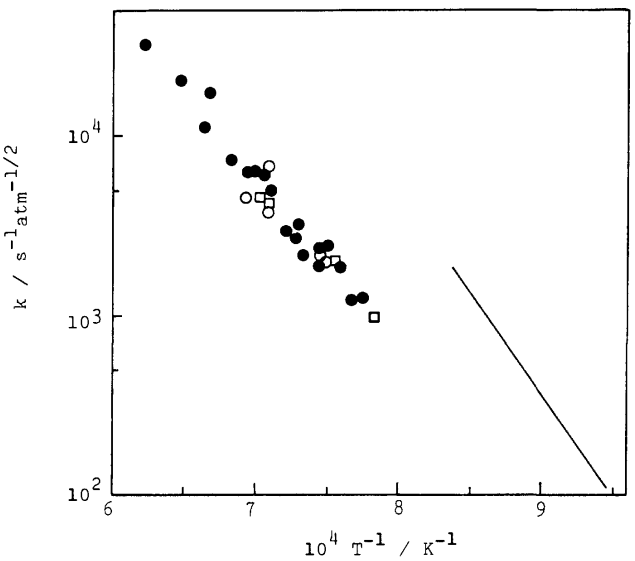

Fig. 2. Arrhenius plots of the pressure independent rate constants for the unimolecular decomposition of silane. k is defined by Eq. I in the text. Pressures of the experimental data are in the range of 0.25—1.2 atm. Closed circle: 500 ppm SiH_4 in Ar, open circle: 500 ppm SiH_4 in Ar with 1.1% H_2, open square: 500 ppm SiH_4 in Ar with 0.31% NO, line: from Ref. 6 (P=5.26 atm, 0.96% SiH_4 in Ar).

The origin of the slowly rising part of the emission profile near the contact surface is not clear. Only the decaying part of the emission intensity which was concluded to be proportional to the concentration of silane is analyzed in the present study. It was found that the first-order rate constants for the silane decay, k_{obs}, were proportional to a square root of the total pressure. Figure 2 shows Arrhenius plots of the pressure independent rate constants, k, which are defined by

$$k=k_{obs}P^{-1/2}, \quad \text{(I)}$$

where P is the total pressure. Irrespective of the total pressure ranging from 0.25 to 1.3 atm, all the experimental points can be very well represented by a single straight line. The least-squares analysis of the data gave the following Arrhenius expression:

$$k=10^{11.1\pm0.8}\exp(-(48.1\pm0.7)\ \text{kcal mol}^{-1}/RT)\ \text{atm}^{-1/2}\,\text{s}^{-1} \quad \text{(II)}$$

A square root pressure dependence of the rate of molecular hydrogen production and of silane decay was also found in static pyrolysis studies at low temperatures.[1,6] This pressure dependence has been well explained by the pressure fall-off behavior of the Reaction 1.[6] However, it is not obvious if the measured rate constants in the present study can be attributed to the rate constant of Reaction 1, because the overall reaction mechanism of the silane decomposition is rather complicated. White et al.[3] proposed the following reaction mechanism for the consecutive reactions of the homogeneous decomposition of silane at static system reaction temperatures.

$$SiH_2+SiH_4 \rightarrow Si_2H_6 \quad (2)$$

$$Si_2H_6 \rightarrow Si_2H_4+H_2 \quad (4)$$

Table 1. Reaction Mechanism

	Reaction				$\log A^{a)}$	$E^{a)}$	Reference
1.	SiH_4		$=SiH_2$	$+H_2$	11.1[b)]	48.1	This work
2.	SiH_2	$+SiH_4$	$=Si_2H_6$		12.45	1.3	3
3.	SiH_2	$+SiH_2$	$=Si_2H_4$		11.2	0.0	3
4.	Si_2H_6		$=Si_2H_4$	$+H_2$	14.4	52.2	3
5.	SiH_2	$+Si_2H_6$	$=Si_3H_8$		12.61	0.4	3
6.	Si_3H_8		$=SiH_3SiH$	$+SiH_4$	14.68	49.24	3
7.	Si_2H_4		$=Si_2H_2$	$+H_2$	14.50	53.0	3
8.	SiH_3SiH		$=Si_2H_4$		12.80	29.2	3
9.	Si	$+H_2$	$=SiH_2$		14.06	2.0	15
10.	SiH_2	$+Si_2$	$=Si_3$	$+H_2$	11.55	2.0	15
11.	SiH_2	$+Si_3$	$=Si_2H_2$	$+Si_2$	11.16	18.8	15
12.	Si_2	$+H_2$	$=Si_2H_2$		13.19	2.0	15
13.	Si_2	$+H_2$	$=SiH$	$+SiH$	13.19	40.0	15
14.	Si_3	$+H_2$	$=Si_2H_2$	$+Si$	12.99	42.6	15

a) Arrhenius parameters for the rate constants in the forward direction written in the form $k=A\exp(-E/RT)$. The units of A depend on the reaction order, but are given in terms of moles, cubic centimeters and seconds. E is in kcal mol^{-1}. b) See text for discussion of the pressure dependence. Listed value is for P=1 atm.

They suggested that the rate acceleration by these reactions might occur when silane conversion was less than 30%. Consequently the induction period on the silane loss was expected. At conversions greater than 40%, a gradual rate deceleration with increasing deviations from first-order kinetics was observed.[3] This rate inhibition was attributed to the contribution of the back reaction of hydrogen and silylene.

$$SiH_2+H_2\rightarrow SiH_4 \qquad (-1)$$

White et al.[3] further suggested that the silylene dimerization-decomposition reactions, 3, −3, and 7, might play a significant role on the silane decay rate over the temperature range of the single pulse shock tube experiments by Newman et al.[5,6]

$$SiH_2+SiH_2 \rightarrow Si_2H_4 \qquad (3)$$

$$Si_2H_4 \rightarrow Si_2H_2+H_2 \qquad (7)$$

In the present study, the induction period on the silane decay was not observed. Moreover, no effect of the addition of molecular hydrogen to the reactant mixtures was observed. This is evident in Fig. 2 in which the pressure independent rate constants obtained with the addition of 1.1% molecular hydrogen are shown. This is consistent with the single exponential decay of sliane during the entire course of the decomposition. This behavior of the silane decay can be explained if the Reaction 3 is much faster than the Reactions 2 and −1 in our experimental conditions. If this is the case, the rate constants for the initial decay observed in the present study correspond directly to the rate constants for the Reaction 1 only. In order to confirm the validity of this prediction, the simultaneous kinetic equations for the various species were numerically solved based on the reaction mechanism and the rate constants listed in Table 1. Each of the reactions listed in the table is reversible. The rate constants for the reverse reactions can be obtained from the reaction thermochemistry. Thermochemical

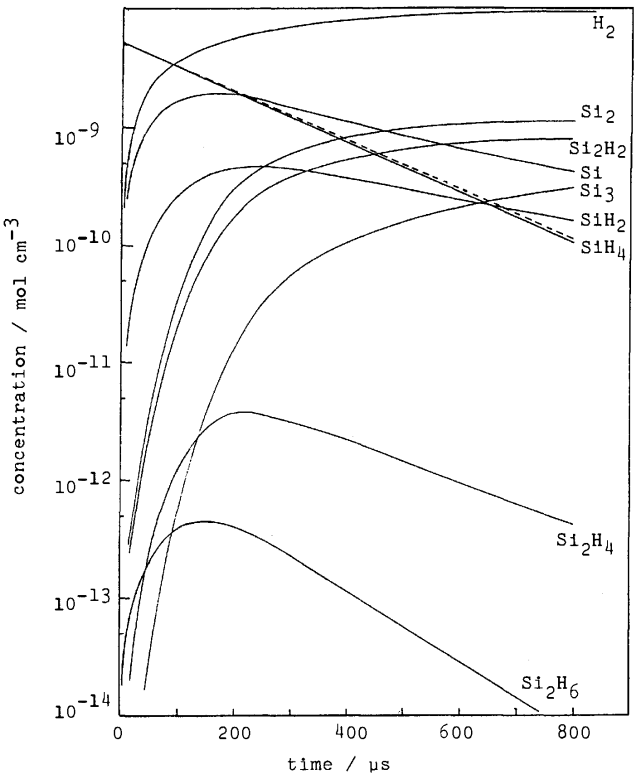

Fig. 3. Calculated concentrations for the mixture of 500 ppm SiH_4 in Ar at T=1400 K and P=1.24 atm.

data for each species involved in the reaction mechanism are taken from the work by Coltrin et al.[15] Although there are no reliable data for the Reactions 9 through 14, these reactions have no sensitivity for the silane loss rate. The rate constants estimated by Coltrin et al.[15] were used for these reactions. An example of the calculated time-concentration profiles of the various species involved in the model is shown in Fig. 3. The dashed curve in the figure represents the analytical solution for the silane concentration calculated by using Reaction 1 only. This curve agrees very well

with that obtained by the numerical integrations of the full kinetic equations. Therefore it is confirmed that the silane decay rate in our experimental conditions is determined by the unimolecular decomposition of silane without any significant contribution of other consecutive reactions.

Another possible silane loss mechanism that is not involved in our model is Si-chain mechanism:

$$SiH_2 (+M) \rightarrow Si + H_2 (+M) \quad (-9)$$
$$Si + SiH_4 \rightarrow SiH_2 + SiH_2 \quad (15)$$

There have been no experimental and theoretical works on the Reaction 15. If we include this reaction with the rate constant estimated by Coltrin et al.[15] in our model, the rate of the silane loss is greatly accelerated and a single exponential decay of silane is no longer obtained. To clarify the contribution of the Si-chain reactions to the rate of the silane decay, nitrogen monoxide was added to the mixtures. Because of the extremely fast reaction between nitrogen monoxide and silicon atom,[16] the silane loss rate might be considerably decelerated if the Si-chain reactions could play an important role. The pressure independent rate constants with the addition of 0.31% nitrogen monoxide are also included in Fig. 2. It was found that the single exponential decay of the silane concentration was not affected by the addition of nitrogen monoxide. No significant deviation of the rate constants from those obtained without the addition of nitrogen monoxide is evident in the figure. The absence of an induction period and the fact that the addition of nitrogen monoxide has no effect on the silane decay provide good evidence that the Si-chain reactions are not responsible for the rate of the silane decay.

The unimolecular rate constants obtained by the single pulse shock tube experiments of Newman et al.[6] are also shown in Fig. 2, where the square root dependence of the rate constants on the total pressure is assumed. The extrapolation of their values to our experimental temperatures gives much higher values than those obtained in this work. Under the conditions of their single pulse shock tube experiments (T=1000—1200 K, P=5.25 atm with 0.96—0.12% SiH_4 in argon), the rate of Reaction 1 is slower than the rates of Reactions 2 and 3. As a result, the decay rate of silane can be accelerated by these consecutive reactions even in a very early stage of the decomposition. If we consider only Reactions 1—3 with an assumption of the steady state concentration of silylene, the following expressions for the initial decay rate of silane are obtained.

$$-d[SiH_4]/dt = k_1[SiH_4](1+F) \quad (III)$$
$$F = g(1+2/g)^{1/2},\ g = (k_2^2/4k_1k_3)[SiH_4] \quad (IV)$$

Using the rate constants listed in Table 1, the value of F is estimated to be equal to 4.2 at T=1100 K and P=5.26 atm for 0.96% SiH_4 in argon. In contrast, F-values in our experimental conditions are always less than 0.14. Although the realistic reaction mechanism is much more complicated because of the reverse process of Reaction 2 and other consecutive reactions, the discrepancy shown in Fig. 2 is caused by the contributions of the consecutive reactions of silylene in the single pulse shock tube experiment.

Recently the rate constant of Reaction 1 has been calculated by Viswanathan et al.[11] They obtained the dissociation rate coefficient at internal energy E, $k(E)$, by means of the Monte-Carlo trajectory calculations. The values of $k(E)$ were fitted to a RRK form:

$$k(E) = \nu[(E-E_0)/E]^{s-1} \quad (V)$$

The values of the RRK parameters obtained by Viswanathan et al. were ν=1.08×10^{13} s^{-1}, E_0=49.6 kcal mol^{-1} and s=2.7. It is interesting to compare the results of their calculations with those of this study. The unimolecular rate coefficient was calculated with the following classical RRK formula.

$$k_1 = \int_{E_0}^{\infty} [f(E)k_d k(E)]dE/[k_d + k(E)], \quad (VI)$$
$$k_d = \lambda zp,$$
$$f(E) = (kT)^{-s}E^{s-1}\exp(-E/kT)/\Gamma(s),$$

where z is the hard-sphere collision frequency, p is the pressure, λ is the deactivation probability upon collision and $\Gamma(s)$ is the Gamma function. In the calculation, hard-sphere collision diameters of 5.76 Å for silane and 3.47 Å for argon were used with a strong collision assumption (λ=1). The pressure dependence of the rate coefficients is compared in Fig. 4. The calculated rate constants with parameters given by Viswanathan et al. show steeper pressure dependence (curve A in Fig. 4) compared with the experimental values. We have searched a new set of RRK parameters

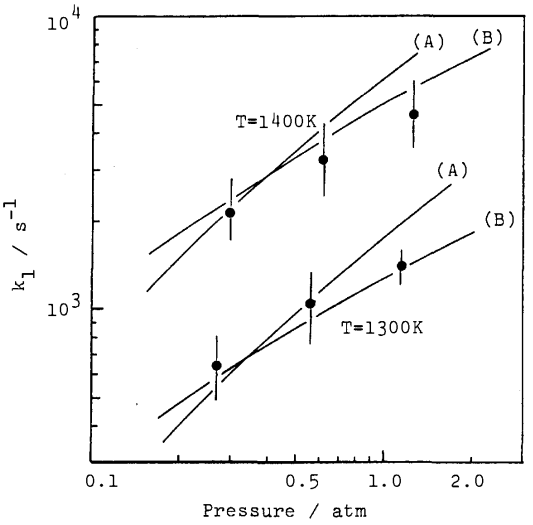

Fig. 4. Pressure dependence of the unimolecular decomposition of silane. Shaded circle with an error bar: Present experimental value, curves A and B: RRK calculations. See text for the RRK parameters used.

which can give better agreement with our experimental results. Although the limited range of the pressure and rather large scatter of the data points prevent the precise determination of parameters, the following set of parameters seems to be reasonable; E_0=55 kcal mol^{-1}, ν=1×10^{13} s^{-1}, and s=4.2. The calculated rate constants with these parameters are shown in Fig. 4 (curve B). The new value for a critical threshold energy is in good agreement with the result of the recent ab initio calculation.[13] The activation energy, E_a, of the unimolecular reaction in the low pressure region will be given by the following equation.[17]

$$E_a = E_0 - (s - 1.5)RT \quad \text{(VII)}$$

Using the RRK parameters obtained in this work, the values of E_a were estimated to be equal to 49.6 kcal mol^{-1} at T=1000 K and 46.7 kcal mol^{-1} at T=1500 K. The observed activation energy in Eq. II agrees well with these estimated values.

Conclusion

In order to obtain the unimolecular rate coefficient for the silane decomposition without any effect of the consecutive reactions, highly diluted silane in argon was decomposed behind shock waves at the temperatures ranging from 1250—1600 K and the intensity of the infrared emission at 4.4 μm which was proportional to the concentration of silane was monitored. The conclusions obtained in the present study are summarized as follows.

(1) In our experimental conditions, the decay of silane is exclusively caused by the unimolocular decomposition of silane. The rate constants for this reaction were determined directly from the time resolved measurements on the silane concentration. (2) No effect on the silane decay rate was observed with the addition of molecular hydrogen nor nitrogen monoxide. (3) The observed pressure fall-off behavior of the rate constant for the silane decomposition is reasonably well explained by a RRK theory with appropriate parameters.

References

1) J. H. Purnell and R. Walsh, *Proc. R. Soc. London, Ser. A.*, **293**, 543 (1966).
2) P. Neudrofl, A. Jodhan, and O. P. Strauz, *J. Phys. Chem.*, **84**, 338 (1980).
3) R. T. White, R. L. Espino-Rios, D. S. Rogers, M. A. Ring, and H. E. O'Neal, *Int. J. Chem. Kinet.*, **17**, 1029 (1985).
4) J. W. Erwin, M. A. Ring, and H. E. O'Neal, *Int. J. Chem. Kinet.*, **17**, 1067 (1985).
5) C. G. Newman, M. A. Ring, and H. E. O'Neal, *J. Am. Chem. Soc.*, **100**, 5945 (1978).
6) C. G. Newman, H. E. O'Neal, M. A. Ring, F. Leska, and N. Shiply, *Int. J. Chem. Kinet.*, **11**, 1167 (1979).
7) P. A. Longeway and W. Lamp, *J. Phys. Chem.*, **87**, 345 (1983).
8) J. M. Jasinski and R. D. Eates, *Chem. Phys. Lett.*, **117**, 495 (1985).
9) R. Robertson, D. Hill, and A. Gallagher, *Chem. Phys. Lett.*, **103**, 397 (1984).
10) H. E. O'Neal and M. A. Ring, *Chem. Phys. Lett.*, **107**, 442 (1984).
11) R. Viswanathan, D. L. Thompson, and L. M. Rapp, *J. Chem. Phys.*, **80**, 4230 (1984).
12) T. N. Bell, K. A. Parkins, and P. G. Perkins, *J. Phys. Chem.*, **88**, 116 (1984).
13) M. S. Gordon, D. R. Gano, J. S. Binkley, and M. J. Frisch, *J. Am. Chem. Soc.*, **108**, 2191 (1986).
14) P. Ho, M. E. Coltrin, J. S. Binkley, and C. F. Melius, *J. Phys. Chem.*, **90**, 3399 (1986).
15) M. E. Coltrin, R. J. Kee, and J. A. Miller, *J. Electrochem. Soc.*, **133**, 1206 (1986).
16) D. Husain and P. E. Norris, *J. Chem. Soc., Faraday Trans. 2*, **74**, 106 (1978).
17) P. V. Robinson and K. A. Holbrook, "Unimolecular reactions," Wiley-Interscience, London (1972).

 © 1987 The Chemical Society of Japan Bull. Chem. Soc. Jpn., 60, 3525—3528 (1987)

Formation of Molecular Complexes of Water-Soluble Porphyrin with Cation-18-Crown-6 Complexes

Masaaki TABATA* and Isao YAMADA
Department of Chemistry, Faculty of Science and Engineering, Saga University, Honjo-machi, Saga 840
(Received May 11, 1987)

The formation of molecular complexes of 5,10,15,20-tetrakis(4-sulfonatophenyl)porphine (H_2tspp) with cation-18-crown-6 (M(18C6)) has been studied spectrophotometrically at I=0.1 mol dm^{-3} (MX and MX_2, M: Na^+, K^+, Cs^+, NH_4^+, Ca^{2+}, Sr^{2+}, Ba^{2+}, X: NO_3^-, Cl^-, Br^-, I^-, SCN^-), and pH 7.0 (*N,N'*-bis(2-sulfonatoethyl)piperazine: PIPES buffer, 2.0×10^{-3} mol dm^{-3}). The absorption spectrum of H_2tspp considerably changed in the presence of both cation and 18-crown-6, but not in the absence of either of them. The formation constants (log K) of the molecular complexes (M(18C6)·H_2tspp) were found to be 2.17±0.05, 2.31±0.03, 2.45±0.03, 2.58±0.02, 1.94±0.03, 2.07±0.02, and 2.12±0.02 for Na^+, K^+, Cs^+, NH_4^+, Ca^{2+}, Sr^{2+}, and Ba^{2+}, respectively at 25.0±0.5 °C and I=0 mol dm^{-3}. Thermodynamic parameters ΔH/(kJ mol^{-1}) and ΔS/(J K^{-1} mol^{-1}) are −19.9, −25.0; −33.0, −66.0; −29.3, −50.8; −48.5, −113.7; −21.9, −34.2 and −32.5, −68.0 for Na^+, K^+, Cs^+, NH_4^+, Sr^{2+}, and Ba^{2+}. The enthalpy changes are linearly correlated to the entropy changes. The equilibrium studies show that charge transfer between M(18C6) and porphyrin π-system is a driving force for the formation of the molecular complex (M(18C6)·H_2tspp) as well as hydrophobic interaction.

The interaction of porphyrins or metalloporphyrins with aromatic ligands such as methyl viologen,[1] 1,10-phenanthrolines,[2] anthraquinones,[3] or DNA[4,5] has been the subject of a number of investigations. The basis for these studies in part is related to the observation that porphyrins can serve as photocatalysts[6] for photoproduction of H_2 and O_2 in water and photosensitizer for destruction of tumor cells[7] (i.e., phototeraphy). The thermodynamic, optical, and physicochemical evidences have suggested the formation of molecular complex by π-π interaction between aromatic donors or acceptors and porphyrin plane. Shelnutt has demonstrated that charge-transfer interaction is a binding force for complexation of metal uroporphyrins with 1,10-phenanthrolines on the basis of the results of resonance Raman differential spectroscopy.[2] Kano et al., concluded that a van der Waals interaction is the predominant binding force and hydrophobic interaction assists the stabilization of the molecular complexes in the reaction of anionic porphyrin with anionic aromatics.[3]

In this studies we describe the formation of molecular complex of 5,10,15,20-tetrakis(4-sulfonatophenyl)-porphine (H_2tspp) with cation-18-crown-6 (M(18C6)), where M is Na^+, K^+, Cs^+, NH_4^+, Ca^{2+}, Sr^{2+}, and Ba^{2+}. 18-Crown-6, of course, does not have π-system. The thermodynamic studies suggest that the formation of the molecular complex ((M(18C6)·H_2tspp)) results from charge transfer between cation-18-crown-6 and π-system of porphyrin as well as hydrophobic interaction of ethylene group of 18-crown-6 with porphyrin. The desolvation of both cation and 18-crown-6 caused by formation of cation-18-crown-6 enables hydrophobic interaction of porphyrin with cation-18-crown-6 and the positive charge in M(18C6) stabilizes the molecular complex.

Experimental

18-Crown-6 (Tokyo Kasei Co. Ltd., Japan) was dried in vacuo at room temperature for 3 days. The inorganic compounds were analytical reagent grade. Porphyrin (H_2tspp) was synthesized and its sodium salt was purified as described previously.[8] The purity was checked by thin-layer chromatography and NMR spectroscopy. Concentrations of calcium(II), strontium(II), and barium(II) in the stock solutions were determined complexometrically. Other stock solutions were prepared by weighing the reagents. Water redistilled in the presence of permanganate was used for all solutions.

The formation constant of the molecular complex was determined spectrophotometrically at pH 7.0 (*N,N'*-bis(2-sulfonatoethyl)piperazine: PIPES buffer) and at given temperatures (20, 25, 30, and 35 °C). Ionic strength was adjusted to 0.1 mol dm^{-1} by cation salts of which molecular complex was studied. Sample solution was prepared by addition of 1 cm^3 H_2tspp (5×10^{-5} mol dm^{-3}) to a solution containing 18C6, PIPES buffer (2.0×10^{-3} mol cm^{-3}) and cation in a 25 cm^3 flask, followed by addition of water to the mark. The solution was kept in a thermostated bath for about 30 min. The absorption spectra were recorded by a Hitachi 323 UV-VIS spectrophotomerter in a 1 cm cell with a thermostated water jacket.

Results

Formation of Molecular Complex of H_2tspp with M(18C6). Absorption spectrum of H_2tspp changed considerably in the presence of both 18-crown-6 and cation as shown in Fig. 1(a), but not in the absence of either of them. The absorption maximum at 413 nm decreased with increasing of 18-crown-6. The isosbestic points were 388 and 420 nm. Similar absorption spectra of porphyrins were also observed in the reaction of H_2tspp with 1,10-phenanthroline[9] and that of 5,10,15,20-tetrakis(4-*N*-methylpyridyl)porphine (H_2tmpyp) with DNA[5] at soret bands.

Under the present experimental conditions (pH 7.0) porphyrin is free base form, because the protonation constants of H_2tspp to form H_3tspp and H_4tspp are $10^{4.99}$ and $10^{4.76}$, respectively (charges on porphyrin are omitted for the simplicity).[10] The formation of the molecular complex decreased at pH lower than 5.

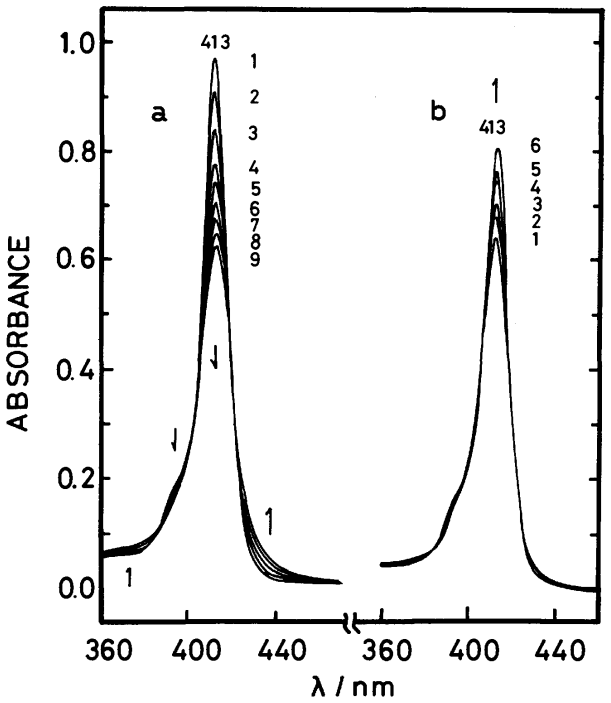

Fig. 1. (a), Absorption spectra of H_2tspp (2.11×10^{-6} mol dm^{-3}) with increasing of 18-crown-6 ((1), 0.000; (2), 1.09×10^{-3}; (3), 2.18×10^{-3}; (4), 3.63×10^{-3}; (5), 5.44×10^{-3}; (6), 7.25×10^{-3}; (7), 1.09×10^{-2}; (8), 1.45×10^{-2}; (9), 1.81×10^{-2}, (unit= mol dm^{-3}) in the presence of K^+ (0.1 mol dm^{-3}) at pH 7.0, and (b) the spectral change of H_2tspp (1.99×10^{-6} mol dm^{-3}) with increasing of ethanol ((1), 0; (2), 2; (3), 4; (4), 6; (5), 8; (6), 10% (v/v)) in the presence of 18-crown-6 (1.97×10^{-2} mol dm^{-3}) and Ba^{2+} (3.47×10^{-2} mol dm^{-3}) at pH 7.0.

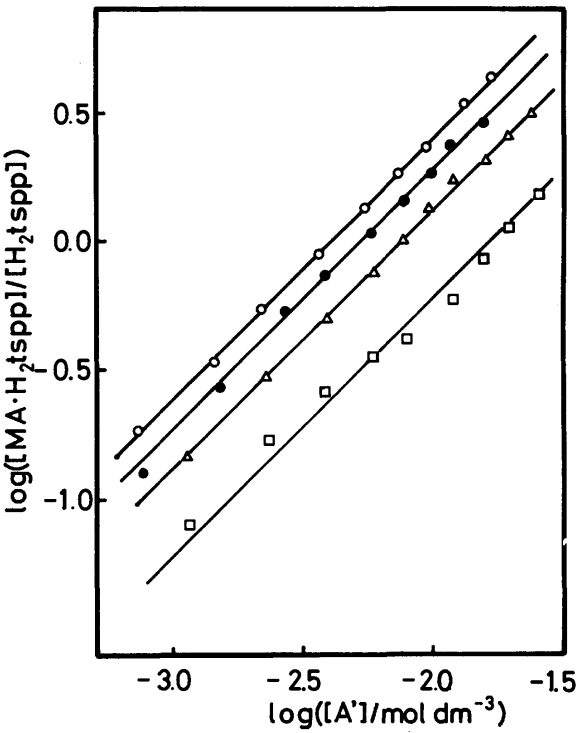

Fig. 2. Plot of $\log([MA\cdot H_2tspp]/[H_2tspp])$ vs. $\log([A']/\text{mol dm}^{-3})$ in the reaction of H_2tspp with NH_4^+ (○), K^+ (●), Ba^{2+} (△), and Na^+ (□) at 25 °C and I=0.1 mol dm^{-3}, where [A'] is the concentration of 18-crown-6 unbound to H_2tspp. $C_{H_2tspp}=2.00\times10^{-6}$ mol dm^{-3}, and pH 7.0.

Cation (M) reacts with 18-crown-6 (A) to form cation-18-crown-6 (MA) as

$$M + A \underset{}{\overset{K_{MA}}{\rightleftharpoons}} MA, \quad (1)$$

and the equilibrium constant is defined by

$$K_{MA}=[MA][M]^{-1}[A]^{-1}. \quad (2)$$

Thus the reaction of H_2tspp with 18-crown-6 in the presence of cation may be given by

$$MA + H_2tspp \overset{K}{\rightleftharpoons} MA\cdot H_2tspp, \quad (3)$$

and the equilibrium constant is written by

$$K=[MA\cdot H_2tspp][MA]^{-1}[H_2tspp]^{-1} \quad (4)$$

From the Eqs. 2 and 4 we obtain Eqs. 5—7:

$$K=[MA\cdot H_2tspp][H_2tspp]^{-1} ([MA]+[A])^{-1}(1+K_{MA}{}^{-1}[M]^{-1}) \quad (5)$$

and

$$K=[MA\cdot H_2tspp][H_2tspp]^{-1}[A']^{-1}\alpha_{MA} \quad (6)$$

$$=\alpha_{MA}K', \quad (7)$$

where A' and α_{MA} denote the total concentration of 18-crown-6 unbound to H_2tspp and side-reaction coefficient of MA, respectively, and they are defined as follows:

$$[A']=[MA]+[A] \quad (8)$$

and

$$\alpha_{MA}=1+K_{MA}{}^{-1}[M]^{-1} \quad (9)$$

Conditional formation constant (K') of the molecular complex can be rearranged in logarithmic form from Eqs. 6 and 7 as follows:

$$\log K'=\log([MA\cdot H_2tspp]/[H_2tspp])-\log[A']. \quad (10)$$

The first term in right-hand side of Eq. 10 was determined from the absorbances in the various concentrations of 18-crown-6, and is plotted against logarithmic concentration of 18-crown-6 in Fig. 2. The plot gives a straight line with a slope of unity and shows that one molecule of MA reacts with an H_2tspp. Thus the formation constants of molecular complexes (K) were calculated from Eqs. 7 and 9, where the logarithmic values of K_{MA} in Eq. 9 were taken from literatures:[11] 0.84, 2.03, 1.01, 1.23, 1.8, 2.71, and 3.83 for Na^+, K^+, Cs^+, NH_4^+, Ca^{2+}, Sr^{2+}, and Ba^{2+}, respectively at I=0.1 mol dm^{-3} and at 25 °C. Table 1 summarizes the formation constants of molecular complexes.

Dependence of the Formation Constant on the Temperature. The formation constants of the molecular complexes for Na^+, K^+, Cs^+, NH_4^+, Ba^{2+}, and Sr^{2+}

Table 1. Formation Constants of Molecular Complexes of MA·H_2tspp at I=0.1 mol dm^{-3} and at 25 °C (A=18-crown-6)

Cation salt	log K / mol^{-1} dm^3	Cation salt	log K / mol^{-1} dm^3
KNO_3	2.31±0.03	NH_4NO_3	2.58±0.02
KCl	2.28±0.03	CsCl	2.45±0.05
KBr	2.40±0.06	$Ca(NO_3)_2$	1.94±0.03
KI	2.32±0.05	$Sr(NO_3)_2$	2.07±0.02
KSCN	2.37±0.04	$Ba(NO_3)_2$	2.12±0.02
$NaNO_3$	2.17±0.05		

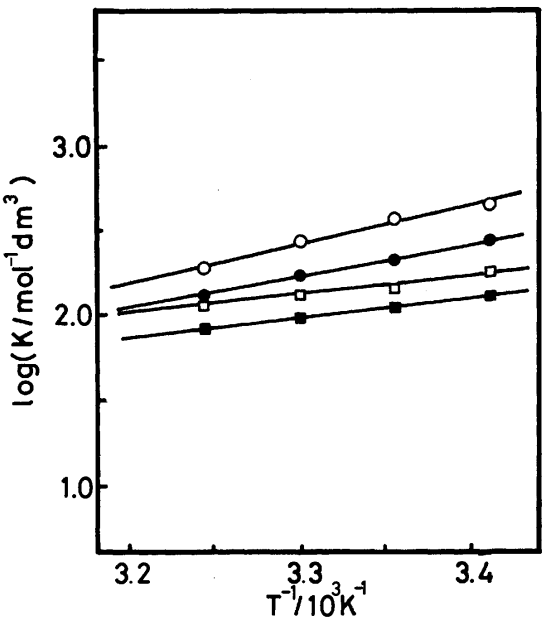

Fig. 3. Temperature dependence of the formation constant of molecular complex between H_2tspp and cations of NH_4^+ (○), K^+ (●), Na^+ (□), and Sr^{2+} (■) at I=0.1 mol dm^{-3}. C_{H_2tspp}=2.00×10^{-6} mol dm^{-3}, and pH 7.0.

were determined at temperatures of 20, 25, 30, and 35 °C. The thermodynamic parameters of enthalpy change (ΔH) and entropy change (ΔS) were calculated from van't Hoff plots of $R\ln K$ vs. T^{-1} and ΔG vs. T, respectively (Fig. 3). The thermodynamic parameters of the formation of the molecular complexes (MA·H_2tspp) are listed in Table 2.

Dependence of the Formation of the Molecular Complex on Ethanol. Addition of ethanol to a solution containing Ba^{2+}, 18-crown-6, and H_2tspp increased the absorbance at 413 nm. At high concentration of ethanol the absorption spectrum is the same as that of H_2tspp in the absence of cation and 18C6 (Fig. 1(b)). The spectral change indicates the dissociation of the molecular complex by addition of ethanol. Since the increase of ethanol decreases dielectric constant of the aqueous solution, the interaction between M(18C6) and H_2tspp does not arise from ion-pair formation. If the molecular complex is ion pair, the formation of the molecular complex may become easier with the decrease of dielectric constant.

Table. 2. Thermodynamic Parameters in the Formation of Molecular Complexes of MA·H_2tspp (A=18-crown-6)

Cation	$-\Delta G$[a)] / kJ mol^{-1}	$-\Delta H$ / kJ mol^{-1}	ΔS / J K^{-1} mol^{-1}
Na^+	12.4	19.9	−25.0
K^+	13.2	33.0	−66.0
Cs^+	14.0	29.3	−50.8
NH_4^+	14.7	48.5	−113.7
Sr^{2+}	11.8	21.9	−34.2
Ba^{2+}	12.1	32.5	−68.0

a) Value at 25 °C.

Discussion

The formation constant of molecular complex is independent of anionic species (Table 1). This shows that anion is not involved in the formation of molecular complex. The formation constants increase in the following order: $Na^+ < K^+ < Cs^+ < NH_4^+$ for univalent and $Ca^{2+} < Sr^{2+} < Ba^{2+}$ for bivalent cations. Comparison of the formation constants of the molecular complexes with those of cation-18-crown-6 shows that the formation of molecular complex is not so affected for different cations as the formation of cation-18-crown-6. Cation size and cavity radius of 18-crown-6 are factors affecting the stability of cation-18-crown-6.[11,12] On the other hand, the molecular complex formation is a weak interaction between porphyrin plane and crown ether complex, and is not so much influenced by the cation size and cavity size of 18-crown-6. As shown in Table 1, the formation constants for bivalent cations are smaller than those for univalent cations. This is the opposite situation compared with the formation of crown ether complex. Since porphyrins trend to associate with organic ligands such as 1,10-phenanthrolines,[2] anthraquinones,[3] and DNA,[4,5] porphyrin plane may be hydrophobic. Thus the large hydration in cation-18-crown-6 may make difficult the interaction between cation-18-crown-6 with porphyrin plane. The hydration free energies ($-\Delta G_h$/(kJ mol^{-1})) are 411.3, 338, 297, 1593, 1447, and 1318 for Na^+, K^+, Cs^+, Ca^{2+}, Sr^{2+}, and Ba^{2+}, respectively.[13] The hydration free energies imply the following relative order for the stabilities of the molecular complexes: $Cs^+ > K^+ > Na^+ > Ba^{2+} > Sr^{2+} > Ca^{2+}$. The hydration enthalpies of

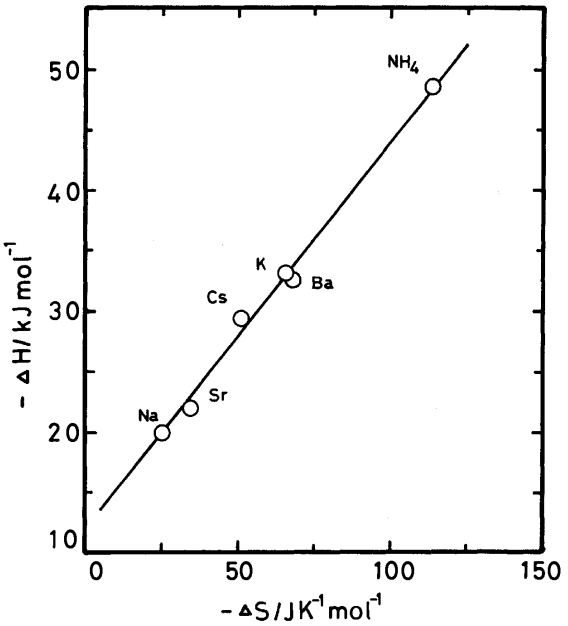

Fig. 4. Plot of $-\Delta H/(\mathrm{kJ\,mol^{-1}})$ vs. $-\Delta S/(\mathrm{J\,K^{-1}\,mol^{-1}})$ for the formation of the molecular complexes of MA·H_2tspp (M=Na^+, K^+, Cs^+, Sr^{2+}, Ba^{2+}, and NH_4^+).

cations also suggest the same order for the formation of the molecular complexes, because the hydration enthalpy is much higher than the hydration entropy.[13] The observed formation constants of the molecular complexes decrease with the order as expected above. This is a reason why the molecular complex of bivalent cation-18-crown-6 is unstabler than that of univalent cation-18C6. Other contribution of cation in the formation of molecular complex is charge-transfer interaction between cation-18-crown-6 and porphyrin π-system.

In Fig. 4, the enthalpy change is plotted against the entropy change in the formation of the molecular complex. The plots give a good straight line. The correlation was generally observed for the charge-transfer complexes such as iodine-aromatic ligands.[14] The enthalpy change is compensated with the entropy change and shows Barcley-Buttler rule. The large contribution of enthalpy change indicates the charge-transfer interaction between cation of M(18C6) and porphyrin π-system. Hydrophobic interaction also contributes to the molecular complex formation. Crown ether does not interact with porphyrin in the absence of cation. Coordination of cation to crown ether releases water molecules from both crown ether and metal ion. The desolvation from 18-crown-6 may increase the hydrophobicity of 18C6, and water around M(18C6) may be structured. In fact the negative entropy change was observed in the reaction of cation with 18-crown-6.[11] The negative enthalpy change in the formation of the molecular complex suggests that water may be structured between cation-18-crown-6 and porphyrin plane. The positive charge in 18-crown-6 complex stabilizes the molecular complex by the charge transfer through porphyrin π-system.

A possible reaction scheme in the formation of molecular complex is given in Scheme 1, in which cation-

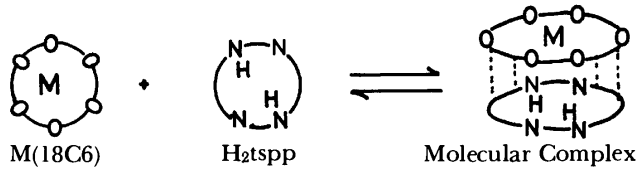

Scheme 1.

18-crown-6 may be parallel to porphyrin plane like "crowned porphyrin."[15] The present studies show, for the first time, the formation of molecular complex of porphyrin with non-aromatic ligands.

The authors thank professor Motoharu Tanaka of Nagoya University, for helpful discussions and gratefully acknowledge the financial support of this study by a Grant-in-Aid from the Ministry of Education, Science and Culture (No. 61540450).

References

1) D. Mauzerall, *Biochemistry*, **4**, 1801 (1965); I. Okura, S. Kusunoki, and S. Aono, *Bull. Chem. Soc. Jpn.*, **57**, 1184 (1984).

2) J. A. Shelnutt, *Inorg. Chem.*, **22**, 2535 (1983).

3) T. Sato, T. Ogawa, and K. Kano, *J. Phys. Chem.*, **88**, 3678 (1984).

4) M. J. Carvlin, N. Datta-Gupta, and R. J. Fiel, *Biochem. Biophys. Res. Commun.*, **108**, 66 (1982).

5) R. F. Pasternack, E. J. Gibbs, and J. J. Villafranca, *Biochemistry*, **22**, 2406 (1983); R. F. Pasternack, E. J. Gibbs, and J. J. Villafranca, *ibid*, **22**, 5409 (1983).

6) I. Okura, S. Kusunoki, and S. Aono, *Inorg. Chem.*, **22**, 3828 (1983); I. Okura, N. Kaji, S. Aono, T. Kita, and A. Yamada, *ibid*, **24**, 451 (1985).

7) J. F. Kelly, M. E. Snell, and M. C. Berenbaum, *Br. J. Cancer*, **31**, 237 (1975).

8) M. Tabata and M. Tanaka, *J. Chem. Soc., Dalton Trans*, **1983**, 1955.

9) M. Tabata and M. Tanaka, unpublished data.

10) M. Tabata and M. Tanaka, *J. Chem. Soc., Chem. Commun.*, **1985**, 43.

11) R. M. Izatt, J. S. Bradshow, S. A. Nielsen, J. D. Lamb, and J. J. Christensen, *Chem. Rev.*, **1985**, 271; R. M. Izatt, R. E. Terry, B. L. Haymore, L. D. Hansen, N. K. Dalley, A. G. Avondet, and J. J. Christensen, *J. Am. Chem. Soc.*, **98**, 7620 (1976); G. Anderegg, *Helv. Chim. Acta*, **64**, 1790 (1981).

12) J. D. Lamb, R. M. Izatt, J. J. Christensen, D. J. Eatough, "Coordination Chemistry of Macrocyclic Compounds," ed by G. A. Melson, Plenum Press, New York (1979), p. 145.

13) H. L. Friedman, C. V. Krishnan, "Water," ed by F. Frank, Plenum, New York (1973), Vol. 3, p. 55.

14) R. M. Keefer and L. J. Andrews, *J. Am. Chem. Soc.*, **77**, 2164 (1955); R. Foster "Organic Charge-Transfer Complexes," Academic Press, New York (1969).

15) C. K. Chang, *J. Am. Chem. Soc.*, **99**, 2819 (1977).

Stereochemistry of a Porphyrin Atropisomer. The Molecular and Crystal Structure of Six-Coordinate [5α,10β-bis(o-nicotinamidophenyl)-15,20-diphenylporphinato]zinc(II)

W. Robert SCHEIDT,* C. W. EIGENBROT, Motoyasu OGISO,† and Keiichiro HATANO*,†
Department of Chemistry, University of Notre Dame, Notre Dame, Indiana 46556, U.S.A.
†Department of Pharmaceutical Sciences, Nagoya City University, Mizuho-ku, Nagoya 467
(Received May 12, 1987)

The synthesis and molecular structure of the title complex was investigated as part of our work into the chemical significance of atropisomerism in porphyrin compounds. The complex crystallizes in the triclinic system, space group $P\bar{1}$, a=11.707 (2) Å, b=12.744 (5) Å, c=9.521 (2) Å, α=102.60 (3)°, β=101.31 (2)°, and γ=100.29 (2)°, Z=1. A total of 3737 reflections (average of two forms) were considered observed and used in the solution and refinement of the structure. The structure was refined to a final R=0.081. The molecule, with a crystallographically imposed inversion center, has disordered nicotinamide side chains. This disorder leads to some ambiguity in defining the relative substitution pattern of the phenyl rings. Independent of the assumptions used to define the disorder, the nicotinamide side chains are found to coordinate the zinc ions of adjacent molecules to form a polymeric, linear chain containing six-coordinate zinc ions. The average equatorial Zn-N bond distance is 2.052 (3) Å and the unique axial bond distance is 2.432 (5) Å.

We and others[1-3] have been exploring strategies for introducing asymmetry in porphyrin species by appropriate substitution of tetraarylporphyrin derivatives. Such asymmetric species could, under appropriate circumstances, be utilized to control reactivity. One such series of asymmetric molecules are *o*-substituted tetraphenylporphyrin complexes in which an adjacent pair of phenyl groups are substituted on opposite sides of the porphyrin plane. The synthesis of one such example, 5α,10β-bis(*o*-aminophenyl)-15,20-diphenylporphyrin has been recently reported.[4] Measurements of the atropisomerization rates of tetrakis(*o*-aminophenyl)porphyrin[5] suggested that such a disubstituted derivative could be manipulated without significant loss of chirality. However, a crystal structure determination[6] of the above diamino derivative showed that the material was profoundly disordered, and suggested that substituents larger than amino groups are required for lattice (solid state) discrimination.

We report in this paper the preparation of a porphyrin derivative bearing much larger *o*-substituents on adjacent phenyls, a bis(nicotinamidophenyl) derivative. We also report the crystal structure of the zinc(II) complex of this porphyrin. Much to our surprise, this derivative also suffers from disorder. However, the disordered porphyrinate species has an interesting structural feature, namely, a six-coordinate zinc(II) ion that results from extended interaction in the solid state. The present complex, like the earlier reported [Zn(TPP)(THF)$_2$],[7] appears to achieve six-coordination purely as a result of solid-state effects. There remain no credible reports for six-coordinate zinc porphyrinates in solution.

Experimental

Syntheses. The preparation and isolation of 5α,10β-bis(*o*-aminophenyl)-15,20-diphenylporphyrin (H_2BADPP) has been described previously.[4] Nicotinoyl chloride hydrochloride (0.3 g, Tokyo Kasei Chem. Co.) was added to a H_2BADPP solution (0.5 g, 50 cm^3 of CH_2Cl_2 and 1 cm^3 pyridine) at room temperature. The resulting green solution was magnetically stirred for 1 h. Aqueous ammonia (8%, 25 cm^3) was poured into the solution and vigorously stirred for 30 min. The solution was then transferred to a separatory funnel and the CH_2Cl_2 layer was washed several times with water and then evaporated to dryness. The resulting solid porphyrin was dissolved in 15 cm^3 of $CHCl_3$ and crystallized by addition of petroleum ether. Yield 520 mg (78%). The product 5α,10β-bis(*o*-nicotinamidophenyl)-15,20-diphenylporphyrin(H_2BNDPP) (250 mg) was reacted with 0.5 g zinc acetate in 25 cm^3 of DMF in a temperature-controlled oil bath (35 °C) for 16 h. TLC of the reaction products confirmed that these conditions led to complete metallation and minimal rotational isomerization.[5] Zn(BNDPP) was obtained by addition of 50 cm^3 of water, followed by filtration of the resulting precipitate. Crystals of Zn(BNDPP) suitable for X-ray analysis were obtained by diffusing pentane into a pyridine-chloroform solution. Found: C, 72.88; H, 3.68; N, 12.06%. Calcd for $C_{66}H_{44}N_{10}O_2Zn$: C, 73.78; H, 4.13; N, 13.04%.

Structure Determination. A single crystal of Zn(BNDPP) with approximate dimensions of 0.35×0.35×0.45 mm was mounted in a thin-walled glass capillary. Preliminary examination on a CAD4 diffractometer established a one-molecule triclinic unit cell. Refined cell constants, a=11.707(2) Å, b=12.744(5) Å, c=9.521(2) Å, α=102.60(3)°, β=101.31(2)°, and γ=100.29(2)°, came from the least-squares refinement of the setting angles of 25 reflections. For a cell content of Zn(BNDPP)·2py (or $ZnO_2N_{10}C_{66}H_{44}$) (F.W.=1074.5), the calculated density is 1.35 g cm^{-3} and the observed density of freshly prepared crystals is 1.36 g cm^{-3}. Intensity data were measured with graphite-monochromated Mo $K\alpha$ radiation at 21±1 °C. Since a completely ordered structure would require that the correct space group be $P1$, the entire triclinic sphere (to 2θ=52.9°) was measured. A total of 10833 reflections were measured. The linear absorption coefficient is 0.52 mm^{-1} and an empirical absorption correction was applied to the entire data set. Relative transmission coefficients ranged from 0.761 to 1.000.

The structure was solved by direct methods (MULTAN):[8] A total of 46 atoms (out of 79) were found in the initially chosen noncentrosymmetric space group $P1$. A few cycles of difference Fourier syntheses located the remaining atoms (except for the solvent molecules). Despite this initial success in the noncentrosymmetric space group, isotropic least-squares refinement led to a number of unsatisfactory interatomic distances and other features more consistent with the presence of inversion centers. Refinement was thus shifted into the centrosymmetric space group $P\bar{1}$. The triclinic data were first averaged assuming Friedel's Law, yielding 3737 observed[9] and averaged reflections (R_{int}=0.019). A certain amount of crystallographic disorder is required in order to describe the Zn(BNDPP) molecule in space group $P\bar{1}$ with Z=1. The zinc atom of the complex was shifted to the inversion center at 0,0,0; this necessarily leads to disorder for the two phenyl substituents. This disorder unfortunately leads to some ambiguity in defining the relative orientations for the two nicotinamide residues. Our analysis assumed the basic molecular structure shown in Fig. 1. The complete structure analysis shows that the terminal pyridine ring of each nicotinamide group coordinates to the zinc atom of an adjacent molecule translated along the c axis. One phenyl ring, C(7)—C(12), had rather large anisotropic thermal parameters and was described by two overlapping rigid groups, a and b. The two rigid groups are almost coplanar but with a C(7a)-C(m2)-C(7b) angle of 17.6°. The occupancy factors of individual atoms of the rigid phenyl groups and amide arms were held fixed at 0.5. The two pyridine solvates (per cell) were found near two separate inversion centers at 1/2,1/2,1/2 and 0,1/2,1/2. Each pyridine ring was close to but disordered around the inversion center. The pyridine near 0,1/2,1/2 was described in terms of two rigid groups. The nitrogen atoms were not conclusively identified and thus the pyridine rings were included in the refinement as three separate, partial occupancy (uniform occupancy factors of 0.25 for each atom) C_6 rigid groups with D_{6h} symmetry. All rigid group refinements were carried out with a locally modified version of ORFLS following the rigid-group description of Scheringer.[10] The hydrogen atoms of the porphyrin ligand were found in difference Fourier maps and were included in fixed idealized positions in the final cycles of least-squares refinement. The final model utilized anisotropic thermal parameters for all non-hydrogen atoms except those of rigid groups. Final values for the discrepancy indices were R_1=0.081 and R_2=0.111.[11] A final differ-

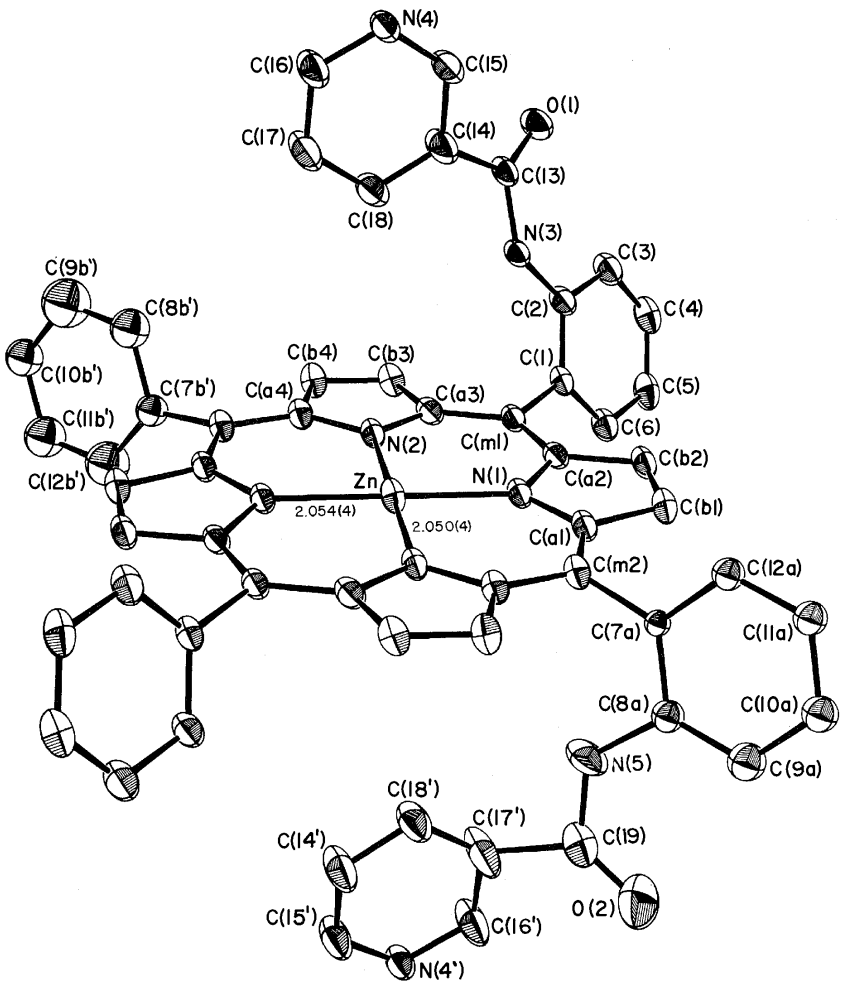

Fig. 1. ORTEP plot (50% ellipsoids) of the Zn(BNDPP) molecule as it exists in the crystal. The atom-labeling scheme for the crystallographically unique atoms are given. Primed (′) atoms are related to unprimed atoms by the inversion center located at the zinc atom.

Table 1. Final Fractional Coordinates and Equivalent Isotropic Temperature Factors for Zn(BNDPP)

Atom	x	y	z	B_{eq}	Atom	x	y	z	B_{eq}
Zn[a]	0.0	0.0	0.0	4.1	C(7a)[a]	−0.2357	−0.3663	−0.0069	2.9
O(1)[a]	−0.3326(7)	0.1452(9)	−0.6490(9)	5.3	C(8a)[a]	−0.2463	−0.3823	0.1313	4.5
O(2)[a]	−0.2259(13)	−0.3502(12)	0.4528(17)	10.0	C(9a)[a]	−0.3142	−0.4807	0.1415	6.0
N(1)	−0.1790(3)	−0.0751(4)	−0.0666(4)	3.6	C(10a)[a]	−0.3727	−0.5647	0.0134	5.3
N(2)	−0.0371(3)	0.1413(4)	−0.0479(5)	3.7	C(11a)[a]	−0.3628	−0.5497	−0.1248	4.6
N(3)[a]	−0.2786(7)	0.1101(8)	−0.4210(9)	3.7	C(12a)[a]	−0.2949	−0.4513	−0.1348	4.3
N(4)	−0.0171(4)	0.0721(4)	−0.7483(5)	4.8	C(7b)[a]	−0.2418	−0.3661	−0.0561	5.2
N(5)[a]	−0.1707(12)	−0.2893(11)	0.2582(12)	6.6	C(8b)[a]	−0.2675	−0.3926	0.0713	8.1
C(a1)	−0.2285(4)	−0.1816(5)	−0.0698(6)	3.8	C(9b)[a]	−0.3373	−0.4955	0.0624	13.0
C(a2)	−0.2709(4)	−0.0307(4)	−0.1247(5)	3.5	C(10b)[a]	−0.3826	−0.5738	−0.0743	7.7
C(a3)	−0.1489(4)	0.1584(5)	−0.0991(6)	3.9	C(11b)[a]	−0.3576	−0.5484	−0.2019	9.4
C(a4)	0.0414(4)	0.2385(4)	−0.0260(6)	4.0	C(12b)[a]	−0.2878	−0.4454	−0.1928	10.5
C(b1)	−0.3571(5)	−0.2063(5)	−0.1331(7)	4.5	C(g1)[b]	0.0881	−0.4707	0.5517	13.4
C(b2)	−0.3811(4)	−0.1139(5)	−0.1678(6)	4.2	C(g2)[b]	0.0529	−0.5212	0.3990	13.4
C(b3)	−0.1367(5)	0.2699(5)	−0.1053(7)	4.7	C(g3)[b]	−0.0603	−0.5904	0.3345	13.4
C(b4)	−0.0203(5)	0.3207(5)	−0.0622(7)	4.6	C(g4)[b]	−0.1403	−0.6101	0.4218	13.4
C(m1)	−0.2570(4)	0.0772(4)	−0.1399(5)	3.6	C(g5)[b]	−0.1062	−0.5603	0.5740	13.4
C(m2)	−0.1674(4)	−0.2588(4)	−0.0245(6)	4.0	C(g6)[b]	0.0071	−0.4911	0.6383	13.4
C(1)	−0.3682(4)	0.1089(4)	−0.2127(6)	3.9	C(g7)[b]	0.2466	−0.3175	0.6983	15.9
C(2)	−0.3774(5)	0.1261(5)	−0.3517(6)	4.4	C(g8)[b]	0.2636	−0.3421	0.5543	15.9
C(3)	−0.4824(5)	0.1509(6)	−0.4216(7)	5.4	C(g9)[b]	0.1672	−0.3940	0.4327	15.9
C(4)	−0.5717(5)	0.1600(6)	−0.3520(8)	5.6	C(g10)[b]	0.0521	−0.4222	0.4532	15.9
C(5)	−0.5624(5)	0.1428(6)	−0.2147(8)	5.6	C(g11)[b]	0.0341	−0.3982	0.5961	15.9
C(6)	−0.4603(5)	0.1172(5)	−0.1456(7)	5.0	C(g12)[b]	0.1306	−0.3463	0.7175	15.9
C(13)[a]	−0.2630(9)	0.1268(10)	−0.5546(12)	3.9	C(g13)[b]	−0.3833	0.3931	0.4011	11.8
C(14)	−0.1340(6)	0.1034(10)	−0.5730(8)	6.8	C(g14)[b]	−0.4774	0.4272	0.4552	11.8
C(15)	−0.1209(6)	0.0638(9)	−0.7136(7)	6.4	C(g15)[b]	−0.4740	0.5390	0.5059	11.8
C(16)	0.0748(6)	0.1291(9)	−0.6393(8)	6.6	C(g16)[b]	−0.3765	0.6187	0.5034	11.8
C(17)	0.0681(7)	0.1680(10)	−0.4953(8)	6.9	C(g17)[b]	−0.2823	0.5858	0.4498	11.8
C(18)	−0.0374(6)	0.1499(8)	−0.4613(7)	6.3	C(g18)[b]	−0.2858	0.4739	0.3992	11.8
C(19)[a]	−0.1632(13)	−0.2868(14)	0.4029(19)	6.8					

The estimated standard deviations of the least significant digits are given in parentheses. a) Site occupancies set to 0.5, see text. b) Site occupancies set to 0.25, see text.

ence Fourier synthesis had its highest peak (0.9 e Å^{-3}) near one of the solvate rigid groups. The atomic coordinates are given in Table 1. Final values for the fixed atoms, rigid group descriptions and anisotropic thermal parameters are available.[12]

Results and Discussion

The molecular structure of Zn(BNDPP) is displayed in Fig. 1 along with the atom labeling scheme. Each nicotinamide pyridine ring is coordinated to a zinc ion above or below its porphyrin plane to create a linear chain along the c axis. Three molecules of the resulting chain of six-coordinate zinc porphyrinates is illustrated in Fig. 2. Bond distances and angles (with estimated standard deviations) in the unique half of the porphinato core are given in Fig. 3. Complete tables of individual bond distances and angles are available.[12] Figure 3 also displays the deviations (in units of 0.01 Å) of each atom from the least-squares plane of the porphinato core. Deviations from exact planarity are unremarkable. The zinc(II) ion is precisely centered in the porphinato plane, as required by the molecular (and crystallographic) inversion center.

The two unique Zn-N_p bond distances are 2.050 (4) and 2.054 (4) Å. This 2.052 (3) Å-average value is larger than the 2.037 Å-average value found for three[13-15] different four-coordinate zinc porphyrinates and significantly shorter than the 2.059 (10) to 2.079 (8) Å range observed in a variety[16-21] of five-coordinate zinc porphyrinates. The 2.052 Å distance is comparable to the 2.057 (1) Å-value observed[7] in the only other known six-coordinate porphinatozinc(II) derivative. In both species, the six-coordinate zinc(II) ion is accommodated by substantial radial expansion of the porphinato central hole.

The axial Zn-N(py) bond distance in Zn(BNDPP) is 2.432 (5) Å. This distance is substantially longer than the Zn-N(ax) distance observed[16-23] in any of the five-coordinate species where the axial distances vary from 2.106 (4) to 2.200 (3) Å. The axial distance is even longer than the 2.380 (2) Å Zn-O distance found in [Zn(TPP)(THF)$_2$].[7] This long distance is consistent with quite weak axial bonding, although the observed porphinate core expansion makes evident that a real axial interaction exists. The coordinated pyridine ring plane makes an 88.2° dihedral angle with the porphinato plane. The dihedral angle between the N(1)-Zn-N(4)′ coordinate plane and the pyridine plane is 5.9°.

The structural analysis of this molecule is like the

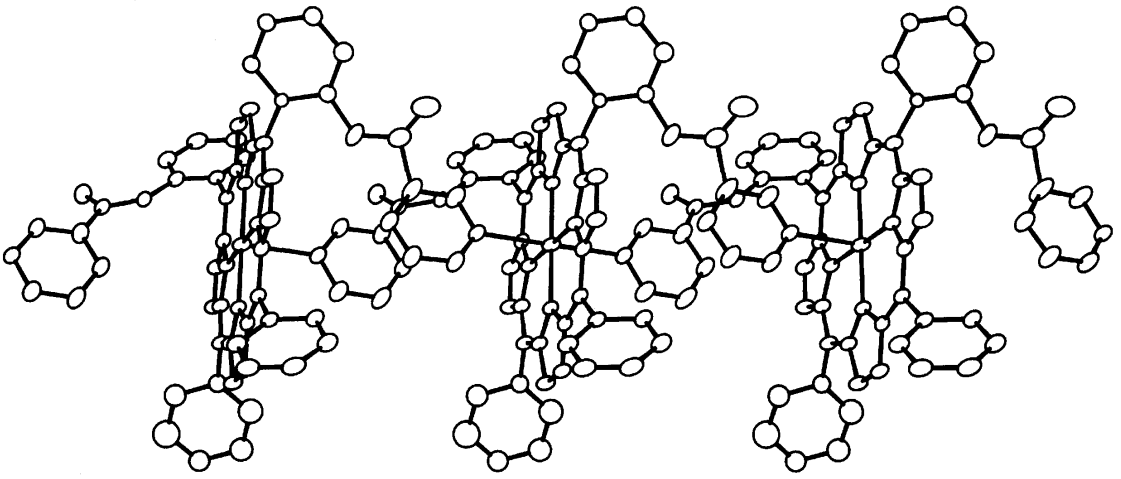

Fig. 2. Computer-drawn plot of the extended structure in crystals of Zn(BNDPP) showing the coordination of the pyridines of the nicotinamide residues on adjacent zinc atoms (c-axis). Only three molecules of the infinite chain are illustrated.

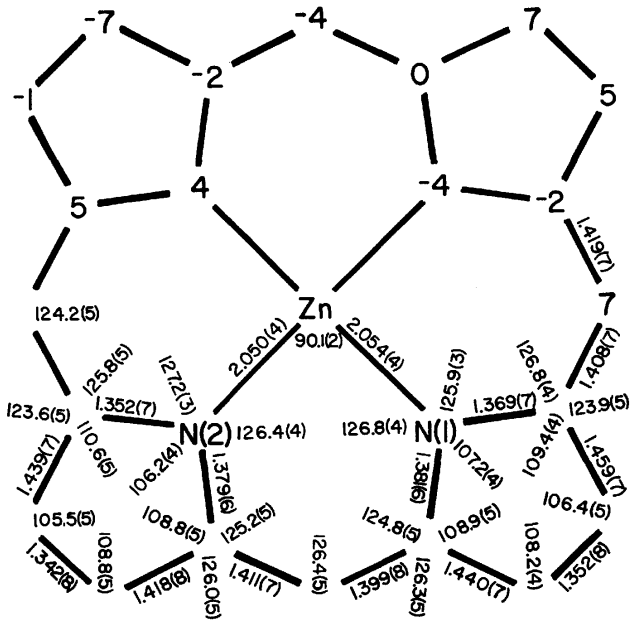

Fig. 3. Formal diagram of the porphinato core illustrating on the top half the displacement of the unique atoms from the mean plane of the 24-atom core. The centrosymmetrically related atoms in the lower half of the diagram have displacements of the same magnitude but opposite sign. All displacement values are in units of 0.01 Å. On the lower half of the diagram are entered the individual values of the bond distances (Å) and angles (°) in the core of the molecule.

resolution of a small puzzle ring. As noted in the Experimental section, the presence of inversion symmetry in the crystal requires a disordered solid-state structure. Unfortunately, this leads to some ambiguity in the complete definition of the molecular structure. However, unless the unlikely assumption—that both amido arms join the porphyrin core to the same pyridine ring—is allowed, the structure determination provides direct evidence that the phenyl substituents are on opposite sides of the porphyrin plane, i.e. the conformation is $\alpha\beta$. Further, unless the assumption that the disorder in the crystal includes two 90° rotational positions (i.e., relative right and left turns) of porphyrin core (in addition to the inversion required disorder), then the structural analysis leads to the conclusion that the substituted phenyl rings on a given molecule must be adjacent. Finally, the six-coordinate nature of the zinc ion is most consistent with this $\alpha\beta$-adjacent substitution of the porphyrin derivative. The disorder in the crystal lattice involves both the chains and the pyridine groups of the nicotinamides, and leads to the enantiomeric disorder. However, although the disorder in the crystal lattice is complex, the $\alpha\beta$-adjacent molecular structure seems to hold in the crystal.

The authors thank the U. S. National Institutes of Health (Grant HL-15627 to WRS) and the Ministry of Education, Science and Culture of Japan (Grant-in-Aid No. 60571024 to KH) for support of this work.

References

1) J. T. Groves and R. S. Meyers, *J. Am. Chem. Soc.*, **105**, 5791 (1983).

2) D. Mansuy, P. Battioni, J.-P. Renaud, and P. Guerin, *J. Chem. Soc., Chem. Commun.*, **1985**, 155.

3) L. R. Milgrom, *J. Chem. Soc., Perkin Trans. 1*, **1984**, 1483.

4) K. Hatano, *Chem. Pharm. Bull.*, **33**, 4116 (1985).

5) K. Hatano, K. Anzai, A. Nishino, and K. Fujii, *Bull. Chem. Soc. Jpn.*, **58**, 3653 (1985).

6) C. E. Eigenbrot, W. R. Scheidt, and K. Hatano, unpublished observations. Crystals of 5α,10β-bis(o-aminophenyl)-15,20-diphenylporphyrin were found to crystallize in the monoclinic system, Z=2, space group $P2_1$ or $P2_1/m$, lattice constants a=13.630 (4) Å, b=11.208 (4) Å, c=11.854 (5) Å, and β=109.32(2)°. The two amino groups were found to be randomly distributed over the eight possible phenyl sites.

7) C. K. Schauer, O. P. Anderson, S. S. Eaton, and G. R. Eaton, *Inorg. Chem.*, **24**, 4082 (1985).

8) Programs used in this study included local modifications of Main, Hull, Lessinger, Germain, Declerq, and Woolfson's MULTAN78, Jacobson's ALLS, Zalkin's FORDAP, Busing and Levy's ORFFE and ORFLS, and Johnson's ORTEP2. Atomic form factors were from: D. T. Cromer and J. B. Mann, *Acta Crystallogr., Sect. A*, **A24**, 321 (1968). Real and imaginary corrections for anomalous dispersion in the form factor of the zinc atom was from: D. T. Cromer and D. J. Liberman, *J. Chem. Phys.*, **53**, 1891 (1970). Scattering factors for hydrogen were from: R. F. Stewart, E. R. Davidson, and W. T. Simpson, *ibid.*, **42**, 3175 (1965). All calculation were performed on a VAX 11/730.

9) Observation criterion, $F>3\sigma(F)$.

10) H. Scheringer, *Acta Crystallogr.*, **16**, 546 (1963).

11) $R_1=\sum||F_o|-|F_c||/\sum|F_o|$ and $R_2=[\sum w(|F_o|-|F_c|)^2/\sum w(F_o)^2]^{1/2}$ The weights used in the least-squares refinement were the usual $1/\sigma^2$, where σ is the estimated standard deviation calculated from counting statistics plus an 'ignorance' factor for large intensity reflections.

12) Final tables of anisotropic thermal parameters, atomic coordinates of the fixed hydrogen atoms, rigid group parameters, bond distances and angles and a table (×10) of observed and calculated structure amplitudes are deposited as Document No. 8760 at the Office of the Editor of Bull. Chem. Soc. Jpn.

13) [Zn(TPP)]·$2C_6H_5CH_3$: Zn-N_p=2.036 (6) Å. W. R. Scheidt, M. E. Kastner, and K. Hatano, *Inorg. Chem.*, **17**, 706 (1978).

14) Zn(TPP): Zn-N_p=2.037 (11) Å. W. R. Scheidt, J. U. Mondal, C. W. Eigenbrot, A. Adler, L. J. Radonovich, and J. L. Hoard, *Inorg. Chem.*, **25**, 795 (1986).

15) [Zn(α-NO_2-OEP)]: Zn-N_p=2.039 Å. W. R. Scheidt, C. W. Eigenbrot, and K. M. Smith, to be submitted for publication.

16) [Zn(TPyP)(Py)]: Zn-N_p=2.073 (8) Å. Zn-N(Py)=2.143 (4) Å. D. M. Collins and J. L. Hoard, *J. Am. Chem. Soc.*, **92**, 3761 (1970).

17) [Zn(OEP)(Py)]: Zn-N_p=2.067 (6) Å, Zn-N(Py)=2.200 (3) Å. D. L. Cullen and E. F. Meyer, Jr., *Acta Crystallogr., Sect. B*, **B32**, 2259 (1976).

18) [Zn(TPP)($OClO_3$)]: Zn-N_p=2.076 (9) Å. L. D. Spaulding, P.G. Eller, J. A. Bertrand, and R. H. Felton, *J. Am. Chem. Soc.*, **96**, 982 (1974).

19) [Zn(TPP-NHCO-$(CH_2)_2$-C_5H_4N]·C_6H_6·0.5C_2H_5OH: Zn-N_p=2.059 (10) Å, Zn-N(Py)=2.147 (7) Å. M. A. Bobrik and F. A. Walker, *Inorg. Chem.*, **19**, 3383 (1980).

20) [Zn(ToCNPP)(Py)]: Zn-N_p=2.076 (12) Å, Zn-N(Py)= 2.151 (4) Å. K. Hatano, K. Kawasaki, S. Munakata, and Y. Iitaka, *Bull. Chem. Soc. Jpn.*, **60**, 1985 (1987).

21) [Zn(OEP)(1-MeIm)]: Zn-N_p=2.068 (7) Å, Zn-N (Im)= 2.106 (4) Å. T. D. Brennan and W. R. Scheidt, to be submitted for publication.

22) [Zn(TPiBc)(Py)]: Zn-N(Py)=2.155 (3) Å. K. M. Barkigia, J. Fajer, L. D. Spaulding, and G. J. B. Williams, *J. Am. Chem. Soc.*, **103**, 176 (1981).

23) [Zn(TPC)(Py)]: Zn-N(Py)=2.171 (2) Å. L. D. Spaulding, L. C. Andrews, and G. J. B. Williams, *J. Am. Chem. Soc.*, **99**, 6918 (1977).

 © 1987 The Chemical Society of Japan Bull. Chem. Soc. Jpn., 60, 3535—3539 (1987)

Nonsteroidal Antiinflammatory Drugs. VI. The Crystal and Molecular Structure of (±)-(2*S**)-2-[4-((1*S**)-2-Oxocyclopentylmethyl)phenyl]-propionic Acid and Force-Field Calculations

Tadashi HATA,* Yuji ŌHASHI,†,†† and Yoshio SASADA†

Analytical and Metabolic Research Laboratories, Sankyo Co. Ltd., 1-2-58 Hiromachi, Shinagawa-ku, Tokyo 140
†Laboratory of Chemistry for Natural Products, Tokyo Institute of Technology, Nagatsuta, Midori-ku, Yokohama 227
(Received May 26, 1987)

The crystal structure of the title compound was determined by X-ray diffraction techniques. The final *R* index was found to be 0.072 for 1187 reflections. The torsional angles of the 2-phenylpropionic acid moiety were comparable to those in other antiinflammatory arylpropionic acids. Force-field energy calculations suggested that the α-methyl substituent to the carboxyl group restricts the rotation of the benzene ring about the C_α-phenyl bond. This restricted conformation may be related to the antiinflammatory activity.

In the search for non-steroidal antiinflammatory drugs, a number of (cycloalkylmethyl)phenylacetic and -propionic acids have been synthesized.[1] Among them, 2-[4-(2-oxocyclopentylmethyl)phenyl]propionic acid (loxoprofen), exhibited particularly potent anti-inflamatory and analgesic activities.[2] This derivative is a mixture of two racemic diastereoisomers having melting points of 102 and 114 °C, respectively. The title compound **1** is the isomer of the lower melting

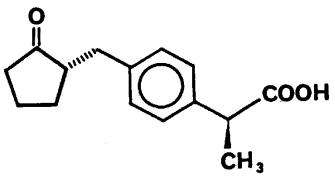

1

point and structure analysis has established the relative configuration.

The potentiating effect of an α-(*S*)-methyl substituent to the carboxyl group has been observed for many antiinflammatory arylacetic acids.[3,4] On the other hand, the substitution of an (*R*)-methyl or two methyls results in manyfold reduction of activity.[5] This must be due to a steric effect at the enzyme surface. It is interesting to compare the conformation of (*S*)-2-phenylpropionic acids with those of phenylacetic and 2-methyl-2-phenylpropionic acids. The present paper deals with the crystal and molecular structure of **1** and the results of empirical force-field calculations for the related molecules based on the crystal structure of **1**.

Experimental

X-Ray Structure Determination of 1. Colorless prisms were grown by slow evaporation of an ether–hexane solution of **1** at room temperature. Diffraction experiments were performed with a crystal, 0.1×0.1×0.6 mm, on a Rigaku AFC-5 diffractometer; monochromated Cu $K\alpha$ radiation being used. The cell parameters were determined from the 2θ values of forty-four reflections in the range with $21° < 2\theta < 49°$. Space group was assigned from systematic absences. The crystal data are as follows; $C_{15}H_{18}O_3$, Mr=246.3, monoclinic, $I2/c$, a=18.276 (1), b=7.5164 (4), c=19.539 (2) Å, β=93.063 (2)°, V=2680.2 (2) Å^3, Z=8, Dc=1.22 g cm^{-3}, μ(Cu $K\alpha$)=6.9 cm^{-1}. An ω-2θ scanning mode was employed up to 2θ=130°. A total of 1842 reflections were measured, of which 1188 unique reflections with $F \geqq 3\sigma(F)$ were used for the analysis. Three references measured every 100 reflections showed no significant variation in intensity. Correction was made for Lorentz and polarization factors, but not for absorption. The structure was solved by the direct method using MULTAN78,[6] and refined by the full-matrix least-squares method with anisotropic thermal parameters. Hydrogen atoms were located on a difference Fourier synthesis and their coordinates were refined with isotropic thermal parameters. One intense low-angle reflection (2,0,−4) seemed to suffer secondary extinction and excluded from the data set. The final refinement converged at R=0.072 and Rw=0.040. The weighting scheme was $w=1/\sigma^2$ (F). Atomic scattering factors were taken from Ref. 7. The final fractional coordinates and equivalent isotropic thermal parameters are given in Table 1.[8]

Table 1. Fractional Coordinates and Equivalent Isotropic Thermal Parameters, with e.s.d.'s in Parentheses

Atom	10^4x	10^4y	10^4z	B_{eq}/Å^2
O(1)	569(2)	6680(6)	3408(2)	6.3(2)
C(2)	612(3)	8134(9)	3665(3)	4.1(2)
C(3)	−27(4)	9319(11)	3829(5)	6.2(3)
C(4)	286(4)	11067(10)	4047(4)	5.3(2)
C(5)	1065(4)	10655(9)	4328(4)	4.6(2)
C(6)	1317(3)	9097(8)	3895(3)	3.5(2)
C(7)	1900(3)	7824(9)	4220(3)	3.4(2)
C(8)	1725(3)	7174(7)	4923(2)	2.9(2)
C(9)	2049(3)	7969(8)	5503(3)	3.6(2)
C(10)	1877(3)	7448(8)	6157(3)	3.6(2)
C(11)	1377(3)	6101(7)	6241(2)	2.6(2)
C(12)	1056(3)	5261(7)	5667(3)	3.2(2)
C(13)	1236(3)	5807(7)	5010(3)	3.0(2)
C(14)	1179(3)	5483(7)	6960(3)	3.0(2)
C(15)	1116(4)	6989(10)	7469(3)	5.0(2)
C(16)	1769(3)	4158(8)	7212(3)	3.0(2)
O(17)	2303(2)	4602(4)	7559(2)	3.9(1)
O(17)	1639(2)	2530(6)	7004(2)	3.7(1)

††Present address: Department of Chemistry, Faculty of Science, Ochanomizu University, Otsuka, Bunkyo-ku, Tokyo.

Force-Field Calculations. The force-field calculations were performed on the model compounds of (*S*)-2-phenylpropionic acid which was constructed based on the crystal structure of **1**, using the MM2′ program.[9] The two torsional angles of τ_1 and τ_2, which correspond to C(10)-C(11)-C(14)-C(16) and C(11)-C(14)-C(16)-O(17) of **1**, were simultaneously varied at intervals of 10 degrees and the conformational energy map for double rotation was calculated. In order to evaluate the effect of the α-methyl group, conformation energy calculations for the two model compounds of phenylacetic acid and 2-methyl-2-phenylpropionic acid which have no and two methyl groups, respectively, were also performed in the same manner as for (*S*)-2-phenylpropionic acid.

Results and Discussion

The Crystal and Molecular Structure of 1. The atom labelling and the thermal ellipsoids are shown in Fig. 1. This racemate crystal of mp 102°C contains molecules with (S, S) and (R, R) configurations. Bond lengths and angles are all normal within the limits of experimental error.

The torsional angles of τ_1[C(12)-C(11)-C(14)-C(16)] and τ_2[C(11)-C(14)-C(16)-O(17)] of the propionic acid side chain are 95.5 (6) and 93.5 (6)°, respectively. These values are compatible with those of other antiinflammatory drugs; 96.4 and 89.3° in ibuprofen,[10] 107.7 and 77.3° in flurbiprofen,[11] 111.7 and 90.2° in naproxen.[12] The torsional angles of other 2-phenylpropionic acids such as 2-(2-isopropyl-5-indanyl)propionic acid (IPIP)[13] and the four racemic diasteroisomers of 2-[4-(2-hydroxycyclopentylmethyl)phenyl]propionic acid (HOPP)[14–16] are listed in Table 2. The corresponding angles of phenylacetic and 2-methyl-2-phenylpropionic acids[17–21] are also included in Table 2. As shown in Table 2, τ_1 and τ_2 of the 2-phenylpropionic acid are localized around angles of 110 and 90°, respectively, with a few exceptions. The corresponding angles for the phenylacetic acid side chain, on the other hand, are 24.4—112.6° and −128.6—25.7°. Therefore, the α-methyl group of the 2-phenylpropionic acid moiety restricts the conformation of this moiety, which should be related to the antiinflammatory activity.

The cyclopentanone ring adopts a half-chair form with the equatorial hydroxyl and methylphenyl groups, in which the C (4) and C (5) atoms are dis-

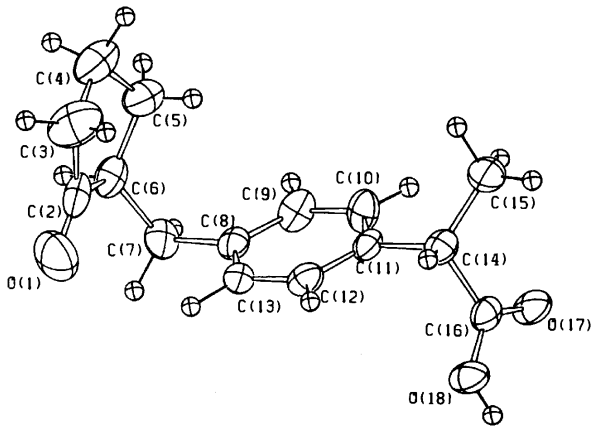

Fig. 1. ORTEP plot of the title compound with thermal ellipsoids at the 50% probability level.

Table 2. Torsional Angles (θ/°) of τ_1 and τ_2

Compound[a]	τ_1	τ_2	Reference
2-Phenylpropionic acid			
Present compound	95.5	93.5	this work
Ibuprofen	96.4	89.3	10)
Flurbiprofen	107.7	77.3	11)
Naproxen	111.7	90.2	12)
IPIP molecule (I)	79.7	102.2	13)
IPIP molecule (II)	119.3	−109.7	13)
HOPP SRS-isomer	108.3	84.0	14)
HOPP SRR-isomer (I)	114.7	94.9	15)
HOPP SRR-isomer (II)	162.6	96.2	15)
HOPP SSR-isomer	122.0	126.5	16)
HOPP SSS-isomer	116.2	95.3	14)
Phenylacetic acid			
EOIA	101.5	25.7	17)
HIPA	24.4	−128.6	18)
BZPA molecule (I)	85.8	−98.4	19)
BZPA molecule (II)	38.2	−90.7	19)
PMPA	112.6	7.7	20)
2-Methyl-2-phenylpropionic acid			
IPIMP	144.4	110.0	21)

a) IPIP; 2-(2-isopropyl-5-indanyl)propionic acid, HOPP; 2-[4-(2-hydroxycyclopentylmethyl)phenyl]propionic acid, EOIA; (2-ethoxy-5-indanyl)acetic acid, HIPA; (*E*)-4-[2-(hydroxyimino)cyclopentylmethyl]phenylacetic acid, BZPA; 4-(benzyloxy)phenylacetic acid, PMPA; 4-(phenoxymethyl)phenylacetic acid, IPIMP; (2-isopropyl-5-indanyl)-2-methylpropionic acid.

placed by −0.22 (9) and 0.30 (9) Å from the plane through C (3), C (2) and C (6). The torsional angles of C(2)-C(6)-C(7)-C(8) and C(5)-C(6)-C(7)-C(8) are −72.5 (7) and 49.2 (8)°, respectively.

The molecules form centrosymmetric dimers by the hydrogen-bonds between the carboxyl groups. The O (18) atom donates a hydrogen to O(17^{i}) [(i) $1/2-x$, $1/2-y$, $3/2-z$]; the hydrogen bond distance being 2.619 (5) Å.

Force-Field Calculations. The conformational energy map for double rotation, τ_1 and τ_2, of the acetic acid residue in phenylacetic acid is given in Fig. 2. The map is cyclic with a period of 180° in τ_1 owing to the two-fold rotation symmetry of the benzene ring and also the two-fold rotation axis at τ_1=180°, τ_2=180° owing to the two equivalent hydrogen atoms at the α-carbon of acetic acid, resulting in four global minima A, A′, A″, and A‴. The rotation around the C_α-phenyl bond is somewhat hindered by a barrier of 5.0 kJ mol^{-1} (between A and A′), whereas the rotation barrier between the global minima A and A″ is only 2.9 kJ mol^{-1}. The values of τ_1 and τ_2 in the crystals of phenylacetic acids, which are plotted by the symbol X in Fig. 2, scatter owing to the low energy barriers. It is suggested that the side chain of acetic acid is freely rotated about the C_α-phenyl and C_α-COOH bonds.

The energy surface of 2-phenylpropionic acid as a function of τ_1 and τ_2 is shown in Fig. 3. Because of the two-fold rotation symmetry of the benzene ring, the map is cyclic with a period of 180° in τ_1, resulting in two global minima A and A′. Local minima B and B′ are 5.9 kJ mol^{-1} higher in energy. The rotation around the C_α-phenyl bond is somewhat hindered by a barrier of 11.3 kJ mol^{-1} (between A and A′), whereas the rotation barrier between the global minimum A and local minimum B is 8.4 kJ mol^{-1}. These values are appreciably higher than those of 5.0 and 2.9 kJ mol^{-1} in 2-phenylacetic acid; 2-phenylpropionic acid has more tendency to take the definite conformation than phenylacetic acid. Smeyer et al.[22] have reported that 2-(4-isobutylphenyl)propionic acid (ibuprofen) presents a preferred conformation with torsional angle τ_1 between 90 and 120°, or between 270 and 300° from CNDO/2 molecular orbital calculations. These coincide with the present global minimum A or A′.

The τ_1 and τ_2 torsional angles in the crystals of some derivatives of 2-phenylpropionic acid are given in Table 2 and plotted by the small circles in Fig. 3. In contrast with phenylacetic acid, these are crowded around τ_1=110° and τ_2=90°, which slightly deviates from the point A. This fact, combined with the higher rotation barrier of the side chain in 2-phenylpropionic acid, indicates that the α-methyl substituent to the carboxyl group restricts rotations about the C_α-phenyl and C_α-COOH bonds. The potentiating effect of α-(*S*)-methyl substituent in many antiinflammatory arylacetic acids may be related to such restricted conformation of propionic acid.

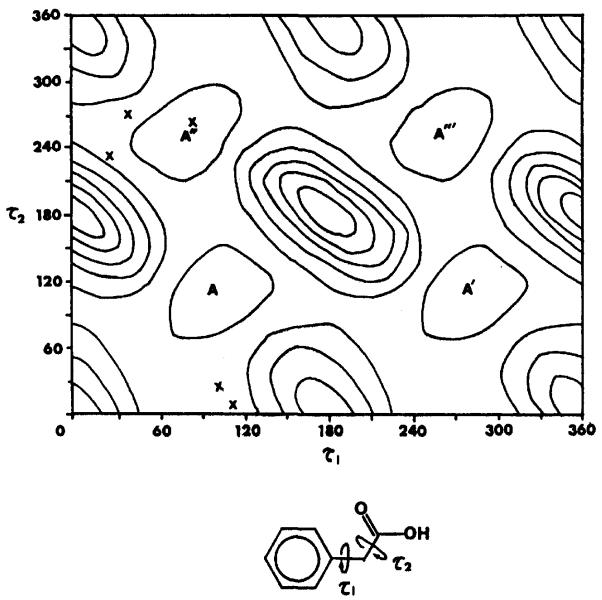

Fig. 2. The conformational energy map for the acetic acid residue in phenylacetic acid by MM2′ calculations. Isobars are drawn at 4.2 kJ mol^{-1} intervals. Four global minimum energy points are A, A′, A″, and A‴. The observed point in the crystal of phenylacetic acids are denoted by the symbol x.

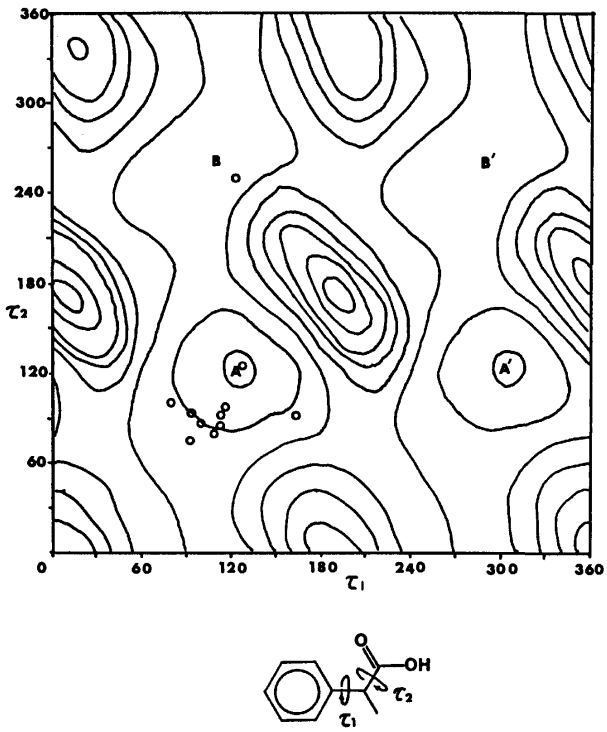

Fig. 3. The conformational energy map for double rotation of the propionic acid residue in 2-phenylpropionic acid by MM2′ calculations. Contours are drawn at 4.2 kJ mol^{-1} intervals. The global minimum points are A and A′ and local ones are B and B′. The observed crystal conformations of 2-phenylpropionic acids are plotted by the small circles.

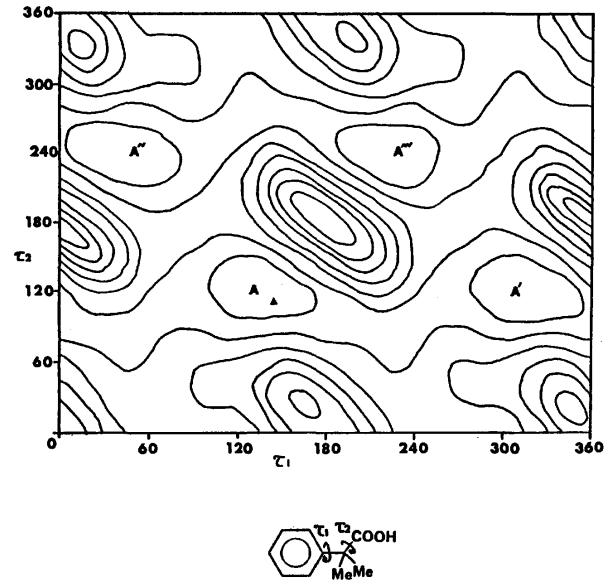

Fig. 4. MM2′ calculated rotational energy surface for the side chain of 2-methyl-2-phenylpropionic acid. Contours are drawn at 4.2 kJ mol^{-1} intervals. The global minimum points are A, A′, A″, and A‴. The observed point of 2-methylpropionic acids in the crystal is denoted by the symbol ▲.

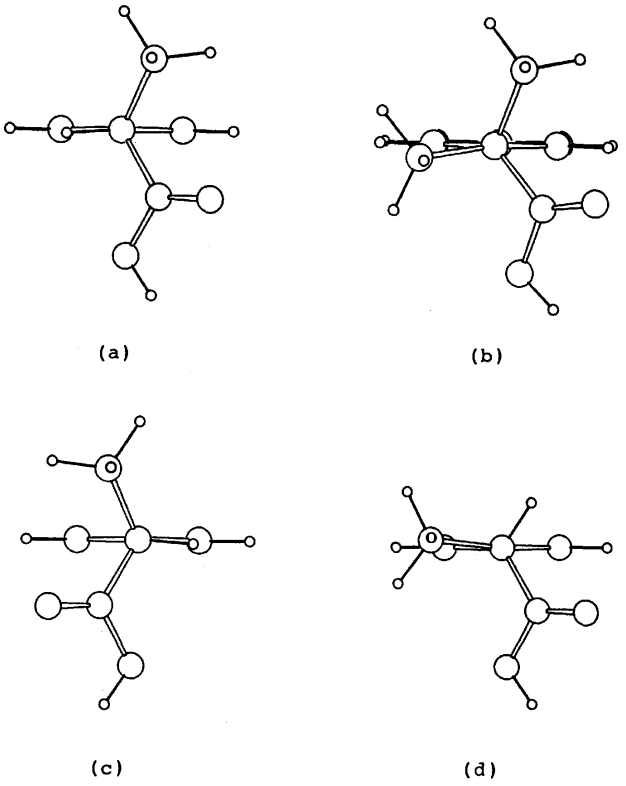

Fig. 5. Perspective projections along the C_α-phenyl axis. (a) The global minimum energy conformation of (*S*)-2-phenylpropionic acid. (b) The global minimum energy conformation of 2-methyl-2-phenylpropionic acid. (c) The global minimum energy conformation of (*R*)-2-phenylpropionic acid. (d) The conformation of (*R*)-2-phenylpropionic acid with torsional angles of τ_1=120° and τ_2=120° corresponding to the global minimum energy conformation of the (S)-isomer.

In order to evaluate the effect of one more methyl group, empirical force-field energy calculations have been performed for 2-methyl-2-phenylpropionic acid. The conformational energy map for double rotation of the 2-methyl-2-phenylpropionic acid is given in Fig. 4. This energy surface map has the four global minima A, A′, A″, and A‴, as in phenylacetic acid. The rotation barriers between the global minima A and A′ and between A″ and A‴ are 7.1 and 9.2 kJ mol^{-1}, respectively. The former is lower by 4.2 kJ mol^{-1} than that in 2-phenylpropionic acid and the latter is higher by 0.8 kJ mol^{-1}. The conformation analysis of 2-methyl-2-phenylpropionic acid has been performed by CNDO/2 molecular orbital calculations.[22] Its results show that the τ_1 torsional angle in the preferred conformation is around 0 or 180° which is different from the global minimum points indicated by the MM2′ calculations. The values of τ_1 and τ_2 in crystals of 2-(2-isopropyl-5-indanyl)-2-methylpropionic acid (IPIMP) are plotted by the symbol ▲ in Fig. 4, close to the global minimum A. It is noted that the bulkier the α-substituent to the carboxyl group is, the larger the value of τ_1 for the global minimum; the τ_1 valules of phenylacetic acid, 2-phenylpropionic acid, and 2-methyl-2-phenylpropionic acid being 100, 120, and 130°, respectively.

The most stable conformations of (*S*)-2-phenylpropionic acid and 2-methyl-2-phenylpropionic acid projected along the C_α-phenyl axis are shown in Fig. 5. For the former the α-hydrogen atom lies in the phenyl plane and one of the two methyl groups of the latter is also located approximately on the phenyl plane. On the other hand, (*R*)-2-phenylpropionic acid presents a preferred conformation with τ_1=60° and τ_2=−120°, which is a mirror image of the structure of the (S)-isomer at the global minimum as shown in Fig. 5. These differences in the torsional angles of the global minimum energy conformation of (*R*)-2-phenylpropionic acids may contribute to the lowering of the antiinflammatory activity of the (R)-isomer. However, in the crystal of the antiinflammatory agent, (*S*)-6-chloro-5-cyclohexyl-1-indancarboxylic acid (clidanac), where the carboxyl group is constrained by attachment to a five-membered ring, the τ_1 torsional angle has been found[23] to be 61.8°, compatible with the value of 60° in the global minimum energy conformation of the (R)-isomer molecule. Therefore, conformations with a τ_1 torsional angle of 60° should be able to exhibit some antiinflammatory activity.

The conformation of the (R)-isomer (τ_1=120° and τ_2=120°) corresponding to the preferred conformation of the (S)-isomer is higher by 7.5 kJ mol^{-1} in energy than the global minimum and the projection is also given in Fig. 5. In this conformation (τ_1=120°), not the α-hydrogen atom but the α-methyl group is approximately in the phenyl ring plane just as 2-

methyl-2-phenylpropionic acid. These projecting methyl groups of both compounds, (*R*)-2-phenylpropionic acid and 2-methyl-2-phenylpropionic acid, may point into the receptor site to prevent binding, giving rise to the manyfold reduction in antiinflammatory activity.

We wish to thank Professor Eiji Ōsawa of Hokkaido University for kindly supplying the MM2′ program and Dr. Atsusuke Terada of The Chemical Research Laboratories of our company for providing samples.

References

1) A. Terada, S. Naruto, K. Wachi, S. Tanaka, Y. Iizuka, and E. Misaka, *J. Med. Chem.*, **27**, 212 (1984).

2) E. Misaka, T. Yamaguchi, Y. Iizuka, K. Kamoshida, T. Kojima, K. Kobayashi, Y. Endo, Y. Misawa, S. Kobayashi, and K. Tanaka, *Oyo Yakuri*, **21**, 753 (1981).

3) T. Y. Shen, *Angew. Chem., Int. Ed. Engl.*, **11**, 460 (1972).

4) P. F. Juby, "Aryl- and Heteroarylalkanoic Acids and Related Compounds," in "Antiinflammatory Agents: Chemistry and Phamacology," ed by R. A. Scherrer and M. W. Whitehouse, Academic Press, New York (1974), Vol. 1, Chap. 2.

5) P. F. Juby, W. R. Goodwin, T. W. Hudyma, and R. A. Partyka, *J. Med. Chem.*, **15**, 1297 (1972).

6) P. Main, S. E. Hull, L. Lessinger, G. Germain, J.-P. Declercq, and M. M. Woolfson, "MULTAN78, A System of Computer Programs for the Automatic Solution of Crystal Structures from X-ray Diffraction Data," Univs. of York, England, and Louvain, Belgium (1978).

7) "International Tables for X-Ray Crystallography," Kynoch Press, Birmingham (1974), Vol. IV.

8) Lists of structure factors, bond lengths, bond angles anisotropic thermal parameters and atomic parameters for hydrogen atoms have been deposited as Document No. 8758 at the Office of the Chemical Society of Japan.

9) C. Jaime and E. Ōsawa, *Tetrahedron*, **39**, 2769 (1983).

10) J. F. McConnell, *Cryst. Struct. Commun.*, **3**, 73 (1974).

11) J. L. Flippen and R. D. Gilardi, *Acta Crystallogr., Sect. B*, **31**, 926 (1975).

12) K. Ravikumar, S. S. Rajan, V. Pattabhi, and E. J. Gabe, *Acta Crystallogr., Sect. C*, **41**, 280 (1985).

13) M. Foulon, F. Baert, and R. Fouret, *Acta Crystallogr., Sect. B*, **35**, 2058 (1979).

14) T. Hata, C. Tamura, Y. Ōhashi, and Y. Sasada, to be published.

15) T. Hata, S. Sato, and C. Tamura, *Acta Crystallogr., Sect. C*, **42**, 1191 (1986).

16) T. Hata, S. Sato, and C. Tamura, *Bull. Chem. Soc. Jpn.*, **59**, 2625 (1986).

17) T. Hata, S. Sato, and C. Tamura, *Acta Crystallogr., Sect. C*, **42**, 449 (1986).

18) T. Hata, S. Sato, and C. Tamura, *Acta Crystallogr., Sect. C*, **42**, 452 (1986).

19) J. Bats and R. Canenbley, *Acta Crystallogr., Sect. C*, **40**, 993 (1984).

20) J. Bats and R. Canenbley, *Acta Crystallogr., Sect. C*, **40**, 995 (1984).

21) T. Hata, S. Sato and C. Tamura, *Acta Crystallogr., Sect. C*, **42**, 96 (1986).

22) Y. G. Smeyer, S. Cuellare-Rodriguez, E. Galvez-Ruano, and M. S. Arias-Perez, *J. Pharm. Sci.*, **74**, 47 (1985).

23) K. Kamiya, Y. Wada, and M. Nishikawa, *Chem. Pharm. Bull.*, **23**, 1589 (1975).

 © 1987 The Chemical Society of Japan Bull. Chem. Soc. Jpn., 60, 3541—3545 (1987)

Surface Properties and Catalytic Activities of Niobic Acid Treated with Diluted Phosphoric Acid

Akito KUROSAKI, Tetsuhiro OKUYAMA, and Susumu OKAZAKI*
Department of Industrial Chemistry, Faculty of Engineering, Ibaraki University, Nakanarusawa-cho, Hitachi 316
(Received February 2, 1987)

A surface treatment of niobic acid using about 1 mol dm^{-3} of phosphoric acid was effective for the enhancement of the surface acidity and the catalytic activity for some acid-catalyzed reactions such as cyclohexanol dehydration and alkylation of benzene with methanol. However, a treatment with phosphoric acid of higher concentration might form a deposit on the surface, which would prevent the penetration of reactants and/or products and, thus, decreased the catalytic activity of niobic acid. The P component added to the niobic acid was hardly removed by steaming at 400 °C, although it could be taken off by soaking in water at room temperature for twelve hours.

Niobic acid is known to exhibit a considerably high acid strength even in the presence of steam and, hence, to be available as an effective catalyst for hydration,[1] esterification,[2] or condensation,[3] which are to be performed in the presence of steam.[4] However, surface acidity of niobic acid remarkably decreases when it is heat-treated at temperatures higher than 400°C, possibly due to the crystallization which is known to be taken place above 435°C.[5] It was previously found that the decrease in the surface acidity lowered the catalytic activity of niobic acid for ethylene hydration and methanol conversion.[6] This limitation on the temperature restricts reaction conditions and the possibility for the reactivation of used catalysts. It was also found in a previous study[6] that the addition of a small amount of phosphoric acid is effective for preventing decreases in the surface acidity and the catalytic activity of niobic acid due to a heat treatment at temperatures higher than 400 °C. Furthermore, the phosphoric acid addition is even effective for increasing the surface acidity or enhancing the catalytic activity of the niobic acid heat-treated at lower temperatures. For uses of niobic acid as an industrial catalyst, the increase in the amount of acid sites seems essential; hence, the effects of a phosphoric acid addition on the surface acidity and on the catalytic activity for an acid-catalyzed reaction were investigated in more detail in this study. Especially, the durability of the P component was examined in terms of the change of the P content in the phosphoric acid-treated sample during a high-temperature (400 °C) steam treatment.

Experimental

Catalyst Preparation. Niobic acid (AD-135) supplied by CBMM was dried in air at 120 °C for 6 h. This material (10 g) was immersed in 30 ml of a phosphoric acid solution prepared so as to have a given concentration (0.05, 0.25, 0.5, 1, 3, or 5 mol dm^{-3} of H_3PO_4). The suspension of niobic acid was allowed to stand for 48 h; the sample was then evaporated to dryness in air at 120 °C. The dried sample was calcined at various temperatures ranging from 200 to 800 °C.

Surface Acidity and Specific Surface Area. The acidity of niobic acid before and after the acid-treatment was determined by adsorptions of ammonia and pyridine at various temperatures. The BET method was applied in order to measure the specific surface area. Constant-volume adsorption of N_2 was carried out at 78 K for samples having sizes of 14—20 mesh.

XRD and XPS Measurements. The XRD measurement was carried out using Geigerflex Diffractometer(Rigaku Denki) (target: Cu; filter: Ni). Some catalyst samples were heat-treated at 400 °C and then subjected to an XPS measurement (using Shimadzu ESCA 750) for the surface composition analysis. Also, ICP (Induction Combined Argon Plasma Emission Spectroscopy) was used to determine the change in the P content during a steam treatment.

Dehydration of Cyclohexanol and Alkylation of Benzene with Methanol. The dehydration of cyclohexanol was performed by using as a catalyst untreated niobic acid as well as niobic acid treated with 1 mol dm^{-3} phosphoric acid. The reaction was carried out at 180 °C under normal pressure using a conventional flow reactor. W/F was kept at 31.0 $g \cdot h \cdot mol^{-1}$ for the catalytic dehydration. The alkylation of benzene with methanol was performed at 400 °C, using a pulse reactor. The pulse size and the catalyst weight were 2 μl and 50 mg, respectively. The molar ratio of methanol/benzene was adjusted at 3 for all the pulse reactions.

Results and Discussion

Surface Area. The surface area of niobic acid sharply dropped when the sample was heat-treated at temperatures above 400 °C, owing to the crystallization which should take place above 435 °C.[5] This decrease in the surface area was prevented by a treatment with 0.5—1.0 mol dm^{-3} of phosphoric acid, similarly to that observed previously.[6] However, treatments with phosphoric acid of higher concentrations were ineffective for the prevention of a decrease in the surface area, (Fig. 1). Especially, a treatment with 5 mol dm^{-3} phosphoric acid decreased rather than increased the surface area of the niobic acid heat-treated at 600 °C. It was possible that some niobium compound, such as niobium phosphate, was formed on the surface of niobic acid, although the XRD measurement did not show any peak ascribable to a newly formed compound on this sample.

Surface Acidity. The acidity changes of phos-

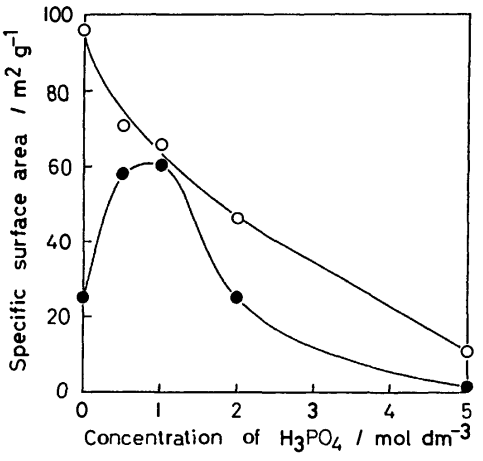

Fig. 1. Effect of H_3PO_4 concentration on specific surface area of niobic acid. Heat treatment temperature; ○: 400 °C, ●: 600 °C.

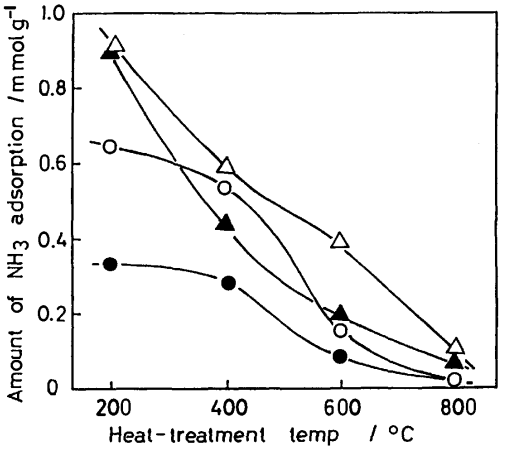

Fig. 2. Effect of heat treatment temperature on surface acidity of niobic acid before and after H_3PO_4 treatment. Concentration of H_3PO_4: 1.0 mol dm^{-3}; ○: adsorption at 100 °C on niobic acid before H_3PO_4 treatment; △: adsorption at 100 °C after treatment; ●: adsorption at 200 °C before treatment; ▲: adsorption at 200 °C after treatment.

phoric acid-treated and untreated niobic acid after heating at various temperatures were determined by the NH_3 adsorptions at 100 and 200 °C. As is shown in Fig. 2, the amount of NH_3 adsorbed at 100 and 200 °C on the acid-treated sample was larger than that adsorbed at a respective temperature on the untreated sample for all the heat-treatment temperatures ranging from 200 to 800 °C. Thus, the phosphoric acid treatment was effective irrespective of the heat-treatment temperature. Especially, adsorption amount of NH_3 at 200 °C was nearly equal to that of NH_3 adsorbed at 100 °C for the sample heat-treated at 200 °C. The evidence suggested that relatively strong acid sites were formed on the sample when the acid-treated sample was heated at a lower temperature such as 200 °C.

To determine the effect of the concentration of phosphoric acid used for the acid treatment on the

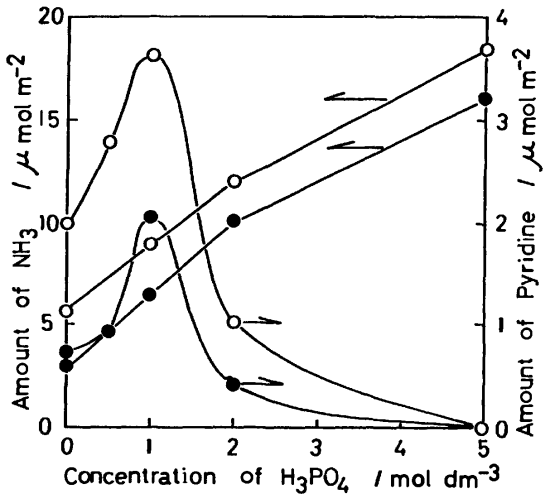

Fig. 3. Effect of H_3PO_4 concentration on surface acidity determined by NH_3 or pyridine adsorption. Ammonia and pyridine adsorptions were carried out by volumetric and gravimetric methods, respectively. Heat treatment temperature: 400 °C. Adsorption temperature: 100 °C (○) or 200 °C (●).

surface acidity of niobic acid, the adsorptions of NH_3 and pyridine on both treated and untreated niobic acid were attempted. The relationship between the amounts of NH_3 and pyridine per unit surface area and the concentration of used phosphoric acid is shown in Fig. 3. The amount of adsorption was similarly changed by changing the heat-treatment temperature, irrespective of the difference of the adsorption temperature. When the determination was carried out by the NH_3 adsorption, both the amounts per unit surface or densities, calculated for the adsorption temperatures of 100 and 200 °C on the niobic acid surface monotonously increased with the phosphoric acid concentration. On the other hand, the densities determined by the pyridine adsorption presented a maximum at a concentration of 1 mol dm^{-3}. This difference between acid site amounts (or densities) determined by NH_3 and pyridine adsorptions may be resulted from the difference in the molecular size of these bases. That is, the smaller molecules of NH_3 may penetrate through the micro pores of the surface layer formed by the phosphoric acid treatment on niobic acid, whereas the larger molecules of pyridine may be unable to penetrate. A similar phenomenon was observed by Itoh and Tada in their study on double adsorption of NH_3 and pyridine on Al_2O_3.[7] The surface possibly came to be covered more compactly as the concentration of the phosphoric acid used for the treatment became higher. On the other hand, the surface of niobic acid treated with less concentrated phosphoric acid might not be fully or less compactly covered by the compound newly formed on the surface. In such a state, the adsorption amount of pyridine was larger than that of NH_3 for the sample treated with phosphoric acid of lower concentration (0.5 and 1

mol dm^{-3}), since the basic strength of pyridine is higher than that of NH_3.[7-8] As a result of the two opposing effects, regarding the basic strength and the molecular size, respectively, a maximum was observed at a 1 mol dm^{-3} concentration of phosphoric acid for the adsorbed amount of pyridine (shown in Fig. 3).

Surface Composition and Structure. The atomic ratio of P/Nb in the surface layer of the catalyst determined by XPS linearly increased with increasing the concentration of phosphoric acid used for the treatment as shown in Fig. 4. The P/Nb ratio shown in the figure was considerably higher than the value calculated from the amount of phosphoric acid added to the niobic acid sample; for example, the value is calculated to be about 0.5 for the treatment with phosphoric acid of 1 mol dm^{-3}, but the experimental value is roughly 1. The evidence again indicated that the P component was concentrated in the surface layer. In spite of the concentration in the surface layer, the P component was slightly removed by a steam treatment at 400°C for 3 h (Fig. 5). The P component was partially removed by soaking in water with vigorous stirring at room temperature for 12 h.

XPS spectra regarding O, Nb, and P components in the surface layer of niobic acid samples containing various amounts of P component is shown in Fig. 6. The numbers in the parentheses indicate the atomic ratio of

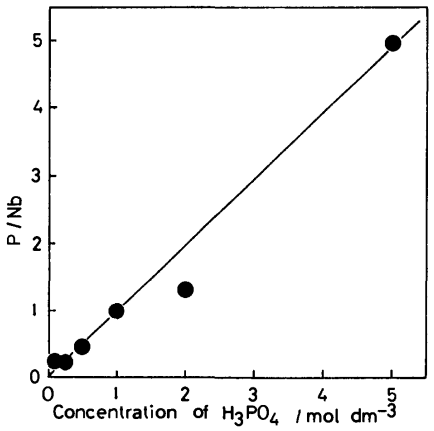

Fig. 4. Effect of H_3PO_4 concentration on atomic ratio P/Nb in surface layer of H_3PO_4-treated niobic acid.

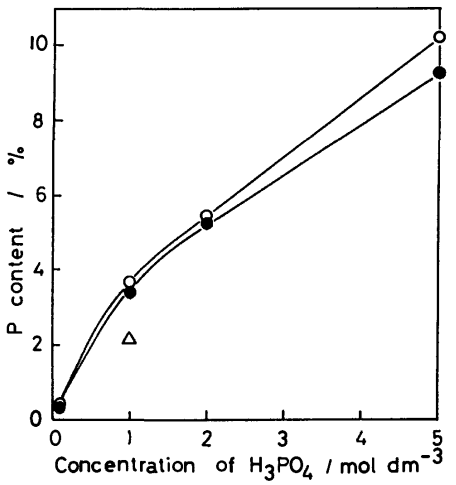

Fig. 5. Change of the P content of the acid treated sample during treatment with steam or water. ○: Untreated; ●: treated with steam. △: Treated with water at room temperature for 12 h. The steam treatment was carried out at 400°C for 3 h by using 106 m mol of steam per g of the niobic acid sample.

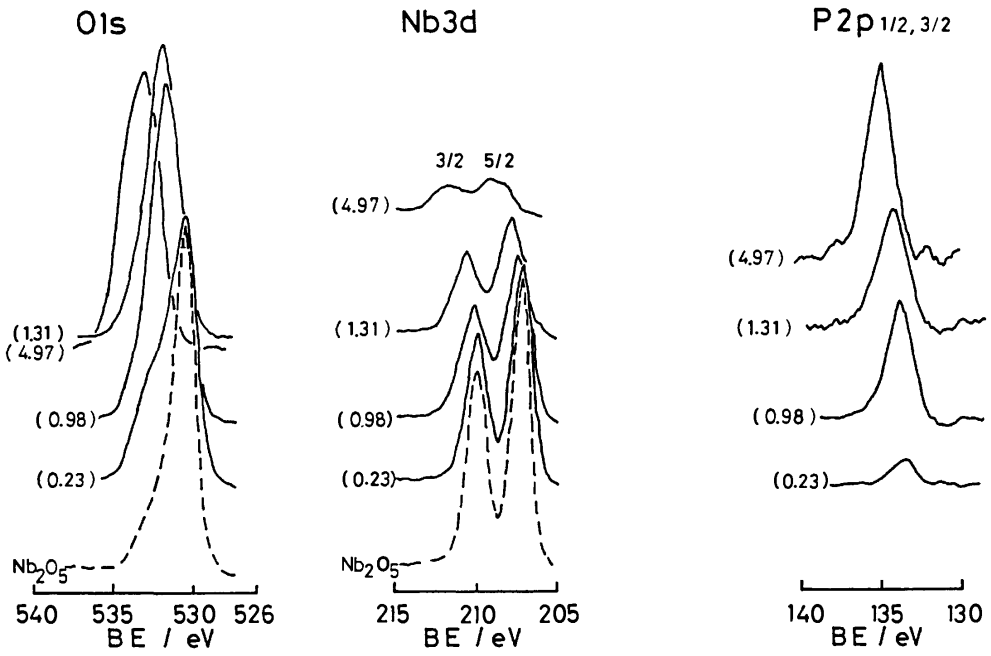

Fig. 6. XPS spectra for niobic acid before and after treatment with phosphoric acid. BE values shown here were obtained by assuming the Cls peak position due to contaminant carbon as 285 eV.

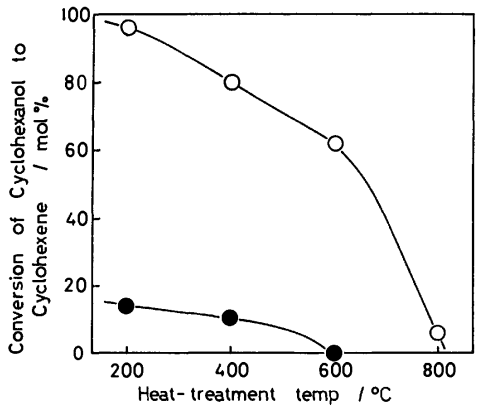

Fig. 7. Catalytic dehydration of cyclohexanol over niobic acid before and after treatment with H_3PO_4. Reaction temperature: 180°C; W/F: 31.0 g·h·mol^{-1}. ●: Before treatment; ○: after treatment with 1.0 mol dm^{-3} H_3PO_4.

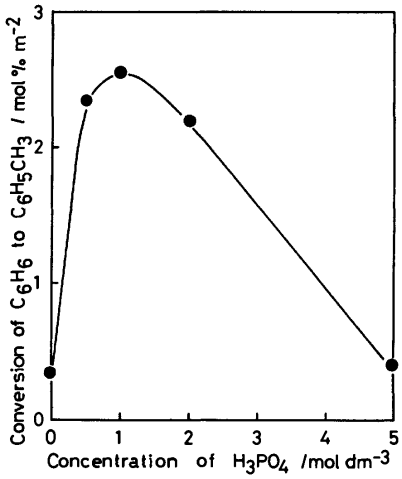

Fig. 8. Catalytic alkylation of benzene with methanol. Reaction temperature: 400°C; molar ratio of MeOH/benzene=0.3; heat treatment temperature of catalyst: 400°C; pulse size: 2 μl; catalyst weight 50 mg.

P/Nb determined by an analysis using XPS. The peak position of P2s for the sample treated with phosphoric acid was, in general, shifted to the lower BE side compared to that observed for P_2O_5 (135.8 eV, which was determined by taking Cls peak position of contaminant C as 285 eV).[9] The extent of the shift increased with decreasing the P content. Thus, the peak positions of samples having various atomic ratios of P/Nb are as follows: 135.8 (P_2O_5), 134.4 (P/Nb=4.97), 134.1 (1.31), 134.0 (0.98), and 133.7 (0.23) eV. The values for samples containing small amounts of the P component almost coincided with that for P^{3+} (134 eV).[9] The evidence suggests that P atoms might contribute to the withdrawal of electrons from the neighbouring Nb atoms; the contribution of individual P atoms might become more remarkable as the amount of phosphoric acid addition decreases. On the other hand, the peak due to Nb3d gradually shifted to the higher bonding energy side upon increasing the amount of the phosphoric acid addition. The result again suggested a withdrawal of electrons from Nb atoms by the phosphoric acid molecules added for the treatment. Thus, the electrons of the Nb atoms surrounded by a larger amount of phosphate molecules might be drawn out to a greater extent; the largest shift to the higher energy side was observed for niobic acid containing the largest amount of the P component (P/Nb=5). However, further details of the induction of electrons of Nb atoms, or the enhancement of the surface acidity due to Nb atoms are not clear at the present stage of this study.

Catalytic Activity in Cyclohexanol Dehydration. Similar to the surface acidity shown in Fig. 2, the catalytic activity of niobic acid in cyclohexanol dehydration, increased with a treatment using phosphoric acid, and gradually decreased upon increasing the heat-treatment temperature (Fig. 7). The change of the catalytic activity described above could be ascribed to a change in the surface acidity. Therefore, the addition of P component should contribute to an increase in the surface acidity, resulting in an enhancement in the catalytic activity in cyclohexanol dehydration.

Catalytic Activity in Alkylation of Benzene with Methanol. The conversion of the alkylation of benzene with methanol over niobic acid before and after a treatment with phosphoric acid of various concentrations is shown in Fig. 8. The catalytic activity of niobic acid, which was shown by the conversion of benzene to toluene, showed a maximum when the sample was treated with 0,5—1.0 mol dm^{-3} of phosphoric acid. As already shown in Fig. 3, a similar maximum value was also obtained for the amount of surface acidity, determined by pyridine adsorption, of H_3PO_4-treated niobic acid, when the phosphoric acid concentration was 1.0 mol dm^{-3}. This fact again suggests that the surface layers formed by the deposition of a phosphorus compound should absorb only small molecules such as N_2 (critical dimension: 3.0 Å[10]) and NH_3 (3.8 Å[10]). On the other hand, larger molecules such as benzene (6.8 Å[10]) might not be able to penetrate through the micro pores of the deposited compound and are, thus, little adsorbed on the H_3PO_4-treated niobic acid. Although the accurate molecular dimension of pyridine is not known, it is considered to be close to that of benzene. This seems to be the reason for obtaining a maximum at about the same concentration of the phosphoric acid to enhance the catalytic activity in the alkylation of benzene with methanol (Fig. 8) and to increase the surface acidity determined by pyridine adsorption (Fig. 3).

The authors are grateful to Mr. Osamu Horie and Mr. Atsushi Uetake for the assistance to perform the catalytic reactions. In addition, we are much obliged to CBMM for the financial support of this study.

References

1) K. Ogasawara, T. Iizuka, and K. Tanabe, *Chem. Lett.*, **1984**, 645.
2) Z. Chen, T. Iizuka, and K. Tanabe, *Chem. Lett.*, **1984**, 1085.
3) Sumitomo Chem. Co., Kokai Tokkyo Koho, 61-167634 (1986).
4) K. Tanabe and T. Iizuka, *Hyomen*, **23**, 471 (1985).
5) B. K. Sen and A. V. Saha, *Mat. Res. Bull.*, **16**, 923 (1981).
6) S. Okazaki, M. Kurimata, T. Iizuka, and K. Tanabe, *Bull. Chem. Soc.Jpn.*, **60**, 37 (1987).
7) H. Itoh and A. Tada, *Shokubai*, **25**, 362 (1983).
8) J. Take, H. Matsumoto, S. Okada, K. Tsutsumi, H. Takahashi, and Y. Yoneda, *Shokubai*, **23**, 344 (1981).
9) Shimadzu Application News, CA148-018 (1980).
10) D. W. Breck, W. G. Eversole, R. M. Milton, T. B. Reed, and T. L. Thomas, *J. Am. Chem. Soc.*, **78**, 5966 (1956).

Syntheses and Characterization of Dinuclear Iron(II, II) and Iron(II, III) Complexes with a Dinucleating Ligand, 2,6-Bis[bis(2-pyridylmethyl)-aminomethyl]-4-methylphenolate (1−)

Masatatu SUZUKI, Akira UEHARA,* Hiroki OSHIO,† Kazutoyo ENDO,††
Makoto YANAGA,†† Sigeo KIDA,† and Kazuo SAITO†
Department of Chemistry, Faculty of Science, Kanazawa University, Kanazawa 920
†Coordination Chemistry Laboratories, Institute for Molecular Science, Okazaki 444
††Department of Chemistry, Faculty of Science, Tokyo Metropolitan University, Fukazawa, Setagaya, Tokyo 158
(Received March 30, 1987)

Dinuclear iron(II, II) complexes, $[Fe_2(L\text{-}py)(RCOO)_2]BF_4 \cdot nH_2O$ (RCOO: CH_3COO (**1a**) and C_6H_5COO (**2a**)), and two types of dinuclear mixed valence iron(II, III) complexes $[Fe_2(L\text{-}py)(RCOO)_2](BF_4)_2 \cdot nH_2O$ (RCOO: CH_3COO (**1b**) and C_6H_5COO (**2b**)) and $[Fe_2(L\text{-}py)(CH_3COO)(OH)](BF_4)_2 \cdot 2H_2O$ (**3**) were prepared, where L-py represents 2,6-bis[bis(2-pyridylmethyl)aminomethyl]-4-methyl-phenolate(1−). Only one of the two iron(II) ions in the iron(II, II) complexes is easily oxidized with molecular oxygen in methanol to form the mixed valence complexes, $[Fe_2(L\text{-}py)(RCOO)_2](BF_4)_2 \cdot nH_2O$, which were characterized by chemical analyses and Mössbauer measurements. Magnetic susceptibility measurements over the temperature range 80—300 K revealed that high-spin iron(II) and iron(III) ions are antiferromagnetically coupled with the spin-exchange coupling constants J=−3—−8 cm^{-1}. The complexes exhibited an ESR signal of $g_{av} \approx 1.7$ near liquid helium temperature. Such an ESR signal arises from an antiferromagnetically spin-coupled high-spin iron(II, III) dimer. An intervalence charge-transfer transition was observed in the region 7000—8500 cm^{-1}. The electron delocalization parameter α is estimated to be ca. 0.08, which corresponds to the class II mixed valence type in the classification of Robin and Day. Cyclic voltammogram of the complex **2b** in acetonitrile showed two reversible couples at +0.05 and +0.73 V (vs. SCE), which were assigned to the redox reactions of Fe(II, III)/Fe(II, II) and Fe(III, III)/Fe(II, III), respectively. The comproportionation constants of **1b** and **2b** at 20 °C are 1.6×10^{12} and 5.0×10^{11}, respectively, implying that the present mixed valence complexes are significantly stabilized.

Dinuclear iron(II, III) mixed valence centers have been found to exist in iron proteins such as *semi-met*hemerythrin,[1-3] pink uteroferrin,[4-8] and the reduced form of bovine spleen acid phosphatase.[4,5,9] They exhibited an ESR signal with g_{av}<2.0 observable only near liquid helium temperature. Such an ESR signal has been interpreted in terms of antiferromagnetic superexchange interaction between high-spin iron(II) and high-spin iron(III) ions.[10] Spin-exchange coupling constants for pink uteroferrin[6,7] and the reduced form of bovine spleen acid phosphatase[9] are ≈−10 and ≈−50 cm^{-1}, respectively. From these data, it was suggested that the former protein had μ-hydroxo bridge[6] and the latter μ-oxo bridge[9]. Recent EXAFS study of the latter protein also suggested the presence of additional bridges such as carboxylato group.[11] For these proteins, phenolato and imidazole groups of tyrosine and histidine residues were proposed as additional coordinating groups;[6,12] possible ligating groups for irons in *semi-met*hemerythrin are imidazole group of histidine residue, and carboxylato groups of aspartic and glutamic acid residues. However, details of structure and function of metal center of these proteins still remain ambiguous.

Synthetic dinuclear mixed valence iron(II, III) complexes with biologically relevant ligands such as imidazole group, carboxylato, and phenolato groups are useful for further elucidation of structure and function of the iron(II, III) centers in the above proteins. In the previous communication, we reported the synthesis and characterization of a mixed valence complex $[Fe_2(L\text{-}Bzim)(C_6H_5COO)_2](BF_4)_2 \cdot 2H_2O$ (L-Bzim=2,6-bis[bis(2-benzimidazolylmethyl)aminomethyl]-4-methylphenolate (1-)) and proposed a dinuclear structure of iron(II) and iron(III) bridged triply by a phenolate and a couple of carboxylato groups.[13] Recently we found a similar triply bridging unit in an analogous dinuclear mixed valence manganese(II, III) complex $[Mn_2(L\text{-}py)(C_6H_5COO)_2](ClO_4)_2 \cdot H_2O$,[14] where L-py is 2,6-bis[bis(2-pyridylmethyl)aminomethyl]-4-methyl-phenolate(1−) (Fig. 1). Reported herein are the syntheses and various physicochemical properties of the two types of dinuclear mixed valence complexes with the dinucleating ligand, L-py, and carboxylate ion(s), $[Fe_2(L\text{-}py)(RCOO)_2](BF_4)_2 \cdot nH_2O$ (RCOO=CH_3COO or C_6H_5COO) and $[Fe_2(L\text{-}py)(CH_3COO)(OH)](BF_4)_2 \cdot 2H_2O$. The L-Bzim and L-py complexes are the first examples of synthetic dinuclear mixed valence high-spin iron(II, III) complexes.

Dinuclear metal complexes with metal ions in sterically and electronically controlled environment are expected to reversibly bind molecular oxygen.

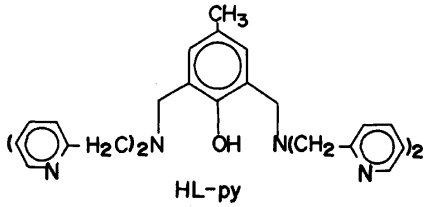

Fig. 1. Dinucleating ligand (HL-py): 2,6-bis[bis(2-pyridylmethyl)aminomethyl]-4-methylphenol.

Recently, we have demonstrated that dinuclear cobalt(II, II) complexes $[Co_2(L\text{-}py)(RCOO)_2]^+$ and $[Co_2(L\text{-}py)(RCOO)]^{2+}$ react reversibly with molecular oxygen to form μ-peroxo complexes $[Co_2(L\text{-}py)(RCOO)(O_2)]^{2+}$.[15] The irreversible oxidation of cobalt ion was much suppressed in the above dioxygen complexes. Such stabilty of the dioxygen complexes must stem from a geometry and donor properties of the ligands. In this study, we also prepared the dinuclear iron(II, II) complexes with L-py and carboxylate ions, $[Fe_2(L\text{-}py)(RCOO)_2]BF_4 \cdot nH_2O$, and their reaction with molecular oxygen was investigated.

Experimental

Materials. HL-py was synthesized as previously described.[15] Iron(II) tetrafluoroborate hexahydrate was prepared according to the method of literature.[16] Other chemicals used were of reagent grade.

Preparation of Iron(II, II) Complexes. $[Fe_2(L\text{-}py)(RCOO)_2]BF_4 \cdot nH_2O$ (RCOO: CH_3COO (1a) or C_6H_5COO (2a)): The complexes were prepared by ordinary Schlenk techniques in an inert atmosphere. A solution of $Fe(BF_4)_2 \cdot 6H_2O$ (1 mmol) in 20 cm^3 of ethanol was added to a solution of HL-py (0.5 mmol), RCOOH (1 mmol), and triethylamine (1 mmol) in 20 cm^3 of ethanol with stirring. The reddish yellow solution was concentrated to a half of the original volume by vacuum evaporation and allowed to stand overnight at 0 °C. Orange-yellow crystals formed were collected by filtration, washed with ethanol and ether, and dried in vacuo.

Preparation of Iron(II, III) Complexes. $[Fe_2(L\text{-}py)RCOO)_2](BF_4)_2 \cdot nH_2O$ (RCOO: CH_3COO (1b) or C_6H_5COO (2b)): A solution of $Fe(BF_4)_2 \cdot 6H_2O$ (1 mmol) in 40 cm^3 of ethanol was added to a mixture of HL-py (0.5 mmol), RCOOH (1 mmol), and triethylamine (1 mmol) in 20 cm^3 of methanol with stirring under a nitrogen atmosphere. The reddish yellow solution was then exposed to an oxygen atmosphere at 10 °C with stirring to cause an instanteneous color change to dark green. The solution was kept at 0 °C for several hours. Dark green crystals thus obtained were collected by filtration, washed with ethanol and ether, and dried in vacuo; they were recrystallized from methanol under a nitrogen atmosphere. The crystals are stable in the open atmosphere. Single crystals suitable for X-ray analysis have not yet been obtained.

$[Fe_2(L\text{-}py)(CH_3COO)(OH)](BF_4)_2 \cdot 2H_2O$ (3): A solution of $Fe(BF_4)_2 \cdot 6H_2O$ (1 mmol) in 20 cm^3 of ethanol was added to a solution of HL-py (0.5 mmol), CH_3COOH (0.5 mmol), and triethylamine (1 mmol) in 20 cm^3 of ethanol under a nitrogen atmosphere. The resulting pale yellow solution was exposed to an oxygen atmosphere with stirring at 10 °C to cause an instanteneous color change to dark blue. The dark blue solution was cooled to 0 °C and allowed to stand for one hour to yield dark blue microcrystalline powders. They were collected by filtration, washed with ethanol and ether, and dried in vacuo. The product is stable in the open atmosphere.

Measurements. The electronic spectra in acetonitrile solution were measured on a Jasco UVIDEC 505 UV/VIS recording digital spectrophotometer and a Hitachi 323 recording spectrophotometer. Infrared spectra were obtained by a KBr-disk method and a Nujol mull method with a Jasco A-3 infrared spectrophotometer. Magnetic susceptibilities were measured with a Shimadzu torsion magnetometer MB-2. The apparatus was calibrated by the use of Hg-$[Co(NCS)_4]$. Diamagnetic corrections were made by using Pascal's constants.[17] Molar conductivities were measured in *N,N*-dimethylformamide or acetonitrile solution (1×10^{-3} mol dm^{-3}) at 25 °C with a Yokogawa Universal Bridge Type BUZ-10A. Mössbauer spectra were measured at 77 K against a $^{57}Co(Pt)$ source moving in a mode of constant acceleration at room temperature. Velocity calibration was carried out by the resonance lines of metallic iron, and isomer shifts were given relative to iron metal at room temperature. Cyclic voltammograms were measured with a Yanagimoto P-900 in a cell containing a glassy carbon working electrode, auxiliary electrode, and a saturated calomel electrode. Applied voltage was measured with a Takeda Riken TR-8651 electrometer. Acetonitrile was used as the solvent and tetrabutylammonium perchlorate as the supporting electrolyte. Ferrocene was added for an internal check on redox potential and reversibility. $E_{1/2}$ of ferrocene was 0.39 V (vs. SCE) with a peak-to-peak separation of 70 mV. ESR spectra above 10 K were measured on a JEOL JES-FE2XG ESR spectrometer (X-band microwave unit, 100 kHz field modulation) equipped with an Air Product LTD-3-110 liquid helium transfer system. The microwave frequency was measured with a Takeda Riken TR5212 microwave counter, and the resonance magnetic field values of the signals were measured with an NMR field meter (ECHO Electronics Co., Ltd.). ESR spectra at 6 K were recorded on a Varian E-112 spectrometer (X-band microwave unit, 100 kHz modulation) equipped with an Oxford cryostat.

Analyses of Iron(II) and Iron(III) Ions. The contents of iron(II) and iron(III) ions in the mixed valence complexes were determined colorimetrically.[18] A weighted quantity of the complex (ca. 40 mg) was dissolved into a solution of 1,10-phenanthroline (200 mg) in 20 cm^3 *N,N*-dimethylformamide under nitrogen atmosphere. The solution was stirred for 1 min and treated with an aqueous suspension (20 cm^3) of excess H_4edta (ca. 100 mg) for preventing the reduction of the iron(III) and masking iron(III)-phenolato complexes.[19] The mixture was diluted to ca. 250 cm^3 with water and the pH of the solution was adjusted to ca. 4 with acetic acid. The volume of the resulting solution was adjusted to 500 cm^3. After filtration, the iron(II) content was determined spectrophotometrically at 510 nm as $[Fe(phen)_3]^{2+}$ (ε=11300 $mol^{-1}\,dm^3\,cm^{-1}$). Total content of iron(II) and iron(III) ions was determined in a similar way after the iron(III) ion had been reduced to divalent state. The iron(III) content was known from the difference. The analytical data are given in Table 1 together with the magnetic moments.

Results and Discussion

Characterization of Complexes. The effective magnetic moments of **1b** and **2b** are 7.7 and 7.3 B. M./Fe_2, respectively, indicating that both iron(II) and iron(III) ions are in high-spin state. The infrared spectra of the complexes in the region of 600—4000 cm^{-1} are almost the same as those of the corresponding manganese(II,III) complexes $[Mn_2(L\text{-}py)(RCOO)_2](ClO_4)_2 \cdot nH_2O$,[14] except for the stretching vibration region of perchlorate and tetrafluoroborate ions.

Table 1. Analytical Data and Effective Magnetic Moments of Complexes

No.	Complex	Found (Calcd)/%					μ_{eff}/B.M.[a]
		C	H	N	Fe(II)	Fe(III)	
1a	$[Fe_2(L\text{-}py)(CH_3COO)_2]$-$BF_4\cdot 0.5H_2O$	52.02 (51.92)	4.62 (4.71)	9.65 (9.82)			7.4
2a	$[Fe_2(L\text{-}py)(C_6H_5COO)_2]$-$BF_4\cdot 3H_2O$	54.99 (55.10)	4.47 (4.82)	8.20 (8.20)			7.2
1b	$[Fe_2(L\text{-}py)(CH_3COO)_2]$-$(BF_4)_2\cdot H_2O$	47.10 (46.70)	4.32 (4.34)	8.90 (8.84)	5.6 (5.87)	5.9 (5.87)	7.7
2b	$[Fe_2(L\text{-}py)(C_6H_5COO)_2]$-$(BF_4)_2\cdot 2H_2O$	51.73 (52.07)	4.13 (4.28)	7.60 (7.75)	4.9 (5.11)	5.2 (5.11)	7.3
3	$[Fe_2(L\text{-}py)(CH_3COO)(OH)]$-$(BF_4)_2\cdot 2H_2O$	44.89 (45.35)	4.22 (4.46)	9.16 (9.07)	5.9 (6.03)	6.0 (6.03)	7.4

a) At room temperature.

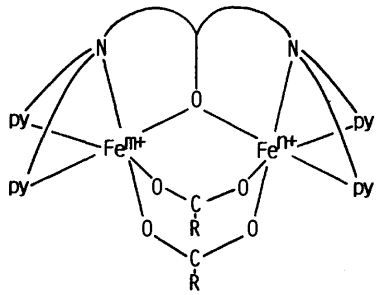

Fig. 2. Possible structure of $[Fe_2(L\text{-}py)(RCOO)_2]^+$ (m=2 and n=2) and $[Fe_2(L\text{-}py)(RCOO)_2]^{2+}$ (m=2 and n=3).

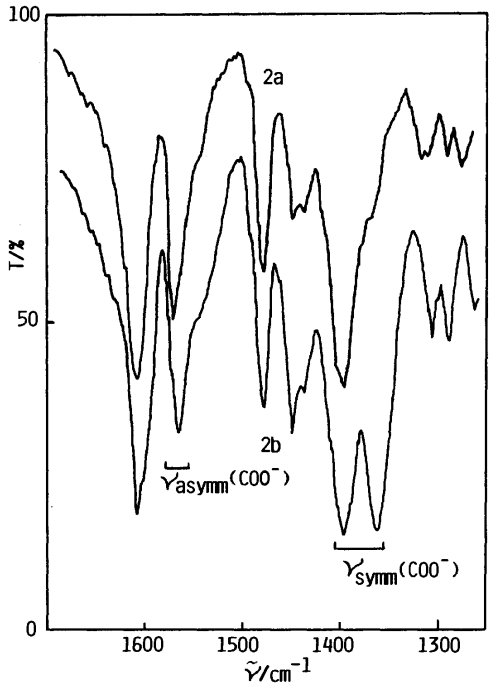

Fig. 3. Infrared spectra of $[Fe_2(L\text{-}py)(C_6H_5COO)_2]$-$BF_4\cdot 3H_2O$ (**2a**) and $[Fe_2(L\text{-}py)(C_6H_5COO)_2](BF_4)_2\cdot 2H_2O$ (**2b**).

From the IR spectral data, both the mixed valence iron and manganese complexes seem to have the same structure. The crystal structure of $[Mn_2(L\text{-}py)(C_6H_5\text{-}COO)_2](ClO_4)_2\cdot H_2O$[14b] showed that manganese(II) and (III) ions are bridged by phenolate and two carboxylate oxygens to form a cofacial bi-octahedral structure. Such triply bridging structure has been found for some dinuclear manganese and iron complexes with bridging groups composed of two carboxylato groups and oxo, hydroxo, or phenolato group.[20-23] A possible structure of **1b** and **2b** is shown in Fig. 2.

Infrared spectra of **2a** and **2b** in the $\nu(COO^-)$ stretching vibration region (Fig. 3) showed that the ν_{symm} (COO^-) of **2b** splits into two bands at 1395 and 1362 cm^{-1}, suggesting the presence of two types of carboxylato groups. A similar splitting of ν_{symm} (COO^-) was also observed in manganese(II,III) complex $[Mn_2(L\text{-}py)(C_6H_5COO)_2](ClO_4)_2\cdot H_2O$[14b] in which two bridging benzoato groups are not equivalent: one symmetrically bridges manganese(II) and (III) ions, and the other unsymmetrically. The Mn(III)-O and Mn(II)-O bond distances, and two C-O bond distances of unsymmetrically bridging benzoato group considerably differ from each other. It has been suggested that $\Delta\tilde{\nu}$ (COO^-) value ($\tilde{\nu}_{asymm}$ (COO^-) $-$ $\tilde{\nu}_{symm}$ (COO^-)) is diagnostically useful for elucidating coordination mode of carboxylato group; a symmetrically bridging carboxylato group gives $\Delta\tilde{\nu}$ smaller than 200 cm^{-1}, whereas an unsymmetrically bridging group a larger $\Delta\tilde{\nu}$.[24] The $\Delta\tilde{\nu}$ values are 150 and 200 cm^{-1} for **1b**, and 173 and 206 cm^{-1} for **2b**. Thus the larger $\Delta\tilde{\nu}$ values correspond to an unsymmetrically bridging carboxylato group and the smaller values to a symmetrically bridging one.

The complex **3** is air-stable in the solid state, but easily oxidized with molecular oxygen in various solvents at room temperature. Its effective magnetic moment is 7.4 B.M./Fe_2 at room temperature, indicating that iron(II) and iron(III) ions are in high-spin state. The molar conductivity (137 Ω^{-1} cm^2 mol^{-1}) in DMF indicates that the complex is a 2:1 electrolyte. From the molar conductivity measurement and elemental analysis, the coordination of hydroxide ion is

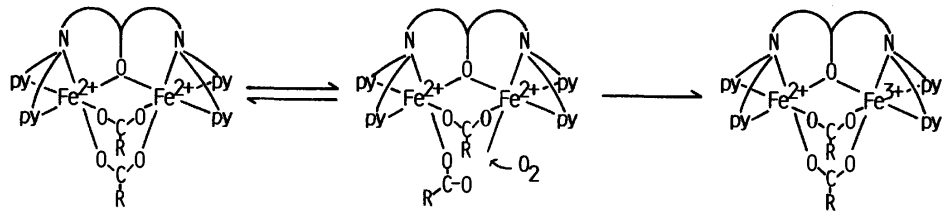

Fig. 4. A possible reaction scheme of oxidation of $[Fe_2(L\text{-}py)(RCOO)_2]^+$ (**1a** and **2a**).

plausible and the complex **3** may be formulated as $[Fe_2(L\text{-}py)(CH_3COO)(OH)](BF_4)_2 \cdot 2H_2O$.

The effective magnetic moments of **1a** and **2a** are 7.4 and 7.2 B.M./Fe_2, respectively, indicating that iron(II) ions are in high-spin state. The infrared spectra of **1a** and **2a** are almost identical to those of the corresponding Co^{II}-Co^{II} complexes, $[Co_2(L\text{-}py)(RCOO)_2]BF_4 \cdot nH_2O$,[15] in which cobalt ions were shown to adopt a six-coordinated structure on the basis of their reflectance spectra. On the analogy with the cobalt complexes, the present complexes seem to have six-coordinated structure. This may also be supported by the reactivity of the complexes with molecular oxygen in various solvents (vide infra). A possible structure is shown in Fig. 2.

The complexes **1a** and **2a** are relatively stable for a day in acetonitrile and dichloromethane under an oxygen atmosphere, whereas they rapidly react with molecular oxygen in methanol and *N,N*-dimethylformamide to form dark brown solution. Addition of tetraethylammonium tetrafluoroborate and ethanol to the above dark brown solution gave the mixed valence complexes **1b** and **2b**.

Reactivity of the Iron(II,II) Complexes with Molecular Oxygen. The effect of solvents on the reactivity of the dinuclear iron(II,II) complexes **1a** and **2a** with molecular oxgyen is quite similar to that of the corresponding cobalt(II,II) complexes $[Co_2(L\text{-}py)(RCOO)_2]^+$.[15] Both cobalt and iron complexes readily react with molecular oxygen in methanol and *N,N*-dimethylformamide but to a much lesser extent in acetonitrile and dichloromethane. The cobalt complexes give reversible oxygenation in the former two solvents to give μ-peroxo complexes, whereas the iron complexes form the mixed valence complexes **1b** and **2b** as mentioned in the preceding section. We suggested that the oxygenation of the cobalt complexes proceeds via a five-coordinated species: one of two carboxylato groups dissociates in the former solvents, but not in the latters. In fact, the five-coordinated complexes $[Co_2(L\text{-}py)(RCOO)]^{2+}$ react reversibly with molecular oxygen both in methanol and acetonitrile as well as in the solid state. This is also the case for the oxidation of iron(II,II) complexes: the oxidation of iron complexes seems to take place in a five-coordinated species. A possible reaction scheme is given in Fig. 4. It is probable that one of two bridging carboxylato groups (a in Fig. 4) dissociates to form a species containing five-and six-coordinated irons and then five-coordinated moiety reacts with molecular oxygen to form a hyperoxo complex as a transient intermediate. This hyperoxo complex is unstable and irreversibly oxidized to form mixed valence complex. In the cobalt complex, however, the hyperoxo complex is relatively stable and the coordinated hyperoxide ion displaces the unidentate carboxylate ion to form a μ-peroxo complex.

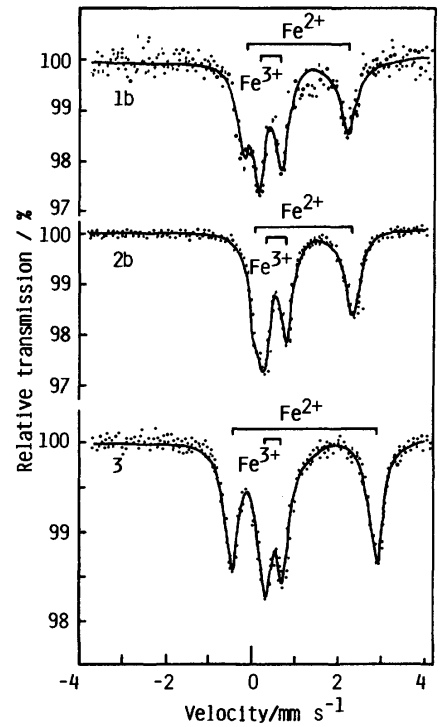

Fig. 5. Mössbauer spectra of $[Fe_2(L\text{-}py)(CH_3COO)_2](BF_4)_2 \cdot H_2O$ (**1b**), $[Fe_2(L\text{-}py)(C_6H_5COO)_2](BF_4)_2 \cdot 2H_2O$ (**2b**), and $[Fe_2(L\text{-}py)(CH_3COO)(OH)](BF_4)_2 \cdot 2H_2O$ (**3**) at 77 K.

Mössbauer Spectra. Mössbauer spectra of the mixed valence complexes are shown in Fig. 5 and their parameters are listed in Table 2. All the spectra were analyzed with a least square fitting program of Lorenztian functions into two sets of quadrupole doublets, each of which was fitted with an equal line width and intensity. The calculated quadrupole splittings ΔE (isomer shifts δ) in mm s^{-1} are 2.06—3.38

Table 2. Mössbauer Parameters of the Mixed Valence Complexes at 77 K[a]

No.	Complex	Fe(II)			Fe(III)			A(Fe(III)/Fe(II))[c]
		δ[b]	ΔE	Γ_{exp}	δ[b]	ΔE	Γ_{exp}	
1b	$[Fe_2(L\text{-}py)(CH_3COO)_2](BF_4)_2\cdot H_2O$	1.16	2.42	0.41	0.47	0.51	0.33	1.03
2b	$[Fe_2(L\text{-}py)(C_6H_5COO)_2](BF_4)_2\cdot 2H_2O$	1.15	2.06	0.56	0.56	0.47	0.28	1.00
3	$[Fe_2(L\text{-}py)(CH_3COO)(OH)](BF_4)_2\cdot 2H_2O$	1.19	3.38	0.34	0.48	0.42	0.43	1.12
	Pink unterrofrin[d]	1.24	2.68	0.28	0.53	1.84	0.43	

a) All data in mm s^{-1} except for A(Fe(III)/(Fe(II)). b) Isomer shift, δ, relative to iron metal. c) Ratios of areas of Fe(III) to Fe(II). d) Data at 60 K from Ref. 8.

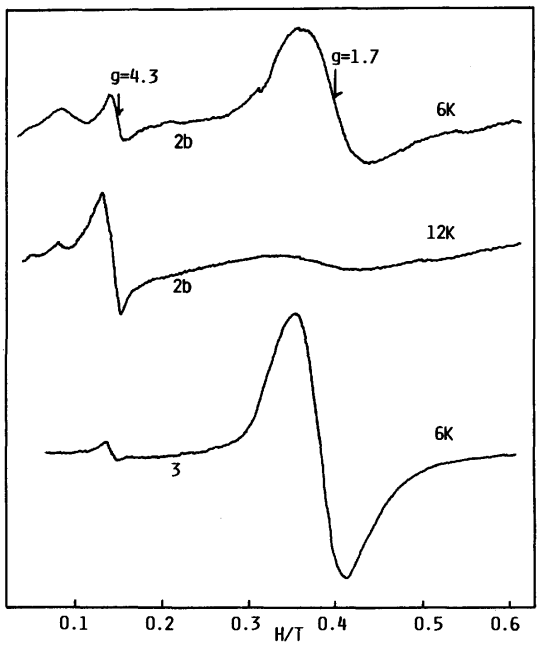

Fig. 6. ESR spectra of $[Fe_2(L\text{-}py)(C_6H_5COO)_2]^{2+}$ (**2b**) and $[Fe_2(L\text{-}py)(CH_3COO)(OH)]^{2+}$ (**3**) in acetonitrile at 6 and 12 K.

(1.16—1.19) and 0.42—0.51 (0.47—0.56), which are assigned to those arising from the high-spin iron(II) and iron(III) moieties, respectively.[25] The presence of iron(II) and iron(III) ions in equimolar ratio is evidenced from the fact that the ratios of areas of two sets of quadrupole doublets are nearly unity (the last columm in Table 2), which is in good agreement with the results of the chemical analyses as described in the Experimental section.

Pink uteroferrin[8] also shows two sets of quadrupole doublets. The reported values are listed in Table 2. The quadrupole splitting of the iron(III) moiety in pink uteroferrin is much larger than those of the present complexes. This fact reflects a remarkable structural difference in iron(III) moieties between the protein and the present complexes. It is well-known that μ-oxo dinuclear iron(III,III) complexes tend to exhibit larger quadrupole splittings.[25,26] However, μ-oxo bridging seems unlikely to occur in pink uteroferrin from its magnetism.[7] Therefore, iron(III) moiety in pink uteroferrin may have a distorted five-coordinated structure which shows a larger quadrupole splitting because of the larger electric field gradient at nucleus.[25,27]

ESR Spectra. ESR spectra of **2b** and **3** at 6 and 12 K are shown in Fig. 6. Both complexes exhibit two signals centered at g=1.7 and 4.3, which are quite similar to those observed in the mixed valence iron proteins such as bovine spleen acid phosphatase.[9] The g=4.3 signal can be assigned to that arising from mononuclear rhombic high-spin iron(III) ion present as impurity which may be produced by a slight decomposition of the complex. The g=1.7 signal is observable only near liquid helium temperature and almost disappears above 12 K as shown in Fig. 6. Such an ESR signal with $g_{av}<2.0$ has been interpreted in terms of antiferromagnetic superexchange interaction between high-spin iron(II) (S=2) and high-spin iron(III) (S=5/2) ions.[10] In contrast to the iron proteins, the present complexes exhibited only a broad isotropic signal even at 6 K, which suggests a rapid electron spin-lattice relaxation.

Magnetic Susceptibilities. The antiferromagnetic interaction was confirmed by the temperature dependence of magnetic susceptibilities. Magnetic susceptibilities of the mixed valence complexes were measured over the temperature range 80—300 K. The results were analyzed by the usual spin-spin interaction model based on the exchange Hamiltonian $H=-2JS_1\cdot S_2$. The molar susceptibility (χ_A) of S_1=2—S_2=5/2 spin exchange coupling dimer is given by Eq. 1,

$$\chi_A=\frac{N\beta^2g^2}{4\kappa T}\times\frac{x^{24}+10x^{21}+35x^{16}+84x^9+165}{x^{24}+2x^{21}+3x^{16}+4x^9+5}+N\alpha \qquad (1)$$

where $x=\exp(-J/\kappa T)$ and the symbols have their usual meanings. The magnetic susceptibilities of the complexes were well interpreted in terms of the above equation. Figure 7 shows temperature dependence of magnetic susceptibilities of **2b**. The solid line is the calculated curve by using the parameters listed in Table 3. The g value used in the fit for magnetic susceptibilities is 2.10, which differs significantly from

Table 3. Magnetic Parameters of the Mixed Valence Complexes

No.	Complex	J/cm^{-1}	g	$N\alpha/10^{-6}$ cgs mol^{-1}
1b	$[Fe_2(L\text{-}py)(CH_3COO)_2](BF_4)_2\cdot H_2O$	−3.2	2.10	0
2b	$[Fe_2(L\text{-}py)(C_6H_5COO)_2](BF_4)_2\cdot 2H_2O$	−8.0	2.10	0
3	$[Fe_2(L\text{-}py)(CH_3COO)(OH)](BF_4)_2\cdot 2H_2O$	−6.5	2.10	0
	Pink uteroferrin[a]	−10		
	Reduced form of bovine spleen acid phosphatase[b]	−50		

a) Refs. 6 and 7. b) Ref. 9.

Table 4. Electronic Spectral Data of the Mixed Valence Complexes[a]

No.	Complex	$\tilde{\nu}_{max}$/cm^{-1} (ε/mol^{-1} dm^3 cm^{-1}) CT band	IT band
1b	$[Fe_2(L\text{-}py)(CH_3COO)_2](BF_4)_2\cdot H_2O$	18000(900)	7700(290)
2b	$[Fe_2(L\text{-}py)(C_6H_5COO)_2](BF_4)_2\cdot 2H_2O$	17400(970)	7400(290)
3	$[Fe_2(L\text{-}py)(CH_3COO)(OH)](BF_4)_2\cdot 2H_2O$	20200(740)	8500(100)

a) In acetonitrile under a nitrogen atmosphere.

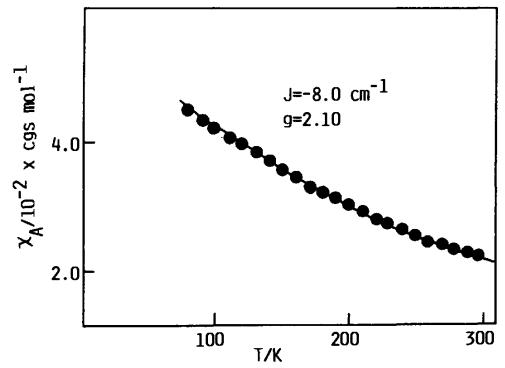

Fig. 7. Temperature dependence of magnetic susceptibilities of $[Fe_2(L\text{-}py)(C_6H_5COO)_2](BF_4)_2\cdot 2H_2O$ (**2b**).

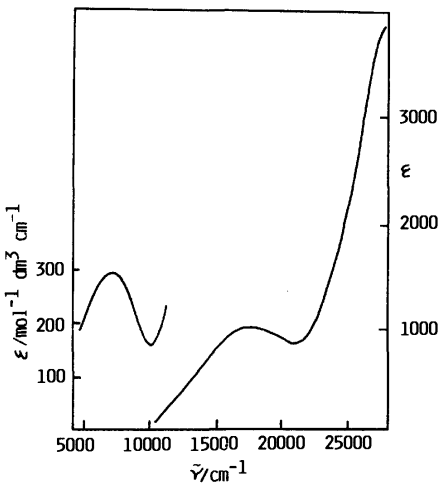

Fig. 8. Electronic spectrum of $[Fe_2(L\text{-}py)(C_6H_5COO)_2](BF_4)_2\cdot 2H_2O$ (**2b**) in acetonitrile under nitrogen atmosphere.

that derived from ESR measurement ($g\approx 1.7$). These two g values are not necessarily the same: the former is the average value derived from the energy separations ($g\beta H$) in the five spin states (S=1/2, 3/2, 5/2, 7/2, 9/2), whereas the latter is that in the S=1/2 ground state. The results indicate that high-spin iron(II) and high-spin iron(III) ions are antiferromagnetically coupled to yield the S=1/2 ground state. The corresponding manganese complexes $[Mn_2(L\text{-}py)(RCOO)_2](ClO_4)_2\cdot nH_2O$ also exhibited weak antiferromagnetic interaction ($J\approx -6$ cm^{-1}).[14] Recently such triply bridging units consisting of two carboxylato groups and oxo, hydroxo, or phenolato group have been found for several iron and manganese complexes.[20-23] The magnitude of spin-exchange interaction in dinuclear iron(III,III) complexes having a triply bridging unit is highly dependent on the nature of the bridging groups. In general, μ-oxo bridged complexes exhibit much stronger antiferromagnetic interaction than μ-hydroxo and μ-phenolato bridged ones.[20,22,28]

The J values of the present complexes are comparable to that for pink uteroferrin ($J\approx -10$ cm^{-1}),[6,7] but much smaller than that for the reduced form of bovine spleen acid phosphatase ($J\approx -50$ cm^{-1}).[9] The oxidized forms of both proteins have been suggested to have a μ-oxo bridge on the basis of their strong antiferromagnetic interactions. The presence of μ-oxo bridge is also suggested in the reduced form of bovine spleen acid phosphatase. A much weaker exchange coupling for pink uteroferrin as compared with that for the reduced form of bovine spleen acid phosphatase may reflect a change in the bridging groups. Lauffer et al.[7] proposed a possibility of hydroxo bridge in pink uteroferrin. It is needed to study extensively the dinuclear iron(II,III) complexes with a μ-oxo or μ-hydroxo bridge for further elucidation of the structure of these proteins.

Electronic Spectra. All the mixed valence complexes exhibit absorption band in the near infrared region (ε=300—100 mol^{-1} dm^3 cm^{-1}/Fe_2) in acetonitrile (Fig. 8 and Table 4). Neither iron(II) nor iron(III) complexes in high-spin state has such intense band in this region,[29] and the band is undoubtedly assigned to

the intervalence charge transfer transition (IT) of the type

$$[Fe^{II}\text{-}Fe^{III}] \xrightarrow{h\nu} [Fe^{III}\text{-}Fe^{II}]^*$$

The complexes also give an band in the visible region (ε=700—1000 mol^{-1} dm^3 cm^{-1}/Fe^{III}). This is the band characteristic of iron(III)-phenolato complexes[30] and is assigned to charge transfer transition from pπ orbital of bridging phenolato group to half filled dπ^* orbital of iron(III) ion. The ligand field bands may be obscured under the above CT band.

According to Hush,[31] the delocalization coefficient, α^2, a measure of mixing of oxidation states, can be calculated by using Eq. 2

$$\alpha^2 = \frac{(4.24\times10^{-4})\cdot\varepsilon_{max}\cdot\Delta\tilde{\nu}_{1/2}}{\tilde{\nu}_{max}\cdot d^2} \quad (2)$$

The α^2 value calculated for **2b** is 6.8×10^{-3} assuming $\tilde{\nu}_{max}$=7300 cm^{-1}, $\Delta\tilde{\nu}_{1/2}$=5000 cm^{-1}, ε_{max}=290 mol^{-1} dm^3 cm^{-1} and d=3.5 Å. The metal-metal distance (d) is estimated from the corresponding manganese(II, III) complex.[14b] The α^2 value implies that delocalization of electron between iron(II) and iron(III) moieties is relatively small and the complex belongs to so-called class II mixed valence system.[32] This is compatible with the results of Mössbauer spectra: all the mixed valence complexes show two sets of quadrupole doublets arising from iron(II) and iron(III) moieties (Fig. 5 and Table 2), indicating that the thermal electron-transfer rate between iron(II) and iron(III) ions are slower than 10^7 s^{-1} (Mössbauer life time).

Loehr et al.[29] reported the electronic spectrum of *semi-met*hemerythrin (*semi-met*)$_R$Hr, where no IT band is detected in the visible and near infrared regions. The absence of IT band in the visible and near infrared regions implies that delocalization of electron in (*semi-met*)$_R$Hr is less than that in the present complexes, and that iron(II) and iron(III) valences in (*semi-met*)$_R$Hr are firmly trapped. It has been suggested that two iron moeities are not equivalent in *deoxy*- and *met*Hr.[33] Such an unsymmetry of two coordination moieties may be responsible for this trapped valence state.

Cyclic Voltammograms. Cyclic voltammograms of the mixed valence complexes **2b** and **3** in acetonitrile at 20 °C are illustrated in Fig. 9 (Table 5). The complex **1b** exhibits two redox couples at 0.68 and −0.03 V (vs. SCE). The constant potential coulometry revealed that these two redox couples correspond to one-electron redox reactions attributable to Fe^{III}-Fe^{III}/Fe^{II}-Fe^{III} (+0.68 V) and Fe^{II}-Fe^{III}/Fe^{II}-Fe^{II} (−0.03 V). Peak-to-peak separations of these two waves are 70 mV at a scan rate of 100 mV s^{-1} and the ratios of the oxidation currents (i_{pa}) for the forward scan to the reduction currents (i_{pc}) for the reverse scan are close to unity for the both couples. These two couples are fairly reversible since ferrocene present in this system as an internal standard showed a peak-to-peak separation of 70 mV. A similar cyclic voltammogram was observed for **1b**. The complex **3** also exhibits two redox couples at ca. +0.7 and −0.1 V (vs. SCE). However, these two couples are not reversible (Fig. 9). This irreversibility suggests a significant structural change upon electron transfer.

Stability of Mixed Valence Complexes. From the separation of the redox potentials of E_1([II, III]/[II, II])

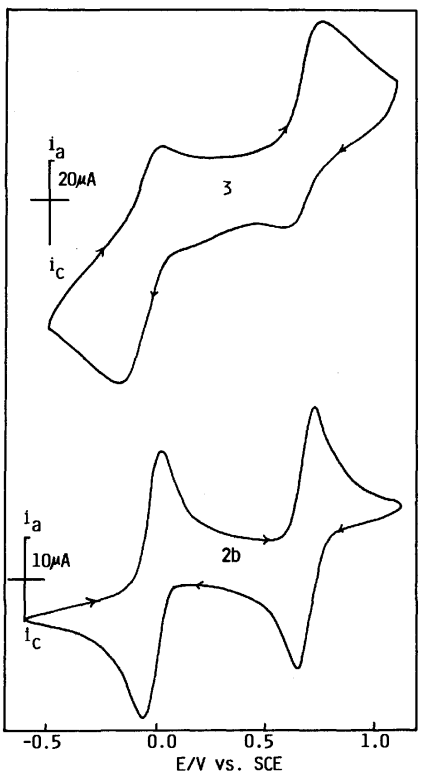

Fig. 9. Cyclic voltammograms of [Fe_2(L-py)-($CH_3COO)_2$]($BF_4)_2\cdot H_2O$ (**1b**) and [Fe_2(L-py)-(CH_3COO)(OH)]($BF_4)_2\cdot 2H_2O$ (**3**) in acetonitrile. The scan rate is 100 mV s^{-1}.

Table 5. Cyclic Voltammetric Data of the Mixed Valence Complexes

No.	Complex	$E_{1/2}$[a] E/V (vs. SCE)	$E_{1/2}$[b] E/V (vs. SCE)	(i_{pa}/i_{pc})[a]	(i_{pa}/i_{pc})[b]	K_c[c]
1b	[Fe_2(L-py)($CH_3COO)_2$]($BF_4)_2\cdot H_2O$	−0.03	+0.68	1.0	1.0	1.6×10^{12}
2b	[Fe_2(L-py)($C_6H_5COO)_2$]($BF_4)_2\cdot 2H_2O$	+0.05	+0.73	1.0	1.0	5.0×10^{11}
3	[Fe_2(L-py)(CH_3COO)(OH)]($BF_4)_2\cdot 2H_2O$	−0.08[d]	+0.67[d]			

a) For Fe(II, III)/Fe(II, II) redox couple. b) For Fe(III, III)/Fe(II, III) redox couple. c) Comproportionation constant at 20 °C. d) Irreversible.

and E_2([III, III])/[II, III]), comproportionation constants (K at 20 °C) of the following reaction are calculated by Eq. 3.

$$(Fe^{III}\text{-}Fe^{III})+(Fe^{II}\text{-}Fe^{II}) \rightleftharpoons 2(Fe^{III}\text{-}Fe^{II})$$
$$E_2-E_1=RT/F\cdot\ln K \quad (3)$$

The values obtained for **1b** and **2b** are 1.6×10^{12} and 5.0×10^{11} (ΔG=−68 and −66 kJ mol^{-1}) respectively, indicating that the present mixed valence complexes are highly stabilized. Others have suggested that factors such as electron delocalization, electrostatic interaction, and steric interaction can contribute to the magnitude of K.[34] The electron delocalization energy (E_e) can be estimated by an analysis of the IT band. The value was calculated to be 600 J mol^{-1} for **2b** by using Eq. 4.

$$E_e=\alpha^2\cdot\tilde{\nu}_{IT}.^{34a)} \quad (4)$$

Thus the electron delocalization energy for the present system is too small to contribute significantly to its stability. When the metal ions are in close proximity, electrostatic interaction may play an important role. A dinuclear metal(II, II) complex will be more readily oxidized than a metal(II, III) species from electrostatic point of view. This will lead to a greater separation of redox potentials and increase of stability of the mixed valence state. In addition, a steric requirement arising from binucleating ligand L-py and two bridging carboxylato groups seems to be important.

Very recently we found that the reaction of an equimolar mixture of iron(III) and manganese(II) ions with L-py and carboxylate ions yields a dinuclear heterometal manganese(II)-iron(III) complex [MnFe(L-py)(RCOO)$_2$]$^{2+}$ in more than 70% yieid.[35] The reaction of iron(III) ion with a dinuclear manganese(II, II) complex [Mn$_2$(L-py)(RCOO)$_2$]$^+$ also resulted in the formation of the above dinuclear heterometal complex with a slight contamination of dinuclear homometal complexes.[35] Thus the present ligand system affords a favorable coordination sites for dinuclear metal(II, III) complexes.

The present work was supported by a Grant-in-Aid for Scientific Research No. 61540443 from the Ministry of Education, Science and Culture.

References

1) R. G Wilkins and P. C. Harrington, *Adv. Inorg. Biochem.*, **5**, 51 (1983).
2) B. B. Muhoberac, D. C. Wharton, L. M. Babcock, P. C. Harrington, and R. G. Wilkins, *Biochim. Biophys. Acta*, **626**, 337 (1980).
3) D. M. Kurtz,Jr., J. T. Sage, M. Hendrich, P. G. Debrunner, and G. S. Lukat, *J. Biol. Chem.*, **258**, 2115 (1983).
4) L. Que, Jr., *Coord. Chem. Rev.*, **50**, 73 (1983).
5) B. C. Antanaitis and P. Aisen, *Adv. Inorg. Biochem.*. **5**, 111 (1983).
6) B. C. Antanaitis, P. Aisen, and H. E. Lilienthal, *J. Biol. Chem.*, **258**, 3166 (1983).
7) R. B. Lauffer, B. C. Antanaitis, P. Aisen, and L. Que, Jr., *J. Biol. Chem.*, **258**, 14212 (1983).
8) P. G. Debrunner, M. P. Hendrich, J. D. Jersey, D. T. Keough, J. T. Sage, and B. Zerner, *Biochim. Biophys. Acta*, **745**, 103 (1983).
9) J. C. Davis and B. A. Averill, *Proc. Natl. Acad. Sci. U.S.A.*, **79**, 4623 (1982).
10) J. F. Gibson, D. O. Hall, J. H, M. Thornley, and F. R. Whatley, *Proc. Natl. Acad. Sci. U.S.A.*, **56**, 987 (1966).
11) S. M. Kauzlarich, B. K. Teo, T. Zirino, S. Burman, J. C. Davis, and B. A. Averill, *Inorg. Chem.*, **25**, 2781 (1986).
12) a) B. P. Gaber, J. P. Sheridan, F. W. Bazer, and R. M. Robert, *J. Biol. Chem.*, **254**, 8340 (1979); b) B. C. Antanaitis, T. Strekas, and P. Aisen, *J. Biol. Chem.*, **257**, 3766 (1982).
13) M. Suzuki. A. Uehara, and K. Endo, *Inorg. Chim. Acta*, **123**, L9 (1986).
14) a) M. Suzuki, S. Murata, A. Uehara, and S. Kida, *Chem. Lett.*, **1987**, 281; b) M. Suzuki, M. Mikuriya, S. Murata, A. Uehara. H. Oshio, S. Kida, and K. Saito, to be submitted.
15) a) M. Suzuki, H. Kanatomi, and I. Murase, *Chem. Lett.*, **1981**, 1745; b) M. Suzuki, I. Ueda, H. Kanatomi, and I. Murase, *Chem, Lett.*, **1983**, 185; c) M. Suzuki, H. Kanatomi, and I. Murase, *Bull. Chem. Soc. Jpn.*, **57**, 36 (1984).
16) C. L. Spiro, S. L. Lambert, T. J. Smith, E. N. Duesler, R, R, Gagne, D. N. Hendrickson, *Inorg. Chem.*, **20**, 1229 (1981).
17) F. E. Mabbs and D. J. Marchin "Magnetisms and Transition Metal Complexes," Chapman and Hall, London, (1973), p. 5.
18) F. D. Snell and C. T. Snell, "Colorimetric Method of Analysis," 3rd ed, D. Van Nostrand; (1957), Vol. 12, p. 316.
19) A slight reduction of iron(III) ion by phenolate of L-py was observed when iron(III) ion, phenanthroline, HL-py, CH_3COONa, and CH_3ONa coexist in molar ratio of 2:10:1:2:1 in *N,N*-dimethylformamide. However, the addition of aqueous suspension of H_4edta prevented the reduction of iron(III) in the above mixture.
20) W. H. Armstrong, A. Spool, G. C. Papaefthymiou, R. B. Frankel, and S. J. Lippard, *J. Am. Chem. Soc.*, **106**, 3653 (1984) and references therein.
21) K. Wieghardt, U. Bossek, D. Ventur, and J. Weiss, *J. Chem. Soc., Chem. Commun.*, **1985**, 347.
22) W. H. Armstrong and S. J. Lippard, *J. Am. Chem. Soc.*, **106**, 4632 (1984).
23) B. P. Murch, F. C. Bradley, and L. Que, Jr., *J. Am. Chem. Soc.*, **108**, 5027 (1986).
24) G. B. Deacon and R. J. Phillips, *Coord. Chem. Rev.*, **23**, 227 (1980).
25) N. N. Greenwood and G. T. Gibbs, "Mössbauer Spectroscopy," Chapman and Hall, London (1971), p. 148.
26) K. S. Murray, *Coord. Chem. Rev.*, **12**, 1 (1974).
27) G. J. Long, J. T. Wrubleski, R. V. Thundathil, D. M. Sparlin, and E. O. Schlemper, *J. Am. Chem. Soc.*, **102**, 6040 (1980).
28) M. Suzuki and A. Uehara, unpublished results.
29) J. S. Loehr, T. M. Loehr, A. G. Mauk, and H. B. Gray, *J. Am. Chem. Soc.*, **102**, 6992 (1980).
30) a) E. W. Aniscough, A. M. Brodie, J. E. Plowman, K. L. Brown, A. W. Addison, and A. R. Gainsford, *Inorg. Chem.*, **19**, 3655(1980); b) J. W. Pyrz, A. L. Roe, L. J. Stern, and L. Que, Jr., *J. Am. Chem. Soc.*, **107**, 614 (1985).

31) N. S. Hush, *Prog. Inorg. Chem.*, **8**, 391 (1967).
32) M. B. Robin and P. Day. *Adv. Inorg. Chem. Radiochem.*, **10**, 247 (1967).
33) a) W. T. Elam, E. A. Stern. J. D. McCallum, and J. S. Loehr, *J. Am. Chem. Soc.*, **105**, 1919 (1983); b) R. E. Stenkamp, L. C. Sieker, and L. H. Jensen, *J. Am. Chem. Soc.*, **106**, 618 (1984).
34) a) J. E. Sutton and H. Taube, *Inorg. Chem.*, **20**, 3129 (1981); b) R. R. Gagne, C. L. Spiro, T. J. Smith, C. A. Hamann, W. R. Thies, and A. K. Shiemke, *J. Am. Chem. Soc.*, **103**, 4073 (1981).
35) M. Suzuki, S. Murata, and A. Uehara, unpublished results.

 © 1987 The Chemical Society of Japan Bull. Chem. Soc. Jpn., 60, 3557—3562 (1987)

Inhibition of Dimerization of Copper(II) Carboxylates by Cyclohexane Ring in Extraction of Copper(II) with Cyclohexanecarboxylic Acid

Hiromichi YAMADA,* Miyuki ITŌ, and Masateru MIZUTA
Faculty of Engineering, Gifu University, 1-1 Yanagido, Gifu 501-11
(Received April 9, 1987)

The extraction of copper(II) with cyclohexanecarboxylic acid in benzene was carried out at 25 °C and at the aqueous ionic strength of 0.1 mol dm^{-3} ($NaClO_4$). The partition constant, $K_{D,HA}$ of cyclohexanecarboxylic acid between benzene and water, and the dimerization constant, $K_{2,HA}$ of cyclohexanecarboxylic acid in benzene were determined: $\log K_{D,HA}=0.90$ and $\log K_{2,HA}=1.54$, respectively. The monomeric and dimeric copper(II) cyclohexanecarboxylates were responsible for the extraction:

$$Cu^{2+}+(HA)_{2,o} \rightleftharpoons (CuA_2)_o+2H^+$$
$$Cu^{2+}+2(HA)_{2,o} \rightleftharpoons (CuA_2(HA)_2)_o+2H^+$$
$$2Cu^{2+}+2(HA)_{2,o} \rightleftharpoons (Cu_2A_4)_o+4H^+$$
$$2Cu^{2+}+3(HA)_{2,o} \rightleftharpoons (Cu_2A_4(HA)_2)_o+4H^+$$

with the extraction constants, $\log K_{ex(10)}=-8.34$, $\log K_{ex(12)}=-7.33$, $\log K_{ex(20)}=-12.47$, and $\log K_{ex(22)}=-11.73$, respectively. By comparing the overall formation constant of the dimeric copper(II) cyclohexanecarboxylate, $Cu_2A_4(HA)_2$ in the aqueous phase with that of copper(II) decanoate and lipoate, the cyclohexane ring was found to inhibit the formation of the dimeric copper(II) carboxylate.

The stability of the dimeric copper(II) carboxylate is so high that no appreciable amount of monomer can be detected in most nonsolvating solvents.[1,2] In the extraction of copper(II) with some sterically crowded carboxylic acids such as trimethylacetic acid,[3] cyclohexanecarboxylic acid,[4] and cyclopentylacetic acid,[5] it was suggested that the monomeric copper(II) species is extracted together with the dimer. But, in the first reference[3] presented by Haffenden and Lawson, they didn't mention the composition of the monomeric copper(II) trimethylacetate. And although the other references[4,5] reported by Brzozka and Rozycki will be later described in detail, there are some doubts about their results. In the previous reports, it has been shown that the monomeric and dimeric copper(II) decanoates are in equilibrium in alcohols[6,7] and ketones,[8] and it has been interpreted according to the regular solution theory that the extraction of the monomeric copper(II) decanoates as well as the dimeric ones can be attributed to the stabilization of the monomeric copper(II) species by the extensive solvation of alcohols or ketones molecules.

The present paper deals with the extraction of copper(II) with cyclohexanecarboxylic acid in benzene, and it was found that the cyclohexane ring at 2-position in cyclohexanecarboxylic acid inhibited the formation of the dimeric copper(II) carboxylate.

Experimental

Reagents. Cyclohexanecarboxylic Acid: Commercial cyclohexanecarboxylic acid (purity: over 97%, Aldrich Chemical Company, Inc.) was dissolved in benzene just before its use. Copper(II) perchlorate,[6] sodium perchlorate,[6] and benzene[9] were the same as employed as previously. All other reagents were reagent grade and used without further purification.

Procedure. Partition was carried out in the same manner as was stated in the previous paper.[10] In the partition of cyclohexanecarboxylic acid between benzene and water, the concentration of the acid in the aqueous phase was determined by potentiometric titration.

Apparatus. Taiyo Incubator M-100^N(Taiyokagaku-Kogyo Co., Tokyo) was used for mechanical shaking in a thermostat. The pH measurements and potentiometric titrations were performed with a Horiba pH Analyzer F-80 (Horiba Seisakusho Ltd., Kyoto). A swing type centrifuge model CD-50SR (Tomy Seiko Co. Ltd., Tokyo) was used for centrifugation.

Results and Discussion

Partition of Cyclohexanecarboxylic Acid. The following equilibria on cyclohexanecarboxylic acid (HA) should be considered: (a) The dissociation of HA in the aqueous phase ($K_a=[H^+][A^-]/[HA]$), (b) the partition of HA into benzene ($K_{D,HA}=[HA]_o/[HA]$), and (c) the dimerization of HA in the organic phase ($K_{2,HA}=[(HA)_2]_o/[HA]_o^2$), where the subscript o refers to the organic phase and $[(HA)_2]_o$ denotes the concentration of the dimeric acid in the organic phase. Then, the distribution ratio of the acid between benzene and water can be written as:

$$D=C_{HA,o}/C_{HA,w}$$
$$=K_{D,HA}(1+2K_{2,HA}K_{D,HA}[HA])/(1+K_a[H^+]^{-1}). \quad (1)$$

In the lower pH region where the dissociation of the acid in the aqueous phase can be neglected, that is, $1 \gg K_a[H^+]^{-1}$, the following equation can be obtained:

$$\log D=\log K_{D,HA}+\log(1+2K_{2,HA}K_{D,HA}[HA]). \quad (2)$$

According to Eq. 2, by comparing the plots of log D against log [HA] with the normalized curve, log $(1+X)$ vs. log X, the dimerization constant in the organic phase and the partition constant can be determined. Benzene solutions of cyclohexanecarboxylic acid ranging from 0.024 to 0.96 mol dm^{-3} were equilibrated with 0.01 mol dm^{-3} perchloric acid solution (ionic strength: 0.1 mol dm^{-3} H, $NaClO_4$). From the plots shown in Fig. 1, the following constants of cyclohexanecarboxylic acid were determined by the curve-fitting method: log $K_{D,HA}$=0.90 and log $K_{2,HA}$=1.54, respectively.

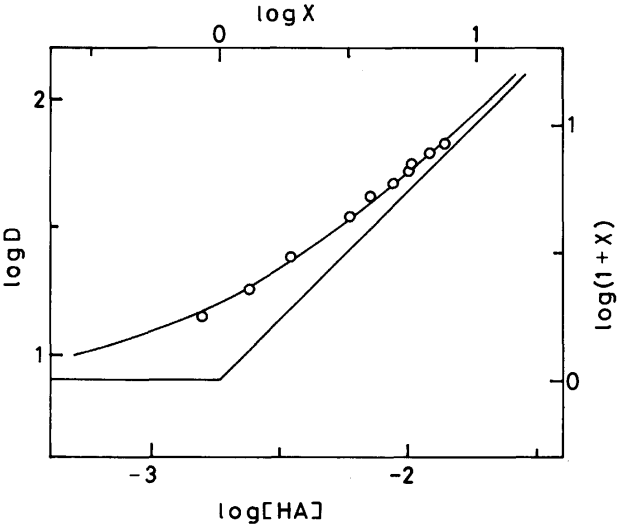

Fig. 1. Determination of the dimerization constant in benzene and the partition constant between benzene and water of cyclohexanecarboxylic acid. Solid curve is the normalized curve, log $(1+X)$ vs. log X. Solid lines are the asymptotes of the normalized curve.

Under the present experimental conditions, the dissociation of cyclohexanecarboxylic acid in the aqueous phase can being neglected, the concentration of the dimeric acid in the organic phase can be written as follows:

$$[(HA)_2]_o = 0.5\,(C_{HA} - [HA]_o - [HA]) \qquad (3)$$

where C_{HA} denotes the total concentration of the acid. Then, the concentration of the dimeric cyclohexanecarboxylic acid in the organic phase was calculated by substituting the dimerization and partition constants of the acid in Eq. 3.

Extraction of Copper(II) with Cyclohexanecarboxylic Acid. If a j-merized copper(II) carboxylate, $Cu_jA_{2j}(HA)_a$ is extracted, the following equilibrium is relevant to the extraction:

$$j\mathrm{Cu}^{2+} + 0.5\,(2j+a)\,(HA)_{2,o} \rightleftharpoons (Cu_jA_{2j}(HA)_a)_o + 2\mathrm{jH}^+$$

with

$$K_{ex(ja)} = [Cu_jA_{2j}(HA)_a]_o[H^+]^{2j}[Cu^{2+}]^{-j}[(HA)_2]_o^{-0.5(2j+a)}. \qquad (4)$$

The following relation can hold for the total concentration of copper in the organic phase, $C_{Cu,o}$:

$$\log C_{Cu,o} = \log \sum_j \sum_a \{jK_{ex(ja)}([Cu^{2+}][H^+]^{-2})^j[(HA)_2]_o^{0.5(2j+a)}\}. \qquad (5)$$

According to Eq. 5, the degree of polymerization of the extracted species can be found from the slope of the plot of log $C_{Cu,o}$ against $(\log[Cu^{2+}] - 2\log[H^+])$ at constant $[(HA)_2]_o$. If two or more species with different degree of polymerization are responsible for the extraction, the plot should give rise to a curve. The results are shown in Fig. 2. The slope lies between unity and two, and tends to approach to two with increasing copper concentration in the organic phase. Therefore, it is expected that the monomeric and dimeric copper(II) carboxylates are responsible for the extraction. Then, the total concentration of copper(II) in the organic phase is expressed as follows:

$$C_{Cu,o} = [CuA_2(HA)_a]_o + 2[Cu_2A_4(HA)_b]_o. \qquad (6)$$

By substituting the extraction constants $K_{ex(1a)}$ and $K_{ex(2b)}$ in Eq. 6, the following expression can be derived:

$$\log C_{Cu,o} - \log[Cu^{2+}] + 2\log[H^+] = 0.5\,(2+a)\log[(HA)_2]_o + \log K_{ex(1a)} + \log\left(1 + \frac{2K_{ex(2b)}}{K_{ex(1a)}}[(HA)_2]_o^{0.5(2+b-a)}[Cu^{2+}][H^+]^{-2}\right). \qquad (7)$$

According to Eq. 7, by comparing the plots of the left-hand side of Eq. 7 against $(\log[Cu^{2+}] - 2\log[H^+])$ at constant $[(HA)_2]_o$ with the normalized curve, log $(1+X)$ vs. log X, the degree of polymerization of cop-

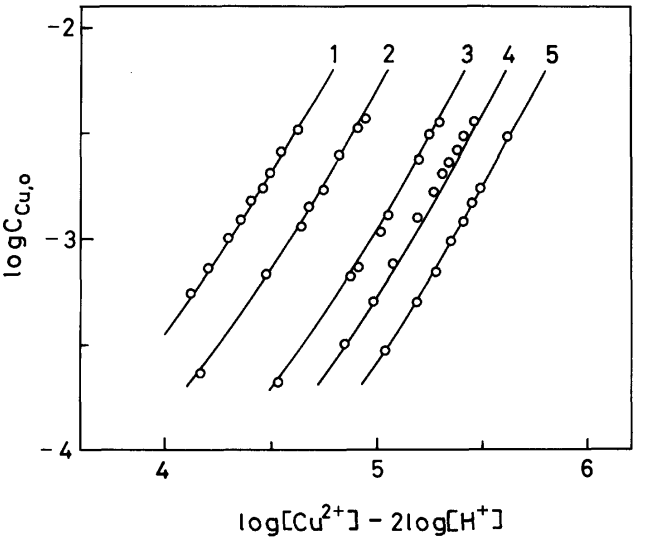

Fig. 2. Determination of the degree of polymerization of copper(II) carboxylate. C_{HA}; 1: 1.47, 2: 0.98, 3: 0.55, 4: 0.40, 5: 0.29 mol dm^{-3}. Solid lines are calculated curves based on the results obtained in this work.

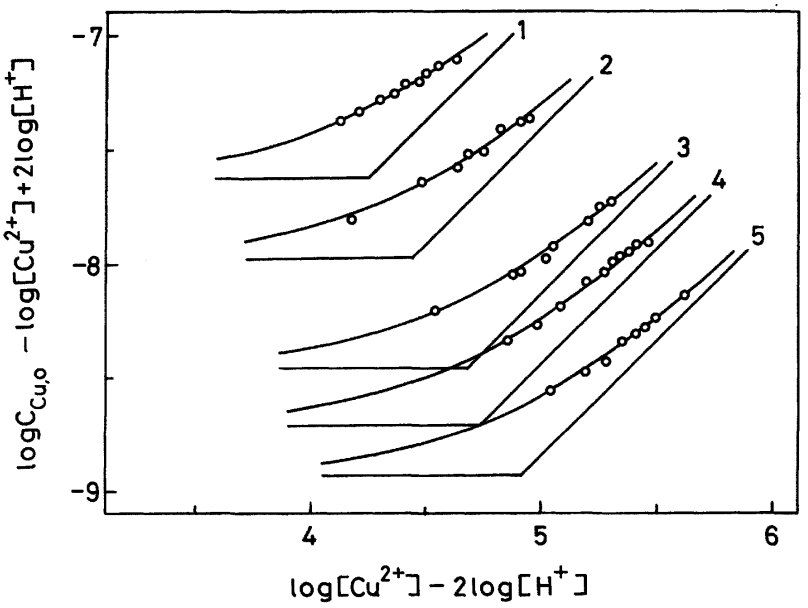

Fig. 3. Identification of the degree of polymerization of copper(II) carboxylate. Solid curves are the normalized curves, $\log(1+X)$ vs. $\log X$. Solid lines are the asymptotes of the normalized curves. Numbers are the same as in Fig. 2.

per(II) species can be identified. As shown in Fig. 3, the plots fit well the normalized curve. Therefore, it was proved that both the dimeric and monomeric copper(II) carboxylates are responsible for the extraction.

In the region, where the plots in Fig. 3 fall along the horizontal asymptotes, the predominant extracted species is the monomer. Then the total concentration of copper(II) in the organic phase can be written as:

$$\log C_{Cu,o} = \log \sum_a (K_{ex(1a)}[Cu^{2+}][H^+]^{-2}[(HA)_2]_o^{0.5(2+a)}). \quad (8)$$

According to Eq. 8, the number of cyclohexanecarboxylic acid molecules involved in the monomeric copper(II) species can be obtained from the slope of the plot of $(\log C_{Cu,o} - \log[Cu^{2+}] + 2\log[H^+])$ against $\log[(HA)_2]_o$. As shown in Fig. 4, the plot deviates upward from the straight line with a slope of two with decreasing $[(HA)_2]_o$. This fact suggests that the two monomeric species are responsible for the extraction in the lower concentration of copper in the organic phase: One of them is $CuA_2(HA)_2$ and the other $CuA_2(HA)_a$ ($a<2$). Under these conditions the total copper concentration in the organic phase can be written as follows:

$$\log C_{Cu,o} - \log[Cu^{2+}] + 2\log[H^+] - 2\log[(HA)_2]_o$$
$$= \log\left(1 + \frac{K_{ex(1a)}}{K_{ex(12)}}[(HA)_2]_o^{-0.5(2-a)}\right) + \log K_{ex(12)}. \quad (9)$$

Comparing the plot of the left-hand side of Eq. 9 against $-\log[(HA)_2]_o$ with the normalized curves, $\log(1+X^n)$ vs. $\log X$, another monomeric species can be determined. As evident from Fig. 5, the plot fits well the normalized curve with $n=1$, $\log(1+X)$ vs. $\log X$, that is, $0.5(2-a)=1$ or $a=0$. Then the monomeric species are CuA_2 and $CuA_2(HA)_2$. By the curve-fitting method from Fig. 5, the respective extraction constants $K_{ex(10)}$ and $K_{ex(12)}$ can be determined: $\log K_{ex(10)} = -8.34 \pm 0.03$, $\log K_{ex(12)} = -7.33 \pm 0.03$, respectively.

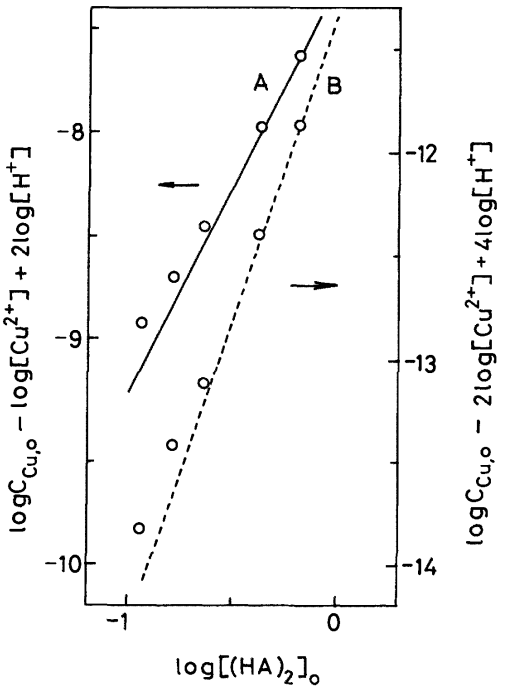

Fig. 4. Determination of the number of carboxylic acid molecules involved in the monomeric and dimeric copper(II) species. A: Monomeric copper(II) carboxylate. B: Dimeric copper(II) carboxylate. Solid and dotted lines are the straight lines with a slope of 2.0 and 3.0, respectively.

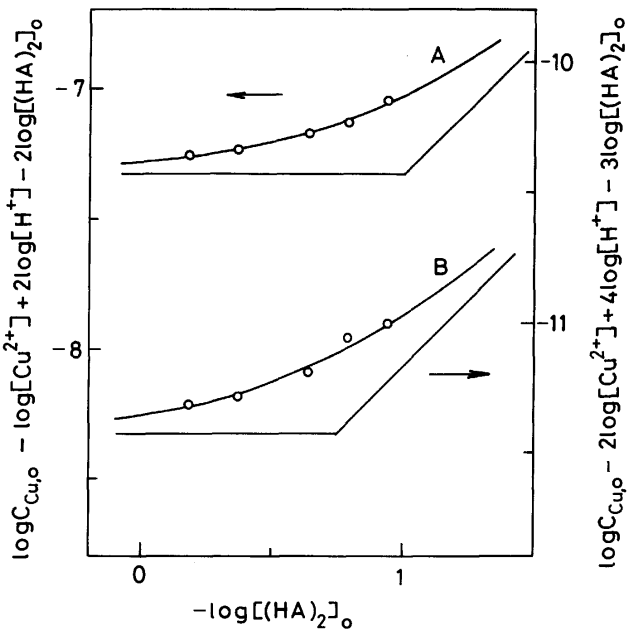

Fig. 5. Determination of the number of carboxylic acid molecules involved in the copper(II) species by curve-fitting method. A and B are the same as in Fig. 4. Solid curves are the normalized curves, $\log(1+X)$ vs. $\log X$. Both solid lines are the asymptotes of the normalized curves.

On the other hand, in the region, where the dimeric copper(II) species is predominant, that is, the plots shown in Fig. 3 fall along the straight line asymptotes with a slope of unity, the total concentration of copper(II) in the organic phase can be represented as:

$$\log C_{Cu,o} = \log(2[Cu^{2+}]^2[H^+]^{-4}) + \log\left(\sum_b (K_{ex(2b)}[(HA)_2]_o^{0.5(4+b)})\right). \quad (10)$$

According to Eq. 10, the number of cyclohexanecarboxylic acid molecules involved in the dimer can be obtained from the slope of ($\log C_{Cu,o} - 2\log[Cu^{2+}] + 4\log[H^+]$) against $\log[(HA)_2]_o$. As shown in Fig. 4, the plot gets to approach the straight line with a slope of 3.0 with increasing the concentration of dimeric cyclohexanecarboxylic acid in the organic phase. As judged from this tendency, the two dimeric species, $Cu_2A_4(HA)_2$ and $Cu_2A_4(HA)_b$ ($b<2$) exist in the higher concentration of copper in the organic phase. Therefore, the following relation can be expected to hold for the total concentration of copper in the organic phase:

$$\log C_{Cu,o} - 2\log[Cu^{2+}] + 4\log[H^+] - 3\log[(HA)_2]_o = \log\left(1 + \frac{K_{ex(2b)}}{K_{ex(22)}}[(HA)_2]_o^{-0.5(2-b)}\right) + \log 2 + \log K_{ex(22)}. \quad (11)$$

In the similar manner as the monomeric species, another dimeric species can be determined. As shown in Fig. 5, the plot of the left-hand side of Eq. 11 against $-\log[(HA)_2]_o$ fits with the normalized curve, $\log(1+X)$ vs. $\log X$, that is, $0.5(2-b)=1$ or $b=0$. Then, Cu_2A_4 is also involved in the extraction together with $Cu_2A_4(HA)_2$ under the present conditions. In addition we can determine the extraction constants $K_{ex(20)}$ and $K_{ex(22)}$ in the similar manner as the monomer: $\log K_{ex(20)} = -12.47 \pm 0.03$ and $\log K_{ex(22)} = -11.73 \pm 0.03$, respectively.

Consequently, in the present extraction system, the corresponding extraction equilibria are described as follows:

$$Cu^{2+} + (HA)_{2,o} \overset{K_{ex(10)}}{\rightleftharpoons} (CuA_2)_o + 2H^+$$

$$Cu^{2+} + 2(HA)_{2,o} \overset{K_{ex(12)}}{\rightleftharpoons} (CuA_2(HA)_2)_o + 2H^+$$

$$2Cu^{2+} + 2(HA)_{2,o} \overset{K_{ex(20)}}{\rightleftharpoons} (Cu_2A_4)_o + 4H^+$$

$$2Cu^{2+} + 3(HA)_{2,o} \overset{K_{ex(22)}}{\rightleftharpoons} (Cu_2A_4(HA)_2)_o + 4H^+.$$

Brzozka and Rozycki found the monomer $CuA_2(HA)_4$ and dimer $Cu_2A_4(HA)_4$ in the extraction of copper(II) with cyclohexanecarboxylic acid in benzene.[4] Judging from the coordination number of copper(II), both extracted species seem unlikely. Because they estimated the composition of the extracted species under the region where both copper(II) species with different degree of polymerization coexist, erroneous results seem to be drawn. In addition, Rozycki reported that only the monomeric species $CuA_2(HA)_2$ was responsible for the extraction of copper(II) with cyclopentylacetic acid in benzene.[5] According to his data, the slope of the plot of $\log C_{Cu,o}$ against ($\log C_{Cu,w} + 2pH$) at constant $[(HA)_2]_o$ (Fig. 1 in Ref. 5) is greater than unity. This suggests that the dimeric copper(II) species is expected to be involved in the extraction. Owing to take no account of a dimeric copper(II) species for analysis of extraction equilibrium, they failed to notice not only dimeric species but also another monomeric species CuA_2.

Recently, the dimeric copper(II) carboxylate $Cu_2A_4(HA)_2$ has been reported to be extracted with 2-bromopentanoic acid in benzene.[11] On the other hand, Bold and Balusescu proposed the monomeric copper(II) carboxylate, $CuA_2(HA)_2$ in the extraction of copper(II) with 2-bromooctadecanoic acid in benzene.[12] Their results appear doubtful. Because recalculation[11] of their data led us to the dimeric species, $Cu_2A_4(HA)_2$. Therefore, it seems likely that bromine at 2-position in the respective carboxylic acid does not inhibit the formation of a dimeric copper(II) carboxylate.

In contrast with these instances, the extraction of monomeric copper(II) species in the present extraction system indicate that the dimerization of copper(II) carboxylate is hindered by the cyclohexane moiety at 2-position in cyclohexanecarboxylic acid.

Effect of Cyclohexane Ring on Dimerization of Carboxylic Acid and Copper(II) Carboxylate in Benzene. The dissociation constant of cyclohexanecar-

Table 1. Comparison of Cyclohexanecarboxylic with Other Carboxylic Acids

Constant \ Acid	Cyclohexanecarboxylic	Heptanoic	Lipoic	Decanoic
pK_a	4.89[a]	4.89[b]	4.85[c]	4.92[d]
$\log K_{D,HA}$	0.90	0.78[e]	1.17[f]	2.80[d]
$\log K_{2,HA}$	1.54	2.61[g]	2.51[f]	2.41[d]
$\log K_{ex(22)}$	−11.73	−11.58[h]	−11.00[f]	−11.36[i]
$\log \beta_{Cu_2A_4(HA)_2}$[j]	12.45	15.81	15.93[f]	15.55[f]
	(12.72)	(16.04)	(16.28)	(16.39)

a) Ref. 13. b) Ref. 14. c) Ref. 17. d) Ref. 18. e) Ref. 15. f) Ref. 9. g) Ref. 16. h) Ref. 1. i) Ref. 2. j) Calculated by Eq. 10 in Ref. 9. The values in the parentheses are evaluated by taking into account the electro-striction of ligands in the complex (Eq. 11 in Ref. 9).

boxylic acid in the aqueous solution is reported to be pK_a=4.89[13] at 25 °C. This value is agreement with that of heptanoic acid[14] with the same carbon number as cyclohexanecarboxylic acid. This implies that the cyclohexane ring has no inductive effect on the carboxylate group. The partition constant of heptanoic acid between benzene and water, and its dimerization constant in benzene can be established from the constants of its homologs as follows: $\log K_{D,HA}$=0.78[15] and $\log K_{2,HA}$=2.61,[16] respectively. Judging from no inductive effect of the cyclohexane moiety, the similar constants for cyclohexanecarboxylic acid as those of heptanoic acid can be expected to be obtained. As expected, the value of the partition constant of cyclohexanecarboxylic acid was found to be close to that of heptanoic acid (see: Table 1). On the other hand, it was proved that the value of its dimerization constant in benzene is smaller by about one order of magnitude than that of heptanoic acid. This fact suggests that the cyclohexane ring would interfere in the dimerization of cyclohexanecarboxylic acid in benzene.

As stated previously,[9] the extraction constant of dimeric copper(II) species, $Cu_2A_4(HA)_2$ can be written as follows:

$$K_{ex(22)}=K_{D,Cu_2A_4(HA)_2}K_{D,HA}^{-6}K_{2,HA}^{-3}\beta_{Cu_2A_4(HA)_2}K_a^4 \quad (12)$$

where $K_{D,Cu_2A_4(HA)_2}$ and $\beta_{Cu_2A_4(HA)_2}$ denote the partition constant of $Cu_2A_4(HA)_2$ between benzene and water, and the overall formation constant of this complex in the aqueous phase, respectively. Then, the overall formation constant can be approximated by Eq. 12. The value is summarized in Table 1 together with other constants. As shown in Table 1, each of these acids has a similar dissociation constant. On the other hand, the overall formation constant of a dimeric copper(II) species, $Cu_2A_4(HA)_2$ for cyclohexanecarboxylic acid are decreased about three orders of magnitude under that for other three acids. It has been shown that the formation of copper(II) cyclohexanecarboxylate is inhibited by cyclohexane ring in the same manner as the dimerization of cyclohexanecarboxylic acid.

It is well-known that the copper(II) carboxylates have dimeric structure not only in the crystalline state but also in various organic solvents. Then, in the extraction of copper(II) carboxylates, only the dimeric copper(II) carboxylate, $Cu_2A_4(HA)_2$ has been widely proved to be responsible for the extraction by numerous investigators.[19] A few studies on the extraction of the monomeric copper(II) carboxylate have been merely published in the extraction systems presented below. In the extraction of copper(II) with decanoic acid in some alcohols[6,7] and ketones,[8] monomeric and dimeric copper(II) species are in equilibrium in these solvents, because of the extensive solvation by these solvents. In addition, the dimerization of copper(II) benzoate does not occur to any appreciable extent in the extraction of copper(II) with benzoic acid.[10] It is reasonable to imagine that the conjugated system in benzoic acid inhibits the dimerization of copper(II) benzoate.

On the other hand, the extraction of the monomeric copper(II) cyclohexanecarboxylates in the present extraction system can be due to the steric hindrance of the cyclohexane moiety on the dimerization of copper(II) carboxylate. The present result is contrast to the facts that "bromine" at 2-position in pentanoic[11] and octadecanoic[12] acids does not inhibit the dimerization of the respective copper(II) carboxylates.

The polymeric metal carboxylates are often involved in the extraction of metal carboxylates.[19] And the polymerization of metal carboxylate can be regarded as a kind of synergistic effect, and would contribute to a good extractability. According to the result obtained from this work, it can be anticipated that the introduction of the more bulky moiety at 2-position in carboxylic acid will also interfere with the polymerization of other metal carboxylates, and will lead to a lowering of the extractability, particularly in the extraction of metal carboxylates into nonsolvating solvents, for which the formation of polymerized species is essential. Therefore, it can be expected that the more crowded substituent at 2-position in carboxylic acid will result in a more favorable selectivity for the extraction of metal carboxylate.

References

1) I. Kojima, M. Uchida, and M. Tanaka, *J. Inorg. Nucl.*

Chem., **32**, 1333 (1970).
2) H. Yamada and M. Tanaka, *J. Inorg. Nucl. Chem.*, **38**, 1501 (1976).
3) W. J. Haffenden and G. J. Lawson, *J. Inorg. Nucl. Chem.*, **29**, 1133 (1967).
4) Z. Brzozka and C. Rozycki, *Chem. Anal. (Warsaw)*, **28**, 585 (1983).
5) C. Rozycki, *Chem. Anal. (Warsaw)*, **26**, 37 (1981).
6) H. Yamada, S. Suzuki, and M. Tanaka, *J. Inorg. Nucl. Chem.*, **43**, 1873 (1981).
7) H. Yamada, R. Kitazaki, and I. Kakimi, *Bull. Chem. Soc. Jpn.*, **56**, 3302 (1983).
8) H. Yamada, K. Takahashi, Y. Fujii, and M. Mizuta, *Bull. Chem. Soc. Jpn.*, **57**, 2847 (1984).
9) H. Yamada, T. Okuda, Y. Fujii, M. Mizuta, and M. Tanaka, *Bull. Chem. Soc. Jpn.*, **59**, 3855 (1986).
10) H. Yamada, K. Adachi, Y. Fujii, and M. Mizuta, *Solvent Extr. Ion Exch.*, **4**, 1109 (1986).
11) Y. Fujii, H. Yamada, and M. Mizuta, *Polyhedron*, **6**, 1203 (1987).
12) A. Bold and L. Balusescu, *Rev. Roum. Chim.*, **23**, 1631 (1978).
13) K. B. Wiberg and B. R. Lowry, *J. Am. Chem. Soc.*, **85**, 3188 (1963).
14) "CRC Handbook of Chemistry and Physics" 67th ed, 1986—1987 (C. W. Robert ed.), CRC Press Inc. (1986).
15) Y. Fujii and M. Tanaka, *Bull. Chem. Soc. Jpn.*, **54**, 3696 (1981).
16) Y. Fujii, Y. Kawachi, and M. Tanaka, *J. Chem. Soc., Faraday Trans. 1*, **77**, 63 (1981).
17) H. Sigel, B. Prijs, D. B. McCormick, and J. C. H. Shin, *Arch. Biochem. Biophys.*, **187**, 208 (1978).
18) M. Tanaka, N. Nakasuka, and S. Sasane, *J. Inorg. Nucl. Chem.*, **31**, 2591 (1969).
19) H. Yamada and M. Tanaka, *Adv. Inorg. Chem. Radiochem.*, **29**, 143 (1986).

1-3-η-Allylpalladium(II) and Platinum(II) Complexes Containing Tris(2,6-dimethoxyphenyl)phosphine Ligand

Hideo KUROSAWA,* Aki TSUBOI, Yoshikane KAWASAKI, and Masanori WADA†
Department of Applied Chemistry, Osaka University, Suita, Osaka 565
†Department of Industrial Chemistry, Tottori University, Koyama-cho, Tottori 680
(Received April 23, 1987)

Neutral and cationic 1-3-η-(2-methylallyl) complexes of Pd and Pt containing tris(2,6-dimethoxyphenyl)-phosphine (abbreviated as $P(2,6)_3$), $M(1\text{-}3\text{-}\eta\text{-}CH_2CMeCH_2)Cl\{P(2,6)_3\}$ and $[M(1\text{-}3\text{-}\eta\text{-}CH_2CMeCH_2)\{P(2,6)_3\}]BF_4$, were prepared. The latter contained a weakly coordinated OMe group of $P(2,6)_3$ which was readily replaced by carbon monoxide to afford $[M(1\text{-}3\text{-}\eta\text{-}CH_2CMeCH_2)(CO)\{P(2,6)_3\}]BF_4$. Owing to large steric bulk and high nucleophilicity of $P(2,6)_3$, addition of $P(2,6)_3$ to these complexes did not result in coordination of the second molecule of the phosphine to the metal atom but ready attack at the metal-bound 2-methylallyl and methoxyl carbon atoms to give the corresponding (2-methylallyl)phosphonium and methylphosphonium ions. From these reactions were isolated a neutral 1-3-η-(2-methylallyl)platinum(II) complex involving chelate coordination of a tertiary phosphine ligand which was derived from the loss of methyl of one methoxyl group in $P(2,6)_3$ and the resulting phenoxo ligand, and a cationic, binuclear Pt(I) carbonyl complex bridged by the 2-methylallyl group. Also prepared in this study were 1-3-η-(2-methylallyl)(acetylacetonato) complexes of Pd and Pt, $M(1\text{-}3\text{-}\eta\text{-}CH_2CMeCH_2)(acac)\{P(2,6)_3\}$. In the platinum analog, the acetylacetonato ligand was suggested to coordinate to the metal in a monodentate fashion via the central carbon atom. Both complexes afforded moderate yields of $CH_2{=}CMeCH_2CH(COMe)_2$ upon treatment with carbon monoxide, while the reaction of $M(1\text{-}3\text{-}\eta\text{-}CH_2CMeCH_2)(CO)\{P(2,6)_3\}^+$ with sodium acetylacetonate failed to give the same coupling product.

A new tertiary phosphine, tris(2,6-dimethoxyphenyl)-phosphine (abbreviated as $P(2,6)_3$) was shown to exhibit unusually high basicity and great nucleophilicity toward some organic electrophiles (e.g. alkyl halides, oxiranes).[1] This electronic property, together with its considerable steric bulk (cone angle= 184°),[1b] prompted us to examine coordination chemistry and catalytic activity of metal complexes containing $P(2,6)_3$ as a ligand. A brief synthesis of two-coordinated complexes, $[M\{P(2,6)_3\}_2]^+$ (M=Cu, Ag) has been reported before.[1b] We describe here synthesis and properties of 1-3-η-(2-methylallyl)palladium(II) and platinum(II) complexes containing $P(2,6)_3$.

Results and Discussion

Coordination and Nucleophilic Attack of $P(2,6)_3$. Dimeric complexes, 1-3-η-(2-methylallyl)(chloro)palladium and platinum reacted with 1 molar quantity of $P(2,6)_3$ to give **1** (see Scheme 1). Treatment of **1** with $AgBF_4$ in acetone gave acetone-free cationic complexes **2**. The very large spin coupling constant between ^{195}Pt and the anti allyl proton cis to the phosphine (H^1) in the ^1H NMR spectrum of **2b** (Table 1) is consistent with coordination of the 2-OMe group having a weak trans influence to Pt.

It seems of particular note that the second molecule of $P(2,6)_3$ did not show any tendency to coordinate to the metal atom of **1**. Thus, when free $P(2,6)_3$ was added to a $CDCl_3$ solution of **1** at room temperature, we could observe no change in ^1H NMR spectra of **1** except for occurrence of a slow attack of $P(2,6)_3$ not on the metal atom but on the different sites, as described below. In the corresponding reaction of $M(1\text{-}3\text{-}\eta\text{-allyl})Cl(PPh_3)$ with PPh_3, there occurred quite ready formation of *trans*-$M(\sigma\text{-allyl})Cl(PPh_3)_2$ or $[M(1\text{-}3\text{-}\eta\text{-allyl})(PPh_3)_2]Cl$.[2] The mixture of **1a** and $P(2,6)_3$ in $CDCl_3$ caused formation of $[P(CH_3)(2,6)_3]Cl$ and $[P(CH_2CMe{=}CH_2)(2,6)_3]Cl$ (each ca. 10%) when kept to stand at room temperature for 12 h. **1b** and $P(2,6)_3$ afforded $[P(CH_3)(2,6)_3]Cl$ still more slowly.

The reaction of $P(2,6)_3$ with **2b** occurred much faster to give $[P(CH_3)(2,6)_3]BF_4$ and a neutral complex **3**. The corresponding reaction of **2a** resulted in rapid, high-yield formation of a mixture of $[P(CH_3)(2,6)_3]BF_4$ and $[P(CH_2CMe{=}CH_2)(2,6)_3]BF_4$ (ca. 1 : 1), but isolation of any palladium-containing product was not successful. Again there was no tendency of the coordination of two molecules of $P(2,6)_3$ to the metal atom in the cationic complexes.

The ready phosphonium ion formation in the reaction of $P(2,6)_3$ with **1** and **2** may have been induced by both steric and electronic causes. The large size of $P(2,6)_3$ would make coordination of two molecules of this ligand highly unfavorable. In addition, its high nucleophilicity facilitates attack at the carbon atom of the OMe and 2-methylallyl groups bound to the metal, with particular ease in the case of the cationic complexes. The methyl abstraction by $P(2,6)_3$ from the OMe group of the coordinated $P(2,6)_3$ ligand in **1** would have occurred via transient coordination of the OMe group to the metal. A quite similar result has been observed in the reaction of MCl_2L_2 (L=PhCN, 1/2COD; M=Pd, Pt) with $P(2,6)_3$ in unsuccessful attempts to prepare $MCl_2\{P(2,6)_3\}_2$.[3]

2 reacted with carbon monoxide to form **4**. **4a** is fairly stable in the solid state for a cationic carbonyl complex of Pd,[4] but reverts to **2a** in $CDCl_3$ in the absence of carbon monoxide. The lower ν(CO) value (2075 cm^{-1}) of **4b** than that[5] (2120 cm^{-1}) of $[Pt(1\text{-}3\text{-}\eta\text{-}$

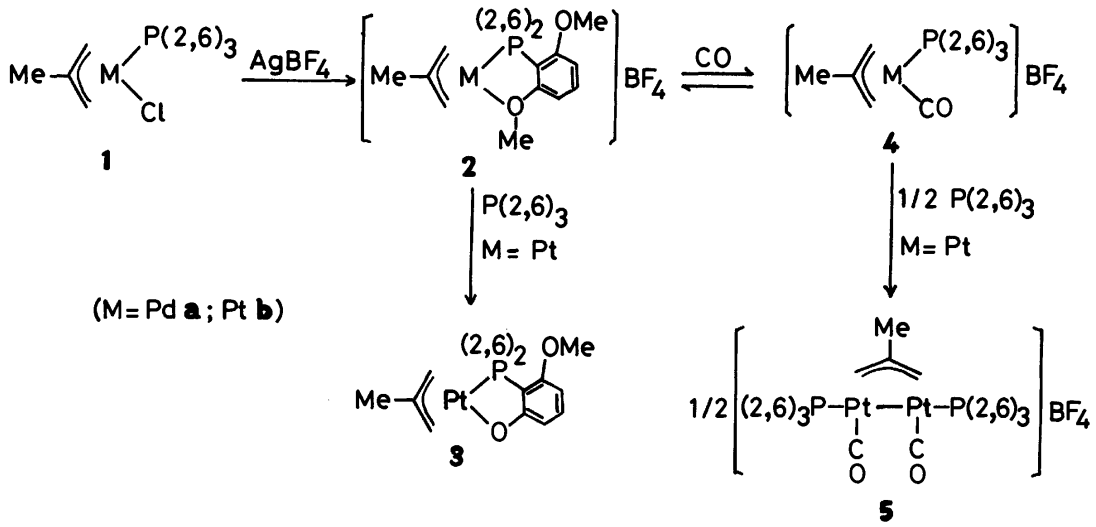

Scheme 1.

TAble 1. ^{1}H NMR Spectral Data[a] of 1-3-η-(2-Methylallyl)metal Complexes

Complex	Methallyl					P(2,6)$_3$		
	H^1	H^2	H^3	H^4	Me	OMe	3-H	4-H
1a[b]	2.46^b	2.90^b	4.07^d J_P=8	3.09^d J_P=12	1.50^s	3.57^s	6.42^{dd} J_H=8 J_P=4	7.18^t
1b	1.82^s J_{Pt}=72	2.62^b	c)	2.36^d J_P=11 J_{Pt}=34	1.49^s J_{Pt}=71	3.55^s	6.40^{dd} J_H=8 J_P=5	7.16^t
2a[b]	2.63^s	3.56^b	4.65^{bd} J_P=6	c)	2.00^s	3.75^s	6.57^{dd} J_H=8 J_P=5	7.37^t
2b	2.33^d J_P=4 J_{Pt}=112	3.20^b	4.40^b	3.40^d J_P=10 J_{Pt}=36	2.06^s J_{Pt}=79	3.82^s	6.58^{dd} J_H=8 J_{Pt}=5	7.37^t
3	1.90^s J_{Pt}=81	3.14^b	3.95^b	2.66^d J_P=10 J_{Pt}=44	1.82^s J_{Pt}=63	3.40^s 3.46^s 3.52^s	5.86^{dd} J_H=8 J_P=3 6.43^m	6.67^{bt} 7.15^m
4a	3.09^b	c)	4.80^{bd} J_P=6	3.42^d J_P=11	1.56^s	3.60^s	6.50^{dd} J_H=8 J_P=5	7.30^t
4b	2.71^b J_{Pt}=31	c)	4.68^b	3.21^d J_P=12 J_{Pt}=33	1.62^s J_{Pt}=74	3.62^s	6.57^{dd} J_H=8 J_P=5	7.38^t
6b[d]	2.07^s J_{Pt}=50	2.60^b	3.20^b	2.34^d J_P=12 J_{Pt}=42	1.60^s J_{Pt}=61	3.50^s	6.41^{dd} J_H=8 J_P=4	7.20^t

a) In $CDCl_3$ at room temperature except as noted. Chemical shifts in ppm, J in Hz. Abbreviations: s=singlet, d=doublet, t=triplet, dd=doublets of doublet, b=broad, m=multiplet. For proton numbering scheme, see below.

b) At −10 °C. c) Obscured by the OMe peak. d) CH_3CO: 1.73^s (J_{Pt}=10) and 1.95^s (J_{Pt}=7). -CH(: 4.43^d (J_P=9, J_{Pt}=115).

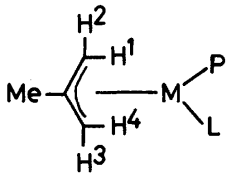

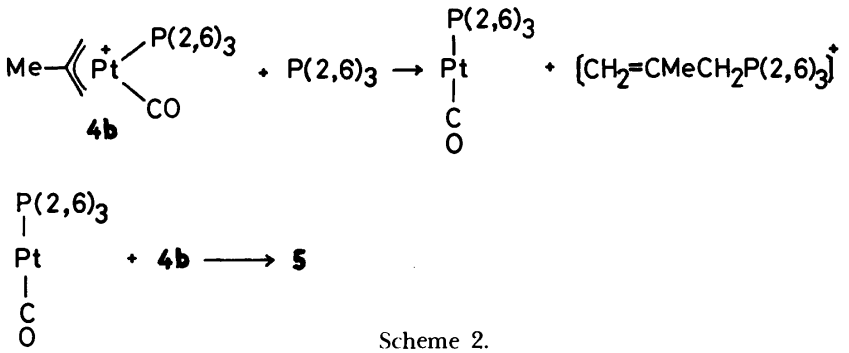

Scheme 2.

$CH_2CMeCH_2)(CO)(PPh_3)]^+$ reflects the more basic nature of $P(2,6)_3$ than PPh_3.

4a rapidly reacted with $P(2,6)_3$ in $CDCl_3$ containing free carbon monoxide to give almost quantitative yield of $[P(CH_2CMe{=}CH_2)(2,6)_3]BF_4$ and palladium metal. In converting **4a** to this phosphonium ion, there was no need to use equimolar amount of $P(2,6)_3$; addition of 10 mol% of $P(2,6)_3$ to **4a** caused formation of the phosphonium ion in ca. 80% yield.

4b also reacted with $P(2,6)_3$ very rapidly in 2 : 1 mole ratio to give a binuclear complex **5** and $[P(CH_2CMe{=}CH_2)(2,6)_3]BF_4$. The structure of **5** was deduced by the following spectral data. The IR spectrum showed ν(CO) bands at 2010 and 2040 cm^{-1} which are in the region expected for the Pt(I)-coordinated carbonyl ligand.[6] In the ^1H NMR spectrum, the 2-methyl proton resonance appeared as a triplet due to coupling with two equivalent ^{31}P nuclei (J_P=2.5 Hz). Furthermore, the resonances of the protons at 3- and 5-positions of $P(2,6)_3$ and the allylic syn protons appeared as double triplets ($1/2[J_P+J_P']$=2 Hz, J_H=8.5 Hz) and a triplet ($1/2[J_P+J_P']$=12 Hz), respectively, owing to virtual coupling arising from strong P-P' coupling, as observed in complexes having the P-M-M-P framework bridged by the allyl group.[7] The structure **5** should also require in ^1H NMR spectra a satellite set of the methyl signal associated with a ^{195}Pt-^{195}Pt framework which is composed of a 1 : 2 : 1 triplet with the central peak overlapping with the main peak. However, we could not observe this set due to low solubility.

A possible route to **5** is shown in Scheme 2. The nucleophilic attack of $P(2,6)_3$ at the 2-methylallyl group of **4b** produces the phosphonium ion and $Pt(CO)\{P(2,6)_3\}$ which subsequently attacks the metal atom of another **4b** to form **5** eventually. The initial step in the corresponding reaction of **4a** with $P(2,6)_3$ may be the same as that shown in Scheme 2, but $Pd(CO)\{P(2,6)_3\}$ formed would be much less stable, releasing free $P(2,6)_3$. It seems of further interest to note that the 2-methylallyl group of **5** underwent no further nucleophilic attack of $P(2,6)_3$ even when excess $P(2,6)_3$ was added to the solution of **5**.

Preparation and Reaction of 1-3-η-(2-Methylallyl)-metal Complexes Containing $P(2,6)_3$ and Acetylacetonato Ligands. Palladium and platinum complexes of PPh_3 are known to be good catalysts for coupling reaction of allylic electrophiles and acetylacetonate anion.[8] However, the $P(2,6)_3$ complexes **1** did not show very good catalytic activity in the reaction of 2-methylallyl acetate with sodium acetylacetonate in acetone where each complex was used either by itself or in combination with free $P(2,6)_3$. Next we looked into stoichiometric reactions of 1-3-η-(2-methylallyl) complexes containing $P(2,6)_3$ with acetylacetonate anion.

The reaction of **1** with thallium acetylacetonate in benzene gave a complex of the formula, $M(C_4H_7)(acac)\{P(2,6)_3\}$ **6**. In the platinum analog, the acetylacetonato ligand may coordinate to the metal via the central carbon atom (see **6b**), as deduced by the following IR and ^1H NMR spectral data. The absence of any IR absorption at 1500—1600 cm^{-1} may exclude the chelating acetylacetonato ligand. Instead, medium to strong absorption bands appeared at 1600—1650 cm^{-1}. In the ^1H NMR spectrum of **6b** (Table 1), the methine proton of the acetylacetonato ligand resonated in the chemical shift region (δ 4.43) considerably higher than where this proton in the bidentate and monodentate oxygen-bonded ligand resonates ($\delta \geqslant$ 5.1).[9] Also, it exhibited a ^{31}P coupling of magnitude similar to those in *cis*-$ML_2(acac\text{-}C)(PR_3)$ (M=Pd, Pt)[9] and a large ^{195}Pt coupling. Moreover, the resonance of the allylic anti proton trans to the acetylacetonato ligand showed a relatively small ^{195}Pt coupling when compared to those in **2b** and **3** containing the oxygen donor, in accord with the presence of a ligand of strong trans influence.

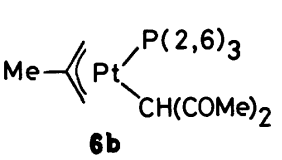

6b

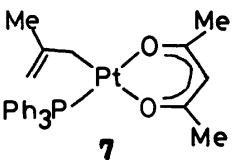

7

It seems notable that the triphenylphosphine analog of **6b** was reported to have the structure **7** having the *O,O*-chelate and the σ-bonded 2-methylallyl group.[8c] It is not certain how the electronic effect of the phosphine ligand controls the mode of the

metal-allyl and -acetylacetonato bonding in these complexes. Adoption of the structure **6b** in the $P(2,6)_3$ analog appears reasonable in terms of the steric cause. Thus, in spite of the presence of the secondary alkyl group ($CH(COMe)_2$), **6b** would contain more room for the bulky $P(2,6)_3$ to coordinate than a structure in which PPh_3 in **7** is replaced by $P(2,6)_3$, primarily due to the smaller bite angle of the 1-3-η-allyl chelate ($\leqslant 70°$)[10] than that of the acetylacetonato chelate (90°).

The IR spectrum of the palladium analog **6a** was much the same as that of **6b**. However, **6a** decomposed relatively rapidly when dissolved in chloroform and dichloromethane (see below), so that the ^1H NMR spectral data were not obtained in these solvents. The spectrum in toluene-d_8 was very broad at room temperature, and the spectra at the lower temperatures (down to −70°C) indicated the presence of free $P(2,6)_3$ and Pd(1-3-η-CH_2CMeCH_2)(acac) in ca. 30% amount. However, the remaining parts of the spectra were still very broad and no definitive structural assignment could be made.

Attempts to isolate a triphenylphosphine analog of **6a** were unsuccessful owing to fast decomposition to give good yields of the coupling product, CH_2=$CMeCH_2CH(COMe)_2$ **8**. Interestingly, however, decomposition of **6a** in methanol or chloroform gave only low yields of **8** (up to ca. 30%). The ^1H NMR spectra of the CD_3OD or $CDCl_3$ solution of **6a** after being kept at room temperature for one day showed the presence of the $[P(CH_2CMe{=}CH_2)(2,6)_3]^+$ ion (ca. 30—50%), although the nature of its counter anion remains to be identified. **6b** is fairly stable in solutions under the similar conditions.

It was reported before[11,12] that addition of phosphine or carbonyl ligand to otherwise stable 1-3-η-allyl (acetylacetonato) complexes of Pd and Pt greatly accelerates the formation of the C-C coupling products. Adding $P(2,6)_3$ to **6a** did not result in the increase of the formation of **8**, but bubbling carbon monoxide through a $CDCl_3$ solution of **6a** somewhat raised the amount of **8** (46%). Addition of $P(2,6)_3$ to **6b** caused no change. On the contrary, it was reported[8c] that **7** reacts with PPh_3 very rapidly to give **8** in good yields. However, **6b** did afford **8** (55—60%) rapidly when carbon monoxide was bubbled through its methanol or chloroform solution. Formation of some 30% amount of the ion, $[P(CH_2CMe{=}CH_2)(2,6)_3]^+$ was also confirmed by ^1H NMR spectroscopy.

When thallium or sodium acetylacetonate was added to **4a** in methanol-chloroform mixture under an atmospheric pressure of carbon monoxide, immediate decomposition of **4a** occurred. However, to our surprise, **8** was obtained in only 3% yields, the major product being $[P(CH_2CMe{=}CH_2)(2,6)_3]BF_4$ (92%). Surprisingly again, in the reaction of **4b** and sodium acetylacetonate in methanol-dichloromethane, **8** was not obtained so efficiently as in the reaction of **6b** with carbon monoxide.

It is possible that the reaction of **6** with carbon monoxide to give **8** does not take a pathway proceeding via an ion pair, $[M(1\text{-}3\text{-}\eta\text{-}CH_2CMeCH_2)(CO)\{P(2,6)_3\}]^+CH(COMe)_2^-$, **9**, as was often postulated in analogous reactions of platinum and palladium complexes.[8c,11b,12] One possible alternative pathway would be intramolecular reductive elimination of **8** from **6** assisted by coordination of carbon monoxide. Or it is also conceivable that the reaction of **6** with carbon monoxide does proceed via **9**, a kind of built-in ion pair, but in the reaction of **4** with sodium acetylacetonate the presence of the counter anion and cation (BF_4^-, Na^+) prohibits close contact of two reacting ions. Evidently, more works are necessary before any definitive conclusion on the mechanistic pathway is attained.

Experimental

Preparation of Complexes. **1a** and **1b** were obtained from the reaction of $[M(1\text{-}3\text{-}\eta\text{-}CH_2CMeCH_2)Cl]_2$ with $P(2,6)_3$ (1 : 1) in chloroform at 0 °C, and recrystallized from dichloromethane-hexane. As for the preparation of **2a**, an acetone solution (1 cm^3) of $AgBF_4$ (1 mmol) was added dropwise to **1a** (1 mmol) in the same solvent (100 cm^3). White precipitates of AgCl obtained immediately were filtered off, and the solution was concentrated to about a half volume by evaporation under vacuum. Hexane was added to cause precipitation of pale-yellow solids. These were recrystallized from dichloromethane-hexane. **2b** was prepared in a similar manner.

4a and **4b** were prepared by passing carbon monoxide through a dichloromethane solution of **2a** or **2b** at 0 °C for 10 min. To the resulting solution was added diethyl ether to give pale-pink **4a** or colorless **4b** precipitates. **4b** was recrystallized from dichloromethane-hexane, but **4a** was used without recrystallization for analysis, spectroscopy, and further reactions. IR (Nujol): **4a** 2098 cm^{-1}; **4b** 2075 cm^{-1}.

6a and **6b** were prepared from the reaction of **1a** and **1b** with thallium acetylacetonate, respectively, in manners similar to that for obtaining **7** described before.[8c] IR (Nujol): **6a** 1610 and 1630 cm^{-1}; **6b** 1624 and 1653 cm^{-1}. The ^1H NMR spectrum of **6a** in toluene-d_8 at −30 °C showed, other than the resonances due to $P(2,6)_3$ and Pd(1-3-η-CH_2CMeCH_2)(acac),[13] broad peaks at δ=1.53, 1.89, and 3.15 and very broad, weak peaks at δ=2.4, 3.9, and 4.6.

Reaction of 2b with $P(2,6)_3$. A chloroform solution (5 cm^3) of **2b** (0.26 mmol) was added to $P(2,6)_3$ (0.26 mmol) at room temperature. The resulting pale-yellow solution was concentrated under vacuum, and hexane was added to cause precipitation of pale-yellow solids. These were extracted with benzene (100 cm^3). Benzene insoluble materials were identified as $[P(CH_3)(2,6)_3]BF_4$ by ^1H NMR spectra ($CDCl_3$). The benzene extract was passed through a short Florisil column. After adding hexane, **3** was obtained as pale-yellow solids (37%). The same reaction as well as the analogous one between **2a** and $P(2,6)_3$ in $CDCl_3$ were also followed by ^1H NMR spectroscopy.

Reaction of 4b with $P(2,6)_3$. A chloroform solution (5 cm^3) of **4b** (0.25 mmol) was added to $P(2,6)_3$ (0.13 mmol) at room temperature. After concentrating the pale-yellow solution by evaporation under vacuum, diethyl ether was added

Table 2. Analytical Data of Complexes

Complex	Mp[a]	C (%)		H (%)	
	θ_m/°C	Found	(Calcd)	Found	(Calcd)
1a[b]	160	52.24	(52.60)	5.39	(5.36)
1b[c]	172	46.38	(46.19)	4.76	(4.70)
2a	150	48.54	(48.69)	4.98	(4.96)
2b	150—153	43.02	(43.15)	4.46	(4.40)
3	168—170	48.25	(47.86)	4.78	(4.61)
4a	150	48.21	(48.46)	4.87	(4.77)
4b	200—205	43.19	(43.14)	4.28	(4.24)
5	180	43.93	(44.03)	4.17	(4.17)
6a	110	56.16	(56.38)	6.11	(5.88)
6b	150—152	49.48	(50.06)	5.38	(5.22)

a) With decomposition. b) Cl (%): 6.22 (5.55). c) Cl (%): 5.25 (4.87).

to cause precipitation of pale-yellow solids. These were dissolved in 20 cm^3 of ethanol, and this solution was kept at −30 °C overnight to give pale-yellow crystals of **5** (36%). This was further recrystallized from dichloromethane-hexane kept in a refrigerator. IR (Nujol): 2010 and 2040 cm^{-1}. ^1H NMR ($CDCl_3$) δ=1.32 (t, J_P=2.5 Hz, J_{Pt}=60 Hz, Me); 1.47 (br s, anti-H); 2.88 (br t, $1/2[J_P+J_P']$=12 Hz, syn-H); 3.51 (s, OMe); 6.45 (dt, $1/2[J_P+J_P']$=2 Hz, J_H=8.5 Hz, 3- and 5-H); 7.25 (t, J_H=8 Hz, 4-H). The stoichiometry of this reaction was also followed by ^1H NMR spectroscopy, and found very clean.

Analytical data of new complexes thus obtained are summarized in Table 2.

Reactions of Other Complexes. The reactions involving **4a** were run in deuterated solvents which had been saturated with an atmospheric pressure of carbon monoxide. The proceeding of all the reactions was followed by ^1H NMR spectroscopy. The reactions of **6**, and those of **4** with sodium acetylacetonate, were also followed by GLC analysis for the determination of the coupling product **8** (SE30, 2 m×3 mm, internal reference, tridecane).

GLC analysis was run on a Hitachi 163 gas chromatograph. ^1H NMR spectra were measured on a JEOL JNM-PS-100 spectrometer, and IR spectra on a Hitachi 215 grating spectrophotometer.

Partial support of this work by a Grant-in-Aid for Special Project Research, Ministry of Education, Science and Culture (No. 61225016) is gratefully acknowledged.

References

1) a) M. Wada and S. Higashizaki, *J. Chem. Soc., Chem. Commun.*, **1984**, 482; b) M. Wada, S. Higashizaki, and A. Tsuboi, *J. Chem. Res., S.*, **1985**, 38; M., **1985**, 467; c) M. Wada and A. Tsuboi, *J. Chem. Soc., Perkin Trans. 1*, **1987**, 151.

2) J. Powell and B. L. Shaw, *J. Chem. Soc. A*, **1967**, 1839; J. Powell and B. L. Shaw, *ibid.*, **1968**, 774; H. Kurosawa and G. Yoshida, *J. Organomet. Chem.*, **120**, 297 (1976).

3) A. Tsuboi, unpublished results.

4) H. C. Clark and K. R. Dixon, *J. Am. Chem. Soc.*, **91**, 596 (1969); R. Uson, J. Fornies, and F. Martinez, *J. Organomet. Chem.*, **112**, 105 (1976); H. Kurosawa, T. Majima, and N. Asada, *J. Am. Chem. Soc.*, **102**, 6996 (1980); F. Ozawa, T. Sugimoto, Y. Yuasa, M. Santra, T. Yamamoto, and A. Yamamoto, *Organometallics*, **3**, 683 (1984).

5) H. Kurosawa, N. Asada, A. Urabe, and M. Emoto, *J. Organomet. Chem.*, **272**, 321 (1984).

6) P. L. Goggin and R. J. Goodfellow, *J. Chem. Soc., Dalton Trans.*, **1973**, 2355; M. P. Brown, R. J. Puddephatt, M. Rashidi, and K. R. Seddon, *ibid.*, **1978**, 1540; C. Couture, D. H. Farrar, D. S. Fisher, and R. R. Gukathasan, *Organometallics*, **6**, 532 (1987).

7) H. Werner, H. J. Kraus, and P. Thometzek, *Chem. Ber.*, **115**, 2914 (1982); A. Kuhn and H. Werner, *J. Organomet. Chem.*, **179**, 421 (1979).

8) a) J. Tsuji,"Organic Synthesis with Palladium Compounds," Springer-Verlag, New York (1980); b) B. M. Trost, *Acc. Chem. Res.*, **13**, 385 (1980); c) H. Kurosawa, *J. Chem. Soc., Dalton Trans.*, **1979**, 939.

9) T. Ito, T. Kiriyama, and A. Yamamoto, *Bull. Chem. Soc. Jpn.*, **49**, 3250 (1976); *idem, Chem. Lett.*, **1976**, 835; S. Okeya, Y. Nakamura, and S. Kawaguchi, *Bull. Chem. Soc. Jpn.*, **54**, 3396 (1981).

10) K. Miki, Y. Kai, N. Kasai, and H. Kurosawa, *J. Am. Chem. Soc.*, **105**, 2482 (1983); K. Miki, K. Yamatoya, N. Kasai, H. Kurosawa, M. Emoto, and A. Urabe, *J. Chem. Soc., Chem. Commun.*, **1984**, 1520.

11) a) Y. Takahashi, S. Sakai, and Y. Ishii, *J. Chem. Soc., Chem. Commun.*, **1967**, 1092; b) T. Hayashi, personal communication.

12) J. E. Bäckvall, R. E. Nordberg, and D. Wilhelm, *J. Am. Chem. Soc.*, **107**, 6892 (1985).

13) S. D. Robinson and B. L. Shaw, *J. Chem. Soc.*, **1963**, 4806.

Synthesis and Chromotropic Behavior of Nickel(II) Complexes with 1,4-Diazacycloheptane-*N,N'*-dicarboxylates in Solution

Yutaka FUKUDA,* Keiko YAMAGATA, and Thomas A. KADEN†
Department of Chemistry, Faculty of Science, Ochanomizu University, Otsuka, Bunkyo-ku, Tokyo 112
†Institute of Inorganic Chemistry, University of Basel, Spitalstr. 51, CH-4056 Basel, Switzerland
(Received April 28, 1987)

A new series of nickel(II) complexes containing 1,4-diazacycloheptane-*N,N'*-dicarboxylates (dachdx, where x=a means the acetate derivative, x=m, e, and p are the α-methyl, α-ethyl, and α-propyl substituents of the carboxyl side chain, respectively) were prepared as solids, Ni(dachdx)L_n (L=H_2O or pyridine, n=0, 1, or 2). These complexes can be classified according to their geometry into three types: (1) Octahedral [Ni(dachda)-$(H_2O)_2$], (2) square planar [Ni(dachdx)](x=m, p, or e) and (3) penta-coordinate [Ni(dachdm)(py)]. In the solid state the strength of the bonds between the metal ion and the carboxylate groups increases in the order: Octahedral < penta-coordinate < square planar. In solution, some of these compounds show chromotropic behavior, e.g. solvatochromism, thermochromism, and inert salt or active salt effects. The stability constants of the Ni^{2+} complexes were determined by pH-titrations and spectrophotometry. The following equilibria were found:

$$[Ni(aq)]^{2+} + dachdx^{2-} \rightleftharpoons [Ni(dachdx)];$$

$$[Ni(dachdx)] + X^- \rightleftharpoons [Ni(dachdx)X]^-;$$

where X^-=NCS^-, Cl^-, or Br^-. It is shown that the substituent of the carboxylate side chain plays an important steric role, thus determining the value of the stability constant of [Ni(dachdx)].

The chemistry of Ni^{2+} complexes with diamino-dicarboxylates is interesting and manifold, since different structures and properties were found. For example the nickel(II) complex of ethylenediamine-*N,N'*-diacetate(edda), [Ni(edda)$(H_2O)_2$], has an octahedral hexa-coordinate geometry in aqueous solution,[1] whereas the nickel(II) complex of 1,5-diazacyclo-octane-*N,N'*-diacetate(dacoda), [Ni(dacoda)(H_2O)], is penta-coordinate.[2] However, there are not many studies on the solution behavior of cyclic diamine-*N,N'*-dicarboxylate complexes (Scheme 1), because of difficulties encountered in the synthesis of such ligands and in the crystallization of their complexes. In particular there is no report about nickel(II) complexes of 1,4-diazacycloheptane-*N,N'*-dicarboxylates except our preliminary communication.[3] In continuation of such studies we describe now several nickel(II) complexes with the ligands dachdx. They show some interesting phenomena in solution, such as solvatochromism, thermochromism and inert salt ($NaClO_4$) or active salt (NCS^-) effects on the electronic spectra. In addition the stability constants of the following two equilibria were determined by means of potentiometric (Eq. 1, in aqueous media) and spectrophotometric methods (Eq. 2, in DMSO solutions):

$$[Ni(aq)^{2+}] + dachdx \rightleftharpoons [Ni(dachdx)(H_2O)_n];\ K_{NiL} \quad (1)$$

$$[Ni(dachdx)] + X^- \rightleftharpoons [Ni(dachdx)X]^-;\ K_{NiLX} \quad (2)$$

Experimental

Syntheses. The synthetic route of the ligands and their Ni^{2+} complexes are shown in Scheme 2.

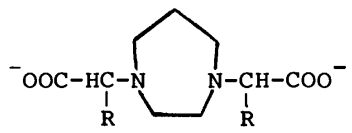

dachdx (L)

R	x	dachdx
H	a	dachda
CH_3	m	dachdm
CH_3CH_2	e	dachde
$CH_3CH_2CH_2$	p	dachdp

Scheme 1.

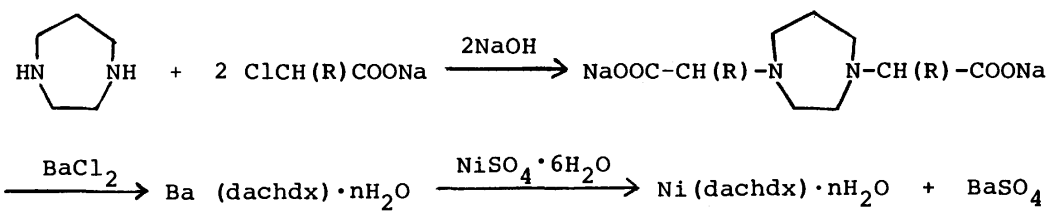

Synthetic route of the complex Ni(L)·nH_2O(L=dachdx)

Scheme 2.

Table 1. Analytical Data, Color and Magnetic Moments of the Ni^{2+} Complexes

Complex	C%	H%	N%	Color	μ_{eff} [b]
Ni(dachda)·$2H_2O$	34.99(34.86)[a]	5.87(5.88)[a]	9.07(9.03)[a]	Green	3.23
Ni(dachdm)	43.90(43.58)	6.03(6.02)	9.31(9.22)	Orange	dia.
Ni(dachde)	47.46(47.01)	6.74(6.83)	8.51(8.43)	Orange	dia.
Ni(dachdp)	50.46(49.76)	7.33(7.40)	7.85(7.73)	Orange	dia.
Ni(dachdm)py	50.56(50.53)	6.10(5.88)	11.06(11.07)	Green	3.22

a) Calculated values are shown in parentheses. b) In B.M., dia.=diamagnetic.

Potentiometric Titrations. To prepare standard solutions of the ligands the recrystallized barium salts of dachdx were treated with a slight excess of 0.1 M H_2SO_4 (1M=1 mol dm^{-3}) to precipitate $BaSO_4$. After centrifugation the clear solutions were diluted to the desired volume and the exact concentration of the ligands was determined acidimetrically with 0.4 M NaOH. Typical concentrations: 2.4×10^{-3} M ligand with no metal addition or with 2.0×10^{-3} M $Ni(NO_3)_2$. The ionic strength was kept constant with KNO_3 to I=0.5 M and the temperature was controlled to 25 °C. The titrations with 0.4 M NaOH were run using the previously described titration unit.[4] The electrode was calibrated with two buffers and checked by titrating a standard mixture of HNO_3 and CH_3COOH in 0.5 M KNO_3. The calculation of the protonation and stability constants was done on a Hewlett-Packard HP 9835 computer using the program TITFIT.[5]

Spectral Measurements. Electronic spectra of solutions were obtained with a Hitachi 340 recording spectrophotometer using 10 mm quartz cells. The procedure for determining the stability constants of the complexes [Ni(dachdx)] with NCS^- ion in DMSO was that reported in the literature.[6] Powder reflectance spectra were recorded with the same instrument, attached with an integrating sphere, using $BaSO_4$ as a reference. Infrared spectra were recorded for Nujol mulls using a JASCO IR-A3 Grating spectrophotometer (5000—400 cm^{-1}).

Results and Discussion

Analytical data, magnetic moments and colors of the Ni^{2+} complexes are shown in Table 1. Since [Ni(dachda)$(H_2O)_2$] is very difficult to crystallize and only a small amount of crystals was obtained, they were used for the determination of the elemental analysis, the magnetic moment and the IR spectrum. For visible spectral measurements we prepared solutions of equimolar amounts of dachda and $[Ni(aq)]^{2+}$, starting from Ba(dachda) and $NiSO_4\cdot6H_2O$ as described previously.[3]

From the analytical data of Table 1 and other data such as magnetic moments, IR and electronic spectra (see later), one can classify the solid nickel(II) complexes according to the coordination geometries into three types. The type 1 complex, [Ni(dachda)$(H_2O)_2$], is a green paramagnetic octahedral complex. The type 2 complex, [Ni(dachdx)] where x=m, e, or p, are orange, diamagnetic and have square planar structure. The type 3 complex, [Ni(dachdm)py] which contains one pyridine, is pentacoordinate, green and paramagnetic.

Because of the different coordination geometries of these complexes, it is interesting to look at the stretching frequencies of the carboxyl groups in the region 1700—1300 cm^{-1}. Table 2 gives the $\nu_{C=O}$ (I) and ν_{C-O} (II) bands of our complexes together with other data reported earlier,[7] as well as the difference between these two bands ($\Delta\nu_{I,II}$). From these data one can see that octahedral nickel(II) complexes with diaminedicarboxylate have $\Delta\nu_{I,II}$ values in the range 168—190 cm^{-1}, the pentacoordinate complex [Ni(dachdm)py] has $\Delta\nu_{I,II}$=246 cm^{-1} and those with square planar geometry have $\Delta\nu_{I,II}$ in the range of 296—373 cm^{-1}. [Ni(dachda)$(H_2O)_2$] and [Ni(dachdm)py] both show a similar IR change, when the complexes are heated. Before heating, the separation $\Delta\nu_{I,II}$ between the two peaks is relatively small, whereas after heating rather large one is observed (Eqs. 3 and 4) as follows (observed values shown in cm^{-1}).

Table 2. Carbonyl Stretching Modes (cm^{-1}) for the Ni(II) Complexes

Complex	I($\nu_{C=O}$)	II(ν_{C-O})	$\Delta\nu_{I,II}$
Ni(dachda)·$2H_2O$	1590	1400	190
Ni(dachdm)(py)	1630	1384	246
Ni(dachdm)	1758	1385	373
Ni(dachde)	1656	1360	296
Ni(dachdp)	1660	1348	312
Ni(edda)·$2H_2O$	1588	1398	190
Ni(edda)$(py)_2\cdot H_2O$	1580	1402	178
	1570		168
$Ni(gly)_2\cdot2H_2O$[a]	1589	1411	178
$Pd(gly)_2$[a]	1642	1374	268

a) Ref. 7.

$$[Ni(dachda)(H_2O)_2] \xrightarrow[\text{heating}]{-2H_2O} [Ni(dachda)] \quad (3)$$

	Oh		square planar	
$\nu_{C=O}$	1590		1670, 1648	
		→ 190($\Delta\nu_{I,II}$)		→ 302 or 280
ν_{C-O}	1400		1368	($\Delta\nu_{I,II}$)

$$[Ni(dachdm)py] \xrightarrow[\text{heating}]{-py} [Ni(dachdm)] \quad (4)$$

	penta-coordinate		square planar
$\nu_{C=O}$ (I)	1630		1658
		→ 246 ($\Delta\nu_{I,II}$)	⋮
ν_{C-O} (II)	1384		(missing)

Table 3. Protonation and Stability Constants($mol^{-1}dm^3$) for the Ligand dachdx at $I=0.5$ M and $T=25°C$. Values in Parentheses are Standard Deviations

	Ligand(L)	dachda	dachdm	dachde	dachdp	edda[a]
H^+	$\log K_{H,1}$	9.87(1)	10.20(1)	9.82(1)	9.88(1)	9.46
	$\log K_{H,2}$	5.98(1)	6.11(1)	5.74(1)	5.67(1)	6.42
Ni^{2+}	$\log K_{NiL}$	6.42(2)	6.22(1)	4.92(1)	5.09(1)	13.5

a) Values taken from Ref. 8.

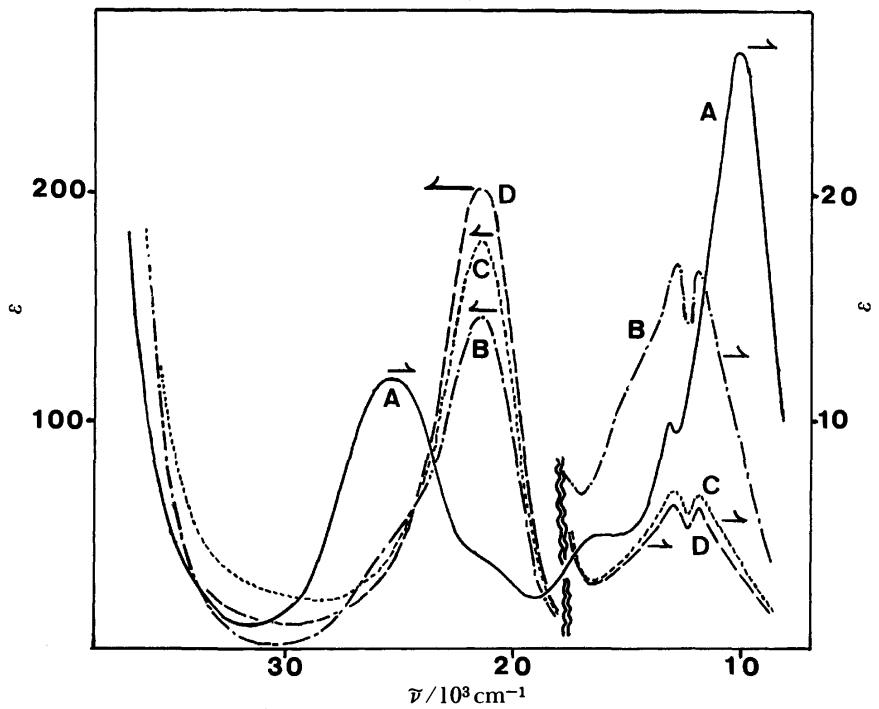

Fig. 1. Electronic absorption spectra of Ni(dachdx) in H_2O at room temperature. A: [Ni(dachda)(H_2O)$_2$] (5.0×10^{-2} M) (——), B: [Ni(dachdm)] (5.2×10^{-3} M) (-·-·-), C: [Ni(dachde)] (5.0×10^{-3} M) (·····), D: [Ni(dachdp)] (4.9×10^{-3} M) (----).

The $\Delta\nu_{I,II}$ values might reflect the strength of the coordinative bond between the metal ion and the carboxylate group. In square planar chelates the metal-ligand bonds are stronger than those in the other two geometries, whereas the bonds in the octahedral structure are the weakest. Since the carboxylate groups in the square planar complex are coordinated more covalently to the metal ion, they become more asymmetrical, whereas the ones in complexes with octahedral geometry being more ionic are less asymmetrical. Consequently the $\Delta\nu_{I,II}$ values reflecting this asymmetry are large for square planar complexes and small for octahedral ones.

The protonation and formation constants of the ligands are given in Table 3. The protonation constants are typical for diamine-*N*,*N*′-dicarboxylates as a comparison with EDDA shows.[8] With Ni^{2+} complexes of the stoichiometry NiL are formed, the stability of which is described by K_{NiL} (Eq. 1). The ligands with small substituent groups, dachda and dachdm, give more stable complexes than dachde and dachdp indicating that steric effects are important (Table 3). However, as we shall discuss later, the complexes NiL formed by these ligands differ from each other, being a mixture of species with different geometies, and this steric effect could play also an important role for determining the predominant species in solution.

The electronic spectra of the Ni^{2+} complexes in aqueous solution are shown in Fig. 1 and the values are given in Table 4. The shapes of the spectra of the complexes with dachdm, dachde, and dachdp (the type 2 complexes) are very similar to each other. Since the peak intensities at 21×10^3 cm^{-1} decrease in the order: [Ni(dachdp)]>[Ni(dachde)]>[Ni(dachdm)], the amount of the square planar species also decreases in the same order. On the other hand, the weak shoulder at 25×10^3 cm^{-1}, which is observed only in the case of dachdm, and the band at ca. 13×10^3 cm^{-1} are due to a pentacoordinate species. This latter species, with an absorption at 13×10^3 cm^{-1} which was also observed more or less distinctly for the complexes of dachde or dachdp, has a spectrum quite similar to that of [Ni-

Table 4. Electronic Absorption Spectra of the Ni(II) Complexes in H_2O

Complex	ν_{max} (10^3 cm^{-1}) and ε_{max} in parentheses (M^{-1} cm^{-1})				
Ni(dachda)·$2H_2O$	10.3	13.2	16.1	21.3	25.6
	(26.4)	(10.6)	(5.1)	(3.9)	(11.9)
Ni(dachdm)	11.9	13.0	21.5	25.3	
	(16.8)	(17.0)	(146.7)	(47.5)	
Ni(dachde)	11.9	13.0	21.5		
	(6.8)	(6.8)	(179.5)		
Ni(dachdp)	11.9	13.0	21.5		
	(6.2)	(6.3)	(202.3)		
Ni(edda)$(H_2O)_2$[a]	9.9	13.2	16.4	27.2	
	(12.6)	(1.9)	(4.2)	(7.2)	
Ni(dacoda)(H_2O)[a]	12.3	13.1	15.8	26.4	
	(21.4)	(25.3)	(28.0)	(86.5)	

a) Values taken from Ref. 2.

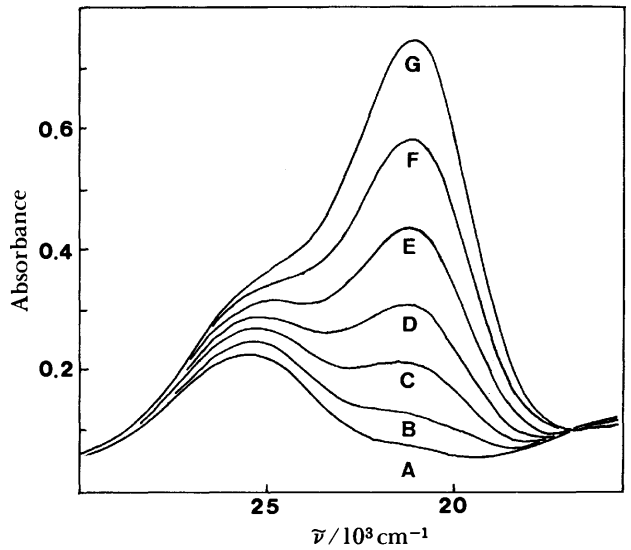

Fig. 2. Temperature effect on the electronic absorption spectra of [Ni(dachda)$(H_2O)_2$] (2.3×10^{-2} M) in H_2O. Curves A to G are the spectra measured at A (293 K), B (313), C (323), D (333), E (343), F (353), and G (363), respectively.

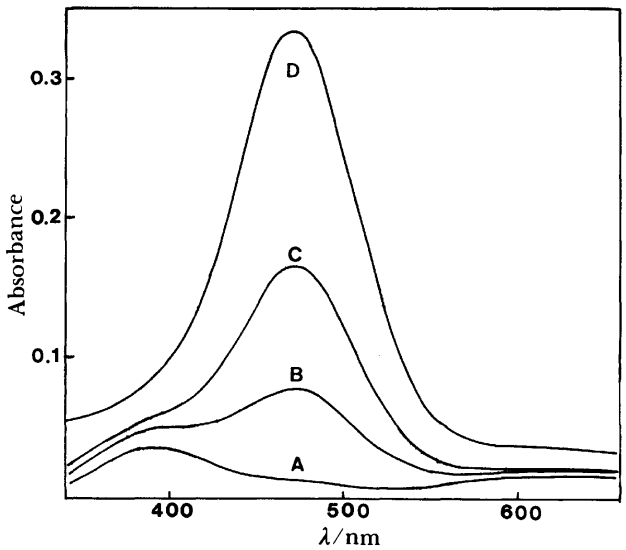

Fig. 3. Inert salt effect on the absorption spectra of [Ni(dachda)$(H_2O)_2$] (4.6×10^{-3} M) in H_2O at room temperature. Concentration of $NaClO_4$ added; A=0.0 M, B=2.0 M, C=3.0 M, and D=large excess amounts of $NaClO_4$.

(dacoda)(H_2O)] in aqueous solution.[2] The order of the amount of penta-coordinate species is the reverse of that for the square planar species given above. The type 2 complexes form equilibrium mixtures of the planar and the penta-coordinate species in aqueous solution, in which the square planar form is predominant. For example, in the case of [Ni(dachdm)] we have Eq. 5.

$$[\text{Ni(dachdm)}] + H_2O \rightleftharpoons [\text{Ni(dachdm)}(H_2O)] \quad (5)$$

Finally, the spectrum of [Ni(dachda)$(H_2O)_2$] is rather different from the other ones. A comparison of this spectrum (Fig. 1) with those typical for planar, penta-coordinate and hexa-coordinate species (Table 4) indicates that in aqueous solution the dachda complex is predominantly a mixture of penta-coordinate and hexa-coordinate species, whereas the square planar form is only present in a minor amount ([Ni(dachda)$(H_2O)_2$] $\rightleftarrows$ [Ni(dachda)(H_2O)]+H_2O). The peak at 17×10^3 cm^{-1} is the second transition expected in octahedral geometry $^3A_{1g} \rightarrow {}^3T_{1g}(F)$,[9] whereas the other two peaks $^3A_{1g} \rightarrow {}^3T_{2g}$, $^3A_{1g} \rightarrow {}^3T_{1g}(P)$ are obscured under the strong bands of the penta-coordinate species.

In addition, the above solutions are thermochromic: The color of the aqueous solution of [Ni(dachda)$(H_2O)_2$] changes from blue-green to orange when the temperature of the solution is raised (Fig. 2). The peak intensity at 21×10^3 cm^{-1} gradually increases as the temperature increases, indicating that Eq. 6 is shifted to the right hand side (where n=1 or 2).

$$\underset{\text{Blue-green (room temp)}}{[\text{Ni(dachda)}(H_2O)_n]} \underset{\text{cool}}{\overset{\text{heat}}{\rightleftharpoons}} \underset{\text{Orange (high temp)}}{[\text{Ni(dachda)}] + nH_2O} \quad (6)$$

Addition of an inert salt such as $NaClO_4$ to an aqueous solution of [Ni(dachda)$(H_2O)_2$] gives rise to this phenomenon more easily. Finally, when a large

excess of $NaClO_4$ is added to this solution, the color of the solution changes already at room temperature from blue-green to orange (Eq. 7, see Fig. 3). This color change (inert salt effect) is explained by decreasing of coordination ability of solvent molecules due to the solvation of large amounts of the inert salt in solution.

$$\underset{\text{Blue-green (room temp)}}{[\text{Ni(dachda)}\,(H_2O)_n]} \xrightarrow{\text{excess } NaClO_4} \underset{\text{Orange(room temp)}}{[\text{Ni(dachda)}]} + nH_2O \quad (7)$$

On the other hand, aqueous solutions of the type 2 compounds show a color change from orange to green when the temperature decreases, e.g. Eq. 8.

$$\underset{\text{Orange (room temp)}}{[\text{Ni(dachdm)}] + H_2O} \xrightarrow{\text{cooling}} \underset{\text{Green (low temp)}}{[\text{Ni(dachdm)}(H_2O)]} \quad (8)$$

We have also noticed that the type 2 complexes, especially the complex [Ni(dachdm)], show solvatochromism. The spectra of this complex in DMSO and H_2O are shown in Fig. 4. The spectrum in DMSO is typical for a planar species, whereas in H_2O there is a mixture of square planar and penta-coordinate species. This is rather strange since from the donor strength of DMSO and H_2O one would expect the opposite.[10] That the species in DMSO solution is square planar and there is no solvent coordination, is probably due to (1) steric effects in solvent coordination, DMSO being larger than H_2O and also (2) the hydrogen bond between carboxylato groups in dachdm and solvent molecules. In other words, the C=O groups can interact with H_2O molecules but not with DMSO molecules, so that H_2O can approach to the central metal ion more easily than DMSO.

The type 2 compounds show an "active salt effect," which means that, when a coordinating anion such as NCS^- is added to the solution, Equilibrium 9 is shifted to the right, i.e. from a square planar species a penta-coordinate one is formed.

$$\underset{\text{Orange, planar}}{[\text{Ni(dachdx)}] + NCS^-} \rightleftharpoons \underset{\text{Green, 5-coordinate}}{[\text{Ni(dachdx)(NCS)}]^-} \quad (9)$$

A typical penta-coordinate spectrum of [Ni(dachdm)-(NCS)]$^-$ is shown in Fig. 5, which was obtained from the DMSO solution with a large excess of NH_4NCS. The formation constants of the penta-coordinate complexes [Ni(dachdx)X]$^-$ (Eq. 2) with three coordinating anions X^-=NCS^-, Br^-, and Cl^- were determined spectrophotometrically in DMSO solutions by the Hildebrand-Benesi method[6] at room temperature (Table 5). The anion coordination decreases in the

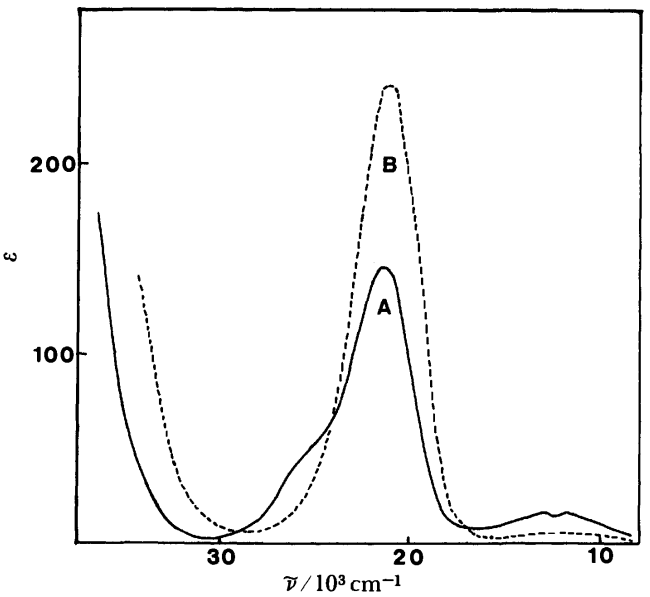

Fi 4. Electronic absorption spectra of [Ni(dachdm)] in H_2O (A; 5.2×10^{-3} M) and in DMSO (B; 2.5×10^{-3} M) at room temperature.

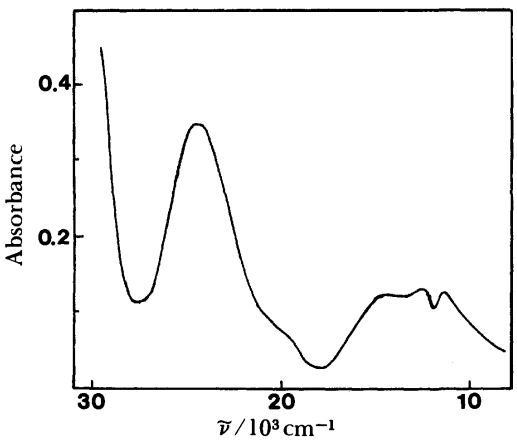

Fig. 5. Electronic absorption spectra of [Ni(dachdm)] (5.0×10^{-2} M) in DMSO with large excess of NH_4-NCS at room temperature.

Table 5. Stability Constants ($mol^{-1}dm^3$) of the Complex [Ni(dachdx)X]$^-$ in DMSO at Room Temperature (25 °C)[a]

		Ni(dachdm)	Ni(dachde)	Ni(dachdp)
Cl^-	NH_4Cl	59(2)	29(1)	26(1)
	$(Et)_4NCl$	55(2)	26(1)	24(1)
NCS^-	NH_4NCS	30(1)	13(1)	12(1)
Br^-	NH_4Br	5(1)	4(1)	—
	$(Et)_4NBr$	5(1)	3(1)	—

a) Values in parentheses are standard deviations.

Conclusion: Some Chromotropic Phenomena of the Chelates, [Ni(dachdx)$(H_2O)_n$]

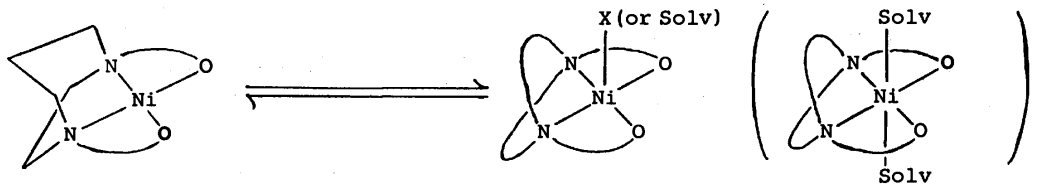

Structure: Square Planar (Sq. Pl.) ⟷ 5-Coord. (or 6-Coord.)
Substituent Effect (R): C_3H_7–, C_2H_5–, CH_3– ⟷ (H–)
Solvent Effect: DMSO ⟷ H_2O
Temperature Effect: High Temp ⟷ Low Temp
Inert Salt Effect ($NaClO_4$ in H_2O): Higher Concn ⟷ Lower Concn
Active Salt Effect (NR_4X in DMSO): Lower Concn ⟷ Higher Concn
Active Salt Effect (Anion Coordination): Br^- ⟷ NCS^- ⟷ Cl^-

Scheme 3.

order $Cl^- > NCS^- > Br^-$, whereas the order of increasing stability of the penta-coordinate species is the following:

[Ni(dachdm)] > [Ni(dachde)] > [Ni(dachdp)].

It is concluded that the substituent at the carboxylate side chain of these ligands plays a very important role in the determination of the structure and the solution behavior of the Ni^{2+} complexes.

Finally, we can summarize the observed chromotropic phenomena due to the structural change between square planar and 5-coordinate structure (or 6-coordinate octahedral one) as shown in Scheme 3.

The authors wish to express their thanks to Professor Kozo Sone of Ochanomizu University for his helpful discussion.

References

1) D. F. Averill, J. I. Legg, and D. L. Smith, *Inorg. Chem.*, **11**, 2344 (1972).

2) J. I. Legg, D. O. Nelson, D. L. Smith, and M. L. Larson, *J. Am. Chem. Soc.*, **90**, 5030 (1968); D. O. Nelson, M. L. Larson, R. D. Willett, and J. I. Legg, *J. Am. Chem. Soc.*, **93**, 5079 (1971); M. Micheloni, P. Paoletti, S. Bürlci, and Th. A. Kaden, *Helv. Chim. Acta*, **65**, 587 (1982).

3) Y. Fukuda, H. Miyamae, K. Yamagata, and K. Sone, *Chem. Lett.*, **1984**, 1309.

4) H. Gampp, M. Maeder, A. D. Zuberbühler, and Th. A. Kaden, *Talanta*, **27**, 573 (1980).

5) A. D. Zuberbühler and Th. A. Kaden, *Talanta*, **29**, 201 (1982).

6) H. A. Benesi and J. H. Hildebrand, *J. Am. Chem. Soc.*, **71**, 2703 (1949); Y. Fukuda, P. R. Michell, and H. Sigel, *Helv. Chim. Acta*, **61**, 638 (1978).

7) K. Nakamoto, "Infrared and Raman Spectra of Inorganic and Coordination Compounds," 3rd ed, John-Wiley & Sons, New York (1978).

8) S. Chaberek and A. E. Martell, *J. Am. Chem. Soc.*, **74**, 6228 (1952).

9) A. B. P. Lever, "Inorganic Electronic Spectroscopy," Elsevier, Amsterdam (1968).

10) V. Gutmann, "Coordination Chemistry in Non-Aqueous Solutions," Springer Verlag, Wien (1968); U. Mayer, "Studies in Physical and Theoretical Chemistry," Vol. 27 ("Ions and Molecules in Solutions"), ed by N. Tanaka, H. Ohtaki, and R. Tamamushi, Elservier, Amsterdam (1983).

Cobalt(III) Complexes of Salen Analog with Thioether Pendant Group. X-Ray Structure Analysis and Thioether Coordination Effects

Kaoru HORIUCHI, Masahiro MIKURIYA,†,§ Hisashi ŌKAWA,* and Sigeo KIDA†
Department of Chemistry, Faculty of Science, Kyushu University, Hakozaki, Higashiku, Fukuoka 812
†Laboratories of Coordination Chemistry, Institute for Molecular Science, Myodaiji, Okazaki 444
(Received May 29, 1987)

A pentadentate salen analog with a pendant thioether group, *N,N'*-disalicylidene-2-methyl-4-ethylthio-1,2-butanediamine (H_2L), formed two types of cobalt(III) complexes, $[Co(L)]ClO_4 \cdot H_2O$ (**1**) and $[Co(L)NH_3]PF_6 \cdot H_2O$ (**2**). Based on infrared and electronic spectra, the complex **1** was revealed to have a square-pyramidal configuration with the pendant sulfur coordination at the apex. The structure of the complex **2** was determined by single-crystal X-ray analysis. The molecule has a six-cooridnate structure with the coordination of the pendant sulfur and the ammonia molecule at the apical sites, the Co-S and Co-N(NH_3) distances being ca. 2.25 and 2.0 Å, respectively. Electrochemical measurements (CV and DPP) for **2** and $[Co(salen)(R\text{-}NH_2)_2]PF_6$ as the reference have revealed that the substitution of thioether sulfur for one of the apical amine ligands results in a positive shift of the Co^{III}/Co^{II} redox potential. It is also found that the Co^{III}/Co^{II} reduction of five-coordinate **1** occurs at a significantly high potential compared with six-coordinate **2** and $[Co(salen)(R\text{-}NH_2)_2]PF_6$.

Pentadentate salen analogs (H_2 salen=*N,N'*-disalicylidenethylenediamine) with a pendant group capable of axial coordination are of current interest because their metal complexes show some characteristics relevant to biological systems, such as formation of reversible oxygen-adducts[1-11] or alkylcobalt(III) complexes[12,13] and catalytic functions in substrate oxidation.[14-18] In a hope to elucidate the effect of the pendant donor atom on the electronic states and the reactivities of the complexes, pentadentate salen analogs with a pendant group of various kinds have been synthesized so far.[19-23] Salen analogs with a thioether in the pendant group, *N,N'*-disalicylidene-2-methyl-4-alkylthio-1,2-butanediamine and *N,N'*-disalicylidene-2-methyl-4-phenylthio-1,2-butanediamine (Fig. 1), were prepared in our laboratory.[22,23] It was shown that the cobalt(II) complexes of these ligands form dioxygen adducts in which the pendant thioether group is coordinated to the trans position to the dioxygen.[22] Further, these ligands form novel μ-oxodiiron(III,IV) complexes composed of high-spin iron(III) and low-spin iron(IV).[23] The unusual low-spin state of the iron(IV) presumably stems from the coordination of the pendant sulfur atom. These findings prompted us to examine the sulfur coordination effect in cobalt(III) complexes of these sulfur-containing salen analogs. This paper deals with synthesis, characterization, structure, and properties of five-coordinate cobalt(III) complex $[Co(L)]ClO_4 \cdot H_2O$ and six-coordinate complex $[Co(L)NH_3]PF_6 \cdot H_2O$ of *N,N'*-disalicylidene-2-methyl-4-ethylthio-1,2-butanediamine (H_2L: Fig. 1, R=C_2H_5).

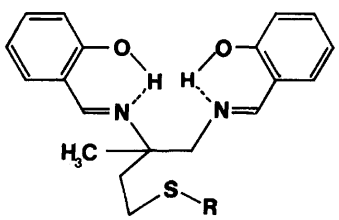

Fig. 1.

Experimental

Preparations. Synthesis of the ligand (H_2L) was described in the preceding paper.[23]

$[Co(L)]ClO_4 \cdot H_2O$ (**1**). Cobalt(II) perchlorate hexahydrate (0.25 g) and H_2L (0.25 g) were dissolved in methanol (30 cm^3), and the mixture was refluxed for 30 minutes to form brownish green solution. It was filtered and the filtrate was left stand in a refrigerator to give a dark green mass. It was crystallized from a chloroform–methanol (1:1) mixture.

Found: C, 46.03; H, 4.99; N, 5.13%. Calcd for $C_{21}H_{26}ClCoN_2O_7S$: C, 46.29; H, 4.81; N, 5.14%.

$[Co(L)NH_3]PF_6 \cdot H_2O$ (**2**). A methanolic solution of cobalt(II) acetate tetrahydrate (0.17 g) and H_2L (0.25 g) was refluxed for two hours. To the resulted deep brown solution was added a methanolic solution of ammonium hexafluorophosphate (excess) to give brown crystals. They were recrystallized from methanol.

Found: C, 41.28; H, 5.00; N, 6.65%. Calcd for $C_{21}H_{29}CoF_6N_3O_3PS$: C, 41.52; H, 4.81; N, 6.92%.

Single-Crystal X-Ray Analysis of 2. On prolonged standing the filtrate of the recrystallization of the complex **2**, the second crop of the complexes was obtained as crystals. From this crop a crystal was picked up and used for the X-ray analysis.

$[Co(L)NH_3]PF_6 \cdot H_2O = C_{21}H_{29}CoSPF_6O_3N_3$, M=607.44, dark brown plates, crystal dimensions 0.15×0.29×0.54 mm, triclinic, a=17.001(2), b=21.388(3), c=11.280(2) Å, α=102.57(1), β=96.71(1), γ=94.38(1)°, V=3954 Å^3, space group $P\bar{1}$ (C_i, No. 2), Z=6, D_m (floatation)=1.53, D_c=1.53 g cm^{-3}, μ(Mo $K\alpha$)=8.52 cm^{-1}, F(000)=1872.

Data collection and processing: RIGAKU AFC-5 diffractometer, $\omega/2\theta$ mode with ω scan width=1.1+0.5 tanθ, ω scan speed 3 deg min^{-1} graphite-monochromated Mo $K\alpha$ radia-

§Present address: School of Science, Kwanseigakuin University, Uegahara, Nishinomiya 663.

Table 1. Atomic Postional Parameters ($\times 10^4$)

	x	y	z		x	y	z	
CoA	3569(1)	−166(1)	8916(2)	C14A	5748(10)	−371(9)	5887(15)	
CoB	5726(1)	4316(1)	6253(2)	C15A	5431(9)	−22(8)	6899(15)	
CoC	9284(1)	7251(1)	1535(2)	C16A	4701(9)	−258(8)	7211(14)	
SA	2773(3)	485(2)	8110(4)	C17A	2064(11)	−1820(9)	6963(18)	
SB	5785(3)	4290(3)	8243(5)	C18A	1740(10)	−687(9)	7068(17)	
SC	8099(3)	7616(2)	1149(4)	C19A	1779(10)	30(9)	7761(18)	
PA	0	0	0	C20A	3042(11)	505(10)	6591(16)	
PB	2274(3)	8617(3)	2945(6)	C21A	2522(14)	959(12)	6029(21)	
PC	5914(4)	2836(3)	1636(6)	C1B	4034(11)	3992(9)	6324(16)	
F1A	−429(7)	565(5)	737(11)	C2B	3298(11)	4190(12)	6561(16)	
F2A	−312(10)	196(6)	−1221(11)	C3B	2637(14)	3756(12)	6630(20)	
F3A	759(7)	490(6)	114(13)	C4B	2730(13)	3131(16)	6493(22)	
F1B	1667(9)	8956(10)	2249(20)	C5B	3461(15)	2856(11)	6210(19)	
F2B	1568(10)	8269(11)	3404(22)	C6B	4149(12)	3317(10)	6118(17)	
F3B	2839(10)	8228(9)	3583(20)	C7B	4893(12)	3053(9)	5833(17)	
F4B	2902(10)	8963(11)	2481(23)	C8B	6318(11)	3083(9)	5622(19)	
F5B	2246(21)	9096(12)	4031(20)	C9B	7017(12)	3539(8)	6379(17)	
F6B	2128(19)	8060(13)	1878(22)	C10B	7415(11)	4633(9)	6263(17)	
F1C	5276(10)	2987(9)	2487(16)	C11B	7307(10)	5317(9)	6321(16)	
F2C	6569(10)	3183(9)	2734(14)	C12B	7994(12)	5703(9)	6209(18)	
F3C	6598(11)	2703(11)	796(17)	C13B	7970(12)	6331(10)	6359(19)	
F4C	5248(12)	2462(12)	603(17)	C14B	7277(12)	6626(9)	6639(18)	
F5C	6011(11)	2202(8)	1996(20)	C15B	6598(12)	6252(9)	6727(17)	
F6C	5807(17)	3452(11)	1266(24)	C16B	6601(11)	5573(8)	6550(15)	
O1A	3977(6)	537(5)	10237(10)	C17B	7779(12)	3323(10)	5869(21)	
O2A	4434(6)	102(5)	8165(9)	C18B	7140(13)	3528(11)	7775(19)	
O1B	4614(7)	4420(6)	6211(11)	C19B	6413(16)	3589(10)	8387(19)	
O2B	5900(7)	5232(5)	6635(10)	C20B	6518(16)	4982(11)	9100(19)	
O1C	9171(7)	7425(5)	3223(10)	C21B	6514(29)	7985(8)	3999(15)	
O2C	8822(7)	6414(6)	1473(11)	C1C	9313(10)	7985(8)	3999(15)	
OWA	4500(17)	1497(13)	8509(28)	C2C	9112(11)	8028(9)	5194(16)	
OWB	5571(17)	2008(11)	7498(22)	C3C	9264(11)	8599(10)	6077(16)	
OWC	8509(11)	3033(10)	−25(20)	C4C	9623(12)	9166(10)	5800(18)	
N1A	2699(8)	−423(7)	9706(12)	C5C	9828(12)	9143(10)	4619(16)	
N2A	3143(7)	−859(6)	7581(12)	C6C	9659(10)	8549(8)	3730(15)	
N3A	4251(7)	−728(6)	9675(12)	C7C	9897(10)	8562(9)	2512(15)	
N1B	5565(9)	3411(7)	5867(13)	C8C	10080(10)	8152(8)	469(15)	
N2B	6836(8)	4201(7)	6281(12)	C9C	9553(10)	7678(8)	−615(16)	
N3B	5622(8)	4329(7)	4460(12)	C10C	9392(11)	6515(9)	−886(18)	
N1C	9782(7)	8078(6)	1596(11)	C11C	9190(11)	5923(9)	−487(17)	
N2C	9408(8)	7072(6)	−148(12)	C12C	9268(12)	5353(9)	−1394(21)	
N3C	10343(9)	6958(7)	1959(14)	C13C	9063(13)	4748(10)	−1118(24)	
C1A	3578(10)	818(8)	11092(14)	C14C	8764(12)	4723(10)	66(23)	
C2A	3917(10)	1421(8)	11839(15)	C15C	8690(11)	5297(9)	891(21)	
C3A	3504(12)	1727(9)	12787(15)	C16C	8911(11)	5902(8)	627(18)	
C4A	2774(11)	1435(10)	13030(17)	C17C	9983(11)	7569(10)	−1766(16)	
C5A	2446(11)	846(9)	12322(15)	C18C	8735(10)	7906(9)	−946(15)	
C6A	2837(10)	519(8)	11348(15)	C19C	8272(10)	8154(9)	107(16)	
C7A	2455(10)	−109(9)	10653(15)	C20C	7444(12)	6939(10)	207(19)	
C8A	2260(10)	−1060(8)	9027(16)	C21C	6592(13)	7135(13)	66(24)	
C9A	2293(9)	−1103(9)	7655(15)	PD1	116(33)	6057(27)	6238(51)	0.1[a]
C10A	3509(9)	−1096(8)	6663(15)	PD2	784(34)	5805(28)	6162(52)	0.1
C11A	4279(9)	−833(8)	6504(15)	PD3	785(49)	5571(40)	4942(74)	0.07
C12A	4616(11)	−1160(9)	5464(16)	PD4	232(22)	5851(18)	5130(34)	0.13
C13A	5328(10)	−941(9)	5181(16)	PD5	−186(30)	6217(25)	3885(46)	0.1

a) Occupancy factor.

tion; 14641 reflections measured ($2.0 \leqq 2\theta \leqq 50.0°$), giving 7623 with $F > 3\sigma(F)$.

The structure was solved by direct method and Fourier technique, and refined by block-diagonal least-squares method. This gave the positions of six $[Co(L)NH_3]^+$ cations, five PF_6^- anions, and six lattice water molecules in the unit cell. At this stage, no remaining peaks as intense as those of a PF_6^- anion could be found. The remaining peaks were eventually assigned to five sites for disordered PF_6^- ion. It was not possible to locate the fluorine atoms of the PF_6^- ion. No attempts were made to locate hydrogen atoms. The weighting scheme was $w=[\sigma_{count}^2+(0.015|F_o|)^2]^{-1}$. Final R and R_w values are 0.093 and 0.167, respectively. The final difference Fourier synthesis showed no peaks higher than 1.3

e Å^{-3}. All the calculations were performed on HITAC M-680H computer of the Computer Centre of the Institute for Molecular Science with the UNICS-III, MULTAN 78, and ORTEP programs. The final atomic parameters are given in Table 1. The anisotropic thermal parameters and the F_o—F_c tables have been deposited as a Document No. 8759 at the Office of the Editor of Bull. Chem. Soc. Jpn.

Other Physical Measurements. Electronic spectra were recorded on a Shimadzu Multipurpose Spectrometer Model MPS-5000 in acetonitrile. Infrared spectra were recorded on a JASCO Infrared Spectrometer Model IR-810 on KBr disks or Nujol mulls. Cyclic voltammograms and differential pulse polarograms were obtained with a Yanagimoto P-1000 voltammetric analyzer in freshly distilled dichloromethane, using a three-electrode cell equipped with a glassy-carbon working electrode, a platinum coil auxiliary electrode, and a calomel electrode as the reference electrode. Tetrabutylammonium perchlorate (0.1 mol dm^{-3}) was added as the supporting electrode. All the potentials were normalized relative to the ferrocenium/ferrocene potential[24] added as the internal standard.

Results and Discussion

Electronic spectra of the complexes in acetonitrile are shown in Fig. 2. The spectrum of **1** is characterized by an absorption ($\varepsilon \approx 700$ dm^3 mol^{-1} cm^{-1}) at 16.9×10^3 cm^{-1}. A similar absorption is observed for five-coordinated salen-cobalt(III) complexes with a soft donor group such as an alkyl anion,[12,25-27] cyanide ion,[18] or triphenylphosphine[28] at the apical site. The spectrum, therefore, suggests the configuration of this complex to be of square-pyramid with the coordination of the pendant sulfur at the apex. The infrared spectrum of the complex indicates non-coordination of the perchlorate ion to the metal ($\nu(ClO_4) \approx 1100$ cm^{-1}).[29] The O-H stretching mode appears near 3400 cm^{-1} when measured on Nujol mulls. This implies that the water molecule is not coordinated but combined in the crystal lattice.[30] It is evident that the complex **1** retains the five-coordinate structure in solid state.

The crystal structure of **2** was determined by single crystal X-ray structure analysis in this study. The crystal contains three crystallographically independent $[Co(L)NH_3]^+$ cations (represented as **A**, **B**, and **C**) which show the essentially same structure. The molecular structure of A is shown in Fig. 3. Selected interatomic distances and bond angles of the cations are given in Table 2. The coordination geometry around the cobalt ion is a distorted octahedron with the thioether sulfur and the ammonia molecule at the apical positions. The in-plane Co-N and Co-O distances are in the range 1.880—1.917 Å, and are comparable to those of salen-complexes.[31] The ethylene chain of the salen skeleton adopts a gauche conformation with the pendant group at the axial orientation so as to allow the sulfur coordination to the metal ion with the Co-S distance of 2.244—2.268 Å. The S-Co-O(1), S-Co-O(2), S-Co-N(1), and S-Co-N(2) angles all are close to 90°, demonstrating that the Co-S bond

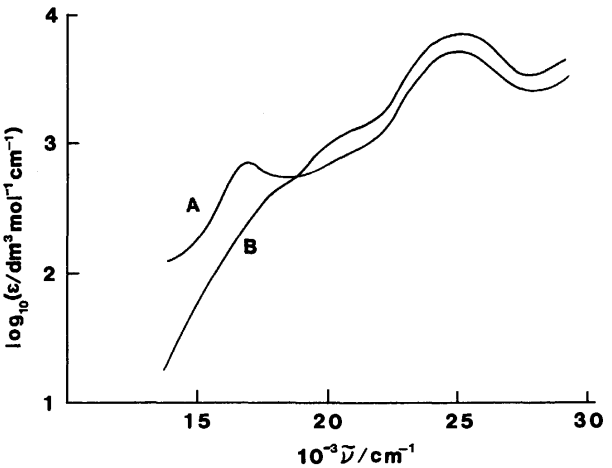

Fig. 2. Electronic spectra of (A) $[Co(L)]ClO_4 \cdot H_2O$ and (B) $[Co(L)NH_3]PF_6 \cdot H_2O$ in acetonitrile.

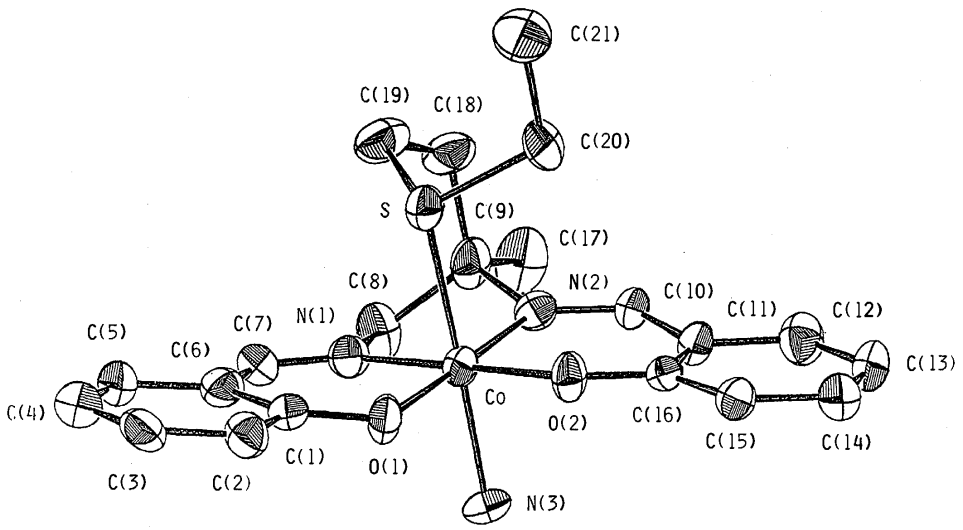

Fig. 3. ORTEP view of the cation **A** with the atomic numbering scheme.

Table 2. Selected Interatomic Distances (l/Å) and Bond Angles with Their Estimated Standard Deviations in Parentheses

	A	B	C
Co-S	2.269(6)	2.248(6)	2.244(6)
Co-O1	1.894(10)	1.915(12)	1.895(12)
Co-O2	1.893(11)	1.904(11)	1.883(12)
Co-N1	1.919(14)	1.881(15)	1.885(13)
Co-N2	1.897(11)	1.921(15)	1.893(14)
Co-N3	1.988(14)	2.016(14)	1.993(15)
S-Co-O1	89.5(4)	89.1(4)	89.1(4)
S-Co-O2	91.7(4)	92.2(4)	93.1(4)
S-Co-N1	88.3(5)	88.2(5)	88.9(4)
S-Co-N2	89.3(4)	91.2(5)	91.6(4)
S-Co-N3	178.1(4)	177.6(4)	177.1(4)
O1-Co-O2	84.8(5)	86.4(5)	85.7(5)
O1-Co-N1	94.0(5)	94.2(6)	94.8(5)
O1-Co-N2	178.8(6)	179.2(5)	179.2(6)
O1-Co-N3	89.4(5)	88.6(6)	88.4(6)
O2-Co-N1	178.8(5)	179.3(6)	178.0(6)
O2-Co-N2	95.4(5)	94.3(6)	94.2(6)
O2-Co-N3	89.7(5)	88.6(6)	88.2(6)
N1-Co-N2	85.8(6)	85.1(6)	85.4(6)
N1-Co-N3	90.3(6)	91.1(6)	89.9(6)
N2-Co-N3	91.8(5)	91.1(6)	90.9(6)

is nearly perpendicular to the least-squares plane defined by the Co, O(1), O(2), N(1), and N(2) atoms (N_2O_2 plane). The Co atom resides on the equatorial plane, the deviation of the cobalt atom from the N_2O_2 least square plane being less than 0.03 Å. The Co-N (NH_3) distance (1.987—2.012 Å) is essentially equivalent to the Co-N (pyridine) distance (2.031 Å) of $[CH_3OCo(salen)py]$[32] and Co-N (amine) distance (2.01 Å) of $[Co(salen)(n\text{-}BuNH_2)_2]^+$ (n-$BuNH_2$=butylamine),[33] but significantly short compared with the Co-N (pyridine) bond (2.15 Å) of [Co(salen)py].[34]

In the related cobalt(II)[20,35] and iron(II)[35] complexes of *N,N'*-disalicylidene-4-(2-pyridyl)-1,2-butanediamine, the coordination of the pendant pyridyl group induces distortions of the MN_2O_2 moiety from square-plane to trigonal bipyramid. Because of this distortion the cobalt complex is high-spin. The cobalt(II) complex of H_2L ([Co(L)]), on the other hand, was revealed to be low-spin based on EPR spectra.[22] In the six-coordinate O_2-adduct, [*N,N'*-disalicylidene-4-(2-pyridyl)-1,2-butanediaminato]superoxocobalt(III),[36] the cobalt atom is still displaced towards the pendant pyridyl nitrogen from the equatorial plane. All these facts suggest that in metal complexes of H_2L the pendant sulfur can occupy the apical position without any significant strain when the salen skeleton coordinates to a metal in the usual planar manner.[31]

Cyclic voltammograms (CV) and differential pulse polarograms (DPP) of **1** and **2** were obtained in order to examine the sulfur coordination effect on their electrochemical properties. Both complexes showed two reduction waves but no oxidation wave up to +1.0 V (see Fig. 4). It is reasonable to assign the reduction

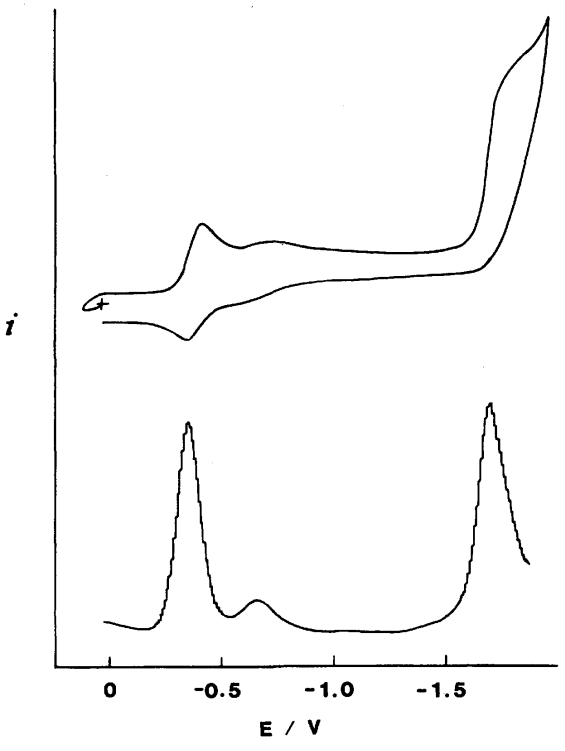

Fig. 4. Cyclic voltammogram (above) and differential pulse polarogram (below) of [Co(L)]$ClO_4 \cdot H_2O$ in dichloromethane ($\approx 1\times10^{-3}$ mol dm^{-3}); scan rate 0.1 V s^{-1} for both CV and DPP.

waves to the Co^{III}/Co^{II} and Co^{II}/Co^{I} processes, respectively.[37] The reduction potentials determined by DPP are given in Table 3. The Co^{III}/Co^{II} process of **1** is quasi-reversible: The separation between the anodic and cathodic peaks is 65 mV. On the other hand, the

Table 3. Redox Potentials of Cobalt(III) Complexes

	Co^{III}/Co^{II}	Co^{II}/Co^{I}
$[Co(L)]ClO_4$	−0.36	−1.70
$[Co(L)NH_3]PF_6$	−0.87	−1.77
$[Co(salen)(CH_3NH_2)_2]PF_6$	−1.03	−1.66
$[Co(salen)(C_2H_5NH_2)_2]PF_6$	−1.06	−1.64
$[Co(salen)(n\text{-}C_3H_7NH_2)_2]PF_6$	−1.00	−1.63

Determined by DPP in dichloromethane and given by V vs. $E(F_c^+/F_c)$.

corresponding process of **2** is irreversible where only anodic peak was observed in the CV spectrum. The Co^{II}/Co^{I} process is irreversible for both **1** and **2**. Esr investigations[2,7] have revealed that the cobalt(II) complexes of salen and its homologs adopt five-coordinate structure even in donative solvents such as pyridine. Such five-coordination has been proved for [Co(salen)py] by single-crystal X-ray analysis.[34] In the case of five-coordinate **1**, no structural change is necessitated to be reduced to the cobalt(II) species [Co(L)]. On the other hand, one of the apical donors (NH_3 or thioether) should be removed in the case of the reduction of **2** to the cobalt(II) species,[38] and such a structural change must be associated with the irreversible Co^{III}/Co^{II} process. The structure of the cobalt(I) species is presumably square planar because of its d^8-electronic configuration. Agin, the structural change on going from the five-coordinate cobalt(II) species to the four-coordinate cobalt(I) species must be the reason for the irreversibility of the Co^{II}/Co^{I} process. It is seen that the Co^{III}/Co^{II} potential of five-coordinate **1** is considerably high relative to the corresponding potential of six-coordinate **2**.

For comparison electrochemical measurements were also made for diamine(*N,N'*-disalicylideneethylenediaminato)cobalt(III) hexafluorophosphate, $[Co(salen)(R\text{-}NH_2)_2]PF_6$,[33] whose structures were shown to be pseudo-octahedral with the coordination of the amine molecules at the apical sites. They also showed two irreversible reductions waves. The reduction potentials determined by DPP are included in Table 3. Inspection of the electrochemical data of **2** and $[Co(salen)(R\text{-}NH_2)_2]PF_6$ indicates that the substitution of the thioether sulfur for the axial amine gives rise to a significant positive shift of the Co^{III}/Co^{II} potential. This is particularily interesting in view of redox potentials of cytochromes, where axial donor groups play an important role in controlling the redox potential required for the enzymes. It is generally known that the redox potential of cytochromes with two histidinyl residues as axial ligands is lower than that of cytochromes with one histidinyl and one methionyl axial ligands.[39]

References

1) T. Tsumaki, *Bull. Chem. Soc. Jpn.*, **13**, 252 (1938).
2) M. J. Carter, D. P. Rillema, and F. Basolo, *J. Am. Chem. Soc.*, **96**, 392 (1974).
3) D. Diemente, B. M. Hoffman, and F. Basolo, *J. Chem. Soc., Chem. Commun.*, **1970**, 467; B. M. Hoffman, D. L. Diemente, and F. Basolo, *J. Am. Chem. Soc.*, **92**, 61 (1970).
4) G. Amiconi, M. Brunori, E. Antonini, G. Tauzher, and G. Costa, *Nature (London)*, **228**, 549 (1970).
5) C. Floriani and F. Calderazzo, *J. Chem. Soc. A*, **1969**, 946.
6) A. Misono and S. Koda, *Bull. Chem. Soc. Jpn.*, **42**, 3048 (1969).
7) E. I. Ochiai, *J. Inorg. Nucl. Chem.*, **35**, 1727 (1973).
8) C. Busetto, C. Neri, N. Palladino, and E. Perrotti, *Inorg. Chim. Acta*, **5**, 129 (1971).
9) R. S. Gall and W. P. Schaefer, *Inorg. Chem.*, **15**, 2758 (1976).
10) A. Avdeef and W. P. Schaefer, *J. Am. Chem. Soc.*, **98** 5153 (1976).
11) E. Cesarotti, M. Gullotti, A. Pasini, and R. Ugo, *J. Chem. Soc., Dalton Trans.*, **1977**, 757.
12) G. Costa, G. Mestroni, and L. Stefani, *J. Organomet. Chem.*, **7**, 493 (1967).
13) G. Costa, G. Mestroni, and G. Pellizer, *J. Organomet. Chem.*, **11**, 333 (1968).
14) L. H. Vogt, Jr., J. G. Wirth, and H. L. Finkbeiner, *J. Org. Chem.*, **34**, 273 (1969).
15) T. J. Fullerton and S. P. Ahern, *Tetrahedron Lett.*, **1976**, 139.
16) A. Nishinaga, K. Watanabe, and T. Matsuura, *Tetrahedron Lett.*, **1974**, 1291.
17) A. Nishinaga, *Chem. Lett.*, **1975**, 273.
18) Y. Aimoto, W. Kanda, S. Megura, Y. Miyahara, H. Ōkawa, and S. Kida, *Bull. Chem. Soc. Jpn.*, **58**, 646 (1985).
19) A. R. Amundsen, J. Whelan, and B. Bosnich, *Inorg. Chem.*, **18**, 206 (1979).
20) J. P. Collman, H. Takaya, B. Winkler, L. Libit, S. S. Koon, G. A. Rodley, and W. T. Robinson, *J. Am. Chem. Soc.*, **95**, 1656 (1973).
21) W. Kanda, H. Ōkawa, and S. Kida, *Bull. Chem. Soc. Jpn.*, **56**, 3268 (1983).
22) K. Nakamoto, H. Oshio, H. Ōkawa, W. Kanda, K. Horiuchi, and S. Kida, *Inorg. Chim. Acta*, **108**, 231 (1985).
23) H. Ōkawa, K. Horiuchi, W. Kanda, H. Oshio, and S. Kida, *Bull. Chem. Soc. Jpn.*, **59**, 2795 (1986).
24) R. R. Gagne, C. A. Koval, and G. C. Lisensky, *Inorg. Chem.*, **19**, 2854 (1980).
25) M. Calvin, R. H. Bailes, and W. K. Wilmarth, *J. Am. Chem. Soc.*, **68**, 2254 (1946).
26) R. H. Bailes and M. Calvin, *J. Am. Chem. Soc.*, **69**, 1886 (1947).
27) M. Calvin and C. H. Barkelew, *J. Am. Chem. Soc.*, **68**, 2267 (1946).
28) C. W. Smith, G. W. Van Loon, and M. C. Baird, *Can. J. Chem.*, **54**, 1875 (1976).
29) K. Nakamoto, "Infrared Spectra of Inorganic and Coordination Compounds," 2nd ed, John-Wiley & Sons, New York (1970), p. 176.
30) K. Nakamoto, "Infrared Spectra of Inorganic and Coordination Compounds," 2nd ed, John-Wiley & Sons, New York (1970), p. 166.
31) M. Calligaris, G. Nardin, and L. Randaccio, *Coord. Chem. Rev.*, **7**, 385 (1972).
32) M. Cesari, C. Neri, G. Perego, E. Perrotti, and A. Zazzetta, *J. Chem. Soc., Chem. Commun.*, **1970**, 276.

33) S. Maeda, M. Nakamura, M. Mikuriya, T. Shinmyozu, H. Ōkawa, and S. Kida, *Mem. Fac. Sci., Kyushu Univ., Ser. C*, **15(1)**, 63 (1985).
34) M. Calligaris, D. Minichelli, G. Nardin, and L. Randaccio, *J. Chem. Soc. A*, **1970**, 2411.
35) G. B. Jameson, F. C. March, W. T. Robinson, and S. S. Koon, *J. Chem. Soc., Dalton Trans.*, **1978**, 185.
36) G. B. Jameson, W. T. Robinson, and G. A. Rodley, *J. Chem. Soc., Dalton Trans.*, **1978**, 191.
37) D. F. Averill and R. F. Broman, *Inorg. Chem.*, **17**, 3389 (1978).
38) J. Hanzlik, A. Puxeddu, and G. Costa, *J. Chem. Soc., Dalton Trans.*, **1977**, 542.
39) A. V. Xavier, "The Coordination Chemistry of Metalloenzymes," ed by I. Bertini, R. S. Drago, and C. Luchinat, D. Reidel Publishing Co., Holland (1983), p. 291.

Possible Fluorescence from the Polycyclic Aromatic Hydrocarbons in the Interstellar Medium

Jun-ichi AIHARA
Department of Chemistry, Faculty of Science, Shizuoka University, Oya, Shizuoka 422
(Received June 1, 1987)

Large compact polycyclic aromatic hydrocarbons (PAHs) are photochemically very stable. These PAHs have been considered as excellent candidates for explaining the interstellar infrared emission lines. Since the large compact PAHs exhibit the first electronic absorption band in a rather low-energy region, it is possible and very probable that fluorescence from such PAHs are responsible for the red emission humps of several nebulae such as the Red Rectangle, a nebula surrounding the binary star HD 44179.

The Red Rectangle is a symmetric biconical nebula centered at the bright binary star HD 44179.[1] Since its discovery in 1975, it has been a target of various spectroscopic observations.[1-4] The visible emission spectrum of the Red Rectangle consists of two major components.[2] They are: (1) The scattered stellar light, which is fairly uniform in intensity over the visible region, and (2) a broad emission hump, which spreads in the wavenumber range 13000—18600 cm^{-1} with a maximum around 15700 cm^{-1}. The latter component gives the red color to the nebula. The rough contour of this red emission hump is reproduced in Fig. 1. Recently several other nebulae were found to exhibit extended red emission similar to that from the Red Rectangle.[5,6]

Duley proposed that the red emission hump of the Red Rectangle could be due to fluorescence from small particles of hydrogenated amorphous carbon (HAC).[7,8] An argument for this hypothesis is the similarity to the observed fluorescence from the HAC particles.[9] Wdowiak attributed the red emission hump to the PAHs clumped together on the surfaces or interiors of grain mantles.[10] He inferred that excimers are formed on the surfaces of grains, and that excimer fluorescence might be responsible for the hump. These explanations require that the molecules responsible for the emission hump must be aggregated on grains.

Discrete infrared lines are emitted coincidentally from the Red Rectange and the like nebulae.[1,5] Léger and Puget and Allamandola et al. ascribed these infrared lines to polycyclic aromatic hydrocarbons (PAHs) in the gas phase, but not in the condensed phase.[11-14] If infrared and red emissions arise from the same source, it must be these PAHs in the gaseous state. In 1986 d'Hendecourt et al. stressed that isolated PAHs can provide broad emission spectra.[15] They suggested that phosphorescence, rather than fluorescence, might be responsible for the red emission hump of the Red Rectangle. Chlewicki and Laureijs also proposed that the most likely source of the red emission hump is phosphorescence from aromatic molecules.[16]

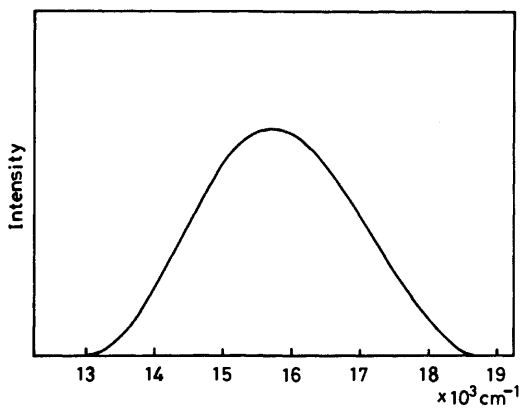

Fig. 1. Rough contour of the red emission hump of the Red Rectangle.

Since the light-emitting interstellar PAHs, if any, are placed in the intense radiation field, they must be fairly resistant to the field. Therefore, photochemically stable PAHs are qualified for explaining the interstellar infrared spectra. In a previous paper,[17] we showed that it is very probable that many of large compact PAHs are stable in the radiation field. They have large percent resonance energies (%REs)[18-20] in the excited state. In this paper, the peculiar red emission hump is interpreted with this characteristic of large compact PAHs in mind. The Hückel molecular orbital model is used throughout this paper.

Results and Discussion

We have developed the graph theory of aromaticity.[18-23] The %RE of a molecule is given as 100 times the graph-theoretically defined resonance energy, divided by the π-electron energy of the olefinic reference structure.[18-20] The %RE can be defined for any conjugated system in any electronic state. It has been established that most of the conjugated molecules with large %REs are stable or fairly unreactive. In the case of polyacenes, naphthalene, anthracene, and naphthacene are relatively stable, but pentacene and higher members are not stable. In general, PAHs with %RE$>$2.15 are stable in our chemical sense.[17]

We previously calculated %REs of a variety of PAHs both in the ground and excited states.[17] As shown in Table 1, **1—14** have the %REs larger than 2.15 both in the ground and excited states. Many large compact

Table 1. The HOMO Energies of the PAHs Having Large %REs in the Excited State

PAH	%RE		m_{HOMO}	$\nu_p/10^3\,cm^{-1}$
	Ground state	Excited state		
1	2.668	2.156	0.271	20.8
2	2.414	2.172	0.186	17.6
3	2.637	2.173	0.251	20.1
4	2.278	2.194	0.134	15.6
5	2.217	2.209	0.095	14.1
6	2.665	2.218	0.249	20.0
7	2.564	2.225	0.209	18.5
8	2.593	2.252	0.213	18.6
9	2.348	2.287	0.118	15.0
10	2.309	2.316	0.076	13.4
11	2.500	2.349	0.150	16.2
12	2.547	2.358	0.162	16.7
13	2.515	2.383	0.138	15.8
14	2.436	2.410	0.091	14.0
15	2.917	1.828	0.465	28.2

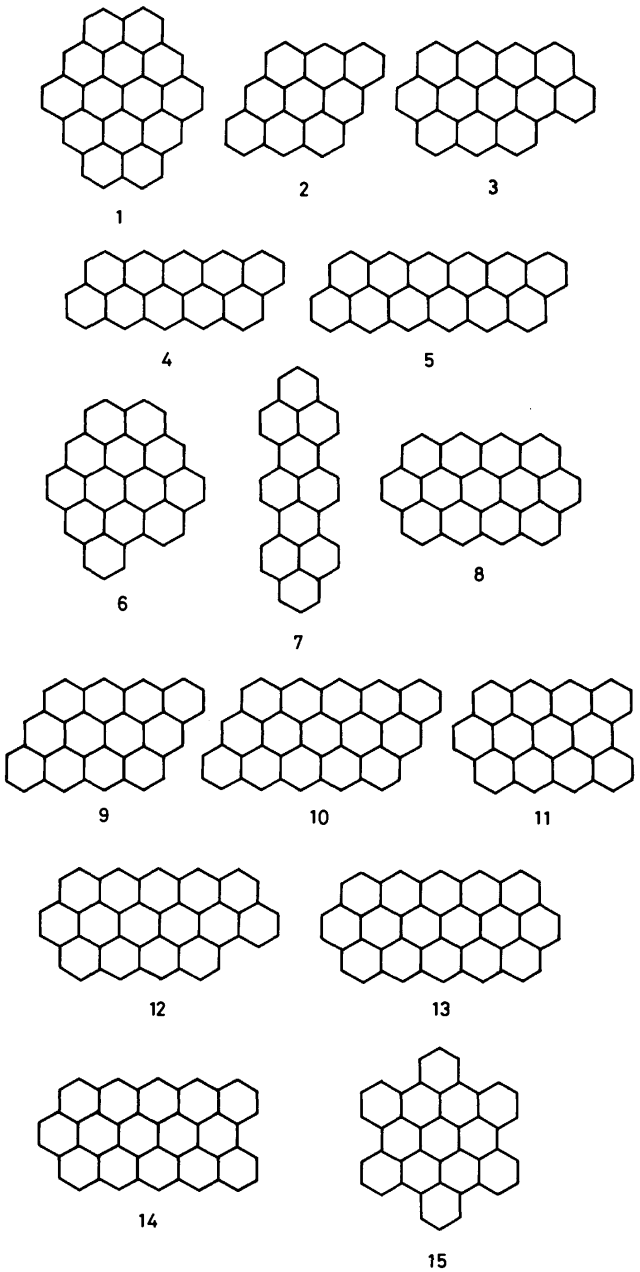

PAHs have large %REs both in the ground and excited states.[17] This implies that these PAHs are possibly stable not only at high temperature but also in the strong radiation field in the interstellar medium. As pointed out by Léger and Puget and Allamandola et al.,[11-14] the PAHs having not a few solo hydrogens are consistent with the infrared emission spectra of the interstellar medium. Therefore, large compact PAHs are the best candidates conceivable for explaining the infrared emission from the interstellar medium.

Fully benzenoid hydrocarbons are the PAHs whose Clar structures consist of aromatic sextets only.[24] There are no formal double bonds in them. This type of PAHs are indeed extremely stable. d'Hendecourt et al. found that the phosphorescence spectrum of hexabenzocoronene (**15**), a typical fully benzenoid hydrocarbon, resembles the red emission hump of the Red Rectangle.[15] However, we previously pointed out that fully benzenoid hydrocarbons are greatly destabilized in the excited state.[17] At present, there is no spectroscopic evidence for the presence of this type of PAHs in the interstellar medium. Compact fully benzenoid hydrocarbons do not have solo hydrogens.[17]

For PAHs having very large %REs or very large resonance energies per π electron in the ground state, the highest occupied molecular orbital (HOMO) is very low in energy,[21,25] and the lowest unoccupied molecular orbital (LUMO) is necessarily very high in energy. This implies that, in general, the energy of the first electronic transition of a fully benzenoid hydrocarbon is too large to exhibit red fluorescence. In other words, fluorescence from such PAHs as **15** cannot reproduce the red emission hump. A situation is essentially the same for relatively small PAHs. It is probably for this reason that Wdowiak and d'Hendecourt et al. were forced to fit excimer fluorescence or phosphorescence to the red emission hump.[10,15] Both excimer fluorescence and phosphorescence are much lower in energy than the fluorescence band of an isolated molecule.

In general, the first electronic absorption band of a PAH can be assigned to the transition from the HOMO to the LUMO. According to Streitwieser,[26] the energy of the first allowed transition (i.e, the p band in Clar's terminology[24]) is linearly related to the energy of the HOMO:

$$\nu_p/\mathrm{cm}^{-1} = 38040\, m_{\mathrm{HOMO}} + 10520 \quad (1)$$

where ν_p is the wavenumber of the p band, and m_{HOMO} is the energy coefficient of the HOMO or the energy of the HOMO given in units of β. This relationship holds for alternant hydrocarbons such as PAHs, for which m_{LUMO} is the negative of m_{HOMO}. It is useful for estimating the absorption edge of an unknown PAH. A p band is sometimes preceded by an α band assignable to a very weak electronic transition.[26] An α band sometimes shifts the absorption edge to a lower-energy side.

In a previous paper, a photochemically stable PAH was defined as the one whose %RE is greater than 2.15 in the excited states.[17] In this sense, **1**—**14** are thermodynamically and photochemically stable. The m_{HOMO} value is less than 0.28 for these PAHs. It follows that the HOMOs of these PAHs are relatively high in energy, as compared with those of fully benzenoid hydrocarbons. Then, photochemically stable PAHs must have the first absorption band in a relatively low-energy region. The m_{HOMO} values of **1**—**14** are listed in Table 1.

For example, m_{HOMO}=0.213 for circumanthracene (**8**).[27] This PAH has been regarded as one of the best candidates for the interstellar molecular species.[17] From Eq. 1 this PAH is predicted to have a p band around 18600 cm^{-1}. Clar et al. devised the relationship between the π-electron ionization potentials and the absorption maximum of the p band,[27] and predicted the location of this band at 2.24 eV or 18100 cm^{-1} in the gas phase. For **8** the p band is the lowest-energy band in the electronic absorption spectrum.[27] The red emission hump appears to give a mirror image of this absorption band. Therefore, it is highly probable that fluorescence from **8** constitutes a part of the red emission hump. Phosphorescence from this PAH is not responsible for it because it is too low in energy.

The wavenumbers of the p bands estimated using Eq. 1 are also presented in Table 1. Fluorescence from **1**—**3**, **6**—**8**, and **11**—**13** might appear in the energy region covered by the red emission hump, and can in principle reproduce the whole or a part of the red emission hump. Thus, there are many qualified large compact PAHs. It is noteworthy that **7** is an exceptionally non-compact PAH with no solo hydrogen. Since these photochemically stable PAHs are expected to exhibit fluorescence in a rather low-energy region, neither phosphorescence nor excimer fluorescence is necessary to explain the red emission hump of the Red Rectangle and other nebulae.

Other PAHs with somewhat larger m_{HOMO} values may also contribute to the red emission hump. If these PAHs coexist with those given in Table 1, the high-energy part of the fluorescence from the former PAHs are absorbed by the latter ones. On the other hand, the PAHs having very small m_{HOMO} values, such as **4**, **5**, **9**, **10**, and **14**, are not desirable as the candidates for explaining the red emission hump. Their fluorescence bands must be located in the infrared region. Among the PAHs in Table 1, these ones have relatively small %REs in the ground state. This might indicate that the ground-state stability is still very important in the interstellar medium.

Aromatic molecules typically have high fluorescence yields.[28] In general, PAHs are much more fluorescent than phosphorescent. Measurements of fluorescence from jet-cooled naphthalene, anthracene, and naphthacene have been made.[29–32] No one has reported the observation of phosphorescence from these PAHs in a supersonic jet. Phosphorescence must follow the intersystem crossing, which is formally a forbidden electronic process for most organic molecules.[28] Therefore, fluorescence is likely to be a much more natural electronic process than phosphorescence even in the interstellar medium. This may further support the assignment of the red emission hump to fluorescence from a group of PAHs.

Concluding Remarks

Large compact PAHs are rich in carbon atoms. If PAHs are formed in a carbon-rich environment, they must be large and compact in shape. Most of them happened to be photochemically very stable.[17] Interestingly, rather large compact PAHs are formed by combustion of light oil in a Diesel engine.[33] This fact might suggest possible formation mechanisms of PAHs in the interstellar medium. As has been seen above, if we accept the existence of abundant large compact PAHs in the interstellar medium, we can rationalize both discrete infrared and broad red emission bands of the Red Rectange and other nebulae in terms of fluorescence spectroscopy. It is very true that most PAHs are more fluorescent than phosphorescent, at least in solution.[28] PAHs emit exclusively from the first excited state.

Hexabenzocoronene (**15**) is a yellow fully benzenoid hydrocarbon of extreme stability.[34,35] Clar reported that this PAH shows an orange-red phosphorescence of very long life at low temperature.[24] If it is generally ture that a large compact PAH tends to undergo intersystem crossing from the singlet excited state to the lowest triplet state at high temperature, the contribution of phosphorescence to the red emission hump must be taken into consideration. At present, it is not at all clear whether there are large compact or fully benzenoid PAHs which are very phosphorescent at high temperature in the gaseous state. This question can only be answered by detailed laboratory measure-

ments of the appropriate materials and processes.

References

1) M. Cohen, C. M. Anderson, A. Cowley, G. V. Coyne, W. M. Fawley, T. R. Gull, E. A. Harlan, G. H. Herbig, F. Holden, H. S. Hudson, R. O. Jakoubek, H. M. Johnson, K. M. Merrill, F. H. Schiffer III, B. T. Soifer, and B. Zuckerman, *Astrophys. J.*, **196**, 179 (1975).
2) G. D. Schmidt, M. Cohen, and B. Margon, *Astrophys. J.*, **239**, L133 (1980).
3) R. E. Warren-Smith, S. M. Scarrott, and P. Murdin, *Nature (London)*, **292**, 317 (1981).
4) "Polycyclic Aromatic Hydrocarbons and Astrophysics," ed by A. Léger, L. d'Hendecourt, and N. Boccara, Reidel, Dordrecht, The Netherlands (1987).
5) K. Sellgren, M. W. Werner, and H. L. Dinerstein, *Astrophys. J.*, **271**, L13 (1983).
6) A. N. Witt and R. E. Schild, *Astrophys. J.*, **294**, 225 (1985).
7) W. W. Duley, *Mon. Not. Roy. Astron. Soc.*, **215**, 259 (1985).
8) W. W. Duley in Ref. 4, pp. 373—386.
9) I. Watanabe, S. Hasegawa, and Y. Kurata, *Jpn. J. Appl. Phys.*, **21**, 856 (1982).
10) T. J. Wdowiak in Ref. 4, pp. 327—328.
11) A. Léger and J. L. Puget, *Astron. Astrophys.*, **137**, L5 (1984).
12) A. Léger and L. d'Hendecourt in Ref 4, pp. 223—254.
13) L. J. Allamandola, A. G. G. M. Tielens, and J. R. Barker, *Astrophys. J.*, **290**, L25 (1985).
14) L. J. Allamandola, A. G. G. M. Tielens, and J. R. Barker in Ref. 4, pp. 255—271.
15) L. B. d'Hendecourt, A. Léger, G. Olofsson, and W. Schmidt, *Astron. Astrophys.*, **170**, 91 (1986).
16) G. Chlewicki and R. J. Laureijs in Ref. 4, pp. 335—337.
17) J. Aihara, *Bull. Chem. Soc. Jpn.*, **60**, 3143 (1987).
18) J. Aihara, *Bull, Chem. Soc. Jpn.*, **52**, 2202 (1979).
19) J. Aihara, *Bull. Chem. Soc. Jpn.*, **53**, 2689 (1980).
20) J. Aihara, *Pure Appl. Chem.*, **54**, 1115, (1982).
21) J. Aihara, *J. Am. Chem. Soc.*, **97**, 2750 (1976).
22) J. Aihara, *J. Am. Chem. Soc.*, **98**, 2048 (1977).
23) I. Gutman, M. Milun, and N. Trinajstić, *J. Am. Chem. Soc.*, **99**, 1692 (1977).
24) E. Clar, "The Aromatic Sextet," Wiley, London (1972).
25) B. A. Hess, Jr., and L. J. Schaad, *J. Am. Chem. Soc.*, **93**, 2413 (1971).
26) A. Streitwieser, Jr., "Molecular Orbital Theory for Organic Chemists," Wiley, New York (1961), Chap. 8.
27) E. Clar, J. M. Robertson, R. Schlögl, and W. Schmidt, *J. Am. Chem. Soc.*, **103**, 1320 (1981).
28) J. B. Birks, "Photophysics of Aromatic Molecules," Wiley-Interscience, London (1970).
29) S. M. Beck, D. E. Powers, J. B. Hopkins, and R. E. Smalley, *J. Chem. Phys.*, **73**, 2019 (1980).
30) S. M. Beck, J. B. Hopkins, D. E. Powers, and R. E. Smalley, *J. Chem. Phys.*, **74**, 43 (1981).
31) A. Amirav, U. Even, and J. Jortner, *Chem. Phys. Lett.*, **71**, 12 (1980).
32) A. Amirav, U. Even, and J. Jortner, *J. Phys. Chem.*, **86**, 3345 (1982).
33) J. C. Fetzer, W. R. Biggs, and K. Jinno, *Chromatographia*, **21**, 439 (1986).
34) E. Clar and C. T. Ironside, *J. Chem. Soc.*, **1959**, 142.
35) W. Hendel, Z. H. Khan, and W. Schmidt, *Tetrahedron*, **42**, 1127 (1986).

Studies on the Interaction of Molybdate Ion and Magnesium Ion Observed in the Raman Spectra of the Mixture Solutions

Toru OZEKI,* Kazuko MURATA, Hiroshi KIHARA, and Seiichiro HIKIME
Hyogo University of Teacher Education, 942-1 Shimokume, Yashiro-cho, Kato-gun, Hyogo 673-14
(Received March 9, 1987)

When alkali metal or alkaline earth metal chloride, (except magnesium chloride) was added to a solution of sodium molybdate, similar Raman spectra were observed. When magnesium chloride was added to the molybdate solution, however, the intensity of the peak (ν_1) based on the symmetric stretching vibration of the tetrahedral molybdate decreased and a new peak (ν_x) appeared at a higher wavenumber than ν_1. The wavenumber of the new peak is almost equal to that observed for solid magnesium molybdate. This suggests that the new peak can be ascribed to the molybdates of the distorted octahedral structure, since the molybdate ion exists as an octahedral in the solid state of magnesium molybdate. The tetrahedral and the octahedral molybdates seem to be in equilibrium in the solution.

The molybdate ion is a typical oxoanion, having a tetrahedral structure in an alkaline or neutral solution.[1,2] The dissolved states of the molybdate ion have been studied under various experimental conditions, e.g., pH, ionic strength, coexisting salt etc.,[2-10] and their typical Raman peaks, based on the fundamental vibrations, have been assigned.[5] However, the number of studies regarding the effect of the coexisting salts on the Raman spectra of the solution have been few. In this study, a change in the Raman spectra was studied, especially when alkaline earth chloride was added to a solution of molybdates.

When magnesium ion was added to a molybdate ion solution, the appearance of a new peak was found in the Raman spectra. This peak seemed to be the result of interaction of these ions in solution.

Experimental

Reagents. Molybdate solutions were prepared using sodium molybdate ($Na_2MoO_4 \cdot 2H_2O$). All reagents used were analytical reagent grade chemicals and were used without further purification.

Equipments. Raman spectra were measured with a laser Raman spectrometer with double monochromators (JASCO R800); the 514.5 nm line of an Ar^+ laser was used as the excitation light source. One ml of sample solution was used for each measurement. The slit widths of the spectrometer for the entrance, intermediate and exit were 300, 500, and 300 μm, respectively.

Results and Discussion

The Effect of Magnesium Ion. The Raman spectra of two 0.1M (1M=1 mol dm^{-3}) sodium molybdate solutions in which lithium chloride and magnesium chloride were added, respectively, are shown in Fig. 1. The Raman spectrum of a magnesium chloride solution is also shown for a reference. In the case of lithium chloride, only the peaks ascribed to the free molybdate were observed. The molybdate ion generally exists as a tetrahedral ion in alkaline or neutral solutions and four peaks characterizing tetrahedral structure have been observed at 900, 850, 310, and 270 cm^{-1} in the Raman spectra. The peak at 900 cm^{-1} (denoted by ν_1) has been assigned to the totally symmetric stretching vibration and the peaks at 850 cm^{-1} (ν_3) to an antisymmetric stretching vibration.[5] When magnesium chloride was added to the molybdate solution, a noticeable change was observed, namely the peak near 900 cm^{-1} decreased and the shape of the peak was deformed. A more detailed change in the shape is indicated by the dotted lines in Fig.2. As the magnesium concentration increased from 0.5 to 4.5M, the intensity of the peak at 900 cm^{-1} (ν_1) decreased, and a new peak (denoted by ν_x) appeared in the region 910 to 930 cm^{-1}. In order to separate the peaks, a nonlinear least-squares wave analysis was applied assuming Lorentz-Gauss sum functions. An algorithm of the calculation was taken from the work of Edgell et al.[11-13] Three peaks were obtained, as shown by the solid lines in Fig. 2. All spectra in Fig. 2 were normalized so that the highest peak in the spectrum had the same intensity. The dependence of the wavenumbers of each peak and that of the area fraction, $\nu_1/(\nu_1+\nu_x)$, upon magnesium concentration are shown in Fig. 3. The area fraction of ν_1 decreased against an increase in the magnesium concentration. This implies a decrease in the concentration of the free molybdate ion and an

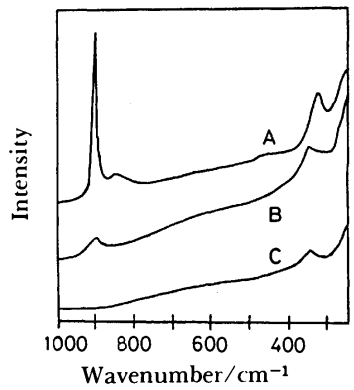

Fig. 1. Raman spectra of molybdate solutions, A: 0.1 M Na_2MoO_4, 1 M LiCl; B: 0.1 M Na_2MoO_4, 4 M $MgCl_2$ and C: 4 M $MgCl_2$.

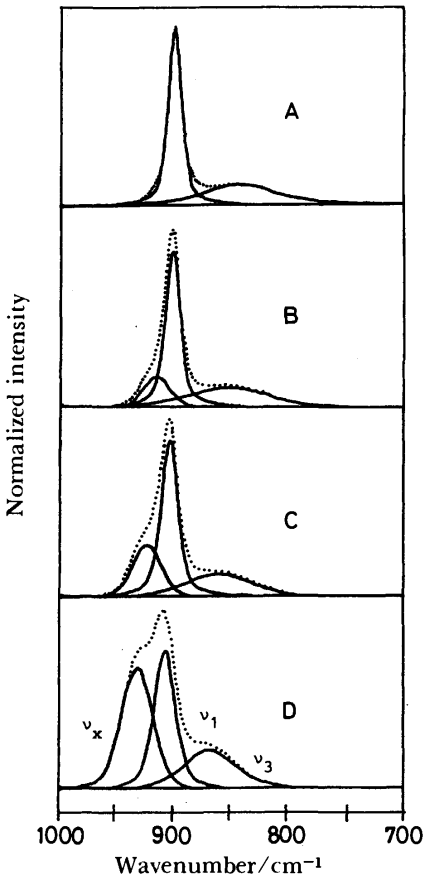

Fig. 2. Effect of $MgCl_2$ concentration on Raman spectra of 0.1 M Na_2MoO_4 solution. A: 0.5; B: 2.5; C: 3.5 and D: 4.5 M $MgCl_2$.

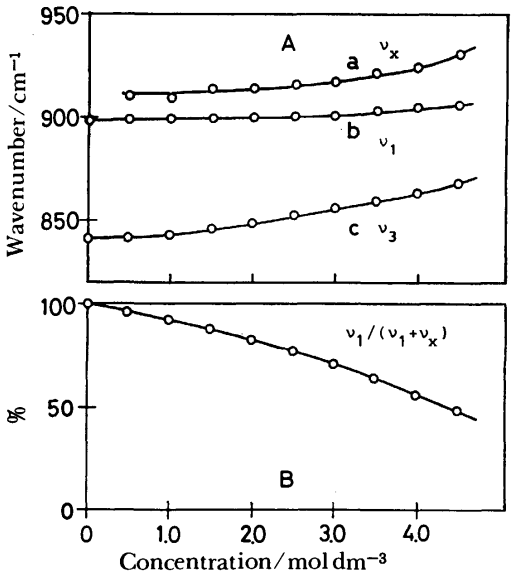

Fig. 3. Effect of $MgCl_2$ concentration on changes of maximum wavenumber of the peaks (A. a: ν_x, b: ν_1, c: ν_3) and B: area fraction, $\nu_1/(\nu_1+\nu_x)$ in 0.1 M Na_2MoO_4 solution.

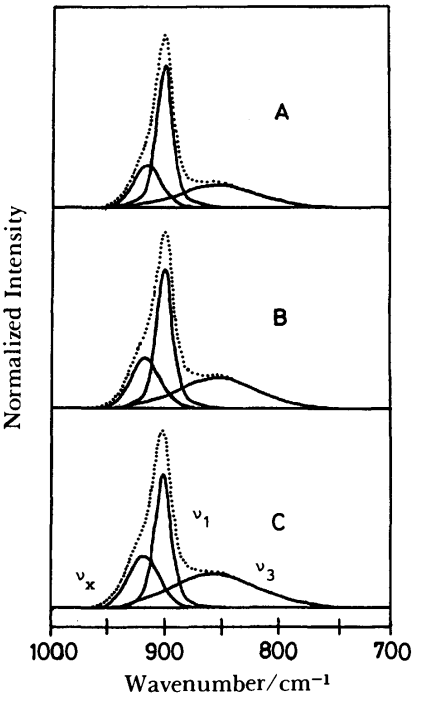

Fig. 4. Effect of Na_2MoO_4 concentration on Raman spectra of 3 M $MgCl_2$ solution. A: 0.05; B: 0.3 and C: 0.5 M Na_2MoO_4.

increase in a new species (ν_x). The peak ν_x appeared at a higher wavenumber than ν_1 and its wavenumber moved to a higher value, accompaning an increase in the magnesium concentration.

In acidic molybdate solutions, the presence of such isopolymolybdates as heptamer and octamer had been known.[14-16] The pH of the solution studied in this work changed from 7.0 (0.1M Na_2MoO_4) to 5.0 (0.1M Na_2MoO_4, 4M $MgCl_2$). Thus, the possibility that the new species might be the isopolymolybdate, was suspected. A study concerning the dissolved states of the isopolymolybdate ions, however, has shown that the peak wavenumbers of the isopolymolybdates are not consistent with ν_x : ν_x=910-930, cf. $\nu(Mo_7O_{24}^{6-})$=945, $\nu(HMo_7O_{24}^{5-})$=957, and $\nu(Mo_8O_{26}^{4-})$=970 cm^{-1}.[17] The new species observed here is not the isopolymolybdate ion, but other species.

The Raman spectra of the solutions in which the concentration of the sodium molybdate was varied and that of magnesium chloride was kept 3M, were shown in Fig. 4. Almost the same spectra were obtained independently of the molybdate concentration, i.e., the peak wavenumbers of each spectra were almost the same and the fraction of the peak areas was nearly constant.

Raman Spectra of Powdered Alkaline Earth Salts of Molybdate. The solubility of calcium, strontium, and barium molybdates are very small, but that of magnesium molybdate is fairly large in water. A precipitate of magnesium molybdate was obtained by concentrating a mixed solution of sodium molybdate and magnesium chloride. The compositions of these freshly prepared precipitates were all 1 : 1 as for the ratio of the

alkaline earth metal ion against the molybdate as a result of a quantitative analysis. After drying them in a desiccator with concentrated sulfuric acid, their Raman spectra were measured. The obtained spectra are shown in Fig. 5. Calcium, strontium, and barium molybdates gave similar Raman spectra. Only magnesium salt gave a different spectrum from the others. From this fact, it is supposed that these alkaline earth salts, except magnesium salt, have a similar crystal structure. In Fig. 6, the X-ray diffraction pattern of these salts are shown. The same analogy was observed among the calcium, strontium and barium molybdates. However, only the pattern of the magnesium molybdate was complex and was different from the others. The crystal salts were divided to two groups. The crystals, except magnesium salt, are all ascribed to Scheelite and only magnesium salt is ascribed to Wolframite.[18-20]

If the salt of molybdate is expressed as XYO_4, the Y atom in Scheelite is surrounded by four oxygen atoms in a tetrahedral structure. On the other hand, the Y atom of XYO_4 in Wolframite type lies in the center of a distorted octahedral structure and is surrounded by six oxygen atoms.[19,21] This suggests that the peak, which is observed in the Raman spectra of magnesium molybdate in solid state, should be ascribed to the molybdate species in a distorted octahedral structure. Even in a such isopolymolybdate ions as heptamer and octamer, it has been reported that each molybdenum atom lies in a center of the octahedral unit.[22,23] The octahedral structure might be a stable structure for molybdate. Figure 3 shows that the wavenumber of the new peak ν_x observed in a mixed solution approaches the peak (930 cm^{-1}) of the solid state magnesium molybdate (Fig. 5) upon increasing the concentration of magnesium chloride. From these facts, it is suggested that both peaks, one for the solid and the other for the solution, must be based on a similar structure; the distorted octahedral structure. Thus, tetrahedral and distorted octahedral ions must be in equilibrium in the solutions.

On the other hand, if the new species formed in the mixture solution is a stoichiometric compound and its shape is constant, then its concentration only depends upon the magnesium concentration and its wavenumber will not shift. However, a shift of ν_x was observed with an increase in the magnesium concentration. This fact implies that the structure of the new species, itself, depends upon the composition. Thus, the formation reaction equation can not be strictly expressed.

However, suppose the stoichiometry and assume the following reaction for the qualitative explanation of the experimental results:

$$Mg^{2+} + Mo(T) = Mg\text{-}Mo(O), \quad (1)$$

where Mo(T) is the free tetrahedral molybdate, and Mg-Mo(O) the distorted octahedral molybdate inte-

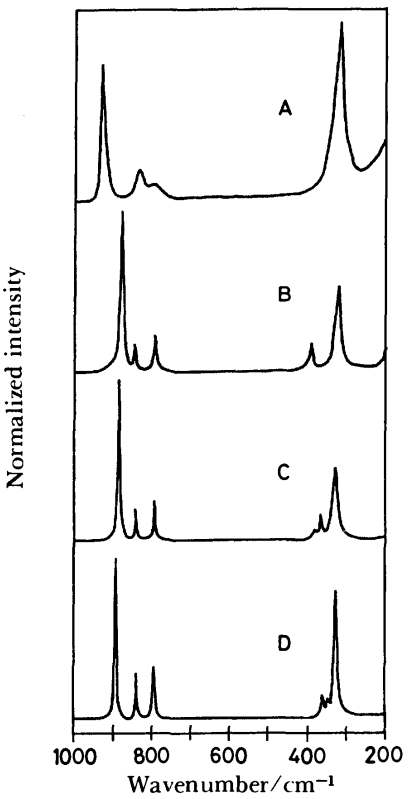

Fig. 5. Raman spectra of solid samples; A: $MgMoO_4$; B: $CaMoO_4$; C: $SrMoO_4$ and D: $BaMoO_4$.

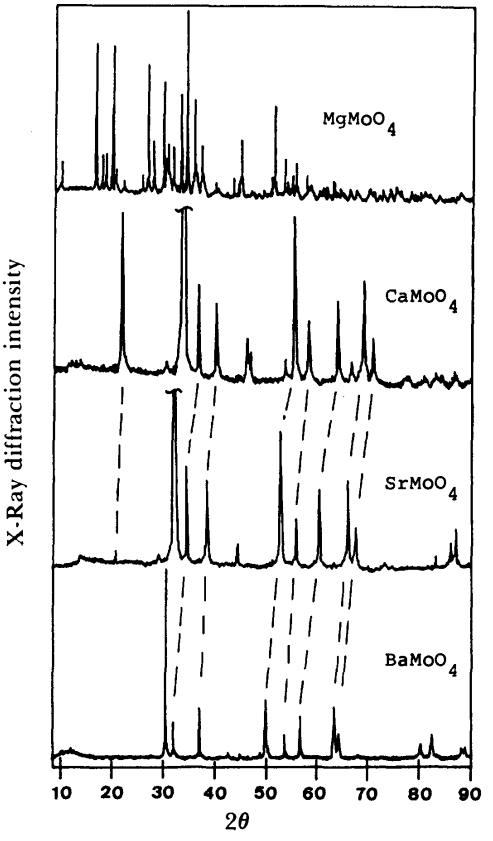

Fig. 6. Comparison of X-ray powder diffraction spectra of A: $MgMoO_4$; B: $CaMoO_4$; C: $SrMoO_4$ and D: $BaMoO_4$.

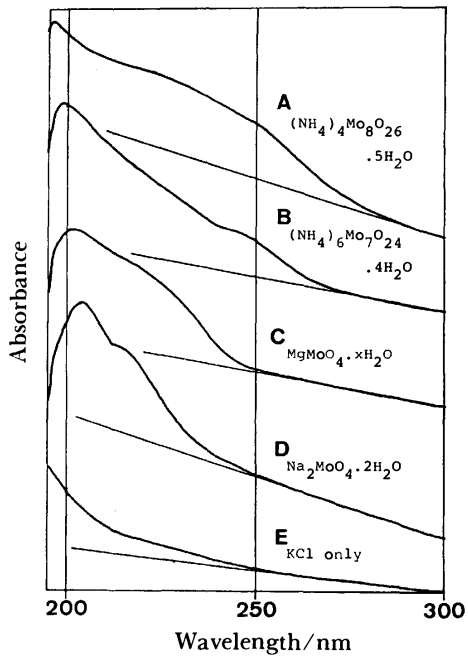

Fig. 7. Comparison of ultraviolet absorption spectra of powder disks containing A: ammonium tetramolybdate; B: ammonium paramolybdate; C: magnesium molybdate and D: sodium molybdate, diluted by KCl powder and E: pure KCl disk.

racting with magnesium ions. Then, the equilibrium constant K is

$$K=[\text{Mg-Mo(O)}]/[\text{Mg}^{2+}][\text{Mo(T)}]. \quad (2)$$

This equation can be rewritten as

$$[\text{Mg-Mo(O)}]/[\text{Mo(T)}]=K[\text{Mg}^{2+}]. \quad (3)$$

This equation indicates that the ratio of the concentration of the new species Mg-Mo(O) against that of free molybdate Mo(T) is in proportion to the total concentration of the magnesium ions, since the latter concentration is in large excess against that of molybdate and is almost identical to the free magnesium ion concentration. If the amount of magnesium is constant and that of molybdate is varied, the fraction of Eq. 3 remains constant. Thus, the results shown in Figs. 2 to 4 are well explained qualitatively by Eq. 3.

Spectroscopic Analysis of the Interaction at Low Concentration Solution. It was expected that the ultraviolet absorption spectra of the molybdate solution would change by the formation of molybdate octahedral species. The absorption spectra of 0.1 mM sodium molybdate solutions in which various concentrations of magnesium chloride were added, were measured; no noticeable change was observed. On the other hand, 3 mg of four kinds of molybdate compounds (sodium molybdate: Na_2MoO_4, magnesium molybdate: $MgMoO_4$, ammonium paramolybdate: $(NH_4)_6Mo_7O_{24}$, and ammonium tetramolybdate: $(NH_4)_4Mo_8O_{26}$), were each mixed with the 0.3 g KCl ground powder, respectively, and their sample disks were prepared by pressing each mixture powders into the disks (1 cm diameter and 1mm thickness) in a vacuum chamber. The measured ultraviolet absorption spectra of these disks are shown in Fig. 7. Two kinds of isopolymolybdates gave different spectra from that of sodium molybdate disk: The former had a definite absorption intensity at 250 nm, but the latter had no absorption there. However, the spectrum of a disk of magnesium molybdate was almost the same as that of sodium molybdate. This indicates that a noticeable difference will not be observed between the absorption spectra of the molybdate tetrahedral ion and that of the octahedral deformed ion. Namely, the fact that the ultraviolet spectra observed in the mixture solutions were almost same as that of free molybdate, does not rule out the presence of the octahedral molybdate species. On the other hand, the fact that the ultraviolet absorption spectra of any isopolymolybdates were shifted to the longer wavelength region, suggests the possibility that the new species is essentially a monomer and, thus, has no direct bonding between each molybdenum atom.

Conclusion

When magnesium chloride is added in greater concentrations than 4.5 M to a 0.1 M sodium molybdate solution, magnesium molybdate precipitates. In the Raman spectra of the mixture solution, a ν_x peak similar to that of a precipitate crystal was already observed, even in a solution of 0.5M $MgCl_2$. This peak shifted to a higher wavenumber. These facts suggest that a crystal-like structure is already formed in a mixture solution of such low concentrations and grows. The new peak was ascribed to the molybdates in the distorted octahedral structure, resulting in the interaction of molybdate and magnesium ions.

We believe that in a precipitation reaction, the ions are all present as free ions before saturation and that they change in structure when the composition reaches a saturated state. Namely, the transformation of the structure occurrs at a saturated composition. However this model is not adequate for explaining the system studied above. This study suggests that before saturation (even in the low concentration solutions) there exists an ion having a structure similar to that of the precipitate crystal. Also, not the free tetrahedral molybdate but, rather, the distorted octahedral molybdates precipitates through a formation reaction of the latter species. This phenomenon was observed for the first time, since the structure of the free molybdate ion in solution happened to be different from that of molybdate ion of magnesium molybdate precipitate. We expect that this is not a unique case but that a similar phenomenon will also be found in the other systems.

References

1) R. H. Busey and O. L. Keller, Jr., *J. Chem. Phys.*, **41**, 215 (1964).
2) J. Aveston, E. W. Anacker, and J. S. Johnson, *Inorg. Chem.*, **3**, 735 (1964).
3) W. P. Griffith, *Coord. Chem. Rev.*, **5**, 459 (1970).
4) F. Gonzalez-Vilchez and W. P. Griffith, *J. Chem. Soc., Dalton Trans.*, **1972**, 1416.
5) N. Weinstock, H. Schulze, and A. Müller, *J. Chem. Phys.*, **59**, 5063 (1973).
6) K. Murata and S. Ikeda, *Polyhedron*, **2**, 1005 (1983).
7) K. Murata and S. Ikeda, *Anal. Chim. Acta*, **151**, 29 (1983).
8) H. Buchwald, P. J. Coope, and W. P. Thistlewalte, *J. Inorg. Nucl. Chem.*, **3**, 300 (1956).
9) G. Jander and K. F. Jahr, *Koll. Beihafte*, **41**, 297 (1934).
10) P. Souchay, *Ann. Chim.*, **2**, 203 (1947).
11) W. F. Edgell, "Infrared and Raman Spectroscopy," ed by E. G. Brame, Jr. and J. Grasselli, Marcel Dekke, New York (1976), Vol. 1, Chap. 4 appendix.
12) R. D. B. Fraser and E. Suzuki, "Spectral Analysis: Methods and Techniques," ed by J. A. Blackburn, Marcel Dekker, New York (1970).
13) P. J. Krueger and B. F. Hawkins, *Can. J. Chem.*, **51**, 3250 (1973).
14) Y. Sasaki, I. Lindqvist, and L. G. Sillén, *J. Inorg. Nucl. Chem.*, **9**, 93 (1959).
15) Y. Sasaki and L. G. Sillén, *Arkiv. Kemi.*, **29**, 253 (1967).
16) W. P. Griffith and P. J. B. Lesniak, *J. Chem. Soc. A*, **1969**, 1066.
17) T. Ozeki, H. Kihara, and S. Hikime, *Anal. Chem.*, **59**, 945 (1987).
18) R. W. G. Wyckoff, "Crystal Structures," 2nd ed, Robert E. Krieger, Florida 1982, Vol. 3, Chap. VIIIA.
19) A. P. Young and C. M. Schwartz, *Science*, **141**, 348 (1963).
20) K. Brandt, *Arkiv. Kemi. Mineral. Geol.*, **17A**, 15 (1943).
21) A. W. Sleight, *Acta Crystallogr., Sect. B*, **28**, 2899 (1972).
22) I. Lindqvist, *Arkiv. Kemi.*, **2**, 325 (1950).
23) I. Lindqvist, *Arkiv. Kimi.*, **2**, 349 (1950).

 © 1987 The Chemical Society of Japan Bull. Chem. Soc. Jpn., 60, 3591—3595 (1987)

Interaction of Cationic Drugs with Nafion on Electrode Surfaces and Its Applicability to Determination of Electroinactive Drugs

Tomokazu MATSUE,* Atsushi AOKI, Isamu UCHIDA,* and Tetsuo OSA†
Department of Applied Chemistry, Faculty of Engineering, and
†Pharmaceutical Institute, Tohoku University, Aramaki Aoba, Sendai 980
(Received May 6, 1987)

The interaction of several electroinactive cationic drugs (hexamethonium, quinidine, neostigmine, nicotine and acetylcholine) with Nafion and the applicability of Nafion-coated electrodes to determination of the drugs have been investigated. The addition of a drug to an electrolyte solution containing (ferrocenylmethyl)trimethylammonium (FA^+) induced a decrease in the peak current and a shift in the apparent half-wave potential of a cyclic voltammogram for FA^+. The decrease in the peak current has been used for determination of the drugs at low concentrations less than 10^{-3} mol dm^{-3}. The ion-selectivity coefficients of Nafion for the drugs have been determined by an electrochemical method. These drugs showed quite large values and the values seemed to be dependent on the hydrophobicity of the drugs.

Du Pont's Nafion, a perfluoro sulfonated ion-exchange polymer, has been receiving a great deal of attention as a modifier for polymer-coated electrodes mainly because of its outstanding chemical stability and excellent ionic conductivity. Among extensive studies[1] dealing with mechanisms of charge and mass transportation as well as catalytic properties, some attempts[2-4] have recently been made to use the Nafion-coated electrodes for determination of electroactive compounds.

Nafion has two important aspects which are useful for electroanalytical purposes. One is its preconcentrating ability[5,6] of cations by electrostatic interaction between the cations and negatively charged sulfonato group in Nafion. Thus, amperometric determination of quite low concentration of electroactive materials becomes possible on the preconcentrated electrodes. Szentirmay and Martin[2] demonstrated that 10^{-8} mol dm^{-3} of methyl viologen could be detected on the Nafion-coated electrode by cyclic voltammetry. This detection limit is about three orders lower than that observed on a bare electrode. The lowering of the effective diffusion coefficient in the Nafion matrix is apparently unfavorable for the electroanalytical purpose, but the favorable preconcentrating effect more than compensates the unfavorable lowering. The other is ionic selectivity. Previous investigations[7,8] have proved that Nafion favors hydrophobic organic cations as compared with hydrophilic inorganic cations. This phenomenon is caused by hydrophobic interaction between fluorocarbon network of the polymer and substrates. There is a possibility for selective determination of organic cations in the presence of hydrophilic cations.

The important advantage of the electrochemical determination over the spectroscopic one widely used currently is that only the vicinity of the electrode surface is necessary in the former method. Therefore, the preconcentrated layer can be very thin; in extreme case, a monolayer is enough to detect the adsorbed species.[9-11] This situation is usually difficult in the spectroscopic method. We report here the indirect determination of electroinactive cationic drugs with Nafion-coated electrodes, taking advantages of the strong interaction of such drugs with Nafion. Indirect electrochemical determination[12,13] is one of the attractive methods since it removes the limitation of direct electrochemical determination. The present method is based on the competitive partitioning effect between an electroactive compound and cationic drugs into Nafion layer, and has been applied to several ammonium drugs using (ferrocenylmethyl)trimethylammonium ion (FA^+) as an electroactive chemical agent. Since the drugs have shown strong affinity with Nafion, the electroinactive drugs less than 10^{-3} mol dm^{-3} level have been determined by voltammetry.

Eperimental

A Nafion solution (Nafion 117, 1100 EW, 5% solution) was obtained from Aldrich Co. and was diluted with methanol to give a 0.025% solution. (Ferrocenylmethyl)trimethylammonium (FA^+) perchlorate was prepared from the iodide salt of FA^+ (Tokyo Kasei Co.) by using aqueous solution of $NaClO_4$ and was recrystallized three times from water. Five drugs were obtained from the commercial sources: hexamethonium chloride (*N*,*N*′-hexamethylenebis(trimethylammonium chloride), autonomic ganglionic blocking drug), Wako chemicals; acetylcholine chloride (parasympathomimetic drug), Kanto Chemicals; neostigmine bromide ([3-(dimethylcarbamoyloxy)phenyl]trimethylammonium-bromide, parasympathomimetic drug), Wako Chemicals; nicotine (autonomic ganglionic blocking drug), Kanto Chemicals; quinidine sulfate (antiarrhythmic drug), Nakarai Chemicals. The structures of these drugs are shown drugs are shown in Fig. 1.

Cyclic voltammetry was carried out with a PAR model 273. The cell was a water-jacket type and kept at 25 °C. The working electrode was a 3 mm diameter glassy carbon (GC) disk (GC-20, Tokai Carbon Co.) mounted in a Teflon rod and was polished finally with alumina powder (50 nm average particle size, Buehler Co.) to give a mirror-like surface. A

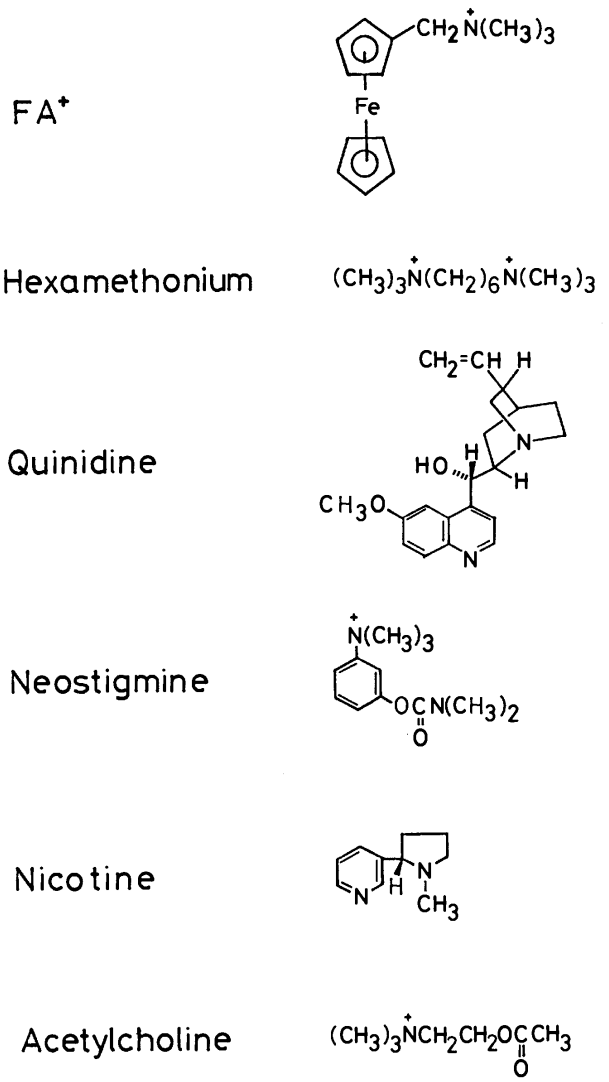

Fig. 1. Structures of drugs.

Pt wire was used as a counter electrode and the potentials were referenced to a saturated calomel electrode (SCE). Nafion coating was prepared by pipetting 2 mm^3 of the 0.025% Nafion solution onto a clean GC surface and allowing the solvent to evaporate at a room temperature. This process was repeated several times using methanol without Nafion to avoid island-like surface coatings. These procedures are important to obtain stable coatings and reproducible results.

Results and Discussion

Voltammetry of FA^+ on the Nafion-Coated Electrode. Figure 2A shows the cyclic voltammograms for FA^+ on the Nafion-coated electrode at different scan rates. The shape indicates near-ideal behavior of a thin film.[14] The peaks are almost symmetrical with very little diffusional tails at the anodic region. The peak current is clearly proportional to the scan rates when the scan rate is less than 200 mV s^{-1} as shown in Fig. 2B. The peak width at half-peak height is 120 mV which is larger than the theoretical value, 90 mV,[14] predicted for a surface species, which may indicate that

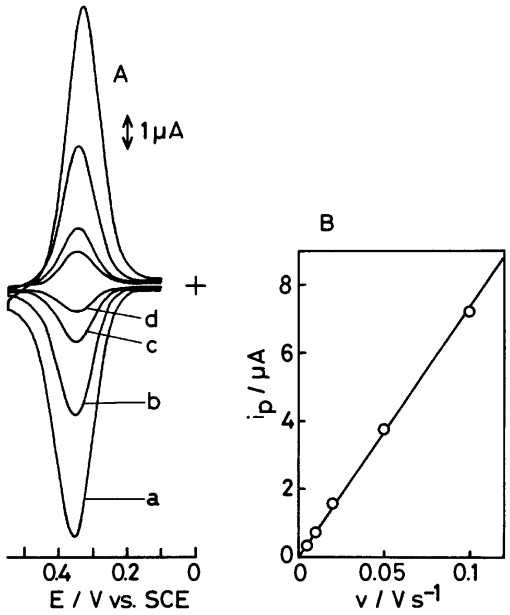

Fig. 2. (A) Cyclic voltammograms of FA^+ on the Nafion-coated GC in 0.1 mol dm^{-3} Na_2SO_4. Scan rate: a, 0.1; b, 0.05; c, 0.02; d, 0.01 V s^{-1}. Concentration of FA^+ in the solution: 7.2×10^{-6} mol dm^{-3}. (B) Relationship between the anodic peak current (i_p) and scan rate (v).

the entrapped FA^+ exists under various circumstances. The small separation between the anodic and cathodic peaks (ca. 15 mV at 50 mV s^{-1}) would be mainly caused by the residual resistance of the polymer film.

The surface concentration of $-SO_3^-$ sites on the electrode is estimated to be 3.4×10^{-9} mol equivalent cm^{-2} from the loading amount of FA^+ entrapped in the Nafion and ion-exchange selectivity coefficient for FA^+.[2] Thus, the average thickness of the film is calculated to be ca. 24 nm by using the density of wet Nafion (1.58 g cm^{-3}) in Na^+ form.[15] This value agrees reasonably with the value (ca. 40 nm) estimated from the amount of the Nafion on the surface. Although the thickness of the Nafion film on the GC surface might be uneven, FA^+ in the outside solution equilibrates fairly rapidly. It takes only ca. 10 min to reach near equilibrium for the cationic exchange between Na^+ and FA^+ after the Nafion-coated electrode is dipped into the electrolyte solution containing 7.2×10^{-6} mol dm^{-3} FA^+. This can be compared with the results reported by Szentirmay and Martin[2] with a 1 μm thick Nafion film. Almost a day was necessary to reach ion-exchange equilibrium between Na^+ and methyl viologen.

The apparent half-wave potential of FA^+ observed on the Nafion-coated electrode is 0.34 V vs. SEC, which is ca. 50 mV negative from the value on a bare GC electrode. This difference in the half-wave potential indicates the stabilization[16-19] of the oxidized species by electrostatic interaction with the negativity charged sulfonato group. This phenomenon contrasts well

with that observed on a perfluorinated carboxylic acid polymer.[17]

Determination of Cationic Drugs on the Nafion-Coated Electrode. The concentration of FA^+ inside the Nafion membrane is susceptible to the presence of cations. Figure 3 shows the cyclic voltammograms observed on the Nafion-coated GC electrode with 7.2×10^{-6} mol dm^{-3} FA^+ and different concentrations of hexamethonium in the electrolyte solution. The addition of hexamethonium resulted in a decrease in the peak current for FA^+. This phenomenon clearly demonstrates that some amount of FA^+ initially trapped inside the Nafion membrane is replaced by hexamethonium added to the electrolyte solution. The extent of the decrease in the peak current is dependent on the concentration of hexamethonium in the solution and thus the determination of the concentration becomes possible by using this phenomenon. As shown in Fig. 3, the presence of 1.0×10^{-6} mol dm^{-3} hexamethonium in solution induces a clear decrease in the peak current for FA^+. We have used several other cationic drugs (acetylcholine, neostigmine, nicotine and quinidine) to clarify the influence of these drugs on the voltammetric response of FA^+ and to investigate the applicability of the Nafion-coated electrodes for determination of these drugs. The drugs induced the decrease in the oxidation peak current for FA^+ as was observed for hexamethonium. Figure 4 demonstrates the relationship between the $i_p/i_{p,o}$ value (where i_p and $i_{p,o}$ are the peak currents with and without drugs, respectively) and the concentration of the several drugs in the electrolyte solution. All drugs investigated here show a clear increase in the $i_p/i_{p,o}$ value in the fairly low concentration ranges of the drugs. Therefore, the concentration of a drug can be determined by using these curves. The detection limits of the drugs in the present procedure are as follows: hexamethonium, 2×10^{-7}; quinidine, 5×10^{-7}; neostigmine, 2×10^{-6}; nicotine, 1×10^{-5}; acetylcholine, 5×10^{-5} mol dm^{-3}.

In these measurements, the cyclic voltammograms were recorded after 5 min of immersion of the Nafion-coated electrode into the sample solution containing a specific amount of a drug. Hexamethonium, acetylcholine and neostigmine equilibrated fairly rapidly and a near equilibrium state was obtained after 5 min of immersion. Only small changes in the voltammetric peak current were observed on the subsequent scans. However, ca. 30 min was necessary to reach a near equilibrium state for quinidine. These differences in the equibration time seem to be mainly dependent on the size of the cation. For analytical purposes it is not necessary to obtain equilibrium response. The same measurements were carried out using a number of Nafion-coated GC electrodes. The results were quite reproducible and the variations of the relative peak current under different runs were within 5%. When the Nafion-coated GC electrode used for these measurements was transferred to the electrolyte solution containing 7.2×10^{-6} mol dm^{-3} FA^+ without any drug, the anodic peak current recovered to its original value. The Nafion film on the GC surface seems to be quite stable and the electrode can be used at least for several times.

Influence of the Added Drugs on the Apparent Half-wave Potentials and Voltammetric Shapes. The apparent half-wave potential ($E_{1/2,app}$) of FA^+ on the Nafion-coated GC is dependent on the loading level of

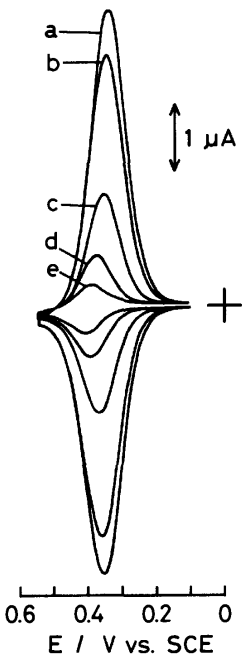

Fig. 3. Cyclic voltammograms of FA^+ in the presence of hexamethonium on the Nafion coated GC in 0.1 mol dm^{-3} Na_2SO_4. Concentration of FA^+ in the solution: 7.2×10^{-6} mol dm^{-3}. Concentration of hexamethonium in the electrolyte solution: a, 0; b, 1.0×10^{-6}; c, 1.0×10^{-5}; d, 1.0×10^{-4}; e, 1.0×10^{-3} mol dm^{-3}. Scan rate: 0.05 V s^{-1}.

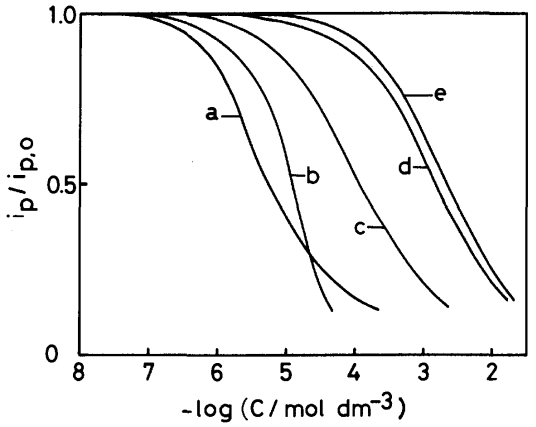

Fig. 4. Relationship between the relative peak current and concentration of drug. a: Hexamethonium. b: Quinidine. c: Neostigmine. d: Nicotine. e: Acetylcholine. Concentration of FA^+ in the solution: 7.2×10^{-6} mol dm^{-3}. Scan rate: 0.05 V s^{-1}.

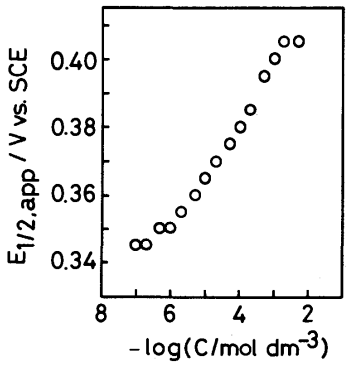

Fig. 5. Relationship between $E_{1/2,app}$ and concentration of hexamethonium in the electrolyte solution.

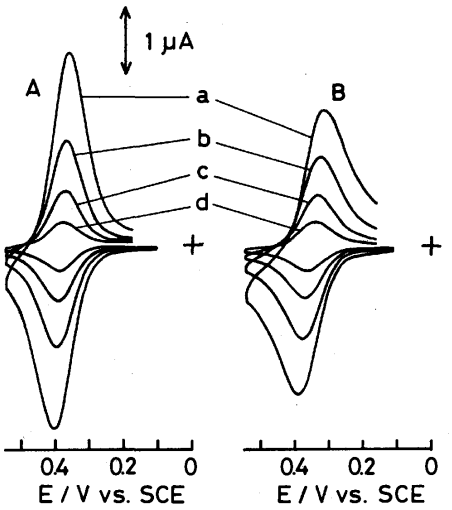

Fig. 6. Cyclic voltammograms of FA^+ on the Nafion coated GC in the presence of 2.0×10^{-4} mol dm^{-3} hexamethonium (A) and 2.0×10^{-5} mol dm^{-3} quinidine (B) in pH 7.0 phosphate buffer. Scan rate: a, 0.2; b, 0.1; c, 0.05; d, 0.02 V s^{-1}. Concentration of FA^+ in the solution: 7.2×10^{-6} mol dm^{-3}.

hexamethonium. Figure 5 shows the relationship between the $E_{1/2,app}$ value and the concentration of hexamethonium in the electrolyte solution. This concentration dependence corresponds well to that of the relative peak current shown in Fig. 4. The half-wave potential (0.34 V vs. SCE) observed on the Nafion-coated GC without hexamethonium is negative compared with the value on a bare GC (0.392 V vs. SCE). The $E_{1/2,app}$ value shifts to positive potentials with increasing concentration of hexamethonium and surpasses the value on a bare GC at hexamethonium concentration higher than 10^{-3} mol dm^{-3}. At the low concentration of hexamethonium, the $E_{1/2,app}$ value is governed by the stabilization[15-19] of the oxidized FA^+ by the favorable electrostatic interaction of the divalent cation (FA^{2+}) with the sulfonato groups in Nafion film. However, the incorporation of hexamethonium into the hydrophilic phase in the Nafion film provides a more hydrophobic environment relative to the original state.[19] This environmental change obviously destabilizes the highly charged species, which implies a positive shift of the $E_{1/2,app}$ of FA^+ entrapped in the Nafion film. Therefore, the shift in $E_{1/2,app}$ is caused by the compensation of extra stability due to electrostatic interaction by the increasing hydrophobicity of the ionic cluster.[19] This trend was also observed for other drugs.

The incorporation of bulky drugs also caused changes in the cyclic voltammetric shapes of FA^+. In Fig. 6 are shown the cyclic voltammograms of FA^+ on the Nafion-coated GC electrodes in the presence of hexamethonium (2.0×10^{-4} mol dm^{-3}) and quinidine (2.0×10^{-5} mol dm^{-3}). The peak heights at 50 mV s^{-1} are about two-tenth of those in the absence of the drugs. A significant difference in the cyclic voltammetric shape was observed. The voltammogram in the presence of quinidine in solution shows obvious diffusional tails after the anodic and cathodic peaks. In addition, the peak separation in this case was ca. 50 mV at 100 mV s^{-1}, which can be compared to ca. 20 mV observed in the original voltammogram. The peak separation gradually increased with increasing concentration of quinidine. These changes in the voltammetric shape are probably caused by the decrease in the apparent diffusion coefficient of FA^+ in the Nafion film since the anodic peak current is no longer linearly dependent on the scan rate. The incorporation of bulky quinidine into the ionic cluster will decrease the hydrodynamic mobility of FA^+ in the hydrophilic region.[19] Therefore, the cyclic voltammetric shape alters from the thin-layer behavior to the diffusion-controlled situation. On the other hand, such an effect on the cyclic voltammetric shape in the presence of hexamethonium in solution is small, suggesting no severe influence of entrapped hexamethonium on the ionic movement of FA^+ in the hydrophilic region. Similarly only small changes in the shape were observed when acetylcholine, neostigmine and nicotine were added to the electrolyte solution. The above may be a reason for the difference in curvature for quinidine in Fig. 4 as compared with those for other drugs.

Ion-Selectivity Coefficient for the Drugs. The present procedure for determination of cationic drugs is based on the competitive partitioning effect between FA^+ and the drug into Nafion, and thus the detection limits are largely dependent on the strength of the interaction. In order to obtain quantitative feature of the drug-Nafion interaction, the determination of steady-state concentration was also carried out. The strength of the interaction can be expressed by the ion-exchange selectivity coefficient, K^D_{Na},[2] which is the equilibrium constant for the following ion-exchange reaction:

$$D^{n+} + n(SO_3^-Na^+)_{Naf} \rightleftharpoons [(SO_3^-)_nD^{n+}]_{Naf} + nNa^+ \quad (1)$$

and given by

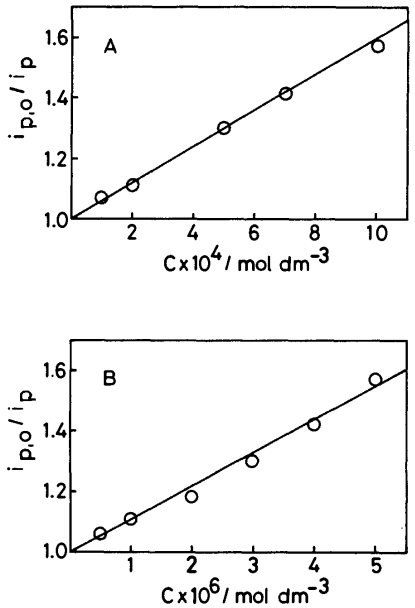

Fig. 7. Relationship between the $i_{p,o}/i_p$ value and concentration of acetylcholine (A) and quinidine (B) in pH 7.0 phosphate buffer. Concentration of FA^+ in the electrolyte solution: 1.0×10^{-5} mol dm^{-3}. Scan rate: 0.05 V s^{-1}.

Table 1. Ion-Selectivity Coefficients for Ammonium Drugs

Drug	Ion-selectivity coefficient
Acethylcholine	5.6×10^2
Hexamethonium	2.0×10^5
Qunidine	1.0×10^5
Neostigmine	2.8×10^4
Nicotine	3.7×10^3
FA^+	$7.3\times10^{4a)}$

a) From Ref. 2.

$$K^D_{Na}=x_D(C_{Na})^n/(x_{Na})^nC_D \quad (2)$$

where C_{Na} and C_D are the concentrations of Na^+ and a drug in an aqueous solution and x_{Na} and x_M are the equilibrium ionic fractions of $-SO_3^-$ sites occupied by each ion, respectively. Thus, for monocationic drugs the following simple equation is derivated:

$$x_{FA,o}/x_{FA}=K^D_{Na}C_D/(C_{Na}+K^{FA}_{Na}C_{FA})+1 \quad (3)$$

where $x_{FA,o}$ and x_{FA} represent the x values for FA^+ without and with a drug, respectively. The $x_{FA,o}/x_{FA}$ value is directly proportional to the ratio of the peak current, $i_{p,o}/i_p$ observed at a steady-state. Figure 7 shows the plots for $i_{p,o}/i_p$ vs. concentrations of quinidine and acetylcholine at low concentration ranges. The plots show quite good linearity and the K^D_{Na} values can be determined from the slopes of the plots by using the K^{FA}_{Na} value (7.3×10^4) reported by Szentirmay and Martin.[2] Since the experimental points deviated from the line at high concentration ranges, the measurements were restricted in the relatively low concentration ranges. The deviation may be indicative of a structural change of Nafion. Hexamethonium is a dicationic drug and the plot does not show a linear relationship. The K^D_{Na} value in this case has been determined by a curve fitting between the experimental and theoretical current ratios. Table 1 shows the ion-selectivity coefficients. It is obvious that these drugs have strong affinity with Nafion. The K^D_{Na} value seems to be related with the hydrophobicity of the drugs. In a series of monocationic drugs, relatively hydrophobic quinidine shows a large value, whereas hydrophilic actylcholine shows a small value.

Since all of these drugs employed here are electroinactive in a practical potential range, the determination by a direct electrochemical method is difficult. In addition, neither acetylcholine nor hexamethonium has a chromophore in the molecule and thus the determination by absorption spectroscopy will also be difficult. It should be emphasized that the simple method proposed here can be used for determination of these drugs and will be applicable to many cationic drugs.

References

1) J. Weber, P. Janda, L. Kavan, and A. Jegorov, *J. Electroanal. Chem.*, **199**, 81 (1986), and references therein.
2) M. N. Szentirmay and C. R. Martin, *Anal. Chem.*, **56**, 1898 (1984).
3) G. Nagy. G. A. .Gerhardt, A. F. Oke, M. E. Rice, R. N. Adams, R. B. Moore, III, M. N. Szentirmay, and C. R. Martin, *J. Electroanal. Chem.*, **188**, 85 (1985).
4) T. Matsue, U. Akiba, and T. Osa, *Anal. Chem.*, **58**, 2096 (1986).
5) C. R. Martin, I. Rubinstein, and A. J. Bard, *J. Am. Chem. Soc.*, **104**, 4817 (1982).
6) N. Oyama and F. C. Anson, *J. Electrochem. Soc.*, **127**, 247 (1980).
7) C. R. Martin and H. Freiser, *Anal. Chem.*, **53**, 902 (1981).
8) H. S. White, J. Leddy, and A. J. Bard, *J. Am. Chem. Soc.*, **104**, 4811 (1982).
9) M. P. Soriaga, J. H. White, and A. T. Hubbard, *J. Phys. Chem.*, **104**, 4811 (1982).
10) K. P. Pang, J. B. Benziger, M. P. Soriaga, and A. T. Hubbard, *J. Phys. Chem.*, **8**, 97 (1984).
11) Y. P. Gui, M. D. Porter, and T. Kuwana, *Anal. Chem.*, **57**, 1474 (1985).
12) Y. Ikariyama and W. R. Heineman, *Anal. Chem.*, **58**, 1803 (1986).
13) J. Ye, R. P. Baldwin, and K. Ravichandran, *Anal. Chem.*, **58**, 2340 (1986).
14) A. J. Bard and L. R. Faulkner, "Electrochemical Methods," John Wiley & Sons, New York (1880), Chap. 12.
15) C. R. Martin and K. A. Dollard, *J. Electroanal. Chem.*, **159**, 127 (1983).
16) H. Braun, W. Storck, and K. Doblhofer, *J. Electrochem. Soc.*, **130**, 807 (1983).
17) Y. H. Tsou and F. C. Anson, *J. Electrochem. Soc.*, **131**, 595 (1984).
18) I. Rubinstein, *J. Electroanal. Chem.*, **176**, 359 (1984).
19) I. Rubinstein, *J. Electroanal. Chem.*, **188**, 227 (1985).

 © 1987 The Chemical Society of Japan Bull. Chem. Soc. Jpn., 60, 3597—3601 (1987)

Alkaline Hydrolysis of *N*-Methyl-2,4-dinitroacetanilide and *N*-Alkyl-*N*-(5-nitro-2-pyridyl)acetamides

Atsushi KIJIMA and Shizen SEKIGUCHI*
Department of Synthetic Chemistry, Faculty of Engineering, Gunma University, Kiryu, Gunma 376
(Received November 21, 1986)

The kinetics of the alkaline hydrolysis of *N*-methyl-2,4-dinitroacetanilide (**2**), *N*-ethyl- (**3**), and *N*-methyl-*N*-(5-nitro-2-pyridyl)acetamide (**4**) was carried out. The reaction path consists of two stages: the first one is the rate-limiting formation of the first tetrahedral intermediate (monoanionic) and the second one the fast decomposition of the intermediate. The latter fast decomposition of the intermediate (monoanionic) involves two processes: one is the direct decomposition of the intermediate to the products and the other is a proton abstraction of the hydroxyl group of the intermediate by $^-$OH giving the second tetrahedral intermediate (dianionic), followed by its deconposition to the products. For the alkaline hydrolysis of **2**—**4**, the decomposition of the first intermediate occurred predominantly via the latter process.

Many reports and reviews have so far appeared on the alkaline hydrolysis of amides.[1] In particular the alkaline hydrolysis of acetanilides has been extensively studied by Schowen et al.,[2-6] Pollack and Bender,[7] Dewolfe and Newcomb,[8] and Eriksson et al.[9] The alkaline hydrolysis of amides is generally considered to be sensitive to both polar and steric effects of acyl substituents. We have already reported the alkaline hydrolysis of *N*-ethyl-2,4-dinitroacetanilide (**1**) and found that the substituents on the amido nitrogen atom and on the phenyl moiety considerably affect its rate of hydrolysis.[10] Although previous studies involved the effects of substituents on the amido nitrogen atom and ring carbon atom of acetanilides, there have been few cases in which both effects are considered[2-9] simultaneously.

This paper reports the effects of substituents of the following acetanilide and *N*-pyridylacetamides on their rates of alkaline hydrolyses to elucidate the nature of these effects (inductive or steric).

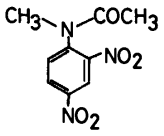

2

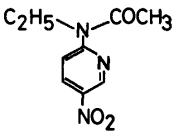

3

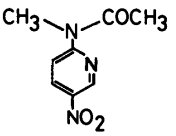

4

Results and Discussion

Absorption Spectra. The time-dependent spectral changes were measured in the reactions of **2** with excess NaOH (Fig. 1). The spectral change was found to be moderate for the reaction rate to be measured, where the absorption (d) was due to *N*-methyl-2,4-dinitroaniline (Fig. 1). For **3** and **4**, similar changes were observed (not shown).

From these results and much information obtained so far,[1-10] the reaction sequence is shown in Scheme 1 in unbuffered solutions.

Order of Reaction. The kinetic order with respect to [NaOH] is important for considering the reaction

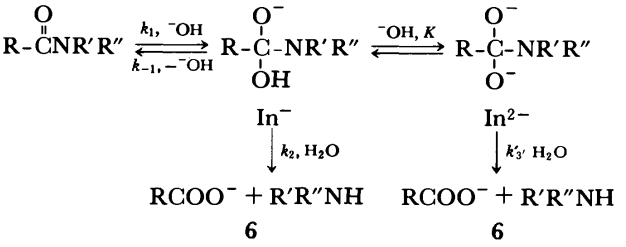

Scheme 1.

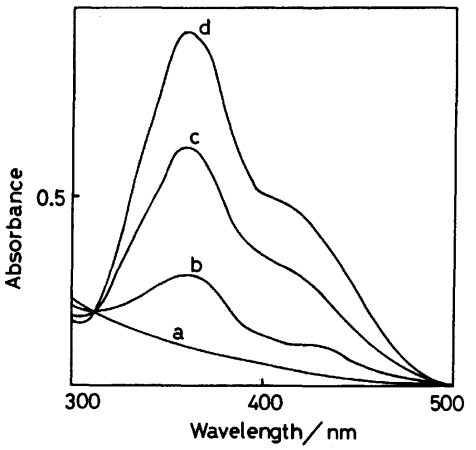

Fig. 1. Time-dependent spectral change in the alkaline hydrolysis of *N*-methyl-2,4-dinitroacetanilide (**2**) at 30°C {[$^-$OH] 0.1 M}: a **2** (3.0×10^{-5} M); b 10 min after addition of NaOH; c 45 min; d 19 h.

mechanism. The relationships between log k_ψ (pseudo first-order rate constant) and log[$^-$OH] (Table 1), therefore, are shown in Fig. 2, together with those of **1** and 4-nitroacetanilide (**7**).[7]

For **7**, the slope varied from ca. 2 at log [$^-$OH] $\leqslant$ ca. -1.0 to ca. 1 at log [$^-$OH] $\geqslant$ ca. -1.0, which shows that at lower log [$^-$OH] the decomposition of In^- to In^{2-} is rate-limiting, whereas at higher log [$^-$OH] the addition of $^-$OH to the carbonyl carbon atom of an amido group is rate-limiting (refer to Eq. 1).

On the other hand, for **1**—**4** the slope was ca. 1 in the

Table 1. Dependence of Pseudo First-Order Rate Constants on Hydroxide Ion Concentrations in the Alkaline Hydrolyses of *N*-Methyl-2,4-dinitroacetanilide (**2**), and *N*-Methyl- (**3**) and *N*-Ethyl-*N*-(5-nitro-2-pyridyl)acetamide (**4**)[a]

[⁻OH] / M	k_ψ / min⁻¹ Obsd[b]	k_ψ / min⁻¹ Calcd[c]	[⁻OH] / M	k_ψ / min⁻¹ Obsd[b]	k_ψ / min⁻¹ Calcd[c]
	2 50°C			**2** 60°C	
0.0095	0.0055	0.0055	0.00185	0.0017	0.0013
0.0190	0.0112	0.0113	0.00090	0.0037	0.0033
0.0285	0.0171	0.0172	0.00585	0.0056	0.0055
0.0380	0.0232	0.0231	0.00780	0.0079	0.0079
0.0475	0.0292	0.0291	0.00975	0.0099	0.0103
0.0570	0.0352	0.0351	0.0117	0.0128	0.0127
0.0665	0.0412	0.0412	0.0136	0.0151	0.0151
0.0760	0.0478	0.0473	0.0156	0.0177	0.0176
0.0855	0.0531	0.0533	0.0176	0.0197	0.0201
0.0950	0.0598	0.0594	0.0195	0.0226	0.0225
0.145	0.0924	0.0916	0.0214	0.0251	0.0249
			0.0254	0.0296	0.0300
	2 70°C		0.0292	0.0354	0.0348
				3	
0.00205	0.00351	0.00408		50°C	
0.00306	0.00552	0.00611			
0.00386	0.00720	0.00769	0.00469	0.0063	0.0070
0.00621	0.0122	0.0124	0.00657	0.0099	0.0099
0.0133	0.0265	0.0266	0.00844	0.0128	0.0128
0.0201	0.0405	0.0404	0.00938	0.0146	0.0143
0.0482	0.0980	0.0980	0.0188	0.0292	0.0293
0.0676	0.138	0.138	0.0281	0.0443	0.0445
0.0772	0.158	0.158	0.0375	0.0605	0.0601
0.0965	0.198	0.198	0.0563	0.0915	0.0915
			0.0750	0.123	0.123
	3 60°C		0.0938	0.155	0.154
				4	
0.00657	0.0191	0.018		60°C	
0.00844	0.0231	0.0237			
0.00938	0.0271	0.0266	0.00201	0.0189	0.0194
0.00188	0.0561	0.0558	0.00302	0.0287	0.0299
0.0281	0.0852	0.115	0.00402	0.0395	0.0405
0.0375	0.116	0.146	0.00503	0.0510	0.0512
0.0469	0.146	0.176	0.00603	0.0609	0.0618
0.0563	0.176	0.236	0.00704	0.0715	0.0726
0.0750	0.238	0.298	0.0101	0.1030	0.1052
0.0938	0.298	0.327	0.0121	0.1253	0.1266
0.103	0.328		0.0141	0.1453	0.1479
			0.0161	0.1691	0.1693

a) [Substrate]$_0$ 2.5×10^{-5} M; μ 0.8 M (NaCl); solvent H_2O–CH_3CN (99.95/0.05 v/y). b) Estimated limit of error ±0.5% for observed k_ψ. c) These k_ψ values were calculated by substituting the data in Table 2 into Eq. 1.

range of [⁻OH] studied, indicating the addition of ⁻OH to the carbonyl carbon atom to be rate-limiting. As will be discussed later, **1**—**4** have an alkyl group on the amide nitrogen atom. This is also expected to exert steric hindrance, in addition to the inductive effect, toward the carbonyl carbon atom in the transition state for formation of In⁻. These effects, therefore, would be expected to make In⁻ less stable.

Rate Constants. According to Scheme 1, the alkaline hydrolysis is catalyzed by ⁻OH to produce the tetrahedral intermediate (In⁻), followed by its decomposition to the products. By applying the steady-state approximation to the concentration of In⁻, the mechanism leads to Eq. 1 for the observed pseudo first-order rate constant, k_ψ, for alkaline hydrolysis (Table 1). In Eq. 1, k_3 (Table 2) means Kk_3'. At present, it is not clear whether the K and k_3' steps are stepwise or simultaneous. Eq. 2 is derived by dividing both sides of Eq. 1 by [⁻OH]. Therefore, the relationship between k_ψ/[⁻OH] and [⁻OH] should be convex upward (not shown),

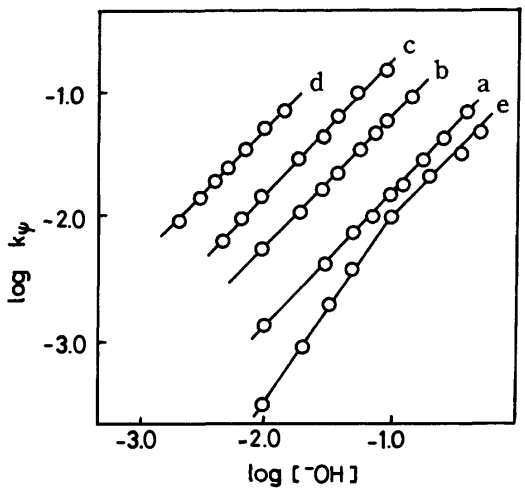

Fig. 2. Relationship between log k_ψ and log[$^-$OH] in the alkaline hydrolyses of acetanilides and pyridylacetamides; a **1** (20 °C); b **2** (60 °C); c **3** (50 °C); d **4** (60 °C); e **7** (25 °C).

which shows the validity of Scheme 1. As a result, k_1 can be obtained as $k_\psi/[^-OH]$ ($=k_1$), when [$^-$OH] is much higher in Eq. 1. Eq. 2 is further derived by rearranging

$$k_\psi = k_1[^-OH]\cdot\frac{k_2+k_3[^-OH]}{k_{-1}+k_2+k_3[^-OH]} \quad (1)$$

$$\frac{k_\psi}{[^-OH]} = k_1\cdot\frac{a+b[^-OH]}{1+a+b[^-OH]} \quad (2)$$

$$a=\frac{k_2}{k_{-1}};\ b=\frac{k_3}{k_{-1}};\ k_3=Kk_3'$$

Eq. 1. Then, the relationship between $k_\psi/(k_1[^-OH]-k_\psi)$ and [$^-$OH] is expected to be linear (Fig. 3). By substituting the k_1 value determined above into Eq. 2, a and b can be estimated from the intercept and slope of the straight line. These k_1, a, and b values were used as the initial ones to calculate k_1, a, and b more accurately. The k_1, a, and b values in Table 2 were derived from Eq. 2 by using the initial values (k_1, a, and b), obtained above, and the non-linear least squares method (Program: SALT Model-F[11]).

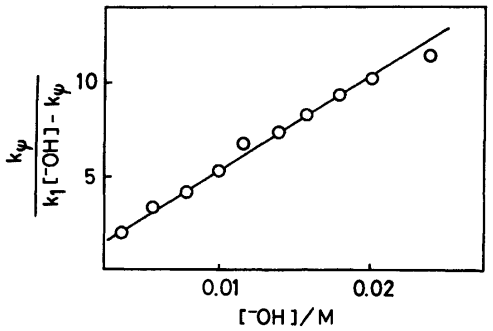

Fig. 3. Relationship between $k_\psi/(k_1[^-OH]-k_\psi)$ and [$^-$OH] in the alkaline hydrolysis of *N*-methyl-2,4-dinitroacetanilide (**2**) at 60 °C [μ 0.8 M (NaCl)].

By applying a similar method to **3** and **4**, the rate constants were determined.

(1) k_1 Values. The k_1 ratio (**2**/**1**) is ca. 2.8, being comparable to ca. 3.3 for that (**4**/**3**) (Run 1, 3, 5, and 6), from which it was found that on changing from an ethyl to a methyl group on the amido nitrogen atom the extent of release of steric compression is similar in both the *N*-pyridylacetamide and the acetanilide. These values are close to the $k_1^{CH_3}/k_1^{C_2H_5}$ values for the alkaline hydrolysis of methyl and ethyl acetates (ca. 2.3 at 0.6—20 °C in 62% acetone-H_2O[12]) and of methyl and ethyl lactates (2.4 at 0 °C in H_2O).[13] These rate ratios are due almost entirely to the inductive effect of the alkyl groups.[12]

As for the k_1 ratio due to the change in the acyl component of esters, Evans et al.[14] showed the $k_1^{CH_3}/k_1^{C_2H_5}$ values of ca. 1.6—1.7 for the alkaline hydrolyses of ethyl acetate and propanoate, and Taft[15] reported 2.0 as a statistical value for the rate ratio of the same esters, which are a little smaller than those described above.

From Table 2 the k_1 value for acetanilide is smaller than that for the corresponding *N*-pyridylacetamide: the k_1 ratio is 7.0 (**3**/**1**) and 8.3 (**4**/**2**) (Run 5 and 1, and 6 and 3). These rate ratios are clearly due to the steric hindrance of 2-substituent toward the steric crowding in the transition state for formation of In$^-$.[10]

On the other hand, Pratt[16] has reported the k_1 value for the alkaline hydrolysis of *N*-methyl-4-nitroacet-

Table 2. Rate Constants and Rate Ratios for the Alkaline Hydrolyses of *N*-Methyl-2,4-dinitroacetanilide (**2**) and *N*-Alkyl-*N*-(5-nitro-2-pyridyl)acetamide (**3** and **4**)

Run No.	Substrate	Temp °C	k_1[a] $M^{-1}min^{-1}$	$a(k_2/k_{-1})$[a]	$b(k_3/k_{-1})$[a] M^{-1}
1	**1**[b]	60	0.460	2.03	5.25
2	**2**	50	0.649	6.95	209
3		60	1.28	0.255	459
		70	2.11	—	—
4	**3**[c]	50	1.71	6.12	238
5		60	3.26	3.22	376
6	**4**[d]	60	10.7	2.23	3484

a) Estimated limit of error ±1.0% for k_1; ±1.3% for a and b. b) *N*-Ethyl-2,4-dinitroacetanilide; cited from Ref. 10. c) *N*-Ethyl-*N*-(5-nitro-2-pyridyl)acetamide. d) *N*-Mehyl-*N*-(5-nitro-2-pyridyl)acetamide.

anilide (**8**) to be 0.0408 M^{-1} min^{-1} ($l\,m^{-1}$ $mol\,dm^{-3}$) at 25 °C, which is smaller than the k_1 value (0.119 M^{-1} min^{-1} at 25 °C) for **2**, derived from the temperature-dependence of log k_1 (E_a=54.8 kJ mol^{-1}).

These results show that the inductive effect (accelerating effect) of 2-NO_2 group is superior to its steric hindrance (retarding effect).

(2) *a* and *b* Values. The b/a value (k_3/k_2) is 2.5 (60 °C) for **1**, and 30 (50 °C) and 1800 (60 °C) for **2**. It is 39 (50 °C) and 117 (60 °C) for **3**, and 1562 (60 °C) for **4**.

From these results, the decomposition of In^- is seen to take place predominantly via the K and k_3' stages, together by considering the b/a value (138 at 30 °C in H_2O) of 4-nitroacetanilide (**7**)[8] and other related acetanilides with electron-withdrawing 4-substituents.[17]

In the case of acetanilide or *N*-pyridylacetamides with electron-withdrawing substituents on the aniline or pyridine moiety, the acidity of the hydroxyl group of In^- becomes stronger,[6] which would make In^- decompose via the K and k_3' stages more often than via the k_2 stage.

Further, on changing from an ethyl to a methyl group on the amido nitrogen atom, the k_3/k_2 (b/a) value increases (2.5 for **1** to 1800 for **2**, and 117 for **3** to 1562 for **4** at 60 °C).

These results indicate that In^- of the substrate with an *N*-methyl group is more stable than In^- of the one with an *N*-ethyl group, because in the former the steric compression is less. Then, proton abstraction of In^- by ^-OH could occur more frequently, that is, the possibility that In^- decomposes to products via the K and k_3' stages would increase.

In conclusion it is found that in the alkaline hydrolysis of nitro-substituted acetanilides or *N*-pyridylacetamides the substituents on the amido nitrogen atom electronically affect the rate of hydrolysis, and those at the 2-position of a ring do so sterically, as well as electronically.

Experimental

Materials. *N*-Methyl-2,4-dinitroacetanilide (2). *N*-Methyl-2,4-dinitroaniline (NMDA) was synthesized from 2,4-dinitrochlorobenzene and methylamine according to the method of Bogoslovskii and Tsil'man[18] (yield 75.1%; recryst. solvent ethanol), mp 174—175 °C (lit,[18] 176—177 °C). The compound **2** was synthesized from NMDA and acetic anhydride in the presence of a small amount of concd. H_2SO_4 (three or four drops) as described in the literature:[10] Yield 63.4%; mp 75—76 °C; ^1H NMR (DMSO-d_6, 60 MHz) δ= 2.17 (3H, s, acetyl CH_3), 3.48 (3H, s, N-CH_3), 7.07 (1H, d, J=4 Hz, ring H^6), and 8.70 (2H, m, ring H^3 and H^5 overlapped). Anal. ($C_9H_9N_3O_5$) C, H, N.

***N*-Ethyl-*N*-(5-nitro-2-pyridyl)acetamide (3).** The synthetic sequence was shown in Scheme 2.

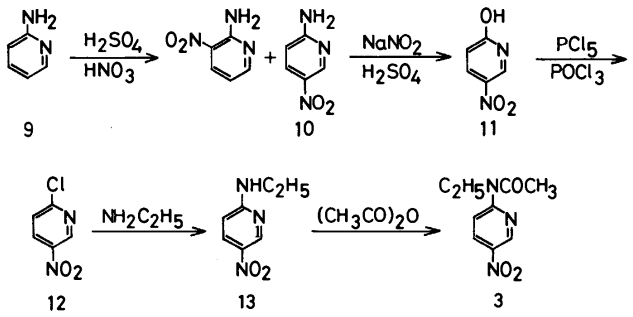

Scheme 2.

9 → 10. Into a 120 ml solution of concd H_2SO_4 was dissolved 2-aminopyridine (27 g, 0.29 mol) by portions under stirring below 90 °C, and the solution was cooled to 0 °C. Then, into this stirred solution was added the cooled mixed acid (concd HNO_3 19.5 ml and concd H_2SO_4 21 ml) at 10 to 20 °C. Stirring was continued and the temperature rose to 65 °C. The mixture was then poured onto 500 ml of ice water and neutralized with Na_2CO_3, giving the precipitate (raw **10**). It was separated by filtration and dried. Althogh it included a small amount of 2-amino-3-nitropyridine, it was used in the next procedure without purification.

10 → 11. To a solution of 24.9 ml of concd. H_2SO_4 in 358 ml of H_2O was added 23.1 g (0.166 mol) of crude **10**, into which 98 g of ice was added. Subsequently a solution of 12.8 g (0.186 mol) of $NaNO_2$ in 40 ml of H_2O was added dropwise under stirring at 0 °C, the solution was stirred for an additional 30 min, and filtered. Recrystallization of the precipitates from H_2O gave 11.9 g (51.2%) of pure **11**: mp 182.5—183.5 °C. Anal. ($C_5H_4N_2O_3$) C, H, N.

11 → 12. To a mixture of 11.9 g (0.085 mol) of **11** and 35 g (0.168 mol) of PCl_5 was added sufficient $POCl_3$ to just cover the mixture. After the mixture was refluxed (at 110 °C) for 3 h, the $POCl_3$ was distilled off under reduced pressure. To the residue was added 144 ml of cooled H_2O, and it was neutralized with NaOH. After the mixture was filtered off, recrystallization of the precipitate from ethanol gave 12.0 g (89.1%) of pure **12**: mp 106—108 °C. Anal. ($C_5H_3ClN_2O_2$) C, H, N.

12 → 13. A solution of 7.9 g (0.05 mol) of **12** in 150 ml of DMSO was added dropwise to a stirred solution of 120 ml $C_2H_5NH_2$ (0.725 mol) in 82.8 ml of DMSO. After the mixture was stirred for 5 h at room temperature, it was neutralized by pouring into a cooled aqueous solution of dilute H_2SO_4 and filtered. Recrystallization of the precipitate from ethanol gave 5.9 g (71.1%) of pure **13**: mp 117—119 °C. Anal. ($C_7H_9N_2O_2$) C, H, N.

13 → 3. After a mixture of 1.5 g (0.009 mol) of **13**, 2 ml of acetic anhydride, and 2 ml of gracial acetic acid was refluxed for 9.5 h, and then the solvent was distilled off under reduced pressure. Recrystallization of the residue from ethanol gave 1.55 g (93%) of **3**: mp 60—61 °C; ^1H NMR (DMSO-d_6, 60 MHz) δ=1.17 (3H, t, *N*-ethyl CH_3), 2.27 (3H, s, acetyl CH_3), 4.05 (2H, q, *N*-ethyl CH_2), 7.87 (1H, d, $J_{H^3\text{-}H^4}$=7.0 Hz, ring H_3), 8.66 (1H, d with each peak finely and doubly split, $J_{H^3\text{-}H^4}$=7.0 Hz, ring H^4), and 9.28 (1H, finely-split d, $J_{H^4\text{-}H^6}$=2 Hz, ring H^6). Anal. ($C_9H_{11}N_3O_3$) C, H, N.

***N*-Methyl-*N*-(5-nitro-2-pyridyl)acetamide (4).** According to the similar method to **3**, **4** was synthesized: mp 96.5—97 °C; ^1H NMR (DMSO-d_6, 60 MHz) δ=2.25 (3H, s, acetyl CH_3), 3.30 (3H, s, N-CH_3), 7.70 (1H, d, $J_{H^3\text{-}H^4}$=7.0 Hz, ring H^3), 8.51 (1H, d with each peak finely and doubly split, $J_{H^3\text{-}H^4}$=7.0 Hz, ring H^4), and 9.11 (1H, finely-split d, $J_{H^4\text{-}H^6}$=2 Hz, ring H^6). Anal. ($C_8H_9N_3O_3$) C, H, N.

Rate Measurements. A sample solution was prepared as follows: After 1.5 μl of an acetonitrile solution of an amide

(0.1 M) was added to a quartz cell containing 3 ml of the prescribed concentration of an aqueous sodium hydroxide solution kept at the constant ionic strength (0.8 M NaCl), the time-dependent increase in the absorption maximum of the corresponding aniline formed were measured with a Hitachi 124 spectrophotometer.

Rate constants were calculated by the Guggenheim method.[19]

References

1) B. C. Challis and J. A. Challis, "The Chemistry of Amides," ed by J. Zabicky, Interscience, London (1970), p. 489; W. P. Jencks, "Catalysis in Chemistry and Enzymology," McGraw-Hill, New York (1968), p. 465; W. P. Jencks, *Acc. Chem. Res.*, **9**, 425 (1976); B. Capon, A. K. Ghosh, and D. M. A. Griene, *Acc. Chem. Res.*, **14**, 306 (1981).

2) R. L. Schowen, H. Jayaramn, and L. Kershner, *J. Am. Chem. Soc.*, **88**, 3373 (1966).

3) R. L. Schowen, H. Jayaraman, L. Kershner, and G. W. Zurick, *J. Am. Chem. Soc.*, **88**, 4008 (1966).

4) R. L. Schowen and G. W. Zurick, *J. Am. Chem. Soc.*, **88**, 1223 (1966).

5) R. L. Schowen, *Progr. Phys. Org. Chem.*, **9**, 275 (1972).

6) L. D. Kershner and R. L. Schowen, *J. Am. Chem. Soc.*, **93**, 2014 (1971).

7) R. M. Pollack and M. L. Bender, *J. Am. Chem. Soc.*, **92**, 7190 (1970).

8) R. H. Dewolfe and R. C. Newcomb, *J. Org. Chem.*, **36**, 3970 (1971).

9) S. P. Eriksson and C. Holst, *Acta Chem. Scand.*, **20**, 1892 (1966); S. O. Eriksson and L. Bratt, *ibid.*, **22**, 892 (1968); S. O. Eriksson, U. Meresaar, and U. Wahlberg, *ibid.*, **22**, 2773 (1968); S. O. Eriksson and M. Kallröt, *Acta Pharm. Suecica*, **6**, 63 (1969); S. O. Eriksson, *ibid.*, **6**, 121 (1969).

10) J. Skarzewski, M. Aoki, and S. Sekiguchi, *J. Org. Chem.*, **47**, 1764 (1982).

11) This program was contrived by Dr. T. Nakagawa, Department of Chemistry, Faculty of Science, Tokyo University, to whom the auther (s.s.) is indebted very much.

12) P. N. Rylander and D. S. Tarbell, *J. Am. Chem. Soc.*, **72**, 3021 (1950).

13) K. H. Vogel and J. C. Warner, *J. Am. Chem. Soc.*, **75**, 6072 (1953).

14) D. P. Evans, J. J. Gordon, and H. B. Watson, *J. Chem. Soc.*, **1938**, 1439.

15) R. W. Taft, Jr., "Steric Effects in Organic Chemistry," ed by M. S. Newman, John Wiley and Sons, New York (1956), Chap. 13 and the literatures cited therein.

16) R. F. Pratt, Ph. D. Dissertation, University of Melbourune, Australia, **1969**.

17) M. L. Bender and R. J. Thomas, *J. Am. Chem. Soc.*, **83**, 4183 (1961).

18) B. M. Bogoslovskii and L. M. Tsill'man, *Org. Chem. Ind. (U. S. R. R.)*, **6**, 445 (1939), *Chem. Abstr.*, **34**, 2360 (1940).

19) E. A. Guggenheim, *Phil. Mag.*, **2**, 538 (1926).

Synthesis and Structural Studies of Remirol

Seiji YAMAGUCHI, Mayumi TAKAI, Isao HANAZOME, Yûko OKADA, and Yoshiyuki KAWASE*
Department of Chemistry, Faculty of Science, Toyama University, Gofuku 3190, Toyama 930
(Received January 21, 1987)

One step cyclization of 2′,4′,6′-trihydroxyacetophenone with 1,4-dibromo-2-methyl-2-butene gave two 2-isopropenyl-2,3-dihydrobenzofuran-4,6-diols and a new 3-methyl-2,5-dihydro-1-benzoxepin-6,8-diol. The structure of natural remirol was confirmed by comparison with monomethylated compounds of the former products. Racemic remirol was synthesized from 3,5-dimethoxyphenol in three steps.

In 1969, Allan et al. isolated a new dihydrobenzofuran from *Remiria maritima* and proposed a structure of 5-acetyl-2-isopropenyl-6-methoxy-2,3-dihydrobenzofuran-4-ol (**1**).[1] A positive Gibbs test was the only reason to propose the structure, and so some possibilities of other structure, 5-acetyl-2-isopropenyl-4-methoxy-2,3-dihydrobenzofuran-6-ol (**2**) or 7-acetyl-2-isopropenyl-4-methoxy-2,3-dihydrobenzofuran-6-ol (**3**), remained for remirol. In this paper, we describe a synthesis and structural reconsideration of remirol.

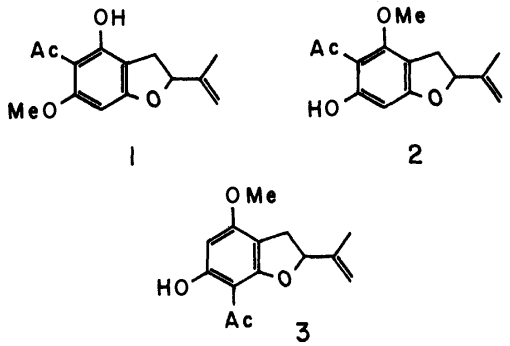

Chart 1.

Cyclization of 2′,4′,6′-trihydroxyacetophenone with 1,4-dibromo-2-methyl-2-butene was already reported by two groups.[2,3] Nickl obtained 7-acetyl-2-isopropenyl-2,3-dihydrobenzofuran-4,6-diol (**5**) in cyclization of the sodium salt of the phenol in cold methanol.[2] Bigi et al. isolated two dihydrobenzofurans, 5-acetyl-2-isopropenyl-2,3-dihydrobenzofuran-4,6-diol (**4**) and **5**, in cyclization of the potassium salt in refluxing toluene.[3] We have reinvestigated these two methods and found that Nickl's method gave a mixture, different from Bigi's, containing 9-acetyl-3-methyl-2,5-dihydro-1-benzoxepin-6,8-diol (**6**). This evidence shows that a different cyclization proceed in a different solvent; the cyclization in nonpolar toluene occurred at 2′- and 4′-hydroxyl groups, while the cyclization in polar methanol occurred mainly at the 2′-hydroxyl group. We have already reported that a similar cyclization of 2′,6′-dihydroxyacetophenone gave a mixture of corresponding dihydrobenzofuran and dihydrobenzoxepin in nonpolar toluene.[4] In these two cases dihydrobenzoxepin derivatives were obtained. Further studies are necessary to establish the formation mechanism of the dihydrobenzoxepin derivatives. In the ^{1}H NMR spectra, two isopropenyldihydrobenzofurans **4** and **5** showed ABX coupling patterns due to protons in their dihydrofuran ring, while **6** showed another coupling mode of the oxepin ring part. The spectral mode of **6** was similar to those of some natural 3-methyl-2,5-dihydro-1-benzoxepin derivatives.[5] Hydrogenation of **6** gave a mixture of 9-acetyl-3-methyl-2,3,4,5-tetrahydro-1-benzoxepin-6,8-diol (**7**) (mp 117—118 °C) and 2′,4′,6′-trihydroxy-3′-(3-methylbutyl)acetophenone (**8**). Nickl already reported that hydrogenation of **5** gave a dihydro compound (mp 153—156 °C) and **8**. The dihydro compound **7** derived from **6** showed only one doublet methyl at δ 0.94 in ^{1}H NMR sectrum. This evidence shows that **6** was not a dihydrobenzofuran derivative but a 3-methyl-2,5-dihydro-1-benzoxepin derivative. In their methylation with diazomethane, **4** gave two mono-methylated

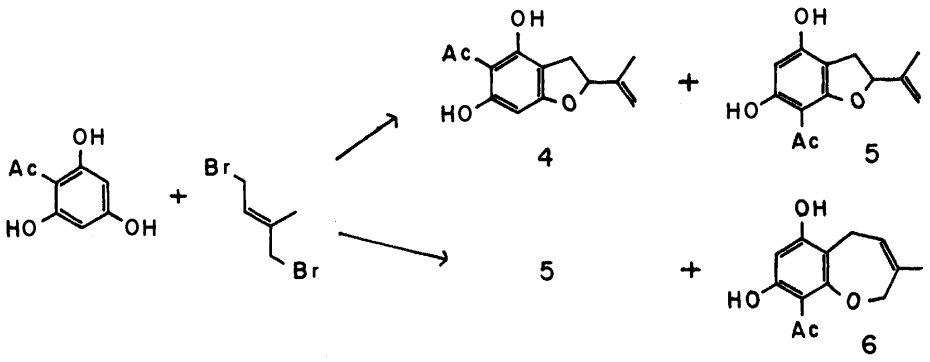

Chart 2.

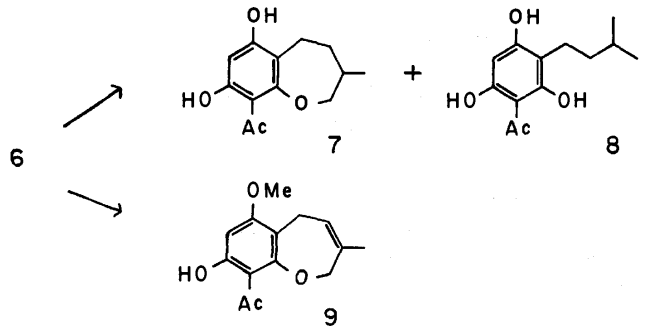

Chart 3.

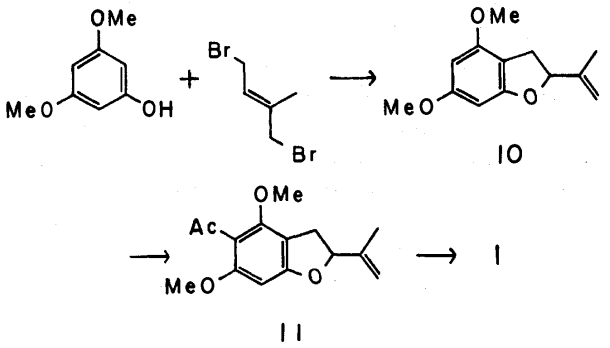

Chart 4.

compounds **1** and **2**, while **5** gave only one monomethylated compound **3**. The methylation of a dihydrobenzoxepin **6** gave one monomethylated compound, 9-acetyl-6-methoxy-3-methyl-2,5-dihydro-1-benzoxepin-8-ol (**9**). Each structure of these monomethylated dihydrobenzofurans **1**—**3** was confirmed by NOE measurements in their ^{1}H NMR spectra. In irradiations at methoxy protons, **1** and **3** showed 39 and 35% area increases, respectively, in their aromatic proton signals (7-H in **1** and 5-H in **3**), but **2** showed only +3 and +4% increases in the two methylene proton signals (3-H). In the UV spectra, **1** and **2** were comparable with 5-acetyl-2-isopropenyl-2,3-dihydrobenzofuran-4-ol and 5-acetyl-2-isopropenyl-2,3-dihydrobenzofuran-6-ol, respectively, while **3** and **9** were comparable with 7-acetyl-2-isopropenyl-2,3-dihydrobenzofuran-6-ol.[4,6] Thus, each structure of the four monomethylated compounds **1**—**3** and **9** was confirmed. The structure of natural remirol whose spectral data were identical with those of **1**, was confirmed to be 5-acetyl-2-isopropenyl-6-methoxy-2,3-dihydrobenzofuran-4-ol.

By a similar procedure,[7] 2-isopropenyl-4,6-dimethoxy-2,3-dihydrobenzofuran (**10**) was prepared from 3,5-dimethoxyphenol and 1,4-dibromo-2-methyl-2-butene. Acylation of **10** with acetic acid and trifluoroacetic anhydride gave only one acylated product, 5-acetyl-2-isopropenyl-4,6-dimethoxy-2,3-dihydrobenzofuran (**11**). Demethylation of **11** with magnesium iodide etherate gave only one demethylated product, the spectrum of which was identical with **1** and natural remirol. This shows that the acylation of **10** occurred only at the 5-position and the demethylation of **11** occurred only at the 4-methoxyl group. It is interesting that the demethylation of **11** occurred only at the 4-methoxyl group, while monomethylation of **4** occurred at two hydroxyl groups with almost equal probability. By this way, racemic remirol was effectively synthesized from 3,5-dimethoxyphenol in three steps.

Experimental

The boiling points (1 mmHg=133.322pa) and melting points are uncorrected. The IR spectra were measured on a Hitachi EPI-S2 spectrophotometer in KBr disks or liquid films, and UV spectra were taken on a Hitachi 220A spectrophotometer in ethanol. The ^{1}H NMR spectra were recorded on a JEOL JNM-MH-60 NMR spectrometer, a JEOL JNM-FX90Q FT NMR spectrometer, or Varian XL-200 FT NMR spectrometer, Mass spectra were determined on a JEOL JMS-OISG-2 mass spectrometer.

Cyclization of 2′,4′,6′-Trihydroxyacetophenone with 1,4-Dibromo-2-methyl-2-butene by Nickl's Procedure.[2] A solution of the sodium salts was prepared by mixing 2′,4′,6′-trihydroxyacetophenone monohydrate (9.95 g, 53.5 mmol) and sodium methoxide (prepared from 2.78 g, 121 mmol of sodium metal) in methanol (200 mL). To the solution , 1,4-dibromo-2-methyl-2-butene (15.5 g, 64.3 mmol) was added and the mixture was stirred at room temperature for 20 h. After removal of the methanol under reduced pressure, the mixture was acidified with 10% hydrochloric acid and extracted with ether. The ethereal layer was extracted with 10% sodium hydroxide solution. The sodium hydroxide solution was acidified with 10% hydrochloric acid and extracted with ether. After removal of the ether, the residue was chromatographed on a silica-gel column to give 7-acetyl-2-isopropenyl-2,3-dihydrobenzofuran-4,6-diol (**5**) (0.90 g, 7.2%) and 9-acetyl-3-methyl-2,5-dihydro-1-benzoxepin-6,8-diol (**6**) (1.48 g, 11.8%). The compounds isolated showed the following data. **5**: mp 185—186 °C (from benzene)(lit,[3] 178—182 °C); IR 1640 cm^{-1}; UV 228.5 (log ε=4.07), 286 (4.26), 327 nm (3.58); ^{1}H NMR (acetone-d_6) δ=1.8 (3H, broad s), 2.6 (3H, s), 3.0 (1H, dd, J=15 and 8 Hz), 3.2 (1H, dd, J=15 and 9.5 Hz), 5.0 (1H, broad s), 5.2 (1H, broad s), 5.5 (1H, dd, J=9.5 and 8 Hz), 6.0 (1H, s), 13.4 (1H, s); all spectra were identical with Bigi's. **6**: mp 192—193 °C (from benzene); IR 1630 cm^{-1}; UV 223.5 (log ε=4.05), 284 (4.11), 328 nm (3.66); ^{1}H NMR (acetone-d_6) δ=1.6 (3H, broad s), 2.7 (3H, s), 3.4 (2H, broad m), 4.6 (1H, broad s), 5.7 (1H, broad m), 6.3 (1H, s), 13.6 (1H, s); MS m/z 234 (M^+), 219, 201. Found: C, 66.56, H, 6.11%. Calcd for $C_{13}H_{14}O_4$: C, 66.65, H, 6.02%.

Hydrogenation of 6. A solution of **6** (330 mg, 1.41 mmol) in ethyl acetate (20 mL) was stirred with Adams catalyst (100 mg) under a hydrogen atmosphere. After the absorption of hydrogen ceased, the catalyst was filtered off. After removal of the ethyl acetate, the residue was chromatographed on a silica-gel column to give 9-acetyl-3-methyl-2,3,4,5-tetrahydro-1-benzoxepin-6,8-diol (**7**) (106 mg, 32%) and 2′,4′,6′-trihydroxy-3′-(3-methylbutyl)acetophenone (**8**) (84 mg, 25%). These two compounds showed following data. **7**: mp 117—118.5 °C (from cyclohexane-benzene); IR 1620 cm^{-1}; ^{1}H NMR ($CDCl_3$) δ=0.94 (3H, d, 3-CH_3), 1.22 (1H, m, 4-Hax), 1.96 (1H, m, 4-Heq), 2.18 (1H, m, 3-Hax), 2.50 (1H, dd, 5-Hax), 2.66 (3H, s, -$COCH_3$), 3.05 (1H, dd, 5-Heq), 3.38 (1H, dd,

2-Hax), 4.29 (1H, dd, 2-Heq), 6.14 (1H, s, 7-H), 6.96 (1H, broad s, 6-OH), 13.54 (1H, s, 8-OH), J=15 (5a-5e), 14 (4a-4e), 12 (2a-2e, 3a-4a, 4a-5a), 9 (2a-3a), 7 (3a-Me, 4e-5e), 4 (2a-3a, 3a-4e), 2 (4a-5e, 4e-5a), 1 Hz (2e-4e); MS m/z 236 (M^+), 221, 181, 165. Found: C, 66.37, H, 6.77%. Calcd for $C_{13}H_{16}O_4$: C, 66.08, H, 6.38%. **8**: mp 190—192 °C (from benzene lit,[2] 185 °C); IR 1640 cm^{-1}; ^1H NMR (acetone-d_6) δ=0.95 (6H, d, J= 6 Hz), 1.2—1.7 (3H, m), 2.57 (2H, t, J=7 Hz), 2.58 (3H, s), 6.00 (1H, s), 8.83 (1H, s), 9.30 (1H, broad s), 13.8 (1H, s).

Methylation of 4—6 with Diazomethane. A solution of **4**, **5**, or **6** in methanol was treated with an ethereal solution containing excess diazomethane at room temperature for one night. After removal of the solvents and the excess of diazomethane, the residual oil was chromatographed. Methylation of **4** gave two monomethyl ether **1** and **2** in 21 and 24%, respectively. 5-Acetyl-2-isopropenyl-6-methoxy-2,3-dihydrobenzofuran-4-ol (racemic remirol) (**1**): mp 72—72.5 °C (from hexane) (natural remirol:[1] 76.5—77 °C); IR 1635 cm^{-1}; UV 238 (log ε=4.11), 293 nm (4.28), (natural remirol:[1] 239 and 294 nm); ^1H NMR ($CDCl_3$) δ=1.76 (3H, s), 2.60 (3H, s), 2.95 (1H, dd, J=15, 8 Hz), 3.30 (1H, dd, J=15, 10 Hz), 3.86 (3H, s), 4.92 (1H, broad s), 5.07 (1H, broad s), 5.29 (1H, broad dd, J=10, 8), 5.97 (1H, s), 14.08 (1H, s); MS m/z 248 (M^+), 233. Found: C, 67.50, H, 6.63%. Calcd for $C_{14}H_{16}O_4$: C, 67.73, H, 6.50% **2**: mp 70.5—71 °C (from hexane); IR 1625 cm^{-1}; UV 233 (log ε=4.12), 241 sh (4.01), 288 (4.20), 323 sh nm. (3.67); ^1H NMR ($CDCl_3$) δ=1.77 (3H, s), 2.62 (3H, s), 3.09 (1H, J=15, 7 Hz), 3.46 (1H, dd, J=15, 9 Hz), 3.94 (3H, s), 4.95 (1H, broad s), 5.08 (1H, broad s), 5.22 (1H, dd, J=9, 7 Hz), 6.15 (1H, s), 13.86 (1H, s); MS m/z 248 (M^+), 233. Found: C, 67.81, H, 6.50%. Calcd for $C_{14}H_{16}O_4$: C, 67.73, H, 6.50%. Methylation of **5** and **6** gave corresponding monomethyl ethers **3** and **9** in 75.4 and 27.6%, respectively. 7-Acetyl-2-isopropenyl-4-methoxy-2,3-dihydrobenzofuran-6-ol (**3**): mp 61—62 °C (from hexane); IR 1640 cm^{-1}; UV 230 (log ε=4.14), 283.5 (4.30), 337 nm (3.52); ^1H NMR ($CDCl_3$) δ=1.82 (3H, s), 2.58 (3H, s), 2.92 (1H, dd, J=15, 8 Hz), 3.17 (1H, dd, J=15, 9 Hz), 3.88 (3H, s), 5.02 (1H, braod s), 5.18 (1H, broad s), 5.38 (1H, dd, J=9, 8 Hz), 6.00 (1H, s), 13.57 ppm (1H, s); MS m/z 248 (M^+), 233. Found: C, 67.90, H, 6.61%. Calcd for $C_{14}H_{16}O_4$: C, 67.73, H, 6.50%. 9-Acetyl-6-methoxy-3-methyl-2,5-dihydro-1-benzoxepin-8-ol (**9**): mp 152—153 °C (from hexane) IR 1630 cm^{-1}. UV 230.5 (log ε=3.99), 280 (4.06), 328 nm (3.84); ^1H NMR ($CDCl_3$) δ=1.55 (3H, broad s), 2.68 (3H, s), 3.37 (2H, broad m), 3.83 (3H, s), 4.45 (2H, broad m), 5.65 (1H, broad m), 6.27 (1H, s), 13.67 (1H, s); MS m/z 248 (M^+), 233. Found: C, 67.93, H, 6.44%. Calcd for $C_{14}H_{16}O_4$: C, 67.73, H, 6.50%.

4,6-Dimethoxy-2-isopropenyl-2,3-dihydroxybenzofuran (10). By a method described in our previous paper,[7] **10** was obtained from 3,5-dimethoxyphenol (25.0 g, 163 mmol) and 1,4-dibromo-2-methyl-2-butene (37.3 g, 163 mmol) in the presence of sodium hydride (7.8 g, 326 mmol) in dry ether (300 mL). After distillation and chromatography, **10** was obtained in pure state in 27% yield. **10**: bp 138—140 °C (3 mmHg); mp 53.5—54.5 °C (from hexane); UV 234 sh (log ε=3.86), 273 nm (3.20); ^1H NMR (CCl_4) δ=1.72 (3H, s), 2.80 (1H, dd, J=15, 8 Hz), 3.03 (1H, dd, J=15, 9 Hz), 3.62 (3H, s), 3.65 (3H, s), 4.73 (1H, broad s), 4.92 (1H, broad s), 4.98 (1H, dd, J=9, 8 Hz), 5.72 (1H, d, J=2 Hz), 5.80 (1H, d, J=2 Hz); MS m/z 220 (M^+), 205. Found: C, 71.15, H, 7.52%. Calcd for $C_{13}H_{16}O_3$: C, 70.89, H, 7.32%.

5-Acetyl-2-isopropenyl-4,6-dimethoxy-2,3-dihydrobenzofuran (11). By the method described in our previous paper,[7] **10** (3.45 g, 15.7 mmol) was acylated with acetic acid (1.90 g, 31.7 mmol) and trifluoroacetic anhydride (6.60 g, 31.4 mmol) to give **11** (1.19 g, 28.3%); bp 225—240 °C (16 mmHg); IR 1685 cm^{-1}; UV 234 sh: 4.02), 274 nm (3.70); ^1H NMR (CCl_4) δ=1.78 (3H, s), 2.33 (3H, s), 3.03 (1H, dd, J=16, 8 Hz), 3.27 (1H, dd, J=16, 9 Hz), 3.78 (6H, s), 4.87 (1H, broad s), 5.05 (1H, broad s), 5.12 (1H, dd, J=8,9 Hz), 6.10 (1H, s); MS m/z 262 (M^+), 245. Found: C, 68.77, H, 6.88%. alcd for $C_{15}H_{18}O_4$: C, 68.68, H, 6.92%.

Demethylation of 11 to Racemic Remirol (1). By the method described in our previous paper,[6] **11** (1.00 g 3.83 mmol) was demethylated with magnesium iodide etherate in refluxing benzene. After purification by silica-gel column chromatography, fractions eluted with hexane-benzene (8:2) gave **1** (431 mg, 42.7%) as colorless crystals (mp 72—72.5 °C). All spectral data were identical with those of **1** obtained from monomethylation of **4** and natural remirol reported by Allan et al.[1]

We wish to thank Dr. Franca Bigi for providing some copies of the spectra of **4** and **5** and also thank Dr. Takashi Tokuyama (Osaka City University) for measuring the NOE data.

References

1) R. D. Allan, R. L. Correll, and R. J. Wells, *Tetrahedron Lett.*, **1969**, 4673.

2) J. Nickl, *Chem. Ber.*, **91**, 553 (1958).

3) F. Bigi, G. Casiraghi, G. Casnati, and G. Sartori, *Tetrahedron*, **39**, 169 (1983).

4) S. Yamaguchi, A. Saitoh, and Y. Kawase, *Bull. Chem. Soc. Jpn.*, **59**, 3983 (1986). Recently, we found, in cyclization of 2′,6′-dihydroxyacetophenone, 9-acetyl-3-methyl-2,5-dihydro-1-benzoxepin was obtained in better yield (4.0%) in methanol.

5) F. M. Dean and D. A. H. Taylor, *J. Chem. Soc. C*, **1966**, 114; P. H. McCabe, F. McCrindle, and R. D. H. Murray, *ibid.*, **1967**, 145; Y. Asakawa, M. Toyota, and T. Takemoto, *Phytochemistry*, **17**, 2005 and 2115 (1978); P. Junior, *ibid.*, **18**, 2053 (1979); M. Takasugi, S. Nagao, and T. Masamune, *Tetrahedron Lett.*, **1979**, 4675; Y. Asakawa, R. Takeda, M. Toyota, and T. Takemoto, *Phytochemistry*, **20**, 858 (1981). B. Epe, U. Oelmann, and A. Mondon, *Chem. Ber.*, **114**, 757 (1981); Y. Asakawa, K. Tanikawa, M. Toyota, and T. Takemoto, *Phytochemistry*, **21**, 2481 (1982).

6) S. Yamaguchi, K. Sugiura, R. Fukuoka, K. Okazaki, M. Takeuchi, and Y. Kawase, *Bull. Chem. Soc. Jpn.*, **57**, 3067 (1984).

7) S. Yamaguchi, A. Miyata, M. Ueno, T. Hase, K. Yamamoto, and Y. Kawase, *Bull. Chem. Soc. Jpn.*, **57**, 617 (1984).

^{13}C and ^{1}H NMR of Arylnitrones. Substituent Effects of α-Phenyl-*N*-(*p*-substituted phenyl)nitrones

Kohji SUDA,* Toshio TSUJIMOTO, and Masashige YAMAUCHI†
Department of Physical Chemistry, Meiji College of Pharmacy, 1-35-23, Nozawa, Setagaya-ku, Tokyo 154
†Faculty of Pharmaceutical Sciences, Josai University, Keyakidai, Sakado, Saitama 350-02
(Received February 2, 1987)

Substituent effects on the chemical shifts of the conjugation sites in α-phenyl-*N*-arylnitrones (**2**) have been investigated. Resonance effects predominate at these positions. The electronic effects of the substituents should be treated separately between electron-donating groups and electron-withdrawing ones. A plausible mechanism for the transmission of the substituent effects in **2** has been proposed.

Recently, the substituent effects of α,*N*-diarylnitrones (**1** and **2**) were investigated by means of ^{13}C and ^{1}H NMR spectroscopy.[1] The analyses, however, seem to be insufficient with regard to the mechanisms of the transmission of the substituent effects. For example, the previous investigators have reported that, while the chemical shifts of C-4′ in α-aryl-*N*-phenylnitrones (**1**) and those of C_α in α-phenyl-*N*-arylnitrones (**2**) are properly correlated with the Hammett σ_p or the Swain-Lupton *F* and *R* parameters, there are poor correlations between these parameters and the chemical shifts of C_α in **1** and those of C-4 in **2**. These results obtained for the conjugation sites of **1** and **2** are inconsistent with their explanation that there are through-resonance effects between the α- and *N*-phenyl rings via the nitrone function; thus, some reasonable explanations of the mechanisms are required.

In a previous paper,[2] the present authors have systematically investigated the substituent effects of **1** and α-aryl-*N*-alkylnitrones, especially the effect of the 4-substituents on the α-position, by means of ^{13}C and ^{1}H NMR spectroscopy. From the good correlations obtained in correlation analyses, we have concluded that 1) inductive effects are predominant at the α-carbon, and 2) a "back-polarized" structure of nitrones is responsible for the anomalous upfield shift of the C_α signals.

The aim of the present work is to understand the nature of the nitrone function and to give an appropriate explanation of the mechanism of the transmission of the substituent effects by assessing the substituent effects of **2**.

Experimental

Materials. α-Phenyl-*N*-(*p*-substituted phenyl)nitrones (**2**): Nitrones **2a**[3] and **2b**[3,4] were synthesized from the corresponding nitrosobenzenes and *N*-benzylpyridinium chloride; they were purified by recrystallization from ethanol-hexane and then from benzene-hexane. Nitrones, **2c—k**, were prepared by the condensation of the appropriate phenylhydrox-

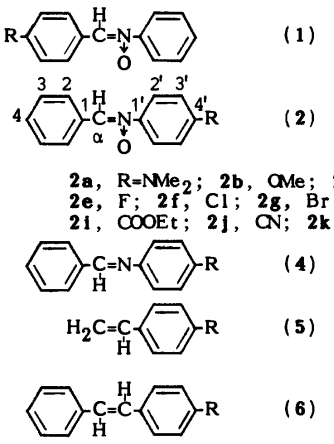

Scheme 1.

Table 1. ^{13}C and ^{1}H SCS Values[a] of α-Phenyl-*N*-(*p*-substituted phenyl)nitrones (**2**)

	R	^{13}C NMR					^{1}H NMR
		C_α	C-1	C-4	C-1′	C-4′	H_α
a	NMe_2	−2.37	0.57	−0.75	−10.80	21.26	−0.08
b	OMe	−0.94	0.19	−0.26	−6.71	30.68	−0.06
c	Me	−0.54	0.10	−0.19	−2.32	10.19	−0.03
d	H	(134.52)[b]	(130.71)[b]	(130.90)[b]	(149.11)[b]	(129.90)[b]	(7.92)[b]
		0.0	0.0	0.0	0.0	0.0	0.0
e	F	−0.08	−0.13	0.16	−3.83	33.16	−0.04
f	Cl	−0.01	−0.21	0.28	−1.61	5.91	−0.02
g	Br	−0.04	−0.24	0.30	−1.16	1.74	−0.02
h	COOMe	0.65	−0.29	0.48	2.88	1.61	0.06
i	COOEt	0.61	−0.27	0.43	2.75	1.92	0.07
j	CN	0.91	−0.58	0.82	2.43	−16.13	0.06
k	NO_2	1.34	−0.64	1.01	3.76	18.35	0.09

a) SCS=δ(X−R)−δ(X−H). b) Chemical shifts δ: in ppm downfield from internal TMS.

ylamines (**3**)[5,6] with benzaldehyde in ethanol and were purified by recrystallization from ethanol-hexane or benzene-hexane. To our knowledge, although nitrones **2a—g**, **2i**, and **2k** are known,[1,7] the physical constants of the following nitrones have not been reported: **2b**, mp 129—130 °C (uncorrected), **2e**, 173—175 °C, **2i**, 130—131 °C, **2k**, 191.5—192 °C. Nitrones **2h** and **2j** are new compounds: **2h** mp 195 °C, Found: C, 70.40; H, 4.94; N, 5.49%. Calcd for $C_{15}H_{13}O_3N$: C, 70.58; H, 5.13; N, 5.49%. **2j** mp 164.5—165 °C, Found: C, 75.47; H, 4.25; N, 12.85%. Calcd for $C_{14}H_{10}ON_2$: C, 75.65; H, 4.54; N, 12.61%. All the compounds obtained were characterized as *Z*-isomers by means of their physical constants and spectral data.[2]

NMR Measurement. The ^{13}C NMR spectra of **2a—d** were measured at 100.4 MHz on a JEOL GX-400 spectrometer under a pulse Fourier transform mode. A spectral width of 25000 Hz was used with 64 K (digital resolution 0.76 Hz) data points. The ^{13}C NMR spectra of **2c—k** were measured at 67.8 MHz on a JEOL GX-270 spectrometer under a pulse Fourier transform mode. A spectral width of 18000 Hz was used with 32 K (digital resolution 1.10 Hz) data points. The ^1H NMR spectra were obtained on the JEOL GX-400 NMR spectrometer operating at 400 MHz for **2a—d** and on the JEOL GX-270 NMR spectrometer for **2c—k** at 270 MHz.

Sample solutions were prepared in a concentration of 0.4 M (mol dm^{-3}), except for **2f—h** and **2k** (0.16 M), with $CDCl_3$ (99.8%, Merck) containing 1% TMS (tetramethylsilane) as the internal standard. Sample tubes with a 5-mm diameter were used, and the probe temperature was 20—25 °C. The chemical shifts were independent of the concentrations of the compounds used within a range of 0.15 to 0.5 M (with a deviation smaller than 5 and 3% in ppm for the ^{13}C and ^1H spectra respectively). The ^{13}C and $^1H_\alpha$ signals of **2** were assigned in a similar manner as described in the previous paper.[2]

Results and Discussion

It is well-accepted that the nitrone function is flush with the two phenyl rings in **1** and **2**.[7a,b] Since C-1′, C_α, and C-4 in **2** are, in contrast to the case of **1**, conjugation sites of the 4′-substituents, we will mainly discuss the substituent effects on these sites. The chemical shifts and substituent-induced chemical shifts (SCS) for C_α, C-1, C-4, C-1′, C-4′, and H_α in **2** are shown in Table 1. All the C_α chemical shifts appear ca. 25 ppm upfield and ca. 20 ppm downfield from the corresponding carbon chemical shifts of imines **4**[8] and styrenes **5**[9] respectively, while they are very close to the corresponding carbon chemical shifts of *trans*-stilbenes **6**.[10] Table 1 reveals that the C_α, C-4, C-1′, and H_α signals of **2** shift downfield as the electron-withdrawing ability of the substituents increases, whereas the C-1 signals shift upfield, showing a reverse substituent effect. This behavior at C-1 is, however, not the characteristic of the nitrone alone; it is also observed in the ^{13}C NMR spectra of **4** and **6**.[8,10]

To ascertain the mechanisms and the extent of the transmission of the substituent effects in **2**, the SCS values for the requisite positions were compared with those for the corresponding sites of **4**, **5**, **6**, and mono-

Table 2. ^{13}C SCS–SCS Correlations between **2** and Reference Systems[a]

Refernce system		Monosubstituted benzenes				**4**				**5**				**6**			
		$SCS=\rho_{Bz}\cdot\delta_{Bz}+C$				$SCS=\rho_{Im}\cdot\delta_{Im}+C$				$SCS=\rho_{Sy}\cdot\delta_{Sy}+C$				$SCS=\rho_{Sb}\cdot\delta_{Sb}+C$			
Position in **2**		n	ρ_{Bz}	C	SD	r	n	ρ_{Im}	C	SD	r	n	ρ_{Sy}	C	SD	r	n	ρ_{Sb}	C	SD	r
C_α		10	0.18 ±0.04	0.12 ±0.22	0.08	0.965[b]	8	0.52 ±0.06	0.03 ±0.12	0.02	0.994	10	0.36 ±0.07	−0.29 ±0.18	0.06	0.974	10	0.38 ±0.07	−0.30 ±0.18	0.06	0.976
C-1							8	0.60 ±0.18	−0.17 ±0.10	0.01	0.960						10	0.59 ±0.05	−0.01 ±0.03	0.00	0.996
C-4		10	0.09 ±0.03	0.30 ±0.15	0.04	0.935[b]	8	0.88 ±0.16	0.00 ±0.09	0.01	0.984						10	0.76 ±0.09	0.03 ±0.06	0.01	0.989
C-1′		10	0.80 ±0.08	−0.70 ±0.45	0.36	0.992[b]	8	0.88 ±0.10	−0.64 ±0.54	0.34	0.994	9	0.88 ±0.09	−0.54 ±0.47	0.30	0.993					
C-4′		10	0.92 ±0.11	0.89 ±2.05	5.37	0.990[c]	8	0.92 ±0.04	0.35 ±0.90	0.43	0.999	9	0.91 ±0.13	1.22 ±2.56	7.03	0.988					

a) n: The number of data, SD: standard deviations, and r: correlation coefficients. The SCS values for the reference systems were obtained from the reported δ values.[8-11] b) Correlations with the $^{13}C_{para}$ SCS of monosubstituted benzenes. c) Correlations with the $^{13}C_{ipso}$ SCS of monosubstituted benzenes.

substituted benzenes.[11] As is shown in Table 2, the SCS-SCS plots gave fairly good correlations with the correlation coefficients of $r>0.960$ at these positions.

However, the slopes, ρ_{Bz}, ρ_{Im}, and ρ_{Sb}, are small, especially at C_α, C-4, and a nonconjugation site, C-1, with the exception of the ρ_{Im} at C-4. Since the magnitude of the rho values is a measure of the relative sensitivity of substituent effects, such smaller values than unity in **2** can be explained by the lower double-bond order of the nitrone function compared with the corresponding side-chain double bonds in **4**, **5**, and **6**.[2] Furthermore, among the SCS-SCS correlations at C_α, the correlation between **2** and a non-planar system **4**,[8a-c] in which the *N*-phenyl ring is twisted from the molecular plane containing the C=N bond, is much better (r=0.994) than the correlations between **2** and the comparable planar molecules, such as monosubstituted benzenes, **5**, and **6** (r=0.965—0.976). In the latter correlations, electron-donating and electron-withdrawing groups have apparently different slopes, as is illustrated in Fig. 1. These findings suggest that the mechanisms of the transmission of substituent effects through the side-chain double bond in **2** are considerably different from those for **5** and **6**.

In the analysis of the substituent effects of **2**, the previous investigators have reported[1] that 1) there is an excellent correlation between the chemical shifts at C_α and Hammett σ_p or Swain-Lupton F and R parameters, 2) the chemical shifts at C-1′ have a poor correlation with the σ_p, but a fair correlation with the σ^+, parameters, and 3) there is no correlation between the chemical shifts at C-4 and these parameters. The

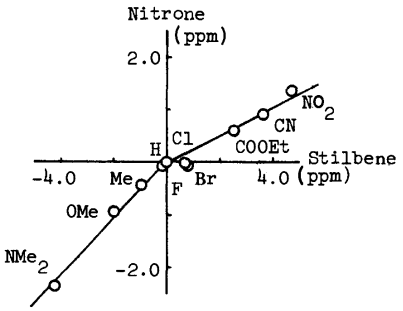

Fig. 1. SCS-SCS correlation at C_α.

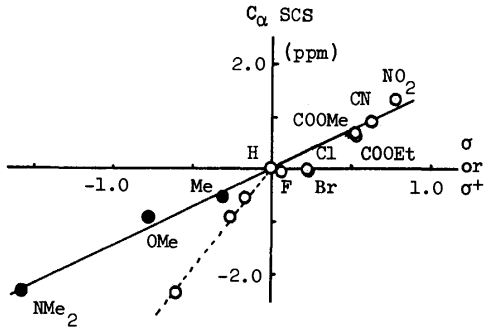

Fig. 2. Plot of C_α SCS vs. Hammett σ (○) or σ^+ (●) constants in **2**.

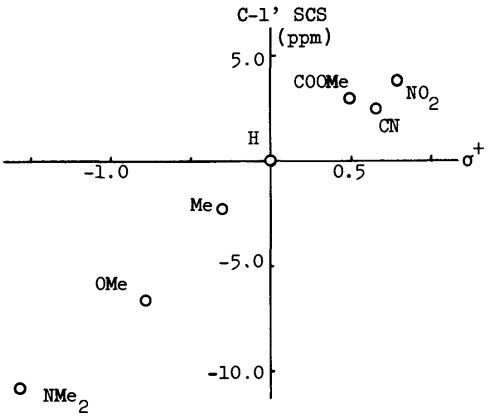

Fig. 3. Plot of C-1′ SCS vs. Hammett σ^+ constants in **2**.

present analyses by the use of our own spectral data are, however, inconsistent with their results at these positions in **2**. As is illustrated in Fig. 2, the SCS values at C_α show an excellent linear relationship with the σ^+ constants, with a correlation coefficient of 0.991, whereas the correlation coefficient with σ_p constants is, at most, 0.976. This can be best interpreted in terms of an enhanced electron density at C_α caused by the electron-donating groups. This also means that the nitrone function is capable of acting either as an electron-donating group or as an electron-withdrawing group, depending on the nature of the substituents on the *N*-phenyl ring, i.e., the electronically amphoteric character of the nitrone function being ascertained. The deviation of halogens from the correlation shown in Fig. 2 might be caused by the well-known electronically amphoteric character of these atoms. Indeed, a principal component analysis of the ^{13}C SCS of monosubstituted benzenes has recently shown that the substituents cluster into four groups: alkyl, halogens, donors, and acceptors; thus, the omission of halogens might be appropriate in the correlation analyses of nitrones.[12]

Although the SCS values at C-1′ in **2** can be correlated fairly well with the σ_p constants (r=0.937), the correlation with the σ^+ constants is much better (r=0.971), and the best correlation coefficient (0.990) is obtained when halogen atoms are omitted from the consideration (Fig. 3). Accordingly, the SCS-SCS correlation between C-1′ and C_α also gives a good linear relationship (r=0.978) when halogens are omitted from the plot.

The SCS values of C-4 in **2** showed a good correlation with σ_p. This supports the idea that the electronic effects of the 4′-substituents are virtually transmitted from the *N*-phenyl ring to the *C*-phenyl ring through the whole conjugation system in **2**. The low sensitivity to resonance effects at C-4 is probably responsible for the lower double bond-order of the nitrone function compared with those of the reference systems, **5** and **6**.[2] The SCS-SCS correlation between C_α and C-4 in **2**, however, gave different slopes between electron-

Table 3. Correlations of ^{13}CSCS Values with Hammett σ_p or Yukawa-Tsuno σ_i and σ_π Constants at Representative Positions in **2**[a)]

	n	SCS=$\rho_p\cdot\sigma_p$+C				SCS=$\rho_\pi^+\cdot\sigma_\pi^+ + \rho_\pi^-\cdot\sigma_\pi^-$+C					SCS=$\rho_i\cdot\sigma_i + \rho_\pi^+\cdot\sigma_\pi^+ + \rho_\pi^-\cdot\sigma_\pi^-$+C					
		ρ_p	C	SD	r	ρ_π^+	ρ_π^-	C	SD	r	ρ_i	ρ_π^+	ρ_π^-	C	SD	r
C_α	11	2.31 ±0.48	−0.45 ±0.21	0.08	0.965	4.41 ±1.12	3.05 ±1.45	0.14 ±0.27	0.05	0.980	1.27 ±0.54	4.34 ±0.53	2.26 ±0.76	−0.10 ±0.16	0.01	0.996
C-1	11	−0.80 ±0.14	0.00 ±0.06	0.01	0.973	−1.28 ±0.75	−1.18 ±0.97	−0.16 ±0.18	0.02	0.920	−0.90 ±0.25	−1.23 ±0.25	−0.62 ±0.36	0.01 ±0.08	0.00	0.993
C-4	11	1.17 ±0.16	0.00 ±0.07	0.01	0.984	1.65 ±1.02	2.04 ±1.31	0.19 ±0.24	0.04	0.931	1.23 ±0.31	1.59 ±0.30	1.28 ±0.43	−0.04 ±0.09	0.00	0.995
C-1′	11	10.00 ±2.80	−3.09 ±1.23	2.72	0.937	20.02 ±2.81	13.58 ±3.63	−0.47 ±0.66	0.32	0.994						
H_α	11	0.13 ±0.04	−0.02 ±0.02	0.00	0.935	0.14 ±0.04	0.33 ±0.06	−0.01 ±0.01	0.00	0.991						

a) n: The number of data, SD: standard deviations, and r: correlation coefficients.

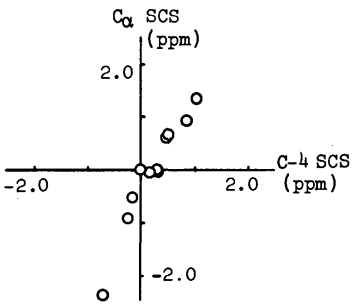

Fig. 4. Plot of C_α SCS vs. C-4 SCS in **2**.

donating and electron-withdrawing substituents (Fig. 4), reflecting different substituent effects at the two sites. Hence, dual parameter analyses will be a better approach to give quantitative information on the balance of electronic substituent effects.

Excellent correlations were obtained between the SCS values and the Yukawa-Tsuno σ_i and σ_π[13] parameters at the positions in **2** being discussed (Table 3).[††] The resonance effects are, as was expected, predominant at the conjugation sites, C-1′ and C_α, except in the case of C-4. The inductive effects can essentially be ignored at C-1′. It should be noticed that the slopes (ρ_π^+) for the electron-donating substituents are much larger than those (ρ_π^-) for the electron-withdrawing substituents at the two positions: ρ_π^+/ρ_π^-=1.5 and 2 at C-1′ and C_α respectively.

The resonance effects are, however, depressed at C-4 and are comparable to inductive effects. Since the ρ_π/ρ_i ratio will be a measure of the relative contribution of resonance effects to inductive effects, we next compared these ratios at C_α and C-4 in **2** with those for the corresponding sites in a reference system **6**. For **6**, the ρ_π^+/ρ_i and ρ_π^-/ρ_i values are nearly constant; i.e., they are 2.3 and 2.5 at C_α, and 1.8 and 2.2 at C-4, respectively. On the other hand, these values in **2** are 3.4 and 1.8 at C_α, and 1.3 and 1.0 at C-4, respectively. It is thus obvious that the resonance effects in **2** are anomalously enhanced at C_α by the electron-donating groups (but depressed by the electron-withdrawing groups), while at C-4 they are much more depressed, especially by electron-withdrawing groups. Therefore, the electronic effects of the 4′-substituents are transmitted to C_α and C-4 in a different fashion in **2**.

On the basis of the above observations of the electronic substituent effects at C-1′, C_α, C-1, and C-4 in **2**, we may propose the mechanisms shown in Scheme 2.

The nitrone function takes a coplanar conformation with the two phenyl groups in **2**, and the double-bond order is lower than those of the corresponding double bonds in **5** and **6**. The observed large shielding at C_α in **2** is best attributable to a "back-polarized" structure, **d**, which predominates over the alternative canonical form, **c**; thus, the positive charge on the nitrone function should be localized mainly on the nitrogen atom. In such situations, resonance effects caused by the electron-donating substituents on the *N*-phenyl ring will be important. The effects are illustrated by the structures shown in the right column of Scheme 2. Among the resonance structures, **g** and **h**, in which a negative charge donated by the substituent R is located on the carbons (i.e., C_α and/or C-1′) next to the positive nitrogen, electrically predominate over such a structure as **i**, in which the negative charge donated by R is delocalized over all the conjugation sites of the molecule (i.e., normal resonance effects are to be expected at the sites). On the other hand, among the resonance structures caused by electron-withdrawing groups, such as **e** and **f**, the **f** structure will show a negligible contribution because of the repulsion between the two neighboring positive charges on the

††A combined treatment of the σ_π^+ and σ_π^- parameters, such as was attempted in the previous paper,[2] is inappropriate in a situation such as this where resonance effects are predominant. Our data also give an excellent correlation with the Swain-Lupton F and R parameters: r=0.993 at C-1; r=0.991 at C_α; and r=0.995 at C-4.

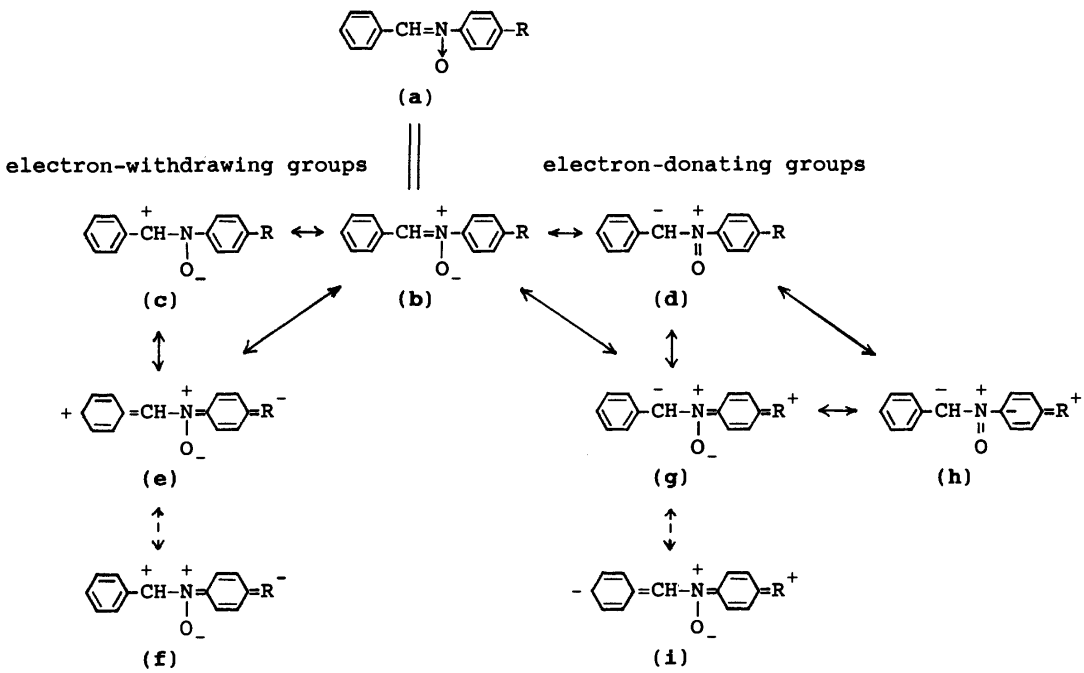

Scheme 2.

carbon and nitrogen atoms; thus, a positive charge is, as is shown by the canonical structure **e**, delocalized over all the conjugation sites of the molecule according to the electron demand of the electron-withdrawing substituents on the C-4′. Resonance effects caused by electron-withdrawing substituents are, hence, normal but depressed at C_α and C-4.

The H_α chemical shifts of **2** appear between the corresponding proton chemical shifts of **4** and **6**. This also supports the idea that the canonical structure **d** predominates over the alternative structure **c** in **2**. The SCS values at H_α also show a fairly good correlation (r=0.935) with the σ_p constants, and a better correlation coefficient of r=0.990 can be estimated when halogens are omitted from the correlation. The resonance effects of the substituents are, therefore, predominant at H_α. However, the sensitivity of H_α SCS is much lower than that of C_α SCS; therefore, correlation analysis based on H_α SCS seems to be less valuable for discussing the precise mechanism of the transmission of substituent effects.

References

1) N. Arumugam, P. Manisankar, S. Sivasubramanian, and D. A. Wilson, *Org. Magn. Reson.*, **22**, 592 (1984).

2) C. Yijima, T. Tsujimoto, K. Suda, and M. Yamauchi, *Bull. Chem. Soc. Jpn.*, **59**, 2165 (1986).

3) G. Palazzo, L. Baiocchi, and G. Picconi, *J. Heterocycl. Chem.*, **16**, 1469 (1979).

4) J. T. Hays, E. H. Butts, and H. L. Young, *J. Org. Chem.*, **32**, 153 (1967).

5) L. Gattermann and T. Wieland, "Die Praxis des Organishen Chemikers," Walter de Gruyter and Co., Berlin (1961), p. 154.

6) I. D. Entwistle, T. Gilkerson, R. A. W. Johnstone, and R. P. Telford, *Tetrahedron*, **34**, 213 (1978).

7) a) T. Kubota, M. Yamanaka, and Y. Mori, *Bull. Chem. Soc. Jpn.*, **36**, 1552 (1963); b) K. Koyano and H. Suzuki, *ibid.*, **42**, 3306 (1969); c) S. R. Sandler and W. Karo, "Organic Functional Group Preparations," Vol. III, Academic Press, New York (1972), Chap. 9; d) F. Kröhnke, *Ber.*, **71**, 2583 (1938); e) S. Hashimoto, I. Furukawa, and S. Fujimoto, *Nippon Kagaku Kaishi*, **1972**, 391.

8) a) R. Akaba, H. Sakuragi, and K. Tokumaru, *Bull. Chem. Soc. Jpn.*, **58**, 1186 (1985); b) *ibid.*, **58**, 1711 (1985); c) K. Tabei and E. Saitou, *ibid.*, **42**, 1440 (1969); d) A. Echevarria, J. Miller, and M. G. Nascimento, *Magn. Reson. Chem.*, **23**, 809 (1985).

9) G. K. Hamer, I. R. Peat, and W. F. Reynolds, *Can. J. Chem.*, **51**, 897 (1973); D. A. R. Happer, *J. Chem. Soc., Perkin Trans. 2*, **1984**, 1673.

10) D. Christoforou and D. A. R. Happer, *Aust. J. Chem.*, **36**, 2083 (1983).

11) G. Miyajima, Y. Sasaki, and M. Suzuki, *Chem. Pharm. Bull. (Tokyo)*, **19**, 2301 (1971); D. F. Ewing, *Org. Magn. Reson.*, **12**, 499 (1979).

12) D. Johnels, U. Edlund, H. Grahn, S. Hellberg, M. Sjostrom, S. Wold, S. Clementi, and W. J. Dunn, III, *J. Chem. Soc., Perkin Trans. 2*, **1983**, 863.

13) Y. Yukawa and Y. Tsuno, *Nippon Kagaku Zasshi*, **86**, 873 (1965); M. Sawada, M. Ichihara, Y. Yukawa, T. Nakachi, and Y. Tsuno, *Bull. Chem. Soc. Jpn.*, **53**, 2055 (1980).

 © 1987 The Chemical Society of Japan Bull. Chem. Soc. Jpn., 60, 3613—3618 (1987)

Enzymatic Reactions in Aqueous-Organic Media. II.[1] Effects of Reaction Conditions and Selectivity in the Esterification of Aromatic Amino Acids by α-Chymotrypsin in Alcohols

Hideo KISE,* Hitoshi SHIRATO, and Hidetaka NORITOMI
Institute of Materials Science, University of Tsukuba, Sakura, Niihari, Ibaraki 305
(Received February 5, 1987)

N-Acetylated aromatic amino acids were esterified by α-chymotrypsin suspended in alcohols. The reaction rate and the yields of the esters depended primarily on the amount of the aqueous buffer solution in which α-chymotrypsin was dissolved. The reaction rate increased but the equilibrium yield of the esters decreased with increasing concentration of water. High substrate selectivity and stereospecificity were observed for L-aromatic amino acids; and therefore, in this system α-chymotrypsin was considered to be an effective catalyst which maintains its native conformation. When the amount of the substrate was increased, the present reactions gave higher yields of the esters than the reactions in chloroform (two-phase method).

Recently, the area of enzymatic reactions in the presence of organic solvents, either miscible or immiscible with water, is rapidly growing and is drawing much attention. These reactions are of great interest in view of both basic studies on the medium effects on enzyme catalysis and the application of enzymatic reactions to organic synthesis. For example, hydrolytic enzymes, such as α-chymotrypsin (CT), have been employed as catalysts for various ester syntheses in aqueous-organic two-phase systems.[2-12] It has been considered that in this system the decreased amount of water and the low solubility of the products in the aqueous phase shift the reaction equilibrium to the synthesis of esters. However, when a hydrophobic (water-immiscible) organic solvent is used, the main drawback of the method is that if one of the reactants RCOOH such as amino acids is hardly soluble in the organic phase, it would be concentrated in the aqueous phase (Fig. 1a). This often causes a substrate inhibition of the enzyme, leading to low yields of the esters.[7,13]

The synthetic reactions by hydrolytic enzymes in water-hydrophilic (water-miscible) organic solvents have also been reported.[9,14-16] By using limited amounts of water in solvents, the equilibrium of the reaction can be shifted to favor the synthesis. However, the catalytic activity of the enzymes is often impaired at high concentrations of organic solvents, and the yields of products have been rather limited. For example, it has been reported that *N*-acetyl-L-tyrosine ethyl ester was obtained in 25—30% yields by CT-catalyzed reactions of *N*-acetyl-L-tyrosine with ethanol in 50—60% water, but that CT was inactivated at lower concentrations of water.[14]

The present study concerns with the esterification of *N*-acetylated aromatic amino acids by CT at very high concentrations of alcohols. The reaction system is heterogeneous containing suspended CT which can be easily separated by filtration like immobilized enzymes. The results for the effects of various reaction conditions on the reaction rate and the yield of the esters, as well as substrate selectivity and stereospecificity of the reaction, are reported.

Experimental

Materials. Bovine pancreatic α-chymotrypsin (CT) (EC 3.4.21.1) having a specific proteinase activity, with *N*-benzoyl-L-tyrosine ethyl ester (BTEE), of 50 units (μmol-min^{-1}) mg^{-1} of protein (pH 7.8 at 25 °C) was purchased from Sigma Chemical Co. *N*-Acetyl-L-tyrosine (ATy), its ethyl ester (ATyE), *N*-acetyl-D-tryptophan, -D-phenylalanine, and -L-alanine were also purchased from Sigma. *N*-Acetyl-L-tryptophan (AT), -L-phenylalanine (AP), their ethyl esters (ATE and APE), and *N*-acetyl-L-leucine were obtained from Nakarai Chemical Co. Alcohols and chloroform of guaranteed grade were also obtained from Nakarai and used without further purification.

Reactions and Measurements. Typically, a solution of CT (0.01 g) in 0.5 ml of phosphate buffer (0.1 M (1M=1 mol dm^{-3}), pH 6.8) was added to a solution of AT (0.05 g, 0.20 mmol) in 20 ml of ethanol. The mixture was incubated with constant reciprocal shaking (140 cycle per min) at 30 °C for 24 h (method A). Unless otherwise stated method A was used throughout this study. Alternatively, AT was first dissolved into the CT solution and then ethanol was added (method B). When chloroform was used as a solvent (two-phase method), the total volume of the organic solution was also 20 ml. In all the methods, after the reaction the solvents were evaporated with a rotary evaporator, and the amounts of AT and ATE in the residue were determined by a HPLC (JASCO Tri Rotar SR-1) using a JASCO Finepak SIL C18 column eluted with water-acetonitrile (50/50 by volume). Acetanilide was used as an internal standard.

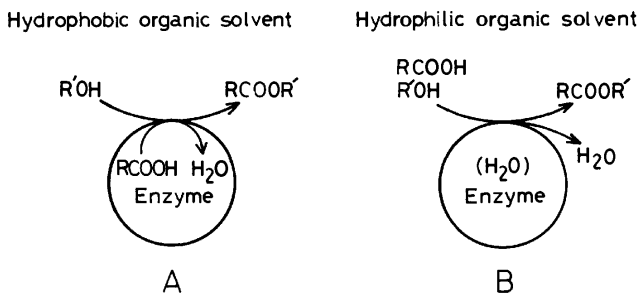

Fig. 1. Schematic representation of enzymatic ester synthesis in two-phase (A) and the present (B) systems.

The initial rate of esterification was measured by a determination of the amounts of AT and ATE in the reaction mixtures at intervals. A 4 μl aliquat of the reaction mixture, from which CT had been removed by filtration with a regenerated cellulose type membrane filter, was injected directly inot HPLC and analyzed under the same conditions as described above.

The CD spectra of CT solutions in ethanol or water were obtained with a JASCO spectropolarimeter model J-20.

Results and Discussion

Ester Synthesis in Chloroform (Two-Phase Method). In order to elucidate the effect of a water-immiscible organic solvent we at first investigated the esterification of AT by CT in chloroform.[1] Figure 2 shows the time courses of esterification with 1 M ethanol in chloroform and with different amounts of buffer solution in which CT was dissolved. It can be seen that the conversion (yield) of ATE at equilibrium increases with the decrease in the amount of the buffer. Although longer reaction time was required to attain the equilibrium with 0.25 ml of the buffer solution, more than 90% conversion was obtained after 24 h. Without water, however, the reaction was totally inhibited, indicating that a minimum amount of water is essential to the catalytic activity of CT. Furthermore, no reaction occurred without CT under the same conditions, ruling out the possibility of catalysis by ionic species in the buffer solutions.

The dependency of the equilibrium conversion on water content may be explained simply by a mass action law which predicts that with decreasing amounts of water the equilibrium shifts to ester synthesis. It is considered that the reaction occurs in the water droplets in which CT is dissolved. With lower water contents the amount of free water available for hydrolysis may be small enough to suppress the hydrolysis.

When the concentration of ethanol in chloroform was increased with a constant total volume of the organic phase (20 ml), the change in ATE yield was found to be rather small (less than 10%); the data are presented in Table 1. It had been considered that high concentration of water-miscible solvents such as ethanol would impair the enzyme activity and for this reason two-phase method has been employed. However, the above result indicates that chloroform can be replaced as a solvent by ethanol without any serious inactivation of CT. In neat ethanol the reaction mixture is a suspension of hydrated CT which can be separated by filtration with a glass or a membrane filter. Since the reactions in alcohols are clean and easy to work up, and, as will be mentioned later, the substrate inhibition is much less than in two-phase method, most of the reactions were carried out in alcohols.

Ester Synthesis in Ethanol. The effects of the reaction conditions on the ester yield were extensively studied in order to obtain optimum conditions. Figures 3 to 5 exhibit plots of the yields of ethyl esters of AT, ATy, and AP after 24 h reactions in ethanol against the volume-% of aqueous buffer solutions in which CT

Table 1. Effect of EtOH Concentration on ATE Yield[a]

EtOH in $CHCl_3$/M	ATE yield/%
1	83
3	86
5	77
8.6 (50 vol-%)	79
17.1 (neat)	78

a) AT 0.05 g (0.20 mmol), CT 0.01 g, organic phase 20 ml, phosphate buffer (0.1 M, pH 6.8) 0.5 ml, 30 °C, 24 h.

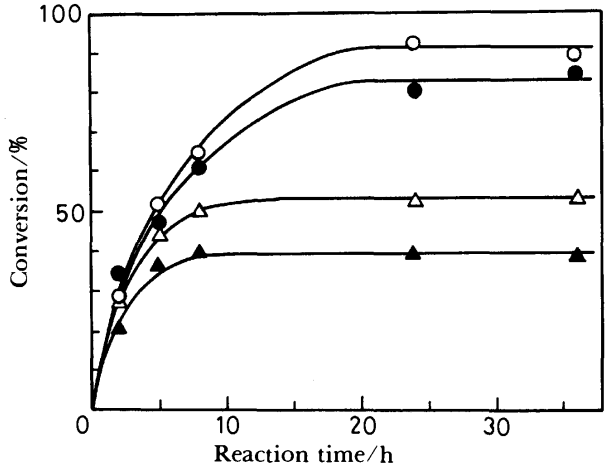

Fig. 2. Time courses of CT-catalyzed esterification of AT in chloroform. AT 0.05 g (0.20 mmol), CT 0.01 g, 1 M EtOH in chloroform (20 ml), 30 °C, phosphate buffer (0.1 M, pH 6.8) ○: 0.25 ml, ●: 0.5 ml, △: 1.0 ml, ▲: 2.0 ml.

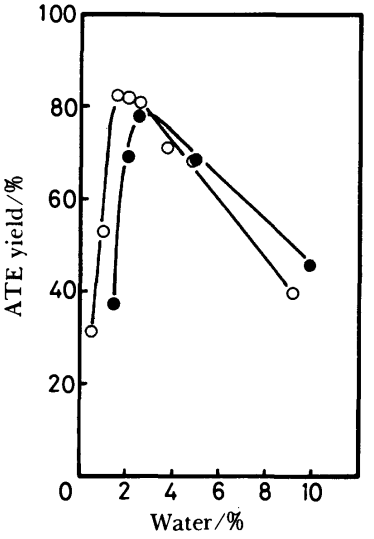

Fig. 3. Effect of water content on ATE yield. AT 0.05 g (0.20 mmol), CT 0.01 g, EtOH 20 ml, phosphate buffer (0.1 M, pH 6.8), 30 °C, 24 h. ○: Method A, ●: method B.

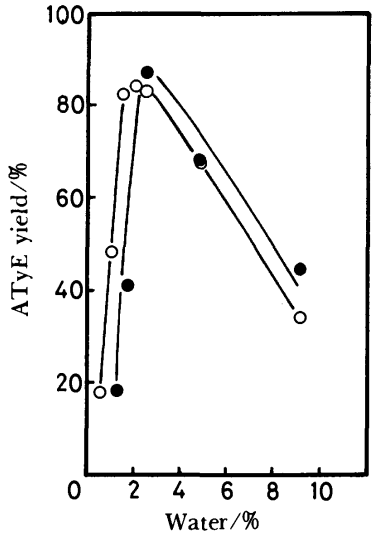

Fig. 4. Effect of water content on ATyE yield. ATy 0.045 g (0.20 mmol). Other reaction conditions and methods are the same as those in Fig. 3.

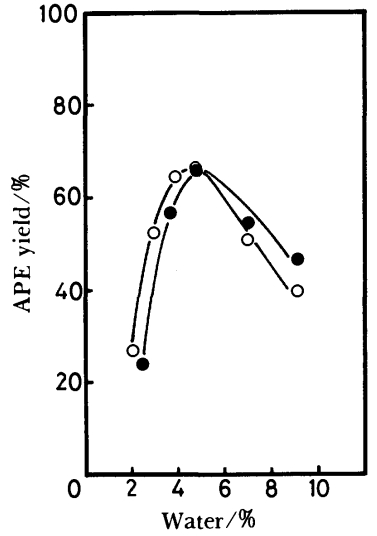

Fig. 5. Effect of water content on APE yield. AP 0.042 g (0.20 mmol). Other reaction conditions and methods are the same as those in Fig. 3.

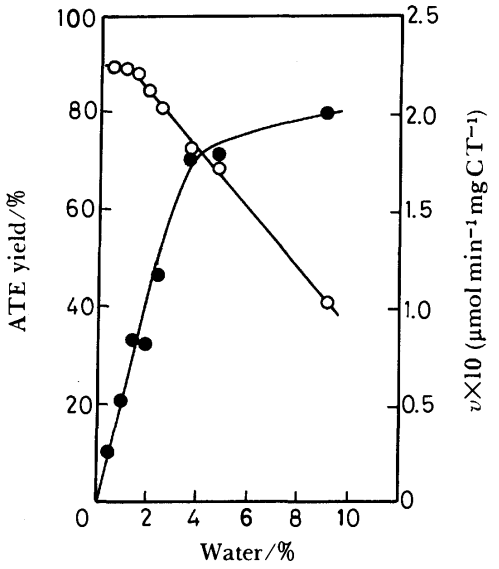

Fig. 6. Effect of water content on ATE yield (○) and the reaction rate (●) of esterification of AT. In the region of low water content, reaction time was increased up to 15 days. AT 0.05 g (0.20 mmol), CT 0.01 g, phosphate buffer (0.1 M, pH 6.8), 30 °C.

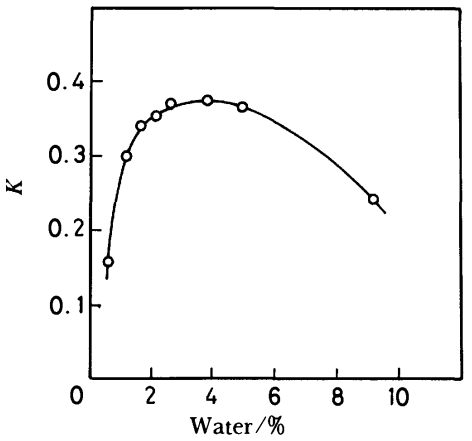

Fig. 7. Change in K with water content. K=[ATE]-[water]/[AT][EtOH].

was dissolved. The results for the two methods (method A and B, see Experimental) are compared in each Figure. The yields of the three esters exhibit a similar dependency on the water content, although the water contents which gave maximum yields are different. Like the reactions in chloroform mentioned above, the decrease in the yield with increasing amount of water may be explained by the shift of the equilibrium to hydrolysis. Alternatively, the increase in the solubility of CT in ethanol-water may be responsible for the decrease in the yield, since, as will be mentioned later, CT loses activity by dissolving in the mixed solvent.

The marked decrease in the yields at lower water concentrations may be the consequence of the slower reaction rate due to the decrease in the degree of hydration of CT which is considered to be essential to the catalytic activity of CT. This consideration may be supported by the fact that, as shown in Fig. 6, the rate of ATE synthesis decreased with a decreasing amount of water. Furthermore, the yield of ATE at prolonged reaction times up to 15 days which were considered to be enough to attain the equilibrium shows quite different dependency on water content from those shown in Fig. 3. In the lower range of water content, a prolonged reaction time gave much higher yields than those for 24 h reactions shown in Fig. 3. This suggests that the amount of active enzyme decreases with the decrease in water content for probably not only ATE but also ATyE and APE synthetic reactions. As in the

Table 2. Effect of Reaction Temperature[a]

Temp/ °C	$v \times 10^2$ μmol min^{-1} mg^{-1}	Yield/% 24 h	48 h	72 h
−3	3.2	73	71	
10	8.3	83	84	
20	12	82	82	
30	12	81	81	
35	12	85		
40	4.9	41	54	60
50	4.7	6.7	7.0	

a) AT 0.05 g, CT 0.01 g, EtOH 20 ml, phosphate buffer (0.1 M, pH 6.8) 0.5 ml.

Table 3. Effect of the Amount of Substrate[a]

AT/g	Reaction time/h	pH	ATE yield/% In EtOH[b]	In $CHCl_3$[c]
0.05	24	6.8	81	78
0.05	48	6.8	81	
0.075	24	6.8	79	
0.075	48	6.8	80	
0.10	24	6.8	86	
0.10	48	6.8	80	
0.15	24	6.8	75	
0.15	48	6.8	81	
0.15	72	6.8	84	
0.20	24	6.8	70	
0.20	48	6.8	85	
0.20	72	6.8	83	
0.20	96	6.8	85	4.4
0.20	96	5.0		2.7
0.20	96	8.6		3.5
0.20	96	9.0		2.0
0.25	24	6.8	26	
0.25	96	6.8	58	3.0

a) CT 0.01 g, phosphate buffer (0.1 M) 0.5 ml, 30 °C. b) EtOH 20 ml. c) 1 M EtOH in $CHCl_3$ 20 ml.

reaction in chloroform, in the absence of water the reaction was totally inhibited.

Figure 7 shows a plot of the calculated equilibrium constant K for ATE synthesis against water content. The K value may be affected by several factors, such as the dielectric constant of the medium; however, much slower reactions at very low concentrations of water are probably responsible for the sharp decrease in K in this region. It was found that CT loses activity at 50 °C, probably due to denaturation; the optimum temperatures for the ester synthesis were between 10 and 35 °C (Table 2).

Effect of the Amount of the Substrate. It was found that an increase in the initial amount of AT caused a decrease in the yield of ATE after 24 h reaction. However, in ethanol the yield of ATE increased upon increasing the reaction time, whereas in chloroform the yield was largely suppressed regardless of the reaction time and pH of the buffer solution. The results are summarized in Table 3.

These results imply that, when the initial amount of AT was increased, for example 0.2 g of AT in 20 ml of

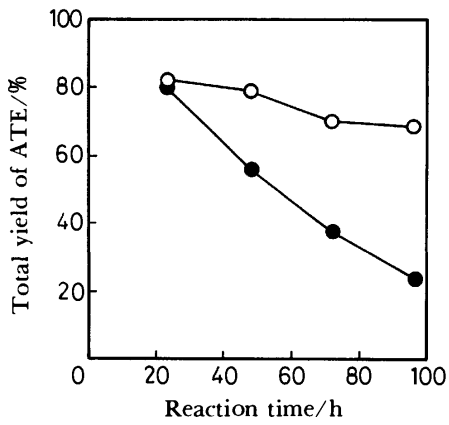

Fig. 8. Change in the yield of ATE in consecutive reactions. 0.05 g each of AT was added every 24 h. CT 0.01 g, EtOH (○) or chloroform (●) 20 ml, phosphate buffer (0.1 M, pH 6.8) 0.5 ml, 30 °C.

solvent, the reaction in ethanol is under kinetic control, but other factors must be taken into consideration for the reactions in chloroform, since the yields were very low even after prolonged reactions (below 5% after 96 h, Table 3). No distinct conclusion can be drawn from the present study, but it is probable that excess AT, which is considered to be concentrated in water phase, hinders CT activity.

Stability of Chymotrypsin. One of the most important aspects of enzymatic reactions is the stability of enzymes in the reaction media. Figure 8 shows the change in the total ATE yield in the course of successive reactions in which an equal amount of AT (0.05 g) was added every 24 h to the reaction mixtures containing constant amounts of CT and water. The total yield in ethanol decreased from 82 to 68% in going from the first reaction with 0.05 g AT for 24 h to the fourth reaction with total 0.20 g AT for 96 h. The yield decreased more rapidly in chloroform than in ethanol. The above result can not be attributed only to the instability of CT in chloroform, since the accumulation of AT may impair CT activity as mentioned above. The result, however, again exhibits the preference of the reaction in ethanol to that in chloroform when larger amounts of AT were employed.

Selectivity in Ester Synthesis. *N*-Acetylated L-alanine and L-leucine could not be esterified under the same conditions as those for aromatic amino acids. Also the yields of ethyl esters of *N*-acetylated D-tryptophan and D-phenylalanine were negligibly low. These results clearly indicate that substrate selectivity, stereospecificity, and therefore the native conformation of CT were strictly maintained in the present reaction system.

Klibanov et al.[17] reported that porcine pancreatic lipase maintained a high stability in various alcohols and that at very low water concentrations the enzyme exhibited a high activity, even at 100 °C. It seems from these results that enzymes require only small amounts

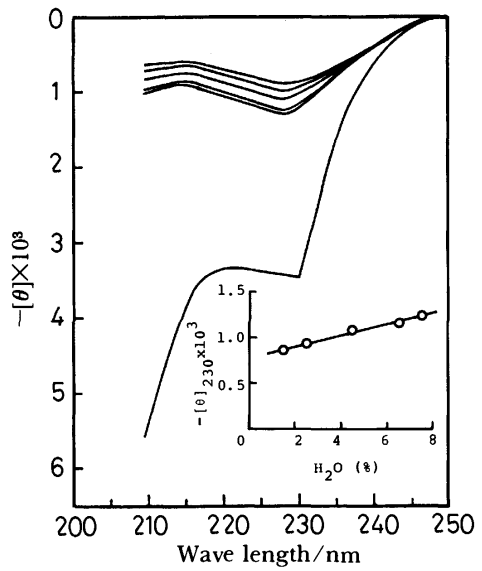

Fig. 9. CD spectra of CT in EtOH. From upper to lower water contents (%) are 1.5, 2.5, 4.5, 6.5, 7.5, and in neat water (pH 6.8). Insertion is the plot of $-[\theta]$ at 230 nm against water content.

Table 4. Effect of Alcohol Structure on AT Ester Synthesis[a)]

Alcohol	$v\times10^2$	Ester yield/%	
	μmol min^{-1} mg^{-1}	24 h	48 h
Methanol	0	0	0
Ethanol	12	81	81
1-Propanol	21	83	82
2-Propanol	17	78	79
1-Butanol	21	83	84
2-Butanol	12	65	78
2-Methyl-1-propanol	17	80	83
2-Methyl-2-propanol	0	0	0
1-Hexanol	0	40	61

a) AT 0.05 g, CT 0.01 g, alcohol 20 ml, phosphate buffer (0.1 M, pH 6.8) 0.5 ml, 30 °C.

of water for the maintenance of their native conformation in alcoholic solutions.

It was found that in the present system about 85% of added CT is suspended in ethanol and the rest of CT which is solubilized in ethanol is inactive. It has been reported that the content of α-helix in CT can be evaluated by the CD band at 230 nm, and the intensity of this band can be correlated with the enzyme activity.[18-20] Our data in ethanol is presented in Fig. 9. The CD spectrum in a phosphate buffer (pH 6.8) is also given in the Figure. It can be clearly seen that the intensity ($-[\theta]$) at 230 nm in ethanol decreases with a decrease in the water content, and is much lower than that in a buffer solution. Thus, the inactivity of solubilized CT in ethanol-water may be interpreted by the change in its conformation, probably due to a hydrophobic interaction between the enzyme and ethanol.

The results for the reactions of AT with different alcohols are summarized in Table 4. It is interesting that methanol and 2-methyl-2-propanol (*t*-butyl alcohol) are specifically inactive, while other alcohols gave esters in fairly good yields. Although no definite conclusion can be derived on the structure-reactivity relationship for the alcohols, it seems that CT exhibits rather a loose selectivity for the structure of alcohols as in the case of peptide synthesis in water where the amine components to some extent affect the reaction rate.[21]

Conclusion

The esterification of *N*-acetylated aromatic amino acids was realized in alcohols containing small amounts of water. The reaction mixture is considered to contain hydrated α-chymotrypsin (CT) suspended in alcohols which catalyzes the reaction, while CT in solution was found to be inactive. The reaction rate and the yield of the esters depended primarily on the water content in the reaction mixtures. The optimum reaction temperatures were between 10 and 35 °C. When the initial amount of AT was increased, CT suffered less of a substrate inhibition in ethanol than in chloroform. From the study of substrate selectivity, CT is considered to maintain its native conformation in this reaction system.

The present work was partially supported by University of Tsukuba Project Research.

References

1) Part I: H. Kise and H. Shirato, *Tetrahedron Lett.*, **26**, 6081 (1985).
2) A. M. Klibanov, G. P. Samokhin, K. Martinek, and I. V. Berezin, *Biotechnol. Bioeng.*, **19**, 1351 (1977).
3) K. Martinek, A. N. Semenov, and I. V. Berezin, *Biotechnol. Bioeng.*, **23**, 1115 (1981).
4) K. Martinek, A. N. Semenov, and I. V. Berezin, *Biochim, Biophys. Acta*, **658**, 76 (1981).
5) K. Martinek and A. N. Semenov, *Biochim. Biophys. Acta*, **658**, 90 (1981).
6) D. Tarquis, P. Monsan, and G. Durand, *Bull. Soc. Chim. Fr.*, **1980**, II-76.
7) J. L. Vidaluc, M. Baboulene, V. Speziale, and A. Lattes, *Tetrahedron*, **39**, 269 (1983).
8) G. Kirchner, M. P. Scollar, and A. M. Klibanov, *J. Am. Chem. Soc.*, **107**, 7072 (1985).
9) H. H. Weetal, *Biotechnol. Bioeng.*, **27**, 124 (1985).
10) G. Langrand, M. Secchi, G. Buono, J. Baratti, and C. Triantaphylides, *Tetrahedron Lett.*, **26**, 1857 (1985).
11) G. Langrand, J. Baratti, G. Buono, and C. Triantaphylides, *Tetrahedron Lett.*, **27**, 29 (1986).
12) S. Osanai, *Yukagaku*, **35**, 955 (1986).
13) B. Cambou and A. M. Klibanov, *Biotechnol. Bioeng.*, **26**, 1449 (1984).
14) R. G. Ingalls, R. G. Squires, and L. G. Butler, *Biotechnol. Bioeng.*, **17**, 1627 (1975).
15) A. Kepune and V. Kasche, *Biochem. Biophys. Res. Commun.*, **80**, 955 (1978).
16) Y. Nakamoto, I. Karube, I. Kobayashi, M. Nishida,

and S. Suzuki, *Arch. Biochem. Biophys.*, **193**, 117, (1979).
17) A. Zaks and A. M. Klibanov, *Science*, **224**, 1249 (1984).
18) G. D. Fasman, R. J. Foster, and S. Beychock, *J. Mol. Biol.*, **19**, 240 (1966).
19) J. McConn, G. D. Fasman, and G. P. Hess, *J. Mol. Biol.*, **39**, 551 (1969).
20) S. Barbaric and P. L. Luisi, *J. Am. Chem. Soc.*, **103**, 4239 (1981).
21) D. D. Petkov and Iv. Stoineva, *Biochem. Biophys. Res. Commun.*, **118**, 317 (1984).

 © 1987 The Chemical Society of Japan Bull. Chem. Soc. Jpn., 60, 3619—3623 (1987)

Excimer Formation and Induced-Fit Type of Complexation of β-Cyclodextrin Capped by Two Naphthyl Moieties

Fumio Moriwaki, Hiromi Kaneko, Akihiko Ueno,* Tetsuo Osa,*
Fumio Hamada,† and Koichi Murai†
Pharmaceutical Institute, Tohoku University, Aobayama, Sendai 980
†Department of Fuel Chemistry, Mining College, Akita University, Gakuen-cho, Tegata, Akita 010
(Received February 16, 1987)

Host-guest complexation of β-Cyclodextrin bearing two naphthyl moieties (**1**) has been studied by circular dichroism and fluorescence spectroscopic methods. The circular dichroism spectrum exhibits a positive band around 225 nm while the fluorescence spectrum exhibits a predominant monomer peak with a shoulder of excimer emission. These data suggest that **1** can take two forms, one of two naphthyl moieties being included in the cavity of the predominant form (A) while both naphthyl moieties being located outside of the cavity in another form (B). With increasing concentration of guests, the dichroism intensity diminishes but the excimer intensity increases. This result indicates that **1** moves the included naphthyl moiety outward from the interior of the cavity during guest binding and then the two naphthyl moieties act as hydrophobic caps. The binding of **1** was stronger for cyclohexanol and 1-adamantanecarboxylic acid but weaker for cyclododecanol than that of the corresponding γ-cyclodextrin derivative in correspondence with size-fitting between the guests and hosts.

Cycloamyloses (Cyclodextrins, CDs) are water-soluble receptors and have been extensively studied as enzyme models, catalysts, miracle additives in pharmacy and food processing, and others.[1] The number of glucopyranose unit is designated by a Greek letter: α for six, β for seven, γ for eight, and so on. The smaller α- and β-CDs have been widely used because of their appropriate cavity sizes for forming 1:1 inclusion complexes with usual organic molecules.[1] However, recently, γ-CD has excited much attention because of the inclusion of two guest molecules in its large cavity.[2-5] As an extension of the works on the two guest accommodation by γ-CD, inclusion phenomena of some γ-CD derivatives have been studied,[6-8] and the γ-CD derivative bearing two naphthyl moieties (**2**) was found to act as a flexible host in which the two naphthyl moieties move outward from the interior of the cavity during guest binding to act as hydrophobic caps (Scheme 1).

In this report, we describe the binding behavior of β-CD bearing two naphthyl moieties **1** in which simultaneous accommodation of the two naphthyl moieties seems impossible because of its smaller cavity size. The guest-dependent excimer formation as well as the solvent-induced conformational changes of **1** will also be shown.

Results

Compound **2** was prepared by the procedure reported previously.[7b] Compound **1** was synthesized in the same manner as that of **2** via azobenzene-capped β-CD (**3**). Figure 1 shows the absorption and circular dichroism spectra of **1** in aqueous 10% ethylene glycol (EG) solutions at various concentrations of 1-adamantanecarboxylic acid (1-ACA). The solvent composition used is due to the poor solubility of **1** in pure

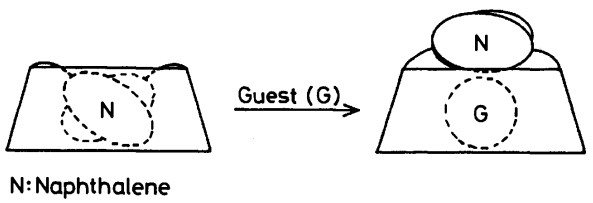

Scheme 1.

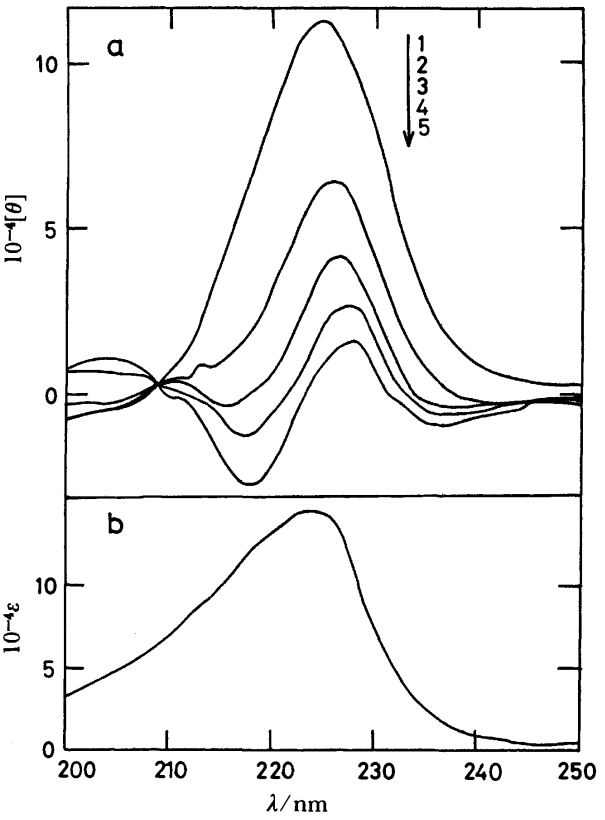

Fig. 1. Circular dichroism (a) and absorption (b) spectra of **1** in aqueous 10% EG solutions (6.5×10^{-6} mol dm^{-3}) at various 1-ACA concentrations (a, 1, 0.0; 2, 3.3×10^{-5}; 3, 6.7×10^{-5}; 4, 1.3×10^{-4}; 5, 3.0×10^{-4} mol dm^{-3}; b, 0.0 mol dm^{-3}).

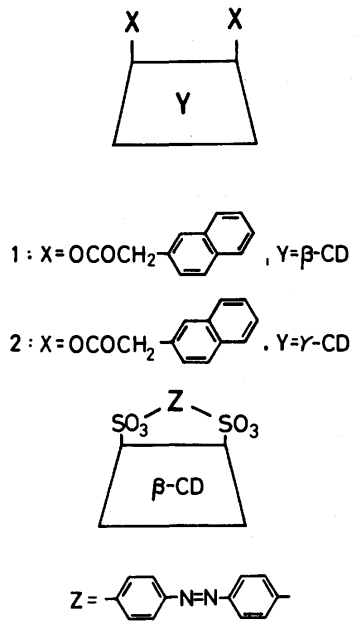

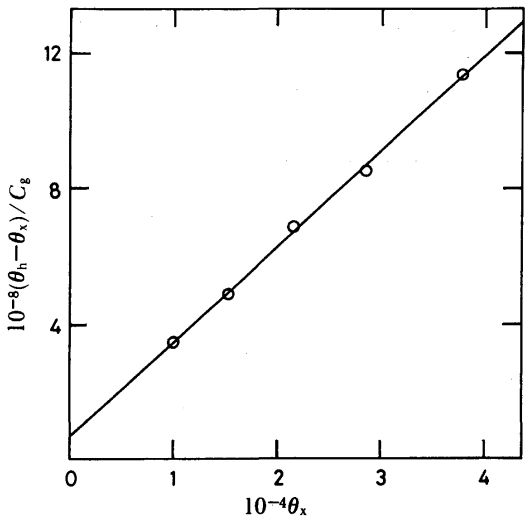

Fig. 2. The plot of $(\theta_h-\theta_x)/C_g$ as a function of θ_x in the system of **1** and 1-ACA.

water. Here, circular dichroism measurements were performed only in the naphthalene ^1B_b transition region. No reliable data in the ^1L_a transition region was obtained due to the limited solubility of **1** and the small circular dichroism ellipticity of the band. The circular dichroism spectrum in the absence of 1-ACA reveals a positive peak around 225 nm with the molar ellipticity of 110000 associated with the naphthalene ^1B_b transition. The intensity of the positive peak diminished with increasing 1-ACA concentration. When (−)-borneol and cyclohexanol were used as guest molecules, similar phenomena were observed. The guest-induced variations in the molar ellipticity were analyzed to obtain binding constants (K) of **1**, by using Eq. 1 which can be used in the presence of large excess

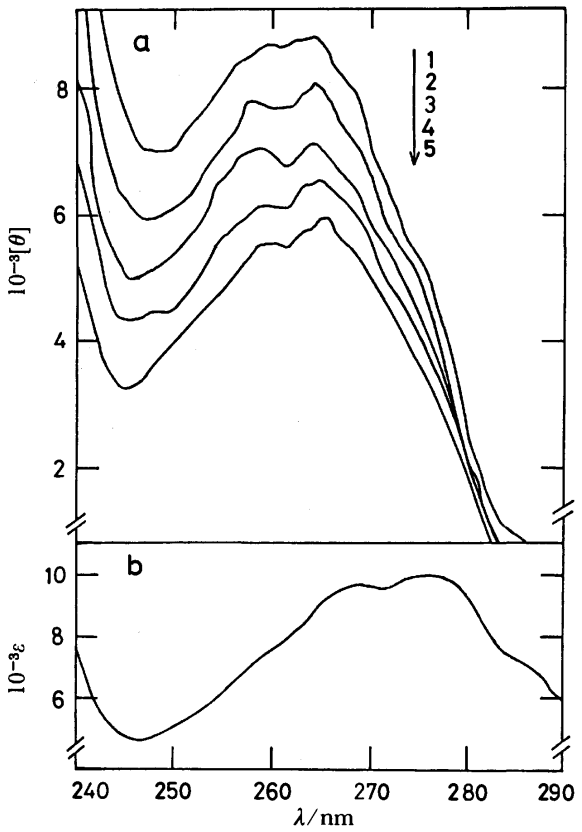

Fig. 3. Circular dichroism (a) and absorption (b) spectra of **1** in aqueous 10% DMSO solutions (6.5×10^{-5} mol dm^{-3}) at various cyclododecanol concentrations (a, 1, 0.0; 2, 3.3×10^{-5}; 3, 6.7×10^{-5}; 4, 1.3×10^{-4}; 5, 2.0×10^{-4} mol dm^{-3}; b, 0.0 mol dm^{-3}).

of guest.[9]

$$\frac{\theta_h-\theta_x}{C_g}=k\theta_x-k\theta_c \qquad (1)$$

Figure 2 shows the plot of $(\theta_h-\theta_x)/C_g$ against θ_x in the case of 1-ACA. Here, θ is molar ellipticity (the molar ellipticity at 225 nm in this study), θ_x for sample, θ_h for host alone, θ_c for complex, and C_g is total guest concentration. Cyclododecanol was also used as a guest molecule. In the case of cyclododecanol, aqueous 10% dimethyl sulfoxide (DMSO) was used as a solvent instead of aqueous 10% EG, because of the poor solubility of cyclododecanol in aqueous 10% EG. Circular dichroism measurements of the aqueous 10% DMSO solutions of **1** were performed in the naphthalene ^1L_a transition region since the measurements in the shorter wavelengths could not be achieved due to the absorption of DMSO. It is noted that the solubility of **1** in aqueous 10% DMSO was large enough to perform the circular dichroism measurements in the naphthalene ^1L_a transition region. The guest-induced variation of the molar ellipticity at 265 nm (Fig. 3) was analyzed by using the curve-fitting method because, in this case, the guest is not in large excess and Eq. 1 cannot be applicable.[7b] The binding constants of **2** for

Table 1. Binding Constants of **1** and **2** at 25 °C[a)]

Guest	Solvent	K/mol^{-1}dm^{3}[b)]	
		1	**2**
1-ACA	10% EG	28000	1000
(−)-Borneol	10% EG	1900	1800
Cyclododecanol	10% DMSO	4600	26000[c)]
Cyclohexanol	10% EG	90	32

a) Values were obtained by the plot of $(\theta_h-\theta_x)/C_g$ vs. θ_x except for the value for cyclododecanol which was obtained by the curve-fitting method. b) Errors are within ±9%. c) Reported in Ref. 7b.

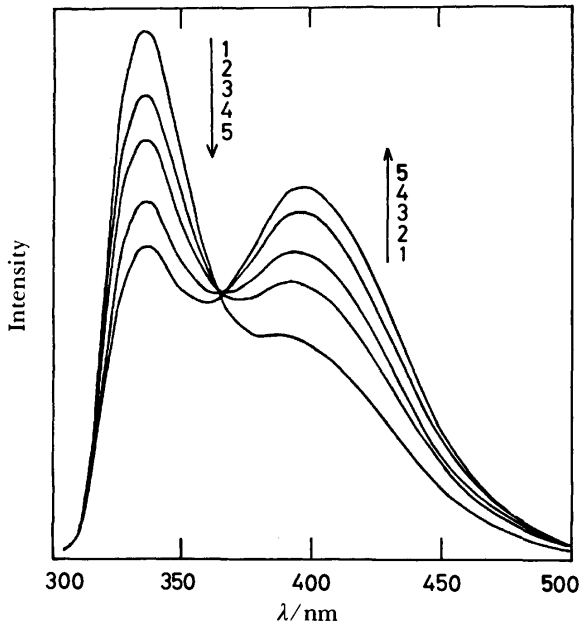

Fig. 4. Fluorescence spectra of **1** in aqueous 10% EG solutions (6.5×10^{-6} mol dm^{-3}) at various 1-ACA concentrations (1, 0.0; 2, 3.3×10^{-5}; 3, 6.7×10^{-5}; 4, 1.3×10^{-4}; 5, 2.3×10^{-4} mol dm^{-3}). Excitation wavelength is 290 nm.

1-ACA, cyclohexanol, and (−)-borneol were also obtained to be compared with those of **1** by the analysis (Eq. 1) of the circular dichroism variations at 215 nm of **2** (6.5×10^{-6} mol dm^{-3}) in aqueous 10% EG solutions. The binding constant of **2** for cyclododecanol in aqueous 10% DMSO solution was reported previously.[7b)] The obtained binding constants are listed in Table 1.

Figure 4 shows the fluorescence spectra of **1** in aqueous 10% EG solutions at various 1-ACA concentrations. The spectrum in the absence of 1-ACA exhibits a predominant monomer fluorescence around 336 nm and a shoulder of excimer emission around 394 nm. With increasing 1-ACA concentration, the intensity of the monomer fluorescence decreases while that of the excimer emission increases. When (−)-borneol and cyclohexanol were used in place of 1-ACA as guests, similar phenomena were observed.

It was found that EG content in the solutions of **1** markedly influences the circular dichroism and fluorescence patterns. The circular dichroism intensity of the positive peak around 225 nm decreased with increasing EG content. The EG-dependency of the fluorescence pattern was more complicated, that is, the intensity of the monomer fluorescence increases monotonously while the intensity of the excimer emission reaches a maximum around 50% of EG and then decreases with increasing EG content (Fig. 5).

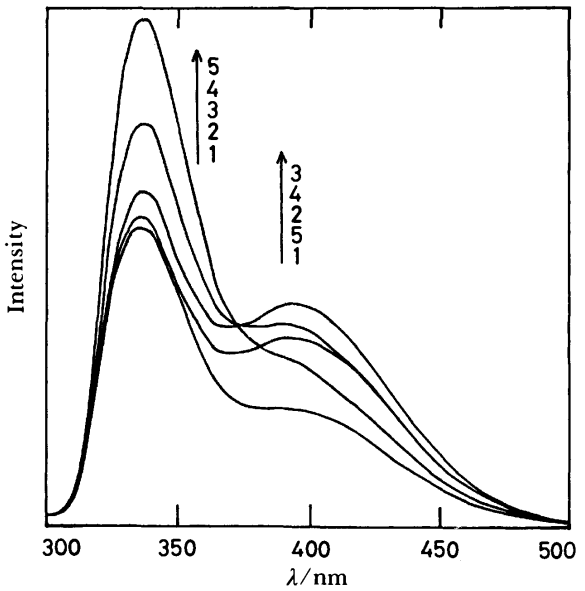

Fig. 5. Fluorescence spectra of **1** (5.4×10^{-6} mol dm^{-3}) at various EG content (1, 10; 2, 30; 3, 50; 4, 80; 5, 100%).

Discussion

The synthesis of **1** was performed via β-CD capped by azobenzene-4,4′-disulfonate moiety (**3**). Therefore, the positions of the two naphthyl moieties are those of primary hydroxyls sulfonated by azobenzene-4,4′-disulfonyl dichloride. When glucose units of CD ring are denoted by A, B, C, D, etc., in the order, primary hydroxyl groups of A and D glucose units of β-CD were reported to be selectively sulfonated by stilbene-4,4′-disulfonyl dichloride.[10)] Similar selectivity may be expected with azobenzene-4,4′-disulfonyl dichloride. The determination of the modified positions of **3** was performed by the reversed-phase high-performance liquid chromatography (HPLC). The diazido-β-CD, which was prepared by the reaction of **3** with sodium azide, was assigned to the AD-isomer by comparing its retention time with those of the AB-, AC-, AD-diazido-β-CD.[11)] Consequently, the modified positions of **1** and **3** are A and D of primary hydroxyls of β-CD.

The circular dichroism and fluorescence spectra of **1** may be used for determing the location of the two naphthyl moieties. By using the spectroscopic data, we first discuss the structural features of **1** in the absence of any guest. Considering the fact that **1** cannot include the two naphthyl moieties simultaneously

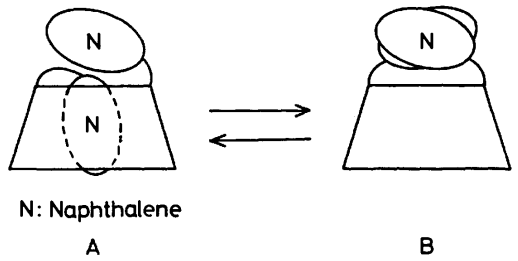

Scheme 2.

because of its small cavity size, the positive peak observed in the region of ^1B_b transition, which is longitudinally polarized, may arise from the form A (Scheme 2), in which one of the two naphthyl moieties is included axially.[12] Since face-to-face interaction between the two naphthyl moieties is not allowed for such a geometry, it is obvious that excimer formation should not occur in the A form. However, excimer emission was observed as shoulder of the main peak of monomer fluorescence; therefore **1** can be either in A or B form as shown in Scheme 2. In the B form, the two naphthyl moieties are both out of the CD cavity, interacting with each other.

The guest-induced decreases in the molar ellipticity suggest that **1** moves one of its pendant naphthyl moieties outward from the interior of the cavity during guest binding. The guest-induced decreases in the monomer fluorescence and increases in the excimer emission suggest that the two naphthyl moieties are close in the complexes. The two naphthyl moieties are likely to contact with the included guest molecule as flexible caps, as illustrated below. It is noted that the

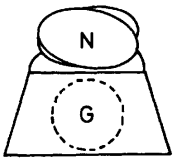

excimer formation in the complex may be compared with the reported base-base interactions in the complexes of β-CD derivatives, which have two nucleobases.[13] The binding constants of **1** and **2** are listed in Table 1. It is noted that the guest-induced circular dichroism variations of **2** as well as those of **1** could be analyzed based on a simple 1 : 1 stoichiometry.[7b] The binding constants of **1** for 1-ACA and cyclohexanol are larger than those of **2**. These results suggest that **1** is a better host for these guests than **2**, in accordance with the fact that the cavity size of **2** is too large to include these guests tightly. The binding constants of **1** and **2** for (−)-borneol are similar in spite of the difference of their cavity sizes. The binding constant of **1** for cyclododecanol is smaller than that of **2**. This result may arise from the fact that **2** has an appropriate cavity to include cyclododecanol while **1** has the cavity too small to include the guest completely. The examination of the Corey-Pauling-Koltun models supports this argument. Consequently, γ-CD derivative **2** seems to exhibit the better binding ability than β-CD derivative **1**, for large guests such as cyclododecanol. This is in contrast with the fact that β-CD derivative **1** is better host than **2** for small guests.

Figure 6 shows the plots of excimer-monomer ratio and circular dichroism intensity at 225 nm against EG content. The solvent-induced decrease in the circular dichroism intensity suggests that EG tends to convert the intramolecular complex form of A into the relaxed form of B (Scheme 2). It is frequently seen that fluorescence of aromatic compounds is solvent-dependent, usually with greater intensity in apolar solvents than in polar solvents. In this case, the monomer fluorescence seems basically to be stronger in EG-rich solutions than in EG-poor solutions. However, the complicated result that there is a maximum ratio of excimer emission around 50% of EG requires an additional explanation. One possible explanation is that the face-to-face interaction needed for excimer formation is attained only in one of three forms of **1** (B in Scheme 3). It is noted that 50% EG is the solvent in

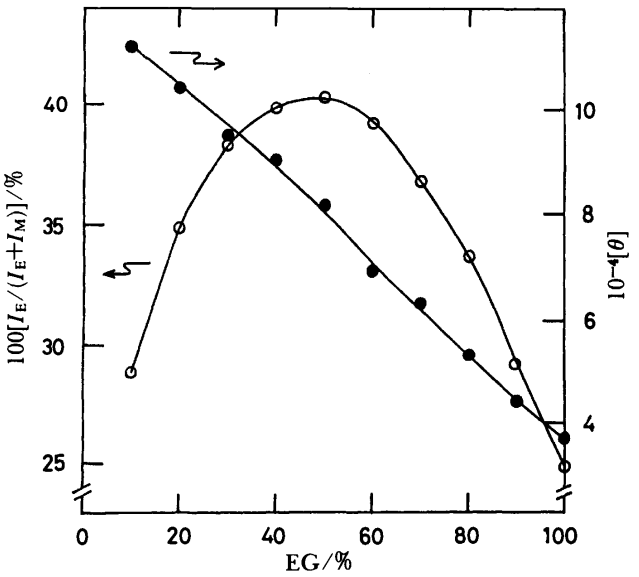

Fig. 6. Plots of excimer-monomer fluorescence ratio (I_M and I_E are intensities at 336 and 394 nm, respectively) and the molar ellipticity at 225 nm of **1** (5.4×10^{-6} mol dm^{-3}) as a function of EG content.

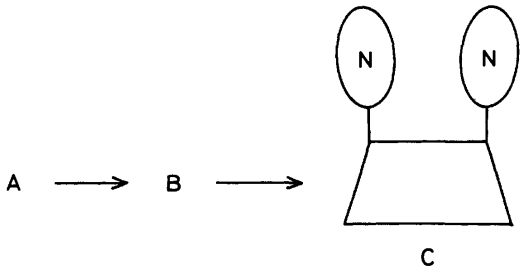

Scheme 3.

which hydrophobic interaction is still important; so two naphthyl moieties tend to interact with each other by the hydrophobic driving force. In the solutions with higher EG contents, the driving force becomes weaker and the two naphthyl moieties are likely to be located apart at the opposite sides of β-CD rim (C in Scheme 3). In the form of A, which mainly exists in the solutions with lower EG contents, excimer formation is stereochemically impossible. Consequently, A converts to C via B with increasing EG content.

Experimental

Materials. The following commercially available reagents (guaranteed grade) were used without further purification, β-CD, 1-ACA, (−)-borneol, cyclododecanol, cyclohexanol, and EG. DMSO was Dotite-spectrosol grade. Azobenzene-4,4′-disulfonyl dichloride and bis(2-naphthylacetyl)-γ-CD (**2**) were prepared by the same methods previously reported.[7b] Isomers of diazido-β-CD were prepared as the standard samples by the method of Fujita et al.[11]

Measurements. HPLC was performed analytically on a JASCO 800 series with a TSKgel ODS 120A column (4.6 ×250 mm, 5 μm, Toyo Soda, Japan). A linear gradient elution of 10% aqueous CH_3CN-25% aqueous CH_3CN was applied, and the diazido-β-CD was detected by monitoring the UV absorption at 210 nm. The circular dichroism, UV and fluorescence spectra were measured at 25 °C using a JASCO J-400X spectrodichrometer, a Shimadzu UV-250 spectrophotometer and a Shimadzu RF-500 spectrofluorophotometer, respectively. The circular dichroism intensities were expressed as molar ellipticity (in degree cm^2 $dmol^{-1}$) on the basis of the total concentration of **1** or **2**.

***trans*-Azobenzene-4,4′-disulfonyl-β-CD (3).** To a stirred solution of dry β-CD (4.0 g, 3.5 mmol) in dry pyridine (100 ml), azobenzene-4,4′-disulfonyl dichloride (1.3 g, 4.1 mmol) was added, and then heated at 60 °C for 1 h. After cooling the reaction mixture, pyridine was removed by evaporation under reduced pressure. Water addition to the residue followed by evaporation was repeated several times until no pyridine odor was detected. The resultant oily residue was dissolved in a small amount of water and subjected to Sephadex G-15 column chromatography. Recrystallization from methanol afforded the product (0.54 g, 10%): R_f=0.33 (5:1 CH_3CN-H_2O); Found: C, 43.47; H, 5.54; N, 1.97; S, 4.47%. Calcd for $C_{54}H_{76}N_2O_{39}S_2 \cdot 3H_2O$: C, 43.37; H, 5.53; N, 1.87; S, 4.29%.

Bis(2-naphthylacetyl)-β-CD (1). A mixture of **3** (0.54 g, 0.36 mmol), sodium 2-naphthyl acetate (0.31 g, 1.5 mmol) and DMSO (10 ml) was stirred at 80 °C for 6 h. After cooling, the reaction mixture was poured into 500 ml acetone. The precipitates were collected by filtration and subjected to column chromatography on silica gel (8:1 CH_3CN-H_2O). Recrystallization from water gave the desired product (0.15 g, 26%): R_f=0.50 (5:1 CH_3CN-H_2O). ^1H NMR (DMSO-d_6, 25 °C) δ=3.2—4.0 (42H, m, CD protons other than C_1H and OH), 4.2—4.6 (9H, m, O_6H and CH_2Ar), 4.7—4.9 (7H, m, C_1H), 5.6—5.9 (14H, m, O_2H and O_3H), 7.4—7.9 (14H, m, ArH); UV (9:1 H_2O-EG) (ε) 224 nm (150000); IR (KBr) 1720 cm^{-1} (CO). Found: C, 48.81; H, 6.01%. Calcd for $C_{66}H_{86}O_{37} \cdot 8H_2O$: C, 49.07; H, 6.36%.

This work was supported by Grant-in-Aid (Nos. 61470152 and 61550585) from the Ministry of Education, Science and Culture.

References

1) M. L. Bender and M. Komiyama, "Cyclodextrin Chemistry," Springer-Verlag (1978).

2) A. Ueno, K. Takahashi, and T. Osa, *J. Chem. Soc., Chem. Commun.*, **1980**, 921; N. Kobayashi, R. Saito, Y. Hino, A. Ueno, and T. Osa, *ibid.*, **1982**, 706; N. Kobayashi, R. Saito, Y. Hino, A. Ueno, and T. Osa, *J. Chem. Soc., Perkin Trans. 2*, **1983**, 1031; A. Harada and S. Nozakura, *Polym. Bull.*, **8**, 141 (1982); T. Yorozu, M. Hoshino, and M. Imamura, *J. Phys. Chem.*, **86**, 4426 (1982); K. Kano, I. Takenoshita, and T. Ogawa, *Chem. Lett.*, **1982**, 321; J. Emert, D. Kodali, and R. Catena, *J. Chem. Soc., Chem. Commun.*, **1981**, 758; N. J. Turro, T. Okubo, and G. C. Weed, *Photochem. Photobiol.*, **35**, 325 (1982); N. Kobayashi, Y. Hino, A. Ueno, and T. Osa, *Bull. Chem. Soc. Jpn.*, **56**, 1849 (1983); R. A. Yellin and D. F. Eaton, *J. Phys. Chem.*, **87**, 5051 (1983); M. Itoh and Y. Fujiwara, *Bull. Chem. Soc. Jpn.*, **57**, 2261 (1984).

3) N. Kobayashi, A. Ueno, and T. Osa, *J. Chem. Soc., Chem. Commun.*, **1981**, 340; N. Kobayashi, R. Saito, A. Ueno, and T. Osa, *Makromol. Chem.*, **184**, 837 (1983).

4) A. Ueno, K. Takahashi, Y. Hino, and T. Osa, *J. Chem. Soc., Chem. Commun.*, **1981**, 194; K. Kano, I. Takenoshita, and T. Ogawa, *J. Phys. Chem.*, **86**, 1833 (1982); K. Takamura, S. Inoue, and F. Kusu, *Chem. Lett*, **1983**, 233; H. Hirai, N. Toshima, and S. Uenoyama, *Bull. Chem. Soc. Jpn.*, **58**, 1156 (1985).

5) T. Tamaki, *Chem. Lett.*, **1984**, 53.

6) A. Ueno, Y. Tomita, and T. Osa, *J. Chem. Soc., Chem. Commun.*, **1983**, 976; A. Ueno, Y. Tomita, and T. Osa, *Tetrahedron Lett.*, **1983**, 5245; A. Ueno, Y. Tomita, and T. Osa, *Chem. Lett.*, **1983**, 1635; A. Ueno, F. Moriwaki, Y. Tomita, and T. Osa, *ibid.*, **1985**, 493.

7) a) A. Ueno, F. Moriwaki, T. Osa, F. Hamada, and K. Murai, *Tetrahedron Lett.*, **26**, 3339 (1985); b) A. Ueno, F. Moriwaki, T. Osa, F. Hamada, and K. Murai, *Bull. Chem. Soc. Jpn.*, **59**, 465 (1986).

8) F. Moriwaki, A. Ueno, T. Osa, F. Hamada, and K. Murai, *Chem. Lett.*, **1986**, 1865.

9) M. P. Pack, R. R. Hendrixson, R. A. Palmer, and R. G. Ghirardelli, *J. Am. Chem. Soc.*, **98**, 7830 (1976).

10) I. Tabushi, K. Yamamura, and T. Nabeshima, *J. Am. Chem. Soc.*, **106**, 5267 (1984).

11) K. Fujita, H. Yamamura, and T. Imoto, *J. Org. Chem.*, **50**, 4393 (1985).

12) K. Harata and H. Uedaira, *Bull. Chem. Soc. Jpn.*, **48**, 375 (1975).

13) K. Nagai, K. Hayakawa, S. Ukai, and K. Kanematsu, *J. Org. Chem.*, **51**, 3931 (1986).

Stereoelectronic Effects in Serine Proteases: Ab Initio Molecular Orbital Calculations

Kazunari TAIRA*,†,†† and David G. GORENSTEIN*
Department of Chemistry, Purdue University, W. Lafayette, Indiana 47907, U.S.A.
†Department of Chemistry, University of Illinois at Chicago, Chicago, Illinois 60680, U.S.A.
(Received February 23, 1987)

Ab initio molecular orbital calculations have been performed on the reaction profile for the addition/elimination reaction between ammonia and formic acid, proceeding via a tetrahedral intermediate: $NH_3+HCO_2H\rightarrow H_2NCH(OH)_2\rightarrow NH_2CHO+H_2O$. For the addition of ammonia two transition state conformations, of which one possesses a lone pair, on the hydroxyl oxygen of formic acid, antiperiplanar to the attacking nitrogen (T1 conformer) and the other possesses a hydrogen atom, of the OH group, antiperiplanar to the nucleophile ammonia (T1′ conformer), have been identified as characteristic transition state structures. Calculated transition state energies for the first addition step of the reaction revealed that a lone pair on the oxygen of the OH group, which is antiperiplanar to the attacking nitrogen (T1 conformer), stabilized the transition state by 7.4 kcal mol^{-1} compared to the T1′ conformer. Similarly, for the second water elimination step of the reaction, two conformers (T2 and T2′) have been identified as transition state structures, of which the T2 conformer possesses a lone pair on the nitrogen, antiperiplanar (app) to the leaving water and the T2′ conformer possesses a hydrogen atom, of the NH_2 group, app to the leaving water molecule. Again, calculated transition state energies for the T2 and T2′ structures revealed that a lone pair on the nitrogen of the NH_2 group, which is app to the scissile C–O bond (T2 conformer), stabilized the transition state by 3.1 kcal mol^{-1}, thus supporting the hypothesis of stereoelectronic control for this reaction. The significance of these stereoelectronic effects for the mechanism of action of serine proteases is discussed and a novel mechanism is proposed.

Stereoelectronic control, or the role of orbital orientation in organic and enzymatic reactions, has been of considerable interest over the last decade.[1–31] Deslongchamps and cowokers[2] in studying tetracovalent carbon species have demonstrated selective cleavage of bonds which are *trans*-antiperiplanar (app) to lone pair on directly bonded oxygen and/or nitrogen atoms. There has been a growing recognition that conformationally-dependent orbital interactions can play a significant role in the structure and reactivity of biomolecules.

Thus, as shown in the reaction below, addition of alkoxide to the acyl carbon, will yield the tetrahedral intermediate **1**. In the stereoelectronic theory, breakdown of this intermediate with cleavage of the C–X bond is facilitated by two non-bonded electron pairs oriented app (shaded) to the C–X bond in conformation **1a**. In conformation **1b** only one non-bonded electron lone pair is oriented app to the scissile C–X bond. In the stereoelectronic theory, cleavage of the C–X bond of the tetrahedral intermediate **1** is presumed to be controlled by the number of *app* lone pairs and thus should proceed through conformation **1a** rather than **1b** (two app paris in **1a** vs. one app pair in **1b**).

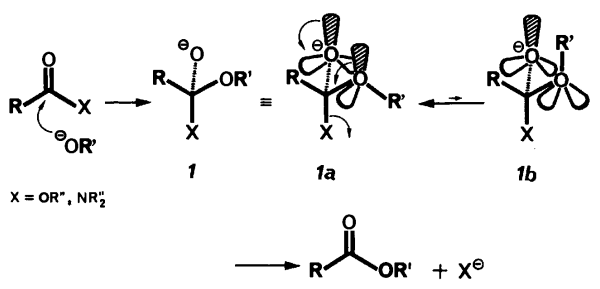

Research groups of Lehn,[5–9] Pople,[10] Gorenstein,[11–17] and others have provided theoretical justification for these stereoelectronic effects in tetracovalent carbon species and phosphates and pentacovalent phosphoranes. We have recently suggested that this stereoelectronic effect has a major impact on the relative energies of transition states, much more so than on ground states or intermediates.[14,15] It is thus important to use calculated transition state energies as a guide in the evaluation of the stereoelectronic effect. Although earlier calculations[1–13] supported the existence of the operation of stereoelectronic effects in tetracovalent species, these comparisons were based only on stable molecular structures that, again, would tend to minimize the stereoelectronic effect. Following the detailed quantum mechanical studies by Oie et al.,[32,33] for the addition-elimination reaction profile between ammonia and formic acid proceeding via a tetrahedral intermediate, we have recently initiated

$$NH_3+HCO_2H\rightarrow H_2NCH(OH)_2\rightarrow NH_2CHO+H_2O \quad (1)$$

an examination of the stereoelectronic effect in the well-characterized transition states.[16] Separate transition states were observed for the first addition step and the second elimination step, with a metastable tetrahedral intermediate.[16,32,33] Related molecular orbital calculations on acyl addition reactions have characterized only a single transition state, failing to find any stabilization of a metastable tetrahedral intermediate.[32,34] Although we could identify for the first

††Present address: Fermentation Research Institute, Agency of Industrial Science & Technology, MITI, Tsukuba Science City, Ibaraki 305.

addition step two transition state structures (T1 and T1′) which were important for the stereoelectronic effect comparison, only one conformer (T2) could be characterized for the second elimination step as a real transition state structure, thus making our work half complete.[16] We report here a complete characterization of all four of the transition state conformers (T1, T1′, T2, and T2′) which are ideal for testing the stereoelectronic theory.

Methods of Calculation

In our original study,[16] the SCF LCAO-MO ab initio molecular orbital calculations utilized the GAUSSIAN 70 series of programs with a STO-3G minimal basis set.[35] Initial structures for the addition-elimination transition states of reaction 1, as shown in Fig. 1, were partially taken from the optimized structures of Oie et al.[32] The geometries for different conformations about the C-N and C-O-H bonds for both transition states were then optimized by sequentially varying all bond lengths, bond angles, and torsional angles until the total energy has been effectively minimized when it was clear that only very small (<0.02 kcal mol^{-1}) decreases in energy were possible by further calculation. For optimization of parameter χ, the following Eq. 2 was used, by calculating three energies (E_1—E_3) around the previously increment of dχ, which assumes a parabolic harmonic vibration function:

$$\chi_{OPT} = \chi_0 - \frac{(E_2 - E_3)d\chi}{2(E_2 + E_3 - 2E_1)} \quad (2)$$

where $E_1 = a\chi_0^2 + b\chi_0 + c$

$E_2 = a(\chi_0 + d\chi)^2 + b(\chi_0 + d\chi) + c$

$E_3 = a(\chi_0 - d\chi)^2 + b(\chi_0 - d\chi) + c$

Since $a=(E_2+E_3-2E_1)/2d\chi^2$, the force constant is negative when the numerator of coefficient a is negative. In those structures (T1, T1′, and T2) identified as transition states (a saddle point with only one negative force constant), the reported energy was maximized with respect to this single geometric parameter defining the reaction coordinate, and all other geometric parameters were relaxed to their minimum energy values.[16] Although this procedure is feasible for calculating stable intermediates or ground state structures, it may not be the best choice for calculations of transition state structures unless one geometric parameter can clearly be identified as the reaction coordinate. In general, however, the reaction coordinate consists of the translating bond coupled with other vibrations. A newer optimization routine of the GAUSSIAN 80 program[36] can now automatically search for the transition state. The initially optimized geometries[16] obtained from the GAUSSIAN 70 program were utilized in the full transition state optimization with the GAUSSIAN 80 program. All four transition state structures (T1, T1′, T2, T2′; see Fig. 1) are now optimized and the final geometries are given in Table 1.

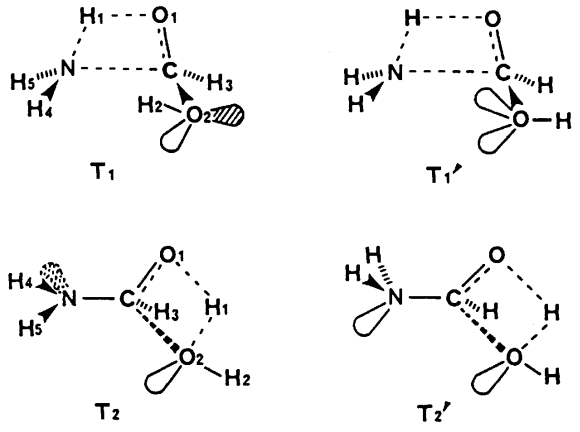

Fig. 1. Structures for different conformations of tetrahedral transition states in the acyl addition-elimination reaction 1.

Table 1. STO-3G Optimized Structures of Transition States and Intermediate Molecule[a]

Parameter[b]	T1	T1′	T2	T2′
C-O_1	1.315 (1.315)	1.308	1.312 (1.312)	1.304
C-O_2	1.402 (1.402)	1.438	1.720 (1.720)	1.678
<O_1CO_2	119.5	121.3	88.09 (88.1)	89.88
C-N	1.756 (1.756)	1.706	1.441 (1.441)	1.486
<NCO_1	89.93 (89.9)	92.25	120.9 (120.6)	122.5
<NCO_2	107.9 (107.9)	101.2	108.6	102.9
H_1-O_1	1.404 (1.404)	1.461		
H_1-O_2			1.078 (1.078)	1.061
<H_1O_1C	79.80 (79.8)	78.37		
<H_1O_2C			72.25 (72.3)	75.73
τ H_1O_1CN	−0.41 (−0.4)	0.81		
τ $H_1O_2CO_1$			−0.70 (−0.5)	−1.11
H_2-O_2	0.990	0.990	0.990	0.991
<H_2O_2C	103.4	103.2	113.9	115.3
τ H_2O_2CN	−88.97	180.0[c]	133.2	129.1
H_3-C	1.112	1.119	1.112	1.112
<H_3CN	101.9	104.0	109.3	108.5
τ $H_3CO_1H_1$	−125.0	−125.1		
<H_3CO_1			122.8	122.7
$H_{4(5)}$-N	1.034	1.034	1.027	1.035
<H_4NC	120.9	117.9	111.3	105.5
τ H_4NCO_1	−110.6	−112.6		
τ H_4NCO_2			63.26	180.0[c]
<H_5NC	119.7	120.3	112.5	105.9
τ H_5NCO_1	111.0	110.9		
<H_5NH_4			109.5	103.5

a) Bond length in Å, bond angles (<XYZ) and torsional angles (τWXYZ) in degrees; see Fig. 1 for definition of atoms W, X, Y, Z. Optimized (at STO-3G level) parameters in parentheses from Ref. 32. b) See Fig. 1 for definition of structures. c) Assumed.

Results

Shown in Fig. 1 are the four optimized transition state structures of which T1 and T1′ correspond to the first addition step of the reaction and T2 and T2′ to the second elimination step. T1 possesses a lone pair on oxygen (shaded), which is antiperiplanar (app) or trans to the attacking nitrogen (nucleophile). Similarly, T2 possesses a lone pair on nitrogen (shaded), which is trans-app to the leaving water molecule. On the other hand, both T1′ and T2′ do not have an app lone pair with respect to the nucleophile (ammonia) or the leaving group (water). Instead they possess a hydrogen atom which is app to the translating bond.

Shown in Fig. 2 are the reaction profiles for formation of the amide bond in the reaction of ammonia and formic acid. The profiles differ with respect to the conformations about the C-N and C-OH bonds. The relative T1 and T2 transition state energies (Table 2) and geometries (Table 1) calculated in the present study agree well with the earlier calculations.[32] The lowest reaction pathway (solid line in Fig. 2) proceeds via T1 and T2 transition states, with T1 being 1.9 kcal mol^{-1} more stable than T2. It is important to note that both T1 and T2 possess a lone pair (shaded), which is app to the translating bond, in agreement with the stereoelectronic theory.[14,15] For the first addition transition state (formation of the C-N bond), the conformation T1 with an oxygen lone pair on $O_{(2)}H$ app to the C-N bond is 7.4 kcal mol^{-1} lower in energy than T1′, which has no lone pair orbital on $O_{(2)}$ app to the C-N bond. We have previously reported[16] that the energy difference between T1 and T1′ is 3.9 kcal mol^{-1}, which is much smaller than the present 7.4 kcal mol^{-1}, indicating the limitation of the stepwise optimization procedure for the characterization of transition state structures. Similarly, for the second elimination transition state, the conformation T2 with a nitrogen lone pair app to the scissile C-$O_{(2)}$ is 3.1 kcal mol^{-1} lower in energy than T2′, which has no lone pair on nitrogen app to the breaking C-$O_{(2)}$ bond. In our previous study,[16] we failed to locate the T2′ transition state when we assumed that we could approximate the 3N-6

Table 2. Ab Initio Energies and Population Analysis for Various Conformations of Transition States T1 and T2

	Conformation			
	T1	T1′	T2	T2′
Rel. energy[a] / kcal mol^{-1}	0.0[a]	7.41	1.87	4.96
bond				
C-O_1	0.6433	0.6595	0.6577	0.6730
C-O_2	0.5400	0.4901	0.1860	0.2131
C-N	0.2286	0.2637	0.6748	0.6048
H_1-O_1	0.1772	0.1533	0.1784	0.1524

a) Total energy of T1 was −241.59257 hartrees.

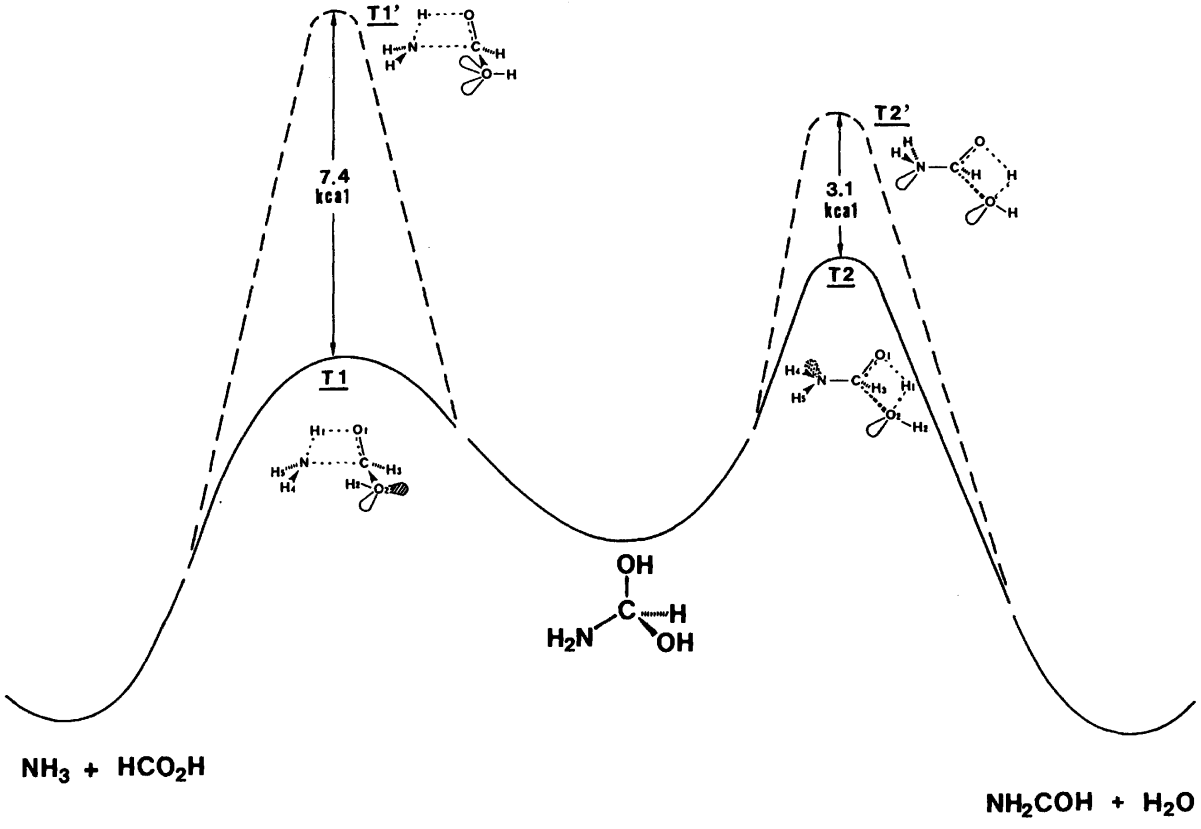

Fig. 2. Reaction profiles for acyl addition-elimination reaction 1 are shown assuming various conformations about the C-N and C-$O_{(2)}$ bonds. All conformations are optimized as transition states.

eigenvectors and eigenvalues of the quadratic force constant matrix by treating them as classical vibrational modes (bond stretches, bends, etc.) and force constants. For a col point or transition state, only one of the eigenvalues (force constant) can be negative, and this corresponds to the imaginary vibration frequency defined as the reaction coordinate. In reality, however, it is an oversimplification to assign a single classical vibrational mode to the reaction coordinate eigenvector, although it has the advantage of giving us better chemical intuition for the nature of chemical reactivity. Apparently, the geometric parameters of T2′ were strongly coupled and thus could not be treated in a classical fashion.[16]

Oie et al. have established that the relative stabilities of the various species were generally unaffected by using more extensive basis sets and inclusion of correlation effects.[32] Because we are only interested in relative energies of transition states differing only in conformation (not atomic bonding), any errors resulting from neglect of correlation and polarization in our study should essentially cancel.[32] The STO-3G optimized geometries, population analyses, and energies for various transition state conformations are shown in Tables 1 and 2.

The stereoelectronic effect is believed to arise from the interaction of an app lone pair (n_{X_1}) on X_1 (oxygen or nitrogen) with the σ^* antibonding Y–X_2 orbital (Scheme 1).[1-28]

In terms of a simple resonance picture for the stereoelectronic effect, stabilization of the structure is thought to derive from an anomeric type, double bond–no bond resonance contribution. The bond opposite to the app lone pair has some no bond character and the bond containing an app lone pair has some double bond character. The overlap population analysis[37] of Table 2 confirms this general picture. As expected, the overlap population of a bond that is app to a lone pair is smaller than the overlap populaton of a bond that is not app to a lone pair (assuming we are comparing otherwise identical structures). Thus the C–N overlap population is 0.264e in the T1′ conformation, whereas it is 0.229e in the T1 conformation (Table 2). The presence of an app lone pair to the scissile C–N bond in T1 conformation weakens this bond (reduces the overlap population). As expected from the double bond–no bond resonance description of the stereoelectronic effect, the C–$O_{(2)}$ overlap population in T1 (0.540e) is larger than in T1′ (0.490). The app lone pair on $O_{(2)}$ to the C–N bond in T1 imparts some double bond character to the C–$O_{(2)}$ bond. Similar overlap population stereoelectronic effects are observed for the T2 and T2′ conformation. T2, with an app lone pair on nitrogen to the scissile C–$O_{(2)}$ bond, has a lower C–$O_{(2)}$ bond overlap population (0.186e) than T2′ (0.213e), and also has a higher C–N bond population (0.675e) than T2′ (0.605e), in accordance with the double bond–no bond resonance structure of Scheme 1.

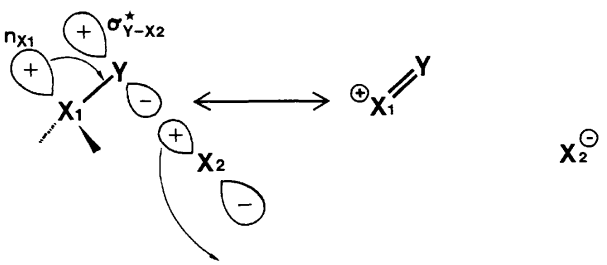

Scheme 1.

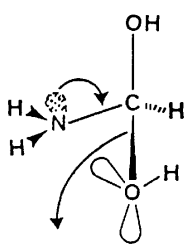

Scheme 2.

Discussion

We have earlier established that the kinetic stereoelectronic effect will largely be manifested in energy differences at the transition state.[14,15,17] On the basis of one-electron molecular orbital theory,[38] the two-electron stabilization from the interaction of a doubly occupied MO(n) with a vacant nondegenerate MO(σ^*) may be approximated as being inversely proportional to the energy separation of the two MO's and directly proportional to the square of their overlap.

$$SE(\mathrm{n},\sigma^*) \propto \frac{S^2_{n\sigma^*}}{\Delta E_{n\sigma^*}} \qquad (3)$$

In the above example, $S_{n\sigma^*}$ is the overlap integral between the app lone-pair orbital(n) on oxygen or nitrogen and the vacant antibonding orbital(σ^*) of the translating bond, and $\Delta E_{n\sigma^*}$ is the energy difference between these orbitals. The app lone-pair stereoelectronic effect presumably derives from this orbital interaction since maximal overlap between n and σ^* is found for the app orientation. Of course, if the stereoelectronic effect does not have its major impact in the transition state, little activation energy differences and no kinetic acceleration will result from these interactions.

By microscopic reversibility, it should be easier to break or make the bond that possesses no bond character (Scheme 1), and indeed as shown in Fig. 2 and Table 2, this has been confirmed in these calculations of transition state structures. For the addition transition state, the conformation T1 with an oxygen lone pair that is app to the translating C–N bond is 7.4 kcal mol^{-1} lower in energy than T1′, which has no lone pair app to the C–N bond. A similar stereoelectronic effect operates on the second water elimination step:

T2 with a nitrogen lone pair app to the scissile C-$O_{(2)}$ bond is 3.1 kcal mol^{-1} lower in energy than T2′, which has no lone pair app to the C-$O_{(2)}$ bond. Note in our discussion we ignore the lone pair orbitals on $O_{(1)}$, which also are app to the C-N or C-$O_{(2)}$ bonds and hence stereoelectronically facilitate C-N or C-$O_{(2)}$ bond translation. Considering also the counterbalancing stereoelectronic effect,[16] the most favored tetrahedral carbon transition state is one that possesses a lone-pair app to the adjacent scissile bond while at the same time does not have a lone pair on the cleaving atom, which is app to a polar adjacent bond (bond which possesses double bond character; see Scheme 2).

This stereoelectronically most favored structure, derived from the comparisons of transition state conformations, supports Lehn and Wipff's similar conclusions[5-9] based upon overlap population and energy differences in stable tetrahedral intermediates.

Reversing the addition-elimination reaction of Eq. 1 (going from right to left in Fig. 2), one can consider this reverse reaction to be a model study of serine proteases, the water molecule representing a serine hydroxyl group and ultimately hydrolyzing a peptide bond. Although enzymic catalysis is believed to derive from the enzyme's special capacity to stabilize (and hence lower the energy of) the transition state of the reaction,[39-41] it is important to recognize that for most enzymatic reactions, and certainly including peptide bond hydrolysis, there is probably no one unique transition state. Thus, as Albery and Knowles[42] have argued, in the "evolutionary perfection" of an enzyme catalyst in facilitating a multistep reaction, eventually the enzyme must find a mechanism that lowers the barrier to each elementary step. Chymotrypsin and most likely all other serine proteases proceed via an acyl enzyme intermediate in which formation of the acyl enzyme intermediate and hydrolysis of the intermediate in turn proceed via tetrahedral intermediates.[43] Concentrating only on the reaction path between Michaelis comple and acyl enzyme, the enzyme must catalyze formation and breakdown of the tetrahedral intermediate in a minimum two-step reaction. If chymotrypsin is "evolutionarily perfect," then each of these steps is partially rate limiting. The enzyme must thus be sufficiently conformationally flexible at its active site to stabilize both transition states in the formation (T2) and breakdown (T1) of the tetrahedral intermediate. If stereoelectronic effects operate for one transition state, they will likely operate for both. Since the optimal stereoelectronic conformation for formation of the tetrahedral intermediate (T2 conformation) must be different from the optimal stereoelectronic conformation for breakdown of the intermediate (T1 conformation), passage from one transition state to the other will require single-bond rotation about C-O and C-N in the tetrahedral intermediate. Although recent papers have addressed the importance of stereoelectronic effects in the mechanism of action of the serine proteases, such as α-chymotrypsin,[29-31] no mention has been made to the important C-O bond rotation, which is required by an additional counterbalancing stereoelectronic effect.[16] We argue that a most important function of the enzyme is to provide for these conformational changes in the tetrahedral intermediate complex.

Experimental support for the stereoelectronic effects in the mechanism of action of α-chymotrypsin is provided by the elegant work of Bizzozero and coworkers.[29-31] Although peptide bonds involving the carbonyl group of amino acid residues with large hydrophobic side chains are known to be easily hydrolyzed by α-chymotrypsin, if the amide nitrogen is contributed by a proline residue, the peptide bond is resistant to chymotryptic cleavage. This finding has led Bizzozero and Zweifel to examine the reactivity of dipeptides, possessing an alkyl substituent on the leaving group nitrogen, such as *N*-acetyl-L-phenylalanyl-L-prolinamide and *N*-acetyl-L-phenylalanyl-sarcosinamide (Scheme 3). Both dipeptides were found to be unreactive but proved to be good competitive inhibitors, indicating that they form enzyme-dipeptide complexes and their unreactivity must be due to some factors arising during the transformation leading to or from the acyl-enzyme intermediate.

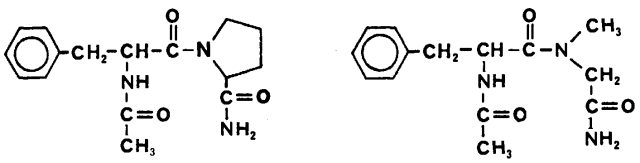

Scheme 3.

Shown in Fig. 3 is our modified description of the catalytic events in the acylation reaction as presented by Dugas and Penny.[31] This modified description is equivalent to Figs. 5 and 6 in our previous article[16] and also to Fig. 4.7 of Deslongchamps' proposal,[31] and this Fig. 3 contains the important C-O bond rotation, in addition to the nitrogen inversion. For the nucleophilic attack by the hydroxyl group of Ser-195, the most stereoelectronically favored transition state is E-T2, which possesses a nitrogen lone pair app to the developing SerO-C_α bond while at the same time does not have a lone pair on the nucleophile serine-oxygen, which is app to a polar N-C_α bond (see also Scheme 2). The important point to be considered here is that the app lone-pair orbital on nitrogen points toward the solvent (backside of the page) and the N-H′ bond toward the inside of the enzyme active site. The distance between the nitrogen and the imidazole ring of His-57 in the E-T2 conformation is only 3.5 Å (based upon model building derived from analogous X-ray crystal structures), and is just sufficient to accommodate a hydrogen atom. When the N-H′ hydrogen is

replaced by an alkyl group, as in the case of a proline residue, this substituent would come too close to the imidazole ring of His-57. Hence it can be argued that a dipeptide containing an alkyl substituent on nitrogen is inactive toward α-chymotrypsin hydrolysis because the steric hindrance prevents formation of the tetrahedral intermediate in the stereoelectronically required E-T2 conformation: In Fig. 3, H′ on nitrogen must be replaced by an alkyl group. The E-T2 conformation is not possible because the distance between the nitrogen and the imidazole ring is only 3.5 Å. Then when H′ is replaced by an alkyl group, the lone pair orbital on the nitrogen can never be app to the nucleophile (Ser-OH), corresponding to the T2′ conformation in Fig. 2-this prevents the nucleophilic attack by Ser-OH.

Note in Fig. 2 that the energy difference between T2 and T2′ is 3.1 kcal mol^{-1}. However, this is the minimum estimate of the corresponding energy difference between E-T2 and E-T2′ (H′ in Fig. 3 is replaced by an alkyl group and rotated to be app to Ser-OH as in the T2′ conformation) since the energy different between T2 and T2′ would have been greater if methyl groups (any alkyl groups) had been used in place of hydrogen on the amide nitrogen. This originates from the expectation that SE (n,σ^*)>SE($\sigma_{O\text{-}H}$,σ^*); SE(n,σ^*)>SE ($\sigma_{C\text{-}H}$,σ^*)>SE ($\sigma_{C\text{-}C}$,σ^*); and SE (n,σ^*)>SE ($\sigma_{N\text{-}C}$, σ^*)>SE ($\sigma_{N\text{-}H}$,n*)[44] in Eq. 3. This implies that electron donation from the $\sigma_{N\text{-}H}$ bond into the σ^* bond is better than the $\sigma_{N\text{-}C}$ bond, resulting in a stabilization of the T2′ conformation compared to the corresponding alkyl substituted counterpart, such as E-T2′ with the replacement of H′ by an alkyl group.

If the E-T2 conformation is stereoelectronically best for lowering the energy of the transition state for SerO-C_α bond formation, as discussed above, it must be the worst for N-C_α bond cleavage. For the cleavage of the N-C_α bond, stereoelectronically the lone pair on the serine oxygen must be app to the translating (scissile) N-C_α bond and no lone pair on the N should be app to the adjacent SerO-C_α bond (E-T1 conformation). This E-T1 conformation is achieved by N-inversion[30] accompanied by torsion about the Ser-195 bonds. The equilibrium between the two intermediates, E-T2 and E-T1 in Fig. 3, is likely to be largely on the side of the E-T1 conformer since E-T2 is destabilized by the unfavorable dipole-dipole repulsion between the N-H group of His-57 and the N-H′ group of the nitrogen. In E-T1 this unfavorable interaction is replaced by a favorable hydrogen bond interaction between the N-H group of His-57 and the lone pair orbital of the nitrogen. It is interesting to note[30] that due to this particular equilibrium position the tetrahedral intermediate is now locked into a conformation (E-T1) where reversion to the enzyme-substrate complex is no longer feasible, since the SerO-C_α bond no longer has an app lone pair on N. Recall that an app lone pair on N is responsible for stabilizing the transition state for C-O cleavage by 3.1 kcal mol^{-1}. This N-inversion step implies that the leaving nitrogen acts as a switch controlling which of the two critical bonds of the tetrahedral intermediate, the C-O bond or the C-N bond, is broken.[30] In the switch position of E-T2, where the lone pair on N points toward the solvent (backside), C-O bond formation is allowed by the stereoelectronic principle, whereas C-N bond cleavage is prevented by lack of an app lone pair on serine oxygen and also by lack of N-protonation by the imidazole. In the other switch position of E-T1, where the lone pair on N points toward the inside of the enzyme active site, C-O bond cleavage is forbidden by the stereoelectronic principle, whereas C-N bond cleavage is facilitated by the app lone pair on the serine oxygen as well as by the N-protonation.

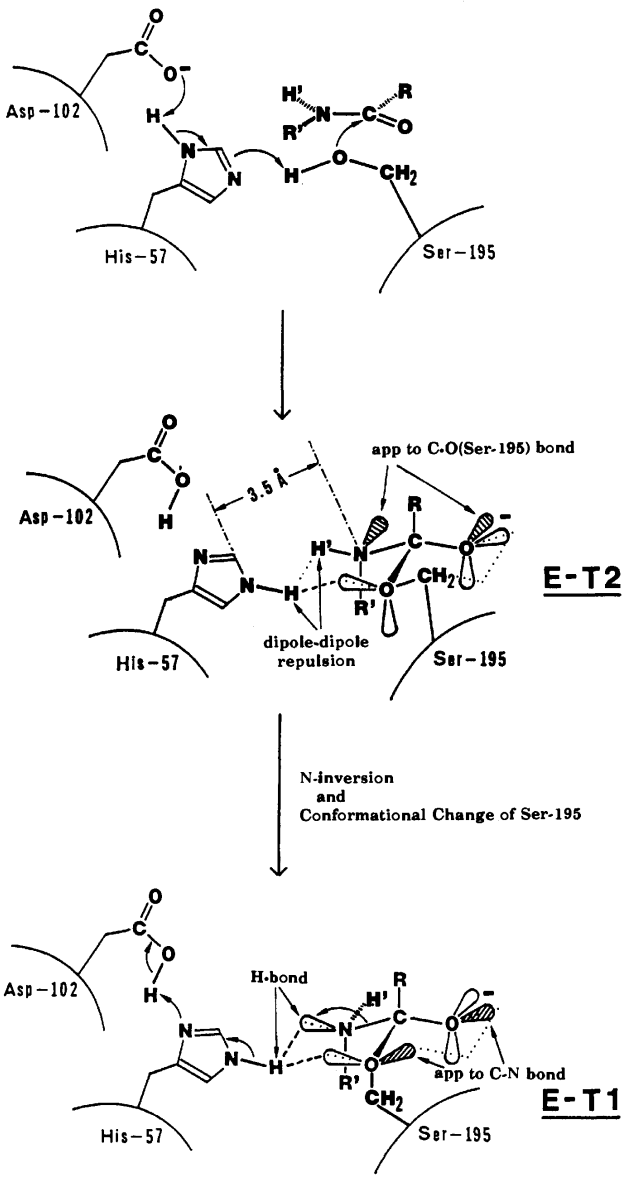

Fig. 3. Schematic drawing of steps in acylation reaction of α-chymotrypsin partially taken from Dugas and Penny.[31] Antiperiplanar lone pairs to the scissile bond are shaded.

Since the tetrahedral intermediate is more stable in E-T1 than in E-T2 (even without considering the dipole-dipole interaction, the T1 transition state is 1.9 kcal mol^{-1} more stable than the T2 transition state; see Table 2), the breakdown of the amide bond (forward direction) is favored over that in the backward direction. Note also the additional important conformational change of Ser-195, going from E-T2 to E-T1, to gain 7.4 kcal mol^{-1} stabilization (Fig. 2) for C-N bond cleavage, which has been missed in the previously recognized literature (actually, the counterbalancing stereoelectronic effect[16] in E-T2 has been ignored in the literature).

The important mobility of the imidazole, to swing between a position allowing formation of a hydrogen bond with the serine oxygen, and one allowing formation of a hydrogen bond with the leaving nitrogen, has been discussed.[16,30] Detailed experimental support for the movement of important atoms has also been given in our earlier publication.[16] Together with the mechanistically required nitrogen inversion, conformational change of the Ser-195, and the observed flexibility of the imidazole group, it would appear as though the serine protease is designed to provide the stereoelectronically optimal transition states for both the acyl addition and elimination steps. These stereoelectronic effects should now be included in a more detailed quantum mechanical calculation of the reaction profile for the serine proteases.

Support by NSF (Chem 83K0098), NIH GM36281 and the John Simon Guggenheim Memorial Foundation for a fellowship (to D.G.G.) and by FRI (to K.T.) is acknowledged. The generous allocation of computing time by the Computer Center, University of Illinois at Chicago, and the help of Dr. Shigeyuki Urano (UIC) with the implementation of GAUSSIAN 80 is also appreciated.

References

1) A. J. Kirby, "The Anomeric Effect and Related Stereoelectronic Effect at Oxygen," Springer-Verlag, Berlin (1983).
2) P. Deslongchamps, "Stereoelectronic Effects in Organic Chemistry," Pergamon Press, Oxford (1983).
3) D. R. Storm and D. E. Koshland, Jr., *J. Am. Chem. Soc.*, **94**, 5815 (1972).
4) W. L. Mock, *Bioorg. Chem.*, **4**, 270 (1975).
5) J. L. Lehn and G. Wipff, *J. Chem. Soc., Chem. Commun.*,**1975**, 800.
6) J. M. Lehn and G. Wipff, *J. Am. Chem. Soc.*, **96**, 4048 (1974).
7) J. M. Lehn and G. Wipff, *J. Am. Chem. Soc.*, **98**, 7498 (1976).
8) J. M. Lehn and G. Wipff, *Helv. Chim. Acta*, **61**, 1274 (1978).
9) J. M. Lehn and G. Wipff, *J. Am. Chem. Soc.*, **102**, 1347 (1980).
10) L. Radom, W. L. Hehre, and J. A. Pople, *J. Am. Chem. Soc.*, **94**, 2371 (1972).
11) D. G. Gorenstein, J. B. Findlay, B. A. Luxon, and D. Kar, *J. Am. Chem. Soc.*, **99**, 3473 (1977).
12) D. G. Gorenstein, B. A. Luxon, J. B. Findlay, and R. Momii, *J. Am. Chem. Soc.*, **99**, 4170 (1977).
13) D. G. Gorenstein, B. A. Luxon, and J. B. Findlay, *J. Am. Chem. Soc.*, **99**, 8048 (1977).
14) D. G. Gorenstein, B. A. Luxon, and J. B. Findlay *J. Am. Chem. Soc.*, **101**, 5869 (1979).
15) D. G. Gorenstein, B. A. Luxon, and E. M. Goldfield, *J. Am. Chem. Soc.*, **102**, 1757 (1980).
16) D. G. Gorenstein and K. Taira, *Biophys. J.*, **46**, 749 (1984).
17) K. Taira and D. G. Gorenstein, *J. Am. Chem. Soc.*, **106**, 7825 (1984).
18) D. G. Gorenstein and R. Rowell, *J. Am. Chem. Soc.*, **101**, 4925 (1979).
19) D. G. Gorenstein, R. Rowell, and J. B. Findlay, *J. Am. Chem. Soc.*, **102**, 5077 (1980).
20) D. G. Gorenstein, R. Rowell, and K. Taira, "Phosphorus Chemistry," p. 69, ACS Symposium No. 171, Washington, D. C. (1981).
21) R. Rowell and D. G. Gorenstein, *J. Am. Chem. Soc.*, **103**, 5894 (1981).
22) D. G. Gorenstein and K. Taira, *J. Am. Chem. Soc.*, **104**, 6130 (1982).
23) K. Taira, T. Fanni, and D. G. Gorenstein, *J. Am. Chem. Soc.*, **106**, 1521 (1984).
24) K. Taira and D. G. Gorenstein, *Tetrahedron*, **40**, 3215 (1984).
25) K. Taira, T. Fanni, and D. G. Gorenstein, *J. Org. Chem.*, **49**, 4531 (1984); D. G. Gorenstein, A. Chang, and J.-C. Yang, *Tetrahedron*, **43**, 469 (1987); J.-C. Yang and D. G. Gorenstein, *Tetrahedron*, **43**, 479 (1987).
26) K. Taira, W. L. Mock, and D. G. Gorenstein, *J. Am. Chem. Soc.*, **106**, 7831 (1984).
27) J.-C. Yang and D. G. Gorenstein, *Tetrahedron Lett.*, **25**, 4627 (1984).
28) K. Taira, K. Lai, and D. G. Gorenstein, *Tetrahedron*, **42**, 229 (1986).
29) S. A. Bizzozero and B. O. Zweifel, *FEBS Lett.*, **59**, 105 (1975).
30) S. A. Bizzozero and H. Dutler, *Bioorg. Chem.*, **10**, 46 (1981).
31) H. Dugas and C. Penney, "Bioorganic Chemistry. A Chemical Approach to Enzyme Action," Springer-Verlag, New York (1981).
32) T. Oie, G. H. Loew, S. K. Burt, J. S. Binkley, and R. D. MacElroy, *J. Am. Chem. Soc.*, **104**, 6169 (1982)
33) T. Oie, G. H. Loew, S. K. Burt, and R. D. MacElroy, *J. Am. Chem. Soc.*, **105**, 2221 (1983).
34) I. H. Williams, D. Spangler, D. A. Femec, G. M. Maggiora, and R. L. Schowen, *J. Am. Chem. Soc.*, **102**, 6621 (1980); H. Yamataka, S. Nagase, T. Ando, and T. Hanafusa, *ibid.*, **108**, 601 (1986).
35) W. J. Hehre, W. A. Lathan, R. Ditchfield, M. D. Newton, and H. A. Pople, Quantum Chemistry Exchange Program, Indiana University, No. 236, W. J. Hehre, R. F. Stewart, and J. A. Pople, *J. Chem. Phys.*, **51**, 2657 (1969).
36) GAUSSIAN 80: Quantum Chemistry Program Exchange University of Indiana.
37) R. S. Mulliken, *J. Chem. Phys.*, **36**, 3428 (1962).
38) W. T. Borden, "Modern Molecular Orbital Theory for

Organic Chemists," Prentice-Hall, Englewood Cliffs, N. J. (1975).
39) L. Pauling, *Chem. Eng. News*, **24**, 1375 (1946).
40) R. Wolfenden, *Acc. Chem. Res.*, **5**, 10 (1972).
41) G. E. Lienhard, *Ann. Rep. Med. Chem. Res.*, **7**, 249 (1972).
42) W. J. Albery and J. R. Knowles, *Biochemistry*, **15**, (1976).
43) A. Fersht, "Enzyme Structure and Mechanism, 2nd ed," Freeman, NY (1985).
44) A. S. Cleplak, *J. Am. Chem. Soc.*, **103**, 4540 (1981).

High-Pressure Cycloaddition Reaction of Tropone with Furans

Shigeru SUGIYAMA, Tohru TSUDA,† Akira MORI, Hitoshi TAKESHITA,* and Mitsuaki KODAMA††
Research Institute of Industrial Science, 86, Kyushu University, Kasuga-koen, Kasuga, Fukuoka 816
†Graduate School of Engineering Sciences, 39, Kyushu University, Kasuga-koen, Kasuga, Fukuoka 816
††Pharmaceutical School of Tokushima Bunri University, Yamashiro-cho, Tokushima 770
(Received March 13, 1987)

Thermal reactions of tropone with furan and 2-methoxyfuran mainly gave the endo-[4+2] cycloadducts, the kinetically controlled products, at 3000 bar. In the latter case, the product further reacted with tropone to yield 2:1-adducts. On the other hand, the reaction with 3,4-dimethoxyfuran under similar conditions yielded mainly the exo-[4+2] adducts, the thermodynamically controlled products. The predominant formation of the endo-Diels-Alder adducts with furans under the high-pressure conditions may be valuable from a synthetic point of view.

We have recently reported the high-pressure kinetic analysis of the electrocyclic reactions of tropone (**1**) to show the normal volume profiles for the cycloadditions of **1**.[1,2] Accordingly, the ordinary pressure effect should apply to **1**, and under the high-pressure conditions, even the hitherto unsuccessful Diels-Alder reaction of **1** with furans, due to a facile cycloreversion, may occur.[3] Here, we describe the reaction of **1** with furan (**2**), 2-methoxyfuran (**3**), and 3,4-dimethoxyfuran (**4**).

Results and Discussion

Thermal Cycloaddition of 1 with Furans. Heating of an isopropylbenzene (IB) solution of **1** and **2** in a Teflon ampule placed in a pressure vessel (3000 bar)[4] at 130 °C for 10 h yielded, after silica-gel column chromatography, two 1:1-adducts (**5** and **6**). A similar treatment of **1** and **3** yielded three 1:1-adducts **7**—**9**, together with six 2:1-adducts **10**—**15**, which were derived from further cycloaddition of **1** to **7a** or **8a**, proto-adducts leading to **7** or **8**. With **4**, **1** afforded two 1:1-adducts **16** and **17** in 8 and 28% yields, respectively. The results are summarized in Table 1.

In comparison with these high-pressure cycloadditions, the reaction of **1** under ordinary pressure yielded inferior results; heating **1** and **2** in a sealed tube at 130 °C caused no reaction, while under similar conditions, **1** and **3** yielded only **7** and **8**, and **1** and **4** yielded a mixture of products too complicated to permit further investigation.

Table 1. High-Pressure Cycloaddition Reactions of Tropone with Furans

Yield/%	endo-[4+2]	exo-[4+2]	endo/exo
1+2	6 (0)[a]	5 (0)	1.2 (—)
1+3	35 (13)	13 (3)	2.7 (4.3)
	45[b]	18[b]	
1+4	8 (0.5)	28 (0.5)	0.29 (1)

a) Figures in parenthesis are yields at room temperature. b) These values are yields including 2:1-cycloadducts.

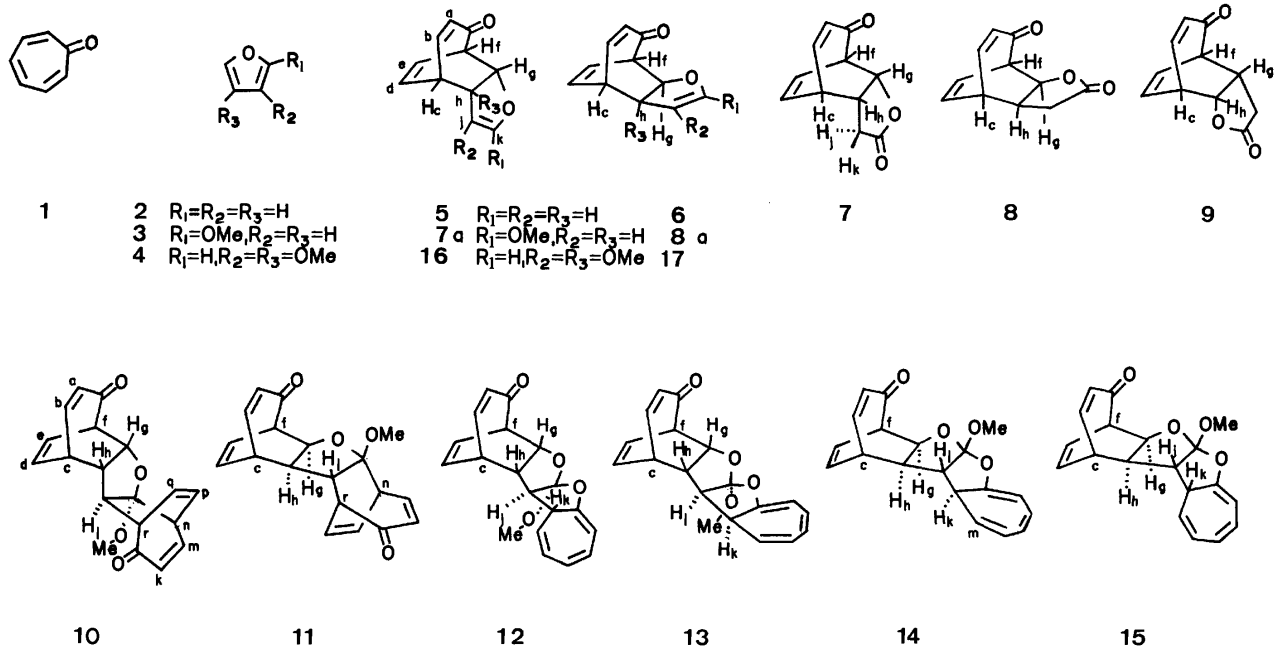

Scheme 1.

Table 2. Selected NMDR Data of **10**

Irradiated frequency at	Behavior of singnal ascribable to										
	H_j	H_h	H_c	H_r	H_f	H_n	H_g	H_a	H_k	H_m	H_b
2.46(H_j)		—[a]	×[b]	○[c]	×	×	×	×	×	×	×
2.67(H_h)	—		J=2[d]	×	×	×	J=8.5	×	×	×	×
3.2 (H_c)	×	J=2		—	—	—	×	J=0.5	×	×	J=8.5
3.4 (H_r)	○	×	—		—	—	×	×	J=2	×	×
3.58(H_f)	×	×	—	—		—	J=1.5	J=2	×	×	×
3.66(H_n)	×	×	—	—	—		×	×	J=1	J=8.5	×
4.74(H_g)	×	J=8.5	×	×	J=1.5	×		×	×	×	×
5.62(H_a)	×	×	J=0.5	×	J=2	×	×		×	×	J=11
5.76(H_k)	×	×	×	J=2	×	J=1	×	×		J=11	×
6.84(H_m)	×	×	×	×	×	J=8.5	×	×	J=11		—
7.02(H_b)	×	×	J=8.5	×	×	×	×	J=11	×	—	

a) Not observable. b) No change in signal shape. c) Appreciable sharpening occurred. d) Figures indicate the confirmed coupling values by NMDR.

Structures of 1 : 1-Adducts. The 1 : 1-adducts from **3** (**7**—**9**) exhibited no methoxyl signals in the ^{1}H NMR spectra to indicate a hydrolytic removal of the methoxyl group under the chromatographic conditions to form γ-lactone functions. Other structural features were parallel with the other adducts from **2** and **4**. The structures of these 1 : 1-adducts were clarified by mutual comparisons of the ^{1}H NMR analysis.[5] Namely, the ^{1}H NMR spectra[6] of all 1 : 1-adducts revealed signals of the α,β-unsaturated keto groups at δ=6.8—7.1 and 5.8—6.2 with the coupling constant of ca. 11 Hz, and the latter signals long-range-coupled with the bridge-head methine protons, being characteristic for the [4+2] adducts from **1**.[5] In addition, the ^{1}H NMR of **5**, **7**, and **16** exhibited the smaller J_{fg} (2.5 Hz for **5** and 2 Hz for **7** and **16**), while those of **6**, **8**, and **17** did larger J_{fg} (7 Hz for **6**, 7.5 Hz for **8**, and 6.5 Hz for **17**). Therefore, endo-[4+2][7] structures could be assigned for the formers and exo-[4+2] ones for the latter.[8]

The remaining **9** was another endo-[4+2] cycloadducts; its spin-spin splitting patterns (J_{gh}=7.5 and J_{ch}=2 Hz) ascribable to the lactonic proton indicated to be a regioisomer of **7**.

Structures of 2 : 1-Adducts. Structures of 2 : 1-adducts from **1** and **3** were determined by detailed 400 MHz-decoupled NMR analysis (NMDR) or measurements of the nuclear Overhauser effect (NOE). The **10** and **11**, having two carbonyl carbon signals in the ^{13}C NMR spectra, were [4+2]-[4+2] cycloadducts. The ^{1}H NMR spectra of **10** and **11** revealed J_{gh}=8.5, J_{fg}=1.5, and J_{jr}=0 Hz for **10** and J_{gh}=8.5, J_{fg}=6.5, and J_{jr}=0 Hz for **11**, and clarified their structures to be endo-[4+2]-endo-[4+2] and exo-[4+2]-endo-[4+2] cycloadducts, respectively. The regiochemistry of the second addition step to tropone was confirmed by NMDR; irradiation of the bridge-head protons (H_r) of **10** and **11** changed the broad doublet of H_j to sharp doublets, respectively. While, H_n of **10** and **11**, spin-coupled with the β-protons (H_m) of α,β-unsaturated keto group, was irradiated, the splitting patterns of H_j did not change at all. Hence, H_j and H_r of **10** and **11** are mutually coupled and their structures are unambiguously clarified as was shown in Scheme 1. The changes in shape of the signals caused by intensive NMDR experiments are tabulated in Tables 2 and 3.

Table 3. Selected NMDR Data of **11**

Irradiated frequency at	Behaviors of signal ascribable to						
	H_h	H_j	H_c	H_r	H_n	H_f	H_g
2.4 (H_h)		—[a]	×[b]	×	×	×	J=8.5[c]
2.58 (H_j)	—		×	○	×	×	○[d]
3.4 (H_c)	×	×		—	×	—	×
3.43 (H_r)	×	○	—		○	○	×
3.75 (H_n)	×	×	—	○		—	○
3.87 (H_f)	×	×	—	○	—		J=6.5
4.65 (H_g)	J=8.5	○	×	×	○	J=6.5	

a) Not observable. b) No change in signal shape. c) Figures indicate the confirmed coupling values by NMDR. d) Appreciable sharpening occurred.

On the other hand, **12**—**15** each revealed only one carbonyl carbon ^{13}C NMR spectrum; one of the tropone molecules had thus reacted as the 8π-cycloaddend. Therefore, they are [4+2]-[8+2] cycloadducts. The observed coupling sequences of the methine protons clarified the stereochemistry, and particularly for analyses of [8+2] adducts, there are good model compounds already investigated;[9,10] e.g., **12** [J_{fg}=2, J_{gh}=8.5, J_{jk}=0, J_{hj}=7, and J_{ch}=2 Hz] and **13** [J_{fg}=2, J_{gh}=8.5, J_{jk}=7.5, and J_{hj}=7.5 Hz] are derived from **7a**, while **14** [J_{fg}=7, J_{gh}=8.5, J_{jk}=1, and J_{hj}=5 Hz] and **15** [J_{fg}=7, J_{gh}=8.5, J_{jk}=7.5, J_{hj}=6, and J_{ch}=5 Hz] are from **8a**. The assignments were supported by NOE observations; i.e., an irradiation with the frequency of H_h-signal of **12** enhanced its H_g- and H_k-signals, and similar irradiations with the frequencies of H_h- and H_j-signals of **14** enhanced the H_g- and H_m-signals. When the isomeric **12**—**15** were separately heated in a sealed NMR tube respectively, although the isolated yields were not sufficiently high due to the instability towards air, stereospecific formation of **10** from **13** and **11** from **15** was confirmed and the identities with

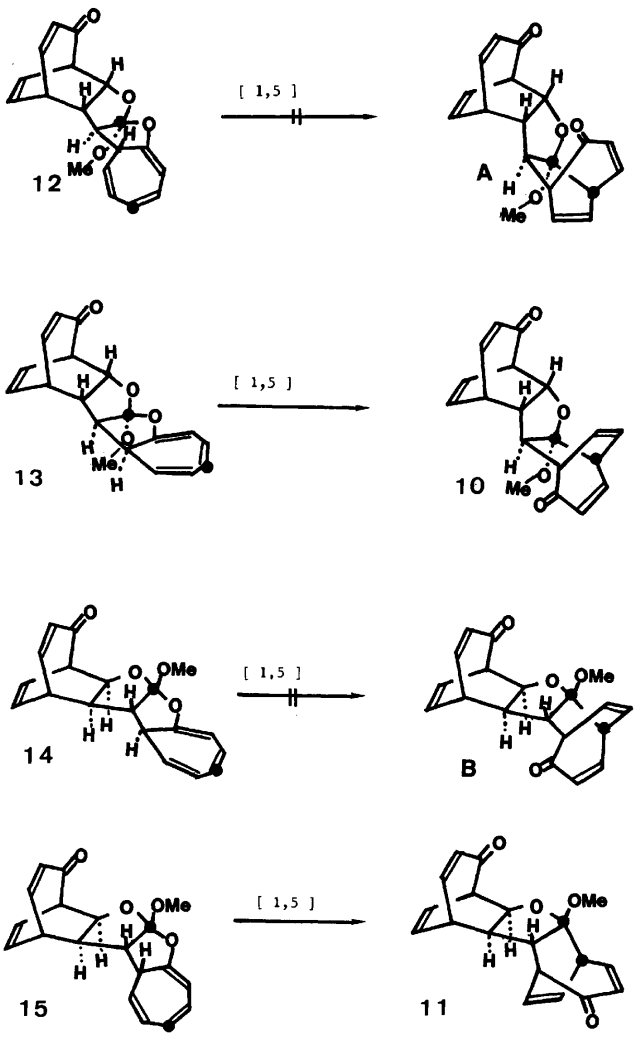

Scheme 2.

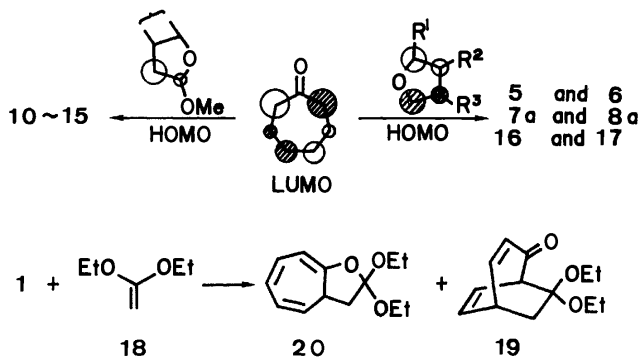

Scheme 3.

authentic **10** and **11** were established by the ^{1}H NMR spectral comparison. Moreover, the stereospecific isomerization without formation of fragmented 1 : 1-adducts eliminated the dissociation-recombination process. Therefore, considering these structural relationships, **13** and **15** were deduced to have endo-[4+2]-cis-[8+2] and exo-[4+2]-cis-[8+2] structures,[11] respectively.

Mechanism of the Cycloaddition. As shown in Table 1, furans only gave [4+2] cycloadducts with **1**, being parallel to cyclopentadiene at 145 °C,[8] but not to 2,5-dimethyl-3,4-diphenylcyclopentadienone, which gave a [4+2] cycloadduct above 100 °C and predominantly a [6+4] cycloadduct at 60 °C.[12] Among 1 : 1-adducts of **1** with furans, there was no [2+4] or [6+4] cycloadduct formed at all, and a predominant occurrence of the endo-[4+2] cycloadducts is noteworthy. In parallel to the previous study of 3,4-dialkoxyfuran with alkyl coumalates,[13] **4** reacted solely as the 2π-component, a dienophile, throughout.

The regioselectivities of these reactions can be explained by consideration of the LUMO(**1**)-HOMO(furans) interactions, where the largest coefficients are at the C-2(7) positions of **1**, the C-2 positions of **2** and **4**, and the C-5 position of **3**.[14]

The reaction of **1** with **3** yielded six 2 : 1-adducts. The second step of tropone incorporation occurred at a dialkoxyethene part of **7a** and **8a** in two different fashions with a high regioselectivity; one is a [4+2] adduct and the other an [8+2] ([8+2]/[4+2]=3.4).[15]

The predominant formation of [8+2] adducts is parallel to the previous result of the reaction of **1** with 1,1-diethoxyethene(**18**).[10] The high regioselectivity in the second step could be reasonably explained by Frontier Orbital interactions.[16] The energies of the HOMO of the dialkoxyethene part in **7a** and **8a** are estimated to be around −7.5 eV, and those of the LUMO around −4.5 eV.[14] Therefore, considering Frontier Orbitals of **1**,[17] the LUMO(**1**)-HOMO(**7a** and **8a**) interactions[16] are primarily important to 2 : 1-adducts formation. However, these could not explain the periselectivity of the second step of cycloaddition; i.e., the LUMO of **1** has the largest coefficient at the C-2 and the next at the C-5, and the coefficient of the carbonyl oxygen is null.[17] Furthermore, the regiochemistry of the second step of the [4+2]-[4+2] addition is opposite to that of the reported [4+2] adduct (**19**) from **1** and **18**.[10,18] Therefore, the [4+2]-[8+2] adducts may be the thermodynamically stable products accumulated by mutual isomerization with the [4+2]-[4+2] adducts via a [1,5] bond migration. As has been stated, **13** and **15** indeed rearranged to **10** and **11**. A failure to isolate the corresponding [4+2]-[4+2] products (**A** and **B**) from **12** or **14**, however, did not contradict but supported the results of the reaction of **1** with **3**. Since the isomerization occurred only with the stereomers having the cis-geometry, the difference in the thermodynamic stability should be critical; as the molecular model suggests, both **12** and **14** possess the stable trans-trans-geometry for H_h-H_j-H_k and as a result, the equilibria could not produce detectable amounts of **A** and **B** while heating.

In addition, although a stepwise rearrangement was unlikely on the basis of the observed stereospecificity, the mechanism should be analyzed carefully. If the [1,5] sigmatropy is operative in this particular case, the trans-cis system present in the reactive diene site of the

molecule forces the migrating group to flight for long distance,[19] but, the doubly-allylic methine hydrogen was inert against the Woodward-Hoffmann rule-allowed [1,5] sigmatropy. At present, due to the instability of our [8+2] adducts,[20] no further study is possible.

Furthermore, the endo/exo ratio is dependent on the substituents on furans, and under higher pressures, the amount of the exo-isomer which is the thermodynamically controlled product increased in the reaction of **1** with **4**.

Finally, although the present pressure, 3000 bar, being a limit of our apparatus, is not high enough in a preparative point of view, yet, the observed pressure effect was significant, and under higher pressures, the yields and the endo/exo-selectivity of the reaction can be improved.[21,22]

Experimental

Elemental analyses were performed by Miss S. Hirashima, of the Research Institute of Industrial Science, Kyushu University. The NMR spectra were recorded either on a JEOL GX 400 Model or on a JEOL FX 100 Model Spectrometer in $CDCl_3$ solution; the chemical shifts were expressed in δ units. The IR spectra were taken in KBr disks or in $CHCl_3$ solution using a Jasco IR-A 102 Spectrometer. The mass spectra were measured on a JEOL OISG-2 Spectrometer. The UV spectra were measured by means of a Hitachi U-3200 Spectrophotometer.

Diels-Alder Reaction of 1 with 2. **a)** An IB solution (3 cm^3) of **1** (103 mg) and **2** (672 mg) was heated at 130 °C for 10 h in a Teflon ampule under 3000 bar. After cooling to room temperature, the mixture was decompressed and chromatographed on a silica-gel column to give unreacted **1** [61.9 mg; 60%] and the mixture of adducts, which was purified via high-pressure liquid chromatography (HPLC; Micropolasil with hexane-AcOEt) to give **5** [a colorless oil, 4.2 mg; 6%. Found: m/z, 174.0682 (M^+). Calcd for $C_{11}H_{10}O_2$: M, 174.0682. ^1H NMR δ=3.28 (H_c,[6] tdm, J=8.5, 2.5 Hz), 3.67 (H_h, dtd, J=10, 2.5, 2 Hz), 3.95 (H_f, dm, J=7 Hz), 4.70 (H_j, td, J=2.5, 1 Hz), 5.00 (H_g, ddd, J=10, 2.5, 1 Hz), 5.72 (H_a, ddd, J=11, 2, 1 Hz), 6.07 (H_e, ddt, J=8.5, 7, 1 Hz), 6.27 (H_k, dd, J=2.5, 2 Hz), 6.40 (H_d, tm, J=8.5 Hz), and 7.10 (H_b, dd, J=11, 8.5 Hz). ^{13}C NMR δ=40.7, 50.4, 59.9, 81.5, 102.9, 125.2, 129.8, 136.7, 148.5, 154.2, and 194.4. IR ν 1670 cm^{-1}. UV λ_{max}^{MeOH} 209 nm (ε=7600)] and **6** [colorless needles, mp 70—72 °C, 3.1 mg; 5%. Found: m/z, 174.0681 (M^+). ^1H NMR δ=3.3—3.5 (H_c and H_h, m), 4.07 (H_f, tm, J=7 Hz), 4.82 (H_j, t, J=2.5 Hz), 5.11 (H_g, dd, J=11, 7 Hz), 5.88 (H_a, dd, J=11, 2 Hz), 5.99 (H_e, ddd, J=8.5, 7, 1 Hz), 6.29 (H_k, dd, J=2.5, 1.5 Hz), 6.53 (H_d, ddd, J=8.5, 7, 1 Hz), and 6.81 (H_b, dd, J=11, 9 Hz). ^{13}C NMR δ=40.9, 49.9, 56.7, 81.9, 102.2, 125.3, 131.6, 139.5, 148.2, 151.4, and 193.9. IR ν 1680 cm^{-1}. UV λ_{max}^{MeOH} 212 nm (ε=7400)].

b) An IB solution (1 cm^3) of **1** (44.4 mg) and **2** (307 mg) was heated at 130 °C for 10 h in a sealed tube. After removal of the volatile material, no compound was isolated other than the recovered **1**.

Diels-Alder Reaction of 1 with 3. **a)** An IB solution (51 cm^3) of **1** (768 mg) and **3** (6.93 g) was heated at 130 °C for 10 h under 3000 bar. Silica-gel column chromatography of the mixture afforded **7** [colorless needles, mp 138—140 °C, 474 mg; 35%. Found: C, 69.35; H, 5.33%; m/z, 190.0627 (M^+). Calcd for $C_{11}H_{10}O_3$: C, 69.45; H, 5.31%; M, 190.0629. ^1H NMR δ=2.28 (H_j, dd, J=18, 5 Hz), 2.88 (H_k, dd, J=18, 11 Hz), 3.26 (H_h, ddddd, J=11, 8, 5, 2, 1 Hz), 3.36 (H_c, ddm, J=8.5, 7 Hz), 3.90 (H_f, dtd, J=7, 2, 1 Hz), 5.04 (H_g, ddd, J=8, 2, 1 Hz), 5.78 (H_a, ddd, J=11, 2, 1 Hz), 6.18 (H_e, ddt, J=8.5, 7, 1 Hz), 6.60 (H_d, ddt, J=8.5, 7, 1 Hz), and 7.14 (H_b, dd, J=11, 8.5 Hz). ^{13}C NMR δ=34.7, 38.9, 39.9, 59.1, 79.7, 127.2, 130.4, 136.2, 152.7, 175.9, and 192.7. IR ν 1780 and 1670 cm^{-1}. UV λ_{max}^{MeOH} 228 nm (ε=7500)], **8** [colorless needles, mp 137—139 °C, 175 mg; 13%. Found: C, 69.39; H, 5.36%; m/z, 190.0628 (M^+). ^1H NMR δ=2.2—3.1 (H_h, H_j, and H_k, m), 3.46 (H_c, ddd, J=8.5, 7, 4 Hz), 4.10 (H_f, tdd, J=7.5, 2, 1 Hz), 5.04 (H_g, dd, J=8, 7.5 Hz), 5.94 (H_a, ddd, J=11, 2, 1 Hz), 6.04 (H_e, ddd, J=8.5, 7.5, 1 Hz), 6.64 (H_d, ddd, J=8.5, 7, 1 Hz), and 6.94 (H_b, dd, J=11, 8.5 Hz). ^{13}C NMR δ=32.6, 39.7, 40.4, 56.3, 78.5, 124.5, 133.5, 140.2, 148.6, 176.0, and 192.7. IR ν 1780 and 1670 cm^{-1}. UV λ_{max}^{MeOH} 227 nm (ε=7100)], and a mixture of adducts, from which, an HPLC fractionation gave **9** [colorless crystals, mp 103—105 °C, 20 mg; 1%. Found: m/z, 190.0631 (M^+). ^1H NMR δ=2.3 (H_g, br m), 2.8—3.2 (H_j and H_k, m), 3.46 (H_f, ddd, J=7.5, 2.5, 1.5 Hz), 3.76 (H_c, dddm, J=9, 7, 2 Hz), 5.02 (H_h, dd, J=7.5, 2 Hz), 5.88 (H_a, ddd, J=11, 2, 1 Hz), 6.22 (H_e, ddt, J=8.5, 7.5, 1 Hz), 6.50 (H_d, ddt, J=8.5, 7, 1 Hz), and 6.98 (H_b, dd, J=11, 9 Hz). ^{13}C NMR δ=34.1, 35.1, 41.4, 57.2, 80.7, 126.2, 132.2, 136.7, 147.2, 175.8, and 194.5. IR ν 1785 and 1670 cm^{-1}. UV λ_{max}^{MeOH} 226 nm (ε=6600)], **10** [colorless needles, mp 192—194 °C, 29.8 mg; 3%. Found: m/z, 310.1161 (M^+). Calcd for $C_{19}H_{18}O_4$: M, 310.1204. ^1H NMR δ=2.46 (H_j, br d, J=4.5 Hz), 2.67 (H_h, ddd, J=8.5, 4.5, 2 Hz), 3.19 (3H, s), 3.2 (H_c, m), 3.4 (H_r, m), 3.58 (H_f, dddm, J=7, 2, 1.5 Hz), 3.66 (H_n, ddt, J=8.5, 7.5, 1 Hz), 4.74 (H_g, dt, J=8.5, 1.5 Hz), 5.62 (H_a, ddd, J=11, 2, 0.5 Hz), 5.76 (H_k, ddd, J=11, 2, 1 Hz), 6.11 (H_q, tm, J=7.5 Hz), 6.16 (H_e, ddt, J=8.5, 7, 1 Hz), 6.50 (H_d, ddd, J=8.5, 7.5, 1.5 Hz), 6.51 (H_p, tm, J=7.5 Hz), 6.84 (H_m, ddm, J=11, 8.5 Hz), and 7.02 (H_b, dd, J=11, 8.5 Hz). ^{13}C NMR δ=39.3, 43.1, 49.1, 52.2, 54.9, 58.7, 60.8, 84.8, 118.1, 125.5, 127.1, 129.7, 130.4, 136.0, 138.1, 148.5, 152.2, 194.8, and 195.2. IR ν 1665 cm^{-1}. UV λ_{max}^{MeOH} 230 nm (ε=11300)], **11** [colorless crystals, mp 180—182 °C, 6 mg; 0.5%. Found: m/z, 310.1201 (M^+). ^1H NMR δ=2.4 (H_h, ddm, J=8.5, 4 Hz), 2.58 (H_j, dm, J=4 Hz), 3.10 (3H, s), 3.4 (H_c, br m), 3.43 (H_r, dm, J=6.5 Hz), 3.75 (H_n, ddt, J=8.5, 7.5, 1 Hz), 3.87 (H_f, dm, J=6.5 Hz), 4.65 (H_g, dd, J=8.5, 6.5 Hz), 5.79 (H_a, ddd, J=11, 2, 1 Hz), 5.93 (H_k, ddd, J=11, 2, 1 Hz), 5.94 (H_e, ddd, J=8.5, 7.5, 1 Hz), 6.18 (H_q, ddm, J=7.5, 6.5 Hz), 6.50 (H_d or H_p, ddd, J=8.5, 7.5, 1 Hz), 6.52 (H_p or H_d, ddd, J=8.5, 7.5, 1 Hz), 6.85 (H_b, dd, J=11, 8.5 Hz), and 6.91 (H_m, dd, J=11, 8.5 Hz). ^{13}C NMR δ=40.4, 43.7, 49.5, 52.4, 54.0, 59.4, 59.5, 85.0, 119.1, 125.9, 126.2, 130.4, 133.0, 137.8, 139.5, 148.6, 149.6, 195.2, and 195.4. IR ν 1662 cm^{-1}. UV λ_{max}^{MeOH} 224 nm (ε=11900)], **12** [a yellow oil, 42.4 mg; 4%. Found: m/z, 310.1193 (M^+).[20] ^1H NMR δ=2.48 (1H, br s), 2.51 (1H, d, J=7 Hz), 2.79 (1H, ddd, J=8.5, 7, 2 Hz), 3.33 (1H, underneath the MeO), 3.38 (3H, s), 3.80 (1H, dtd, J=7, 2, 1.5 Hz), 4.84 (1H, ddd, J=8.5, 2, 1 Hz), 5.06 (1H, dd, J=9, 4 Hz), 5.68 (1H, dd, J=11, 2 Hz), 5.68 (1H, br d, J=6 Hz), 6.0—6.3 (3H, m), 6.36 (1H, dd, J=9, 6 Hz), 6.60 (1H, tm, J=8 Hz), and 7.03 (1H, dd, J=11, 8 Hz). ^{13}C NMR δ=38.6, 47.4, 51.3, 51.8, 54.0, 59.1, 80.0, 97.1, 121.4, 124.7, 126.8, 128.1, 129.5, 130.1, 134.1, 135.7, 149.3, 152.6, and 193.8. IR ν 1670 and 1633 cm^{-1}], **13** [a yellow oil, 36.1 mg; 3%. Found: m/z, 310.1210 (M^+).

^{1}H NMR δ=2.51 (1H, t, J=7.5 Hz), 3.1—3.6 (3H, m), 3.45 (3H, s), 3.78 (1H, dtd, J=7, 2, 1.5 Hz), 4.71 (1H, ddd, J=8.5, 2, 1 Hz), 5.00 (1H, dd, J=9, 3 Hz), 5.7 (1H, br m), 5.71 (1H, dd, J=11, 2 Hz), 6.0—6.2 (3H, m), 6.28 (1H, ddt, J=9.5, 7, 1 Hz), 6.58 (1H, tm, J=7.5 Hz), and 7.10 (1H, dd, J=11, 8.5 Hz). ^{13}C NMR ν=39.1, 42.6, 45.5, 50.2, 51.7, 58.8, 80.1, 99.9, 118.3, 123.9, 128.2, 128.3, 129.4, 130.2, 131.6, 135.5, 152.4, 152.7, and 193.8. IR ν 1670 and 1632 cm^{-1}], and **14** [a yellow oil, 37.4 mg; 3%. Found: m/z, 310.1202 (M^+). ^{1}H NMR δ=2.4—2.6 (2H, m), 2.68 (1H, dd, J=5, 1 Hz), 3.35 (3H, s), 3.5 (1H, br m), 4.00 (1H, tdd, J=7, 2, 1 Hz), 4.80 (1H, dd, J=8.5, 7 Hz), 5.10 (1H, ddd, J=8.5, 4.5, 1 Hz), 5.67 (1H, d, J=5.5 Hz), 5.98 (1H, ddd, J=11, 2, 1 Hz), 6.05 (1H, ddd, J=7.5, 2, 1 Hz), 6.1—6.5 (3H, m), 6.56 (1H, ddd, J=8, 7, 1 Hz), and 6.98 (1H, dd, J=11, 8.5 Hz). ^{13}C NMR δ=39.9, 48.0, 51.9, 52.1 (2C), 56.8, 78.8, 96.5, 121.4, 124.6, 125.2, 126.7, 128.4, 129.5, 132.9, 134.5, 139.8, 149.4, and 194.2. IR ν 1670 and 1633 cm^{-1}], and **15** [a yellow oil, 22.6 mg; 2%. Found: m/z, 310.1205 (M^+). ^{1}H NMR δ=2.69 (1H, dd, J=7.5, 6 Hz), 2.90 (1H, ddd, J=8.5, 6, 5 Hz), 3.3—3.7 (2H, m), 3.42 (3H, s), 3.98 (1H, dddd, J=7.5, 7, 2, 1 Hz), 4.61 (1H, dd, J=8.5, 7 Hz), 5.00 (1H, ddm, J=9, 3 Hz), 5.66 (1H, dm, J=5 Hz), 5.98 (1H, ddd, J=11, 2, 1 Hz), 6.0—6.4 (4H, m), 6.61 (1H, ddd, J=9, 7, 1 Hz), and 6.97 (1H, dd, J=11, 8.5 Hz). ^{13}C NMR δ=40.4, 42.7, 45.8, 48.5, 51.8, 56.9, 78.8, 99.6, 119.1, 123.8, 125.3, 128.2, 129.2, 131.7, 132.7, 139.7, 150.0, 153.1, and 194.5. IR ν 1670 and 1632 cm^{-1}].

b) An IB solution (5 cm^3) of **1** (67 mg) and **3** (613 mg) was heated at 130 °C for 10 h in a sealed tube. Silica-gel column chromatography of the mixture afforded recovered **1** [14.6 mg; 22%], **7** [11.8 mg; 13%], and **8** [2.6 mg; 3%].

Diels-Alder Reaction of 1 with 4. a) An IB solution (5 cm^3) of **1** (94 mg) and **4** (126 mg) was heated at 130 °C for 10 h under 3000 bar. The silica-gel column chromatography afforded, together with the recovered **1** [59.2 mg; 63%], a mixture of products, whose HPLC purification gave **16** [colorless crystals, mp 82—84 °C, 6.4 mg; 8%. Found: m/z, 234.0897 (M^+). Calcd for $C_{13}H_{14}O_4$: M, 234.0892. ^{1}H NMR δ=3.24 (3H, s), 3.54 (3H, s), 3.69 (1H, t, J=8.5 Hz), 3.77 (1H, dtd, J=7, 2, 1.5 Hz), 4.58 (1H, d, J=2 Hz), 5.82 (1H, dd, J=11, 2 Hz), 6.06 (1H, tt, J=7, 1 Hz), 6.09 (1H, s), 6.36 (1H, ddd, J=8.5, 7, 1.5 Hz), and 7.00 (1H, dd, J=11, 8.5 Hz). ^{13}C NMR δ=42.2, 51.6, 57.9, 60.4, 81.4, 94.1, 125.8, 128.2, 130.7, 136.1, 140.5, 152.5, and 193.5. IR ν 1660 and 1090 cm^{-1}. UV λ_{max}^{MeOH} 220 nm (ε=8800) and 302 (850)] and **17** [colorless crystals, mp 126—128 °C, 21.2 mg; 28%. Found: C, 66.25; H, 5.97%; m/z, 234.0922. Calcd for $C_{13}H_{14}O_4$: C, 66.65; H, 6.04%. ^{1}H NMR δ=3.23 (3H, s), 3.52 (3H, s), 3.52 (1H, dddt, J=9, 7, 1.5, 1 Hz), 3.95 (1H, dddd, J=7.5, 6.5, 2, 1 Hz), 4.58 (1H, dd, J=6.5, 1.5 Hz), 5.80 (1H, ddd, J=11, 2, 1 Hz), 5.97 (1H, ddd, J=8.5, 7.5, 1 Hz), 6.03 (1H, s), 6.59 (1H, ddd, J=8.5, 7, 1 Hz), and 6.89 (1H, dd, J=11, 9 Hz). ^{13}C NMR δ=44.5, 51.9, 56.0, 57.8, 81.5, 92.8, 123.0, 127.4, 131.7, 137.8, 140.8, 148.8, and 193.7. IR ν 1665 and 1080 cm^{-1}. UV λ_{max}^{MeOH} 221 nm (ε=7600) and 316 (250)].

b) An IB solution (1 cm^3) of **1** (31.6 mg) and **4** (38.9 mg) was heated at 130 °C in a sealed tube. Silica-gel column chromatography of the mixture afforded, other than the recovered **1** [21.3 mg; 67%] and **4** [19 mg; 49%], a complicated mixture of products, 3.8 mg, whose HPLC revealed more than ten compounds.

Thermal Rearrangement of 13. A benzene-d_6 (C_6D_6) solution (0.3 cm^3) of **13** (13 mg) was heated in a sealed NMR tube at 100 °C for 5 d. The HPLC of the mixture afforded **10** [0.3 mg; 3%], which was identical with the authentic sample prepared directly from **1** and **3**.

Thermal Rearrangement of 15. A C_6D_6 solution (0.3 cm^3) of **15** (9 mg) was similarly heated in a sealed tube at 100 °C for 5 d. The HPLC of the mixture afforded **11** [0.1 mg; 1%], identical with the authentic sample.

Attempted Thermal Rearrangement of 12 and 14. An each C_6D_6 solution (0.3 cm^3) of **12** (17 mg) and **14** (27 mg) was heated in a sealed NMR tube at 100 °C for 5 d. Despite a careful NMR inspection, every chromatographic fraction gave no identifiable product.

We thank The Ministry of Education, Science and Culture for a Grant-in-Aid for Scientific Research given to S. S. (No. 61740294).

References

1) H. Takeshita, S. Sugiyama, and T. Hatsui, *Chem. Lett.*, **1984**, 1855; *Bull. Chem. Soc. Jpn.*, **58**, 2490 (1985).

2) H. Takeshita, S. Sugiyama, and T. Hatsui, *J. Chem. Soc., Perkin Trans. 2*, **1986**, 1491.

3) I. Saito (D. Sc. Thesis, Tohoku University, 1975) observed a formation of cycloadducts in the reaction of **1** with **2** in a methanolic $HClO_4$. This could be, however, the reaction of **1** with 5-methoxyoxolene formed in situ.

4) In this study, the same apparatus was used as in the previous study.

5) S. Ito, H. Takeshita, and Y. Shoji, *Tetrahedron Lett.*, **1969**, 1815.

6) To specify the protons, Roman characters were used as depicted.

7) For a convenience, we adopted the expression, [m+n], as the cycloadducts with $m\pi$ system of **1** to $n\pi$ system of furans.

8) A high-field shift of H_b-signals in the exo-[4+2] adducts is parallel to the cyclopentadiene adducts of **1**. See S. Ito, K. Sakan, and Y. Fujise, *Tetrahedron Lett.*, **1970**, 2873.

9) R. Gomper, A. Studeneer, and W. Elser, *Tetrahedron Lett.*, **1968**, 1019.

10) T. S. Cantrell, *Tetrahedron Lett.*, **1975**, 907.

11) The [8+2] mode found in the 2:1-adducts should be explained by the reaction of **1** with a 1,1-dialkoxyethene.

12) K. N. Houk and R. B. Woodward, *J. Am. Chem. Soc.*, **92**, 4145 (1970).

13) M. E. Jung, L. J. Street, and Y. Usui, *J. Am. Chem. Soc.*, **108**, 6810 (1986).

14) K. N. Houk, *J. Am. Chem. Soc.*, **95**, 4092 (1973).

15) The figure, 3.4, might be smaller than the actual value. All [4+2]-[8+2] adducts were unstable under workup conditions, and even polymerized in $CDCl_3$ solution.

16) e.g., I. Fleming, "Frontier Orbitals and Organic Chemical Reactions," John Wiley & Sons, Ltd., New York (1976), pp. 87—181.

17) D. Mukherjee, C. R. Watts, and K. N. Houk, *J. Org. Chem.*, **43**, 817 (1978).

18) Should the proposed structure for **19** be correct, no mutual isomerization process should be present between the [8+2] adduct, **20** and **19**, and they should have been formed independently. Reinvestigations of the reaction of **18** and **1** seem to be desirable.

19) Recently, we have noticed the volume profiles in sigmatropies were dependent on the flight distance of the migrating groups. See S. Sugiyama, A. Mori, and H.

Takeshita, *Chem. Lett.*, **1987**, 1247.

20) These cycloadducts were extremely sensitive towards light and air, and elemental analyses were difficult.

21) A recent paper described the high-pressure reactions of oxazoles with ethylenic dienophiles showing the pressure-dependent temperature and solvent effects. See T. Ibata, H. Nakawa, Y. Isogami, and K. Matsumoto, *Bull. Chem. Soc. Jpn.*, **59**, 3197 (1986).

22) J. Jurczak, T. Kozluk, M. Tkacz, and C. H. Eugster, *Helv. Chim. Acta*, **66**, 218 (1983).

 © 1987 The Chemical Society of Japan Bull. Chem. Soc. Jpn., 60, 3639—3643 (1987)

The Synthesis of Lycoxanthol and Its C-15 Epimer

Takashi MATSUMOTO,* Sachihiko IMAI, and Takashi YOSHINARI
Department of Chemistry, Faculty of Science, Hiroshima University, Higashisenda-machi, Naka-ku, Hiroshima 730
(Received March 28, 1987)

In order to elucidate the absolute configuration of C-15 in natural lycoxanthol, (15*R*)-11,16-dihydroxy-12-methoxymethoxy-8,11,13-abietatrien-7-one and its (15*S*)-epimer were transformed into (15*R*)-12,16-epoxy-6,11,14-trihydroxy-5,8,11,13-abietatetraen-7-one (**1a**) and its (15*S*)-epimer, respectively. The synthetic **1a** was identical with natural lycoxanthol. Thus, the stereochemistry of C-15 in the natural compound was conclusively assigned as R-configuration.

Lycoxanthol, a highly oxygenated abietane-type diterpene possessing a dihydrofuran moiety, has been isolated from *Lycopodium lucidulum* by Burnell et al.[1,2] On the basis of chemical and spectroscopic studies, they deduced the structure of lycoxanthol to be 12,16-epoxy-6,11,14-trihydroxy-5,8,11,13-abietatetraen-7-one (**1**). However, the absolute configuration of C-15 in the natural compound remained unsettled. In order to elucidate the unknown stereochemistry at C-15, we have now attempted the syntheses of (15*R*)-12,16-epoxy-6,11,14-trihydroxy-5,8,11,13-abietatetraen-7-one (**1a**) and its (15*S*)-epimer (**1b**). For this purpose, (15*R*)-11,16-dihydroxy-12-methoxymethoxy-8,11,13-abietatrien-7-one (**2a**)[3] and its (15*S*)-epimer (**2b**)[3] were chosen as convenient relay intermediates, because these compounds have recently been synthesized in our laboratory by an unambiguous method starting from (+)-dehydroabietic acid.

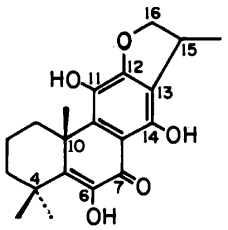

1

Mesylation of the 12-methoxymethyl ether **2a** with methanesulfonyl chloride in pyridine afforded a mesylate **3a** which was converted into 12,16-epoxy-11-hydroxy-8,11,13-abietatrien-7-one (**4a**) by refluxing with sodium iodide in ethyl methyl ketone and then with anhydrous potassium carbonate in ethyl methyl ketone in 87.2% yield from **2a**. The ^{1}H NMR spectrum of **4a** showed signals at δ 1.30 (3H, doublet), ca. 3.5 (1H, multiplet), 4.13 (1H, double doublet), and 4.75 ppm (1H, triplet) due to a dihydrofuran moiety. For the protection of the hydroxyl group, the dihydrobenzofuran derivative **4a** was acetylated with acetic anhydride in pyridine to give an acetate **5a** in 95.0% yield. This was reduced with sodium borohydride in a mixture of ether and methanol at room temperature, and the resulting crude product was immediately refluxed with *p*-toluenesulfonic acid in benzene to give 11-acetoxy-12,16-epoxy-6,8,11,13-abietatetraene (**6a**) in 93.1% yield. Epoxidation of **6a** with *m*-chloroperbenzoic acid in dichloromethane followed by treatment with *p*-toluenesulfonic acid in refluxing benzene afforded 11-acetoxy-12,16-epoxy-8,11,13-abietatrien-6-one (**7a**) in 63.1% yield. To introduce an oxygen function at the C-14 position, the 6-oxo compound **7a** was reduced with lithium aluminium hydride in ether and the resulting 6β,11-diol (**8a**: 94.5%) was then oxidized with *m*-chloroperbenzoic acid in tetrahydrofuran at room temperature to give a *p*-quinone, 12,16-epoxy-6β-hydroxy-8,12-abietadiene-11,14-dione (**9a**) in 19% yield.[4] In the ^{1}H NMR spectrum of **8a**, the downfield shift of a signal (δ 1.70) due to the methyl group at C-10 relative to the corresponding signal (δ 1.33) for **7a** suggested a 1,3-diaxial-*cis*-relationship between the methyl group and the hydroxyl group at C-6. For the protection of the *p*-quinone moiety, the hydroxy quinone **9a** was subjected to reductive acetylation with zinc powder and acetic anhydride in pyridine, and the resulting crude product was immediately oxidized with Jones reagent at 0—5 °C to give 11,14-diacetoxy-12,16-epoxy-8,11,13-abietatrien-6-one (**10a**) in 20% yield. To introduce a final oxygen function at the C-7 position, the diacetate **10a** was further oxidized with Jones reagent at room temperature and the crude product, without purification, was hydrolyzed with dilute hydrochloric acid in refluxing ethanol to give the desired (15*R*)-12,16-epoxy-6,11,14-trihydroxy-5,8,11,13-abietatetraen-7-one (**1a**), mp 250—251 °C, in 31% yield. The synthetic **1a** was identical with natural lycoxanthol (mp 249 °C).

For direct comparison with **1a**, the synthesis of (15*S*)-12,16-epoxy-6,11,14-trihydroxy-5,8,11,13-abietatetraen-7-one (**1b**) was also carried out in the same manner to that described for the preparation of **1a**. Mesylation of (15*S*)-11,16-dihydroxy-12-methoxymethoxy-8,11,13-abietatrien-7-one (**2b**) with methanesulfonyl chloride in pyridine, followed by treatment of the resulting mesylate **3b** with sodium iodide in refluxing ethyl methyl ketone and then with anhydrous potassium carbonate in refluxing ethyl methyl ketone afforded 12,16-epoxy-11-hydroxy-8,11,13-abietatrien-7-one (**4b**) in 97.8% yield from **2b**. The 11-

hydroxy compound **4b** was acetylated with acetic anhydride in pyridine and the acetate (**5b**: 94.8%) was then transformed into 11-acetoxy-12,16-epoxy-6,8,11,13-abietatetraene (**6b**: 83.0%) by sodium borohydride reduction and acid-catalyzed dehydration. Oxidation of **6b** with *m*-chloroperbenzoic acid followed by treatment with *p*-toluenesulfonic acid led to 11-acetoxy-12,16-epoxy-8,11,13-abietatrien-6-one (**7b**) in 58.0% yield. This was reduced with lithium aluminium hydride to give the corresponding 6β,11-diol (**8b**: 99.2%) which was then converted into 12,16-epoxy-6β-hydroxy-8,12-abietadiene-11,14-dione (**9b**: 16.4%[4]) by oxidation with *m*-chloroperbenzoic acid. Reductive acetylation of **9b** with zinc powder and acetic anhydride in pyridine, followed by oxidation with Jones reagent at 0—5 °C produced 11,14-diacetoxy-12,16-epoxy-8,11,13-abietatrien-6-one (**10b**) in 28.7% yield. Further oxidation of **10b** with Jones reagent at room temperature and subsequent hydrolysis with dilute hydrochloric acid afforded the desired **1b** (40%), mp 219—220 °C, which was not identical with natural lycoxanthol.

From the present study, the stereochemistry of C-15 in natural lycoxanthol was conclusively assigned as R-configuration.

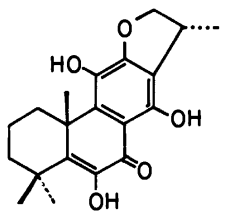

1a

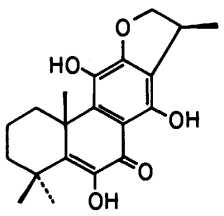

1b

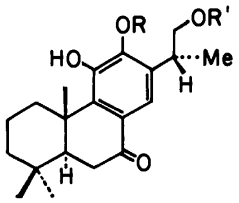

2a R=CH_2OMe, R'=H **2b**
3a R=CH_2OMe, R'=Ms **3b**

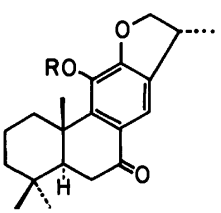

4a R=H **4b**
5a R=Ac **5b**

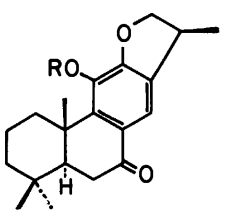

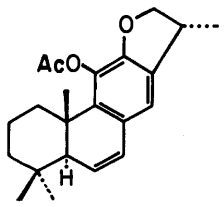

6a

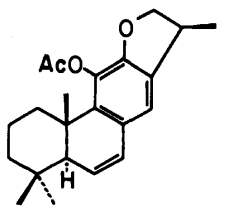

6b

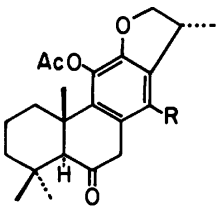

7a R=H **7b**
10a R=OAc **10b**

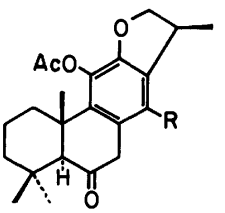

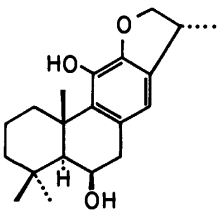

8a

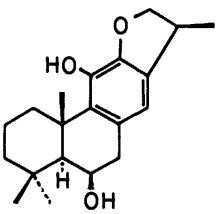

8b

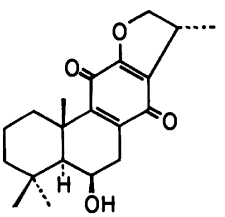

9a

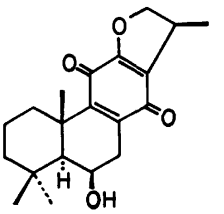

9b

Experimental

All melting points are uncorrected. The IR spectra and optical rotations were measured in chloroform, and the ^1H NMR spectra in deuteriochloroform at 60 MHz, with tetramethylsilane as an internal standard, unless otherwise stated; s: singlet, bs: broad singlet, d: doublet, bd: broad doublet, dd: double doublet, t: triplet, m: multiplet. The column chromatography was performed using Merck silica gel (0.063 mm).

(15*R*)-12,16-Epoxy-11-hydroxy-8,11,13-abietatrien-7-one (4a) and Its (15*S*)-Epimer (4b). a) A mixture of (15*R*)-11,16-dihydroxy-12-methoxymethoxy-8,11,13-abietatrien-7-one (**2a**)[3] (4.485 g) and methanesulfonyl chloride (1.1 ml) in pyridine (10 ml) was allowed to stand at room temperature for 15 h and then poured into a mixture of ice and dilute hydrochloric acid. The mixture was extracted with ether.

The ether extract was washed with brine, dried over sodium sulfate, and evaporated in vacuo to give a crude mesylate (**3a**), IR 3490—3325, 1670, 1360, and 1170 cm^{-1}; ^1H NMR δ=0.95 (3H, s) and 0.98 (3H, s) (-C(CH$_3$)$_2$), 1.32 (3H, d, J=7 Hz, C_{15}-CH$_3$), 1.41 (3H, s, C_{10}-CH$_3$), 2.91 (3H, s, -OSO$_2$-CH$_3$), 3.67 (3H, s, -OCH$_3$), 4.22 (2H, bd, J=7 Hz, -CH$_2$-OSO$_2$CH$_3$), 5.03 (2H, s, -OCH$_2$O-), 7.45 (1H, s) and 7.51 (1H, s) (C_{11}-OH and C_{14}-H).

A stirred mixture of the above crude **3a** and sodium iodide (3.572 g) in ethyl methyl ketone (40 ml) was refluxed for 4 h. After cooling, the mixture was poured into water and extracted with ether. The ether extract was washed successively with aqueous sodium thiosulfate and brine. The dried solution was evaporated in vacuo. The residue was further refluxed with anhydrous potassium carbonate (3.5 g) in ethyl methyl ketone (20 ml) for 2.5 h. After cooling, the mixture was poured into dilute hydrochloric acid and extracted with ether. The ether extract was washed successively with aqueous sodium thiosulfate and brine, dried, and evaporated in vacuo. The crude product was purified by column chromatography on silica gel (100 g), using ether-benzene (1 : 99) as eluent, to give an oily **4a** (3.268 g: 87.2% yield from **2a**), $[\alpha]_D$ +17.1° (*c* 12.35), IR 3560, 3320, and 1668 cm^{-1}; ^1H NMR δ=0.94 (3H, s) and 0.97 (3H, s) (-C(CH$_3$)$_2$), 1.30 (3H, d, J=7 Hz, C_{15}-CH$_3$), 1.39 (3H, s, C_{10}-CH$_3$), ca. 3.5 (1H, m, C_{15}-H), 4.13 (1H, dd, J=7 and 8 Hz) and 4.75 (1H, t, J=7 Hz) (-OCH$_2$-), 5.36 (1H, s, C_{11}-OH), 7.60 (1H, bs, C_{14}-H). Found: C, 76.54; H, 8.64%. Calcd for $C_{20}H_{26}O_3$: C, 76.40; H, 8.34%.

b): A mixture of (15*S*)-11,16-dihydroxy-12-methoxy-methoxy-8,11,13-abietatrien-7-one (**2b**)[3] (4.104 g) and methanesulfonyl chloride (0.93 ml) in pyridine (10 ml) was treated as described in **a**) to give a crude mesylate **3b**, IR 3490—3325, 1678, 1360, and 1170 cm^{-1}; ^1H NMR δ=0.96 (3H, s) and 0.99 (3H, s) (-C(CH$_3$)$_2$), 1.29 (3H, d, J=7 Hz, C_{15}-CH$_3$), 1.42 (3H, s, C_{10}-CH$_3$), 2.93 (3H, s, -OSO$_2$CH$_3$), 3.68 (3H, s, -OCH$_3$), 4.26 (2H, bd, J=7 Hz, -CH$_2$OSO$_2$CH$_3$), 5.04 (2H, s, -OCH$_2$O-), 7.48 (1H, s) and 7.53 (1H, s) (C_{11}-OH and C_{14}-H).

A stirred mixture of the above crude **3b** and sodium iodide (3.268 g) in ethyl methyl ketone (40 ml) was refluxed for 4 h. After the work-up as described in **a**), the crude product was further refluxed with anhydrous potassium carbonate (3.0 g) in ethyl methyl ketone (20 ml) for 2.5 h. The crude product was purified by column chromatography on silica gel (100 g), using ether-benzene (1 : 99) as eluent, to give an oily **4b** (3.352 g: 97.8% yield from **2b**), $[\alpha]_D$ +33.3° (*c* 8.95), IR 3560, 3320, and 1669 cm^{-1}; ^1H NMR δ=0.95 (3H, s) and 0.97 (3H, s) (-C(CH$_3$)$_2$), 1.33 (3H, d, J=7 Hz, C_{15}-CH$_3$), 1.40 (3H, s, C_{10}-CH$_3$), *ca.* 3.5 (1H, m, C_{15}-H), 4.14 (1H, dd, J=7 and 8 Hz) and 4.78 (1H, t, J=8 Hz) (-OCH$_2$-), 5.33 (1H, s, C_{11}-OH), 7.62 (1H, bs, C_{14}-H). Found: C, 76.13; H, 8.54%. Calcd for $C_{20}H_{26}O_3$: C, 76.40; H, 8.34%.

(15*R*)-11-Acetoxy-12,16-epoxy-8,11,13-abietatrien-7-one (5a) and Its (15*S*)-Epimer (5b). **a**): A mixture of **4a** (1.403 g) and acetic anhydride (3.0 ml) in pyridine (4.0 ml) was heated at 75—80 °C for 2.5 h. After the usual work-up, the crude product was chromatographed on silica gel (50 g), using ether-benzene (1 : 99 and then 5 : 95) as eluents, to give **5a** (1.511 g: 95.0%) which was recrystallized from hexane, mp 165—166.5 °C, IR 1770 and 1668 cm^{-1}, ^1H NMR δ=0.94 (3H, s) and 0.97 (3H, s) (-C(CH$_3$)$_2$), 1.32 (3H, d, J=7 Hz, C_{15}-CH$_3$), 1.33 (3H, s, C_{10}-CH$_3$), 2.32 (3H, s, -OCOCH$_3$), ca. 3.5 (1H, m, C_{15}-H), 4.13 (1H, dd, J=7 and 9 Hz) and 4.73 (1H, t, J=9 Hz) (-OCH$_2$-), 7.88 (1H, d, J=1 Hz, C_{14}-H). Found: C, 74.33 H, 8.18%. Calcd for $C_{22}H_{28}O_4$: C, 74.13; H, 7.92%.

b): A mixture of **4b** (3.047 g) and acetic anhydride (7.0 ml) in pyridine (7.0 ml) was heated at 75—80 °C for 2 h. After the usual work-up, the crude product was chromatographed on silica gel (100 g), using ether-benzene (1 : 99 and then 5 : 95) as eluents, to give **5b** (3.273 g: 94.8%) which was recrystallized from hexane, mp 156.5—158 °C, $[\alpha]_D$ +64.4° (*c* 4.64), IR 1770 and 1668 cm^{-1}, ^1H NMR δ=0.99 (6H, s, -C(CH$_3$)$_2$), 1.36 (3H, s, C_{10}-CH$_3$), 1.36 (3H, d, J=7 Hz, C_{15}-CH$_3$), 2.33 (3H, s, -OCOCH$_3$), *ca.* 3.5 (1H, m, C_{15}-H), 4.12 (1H, dd, J=7 and 9 Hz) and 4.79 (1H, t, J=9 Hz) (-OCH$_2$-), 7.91 (1H, d, J=1 Hz, C_{14}-H). Found: C, 74.26; H, 8.17%. Calcd for $C_{22}H_{28}O_4$: C, 74.13; H, 7.92%.

(15*R*)-11-Acetoxy-12,16-epoxy-6,8,11,13-abietatetraene (6a) and Its (15*S*)-Epimer (6b). **a**): A suspension of **5a** (648 mg) and sodium borohydride (69 mg) in ether-methanol (2 : 1) (9.0 ml) was stirred at 0—5 °C for 15 min and at room temperature for 1 h. The mixture was acidified with dilute hydrochloric acid and extracted with ether. The ether extract was washed with brine, dried, and evaporated in vacuo. The residue was refluxed with *p*-toluenesulfonic acid (50 mg) in dry benzene (10 ml) for 1 h, cooled, and diluted with ether. The ether solution was washed with water, dried, and evaporated in vacuo. The crude product was chromatographed on silica gel (50 g), using benzene as eluent, to give an oily **6a** (576 mg: 93.1%), $[\alpha]_D$ −55.9° (*c* 1.67), IR 1750 cm^{-1}, ^1H NMR δ=0.95 (3H, s), 1.01 (3H, s), and 1.10 (3H, s) (-C(CH$_3$)$_2$ and C_{10}-CH$_3$), 1.27 (3H, d, J=6.5 Hz, C_{15}-CH$_3$), 2.28 (3H, s, -OCOCH$_3$), ca. 3.5 (1H, m, C_{15}-H), 4.03 (1H, dd, J=7 and 9 Hz) and 4.63 (1H, t, J=9 Hz) (-OCH$_2$-), 5.79 (1H, dd, J=3 and 9.5 Hz, C_6-H), 6.42 (1H, dd, J=3 and 9.5 Hz, C_7-H), 6.72 (1H, s, C_{14}-H). Found: C, 77.91; H, 8.56%. Calcd for $C_{22}H_{28}O_3$: C, 77.61; H, 8.29%

b): A suspension of **5b** (3.273 g) and sodium borohydride (348 mg) in ether-methanol (2 : 1) (15 ml) was stirred at 0—5 °C for 15 min and at room temperature for 2 h. After the work-up as described in **a**), the crude product was refluxed with *p*-toluenesulfonic acid (200 mg) in dry benzene (30 ml) for 1 h. The mixture was cooled and diluted with ether. The ether solution was washed with water, dried, and evaporated in vacuo. The residue was chromatographed on silica gel (60 g), using benzene as eluent, to give an oily **6b** (2.594 g: 83.0%), $[\alpha]_D$ −102.8° (*c* 6.48), IR 1752 cm^{-1}, ^1H NMR δ=0.96 (3H, s), 1.01 (3H, s), and 1.11 (3H, s) (-C(CH$_3$)$_2$ and C_{10}-CH$_3$), 1.30 (3H, d, J=6.5 Hz, C_{15}-CH$_3$), 2.29 (3H, s, -OCOCH$_3$), ca. 3.5 (1H, m, C_{15}-H), 4.02 (1H, t, J=9 Hz) and 4.69 (1H, t, J=9 Hz) (-OCH$_2$-), 5.81 (1H, dd, J=3 and 9.5 Hz, C_6-H), 6.44 (1H, dd, J=3 and 9.5 Hz, C_7-H), 6.72 (1H, s, C_{14}-H). Found: C, 77.41; H, 8.52%. Calcd for $C_{22}H_{28}O_3$: C, 77.61; H, 8.29%.

(15*R*)-11-Acetoxy-12,16-epoxy-8,11,13-abietatrien-6-one (7a) and Its (15*S*)-Epimer (7b). **a**): A mixture of **6a** (508 mg) and *m*-chloroperbenzoic acid (80%: 483 mg) in dichloromethane (5.0 ml) was stirred at 0—5 °C for 30 min and at room temperature for 17 h. The mixture was diluted with ether and washed successively with aqueous potassium iodide, aqueous sodium thiosulfate, aqueous sodium hydrogencarbonate, and brine. The dried solution was evaporated in vacuo. The residual oil was refluxed with *p*-toluenesulfonic acid (50 mg) in dry benzene (5.0 ml) for 1 h,

cooled, and diluted with ether. The ether solution was washed successively with water, aqueous sodium hydrogencarbonate, and water. The dried solution was evaporated in vacuo. The crude product was chromatographed on silica gel (50 g), using ether-benzene (1 : 99) as eluent, to give an oily **7a** (332 mg: 63.1%), $[\alpha]_D$ +44.8° (*c* 4.58), IR 1763 and 1716cm^{-1}, ^{1}H NMR δ=1.03 (3H, s) and 1.22 (3H, s) (-C(CH$_3$)$_2$), 1.29 (3H, d, *J*=7 Hz, C_{15}-CH$_3$), 1.33 (3H, s, C_{10}-CH$_3$), 2.32 (3H, s, -OCOCH$_3$), 2.60 (1H, s, C_5-H), 3.34 (1H, bd, *J*=21 Hz) and 3.76 (1H, d, *J*=21 Hz) (-COCH$_2$-), 4.08 (1H, dd, *J*=7 and 9 Hz) and 4.67 (1H, t, *J*=9 Hz) (-OCH$_2$-), 6.72 (1H, s, C_{14}-H). Found: C, 73.92; H, 8.09%. Calcd for $C_{22}H_{28}O_4$: C, 74.13; H, 7.92%.

b): A mixture of **6b** (2.820 g) and *m*-chloroperbenzoic acid (80%: 2.680 g) in dichloromethane (20 ml) was stirred at 0—5 °C for 30 min and at room temperature for 13 h. After the work-up as described in **a**), the crude product was refluxed with *p*-toluenesulfonic acid (100 mg) in dry benzene (20 ml) for 1 h. The mixture was cooled, diluted with ether, and washed successively with water, aqueous sodium hydrogencarbonate, and water. The dried solution was evaporated in vacuo. The residue was chromatographed on silica gel (50 g), using ether-benzene (1 : 99) as eluent, to give an oily **7b** (1.712 g: 58.0%), $[\alpha]_D$ +54.6° (*c* 6.54), IR 1761 and 1712 cm^{-1}, ^{1}H NMR δ=1.02 (3H, s) and 1.22 (3H, s) (-C(CH$_3$)$_2$), 1.29 (3H, d, *J*=7 Hz, C_{15}-CH$_3$), 1.31 (3H, s, C_{10}-CH$_3$), 2.28 (3H, s, -OCOCH$_3$), 2.55 (1H, s, C_5-H), 3.31 (1H, d, *J*=21 Hz) and 3.71 (1H, d, *J*=21 Hz) (-COCH$_2$-), 4.00 (1H, t, *J*=8 Hz) and 4.68 (1H, t, *J*=8 Hz) (-OCH$_2$-), 6.66 (1H, s, C_{14}-H). Found: C, 74.26; H, 7.79%. Calcd for $C_{22}H_{28}O_4$: C, 74.13; H, 7.92%.

(15*R*)-12,16-Epoxy-8,11,13-abietatriene-6β,11-diol (8a) and Its (15*S*)-Epimer (8b). **a**): A mixture of **7a** (434.0 mg) and lithium aluminium hydride (69.3 mg) in dry ether (7.0 ml) was refluxed for 1.5 h. The mixture was poured into ice-dilute hydrochloric acid and extracted with ether. The ether extract was washed with brine, dried, and evaporated in vacuo to give a crude **8a** as a solid (364.3 mg: 94.5%) which was recrystallized from acetone-hexane, mp 216—218 °C, IR (KBr) 3580 and 3380 cm^{-1}, ^{1}H NMR δ=1.03 (3H, s) and 1.27 (3H, s) (-C(CH$_3$)$_2$), 1.28 (3H, d, *J*=7 Hz, C_{15}-CH$_3$), 1.70 (3H, s, C_{10}-CH$_3$), 4.02 (1H, t, *J*=8 Hz) and 4.63 (1H, t, *J*=8 Hz) (-OCH$_2$-), 4.55 (1H, overlap, C_6-H), 5.03 (1H, s, C_{11}-OH), 6.42 (1H, s, C_{14}-H). Found: C, 76.16; H, 9.13%. Calcd for $C_{20}H_{28}O_3$: C, 75.91; H, 8.92%.

b): A mixture of **7b** (1.252 g) and lithium aluminium hydride (133 mg) in dry ether (10 ml) was refluxed for 1.5 h to give a crude **8b** as a solid (1.102 g: 99.2%). This was recrystallized from acetone-hexane, mp 212—214.5 °C, IR (KBr) 3490 and 3230 cm^{-1} ^{1}H NMR δ=1.03 (3H, s) and 1.27 (3H, s) (-C(CH$_3$)$_2$), 1.27 (3H, d, *J*=7 Hz, C_{15}-CH$_3$), 1.70 (3H, s, C_{10}-CH$_3$), 4.00 (1H, t, *J*=8 Hz) and 4.66 (1H, t, *J*=8 Hz) (-OCH$_2$-), 4.55 (1H, overlap, C_6-H), 5.01 (1H, s, C_{11}-OH), 6.42 (1H, s, C_{14}-H). Found: C, 76.20; H, 9.15%. Calcd for $C_{20}H_{28}O_3$: C, 75.91; H, 8.92%.

(15*R*)-12,16-Epoxy-6β-hydroxy-8,12-abietadiene-11,14-dione (9a) and Its (15*S*)-Epimer (9b). **a**): A mixture of the above crude **8a** (56.2 mg) and *m*-chloroperbenzoic acid (80%: 42.1 mg) in tetrahydrofuran (2.0 ml) was stirred at room temperature for 18 h. The mixture was diluted with ether and washed successively with aqueous potassium iodide, aqueous sodium thiosulfate, aqueous sodium hydrogencarbonate, and brine. The dried solution was evaporated in vacuo. The residue was chromatographed on silica gel (7.0 g), using chloroform as eluent, to give the starting **8a** (19.1 mg) and a *p*-quinone **9a** (7.2 mg: 12%). The *p*-quinone **9a** was recrystallized from acetone-hexane, mp 224—225 °C, $[\alpha]_D$ +39° (*c* 0.51), IR 3620, 3530, 1669sh, 1652, and 1636 cm^{-1}; ^{1}H NMR δ=1.00 (3H, s) and 1.25 (3H, s) (-C(CH$_3$)$_2$), 1.29 (3H, d, *J*=7 Hz, C_{15}-CH$_3$), 1.63 (3H, s, C_{10}-CH$_3$), 4.17 (1H, dd, *J*=6 and 9.5 Hz) and 4.72 (1H, t, *J*=9.5 Hz) (-OCH$_2$-), ca. 4.6 (1H, overlap, C_6-H). Found: C, 72.47; H, 7.69%. Calcd for $C_{20}H_{26}O_4$: C, 72.70; H, 7.93%.

b): A mixture of the crude **8b** (880 mg) and *m*-chloroperbenzoic acid (80%: 660 mg) in tetrahydrofuran (5.0 ml) was stirred at room temperature for 17.5 h. After the work-up as described in **a**), the crude product was chromatographed on silica gel (30 g), using chloroform as eluent, to give the starting **8b** (144 mg) and a *p*-quinone **9b** (126 mg: 13.7%). The *p*-quinone **9b** was recrystallized from acetone-hexane, mp 225—226.5 °C, $[\alpha]_D$ +20.6° (*c* 1.41), IR 3615, 3540, 1670 sh, 1650, and 1637 cm^{-1}; ^{1}H NMR δ=1.01 (3H, s) and 1.26 (3H, s) (-C(CH$_3$)$_2$), 1.29 (3H, d, *J*=7 Hz, C_{15}-CH$_3$), 1.66 (3H, s, C_{10}-CH$_3$), 4.18 (1H, dd, *J*=6 and 9.5 Hz) and 4.70 (1H, t, *J*=9.5 Hz) (-OCH$_2$-), ca. 4.6 (1H, overlap, C_6-H). Found: C, 72.58; H, 7.79%. Calcd for $C_{20}H_{26}O_4$: C, 72.70; H, 7.93%.

(15*R*)-11,14-Diacetoxy-12,16-epoxy-8,11,13-abietatrien-6-one (10a) and Its (15*S*)-Epimer (10b). **a**): A mixture of **9a** (33.3 mg), acetic anhydride (1.0 ml), and zinc powder (50 mg) in pyridine (1.0 ml) was stirred at 0—5 °C for 1 h. After the addition of ether, the zinc powder was removed and the organic solution was washed successively with dilute hydrochloric acid, aqueous sodium hydrogencarbonate, and brine. The dried solution was evaporated in vacuo. The residue was oxidized with Jones reagent (2.5 mol dm^{-3}: 0.06 ml) in acetone (2.0 ml) with cooling in an ice-water bath for 3 min. After the addition of ether, the mixture was washed with water, dried, and evaporated in vacuo. The crude product was chromatographed on silica gel (5.0 g), using ether-benzene (3 : 97) as eluent, to give an oily **10a** (8.5 mg: 20%), IR 1763 and 1718 cm^{-1}, ^{1}H NMR (90 MHz) δ=1.01 (3H, s), 1.21 (3H, s), and 1.32 (3H, s) (-C(CH$_3$)$_2$ and C_{10}-CH$_3$), 1.23 (3H, d, *J*=7 Hz, C_{15}-CH$_3$), 2.29 (6H, s, C_{11}-OCOCH$_3$ and C_{14}-OCOCH$_3$), 2.62 (1H, s, C_5-H), 3.08 (1H, d, *J*=21 Hz) and 3.47 (1H, d, *J*=21 Hz) (-COCH$_2$-), 3.57 (1H, m, C_{15}-H), 4.13 (1H, dd, *J*=6.5 and 9 Hz) and 4.66 (1H, t, *J*=9 Hz) (-OCH$_2$-). Found: C, 69.25; H, 7.11%. Calcd for $C_{24}H_{30}O_6$: C, 69.54; H, 7.30%.

b): A mixture of **9b** (81.8 mg), acetic anhydride (1.0 ml), and zinc powder (30 mg) in pyridine (1.0 ml) was stirred at 0—5 °C for 1 h. After the work-up as described in **a**), the crude product was oxidized with Jones reagent (2.5 mol dm^{-3}: 0.15 ml) in acetone (1.0 ml) with cooling in an ice-water bath for 3 min. After the addition of ether, the mixture was washed with water, dried, and evaporated in vacuo. The residue was chromatographed on silica gel (10 g), using ether-benzene (3 : 97) as eluent, to give an oily **10b** (29.4 mg: 28.7%), $[\alpha]_D$ +48.2° (*c* 1.23), IR 1761 and 1718 cm^{-1}, ^{1}H NMR (90 MHz) δ=1.00 (3H, s), 1.21 (3H, s), and 1.31 (3H, s) (-C(CH$_3$)$_2$ and C_{10}-CH$_3$), 1.23 (3H, d, *J*=7 Hz, C_{15}-CH$_3$), 2.28 (6H, s, C_{11}-OCOCH$_3$ and C_{14}-OCOCH$_3$), 2.61 (1H, s, C_5-H), 3.15 (1H, d, *J*=21 Hz) and 3.42 (1H, d, *J*=21 Hz) (-COCH$_2$-), 3.57 (1H, m, C_{15}-H), 4.09 (1H, dd, *J*=6.5 and 9 Hz) and 4.69 (1H, t, *J*=9 Hz) (-OCH$_2$-). Found: C, 69.81; H, 7.59%. Calcd for $C_{24}H_{30}O_6$: C, 69.54; H, 7.30%.

(15*R*)-12,16-Epoxy-6,11,14-trihydroxy-5,8,11,13-abietate-

traen-7-one (Lycoxanthol) (1a) and Its (15*S*)-Epimer (1b). **a**): A stirred solution of **10a** (8.5 mg) in acetone (1.0 ml) was oxidized with Jones reagent (1 mol dm^{-3}: 0.1 ml) at room temperature for 2 h. The mixture was diluted with ether, washed with water, and evaporated in vacuo. The residue was dissolved in ethanol (1.0 ml) containing dilute hydrochloric acid (15%: 0.1 ml). The solution was refluxed for 5 h, cooled, and then diluted with ether. The ether solution was washed with water, dried, and evaporated in vacuo. The crude product was chromatographed on silica gel (Mallinckrodt CC-4, 7 g), using hexane-chloroform (1 : 2) as eluent, to give **1a** (2.2 mg: 31%) which was recrystallized from acetone-hexane, mp 250—251 °C, IR (KBr) 3485, 1640, and 1615 cm^{-1}; ^{1}H NMR (90 MHz) δ=1.40 (3H, d, J=7 Hz, C_{15}-CH_3), 1.44 (6H, s, -C(CH$_3$)$_2$), 1.65 (3H, s, C_{10}-CH_3), 3.80 (1H, m, C_{15}-H), 4.28 (1H, dd, J=9 and 6 Hz) and 4.81 (1H, t, J=9 Hz) (-OCH_2-), 12.55 (1H, s, C_{14}-OH); MS m/z 344 (M^+). The synthetic **1a** was identical with natural lycoxanthol (mp 249 °C).

b): A stirred solution of **10b** (29.4 mg) in acetone (2.0 ml) was oxidized with Jones reagent (2.5 mol dm^{-3}: 0.14 ml) at room temperature for 2 h. The crude product was hydrolyzed with dilute hydrochloric acid (15%: 0.1 ml) in refluxing ethanol (1.0 ml) for 5 h. After the work-up as described in **a**), the crude product was chromatographed on silica gel (Mallinckrodt CC-4, 7 g), using hexane-chloroform (1 : 2) as eluent, to give **1b** (9.8 mg: 40%). This was recrystallized from acetone-hexane, mp 219—220 °C, IR (KBr) 3395, 1637, and 1611 cm^{-1}; ^{1}H NMR (90 MHz) δ=1.42 (3H, d, J=7 Hz, C_{15}-CH_3), 1.44 (6H, s, -C(CH$_3$)$_2$), 1.66 (3H, s, C_{10}-CH_3), 3.75 (1H, m, C_{15}-H), 4.28 (1H, dd, J=9 and 6 Hz) and 4.80 (1H, t, J=9 Hz) (-OCH_2-), 12.55 (1H, s, C_{14}-OH); MS m/z 344 (M^+).

References

1) R. H. Burnell and M. Moinas, *Chem. Commun.*, **1971**, 897.

2) R. H. Burnell, L. Mo, and M. Moinas, *Phytochemistry*, **11**, 2815 (1972).

3) T. Matsumoto, S. Imai, and T. Yoshinari, *Bull. Chem. Soc. Jpn.*, **60**, 2435 (1987).

4) Yields are based on the starting material consumed.

 © 1987 The Chemical Society of Japan Bull. Chem. Soc. Jpn., 60, 3645—3653 (1987)

The 1,3-Dipolar Cycloaddition Reactions of Heteroaromatic Dicyanomethylides with Phenylsulfinylethene and Bis(trimethylsilyl)ethyne: Synthesis of 1,2-Unsubstituted 3-Cyanoindolizines

Kiyoshi MATSUMOTO,* Takane UCHIDA,† Yukio IKEMI, Toshio TANAKA,† Momoyo ASAHI,††
Tomoe KATO,† and Hideyuki KONISHI†††
Department of Chemistry, College of Liberal Arts and Sciences, Kyoto University, Kyoto 606
†Laboratory of Chemistry, Faculty of Education, Fukui University, Fukui 910
††Fukui Prefectural College, Fukui 910
†††Department of Chemistry, Aichi Kyoiku University, Kariya, Aichi 448
(Received April 1, 1987)

Pyridinium and diazinium dicyanomethylides underwent 1,3-dipolar cycloaddition-extrusion reactions with phenylsulfinylethene, producing the corresponding 3-cyanoindolizines in moderate to good yields. 1,3-Dipolar cycloadditions of these ylides with bis(trimethylsilyl)ethyne gave either the 1,2-bis(trimethylsilyl)-3-cyanoindolizines or the 1-trimethylsilyl-3-cyanoindolizines, or mixtures of these, depending on the substituents and the presence of another nitrogen atom in the pyridine ring. 1,2-Bis(trimethylsilyl)-3-cyanoindolizines underwent regiospecific protodesilylation at the 2-position upon a treatment with silica gel in refluxing chloroform, yielding 1-trimethylsilyl-3-cyanoindolizines. The 1,2-bis(trimethylsilyl)-, and 1-trimethylsilyl-3-cyanoindolizines suffered from quantitative protodesilylation under catalysis by tetrabutylammonium fluoride to afford 1,2-unsubstituted 3-cyanoindolizines.

The preparation of indolizines and their aza analogues[1] has been the subject of considerable interest from physical, chemical, and biological points of view.[2] Controlled reductions of appropriate indolizines would provide a stereospecific and general route to indolizidine alkaloids that comprise a large family of naturally occuring molecules with important medicinal and agricultural properties.[3] In the course of our studies on cycl[3.2.2]azine derivatives, it became necessary to know whether 1,2-unsubstituted 3-cyanoindolizines could serve as key intermediates in cycl[3.2.2]azine synthesis.[4] Unfortunately, however, there are few precedents for 3-substituted indolizines substituted only in the pyridine ring.[5]

In this paper we wish to report in full detail on the simple preparation of 1,2-unsubstituted 3-cyanoindolizines by 1,3-dipolar cycloaddition of heteroaromatic dicyanomethylides with phenylsulfinylethene and bis(trimethylsilyl)ethyne, followed by protodesilylation in the latter case.[6]

Results and Discussion

Although a wide variety of acetylene equivalents in cycloaddition reactions have been devised,[7] only few are suitable for the preparation of nitrogen heterocycles since most of the acetylene equivalents require either an oxidative or reductive procedure after cycloaddition in order to remove the functional groups. For example, in the case of 1,2-bis(methoxycarbonyl)-3-cyanoindolizine (**1**) that was prepared in good yield by a reaction of bis(methoxycarbonyl)ethyne with pyridinium dicyanomethylide (**2a**), a procedure employing LiBr/HMPA that is amenable to the demethoxycarbonylation of tetraheterafulvalenes[8] was unsuccessful, resulting in the formation of a complex reaction mixture. On the other hand, the reaction

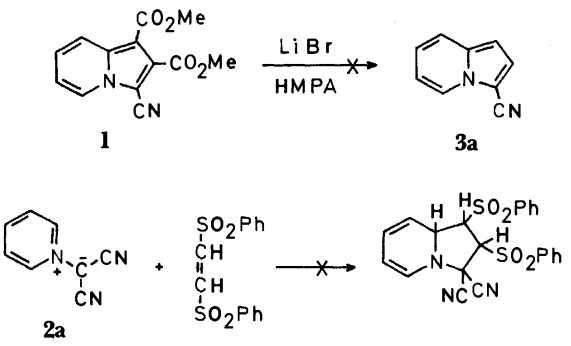

of (*Z*)- and (*E*)-1,2-bis(phenylsulfonyl)ethenes, excellent acetylene equivalents in cycloadditions of acyclic compounds[7,9] with pyridinium dicyanomethylide was extremely sluggish, producing a complex mixture after 4 days in refluxing toluene.

We have found that both phenylsulfinylethene (PVSO) and bis(trimethylsilyl)ethyne (BTMSA) serve as reliable acetylene equivalents in 1,3-dipolar cycloadditions. The reaction of pyridinium dicyanomethylide (**2a**) with PVSO[10] produced 3-cyanoindolizine (**3a**) in 43% yield. The elemental and mass spectral analyses as well as IR, ^{1}H and ^{13}CNMR spectra are in agreement with structure **3a** (Tables 2 and 3). The generality of this cycloaddition-extrusion reaction follows from Table 1; the yields are moderate to good. These 3-cyanoindolizines are highly fluorescent in solution. Those possessing an electron-withdrawing group in the pyridine moiety are pale yellow and stable, whereas indolizines like **3a** and **3b** form colorless crystals which turn dark brown on standing.

A comparison of the NMR data of **3** with those of the parent indolizine (**4**)[11,12] deserves to be mentioned. In general, δ(H-2) and δ(H-5) appear in a lower field than those of **4** due to conjugation with the electron-withdrawing 3-CN. Similar to the cyano-substituted

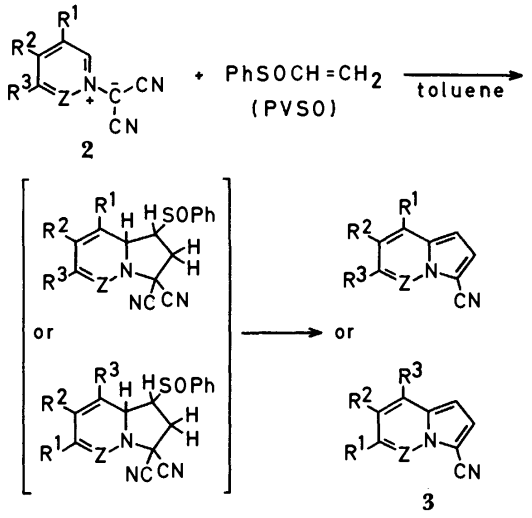

2 and 3:

a: Z=CH, R^1=R^2=R^3=H
b: Z=CH, R^1=R^3=H, R^2=Me
c: Z=CH, R^1=R^3=H, R^2=$PhCH_2$
d: Z=CH, R^1=R^3=H, R^2=Ph
e: Z=CH, R^1=R^3=H, R^2=PhCO
f: Z=CH, R^1=R^3=H, R^2=MeOCO
g: Z=CH, R^1=R^3=H, R^2=CN
h: Z=CH, R^1=R^2=Me, R^3=H
i: Z=CH, R^1=R^3=Me, R^2=H
j: Z=CH, R^1=—$(CH=CH)_2$—=R^2, R^3=H
k: Z=N, R^1=R^2=R^3=H

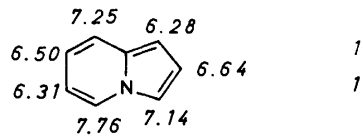

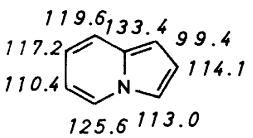

4(^{13}C NMR)

J (Hz)

1 - 2 = 3.9	1 - 3 = 1.2
2 - 3 = 2.7	5 - 6 = 6.8
5 - 7 = 1.0	6 - 7 = 6.4
6 - 8 = 1.0	7 - 8 = 8.9

4(^{1}H NMR: δ & J)

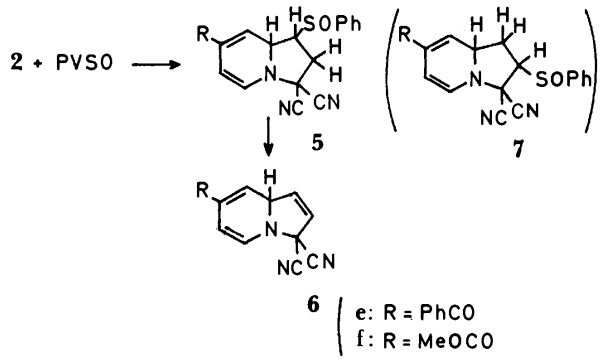

The reaction of pyridinium dicyanomethylide (**2a**) with BTMSA in refluxing toluene afforded a mixture of 1,2-bis(trimethylsilyl)-3-cyanoindolizine (**8a**) and 1-trimethylsilyl-3-cyanoindolizine (**9a**) each in 2% yield (^{1}H NMR analysis). They could be separated by medium-pressure liquid chromatography (MPLC), though accompanied by some protodesilylation, **8a**→**9a**. One run (Entry 2, Table 4) gave a 1 : 5 mixture of **8a** and **9a** in 24 % yield (^{1}H NMR analysis). The MPLC separation of crude **8a** afforded a mixture of **8a** and **9a** in the ratio of 1 : 8; the ratio did not change appreciably upon refluxing the mixture in xylene. 4-Methyl- and 4-(*t*-butyl)pyridinium dicyanomethylide, (**2b**) and (**2l**), reacted sluggishly with BTMSA in refluxing toluene, giving **9b** and a mixture of **8l** and **9l** respectively (Table 4). The low yield could be improved when the reaction was performed in refluxing xylene (Entry 9). In contrast, the pyridinium dicyanomethylides (**2e, f, g, m**) having an electron-withdrawing substituent gave better yields of the indolizines (**8e, f, g, m**) and (**9e**). For instance, heating of 4-cyanopyridinium dicyanomethylide (**2g**) with BTMSA in refluxing toluene produced 1,2-bis(trimethylsilyl)-3-cyanoindolizine (**8g**) in 65% isolated yield. Diazinium ylides (**2k, n, o**) that are more π-deficient than the pyridinium analogues reacted smoothly with BTMSA affording the

benzene series, the cyano causes higher field shifts of δ(C-3) by 14—18 ppm (16 ppm in benzonitrile). The ^{13}C resonances at the 6-, 7-, and 8-positions appear lower than those of **4**.

Although no initial adducts **5** have been isolated, a probable mechanism for the formation of **3** involves a 1,3-dipolar cycloaddition of **2** to PVSO to give a primary adduct **5** followed by the elimination of benzenesulfenic acid and hydrogen cyanide. Indeed, the intermediates **6e, f** were isolated in reactions of 4-benzoyl- and 4-methoxycarbonylpyridinium dicyanomethylides (**2e, f**) in yields as poor as 4 and 3%, respectively. The regioisomeric structure **7** might be unlikely, both on steric and electronic grounds (see discussion below).

Although silylacetylenes could be employed as an acetylene equivalent,[7] they usually do not exceed the unsilylated acetylenes in reactivity.[13]

Table 1. Preparation of 3-Cyanoindolizines **3a**—i and Their Analogues **3j, k** from Heteroaromatic Dicyanomethylides **2a**—**k** and Phenylsulfinylethene (PVSO)

Product	Reaction Time/h	Yield/%[a]	Mp θ_m/°C
3a	20	43	49—52
3b	15	37	58—60
3c	15	73	60—62
3d	19	33	114—115
3e	20	22	141—142
3f	11	20	167—168
3g	20	19	187—189
3h[b]	14	33	78—82
3i	20	58	108—109
3j	30	51	102—104
3k	8	42	66—68

a) Isolated yield. b) Mixture of 6,7- and 7,8-dimethyl-3-cyanoindolizine.

Table 2. IR and ^{1}H NMR Spectroscopic Data of 3-Cyanoindolizines **3a—i** and Their Analogues **3j, k**

Compound	ν(KBr)/cm^{-1}		Chemical shift ($CDCl_3$)/δ							Coupling constant; J/Hz					
	CN	CO	H-1	H-2	H-5	H-6	H-7	H-8	Others	1-2	5-6	5-7	6-7	6-8	7-8
3a	2210	—	6.37	7.19	8.15	6.68	6.91	7.41	—	3.9	6.4	1.1	6.0	1.5	7.1
3b	2220	—	6.23	7.14	8.02	6.53	—	7.15	2.29(Me)	4.2	6.8	—	—	1.3	—
3c	2230	—	6.28	—[a]	8.10	6.56	—	—[a]	3.89 (CH_2) 7.0—7.5 (Ph+H-2, 8)	4.5	7.1	—	—	1.5	—
3d	2220	—	6.43	—[a]	8.21	7.00	—	—[a]	7.2—7.8 (Ph+H-2, 8)	3.9	6.4	—	—	1.5	—
3e	2220	1620 1640	6.69	—[a]	8.26	—[a]	—	—[a]	7.2—7.8(Ph+H-2, 5, 8)	4.2	7.2	—	—	—	—
3f	2215	1715	6.74	7.43	8.25	7.36	—	8.30	3.96 (MeO)	4.0	7.8	—	—	1.2	—
3g	2230	—	6.71	7.36	8.26	6.87	—	7.38	—	4.1	6.8	—	—	1.0	—
3h	2220	—	6.27	7.10	7.96	6.54	—	—	2.24, 2.26, 2.29 (Me)	4.5	6.6	—	—	—	—
3h′			6.19	6.86	7.92	—	—	7.19		3.8	—	—	—	—	—
3i	2250	—	6.35	7.19	7.93	—	6.63	—	2.26, 2.40 (Me)	4.1	—	—	—	—	—
3j[b]	2230	—	—[a]	—[a]	8.10	—[a]	—	—	6.9—7.7 (Ar)	—	5.0	—	—	—	—
3k[b]	2260	—	6.50	7.27	—	8.26	6.80	7.83	—	4.5	—	—	2.9	1.5	8.6

a) Overlapped with aromatic protons. b) For convenience, the numberings are formally based upon indolizine system.

Table 3. ^{13}C NMR Spectroscopic Data of 3-Cyanoindolizines **3a—i** and Their Analogues **3j, k**[a]

Compound	C-1	C-2	C-3	C-5	C-6	C-7	C-8	C-8a	CN	Other substituent
3a	101.2	122.5	95.3	129.3	113.1	119.4	121.7	131.3	113.9	——
3b	99.9	122.8	94.4	124.6	115.8	137.0	117.9	132.6	114.4	21.1 (Me)
3c	100.6	122.9	94.7	125.0	115.9	136.0	118.0	135.8	114.2	41.2 (CH_2); 139.1 (s) 126.7, 128.7, 129.0 (each d)
3d	101.9	123.2	94.9	125.2	113.0	136.8	116.3	134.7	114.1	138.2 (s) 126.5, 128.3, 129.1 (each d)
3e	106.0	123.5	97.3	125.1	112.7	137.0	123.8	134.6	113.1	193.9 (CO); 132.7(s) 128.6, 129.6, 130.4 (each d)
3f	105.3	122.4	97.6	124.1	112.0	122.4	122.3	134.8	112.3	52.5 (MeO); 163.9 (CO)
3g	105.7	123.8	99.0	126.1	112.8	104.9	125.7	134.0	112.3	117.4 (CN)
3i	99.3	123.0	95.1	124.3	120.8	136.1	121.5	136.1	114.4	17.8, 18.2 (each Me)
3j[b]	101.3	122.9	97.6	127.7	113.5	124.9	127.5	134.0	113.7	121.6, 122.4, 127.1, 127.7 (each d)
3k[b]	101.2	120.7	100.2	—	143.5	113.9	127.4	129.9	112.6	——

a) In ppm relative to TMS in $CDCl_3$. b) For convenience, the numberings are formally based upon indolizine system.

azaindolizines (**8k**, **n**, **o**) and (**9n**); e.g., pyridazinium dicyanomethylide (**2k**) with BTMSA in refluxing toluene gave 92% of **8k**.

In some cases (Entries 5, 6, 7, and 10), protodesilylation was not observed (Table 4). The higher temperature improved the yield, but also promoted protodesilylation, as exemplified with Entry **11**.

The structures of **8** and, partially, **9** were confirmed by elemental (see Experimental) and mass analyses as well as ^{1}H and ^{13}C NMR data (Tables 5 and 6). However, the spectral data did not permit an unambiguous determination of the position of the trimethylsilyl group in **9**. The 1,2-bis(trimethylsilyl)-3-cyanoindolizines (**8**) underwent regiospecific protodesilylation in refluxing chloroform with suspended silica gel yielding **9**; as an exception, **8k** did not undergo protodesilylation under these conditions. The regiochemistry of **9a** was mainly based on the probable regioselectivity in the reaction of **2a** with trimethylsilylethyne (see below). Attempts to convert **8a** to the known 1-methoxycarbonyl-3-cyanoindolizine (**10**)[14] with

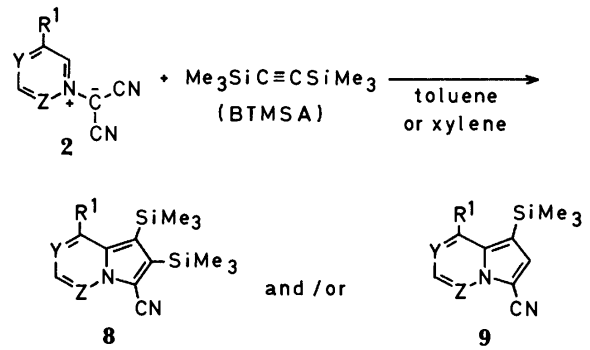

2, **8**, and **9**:

a: Z=Y=CH, R^1=H
b: Z=CH, Y=CMe, R^1=H
e: Z=CH, Y=CCOPh, R^1=H
f: Z=CH, Y=CCO_2Me, R^1=H
g: Z=CH, Y=CCN, R^1=H
k: Z=N, Y=CH, R^1=H
l: Z=CH, Y=$CCMe_3$, R^1=H
m: Z=CH, Y=CCOMe, R^1=H
n: Z=N, Y=C-$(CH{=}CH)_2$-=R^1
o: Z=CH, Y=N, R^1=H

Table 4. Reactions of Heteroaromatic Dicyanomethylide with Bis(trimethylsilyl)ethyne (BTMSA)

Entry	Ylide	Reaction condition		Product	Yield/%[a]	Mp	IR (KBr)/cm^{-1}	
		Solvent	Reflux time/h			θ_m/°C		
1	**2a**	toluene	62	**8a**	2.4 (30)	106—107	2210	
				9a	2.1 (27)	95—96	2180	
2		xylene	45.5	**8a**	4 (14)			
				9a	20 (61)			
3	**2b**	toluene	72	**9b**	4.9 (44)	59—60	2200	
4	**2e**	toluene	68	**8e**	20 (66)	152—153	2200	1620, 1610 (sh)
				9e	0.7 (2)	130—133	2225	1640, 1620 (sh)
5	**2f**	toluene	72	**8f**	36 (93)	160—161	2250	1715
6	**2g**	toluene	72	**8g**	65 (72)	129—130	2250, 2225	
7	**2k**	toluene	56	**8k**	92 (—)[b]	73—74	2250	
8	**2l**	toluene	72	**8l**	5.7 (33)	105—107	2200	
				9l	3.4 (20)	84—86	2180	
9		xylene	85	**9l**	45 (86)			
10	**2m**	toluene	72	**8m**	22 (69)	189—190	2210	1682
11		xylene	88.5	**8m**	48 (58)			
				9m	16 (19)	124—125	2250	1720
12	**2n**	toluene	56	**8n**	71 (—)[b]	152—153	2220	
				9n	19 (—)[b]	205—206	2195	
13	**2o**	toluene	86	**8o**	96 (98)	136—137	2250	

a) Parentheses indicate yields based on the consumed ylides. b) Not be recovered.

Table 5. ^{1}H NMR Spectroscopic Data of 3-Cyanoindolizines and Their Analogues **8** and **9**[a]

Compound	H-2	H-5	H-6	H-7	H-8	$J_{5\text{-}6}$[b]	$J_{6\text{-}8}$[b]	$J_{7\text{-}8}$[b]	TMS		Other substituent
8a	—	8.36	6.85	7.02	7.77	6.2	—	7.7	0.43	0.50	—
8e	—	8.35	7.34	—	8.16	7.2	1.2	—	0.37	0.50	7.4—7.7 (3H), 7.7—7.9 (2H)
8f	—	8.32	7.36	—	8.52	7.3	1.2	—	0.46	0.50	3.90 (Me)
8g	—	8.28	6.82	—	8.04	7.2	1.2	—	0.47	0.51	—
8k[d]	—	—	8.26	6.77	8.06	4.2[c]	1.5	9.2	0.43	0.50	—
8l	—	8.32	6.94	—	7.71	7.4	1.9	—	0.43	0.49	1.33 (Me)
8m	—	8.31	7.35	—	8.39	6.8	1.7	—	0.50	0.51	2.62 (Me)
8n[d]	—	8.61	—	—	—	—	—	—	0.51	0.56	7.62—8.03 (3H), 8.13—8.38 (1H)
8o[d]	—	7.89	7.93	—	9.26	4.2	1.3	—	0.51	0.52	—
9a	6.52	8.28	6.86	6.98	7.49	6.2	—	7.8	0.39		—
9b	6.31	8.09	6.55	—	7.17	7.0	1.7	—	0.36		2.31 (Me)
9e	6.75	8.29	7.35	—	7.90	7.2	2.7	—	0.40		7.5—7.8 (Ar)
9f	6.76	8.26	7.34	—	8.24	7.2	1.8	—	0.38		3.93 (Me)
9g	6.75	8.26	6.84	—	7.84	8.0	1.8	—	0.41		—
9l	6.50	8.28	6.91	—	7.45	7.4	1.6	—	0.39		1.34 (Me)
9m	6.82	8.25	7.35	—	8.10	7.6	2.0	—	0.42		2.63 (Me)
9n[d]	6.94	8.54	—	—	—	—	—	—	0.39		7.54—8.19 (Ar)

a) δ in $CDCl_3$. b) Coupling constants; Hz. c) $J_{6\text{-}7}$. d) For convenience, the numberings are formally based upon indolizine system.

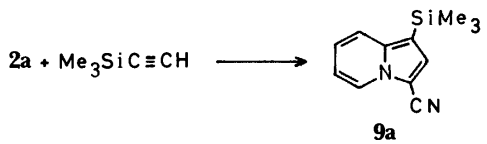

9a

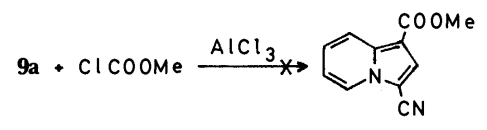

10

methyl chloroformate catalyzed either by aluminium (III) chloride[15] or by potassium fluoride/18-crown-6[16] were unsuccessful, resulting in the formation of 3-cyanoindolizine (**3a**) in low yields. 7-(*t*-Butyl)-1,2-bis(trimethylsilyl)-3-cyanoindolizine (**8l**) readily lost the trimethylsilyl moiety at 2-position in deuteriochloroform even at room temperature. The reaction is presumably acid-catalyzed.

Tetrabutylammonium fluoride catalyzed the protodesilylation of the trimethylsilylindolizines **8** and/or **9** to give the 3-cyanoindolizines **3** in excellent yields (see Experimental).

The ^{29}Si NMR chemical shifts of **8** reveal a mutual deshielding of the ortho trimethylsilyl groups, as established in the benzene analogues.[17a] the magnitude (0.2—0.3 ppm) is here slightly smaller than in the benzene analogues (ca. 0.6 ppm).[17]

It is now well-documented that, to a more or less extent, most 1,3-dipolar cycloadditions[18] receive

Table 6. ^{13}C NMR Spectroscopic Data of 3-Cyanoindolizines and Their Analogues **8** and **9**[a]

Compound	C-1	C-2	C-3	C-5	C-6	C-7	C-8	C-8a	CN	TMS	Other substituent
8a	139.7	115.4	103.3	125.2	112.9	120.5	122.0	142.4	115.6	1.9 2.7	—
8e	140.4	121.5	105.4	128.4	112.2	137.0	125.0	141.1	114.8	1.8 2.6	130.0 (s), 128.4, 129.5, 132.5 (each d), 193.9 (s)
8f	140.9	114.9	105.2	124.8	111.8	120.9	123.4	140.9	114.5	1.8 2.7	52.4 (q), 165.6 (s)
8g	140.5	118.6	105.5	127.7	113.1	107.2	126.5	142.7	115.0[b]	2.3 2.4	115.0[b]
8k[c]	138.1	116.3	100.5	—	143.2	113.9	128.3	135.6	114.4	1.7 2.7	—
8m	140.6	121.5	105.4	124.8	110.4	130.3	122.6	141.2	114.7	1.7 2.7	26.0 (q), 195.2 (s)
8n[c]	137.6	117.5	110.3	—	145.5	122.0	127.7	133.1	114.6	2.1 2.8	126.1, 128.0, 128.1, 131.8 (each d)
8o[c]	136.6	120.7	105.1	129.6	117.8	—	146.2	140.2	113.8	1.7 2.7	—
9a	134.7	122.9	99.2	124.9	107.0	113.0	119.2	137.6	115.1	−1.0	—
9b	134.9	117.5	98.4	124.3	105.6	132.3	115.7	137.4	115.5	−0.9	21.1 (q)
9e	136.2	123.5	101.7	124.7	111.9	135.1	112.5	127.1	114.2	−1.0	130.1 (s), 128.5, 129.6, 132.6 (each d), 193.9 (s)
9f	135.5	122.3	101.6	124.4	111.2	123.2	112.0	136.0	114.2	−1.0	52.6 (q), 165.4 (s)
9g	134.4	125.4	102.7	125.8	111.5	104.4	112.6	136.8	113.6	−1.1	117.7 (s)
9l	134.6	124.1	98.0	113.4	106.2	145.2	112.3	137.0	115.1	−1.1	30.1 (q), 34.3(s)
9m	135.3	121.4	101.8	124.6	110.6	130.1	112.0	136.1	114.1	−1.1	26.0 (q), 195.2 (s)
9n[c]	131.4	122.1	105.1	—	145.3	120.6	126.8	127.6	114.1	−0.9	105.5, 128.0, 128.1, 133.0 (each d)

a) In ppm relative to tetramethylsilane in $CDCl_3$. b) Overlapped with another cyano group. c) For convenience, the numberings are formally based upon indolizine system.

Table 7. ^{29}Si NMR Chemical Shifts of **8** and **9**[a]

Compound	1-TMS[b]	2-TMS[b]	Compound	1-TMS
8a	−7.40	−9.54	**9a**	−7.62
8b	—[c]		**9b**	−7.68
8e	−6.98	−8.99	**9e**	−7.21
8f	−7.07	−8.94	**9f**	−7.29
8g	−6.64	−8.67	**9g**	−6.88
8k	−6.90	−9.09		
8l	—[c]		**9l**	−7.86
8m	−6.94	−8.89	**9m**	−7.24
8n	−6.80	−8.60	**9n**	−7.13
8o	−6.69	−8.72		

a) In ppm relative to tetramethylsilane. b) Tentatively assigned. c) Could not be taken for the instability in solution.

Table 8. Energy Levels of HOMO and LUMO of the Ylides **2**[a]

Ylide	HOMO/eV	LUMO/eV
2a	−8.677	1.016
2b	−8.473	1.030
2l	−8.381	1.177
2g	−8.830	0.349
2m	−8.815	0.168

a) Calculated by the CNDO/2 method.

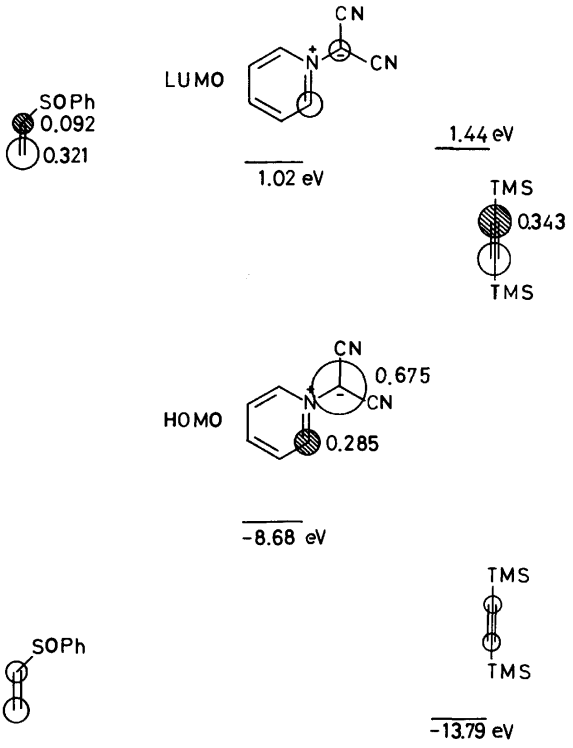

Fig. 1. Frontier molecular orbital interactions in 1,3-dipolar cycloadditions of **2a** with PVSO and BTMSA.

contributions from HOMO-LUMO interactions.[19] Clearly, cycloadditions of highly electron-deficient PVSO with **2** are predominantly HOMO (1,3-dipole)-LUMO(dipolarophile) controlled [type I in Sustmann's classification],[20] whereas those of BTMSA with **2** tend to be under major HOMO(1,3-dipole) control and partial LUMO(1,3-dipole) control when an electron-withdrawing group is introduced in the pyridine ring of **2** (Fig. 1);[21] CNDO/2 calculations of some ylides **2** show that LUMO energy levels are highly affected by a 4-substituent of **2**, while HOMO energy levels vary much less (Table 8).

A consideration of the LUMO-HOMO coefficient would lead to the regioselective formation of **9a** in a reaction of **2a** with trimethylsilylethyne when this reaction is HOMO(1,3-dipole)-LUMO(dipolarophile) controlled, as depicted in Fig. 2.[21]

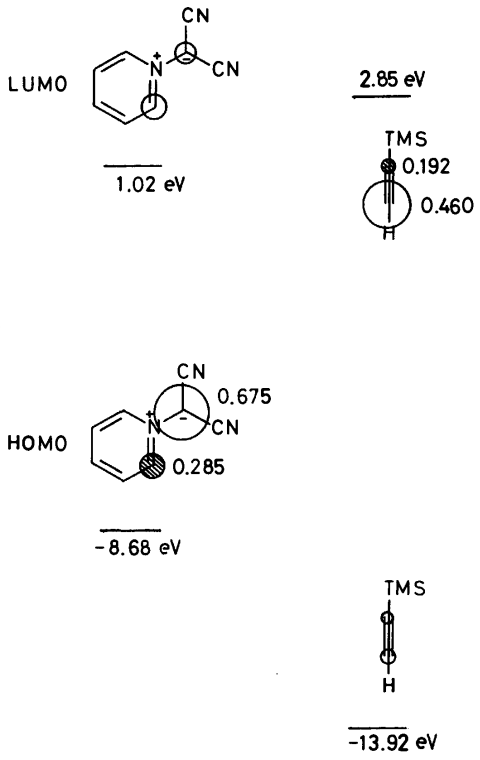

Fig. 2. Frontier molecular orbital interactions in 1,3-dipolar cycloaddition of **2a** with trimethylsilylethyne.

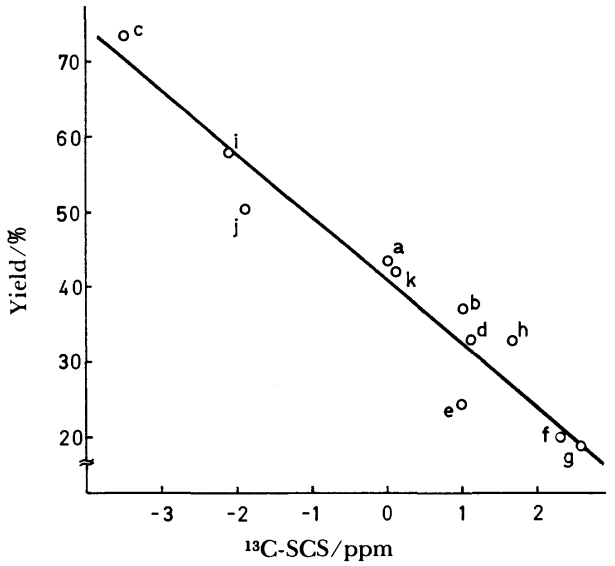

Fig. 3. Plot of the isolated yields of **3** vs ^{13}C-SCS of C-2 of **2**. Yields=−8.26(^{13}C-SCS)+40.91 (r=0.959).

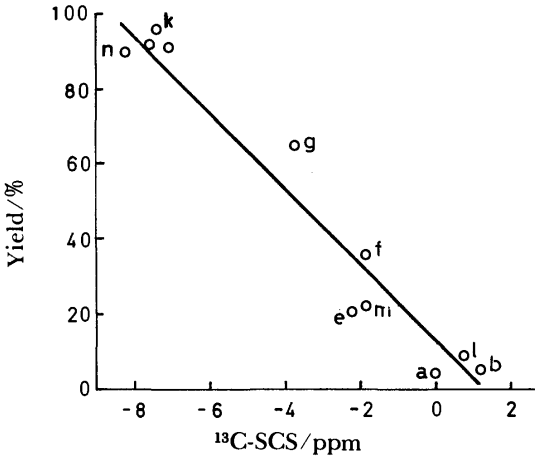

Fig. 4. Plot of the total yields of **8** and **9** (in refluxing toluene) vs. ^{13}C-SCS of the ylidic carbons of **2**. Yields=−10.42(^{13}C-SCS)+11.63 (r=0.971).

Surprisingly, linear correlations have been observed between the yields of **3** and (**8**+**9**) with the ^{13}C-SCS of the C-2 and ylidic carbons, respectively (Figs. 3 and 4). Yields are just determined by the rate ratio of the desired and undesired reactions. Only if the rate of all the side reactions remains constant upon substituent variation, yields may reflect the rate constants. The linear correlations (Figs. 3 and 4) give examples that are amusing, although we do not ascribe much value to them.

In view of the ready availability of cycloiminium ylides, PVSO, and BTMSA, the present two methods for the preparation of 1,2-unsubstituted 3-cyanoindolizines that are otherwise difficult to obtain directly, seem to be practical even in those cases in which only moderate yields are realized. Thus, both PVSO and BTMSA constitute reliable and complementary acetylene equivalents in 1,3-dipolar cycloadditions.

Experimental

General. Melting points were taken on a Yanagimoto micro melting point apparatus and uncorrected. IR spectra were obtained on a Jasco IR-G or a Hitachi EPI-G spectrometer. ^{1}H NMR spectra were measured on a JEOL JNM-C-60HL (60 MHz) or Hitachi R40 (90 MHz) instrument. ^{13}C and ^{29}Si NMR spectra were recorded on a JEOL FX-90Q pulsed Fourier-transform spectrometer operating at 22.49 and 17.75 MHz, respectively. Chemical shifts are expressed in parts per million downfield from internal tetramethylsilane. Partial proton decoupling was used to distinguish between individual carbon atoms. Mass spectra were obtained on a JEOL 01SG-2 spectrometer at 75 eV of ionization energy. Thin-layer chromatography (TLC) was performed on Kiessel-gel PF-254 (0.25 mm; Merck). Preparative medium-pressure liquid chromatography (MPLC) was carried out using a column (25×310 mm) pre-packed with silica gel (Lobar; LiChroprep Si 60; Merck).

Toluene and xylene were dried over sodium or Drierite. The dicyanomethylides **2** were prepared according to the method of Linn et al.[22]

Action of Lithium Bromide on 1. A magnetically stirred mixture of **1** (0.10 g; 0.4 mmol), lithium bromide (0.53 g; 6 mmol), and HMPA (12 ml) was heated to about 100 °C for 1.5 h. The resultant mixture was poured into cold water (15 ml) and extracted with two portions of cyclohexane containing five percent benzene (total 50 ml). The combined organic layer was dried over anhydrous magnesium sulfate and evaporated, leaving an oil which was fractionated by MPLC (elution with hexane-ethyl acetate (1 : 1)). With the

recovered **1** (20 %), many other fractions were obtained, the amounts of which were too small to determine their structures.

Reaction of 2a with (*Z*)- and (*E*)-1,2-Bis(phenylsulfonyl)-ethenes. A solution of **2a** (118 mg; 0.83 mmol) and the ethenes (254 mg; 0.83 mmol) in dry toluene (20 ml) was heated at reflux for 95 h. The solvent was evaporated and the residue was fractionated by MPLC (elution with hexane-ethyl acetate (2 : 1)) to give very complex fractions. A 20 % of **2a** was recovered.

General Procedure for the Reactions of 2 with PVSO. A solution of **2** (6 mmol) and PVSO (9—12 mmol) in dry toluene (35—50 ml) was refluxed under nitrogen with stirring for the time periods given in Table 1. The resulting mixture was concentrated and chromatographed on silica gel (Wako-gel C-100). Elution with hexane and hexane-benzene (1 : 1) gave diphenyl disulfide in the first fraction. Further elution of the column with benzene or hexane-ethyl acetate (2 : 1) gave the 3-cyanoindolizines **3**, which was purified by recrystallization from hexane containing a small portion of ethanol. Yields of the reactions and the physical properties of **3** are shown in Tables 1—3. The analytical data are tabulated in Table 9. In the cases of the reactions of **2e** and **2f** with PVSO, the third elution of the column with benzene-ethyl acetate (1 : 1) gave **6e** and **6f**, respectively. **6e** (4%): Dark red needles (ethanol-ethyl acetate); mp 182—183 °C; IR (KBr) 2200, 1647, 1605 cm^{-1}; ^1H NMR ($CDCl_3$) δ=6.22 (d, J=7 Hz, H-8a), 7.1—7.9 (m, 9H, Ph-H+H-1, -2, -5, -6), 9.32 (d, J=7 Hz, 1H, H-8); ^{13}C NMR ($CDCl_3$) δ=93.6 (s, C-3), 101.7 (d, C-8a), 114.2 (d, C-1), 117.8 (s, CN), 127.9 (d, C-2), 128.9 (d, C-ortho), 129.8 (d, C-meta), 133.9 (d, C-para), 135.4 (s, C-ipso), 139.5 (d, C-6), 140.2 (s, C-7), 144.4 (d, C-8), 154.6 (d, C-5), 192.7 (CO); MS m/z (rel intensity, %) 273 (M^+, 100), 237 (32, M^+—HCN). Found: C, 75.04; H, 4.20; N, 15.43%. Calcd for $C_{17}H_{11}N_3O$: C, 74.73; H, 4.03; N, 15.38%. **6f** (3%): Dark brown crystals (hexane-benzene); mp 184—186 °C; IR (KBr) 2205, 2150, 1725 cm^{-1}; ^1H NMR ($CDCl_3$) δ=4.01 (s, 3H, OCH_3), 6.31 (br d, J=8 Hz, 1H, H-8a), 7.41 (dd, J=7.5 and 1.5 Hz, 1H, H-1), 7.53 (d, J=7.5 Hz, 1H, H-2), 8.04 (d, J=8 Hz, 1H, H-6), 8.45 (d, J=8 Hz, 1H, H-5), 9.34 (d, J=8 Hz, 1H, H-8); MS m/z (rel intensity, %), 227 (M^+, 100), 200 (58, M^+—HCN), 169 (40, M^+—HCN—OMe) (MW=227.2; Calcd for $C_{12}H_9N_3O_2$).

General Procedure for the Reactions of 2 with BTMSA. A solution of **2** (5 mmol) and BTMSA (50 mmol) in dry toluene or xylene (40 ml) was refluxed with stirring for the time periods stated in Table 4. The solvent and the excess BTMSA were removed in vacuo giving a dark-brown residue, which was subjected to chromatography on Florisil (Wako; 100—200 mesh). Elution with hexane, benzene, and then benzene-ethyl acetate (10 : 1) gave **8** or a mixture of **8** and **9** as pale-yellow crystals. In the cases of Entries 1, 2, 8, and 11, **8** and **9** were isolated by MPLC (elution with hexane-ethyl acetate (9 : 1)) and purified by recrystallization from hexane. The results of the reactions and physical properties are given in Tables 4—6. The analytical data are tabulated in Table 9. In the cases of the reactions of **2a** and **2m** with BTMSA in xylene, the addition of paradium/carbon

Table 9. Analytical Data of Indolizines **3**, **8**, and **9**

Compound	Found/%			Calcd/%			Formula
	C	H	N	C	H	N	
3a	75.83	4.17	19.49	76.04	4.25	19.71	$C_9H_6N_2$
3b	76.82	5.10	17.73	76.90	5.16	17.94	$C_{10}H_8N_2$
3c	82.70	5.18	11.97	82.73	5.21	12.06	$C_{16}H_{12}N_2$
3d	82.28	4.57	12.87	82.54	4.62	12.84	$C_{15}H_{10}N_2$
3e	78.23	4.28	11.50	78.03	4.09	11.38	$C_{16}H_{10}N_2O$
3f	66.23	3.77	13.89	65.99	4.03	13.99	$C_{11}H_8N_2O_2$
3g	72.03	2.85	25.00	71.85	3.01	25.14	$C_{10}H_5N_3$
3h[a]	77.84	6.11	16.31	77.62	5.92	16.46	$C_{11}H_{10}N_2$
3i	77.38	5.65	16.70	77.62	5.92	16.46	$C_{11}H_{10}N_2$
3j	80.96	4.15	14.64	81.23	4.19	14.58	$C_{13}H_8N_2$
3k	67.20	3.53	29.47	67.12	3.52	29.36	$C_8H_5N_3$
3m	71.60	4.35	15.00	71.73	4.38	15.21	$C_{11}H_8N_2O$
3n	74.54	3.69	21.38	74.60	3.65	21.75	$C_{12}H_7N_3$
8a	62.51	7.69	9.99	62.88	7.74	9.78	$C_{15}H_{22}N_2Si_2$
8e	67.69	6.75	7.20	67.65	6.71	7.17	$C_{22}H_{26}N_2OSi_2$
8f	59.58	7.18	7.92	59.26	7.02	8.13	$C_{17}H_{24}N_2O_2Si_2$
8g	62.02	7.01	13.66	61.69	6.79	13.49	$C_{16}H_{21}N_3Si_2$
8k	58.36	7.31	14.63	58.48	7.36	14.62	$C_{14}H_{21}N_3Si_2$
8m	62.16	7.23	8.29	62.14	7.36	8.53	$C_{17}H_{24}N_2OSi_2$
8n	64.20	6.66	12.60	64.04	6.87	12.45	$C_{18}H_{23}N_3Si_2$
8o	58.74	7.37	14.63	58.48	7.36	14.62	$C_{14}H_{21}N_3Si_2$
9a	67.49	6.62	13.10	67.24	7.06	13.07	$C_{12}H_{14}N_2Si$
9b	68.41	7.15	12.02	68.37	7.06	12.27	$C_{13}H_{16}N_2Si$
9e	71.38	5.58	8.63	71.66	5.70	8.80	$C_{19}H_{18}N_2OSi$
9f	61.81	5.88	10.17	61.73	5.92	10.29	$C_{14}H_{16}N_2O_2Si$
9g	65.35	5.31	17.78	65.23	5.48	17.56	$C_{13}H_{13}N_3Si$
9l	71.18	8.18	10.34	71.06	8.20	10.39	$C_{16}H_{22}N_2Si$
9m	65.41	6.38	10.72	65.59	6.29	10.93	$C_{14}H_{16}N_2OSi$
9n	67.80	5.58	15.94	67.89	5.70	15.83	$C_{15}H_{15}N_3Si$

a) A mixture of 6,7- and 7,8-dimethyl-3-cyanoindolizine.

(10%; the same weight to the ylide) raised the yields as follows: **8a** (15%) and **9a** (34%); **8m** (58%) and **9m** (27%).

Reaction of 2a with Trimethylsilylethyne. A mixture of **2a** (0.36 g; 2.5 mmol) and trimethylsilylethyne (1.3 g; 14 mmol) in dry toluene (40 ml) was refluxed with stirring for 50 h. The reaction mixture was allowed to stand at room temperature and filtered to recover **2a** (75%). The solids were rinsed with a small portion of toluene and the combined filtrate was concentrated and chromatographed on silica gel (Wakogel C-100; elution with hexane-ethyl acetate (1 : 9)) to give the crude product, which was purified by MPLC (elution with hexane-ethyl acetate (1 : 9)) to afford **9a** (53 mg; 42% based upon the consumed ylide).

Attempts to Transform 9a to 10. 1. To an ice-cold mixture of anhydrous aluminium chloride (53 mg; 0.4 mmol) in dry tetrachloromethane (10 ml) were added methyl chloroformate (38 mg; 0.4 mmol) and **9a** (43 mg; 0.2 mmol). After 20 min, the reaction mixture was heated at the reflux temperature for 4 d and poured into cold water (20 ml). The aqueous phase was extracted with dichloromethane (total 40 ml). The combined organic layers were dried over anhydrous magnesium sulfate and evaporated to leave a dark brown oil that was fractionated by MPLC (elution with hexane-ethyl acetate (4 : 1)). There was isolated a small amount of crude **3a** (ca. 6 mg).

2. A mixture of **9a** (22 mg; 0.1 mmol), methyl chloroformate (19 mg; 0.2 mmol), potassium fluoride (5.8 mg; 0.1 mmol), 18-crown-6 (1,4,7,10,13,16-hexaoxacyclooctadecane) (26 mg; 0.1 mmol) in dry tetrahydrofuran (4 ml) was stirred at room temperature for 51 h and then refluxed for 6 h under a nitrogen atmosphere. There was no detectable product by TLC of the reaction mixture.

3. A mixture of **9a** (22 mg; 0.1 mmol), methyl chloroformate (19 mg; 0.2 mmol), anhydrous zinc chloride (27 mg; 0.2 mmol) in dry dichloromethane (5 ml) was reacted with stirring at room temperature for 22 h and heated to the reflux temperature under a nitrogen atmosphere. The expected product was not detected by TLC of the solution.

Regioselective Protodesilylations of 8. A magnetically stirred mixture of **8** (1.5 mmol) and silica gel (Wakogel C-100; 0.5 g) in trichloromethane (5 ml) was heated at the reflux temperature for 14 h, filtered, and rinsed with dichloromethane. The combined organic solutions were purified by recrystallizations from hexane. The yields of each reaction and various physical properties are given as follows: **9a** (100%), **9f** (93%): mp 124—125 °C; IR (KBr) 2250, 1720 cm^{-1}, **9g** (89%): mp 133—134 °C; IR (KBr) 2225 cm^{-1}, **9m** (95%), **9n** (83%). The other spectral data and analytical data are shown in Tables 5, 6, and 9.

Complete Protodesilylations of 8 with Tetrabutylammonium Fluoride. A cold (0 °C) solution of **8** (1.0 mmol) in dry tetrahydrofuran (7 ml) was treated with tetrabutylammonium fluoride (0.5 ml of 1.0 mol dm^{-3} in tetrahydrofuran). The mixture was stirred at room temperature for 1 d and treated with cold water (20 ml). The aqueous layer was extracted with benzene (total 80 ml), and the combined organic layers were dried over anhydrous sodium sulfate and evaporated to give the crude products **3**, which were identified as **3** by the ^1H NMR and IR spectroscopic data except **3m** and **3n**. The yields of each reactions and some physical properties are given as follows: **3f** (100%), **3k** (86%), **3m** (93%): mp 149—150 °C; IR (KBr) 2240, 1655, 1620 cm^{-1}; ^1H NMR (δ; $CDCl_3$) 2.62 (s, 3H, Me), 6.75 (d, J=4.5 Hz, 1H, H-2), 7.33 (d, J=4.5 Hz, 1H, H-1), 7.35 (dd, J=7.2, 2.7 Hz, 1H, H-6), 8.09 (d, J=2.7 Hz, 1H, H-8), 8.22 (d, J=7.2 Hz 1H, H-5); ^{13}C NMR (ppm from TMS; $CDCl_3$) 26.0 (q, Me), 97.9 (s, C-3), 106.1 (d, C-1), 110.8 (d, C-2), 113.0 (s, CN), 121.7 (d, C-6), 123.4 (d, C-8), 124.9 (d, C-5), 130.3 (s, C-7), 134.8 (s, C-8a), 195.1 (s, CO). **3n** (100 %): mp 158—159 °C; IR (KBr) 2250 cm^{-1}; ^1H NMR (δ; $CDCl_3$) 6.87 (d, J=4.8 Hz, 1H, H-2), 7.25 (d, J=4.8 Hz, 1H, H-1), 7.5—8.1 (m, 4H, Ar-H), 8.54 (bs, 1H, H-6); ^{13}C NMR (ppm from TMS; $CDCl_3$) 99.8 (d, C-1), 101.2 (s, C-3), 112.9 (s, CN), 119.8 (d, C-2), 120.6 (s, C-7), 127.0 (s, C-8), 130.9 (s, C-8a), 145.5 (d, C-6), 122.2, 128.1, 128.3, 133.2 (each d, Ar-C).

Molecular Orbital Calculations. Molecular orbitals were calculated by the CNDO/2 method.[23] The geometry of **2a** was approximated using data for the crystalline state[24] with a slight modification involving a reforming of the molecule planar. Regarding the substituted compounds, the geometries were assumed by means of standard geometrical models,[25] except for the ylide structure which was kept unchanged. The HMO calculations were performed according to the established method.[26]

The authors wish to thank Professor Rolf Huisgen (University of Munich, West Germany) for his kind and helpful comments. They also extend their gratitude to the Institute for Molecular Science for allotment of CPU time on the HITAC M-680H Computer. This work was supported by Grant-in-Aid for Scientific Research from the Ministry of Education, Science and Culture (Nos. 61840017 and 62540377).

References

1) Some reviews on indolizines and aza-analogues: K. Matsumoto and T. Uchida, *Yuki Gosei Kagaku Kyokai Shi* **32**, 731 (1974); T. Uchida and K. Matsumoto, *Synthesis*, 209 (1976); F. J. Swinbourne, J. H. Hunt, and G. Klinkert, *Adv. Heterocycl. Chem.*, **23**, 103 (1978); Y. Tamura and M. Ikeda, *Adv. Heterocycl. Chem.*, **29**, 71 (1981).

2) Recent examples on these aspects: H. Duerr, C. Schommer, and T. Muenzmay, *Angew. Chem., Int. Ed. Engl.*, **25**, 572 (1986); Japan Kokai Tokkyo Koho JP 6071296, *Chem. Abstr.*, **103**, 132469q (1985); I. Antonini, F. Claudi, U. Gulini, L. Miscossi, and F. Venturi, *J. Pharm. Sci.*, **68**, 321 (1979).

3) Review: "The Alkaloids, Chemistry and Physiology," ed by R. H. F. Manske, Academic Press, New York, Vol. I—XV.

4) T. Uchida and K. Matsumoto, *Chem. Lett.*, **1980**, 149.

5) To our knowledge, only 3-dialkylaminoindolizines have been reported: A. Ohsawa, Y. Abe, and H. Igeta, *Chem. Lett.*, **1979**, 241.

6) Presented in part at the 9th International Congress of Heterocyclic Chemistry; Aug. 1983; Tokyo; Abstract P-161.

7) O. De Lucchi and G. Modena, *Tetrahedron*, **40**, 2585 (1984).

8) C. U. Pittman, M. Narita, and Y. F. Liang, *J. Org. Chem.*, **41**, 2855 (1976); M. V. Lakshmikanthan and M. P. Cava, *J. Org. Chem.*, **41**, 882 (1976).

9) O. De Lucchi, V. Lucchini, L. Pasquato, and G. Modena, *J. Org. Chem.*, **49**, 596 (1984).

10) L. A. Paquette, R. E. Moerck, H. Harirchian, and P. D. Magnus, *J. Am. Chem. Soc.*, **100**, 1597 (1978); A novel

1,3-diploar cycloaddition of tetrasulfur tetranitrite with PVSO has been recently described: R. Jones, J. L. Morris, C. W. Rees, and D. J. Williams, *J. Chem. Soc., Chem. Commun.*, **1985**, 1654.

11) P. J. Black, M. L. Heffernan, L. M. Jackman, Q. N. Porter, and G. R. Underwood, *Aust. J. Chem.*, **17**, 1128 (1964).

12) R. J. Pugmire, M. J. Robins, D. M. Grant, and R. K. Robins, *J. Am. Chem. Soc.*, **93**, 1887 (1971).

13) W. P. Weber, "Silicon Reagents for Organic Synthesis" Springer Verlag, New York (1983), p. 148.

14) R. M. Acheson, M. G. Bite, and M. W. Cooper, *J. Chem. Soc., Perkin Trans. 1*, **1976**, 1908.

15) F. Effenberger and A. Krebs, *J. Org. Chem.*, **49**, 4687 (1984).

16) A. Ricci, A. Del'innocenti, M. Florenza, M. Taddei, M. Spartera, and D. R. W. Walton, *Tetrahedron Lett.*, **23**, 577 (1982).

17) a) J. Schraml, V. Chvalovsky, M. Magi, E. Lippmaa, B. Calas, J. Dungues, and P. Bourgeois, *J. Organomet. Chem.*, **120**, 41, (1976); b) K. Mach, H. Antropiusova, L. Petrusova, F. Turecek, V. Hanus, P. Sedmera, and J. Schraml, *J. Organomet. Chem.*, **289**, 331 (1985).

18) R. Huisgen, *J. Org. Chem.*, **41**, 403 (1976); "1,3-Dipolar Cycloaddition Chemistry," ed by A. Padwa, Wiley-Interscience, New York (1984).

19) W. Bihlmaier, R. Huisgen, H.-U. Reissig, and S. Voss, *Tetrahedron Lett.*, **1979**, 2621 and references cited.

20) R. Sustmann, *Tetrahedron Lett.*, **1971**, 2717.

21) Sofar, the CNDO/2 calculation of PVSO has been unsuccessful in our hands. The coefficients described in Fig. 1 were obtained by HMO method.[26] The energy levels shown are only qualitative.

22) W. J. Linn, O. W. Webster, and R. E. Benson, *J. Am. Chem. Soc.*, **87**, 3651 (1965).

23) J. A. Pople and G. A. Segal, *J. Chem. Phys.*, **44**, 3289 (1966).

24) C. Bugg and R. L. Sass, *Acta Cryst.*, **18**, 591 (1965).

25) J. A. Pople and D. L. Beveridge, "Approximate Molecular Orbital Theory," McGraw-Hill, New York (1970), p. 110

26) T. Yonezawa, C. Nagata, H. Kato, A. Imamura, and K. Morokuma, "Ryoushi Kakagu Nyuumon," 3rd ed, Kagaku Doujin, Kyoto (1983), pp. 55—73.

 © 1987 The Chemical Society of Japan Bull. Chem. Soc. Jpn., 60, 3655—3658 (1987)

Molecular Recognition in the Formation of Conglomerate Crystal. The Role of Cinnamic Acid in the Conglomerate Crystals of 1-Phenylethylamine and 1-(4-Isopropylphenyl)ethylamine Salts

Kazuhiko SAIGO,* Hiroki KIMOTO, Hiroyuki NOHIRA,† Kazunori YANAGI,†† and Masaki HASEGAWA
Department of Synthetic Chemistry, Faculty of Engineering, The University of Tokyo, Hongo, Bunkyo-ku, Tokyo 113
†Department of Applied Chemistry, Faculty of Engineering, Saitama University, Shimo-ohkubo, Urawa, Saitama 338
††The Takatsuki Research Laboratory, Sumitomo Chemical Co. Ltd., Tsukahara, Takatsuki, Osaka 569
(Received April 9, 1987)

The Crystal structures of (+)-1-phenylethylamine·cinnamic acid salt and (+)-1-(4-isopropylphenyl)-ethylamine·cinnamic acid salt were determined by X-ray analysis. The crystal structures of these two salts provided for the first time some insights into the mechanism of the formation of a conglomerate crystal. In each crytal, two amine components and two acid components form a helical column by hydrogen bonds. On the basis of this similarity in the molecular arrangements, the role of cinnamic acid, an achiral acid, is discussed, and the criteria for the choice of an achiral acid in the transformation of the racemic modification of an amine into a conglomerate crystal is proposed.

The optical resolution of the racemic modification of an amine or a carboxylic acid is usually carried out by the diastereomeric salt method.[1] But, in this resolution, a stoichiometric amount of an optically pure enantiomer is required as a resolving agent, and it is difficult to get both enantiomers of the racemic modification by a simple operation. This difficulty can be solved by the preferential crystallization method. Despite the practical importance, the technique is known to be applicable for the optical resolution of only about 300 racemic modifications, since only conglomerates can be resolved by the method.[1] Moreover, rational explanation has not been proposed for the experimental results. Then, the successful resolution by the preferential crystallization method can only be achieved by a time-consuming trial-and-error procedure.

In the previous papers, we reported that the cinnamic acid salts of α-substituted benzylamine derivatives such as 1-phenylethylamine,[2] 1-phenyl-2-(*p*-tolyl)ethylamine,[2] *erythro*-2-amino-1,2-diphenylethanol,[3] and 1-(4-isopropylphenyl)ethylamine[4] are conglomerates and that these salts can be resolved into pairs of enantiomers by the preferential crystallization. These results seem to suggest the presence of some structural relationship between the chiral amines and the achiral acid. We report here the crystal structures of two conglomerates, 1-phenylethylamine·cinnamic acid salt and 1-(4-isopropylphenyl)ethylamine·cinnamic acid salt that provide considerable insight into the mechanism of the formation of a conglomerate.

Table 1. Crystal Data and Details of Refinement

	1	2
Formula	$C_8H_{11}N\cdot C_9H_8O_2$	$C_{11}H_{17}N\cdot C_9H_8O_2$
M	269.35	311.43
Crystal system	orthorhombic	orthorhombic
Space group	$P2_12_12_1$	$P2_12_12_1$
a/Å	9.368 (1)	13.868 (1)
b/Å	26.703 (2)	20.457 (1)
c/Å	6.043 (1)	6.471 (1)
V/Å^3	1511.8 (5)	1835.7 (6)
Z	4	4
D_c/g cm^{-3}	1.183	1.127
μ(Cu $K\alpha$)/cm^{-1}	5.808	5.158
Crystal size/mm^3	0.45×0.40×0.30	0.30×0.30×0.40
Number of unique reflections	1701	2015
Number of observed reflections	1433	1565
Number of parameters	258	309
$\Delta\rho_{max}$/e Å^{-3}	+0.14	+0.18
$\Delta\rho_{min}$/e Å^{-3}	−0.15	−0.13
$(\Delta/\rho)_{max}$	0.29	0.24
R_w	0.049	0.059
R	0.036	0.042

Experimental

Materials. (+)-1-Phenylethylamine[3] and (+)-1-(4-isopropyl)ethylamine[4] were obtained by the optical resolution of the corresponding racemic modifications according to the

Table 2. Fractional Atomic Coordinates and Equivalent Isotropic Thermal Parameters for 1

Atom	x	y	z	B_{eq}[6]/Å^2
O(1)	0.5697(2)	0.42478(6)	0.4982(3)	6.77(4)
O(2)	0.6843(2)	0.44281(5)	0.8082(3)	4.58(3)
N(1)	0.9024(2)	0.50408(5)	0.6814(3)	3.68(3)
C(1)	0.6018(2)	0.41643(6)	0.6939(4)	3.86(3)
C(2)	0.5356(2)	0.37105(7)	0.7927(4)	4.18(4)
C(3)	0.5608(2)	0.35539(7)	0.9950(4)	4.06(4)
C(4)	0.5050(2)	0.30988(6)	1.1025(3)	4.08(4)
C(5)	0.5639(3)	0.29638(8)	1.3022(4)	5.29(5)
C(6)	0.5207(3)	0.25344(9)	1.4126(4)	6.23(6)
C(7)	0.4170(3)	0.22367(8)	1.3212(5)	6.53(6)
C(8)	0.3567(3)	0.23651(9)	1.1243(5)	6.31(6)
C(9)	0.3993(2)	0.27997(8)	1.0130(4)	5.14(5)
C(10)	1.0466(2)	0.48095(7)	0.6639(3)	3.61(3)
C(11)	1.1530(2)	0.52163(7)	0.6005(4)	4.55(4)
C(12)	1.0496(2)	0.43768(6)	0.5022(3)	3.59(3)
C(13)	0.9633(2)	0.43453(7)	0.3193(4)	4.56(4)
C(14)	0.9771(3)	0.39551(8)	0.1686(4)	5.34(5)
C(15)	1.0807(3)	0.35967(7)	0.1984(4)	5.36(5)
C(16)	1.1688(3)	0.36256(8)	0.3802(5)	5.69(5)
C(17)	1.1526(2)	0.40086(8)	0.5330(4)	4.76(4)

methods in the literatures.

Crystal Structure Determination. Colorless crystals **1** and **2** were grown from a saturated solution of an equimolar mixture of the amine and cinnamic acid in methanol, respectively. The specimen used was a fragment of a plate. Data were collected up to $2\theta=140°$ on an Enraf-Nonius CAD-4 diffractometer using graphite-monochromated Cu $K\alpha$ (1.5418 Å) radiation by ω—2θ scan. Standard reflections showed no

Table 3. Fractional Atomic Coordinates and Equivalent Isotropic Thermal Parameters for **2**

Atom	x	y	z	B_{eq}[6]/Å^2
O(1)	0.1563(2)	0.3929(1)	0.1739(3)	5.96(5)
O(2)	0.1974(1)	0.4288(1)	0.4829(3)	5.26(4)
N(1)	0.3393(1)	0.5147(1)	0.3670(3)	3.96(4)
C(1)	0.1507(2)	0.3916(1)	0.3665(4)	3.98(5)
C(2)	0.0843(2)	0.3424(2)	0.4530(5)	5.16(6)
C(3)	0.0883(2)	0.3184(1)	0.6391(5)	4.91(6)
C(4)	0.0203(2)	0.2704(1)	0.7306(5)	4.75(6)
C(5)	0.0337(3)	0.2519(2)	0.9316(6)	5.96(7)
C(6)	−0.0295(3)	0.2108(2)	1.0291(6)	7.21(9)
C(7)	−0.1097(3)	0.1875(2)	0.9314(7)	6.97(9)
C(8)	−0.1244(3)	0.2047(2)	0.7290(7)	6.67(9)
C(9)	−0.0598(2)	0.2456(2)	0.6311(6)	5.87(7)
C(10)	0.4261(2)	0.4720(1)	0.3692(5)	4.40(5)
C(11)	0.4405(2)	0.4462(2)	0.5870(6)	6.40(7)
C(12)	0.5135(2)	0.5070(1)	0.2826(4)	3.94(5)
C(13)	0.5500(2)	0.5638(1)	0.3730(5)	4.33(5)
C(14)	0.6303(2)	0.5943(1)	0.2901(5)	4.34(5)
C(15)	0.6769(2)	0.5692(1)	0.1179(5)	4.51(6)
C(16)	0.6408(2)	0.5129(2)	0.0307(5)	5.93(7)
C(17)	0.5603(2)	0.4823(2)	0.1111(5)	5.34(6)
C(18)	0.7651(2)	0.6018(2)	0.0205(5)	5.82(7)
C(19)	0.8151(2)	0.6501(2)	0.1580(7)	6.90(9)
C(20)	0.7381(3)	0.6332(2)	−0.1884(6)	8.5 (1)

Table 4. Bond Distances (l/Å)

	1	**2**
O(1)-C(1)	1.241(2)	1.249(3)
O(2)-C(1)	1.253(2)	1.251(2)
N(1)-C(10)	1.489(2)	1.488(3)
C(1)-C(2)	1.486(2)	1.475(3)
C(2)-C(3)	1.314(3)	1.302(4)
C(3)-C(4)	1.473(2)	1.485(3)
C(4)-C(5)	1.375(3)	1.367(4)
C(4)-C(9)	1.383(3)	1.381(4)
C(5)-C(6)	1.387(3)	1.367(5)
C(6)-C(7)	1.372(4)	1.366(5)
C(7)-C(8)	1.361(4)	1.371(5)
C(8)-C(9)	1.399(3)	1.379(4)
C(10)-C(11)	1.523(2)	1.519(4)
C(10)-C(12)	1.514(2)	1.514(3)
C(12)-C(13)	1.372(2)	1.395(3)
C(12)-C(17)	1.390(2)	1.381(3)
C(13)-C(14)	1.390(3)	1.386(3)
C(14)-C(15)	1.375(3)	1.386(3)
C(15)-C(16)	1.376(3)	1.377(3)
C(16)-C(17)	1.386(3)	1.382(3)
C(15)-C(18)		1.529(3)
C(18)-C(19)		1.500(5)
C(18)-C(20)		1.543(5)

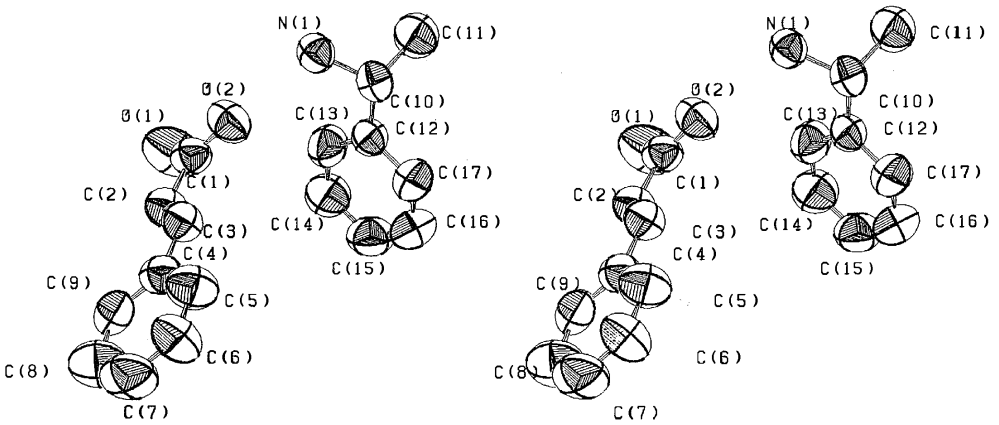

Fig. 1. Labeled Stereoscopic Drawing of **1**.

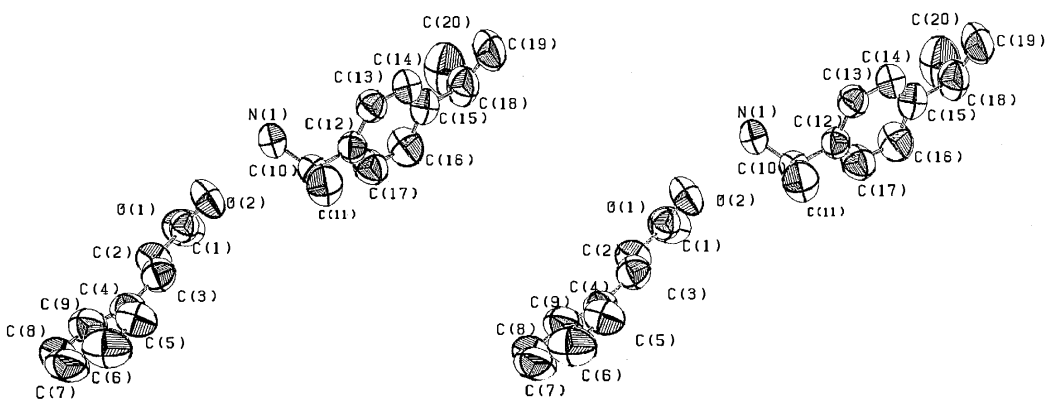

Fig. 2. Labeled Stereoscopic Drawing of **2**.

significant intensity change. Of unique reflections measured, those as observed with $I > 3\sigma(I)$ were used. The intensities were corrected for Lorentz, polarization, and extinction but not for absorption. The structure was solved by the direct method (MULTAN 11/82) and was refined by the full-matrix least-squares. Scattering factors were taken from "International Tables for X-Ray Crystallography (1974)." Computations were performed by using Enraf-Nonius SDP v3.0. Crystal data and details of refinement are summarized in Table 1.

Results and Discussion

Fractional coordinates for the crystals of (+)-1-phenylethylamine · cinnamic acid salt (**1**) and (+)-1-(4-isopropylphenyl)ethylamine · cinnamic acid salt (**2**) are given in Tables 2 and 3, respectively.[5] Labeled stereoscopic drawings of cinnamic acid and (+)-1-phenylethylamine in the crystal of **1** and those of cinnamic acid and (+)-1-(4-isopropylphenyl)ethylamine in the crystal of **2** are given in Figs. 1 and 2, respectively. Bond distances of **1** and **2** are given in Table 4.

In the crystal of **1**, two amine components and two acid components form a helical column by hydrogen bonds along the *c* axis (Fig. 3). The lengths of the hydrogen bonds are 2.727(2) Å for $O(2)^{i} \cdots N(1)^{i}$, 2.709(2) Å for $N(1)^{i} \cdots O(1)^{ii}$, and 2.785(2) Å for $O(2)^{i} \cdots N(1)^{ii}$. But, no hydrogen bond exists between the columns. Excluding the hydrogen bonds, the shortest intermolecular distance is 3.618(1) Å which is a little larger than the sum of ordinary van der Waals radii.

In the crystal of **2**, two amine components and two acid components are also arranged to form a helical column by hydrogen bonds along the *c* axis (Fig. 4). The lengths of the hydrogen bonds are 2.743(2) Å for $O(2)^{i} \cdots N(1)^{i}$, 2.741(3) Å for $N(1)^{i} \cdots O(1)^{ii}$, and 2.787(3) Å for $O(2)^{i} \cdots N(1)^{ii}$. There is no hydrogen bond between the columns. Other than the hydrogen bonds,

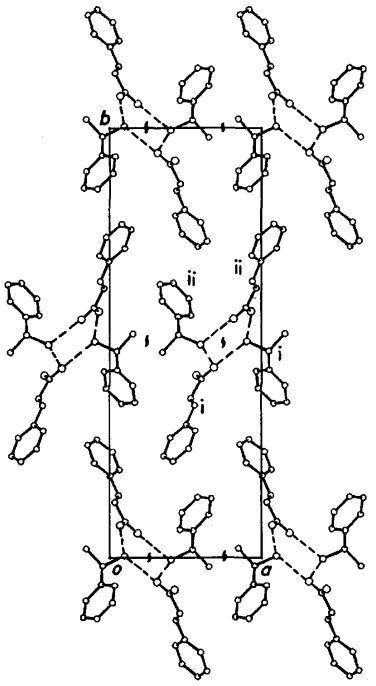

Fig. 3. The Crystal Structure of **1** viewed along the *c* axis. Hydrogen bonds are shown by dashed lines. The numbers i, ii denote the operations, i: *x*, *y*, *z*; ii: 3/2−*x*, 1−*y*, 1/2+*z*.

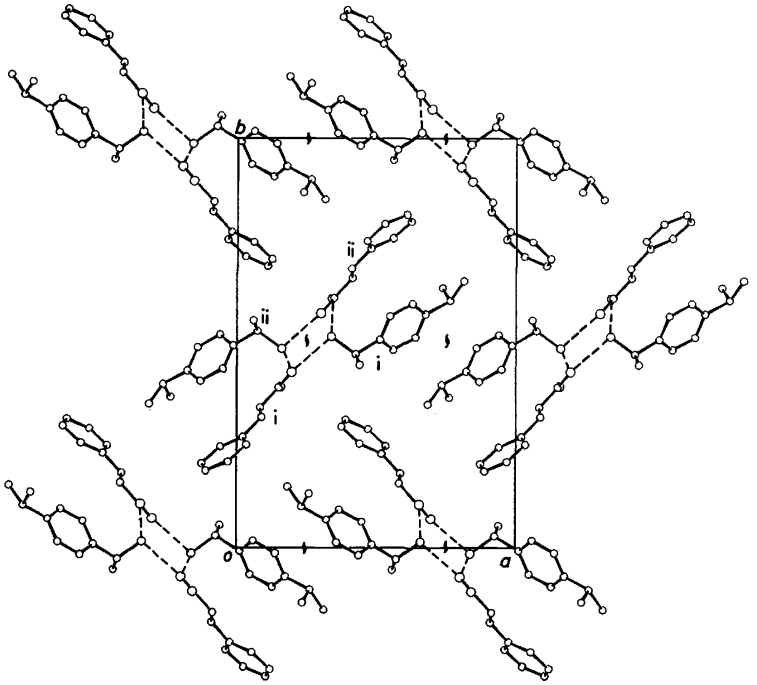

Fig. 4. The Crystal Structure of **2** viewed along the *c* axis. Hydrogen bonds are shown by dashed lines. The numbers i, ii denote the operations, i: *x*, *y*, *z*; ii: 1/2−*x*, 1−*y*, 1/2+*z*.

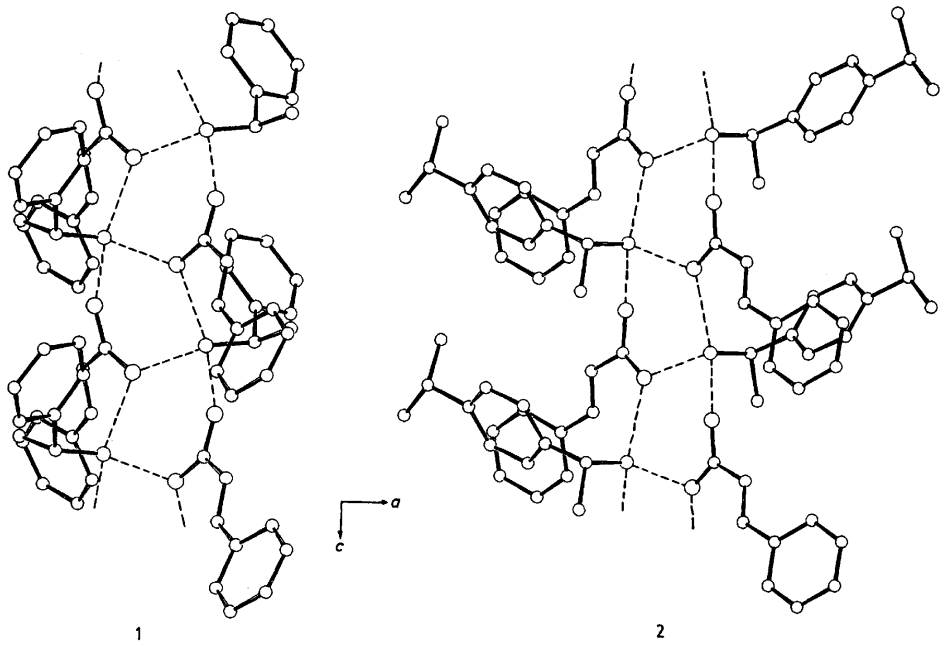

Fig. 5. The Crystal Structures of **1** and **2** viewed along the *b* axis. Hydrogen bonds are shown by dashed lines.

the short intermolecular distances are 3.432(1) Å for C(3)^{i}–C(13)^{ii} and 3.489(0) Å for C(4)^{i}–C(14)^{ii}, which are nearly equal to the sum of van der Waals radii.

As mentioned above, the crystal structures of **1** and **2** are very close. Namely, the crystals of **1** and **2** are built up by the hydrogen bonds between two amine components and two acid components to form columns along the *c* axis. Figure 5 shows the hydrogen bond columns in **1** and **2**. The arrangements of the acid components are very similar to each other in the two columns, whereas those of the amine components are differed from one another. In the structure of **1**, the phenyl group of (+)-**1**-phenylethylamine is parallel to the axis of the column, whereas in the structure of **2** the isopropylphenyl group of (+)-**1**-(4-isopropylphenyl)ethylamine is nearly perpendicular to the column axis. Such different arrangements may be interpreted by steric requirement. The parallel arrangement of isopropylphenyl group would be unfavorable for the formation of the hydrogen bonds. In other words, unusually short contacts less than 2 Å appear between the isopropyl group and the methyl group of the neighboring amine in the hydrogen bond columns, if the phenyl group is replaced by the isopropylphenyl one. The formation of these rigid hydrogen bonds would result in the high selectivity for only one enantiomer of the chiral amine in the course of crystallization. On the other hand, the phenyl group and double bond of cinnamic acid play a significant role for crystal packing to offer suitable space for the amine molecules and to fix it well. In addition, a similar size between the molecules of the amine and cinnamic acid seems to be very important in order to form the column by the hydrogen bonds and to make it rigid.

On the basis of structural similarity of the two conglomerates it is suggested that an achiral acid satisfying the following structural requirement is favorable for the transformation of a racemic modification of an amine into a conglomerate crystal: (a) The achiral acid can form a helical column by hydrogen bonds with the amine; (b) the acid should be rigid and flat to limit the orientation of the amine; (c) the sizes of the amine and the acid are similar to each other.

These working hypotheses are the first insights for the structure of a conglomerate crystal, and they are regarded at the first step for the prediction of the transformation from a racemic modification into a conglomerate crystal.

References

1) J. Jacques, A. Collet, and S. H. Wilan, "Enantiomers, Racemates and Resolutions," John Wiley & Sons, New York (1981).

2) H. Nohira, M. Kai, M. Nohira, J. Nishikawa, T. Hoshiko, and K. Saigo, *Chem. Lett.*, **1981**, 951.

3) K. Saigo, S. Ogawa, S. Kikuchi, A. Kasahara, and H. Nohira, *Bull. Chem. Soc. Jpn.*, **55**, 1568 (1982).

4) K. Saigo, M. Kai, N. Yonezawa, M. Hasegawa, and H. Nohira, *Synthesis*, **1985**, 214.

5) F_o—F_c Tables, anisotropic thermal temperature factors, fractional atomic coordinates of hydrogen atoms, and bond angles are deposited as Document No. 8757 at the Office of the Editor of Bull. Chem. Soc. Jpn.

6) The equivalent isotropic temperature factors were computed using the following expression; $B_{eq}=4/3(B_{11}a^2+B_{22}b^2+B_{33}c^2)$.

Practical Method for the Synthesis and Optical Resolution of Axially Dissymmetric 6,6′-Dimethylbiphenyl-2,2′-dicarboxylic Acid

Shigeyoshi KANOH, Hiroki MURAMOTO, Natsumi KOBAYASHI, Masatoshi MOTOI, and Hiroshi SUDA*
Department of Chemistry and Chemical Engineering, Faculty of Technology, Kanazawa University, 2-40-20 Kodatsuno, Kanazawa 920
(Received April 9, 1987)

Racemic 6,6′-dimethylbiphenyl-2,2′-dicarboxylic acid (**1**) could be conveniently synthesized and efficiently resolved by the recrystallization of the brucine salts in satisfactory yields. Each enantiomer, thus obtained, was confirmed to be optically pure from a high-performance liquid chromatographic (HPLC) analysis on an optically active column.

N,N- and *N,N*:*N′,N′*-[(Axially dissymmetric biphenyl-2,2′-diyl)dimethylene]-substituted ethylenediamines, such as **2** and **3**, have been found to serve as very efficient chiral ligands for organolithium compounds in the asymmetric polymerization of triphenylmethyl methacrylate[1,2] and the enantioface-differentiating alkylation of aldehydes.[3] A highly asymmetric induction in these reactions is considered to be due to a complementary effect between the high ability of the biphenyl unit for chiral recognition[4] and the flexibility of the tetramethylethylenediamine sidearm for chelation with organolithium compounds.[5] The key intermediate in the syntheses of ligands **2** and **3** is axially dissymmetric 6,6′-dimethylbiphenyl-2,2′-dicarboxylic acid (**1**) as optically pure forms. Therefore, the development of a convenient method for the synthesis and optical resolution of the diacid is practically important from the viewpoint of a ready application of such ligands to asymmetric reactions.

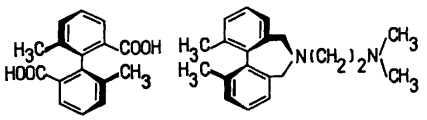

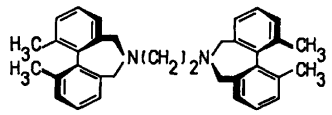

Recently, we have reported asymmetric polymerizations of triphenylmethyl methacrylate by using chiral complexes of organolithium with **2** or **3**.[1,2] During the course of these investigations, we intended to develop a more convenient preparation of the chiral ligands. In this paper, we wish to describe a facile synthesis of (*RS*)-**1** and its efficient optical resolution through the recrystallization of the brucine salt. The resolved acids were confirmed to be optically pure by means of a high-performance liquid chromatography (HPLC) with an optically active column.

The synthesis of (*RS*)-**1** has been outlined briefly by two research groups.[6,7] However, these papers failed

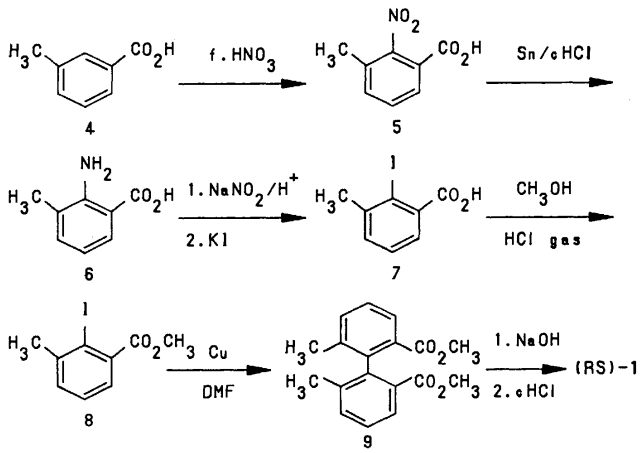

Scheme 1.

to give the detailed procedures. Our approach to (*RS*)-**1** is represented in the above scheme; details are described in Experimental. The first stage of the synthesis is the nitration of *m*-toluic acid. Even after the optimization of the reaction conditions, the yield was as low as 49%, owing to an inevitable formation of nitrated isomers. However, the poor solubility of 2-nitro-3-methylbenzoic acid (**5**) in cold fuming nitric acid facilitated the separation of **5** from undesirable isomers by a simple suction-filtration. The subsequent steps were conducted in a combination of common procedures, resulting in satisfactory yields.

The first optical resolution of (*RS*)-**1** was carried out with morphine by Bell.[7] Since then, this method has been followed essentially by later investigators.[8,9] However, different specific rotations ranging from +15 to +25° in methanol at 589 nm have been reported for the (+)-acid resolved.[7-9] Moreover, it has been very difficult to obtain optically pure (−)-enantiomer, since the recrystallization of morphine salt of (−)-**1** was not successful.[7]

Bell[7] also reported that an attempt to resolve (*RS*)-**1** with brucine was unsuccessful. We succeeded to resolve the diacid by using this alkaloid.[1] Details of the procedure is as follows. A reaction of (*RS*)-**1** with an equimolar amount of brucine gave a mixture of the diastereomeric salts. In order to effectively separate

this mixture into each salt, it was found that solvent systems for recrystallization were extremely important. One recrystallization of the diastereomeric salts from a mixture of methanol–acetone (7/3 v/v) gave levorotatory brucine salt of (*S*)-**1**, the yield of which was 40% based on (*RS*)-**1** used. The optical purity of this salt seemed to be nearly 100%, since further recrystallization did not cause any noticeable change in the optical rotation. Subsequently, when the solvents of the mother liquor were replaced with acetone alone, crystallization of another diastereomeric salt started. The (+)-salt obtained was recrystallized from acetone containing a small amount of methanol to give pure brucine salt of (*R*)-**1** in 43% yield. Further recrystallizations of the last residue remaining in the acetone solution led to additional yields of the individual salts. The decomposition of each salt with diluted hydrochloric acid gave (*S*)- and (*R*)-**1** in 43 and 42% overall yields, respectively; the absolute configuration has been established.[9] As a matter of course, most of the resolving agent was recovered.

Optical purities of (+)- and (−)-**1**, thus resolved, were determined from HPLC analyses of the dimethyl esters **9** derived from the diacids. The column used was an optically active column, **CHIRALCEL OC**, which is commercially available from *Daicel Chemical Industries Ltd.*; the packing material is cellulose tris-(phenylcarbamate) coated on a macroporous silica gel.[10] Base-line resolution of racemic **9** was accomplished with this column, using hexane–2-propanol (9/1 v/v) as an eluent.[11] Figure 1 shows the chromatograms of (+)- and (−)-**9** under the same operation conditions as those for the racemate. Each major peak in the curves appeared at a different retention volume,

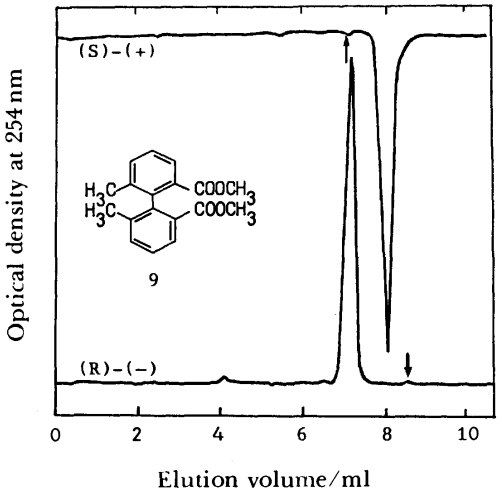

Fig. 1. Chromatograms of the dimethyl esters **9** derived from optically resolved **1**. The peaks marked with arrows are probably due to the minor enantiomers. Column: **CHIRALCEL OC** (*Daicel Chemical Industries Ltd.*), 25×0.46 (i.d.) cm; eluent: hexane–2-propanol (9/1 v/v); flow rate: 0.2 ml min^{-1} at 25 °C; detector: UV at 254 nm.

which is nearly in agreement with that of either two peaks in the enantiomeric separation observed for the racemate. An inspection of the curves reveals that each of the samples probably contains a very small amount of the opposite enantiomer. Based on the relative peak area, the optical purities of (+)- and (−)-diesters were estimated to be 99.1 and 99.6%, respectively. From the chromatographic results, each of the diacids **1** resolved in the present study may be regarded as almost optically pure. The completely pure enantiomers, if required, are obtainable by a recrystallization from benzene.

The present procedure for the optical resolution of (*RS*)-**1** seems advantageous regarding the use of cheaper brucine, an easy access of nicely recrystallizable salts with both enantiomers and, above all, an operational simplicity and high efficiency of the resolution.

Experimental

Melting points are uncorrected. IR and ^{1}H NMR spectra were recorded on a JASCO A-202 and a JEOL JNM-FX-100S (100 MHz) spectrometer, respectively. Optical rotations were measured on a JASCO DIP-360 digital polarimeter. A determination of the optical purities of (+)- and (−)-**9** was performed by using an HPLC on an optically active column, **CHIRALCEL OC** (*Daicel Chemical Industries Ltd.*; 25×0.46 (i.d.) cm). Resolution was carried out with hexane–2-propanol (9/1 v/v) at a flow rate of 0.2 ml min^{-1} at 25 °C.

Preparation of (*RS*)-2,2′-Dimethylbiphenyl-6,6′-dicarboxylic Acid (1). 2-Nitro-3-methylbenzoic Acid (5): *m*-Toluic acid (**4**) (200 g, 1.47 mol) was added in small portions to 500 ml of fuming nitric acid (d=1.52) with stirring at −10 °C. Stirring was continued for an additional 1 h at this temperature. The precipitate was collected by a suction-filtration with a large sintered-glass filter as quickly as possible, and thoroughly washed with water. Recrystallization from ethanol yielded 130 g (49%) of **5**. Mp 218—219 °C (lit,[12] 219 °C); IR (KBr) 3200—2400, 1690, 1550, 1375, and 1300 cm^{-1}; ^{1}H NMR (DMSO-d_6/D_2O) δ=2.32 (s, 3H), 7.5—7.9 (m, 3H).

2-Amino-3-methylbenzoic Acid (6): Tin powder (220 g, 1.85 mol) was suspended in a solution of **5** (120 g, 0.66 mol) in ethanol (500 ml). To the stirred mixture was added dropwise 1.3 l of 9 mol dm^{-3} hydrochloric acid at 50—60 °C. The resulting solution was stirred for 1.5 h at 70 °C, cooled, and then made alkaline by the addition of concd. aqueous NH_3. Inorganic precipitates were removed and the filtrate was freed from ethanol by evaporation under reduced pressure. The resulting solution was acidified with acetic acid (pH=5). The precipitate was collected and dissolved in acetone. After the removal of insoluble materials and then the solvent, recrystallization of the residue from ethanol gave 89 g (89%) of **6**. Mp 174—175 °C (lit,[12] 172 °C); IR (KBr) 3500, 3380, 3200—2400, 1670, 1575, and 1240 cm^{-1}; ^{1}H NMR ($CDCl_3$/D_2O) δ=2.18 (s, 3H), 6.5—7.9 (m, 3H).

2-Iodo-3-methylbenzoic Acid (7): A suspension of **6** (75 g, 0.5 mol) in a mixture of concd. H_2SO_4 (300 ml) and water (600 ml) was stirred for 1 h at room temperature, and then a solution of $NaNO_2$ (45 g, 0.65 mol) in 75 ml of water was

added drop by drop at 10 °C. The excess nitrite was decomposed with urea. To the solution were added in one portion a saturated aqueous solution of KI (420 g, 2.5 mol) and a small amount of copper powder,[13] which was prepared by the reduction of copper(II) sulfate with zinc powder. Vigorous stirring was continued for 3 h at about 30 °C, and the mixture was allowed to stand overnight. The supernatant solution was decanted and a brownish precipitate was dissolved in benzene. The benzene solution was decolorized with aqueous $NaHSO_3$, followed by evaporation under reduced pressure. Recrystallization from aqueous ethanol yielded 106 g (81%) of **7**. Mp 143—144 °C (lit,[6] 145—146 °C); IR (KBr) 3200—2400, 1700, and 1290 cm^{-1}; ^1H NMR ($CDCl_3$) δ=2.56 (s, 3H), 7.2—7.7 (m, 3H), 9.5 (br s).

Methyl 2-Iodo-3-methylbenzoate (8): A solution of **7** (129 g, 0.49 mol) in 650 ml of methanol was saturated with hydrogen chloride; the gas was then passed through the refluxing solution for 1 h. The usual extractive work-up, followed by distillation under reduced pressure, gave 128 g (94%) of **8**. Bp 130—140 °C (5 mmHg (1 mmHg=133.322 Pa)) (lit,[8] 156.5—157.5 °C (13 mmHg)); IR (liquid film) 1730, 1295, and 1145 cm^{-1}; ^1H NMR ($CDCl_3$) δ=2.50 (s, 3H), 3.92 (s, 3H), 7.2—7.4 (m, 3H).

Methyl 6,6′-Dimethylbiphenyl-2,2′-dicarboxylate (9): A solution of **8** (209 g, 0.76 mol) in 210 ml of *N*,*N*-dimethylformamide was mixed with activated copper powder[14] (100 g), and gently refluxed for 5 h. The copper was filtered off and thoroughly washed with hot benzene. The combined filtrates were washed with water, 1 mol dm^{-3} HCl, aqueous $NaHCO_3$, and then brine. After the solvents were removed, distillation under reduced pressure gave 91 g (80%) of **9**. Bp 150—160 °C (0.05 mmHg) (lit,[8] 197—198 °C (13 mmHg)); IR (liquid film) 1735, 1280, and 1150 cm^{-1}; ^1H NMR ($CDCl_3$) δ=1.91 (s, 6H), 3.57 (s, 6H), 7.2—7.9 (m, 6H).

6,6′-Dimethylbiphenyl-2,2′-dicarboxylic Acid (1): The diester **9** (116 g, 0.39 mol) was refluxed in a solution of 150 g of NaOH in 800 ml of water for 5 h. The mixture was acidified by the addition of concd. HCl with cooling and the precipitate was collected. Recrystallization from aqueous ethanol yielded 100 g (95%) of **1**. Mp 240—241 °C (lit,[9] 236—237.5 °C); IR (KBr) 3300—2400, 1700, and 1280 cm^{-1}; ^1H NMR (DMSO-d_6/D_2O) δ=1.81 (s, 6H), 7.3—7.8 (s, 6H). Found: C, 71.06; H, 5.05%. Calcd for $C_{16}H_{14}O_4$: C, 71.10; H, 5.22%.

Optical Resolution of (*RS*)-1. Brucine (100 g, 0.26 mol) and (*RS*)-**1** (69 g, 0.26 mol) were dissolved in a refluxing mixture of methanol (420 ml) and acetone (180 ml). After the solution was cooled at room temperature overnight, the colorless needles deposited were collected by filtration and washed with cold methanol: Brucine salt of (*S*)-**1**, 68 g (40% yield); $[\alpha]_D^{25}$ −39.2° (*c* 1.0, methanol). When a part of the first crop was recrystallized from acetone, the resulting salt showed a similar rotation of $[\alpha]_D^{25}$ −38.9°. The solvents of the mother liquor were evaporated under reduced pressure and the oily residue was dissolved in 200 ml of acetone on heating. Cooling the solution in a refrigerator overnight gave 78 g of colorless cubics, which showed $[\alpha]_D^{25}$ +37.1° (*c* 1.0, methanol). After the recrystallization of the (+)-salt from acetone containing a small amount of methanol, the resulting (+)-salt showed a slightly higher rotation of $[\alpha]_D^{25}$ +38.1 (*c* 1.0, methanol), and the rotation was not changed by further recrystallization. The yield of brucine salt of (*R*)-**1** was 43% (73 g). Additional recrystallizations of the last residue, in turn from methanol–acetone (7/3 v/v) and acetone alone, gave small amounts of the (−)- and (+)-salts in 5 and 2%, respectively.

The combined (−)-salts (77 g, 0.12 mol) were decomposed in 250 ml of 1 mol dm^{-3} HCl and the equal volume of ethyl acetate with stirring at 50 °C. The organic extracts were washed with 1 mol dm^{-3} HCl and brine, dried over Na_2SO_4, and evaporated under reduced pressure. The residual oil, which gradually solidified, was dried under reduced pressure to give 30 g of (*S*)-**1** (43% yield based on (*RS*)-**1** used).[15] It was possible to recrystallize the diacid from benzene. Mp 211—212 °C (lit,[9] 211.5—213.5 °C); $[\alpha]_D^{25}$ +22.1° (*c* 1.0, methanol) (lit,[9] $[\alpha]_D^{25}$ +25° (*c* 1.2)).

The (+)-salt (76 g, 0.11 mol) was similarly converted back to (*R*)-**1** in 42% yield.[15] Mp 213—214 °C (lit,[9] 207—211 °C); $[\alpha]_D^{25}$ −21.3° (*c* 1.0, methanol) (lit,[9] $[\alpha]_D^{23}$ −22° (*c* 1.0)). More than 90% of brucine used were recovered from the acid extracts combined, by the recrystallization from ethanol.

In order to determine the optical purity of the resolved **1**, it was converted to the dimethyl ester **9**. Thus, an ethereal suspension of optically active **1** before recrystallization was treated with a large excess of diazomethane in tetrahydrofuran at room temperature; then, the solvents were removed. The chromatographic sample was purified by a simple distillation of the residue under reduced pressure. The yield of **9** was nearly quantitative. (*R*)-**9**, $[\alpha]_D^{25}$ −55.3° (*c* 2.0, benzene) (lit,[8] $[\alpha]_D^{25}$ −45.1° (*c* 1.3)). (*S*)-**9**, $[\alpha]_D^{25}$ +55.8° (*c* 2.0, benzene) (lit,[8] $[\alpha]_D^{25}$ +55.2° (*c* 2.0)).

The authors are indebted to Dr. Akito Ichida of Daicel Chemical Industries Ltd. for the chromatographic resolution of **9** on the optically active column. This work was supported in part by a Grant-in-Aid for Scientific Research No. 61470105 from the Ministry of Education.

References

1) S. Kanoh, H. Suda, N. Kawaguchi, and M. Motoi, *Makromol. Chem.*, **187**, 53 (1986).
2) S. Kanoh, N. Kawaguchi, T. Sumino, Y. Hongoh, and H. Suda, *J. Polym. Sci., Part A, Polym. Chem.*, **25**, 1603 (1987).
3) When the ligands, (*S*)-**2** and (*S,S*)-**3**, complexed to butyllithium were reacted with, for example, benzaldehyde in dry diethyl ether at −78 °C, according to the Cram's alkylation conditions, (*S*)-enriched 1-phenyl-1-pentanols were obtained in both cases in the optical yields of 56 and 89%, respectively; J.-P. Mazaleyrat and D. J. Cram, *J. Am. Chem. Soc.*, **103**, 4585 (1981).
4) S. Kanoh, N. Kawaguchi, and H. Suda, *Makromol. Chem.*, **188**, 463 (1987).
5) A. W. Langer Jr., *Adv. Chem. Ser.*, **1974**, 1.
6) F. Mayer, *Ber. Dtsch. Chem. Ges.*, **44**, 2298 (1911).
7) F. Bell, *J. Chem. Soc.*, **1934**, 835.
8) G. Wittig and H. Zimmermann, *Chem. Ber.*, **86**, 629 (1953).
9) M. Siegel and K. Mislow, *J. Am. Chem. Soc.*, **80**, 473 (1957).
10) Y. Okamoto, M. Kawashima, and K. Hatada, *J. Chromatogr.*, **363**, 173 (1986).
11) Results of the chromatographic resolution of (*RS*)-**9**:

capacity factors, k_1' (to less retained (*R*)-**9**)=1.22 and k_2'=1.51; separation factor, α=1.24; resolution factor, R_S=1.84; the void volume of the column was estimated to be 3.23 ml with a nonretained compound, 1,3,5-tri-*t*-butylbenzene.

12) W. Findeklee, *Ber. Dtsch. Chem. Ges.*, **38**, 3553 (1905).
13) F. B. Dains and F. Eberly, *Org. Synth.*, Coll. Vol. II, 355 (1943).
14) R. C. Fuson and E. A. Cleveland, *Org. Synth.*, Coll. Vol. III, 339 (1955).
15) It may be recommended that the resolved acid, without recrystallization, is esterified with methanolic hydrogen chloride and the resulting diester **9** is purified by distillation (the yield > 95%).

 © 1987 The Chemical Society of Japan Bull. Chem. Soc. Jpn., 60, 3663—3666 (1987)

Regeneration of NADPH and Hydrogenation of Ketones to Alcohols with the Combination of Hydrogenase, Ferredoxin-NADP Reductase, and Alcohol Dehydrogenase

Ichiro Okura,* Katsumi Kurabayashi, and Shigetoshi Aono
Department of Bioengineering, Tokyo Institute of Technology, Meguro-ku, Tokyo 152
(Received April 14, 1987)

The regeneration of nicotinamide-adenine dinucleotide phosphate (reduced form, NADPH) by the reduction of NADP by hydrogen gas was carried out with the [hydrogenase-ferredoxin-NADP reductase (FNR)] system. Ketone hydrogenation was tried by the combination of the above system and alcohol dehydrogenase (ALDH), as shown in the following scheme:

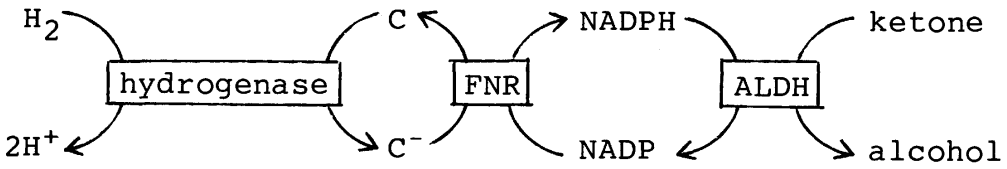

C: electron carrier

Scheme 1.

In the [hydrogenase-FNR] system, NADP was easily reduced by hydrogen to form NADPH. By adding ALDH to the above system, the hydrogenation of ketone to alcohol was observed. The ketones used in this study were 2-butanone, 2-pentanone, and 2-hexanone. After 8 h, the turnover number of NADP was 13 for 2-butanone, 15 for 2-pentanone, and 10 for 2-hexanone, showing a recurrence of NADP by hydrogen gas.

Some photochemical,[1-3] electrochemical,[4-7] and enzymatic[7-9] systems for NAD(P)H regeneration have been reported. Among these systems, enzymatic systems are of great advantage to produce compounds with a high optical purity, and to the simplicity of the systems.

In this study the [hydrogenase-FNR] system for the regeneration of NADPH from NADP was established by using hydrogen gas as a reducing agent; ketone hydrogenation was tried by a combination of the system with ALDH as shown in Scheme 1.

Experimental

The bipyridinium compounds used in this experiment are listed in Fig. 1. Compounds **A**, **B**, and **C** were synthesized according to the literature.[10,11] The hydrogenase from *Desulfovibrio vulgaris* (Miyazaki type, IAM 12604) was purified according to Yagi's method.[12] The activity (1 unit) of hydrogenase used was to reduce 1 μmol of methyl viologen for 1 min in the system containing hydrogenase and methyl viologen (3.7×10^{-2} mol dm^{-3}) in 5.0 ml of a 0.02 mol dm^{-3} Tris-HCl buffer (pH 7.0) under 1 atmospheric pressure of hydrogen at 30 °C. FNR from spinach leaves was purified by Shin's method.[13] The concentration of FNR is not known but it had the ability to reduce 0.37 μmol of 2,6-dichlorophenol-indophenol (DPIP) in the following system: NADPH (1.2×10^{-4} mol dm^{-3})-DPIP (7.4×10^{-5} mol dm^{-3})-FNR (2.0%) in 5.0 ml of 0.05 mol dm^{-3} Tris-HCl buffer (pH 7.0) at 30 °C for 1 min. ALDH from *Thermoanaerobium brockii* was obtained from SIGMA Co.

The sample solution, which consisted of hydrogenase, bipyridinium salt, FNR, NADP, and ketone (if included) in a Tris-HCl buffer (pH 7.0), was deaerated by repeated freeze-pump-thaw cycles. The reaction was carried out at 30 °C by the introduction of hydrogen gas into the above system.

Ketones and alcohols were analyzed by gas chromatography with a 3-m long column of PEG 6000 at 80 °C by using nitrogen as a carrier gas. The electronic spectra were measured using a Shimadzu MPS 5000 spectrometer, and the concentration of NADPH was determined from the absorbance at 340 nm.

Results and Discussion

Reduction of Bipyridinium Compounds by Hydrogen. When hydrogen gas was introduced into a system containing hydrogenase and methyl viologen, a

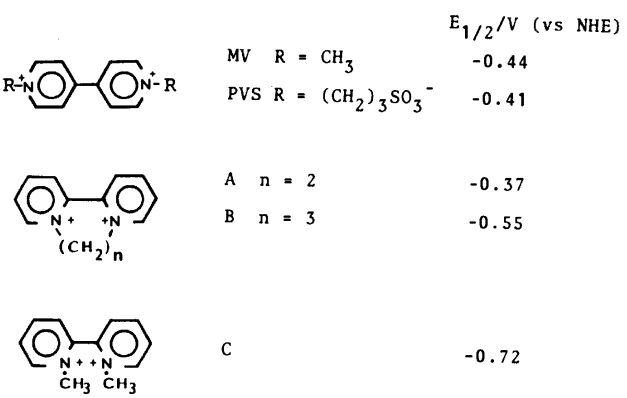

Fig. 1. Bipyridinium salts as electron carriers.

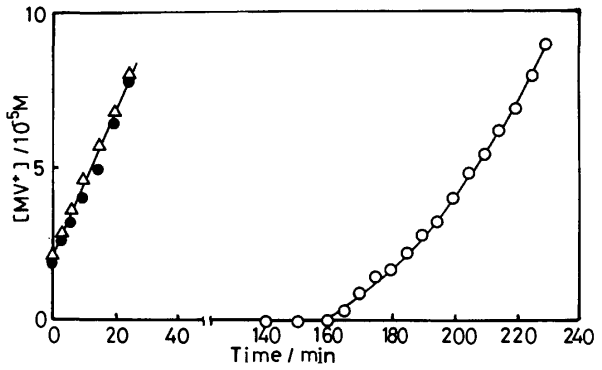

Fig. 2. Reduction of methyl viologen by hydrogen gas with hydrogenase. Reaction conditions: Methyl viologen, 3.7×10^{-2} mol dm^{-3}; hydrogenase, 4.9 units dm^{-3}; hydrogen, 0.97 atm; Tris-HCl buffer, 0.4 mol dm^{-3}, pH 7.0; reaction temp, 30°C. a (○): No pretreatment, b (△): pretreated with RSH (2.0×10^{-4} mol dm^{-3}) for 1 h, c (●): pretreated with $Na_2S_2O_4$ (5.0×10^{-4} mol dm^{-3}) for 1 h.

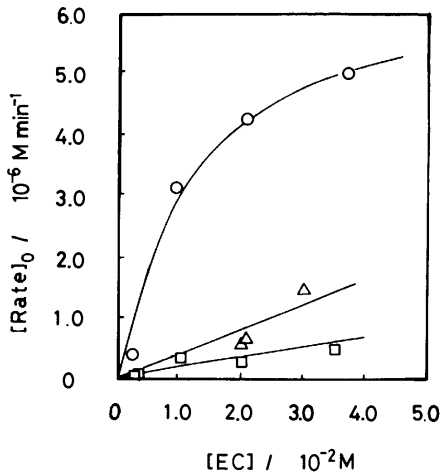

Fig. 3. Initial reduction rate vs. bipyridinium salt concentration. Reaction conditions: Hydrogenase pretreated with RSH, 4.9 units dm^{-3}, hydrogen, 0.97 atm; Tris-HCl buffer, 0.4 mol dm^{-3}, pH 7.0; reaction temp, 30°C. ○: Methyl viologen; △: A; □: PVS.

reduced type of methyl viologen was detected as shown in Fig. 2-(a). The induction period, ca. 150 min, was observed for the reduction. When the hydrogenase was pretreated with $Na_2S_2O_4$ or 2-mercaptoethanol, the induction period disappeared and a reduced form of methyl viologen was detected, as shown in Fig. 2-(b) and (c). As $Na_2S_2O_4$ and 2-mercaptoethanol are well-known reducing agents, the hydrogenase may be activated by reduction. The hydrogenase, sensitive to oxygen,[12,14] may be inactivated during the purification of the enzyme. The inactivated hydrogenase, however, may be re-activated by treatment with a reducing agent. Though hydrogen is also a reducing agent, it takes time to re-activate the hydrogenase. A long induction time appeared when hydrogen was used, as shown in Fig. 2-(a). In the following experiments, the hydrogenase pretreated by 2-mercaptoethanol was used.

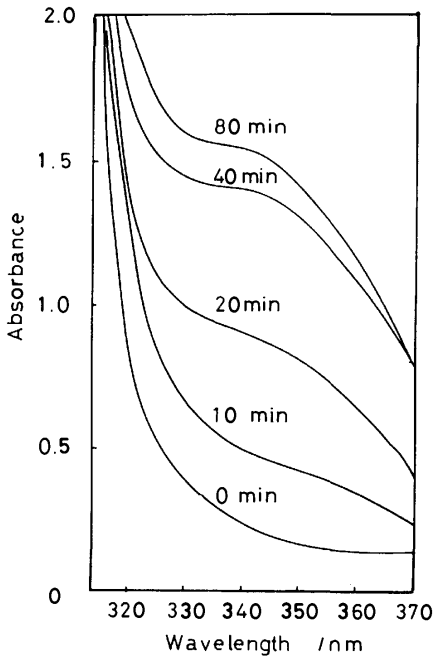

Fig. 4. Typical spectrum change during the reaction. Reaction conditions: Methyl viologen, 3.7×10^{-2} mol dm^{-3}; hydrogenase pretreated with RSH, 20.2 units dm^{-3}, hydrogen, 0.97 atm; FNR, 1.0 ml; NADP, 9.7×10^{-4} mol dm^{-3}; Tris-HCl buffer, 0.4 mol dm^{-3}, pH 7.0; reaction temp, 30°C.

When 3-sulfonatopropyl viologen (PVS) or compound A was used in place of methyl viologen, these compounds were also reduced by hydrogen with hydrogenase. The dependence of the initial reduction rate on the concentration of these compounds is shown in Fig. 3. The order of the reduction rate does not coincide with that of the redox potential (see Fig. 1) of these compounds, suggesting that methyl viologen is the most effective substrate of the hydrogenase among these compounds.

Reduction of NADP by Hydrogen. When hydrogen gas was introduced to a system containing hydrogenase, FNR, and NADPH, the spectrum of the solution changed with reaction time (Fig. 4). The characteristic absorption band of the reduced form (NADPH) of NADP was observed at 340 nm.

As shown in Fig. 5, the NADPH concentration increased linearly with the reaction time at low NADP conversion; then, the NADPH formation rate decreased. The rate decrease was caused by a decrease in the concentration of the starting material, NADP. When 4.5×10^{-3}, 9.7×10^{-4}, and 4.9×10^{-4} mol dm^{-3} of NADP were used, the conversion of NADP after 1 h was 26, 67, and 70%, respectively. In the case of the system shown in Fig. 5-(a), NADPH formed with the reaction time and no deactivation of the enzymes was observed within the reaction time.

The time dependence of the amount of NADPH

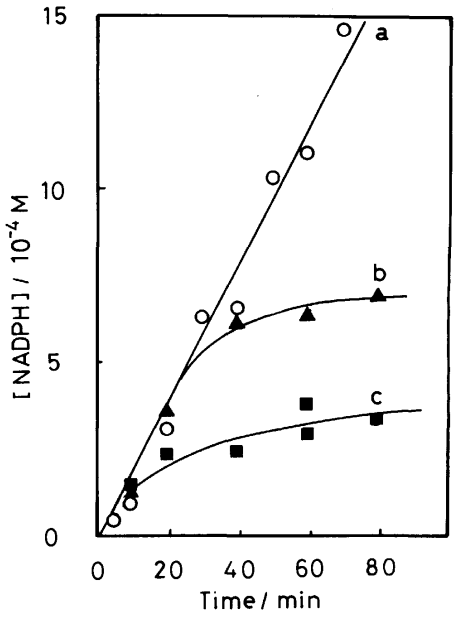

Fig. 5. Time dependence of NADPH formation. Reaction conditions: Methyl viologen, 3.7×10^{-2} mol dm^{-3}; hydrogenase pretreated with RSH, 20.2 units dm^{-3}, hydrogen, 0.97 atm; FNR, 1.0 ml; NADP, 4.5×10^{-3} mol dm^{-3} (○), 9.7×10^{-4} mol dm^{-3} (▲), 4.9×10^{-4} mol dm^{-3} (■); Tris-HCl buffer, 0.4 mol dm^{-3}, pH 7.0; reaction temp, 30°C.

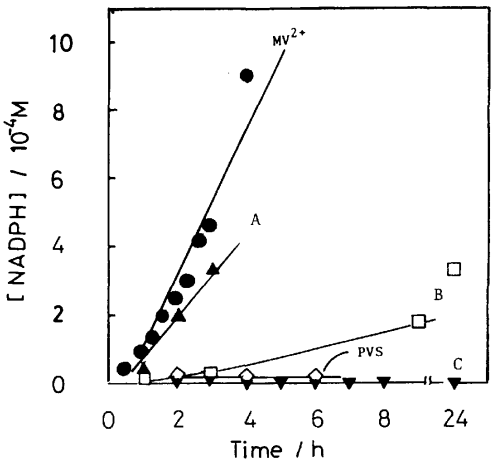

Fig. 6. Time dependence of NADPH formation. Reaction conditions: Bipyridinium salt 1.9×10^{-3} mol dm^{-3}; hydrogenase pretreated with RSH, 7.4 units dm^{-3}, hydrogen, 0.97 atm; FNR, 1.0 ml; NADP, 3.3×10^{-2} mol dm^{-3}; Tris-HCl buffer, 0.4 mol dm^{-3}, pH 7.0; reaction temp, 30°C. ●: Methyl viologen, ▲: A, □: B, ▼: C, ◇: PVS.

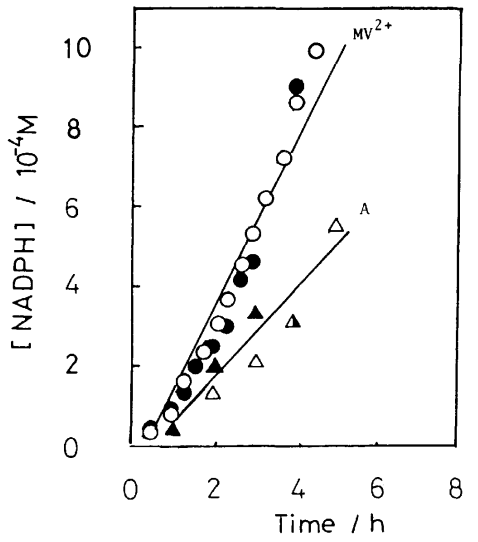

Fig. 7. Time dependence of NADPH formation. Reaction conditions: Same as the caption of Fig. 6 except for the amount of FNR. FNR: 1 ml (●,▲), 2 ml (○,△), 3 ml (▲).

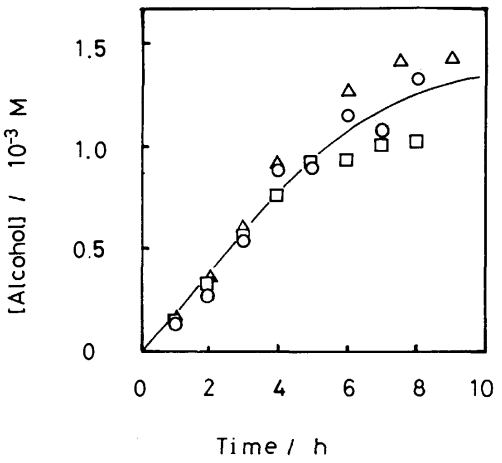

Fig. 8. Time dependence of alcohol formation. Reaction conditions: Methyl viologen, 3.7×10^{-2} mol dm^{-3}; hydrogenase pretreated with RSH, 5.25 units dm^{-3}, hydrogen, 0.97 atm; FNR, 2.0 ml; NADP, 1.0×10^{-4} mol dm^{-3}; NADP, 1.0×10^{-4} mol dm^{-3}; ALDH, 500 units dm^{-3}; Tris-HCl buffer, 0.4 mol dm^{-3}, pH 7.0; reaction temp, 30°C. ○: 2-Butanone (3.15×10^{-2} mol dm^{-3}), △: 2-pentanone (1.24×10^{-2} mol dm^{-3}), □: 2-hexanone (3.6×10^{-3} mol dm^{-3}).

formation is shown in Fig. 6, when various bipyridinium compounds were used as electron carriers. Among these compounds, methyl viologen, compounds **A** and **B**, were effective for NADPH formation. PVS and compound **C** were inactive. As PVS was easily reduced by hydrogen with hydrogenase and its reduced form has a sufficient redox potential (see Fig. 1) to reduce NADP, it is apparent that PVS cannot be a substrate of FNR.

When other concentrations of methyl viologen and compound **A** were used, no change in the reduction rate of NADP was observed (Fig. 7). From the above results, it can be seen that the rate determining step of NADPH formation by hydrogen is not the reduction step of NADP with FNR, but the reduction step of a bipyridinium compound by hydrogen with hydrogenase.

Reduction of Ketone by Hydrogen. When NADP is reduced in a [hydrogenase-FNR] system, the

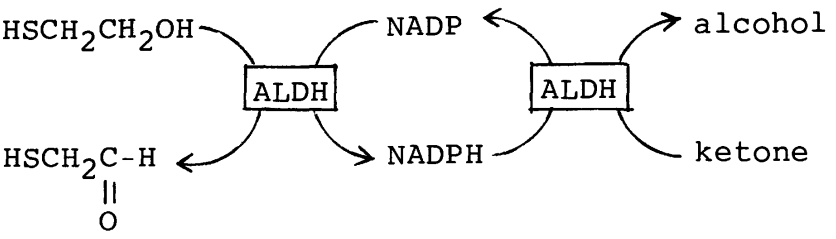

Scheme 2.

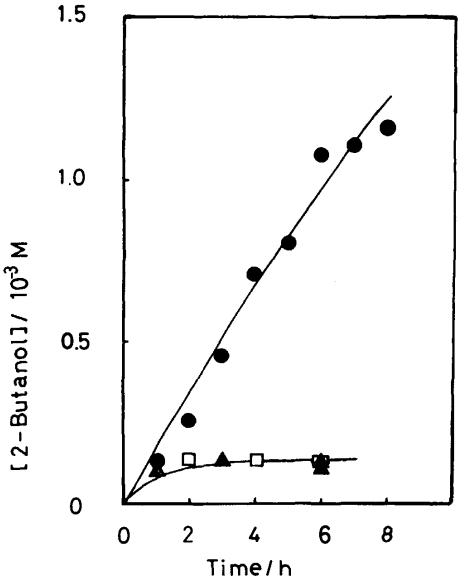

Fig. 9. Effect of RSH for alcohol formation. The system (shown by ●) contains methyl viologen (3.7×10^{-2} mol dm^{-3}), hydrogenase (5.25 units dm^{-3}), RSH (1.0×10^{-2} mol dm^{-3}), hydrogen (0.97 atm), FNR (2.0 ml), NADP (1.0×10^{-4} mol dm^{-3}), ALDH (500 units dm^{-3}), 2-butanone (0.18 mol dm^{-3}), Tris-HCl buffer (0.4 mol dm^{-3}, pH 7.0); reaction temp, 30°C. The systems (shown by ▲,□) contain RSH (1.0×10^{-2} mol dm^{-3}), hydrogen (0.97 atm), FNR (2.0 ml), NADP (3.0×10^{-3} mol dm^{-3}, (▲), 1.6×10^{-3} mol dm^{-3} (□)); ALDH (500 units dm^{-3}), 2-butanone (0.18 mol dm^{-3}), Tris-HCl buffer (0.4 mol dm^{-3}, pH 7.0); reaction temp, 30°C.

hydrogenation of ketones to alcohols could be accomplished by adding ALDH to the above system. The hydrogenation of some ketones were tried. The results are shown in Fig. 8. As ketones, 2-butanone, 2-pentanone, and 2-hexanone were used. All the ketones were hydrogenated and the corresponding alcohols were formed. The turnover numbers of NADP against alcohols after an 8-h reaction were 13, 15 and 10 for 2-butanone, 2-pentanone, and 2-hexanone, respectively. The results show that NADP recycled catalytically in this system, and that ketone hydrogenation by hydrogen gas was accomplished.

Since 2-mercaptoethanol was used in order to avoid the induction period of the hydrogenase activation (Fig. 2) in the system, there is a possibility of ketone hydrogenation through the following reaction:

Thus, the hydrogenation of ketone was tried using a system containing 2-mercaptoethanol, ALDH, NADP, and 2-butanone. The results are shown in Fig. 9-(a). The above reaction proceeded and 2-butanol formation was observed. The amount of 2-butanol, however, was much less compared with that of the 2-butanone formed by a reduction with hydrogen gas as (Fig. 9-(b)). Ketone hydrogenation by 2-mercaptoethanol is neglected in this system.

The authors wish to express their thanks to Professor Yoshio Ono for his helpful discussions. This work was supported by a Grant-in-Aid for Scientific Research on Priolity Areas No. 62612505 "Dynamic Interactions and Electronic Processes of Macromolecular Complexes" from the Ministry of Education, Science and Culture.

References

1) D. Mandler and I. Willner, *J. Am. Chem. Soc.*, **106**, 5352 (1984).
2) P. Cuendet and M. Gratzel, *Photochem. Photobiol.*, **39**, 609 (1984).
3) R. Wienkamp and E. Steckhan, *Angew. Chem., Int. Ed. Engl.*, **22**, 497 (1983).
4) Z. Shaked, J. J. Barber, and G. M. Whitesides, *J. Org. Chem.*, **46**, 4101 (1981).
5) R. DiCosimo, C.-H. Wong, L. Daniels, and G. M. Whitesides, *J. Org. Chem.*, **46**, 4623 (1981).
6) R. Wienkamp and E. Steckhan, *Angew. Chem., Int. Ed. Engl.*, **21**, 782 (1982).
7) H. Simon, J. Bader, H. Gunther, S. Neumann, and J. Thanos, *Angew. Chem., Int. Ed. Engl.*, **24**, 539 (1985), and the references therein.
8) C.-H. Wong and G. H. Whitesides, *J. Am. Chem. Soc.*, **103**, 4890 (1981); **105**, 5012 (1983).
9) Z. Shaked and G. M. Whitesides, *J. Am. Chem. Soc.*, **102**, 7104 (1980).
10) K. J. Schmalzl and L. A. Summers, *Aust. J. Chem.*, **30**, 657 (1977).
11) R. F. Homer and T. E. Tolinson, *J. Chem. Soc.*, **1960**, 2498.
12) T. Yagi, *J. Biochem.*, **68**, 649 (1970).
13) M. Shin, *Tanpakushitsu Kakusan Koso, Bessatsu*, **76**, 226 (1976).
14) H. M. Fisher, A. E. Krasna, and D. Rittenberg, *J. Biol. Chem.*, **209**, 569 (1954).

 © 1987 The Chemical Society of Japan Bull. Chem. Soc. Jpn., 60, 3667—3671 (1987)

Synthesis of (−)-8a-*epi*-Swainsonine, (1*S*,2*R*,8*R*,8a*S*)-Octahydro-1,2,8-indolizinetriol

Kin-ichi TADANO,* Yukinori HOTTA, Masahiro MORITA, Tetsuo SUAMI,†
Bryan WINCHESTER,†† and Isabello Centi di BELLO††
Department of Applied Chemistry, Faculty of Science and Technology, Keio University, Hiyoshi, Kohoku-ku, Yokohama 223
††Department of Biochemistry, King's College London, University of London, Campden Hill Road, Kensington, London W8 7AH, U. K.
(Received April 15, 1987)

(−)-8a-*epi*-Swainsonine (**4**), one of the stereocongeners of physiologically interesting indolizidine alkaloid (−)-swainsonine (**1**), has been synthesized starting from known methyl 3-azido-4,6-*O*-benzylidene-3-deoxy-α-D-altropyranoside. The α-D-mannosidase inhibitory activity of **4** was compared with natural **1**.

Swainsonine (**1**), which was isolated from some plants[1-3] and a microorganism,[4] is a novel indolizidine alkaloid. This alkaloid exhibits remarkable physiological effects such as an α-D-mannosidase inhibitory activity and immunoregulating activity.[5] The structure of **1** including absolute configuration was established by Harris and coworkers to be (1*S*, 2*R*, 8*R*, 8a*R*)-octahydro-1,2,8-indolizinetriol.[3] Owing to this structural novelty and the interesting physiological effects of **1**, extensive efforts have been made toward the total synthesis of **1**[6] and its stereocongeners.[7] After completion of the total synthesis of **1**,[6a] we have synthesized two stereocongeners of **1**, namely (−)-8-*epi*- (**2**) and (−)-1,8-di*epi*-swainsonine (**3**), from 3-amino-3-deoxy-D-glucose and -D-galactose derivatives.[8] Herein, we wish to describe a synthesis of another stereocongener, (−)-8a-*epi*-swainsonine (**4**), from readily available methyl 3-azido-4,6-*O*-benzylidene-3-deoxy-α-D-altropyranoside (**6**).[9]

Compound **4** was retro-synthesized to an azido group containing α,β-unsaturated ester (**5**-*E* and **5**-*Z*) by twice C-N bond disconnection as shown in Scheme 1. Hydrogenation of the both geometrical isomers **5** would give a disubstituted 2-piperidinone **13** via a 5-aminooctanoic acid ethyl ester **12**, which tends to cyclize simultaneously resulting a δ-lactam formation. The 2-indolizinone formation of **13** would be achieved by introduction of a suitable leaving group at the primary hydroxyl group in an intramolecular *N*-alkylation fashion. Reduction of the amido group in the resulting **14** would give 1,8-di-*O*-benzylated 8a-*epi*-swainsonine (**15**) and deprotection of **15** would furnish the desired **4**.

The configurations of the four continuous chiral centers in **5** are corresponding to those of C-2 to C-5 of 3-azido-3-deoxy-D-altrose. Therefore, our synthesis of

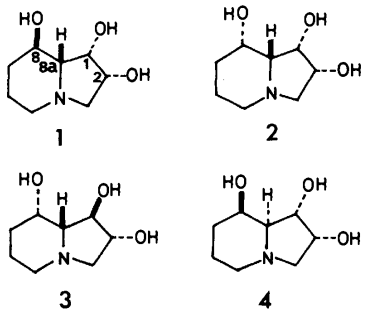

Fig. 1.

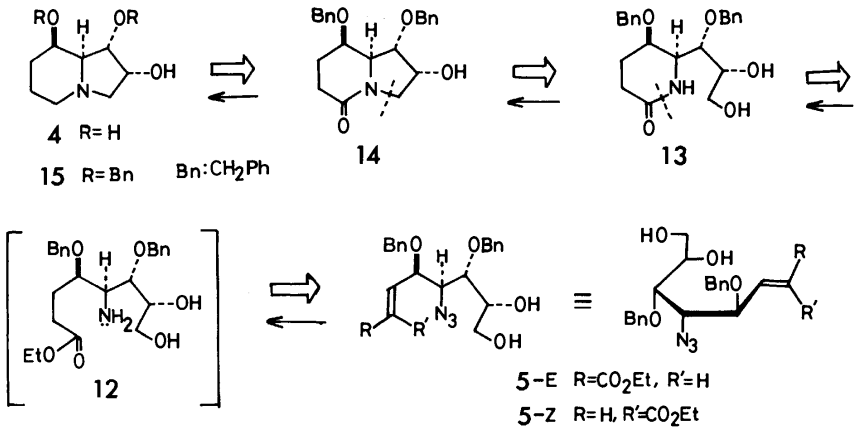

Scheme 1.

†Present address: Department of Chemistry, Faculty of Science and Technology, Meisei University, Hodokubo, Hino, Tokyo 191.

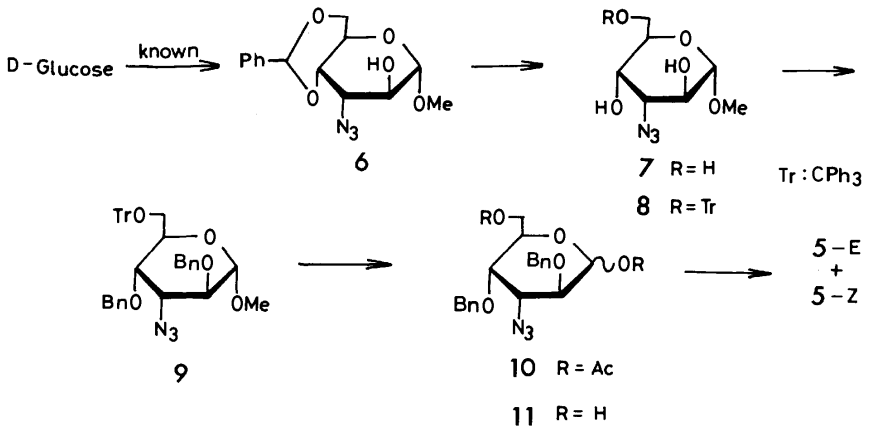

Scheme 2.

4 was started from the known 3-azido sugar **6**, which was readily prepared by regioselective diaxial epoxy ring opening of methyl 2,3-anhydro-4,6-*O*-benzylidene-α-D-mannopyranoside[10] (Scheme 2). Hydrolysis of **6** in 50% aqueous acetic acid at 100 °C gave *O*-debenzylidene derivative **7**, and the primary hydroxyl group in **7** was preferentially protected as a trityl ether by treatment with trityl chloride in pyridine in the presence of 4-(dimethylamino)pyridine to provide 6-*O*-trityl derivative **8** in 82% yield. *O*-Benzylation of **8** with excess benzyl bromide in the presence of sodium hydride gave 2,4-di-*O*-benzyl derivative **9** in 94% yield. Acetolysis of **9** in acetic anhydride in the presence of a catalytic amount of sulfuric acid at 0 °C gave an anomeric mixture of **10** in 80% combined yield. The anomeric mixture **10** was *O*-deacetylated with sodium methoxide to provide an anomeric mixture **11**, which was subjected to Wittig olefination for a two-carbon elongation. Treatment of the mixture **11** with (ethoxycarbonylmethylene)triphenylphosphorane in refluxing benzene gave a mixture of ***E***- and ***Z***-α,β-unsaturated esters **5-*E*** and **5-*Z***, which was separated by chromatography on silica gel, in 54% combined yield. The geometrical stereochemistry of each compound was determined by the ^{1}H NMR spectrum. In the ^{1}H NMR of **5-*E***, H-3 (α-olefinic proton of the α,β-unsaturated ester) appeared at δ 6.91 as a double doublet with $J_{2,3}$=18 Hz and $J_{3,4}$=7 Hz supporting a trans geometry of the double bond. On the other hand, H-3 of **5-*Z*** appeared at δ 6.33 as a double doublet with $J_{2,3}$=12 Hz and $J_{3,4}$=8 Hz. The ratio of **5-*E*** and **5-*Z*** was 10:8.5, and no preferential formation of the ***E***-isomer was observed in this Wittig olefination of **11** by stabilized ylide. As expected, hydrogenation of each **5-*E*** and **5-*Z*** in the presence of Raney nickel gave 2-piperidinone derivative **13** in 67 and 73% yields, respectively. No other products were detected in both reaction mixtures. Next, the intramolecular cyclization of **13** for trisubstituted indolizinone **14** was attempted under several conditions (TsCl in pyridine or MsCl in pyridine). The best result was obtained under *O*-tosylation conditions as follows. A solution of **13** in pyridine was stirred with 3.4 mol equivalent of *p*-toluenesulfonyl chloride, which was added in a five portion at 10 h interval, at 70 to 100 °C in the presence of 4-(dimethylamino)pyridine. Consequently, compound **14** was obtained in 60% yield. When *p*-toluenesulfonyl chloride (3.0 mol equiv) was added to a pyridine solution of **13** all at once, and the mixture was stirred at room temperature for 24 h, compound **14** was obtained in 41% yield along with a further *O*-tosylated product of **14** (30%). No intermediate of the reaction was detected, however, the cyclization seems to proceed via a *O*-tosyl derivative of **13** at the primary hydroxyl group. The *O*-tosyl derivative was attacked by amide nitrogen in **13** instantly. Reduction of **14** with borane-Me_2S complex in THF at room temperature, followed by stirring the product in pyridine gave 1,8-dibenzylated 8a-*epi*-swainsonine **15** in 84% yield. For conversion of the initially formed amine-borane complex to **15**, the pyridine-treatment is essential. *O*-Debenzylation of **15** by hydrogenolysis in the presence of 10% Pd on charcoal, or by treatment with refluxing cyclohexene-ethanol in the presence of 20% $Pd(OH)_2$/C, gave a mono-*O*-benzyl derivative. The structure of the mono-*O*-benzyl derivative was not determined. The complete deprotection was achieved by treatment of **15** with iodotrimethylsilane,[11] and purification of the product by PTLC gave the desired **4** as crystals in 75% yield. The structure of **4** was supported by spectral means (IR, ^{1}H and ^{13}C NMR, and mass spectra). The overall yield from **6** to **4** was 9%.

A preliminary assay of **4** for α-D-mannosidase inhibitory activity was investigated. Against a human α-D-mannosidase, compound **4** exhibits a 93% inhibition at 1 mM concentration at pH 4 (optimal pH value). Under the same conditions, swainsonine **1** shows a 99% inhibition.

Experimental

General Procedures. Reactions were carried out at room temperature unless otherwise stated. Reaction mixture, extract, and fraction of chromatography were concentrated under a reduced pressure below 40 °C with a bath by

an evaporator. Melting points were determined with a Mitamura Riken micro mp apparatus and are uncorrected. Specific rotations were measured in a 10 mm cell with a Jasco DIP-4 polarimeter. Column chromatography was performed on Kieselgel 60 (Merck), and thin-layer chromatography (TLC) was performed on a glass plate coated with Kieselgel 60 GF_{254} (Merck), followed by detection by UV light and charring with sulfuric acid. Preparative TLC (PTLC) was performed on a glass plate (20×20 cm) coated with Kieselgel PF_{254} (Merck). IR spectra were recorded with a Hitachi Model 225 (KBr) or with a Jasco Model A-202 ($CHCl_3$) spectrometer. ^{1}H NMR spectra were recorded with a Varian EM-390 (90 MHz) spectrometer in $CDCl_3$ solutions with internal tetramethylsilane. ^{13}C NMR spectra were recorded with a JEOL FX-200 spectrometer in CD_3OD solution with internal tetramethylsilane. High-resolution mass spectra were obtained using a Hitachi M-80 mass spectrometer.

Pyridine was distilled over NaOH, *N*,*N*-dimethylformamide (DMF) was distilled over CaH_2, benzene was distilled over $LiAlH_4$, and tetrahydrofuran (THF) was distilled over $LiAlH_4$ and then over sodium-benzophenone.

Methyl 3-Azido-4,6-*O*-benzylidene-3-deoxy-α-D-altropyranoside (6). This compound was prepared according to the reported pocedure.[10] **6**: Mp 133—134 °C; lit,[10] mp 135—136 °C; $[\alpha]_D^{21}$ +34.2° (*c* 0.85, $CHCl_3$); lit,[10] $[\alpha]_D^{18}$ +37.9° (*c* 1.00, $CHCl_3$).

Methyl 3-Azido-3-deoxy-6-*O*-trityl-α-D-altropyranoside (8). A solution of **6** (2.02 g, 6.56 mmol) in 50% aqueous acetic acid (10 ml) was stirred at 100 °C for 90 min, and diluted with ethyl acetate (60 ml). The solution was extracted with water (50 ml×4), and the combined aqueous layers were concentrated with ethanol. The residue, which consisted of *O*-debenzylidene derivative **7**, was dissolved in pyridine (10 ml) and trityl chloride (4.58 g, 16.4 mmol) and 4-(dimethylamino)-pyridine (0.16 g, 1.31 mmol) were added. The mixture was stirred at 70 °C for 150 min and concentrated with toluene. The residue was partitioned between dichloromethane (60 ml) and water (60 ml). The aqueous layer was extracted with dichloromethane (60 ml×3). The organic layer was dried over Na_2SO_4 and concentrated. The residue was chromatographed on silica gel (180 g, ethyl acetate-hexane=1 : 4 containing 1% triethylamine), and the fraction corresponding to R_f 0.53 (ethanol-toluene=1 : 5) was concentrated to give **8** (2.48 g, 82%) as a colorless syrup. **8**: $[\alpha]_D^{27}$ +31.5° (*c* 1.35, $CHCl_3$); IR $\nu_{max}^{CHCl_3}$ 3760, 2950, 2130, 1460, 1270 cm^{-1}; ^{1}H NMR δ=2.32—2.63 (2H, m, 2×OH), 3.36—3.41 (2H, m, H-6, 6′), 3.43 (3H, s, OCH_3) 3.68—4.09 (4H, m, H-2,3,4,5), 4.56 (1H, d, *J*=2.5 Hz, H-1), 7.16—7.55 (15H, m, $C(C_6H_5)_3$). Found: C, 67.39; H, 5.92; N, 8.84%. Calcd for $C_{26}H_{27}N_3O_5$: C, 67.66; H, 5.90; N, 9.10%.

Methyl 3-Azido-2,4-di-*O*-benzyl-3-deoxy-6-*O*-trityl-α-D-altropyranoside (9). Sodium hydride (60% emulsion in mineral oil, 967 mg, 24.2 mmol) was washed with hexane (2 ml×4), dried and suspended in DMF (8 ml). To the suspension was added a DMF solution (8 ml) of **8** (2.48 g, 5.37 mmol), and the mixture was stirred at 0 °C for 15 min. Benzyl bromide (2.88 ml, 24.2 mmol) was added to the mixture, and stirred for 19 h. The excess base was destroyed by addition of ethanol. After concentration of the mixture, the residue was partitioned between dichloromethane (80 ml) and water (80 ml). The aqueous layer was extracted with dichloromethane (80 ml×3). The combined extracts were dried over Na_2SO_4 and concentrated. The residue was chromatographed on silica gel (hexane containing 1% triethylamine), and the fraction corresponding to R_f 0.74 (ethyl acetate-hexane=1 : 5) was concentrated to give **9** (3.24 g, 94%) as a colorless syrup. 9: $[\alpha]_D^{27.5}$ +28.4° (*c* 0.98, $CHCl_3$); IR $\nu_{max}^{CHCl_3}$ 3060, 3000, 2930, 2110, 1490, 1450, 1260 cm^{-1}; ^{1}H NMR δ=3.00—3.38 (2H, m, H-6,6′), 3.42 (3H, s, OCH_3), 3.57—4.28 (4H, m, H-2,3,4,5), 4.33—4.77 (5H, m, H-1, 2×$OC\underline{H}_2C_6H_5$), 6.98—7.67 (25H, m, 2×$OCH_2C_6\underline{H}_5$, $C(C_6H_5)_3$).

Anomeric Mixture of 1,6-Di-*O*-acetyl-3-azido-2,4-di-*O*-benzyl-3-deoxy-D-altropyranose (10) To a solution of **9** (1.91 g, 2.87 mmol) in acetic anhydride (16 ml) was added concd sulfuric acid (0.3 ml), and the solution was stirred for 2 h at 0 °C. The solution was diluted with water (90 ml) and extracted with dichloromethane (90 ml×3). The extract was washed with 10% aqueous $NaHCO_3$ (50 ml×2), dried over Na_2SO_4 and concentrated. The residue was acetylated with acetic anhydride (5 ml) in pyridine (10 ml) for 1 h. After concentration of the mixture with toluene, the residue was chromatographed on silica gel (150 g, ethyl acetate-hexane=1 : 8). The fractions corresponding to R_f 0.40 and 0.31 (ethyl acetate-hexane=1 : 5) were combined and concentrated to give **10** (1.12 g, 80%) as a colorless syrup. IR $\nu_{max}^{CHCl_3}$ 3000, 2920, 2870, 2120, 1735 1450, 1370 cm^{-1}; ^{1}H NMR δ=1.98, 2.00, 2.06, 2.07 (total 6H, each s, 2×$OCOCH_3$), 3.60—4.85 (10H, m, H-2,3,4,5,6,6′, 2×$OC\underline{H}_2C_6H_5$), 6.00, 6.03 (total 1H, each d, *J*=2.5 Hz, H-1), 7.35 (10H, s, 2×$OCH_2C_6\underline{H}_5$). Found: C, 61.24; H, 5.87; N, 8.86%. Calcd for $C_{24}H_{27}N_3O_7$: C, 61.40; H, 5.80; N, 8.95%.

Ethyl (*E*)- and (*Z*)-5-Azido-4,6-di-*O*-benzyl-2,3,5-trideoxy-altro-2-octenonate, (5-*E*) and (5-*Z*). To a solution of **10** (1.94 g, 4.13 mmol) in dichloromethane (15 ml) was added sodium methoxide (1 mol dm^{-3} in methanol, 9.08 ml, 9.08 mmol) at 0 °C with stirring. After stirring at 0 °C for 30 min, the solution was neutralized with Amberlite IR-120B (H^+). The resin was removed by filtration, washed with methanol, and the combined filtrate and washing were concentrated to give crude **11** (R_f 0.03, ethyl acetate-hexane=1 : 3) as a syrup. To a benzene solution (14 ml) of the crude **11** was added (ethoxycarbonylmethylene)triphenylphosphorane (3.60 g, 10.5 mmol), and the mixture was refluxed for 2 h, and then concentrated. The residue was chromatographed on silica gel (120 g, ethyl acetate-hexane=1 : 4). The fraction corresponding to R_f 0.23 (ethyl acetate-hexane=1 : 2) was concentrated to give **5-*Z*** (410 mg, 22%), and the fraction corresponding to R_f 0.19 was concentrated to give **5-*E*** (511 mg, 27%). A mixture of **5-*Z*** and **5-*E*** was obtained (99 mg; total **5-*Z*** and **5-*E***, 1.02 g, 54%). **5-*E*** as a colorless syrup: $[\alpha]_D^{20}$ −14.7° (*c* 1.06, $CHCl_3$); IR $\nu_{max}^{CHCl_3}$ 2925, 2870, 2100, 1720, 1450, 1365, 1300, 1270, 1175 cm^{-1}; ^{1}H NMR δ=1.27 (3H, t, *J*=7 Hz, $COOCH_2C\underline{H}_3$), 3.46—4.05 (8H, m, H-4,5,6,7,8,8′,2×OH), 4.22 (2H, q, *J*=7 Hz, $COOC\underline{H}_2CH_3$), 4.38—4.75 (4H, m, 2×$OC\underline{H}_2C_6H_5$), 6.12 (1H, d, *J*=18 Hz, H-2), 6.91 (1H, dd, *J*=18 and 7 Hz, H-3), 7.34 (10H, s, 2×$OCH_2C_6\underline{H}_5$). **5-*Z*** as a colorless syrup: $[\alpha]_D^{20}$ −64.1° (*c* 1.13, $CHCl_3$); IR $\nu_{max}^{CHCl_3}$ 2930, 2110, 1710, 1455, 1410, 1385, 1190 cm^{-1}; ^{1}H NMR δ=1.27 (3H, t, *J*=7 Hz, $COOCH_2C\underline{H}_3$), 3.00—3.42 (1H, br, OH), 3.58—4.38 (6H, m, H-5,6,7,8,8′, OH), 4.18 (2H, q, *J*=7 Hz, $COOC\underline{H}_2CH_3$), 4.40—4.74 (4H, m, 2×$OC\underline{H}_2C_6H_5$), 5.40 (1H, dd, *J*=8 and 4 Hz, H-4), 6.04 (1H, d, *J*=12 Hz, H-2), 6.33 (1H, dd, *J*=12 and 8 Hz, H-3), 7.48 (10H, s, 2×$OCH_2C_6\underline{H}_5$). Found: C, 63.00; H, 6.61; N, 9.07%. Calcd for $C_{24}H_{29}N_3O_6$ (as a mixture of **5-*E*** and **5-*Z***): C, 63.28; H, 6.42; N, 9.23%.

(5*R*,6*S*)-5-Benzyloxy-6-[(1*S*,2*R*)-1-benzyloxy-2,3-dihydroxypropyl]-2-piperidinone (13). From compound **5-*E***. A solution of **5-*E*** (170 mg, 0.37 mmol) in ethanol (10 ml) was hydrogenated in the presence of Raney nickel T-4 under an atmospheric hydrogen pressure for 15 h. After removal of the catalyst with a Celite pad and washing with ethanol, the combined filtrate and washing were concentrated. The residue was chromatographed on silica gel (15 g, ethanol-toluene=1 : 10), and the fraction corresponding to R_f 0.34 (ethanol-toluene=1 : 5) was concentrated to give **13** (96 mg, 67%) as crystals. **13**: Mp 145—146 °C; $[\alpha]_D^{27}$ −87.9° (*c* 1.00, $CHCl_3$); IR $\nu_{max}^{CHCl_3}$ 3400, 3290, 2910, 1640, 1620, 1470, 1450, 1390, 1325, 1295, 1270, 1210 cm^{-1}; ^1H NMR δ=1.50—2.58 (4H, m, H-3,3′,4,4′), 3.48—4.30 (8H, m, H-5,6, H-1,2,3,3′ of the side chain, 2×OH), 4.32—4.82 (4H, m, 2×$OCH_2C_6H_5$), 7.33 (10H, s, 2×$OCH_2C_6H_5$), 8.04 (1H, s, NH). High-resolution mass spectrum, Found: *m/z* 385.1884, Calcd for $C_{22}H_{27}NO_5$: M, 385.1887. Found: C, 68.32; H, 7.03; N, 3.45%. Calcd for $C_{22}H_{27}NO_5$: C, 68.55; H, 7.06; N, 3.68%. From compound **5-*Z***. Hydrogenation of **5-*Z*** (402 mg) and purification on silica gel as described in the case of **5-*E*** gave **13** (204 mg, 73%).

(1*S*,2*R*,8*R*,8a*S*)-1,8-Bis(benzyloxy)-2-hydroxyoctahydro-5-indolizinone (14). To a solution of **13** (68 mg, 0.16 mmol) in pyridine (3 ml) were added *p*-toluenesulfonyl chloride (24 mg) and 4-(dimethylamino)pyridine (4 mg). The mixture was stirred at 70 °C for 3 h, then at 100 °C. *p*-Toluenesulfonyl chloride was added after 25 h (18 mg), 40 h (30 mg), 50 h (15 mg), and 74 h (15 mg), successively. 4-(Dimethylamino)pyridine (4 mg) was added also after 44 h. The mixture was stirred at room temperature additional 41 h. The mixture was concentrated with toluene. The residue was partitioned between dichloromethane (20 ml) and water (20 ml), and the aqueous layer was extracted with dichloromethane (20 ml×2). The combined organic layers were dried over Na_2SO_4 and concentrated. The residue was chromatographed on silica gel (10 g, ethanol-toluene=1 : 40), and the fraction corresponding to R_f 0.43 (ethanol-toluene=1 : 5) was concentrated to give **14** (37.5 mg, 60%) as crystals. **14**: Mp 88—90 °C; $[\alpha]_D^{22}$ −78.4° (*c* 1.01, $CHCl_3$); IR $\nu_{max}^{CHCl_3}$ 3540, 3000, 2875, 1630, 1455, 1370, 1355, 1325, 1295, 1090 cm^{-1}; ^1H NMR δ=1.66—2.49 (4H, m, H-6,6′,7,7′), 2.53—2.84 (1H, OH), 3.38—3.82 (3H, m, H-3,3′, 8a), 3.84—4.29 (3H, m, H-1,2,8), 4.30—4.72 (4H, m, 2×$OCH_2C_6H_5$), 7.10—7.58 (10H, m, 2×$OCH_2C_6H_5$). High-resolution mass spectrum, Found: *m/z* 367.1776, Calcd for $C_{22}H_{25}NO_4$: M, 367.1781. Found: C, 68.38; H, 6.97; N, 3.48%. Calcd for $C_{22}H_{25}NO_4 \cdot H_2O$: C, 68.56; H, 7.06; N, 3.63%.

(1*S*,2*R*,8*R*,8a*S*)-1,8-Di-*O*-benzyloctahydro-1,2,8-indolizinetriol (15). To a solution of **14** (20.1 mg, 0.055 mmol) in THF (2 ml) was added borane-Me_2S complex (10 mol dm^{-3} in BH_3, 0.02 ml, 0.2 mmol) at 0 °C with stirring. The mixture was stirred at room temperature for 3 h, and then water (8 ml) was added. The aqueous solution was extracted with dichloromethane (15 ml×5), and the extract was washed with water (7 ml). The organic layer was dried over Na_2SO_4 and concentrated. The residue was dissolved in pyridine (2 ml) and the solution was stirred for 17 h. After the mixture was concentrated, the residue was chromatographed on silica gel (ethyl acetate-hexane=1 : 2, then ethanol-toluene=1 : 20). The fraction corresponding to R_f 0.45 (ethanol-toluene=1 : 3) was concentrated to give **15** (16.3 mg, 84%) as a colorless syrup. **15**: $[\alpha]_D^{22}$ −61.1° (*c* 0.97, $CHCl_3$); IR $\nu_{max}^{CHCl_3}$ 2875, 1480, 1435, 1340, 1305, 1220, 1195 cm^{-1}; ^1H NMR δ=1.06—2.25 (7H, m, H-3,5,6,6′,7,7′,8a), 2.30—2.72 (1H, br s, OH), 2.87—3.21 (1H, m, H-5′), 3.48 (1H, dd, *J*=11 and 7 Hz, H-3′), 3.35—4.73 (7H, m, H-1,2,8,2×$OCH_2C_6H_5$), 7.12—7.64 (10H, m, 2×$OCH_2C_6H_5$). High-resolution mass spectrum, Found: *m/z* 353.1995, Calcd for $C_{22}H_{27}NO_3$: M, 353.1989.

(1*S*,2*R*,8*R*,8a*S*)-Octahydro-1,2,8-indolizinetriol, 8a-*epi*-Swainsonine (4). A solution of **15** (19.5 mg, 0.065 mmol) in chloroform (0.5 ml) in the presence of iodotrimethylsilane (0.09 ml, 0.65 mmol) was stirred in dark for 15 h. To the mixture was added methanol (2 ml), and the solution was stirred for 2 h and concentrated. The residue was partitioned between dichloromethane (10 ml) and water (10 ml), and the organic layer was extracted with water (10 ml). The combined aqueous layers were concentrated. The residue was purified on PTLC (aqueous ammonia-1-butanol-chloroform-ethanol=1 : 4 : 4 : 4), and a ninhydrin positive band (R_f 0.39 on the same solvents) was extracted with methanol to give **4** as crystals (7.2 mg, 75%). Analytical sample was obtained by recrystallization from chloroform. **4**: Mp 122—124 °C (decomp); $[\alpha]_D^{19}$ −64.5° (*c* 0.95, MeOH); IR ν_{max}^{KBr} 3440, 3320, 2940, 2830, 2820, 1445, 1385, 1345, 1330, 1320, 1240, 1205, 1160, 1130, 1110 cm^{-1}; ^1H NMR (D_2O) δ=1.31—2.40 (6H, m, H-5,6,6′,7,7′,8a), 2.81—3.17 (1H, br s, H-3), 3.22—3.60 (2H, m, H-3′,5′), 3.79—4.48 (3H, m, H-1,2,8). ^{13}C NMR δ=20.87, 32.26, 54.10, 62.83, 64.71, 68.18, 70.91, 72.51, High-resolution mass spectrum, Found: *m/z* 173.1050, Calcd for $C_8H_{15}NO_3$: M, 173.1050.

We are grateful to Professor Anthony C. Richardson (Queen Elizabeth College, University of London) for his continuous interest and encouragement to this work. One of us (B. W.) also thanks to the International Children's Aid and Research Endowment for Mannosidosis for support to this work. We also thank to Mr. Akio Takahashi for his elemental analyses.

References

1) S. M. Colegate, P. R. Dorling, and C. R. Huxtable, *Aust. J. Chem.*, **32**, 2257 (1979).

2) R. J. Molyneux and L. F. James, *Science*, **216**, 190 (1982).

3) M. J. Schneider, F. S. Ungemach, H. P. Broquist, and T. M. Harris, *Tetrahedron*, **39**, 29 (1983).

4) T. Kino, N. Inamura, K. Nakahara, S. Kiyoto, T. Goto, H. Terano, M. Kohsaka, H. Aoki, and H. Imanaka, *J. Antibiot.*, **38**, 936 (1985).

5) P. R. Dorling, C. R. Huxtable, and S. M. Colegate, *Biochem. J.*, **191**, 649 (1980); A. D. Elbein, R. Solf, P. R. Dorling, and K. Vosbeck, *Proc. Natl. Acad. Sci. U. S. A.*, **78**, 7393 (1981) and also see Refs. 1—4.

6) a) T. Suami, K. Tadano, and Y. Iimura, *Chem. Lett.*, **1984**, 513; *Carbohydr. Res.*, **136**, 67 (1985). b) M. H. Ali, L. Hough, and A. C. Richardson, *J. Chem. Soc., Chem. Commun.*, **1984**, 447; *Carbohydr. Res.*, **136**, 225 (1985). c) G. W. J. Fleet, M. J. Gough, and P. W. Smith, *Tetrahedron Lett.*, **25**, 1853 (1984). d) N. Yasuda, H. Tsutsumi, and T. Takaya, *Chem. Lett.*, **1984**, 1201. e) C. E. Adams, F. J. Walker, and K. B. Sharpless, *J. Org. Chem.*, **50**, 421 (1985). f) H. Setoi, H. Takano, and M. Hashimoto, *J. Org. Chem.*, **50**, 3948 (1985).

7) The syntheses of 8-*epi*- (**2**) and 2,8-di-*epi*-swainsonine have been achieved recently: N. Yasuda, H. Tsutsumi, and

T. Takaya, *Chem. Lett.*, **1985**, 31.

8) Y. Iimura, Y. Hotta, C. Fukabori, K. Tadano, and T. Suami, *J. Carbohydr. Chem.*, **5**, 147 (1986); *Bull. Chem. Soc. Jpn.*, **59**, 3885 (1986). The α-D-mannosidase inhibitory activities of compounds **2** and **3** are approximately 15 and 20% of swainsonine (**1**), respectively.

9) The present work has been published as a preliminary communication form: K. Tadano, Y. Hotta, M. Morita, T. Suami, B. Winchester, and I. C. di Bello, *Chem. Lett.*, **1986**, 2105.

10) R. D. Guthrie and D. Murphy, *J. Chem. Soc.*, **1963**, 5288.

11) M. E. Jung and M. A. Lyster, *J. Org. Chem.*, **42**, 3761 (1977).

 © 1987 The Chemical Society of Japan Bull. Chem. Soc. Jpn., 60, 3673—3678 (1987)

Transformation of D-Xylose to (1*R*,2*R*,3*R*,4*R*)-2,3,4-Trihydroxy-1-(hydroxymethyl)cyclopentane, Pseudo-β-D-arabinofuranose

Kin-ichi TADANO,* Hiroshi KIMURA, Masahide HOSHINO, Seiichiro OGAWA,* and Tetsuo SUAMI†
Department of Applied Chemistry, Faculty of Science and Technology, Keio University, Hiyoshi, Kohoku-ku, Yokohama 223
(Received April 21, 1987)

The known 3-*O*-benzyl-D-xylose was converted into methyl (4*S*,5*R*,6*R*)-4,6,7-triacetoxy-5-benzyloxy-2-(methoxycarbonyl)heptanoate (**8**) by employing Knoevenagel condensation of 2,4,5-tri-*O*-acetyl-3-*O*-benzyl-*aldehydo*-D-xylose with dimethyl malonate as a key reaction. *O*-Deacetylation of **8** and successive glycol cleavage followed by acetylation gave a mixture of (1*S*,4*R*,5*R*,6*R*)-5-acetoxy-6-benzyloxy-4-methoxycarbonyl-2-oxobicyclo[2.2.1]heptan-3-one and dimethyl (2*R*,3*R*,4*S*)-2,4-diacetoxy-3-benzyloxy-1,1-cyclopentanedicarboxylate (**12**), which was converted into **12** exclusively. This enantiomerically pure highly oxygenated cyclopentane dicarboxylate **12** was converted into (3*S*,4*S*)-3-benzyloxy-1-(*t*-butyldiphenylsilyloxymethyl)-4-hydroxy-1-cyclopentene (**15**) by 1) thermal demethoxycarbonylation accompanied by β-elimination of the acetoxyl group, 2) diisobutylaluminium hydride reduction, and 3) selective protection of thus formed 1-cyclopentene-1-methanol. Pyridinium chlorochromate oxidation of **15** followed by reduction with sodium borohydride gave a 6.4 : 1 mixture of (3*S*,4*R*)-3-benzyloxy-1-(*t*-butyldiphenylsilyloxymethyl)-4-hydroxy-1-cyclopentene (**18**) and **15**. Hydroboration of *O*-desilyl derivative of **18** proceeded stereoselectively from the less hindered α-face, and (1*R*,2*R*,3*R*,4*R*)-2,4-diacetoxy-1-acetoxymethyl-3-(benzyloxy)cyclopentane (**21**) was obtained after acetylation. Deprotection of **21** gave pseudo-β-D-arabinofuranose.

In our consecutive synthetic efforts on the access to enantiomerically pure highly oxygenated six- and five-membered carbocycles from carbohydrates, we developed several novel approaches to pseudo-sugars [stereoisomers of 2,3,4,5-tetrahydroxy-1-(hydroxymethyl)cyclohexane and those of 2,3,4-trihydroxy-1-(hydroxymethyl)cyclopentane][1a-f] and shikimate[1g] syntheses. In recent articles,[1e] we described the synthesis of (1*S*,2*S*,3*S*,4*S*)-2,3,4-trihydroxy-1-(hydroxymethyl)-cyclopentane, pseudo-β-L-arabinofuranose (**1**), starting from D-erythrose. The synthetic utility of **1** was verified by conversion of **1** into some enantiomerically pure pseudo-pentofuranoses and a key intermediate for the carbocyclic antibiotic (−)-aristeromycin synthesis, (1*R*,2*S*,3*R*,4*R*)-2,3-dihydroxy-4-hydroxymethyl-1-cyclopentanamine (**2**).[2] In this article, we describe a synthesis of (1*R*,2*R*,3*R*,4*R*)-2,3,4-trihydroxy-1-(hydroxymethyl)cyclopentane (**3**), an enantiomer of pseudo-β-L-arabinofuranose **1**. The synthesis of **3** was started from the known 3-*O*-benzyl-D-xylose, and the crucial cyclopentane ring formation was accomplished by an intramolecular aldol cyclization strategy, which has been developed in our laboratory for the synthesis of **1**.[1e]

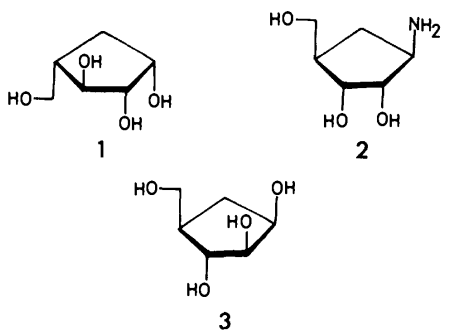

Results and Discussion

The starting material, 3-*O*-benzyl-D-xylose (**4**), was prepared from D-glucose by a modified known procedure (Scheme).[3] Dithioacetal formation of **4** with ethanethiol in concd HCl followed by acetylation gave an acyclic diethyl dithioacetal **5** in 95% yield. An aldehyde group was regenerated by treatment of **5** with mercury(II) chloride in an aqueous acetonitrile giving 2,4,5-tri-*O*-acetyl-3-*O*-benzyl-*aldehydo*-D-xylose (**6**). The Knoevenagel condensation of **6** with dimethyl malonate in a mixture of acetic anhydride and pyridine resulted in a formation of α,β-unsaturated diester **7**, which was reduced with sodium borohydride at −15 °C to give the key intermediate **8** by a 1,4-conjugate addition of the hydride. The overall yield of **8** from **5** was 62%. *O*-Deacetylation of **8** with sodium methoxide provided an inseparable mixture of (4*S*,5*R*,6*R*)-5-benzyloxy-4,6,7-trihydroxy-2-(methoxycarbonyl)heptan-1,4-olide (**9**) and methyl (4*S*,5*R*,6*R*)-5-benzyloxy-4,6,7-trihydroxy-2-(methoxycarbonyl)heptanoate (**10**). The stereochemistry at C-2 of **9** was not determined. The glycols at C-6 and C-7 of the mixture **9** and **10** were cleaved by sodium periodate in an aqueous dioxane and the products were acetylated to give a mixture of (1*S*,4*R*,5*R*,6*R*)-5-acetoxy-6-benzyloxy-4-(methoxycarbonyl)-2-oxabicyclo[2.2.1]heptan-3-one (**11**) and dimethyl (2*R*,3*R*,4*S*)-2,4-diacetoxy-3-benzyloxy-1,1-cyclopentanedicarboxylate (**12**). The mixture was separated by silica-gel chromatography, and the ratio of **11** and **12** was approximately 8 : 1. As expacted, the desired intramolecular aldol cyclization occurred under the conditions of glycol cleavage. Based on this

†Present address: Department of Chemistry, Faculty of Science and Technology, Meisei University, Hodokubo, Hino, Tokyo 191.

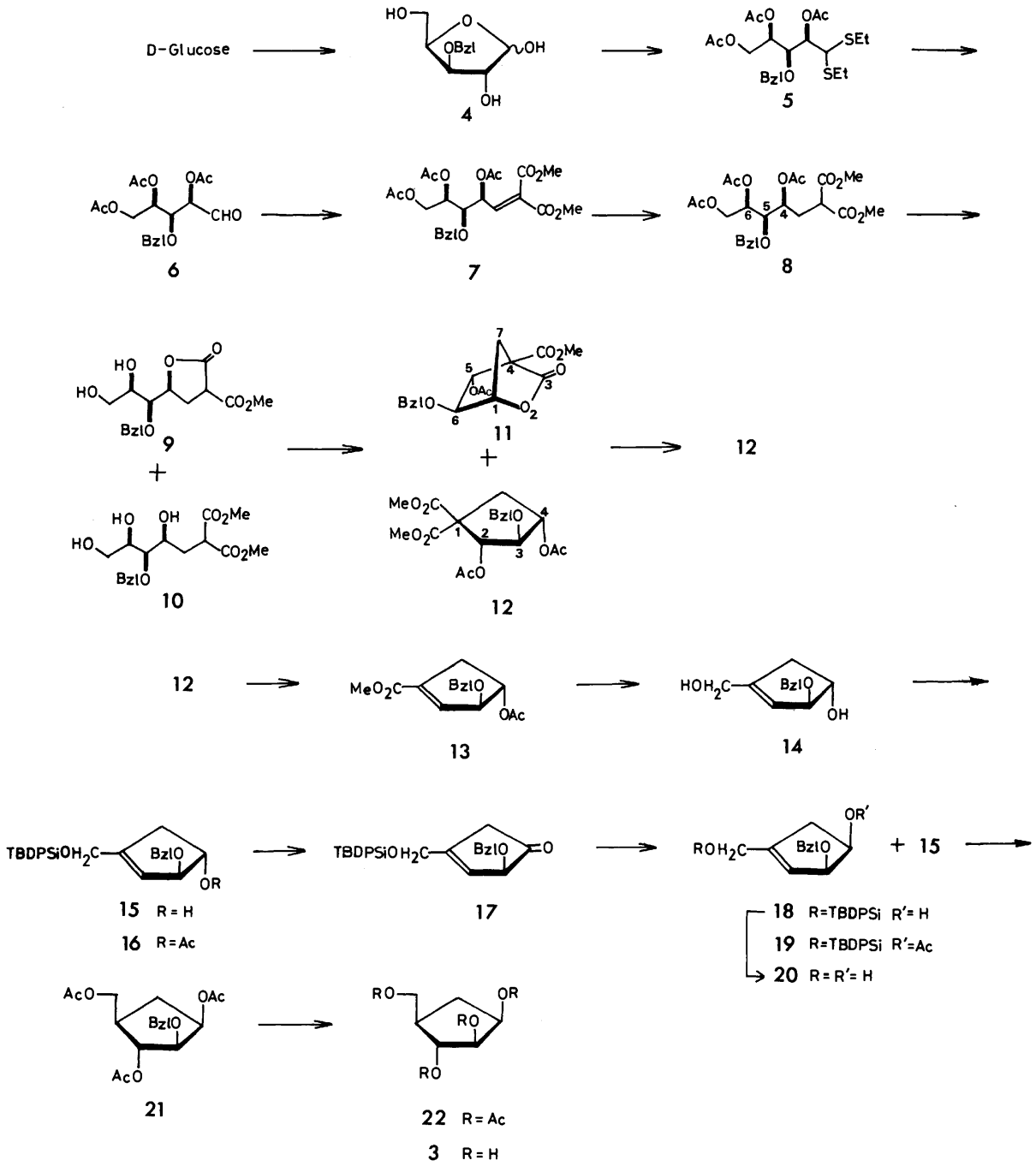

Scheme.

result, we assume that the ratio of **9** and **10** is same as that of **11** and **12**. On the ^{1}H NMR spectrum of **11**, H-5 (H-C-OAc) appeared at δ 5.56 as a broad singlet. This indicates that H-5 and H-6 (H-C-OBzl) is an endo-exo relationship as depicted.[4] The stereochemistry of the newly introduced chiral center on **12** (C-2) was assigned to be (R) based on the ^{1}H NMR spectrum, in which H-2 appeared at δ 5.90 as a doublet with $J_{2,3}$=3 Hz.[5] When a methanol solution of the mixture **11** and **12** in the presence of Amberlite IR-120 (H^+) resin was refluxed, the bicyclic compound **11** was converted into **12** after acetylation. The overall yield of **12** from **8** was 59% without separation of the mixture **11** and **12**. The fact that the sterically less crowded products **11** and **12** were formed predominantly on the aldol cyclization is parallel to our previous result on the aldol cyclization performed for the similar model.[1e]

Thermal demethoxycarbonylation of **12** in an aqueous DMSO at 110—160 °C in the presence of NaCl accompanied a β-elimination of the acetoxyl group to give methyl (3*S*,4*S*)-4-acetoxy-3-benzyloxy-1-cyclopentene-1-carboxylate (**13**) as a somewhat volatile liquid. The crude **13** was reduced with diisobutylaluminium hydride (DIBAL-H) at −78 °C to give (3*S*,4*S*)-3-benzyloxy-4-hydroxy-1-cyclopentene-1-methanol (**14**) in 75% yield. The primary hydroxyl group in **14** was

protected as a silyl ether with *t*-butylchlorodiphenylsilane and imidazole to provide **15** in 73% yield. Compound **15** was oxidized with pyridinium chlorochromate (PCC) giving (3*S*)-3-benzyloxy-1-(*t*-butyldiphenylsilyloxymethyl)-1-cyclopenten-4-one (**17**), which was reduced with sodium borohydride in methanol solution. The reduction gave (3*S*,4*R*)-1-cyclopentene-1-methanol **18** and **15** in 64 and 10% yield, respectively. The stereoselectivity of the reduction was 6.4 : 1 with preferential hydride attack from the less hindered α-side. The inversion at C-4 in **15** to *R* configuration was apparent by comparing the ^{1}H NMR sectra of the corresponding acetates **16** and **19**, both of which were prepared by acetylation of **15** and **18**. The *t*-butyldiphenylsilyl group was deprotected with tetrabutylammonium fluoride to give **20** as crystals in 90% yield. Hydroboration of **20** with borane–THF complex, oxidation of the product with hydrogen peroxide in an aqueous NaOH solution followed by acetylation gave a fully protected pseudo-β-D-arabinofuranose, (1*R*,2*R*,-3*R*,4*R*)-2,4-diacetoxy-1-acetoxymethyl-3-(benzyloxy)-cyclopentane (**21**), in 65% yield. The hydroboration occurred stereoselectively from the less hindered α-face of **20**, and the (1*S*,2*S*,3*R*,4*R*)-diastereomer, a derivative of pseudo-α-L-ribofuranose, was not detected. Removal of the benzyl group in **21** with cyclohexene in the presence of 20% $Pd(OH)_2$ on charcoal[6] followed by acetylation gave a fully acetylated pseudo-β-D-arabinofuranose **22** in 90% yield. The ^{1}H NMR spectrum of **22** was identical with that of the L-enantiomer,[1e] and the $[\alpha]_D$ value of **22** ($[\alpha]_D^{23}$ −4.8°) coincided with that of the L-enantiomer ($[\alpha]_D^{23}$ +4.1°). *O*-Deacetylation of **22** with sodium methoxide gave pseudo-β-D-arabinofuranose (**3**) in a quantitative yield.[7]

Experimental

Gereral. Reactions were carried out at room temperature unless otherwise described. Reaction mixture, extracts, and fraction of column chromatography were concentrated under a reduced pressure at below 40 °C with a bath. Melting points were determined with a Mitamura Riken micro melting point apparatus and are uncorrected. Specific rotation was measured by a Jasco DIP-4 polarimeter with a 10 mm cell. Column chromatography was performed with Silicagel 60 (Katayama Chemicals, K070), and thin-layer chromatography (TLC) by a glass plate coated with Kieselgel 60 GF_{254} (Merck), followed by UV light detection and charred with sulfuric acid. IR spectra were recorded with a Hitachi 225 spectrometer or with a Jasco A-202 spectrometer. ^{1}H NMR spectra were recorded with a Varian EM-390 (90 MHz) spectrometer for solutions in $CDCl_3$ with an internal standard of Me_4Si. High resolution mass spectra were obtained by a Hitachi M-80 spectrometer.

Dichloromethane and *N*,*N*-dimethylformamide (DMF) were dried over CaH_2 and distilled. Pyridine was distilled over NaOH. Tetrahydrofuran (THF) was distilled over $LiAlH_4$ and then over Na-benzophenone.

3-*O*-Benzyl-D-xylose (4). This compound was prepared from D-glucose according to the reported procedure.[3] In our case, acid hydrolysis of the intermediate, 3-*O*-benzyl-1,2-*O*-isopropylidene-α-D-xylofuranose, was performed in refluxing 80% aqueous acetic acid in place of the reported sulfuric acid in refluxing 50% methanol. The overall yield of **4** from 1,2 : 5,6-di-*O*-isopropylidene-α-D-glucofuranose was 51%. **4**: Mp 115—116 °C, lit,[3] 89—91 °C. Found: C, 59.92; H, 6.67%. Calcd for $C_{12}H_{16}O_5$: C, 59.99; H, 6.71%.

2,4,5-Tri-*O*-acetyl-3-*O*-benzyl-D-xylose Diethyl Dithioacetal (5). A solution of **4** (23.5 g, 98.0 mmol) in concd HCl (80 ml) in the presence of ethanethiol (120 ml) was stirred at −15 °C for 30 min, and neutralized by addition of aqueous ammonia. The solution was concentrated, and the residue was suspended in ethanol, then concentrated. Ethanol (1 l) was added to the residue, and insoluble solids were removed by filtration, washed with ethanol (1 l). The combined filtrate and washing were concentrated, and the residue was acetylated with acetic anhydride (100 ml) in pyridine (100 ml) for 13 h. The mixture was concentrated, and the residue was chromatographed on silica gel (500 g, ethyl acetate–hexane=1 : 15), and the fraction corresponding to R_f 0.78 (ethyl acetate–hexane=1 : 3) was concentrated to give **5** (44.1 g, 95%) as a colorless syrup. **5**: $[\alpha]_D^{24.5}$ −5.3° (*c* 0.71, $CHCl_3$); IR $\nu_{max}^{CHCl_3}$ 2950, 2860, 1740, 1490, 1450, 1370, 1210, 1110, 1070 cm^{-1}; ^{1}H NMR δ=1.21, 1.23 (3H×2, each t, *J*=6 Hz, 2×$SCH_2C\underline{H}_3$), 2.01, 2.04, 2.10 (3H×3, each s, 3×$OCOCH_3$), 2.48—2.86 (4H, m, 2×$SC\underline{H}_2CH_3$), 3.93—4.53 (4H, m, H-1,3,5,5′), 4.73 (2H, s, $OC\underline{H}_2C_6H_5$), 5.18—5.39 (2H, m, H-2,4), 7.31 (5H, s, $OCH_2C_6\underline{H}_5$). Found: C, 56.00; H, 6.73%. Calcd for $C_{22}H_{32}O_7S_2$: C, 55.91; H, 6.83%.

Methyl (4*S*,5*R*,6*R*)-4,6,7-Triacetoxy-5-benzyloxy-2-(methoxycarbonyl)heptanoate (8). A solution of **5** (8.39 g, 17.6 mmol) in a mixture of acetonitrile (200 ml) and water (200 ml) in the presence of mercury(II) chloride (48.2 g, 176.0 mmol) and calcium carbonate (20.25 g, 202 mmol) was stirred for 30 min. Insoluble solids were removed by filtration with a Celite-pad, washed with ethyl acetate (1 l). The combined filtrate and washing were washed with 1 mol dm^{-3} aqueous KI solution (400 ml×5), 20% aqueous sodium thiosulfate solution (400 ml×3), and brine (400 ml×2) successively. The organic layer was dried over Na_2SO_4 and concentrated to give crude **6**, which was subjected to the Knoevenagel condesation directly. **6**: ^{1}H NMR δ=2.00, 2.19 (6H and 3H, each s, 3×$OCOCH_3$), 3.90—4.45 (3H, m, H-3, 5,5′), 4.70 (2H, s, $OC\underline{H}_2C_6H_5$), 5.20—5.45 (2H, m, H-2, 4), 7.36 (5H, s, $OCH_2C_6\underline{H}_5$), 9.60 (1H, s, CHO).

A solution of the crude **6** and dimethyl malonate (20.1 ml, 176 mmol) in a mixture of acetic anhydride (63 ml) and pyridine (90 ml) was stirred for 36 h. The mixture was diluted with ethyl acetate (900 ml) and washed with water (300 ml×3). The aqueous layer was extracted with ethyl acetate (300 ml×3). The combined organic layers were dried over Na_2SO_4 and concentrated to give crude **7**, which was used to next step without purification. In a separate small scale experiment, the crude **7** was purified on silica-gel chromatography (ethyl acetate–hexane=1 : 3). **7** as a colorless syrup, TLC R_f 0.31 (ethyl acetate–hexane=1 : 3): $[\alpha]_D^{24}$ +10.0° (*c* 1.15, $CHCl_3$); IR $\nu_{max}^{CHCl_3}$ 2925, 1730, 1650, 1490, 1425, 1360, 1210, 1060^{-1}; ^{1}H NMR δ=2.00, 2.05 (3H and 6H, each s, 3×$OCOCH_3$), 3.79 (6H, s, 2×$COOCH_3$), 3.66—4.53 (3H, m, H-5,7,7′), 4.65 (2H, s, $OC\underline{H}_2C_6H_5$), 5.10—5.53 (1H, m, H-6), 5.72—5.95 (1H, m, H-4), 6.92 (1H, d, *J*=7 Hz, H-3), 7.33 (5H, s, $OCH_2C_6\underline{H}_5$).

A solution of the crude **7** in methanol (150 ml) containing

sodium borohydride (799 mg, 21.1 mmol) was stirred at −15 °C for 30 min. After concentration of the mixture to ca. 50 ml, water (300 ml) was added. This aqueous solution was extracted with dichloromethane (300 ml×3), and the extracts were dried over Na_2SO_4, then concentrated. The residue was chromatographed on silica gel (500 g,. ethyl acetate-hexane=1 : 5). The fraction corresponding to R_f 0.47 (ethyl acetate-hexane=2 : 3) was concentrated to give **8** (5.24 g, 62%) as a colorless syrup. **8**: $[\alpha]_D^{25.5}$ −0.6° (*c* 1.32, $CHCl_3$); IR $\nu_{max}^{CHCl_3}$ 2950, 1735, 1435, 1370, 1225 cm^{-1}; ^1H NMR δ=1.98, 2.01, 2.05 (3H×3, each s, 3×$OCOCH_3$), 1.86—2.30 (2H, m, H-3,3′), 3.30 (1H, dd, *J*=6 and 9.5 Hz, H-2), 3.61—4.45 (3H, m, H-5,7,7′), 3.70, 3.72 (3H×2, each s, 2×$COOCH_3$), 4.65 (2H, s, $OCH_2C_6H_5$), 5.00—5.45 (2H, m, H-4, 6), 7.32 (5H, s, $OCH_2C_6H_5$). Found: C, 57.16; H, 6.26%. Calcd for $C_{23}H_{30}O_{11}$: C, 57.26; H, 6.27%.

Dimethyl (2*R*,3*R*,4*S*)-2,4-Diacetoxy-3-benzyloxy-1,1-cyclopentanedicarboxylate (12). A solution of **8** (6.50 g, 13.5 mmol) in methanol (160 ml) containing sodium methoxide (1 mol dm^{-3} in methanol, 20.0 ml, 20.0 mmol) was stirred at 0 °C for 2 h. The mixture was neutralized with Amberlite IR-120 (H^+), and the resin was removed by filtration, washed with methanol. The combined filtrate and washing were concentrated to give an approximately 8 : 1 mixture of **9** and **10**, which was used directly to next step.

To a solution of the mixture of **9** and **10** in dioxane (190 ml), an aqueous solution (22 ml) of sodium periodate (4.28 g, 20.0 mmol) was added with stirring. After stirring the mixture for 50 min, an aqueous solution (15 ml) of the oxidizing reagent (2.89 g, 13.5 mmol) was added. The mixture was stirred additional 1 h, and insoluble solids were removed by filtration. The filtrate was diluted with water (500 ml), and extracted with dichloromethane (800 ml×3). The extract was dried over Na_2SO_4 and concentrated. The residue was acetylated with acetic anhydride (60 ml) in pyridine (60 ml) for 18 h. The mixture was concentrated, and the residue was dissolved in toluene and then concentrated to give a mixture of **11** and **12**, which was subjected to next step without separation. In a separate experiment, **8** (456 mg) was converted to the mixture of **11** and **12** by the same procedure as described above. The mixture was separated by chromatography on silica gel (ethyl acetate-hexane=1 : 10) to give **11** (147 mg, 47%) and **12** (24 mg, 6%). **11** as a colorless syrup, TLC R_f 0.55 (ethyl acetate-hexane=1 : 2): $[\alpha]_D^{25}$ +87.8° (*c* 1.32, $CHCl_3$); IR $\nu_{max}^{CHCl_3}$ 2960, 1800, 1740, 1450, 1440, 1375, 1350, 1330, 1310, 1280, 1220, 1165, 1090 cm^{-1}; ^1H NMR δ=2.10 (3H, s, $OCOCH_3$), 2.53—2.72 (2H, m, H-7,7′), 3.66—4.00 (1H, m, H-6), 3.79 (3H, s, $COOCH_3$), 4.62 (1H, broad s, H-1), 4.70 (2H, ABq, *J*=11 Hz, $OCH_2C_6H_5$), 5.56 (1H, broad s, H-5), 7.32 (5H, s, $OCH_2C_6H_5$). Found: C, 61.04; H, 5.57%. Calcd for $C_{17}H_{18}O_7$: C, 61.05; H, 5.43%.

A solution of the crude mixture of **11** and **12** in methanol (200 ml) was refluxed in the presence of Amberlite IR-120 (H^+) (30 g). The resin was added after 6 h (20 g), 12 h (30 g), 16 h (15 g), 17 h (20 g), and 19 h (20 g) successively, and the mixture was refluxed additional 4 h. After removal of the resin by filtration and washing with methanol, the combined filtrate and washing were concentrated. The residue was acetylated with acetic anhydride (110 ml) in pyridine (110 ml) for 18 h. The mixture was concentrated with toluene. The residue was chromatographed on silica gel (130 g, ethyl acetate-hexane=1 : 7), and the fraction corresponding to R_f 0.59 (ethyl acetate-hexane=1 : 2) was concentrated to give **12** (3.26 g, 59%) as a colorless syrup. **12**: $[\alpha]_D^{27}$ +40.8° (*c* 0.53, $CHCl_3$); IR $\nu_{max}^{CHCl_3}$ 2950, 2910, 2850, 1730, 1430, 1370, 1230 cm^{-1}; ^1H NMR δ=2.02 (6H, s, 2×$OCOCH_3$), 2.30—2.45, 2.75—3.10 (1H×2, each m, H-5,5′), 3.69, 3.73 (3H×2, each s, 2×$COOCH_3$), 3.97 (1H, t, *J*=3 Hz, H-3), 4.63 (2H, d, *J*=1.5 Hz, $OCH_2C_6H_5$), 4.83—5.15 (1H, m, H-4), 5.90 (1H, d, *J*=3 Hz, H-2), 7.30 (5H, s, $OCH_2C_6H_5$). Found: C, 58.58; H, 6.04%. Calcd for $C_{20}H_{24}O_9$: C, 58.82; H, 5.92%.

(3*S*,4*S*)-3-Benzyloxy-4-hydroxy-1-cyclopentene-1-methanol (14). A solution of **12** (556 mg, 1.36 mmol) in a mixture of DMSO (44 ml) and water (2 ml) containing NaCl (239 mg, 4.09 mmol) was heated from 110 to 160 °C for 2 h. The mixture was heated at 160 °C additional 4 h. After cooling to room temperature, water (300 ml) was added. The aqueous mixture was extracted with dichloromethane (300 ml×2). The extract was dried over Na_2SO_4 and concentrated at below 9 °C until ca. 10 ml volume. The remaining liquid contained **13**, which was reduced directly. In a separate experiment, the crude **13** was purified on silica gel chromatography (ethyl acetate-hexane=1 : 15). **13** as a somewhat volatile colorless liquid, TLC R_f 0.73 (ethyl acetate-hexane=1 : 2): $[\alpha]_D^{27}$ +94.7° (*c* 0.44, $CHCl_3$): IR $\nu_{max}^{CHCl_3}$ 2950, 1720, 1630, 1435, 1370, 1290, 1240, 1220, 1170 cm^{-1}; ^1H NMR δ=2.01 (3H, s, $OCOCH_3$), 2.25—2.60, 3.04—3.40 (1H×2, each m, H-5,5′), 3.75 (3H, s, $COOCH_3$), 4.53—4.70 (1H, m, H-3), 4.63 (2H, s, $OCH_2C_6H_5$), 5.20—5.39 (1H, m, H-4), 6.60—6.75 (1H, m, H-2), 7.33 (5H, s, $OCH_2C_6H_5$). High-resolution mass spectrum, Found: *m/z* 290.1147, Calcd for $C_{16}H_{18}O_5$: M, 290.1152.

To a solution of the above concentrate in dichloromethane (14 ml), DIBAL-H (1.5 mol dm^{-3} in toluene, 18.1 ml, 27.2 mmol) was added at −78 °C with stirring under an argon atmosphere. The reducing reagent was added after 100 min (18.1 ml), 140 min (18.1 ml), and 160 min (9.1 ml) successively at −78 °C. The mixture was stirred at the same temperature additional 80 min and diluted with water (70 ml). The resulting insoluble solids were removed by filtration. The filtrate was diluted with water (200 ml) and extracted with dichloromethane (300 ml×6). The extract was dried over Na_2SO_4 and concentrated. The residue was chromatographed on silica gel (15 g, ethyl acetate-hexane=2 : 3) and the fraction corresponding to R_f 0.18 (ethyl acetate-hexane=1 : 1) was concentrated to give **14** (225 mg, 75%) as a colorless syrup. **14**: $[\alpha]_D^{25}$ +100.0° (*c* 0.99, $CHCl_3$); IR $\nu_{max}^{CHCl_3}$ 3350, 2900, 2850, 1650, 1490, 1455 cm^{-1}; ^1H NMR δ=1.95—2.26, 2.50—2.87 (1H×2, each m, H-5,5′), 3.15—3.65 (2H, broad s, 2×OH), 4.01 (2H, s, CH_2OH), 4.20—4.43 (2H, m, H-3,4), 4.54 (2H, s, $OCH_2C_6H_5$), 5.60 (1H, broad s, H-2), 7.30 (5H, s, $OCH_2C_6H_5$). High-resolution mass spectrum, Found: *m/z* 220.1097, Calcd for $C_{13}H_{16}O_3$: M, 220.1073.

(3*S*,4*S*)-3-Benzyloxy-1-(*t*-butyldiphenylsilyloxymethyl)-4-hydroxy-1-cyclopentene (15). To a solution of **14** (218 mg, 0.99 mmol) in DMF (4 ml), *t*-butylchlorodiphenylsilane (0.16 ml, 0.60 mmol) and imidazole (81 mg, 1.19 mmol) were added with stirring. Each 0.08 ml of the silylating reagent and 40.5 mg of imidazole was added after 5, 24, and 29 h. The mixture was stirred totally 31 h, and diluted with ethyl acetate (300 ml). The solution was washed with water (50 ml×3). The organic layer was dried over Na_2SO_4 and concentrated. The residue was chromatographed on silica gel (15 g, ethyl acetate-hexane=1 : 8), and the fraction corresponding to R_f 0.45 (ethyl acetate-hexane=1 : 3) was concentrated to give **15** (332 mg, 73%) as a colorless syrup. **15**: $[\alpha]_D^{20}$

+50.4° (*c* 1.00, $CHCl_3$); IR $\nu_{max}^{CHCl_3}$ 3420, 3075, 3055, 2960, 2940, 2860, 1590, 1500, 1470, 1460, 1430, 1390, 1360 cm^{-1}; ^1H NMR δ=1.02 (9H, s, $OSiC(CH_3)_3$), 1.88—2.22 (2H, m, H-5, OH), 2.45—2.82 (1H, m, H-5′), 4.08 (2H, s, CH_2OSi), 4.13—4.40 (2H, m, H-3,4), 4.49 (2H, s, $OC\underline{H}_2C_6H_5$), 5.60 (1H, m, H-2), 7.20—7.75 (15H, m, $OCH_2C_6\underline{H}_5$, $OSi(C_6\underline{H}_5)_2$). Found: C, 76.02; H, 7.55%. Calcd for $C_{29}H_{34}O_3Si$: C, 75.94; H, 7.47%.

(3*S*,4*S*)-4-Acetoxy-3-benzyloxy-1-(*t*-butyldiphenylsilyloxymethyl)-1-cyclopentene (16). Compound **15** (15 mg, 0.032 mmol) was acetylated with acetic anhydride (1 ml) in pyridine (1 ml) for 2 h. The mixture was concentrated, and the residue was purified on preparative TLC (20×20 cm, Merck Kieselgel 60 PF_{254}, ethyl acetate-hexane=1 : 3). The band corresponding to R_f 0.85 (ethyl acetate-hexane=1 : 3) was extracted with $CHCl_3$ and concentrated to give **16** (14 mg, 87%) as a colorless syrup. **16**: $[\alpha]_D^{19.5}$ +45.8°(*c* 0.65, $CHCl_3$); IR $\nu_{max}^{CHCl_3}$ 2930, 2860, 1725, 1450, 1430, 1370, 1250, 1170, 1110 cm^{-1}; ^1H NMR δ=0.85 (9H, s, $OSiC(CH_3)_3$), 1.83 (3H, s, $OCOCH_3$), 1.75—2.10, 2.50—2.90 (1H×2, each m, H-5,5′), 4.00 (2H, s, CH_2OSi), 4.20—4.50 (1H, m, H-3), 4.41 (2H, d, *J*=3 Hz, $OC\underline{H}_2C_6H_5$), 4.98—5.23 (1H, m, H-4), 5.55 (1H, d, *J*=2 Hz, H-2), 7.10—7.60 (15H, m, $OCH_2C_6\underline{H}_5$, $OSi(C_6\underline{H}_5)_2$). Found: C, 74.18; H, 7.32%. Calcd for $C_{31}H_{36}O_4Si$: C, 74.36; H, 7.25%.

(3*S*,4*R*)-3-Benzyloxy-1-(*t*-butyldiphenylsilyloxymethyl)-4-hydroxy-1-cyclopentene (18). To a solution of **15** (251 mg, 0.55 mmol) in dichloromethane (24 ml), PCC (2.36 g, 10.9 mmol) and molecular sieves (4A, powder, 1 g) were added. The mixture was stirred for 30 min. The mixture was applied on silica-gel column (40 g), and eluted with ether. The fraction corresponding to R_f 0.79 (ethyl acetate-hexane =1 : 4) was concentrated to give **17** (223 mg) as a colorless syrup. To a solution of **17** in methanol (8 ml), sodium borohydride (31 mg, 0.82 mmol) was added with stirring at 0 °C. After stirring at 0 °C for 1 h, the mixture was neutralized with 1 mol dm^{-3} HCl and diluted with water (50 ml). The solution was extracted with dichloromethane (80 ml×4), and the extracts were combined, dried over Na_2SO_4, and concentrated. The residue was chromatographed on silica gel (11 g, ethyl acetate-hexane=1 : 25), and the fraction corresponding to R_f 0.53 (ethyl acetate-hexane=1 : 4) was concentrated to give **18** (160 mg, 64%) as a colorless syrup. The fraction corresponding to R_f 0.33 was concentrated to give **15** (25 mg, 10%) **18**: $[\alpha]_D^{21.5}$ +33.1° (*c* 1.17, $CHCl_3$); IR $\nu_{max}^{CHCl_3}$ 3550, 2940, 2860, 1650, 1590, 1470, 1430, 1390, 1160, 1110 cm^{-1}; ^1H NMR δ=1.09 (9H, s, $OSiC(CH_3)_3$), 2.28—2.50 (2H, m, H-5,5′), 2.00—3.00 (1H, broad, OH), 4.15—4.50 (4H, m, CH_2OSi, H-3,4), 4.66 (2H, s, $OC\underline{H}_2C_6H_5$), 5.70—5.85 (1H, m, H-2), 7.25—7.75 (15H, m, $OCH_2C_6\underline{H}_5$, $OSi(C_6\underline{H}_5)_2$). Found: C, 75.67; H, 7.50%. Calcd for $C_{29}H_{34}O_3Si$: C, 75.94; H, 7.47%.

(3*S*,4*R*)-4-Acetoxy-3-benzyloxy-1-(*t*-butyldiphenylsilyloxymethyl)-1-cyclopentene (19). Compound **18** (11 mg, 0.024 mmol) was acetylated with acetic anhydride (1 ml) in pyridine (1 ml) for 13 h. The mixture was concentrated, and the residue was chromatographed on silica gel (1 g, ethyl acetate-hexane=1 : 30). The fraction corresponding to R_f 0.47 (ethyl acetate-hexane=1 : 8) was concentrated to give **19** (11 mg, 90%) as a colorless syrup. **19**: $[\alpha]_D^{22.5}$ +35.1° (*c* 0.49, $CHCl_3$); IR $\nu_{max}^{CHCl_3}$ 3000, 2960, 2930, 2860, 1725, 1250, 1170, 1110 cm^{-1}; ^1H NMR δ=1.05 (9H, s, $OSiC(CH_3)_3$), 2.03 (3H, s, $OCOCH_3$), 2.40—2.65 (2H, m, H-5,5′), 4.21 (2H, s, CH_2OSi), 4.50—4.68 (3H, m, $OC\underline{H}_2C_6H_5$, H-3), 5.30 (1H, q, *J*=6.5 Hz, H-4), 5.73—5.86 (1H, m, H-2), 7.30—7.80 (15H, m, $OCH_2C_6\underline{H}_5$, $OSi(C_6H_5)_2$). Found: C, 74.46; H, 7.28%. Calcd for $C_{31}H_{36}O_4Si$: C, 74.36; H, 7.25%.

(3*S*,4*R*)-3-Benzyloxy-4-hydroxy-1-cyclopentene-1-methanol (20). To a solution of **18** (156 mg, 0.34 mmol) in THF (10 ml), tetrabutylammonium fluoride (1 mol dm^{-3} in THF, 0.51 ml, 0.51 mmol) was added with stirring. After stirring for 2 h, the mixture was concentrated. The residue was chromatographed on silica gel (6 g, ethyl acetate-hexane=1 : 2), and the fraction corresponding to R_f 0.14 (ethyl acetate-hexane=1 : 1) was concentrated to give crystals of **20** (68 mg, 90%), mp 74—75 °C. **20**: $[\alpha]_D^{23}$ +75.4° (*c* 0.985, $CHCl_3$), IR $\nu_{max}^{CHCl_3}$ 3400, 2925, 2860, 1650, 1495, 1450, 1395, 1330, 1210, 1160 cm^{-1}; ^1H NMR δ=2.39 (2H, broad s, H-5,5′), 2.91 (2H, broad s, 2×OH), 4.10 (2H, broad s, CH_2OH), 4.25—4.50 (2H, m, H-3,4), 4.60 (2H, s, $OC\underline{H}_2C_6H_5$), 5.69 (1H, broad s, H-2), 7.34 (5H, s, $OCH_2C_6\underline{H}_5$). High-resolution mass spectrum, Found: *m/z* 220.1104, Calcd for $C_{13}H_{16}O_3$: M, 220.1098.

(1*R*,2*R*,3*R*,4*R*)-2,4-Diacetoxy-1-acetoxymethyl-3-(benzyloxy)cyclopentane (21). To a solution of **20** (65 mg, 0.29 mmol) in THF (5 ml), borane-THF complex (1 mol dm^{-3} in THF, 1.19 ml, 1.19 mmol) was added at 0 °C with stirring under an argon atmosphere. After 90 min stirring, borane-THF (0.59 ml) was added. The mixture was stirred additional 90 min at 0 °C, and water (1.8 ml), aqueous NaOH (3 mol dm^{-3}, 2.1 ml) and aqueous hydrogen peroxide (35%, 2.3 ml) were added successively. After stirring at room temperature for 3 h, saturated aqueous sodium sulfite (2.5 ml) was added and the mixture was concentrated with ethanol. The residue was passed through a short column of silica gel (3 g), and eluted with ethanol. The fraction corresponding to R_f 0.35 (ethanol-toluene=1 : 5) was concentrated. The residue was acetylated with acetic anhydride (5 ml) in pyridine (5 ml) for 18 h. The mixture was diluted with water (50 ml) and extracted with dichloromethane (50 ml×3). The extracts were dried over Na_2SO_4 and concentrated. The residue was chromatographed on silica gel (6 g, ethyl acetate-hexane=1 : 10), and the fraction corresponding to R_f 0.42 (ethyl acetate-hexane=1 : 3) was concentrated to give **21** (71 mg, 65%) as a colorless syrup. **21**: $[\alpha]_D^{23.5}$ −2.2° (*c* 0.9, $CHCl_3$); IR $\nu_{max}^{CHCl_3}$ 2930, 1740, 1730, 1450, 1365, 1230, 1220 cm^{-1}; ^1H NMR δ=2.03, 2.06 (6H, 3H, each s, 3×$OCOCH_3$), 1.95—2.40 (3H, m, H-1,5,5′), 3.89 (1H, t, *J*=4.5 Hz, H-3), 4.18 (2H, dd, *J*=3 and 6 Hz, $C\underline{H}_2OAc$), 4.59 (2H, s, $OC\underline{H}_2C_6H_5$), 5.00—5.30 (2H, m, H-2,4), 7.31 (5H, s, $OCH_2C_6\underline{H}_5$). Found: C, 62.75; H, 6.77%. Calcd for $C_{19}H_{24}O_7$: C, 62.63; H, 6.64%.

(1*R*,2*R*,3*R*,4*R*)-2,3,4-Triacetoxy-1-(acetoxymethyl)cyclopentane (22). A solution of **21** (68.5 mg, 0.19 mmol) in a mixture of ethanol (3 ml) and distilled cyclohexene (6.5 ml) in the presence of 20% $Pd(OH)_2$ on charcoal (150 mg) was refluxed for 4 h. The catalyst was removed by filtration with a Celite-pad, and the filtrate was concentrated. The residue was chromatographed on silica gel (3 g, ethyl acetate-hexane=1 : 4), and the fraction corresponding to R_f 0.19 (ethyl acetate-hexane=1 : 2) was concentrated. The residue was acetylated with acetic anhydride (1 ml) in pyridine (1 ml) for 2 h. The mixture was concentrated, and the residue was chromatographed on silica gel (3 g, ethyl acetate-hexane=1 : 6). The fraction corresponding to R_f 0.44 (ethyl acetate-hexane=1 : 2) was concentrated to give **22** (53.5 mg, 90%) as a colorless syrup. $[\alpha]_D^{23}$ −4.8° (*c* 0.87, $CHCl_3$), $[\alpha]_D^{23}$ +4.1° (*c* 1.07, $CHCl_3$) for the enantiomer of **22**.[1e] The IR and

^{1}H NMR spectra of **22** were identical with those of the (1*S*,2*S*,3*S*,4*S*)-enantiomer. Found: C, 53.37; H, 6.18%. Calcd for $C_{14}H_{20}O_8$: C, 53.16; H, 6.34%.

(1*R*,2*R*,3*R*,4*R*)-2,3,4-Trihydroxy-1-(hydroxymethyl)cyclopentane, Pseudo-β-D-arabinofuranose (3). To a solution of **22** (47 mg, 0.15 mmol) in methanol (2 ml), sodium methoxide (1 mol dm^{-3} in methanol, 0.45 ml, 0.45 mmol) was added at 0 °C with stirring. After stirring at 0 °C for 2 h, the mixture was neutralized by addition of Amberlite IR-120 (H^+). The resin was removed by filtration, washed with methanol. The filtrate and washing were concentrated to give **3** (22 mg, quantitatively). An analytical sample was obtained by PTLC (chloroform-methanol=2:1). **3** as a colorless syrup, TLC R_f 0.41 (chloroform-methanol=2:1): $[\alpha]_D^{22}$ +9.7° (*c* 0.72, MeOH), $[\alpha]_D^{14}$ −8.8° (*c* 0.56, MeOH) for the (1*S*,2*S*,3*S*,4*S*)-enantiomer **1**.[1e,8] The ^{1}H NMR sepctrum of **3** was identical with that of **1**. High-resolution mass spectrum, Found: *m/z* 149.0781. Calcd for $C_6H_{13}O_4$: M+H, 149.0812.

We thank to Mr. Akio Takahashi of our university for his elemental analyses.

References

1) a) T. Suami, K. Tadano, Y. Kameda, and Y. Iimura, *Chem. Lett.*, **1984**, 1919; *J. Carbohydr. Chem.*, **6**, 231 (1987). b) T. Suami, K. Tadano, Y. Ueno, and C. Fukabori, *Chem. Lett.*, **1985**, 1557. c) K. Tadano, Y. Ueno, C. Fukabori, Y. Hotta, and T. Suami, *Bull. Chem. Soc. Jpn.*, **60**, 1727 (1987). d) K. Tadano and T. Suami, *Yuki Gosei Kagaku Kyokai Shi*, **44**, 633 (1986). e) K. Tadano, H. Maeda, M. Hoshino, Y. Iimura, and T. Suami, *Chem. Lett.*, **1986**, 1081; *J. Org. Chem.*, **52**, 1946 (1987). f) K. Tadano, C. Fukabori, M. Miyazaki, H. Kimura, and T. Suami, *Bull. Chem. Soc. Jpn.*, **60**, 2189 (1987). g) T. Suami, K. Tadano, Y. Ueno, and Y. Iimura, *Chem. Lett.*, **1985**, 37; *J. Carbohydr. Chem.*, **6**, 245 (1987).

2) K. Tadano, M. Hoshino, S. Ogawa, and T. Suami, *Tetrahedron Lett.*, **28**, 2741 (1987).

3) T. Nakagawa, H. Tokuoka, K. Shinoto, J. Yoshimura, and T. Sato, *Bull. Chem. Soc. Jpn.*, **40**, 2150 (1967).

4) In regard to the ^{1}H NMR spectral interpretation of bicyclo[2.2.1]heptanes: L. M. Jackman and S. Sternhell, "Applications of Nuclear Magnetic Resonance Spectroscopy in Organic Chemistry," 2nd ed, Pergamon Press, Oxford (1969), p. 289.

5) In regard to the ^{1}H NMR sectral interpretation on the cyclopentanoids: see the book cited in Ref. 4, pp. 286—288.

6) S. Hanessian, T. J. Liak, and B. Vanasse, *Synthesis*, **1981**, 396.

7) Compound **1**, the L-enantiomer of **3**, was obtained as crystals (mp 103—104 °C),[1e] however, we can not crystallize compound **3** up to now.

8) In the previous paper,[1e] the $[\alpha]_D$ of compound **1** was incorrectly presented. Remeasurement of the crystalline (mp 103—104 °C) **1** gave $[\alpha]_D$ value described in this article.

 © 1987 The Chemical Society of Japan Bull. Chem. Soc. Jpn., 60, 3679—3685 (1987)

Influence of Hexasulfonated Calix[6]arenes on the Reactivities of Arenediazonium Ions in an Aqueous System

Seiji SHINKAI,* Seiichi MORI, Koji ARAKI, and Osamu MANABE
Department of Industrial Chemistry, Faculty of Engineering, Nagasaki University, Nagasaki 852
(Received April 17, 1987)

The pK_a of Phenol Blue shifted from 4.6 to 6.2 because of complexation of protonated Phenol Blue in the cavity of hexasulfonated calix[6]arene with dodecyl substituents (**2C**$_{12}$). The finding stimulated us to examine whether the analogs (**2C**) suppress the dediazoniation of arenediazonium ions in an aqueous system as crown ethers do in organic solvents. We have found that **2C** can suppress the dediazoniation in an aqueous system where neither 18-crown-6 nor anionic micelles are effective. The magnitude of the inhibition effect was 4—5 fold. The reaction rate of the diazo coupling with *N,N*-dimethylaniline was significantly suppressed in the presence of **2C**, suggesting that arenediazonium ions are deactivated through complexation with **2C**. The novel stabilization effects were explained by the strong anionic reaction field which neither 18-crown-6 nor anionic micelles have: that is, **2C** has a peculiar architecture that six sulfonato groups are circularly arranged on the edge of the calixarene cavity.

Recently, Gutsche and co-workers[1,2] have reported on a series of new cyclic molecules called "calixarenes" which are cyclic oligomers made up of benzene units as cyclodextrins are made up of glucose units. Several groups have reported on the ionophoric properties of calixarenes,[3-7] but almost nothing is known with certainty as to the inclusion properties of calixarenes in solution. In 1984, we reported the synthesis and properties of hexasulfonated calix[6]arenes, the first example of water-soluble calixarenes.[8] The subsequent investigations on these calixarenes established that they can form host-guest-type complexes with a variety of guest molecules in an aqueous system.[9-12] During these studies, we noticed an interesting spectral change in Phenol Blue: In the presence of hexasulfonated calix[6]arene (**2C**$_{12}$), the absorption maximum (658 nm in water) moves to 592 nm at low concentration region followed by a relatively small blue shift (630 nm) at high concentration region.[9] The λ_{max} 630 nm was equal to the blue shift induced by the sodium dodecyl sulfate(SDS) micelle,[9] but the origin of the unusually large blue shift to 592 nm was not explained until recently. We found, as described in this paper, that this blue shift is due to "protonation" of Phenol Blue in neutral aqueous solution (Eq. 1). The finding suggests that hexasulfonated calix[6]arenes, which have six anionic groups on the upper rim of the calixarene cavity, have some special architecture effecive to stabilize included cationic species.

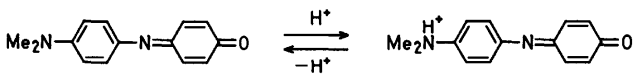

(1)

In 1973, Gokel and Cram[13] found that crown ethers of the proper dimensions can solubilize several arenediazonium salts in nonpolar media (e.g., chloroform). Subsequent spectroscopic studies established that the solubilization is caused by complexation, like complexation between crown and metal cation, the linear Ar-N^+≡N inserting into the hole of the crown ring with its oxygen atoms turned inward toward the positive charge as shown in structure **1**.[13-19] As expected from the complex structure, the association constants (K) for crown-arenediazonium complexes are affected by both electronic effects and steric effects:[13-20] for example, strongly electron-donating groups (e.g, Et_2N-) in arenediazonium salts depress complexation to such extent that the K values cannot be determined[20] and the sterically hindered 2,6-dimethylbenzenediazonium salt is not complexed by crown ethers.[14] Of additional interest is the finding that the thermal decomposition of arenediazonium salts is slowed down when the salts are complexed by crown ethers.[17-19,21-23] This stabilization effect is attributed to the attenuation of the positive charge at the diazonium group in the complex[13,14,19] and to the retardation of the decomplexation rate.[23]

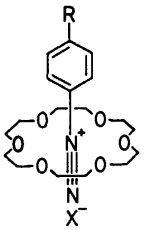

1

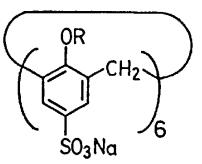

2C
2C$_1$: R=Me-
2C$_6$: R=Me$(CH_2)_5$-
2C$_{12}$: R=Me$(CH_2)_{11}$-

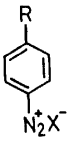

3R
3H: R=H-
3C$_6$: R=Me$(CH_2)_5$-
3Cl: R=Cl

Based on the foregoing results, we considered that **2C** may form stable complexes with arenediazonium salts (**3R**) and may stabilize them even in an aqueous system.[24] We here report that (i) the absorption maximum of Phenol Blue undergoes the unusual blue shift in the presence of **2C**$_{12}$ due to electrostatic stabilization of protonated Phenol Blue, (ii) the dediazoniation of **3R** is significantly suppressed by complexation with **2C** even in an aqueous system where neither crown ethers nor anionic micelles are effective, and (iii) the rates of diazo coupling with *N,N*-dimethyl-

aniline and 3-hydroxy-2,7-naphthalenedisulfonate (R-acid) are selectively slowed down.

Experimental

Materials. Preparations of 5,11,17,23,29,35-hexasulfonato-37,38,39,40,41,42-hexamethoxycalix[6]arene (**2C**$_1$), 5,11,17,23,29,35-hexasulfonato-37,38,39,40,41,42-hexakis(hexyloxy)calix[6]arene (**2C**$_6$), and 5,11,17,23,29,35-hexasulfonato-37,38,39,40,41,42-hexakis(dodecyloxy)calix[6]arene (**2C**$_{12}$) were described in a previous paper of this series.[9]

Kinetic Measurements. The rate constants for the dediazoniation were estimated as follows. Compound **3R** was prepard from aniline (or *p*-hexylaniline) by the reaction with $NaNO_2$ in 0.05 M† H_2SO_4 solution at 0—5 °C and then diluted with 0.024 M H_2SO_4 solution. This solution (containing [**3R**]=1.00×10^{-3} M) was mixed with **2C** and maintained in the dark at 30 °C in a thermostated water bath. Aliquots were withdrawn from the reaction mixture and treated with 3-hydroxy-2,7-naphthalenedisulfonate in 0.10 M Na_2CO_3 solution. The concentration of unreacted **3R** was determined using a calibration curve by the absorption band (490 nm) of the diazo-coupling product. The plots of OD_{490} vs. reaction time were first-order for up to three half-lives.

The reaction between *p*-chlorobenzenediazonium ion **3Cl** and *N,N*-dimethylaniline (or 3-hydroxy-2,7-naphthalenedisulfonate) was followed spectrophotometrically at 30 °C. *p*-Chloroaniline was diazotized with $NaNO_2$ and diluted with an aqueous solution buffered to pH 6.92 (0.05 M phosphate) for *N,N*-dimethylaniline and to pH 4.80 (0.05 M acetate) for 3-hydroxy-2,7-naphthalenedisulfonate. This solution was equilibrated to 30 °C in a spectrophotometer and then mixed with 100 μl of aqueous *N,N*-dimethylaniline (or 3-hydroxy-2,7-naphthalenedisulfonate): [*p*-chlorobenzenediazonium ion]=4.96×10^{-5} M, [*N,N*-dimethylaniline]=1.51×10^{-3} M, [3-hydroxy-2,7-naphthalenedisulfonate]=1.10×10^{-3} M. The pseudo-first-order rate constants were estimated from the time-dependent appearence of a new absorption band for the product (440 nm for *N,N*-dimethylaniline and 490 nm for 3-hydroxy-2,7-naphthalenedisulfonate).

Results and Discussion

Absorption Spectra of Phenol Blue in the Presence of 2C. Brooker and Sprauge[25] suggested the use of Phenol Blue (PB) as a solvent property indicator; the absorption maximum (668 nm in water;[25] 658 nm according to our measurement at 30 °C) shifts to shorter wavelengths in nonpoler solvents e.g., 552 nm in cyclohexane). The blue shift is attributed to destabilization of the charge-separated excited state PB$^{\pm}$.

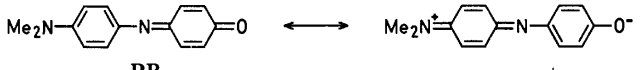

PB PB$^{\pm}$ (2)

In the presence of **2C**$_{12}$ at pH 5.6 (no buffer), the λ_{max} of PB shifts to 592 nm at around [**2C**$_{12}$]/[PB]≈1 and then moves to 630 nm at [**2C**$_{12}$]/[PB]>1 (Fig. 1). The absorption band at 592 nm is attributable to protonated species of PB, because (i) the similar absorption

† 1 M=1 mol dm^{-3}.

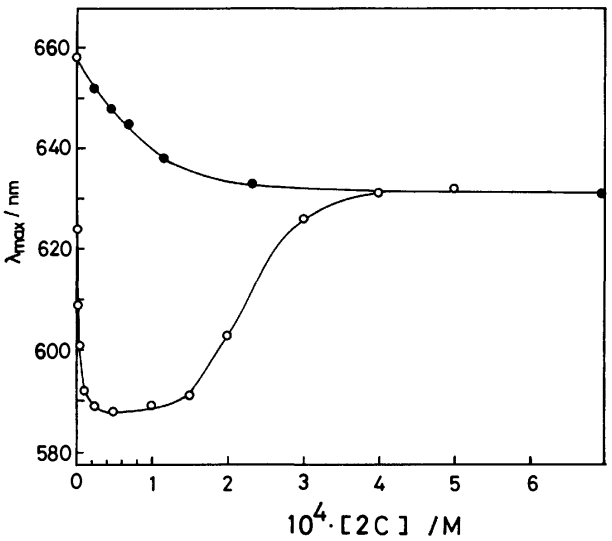

Fig. 1. Absorption maximum of Phenol Blue vs. 2C$_{12}$ concentration: ○ at pH 5.6 (no buffer), ● at pH 8.7 with 0.02 M borate buffer. 30 °C, [Phenol Blue]=1.00×10^{-5} M.

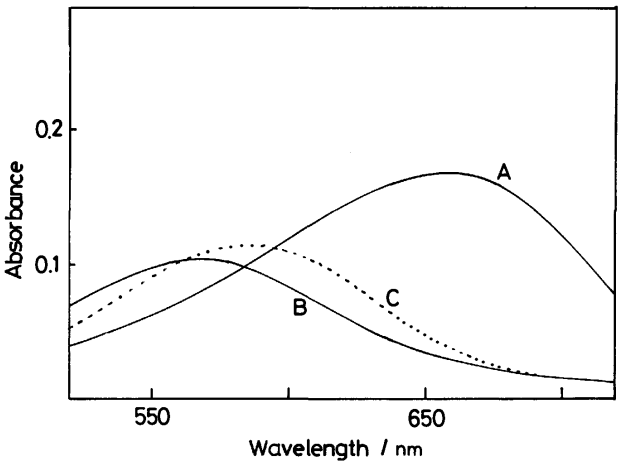

Fig. 2. Absorption spectra of Phenol Blue (1.00×10^{-5} M) at 30 °C: (A) pH 5.6 (no buffer), (B) pH 3.2 (with HCl), (C) pH 5.6 (no buffer, [**2C**$_{12}$]=1.00×10^{-4} M).

spectra (λ_{max} 570—590 nm) can be reproduced in acidic aqueous solution in the absence of **2C**$_{12}$ (Fig. 2) and (ii) the biphasic dependence of λ_{max} disappears in buffered aqueous solution (pH 8.7 with 0.02 M borate) (Fig. 1). This finding supports that protonated PB is strongly stabilized through inclusion in the cavity of **2C**$_{12}$. In Fig. 3, OD_{650} is plotted against pH. The solution pH was adjusted by HCl below pH 6 and aqueous NH_3 above pH 6. Thus, the pK_a of PB was estimated to be 4.6. In the presence of **2C**$_{12}$ the pK_a shifted to 6.2 (ΔpK_a=1.6), indicating that the included PB behaves as an apparently stronger base. The similar pK_a shift was also observed in the presence of the SDS micelle (pK_a=5.4; ΔpK_a=0.8), but the magnitude of the pK_a shift was about one-half.

The remarkable stabilization effect of $2C_{12}$ would be explained in two ways: That is, (i) oxonium ions are locally concentrated around $2C_{12}$ owing to the electrostatic interaction, resulting in a facile protonation of PB and (ii) hexa-anionic sulfonato groups stabilized the included, protonated PB through the host-guest-type electrostatic interaction. The effect (i) should be operative in the present system because addition of inorganic salts (e.g., NaCl) reduces the magnitude of the pK_a shift. This can be rationalized in terms of competitive binding of Na^+ and H_3O^+ to the anionic sulfonato groups. The effect (ii) should be also important. We have found that the "cone" conformation is favorably adopted when a guest molecule is included in the cavity of calixarenes.[26] When **2C** adopts the cone conformation, six sulfonato groups are circularly arranged on one side of the calixarene cavity (Scheme 1). This unusual architecture would exert the remarkable stabilization effect on included cationic species. It is not easy to distinguish two effects on the basis of the present qualitative experiments. Probably, it is reasonable to consider that two effects are operative synergisticallly. If the effect (ii) contributes to the pK_a shift to a significant extent, one can extend this study to an interesting idea: That is, arenediazonium ions could be also stabilized through complexation with **2C**.

Stabilization of Arenediazonium Ions. In the thermal decomposition of **3H**, we found by a GLC method that phenol is afforded in 58—65% yield as a sole detectable product in the absence and the presence of **2C**([$2C_{12}$]=2.00 mM, 50 °C, 24 h). This indicates that the dediazoniation proceeds according to the ionic reaction path and the radical reaction path is not included.

The first-order rate constants (k_d) for the dediazoniation of **3H** and $3C_6$ are summarized in Table 1 and plots of k_d vs. [**2C**] for **3H** are illustrated in Fig. 4. Examination of Table 1 leads to the following conclusions: (i) in an aqueous system, neither 18-crown-6 nor anionic micelles suppress the thermal decomposition

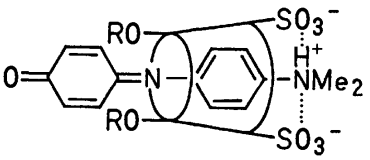

Scheme 1.

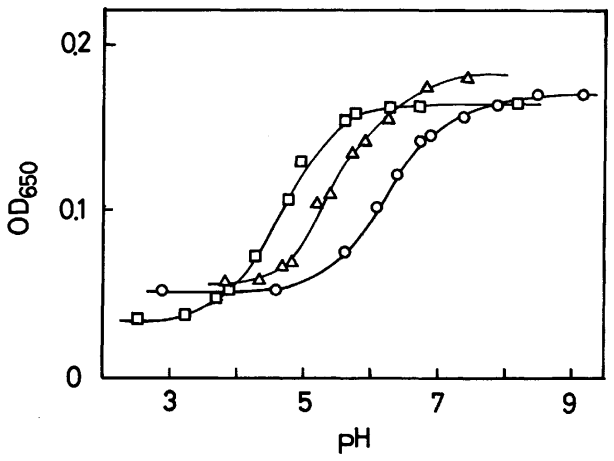

Fig. 3. pH-Dependence of the absorption band (650 nm) of Phenol Blue (1.00×10^{-5} M) at 30 °C: □ no additive, △ SDS (2.00×10^{-2} M), ○ $2C_{12}$ (1.00×10^{-5} M).

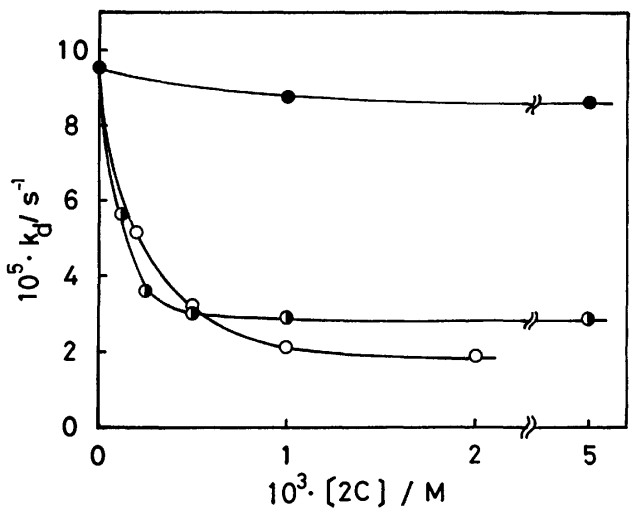

Fig. 4. Dediazoniation of **3H** (5.00×10^{-4} M) in the presence of **2C** at 30 °C: ● $2C_1$, ◑ $2C_6$, ○ $2C_{12}$.

Table 1. First-Order Rate Constants (k_d) for Thermal Decomposition of Arenediazonium Salts (**3R**) at 30 °C

Additive (concn/mM)	**3H**		$3C_6$	
	$10^5 \cdot k_d/s^{-1}$	k_d/k_0	$10^5 \cdot k_d/s^{-1}$	k_d/k_0
None	9.52(=k_0)	1.00	1.60(=k_0)	1.00
$2C_1$ (5.00)	8.62	0.91	1.27	0.79
$2C_6$ (5.00)	2.92	0.31	0.37	0.23
$2C_{12}$ (2.00)	1.91	0.20	0.37	0.23
18-Crown-6 (24.4)	9.25	0.97	—	—
SDS[a] (20.0)	8.84	0.93	—	—
SDBS[b] (47.0)	8.72	0.92	—	—
Sodium *p*-toluenesulfonate (5.00)	9.46	0.99	—	—
Disodium 1,5-naphthalenedisulfonate (4.58)	9.60	1.01	—	—

a) Sodium dodecylsulfate: the cmc is 6.6 mM. b) Sodium dodecylbenzenesulfonate: the cmc is 1.2 mM.

of **3R** to a significant extent, (ii) 1,5-naphthalenedisulfonate, which is used as a stabilizer for arenediazonium salts in the solid state, is also ineffective, and (iii) the k_d values decrease with increasing concentration of **2C** and in particular, $2C_{12}$ can reduce the k_d to 20—23% of those observed in the absence of **2C**. The fact (iii) is sharply contrastive to the fact (i) that 18-crown-6 can stabilize arenediazonium salts only in certain organic solvents but not at all in an aqueous system. These findings suggest that hexasulfonato calixarene derivatives have some specific architecture to stabilize **3R** even in an aqueous system. From the scheme depicted in Eq. 3, we estimated the association constans (K) and the intra-complex dediazoniation rate constants ($k_{complex}$) for 3H assuming the formation of a 1 : 1 complex:[††] K=ca. 10^2 M^{-1} for $2C_1$, 4.2×10^6 M^{-1} for $2C_6$, and 5.6×10^4 M^{-1} for $2C_{12}$; $k_{complex}=8.62\times10^{-5}$ s^{-1} for $2C_1$, 2.92×10^{-5} s^{-1} for $2C_6$, and 1.91×10^{-5} s^{-1} for $2C_{12}$. These results support that hexa-anionic **2C** can form stable complexes with cationic **3H**. Since the K values for $2C_6$ and $2C_{12}$ are much greater than that for $2C_1$, not only the electrostatic interaction but also the hydrophobic force is operative in the association with **3H**. We previously found that $2C_6$ forms micelle-like aggregates, the cmc being detected at 0.6 mM while $2C_{12}$ acts as a "unimolecular" micelle at 10^{-5}—10^{-3} M region forming host-guest type 1 : 1 complexes with guest molecules.[9] The fact that the K for $2C_6$ is greater by a factor of 75 than that for $2C_{12}$ may be due to the aggregate formation of $2C_6$.

$$\begin{array}{ccc} 3H + 2C & \overset{K}{\rightleftharpoons} & 3H\cdot 2C \\ \downarrow k_0(=9.52\times10^{-5}s^{-1}) & & \downarrow k_{complex} \\ \text{product} & & \text{product} \end{array} \qquad (3)$$

To obtain an insight into the binding mode of **3R** into the calixarene cavity, we examined the solvent effect on the dediazoniation rate because the hydrophobic effect in an aqueous system is partly reproduced by the solvent effect. We used 4-(4-dimethylaminophenylazo)benzenediazonium tetrafluoroborate (**4**) as a spectroscopic probe. The absorption maximum of **4** shifts to shorter wavelengths in nonpolar solvents: For example, λ_{max} 612 nm in water, 579 nm in tetrahydrofuran, and 558 nm in dioxane (30 °C). In Fig. 5, the λ_{max} is plotted against the dioxane concentration in water. The λ_{max} shifts to shorter wavelengths with increase in the dioxane concentration. In an aqueous system, the λ_{max} was not affected by the addition of $2C_1$ (2.00 mM) but shifted to 609 and 595 nm in the presence of $2C_6$ and $2C_{12}$ (2.00 mM), respectively. These wavelenghts correspond to the aqueous solutions containing 25 and 85 vol% of dioxane. This implies that **3R** is bound to the relatively hydrophobic site in the calixarene cavity.

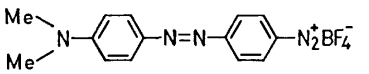

4

In Fig. 6, the k_d values are plotted against the λ_{max} of **4**. The open circles indicate the rate constants obtained for **3H** in an aqueous system in the presence of additives, and the filled circles indicate the rate constants obtained for benzenediazonium tetrafluoroborate in a dioxane-water system. It is seen from Fig. 6 that the plots for most additives are not so different from those for a dioxane-water system, but two plots

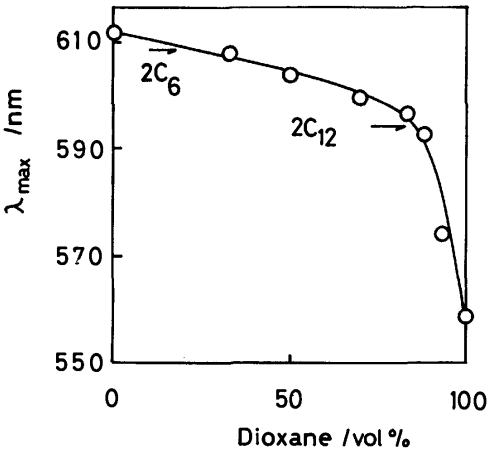

Fig. 5. Absorption maximum of **4** (1.78×10^{-5} M) in water-dioxane at 30 °C. The arrows indicate the "hydrophobicity" of **2C** in an aqueous system.

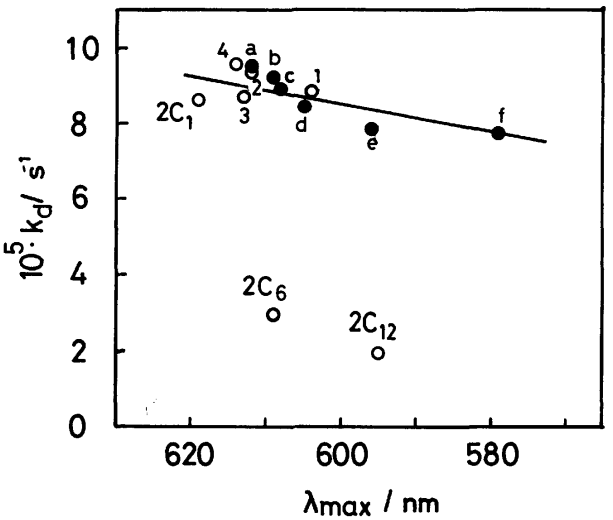

Fig. 6. First-order rate constant for the dediazoniation of **3H** vs. absorption maximum of **4** (the longer the wavelength, the more hydrophobic): (1) SDS (2.00×10^{-2} M), (2) sodium *p*-toluenesulfonate (5.00×10^{-3} M), (3) sodium dodecylbenzenesufonate (4.70×10^{-2} M), (4) disodium naphthalene-1,5-disulfonate (4.58×10^{-3} M). (a)—(f) indicate a water-dioxane system; the dioxane concentrations (vol%) are (a) 0, (b) 25, (c) 33, (d) 49, (e) 82, (f) 93.

[††]The detailed calculation method equivalent to Eq. 3 was described previously: S. Shinkai, T. Minami, Y. Kusano, and O. Manabe, *J. Am. Chem. Soc.*, **105**, 1851 (1983).

for $2C_6$ and $2C_{12}$ are distinctly deviated from this relationship. This implies that the stabilization effect of $2C_6$ and $2C_{12}$ is not fully explained by the hydrophobic effect. We believe that the specific stabilization is due to the strong anionic field brought about by six sulfonato groups on the edge of the calixarene cavity. Therefore, the hexasulfonated calix[6]arene has an architecture very favorable to stabilize the complexed arenediazonium ions.

Influence on the Diazo-Coupling Reactions. The decomposition of arenediazonium ions is efficiently suppressed through complexation with hexasulfonated calix[6]arenes. As a next stage, it is of a great significance to examine the reactivity of these stabilized arenediazonium ions in the diazo-coupling reactions. However, this seems fairly difficult because in contrast to the unimolecular dediazoniation the rate of the bimolecular diazo-coupling reaction reflects not only the reactivity of arenediazonium ions but also the local concentration effect. We chose the reaction with neutral species, *N*,*N*-dimethylaniline (DA) in order to obviate at least the complexity arising from the electrostatic interaction and repulsion between charged reactants. As **3H** and $3C_6$ did not exhibit a measurable reactivity toward DA, we employed more reactive arenediazonium ion, *p*-chlorobenzenediazonium (**3Cl**).

First, we tested whether the dediazoniation of **3Cl** is really suppressed by **2C**. The reaction was carried out at 60 °C because **3Cl** decomposed very slowly at 30 °C. As shown in Fig. 7, this reaction is also slowed down in the presence of $2C_6$ and $2C_{12}$: $K=5.0\times10^4$ M and $k_d/k_0=0.18$ for $2C_6$ (2.00 mM) and $K=5.2\times10^4$ M and $k_d/k_0=0.30$ for $2C_{12}$ (2.50 mM). In Fig. 8, the pseudo-first-order rate constants (k_c) for the diazo-coupling reaction at 30 °C are plotted against the calixarene concentrations. The k_c for sodium dodecyl sulfate (SDS; the cmc is 6.6 mM) sharply increased at 0—7 mM region and then decreased at higher concentration region. The biphasic dependence can be explained by the micellar effect on the bimolecular reaction:[27] The rate acceleration at the low concentration region would be due to the formation of a hydrophobic ion pair[27,28] between **3Cl** and SDS leading to the enhancement in the local concentration, whereas the rate retardation at the high concentration region would be due to the so-called dilution effect caused by the micellar aggregates.[27] The effect of added **2C** is quite contrasting: $2C_6$ and $2C_{12}$ which strongly associated with arenediazonium ions decelerated the reaction monotonously, while $2C_1$, which associated with arenediazonium ions only weakly accelerated the reaction to some extent. The typical rate constants are summarized in Table 2.

Probably, one has to take two different effects into consideration to account for the kinetic results in Fig. 8. The first is the stabilization of **3Cl** through complexation with **2C**, leading to the rate retardation. The second effect is the concentration of reactants in the calixarene cavity, leading to the rate acceleration as seen for the SDS system. As shown in Fig. 8 and Table 2, the k_c values were decreased by 11—13 fold in the presence of $2C_6$ and $2C_{12}$ in spite of the expected, positive contribution of the concentration effect. This suggests that arenediazonium ions included in the calixarene cavity are considerably deactivated. However, it is also possible to explain the kinetic data in a different way on the basis of the concentration effect: For example, possible explanations are (i) the cavity of **2C** can accept only one guest molecule and therefore

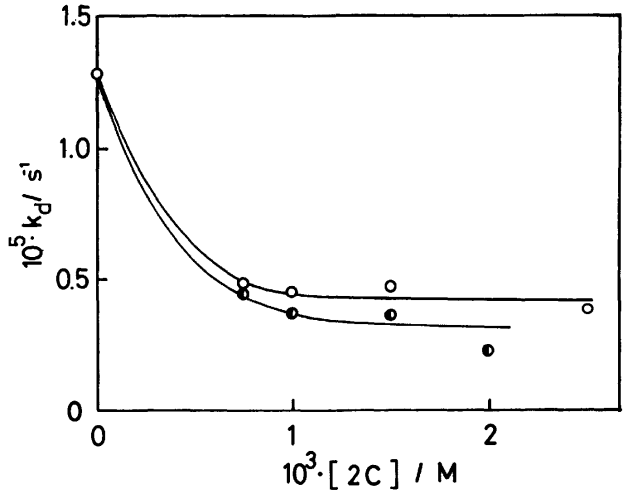

Fig. 7. Dediazoniation of **3Cl** (5.00×10^{-4} M) in 0.024 M H_2SO_4 at 60 °C: ◐ $2C_6$, ○ $2C_{12}$.

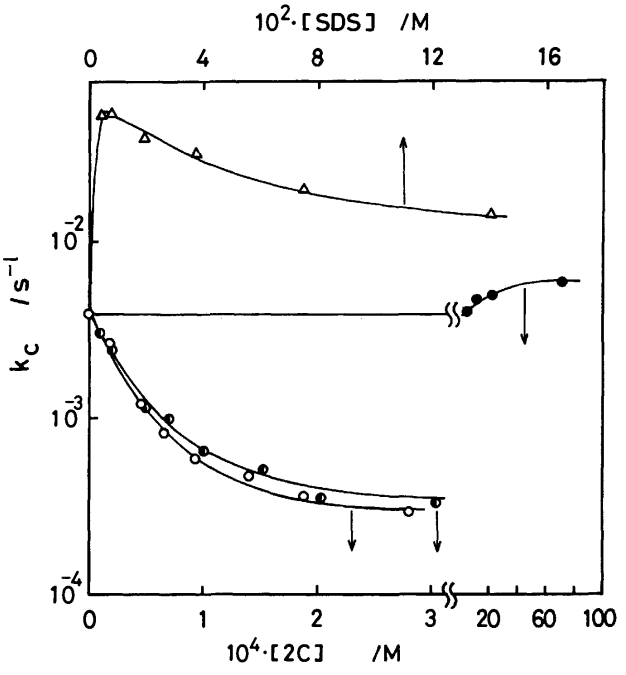

Fig. 8. Semi-log plots for diazo coupling of **3Cl** (4.96×10^{-5} M) with *N*,*N*-dimethylaniline (1.51×10^{-3} M) at 30 °C and pH 6.92 with 0.05 M phosphate buffer. ● $2C_1$, ◐ $2C_6$, ○ $2C_{12}$, △ SDS.

Table 2. Pseudo-First-Order Rate Constants (k_c) for the Diazo-Couping Reactions at 30 °C

Calixarene (concn/mM)	*N*,*N*-Dimethylaniline		3-Hydroxy-2,7-naphthalenedisulfonate	
	$10^3 \cdot k_c/s^{-1}$	k_c/k_0	$10^4 \cdot k_c/s^{-1}$	k_c/k_0
None	3.86 (=k_0)	1.00	3.56 (=k_0)	1.00
$2C_1$ (7.04)	5.90	1.53	2.15	0.60
$2C_6$ (0.271)	0.350	0.091	0.087	0.024
$2C_{12}$ (0.297)	0.297	0.077	0.058	0.016
SDS (7.51)	52.7	14	0.715	0.20
SDS (108)	15.9	4.12	0.070	0.020

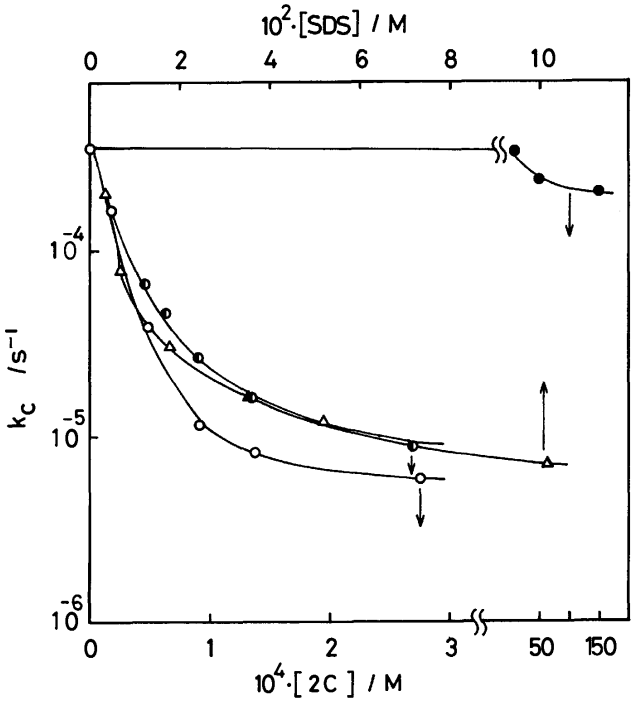

Fig. 9. Semi-log plots for diazo coupling of **3Cl** (4.96×10^{-5} M) with 3-hydroxy-2,7-naphthalenedisulfonate (1.10×10^{-3} M) at 30 °C and pH 4.80 with 0.05 M acetate buffer. ● $2C_1$, ◐ $2C_6$, ○ $2C_{12}$, △ SDS.

retards the rate of the bimolecular diazo coupling and (ii) **2C** has two binding sites, one consisting of sulfonated benzene rings suitable to bind a cationic guest molecule (e.g., **3Cl**) and the other consisting of alkyl (hexyl or dodecyl) groups suitable to bind a neutral guest molecule (e.g., DA). In either case, the reaciton rate should be suppressed by the apparent dilution of reactants. In particular, the case (ii) is likely because $2C_1$, in which the binding site consisting of alkyl (methyl) groups is relatively weak accelerates the reaction rate (Fig. 8). At present we believe that the efficient rate retardation results from both the deactivation of **3Cl** and the dilution of **3Cl** and DA.

The effect of added **2C** may be shown more clearly by the combination with the electrostatic repulsion. This combination may be of some significance because the diazo-coupling reaction usually includes the attack of cationic arenediazonium ions at anionic species (e.g., phenolate anion). We chose 3-hydroxy-2,7-naphthalenedisulfonate (pK_a 9.42 under the present reaction conditions). The kinetic results are illustrated in Fig. 9. We found that the reaction is strongly inhibited by $2C_6$ and $2C_{12}$, the rate constants being smaller by 42—63 fold than that in a non-additive system (Table 2). A similar rate retardation was observed for SDS, the inhibition effect (50 fold) being comparable with that for $2C_6$ and $2C_{12}$. One can thus envisage a reaction mode such **3Cl** is bound to the anionic calixarene or to the SDS micelle by the electrostatic interaction and 3-hydroxy-2,7-naphthalenedisulfonate is separated by the electrostatic repulsion. Since the inhibition effect is comparable between **2C** and SDS, this reaction should be primarily governed by the electrostatic effect and the stabilization of **3Cl** by **2C** should play only a secondary role. It is worthy mentioning, however, that $2C_6$ and $2C_{12}$ sufficiently inhibit the reaction at 10^{-4} M region while the same inhibition is attained by 10^{-2} M SDS. This implies that the electrostatic effect of **2C** is much superior to that of the SDS micelle.

Conclusion

The present study demonstrated that hexasulfonated calixarene can provide a very strong anionic environment which is effective to suppress the dediazoniation and the diazo coupling. The novel behaviors arise from the peculiar architecture of **2C** which has six anionic charges on the upper rim of the calixarene cavity. Further applications to host molecules, catalysts, etc. are now continued in this laboratory.

This research was supported by the Grant-in-Aid from the Ministry of Education.

References

1) C. D. Gutsche, *Acc. Chem. Res.*, **16**, 161 (1983).
2) C. D. Gutsche, "Host Guest Complex Chemistry/Macrocycles," Springer-Verlag, Berlin (1985), p. 375.
3) S.-K. Chang, *Chem. Lett.*, **1984**, 477.
4) R. Ungaro, A. Pochini, and G. D. Andreetti, *J. Inclusion Phenom.*, **2**, 199 (1984).
5) M. A. McKervey, E. M. Seward, G. Ferguson, B. Ruhl, and S. J. Harris, *J. Chem. Soc., Chem. Commun.*, **1985**, 388.
6) R. M. Izatt, J. D. Lamb, R. T. Hawkins, P. R. Brown, S. R. Izatt, and J. J. Christensen, *J. Am. Chem. Soc.*, **105**, 1782 (1983).

7) S. R. Izatt, R. T. Hawkins, J. J. Christensen, and R. M. Izatt, *J. Am. Chem. Soc.*, **107**, 63 (1985).
8) S. Shinkai, S. Mori, T. Tsubaki, T. Sone, and O. Manabe, *Tetrahedron Lett.*, **25**, 5315 (1984).
9) S. Shinkai, S. Mori, H. Koreishi, T. Tsubaki, and O. Manabe, *J. Am. Chem. Soc.*, **108**, 2409 (1986).
10) S. Shinkai, H. Koreishi, S. Mori, T. Sone, and O. Manabe, *Chem. Lett.*, **1985**, 1033.
11) S. Shinkai, H. Koreishi, K. Ueda, and O. Manabe, *J. Chem. Soc., Chem. Commun.*, **1986**, 233.
12) S. Shinkai, K. Araki, H. Koreishi, T. Tsubaki, and O. Manabe, *Chem. Lett.*, **1986**, 1351.
13) G. W. Gokel and D. J. Cram, *J. Chem. Soc., Chem. Commun.*, **1973**, 482.
14) E. P. Kyba, R. C. Helgeson, K. Madan, G. W. Gokel. T. L. Tarnowski, S. S. Moore, and D. J. Cram, *J. Am. Chem. Soc.*, **99**, 2564 (1977).
15) B. L. Haymore, J. A. Ibers, and D. W. Meek, *Inorg. Chem.*, **14**, 541 (1975).
16) S. H. Korzeniowski, R. J. Petcavich, M. M. Coleman, and G. W. Gokel, *Tetrahedron Lett.*, **1977**, 2647; J. R. Beadle, R. K. Khanna, and G. W. Gokel, *J. Org. Chem.*, **48**, 1242 (1983).
17) R. A. Bartsch, H. Chen, N. F. Haddock, and P. N. Juri, *J. Am. Chem. Soc.*, **98**, 6753 (1976).
18) R. A. Bartsch and P. N. Juri, *J. Org. Chem.*, **45**, 1011 (1980).
19) G. W. Gokel, S. H. Korezeniowski, and L. Blum, *Tetrahedorn Lett.*, **1977**, 1633; S. H. Koreniowski and G. W. Gokel, *ibid.*, **1977**, 1637.
20) R. M. Izatt, J. D. Lamb, B. E. Rossiter, N. E. Izatt, and J. J. Christensen, *J. Chem. Soc., Chem. Commun.*, **1978**, 386; R. M. Izatt, J. D. Lamb, C. S. Swain, J. J. Christensen, and B. L. Haymore, *J. Am. Chem. Soc.*, **102**, 3032 (1980).
21) P. N. Juri and R. A. Bartsch, *J. Org. Chem.*, **44**, 143 (1979).
22) J. R. Beadle and G. W. Gokel, *Tetrahedron Lett.*, **25**, 1681 (1984).
23) H. Nakazumi, I. Szele, K. Yoshida, and H. Zollinger, *Helv. Chim. Acta*, **66**, 1721 (1983).
24) S. Shinkai, S. Mori, T. Arimura, and O. Manabe, *J. Chem. Soc., Chem. Commun.*, **1987**, 238.
25) L. G. S. Brooker and R. H. Sprauge, *J. Am. Chem. Soc.*, **63**, 3214 (1941).
26) S. Shinkai and K. Araki, unpublished results.
27) J. H. Fendler and E. J. Fendler, "Catalysis in Micellar and Macromolecular Systems," Academic Press, New York (1975).
28) T. Kunitake and S. Shinkai, *Adv. Phys. Org. Chem.*, **17**, 435 (1980).

 © 1987 The Chemical Society of Japan Bull. Chem. Soc. Jpn., 60, 3687—3691 (1987)

Asymmetric Radical Reaction in the Coordination Sphere. III.[1] Asymmetric Addition of Trichloromethanesulfonyl Chloride and Carbon Tetrachloride to Olefins Catalyzed by a Ruthenium(II) Complex with Chiral Ligand

Masayuki KAMEYAMA and Nobumasa KAMIGATA*
Department of Chemistry, Faculty of Science, Tokyo Metropolitan University, Fukazawa, Setagaya-ku, Tokyo 158
(Received April 23, 1987)

The asymmetric addition of trichloromethanesulfonyl chloride to styrene in the presence of a catalytic amount of a ruthenium(II) complex with chiral ligands, Ru_2Cl_4[(−)-diop]$_3$ or Ru_2Cl_4[(+)-diop]$_3$, proceeds under mild conditions to give optically active 1 : 1 adducts, 1,1,1,3-tetrachloro-3-phenylpropane (**2**), with the extrusion of sulfur dioxide. When (−)-DIOP or (+)-DIOP was used as a chiral ligand of the ruthenium(II) complex, (*R*)-(+)-(**2**) or (*S*)-(−)-(**2**), was obtained with about 10% enantiomeric excess, respectively. A reaction mechanism involving a radical redox transfer mechanism was proposed; the asymmetric induction was attributed to the restricted configuration of the radical intermediates confined in the coordination sphere of the ruthenium complex with chiral ligands.

We recently reported that the addition reaction of arene- and alkanesulfonyl chlorides with olefins catalyzed by a dichlorotris(triphenylphosphine)ruthenium(II) under mild conditions affords 2-chlorosulfones in high yield.[2] On the other hand, the addition of trichloromethanesulfonyl chloride to olefins catalyzed by the ruthenium(II) complex affords 1 : 1 adducts, 1,1,1,3-tetrachloropropanes, with the extrusion of sulfur dioxide.[3] A reaction mechanism involving a radical redox transfer process is proposed. The intermediate radicals generated by interactions of sulfonyl chlorides with the ruthenium(II) complexes are considered to be confined in the coordination sphere of the metal complexes and to have different features from such a free radical as that initiated by irradiation or decomposition of peroxides.

We suppose that the relation between a free radical and the radical in the coordination sphere of the metal complex closely resembles the relation between a carbene and a carbenoid. Nozaki and Noyori first reported that an asymmetric addition of alkyl diazoacetate with olefins catalyzed by a copper complex with chiral ligand gave optically active cyclopropanes.[4] This reaction involves a carbenoid intermediate generated by an interaction of the diazoacetate with the metal complex. The carbenoid was affected by the chiral ligand and differentiated the enantioface of the olefin in the addition step. Thus, an asymmetric induction is expected in the reaction of sulfonyl chloride with olefin, which proceeds by a radical reaction in the coordination sphere. In a preliminary paper, we reported that arene- and alkanesulfonyl chlorides reacted with styrenes in the presence of a ruthenium(II) complex with chiral ligand, Ru_2Cl_4[(−)-diop]$_3$ ((−)-**1**) or Ru_2Cl_4[(+)-diop]$_3$ ((+)-**1**), as a catalyst to give optically active 1 : 1 adducts.[5] We report, herein, an asymmetric radical addition of trichloromethanesulfonyl chloride to olefins catalyzed by the ruthenium(II) complex with chiral ligand **1**.

Results and Discussion

The reaction of trichloromethanesulfonyl chloride with olefin was carried out by using the ruthenium(II)-DIOP complex **1** as a catalyst. When Ru_2Cl_4-[(−)-diop]$_3$ ((−)-**1**) was used, the reaction of trichloromethanesulfonyl chloride with styrene at 100 °C for 6 h in a degassed tube gave 1 : 1 adduct (**2a**) quantitatively with extrusion of sulfur dioxide. The adduct showed a specific rotation $[\alpha]_D$ +12° (*c* 12, benzene). Similarly, the reaction of trichloromethanesulfonyl chloride with styrene in the presence of Ru_2Cl_4[(+)-diop]$_3$ ((+)-**1**) was carried out; adduct **2a** was obtained quantitatively and showed $[\alpha]_D$ −10° (*c* 11, benzene).

$$Cl_3CSO_2Cl + ArCH{=}CH_2 \xrightarrow[-SO_2]{Ru_2Cl_4(diop)_3\ (1)} Ar\overset{*}{C}HCH_2CCl_3 \quad (Cl)$$

2

The enantiomeric excess and absolute configuration of products **2** in the present reactions were estimated by converting to a known optically active compound. The adduct (−)-**2a**, which showed $[\alpha]_D$ −10° (*c* 11, benzene), was treated with sodium azide to give 3-azido-1,1,1-trichloro-3-phenylpropane (**3a**),[6] which was reduced with lithium aluminum hydride to afford 1-amino-1-phenylpropane (**4a**).[7] Amine **4a** showed $[\alpha]_D$ +2.1° (*c* 2.3, benzene) and was determined to be 10% enantiomeric excess and (R)-configuration. In a similar way, the adduct (+)-**2a** ($[\alpha]_D$ +12° (*c* 12, benzene)) was converted to amine **4a**, which showed $[\alpha]_D$ +3.1° (*c* 1.7, benzene) and corresponded to 14% ee of (S)-isomer.

The optical yield of **2a** was also determined by a HPLC analysis of the diastereomer (**5a**) derived from the amine **4a**. Amine **4a** was treated with (*S*)-MTPA-Cl,[8] prepared by the reaction of (*S*)-MTPA (MTPA=2-methoxy-2-trifluoromethylphenylacetic acid) with thionyl chloride, to give the diastereomeric MTPA-

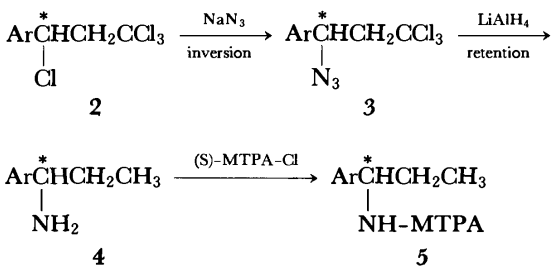

amide (**5a**). The diastereomer **5a** was separated into two isomer peaks by HPLC. Thus, the optical yield of adduct **2a** was estimated to be 14% ee. Similarly, the addition of trichloromethanesulfonyl chloride to several styrenes was carried out, and the optical purity of the products (**2b—d**) was also determined by HPLC analysis of the diastereomeric MTPA-amide. The results are summarized in Table 1.

The reaction products, 1,1,1,3-tetrachloro-3-arylpropanes, in the reaction of trichloromethanesulfonyl chloride with olefins corresponded to the adducts obtained by the addition of carbon tetrachloride to olefins. Matsumoto and Nagai have reported that a radical addition reaction of carbon tetrachloride with olefin catalyzed by the ruthenium(II) complex proceeds by a radical redox transfer mechanism and the intermediate radicals are considered to be confined in the coordination sphere of the ruthenium complex.[9] Thus, an asymmetric radical addition of carbon tetrachloride to olefins can also be expected by using the ruthenium(II) complex with chiral ligands as a catalyst.

When the ruthenium(II)-(−)-DIOP complex (−)-**1** was used as a catalyst, the addition reaction of carbon tetrachloride with styrene at 100 °C for 6 h gave 1 : 1 adduct (**2a**) in 73% yield.

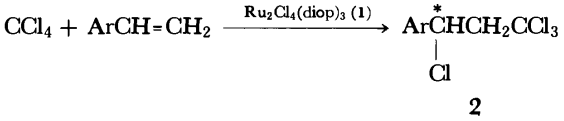

Adduct **2a** showed a specific rotation $[\alpha]_D$ +12° (*c* 6.1, benzene). Similarly, when (+)-**1** was used as a catalyst, adduct **2a** was obtained in 68% yield and showed $[\alpha]_D$ −10° (*c* 5.3, benzene). The optical yields and absolute configurations of products **2** were determined by comparing the optical rotation of **4**, which was derived

Table 1. Reaction of Trichloromethanesulfonyl Chloride with Styrene Derivatives

Ar	DIOP	Product	$[\alpha]_D$/° (*c*, in PhH)	Chemical yield/%	Optical yield/%ee[a]	Absolute configuration
C_6H_5	(−)	**2a**	+12 (12)	97	13 (14)	R
C_6H_5	(+)	**2a**	−10 (11)	100	7 (10)	S
p-$CH_3C_6H_4$	(−)	**2b**	+11 (24)	98	—[c]	R
p-$CH_3C_6H_4$	(+)	**2b**	− 9 (23)	100	—[c]	S
p-ClC_6H_4	(−)	**2c**	+ 7 (23)	89	13	R
p-ClC_6H_4	(+)	**2c**	− 7 (23)	87	9	S
m-$O_2NC_6H_4$	(−)	**2d**	+ 7 (36)[b]	79	—[d]	R
m-$O_2NC_6H_4$	(+)	**2d**	− 7 (39)[b]	87	—[d]	S

a) Optical yields were estimated by HPLC of MTPA-amides and optically pure sample reported as $[\alpha]_D$+21.7° (PhH) in parentheses. b) The reaction was carried out for 24 h. c) The amine **4b**, which was converted from the adduct **2b**, did not show any optical rotation. Racemization in the reaction of **2b** with sodium azide may be caused. d) The azide **3d** was reduced by sodium borohydride to the amine **4d** remaining trichloromethyl moiety. However, the diastereomer **5d** formed from **4d** did not show a pure chromatogram by HPLC analysis.

Table 2. Reaction of Carbon Tetrachloride with Styrene Derivatives

Ar	DIOP	Product	$[\alpha]_D$/° (*c*, in PhH)	Chemical yield/%	Optical yield/%ee[a]	Absolute configuration
C_6H_5	(−)	**2a**	+12 (6.1)	73	13 (13)	R
C_6H_5	(+)	**2a**	−10 (5.3)	68	7 (11)	S
p-$CH_3C_6H_4$	(−)	**2b**	+10 (3.4)	79	—[c]	R
p-$CH_3C_6H_4$	(+)	**2b**	− 7.8 (3.0)	80	—[c]	S
p-ClC_6H_4	(−)	**2c**	+ 5.2 (3.9)	70	10	R
p-ClC_6H_4	(+)	**2c**	− 4.9 (2.9)	68	6	S
m-$O_2NC_6H_4$	(−)	**2d**	+ 5.2 (1.9)	54[b]	—[d]	R
m-$O_2NC_6H_4$	(+)	**2d**	− 3.7 (2.6)	57[b]	—[d]	S

a) Optical yields were estimated by HPLC of MTPA-amides and optically pure sample reported as $[\alpha]_D$+21.7° (PhH) in parentheses. b) The reaction was carried out for 24 h. c) The amine **4b**, which was converted from the adduct **2b**, did not show any optical rotation. Racemization in the reaction of **2b** with sodium azide may be caused. d) The azide **3d** was reduced by sodium borohydride to the amine **4d** remaining trichloromethyl moiety. However, the diastereomer **5d** formed from **4d** did not show a pure chromatogram by HPLC analysis.

from **2**, with that of known optically active amine and by HPLC analysis of the MTPA-amides **5**. The reaction of carbon tetrachloride with various styrenes was carried out in a similar way and the results are summarized in Table 2.

There are a few reports in an asymmetric addition of polyhaloalkane to olefin. Boutevin and Dongala have reported the addition of carbon tetrachloride to an optically active olefin, menthyl acrylate, catalyzed by iron or copper salts.[10] Murai and Sonoda studied the asymmetric addition of bromotrichloromethane to styrene catalyzed by RhCl[(−)-diop].[11] They obtained optically active (*S*)-(−)-3-bromo-1,1,1-trichloro-3-phenylpropane with 32% ee when the rhodium-DIOP complex was employed as the catalyst. However, no mechanistic aspects are described.

The addition reaction catalyzed by the ruthenium(II) complex can be explained by the following mechanism involving a radical redox transfer process in the coordination sphere of the ruthenium(II) complexes (Scheme 1). In the case of the reaction of trichloromethanesulfonyl chloride, the ruthenium(II) catalyst **1** selectively activates a sulfur-chlorine bond of trichloromethanesulfonyl chloride, which is weaker than a carbon-chlorine bond, to give a trichloromethanesulfonyl radical confined to the coordination sphere of the ruthenium(III) species (**6**). The intermediate **6** readily loses sulfur dioxide to give a trichloromethyl radical confined to the ruthenium(III) species (**7**). Then, the intermediate **7** forms a π-complex (**8**) with styrene and the coordinated styrene reacts with the confined carbon radical to give 3,3,3-trichloro-1-phenylpropyl radical confined to the ruthenium(III) species (**9**). The carbon radical in **9** abstracts the chlorine atom from the ruthenium(III) species containing chiral ligands to give the adduct **3** and regenerate the ruthenium(II) catalyst **1**. It also may be probable that

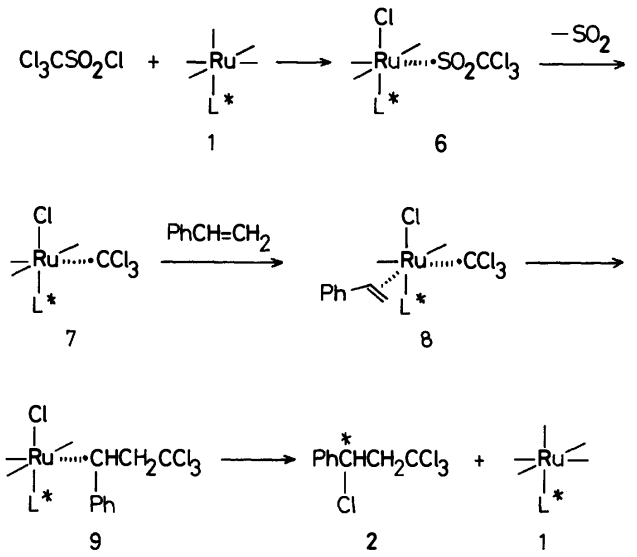

Scheme 1.

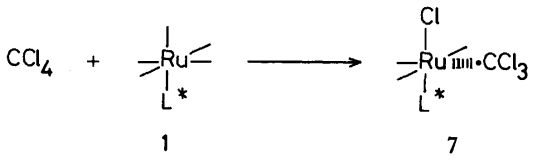

Scheme 2.

7 directly reacts with styrene to give **9** without forming the intermediate **8**. As shown in Scheme **1**, the trichloromethanesulfonyl, trichloromethyl, and 3,3,3-trichloro-1-phenylpropyl radical are considered to be confined in the coordination sphere of the ruthenium complexes containing chiral ligands. An enantioface differentiation may be occurred in the last step in Scheme **1**, abstracting the chlorine atom from the ruthenium(III) species **9** with chiral ligand by the carbon radical. The asymmetric addition in the reaction of carbon tetrachloride with olefin will be similar to that of the reaction of trichloromethanesulfonyl chloride with olefin. Carbon tetrachloride reacts with the ruthenium(II) complex **1** to give the intermediate **7**, (Scheme 2) which reacts with styrene and to afford optically active **2** in a similar way as shown in Scheme **1**.

In conclusion, asymmetric induction was definitely observed in the addition of sulfonyl chloride or carbon tetrachloride to olefin catalyzed by the ruthenium(II) complex containing chiral ligand such as (−)-DIOP or (+)-DIOP. The results support our assumption that the radicals generated by interaction of the ruthenium(II) complexes are confined in the coordination sphere of the metal complexes. The radical in the coordination sphere should be called "RADICALOID" since a carbene-metal complex is called a carbenoid. The enantiomeric excess of the products obtained in the present reaction was not satisfied, while high enantioselective addition was achieved in the chiral copper carbenoid reaction and applied to the synthesis of industrially valuable chrysanthemic acid.[12] This suggests that the "RADICALOID" coordinates to the metal complex more loosely compared with that of carbenoid.

The present work has been supported by a Grant-in-Aid for Scientific Research No. 60470027 from the Ministry of Education, Science and Culture.

Experimental

Measurement. Melting points and boilng points were uncorrected. The infrared absorption spectra were determined on a Hitachi Model 260-10 spectrophotometer with samples as either neat liquids or KBr disks. The proton magnetic resonance spectra were recorded at 60 MHz by using a JNM-PMX 60 SI spectrometer with Me_4Si as an internal standard in $CDCl_3$. The optical rotations were measured with a JASCO DIP-140 polarimeter. The high-performance liquid chromatography system consisted of a

Hitachi 655 liquid chromatograph equipped with a Rhedyne 7125 sample injector. Elutions were monitored at 260 nm using a Hitachi 638-41 variable-wavelength UV monitor. The gel permeation chromatography was performed by using a JAI LC-08 liquid chromatograph with a JAIGEL-1H column (20ϕ×600 mm×2, chloroform as an eluent). Mass spectra were determined with a JEOL JMX-DX 300 mass spectrometer with JEOL JMA 5000 Mass Data System at an ionizing voltage of 20—70 eV.

Materials. The ruthenium(II) complexes such as Ru_2Cl_4-[(−)-diop]$_3$ ((−)-**1**) and Ru_2Cl_4[(+)-diop]$_3$ ((+)-**1**) were prepared by the methods described in the literature.[13] Trichloromethanesulfonyl chloride, carbon tetrachloride, styrene, *p*-methylstyrene, *p*-chlorostyrene (Tokyo Kasei Chemicals), and *m*-nitrostyrene (Aldrich Chemicals) were purified by distillation under nitrogen prior to use.

General Procedure for the Reaction of Trichloromethanesulfonyl Chloride with Olefins. A solution containing of 5.0 mmol of trichloromethanesulfonyl chloride, 7.5 mmol of olefin, 0.05 mmol of **1** in 10 cm^3 of benzene was degassed and heated in a sealed tube at 100 °C for 6—24 h. The reaction mixture was chromatographed on silica gel using benzene as an eluent. The products were identified by their infrared absorption spectra, proton magnetic resonance spectra, mass spectra, and high-resolution mass spectra. The physical and spectral data of the compounds (**2a**—d) are as follows.

(*R*)-(+)-1,1,1,3-Tetrachloro-3-phenylpropane (2a): Bp 85—88 °C/0.3 mmHg† (Kugelrohr); IR (neat) 1490, 1450, 1420, 1200, and 970 cm^{-1}; ^{1}H NMR (CCl_4) δ=3.49 (2H, d, J=6.0 Hz), 5.17 (1H, t, J=6.0 Hz), and 7.25 (5H, s); MS m/z 256 (M$^+$); HRMS m/z 255.9428 ($C_9H_8Cl_4$ requires 255.9380).

(*S*)-(−)-1,1,1,3-Tetrachloro-3-phenylpropane (2a): Bp 88—90 °C/0.3 mmHg (Kugelrohr); IR (neat) 1490, 1450, 1420, 1200, 970 cm^{-1}; ^{1}H NMR (CCl_4) δ=3.49 (2H, d, J=6.0 Hz), 5.17 (1H, t, J=6.0 Hz), and 7.25 (5H, s); MS m/z 256 (M$^+$), HRMS m/z 255.9356 ($C_9H_8Cl_4$ requires 255.9380).

(*R*)-(+)-1,1,1,3-Tetrachloro-3-(*p*-tolyl)propane (2b): Bp 90—95 °C/0.3 mmHg (Kugelrohr); IR (neat) 1510, 1420, 1200, and 970 cm^{-1}; ^{1}H NMR (CCl_4) δ=2.30 (3H, s), 3.50 (2H, d, J=6.0 Hz), 5.17 (1H, t, J=6.0 Hz), and 6.97—7.30 (4H, m); MS m/z 270 (M$^+$); HRMS m/z 269.9496 ($C_{10}H_{10}Cl_4$ requires 269.9537).

(*S*)-(−)-1,1,1,3-Tetrachloro-3-(*p*-tolyl)propane (2b): Bp 90—95 °C/0.3 mmHg (Kugelrohr); IR (neat) 1515, 1420, 1200, and 970 cm^{-1}; ^{1}H NMR (CCl_4) δ=2.30 (3H, s), 3.50 (2H, d, J=6.0 Hz), 5.18 (1H, t, J=6.0 Hz), and 6.97—7.30 (4H, m); MS m/z 270 (M$^+$); HRMS m/z 269.9464 ($C_{10}H_{10}Cl_4$ requires 269.9537).

(*R*)-(+)-1,1,1,3-Tetrachloro-3-(*p*-chlorophenyl)propane (2c): Mp 41—42 °C; Bp 105—110 °C/0.4 mmHg (Kugelrohr); IR (neat) 1500, 1420, 1200, 1100, and 970 cm^{-1}; ^{1}H NMR (CCl_4) δ=3.40—3.50 (2H, m), 5.17 (1H, t, J=6.0 Hz), and 7.25 (4H, s); MS m/z 290 (M$^+$); HRMS m/z 289.9010 ($C_9H_7Cl_5$ requires 289.8990).

(*S*)-(−)-1,1,1,3-Tetrachloro-3-(*p*-chlorophenyl)propane (2c): Mp 41—42 °C; bp 103—105 °C/0.3 mmHg (Kugelrohr); IR (neat) 1500, 1425, 1210, 1100, and 970 cm^{-1}; ^{1}H NMR (CCl_4) δ=3.40—3.50 (2H, m), 5.17 (1H, t, J=6.0 Hz), and 7.25 (4H, m); MS m/z 290 (M$^+$); HRMS m/z 289.9045 ($C_9H_7Cl_5$ requires 289.8990).

(*R*)-(+)-1,1,1,3-Tetrachloro-3-(*m*-nitrophenyl)propane (2d): IR (neat) 1530 and 1350 cm^{-1}; ^{1}H NMR (CCl_4) δ= 3.50—3.62 (2H, m), 5.32 (1H, t, J=6.0 Hz), and 7.34—8.30 (4H, m); MS m/z 301 (M$^+$); HRMS m/z 300.9243 ($C_9H_7O_2NCl_4$ requires 300.9231).

(S)-(−)-1,1,1,3-Tetrachloro-3-(*m*-nitrophenyl)propane (2d): IR (neat) 1530 and 1350 cm^{-1}; ^{1}H NMR (CCl_4) δ= 3.50—3.62 (2H, m), 5.33 (1H, t, J=6.0 Hz), and 7.36—8.30 (4H, m); MS m/z 301 (M$^+$); HRMS m/z 300.9200 ($C_9H_7O_2NCl_4$ requires 300.9231).

General Procedure for the Reaction of Carbon Tetrachloride with Olefins. A solution containing 5.0 mmol of carbon tetrachloride, 20.0 mmol of olefin, 0.05 mmol of **1** in 10 cm^3 of benzene was degassed and heated in a sealed tube at 100 °C for 6—24 h. The reaction mixture was chromatographed on silica gel using benzene as an eluent. The products were identified by comparing their boiling points, IR spectra, ^{1}H NMR spectra, mass spectra with that of the products **2** obtained by the reaction of trichloromethanesulfonyl chloride with olefins.

Preparation of 1-Amino-1-arylpropane (4). A solution of 1.4 g (5.4 mmol) of 1,1,1,3-tetrachloro-3-phenylpropane (**2a**) which showed $[\alpha]_D$ −10° (*c* 11, benzene) and 1.0 g (15 mmol) of sodium azide in 15 cm^3 of ethanol-water=4:1 (v/v) was heated at 70—75 °C for 5 d. After cooling, 50 cm^3 of water and 100 cm^3 of ether were added to the reaction mixture. The organic layer was extracted and dried over sodium sulfate. The solvent was removed to give 1.0 g of an oil which was found to contain a starting material **2a** by TLC analysis. Purification by gel permeation liquid chromatography using chloroform as an eluent gave 0.75 g (65%) of 3-azido-1,1,1-trichloro-3-phenylpropane (**3a**) as a yellow oil: IR (neat) 2100 cm^{-1}; ^{1}H NMR (CCl_4) δ=3.07—3.14 (2H, m), 4.90 (1H, t, J=6.0 Hz), 7.29 (5H, s); MS m/z 263 (M$^+$).

A solution of 0.69 g (2.6 mmol) of the azide **3a** in 60 cm^3 of dry dibutyl ether was added dropwise to a stirred suspension of 2.0 g (53 mmol) of lithium aluminum hydride in 40 cm^3 of dry dibutyl ether at room temperature. After the addition was completed, the mixture was heated at 100 °C for 24 h, then cooled in an ice bath, and treated with 2.0 cm^3 of 15% sodium hydroxide, and 6.0 cm^3 of water. After stirring for additional 30 min, the mixture was filtered, and the precipitate was washed with ether. The combined ethereal solution was washed with 15% hydrochloric acid, the acidic aqueous layer was made basic with 15% sodium hydroxide, and the aqueous layer was extracted with ether. The organic layer was dried over sodium sulfate and the solvent was removed to give 0.15 g (43%) of 1-amino-1-phenylpropane (**4a**): $[\alpha]_D$ +2.1° (*c* 2.3, benzene); IR (neat) 3300 cm^{-1}; ^{1}H NMR ($CDCl_3$) δ=0.84 (3H, t, J=6.0 Hz), 1.45—1.92 (4H, m), 3.64—3.86 (1H, m), and 7.22 (5H, s); MS m/z 134 (M$^+$−1).

Preparation of 2-Methoxy-2-trifluoromethylphenylacetic Acid (MTPA) Amides (5). The sample of optically active (*R*)-(+)-1-amino-1-phenylpropane **4a** (45 mg, 0.33 mmol) was added to a solution of 42 mg (0.17 mmol) of (*S*)-(−)-2-methoxy-2-trifluoromethylphenylacetyl chloride (MTPA-Cl), which was prepared by refluxing (*S*)-(−)-MTPA, excess thionyl chloride, and sodium chloride in 3 cm^3 of dichloromethane for 2 d and then removing the excess thionyl chloride in vacuo. The mixture was stirred at room temperature for 24 h. The amine hydrochloride precipitated was filtered off and the solvent was removed under reduced pressure to give 75 mg of the crude MTPA amide (**5a**) as a yellow oil: IR (neat) 3400, 3300, 2950, 1690, 1510, 1270, 1170, and

† 1 mmHg=133.322 Pa.

1110 cm^{-1}; ^1H NMR ($CDCl_3$) δ=0.73—1.05 (3H, m), 1.50—2.00 (2H, m), 3.29—3.40 (3H, m), 4.68—5.07 (10H, m); MS *m/z* 351 (M^++1).

Separation of the MTPA Amides (5). The HPLC separation of the MTPA amides **5** was performed with a Waters Radial PAK Cartridge Silica Column (8mm×10 cm, particle size 10 μm) using hexane–ethyl acetate=30 : 1 (v/v) as an eluent at a flow rate of 1.0 $cm^3\,min^{-1}$.

References

1) For Part 2, see: M. Kameyama, N. Kamigata, and M. Kobayashi, *J. Org. Chem.*, **52**, 3312 (1987).

2) N. Kamigata, H. Sawada, and M. Kobayashi, *J. Org. Chem.*, **48**, 3793 (1983); N. Kamigata, H. Sawada, N. Suzuki, and M. Kobayashi, *Phosphorus and Sulfur*, **19**, 199 (1984).

3) N. Kamigata, H. Sawada, J. Ozaki, and M. Kobayashi, *Sulfur Lett.*, **1**, 131 (1983).

4) H. Nozaki, S. Moriuti, H. Takaya, and R. Noyori, *Tetrahedron Lett.*, **1966**, 5239.

5) M. Kameyama, N. Kamigata, and M. Kobayashi, *Chem. Lett.*, **1986**, 527; M. Kameyama, N. Kamigata, and M. Kobayashi, *J. Org. Chem.*, **52**, 3312 (1987).

6) Reaction of 1-chloro-1-phenylethane with sodium azide in 80% ethanol has been reported to proceed with 30% racemization; F. Hiron and E. D. Hughes, *J. Chem. Soc.*, **1960**, 795.

7) The highest value of optical rotation of (R)-(+)-**4a** was reported as $[\alpha]_D$ +21.7 (benzene); K. Harada and J. Ohhashi, *Bull. Chem. Soc. Jpn.*, **43**, 960 (1970).

8) J. A. Dale, D. L. Dull, and H. S. Mosher, *J. Org. Chem.*, **34**, 2543 (1969).

9) H. Matsumoto, T. Nakano, and Y. Nagai, *Tetrahedron Lett.*, **1973**, 5147; **1975**, 899; *idem.*, *J. Org. Chem.*, **41**, 396 (1976).

10) B. Boutevin and E. B. Dongala, *Tetrahedron Lett.*, **1977**, 4315.

11) S. Murai, R. Sugise, and N. Sonoda, *Angew. Chem., Int. Ed. Engl.*, **20**, 475 (1981).

12) T. Aratani, *Yuki Gosei Kagaku Kyokai Shi*, **43**, 1134 (1985).

13) B. R. James, D. K. Wang, and R. F. Voight, *J. Chem. Soc., Chem. Commun.*, **1975**, 574.

 © 1987 The Chemical Society of Japan Bull. Chem. Soc. Jpn., 60, 3693—3696 (1987)

Anodic Cyanation of 1-Methylimidazoles

Kunihisa YOSHIDA* and Hirohito KITABAYASHI
Department of Chemistry, Faculty of Engineering Science, Osaka University, Toyonaka, Osaka 560
(Received April 30, 1987)

The electrooxidation of several 1-methylimidazoles was performed in MeOH that contains NaCN at a platinum anode in a divided cell. Replacement of an aromatic hydrogen by a cyano group occurred. With 1,2,4,5-tetramethylimidazole, the 2,5-addition of cyano groups to the imidazole ring was achieved, and besides side-chain substitution occurred concurrently.

It has been shown that an electrochemical technique makes possible the direct introduction of cyano groups either by substitution or addition into aromatic compounds.[1,2] This method is especially useful for five-membered heterocycles.[3]

The present paper describes synthetic application of the method to 1-methylimidazoles. The possible products α-amino nitriles are useful as the synthetic intermediates. Heretofore, in electrooxidation reactions, imidazoles were often used as nucleophiles rather than as substrates.[4,5]

Results

Controlled-Potential Electroreaction (CPE). The potentiostatic oxidations of 1-methylimidazoles were performed in a divided cell with a Pt anode at room temperature. The reference electrode was an SCE. The electroreaction medium was MeOH–0.4 M NaCN (1 M=1 mol dm^{-3}). After the theoretically calculated amount of charge had passed, the solvent was removed. The residue was triturated with chloroform, filtered, concentrated, and analyzed by GLC. The products reported in Table 1 were isolated by preparative GLC. They were identified by the elemental and ^{1}H NMR, IR, and mass spectroscopic analyses and by comparison with the authentic samples prepared by other routes. Current efficiencies (CEs) are based on the total charge passed; the formation of 1 mol of each product is assumed to require 2 F.

The replacement of an aromatic hydrogen by a cyano group occurred at a position lacking the substituent on the imidazole ring. MI gives all three possible ring-substitution products, 5-, 2-, and 4-cyano isomers in an approximate ratio of 5 : 2 : 1. A similar product distribution has been reported for the electroreaction in aqueous cyanide (presumably as a potassium salt, experimental details including melting points of some products were not furnished).[6] The reaction point in the present anodic reaction is of particular interest because conventional electrophilic substitution by a cyano group occurs exclusively at the 2 position.[7]

For TEMI obstructed all of the replaceable positions by the methyl substituents, the 2,5-addition of cyano groups across the diene system of an imidazole was achieved, and besides side-chain substitution occurred concurrently at the substituent methyl group in the 5 position. The transformation of the adduct **2** to the side-chain-cyanation product **1h** during GLC analysis was not observed. For the 2,5-dicyano adduct of 1,2,5-trimethylpyrrole, such a rearrangement of a cyano group has been reported.[8]

The CE for the formation of these carbonitriles

Table 1. Anodic Cyanation of 1-Methylimidazoles. Voltammetric Data and Products

Reactant	E_p[a] / V	PCPE[b] / V	n[c] / F mol^{-1}	Product	CE[d] / %
1-Methylimidazole (MI)	≈1.75	1.80	2.7	1-Methyl-2-imidazolecarbonitrile (**1a**)	17
				1-Methyl-4-imidazolecarbonitrile (**1b**)	8
				1-Methyl-5-imidazolecarbonitrile (**1c**)	42
1,2-Dimethylimidazole (1,2-DIMI)	1.54	1.54	2.1	1,2-Dimethyl-4-imidazolecarbonitrile (**1d**)	7.5
				1,2-Dimethyl-5-imidazolecarbonitrile (**1e**)	79
1,5-Dimethylimidazole (1,5-DIMI)	1.47	1.47	2.1	1,5-Dimethyl-2-imidazolecarbonitrile (**1f**)	32
				1,5-Dimethyl-4-imidazolecarbonitrile (**1g**)	36
1,2,4,5-Tetramethylimidazole (TEMI)	1.12	1.10	2.1	2,5-Dihydro-1,2,4,5-tetramethyl-2,5-imidazoledicarbonitrile (**2**)	13
				1,2,4-Trimethylimidazole-5-acetonitrile (**1h**)	11

a) Peak potential for cyclic voltammetry; Pt anode, MeOH, 0.4 M NaCN, SCE. Scan rate is 0.1 V s^{-1}. Substrate concentration is 2×10^{-2} M. All voltammograms showed no cathodic peak corresponding to reversible reduction of an initially formed cation radical. b) Potential for controlled-potential electroreaction. c) Controlled-potential coulometry. d) Current efficiency (based on **2e** process). This value corresponds to the yield based on imidazole used since the reaction was terminated at the stage when 2 F mol^{-1} of electricity was passed.

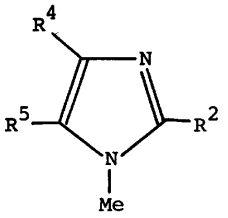

1a, R^2=CN; R^4=R^5=H
b, R^2=R^5=H; R^4=CN
c, R^2=R^4=H; R^5=CN
d, R^2=Me; R^4=CN; R^5=H
e, R^2=Me; R^4=H; R^5=CN
f, R^2=CN; R^4=H; R^5=Me
g, R^2=H; R^4=CN; R^5=Me
h, R^2=R^4=Me; R^5=CH_2CN

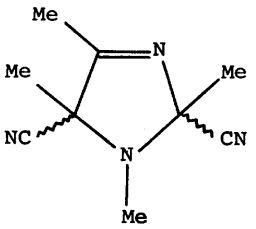

2

increases with decreasing amounts of passed electricity. It would be ascribable to that, the oxidation of the background solvent-electrolyte system becomes conspicuous with decreasing concentration of the electroactive substrate.

The GLC retention time of 4-carbonitriles is remarkably long compared with that of the other positional isomers (e.g., t_R=14, 14, and 98 min for **1a**, **1c**, and **1b**, respectively; PEG 6000 column, 190 °C).

The intensity of C≡N stretching vibration in IR spectra varied with structure. Ring substitution products have a strong band in the region of the C=N stretching vibration, whilst the intensity of the nitrile absorption band in 2,5-addition or side-chain-substitution product is weaker.

Preparative-Scale Electroreaction. The larger preparative electroreactions were conducted at constant current of 0.05 A. After usual workup, the products were separated by column chromatography. The CEs for constant-current electroreaction were lower than those for CPE. There was some difference in product ratios using the different reaction conditions. At the nonpotentiostatic conditions, a portion of the primary product would be consumed by further oxidations.

Experimental

General. Spectrometers and electrochemical equipment have been described previously.[9]

Materials. MeOH and reagent grade NaCN were used without purification.

MI and 1,2-DIMI were obtained commercially and were purified by distillation. TEMI was also a commercial sample and was purified by column chromatography on silica gel using pentane–chloroform (1:2) as an eluent and by recrystallization; mp 58.0—61.0 °C (from petroleum ether, lit,[10] mp 51—54 °C).

1,5-DIMI was prepared by the hydrazine reduction of 1-methyl-5-imidazolecarbaldehyde according to the method of Martin, et al.[11] The desired aldehyde was obtained by oxidation of the corresponding alcohol with activated manganese dioxide in benzene according to the method of Loozen, et al.[12] The procedures of Jones and McLaughlin were followed for the preparation of 1-methyl-5-(hydroxymethyl)-imidazole.[13-15]

^{1}H NMR ($CDCl_3$): MI, δ=3.66 (3H, s), 6.84 (1H, m), 7.00 (1H, m), 7.38 (1H, br s); 1,2-DIMI, δ=2.37 (3H, s), 3.56 (3H, s), 6.78 (1H, d, J=1.2), 6.86 (1H, d, J=1.2); 1,5-DIMI, δ=2.17 (3H, d, J=1.0), 3.50 (3H, s), 6.72 (1H, br s), 7.32 (1H, s); TEMI, δ=2.07 (3H, s), 2.09 (3H, s), 2.30 (3H, s), 3.35 (3H, s).

The following reference materials were obtained by dehydration of the oximes with acetic anhydride according to the procedure of Anderson,[16] which describes the preparation of 2-pyrrolecarbonitrile from the corresponding oxime: **1a—c** and **1e**. Their precursors aldehydes were prepared according to the literature. 1-Methyl-2-imidazolecarbaldehyde[12] was obtained from oxidation of the corresponding alcohol[17,18] with active manganese dioxide. 1-Methyl-4-imidazolecarbaldehyde was prepared by an eight-step method of Martin, et al.[11] The desired α-acetamidoacrylic acid was obtained according to the literature.[19,20] The preparation of 1-methyl-5-imidazolecarbaldehyde was described above. 1,2-Dimethyl-5-imidazolecarbaldehyde was made by the literature procedure.[12,21]

Cyclic Voltammetry. Voltammograms were recorded for each compound as described previously.[9] The E_p value are in Table 1.

CPE. The cell and general procedure have been described.[9] Oxidations in MeOH, 0.4 M NaCN were performed at controlled potentials as indicated in Table 1. The reactions were usually terminated after passage of ≈2 F mol^{-1} of added imidazole. The workup procedure consisted of evaporation of much of the MeOH (*caution*: HCN), addition of chloroform, and filtration of NaCN. The chloroform extract was concentrated and analyzed by GLC using a PEG 6000 column. Each isomeric product was separated in pure form by preparative GLC.[22] They were identified by the elemental and ^{1}H NMR, IR, and mass spectroscopic analyses (Table 2).

Preparative-Scale Electroreaction of MI. The electroreaction was carried out in a two-compartment H-type cell with glass frit separating the compartments fitted with Pt foil electrodes (2×2 cm). The anolyte was made up of 3.3 g (0.04 mol) of MI, 2.5 g (0.05 mol) of NaCN, and 50 ml of MeOH. The catholyte was the same medium in the absence of the substrate. The anode and cathode compartments were kept under a nitrogen atmosphere and the anolyte was stirred magnetically. The reaction was performed at 0.05 A of constant current by using a direct-current power supply at room temperature until ≈2 F mol^{-1} of added imidazole had passed through the electrolyte, which generally took 24 h.

After completion of the oxidation, the solvent was removed under aspirator vacuum. The residue was triturated with chloroform, filtered, concentrated,[25] and chromatographed on silica-gel column using chloroform as the eluant. The elution of products was followed by IR spec-

troscopy. The first product to elute was **1a**, the second **1c**, followed by unreacted substrate and successive elution of **1b**. Separation of the isomers was accomplished without loss.

Preparative-Scale Electroreaction of TEMI. The method of oxidation, workup, and product isolation was identical to that described for MI. 2,5-Dihydro-1,2,4,5-tetramethyl-2,5-imidazoledicarbonitrile (**2**; 0.35 g, 5% CE) was isolated as the first fraction by column chromatography, followed by unidentified substances. 1,2,4-Trimethylimidazole-5-acetonitrile (**1h**) as well as the adduct **2** could be separated from the reaction mixture by preparative GLC using a PEG 6000 column at 190 °C.

References

1) K. Yoshida, "Electrooxidation in Organic Chemistry," Wiley-Interscience, New York (1984), Chap. 4.

2) K. Yoshida, "The Chemistry of Functional Groups, Suppl. C," ed by S. Patai and Z. Rappoport, Wiley-Interscience, London (1983), p. 221.

3) K. Yoshida, *J. Am. Chem. Soc.*, **99**, 6111 (1977); K. Yoshida, *J. Chem. Soc., Chem. Commun.*, **1978**, 1108; K. Yoshida, *J. Am. Chem. Soc.*, **101**, 2116 (1979).

4) G. M. Blackburn and J. P. Will, *J. Chem. Soc., Chem. Commun.*, **1974**, 67.

5) Ref. 1, Chap. 6.

6) C. Oldenhof and J. Cornelisse, *Recl. Trav. Chim. Pays-Bas*, **97/2**, 35 (1978).

7) J. R. McCarthy, D. P. Matthews, and J. P. Whitten, *Tetrahedron Lett.*, **26**, 6273 (1985).

8) L. Eberson, *Acta Chem. Scand., B*, **34**, 747 (1980).

9) K. Yoshida and T. Fueno, *Bull. Chem. Soc. Jpn.*, **60**, 229 (1987).

10) M. Guntensperger and A. D. Zuberbuhler, *Helv. Chim. Acta*, **60**, 2584 (1977).

11) P. K. Martin, H. R. Matthews, H. Rapoport, and G. Thyagarajan, *J. Org. Chem.*, **33**, 3758 (1968).

12) H. J. J. Loozen, E. F. Godefroi, and J. S. M. M. Besters, *J. Org. Chem.*, **40**, 892 (1975).

13) R. G. Jones, *J. Am. Chem. Soc.*, **71**, 644 (1949).

14) R. G. Jones and K. C. McLaughlin, *J. Am. Chem. Soc.*, **71**, 2444 (1949).

15) D. S. Noyce and G. T. Stowe, *J. Org. Chem.*, **38**, 3762 (1973).

16) H. J. Anderson, *Can. J. Chem.*, **37**, 2053 (1959).

17) R. Grindley and F. L. Pyman, *J. Chem. Soc.*, **1927**, 3128.

18) P. E. Iversen and H. Lund, *Acta Chem. Scand.*, **20**, 2649 (1966).

19) M. Bergmann and K. Grafe, *Z. Physiol. Chem.*, **187**, 187 (1930); *Chem. Abstr.*, **24**, 2150 (1930).

20) D. McHale, P. Mamalis, and J. Green, *J. Chem. Soc.*, **1960**, 2847.

21) E. F. Godefroi, H. J. J. Loozen, and J. Th. J. Luderer-Platje, *Recl. Trav. Chim. Pays-Bas*, **91**, 1383 (1972).

22) The isomeric **1a** and **1c** could not be separated by GLC. The mixed isomers were taken out by preparative GLC and their ratio was determined by NMR spectroscopy. Separation to the individual isomers was made by column chromatography on silica gel with chloroform (see

Table 2. Melting points and Spectroscopic Data of Cyanation Products

Product	Mp θ_m/°C	^{1}H NMR,[a] δ/ppm (J in Hz)	MS m/z (M^+)	IR[b] ν/cm^{-1}
1a	Oil (bp 65—70 °C/0.4 mmHg[c] (1 mmHg=133.322 Pa))	3.86 (3H, s) 7.08 (1H, d, J=0.8) 7.13 (1H, d, J=0.8)	107	2210 (C≡N)
1b	73.5—74.5, from $CHCl_3$-hexane (72—73[d])	3.78 (3H, s) 7.46 (2H, br s)[e]	107	2240 (C≡N)
1c	53.0—53.5, from CCl_4 (48—50[f])	3.80 (3H, s) 7.57 (1H, s) 7.61 (1H, s)	107	2260 (C≡N)
1d	139.0—140.0, from hexane	2.38 (3H, s) 3.60 (3H, s) 7.32 (1H, s)	121	2240 (C≡N)
1e	66.0—67.0, from CCl_4 (54—57[g])	2.44 (3H, s) 3.66 (3H, s) 7.50 (1H, br s)	121	2260 (C≡N)
1f	75.0—78.0, from CCl_4	2.23 (3H, d, J=0.8) 3.69 (3H, s) 6.90 (1H, m)	121	2240 (C≡N)
1g	94.0—97.0, from $CHCl_3$-CCl_4 (1 : 5)	2.37 (3H, s) 3.60 (3H, s) 7.40 (1H, br s)	121	2220 (C≡N)
1h	32.5—33.5, from hexane	2.16 (3H, br s) 2.32 (3H, s) 3.38 (3H, s) 3.56 (2H, br s)	149	2240 (C≡N)
2	79.5—81.5, from petroleum ether	1.84 (3H, s) 1.86 (3H, s) 2.01 (3H, s) 2.90 (3H, s)	176	2220 (C≡N) 1590 (C=N)

a) 100 MHz, $CDCl_3$ solution. b) Uncorrected. c) Ref. 7. d) Ref. 23. e) Divided into two peaks in the dilute solution, δ 7.47 (1H, s), 7.45 (1H, s). f) Ref. 6. g) Ref. 24.

Preparative-Scale Electroreaction).
23) S. Wakamatsu, J. A. Barltrop, and A. C. Day, *Chem. Lett.*, **1982**, 667.
24) G. J. Durant, M. E. Foottit, C. R. Ganellin, J. M. Loynes, E. S. Pepper, and A. M. Roe, *Chem. Commun.*, **1968**, 108.
25) At this stage, yields were estimated by GLC combined with NMR spectral analysis (**1a**, 0.26 g, 6% CE; **1b**, 0.20 g, 4.6% CE; **1c**, 0.58 g, 13.5% CE).[22]

 © 1987 The Chemical Society of Japan Bull. Chem. Soc. Jpn., 60, 3697—3704 (1987)

Asymmetric Allylation with a New Chiral Allylating Agent Prepared from Tin(II) Triflate, Chiral Diamine, and Allylaluminum

Nobuto MINOWA and Teruaki MUKAIYAMA
Department of Chemistry, Faculty of Science, The University of Tokyo, Hongo, Bunkyo-ku, Tokyo 113
(Received May 2, 1987)

A chiral allylating agent, readily generated from tin(II) trifluoromethanesulfonate (tin(II) triflate), chiral diamines derived from (S)-proline and allylaluminum, is efficiently employed in the asymmetric allylation of aldehydes and an epoxide. Reaction of a chiral 2-methyl-2-propenylating (methallylating) agent with aldehydes also proceeds smoothly to afford the corresponding homoallylic alcohols in good yields with high enantioselectivities. According to a similar procedure, asymmetric propargylation of aldehydes affords homopropargylic alcohols in good optical purities.

Asymmetric synthesis is one of the most important approaches for producing optically active substances and recently a wide variety of methods have been reported by many research groups.[1] Asymmetric synthesis may be divided into two distinct sections; those processes in which, (i) the chiral auxiliary is incorporated into either (or both) reacting partners (ii) the chiral auxiliary is not covalently bonded to either of the reactants. Incorporation of a chiral source into either (or both) of the reactants has met with great success and many examples have been reported.[1] However, incorporation of the chiral auxiliary into reactants and the subsequent necessary removal of it from the reaction products is a disadvantage of this method.

The latter of these two approaches should be a very convenient method for asymmetric synthesis and seems to warrant concentrated investigation, however, so far it has not met with much success.[1] Utilization of metal chelates for inter- or intramolecular interactions seems to be one of the solutions leading to successful asymmetric synthesis of this type, in which the chiral auxiliary is not covalently bonded to the reactants. During the course of our synthetic investigation, we found that utilization of the chelation of chiral diamines derived from (*S*)-proline to tin(II) enolate enables a highly efficient asymmetric cross aldol reaction.[2] Thus, divalent tin, having vacant d orbitals, is able to accept a bidentate ligand, and chiral diamines are efficient ligands in certain asymmetric reactions by virtue of forming a rigid five-five membered fused ring chelate in the transition state. In an extension of this concept, we have reported a convenient and efficient asymmetric acylation[3] and asymmetric reduction[4] using a new chiral reducing agent prepared from tin(II) chloride, chiral diamine derived from (*S*)-proline and diisobutylaluminum hydride as the reductant. It was considered that this new method for asymmetric reduction should be applicable to asymmetric carbon-carbon bond forming reactions and hence we examined asymmetric allylation of carbonyl compounds utilizing tin(II) compound, chiral diamine and allylating reagent. The asymmetric allylation reaction is useful for asymmetric carbon-carbon bond formation,[5] and several successful methods have been reported using chiral allylic organometallics as the allylating agent[6] or , using chiral acetals as chiral acceptors.[7] However, in these reactions tedious procedures for the attachment and removal of the chiral sources are necessary. Hence a simple procedure for the asymmetric allylation utilizing chiral chelating agents is desirable. We investigated the effective combination of tin(II) compound, chiral diamine and allylating reagent, and found that a new chiral allylating agent prepared by the treatment of tin(II) triflate, chiral diamine derived from (*S*)-proline and allyldialkylaluminum as the allylating reagent is efficient for asymmetric allylation of aldehydes, as we have briefly reported in a preliminary communication.[8] We now describe in full the results of our investigation on asymmetric allylation with this new reagent and the application of the present method to asymmetric methallylation and propargylation.

Results and Discussion

Asymmetric Allylation of Aldehydes with Chiral Allylating Agent. Allyldialkylaluminum is easily prepared by treatment of allylmagnesium bromide with dialkylaluminum chloride at 0 °C in Et_2O,[9] followed by exchange of solvent from Et_2O to CH_2Cl_2. This solution of allyldialkylaluminum in CH_2Cl_2 was employed in the reactions described below. In the first place, we examined suitable reaction conditions using benzaldehyde as a model substrate, and these results are summarized in Table 1.

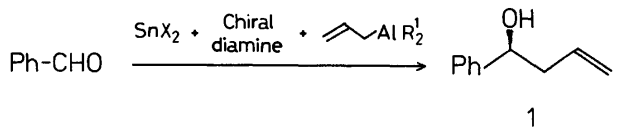

1

The reactions were carried out as follows: To a suspension of tin(II) compound in CH_2Cl_2 was added chiral diamine in CH_2Cl_2 at room temperature. After the solution was cooled to −78 °C, allyldialkylaluminum was added, followed by the addition of benzalde-

Table 1. Asymmetric Allylation of Benzaldehyde with Chiral Allylating Agent under Various Conditions[a)]

Entry No.	R^1	SnX_2	Chiral diamine	Molar ratio[b)]	Solvent	Yield[c)]/%	% ee
1	Et	—	**2**	A	CH_2Cl_2	62	0
2	Et	$SnCl_2$	**2**	A	CH_2Cl_2	76	0
3	Et	$SnBr_2$	**2**	A	CH_2Cl_2	85	0
4	Et	SnF_2	**2**	A	CH_2Cl_2	71	10[d)]
5	Et	$Sn(OAc)_2$	**2**	A	CH_2Cl_2	82	0
6	Et	$Sn(OTf)_2$	**2**	A	CH_2Cl_2	81	42[d)]
7	Et	$Sn(OTf)_2$	**2**	A	$PhCH_3$	69	0
8	Et	$Sn(OTf)_2$	**2**	A	THF	64	4[d)]
9	Et	$Sn(OTf)_2$	**2**	A	CH_2Cl_2	83	52[d)]
10	Et	$Sn(OTf)_2$	**2**	B	CH_2Cl_2	75	61[d)]
11	Et	$Sn(OTf)_2$	**3**	B	CH_2Cl_2	88	3[d)]
12	Et	$Sn(OTf)_2$	**4**	B	CH_2Cl_2	65	21[d)]
13	Et	$Sn(OTf)_2$	**5**	B	CH_2Cl_2	84	8[d)]
14	Ph	$Sn(OTf)_2$	**2**	B	CH_2Cl_2	77	59[d)]
15	Bu^i	$Sn(OTf)_2$	**2**	B	CH_2Cl_2	91	84[e)] 82[d)]
16	Bu^i	$Sn(OTf)_2$	**2**	C	CH_2Cl_2	78	82[e)]
17	Bu^i	$Sn(OTf)_2$	**2**	D	CH_2Cl_2	90	82[e)]
18	Bu^i	$Sn(OTf)_2$	**2**	E	CH_2Cl_2	86	80[e)]
19	Bu^i	$Sn(OTf)_2$	**2**	F	CH_2Cl_2	73	67[e)]
20	Bu^i	$Sn(OMs)_2$	**2**	B	CH_2Cl_2	63	2[d)]

a) The mixture of tin(II) compound, divalent tin, chiral diamine, and allylaluminum was run for 30 min at −78 °C, before benzaldehyde was added. (Entries 9—20). All reactions were carried out at −78 °C for 1 h. b) Tin(II) compound-chiral diamine-allylalminum-benzaldehyde A=1.0 : 1.0 : 1.0 : 0.7, B=1.3 : 1.3 : 1.0 : 0.7 C=2.0 : 2.0 : 1.0 : 0.7, D=1.6 : 1.6 : 1.0 : 0.7, E=1.1 : 1.1 : 1.0 : 0.7, F=0.8 : 0.8 : 1.0 : 0.7. c) Isolated yield. Yields are based on benzaldehyde. All the products have S-configuration. d) Based on $[\alpha]_D^{18}$ −48.7° (*c* 6.92, PhH) for (*S*)-1-phenyl-3-buten-1-ol.[6c)] e) Determined by ^{19}F NMR measurement of the ester from (*R*)-(+)-α-methoxy-α-(trifluoromethyl)phenylacetyl chloride.

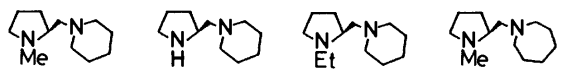

2 3 4 5

hyde at the same temperature, and the reaction mixture was stirred for an additional hour at −78 °C. Usual workup of the reaction mixture afforded 1-phenyl-3-buten-1-ol (**1**). The substituents of the tin(II) compound influenced remarkably the optical purity of the homoallylic alcohol **1** produced by the present allylation reaction (Entries 2—6). When tin(II) chloride or bromide was used, the enantioselectivity of the reaction was low, however, introduction of electron-withdrawing group such as trifluoromethanesulfonate as substituents of the tin(II) species increased the enantioselectivity of the reaction. Thus, when tin(II) triflate was used, good optical purities were attained, while the optical purity of the product dramatically decreased on use of tin(II) methanesulfonate instead of tin(II) triflate (Entries 20). It is assumed that as tin(II) triflate has electron-withdrawing group such as trifluoromethanesulfonate as substituents, that the tin(II) compound can strongly bind to the chiral diamine leading to effective enhancement of the enantioselectivity of the reaction.

In order to find the most suitable solvent for the present allylation reaction, the influence of various solvents on the reaction was examined (Entries 6—8). These results indicate that CH_2Cl_2 is the preferred solvent and that using THF, a highly coordinating solvent, led to a sharp decrease in the optical purity of the product. This implies that the chelate structure existing in the transition state plays an important role in the enantioselectivity. It was also found that reverse addition of the reactants also affects the optical purity. That is, when allyldiethylaluminum was added to the mixture of tin(II) triflate, chiral diamine and benzaldehyde at −78 °C, the optical purity decreased dramatically from 42 to 6% ee. In addition, when benzaldehyde was added at −78 °C, after the mixture of tin(II) triflate, chiral diamine and allyldiethylaluminum was run for 30 min at −78 °C, optical purity increased from 42 to 52% ee. (Entry 9) Judging from these results, initial formation of the complex, chiral allylating agent, prepared from tin(II) triflate, chiral diamine and allylaluminum seems to be important for this asymmetric allylation. The effect of the *N*-substituents in the ligand diamines on the enantioselectivity in the present allylation reaction was also examined by using *N*-substituted diamines (Entries 10—13). Relatively high enantioselectivity was achieved when (*S*)-1-methyl-2-[(1-piperidinyl)methyl]pyrrolidine (**2**) was used as the ligand diamine. It was also found that the substituents of the allylaluminum had a

significant effect on the enantioselectivity of the product (Entries 13—15). When allyldiisobutylaluminum (**6**) having bulky substituents was employed as the allylaluminum, the enantioselectivity of the reaction increased from 61 to 84% ee. In contrast, the molar ratio of each reactant did not have any remarkable effect on the enantioselectivity of the reaction, however, the enantioselectivity of the reaction decreased from 80 to 67% ee, when the molar ratio of tin(II) triflate and diamine decreased from 1.1 to 0.8 (Entries 15—19). These results indicate that this chiral allylating agent consists of a 1 : 1 : 1 complex of tin(II) triflate, diamine and allylaluminum. Finally, the use of other allylic organometallics instead of allylaluminum was studied. When trisallyl borane,[10] allyllithium,[11] allylmagnesium bromide and allyltriphenyltin was used, asymmetric induction could not be observed indicating that the aluminum atom of allyla luminum plays an important role in the present reaction.

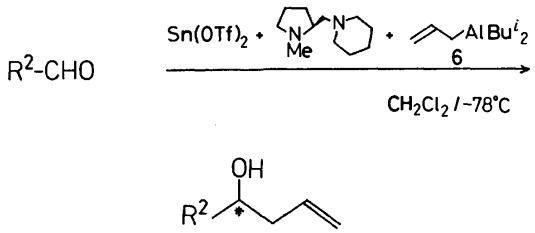

Having optimized the reaction conditions, the reaction with various aldehydes was examined and these results are summarized in Table 2. The allylation with other aldehydes proceeded smoothly to afford the corresponding homoallylic alcohols in high yield in any case. In the cases of aromatic aldehydes, fairly good optical purities were achieved. Electron-withdrawing groups or electron-donating groups in the aryl substituent did not have any remarkable effect either on the synthetic or on the optical yield. On the other hand, in the case of aliphatic aldehydes, satisfactory results could not be obtained, however, relatively good optical purities were attained when α,β-unsaturated aldehydes were employed.

Asymmetric Allylation of Epoxide with Chiral Allylating Agent. Highly selective transformations of enantiotopic groups in prochiral or meso compounds are well-known in enzymatic processes,[12] however, only a few enantioselective chemical approaches have been reported.[13] In order to study the asymmetric carbon-carbon bond forming reaction to meso compound, we examined the asymmetric reaction of the chiral allylating agent with a meso *cis*-epoxide. The allylation was carried out using *cis*-stilbene oxide (**7**) as a *cis*-epoxide. The research mixture of tin(II) triflate and chiral diamine **2** was cooled to 0 °C, and

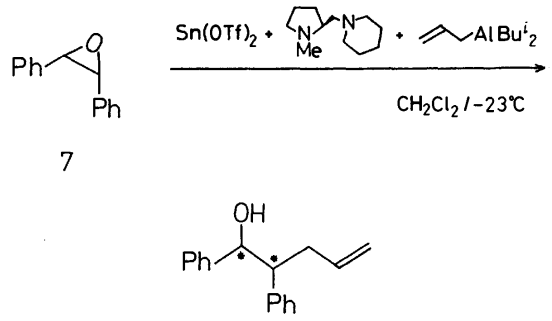

allylaluminum **6** and *cis*-stilbene oxide (**7**) were added successivly at 0 °C. The mixture was stirred for 1 h at

Table 2. Asymmetric Allylation of Aldehydes with Chiral Allylating Agent[a]

Entry No.	Aldehyde	Yield[b] %	$[\alpha]_D$ (c, solvent)	% ee (Configuration)
1	Benzaldehyde	91	$[\alpha]_D^{21}$—39.9° (2.48, PhH)	84[c] 82[d](S)[d]
2	4-Chlorobenzaldehyde	92	$[\alpha]_D^{23}$—28.4° (3.03, PhH)	84[e]
3	4-Nitrobenzaldehyde	65	$[\alpha]_D^{23}$—19.3° (2.14, PhH)	84[e]
4	4-Methylbenzaldehyde	85	$[\alpha]_D^{25}$—37.3° (2.00, PhH)	82[c]
5	4-Methoxybenzaldehyde	93	$[\alpha]_D^{23}$—65.8° (3.56, PhH)	80[c]
6	1-Naphthaldehyde	80	$[\alpha]_D^{24}$—77.5° (2.98, PhH)	80[c]
7	3-Phenyl-2-propenal	84	$[\alpha]_D^{19}$+9.29° (1.41, Et_2O)	64[e] (S)[f]
8	3-Phenylpropanal	86	$[\alpha]_D^{23}$+11.1° (3.14, $CHCl_3$)	53[c] (R)[g]
9	Cyclohexanecarbaldehyde	78	$[\alpha]_D^{25}$—1.78° (0.79, CH_2Cl_2)	56[c]
10	Nonanal	86	$[\alpha]_D^{23}$+5.22° (3.12, PhH)	40[c]

a) All reactions were carried out as described in Entry 15 in Table 1. b) Isolated yield. Yields are based on carbonyl compounds. c) The % ee was determined by ^{19}F NMR measurement of the ester from (*R*)-(+)-α-methoxy-α-(trifluoromethyl)phenylacetyl chloride. d) Optically pure (*S*)-1-phenyl-3-buten-1-ol gives $[\alpha]_D^{18}$—48.7° (*c* 6.92, PhH).[6c] e) Determined by ^{19}F NMR measurement of the ester from (*R*)-(+)-α-methoxy-α-(trifluoromethyl)phenylacetyl chloride in the presence of $Eu(fod)_3$. f) Optically active (*S*)-1-phenyl-1,5-hexadien-3-ol gives $[\alpha]_D^{20}$+3.60° (*c* 10.08, Et_2O).[6c] g) Optically active (*R*)-1-phenyl-5-hexen-3-ol gives $[\alpha]_D^{20}$+16.9° (*c* 1, $CHCl_3$).[6c]

the same temperature to gave 1,2-diphenyl-4-penten-1-ol (**8**) in 69% yield with optical purity of 40% based on NMR analysis of the corresponding MTPA ester. Examination of effect of temperature shows that lowering the temperature from 0 to −23 °C increased the enantioselectivity of the reaction from 40 to 50% ee. However, at the temperature lower than −23 °C, the reaction did not produce the corresponding bis homoallylic alcohol. Although the enantioselective deprotonation[13b,d] and ring-opening with thiols[13i] of a meso epoxide have been accomplished, the present result is, to our knowledge, the first example of an enantioselective allylation of a meso epoxide.

Asymmetric Methallylation of Aldehyde with Chiral Methallylating Agent. Next, we examined the asymmetric methallylation reaction with aldehyde based on the above mentioned consideration: Diisobutyl(2-methyl-2-propenyl)aluminum (diisobutylmethallylaluminum) (**9**) is readily prepared by treatment of diisobutylaluminum chloride with methallyl magnesium chloride at 0 °C in Et_2O, followed by exchange of solvent to CH_2Cl_2 in a similar procedure to that for allylaluminum. This solution of methallylaluminum **9** in CH_2Cl_2 was used for the reactions with aldehyde. The

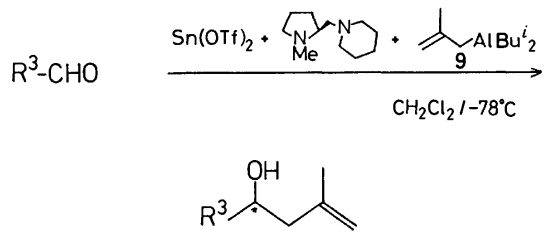

reactions were carried out according to a procedure similar to the previous asymmetric allylation and the results are summarized in Table 3. The reaction of aldehyde with chiral methallylating agent affords the corresponding methallylated product in good yields with high optical purities. The absolute configuration of the product which was obtained by the reaction with benzaldehyde was S-configuration as that of allylation. In the case of both aromatic and aliphatic aldehydes, relatively high optical purities were attained compared with those observed in the asymmetric allylation. Interestingly, in the case of nonanal, the enantioselectivity of the reaction increased from 40 to 73% ee.

Asymmetric Propargylation of Aldehyde with Chiral Propargylating Agent. Asymmetric propargylation is as useful as asymmetric allylation for asymmetric carbon-carbon bond forming reaction. The successful asymmetric propargylation of aldehydes with chiral allenylboronic ester has been reported by Yamamoto.[14] In this reaction, the chiral auxiliary is incorporated into the propargylating reagent. In order to explore the scope of the asymmetric carbon-carbon bond formation utilizing a chiral chelating agent, the asymmetric propargylation with aldehydes was studied. Asymmetric propargylation could be achieved by use of propargylaluminum instead of allylaluminum. The propargylaluminum derivative **10** was prepared as follows: To a solution of diisobutylaluminum chloride in hexane was added the Grignard reagent prepared from propargyl bromide and magnesium in Et_2O at 0 °C and the solvent was changed to CH_2Cl_2. In the first place, the reaction of benzaldehyde with the above solution of **10** afforded the desired homopropargylic alcohol and none of the allenic alcohol was obtained. The same results are reported by Eiter in the reaction of propargylaluminum derivative, derived from aluminum amalgam and propargyl bromide, with carbonyl compounds.[15] It is recognized that the propargylic organometallics are in equilibrium with allenic organometallic and that propargylic alcohols are obtained by the reaction of allenic organometallics with carbonyl compounds via a allylic rearrangement of the allenic organometallics.[16] These results indicate that allenic structure predominates in the above solution of propargylaluminum derivative. The reaction of the propargylating agent, prepared from **10**, tin(II) triflate, and chiral diamine, with aldehyde were carried out according to a procedure similar to that for the asymmetric allylation. We examined the effect of the *N*-substituents in the ligand diamines on the enantioselectivity by using some *N*-substituted diamines. When chiral diamine **2** was used, relatively high enantioselectivity was attained. The reaction with benzaldehyde under these condi-

Table 3. Asymmetric Methallylation of Aldehydes with Chiral Methyllylating Agent

Entry No.	Aldehyde	Yield[a] %	$[\alpha]_D$ (c, solvent)	% ee[b]
1	Benzaldehyde	80	$[\alpha]_D^{21}$−46.6° (1.97, PhH)	87[c]
2	4-Chlorobenzaldehyde	84	$[\alpha]_D^{21}$−40.4° (3.15, PhH)	88
3	3-Phenyl-2-propenal	85	$[\alpha]_D^{22}$−1.69° (2.43, Et_2O)	71
4	3-Phenylpropanal	85	$[\alpha]_D^{23}$+16.6° (2.66, $CHCl_3$)	67
5	Nonanal	70	$[\alpha]_D^{21}$+9.74° (2.71, PhH)	73

a) Isolated yield. Yields are based on aldehydes. b) The % ee was determined by ^{19}F NMR measurement of the ester from (*R*)-(+)-α-methoxy-α-(trifluoromethyl)phenylacetyl chloride. c) S-Configuration. Based on Ref. 6a.

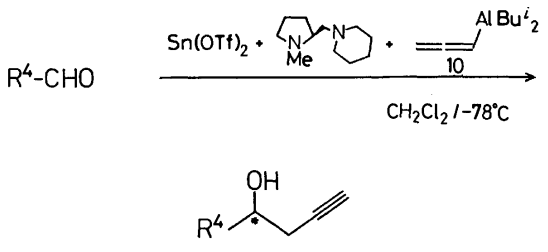

tions affords (*S*)-1-phenyl-3-butyn-1-ol in 60% ee. The reaction with other aldehydes also affords the corresponding homopropargylic alcohols in good yield with good optical purity as shown in Table 4. Interestingly, none of the allenic alcohols were obtained in any case as same as the reaction of **10** with aldehyde.

A highly enantioselective allylation of aldehydes has been accomplished by this new chiral allylating agent. The precise mechanism of the present allylation reaction that enables high enantioselectivity is not clear, however, the high enantioselectivity in the present reaction is assumed to be dependent on the following factors: The chiral allylating agent is generated from a 1 : 1 : 1 complex of chiral diamine **2**, tin(II) triflate and allylaluminum **6**. In this complex, **2** is coordinated to the tin(II) metal center, and in addition one of the oxygen atoms of tin(II) triflate is coordinated to the aluminum of **6** as shown in Fig. 1. Tin(II) triflate, **2** and **6** can form a rigid complex, because tin(II) triflate can strongly bind to the chiral diamine and aluminum has a strong affinity for oxygen. Thus, the chiral diamine **2** as chiral auxiliary and allylaluminum **6** as allylating reagent are brought into proximity by the chelation with tin(II) triflate. As a result, the direction of approach of the aldehyde to this complex is limited by the chiral diamine **2** and the isobutyl group, bulky substituents of the allylaluminum **6** in this complex

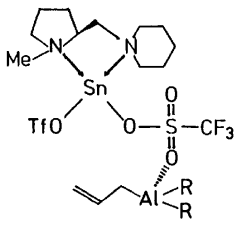

Fig. 1.

leading to high optical purities. In the case of the asymmetric methallylation, relatively high optical purities were attained compared with those of the asymmetric allylation. In this case, the direction of approach of the aldehyde to the complex is extremely restricted by **2** and the isobutyl and methallyl group of **9** leading to relatively high optical purities.

It is noted that treatment of tin(II) triflate, chiral diamine, and allylaluminum generates a new chiral allylating agent. This chiral agent is efficient for the enantioselective synthesis of homoallylic alcohols with satisfactory chemical and optical yields. The present procedure is the first example of the asymmetric allylation reaction with high optical purity induced by the chelation of a chiral auxiliary to active intermediate species. Furthermore, this newly introduced method is applicable to asymmetric methallylation and propargylation.

Experimental

IR spectra were recorded on a Hitachi 260-30 spectrometer. ^{1}H NMR spectra were recorded on a Hitachi R-24B (60 MHz) using TMS as an internal standard. ^{19}F NMR spectra were recorded on a Varian EM-390 (90 MHz) using hexafluorobenzene as an internal standard. Optical rotations were recorded on a JASCO DIP-181 automatic polarimeter using 1-dm thermostated microcell.

All reactions were carried out under an atmosphere of argon. CH_2Cl_2 was distilled successively from P_2O_5 and calcium hydride. Et_2O was freshly distilled from sodium metal using benzophenone ketyl as indicator. The (*R*)-3,3,3-trifluoro-2-methoxy-2-phenylpropionates (MTPA esters) were prepared according to Mosher's procedure[17] using the acid chloride derived from (*R*)-(+)-MTPA supplied from Aldrich (99+%).

Optical purity was determined by ^{19}F NMR of the MTPA esters of the alcohols or ^{19}F NMR of the MTPA esters in the presence of Eu(fod)$_3$.

Tin(II) Trifluoromethanesulfonate (Tin(II) Triflate). Tin(II) triflate was prepared from $SnCl_2$ and trifluoromethanesulfonic acid according to a procedure similar to that of Ref. 2. All handling of tin(II) triflate was carried out under argon atmosphere.

Preparation of Chiral Diamine. Chiral diamines were prepared from (*S*)-proline by a procedure similar to that of Ref **2**.

(*S*)-1-Methyl-2-[(1-piperidinyl)methyl]pyrrolidine: bp 116—

Table 4. Asymmetric Propargylation of Aldehydes with Chiral Propargylating Agent

Entry No.	Aldehyde	Yield[a] %	$[\alpha]_D$ (*c*, MeOH)	% ee[b]
1	Benzaldehyde	77	$[\alpha]_D^{21}$−6.93° (2.18)	60[c]
2	1-Naphthaldehyde	68	$[\alpha]_D^{28}$−29.7° (1.89)	52
3	3-Phenylpropanal	61	$[\alpha]_D^{25}$+21.4° (1.55)	54
4	3-Phenyl-2-propenal	45	$[\alpha]_D^{17}$+17.3° (1.65)	48

a) Isolated yield. Yields are based on aldehyde. b) The % ee was determined by ^{19}F NMR measurement of the ester from (*R*)-(+)-α-methoxy-α-(trifluoromethyl)phenylacetyl chloride. c) S-Configuration. Based on Ref. 14.

118 °C/20 mmHg (1 mmHg=133.322 Pa); IR (neat) 2935, 2770, 1450 cm^{-1}; ^1H NMR ($CDCl_3$) δ=1.28—1.88 (m, 10H), 1.88—2.50 (m, 8H), 2.4 (s, 3H), 2.92—3.15 (m, 1H); $[\alpha]_D^{21}$ −66.9° (*c* 0.32, EtOH).

Preparation of Allyldiisobutylaluminum. To a solution of diisobutylaluminum chloride (6.25 mmol) in 10 ml of hexane was added dropwise allylmagnesium bromide (6.25 mmol) in 10 ml of Et_2O at 0 °C under argon atmosphere. After warming to room temperature, the reaction mixture was stirred for 3 h at this temperature and evaporated. A minimum amount of CH_2Cl_2 was added to the residue and the mixture was evaporated in vacuo. The same operation was repeated again and finally 25.0 ml of CH_2Cl_2 was added. The resulting suspension was decanted and the supernatant used for the reaction.

Methallyldiisobutylaluminum was prepared from methallylmagnesium chloride and diisobutylaluminum chloride by an analogous procedure. Propargyldiisobutylaluminum derivative was prepared from propargylmagnesium bromide and diisobutylaluminum chloride by an analogous procedure.

Asymmetric Allylation of Aldehydes with Chiral Allylating Agent (Table 2). A typical reaction procedure is described for the reaction of benzaldehyde using (*S*)-1-methyl-2-[(1-piperidinyl)methyl]pyrrolidine (Entry 1); to a suspension of tin(II) triflate (224 mg, 0.54 mmol) and (*S*)-1-methyl-2-[(1-piperidinyl)methyl]pyrrolidine (97.9 mg, 0.54 mmol) in 4 ml of CH_2Cl_2 was added dropwise allyldiisobutylaluminum (2.1 ml of a stock solution in CH_2Cl_2, 0.42 mmol) at −78 °C under argon atmosphere. After the yellow solution was stirred for 30 min, benzaldehyde (29.5 mg, 0.28 mmol) in 2 ml of CH_2Cl_2 was added dropwise at −78 °C. The resulting mixture was stirred for 1 h at the same temperature, then quenched with sat. NH_4Cl aq and 1M HCl (1M=1 mol dm^{-3}). The organic layer was extracted with CH_2Cl_2 and dried over anhydrous Na_2SO_4. After concentration in vacuo the resulted oily substance was purified by preparative TLC (hexane-Et_2O=8:3) to yield 1-phenyl-3-buten-1-ol (37.2 mg, 91%). IR (neat) 3400, 1640, 1490, 1450 cm^{-1} ^1H NMR (CCl_4) δ=2.02 (s, 1H), 2.28 (t, *J*=6.6 Hz, 2H), 4.45 (t, *J*=6.6 Hz, 1H), 4.70—6.00 (m, 3H), 7.16 (s, 5H).

Other spectral data are presented: 1-(4-Chlorophenyl)-3-buten-1-ol (Entry 2). IR (neat) 3400, 1640, 1600, 1500 cm^{-1}; ^1H NMR (CCl_4) δ=2.02 (s, 1H), 2.26 (dd, *J*=6.2 Hz, 2H), 4.46 (t, *J*=6.2 Hz, 1H), 4.68—6.00 (m, 3H), 7.13 (s, 4H).

1-(4-Nitrophenyl)-3-buten-1-ol (Entry 3). IR (neat) 3400, 1640, 1600, 1520, 1350 cm^{-1}; ^1H NMR (CCl_4) δ=2.00 (br s, 1H), 2.40 (dd, *J*=6.2, 6.2 Hz, 2H), 4.71 (t, *J*=6.2 Hz, 1H), 4.85—6.10 (m, 3H), 7.38 (d, *J*=8.6 Hz, 2H), 8.05 (d, *J*=8.6 Hz, 2H).

1-(4-Methylphenyl)-3-buten-1-ol (Entry 4). IR (neat) 3400, 1640, 1520 cm^{-1}; ^1H NMR (CCl_4) δ=1.89 (s, 1H), 2.32 (s, 3H), 2.38 (dd, *J*=6.2, 6.2 Hz, 2H), 4.52 (t, *J*=6.2 Hz, 1H), 4.80—6.10 (m, 3H), 7.08 (s, 4H).

1-(2-Methoxyphenyl)-3-buten-1-ol (Entry 5). IR (neat) 3400, 1640, 1600, 1580, 1490, 1460 cm^{-1}; ^1H NMR (CCl_4) δ=2.02 (s, 1H), 2.20—2.55 (m, 2H), 3.80 (s, 3H), 4.86—6.05 (m, 3H), 6.60—7.40 (m, 4H).

1-(1-Naphthyl)-3-buten-1-ol (Entry 6). IR (neat) 3400, 1640, 1600, 1520 cm^{-1}; ^1H NMR (CCl_4) δ=2.12 (s, 1H), 2.35—2.75 (m, 2H), 4.84—6.25 (m, 4H), 7.15—8.10 (m, 7H).

1-Phenyl-1,5-hexadien-3-ol (Entry 7). IR (neat) 3350, 1640, 1600, 1490, 1450 cm^{-1}; ^1H NMR (CCl_4) δ=1.87 (s, 1H), 2.22 (dd, *J*=6.2, 6.2 Hz, 2H), 4.13 (dt, *J*=6.2, 6.2 Hz, 1H), 4.75—5.22 (m, 2H), 5.30—6.70 (m, 3H), 7.18 (s, 5H).

1-Phenyl-5-hexen-3-ol (Entry 8). IR (neat) 3400, 2920, 1640, 1600, 1500, 1460 cm^{-1}; ^1H NMR (CCl_4) δ=1.45 (s, 1H), 1.55—1.90 (m, 2H), 1.95—2.32 (m, 2H), 2.40—2.85 (m, 2H), 3.48 (tt, *J*=6.0, 6.0 Hz, 1H), 4.80—6.20 (m, 3H), 7.09 (s, 5H).

1-Cyclohexyl-3-buten-1-ol (Entry 9). IR (neat) 3400, 2930, 2860, 1640, 1450 cm^{-1}; ^1H NMR (CCl_4) δ=0.80—2.10 (m, 12H), 2.10—2.40 (m, 2H), 3.10—3.50 (m, 1H), 4.80—6.10 (m, 3H).

1-Dodecen-4-ol (Entry 10). IR (neat) 3350, 2920, 2850, 1640, 1460 cm^{-1}; ^1H NMR (CCl_4) δ=0.88 (t, *J*=5.0 Hz, 3H), 1.30 (br s, 15H), 1.95—2.30 (m, 2H), 3.25—3.70 (m, 1H), 4.80—6.10 (m, 3H).

Asymmetric Allylation of *cis*-Stilbene Oxide with Chiral Allylating Agent. To a suspension of tin(II) triflate (202 mg, 0.49 mmol) and (*S*)-1-methyl-2-[(1-piperidinyl)methyl]-pyrrolidine (88.5 mg, 0.49 mmol) in 4 ml of CH_2Cl_2 was added dropwise allyldiisobutylaluminum (1.9 ml of a stock solution in CH_2Cl_2, 0.37 mmol) at −23 °C under argon atmosphere. After the yellow solution was stirred for 5 min, *cis*-stilbene oxide (43.3 mg, 0.22 mmol) in 2 ml of CH_2Cl_2 was added dropwise at −23 °C. The resulting mixture was stirred for 1 h at the same temperature, then quenched with sat. NH_4Cl aq and 1M HCl. The organic layer was extracted with CH_2Cl_2 and dried over anhydrous Na_2SO_4. After evaporation of the solvent, the crude product was purified by (hexane-Et_2O=7 : 4) preparative TLC to afford 1,2-diphenyl-4-penten-1-ol (33.2 mg, 63%). IR (neat) 3400, 1640, 1600, 1500 cm^{-1}; ^1H NMR (CCl_4) δ=1.34 (s, 1H), 1.80—2.20 (m, 2H), 3.69 (d, *J*=8.0 Hz, 1H), 3.90—4.40 (m, 1H), 4.58—6.20 (m, 3H), 7.12 (s, 10H); $[\alpha]_D^{17}$ −7.24° (*c* 2.21, CH_2Cl_2).

The optical purity of the product was determined by conversion to the diastereoisomeric mixture of (*R*)-(+)-α-methoxy-α-(trifluoromethyl)phenylacetic acid esters. ^{19}F NMR analysis showed two clearly separated peaks with a ratio of 75 : 25.

Asymmetric Methallylation of Aldehydes with Chiral Methallylating Agent (Table 3). A typical reaction procedure is described for the reaction of benzaldehyde (Entry 1); to a suspension of tin(II) triflate (184 mg, 0.44 mol) and (*S*)-1-methyl-2-[(1-piperidinyl)methyl]pyrrolidine (80.4 mg, 0.44 mmol) in 4 ml of CH_2Cl_2 was added dropwise methallyldiisobutylaluminum (1.7 ml of a stock solution in CH_2Cl_2, 0.34 mmol) at −78 °C under argon atmosphere. After the yellow solution was stirred for 30 min, benzaldehyde (24.3 mg, 0.23 mmol) in 2 ml of CH_2Cl_2 was added dropwise at −78 °C. The resulting mixture was stirred for 1 h at the same temperature, then quenched with sat. NH_4Cl aq and 1M HCl. The organic layer was extracted with CH_2Cl_2 and dried over Na_2SO_4. After evaporation of the solvent, the crude product was purified by preparative TLC (hexane-Et_2O=7 : 3) to yield 1-phenyl-3-methyl-3-buten-1-ol (29.5 mg, 80%). IR (neat) 3400, 1650, 1500, 1450 cm^{-1}; ^1H NMR (CCl_4) δ=1.75 (s, 3H), 1.91 (s, 1H), 2.32 (d, *J*=7.0 Hz, 2H), 4.67 (t, *J*=7.0 Hz, 1H), 4.76 (br s, 2H), 7.19 (s, 5H).

Other spectral data are presented: 1-(4-Chlorophenyl)-3-methyl-3-buten-1-ol (Entry 2). IR (neat) 3400, 1650, 1500, 1450 cm^{-1}; ^1H NMR (CCl_4) δ=1.62 (s, 3H), 1.95 (s, 1H), 2.18 (d, *J*=7.0 Hz, 2H), 4.55 (t, *J*=7.0 Hz, 1H), 4.60—4.90 (m, 2H), 7.14 (s, 4H); Found: *m/z* 196.0629. Calcd for $C_{11}H_{13}OCl$: M, 196.0653.

1-Phenyl-5-methyl-5-hexen-3-ol (Entry 4). IR (neat) 3400, 2940, 1650, 1600, 1500, 1460 cm^{-1}; ^1H NMR (CCl_4) δ=1.30—1.90 (m, 6H), 2.10 (d, J=7.0 Hz, 2H), 2.50—3.00 (m, 2H), 3.62 (tt, J=7.0, 7.0 Hz,1H), 4.50—5.10 (m, 2H), 7.12 (s, 5H); Found: m/z 190.1397. Calcd for $C_{13}H_{18}O$: 190.1357.

1-Phenyl-5-methyl-1,5-hexadien-3-ol (Entry 3). IR (neat) 3400, 1650, 1600, 1500, 1450 cm^{-1}; ^1H NMR (CCl_4) δ=1.78 (s, 3H), 1.94 (s, 1H), 2.25 (d, J=7.0 Hz, 2H), 4.30 (dt, J=6.0, 6.0 Hz, 1H), 4.79 (br s, 2H), 5.8—6.8 (m, 2H), 7.22 (s, 5H).

2-Methyl-1-dodecen-4-ol (Entry 5). IR (neat) 3400, 2930, 1640, 1450 cm^{-1}; ^1H NMR (CCl_4) δ=0.88 (t, J=6.0 Hz, 3H), 1.30 (br s, 15H), 1.74 (s, 3H), 1.90—2.20 (m, 2H), 3.30—3.80 (m, 1H), 4.60—4.90 (m, 2H).

Asymmetric Propargylation of Aldehydes with Chiral Propargylating Agent (Table 4). A typical reaction procedure is described for the reaction of benzaldehyde (Entry 1); to a suspension of tin(II) triflate (208.5 mg, 0.50 mmol) and (*S*)-1-methyl-2-[(1-piperidinyl)methyl]pyrrolidine (91.2 mg, 0.50 mmol) in 4 ml of CH_2Cl_2 was added dropwise propargylaluminum derivative (2.0 ml of a stock solution in CH_2Cl_2, 0.39 mmol) at −78 °C under argon atmosphere. After the yellow solution was stirred for 30 min, benzaldehyde (30.2 mg, 0.29 mmol) in 2 ml of CH_2Cl_2 was added dropwise at −78 °C. The resulting mixture was stirred for 2 h at the same temperature, then quenched with sat. NH_4Cl aq and 1M HCl. The organic layer was extracted with CH_2Cl_2 and dried over Na_2SO_4. After concentration in vacuo the resulted oily substance was purified by preparative TLC (hexane-Et_2O=7 : 3) to yield 1-phenyl-3-butyn-1-ol (32.2 mg, 77%). IR (neat) 3400, 3300, 2100, 1500, 1460 cm^{-1}; ^1H NMR (CCl_4) δ=1.88 (t, J=2.5 Hz, 1H), 2.50 (dd, J=2.5, 6.6 Hz, 2H), 2.40 (s, 1H), 4.72 (t, J=6.6 Hz, 1H), 7.26 (s, 5H). Other spectral data are presented.

1-(1-Naphthyl)-3-butyn-1-ol (Entry 2). IR (neat) 3400, 3300, 2100, 1600, 1500 cm^{-1}; ^1H NMR (CCl_4) δ=1.90 (t, J=2.5 Hz, 1H), 2.40—2.95 (m, 3H), 5.10—5.55 (m, 1H), 7.05—8.10 (m, 7H); Found: m/z 196.0825. Calcd for $C_{14}H_{12}O$: M, 196.0887.

1-Phenyl-5-hexyn-3-ol (Entry 3). IR (neat) 3400, 3300, 2920, 2100, 1600, 1500, 1450 cm^{-1} ^1H NMR (CCl_4) δ=1.50—2.00 (m, 3H), 2.27 (dd, J=2.5, 6.0 Hz, 2H), 2.40—3.00 (m, 3H), 3.30—3.90 (m, 1H), 7.08 (s, 5H); Found: m/z 174.1039. Calcd for $C_{12}H_{14}O$: M, 174.1043.

1-Phenyl-1-hexen-5-yn-3-ol (Entry 4). IR (neat) 3400, 3300, 2100, 1650, 1490, 1450 cm^{-1}; ^1H NMR (CCl_4) 1.92 (t, J=2.5 Hz, 1H), 2.43 (dd, J=2.5, 6.0 Hz, 2H), 2.72 (s,1H), 4.05—4.50 (m, 1H), 5.75—6.70 (m, 2H), 7.15 (s, 5H); Found; m/z 172.0934. Calcd for $C_{12}H_{12}O$: M, 172.0887.

References

1) J. D. Morrison, "Asymmetric Synthesis;" ed by Academic Press, New York (1983), Vol. 1—4.

2) N. Iwasawa and T. Mukaiyama, *Chem. Lett.*, **1982**, 1441; **1983**, 297; R. W. Stevens and T. Mukaiyama, *ibid.*, **1983**, 1799; T. Mukaiyama and N. Iwasawa, *ibid.*, **1984**, 753; T. Mukaiyama, N. Iwasawa, R. W. Stevens, and T. Haga, *Tetrahedron*, **40**, 1381 (1984).

3) J. Ichikawa, M. Asami, and T. Mukaiyama, *Chem. Lett.*, **1984**, 949.

4) T. Oriyama and T. Mukaiyama, *Chem. Lett.*, **1984**, 2071; T. Mukaiyama, K. Tomimori, and T. Oriyama, *ibid.*, **1985**, 813, 1359.

5) S. Masamune, G. S. Bates, and J. W. Corcoran, *Angew. Chem., Int. Ed. Engl.*, **16**, 585 (1977).

6) a) B: T. Herold and R. W. Hoffmann, *Angew. Chem., Int. Ed. Engl.*, **17**, 768 (1978); R. W. Hoffmann and T. Herold, *Chem. Ber.*, **114**, 375 (1981); T. Herold, U. Schrott, and R. W. Hoffmann, *ibid.*, **114**, 359 (1981); M. M. Midland and S. B. Preston, *J. Am. Chem. Soc.*, **104**, 2330 (1982); H. C. Brown and P. K. Jadhar, *J. Am. Chem. Soc.*, **105**, 2092 (1983); H. C. Brown, P. K. Jadhar, and P. T. Perumal, *Tetrahedron Lett.*, **25**, 5111 (1984); H. C. Brown and P. K. Jadhar, *ibid.*, **25**, 1215 (1984); P. K. Jadhav, K. S. Bhat, P. T. Perumal, and H. C. Brown, *J. Org. Chem.*, **51**, 432 (1986); H. C. Brown and K. S. Bhat, *J. Am. Chem. Soc.*, **108**, 293, 5919 (1986); W. R. Roush and R. L. Halterman, *J. Am. Chem. Soc.*, **108**, 294 (1986). b) Si: T. Hayashi, M. Konishi, and M. Kumada, *J. Am. Chem. Soc.*, **104**, 4962; 4963 (1982); T. Hayashi, M. Konishi, and M. Kumada, *J. Org. Chem.*, **48**, 281 (1983); T. Hayashi, K. Kabeta, T. Yamamoto, K. Tamao, and M. Kumada, *Tetrahedron Lett.*, **24**, 5661 (1983); S. J. Hathaway and L. A. Paquette, *J. Org. Chem.*, **48**, 3351 (1983); L. Coppi, A. Mordini, and M. Taddei, *Tetrahedron Lett.*, **28**, 969 (1987). c) Sn: J. Otera, Y. Kawasaki, H. Mizuno, and Y. Shimizu, *Chem. Lett.*, **1983**, 1529; J. Otera, Y. Yoshinaga, T. Yamaji, T. Yoshioka, and Y. Kawasaki, *Organometallics*, **4**, 1213 (1986); G. P. Boldrini, E. Tagliavini, C. Trombini, and A. Umani-Ronchi, *J. Chem. Soc., Chem. Commun.*, **1986**, 685. d) Cr: B. Cazes, C. Verniere, and J. Gore, *J. Synth. Commun.*, **13**, 73 (1983).

7) a) I. Ojima, Y. Miyazawa, and K. Kumagai, *J. Chem. Soc., Chem. Commun.*, **1976**, 927; K. Soai and M. Ishizaki, *ibid.*, **1984**, 1016; *idem*, *J. Org. Chem.*, **51**, 3290 (1986); K. Soai, M. Ishizaki, and S. Yokoyama, *Chem. Lett.*, **1987**, 341. b) J. M. McNamara and Y. Kishi, *J. Am. Chem. Soc.*, **104**, 7371 (1982); P. A. Bartlett, W. S. Johnson, and J. D. Elliott, *ibid.*, **105**, 2088 (1983); S. H. Mashraqui, and R. M. Kellogg, *J. Org. Chem.*, **49**, 2513 (1984); R. Imwinkelried and D. Seebach, *Angew. Chem., Int. Ed. Engl.*, **24**, 765 (1985); T. Mukaiyama, M. Ohshima, and N. Miyoshi, *Chem. Lett.*, **1987**, 1121.

8) T. Mukaiyama, N. Minowa, T. Oriyama, and K. Narasaka, *Chem. Lett.*, **1986**, 97.

9) H. Lehmkuhl and D. Reinehr, *J. Organomet. Chem.*, **23**, C25 (1970).

10) A. Stefani and P. Pino, *Helv. Chim. Acta*, **55**, 1110 (1970).

11) D. Seyferth and M. A. Weiner, *J. Org. Chem.*, **26**, 4797 (1961).

12) For example: J. B. Jones, *Ciba Found. Symp.*, **111**, 3 (1985); Y. F. Wang, C. S. Chen, G. Girdaukas, and D. J. Sih, *ibid.*, **111**, 128 (1985); M. Ohno, *ibid.*, **111**, 171 (1985).

13) a) N. Cohen, *Acc. Chem. Res.*, **9**, 412 (1976); b) J. K. Whitsell and S. W. Felman, *J. Org. Chem.*, **45**, 755 (1980); c) K. Osakada, M. Obana, T. Ikariya, M. Saburi, and S. Yoshikawa, *Tetrahedron Lett.*, **22**, 4297 (1981); d) M. Asami, *Chem. Lett.*, **1984**, 829; e) J. Ichikawa, M. Asami, and T. Mukaiyama, *ibid.*, **1984**, 949; f) S. Hanessian, D. Delorme, S.Beaudoin, and Y. Leblanc, *J. Am. Chem. Soc.*, **106**, 5754 (1984); g) N. S. Simpkins, *J. Chem. Soc., Chem. Commun.*, **1986**, 88; h) R. Shirai, M. Tanaka, and K. Koga, *J. Am. Chem. Soc.*, **108**, 543 (1986); i) H. Yamashita and T. Mukaiyama, *Chem. Lett.*, **1985**, 1643.

14) R. Haruta, M. Ishiguro, N. Ikeda, and H. Yamamoto,

J. Am. Chem. Soc., **104**, 7667 (1982); N. Ikeda, I. Arai, and H. Yamamoto, *ibid.*, **108**, 483 (1986).

15) K. Eiter and H. Oediger, *Justus Liebigs Ann. Chem.*, **682**, 62 (1965); R. G. Daniels and L. A. Paquette, *Tetrahedron Lett.*,**22**, 1579 (1981).

16) J. L. Moreau "The Chemistry of Ketenes, Allenes, and Related Compounds," ed by S. Patai, Wiley, New York (1980).

17) J. A. Dale, D. L. Dull, and H. S. Mosher, *J. Org. Chem.*, **34**, 2543 (1969).

 © 1987 The Chemical Society of Japan Bull. Chem. Soc. Jpn., 60, 3705—3711 (1987)

400 MHz Two-Dimensional NMR Studies of Cyclodextrin Derivatives for ^{1}H and ^{13}C Chemical Shift Determination

Iwao TABUSHI, Tatsuya NABESHIMA, Kazuo YAMAMURA,* and Haruo FUJITA
Department of Synthetic Chemistry, Kyoto University, Sakyo-ku, Kyoto 606
(Received May 2, 1987)

Two-dimensional (2D) NMR spectroscopies, proton (400 MHZ)- proton (400 MHz) and carbon (100 MHz)-proton (400 MHz) chemical shift correlation spectroscopy, were developed as a reliable technique for the strict assignment of crowded and complicated NMR absorptions of substituted cyclodextrin derivatives, pentakis[2,6-*O*-(*t*-butyldimethylsilyl)]-*A*,*B*-bis-[2-*O*-(*t*-butyldimethylsilyl)-6-deoxy-6-(methylthio)]-β-cyclodextrin (**2**) and *A*,*B*-bis[6-deoxy-6-(methylthio)]-β-cyclodextrin (**1**).

Cyclodextrins bind a large variety of guest molecules of appropriate shapes and sizes in their "hydrophobic" cavities in aqueous solution.[1] This concept of molecular recognition in water has led the authors to a new concept of artificial enzymes or artificial receptors[2,3] and the approaches to realize these have been attempted via attachment of appropriate functional groups onto the "rim" of cyclodextrins. For specific derivatization of cyclodextrins, the explicit determination of the product structures is necessary and important. For the purpose, ^{13}C and ^{1}H NMR[4–16] have been especially useful.

More important, however, is the macrocyclic regiochemistry (see Scheme 1), since it seems very crucial to the development of artificial enzymes or receptors.[17,18] Nevertheless, this regiochemistry on cyclodextrins is not explicitly determined by simple spectroscopies[16,19] other than NMR (high magnetic field) spectroscopy. But instead, a great deal of effort of synthetic[19] or enzymatic[20,21] approach has been made to overcome the drawback.

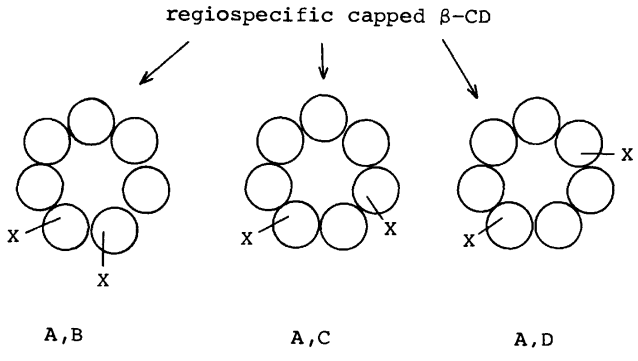

Scheme 1. Regiochemistry of prim-disubstituted β-cyclodextrin.

Recently two-dimensional (2D) NMR spectroscopy[22] has been developed rapidly for the structure determinations of complicated molecules such as natural products,[23] proteins,[24] or carbohydrates.[25] 2D NMR gives much more reliable and well defined informations of chemical shifts or coupling constants than the convensional one-dimensional NMR. Parent α- and β-cyclodextrins were studied by 250 or 270 MHz 2D NMR, and the assignments of individual ^{13}C absorptions of C_1 to C_6[25c] have been successfully made. Substituted cyclodextrins, however, usually show finely separated and delicately overlapped complex absorptions of ^{13}C (or ^{1}H), probably due to appreciable remote substituent effects on chemical shifts and also due to minor but often important conformational changes.

Now we wish to report a complete study of pentakis[2,6-*O*-(*t*-butyldimethylsilyl)]-*A*,*B*-bis[2-*O*-(*t*-butyldimethylsilyl)-6-deoxy-6-(methylthio)]-β-cyclodextrin (**2**) by using 400 MHz 2D NMR by taking proton-proton[27] (400 MHz) and proton-carbon chemical shift correlation[28] (400—100 MHz). Explicit assignments of C_1–C_6 carbons are presented herein.

Results and Discussion

Per(2,6-*O*-disilylation) of disubstituted cyclodextrin derivative **1** with *t*-$BuMe_2SiCl$[14] was carried out (see

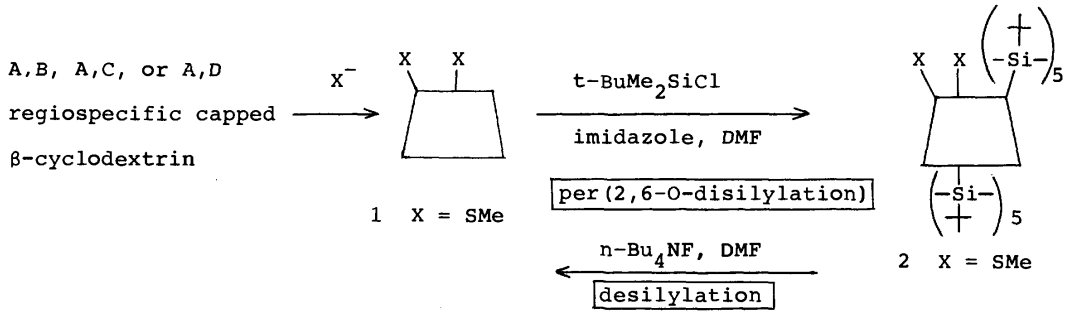

Scheme 2.

Scheme 2). This persilylation is important because of the following reasons; (a) separation and isolation of the silylated derivatives are easily achieved by a usual silica-gel column chromatography, (b) the silylated compounds are satisfactorily stable under weak acidic or from weak to strong basic conditions, (c) an appropriate substituent can be conveniently introduced into the unsilylated C_3-OH groups, and (d) desilylation is readily carried out by treatment with n-Bu_4NF in DMF at room temperature (Scheme 2). By use of this silylation-desilylation technique, a promising possibility of constructing sophisticated enzyme models or receptor models through preparation of regiospecific prim,prim-disubstituted cyclodextrins with or without additional appropriate functional group at the secondary position can be done without serious difficulty (Fig. 1).

Pentakis[2,6-*O*-(*t*-butyldimethylsilyl)]-*A*,*B*-bis[2-*O*-(*t*-butyldimethylsilyl)-6-deoxy-6-(methylthio)]-β-cyclodextrin (**2**), which was prepared according to Scheme 2, gave a very crowded conventional ^1H NMR spectrum (400 MHz) (Fig. 2) like other cyclodextrin derivatives. Direct analysis of the spectrum does not afford enough informations to determine the structure of **2** explicitly. Only ^1H absorptions for C_1-H bond appeared at δ 4.80—4.89 separately from other ^1H absorptions. The assignment is based on the comparison with the known ^1H chemical shift for C_1-H protons of the parent cyclodextrin. The ^1H absorptions at δ 2.73—3.04 may be ascribed to H_{6A} ($H_{6A'}$) and H_{6B} ($H_{6B'}$) protons tentatively (Fig. 3), since these are reasonable as CH_2 protons α to the SMe substituent. For other ^1H absorptions, however, explicit assignments were difficult, particularly for other protons attached

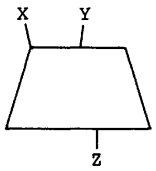

X, Y = substituent at primary rim of cyclodextrin

Z = substituent at C_3

Fig. 1. Regiospecific prim-disubstituted β-cyclodextrin with an appropriate functional groups at secondary C_3 carbon.

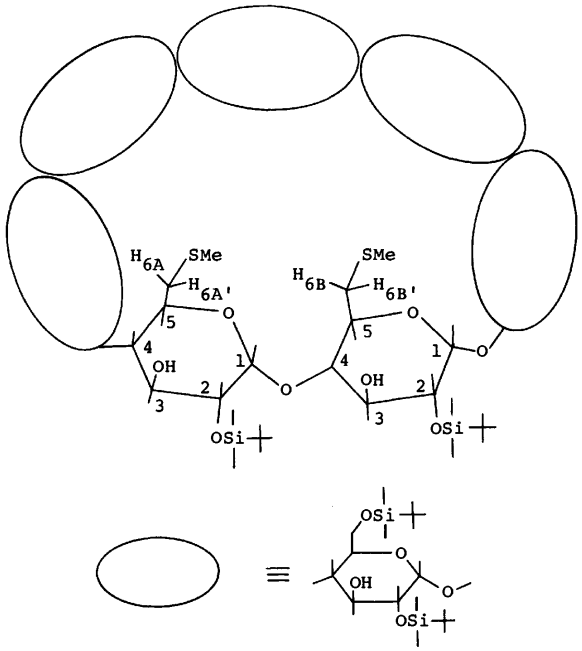

Fig. 3. Structure of **2**. Two H_6 protons on the same ring are interchangeable in the NMR assignment.

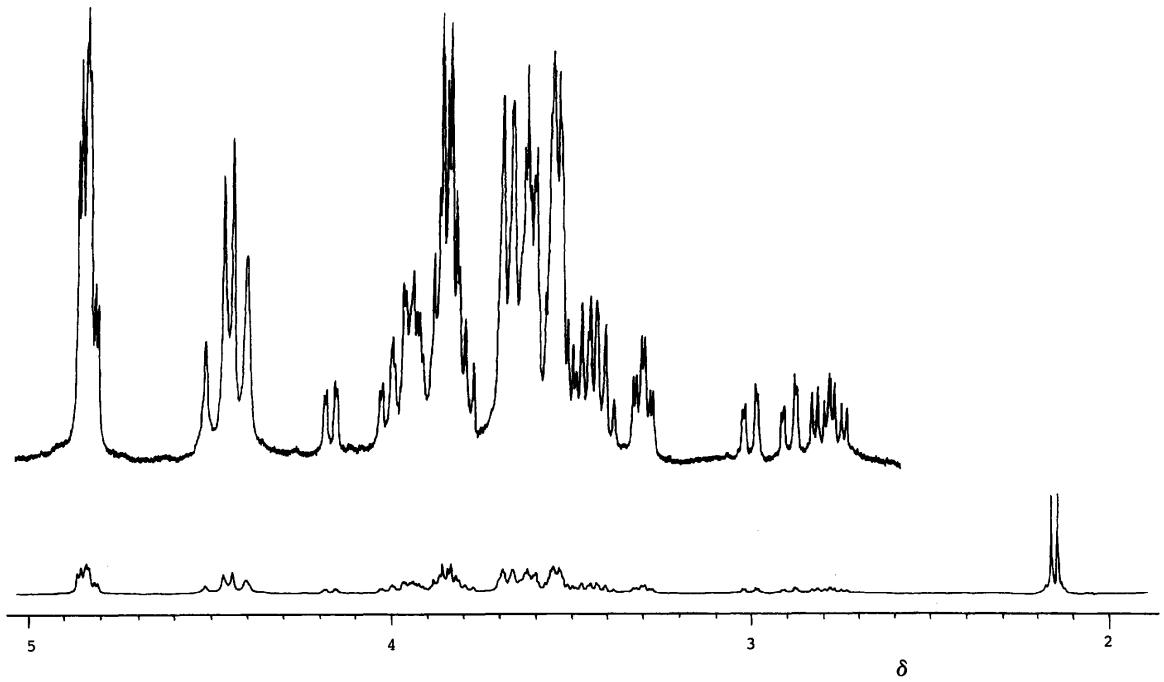

Fig. 2. 400 MHz ^1H NMR spectrum of **2**.

to carbons of cyclodextrin skeleton, because of the extreme complexity of the spectrum.

^{13}C NMR, satisfactorily well-separated absorptions were obtained at 100 MHz NMR (Fig. 4), in which fine structures of the ^{13}C absorptions provide a useful information not only as to the skeletal structure but also as to the possible conformation. Clearly, groups of the ^{13}C absorptions which appeared at well-separated magnetic fields centered at δ 103.0, 82.1, and 62.0 are to be assigned to C_1, C_4, and C_6, respectively, by comparison with ^{13}C absorptions of parent β-cyclodextrin. Thus, $C_{4A,B}$ and $C_{6A,B}$ carbons are tentatively ascribed to the carbon absorption peaks centered at δ 86.4 and 35.9 respectively, by considering the substituent effect of MeS group, while unequivocal determinations of C_2, C_3, C_5, and $C_{5A,B}$ are not feasible from the present one-dimensional NMR spectrum. The lack of NMR data of related compounds suitable for mutual comparison makes the further assignment difficult. Therefore, it is important and necessary to obtain a series of different types of well resolved NMR spectra and to combine information of ^{13}C and

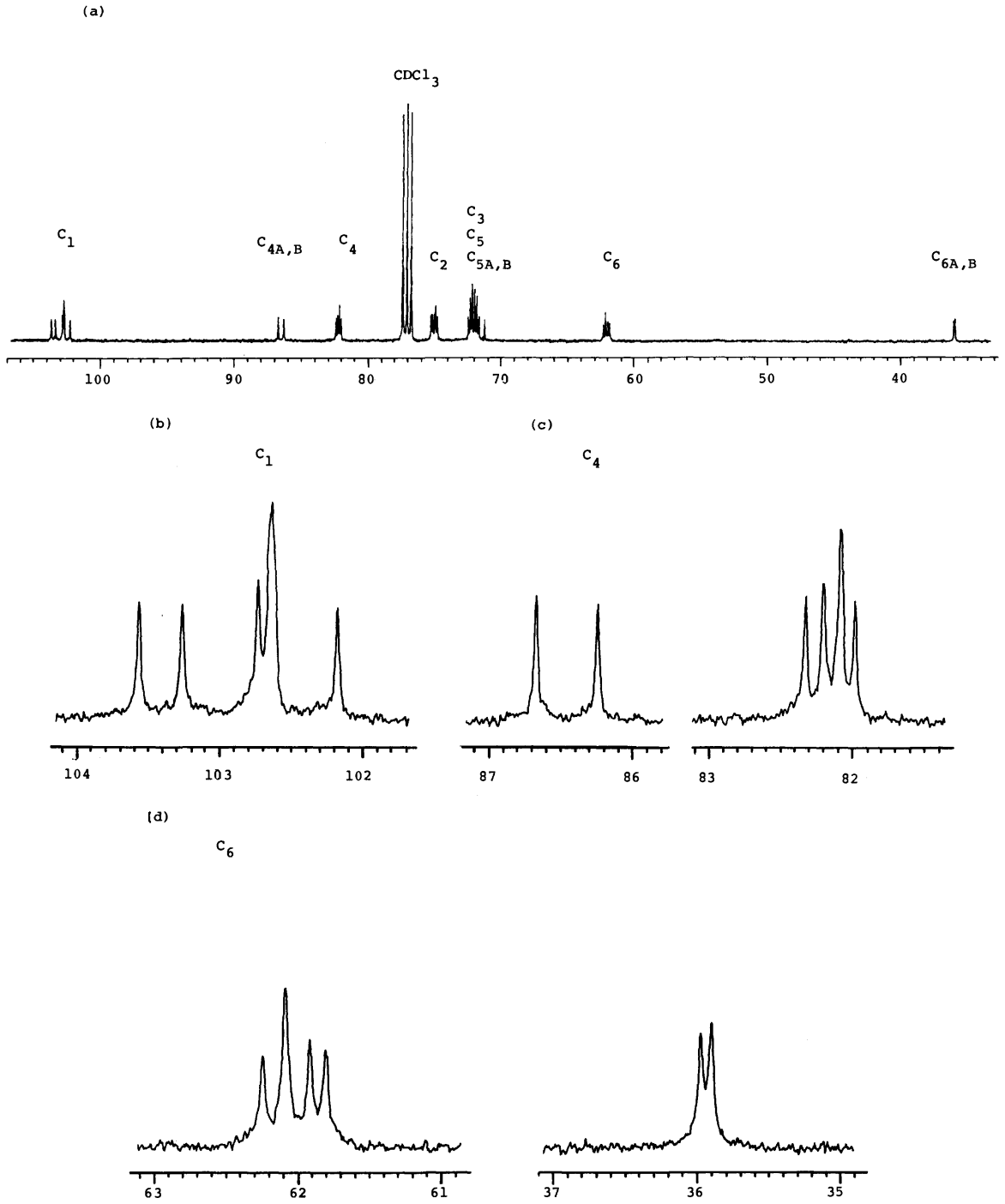

Fig. 4. 100 MHz ^{13}C NMR spectrum of **2**.

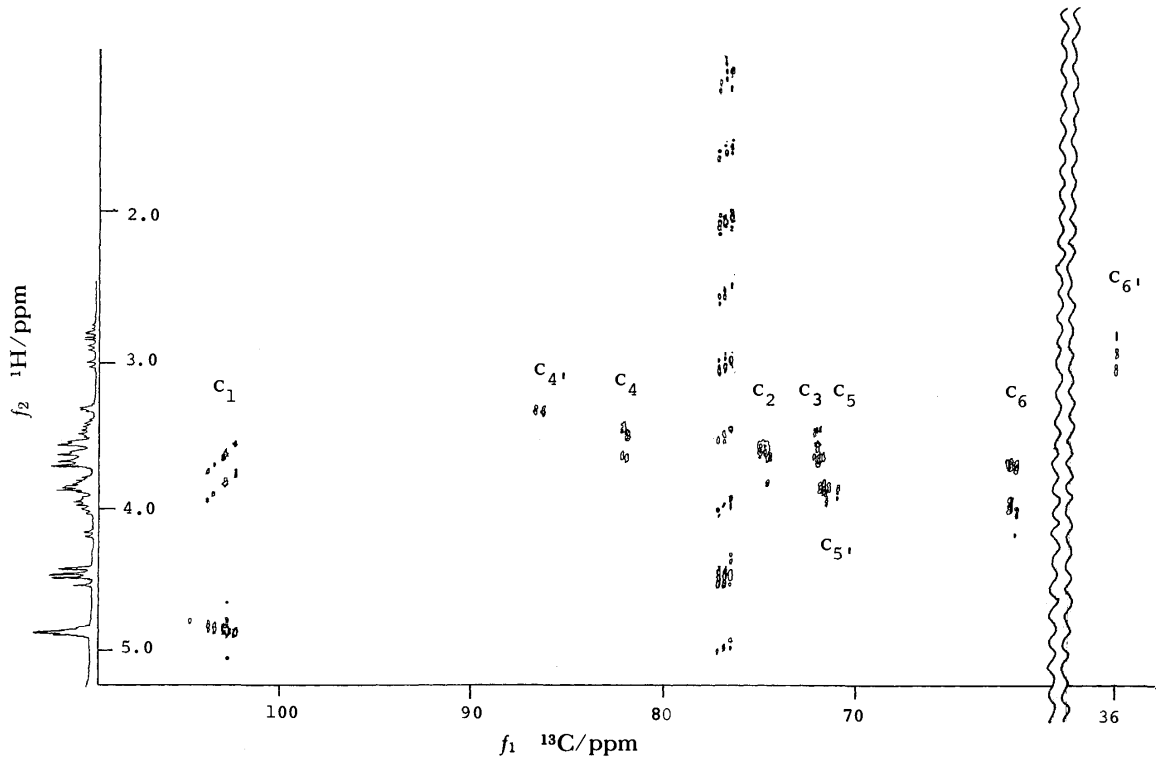

Fig. 5. Contour plot of the two-dimensional (2D) ^{1}H–^{13}C shift correlation of **2** in $CDCl_3$, 30°C.

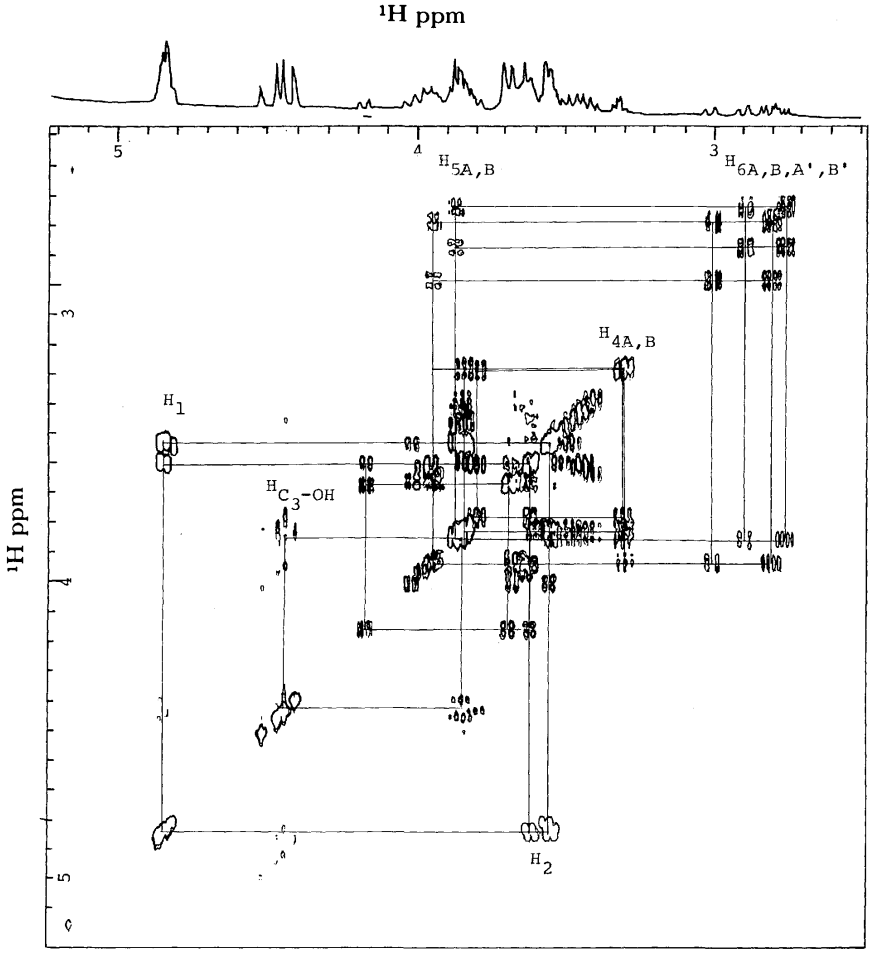

Fig. 6. Contour plot obtained in the 400 MHz ^{1}H COSY of **2**.

Table 1. ^{13}C NMR Chemical Shift (δ from TMS) of Pentakis[2,6-*O*-(*t*-butyldimethylsilyl)]-*A*,*B*-bis[2-*O*-(*t*-butyldimethylsilyl)-6-deoxy-6-(methylthio)]-β-cyclodextrin (**2**) and *A*,*B*-Bis[6-deoxy-6-(methylthio)]-β-cyclodextrin (**1**)

	C_1 $C_{1A,B}$	C_4	C_{4A} C_{4B}	C_2 $C_{2A,B}$	C_3 C_5 $C_{3A,B}$ $C_{5A,B}$	C_6	C_{6A} C_{6B}
2	103.57	82.32	86.67	75.22	72.42	62.24	35.98
	103.27	82.20	86.24	75.17	72.28	62.08	35.90
	102.74	82.08		75.08	72.14	61.91	
	102.64	81.97		74.95	71.93	61.80	
	102.18			74.86	71.77		
				74.75	71.63		
					71.20		
1	103.40	82.65	86.29	74.09		60.98	36.28
	103.22	82.57	86.20	74.04			36.12
	103.02			73.99			
	102.75			73.94			
				73.70			
				73.47			
				73.19			
				73.10			
				72.33			
				71.87			

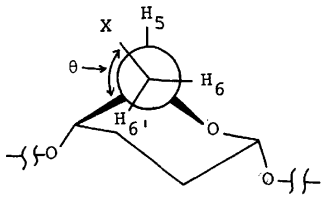

Fig. 7. Dihedral angle between C_4-C_5 axis and C_6-X axis.

Table 2. The Observed Coupling Constants (Hz) between H_6 and $H_{5(6)}$ of the MeS-Substituted Glucose Rings of **2**[a)]

	$H_{6A',B}$	$H_{6B',B}$	H_{5A}	H_{5B}
$H_{6A,A'}$	14	—	6.0	—
			2.5	
$H_{6B,B'}$	—	14	—	6.5
				2.5

a) Assignments A and B are tentative and interchangeable.

^1H NMR spectra for strict structure and conformation determination of cyclodextrin derivatives.

Figures 5 and 6 depict the 2D ^1H-^{13}C chemical shift correlation spectrum and 400 MHz ^1H COSY spectrum of **2**, respectively. Figure 5 displays proton chemical shift information in f_1 (vertical axis) and carbon shifts in f_2 (horizontal axis), one signal appearing for each directly bonded carbon-proton pair. Thus, in the ^1H-^{13}C shift correlation, H_{4A}-C_{4A} correlation and H_{6A}-C_{6A} correlation are clearly seen (Fig. 5), suggesting that the ^1H absorptions at δ 3.28—3.34 and 2.73—3.04 (see also Fig. 2) are assigned unambiguously to H_{4A} (H_{4B}) and H_{6A} (H_{6B}), respectively. Similarly, ^1H COSY spectrum clearly depicts the H_6-H_5 correlation (see Fig. 6), strongly indicating that H_{5A} (H_{5B}) proton absorbs at δ 3.88 (3.95) though hidden by a very complicated ^1H absorptions. Finally the H_{5A}-C_{5A} correlation found in Fig. 5 strongly indicates that C_{5A} and C_{5B} carbons absorb at δ 71.2 and 71.8, one of which is overlapped by the ^{13}C absorptions of C_3 carbons. The presence of H_{5A}-H_{4A} correlation observed (Fig. 6) also supports the mutual consistency of the present assignment. It is clear that the H_4-H_5-H_6 network on A and B rings of **2** has been successfully solved by the 2D NMR technique, providing considerable increase in resolving power and information content over that obtainable using conventional methods.

The 2D NMR technique was found also effective in the assignment of H_1-H_2-C_2 network of **2**. Thus, from ^1H COSY spectrum, H_1-H_2 correlation has led to the clear assignment of H_2 protons (Fig. 6). Therefore, a decisive assignment, ^{13}C absorption at δ 74.8—75.2 due to C_2 carbons, was made clearly. The complete ^{13}C absorptions together with their assignments are summarized in Table 1.

The absorptions due to C_3-OH protons were concluded to have appeared at δ 4.3—4.6 region (see Fig. 2), since a clear correlation was seen between H-C_3 and C_3-O-H in the ^1H COSY spectrum.

H_{6A} (H_{6B}) (see Fig. 7) are coupled to $H_{6A'}$ ($H_{6B'}$) with the coupling constant of J=14 Hz and the two $H_{6A,A'}$ ($H_{6B,B'}$) protons coupled again to H_{5A} (H_{5B}) but with different coupling constants of 6 and 2.5 Hz (6.5 and 2.5 Hz) (see Table 2), suggesting the preference of rotamers around the C_5 -C_6 axis (most populated position in the freely or restrictedly rotating substituted methylene) at certain angle (ca. 40° or ca. 200°) twisted from C_5-C_4. One H_6 proton absorbing at δ 4.14—4.23 obviously belongs to the unsubstituted glucose ring. Therefore, H_6 protons may be used as the rotamer probe for the dihedral angle change.

In conclusion, the 2D NMR technique was very effective, particularly for the explicit assignment of ^{13}C NMR absorptions of the glucose ring carrying the substituent (SMe) at C_6 carbons of *A,B*-disubstituted cyclodextrin derivative, **2**. The technique was found also powerful for the desilylated compound, *A,B*-bis[6-deoxy-6-(methylthio)]-*β*-cyclodextrin (**1**), which was obtained via the desilylation of **2** (Scheme 2). The ^{13}C NMR absorptions of **1** together with their assignments are given in Table 1. The correlation of ^{13}C NMR assignments between **1** and **2** was satisfactory as shown in Table 1.

Experimental

Instruments and Apparatus. ^1H (400 MHz), ^{13}C (100 MHz), and 2D correlation NMR spectra were recorded on a JEOL JNM-GX 400 spectrometer. Chemical shifts in $CDCl_3$ are given in *δ* values from tetramethylsilane (TMS) used as an internal standard. ^{13}C and 2D NMR spectra were obtained with a coaxial dual cell. The inner tube (5 mm*φ*) contained 1% TMS in $CDCl_3$, which was used as an external standard by taking the chemical shift of the central peak of $CDCl_3$ from TMS as *δ* 77.02. The outer tube (10 mm*φ*) contained a DMSO-d_6 solution of a cyclodextrin derivative to be measured. Both tubes were purchased from Wilmad Glass Co. 2D homonuclear chemical shift correlation (COSY) spectrum (512×1024 matrix after Fourier transformation) was obtained from 512 spectra of 2048 points. The spectral width was 2200 Hz, and 90° pulse of ^1H was 9.1 μs. In carbon-proton chemical shift correlation spectra, spectral widths of two axes were 2200 Hz (^1H axis) with 512 data points and 12000 Hz (^{13}C axis) with 4096 data points. 90° pulse widths of ^{13}C and ^1H were 19.4 and 26.5 μs, respectively. All measurements were carried out at 30±1 °C.

IR spectra were obtained using a Hitachi model 260-50 spectrophotometer. $CDCl_3$ (99.8%), DMSO-d_6 (99.9%), and TMS were purchased from Aldrich or E. Merck.

Materials. Commercially available *N,N*-dimethylformamide was kept standing over CaH_2 overnight at room temperature, and then distilled under reduced pressure (ca. 20 mmHg (1 mmHg=133.322Pa)) before use. Imidazole was freshly recrystallized from benzene, and then dried in vacuo at room temperature before use. Methanethiol sodium salt (15% aqueous solution, Tokyo Kasei) was used without further purification.

Per(2,6-*O*-disilylation) of cyclodextrin derivatives were carried out by treatment of the corresponding unsilylated cyclodextrin derivatives with a mixture of *t*-butyldimethylchlorosilane and dry imidazole in dry DMF according to the reported procedure.[14] The persilylated compounds were purified by silica-gel column chromatography (3×30 cm) at least twice using $CHCl_3$ as an eluent. The purity was checked by TLC using $CHCl_3$ or benzene-AcOEt (100 : 1, v/v).

A typical procedure for desilylation of silylated cyclodextrins—A silylated cyclodextrin derivative (0.5 g) was treated with tetrabutylammonium fluoride (1.0 g) in 30 mL of DMF at room temperature overnight. After the mixture was evaporated to dryness in vacuo, 30 mL of water and 1 mL of tetrachloroethylene were added to the residue. The mixture was stirred for 1 h at 0 °C to afford white precipitates, which were collected by suction filtration. The precipitates were dissolved in ca. 100 mL of 30—40% aqueous EtOH, and then tetrachloroethylene and the solvent were evaporated to dryness at 30 °C, finally at 80 °C at 20 mmHg. This procedure was repeated at least three times for the complete removal of tetrachloroethylene included in the cyclodextrin cavity.

***A,B*-Bis[6-deoxy-6-(methylthio)]-*β*-cyclodextrin (1).** *m*-Benzenedisulfonyl-capped *β*-cyclodextrin[20] (2.8 g, 2.1 mmol) was treated with 20 g (43 mmol) of a 15% aqueous MeSNa solution at 80 °C for 14 h under Ar. The mixture was acidified to pH 4 by the addition of 3M hydrochloric acid (1M=1 mol dm^{-3}) to give a pale yellow precipitates, which were collected by filtration. The filtrate was stirred with 1 mL of tetrachloroethylene at 0 °C for 1 h. The precipitates thus formed (containing tetrachloroethylene) were collected. Tetrachloroethylene included in the precipitates was removed as described above. The removal of tetrachloroethylene was ascertained by IR, viz., by the disappearance of the 775, 910 cm^{-1} absorptions. The precipitates were combined and dried in vacuo at 90 °C overnight, giving 0.9 g of **2**: IR (KBr) 3350 (br), 2910, 1150, 1030, 935, 755 cm-1; ^1H NMR (DMSO-d_6) *δ*=2.06 (s, Me-S, 3H), 2.10 (s, Me-S, 3H), 2.63 (dd, S-C(6)-H, *J*=8, 14 Hz, 1H), 2.75 (dd, S-C(6)-H, *J*=8, 14 Hz, 1H), 3.01 (d, S-C(6)-H, *J*=14 Hz, 1H), 3.13 (d, S-C(6)-H, *J*=14 Hz, 1H), 3.23—3.86 (m, other H), 4.40—4.56 (m, C(6)-OH, 5H), 4.80—4.91 (m, C(1)-H, 7H), 5.67—5.93 (m, C(2)-OH and C(3)-OH, 14H).

Pentakis[2,6-*O*-(*t*-butyldimethylsilyl)]-*A,B*-bis[2-*O*-(*t*-butyl dimethylsilyl)-6-deoxy-6-(methylthio)]-*β*-cyclodextrin (2). *A,B*-Bis[6-deoxy-6-(methylthio)]-*β*-cyclodexttrin (0.9 g, 0.75 mmol) was treated with *t*-butyldimethylchlorosilane (4.5 g, 30 mmol) and dry imidazole (4.3 g, 63 mmol) in 40 mL of dry DMF in a reported way,[14] giving 250 mg of the corresponding per(2,6-*O*-disilylated) compound **2** after the chromatographic purification as described above. **2**: IR (KBr) 3455 (br), 2960, 2940, 2900, 2865, 1470, 1365, 1260 (Si-CH_3), 1160, 1140, 1095, 1045, 1010, 860, 840, 785 cm^{-1}; ^1H NMR ($CDCl_3$) *δ*=0.01—0.07 (m, Me_2Si-O-C(6), 30H), 0.12—0.19 (m, Me_2 Si-O-C(2), 42H), 0.85—0.90 (m, *t*-BuSi-O-C(6), 45H), 0.90—0.96 (m, *t*-Bu-O-C(2), 63H), 2.15 (s, Me-S-C(6), 3H), 2.17 (s, Me-S-C(6), 3H), 2.76 (dd, S-C(6)-H, *J*=6, 14 Hz, 1H), 2.81(dd, S-C(6)-H, *J*=6.5, 14 Hz, 1H), 2.89 (dd, S-C(6)-H, *J*=2.5, 14 Hz, 1H), 3.00 (dd, S-C(6)-H, *J*=2.5, 14 Hz, 1H), 3.25—4.21 (m, other H, 49 H), 4.39—4.67 (m, C(3)-OH, 7H), 4.80—4.89 (m, C(1)-H, 7H); Found : C, 53.76 ; H, 9.54%. Calcd for $C_{116}H_{242}O_{33}S_2Si_{12}$: C, 54.29 ; H, 9.51%.

References

1) E.g., F. Cramer, *Angew. Chem.*, **5**, 115 (1956).

2) For reviews see a) I. Tabushi, *Tetrahedron*, **40**, 269 (1984); b) I. Tabushi and K. Yamamura, "Cyclophanes. I," ed by F. Voegtle, Springer Verlag, New York (1983), p. 145; c) "Host Guest Complex Chemistry, I and II," ed by F. Voegtle, Springer Verlag, New York (1981) and (1982).

3) For reviews see I. Tabushi and Y. Kuroda, *Adv. Catal.*, **32**, 417 (1983); M. L. Bender and M. Komiyama, "Cyclodextrin Chemistry," Springer Verlag, New York (1978); R. Breslow, *Acc. Chem. Res.*, **13**, 170 (1980); I. Tabushi, *ibid.*, **15**, 66 (1982); R. Breslow, *Science*, **218**, 532 (1982); W. Saenger, *Angew. Chem., Int. Ed. Engl.*, **19**, 344 (1980); J. Szejtli, "Cyclodextrins and Their Inclusion Complexes," Akademiai Kiado, Budapest (1982).

4) K. Takeo, K. Hirose, and T. Kuge, *Chem. Lett.*, **1973**, 1233.

5) R. J. Bergeron, M. P. Meeley, and Y. Machida, *Bioorg. Chem.*, **5**, 121 (1976).
6) A. Harada, M. Furue, and S. Nozakura, *Macromolecules*, **9**, 701 (1976).
7) T. Ogawa and M. Matsui, *Carbohydr. Res.*, **56**, C1-6 (1977).
8) B. Siegel, A. Pinter, and R. Breslow, *J. Am. Chem. Soc.*, **99**, 2309 (1977).
9) D. Gagnaire, D. Mancier, and M. Vincendon, *Org. Magn. Reson.*, **11**, 344 (1978).
10) J. Boger, R. J. Corcoran, and J.-M. Lehn, *Helv. Chim. Acta*, **61**, 2190 (1978).
11) I. Tabushi, Y. Kuroda, and K. Shimokawa, *J. Am. Chem. Soc.*, **101**, 1614 (1979).
12) J. Boger, D. G. Brenner, J. Knowles, *J. Am. Chem. Soc.*, **101**, 7630 (1979).
13) I. Tabushi, L.C. Yuan, K. Shimokawa, K. Yokota, T. Mizutani, and Y. Kuroda, *Tetrahedron Lett.*, **24**, 2273 (1981).
14) R. L. Wife, D. E. Reed, D. P. Leworthy, D. M. Barnett, P. D. Regen, and H. C. Volger, *Int. Symp. on Cyclodextrins, Budapest*, **1981**, 301.
15) A. Ueno and R. Breslow, *Tetrahedron Lett.*, **23**, 3451 (1982).
16) H.-R. Schulten, T. Komori, K. Fujita, A. Shinoda, T. Imoto, and T. Kawasaki, *Carbohydr. Res.*, **107**, 177 (1982).
17) K. Hirotsu, T. Higuchi, K. Fujita, T. Ueda, A. Shinoda, and T. Imoto, *J. Org. Chem.*, **47**, 1143 (1982).
18) Y. Iwakura, K. Ueno, F. Toda, S. Onozuka, K. Hattori, and M. L. Bender, *J. Am. Chem. Soc.*, **97**, 4432 (1975); S. Onozuka, M. Kojima, K. Hattori, and F. Toda, *Bull. Chem. Soc. Jpn.*, **53**, 3225 (1980).
19) I. Tabushi, Y. Kuroda, K. Yokota, and L.C. Yuan, *J. Am. Chem. Soc.*, **103**, 711 (1981).
20) I. Tabushi, T. Nabeshima, K. Fujita, A. Matsunaga, and T. Imoto, *J. Org. Chem.*, **50**, 2638 (1985).
21) K. Fujita, A. Matsunaga, and T. Imoto, *J. Am. Chem. Soc.*, **106**, 5740 (1984).
22) A. Bax, "Two-Dimensional Nuclear Magnetic Resonance in Liquids," Reidel Publishing Co., Boston (1982).
23) E.g., a) A. Pardi, R. Walker, H. Rappoport, G. Wider, and K. Wuethrich, *J. Am. Chem. Soc.*, **105**, 1652 (1983); b) N. S. Bhacca, M. F. Balandrin, A. D. Kinghorn, T. A. Frenkiel, R. Freeman, and G. A. Morris, *ibid.*, **105**, 2538 (1983); c) M. A. Weiss, D. J. Patel, R. T. Sauer, and M. Karplus, *Proc. Natl. Acad. Sci., U.S.A.*, **81**, 130 (1984).
24) For a review see G. Wider, S. Macura, A. Kumar, R. Ernest, and K. Wuethrich, *J. Magn. Reson.*, **56**, 207 (1984).
25) a) L. D. Hall and G. A. Morris, *Carbohydr. Res.*, **82**, 175 (1980); b) G. A. Morris, *J. Magn. Reson.*, **44**, 277 (1981); c) G. A. Morris and L.D. Hall, *J. Am. Chem. Soc.*, **103**, 4703 (1981); d) D. Y. Gagnaire, F.R. Taravel, and M. R. Vignon, *Macromolecules*, **15**, 126 (1982); e) G. A. Morris and L. D. Hall, *Can. J. Chem.*, **60**, 2431 (1982); f) W. Curatolo, L. J. Neuringer, D. Ruben, and R. Haberkorn, *Carbohydr. Res.*, **112**, 297 (1983); g) P. J. Card and G.S. Reddy, *J. Org. Chem.*, **48**, 4734 (1983); h) B, Coxon, *Anal. Chem.*, **55**, 2361 (1983); i) G. Batta and A. J. Liptak, *J. Am. Chem. Soc.*, **106**, 248 (1984).
26) F. R. Travel and M. R. Vignon, *Polym. Bull. (Berlin)*, **7**, 153 (1982).
27) a) K. Nagayama, K. Wuethrich, and R. R. Ernst, *Biochem. Biophys. Res. Commun.*, **90**, 305 (1979); b) K. Nagayama, A. Kumar, K. Wuethrich, and R. R. Ernst, *J. Magn. Reson.*, **40**, 321 (1980); c) A. Kumar, G. Wagner, R. R. Ernst, and K. Wuethrich, *Biochem. Biophys. Res. Commun.*, **96**, 1156 (1980); d) A. Bax, R. Freeman, and G. A. Morris, *J. Magn. Reson.*, **42**, 164 (1981).
28) a) A. A. Mandsley and R. R. Ernst, *Chem. Phys. Lett.*, **50**, 368 (1977); b) A. A. Mandsley, L. Mueller, and R. R. Ernst, *J. Magn. Reson.*, **28**, 463 (1977); c) G. Bodenhausen and R. Freeman, *ibid.*, **28**, 471 (1977); d) G. Bosenhausen and R. Freeman, *J. Am. Chem. Soc.*, **100**, 320 (1978); e) R. Freeman and G. A. Morris, *J. Chem. Soc., Chem. Commun.*, **1978**, 684; f) L. Mueller and R. R. Ernst, *Mol. Phys.*, **38**, 963 (1979); g) L. D. Hall, G. A. Morris, and S. Sukumar, *J. Am. Chem. Soc.*, **102**, 1745 (1980); h) A. Bax and G. A. Morris, *J. Magn. Reson.*, **42**, 501 (1981).

Preparation of New Nitrogen-Bridged Heterocycles. 16.[1] Facile Synthesis of Thieno[2,3-*b*]indolizine Derivatives

Akikazu KAKEHI,* Suketaka ITO, Yasuhiro OHNO, Shouji SHIBA, and Sakashi KAMATA
Department of Industrial Chemistry, Faculty of Engineering, Shinshu University, Wakasato, Nagano 380
(Received May 6, 1987)

2-Ethoxycarbonyl-3-methyl- and 3-phenylthieno[2,3-*b*]indolizine derivatives were first synthesized in moderate to good yields by the treatment of tricyclic 5,5a-dihydropyrido[2,1-*c*]thieno[3,2-*e*][1,4]thiazines with a dehydrogenating agent. In contrast to the cases of bicyclic 1,9a-dihydropyrido[2,1-*c*][1,4]thiazines, all of the thienoindolizines obtained here were rearranged products and no desulfurized product could be obtained.

Our recent papers in this series have described the novel ring contraction reactions of pyrido[2,1-*c*]-[1,4]thiazines and pyrido[1,2-*d*][1,3,4]thiadiazines generated in situ from their dihydro compounds.[1,2] These reactions are not only convenient preparative methods for some indolizines and pyrazolo[1,5-*a*]-pyridines which are not obtainable by other methods but also good models for studying the behavior of the heterocyclic compounds having a $4n\pi$ electron system.[3] The wide versatility and the ready availability of starting materials and the synthetic and mechanistic interests prompted us to extend these reactions to a fused system with an aromatic ring in anticipation of the stabilization of reaction intermediates and of a new skeletal synthesis. In this paper we wish to report the isolations of some stable dihydropyridothiazines fused with a thiophene ring and their transformations to the corresponding thieno[2,3-*b*]indolizine derivatives and will also discuss about the effect of the fused aromatic ring on the reaction courses.

Results and Discussion

Preparations of 3-(1-Pyridinio)thiophene-2-thiolates. These pyridinium betaines **3a—e** bearing a thiophene ring were synthesized in 54—90% yields by the intramolecular condensations of pyridinium 1-methylides **2a—e**, readily obtainable from the reactions of 1-acetonyl- **1a** and **1b** and 1-phenacylpyridinium chlorides **1c—e**, carbon disulfide, and ethyl bromoacetate in the precence of base (Scheme 1).

The structures of pyridinium methylides **2a—e** and 3-(1-pyridinio)thiophene-2-thiolates **3a—e** were decided by their elemental analyses and by their spectral comparisons with those of analogous types of compounds.[4]

Preparations of 5,5a-Dihydropyrido[2,1-*c*]thieno-[3,2-*e*][1,4]thiazines. When the *S*-alkylations of pyridinium betaines **3a—d** with reagents such as bromoacetonitrile **4a**, methyl bromoacetate **4b**, ethyl bromoacetate **4c**, phenacyl bromide **4d**, *p*-chlorophenacyl bromide **4e**, and *p*-bromophenacyl bromide **4f** in chloroform followed by the treatment of the resulting pyridinium salts **5a—x** with 1,8-diazabicyclo[5.4.0]-undec-7-ene (DBU) in chloroform at 0 °C were carried out, the corresponding 2-ethoxycarbonyl-1-methyl- and 1-phenyl-5,5a-dihydropyrido[2,1-*c*]thieno[3,2-*e*]-[1,4]thiazines **6a—l** and **7a—x** were formed in considerable yields as crystalline compounds, respectively. On the other hand, the expected tricyclic adducts **6y**+**7y** and **6z**+**7z** could not be obtained by the alkaline treatment of pyridinium salts **5y** and **5z** which were

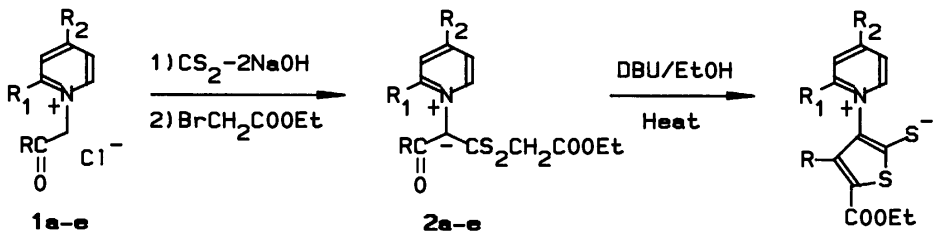

1	R	R_1	R_2
a	Me	H	H
b	Me	H	Me
c	Ph	H	H
d	Ph	H	Me
e	Ph	Me	H

2	R	R_1	R_2
a	Me	H	H
b	Me	H	Me
c	Ph	H	H
d	Ph	H	Me
e	Ph	Me	H

3	R	R_1	R_2
a	Me	H	H
b	Me	H	Me
c	Ph	H	H
d	Ph	H	Me
e	Ph	Me	H

Scheme 1.

similarly obtained from the reactions of pyridinium betaine **3e** bearing a methyl group at the 2-position with bromoacetonitrile **4a** and ethyl bromoacetate **4c**. (Scheme 2) The inaccessibility of adducts **6y+7y** and **6z+7z** from 2-methylpyridinium salts **5y** and **5z** suggested a large steric hinderance against the cyclization between the 2-methyl group and the bulky thiophene moiety.

In contract to bicyclic dihydropyridothiazines[1] the adducts **6a—l** and **7a—x** were fairly stable compounds and scarcely decomposed at room temperature. The elemental analyses of adducts **6a—l** and **7a—x** were in good accord with the proposed compositions, and the chemical shifts and the signal patterns due to the dihydropyridothiazine moiety in their proton NMR (^{1}H NMR) spectra (see Table 1) were similar to those of bicyclic ones.[1] The latter also showed that adducts **6a—l** and **7a—l** were cis and trans mixtures with respect to the 8a and 9 positions and **7m—x** only trans isomers. The isomer ratios are shown in Scheme 2.

Preparations of 2-Ethoxycarbonyl-3-methyl- and 3-phenylthieno[2,3-*b*]indolizines. Although the reactions of dihydropyridothienothiazines **6a—l** and **7a—x** with lead tetraacetate did not afford the expected ring

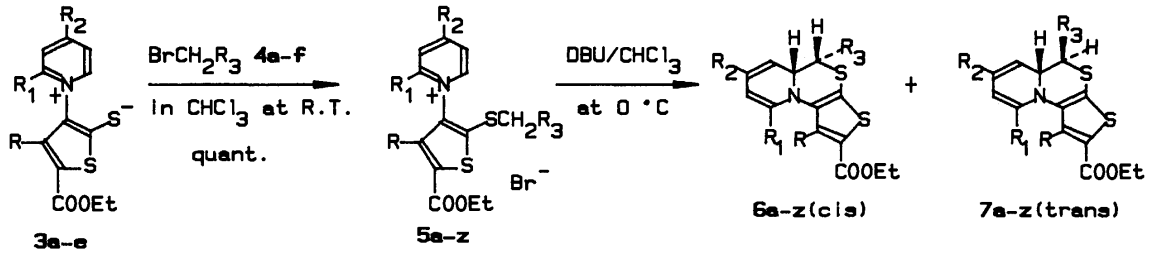

3a-e 5a-z

4	R_3
a	CN
b	COOMe
c	COOEt
d	Bz
e	*p*-ClBz
f	*p*-BrBz

Bz=benzoyl

Prod.	Salt	R	R_1	R_2	R_3	6/7
6a+7a	5a	Me	H	H	CN	4/7
6b+7b	5b	Me	H	Me	CN	4/5
6c+7c	5c	Ph	H	H	CN	1/1
6d+7d	5d	Ph	H	Me	CN	2/1
6e+7e	5e	Me	H	H	COOMe	1/2
6f+7f	5f	Me	H	Me	COOMe	1/2
6g+7g	5g	Ph	H	H	COOMe	5/6
6h+7h	5h	Ph	H	Me	COOMe	5/7
6i+7i	5i	Me	H	H	COOEt	3/10
6j+7j	5j	Me	H	Me	COOEt	1/3
6k+7k	5k	Ph	H	H	COOEt	5/9
6l+7l	5l	Ph	H	Me	COOEt	2/5
7m	5m	Me	H	H	Bz	0/1

Prod.	Salt	R	R_1	R_2	R_3	6/7
7n	5n	Me	H	Me	Bz	0/1
7o	5o	Ph	H	H	Bz	0/1
7p	5p	Ph	H	Me	Bz	0/1
7q	5q	Me	H	H	*p*-ClBz	0/1
7r	5r	Me	H	Me	*p*-ClBz	0/1
7s	5s	Ph	H	H	*p*-ClBz	0/1
7t	5t	Ph	H	Me	*p*-ClBz	0/1
7u	5u	Me	H	H	*p*-BrBz	0/1
7v	5v	Me	H	Me	*p*-BrBz	0/1
7w	5w	Ph	H	H	*p*-BrBz	0/1
7x	5x	Ph	H	Me	*p*-BrBz	0/1
(6y+7y)	5y	Ph	Me	H	CN	
(6z+7z)	5z	Ph	Me	H	COOEt	

Scheme 2.

Table 1. ^{1}H NMR Spectral Data of Dihydropyridotienothiazines in $CDCl_3$

Compound[a] No.	C-5	C-6	C-7	C-8	C-8a	C-9	R	R_3	COOEt	
6a	6.44	b)	6.30	b)	c)	6.44	2.53	—	1.36	4.33
	d		br q			d	s		t	q
7a	6.13	b)	6.30	b)	c)	c)	2.47	—	1.36	4.33
	d		br q				s		t	q
6b	6.40	4.86	1.89	5.21	d)	3.60	2.52	—	1.36	4.33
	d	dd	s	br s		d	s		t	q
7b	6.08	5.04	1.89	5.43	d)	d)	2.46	—	1.36	4.33
	d	dd	d	br s			s		t	q
6c	5.80	e)	6.10	f)	e)	3.61	7.42	—	1.14	4.16
	d		m			d	s		t	q
7c	5.59	e)	6.10	f)	e)	e)	7.42	—	1.14	4.16
	d		m				s		t	q
6d	5.71	c)	1.71	5.00	c)	3.55	7.37	—	1.13	4.13
	d		s	br s		d	s		t	q
7d	5.50	c)	1.71	5.30	c)	c)	7.37	—	1.13	4.13
	d		s	br s			s		t	q

Table 1. (Continued)

Compound[a] No.	C-5	C-6	C-7	C-8	C-8a	C-9	R	R_3		COOEt	
6e	g)	h)	g)	4.1—5.5 m		3.56 d	2.52 s	3.68 s		1.36 t	4.31 q
7e	g)	h)	g)	— 4.1—5.5 — m			2.47 s	3.81 s		1.36 t	4.31 q
6f	6.20 d	4.68 dd	1.79 s	5.07 br s	d)	3.50 d	2.50 s	3.64 s		1.34 t	4.32 q
7f	6.08 d	4.90 dd	1.79 s	5.07 br s	d)	d)	2.46 s	3.80 s		1.34 t	4.32 q
6g	5.59 d	c)	5.93 q	5.26 br q	c)	3.59 d	7.43 s	3.63 s		1.14 t	4.17 q
7g	5.59 d	c)	5.93 q	5.26 br q	c)	c)	7.43 s	3.80 s		1.14 t	4.17 q
6h	5.57 d	e)	1.65 s	5.00 br s	e)	3.52 d	7.42 s	3.61 s		1.13 t	4.16 q
7h	5.57 d	e)	1.65 s	5.00 br s	e)	e)	7.42 s	3.81 s		1.13 t	4.16 q
6i	g)	5.01 br t	g)	5.35 m	c)	3.53 d	2.50 s	1.30 t	4.30 q	1.34 t	4.31 q
7i	g)	5.01 br t	g)	5.35 m	c)	c)	2.46 s	1.30 t	4.30 q	1.34 t	4.31 q
6j	6.23 d	4.63 dd	1.79 s	5.10 br s	c)	3.52 d	2.52 s	1.31 t	4.27 q	1.36 t	4.32 q
7j	6.08 d	4.92 dd	1.81 s	5.10 br s	c)	c)	2.47 s	1.31 t	4.27 q	1.36 t	4.32 q
6k	5.60 d	e)	5.93 q	5.27 br q	e)	3.57 d	7.43 s	1.31 t	4.28 q	1.17 t	4.17 q
7k	5.60 d	e)	5.93 q	5.27 br q	e)	e)	7.43 s	1.31 t	4.28 q	1.17 t	4.17 q
6l	5.60 d	d)	1.67 s	5.04 br s	d)	3.53 d	7.43 s	1.31 t	4.28 q	1.15 t	4.17 q
7l	5.60 d	d)	1.67 s	5.04 br s	d)	d)	7.43 s	1.31 t	4.28 q	1.15 t	4.17 q
7m	6.21 d	5.02 br t	6.00 q	5.38 br q	4.63 br d	5.40 d	2.50 s	7.3—8.3 m		1.34 t	4.33 q
7n	6.07 br d	i)	1.57 s	— 4.3—5.5 — m			2.47 s	7.3—8.3 m		1.33 t	4.31 q
7o	5.67 br d	j)	5.67 br	5.25 br	j)	5.29 br d	7.45 s	7.3—8.3 m		1.17 t	4.18 q
7p	5.50 br d	k)	1.43 s	— 4.4—5.3 — m			7.45 s	7.3—8.2 m		1.16 t	4.17 q
7q	6.22 br d	5.05 br t	6.00 br q	l)	4.62 br d	5.32 br d	2.50 s	7.3—8.3 m		1.35 t	4.34 q
7r	5.90 br d	k)	1.57 s	— 4.4—5.3 — m			2.47 s	7.3—8.2 m		1.32 t	4.28 q
7s	5.67 br d	— 4.4—5.4 — m					7.39 s	7.3—8.1 m		1.34 t	4.13 q
7t	5.30 br d	m)	1.43 s	— 4.3—5.2 — m			7.44 s	7.3—8.2 m		1.14 t	4.15 q
7u	6.21 br d	5.06 br t	5.99 br q	l)	4.57 br d	5.30 br d	2.50 s	7.5—8.2 m		1.34 t	4.33 q
7v	5.93 br	k)	1.59 s	— 4.4—5.3 — m			2.49 s	7.5—8.1 m		1.35 t	4.32 q
7w	5.71 br d	n)	5.67 br	— 4.4—5.4 — m			7.43 s	7.5—8.1 m		1.16 t	4.17 q
7x	5.30 br	o)	1.43 s	— 4.4—5.2 — m			7.39 s	7.5—8.1 m		1.15 t	4.15 q

a) The coupling constants are as follows: $J_{8a,9}$(cis)=2.0, $J_{8a,9}$(trans)=8.0, $J_{5,6}$=7.0, $J_{6,7}$=6.0, $J_{7,8}$=10.0, $J_{8,8a}$=4.0, $J_{5,7}$=2.0, and J_{Et}=7.0 Hz. b) Overlapped with the other signals at δ 4.8—5.9. c) Overlapped with the signals at δ 4.0—4.8. d) Overlapped with the other signals at δ 4.0—4.7. e) Overlapped with the other signals at δ 4.0—4.9. f) Overlapped with the other signals at δ 5.0—5.5. g) Overlapped with the other signals at δ 5.9—6.4. h) Overlapped with the other signals at δ 4.1—5.5. i) Overlapped with the other signals at δ 4.3—5.5. j) Overlapped with the other signals at δ 4.4—4.9. k) Overlapped with the other signals at δ 4.4—5.3. l) Overlapped with the other signals at δ 4.8—5.6. m) Overlapped with the other signals at δ 4.3—5.2. n) Overlapped with the other signals at δ 4.4—5.4. o) Overlapped with the other signals at δ 4.4—5.2.

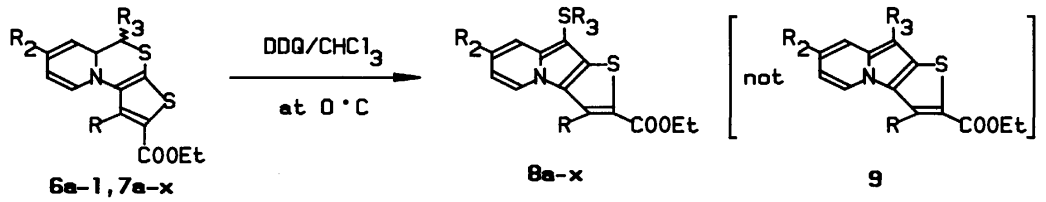

Prod.	React.	R	R_2	R_3	Prod.	React.	R	R_2	R_3
8a	6a+7a	Me	H	CN	**8m**	7m	Me	H	Bz
8b	6b+7b	Me	Me	CN	**8n**	7n	Me	Me	Bz
8c	6c+7c	Ph	H	CN	**8o**	7o	Ph	H	Bz
8d	6d+7d	Ph	Me	CN	**8p**	7p	Ph	Me	Bz
8e	6e+7e	Me	H	COOMe	**8q**	7q	Me	H	*p*-ClBz
8f	6f+7f	Me	Me	COOMe	**8r**	7r	Me	Me	*p*-ClBz
8g	6g+7g	Ph	H	COOMe	**8s**	7s	Ph	H	*p*-ClBz
8h	6h+7h	Ph	Me	COOMe	**8t**	7t	Ph	Me	*p*-ClBz
8i	6i+7i	Me	H	COOEt	**8u**	7u	Me	H	*p*-BrBz
8j	6j+7j	Me	Me	COOEt	**8v**	7v	Me	Me	*p*-BrBz
8k	6k+7k	Ph	H	COOEt	**8w**	7w	Ph	H	*p*-BrBz
8l	6l+7l	Ph	Me	COOEt	**8x**	7x	Ph	Me	*p*-BrBz

Scheme 3.

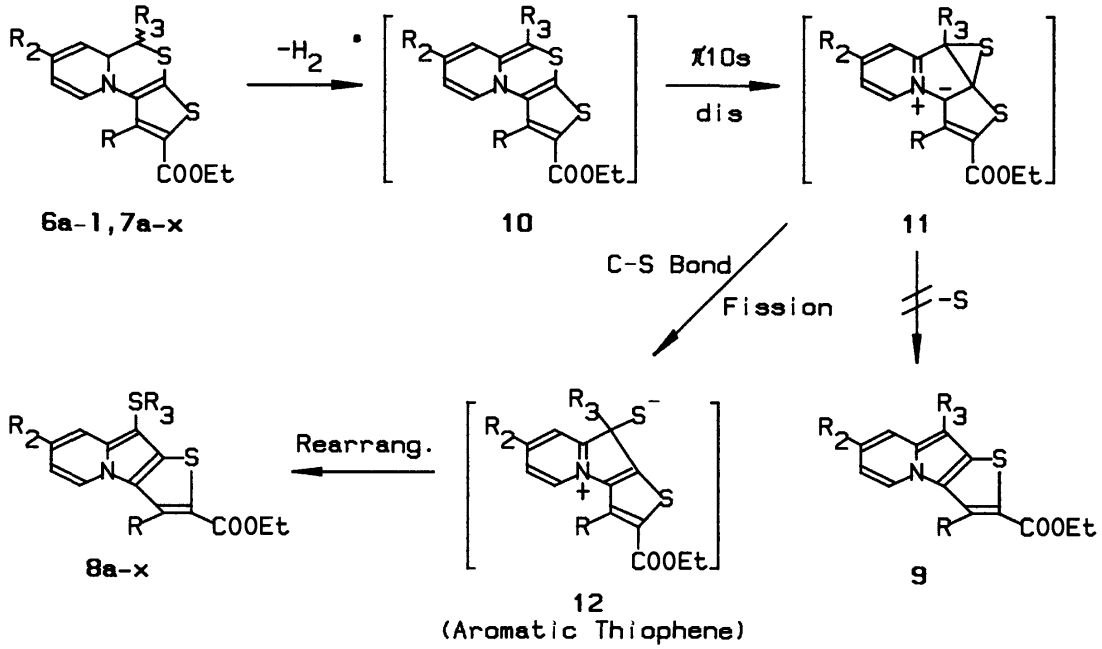

Scheme 4.

contraction products, the treatment with 2,3-dichloro-5,6-dicyano-*p*-benzoquinone (DDQ) in chloroform at 0 °C formed the corresponding thieno[2,3-*b*]indolizine derivatives **8a—z** as dark red or black crystals in 19—96% yields. Furthermore, the same products **8a—z** could be also obtained from adducts **6a—l** and **7a—x** by the action of palladium on carbon at room temperature, but their yields were low in compared with those using DDQ (Scheme 3).

Very interestingly, all of products **8a—x** were not the desulfurized thienoindolizines such as **9** but the rearranged ones regardless of the kinds of the substituent (R_3).[1,2]

The thienoindolizines, **8a—x**, were comparatively stable compounds at room temperature, but their 3-phenyl derivatives **8c**, **8d**, **8g**, **8h**, **8k**, **8l**, **8o**, **8p**, **8s**, **8t**, **8w**, and **8x**, in particular, were easily decomposed at the refluxing temperature of ethanol to give polymeric substances. The instability of these thienoindolizines **8a—x** must be caused by both the strained thiaazapenta-

Table 2. ^{1}H NMR Spectral Data of Thieno[2,3-*b*]indolizines in $CDCl_3$

Compound[a] No.	C-5	C-6	C-7	C-8	R	R_3	COOEt	
8a	7.28	6.11	6.6—7.2		2.49	—	1.35	4.34
	br d	m	m		s		t	q
8b	7.19	5.97	2.12	6.80	2.48	—	1.34	4.32
	d	dd	s	br s	s		t	q
8c	6.53	5.43	6.77	6.98	7.0—7.6	—	1.15	4.15
	br d	br t	br t	br d	m		t	q
8d	6.44	5.28	2.00	6.73	6.9—7.6	—	1.13	4.12
	d	dd	s	br s	m		t	q
8e	7.28	6.18	6.92	8.28	2.45	3.76	1.35	4.33
	br d	dt	br t	br d	s	s	t	q
8f	7.18	6.05	2.16	8.09	2.43	3.71	1.32	4.29
	d	dd	s	br s	s	s	t	q
8g	6.58	5.51	6.72	8.21	6.9—7.6	3.74	1.12	4.13
	br d	dt	br t	br d	m	s	t	q
8h	6.58	5.44	2.04	8.11	6.9—7.6	3.77	1.13	4.15
	d	dd	s	br s	m	s	t	q
8i	7.22	6.11	6.83	8.21	2.41	1.28 4.18	1.33	4.30
	br d	dt	br t	br d	s	t q	t	q
8j	7.21	6.06	2.17	8.11	2.43	1.29 4.20	1.34	4.31
	d	dd	s	br s	s	t q	t	q
8k	6.53	5.50	6.70	8.19	7.0—7.6	1.33 4.21	1.15	4.15
	br d	br t	br t	br d	m	t q	t	q
8l	6.55	5.42	2.03	8.10	7.0—7.6	1.32 4.21	1.14	4.15
	d	dd	s	br s	m	t q	t	q
8m	b)	6.48	7.08	7.98	2.52	7.3—7.8	1.35	4.34
		dt	br t	br d	s	m	t	q
8n	b)	6.39	2.22	8.03	2.50	7.3—7.7	1.34	4.30
		dd	s	br s	s	m	t	q
8o	6.92	5.82	b)	8.00	7.0—7.8	7.0—7.8	1.16	4.15
		dt		br d	m	m	t	q
8p	6.91	5.82	2.09	8.09	7.0—7.9	7.0—7.9	1.13	4.17
	d	dd	s	br s	m	m	t	q
8q	b)	6.57	7.19	8.10	2.53	7.3—7.8	1.37	4.35
		dt	br t	br d	s	m	t	q
8r	b)	6.51	2.27	8.16	2.51	7.2—7.7	1.34	4.32
		dd	s	br s	s	m	t	q
8s	6.94	5.92	b)	8.13	7.0—7.8	7.0—7.8	1.15	4.17
	br d	br t		br d	m	m	t	q
8t	6.99	5.92	2.18	8.26	7.0—8.0	7.0—8.0	1.16	4.19
	d	dd	s	br s	m	m	t	q
8u	b)	6.57	7.19	8.13	2.51	7.3—7.8	1.34	4.33
		dt	br t	br d	s	m	t	q
8v	b)	6.47	2.27	8.17	2.49	7.2—7.7	1.33	4.30
		dd	s	br d	s	m	t	q
8w	6.94	5.93	b)	8.13	7.0—7.7	7.0—7.7	1.15	4.17
	br d	br t		br d	m	m	t	q
8x	7.00	5.93	2.17	8.27	7.0—7.9	7.0—7.9	1.14	4.18
	d	dd	s	br s	m	m	t	q

a) The coupling constants are as follows: $J_{5,6}=J_{6,7}=7.0$, $J_{7,8}=10.0$, $J_{6,8}=2.0$ Hz, and $J_{Et}=7.0$ Hz.
b) Overlapped with the phenyl proton signals.

lene skeleton and the steric repulsion between the 3-substituent (R) and the 5-proton.

The elementary analyses of these products **8a—x** were in accord with the compositions of the thieno[2,3-*b*]indolizines carrying a thio group at the 9-position. The IR spectra of thienoindolizines **8a—d** exhibited also clearly the precence of a thiocyanato group (2141—2151 cm^{-1}). The proton signals (Table 2) on the pyridine ring in compounds **8a—x** appeared in the range of δ 5.28—8.28, and the values (δ 5.97—8.28) except those (δ 5.28—5.93) due to the 5- and 6-protons of 3-phenyl derivatives **8c**, **8d**, **8g**, **8h**, **8k**, **8l**, **8o**, **8p**, **8s**, **8t**, **8w**, and **8x** are not contradictory to those of aromatic indolizine derivatives.[1,5] These high field shifts observed largely for the 5- and 6-protons in 3-phenyl derivatives must be caused by the shielding effect of the 3-phenyl group whose resonance-stabilized planar conformation is prevented owing to the proximity of great extent between the 3-phenyl group and the 5-proton. From these data, the products

Table 3. Some Data of Dihydropyridothienothiazines

Compd. No.	Salt(S.M.)[a]	Yield %	Mp θ_m/°C	IR^{KBr}/cm^{-1}	Formula	Calcd/% (Found/%) C	H	N
6a+7a	5a(**3a**, **4a**)	71	b)	2235 1709	$C_{15}H_{14}N_2O_2S_2$	56.58 (56.40)	4.43 4.46	8.80 9.08)
6b+7b	**5b**(**3b**, **4a**)	64	b)	2239 1690	$C_{16}H_{16}N_2O_2S_2$	57.81 (57.98)	4.85 4.86	8.43 8.40)
6c+7c	**5c**(**3c**, **4a**)	77	b)	2215 1710	$C_{20}H_{16}N_2O_2S_2$	63.13 (63.10)	4.24 4.31	7.36 7.33)
6d+7d	**5d**(**3d**, **4a**)	74	b)	2210 1710	$C_{21}H_{18}N_2O_2S_2$	63.93 (63.72)	4.60 4.55	7.10 7.12)
6e+7e	**5e**(**3a**, **4b**)	56	b)	1720 1695	$C_{16}H_{17}NO_4S_2$	54.68 (54.86)	4.88 4.89	3.99 3.94)
6f+7f	**5f**(**3b**, **4b**)	44	b)	1716 1690	$C_{17}H_{19}NO_4S_2$	55.87 (55.89)	5.24 5.11	3.83 3.94)
6g+7g	**5g**(**3c**, **4b**)	97	b)	1733 1675	$C_{21}H_{19}NO_4S_2$	61.00 (61.07)	4.63 4.62	3.39 3.33)
6h+7h	**5h**(**3d**, **4b**)	88	b)	1735 1680	$C_{22}H_{21}NO_4S_2$	61.81 (62.08)	4.95 4.87	3.28 2.99)
6i+7i	**5i**(**3a**, **4c**)	54	b)	1728 1680	$C_{17}H_{19}NO_4S_2$	55.87 (55.90)	5.24 5.21	3.83 3.69)
6j+7j	**5j**(**3b**, **4c**)	26	b)	1723 1700	$C_{18}H_{21}NO_4S_2$	56.97 (57.18)	5.58 5.31	3.69 3.83)
6k+7k	**5k**(**3c**, **4c**)	83	b)	1732 1702	$C_{22}H_{21}NO_4S_2$	61.81 (61.77)	4.95 4.91	3.28 3.24)
6l+7l	**5l**(**3d**, **4c**)	80	b)	1732 1682	$C_{23}H_{23}NO_4S_2$	62.56 (62.68)	5.25 5.29	3.17 3.00)
7m	**5m**(**3a**, **4b**)	80	108—110	1703 1680	$C_{21}H_{19}NO_3S_2$	63.45 (63.45)	4.82 4.82	3.52 3.43)
7n	**5n**(**3b**, **4d**)	54	107—109	1704 1675	$C_{22}H_{21}NO_3S_2$	64.21 (64.20)	5.14 5.15	3.40 3.23)
7o	**5o**(**3c**, **4d**)	89	178—180	1681 1670	$C_{26}H_{21}NO_3S_2$	67.95 (67.92)	4.61 4.67	3.05 2.86)
7p	**5p**(**3d**, **4d**)	89	170—172	1710 1662	$C_{27}H_{23}NO_3S_2$	68.47 (68.57)	4.90 5.09	2.96 2.67)
7q	**5q**(**3a**, **4e**)	91	152—155	1680 1665	$C_{21}H_{18}ClNO_3S_2$	58.39 (58.09)	4.20 4.16	3.24 3.54)
7r	**5r**(**3b**, **4e**)	51	147—150	1701 1679	$C_{22}H_{20}ClNO_3S_2$	59.25 (59.16)	4.52 4.47	3.14 3.42)
7s	**5s**(**3c**, **4e**)	66	142—144	1720 1683	$C_{26}H_{20}ClNO_3S_2$	63.21 (63.32)	4.08 4.07	2.84 2.80)
7t	**5t**(**3d**, **4e**)	54	147—149	1720 1680	$C_{27}H_{22}ClNO_3S_2$	63.83 (63.54)	4.36 4.27	2.76 3.04)
7u	**5u**(**3a**, **4f**)	70	157—159	1690 1663	$C_{21}H_{18}BrNO_3S_2$	52.94 (52.92)	3.81 3.83	2.94 3.11)
7v	**5v**(**3b**, **4f**)	46	152—154	1703 1679	$C_{22}H_{20}BrNO_3S_2$	53.88 (53.87)	4.11 3.95	2.86 3.03)
7w	**5w**(**3c**, **4f**)	77	161—163	1710 1679	$C_{26}H_{20}BrNO_3S_2$	57.99 (57.80)	3.74 3.72	2.60 2.77)
7x	**5x**(**3d**, **4f**)	89	168—170	1720 1666	$C_{27}H_{22}BrNO_3S_2$	58.70 (58.51)	4.01 3.97	2.54 2.77)
(**6y+7y**)	**5y**(**3e**, **4a**)	0						
(**6z+7z**)	**5z**(**3e**, **4c**)	0						

a) Starting materials. b) This compound is a cis and trans mixture.

were concluded to be 5-thiocyanato- **8a—d**, 9-(alkoxycarbonylthio)-**8e—l**, and 9-(aroylthio)thieno-[2,3-*b*]indolizine derivatives **8m—x**, respectively.

Reaction Mechanisms. Possible mechanisms for the formation of the rearranged thienoindolizines **8a—x** from the corresponding dihydropyridothienothiazines **6a—l** and **7a—x** are shown in Scheme 4. The most remarkable feature in these ring contraction reactions is that only the rearranged tricyclic indolizines were formed regardless of the kinds of the R_3 group and the desulfurized compounds as described in similar reactions of bicyclic dihydropyridothiazines were not at all.[1] The reason why the desulfurized indolizines were not afforded in this tricyclic system is still uncertain, but, perhaps, the rapid ring opening from tetracyclic thiirane **11** to indolizinium 9-thiolate **12** possessing an aromatic thiophene ring may take place prior to the desulfurization to **9**.

Table 4. Some Data of Thieno[2,3-*b*]indolizines

Compd. No.	React.	Yield %	Mp θ_m/°C	IR^{KBr}/cm^{-1}	Formula	Calcd/% (Found/%) C	H	N
8a	**6a+7a**	81	159—162	2151 1680	$C_{15}H_{12}N_2O_2S_2$	56.94 (57.00	3.82 3.67	8.85 8.94)
8b	**6b+7b**	49	157—159	2144 1702	$C_{16}H_{14}N_2O_2S_2$	58.16 (58.21	4.27 3.97	8.48 8.73)
8c	**6c+7c**	94	146—148	2141 1711	$C_{20}H_{14}N_2O_2S_2$	63.47 (63.35	3.73 3.94	7.40 7.31)
8d	**6d+7d**	56	131—132	2150 1674	$C_{21}H_{16}N_2O_2S_2$	64.26 (64.42	4.11 4.14	7.14 6.95)
8e	**6e+7e**	77	125—127	1701 1670	$C_{16}H_{15}NO_4S_2$	55.00 (55.03	4.33 4.14	4.01 4.13)
8f	**6f+7f**	37	133—135	1695	$C_{17}H_{17}NO_4S_2$	56.18 (56.24	4.71 4.68	3.85 3.83)
8g	**6g+7g**	54	122—124	1678	$C_{21}H_{17}NO_4S_2$	61.30 (61.35	4.16 4.05	3.40 3.46)
8h	**6h+7h**	51	144—146	1690	$C_{22}H_{19}NO_4S_2$	62.10 (61.98	4.50 4.46	3.29 3.44)
8i	**6i+7i**	72	124—126	1700	$C_{17}H_{17}NO_4S_2$	56.18 (56.41	4.71 4.68	3.85 3.82)
8j	**6j+7j**	38	132—134	1690	$C_{18}H_{19}NO_4S_2$	57.27 (57.47	5.07 4.82	3.71 3.69)
8k	**6k+7k**	84	132—135	1709	$C_{22}H_{19}NO_4S_2$	62.10 (61.87	4.50 4.52	3.29 3.51)
8l	**6l+7l**	68	126—128	1689	$C_{23}H_{21}NO_4S_2$	62.85 (62.66	4.82 5.01	3.19 3.19)
8m	**7m**	43	141—142	1690	$C_{21}H_{17}NO_3S_2$	63.78 (63.91	4.33 4.07	3.54 3.67)
8n	**7n**	38	144—146	1683	$C_{22}H_{19}NO_3S_2$	64.52 (64.59	4.68 4.88	3.42 3.16)
8o	**7o**	66	104—106	1705	$C_{26}H_{19}NO_3S_2$	68.25 (68.25	4.19 4.28	3.06 2.97)
8p	**7p**	56	133—135	1710	$C_{27}H_{21}NO_3S_2$	68.77 (68.92	4.49 4.53	2.97 2.78)
8q	**7q**	29	139—141	1691	$C_{21}H_{16}ClNO_3S_2$	58.67 (58.54	3.75 3.74	3.26 3.07)
8r	**7r**	35	143—145	1705	$C_{22}H_{18}ClNO_3S_2$	59.52 (59.53	4.09 4.05	3.15 3.18)
8s	**7s**	78	136—138	1710	$C_{26}H_{18}ClNO_3S_2$	63.47 (63.24	3.69 3.82	2.85 2.96)
8t	**7t**	71	152—155	1713	$C_{27}H_{20}ClNO_3S_2$	64.09 (64.12	3.98 3.98	2.77 2.74)
8u	**7u**	19	149—151	1685	$C_{21}H_{16}BrNO_3S_2$	53.17 (53.04	3.40 3.32	2.95 3.17)
8v	**7v**	27	146—148	1685	$C_{22}H_{18}BrNO_3S_2$	54.10 (54.17	3.71 3.58	2.87 2.93)
8w	**7w**	96	151—153	1708	$C_{26}H_{18}BrNO_3S_2$	58.21 (58.02	3.38 3.39	2.61 2.79)
8x	**7x**	62	141—143	1710 1686	$C_{27}H_{20}BrNO_3S_2$	58.91 (59.04	3.66 3.79	2.54 2.56)

In contract to the observations obtained by other investigators,[3,6] a strong trend toward the rearrangement was found in our pyrido[2,1-*c*][1,4]thiazine system, and further efforts to explain this phenomenon will be done.

Experimental

Melting points were measured with a Yanagimoto micro-melting point apparatus and are uncorrected. Microanalyses were carried out on a Perkin-Elmer 240 Elemental Analyzer. The ^{1}H NMR spectra were determined with a Varian EM360A spectrometer in deuteriochloroform with tetramethylsilane as an internal standard. The chemical shifts are expressed in δ values. The IR spectra were taken with a Hitachi 260-10 Infrared spectrophotometer.

Preparations of Pyridinium Methylides 2a—e. These pyridinium 1-(dithiocarboxy)methylides **2a—e** were prepared from the reactions of 1-acetonyl- **1a** and **1b** and 1-phenacylpyridinium chlorides **1c—e**, carbon disulfide, and ethyl bromoacetate in the presence of base according to the procedure described in the literature.[4] Some data of compounds **2a—e** are as follows: **2a**, 90%, yellow flakes (from ethanol), mp 162—164 °C, IR (KBr) 1730 cm^{-1} (CO). Found: C, 52.48; H, 5.06; N, 4.76%. Calcd for $C_{13}H_{15}NO_3S_2$: C, 52.50; H, 5.08; N, 4.71%. **2b**, 76%, yellow flakes (from ethanol), mp

170—172 °C, IR (KBr) 1730 cm^{-1} (CO). Found: C, 53.77; H, 5.47; N, 4.76%. Calcd for $C_{14}H_{17}NO_3S_2$: C, 54.00; H, 5.50; N, 4.50%. **2c**, 73%, yellow needles (from ethanol), mp 190—192 °C, IR (KBr) 1720 cm^{-1} (CO). Found: C, 59.98; H, 4.93; N, 3.90%. Calcd for $C_{18}H_{17}NO_3S_2$: C, 60.14; H, 4.77; N, 3.90%. **2d**, 84%, yellow needles (from ethanol), mp 191—193 °C, IR (KBr) 1730 cm^{-1} (CO). Found: C, 61.26; H, 4.79; N, 3.93%. Calcd for $C_{19}H_{19}NO_3S_2$: C, 61.10; H, 5.13; N, 3.75%. **2e**, 54%, yellow prisms (from ethanol), mp 183—185 °C, IR (KBr) 1720 cm^{-1} (CO). Found: C, 60.93; H, 5.11; N, 3.95%. Calcd for $C_{19}H_{19}NO_3S_2$: C, 61.10; H, 5.13; N, 3.75%.

Preparations of 3-(1-Pyridinio)thiophene-2-thiolates 3a—e. General Method: An ethanolic solution (100 ml) of pyridinium 1-methylide (10 mmol) and DBU (1.82 g, 12 mmol) was heated under the reflux temperature on a water bath until the disappearance of yellow spot of pyridinium 1-methylide was confirmed by the TLC monitoring of the reaction solution. (2—5 h) The resulting red solution was cooled to room temperature and then the product crystallized was collected by filtration. Recrystallizations from ethanol gave 3-(1-pyridinio)thiophen-2-thiolates **3a—e** as red needles. Some data of compounds **3a—e** are shown below. **3a**, 68%, mp 205—207 °C, IR (KBr) 1685 cm^{-1} (CO). Found: C, 55.80; H, 4.70; N, 5.09%. Calcd for $C_{13}H_{13}NO_2S_2$: C, 55.89; H, 4.69; N, 5.01%. **3b**, 83%, mp 202—205 °C, IR (KBr) 1670 cm^{-1} (CO). Found: C, 57.47; H, 5.08; N, 4.68%. Calcd for $C_{14}H_{15}NO_2S_2$: C, 57.31; H, 5.15; N, 4.77%. **3c**, 87%, mp 244—246 °C, IR (KBr) 1675 cm^{-1} (CO). Found: C, 63.09; H, 4.44; N, 4.16%. Calcd for $C_{18}H_{15}NO_2S_2$: C, 63.32; H, 4.43; N, 4.10%. **3d**, 76%, mp 242—244 °C, IR (KBr) 1685 cm^{-1} (CO). Found: C, 64.32; H, 4.69; N, 3.95%. Calcd for $C_{19}H_{17}NO_2S_2$: C, 64.20; H, 4.82; N, 3.94%. **3e**, 60%, mp 217—221 °C, IR (KBr) 1690 cm^{-1} (CO). Found: C, 63.99; H, 4.93; N, 4.04%. Calcd for $C_{19}H_{17}NO_2S_2$: C, 64.20; H, 4.82; N, 3.94%.

Preparations of 5,5a-Dihydropyrido[2,1-*c*]thieno[3,2-*e*]-[1,4]thiazines 6a—l and 7a—x. General Method. A mixture of pyridinium betaine (2 mmol) and alkyl bromide (2.2 mmol) was dissolved in chloroform (20 ml) and the resulting solution was kept at room temperature until the spot of pyridinium betaine disappeared (1—7 d, by TLC monitoring). The solution was concentrated under reduced pressure and the residue was washed three times with ether to remove the unaltered alkylating agent. To the chloroform solution (50 ml) of the pyridinium salt prepared above DBU (0.38 g, 2.5 mmol) was added dropwise at 0 °C in an ice bath, and then stirred for further 10 min at the temperature. The resulting solution was concentrated under reduced pressure and the residue was separated by column chromatography (alumina) using chloroform as an eluent. The chloroform layer was concentrated under reduced pressure. Recrystallizations from chloroform-hexane or ether-hexane gave pure products as pale yellow prisms (**6a+7a** and **6f+7f**). pale yellow needles (**6b+7b—6e+7e**, **6g+7g—6i+7i**, and **7m**), yellow prisms (**6j+7j** and **7v**), yellow needles (**6k+7k**, **6l+71**, **7n—7s**, and **7u**), or orange needles (**7t**, **7w**, and **7x**).

On the other hand, similar treatment of pyridinium salts **5y** and **5z** gave complex mixtures and any significant product could not be isolated.

There results and some physical and spectral data are summarized in Tables 1 and 3.

Preparations of Thieno[2,3-*b*]indolizines 8a—x. General Method. To a chloroform solution (50 ml) of dihydropyridothienothiazine (0.2—0.5 g) an equimolar amount of DDQ was added under stirring at 0 °C in an ice bath and the resulting mixture was stirred at the temperature until the material was disappeared (TLC monitoring). (about 2—4 h) The solution was filtered to remove insoluble substances and then the filtrate was concentrated under reduced pressure at below 40 °C. The residual oil was separated by column chromatography (alumina) using chloroform as an eluent. The evaporation of the solvent and recrystallization of the residue from chloroform-hexane gave the corresponding thieno[2,3-*b*]indolizine derivatives as dark red needles (**8a—c**, **8j**, **8n**, **8t**, and **8v**) or black needles (**8d—i**, **8k—m**, **8o—s**, **8u**, **8w**, and **8x**).

These thienoindolizines could be also obtained in moderate yields from the reactions of dihydropyridothienothiazines with palladium on carbon (5%) in dry benzene at room temperature.

These results and some data are listed in Tables 2 and 4.

References

1) For part 15 of this series, see A. Kakehi, S. Ito, S. Yonezu, K. Maruta, K. Yuito, M. Shiohara, and K. Adachi, *Bull. Chem. Soc. Jpn.*, **60**, 1867 (1987).

2) A. Kakehi, S. Ito, and T. Yotsuya, *Heterocycles*, **22**, 2237 (1984); A. Kakehi, S. Ito, S. Yonezu, K. Maruta, and K. Yuito, *ibid*, **23**, 33 (1985); A. Kakehi, S. Ito, T. Yotsuya, and K. Nagata, *Bull. Chem. Soc. Jpn.*, **58**, 1432 (1985); A. Kakehi, S. Ito, K. Nagata, N. Kinoshita, and N. Kakinuma, *Chem. Pharm. Bull.*, **35**, 156 (1986).

3) H. Beyer, *Z. Chem.*, **9**, 361 (1969); H. Beyer, H. Honeck, and L. Reichelt, *Justus Liebigs Ann. Chem.*, **741**, 45 (1970); R. R. Schmidt, *Angew. Chem., Int. Ed. Engl.*, **14**, 581 (1975); R. R. Schmidt and H. Huth, *Tetrahedron Lett.*, **1975**, 33; K. Kaji, H. Nagashima, S. Nagao. K. Tabashi, and H. Oda, *Chem. Pharm. Bull.*, **32**, 4437 (1984); K. Kaji, H. Nagashima, Y. Ohta, S. Nagao, Y. Hirose, and H. Oda, *Heterocycles*, **22**, 479 (1984).

4) Y. Tominaga, H. Fujito, H. Norisue, A. Ushirogochi, Y. Masuda, and G. Kobayashi, *Yakugaku Zasshi*, **99**, 1081 (1979).

5) C. Maseda, M. Sone, Y. Tominaga, R. Natsuki, Y. Matsuda, and G. Kobayashi, *Yakugaku Zasshi*, **94**, 839 (1974); A. Kakehi and S. Ito, *Bull. Chem. Soc. Jpn.*, **47**, 938 (1974); Y. Tominaga, H. Fujito, K. Mizuyama, Y. Matsuda, and G. Kobayashi, *Chem. Pharm. Bull.*, **25**, 1519 (1977); H. Pauls and F. Krohnke, *Chem. Ber.*, **110**, 1294 (1977); A. Kakehi, S. Ito, T. Maeda, R. Takeda, M. Nishimura, M. Tamashima, and T. Yamaguchi, *J. Org. Chem.*, **43**, 4837 (1978); E. K. Pohjara, *J. Heterocycl. Chem.*, **15**, 955 (1978).

6) L. F. Lee and R. K. Howe, *J. Org. Chem.*, **49**, 4780 (1984).

 © 1987 The Chemical Society of Japan Bull. Chem. Soc. Jpn., 60, 3721—3730 (1987)

Autoxidation of 1-Methyl- and 1,3-Dimethylazulenes in Polar Aprotic Solvents: Structural Proof for Products and Reaction Pathways[1)]

Shin-ichi TAKEKUMA, Yoshiharu MATSUBARA,* Hiroshi YAMAMOTO,†,* and Tetsuo NOZOE††
Department of Applied Chemistry, Faculty of Science and Engineering, Kinki University, Kowakae, Higashi-Osaka 577
†Deparment of Chemistry, Okayama University, Okayama 700
††Tokyo Research Laboratories, Takasago Corporation, 5-36-31 Kamata, Ohta-ku, Tokyo 144
(Received May 11, 1987)

Autoxidation of the title azulenes at 100 °C in HMPA or DMF afforded a wide variety of products: Namely, the oxidation products of the side-chains, 1-substituted azulenes, 1*H*-inden-1-ols, naphthoquinones, benzenoids, and dimeric and trimeric compounds, with or without rearrangements. ^{1}H NMR (200-MHz) parameters of various azulene derivatives are given for comparative study. Possible reaction pathways for the formation of these products are discussed in comparison with the results of the previous studies on guaiazulene and 4,6,8-trimethylazulene.

We reported recently[2-4)] that autoxidation of naturally occurring guaiazulene (**3**) and synthetic 4,6,8-trimethylazulene (**4**) in *N*,*N*-dimethylformamide (DMF) or hexamethylphosphoric triamide (HMPA) gave a wide variety of products possessing interesting structures of azulenequinone, naphthoquinone, 1-indenone, and dimeric forms. It has been presumed[4)] that the oxidation is initiated by the formation of an electron-transferred complex **5**, which would then lead to a covalent linkage between the azulene nucleus and active radical species (produced during the oxidation) at various positions according to the ease of their affinity and steric requirement. Consequently, the autoxidation of **3** and **4** can be classified into such several types of reactions as oxidative dimerization, oxidation of side chains, azulenequinone formation, intermolecular one-carbon transfer reactions, and rearrangements to naphthalenoids, benzenoid, and 1*H*-inden-1-one derivatives. In these oxidation and coupling reactions, the facility of the radical attack on the C-1 and C-3 position of the azulene nucleus appeared to exceed usually that on various positions of the seven-membered ring,[5)] as in the case of many other electrophilic reactions of azulenes.[6)]

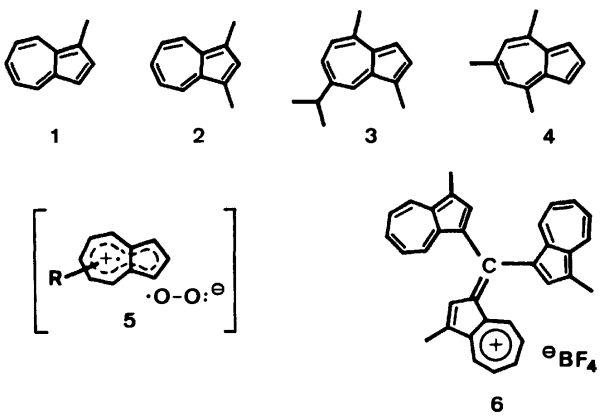

We now wish to report in this paper the detailed study on autoxidation of two other alkylazulenes **1** and **2** having methyl substituent(s) on the C-1 and C-3 position(s). This study was conducted to compare the mode of the oxidation with that of the trialkylazulenes **3** and **4** and to establish a further general aspect of the reaction mechanism of oxidation of azulenes. This information would in turn become important in view of an increasing interest in the potential utility of the physicochemical properties as well as biological activity of some synthetic azulene derivatives, exemplified by polyazulenes[7)] and azulenequinones.[8)]

Results and Discussion

Autoxidation of 1-Methylazulene (1). The oxidation was conducted in a manner similar to that described for the trialkylazulenes **3** and **4**.[2-4)] Thus, finely bubbling oxygen was passed into a soln of the substrate **1** in HMPA (or DMF) at 100 °C, while the reaction was monitored by the use of the reversed phase high-pressured liquid chromatography (HPLC) or silica-gel TLC. As in the case of the previous study, the reaction products were separated into each compo-

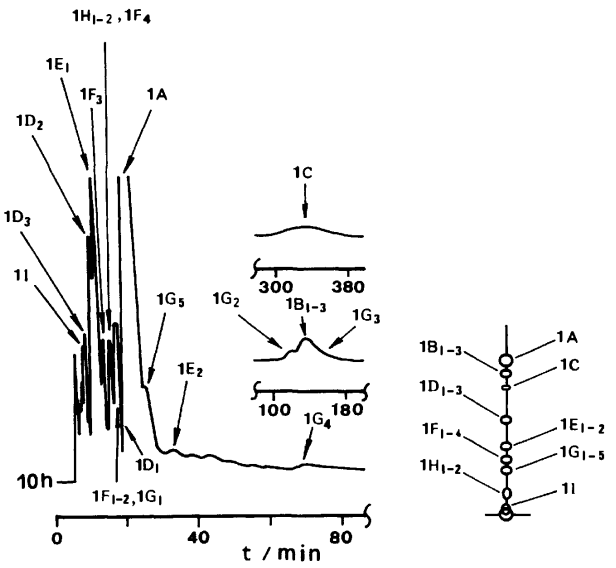

Fig. 1. HPLC and TLC diagrams of the autoxidation products from **1**.

nent by using chromatography, when about a half of the starting material was consumed (10 h); see HPLC and TLC diagrams in Fig. 1. The products thus obtained as pure components [19 altogether besides the recovered starting material **1** (**1A**)] are referred to as Compounds **1A—I** according to the same definition employed in the previous study.[2-4]

In Chart 1 are summarized structures of these products which were established by spectroscopy and chromatography as will be explained below; for the purpose of comparison in determining the structures of the oxidation products, the 200-MHz ^{1}H NMR parameters[9] for azulene derivatives obtained in the present study are summarized in Table 1. Amont these products, the followings were identified as all known compounds: **1B$_1$**,[10] **1D$_1$**,[11] **1D$_2$**, **1D$_3$**,[12] **1E$_1$**,[13] **1F$_1$**,[14] **1F$_2$**,[15] **1G$_1$**,[14] **1H$_1$**,[16] **1H$_2$**,[17] and **1I**[18] (for their spectral and other data, see Table 1 and the Experimental Section). The theoretical yields of these isolated products totaled to 25.2%; besides these, ca. 60% (w/w) yield of unidentified resinous polar products of rather high molecular weights were obtained.

Both Compounds **1B$_2$** and **1B$_3$** were shown to have a composition of $C_{22}H_{18}$ by MS and structures of 1′,3-dimethyl-1,2′-biazulene and 3,3′-dimethyl-1,1′-biazulene were respectively assigned to these minor products by the careful comparison of the ^{1}H NMR spectral data (see Table 1) with those of the starting material **1**.

Compound **1C** ($C_{34}H_{28}$ by MS), a major product, was found by spectroscopy to be 1,1′,1″-methylidynetris[3-methylazulene]; while the chemical shifts of other signals of **1C** in the ^{1}H NMR spectrum (Table 1) closely resembled those of **1**, an appreciable upfield shift (ca. 0.5 ppm) was observed for the H-2 signal presumably due to an electronic as well as an anisotropic effect by a nonplanar conformation of the three azulene nuclei owing to the steric repulsion. Although on allowing to stand at room temperature **1C** was gradually converted into a blue, polar substance (R_f=0.0), it remained stable when kept with a small proportion of an antioxidant (hydroquinone). Treatment of **1C** with triphenylmethylium tetrafluoroborate afforded the tetrafluoroborate **6**.[19]

Compound **1E$_2$** was an extremely minor product which possessed a dimeric composition ($C_{23}H_{20}O$ by MS) having an extra-carbon atom and a carbonyl group (1690 cm^{-1}). The ^{1}H NMR data indicated the presence of a 3-methyl-1-azulenylmethyl moiety attached to a certain nucleus ($C_{11}H_9O$) that exhibited a methyl group (at δ 1.78, doublet, J=1.0 Hz, coupling with a ring-proton at 6.56, quartet), a methine proton (at 5.38, singlet), and four olefinic ring-protons (6.04—6.56); the methylene proton signals of an AB type (at 3.31 and 3.37, J=14 Hz) should also be noticed. All of

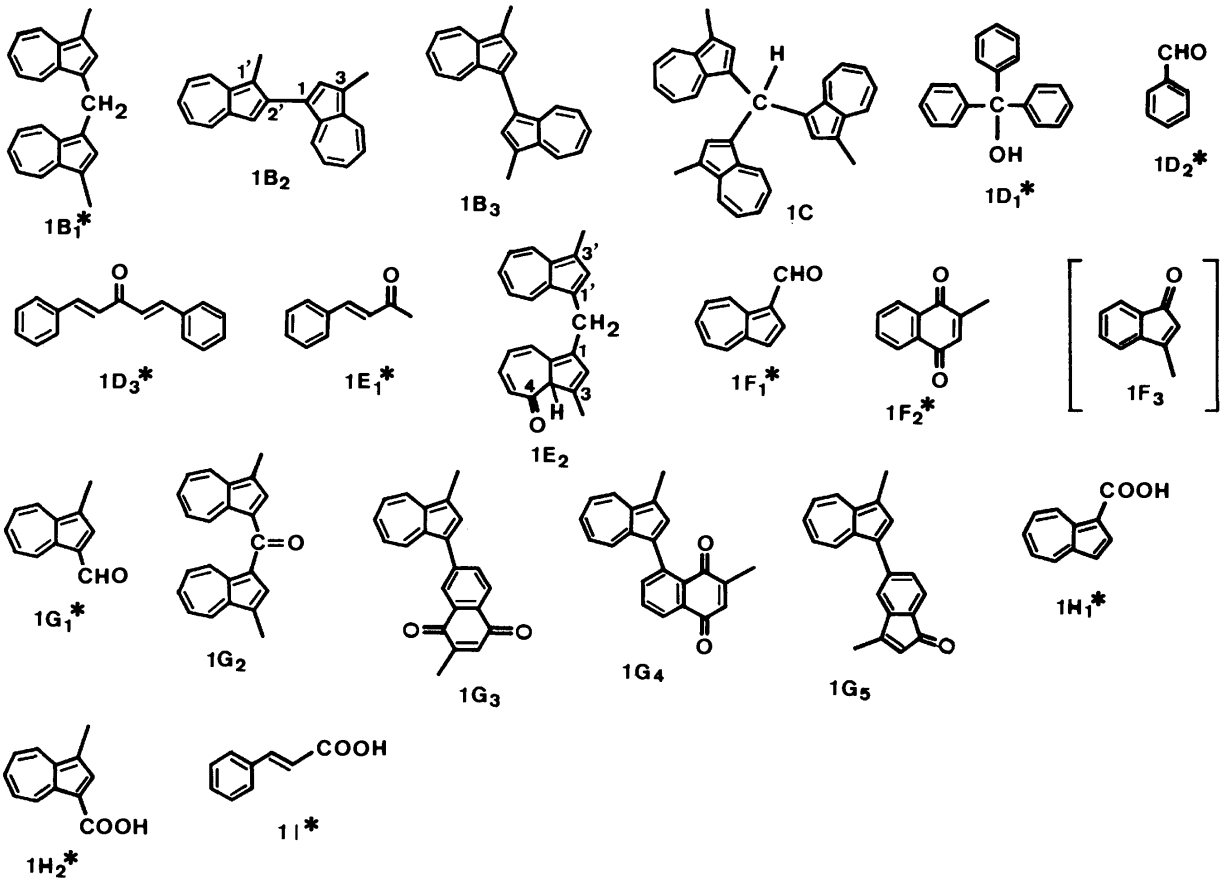

Chart 1. Structures of the autoxidation products from **1**; *previously known compounds.

Table 1. ^{1}H NMR (200 MHz) Parameters for Azulene Derivatives[a)]

Compound	H-1 (H-1′)	H-2 (H-2′)	H-3 (H-3′)	H-4 (H-4′)	H-5 (H-5′)	H-6 (H-6′)	H-7 (H-7′)	H-8 (H-8′)	J J
1	2.59[b)]	7.68	7.24	8.09	6.92	7.36	6.88	8.09	c, d)
1B$_1$	4.75[e)]	7.37	2.54[b)]	8.05	6.87	7.38	6.89	8.20	d)
1B$_2$	—	7.94	2.50[b)]	7.82	6.98	7.34	7.08	8.20	d)
	(2.76)[b)]	—	(7.34)	(8.25)	(7.03)	(7.49)	(7.03)	(8.24)	d)
1B$_3$	—	7.94	2.76[b)]	8.25	6.93	7.50	7.03	8.25	d)
1C	7.20[f)]	7.20	2.52[b)]	8.09	6.77	7.36	6.91	8.11	g)
1E$_2$	3.31[h)]	6.56	1.78[b)]	5.37[i)]	6.31	6.56	6.25	6.04	j)
	3.37[h)]	(7.30)	(2.52)[b)]	(7.99)	(6.88)	(7.37)	(6.88)	(8.04)	d)
1F$_1$	10.34[k)]	8.27	7.33	8.50	7.53	7.86	7.63	9.59	c, d)
1G$_1$	10.22[k)]	8.02	2.59[b)]	8.30	7.40	7.72	7.45	9.35	d)
1G$_2$	—	8.02	2.67[b)]	8.38	7.37	7.74	7.42	9.51	d)
1G$_3$	2.72[b)]	7.98	—	8.50	7.19	7.63	7.17	8.26	d)
	—	(6.88)	(2.24)[b)]	—	(8.32)	—	(7.96)	(8.21)	l, m)
1G$_4$	2.75[b)]	7.71	—	8.26	7.09	7.50	6.91	7.85	d)
	—	(6.84)	(2.03)[b)]	—	—	(7.65)	(7.73)	(8.18)	l, n)
1G$_5$	2.72[b)]	7.90	—	8.45	7.13	7.58	7.10	8.27	d)
	—	(5.78)	(2.29)[b)]	(7.34)	—	(7.46)	(7.53)	—	l, o)
1H$_1$	1.58[p)]	8.46	7.32	8.50	7.50	7.85	7.62	9.70	c, d)
1H$_2$	1.70[p)]	8.20	2.62[b)]	8.31	7.38	7.72	7.44	9.51	d)
2	2.59[b)]	7.49	2.59[b)]	8.00	6.84	7.34	6.84	8.00	g)
2B$_1$	—	7.74	2.74[b)]	8.20	6.90	7.46	7.04	7.73	d)
	(2.46)[b)]	—	(2.46)[b)]	(8.10)	(6.95)	(7.38)	(6.95)	(8.10)	d)
2D	2.62[b)]	7.54	2.69[b)]	8.51	9.86[k)]	7.85	6.96	8.05	q)

a) Chemical shifts (δ) are parts per million from Me_4Si measured in $CDCl_3$ (concn <ca. 0.5% v/v). Coupling constants (J, Hz) were confirmed by double resonance. b) Me. c) $J_{2,3}$=4.0 Hz. d) $J_{4,5}$, $J_{5,6}$, $J_{6,7}$, and $J_{7,8}$: 10.0 Hz. $J_{4,6}$, $J_{5,7}$, and $J_{6,8}$: 1 Hz. e) CH_2-1. f) CH-1. g) $J_{4,5}$, $J_{5,6}$, $J_{6,7}$, and $J_{7,8}$: 9.5 Hz. h) CH_2-1, J=14 Hz. i) H-3a, singlet. j) $J_{2,Me(3)}$=1.0 Hz, $J_{5,6}$=$J_{6,7}$=6.0 Hz, $J_{7,8}$=10 Hz. k) CHO. l) $J_{2,Me(3)}$=1.5 Hz. m) $J_{5,7}$=2.0 Hz, $J_{7,8}$=8.0 Hz. n) $J_{6,7}$=7.5 Hz, $J_{6,8}$=2.0 Hz, $J_{7,8}$=8.0 Hz. o) $J_{4,6}$=1.5 Hz, $J_{6,7}$=7.5 Hz. p) COOH. q) $J_{4,5}$=1.5 Hz, $J_{6,7}$=10.0 Hz, $J_{6,8}$=1.0 Hz, $J_{7,8}$=9.5 Hz.

these signals appeared at slightly up-field compared with the corresponding proton signals of other azulene derivatives described in this paper. Based on these spectral data, 3-methyl-1-[(3-methyl-1-azulenyl)methyl]-4(3aH)-azulenone was tentatively assigned to **1E$_2$** as the most likely structure;[20] see Table 1 for the assignments of the ^{1}H NMR signals of **1E$_2$**.

Compound **1F$_3$** was a pale yellow oil which appeared to be hitherto unknown 3-methyl-1*H*-inden-1-one by judging from the R_f values (on HPLC and TLC) in comparison with those of 5-isopropyl-3,8-dimethyl-1*H*-inden-1-one.[2,4] However, on allowing to stand at room temp **1F$_3$** gradually changed into a rather unstable dimer (**1F$_4$**, $C_{20}H_{16}O_2$ by MS).[21]

Compound **1G$_2$** ($C_{23}H_{18}O$ by MS) was a minor product which showed a similar ^{1}H NMR spectrum to that of **1G$_1$** (except for the aldehyde signal of the latter). Therefore, structure of bis(3-methyl-1-azulenyl) ketone was assigned for **1G$_2$**. Both Compounds **1G$_3$** and **1G$_4$** ($C_{22}H_{16}O_2$) were found spectroscopically to possess a 3-methyl-1-azulenyl group attached to a 2-methyl-1,4-naphthoquinone moiety; a careful analysis of the ^{1}H NMR data (Table 1) led to the most likely coupling positions of **1G$_3$** and **1G$_4$** at C-6 and C-5 of the naphthoquinone nucleus, respectively. Compound **1G$_5$** ($C_{21}H_{16}O$ by MS), on the other hand, was found to possess a 3-methyl-1-azulenyl group attached to a 3-methyl-1*H*-inden-1-one moiety at C-5 on the evidence of ^{1}H NMR spectral data (Table 1).

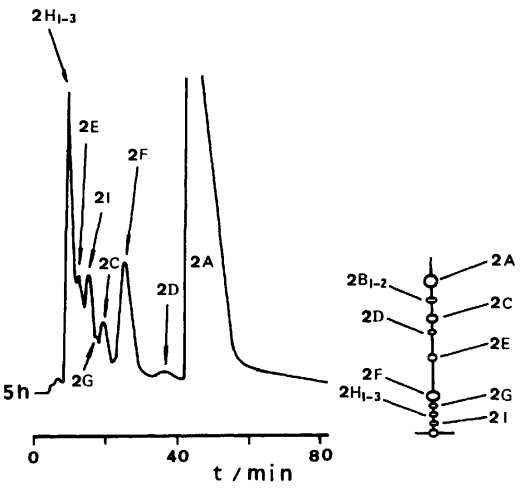

Fig. 2. HPLC and TLC diagrams of the autoxidation products from **2**.

Autoxidation of 1,3-Dimethylazulene (2). The oxidation was carried out in HMPA or DMF at 100 °C for 5 h in a manner similar to that described for **1**; compared with that of **1**, the oxidation of **2** was observed to take place slightly faster at 100 °C (HPLC). The resulting mixture (see HPLC and TLC in Fig. 2)

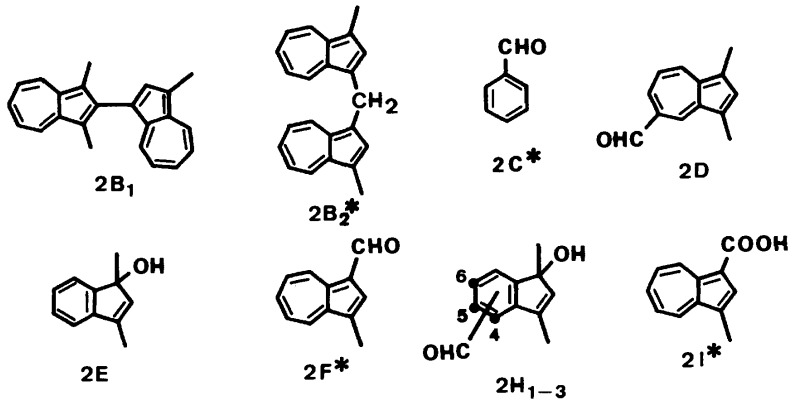

Chart 2. Structures of the autoxidation products of 2; *previously known compounds.

was carefully separated by using chromatography, and 11 products (**2A—I**) were obtained besides the recovered starting material **2** (**2A**). Structures of these products which have been similarly established are shown in Chart 2; among these, Compounds **2B**$_2$,[10] **2C**, **2F**,[14] and **2I**[17] were identified to be already known. The total theoretical yields of these isolated products were 35.4%. Besides these, a large amount (ca. 60%, w/w) of unidentified polar products of relatively high molecular weights were obtained.

Compound **2B**$_1$ ($C_{23}H_{20}$ by MS) was readily found to possess an asymmetric structure, 1′,3,3′-trimethyl-1,2′-biazulene, on the basis of the ^{1}H NMR data (Table 1) which closely resembled those of **1B**$_2$ except for the presence of a Me-3′ signal of **2B**$_1$.

Compound **2D** ($C_{13}H_{12}O$), a minor product, was proved to be 1,3-dimethyl-5-azulenecarbaldehyde on the evidence of spectral data (UV, ^{1}H NMR, and MS).

Compound **2E** ($C_{11}H_{12}O$ by MS) possessed the structure of 1,3-dimethyl-1*H*-inden-1-ol on the evidence of UV, IR, and ^{1}H NMR data, whereas Compounds **2H**$_{1\text{-}3}$ which remained inseparable by chromatography were found spectroscopically to be a mixture of 1-hydroxy-1,3-dimethyl-1*H*-indene-4-, 5-, and 6-carbaldehydes in an approximate ratio of 1 : 2 : 1, respectively.

Compound **2G** was an extremely minor product but its structure has remained to be clarified owing to the limited amount for sufficient spectroscopic data.

Possible Reaction Pathways for the Formation of Autoxidation Products of 1 and 2. As was observed for the trialkylazulenes **3** and **4**, the autoxidation of **1** and **2** has resulted in the simultaneous formation of many kinds of products by competitive processes. An attempt will now be made here to suggest the most probable reaction pathways for the formation of the major products (and in some cases minor products as well) after having been divided into four groups according to the type of reactions involved: (a) Side chain oxidation, (b) one-carbon transfer reactions, (c) rearrangement reactions to naphthoquinonoids, benzenoids, and indenols, and (d) oxidative dimerization, as illustrated in Schemes 1 and 2. Although the yield of each product may not necessarily reflect the ease of the corresponding reaction pathway, the combined yields of the products formed by the above reactions from alkylazulenes **1**—**4** are summarized in Table 2 for comparison.

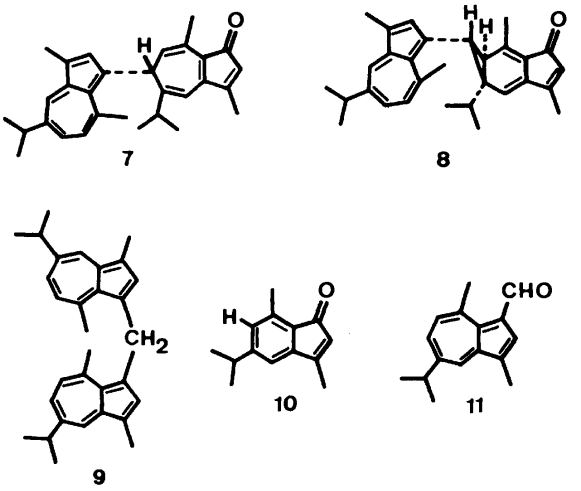

Table 2. Combined Yields (%, Isolated) of the Autoxidation[a] Products Classified into the Reaction Pathways

Reaction pathways	Starting alkylazulene			
	1	**2**	**3**[b]	**4**[c]
[a]	4	20.7	9.7	0.5
[b]	14.8	0.7	21.3	17.5
[c]	5.6	6.7	12.8	1.3
[d]	0.6	6.6	7.7	0
[e]	0	0	1.5	4.6
[f]	60	60	34	59

Reaction pathways: [a], side-chain oxidation; [b], one-carbon transfer reactions; [c], rearrangement reactions to naphthalenoids, benzenoids, and indene derivatives; [d], oxidative dimerization; [e], 1,5- and 1,7-azulenequinone formation; [f] polar resinous substance formation. a) Oxygenation in DMF or HMPA at 100 °C. b) From Refs. 2 and 4. c) From Refs. 3 and 4 (oxygenation at 120 °C).

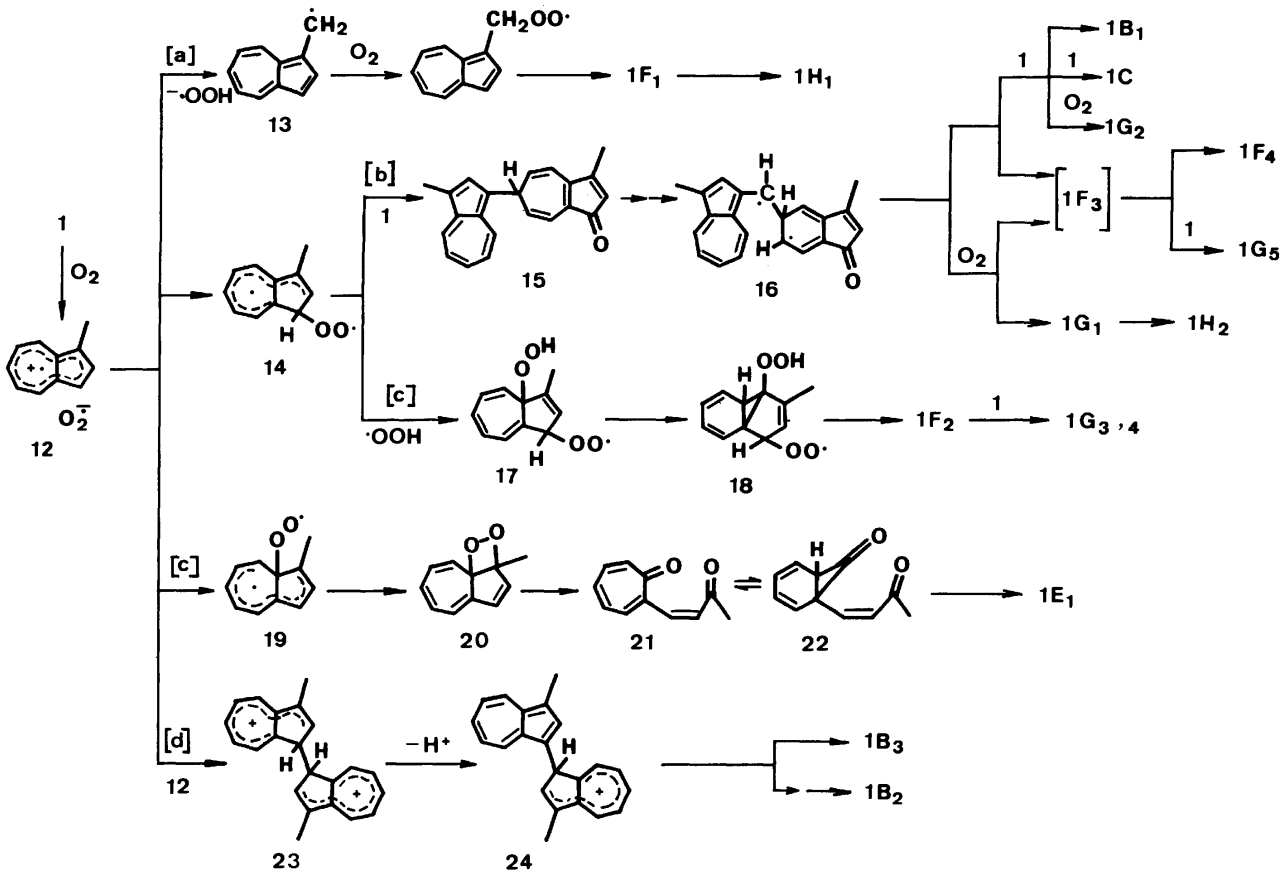

Scheme 1. Possible reaction pathways for the autoxidation products from **1**.

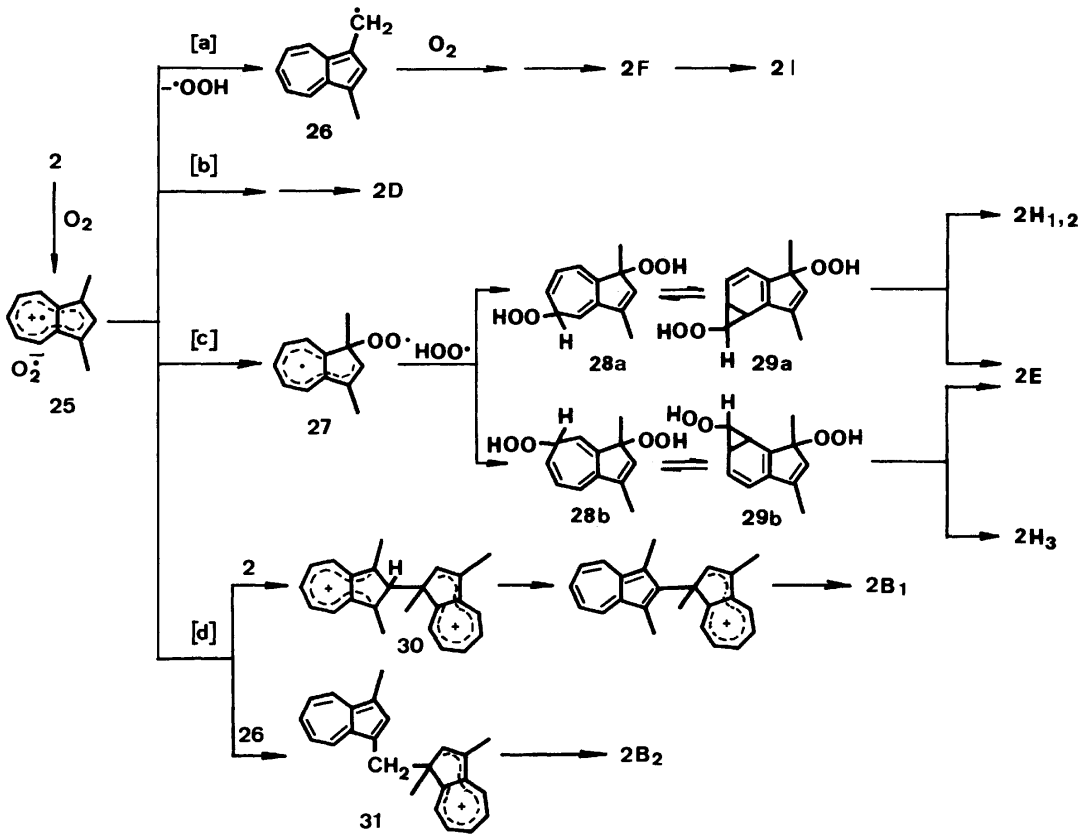

Scheme 2. Possible reaction pathways for the autoxidation products from **2**.

a) As was postulated in the case[4] of **3** and **4**, the facile oxidation of **1** and **2** with molecular oxygen is likely to form the radical cation complexes **12** and **25**, respectively, from which various products are derived (see Schemes 1 and 2). Then the transformation of these complexes into the radical intermediates **13** and **26** (path [a]) would result in the oxidation of the side chain, thus yielding 1-azulenecarbaldehydes **1F**$_1$ and **2F**, respectively, by the consecutive oxidation with another molecule of oxygen in a manner similar to the well-accepted mechanism for the autoxidation of side chains of alkylbenzenes and naphthalene.[22] Further autoxidation of these aldehydes in the usual way gives the 1-azulenecarboxylic acids **1H**$_1$ and **2I**. It is particularly a characteristic feature, in comparison with the case[4] of **3** and **4**, that oxidation of a side chain on the C-1 and 3 positions of azulene nucleus constitutes an exclusive process in the autoxidation of **2**, while it takes place only moderately in **1** under the present conditions (see Table 2).

b) It is significant in the present autoxidation that compounds having extra-carbon(s) such as 1,1′-methylenebis[3-methylazulene] (**1B**$_1$), and related compounds **1C**, **1G**$_1$, **1G**$_2$, and **1H**$_2$ have been obtained in relatively high yields from **1**, whereas **2** has afforded 1,3-dimethyl-5-azulenecarbaldehyde (**2D**) as the only compound of this type in an extremely low yield.

Meanwhile, we have recently isolated[23] both the dimeric cycloheptatriene form **7** and its norcaradiene isomer **8** on autoxidation of guaiazulene (**3**) either at 85 °C in DMF–0.5 M sulfuric acid (1 M=1 mol dm^{-3}) or at 25—35 °C on the surface of a filter paper. These compounds were shown to exist in an equilibrium and to constitute important intermediates for the intermolecular one-carbon transfer reactions. For examples, treatment of **8** with one equivalent of **3** under nitrogen exclusively yields 3,3′-methylenebis[guaiazulene] (**9**) and 5-isopropyl-3,7-dimethyl-1*H*-inden-1-one (**10**), whereas **8** is transformed into 3-guaiazulenecarbaldehyde (**11**) and indenone **10** on exposure to air.

From these facts, similar dimeric cycloheptatriene **15** (formed by the coupling of the 3-methyl-1-azulenylperoxyl diradical **14** with **1**) and its equilibrated norcaradiene isomer (similar to the structural formula **8**) are also considered to be the most likely key intermediates for the one-carbon transfer reactions (path [b] in Scheme 1). The fragmentation of the latter intermediate through a dimeric diradical **16** in the presence of **1** would give 1,1′-methylenebis(3-methylazulene) (**1B**$_1$) and 3-methyl-1*H*-inden-1-one (**1F**$_3$); the latter is unstable and gradually changes to its dimer **1F**$_4$. Further oxidative coupling of **1B**$_1$ (or of its precursor) with another molecule of **1** would form the trimer **1C**. Concomitantly, oxidative cleavage of **16** would give 3-methyl-1-azulenecarbaldehyde **1G**$_1$ (and its carboxylic acid derivative **1H**$_2$) and **1F**$_3$, whereas bis(3-methyl-1-azulenyl) ketone (**1G**$_2$) appears to be derived from **16** through oxidation of a subsequent, yet unclarified intermediate (Scheme 1). It should be noticed that this type of reaction involving one-carbon transfer constitutes the major pathway in the oxidation of **1** (see Table 2).

In contrast, **2D** apparently formed as the result of the intermolecular one-carbon transfer reaction (path [b] in Scheme 2) was isolated in an extremely small amount (Table 2). Although this pathway seems to be of interest in view of the reactivity of the azulene nucleus, the exact mechanism has remained to be clarified.

c) As in the case[4] of the oxidative rearrangement of guaiazulene **3** to naphthoquinonoids, addition of another molecule of oxygen (or ·OOH) to C-3a of **14** (Scheme 1) is expected to give the intermediate **17** (path [c]) that can be converted into 2-methyl-1,4-naphthoquinone (**1F**$_2$) through the equilibrated norcaradiene form **18**. It is more likely that (*Z*)-4-phenyl-3-buten-2-one (**1E**$_1$) obtained from **1** in the highest yield among the benzenoid compounds is derived by transformation of **12** into the diradical **19** (path [c]) and then into the dioxetane intermediate **20**, followed by the ring opening, the tropone-norcaradiene dicarbonyl equilibrium between **21** and **22**, and then by facile decarbonylation of **22** accompanied by isomerization of the olefinic side chain.

On the other hand, possible reaction pathways for the formation of the rearrangement products (1-indenols **2E** and **2H**$_{1\text{-}3}$) from **2** are shown as path [c] in Scheme 2: transformation of **25** into 1,3-dimethyl-1-azulenylperoxyl diradical **27**, followed by addition of peroxyl radical to the C-5 (or C-7) position, would give an intermediate such as hydroperoxide **28a** (or **28b**) that rearranges into 1,3-dimethyl-1*H*-inden-1-ols **2E** and **2H**$_{1\text{-}3}$ presumably through the equilibrated norcaradiene form **29a**/**29b**.

d) Dimerization of the radical cation **12** is expected to give **23**, from which the proton loss would lead to the intermediate **24** (path [d] in Scheme 1). This yields then 3,3′-dimethyl-1,1′-biazulene (**1B**$_3$) and a smaller proportion of the 1,2′-isomer **1B**$_2$ through a 1,2-rearranged intermediate as in the case of guaiazulene **3**.[4] It is another significant feature that these dimers from **1** were isolated in extremely small proportions in comparison with the case of the oxidation of **3**. On the other hand, the radical coupling of **25** with **2** and **26** is likely to afford dimeric intermediates **30** and **31**, respectively, and then loss of the methyl group on C-1 from these dimeric intermediates would result in the formation of the oxidative dimers **2B**$_1$ and **2B**$_2$ as illustrated in Scheme 2 (path [d]). The dimers **1G**$_{3\text{-}5}$ are apparently derived as the result of oxidative couplings of **1** with the rearranged monomers **1F**$_2$ and **1F**$_3$, as illustrated in Scheme 1.

It is noteworthy that neither 3-methyl-1,5- nor 1,7-azulenequinone was isolated in the present autoxidation of **1** or **2** (Table 2). This is most likely due to lability of these unknown azulenequinones under the

reaction conditions presently employed (at 100 °C),[24] taking into account the melting points of e.g. parent 1,5- and 1,7-azulenequinones: both mp 100 °C decomp.[8d]

The detailed mechanistic consideration for the formation of other minor compounds is not made here because of the limited evidences at this stage with regard to the reaction pathways. Besides these isolated compounds described so far, considerable amounts (ca. 60%) of intractable resinous substances are accompanied also by the present autoxidation of **1** and **2** as was observed particularly in the case[3,4] of **4** (Table 2).

Nevertheless, it has now become apparent that the autoxidation of the alkylazulenes **1** and **2** is highly competitive involving oxidation of the nucleus and side chains (exclusively at C-1 position), substitutions, ring contraction, and other reactions such as rearrangement to naphthoquinones in a similar manner to the oxidation of the previously studied trialkylazulenes in many respects. However, depending upon the kinds and positions of alkyl substituents on the azulene nucleus, some significant differences in the reactivities between them were also observed as described above. Thus, although the exact mechanism is under further investigation in detail by employing azulene itself and other alkylazulenes under various reaction conditions, the present findings are believed to provide valuable information on autoxidation of azulenoid compounds.[24]

Experimental

Melting points were determined with a Yanagimoto MP-S3 instrument and are uncorrected. Column chromatography was performed with Wako C-300 silica-gel. TLC was conducted on plates precoated with silica-gel 60F-254 (0.25 mm, Merck) by using 15:85 AcOEt–hexane as eluant. HPLC was carried out with Hitachi gel #3011 packed in a Pyrex column (ϕ 5 mm, 500 mm length) with 1:9 hexane-MeOH as solvent.

UV and IR (both in $CHCl_3$ unless otherwise stated) spectra were taken on a Hitachi 323 spectrophotometer and a Nihonbunko IR-A-202 Grating spectrometer, respectively. NMR spectra were recorded in $CDCl_3$ (unless otherwise stated) with a JEOL-FX200 cryospectrometer (200-MHz for ^1H and 50-MHz for ^{13}C) at 27 °C. Chemical shifts are reported as δ values in parts per million rel to tetramethylsilane (δ 0.0) as the internal standard. The assignments of all signals were made by employing a first-order analysis with the aid of decoupling technique and the parameters were confirmed by a computer-assisted simulation analysis; those values for azulene derivatives are summarized in Table 1. Mass spectra were taken on a JEOL JMS-HX100 (with a JEOL JMA-DA5000 mass data system) high-resolution instrument and are given in terms of m/z (rel intensity) compared with the base peak.

Oxidation of 1-Methylazulene (1) in HMPA. A soln of **1**[25] (1.00 g) in freshly distilled HMPA (20 g) was placed in a Pyrex flask (ϕ 1.8 cm, 60 cm height) and subjected to autoxidation by allowing finely bubbling oxygen to pass through the soln (from the bottom of the flask) for 10 h at 100±5 °C. After cooling, the mitxture was diluted with water (200 cm^3) and extracted with ether (4×50 cm^3). The combined organic layers were washed with water, dried (Na_2SO_4), and evaporated in vacuo, giving a brown oil (0.96 g); the HPLC and TLC diagrams of this crude mixture are given in Fig. 1. This oil was preliminarily separated into five fractions by means of preparative HPLC with Hitachi gel #3019 (100 g) using methanol as eluant. Then each fraction was carefully separated by silica-gel column or thin layer with AcOEt-hexane; when necessary, this chromatographic procedure was repeated. Thus, the following 19 products were obtained as pure substances (**1A—I**), besides the reccovered starting material **1** (**1A**: 0.50 g; R_f=0.83; ^1H NMR, see Table 1) and polar resinous substances [0.30 g, 60% (w/w); R_f=0.0]. The yield of each product is based on the consumed starting material (0.50 g).

1,1′-Methylenebis[3-methylazulene][10] **(1B$_1$):** Dark blue prisms; 30 mg (6.0% yield); mp 79 °C (Ref. 10, 79—80 °C); R_f=0.76; UV 245 (log ε 4.65), 288 (4.83), 345 (sh, 4.23), 355 (4.29), 410 (sh, 2.80), 430 (sh, 2.70), 590 (sh, 2.70), 640 (sh, 2.80), and 652 nm (2.81); MS m/z 296 (M^+; 100), 281 (65), 265 (55), 252 (11), 239 (6), and 155 (24); ^1H NMR, see Table 1. (Found: m/z 296.1549).

1′,3-Dimethyl-1,2′-biazulene (1B$_2$): A yellow-green oil; 1 mg (0.2%); R_f=0.76; UV 245 (log ε 4.69), 251 (4.72), 257 (4.74), 263 (4.76), 272 (4.76), 301 (4.70), 315 (4.68), 350 (sh, 4.35), 410 (3.91), 580 (sh, 2.94), 634 (3.04), and 676 nm (sh, 3.02); MS m/z 282 (M^+; 100), 265 (26), and 252 (11); ^1H NMR, see Table 1.

Found: m/z 282.1446. Calcd for $C_{22}H_{18}$: M, 282.1409.

3,3′-Dimethyl-1,1′-biazulene (1B$_3$): Dark green paste; 2 mg (0.4%); R_f=0.76; MS m/z 282 (M^+; 100), 276 (5), 265 (31), 252 (20), 239 (7), 141 (13), 132 (9), 126 (8), and 119 (4); ^1H NMR, see Table 1.

Found: m/z 282.1421. Calcd for $C_{22}H_{18}$: M, 282.1409.

1,1′,1″-Methylidynetris[3-methylazulene] (1C): Dark blue prisms; mp 138 °C; 20 mg (4.0%); R_f=0.68; UV 245 (log ε 4.50), 280 (sh, 4.54), 290 (4.55), 349 (sh, 4.26), 358 (4.29), 370 (4.29), 596 (sh, 2.76), and 636 nm (2.80); MS m/z 436 (M^+; 100), 421 (41), 405 (13), 391 (12), 377 (5), 294 (25), 279 (80), 265 (23), 252 (10), 239 (5), 218 (8), 195 (7), 155 (13), 141 (10), 115 (7), 83 (4), 71 (6), 57 (9), and 43 (6); ^1H NMR, see Table 1; ^{13}C NMR 139.45, 137.06, 134.78, 133.44, 132.97, 132.74, 124.56, 120.88, 120.53, 35.21, and 12.73.

Found: m/z 436.2262. Calcd for $C_{34}H_{28}$: M, 436.2191.

Treatment of **1C** with an equivalent of triphenylmethylium tetrafluoroborate in dry acetonitril at 20 °C for 1 h gave the tetrafluoroborate (**6**) as dark blue-green crystals: mp>300 °C; UV 643 nm.

Triphenylcarbinol[11] **(1D$_1$):** Colorless prisms; 5 mg (1.0%); mp 163 °C (Ref. 11, 161—162 °C); R_f=0.49; MS m/z 260 (M^+; 100); ^1H NMR, identical with the spectrum of the authentic sample.

Benzaldehyde (1D$_2$): Colorless oil; 1 mg (0.2%); R_f= 0.49; MS m/z 106 (M^+; 100); ^1H NMR, identical with the spectrum of the authentic sample.

(1*Z*),(4*Z*)-1,5-Diphenyl-1,4-pentadien-3-one[12] **(1D$_3$):** Colorless prisms; 1 mg (0.2%); mp 103 °C (Ref. 12, 104—107 °C); R_f=0.49; MS m/z 234 (M^+; 100); ^1H NMR, identical with that of the authentic sample.

(*Z*)-1-Phenyl-1-buten-3-one[13] **(1E$_1$):** Colorless prisms; 5 mg (1.0%); mp 41 °C (Ref. 13, 39—41 °C); R_f=0.36; MS m/z 146 (M^+; 100); ^1H NMR, identical with that of the authentic sample.

3-Methyl-1-[(3-methyl-1-azulenyl)methyl]-4(3a*H*)-azulenone[20] **(1E$_2$):** Green prisms; 2 mg (0.4%); mp 143 °C; R_f=0.36; UV (MeOH) 243 (log ε 4.55), 285 (4.57), 340 (sh, 4.17), 351 (4.22), 380 (sh, 3.37), 430 (sh, 3.20), 580 (sh, 2.80), 600 (sh, 2.84), 626 (2.87), 650 (sh, 2.81), and 684 nm (sh, 2.80); MS *m/z* 312 (M^+; 4%), 297 (1), 279 (1), 265 (1), 252 (1), 170 (1), 155 (100), 141 (4), 128 (3), and 115 (3); IR (KBr) 1690 cm^{-1} (C=O); ^1H NMR, see Table 1.

Found: *m/z* 312.1575. Calcd for $C_{23}H_{20}O$: M, 312.1635.

1-Azulenecarbaldehyde[14] **(1F$_1$):** Red oil; 15 mg (3.0%); R_f=0.28; MS *m/z* 156 (M^+; 100); ^1H NMR, identical with the reported spectrum.[14]

2-Methyl-1,4-naphthoquinone[15] **(1F$_2$):** Pale yellow needles; 5 mg (1.0%); mp 105 °C (Ref. 15, 105—107 °C; R_f=0.28; MS *m/z* 172 (M^+; 100); ^1H NMR, identical with that of the authentic sample.

Compound 1F$_3$: Pale yellow oil; 1 mg (0.2%); R_f=0.28. This product, which was presumed to be hitherto unknown 3-methyl-1*H*-inden-1-one, gradually changed to Compound **1F$_4$**:[21] colorless oil; R_f=0.28; UV 242 (log ε 3.17), 255 (sh, 3.13), and 285 nm (sh, 2.82); IR 1730—1680 cm^{-1} (C=O); MS *m/z* 288 (M^+; 24%), 144 (100), and 116 (8).

Found: *m/z* 288.1169. Calcd for $C_{20}H_{16}O_2$: M, 288.1150.

3-Methyl-1-azulenecarbaldehyde[14] **(1G$_1$):** Dark violet needles; 10 mg (2.0%); mp 73 °C (Ref. 14, 73 °C); R_f=0.23; MS *m/z* 170 (M^+; 100); ^1H NMR, identical with the reported spectrum.[14]

Bis(3-methyl-1-azulenyl) Ketone (1G$_2$): Dark green prisms; 3 mg (0.6%); mp 163 °C; R_f=0.23; UV 242 (log ε 4.48), 280 (sh, 4.51), 295 (4.60), 315 (4.54), 327 (sh, 4.46), 422 (4.39), 566 (2.71), and 596 nm (sh, 2.65); MS *m/z* 310 (M^+; 100), 295 (63), 281 (12), 267 (27), 252 (27), 239 (6), 215 (2), 189 (2), 169 (13), 153 (11), 141 (34), 126 (11), 115 (40), 97 (9), 85 (11), 71 (18), 57 (30), and 43 (28); IR 1720 cm^{-1} (C=O); ^1H NMR, see Table 1.

Found: *m/z* 310.1354. Calcd for $C_{23}H_{18}O$: M, 310.1357.

2-Methyl-7-(3-methyl-1-azulenyl)-1,4-naphthoquinone (1G$_3$): Dark violet prisms; 5 mg (1.0%); mp 122 °C; R_f=0.23; UV (MeOH) 250 (log ε 4.37), 294 (4.34), 360 (sh, 3.44), 380 (sh, 3.43), and 500 nm (3.35); MS *m/z* 312 (M^+; 100), 295 (9), 239 (8), 215 (11), 165 (5), 141 (20), 118 (17), 108 (5), 97 (7), 83 (8), 69 (8), 55 (9), and 44 (16); IR 1655 cm^{-1} (C=O); ^1H NMR, see Table 1.

Found: *m/z* 312.1057. Calcd for $C_{22}H_{16}O_2$: M, 312.1150.

1-Methyl-3-(3-methyl-1,4-dioxo-5-naphthyl)azulene (1G$_4$): dark blue violet prisms; 5 mg (1.0%); mp 192 °C; R_f=0.23; UV 245 (sh, log ε 4.52), 251 (4.53), 257 (4.52), 263 (4.52), 290 (4.53), 340 (sh, 4.11), 375 (3.40), 590 (3.13), and 670 nm (sh, 3.00); MS *m/z* 312 (M^+; 100), 297 (61), 286 (11), 269 (4), 260 (1), 243 (2), 228 (2), 215 (4), 141 (2), 71 (1), and 57 (1); IR 1665 and 1660 cm^{-1} (C=O); ^1H NMR, see Table 1.

Found: *m/z* 312.1163. Calcd for $C_{22}H_{16}O_2$: M, 312.1150.

3-Methyl-5-(3-methyl-1-azulenyl)-1*H*-inden-1-one (1G$_5$): Dark brown prisms; 5 mg (1.0%); mp 80 °C; R_f=0.23; UV 246 (log ε 4.11), 299 (4.09), 306 (sh, 4.08), 353 (3.25), 458 (3.24), 620 (2.42), and 670 nm (sh, 2.34); MS *m/z* 284 (M^+; 100), 253 (5), 239 (18), 215 (7), and 141 (16); IR 1700 cm^{-1} (C=O); ^1H NMR, see Table 1.

Found: *m/z* 284.1208. Calcd for $C_{21}H_{16}O$: M, 284.1201.

1-Azulenecarboxylic Acid[16] **(1H$_1$):** Red needles; 5 mg (1.0%); mp 182 °C (Ref. 16, 181—182 °C); R_f=0.10; MS *m/z* 172 (M^+; 100); ^1H NMR, identical with the reported spectrum.[16]

3-Methyl-1-azulenecarboxylic Acid[17] **(1H$_2$):** Dark violet needles; 5 mg (1.0%); mp 196 °C (Ref. 17, 196 °C); R_f=0.10; MS *m/z* 186 (M^+; 100); ^1H NMR, identical with the reported spectrum.[17]

Cinnamic Acid[18] **(1I):** Colorless prisms; 1 mg (0.2%); mp 130 °C (Ref. 18, 132—133 °C); R_f=0.04; MS and ^1H NMR, identical with those of the authentic sample.

Autoxidation of 1 in DMF. The same oxidation procedure was employed, and virtually the same products were obtained as in the case of the oxidation in HMPA described above.

Oxidation of 1,3-Dimethylazulene (2) in HMPA. Autoxidation of **2**[25] (0.40 g) in HMPA (16 g) was carried out for 5 h at 100±5 °C in a manner similar to that described for **1**, thus affording, after the careful chromatographic separation, 11 products (**2A—I**; see Fig. 2 for HPLC and TLC), besides the recovered starting material **2** (**2A**, 0.25 g, R_f 0.83: ^1H NMR, see Table 1) and polar resinous substances [0.09 g, 60% (w/w); R_f 0.0]; the yield of each product is based on the consumed starting material (0.15 g).

1′,3,3′-Trimethyl-1,2′-biazulene (2B$_1$): Green prisms; 5 mg (3.3%); mp 78 °C; R_f=0.74; UV 245 (log ε 4.37), 277 (4.52), 300 (4.51), 310 (sh, 4.47), 355 (4.18), 436 (3.25), 572 (sh 2.62), 624 (2.67), and 680 nm (sh, 2.65); MS *m/z* 296 (M^+; 100), 281 (17), 279 (17), 265 (44), and 252 (8); ^1H NMR, see Table 1.

Found: *m/z* 296.1562. Calcd for $C_{23}H_{20}$: M, 296.1564.

1,1′-Methylenebis[3-methylazulene][10] **(2B$_2$):** Dark blue prisms; 5 mg (3.3%); mp 79 °C; R_f=0.74; MS and ^1H NMR, identical with those of **1B$_1$** obtained by the oxidation of **1** in HMPA or DMF as described above.

Benzaldehyde (2C): Colorless oil; 1 mg (0.7%); R_f=0.64; MS and ^1H NMR, identical with those of the authentic sample.

1,3-Dimethyl-5-azulenecarbaldehyde (2D): Yellow green oil; 1 mg (0.7%); R_f=0.56; UV 245 (log ε 4.03), 284 (sh, 4.09), 292 (4.13), 304 (sh, 4.12), 332 (sh, 3.74), 415 (3.42), 620 (2.76), and 672 nm (sh, 2.72); MS *m/z* 184 (M^+; 100), 169 (41), and 155 (19); IR 1690 cm^{-1} (C=O); ^1H NMR, see Table 1.

Found: *m/z* 184.0881. Calcd for $C_{13}H_{12}O$: M, 184.0888.

1,3-Dimethyl-1-indenol (2E): Colorless oil; 7 mg (4.7%); R_f=0.42; UV 248 (sh, log ε 4.17), 253 (4.18), 265 (sh, 4.12), 271 (sh, 4.08), 276 (sh, 4.06), 282 (sh, 4.04), and 294 nm (sh, 3.86); MS *m/z* 160 (M^+; 61%), 145 (100), 128 (12), 127 (12), and 115 (32); IR 3750—3100 cm^{-1} (OH); ^1H NMR 1.55 (3H, s, Me-1), 1.66 (1H, brs, HO-1), 2.02 (3H, d, $J_{2,Me(3)}$=1.5 Hz, Me-3), 5.92 (1H, q, H-2), 7.06 (1H, ddd, $J_{6,7}$=7.0 Hz, $J_{5,7}$=1.3 Hz, $J_{4,7}$=0.6 Hz, H-7), 7.12 (1H, ddd, $J_{5,6}$=7.2 Hz, $J_{4,5}$=7.0 Hz, H-5), 7.19 (1H, ddd, H-6), and 7.31 (1H, ddd, H-4).

Found: *m/z* 160.0885. Calcd for $C_{11}H_{12}O$: M, 160.0888.

3-Methyl-1-azulenecarbaldehyde[14] **(2F):** Dark violet needles; 30 mg (20%); R_f=0.19; MS and ^1H NMR, identical with the spectra of **1G$_1$** described above.

Compound 2G: Yellow crystals; R_f=0.14; UV 245 (sh, log ε 3.90), 255 (3.94), 360 (sh, 3.46), 378 (3.49), 398 (sh, 3.45), 430 (sh, 2.97), 460 (sh, 2.76), 496 (sh, 2.48), and 530 nm (sh, 2.13); MS *m/z* 160 (MS^+; 100), 131 (63), 104 (20), 103 (20), 78 (19), 77 (20), and 51 (20).

1-Hydroxy-1,3-dimethyl-1*H*-indene-4-, 5-, and 6-carbaldehyde (2H$_1$, 2H$_2$, and 2H$_3$): (as a ca. 1:2:1 mixture, respectively): Colorless oil; 3 mg (2.0%); R_f=0.10; MS *m/z* 188 (M^+; 100), 173 (89), 159 (50), 145 (59), 128 (22), 127 (22), and 115 (59); IR 3750—3150 (OH) and 1690 cm^{-1} (C=O); ^1H NMR (DMSO-d_6) **2H$_1$** δ= 1.41 (3H, s, Me-1), 2.27 (3H, d,

$J_{2,Me(3)}$=1.5 Hz, Me-3), 5.10 (1H, brs, HO-1), 6.20 (1H, q, H-2), 7.24 (1H, t, $J_{5,6}=J_{6,7}$=7.5 Hz, H-6), 7.51 (1H, dd, $J_{5,7}$=1.5 Hz, H-7), 7.69 (1H, dd, H-5), and 10.40 (1H, s, CHO-4), **2H**$_2\delta$=1.43 (3H, s, Me-1), 2.02 (3H, d, $J_{2,Me(3)}$=1.5 Hz, Me-3), 5.10 (1H, brs, OH-1), 6.17 (1H, q, H-2), 7.27 (1H, brd, $J_{6,7}$=8.0 Hz, H-7), 7.72 (1H, brd, $J_{4,6}$=1.5 Hz, H-4), 7.74 (1H, dd, H-6), and 9.88 (1H, s, CHO-5), and **2H**$_3\delta$=1.41 (3H, s, Me-1), 2.03 (3H, d, $J_{2,Me(3)}$=2.0 Hz, Me-3), 5.10 (1H, brs, HO-1), 6.04 (1H, q, H-2), 7.46 (1H, brd, $J_{4,5}$=8.0 Hz, H-4), 7.55 (1H, d, $J_{5,7}$=1.5 Hz, H-7), 7.61 (1H, dd, H-5), and 9.88 (1H, s, CHO-6).

Found (for the mixture of **2H**$_{1,3}$): *m/z* 188.0839. Calcd for $C_{12}H_{12}O_2$: M, 188.0837.

3-Methyl-1-azulenecarboxylic Acid[17] **(2I):** Dark violet needles; mp 196 °C (Ref. 17, 196 °C); 1 mg (0.7%); R_f=0.06; MS and ^{1}H NMR, identical with the spectra of **1H**$_2$ described above.

Autoxidation of 2 in DMF. The same procedures as those for **2** in HMPA were employed, and virtually the same products were obtained.

We wish to thank Professors Kahei Takase (Tohoku Univ.) and Ichiro Murata (Osaka Univ.) for valuable discussion.

References

1) A part of the results have been preliminarily presented: S. Takekuma, O. Okabe, Y. Matsubara, H. Yamamoto, and T. Nozoe, 50th National Meeting of the Chemical Society of Japan, Tokyo, April 1985, Abstr. No. 1T11; Y. Matsubara, S. Takekuma, K. Kitajima, H. Yamamoto, and T. Nozoe, 52nd National Meeting of the Chemical Society of Japan, Kyoto, April 1986, Abstr. No. 2V28.

2) T. Nozoe, S. Takekuma, M. Doi, Y. Matsubara, and H. Yamamoto, *Chem. Lett.*, **1984**, 627

3) Y. Matsubara, S. Takekuma, K. Yokoi, H. Yamamoto, and T. Nozoe, *Chem. Lett.*, **1984**, 631

4) Y. Matsubara, S. Takekuma, K. Yokoi, H. Yamamoto, and T. Nozoe, *Bull. Chem. Soc. Jpn.*, **60**, 1415 (1987).

5) These experimental results are also in agreement with a preliminary theoretical calculation: T. Kurihara, S. Ishikawa, and T. Nozoe, 52nd National Meeting of the Chemical Society of Japan, Kyoto, April 1986, Abstr. No. 2V26.

6) For reviews and monographs, see K. Hafner, *Angew. Chem.*, **70**, 419 (1958); *Angew. Chem., Int. Ed. Engl.*, **3**, 167 (1964); T. Nozoe and S. Ito, *Fortschr. Chem. Org. Naturst.*, **19**, 33 (1961); A. G. Anderson and R. G. Anderson, *J. Org. Chem.*, **27**, 3578 (1962), and references cited therein; K. Takase and M. Yasunami, *Yuki Gosei Kagaku Kyokai Shi*, **39**, 1172 (1981); D. Lloyd, "Non-Benzenoid Conjugated Carbocyclic Compounds," Elsevier, Amsterdam (1984), pp. 351—377.

7) R. J. Waltman and J. Bargon, *Can. J. Chem.*, **64**, 76 (1986) and references cited therein.

8) a) L. T. Scott, M. D. Rozeboom, K. N. Houk, T. Fukunaga, H. J. Lindner, and K. Hafner, *J. Am. Chem. Soc.*, **102**, 5169 (1980), and references cited therein; b) L. T. Scott, *Pure Appl. Chem.*, **1983**, 363; c) L. T. Scott, P. Grutter, and R. Chamberlain, III, *J. Am. Chem. Soc.*, **106**, 4852 (1984); d) L. T. Scott and C. M. Adams, *ibid.*, **106**, 4857 (1984); e) T. Morita, M. Karasawa, and K. Takase, *Chem. Lett.*, **1980**, 197; f) T. Morita, F. Ise, and K. Takase, *ibid.*, **1982**, 1303.

9) Slightly different, unresolved values have been reported for a few of these azulenes (mostly measured at 60-MHz in much concentrated CCl_4 or $CDCl_3$ soln); see the Exptl section.

10) K. Hafner and W. Senf, *Justus Liebigs Ann. Chem.*, **656**, 34 (1962).

11) W. E. Bachmann and H. P. Hetzner, *Org. Synth.*, Coll. Vol. III, 839 (1955).

12) C. R. Conard and M. A. Dolliver, *Org. Synth.*, Coll. Vol. II, 167 (1943).

13) N. L. Drake and P. Allen, Jr., *Org. Synth.*, Coll. Vol. I, 77 (1932).

14) K. Hafner and C. Bernhard, *Angew. Chem.*, **69**, 533 (1957); *Justus Liebigs Ann. Chem.*, **625**, 108 (1959); W. Treibs, J. Hiebsch, and H.-J. Neupert, *Naturwiss.*, **44**, 352 (1957); W. Treibs, H.-J. Neupert, and J. Hiebsch, *Chem. Ber.*, **92**, 141 (1959).

15) L. F. Fieser, M. Tishler, and W. L. Sampson, *J. Am. Chem. Soc.*, **62**, 996 (1940).

16) W. Treibs, H.-J. Neupert, and J. Hiebsch, *Chem. Ber.*, **92**, 1216 (1959); A. G. Anderson, Jr., R. G. Anderson, and L. L. Roplogle, *Proc. Chem. Soc.*, **1960**, 72.

17) R. N. McDonald, R. R. Reitz, and J. M. Richmond, *J. Org. Chem.*, **41**, 1822 (1976).

18) J. R. Johnson, *Organic Reactions*, **1**, 210 (1942).

19) The chloride of this cation has been reported: K. Hafner, H. Pelster, and J. Schneider, *Justus Liebigs Ann. Chem.*, **650**, 62 (1961).

20) Autoxidation of 1,1′-methylenebis[3-methylazulene] (**1B**$_1$) under similar conditions has been found to produce **1E**$_2$ besides other products. Moreover, on oxidation of 3,3′-methylenebisguaiazulene with peracetic acid in hexane at 25 °C, we have recently isolated a structurally similar compound 5-isopropyl-3,8-dimethyl-1-[(3-guaiazulenyl)methyl]-4(3a*H*)-azulenone (dark green prisms, mp 117 °C, 61% yield), which is presumed on the molecular model inspection to exist in a favorable conformation **32** in $CDCl_3$. ^{1}H NMR parameters of **1E**$_2$ closely resemble those of the corresponding positions of **32**. Problems of keto-enol equilibria of these compounds and related other azulene analogues will be reported elsewhere together with their preparation and detailed structural determination.

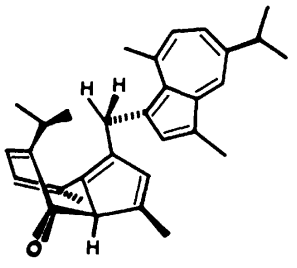

32

21) Although composition of the dimer **1F**$_4$ was confirmed by MS, its purification and structural determination are currently under investigation.

22) E.g. See J. Santamaria, *Tetrahedron Lett.*, **22**, 4511 (1981); H. Iwamoto, M. Kanehiro, and Y. Matsubara, *Yukagaku*, **31**, 222 (1982); S. Takekuma, Y. Matsubara, H. Yamamoto, and T. Nozoe, *ibid.*, **34**, 1026 (1985).

23) Y. Matsubara, S. Takekuma, K. Ueno, H. Yamamoto, and T. Nozoe, 52nd National Meeting of the Chemical Society of Japan, Kyoto, April 1986, Abstr. No. 2V27; Y. Matsubara, S. Takekuma, K. Kitajima, H. Yamamoto, and T. Nozoe, 53rd National Meeting of the Chemical Society of Japan, Nagoya, October 1986, Abstr. No. 3D07; Y. Matsubara, S. Takekuma, H. Yamamoto, and T. Nozoe, *Chem. Lett.*, **1987**, 455.

24) Studies on more selective, aerobic, as well as anodic, oxidation of azulenes at lower temps or under more dilute conditions are in progress.

25) We are grateful to Professor Masafumi Yasunami (Tohoku University) for a generous gift of 1-methyl- and 1,3-dimethylazulene.

 © 1987 The Chemical Society of Japan Bull. Chem. Soc. Jpn., 60, 3731—3738 (1987)

Effect of Substituents on the Oxidation Potential of Phthalocyanines and Electrocrystallization

Yuji ORIHASHI, Michinori NISHIKAWA, Hiroyuki OHNO, Eishun TSUCHIDA,* Hiro MATSUDA,†
Hachiro NAKANISHI,† and Masao KATO†
Department of Polymer Chemistry, Waseda University, Tokyo 160
†Research Institute for Polymers and Textiles, Tsukuba 305
(Received May 14, 1987)

A series of tetra- or octasubstituted phthalocyaninatocobalt derivatives were prepared and their oxidation behaviors were examined in relation to the nature of substituents. The oxidation potentials of phthalocyanines, especially those of rings were affected by the nature of both substituents and axial ligands. These oxidation potentials were in a linear relation with the Hammett's constants for substituents or axial ligands. The electrocrystallization proceeded when an oxidation potential higher than that for the phthalocyanine ring was given to the solution. This potential shift was therefore revealed to be an important factor to control the electrocrystallization of these phthalocyanines.

Phthalocyanines are being widely used as dyes, catalysts, photocatalysts, major component for solar energy conversion systems, conductive materials, and so on. The redox processes of metallophthalocyanines have been well analyzed in detail,[1] because it is quite important to design geared redox cycles as well as models for biologically active metalloporphyrins. On the other hand, we have reported the preparation of inherently conductive crystals of metallophthalocyanine by way of the electrocrystallization technique.[2] The applied potential was revealed to have a considerable effect on the efficiency of the crystal growth.[2c] These experimental results triggered us to examine the relation between the structure and the oxidation potential of phthalocyanines to get the best conditions for the electrocrystallization. The redox reaction of phthalocyanine occurs both at the central metal ion and on the phthalocyanine ring. The redox processes of some unsubstituted phthalocyanines have clearly been identified by cyclic voltammetry, coulometry, UV/Visible spectroscopy, and ESR spectroscopy.[3,4] Indeed, two successive oxidations and four successive reductions of the ring have been reported.[3] Effects of solvent, chemical environment or axial ligand on the redox potentials of metallophthalocyanines have also been reported.[4] Substituents to the phthalocyanine ring are also expected to be effective for the shift of oxidation potential, but only a few examples have hitherto been reported, such as tetrasulfonated compounds.[1a,3]

The effects of substituents on the oxidation potential of the ring of phthalocyaninatocobalt derivatives were examined in this paper for the purpose of obtaining useful data with regard to electrocrystallization.

Experimental

Materials. Substituted phthalocyaninatocobalt(II) derivatives prepared in this study are summarized in Table 1.

Phthalocyaninatocobalt(II).[5] Phthalonitrile (29.0 g: 0.23 mol) and cobalt(II) acetate (12.0 g: 0.07 mol) were dissolved in 1000 ml of dehydrated methanol. 1,8-Diazabicyclo[5.4.0]-undec-7-ene (DBU) (38 ml) was added dropwise into the methanol solution under stirring at room temperature, then the solution was refluxed for 24 h. After cooling, the red-purple colored precipitate was filtered. The crude product was boiled in 10%-HCl then in 10%-NaOH aqueous solution, washed with water until the aqueous solution reached neutral. The washed precipitate was dried in vacuo. Ten grams of phthalocyaninatocobalt(II) was obtained with 30% yield. Calcd for $C_{32}H_{16}N_8Co$: C, 67.3; H, 2.8; N, 19.6; Co, 10.3%. Found: C, 68.1; H, 2.7; N, 20.0; Co, 9.1%.

Tetranitrophthalocyaninatocobalt(II).[6] **(a) 4-Nitrophthalonitrile:** A total of 30.0 g (0.16 mol) of 4-nitrophthalic anhydride and 84.0 g (1.40 mol) of urea was suspended in 500 ml of 1,2,4-trichlorobenzene, heated at 150 °C for 72 h under stirring. The precipitate was filtered and then washed with aqueous ammonia, yielding 16.6 g of 4-nitrophthalamide with 49.6% yield.

4-Nitrophthalamide (16.0 g: 0.08 mol) was suspended in 200 ml of dehydrated *N,N*-dimethylformamide. Trichloromethyl chloroformate (30 ml) was added dropwise to the solution under vigorous mixing at 5 °C, and kept under moderate stirring for 72 h. The solution was poured into 1000 ml of ice water, and then the phase-separated precipitate was filtered. A crude product was purified as light yellow needle with 73% yield by sublimation at 150 °C under

Table 1. Substituted Phthalocyanines

Compound		
Abb.	R_1	R_2[a]
$(CN)_8PcCo$	CN	CN
$(HOOC)_8PcCo$	COOH	COOH
PcCo	H	H
$(H_3CO)_8PcCo$	OCH_3	OCH_3
$(H_3C)_8PcCo$	CH_3	CH_3
$(O_2N)_4PcCo$	NO_2	H
$(HOOC)_4PcCo$	COOH	H
$(H_3CO)_4PcCo$	OCH_3	H
$(H_2N)_4PcCo$	NH_2	H

a) 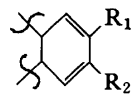

10^{-2} Torr (1 Torr=133.322 Pa). Mp 140 °C. IR (cm^{-1}) 2240 (C≡N).

(b) Tetranitrophthalocyaninatocobalt(II): A total of 8.6 g (0.04 mol) of 4-nitrophthalonitrile and 2.1 g (0.01 mol) of cobalt(II) acetate was dissolved in 300 ml of freshly distilled nitrobenzene and stirred at 150 °C for 24 h. The precipitate was filtered and washed with methanol. The crude product was washed with 10%-HCl then with 10%-NaOH as described above. Yield 20%. Calcd for $C_{32}H_{12}N_{12}O_8Co$: C, 51.1; H, 1.6; N, 22.4; Co, 7.8%. Found: C, 50.0; H,1.9; N, 21.6; Co, 8.1%. IR (cm^{-1}): 1530, 1340 (NO_2).

Tetraaminophthalocyaninatocobalt(II).[7] Tetranitrophthalocyaninatocobalt(II) (2.0 g: 2.7×10^{-4} mol) was mixed with sodium hydrogensulfide (1.5 g: 2.7×10^{-2} mol) in 100 ml of *N,N*-dimethylformamide at 100 °C for 5 h. After cooling, 6 M-NaOH (1M=1 mol dm^{-3}) was slowly added until the pH reached 10 to precipitate the product. A dark-blue product was filtered and washed with distilled water until the solution was completely neutralized. Yield 65%. Calcd for $C_{32}H_{20}N_{12}Co$: C, 60.9; H, 3.2; N, 26.6; Co, 9.3%. Found: C, 61.9; H, 3.0; N, 25.8; Co, 9.3%. IR (cm^{-1}): 3400, 3200, 1600(NH_2).

Tetracarboxyphthalocyaninatocobalt(II).[8] Trimellitic anhydride (20.0 g: 0.10 mol), urea (48.0 g: 0.80 mol), cobalt(II) acetate (6.9 g: 0.45 mol) and ammonium molybdate (0.20 g: 1.7×10^{-1} mol) were suspended in 300 ml of freshly distilled nitrobenzene, then the suspension was heated at 150 °C with stirring for 24 h. After cooling, the precipitate was filtered and washed with dehydrated methanol. Crude tetracarbamoylphthalocyaninatocobalt(II) (10.0 g) was obtained as a blue-purple precipitate. Then it was treated with 2 M-KOH aqueous solution under reflux. After the gas evolution ceased, 200 ml of pure water was further added, then filtered again. The filtrate was acidified to pH 2 with 6 M-HCl aqueous solution to precipitate the product. The precipitate thus obtained was washed with distilled water for several times. The product was dissolved in 500 ml of KOH aqueous solution (pH 10). The filtrate was again acidified to pH 2. This purification procedure was repeated three times. A red-purple product was obtained with 35% yield. Calcd for $C_{36}H_{16}N_8O_8Co$: C, 57.8; H, 2.1; N, 15.0; Co, 7.9%. Found: C, 56.0; H, 2.3; N, 14.6; Co, 8.3%. IR (cm^{-1}), 1720 (COOH).

Octacyanophthalocyaninatocobalt(II).[9] Tetracyanobenzene (6.0 g: 0.31 mol) and cobalt(II) acetate (0.74 g: 4.8×10^{-3} mol) were dissolved in 500 ml of *N,N*-dimethylformamide and heated at 150 °C for 2 h. The solution was slowly dropped into 2000 ml of diethyl ether under stirring, then the obtained precipitate was filtered and washed with dehydrated methanol. Yield 50%. Calcd for $C_{40}H_8N_{16}Co$: C, 62.3; H, 1.0; N, 29.1; Co, 7.6%. Found: C, 61.9; H, 1.2; N, 28.9; Co, 8.0%. IR (cm^{-1}): 2225 (C≡N).

Octacarboxyphthalocyaninatocobalt(II).[9] Octacyanophthalocyaninatocobalt(II) (0.5 g: 6.5×10^{-4} mol) was treated with KOH in ethylene glycol-water mixture (15/2 by vol) at 160 °C for 24 h. The reaction mixture was diluted with 100 ml of water and then filtered. The filtrate was acidified to pH 2 to precipitate the product. The blue product was filtered and purified by the same procedure as that for tetracarboxy derivative. Yield 50%. Calcd for $C_{36}H_{16}N_8O_{16}Co$: C, 49.4; H, 1.8; N, 12.8; 0, 29.3; Co, 6.7%. Found: C, 49.2; H, 1.7; N, 13.0; O, 29.2; Co, 6.7%. IR (cm^{-1}) 1700 (COOH).

Octamethylphthalocyaninatocobalt(II).[10] **(a) 1,2-Dibromo-4,5-dimethylbenzene:**[11] A few mg of iron powder and iodide were added to a cooled (5 °C) *o*-xylene (220 g: 2.06 mol). When the characteristic color for iodine disappeared, 660 g (4.1 mol) of bromine was added dropwise. When a half amount of bromine was added, 200 ml of dichloromethane was added to dilute the reaction medium. A residual amount of bromine was added slowly and the solution was maintained at 5 °C for 72 h. Dichloromethane (200 ml) was added and the excess bromine was neutralized with sodium bisulfite. An organic extract was washed with distilled water and dried over $MgSO_4$, evaporated to complete dryness. Recrystallization from hexane yielded white crystals with 40% yield. Mp 87.5—88 °C. ^1H NMR (CCl_4) δ=2.1 (s, 6H, $-CH_3$), 7.15 (s, 2H, arom).

(b) 1,2-Dicyano-4,5-dimethylbenzene: 1,2-Dibromo-4,5-dimethylbenzene (90.0 g: 0.34 mol) was heated under reflux for 5 h with CuCN (86.0 g: 0.96 mol) in 950 ml of *N,N*-dimethylformamide. After cooling, the reaction mixture was poured slowly into 1000 ml of aqueous ammonia and stirred for 12 h with air bubbling agitation. The blue solution was filtered and washed with distilled water until the filtrate was neutralized. The product was extracted with ether by Soxhlet extractor. Recrystallization from methanol yielded 24 g of white crystals. Yield 45%. Mp 117—117.5 °C. ^1H NMR ($CDCl_3$)δ=2.3 (s, 6H, $-CH_3$), 7.5 (s, 2H, arom).

(c) Octamethylphthalocyaninatocobalt(II): 1.2-Dicyano-4,5-dimethylbenzene (8.0 g: 0.05 mol) and cobalt(II) acetate (2.70 g: 0.02 mol) were heated under reflux for 24 h in 400 ml of ethylene glycol. After cooling, the blue-purple product was filtered and purified by treating with 1M-NaOH aqueous solution and then with 1M-HCl aqueous solution. Yield 30%. Calcd for $C_{40}H_{32}N_8Co$: C, 70.3; H, 4.7; N, 16.4; Co, 8.6%. Found: C, 70,3 ; H, 4.8 ; N, 15.9 ; Co, 9.0%.

Octamethoxyphthalocyaninatocobalt(II).[6] **(a) 1,2-Dibromo-4,5-dimethoxybenzene:** Veratrole (75.0 g: 0.54 mol) was dissolved in carbon tetrachloride (220 ml), then bromine (29 ml: 1.1 mol) was added dropwise into the solution at 0—5 °C. The mixed solution was stirred for 48 h. The reaction mixture was washed with 10%-NaOH aqueous solution and then with distilled water. The solvent was evaporated, and the obtained white product was recrystallized from chloroform. Yield 71%. Colorless plate crystals. Mp 81.5—82 °C. ^1H NMR (d_6-acetone)δ=3.9 (s, 6H, OCH_3), 7.0 (s, 2H, arom).

(b) 1,2-Dicyano-4,5-dimethoxybenzene: The reaction conditions were very close to those for 1,2-dicyano-4,5-dimethylbenzene. A mixture of 1,2-dibromo-4,5-dimethoxybenzene (15.8 g: 0.05 mol) and CuCN (13.4 g: 0.15 mol) was heated under reflux for 5 h in 200 ml of *N,N*-dimethylformamide. The follow-up procedure was the same as that for 1,2-dicyano-4,5-dimethylbenzene described above. Recrystallization from methanol yielded 6.0 g of white needles. Yield 64%. Mp 180—180.5 °C. ^1H NMR ($CDCl_3$) δ=3.9 (s, 6H, OCH_3), 7.1 (s, 2H, arom).

(c) Octamethoxyphthalocyaninatocobalt(II): 1,2-Dicyano-4,5-dimethoxybenzene (2.60 g: 1.5×10^{-2} mol) and cobalt(II) acetate (0.80 g: 4.5×10^{-3} mol) were mixed in 100 ml of ethylene glycol and refluxed for 24 h. The reaction mixture was cooled and filtered, then washed with methanol. The purification procedure with 1M-NaOH and 1M-HCl aqueous solution was the same as described above. Calcd for $C_{40}H_{32}N_8O_8Co$: C, 59.2; H, 3.9; N, 13.8; O, 15.8; Co, 7.3%. Found: C, 58.6; H, 4.0; N, 13.4; 0, 16.0; Co, 8.0%.

Potassium (dicyanophthalocyaninato)cobaltate(III).[12] As tetra- or octasubstituted (dicyanophthalocyaninato)cobaltate(III) derivatives were synthesized and purified with the same procedure, a representative method is mentioned here.

Procedure (a): Phthalocyaninatocobalt(II) (2.1 g: 3.7×10^{-3} mol) was suspended in 70 ml of nitrobenzene with thionyl chloride (14 ml: 0.2 mol) and heated at 60 °C for 6 h. After cooling, the mixture was filtered and washed with dehydrated methanol. Dichlorophthalocyaninatocobalt(III) obtained as a brown precipitate,[13] was dried in vacuo. Yield 76%. Calcd for $C_{32}H_{16}N_8Cl_2$: C, 59.8; H, 2.5; N, 17.5; Co, 9.2; Cl, 11.1%. Found: C, 58.7; H, 2.6; N, 17.1; Co, 10.3; Cl, 11.3%.

Dichlorophthalocyaninatocobalt(III) (3.80 g: 6.0×10^{-3} mol) and KCN (5.85 g: 9.0×10^{-3} mol) were mixed in 200 ml of ethanol and was heated under reflux for 72 h. The blue-purple product was filtered and washed with cold water. The product was placed in a thimble of Soxhlet extractor and extracted with dehydrated acetone for 72 h. The extract was evaporated and the product was recrystallized from dehydrated acetone to yield purple crystals with 78% of yield.

Procedure (b): Phthalocyaninatocobalt(II) (3.4 g: 6×10^{-3} mol) was mixed with KCN (7.5 g: 0.12 mol) in 350 ml of ethanol and heated for 72 h. After cooling, the product was filtered and washed with cold water. The purification procedure was the same as that for procedure (a). Yield 50%. Calcd for $C_{34}H_{16}N_{10}CoK$: C, 61.6; H, 2.4; N, 21.1; Co, 8.9; K, 5.9%. Found: C, 61.8; H, 3.0; N,20.5; Co, 8.7; K, 5.9%. IR (cm^{-1}) 2130 (C≡N).

Potassium (dithiocyanatophthalocyaninato)cobaltate(III). Dichlorophthalocyaninatocobalt(III) (1.65 g: 2.6×10^{-3} mol) was suspended in 200 ml of dehydrated ethanol with KSCN (0.75 g: 7.7×10^{-3} mol) for 6 h. After cooling, the blue-purple product was filtered and washed with cold water. The product was purified with the same procedure as that for potassium (dicyanophthalocyaninato)cobaltate(III). Yield 82%. Calcd for $C_{34}H_{16}N_{10}S_2K$: C, 56.2; H 2.2; N, 19.3; S, 8.8; Co, 8.1; K, 5.4%. Found: C, 56.4; H, 2.1; N, 19.4; S, 8.3; K, 5.6%. IR (cm^{-1}) 2100 (C≡N).

Cyclic Voltammetry. Cyclic voltammograms were obtained with a Pt plate electrode coated with phthalocyaninatocobalt(II) derivatives in an acetonitrile solution containing 0.1 M tetraethylammonium chloride (TEAC). In case of soluble potassium [dicyano(or dithiocyanato)phthalocyaninato]cobaltate(III) derivatives, a Pt wire was used as working electrode in an acetonitrile solution of phthalocyanine. Cyclic voltammetry was carried out with a Hokuto Denko HA-501G potentiostat and a Hokuto Denko HB-105 function generator, at a scan rate of 50 mV s^{-1}.

Spectroscopies. IR spectra were obtained with Hitachi 260-30. ESR spectra were obtained with JES-FE-3X, Nippon Denshi Co. Ltd. UV/Visible spectra were obtained with Varian Cary 17D. Details of the spectroscopic measurements were mentioned in previous papers.[2]

Results and Discussion

I) Oxidation Behaviors of Substituted Phthalocyanine Derivatives. The oxidation potentials of metallophthalocyanines have been reported by Lexa et al.,[14] and Wolberg et al.[15] They measured the oxidation potentials of metallophthalocyanines in *N,N*-dimethylformamide or 1-chloronaphthalene by cyclic voltammetry. The oxidation potential of the phthalocyanine ring was about 1.0 V vs. SCE. The oxidation potential of 0.9 V vs. Ag-AgCl in acetonitrile was obtained in our measurements, this result seemed reasonable comparing with the data in Table 2. The oxidation or reduction of the phthalocyanine ring directly reflects the electrostatic interaction between the ring and metal.[3] For OTi(IV), OV(IV), Ni(II), Cu(II), or Zn(II) complexes, the central metal ions do not show its oxidation until the phthalocyanine ring was oxidized. On the other hand, Fe(II) and Co(II) derivatives showed the ring oxidation at oxidation potentials after the oxidation of central metal ions and the reduction was also followed by the reduction of metal.[1a,14-17] In the potential range from 0 to +2.0 V (vs. Ag-AgCl) the oxidation between Co(II)/Co(III) occurred, but the oxidation processes for the phthalocyanine ring and metal were clearly distinguished with each other.

Only a few redox processes for octasubstituted phthalocyanine have hitherto been reported. Redox processes for octa-*t*-butyl-[18] and octacyanophthalocyaninatozinc(II)[19] have been reported, and the latter showed reversible four step one-electron redox reac-

Table 2. Metallophthalocyanine Electrochemistry

Complex	P^+/P (V vs. Ag-AgCl)	Solvent	Ref.
H_2Pc	1.143	CLN	15
	0.668	DMF	1k
	0.77	MeCN	This work
MgPc	0.743	DMF	22
	0.693	DMF	1f, 3
	0.653	DMF	14, 17b
AlPcCl	1.193	DMAc	22
	0.983	DMF	14, 17b
	0.958	DMF	16
	0.953	DMF	1k
$SiPc(OR)_2$[a]	1.44	CHC	1 l
FePc	0.78	MeCN	This work
	0.234[b]	CLN	15
	0.703	DMF	1h
CoPc	0.90	MeCN	This work
	0.843	DMAc	22
	0.814	CLN	15
	0.683	DCB	3, 26
NiPc	0.69	MeCN	This work
	1.093	CLN	15
CuPc	0.68	MeCN	This work
	1.023	CLN	15
ZnPc	0.65	MeCN	This work
	0.723	CLN	1g, 15
	0.823	DMF	22
GaPcCl	0.908	DMF	1f, 3
CdPc	0.583	DMF	1f, 3, 14, 17
InPcCl	0.873	DMF	1f
	0.883	DMF	1k
BaPc	0.498	DMF	3
HgPc	0.293	DMF	1f, 3
PbPc	0.713	DMF	1f, g, k

a) R: $Si(n\text{-}C_6H_{13})_3$, b) Fe(II) ↔ Fe(III), solvent CLN: 1-chloronaphthalene, DMF: *N,N*-dimethylformamide, MeCN: acetonitrile, DMAc: *N,N*-dimethylacetamide, CHC: dichloromethane, DCB: dichlorobenzene.

Table 3. Oxidation Potentials of Octasubstituted Phthalocyaninatocobalt(II)

Compound	P^+/P[a] (V vs. Ag-AgCl)	Hammett's constant[b]
$(CN)_8PcCo$	1.80	0.70
$(COOH)_8PcCo$	1.65	0.44
PcCo	0.90	0
$(CH_3O)_8PcCo$	0.77	−0.12
$(CH_3)_8PcCo$	0.83	−0.14

a) In acetonitrile solution, 10 mM TEAC, 25 °C.
b) For benzene derivatives from Ref. 20.

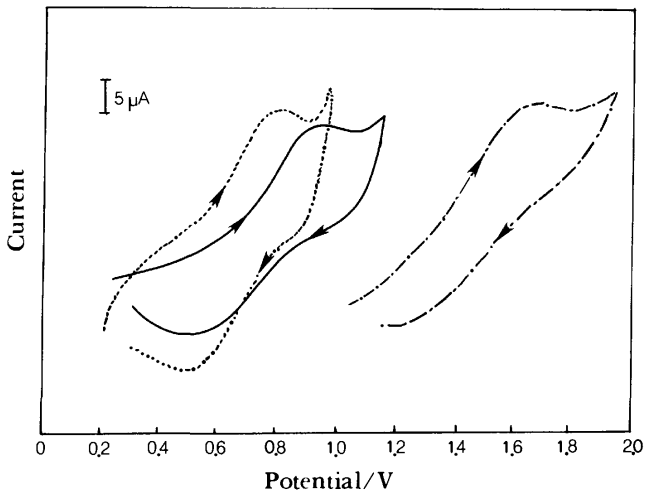

Fig. 1. Cyclic voltammograms for octasubstituted phthalocyanine in acetonitrile solution. 10mM TEAC, scan rate: 50mv s^{-1}.
Phthalocyaninatocobalt(II): (——), octamethylphthalocyaninatocobalt(II): (----), octacarboxyphthalocyaninatocobalt(II): (-·-·-). The electrode potential was measured vs. Ag-AgCl.

tions. The oxidation potentials of the phthalocyanine ring we measured are summarized in Table 3, and some of the cyclic voltammograms are shown in Fig. 1. Electron-withdrawing groups, such as cyano and carboxyl groups were expected to reduce the negative charge on the phthalocyanine ring. On the contrary, electron-donating groups, such as methoxyl and methyl groups were expected to increase it. Octacyano derivative showed the oxidation peak of the ring at +1.80 V and octacarboxy derivative at +1.65 V, as expected. On the contrary, methoxyl groups shifted it negatively by 0.13 V as shown in Table 3. The oxidation potential of octasubstituted derivatives was in the order of the following substituents;

$$-CN > -COOH > -H > -OCH_3 > -CH_3. \quad (1)$$

A good linear relation between the oxidation potential and the Hammett's constant for benzene derivatives[20] is observed as shown in Fig. 2. This suggests that the Hammett's constant for benzene derivatives is effective for the estimation of the oxidation potential of substituted phthalocyanine derivatives. The oxidation potential (E_{ox}) was expressed as a function of the

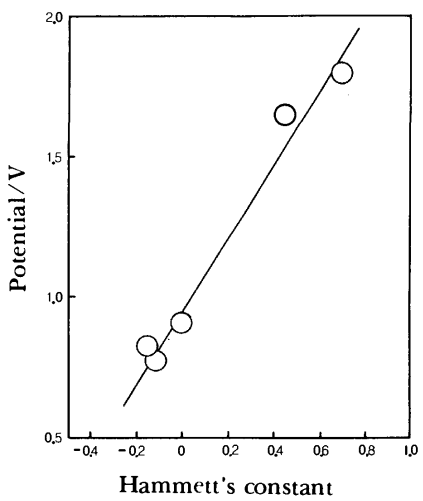

Fig. 2. Relation between the oxidation potential and the Hammett's constant of substituent for octasubstituted phthalocyaninatocobalt(II).

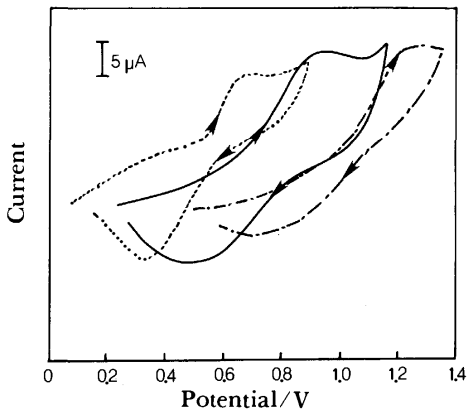

Fig. 3. Cyclic voltammograms for tetrasubstituted phthalocyanine in acetonitrile solution. 10mM TEAC, scan rate: 50mV s^{-1}.
Phthalocyaninatocobalt(II): (——), tetramethoxyphthalocyaninatocobalt(II): (----), tetracarboxyphthalocyaninatocobalt(II): (-·-·-). The electrode potential was measured vs. Ag-AgCl.

Hammett's constant (K) as shown in Eq. 2.

$$E_{ox} = 1.30\,K + 0.96 \quad (2)$$

This relationship should be useful not only for the estimation of a suitable potential for electrocrystallization as described later but also for the regulation of oxidation potential of phthalocyanines for the design of some catalytic systems.

For tetrasubstituted derivatives, the substituents also affect the oxidation potential just as the octasubstituted derivatives do. Though the redox processes of tetrasubstituted phthalocyanines such as tetra-*t*-butyl-, tetrasulfo-, and tetrakis(dodecanesulfonylamino)phthalocyanine have also been reported,[1a,3,21] the effects of substituent on the oxidation have not been summarized yet. The oxidation potentials of tetrasubstituted phthalocyaninatocobalt(II) derivatives were measured with cyclic voltammetry (Fig. 3), and are

Table 4. Oxidation Potentials of Tetrasubstituted Phthalocyaninatocobalt(II)

Compound	P^+/P[a] (V vs. Ag-AgCl)	Hammett's constant[b]
$(NO_2)_4PcCo$	1.30	0.81
$(COOH)_4PcCo$	1.24	0.44
PcCo	0.90	0
$(CH_3O)_4PcCo$	0.73	−0.12
$(NH_2)_4PcCo$	0.72	−0.30

a) In acetonitrile solution, 10 mM TEAC, 25 °C.
b) For benzene derivatives from Ref. 20.

Table 5. Tetrasubstituted Phthalocyanine Electrochemistry

Compound	P^+/P (V vs. Ag-AgCl)	Solvent	Ref.
$TsPcH_2$	0.943	DMSO	1a
TsPcCr	0.764	DMF	1f
TsPcCo	1.134	DMSO	1a
	0.443	DMF	3
TsPcNi	1.024	DMSO	1a
	0.993	DMF	3, 21a
TsPcCu	1.154	DMSO	1a
	0.993	DMF	3
TdPcFe	0.643	DMF	3
$(COOH)_4PcFe$	1.26	MeCN	This work
$(COOH)_4PcCo$	1.24	MeCN	This work
$(COOH)_4PcCu$	1.22	MeCN	This work
$TbPcH_2$	0.668	CHC	3
TbPcTiO	0.893	DMF	3
TbPcVO	0.983	DMF	3
TbPcCr	0.748	DMF	3
TbPcCo	0.683	DMF	22

Solvent DMSO: dimethyl sulfoxide, DMF: *N,N*-dimethylformamide, MeCN: acetonitrile, CHC: dichloromethane Ts: tetrasulfo-, Td: tetrakis(dodecylsulfonyl)-, Tb: tetra-*t*-butyl-.

summarized in Table 4. The solvents are weak donors, but the solvent coordination does not perturb strongly the oxidation as summarized in Table 5. Tetranitro and tetracarboxy derivatives showed positive oxidation potentials than unsubstituted phthalocyaninatocobalt(II) as expected from the results for octasubstituted ones. For tetrasubstituted derivatives, nitro groups shifted its oxidation potential to more positive side by 0.40 V, and carboxyl groups by 0.34 V. It was found as well that tetramethoxy and tetraamino derivatives which showed their oxidation peak at +0.73 V and +0.72 V, respectively, which is smaller than it for unsubstituted one. The oxidation potential for tetrasubstituted compound was shifted by their substituents as the following order;

$$-NO_2 > -COOH > -H > -OCH_3 > -NH_2. \quad (3)$$

This sequence was also characterized by the Hammett's constant. The relation between the oxidation potential of tetrasubstituted phthalocyaninatocobalt(II) and the Hammett's constant for benzene derivatives is shown in Fig. 4. It is a similar relationship to that for octasubstituted ones as shown in Fig. 2. This also delivers the following equation:

$$E_{ox} = 0.59\,K + 0.88 \quad (4)$$

The potentials of tetra-*t*-butyl- and tetrasulfophthalocyaninatocobalt(II) which have been measured in dichlorobenzene and *N,N*-dimethylformamide, respectively,[3,22] are also shown in Table 5. These data also lied on this relation as shown in Fig. 4. As mentioned above, the oxidation potentials of substituted metallophthalocyanine have not been investigated substantially. For the potentials of substituted derivatives examined here, a good linear relationship between the oxidation potential and the Hammett's constant of substituent was firstly found for both tetra- and octasubstituted complexes. In our experimental data a potential shift as much as about 1.0 V is noted, though it has been reported that the redox potential shift was generally seen within 100 mV by substituent such as chloro, methyl, *t*-butyl, sulfo, and carboxyl group.[3]

The oxidation potentials of potassium dicyano derivatives were also analyzed by cyclic voltammetry. The results are summarized in Table 6. The relation between the oxidation potential and the Hammett's constant of substituent which was found for octa- and tetrasubstituted derivatives was also available for these compounds. A similar linear relationship should be observed as long as the compounds had the same axial ligands.

Table 6. Oxidation Potentials of $K^+[R_nPcCoX_2]^-$ in Acetonitrile Solution[a]

Compound	P^+/P (V vs. Ag-AgCl)
$K^+[PcCo(CN)_2]^-$	1.10
$K^+[(CH_3O)_8PcCo(CN)_2]^-$	0.65
$K^+[(CH_3)_8PcCo(CN)_2]^-$	0.63
$K^+[(NH_2)_4PcCo(CN)_2]^-$	0.59
$K^+[PcCo(SCN)_2]^-$	0.98

a) No supporting electrolyte was added.

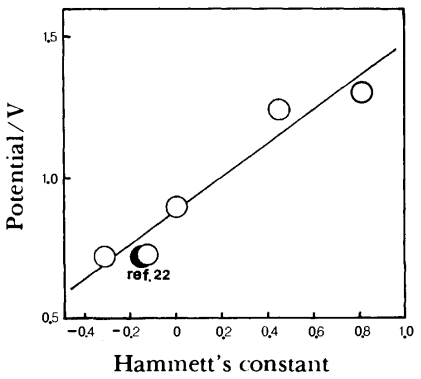

Fig. 4. Relation between the oxidation potential and the Hammett's constant of substituent for tetrasubstituted phthalocyaninatocobalt(II).

II) Effect of Axial Ligand on the Oxidation Behavior Effects of axial ligand on the oxidation potentials of metallophthalocyanine have been reported widely by Lever et al.,[1e,3,23] and Dolphin et al.,[24] through the analyses in several coordinating solvents. The effects of coordinating solvents on the oxidations are recognized for the strength of σ-donor ability of solvent, which means the occurrence of π-back donation. The stronger the σ-donor ability of solvent, the lower the potential shifts. The oxidations at the central metal ion are considered to be affected similarly, for example when strong σ-donor solvents bind to the Co(II) or Fe(II) complex, electrons in dz^2 orbital of metal are destabilized and the oxidation of metal (d^6-d^7) should occur more easily. The potential shift and the strength of σ-donor ability of solvent are the following.

$$\text{DMAc} = \text{DMF} > \text{DMSO} > \text{pyridine (redox potential)} \quad (5)$$

$$\text{DMAc} = \text{DMF} < \text{DMSO} < \text{pyridine } (\sigma\text{-donor ability}) \quad (6)$$

For these solvent systems, relation between the Gutmann Donicity Number[25] of solvent and the oxidation potential is depicted as linear.[26] For the reduction of Co(II)/Co(I) system, the same tendency was observed.[26] But contrary to these results, the potential is more positive with the strength of σ-donor ability for Fe(III)/Fe(II) system. This seemed to be the reason that the π-back donation in d^6 state (Fe(II)) was stronger than that in d^5 state (Fe(III)) by higher charge density in metal ion.[26]

Similar effects are expected for the phthalocyanine complexes which have the same two axial ligands, such as CN^- or SCN^-. With CN^- which is an electron-withdrawing group bound to metallophthalocyanine, the oxidation potential of the ring shifted to more positive side than that for uncoordinated complex. Furthermore, the CN^- coordinated derivative gave more positive oxidation potential than the SCN^- coordinated one as shown in Fig. 5. This is because CN^- withdraws electrons more strongly than SCN^-. For these phthalocyanine compounds, only one axial ligand can be replaced, for example to pyridine. It has been found that the stronger σ-donor axial ligand shifts the CN band to lower frequency in the IR spectrum.[12,27] This is one of the proofs that σ-donor ability of axial ligand affects the oxidations.

III) Effect of Central Metal Ion on the Oxidation Potentials of Substituted Metallophthalocyanines. We prepared tetracarboxyphthalocyaninatoiron(II) and that of copper(II). Their oxidation potentials of the phthalocyanine ring were +1.26 and +1.22 V vs. Ag-AgCl, respectively. Fe, Co, or Cu was introduced into tetracarboxy derivatives as central metal ion, the sequence of the oxidation potential (Fe> Co> Cu) was the same as that for unsubstituted metallophthalocyanines. This suggests that though an interaction between the central metal ion and the phthalocyanine ring did affect the oxidation potential, its magnitude was much less than that of the effect of substitution on rings. The relation between the metal and the oxidation potential of the ring might be explained as follows. The increase in the number of d-electrons of transition metal shifted the oxidation potential to a lower side, suggesting a strong coordination of nitrogen atoms in the ring to metal ion. When the $3dx^2$-y^2 orbital was empty as for Fe(II) and Co(II) complexes, this coordination bond should accommodate the oxidation of the ring. On the other hand, when the $3dx^2$-y^2 orbital was filled as for Cu(II) complex, charges on the metal made it easier to ionize the ring, i.e., oxidize.[15] This could be the main reason for the unusual oxidation potential of phthalocyaninatocopper(II).

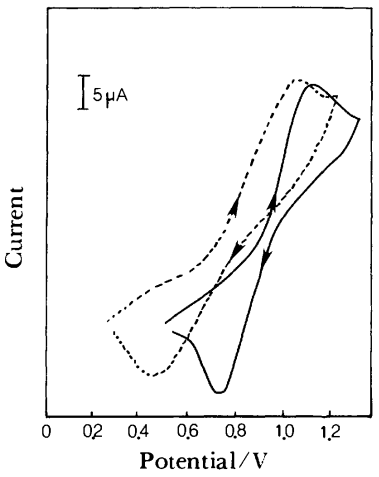

Fig. 5. Cyclic voltammograms for $K^+[PcCo(X)_2]^-$ in acetonitrile solution. Scan rate: 50 mV s^{-1}. X= CN: (——), X=SCN: (----). The electrode potential was measured vs. Ag-AgCl.

IV) Control of Electrocrystallization with Applied Potential. Electrocrystallization was carried out for potassium (substituted dicyanophthalocyaninato)cobaltate(III) in acetonitrile. A cell construction has already been shown elsewhere.[2b] It was found that electrocrystallization occurred when the solution was stored under the oxidative moiety of the phthalocyanine ring in the case of cyanophthalocyaninatocobalt(III).[2] The relation between the yield of crystals and applied potential for substituted phthalocyanine was shown in Fig. 6. Not all phthalocyanine derivatives could be crystallized in electric field because of the presence of structural isomers for tetrasubstituted derivatives. Even though, those were crystallized when the solution was stored under the oxidative moiety of the ring. It was clear that the drastic decrease in the solubility of phthalocyanines through the oxidation of phthalocyanine rings was the essential factor for the electrocrystallization. The difference in the crystal yield as shown in Fig. 6 is therefore attributed to the difference in the solubility of oxidized compounds. Though cyanophthalocyaninatocobalt(III) obtained

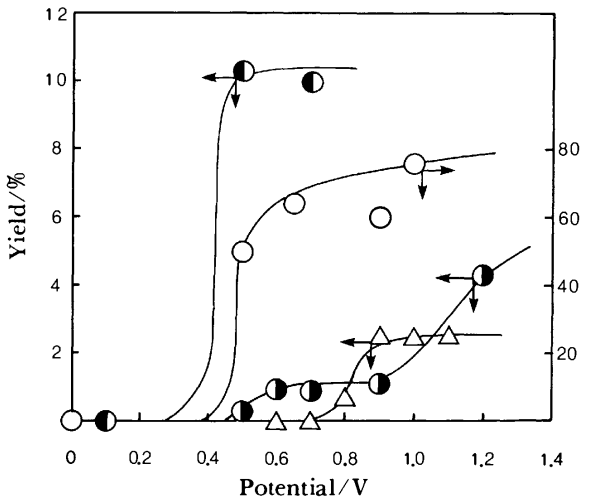

Fig. 6. Relation between the yield of crystals and the applied potential for electrocrystallization of substituted phthalocyanines.
○: Cyanophthalocyaninatocobalt(III), ◑: octamethyl-substituted derivative, ◐: octamethoxy-substituted derivative, △: thiocyanatophthalocyaninatocobalt(III).

through electrocrystallization was insoluble in organic solvents, introducing substituents to phthalocyanine ring probably made the solubility higher. For this reason, the crystals were partially soluble in the solution which made the yield low. The lower yield for the system having thiocyanato group as axial ligand could also be explained in terms of this. There are four structural isomers in the case of tetrasubstituted derivatives. They are generally more soluble than octasubstituted ones owing to the decrease of symmetry (except the increased solubility by the nature of functional group). But it is clear that the existence of isomers is a negative factor for electrocrystallization. Octasubstituted derivatives gave better results on electrocrystallization. The mechanism of electrocrystallization seemed therefore to be as follows.

$$\text{anode} \quad [Pc^{2-}Co^{3+}(CN)_2]^- \xrightarrow{-e} [Pc^{1-}Co^{3+}(CN)_2] \longrightarrow Pc^{2-}Co^{3+}CN + \cdot CN$$

$$\text{cathode} \quad K^+ \xrightarrow{+e} K$$

At first, $[Pc^{2-}Co^{3+}(CN)_2]^-$ anion was oxidized at the anode surface to produce $[Pc^{1-}Co^{3+}(CN)_2]$. This complex seemed to be unstable, and it immediately changed to $[Pc^{2-}Co^{3+}CN]$, and the CN radical changed to $(CN)_2$. On the other hand, metallic potassium deposited on the cathode. As crystal growth was observed only on the anode surface, this oxidation should occur on the crystal surface through the electron-transfer reaction in the crystals. However, stable phthalocyaninatocobalt(III) radical complexes such as $Pc^{1-}Co^{3+}Cl_2$ and $Pc^{1-}Co^{3+}Br_2$ were reported,[14] and no $Pc^{1-}Co^{3+}(CN)_2$ was obtained when $K^+[PcCo(CN)_2]^-$ was prepared from $Pc^{1-}Co^{3+}Cl_2$. This suggests strongly that $[Pc^{1-}Co^{3+}(CN)_2]$ should be unstable. Though $(CN)_2$ have not been detected yet, the mechanism described above is considered reasonable. The molecular arrangements and conductivities of crystals will be reported elsewhere.

Conclusion

A series of tetra- or octasubstituted phthalocyaninatocobalt(II) were synthesized, and the effect of substituent group on the oxidation was examined in terms of the Hammett's constant. A linear relationship between the oxidation potential of the ring and the Hammett's constant of substituent was confirmed for all cases of tetra-, octasubstituted derivatives and even for derivatives with different axial ligands. Electrocrystallization of phthalocyanine derivatives was initiated by the oxidation of the phthalocyanine ring, that was suggested from the effect of applied potential on the crystal yield for a series of substituted phthalocyanines.

This work was partially supported by a Grant-in-Aid for Scientific Researches No. 61103002 and for Scientific Research on Priority Area "Macromolecular Complexes No. 62612005" from the Ministry of Education, Science and Culture.

References

1) a) L. D. Rollmann and R. Iwamoto, *J. Am. Chem. Soc.*, **90**, 1455(1968); b) J. R. Darwent, P. Douglas, A. Harrimann, G. Porter, and M.-C. Richoux, *Coord. Chem. Rev.*, **44**, 83(1982); c) D. Wöhrle and G. Meyer, *Kontakte*, **3**, 38 (1985); d) C. D. Jaeger, F.-R. F. Fan, and A. J. Bard, *J. Am. Chem. Soc.*, **102**, 2592 (1980); e) A. B. P. Lever, P. C. Minor, and J. P. Wilshire, *Inorg. Chem.*, **20**, 2550(1981); f) A. B. P. Lever, S. R. Pickens, P. C. Minor, S. Licoccia, B. S. Ramaswamy, and K. Magnell, *J. Am. Chem. Soc.*, **103**, 6800 (1981); g) A. B. P. Lever and P. C. Minor, *Inorg. Chem.*, **20**, 4015 (1981); h) V. R. Shepard, Jr., and N. R. Armstrong, *J. Phys. Chem.*, **83**, 1268 (1979); i) A. B. P. Lever and J. P. Wilshire, *Inorg. Chem.*, **17**, 1145 (1978); j) T. M. Mezza,N. R. Armstrong, G. W. Litter, II, J. P. Iafalice, and M. E. Kenny, *J. Electroanal. Chem.*, **137**, 227(1982); k) O. R. Loutfy and Y. C. Cheng, *J. Phys. Chem.*, **74**, 2902 (1980); l) B. L. Wheeler, G. Nagasubramanian, A. J. Bard, L. A. Schechtmann, D. R. Dininny, and M. E. Kenny, *J. Am. Chem. Soc.*, **106**, 7404 (1984).

2) a) Y. Orihashi, N. Kobayashi, E. Tsuchida, H. Matsuda, H. Nakanishi, and M. Kato, *Chem. Lett.*, **1985**, 1617; b) Y. Orihashi, H. Ohno, E. Tsuchida, H. Matsuda, H. Nakanishi, and M. Kato, *ibid.*, **1987**, 601; c) E. Tsuchida, Y. Orihashi, N. Kobayashi, and H. Ohno, *Synth. Met.*, **15**, 201 (1986); d) Y. Orihashi, N. Kobayashi, H. Ohno, H. Matsuda, H. Nakanishi, and M. Kato, *ibid.*, **19**, 751 (1987).

3) A. B. P. Lever, S. Licoccis, K. Magnell, and B. S. Ramasnamy, *Adv. Chem. Ser.*, **201**, 237 (1982).

4) A. B. P. Lever and J. P. Wilshire, *Can. J. Chem.*, **54**, 2514 (1976).

5) a) A. B. P. Lever, *Adv. Inorg. Chem. Radiochem.*, **7**, 27 (1965); b) H. Tomoda, S. Saito, S. Ogawa, and S. Shiraishi, *Chem. Lett.*, **1980**, 1277.
6) J. Metz, O. Schneider, and M. Hanack, *Inorg. Chem.*, **23**, 1065 (1984).
7) B. N. Achar, G. M. Fohlen, and J. A. Parker, *J. Polym. Sci., Polym. Chem. Ed.*, **20**, 2773 (1982).
8) H. Shirai, A. Maruyama, K. Kobayashi, and N. Hojo, *Makromol. Chem.*, **181**, 575 (1980).
9) D. Wöhrle and G. Meyer, *Makromol. Chem.*, **181**, 2127 (1980); D. Wöhrle, *Tetrahydron Lett.*, **1979**, 227.
10) E. A. Cuellar and T. J. Marks, *Inorg. Chem.*, **20**, 3766 (1981).
11) C. Piechocki and J. Simon, *Nouveau J. Chim.*, **9**, 159 (1985).
12) J. Metz and M. Hanack, *J. Am. Chem. Soc.*, **105**, 828 (1983).
13) J. F. Myers, G. W. R. Canham, and A. B. P. Lever, *Inorg. Chem.*, **14**, 461 (1975).
14) D. Lexa and M. Reix, *J. Chim. Phys.*, **71**, 511 (1974).
15) A. Wolberg and J. Manassen, *J. Am. Chem. Soc.*, **92**, 2982 (1970).
16) D. W. Clark, N. S. Hash, and I. S. Wooley, *Inorg. Chim. Acta*, **19**, 129 (1976).
17) D. Lexa and M. Reix, *J. Chim. Phys.*, **71**, 517 (1974).
18) D. Wöhrle, personal communication in 1986.
19) A. Giraudeau, A. Louati, M. Gross, J. J. Andre, J. Simon, C. H. Su, and K. M. Kadish, *J. Am. Chem. Soc.*, **105**, 2917 (1983).
20) F. A. Carey and R. J. Sundberg, "Advanced Organic Chemistry," Plenum, New York (1984).
21) F. Beck, Ber. Bunsenges. *Phys. Chem.*, **77**, 35 (1973); K. Schmatz, S. Muralidharan, K. Madden, R. Fessenden, and G. Ferraudi, *Inorg.Chim. Acta*, **64**, L23 (1981).
22) A. Giraudeau, F.-R. F. Fan, and A. J. Bard, *J. Am. Chem. Soc.*, **102**, 5137 (1980).
23) A. B. P. Lever and J. P. Wilshire, *Inorg. Chem.*, **17**, 1145 (1978).
24) D. Dolphin, B. R. James, A. J. Murray, and J. R. Thornback, *Can. J. Chem.*, **58**, 1125 (1980).
25) V. Gutmann, "The Donor Acceptor Approach to Molecular Interaction," Plenum, New York (1978).
26) A. B. P. Lever and P. C. Minor, *Adv. Mol. Relax. Inter. Proc.*, **18**, 115 (1980).
27) A. Diaz, J. Metz, O. Schneider, and M. Hanack, *Synth. Met.*, **9**, 31 (1984).

 © 1987 The Chemical Society of Japan Bull. Chem. Soc. Jpn., 60, 3739—3750 (1987)

Oxidation of $(CD_3)_2\dot{C}X$ Radicals. I. Reaction of Propane and Isopropyl Radicals with Atomic Oxygen

Nobuaki WASHIDA
Division of Atmospheric Environment, The National Institute for Environmental Studies,
P.O. Tsukuba-gakuen, Ibaraki 305
(Received April 10, 1987)

The reaction of oxygen atoms with propane-1,1,1,3,3,3-d_6, $(CD_3)_2CH_2$, in a fast-flow system was studied with a photoionization mass spectrometer. Isopropyl-d_6 radicals, $(CD_3)_2\dot{C}H$, formed by the initial hydrogen abstraction at the 2-position were detected directly.

$$(CD_3)_2CH_2 + O(^3P) \rightarrow (CD_3)_2\dot{C}H + OH \quad (3)$$

The subsequent reaction of $(CD_3)_2\dot{C}H$ radicals with atomic oxygen proceeds by both an deuterium abstraction (61%) and an oxygen addition reaction (39%). The product in the deuterium abstraction was CD_2CHCD_3 and those in the oxygen addition were $(CD_3)_2CO$ (18%) and CD_3CHO (21%).

$$(CD_3)_2\dot{C}H + O(^3P) \rightarrow \begin{cases} CD_2CHCD_3 + OD & (4a) \\ (CD_3)_2CO + H & (4b) \\ CD_3CHO + CD_3 & (4c) \end{cases}$$

Competition experiments show that $(CD_3)_2\dot{C}H$ radicals react (0.029 ± 0.004) times as fast with O_2 as with $O(^3P)$. In the presence of an excess of O_2, CD_2CHCD_3 was observed in decreased yield (20%) and $(CD_3)_2CO$ and CD_3CHO increased to 32 and 44%, respectively. The rate data for Reaction 3 were fitted by an Arrhenius expression:

$$k_3 = (2.0^{+1.0}_{-0.7}) \times 10^{-10} \exp[-(6086 \pm 392 \text{ cal mol}^{-1})/RT]^{\dagger}$$

$cm^3 molecule^{-1} s^{-1}$ (381—627 K). The rate constant of Reaction 3 obtained from the yields of products was 7.9×10^{-15} $cm^3 molecule^{-1} s^{-1}$ at 298K.

Reaction of alkyl radicals with atomic oxygen, $O(^3P)$, has been investigated for t-C_4H_9[1] and *cyclo*-C_6H_{11}[2] using the technique of discharge-flow-photoionization mass spectrometry. In the case of t-C_4H_9, it has been suggested[1] that the reaction of $O(^3P)$ with t-C_4H_9 is very fast, and that the large rate constant was explained by the hydrogen abstraction from nine equivalent hydrogen atoms in the t-C_4H_9 radical (formation of isobutene was 80% of the total reaction). Formation of acetone (20%) by the addition of an oxygen atom to the radical was observed as an alternative channel. Similar results have been obtained in the reaction of *cyclo*-$C_6H_{11}+O(^3P)$.[2] Formation of the two types of products (olefins by hydrogen abstraction and aldehydes or ketones by the oxygen addition reaction) has also been reported in reactions of C_3H_7+O,[3,4] t-C_4H_9+O,[4-6] and *neo*-$C_5H_{11}+O$,[6] although Hoyerman and Sievert[7] reported no formation of olefins.

The primary attack of ground state $O(^3P)$ atoms to propane is expected to be hydrogen abstraction producing a propyl radical:

$$O(^3P) + C_3H_8 \rightarrow C_3H_7 + OH \quad (1)$$

Propyl radicals should react with oxygen atoms very rapidly and produce several products:

$$C_3H_7 + O(^3P) \rightarrow \text{Products} \quad (2)$$

In the discharge-flow experiments reported previously,[3,4] the formation of CH_3CHO, $(CH_3)_2CO$, C_3H_6, C_2H_5CHO, C_2H_6, C_2H_4, CH_2O, CH_4, CO_2, H_2O, and H_2 (including both primary and secondary products) has been reported.

In the previous $O+C_3H_8$ studies, however, it was not clear whether propyl or isopropyl radicals (or both) were produced by Reaction 1. Also it was not possible to clarify the reaction mechanism of the $O(^3P)+C_3H_7$ reaction. In the present study, the reaction of oxygen atoms with propane-1,1,1,3,3,3-d_6, $(CD_3)_2CH_2$, is studied by using a photoionization mass spectrometer[8,9] coupled with a fast-flow reactor. In this case the primary attack of O atoms can be identified by measuring the mass number of the propyl radicals produced. Subsequent reactions of propyl radicals with atomic and molecular oxygen are then analyzed.

Experimental

A schematic diagram of a fast-flow reactor and a photoionization mass spectrometer is shown in Fig. 1. Most of the components are as described previously[10-12] except for two improvements; 1) three diffusion pumps (10, 4, and 6 inches in diameter for A, B, and C, respectively) with liquid nitrogen traps were used to evacuate the ionization chamber, the quadrupole mass filter, and the detector region; 2) a 0.4 mm (in diameter) Pyrex orifice was used to sample the gases into the ionization region. About 5×10^4 counts s^{-1} of signal was obtained for 1 mTorr NO(1 Torr=133.322 Pa) in the flow reactor when it was ionized by a Kr lamp having a MgF_2 window.

Oxygen atoms were generated by a microwave discharge in a helium-oxygen mixture (0.05—2% in helium), and their concentration was determined by titration with NO_2 according to the reaction $O+NO_2 \rightarrow NO+O_2$. Then known partial

†1 cal=4.184 J.

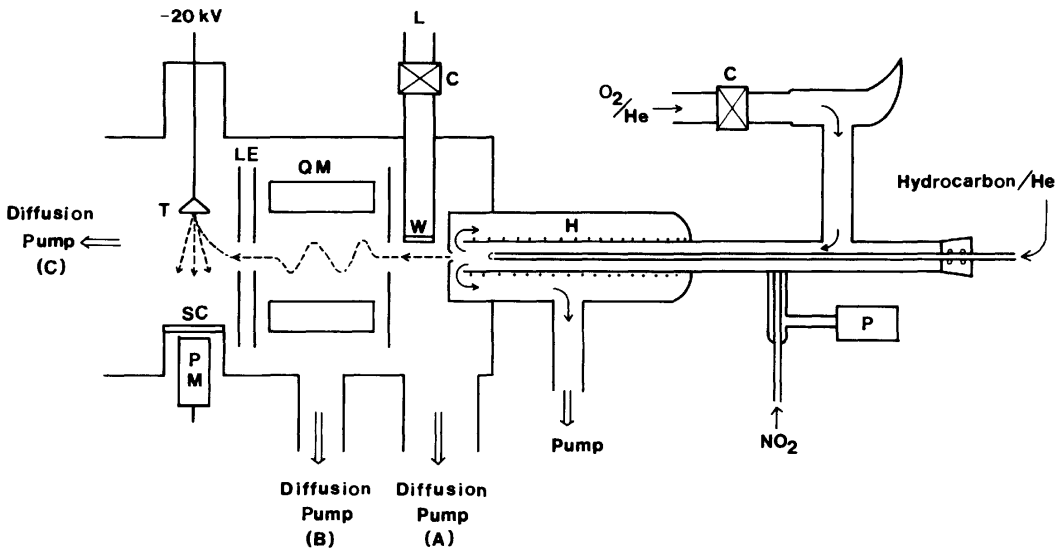

Fig. 1. Schematic diagram of the apparatus; C, microwave cavity; P, MKS Baratron pressure gauge; H, coiled Nichrome wire heater; L, VUV lamp; W, window; QM, quadrupole mass filter; LE, lens; T, Al coated Stainless steel target; SC, Al coated plastic scintillator; PM, photomultiplier.

pressures of NO were added to calibrate the instrument sensitivity. Propane-1,1,1,3,3,3-d_6, $(CD_3)_2CH_2$, was diluted in helium (about 10% in helium) and entered the main flow through a movable inlet with six small radially directed holes. Total and partial pressures of gases were measured by a capacitance manometer (MKS Baratron 170M-35). These pressures were converted to concentrations by using a separate calibration of the flow as a function of pressure and temperature. The linear flow velocity measured with a bubble meter was 16.5 m s^{-1} at 2 Torr, 19.9 m s^{-1} at 4 Torr, and 21.4 m s^{-1} at 6 Torr at 298K. The various photoionization lamps used to ionize radicals and molecules were powered by a microwave discharge. Most of the measurements were done at room temperature, 298±3K. Some experiments were carried out at high temperature, 420—630K. The reaction zone was heated with a coiled Nichrome wire heater. Temperature was measured with a pair of Alumel Chromel thermocouples suspended in the central reactant-inlet tube. Temperature uniformity was ±2K.

The gases O_2 (Nippon Sanso, 99.99%), He (Nippon Sanso, 99.9999%), NO (Matheson, 99.0%), NO_2 (Matheson, 99.5%) were used without further purification. The propane-1,1,1,3,3,3-d_6, $(CD_3)_2CH_2$, (98%) was from Merck Sharp & Dohme. Part of the $(CD_3)_2CH_2$ used was synthesized[13] in this laboratory from $(CD_3)_2CO$. Both $(CD_3)_2CH_2$ from Merck Sharp & Dohme and the synthesized material contained 1—2% of olefins (mostly CD_2CHCD_3). These were removed by passing the sample through a solution of $KMnO_4$ and drying on a column of $CaCl_2$. After this purification, the CD_2CHCD_3 contained in the $(CD_3)_2CH_2$ was less than 0.005%. Oxygen-18($^{36}O_2$ about 20%) from Merk Sharp & Dohme was analyzed by the mass spectrometer, and the $^{36}O_2$ content was determined to be 19.2±0.7%. All measurements were done under the condition $[O] > 0.5[(CD_3)_2CH_2]$.[14]

Results

A. Radicals and Molecules Detected in the Reaction of $(CD_3)_2CH_2+O(^3P)$. Preliminarily, the measurement of radicals and molecules produced in the reaction of C_3H_8+O was investigated. A signal at $m/z=43$ was detected by using a Xe resonance lamp with a sapphire window (8.44 eV) as a photoionization light source. When a Kr lamp with a CaF_2 window (10.03 eV) was used, signal at $m/z=42$ and 58 were also observed. The signal at $m/z=44$ was observed in addition to the above signals when a Kr lamp with a MgF_2 window (10.03 and 10.64 eV) was used. Mass spectra of these signals are shown in Fig. 2. Ionization potentials together with values of heats of formation for possible radicals and molecules are listed in Table 1. The signal at $m/z=43$ shown in Fig. 2c should be from C_3H_7 radicals produced in the reaction of C_3H_8+O.[29] However, it was not possible to identify the radical as either an *n*-propyl or an isopropyl radical. The signal at $m/z=42$ might be from C_3H_6 and/or CH_2CO and at $m/z=58$ from $(CH_3)_2CO$ and/or C_2H_5CHO produced by the reaction of propyl radicals with the excess of oxygen atoms.[29] The signal at $m/z=44$ shown in Fig. 2a should be from CH_3CHO.[29] In addition to the signals shown in Fig. 2, signals for CH_3 (Kr lamp), C_2H_4 (Ar lamp), and CH_2O (Ar lamp) were observed at $m/z=15$, 28, and 30, respectively. Although the radicals and molecules were observed as expected, the kinetic analysis of the reaction is not possible because of the failure to determine the branching ratio for the formation of *n*-propyl and isopropyl radicals.

Isopropyl-d_6 radicals, $(CD_3)_2\dot{C}H$ were observed at $m/z=49$ when oxygen atoms reacted with propane-1,1,1,3,3,3-d_6, $(CD_3)_2CH_2$. The radical was detected by using a Xe resonance lamp with a sapphire window (8.44 eV). The mass spectra are shown in Fig. 3. No significant signal of propyl-1,1,3,3,3-d_5 radicals, $\cdot CD_2CH_2CD_3$, was observed at $m/z=48$. Other prod-

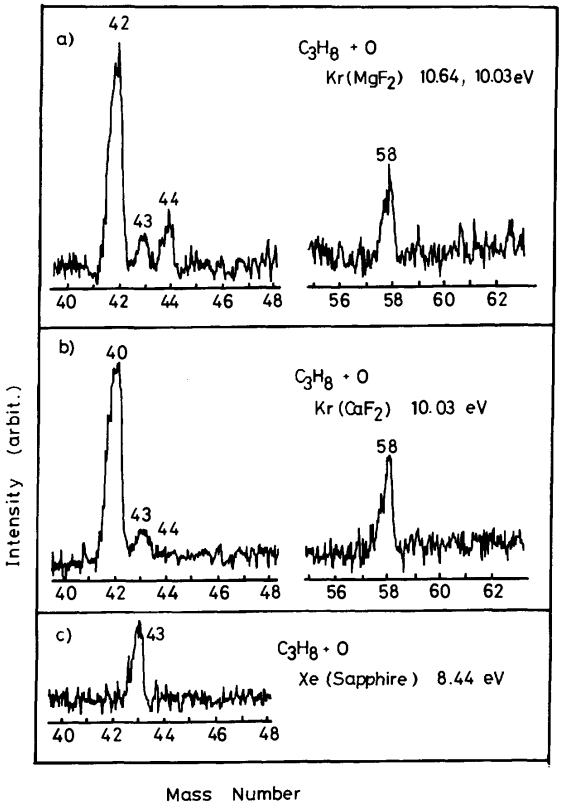

Fig. 2. Mass spectra of the reaction products produced in O+C_3H_8. Kr lamps having a MgF_2 window (10.64 and 10.03 eV) and a CaF_2 window (10.03 eV), and a Xe lamp having a sapphire window (8.44 eV) were used. The conditions: $[O]_0$= 3.6 mTorr; $[C_3H_8]_0$=1.4 mTorr; reaction time 4.5 ms; total pressure 4.3 Torr.

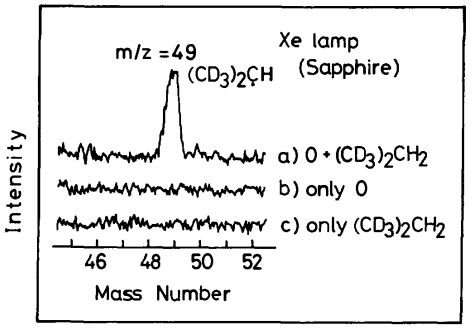

Fig. 3. Mass spectra of the $(CD_3)_2\dot{C}H$ radical produced in O+$(CD_3)_2CH_2$. A Xe lamp with a sapphire window (8.44 eV) was used for the photoionization. The conditions: partial pressure (mTorr), $[O]_0$=3.7, $[(CD_3)_2CH_2]$=1.5; reaction time=4.5 ms; total pressure=4.3 Torr.

ucts produced by subsequent reactions and the parent molecule were not photoionized by this lamp.

$$(CD_3)_2CH_2 + O(^3P) \rightarrow (CD_3)_2\dot{C}H\ (m/z=49) + OH \quad (3)$$

From the ratio of the signal at m/z=49 to the back ground noise at m/z=48, it was concluded that more than 95% of the total reaction of $(CD_3)_2CH_2$+O forms $(CD_3)_2\dot{C}H$ radicals by abstraction of the 2-hydrogen from $(CD_3)_2CH_2$.

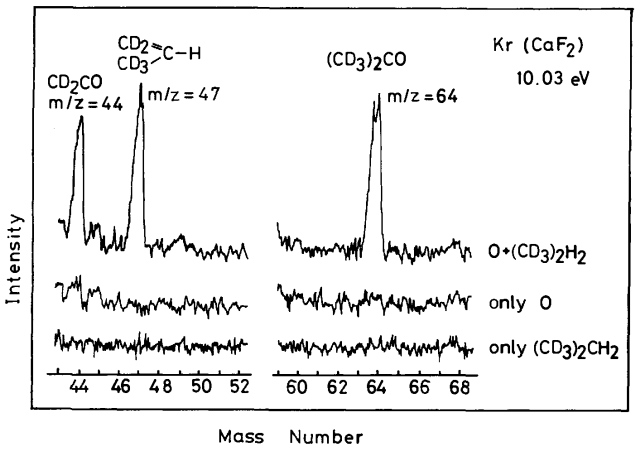

Fig. 4. Mass spectra of the reaction products produced in O+$(CD_3)_2CH_2$. A Kr lamp having a CaF_2 window (10.03 eV) was used for the photoionization. The conditions: partial pressure (mTorr), $[O]_0$=3.5, $[(CD_3)_2CH_2]$=0.7; reaction time=4.5 ms; total pressure=4.3 Torr.

Table 1. Ionization Potentials and Heat of Formations of Radicals and Molecules[a)]

m/z	Molecule	I.P. / eV	ΔH^0_{f298} (g) / kcal mol^{-1}
42	C_3H_6	9.7	4.88
42	CH_2CO	9.6	−14.6
43	n-C_3H_7	8.1	20.7
43	i-C_3H_7	7.5	17.6
44	C_3H_8	11.0	−24.8
44	CH_3CHO	10.2	−39.7
48	$(CH_3)_2CO$	9.7	−52.0
58	C_2H_5CHO	9.9	−45.9

a) Quoted from Ref. 28.

Possible products produced by the reaction of O+$(CD_3)_2\dot{C}H$ are as follows:

$$(CD_3)_2\dot{C}H + O \rightarrow \begin{cases} CD_2CHCD_3\ (m/z=47) + OD & (4a) \\ (CD_3)_2CO\ (m/z=64) + H & (4b) \\ CD_3CHO\ (m/z=47) + CD_3 & (4c) \end{cases}$$

where Reaction 4a is deuterium abstraction, 4b and 4c result from the addition reaction of an oxygen atom to carbon. Signals at m/z=44, 47, and 64 were observed when the Kr lamp having a CaF_2 window (10.03 eV) was used (see Fig. 4). Among the signals observed, the signal at m/z=64 should be from $(CD_3)_2CO$. The signal at m/z=47 should be from CD_2CHCD_3 not from CD_3CHO, since as shown in Table 1, the ionization potential of propene is 9.7 eV, while that of acetaldehyde is 10.2 eV. The signal at m/z=44 would be from ketene, CD_2CO, produced in the secondary reaction of CD_3CHO+O.[29)]

As mentioned before, since acetaldehyde was observed in the reaction of O+C_3H_8, CD_3CHO (m/z=47) should be observed in the present case when the Kr lamp having a MgF_2 window (10.03 and 10.64 eV) was used. However, it is difficult to distinguish CD_2-$CHCD_3$ and CD_3CHO, because these have the same

mass number. In order to distinguish between these two molecules, $(CD_3)_2CH_2$ was reacted with ^{18}O (19.2% of $^{36}O_2$ in $^{32}O_2$ was diluted in helium and discharged by microwave). Mass spectra observed in the region from m/z=43 to 53 by using the Kr lamp with the MgF_2 window are shown in Fig. 5. Possible molecules corresponding to the significant signals observed are listed in Table 2. Signals of ketene, CD_2CO, propene, CD_2CHCD_3, and acetaldehyde, CD_3CHO was observed as expected. In addition, the signal of CD_3CDO was observed. CD_3CDO might be a secondary product in the reaction of CD_2CHCD_3+O (reaction mechanisms will be discussed later). Among the above signals, the signal at m/z=49 ($CD_3CH^{18}O$) can be used to monitor the concentration of acetaldehyde produced in Reaction 4c because, as will be described later, the concentration of $(CD_3)_2\dot{C}H$ radicals is in the steady-state concentration under the present experimental conditions (the signal intensity of $(CD_3)_2\dot{C}H$ is independent of the reaction time), while the concentration of $CD_3CH^{18}O$ increases linearly with reaction time. In this way the signals from $CD_3C^{18}O$ and $(CD_3)_2\dot{C}H$ can be distinguished.

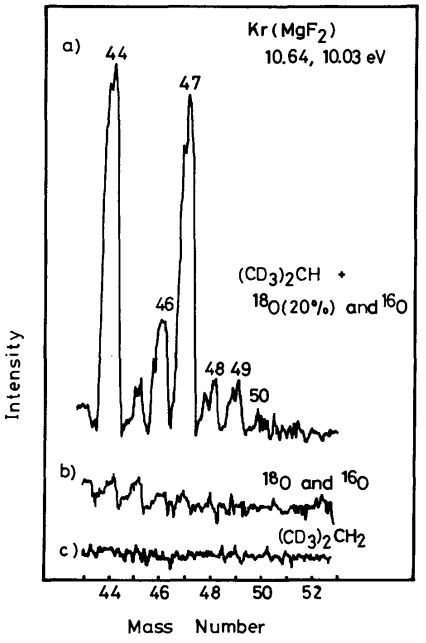

Fig. 5. Mass spectra of the reaction products produced in $(CD_3)_2CH_2$+^{18}O(20%)+^{16}O(80%). A Kr lamp with a MgF_2 window (10.64 and 10.03 eV) was used to photoionize molecules. The conditions: partial pressure (mTorr), $[O]_0$=3.4, $[(CD_3)_2CH_2]$= 0.9; reaction time=4.5 ms; total pressure=4.3 Torr.

Table 2. Signals Observed and Possible Molecules in the Reaction of ^{18}O+$(CD_3)_2CH_2$ (19.2%) and ^{16}O+ $(CD_3)_2CH_2$ (80.8%) over the Mass Number Region from 43 to 53. The Kr Lamp with a MgF_2 Window Was Used as a Photoionization Light Source

m/z	Possible molecule
44	CD_2CO
45	Isotope (^{13}C) signal of m/z=44
46	$CD_2C^{18}O$
47	CD_2CHCD_3, CD_3CHO
48	CD_3CDO, isotope (^{13}C) signal of m/z=47
49	$CD_3CH^{18}O$, $(CD_3)_2CH$ radical
50	$CD_3CD^{18}O$

B. Competition between $O(^3P)$ and O_2 for $(CD_3)_2\dot{C}H$. The time dependence of the $(CD_3)_2\dot{C}H$ radical signal was measured by changing the reaction time of $(CD_3)_2CH_2$ and oxygen atom. No significant change of signal was observed for the conditions of 3—6 mTorr of oxygen atoms, 1 mTorr of $(CD_3)_2CH_2$, and 0.5—10 ms of reaction time. When the concentration of $(CD_3)_2CH_2$ was increased, the signal for $(CD_3)_2\dot{C}H$ increased in proportion to the $(CD_3)_2CH_2$ concentration. This means that Reaction 4 is very rapid and that $(CD_3)_2\dot{C}H$ radicals are in their steady-state concentration

$$[2\text{-pr}]_{ss} = \frac{k_3}{k_4}[P]. \tag{5}$$

Here $[2\text{-pr}]_{ss}$ and [P] represent the steady-state concentration of $(CD_3)_2\dot{C}H$ radicals and the initial concentration of $(CD_3)_2CH_2$, respectively. When molecular oxygen was added to the system, the steady-state concentration of $(CD_3)_2\dot{C}H$ decreased. This decrease is caused by the competition between $O(^3P)$ and O_2 for $(CD_3)_2\dot{C}H$ radicals and the competition results in a Stern-Volmer-type of equation.

$$\frac{[2\text{-pr}]^0_{ss}}{[2\text{-pr}]_{ss}} = 1 + \frac{k_7[O_2]}{k_4[\bar{O}]}, \tag{6}$$

where the superscript zero refers to the conditions in the absence of O_2 and k_7 is the effective second-order rate constant for the reaction of $(CD_3)_2\dot{C}H+O_2$.

$$(CD_3)_2\dot{C}H + O_2 \rightarrow \text{Products} \tag{7}$$

The results of the O_2 addition for two different conditions are presented in Fig. 6. The average concentration of oxygen atoms, $[\bar{O}]$, was calculated[36] using a stoichiometric factor of n=6. The correction for oxygen-atom consumption was 0.5% or less. The concentration of O_2 was calculated from $[O_2]_{added}+[O_2]_0 - 1/2[O]_0$, where $[O_2]_0$ and $[O]_0$ refer to the original concentraiton of O_2 in the O_2/He mixture before the discharge, and the original oxygen-atom concentration produced in the O_2/He discharge, respectively. The value of $[O_2]_0-1/2[O]_0$ corresponds to the concentration of O_2 surviving from the O_2/He discharge. The two points shown on the left-hand side in Fig. 6 are obtained with just $[O_2]_0-1/2[O]_0$ present.

Values for $[2\text{-pr}]^0_{ss}$ were determined by plotting $([2\text{-pr}]_{ss})^{-1}$ against $[O_2]/[\bar{O}]$ and then determining $([2\text{-pr}]^0_{ss})^{-1}$ from the intercept of a least-square fit in order to remove the effect of the O_2 surviving from the discharge. The value for k_7/k_4 calculated from the slope in Fig. 6 is 0.029±0.004. Error limits due to the scattering of plots were calculated by the least square with

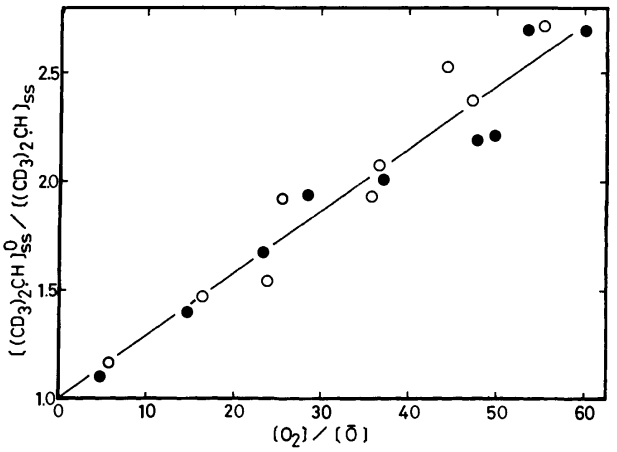

Fig. 6. Stern-Volmer plot for the competition between O_2 and $O(^3P)$ for the $(CD_3)_2CH$ radicals. Conditions for the open symbols: partial pressure (mTorr), $[O]_0$=3.32, $[\bar{O}]$=3.30, $[(CD_3)_2CH_2]$=1.31, $[O_2]_0$=19.44; total pressure 4.151 Torr; reaction time=4.46 ms. Conditions for the filled symbols: partial pressure (mTorr), $[O]_0$=2.99, $[\bar{O}]$=2.97, $[(CD_3)_2CH_2]$=1.003, $[O_2]_0$=15.43; total pressure= 4.32 Torr; reaction time=4.51 ms. $[O_2]$ was calculated from $[O_2]_{added.}+[O_2]_0-1/2[O]_0$.

the 95% confidence limits.

C. Yields of CD_2CHCD_3 and $(CD_3)_2CO$. The dependence of the CD_2CHCD_3 (m/z=47) and $(CD_3)_2CO$ (m/z=64) signals on the reaction time was measured by using a Kr lamp having a CaF_2 window and is shown in Fig. 7. The signal of $(CD_3)_2CO$ (open triangles) rises linearly with reaction time, while the signal of CD_2CHCD_3 (solid circles) increased but not linearly. The nonlinear increase of CD_2CHCD_3 with reaction time results from the consumption of CD_2CHCD_3 by Reaction 8.

$$CD_2CHCD_3 + O(^3P) \rightarrow \text{Products} \qquad (8)$$

If CD_2CHCD_3 is produced in Reaction 3 followed by Reaction 4a and consumed in Reaction 8, the concentration of CD_2CHCD_3 observed is given by Eq. 9, assuming that Reaction 4 is much faster than Reaction 3,

$$[CD_2CHCD_3] = \frac{k_3 f_{4a}[P]_0}{(k_8 - k_3)} (e^{-k_3[\bar{O}]t} - e^{-k_8[\bar{O}]t}) \qquad (9)$$

where f_{4a}, $[P]_0$, and $[\bar{O}]t$ represent the fraction of Reaction 4a in the total reaction of $(CD_3)_2\dot{C}H+O$, the original concentration of $(CD_3)_2CH_2$, and the product of the average oxygen-atom concentration and the reaction time,[36] respectively. In the present study, since the rate constant for Reaction 3 is very small, 7.91×10^{-15} cm^3 molecule^{-1} s^{-1} at 298K as will be described later, and the rate of Reaction 8, $(3.3—4.50)\times10^{-12}$ cm^3 molecule^{-1} s^{-1} [16,38] for $O+C_3H_6$, is 500 times faster than that of Reaction 3, the value of $\exp(-k_3[\bar{O}]t)$ is nearly 1 and k_8-k_3 is nearly equal to k_8 under the present experimental conditions; $[\bar{O}]t<1.5\times10^{12}$ molecule s cm^{-3}. Thus Eq. 9 is simplified to Eq. 10.

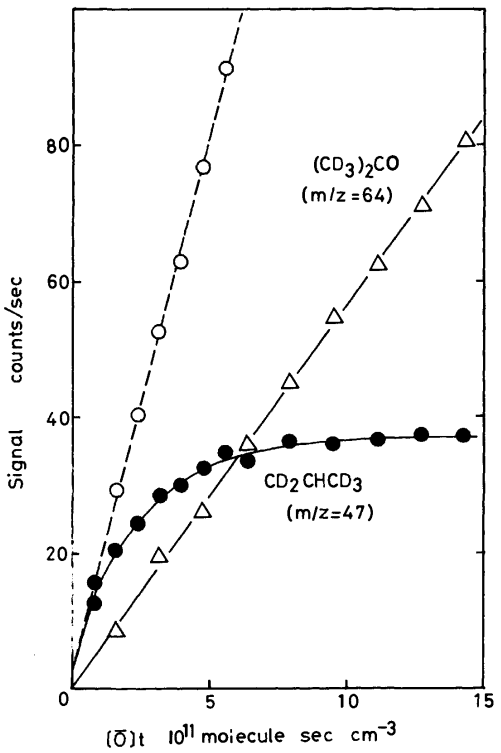

Fig. 7. Time dependence of CD_2CHCD_3 (solid circles) and $(CD_3)_2CO$ (open triangles) signals produced in the $O+(CD_3)_2CH_2$ reaction. A Kr lamp with a CaF_2 window (10.03 eV) was used for the photoionization. The conditions: partial pressure (mTorr), $[O]_0$=5.34, $[(CD_3)_2CH_2]$=0.95, $[O_2]_0$=24.60; total pressure=4.46 Torr. $[O_2]_0$ refers the amount of O_2 added to the O_2/He discharge. Reaction times used were 0.5—8.1 ms. Corrections for $[\bar{O}]$ were 1% or less. The CD_2CHCD_3 signals are corrected for the subsequent reaction to give $[CD_2CHCD_3]_T$ as indicated by open circles.

$$[CD_2CHCD_3] = \frac{f_{4a}k_3}{k_8}[P]_0(1-e^{-k_8[\bar{O}]t}) \qquad (10)$$

Equation 10 shows the CD_2CHCD_3 approaches a constant concentration at long reaction time. When the plots of CD_2CHCD_3 shown in Fig. 6 are fitted to Eq. 10, a value for k_8 of $(4.06\pm0.18)\times10^{-12}$ cm^3 molecule^{-1} s^{-1} was calculated, which agrees well with the reported rate constants for $O+C_3H_6$.[16,38] The indicated errors due to the scattering of plots were calculated by the least square with the 95% confidence limits. The best fit line for Eq. 10 is shown as a solid line in Fig. 7. The total amount of CD_2CHCD_3 produced by Reaction 4a, $[CD_2CHCD_3]_T$, is given by Eq. 11,

$$[CD_2CHCD_3]_T = f_{4a}k_3[P]_0[\bar{O}]t \qquad (11)$$

Therefore, the total amount of CD_2CHCD_3 can be calculated by multiplying each observed CD_2CHCD_3 signal by $k_8[\bar{O}]t[1-\exp(-k_8[\bar{O}]t)]^{-1}$. These corrected points are shown as open circles in Fig. 7, and they are represented by the dashed straight line. The ratio of the slope of the dashed straight line to that for $(CD_3)_2CO$ is 2.8. The relative sensitivity of the photoi-

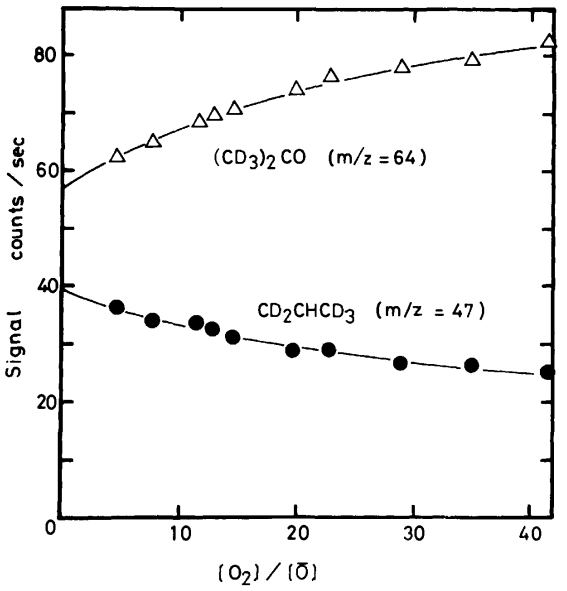

Fig. 8. Change of signals of CD_2CHCD_3 and $(CD_3)_2CO$ with the addition of O_2. Conditions: partial pressure (mTorr) $[O]_0$=5.34, $[\bar{O}]$=5.32, $[(CD_3)_2CH_2]$=0.95, $[O_2]_0$=27.27; reaction time= 6.30 ms; total pressure=4.46 Torr. $[O_2]$ was calculated from $[O_2]_{added.}+[O_2]_0-1/2[O]_0$. The points shown on the left-hand side are obtained from just $[O_2]_0-1/2[O]_0$ (no $[O_2]_{added.}$).

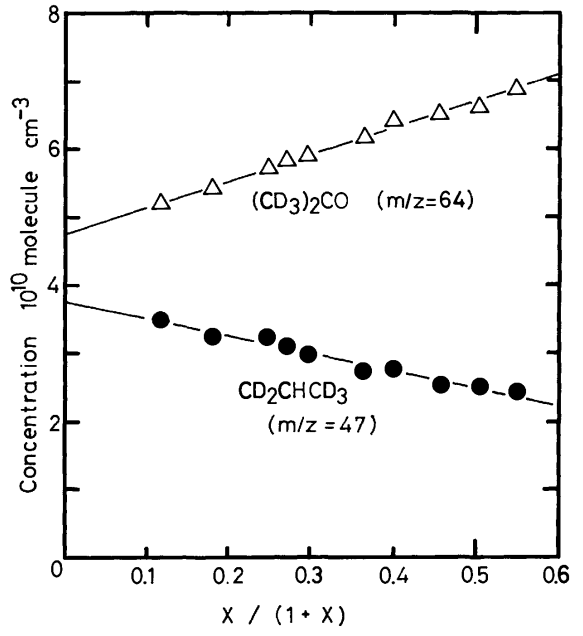

Fig. 9. The absolute concentrations of CD_2CHCD_3 and $(CD_3)_2CO$ are plotted against $X/(1+X)$ (see the text). Conditions are the same as in Fig. 8.

onization mass spectrometer for NO, C_3H_8, and $(CH_3)_2CO$ was mesured as 1 : 7.1 : 8.1 by using a Kr lamp (CaF_2). Assuming that the sensitivities of CD_2CHCD_3 and $(CD_3)_2CO$ are equal to those of C_3H_8 and $(CH_3)_2CO$, respectively, the ratio of the rate of formation of these two products was CD_2CHCD_3: $(CD_3)_2CO$=3.2 : 1 for the above conditions. Corrections for the consumption of acetone in the reactor is not important because the rate of the O+acetone reaction is very slow at room temperature[39] (5—7×10^{-16} cm^3 $molecule^{-1}s^{-1}$).

The effect of the O_2 surviving from the O_2/He discharge on the yield of products might not be neglected. The CD_2CHCD_3 and $(CD_3)_2CO$ signals were measured when molecular oxygen was added to the system. The signal of CD_2CHCD_3 decreased and that of $(CD_3)_2CO$ increased when O_2 was added, as shown in Fig. 8. The two points on the left-hand side are obtained with only the O_2 surviving from the O_2/He discharge (no addition of O_2). In Fig. 8, CD_2CHCD_3 is in its steady-state concentration and $(CD_3)_2CO$ is not under these experimental conditions. If the fraction of CD_2CHCD_3 produced in Reaction 7 is represented by s_{7a}, the steady-state concentration of CD_2CHCD_3 is given by Eq. 12 when both $O(^3P)$ and O_2 are present, where X is defined in Eq. 13.

$$[CD_2CHCD_3]_{ss} = \left\{f_{4a} + \frac{(s_{7a}-f_{4a})X}{1+X}\right\}\frac{k_3}{k_8}[P] \quad (12)$$

$$X = \frac{k_7}{k_4}\frac{[O_2]}{[\bar{O}]} \quad (13)$$

Similarly, the concentration of $(CD_3)_2CO$ at reaction time t is represented by Eq. 14;

$$[(CD_3)_2CO] = \left\{f_{4b} + \frac{(s_{7b}-f_{4b})X}{1+X}\right\}k_3[P][\bar{O}]t \quad (14)$$

where s_{7b} refers to the fraction of $(CD_3)_2CO$ produced in Reaction 7. Since the ratio of k_7/k_4 was determined previously, the concentrations of CD_2CHCD_3 and $(CD_3)_2CO$ can be plotted against $X/(1+X)$, as are shown in Fig. 9. The absolute concentrations of CD_2CHCD_3 and $(CD_3)_2CO$ were calculated using the instrumental sensitivities to propylene, C_3H_6 and acetone, $(CH_3)_2CO$, as measured by adding known partial pressures of both molecules to the reactor. Since the initial concentration of $(CD_3)_2CH_2$ and reaction time are known, values for f_{4a} and f_{4b} can be determined from the intercepts of the two lines and those for s_{7a} and s_{7b} are determined from the slopes. Here the value for k_3 of 7.91×10^{-15} cm^3 $molecule^{-1}s^{-1}$ was used, as will be discussed later, and the value for k_8 of 4.06×10^{-12} cm^3 $molecule^{-1}s^{-1}$ was used. Values obtained are (0.61±0.07), (0.17±0.01), (0.20±0.02), and (0.31±0.02), for f_{4a}, f_{4b}, s_{7a}, and s_{7b}, respectively. The indicated errors due to the scattering of plots were calculated by the least square with the 95% confidence limits.

D. Yield of CD_3CHO. The dependence of the signal at m/z=49 shown in Fig. 4 on the reaction time was measured by using a Kr lamp having a MgF_2 window and is shown in Fig. 10. The signal at m/z=66, $(CD_3)_2C^{18}O$, is also plotted as a reference. The signal at m/z=49 increased with reaction time but the increase was not linear. The nonlinear increase results

from the consumption of $CD_3CH^{18}O$ by Reaction 15, and so the concentration of $CD_3CH^{18}O$ can be expressed by Eq. 16,

$$CD_3CHO + O(^3P) \rightarrow \text{Products} \quad (15)$$

$$[CD_3CH^{18}O] = \frac{0.192\, f_{4c} k_3}{k_{15}} [P](1-e^{-k_{15}[\bar{O}]t}) \quad (16)$$

where the value of 0.192 represents the fraction of $^{18}O(^3P)$ in the sum of $^{18}O(^3P)$ and $^{16}O(^3P)$. When the measured values of $CD_3CH^{18}O$ shown in Fig. 10 are fitted to Eq. 16, a value for k_{15} of $(5.6\pm0.5)\times10^{-13}$ cm^3 molecule^{-1} s^{-1} was calculated, which agrees well with the reported rate constants for $O+CH_3CHO$,[16,33,40] $(4.3—5)\times10^{-13}$ cm^3 molecule^{-1} s^{-1}. The indicated errors due to the scattering of plots were calculated by the least square with the 95% confidence limits. The best fit line for Eq. 16 is shown as a solid line in Fig. 10. The large intercept results from the signal due to $(CD_3)_2\dot{C}H$ radicals. As described before, the $(CD_3)_2\dot{C}H$ radicals should be in the steady-state concentration and the signals of $(CD_3)_2\dot{C}H$ are independent of the reaction time under the experimental conditions shown in Fig. 10. Each signal at m/z=49 minus the intercept is taken to be the signal of $CD_3CH^{18}O$. The total amount of $CD^3CH^{18}O$ produced in Reaction 4c, $[CD_3CH^{18}O]_T$, can be calculated by multiplying each observed $CD_3CH^{18}O$ signal by $k_{15}[\bar{O}]t[1-\exp(-k_{15}[\bar{O}]t)]^{-1}$. These corrected points are shown as open circles in Fig. 10, and they are represented by the dashed straight line. The ratio of the slope of the dashed line to that for $(CD_3)_2C^{18}O$ is 0.12. The relative sensitivity of the photoionization mass spectrometer for CH_3CHO, and $(CD_3)_2CO$ was measured as 1:9.87 by using a Kr lamp with a MgF_2 window. The ratio of the rate of formation of these two products was estimated to be $CD_3CH^{18}O$: $(CD_3)_2C^{18}O$=1 : 0.86 for the above conditions.

Signals at m/z=49 and 66 were measured when molecular oxygen containing 19.2% of $^{36}O_2$ in O_2 was added to the system. The results are listed in Table 3. The signal at m/z=66, $(CD_3)_2C^{18}O$, increased with addition of O_2 but the apparent signal at m/z=49 was nearly constant. As shown in Fig. 10, the signal at m/z=49 consists of $CD_3CH^{18}O$ and $(CD_3)_2\dot{C}H$. Between them, the signal of $(CD_3)_2\dot{C}H$ should decrease by the addition of O_2. This decrease is given by Eq. 6. Since the value for k_7/k_4 of 0.029 was determined previously and the signal intensity for the steady-state concentration of $(CD_3)_2\dot{C}H$ ($[2\text{-pr}]_{ss}$=17.2 counts s^{-1}) under the condition of $[O_2]/[\bar{O}]$=3.66 was determined from the intercept of the line in Fig. 10, the signal intensity for $[2\text{-pr}]^0_{ss}$, of 19.2 counts s^{-1} was calculated by Eq. 6. Using this value of $[2\text{-pr}]^0_{ss}$, the signal intensity for $[2\text{-pr}]_{ss}$ was calculated for each $[O_2]/[\bar{O}]$ by Eq. 6 as is shown in Table 3. The signal for $CD_3CH^{18}O$ was obtained from the difference between the total signal at m/z=49 and the calculated signal of $[2\text{-pr}]_{ss}$.

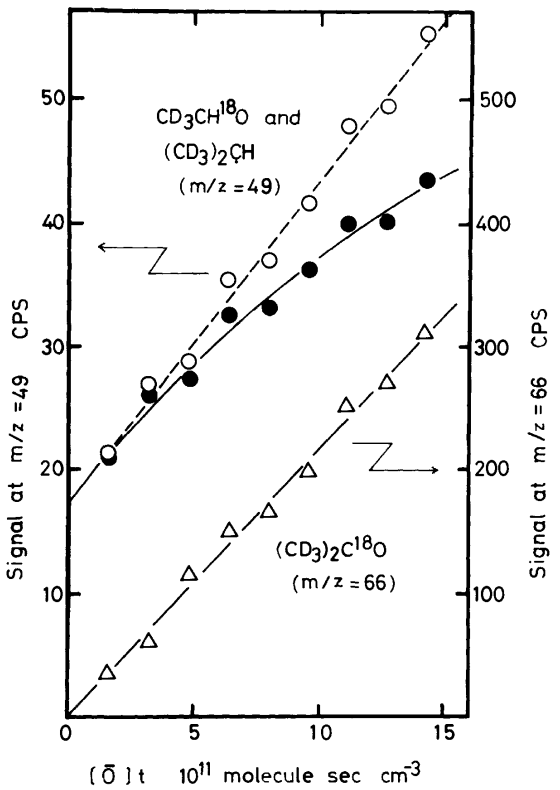

Fig. 10. Time dependence of $CD_3CH^{18}O$ (solid circles) and $(CD_3)_2C^{18}O$ (open triangles) signals produced in the $^{18}O+(CD_3)_2CH_2$ reaction. 19.2% of $^{36}O_2$ in O_2 was diluted in He and discharged. A Kr lamp with a MgF_2 window (10.64 and 10.03 eV) was used for the photoionization. The conditions: partial pressure (m Torr), $[O]_0$=5.42, $[(CD_3)_2CH_2]$=2.37, $[O_2]_0$=22.28; total pressure=4.48 Torr. $[O_2]_0$ refers to the amount of O_2 added to the O_2/He discharge. Reaction times used were 0.9—8.1 ms. Corrections for $[\bar{O}]$ were 1.5% or less. The $CD_3CH^{18}O$ signals are corrected for subsequent reaction to give $[CD_3CH^{18}O]_T$ as indicated by open circles. The large intercept for the signal at m/z=49 resulted from the signal of $(CD_3)_2\dot{C}H$ radicals.

The signal of $CD_3CH^{18}O$ increased with the addition of O_2 as shown in Table 3. The absolute concentrations of $CD_3CH^{18}O$ and $(CD_3)_2C^{18}O$ were determined using the measured instrumental sensitivities to CH_3CHO and $(CD_3)_2CO$.

As shown in Table 3, the formation of both $CD_3CH^{18}O$ and $(CD_3)_2C^{18}O$ increased when molecular oxygen was added to the system. The concentrations of $CD_3CH^{18}O$ and $(CD_3)_2C^{18}O$ were plotted against $X/(1+X)$, where X is given by Eq. 13. The plots are shown in Fig. 11. As described before, from the slopes and intercepts of these straight lines values for f_{4b}, f_{4c}, s_{7b}, and s_{7c} can be determined,[41] where s_{7c} refers to the fraction of CD_3CHO produced in Reaction 7. In these calculations, the fraction of ^{18}O in O (19.2%) was used and the effect of the consumption of $CD_3CH^{18}O$ by Reaction 15 was taken into account.[41] The values calculated are (0.18±0.02), (0.21±0.03), (0.32±0.03), and (0.44±0.08), for f_{4b}, f_{4c}, s_{7b}, and s_{7c}, respectively.

Table 3. Observed Signals at m/z=49 and 66 and Absolute Concentrations of $CD_3CH^{18}O$ and $(CD_3)_2C^{18}O$ in the Reaction of $(CD_3)_2CH_2+{}^{18}O+{}^{18}O_2$[a]

O_2 added mTorr	$[O_2]/[\bar{O}]$[b]	Signal at m/z=49 cps	$[2\text{-pr}]_{ss}$[c] cps	$[CD_3CH^{18}O]$[d] cps	$[CD_3CH^{18}O]$[e] 10^{10}molecule cm^{-3}	Signal at m/z=66 cps	$[(CD_3)_2C^{18}O]$[e] 10^{10}molecule cm^{-3}
0	3.66	40.03	17.30	22.73	2.24	255.23	2.55
19.58	7.31	41.18	15.87	25.31	2.50	271.25	2.71
47.65	12.55	40.33	14.12	26.21	2.59	283.26	2.83
65.74	15.93	42.16	13.15	29.01	2.86	249.27	2.94
87.90	20.07	40.93	12.15	28.78	2.84	305.28	3.05
113.01	24.76	41.99	11.16	30.83	3.04	310.29	3.10
151.61	31.97	42.97	9.95	33.02	3.26	331.30	3.31
207.00	42.31	41.47	8.61	32.86	3.24	335.31	3.35

a) Experimental conditions are: $[{}^{18}O]/([{}^{18}O]+[{}^{16}O])=0.192$, $[{}^{36}O_2]/([{}^{36}O_2]+[{}^{32}O_2])=0.192$, $[O]_0=5.42$ mTorr, $[(CD_3)_2CH_2]=2.37$ mTorr, $[O_2]_0=22.28$ mTorr, reaction time=6.299 ms, $[\bar{O}]=5.36$ mTorr, and total pressure=4.48 Torr. b) $[O_2]$ was calculated by $[O_2]_s+[O_2]_{added}$, where $[O_2]_s=[O_2]_0-1/2[O]_0$ refers to the O_2 surviving from the O_2/He discharge. c) The value for $[2\text{-pr}]_{ss}$ were calculated form Eq. 6 as follows; each value for $[2\text{-pr}]^0_{ss}/[2\text{-pr}]_{ss}$ can be calculated by using the known values of k_7/k_4 and $[\bar{O}_2]/[O]$. The absolute intensity for $[2\text{-pr}]^0_{ss}$ of 19.2 counts s^{-1} was determined from the intercept of the line shown in Fig. 10, in which the values for $[O_2]/[\bar{O}]$ and $[2\text{-pr}]_{ss}$ were 3.66 and 17.2 counts s^{-1},respectively. d) Signal intensity for $CD_3CH^{18}O$ was determined from (signal at m/z=49)−(signal for $[2\text{-pr}]_{ss}$). e) The absolute concentrations for $CD_3CH^{18}O$ and $(CD_3)_2C^{18}O$ were determined by the instrumental sensitivities to CH_3CHO and $(CH_3)_2CO$ as measured by adding known partial pressures of both gases to the reactor.

These values for f_{4b} and s_{7b} are in good agreement with the values obtained from Fig. 9. Combining the results obtained from Figs. 9 and 11, the branching fractions in Reactions 4 and 7 are:

$$(CD_3)_2\dot{C}H+O \xrightarrow{(61\pm7)\%} CD_2CHCD_3$$
$$\xrightarrow{(18\pm2)\%} (CD_3)_2CO$$
$$\xrightarrow{(21\pm3)\%} CD_3CHO \quad (4)$$

$$(CD_3)_2\dot{C}H+O_2 \xrightarrow{(20\pm2)\%} CD_2CHCD_3$$
$$\xrightarrow{(32\pm3)\%} (CD_3)_2CO$$
$$\xrightarrow{(44\pm8)\%} CD_3CHO \quad (7)$$

The values for f_{4b} and s_{7b} are averaged for the two measurements.

E. Rate Constant for $(CD_3)_2CH_2+O(^3P)$ Reaction. As described before, the determination of the rate constant for Reaction 3 is necessary in order to determine the fractions in Reaction 4. Since the rate of Reaction 3 at room temperature is too slow to measure by the pseudo-first-order decay of $(CD_3)_2CH_2$ under the present experimental conditions, the pseudo-first-order decay of $(CD_3)_2CH_2$ was measured over a temperature range of 381—627K in a large excess of oxygen atoms $[O]\gg[(CD_3)_2CH_2]$ by changing the contact time of $(CD_3)_2CH_2$ with oxygen atoms. An Ar lamp having a LiF window (11.83 and 11.62 eV) was used to photoionize $(CD_3)_2CH_2$. Since there was no signal from reaction product at m/z=50 when $(CD_3)_2CH_2$ reacted with atomic oxygen (see Fig. 4), the bimolecular rate of Reaction 3 can be measured from the decay of the signal of $(CD_3)_2CH_2$ at m/z=50. The results are presented in Table 4. The 95% confidence limits were calculated from the least squares line using ten points (ten different reaction times) for each run.

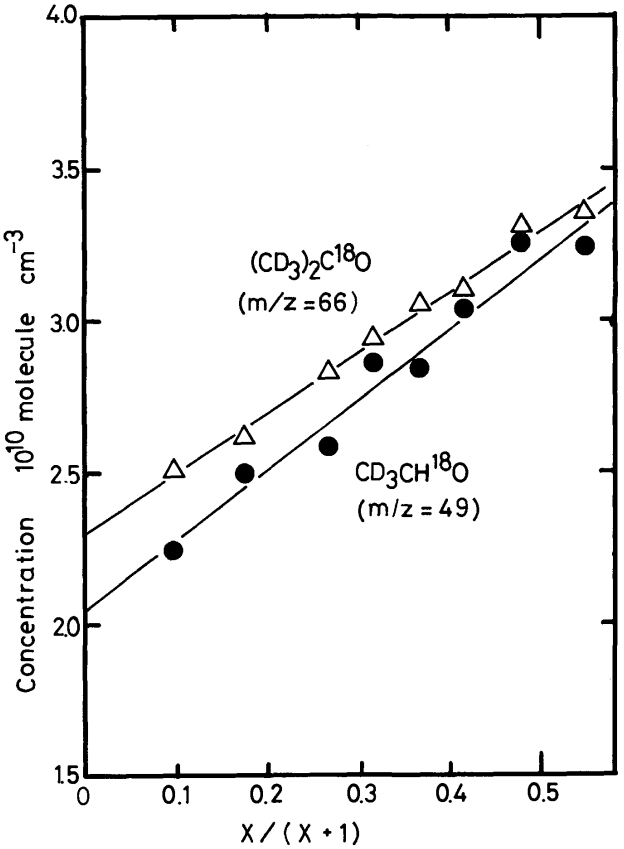

Fig. 11. The absolute concentrations of $CD_3CH^{18}O$ (solid circles) and $(CD_3)_2C^{18}O$ (open triangles) are plotted against $X/(1+X)$. Conditions are the same as those in Table 3.

The bimolecular rate constants of k_3 are plotted in

Table 4. Rate Data[a] for $O(^3P)+(CD_3)_2CH_2$ at 385—627 K

T	$[P]_0$[b]	$[O]_0$	Total pressure	Flow rate	k_3
K	mTorr	mTorr	Torr	m s^{-1}	10^{-14} cm^3molecule^{-1} s^{-1}
627	0.052	1.681	5.68	43.4	198±22
605	0.073	3.837	5.26	40.9	113±18
573	0.101	4.129	5.83	41.2	93.8±9.6
561	0.103	6.836	5.73	41.0	80.2±6.5
491	0.114	5.801	5.62	36.2	34.6±4.2
485	0.102	7.026	5.31	36.1	36.4±5.3
426	0.098	8.381	6.18	31.7	15.1±1.3
421	0.182	10.79	6.07	31.9	14.0±1.6
385	0.146	12.52	6.68	28.3	6.71±0.73
381	0.102	13.32	6.65	28.1	7.46±0.66

a) The rate constant was calculated from the equation of $\ln [P]/[P]_0=-k_3[\bar{O}]t$, where [P] and $[P]_0$ represent the signal of $(CD_3)_2CH_2$ in the presence and absence of oxygen atoms, respectively. b) $[P]_0$ represents the original concentration of $(CD_3)_2CH_2$.

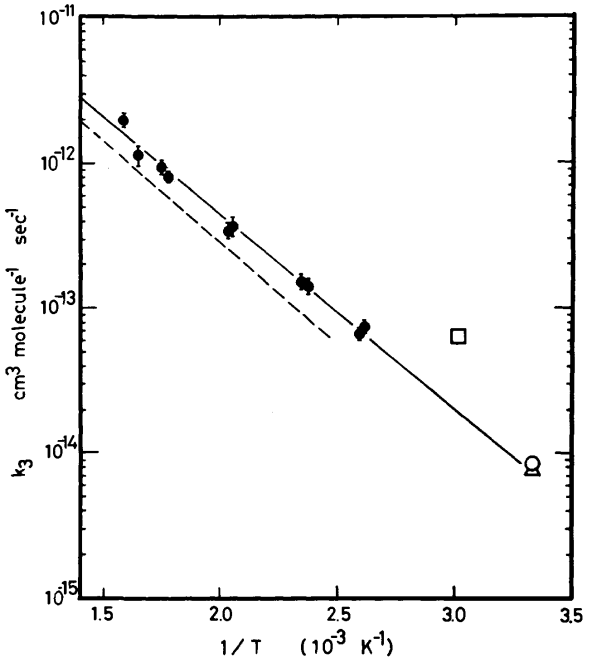

Fig. 12. Arrhenius plot for reaction O+propane. ● This work for $O+(CD_3)_2CH_2$; solid line drawn is obtained by the least-square fit. □: Harker and Burton[46] for $O+C_3H_8$. △: Jewell et al.[3] for $O+C_3H_8$. Dashed line is consensus rate constant for $O+C_3H_8$ by Klemm et al.[47] The open circle is obtained in this work from the yields of reaction products.

Fig. 12 vs. the reciprocal of the absolute temperature. A linear least square treatment yields the Arrhenius expression:

$$k_3 = (2.0^{+1.0}_{-0.7}) \times 10^{-10} \exp\left(\frac{-6086 \pm 392 \text{ cal mol}^{-1}}{RT}\right) \quad (17)$$

in units of cm^3 molecule^{-1} s^{-1}. The indicated errors were calculated by the least-square with 95% confidence limits. The rate constant for Reaction 3 at 298K calculated from Eq. 17 is 6.94×10^{-15} cm^3 molecule^{-1} s^{-1}.

The rate constant for Reaction 3 can also be calculated from the sum of the absolute yields of the three reaction products; CD_2CHCD_3, $(CD_3)CO$, and CD_3CHO. The value for k_3 of 7.9×10^{-15} cm^3 molecule^{-1} s^{-1} was calculated[42] from absolute concentrations of products produced initially by Reaction 4. The value is in reasonable agreement with that calculated from Eq. 17. Therefore, the value of 7.91×10^{-15} cm^3 molecule^{-1} s^{-1} was used for k_3 in all calculations in this study.

Discussion

The observation of propyl radicals by photoionization using the Xe resonance lamp (8.44 eV) is reasonable because the ionization potentials for the propyl radicals are low (Table 1). The detection of propyl radicals using photoionization by the Xe lamp has been reported by Bayes et al.[43] Only the $(CD_3)_2\dot{C}H$ radical was formed in the reaction of $O+(CD_3)_2CH_2$. For comparison, the reaction of oxygen atoms with propane-2,2-d_2, $(CH_3)_2CD_2$, gave both $\cdot CH_2CD_2CH_3$ (m/z=45) and $(CH_3)_2\dot{C}D$ (m/z=44). The ratio of the signal at m/z=44 to 45 was about 3 : 2. Therefore, the abstraction of the 1- or 2-hydrogen from propane is very sensitive to the small difference in the bond dissociation energies of C-H and C-D. Jewell et al.[3] observed the formation of $(CH_3)_2CO$ and C_2H_5CHO in the $O+C_3H_8$ system. This result also suggests that both n-propyl and isopropyl radicals are produced by the primary attack of O atoms on C_3H_8.[29]

CD_2CHCD_3, $(CD_3)_2CO$, and CD_3CHO were observed as major products of the $O+(CD_3)_2\dot{C}H$ reaction. In addition, the signal of CD_2CO was observed in this study. Since the signals for CD_2CO were proportional to the square of $[\bar{O}]t$, CD_2CO probably is produced by secondary reactions.[29] In the previous discharge-flow experiments involving $O+C_3H_8$,[3,4] the formation of C_2H_5CHO, C_2H_6, C_2H_4, CH_2O, CH_4, CO_2, CO, H_2O, and H_2 has been reported in addition to propene, acetone and acetaldehyde. These products, except for C_2H_5CHO, are probably produced in secondary reactions.

Propene, CD_2CHCD_3, was a major product of the $O+(CD_3)_2CH$ reaction. Propene can be produced by

hydrogen abstraction, Reaction 4a. Similar hydrogen abstraction reactions were found for O+t-C_4H_9[1] and O+$cyclo$-C_6H_{11}.[2] These results disagree with the findings by Hoyerman and Sievert,[7] who observed no formation of olefins in the reactions of O+alkyl radicals.

As shown in Table 2 and Fig. 5, the products CD_3CDO (m/z=48) and $CD_3CD^{18}O$ (m/z=50) were observed in the ^{16}O and ^{18}O+$(CD_3)_2CH_2$ systems. These products might be produced by secondary reactions following O+CD_2CHCD_3. According to the previous studies on O+C_3H_6,[37,44,45] Reaction 8 proceeds as follows:

$$CD_2CHCD_3 + O \rightarrow (CD_3CHDCDO)^* \rightarrow CD_3CHD + CDO \quad (8a)$$

$$CD_2CHCD_3 + O \rightarrow (CD_3(CO)CHD_2)^* \rightarrow CD_3 + CHD_2CO \quad (8b)$$

$$(CD_3(CO)CHD_2)^* \rightarrow CHD_2 + CD_3CO \quad (8c)$$

Since no signals at m/z=63 were observed as shown in Fig. 4, the vibrationally hot $CD_3CHDCDO$ and CD_3COCHD_2 were not stabilized for the present experimental conditions. CD_3CHD produced in Reaction 8a reacts with oxygen atoms and can produce CD_3CHO and CD_3CDO.

$$CD_3CHD + O \rightarrow CD_3CDO + H \ (m/z=48) \quad (18a)$$

$$CD_3CHD + O \rightarrow CD_3CHO + D \ (m/z=47) \quad (18b)$$

CD_3CDO shown in Table 2 and Fig. 5 might be produced in Reaction 18a. As described before, yields of acetaldehyde were determined from the signals of $CD_3CH^{18}O$ (m/z=49). If Reaction 18b occurred, the yield of $CD_3CH^{18}O$ was overestimated. The fraction of Reaction 18b should be less than 18a because of the difference of the bond energy of C-H and C-D. Therefore, the signal of $CD_3CH^{18}O$ from Reaction 18b should be smaller than that of $CD_3CD^{18}O$ (m/z=50). From the measurement of the signal intensities at m/z=49 and 50 in the ^{18}O+$(CD_3)_2CH_2$ reaction, it was determined that the effect of Reaction 18b on the total signal of $CD_3CH^{18}O$ was less than 20%. Thus the lower error limit of the yield of acetaldehyde should be increased in 20%; $f_{4c}=0.21^{+0.03}_{-0.07}$.

The value for k_7/k_4 of 0.029±0.004 was obtained from the competition experiment between O and O_2 for the $(CD_3)_2\dot{C}H$ radical. The rate constant for the reaction of isopropyl radicals, i-C_3H_7, with molecular oxygen has been reported[43], to be $(14.1\pm2.4)\times10^{-12}$ cm^3 $molecule^{-1}$ s^{-1} at 298K. Assuming that the rates of reactions of $(CD_3)_2CH+O_2$ and i-$C_3H_7+O_2$ are equal, the value for k_4 can be calculated as 4.9×10^{-10} cm^3 $molecule^{-1}$ s^{-1}. The rate of Reaction 4 is very rapid, but slower than the rate of reaction of t-butyl radical+O,[1] 8.7×10^{-10} cm^3 $molecule^{-1}$ s^{-1}.

Propene, CD_2CHCD_3, was produced by deuterium abstraction. The excess energy of Reaction 4a is about 63 kcal mol^{-1}. The yield of propene was 61% of the total O+$(CD_3)_2CH$ reaction. Yields of olefins from other O+alkyl radical reactions were 80% (isobutene) from O+t-C_4H_9,[1] and 52% (cyclohexene) from O+$cyclo$-C_6H_{11}.[2] These yields appear to correlate with the number of hydrogen atoms which can be abstracted; nine equivalent hydrogen atoms in the t-butyl radical to produce isobutene, six in the isopropyl radical to produce propene, and four in the cyclohexyl radical to produce cyclohexene.

Acetone, $(CD_3)_2CO$, and acetaldehyde, CD_3CHO, were formed by the oxygen atom addition. The isopropoxyl radical, $(CD_3)_2CH$-O·, formed in Reaction 4 would have approximately 90 kcal mol^{-1} excess energy and should rapidly decompose to $(CD_3)_2CO$+H and $CD_3CHO+CD_3$. Excess energies for Reactions 4b and 4c are 77.1 and 82.9 kcal mol^{-1}, respectively. Yields of acetone (18%) and acetaldehyde (21%) are similar, reflecting the similar exothermicities. The ratio of deuterium abstraction to oxygen atom addition was 1.6:1.

In the presence of an excess of O_2 the same products were observed but in different proportions; propene decreased to 20% and acetone and acetaldehyde increased to 32 and 44%, respectively. This trend is very similar to the case of the t-butyl radical.[11] It is proposed that the formation of these products occurs by the reaction of propylperoxyl radicals with atomic oxygen.

$$(CD_3)_2\dot{C}H + O_2 \xrightarrow{+M} (CD_3)_2C(H)OO \quad (7')$$

$$(CD_3)_2C(H)OO + O \rightarrow CD_2CHCD_3 + OD + O_2 \quad (19a)$$

$$(CD_3)_2C(H)OO + O \rightarrow (CD_3)_2CO + H + O_2 \quad (19b)$$

$$(CD_3)_2C(H)OO + O \rightarrow CD_3CHO + CD_3 + O_2 \quad (19c)$$

Here Reaction 19a is a deuterium abstraction reaction from the peroxyl radical by $O(^3P)$; after abstraction, O_2 departs from the peroxy biradical (·$CD_2CH(CD_3)OO$·) and propene is produced. In Reactions 19b and 19c oxygen atoms attack the radical oxygen (-O-O·). The resulting hot propoxyl radical decomposes to the fragements $(CD_3)_2CO$+H and $CD_3CHO+CD_3$. Reactions 19a and 19c are 49 and 55 kcal mol^{-1} exothermic, respectively.

Various studies of the rate of the O+C_3H_8 reaction are summarized in Fig. 12. Harker and Burton[46] measured the OH radical produced by Reaction 1 by molecular modultion spectroscopy. They obtained a value for k_1 of 6.5×10^{-14} cm^3 $molecule^{-1}$ s^{-1} at 329K. Jewell et al.[3] measured the decay of O-atoms and also propane in the O+C_3H_8 discharge-flow system and proposed a value for k_1 of 7.8×10^{-15} cm^3 $molecule^{-1}$ s^{-1} at 306K. In a recent article, Klemm et al.[47] reported the measurement of the rate of the O+C_3H_8 reaction by both flash photolysis-resonance fluorescence and discharge flow-resonance fluorescence techniques over a temperature range of 411—1018K; they proposed the Arrhenius expression: $k_1=(1.66\pm0.16)\times10^{-10}$ exp[$(-6290\pm120$ cal $mol^{-1})/RT$] in unit of cm^3 $molecule^{-1}$

s^{-1}. Rate constants for $O+(CD_3)_2CH_2$ obtained in this study agree well with the value by Klemm et al. in both activation energy and frequency factor considering the error of the measurements. The rate constant extrapolated to room temperature, 6.94×10^{-15} cm^3 $molecule^{-1}$ s^{-1}, using Eq. 17 differs by 1.6 factor with the value of k_3 calculated from the absolute yields of products, 7.81×10^{-15} cm^3 $molecule^{-1}$ s^{-1}. Both values of k_3 at room temperature agree well with the rate constant for $O+C_3H_8$ at 306K reported by Jewell et al.

Conclusion

(1) Isopropyl-d_6 radicals, $(CD_3)_2CH$, produced in the reaction of propane-1,1,1,3,3,3-d_6, $(CD_3)_2CH_2$, with atomic oxygen were detected directly by the photoionization mass spectrometer.

(2) The reaction of $(CD_3)_2\dot{C}H$ radicals with atomic oxygen proceeds by deuterium abstraction (61%) and by an oxygen atom addition reaction (39%).

(3) The product in the deuterium abstraction was propene-1,1,3,3,3-d_5, CD_2CHCD_3. Acetone-d_6, $(CD_3)_2CO$ and acetaldehyde-2,2,2-d_3, CD_3CHO were produced by the oxygen atom addition reaction with yields of 18 and 21%, respectively.

(4) The reaction of $(CD_3)_2\dot{C}H$ radicals with molecular oxygen was 0.029 ± 0.004 times as fast as that with atomic oxygen. From the rate constant for the $O_2+C_3H_7$ reaction reported, the rate constant for the reaction of O+isopropyl radicals was estimated to be 4.9×10^{-10} cm^3 $molecule^{-1}$ s^{-1}.

(5) In the reaction of isopropylperoxyl radicals with molecular oxygen, the yield of CD_2CHCD_3 decreased to 20% and the yields of $(CD_3)_2CO$ and CD_3CHO increased to 32 and 44%, respectively.

(6) The rate data for the reaction of $O+(CD_3)_2CH_2$ were fitted by an Arrhenius expression; $k_3=(2.01^{+1.0}_{-0.7})\times 10^{-10}\exp[(-6086\pm392\ \text{cal mol}^{-1})/RT]$ cm^3 $molecule^{-1}$ s^{-1} (381—627 K). The rate constant obtained from the yields of products was 7.9×10^{-15} cm^3 $molecule^{-1}$ s^{-1} at 298K.

The author wishes to thank Professor Kyle D. Bayes of UCLA for his kind and helpful suggestions and discussions. The assistance of Hiroo Takagi in the early stage of this work is gratefully acknowledged.

References

1) N. Washida and K. D. Bayes, *J. Phys. Chem*, **84**, 1309 (1980).

2) N. Washida and H. Takagi, *J. Am. Chem. Soc.*, **104**, 168 (1982).

3) S. P. Jewell, K. A. Holbrook, and G. A. Oldershaw, *Int. J. Chem. Kinet.*, **13**, 69 (1981).

4) F. J. Wright, *Symp. (Int.) Combust. [Proc.]*, **10**, 387 (1965).

5) F. J. Wright, *J. Chem. Phys.*, **38**, 950 (1963).

6) S. P. Jewell, K. A. Holbrook, and G. A. Oldershaw, *Int. J. Chem. Kinet.*, **14**, 585 (1982).

7) K. Hoyerman and R. Sievert, *Symp. (Int.) Combust. [Proc.]*, **17**, 517 (1978): *Ber. Bunsenges. Phys. Chem.*, **83**, 732 (1979).

8) I. T. N. Jones and K. D. Bayes, *J. Am. Chem. Soc.*, **94**, 6869 (1972).

9) J. R. Kanofsky and D. Gutman, *Chem. Phys. Lett.*, **15**, 236 (1972).

10) N. Washida and K. D. Bayes, *Int. J. Chem. Kinet.*, **8**, 777 (1976).

11) N. Washida, H. Akimoto, and M. Okuda, *J. Phys. Chem.*, **82**, 2293 (1978).

12) N. Washida, *J. Chem. Phys.*, **73**, 1665 (1980).

13) A. Murray III and D.L. Williams, "Organic Syntheses with Isotopes," Part II., Interscience: New York (1958), pp. 1408—1410.

14) Reaction of propane with atomic oxygen starts by the hydrogen abstraction reaction

$$C_3H_8+O\rightarrow C_3H_7+OH \quad (A)$$

OH radicals can also be produced by the subsequent radical-atom reactions. OH radicals can react with C_3H_8 faster than Reaction A

$$C_3H_8+OH\rightarrow C_3H_7+H_2O \quad (B)$$

The rate constants for Reactions A and B at 298K have been reported to be $(8—15)\times10^{-15}$ (Refs. 3, 15, 16) and $(0.8—2)\times10^{-12}$ cm^3 $molecules^{-1}$ s^{-1} (Refs. 17—23), respectively. OH radicals are destroyed by the following two reactions:

$$OH+O\rightarrow H+O_2 \quad (C)$$

$$OH+\text{wall}\rightarrow\text{removal of OH} \quad (D)$$

Therefore, in order to avoid an effect of the OH radicals on the formation of C_3H_7 radicals, the ratio of $k_B[C_3H_8]/k_C[O]$ must be less than 0.1. The rate constant of Reaction C has been reported to be $(3—4)\times10^{-11}$ cm^3 $molecule^{-1}$ s^{-1} (Refs. 24—27) at 298K. The above requirement means that the kinetic experiments should be done under the condition that the concentration of oxygen atoms must be at least twice as large as the concentration of propane.

15) D. Sanders and J. Heicklen, *J. Phys. Chem.*, **70**, 1950 (1966).

16) J. T. Herron and R. E. Huie, *J. Phys. Chem. Ref. Data*, **2**, 467 (1973).

17) N. R. Greiner, *J. Chem. Phys.*, **53**, 1070 (1970).

18) J. N. Bradley, W. Hack, K. Hoyermann, and H. Gg. Wagner, *J. Chem. Soc., Faraday Trans. 1*, **69**, 1889 (1973).

19) R. A. Gorse and D. H. Volman, *J. Photochem.* **3**, 115 (1974).

20) R. P. Overend, G. Paraskevopoulos, and R. J. Cvetanovic, *Can. J. Chem.*, **53**, 3374 (1975).

21) R. Atkinson, D. R. Darnall, A. C. Lloyd, A. M. Winer, and J. N. Pitts, Jr., "Advances in Photochemistry," ed by J. N. Pitts, Jr., G. S. Hammond, and W. A. Noyes, Jr., Interscience, New York, **11**, 375 (1979).

22) K. R. Darnall, R. Atkinson, and J. N. Pitts, Jr., *J. Phys. Chem.*, **82**, 1581 (1978).

23) R. Atkinson, S. M. Ashmann, W. P. L. Carter, A. M. Winer, and J. N. Pitts, Jr., *Int. J. Chem. Kinet.*, **14**, 781 (1982).

24) J. E. Breen and G. P. Glass, *J. Chem. Phys.*, **52**, 1082 (1970).

25) A. A. Westenberg, N. de Haas, and J. M. Roscoe, *J. Phys. Chem.*, **74**, 3431 (1970).

26) I. M. Campbell and B. J. Handy, *Chem. Phys. Lett.*, **47**, 475 (1977).

27) M. J. Howard and I. W. M. Smith, *Chem. Phys. Lett.*, **69**, 40 (1980): *J. Chem. Soc., Faraday Trans. 2*, **77**, 997 (1981).

28) H. M. Rosenstock, K. Draxl, B. W. Steiner, and J. T. Herron, "Energetics of Gaseous Ions," *J. Phys. Chem. Ref. Data*, **6**, Suppl. 1. (1977).

29) The reaction of $O+C_3H_8$ might proceed as follows:

$$O + C_3H_8 \begin{cases} \rightarrow n\text{-}C_3H_7 + OH & (E) \\ \rightarrow i\text{-}C_3H_7 + OH & (F) \end{cases}$$

$$n\text{-}C_3H_7 + O \begin{cases} \rightarrow C_3H_6 + OH & (G) \\ \rightarrow C_2H_5CHO + H & (H) \\ \rightarrow CH_2O + C_2H_5 & (I) \end{cases}$$

$$i\text{-}C_3H_7 + O \begin{cases} \rightarrow C_3H_6 + OH & (J) \\ \rightarrow (CH_3)_2CO + H & (K) \\ \rightarrow CH_3CHO + CH_3 & (L) \end{cases}$$

Ketene, CH_2CO (see Ref. 30), can be produced by a secondary reaction (Ref. 31) such as;

$$CH_3CHO + O \rightarrow CH_3CO + OH \quad (M)$$
$$CH_3CO + O \rightarrow CH_2CO + OH \quad (N)$$

30) Since the photoionization mass spectrometer is very sensitive to ketene (5—20 times more sensitive than other organic compounds), its absolute concentration is much smaller than is suggested by the signal intensity.

31) N. Washida and K.D. Bayes, unpublished data.

32) $CH_3CO+O \rightarrow CH_3+CO_2$ (Refs. 31 and 33) subsequent to Reaction M in Ref. 29.

33) G. P. R. Mack and B. A. Thrush, *J. Chem. Soc., Faraday Trans. 1*, **70**, 178 (1974).

34) $CH_3+O \rightarrow CH_2O+H$ from Refs. (13 and 35).

35) H. Niki, E. E. Daby, and B. Weinstock, *J. Chem. Phys.*, **48**, 5729 (1968).

36) The consumption of oxygen atoms in the reactor was corrected as follows: Oxygen atoms are destroyed by Reactions 3, 4, O, and P.

$$OD + O \rightarrow O_2 + D \quad (O)$$
(or $OH + O \rightarrow O_2 + H$)
$$CD_3 + O \rightarrow CD_2O + D \quad (P)$$

Further, a major part of the CD_2CHCD_3 produced in Reaction 4a and a small part of the CD_3CHO produced in Reaction 4c react with atomic oxygen. According to the results by Kanofsky et al. (Ref. 37), the major routes of the $O+C_3H_6$ reaction are:

$$O + C_3H_6 \begin{cases} \rightarrow CHO + C_2H_5 & (Qa) \\ \rightarrow CH_3 + CH_3CO & (Qb) \end{cases}$$

Therefore, the stoichiometric factor, n, for the number of oxygen atoms consumed per $(CD_3)_2CH_2$ reacted varies from 2.5 to 8 depending on the reaction time. A value $n=6$ was used for all experiments in the present study. The value of $[\bar{O}]t$, which is a product of the average oxygen-atom concentration and the reaction time, were calculated by Eq. R.

$$[\bar{O}]t = [O]_0 \int_0^t \exp(-nk_3[P]t)\,dt \quad (R)$$

where, $[O]_0$, k_3, and [P] are the original oxygen-atom concentration, the rate constant for Reaction 3, and the concentration of $(CD_3)_2CH_2$, respecrively. The value for k_3 of 7.91×10^{-15} cm^3 molecule^{-1} s^{-1} was used for this calculations as will be discussed later.

37) J. R. Kanofsky, D. Lucas, and D. Gutman, *Symp. (Int.) Combust., [Proc.]*, **14**, 285 (1973).

38) F. Stuhl and H. Niki, *J. Chem. Phys.*, **55**, 3954 (1971); M. J. Kurylo, *Chem. Phys. Lett.*, **14**, 117 (1971); R. E. Huie, J. T. Herron, and D. D. Davis, *J. Phys. Chem.*, **76**, 3311 (1972); S. Furuyama, R. Atkinson, A. J. Colussi, and R. J. Cvetanović, *Int. J. Chem. Kinet.*, **6**, 741 (1974); R. Atkinson and J. N. Pitts, Jr., *Chem. Phys. Lett.*, **27**, 467 (1974); R. Atkinson and J. N. Pitts, Jr., *J. Phys. Chem.*, **78**, 1780 (1974); D. L. Singleton and R. J. Cvetanovic, *J. Am. Chem. Soc.*, **98**, 6812 (1976); R. Atkinson and J. N. Pitts, Jr., *J. Chem. Phys.*, **67**, 38 (1977).

39) P. F. Ambridge, J. N. Bradley, and D. A. Whytock, *J. Chem. Soc., Faraday Trans. 1*, **72**, 1870 (1976); J. H. Lee and R. B. Timmons, *Int. J. Chem. Kinet.*, **9**, 133 (1977).

40) D. L. Singleton, R. S. Irwin, and R. J. Cvetanovic, *Can. J. Chem.*, **55**, 3321 (1977).

41) For $(CD_3)_2C^{18}O$, since ^{18}O used is 19.2% in O, f_{4b} and s_{7b} were determined by Eq. S.

$$[(CD_3)_2C^{18}O] = \left\{f_{4b} + \frac{(s_{7b}-f_{4b})X}{1+X}\right\} 0.192k_3[P][\bar{O}]t \quad (S)$$

For $CD_3CH^{18}O$, f_{4c} and s_{7c} were calculated by Eq. T since a correction of the consumption of $CD_3CH^{18}O$ by Reaction 15 is necessary.

$$[(CD_3)_2C^{18}O] = \left\{f_{4c} + \frac{(s_{7c}-f_{4c})X}{1+X}\right\} 0.192k_3[P][\bar{O}]t \, \frac{1-e^{-k_{15}[\bar{O}]t}}{k_{15}[\bar{O}]t} \quad (T)$$

42) The amount of $(CD_3)_2CO$ produced when $[O_2]$ is zero was calculated to be 4.76×10^{10} molecule cm^{-3} in the case of Fig. 9. In the case of Fig. 11, the total amount of actone produced when $[O_2]$ is zero was 12.36×10^{10} molecule cm^{-3} (the amount of $(CD_3)_2C^{18}O$ was 2.37×10^{10} molecule cm^{-3}). The ratio of the yield of three reaction products produced initially by Reaction 4, $f_{4a}:f_{4b}:f_{4c}$, was 3.56 : 1 : 1.16. Therefore, the sums of the amounts of three products are 27.24 and 69.36×10^{10} molecule cm^{-3} in cases of Figs. 9 and 11, respectively. Since the values for $[O]t$ were 11.06 and 11.14×10^{11} molecule s cm^{-3} for Figs. 9 and 11, respectively, values for k_3 calculated from $k_3[O][(CD_3)_2CH_2]t$=[total products] are 7.86 and 7.96×10^{-15} cm^3 molecule^{-1} s^{-1} for Figs. 9 and 11, respectively. The average value of 7.91×10^{-15} cm^3 molecule^{-1} s^{-1} was used for all subsequent calculations.

43) R. P. Ruiz and K. D. Bayes, *J. Phys. Chem.*, **88**, 2592 (1984).

44) R. J. Cvetanovic, "Advances in Photochemistry," ed by W. A. Noyes, Jr., G. S. Hammond, and J. N. Pitts, Jr., Interscience, New York, **1**, 115 (1963).

45) R. E. Huie and J. T. Herron, *Prog. Reaction Kinet.*, **8**, 1 (1975).

46) A. B. Harker and C. S. Burton, *Int. J. Chem. Kinet.*, **7**, 907 (1975).

47) J. V. Michael and D. G. Keil, and R. B. Klemm, *Int. J. Chem. Kinet.*, **15**, 705 (1983).

 © 1987 The Chemical Society of Japan Bull. Chem. Soc. Jpn., 60, 3751—3756 (1987)

Oxidation of $(CD_3)_2\dot{C}X$ Radicals. II. Reaction of $(CD_3)_2CHCl$ and $(CD_3)_2\dot{C}Cl$ Radicals with Atomic Oxygen

Nobuaki WASHIDA* and Shiro HATAKEYAMA
Division of Atmospheric Environment, The National Institute for Environmental Studies,
P.O. Tsukuba-gakuen, Ibaraki 305
(Received April 10, 1987)

The reaction of oxygen atoms with $(CD_3)_2CHCl$ in a fast flow system was studied with a photoionization mass spectrometer. The $(CD_3)_2\dot{C}Cl$ radical formed by the initial hydrogen abstraction at the 2-position was detected directly.

$$(CD_3)_2CHCl + O(^3P) \rightarrow (CD_3)_2\dot{C}Cl + OH \quad (1)$$

The rate data for Reaction 1 were fitted by an Arrhenius expression: $k_1=(3.5^{+1.2}_{-0.9})\times10^{-11}$ exp[(−4973±278 cal mol^{-1})/RT]† cm^3 molecule^{-1} s^{-1} (399—628 K). Among the products formed in the subsequent reaction of $(CD_3)_2\dot{C}Cl$ radicals with atomic oxygen, $CD_3CCl=CD_2$ (31%) produced by the deuterium abstraction and $(CD_3)_2CO$ (24%) by the oxygen addition were observed. Competition experiments show that $(CD_3)_2\dot{C}Cl$ radicals react (0.0079 ±0.0010) times as fast with O_2 as with $O(^3P)$. In the presence of an excess of O_2, $CD_3CCl=CD_2$ was observed in decreased yield (3.5%) and $(CD_3)_2CO$ increased to 56%.

Since the formation of $(CD_3)_2\dot{C}H$ radicals was confirmed in the reaction of atomic oxygen with $(CD_3)_2CH_2$, the reaction of $(CD_3)_2CHCl$ with atomic oxygen is investigated in the present study as an analogy of the reaction. In the reaction of O+$(CD_3)_2CHCl$, it is supposed that the $(CD_3)_2\dot{C}Cl$ radical is produced by the initial attack of $O(^3P)$ on $(CD_3)_2CHCl$.

$$(CD_3)_2CHCl\ \ O(^3P) \rightarrow (CD_3)_2\dot{C}Cl + OH \quad (1)$$

The subsequent reaction of the $(CD_3)_2\dot{C}Cl$ radicals with atomic oxygen can be considered as follows by the analogy of the O+propyl radical reaction:

$$(CD_3)_2\dot{C}Cl + O(^3P) \rightarrow \begin{cases} CD_3CCl=CD_2 + OD & (2a) \\ (CD_3)_2CO + Cl & (2b) \\ CD_3CClO + CD_3 & (2c) \end{cases}$$

A question of interest is the change of the branching ratio of each process, 2a—c, due to a chlorine substitution for a hydrogen at 2-position of propane.

Experimental

The experimental setup and procedures were the same as those mentioned before.[1] $(CD_3)_2CHCl$ was synthesized[2] in this laboratory. All measurements were done at room temperature, 298±3 K, under the conditions [O]>0.5 $[(CD_3)_2CHCl]$.[3]

Results and Discussion

A. Radicals and Molecules Detected in the $(CD_3)_2CHCl$+O Reaction. Radicals produced in the reaction of $(CD_3)_2CHCl$ with atomic oxygen were detected at m/z=83 and 85 when a Xe lamp with a sapphire window (8.44 eV) was used as a photoionization light source. Mass spectra measured are shown in Fig. 1. Other products produced by subsequent reactions and the parent $(CD_3)_2CHCl$ were not photoionized by this lamp. Radicals observed at m/z=83 and 85 are $(CD_3)_2\dot{C}^{35}Cl$ and $(CD_3)_2\dot{C}^{37}Cl$, respectively. The ratio of the signal intensities at m/z=83 and 85 corresponds to the ratio of the natural abundance of ^{35}Cl (75.5%) and ^{37}Cl (24.5%). No observation of the signals at

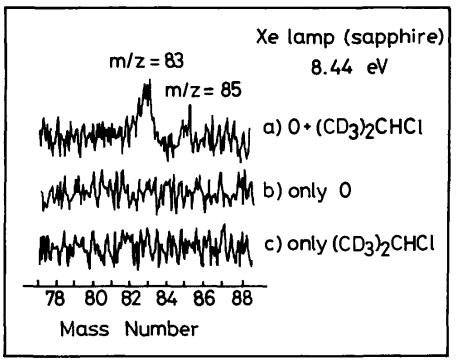

Fig. 1. Mass spectra of the $(CD_3)_2\dot{C}Cl$ radical produced in the O+$(CD_3)_2CHCl$ reaction. A Xe lamp having a sapphire window (8.44 eV) was used for the photoionization. The conditions: Partial pressure (mTorr), $[O]_0$=3.5, $[(CD_3)_2CHCl]$=0.82; reaction time=4.6 ms; total pressure=3.6 Torr.

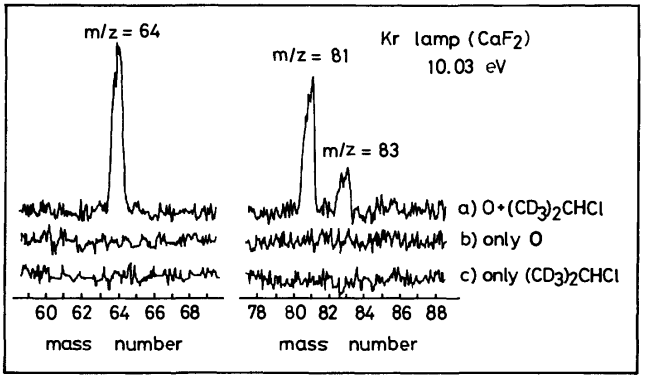

Fig. 2. Mass spectra of the reaction products produced in the O+$(CD_3)_2CHCl$ reaction. A Kr lamp having a CaF_2 window (10.03 eV) was used for the photoionization. The conditions: partial pressure (mTorr), $[O]_0$=3.1, $[(CD_3)_2CHCl]$=0.63; reaction time=4.6 ms; total pressure=3.6 Torr.

† 1 cal=4.184 J.

Table 1. Rate Data for $O(^3P)+(CD_3)_2CHCl$ at 399—628 K

T	$[P\text{-}Cl]_0$[a]	$[O]_0$	Total pressure	k_3
K	mTorr	mTorr	Torr	10^{-14} cm^3 molecule^{-1} s^{-1}
628	0.102	6.211	5.38	67.2±5.3
621	0.099	5.689	5.21	57.1±5.2
606	0.081	6.338	5.54	62.9±6.6
588	0.113	4.996	5.61	48.2±5.2
513	0.121	5.932	5.38	25.8±4.1
496	0.098	6.018	6.07	24.6±3.6
421	0.123	6.230	6.12	9.02±0.81
414	0.139	8.440	6.80	8.11±0.74
408	0.114	6.795	6.65	8.83±0.44
399	0.141	6.833	6.83	6.31±0.73

a) $[P\text{-}Cl]_0$ represents the original concentration of $(CD_3)_2CHCl$.

m/z=82 and 84 (deuterium abstraction by $O(^3P)$) shows that the initial attack of $O(^3P)$ on $(CD_3)_2CHCl$ occurs in selective abstraction of a hydrogen at 2-position of $(CD_3)_2CHCl$; Reaction 1.

Products produced in the reaction of oxygen atoms with $(CD_3)_2\dot{C}Cl$ radicals were measured by using a Kr lamp having a CaF_2 window (10.03 eV). Mass spectra obtained are shown in Fig. 2. Signals for $(CD_3)_2CO$ (m/z=64), $CD_3C^{35}Cl{=}CD_2$ (m/z=81), and $CD_3C^{37}ClCD_2$ (m/z=83) were observed as expected in Reaction 2.

Since ionization potential for acetyl chloride, CH_3COCl, has been reported[4] to be 11.02 eV, CD_3COCl formed by Reaction 2c cannot be ionized by the Kr resonance line but should be ionized by the Ar resonance lines (11.83 and 11.62 eV). Detection of CD_3COCl was investigated by using an Ar lamp with a LiF window. Since mass numbers of CD_3COCl and $CD_3CCl{=}CD_2$ are identical in the present case, $(CD_3)_2CHCl$ was reacted with ^{18}O (19.2% of $^{36}O_2$ in $^{32}O_2$ was diluted in helium and discharged by microwave) and the measurement of the signals for $CD_3C^{18}O^{37}Cl$ at m/z=85 was investigated. However, no significant signal at m/z=85 was observed except the isotope (^{13}C) signal of the parent $(CD_3)_2CH^{35}Cl$ molecule. In order to determine whether CD_3COCl is produced in Reaction 2 or not, the sensitivity measurement of acetyl chloride to the instrument when the Ar lamp was used as a photoionization light source was carried out by adding known partial pressures of CH_3COCl to the reactor. Surprisingly, no signal was observed even when up to 1 mTorr†† of CH_3COCl was added to the reactor. Since about 5×10^4 counts s^{-1} signals were obtained for 1 mTorr of NO in the reactor, we have to conclude that acetyl chloride cannot be ionized by the Ar resonance lines, and it cannot be determined whether Reaction 2c occurs or not.

B. Rate Constant for the $(CD_3)_2CHCl$ Reaction. The pseudo-first-order decay rates of $(CD_3)_2CHCl$ by Reaction 1 were measured over a temperature range of 399—628 K in a large excess of oxygen atoms by changing the contact time of $(CD_3)_2CHCl$ with oxygen atoms. An Ar lamp with a LiF window was used to photoionize $(CD_3)_2CHCl$ and the bimolecular rates of Reaction 1 were measured from the decay of the signal of $(CD_3)_2CH^{37}Cl$ at m/z=86. Values for k_1 obtained are listed in Table 1. The 95% confidence limits were calculated from the least squares line using ten points for each run. The concentration of oxygen atoms was corrected using a stoichiometric factor of n=6 as described in the preceeding paper.[1] The correction for oxygen atom consumption was 5% or less.

The linear least square treatment for the values of k_1 shown in Table 1 yields the Arrhenius expression of $k=A\exp(-E_a/RT)$.

$$k_1 = (3.5^{+1.2}_{-0.9}) \times 10^{-11} \exp\left(\frac{-4973\pm278 \text{ cal mol}^{-1}}{RT}\right); \quad (3)$$

in unit of cm^3 molecule^{-1} s^{-1}. The indicated errors were calculated by the least-square with 95% confidence limits. The rate constant for Reaction 1 at 298K calculated by Eq. 3 is 7.8×10^{-15} cm^3 molecule^{-1} s^{-1}.

The rate constants for the reaction of atomic oxygen with 2-chloropropane, $(CH_3)_2CHCl$, have been measured over a temperature range of 336—622K by Herron and Huie.[5] The Arrhenius expression obtained from their data was $k=(4.3^{+0.9}_{-0.6})\times10^{11}\exp[(-5206\pm139)/RT]$ cm^3 molecule^{-1} s^{-1} with a value at 298K of $k=6.5\times10^{-15}$ cm^3 molecule^{-1} s^{-1}. Values of Arrhenius activation energy, frequency factor, and the rate at 298K obtained in the present study for the $O+(CD_3)_2CHCl$ reaction are in good agreement with those measured in the $O+(CH_3)_2CHCl$ reaction by Herron and Huie.

C. Competition between $O(^3P)$ and O_2 for $(CD_3)_2\dot{C}Cl$. The steady-state concentrations of $(CD_3)_2\dot{C}Cl$ radicals were evidenced by no change of signals by changing the contact time of the reaction of $(CD_3)_2CHCl$ with oxygen atoms. The competition between $O(^3P)$ and O_2 for the $(CD_3)_2\dot{C}Cl$ radicals was measured by adding molecular oxygen to the system. The steady-state concentration of $(CD_3)_2\dot{C}Cl$ was decreased by the addition of O_2 and the competition results in a Stern-Volmer-type of equation,

†† 1 Torr=133.322 Pa.

$$\frac{[\text{pr-Cl}]^0_{ss}}{[\text{pr-Cl}]_{ss}} = 1 + \frac{k_5[O_2]}{k_2[O]} \quad (4)$$

where $[\text{pr-Cl}]_{ss}$ represents the steady-state concentration of $(CD_3)_2\dot{C}Cl$ radicals, the superscript zero refers to the condition in the absence of O_2 and k_5 is the effective second-order rate constant for the reaction of $(CD_3)_2\dot{C}Cl$ radicals with molecular oxygen.

$$(CD_3)_2\dot{C}Cl + O_2 \rightarrow \text{Products} \quad (5)$$

Figure 3 shows the result of an O_2 addition experiment. The concentration of $(CD_3)_2\dot{C}Cl$ radical was monitored by the signal at m/z=83, $(CD_3)_2\dot{C}^{35}Cl$. A value for $[(CD_3)_2\dot{C}Cl]^0_{ss}$ was determined by the method mentioned before.[5] The concentration of oxygen atoms, $[\bar{O}]$, was corrected using a stoichiometric factor of n=6 (the correction was 0.4%). The value for k_5/k_2 calculated from the slope is 0.0079±0.0010. Error limits due to the scatter of plots were calculated by the least square with the 95% confidence limits.

The value for k_5/k_2 suggests that the rate of the reaction of $(CD_3)_2\dot{C}Cl+O_2$ is 127 times slower than that of the $(CD_3)_2\dot{C}Cl+O$ reaction. This competition ratio of 127 is larger than that in the case of $(CD_3)_2\dot{C}H$ radicals where the ratio was 35. This result suggests that the rate of the reaction of $(CD_3)_2\dot{C}Cl+O_2$ is much slower than that of $(CD_3)_2\dot{C}H+O_2$ if the rate of the reaction of $(CD_3)\dot{C}Cl+O(^3P)$ and that of $(CD_3)_2\dot{C}H+O$ are close.

D. Time Dependence of Products. The dependence of the $(CD_3)_2CO$ and $CD_3CCl=CD_2$ signals on the reaction time was measured. Solid circles in Fig. 4 show the $CD_3C^{35}Cl=CD_2$ signal at m/z=81 in the $O+(CD_3)_2CHCl$ reaction. $CD_3CCl=CD_2$ approaches a constant concentration at long reaction time. This results from the fast reaction of $O+CD_3CCl=CD_2$, Reaction 6,

$$CD_3CCl=CD_2 + O \rightarrow \text{Products} \quad (6)$$

This approach to the steady-state concentration is

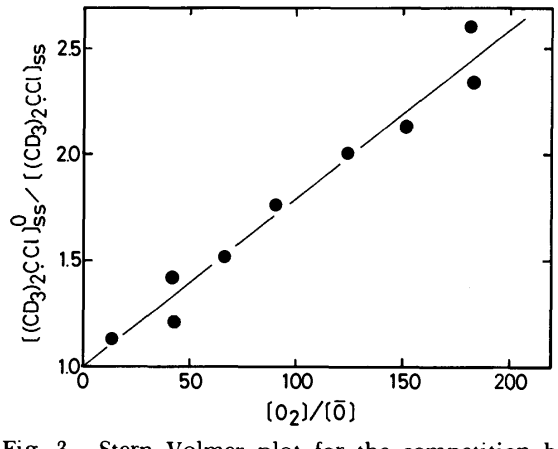

Fig. 3. Stern-Volmer plot for the competition between O_2 and $O(^3P)$ for the $(CD_3)_2\dot{C}Cl$ radicals. Conditions: Partial pressure (mTorr), $[O]_0$=2.03, $[\bar{O}]$=2.02, $[(CD_3)_2CHCl]_0$=0.71; $[O_2]_0$=29.65; total pressure=3.58 Torr; reaction time=4.59 ms. $[O_2]$ was calculated from $[O_2]_{added}+[O_2]_0-1/2[O]_0$.

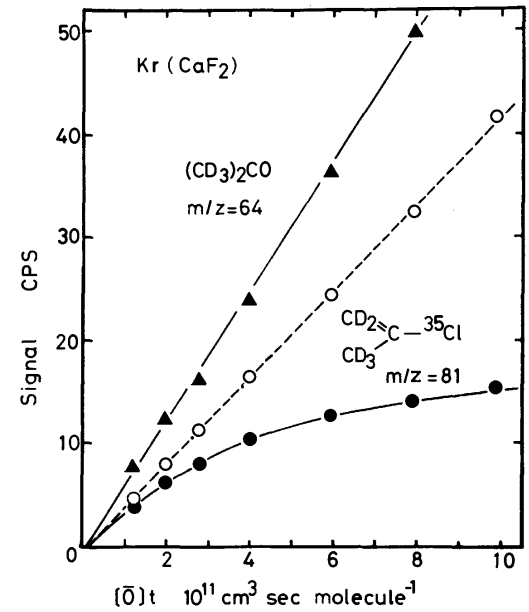

Fig. 4. Time dependence of $CD_3CCl=CD_2$ (solid circles) and $(CD_3)_2CO$ (solid triangles) signals produced in the $O+(CD_3)_2CHCl$ reaction. A Kr lamp with a CaF_2 window (10.03 eV) was used for the photoionization. The conditions: partial pressure (mTorr), $[O]_0$=2.62, $[(CD_3)_2CHCl]_0$=0.75, $[O_2]_0$=26,53; total pressure=3.55 Torr. Reaction times used were 1.4—11.5 ms. Correction for $[\bar{O}]$ were 0.7% or less. The $CD_3CCl=CD_2$ signals are corrected for the subsequent reaction to give $[CD_3CCl=CD_2]_T$ as indicated by open circles.

given by Eq. 7, assuming that Reaction 2 is much faster than Reactions 1 and 6.

$$[CD_3CCl=CD_2] = \frac{f_{2a}k_1}{k_6}[\text{P-Cl}][1-\exp(-k_6[\bar{O}]t)] \quad (7)$$

Here f_{2a} and [P-Cl] represent the fraction of Reaction 2a in the total reaction of $(CD_3)_2\dot{C}Cl$ radicals with atomic oxygen, Reaction 2, and the original concentration of $(CD_3)_2CHCl$. The values of $[\bar{O}]t$, which is a product of the average oxygen atom concentration and the reaction time, were calculated by using a stoichiometric factor n=6 as described before. The correction for oxygen atom consumption was less than 0.7%. When the plots shown by solid circles are fitted to Eq. 7, a value for k_6 of $(2.5\pm0.1)\times10^{-12}$ cm^3 molecule^{-1} s^{-1} is calculated. The best fit line for Eq. 7 is shown as a solid line in Fig. 4. The total amount of $CD_3CCl=CD_2$ produced by Reaction 2a, $[CD_3CCl=CD_2]_T$, is given by Eq. 8.

$$[CD_3CCl=CD_2]_T = f_{2a}k_1[\text{P-Cl}][\bar{O}]t \quad (8)$$

Therefore, the total amount of $CD_3CCl=CD_2$ can be calculated by multiplying each observed $CD_3CCl=CD_2$ value by $k_6[\bar{O}]t[1-\exp(-k_6[\bar{O}]t)]^{-1}$. These corrected points are shown as open circles in Fig. 4, and they are represented by the dashed straight line.

The time dependence of the $(CD_3)_2CO$ signal at m/z=64 produced in the $O+(CD_3)_2CHCl$ reaction is

shown as triangles in Fig. 4. Since the reaction of $O+(CD_3)_2CO$ is slow on the time scale shown, $(CD_3)_2CO$ rises linearly.

The rate constant for the $O+CD_3CCl=CD_2$ reaction was determined to be $(2.5\pm0.1)\times10^{-12}$ cm^3 molecule^{-1} s^{-1}. There is no previous determination of the rate constant for the reaction of O+2-chloropropene, $CH_3CCl=CH_2$, with which the value of k_6 can be compared. Since the standard sample of 2-chloropropene was not available, the pseudo-first-order decays were measured for the reaction of oxygen atoms with 1-chloro-1-propene, $CH_3CH=CHCl$ (cis- and trans-mixture from Tokyo Kasei), and 3-chloro-1-propene, $CH_2ClCHCH_2$ (from Tokyo Kasei). Results are listed in Table 2 with the value of the rate constants for $O+CD_3CCl=CD_2$ and $CD_3CH=CD_2$ reactions obtained by the steady-state approach method. In the measurements, since $CH_3CH=CHCl$ can be ionized by a Kr lamp with a CaF_2 window (10.03 eV) but $CH_2ClCH=CH_2$ cannot, an Ar lamp with a LiF window (11.83 and 11.62 eV) was used to ionize $CH_2ClCH=CH_2$. The rate for the $O+CD_3CCl=CD_2$ reaction is faster than that for the $O+CH_2ClCH=CH_2$, slower than that for the $O+CD_3CH=CD_2$, and close to that for the $O+CH_3CH=CHCl$ reaction. The rate constants for the reactions of 2-fluoro-1-propene and 3-fluoro-1-propene with oxygen atoms have been reported.[6,7] These values are close to those of chloropropenes and are also listed in Table 2.

It has been noted[8-10] for olefins that there is a good correlation between the rate constant with atomic oxygen and ionization potential. In the present case, since the rate constant for the $O+CH_3CH=CHCl$ reaction is close to that for $O+CD_3CCl=CD_2$, tentatively $CH_3CH=CHCl$ can be used as a standard sample to estimate the absolute concentration of $CD_3CCl=CD_2$. Supposing that the ionization cross sections of $CH_3CH=CHCl$ and $CD_3CCl=CD_2$ for the Kr resonance line of 10.03 eV are equal, the absolute concentrations of $CD_3CCl=CD_2$ were calculated using the instrumental sensitivity of $CH_3CH=CHCl$. The ratio of the slope of the dashed straight line to that for $(CD_3)_2CO$ is 0.67. The relative sensitivity of the instrument for $CH_3CHCH^{35}Cl$ and acetone was measured as 1 : 1.8 by using a Kr lamp (CaF_2). Thus the ratio of the rate of formation of these two products was tentatively $CD_3CCl=CD_2$:$(CD_3)_2CO$=1.2 : 1 considering the natural abundance of ^{35}Cl and ^{37}Cl.

E. Yields of the Products. The effect of the O_2 on the products was measured by adding O_2 to the system. The signal of $CD_3CCl=CD_2$ decreased and that of $(CD_3)_2CO$ increased when O_2 was added. Results are shown in Fig. 5. The two points on the left-hand side

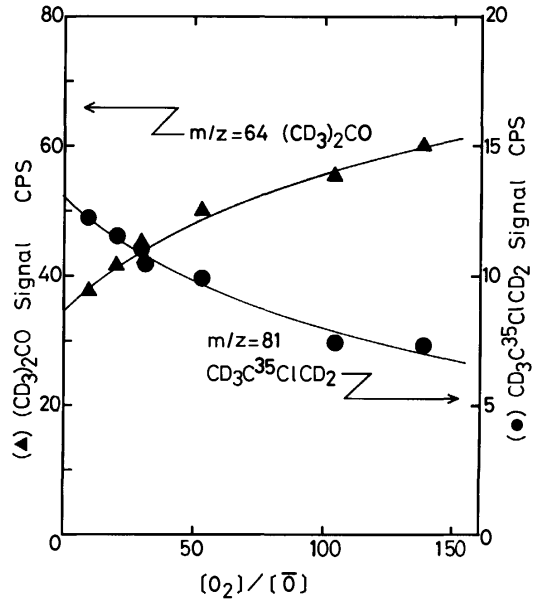

Fig. 5. Changes of signals of $(CD_3)_2CO$ at m/z=64 and $CD_3C^{35}Cl=CD_2$ at m/z=81 by the addition of O_2. Conditions: partial pressure (mTorr) $[O]_0$= 2.63, $[\bar{O}]$=2.62, $[(CD_3)_2CHCl]_0$=0.75, $[O_2]_0$= 26.53; reaction time=6.89ms; total pressure= 3.55 Torr. $[O_2]$ was calculated from $[O_2]_{added}+[O_2]_0-1/2[O]_0$. The points shown on the left-hand side are obtained from just $[O_2]_0-1/2[O]_0$ (no $[O_2]_{added}$).

Table 2. Rate Constants for the Reaction of $O(^3P)$+Chloro- and Fluoro-Propene at 298 K

Reaction	Rare constant at 298K / 10^{12} cm^3 molecule^{-1} s^{-1}	Method	Reference
$O+CH_3CH=CHCl$ (Cis- and trans-mixture)	(2.1±0.2)	Pseudo-first-order decay[a]	This work
$O+CH_2ClCH=CH_2$	(0.77±0.05)	Pseudo-first-order decay[b]	This work
$O+CD_3CCl=CD_2$	(2.5±0.1)	Steady-state approach	This work
$O+CD_3CH=CD_2$	(4.1±0.2)	Steady-state approach	Ref. 1
$O+CH_2FCH=CH_2$	0.73	Hg photosens. decomp of N_2O	Refs. 6, 7
$O+CH_3CF=CH_2$	1.7	Hg photosens. decomp of N_2O	Refs. 6, 7

a) The pseudo-first-order decay of $CH_3CH=CHCl$ was measured under the conditions: $[CH_3CH=CHCl]_0$= 0.023 Torr, $[O]_0$=1.24 mTorr, total pressure=4.5 Torr and reaction time 0.9—7.3 ms. A Kr lamp with a CaF_2 window (10.03 eV) was used to photoionize $CH_3CH=CHCl$. The decay of the signal was measured at m/z=76. b) The pseudo-first-order decay of $CH_2ClCH=CH_2$ was measured under the conditions: $[CH_2ClCH=CH_2]_0$=0.022 Torr, $[O]_0$=2.14 mTorr, total pressure=4.5 Torr and reaction time 0.9—7.3 ms. An Ar lamp with a LiF window (11.83 eV and 11.62 eV) was used to photoionize $CH_2ClCH=CH_2$. The decay of the signal was measured at m/z=76.

are the points obtained by the O_2 just surviving from the O_2/He discharge (no addition of O_2). If the fraction of $CD_3CCl{=}CD_2$ produced in Reaction 5 is represented by s_{5a}, the concentration of $CD_3CCl{=}CD_2$ at reaction time t is given by Eqs. 9 and 10 when both $O(^3P)$ and O_2 are present.

$$[CD_3CCl{=}CD_2] = f_{2a} + \left\{\frac{(s_{5a}-f_{2a})X}{1+X}\right\}\frac{k_1}{k_6}[\text{P-Cl}]\times [1-\exp(-k_6[\bar{O}]t)] \quad (9)$$

$$X = \frac{k_5}{k_2}\frac{[O_2]}{[\bar{O}]} \quad (10)$$

Similarly, the concentration of $(CD_3)_2CO$ at reaction time t is represented by Eq. 11;

$$[(CD_3)_2CO)] = f_{2b} + \left\{\frac{(s_{5b}-f_{2b})X}{1+X}\right\}k_1[\bar{O}][\text{P-Cl}]\,t \quad (11)$$

where s_{5b} refers to the fraction of $(CD_3)_2CO$ produced in Reaction 5 and [P-Cl] represents the concentration of $(CD_3)_2CHCl$. Since the value for k_5/k_2 was determined before, the concentrations of $CD_3CCl{=}CD_2$ and $(CD_3)_2CO$ can be plotted against $X/(1+X)$, as shown in Fig. 6. Using the values for k_1 and k_6 determined before and known initial concentration of $(CD_3)_2CHCl$ and the reaction time, values for f_{2a} and f_{2b} can be determined from the intercepts of the two lines. The values for s_{5a} and s_{5b} can be calculated from the slopes of the two straight lines in Fig. 6. Here, the instrumental sensitivity of $CH_3CH{=}CHCl$ was used in order to estimate the absolute concentrations of $CD_3CCl{=}CD_2$ ($^{35}Cl{+}^{37}Cl$). Values obtained are 0.31±0.03 for f_{2a}, 0.24±0.03 for f_{2b}, 0.035±0.003 for s_{5a}, and 0.56±0.05 for s_{5b}.

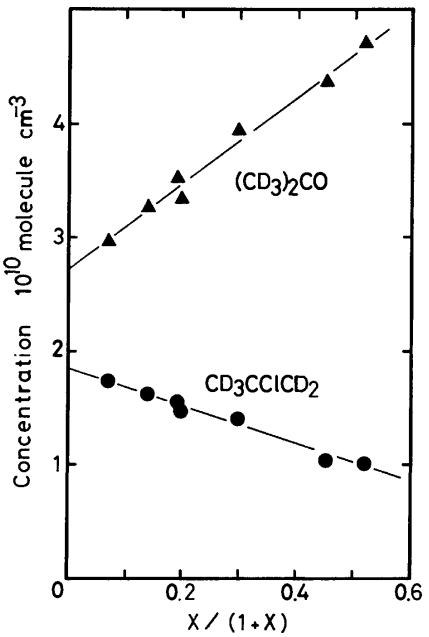

Fig. 6. The absolute concentrations of $(CD_3)_2CO$ and $CD_3CCl{=}CD_2$ ($^{35}Cl{+}^{37}Cl$) are plotted against $X/(1+X)$. Conditions are the same as the case of Fig. 5.

Table 3. Sum of the Heat of Formation of the Products of Reaction of $(CH_3)_2CH{+}O$ and $(CH_3)_2CCl{+}O$

Reaction	ΔH/kcal mol^{-1} a)
$C_3H_6{+}OH$	14.2
$(CH_3)_2CO{+}H$	−0.9
$CH_3CHO{+}CH_3$	−5.7
$CH_3CCl{=}CH_2$ b)$+OH$	3.3
$(CH_3)_2CO{+}Cl$	−22.9
$CH_3COCl{+}CH_3$	−24.2

a) Values of H^0_{298} are from Ref. 4. b) Calculated by the group additivity rule, Ref. 11.

$$(CD_3)_2\dot{C}Cl + O \xrightarrow{31\pm3\%} CD_3CCl{=}CD_2$$
$$\xrightarrow{24\pm3\%} (CD_3)_2CO \quad (2)$$

$$(CD_3)_2\dot{C}Cl + O_2 \xrightarrow{3.5\pm0.3\%} CD_3CCl{=}CD_2$$
$$\xrightarrow{56\pm5\%} (CD_3)_2CO \quad (5)$$

The yield of $CD_3CCl{=}CD_2$ from the oxygen atom reaction was 31%. This yield is smaller than the corresponding formation of $CD_3CH{=}CD_2$ (61%) in the reaction of $O{+}(CD_3)_2\dot{C}H$. On the other hand the yield of $(CD_3)_2CO$ (24%) is larger than that obtained in the $O{+}(CD_3)_2\dot{C}H$ reaction (18%). The results suggest that the probability of the deuterium abstraction from the radicals is decreased by the chlorine substitution for a hydrogen at 2-position of the isopropyl radical. The results might be explained from the exothermicity of the product channels shown in Table 3. The exothermicity of the addition routes was relatively raised by the chlorine substitution. Although the formation of CD_3COCl could not be observed, the most probable product corresponding to the residual 45% is CD_3COCl.

The channel of the deuterium abstraction (the $CD_3CCl{=}CD_2$ formation) decreased by the addition of O_2 and that of the oxygen atom addition (the $(CD_3)_2CO$ formation) increased as the case of the $(CD_3)_2\dot{C}H$ radical. These products are probably produced by the reaction of oxygen atoms with $(CD_3)_2CCl(O_2\cdot)$ radicals as described in the case of the $(CD_3)_2\dot{C}H$ radical.

$$(CD_3)_2\dot{C}Cl + O_2 \xrightarrow{+M} (CD_3)_2CCl(O_2\cdot) \quad (5)$$

$$(CD_3)_2CCl(O_2\cdot) + O \rightarrow \begin{cases} CD_3CCl{=}CD_2 + OD + O_2\ (3.5\%) & (12a) \\ (CD_3)_2CO + Cl + O_2\ (56\%) & (12b) \\ CD_3COCl + CD_3 + O_2\ (40\%) & (12c) \end{cases}$$

In the case of Reaction 12, product channels are affected more directly by the exothermicity.

Referenses

1) N. Washida, Preceeding paper.
2) A. Murray III and D. L. Williams, "Organic Syntheses

with Isotopes" Part II, Interscience, New York (1958), p. 1408.

3) This condition was determined by the same reason as Ref. 14 in paper I.

4) H. M. Rosenstock, K. Draxl, B. W. Steiner, and J. T. Herron, "Energetics of Gaseous Ions," *J. Phys. Chem. Ref. Data*, **6**, Suppl. 1, 1 (1977).

5) J. T. Herron and R. E. Huie, *J. Phys. Chem.*, **73**, 1326 (1969).

6) S. J. Moss and K. R. Hennings, *Trans. Faraday Soc.*, **65**, 415 (1969).

7) J. T. Herron and R. E. Huie, *J. Phys. Chem. Ref. Data*, **2**, 467 (1973).

8) R. J. Cvetanovic, "Advances in Photochemistry," ed by W. A. Noyes, Jr., G. S. Hammond, and J. N. Pitts, Jr., Interscience, New York, **1**, 115 (1963).

9) R. E. Huie and J. T. Herron, *Prog. React. Kinet.*, **8**, 1 (1975).

10) R. Atkinson and J. N. Pitts, Jr., *J. Chem. Phys.*, **67**, 2492 (1977).

11) S. W. Benson "Thermochemical Kinetics, Method for the Estimation of Thermochemical Data and Rate Parameters," 2nd ed, John Wiley & Sons, New York (1976), p. 272.

 © 1987 The Chemical Society of Japan Bull. Chem. Soc. Jpn., 60, 3757—3764 (1987)

Oxidation of $(CD_3)_2\dot{C}X$ Radicals. III. Reaction of 2-Propanol and $(CD_3)_2\dot{C}(OH)$ Radicals with Atomic Oxygen

Nobuaki WASHIDA
Division of Atmospheric Environment, The National Institute for Environmental Studies,
P.O. Tsukuba-gakuen, Ibaraki 305
(Received April 10, 1987)

The reaction of oxygen atoms with 2-propanol was studied in a fast flow system coupled with a photoionization mass spectrometer. Radicals formed in the primary attack of $O(^3P)$ atoms on 2-propanol were photoionized by the Xe lamp and identified as the $(CH_3)_2\dot{C}(OH)$ radical from $(CH_3)_2CH(OH)$ and $(CH_3)_2CD(OH)$ and the $(CD_3)_2\dot{C}(OH)$ radical from $(CD_3)_2CH(OH)$. The major primary product in the subsequent reaction of $O+(CD_3)_2\dot{C}(OH)$ was found to be acetone, $(CD_3)_2CO$, (62±4%). Formation of 1-propen-2-ol, $CD_3C(OH)=CD_2$, by deuterium abstraction and acetic acid, CD_3COOH, by oxygen addition were observed in the reaction of $O+(CD_3)_2\dot{C}(OH)$. In the reaction of $^{18}O+(CD_3)_2\dot{C}(OH)$, the acetone produced was mostly $(CD_3)_2CO$. This fact shows that acetone is produced predominantly by the hydrogen abstraction by $O(^3P)$ from the O-H in the $(CD_3)_2\dot{C}(OH)$ radical. A part of the acetone is produced also by the addition of $O(^3P)$ to the $(CD_3)_2\dot{C}(OH)$ radical; i.e., a small but significant signal of $(CD_3)_2C^{18}O$ was observed in the reaction of $^{18}O+(CD_3)_2\dot{C}(OH)$. The competition experiment between $O(^3P)$ and O_2 for the $(CD_3)_2\dot{C}(OH)$ radical shows that $(CD_3)_2\dot{C}(OH)$ react (0.16±0.02) times as fast with O_2 as with $O(^3P)$. This result suggests that the reaction of $(CD_3)_2\dot{C}(OH)$ with O_2 is very rapid. It is proposed that the rapid reaction is hydrogen abstraction by O_2 from the O-H in the $(CD_3)_2\dot{C}(OH)$ radical to form acetone and HO_2.

The study is extended[1] to reactions of oxygen atoms with 2-propanol and $(CD_3)_2\dot{C}(OH)$ radicals. There have been a few reports on the mechanism and the rate of the O+2-propanol reaction. Kato and Cvetanovic[2] studied the reaction of 2-propanol with oxygen atoms produced by the mercury photosensitized decomposition of dinitrogen monoxide. They suggested that abstraction of an α-hydrogen atom from 2-propanol to give $(CD_3)_2\dot{C}(OH)$ radicals takes place in the primary step, because they found the formation of pinacol, $[C(CH_3)_2OH]_2$, as a product. A large amount of acetone observed in the system was explained as a product of the radical-radical reaction. A kinetic investigation[3] reports that the rate constant for the reaction of $O(^3P)$ with 2-propanol is 1.3×10^{-14} cm^3 molecule^{-1} s^{-1} at 298K with an activation energy of 2.2 kcal mol^{-1}.

$$(CH_3)_2CH(OH)+O(^3P)\rightarrow(CD_3)_2\dot{C}(OH)+OH \quad (1)$$

In the present study, the reaction of oxygen atoms with 2-propanol was investigated in a fast-flow reactor coupled with a photoionization mass spectrometer in order to examine the following questions: (1) Can the $(CD_3)_2\dot{C}(OH)$ radical produced by the selective abstraction of an α-hydrogen suggested by Kato and Cvetanovic be detected by the photoionization mass spectrometry ?; (2) What products are produced by the radical-atom reaction ? Possible radical-atom reaction processes in both hydrogen abstraction and the oxygen atom addition are:
abstraction;

$$(CD_3)_2\dot{C}(OH)+O\rightarrow\begin{cases}(CH_3)_2CO\ (m/z=58)+OH & (2a)\\ CH_3C(OH)CH_2\ (m/z=58)+OH & (2b)\end{cases}$$

addition;

$$(CD_3)_2\dot{C}(OH)+O\rightarrow\begin{cases}(CH_3)_2CO\ (m/z=58)+OH & (2c)\\ CH_3COOH\ (m/z=60)+CH_3 & (2d)\end{cases}$$

subsequent to Reaction 1. In the previous study of the reaction of oxygen atoms with 1-hydroxyethyl radicals,[4] formation of acetaldehyde produced by hydrogen abstraction, a type of Reaction 2a, was observed as a major product (80%). Formation of vinyl alcohol, and formic and acetic acids, types of Reactions 2b and 2d, respectively, could not be observed.

Experimental

The experimental apparatus and procedures were the same as those mentioned before.[1] 2-Propanol (from Wako Pure Chemical Ind.), propan-2-*d*-2-ol, $(CH_3)_2CD(OH)$, and propan-1,1,1,3,3,3-d_6-2-ol, $(CD_3)_2CH(OH)$, (both from Merck Sharp & Dohm) were used without further purification except degassing. All measurements were done at room temperature, 298±3K, under the conditions $[O]>2[2\text{-propanol}]$.[5]

Results

A. Reaction of 2-Propanol with $O(^3P)$. Radicals produced by the initial attack of $O(^3P)$ on three different 2-propanols such as $(CH_3)_2CH(OH)$, $(CH_3)CD(OH)$, and $(CD_3)_2CH(OH)$ were detected when a Xe resonance lamp having a sapphire window (8.44 eV) was used as a photoionization light source. Radical signals observed are shown in Fig. 1. Possible radicals produced by abstraction of an α-hydrogen (a) and a β-hydrogen (b) in each 2-propanol are as follows:

$$(CH_3)_2CH(OH)+O\rightarrow\begin{cases}(CD_3)_2\dot{C}(OH)\ (m/z=59)+OH & (1a)\\ \cdot CH_2CH(CH_3)(OH)\ (m/z=59)+OH & (1b)\end{cases}$$

$$(CH_3)_2CD(OH)+O \rightarrow (CD_3)_2\dot{C}(OH)\ (m/z=59)+OD \quad (3a)$$
$$\rightarrow \cdot CH_2CD(CH_3)(OH)\ (m/z=60)+OH \quad (3b)$$

$$(CH_3)_2CH(OH)+O \rightarrow (CD_3)_2\dot{C}(OH)\ (m/z=65)+OH \quad (4a)$$
$$\rightarrow CD_2CH(CD_3)(OH)\ (m/z=64)+OD \quad (4b)$$

Isotopic measurements shown in Fig. 1 demonstrate that the radicals observed are produced by selective abstraction of an α-hydrogen in 2-propanol as suggested by Kato and Cvetanovic.[2] Since no significant signals were observed at m/z=60 and 64 in Reactions 3 and 4 considering the natural abundance of ^{13}C (1.11%) and the background noise, it is concluded that more than 99% of the primary attack of $O(^3P)$ atoms on 2-propanol is abstraction of α-hydrogen (or deuterium).

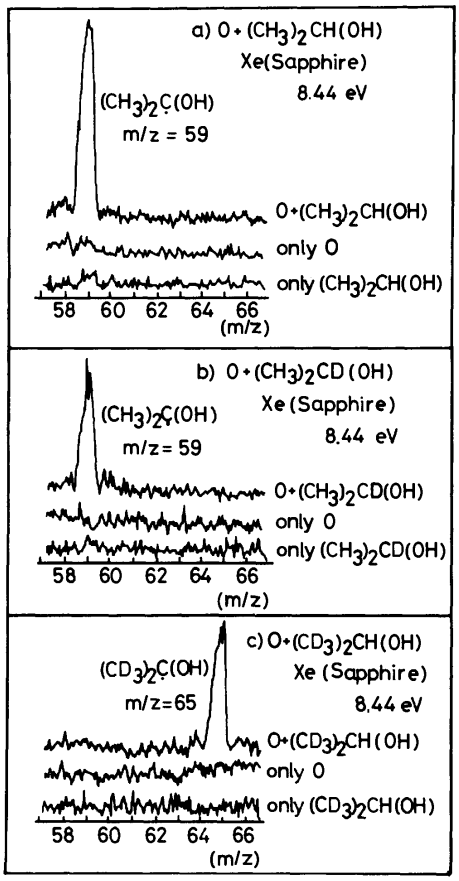

Fig. 1. Mass spectra of $(CH_3)_2C(OH)$ and $(CD_3)_2C(OH)$ radicals produced in O+2-propanol. A Xe lamp with a sapphire window (8.44eV) was used for the ionization. a) O+$(CH_3)_2$CH(OH); b) O+$(CH_3)_2$CD(OH); c) O+$(CD_3)_2$CH(OH). The conditions: $[O]_0$=0.87 mTorr; [2-propanol]$_0$=0.41 mTorr; reaction time 4.4 ms; total pressure 3.8 Torr.

The pseudo-first-order decay rates of $(CD_3)_2CH(OH)$ were measured in the presence of a large excess of oxygen atoms. $(CD_3)_2CH(OH)$ was photoionized by the Ar lamp with a LiF window (11.83 and 11.62 eV) and measured at m/z=66 (M^+). Values for k_4 obtained are listed in Table 1. The 95% confidence limits were calculated form the least-squares line using 8 points for each run and 24 points for the average values. The value of $(4.3\pm0.4)\times10^{-13}$ cm^3 molecule^{-1} s^{-1} for k_4 is 33 times larger than the rate for the reaction $(CD_3)_2$CH(OH)+O reported by Ayub and Roscoe.[3] The rate constant for the reaction O+$(CD_3)_2$CD(OH) was also measured and shown in Table 1. The rate for Reaction 3 was about 40% slower than that for Reaction 4 at 298K. The rate of reaction O+$(CH_3)_2$CH(OH) could not be measured[8] because signals for $(CD_3)_2CH(OH)$ coincide with one of the signals of products formed in the reaction of O+$(CH_3)\dot{C}$(OH) as will be described later.

B. Radical-Atom Reactions. Products produced in the reaction of oxygen atoms with radicals produced in Reactions 1, 3, and 4 were measured by using a Kr lamp having a CaF_2 window (10.03 eV). Mass spectra observed in the reaction of $(CH_3)_2CH(OH)+O$ are shown in Fig. 2a. The signal observed at m/z=58 should be from acetone, $(CH_3)_2CO$, and/or 1-propen-2-ol, $CH_3C(OH)CH_2$, which are expected in Reaction 2. The signal at m/z=59 is the isotope (^{13}C) signal of the molecule at m/z=58. The same mass spectra were observed in the reaction of $(CD_3)_2CD(OH)+O$. A small signal at m/z=63 and a large signal at m/z=64 were observed when $(CD_3)_2CH(OH)$ reacted with oxygen atoms (Fig. 2b). Possible reaction processes of the reaction $(CD_3)_2\dot{C}(OH)+O$ in both hydrogen abstraction and the oxygen addition reaction are:
abstraction;

$$O+(CD_3)_2\dot{C}(OH) \rightarrow (CD_3)_2CO\ (m/z=64)+OH \quad (5a)$$
$$\rightarrow CD_3C(OH)CD_2\ (m/z=63)+OH \quad (5b)$$

addition;

Table 1. First-Order Decay Rate for the Reaction[a] of 2-Propanol with Atomic Oxygen at 298K

	Total pressure	Flow velocity	$[O]_0$	[2-propanol]$_0$	$k\times10^{13}$
	Torr	m s^{-1}	mTorr	mTorr	cm^3 molecule^{-1} s^{-1}
O+$(CD_3)_2$CH(OH)	4.593	22.3	6.192	0.101	4.1±0.6
	4.642	22.3	4.127	0.0837	4.5±0.4
	4.638	22.3	8.236	0.0842	4.2±0.5
					Av. 4.3±0.4
O+$(CH_3)_2$CD(OH)	4.602	22.3	6.827	0.0923	2.7±0.3

a) Reaction time used was 0.9—9 ms for each run.

$$O+(CD_3)_2\dot{C}(OH)\rightarrow (CD_3)_2CO\ (m/z=64)+OH \quad (5c)$$
$$\rightarrow CD_3COOH\ (m/z=63)+CD_3 \quad (5d)$$

subsequent to Reaction 4. Since the ionization potential of acetic acid has been reported[9] to be 10.4 eV, acetic acid cannot be ionized by the Kr lamp with the CaF_2 window (10.03 eV). This was confirmed by the test that no signal of CH_3COOH was observed by adding known partial pressures of CH_3COOH to the reactor. Therefore, the signal observed at m/z=63 in Fig. 2b should be from 1-propen-2-ol $CD_3C(OH)=CD_2$. Since the signal intensity of $CD_3C(OH)=CD_2$ is much weaker than that of $(CD_3)_2CO$, most of the signal at m/z=58 in Fig. 2a might be from $(CH_3)_2CO$.

Signals obtained when the Ar lamp with the LiF window (11.83 and 11.62 eV) was used are shown in Fig. 3. Figures 3a′, 3b′, and 3c′ show mass spectra of three different isotopic 2-propanols. Parent ions of 2-propanols were observed in all cases. In addition to the parent ions, fragment ions produced by an α-hydrogen (deuterium) elimination from the 2-propanols are observed. In reactions of atomic oxygen with each 2-propanol, signals of acetic acid, CH_3COOH (m/z=60) for $(CH_3)_2CH(OH)$ and $(CH_3)_2CD(OH)$, and CD_3COOH (m/z=63) for $(CD_3)_2CH(OH)$, were observed in addition to the large signals of acetones. Since the instrumental sensitivities to acetone and acetic acid are 45 and 25 times higher than that for 2-propanol, respectively, the real concentrations of the products are much lower than they appear in Fig. 3.

In the reaction O+2-propanol, three products (acetone, acetic acid, and 1-propen-2-ol were observed as expected. Among them, acetone is the largest. Ace-

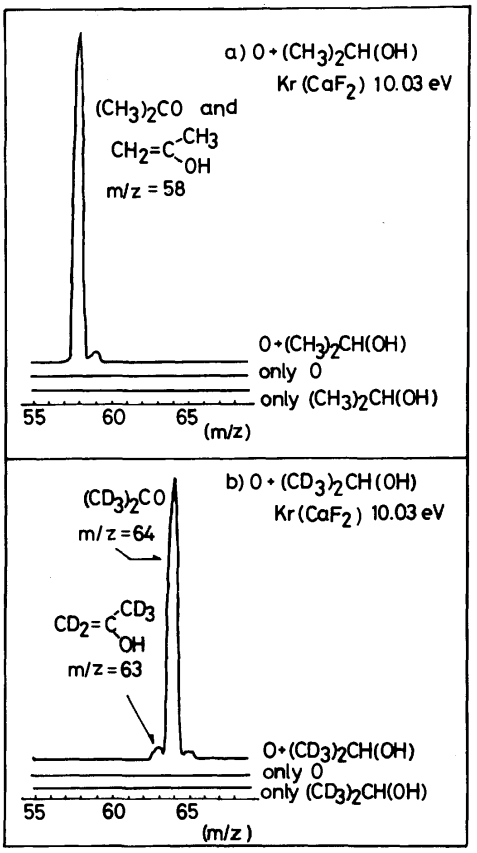

Fig. 2. Mass spectra of the reaction products produced in O+2-propanol. A Kr lamp having a CaF_2 window (10.03 eV) was used. a) O+$(CH_3)_2CH(OH)$; b) O+$(CD_3)_2CH(OH)$. The conditions: $[O]_0$=0.84 mTorr; [2-propanol]$_0$=0.27 mTorr; $[O_2]_0$=15 mTorr; reaction time 4.4 ms; total pressure 3.9 Torr.

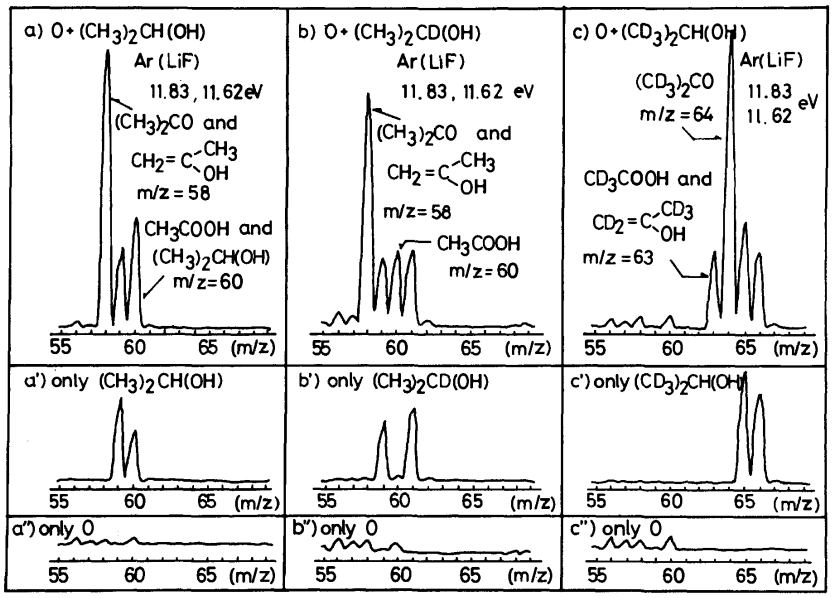

Fig. 3. Mass spectra of the reaction products produced in O+2-propanol. An Ar lamp with a LiF window (11.83 and 11.62 eV) was used. a) O+$(CH_3)_2CH(OH)$; b) O+$(CH_3)_2CD(OH)$; c) O+$(CD_3)_2CH(OH)$. The conditions: $[O]_0$=0.98 mTorr; [2-propanol]$_0$=0.28 mTorr; $[O_2]_0$=5.8 mTorr; reaction time 4.3 ms; total pressure 4.0 Torr.

tone can be produced by both hydrogen abstraction and oxygen addition reactions. In order to distinguish these two possibilities, 2-propanol was reacted with ^{18}O (19.2% of $^{36}O_2$ in $^{32}O_2$ was diluted in helium and discharged). When the $(CH_3)_2\dot{C}(OH)$ and $(CD_3)_2\dot{C}(OH)$ radicals react with the $^{18}O(^3P)$, the acetone produced by hydrogen abstraction and by oxygen addition should be different:

$$(CH_3)_2\dot{C}(OH)+{}^{18}O \rightarrow \begin{cases} (CH_3)_2CO(m/z=58)+{}^{18}OH & \text{abstraction} \quad (2a') \\ (CH_3)_2C^{18}O(m/z=60)+OH & \text{addition} \quad (2c') \end{cases}$$

$$(CD_3)_2\dot{C}(OH)+{}^{18}O \rightarrow \begin{cases} (CD_3)_2CO(m/z=64)+{}^{18}OH & \text{abstraction} \quad (5a') \\ (CD_3)_2C^{18}O(m/z=66)+OH & \text{addition} \quad (5c') \end{cases}$$

The mass spectra obtained are shown in Fig. 4. Weak signals at $m/z=60$ and 66 were observed in $^{18}O+(CH_3)_2\dot{C}(OH)$ and $^{18}O+(CD_3)_2\dot{C}(OH)$ reactions, respectively. Relative signal intensities at $m/z=58$ and 60 in the $(CH_3)_2\dot{C}(OH)+{}^{18}O$ reaction and at $m/z=64$ and 66 in the $(CD_3)_2\dot{C}(OH)+{}^{18}O$ reaction were observed to be 100 : 3.04±0.02 and 100 : 3.10±0.04, respectively. Since the 19.2% oxygen-18 was used in this study, acetone produced by the oxygen addition reaction is about 15% of the total acetone produced under these particular conditions and most of acetone is produced by the hydrogen abstraction from the OH of the radicals.

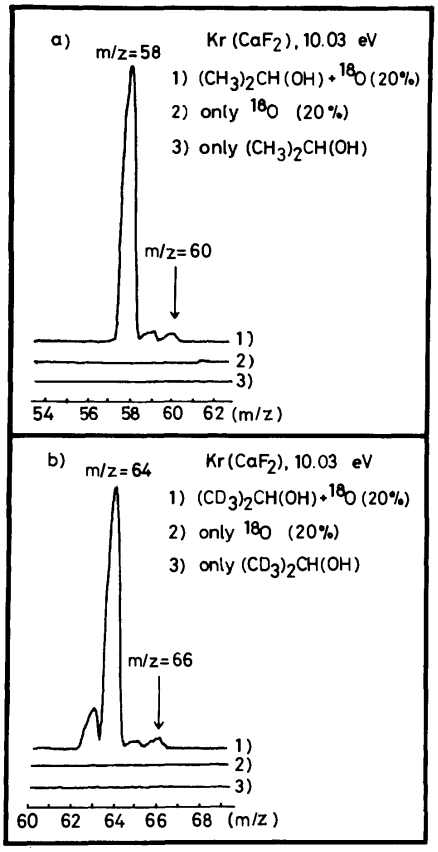

Fig. 4. Mass spectra of the reaction products produced in 2-propanol+^{18}O (19.2% of $^{36}O_2$ in $^{32}O_2$ was diluted in He and discharged). A Kr lamp with a CaF_2 window (10.03 eV) was used for the photoionization. a) $(CH_3)_2CH(OH)+{}^{18}O$; b) $(CD_3)_2CH(OH)+{}^{18}O$. The conditions: $[O]_0$= 0.61 mTorr; [2-propanol]$_0$=0.26 mTorr; $[O_2]_0$=3 mTorr; reaction time 4.4 ms; total pressure 3.9 Torr.

C. Competition between $O(^3P)$, O_2, and NO for $(CD_3)_2\dot{C}(OH)$. The signal obtained by Reaction 4a increased linearly with $(CD_3)_2CH(OH)$ partial pressure up to a few mTorr. The $(CD_3)_2\dot{C}(OH)$ signal was almost independent both of reaction time (0.5—5 ms) and oxygen atom concentration (0.2—1 mTorr†). This means that $(CD_3)_2\dot{C}(OH)$ radicals are in their steady-state concentration due to the balance between Reactions 4 and 5. The steady-state concentration of $(CD_3)_2\dot{C}(OH)$ radicals decreased when molecular oxygen was added to the system. This decrease is caused by the competition between $O(^3P)$ and O_2 for the $(CD_3)_2\dot{C}(OH)$ radicals and the competition would result in a Stern-Volmer type of equation,

$$\frac{[(CD_3)_2\dot{C}(OH)]^0_{ss}}{[(CD_3)_2\dot{C}(OH)]_{ss}} = 1 + \frac{k_7[O_2]}{k_5[\bar{O}]} \qquad (6)$$

where the superscript zero indicates the conditions with no O_2 present and k_7 is the effective second-order rate constant for the reaction of $(CD_3)_2\dot{C}(OH)$ with O_2.

$$(CD_3)_2\dot{C}(OH)+O_2 \rightarrow \text{Products} \qquad (7)$$

Results of O_2 addition experiment are presented in Fig. 5 by an open triangle and open circles. A value for $[(CD_3)_2\dot{C}(OH)]^0_{ss}$ was determined by plotting $([(CD_3)_2\dot{C}(OH)]_{ss})^{-1}$ against $[O_2]/[\bar{O}]$ and then determining $([(CD_3)_2\dot{C}(OH)]^0_{ss})^{-1}$ from the intercept of a least-square fit in order to remove the effect of O_2 surviving from the discharge. The average oxygen-atom concentration, $[\bar{O}]$, was calculated by the method mentioned before[1] using the value of $n=5$[10] (the correction was 4.6%). The amount of O_2 in the system was calculated from $[O_2]_{added}+[O_2]_0-1/2[O]_0$, where $[O_2]_0$ and $[O]_0$ represent the concentration of O_2 in the O_2-He mixture before discharge and the original concentration of oxygen atoms when the O_2-He mixture was discharged, respectively. The open triangle in Fig. 5 is the point which was obtained with no added O_2 (effect of O_2 just surviving from the discharge). The value for k_7/k_5 calculated from the slope of the plots (an open triangle and open circles) in Fig. 5 is (0.16±0.02). Error limits due to the scatter of plots were calculated by the least square with the 95% confidence limits. The value for k_7/k_5 suggests that the rate of the reaction of $(CD_3)_2\dot{C}(OH)+O_2$ is 6.4 times slower than that of the $(CD_3)_2\dot{C}(OH)+O(^3P)$ reaction.

When oxygen atoms were produced by NO titration of N atoms formed in a microwave discharge through

† 1 Torr=133.322 Pa.

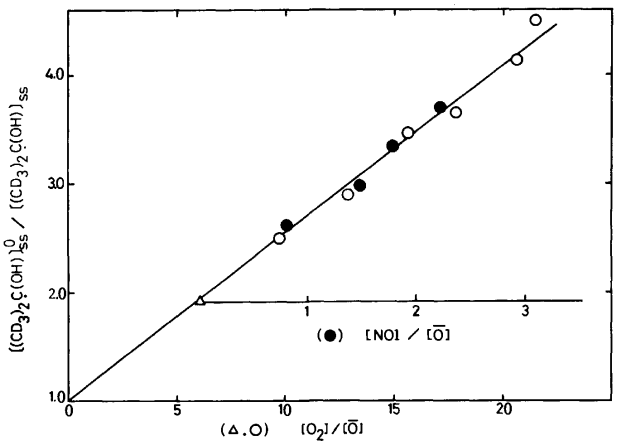

Fig. 5. Stern-Volmer plot for the competition between O_2 and $O(^3P)$ (open symbols), and NO and $O(^3P)$ (filled symbols) for $(CD_3)_2C(OH)$ radicals. A Xe lamp with a sapphire window (8.44 eV) was used to photoionize $(CD_3)_2C(OH)$. The conditions: $[O]_0$=0.632 mTorr; $[\bar{O}]$=0.588 mTorr; $[(CD_3)_2CH(OH)]$=0.288 mTorr; $[O_2]_0$=4.073 mTorr; reaction time=4.540 ms; total pressure= 3.909 Torr. $[O_2]$ was calculated from $[O_2]_{added}+[O_2]_0-1/2[O]_0$.

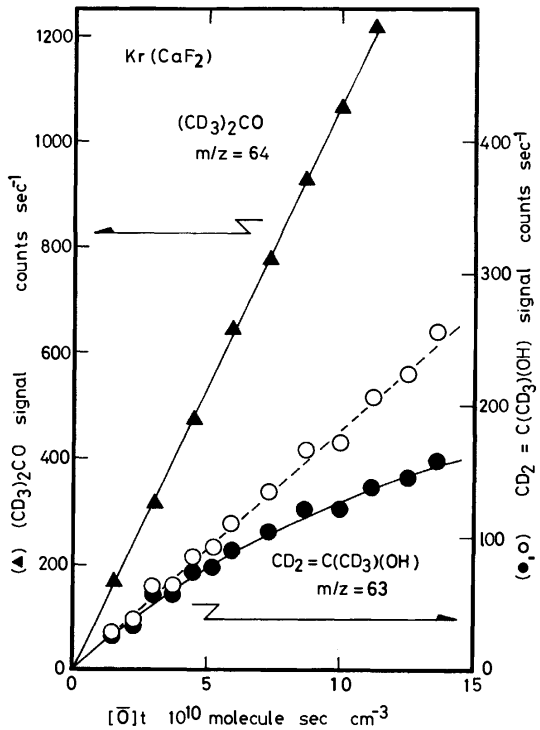

Fig. 6. Time dependence of $(CD_3)_2CO$ and $CD_3C(OH)=CD_2$ produced in the $O+(CD_3)_2CH(OH)$ reaction. A Kr lamp with a CaF_2 window (10.03 eV) was used for the photoionization. The conditions: $[O]_0$=0.517 mTorr; $[(CD_3)_2CH(OH)]_0$= 0.362 mTorr; $[O_2]_0$=1.667 mTorr; total pressure= 3.699 Torr. Reaction time used was 0.91—9.11 ms. Corrections for [O] were 12% or less. The $CD_3C(OH)=CD_2$ signals are corrected for the subsequent reaction to give $[CD_3C(OH)=CD_2]_T$ as indicated by open circles (see the text).

N_2-He mixture and were reacted with $(CD_3)_2CH(OH)$, signals of $(CD_3)_2\dot{C}(OH)$ radicals were quenched by the excess of NO. This means that the reaction of $(CD_3)_2\dot{C}(OH)+NO$ should be extremely fast. In order to measure the rate of the reaction $(CD_3)_2\dot{C}(OH)+NO$, small amount of NO were added to the system of $(CD_3)_2\dot{C}(OH)+O+O_2$. In these experiments, NO was added under the conditions shown by an open-triangle in Fig. 5 (the O_2 present in the reactor is just from the O_2 surviving from the discharge). The decrease of the steady-state concentrations of $(CD_3)_2\dot{C}(OH)$ radicals by the addition of the small amounts of NO are shown by the value of $[(CD_3)_2\dot{C}(OH)]^0_{ss}/[(CD_3)_2\dot{C}(OH)]_{ss}$ (solid circles in Fig. 5). From the slope of the plots of solid circles, the value for k_8/k_5 of (0.780±0.085) was obtained. Here, k_8 is the rate of the reaction $(CD_3)_2\dot{C}(OH)+NO$.

$$(CD_3)_2\dot{C}(OH)+NO \rightarrow (CD_3)_2CO+HNO \qquad (8)$$

The rate of the reaction of $(CD_3)_2\dot{C}(OH)+NO$ is extremely rapid. The rate is close to that of the $(CD_3)_2\dot{C}(OH)+O$ reaction. The large rate constant can be explained by a hydrogen atom abstraction by NO from the $(CD_3)_2\dot{C}(OH)$ radical. This was confirmed by measuring the signals of products. In the presence of NO, signals of acetic acid and 1-propen-2-ol disappeared and only the signal of acetone was observed.

D. Yields of the Products. Two products, $(CD_3)_2CO$ and $(CD_3)_2C(OH)CD_2$, were observed during the $O+(CD_3)_2CH(OH)$ reaction when the Kr lamp with the CaF_2 window was used. The time dependences of these products are shown in Fig. 6. On the time scale shown, $(CD_3)_2CO$ rises linearly with reaction time, while $CD_3C(OH)=CD_2$ increases not linearly. The time dependence of the $CD_3C(OH)=CD_2$ can be understood as the result that the $CD_3C(OH)=CD_2$ can react further with oxygen atoms.

$$CD_3C(OH)=CD_2+O \rightarrow \text{Products} \qquad (9)$$

The concentration of $CD_3C(OH)=CD_2$ is expressed by Eq. 10.

$$[CD_3C(OH)=CD_2] = \frac{f_{5b}k_4[(CD_3)_2CH(OH)]}{k_9 - k_4} \times (e^{-k_4[\bar{O}]t} - e^{-k_9[\bar{O}]t}) \qquad (10)$$

Here f_{5b} represents the fraction of Reaction 5b in the total reaction of $(CD_3)_2C(OH)+O$. Since the value for k_4 of 4.3×10^{-13} cm^3 $molecule^{-1}$ s^{-1} was determined, the plots of $CD_3C(OH)=CD_2$ shown in Fig. 6 can be fitted to Eq. 10. The best fit line is shown by a solid line in Fig. 6, and a value for k_9 of $(7.1\pm0.5)\times10^{-12}$ cm^3 $molecule^{-1}s^{-1}$ was calculated. The indicated errors due to the scattering of plots were calculated by the least square with the 95% confidence limits. The rate for Reaction 9 is 1.7 times faster than the rate for the reac-

tion O+ propene. It is possible to correct the observed $CD_3C(OH)=CD_2$ signals for subsequent reactions by multiplying each observed value by $k_9[\bar{O}]t[1-\exp(-k_9[\bar{O}]t)]^{-1}$ in order to give the total amount of $CD_3C(OH)=CD_2$ formed, $[CD_3C(OH)=CD_2]_T$. These corrected points are shown as open circles in Fig. 6, and they are well represented by the dashed straight line.

Signals for $(CD_3)_2CO$ at $m/z=64$ and CD_3COOH+ $CD_3C(OH)=CD_2$ at $m/z=63$ observed by using the Ar lamp with a LiF window are shown in Fig. 7. Since the rate for the reaction of acetic acid with atomic oxygen is expected to be very slow, the signal only from CD_3COOH should rise linearly with reaction time. This was confirmed in the reaction $O+(CH_3)_2\dot{C}D(OH)$, in which the signal of CH_3COOH can be observed without overlapping of other signals (see Fig. 3b).

The effect of O_2 on the yield of products was measured by adding O_2 to the system. The results are shown in Fig. 8. The signal of $(CD_3)_2CO$ increased while signals of $CD_3C(OH)=CD_2$ and CD_3COOH decreased[11] when O_2 was added. The two points on the left-hand side in each Figs. 8a and 8b are the points obtained from the O_2 just surviving from the O_2/He discharge (no addition of O_2). Since the standard sample gas of 1-propen-2-ol is not available, the absolute concentration of $CD_3C(OH)=CD_2$ cannot be determined. The absolute concentration of $(CD_3)_2CO$ was determined from the sensitivity of acetone to the instrument. The concentration of $(CD_3)_2CO$ is represented by Eqs. 11 and 12 when both $O(^3P)$ and O_2 are present in the system.

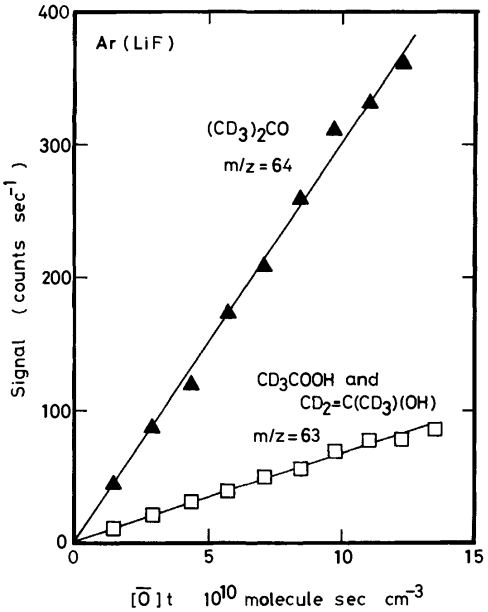

Fig. 7. Time dependence of signals at $m/z=63$ and 64 in the O+$(CD_3)_2CH(OH)$ reaction. An Ar lamp with a LiF window (11.83 and 11.62 eV) was used. The conditions: $[O]_0=0.496$ mTorr; $[(CD_3)_2CH(OH)]_0=0.289$ mTorr; $[O_2]_0=1.748$ mTorr; total pressure=3.791 Torr. Reaction time used was 0.91—9.11 ms. Corrections for $[\bar{O}]$ were 5% or less.

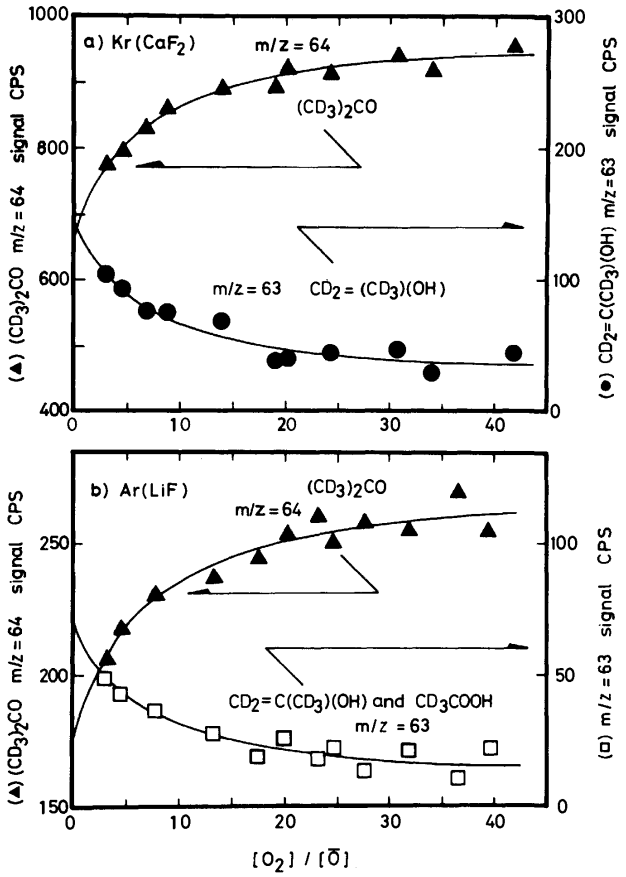

Fig. 8. Change of signals at $m/z=63$ and 64 with the addition of O_2. A Kr lamp with a CaF_2 window (a) and an Ar lamp with a LiF window (b) were used for the photoionization. The conditions for (a): $[O]_0=0.517$ mTorr; $[\bar{O}]=0.487$ mTorr; $[(CD_3)_2CH(OH)]_0=0.362$ mTorr; $[O_2]_0=1.667$ mTorr; reaction time=4.556 ms; total pressure=3.699 Torr. The conditions for (b): $[O]_0=0.496$ mTorr; $[O]_0=0.473$ mTorr; $[(CD_3)_2CH(OH)]_0=0.289$ mTorr; $[O_2]_0=1.748$ mTorr; reaction time=4.556 ms; total pressure=3.791 Torr. $[O_2]$ was calculated from $[O_2]_{added}+[O_2]_0-1/2[O]_0$. The points shown on the left-hand side are obtained from just $[O_2]_0-1/2[O]_0$ (no $[O_2]_{added}$).

$$[(CD_3)_2CO] = \left\{(f_{5a}+f_{5c})+\frac{(s_{7a}-f_{5a}-f_{5c})X}{1+X}\right\}\times k_4[(CD_3)_2CH(OH)][\bar{O}]t \quad (11)$$

$$X=\frac{k_7}{k_5}\frac{[O_2]}{[\bar{O}]} \quad (12)$$

Here s_{7a} is the fraction of $(CD_3)_2CO$ produced in Reaction 7. Using the value for k_7/k_4 determined before, the absolute concentrations of $(CD_3)_2CO$ are plotted against $X/(1+X)$ and are shown in Fig. 9. Under each experimental condition, values for $(f_{5a}+f_{5c})$ determined from the intercepts of lines in Figs. 9a and 9b are (0.64±0.05) and (0.60±0.06), respectively. From the

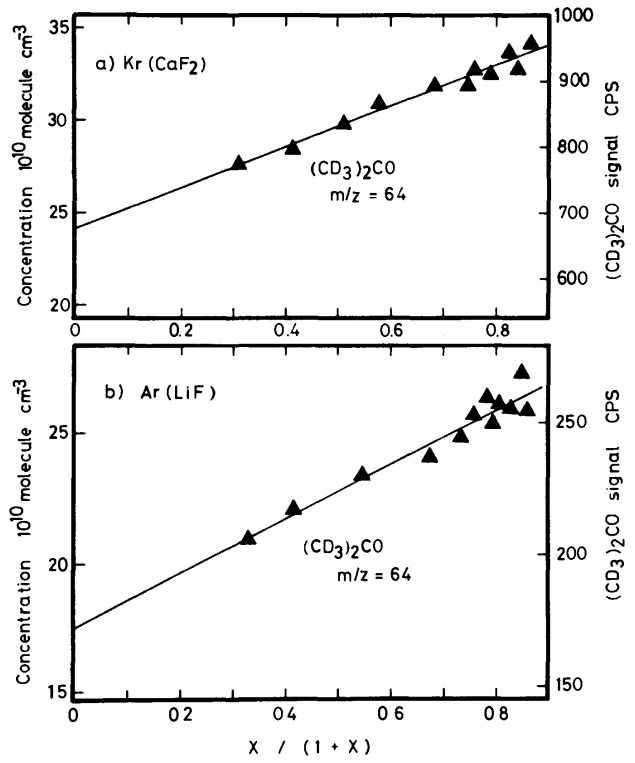

Fig. 9. The absolute concentrations of $(CD_3)_2CO$ are plotted against $X/(1+X)$. The conditions for (a) and (b) are the same as the cases of (a) and (b) in Fig.8, respectively.

slopes of straight lines shown in Figs. 9a and 9b, values for s_{7a} of (0.94±0.07) and (0.96±0.14) were calculated, respectively. The indicated errors due to the scattering of plots were calculated by the least square with the 95% confidence limits.

$$(CD_3)_2C(OH)+O \xrightarrow{(62\pm4)\%} (CD_3)_2CO \qquad \text{(5a) and (5c)}$$

$$(CD_3)_2C(OH)+O_2 \xrightarrow{(95\pm8)\%} (CD_3)_2CO \qquad \text{(7a)}$$

Signals at m/z=63 observed by the use of the Ar lamp consist of the signals of $CD_3C(OH)=CD_2$ and CD_3COOH. From the mass spectra shown in Figs. 3a, b, and c, however, it is probable that the greater part of the signal at m/z=63 is from CD_3COOH. Supposing that all the signals at m/z=63 is from acetic acid, the absolute concentrations of CD_3COOH were determined from the instrumental sensitivity of acetic acid. From the slope and intercept of the plots of $X/(1+X)$ vs. absolute concentrations of CD_3COOH, values for f_{5d} and s_{7d} can be calculated to be (0.28±0.04) and (0.02±0.06), respectively. Therefore, tentatively;

$$(CD_3)_2\dot{C}(OH)+O \xrightarrow{(28\pm4)\%} CD_3COOH \qquad \text{(5d)}$$

$$(CD_3)_2\dot{C}(OH)+O_2 \xrightarrow{(2\pm6)\%} CD_3COOH \qquad \text{(7d)}$$

Discussion

The selective abstraction of an α-hydrogen (deuterium) in the primary attack of $O(^3P)$ atoms on 2-propanol agreed well with the suggestion of Kato and Cvetanovic.[2] The result of the α-hydrogen abstraction agreed also with the case of O+ethanol reaction.[4] The rate constant for the reaction $O+(CD_3)_2CH(OH)$ at 298K, $(4.3\pm0.4)\times10^{-13}$ cm^3 $molecule^{-1}$ s^{-1}, was 33 times larger than the rate constant for $O+(CH_3)_2CH(OH)$ reaction reported by Ayub and Roscoe.[3] In the present study, the rate measurements were carried out under the conditions of $[O]_0/[2\text{-propanol}]_0 \geqslant 50$. Under these conditions, the consumption of oxygen atoms in the reactor (reaction time was 0.9—10 ms) was less than 5% of the original oxygen atom concentration on the basis of a stoichiometric factor of n=5.[10] On the other hand, the rate measurements by Ayub and Roscoe were done by observing the decay of oxygen atoms under a large excess of 2-propanol. Probably, many subsequent reactions are possible under their experimental conditions and their estimation of the stoichiometric factor for the decay of oxygen atoms is not correct.

The major primary product in the subsequent reaction of $(CD_3)_2\dot{C}(OH)$ radicals with atomic oxygen was found to be acetone (62±4%). Formation of 1-propen-2-ol and acetic acid was observed in addition to $(CD_3)_2CO$. In the previous work of the O+ethanol reaction system[4] acetaldehyde (79±8%), which is equivalent to acetone in the present reaction system, was found to be major primary product in the reaction of 1-hydroxyethyl radical with atomic oxygen. No formation of vinyl alcohol, formic and acetic acids were observed. In the present study, however, it was demonstrated that the yield of products was largely affected by the amount of O_2 surviving from the discharge; i.e., the yield of acetone (acetaldehyde for O+ethanol) increased and yields of 1-propen-2-ol (vinyl alcohol for O+ethanol) and acetic acid (formic or acetic acids for O+ethanol) decreased in the presence of O_2. Therefore, in the previous O+ethanol system, vinyl alcohol and formic or acetic acids probably could be observed if the measurements were carried out carefully taking notice of the effect of O_2.

The isotope (^{18}O) experiments showed that acetone was produced predominantly by the hydrogen abstraction by $O(^3P)$ from the O-H in the $(CD_3)_2\dot{C}(OH)$ radical, Reaction 5a′. The result is consistent with that obtained in the O+ethanol system. In the present study, however, it was found that acetone can also be produced by the addition of $O(^3P)$ to the $(CD_3)_2\dot{C}(OH)$ radical, Reaction 5c′, in small but significant yield.

The reaction of $(CD_3)_2\dot{C}(OH)$ radicals with molecular oxygen was very rapid. The rate of the reaction of $(CD_3)_2\dot{C}(OH)+O_2$ was just 6.4 times slower than that of the $(CD_3)_2\dot{C}(OH)+O(^3P)$ reaction. This competition ratio is quite similar to the case of the 1-hydroxyethyl radical.[4] The rate of the reaction of $(CD_3)_2\dot{C}(OH)$+NO was found to be much faster. The reaction proceeds as fast as with atomic oxygen. These rapid reactions can be explained by the two body reactions to form acetone and HO_2 (HNO), Reactions 7a

and 8.

$$(CD_3)_2\dot{C}(OH) + O_2 \rightarrow (CD_3)_2CO + HO_2 \qquad (7a)$$

Reaction 7a was proved by the isotope (^{18}O) experiment; that is, in the experiment shown in Fig. 4b, the signal at m/z=66, $(CD_3)_2C^{18}O$, disappeared by adding the $^{18}O_2$ (20%)/$^{16}O_2$ mixture gas. The formation of acetone by Reaction 7a is consistent with the results obtained from the photooxidation of 2-propanol in air.[12]

Conclusion

(1) $(CD_3)_2\dot{C}(OH)$ and $(CD_3)_2\dot{C}(OH)$ radicals produced by a selective abstraction of an α-hydrogen in the primary attack of $O(^3P)$ atoms on 2-propanol were detected directly by the photoionization mass spectrometer. The results of the present and earlier study[4] show that $O(^3P)$ atoms react with simple alcohols by abstracting the most weakly bonded hydrogen atoms in the alcohol molecules.

(2) The major primary product in the reaction of $(CD_3)_2\dot{C}(OH)$ radicals with atomic oxygen is acetone, $(CD_3)_2CO$, (62%). Formation of 1-propen-2-ol and acetic acid was also observed.

(3) Acetone is produce predominantly by the hydrogen abstraction by $O(^3P)$ from the O-H in the $(CD_3)_2\dot{C}(OH)$ radical. A part of acetone is produced also by the addition of $O(^3P)$ to the $(CD_3)_2\dot{C}(OH)$ radical.

(4) The rate of the reaction of $(CD_3)_2\dot{C}(OH)$ radicals with molecular oxygen is 6.4 times slower than the reaction with atomic oxygen. This rapid reaction is explained by the hydrogen abstraction by O_2 from the O-H in the $(CD_3)_2\dot{C}(OH)$ radical.

References

1) N. Washida, preceeding papers.

2) A. Kato and R. J. Cvetanovic, *Can. J. Chem.*, **46**, 235 (1968).

3) A. L. Ayub and J. M. Roscoe, *Can. J. Chem.*, **57**, 1269 (1979).

4) N. Washida, *J. Chem. Phys.*, **75**, 2715 (1981).

5) The reaction of 2-propanol with atomic oxygen is initiated by hydrogen abstraction, Reaction 1. The OH radicals produced react with 2-propanol faster than atomic oxygen. The rate constant of the 2-propanol+OH reaction has been reported[6,7] to be $(5—7)\times10^{-12}$ cm^3 molecule^{-1} s^{-1}. OH radicals are destroyed by the reaction OH+O→H+O_2 with a rate constant of $(3—4)\times10^{-11}$ cm^3 molecule^{-1} s^{-1}. Therefore, in order to make the effect of OH radicals on the formation of $(CD_3)_2\dot{C}(OH)$ radicals less than 10%, the concentration of oxygen atoms must be at least twice as large as the 2-propanol concentration.

6) A. C. Lloyd, K. R. Darnall, A. M. Winer, and J. N. Pitts, Jr., *Chem. Phys. Lett.*, **42**, 205 (1976).

7) R. Overend and G. Paraskevopoulos, *J. Phys. Chem.*, **82**, 1329 (1978).

8) Signals at m/z=59 ($M-1^+$) and 60 (M^+) were observed when $(CH_3)_2CH(OH)$ was photoionized by the Ar lamp with the LiF window (11.83 and 11.62 eV). As will be demonstrated later in Fig. 3, signals for $(CH_3)_2CO$ and CH_3COOH were observed at m/z=58 and 60, respectively when $(CH_3)_2CH(OH)$ was reacted with oxygen atoms. Further, the isotope (^{13}C) signal of $(CD_3)_2CO$ appeared at m/z=59. Since the sensitivities of the instrument to $(CH_3)_2CO$ and CH_3COOH were 45 and 25 times higher than that to $(CH_3)_2CH(OH)$, respectively, when the Ar lamp was used, the effect of the signals of both products on the $(CD_3)_2CH(OH)$ signals at m/z=59 and 60 can not be neglected. In the rate measurements of the reaction $(CH_3)_2CD(OH)$+O, signals for $(CH_3)_2CD(OH)$ were measured at m/z=61. The signal at m/z=61 coincides with the isotope (^{13}C) signal of CH_3COOH. In this case, however, since the signal of CH_3COOH was not so strong as $(CH_3)_2CO$, the effect of the isotope signal of CH_3COOH on the $(CH_3)_2CD(OH)$ signal at m/z=61 was less than 6% even when the 50% of $(CH_3)_2CD(OH)$ ws consumed in the reactor.

9) H. M. Rosenstock, K. Draxl, B. W. Steiner, and J. T. Herron, "Energetics of gaseous ions," *J. Phys. Chem. Ref. Data*, **6**, Suppl. 1, 1 (1977).

10) A stoichiometric factor of n=5 was used in the present study, because, as will be described later, the yield of acetone in the O+2-propanol reaction is much higher than that in the O+propane reaction, and acetone produced does not react further under the present experimental conditions.

11) The decrease of acetic acid by the addition of O_2 was confirmed also in the reaction of O+$(CH_3)_2CD(OH)$, in which the signal of CH_3COOH can be observed without the overlapping of the 1-propen-2-ol signal.

12) T, Ohta, H. Bandow, and H. Akimoto, *Int. J. Chem. Kinet.*, **14**, 173 (1982).

 © 1987 The Chemical Society of Japan Bull. Chem. Soc. Jpn., 60, 3765—3769 (1987)

Heat Capacity and Thermodynamic Properties of Bismuth in the Range 333 to 923 K

Walid Ahmad BADAWI,*,† H. A. BROWN-ACQUAYE, and Ali Esa EID
Department of Chemistry, Faculty of Science, Al-Fateh University, Tripoli, Libya
†P. O. Box 13539, Tripoli, Libya
(Received May 9, 1986)

Calorimetric studies on the behavior of the heat capacity of bismuth have been carried out in the range 333 to 923 K. Values of the enthalpy and entropy have been determined for selected temperatures. The enthalpy and entropy of fusion at 544.54 K are 11.360±0.014 kJ mol^{-1} and 20.86±0.03 JK^{-1} mol^{-1}, respectively. Appropriate polynomial temperature functions of the C_p for solid and liquid bismuth are given. Earlier reported increasing C_p at temperatures above 800 K proved not to be reliable. The heat capacity at constant volume decreased from 25.80 to 21.14 JK^{-1} mol^{-1} over the region 544.54 to 873 K. Due to beginning of higher-order transformation, the C_v of solid bismuth showed an excess over the harmonic value (3R).

Studies on the heat capacity and thermodynamic properties of solid and liquid bismuth have been undertaken with the views to obtain more accurate values of the C_p and of enthalpy and entropy of fusion since earlier ones showed discrepancies.[1-4]

Earlier works[4] on liquid bismuth showed increasing heat capacity at temperatures above 800 K. This was a somewhat surprising observation since decreasing C_p behavior is common for liquid metals. In order to understand this unusual behavior, we have been studying bismuth in the range 333 to 923 K.

The most recent study on solid bismuth[3] showed an excess of the C_v over the harmonic value ($3R$). This behavior was attributed to beginning of higher-order transformation. On the other hand, the curve of the C_v against temperature has not indicated any signal (such as a bend) which points to beginning transformation. This phenomenon has attracted our interest to investigate the C_v behavior in the solid region using adiabatic calorimeter for the C_p measurements.

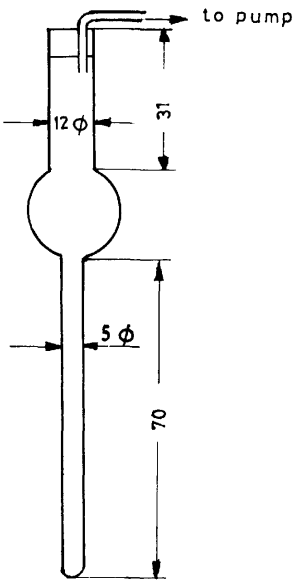

Fig. 1. Zintl funnel.

Experimental

Metal. Bismuth of extra purity grade procured from E. Merck Company was further purified by means of a melting device (similar to a Zintl funnel: Fig. 1). By this melting device, while the clean metal flows down into the lower tube of silica glass, the oxide layer remains apart in the first one. Analysis of the metal showed the presence of the following impurities in ppm by mass: Na: 0.1, Be: 0.1, Zn: 0.1, Pb: 0.1, Ag: 0.1.

Sample. The cylindrical metallic sample (ϕ=5 mm, h=20 mm) weighing 65.288 g was sealed in the sample container of Pyrex glass. Since bismuth expands on solidification after completion of the measurements, a cord of Pyrex glass was coiled spirally in the space of the sample to prevent breakage of the container. The external dimensions of the sample container were similar to the internal ones of the calorimeter (small corrections for small C_p).

Procedure and Calorimetric Technique. The measurement technique and calorimeter were described before.[5] The procedure employed depended on the method of primary indirect provision of energy under adiabatic conditions. The slightly modified calorimeter was tested by measurements on the heat capacity of a standard α-Al_2O_3 sample. The accuracy was estimated to 0.3%. The heating of the calorimeter occured with a speed of 0.6 K min^{-1} while that of the adiabatic shield was regulated to a speed of 0.5 K min^{-1}.

The sample container with a cover possessing holes for heater and thermopile was sealed in a calorimeter of silver which was suspended inside the shield of Cu-Al alloy (90 at-% Cu) with enclosed heater. Both calorimeter and shield were placed in a vertical tube furnace which in turn was protected by another larger one (principle of double shielding).

The temperature differences between the calorimeter and the shield were measured by means of a set of twelve differential Pt-to-(Pt+10 pass per cent Rh) thermopiles. These were connected in series and calibrated as follows: On comparing the thermal potential of these thermopiles with that of a standard Pt-Pt/Rh, we obtain a calibration curve giving the values of temperature with an accuracy of ±0.1 K. The measurement of the thermal potential of the thermopiles was made by means of a digital millivoltmeter (Hewlett-Packard Model 2401 C). The temperature drifts of the shield from the calorimeter temperature were of negligible importance. The observed short-term fluctuation of the null-point was mea-

Table 1. Experimentally Determined Constant Pressure Heat Capacity of Bismuth
M(Bi)=208.96 g mol^{-1}

T/K	C_p/JK^{-1}mol^{-1}	T/K	C_p/JK^{-1}mol^{-1}	T/K	C_p/JK^{-1}mol^{-1}	T/K	C_p/JK^{-1}mol^{-1}	T/K	C_p/JK^{-1}mol^{-1}
Series 1		Series 4 (continued)		Series 7		Series 9 (continued)		Series 11 (continued)	
332.98	27.14	542.26	29.35	462.97	28.19	544.54	134500	733.09	28.12
343.02	27.19	543.567	46.61	473.01	28.29	544.57	13278	743.21	28.07
353.01	27.22	544.256	145.96	483.11	28.41	545.10	130.8	Series 12	
362.81	27.27	544.516	1462.40	493.21	28.62	547.35	29.95	752.81	27.94
373.02	27.30	Series 5		502.92	28.57	553.17	29.93	763.13	27.85
383.11	27.40	532.17	28.85	513.31	28.73	Series 10		773.07	27.75
Series 2		539.48	29.28	Series 8		332.89	27.14	782.90	27.69
382.94	27.50	541.94	30.50	533.44	28.92	343.21	27.20	793.41	27.67
402.97	27.60	543.85	57.43	539.69	32.55	353.19	27.23	803.22	27.56
413.01	27.70	544.60	5488	544.69	5042.10	Series 11		813.11	27.50
423.12	27.80	544.54	161111	546.18	3405	613.13	29.45	823.39	27.47
432.97	27.90	544.55	62286	550.24	29.95	623.09	29.33	832.96	27.38
443.03	28.00	544.55	9673333	553.01	29.93	633.01	29.22	843.21	27.29
453.11	28.10	544.56	1453000	558.23	29.92	643.09	29.00	853.32	27.20
462.95	28.20	548.68	105.42	563.01	29.90	653.17	28.85	863.04	27.08
483.01	28.40	560.255	29.91	568.31	29.85	663.54	28.73	872.83	27.01
Series 3		Series 6		573.02	29.81	672.91	28.70	883.32	26.83
492.96	28.50	593.01	29.58	578.24	29.75	683.15	28.60	893.11	26.81
503.01	28.60	602.98	29.54	583.21	29.75	692.93	28.51	903.07	26.71
Series 4		613.02	29.45	Series 9		702.77	28.37	913.35	26.63
513.02	28.70	623.10	29.34	541.93	1897	712.86	28.29	923.04	26.51
523.11	28.80	633.02	29.23	544.54	364429	723.31	28.19		
533.09	28.90			544.54	253333				

sured to 2.5×10^{-4} K min^{-1}. The time needed to reach the adiabatic state was registered to 20 min. Excellent regulation of the temperature was obtained by means of a p-regulator.[6] A constant current supply (John Fluke Calibrator Model 382 A) was used in the measurement processes. The mueller bridge (Leeds & Northrup Model 8072, used in the current circuit) and other instruments were controlled by a digital computer. The thermometer resistance was measured with a Mueller bridge automated with stepping motors and a gated null-detector, operated by a computer of the type Hewlett-Packard 2224 B. Calibration of the platinum resistance thermometer used for determination of the fusion temperature of bismuth was made at the triple point of water and the melting points of tin and zinc on IPTS-68.[7] The derived temperatures were judged to correspond to the IPTS-68 to within 0.01 at 500 K and 0.1 at 1000 K. In fact the temperature increments were precisely measured to 0.0002 K.

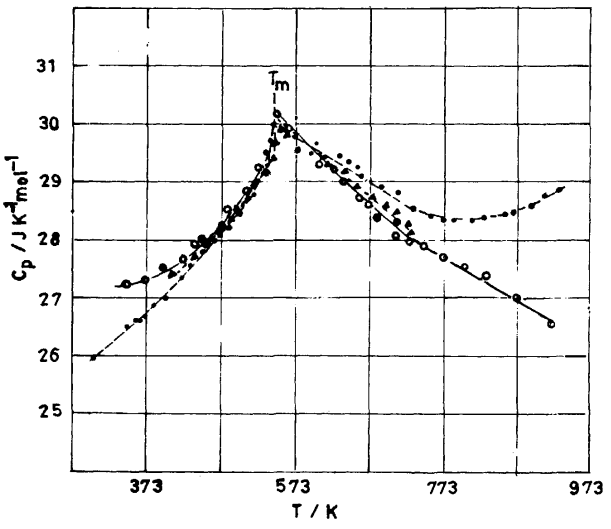

Fig. 2. Heat capacity of bismuth, —○— represents present results, —●— results by Grønvold,[4] —▲— results by Okhotin.[3]

The heat capacity of the empty calorimeter which represented 10 to 15% of the total heat capacity was indirectly measured: From measurements of the heat capacity for samples of silver of different masses and comparing these results with each other, the C_p of the empty calorimeter was calculated at the temperature of measurement. Neglect of this C_p value in the calculation of the total C_p would cause an error of about 0.10 to 0.15%. For this reason small corrections were derived to obtain accurate values of the C_p of bismuth.

From the calibration of the calorimeter on the exactly measured enthalpy of a standard sample of tin (Ref. 5), the "Interchange of heat constant" of the calorimeter has been determined in the whole region of temperature.

Results and Discussion

Heat Capacity of Bismuth. In Table 1 are listed the values of the heat capacity of bismuth in chronological order as determined in the present study. The reader can infer the approximate temperature increments in the determinations from the adjacent mean temperature in the table.

Figure 2 shows the curves of the C_p of solid and liquid bismuth, versus temperature. From curve-fitting calculations of the C_p values illustrated in Table 1, the appropriate temperature functions for solid and liquid bismuth were derived, respectively as

$$C_p = 24.081 + 9.023\times10^{-3}\,T - 3.1\times10^{-7}\,T^2 \quad \text{J K mol}^{-1},$$

$$C_p = 35.000 - 9.023\times10^{-3}\,T - 3.1\times10^{-7}\,T^2 \quad \text{J K mol}^{-1}.$$

The deviations ranged from 0 to 0.36% for solid bismuth and from 0.2 to 0.365% for liquid bismuth.

The most recently reported heat capacity measurements by Okhotin[3] carried out in the region 417 to 733 K, are in agreement with the present ones.

In the region 333 to 400 K, the values of the heat capacity of bismuth reported by Grønvold[4] differ from our values, although comparable results are obtained in the melting point region and in the liquid state from 545 to 634 K. The differences in the two results could not have been caused by temperature gradients in the calorimeter used in the present study since the temperature excursions of the shield from calorimeter in the null-point period were found to be negligible. Another area of differing results in the region 840 to 923 K, where the present studies show decreasing heat capacity while increasing C_p is reported by others.[4,8] To decide the dependency of the C_p on temperature and to shed light on the factors determining the behavior of the C_p in this striking region of temperature, we redetermined the measurements of the heat capacity in the whole range of temperature. It was found that the deviations of the comparable C_p values in both series of experiments which ranged from 0 to 0.05% are of negligible importance. Furthermore, C_p measurements were carried out in a wider range of temperature (333 to 960 K). The C_p value at 940, 950, and 960 K were measured to 26.20, 26.10, and 26.00 $JK^{-1}mol^{-1}$, respectively. This means that the C_p of liquid bismuth does not show the tendency to increase at high temperatures. Such behavior of the C_p is common to many metallic liquids. The decreasing heat capacity at high temperatures can be related to the pair correlation behavior. In the case of bismuth, the bonding changes into that of a mono-atomic gas with heat capacity decreasing toward $5R/2$ (20.35 $JK^{-1}mol^{-1}$). Taking this theory by Kincaid and Eyring[9] into consideration, the present C_p data at temperatures above 800 K seemed to be more reliable. It is also noteworthy that the existence of mono-atomic liquid bismuth was decided by other authors.[10] Also the present study could confirm the existence of mono-atomic liquid bismuth through X-ray diffraction study (to be published). It was observed that the neighbour distances of the straight chains in the structure decreased regularly with increasing temperature as follows: 850 K: 3.43 Å, 900 K: 3.60 Å, 950 K: 3.81 Å. This means that the potential energy of the system decreased with increasing temperature to reach the value of zero for a mono-atomic gas. As a result of this the C_p must decrease with increasing temperature to reach a certain value at $E_{pot}=0$. On the basis of the above discussion, earlier reported[4,8] increasing heat capacity at temperatures above 800 K proved not to be reliable.

Thermodynamic properties of bismuth. The values of C_p, $H°(T)-H°$ (298.15 K), and $S°(T)-S°$ (298.15 K) are collected in Table 2 for selected temperatures. For the solid region up to 542.52 K, the results have been least squares fitted by a polynomial expression, with a standard deviation of 0.29% for a single measurement. Similarly fitted expression with a standard deviation of 0.28% has been derived for liquid bismuth in the region beginning from 646.98 K. The accuracy of the obtained thermodynamic functions values was estimated to 0.2%. The present results of the enthalpy and entropy vary between 1 and 3% from those reported by other workers[1,2] and are in reasonable agreement with the values obtained by some researchers.[3,4]

In Table 3 are presented the results of the fractional enthalpy of fusion determination on bismuth. The values of the enthalpy and entropy of fusion are found to be

$$\Delta H°_{fus} = 11.360 \pm 0.14 \text{ kJ mol}^{-1},$$
$$\Delta S°_{fus} = 20.86 \pm 0.03 \text{ J mol}^{-1}.$$

As reported by Westrum,[11] the pre-melting excess heat capacity can be calculated through the following equation:

Table 2. Thermodynamic Properties of Bismuth

T/K	C_p/$JK^{-1}mol^{-1}$	$H°(T)-H°$(298.15 K)	$S°(T)-S°$(298.15 K)
298.15	26.80[a]	0	0
333	27.15	(0.93)	(3.00)
383	27.40	2.28	6.84
433	27.90	3.62	10.33
483	28.40	5.09	13.66
533	28.90	6.53	15.83
544.54(s)	29.40	6.77	16.46
544.54(l)	30.00	17.90	36.87
583	29.69	19.04	38.90
633	29.23	20.50	41.43
683	28.60	21.77	43.10
733	28.12	23.01	45.06
783	27.70	24.41	46.37
833	27.38	25.67	48.10
883	26.90	26.87	49.39
923	26.50	27.79	50.37

a) Extrapolated value. The values in brackets depend on the extrapolated C_p value at 298.15 K.

Table 3. Fractional Enthalpy of Fusion Determinations on Bismuth

T/K	$(\Delta T/2)$/K	C_p/JK^{-1}mol^{-1}	Δt/min	$\sum\Delta H$/J mol^{-1}	T_{fin}/K	$\Delta H_{fus}/\sum\Delta H$
Series 4, run 4—7						
542.255	0.547	29.35	14	0	543.102	
543.567	0.464	46.61	25	16.7	544.031	679
544.256	0.223	145.96	45	81.8	544.479	138.9
544.516	0.0366	1462.4	26	188.7	544.553	60.19
Series 5, run 2—11						
539.475	1.2375	29.28	46	0	540.712	
541.936	1.2235	30.5	50	30	543.159	4111
543.848	0.69	57.43	33	109	544.538	124.98
544.559	0.0215	5488	30	345	544.580	33.99
544.543	0.0045	161111	70	1795	544.588	6.279
544.553	0.0041	622857	79	6155	544.556	1.81
544.553	0.0002	9673333	117	9057	544.556	1.229
544.557	0.0005	1453000	39	10510	544.557	1.519
548.676	4.098	105.42	57	11374	552.774	1.000
560.255	7.43	29.91	52	11374	567.685	1.000
Sries 8, run 1—5						
533.443	0.723	28.92	91	0	534.889	
539.687	4.798	32.55	73	32.23	544.485	351.998
544.49	0.054	5042.1	26	539.5	544.544	21.099
546.181	1.587	3405	137	11346	547.768	1.000
550.235	2.454	29.94	28	11346	552.689	1.000
Sries 9, run 1—7						
541.934	2.697	1897	151	10234	544.541	1.110
544.542	0.0004	364429	35	10489	544.54	1.083
544.543	0.0005	253333	49	10717	544.543	1.060
544.544	0.001	134500	48	10986	544.545	1.034
544.565	0.009	13278	39	11225	544.574	1.012
545.101	0.516	130.8	147	11360	545.617	1.000
547.353	0.7465	29.95	27	11360	548.099	1.000

$\Delta H_{fus}=11360\pm14$ J mol^{-1}; $\Delta S_{fus}=20.86\pm0.03$ JK^{-1}mol^{-1}; $T_f=544.54$ K.

Table 4. Constant Volume Heat Capacity of Bismuth

T/K	C_p/JK^{-1}mol^{-1}	$(\alpha^2/x)vT$ / JK^{-1}mol^{-1}	C_v/JK^{-1}mol^{-1}
373	27.30	0.47	26.83
473	28.30	0.57	27.73
544.54(s)	29.40	0.70	28.70
544.54(l)	30.00	4.20	25.80
573	29.80	4.30	25.50
673	28.70	4.86	23.84
773	27.75	5.37	22.38
873	27.00	5.86	21.14

$$C_i(\text{prem}) = x'RT_f^2/[(T_f - T_i)^2 - (\Delta T/2)^2],$$

where x' is the total mole fraction of impurities, T_i the temperature and ΔT the temperature interval to which C_i (prem) refers. It was found that the pre-melting excess heat capacity is caused by impurities of about 1×10^{-4} M (1 M=1 mol dm^{-3}). These liquid-soluble and solid-insoluble impurities in the sample constrain 0.1 of bismuth to melt 1.1 K below the ideal melting point. This was taken into consideration to include slight pre- and post-melting contributions above the extrapolated heat capacities of solid and liquid bismuth in the above given enthalpy and entropy of fusion values. These values differ 2% from those obtained in earlier studies. On the basis of fractional melting experiments (Table 3), about 96% of the bismuth sample fused at 544.54 K and zero pressure. The calibration of the platinum resistance thermometer used for the determination of the T_f occured as described before. The observed melting point of bismuth is in good agreement with that one reported earlier.[3]

Constant volume heat capacity of bismuth. Table 4 represents the values of the heat capacity at constant volume for selected temperatures, calculated according to the following equation:

$$C_v = C_p - (\alpha^2/x)vT,$$

where α is the thermal coefficient, x the compressibility, and v the molar volume. The curve of the C_v against temperature is shown in Fig. 3.

The molar volume of solid and liquid bismuth was computed from the lattice data, while the study by Lucas[12] provided the data for liquid bismuth and for the thermal coefficient values. The compressibility values were derived from many sources.[13-19]

An excess over the harmonic value $3R$ is shown in the present estimate of the C_v of solid bismuth. This behavior is not common for all metals. In the case of bismuth, the expansion on solidification would cause a considerable dilation contribution in the C_v value due to lattice vibrations. On the other hand, the anharmonic contributions are small if compared with

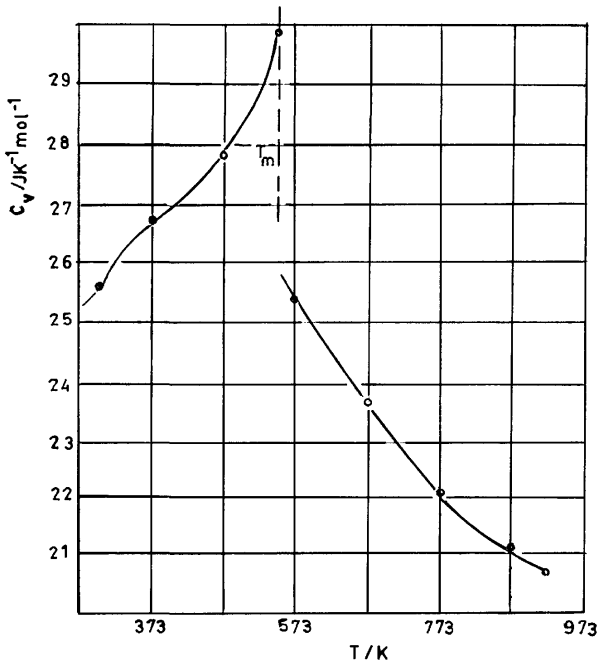

Fig. 3. Constant volume heat capacity of bismuth.

the dilation contributions observed in our study. This is due to the fact that the excess heat capacity from the disorder in the structure of the low-melting bismuth is small. Therefore, the excess over the harmonic value could be attributed to a beginning higher-order transformation. It is also noteworthy that the transformation to a new metallic phase was reported earlier.[10]

For liquid bismuth, the present C_v value is as low as 21.14 $JK^{-1}mol^{-1}$ at 873 K, calculated on decreasing C_p value over the region 840 to 900 K as compared to a value of 22.6 $JK^{-1}mol^{-1}$ at 900 K by Grønvold[4] who based his calculations on values of increasing C_p over the same region of temperature. The present value of C_v at 900 K seemed to be close to that limiting value given by Brillouin.[10] The observed drop in the C_v value over the region 540 to 900 K points to eventual radial distribution in this range of temperature.

References

1) K. K. Kelley, "Contributions to the Data on Theoretical Metallurgy. xiii," U. X. Bureau of Mines Bull. 584, Wash. D. C. (1960).
2) R. Hultgren, R. Li Or, P. D. Anderson, and K. K. Kelley, "Selected Values of Thermodynamic Properties of Metals and Alloys," Wiley, New York (1963).
3) V. S. Okhotin, et al. Tr. M. K. Energ. Inst. (1982).
4) F. Grønvold, *Acta Chem. Scand., Ser. A*, **29**, 945 (1975).
5) F. E. Wittig and A. Z. f. Stingle, *Angew. Phys.*, **23**, 1 Heft (1967).
6) F. E. Wittig, *Chem.-Ing.-Tech.*, **32** (1960).
7) The International Practical Temperature Scale of 1968, *Metrologia*, **5**, 35 (1969).
8) F. Wüst, A. Meuthen, and R. Durrer, *Forschungsarb. Ver. Deutsch. Ing.*, Heft 204 (1918).
9) J. F. Kincaid and H. J. Eyring, *Chem. Phys.*, **5**, 587 (1937); **6**, 620 (1938).
10) L. Brillouin, *Trans. Faraday Soc.*, **1937**, 54.
11) E. F. Westrum, Jr., G. T. Furukawa, and J. P. McCullough, "Experimental Thermodynamics," Butterworths, London (1968), Vol. 1, p. 189.
12) L. D. Lucas, *Mem. Sci. Rev. Metall.*, **1964**, 61.
13) "Gmelins Handbuch der Anorganischen Chemie," 8th ed., Wismuth, Ergänzungsband, Verlag Chemie (1964).
14) A. H. Jay, *Roy. Soc. (London)*, **A143**, 465 (1934).
15) R. B. Jacobs and A. Goetz, *Phys. Rev.*, **51**, 159 (1937).
16) E. R. Cave and L. V. Holroyd, *J. Appl. Phys.*, **31**, 1375 (1960).
17) G. K. White, *J. Phys. C*, **2**, 573 (1969).
18) O. J. Kleppa, *J. Chem. Phys.*, **18**, 1331 (1950).
19) S. I. Fillipov, N. B. Kazakov, and A. Pronin, *Izv. Vyssh. Uchebn. Zaved., Chern., Metall.*, **9**, 8 (1966).

Behavior of the Enthalpy of Formation in the Tin-Antimony System

Walid Ahmad BADAWI*,† and Ali Esa EID
Department of Chemistry, Faculty of Science, Al-Fateh University, Tripoli, Libya
†P. O. Box 13539, Tripoli, Libya
(Received May 9, 1986)

Calorimetric studies on the behavior of the enthalpy of formation in the tin-antimony system have been carried out at five different compositions (43.3—55 at -% Sb). The enthalpy of dissolution has been determined at 796.15 and 768.15 K. The enthalpy of formation is negative and takes a maximum value (2.906±0.002 kJ mol^{-1}) at 298.15 K for 50 at-% Sb. The molar enthalpy of mixing is more positive than that of formation. On comparing with partial molar enthalpy of mixing, the partial molar enthalpy of formation of tin is shifted to more negative values, while that of antimony to more positive values.

In recent years, the study of thermodynamic properties of binary systems of metals has attracted much interest. One such system, namely tin-antimony has been studied by some researchers eg. phase diagram by Predel and Schwermann[1] and heat of mixing by Wittig and Gehring[2] and other authors.[3] Also in this laboratory, work has been carried out in order to study the behavior of the enthalpy of formation of the β'-phase in the tin-antimony system[4] and to obtain the ratio of the enthalpies of formation to those of mixing. This would facilitate interpolation of the behavior of the enthalpy of formation at positions having indefinite structures.

Experimental

Sample. The metals used were of extra purity grade. These were procured from Riedel de Haen Co. The alloys samples were produced in cylindrical forms (ϕ=4.5—5mm; h=12—16 mm) by means of a melting device (Fig. 1). By this melting device, while the clean liquid metal flows down into the lower tube of quartz, the oxide layer remains apart in the first one. The mixture of tin and antimony was stirred mechanically with a stirrer made of ceramic for 30 min at 873 K. In order to reduce the effect of oxidation, argon gas was used as a protector during the melting process. The samples were tempered for 6 h at 673 K, 6 h at 623 K, and 192 h at 483 K.

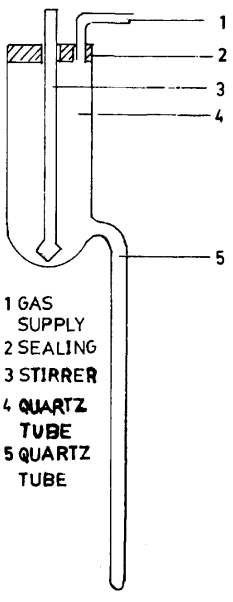

Fig. 1. Melting device.

Table 1. Lattice Constant of the β'-Phase in Sn Sb System (Found/Ref.)

x_{Sb}	a in Å (Found)	a in Å	(Ref.)
0.433	6.118	6.133	6
0.450	6.103	[6.136]	7
0.500	6.116	[6.120]	8
0.525	6.100	[6.136]	8
0.550	6.118	[6.134]	1

The values between the brackets were calculated from KX. The reported a values for 50 at-% Sb are different. They fluctuate between 6.104 and 6.138 Å.

The homogeneity of all the composition studied was established through testing the polished pictures prepared as described by Czochralski and Przyjemski.[5] Also X-ray (powder) photograph of the samples was taken and lattice constants have been determined (Table 1).

Calorimeter. The calorimeter used was a slightly modified version of the type described by Wittig and Gehring.[2]

Theory and Procedure

The enthalpy of dissolution of solid antimony in liquid tin can be determined at the temperature T_1 through the equations

$$-(1-x_2)\cdot \mathrm{Sn}(l, T_1)-x_2\cdot \mathrm{Sb}(s, T_1)+\mathrm{Sn}_{1-x_2}\mathrm{Sb}_{x_2}(l, T_1)=0, \quad (1)$$

$$h^s=-(1-x_2)\cdot h_1(T_1)-x_2\cdot h_2(T_1)+h_3(T_1), \quad (2)$$

where, h^s is the enthalpy of dissolution of solid antimony in liquid tin, h_3 the enthalpy of the alloy at the mole fraction of antimony x_2.

The enthalpy of dissolution has been determined at 796.15 and 768.15 K.

The enthalpy of formation is the special form of the enthalpy of reaction evolved by the formation of the substance from the elements. In the case of the tin-antimony alloy, the formation reaction is

$$-(1-x_2)\cdot \mathrm{Sn}(s, T_0)-x_2\cdot \mathrm{Sb}(s, T_0)+\mathrm{Sn}_{1-x_2}\mathrm{Sb}_{x_2}(s, T_0)=0, \quad (3)$$

where, T_0 is the initial temperature.

The enthalpy of formation is then

$$h^F=-(1-x_2)\cdot h_1(T_0)-x_2\cdot h_2(T_0)+h_3(T_0). \quad (4)$$

The indices 1, 2, and 3 indicate tin, antimony, and the alloy, respectively.

Subtraction of Eq. 4 from Eq. 2 yields

$$h^s-h^F=-(1-x_2)\cdot[h_1(T_1)-h_1(T_o)]-x_2[h_2(T_1)-h_2(T_o)]+[h_3(T_1)-h_3(T_o)]. \quad (5)$$

The term $h_3(T_1)-h_3(T_o)$ which appears in Eq. 5 is the enthalpy difference of the alloy; this was measured between 298.15 and 768.15 K; between 483.15 and 796.15 K. The enthalpy differences $h_1(T_1)-h_1(T_o)$ and $h_2(T_1)-h_2(T_o)$ are measured accurately (s. Table 3).

This procedure can be illustrated with reference to the following scheme:

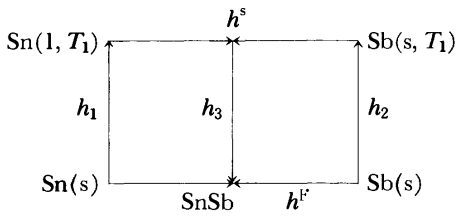

The non-measurable process of the enthalpy of formation at T_o will be substituted by (1) heating of tin and antimony at T_1, (2) measurement of the enthalpy difference of the single miscible phase between T_o and T_1 and (3) measurement of the enthalpy of dissolution at T_1. Employing the present procedure, the enthalpy of formation has been experimentally determined at five different compositions. From the obtained values of the enthalpy of formation an appropriate polynomial function is given (Eqs. 6 and 7).

Results and Discussion

(i) Lattice Constants. Results of the lattice constant determinations are presented in Table 1 together with the values reported by other authors.[1,6-8] The quoted lattice constants of the β'-Sn Sb vary regularly with the composition. The a value for 50 at-% Sb is in agreement with that reported by Osawa,[8] while those for other compositions differ 0.245 to 0.59% from earlier ones.

(ii) Enthalpy of Dissolution. Table 2 represents values of the enthalpy of dissolution of solid antimony in liquid tin at 768.15 and 796.15 K. The results have been least squares fitted by a polynomial expression, with a standard deviation of 0.4% for a single measurement. The enthalpy of dissolution varies regularly with the composition as the associated lattice constant data do.

(iii) Enthalpies. Table 3 represents values of $h_1(T)-h_1$(298.15 K); $h_1(T)-h_1$(483.15 K) and $h_2(T)-h_2$(298.15 K); $h_2(T)-h_2$(483.15 K) as determined by the present study. The average error of the individual measurement was found to be 0.32%, while the deviation of the single measurement of the earlier reported data (s. Ref. 9) was estimated to be 1—2%.

Values of $h°$(768.15 K)$-h°$(298.15 K) and $h°$(796.15 K)$-h°$(483.15 K) of the alloys are collected in Table 4 at five compositions. The deviation is 0.3% for a single measurement.

(iv) Integral and Partial Molar Enthalpy of Formation. The integral and partial molar enthalpies of formation at 298.15 and 483.15 K are illustrated in Table 5 for five different compositions. The average error of the individual measurement was found to be 0.41% for T=298.15 K and 0.3% for T=483.15 K.

Using the data in Table 5, it was possible to derive empirically, equations which represent the shapes of the curves drawn in Figs. 2 and 3 as follows:

Table 2. Experimentally Determined Enthalpy of Dissolution of Solid Antimony in Liquid Tin in J mol^{-1}
M(Sn)=118.7 g mol^{-1}; M(Sb)=121.76 g mol^{-1}

x_2	0.433	0.450	0.500	0.525	0.550
h^s(796.15 K)	7382	7729	8753	9281	9821
h^s(768.15 K)	7212	7552	8549	9113	9590

Table 4. Enthalpy Difference of the Alloys in J mol^{-1}
M(Sn)=118.7 g mol^{-1}; M(Sb)=121.76 g mol^{-1}

x_{Sb}	$h°$(796.15)$-h°$(483.15 K)	$h°$(768.15)$-h°$(298.15 K)
0.433	23790	28067
0.450	23796	28091
0.500	23822	28057
0.525	23903	28066
0.550	23816	28040

Table 3. Experimentally Determined Enthalpy Differences of Tin and Antimony
M(Sn)=118.7 g mol^{-1}; M(Sb)=121.76 g mol^{-1}

T/K	$h_1(T)-h_1$(298.15 K)	$h_1(T)-h_1$(483.15 K)	$h_2(T)-h_2$(298.15 K)	$h_2(T)-h_2$(483.15 K)
	J mol^{-1}	J mol^{-1}	J mol^{-1}	J mol^{-1}
298.15	0	—	0	—
400	2850	—	2612	—
500	5820	458	5239	410
505.11(s)	5985	623	—	—
505.11(l)	13010	7648	—	—
600	15755	10393	7912	3083
700	18617	13255	10670	5841
768.15	20550	15188	12654	7825
796.15	21354	15275	13432	8723
800	21462	16100	13541	8842
900	24309	18947	16552	11723

Table 5. Enthalpy of Formation of the β'-Phase in the Tin-Antimony System in $J\,mol^{-1}$, (Calcd) Found

x_{Sb}	$T=298.15$ K			$T=483.15$ K		
	$-h^F$	$-h_1^F$	$+h_2^F$	$-h^F$	$-h_1^F$	$+h_2^F$
0.433	(3736) 3724	8540	2625	(3960) 3970	9043	2698
0.450	(3541) 3542	8851	2950	(3755) 3741	9316	3042
0.500	(2908) 2906	9664	3849	(3092) 3070	10178	3995
0.525	(2559) 2549	10103	4266	(2726) 2787	10643	4437
0.550	(2189) 2200	10563	4662	(2338) 2324	11130	4856

$$h^F=-5.387-3.606x_2+17.12x_2^2;\ T=298.15\ K, \quad (6)$$

$$h^F=-5.642-3.970x_2+18.14x_2^2;\ T=483.15\ K. \quad (7)$$

It is apparent that the enthalpy of formation depends insignificantly on the temperature (Figs. 2 and 3).

The data in Table 5 clearly indicate that the enthalpy of formation increased with the increase of antimony mole fraction. This behavior is expected due to the charging of the Brillouin zones.

For a heteropolar behavior, a minimum of the enthalpy of formation is expected to appear at 40 at-% Sb. This minimum could not be observed in the normally experimental values. This is due to the fact that the deformation energy constrains the minimum of the enthalpy of formation to shift from a stoichiometric composition to other mole fraction of antimony.

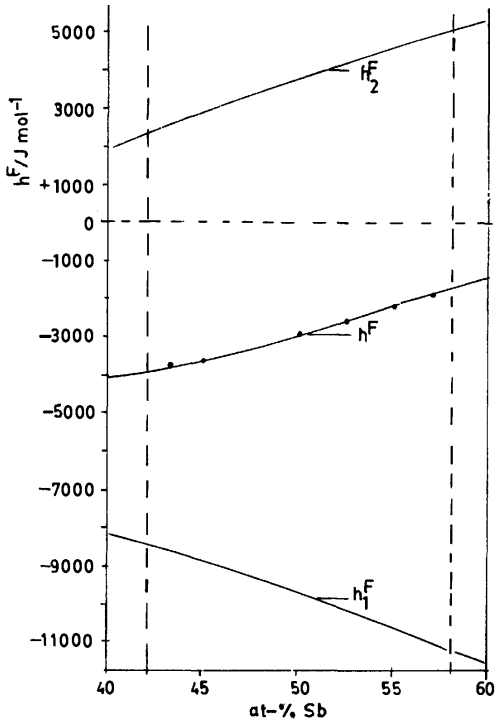

Fig. 2. Integral and partial enthalpy of formation in the tin-antimony system at 298.15 K.

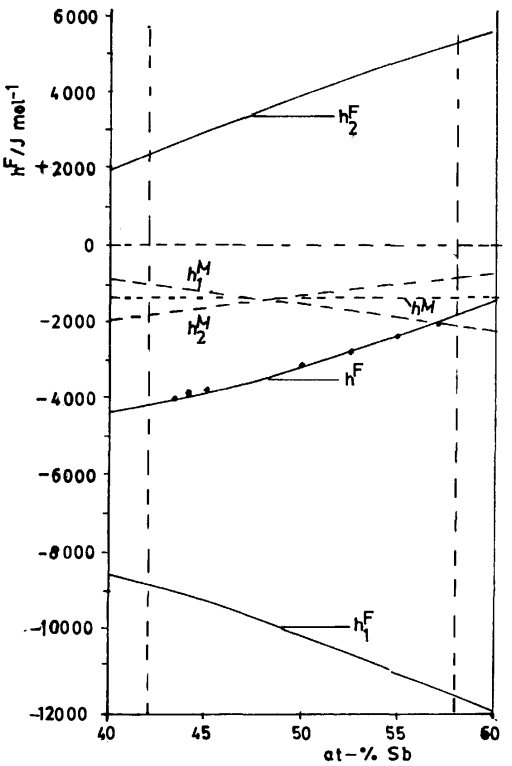

Fig. 3. Integral and partial enthalpy of formation in the tin-antimony system at 483.15 K.

The partial molar enthalpies of formation of tin and antimony are given by

$$h_1^F=h^F-x_2\cdot(\partial h^F/\partial x_2)_{T,p}, \quad (8)$$

and

$$h_2^F=h^F-(x_2-1)\cdot(\partial h^F/\partial x_2)_{T,p}. \quad (9)$$

Using Eqs. 6, 7, 8, and 9, we have

$$h_1^F=-5.385-17.12\,x_2^2 \quad h_2^F=+8.13-17.12\,(x_2-1)^2 \quad T=298.15\ K, \quad (10)$$

$$h_1^F=-5.642-18.14\,x_2^2 \quad h_2^F=+8.527-18.14(x_2-1)^2 \quad T=483.15\ K. \quad (11)$$

The curve in Fig. 3 shows that the partial molar enthalpy of antimony is positive and shifts to more positive values at higher composition. This is due to the insertion of the larger antimony atom in the structure of Sn Sb which becomes instable at higher mole fraction of antimony. The structure exhibits a higher tension resulting from the deformation work which is associated with the insertion of the antimony atom in th structure.

The partial molar enthalpy of tin is negative and becomes more negative at higher composition.

A hypothetical illustration of this behavior is probably that a poor fraction of tin p-electrons builds a weak bond with antimony ions. At higher mole fraction of antimony, the equilibrium shifts for the benefit of the delivery of further electrons on antimony.

On the basis of the above discussion, we come to the

following conclusion:

(1) The average molar enthalpy of mixing is more positive than that of formation.

(2) On comparing with partial molar enthalpy of mixing, the partial molar enthalpy of formation of tin is shifted to more negative values, while that of antimony to more positive values.

References

1) B. Predel and W. Schwermann, *J. Inst. Metals*, **99**, 169 (1971).

2) F. E. Wittig and E. Z. f. Gehring, *Naturforshung*, **18a**, 351 (1963).

3) A. Yazawa, T. Kawashima, K. Itagaki, *Nippon Kinzoku Gakkaishi*, **32**, 1288 (1968).

4) B. C. Ellwood, "The Equilibrium Diagram of the System Tin-Antimony," J. Wiley, London (1956) 1/6.

5) J. Czochralski and E. Przyjemski, *Wiadomosci Inst. Metallurg. Metaloznawstwa*, **3**, 113 (1936).

6) C. A. McKay, *J. Appl. Crystallogr.*, **2**, 295/7 (1969).

7) E. G. Bowen and W. Morris-Jones, *Philos. Mag.*, 7/12 (1931) 441/62, 446.

8) A. Osawa, *Nature*, 2124 (1929) 14.

9) Hultgren et al., "Selected Values of the Thermodynamic Properties of Metals and Alloys," American Society for Metals, Metals Park, Ohio (1973).

The Study of Planarized and Planar Cyclohexane Rings on the Basis of Molecular Mechanics

Helena Dodziuk
Institute of Organic Chemistry, Polish Academy of Sciences Warsaw 00-961, Kasprzaka 44, Poland
(Received June 25, 1986)

Recent rapid development of synthetic and theoretical methods has yielded molecules with unusual stereochemistry on carbon atom. One of the most interesting examples of such earlier unsought of arrangements is provided by planar cyclohexane rings. Few molecules of this kind have been synthesized and two others have been postulated on the basis of molecular mechanics calculations. In the present article a critical review of existing experimental and theoretical results is supplemented with a molecular mechanics study of a series of cyclohexanes fused with up to six 3-, 4-, and 5-membered rings causing the flattening of C_6 ring. The existing experimental data and the results of the calculations seem to indicate that the flattening is more pronounced when smaller and/or larger number of rings are fused. The applicability and limitations of molecular mechanics with the MM2 parameterization to the study of the flattening of cyclohexane ring have been critically analyzed. The synthetic efforts in this field seem to indicate that some results calculated for hypothetical molecules will be checked in the near future. Similarly to hypothetical [6]asterane and hexaprismane, the planarity of [6.3]coronane has been postulated.

Until recently, the following stable conformations of a cyclohexane ring has been taken into account: chair, twist, boat (and half-chair for a ring with a double bond). In their review on the nonchair conformations of cyclohexane rings published in 1974 Kellie and Riddell[1] limited themselves with the former three conformations. The half-chair and boat rings have been also lately discussed by Vereshchagin.[2] Due to a rapid development of synthetic and theoretical methods in the last 15 years molecules with considerable distortions from a standard cyclohexane geometry toward a planar cyclohexane ring or even those with completely planar rings have been reported. Several derivatives of *cis*- and *trans*-tris-σ-homobenzenes (**1**—**3**, complexes of **4**) have been found to exhibit planar sixmembered rings by means of X-ray analysis.[3-6] *trans*-Tris-σ-homobenzene **5** has been synthesized by Engelhardt and Lüttke.[7] The authors claimed that the central ring in the molecule is planar but no sound arguments in favor of the planarity have been given. A highly strained diplanar structure of hexamethylated derivative **6** with the torsional angle between the planes close to 180°[8] seems to validate the planarity of the parent molecule **5**. Planar C_6 rings have been also postulated for other types of hypothetical molecules by Osawa and Musso **7**[9] and Allinger and Eaton **8**[10] on the basis of molecular mechanics calculations.

Molecules with flattened but not completely planar cyclohexane rings are much more common. A *cis*-fusion of a 4- or 5-membered ring in **9** and **10**[11,12] was reported to yield a distorted C_6 ring with a flattening along the junction and an enhanced twisting in the other part of the ring and a fusion with cyclopropane is known to result in a half-chair conformation.[2,13] The overall flattening effect of a cis-fusion can be estimated by means of a sum of the absolute values of torsional angles within the C_6 ring α. The lowering of the α value from the cyclohexane value of 336°[14] is small for bicyclo[4.3.0]nonane (**9**), it increases for bicyclo[4.2.0]octane (**10**) and is the biggest for bicyclo[4.1.0]heptane (**11**) where the six-membered ring assumes a half-chair conformation (the corresponding values are given in Table 1). A cis-substitution of subsequent small rings seem to cause further flatten-

Table 1. The Calculated Steric Energies, Heats of Formation (in kcal mol^{-1}) and α Values and the Corresponding Experimental Data

Molecule	E_s	HOF	α calcd degrees	α exp. degrees
9[a]	18.3	−30.5 calcd −30.4 exp.[j]	317.6	314.0[b]
10	36.6	−5.7 calcd −6.4 exp.[j]	280.6	280.6[c]
11	16.6	1.2 calcd 0.4 exp.[d]	203.8	
cis-**13**[e]	27.1	29.6	153.3	
trans-**13**[e]	24.6	27.1	116.9	
cis-**5**	39.8	57.5[i]	7.8	
trans-**5**	36.3	54.0	15.8	
trans-**6**	55.6	20.8	58.6	f)
14	82.9	−20.1	201.0	
15	161.1	90.2	144.4	163.3[g]
16	98.9	−18.5	236.2	
17	193.2	114.4	135.9	
18	77.8	161.0	34.8	
19	100.0	215.6	0.1	
21	95.5	−24.9	238.5	256.8[h]

a) For the less stable *cis*-isomer studied in this work. b) Ref. 11. c) Ref. 12. d) Ref. 21. e) Favoured conformer with H(1) and H(2) in diequatorial disposition for *trans*-**13**. The experimental data of Ref. 17 are insufficient for α determination. See text for discussion of the α value. f) As above, the experimental data of Ref. 8 are insufficient for the α determination. See text for discussion of the α value. g) The experimental value refers to 13-(3,5-dinitrobenzoyloxy)hexacyclo-[12.2.0.0^{1,4}.0^{4,7}.0^{7,10}.0^{10,13}]hexadecane (**22**) reported in Ref. 18. h) The experimental value refers to the analogous compound **20**.[19] i) A MINDO/3 value of 52.7 kcal mol^{-1} has been reported.[32] j) Ref. 31.

ing of the ring under investigation. Examples of this type include several derivatives of *cis*- and *trans*-tricyclo[5.1.0.0^{3,5}]octanes (**12**) and those of *cis*- and *trans*-tricyclo[5.1.0.0^{2,4}]octanes (**13**).[2,15-17]

Recent elegant syntheses carried out by Fitjer and coworkers[18,19] yielded derivatives of polycycles **14** and **15** (exhibiting a considerable flattening of the C_6 rings) with the purpose to obtain the corresponding coronanes **16** and **17**.

Some molecular mechanics[20] studies of the molecules under investigation have been reported but they are inconsistent and deal only with some particular aspects. Boyd and coworkers[21] calculated thermochemical properties of a series of bicyclic molecules using their own force field. They have reported the calculated values of bond angles and torsional angles for the molecules **9**—**11** but, having no experimental data to compare with, they did not discuss the geometrical results obtained. In their electron diffraction study of *cis*- and *trans*-bicyclo[4.3.0]nonanes (**9**) Enden and Geise[11] repeated the molecular mechanics calculations for the molecules using the force field proposed by Ermer and Lifson.[22] Spelbos et al. repeated[12] the Boyd force field calculations similarly, in addition to their electron diffraction study of *cis*- and *trans*-fused bicyclo[4.2.0]octanes. An old diffraction work on bicyclo[4.1.0]heptane (**11**) has also been accompanied by simplified molecular mechanics calculations using still another force field.[13]

Heat of formation values (HOF) for **9** and **10** have been also calculated by Allinger[24] using his MM2 parameterisation[23] and the MM2 calculations for **11** has been only cited as unpublished results.[25] The same force field used by Osawa and coworkers[26] for tricyclic systems *cis*- and *trans*-**13** yielded results somewhat different from these reported in the present paper. They will be discussed below in some detail.

The aim of this work was to analyze by means of molecular mechanics[20] with the MM2 parameterization[23] the flattening of cyclohexane ring forced by *cis*-fusion of small ring(s) to find out regularities and to check the applicability of the method to the study of this interesting problem. For the sake of completeness the following series of molecules has been studied: **9**—**11**, *cis*- and *trans*-**13**, *cis*- and *trans*-**5**, *tarans*-**6**, **14**—**19**, and **21**. *cis*- and *trans*-tricyclo[5.1.0.0^{3,5}]octanes (**12**) have not been included into the series in view of the unreliability of one parameter involved in the calculations which will be discussed below.

The available experimental data and the results of the calculations carried out in the present work seem to indicate that *cis*-fusion of a small ring flattens cyclohexane ring and the flattening is more pronounced when more and smaller rings are involved in fusion with the C_6 ring. In the limiting case of *cis*- and *trans*-tris-σ-homobenzenes (**5**) and that of the hypothetical [6.3]coronane (**19**) the cyclohexane ring is completely planar. The calculations yielded also the HOF values

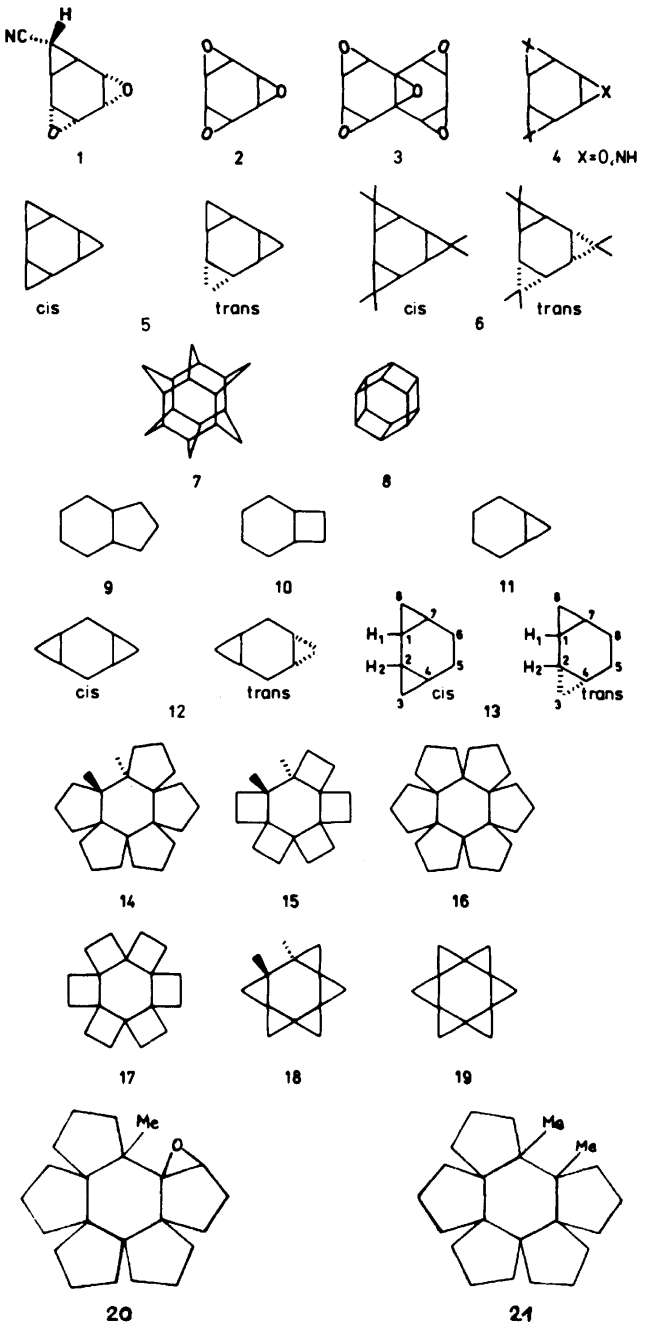

for the molecules under investigation.

Method

The calculations have been carried out using MM2-type program KNOW[27] on Mera 400 computer with the standard MM2 parameterization.[23] The molecules *cis*- and *trans*-**5**, *trans*-**6**, *cis*- and trans-**13**, **14**—**19**, and **21** represent highly strained systems for which the method could be of limited accuracy[28,29] or even fail since minor inaccuracies in potential functions and/or parameters used, which do not impair results for less congested molecules, can influence them for highly strained systems. Therefore, the calculations are also of value for detection of deficiencies and limitations of

the method itself. The problem is further complicated by the fact that the corresponding experimental data to compare with are scarce and the ones at our disposal often refer to solid state X-ray of derivatives of the molecules under investigation. In cases when such a comparison could be carried out (*trans*-**6**, **13**—**15**, **20**, **21**)† the results of the calculations performed in the present work seem to indicate that (1) the method yields reliable estimation of torsional angles (see Tables and discussion below) and, therefore, seems suitable for the analysis of planarity of cyclohexane ring. (2) On the other hand, it performs badly for bond lengths in highly congested systems. In particular, contrary to the report by Osawa et al.[26] we were not able to reproduce the bond lengths for *cis*- and *trans*-**13**.†† Consequently, (3) poor reproducibility of bond lengths and the condition for ring closure lead to wrong values of bond angles. Therefore, the calculations reported here seem to underline the need for further refinement of the MM2 force field parameters involving cyclopropane ring. On the other hand, the magnitude of the V_3 torsional constant of the type 22-22-1-22 chosen in Ref. 25 raises more serious objections. The value of 4.5 kcal mol^{-1} assigned to this constant in the MM2 parameterization has been questioned by Rüchardt et al.[28] We also believe that this value is unreliable since it is about 10 times bigger than other constants of similar type. Thus, as stated above, the lack of this constant precluded the performance of the calculations for the *cis*- and *trans*-tricyclo[5.1.0.0^{3,5}]octanes (**12**).

It is well-known that local minima pose a serious problem in molecular mechanics calculations.[20,30] In our case for the molecules **14** and **15** (and for the hypothetical molecules **17**—**19** and **21**) the minimization ends at local minima if one starts from a cyclohexane chair geometry. Only the use of the strongly planarized C_6 rings as input geometry guarantees the achievement of the absolute minimum.

Results and Discussion

The calculated steric energies E_s, heats of formation HOF, and the values of the sum of torsional angles within the C_6 ring in the molecules under investigation α are collected in the Table 1 together with the available experimental results and the calculated data from the literature. The trends exhibited by some torsional angles within the series **9**—**11** and **16**, **17**, and **19** are given in Table 2.

Some remarks should be made on the calculated steric energies. E_s values represent actually energies relative to hypothetical reference system. As such they can be compared on a physically sound basis only for isomers. For obvious reason the values calculated for the *cis*-compounds **5** and **13** are higher than those for the *trans*-molecules. More interesting seems the fact that the closure of the last ring in polycycles **14**—**19** yielded a higher value of the steric energy of [6.4]coronane **17** than the value for **15** while the corresponding values for [6.5]coronane (**16**) and [6.3]coronane (**19**) are lower than the ones for the molecules **14** and **18**, respectively.

Table 2. Calculated and Experimental (in Parentheses) Values of Selected Torsional Angles (in Degrees)

		ϕ_1	ϕ_2
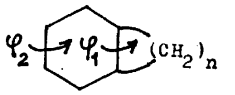	n=1 (**11**)	−2.9	64.4
	n=2 (**10**)	−30.1	63.8
		(−32.8)[12]	(64.4)[11a]
	n=3 (**9**)	−47.5	58.0
		(−46.6)	(58.2)[11]
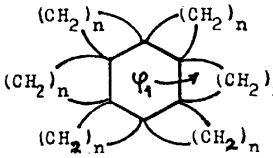	n=1 (**19**)	0.0	
	n=2 (**17**)	22.6	
	n=3 (**16**)	39.5	

a) This value has not been given in the original Ref. 12 and is incorrectly cited as C5-C9-C8-C7 angle in the Table 5 of the Ref. 11 but the model calculations cited in the former reference prove that this is the largest torsional angle in the C_6 ring.

As was stated above, very few experimental data are known to compare with. Experimental heats of formation values have been reported only for the molecules **9**—**11**[31] and the HOF values for *cis*- and *trans*-**5**, *trans*-**6**, *cis*- and *trans*-**13**, **14**—**19**, and **21** can be considered as an estimation of the values which are very difficult, if possible, to obtain experimentally. The calculated MM2 HOF values for the molecule *cis*-**5** is reasonably close to the corresponding MINDO/3 value calculated in Ref. 32 (see footnote i to the Table 1).

An inspection of the α values collected in the Table 1 seems to indicate that in the cases where the corresponding experimental data have been published there is a reasonable agreement between the calculated and experimental results. The difference is equal to 5° for bicyclo[4.2.0]octane (**10**) and is equal to ca. 20° between the analogous molecules **14** and 13-(3,5-dinitrobenzoyloxy)hexacyclo[12.2.0.0^{1,4}.0^{4,7}.0^{7,10}.0^{10,13}]hexadecane (**22**), and **20** and **21**. It seems that even the last value of 20° is not big since (a) it corresponds to an average error of less than 4° and (b) the molecules in comparison are not identical but rather close analogues.

For the molecules *trans*-**6** and *cis*- and *trans*-**13** the reported experimental data are insufficient to calculate the corresponding α values but the results of the calculations reproduce with a reasonable accuracy the available experimental torsional angles. For example,

†The calculated results of the present paper as well as those of references **11**—**13** for the molecules **9**—**11** reproduce all available experimental data satisfactorily.

††The values of the C_1-C_2 bond length for *cis*- and *trans*-**13** calculated in Ref. 26 are lower than the natural bond lengths which is very unusual.

for *trans*-**6** the central ring has been found to be approximately diplanar with the interplane angle of 163° and the corresponding calculated value is equal to 158°. Similarly, the calculated and experimental values of torsional angles for *cis*- and *trans*-**13** are very close. The angle $\varphi_{4,2,1,7}$ is equal to 16.7° (exp.[17]), 14.9° (calcd MM2, this work), and 14.4° (calcd MM2[26]) for *trans*-**13**; and to 17.9° (exp.[17]), 18.0° (calcd MM2, this work), and 18.8° (calcd MM2[26]) for *cis*-**13**.

The reasonable results obtained for **9**, **10**, **13**, **14**, and **21** and especially those for *trans*-**6** seem to validate the use of molecular mechanics method with the MM2 parameterization to analysis of the flattening in even highly strained cyclohexane rings. The available experimental data and the results of the calculations seem to indicate that fusion of a 3-membered ring or fusion of several 4- and 5-membered rings leads to a similar flattening since the corresponding values are similar for **11** and **15** ($\alpha \cong 135°$) and for *cis*- and *trans*-**13** and for **16** and **18** ($\alpha \cong 200°$). The experimental data for the molecule **15** and **17** are not known at present but synthetic effort by Prof. Fitjer and his group allows to hope that they will be available in the near future. Similarly, the synthesis of *cis*-**5** carried out at present by the Prof. Prinzbach's group should yield another check of the predictive power of the method if the substances will crystallize enabling X-ray analysis to be carried out.

As was stated in Chapter 2, the calculated values for bond angles do not reproduce the experimental ones, but a general trend of enlarging the angles upon ring planarization holds since it is enforced by the conditions of ring closure.

Conclusion

In spite of the inaccuracies in the MM2 parameterization involving cyclopropane ring molecular mechanics calculations seem to reproduce the flattening of a cyclohexane ring upon fusion with small ring(s). The experimental data and the results of the calculations presented in this work seem to indicate that the flattening is more pronounced when smaller and/or more ring(s) are fused to a cyclohexane ring. On the basis of calculations a hypothetical [6.3]coronane is postulated to exhibit a planar C_6 ring. The calculations yielded also an estimation of the HOF values for the molecules *cis*- and *trans*-**13**, **14**—**19**, **21** which are unavailable at present. The value of 4.5 kcal mol^{-1} for the V_3 parameter of the type 22-22-1-22 proposed in the MM2 parameterization is questioned and further refinement of other parameters for highly strained and/or cyclopropane containing molecules is postulated.

Further studies of the molecules with planar cyclohexane rings are in prospects. The synthetic efforts by the Prof. Prinzbach's group in the field of heteroanalogues of *cis*-tris-σ-homobenzenes and those by the Prof. Fitjer's group in the field of coronanes seem especially promising in this respect. If the substances will crystallize they will enable an additional check of the present calculations in the near future.

I thank Prof. Fitjer for providing me with the results of X-ray analysis of **20** prior to its publication. Critical remarks by Prof. A. Zamojski and Dr. L. Stefaniak are gratefully acknowledged.

This work is a part of the Polish Academy of Sciences Research Project CPBP 01.12.

References

1) G. M. Kellie and F. G. Riddell, *Top. Stereochem.*, **8**, 225 (1974).
2) A. N. Vereshchagin, *Usp. Khim.*, **52**, 1879 (1983), Chapters 3, 4.
3) Ch. Kabuto, M. Yagihara, T. Asso, and Y. Kitahara, *Angew. Chem.*, **85**, 860 (1973).
4) W. Littke and U. Drück, *Angew. Chem.*, **86**, 557 (1974).
5) L. K. Liu and E. Davies, *Angew. Chem.*, **89**, 175 (1977).
6) R. Schwesinger, K. Piontek, W. Littke, and H. Prinzbach, *Angew. Chem.*, **97**, 344 (1985), and references cited therein.
7) M. Engelhardt and W. Lüttke, *Angew. Chem.*, **84**, 345 (1972).
8) C. Krüger and P. J. Roberts, *Cryst. Struct. Commun.*, **3**, 459 (1974).
9) E. Osawa and H. Musso, *Angew. Chem.*, **95**, 1 (1983).
10) N. L. Allinger and P. E. Eaton, *Tetrahedron Lett.*, **24**, 3697 (1983).
11) L. Enden and H. J. Geise, *J. Mol. Struct.*, **74**, 309 (1981).
12) A. Spelbos, F. C. Mijlhoff, W. H. Bakker, R. Baden, and L. Enden, *J. Mol. Struct.*, **38**, 155 (1977).
13) V. A. Naumov, *DAN SSSR*, **186**, 599 (1968).
14) R. Bucourt, *Top. Stereochem.*, **8**, 159 (1974).
15) W. R. Dolbier, *Tetrahedron*, **40**, 3945 (1984).
16) W. Cocker, P. D. Cunningham, N. W. A. Geraghty, T. Higgins, and P. J. McArdle, *Tetrahedron Lett.*, **25**, 5441 (1984).
17) S. Braun and M. Traetteberg, *J. Mol. Struct.*, **39**, 101 (1977).
18) L. Fitjer, D. Wehle, M. Noltenmeyer, E. Egert, and G. M. Sheldrick, *Chem. Ber.*, **117**, 203 (1984).
19) L. Fitjer, private communication.
20) N. L. Allinger, *Adv. Phys. Prg. Chem.*, **13**, 1 (1976); A. I. Kitajgorodsky, *Chem. Soc. Rev.*, **7**, 133 (1978); O. Ermer, *Struct. Bonding (Berlin)*, **27**, 161 (1976).
21) S. Chang, D. McNally, S. Shary-Tehrany, M. J. Hickey, and R. H. Boyd, *J. Am. Chem. Soc.*, **92**, 3109 (1970).
22) O. Ermer and S. Lifson, *J. Am. Chem. Soc.*, **95**, 4121 (1973).
23) "Operating instructions for MM2 and MMP2 program." Updated as of January (1980). N. L. Allinger, Y. H. Yuh, University of Georgia, Athens, USA.
24) U. Burkert and N. L. Allinger, "ACS Monograph 177," Am. Chem. Soc., Washington, D. C. (1982).
25) R. Greengard, R. Chang, Y. Yuh, and N. L. Allinger, unpublished results cited in Ref. 24.
26) E. Osawa, G. Szalontai, and A. Tsurumoto, *J. Chem. Soc., Perkin Trans. 2*, **1983**, 1209.

27) K. Nowiński, "Operating instruction to molecular mechanics program KNOW," to be published. The program adapted at present for IBM PC computer differs from the MM2 one in three points: a) It utilizes a more efficient minimization procedure avoiding the MM2 dead-ends signaled by a message "Minimization can not continue due to abnormal bond lengths." b) It utilizes display for data preparation and enables visualizing the molecule from different points of view. c) Some errors in parameters choice exhibited by the MM2 program, i.e. for small-ring propellanes, are cleared away. This program was designed for use on mini- and microcomputers, therefore, it requires no large memory retaining reasonable minimization speed.

28) W. Berlohr, H.-D. Beckhaus, K. Peters, H.-G. Schnering, and Ch. Rüchardt, *Chem. Ber.*, **117**, 1013 (1984).

29) E. M. Engler, J. D. Andose, and P. von R. Schleyer, *J. Am. Chem. Soc.*, **95**, 8005 (1973).

30) F. A. L. Anet and R. Anet, *Tetrahedron Lett.*, **26**, 5355 (1985).

31) J. D. Cox and G. Pilcher, "Thermochemistry of Organic and Organometallic Compounds," Academic Press, London (1970).

32) J. Spanget-Larsen and R. Gleter, *Angew. Chem.*, **90**, 471 (1978).

Aryliminodimagnesium Reagents. XII. The Distribution of Products in the Condensation with Nitrobenzothiazoles. Reduction of Electron-Donating Ability of Reagent by the Interaction with Thiazolyl Group

Masao Ōkubo,* Keiko Asao, and Hiroyuki Hyakutake
Department of Chemistry, Faculty of Science and Engineering, Saga University, Honjō-machi, Saga 840
(Received April 2, 1987)

The 4-, 5-, 6-, and 7-nitro derivatives of benzothiazole condense with $ArN(MgBr)_2$ giving unsym-azoxy and -azo products. The product distribution indicated the mild nature of the reaction, and could be explained in terms of a reduced electron-donating ability of the reagent due to an interaction with thiazolyl group.

The electron transfer initiated condensation of aryliminodimagnesium reagent($ArN(MgBr)_2$, aryl-IDMg) with nitroarenes[1] and diaryl ketones[2] has been developed in our laboratory. Independently of the manners of reactions of IDMg (condensation) and ArMgBr (addition) as well as those of other magnesium reagents, the principal factor governing the distribution of normal and abnormal (radical) products is a combination of electron-donating and -accepting abilities (EDA and EAA) of reactants:[3,4] The combination represents the relative efficiency of an electron transfer. The efficiency is generally estimated (as the first approximation in fifteen reactions of various magnesium reagents with aromatic substrates) by the value of the difference between the oxidation and reduction potentials of reactants.[4]

A Grignard reaction with nitroarenes had attracted no attention until 1977, since the formation of a large amount of radical product was unavoidable.[5] However, during the past decade, Bartoli and his coworkers have investigated the reaction at lower temperatures, and have established the deoxygenative conjugate addition mechanism involving an electron transfer.[6] Among a lot of nitroarenes, nitrobenzothiazoles, which were first used by the Italian authors,[7] attracted our attention from the EDA-EAA viewpoint since these substrates seemed to be favorable for affording "normal" conjugate addition product as the result of a moderate electron transfer.

The IDMg reagent has a weaker EDA than that of ArMgBr.[8] If IDMg condense with nitrobenzothiazoles in the usual manner,[1] the product distribution is expected to be similarly explainable by a much milder

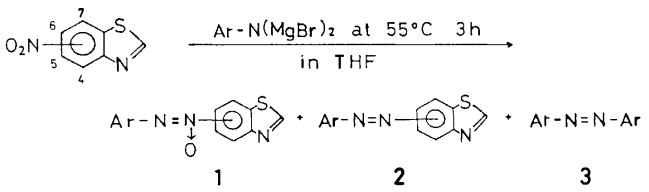

Scheme 1.

Table 1. Product Distribution in IDMg Reaction with Nitrobenzothiazoles

Run No.	Substr.	*p*-RC_6H_4-IDMg (R)	[IDMg]/[Substr.]	Yield[c]/% *unsym*-azoxy **1**	*unsym*-azoxy **2**	*sym*-azoxy **3**	Recov. %
1	4-NBT[a]	MeO	2.0	27	6	27	13
2	4-NBT	Me	2.0	28	3	24	10
3	4-NBT	Cl	2.0	17	0	16	72
4	5-NBT	MeO	2.0	46	15	31	7
5	5-NBT	Me	2.0	36	7	5	31
6	5-NBT	Me	5.0	62	8	12	0
7	5-NBT	Cl	2.0	21	6	4	29
8	5-NBT	Cl	7.0	74	7	5	0
9	6-NBT	MeO	2.0	50	11	28	trace
10	6-NBT	Me	2.0	45	8	10	13
11	6-NBT	Me	5.0	49	0	20	13
12	6-NBT	Cl	2.0	22	0	10	54
13	6-NBT	Cl	7.0	73	6	11	0
14	7-NBT	MeO	2.0	47	3	12	3
15	7-NBT	Me	2.0	40	6	7	—
01	4-MeNB[b]	MeO	2.0	39	34	10	0
02	4-MeNB	Me	2.0	64	[36]		0
03	4-ClNB	MeO	2.0	50	12	9	0
04	4-ClNB	Cl	2.0	71	[24]		0

a) NBT=nitrobenzothiazole. b) NB=nitrobenzene. c) Yields, based on the amount of NBT used, are obtained after stirring at 55 °C for 3 h.

electron transfer. This expectation was verified. The effect of the thiazolyl group on the reaction is discussed in this paper.

Results and Discussion

Product Distribution in IDMg Reaction with Nitrobenzothiazoles. In a reaction of aryl-IDMg with 4-, 5-, 6-, and 7-nitrobenzothiazoles (Scheme 1), unsymmetrical(*unsym*-) azoxy- and azobenzothiazoles (**1** and **2**) and symmetrical (*sym*-) azobenzenes (**3**) were obtained. The product **1** was formed via condensation with IDMg, **2** via a subsequent deoxygenation of **1** with excess IDMg, and **3** via an oxidative coupling of reagent molecules. The types of products are same with those obtained in reactions with nitrobenzenes.[1] The yields of **1**—**3** obtained under fixed reaction conditions are summarized in Table 1 (Runs 1—15); four previous results (Runs 01—04)[1] are also listed for a comparison. As described in the following, the notable features of product distribution meet the expectation given above.

The first feature is that the recovery of the substrate was observed in all cases using two molar equuivalents of reagents. Two molar equivalents of *p*-ClC_6H_4-IDMg, having the weakest EDA,[8] leads to a large amount of recovery (Runs 7 and 12), and seven molar equivalents are needed for a complete conversion (Runs 8 and 13). In the case of *p*-MeC_6H_4-IDMg, having a stronger EDA,[8] five molar equivalents are needed (Run 6). In contrast, in cases of nitrobenzenes (Runs 01—04), no recovery was observed, even upon using two molar equivalents of *p*-ClC_6H_4-IDMg (Run 04).

The second feature is that, even in Runs 6, 8, 11, and 13 using a large excess of IDMg, the yield of *unsym*-azoxy product **1** was always much higher than those of the corresponding *unsym*-azo product **2**. This indicates that **1** was quite sluggishly deoxygenated by IDMg, as compared to the previous results (Runs 01—03).[1] As previously reported, the IDMg deoxygenation of azoxyarenes is accelerated and/or retarded, depending on their EAA's.[1,9]

Table 2. Melting Points and ^1H NMR Data of Azoxy- and Azobenzothiazoles

No.	Mp θ_m/°C	^1H NMR data[b] δ
$\mathbf{1}_4^{MeO}$	137—138	9.18(1H, s), 8.44 & 7.03(4H, ABq), 8.12(1H, d), 8.01(1H, d), 3.91(3H, s).
$\mathbf{2}_4^{MeO}$	101—105	9.28(1H, s), 8.23—8.09(3H, m), 7.89(1H, d), 7.63(1H, t), 7.12(2H, d), 3.94(3H, s).
$\mathbf{1}_4^{Me}$	105—105.5	9.24(1H, s), 8.28 & 7.36(4H, ABq), 8.16(1H, d), 8.04(1H, d), 7.60(1H, t), 2.24(3H, s).
$\mathbf{2}_4^{Me}$	135—136	9.45(1H, s), 8.11(1H, d), 8.05 & 7.38(4H, ABq), 7.90(1H, d), 7.61(1H, t), 2.46(3H, s).
$\mathbf{1}_4^{Cl}$	127.5—129	9.20(1H, s), 8.29 & 7.49(4H, ABq), 8.17(1H, d), 8.03(1H, d), 7.60(1H, t).
$\mathbf{2}_4^{Cl}$	—[a]	9.26(1H, s), 8.20—8.04(4H, m), 7.60—7.51(3H, m).
$\mathbf{1}_5^{MeO}$	162—163	9.07(1H, s), 8.49 & 7.98(2H, ABq), 8.34 & 6.97(4H, ABq), 3.87(3H, s).
$\mathbf{2}_5^{MeO}$	122.5—123	9.06(1H, s), 8.65(1H, d), 8.05(2H, s), 7.96 & 7.02(4H, ABq), 3.90(3H, s).
$\mathbf{1}_5^{Me}$	192—192.5	9.09(1H, s), 9.06(1H, d), 8.44 & 8.18(2H, ABq), 7.97 & 7.31(4H, ABq), 2.45(3H, s).
$\mathbf{2}_5^{Me}$	174—175	9.06(1H, s), 8.67(1H, d), 8.06(2H, s), 7.90(2H, s), 7.90 & 7.33 (4H, ABq), 2.49(3H, s).
$\mathbf{1}_5^{Cl}$	201—202	9.12(1H, s), 9.05(2H, d), 8.44 & 8.05(2H, ABq), 8.21 & 7.45(4H, ABq).
$\mathbf{2}_5^{Cl}$	212—213	9.06(1H, s), 8.65(1H, d), 8.059(2H, s), 7.92 & 7.48(4H, ABq).
$\mathbf{1}_6^{MeO}$	153—153.5	9.17(1H, s), 8.96(1H, d), 8.54 & 8.22(2H, ABq), 8.40 & 7.04(4H, ABq), 3.90(3H, s).
$\mathbf{2}_6^{MeO}$	143—144	9.08(1H, s), 8.51(1H, d), 8.28 & 8.09(2H, ABq), 7.98 & 7.03(4H, ABq), 3.90(3H, s).
$\mathbf{1}_6^{Me}$	122—124	9.15(1H, s), 8.97(1H, d), 8.54 & 8.22(2H, ABq), 8.20 & 7.33(4H, ABq), 2.43(3H, s).
$\mathbf{2}_6^{Me}$	132—134	9.05(1H, s), 8.50(1H, d), 8.23 & 8.10(2H, ABq), 7.87 & 7.31(4H, ABq), 2.43(3H, s).
$\mathbf{1}_6^{Cl}$	146—147	9.18(1H, s), 8.95(1H, d), 8.53 & 8.22(2H, ABq), 8.20 & 7.48(4H, ABq).
$\mathbf{2}_6^{Cl}$	130—132	9.15(1H, s), 8.57(1H, d), 8.30 & 8.16(2H, ABq), 7.96 & 7.55(4H, ABq).
$\mathbf{1}_7^{Me}$	125—126.5	9.10(1H, s), 8.51(1H, d), 8.29(1H, d), 8.24 & 7.30(4H, ABq), 7.62(1H, t), 2.42(3H, s).
$\mathbf{2}_7^{Me}$	147—148	9.18(1H, s), 8.31(2H, d), 8.00 & 7.39(4H, ABq), 7.79 (1H, t), 2.49(3H, s).
$\mathbf{1}_7^{MeO}$	—[a]	9.11(1H, s), 8.52(1H, d), 8.29(1H, d), 8.41 & 7.00(4H, ABq), 7.65(1H, t), 3.91(3H, s).
$\mathbf{2}_7^{MeO}$	—[a]	9.13(1H, s), 8.32(2H, d), 8.07 & 7.05(4H, ABq), 7.76 (1H, t), 7.62(1H, t), 3.92(3H, s).

a) Melting points are undetermined because the trace amounts of samples were not purified completely.
b) For AB-quartets of aromatic protons, all the ΔJ values are 8—9 Hz.

The third feature is that the yields of **1** and **2** in reactions of the 4-nitro isomer (Runs 1—3) having neighboring nitrogen atom are lower than those in cases of other isomers (Runs 4, 5, 7, 9, 12, 14, and 15). Even the 7-nitro isomer, having a neighboring sulfur atom, gave **1** and **2** in yields comparable to those in cases of 5- and 6-nitro isomers. Thus, the anomaly indicates that 4-nitro group is less favorable for the condensation with IDMg, probably due to a steric repulsion caused by the neighboring nitrogen atom, whereas the "normal" yields in cases of the 7-isomer may be ascribed to the long C_{Ar}-S bond causing no appreciable repulsion. The retardation of IDMg condensation by some ortho substituents of nitrobenzene was observed.[10] In this connection, the Grignard reagent[7] converts the 4-nitro isomer into a non-deoxygenative product(*vide supra*) different from the deoxygenative ones obtained in cases involving the other isomers.

Reduction of EDA of Reagent Caused by Coordination of Thiazolyl Group to Mg Atom. The first and second features of the product distribution seem to indicate that the electron transfer involved in the reaction of Scheme 1 is milder than those in the IDMg reaction with nitro- and azoxybenzenes.[1,9] However, the normalized reduction potentials of the nitro- and azoxybenzothiazoles are lower than or comparable to those of the corresponding benzene derivatives, as shown below(BT=benzothiazolyl).

Nitroarenes ($ArNO_2$):

Ar	V (redox)
p-$MeOC_6H_4$	−1.508
p-MeC_6H_4	−1.418
p-ClC_6H_4	−1.254
4-BT	−1.314
5-BT	−1.299
6-BT	−1.220
7-BT	−1.142

Azoxyarenes (Ar^1-N(O)=N-Ar^2):

Ar^1	Ar^2	V (redox)
p-$MeOC_6H_4$	*p*-$MeOC_6H_4$	−1.748
p-$MeOC_6H_4$	C_6H_5	−1.642
C_6H_5	C_6H_5	−1.596
p-$MeOC_6H_4$	*p*-ClC_6H_4	−1.574
p-MeC_6H_4	*p*-ClC_6H_4	−1.524
C_6H_5	*m*-ClC_6H_4	−1.423
5-BT	*p*-$MeOC_6H_4$	−1.608
5-BT	*p*-ClC_6H_4	−1.443
6-BT	*p*-$MeOC_6H_4$	−1.732
6-BT	*p*-ClC_6H_4	−1.359

The lower values of the reduction potentials indicate a stronger EAA; this seems to be in conflict with the suggestion of a mild electron transfer. However, when the oxidation peak potential of *p*-MeC_6H_4-IDMg in THF was measured in the presence of an equimolar amount of unsubstituted benzothiazole, the normalized potential value (1.055 V) was reproducible and was found to be higher than that (0.941 V) obtained in its absence.[8] This indicates that (in the reaction of Scheme 1) the actual EDA is much weaker, due to an interaction with the thiazolyl group, and gives rise to a mild electron transfer.

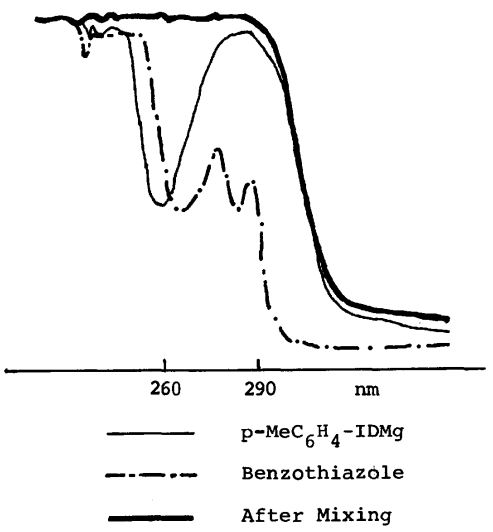

Fig. 1. Shift of n→π* transition band of benzothiazole by mixing with *p*-MeC_6H_4-IDMg.

The interaction arises from a coordination of the thiazolyl group to Mg atom of IDMg, as shown by the electronic absorption spectra measured in degassed THF solutions (Fig. 1). The λ_{max} of n→π* transition of *p*-MeC_6H_4-IDMg is observed at 290 nm and that of benzothiazole at 275 nm. By mixing two equimolar solutions through breaking the seal, the dip between the n→π* and π→π* bands of the reagent disappeared. The spectrum change is attributed to an overlap of the n→π* band of benzothiazole, shifted by 20—30 nm toward blue, due to coordination of the thiazolyl group (probably via nitrogen atom) to Mg atom of IDMg. Undoubtedly, the coodination gives rise to the first and second features of product distribution, i.e., an appreciable recovery and a sluggish deoxygenation. Among the two reagent molecules, tentatively depicted in Fig. 2, the one is coordinated and deactivated while the other is responsible for the condensation with the nitro group.

According to the discussion given above, Bartoli's Grignard reaction[7] owes its first success (as at least one of the reasons) to the reduction of EAA arising from a similar interaction of the thiazolyl group with the reagent. The EDA-EAA concept is useful for characterizing the reactions of aromatic substrates and magnesium reagents of simple molecular structures,[3,4]

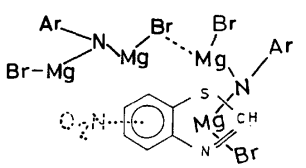

Fig. 2. Schematic depiction for coordination of thiazolyl group to Mg atom of reagent.

however, the modification of the concept on the basis of special molecular structures of substrates must be taken into account.

Experimental

Melting points are uncorrected.

Materials and Procedures. Four isomeric nitrobenzothiazoles were prepared by the nitration of benzothiazole, and separated by recrystallization, steam distillation, and repeated column chromatography on silica gel.[11]

The IDMg reactions were carried out according to the reported procedures; the reaction mixtures of substrates (3.0 or 5.0 mmol) with the given molar amounts of IDMg in THF (30 or 50 ml) were stirred at 55 °C for 3 h. The products were separated by column and thin-layer chromatographies on silica gel(Wako Gel C-200, C-300, and Merck's Kiesel Gel 60G).

Elemental analyses of the products gave satisfactory results. The melting points and ^{1}H NMR data of azoxy- and azobenzothiazoles (**1** and **2**) are summarized in Table 2.

The measurement of reduction potentials of nitro and azoxy compounds using bis(biphenyl)chromium(I) tetraphenylborate (BCTB) as internal reference was carried out according to the reported procedures.[4,9]

The gift of samples of BCTB by Prof. Gerhard Gritzner, University of Linz, is gratefully acknowledged. The authors thank Mr. Toshiki Tsutsumi and Mr. Kōji Matsuo for their assistance in polarographic measurements. The authors are grateful to the Ministry of Education, Science, and Culture for a financial support by a Grant-in-Aid for Scientific Research (No. 60470026).

References

1) M. Ōkubo, T. Takahashi, and K. Koga, *Bull. Chem. Soc. Jpn.*, **56**, 199 (1983); M. Ōkubo and K. Koga, *ibid.*, **56**, 203 (1983).
2) M. Ōkubo, *Bull. Chem. Soc. Jpn.*, **58**, 3108 (1985).
3) M. Okubo, M. Yoshida, K. Horinouchi, H. Nishida, and Y. Fukuyama, *Bull. Chem. Soc. Jpn.*, **56**, 1196 (1983).
4) M. Ōkubo, T. Tsutsumi, and K. Matsuo, *Bull. Chem. Soc. Jpn.*, **60**, 2085 (1987).
5) D. N. Kursanov and P. A. Solodkov, *Chem Abstr.*, **30**, 2181 (1936).
6) G. Bartoli, *Acc. Chem. Res.*, **17**, 109 (1984).
7) G. Bartoli, R. Leardini, M. Lelli, and G. Rosini, *J. Chem. Soc. Perkin I*, **1977**, 884.
8) M. Ōkubo, T. Tsutsumi, A. Ichimura, and T. Kitagawa, *Bull. Chem. Soc. Jpn.*, **57**, 2679 (1984).
9) M. Ōkubo, C. Sugimori, M. Tokisada, and T. Tsutsumi, *Bull. Chem. Soc. Jpn.*, **59**, 1644 (1986).
10) M. Ōkubo, Y. Inatomi, and N. Taniguchi, unpublished results.
11) E. R. Ward and W. H. Poesche, *J. Chem. Soc.*, **1961**, 2825.

An Ab Initio Molecular Orbital Study of Lithiopyridines

Osamu KIKUCHI,* Hideo TOGO, and Naomichi FURUKAWA
Department of Chemistry, The University of Tsukuba, Sakura, Ibaraki 305
(Received May 9, 1987)

Synopsis. Ab initio molecular orbital calculations were performed for 2-, 3-, and 4-lithiopyridine monomers, and the molecular and electronic structures of lithiopyridines and their reactivity with electrophiles were examined.

Aryllithium compounds react with various electrophiles to afford the corresponding substituted compounds, and they are very important species for synthetic purposes.[1,2] Lithiopyridines are considered to be the intermediates in the following synthetic route to the substituted pyridines.[2] Since phenyllithium, **1**, is

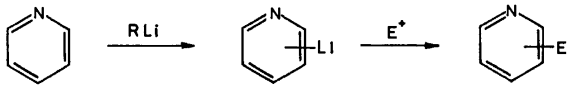

tetrametric in the solid phase and in solution,[3] lithiopyridines may exist in the aggregation state with a solvent in solution. However, the study of the lithiopyridine monomers is essential to understand the electronic properties of lithiopyridines. The present note will examine the molecular and electronic structures and reactivity of 2-, 3-, and 4-lithiopyridines on the basis of MO calculations.

The molecular structures of phenyllithium, **1**, and of lithiopyridines, **2**—**4**, were optimized by means of ab initio calculations with the STO-3G basis set[4] by assuming planar molecular structures. Their energies were obtained with the 6-31G basis set.[5] The molecular strcture of **1** is shown in Fig. 1, while those of **2**—**4** are shown in Fig. 2. The energies of **2**—**4** and some electronic properties of **1**—**4** are listed in Table 1.

The molecular structures of **3** and **4** can be estimated from those of phenyllithium and pyridine; the STO-3G structure of pyridine has 1.352 Å for the CN bond and 115.6° for the CNC angle. The structures around the N atom in **3** and **4** resemble that of pyridine, while those around the C-Li bond resemble that of phenyllithium. The calculated C-Li bond lengths of **1**, **3**, and

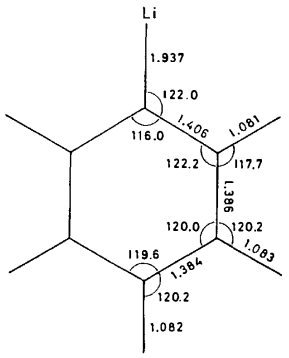

1

Fig. 1. The STO-3G structure of phenyllithium. Bond lengths are in Å, and bond angles are in degrees.

4 are shorter than the C-Li bond in alkyllithium, 2.001,[6] and longer than those between the Li atom and the olefinic carbon atom, 1.776—1.863.[7] The structure of **2** was found to be very different from **3** and **4**; the interaction between the Li atom and the lone-pair electrons of the N atom is strong enough to give the bridged structure. A similar bridged structre has been reported for LiHNOH.[8] The energies of **3** and **4** are comparable and are higher than **2** by about 50 kJ mol^{-1}. The lower energy of **2** is due to the stabilization of the Li atom by the lone-pair electrons. As was pointed out above, lithiopyridines may be stabilized in solution by the Li-solvent interaction; the relative stabilities among the three isomers in solution can not, however, be estimated here.

Since the electrophilic substitution at the C-Li carbon atom is a typical reaction of lithiopyridines, the reactivity of **1**, **3**, and **4** with electrophiles was com-

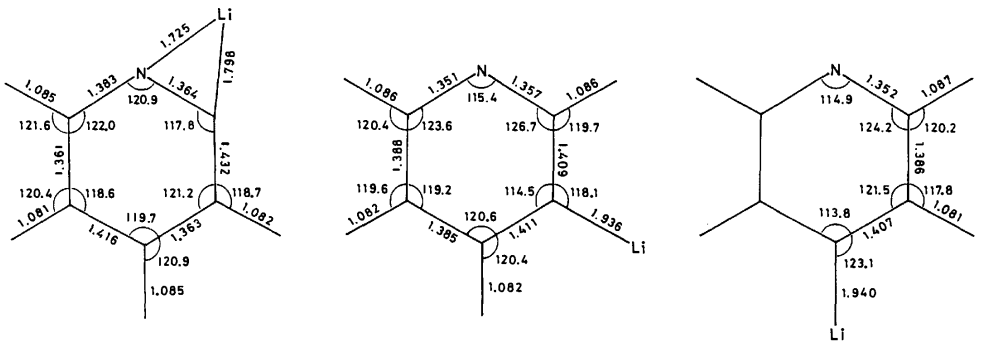

2 3 4

Fig. 2. The STO-3G structures of 2-lithiopyridine (**2**), 3-lithiopyridine (**3**), and 4-lithiopyridine (**4**). Bond lengths are in Å, and bond angles are in degrees.

Table 1. Energies and Some Electronic Properties of 2-, 3-, and 4-Lithiopyridines and Phenyllithium

Compound	Energy[a]	Q(Li)[b]	q(C)[c]	q_π(C)[d]	$\varepsilon_{HOMO}(\pi)$[e]
2-Lithiopyridine (**2**)	−253.44542 (0.0)	0.088	5.932	0.678	−7.52
3-Lithiopyridine (**3**)	−253.42588 (51.5)	0.217	6.054	0.851	−6.68
4-Lithiopyridine (**4**)	−253.42633 (50.2)	0.228	6.035	0.816	−7.06
Phenyllthium (**1**)		0.190	6.042	0.849	−6.23

a) The 6-31G calculation for the STO-3G structures. The values are in atomic units, and the values in parentheses are relative energies in kJ mol^{-1}. b) Charge at the Li atom. c) Electron population at the carbon atom of the C-Li bond.
d) π-Electron population at the carbon atom of the C-Li bond. e) Orbital energy of the highest occupied π-orbital. The values are in eV.

pared. As may be seen from Table 1, the electron population on the C-Li carbon atom is in the order of **3**>**1**>**4**, while the π-electron population on the carbon atom in the order of **3**≅**1**>**4**. These findings suggest that the S_E2-type displacement of the Li atom occurs in **3** more easily than in **4**. The orbital energies of HOMO(π) of **3** and **4** are more negative than **1**; this indicates that the reactivity of **3** and **4** is lower than **1** for the orbital-controlled reaction. The calculated positive charges of the Li atom are in the order of **4**>**3**>**1**≫**2**. The small value in **2** is due to the participation of the lone-pair electrons of nitrogen.

All the calculations were performed on the FACOM M-380 computer at The University of Tsukuba using the ABINIT program written by our group. The work was supported by University of Tsukuba Project Research.

References

1) M. Yamamoto, K. Suzuki, S. Tanaka, and K. Yamada, *Bull. Chem. Soc. Jpn.*, **60**, 1523 (1987); L. S. Chen, G. J. Chen, and C. Tamborski, *J. Organoment. Chem.*, **251**, 139 (1983).
2) W. G. Gribble and M. G. Saulnier, *Tetrahedron Lett.*, **21**, 4137 (1980); F. Marsais. G. Le Nard, and G. Quéguiner, *Synthesis*, **1982**, 235; A. I. Meyers and R. A. Gabel, *J. Org. Chem.*, **47**, 2633 (1982).
3) H. Hope and P. P. Power, *J. Am. Chem. Soc.*, **105**, 5320 (1983); L. M. Jackman and L. M. Scarmountzos, *J. Am. Chem. Soc.*, **106**, 4627 (1984).
4) W. J. Hehre, R. F. Stewart, and J. A. Pople, *J. Chem. Phys.*, **51**, 2657 (1969).
5) W. J. Hehre, R. Ditchfield, and J. A. Pople, *J. Chem. Phys.*, **56**, 2257 (1972); J. D. Dill and J. A. Pople. *ibid.*, **62**, 2921 (1975).
6) E. Kaufmann, T. Clark, and P. v. R. Schleyer, *J. Am. Chem. Soc.*, **106**, 1856 (1984).
7) A. J. Kos and P. v. R. Schleyer, *J. Am. Chem. Soc.*, **102**, 7928 (1980).
8) M. L. McKee, *J. Am. Chem. Soc.*, **107**, 859 (1985).

Theoretical Estimation of the Solubilities of Lanthanoid Iodates in Dimethyl Sulfoxide-Water Mixtures

Takehiro ABE
College of General Education, Tohoku University, Kawauchi, Sendai 980
(Received March 14, 1987)

Synopsis. By using a Modified Born equation, the solubilities of sparingly soluble lanthanoid iodates in dimethyl sulfoxide-water mixtures have been successfully estimated.

Recently Miyamoto et al.[1] have reported the solubilities of lanthanoid iodates in dimethyl sulfoxide (DMSO)-water mixtures. They have qualitatively accounted for these values of solubilities, using the theory of Davis, Ricci, and Sauter[2] for solubility. In their theory, the famous Born equation[3] is applied to the calculation of the interaction energy of an ion with a solvent. Recently, Abe[4] has modified the Born equation by considering a distance-dependent relative permittivity of a solvent. The modified equation better reproduces the observed solvation free energies of ions than does the Born equation. Moreover, Ehrenson[5] has shown that the solvent parameter in Abe's equation is the best in the inverse exponential radial dielectric function family of the modified Born equations for the correlation of the free energies of solvation. In this paper, therefore, an attempt has been made to account quantitatively for the solubilities of lanthanoid iodates by using Abe's equation instead of the Born equation in the theory of Davis, Ricci, and Sauter.

Theoretical Treatment

Let us consider that a sparingly soluble salt, $A_{\nu+}B_{\nu-}$, dissolves in a given solvent i at a concentration of c_i (molarity) and that the salt is completely dissociated into spherical ions:

$$A_{\nu+}B_{\nu-} \longrightarrow \nu_+ A^{(z_+)+} + \nu_- B^{(z_-)-} \tag{1}$$

Following the theoretical treatment of Davis et al.[2] one obtains the following final equation by replacing the Born equation with Abe's equation:[4]

$$\ln\left(\frac{c_2}{c_1}\right) = \frac{e^2}{2kT} \times \frac{z_+z_-}{z_+ + z_-} \times \left(\frac{z_+}{r_+} + \frac{z_-}{r_-}\right) \times \{\eta'_1(\varepsilon_{r,1}) - \eta'_2(\varepsilon_{r,2})\} - A \times (z_+z_-) \times \left\{\frac{I_1^{1/2}}{(T\varepsilon_{r,1})^{3/2}} - \frac{I_2^{1/2}}{(T\varepsilon_{r,2})^{3/2}}\right\}, \tag{2}$$

where e the charge of the proton; k, the Boltzmann constant; T, the temperature (K); r_+ and r_-, the radii of the cation and the anion respectively; $\varepsilon_{r,i}$, the relative permittivity of the solvent i, and $A=4.2013\times10^6$ $mol^{-1/2}\,dm^{1/2}\,K^{3/2}$. Here,

$$\eta'_i(\varepsilon_{r,i}) = \frac{1}{\ln\varepsilon_{r,i}} - \frac{1}{\varepsilon_{r,i}\ln\varepsilon_{r,i}}, \tag{3}$$

and

$$I_i = \frac{1}{2} \times (\nu_+ z_+^2 + \nu_- z_-^2) c_i. \tag{4}$$

The second term on the right-hand side of Eq. 2 is the logarithmic mean activity coefficients, that have been calculated by the limiting Debye-Hückel equation on the assumption that the activity coefficients corresponding to the molarity and mole fraction are approximately the same for sufficiently dilute solutions of the salt.[6] When the Born equation is used instead of Abe's, one obtains an equation corresponding to Eq. 2 in which $\{\eta'_1(\varepsilon_{r,1})-\eta'_2(\varepsilon_{r,2})\}$ is replaced with $(1/\varepsilon_{r,1}-1/\varepsilon_{r,2})$.

In applying Eq. 2, as the solvent 1 we must choose a standard solvent whose c_1 value is already known. It is, however, impossible to evaluate explicitly the c_2 value by using the $\varepsilon_{r,2}$ value, because the c_2 value is contained not only in $\ln(c_2/c_1)$ but also in the ionic strength of I_2, according to Eq. 4. The c_2 value was, therefore, numerically obtained as follows. The pure solvent of water for which the solubility of the lanthanoid iodate is the highest was chosen as the standard solvent. The solubility, therefore, decreases in the DMSO-water mixture with an increase in the component of DMSO. Accordingly, by gradually decreasing the c_2 value, independent calculations of the values of both the right- and left-hand sides of Eq. 2 could be repeated by means of a computer until a close agreement (within 10^{-4}) between the values of the two sides was obtained. Thus, the c_2 value was evaluated.

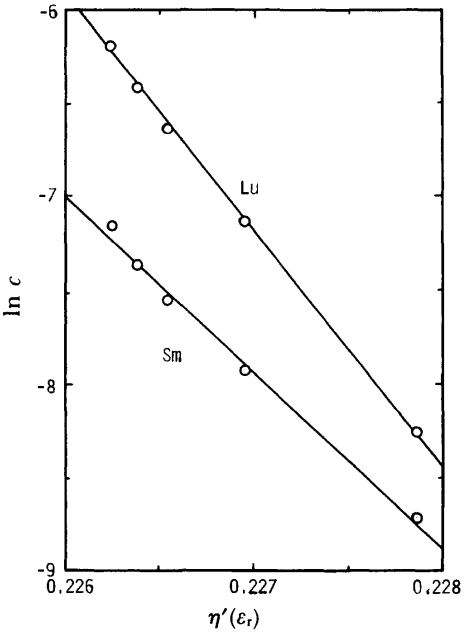

Fig. 1. Relation between $\ln c$ and $\eta'(\varepsilon_r)$ for samarium and lutetium iodates in DMSO-water mixtures.

Table 1. Solubilities of Representative Lanthanoid Iodates in DMSO-Water Mixtures at 25 °C

DMSO	c_{obsd}[a)]	c_{calcd}
mass %	10^{-3}mol dm^{-3}	10^{-3}mol dm^{-3}
$Ce(IO_3)_3$		
0	1.963	—
5.03	1.495	1.558
10.03	1.261	1.397
20.09	0.905	1.037
40.03	0.428	0.537
$Gd(IO_3)_3$		
0	0.893	—
5.03	0.747	0.732
10.03	0.614	0.650
20.09	0.422	0.470
40.03	0.185	0.230
$Lu(IO_3)_3$		
0	2.036	—
5.03	1.629	1.581
10.03	1.304	1.389
20.09	0.794	0.976
40.03	0.258	0.448

a) Data from Ref. 1.

Results and Discussion

In applying Eq. 2 to the data of solubilities for the lanthanoid iodates in DMSO-water mixtures,[1)] the crystal radii of the trivalent rare earth ions[7)] were used as the r_+ values. The reported radius of 0.182 nm[8)] for IO_3^- was used as the r_- value. The ε_r values used for the DMSO-water mixtures were those indicated in a previous paper.[1)] Miyamoto et al. have shown examples of the relation between ln c and $1/\varepsilon_r$ for samarium and lutetium iodates.[1)] The corresponding relation between ln c and $\eta'(\varepsilon_r)$ is shown in Fig. 1. The figure shows that the values of ln c are linearly proportional to the values of $\eta'(\varepsilon_r)$. This means that the first term in Eq. 2 contributes dominantly to the value of ln (c_2/c_1) in the present case. The observed and calculated solubilities (c_2) for the three representative lanthanoid iodates are shown in Table 1. Table 1 shows that the solubilities calculated by the use of Eq. 2 agree, to a gross approximation, with the corresponding observed values. When the Born equation was used, similar calculations gave solubilities too much higher for the mixtures of high-DMSO components.

Binary solvent mixtures, such as the DMSO-water mixture, are accompanied by the problem of selective solvation.[9)] The observed solubilities of the lanthanoid iodates may be influenced to some extent by the selective solvation. However, the finding that Eq. 2 gives grossly approximate values of the observed solubilities means that the effects of the selective solvation are small in the present case. This is supported by the following facts. The selective solvation of ions in binary solvent mixtures depends on the standard increase of molar Gibbs function ($\Delta G°$) for the solvation of the ions in the two pure solvents.[9b)] Up to 10 mol% of DMSO, $d\Delta G_t°/dx_{DMSO}$ is nearly zero for some ions in the mixtures of DMSO and water,[9c)] where $\Delta G_t°$ is the $\Delta G°$ value of the transfer of an ion from water to the mixture and x_{DMSO}, the mole fraction of DMSO.

Thus, by using Eq. 2, one may calculate the approximate solubilities for a sparingly soluble salt in binary mixtures, as long as there is no strong selective solvation.

References

1) H. Miyamoto, H. Iijima, and M. Sugawara, *Bull. Chem. Soc. Jpn.*, **59**, 2973 (1986).
2) T. W. Davis, J. E. Ricci, and C. G. Sauter, *J. Am. Chem. Soc.*, **61**, 3274 (1939).
3) M. Born, *Z. Phys.*, **1**, 45 (1920).
4) T. Abe, *J. Phys. Chem.*, **90**, 713 (1986).
5) S. Ehrenson, *J. Phys. Chem.*, **91**, 1868 (1987).
6) For example, see: "Physical Chemistry of Organic Solvent Systems," ed by A. K. Covington and T. Dickinson, Prenum Press, London (1973), pp. 31, 183.
7) D. H. Templeton and C. H. Dauben, *J. Am. Chem. Soc.*, **76**, 5237 (1954).
8) A. F. Kapustiuski, *Dokl. Akad. Nauk. SSSR*, **32**, 59 (1941).
9) For example, see: a) C. Reichardt, "Solvent Effects in Organic Chemistry," Verlag Chemie, Weinheim-New York (1979), p. 26. b) H. Schneider, "Solute-Solvent Interactions," ed by J. F. Coetzee and C. D. Ritchie, Marcel Dekker, New York-London (1969), p. 301. c) H. Schneider, "Solute-Solvent Interactions. Vol. 2," ed by J. F. Coetzee and C. D. Ritchie, Marcel Dekker, New York-Basel (1976), p. 155.

Effects of $CH_3 \cdots O$ Hydrogen Bond on the Rotamer Populations in 9-(Alkoxymethyl)-1,4-dimethyltriptycenes

Yoshio TAMURA, Gaku YAMAMOTO, and Michinori ŌKI*
Department of Chemistry, Faculty of Science, The University of Tokyo, Bunkyo-ku, Tokyo 113
(Received March 24, 1987)

Synopsis. Rotamer populations in 9-(alkoxymethyl)-1,4-dimethyltriptycenes, where the alkyl is an ethyl, a methyl, or a 2,2,2-trifluoroethyl, were examined by ^1H NMR spectra. The populations of the *sc* isomer decreased as the alkyl group becomes electronegative. The population ratio, *sc*/*ap*, of the methyl compound was almost the same with that for 1,4-dimethyl-9-(phenoxymethyl)triptycene to indicate that the populations of the rotamers in this and related series of compounds are determined on a delicate balance of various factors such as van der Waals repulsive and charge-transfer attractive interactions.

As an extension of the investigation on the factors affecting the rotamer populations, we have prepared 9-(methoxymethyl)-1,4-dimethyltriptycene to find that the population ratio, *sc*/*ap*, was 0.45 at −49.6 °C. The result was surprising because the corresponding 9-(phenoxymethyl) compound gave the ratio of 0.44 at −49.4 °C:[1] Though the electron-density of the phenolic oxygen is supposed to be lower than that of methanol-oxygen, the rotamer populations in these compounds were almost the same. The results may imply that, though the basicity of the oxygen atom in the methoxy compound is higher than that of the phenoxy compound, the van der Waals radius of the methoxy-oxygen is larger than the phenoxy-oxygen to counterbalance the attractive $CH_3 \cdots O$ interactions with the van der Waals repulsion, since high electron-density of an atom means a large steric size. Thus we felt it would be worthwhile to examine the electronic effects on the rotamer populations in 9-(alkoxymethyl)-1,4-dimethyltriptycenes to find whether the effects again would support the existence of the $CH_3 \cdots O$ hydrogen bond. This paper reports the results of such an investigation.

Syntheses of the compounds in question were carried out in analogous ways to those reported previously:[1] 9-(Chloromethyl)anthracene (**1**) was treated with the corresponding alcohol, in the presence of a base if necessary, and the resulting 9-(alkoxymethyl)-anthracene (**2**) was treated with 3,6-dimethylbenzyne to produce the desired 9-(alkoxymethyl)-1,4-dimethyltriptycene (**3**). As alkyl groups, other than a methyl, an ethyl and a 2,2,2-trifluoroethyl were chosen, the former giving a more basic oxygen and the latter giving a less basic oxygen than the methoxy-oxygen.

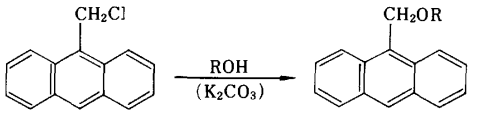

1 2

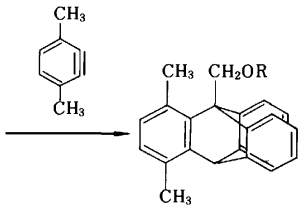

3

The rotamer populations were determined by 400 MHz ^1H NMR spectra at low temperatures. Assignment of the conformations was straightforward from the methylene signals (see Scheme 1).[1] The results are shown in Tables 1 and 2. The population of the *sc* form was divided by 2 to accommodate the fact that there are two (+ and −) equivalent conformations for the *sc* form.

The results clearly indicate that, as the alkyl group becomes electronegative and consequently the proton affinity of the oxygen atom in the 9-substituent decreases, the population ratios (*sc*/*ap*) become small and the free energy differences between the *sc* and the *ap* rotamers become large. The results are consistent with the presence of the $CH_3 \cdots O$ hydrogen bond, if we compare the populations in the 9-(alkoxymethyl)-1,4-

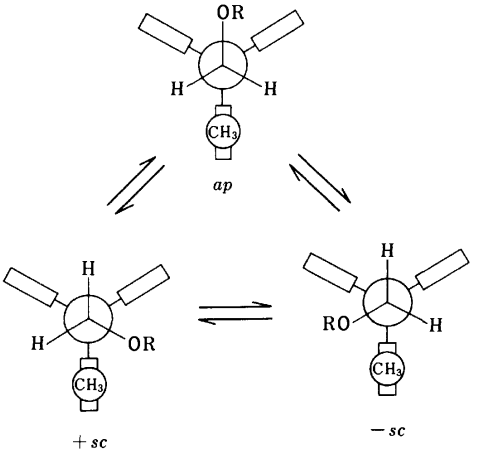

Scheme 1. Rotational circuit.

Table 1. Rotamer Populations in 9-(Alkoxymethyl)-1,4-dimethyltriptycenes in $CDCl_3$ at Various Temperatures

Alkyl	Population ratio[a] (Temperature/°C)
CH_3CH_2	0.346 (−49.5) 0.354 (−39.6) 0.372 (−9.7)
CH_3	0.225 (−49.6) 0.240 (−39.6) 0.269 (−29.6) 0.278 (−19.7) 0.304 (−9.7)
CF_3CH_2	0.149 (−49.5) 0.163 (−39.6) 0.175 (−29.6) 0.188 (−19.7)

a) +(or −) *sc*/*ap*: see text.

Table 2. Thermodynamic Parameters for the Equilibrium, $ap \rightleftharpoons sc$, in 9-(Alkoxymethyl)-1,4-dimethyltriptycenes in $CDCl_3$ and Related Data

Alkyl	$\Delta H°$	$\Delta S°$	PA[b]
	kcal mol^{-1}[a]	cal mol^{-1} K^{-1}	kcal mol^{-1}
CH_3CH_2	0.21±0.05	−1.2±0.2	190.3
CH_3	0.88±0.16	1.0±0.7	184.9
CF_3CH_2	0.87±0.05	0.1±0.2	174.9

a) 1 cal≒4.184 J. b) Proton affinity of the corresponding alcohols obtained from the gas phase equilibrium.[2]

dimethyltriptycene series.

As was discussed previously, the 9-(alkoxymethyl) group in these compounds is placed in a space where other neighboring groups are in close proximity. Therefore, the repulsive interactions between the alkoxy-oxygen and the 1-methyl group is especially severe in the *sc* conformation, where the attractive $CH_3 \cdots O$ interaction is also possible. We believe that the bulkiness effects of the methoxy-oxygen compensate the stabilization by the $CH_3 \cdots O$ hydrogen bond in 9-(methoxymethyl)-1,4-dimethyltriptycene to make the apparent rotameric populations of the compound about the same with that of 1,4-dimethyl-9-(phenoxymethyl)triptycene.

We conclude that the $CH_3 \cdots O$ hydrogen-bond effects on the rotamer populations do exist in this series but care should be exercised in comparing the population ratios of rotamers in different series of compounds, if the molecules are in congested states.

Experimental

Determination of Population Ratios. The ^1H NMR spectra at low temperatures were obtained with the use of a JEOL GX-400 NMR spectrometer. The indicated temperatures were calibrated with a thermocouple. For the determination of populations, the integrated intensities were obtained by cutting the chart papers and weighing them for several times. The peaks for the integration were those due to 9-methylene protons.

9-(Ethoxymethyl)anthracene. A solution of 0.15 g (0.66 mmol) of 9-(chloromethyl)anthracene[3] in 20 mL of ethanol was stirred for 10 h at room temperature. The mixture was poured into water and extracted with dichloromethane. The solvent was evaporated, after drying over magnesium sulfate, to afford 0.14 g (90%) of practically pure 9-(ethoxymethyl)-anthracene. This compound was directly used for the syntheses of the corresponding triptycene. The following ^1H NMR data ($CDCl_3$, δ) were recorded: 1.27 (3H, t, J=6.0 Hz), 3.70 (2H, q, J=6.0 Hz), 5.43 (2H, s), 7.1—8.6 (8H, m), 8.43 (1H, s).

9-[(2,2,2-Trifluoroethoxy)methyl]anthracene. A mixture of 0.20 g (0.88 mmol) of 9-(chloromethyl)anthracene, 1.30 g (13.0 mmol) of 2,2,2-trifluoroethanol, and 0.12 g (0.86 mmol) of potassium carbonate in 40 mL of acetone was refluxed for 3 d. The precipitate was filtered off and the product was taken up into dichloromethane by shaking the filtrate with a mixture of water and dichloromethane. The organic layer was washed with aqueous sodium hydroxide and dried over magnesium sulfate. Evaporation of the solvent afforded 0.20 g of the crude product which was recrystallized from dichloromethane-hexane. The mother liquor was submitted to preparative TLC (silica gel, 2:1 hexane-dichloromethane) to afford a further crop. The desired product was obtained in 0.16 g (62%) yield. This compound was directly used for the triptycene synthesis. The following ^1H NMR data ($CDCl_3$, δ) were recorded: 3.89 (2H, q, J=9.0 Hz), 5.66 (2H, s), 7.3—8.6 (8H, m), 8.48 (1H, s).

9-(Methoxymethyl)-1,4-dimethyltriptycene. To a boiling solution of 0.46 g (2.1 mmol) of 9-(methoxymethyl)anthracene[3] in 20 mL of dichloromethane, were simultaneously added from two separatory funnels a solution of 2.23 g (13.5 mmol) of 3,6-dimethylanthranilic acid[4] in 70 mL of acetone and that of 3.92 g (33.5 mmol) of isopentyl nitrite in 70 mL of dichloromethane in 3 h. The whole was refluxed for further 30 min and the solvent was evaporated. The residue was submitted to chromatography on alumina with a 4:1 hexane-dichloromethane eluent. The desired product, mp 219—220 °C, was obtained in 20% yield after recrystallization of the product from dichloromethane-hexane. Found: C, 88.50; H, 6.49%. Calcd for $C_{24}H_{22}O$: C, 88.31; H, 6.79%. ^1H NMR ($CDCl_3$) δ=2.43 (3H, s), 2.52 (3H, s), 3.70 (3H, s), 5.03 (2H, br s), 5.56 (1H, s), 6.58 and 6.66 (2H, ABq, J=8.1 Hz), 6.8—7.8 (8H, m).

9-(Ethoxymethyl)-1,4-dimethyltriptycene. Mp 167.5—169 °C, was prepared in 84% yield similarly. Found: C, 88.24; H, 7.27%. Calcd for $C_{25}H_{24}O$: C, 88.19; H, 7.11%. ^1H NMR ($CDCl_3$) δ=1.33 (3H, t, J=6.3 Hz), 2.40 (3H, s), 2.50 (3H, s), 3.83 (2H, q, J=6.3 Hz), 5.03 (2H, br s), 5.54 (1H, s), 6.4—8.0 (10H, m).

1,4-Dimethyl-9-[(2,2,2-trifluoroethoxy)methyl]triptycene. Mp 151—152 °C, was prepared similarly in 41% yield. Found: C, 76.01; H, 5.67%. Calcd for $C_{25}H_{21}F_3O$: C, 76.13; H, 5.37%. ^1H NMR ($CDCl_3$) δ=2,44 (3H, s), 2.50 (3H, s), 4.18 (2H, q, J=9.0 Hz), 5.34 (2H, br s), 5,58 (1H, s), 6.4—7.6 (10H, m).

We thank Dr. Shigeru Murata, Institute for Molecular Science, for the measurement of the ^1H NMR spectra.

References

1) Y. Tamura, G. Yamamoto, and M. Ōki, *Bull. Chem. Soc. Jpn.*, **60**, 1781 (1987).

2) J. Gasteiger and M. G. Hutchings, *J. Am. Chem. Soc.*, **106**, 6489 (1984).

3) F. H. C. Stewart, *Aust. J. Chem.*, **13**, 478 (1960).

4) S. Gronowitz and G. Hansen, *Ark. Kemi*, **27**, 145 (1967).

(3*E*)-Laureatin and (3*E*)-Isolaureatin, Halogenated C-15 Non-Terpenoid Compounds from the Red Alga *Laurencia nipponica* Yamada[1)]

Minoru SUZUKI* and Etsuro KUROSAWA
Department of Chemistry, Faculty of Science, Hokkaido University, Sapporo 060
(Received May 2, 1987)

Synopsis. (3*E*)-Laureatin and (3*E*)-isolaureatin have been isolated as major metabolites from the red alga *Laurencia nipponica* Yamada, and their structures were confirmed on the basis of spectral and chemical evidence.

In the course of our continuing studies on the constituents of the red marine algae of the genus *Laurencia* (family Rhodomelaceae), we have reported that *L. nipponica* Yamada ("Ura-sozo"), one of the Japanese species, displayed a marked variation in the major chemical components which seems to be mainly dependent upon the growth locality. The major metabolites from this species collected in the warm current region in Hokkaido are, with some exception,[2,3)] composed of halogenated C-15 non-terpenoids.[4)] As part of our investigations for this species, we have newly collected at several separate locations in Hokkaido and at two locations in Honshū, Oga (Akita Prefecture), and Shichigahama (Miyagi Prefecture). The specimens collected in Hokkaido, as anticipated, contained C-15 non-terpenoids as major metabolites. Laurencin (**1**),[4a)] laureatin (**2**),[4b)] and epilaurallene (**3**)[4c)] were obtained from the specimens of six collecting sites, single site, and two sites, respectively. The major metabolite of Oga's specimen was also C-15 non-terpenoid, laureatin (**2**). On the other hand, the Shichigahama's specimen contained (3*E*)-laureatin (**4**) and (3*E*)-isolaureatin (**5**) as major metabolites, which have previously been obtained as minor components from this species.[5)] We report here the isolation and structural confirmation of these compounds.

(3*E*)-Laureatin (**4**), $C_{15}H_{20}O_2Br_2$, showed the ^1H NMR spectrum very similar to that of laureatin (**2**),[4b)] which has previously been isolated from this species collected at Moheji, except for the signals due to acetylenic and olefinic protons. In the ^1H NMR spectrum of **4**, the signal due to the acetylenic proton was observed in upfield region (δ=2.84) compared with that (δ=3.13) in **2** and the coupling constant between the olefinic protons was 16 Hz. Above-mentioned data coupled with the close resemblance of the ^{13}C NMR spectra (Table 1) of **4** and **2** indicate that **4** is the geometric isomer of the double bond at C-3 of laureatin (**2**). Hydrogenation of **4** over platinum oxide in ethyl acetate gave the hexahydro derivative, $C_{15}H_{26}O_2Br_2$, which was identical with hexahydrolaureatin (**6**)[4b)] in all respects.

Table 1. ^{13}C NMR Chemical Shifts[a)] for **2**, **4**, **5**, and **7**

Carbon No.	2	4	5	7
1	82.6	77.2	76.6	82.2
2	79.6	81.5	81.6	79.7
3	110.7	111.7	111.5	110.4
4	141.5	141.2	141.6	141.5
5	40.8	41.1	34.4	34.7
6	75.7	76.9	75.2§	75.3‡
7	81.5#	80.7†	80.2	81.2
8	21.8	21.5	33.7	31.1
9	80.8#	80.5†	47.0	47.2
10	51.0	50.7	76.0§	75.7‡
11	29.2	31.8	33.7	33.3
12	73.2	73.4	72.2	71.9
13	65.2	64.5	62.3	63.1
14	28.9	28.3	27.9	28.4
15	12.6	12.7	12.8	12.8

a) Measured at 25.0 MHz in $CDCl_3$ (TMS=0).
#, †, §, ‡; Assignments may be reversed.

The ^1H and ^{13}C NMR (Table 1) spectra of (3*E*)-isolaureatin (**5**), $C_{15}H_{20}O_2Br_2$, again were very similar to those of isolaureatin (**7**),[4b)] an isomer of **2**, except for the signals due to the acetylenic and olefinic protons, thus indicating that **5** is also the geometric isomer of the double bond at C-3 of **7**. Confirmation of the structure of **5** was also obtained by hydrogenation reaction. Hydrogenation of **5** gave the same hexahydro derivative (**8**)[4b)] as that derived from **7**. Accordingly, the structures of (3*E*)-laureatin and (3*E*)-isolaureatin were established as formulae **4** and **5**, respectively.

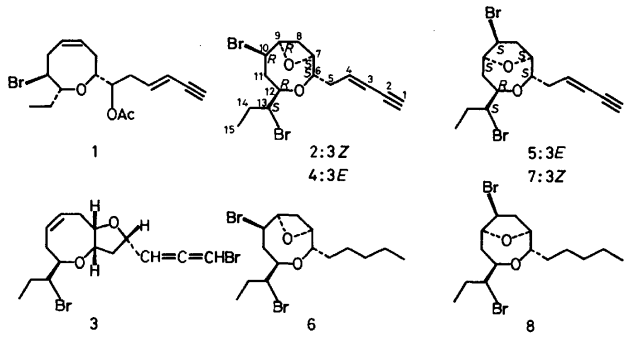

Experimental

The melting point was uncorrected. The IR spectra were recorded on a JASCO A-102 spectrophotometer and the UV spectra on a Shimadzu UV-240 spectrophotometer. The ^1H and ^{13}C NMR spectra were measured on a JEOL JNM-FX 100 spectrometer, using $CDCl_3$ as the solvent and tetramethylsilane as the internal standard. The low and high resolution mass spectra were obtained by a JEOL JMS-D300 spectrometer. Specific rotations were measured on a JASCO DIP-140 polarimeter in $CHCl_3$ unless otherwise stated. Aluminium oxide (Merck, activity II—III) and silica gel (Merck, Kieselgel 60, 70—230 mesh) were used for column chromatography. Silica gel 60 F_{254} (Merck) was used for preparative thin-layer chromatography. All known com-

pounds were identified by comparison of the spectral data with those of the authentic specimens.

Collection. Algae were collected in Hokkaido at Kabutosaki ('Kabutoiwa')[4a,6] (Oshoro Bay, near Otaru, May 7, 1982), Ebisuiwa (Oshoro Bay, May 7, 1982), Poromaisaki (Oshoro Bay, May 7, 1982), Bikuni (East Shakotan, June 30, 1982), Moiwa (Tomari, West Shakotan, June 30, 1982), Terugishi (West Shakotan, June 30, 1982), Raiden (near Iwanai, June 24, 1982), Sametorima (near Raiden, June 24, 1982), and Benkei Point (Suttsu, June 24, 1982). Furthermore, algae were collected in Honshū at Oga (Akita Prefecture, July 20, 1981) and Shichigahama (near Shiogama, Miyagi Prefecture, April 26, 1982).

Extraction and Isolation. Extraction and isolation were carried out by conventional methods as described in the case of Shichigahama's specimen. Major metabolites; laurencin (**1**): Kabutosaki (10% of the extract), Bikuni (13%), Terugishi (15%), Raiden (15%), Sametorima (10%), and Benkei Point (15%); laureatin (**2**): Moiwa (15%, isolaureatin 5%) and Oga (17%, isolaureatin 5%); epilaurallene (**3**): Ebisuiwa (20%) and Poromaisaki (13%, laurencin 5%).

Isolation of (3*E*)-Laureatin (4) and (3*E*)-Isolaureatin (5). Dried alga (150 g) collected at Shichigahama was extracted with methanol, and the methanol extract was treated with 10% aqueous Na_2CO_3 in the usual manner to give a neutral brown oil (3 g). The neutral oil (1.2 g) was chromatographed over alumina column. The earlier benzene fraction was further chromatographed over silica-gel column to yield crude (3*E*)-isolaureatin (**5**) (60 mg as a pale yellow oil) and (3*E*)-laureatin (**4**) (130 mg as crystals). The successive benzene fraction was subjected to repeated preparative TLC to afford prepacifenol (20 mg),[7] pacifenol (70 mg),[8] and diacetate of laurediol (20 mg).[5] Purification of **4** and **5** was performed by recrystallization and preparative TLC, respectively.

4: Mp 77—78 °C (methanol); $[\alpha]_D^{18}$ +36.6° (*c* 0.95); UV (ethanol), λ_{max} 224 nm (ε 16000) and λ_{inf} 215 (ε 13000) and 231 nm (ε 13000); IR ($CHCl_3$), ν_{max} 3310, 1285, 1140, 1085, 1045, 967, 947, 905, and 803 cm^{-1}: ^1H NMR (100 MHz), δ=1.08 (3H, t, *J*=7 Hz, H-15), 1.7—2.0 (2H, m, H-14), 2.4—3.1 (6H, m, H-5, H-8, and H-11), 2.84 (1H, d, *J*=2 Hz, H-1), 3.7—4.0 (2H, m, H-6 and H-13), 4.21 (1H, ddd, *J*=10, 7, 3 Hz, H-10), 4.45 (1H, ddd, *J*=5, 5, 4 Hz, H-12), 4.65 (1H, ddd, *J*=8, 5.5, 1.5 Hz, H-7), 4.97 (1H, ddd, *J*=8, 5.5, 3 Hz, H-9), 5.47 (1H, br dd, *J*=16, 2 Hz, H-3), and 6.18 (1H, ddd, *J*=16, 7, 7 Hz, H-4); ^{13}C NMR, in the Table 1; EI-MS (70 eV), *m/z* (rel intensity) 394, 392, 390 (0.2:0.4:0.2; M^+), 329, 327, 325 (0.6:1.3:0.7; $M^+-C_5H_5$), 313, 311 (0.9:0.8; M^+—Br), 247, 245 (21:22), 179, 177 (25:27), 165 (66), 149 (19), 147 (44), 119 (37), 107 (35), 105 (27), 93 (47), 91 (33), 81 (24), 79 (43), 77 (38), 71 (20), 69 (30), 67 (59), 65 (44), 57 (22), 55 (54), 53 (28), 44 (37), 43 (27), and 41 (100). Found: *m/z* 391.9815. Calcd for $C_{15}H_{20}O_2{}^{79}Br^{81}Br$: M, 391.9809.

5: Colorless oil; $[\alpha]_D^{15}$ −8.73° (*c* 1.11); UV (ethanol), λ_{max} 224 nm (ε 14000) and λ_{inf} 214 (ε 11000) and 232 nm (ε 11700); IR ($CHCl_3$), ν_{max} 3310, 2150, 1287, 1135, 1110, 963, 945, and 842 cm^{-1}; ^1H NMR (100 MHz), δ=1.07 (3H, t, *J*=7 Hz, H-15), 1.6—2.7 (8H, m, H-5, H-8, H-11, and H-14), 2.83 (1H, d, *J*=2 Hz, H-1), 3.56 (1H, dd, *J*=7, 7 Hz, H-6), 3.8—4.5 (5H, m, H-7, H-9, H-10, H-12, and H-13), 5.55 (1H, br dd, *J*=16, 2 Hz, H-3), and 6.23 (1H, ddd, *J*=16, 7, 7 Hz, H-4); ^{13}C NMR, in the Table 1; EI-MS, *m/z* 394, 392, 390 (0.5:0.9:0.4; M^+), 329, 327, 325 (0.4:0.9:0.5; $M^+-C_5H_5$), 313, 311 (1.6:1.6; M^+—Br), 247, 245 (45:47), 179, 177 (32:33), 165 (80), 149 (20), 147 (46), 119 (33), 109 (18), 107 (29), 105 (21), 95 (25), 93 (44), 91 (22), 81 (27), 79 (31), 77 (21), 69 (38), 68 (22), 67 (53), 65 (30), 55 (60), 53 (21), 43 (31), and 41 (100). Found: *m/z* 389.9847. Calcd for $C_{15}H_{20}O_2{}^{79}Br^{79}Br$: M, 389.9830.

Hydrogenation of (3*E*)-Laureatin (4). **4** (12 mg) was hydrogenated in ethyl acetate over PtO_2-catalyst to give **6** (10 mg); oil; $[\alpha]_D^{20}$ +26.5° (*c* 1.00) and $[\alpha]_D^{18}$ +28.3° (*c* 0.78, CCl_4); whose spectral data were consistent with those of hexahydrolaureatin (**6**)[4b] derived from laureatin (**2**).

Hydrogenation of (3*E*)-Isolaureatin (5). **5** (9 mg) was hydrogenated in ethyl acetate over PtO_2-catalyst to yield **8** (9 mg); oil; $[\alpha]_D^{18}$ +5.79° (*c* 0.97) and $[\alpha]_D^{19}$ −0.62° (*c* 0.69, CCl_4); whose spectral data were identical with those of hexahydroisolaureatin (**8**)[4b] derived from isolaureatin (**7**).

We are grateful to Dr. Yuzuru Saito, Faculty of Fisheries, Hokkaido University, for collection and identification of the algae.

References

1) Part 68 of "Constituents of Marine Plants." Part 67; T. Suzuki, S. Takeda, M. Suzuki, E. Kurosawa, A. Kato, and Y. Imanaka, *Chem. Lett.*, **1987**, 361.

2) T. Suzuki, H. Kikuchi, and E. Kurosawa, *Bull. Chem. Soc. Jpn.*, **55**, 1561 (1982).

3) M. Suzuki, M. Segawa, H. Kikuchi, T. Suzuki, and E. Kurosawa, *Phytochemistry*, **24**, 2011 (1985).

4) a) T. Irie, M. Suzuki, and T. Masamune, *Tetrahedron*, **24**, 4193 (1968); M. Suzuki and E. Kurosawa, *Bull. Chem. Soc. Jpn.*, **52**, 3349 (1979); b) T. Irie, M. Izawa, and E. Kurosawa, *Tetrahedron*, **26**, 851 (1970); H. Kikuchi, T. Suzuki, M. Suzuki, and E. Kurosawa, *Bull. Chem. Soc. Jpn.*, **58**, 2437 (1985); c) M. Suzuki, K. Koizumi, H. Kikuchi, T. Suzuki, and E. Kurosawa, *Bull. Chem. Soc. Jpn.*, **56**, 715 (1983); d) T. Suzuki, K. Koizumi, M. Suzuki, and E. Kurosawa, *Chem. Lett.*, **1983**, 1639, 1643; M. Suzuki, M. Segawa, T. Suzuki, and E. Kurosawa, *Bull. Chem. Soc. Jpn.*, **56**, 3824 (1983); e) M. Suzuki, K. Kurata, T. Suzuki, and E. Kurosawa, *Bull. Chem. Soc. Jpn.*, **59**, 2953 (1986).

5) E. Kurosawa, A. Fukuzawa, and T. Irie, *Tetrahedron Lett.*, **1972**, 2121.

6) *L. glandulifera* Kützing[4a] has not grown in Japan, and *L. glandulifera* should be revised to *L. nipponica* Yamada: Y. Saito, *Mem. Fac. Fish., Hokkaido Univ.*, **15**, 1 (1967); Y. Saito, *Jap. J. Phycol.*, **33**, 167 (1985).

7) J. J. Sims, W. Fenical, R. M. Wing, and P. Radlick, *J. Am. Chem. Soc.*, **95**, 972 (1973).

8) J. J. Sims, W. Fenical, R. M. Wing, and P. Radlick, *J. Am. Chem. Soc.*, **93**, 3774 (1971).

(*E*)-2-Tridecyl-2-heptadecenal, an Unusual Metabolite from the Red Alga *Laurencia* Species[1)]

Minoru SUZUKI,* Etsuro KUROSAWA, and Kazuya KURATA*,†
Department of Chemistry, Faculty of Science, Hokkaido University, Sapporo 060
†Department of Industrial Chemistry, Hakodate Technical College, Hakodate 042
(Received May 2, 1987)

Synopsis. The structure of an unusual α,β-unsaturated aldehyde isolated from the red algae *Laurencia undulata* and *L. papillosa* was established as (*E*)-2-tridecyl-2-heptadecenal by synthetic method.

In connection with our interest on the halogenated metabolites of the marine seaweeds, we have investigated various Japanese species of the genus *Laurencia* (Rhodomelaceae; Rhodophyta) and found as the major metabolites many halogenated compounds with unique structural features in the extracts of *L. nipponica* Yamada (Ura-sozo),[2)] *L. okamurai* Yamada (Mitsude-sozo),[3,4)] *L. venusta* Yamada (Hime-sozo),[5)] *L. majuscula* Harvey (Aka-sozo),[6)] and *L. pinnata* Yamada (Hane-sozo).[7)] On the other hand, *L. intermedia* Yamada (Kuro-sozo),[3a)] *L. capituliformis* Yamada (Maru-sozo),[3a)] and *L. cartilaginea* Yamada (Kata-sozo)[8)] displayed no halogenated metabolite in their extracts. Furthermore, *L. undulata* Yamada (Kobu-sozo) and *L. papillosa* (Forsk.) Greville (Papira-sozo) also contained no halogenated compound and instead an unusual α,β-unsaturated aldehyde **1**, whose structure is described in this note.

The neutral methanol extract was subjected to repeated column and thin-layer chromatography to give a new aldehyde **1** in 5% yield of the extract along with fatty acid esters.

Compound **1**, $C_{30}H_{58}O$, showed in its ^{1}H NMR spectrum the signals due to two methyl groups at δ=0.88 (6H, br t, J=7 Hz), a vinyl proton at δ=6.43 (1H, dd, J=7, 7 Hz), and an aldehyde proton at δ=9.35 (1H, s). The presence of a disubstituted α,β-unsaturated aldehyde moiety was evident on the basis of UV (λ_{max} 230 nm (ε 10800)), IR (ν_{max} 2730, 1680, and 1640 cm^{-1}), and ^{13}C NMR (δ=195.3 (s), 155.2 (d), and 143.9 (s)) spectra. Furthermore, ^{13}C NMR spectrum (INEPT method) revealed the presence of methyl groups at δ=14.1, methylene groups at δ=22.7—32.0, and no methine group and no other double bonds except for the above-mentioned trisubstituted double bond. Therefore, compound **1**, having two degrees of unsaturation, must be composed of branched-chain carbon skeleton, permitting a formula **2** (m+n=25) to be assigned to this unique aldehyde.

At this stage we noticed the previous report[9)] that 2-dodecyl-2-hexadecenal (formula **2**: m=12 and n=11) was isolated as the major constituent from *L. spectabilis* collected from Southern California along with other α,β-unsaturated aldehydes (range from C_{22} to C_{34}). Thus, formula **2** (m=13 and n=12) could be assigned to our aldehyde. The stereochemistry of the double bond was established as *E*-configuration by the observation of a strong NOE between the aldehyde proton and the vinyl proton on the NOE difference spectra. Confirmation of the structure of **1**, 2-tridecyl-2-heptadecenal, was obtained by synthesis from pentadecanal.

Aldol condensation of pentadecanal, which was obtained from commercially available 1-pentadecanol by oxidation with the chromium trioxide–pyridine complex,[10)] gave (*E*)-2-tridecyl-2-heptadecenal[11)] in 83% yield which was identical with natural aldehyde **1** in all respects.

Consequently, the structure of the unique aldehyde is represented by formula **1**.

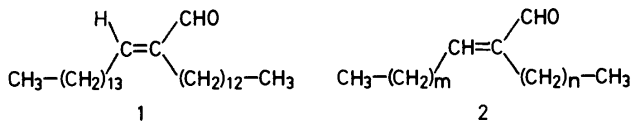

1 **2**

Experimental

The IR spectra were measured on a JASCO IR-S or a JASCO A-102 spectrophotometer. The UV spectrum was taken with a Shimadzu UV-240 spectrophotometer. The ^{1}H and ^{13}C NMR spectra were recorded on a JEOL JNM-FX 100 or a JEOL JNM-GX 270 spectrometer, using tetramethylsilane as an internal standard. The low and high resolution mass spectra were measured by a JEOL JMS-D300 spectrometer. Silica gel (Merck, Kieselgel 60, 70—230 mesh) and silica gel 60 F_{254} (Merck) were used for column and thin-layer chromatography, respectively.

Collection. *Laurencia undulata* Yamada were collected at Zagashima, Ago Bay, Mie Prefecture, late in June 1983, and at Shirahama, Wakayama Prefecture, late in May 1976. *Laurencia papillosa* (Forsk.) Greville was collected at Hedomisaki, Okinawa Prefecture, late in May 1976. These three specimens showed almost identical thin-layer chromatogram.

Isolation of (*E*)-2-Tridecyl-2-heptadecenal (1). Half-dried alga (40 g) collected at Ago Bay was extractcd with methanol, and the methanol extract was percolated with ether. The ethereal solution was shaken with 0.5M aqueous KOH (1 M=1 mol dm^{-3}) and saturated brine. After drying over anhydrous Na_2SO_4, the ether was evaporated to give a neutral brown oil (160 mg) which was chromatographed on silica-gel column. The earlier benzene fraction was further subjected to preparative thin-layer chromatography to yield **1** (10 mg) as white crystals. Recrystallization of **1** has been unsuccessful.

1: UV (C_2H_5OH), λ_{max} 230 nm (ε 10800); IR ($CHCl_3$), ν_{max} 2730, 1680, and 1640 cm^{-1}; ^{1}H NMR (100 MHz; $CDCl_3$), δ=0.88 (6H, br t, J=7 Hz), 1.0—1.7 (46H, br s), 2.0—2.5 (4H, m), 6.43 (1H, dd, J=7, 7 Hz), and 9.35 (1H, s); ^{13}C NMR (67.9 MHz; $CDCl_3$) (INEPT), CH_3: δ=14.1; CH_2: δ=22.7, 24.1, 28.7, 28.8, 29.0, 29.4, 29.5, 29.6, 29.7, and 32.0; CH: δ=155.2; C: δ=143.9 and 195.3; LR-EI-MS (70 eV), m/z (rel intensity)

434 (19; M^+), 265 (9), 255 (11), 237 (20), 169 (16), 149 (11), 135 (17), 123 (14), 121 (19), 119 (15), 111 (21), 109 (25), 98 (38), 97 (38), 95 (41), 83 (46), 81 (48), 71 (40), 69 (55), 67 (46), 57 (93), 55 (78), and 43 (100). HR-EI-MS; Found: *m/z* 434.4481. Calcd for $C_{30}H_{58}O$: M, 434.4487.

Aldol Condensation of Pentadecanal. To a solution of pentadecanal (100 mg) in ethanol (1 ml) was added saturated methanolic KOH solution (4 ml), and the mixture was stirred at room temperature for 1 h, acidified with 6M HCl, and extracted with ether. The ethereal solution was washed with 1M HCl and water. After drying over anhydrous Na_2SO_4, the ether was evaporated to give an oily substance which was chromatographed on silica-gel column to yield (*E*)-2-tridecyl-2-heptadecenal (**1**) (42 mg) as crystals, whose spectral properties were consistent with those of natural **1**.

We are grateful to Dr. Yuzuru Saito, Faculty of Fisheries, Hokkaido University, and Dr. Washiro Kida, Mie University, for collection and identification of *L. undulata*, and also to Dr. Hiroshi Yabu, Faculty of Fisheries, Hokkaido University, for collection and identification of *L. papillosa*.

References

1) Part 69 of "Constituents of Marine Plants." Part 68; Ref. 2.

2) M. Suzuki and E. Kurosawa, *Bull. Chem. Soc. Jpn.*, **60**, 3791 (1987) and references cited.

3) a) M. Suzuki and E. Kurosawa, *Bull. Chem. Soc. Jpn.*, **52**, 3352 (1979); b) M. Suzuki and E. Kurosawa, *Tetrahedron Lett.*, **22**, 3853 (1981); c) M. Suzuki and E. Kurosawa, *Phytochemistry*, **24**, 1999 (1985).

4) *L. okamurai* Y., collected in Kyūshū at Hananose and Sakurajima, Kagoshima Prefecture, late in March 1986, also contained laurinterol[3a] as the major metabolite.

5) a) M. Suzuki and E. Kurosawa, *Chem. Lett.*, **1980**, 1177; b) M. Suzuki, E. Kurosawa, A. Furusaki, and T. Matsumoto, *Chem. Lett.*, **1983**, 779.

6) a) M. Suzuki and E. Kurosawa, *Tetrahedron Lett.*, **1978**; 4805; b) M. Suzuki, A. Furusaki, N. Hashiba, and E. Kurosawa, *Tetrahedron Lett.*, **1979**, 879.

7) Contrary to the previous reports,[12] *L. pinnata* Y., collected in Kyūshū at Matsushima, Nagasaki Prefecture, in April 1, 1986, contained as the main component (10% of the extract) a unique sesquiterpene, cupalaurenol, which has recently been isolated from the sea hare *Aplysia dactylomela*.[13] We thank to Prof. Tatsuo Higa, University of the Ryukyus, for providing us with preprint and spectral data.

8) *L. cartilaginea* Y. was collected at Sakurajima, Kagoshima Prefecture, late in March 1986.

9) R. P. Maiden and J. A. Pettus, Jr., ACS/JCS Chemical Congress, Honolulu, Hawaii, April 1979, Abstr. (Part II) (Org. Chem.), No. 575.

10) R. Ratcliffe and R. Rodehorst, *J. Org. Chem.*, **35**, 4000 (1970).

11) It is well-known that the α,β-unsaturated aldehydes derived from aldols are trans isomers with trans disposition of the β-alkyl group and the α-formyl group.[14]

12) a) A. Fukuzawa and T. Masamune, *Tetrahedron Lett.*, **22**, 4081 (1981); b) A. Fukuzawa, Y. Kumagai, T. Masamune, A. Furusaki, T. Matsumoto, and C. Katayama, *Chem. Lett.*, **1982**, 1389; c) A. Fukuzawa, M. Miyamoto, Y. Kumagai, A. Abiko, Y. Takaya, and T. Masamune, *Chem. Lett.*, **1985**, 1259; d) A. Fukuzawa, Y. Takaya, H. Matsue, and T. Masamune, *Chem. Lett.*, **1985**, 1263.

13) T. Ichiba and T. Higa, *J. Org. Chem.*, **51**, 3364 (1986).

14) A. T. Nielsen and W. J. Houlihan, *Org. React. (N.Y.)*, **16**, 12 (1968).

Majusculone, a Novel Norchamigrane-Type Metabolite from the Red Alga *Laurencia majuscula* Harvey[1)]

Minoru SUZUKI,* Etsuro KUROSAWA, and Kazuya KURATA*,†
Department of Chemistry, Faculty of Science, Hokkaido University, Sapporo 060
†Department of Industrial Chemistry, Hakodate Technical College, Hakodate 042
(Received May 2, 1987)

Synopsis. The structure of majusculone, a novel norchamigrane-type terpene isolated from the red alga *Laurencia majuscula* Harvey, was deduced from the spectral data.

As part of our continuing studies on the constituents of the red algae genus *Laurencia* (family Rhodomelaceae), we have reported in the previous papers[2)] the structures of two halogenated chamigrene derivatives, **1** and **2**, with an unique vinyl bromide moiety at C-3(15) double bond which have been isolated as the major metabolites from the red alga *L. majuscula* Harvey ("Aka-sozo"). Further investigation of the minor components of this alga has led to the isolation of a novel norchamigrane-type metabolite **3**, designated as majusculone, along with *E*-isomers, **4** and **5**,[3,4)] and also microcladallene C,[3,5)] a non-terpenoid C-15 compound which has previously been obtained from *L. microcladia* collected on the French coast at Cap Ferrat. We wish to describe herein the isolation and structural elucidation of majusculone (**3**).

A combination of column and thin-layer chromatography of the neutral methanol extract afforded majusculone (**3**) in 1.6% yield.

Majusculone (**3**) had the molecular formula of $C_{14}H_{18}O_2$. Its ^{1}H NMR spectrum revealed the presence of two tertiary methyl groups at δ=1.10 and 1.12 (each 3H, s), one vinyl methyl group at δ=1.97 (3H, d, J=1.5 Hz), and three vinyl protons at δ=5.98 (1H, br s), 6.29 (1H, d, J=10.5 Hz), and 6.78 (1H, d, J=10.5 Hz). The IR spectrum exhibited an absorption maximum at ν_{max} 1660 cm^{-1} characteristic of α,β-unsaturated carbonyl group. The ^{13}C NMR spectrum (Table 1) of **3** showed the signals due to two carbonyl carbon atoms at δ=197.3 and 197.5, thus indicating the presence of two α,β-unsaturated ketone moieties which was supported by the UV spectrum, λ_{max} 241 nm (ε 19900). Furthermore, the ^{13}C NMR spectrum revealed the presence of two quaternary carbons at δ=47.4 and 41.0 and three methylene carbons at δ=48.6, 35.1, and 27.5. Above-

Table 1. ^{13}C NMR Chemical Shifts of **2**, **3**, and **5**[a)]

Carbon No.	2	3	5
1	133.4 (d)	149.8 (d)	130.1 (d)
2	128.1 (d)	131.9 (d)	129.7 (d)
3	135.4 (s)	197.3 (s)‡	137.7 (s)
4	28.5 (t)	35.1 (t)	25.5 (t)
5	28.5 (t)	27.5 (t)	27.3 (t)
6	47.6 (s)	47.4 (s)	47.3 (s)
7	165.9 (s)	163.0 (s)	166.1 (s)
8	126.2 (d)	127.4 (d)	126.2 (d)
9	198.0 (s)	197.5 (s)‡	198.1 (s)
10	48.7 (t)	48.6 (t)	48.6 (t)
11	40.3 (s)	41.0 (s)	40.2 (s)
12	25.4 (q)#	25.5 (q)§	25.4 (q)†
13	24.8 (q)#	25.0 (q)§	24.9 (q)†
14	23.3 (q)	23.0 (q)	23.3 (q)
15	102.9 (d)		107.0 (d)

a) Measurcd at 25.0 MHz in $CDCl_3$ (TMS=0).
#, †, §, ‡; Assignments may be reversed.

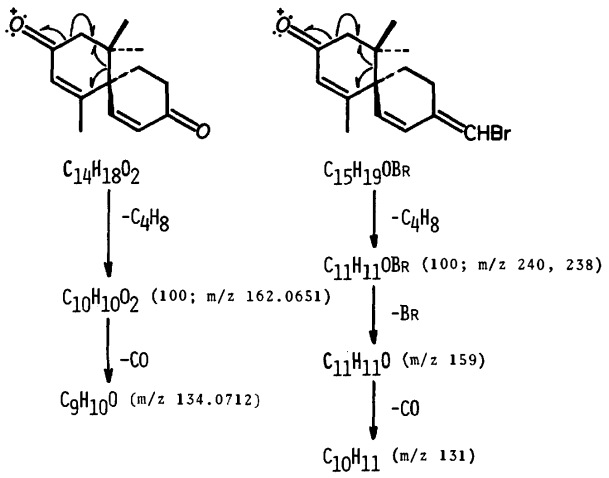

Scheme 1.

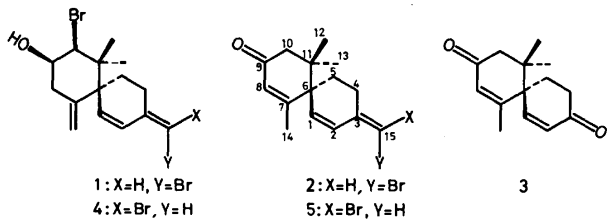

Fig. 1. Partial structures (■; quaternary carbon).

-CO-CH=C(CH$_3$)-■ -CO-CH=CH-■ ■-CH$_2$-CH$_2$-■
■-CH$_2$-■ ■-CH$_3$X2 ■X2

mentioned spectral properties coupled with ^{1}H-^{1}H 2D COSY spectrum indicated the presence of the following partial structures (Fig. 1) in the molecule of **3**. Moreover, the ^{13}C NMR spectrum of **3** showed ten carbon signals compatible with those of **2** and **5**. In view of the above-mentioned data together with co-occurrence of **2**, **3**, and **5** in the same alga, formula **3** could readily be assigned for majusculone. The gross structure **3** was further supported by the mass spectrum. The EI-MS spectrum of **3** displayed a base peak at m/z 162 due to $C_{10}H_{10}O_2$, derived from a loss of C_4H_8 which was resulted from cleavage at C_9-C_{10} and C_{11}-C_6 bonds (Scheme 1). On the other hand, compounds **2**

and **5** revealed in their mass spectra the base peak at *m/z* 240 and 238 ($M^+-C_4H_8$).

Majusculone (**3**) may be biosynthesized from **2** or **5** via epoxidation at C-3(15) double bond.

Majusculone (**3**) is the first example of sesquiterpenoid with a norchamigrane skeleton from marine or terrestrial organisms.

Experimental

The melting point was uncorrected. The IR spectrum was measured on a JASCO A-102 spectrophotometer and the UV spectrum on a Shimadzu UV-240 spectrophotometer. The ^1H and ^{13}C NMR spectra were recorded on a JEOL JNM-FX 100 or a JEOL JNM-GX 270 spectrometer, using tetramethylsilane as an internal standard. The low and high resolution mass spectra were taken with a JEOL JMS-D300 spectrometer. Specific rotation was measured on a JASCO DIP-140 polarimeter. Aluminium oxide (Merck, activity II—III) and silica gel (Merck, Kieselgel 60, 70—230 mesh) were used for column chromatography. Silica gel 60 F_{254} (Merck) was used for preparative thin-layer chromatography.

Isolation of Majusculone (3). *Laurencia majuscula* Harvey was collected at Nyudogatane, Okino-shima, Kochi Prefecture, early in June 1977, and extracted with methanol. The neutral methanol extract (8.5 g) obtained by the conventional methods was fractionated by column chromatography over alumina. The fraction eluted with ethyl acetate gave an oily substance (850 mg) which was repeatedly subjected to silica-gel column and thin-layer chromatography to give majusculone (**3**) as crystals (140 mg).

Majusculone (3): Mp 91.1—92.0 °C (diisopropyl ether); $[\alpha]_D^{19}$ +145° (*c* 0.965, $CHCl_3$); UV (EtOH), λ_{max} 241 nm (ε 19900); IR ($CHCl_3$), ν_{max} 1660, 1615, 1469, 1450, 1437, 1427, 1390, 1377, 1328, 1280, 1269, 963, 905, 855, and 833 cm^{-1}; ^1H NMR (270 MHz; $CDCl_3$), δ=1.10 (3H, s), 1.12 (3H, s), 1.97 (3H, d, *J*=1.5 Hz), 2.08 (1H, m), 2.3—2.7 (5H, m), 5.98 (1H, br s), 6.29 (1H, d, *J*=10.5 Hz), and 6.78 (1H, d, *J*=10.5 Hz); ^{13}C NMR, in the Table 1; EI-MS (70 eV), *m/z* (rel intensity) 162 (100; $M^+-C_4H_8$), 147 (11; $M^+-C_4H_8-CH_3$), 134 (52; $M^+-C_4H_8-CO$), 133 (19), 119 (11), 91 (25), 77 (11), 57 (15), 55 (13), 44 (37), 43 (24), 41 (17), and 40 (47). FI-HR-MS; Found: *m/z* 218.1279. Calcd for $C_{14}H_{18}O_2$: M, 218.1305.

We are grateful to Dr. Yuzuru Saito, Faculty of Fisheries, Hokkaido University, for collection and identification of the alga.

References

1) Part 70 of "Constituents of Marine Plants." Part 69; M. Suzuki, E. Kurosawa, and K. Kurata, *Bull. Chem. Soc. Jpn.*, **60**, 3793 (1987).

2) a) M. Suzuki and E. Kurosawa, *Tetrahedron Lett.*, **1978**, 4805; b) M. Suzuki, A. Furusaki, N. Hashiba, and E. Kurosawa, *Tetrahedron Lett.*, **1979**, 879.

3) Compound **4** (acetate; $[\alpha]_D^{23}$ −47.3° (*c* 1.17; $CHCl_3$)), compound **5** ($[\alpha]_D^{20}$ +69.7° (*c* 1.25; $CHCl_3$)), and microcladallene C ($[\alpha]_D^{21}$ +122° (*c* 1.19; $CHCl_3$) and $[\alpha]_D^{21}$ +155° (*c* 0.814; acetone)) have been isolated in 1, 1.5, and 0.1% yields, respectively. The spectral data of these metabolites were consistent with those[2a,4,5] reported. Compounds **4** and **5** may be artefacts, which were formed during extraction or separation process, because the *Z*-isomers **1** and **2** easily isomerize.[2a,4]

4) F. J. Schmitz, D. P. Michaud, and P. G. Schmidt, *J. Am. Chem. Soc.*, **104**, 6415 (1982).

5) D. J. Kennedy, I. A. Selby, H. J. Cowe, P. J. Cox, and R. H. Thomson, *J. Chem. Soc., Chem. Commun.*, **1984**, 153.

Autoxidation of Indolo[3,2,1-*de*][1,5]naphthyridines

Hajime IRIKAWA* and Yasuaki OKUMURA
Department of Chemistry, Faculty of Science, Shizuoka University, Oya, Shizuoka 422
(Received May 9, 1987)

Synopsis. The yellow keto lactam and the blue dimeric pigment were formed by the autoxidation of indolo[3,2,1-*de*]-[1,5]naphthyridines.

Autoxidation of indole compounds gave various products via indoleninyl hydroperoxides.[1] The well known conversion of indoxyl into indigo and the synthesis of trichotomine dimethyl ester (**3**)[2,3] prompted us to study the autoxidation of indolo[3,2,1-*de*][1,5]-naphthyridines **2c** and **7**.

L-Tryptophan was condensed with 2-oxoglutaric acid to give **1a** and **2a**,[4] which were converted into **1b**[5] and **2b** with methanolic hydrogen chloride. The proton at C-3a in **2b** was suggested to have the same β-configuration as the corresponding proton in **1b** had, since the CD spectrum of **2b** ($[\theta]_{221}$−28800) was similar to that of **1b** ($[\theta]_{232}$−22600).[6]

When **1b** (mp 202—203 °C) was heated at 205—208 °C for 30 min, it changed into blue oil. Separation of the colored product afforded the blue pigment **3** (1%), which was identical with **3** synthesized by the procedure of Iwadare et al. (TLC, IR, and ^{1}H NMR).[2]

Similarly, **2b** was heated above its melting point, but no blue spot was detected on the TLC. In order to protect the NH group, **2b** was converted into the acetate **2c**. When **2c** was heated at 168—172 °C for 30 min, it changed into green oil, which showed the yellow and blue spots on the TLC. Separation of the colored products gave the yellow compound **4** and the blue pigment **5** in very low yields.

On the other hand, pyridinium dichromate oxidation of **2c** in *N*,*N*-dimethylformamide (20 °C, 18 h) afforded **4** (20%), which showed the same R_f value on the TLC as **4** obtained above. The structure of **4** was in agreement wih the spectral data: UV 402 nm (ε 11400); ^{1}H NMR ABX signals of C-1 and C-2 protons and a singlet of C-4 proton at δ=6.49; ^{13}C NMR signals of four carbonyl carbons at δ=152.1, 169.8, 170.6, and 177.6.

The dimeric structure **5** was suggested for the blue pigment, since the coloration of **1b** above its melting point resulted from the formation of **3**. In order to confirm the structure, **5** was synthesized as follows.

Shono et al. reported the α-methoxylation of carbamates by electrolysis.[7] Since **2c** showed the anodic peak at 1.57 V vs. SCE in the cyclic voltammetry, it was electrolyzed at 1.3 V vs. SCE in methanol to give **6**, which showed a singlet at δ=3.00 (3H, OCH_3) in the ^{1}H NMR spectrum. Treatment of **6** with formic acid in chloroform under argon afforded **7**. When a colorless solution of **7** in 1-butanol was stirred at room temperature for 47 h, it became blue. Separation of the products gave **4** (6%) and **5** (12%), the latter of which was identical with that obtained by the autoxidation of **2c** (TLC, IR). The structure of **5** was in line with the spectral data: UV 648 nm (ε 38700); ^{1}H NMR ABX signals of C-1 and C-2 protons and a singlet of C-4 proton at δ=8.57; MS *m*/*z* 644 (M^+).

The autoxidation of **2c** at elevated temperature might proceed via **7**. Formation of **4** and **5** from **7** seemed to proceed via the plausible intermediate **8**, since the autoxidation of **7** is similar to that of indoxyl.[8]

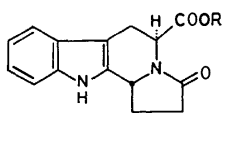

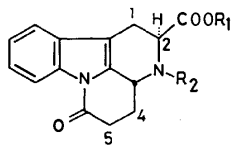

1a R=H
1b R=Me

2a R_1=R_2=H
2b R_1=Me R_2=H
2c R_1=Me R_2=Ac

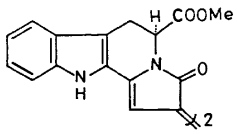

3

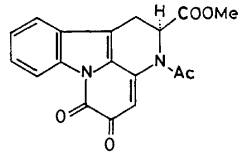

4

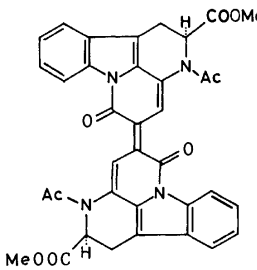

5

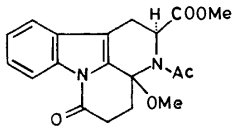

6

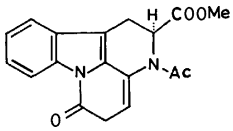

7

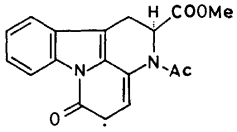

8

Experimental

All melting points were uncorrected. IR spectra were recorded on a Hitachi EPI-G_3 in $CHCl_3$. ^{1}H NMR spectra were obtained on a Varian EM-390 (90 MHz) in $CDCl_3$, and ^{13}C NMR on a JNM-PFT-60 (15 MHz) or a JNM-FX-99 (22.5 MHz) in $CDCl_3$. UV spectra were measured on a JASCO UVIDEC-510 in CH_3OH, and CD spectra on a JASCO J-500 in CH_3OH. Mass spectra were obtained on a Hitachi M-52 or M-80 operating with an ionization energy (70 eV). The cyclic voltammetry of **2c** was recorded on a Yanaco P-1100 in

acetonitrile containing tetrabutylammonium perchlorate (0.10 mol dm^{-3}). Preparative and analytical TLC were carried out on silica-gel plates (Kieselgel 60 F_{254}, E. Merk).

Preparation of 2b. According to the literature,[4] a solution of L-tryptophan (25.0 g) and 2-oxoglutaric acid in 4 mol dm^{-3} hydrochloric acid (250 ml) was heated at 87—91 °C for 2 h. The precipitate was collected and dried. A suspension of the precipitate in 4 wt% hydrogen chloride-CH_3OH (500 ml) was refluxed for 6 h and cooled to room temperature to give the hydrochloride of **2b** (13.1 g), which was freed with aqueous $NaHCO_3$ and crystallized from CH_3OH to give **2b**: mp 154—156 °C; UV 240 (ε 20300), 264 (10400), 292 (4360), and 301 nm (4220); IR 1742 and 1710 cm^{-1}; ^1H NMR δ=1.5—3.2 (7H, m), 3.81 (3H, s), 3.7—4.1 (2H, m), 7.1—7.5 (3H, m), and 8.32 (1H, m); ^{13}C NMR δ=24.9, 28.9, 33.0, 50.2, 52.3, 56.6, 111.8, 116.1, 118.0, 124.0, 124.6, 129.4, 134.8, 135.7, 167.8, and 172.8; MS m/z 284 (M^+); CD $[\theta]_{300}$ −9600, $[\theta]_{276}$ 0, $[\theta]_{267}$ +5100, $[\theta]_{253}$ 0, $[\theta]_{221}$ −28800, and $[\theta]_{211}$ 0. Anal. ($C_{16}H_{16}N_2O_3$) C, H, N.

The mother liquor was concentrated. The residue was neutralized with aqueous $NaHCO_3$, followed by isolation with $CHCl_3$ to give **1b** (3.9 g).[5]

Preparation of 2c. A solution of **2b** (0.91 g) in acetic anhydride (8 ml) and pyridine (8 ml) was allowed to stand at 11—13 °C for 18 h, and concentrated. The residue was crystallized from CH_3OH to give **2c** (1.0 g): mp 168—169 °C; $[\alpha]_D$ +165° (c 0.185, CH_3OH); UV 240 (ε 20800), 264 (10700), 292 (4620), and 300 nm (4480); IR 1747, 1713, 1659, and 1644 cm^{-1}; ^1H MNR δ=2.25 (3H, s), and 3.53 (3H, s); ^{13}C NMR δ=22.7, 23.9, 27.1, 33.4, 49.2, 52.6, 56.2, 110.5, 116.2, 118.2, 124.1, 124.9, 128.5, 133.0, 135.2, 167.8, and 170.8; MS m/z 326 (M^+); CD $[\theta]_{301}$ −8300, $[\theta]_{281}$ 0, $[\theta]_{268}$ +17800, $[\theta]_{255}$ +10400, $[\theta]_{250}$ +15000, $[\theta]_{243}$ 0, $[\theta]_{221}$ −53500, and $[\theta]_{210}$ 0. Anal. ($C_{18}H_{18}N_2O_4$) C, H, N.

Autoxidation of 1b. Colorless crystals of **1b** (103 mg) were placed in a 100 ml Erlenmeyer flask and heated at 205—208 °C for 30 min, open to the atmosphere. Separation of the resulting blue oil with column chromatography afforded **3**[2] (1 mg) in addition to **1b** (77 mg).

Autoxidation of 2c. Colorless crystals of **2c** (104 mg) were placed in a 100 ml Erlenmeyer flask and heated at 168—172 °C for 30 min, open to the atmosphere. The resulting green oil showed the yellow spot of **4** (R_f 0.59), the blue spot of **5** (R_f 0.74), and the spot of **2c** (R_f 0.45) on TLC (ethyl acetate). Separation with column and thin-layer chromatography afforded **4** (<0.1 mg) and **5** (<0.3 mg), respectively, in addition to **2c** (83 mg).

Oxidation of 2c with Pyridinium Dichromate. To a solution of **2c** (98 mg) in DMF (4 ml) was added PDC (1.7 g). The mixture was stirred at 20 °C for 18 h, and poured into water. Isolation in a usual way, purification with column chromatography, and crystallization with $CHCl_3$-hexane afforded **4** (20 mg) in addition to the starting material **2c** (12 mg). **4**: mp 188—190 °C; UV 211 (ε 35400), 248 (12600), 275 (13400), 324 (10600), and 402 nm (11400); IR 1745, 1722, 1697, 1663, 1615, and 1606 cm^{-1}; ^1H NMR δ=2.49 (3H, s), 3.22 (1H, dd, J=18.0 and 6.0 Hz), 3.66 (1H, dd, J=18.0 and 1.8 Hz), 3.71 (3H, s), 5.79 (1H, dd, J=6.0 and 1.8 Hz), 6.49 (1H, s), 7.2—7.7 (3H, m), and 8.33 (1H, m); ^{13}C NMR δ=23.4 (t), 24.7 (q), 53.4 (q), 55.4 (d), 112.3 (d), 117.0 (d), 121.5 (d), 122.7 (s), 125.9 (d), 127.7 (s), 129.7 (d), 138.6 (s), 143.7 (s), 152.1 (s), 169.8 (s), 170.6 (s), and 177.6 (s). Found: C, 63.79; H, 4.23; N, 7.94%. Calcd for $C_{18}H_{14}N_2O_5$: C, 63.90; H, 4.17; N, 8.28%.

Anodic Oxidation of 2c. A mixture of **2c** (74 mg), tetrabutylammonium tetrafluoroborate (330 mg), and CH_3OH (80 ml) was placed in a beaker-type undivided cell, and glassy carbon rods were used as an anode and a cathode, respectively. After electrolysis at constant potential of 1.3 V vs. SCE (electricity: ca. 3 F mol^{-1} (1 F=96480 C)), the electrolytic solution was concentrated. The residue was dissolved in benzene, washed with water, and dried over Na_2SO_4. Evaporation of the solvent and crystallization from CH_3OH gave **6** (45 mg): mp 130—134 °C; UV 238 (ε 21200), 263 (11500), 292 (6200), and 302 nm (6570); IR 1749, 1716, 1661, and 1643 cm^{-1}; ^1H NMR δ=2.50 (3H, s), 2.6—3.5 (4H, m), 3.00 (3H, s), 3.07 (1H, dd, J=16.8 and 5.7 Hz), 3.50 (1H, dd, J=16.8 and 2.1 Hz), 3.57 (3H, s), 5.85 (1H, m), 7.2—7.6 (3H, m), and 8.43 (1H, m); ^{13}C NMR δ=22.8 (t), 24.0 (q), 31.5 (t), 33.3 (t), 49.2 (q), 52.5 (q), 56.3 (d), 84.2 (s), 116.4 (s), 116.8 (d), 118.9 (d), 124.3 (d), 126.2 (d), 126.9 (s), 129.8 (s), 135.7 (s), 167.6 (s), 171.6 (s), and 173.0 (s). Found: m/z 356.1393. Calcd for $C_{19}H_{20}N_2O_5$: M, 356.1371.

Treatment of 6 with HCOOH. To a solution of **6** (40 mg) in $CHCl_3$ (10 ml) was added 99% HCOOH (0.2 ml) under argon. The solution was kept at 20 °C for 24 h, washed with aqueous $NaHCO_3$, and dried over Na_2SO_4. Evaporation of the solvent gave **7** in almost quantitative yield. **7**: IR 1743, 1703, 1659, and 1605 cm^{-1}; ^1H NMR δ=2.38 (3H, s), 3.06 (1H, dd, J=16.8 and 6.0 Hz), 3.51 (1H, d, J=16.8 Hz), 3.62 (3H+2H, s), 5.5—6.2 (2H, m), 7.2—7.6 (3H, m), and 8.37 (1H, m); ^{13}C NMR δ=23.3, 23.4, 35.4, 52.8, 53.8, 110.3, 112.4, 116.3, 119.0, 124.6, 126.0, 126.5, 128.8, 134.8, 165.2, 170.0, and 170.6. Found: m/z 324.1096. Calcd for $C_{18}H_{16}N_2O_4$: M, 324.1108.

Without further purification, **7** was subjected to the next autoxidation.

Autoxidation of 7. A solution of **7**, obtained above, in 1-butanol (20 ml) was stirred at 15—20 °C for 47 h. The resulting blue solution was concentrated. Separation with column and thin layer chromatography afforded **4** (2.2 mg) and the blue oil, which was precipitated with $CHCl_3$ and hexane to give **5** (4.6 mg): UV 228 (ε 59600), 264 (22300), 302 (15200), 348 (12900), 607 (40500), and 648 nm (38700); IR 1742, 1671, 1615, and 1601 cm^{-1}; ^1H NMR δ=2.17 (1H×2, dd, J=18.0 and 6.0 Hz), 2.94 (3H×2, s), 3.20 (1H×2, d, J=18.0 Hz), 3.52 (3H×2, s), 5.87 (1H×2, d, J=6.0 Hz), 7.2—7.5 (3H×2, m), 8.38 (1H×2, m), and 8.57 (1H×2, s). ^{13}C NMR δ=22.8, 24.6, 52.8, 53.7, 115.1, 116.3, 116.6, 120.2, 125.1, 127.1, 128.0, 128.3, 129.5, 130.8, 137.3, 159.9, 170.5, and 170.8; MS m/z 644 (M^+). Found: m/z 644.1887. Calcd for $C_{36}H_{28}N_4O_8$: M, 644.1905.

We would like to thank Professor Akira Tatematsu and Dr. Hiroshi Sakurai of Meijo University, and Dr. Yoshikazu Shizuri of Keio University for obtaining the mass spectra. We also express our thanks to Dr. Kanzo Sakata and Mr. Akihito Yagi of Shizuoka University for measuring the ^{13}C NMR spectra.

References

1) S. Mclean and G. I. Dmitrienko, *Can. J. Chem.*, **49**, 3642 (1971), and references cited therein.

2) S. Iwadare, Y. Shizuri, K. Yamada, and Y. Hirata, *Tetrahedron*, **34**, 1457 (1978).

3) G. J. Kapadia and R. E. Rao, *Tetrahedron Lett.*, **1977**, 975.

4) J. D. Hobson, J. Raines, and R. J. Whiteoak, *J. Chem. Soc.*, **1963**, 3495.

5) Y. Toyoda, H. Kumagai, H. Irikawa, and Y. Okumura, *Chem. Lett.*, **1982**, 903.

6) Detailed discussion will be published elsewhere.

7) T. Shono, H. Hamaguchi, and Y. Matsumura, *J. Am. Chem. Soc.*, **97**, 4264 (1975).

8) G. A. Russell and G. Kaupp, *J. Am. Chem. Soc.*, **91**, 3851 (1969).

The Crystal Structure of 9-Ethyl-8-hydroxyguanine

Hiroshi KASAI,* Susumu NISHIMURA, Yoshiharu TORIUMI,† Akiko ITAI,† and Yoichi IITAKA†
Biology Division, National Cancer Center Research Institute, Chuo-ku, Tokyo 104
†Faculty of Pharmaceutical Sciences, University of Tokyo, Bukyo-ku, Tokyo 113
(Received May 25, 1987)

Synopsis. Analysis of the crystal structure of 9-ethyl-8-hydroxyguanine using X-ray diffraction showed that it is in C-8 keto form. As compared with 9-ethylguanine, significant differences were observed in bond lengths and bond angles of the imidazole ring.

8-Hydroxyguanine (8-OH-Gua) in DNA, induced by oxygen radicals,[1] is a newly encountered form of DNA damage. Many mutagens or carcinogens which form oxygen radicals produce an 8-OH-Gua moiety in DNA in vitro. These agents include mutagenic reducing agents (ascorbic acid, hydrazine, hydroxylamine),[1] asbestos-H_2O_2,[2] polyphenol-H_2O_2-Fe^{3+},[3] and ionizing radiation.[4] The modified base, 8-OH-Gua, is also produced in cellular DNA by ionizing radiation,[5] and it is reasonable to speculate that it may be one of the forms of DNA damage responsible for mutation or carcinogenesis. In fact, misreading was observed during DNA replication in vitro at 8-OH-Gua residue and at adjacent residues.[6] To elucidate the mechanism of mispairing by the 8-OH-Gua residue in DNA, it is important to compare the molecular structure of 8-OH-Gua with that of Gua. It is also important to determine which tautomer of 8-OH-Gua, the 8-enol form or the 8-keto form, is favoured in solution, although the 8-keto form has been proposed for 8-hydroxyguanosine based on ^{13}CNMR shift.[7] This communication describes the analysis of the crystal structure of 9-ethyl-8-hydroxyguanine (9-Et-8-OH-Gua), a model compound of N-9 substituted 8-OH-Gua.

Experimental

9-Et-8-OH-Gua was prepared from *N*-9-ethylguanine (9-Et-Gua, SIGMA) by the treatment with 1 mM $FeSO_4$ (1 M=1 mol dm^{-3}), 5 mM EDTA, 10 mM ascorbic acid, 100 mM phosphate buffer (pH 6.8) in the presence of oxygen gas (Udenfriend system[8]). A 15% yield of pure 9-Et-8-OH-Gua was obtained after fractionation of the reaction mixture using high-performance liquid chromatography. Crystals of 9-Et-8-OH-Gua were then grown in an aqueous solution.

A crystal of approximate dimensions 0.6×0.1×0.1 mm was mounted on a Philips PW1100 diffractometer. The Setting angles for twenty-five high angle reflections and intensity data were measured using Cu $K\alpha$ monochromatic radiation reflected by a graphite plate. Crystal data: 9-Ethyl-8-hydroxyguanine monohydrate (9-Et-8-OH-Gua monohydrate), $C_7H_9O_2N_5$ H_2O, MW=213.2. Triclinic, space group $P\bar{1}$, Z=2. Lattice constants, a=9.937(5), b=9.745(5), c=5.304(6) Å, α=99.95(5), β=92.52(4), γ=114.09(6)°, U=458.1 Å^3. Dcal=1.546 g cm^{-3}, μ for Cu $K\alpha$=1.54 cm^{-1}. Intensities were measured using a 2θ—ω scan method with a scan speed of 4° $2\theta s^{-1}$. The reflections having net intensities (I) above the $2\sigma(I)$ level were recorded as observed. Intensities of three standard reflections, whose values remained within ±2.5%, were monitored every 2 h. 1574 Independent structure factors, out of a theoretically possible 1879, were obtained within the 2θ range from 6—156°. The crystal structure was solved by the direct method, using the computer program MULTAN, and refined by the least-squares method with block-diagonal-matrix approximations. All eleven hydrogen atoms were located on a difference electron-density map and their positional and isotropic thermal parameters were included in the least-squares refinement. The final R value was 0.038 for the 1574 observed structure factors.

Results and Discussion

Analysis of the crystal structure of 9-Et-8-OH-Gua clearly shows it to be in the C-8 keto form, with a

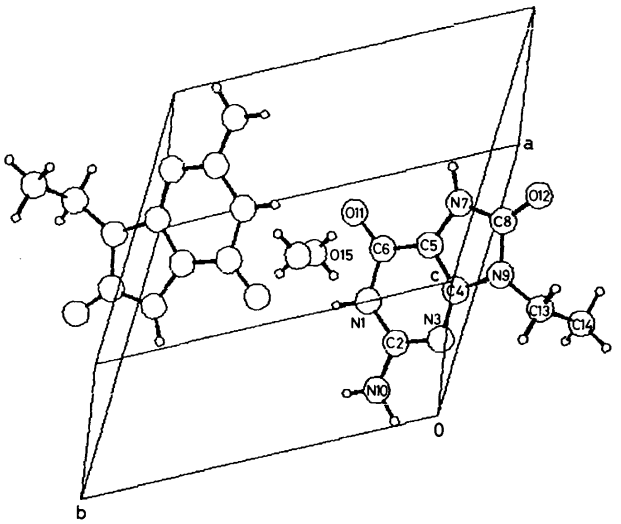

Fig. 1. Projection of the crystal structure of 9-Et-8-OH-Gua.

Table 1. Comparison of Bond Lengths (l/Å) in 9-Et-8-OH-Gua and 9-Et-Gua.

	9-Et-8-OH-Gua	9-Et-Gua	Deviation
	(±0.002)[a]	(±0.004)[a]	
N(1)-C(2)	1.369	1.370	−0.001
N(1)-C(6)	1.369	1.394	0.003
C(2)-N(3)	1.332	1.321	0.011
C(2)-N(10)	1.338	1.344	−0.006
N(3)-C(4)	1.350	1.350	−0.000
C(4)-C(5)	1.373	1.377	−0.004
C(4)-N(9)	1.376	1.375	0.001
C(5)-C(6)	1.395	1.406	0.013
C(5)-N(7)	1.395	1.384	0.005
C(6)-O(11)	1.249	1.238	0.011
N(7)-C(8)	1.358	1.312	0.046
C(8)-N(9)	1.391	1.369	0.022
C(8)-O(12)	1.237	—	—

a) Estimated SD.

Table 2. Comparison of Bond Angles (ϕ/°) in 9-Et-8-OH-Gua and 9-Et-Gua

	9-Et-8-OH-Gua	9-Et-Gua	Deviation
	(±0.2)[a]	(±0.5)[a]	
C(2)-N(1)-C(6)	125.0	124.8	0.2
N(3)-C(2)-N(1)	123.1	124.2	−1.1
N(3)-C(2)-N(10)	119.5	119.4	0.1
N(1)-C(2)-N(10)	117.4	116.4	1.0
C(4)-N(3)-C(2)	112.6	111.7	0.9
C(5)-C(4)-N(3)	127.5	128.5	−1.0
C(5)-C(4)-N(9)	107.4	105.7	1.7
N(3)-C(4)-N(9)	125.1	125.9	−0.8
C(6)-C(5)-C(4)	120.1	119.3	0.8
C(6)-C(5)-N(7)	132.1	130.1	2.1
C(4)-C(5)-N(7)	107.7	110.7	−3.0
O(11)-C(6)-N(1)	120.0	119.8	−0.2
O(11)-C(6)-N(5)	128.4	128.7	−0.3
N(1)-C(6)-C(5)	111.6	111.6	0
C(8)-N(7)-C(5)	108.9	104.4	4.5
N(9)-C(8)-N(7)	107.0	113.0	−6.0
N(9)-C(8)-O(12)	124.7	—	—
N(7)-C(8)-O(12)	128.3	—	—
N(13)-N(9)-C(4)	127.6	126.0	1.6
C(13)-N(9)-C(8)	123.5	127.7	−4.2
C(4)-N(9)-C(8)	109.0	106.4	2.6

a) Estimated SD.

proton attached to the N-7 position and with a C(8)-O(12) bond length of 1.237 Å (Fig. 1). Within the crystal, the molecules of 9-Et-8-OH-Gua are linked together and to water molecules by the seven kinds of hydrogen bonds. When the bond lengths and bond angles of 9-Et-8-OH-Gua were compared with those of 9-Et-Gua,[9] significant differences were observed in the imidazole ring due to the 8-keto structure (Tables 1 and 2). Bond lengths, C(8)-N(7) and C(8)-N(9) of 9-Et-8-OH-Gua are considerably longer than those of 9-Et-Gua, and there is a highly significant deviation in the bond angles C(8)-N(7)-C(5), N(9)-C(8)-N(7), and C(13)-N(9)-C(8) from the corresponding bond angles in 9-Et-Gua. In contrast, the structure of pyrimidine ring of 9-Et-8-OH-Gua is very similar to that of 9-Et-Gua. Based on ^{13}C NMR studies, it has been reported that 8-hydroxyguanosine favors the syn-conformation.[7] Our finding based on ^{1}H and ^{13}C NMR spectra suggest 8-OH-dG can also adopt the syn-conformation (unpublished results). From these results it is concluded that misreading by 8-OH-dG observed during DNA replication in vitro,[6] may be due either to formation of Hoogsteen type base-pairing by 8-OH-dG (6,8-diketo form and syn-conformation) or to disturbance of the tertially structure of DNA around 8-OH-dG residues. To elucidate the actual effect of the 8-OH-Gua residue in DNA, the tertiary structure of selfcomplementary oligodeoxynucleotides containing 8-OH-Gua at specific position need to be studied, and work on this line is now in progress.

References

1) H. Kasai and S. Nishimura, *Nucleic Acids Res.*, **12**, 2137 (1984).
2) H. Kasai and S. Nishimura, *Gann*, **74**, 841 (1984).
3) H. Kasai and S. Nishimura, *Gann*, **75**, 565 (1984).
4) H. Kasai, H. Tanooka, and S. Nishimura, *Gann* **75**, 1037 (1984).
5) H. Kasai, P. F. Crain, Y. Kuchino, S. Nishimura, A. Ootsuyama, and H. Tanooka, *Carcinogenesis*, **7**, 1849 (1987).
6) Y. Kuchino, F. Mori, H. Kasai, H. Inoue, S. Iwai, K. Miura, E. Ohtsuka, and S. Nishimura, *Nature (London)*, **327**, 77 (1987).
7) S. Uesugi and M. Ikehara, *J. Am. Chem. Soc.*, **99**, 3250 (1977).
8) S. Udenfriend, C. T. Clark, J. Axelrod, and B. B. Brodie, *J. Biol. Chem.*, **208**, 731 (1954).
9) R. Destro, T. J. Kistenmacher, and R. E. Marsh, *Acta Crystallogr., Sect. B*, **30**, 79 (1974).

The Simple Synthesis of Cordiachrome B, a Terpenoid Benzoquinone from Cordia Millenii

Takashi WATABE, Yasushi HOSODA, Keiji OKADA, and Masaji ODA*
Department of Chemistry, Faculty of Science, Osaka University, Toyonaka, Osaka 560
(Received May 27, 1987)

Synopsis. Cordiachrome B, a tricyclic terpenoid *p*-benzoquinone isolated from Cordia millenii, was synthesized in three steps from 1,2-dihydro-3,6-dimethoxybenzocyclobutene employing a Diels-Alder reaction in a key step.

Cordiachrome B (**1**) is a tricyclic sesquiterpene quinone isolated from the heartwood of *Cordia millenii*.[1] Its structure is featured by the cis configuration at the B-C ring juncture, which could be advantageously constructed by a Diels-Alder reaction. In the course of our studies on benzocyclobutene-3,6-quinones,[2] we have prepared 1,2-dihydro-3,6-dimethoxybenzocyclobutene (**2**) which would be a useful synthon for **1** and other polycyclic benzoquinones owing to its thermal isomerization to 1,4-dimethoxy-5,6-dimethylene-1,3-cyclohexadiene (**3**), a reactive *o*-quinodimethane. Generation of **3** through debromination of 3,6-dimethoxy-α,α'-dibromo-*o*-xylene and its trapping with typical dienophiles have been reported by Laduranty et al.;[3] however, the *o*-quinodimethane **3** thus generated seems not suitable for Diels-Alder reactions with weak dienophiles, since it will undergo ring-closure to **2** and oligomerization in competition with the Diels-Alder reaction. This situation would be improved by employing **2** as a synthetic equivalent because **3** can be thermally and reversibly generated from **2** under a high concentration of dienophiles. We here describe the first, short-step synthesis of **1** starting from **2**.

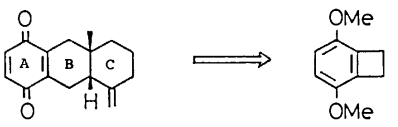

1 2

At first, thermolytic Diels-Alder reaction of **2** with 2-methyl-2-cyclohexen-1-one (**4**) was examined. Reaction of **2** and **4** (5 equivalents) in *o*-dichlorobenzene at 200 °C in an ampoule gave the cycloadduct **5** in a good yield of 75%. Less reactive 3-methyl-2-cyclohexen-1-one (**6**) required somewhat more forced conditions (8.8—10 equivalents of **6** at neat) for satisfactory cycloaddition and afforded a rather complex mixture mainly composed of the desired adduct **7** (16—28% isolated yield) and its trans-isomer **8** (30—40%). The trans adduct **8** was probably formed by epimerization of the cis adduct **7** under the reaction conditions. The higher thermodynamic stability of **8** over **7** was actually demonstrated by smooth epimerization of **7** to **8** on treatment with methanolic sodium hydroxide. Methylenation of **7** with methylenetriphenylphosphorane gave the *exo*-methylene compound **9** in 68% yield without noticeable epimerization. Finally, oxidation of **9** with ammonium cerium(IV) nitrate[4] afforded Cordiachrome B (**1**) in 74% yield. The synthetic quinone **1** was identical with the authentic sample in all respects (Mp, TLC, IR, and ^{1}H NMR).

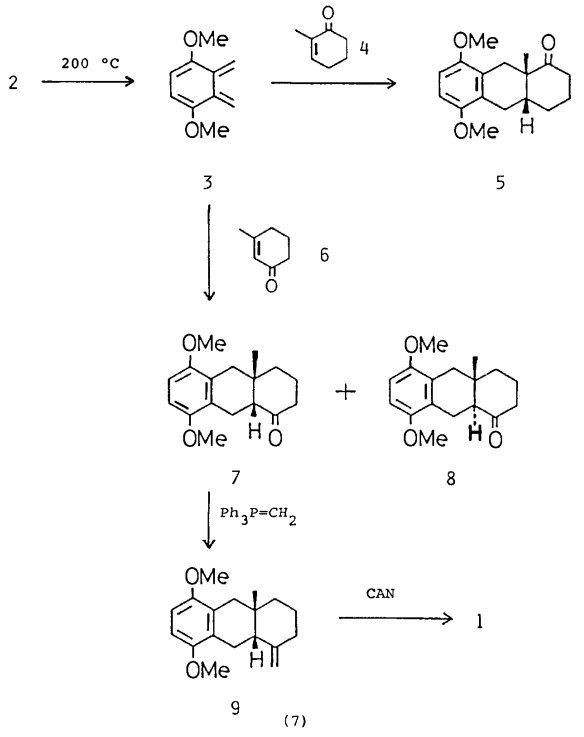

Experimental

Melting points were measured on a Mettler FP2 apparatus and are uncorrected. IR spectra were recorded on a Hitachi EPI-G3 grating spectrophotometer. ^{1}H NMR spectra were taken on a Varian XL-100 or JEOL PMX-60SI spectrometer. Column chromatography was performed with Merck Kieselgel 60.

Thermolytic Diels-Alder Reaction of 1,2-Dihydro-3,6-dimethoxybenzocyclobutene (2) with 2-Methyl-2-cyclohexen-1-one (4). A solution of **2** (164 mg, 1.0 mmol) and **4** (550 mg, 5.0 mmol) in *o*-dichlorobenzene (3 cm^3) was heated at 200 °C in an ampoule for 15 h. The solvent and excess **4** were removed in vacuo. Chromatography of the residue on silica gel eluted with hexane-ethyl acetate (95:5 v/v) gave the cycloadduct **5** (205 mg, 75%). Recrystallization from hexane gave colorless prisms; mp 102—103 °C; IR (KBr) 1703, 1599, 1481, 1264, 1080, 952, 808 cm^{-1}; ^{1}H NMR ($CDCl_3$), δ=1.04 (s, 3H), 1.3—3.1 (m, 11H), 3.67 (s, 6H), 6.43 (s, 2H). Found: C, 74.14; H, 8.08%. Calcd for $C_{17}H_{22}O_3$: C, 74.42; H. 8.08%.

Thermolytic Diels-Alder Reaction of 2 with 3-Methyl-2-cyclohexen-1-one (6). A mixture of **2** (492 mg, 3.0 mmol) and **6** (3.0 cm^3, 26.4 mmol) was heated at 210 °C in an ampoule for 22 h. Excess **6** was recovered by distillation in vacuo and the residue was chromatographed on silica gel to give the cis adduct **7** (130 mg, 16%) and trans adduct **8** (327

mg, 40%) in the order of elution. Other minor components were not persued.

Cis adduct **7**: Mp 85—86 °C; IR (KBr) 1710, 1602, 1484, 1260, 1083, 790 cm^{-1}; ^1H NMR ($CDCl_3$) δ=1.06 (s, 3H), 1.6—3.5 (m, 11H), 3.68 (s, 3H), 3.75 (s, 3H), 6.52 (s, 2H). Found: C, 74.22; H, 8.06%. Calcd for $C_{17}H_{22}O_3$: C, 74.42; H, 8.08%.

Trans adduct **8**: Mp 166—168 °C; IR (KBr) 1713, 1600, 1482, 1262, 1083, 945, 808 cm^{-1}; ^1H NMR ($CDCl_3$) δ=0.75 (s, 3H), 1.8—3.1 (m, 11H), 3.72 (s, 6H), 6.53 (s, 2H).

Methylenation of The Cis Adduct 7. To a suspension of methyltriphenylphosphonium iodide (545 mg, 1.35 mmol) in dry tetrahydrofuran (8 cm^3) was added a hexane solution of butyllithium (1.25 mmol) under nitrogen atmosphere at 0 °C. A solution of **7** (124 mg, 0.45 mmol) in dry tetrahydrofuran (2 cm^3) was added and the mixture was stirred for 2.5 h during which time temperature was allowed to rise to room temperature. Aqueous ammonium chloride was added and products were extracted with ether. After removal of the solvents, the residue was chromatographed on silica gel to give the exo-methylene compound **9** (84 mg, 70%): Colorless prisms from hexane; Mp 87—88 °C; IR (KBr) 1645, 1602, 1482, 1257, 1088, 890, 794 cm^{-1}; ^1H NMR ($CDCl_3$) δ=0.98 (s, 3H), 3.72 (s, 3H), 3.75 (s, 3H), 4.38 (br. s, 1H), 4.62 (br. s, 1H), 6.54 (s, 2H). Found: C, 79.36; H, 8.92%. Calcd for $C_{18}H_{24}O_2$: C, 79.37; H, 8.88%.

Cordiachrome B(1). To a solution of the compound **9** (84 mg, 0.31 mmol) and 2,6-pyridinedicarboxylic acid *N*-oxide (150 mg, 0.78 mmol) in 20% aqueous acetonitrile (2 cm^3) was added a solution of ammonium cerium(IV) nitrate (425 mg, 0.78 mmol) in 50% aqueous acetonitrile (2 cm^3) at 0 °C. After stirring for 1 h, the mixture was diluted with water and extracted with dichloromethane. Removal of the solvents and chromatographic purification of the product on silica gel column gave **1** as yellow crystals; Mp 63—64 °C (lit,[1] 64—65 °C). The IR and ^1H NMR spectra of the synthetic material were superimposable to those of the authentic sample given from Prof. R. H. Thomson.

The authors are grateful to Prof. Ronald H. Thomson for a generous gift of natural Cordiachrome B and a copy of its ^1H NMR spectrum.

References

1) M. Moir and R. H. Thomson, *J. Chem. Soc. Perkin I*, **1973**, 1352.

2) M. Oda and Y. Kanao, *Chem. Lett.*, **1981**, 37, 1547; Y. Kanao, M. Iyoda, and M. Oda, *Tetrahedron Lett.*, **24**, 1727 (1983); T. Watabe, Y. Takahashi, and M. Oda, *ibid.*, **24**, 5623 (1983); Y. Kanao and M. Oda, *Bull. Chem. Soc. Jpn.*, **57**, 615 (1984); T. Watabe and M. Oda, *Chem. Lett.*, **1984**, 1791.

3) J. Laduranty, L. Lepage, and Y. Lepage, *Can. J. Chem.*, **58**, 1161 (1980).

4) L. Syper, K. Kloc, J. Mlochowski, and Z. Szulc, *Synthesis*, **1979**, 521.

The Synthesis of 12-Ethoxy-4,9-methanoaza[12]annulene, a 12π-Electron Vinylogue of Pyridine

Jūro Ojima,* Masayuki Masumoto, Shigeyasu Kuroda,† Shuji Hirooka,† and Yoshihiko Nozawa†
Department of Chemistry, Faculty of Science, Toyama University, Gofuku, Toyama 930
†Department of Industrial Chemistry, Faculty of Engineering, Toyama University, Gofuku, Toyama 930
(Received May 29, 1987)

Synopsis. The title aza[12]annulene has been synthesized by Beckmann rearrangement of the oxime from the methano[11]annulenone, followed by alkylation of the resulting lactam. Examination of the ^{1}H NMR spectrum indicates that the aza[12]annulene is slightly paratropic.

Several diatropic methano-bridged aza[10]annulene derivatives (e.g. **1**) were prepared previously.[1] Also, the bisdehydroaza[14]annulene **2** as well as its higher analogs was prepared and proved to sustain ring current.[2] Of these azaannulene family of pyridine type, the 12π-analogue is unknown. We have now synthesized the title aza[12]annulene derivative by the reaction sequence used to prepare **2**,[2] in order to discover whether the same alternation of tropicity between $(4n+2)\pi$- and $(4n)\pi$-electron systems occurs in the azaannulene series as has already been demonstrated in the carbocyclic annulene series.[3] This synthetic objective has been verified experimentally.

1

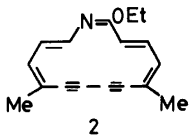

2

Although several attempts of rearrangement reactions with phosphorus pentachloride were fruitless, the oxime **3**, obtained from 4,9-methano[11]-annulenone,[4] when heated with *p*-toluenesulfonyl chloride in pyridine,[5] gave Beckmann rearrangement product, the lactam **4**, in 26% yield. The alkylation of **4** with triethyloxonium tetrafluoroborate gave the desired aza[12]annulene **5** in 10% yield. The substance was unstable to diffused light and air.

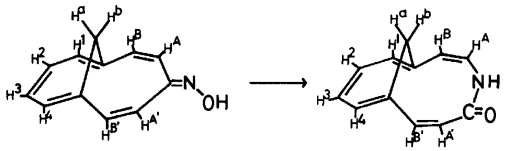

3

4

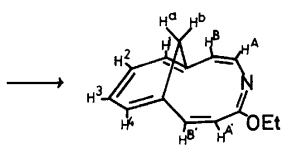

5

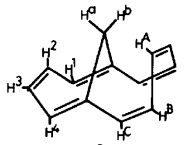

6

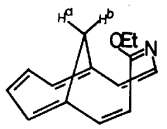

5a

The ^{1}H NMR chemical shifts of **5** are listed in Table 1, together with those of the closely related methano-[12]annulene **6**. Table 1 shows that **5** is slightly paratropic as espected for a 12π-electron system, since the annulene outer protons resonate at relatively high field and the H^b proton of the bridged methylene group do at relatively low field, as compared with the usual olefinic and methylene protons. This also suggests that **5** exists in syn-form **5a** as similarly to the case of **6**.[6] However, comparison of the chemical shifts of the corresponding protons between **5** and **6** shows that the paratropicity of **5** is smaller than that of **6**, revealing that an incorporation of a nitrogen atom and a substitution of ethoxyl group into and upon the molecular perimeter of **6** hinder conjugation of π-electrons to some extent.

Variable-temperature ^{1}H NMR spectra of the aza[12]-annulene **5** were run over the range from −60 to 60 °C, and the results show all the spectra to be essentially temperature-independent, ruling out a change in the conformation **5a** between these temperatures.

Experimental

All melting points are uncorrected. IR spectra were measured on Hitachi 260-50 spectrophotometer as KBr disk; only significant maxima are reported. UV spectra were taken on Hitachi 220A spectrophotometer and were recorded in nm, in tetrahydrofuran solution. ε-Values are given in parentheses, the shoulders being denoted by sh. Mass spectra were measured with JEOL JMS-200 spectrometer at 75 eV using a direct inlet system. ^{1}H NMR spectra were taken on JEOL FX-90Q (90 MHz) or GX-270 (270 MHz) spectrometer, and refer to solutions in $CDCl_3$, unless otherwise stated, in δ-values with TMS as an internal standard. The coupling constants (J) are given in Hz. Alumina (II—III) was used for column chromatography. Preparative TLC was carried out on 20×20 cm silica-gel plates (Merck, 0.5 mm thick). Dichloromethane was distilled over calcium hydride before use. Organic extracts were dried over anhyd sodium sulfate prior to solvent removal.

Table 1. ^{1}H NMR Chemical Shifts of Methanoaza[12]annulene **5** (270 MHz) and Methano-[12]annulene **6** (90 MHz) in $CDCl_3$ (δ Value: Internal Standard TMS)

Compd	H^2	H^3	H^4	H^1	$H^{B'}$	$H^{A'}$	H^C	H^B	H^A	H^b	H^a	$-CH_2CH_3$	$-CH_2CH_3$
5	6.56	6.41	6.13	5.97	6.41	5.09		—6.40—		5.39	1.62	4.35—4.05	1.36
6	6.28—6.22		5.86—5.77				5.59——5.52			7.10	2.35		

1-Hydroxyimino-4,9-methanocycloundeca-2,4,6,8,10-pentaene (3). To a stirred soln of the 4,9-methano[11]-annulenone[4] (586 mg, 3.44 mmol) in methanol (40 ml) and THF (10 ml) was added a soln of hydroxylamine hydrochloride (4.8 g) in water (10 ml) at 38 °C in one portion. After stirring for further 10 h at the same temp, further quantities of hydroxylamine hydrochloride (each 5.0 g in water (10 ml)) were added after every 40 h. After stirring for a total of 5 d at 38 °C, the soln was poured into water. The precipitates formed were filtered off under suction, giving **3** (444 mg, 70%). Recrystallization from chloroform afforded orange needles: Mp 196—197 °C; MS *m/z* 185, (M^+, 96%) and 141 100); mol wt 185.2; IR 3140 (OH), 1610 (C=N), and 680 cm^{-1} (cis C=C); UV λ_{max} 213 sh (9710), 229 (14400), 280 (36700), and 341 nm (3220); ^1H NMR (90 MHz, DMSO-d_6) δ=11.31 (s, 1H, OH, exchangeable with D_2O), 7.03—6.96 (m, 2H, H^2, H^3), 6.89 (d, 12, 1H, H^B), 6.71 (d, 12, 1H, $H^{B'}$), 6.69—6.59 (m, 2H, H^1, H^4), 6.09 (d, 12, 1H, $H^{A'}$), 5.86 (d, 12, 1H, H^A), 6.84 (d, 11, 1H, H^b), and 0.54 (d, 11, 1H, H^a).

Found: C, 77.89; H, 5.93; N, 7.40%. Calcd for $C_{12}H_{11}NO$: C, 77.81; H, 5.99; N, 7.56%.

5,10-Methanoazacyclododeca-3,5,7,9,11-pentaen-2-one (4). A soln of *p*-toluenesulfonyl chloride (1.75 g, 9.20 mmol) in pyridine (10 ml) was added to a stirred soln of the oxime **3** (340 mg, 1.84 mmol) in pyridine (50 ml). After stirring for 6 h at 90 °C, further quantities (1.5 g) of the chloride were added and stirring was continued for further 6 h at 90 °C. Then the mixture was poured onto water and extracted with benzene. The extracts were washed with 2M-hydrochloric acid (1 M=1 mol dm^{-3}), aq sodium hydrogencarbonate soln, and aq sodium chloride soln, and dried. The dark red semisolid obtained after solvent removal was chromatographed on alumina (4.3×8 cm). The fractions eluted with dichloromethane afforded the lactam **4** (87 mg, 26%). Recrystallization from hexane-benzene afforded yellow needles: Mp 146—147 °C; MS *m/z* 185 (M^+, 72%) and 156 (100); mol wt 185.2; IR 3140 (NH), 1640, and 1605 cm^{-1} (C=O, C=C); UV λ_{max} 249 (25300) and 344 nm (2300); ^1H NMR (270 MHz) δ=6.89 (d, 11.7, 1H, $H^{B'}$), 6.74—6.10 (m, 7H, H^1, H^2, H^3, H^4, H^A, H^B, NH), 5.98 (d, 11.7, 1H, $H^{A'}$), 3.08 (d, 13.5, 1H, H^b), and 2.18 (d, 13.5, 1H, H^a).

Found: C, 78.07; H, 6.02; N, 7.80%. Calcd for $C_{12}H_{11}NO$: C, 77.81; H, 5.99; N, 7.56%.

The following fractions eluted with 10% ethanol in dichloromethane gave the recovered oxime **3** (107 mg).

12-Ethoxy-4,9-methanoaza[12]annulene (5). To a stirred soln of the lactam **4** (50 mg, 0.27 mmol) in dry dichloromethane (14 ml) was added dropwise a soln of triethyloxonium tetrafluoroborate (1.54 g, 8.10 mmol) in dry dichloromethane (14 ml) during 40 min at room temp. After stirring for 5 h at room temp, the soln was cooled in an ice-bath and aq. 50% potassium carbonate soln (8 ml) was cautiously added. Then the mixture was poured into water and extracted with dichloromethane. The residue after solvent removal was chromatographed on alumina (4.2×8.5 cm). The fractions eluted with hexane gave a semisolid, which was further purified by preparative plate chromatography (dichloromethane-hexane (1 : 1) as eluent). The fast moving, yellow band gave the azaannulene **5** (6.0 mg, 10%). Recrystallization from hexane-benzene afforded yellow needles: Mp 67—68 °C; IR 1200 1120, and 1070 cm^{-1} (-O-); UV λ_{max} (ε) 252 (41900) and 310 nm sh (18600); ^1H NMR (270 MHz) δ=6.56 (dd, 10.5, 5.6, 1H, H^2), 6.41 (dd, 10.5, 5.6, 1H, H^3), 6.41 (d, 10, 1H, $H^{B'}$), 6.13 (d, 5.6, 1H, H^4), 6.04 (s, 2H, H^A, H^B), 5.97 (d, 5.6, 1H, H^1), 5.39 (d, 12.1, 1H, H^b), 5.09 (d, 10, 1H, $H^{A'}$), 4.35—4.23 (m, 1H, $-CH_2CH_3$), 4.17—4.05 (m, 1H, $-CH_2CH_3$), 1.62 (d, 12.1, 1H, H^a), and 1.36 (t, 7, 3H, $-CH_2CH_3$).

HRMS: Found: *m/z* 213.1120. Calcd for $C_{14}H_{15}NO$: M, 213.1151.

This work was financially supported by a Grant-in-Aid for Scientific Research No. 61470023 from the Ministry of Education, Science and Culture.

References

1) M. Schätter-Ridder, A. Wagner, M. Schwamborn, E. Schreiner, F. Devrout, and E. Vogel, *Angew. Chem.*, **90**, 894 (1978); H. J. Golz, J. W. Muchowski, and M. L. Maddox, *ibid.*, **90**, 896 (1978); W. J. Lipa, H. J. Crawford, P. C. Radlick, and G. K. Helmkamp, *J. Org. Chem.*, **43**, 3813 (1979).

2) J. Ojima, T. Nakada, E. Ejiri, and M. Nakamura, *J. Chem. Soc., Perkin Trans. 1*, **1986**, 933.

3) For reviews, a) F. Sondheimer, *Acc. Chem. Res.*, **5**, 81 (1972); b) M. Nakagawa, *Pure Appl. Chem.*, **44**, 885 (1975).

4) E. Vogel, "Topics in Nonbenzenoid Aromatic Chemistry," Hirokawa, Tokyo (1977), Vol. 2, pp. 243—281.

5) W. D. Burrow and R. H. Eastman, *J. Am. Chem. Soc.*, **79**, 3756 (1957).

6) E. Vogel, M. Mann, Y. Sakata, K. Müllen, and J. M. F. Oth, *Angew. Chem.*, **86**, 231 (1974); K. Yamamoto, S. Kuroda, Y. Nozawa, S. Fujita, and J. Ojima, *J. Chem. Soc., Chem. Commun.*, **1987**, 199.

Effect of 1-Methoxy-5-methylphenazinium Methyl Sulfate on Photocurrent Produced by *Rhodospirillum rubrum* Chromatophores

Tatsuo ERABI,* Kiyoharu MATSUMOTO, Hideki ITOH, Noritaka TAKAHASHI, Kumiko NISHIMURA, and Masanori WADA
Department of Industrial Chemistry, Faculty of Engineering, Tottori University, Koyama, Tottori 680
(Received April 22, 1987)

Synopsis. A cathodic photocurrent produced by chromatophores was measured in the presence of 1-methoxy-5-methylphenazinium methyl sulfate (methoxy-PMS). The magnitude of the photocurrent was a function of the wavelength of the incident light, and the photocurrent action spectrum was in agreement with the absorption spectrum of chromatophores. The photocurrent also depended on the concentration of methoxy-PMS or of chromatophores.

Many studies have demonstrated the possibility of employing photoactive biological components in photoelectrochemical cells, in connection with studies regarding the mechanism of photosynthetic primary process as well as solar energy conversion projects. From this viewpoint, we[1] reported that a cathodic photocurrent was produced, upon illumination, at a platinum electrode immersed in a chromatophore suspension under potentiostatic conditions. This phenomenon was largely enhanced by adding 1-methoxy-5-methylphenazinium methyl sulfate (methoxy-PMS) to the suspension. Although an enhancement of the photocurrent was presumed, that methoxy-PMS functioned as a mediator between the electrode and chromatophore particles, a further discussion was not given because of insufficient data. This paper reports on subsequent measurements of the photocurrent in the presence of methoxy-PMS.

Experimental

The carotenoid-less blue-green mutant strain (G-9) of *Rhodospirillum rubrum* was used throughout the present study. The cells were grown anaerobically at 30 °C for 3 days under continuous illumination from tungsten lamps.[2] Chromatophores were prepared from light-grown cells by sonication,[3] suspended in a 0.12 M (M=mol dm^{-3}) GTA buffer (pH 8.0) which consisted of an equimolar mixture of 3,3-dimethylglutaric acid, tris(hydroxymethyl)aminomethane and 2-amino-2-methyl-1,3-propanediol, and stored at 4 °C in the dark. The concentration of chromatophores was expressed in terms of absorbance of bound bacteriochlorophyll at 873 nm (A_{873}; corresponding to 7.1 μM of bound bacteriochlorophyll[4]).

A schematic diagram of a photoelectrochemical measurement is shown in Fig. 1. The experimental cell, in which the light path length was 0.4 mm, consisted of a platinum plate working electrode (2×3 cm^2 of surface area), a platinum wire counter electrode and a saturated calomel reference electrode. All potentials listed in this paper are corrected against the normal hydrogen electrode. For a potentiostatic measurement, the potential of the electrode was controlled with a Hokuto Model potentiostat HA-101 or HA-501 and the resulting current was recorded. A photocurrent was measured after electrolyzing for 30 minutes in the dark at an arbitrary potential. As the light source, a 60 W tungsten lamp was usually used in combination with a 12 cm thick water filter in order to eliminate the thermal effect; a 500 W

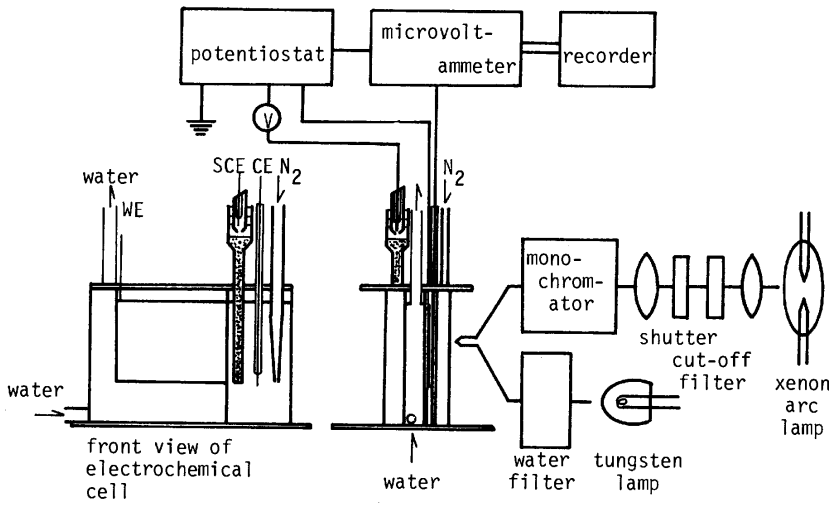

Fig. 1. Electrolytic cell arrangement for measuring photocurrent. The experimental cell was all made of borosilicate glass. A cellulose membrane divides between main compartment (chromatophore suspension) and subcompartment (buffer solution). WE, working electrode; CE, counter electrode; SCE, saturated calomel reference electrode.

xenon arc lamp (Wacom Model MX-500) was used in combination with a JASCO Model CT-25N grating monochromator equipped with a cut-off filter UV-39 or VR-69 for measuring the photocurrent action spectrum. 10 Units ml^{-1} of glucose oxidase, 2 mM of glucose and 13 units/ml of catalase were added to the suspension in order to remove dissolved oxygen and oxygen-free nitrogen was passed through into the suspension for 30 minutes. The suspension was kept constant at 25°C with a help of a thermostat. Methoxy-PMS was synthesized as described.[5,6]

Results and Discussion

When the cathodic photocurrent by chromatophores was measured in the presence of methoxy-PMS, it was largely enhanced.[1] The photocurrent increased with a greater cathodic shift of the applied potential up to about −200 mV and then gradually decreased. Since methoxy-PMS showed a large enhancing effect of the photocurrent, the behavior of the photocurrent in the presence of methoxy-PMS was examined in some detail. The magnitude of the cathodic photocurrent was a function of the wavelength of the incident light. The resulting action spectrum is shown in Fig. 2. There are three maxima (600, 800, and 875 nm) in agreement with the maxima of the absorption spectrum (588, 804, and 873 nm, ascribed to chromatophore-bound bacteriochlorophyll[7]) of the chromatophore suspension, and not with that of methoxy-PMS solution (508 nm). This suggests that the enhanced photocurrent is independent of the photoexcitation of methoxy-PMS: that is, the photocurrent is not due to a light-induced electron transfer from the electrode to methoxy-PMS, and the photocurrent is actually due to the light absorbed by chromatophores.

The effect of the concentration change of methoxy-PMS or of chromatophores on the photocurrent is shown in Fig. 3. In this figure, a linear relationship can be observed between the photocurrent and the concentration of methoxy-PMS or of chromatophores. If

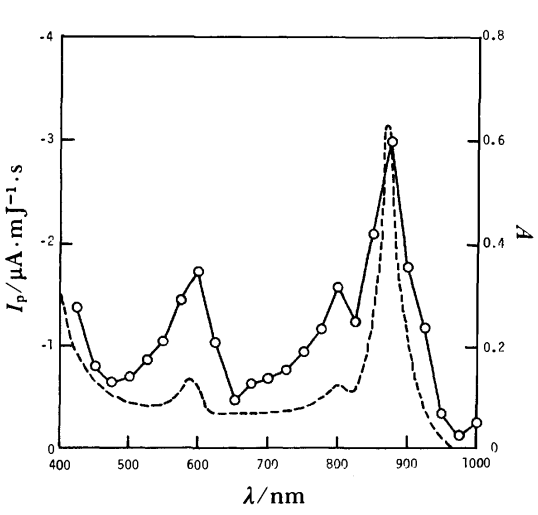

Fig. 2. Comparison of photocurrent action spectrum with absorption spectrum. The concentrations of chromatophores and methoxy-PMS were kept constant at A_{873}=75 and 100 μM, respectively. The photocurrent was measured at −200 mV of applied potential. The dotted line shows the absorption spectrum of chromatophore suspension.

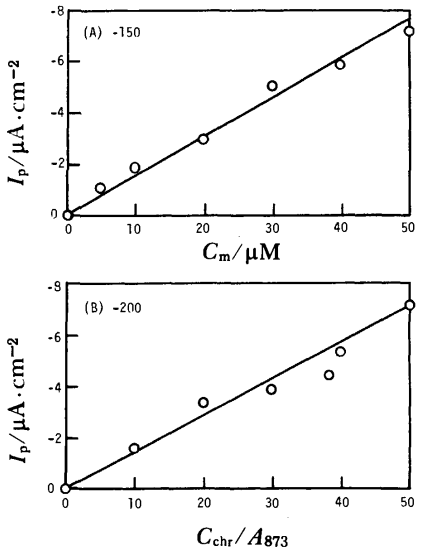

Fig. 3. Dependence of photocurrent on concentration of methoxy-PMS (A) or of chromatophores (B). Numbers in the figure represent the applied potential by mV. The concentration of chromatophores (A) and that of methoxy-PMS (B) were kept constant at A_{873}=75 and at 100 μM, respectively. The illumination was carried out at 6000 lx of illuminance.

the enhancing effect of the photocurrent is based on the ability of methoxy-PMS as the electron mediator,[1] the concept of a catalytic current[8] can be applied to an analysis of the reaction. According to the concept of a reaction layer as a maximal approximation for the treatment of the catalytic current, the enhanced photocurrent is

$$I_p = nF\mu k_f C_{chr} C_m,$$

where I_p, C_{chr}, and C_m are the enhanced photocurrent, bulk concentration of chromatophores and that of methoxy-PMS, respectively. Thus, I_p comes to be proportional to C_{chr} or C_m. As shown in Fig. 3, the result that linear relationship was observed between the photocurrent and the concentration of chromatophores or methoxy-PMS suggests that the methoxy-PMS function as the mediator between the platinum electrode and chromatophore particle, as expected. Moreover, the photocurrent increased with an increasing concentration of the reduced form of methoxy-PMS.[1] This suggests that the main reactant with chromatophores in the production of photocurrent is the reduced form of methoxy-PMS. This suggestion is supported by a study[9] on flash photolysis and electron paramagnetic resonance, in which an electron transfer from PMS in reduced form to reaction center bacteriochlorophyll (BChl) cation was observed.

In conclusion, it has become clear that the photocurrent produced by chromatophores at a platinum electrode under potentiostatic conditions is greatly enhanced in the presence of methoxy-PMS, and that the enhancing effect is based on the ability of methoxy-PMS as an electron mediator. A possible mechanism for the production of photocurrent is shown below.

$$BChl \cdot I \cdot Q \cdot Fe \xrightarrow{h\nu} BChl^* \cdot I \cdot Q \cdot Fe \longrightarrow BChl^+ \cdot I \cdot Q^- \cdot Fe \text{(in chromatophores}^{10)})$$

$$BChl^+ \cdot I \cdot Q^- \cdot Fe + \text{methoxy-PMS (reduced)} \longrightarrow BChl \cdot I \cdot Q^- \cdot Fe + \text{methoxy-PMS (oxidized)}$$

$$\text{methoxy-PMS (oxidized)} + e \longrightarrow \text{methoxy-PMS (reduced) (production of photocurrent)}$$

References

1) T. Erabi, H. Hiura, M. Yamada, T. Endo, J. Yamashita, M. Tanaka, and T. Horio, *Chem. Lett.*, **1978**, 341.

2) T. Horio, K. Nishikawa, M. Katsumata, and J. Yamashita, *Biochim. Biophys. Acta*, **94**, 371 (1965).

3) N. Nishi, M. Kataoka, G. Soe, T. Kakuno, T. Ueki, J. Yamashita, and T. Horio, *J. Biochem.*, **86**, 1211 (1979).

4) T. Kakuno, R. G. Bartsch, K. Nishikawa, and T. Horio, *J. Biochem.*, **70**, 79 (1971).

5) I. Yoshioka, *Yakugaku Zasshi*, **72**, 1128 (1952).

6) A. R. Surrey, *Org. Synth.*, Coll. Vol. 3, 753 (1955).

7) K. Hosoi, G. Soe, and T. Horio, "Seitaimaku Jikkenho," Kyoritsu Shuppan, Tokyo (1974), pp. 321—326.

8) P. Delahay, "New Instrumental Methods in Electrochemistry," Wiley (Interscience), New York (1954), pp. 100—114.

9) K. Cost and J. R. Bolton, *Photochem. Photobiol.*, **18**, 423 (1973).

10) G. Feher and M. Y. Okamura, "The Photosynthetic Bacteria," ed by R. K. Clayton and W. R. Sistrom, Plenum Press, New York (1978), pp. 349—386.

Effect of Post-Treatments on the Stability of the Langmuir-Blodgett Film of Fatty Acid Salt in Vacuum

Makio IWAHASHI,* Yoshimi YAMAGUCHI, Koichi KOBAYASHI,† and Tsutomu SEIMIYA††
Department of Chemistry, School of Hygienic Sciences, Kitasato University, Sagamihara, Kanagawa 228
†Laboratory of Chemistry, Musashi Institute of Technology, Setagaya-ku, Tokyo 158
††Department of Chemistry, Faculty of Sciences, Tokyo Metropolitan University, Setagaya-ku, Tokyo 158
(Received April 24, 1987)

Synopsis. The effects of the following treatments on the stability of the Langmuir-Blodgett (L/B) film of fatty acid salt in vacuo have been investigated by radiotracer method: (I) Skeletonization of the L/B film. (II) Transformation of the fatty acid molecules remaining in the L/B film into its soap molecules. (III) Perfect formation and deposition of the metal soap monolayer.

Langmuir-Blodgett (L/B) films of tritiated fatty acid are expected to be an excellent ^{3}H-source for the measurement of the electron anti-neutrino mass:[1] The measurement requires a source that is highly radioactive, homogeneous, very thin, uniform and nonvolatile in vacuo. Concerning the volatility in vacuo, however, the L/B film of fatty acid is not so stable,[2-4] and the desorption of the source molecules becomes the origin of the main background in the measurement.

Roberts and Gaines[2] reported that almost 90% of the ^{14}C-octadecanoic acid film on a quartz backing was evaporated after one hour evacuation at a pressure of 10^{-4} Pa and room temperature, while only 10% of the barium ^{14}C-octadecanoate film was evaporated at the same conditions. This suggests that the L/B film of metal soap is more stable in vacuo than that of the free acid. Most of L/B films of metal soap, in addition, do not consist of only pure metal soap molecules: They include more or less the original acid molecules which evaporate easily.[5] The increase of the metal soap content in the molecules consisting the L/B film is therefore expected to make the L/B film more stable even under high vacuum conditions.

In the present study we investigated the desorption behaviours of ^{3}H-molecules from the L/B films of barium or cadmium $^3H_2$-octadecanoate in solvent and/or in vacuo, trying to improve the stability of the L/B film with various procedures such as (I) preremoval of the free acid molecules by rinsing the L/B film in a solvent (skeletonization), (II) transformation of the free acid molecules in the L/B film to the metal soap molecules by immersing the L/B film in a concentrated $BaCl_2$ aqueous solution under high pH conditions, and (III) complete formation and deposition of monolayer of pure metal soap.

Experimental

A sample of 9,10-$^3H_2$-octadecanoic acid (sp. ac. of 16 Ci mol^{-1}) was synthesized[6] the addition of hydrogen gas to 9,10-$^3H_2$-octadecenoic acid (sp. ac. of 5700 Ci mol^{-1}, Amersham Co.) diluted with pure 9-octadecenoic acid (purity $\gg$ 99.5%, Merck Co.). The sample was purified by repeated recrystallization from hexane and dissolved in benzene to make a spreading solution of 1×10^{-3} mol dm^{-3}.

Organic solvents and inorganic salts were the purest grade reagents of Wako Pure Chemical Co., Osaka. The former were distilled prior to use and the latter were used without further purification. Iron(III) octadecanoate (the purest grade of Tokyo Kasei Industry Co., Tokyo) was used for the pretreatment of surface of substrate plate (ferrotype plate whose size was 15 mm ×25 mm×0.8 mm).

Water for the subphase solution was triply distilled, the second distillation being from alkaline permanganate, and was contained in a Teflon trough (8 cm×20 cm×1 cm) with a waxed silk thread as the movable barrier. The trough had a pocket (1.5 cm×4 cm×1 cm) in its bottom for the dipping of the substrate plate. The pH of the solution was adjusted by adding a solution of NaOH or $Ba(OH)_2$. All the solutions were not buffered. The pH value was determined prior to and after the built-up procedure. The change of pH was less than 0.3 unit. L/B films were deposited at a surface pressure of 29.5 mN m^{-1} using 9-octadecenoic acid (Merck reagent grade) as a piston oil. The plate was dipped to 10 mm in depth of the subphase water and withdrawn through the monolayer at a velocity of 0.1—0.5 cm s^{-1} by means of a synchronous motor. In order to determine the transfer ratio of the monolayer onto the substrate plate, we used an another Teflon trough (2.5 cm×20 cm×2 cm) with an inside that was hydrophilic.[7] A thin mica plate (23 mm×30 mm×0.1 mm) coated with paraffin was placed on the surface of the solution in the trough and used as a movable barrier. The floating barrier can move smoothly by the repulsion[8] between the hydrophilic trough and the hydrophobic ends of the movable barrier. From the movement of the barrier in the deposition process we evaluated the transfer ratio of the monolayer. The transfer ratio, thus obtained, for each deposition process was almost unity (0.97—1.00).

The radioactivity of the L/B films of Ba- or Cd-$^3H_2$-octadecanoate was measured with a 2π-windowless gas flow counter (Aloka Model FC-1E) using Q-gas as the counting gas.

Results and Discussion

A good linear relationship was obtained between the radioactivity and the number of layers of barium $^3H_2$-octadecanoate film deposited on the ferrotype plate under the conditions of pH=6.2—11.2. From the radioactivity results and the movements of the movable barrier, it was confirmed that two monolayers were always deposited onto the substrate plate in one dipping and withdrawing process of the plate even at high pH region. Autoradiographs of the other samples with two molecular films of Ba-$^3H_2$-octadecanoate similarly prepared were taken using LKB Biofilm-^{3}H (Akom Co., Tokyo); they were fairly uniform.

Five kinds of L/B films were prepared under the following depositional conditions and by post-treat-

Table 1. The Effects of Immersing in $BaCl_2$ Solution and Rinsing in Benzene on the Stability for the L/B Film of Octadecanoic Acid

Film	No. of monolayer	Built-up condition[a)]	Fraction of remaining radioactivity after immersing in $BaCl_2$ solution of 1×10^{-3} mol dm^{-3} at pH=9.2	Fraction of remaining radioactivity after rinsing in benzene for 30 s
(a)	4	pH=6.2		
(b)	4	pH=9.0		
(c)	4	pH=6.2		0.885
(d)	2	pH=11.2		0.940
(e)	4	pH=6.2	1.00 (1 min immersing)	0.679
(f)	4	pH=6.2	0.935 (1.5 h immersing)	0.822

a) Built-up process for these L/B film was carried out at the surface of $BaCl_2$ solution of 1×10^{-4} mol dm^{-3} at ca. 288K.

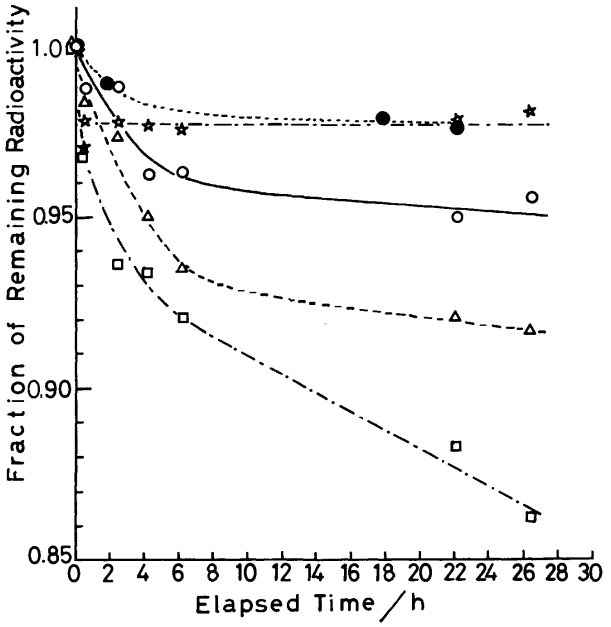

Fig. 1. The effect of post-treatments of the L/B film on its removal at a pressure of 133 Pa and a source temperature of 288 K; ○, L/B film (a) was composed of four molecular layers transfered from the $^3H_2$-octadecanoic acid monolayer spread on an aqueous $BaCl_2$ solution of 1×10^{-4} mol dm^{-3} at pH=6.2; ●, film (b), four layers transfered from the acid monolayer spread on $BaCl_2$ solution of 1×10^{-4} mol dm^{-3} at pH=9; △, film (c), the same as the film (a), but was rinsed in benzene for 30 seconds; □, film (e), the same as the film (a), but was immersed in $BaCl_2$ solution of 1×10^{-3} mol dm^{-3} at pH=9.2 for one minute and then rinsed in benzene for 30 seconds; ☆, film (f), the same as the film (a), but was immersed in the above $BaCl_2$ solution for 1.5 hours and then rinsed in benzene for 30 seconds.

ments. Film (a): four-layers film deposited from the $^3H_2$-octadecanoic acid monolayer spread on the aqueous $BaCl_2$ solution of 1×10^{-4} mol dm^{-3} at pH=6.2, film (b): four-layers film deposited from the acid monolayer spread on a $BaCl_2$ solution of 1×10^{-4} mol dm^{-3} at pH=9, film (c): the same as the film (a) but was rinsed in benzene for 30 seconds, film (d): two-layers film deposited from the acid monolayer spread on a $BaCl_2$ solution of 1×10^{-4} mol dm^{-3} at pH=11.2 and then rinsed in benzene for 30 seconds, film (e): the same as the film (a) but was immersed in a $BaCl_2$ solution of 1×10^{-3} mol dm^{-3} at pH=9.2 for one minute and then rinsed in benzene for 30 seconds, film (f): the same as the film (a) but was immersed in the above $BaCl_2$ solution for 1.5 hours and then rinsed in benzene for 30 seconds.

The desorption ratio of the above films (c—f) into solvent are tabulated in Table 1 as a remaining fraction of the radioactivity. Film (d) deposited at high pH was more stable against rinsing in benzene than film (c) deposited at low pH. Barium octadecanoate, being resistant against dissolution in benzene,[5)] might be easily formed at a high pH region. The fatty acid monolayer, however, tends to desorb into the subphase solution at the highest pH region, even during the deposition process. The radioactivity of the film (e) was not changed by one-minute immersing in the $BaCl_2$ solution of pH=9.2. The succeeding rinsing of the film (e) in benzene, however, decreased its radioactivity considerably. The one-minute immersing of the L/B film of fatty acid in $BaCl_2$ solution of high pH does not improve the conversion of fatty acid to its barium soap in the film, but seems to distort the arrangement of the acid molecules and to loosen the lateral bondings among the molecules by the electrical repulsions of their dissociated carboxyl groups. Although the long period of immersing of the L/B film in the $BaCl_2$ solution is expected to progress the conversion, a slight removal of the film material was resulted.

Figure 1 shows the evaporation profiles of the $^3H_2$-octadecanoic acid from the L/B films under a condition of 133 Pa and 288 K. For the films (c), (e), and (f), the initial radioactivity is defined as that obtained just after their rinsing in benzene. Evaporation of the acid molecules from the film (e), was most significant. This is also due to the distortion of the arrangement of the molecules. Film (b) strongly resisted the removal of molecules. The evaporation rate for the skeletonizated film (c) was much higher than that for film (a); the skeletonized films did not resist the thermal desorption of the film molecules. Beischer[9)] reported that copper 1-^{14}C-octadecanoate molecules, whose neighboring octadecanoic acid molecules were excluded, evaporated much easier than copper octadecanoate molecules in the pure L/B film.

Film (f) seems to be better than film (a) in the resistance against the thermal removal of film molecules. However, the total remaining fraction of the radioactivity (0.749=0.935×0.822×0.975) of film (f) is smaller than that (0.929) of film (a).

Consequently, an increase of the metal soap content in the film is essential to obtain a L/B film stable in vacuum without the skeletonization for the film.

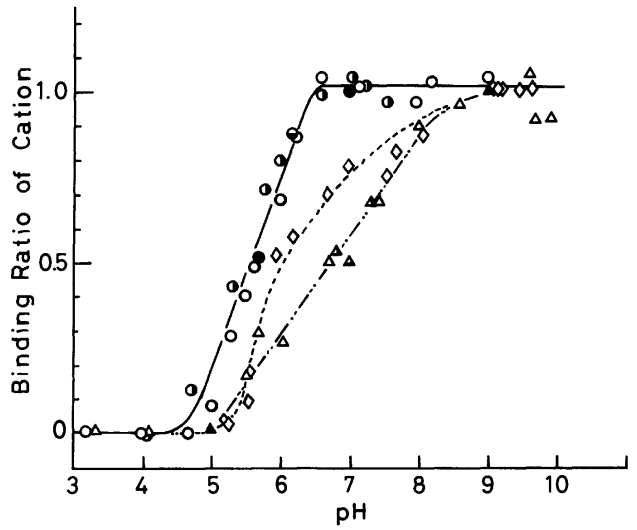

Fig. 2. The pH dependence of the ratio of binding of divalent cations to fatty acid monolayers. Circles denote the ratio of binding for cadmium ion, diamonds that for calcium ion and triangles that for barium ion. The marks ○ and △ are from neutron activation analysis study[10] for icosanoic acid; ● and ▲ are the Blodgett's data[11] for icosanoic acid and ◭ is the Ehlert's data[12] for octadecanoic acid (both data were obtained by the skimming method); ▲ and ◇ are IR-spectroscopic data[13,14] for octadecanoic acid; ◒ is from the photometric study of dissolved multilayers of icosanoic acid;[15] ◑ is the Kobayashi's data[16] for icosanoic acid by ESCA.

Figure 2 shows the metal-ion bindings in the monomolecular films of octadecanoic and icosanoic acids[10-16] in their L/B films. The binding ratio of the barium cation to the above fatty acids is only 0.4 at pH=6.2, that is, ca. 60 mole-percent of the fatty acid seems to remain as the original fatty acid at the surface of the barium solution of pH=6.2. Cadmium cation binds perfectly in the icosanoic acid monolayer above at pH=6.5, whereas both calcium and barium cations do above pH=9. The former pH is close to the pH of distilled water (pH=5.8): This is suitable for preparing a perfect metal soap L/B film because we need not use much undesirable ions such as Na^+, K^+, PO_4^-, or CO_3^{2-} for adjusting the pH of the subphase solution. New samples of L/B film of Cd-$^3H_2$-octadecanoate were therefore prepared by using a $CdCl_2$ solution of 1×10^{-3} mol dm^{-3} (pH=7.2; the NaOH concentration of the solution was ca. 1.7×10^{-6} mol dm^{-3}) as the subphase solution and evacuated under the pressure of 133 Pa and temperature 288 K. The radioactivities of the L/B films remained unaltered for two days within an error of ±3%; the fatty acid molecule anchored by the cadmium ion seems not to evaporate from the L/B film.

Concequently, in order to obtain a L/B film stable in vacuum, the increase of metal soap content in the L/B film is absolutely essential without skeletonization of the film or without new formation of metal soap. For the increase of the metal soap content, in addition, the cadmium solution can be more advantageously used than the calcium or barium solution.

References

1) V. A. Lubimov, E. G. Novikov, V. Z. Nozik, E. F. Tretyakov, and V. S. Kosik, *Phys. Lett.*, **94B**, 266 (1980).
2) R. W. Roberts and G. L. Gaines Jr., Trans. Ninth Natl. Vacuum Symp., Am. Vacuum Soc., 515, (1962); *Nature (London)*, **197**, 787 (1963).
3) H. Schonohorn, *J. Colloid Soi.*, **18**, 445 (1963).
4) J. A. Spink, *J. Colloid Interface Sci.*, **24**, 61, (1967).
5) J. E. Young, *Australian J. Chem.*, **8**, 173 (1955).
6) M. Iwahashi and K. Tajima, *J. Labelled Comp.*, **7**, 501 (1971).
7) M. Iwahashi, F. Naito, N. Watanabe, T. Seimiya, N. Morikawa, N. Nogawa, T. Ohshima, H. Kawakami, K. Ukai, I. Sugai, S. Shibata, T. Yasuda, Y. Shoji, T. Suzuki, T. Nagafuchi, H. Taketani, T. Matsuda, Y. Fukushima, M. Fujioka, and K. Hisatake, *Bull. Chem. Soc. Jpn.*, **58**, 2093 (1985).
8) J. J. Bikerman, "Physical Surfaces," Academic Press, New York (1970), p. 39.
9) D. E. Beischer, *J. Phys. Chem.*, **57**, 134 (1953).
10) J. G. Petrov, I. Kuleff, and D. Platikanov, *J. Colloid Interface Sci.*, **88**, 29 (1982).
11) K. B. Blodgett, *Phys. Rev.*, **55**, 391 (1939).
12) R. S. Ehlert, *J. Colloid Sci.*, **20**, 387 (1965).
13) J. W. Ellis and J. L. Pauley, *J. Colloid Sci.*, **19**, 755 (1964).
14) J. Bagg, M. B. Abramson, M. Fichman, M. D. Haber, and H. P. Gregor, *J. Am. Chem. Soc.*, **86**, 2759 (1964).
15) J. G. Petrov, H. Kuhn, and D. Möbius, *J. Colloid Interface Sci.*, **73**, 66 (1980).
16) K. Kobayashi and K. Takaoka, *Bull. Chem. Soc. Jpn.*, **59**, 933 (1986).

Measurement of Concentration Profile of Dye at Glass-Solution Interface by Photoacoustic Spectrometry Coupled with Total Internal Reflection Technique

Teruo HINOUE,* Masaaki KAWABE, and Yu YOKOYAMA
Department of Chemistry, Technological University of Nagaoka, Nagaoka 940-21
(Received April 18, 1987)

Synopsis. Photoacoustic signals were measured as a function of a penetration depth by changing an angle of incidence of an excitation beam. Concentration profiles were obtained from a relationship between the signal magnitude and the penetration depth by an inverse Laplace transformation. The smallest value of the penetration depth used was 34 nm.

In the previous works,[1-4] we developed photoacoustic spectrometry coupled with a total internal reflection technique (PAS-TIR) and could measure dye concentrations in a solution layer of submicrometer from a glass-solution interface. In the present paper, we demonstrate measurement of the photoacoustic signal (PAS) as a function of an angle of incidence of the excitation beam in PAS-TIR and discuss relationships between the PAS magnitude and concentration profile in the solution layer at the interface.

Experimental

Apparatus. A spectrometer and cell design used in the present study is similar to that used previously[3] except an argon ion laser (Spectra-Physics, 162D) and an active band path filter (NF Co., Ltd., UF-1BP). The laser of 15 mW at 488.0 nm was modulated at 40 Hz by an optical chopper and the plane of polarization of the laser was perpendicular to that of incidence. The laser beam passed through a convex lens (f=300 mm), entered a hemicylindrical internal reflection element made of dense flint glass from the cylindrical surface, and was focused on the axis of the hemicylinder on the opposite plane in contact with the solution. The PAS caused by absorption of the intermittent laser beam was detected by a piezoelectric transducer (MURATA MFG. Co., Ltd., 7D-15-4000 BKA) and was amplified by a lock-in amplifier (NF Co., Ltd., LI 574A) through a preamplifier (NF Co., Ltd., LI 75A) and the band path filter. The angle of incidence was changed by a rotary optical stage driven by a stepping motor (Oriental Motor Co., Ltd., UPD 569) and a programmable controller (Oriental Motor Co., Ltd., PC 100). The angle of incidence was changed stepwise and the corresponding PAS magnitudes were recorded on a Y-t recorder.

Reagents and Optical Parameters. New Coccine (NC) supplied from Tokyo Kasei Co., Ltd. was used without further purification. A 0.1 M (M=mol dm^{-3}) NC aqueous solution was prepared from distilled water for the measurement. The penetration depth of the beam was calculated according to expressions derived by Hansen.[5] Optical parameters used in the calculation are listed in Table 1. In general the refractive index of a solution containing light absorbing species is affected by the extinction coefficient of the solution due to anomalous dispersion.[5-7] However, the extinction coefficient of the 0.1 M NC solution is so small that the refractive index is not virtually susceptible to the anomalous dispersion.[6,7] Thus the refractive index of the NC solution was estimated to be equal to that of pure water at 488.0 nm.

Results and Discussion

Figure 1 schematically illustrates a total internal reflection. When the light beam progresses from the glass internal reflection element with a higher refractive index, n_1, toward the solution with a lower refractive index, n_2, at the angle of incidence, θ_1, beyond the critical angle, θ_c, the light beam is totally reflected and the evanescent wave emerges from the interface toward the solution. A mean square electric field strength of the evanescent wave exponentially attenuates with distance, x, from the interface. The distance at which the strength is reduced to 1/e of that at the interface is called the penetration depth, d, and is expressed by[5]

$$d=(-\lambda/4\pi)/\mathrm{Im}\{[(n_2-ik_2)^2-n_1^2\sin^2\theta_1]^{1/2}\}. \quad (1)$$

Here the extinction coefficient of the solution, k_2, is equal to $2.303\cdot\varepsilon c\lambda/4\pi$, where ε, c, and λ denote the molar absorption coefficient, the concentration of the light absorbing species, and the wavelength of the light in vacuum, respectively. That is, the penetration depth at a constant wavelength is a function of the angle of incidence, the refractive indices of the internal reflection element and the solution, and the extinction coefficient. Therefore, the penetration depth depends only on the angle of incidence for a particular internal reflection system. Figure 2(a) shows the PAS magni-

Table 1. Optical Parameters Used in the Calculation of the Penetration Depth

	Refractive index	Extinction coefficient
0.1 M NC solution	1.337	0.0172
Dense flint glass	1.819	0[a]

a) Assumed value.

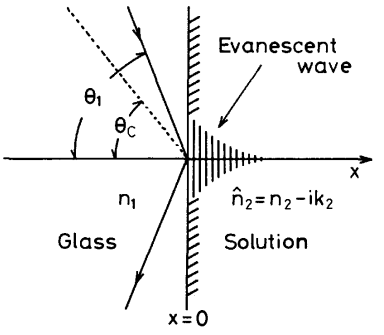

Fig. 1. Illustration of total internal reflection. n_1: refractive index of internal reflection element, n_2: refractive index of solution, k_2: extinction coefficient of solution, $\hat{n}_2$: complex refractive index of solution, θ_1: angle of incidence, θ_c: critical angle.

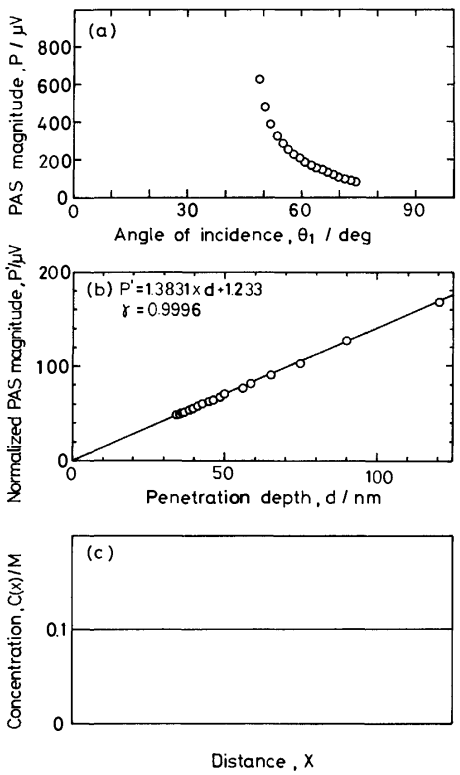

Fig. 2. (a) Relationship between PAS magnitude and angle of incidence, (b) relationship between normalized PAS magnitude and penetration depth, (c) concentration profile.

tudes for a 0.1 M NC aqueous solution against the angle of incidence from 49 to 74.5 degree.

On the other hand, the mean square electric field strength at a given position of x (see Fig. 1) is expressed by $S \cdot \exp(-x/d)$, where S is a sensitivity factor, depending on an optical coupling at the interface,[5,6,8] and was calculated from the optical parameters of the system in a similar manner to the calculation for the penetration depth.[5] The absorbed light power at x is, therefore, proportional to $\varepsilon cS \cdot \exp(-x/d)$. The overall absorption is expressed by the integration from $x=0$ to $x=\infty$. Thus the PAS magnitude, P, is given as follows:

$$P = S\int_0^\infty K\varepsilon c \cdot \exp(-x/d)\mathrm{d}x, \quad (2)$$

where K is a coefficient depending on instrumental parameters and photoacoustic characteristics of the internal reflection system.[3] When the molar absorption coefficient and the photoacoustic characteristics of the solution are constant over the full range, Eq. 2 is rearranged to

$$P' = P/SK\varepsilon = \int_0^\infty c(x) \cdot \exp(-x/d)\mathrm{d}x. \quad (3)$$

Hereafter P' is called the normalized PAS magnitude. The right hand side of Eq. 3 expresses a Laplace transformation of the concentration profile, $c(x)$, when $1/d$ is considered as a parameter. Consequently, the concentration profile can be obtained by the inverse Laplace transformation of the normalized PAS magnitude as a function of the penetration depth. In practice, three concentration profiles were assumed and compared with a regression function for a plot of the

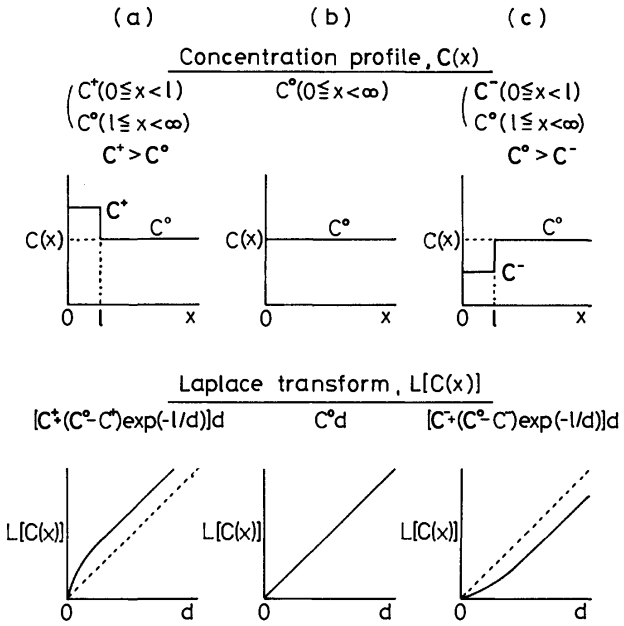

Fig. 3. Assumed concentration profiles, $c(x)$, and the corresponding Laplace transformations, $L[c(x)]$.

normalized PAS magnitude against the penetration depth at each angle of incidence. Figure 3 shows the assumed concentration profiles and the corresponding Laplace transformations. The first (a) represents the enrichment of the species at the interface accompanying an interfacial phenomenon such as adsorption, the second (b) corresponds to the concentration profile of uniform distribution over the range considered, and the last (c) is the reverse case to the first. The plot derived from the results in Fig. 2(a) and the corresponding regression function are shown in Fig. 2(b). As can be seen in Fig. 2(b), the regression function can be regarded as a straight line through the origin, that is, the normalized PAS magnitude is directly proportional to the penetration depth. Accordingly, the present case corresponds to (b) in Fig. 3 and it is concluded that the concentration of the dye is constant over the solution range from the interface to the bulk. Here it should be noted that the distance from the interface, x, is a different variable from the penetration depth, d, and that graduations on the abscissa in Fig. 2(c) can not be determined, because of the nature of the Laplace transformation. However, it is significant that the above conclusion can be derived from the measurement of the PAS magnitude against the penetration depth of submicrometer.

As described previously, the available range of the penetration depth is limited by the optical parameters of the internal reflection system examined and the angle of incidence. In this study, the smallest penetration depth was 34 nm. This limit is still inadequate for exact observation of a thinner layer adjacent to the interface, such as an adsorption layer. Figure 4 shows a dependence of the relative penetration depth, d/λ, on the angle of incidence for two internal reflection elements with the different refractive indices, that is, (a) 1.819 and (b) 2.417. As expected from Fig. 4, the shorter penetration depth will be approached by using the

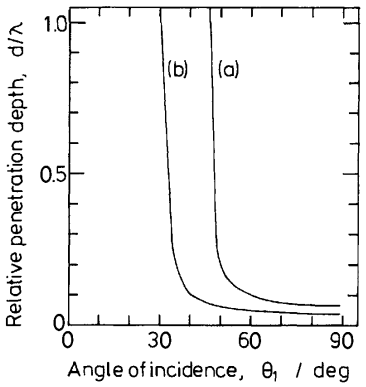

Fig. 4. Dependence of relative penetration depth on angle of incidence. (a) Refractive index of internal reflection element, n_1=1.819 and refractive index of solution, n_2=1.337, (b) n_1=2.417 and n_2=1.337.

larger angle of incidence, the higher refractive index of the internal reflection element, and the shorter wavelength of the laser. The complex concentration profiles, which are due to adsorption, electrochemical operation, and mass transfer of species in membrane, will be examined by the proposed spectrometric technique.

This work was supported by a Grant-in-Aid for Scientific Research No. 60840017 from the Ministry of Education, Science and Culture.

References

1) T. Hinoue, Y. Shimahara, and Y. Yokoyama, *Chem. Lett.*, **1983**, 225.
2) T. Hinoue, Y. Shimahara, H. Murata, and Y. Yokoyama, *Bunseki Kagaku*, **33**, E459 (1984).
3) T. Hinoue, H. Murata, and Y. Yokoyama, *Anal. Sci.*, **2**, 401 (1986).
4) T. Hinoue, H. Murata, M. Kawabe, and Y. Yokoyama, *Anal. Sci.*, **2**, 407 (1986).
5) W. N. Hansen, "Advances in Electrochemistry and Electrochemical Engineering," ed by P. Delahay and C. W. Tobias, John Wiley & Sons, New York (1977), Vol. 9, pp. 1—60.
6) N. J. Harrick, "Internal Reflection Spectroscopy," Wiley-Interscience, New York (1967).
7) W. N. Hansen, *ISA Trans.*, **4**, 263 (1965).
8) T. Kuwana, "Electroanalytical Chemistry," ed by A. J. Bard, Marcell Dekker, New York (1974), Vol. 7, pp. 2—78.

Preparations and Structures of 3-Chloro-ONN-4′-methylazoxybenzene and 4-Methoxy-ONN-4′-methylazoxybenzene†

Jiro YAMAMOTO,* Takashi TSUBOI, Yasunori SUMI, Noriyasu ODA, and Keiichi FUKUYAMA††
Department of Industrial Chemistry, Faculty of Engineering, Tottori University, Tottori 680
(Received March 26, 1987)

Synopsis. A treatment of 3-chloro-NNO-4′-methylazoxybenzene (**1β**) with CrO_3 in acetic acid gave 3-chloro-**ONN**-4′-methylazoxybenzene (**1α**) in good yield, whereas 4-methoxy-**ONN**-4′-methylazoxybenzene (**2α**) isomerized partially to 4-methoxy-**NNO**-4′-methylazoxybenzene (**2β**) under the same conditions. The structures of **1α** and **2α** have been determined by X-ray analysis.

The transformations of azoxybenzene into 4-hydroxyazobenzene[1] and small amounts of 2-hydroxyazobenzene[2] were discovered by Wallach and Belli, respectivelly. A number of investigations on the Wallach rearrangement for various substituted azoxybenzenes have since followed. However, little has been studied regarding the Wallach rearrangement of unsymmetrically substituted azoxybenzenes or on the isomerization of the azoxybenzenes under the conditions of the Wallach rearrangement.[3-5] Recently, the α,β-isomerization††† based on a migration of an azoxy-oxygen atom was found in the reaction of some unsymmetrically substituted azoxybenzenes with sulfuric acid.[6-8] In order to reveal the mechanism of the Wallach rearrangement through the behavior of unsymmetrically substituted azoxybenzenes, it is necessary to determine their structure unambiguously, i.e. the relative position of the oxygen atom on the azoxy group. Here, we report on the preparation of 3-chloro-**ONN**-4′-methylazoxybenzene (**1α**) and 4-methoxy-**ONN**-4′-methylazoxybenzene (**2α**) and the structures of **1α** and **2α** determined by X-ray crystallographic analysis.

Results and Discussion

It was shown that some β-isomers converted into α-isomers upon treating with CrO_3 in acetic acid [4-(phenyl-**NNO**-azoxy)beozoic acid,[9] 4-nitro-**NNO**-azoxybenzene[10]]. When **1β** was warmed with CrO_3 in acetic acid, an oxygen atom of it transfered to a nitrogen atom, binding with 4-tolyl group (β,α-isomerization). In the reaction of a mixture of **2α** and **2β** with CrO_3 under some conditions (i.e. by using four different starting mixtures in molar ratio and changing the reaction time, adding amounts of CrO_3, and volume of AcOH), the preparation of pure **2α** was unsuccessful. However, an azoxy-oxygen atom partialy transfered to a remote nitrogen atom from the 4-tolyl group in a α,β-ratio (2α : 2β=0.5 : 1.0) in each case (Table 1).

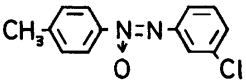

3-Chloro-**ONN**-4′-methylazoxybenzene
1α

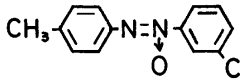

3-Chloro-**NNO**-4′-methylazoxybenzene
1β

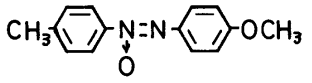

4-Methoxy-**ONN**-4′-methylazoxybenzene
2α

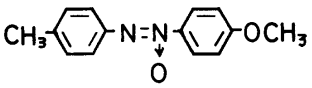

4-Methoxy-**NNO**-4′-methylazoxybenzene
2β

In order to separate the α and β-isomer of unsymmetrically substituted azoxybenzenes from each other, a fractional crystallization technique was spplied using ethanol [methyl 4-(phenylazoxy) benzoates,[9] 4-methylazoxybenzenes,[7] 4-phenylazoxybenzoic acid[9]]. When a hot equimolar ethanol solution of **2α** and **2β** was allowed to stand at room temperature, deposited first crystals had the same isomeric ratio as the starting mixture. In an effective separation of **2α** from a mixture of **2α** and **2β**, the deposited crystalline substance are filtered off from an ethanol solution at 50 °C. The structures of **1α** and **2α**, determined by the X-ray analyses, are shown in Fig.1. It could be guaranteed that both **1α** (δ 1.97) and **2α** (δ 1.98) had an azoxy-oxygen atom on the nitrogen atom, binding the 4-tolyl group, respectively.

Experimental

Preparation of 3-Chloro-4′-methylazoxybenzene (3). *p*-Nitrosotoluene (**4**) (6.3 g, 52.0 mmol) was dissolved in an equal volume solution of acetic acid and ethanol (40 ml in each) with warming; was added an acetic acid solution of *m*-chloroaniline (4.6 g, 45.6 mmol) to it. After the reaction, the mixture was kept at 50 °C for 30 min, and then allowed to stand overnight. A dark brown precipitate was filtered and washed throughly with water. The precipitate was dissolved in ether and the ether solution was washed with water: 3% NaOH aq soln, 5% HCl aq soln, and water. After the ether solution was dried, crude **3** was obtained by recrystallization with ethanol (150 ml). Mp 106.0—107.0 °C. Methyl signal δ=2.05. 4-Methyl-4′-methoxyazobenzene (**5**) (86.5%) was also

†Reactivities of Azoxybenzenes. 17.

††Present Address: Department of Biology, Faculty of Science, Osaka University, Toyonaka, Osaka 560.

†††Although the IUPAC nomenclature on unsymmetrically substituted azoxybenzenes is not used the terms of α and β, we use these signs in this paper for convenience.

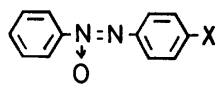

α-Isomer

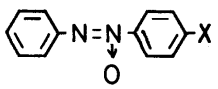

β-Isomer

Table 1. The Reaction of the Mixture of 4-Methoxy-**ONN**- (2α) and 4-Methoxy-**NNO**-4'-methylazoxybenzene (**2**β) with CrO_3

Starting 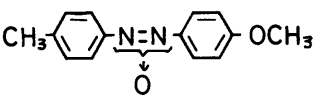	Reaction condition[a]			Product[b] 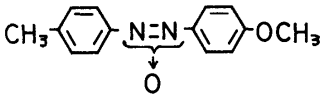
	Time	CrO_3	AcOH	
g (mmol)	h	g (mmol)	ml	g (%)
2.51 (10.36) ($\alpha:\beta$=0.98:1.00)	3.0	2.0 (20.0)	100	2.00 (80.0) ($\alpha:\beta$=0.50:1.00)
3.29 (13.58) ($\alpha:\beta$=0.40:1.00)	4.0	3.5 (35.0)	100	2.60 (79.1) ($\alpha:\beta$=0.50:1.00)
3.90 (16.10) ($\alpha:\beta$=0.66:1.00)	4.5	2.5 (25.0)	100	3.29 (84.4) ($\alpha:\beta$=0.50:1.00)
2.60 (10.73) ($\alpha:\beta$=0.50:1.00)	6.0	6.0 (60.0)	150	0.90 (34.6) ($\alpha:\beta$=0.50:1.00)

a) Reaction temperature: 60 °C. b) In high reaction temperature, benzene insolubles were found.

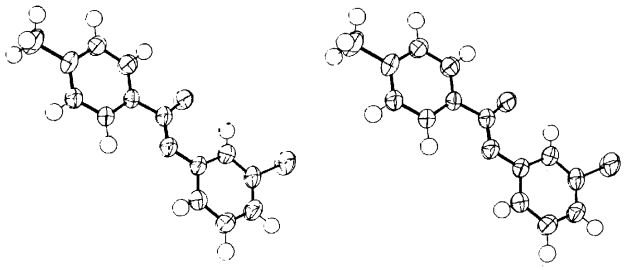

Fig. 1(a).

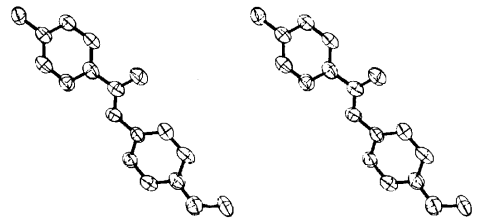

Fig. 1(b).

Fig. 1. Stereoscopic views of (a) **1**α and (b) **2**α.

prepared in a reaction of 4 with *p*-anisidine: mp 111.0 °C (lit,[11] 110.0—111.0 °C) δ=2.07.

Preparation of 3-Chloro-ONN-4'-methylazoxybenzene (1α). An acetic acid solution (500 ml) of **3** (5.0 g, 24.2 mmol) was kept at around 65 °C with 30% H_2O_2 (50 ml). When the orange-reddish solution changed to yellow, the reaction mixture was poured into water. The precipitate was filtered and washed with water until the smell of acetic acid disappeared. An equimolar mixture of **1**α (δ=1.97) and 4-methyl-**ONN**-3'-chloroazoxybenzene (**1**β) (δ=2.09) was obtained (5.3 g, 97.1%) mp 76.5—77.0 °C. The mixture (5.0 g, 22.3 mmol) was kept in the range 30—40 °C in acetic acid and CrO_3 (5.1 g, 51.0 mmol) was added in three portions during 30 minutes. After the reaction mixture was warmed in the range 55—60 °C for 3 h and allowed to stand over night, it was poured into cold water and filtered. **1**α was thoroughly washed with water and dried (4.25 g, 85.0%). The oxidation of **5** with H_2O_2 was carried out by the same procedure and an equimolar mixture (85.0%) of **2**α (δ=1.98) and **2**β (δ=2.08) was obtained. An ethanol solution (80 ml) of the mixture was kept in the range 60—70 °C. When the temperature of the solution dropped to 50 °C, the deposited crystals were filtered and dried (5.1 g, 81.0%), (**2**α:**2**β=5.67:1.00). The same procedure was applied for a mixture (5.1 g, 24.6 mmol) using ethanol (100 ml) again. After being worked up, pure **2**α (2.86 g, 55.0%) was obtained mp 110.5—111.0 °C (δ=1.98).

Crystallographic Measurements. The diffraction data of the crystals of **1**α and **2**α were measured at room temperature on a microcomputer-controlled four-circle diffractometer.[12] The crystal data are as follows: **1**α; $C_{13}H_{11}N_2OCl$, M=246.7, monoclinic, space group $P2_1/n$, a=12.133(5), b=12.805(5), c=7.738(4) Å, β=93.69(5)°, V=1199.7 Å^3, Z=4, D_c=1.37 g cm^3. **2**α: $C_{14}H_{14}N_2O_2$, M=242.3 monoclinic, space group $C2$, a=25.485(7), b=3.986(3), c=13.428(5) Å, β=116.42(5)°, V=1221.6 Å^3 Z=4, D_c=1.32 g cm^3. The intensities were measured up to 2θ=120° by a θ—2θ scan technique using Ni-filtered Cu $K\alpha$ radiation. The reflections with $F>2\sigma_F$ were used for subsequent caluculations. The numbers of measured and significant reflections were 1784 and 1368, respectivelvely,for **1**α, and 1019 and 778, respectively for **2**α. Periodically monitored reflections showed no significant change in intensity. The intensities were corrected for the Lorenz and polarization factors.

Structure Determination. The structure of **1**α was solved by the direct method.[13] Since an attempt to solve the structure of **2**α by a direct method was unsuccessful, the vector search method[14] was applied; the parameters of the orientation and the translation of azoxybenzene were deter-

Table 2. Final Atomic Coordinates of **1**α with Their Estimated Standard Deviations in Parentheses

	x	y	z
C(1)	0.0376(3)	0.6938(3)	0.7470(5)
C(2)	0.0106(4)	0.7969(4)	0.7311(6)
C(3)	−0.0328(4)	0.8482(4)	0.8703(6)
C(4)	−0.0480(4)	0.7939(4)	1.0231(5)
C(5)	−0.0205(4)	0.6892(4)	1.0340(5)
C(6)	0.0232(4)	0.6379(3)	0.8960(6)
C(7)	0.1671(3)	0.4937(3)	0.4906(5)
C(8)	0.1934(4)	0.3940(4)	0.5428(6)
C(9)	0.2456(4)	0.3247(4)	0.4367(6)
C(10)	0.2734(4)	0.3586(4)	0.2743(6)
C(11)	0.2482(4)	0.4576(4)	0.2242(6)
C(12)	0.1939(4)	0.5281(3)	0.3249(6)
C(13)	−0.0951(5)	0.8497(4)	1.1767(7)
N(1)	0.0846(3)	0.6421(3)	0.5970(4)
N(2)	0.1162(3)	0.5496(3)	0.6216(4)
O(1)	0.0878(3)	0.6949(3)	0.4598(4)
Cl	0.2845(1)	0.4998(1)	0.0214(2)

Table 3. Final Atomic Coordinates of **2α** with Their Estimated Standard Deviations in Parentheses

	x	*y*	*z*
C(1)	0.1655(4)	0.0104(31)	0.2794(7)
C(2)	0.1083(4)	0.1102(29)	0.2273(6)
C(3)	0.0709(4)	0.0563(30)	0.2778(7)
C(4)	0.0924(4)	−0.0963(29)	0.3816(7)
C(5)	0.1511(4)	−0.1950(29)	0.4326(7)
C(6)	0.1879(4)	−0.1408(31)	0.3826(7)
C(7)	0.2948(4)	0.0000(29)	0.2299(6)
C(8)	0.3480(4)	−0.1419(31)	0.2984(7)
C(9)	0.3949(4)	−0.1292(32)	0.2718(7)
C(10)	0.3876(4)	0.0319(29)	0.1742(7)
C(11)	0.3339(4)	0.1754(29)	0.1051(7)
C(12)	0.2873(4)	0.1552(27)	0.1320(7)
C(13)	0.0512(4)	−0.1609(34)	0.4356(8)
C(14)	0.4310(4)	0.2096(40)	0.0564(7)
N(1)	0.2024(3)	0.0607(24)	0.2242(5)
N(2)	0.2548(3)	−0.0402(25)	0.2756(5)
O(1)	0.1790(3)	0.2105(26)	0.1308(5)
O(2)	0.4354(3)	0.0413(22)	0.1549(5)

mincd by the program RICS.[15] The renaining non-hydrogen atoms were located in a successive Fourier synthesis. Positional and anistropic temperature factors for **1α** and **2α** were refined by a block diogonal least-squares method.[16] All hydrogen atoms of **1α** were located in the difference Fourier synthesis and included in the subsequent refinement. The positions of the hydrogen atoms of **2α**, except those of the methyl group, were caluculated geometrically and included in the refinement. The isotopic temperature factors of these hydrogen atoms of **2α** were fixed to those of the atoms to which they were bonded. The weighting scheme used in the final cycle of the refinement for **1α** was $w=1.0$ for $F_o \leqq 18$ and $w=[1.0+0.25(F_o-18)]^{-1}$, for $F_o>18$ and that for **2α** was $w=1.0$ for $F_o \leqq 30$ and $w=[1.0+0.2(F_o-30)]^{-1}$ for $F_o>30$. The final R values are 0.071 and 0.083 for **1α** and **2α**, respectivelly. The final atomic parameters are given in Tables 2 and 3.[17] The atomic scattering factors were taken from the International Tables for X-Ray Crystallography.[18]

We thank Shigeo Fujii and Yoshikuni Takiyama for the assistance of X-ray analysis.

References

1) O. Wallach and L. Belli, *Ber.*, **13**, 525 (1880).
2) E. Bamberger, *Ber.*, **35**, 1614 (1900).
3) E. Buncel, "Mechanism of Molecular Migrations," ed by B. S. Thyagarajan, Interscience, New York (1968), Vol. 1 p. 61.
4) E.Buncel, and R. B. Cox, "The chemistry of hydrazo, azo and azoxy groups" ed by S. Patti, Interscience, London (1975), Part 2, p. 808.
5) H. J. Shine "Aromatic rearrangements," Elsivier Amsterdam (1976), p. 272.
6) J. Yamamoto, T. Sakamoto, K. Kusunoki, M. Umezu, and T. Matsuura, *Nippon Kagaku Kaishi*, **1977**, 66.
7) J. Yamamoto, H. Aimi, Y. Masuda, T. Sumida, M. Umezu, and T. Matsuura, *J. Chem. Soc., Perkin Trans., 2*, **1982**, 1565.
8) J. Yamamoto, N. Tanaka, M. Yamamoto, T. Nakagawa, and H. Aimi, *Nippon Kagaku Kaishi*, **1987**, 851.
9) A. Angeli and B. Valori, *Atti Accad Lincei*, **22, I**, 132 (1912); *Chem. Abstr.*, **7**, 2223 (1913).
10) A. Angeli and B. Valori, *Atti Accad. Lincei*, **21, I**, 729 (1911); *Chem. Abstr.*, **6**, 2747 (1912).
11) H. Wieland, *Ber.*, **48**, 1107 (1915).
12) Y. Katsube, *J. Cryst. Soc. Jpn.*, **24**, 132 (1982).
13) G. Germain, P. Main, and M. M. Woolfson, *Acta. Crystallgr., Sect. A*, **27**, 368 (1971).
14) R. Huber, "Crystallographic Computing," ed by F. R. Ahmed. Munksgaard, Copenhagen (1970), p. 96.
15) I. Tanaka, personal communication.
16) T. Ashida, HBLS-V, The Universal Crystallographic Computing System, p. 55. The Computation Center, Osaka University 1973.
17) The Coordinates of hydrogen atoms, the anisotropic temperature, bond lengths and angles, and the list of observed and caluculated structure factors (×10) for **1α** and **2α** are deposited as Document No. 8764 at the Office of the Editor of Bull. Chem. Soc. Jpn.
18) "International Tables for X-Ray Crystallography," Brimingham, Kynoch Press (1974), Vol. IV, p. 71.

Synthetic Photochemistry. XXXIX.[1] Sensitized-Photooxygenation of 2-Benzyltropone, 2-[Hydroxy(4-nitrophenyl)methyl]tropone, and 2-(1-Hydroxy-2-oxo-2-phenylethyl)tropone. A Quenching Effect of Hydroxyl Group in the Vicinity of the Reaction Site

Akira MORI,* Hiroshi SUIZU,† and Hitoshi TAKESHITA*
Research Institute of Industrial Science, 86, Kyushu University, Kasuga-koen, Kasuga, Fukuoka 816
†Graduate School of Engineering Sciences, 39, Kyushu University, Kasuga-koen, Kasuga, Fukuoka 816
(Received April 24, 1987)

Synopsis. Singlet-oxygen oxidation of 2-[hydroxy(4-nitrophenyl)methyl]tropone gave 6,7-dioxabicyclo[3.2.2]-nona-3,8-dien-2-one derivatives in good yields. A change of regioselectivity of the oxygenation with a remarkable rate of enhancement (23 times) in deuteriomethanol vs. methanol could be best explained in terms of the quenching of singlet oxygen by the free hydroxyl group in the vicinity of the reaction site. Similarly studied were 2-(1-hydroxy-2-oxo-2-phenylethyl)tropone and 2-benzyltropone. The stereochemistry of the oxygen adducts was elucidated by a ^{1}H NMR chemical-shift comparison.

Sensitized photooxygenation of tropones is a useful method for preparing 2,5-dihydroxytropones which are important starting materials for functionalized troponoids such as *p*-tropoquinones.[2] Among those, tropone (**1**)[3] and 2-methoxytropone (**2**)[4] gave corresponding single endoperoxides, 6,7-dioxabicyclo[3.2.2]-nona-3,8-dien-2-one and its 1-methoxy derivative (**3** and **4**), while 2-aryltropones (**5**) gave two regioisomers, 1- and 3-aryl derivatives (**6** and **7**), the former of which was predominant (ca. 2.3 : 1).[5] Thus, the oxygenation takes place predominantly at electron-rich 2,5-positions rather than less-hindered 4,7-positions. Contrary to the previous cases, 2-[hydroxy-(4-nitrophenyl)methyl]tropone (**8**)[6] and 2-(1-hydroxy-2-oxo-2-phenylethyl)tropone (**9**),[7] have now been found to react predominantly at the 4,7-positions, while 2-benzyltropone (**10**) reacted at both positions in a 1 : 1-ratio. Herein, we describe the findings.

First of all, **10** gave a 1 : 1-mixture of photooxygenation products (**11** and **12**) upon irradiation with a tungsten lamp in the presence of a sensitizer, hematoporphyrin (HMP), under an oxygen atmosphere. The reaction rate was considerably larger than those of the other substrates taken in this study. The structures of **11** and **12** were elucidated by a ^{1}H NMR analysis to be 3-benzyl-6,7-dioxabicyclo[3.2.2]nona-3,8-dien-2-one and 1-benzyl-6,7-dioxabicyclo[3.2.2]nona-3,8-dien-2-one, respectively; in **11**, there were three vinylic proton signals together with the five-proton singlet for the phenyl group, and in **12**, there were four vinylic proton signals together with rest of signals which closely resembled those of **11**. No other product was detectable in spite of the careful check of every chromatographic fraction.

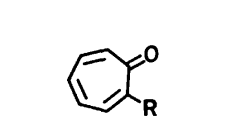

1 R=H
2 R=OMe
5 R=Ar
8 R=CH(OH)-C$_6$H$_4$-NO$_2$
9 R=CH(OH)-C(=O)-C$_6$H$_5$
10 R=CH$_2$Ph
21 R=C(=O)-C$_6$H$_4$-NO$_2$

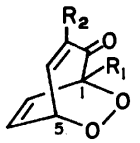

3 R$_1$=R$_2$=H
4 R$_1$=OMe, R$_2$=H
6 R$_1$=Ar, R$_2$=H
7 R$_1$=H, R$_2$=Ar
11 R$_1$=H, R$_2$=CH$_2$Ph
12 R$_1$=CH$_2$Ph, R$_2$=H

Chart 1.

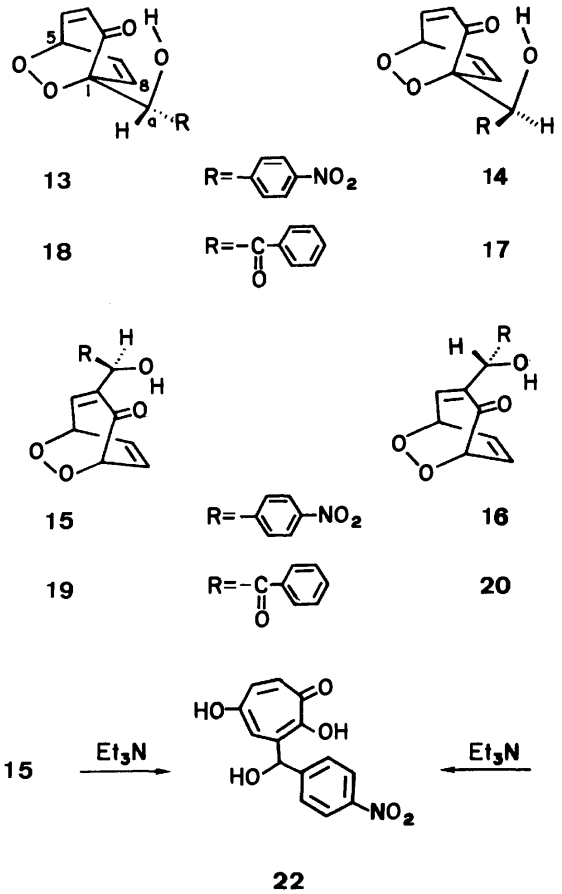

13 R=-C$_6$H$_4$-NO$_2$ 14
18 R=-C(=O)-C$_6$H$_5$ 17
15 R=-C$_6$H$_4$-NO$_2$ 16
19 R=-C(=O)-C$_6$H$_5$ 20
15 —Et$_3$N→ 22 ←Et$_3$N— 16

Chart 2.

Table 1. The ^{1}H NMR Chemical Shifts[8] of Photoproducts

Compd	H-C_1	H-C_3	H-C_4	H-C_5	H-C_8	H-C_9	H-C_a	Aryl-H
11	—	6.02	6.94	4.96	6.06	6.90	3.07, 3.40	7.1—7.4(5H)
12	5.05	—	a)	5.00	a)	a)	3.57(2H)	a)
13	—	6.02	7.02	4.96	6.42	6.97	5.22	7.66(2H), 8.17(2H)
14	—	6.02	6.98	5.03	6.26	7.05	5.31	7.70(2H), 8.21(2H)
15	5.02	—	7.12	5.19	6.50	7.02	5.58	7.56(2H), 8.18(2H)
16	5.00	—	7.09	5.17	6.54	7.04	5.73	7.56(2H), 8.20(2H)
17	—	5.95	6.92	5.02	6.73	7.05	5.24	7.4(3H), 8.0(2H)
18	—	5.95	6.92	4.96	6.65	7.05	5.62	7.4(3H), 8.0(2H)
19	b)	—	7.18	b)	6.43	6.84	5.68	7.4(3H), 8.0(2H)
20	b)	—	7.03	b)	6.47	6.91	5.84	7.4(3H), 8.0(2H)
3	5.00	6.00	7.06	5.00	6.50	7.02		

a) Appeared as overlapped signals at 6.4—6.7(2H) and 6.9—6.3(6H). b) Appeared as overlapped signals at 4.9.

The oxygenation of **8** gave four endoperoxides **13**—**16** in good yields. They were all of the possible [4+2] cycloadducts, and their structures were easily identified by the ^{1}H NMR spectroscopy; the less polar **13** and **14** were 1-substituted 6,7-dioxabicyclo[3.2.2]nona-3,8-dien-2-ones, while the more polar **15** and **16** were 3-substituted derivatives.

Similarly, **9** gave diastereomeric mixtures of 1-substituted products **17** and **18** and 3-substituted products **19** and **20**. Their stereostructure was deduced by chemical-shift comparisons; i.e., one can assume that the preferential conformer of each product must possess the internally-hydrogen-bonded structure for the C-2 carbonyl and the benzylic hydroxyl groups. As a result, one of the isomers should have the up-field shifted C-8 proton signal and a low-field shifted C-a proton signal, depending on the relative geometry to the anisotropic phenyl group. The cases were two pairs of 1-substituted derivatives: **13** and **14** and **17** and **18**. In the 3-substituted derivatives, the chemical shifts of the a-protons led to an assignment of their orientation as depicted in Chart 2.

Thus, the photooxygenation reaction of **10** yielded a 1 : 1-mixture of **11** and **12**. However, the hydroxyl-carrying substrates all produced the 3-substituted products preferably, and retardations in the rates of the oxygenation were recognized to some extent. This would be due to a quenching effect of the hydroxyl group to singlet oxygen. This has been confirmed when the photooxygenation of **9** was carried out in methanol-d_4: the rate was much improved, as large as 23 times that in methanol; the product distribution, the ratio of (**17**+**18**) : (**19**+**20**), was changed to 44:56. The rate enhancement in deuterio solvent is interpreted in terms of an increased lifetime of the singlet oxygen; the degree of the rate-enhancement effect by the medium was theoretically estimated as being ca. 8—10.[9] The present figure is, therefore, attributable to not only the medium effect, but also a quenching effect of the hydroxyl group in the vicinity of the reaction site.[10] This is related to the inversed ratio of the formation of **19** and **20** vs. **17** and **18**. The results are cited in Table 2.

2-(4-Nitrobenzoyl)tropone (**21**) gave no photooxygenation product after prolonged irradiation; this is parallel to the general tendency of the reaction with singlet oxygen, e.g., an introduction of the electron-withdrawing substituent into tropones retarded the oxygenetion.[11]

Table 2. The Product Distributions of the Photooxygenation of **9**

Solv.	Yield/%		Recovery
	(**19**+**20**)	(**17**+**18**)	
Acetone	64	36	
CH_3OH	5.7	7.3	87
CD_3OD	51	40	9

A mild base treatment of **15** and **16** gave 5-hydroxytropolone derivative **22** quantitatively; unfortunately, its attempted conversion to the tropoquinone derivative has not yet been successful.[2]

Experimental

Sensitized Photooxygenation of 2-Benzyltropone (10). Formation 11 and 12. An acetone solution of **10** (114.8 mg) was oxygenated with HMP (10.5 mg) by a 500-W tungsten lamp under oxygen stream. After 4 h, the mixture was chromatographed on a silica-gel column to give **11** [a yellow oil, 43 mg; 32%. Found: C, 73.41; H, 5.29%; *m/z*, 228.0745 (M^+). Calcd for $C_{14}H_{12}O_3$: C, 73.67; H, 5.30%; M, 228.0787. ^{13}C NMR δ[8]= 37.8, 74.8, 90.3, 126.0, 127.1, 128.5 (2C), 130.9 (2C), 131.7, 134.8, 139.0, 142.8, and 195.7. IR ν: 3040, 1680, 1495, 1450, 1240, 1005, 965, 825, 750, and 700 cm^{-1}. UV λ_{max}^{MeOH}: 208 (ε=13900), 241 (1400, sh), and 383 (1000)] and **12** [a yellow oil, 41.2 mg; 31%. Found: C, 73.74; H, 5.40%; *m/z* 228.0787 (M^+). ^{13}C NMR δ=36.3, 75.5, 85.8, 123.5, 126.7, 128.8 (2C), 129.4 (2C), 138.1, 138.8, 140.7, 142.1, and 195.5. IR ν: 3025, 1675, 1490, 1450, 1365, 1220, 960, 790, 730, and 695 cm^{-1}. UV λ_{max}^{MeOH}: 206 nm (ε=13900, sh) and 260 (2200)].

Sensitized Photooxidation of 8. An acetone solution (50 cm^3) of **8** (617 mg) was irradiated for 8.5 h with HMP (22 mg) under an O_2 stream. The reaction mixture was evaporated in vacuo and the residue was chromatographed on a silica-gel column to give **13**[pale yellow needles, mp 110—114 °C, 87.2 mg; 14%. Found: C, 58.00; H, 3.85; N, 5.10%. Calcd for $C_{14}H_{11}NO_6$: C, 58.13; H, 3.83, N, 4.84%. ^{13}C NMR δ=71.1, 75.8, 89.2, 122.6, 123.1 (2C), 128.8 (2C), 131.3, 139.9, 144.3, 144.5, 147.6, and 197.5. IR ν: 3480, 3080, 1660, 1600, 1515, 1400, and 1345 cm^{-1}; UV λ_{max}^{MeOH}: 214 nm (ε=15200), 268 (11300), 344 (2900), and 388 (2500)], **14** [pale yellow needles, mp 129—131 °C, 113.4 mg; 18%. Found: C, 58.25; H, 3.89; N, 5.14%. ^{13}C NMR δ=75.1 (2C), 89.9, 123.5 (2C), 123.8, 129.8 (2C), 131.7, 140.3, 143.3, 144.5, 148.1, and 197.2. IR ν: 3580, 3070, 1680, 1600, 1510, and 1345 cm^{-1}. UV λ_{max}^{MeOH}: 213 nm (ε=14300), 268 (11300), and 340 (1100)], **15** [pale yellow nee-

dles, mp 131—134 °C, 127 mg; 21%. Found: C, 57.84; H, 3.88; N, 5.09%. ^{13}C NMR δ=72.0, 75.3, 85.7, 123.5 (2C), 123.9 (2C), 127.4 (2C), 138.6, 141.9, 142.4, 148.5, and 195.6. IR ν: 3550, 1675, 1600, 1505, and 1340 cm^{-1}. UV λ_{max}^{MeOH}: 211 nm (ε=14700) and 273 (11600)], and **16** [pale yellow needles, mp 127—130 °C, 162.6 mg; 26%. Found: C, 58.25; H, 3.87; N, 5.14%. ^{13}C NMR δ=70.8, 75.3, 85.6, 123.5, 123.7, 124.0 (2C), 127.9 (2C), 138.7, 140.8, 142.7, 148.0, and 195.5. IR ν: 3500, 1655, 1600, 1510, and 1345 cm^{-1}. UV λ_{max}^{MeOH}: 214 nm (ε=14700) and 271 (12500)], together with recovered **8** [70.2 mg; 11%].

Sensitized Photooxygenation of 9. An acetone solution (10 cm^3) of **9** (160 mg) was oxygenated similarly. The reaction mixture was heated in vacuo to remove the solvent, and chromatographed on a silica-gel column to give a 4:1-mixture of **17** and **18** [a yellow oil, 54.5 mg; 30%. Found: *m/z*, 272.0688 (M$^+$). Calcd for $C_{15}H_{12}O_5$: M, 272.0684. ^{13}C NMR δ=73.8, 75.2, 90.0, 124.2, 128.7 (2C), 129.4 (2C), 131.5, 133.8, 135.9, 139.0, 141.3, 195.9, and 196.5 for **17**; δ=73.8, 75.2, 90.0, 123.6, 128.7 (2C), 129.4 (2C), 131.1, 133.8, 135.2, 138.6, 143.5, 195.9, and 196.5 for **18**. IR ν: 3400, 1680, 1665, 1595, 1575, 1450, 1370, and 1335 cm^{-1} UV λ_{max}^{MeOH}: 247 nm (ε=15200) and 345 (900)] and a 2:1-mixture of **19** and **20** [a yellow oil, 97.6 mg; 54%. Found: *m/z*, 272.0641 (M$^+$). ^{13}C NMR δ=71.5, 75.2, 85.5, 123.5, 129.4 (4C), 133.7, 134.4, 138.2, 140.7, 144.7, 193.8, and 198.0 for **19**; δ=70.9, 75.2, 85.5, 123.5, 129.0 (4C), 133.7, 134.4, 138.2, 140.5, 144.7, 194.3, and 198.4 for **20**. IR ν: 3450, 1690, 1600, 1580, 1450, and 1380 cm^{-1}. UV λ_{max}^{MeOH}: 246 nm (ε=13300) and 292 (1200)].

Sensitized Photooxygenation of 9 in CD_3OD. An anhydrous CD_3OD solution (0.5 cm^3) of **9** (13.3 mg) was irradiated by a 500-W tungsten lamp in the presence of HMP (1.4 mg) under an O_2 stream for 3 h. The rate of the oxygenation was ca. 23 times larger than in MeOH. The ratio of (**17**+**18**) and (**19**+**20**) was analyzed to be 44:56 according to ^{1}H NMR spectrometry.

Sensitized Photooxygenation of 9 in CH_3OH. An MeOH solution (0.5 cm^3) of **9** (13.3 mg) was irradiated in the presence of HMP (1.3 mg) under an O_2 stream for 10 h. The ratio of (**17**+**18**): (**19**+**20**) was analyzed to be 56:44.

Base-Catalyzed Isomerization of 15. A benzene solution (7 cm^3) of **15** (21.5 mg) was stirred in the presence of Et_3N (1 mg) for 2 d at room temperature. The precipitates were filtered off and washed with benzene to give **22** [yellow powders, 20.2 mg; 93%. Found: *m/z*, 289.0621 (M$^+$). Calcd for $C_{14}H_{11}NO_6$: M, 289.0586. ^{1}H NMR (CD_3OD) δ=6.36 (1H, s), 6.95 (1H, dd, *J*=11, 3 Hz), 7.26 (1H, d, *J*=11 Hz), 7.66 (2H, d, *J*=9 Hz), 7.79 (1H, d, *J*=3 Hz), and 8.10 (2H, d, *J*=9 Hz). ^{13}C NMR (CD_3OD) δ=71.7, 123.9, 124.1, 124.5 (2C), 127.2, 129.0 (2C), 145.9, 148.8, 152.4, 160.4, 165.8, and 169.9. IR ν: 3600—3200, 1590, 1510, 1400, and 1345 cm^{-1}. UV λ_{max}^{MeOH}: 219 nm (ε=19100), 241 (22500), 266 (13300, sh), 340 (8300), 380 (8500, sh), and 394 (8800)].

Base-Catalyzed Isomerization of 16. A benzene solution (13 cm^3) of **16** (38.0 mg) was similarly treated with Et_3N (1 mg) at room temperature for 2 d to give **22** [35.0 mg; 94%], which was identical with the sample prepared from **15**.

Attempted Oxygenation of 21. An acetone solution (2 cm^3) of **21** (16.2 mg) and HMP (2 mg) was photooxygenated under an O_2 stream at room temperature for 15 h. The silica-gel column chromatogram of the mixture gave **21** quantitatively.

Attempted DDQ-Dehydrogenation of 22. An acetone solution (5 cm^3) of **22** (52.5 mg) and DDQ (74.2 mg) was stirred at room temperature for 1.5 h. The thin-layer chromatography of the mixture confirmed that no reaction occurred.

We wish to thank The Ministry of Education, Science and Culture for a financial assistance through a Grant-in-Aid for Scientific Research to A. M. (No. 60470025).

References

1) Part XXXVIII: A. Mori and H. Takeshita, *Bull. Chem. Soc. Jpn.*, **60**, 3037 (1987).

2) S. Itô, Y. Shoji, M. Hirama, H. Takeshita, and K. Takahashi, *Tetrahedron Lett.*, **1975**, 1075; H. Takeshita, T. Kusaba, and A. Mori, *Chem. Lett.*, **1982**, 701; **1983**, 1371; *Bull. Chem. Soc. Jpn.*, **55**, 1659 (1982); H. Takeshita, A. Mori, Y. Isayama, and T. Kusaba, *Kyushu Daigaku Sogo Rikogaku Kenkyuka Hokoku*, **6**, 185 (1985); H. Takeshita, A. Mori, and Y. Isayama, *Bull. Chem. Soc. Jpn.*, **58**, 1678 (1985).

3) M. Oda and Y. Kitahara, *Tetrahedron Lett.*, **1969**, 3295.

4) E. J. Forbes and J. Griffiths, *J. Chem. Soc.*, **1968**, 575.

5) T. Tezuka, R. Miyamoto, T. Mukai, C. Kabuto, and Y. Kitahara, *J. Am. Chem. Soc.*, **94**, 9280 (1972).

6) H. Takeshita, A. Mori, and H. Suizu, *Chem. Lett.*, **1986**, 593.

7) H. Takeshita, A. Mori, and H. Suizu, *Bull. Chem. Soc. Jpn.*, **60**, 1429 (1987).

8) The NMR spectra were measured in $CDCl_3$ unless otherwise stated, and the chemical shifts were expressed in δ unit.

9) D. R. Kearns, "Singlet Oxygen," ed by H. H. Wassermann and R. W. Murray, Academic Press, New York (1979), p. 115.

10) A change of life-time of $^1O_2$ by the deuteration of the solvent in bulk may not cause an inversed change in the product distributions. And a change of hydroxyl- to deuteroxyl group on the ethereal substituents of 2-alkoxytropones is least likely to alter the steric effect or electronic properties of the reactant tropones. It is true that the reactivity of $^1O_2$ is known to decrease by introducting oxygen functions; e.g., 3-hydroxyalkenes. A duallity due to the cyclic structures in present cases verified this in terms of the product distributions.

11) I. Saito and T. Matsuura, "Singlet Oxygen," ed by H. H. Wassermann and R. W. Murray, Academic Press, New York (1979), pp. 511—574.

A Convenient One-Pot Cyanosilylation of Aldehydes and Ketones Using Potassium or Sodium Cyanide Impregnated on Amberlite XAD Resin and Trimethylsilyl Chloride

Kazuaki SUKATA
Nihon Tokushu Kagaku Kogyo Co., Ltd., 1 Takijiri-aza-hashimoto, Izumi-cho, Iwaki, Fukushima 970-04
(Received May 22, 1987)

Synopsis. In the cyanosilylation of benzaldehyde, the combination of potassium or sodium cyanide impregnated on Amberlite XAD resin and trimethylsilyl chloride has been found to be a good one-pot cyanosilylation agent. Although acetonitrile is the best solvent, substantial yields of the product is obtained even in a nonpolar solvent or without any solvent. In the reaction with other aldehydes or ketones, this method gives the corresponding silylated cyanohydrins in extremely high yields.

Cyanosilylation of aldehydes and ketones using trimethylsilyl cyanide (Me_3SiCN) gives the corresponding α-trimethylsilyloxy nitriles which are versatile and important as acyl anion equivalents[1] and intermediates.[2] Although this reaction gives good yields of the products,[3] independently prepared Me_3SiCN, which is toxic and moisture sensitive, has been used. Furthermore, in general, the synthesis of Me_3SiCN is tedious and the isolated yields are not very good.[2,4] To overcome this disadvantage, a one-pot cyanosilylation using trimethylsilyl chloride (Me_3SiCl) and KCN with or without catalysts has been reported.[5] This method, however, requires very long reaction times and high reaction temperatures in acetonitrile or *N,N*-dimethylformamide, even in the presence of 18-crown-6 or ZnI_2 as a catalyst.

On the other hand, in a previous paper,[6] it has been shown that the reaction of alkylsilyl chloride with KCN or NaCN impregnated on Amberlite XAD resins (KCN/XAD, NaCN/XAD) produces good yields of alkylsilyl cyanide. This paper describes a mild and convenient method for the one-pot cyanosilylation of aldehydes and ketones using KCN/XAD or NaCN/XAD and Me_3SiCl.

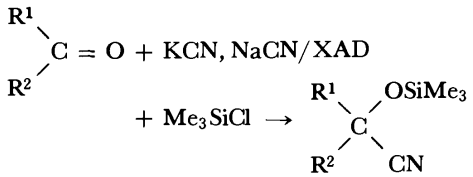

Results and Discussion

In a preliminary experiment, the one-pot cyanosilylation was performed with benzaldehyde, Me_3SiCl, and KCN/XAD-4 in various solvents. Table 1 shows the results. In acetonitrile, the reaction was very fast and the complete conversion of the aldehyde occured at 60 °C in 4 h. Interestingly, in nonpolar solvents or without any solvent, 50—63% of the product was obtained at 60 °C in 8 h and the reaction was substantially faster than those in more polar solvents such as 1,2-dimethoxyethane (DME) and tetrahydrofuran (THF). The order of reaction rates was acetonitrile ≫ hexane ≥ benzene ≈ none > dichloromethane > DME ≈ THF. This order is in contrast to that in the reaction of Me_3SiCl with KCN/XAD-4, that is, acetonitrile ≫ DME ≈ THF ≈ none > benzene ≈ hexane.[6]

Table 1. Cyanosilylation of Benzaldehyde with KCN/XAD-4 and Me_3SiCl in Various Solvents[a]

Solvent	Time/h	Temp/°C	Yield/%[b]
Acetonitrile	4	60	≈98
	4	60	≈98[c]
DME	8	60	27
THF	8	60	21
CH_2Cl_2	8	40	20
	24	40	30
Benzene	8	60	55
	8	40	36
	24	40	43
Hexane	8	60	63
None	8	60	50

a) Unless otherwise noted, reactions were carried out with benzaldehyde (5 mmol), KCN (15 mmol)/XAD-4 (3.75 g), Me_3SiCl (7.5 mmol), and a solvent (20 ml). b) Determined by GLC. c) Sodium cyanide (15 mmol) was used.

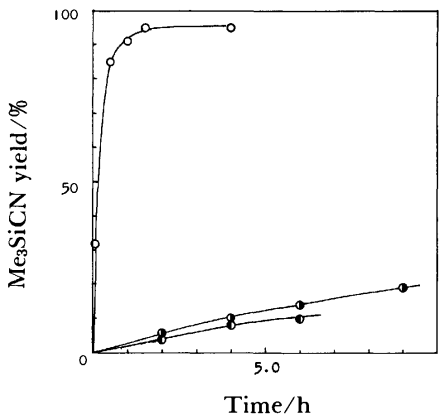

Fig. 1. Plots of Me_3SiCN yield vs time. Reactions were carried out with KCN (15 mmol)/XAD-4 (3.75 g), Me_3SiCl (7.5 mmol), and a solvent (20 ml) at 60 °C. ○: In acetonitrile; ◑: in DME; ◐: in benzene.

Figure 1 shows the relationship between the yield of Me_3SiCN and reaction time in the reaction of Me_3SiCl with KCN/XAD-4. The yields of Me_3SiCN in acetonitrile and other solvents were ca. 85% (0.5 h) and 1—2% (0.5 h), respectively. This finding indicates that the cyanosilylation of benzaldehyde in acetonitrile is performed predominantly by the process of Eq. 1, whereas those in the other solvents are performed mainly by the process of Eq. 2.

$$Me_3SiCl \xrightarrow{KCN/XAD} Me_3SiCN \xrightarrow{PhCHO} PhCH(OSiMe_3)CN \quad (1)$$

$$PhCHO \xrightarrow{KCN/XAD} PhCH(O^-K^+)CN \xrightarrow{Me_3SiCl} PhCH(OSiMe_3)CN \quad (2)$$

This also indicates that the cyanosilylation in acetonitrile occurs in the bulk organic phase, while those in the other solvents occur on the surface of the XAD resin. In the reaction using other solvents with the exception of acetonitrile, mass transfer seems to be important similar to the reaction of acyl chloride with KCN/XAD.[7]

Figure 2 shows the relationship between the conversion of benzaldehyde and the molar ratio Me_3SiCl/KCN. The reactions were carried out in acetonitrile. In both cases of the molar ratio KCN/benzaldehyde=3 and Me_3SiCl/benzaldehyde=1.5, the conversion of benzaldehyde rapidly slowed down over the molar ratio Me_3SiCl/KCN=0.5. Although at present I have no explanation for this fact, it is clear that the molar ratio Me_3SiCl/KCN=0.5 is the optimum value.

The method using Me_3SiCl and KCN/XAD was applied to the cyanosilylation of other aldehydes and ketones. Table 2 shows the results. In both cases of aliphatic and aromatic carbonyl compounds, the reaction was smooth and gave the corresponding silylated cyanohydrins in extremely high yields in the absence of any catalyst such as crown ether or Lewis acids. The impregnated KCN, which has strong nucleophilicity,[8] catalyzed the reaction. In the reaction of enolizable carbonyl compounds, it is predicted that silyl enol ethers are formed as by-products.[5] The present method, however, gave substantially no silyl enol ethers. In the case of crotonaldehyde, only 1,2-adduct was obtained as expected.[3] The reaction of fluorenone required higher reaction temperature than those of the other carbonyl compounds probably because of its

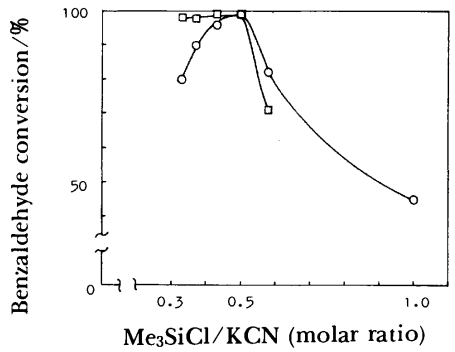

Fig. 2. Plots of benzaldehyde conversion vs. Me_3SiCl/KCN molar ratio. Reactions were carried out in acetonitrile. □: Me_3SiCl/benzaldehyde=1.5, ○: KCN/benzaldehyde=3.0.

Table 2. Cyanosilylation of Aldehydes and Ketones Using KCN/XAD and Me_3SiCl[a]

$$R^1(R^2)C{=}O \xrightarrow{Me_3SiCl+KCN/XAD} R^1(R^2)C(OSiMe_3)CN$$

R^1	R^2	Resin[c]	Time h	Yield[b] %	Bp(θ_b/°C)/mmHg (Mp(θ_m/°C)) Found	Lit
CH_3CH_2	H	A	4	81 (97)	87—9/29	168—70/760[3c]
		B	4	82 (97)		
CH_3CH=CH	H	A	4	85 (97)	80—1/12	80.5/12[3b]
		B	4	80 (95)		
C_6H_5	H	A	4	93 (98)	89—90/2	64/0.5[3b]
		B	8	95 (98)		
4-$CH_3C_6H_4$	H	A	6	96 (99)	84—5/0.35	87/0.45[5]
		B	8	(92)		
4-$CH_3OC_6H_4$	H	A	6	95 (97)	103—4/0.35	95/0.13[5]
		B	8	(92)		
2-ClC_6H_4	H	A	6	91 (96)	85—6/0.4	92—3/0.45[5]
		B	8	(84)		
CH_3CH_2	CH_3	A	6	83 (98)	86—8/30	165—6/760[3c]
-$(CH_2)_5$-		A	6	92 (99)	96—7/14	92.5/12[3b]
-$(CH_2)_4$-		A	6	93 (99)	85—6/13.5	197—8/760[3c]
C_6H_5	CH_3	A	8	97 (≈100)	84—5/3	237—8/760[3c]
		B	8	90 (94)		
C_6H_5	C_6H_5	A	6	97 (99)	105—6/0.3	104/0.5[3b]
		B	8	(92)		
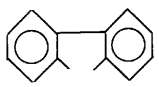		A	25	93 (98)	(94.5—95.5)	(95—6)[3b]
		A	8[d]	90 (96)		

a) Unless otherwise noted, reactions were carried out with carbonyl compound (10 mmol), KCN (30 mmol)/XAD (7.5 g), Me_3SiCl (15 mmol) in acetonitrile (40 ml) at 60 °C. b) Isolated yields. Values in parentheses are the yields determined by GLC. c) A: XAD-4, B: XAD-2. d) The reaction was carried out at 80 °C.

steric hindrance. In general, XAD-4 more rapidly produced products than XAD-2, which was probably due to the difference in the surface area.

In conclusion, the combination of Me_3SiCl and KCN or NaCN/XAD was found to be a good reagent for the cyanosilylation of aldehydes and ketones. This reagent can be used for other cyanosilylations in substitution for Me_3SiCN.

Experimental

Materials. Actonitrile, benzene, and hexane were dried with molecular sieves 4A. Tetrahydrofuran was passed through an alumina column, distilled, and dried with molecular sieves 4A. 1,2-Dimethoxyethane was refluxed with Na and distilled. Dichloromethane was washed with aqueous Na_2CO_3, distilled, and dried with molecular sieves 3A. Trimethylsilyl chloride (Toray Silicone Co.) was used as obtained. Carbonyl compounds (Wako Pure Chemicals Ind. Co.) were used without further purification. Amberlite XAD resins (Organo Co.) were washed with methanol, methanol-benzene, and methanol, and then dried under vacuum. KCN/XAD and NaCN/XAD were prepared by the method previously reported:[8] To a solution of KCN or NaCN (15 mmol) in 4 ml of aqueous methanol (50 vol%) was added XAD resin (3.75 g) and then the solvent was removed under reduced pressure (≈15 mmHg, 1 mmHg=133.322Pa) at 60 °C with vigorous shaking. The half-dried KCN or NaCN/XAD was further dried under vacuum (0.1 mmHg) for 4 h at 90 °C.

Typical Procedure for the Cyanosilylation with KCN or NaCN/XAD and Me_3SiCl. In all reactions, Me_3SiCl and carbonyl compounds were added directly to the flask in which the KCN or NaCN/XAD had been made and dried. All the products were known compounds and satisfactory IR spectra for these compounds, which had no CN absorption band, were obtained.[3c]

Cyanosilylation of Benzaldehyde Using Me_3SiCl and KCN/XAD-4 in Various Solvents. After a mixture of KCN (0.98 g, 15 mmol)/XAD-4 (3.75 g), Me_3SiCl (0.81 g, 7.5 mmol), and a solvent (20 ml) was stirred for several minutes, benzaldehyde (0.53 g, 5.0 mmol) was added to the mixture. The resulting mixture was stirred at 60 °C for the indicated time. The yield of the product was determined by GLC (Silicone OV-17, 3 m×3 mm, 160 °C) using tetradecane as an internal standard.

Crotonaldehyde Cyanohydrin Trimethylsilyl Ether: A mixture of KCN (1.95 g, 30 mmol)/XAD-4 (7.5 g), Me_3SiCl (1.62 g, 15 mmol), and acetonitrile (40 ml) was stirred for several minutes at room temperature, followed by the addition of crotonaldehyde (0.70 g, 10 mmol). The mixture was stirred at 60 °C for 4 h. GLC (Silicone OV-17, 3 m×3 mm, 140 °C) showed almost complete conversion of the aldehyde. The solid material was filtered and washed well with benzene (100 ml). After removal of the solvent, the residue was distilled under reduced pressure, giving 1.44 g (85%) of the product, bp 80—81 °C/12 mmHg (lit,[3b] 80.5 °C/12 mmHg). IR (neat): 1670 (C=C), 1253, 1100, 1056, 960, 870, 844, 752 cm^{-1} no CN.

4-Methoxybenzaldehyde Cyanohydrin Trimethylsilyl Ether: A mixture of KCN (1.95 g, 30 mmol)/XAD-4 (7.5 g), Me_3SiCl (1.62 g, 15 mmol), and acetonitrile (40 ml) was stirred for several minutes at room temperature followed by the addition of 4-methoxybenzaldehyde (1.36 g, 10 mmol). The mixture was stirred at 60 °C for 6 h. After the same treatment as crotonaldehyde, the solvent was removed and the residue was distilled under reduced pressure, giving 2.23 g (95%) of the product, bp 103—104 °C/0.35 mmHg (lit,[5] 95 °C/0.13 mmHg). IR (neat): 1250, 1088, 872, 844, 760 cm^{-1} no CN.

Cyclohexanone Cyanohydrin Trimethylsilyl Ether: The reaction of cyclohexanone (0.98 g, 10 mmol) similar to that of 4-methoxybenzaldehyde was performed. The same treatment as 4-methoxybenzaldehyde gave 1.81 g (92%) of the product, bp 96—97 °C/14 mmHg (lit,[3b] 92.5 °C/12 mmHg). IR (neat): 1250, 1122, 878, 844, 754 cm^{-1} no CN and no C=C.

Acetophenone Cyanohydrin Trimethylsilyl Ether: The reaction of acetophenone (1.20 g, 10 mmol) similar to that of 4-methoxybenzaldehyde was performed. The same treatment as 4-methoxybenzaldehyde gave 2.12 g (97%) of the product, bp 84—85 °C/3mmHg (lit,[3c] 237—238 °C/760 mmHg). IR (neat): 1252, 1116, 845, 758 cm^{-1} no CN and no C=C.

Fluorenone Cyanohydrin Trimethylsilyl Ether: The reaction of fluorenone (1.80 g, 10 mmol) similar to that of 4-methoxybenzaldehyde was performed at 80 °C for 8 h. The solid material was filtered and washed well with benzene (100 ml). Removal of the solvent gave 2.80 g of the crude product as the residual solid, mp 88—94 °C, recrystallization of which gave 2.51 g (90%) of the pure product, mp 94.5—95.5 °C (lit,[3b] 95—96 °C). IR (Nujol): 1250, 1114, 1096, 868, 844, 764, 752, 726 cm^{-1} no CN.

I thank Nihon Tokushu Kagaku Kogyo Co., Ltd., for permission to publish this article.

References

1) K. Deuchert, U. Hertenstein, and S. Hünig, *Synthesis*, **1973**, 777; S. Hünig and G. Wehner, *ibid.*, **1975**, 180; S. Hünig and G. Wehner, *ibid.*, **1975**, 391.

2) D. A. Evans, G. L. Carroll, and L. K. Truesdale, *J. Org. Chem.*, **39**, 914 (1974).

3) a) D. A. Evans, L. K. Truesdale, and G. L. Carroll, *J. Chem. Soc., Chem. Commun.*, **1973**, 55; b) W. Lidy and W. Sundermeyer, *Chem. Ber.*, **106**, 587 (1973); c) H. Neef and R. Müller, *J. Prakt. Chem.*, **315**, 367 (1973).

4) J. W. Zubrick, B. I. Dunbar, and H. D. Durst, *Tetrahedron Lett.*, **1975**, 71; S. Hünig and G. Wehner, *Synthesis*, **1979**, 522; J. K. Rasmussen and S. M. Heilmann, *ibid.*, **1979**, 523; M. T. Leetz and I. Chatziiosifidis, *ibid.*, **1982**, 330; T. Livinghouse, *Org. Synth.*, **60**, 126 (1981).

5) J. K. Rasmussen and S. M. Heilmannn, *Synthesis*, **1978**, 219.

6) K. Sukata, *Bull. Chem. Soc. Jpn.*, **60**, 2257 (1987).

7) K. Sukata, *Bull. Chem. Soc. Jpn.*, **60**, 1085 (1987).

8) K. Sukata, *J. Org. Chem.*, **50**, 4388 (1985).

1*H*,1*H*-Perfluoroalkylation of Enol Silyl Ethers with (1*H*,1*H*-Perfluoroalkyl)-phenyliodonium Triflates. A New Method for the Preparation of β- and δ-Trifluoromethyl Carbonyl Compounds and Their Higher Perfluoroalkyl Homologues[1]

Teruo UMEMOTO* and Yoshihiko GOTOH
Sagami Chemical Research Center, Nishi-Ohnuma 4-4-1, Sagamihara, Kanagawa 229
(Received April 30, 1987)

Synopsis. The reaction of enol trimethylsilyl ethers of carbonyl compounds with (1*H*,1*H*-perfluoroalkyl)phenyliodonium triflates was promoted successfully by potassium fluoride in dichloromethane at room temperature, giving β-perfluoroalkyl (Rf; CF_3, C_2F_5, *i*-C_3F_7, *n*-C_7F_{15}) carbonyl compounds in good yields. An enol silyl ether of an α,β-unsaturated carbonyl compound gave a δ-Rf-α,β-unsaturated carbonyl compound selectively.

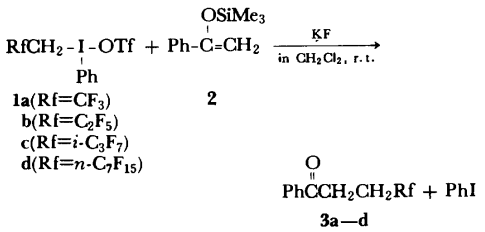

Much attention is being denoted to polyfluoroalkyl groups from the viewpoint of the development of new chemicals or materials having characteristic properties, because they have high electronegativity, stability, lipophilicity, strong surface intension- and refractive index-decreasing effects, and so on.[2] Among them, trifluoromethyl (CF_3) or 2,2,2-trifluoroethyl (CF_3CH_2) group in particular has been of increasing importance in the development of new medicines or agricultural chemicals owing to its unique effects on the bioactivity.[2,3] However, the introduction of the fluoroalkyl groups into the desired sites of the organic molecules was troublesome.[4]

Recently we have developed (1*H*,1*H*-perfluoroalkyl)-phenyliodonium triflates **1** (FMITS) as the most reactive reagents for the source of $RfCH_2$ cations.[5,6] In this paper, we described potassium fluoride-promoted 1*H*,1*H*-perfluoroalkylation of enol silyl ethers with FMITS under mild conditions, giving β- or δ-CF_3 carbonyl compounds or their higher perfluoroalkyl (Rf) homologues in good yields.[7]

Results and Discussion

We examined the reaction of **1** with α-(trimethylsiloxy)styrene (**2**), and the results are shown in Table 1. It was found that **1a** smoothly reacted with an equimolar amount of **2** in dichloromethane at room temperature in the presence of a large excess of potassium fluoride (KF) as an additive to give phenyl 3,3,3-trifluoropropyl ketone (**3a**) in a high yield along with an almost quantitative yield of iodobenzene (Run 1). The product **3a** was also contaminated with the starting acetophenone, the amount of which increased as the yield of **3a** decreased. **3a** was easily purified by chromatography on silica gel. When **1a** was treated with **2** without an additive, the yield of **3a** was low (Run 10). When using 2,4,6-collidine, *N*-(2,2,2-trifluoroethyl)-pyridinium triflate was obtained in a 60% yield along with **3a** (30%) (Run 9). Sodium bicarbonate as a solid base afforded a trace of **3a** (Run 7). Since the treatment of an enol trimethylsilyl ether with methyllithium in tetrahydrofuran (THF) has been known as the effective method for the generation of an enolate anion,[8,9] the results of Run 8 indicated that the direct reaction of **1a** with an enolate anion of acetophenone in THF resulted in the low yield of **3a**. One of the causes may be that the enolate anion competitively abstracted a proton from the acidic CH_2 protons of **1a**, since triflates **1** were found to be easily deprotonated with such a base as sodium hydride.[5b] KF is insoluble in dichloromethane and the reaction of **1a** with **2** proceeded slightly without an additive. Moreover, it is reasonable that electron-deficient iodine atom-containing **1** forms a complex with electron-rich double bond-containing **2**. From the above facts and discussion, it may be suggested that solid KF successfully promoted

Table 1. 2,2,2-Trifluoroethylation of **2** with **1a**

Run	Additive(equiv)[a]	Solv.	Temp	Time/h	Yield/%[b]/**3a**
1	KF(5.2)	CH_2Cl_2	R.t.	1.5	87
2	KF(2)	CH_2Cl_2	R.t.	3	40
3	KF(5.5)	$CHCl_3$	R.t.	4	45
4	KF(5.5)	Et_2O	R.t.	4	39
5	KF(5.5)	THF	R.t.	5	38
6	CsF(3)	CH_2Cl_2	R.t.	11[c]	23
7	$NaHCO_3$(1.2)	CH_2Cl_2	R.t.	5	<7
8[c]	MeLi (1)	THF	0 °C→R.t.	1	27
9	2,4,6-Collidine(1)	CH_2Cl_2	R.t.	1	30[d]
10	None	CH_2Cl_2	R.t.	5	16

a) KF used was spray-dried KF.[10] The values in parentheses mean the molar equivalency of the additive to **1a**. An equimolar amount of **2** to **1a** was used in all the runs. b) Isolated Yields except for Run 6 (GC Yield). c) **1a** was added after **2** was allowed to react with MeLi at 0 °C in THF for 15 min. d) *N*-(2,2,2-Trifluoroethyl)pyridinium triflate as another product was obtained in a 60% yield. e) Overnight.

Table 2. 2,2,2-Trifluoroethylation of Enol Silyl Ethers with **1a**

Run[a]	Silyl ether	Product		Yield/%[b]
1	$PhC(OSiMe_3)=CHCH_3$	$PhC(=O)CH(CH_2CF_3)CH_3$	(**4**)	55
2	$PhCH=CHC(OSiMe_3)=CH_2$	$PhCH=CHC(=O)CH_2CH_2CF_3$	(**5**)[c]	75
3	$PhC(OSiMe_3)=CHCH=CH_2$	$PhC(=O)CH=CHCH_2CH_2CF_3$	(**6**)[d]	42
		$PhC(=O)CH(CH_2CF_3)CH=CH_2$	(**7**)	0.8
4	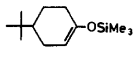	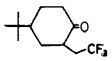	(**8**)	53
5	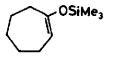	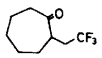	(**9**)	49
6	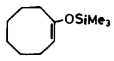	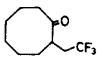	(**10**)	71
7	$n\text{-}C_6H_{13}C(OSiMe_3)=CH_2$	$n\text{-}C_6H_{13}C(=O)CH_2CH_2CF_3$	(**11**)	80
8	$n\text{-}C_6H_{13}CH=C(OSiMe_3)CH_3$	$n\text{-}C_6H_{13}CH(CH_2CF_3)COOCH_3$	(**12**)	76
9	$PhCH=C(OSiMe_3)CH_2CH_3$	$PhCH(CH_2CF_3)COOCH_2CH_3$	(**13**)	92

a) The reaction conditions were the same as for Run 1 in Table 1. b) Isolated Yields except for Run 8 (GC yield). c) Trans-isomer. d) The configuration around the double bond was not determined.

Table 3. 1*H*,1*H*-Perfluoroalkylation of Enol Silyl Ethers with **1b**—d

Run[a]	Ether	1	Temp	Time/h	Product	Yield/%[b]
1	**2**	**1b**	R.t.	4	**3b**	67
2	**2**	**1b**	Reflux	3	**3b**	87
3	**2**	**1c**	R.t.	8	**3c**	18
4	**2**	**1c**	Reflux	7	**3c**	32
5	**2**	**1d**	R.t.	12	**3d**	50
6	**2**	**1d**	Reflux	10	**3d**	54
7	$n\text{-}C_6H_{13}C(OSiMe_3)=CH_2$	**1b**	R.t.	4	$n\text{-}C_6H_{13}C(=O)CH_2CH_2C_2F_5$ (**14**)	63
8	$n\text{-}C_6H_{13}C(OSiMe_3)=CH_2$	**1d**	R.t.	8	$n\text{-}C_6H_{13}C(=O)CH_2CH_2C_7F_{15}{}^n$ (**15**)	45
9	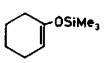	**1d**	R.t.	7	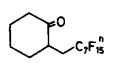 (**16**)	21

a) In all the runs, 5—5.5 equimolar amounts of spray-dried KF and dichloromethane as a solvent were used. b) Isolated yields.

the reaction of the complex of **1** with **2** giving **3**, by attacking the silyl site of the enol silyl ether moiety of the complex under the conditions of Run 1. The use of cesium fluoride (CsF) which is expected to have better solubility than KF resulted in the low yield of **3a** (Run 6). This may be explained by the high reactivity of CsF, compared to KF, which can disturb the triple-molecular reaction.

This method was successfully applied to the 2,2,2-trifluoroethylation of a variety of carbonyl compounds (Table 2). An enol trimethylsilyl ether of an α,β-unsaturated ketone underwent selective γ-trifluoroethylation (Run 3). Only a trace of the α-trifluoroethylated product was obtained. Similarly, keten trimethylsilyl acetals derived from esters gave α-CF_3CH_2 esters in good yields.

We also examined the reaction of **1** having a long chain of Rf group with the enol silyl ethers in the presence of KF (Table 3). Since the reactivity decreased as the carbon number of Rf group increased, the high reaction temperature or long reaction time was needed.

Since a variety of the enol silyl ethers can easily be prepared by the advanced synthetic methods,[9] our technique with FMITS reagents is expected to be widely utilized for the preparation of the β- and δ-Rf carbonyl compounds.

Experimental

General. Melting points were uncorrected. ^1H NMR spectra were recorded with a Varian XL-100 NMR spectrometer, a Varian EM 390 NMR spectrometer, or a Bruker AM-400 NMR spectrometer with chloroform-*d* as a solvent and tetramethylsilane as an internal standard. ^{19}F NMR spectra were measured with a Varian XL-100 NMR spectrometer or a Hitachi R-20 B NMR spectrometer, and chloroform-*d* as a solvent. ^{19}F NMR chemical shifts were

reported in ppm upfield from trichlorofluoromethane as an internal standard. IR spectra were measured on a Jasco A-202 diffraction grating infrared spectrometer. Mass spectra were recorded on a Hitachi RMU-6MG spectrometer at 70 eV and 100 °C.

Materials. FMITS reagents were prepared according to the method reported previously.[5] The enol silyl ethers were prepared by the usual methods.[9] Spray-dried KF[10] commercially available from Morita Kagaku Company, Japan, was dried under vacuum at 140 °C for 11 h before use.

1*H*,1*H*-Perfluoroalkylation of Enol Silyl Ethers with 1. General Procedure; **1** (1 mmol) was added into a mixture of an enol silyl ether (1 mmol) and spray-dried KF (5—5.5 mmol) in 3 ml of dry dichloromethane under argon atmosphere and the mixture was stirred for 1.5 h at room temperature. After the filtration through the short column of silica gel, the resulting residue was purified by thin-layer chromatography on silica gel to give the Rf carbonyl compounds. **3a**: Mp 59—60 °C; ^{1}H NMR δ=2.20—2.80 (2H, m, CH_2), 3.10—3.35 (2H, m, CH_2), 7.30—7.70 (3H, m, *m,p*-PhH), 7.83—8.10 (2H, m, *o*-PhH); ^{19}F NMR 65.3 (t, J=11 Hz, CF_3); IR (KBr, cm^{-1}) 1690 (CO); MS 202 (M^+). Found: C, 59.46; H, 4.46%. Calcd for $C_{10}H_9F_3O$: C, 59.41; H, 4.49%. **3b**: Mp 67—68 °C; ^{1}H NMR δ=2.20—2.90 (2H, m, CH_2), 3.13—3.43 (2H, m, CH_2), 7.30—7.76 (3H, m, *m,p*-PhH), 7.83—8.13 (2H, m, *o*-PhH); ^{19}F NMR 85.9 (3F, s, CF_3), 117.0 (2F, t, J=16.9 Hz, CF_2); IR (KBr, cm^{-1}) 1690 (CO); MS 252 (M^+). Found: C, 52.12; H, 3.63%. Calcd for $C_{11}H_9F_5O$: C, 52.39; H, 3.60%. **3c**: Mp 28—29 °C; ^{1}H NMR δ=2.33—2.87 (2H, m, CH_2), 3.13—3.43 (2H, m, CH_2), 7.31—7.71 (3H, m, *m,p*-PhH), 7.80—8.10 (2H, m, *o*-PhH); ^{19}F NMR 76.5 (6F, d, J=7 Hz, CF_3), 184.1 (1F, m, CF); IR (KBr, cm^{-1}) 1690 (CO); MS 302 (M^+). Found: C, 47.59; H, 3.02%. Calcd for $C_{12}H_9F_7O$: C, 47.69; H, 3.00%. **3d**: Mp 80—81 °C; ^{1}H NMR δ=2.20—2.90 (2H, m, CH_2), 3.10—3.43 (2H, m, CH_2), 7.30—7.68 (3H, m, *m,p*-PhH), 7.80—8.13 (2H, m, *o*-PhH); ^{19}F NMR 81.5 (3F, t, J=10 Hz, CF_3), 114.6 (2F, m, CF_2), 122.4 (4F, m, CF_2), 123.3 (2F, m, CF_2), 123.8 (2F, m, CF_2), 126.7 (2F, m, CF_2); IR (KBr, cm^{-1}) 1690 (CO); MS 502 (M^+). Found: C, 38.03; H, 1.84%. Calcd for $C_{16}H_9F_{15}O$: C, 38.26; H, 1.81%. **4**: Oil; ^{1}H NMR δ=1.30 (3H, d, J=6 Hz, CH_3), 1.90—3.20 (2H, m, CH_2), 3.60—4.00 (1H, m, CH), 7.30—7.70 (3H, m, *m,p*-PhH), 7.85—8.10 (2H, m, *o*-PhH); ^{19}F NMR 64.5 (t, J=11 Hz, CF_3); IR (neat, cm^{-1}) 1690 (CO); MS 216 (M^+). Found: C, 61.27; H, 5.17%. Calcd for $C_{11}H_{11}F_3O$: C, 61.11; H, 5.13%. **5**: Bp 140 °C (bath temperature)/400 Pa, mp 48—49 °C; ^{1}H NMR δ=2.20—2.78 (2H, m, CH_2), 2.80—3.10 (2H, m, CH_2), 6.73 (1H, d, J=16.5 Hz, olefin proton), 7.30—7.73 (6H, m, PhH and olefin proton); ^{19}F NMR 66.8 (t, J=10 Hz, CF_3); IR (KBr, cm^{-1}) 1700 (CO); MS 228 (M^+). Found: C,62.86; H, 4.80%. Calcd for $C_{12}H_{11}F_3O$: C, 63.15; H, 4.86%. **6**: Mp 37 °C; ^{1}H NMR δ=2.20—2.80 (4H, m, CH_2), 6.80—7.03 (2H, m, olefin protons), 7.25—7.65 (3H, m, *m,p*-PhH), 7.80—8.05 (2H, m, *o*-PhH); ^{19}F NMR 66.0 (t, J=10 Hz, CF_3); IR (neat, cm^{-1}) 1675 (CO); MS 228 (M^+). Found: C, 62.91; H, 4.47%. Calcd for $C_{12}H_{11}F_3O$: C, 63.15; H, 4.86%. **7**: Oil; ^{1}H NMR δ=2.20—3.10 (2H, m, CH_2), 4.20—4.55 (1H, m, CH), 5.10—5.40 (2H, m, =CH_2), 5.60—6.10 (1H, m, olefin proton), 7.35—7.70 (3H, m, *m,p*-PhH), 7.83—8.06 (2H, m, *o*-PhH); ^{19}F NMR 64.0 (t, J=11 Hz, CF_3); MS 228 (M^+). **8**: Oil; ^{1}H NMR δ=0.90 (9H, s, *t*-Bu), 1.20—3.00 (9H, m); ^{19}F NMR 64.1 (t-d, J=10, 1.4 Hz, CF_3); IR (neat, cm^{-1}) 1720 (CO); MS 236 (M^+). Found: C, 60.74; H, 7.82%. Calcd for $C_{12}H_{19}F_3O$: C, 61.00; H, 8.11%. **9**: Oil; ^{1}H NMR δ=1.00—2.35 (10H, m), 2.35—3.16 (3H, m); ^{19}F NMR 64.1 (t, J=10 Hz, CF_3); IR (neat, cm^{-1}) 1710 (CO); MS 194 (M^+). Found: C, 55.46; H, 6.74%. Calcd for $C_9H_{13}F_3O$: C, 55.66; H, 6.75%. **10**: Oil; ^{1}H NMR δ=1.30—3.20 (m); ^{19}F NMR 64.9 (t, J=10 Hz, CF3); IR (neat, cm^{-1}) 1715 (CO); MS 208 (M^+). Found: C, 57.89; H, 7.03%. Calcd for $C_{10}H_{15}F_3O$: C, 57.68; H, 7.26%. **11**: Oil; ^{1}H NMR δ=0.78—1.06 (3H, m, CH_3), 1.13—1.83 (8H, m, CH_2), 2.23—2.80 (6H, m, CH_2); ^{19}F NMR 66.8 (t, J=9.9 Hz, CF_3); IR (neat, cm^{-1}) 1725 (CO); MS 210 (M^+). Found: C, 57.11; H, 8.14%. Calcd for $C_{10}H_{17}F_3O$: C, 57.13; H, 8.15%. **12**: Oil; ^{1}H NMR δ=0.75—1.00 (3H, m, CH_3), 1.10—1.80 (10H, m, CH_2), 1.95—2.80 (3H, m, CH_2CH), 3.70 (3H, s, OCH_3); ^{19}F NMR 65.3 (t, J=10 Hz, CF_3); IR (neat, cm^{-1}) 1740 (CO); MS 240 (M^+). Found: C, 55.24; H, 7.83%. Calcd for $C_{11}H_{19}F_3O_2$: C, 54.99; H, 7.94%. **13**: Bp 78 °C/400 Pa; ^{1}H NMR δ=1.20 (3H, t, J=6.6 Hz, CH_3), 2.10—3.50 (2H, m, CH_2), 3.80—4.00 (1H, m, CH), 4.16 (2H, q-d, J=6.6, 2.4 Hz, OCH_2), 7.33 (5H, s, Ph); ^{19}F NMR 65.3 (t, J=11 Hz, CF_3); IR (neat, cm^{-1}) 1740 (CO); MS 246 (M^+). Found: C, 58.23; H, 5.28%. Calcd for $C_{12}H_{13}F_3O_2$: C, 58.53; H, 5.02%. **14**: Oil; ^{1}H NMR δ=0.78—1.03 (3H, m, CH_3), 1.13—1.80 (8H, m, CH_2), 2.00—2.83 (6H, m, CH_2); ^{19}F NMR 85.9 (3F, s, CF_3), 117.8 (2F, t, J=17 Hz, CF_2); IR (neat, cm^{-1}) 1720 (CO); MS 260 (M^+). Found: C, 50.76; 6.64%. Calcd for $C_{11}H_{17}F_3O$: C, 50.77; H, 6.58%. **15**: Mp 43—44 °C; ^{1}H NMR δ=0.80—1.00 (3H, m, CH_3), 1.13—1.81 (8H, m, CH_2), 2.20—2.88 (6H, m, CH_2); ^{19}F NMR 81.0 (3F, t, J=10 Hz, CF_3), 113.6 (2F, m, CF_2), 121.5 (6F, m, CF_2), 123.0 (2F, m, CF_2), 125.6 (2F, m, CF_2); IR (KBr, cm^{-1}) 1720 (CO); MS 510 (M^+). Found: C, 37.60; H, 3.40%. Calcd for $C_{16}H_{17}F_{15}O$: C, 37.66; H, 3.36%. **16**: Oil; ^{1}H NMR δ=1.30—3.30 (m); ^{19}F NMR 81.2 (3F, m, CF_3), 111.5 (1F, A part of AB system, J=283 Hz, CF_2), 114.8 (1F, B part of AB system, J=283 Hz, CF_2), 122.4 (4F, m, CF_2), 123.2 (2F, m, CF_2), 124.0 (2F, m, CF_2), 126.6 (2F, m, CF_2); IR (neat, cm^{-1}) 1720 (CO); MS 480 (M^+). Found: C, 35.07; H, 2.37%. Calcd for $C_{14}H_{11}F_{15}O$: C, 35.01; H, 2.31%.

References

1) Presented at 52th National Meeting of Japanese Chemical Society, Abstract II, p. 1588 (1Z03), Apr. 1, 1986 (Kyoto).

2) N. Ishikawa and Y. Kobayashi, "Fusso no Kagōbutsu — sono Kagaku to Ōyō," Kodansha, Tokyo (1979); "Biomedicinal Aspects of Fluorine Chemistry," ed by R. Filler and Y. Kobayashi, Kodansha Ltd., Tokyo (1982); R & D Report No. 6, "Fusso Kagōbutsu no Saisentan Ōyō Gijutsu," ed by N. Ishikawa, CMC, Tokyo (1981); "Preparation, Properties, and Industrial Applications of Organofluorine Compounds," ed by R. E. Banks, Ellis Horwood Ltd., 1982 (Chichester).

3) *Chem. Eng. News*, Sept. 10, pp. 32—33 (1984).

4) "Fusso Kagōbutsu no Gōsei to Kinō," ed by N. Ishikawa, CMC, Tokyo (1987).

5) a) T. Umemoto and Y. Gotoh, *J. Fluorine Chem.*, **28**, 235 (1985). b) *Idem, Bull. Chem. Soc. Jpn.*, **60**, 3307 (1987).

6) T. Umemoto and Y. Gotoh, *J. Fluorine Chem.*, **31**, 231 (1986).

7) It was described in the patent [R. L. Hansen, U.S. Patent 3,419,595 (1968)] that the reaction of enamines with 1*H*,1*H*-perfluoroalkyl ($RfCH_2$) triflates followed by acid hydrolysis gave β-Rf carbonyl compounds, but neither yields nor spectral data of the products were reported.

8) H. O. House, D. S. Crumrine, A. Y. Teranishi, and H. D. Olmstead, *J. Am. Chem. Soc.*, **95**, 3310 (1973).

9) H. O. House, L. J. Czuba, M. Gall, and H. D. Olmstead, *J. Org. Chem.*, **34**, 2324 (1969); G. H. Posner, J. J. Sterling, C. E. Whitten, G. M. Lentz, and D. J. Brunelle, *J. Am. Chem. Soc.*, **97**, 107 (1975); E. Nakamura, E. Murofushi, M. Shimizu, I. Kuwajima, *J. Am. Chem. Soc.*, **98**, 2346 (1976); G. Simchen and W. Kober, *Synthesis*, **1976**, 259 and references cited therein.

10) T. Kitazume and N. Ishikawa, *Chem. Lett.*, **1981**, 1259.

 © 1987 The Chemical Society of Japan Bull. Chem. Soc. Jpn., 60, 3827—3833 (1987)

Synthetic Polyether Dicarboxylic Acids Exhibiting Lithium Ion-Selective Transport[1)]

Kazuhisa HIRATANI* and Kazuhiro TAGUCHI
Industrial Products Research Institute, Higashi 1-chome, Yatabe-machi, Tsukuba-gun, Ibaraki 305
(Received January 29, 1987)

Polyether dicarboxylic acid carriers with several alternate units of oxytrimethylene and oxy-*o*-phenylene groups have been synthesized. They exhibit lithium ion selectivity in the competitive cation transport among lithium, sodium, and potassium ions through liquid membranes. On the basis of the cation extraction and the spectroscopic behavior, it is proposed that these carriers form a coiled structure into which the lithium ion becomes selectively incorporated to exhibit lithium ion-selective transport.

Since Pedersen has reported for the macrocyclic polyethers, the so-called crown ethers,[2)] a large number of macrocyclic polyethers exhibiting cation-selectivity have been synthesized.[3)] On the other hand, it has attracted considerable attention that naturally-occurring antibiotic ionophores can transport cations through biomembranes.[4)] One of the properties of both such artificial and natural ionophores is that they incorporate cations into the cavity by means of the electrostatic interactions of electron-donating hetero atoms. It should be noted that there are a number of noncyclic polyether carboxylic acids among such natural ionophores which exhibit a high selectivity toward alkali and alkaline earth metal ions. We have now studied these structures and functions and have synthesized a series of noncyclic polyether compounds.[5)]

In general, the cation complexes of synthetic and noncyclic polyethers have low stability constants and have less ability to extract cation from aqueous to organic solutions compared with cyclic ones.[6)] Therefore, these compounds have attracted less attention than have macrocyclic polyethers. However, as has been reported by the works of Vögtle, Simon, and other groups, various functionalized noncyclic polyethers have been synthesized.[7,8)] Noncyclic polyethers with carboxyl end groups have been reported as carriers for the cation transport through liquid membranes.[9–12)] The introduction of carboxyl groups results in the rapid formation of salts with cations, and it is particularly useful for cation transport and also for cation extraction into an organic solvent from an aqueous solution. It has been found that cation selectivity with the polyether carboxylic acids depends on the residual parts of polyether structures.

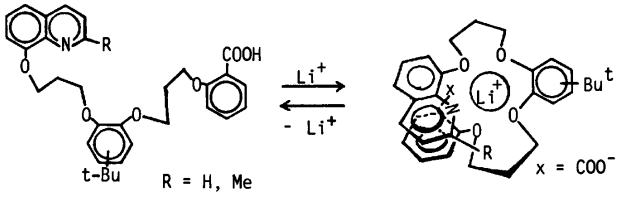

Fig. 1. Uptake of Li^+ ion by the conformational change of **5**.

As previously reported, the noncyclic polyether **5** is an ionophore which can selectively transport lithium ions through liquid membranes against the concentration gradient.[13)] In this case, it has been inferred that lithium ions form the salt with the carboxyl group and become incorporated into the pseudocavity thus formed, as is shown in Fig. 1. Such a conformation has been suggested on the basis of the CPK model building and supported spectroscopically.[14)]

By the way, the lithium ion has the smallest naked ionic radius among the alkali metal ions, while it has the largest hydrated ionic radius and the largest hydration energy. There is no naturally-occurring ionophore which exhibits an excellent lithium ion-selectivity, but several synthetic lithium ion-selective ionophores have been reported in noncyclic,[15,16)] cyclic,[17–21)] and bicyclic[22)] compounds. Wide applications can be expected for lithium ion-selective ionophores, e.g., in the selective separation of lithium ions by transport through liquid membranes and by solvent extraction, and also in monitoring lithium-ion activity in blood during therapy for manic-depressive psychosis.[23)]

If the carrier **5** can wrap around the lithium ion by means of conformational change, as is shown in Fig. 1, even polyethers with fairly long chain structures can be expected to transport lithium ions selectively. In this paper, we wish to report on the synthesis of polyethers with long polyether chains and on their transport of alkali metal ions through liquid membranes.

Experimental

General. The IR and the UV spectra were recorded with JASCO A-3 Infrared and Hitachi 330 spectrophotometers respectively. The ^1H NMR spectrum was recorded with a Varian EM-360 spectrometer. The chemical shifts for the $CDCl_3$ solution are reported from internal tetramethylsilane (TMS).

Synthesis of Noncyclic Polyethers. The ethyl salicylate, 4-*t*-butylcatechol, and potassium *t*-butoxide used were extra-pure-grade reagents of Wako Pure Chemical Industries, Ltd.

Extra pure-grade *N,N*-dimethylformamide (DMF) was used as the solvent after having been dried with molecular sieves. The 1,2-bis(3-chloropropoxy)-4-*t*-butylbenzene (**7**), 1-[3-(*o*-ethoxycarbonylphenoxy)propoxy]-2-(3-chloropropoxy)-4(or 5)-*t*-butylbenzene (**9**), and 2-[3-(*o*-ethoxycarbonylphenoxy)-propoxy]-4(or 5)-*t*-butylphenol (**10**) were prepared as previously reported.[13] The 1,2-bis[3-(*o*-carboxyphenoxy)-propoxy]-4-*t*-butylbenzene (**1**)[22] and 1-[3-(*o*-carboxyphenoxy)propoxy]-2-[3-(8-quinolyloxy)propoxy]-4(or 5)-*t*-butylbenzene (**5**)[13] which were used in the transport experiment for comparison were also prepared as previously reported. Compounds **2**—**4**, with long polyether chains, were prepared by the reaction process shown in Scheme 1.

1,3-Bis[1-[2-(*o*-carboxyphenoxy)propoxy]-4(or 5)-*t*-butylphenoxy]propane (2). A mixture of 1.9 g (5 mmol) of 2-[3-(*o*-ethoxycarbonylphenoxy)propoxy]-4(or 5)-*t*-butylphenol (**10**) and 0.56 g (5 mmol) of potassium *t*-butoxide was stirred in 30 ml of DMF until it became homogeneous. To the solution we then added 2.3 g (5 mmol) of 1-[3-(*o*-ethoxycarbonylphenoxy)propoxy]-2-(3-chloropropoxy)-4(or 5)-*t*-butylbenzene (**9**) and a small amount of KI, after which the mixture was stirred at 80 °C for 24 h. Then, after cooling, 150 ml of water was added to the solution after and extraction with benzene (100 ml) was carried out. The benzene layer was washed with water three times and dried with $MgSO_4$. After the removal of the benzene, the residue was submitted to column chromatography on silica gel, with ethyl acetate–hexane as the eluent, to give 1.4 g (36%) of the ethyl ester of **2** as a viscous, clear oil. A solution of the diethyl ester of **2** (1.0 g, 1.3 mmol) in ethanol (70 ml) and potassium hydroxide (0.5 g) was mixed and heated at reflux overnight. After the solvent has evaporated, water (100 ml) was added. The aqueous phase was acidified with concentrated hydrochloric acid and extracted with chloroform (3×50 ml). The combined organic phase was washed with water, dried with $MgSO_4$, and evaporated. The residue was submitted to column chromatography on silica gel, with chloroform–ethanol as the eluent, to give 0.8 g (85%) of **2** as a pale yellow, glassy solid: IR (KBr) 3300 and 2600 (COOH), 1735 and 1700 (C=O), 1605 and 1580 (aromatic C=C), 1055 cm^{-1} (C–O); ^1H NMR ($CDCl_3$) δ=1.29 (18H, s, $C(CH_3)_3$), 2.0—2.6 (6H, m, $OCH_2C\underline{H}_2CH_2O$), 4.0—4.7 (12H, m, $OC\underline{H}_2CH_2C\underline{H}_2O$), 6.8—7.8 (12H, m, aromatic), 8.17—8.4 (2H, m, aromatic); UV ($CHCl_3$), λ_{max}=283 nm, ε=10000. Found: C, 70.25; H, 6.98%. Calcd for $C_{43}H_{52}O_{10}$ (MW 728.88): C, 70.86; H, 7.19%.

1,2-Bis[3-[2-[3-(*o*-carboxyphenoxy)propoxy]-4(or 5)-*t*-butylphenoxy]propoxy]-4(or 5)-*t*-butylbenzene (3). A mixture of 3.7 g (10 mmol) of 2-[3-(*o*-ethoxycarbonylphenoxy)propoxy]-4(or 5)-*t*-butylphenol (**10**) and 1.1 g (10 mmol) of potassium *t*-butoxide was stirred in 30 ml of DMF until it became homogeneous. To the solution we then added 1.6 g (5 mmol) of 1,2-bis(3-chloropropoxy)-4-*t*-butylbenzene (**7**) and a small smount of KI, after which the mixture was stirred at 80 °C for 48 h. After the same post-treatment as in the case of **2**, 1.5 g (32%) of the ethyl ester of **3** was obtained as a viscous, pale yellow oil. In a manner similar to the hydrolysis described above, **3** (1.2 g, 85%) was obtained as a pale yellow, glassy solid: IR (KBr) 3300 and 2500 (COOH), 1740 and 1700 (C=O), 1605 and 1580 (aromatic C=C), 1050 cm^{-1} (C–O); ^1H NMR ($CDCl_3$) δ=1.30 (27H, s, $C(CH_3)_3$), 2.0—2.6 (8H, m, $OCH_2C\underline{H}_2CH_2O$), 4.0—4.7 (16H, m, $OC\underline{H}_2CH_2C\underline{H}_2O$), 6.8—7.8 (15H, m, aromatic), 8.2—8.45 (2H, m, aromatic); UV ($CHCl_3$) λ_{max}=282 nm, ε=12000. Found: C, 71.23; H, 7.84%. Calcd for $C_{56}H_{70}O_{12}$ (MW 935.16): C, 71.93; H, 7.55%.

1,2-Bis[3-[2-[3-[2-[3-(*o*-carboxyphenoxy)propoxy]-4(or 5)-*t*-butylphenoxy]propoxy]-4(or 5)-*t*-butylphenoxy]propoxy]-4(or 5)-*t*-butylbenzene (4). A mixture of 1.7 g (10 mmol) of *t*-butylcatechol (**6**) and 2.3 g (20 mmol) of potassium *t*-butoxide was stirred in 50 ml of DMF under a nitrogen atmosphere until it became homogeneous. To the solution we then added 10 g (31 mmol) of 1,2-bis(3-chloropropoxy)-4-*t*-butylbenzene (**7**) and a small amount of KI, after which the mixture was stirred at 80 °C for 24 h. After the post-treatment described above, 3.1 g (42%) of 1,2-bis[3-[2-(3-chloropropoxy)-4(or 5)-*t*-butylphenoxy]propoxy]-4(or 5)-*t*-butylbenzene (**11**) were obtained. Then a mixture of 2.8 g

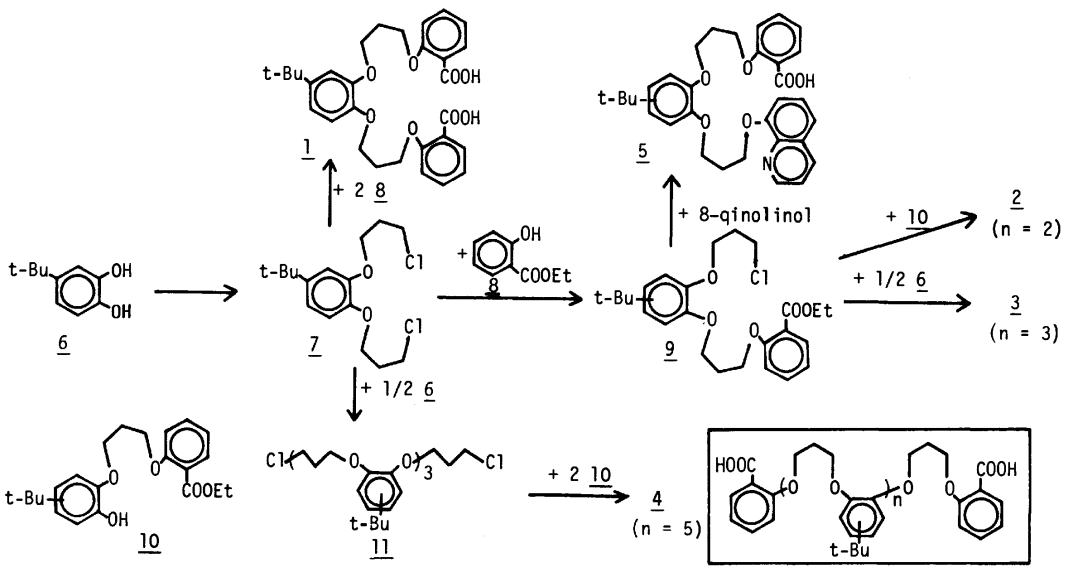

Scheme 1.

(7.5 mmol) of 2-[3-(*o*-ethoxycarbonylphenoxy)propoxy]-4-(or 5)-*t*-butylphenol (**10**) and potassium *t*-butoxide (0.85 g, 7.5 mmol) was stirred in 50 ml of DMF until it became homogeneous. To the solution we then added 1.8 g (2.5 mmol) of **11** and a small amount of KI, after which the mixture was stirred at 80 °C for 48 h. After the same post-treatment, 1.2 g (34%) of the ethyl ester of **4** were obtained. The hydrolysis of the ethyl ester as described above gave **4** (0.9 g, 78%) as a pale yellow, glassy solid: IR (KBr) 3300 and 2550 (COOH), 1740 and 1700 (C=O), 1605 and 1580 (aromatic C=C), 1050 cm^{-1} (C-O); ^1H NMR ($CDCl_3$) δ=1.30 (45H, s, $C(CH_3)_3$), 2.0—2.6 (12H, m, $OCH_2\underline{C}H_2\underline{C}H_2O$), 4.05—4.7 (24H, m, $OC\underline{H}_2CH_2C\underline{H}_2O$), 6.9—7.8 (18H, m, aromatic), 8.25—8.5 (2H, m, aromatic); UV ($CHCl_3$) λ_{max}=282 nm, ε=17000. Found: C, 72.69; H, 8.26%. Calcd for $C_{82}H_{106}O_{16}$ (MW 1347.73): C, 73.08; H, 7.93%.

General Procedure of Cation Transport. Reagents: Chloroform (extra-pure grade) was used without further purification. Each aqueous solution which was used in either the source or receiving phase was prepared by the dilution of one normal alkali hydroxide and/or one normal acid.

Procedure: A U-type or H-type glass tube as previously reported was used for measuring the transport of alkali metal ions.[13] In the case of the use of chloroform as the membrane solvent, a U-type glass tube was used. First, 30 ml of chloroform containing the carrier (0.03—0.15 mmol) was poured into the tube. Then, 15 ml of a solution of 0.1 M† LiOH+0.1 M NaOH+0.1 M KOH+0.1 M H_2SO_4 and 15 ml of a solution of 0.05 M H_2SO_4 were simultaneously poured into the source and receiving phases respectively. The tube was then placed in a water bath whose temperature was kept at 25±0.2 °C. Each phase was agitated at 200 min^{-1} mechanically with a pair of glass stirrers. On the other hand, in the case of the use of toluene, an H-type glass tube was used. In this case, first the aqueous solution containing metal hydroxides described above and an acidic solution (0.05 M H_2SO_4) were poured into the source and receiving phases respectively. Subsequently, a 30-ml portion of chloroform containing the carrier was poured into the tube.

The transport of cations was initiated by the addition of the solutions and by then stirring each phase. At each time point, 50 μl of the solution was withdrawn from each aqueous phase and the concentration of each cation was adjusted by using a measuring flask and determined by means of a Shimadzu AA-646 atomic absorption spectrometer.

The transport of cations in the blank systems was negligible. The detailed conditions are shown in the table.

Extraction of Cations. Polyether (0.05 mmol) was added to 5 ml of a 0.1 M LiOH aqueous solution in a 30-ml Erlenmeyer flask. The mixture was stirred overnight at room temperature. Then, 10 ml of chloroform was added to it. After the mixture had been vigorously stirred for 6 h, the amounts of the lithium salt of the polyethers in the aqueous solution were measured by means of the UV spectrum.

Results and Discussion

Cation Transport through Liquid Membranes. Cation transport through liquid membranes was carried out by using the **2**—**4** carriers, and also for the sake of comparison, **1** and **5** which were previously reported. Figure 2 shows the plots of the amounts of cation transported versus the running time in the case of carrier **4**, which has five repeating units of the 2-propoxy-4(or 5)-*t*-butylphenoxy group. Apparently, among the three alkali metal ions, the lithium ion can be transported with the most appreciable selectivity in the competitive transport. The cation transport by this carrier ceased within 1 day under these conditions because of the pH-decrease in the source phase. The results for cation transport by **1**—**5** are summarized in Table 1. Carrier **1**, which has the shortest chain structure, with two carboxyphenyl terminal groups, transported hardly any alkali metal ions although **1** can selectively transport either Ca^{2+} or Mg^{2+}, depending on the transport conditions[24] It should be noted that the longer the polyether chain, the better the ability of transport for monovalent cations, especially the lithium ion, by carriers which have two

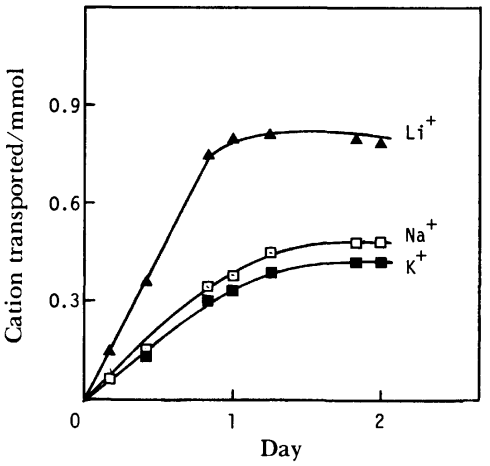

Fig. 2. Plots of amounts of cation transported by carrier **4** vs. the running time.

Table 1. Cation Transport through Liquid Membranes

Carrier	Transport rate/μmol h^{-1}			Selectivity	
	Li	Na	K	Li/Na	Li/K
1	0.1	<0.1	0	—	—
2	11.3	3.4	2.6	3.3	4.3
3	35.6	18.7	16.9	1.9	2.1
4	36.6	15.0	13.1	2.4	2.8
5	18.8	6.3	3.4	3.0	5.5

Reproducibility: ±10% or better.
Initial transport conditions (25 °C):

Source phase	Chloroform membrane	Receiving phase
0.1 M LiOH	Carrier	0.05 M H_2SO_4
0.1 M NaOH	1.5×10^{-4} mol	15 ml
0.1 M KOH	$CHCl_3$ 30 ml	
0.1 M H_2SO_4		
15 ml		

† 1 M=1 mol dm^{-3}.

carboxyphenyl terminal groups. Carrier **5**, which can selectively transport the lithium ion, as has previously been reported,[13] exhibits the selectivity ratios of Li/Na=3.0 and Li/K=5.5 under these transport conditions. Carrier **2**, with a relatively short chain, has a small cation-transport rate compared with carrier **5**, which has one carboxyl group, whereas carriers **3** and **4**, which have longer polyether chains, show a more than 2-fold enhancement in the transport of monovalent cations over **5**. However, the lithium-ion selectivity has a tendency to be reduced as the polyether chain lengthens. The lithium-ion transport rate by **3** and **4** is nearly two times larger than that by **5**. It is presumed that the two carboxyl groups on **3** and **4** act effectively in cation transport. That is, it is probable that one carrier has the ability to carry two cations at the same time in the case of carriers **3** and **4**. The relatively long polyether chain in these carriers, which can form a looser conformation for the uptake of cations, may be responsible for the increase in the ability of sodium- and potassium-ions transport.

In Table 2, the influence of the carrier concentration and the liquid-membrane solvent on the cation transport are summarized. The greater the concentration of **4** in chloroform, the larger both the transport rate and the amounts of cations transported after 2 days. When toluene was used as the liquid-membrane solvent in the H-type glass tube, the transport rates of cations by **4** are relatively small compared with those in the same concentration of **4** in chloroform (see Runs 2 and 3 in Table 2). However, it should be noted that appreciable cation transport by **4** through toluene (Run 3) can occur, whereas **5** in toluene transports scarcely no cations. This means that carriers with long polyether chains, such as **4**, can selectively transport lithium ion even in the more nonpolar solvent, toluene.

Thus, it is noteworthy that compounds **3** and **4**, with relatively long polyether chains can exhibit the selective transport of the lithium ion, which has the smallest naked ion radius among alkali metal ions. We have proposed the hypothesis that carrier **5** forms a pseudocyclic conformation to pass through an organic solvent, and that then the ion (i.e., the lithium ion), which can be well incorporated into the pseudocavity[13], can be selectively transported. Can compounds **3** and **4**, with long polyether chains, form such a conformation? The length between the two carboxyl groups of **1** is too short to take the conformation incorporating the lithium ion. In this case, the electrostatic repulsion between the two terminal carboxylato anions occurs inevitable when **1** forms a complex with two lithium ions. In the case of **2**, with a polyether chain of an intermediate length, it is also difficult for the carrier to wrap two lithium ions at the same time. Nevertheless, it is possible for one cation to be incorporated by **2**, though the salt of **2** with the lithium ion might not have enough solubility in organic solvents. Therefore, the transport ability of **2** is considered to decrease compared with that of **5**. On the contrary, carriers **3** and **4** are expected to have chains long enough to be able to wrap two lithium ions inside the pseudocavity formed. Recently, Nakahama et al. have also reported that a synthetic carboxylic ionophore with eight ether oxygens and five aromatic rings can complex with the potassium ion, and that the resulting complex has a coiled conformation, with coordination of the ether oxygen atoms to the potassium ion. This was presumed by means of the NMR spectrum.[25]

From these results, it can be inferred that the lithium complex of carriers **3** and **4** becomes more lipophilic than that of **1** and **2**. The lithium-ion complexes of **3** and **4** can be expected to dissolve more easily in an organic solvent than in water because of their lipophilicity. Therefore, their ability of cation extraction was investigated.

Cation Extraction. All carriers except **4** (0.05 mmol) are completely soluble in 5 ml of an aqueous solution containing 0.1 M LiOH after it has been stirred overnight at room temperature. Carrier **4**, with sufficiently hydrophobic groups, is insoluble in such a solution, while carrier **3** becomes foamy on the surface of an aqueous solution; that is, **3** seems to have surface activity. Then, chloroform (10 ml) was added to this alkaline solution or mixture containing the carrier, and the mixture was stirred. After that, the amounts of lithium salt of carriers remaining in the aqueous solution were determined by means of the UV spectrum. It was confirmed that one polyether formed

Table 2. Effects of Carrier Concentration and Membrane Solvent on the Cation Transport

Run	Concn of carrier	(mM)	Membrane solvent	Transport rate/μmol h^{-1} Li	Na	K
1	**4**	1.0	$CHCl_3$	5.5	1.7	1.3
2	**4**	2.5	$CHCl_3$	13.1	4.4	3.0
3	**4**	2.5	Toluene	9.7	4.4	3.4
4	**4**	5.0	$CHCl_3$	36.6	15	13.1
5	**5**	5.0	Toluene	0	0	0

Initial transport conditions: see Table 1.
Reproducibility: ±10% or better.

Table 3. Partition of Li^+ Salt of Polyethers between Aqueous and Chloroform Phases

Polyether	**1**	**2**	**3**	**4**	**5**
In aqueous phases/%	100	51	8	≈3	≈1

Initial conditions
Aqueous phase: 5 ml of 0.1 M LiOH solution.
$CHCl_3$ phase: 10 ml of $CHCl_3$ containing 0.5×10^{-4} mol of carrier.

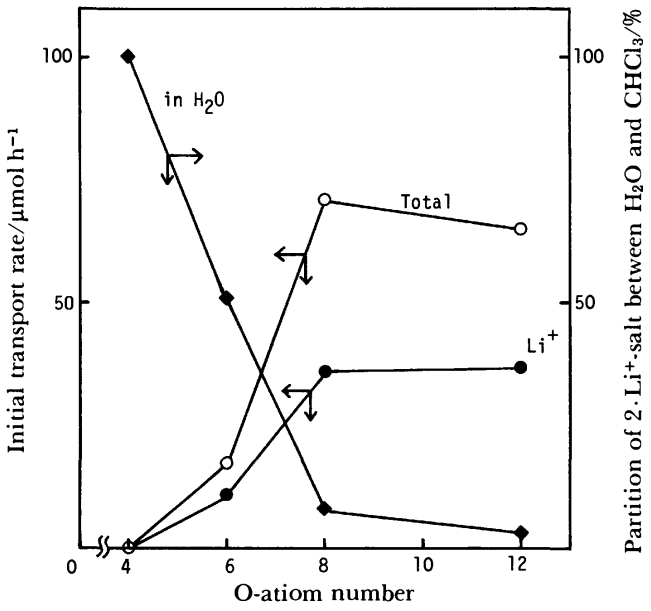

Fig. 3. Plots of initial transport rate and partition ratio of lithium salt of carriers vs. the number of ether oxygen atom of each carrier; O-atom number=4: **1**, 6: **2**, 8: **3**, 12: **4**.

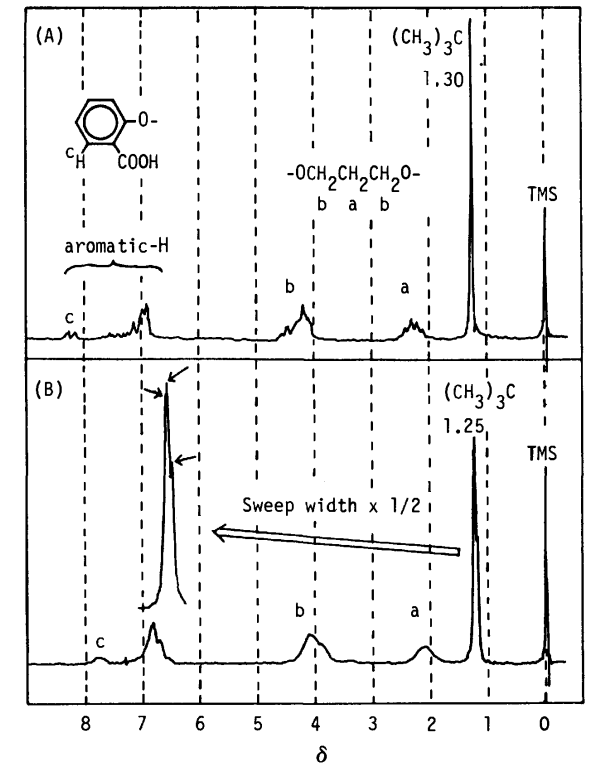

Fig. 4. Proton NMR spectrum of **3** and Li+ salt of **3** in $CDCl_3$; (A): **3**, (B): Li+ salt of **3**.

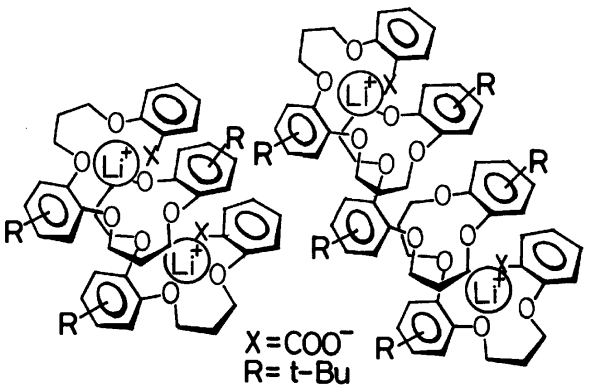

Fig. 5. Posturated strucutre of Li+ salts of polyethers **3** and **4** in chloroform liquid membrane.

salts with two lithium ions under these conditions. These results, shown in Table 3, are in good agreement with favorably those of the cation transport. Two equimolar lithium salts of **1** are not at all removed from the aqueous to the chloroform phase. The lithium salt of **2** has small solubility in chloroform. On the contrary, carriers **3** and **4** can extract two equimolar lithium ions almost quantitatively from aqueous to chloroform phase. Carrier **5**, with one carboxyl group, can also extract the lithium ion completely to the chloroform phase. These results reflect the cation-transport rate and the amounts of cation transported, as is shown in Table 1.

Figure 3 depicts the plots of the initial lithium ion-transport rate and the partition ratio of lithium salt of carriers between chloroform and aqueous solutions versus the number of ether oxygen atoms of each carrier. Apparently carriers **3** and **4** are superior to carriers **1** and **2** in both the distribution to chloroform and in the ability of lithium ion transport through liquid membranes.

Conformations of Cation Salts of Carriers in Chloroform. As has been indicated for the cation transport and cation extraction, **3** and **4** exhibited an appreciable selectivity toward the lithium ion, although **3** and **4** have rather long polyether chains, containing 8 and 12 ether oxygens respectively. Furthermore, carriers **3** and **4** can transport about twice as many cations as the polyether monocarboxylic acid **5** and can capture two equivalent lithium ions at the same time by means of the two carboxyl terminal groups.

Figure 4 shows the signal for the methyl protons on three *t*-butyl groups in **3** and its lithium salt. One sharp singlet for the methyl protons in free **3** becomes appreciably broad, when free **3** becomes its lithium salt. It can be inferred that the splitting of the proton signal for *t*-butyl groups is attributable to the proton-nonequivalency of each *t*-butyl group when **3** forms a complex with the lithium ion in chloroform. Such a change in the NMR spectrum was also observed in the case of carrier **4**. Additionally, a study of the NMR spectra confirms that the lithium salts of **3** and **4** do not contain water.

From these results, we would like to propose that **3** and **4** take the conformation shown in Fig. 5, where

two lithium ions become incorporated into the pseudocavity formed and can selectively transport lithium ions through liquid membranes. When the carriers take such a conformation, the protons for the *t*-butyl groups situated adjacent to the carboxyl terminal groups and those in the middle position seem to be at least nonequivalent. Therefore, the lithium salts can dissolve in a hydrophobic solvent and transport lithium ions selectively. An inspection of the CPK models suggests the formation of a small pseudocavity in which the lithium ion best fits. However, in carrier **1**, with the shortest polyether chain, electrostatic repulsion between lithium salts of two terminal carboxylato groups results in the deformation of the pseudocavity. Therefore, water molecules around the lithium ion presumably cannot be removed, and the salt of **1** does not dissolve in organic liquid membranes. Because the lithium salt of carrier **2**, with a medium chain length, is soluble in the organic phase, at least to some extent, it is considered that **2** can transport cations, although the ability of ion-transport is smaller even than that of monocarboxylic acid **5**.

Conclusion

Thus, we could show that compounds with rather long polyether chains can recognize the lithium ion as a guest, accompanied by a drastic conformational change. Cyclic polyether (crown ethers), cryptands, and spherands,[26] which have a preorganized cavity, can selectively incorporate ions which fit well inside. On the contrary, the noncyclic compounds with long polyether chains used in this study can wrap around cations by changing their conformation, as is shown in Scheme 2. Such a conformational change accompanies a large energetic loss and causes a decrease in the complex stability and in the rate of cation uptake compared with those of preorganized compounds. Such a dynamic conformational change reminds us of the induced-fit theory in enzymatic reactions proposed by Koshland,[27] although an enzyme has a much larger molecular weight and can recognize a substrate much more precisely compared with the noncyclic polyethers reported here.

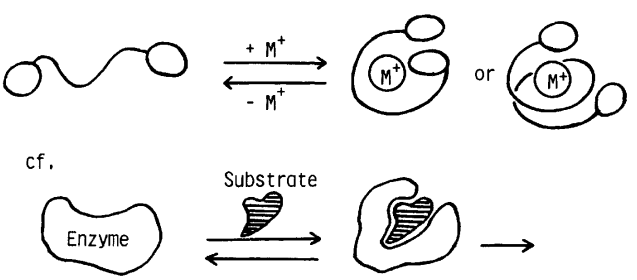

Scheme 2.

It should be noted that the selectivity for cations can change when the chain structures on the carriers change appropriately. In this study, the chain structures containing oxytrimethylene groups can result in the lithium-ion selectivity, whereas those containing oxyethylene groups can exhibit potassium- ion selectivity, as has been reported by Nakahama et al.[25] Thus, the importance of the chain structure in producing ion-selectivity should also be pointed out.

References

1) Part XVI: "Synthesis and Properties of Noncyclic Polyether Compounds." Part XV: K. Hiratani, K. Taguchi, H. Sugihara, and K. Iio, *J. Membr. Sci.*, in press.

2) C. J. Pedersen, *J. Am. Chem. Soc.*, **89**, 7017 (1967).

3) G. W. Gokel and S. H. Korzeniowski, "Macrocyclic Polyether Synthesis," Springer-Verlag, Berlin Heidelberg (1982).

4) Yu. A. Ovchinnikov, V. T. Ivanov, and A. M. Shkrob, "Membrane-active Complexones," B. B. A. Library, Vol. 12, Elsevier Scientific Publishing Co., Amsterdam (1974), Chap. 6.

5) K. Hiratani, *Maku (Membrane)*, **10**, 107 (1985).

6) D. J. Cram and K. N. Trueblood, "Host Guest Complex Chemistry I," ed by F. Vögtle, Springer-Verlag, Berlin (1981), p. 43.

7) F. Vögtle and E. Weber, *Angew. Chem., Int. Ed. Engl.*, **18**, 753 (1979); N. S. Poonia and A. V. Bajaj, *Chem. Rev.*, **79**, 389 (1979).

8) D. Ammann, W. E. Morf, P. Anker, P. C. Meier, E. Pretsch, and W. Simon, *Ion-selective Electrode Rev.*, **5**, 3 (1983).

9) N. Yamazaki, A. Hirano, and S. Nakahama, *J. Macromol. Sci. Chem.*, **A13**, 321 (1979).

10) K. Hiratani, S. Aiba, and T. Nakagawa, *Chem. Lett.*, **1980**, 477.

11) W. Wierenga, B. R. Evans, and J. A. Woltersom, *J. Am. Chem. Soc.*, **101**, 1334 (1979).

12) S. I. Kang, A. Czech, B. P. Czech, L. E. Stewart, and R. A. Bartsch, *Anal. Chem.*, **57**, 1713 (1985); W. Walkowiak, L. E. Stewart, H. K. Lee, B. P. Czech, and R. A. Bartsch, *ibid.*, **58**, 188 (1986).

13) K. Hiratani, *Chem. Lett.*, **1982**, 1021; K. Hiratani, K. Taguchi, H. Sugihara, and K. Iio, *Bull. Chem. Soc. Jpn.*, **57**, 1976 (1984).

14) K. Hiratani, *Bull. Chem. Soc. Jpn.*, **58**, 420 (1985).

15) N. N. L. Kirsch, R. J. J. Funck, E. Pretsch, and W. Simon, *Helv. Chim. Acta*, **60**, 2326 (1977).

16) A. Shanzer, D. Samuel, and R. Korenstein, *J. Am. Chem. Soc.*, **105**, 3815 (1983).

17) K. Kimura, H. Sakamoto, S. Kitazawa, and T. Shono, *J. Chem. Soc., Chem. Commun.*, **1985**, 669.

18) K. Kobori, T. Matsuoka, S. Takada, K. Kakiuchi, Y. Tobe, and Y. Odaira, *Chem. Lett.*, **1986**, 713.

19) R. A. Bartsch, B. P. Czech, S. I. Kang, L. E. Stewart, W. Walkowiak, W. A. Charewicz, G. S. Heo, and B. Son, *J. Am. Chem. Soc.*, **107**, 4997 (1985).

20) D. J. Cram, T. Kaneda, R. C. Helgeson, S. B. Brown, C. B. Knobler, E. Marverick, and K. N. Trueblood, *J. Am. Chem. Soc.*, **107**, 3645 (1985).

21) T. Kaneda, S. Umeda, H. Tanigawa, S. Misumi, Y. Kai, H. Mori, K. Miki, and N. Kasai, *J. Am. Chem. Soc.*, **107**, 4802 (1985).
22) J.-M. Lehn and J.-P. Sauvage, *J. Chem. Soc., Chem. Commun.*, **1971**, 440.
23) D. C. Tosteson, *Sci. Am.*, **244**, 164 (1981).
24) K. Hiratani, K. Taguchi, and H. Sugihara, *Chem. Lett.*, **1983**, 1657.
25) H. Kuboniwa, S. Nagami, K. Yamaguchi, A. Hirao, S. Nakahama, and N. Yamazaki, *J. Chem. Soc., Chem. Commun.*, **1985**, 1468.
26) D. J. Cram, *Angew. Chem., Int. Ed. Engl.*, **25**, 1039 (1986).
27) D. E. Koshland, Jr., and K. E. Neet, *Ann. Rev. Biochem.*, **37**, 359 (1960).

 © 1987 The Chemical Society of Japan Bull. Chem. Soc. Jpn., 60, 3835—3842 (1987)

The Trapping and Release of Injected Hydrogen Isotopes in Vitreous Silica

Naoto AZUMA, Tetsuo MIYAZAKI,* Kenji FUEKI, Katsutoshi FURUKAWA,† Yasuyuki ARATONO,† Shin-ichi OHNO,† Masakatsu SAEKI,† and Enzo TACHIKAWA†

Department of Synthetic Chemistry, Faculty of Engineering, Nagoya University, Chikusa-ku, Nagoya 464

†Department of Chemistry, Japan Atomic Energy Research Institute, Tokai-mura, Ibaraki 319-11

(Received March 31, 1987)

The behavior in vitreous silica of hydrogen isotopes, which had been introduced by 80-keV D^+-ion implantation, thermal D_2 doping, or recoil tritium implantation (2.7 MeV), was studied by means of FT-IR spectroscopy, ESR spectroscopy, and radioassay with a liquid scintillation counter. The hydrogen isotopes are trapped by forming hydroxyl bonds (OD, OT). In the D^+-ion implantation, OD bonds are formed mainly by the rupture of the ≡Si-O-Si≡ bonds. In the thermal D_2 doping, however, OD bonds are formed mainly by the isotope-exchange reaction between the preexisting OH bonds and D_2 molecules. When vitreous silica implanted by recoil tritium is heated to about 1150 K, HTO and HT are released. The OD bonds produced by D^+ implantation decrease upon annealing at 1150 K. The OD bond-rupture is controlled by the diffusion of hydrogen isotopes trapped as OD(OT) bonds to the surface of vitreous silica. The mechanism of the diffusion of the hydrogen isotopes through vitreous silica was explained in terms of a repetition of the chemical reaction of ≡SiOD(OT)+≡SiOSi≡ ⟶ ≡SiOSi≡+≡SiOD(OT). The diffusion coefficient (D_T(HTO)) of tritium according to the above mechanism was obtained as:

$$D_T(\mathrm{HTO}) = 2.3 \times 10^{-4} \exp[-1.7 \times 10^2(\mathrm{kJ\ mol^{-1}})/RT]\ \mathrm{cm^2\ s^{-1}}$$

Nonmetallic materials are used in fusion reactors as tritium diffusion barriers, first-wall coatings, or diagnostic window materials for the reactors. Hydrogen generally diffuses much more slowly in oxides than in metals. The first-wall materials are irradiated with high-energy tritium, neutrons, and high levels of γ-rays. The high energy tritium, injected into the material, is trapped there or diffuses through the material. In order to prevent tritium fuel from permeating through the fusion material, it is very important to elucidate the interactions between the high-energy hydrogen and the material.

Previous studies of the interaction, however, have been concerned mainly with the physical interaction, such as the sputtering of the solid surface, the production of radiation damage, and a depth-profile of the injected hydrogen. Since hydrogen isotopes are reactive species, the chemical interactions between injected hydrogen and the materials also play a significant role. The chemical interactions consist of several microscopic processes, such as hydrogen trapping, detrapping, diffusion, and desorption. The role of chemical reactions in these processes is shown in Fig. 1. Though physical interactions are not neglected in these processes, they are omitted from Fig. 1. When hydrogen isotopes with a high energy are injected into a material, they are trapped by the formation of chemical bonds. Since the first-wall material is held at a high temperature or under the high radiation field, the hydrogen isotopes are detrapped by the rupture of the chemical bonds and diffuse through the material to its surface, where the diffusion involves a chemical reaction in some cases. The hydrogen isotopes are released from the surface by surface reactions. Since the chemical interactions have been studied in only a few cases, the chemical

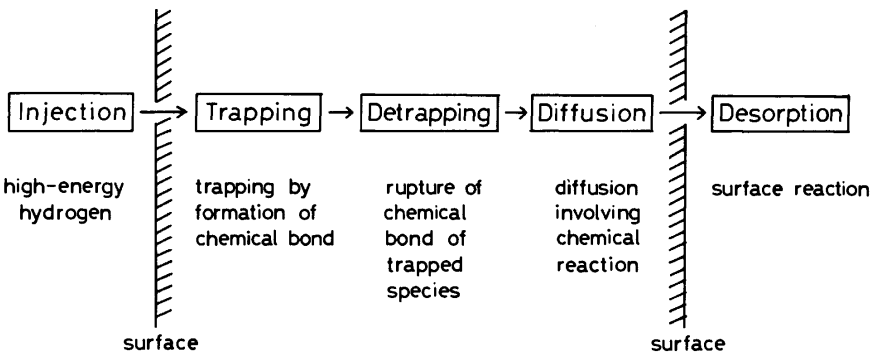

Fig. 1. The role of chemical interactions between high-energy hydrogen and materials.

interactions between hydrogen isotopes and vitreous silica (silica) will be reported here.

Silica, one of the most popular oxides, has the following characteristic properties: a relatively simple structure, a high softening point, transparent properties, a low cross-section for neutron-capture reactions, and a high activation energy for tritium diffusion.[1] In addition, the impurity content of silica can be controlled. Since the presence of OH bonds may affect the chemical interactions of hydrogen isotopes, the concentration of the OH bonds in silica was varied from 5 to 4000 ppm in this study. Several studies of silica have been reported previously. The compaction effects on silica by irradiation were reviewed by Primak.[2] The diffusion of hydrogen isotopes in silica have also been studied,[3,4] as has the hydrogen-ion implantation in SiO_2.[5,6] The presence of the radiation damage produced by the ion-implantation protects the radiation-induced detrapping of D atoms.[6] Moreover, the kinetic behavior of H and D atoms in silica has been investigated by means of ESR spectroscopy.[7]

In this study, hydrogen is introduced into silica by 80-keV D^+-ion implantation, 2.7 MeV-recoil tritium implantation, and D_2 gas-doping at high temperatures. The interaction between the hydrogen isotopes and silica was studied here by means of infrared Fourier transform spectroscopy (FT-IR), electron spin resonance spectroscopy (ESR), and tritium analysis using a liquid scintillation counter. Since it is difficult to elucidate the microscopic processes in Fig. 1 by using only one method, we have here studied these processes by a combination of the several methods mentioned above. The elucidation of the following problems is the main purpose of this study: (1) It was reported previously[8,9] that D_2 gas is trapped thermally in silica to form OD bonds by an isotope-exchange reaction between preexisting OH bonds (as inherent impurities) and D_2. Is the efficiency of the trapping of deuterium or tritium, injected with a high energy, affected by the preexisting OH bonds? If deuterium with a high energy is trapped to form OD bonds,[6] what is the mechanism of the formation of the OD bonds? (2) The deuterium and tritium trapped as OD (OT) bonds are released by thermal heating above 700 K. What is the mechanism of the release of hydrogen isotopes from the trapping sites? (3) How much is the value of the diffusion coefficient of tritium in silica?

Experimental

The four types of vitreous silica used here are Spectrosil, obtained from the Thermal American Fused Quartz Co.; Fused silica glass, obtained from the Asahi Glass Co., and Silica T1030 and Silica T2230, obtained from the Toshiba Ceramic Co. The concentrations of preexisting hydroxyl bonds in the four kinds of silica range from 5 to 4000 ppm.[10] The OH-bond concentration of the sample was measured by means of an infrared Fourier transform spectrometer (FT-IR)[11] at room temperature. It was estimated from the O-H stretching band at 3670 cm^{-1} [8,9] taking the extinction coefficient at the wavenumber as 77.5 l/mol cm.[12] The amounts of the OH bond and metal impurities[13] contained in the samples are summarized in Table 1. The samples which contain the OH bonds at 5, 610, 960, and 4000 ppm will be denoted hereafter as silica A, B, C, and D respectively. The samples for deuterium implantation were cut in the form of plates measuring 3.3×9×0.3 mm, while those for tritium implantation were cut in the form of plates measuring 5×10×1 mm.

The deuterium implantation was performed with a low-energy ion accelerator which has previously been described in detail.[14] Deuterium ions accelerated to 80-keV were injected into the target at an ion-beam flux of 2.5×10^{14} ions $s^{-1}cm^{-2}$. The compositions of the deuterium ions were D^+(78%), D_2^+(13%), and D_3^+(9%). The total deuteron fluence was 2.7×10^{18} D/sample. The sample chamber was evacuated to 10^{-5} Pa during irradiation.

The tritium implantation was performed by the use of recoil tritium atoms from the reaction of ^6Li (n, α) T, where ^6Li-enriched lithium chloride was used as the tritium source. It was prepared from lithium metal obtained from Oak Ridge National Laboratory; the ^6Li content was 95%. An aliquot of lithium chloride solution was dried on a 7×12×1 mm polyethylene plate. Then it was wrapped with a mylar sheet. The wrapped plate was tightly attached to the sample. The assembly was put into a quartz ampoule which was sealed in vacuo. The ampoules were irradiated by neutrons in the JRR-4 reactor in JAERI for 10 min at the ambient temperature. The thermal neutron flux was 8×10^{13} n_{th} cm^{-2} s^{-1} at the irradiation port. The amount of tritium activity doped in the sample was about 37 kBq (1 μCi).

Thermal-deuterium doping was performed by the

Table 1. Impurity Content (ppm) of Vitreous Silica

Impurity	Sample (vitreous silica)[a]			
	Silica A (T2230)	Silica B (Silica glass)	Silica C T1030	Silica D (Spectrosil)
B	nd	nd	nd	nd
Mg	11	13	8.7	10
Al	nd	27	nd	nd
Ti	2.3	0.9	2.7	nd
Cr	1.6	nd	1.7	nd
Mn	0.2	0.4	0.1	nd
Fe	3.5	4.6	3.2	2.1
Ni	nd	nd	nd	nd
Cu	nd	nd	nd	nd
Zn	4.7	9.7	6.1	2.4
Zr	nd	6.1	0.7	nd
Sn	nd	nd	nd	nd
Na	15	9.2	nd	nd
K	nd	7.4	nd	nd
Ca	9.4	6.7	3.7	5.9
Ba	0.2	nd	nd	nd
O-H	5	610	960	4000

a) nd: undetected.

following method. The sample was saturated with D_2 gas of 7.5×10^5 Pa for 280 h at 723 K or for 1—5 h at 923—1173 K.

After deuterium-implantation or thermal-D_2 doping, the infrared absorption spectra of the sample were measured at room temperature with an infrared Fourier transform spectrometer.[11] The ESR spectra of the sample were also measured at 77 K with an ESR spectrometer.[15] In the study of the thermal desorption of trapped deuterium, the samples were held for 6 h at 1173 K in vacuo.

After tritium implantation, the sample was heated at a constant rate (5 K min^{-1}) from room temperature to 1373 K and was then held for 180 s at the maximum temperature. The HTO and HT released during the annealing were measured.[16] Then the release rate of the HTO and HT components were calculated as a function of the heating temperature. The device for the isochronal annealing of the tritium-implanted sample has previously been described in detail.[17] The tritium component, which remained in the sample even after the thermal treatment, was measured by means of a liquid scintillation counter after the sample has been chemically etched by using a hydrofluoric acid solution.

In order to measure the initial distribution of tritium contained in a tritium-implanted specimen, the samples were gradually etched from the surface by 2% hydrofluoric acid to release the trapped tritium. The distribution of tritium in the sample was determined by measuring both the released tritium and the thickness of the sample. In this measurement, the amount of tritium was radioassayed by the use of a liquid scintillation counter.

Results

When hydrogen isotope was injected into silica, the spatial distribution and the range of the trapped hydrogen depend on both the injection energy and the injection method. Figure 2 shows the results of chemical-etching experiments on tritium-implanted silica. The experimentally measured range of recoil tritium with 2.7 MeV is about 39 μm, which coincides with the calculated value (39 μm) for recoil tritium in SiO_2.[18] The distribution of the recoil-injected tritium into the silica shows a linearly decreasing distribution with the distance from the surface.

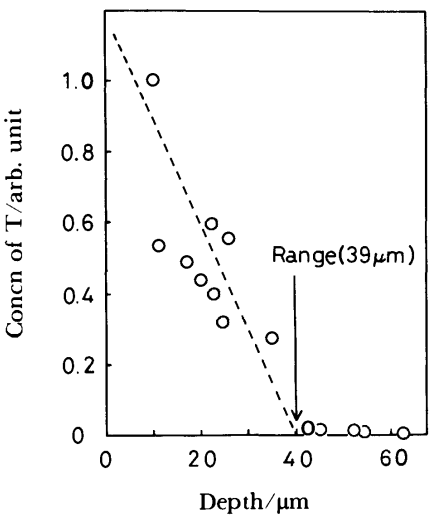

Fig. 2. Depth profile of tritium-implanted silica by ^6Li (n, α)T (2.7 MeV) reaction.

In the 80-keV D^+-ion implantation, we did not measure the distribution of the trapped deuterium. The trapped depth of the deuterium was calculated, using the TRIM code,[19] as about 0.5 μm from the surface. According to the study of 20-keV D^+ implantation in vitreous silica by Arnold et al.,[5] the deuterium is trapped between 0.2 and 0.5 μm from the surface.

In the thermal-D_2 doping, the distribution of the trapped deuterium can be expressed by a model of a tarnishing reaction,[20,21] in which the range (d) of trapped deuterium from the surface in the partially deuterated silica is estimated by the use of Eq. 1:

$$d = L \cdot C/(2C_f) \quad (1)$$

where L, C, and C_f are the thickness of silica, the concentration of OD bonds of partially deuterated silica, and the OD concentration of completely deuterated silica respectively. The ranges of the trapped deuterium in this study were varied from 7 to 125 μm from the surface by controlling the amount of deuteration at 923 K, where a model of the tarnishing reaction can be applied.[21]

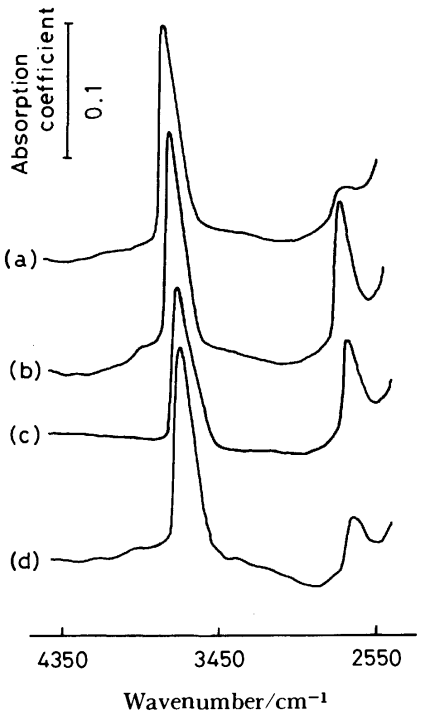

Fig. 3. Infrared absorption spectra of fused silica B (OH 610 ppm). (a) Before deuterium treatment, (b) after 80-keV D^+ ion implantation, (c) after thermal D_2 doping in which silica was stored in 7.5×10^5 Pa gas at 723 K, and (d) after annealing the sample of Fig. 3(b) at 1173 K for 6 h.

Figure 3(a) shows the infrared absorption (IR) spectrum of silica B before deuterium treatment. The absorption band at 3670 cm^{-1} in the figure is the O-H stretching band, which agrees with the previously reported values (3690,[8] 3640[9] cm^{-1}) of the O-H stretching band. When the silica is implanted with 80-keV D^+ ions or doped by D_2 gas at a high temperature, OD bonds are formed.[6] In a previous study,[6] however, the amount of deuteration was very small. In order to examine the effect of deuteration on the preexisting OH bonds, the OD bonds were produced in very high yields in this study. Figure 3(b) shows an IR spectrum of silica B after 80-keV D^+-ion implantation. The appearance at 2670 cm^{-1} of the absorption band, which is identified as the O-D stretching band in silica on the basis of previous studies,[6,8,9] indicates the formation of OD bonds in the sample by the ion-implantation, while the amounts of the preexisting OH bonds are not changed by the OD-bond formation. Figure 3(c) shows an IR spectrum of silica B after thermal-D_2 doping at 723 K for 280 h. The absorption band at 2670 cm^{-1} indicates the formation of OD bonds by such treatment in silica B, where the amounts of the OH bonds decrease. The amount of OD bonds in the silica was estimated from the intensity of the O-D stretching band at 2670 cm^{-1}, where the extinction coefficient (ε_{OD}) of the OD band was taken as $0.53 \times \varepsilon_{OH}$.[22] Figure 3(d) shows the spectrum of the sample of Fig. 3(b) after annealing at 1173 K for 6 h. The amounts of OD bonds decrease drastically upon the thermal annealing.

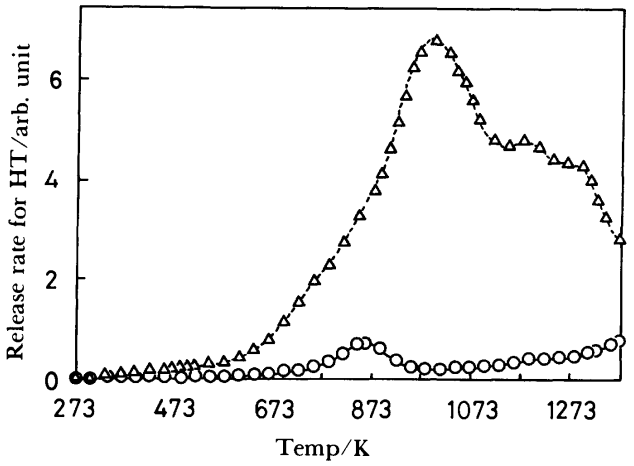

Fig. 4. Release spectra of HT in annealing at the same heating rate (5 K min^{-1}) from T-irradiated silica A (OH 5 ppm: Δ----Δ), and from T-irradiated silica D (OH 4000 ppm: O—O).

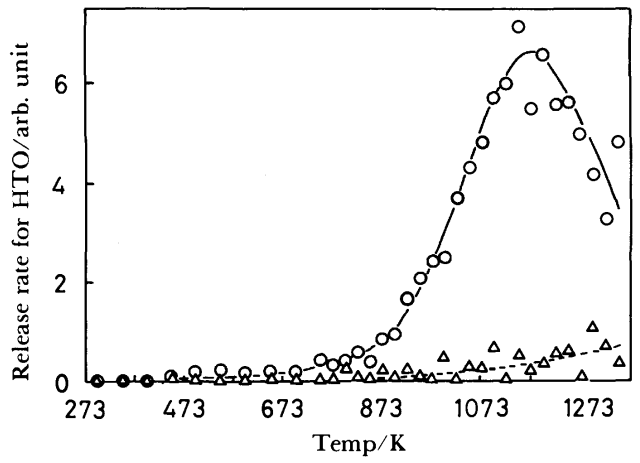

Fig. 5. Release spectra of HTO in annealing at the same heating rate (5 K min^{-1}) from T-irradiated silica A (OH 5 ppm: Δ----Δ), and from T-irradiated silica D (OH 4000 ppm: O—O).

When the recoil tritium-implanted silica is heated at a high temperature, the trapped tritium is released from the silica as HT and HTO. Figure 4 shows the releasing behavior of HT from tritium-implanted silica A and D at a heating rate of 5 K min^{-1}. The evolution of HT begins around 700 K and reaches a peak at 970 K.

Figure 5 shows the releasing behavior of HTO from tritium-implanted silica A and D at the same heating rate as that in Fig. 4. HTO is released gradually around 900 K and reaches a peak around 1150 K. It can be seen from the results in Figs. 4 and 5 that tritium from silica A, which contains OH bonds at 5 ppm, is released almost entirely as HT, whereas tritium from silica D, which contains 4000-ppm OH bonds, is released as HTO.

Discussion

Trapping of Hydrogen Isotopes in 80-keV D^+-Ion Implantation, Thermal D_2 Doping, and Recoil T Implantation.

1. Trapping Efficiency and Preexisting Hydroxyl Bonds. When deuterium is injected into silica by 80-keV D^+ implantation or thermal D_2 doping deuterium is trapped by the formation of OD bonds (cf. Figs. 3(b) and 3(c)). The hydroxyl-bond formation by ion implantation and hydrogen gas-doping was reported previously.[5,6] The OD-bond formation may be the main trapping process in the D^+-ion implantation for the following reasons. First, since trapped D atoms were not observed in the D^+ ion-implanted silica by ESR spectroscopy, deuterium must be trapped in silica by the formation of a chemical bond. Second, the SiD-bond formation is another possible process of trapping. The IR absorption spectrum of SiD bonds is expected to appear around 1600 cm^{-1},[23] but the spectrum of the SiD bonds could not be observed in D^+-implanted silica (silica B), not even by the subtraction of the spectrum of silica before the implantation from that after the implantation. Third, the total amount of OD

bonds in D^+-implanted silica is about 2.4×10^{21} bonds cm^{-3}, which is approximately the same as the saturation value (2.1×10^{21} D atoms cm^{-3})[5] of the total trapped deuterium in D^+-implanted silica. Fourth, when T-implanted silica is heated, HT is released at a high temperature such as 970 K. If HT molecules are trapped physically in the implanted silica, HT is released, probably at a much lower temperature. Thus, tritium is not trapped as hydrogen molecules after T-implantation. HT is produced by some chemical reaction upon thermal annealing.

The effect of preexisting OH bonds on the deuterium-trapping has been studied here by the use of silica containing the OH bonds at different concentrations. The relative yields of OD bonds produced by D^+ implantation and D_2 doping are summarized in Table 2, where the yields in silica A is taken as 1.0. A radiation-damage center produced by 80-keV D^+-implantation can be observed clearly by means of ESR spectroscopy.[6] The relative yields of the radiation-damage center, also shown in Table 2, do not depend on the OH-bond concentration. In the recoil tritium-implantation, the total amount of tritium trapped in silica can be measured by the use of a liquid scintillation counter after the irradiated sample has been etched. The relative yields of the total trapped tritium are also shown in Table 2. The total amounts of trapped tritium are almost independent of the concentration of preexisting OH bonds. The yields of the OD bonds produced by D^+-implantation also do not depend on the concentration of preexisting OH bonds. In the thermal D_2-gas doping, however, the yields of OD bonds increase with an increase in the preexisting OH bonds, though the OD-bond yields are not linearly proportional to the concentration of the OH bonds.

2. Mechanism of Trapping Reaction. The production of OD bonds is an important process for the trapping of deuterium in the D^+-ion implantation or the D_2-gas doping. The injected D^+ ions are neutralized in the silica and change into D atoms. Thus, the production mechanisms of the OD bonds in the D^+-implantation and the D_2-doping may be given as follows:

$$\equiv\text{Si-O-Si}\equiv + D(D_2) \longrightarrow \equiv\text{Si-OD} + P \quad (2)$$

$$\equiv\text{Si-OH} + D(D_2) \longrightarrow \equiv\text{Si-OD} + Q \quad (3)$$

where P and Q are some other products in these reactions. Reaction 2 represents the OD-bond formation by the insertion reaction accompanying the scission of the $\equiv$Si-O-Si$\equiv$ bonds. Reaction 3 represents the substitutional reaction between H in preexisting hydroxyl bonds and $D(D_2)$, where the formation of OD bonds accompanies the decrease in the amount of the OH bonds.[24]

Figures 3(a) and 3(b) show that the amounts of preexisting OH bonds are not affected by the formation of OD bonds in the D^+-implantation, but Figs. 3(a) and 3(c) show that those of the OH bonds decrease in the D_2-gas doping. In order to analyze the results in Figs. 3(a), (b), and (c) quantitatively, the relation between the increase in the OD bonds and the decrease in the OH bonds is shown in Table 3. The values of $-\Delta OH/\Delta OD$ in silica represent the fraction of Reaction 3 to the total OD-bond formation in the deuterium treatment. The formation of OD bonds in the D^+-implantation is not accompanied by a drastic decrease in the preexisting OH bonds. Therefore, in the ion-implantation, hydroxyl bonds are formed mainly by the insertion reaction (cf. Reaction 2). D^+ ions, implanted into silica, are neutralized in silica and so become hot D atoms. The hot atoms may react with $\equiv$Si-O-Si$\equiv$ bonds to form $\equiv$Si-OD bonds. A part of the hot D atoms are thermalized and may react with $\equiv$Si-O radicals, which are produced along the trajectory of hot D atoms by the radiolysis of the $\equiv$Si-O-Si$\equiv$ bond, to form $\equiv$Si-OD bonds. Both possibilities are represented by Reaction 2.

In the D_2-doping, however, about 60% of the OD-bond yields correspond to the decrement of the preexisting OH bonds. Thus, the OD bonds in the thermal doping are produced mainly by the substitu-

Table 2. Trapping of D (T) in Silica

Silica	Impurity		Method of injection[a]			
			80-keV D^+-implantation		Thermal D_2-doping	Recoil T-implantation
	OH ppm	Metal ppm	Yield of radiation damage	Yield of OD bond	Yield of OD bond	Total T yield
Silica A	5	23	1.0	1.0[b]	1.0	1.0[c]
Silica B	610	62	2.1	0.8	3.3	0.9
Silica C	960	23	1.5	0.9	2.5	1.1
Silica D	4000	15	1.2	1.1	5.6	1.4

a) Yields are expressed by relative values. The yield in silica A is taken as 1.0. b) The amount of OD bonds is 1.2×10^{-7} mol/sample. c) The amount of tritium is 1.1 μCi, that is, 3.8×10^{-11} mol/sample.

tional reaction (cf. Reaction 3). Since some metal ions may exist near OH bonds as impurities, D_2 gas may react with the OH bonds by some catalytic effect of the metal ions to form OD bonds.

Release of Trapped Hydrogen Isotopes.

1. Diffusion-Controlled Release of OD Bonds. As is shown clearly in Figs. 3(b) and (d), the amounts of OD bonds produced by the D^+-ion implantation decrease upon the thermal annealing at 1173 K for 6 h to become about 30% of the initial amounts of the OD bonds. The question of whether the process of the detrapping of deuterium from OD-bond sites is a reaction-controlled process or a diffusion-controlled one will be discussed here. In order to solve this problem, the distributions of OD bonds in silica were varied by partial D_2-doping. The silicas with OD bonds distributed at different depths from the surface were annealed at 1173 K for 6 h in vacuo. The efficiency of the decrease in OD bonds by the annealing are shown in Table 4, together with that for the OD bonds produced by D^+-ion implantation and that for the preexisting OH bonds.

If the dissociation reaction of the OD bond is a rate-determining process, the efficiency of the decrease in OD bonds should be independent of the depth of the OD-bond distribution. The results in Table 4, however, show clearly that the efficiency of the decrease depends on the depth of the OD-bond distribution. The efficiency increases with a decrease in the depth of the OD-bond distribution. The D, as OD bonds near the surface, can easily diffuse to the surface and decompose there to form some product, such as HDO. Therefore, it may be concluded that the process of the detrapping of deuterium from OD bond sites, followed by the formation of HDO, is not a reaction-controlled (bond-rupture) process, but a diffusion-controlled one.

2. HTO and HT Formation from Tritiated Silica. In order to detect thermally-released products from hydrogen-implanted silica, tritium analysis is the most convenient method because of its high sensitivity. When silica implanted by recoil tritium is annealed from room temperature to 1373 K, HTO and HT are released from the silica (cf. Figs. 4 and 5). Since HTO is released at a higher temperature (1150 K) than that for HT (970 K), HTO and HT must be produced by different mechanisms.

The amount of OD bonds, which are one of the main trapped species in D^+-implanted silica, decreases upon thermal annealing. Table 5 compares the release of trapped tritium in the recoil T-implanted silica with the decrease in the OD bonds in the D^+-implanted silica. Both the release of the trapped tritium and the decrease in the OD bonds take place efficiently upon heating at 1200—1300 K. If it is assumed that HTO is produced by the thermal decomposition of OT bonds, the HTO formation corresponds to the decrease in the OT bonds in the thermal annealing. Since the decrease in OD bonds is a diffusion-controlled process, the decrease in OT

Table 3. Ratio of Decrement of the OH Bond to the Increment of the OD Bond in 80 keV D^+-Implantation and Thermal D_2-Doping in Silica[a)]

Silica OH/ppm	$-\Delta OH/\Delta OD$	
	80 keV D^+-implantation	Thermal D_2-doping
610	0.1	0.58
960	0.2	0.75

a) $-\Delta OH$ represents the decrement of the amount of preexisting OH bonds on the D^+-implantation or the D_2-doping. ΔOH represents the increment of the amount of OD bonds on the same deuterium treatment.

Table 4. Efficiency of Decrease of the OD Bond and Depth of OD-Bond Distribution from the Surface[a)]

Method of injection	Hydroxyl group	Depth μm	Efficiency of decrease[d)]
D^+-implantation	OD	0.5[b)]	≈0.7
Thermal	OD	7[c)]	0.61
D_2-doping	OD	13[c)]	0.42
	OD	23[c)]	0.27
	OD	125[c)]	0.11
Inherent impurity	OH	125	0.13

a) Silica was heated at 1173 K for 6 h. Silica D was used here. b) Estimated theoretically.[19)] c) Estimated by a model of a tarnishing reaction.[21)] d) 1−[(amount of OD(OH) after heating)/(amount of OD(OH) before heating)].

Table 5. Release of Trapped Tritium from T-Implanted Silica and Decrease of OD Bonds from D^+-Implanted Silica on Thermal Annealing

Sample	D^+-implantation[a)]		Recoil T-implantation[b)]	
	Efficiency of decrease in OD bonds[c)]	Efficiency of release of trapped tritium[d)]	Composition of released tritium/%	
			HTO	HT
Silica A	0.72	0.89	4	96
Silica B	0.79	0.45	23	77
Silica C	0.55	0.34	41	59
Silica D	0.66	0.53	71	29

a) D^+-implanted silica is heated at 1173 K for 6 h. b) HTO and HT are produced when T-implanted silica is heated from room temperature to 1373 K. c) The efficiency is 1−[(amount of OD after heating)/(amount of OD before heating)]. d) The efficiency is (amount of released tritium)/(amount of total trapped tritium before heating).

bonds and the HTO formation may also be controlled by diffusion to the surface. Therefore, the diffusion coefficient of tritium trapped in silica can be estimated from the releasing behavior of HTO.

From the results of the measurement of the depth profile of tritium, implanted into silica by the recoil reaction of ^{6}Li(n,α)T(2.7 MeV) (cf. Fig. 2), the distribution of the recoil-injected tritium in silica is shown to be that of tritium, implanted from a tritium source of infinite size. In this depth profile, the solution of Fick's second law can be given by the following equation:[25,26]

$$F(t) = 4[D \cdot t/(\pi \cdot R^2)]^{1/2} \quad (4)$$

where $F(t)$ is the fractional release of HTO at an annealing time of t at a constant temperature, while R represents the recoil range of tritium (39 μm) in silica. The diffusion coefficients (D_T(HTO)) can be obtained from the slope of the plot of $t^{1/2}$ vs. $F(t)$ in the isothermal annealing of tritium-implanted silica; they are shown in Fig. 6 in relation to $10^3/T$. They are expressed by the following equation:

$$D_T(\mathrm{HTO}) = 2.3 \times 10^{-4} \exp[-1.7 \times 10^2 (\mathrm{kJ\ mol^{-1}})/RT]\ \mathrm{cm^2\ s^{-1}} \quad (5)$$

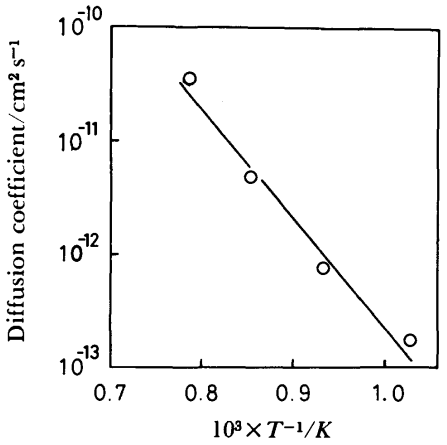

Fig. 6. Arrhenius plot for tritium diffusion in vitreous silica. (O) tritium released as HTO in isothermal annealing from T-irradiated silica C (OH 960 ppm).

Table 6. Activation Energy for the Diffusion of Hydrogen Isotopes in Vitreous Silica

Species	E_d / kJ mol^{-1}	Temperature range/K	Reference
H	15	77— 110	7
D	15	77— 110	7
H_2	37.8	573—1273	28
D_2	39.2	573—1273	28
D_2	37.0	497—1066	4
H_2O	76.7	873—1473	29
"HTO"	171	973—1273	This work

Table 6 compares an activation energy for the diffusion in this work with the reported values of hydrogen diffusion in silica. The activation energy for diffusion in Eq. 5 is much larger than the energies for the diffusions of H(D) atoms, H_2, D_2, and H_2O molecules. Thus, the diffusing species for the HTO formation in silica can not be these atoms and molecules, but must be some other species. The diffusing species has not yet been conclusively identified. As has discussed in the previous section, the decrease in OD bonds upon heating is controlled by their diffusion to the surface, where the OD bonds do not rupture during diffusion, but decompose only at the surface. Thus, one plausible mechanism is that tritium in an OT bond migrates from one oxygen site to a neighboring oxygen site as a consequence of the forllowing chemical reaction, and then repeats this reaction to the surface of silica. Then, the OT bond decomposes into HTO at the surface, and tritium is released from silica:

$$\equiv\mathrm{Si\text{-}OT} + \equiv\mathrm{Si\text{-}O\text{-}Si}\equiv \longrightarrow \equiv\mathrm{Si\text{-}O\text{-}Si}\equiv + \mathrm{TO\text{-}Si}\equiv \quad (6)$$

$$\equiv\mathrm{Si\text{-}OT} \xrightarrow{\text{at surface}} \mathrm{HTO} + \mathrm{S} \quad (7)$$

where S represents some products at the surface. Tritium migration by the repetition of a chemical reaction like Reaction 6 was also suggested for the tritium migration in MgO.[27]

The authors wish to thank Mr. Nobuhiko Kuribayashi of the Japan Atomic Energy Research Institute for his help in the measurement of metal impurities in the sample, and Mr. Kazuo Kobayashi of Nagoya University for his help in the experiment on thermal D_2-doping. This work was supported in part by a Grant-in-Aid for Scientific Research from the Japanese Ministry of Education, Science and Culture. This work was done under the Collaboration Program between the Japan Atomic Energy Research Institute and Nagoya University, and under the Collaboration Research Program of the Research Center for Resource and Energy Conservation, Nagoya University.

References

1) Hj. Matzke, *Z. Naturforschg*, **22a**, 965 (1967).
2) W. Primak, No. ANL/FPP/TM-146, Argonne National Laboratory, July 1981. Available from National Technical Information Service, US Department of Commerce.
3) D. L. Griscom, *J. Appl. Phys.*, **58**, 2524 (1985).
4) J. E. Shelby, *J. Appl. Phys.*, **48**, 3387 (1977).
5) G. W. Arnold and B. L. Doyle, *Nucl. Instrum. Methods*, **194**, 491 (1982).
6) M. Saeki, S. Ohno, E. Tachikawa, N. Azuma, T. Miyazaki, and K. Fueki, *J. Am. Ceram. Soc.*, **68**, 151 (1985).
7) T. Miyazaki, N. Azuma, and K. Fueki, *J. Am. Ceram. Soc.*, **67**, 99 (1984).
8) J. E. Shelby, P. L. Mattern, and D. K. Ottesen, *J. Appl.*

Phys., **50**, 5533 (1979).

9) B. Kumar, N. Fernelius, and J. A. Detrio, *J. Am. Ceram. Soc.*, **64**, C-178 (1981).

10) 1 ppm means the ratio of one molecule of an impurity to 10^6 of the SiO_2 unit.

11) NICOLET MX-1, Nicolet Zeta Corp., CA

12) G. Hetherington and K. H. Jack, *Phys. Chem. Glass*, **3**, 129 (1962).

13) The concentrations of metal impurities were measured by the following method: a sample was dissolved in a solvent, and then the amounts of the metal ions were measured by means of Inductively Coupled Plasma (ICP) Emission Spectrometry.

14) K. Furukawa and S. Ohno, JAERI-M 85-110 (in Japanese).

15) JES-3BX, Japan Electronic Optical Laboratory, Tokyo, Japan.

16) The release gases were first filtered in a water bubbler which traps HTO components. An aliquot of the tritiated water was taken from the water bubbler at regular time intervals and radioassayed by means of a liquid scintillation counter. After removing the HTO components from the release gases, the gases were lead to an ionization chamber after they had been passed through a column packed with silica gel to remove vaporous water. The HT components were measured at 20-sec intervals. Finally, HT gases were collected in the water bubbler, after having been oxidized to tritiated water by the use of a CuO column heated to 873 K, in order to measure the total amount of HT components.

17) M. Saeki, *J. Nucl. Mater.*, **99**, 100 (1981).

18) H. H. Anderson and J. F. Ziegler, "Hydrogen-stopping Powers and Ranges in All Elements," organized by J. F. Ziegler, Pergamon Press, New York (1977), **3**, 16.

19) J. P. Biersack and L. G. Haggmark, *Nucl. Instrum. Methods*, **174**, 257 (1980).

20) J. Crank, "The Mathematics of Diffusion," Clarendon, Oxford (1975), p. 305.

21) J. E. Shelby, *J. Appl. Phys.*, **51**, 2589 (1980).

22) S. Pinchas and I. Laulicht, "Infrared Spectra of Labelled Compounds," Academic Press, New York (1971), p. 297.

23) K. H. Beckmann and N. J. Harrick, *J. Electrochem. Soc.*, **118**, 614 (1971). Since the absorption spectrum of the SiH bond is observed at 2300 cm^{-1}, the absorption of the SiD bond may be expected around 1600 cm^{-1} from the difference in the mass.

24) Reactions 2 and 3 represent only the overall reaction schemes concerning the ≡Si-O-Si≡ and ≡Si-OH bonds respectively.

25) G. Dicola and Hj. Matzke, *Nucl. Instrum. Methods*, **57** 341 (1967).

26) M. Saeki, *J. Nucl. Mater.*, **131**, 32 (1985).

27) K. T. Scott and L. L. Wassell, *Proc. Br. Ceram. Soc.*, **7**, 375 (1967).

28) R. W. Lee, *J. Chem. Phys.*, **38**, 448 (1963).

29) A. J. Moulson and J. P. Roberts, *Trans. Brit. Ceram. Soc.*, **59**, 338 (1966).

 © 1987 The Chemical Society of Japan Bull. Chem. Soc. Jpn., 60, 3843—3847 (1987)

Pressure Dependence of the Reaction of Thiolane with H and D Atom

Jie TANG,* Tohru KAMO, Muneyoshi YAMADA, and Akira AMANO
Department of Applied Chemistry, Faculty of Engineering, Tohoku University,
Aoba, Aramaki, Sendai 980
(Received April 2, 1987)

The title reaction was investigated at room temperature and under pressures ranging from 133 to 2660 Pa, using a conventional discharge flow reactor. 1-Butanethiol, butane, and 1-butene were the main products, whose compositions varied according to the pressure. In the reaction with deuterium atom, 1-butene was monodeuterated, while 1-butanethiol and butane were dideuterated. The following mechanism was proposed to account for the product compositions and their pressure dependencies as well as the deuterium labeling of the products.

$$(CH_2)_4S + H \longrightarrow CH_2(CH_2)_3SH \quad (1)$$
$$CH_2(CH_2)_3SH + H \longrightarrow CH_3CH_2CH_2CH_2SH^* \quad (2)$$
$$CH_3CH_2CH_2CH_2SH^* \longrightarrow CH_3CH_2CH_2CH_2SH \quad (3)$$
$$\longrightarrow CH_3CH_2CHCH_2 + H_2S \quad (4)$$
$$\longrightarrow CH_3CH_2CH_2CH_2 + HS \quad (5)$$
$$CH_3CH_2CH_2CH_2 + H \longrightarrow CH_3CH_2CHCH_2 + H_2 \quad (6)$$
$$\longrightarrow CH_3CH_2CH_2CH_3 \quad (7)$$

In the comparatively few mechanistic studies, the common initial step being characteristic of direct attack on sulfur has been proposed for the reactions of hydrogen atom with cyclic sulfides. The subsequent decomposition paths of trivalent sulfur complexes so formed, however, were quite different from each other. With the thiirane[1] and thietane[2] the concerted decomposition mechanisms were proposed as

$$(CH_2)_2S + H \longrightarrow CH_2CH_2 + SH$$
$$(CH_2)_3S + H \longrightarrow CH_3CHCH_2 + SH.$$

With thiolane, to account for the predominant formation of 1-butanethiol, the distinct C-S bond cleavage and subsequent reactions, Reactions 1—4, were proposed in our previous study[3]

$$(CH_2)_4S + H \longrightarrow CH_2(CH_2)_3SH \quad (1)$$
$$CH_2(CH_2)_3SH + H \longrightarrow CH_3CH_2CH_2CH_2SH^* \quad (2)$$
$$CH_3CH_2CH_2CH_2SH^* \longrightarrow CH_3CH_2CH_2CH_2SH \quad (3)$$
$$\longrightarrow CH_3CH_2CHCH_2 + H_2S. \quad (4)$$

An asterisk denotes a vibrational energized species. Reaction 4, a molecular H_2S elimination channel for the decomposition of chemically activated 1-butanethiol, was tentatively proposed on the analogue to the decomposition of alkyl halide or aliphatic alcohol to interpret the formation of 1-butene, one of the hydrocarbon products. Butane, another hydrocarbon product, was interpreted to be produced via secondary reactions of 1-butanethiol and 1-butene.

In very little studies up to date of our study on 1-butanethiol, thermal reactions of thiols have been reported to proceed either by a free radical chain mechanism or by a molecular H_2S elimination mechanism, neither of which have conclusive evidence for the validity.[4,5] Recently, we have studied the thermal decomposition of 1-butanethiol, using low pressure pyrolysis technique combined with deuterium labeling method, and reached the conclusion that the decomposition is through two parallel channels, Reactions 4′ and 5′[5]

$$CH_3CH_2CH_2CH_2SH \longrightarrow CH_3CH_2CHCH_2 + H_2S \quad (4')$$
$$CH_3CH_2CH_2CH_2SH \longrightarrow CH_3CH_2CH_2CH_2 + HS. \quad (5')$$

On the other hand, we have studied the reaction of dibutyl disulfide with hydrogen atom,[6] and found that we have to propose another parallel decomposition channel to Reaction 4, Reaction 5

$$CH_3CH_2CH_2CH_2SH^* \longrightarrow CH_3CH_2CH_2CH_2 + HS \quad (5)$$

of chemically activated 1-butanethiol formed in the reaction to give a satisfactory explanation on the product compositions and their pressure dependencies as well as deuterium distributions in the products. Reactions 4 and 5 were also shown to be flexible in giving an explanation of reaction of 1-butanethiol with hydrogen atom,[7] where chemically activated 1-butanethiol was also considered to be formed.

These facts aroused our attempt to reinvestigate the reaction of thiolane with hydrogen (and deuterium) atom over a wide pressure range for acquiring a clearer picture of the chemically activated species in this reaction.

Experimental

The adopted apparatus and procedure were similar to those described in our previous work.[3] In brief, the apparatus consisted of discharge flow reactor, reactant vaporizer, liq. N_2 chilling traps for trapping product, flow

control line, and evacuation system. Thiolane and H_2 (or D_2), both diluted in excess of He, were introduced into a Pyrex reactor of 400 mm in length and 27 mm in inside diameter. Flow rate of thiolane, H_2 (or D_2), and He were 0.001 ml(NTP) s^{-1}, 0.01 ml(NTP) s^{-1}, and 0.72—14.4 ml (NTP) s^{-1}, respectively. Hydrogen atom (or deuterium atom) was generated by passing H_2 (or D_2) through a microwave cavity at upstream side of reactor. To prevent hydrogen atom (or deuterium atom) from recombination, the reactor surface was coated with boric acid.

The reaction was carried out at room temperature and under pressures ranging from 133 to 2660 Pa. Many attempts were made to get observation at low conversions. Reaction gas mixture was intermittently withdrawn through a nozzle and was isolated into an arm chilled by liq. N_2. The isolated sample was then analyzed by gas chromatography (GC) and gas chromatograph-mass spectrometer (GC-MS), using VZ-10 column (2 m, 55 °C) for hydrocarbons and polyethylene glycol (3 m, 80 °C) for organosulfur compounds.

Commercially available purest grade thiolane was purified by trap-to-trap distillation, and the middle one third fraction of better than 99% purity was used. Cylindered gases of H_2, D_2, and He were dried by passing through a train of liq. N_2 traps.

Results

Course of reaction was followed up to conversion of 60%. Product composition vs. conversion relations observed under 133, 530, and 2660 Pa are shown in Figs. 1, 2, and 3, respectively. Although 1-butanethiol was by far the most important, all the three major components including 1-butene and butane were evidently the initial products. The adequacy of interpretation that butane was an initial product will be presented in detail later in discussion. Small amounts of fragmental products such as propane, propylene, ethane, and ethylene were also formed. However, they all decreased to a negligible amount as pressure increased.

When deuterium atom was used instead of

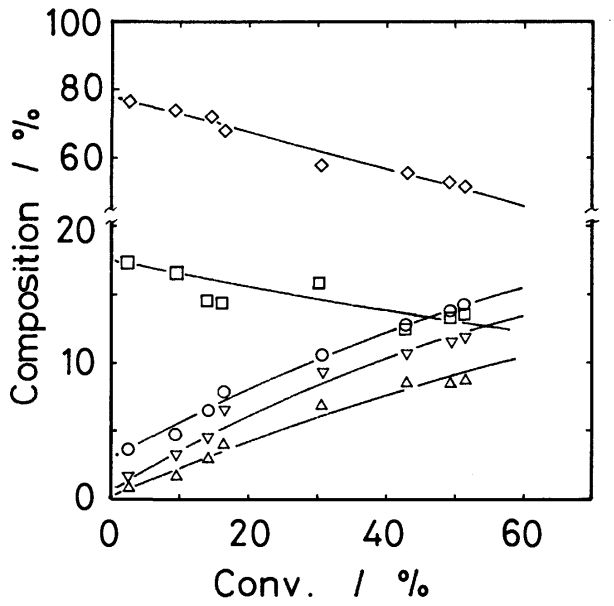

Fig. 1. Composition vs. conversion relation under 133 Pa.
◇: 1-Butanethiol, ○: butane, □: 1-butene, △: C_2 hydrocarbons, ▽: C_3 hydrocarbons.

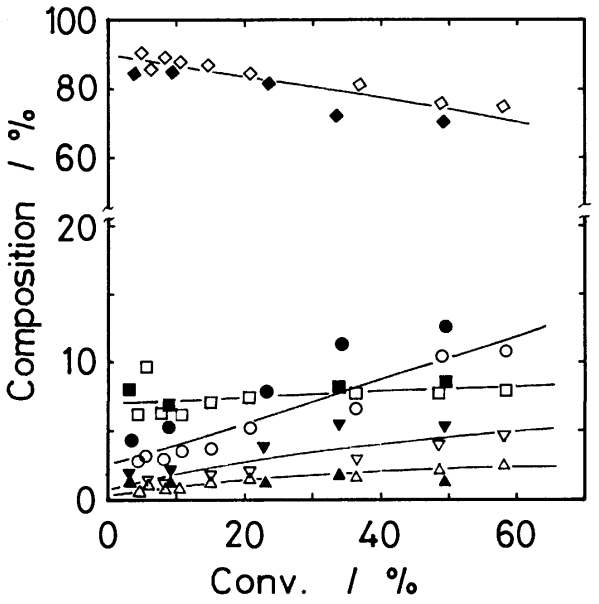

Fig. 2. Composition vs. conversion relation under 530 Pa.
◇: 1-Butanethiol, ○: butane, □: 1-butene, △: C_2 hydrocarbons, ▽: C_3 hydrocarbons.
(Filled points denote reaction with deuterium atom.)

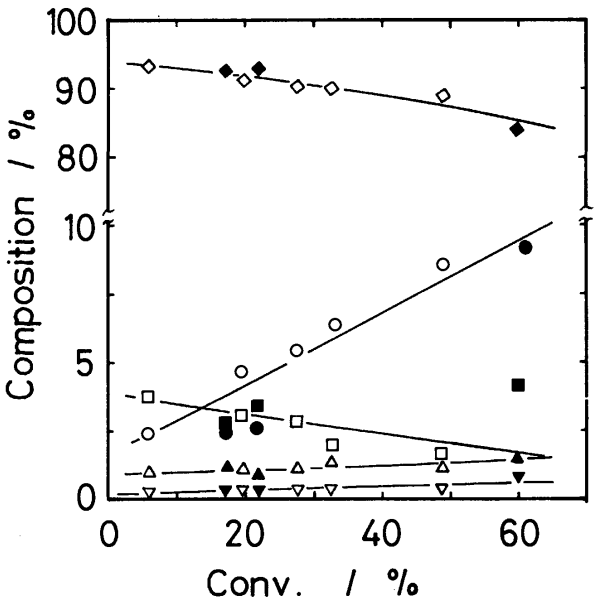

Fig. 3. Composition vs. conversion relation under 2660 Pa.
◇: 1-Butanethiol, ○: butane, □: 1-butene, △: C_2 hydrocarbons, ▽: C_3 hydrocarbons.
(Filled points denote reaction with deuterium atom.)

hydrogen atom, quite similar results were obtained with respect to the composition-conversion behavior as shown in Figs. 2 and 3 by filled points. Practically no isotopic mixing was observed with thiolane left unreacted in the reaction with deuterium atom. Deuterium distributions observed with butane and 1-butene are listed in Table 1 for a few different conversions. Two deuterium atoms were introduced into each butane molecule produced, and one into each 1-butene. 1-Butene[D_2] and butane[D_3] were observed as progressively important with the increase of conversion. The GC-MS analysis also showed that only one deuterium atom was introduced into each 1-butanethiol molecule produced.

Both butane/1-butanethiol and 1-butene/1-butanethiol ratios tend to increase linearly as the conversion increases. The trend is illustrated in Fig. 4. The

Table 1. Deuterium Distribution in Butane and 1-Butene

Press.	Conv.	Butane			1-Butene		
Pa	%	d_1	d_2	d_3	d_0	d_1	d_2
530	2.0	0	100	0	0	100	7
530	3.0	0	100	12	1	100	12
133	6.5	14	100	11	0	100	7
2660	10.7	15	100	9	4	100	18
530	12.1	10	100	26	3	100	20
530	30.3	10	100	33	9	100	22
2660	43.5	14	100	22	3	100	20

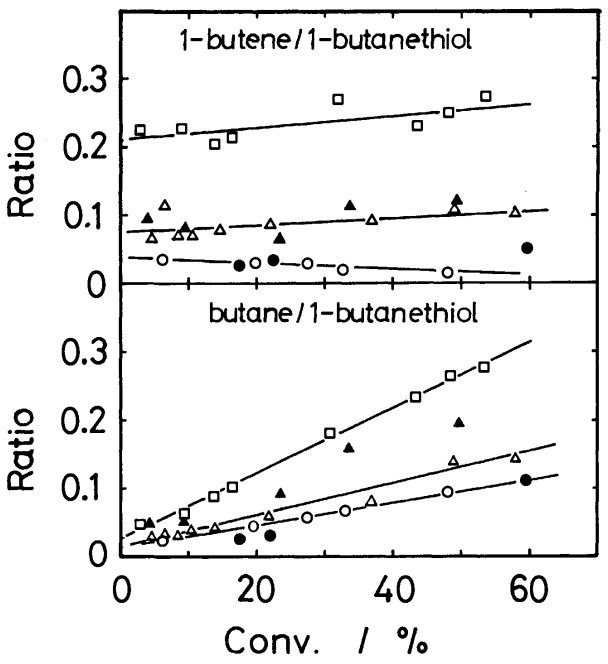

Fig. 4. Amounts of 1-butene and butane relative to 1-butanethiol.
□: 133 Pa, △: 530 Pa, ○: 2660 Pa.
(Filled points denote reaction with deuterium atom.)

values of 0.020, 0.016, 0.006 for butane/1-butanethiol, and of 0.239, 0.077, 0.029 for 1-butene/1-butanethiol at 133, 530, 2660 Pa were obtained when extrapolating the ratios at various pressures to zero conversion. Clearly these values exhibit certain pressure dependencies of the initial product compositions.

Discussion

Primary Reaction. The fact that no isotopic mixing was observed with thiolane left unreacted in the reaction with deuterium atom eliminated the possibility of hydrogen abstraction-addition on ring. This approved the characteristic hydrogen atom attack on sulfur proposed previously to be valid. Thus the Reactions 1—4 proposed previously kept their validity for reasons that they give a proper interpretation of primary formations of 1-butanethiol and 1-butene.[3] However, butane is not referred to in Reactions 1—4. In fact, butane was shown not to be formed from the reactions of 1-butene and 1-butanethiol with hydrogen atom, the conclusive diagnosis of which will be presented in the discussion on secondary reaction later. Thus, to interpret the primary formation of butane, we add Reaction 5, a parallel decomposition channel to Reaction 4 for chemically activated 1-butanethiol, and subsequent Reactions 6 and 7. The reaction formulas 1—7 should be written as follows,

$$(CH_2)_4S + D \longrightarrow CH_2(CH_2)_3SD \quad (1)$$

$$CH_2(CH_2)_3SD + D \longrightarrow CH_2DCH_2CH_2CH_2SD^* \quad (2)$$

$$CH_2DCH_2CH_2CH_2SD^* \longrightarrow CH_2DCH_2CH_2CH_2SD \quad (3)$$

$$\longrightarrow CH_2DCH_2CHCH_2 + HDS \quad (4)$$

$$\longrightarrow CH_2DCH_2CH_2CH_2 + DS \quad (5)$$

$$CH_2DCH_2CH_2CH_2 + D \longrightarrow CH_2DCH_2CHCH_2 + HD \quad (6)$$

$$\longrightarrow CH_2DCH_2CH_2CH_2D. \quad (7)$$

For the sake of clearity, we hereafter write D standing for both hydrogen and deuterium atoms.

According to this scheme, 1-butene[D_1], butane[D_2], and 1-butanethiol[D_2] should be given when deuterium atom was used. The initial deuterium distribution of 1-butene and butane was in conformity with this inference, while the GC-MS observation on 1-butanethiol was apparently inconsistent with this inference. However, by a contrast analysis of the separately prepared 1-butanethiol[S-D] using a direct sampling quadrupole mass spectrometer, we verified that, even if the mercapto-hydrogen is deuterated perfectly, conventional GC-MS analysis can not give any evidence about the mercapto-deuterium due to the retro H–D exchange with residual water in the column and in the ionization chamber. It may therefore be concluded that 1-butanethiol was actually dideuterated in the course of reaction, and that the

Table 2. Rate Constants and Activation Energy of the Reactions of Related Species with Hydrogen Atom

Reactant	log A	E_a / kJ mol^{-1}	Rate constant at 300 K / cm^3 mol^{-1} s^{-1}	Ref.
Thiolane	9.93	8.4	$2.92*10^{11}$	3
1-Butanethiol (a)	9.20	9.3	$3.84*10^{10}$	3
(b)	10.11	13.3	$6.27*10^{10}$	3
1-Butene	13.17	6.2	$1.32*10^{12}$	10
Butane	13.3—14.4	6.7—8.5	ca. $2*10^8$	11

(a): for Reaction 8. (b): for Reaction 9.

Table 3. Comparison of k_4/k_5 Ratios of 1-Butanethiol

Reaction	k_4/k_5	Energized level / kJ mol^{-1}	Ref.
Thermal decomposition	0.18	310[a]	5
Dibutyl disulfide+H	0.43	385[b]	6
Thiolane+H	3.0—9.7	410[c]	This work

a) Calculated by E_0+RT, E_0 is activation energy; b) bond dissociation energy of S-H bond; c) bond dissociation energy of primary C-H bond.

result as observed with GC-MS just should be interpreted as monodeuteration of butyl group of 1-butanethiol.

The Reactions 6 and 7 are the well-known disproportionation and recombination reactions for an alkyl radical with hydrogen atom. From the reported values for the reactions of ethyl radical with hydrogen atom[8] and of propyl radical with methyl radical,[9] we can reasonably estimate the k_6/k_7 to be about 0.05. Thus, the predominant source of 1-butene was plausibly molecular H_2S elimination of chemically activated 1-butanethiol, Reaction 4, rather than Reaction 6.

Secondary Reaction. Table 2 shows rate constants of some related species with hydrogen atom at room temperature. Thiolane, 1-butanethiol, and 1-butene all have a much higher reactivity over butane toward hydrogen atom. We may therefore ignore the reaction of butane with hydrogen atom in formulating a group of secondary reactions.

Conceivable reactions of 1-butanethiol with hydrogen atom can be cited from our study[7] on the reaction of 1-butanethiol with hydrogen atom as follows

$$CH_2DCH_2CH_2CH_2SD + D \longrightarrow CH_2DCH_2CH_2CH_2S + D_2 \quad (8)$$

$$\longrightarrow CH_2DCH_2CH_2CH_2 + D_2S. \quad (9)$$

Reactions subsequent to Reaction 8 are

$$CH_2DCH_2CH_2CH_2S + D \longrightarrow CH_2DCH_2CH_2CH_2SD^* \quad (10)$$

and Reactions 3—5. Reactions subsequent to Reaction 9 are Reactions 6 and 7. For 1-butene, the secondary reaction with hydrogen atom is the well-known addition to double bond giving butyl and *s*-butyl radicals. The reactions of these radicals with hydrogen atom result in the formation of butane, 2-butenes, and regeneration of 1-butene.

The decreases of the composition of 1-butanethiol and 1-butene with the increase of conversion shown in Figs. 1, 2, and 3 indicate the secondary reactions of 1-butanethiol and 1-butene with hydrogen atom. Moreover, from Fig. 4, the almost fixed 1-butene/1-butanethiol ratio relative to the conversion exhibits the similar reactivity toward hydrogen atom of both. This fact is also in quite accord with the reported rate constant data listed in Table 2. As a net result of secondary reactions of 1-butene and 1-butanethiol, butane/1-butanethiol solely increased with the increase of conversion, as shown in Fig. 4.

On account of secondary reaction, one may predict the change of deuterium distribution in products when deuterium atom was used. Secondary reaction of 1-butanethiol can not introduce any additional deuterium into 1-butene, butane, and itself, while the secondary reaction of 1-butene introduces two more deuterium atoms into butane, one more into 1-butene, leading to the formation of butane[D_3] and 1-butene[D_2]. Table 1 shows that the abundances of butane[D_3] and 1-butene[D_2] increased as conversion increased, and the both approached to zero at low conversion. The latter fact makes primary formation of butane evident, because 1-butanethiol is known to be never more reactive toward hydrogen atom than 1-butene.

Pressure Dependence of Primary Products and Decomposition of Chemically Activated 1-Butanethiol. The pressure dependence of the initial proportion of 1-butene gives an undoubted evidence for the formation of chemically activited 1-butanethiol in this reaction. The initial proportion of butane was so small that its pressure dependence was submerged into experimental error. Therefore we can not say any about its pressure dependency arbitrarily, but we can conclude that the chemically activated 1-butanethiol formed in this reaction has a higher selectivity to the concerted channel of 4 over 5.

According to the proposed reaction mechanism, the following formula may be deduced to relate the initial products composition with k_4/k_5.

$$\frac{[\text{1-butene/1-butanethiol}]}{[\text{butane/1-butanethiol}]} = \frac{k_6}{k_7} + \frac{k_4}{k_5}\left(1+\frac{k_6}{k_7}\right)$$

Table 3 listed the evaluated values of k_4/k_5 for thermal decomposition of 1-butanethiol and decomposition of chemically activated 1-butanethiol created from different reactions. A comparison can be made between the values of k_4/k_5 and the energized level of

1-butanethiol. The relevancy between the two may give a rough explanation of the difference in the values of k_4/k_5.

References

1) T. Yokota, M. G. Ahmed, I. Safarik, O. P. Strausz, and H. E. Gunning, *J. Phys. Chem.*, **79**, 1756 (1975); J. Nishino and M. Yamada, *Nippon Kagaku Kaishi*, **1982**, 1735.

2) M. Yamada, T. Kamo, J. Nishino, and A. Amano, *Nippon Kagaku Kaishi*, **1983**, 1475.

3) O. Horie, K. Onuki, and A. Amano, *J. Phys. Chem.*, **81**, 1706 (1977); O. Horie, J. Nishino, and A. Amano, *Int. J. Chem. Kinet.*, **10**, 1043 (1978).

4) O. P. Strausz, H. E. Gunning, and J. W. Lown, in "Comprehensive Chemical Kinetics," ed by C. H. Bamford and C. F. H. Tipper, Elsevier, Amsterdam (1972), Vol. 5, pp. 697—731.

5) M. Yamada, Y. Takahashi, T. Kamo, Y. Ohshima, and A. Amano, *Nippon Kagaku Kaishi*, **1985**, 1560; M. Yamada, T. Kamo, J. Tang, Y. Ohshima, and A. Amano, *ibid.*, **1985**, 2283.

6) J. Tang, T. Kamo, M. Yamada, Y. Ohshima, and A. Amano, *Bull. Chem. Soc. Jpn.*, **60**, 2019 (1987).

7) T. Kamo, J. Tang, M. Yamada, and A. Amano, *Nippon Kagaku Kaishi*, **1987**, 335.

8) J. O. Terry and J. H. Futrell, *Can. J. Chem.*, **45**, 2327 (1967).

9) J. W. Kraus and J. G. Calvert, *J. Am, Chem, Soc.*, **79**, 592 (1957).

10) T. Kyogoku, T. Watanabe, S. Tsunashima, and S. Sato, *Bull. Chem. Soc. Jpn.*, **56**, 19 (1983).

11) W. E. Jones, S. D. Macknight, and L. Teng, *Chem. Rev.*, **73**, 407 (1973).

 © 1987 The Chemical Society of Japan Bull. Chem. Soc. Jpn., 60, 3849—3853 (1987)

Interactions between a Synthetic Phospholipid Vesicle and Cationic Surfactants

Mitsuhiro TAKASAKI, Noboru TAKISAWA, and Keishiro SHIRAHAMA*
Department of Chemistry, Faculty of Science and Engineering, Saga University, Saga 840
(Received April 9, 1987)

The interaction between a synthetic phospholipid derivative, the 1,3-ditetradecyl-*rac*-glycerophosphatidylcholine ($2C_{14}$-Gly-PC) vesicle, and two cationic surfactants, *N*-tetradecylpyridinium bromide (TDPBr) and *N*-tetradecyltrimethylammonium bromide (TDTMABr), were investigated in the hope of obtaining a better understanding of the mechanism of the growth of the vesicle size by the "surfactant-removal" method. The binding isotherms of these surfactants to the lipid vesicle obtained by the surfactant selective electrode were characterized by two-step binding processes; the Langmuir adsorption mechanism in the initial binding, followed by a markedly positive cooperative process. The variation in the hydrodynamic radius, as measured by quasi-elastic light scattering, and the quenching kinetics of pyrene fluorescence with the TDPBr surfactant solution as measured by a stopped-flow method, share a tendency with the binding behavior. The van't Hoff plots of the initial binding data give a slightly negative enthalpy change, $\Delta H°$, for TDPBr and a relatively large positive $\Delta H°$ for TDTMABr. The microenvironmental polarity around pyrene in the molecular assemblies was assessed by means of fluorescence spectroscopy.

When amphiphiles such as lecithin are dispersed in water, they form molecular assemblies with a bilayer structure called a vesicle, which is excellent in mimicking biological membranes.[1-3] Vesicles comparable in size with a biological cell will facilitate study of the mechanism of cellular reaction. A vesicle formed in water is usually much smaller than biocells and a multilamellar structure, even if the vesicle is prepared by the sonication method. It is known that a vesicle is solubilized by a surfactant, which is subsequently removed by dialysis or some other method above the transition temperature of the gel-liquid crystal, T_C of the lipid; there, then produced a large homogeneous, unilamellar vesicle. However, the "surfactant-removal" method has not been well understood yet[4-6] in spite of its biochemical significance.[7-9] We have investigated the interaction of the 1,3-ditetradecyl-*rac*-glycerophosphatidylcholine ($2C_{14}$-Gly-PC) vesicle with two cationic surfactants, *N*-tetradecylpyridinium bromide (TDPBr) and *N*-tetradecyltrimethylammonium bromide (TDTMABr). It has been known that $2C_{14}$-Gly-PC behaves much like lecithin, having the corresponding alkyl chains,[10] and it is chemically stable and suitable for investigating the vesicle-surfactant interaction, since the ether bond between two alkyl chains and the phosphatidylcholine group is resistant against hydrolysis.

The binding of TDPBr and TDTMABr to the vesicle was measured by using surfactant-electrodes which have been successfully utilized in our laboratory,[11-13] and the thermodynamic aspects of binding were discussed. The hydrodynamic radii of the vesicle were obtained by means of quasi-elastic light scattering (QELS). Pyrene fluorometry was useful in the static and kinetic study of the interaction mechanism.

Experimental

Materials. The $2C_{14}$-Gly-PC (Fig. 1) was purchased from Sogo Pharmaceutical, Tokyo, and was used as received. The TDPBr was synthesized by a method similar to that used for dodecylpyridinium bromide[12] and was recrystallized three times from acetone. A triple recrystallization of TDTMABr (Tokyo Kasei) from acetone was also carried out. The critical micelle concentrations (cmc) in an aqueous solution, as determined by the electric conductivity method, are 2.82 and 3.60 mmol dm^{-3} at 30 °C for TDPBr and TDTMABr respectively; these values are in good agreement with the literature.[14] For convenience, we use the abbreviation 1 M=1 mol dm^{-3} throughout this paper.

Sample Preparation. The vesicle-forming agent, $2C_{14}$-Gly-PC, was dispersed in doubly distilled water and treated in a bath-type sonicater (VELVO CLEAR VS-20, Iuchi) for 1 hour at about 50 °C. Surfactant-containing samples were incubated at about 50 °C and used after they had been allowed to stand for a day or so for a complete equilibration of the system.

Surfactant-Selective Electrode. Poly(vinyl chloride) (PVC; 0.9 g) and bis(2-ethylhexyl) phthalate (2.1 g) were mixed well, after which 6 ml of tetrahydrofuran was added to the slurry mixture. The whole mixture was then heated at 60 °C. After a while, a clear and viscous solution was obtained; it was cast on a flat glass plate. The solvent was gradually removed in a silica-gel desiccator for two days, and then the gel membrane (about 0.2 mm thick) was obtained. The membrane was cut out and glued on one end

1,3-ditetradecyl-rac-glycero-phosphatidyl choline
($2C_{14}$-Gly-PC)

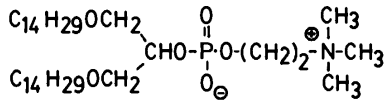

Fig. 1. Structure of $2C_{14}$-Gly-PC amphiphile.

of a PVC tube (9 mm in inner diameter, 11 cm long) and "annealed" at 40—50 °C under reduced pressure.

The binding of the surfactant to the vesicle was measured by using the surfactant-selective electrode in a thermostated cocylindrical cell. The concentration cell formula was as follows.

Ag/AgCl	KCl agar bridge	C_0 mM surfactant	M	C_1 mM surfactant (+vesicle)	KCl agar bridge	AgCl/Ag

in which M is the surfactant-selective electrode membrane; C_0, the inner (reference) surfactant concentration, and C_1, the outer surfactant concentration. The electromotive force, emf, was measured with a digital multimeter (Advantest TR-6845).

Pyrene Fluorometry. The fluorescence of pyrene was measured by means of a Shimadzu digital spectrophotomerer RF-510 (temperature controlled with LAUDA RM3 MODEL S-1 thermostat). The fluorometry was carried out from both static and kinetic points of view. The static experiment was done only with the system using TDTMABr. The variation in the I/III ratio found in the vibronic fine structure in the pyrene fluorescence spectrum was measured by changing the surfactant concentration in the 350—450 nm emission-wavelength region.[15] As for the kinetic experiment, the vesicle dispersions containing pyrene (p-dispersion) and TDPBr as a fluorescent quencher (q-dispersion) were quickly mixed by the used of a stopped-flow mixer (Union Giken MX-7) and the fluorescence intensity was followed with time, where the excitation wavelength, λ_{ex}=337 nm, and the emission one, λ_{em}=391 nm, were both used. The mixing was also carried out by a conventional "manual fast mixing"; i.e., the q-dispersion was poured into the p-dispersion in a cuvette cell, and the mixture was stirred with a tiny plastic rod as quickly as possible.

Quasi-Elastic Light Scattering (QELS). The hydrodynamic radii of the molecular assemblies were measured for the TDPBr system by the QELS method.

Results and Discussion

Figure 2 shows the relation between the emf and the logarithm of the TDPBr concentration. The electrode exhibits the Nernstian response for the TDPBr surfactant without a vesicle. In the coexistence of the $2C_{14}$-Gly-PC vesicle, however, a deviation from linearity is observed. The deviation may result from a partial binding of TDPBr to the vesicle. From the deviation, we can obtain the equilibrium surfactant concentration, C_f, and the bound surfactant concentration, $C_b=C_t-C_f$, where C_t is the concentration actually weighed-in. The surfactant-selective electrode responds equally well to TDTMABr. The binding isotherms were obtained by plotting the amount of binding per unit of lipid concentration, C_b/C_v, against C_f; they are shown in Figs. 3 and 4 for TDPBr and TDTMABr respectively. In the lower C_f region, the C_b/C_v amount is not so large, and it increases gradually with C_f before increasing sharply.

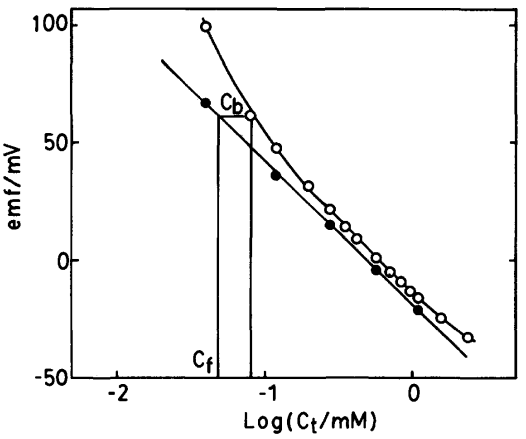

Fig. 2. Potentiogram of TDPBr at 303 K.
●: Without vesicle O: with 0.616 mM vesicle.

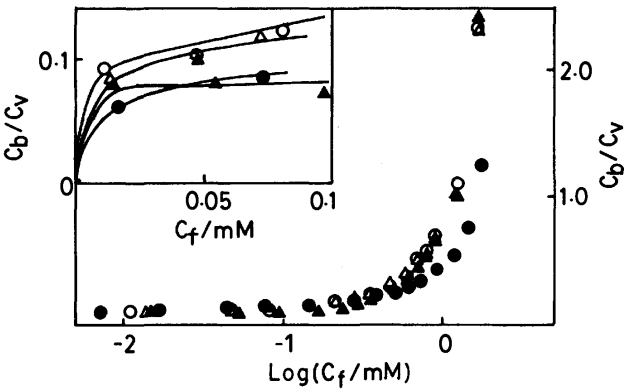

Fig. 3 Binding isotherms for TDPBr.
Temperature at ▲: 283 K, △: 293 K, O: 303 K, ●: 313 K.

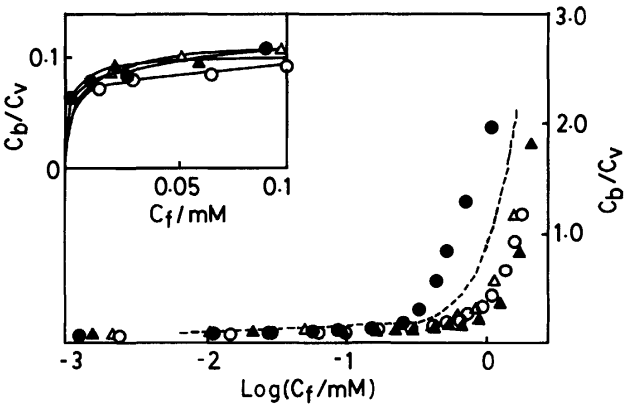

Fig. 4. Binding isotherms for TDTMABr.
Temperature at ▲: 283 K, △: 293 K, O: 303 K, ●: 313 K. ----: For TDPBr at 303 K.

In Fig. 4, a typical isotherm for TDPBr at 303 K is also shown by a dashed line for the sake of comparison. It appears that the C_b/C_v amount for TDPBr are slightly larger than those of TDTMABr, indicating a stronger

affinity of the pyridinium analog to the lipid vesicle. These isotherms depend a little on the temperature.

When the surfactants bind multiply and independently to the binding sites, which are mainly located on the surface of the vesicle, binding is expressed by the Langmuir isotherm:[16]

$$C_b/C_v = \frac{mKC_f}{1+KC_f} \quad (1)$$

where m is the maximum amount of binding and K, a sort of equilibrium constant. The Scatchard equation[16] derived from Eq. 1,

$$\frac{C_b/C_v}{C_f} = -K(C_b/C_v) + Km \quad (2)$$

is plotted for TDPBr and TDTMABr in Fig. 5. The data points support a straight line, with a negative slope at the lower concentrations; a different behavior

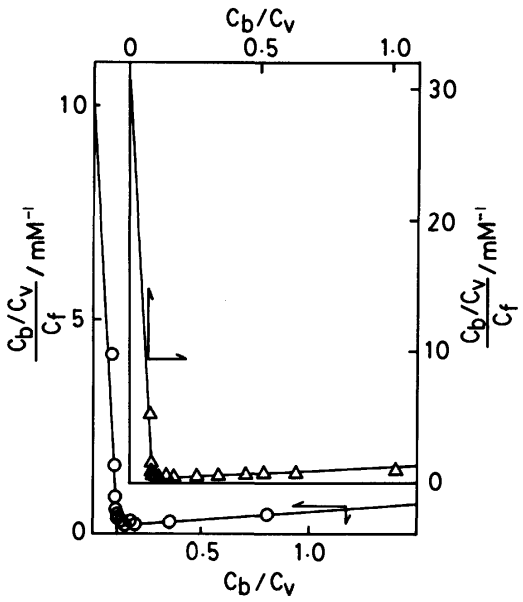

Fig. 5. Scatchard plots at 283 K.
△: For TDPBr, ○: for TDTMABr.

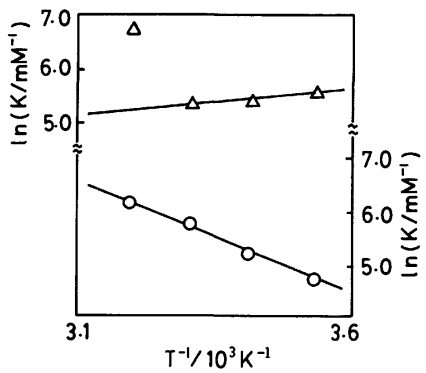

Fig. 6. The temperature dependence of K.
△: TDPBr, ○: TDTMABr.

with a positive slope is seen in the higher-concentration region, indicative of cooperative binding.[16,17] From the straight line in the lower-concentration region, the equilibrium constant, K, and the maximum amount of binding, m, were obtained. The maximum amount of binding is about 10 mol% irrespective of the kind of surfactant and the temperature; the further addition of a surfactant exceeding m may induce the formation of a mixed micelle. The van't Hoff plot for TDPBr in Fig. 6 has a slightly positive slope from 283 to 303 K, and the point at 313 K deviates from linearity, while all the data points for the TDTMABr system support linearity, with a relatively large negative slope. The different behavior at 313 K between the two systems may be related to the difference in the binding enthalpy, which is very much affected near the gel-liquid crystal transition temperature[10] of the vesicle, but the details remain still to be studied. The Langmuir parameters and ΔH°'s are listed in Table 1. In the Langmuir region, TDPBr binds to the vesicle exothermically, and TDTMABr, endothermically. This difference probably originates from the difference in the head group, since the two surfactants have the same hydrophobic chain-length. The difference in the ΔH° of binding between the surfactants, $\Delta\Delta H^\circ = \Delta H^\circ_{\text{TDPBr}} - \Delta H^\circ_{\text{TDTMABr}}$, may be governed by the electrostatic interaction between the phosphate anion and the cationic head group of each surfactant, and may result from the electrostatic energy difference. The phosphate ion group may approach the pyridinium ring plane closer so that electrostatic energy becomes less. The three bulky methyl groups of TDTMABr may interfere with such a close approach to the vesicular phosphate group.

QELS Measurement. The hydrodynamic radii, R_H, are obtained from the observed autocorrelation function, which decays single-exponentially, as

Table 1. Thermodynamic Parameters in the Langmuir Binding Process for (a) TDPBr and (b) TDTMABr Systems

(a)

T/K	m	K/mM^{-1}	ΔH°/kJ mol^{-1}
283	0.093	258	-7.7×10^0
293	0.112	220	
303	0.125	209	
313	0.105	801	

(b)

T/K	m	K/mM^{-1}	ΔH°/kJ mol^{-1}
283	0.107	115	3.43×10^1
293	0.118	183	
303	0.092	313	
313	0.096	450	

shown by an insert in Fig. 7. The variation in the R_H with C_f is shown in Fig. 7. In the lower-surfactant-concentration region, the R_H's are nearly invariant with C_f; the growth in the molecular assembly size appears above the same concentration range, where the binding deviates from the Langmuir isotherm. A similar constancy was previously observed with the system of a synthetic surfactant vesicle and nonionic surfactants.[4]

Pyrene Fluorescence. Pyrene shows a significant fine structure: the five well-defined peaks are numbered I—V from th lowest wavelength.[15] Since the intensity ratio, I/III, changes with the microenvironmental polarity around a pyrene molecule,[15] it will be used to assess the environment of pyrene molecules. Figure 8 shows how the polarity changes with the surfactant concentration. Pyrene dissolved in water shows a I/III ratio of about 1.5, as is indicated by the arrow in Fig. 8. The pyrene containing TDTMABr solution shows a sharp decrease in its I/III ratio near the cmc of TDTMABr and then a leveling-off. In contrast, pyrene shows a very low polarity in the vesicular medium at a low TDTMABr concentration, but its polarity increases to as much as that of pure micelle with an increase in the TDTMABr concentration, suggesting the formation of mixed micelles with the lipid molecules.

Quenching Kinetics of Pyrene Fluorescence. As soon as the pyrene-containing vesicle (p-vesicle) and the quencher-containing vesicle (q-vesicle) are mixed, quenching begins. It is considered to be controlled by the collision between the two kinds of vesicles. The frequency of collision may be very slow because of the large vesicular size, and so the quenching may also be very slow. The fluorescent intensity, $I(t)$ at 391 nm, decayed immediately until it reached about half the initial intensity. This may be due to the quenching of the free pyrene by the free quencher. Following this very rapid process, a relatively slow single-exponential decay was observed in the lower-TDPBr-concentration region, while in the higher-surfactant-concentration region the quenching kinetic trace seems a double-exponential process. By plotting the quantity, $\ln(I(t)-I(\infty))/(I(0)-I(\infty))$ against the time, the first order reaction constant, k, is obtained; it is shown in Fig. 9, where it may be seen that k is independent of C_f when C_f is low, but the k value increases rather abruptly at higher C_f values. It may be considered that the slow process results from a collision between the p-vesicle and the q-vesicle. At a higher cationic surfactant concentration, a part of the lipid is solubilized to form mixed micelles with the lipid and pyrene; the small molecular assemblies are efficient for quenching since they are moving quickly. The labile structure of a mixed micelle may also be preferable for efficient quenching.

All these experimental results for TDPBr are summarized in Fig. 10, where the various observed

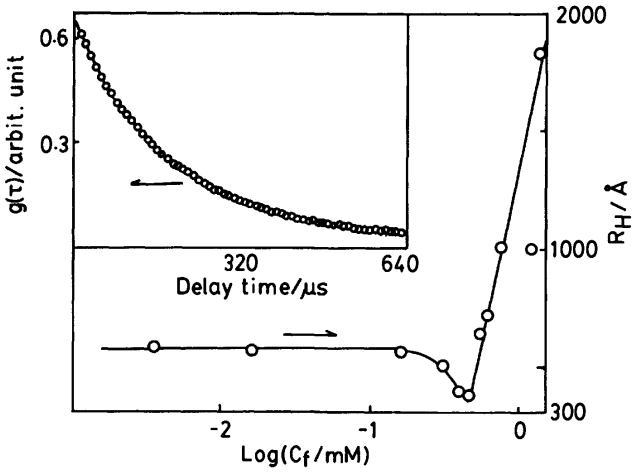

Fig. 7. An autocorrelation function and the variation of R_H with log C_f measured at 303 K.

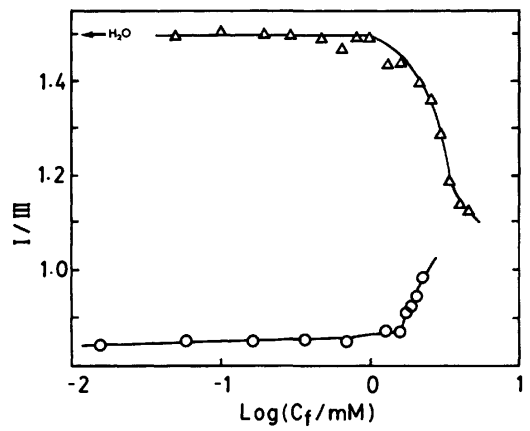

Fig. 8. The change of I/III ratio of pyrene molecule with C_f measured at 303 K.
○: With 0.616 mM lipid, △: without lipid.

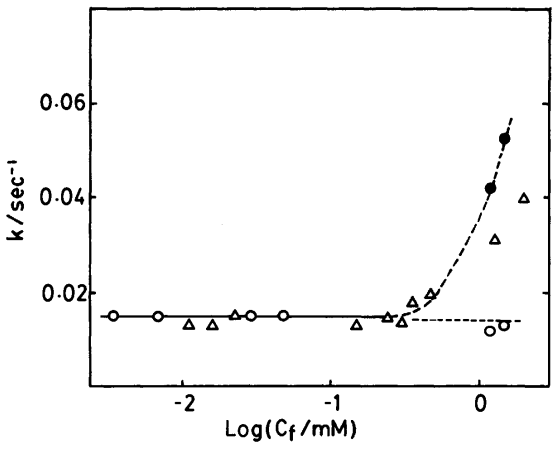

Fig. 9. Variation of quenching rate constant of pyrene fluorescence with logarithm of C_f.
○●: Stopped-flow method, △: manual mixing.

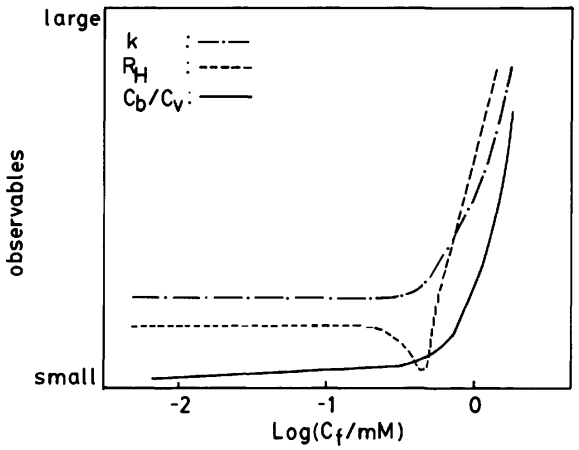

Fig. 10. Various observable vs. log C_f plot for TDPBr. —·—; k, ----; C_b/C_v, ——; R_H.

results are plotted as a function of the logarithm of C_f. It is notable that there is a close resemblance among the tendencies of all these observed data; the addition of the surfactant to the Langmuir binding limit causes drastic change in the behavior of the system. It may be concluded that the cationic surfactants are bound to the vesicle that remains the original vesicular structure in the lower-surfactant-concentration regions, and that, with an increase in the surfactant concentration, the sudden change in the observables in the present work may result from the formation of the mixed micelle. The growth of the vesicular size may also occur by the collision between the mixed micelle and the vesicular aggregation.[18]

In the QELS measurements we are grateful to the kind support of Professor Mitsuru Tanaka's laboratory of Fukuoka University. We are also thankful to Professor Masao Okubo of Saga University for lending the stopped-flow mixer. The author (K.S.) thanks "the Asahi Glass Foundation for Industrial Technology" for partially supporting this work.

References

1) J. H. Fendler, *Acc. Chem. Res.*, **1**, 7 (1980).
2) C. Tanford, "The Hydrophobic Effect: Formation of Micelles and Biological Membranes," John Wiley & Sons, New York (1973).
3) L. Stryer, "Biochemistry," Freeman, San Francisco (1981), p. 205.
4) K. Shirahama, K. Takashima, N. Takisawa, K. Kameyama, and T. Takagi, "Phenomena in Mixed Surfactant Systems," ed by John F. Scamehorn, American Chemical Society, Washington D.C. (1985), p. 299.
5) G. C. Kresheck, K. Kale, and J. Erman, "Solution Behavior of Surfactants," ed by K. L. Mittal and E. J. Fendler, Plenum, New York (1982), Vol. 1, p. 677.
6) P. Schurtenberger, N. Mazer, and W. Kanzig, *J. Phys. Chem.*, **89**, 1042 (1985).
7) H. Hauser, N. Gains, H.-J. Eibl, M. Muller, and E. Wehrli, *Biochemistry*, **25**, 2126 (1986).
8) S. Almog, T. Kushner, S. Nir, and D. Lichtenberg, *Biochemistry*, **25**, 2597 (1986).
9) R. Schubert, K. Beyer, H. Wolburg, and K.-H. Schmidt, *Biochemistry*, **25**, 5263 (1986).
10) T. Kunitake, Y. Okahata, and S. Tawaki, *J. Colloid Interface Sci.*, **103**, 190 (1983).
11) K. Shirahama, and M. Tashiro, *Bull. Chem. Soc. Jpn.*, **57**, 377 (1984).
12) K. Shirahama, T. Masaki, and T. Takashima, "Microdomains in Polymer Solutions," ed by P. Dubin, Plenum, New York (1985), p. 299.
13) K. Shirahama, K. Takashima, and N. Takisawa, *Bull. Chem. Soc. Jpn.*, **60**, 43 (1987).
14) P. Mukerjee and K. J. Mysels, "Critical Micelle Concentrations of Aqueous Surfactant Solutions," U.S. Government Printing Office, Washington D.C. (1971).
15) J. K. Thomas, *Chem. Rev.*, **80**, 283 (1980).
16) G. M. Barrow, "Physical Chemistry," ed by D. C. Jackson and S. Wagley, McGraw-Hill, Auckland (1979), p. 731.
17) K. E. Van Holde, "Physical Biochemistry," ed by L. Hager and F. Wold, Prentice-Hall, Englewood Cliffts, New Jersey (1971), Chap. 3.
18) D. Lasic, *Biochim. Biophys. Acta*, **692**, 501 (1982).

 © 1987 The Chemical Society of Japan Bull. Chem. Soc. Jpn., 60, 3855—3863 (1987)

Excited-State Reactions of Coumarins in Aqueous Solutions. IV. The Fluorescence Quenching of 7-Ethoxycoumarins by Inorganic Ions in Micellar Solutions of Sodium Dodecyl Sulfate

Tetsuo MORIYA
Electrotechnical Laboratory, 1-1-4 Umezono, Sakura-mura, Niihari-gun, Ibaraki 305
(Received April 18, 1987)

The effect of added salts (NaCl, NaBr, CsCl) on the fluorescence behavior of 7-ethoxycoumarin (7EC) and 7-ethoxy-4-methylcoumarin (7E4MC) has been studied in aqueous micellar solutions of sodium dodecyl sulfate (SDS). Data on the fluorescence quenching as a function of the salt concentration are analyzed in terms of a proposed two-reactive-state (aqueous and micellar phases) model. The results are in good accord with the model and permit the evaluation of the quenching-rate constants attributable to Br^- and Cs^+ respectively in the two phases. Quenching mechanisms influencing the fluorescence yield are discussed on the basis of the electrostatic force among micelles and quenchers, the electron-transfer reaction from anion to fluorescer, and the hydration degree of the quencher ions.

Since most coumarin derivatives in solutions have a strong fluorescence which depends on interactions with the surroundings, they can be used as fluorescent probes for the investigation of various reactions among organic molecules, inorganic ions, and molecular aggregations. In previous papers,[1,2] the fluorescence quenching of 7-ethoxycoumarin (7EC) and 7-ethoxy-4-methylcoumarin (7E4MC) by halide ions has been studied in aqueous solutions. Generally, halide ions are able to quench the fluorescence of dissolved fluorophores by the external heavy-atom effect[3] or the charge-transfer interaction.[4,5] It has been revealed that bromide and iodide ions in neutral aqueous solutions are very efficient fluorescence quenchers of 7EC and 7E4MC, whereas a chloride ion showed no such effect.[1] In acidic aqueous solutions, however, a chloride ion, as well as bromide and iodide ions, had a pronounced quenching effect on the fluorescence, because the photo-excited state of 7EC and 7E4MC preferred to associate with a proton in the solution, and, subsequently, the generated cationic fluorophore interacted attractively with the chloride ion.[2] In addition to these interactions of the fluorescers with inorganic ions, it has recently been found that 7EC and 7E4MC are easily solubilized into the micelle formed in an aqueous solution of sodium dodecyl sulfate (SDS).[6] The solubilization property of fluorescers and their microenvironment in micelles will be made clear by a spectroscopic investigation of the fluorophores distributed in the aqueous and micellar phases respectively.

In the present work, the absorption and fluorescence spectra of aqueous micellar solutions containing 7EC and 7E4MC are measured precisely upon the addition of several inorganic fluorescence quenchers. Since SDS forms anionic micelles, the solubilized fluorophore is protected from the quenching reaction with anionic quenchers. On the other hand, the quenching by cationic ions is enhanced because the quencher concentration near the surface of SDS micelles becomes higher as a result of electrostatic attraction. Based on a generalized scheme for quenching reactions in aqueous micellar systems, these aspects will be proved quantitatively through the determination of the quenching-rate constants for typical inorganic ions.

Experimental

Materials. The high-purity-grade reagents of 7-ethoxycoumarin (7EC) and 7-ethoxy-4-methylcoumarin (7E4MC) were obtained from Molecular Probes, Inc., and were used without further purification. The sodium dodecyl sulfate (SDS, Wako) was of a biochemical grade. The sodium chloride, sodium bromide, and cesium chloride were pure in quality (Wako). The water was permeated and distilled.

Methods. The UV-absorption spectra were obtained on a Hitachi 323 spectrophotometer, while the measurements of the fluorescence spectra and the fluorescence yields were made on a Hitachi MPF 4 spectrofluorometer with an S-5 type photomultiplier. The temperature of the sample cuvette was thermostated with circulating water from a constant-temperature bath (25±0.1 °C).

The wavelengths of the excitation light were chosen to be 326 nm for 7EC and 323 nm for 7E4MC; these values nearly coincided with their absorption maxima under various conditions, and there was no disturbing absorption of surfactants or ions at these wavelengths. The aqueous micellar solutions in high ionic concentrations were so labile that ultrasonic agitation and warming-up procedures of the solution were necessary to ensure homogeneity, and the fluorescence measurement was done as quickly as possible so as not to change the equilibrium conditions of the sample. The concentration of 7EC and 7E4MC was $4—5\times10^{-5}$ mol dm^{-3} unless otherwise mentioned.

Results

When 7EC and 7E4MC are dissolved in aqueous SDS solutions with concentrations higher than the critical micelle concentration (cmc),[7] they become distributed between the micellar and aqueous phases. The absorption spectra of 7EC and 7E4MC are

changed from those in the absence of SDS with a peak-position red-shifted by ≈1.5 nm and with a slightly decreased peak-value of the molar extinction coefficient (ε). Compared to this, the dependence of the fluorescence spectra on the SDS concentration becomes much larger, as may be seen from Fig. 1. By the addition of 0.025 mol dm^{-3} SDS, the fluorescence intensities are decreased to 74% (7EC) and 88% (7E4MC) at 25 °C, and the peak position of a fluorescence band is blue-shifted by ≈4 nm without changing the original spectral shape.[6] The 7EC and 7E4MC solubilized in the micellar phase are believed to have lower fluorescence yields than in the aqueous phase, because those in less polar water-organic mixed solvents such as water-dioxane are also low; in them a microenvironment similar to the micellar interior may be realized.[6]

The fluorescence quenching phenomena of these fluorophores by halide ions in aqueous solutions have been investigated in a previous paper.[1] The addition of NaCl to the solution did not result in any noticeable change in the fluorescence spectrum (at least for [NaCl]≦0.5 mol dm^{-3}), while NaBr could strongly quench the fluorescence, whose dependence on the salt concentration approximately followed the linear Stern-Volmer relation in the concentration range of interest, if we neglect a small deviation (a few percent) which becomes a discernible amount only for [NaBr]>0.3 mol dm^{-3}. The order of the quenching ability of the halide ions homogeneously distributed in the aqueous phase was shown to be: $I^- > Br^- \gg Cl^- \approx 0$.[4] CsCl also quenches the fluorescence, but the degree of quenching is very low compared to that in the case of NaBr. Taking into consideration the fact that NaCl (the pair of Na^+ and Cl^-) does not contribute to the quenching in the aqueous phase, Br^- is classified as a very efficient quencher, and Cs^+, as a very weak one. Usually the quenching ability of halide ions for coumarin derivatives of a neutral form is much greater than that of alkali ions with similar atomic weights, e.g., $I^- \gg Cs^+$ (I=53, Cs=55). Therefore, the fluo-

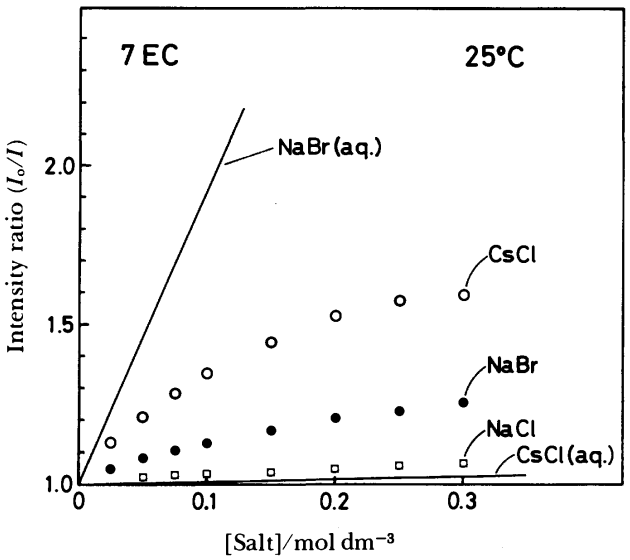

Fig. 2. Dependence of the fluorescence intensity ratio, I_0/I, of 7EC on the concentration of salts in aqueous solutions (solid lines) and in 0.025 mol dm^{-3} SDS solutions (data points) at 25 °C.

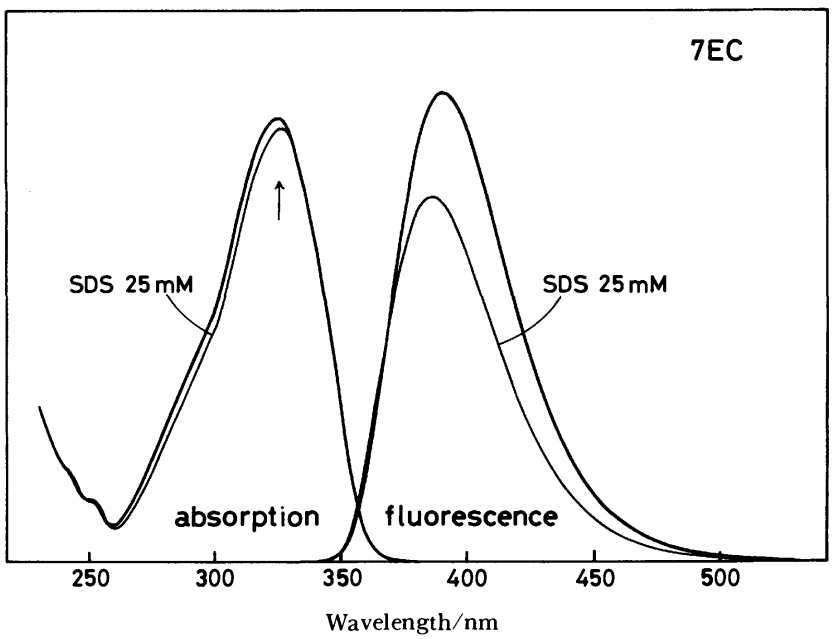

Fig. 1. UV absorption and emission spectra of 7EC in the pure water (thick lines) and in the aqueous solution of 0.025 mol dm^{-3} SDS (thin lines), respectively. The arrow indicates the wavelength of excitation for the emission spectra.

rescence quenching attributable to these inorganic ions cannot be explained consistently by the external heavy-atom effect; rather, it is possibly attributable to a charge-transfer interaction or an electrically induced perturbation among fluorophores and ions. Figures 2 and 3 show, by thin solid lines, the Stern-Volmer plots for I_0/I vs. [NaBr] and [CsCl], where I and I_0 are the fluorescence intensities in the presence and in the absence of added salts respectively. The quenching constants, K_{sv}, evaluated for Br^- and Cs^+ in the aqueous phase at 25 °C are cited in Table 1.

The solubilization phenomena of fluorophores combined with the fluorescence quenching due to inorganic ions bring about additional complexities in the fluorescence analysis, but these complexities will permit the study of various reaction mechanisms occurring in the solution. When NaCl, NaBr, and CsCl are added to the aqueous 7EC and 7E4MC solutions in which 0.025 mol dm^{-3} SDS has been dissolved, the absorption spectra do not change very much except for a slight decrease in ε (a few percent). In spite of the similar absorption spectra, the fluorescence intensity is appreciably decreased by the addition of NaBr and CsCl, which have the fluorescence quenching ability attributable to Br^- and Cs^+ in aqueous solutions without any surfactant. Figures 2 and 3 show plots of I_0/I vs. the concentration of salts in the presence of SDS micelles at 25 °C. It can readily be seen, by comparing the data with the thin solid line (upper), that the quenching ability of NaBr is suppressed by the micelle formation, while, on the contrary, that of CsCl is enhanced. These results can be understood qualitatively, considering that the electrostatically attractive force between the anionic SDS micelle and Cs^+ catalyzes the fluorescence-quenching reaction of the fluorophore embedded in the micelle interior, whereas the repulsive interaction between the micelle and Br^- decreases the probability of a quenching reaction. For Br^- and Cs^+ quenchers in micellar solutions, the Stern-Volmer relation does not hold any more to show nonlinear downward deviations (Figs. 2 and 3).

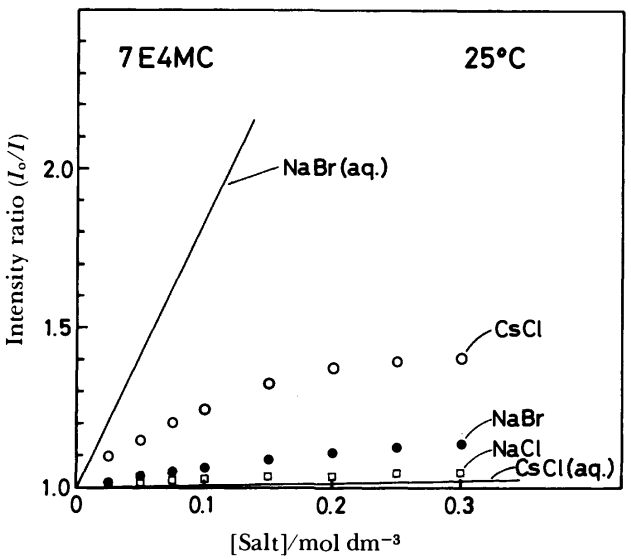

Fig. 3. Dependence of the fluorescence intensity ratio, I_0/I, of 7E4MC on the concentration of salts in aqueous solutions (solid lines) and in 0.025 mol dm^{-3} SDS solutions (data points) at 25 °C.

The addition of NaCl has also induced a decrease of several percent in the fluorescence intensity, probably caused by the change in such micelle parameters as cmc, the aggregation number (n), and the degree of ionization of a micelle (α). These factors are subtly affected by the ionic strength of the solution and will determine the micelle density and the microenvironment around the solubilization site of fluorophores. Since Cl^- has no quenching ability in the aqueous phase and is electrically repelled from the negatively charged head-group of SDS on the surface of sphere-like micelles, we need not think of the quenching from Cl^-. While Na^+ also has no quenching ability in the aqueous phase, there is a possibility that the quenching of the solubilized fluorophore may take place as a consequence of a number of Na^+ ions being attracted onto the negatively charged micelle surface. However, by using the optical detection of magnetic resonance (ODMR), Ghosh et al.[8] proved the absence of perturbation on the π-electron distribution of the fluorophore due to added Na^+ in a naphthalene-sodium n-alkyl sulfate micelle system, in spite of the

Table 1. Quenching Constants, K_{sv} and K'_{sv}, and Quenching-Rate Constants, k_q and k'_q, in the Aqueous and Micellar Phases Respectively of the 0.025 mol dm^{-3} SDS Solution at 25 °C

Quencher	Substance	K_{sv} / mol^{-1} dm^3	K'_{sv} / mol^{-1} dm^3	$k_q \times 10^{-9}$ a) / mol^{-1} dm^3 s^{-1}	$k'_q \times 10^{-9}$ a) / mol^{-1} dm^3 s^{-1}
Br^-	7EC	9.24	0.21	5.13	0.16
	7E4MC	8.38	0.24	3.99	0.13
Cs^+	7EC	0.08	9.84	0.04	7.39
	7E4MC	0.07	8.36	0.03	4.52

a) $\tau = 1.8$ ns (7EC) and $\tau = 2.1$ ns (7E4MC) at 25 °C were used,[1] and τ' was estimated by the use of $\tau' = \tau \cdot (\eta'/\eta)$.

large effect from Cs^+. Furthermore, the addition of NH_4Cl, $NaClO_4$, and Na_2SO_4 with the same ionic strength as NaCl, all of which are, in many cases, thought to have little or no quenching efficiency against coumarin derivatives, induced small changes in the fluorescence intensity, very similar to the case of NaCl. Therefore, Na^+, NH_4^+, Cl^-, ClO_4^-, and SO_4^{--} are not 'fluorescence quenchers,' although a small effect attributable to the ionic-strength change is found for all these ions and cannot be neglected.

Discussion

Model for the Fluorescence Change. To analyze the fluorescence quenching phenomena of fluorophores in an aqueous micellar solution containing various salts as quenchers, we may adopt the following general scheme of the light-emitting mechanism (two-reactive-state model):

$$\begin{array}{l} \mathrm{N} \xrightarrow{G\frac{\varepsilon[\mathrm{N}]}{\varepsilon[\mathrm{N}]+\varepsilon'[\mathrm{D_nN}]}} \overset{*}{\mathrm{N}} \begin{cases} \xrightarrow{k} \mathrm{N}+h\nu \\ \xrightarrow{k_n} \mathrm{N} \end{cases} \\ \qquad\qquad \overset{*}{\mathrm{N}} + \mathrm{Q} \xrightarrow{k_q} \mathrm{N} + \mathrm{Q} \\ \mathrm{D_nN} \xrightarrow{G\frac{\varepsilon'[\mathrm{D_nN}]}{\varepsilon[\mathrm{N}]+\varepsilon'[\mathrm{D_nN}]}} \mathrm{D_n}\overset{*}{\mathrm{N}} \begin{cases} \xrightarrow{k'} \mathrm{D_nN}+h\nu' \\ \xrightarrow{k_n'} \mathrm{D_nN} \end{cases} \\ \qquad\qquad \mathrm{D_n}\overset{*}{\mathrm{N}} + \mathrm{Q} \xrightarrow{k_q'} \mathrm{D_nN} + \mathrm{Q} \end{array} \tag{1}$$

$$\mathrm{D_n} + \mathrm{N} \overset{K_{eq}}{\rightleftharpoons} \mathrm{D_nN} \tag{2}$$

Here, D_n represents the micelle formed of n surfactants. N and D_nN are the ground states of the fluorophore in the aqueous and micellar phases respectively; $\overset{*}{N}$ and $D_n\overset{*}{N}$ are their excited states generated on light illumination. G is the flux of illuminating light, and ε and ε' are the molar extinction coefficients of N and D_nN respectively at the excitation wavelength. $h\nu$ and $h\nu'$ are the light quanta emitted from each molecular species. k's are the rate constants for the radiative transition of $\overset{*}{N}$ and $D_n\overset{*}{N}$ to their ground states, and k_n's are the rate constants for the nonradiative transition. k_q's are the bimolecular quenching-rate constants resulting from the collision with added quencher ions, Q. Assuming that the fluorophore in the aqueous phase is in equilibrium with that in the micellar phase (Eq. 2), the equilibrium constant is given by $K_{eq}=[D_nN]/[D_n][N]$.[6] It may be noted that the fluorophore cannot be transferred between the aqueous and micellar phases in its lifetime of the optically excited state because the time constant needed to attain such equilibriation is of the order of microseconds,[9] while the fluorescence lifetime is about 2 ns, as will be discussed later.

When N and D_nN are excited by the light at a fixed wavelength with a flux, G, the generation rates of $\overset{*}{N}$ and $D_n\overset{*}{N}$ are in proportion to ε and ε' respectively. Therefore, based on the fact the fluorescence spectrum of $\overset{*}{N}$ bears a close resemblance to that of $D_n\overset{*}{N}$, the total fluorescence intensity is given by the summation of the respective intensities at the peak position:

$$I = I_N + I_{D_nN} = \frac{G}{\varepsilon[\mathrm{N}]+\varepsilon'[\mathrm{D_nN}]} \times \left\{\frac{\varepsilon\eta[\mathrm{N}]}{1+K_{sv}[\mathrm{Q}]} + \frac{\varepsilon'\eta'[\mathrm{D_nN}]}{1+K'_{sv}[\mathrm{Q}]}\right\} \tag{3}$$

where the quantum efficiencies of the fluorescers in the aqueous and micellar phases are defined by $\eta=k/(k+k_n)$ and $\eta'=k'/(k'+k_n')$ respectively; their fluorescence lifetimes are $\tau=1/(k+k_n)$ and $\tau'=1/(k'+k_n')$, and the quenching constants are given by $K_{sv}=k_q\tau$ and $K'_{sv}=k_q'\tau'$. Using Eq. 2 and letting the value of I at $[Q]=0$ be I_0, the relative fluorescence intensity is written as:

$$\frac{I}{I_0} = \frac{1+\frac{\varepsilon'}{\varepsilon}K^0_{eq}[\mathrm{D_n}]^0}{1+\frac{\varepsilon'}{\varepsilon}K_{eq}[\mathrm{D_n}]} \cdot \frac{1}{1+\frac{\varepsilon'\eta'}{\varepsilon\eta}K^0_{eq}[\mathrm{D_n}]^0} \times \left\{\frac{1}{1+K_{sv}[\mathrm{Q}]} + \frac{\frac{\varepsilon'\eta'}{\varepsilon\eta}K_{eq}[\mathrm{D_n}]}{1+K'_{sv}[\mathrm{Q}]}\right\} \tag{4}$$

where K^0_{eq} and $[D_n]^0$ are the equilibrium constant and the density of micelles at $[Q]=0$. Apparently, $I_0/I\to 1$ at $[Q]\to 0$. If the dependence of $K_{eq}[D_n]$ on [Q] is small, the first term on the right-hand side of Eq. 4 reaches to unity. Then, at $K_{sv}[Q]$, $K'_{sv}[Q]\ll 1$, $I_0/I\approx 1+aK_{sv}[Q]+bK'_{sv}[Q]$, where $a=1/(1+\frac{\varepsilon'\eta'}{\varepsilon\eta}K_{eq}[D_n])$ and $b=\frac{\varepsilon'\eta'}{\varepsilon\eta}K_{eq}[D_n]/(1+\frac{\varepsilon'\eta'}{\varepsilon\eta}K_{eq}[D_n])$. A more careful inspection of Eq. 4 leads to the prediction that the plot of I_0/I vs. [Q] curves nonlinearly downward apart from the linear relation, $I_0/I=1+aK_{sv}[Q]+bK'_{sv}[Q]$.

If the effect of the ionic strength, i.e., the dependence of $K_{eq}[D_n]$ on [Q], cannot be ignored, the reference of the fluorescence intensity must be replaced, in order to get a tractable formula, by the value under a hypothetical condition, $K_{sv}=K'_{sv}=0$, where no quenching reaction occurs. Letting this reference intensity be $\bar{I}_0$, Eq. 4 is, therefore, rewritten as:

$$\frac{I}{\bar{I}_0} = \frac{1}{1+\frac{\varepsilon'\eta'}{\varepsilon\eta}K_{eq}[\mathrm{D_n}]} \cdot \left\{\frac{1}{1+K_{sv}[\mathrm{Q}]} + \frac{\frac{\varepsilon'\eta'}{\varepsilon\eta}K_{eq}[\mathrm{D_n}]}{1+K'_{sv}[\mathrm{Q}]}\right\} \tag{5}$$

Finally, we attain:

$$\frac{1}{(I/\bar{I}_0)(1+K_{sv}[Q])-1} = \frac{1+\frac{\varepsilon'\eta'}{\varepsilon\eta}K_{eq}[D_n]}{\frac{\varepsilon'\eta'}{\varepsilon\eta}K_{eq}[D_n]} \cdot \times\left(\frac{K'_{sv}}{K_{sv}-K'_{sv}}+\frac{1}{K_{sv}-K'_{sv}}\cdot\frac{1}{[Q]}\right) \quad (6)$$

Equation 6 shows that the plot of $1/\{(I/\bar{I}_0)(1+K_{sv}[Q])-1\}$ vs. $1/[Q]$ is linear if the first term on the right-hand side of Eq. 6 is insensitive to [Q]. Therefore, the quenching constants can be known by means of the slope and intercept of this plot.

Interpretation of the Fluorescence-Quenching Data. The concentrations of 7EC and 7E4MC (C_N) for fluorescence measurements are fixed around 4—5×10^{-5} mol dm^{-3}. Above the cmc, it can reasonably be assumed that a spherical micelle of n surfactant molecules with a diameter of about 4 nm is generated in the solution and that the surfactant-monomer concentration in the bulk-water phase remains constant. Then, the number-density of micelles (C_M) is estimated by using the total concentration of the added surfactant (C_S) as $C_M=(C_S-\text{cmc})/n$. For the aqueous solution of SDS at 25 °C, the cmc and n are 8×10^{-3} mol dm^{-3} and 62 respectively.[10,11] As $C_S=2.5\times10^{-2}$ mol dm^{-3}, C_M is estimated to be $\approx3\times10^{-4}$ mol dm^{-3}, which is greater than the added fluorophore concentration (C_N) by one order of magnitude. Under such conditions, almost all fluorophores are solubilized into the micelle,[6] and the concentration of empty micelles is given simply by $[D_n]\approx C_M-C_N\approx2.5\times10^{-4}$ mol dm^{-3}. The molar extinction coefficients of 7EC and 7E4MC in the micelle (ε') and in the bulk water (ε) are independently measurable at $C_S\gg$cmc and at $C_S=0$ respectively. The ε'/ε values in an aqueous SDS micellar solution at the excitation wavelength are 0.972 (7EC) and 0.965 (7E4MC). The ratio of the quantum efficiencies, η'/η, can be estimated, by the use of a method described earlier,[6] as 0.74 (7EC) and 0.88 (7E4MC). Anyhow, if the salt effect does not seriously change the situation, the factor, $\varepsilon'\eta'/\varepsilon\eta$, in Eq. 4 should be a constant slightly less than unity.

The fluorescence-yield change shown in Figs. 2 and 3 as a function of the concentration of added salts is essentially explained by Eq. 4. However, such nonlinear plots for micelle-quencher systems are so complex to analyze that a more convenient expression to argue quantitatively (Eq. 6) has been proposed. First, the reference intensity ($\bar{I}_0$) corresponding to the case of $K_{sv}=K'_{sv}=0$ must be determined in accordance with the experiments. As has been mentioned earlier, the addition of NaCl to the micellar system induces a slight decrease in the fluorescence intensity. Since Cl^- has no quenching ability in the aqueous phase and is repelled from the negatively charged SDS micelle, this ion, apparently, cannot contribute to the fluorescence quenching in the micellar phase. In spite of the attractive interaction with SDS micelles, Na^+ has been proved to cause no electronic reaction against the molecule embedded in SDS micelles; this is in contrast to the case of Cs^+, which is confirmed by means of the ODMR technique.[8] Therefore, the fluorescence decrease upon the addition of NaCl is not caused by the quenching effect, but by the change in ionic strength, forcing micelles to alter their characteristic parameters (cmc, n, and α). Thus, $\bar{I}_0$ can be determined as the fluorescence intensity of the solution in which NaCl of the same ionic strength as the quenchers employed (NaBr and CsCl) is dissolved. Experimentally, C_M and, consequently, $[D_n]$ do depend on the amount of salt added through the change in cmc and n. Moreover, the salt effect on K_{eq} may also be important.[12] It is very difficult, at present, to know quantitatively the exact effect from the ionic-strength changes. Irrespective of all such complexities, however, it should be noted that the standard of the fluorescence intensity has always been taken from the solution with an appropriate amount of NaCl.

As the $I/\bar{I}_0$ appearing on the left-hand side of Eq. 6 can thus be calculated at each [Q] by using the experimentally determined $\bar{I}_0$ value, and since K_{sv} has already been known from an independent experiment in a simple aqueous solution (Table 1), it now becomes possible to plot $1/\{(I/\bar{I}_0)(1+K_{sv}[Q])-1\}$ vs. $1/[Q]$. These plots are shown for Br^- in Fig. 4 and for Cs^+ in Fig. 5. The signs on both sides of Eq. 6 are reversed for the Cs^+ quencher because the sign of $K_{sv}-K'_{sv}$ depends on the charge of the quencher ions. The data points in Figs. 4 and 5 obey very well the expected linear relationship, thus showing the good applicability of the proposed model irrespective of the charge type of the inorganic quenchers. The quenching constants (K'_{sv}) of the fluorescer solubilized in SDS micelles due to Br^- and Cs^+ are calculated by dividing the intercept by the slope of the plots in Figs. 4 and 5; they are cited in Table 1. For Br^-, K'_{sv} is much less than K_{sv}. This reduction is caused by the repulsive force between the anionic micelle and the anionic quencher. For Cs^+, on the contrary, K'_{sv} becomes larger by about two orders of magnitude than K_{sv}, the change being more drastic than in the case of Br^-. The associative interaction of the positively charged Cs^+ ion with the anionic micelle catalyzes to quench the fluorescence. Similar phenomena were observed by Eftink and Ghiron[13] for indole derivatives in a SDS micelle-Cs^+ system, but their analysis was only a primitive one insufficient for discussing the quenching mechanism in detail.

The lifetimes (τ) of 7EC and 7E4MC in the aqueous solution have been measured in Ref 1. The lifetimes (τ') in the micelle can be calculated by the use of $\tau'=\tau\cdot(\eta'/\eta)$. Then the quenching-rate constants k_q

($=K_{sv}/\tau$) and k_q' ($=K_{sv}'/\tau'$) are obtained as is shown in Table 1. It is reasonable that 7EC and 7E4MC have the same order of k_q values, for these molecules are different only in the substituent at the 4-position. The k_q and k_q' values of 7EC are always larger than those of 7E4MC. Since this tendency is independent of the charge on quencher ions, and also of the environmental conditions in the aqueous and micellar phases, the quenching reaction seems to be partly screened off by the 4-methyl substituent. The ratio of k_q values for 7EC and 7E4MC in the aqueous phase is nearly equal to the ratio in the micellar phase, irrespective of whether the quencher is Br^- or Cs^+. If the screening effect of the 4-methyl substituent is equally operative in both phases, this parallelism shows that the solubilization sites of the fluorophore should be essentially identical in position. It has already been shown that the polarities felt by these fluorophores

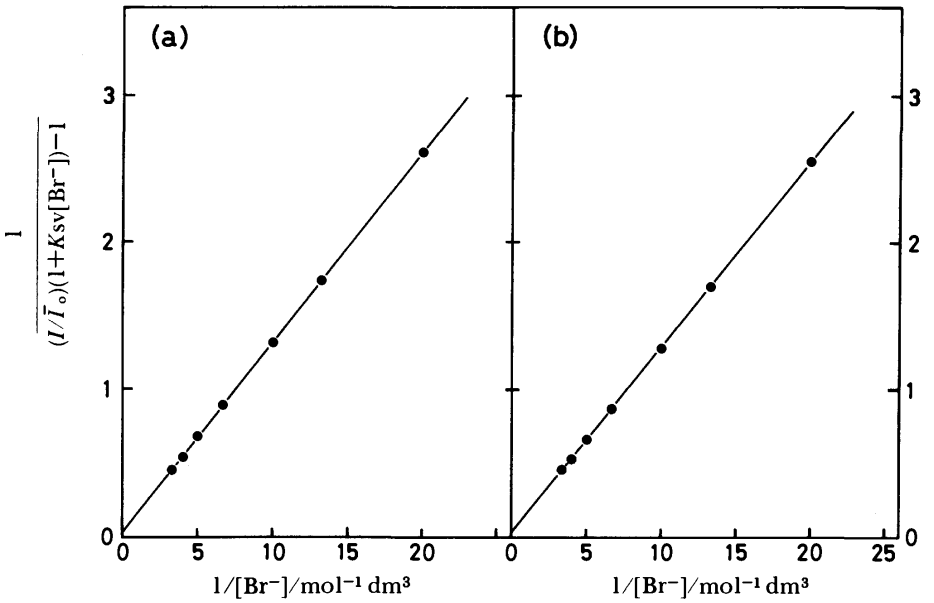

Fig. 4. Plots of $1/\{(I/\bar{I}_0)(1+K_{sv}[Br^-])-1\}$ vs. $1/[Br^-]$ in the 0.025 mol dm^{-3} SDS solution at 25 °C. (a), 7EC; (b), 7E4MC.

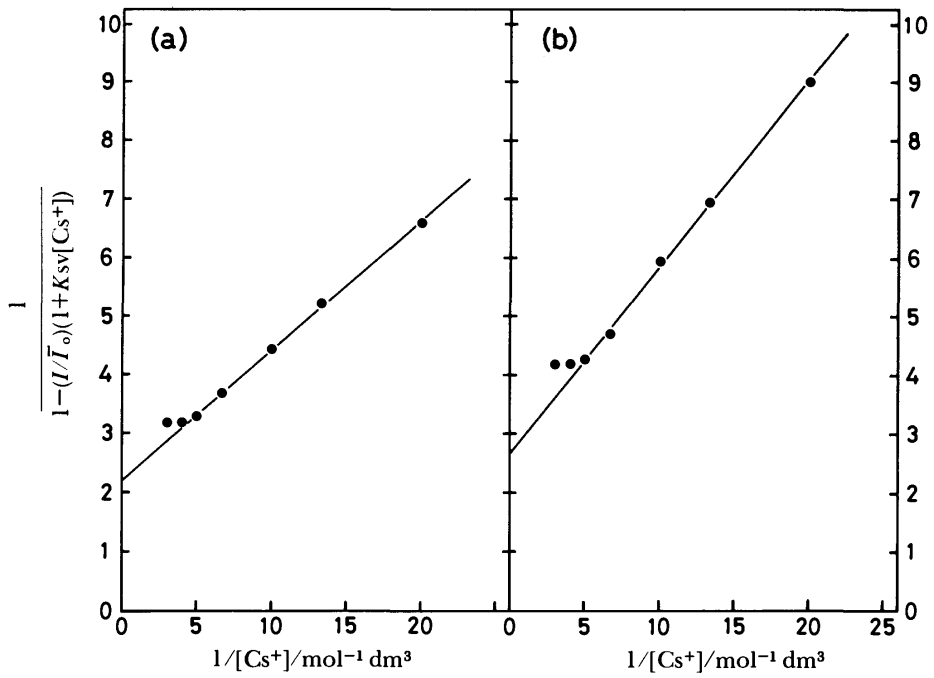

Fig. 5. Plots of $1/\{1-(I/\bar{I}_0)(1+K_{sv}[Cs^+])\}$ vs. $1/[Cs^+]$ in the 0.025 mol dm^{-3} SDS solution at 25 °C. (a), 7EC; (b), 7E4MC.

within the SDS micelle are very similar,[6] a finding which supports the conclusion presented above.

The most probable quenching mechanism for Br^- is the charge-transfer interaction between the ion and the fluorophore, as has been pointed out in earlier works.[1,4,5] If the encounter distance between the fluorescer and quencher, R, and the sum of the diffusion coefficients of each species in aqueous solutions, D, at 25 °C are reasonably assigned as 0.7 nm and 1.5×10^{-5} cm^2 s^{-1} by means of the Stokes-Einstein relation (fluorophore radius ≈0.47 nm; van der Waals radius of Br^-≈0.23 nm), the diffusion-limited value of the quenching-rate constant (k_1) for Br^- is estimated to be $\approx8\times10^9$ mol^{-1} dm^3 s^{-1}, with $k_1=4\pi NRD$, where N is the Avogadro number. If all collisional events among fluorescers and quenchers result in the quenching reaction, k_q will coincide with k_1 and the quenching efficiency (γ) will become unity. Since the experimentally obtained k_q for Br^- (Table 1) is about one-half of k_1, $\gamma\approx0.5$. In contrast to this, k_q' for Br^- is only 1.5—2% of k_1 (Table 1). Such a situation can readily be understood on the basis of the idea that Br^- impinging on the micelle surface is repelled instantaneously by the negatively charged SDS head-groups as a result of electrostatic repulsion and the quenching reaction with the solubilized fluorophore rarely occurs. When I^- is employed as a quencher instead of Br^-, large quenching effects have been observed in both the aqueous and micellar phases. Because the quenching ability of I^- against 7EC and 7E4MC is very high, and because the Stern-Volmer relation does not hold even in a simple aqueous solution,[1] it has been impossible to treat the case of I^- quantitatively within the framework developed here. Quina et al.[14] have investigated the I^- quenching of a pyrene derivative in SDS micelles; they have analyzed it in terms of a two-reactive-state model in which only one of the states (the aqueous phase) is quenchable. This assumption, which represents a special case of the generalized scheme given by Eq. 1, is insufficient for the analysis of a coumarin derivative-SDS micelle system, as is apparent from the investigation of Br^-.

The fluorescence-quenching mechanism due to inorganic cations in aqueous solutions has not been so clear as in the case of inorganic anions, such as halides and pseudohalides.[4,5] As is cited in Table 1, the k_q values for Cs^+ in the aqueous phase are smaller than the values for Br^- by about two orders of magnitude. 7EC and 7E4MC are neutral molecules, and the cations and anions of interest (e.g., Rb^+, Cs^+, Br^-, and I^-) have similar mobilities in aqueous solutions.[15] Therefore, the collisions between the fluorescer and the various quenchers will be nearly equal in probability; if so, the heavy-atom effects from Rb^+ and Br^- and from Cs^+ and I^- should be of the same order. Nevertheless, the experimentally determined quenching-ability order is $I^->Br^-\gg Cs^+>Rb^+$, irrespective of the order of the atomic weights, which are rough measures of the spin-orbit coupling. Further, the ionic radii and the enthalpy changes for the hydration of Br^- and Cs^+ are so similar that there is no positive explanation for the widely different quenching abilities of Cs^+ and Br^- in terms of the participation of heavy-atom effect. The charge-transfer mechanism may, instead, be operative for the cation-quenching. The quenching ability of halide ions is known to increase as the ionization energy of the ion ($X^-\rightarrow X$) is decreased; therefore, the origin of quenching was concluded to be the electron transfer from the quencher to the fluorescer.[4,5] Since the electron-affinity order of alkali ions ($M^+\rightarrow M$) is $Na^+>K^+>Rb^+>Cs^+$, the quenching ability caused by the charge-transfer from the fluorescer to the quencher, if possible, must align in the same order. This idea is not applicable to the present problem, however, because the quenching ability is ordered experimentally as $Cs^+>Rb^+>K^+\approx Na^+\approx0$. The electron-transfer from the cation to the fluorescer that generates dication is energetically more improbable. Although these contradictions will be partly mitigated by the subtle hydration effect that depends on the ionic radius, it is unreasonable to think that either the heavy-atom effect or the charge-transfer interaction is mainly responsible for the weak cationic quenching in the aqueous phase. The most natural explanation possible at present is that the weaker hydration of Cs^+ than of the other cations, indicated by the smaller Stokes' radius for hydrated ions,[15] enables it to come in closer contact with the fluorescer; consequently, an induced electronic perturbation increases the non-radiative deactivation of the fluorescer.

The quenching-rate constant of Cs^+ for the fluorescer in micelles (k_q') becomes larger than k_q by more than two orders of magnitude. This increase in k_q' is qualitatively expected from the attractive interaction between the SDS micelle and Cs^+. However, there occurs the problem which of 'static' and 'bimolecular' quenching mechanisms will really operate in the solution. When the Na^+ of the original counterion of SDS is gradually replaced by Cs^+ by adding CsCl, the concentration of Cs^+ near the micelle surface steadily becomes higher than that in the bulk water. Under such circumstances, it is predictable for a ground-state complex like D_nN-Cs^+ to be generated, thus leading to an instantaneous deactivation of the optically excited state. However, it has not been detected by the measurement of the absorption spectra at any high concentration of added Cs^+. The 'static' or ground-state-complex induced quenching, therefore, can be discarded or need not be taken into account. It can be justified, on the basis of this result, that, at the beginning of analysis, the quenching effect predicted by Eq. 1 is based on the bimolecular interaction

between fluorescers and quenchers. Using the van der Waals radius of Cs^+ ($r_v \approx 0.2$ nm), the diffusion-limited value of the quenching constant, k_1, becomes $\approx 9\times10^9$ $mol^{-1}\,dm^3\,s^{-1}$. The k_q values are so small compared to k_1 that the Cs^+ in the aqueous phase is only a weak quencher. Since the SDS micelle is a spherical particle with a radius of about 2 nm, the collisional rate between the micelle and ion amounts to $\approx 2\times10^{10}$ $mol^{-1}\,dm^3\,s^{-1}$. Considering that the k_q' values for Cs^+ are several tenths of this value, the collisions between Cs^+ and the micelle would lead to a nonradiative deactivation of the excited state only when Cs^+ has come close to the solubilized fluorophore, possibly residing in the micelle interior, but very near the surface. Among bimolecular mechanisms, a contact-type interaction of Cs^+ such as a heavy-atom effect cannot be effective for a fluorescer embedded in the micelle interior across the palisade layer with an interfacial potential barrier. As has been mentioned in the case of the bulk-water phase, there is also no physical reason for the effective occurrence of charge-transfer interaction between the fluorescer and Cs^+. Ghosh et al.[8] have shown that the association of Cs^+ ions with SDS micelles can serve to decrease the extent of the hydration of the micelle, making a less polar environment for the fluorophore. Since the fluorescence yield of 7EC and 7E4MC is sensitively dependent on the polarity of the microenvironment,[6] the polarity change due to the cation becomes a possible candidate for a reasonable explanation. The quenching ability of Cs^+ in the aqueous phase is very low, but it becomes very large for the solubilized fluorophore by virtue of the incident flux of Cs^+ ions toward the micelle surface. Cs^+ impinges against the surface by thermal agitation and electrostatic attraction, and will be exchanged with loosely bounded counterions. Since Cs^+ has a smaller hydrated Stokes' radius than Na^+,[15] it can approach closer to the micelle interface to induce the environmental-polarity change around the fluorophore. It is instructive to notice that the photoionization yields of perylene in SDS micelles was decreased by the addition of monovalent inorganic salts,[16] although the electron-liberation process occurring under a high-energy UV excitation has no direct correlation with the quenching process of the present problem. The binding degree of the counterion at the micelle interface seems to depend on the size of the hydrated ions, and the change in the photoionization efficiency has been understood in terms of the expectation that smaller hydrated ion radii favor a closer approach to the surface and decrease the interfacial electric potential extensively. Considering these results and the difficulty that hydrated inorganic ions have in penetrating deep into the hydrophobic core region of micelles, the solubilization site of the fluorophore must be near to the micelle interface rather than in the micelle core in order that the Cs^+ quenching caused by the collision of Cs^+ against the micelle surface operates efficiently. In addition, it may be possible to generate an activated encounter-complex described by a structure like $D_n^*N\cdots Cs^+\cdots(H_2O)_n$, where D_n^*N is the fluorescer in the micelle, H_2O is solvated water, and the dots describe loose couplings as presented in the 'outer-sphere' reaction between a metal ion and a ligand of metal-complexes. The role of such a cation-bridged complex was emphasized by Shporer et al.[17] to explain the electron-transfer reaction between cyano-metal complexes in a solution in which cations have been dissolved as catalysts; they found that the reaction rate increases from Li^+ to Cs^+. In the present case, although it seems unlikely that the electron transfer really occurs between the fluorescer and solvated water, the cation-assisted complexation may contribute effectively to the nonradiative deactivation of excited fluorophores. It is believed that the polarity change and the formation of the excited-state complex will act in concert to enhance the quenching ability of Cs^+ in the anionic micellar system.

Limitation on the Applicability of the Proposed Model. The discussion has hitherto proceeded by assuming that the first term on the right-hand side of Eq. 6, $\left(1+\frac{\varepsilon'\eta'}{\varepsilon\eta}K_{eq}[D_n]\right)/\frac{\varepsilon'\eta'}{\varepsilon\eta}K_{eq}[D_n]$, is independent of the added salt concentration. If $(\varepsilon'\eta'/\varepsilon\eta)K_{eq}[D_n] \gg 1$, this assumption is valid no matter how much the term depends on the salt concentration. By means of the slope of the plots in Fig. 4 and the obtained K_{sv} and K_{sv}' values shown in Table 1, the value for Br^- can be estimated to be $(\varepsilon'\eta'/\varepsilon\eta)K_{eq}[D_n] \approx 6.1$ (7EC) and ≈ 38.6 (7E4MC), which satisfy the assumption. Further, the C_M ($=(C_S-\text{cmc})/n$) necessary for the estimation of $[D_n]$ is only weakly dependent on the ionic strength under the experimental condition employed, as cmc is decreased while, on the contrary, n is increased by the addition of salts. These two reasons for the insensitiveness of the first term in Eq. 6 to the ionic strength confirm that the data follow very generally the theoretically predicted linear relationship. Since the counterion of an aqueous SDS micelle, Na^+, is not changed by the addition of NaBr, the factor of $\varepsilon'\eta'/\varepsilon\eta$ can be approximated by the value with no added salt (salt-free conditions).[6] Then, the $K_{eq}[D_n]$ values are 8.4 (7EC) and 45.7 (7E4MC). When the 'solubilization ratio' of the fluorophore is defined by $p=[D_nN]/([D_nN]+[N])$, p is rewritten as $p=K_{eq}[D_n]/(K_{eq}[D_n]+1)$; its values are estimated to be 0.89 (7EC) and 0.98 (7E4MC). These p values are very close to those in a salt-free SDS micelle[6] and show that the majority of fluorophores exist in the micelle even in NaBr is added to the solution. If $[D_n]$ should be approximated by $[D_n] \approx C_M - C_N \approx 2.5\times10^{-4}$ mol dm^{-3}, as carried out before under salt-free conditions, the K_{eq} values can be calculated as 3.4×10^4 $mol^{-1}\,dm^3$ (7EC) and 1.8×10^5

$mol^{-1}\,dm^3$ (7E4MC); these values are in good accord with the value based on a different method[6] in spite of the approximations used here and the existence of the additive.

From Fig. 5, the $(\varepsilon'\eta'/\varepsilon\eta)K_{eq}[D_n]$ values for Cs^+ are calculated to be 0.85 (7EC) and 0.61 (7E4MC), smaller than the values for Br^- by one or more orders of magnitude. If the first term of Eq. 6 varies through the dependence of $K_{eq}[D_n]$ on $[Cs^+]$, the applicability of the linear relationship is restricted. As may be seen in Fig. 5, data have deviated systematically from the theory at high concentrations of CsCl (at small $1/[Cs^+]$). The region where the proposed model seems valid is, at most, from $[Cs^+]=0.05$ to $0.2\,mol\,dm^{-3}$. There may be another possibility that the static quenching process mentioned earlier begins to contribute at higher Cs^+ concentrations, although no sign of the ground-state complex formation has yet been detected spectroscopically. When the counterions of the micelle are changed from Na^+ to Cs^+, ε' shows no observable change. η' will decrease with this change through the generation of a less polar environment by the Cs^+ attachment to the micelle surface. However, the amount of decrease is believed to be not very large, for the fluorescence yields of 7EC and 7E4MC are a smoothly varying function of the environmental polarity,[6] which cannot explain the drastic decrease in $(\varepsilon'\eta'/\varepsilon\eta)K_{eq}[D_n]$. Possibly, $K_{eq}[D_n]$ or p is affected by the polarity change around the solubilization site, which serves to make the state of the solubilized fluorophores unstable. The latter may be the main reason for the observed decrease in the solubilization ratio. It must be mentioned in this connection that, if η' is decreased by adding CsCl instead of NaCl or NaBr, the k_q' value for Cs^+ in Table 1 understimates the quenching reaction, for η' under salt-free conditions is employed in the estimation.

Hautala et al.[18] have reported large and complex effects of oxygen on the fluorescence lifetimes of naphthalene in aqueous micellar solutions in addition to the fluorescence-quenching effects attributable to inorganic ions. The situation is different from the case of coumarin derivatives because the fluorescence lifetimes of 7EC and 7E4MC ($\tau\approx2$ ns) are too short to be affected by a quenching process caused by oxygen in comparison with the case of naphthalene ($\tau\approx40$ ns). Experimentally, no quenching phenomenon caused by dissolved oxygen has been found through the examination of deaerated samples.

The author wishes to thank Dr. Hiroyuki Anzai of this laboratory for his helpful advice and stimulating discussions. This work was supported by the special research program on "Molecular Electronics" of the Ministry of International Trade and Industry, Agency of Industrial Science and Technology.

References

1) T. Moriya, *Bull. Chem. Soc. Jpn.*, **57**, 1723 (1984).
2) T. Moriya, *Bull. Chem. Soc. Jpn.*, **59**, 961 (1986).
3) N. Mataga and T. Kubota, "Molecular Interactions and Electronic Spectra," Marcel Dekker, New York (1970), Chap. 9, p. 470.
4) R. Beer, K. M. C. Davis, and R. Hodgson, *J. Chem. Soc., Chem. Commun.*, **1970**, 840.
5) A. R. Watkins, *J. Phys. Chem.*, **78**, 2555 (1974).
6) T. Moriya, *Bull. Electrotech. Lab.*, **50**, 1123 (1986).
7) P. Mukerjee and K. J. Mysels, *Nat. Stand. Ref. Data Ser.*, **NBS36**, 51 (1971).
8) S. Ghosh, M. Petrin, and A. H. Maki, *J. Phys. Chem.*, **90**, 5206 (1986).
9) N. M. Atherton and S. J. Strach, *J. Chem. Soc., Faraday Trans. 2*, **68**, 374 (1972).
10) H. Coll, *J. Phys. Chem.*, **74**, 520 (1970).
11) K. Granath, *Acta Chem. Scand.*, **7**, 297 (1953).
12) S. Glasstone, K. J. Laidler, and H. Eyring, "The Theory of Rate Processes," McGraw-Hill, New York (1964), Chap. 8.
13) M. R. Eftink and C. A. Ghiron, *J. Phys. Chem.*, **80**, 486 (1976).
14) F. H. Quina and V. G. Toscano, *J. Phys. Chem.*, **81**, 1750 (1977).
15) P. Mukerjee, K. J. Mysels, and P. Kapauan, *J. Phys. Chem.*, **71**, 4166 (1976).
16) S. Hautecloque, D. Grand, and A. Bernas, *J. Phys. Chem.*, **89**, 2705 (1985).
17) M. Shporer, G. Ron, A. Loewenstein, and G. Navon, *Inorg. Chem.*, **4**, 361 (1965).
18) R. H. Hautala, N. E. Schore, and N. J. Turro, *J. Am. Chem. Soc.*, **95**, 5508 (1973).

Energetics of the Sequential Electroreduction and Electrooxidation Steps of Benzenoid Hydrocarbons[1)]

Tanekazu KUBOTA,* Kenji KANO, Bunji UNO, and Tomonori KONSE
Gifu Pharmaceutical Universtiy, 5-6-1 Mitahora-higashi, Gifu 502
(Received May 6, 1987)

The first and second reduction ($E^{red}_{1/2\cdot1}$, $E^{red}_{1/2\cdot2}$) and the first oxidation ($E^{oxd}_{1/2\cdot1}$) standard potentials of benzenoid alternant hydrocarbons (BAH) were experimentally determined by means of cyclic voltammetry (CV) in nonaqueous solvents. The second standard oxidation potential ($E^{oxd}_{1/2\cdot2}$) was, however, estimated by checking the scan rate dependence of the irreversible CV curve. The equations pertinent to these potentials and their mutual relations were formulated from the points of view of the Born-Haber-type thermodynamic energy cycle and SCFMO calculations. Of the SCFMO calculations, the MO-paring property established in the PPP-type π-electron theory was very successful in the discussion of the equations given above. Under the acceptable assumptions that the solvation energies due to mono- and dications are put equal to those of the mono- and dianions respectively, and using the MO-pairing property, the equation of $(E^{oxd}_{1/2\cdot1}+E^{red}_{1/2\cdot1})=(E^{oxd}_{1/2\cdot2}+E^{red}_{1/2\cdot2})$ was derived. The experimental results were well described by this equation. The solvation-energy values were evaluated by applying the experimentally determined reduction or oxidation potentials to the theoretical equations. An examination of the solvation energies has shown that these values can be interpreted by means of the Born-type equation.

It is well-known that the voltammetric reduction and oxidation of usual organic substances show two waves in nonaqueous solvents;[2-5)] these waves are correlated with the formation of the monoanion radical R^- and the dianion $R^=$ for the reduction and the monocation radical R^+ and the dication R^{++} for the oxidation. Especially, the voltammetric reduction and oxidation behavior of aromatic hydrocarbons in nonaqueous solvents has been studied by many workers in connection with their investigations of the radical ions themselves or electrochemical and chemical reactions immediately following the radical-ion formation.[6-8)] The molecular orbital description for the first half-wave reduction ($E^{red}_{1/2\cdot1}$) and oxidation ($E^{oxd}_{1/2\cdot1}$) potentials was also discussed[6-15)] and written by the sum of the LUMO (ε_{lu}) or HOMO (ε_{ho}) energy and the solvation energy, as is given by Eqs. 1 and 2:[7-15)]

$$FE^{red}_{1/2\cdot1}(R^-/R) = \Delta G^\circ - \varepsilon_{lu} - \Delta E^-_{solv} \quad (1)$$

$$FE^{oxd}_{1/2\cdot1}(R^+/R) = \Delta G^\circ - \varepsilon_{ho} + \Delta E^+_{solv} \quad (2)$$

where the absolute potential of a reference electrode is denoted by ΔG°[16)] and where $\Delta E^-_{solv}=(E^-_{solv}-E_{solv})$ and $\Delta E^+_{solv}=(E^+_{solv}-E_{solv})$ are the solvation-energy difference between monoanion and neutral species and that between monocation and neutral species respectively. The linear relation of the $E^{red}_{1/2\cdot1}$ vs. ε_{lu} plot or the $E^{oxd}_{1/2\cdot1}$ vs. ε_{ho} plot has been reported using HMO or semiempirical SCFMO;[6-15,17-19)] also, the values of ΔE^-_{solv} and ΔE^+_{solv} have been estimated by means of Eqs. 1 and 2.[12)] In turn, Hush and Blackledge[20)] discussed first the reduction potential difference between $E^{red}_{1/2\cdot1}$ and $E^{red}_{1/2\cdot2}$ (the second half-wave reduction potential) by using π-SCFMO in neutral species, showing that the difference stands for the free-energy change pertinent to the disproportionation $2R^- \rightleftarrows R+R^=$ and is in intimate correlation with the two-electron-repulsion-integral γ_H at LUMO.[20,21)] However, the monoanion and dianion are necessarily in a quite different electronic structure from that of the neutral species, so that their discussion is only qualitative. Keeping this fact in mind, in a previous paper[19)] we ourselves again discussed and formulated the mutual relation between $E^{red}_{1/2\cdot1}$ and $E^{red}_{1/2\cdot2}$ from the points of view of the Born-Haber-type thermodynamic energy cycle and SCFMO calculation under the assumption that the above reduction waves are for a reversible system. The theoretical equations thus formulated were experimentally examined using stilbene derivatives as model substances, with the result that the theoretical and experimental outcomes were found to be reasonably compatible.[19)] Here we have newly derived the equations with regard to the mutual relation between the first ($E^{oxd}_{1/2\cdot1}$) and the second ($E^{oxd}_{1/2\cdot2}$) half-wave oxidation potentials. The equations mentioned above on the first and second reduction and oxidation potentials and their mutual correlations have been quantitatively examined using benzenoid alternant hydrocarbons (BAH) in order to verify their reliability, because the BAH's are the fundamental substances for testing a theoretical treatment. In addition, the solvation energies of the monoanion, monocation, dianion, and dication were evaluated using the above equations. The details of these examinations will be reported here.

Experimental

Cyclic Voltammetry. The half-wave reduction potentials of various kinds of BAH were polarographically reported by Hoytink et al.[2,6)] and later by other workers in nonaqueous solvents.[7-12,22,23)] Hoytink's data were mainly obtained in 75 and 96 % aqueous dioxanes vs. a saturated calomel electrode (SCE).[2,6)] However, the data of $E^{red}_{1/2\cdot2}$ were not sufficient. Parker and his colleagues[8,15)] also carried out

much work on the nonaqueous voltammetries of BAH and other organic substances; they recommended the use of neutral alumina,[24] which is added in a nonaqueous sample solution in order to remove the moisture thoroughly from nonaqueous solvents so that one can record the reversible cyclic voltammograms (CV) for $E^{red}_{1/2\cdot2}$ as well as the $E^{red}_{1/2\cdot1}$ and $E^{oxd}_{1/2\cdot1}$, and also for $E^{oxd}_{1/2\cdot2}$ in some organic substances. For our present purpose, the measurement of reduction and oxidation potentials in reversible redox systems of BAH is, of course, to be hoped for, so much effort was made along these lines using Parker's alumina method.[24] Our experiments were as follows: The instruments used for the CV measurements were the same as were employed in our foregoing study.[19] In the present experiment, however, positive feedback circuits were added to the above instruments for a so- called IR-drop compensation, though the instruments consist of a three-electrode system.[19,25,26] The CV curves were recorded at various sweep rates. The working electrode was a platinum rod, 1 mm in diameter and sealed in a soft glass tube with a diameter of ca. 6.5 mm.[27] Just before use, we polished the plane head of the platinum electrode with a polishing powder, "Royal Diamond Compound," commercially available. The nonaqueous electrolysis cell used here was the same as that previously reported.[18,19,26,28] A saturated calomel electrode (SCE) was employed as a reference electrode.

Purification of Solvents. The solvents for the reduction and oxidation CV measurements were *N,N*-dimethylformamide (DMF) and acetonitrile (AN) respectively, in which 0.1 mol dm^{-3} of tetrapropylammonium perchlorate (TPAP) had been dissolved as a supporting electrolyte. The purification of DMF (Dotite Spectrosol) was carefully done by the method recommended by Juillard;[29] i. e. the impurities were removed by treatment with P_2O_5, KOH, and picric acid, its distillation always being carried out in reduced pressure under a nitrogen atmosphere. Just after the purification, we used the DMF for our experiments. AN of Dotite Spectrosol was first treated overnight with CaH_2 and then distilled, all the operations being done in a stream of N_2.[19,26] According to the method of Hammerich and Parker,[24] the AN was then passed through a column of a neutral alumina (Woelm W 200, active-grade Super I; water addition, 0%; ICN Biomedicals) into the vessel under an N_2 atmosphere.

Experimental Procedure. The sample solutions were prepared as follows. The necessary amounts of the samples and TPAP were weighed into a 20-ml volumetric flask; then the flask as well as a nonaqueous electrolysis cell were dried overnight in a vacuum desiccator. In a dry box completely filled with N_2 gas, the samples in the flask were dissolved with DMF or AN, and then transferred into the electrolysis cell, containing about 10 g of the above neutral alumina, a good suspension of which is required, before recording the CV curves. All the measurements were carried out at 25±0.1 °C at a concentration of 0.5—1×10^{-3} mol dm^{-3}. The dissolved oxygen was removed by bubbling N_2 gas through the sample solution, and then the inactive gas was passed over the solution surface during the measurement. The trace of moisture in the N_2 gas was removed by immersing the N_2-gas guide tube into a liquid-nitrogen bath. The method of purifying TPAP was the same as previously reported.[18,19,26,28] The neutral alumina was always kept in a nitrogen atmosphere.

Samples. The hydrocarbons employed in the present study are listed in Table 1. All of them were commercially available from Aldrich and Wako Chemical Co. The samples were recrystallized several times from ether, methanol, ethanol, benzene, benzene plus ethanol, benzene plus methanol, and toluene for Samples No. (**1**), (**2**), (**5**,**6**,**10**,**13**), (**7**,**12**), (**3**), (**11**), and (**9**) respectively.[30] High-vacuum sublimation was also used to purify Samples **3**, **4**, **8**, and **9**. All the melting points agreed well with those in the literature, and the elemental analyses of all the samples were in good agreement with the calculated values.

MO Calculation

In order to interpret the relations between $E^{red}_{1/2\cdot1}$ and $E^{red}_{1/2\cdot2}$ and also between $E^{oxd}_{1/2\cdot1}$ and $E^{oxd}_{1/2\cdot2}$ values, MO calculations were carried out by using the methods of Pariser-Parr-Pople (PPP), CNDO/2, and the ab initio STO-3G basis set for closed shell systems, such as neutral molecules and their dianions and dications.[31,32] In the case of monoanion and monocation radicals in their doublet ground states, we have applied a restricted Longuet-Higgins-Pople type open-shell SCFMO (LP-SCFMO) calculation for π-electron systems.[33,34] The molecular geometries of BAH were determined using the Nishimoto-Forster equation,[35] $r_{cc}=1.517-0.180P_{cc}$, where r_{cc} and P_{cc} are the bond distance and the π-bond order on the nearest neighbor carbon atoms. PPP calculations of neutral species started from the regular hexagon of $r_{cc}=1.396$ Å. After repeating the calculation, final r_{cc} values in the self-consistent as regards P_{cc} were obtained. In this case, the bond angles were altered within 120±2° so as to keep the molecular symmetry.[36] In the PPP- and LP-SCFMO calculations, Nishimoto-Mataga's equation[37] was employed for the evaluation of the two-center-repulsion-integrals, and the core resonance integral, β^{core}_{cc}, was fixed as −2.37 eV for the sake of convenience.[36] The total energies were calculated using the CNDO/2 and ab initio STO-3G methods. The PPP calculation was carried out with an NEC PC-9801 microcomputer, but the other calculations were performed with the FACOM M-382 and HITAC M-680H computers in the Nagoya University Computation Center and the Okazaki Institute for Molecular Science respectively.

Results and Discussion

Theoretical Correlation of the First and Second Half-Wave Potentials Pertinent to Reversible Reduction or Oxidation Processes. In the foregoing paper we discussed the physical meaning of $E^{red}_{1/2\cdot2}$, $(E^{red}_{1/2\cdot1}+E^{red}_{1/2\cdot2})$, and $(E^{red}_{1/2\cdot1}-E^{red}_{1/2\cdot2})$ from the points of view of the thermodynamical energy cycle and the MO calculation, and also by referring to the derivation of Eq. 1. Equations 3—5 were thus obtained:[19]

$$FE^{red}_{1/2\cdot2}(R^{=}/R^{-}) = \Delta G^{\circ} - \varepsilon^{-}_{so} - \gamma^{-}_{ss} - \Delta E^{=}_{solv} \qquad (3)$$

$$F(E^{red}_{1/2\cdot1} + E^{red}_{1/2\cdot2}) = 2\Delta G^\circ - (\varepsilon^-_{so}+\varepsilon_{1u}+\gamma^-_{ss}) - (\Delta E^-_{solv}+\Delta E^=_{solv}) \quad (4)$$

$$F(E^{red}_{1/2\cdot1} - E^{red}_{1/2\cdot2}) = (\varepsilon^-_{so}-\varepsilon_{1u}+\gamma^-_{ss}) + (\Delta E^=_{solv}-\Delta E^-_{solv}) \quad (5)$$

where the electronic structures of neutral species, monoanion, and dianion are considered separately, ε_{lu} and ε^-_{so} being the LUMO and SOMO (singly occupied MO) energies for neutral and anion radical species respectively. The Coulomb-repulsion integral caused by the two electrons in the SOMO of a monoanion is written as γ^-_{ss}. The solvation energy terms, $\Delta E^=_{solv}$, $(\Delta E^=_{solv}-\Delta E^-_{solv})$, and $(\Delta E^-_{solv}+\Delta E^=_{solv})$, are given by $(E^=_{solv}-E^-_{solv})$, $(E^=_{solv}+E_{solv}-2E^-_{solv})$, and $(E^=_{solv}-E_{solv})$ respectively.[38] Equation 4 is very important for evaluating the solvation energy of a dianion (see below), and Eq. 5 is in intimate correlation with the disproportionation equilibrium of a monoanion, as Hush and Blackledge pointed out qualitatively.[20] In this paper we have newly established the mutual relation of the first and the second half-wave oxidation potentials, $E^{oxd}_{1/2\cdot1}$ and $E^{oxd}_{1/2\cdot2}$, by applying a Born-Haber-type thermodynamical cycle. The $E^{oxd}_{1/2\cdot1}$ value for a reversible redox couple is expressed by Eq. 2, where the energy level is put in vacuo. The energy (IE^+) necessary to produce a dication from a monocation can now be represented by the orbital approximation as $IE^+=-\varepsilon^+_{so}-\varepsilon_{coul}$; here, ε^+_{so} is the SOMO energy of the monocation radical, while $-\varepsilon_{coul}$ is the extra energy needed in order to eject an electron from the cation species by overcoming the Coulomb-stabilization energy, ε_{coul}, between the electron and the cationic core field. This $-\varepsilon_{coul}$ term may be put equal to the two-center-repulsion integral, γ^+_{ss}, using SOMO, as the CNDO/2 semiempirical theory adopted this model also. Thus, $IE^+=-\varepsilon^+_{so}+\gamma^+_{ss}$; also, the IE^+ should correspond to the LUMO energy, ε^{++}_{lu}, of the singlet dication from the point of view of the orbital approximation. The solvation energy term, ΔE^{++}_{solv}, is now given by $\Delta E^{++}_{solv}=E^{++}_{solv}-E^+_{solv}$, E^{++}_{solv} being the solvation energy of the dication. $E^{oxd}_{1/2\cdot2}$ is thus written as Eq. 6 with reference to the derivation of Eq. 2:

$$FE^{oxd}_{1/2\cdot2}(R^{++}/R^+) = \Delta G^\circ - (\varepsilon^+_{so}-\gamma^+_{ss}) + \Delta E^{++}_{solv} \quad (6)$$

The combination of Eqs. 6 and 2 leads to:

$$F(E^{oxd}_{1/2\cdot1} + E^{oxd}_{1/2\cdot2}) = 2\Delta G^\circ - (\varepsilon_{ho}+\varepsilon^+_{so}-\gamma^+_{ss}) + (\Delta E^+_{solv}+\Delta E^{++}_{solv}) \quad (7)$$

and:

$$F(E^{oxd}_{1/2\cdot2}-E^{oxd}_{1/2\cdot1}) = (\varepsilon_{ho}-\varepsilon^+_{so}+\gamma^+_{ss}) + (\Delta E^{++}_{solv}-\Delta E^+_{solv}) \quad (8)$$

The same consideration as is given in Eqs. 3—5 indicates that the solvation energy terms in Eqs. 7 and 8 are given by $(\Delta E^+_{solv}+\Delta E^{++}_{solv})=(E^{++}_{solv}-E_{solv})$ and $(\Delta E^{++}_{solv}-\Delta E^+_{solv})=(E^{++}_{solv}+E_{solv}-2E^+_{solv})$. The physical meaning of Eqs. 7 and 8 is the same as that of Eqs. 4 and 5 except that the former is for the cation species. Equation 7 is especially important for estimating the solvation energy of the dication.

Correlation between Orbital Energy Approximation and Overall Calculations. Here it should be pointed out that $(\gamma^+_{ss}-\varepsilon_{ho}-\varepsilon^+_{so})$ in Eq. 7 is equivalent to the $(E^{++}_t-E_t)$, where E^{++}_t and E_t are the total energies of the dication and the neutral molecules respectively. This is because, under Koopmans' theorem,[39] $IE=-\varepsilon_{ho}$, and $IE^+=\gamma^+_{ss}-\varepsilon^+_{so}$ are the quantities pertinent to the total energy difference, expressed by $(E^+_t-E_t)$ and $(E^{++}_t-E^+_t)$ respectively.[19] Similarly, $(\varepsilon^+_{so}-\gamma^+_{ss})$ should correspond to ε^{++}_{lu}, which is the LUMO energy derived from the overall calculation of the dication. The correlation of the $(\gamma^+_{ss}-\varepsilon_{ho}-\varepsilon^+_{so})$ to $(E^{++}_t-E_t)$, and also that of $(\varepsilon^+_{so}-\gamma^+_{ss})$ to ε^{++}_{lu}, were checked by the actual MO calculation of the present BAH's. The total energy values were obtained by the use of the CNDO/2 and ab initio STO-3G methods, while the other quantities were evaluated by means of the PPP-SCF and LP-SCF methods (vide supra). All the calculation results are listed in Table 1. The application of the least-squares method led to the following results:

$$\varepsilon^{++}_{lu} = 0.852(\varepsilon^+_{so}-\gamma^+_{ss}) - 0.104 \quad (9)$$

with r (correlation coefficient) = 0.998 for n=11 (Compounds **1**—**11**).

$$(E^{++}_t-E_t) = a(\gamma^+_{ss}-\varepsilon_{ho}-\varepsilon^+_{so}) - c \quad (10)$$

with a=1.749, c=16.961, r=0.988 (n=11, Compounds **1**—**11**) for the CNDO/2 total energies, and with a=1.366, c=17.526, and r=0.986 (n=10, Compounds **1**—**11** except **5**) for the STO-3G calculation. As was discussed in the foregoing paper,[19] we have similarly obtained Eqs. 11 and 12:

$$\varepsilon^=_{ho} = 0.852(\varepsilon^-_{so}+\gamma^-_{ss}) - 1.655 \quad (11)$$

with r=0.998 for 11 compounds **1**—**11** and:

$$(E^=_t-E_t) = a(\varepsilon_{1u}+\varepsilon^-_{so}+\gamma^-_{ss}) + c \quad (12)$$

with a=1.546, c=6.538, and r=0.977 (n=11, Compounds **1**—**11**) for the CNDO/2 calculation, and with a=1.454, c=13.617, and r=0.985 (n=10, Compounds **1**—**11** except **5**) for the STO-3G calculation. The mutual correlation shown in Eqs. 9—12 is surprisingly good despite the adoption of different calculation methods, indicating that the orbital approximation employed here is quite good for the present systems. It may also be noted that the relations of Eqs. 9—12 are especially good for such polyacenes as Substances **1**—**4**, the correlation coefficient for these cases being more than 0.99976.

Table 1. The Values of the Orbital Energies (ε) and Two-Center-Repulsion Integrals (γ) Obtained by PPP-Type Approximation for Neutral and Ion Species, and the Total Energy (E_t) Differences between Neutral and Ion Species, as Calculated by CNDO/2 and STO-3G Methods on Benzenoid Hydrocarbons[a)]

No.	Compound	ε_{ho}[b)]	ε_{lu}[c)]	ε_{so}^{-}[d)]	γ_{ss}^{-}[e)] (γ_{ss}^{+})[l)]	$\varepsilon_{ho}^{=}$[f)]	ε_{so}^{+}[g)]	ε_{lu}^{++}[h)]	$\varepsilon_{so}^{-}-\varepsilon_{lu}$ ($\varepsilon_{ho}-\varepsilon_{so}^{+}$)[l)]	$\varepsilon_{so}^{-}+\gamma_{ss}^{-}-\varepsilon_{lu}$ ($\varepsilon_{ho}-\varepsilon_{so}^{+}+\gamma_{ss}^{+}$)[l)]	$\varepsilon_{ho}^{=}-\varepsilon_{lu}$ ($\varepsilon_{ho}-\varepsilon_{lu}^{++}$)[l)]	$E_t^{=}-E_t$[i,j)]	$E_t^{++}-E_t$[i,k)]
1	Naphthalene	−9.4819	−2.3581	−0.1487	4.5571	2.0818	−11.6913	−13.9218	2.2094	6.7665	4.4399	9.2353	27.6907
												(16.2989)	(17.3765)
2	Anthracene	−8.8272	−3.0128	−1.1100	4.0332	0.7942	−10.7299	−12.6341	1.9028	5.9360	3.8070	5.9961	23.9056
												(13.2244)	(14.4799)
3	Naphthacene	−8.4152	−3.4248	−1.7274	3.6959	−0.0374	−10.1126	−11.8025	1.6974	5.3933	3.3874	3.8021	21.4333
												(11.1659)	(12.5183)
4	Pentacene	−8.1454	−3.6945	−2.1496	3.4416	−0.6184	−9.6904	−11.2216	1.5449	4.9865	3.0761	2.2299	19.8724
												(9.6903)	(11.1014)
5	Phenanthrene	−9.3915	−2.4485	−0.5684	4.0326	1.2953	−11.2716	−13.1353	1.8801	5.9127	3.7438	8.2488	26.3596
6	Benz[*a*]-anthracene	−8.9179	−2.9220	−1.2098	3.7529	0.4736	−10.6302	−12.3136	1.7122	5.4651	3.3956	5.9962	23.7719
												(13.0973)	(14.3124)
7	Chrysene	−9.1027	−2.7373	−1.0691	3.6339	0.5786	−10.7709	−12.4185	1.6682	5.3021	3.3159	6.7839	24.5645
												(13.7730)	(14.8412)
8	Dibenz[*a*,*h*]-anthracene	−8.9553	−2.8847	−1.3630	3.4277	0.1074	−10.4770	−11.9473	1.5217	4.9494	2.9921	5.8799	23.5113
												(12.8313)	(14.0020)
9	Perylene	−8.5180	−3.3220	−1.7119	3.4588	−0.0999	−10.1281	−11.7401	1.6101	5.0689	3.2221	4.3019	21.8273
												(11.4477)	(12.8763)
10	Pyrene	−8.8265	−3.0135	−1.2082	3.7738	0.6031	−10.6318	−12.4430	1.8053	5.5791	3.6166	6.0627	23.8771
												(13.1492)	(14.4643)
11	Benzo[*a*]pyrene	−8.5683	−3.2717	−1.6517	3.5229	−0.0407	−10.1883	−11.7993	1.6200	5.1429	3.2311	4.6095	22.1943
												(11.7603)	(13.1310)
12	Coronene	−9.0237	−2.8163	—	—	—	—	—	—	—	—	—	—
13	9,10-Dimethyl-anthracene[m)]	−8.6063	−2.8547	−0.9948	3.9211 (3.9743)[m)]	0.8693	−10.4735	−12.3430	1.8599 (1.8672)[m)]	5.7811 (5.8415)[m)]	3.7240 (3.7366)[m)]	5.5455	22.3678

a) All the values are in eV units. b) HOMO energy of neutral species. c) LUMO energy of neutral species. d) SOMO energy of monoanion species. e) Values at SOMO calculated by the Nishimoto-Mataga equation for anion and cation species, both of which values come out the same because of the pairing theorem (see text). f) HOMO energy of dianion species. g) SOMO energy of monocation species. h) LUMO energy of dication speies. i) Ab initio STO-3G values are given in parentheses. j) Total energy difference between dianion and neutral species. k) Total energy difference between dication and neutral species. l) These values are the same for the cation and anion species because of the MO-pairing property (see text). m) The MO-pairing theorem is broken for this compound. The values in parentheses are for the energies given in the parentheses in the title.

Examination of the First and Second Reduction Potentials of Benzenoid Alternant Hydrocarbons by Means of MO Calculations. When we use the experimental method employed here, reversible or quasireversible reduction voltammograms for all the BAH's, except for naphthalene and phenanthrene, have been recorded not only for the first wave, but also for the second reduction wave under the voltage sweep rates of 50 mV s^{-1}—250 V s^{-1}, in depending on the substance. However, only the first reduction wave was observed as a reversible voltammogram on naphthalene and phenanthrene. An example of cyclic voltammograms is illustrated in Fig. 1 for perylene. The reversible half-wave reduction potentials were determined using the equation $E^{red}_{1/2}=(E_{cp}+E_{ap})/2$, where E_{cp} and E_{ap} are the cathodic and anodic peak potentials of a CV curve. All of these experimental data are listed in Table 2.[27] It should be noted that the $E^{red}_{1/2.1}$ and $E^{red}_{1/2.2}$ values listed in Table 2 are consistent with those reported by Jensen and Parker[40] for Compounds **2**, **6**, **7**, **9**, and **12**, though their data were obtained at 11 °C and with 0.2 mol dm^{-3} tetramethylammonium bromide as the supporting electrolyte.[41]

Let us now discuss the application of Eqs. 1, 3, 4, and 5 to the present experimental results. As has already been reported by other authors,[6,13-15,17] the

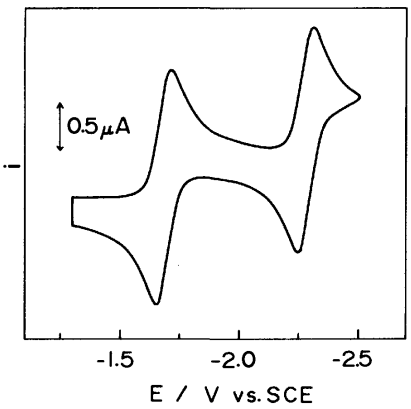

Fig. 1. Cyclic voltammogram of perylene in reduction process at a Pt electrode. Solvent is DMF containing 0.1 mol dm^{-3} TPAP and ca. 10 g of neutral alumina, the sample concentration being 9.3×10^{-4} mol dm^{-3}. The voltammogran was recorded at $v=$ 50 mV s^{-1} and 25 °C.

Table 2. First and Second Reduction and Oxidation Potentials, Ionization Potentials, and Electron Affinities of Benzenoid Hydrocarbons

No.	Compound	Reduction potential[a] (V vs. SCE)		Oxidation potential[b] (V vs. SCE)					
		$E^{red}_{1/2.1}$	$E^{red}_{1/2.2}$	$E^{oxd}_{1/2.1}$	$E^{oxd}_{1/2.2}$	$(E^{oxd}_{1/2.1}+E^{red}_{1/2.1})/2$	I_P/eV[c]	E_A/eV[d]	$(I_P+E_A)/2$
1	Naphthalene	−2.557	—	—[e]	—	—	8.15	0.152	4.151
2	Anthracene	−1.985	−2.740	1.321	1.76	−0.332	7.47	0.552	4.011
3	Naphthacene	−1.595	−2.245	0.980	1.47	−0.308	7.04	—	—
4	Pentacene	−1.325	−1.910	—[f]	—	—	6.74	—	—
5	Phenanthrene	−2.480	—	—[e]	—	—	7.86	0.308	4.084
6	Benz[*a*]-anthracene	−2.028	−2.687	1.388	1.90	−0.320	7.47	0.696	4.083
7	Chrysene	−2.295	−2.870	1.587	2.02	−0.354	7.60	0.419	4.010
8	Dibenz[*a*,*h*]-anthracene	−2.068	−2.628	1.425	1.80	−0.322	7.38	—	—
9	Perylene[h]	−1.686 (−1.692)	−2.281 (−2.246)	1.040	1.59	−0.323 (−0.326)	7.00	—	—
10	Pyrene	−2.089	−2.792	1.283	—	−0.403	7.41	0.579	3.995
11	Benzo[*a*]-pyrene	−1.865	−2.510	1.160	1.61	−0.353	7.12	—	—
12	Coronene	−2.078	−2.695	1.350	—[g]	−0.364 (−0.342± 0.030)[i]	7.36	—	— (4.056± 0.061)[i]
13	9,10-Dimethyl-anthracene	−2.002	−2.708	1.098	1.538	−0.452	—	—	—

a) These values were obtained from reversible or quasireversible CV curves using a Pt electrode in DMF containing 0.1 mol dm^{-3} TPAP. b) These values were obtained by CV measurements with a Pt electrode in AN containing 0.1 mol dm^{-3} TPAP. Although the first oxidation waves are reversible or quasireversible, the second ones are irreversible for all the samples employed except for Compound **13**, which gave a quasireversible one. See text for the method of evaluating $E^{oxd}_{1/2.2}$. c) Ionization potentials.[52] d) Electron affinities.[43] e) The first oxidation wave was irreversible at $v<200$ V s^{-1}. f) Insoluble in AN. g) Three or four oxidation waves were observed. h) Reduction potentials were also measured in AN containing 0.1 mol dm^{-3} TPAP. These are given in parentheses. i) Average values are given in parentheses.

data in Tables 1 and 2 indicate a good linear relation to satisfy Eq. 1, written as $E^{red}_{1/2\cdot1}=-0.895\varepsilon_{lu}-4.681$, with $r=0.985$ and $n=12$ (Compounds **1—12**). The absolute value (0.895) of the slope is near to the theoretical value of unity. The first reduction potential, $E^{red}_{1/2\cdot1}$, is then well expressed by Eq. 1.[42,43] We next test Eq. 3 again using the data in Tables 1 and 2. The $E^{red}_{1/2\cdot2}$ vs. $(\varepsilon^{-}_{so}+\gamma^{-}_{ss})$ plot is $E^{red}_{1/2\cdot2}=-0.549\ (\varepsilon^{-}_{so}+\gamma^{-}_{ss})-1.327$, with $r=0.897$ and $n=9$ (Compounds **2—4, 6—11**). Since $\varepsilon^{=}_{ho}$ is in a good correlation with $(\varepsilon^{-}_{so}+\gamma^{-}_{ss})$, as may be understood from Eq. 11, we attempted to establish the plot of $E^{red}_{1/2\cdot2}$ against $\varepsilon^{=}_{ho}$; it is illustrated in Fig. 2 along with the correlation equation.[44] The above linearity seems to be relatively good, but the absolute values of the slope and the correlation coefficients are both smaller than those of the $E^{red}_{1/2\cdot1}$ vs. ε_{lu} plot. As would be expected, one of these factors may be attributed to the lower accuracy of the orbital-energy calculations of the mono- and dianion species in comparison with those of the neutral one. However, another important reason is the different contribution from the molecular electronic states and the solvation-energy terms between the redox systems of $R+e\rightleftarrows R^{-}$ (Eq. 1) and $R^{-}+e\rightleftarrows R^{=}$ (Eq. 3). It is well known that the π-electron distribution on each carbon atom in neutral alternant hydrocarbon is the same,[45] so that their π-dipole moment is zero, thus leading to a small solute-solvent interaction. However, generally speaking, the electron density of the anion radical of BAH is not uniformly distributed in the molecules,[46] because π-electrons in the LUMO are distributed mainly over the atomic orbitals determined by its orbital symmetry.[44] This tendency turns out to be much larger for the dianion than for the monoanion, so the possibility of a specific solute (ion)-solvent interaction seems to be larger for the former than the latter.[47] This must play an important role for that the correlation coefficient of the $E^{red}_{1/2\cdot2}$ vs. $(\varepsilon^{-}_{so}+\gamma^{-}_{ss})$ or $\varepsilon^{=}_{ho}$ plot is less than that of the $E^{red}_{1/2\cdot1}$ vs. ε_{lu} plot. In addition, the BAH's studied here extend from small-ring-size molecules (small cavity radius in solution) to large ones (large cavity radius). Therefore, a Born-type equation[48] indicates that the contribution from the solvation-energy term is not constant in the strict sense; this tendency is more important in the $E^{red}_{1/2\cdot2}$ step than in the $E^{red}_{1/2\cdot1}$ step (see below). This fact is discussed in the Appendix from the point of view of multivariate analysis. As a result, we can expect a positive correlation of $E^{red}_{1/2\cdot2}$ to $\Delta E^{=}_{solv}$ (Eq. 3). In other words, the values of both $E^{red}_{1/2\cdot2}$ and $\Delta E^{=}_{solv}$ move to a small negative value with an increase in the ring size (vide infra). This may cause the decrease in the slope value of the $E^{red}_{1/2\cdot2}$ vs. $(\varepsilon^{-}_{so}+\gamma^{-}_{ss})$ or $\varepsilon^{=}_{ho}$ plot.

Let us now turn to a discussion of Eq. 4. Using the linear relations of Eqs. 11 and 12, the plots of $(E^{red}_{1/2\cdot1}+E^{red}_{1/2\cdot2})$ to $(E^{=}_{t}-E_{t})$, $(\varepsilon_{lu}+\varepsilon^{=}_{ho})$, and $(\varepsilon_{lu}+\varepsilon^{-}_{so}+\gamma^{-}_{ss})$ led to good linear relations as follows: $(E^{red}_{1/2\cdot1}+E^{red}_{1/2\cdot2})=-a(E^{=}_{t}-E_{t})-b$ with $a=0.417$ (0.459), $b=2.287$ (−1.212), and $r=0.990$ (0.987) for the CNDO/2 and ab initio STO-3G calculations (the latter is given in parentheses); $(E^{red}_{1/2\cdot1}+E^{red}_{1/2\cdot2})=-0.808(\varepsilon_{lu}+\varepsilon^{=}_{ho})-6.781$ with $r=0.962$; $(E^{red}_{1/2\cdot1}+E^{red}_{1/2\cdot2})=-0.734(\varepsilon_{lu}+\varepsilon^{-}_{so}+\gamma^{-}_{ss})-5.113$ with $r=0.942$. The compounds employed are Nos. **2—4** and **6—11**. An example is illustrated in Fig. 3. We think that the theoretical Eq. 4 is quite well satisfied from the experimental point of view. The relatively large difference in the slope values between the orbital-energy approximation and the total energy calculations may be attributed to the different models adopted here; i. e., the "*a*" value of Eq. 12 shows large deviation from 1.

Let us next consider the physical meaning of the $(E^{red}_{1/2\cdot1}-E^{red}_{1/2\cdot2})$ given by Eq. 5, where we can easily understand that the γ^{-}_{ss} values make the largest

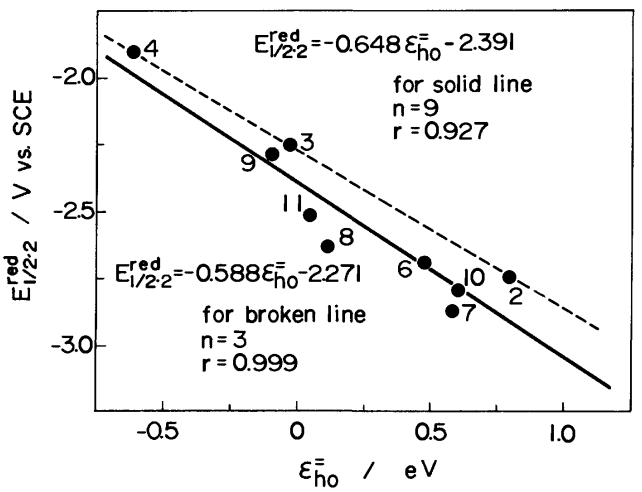

Fig. 2. Linear relation of $E^{red}_{1/2\cdot2}$ values to $\varepsilon^{=}_{ho}$ for BAH's. Each sample number is the same as given in Table 1. See text for detail.

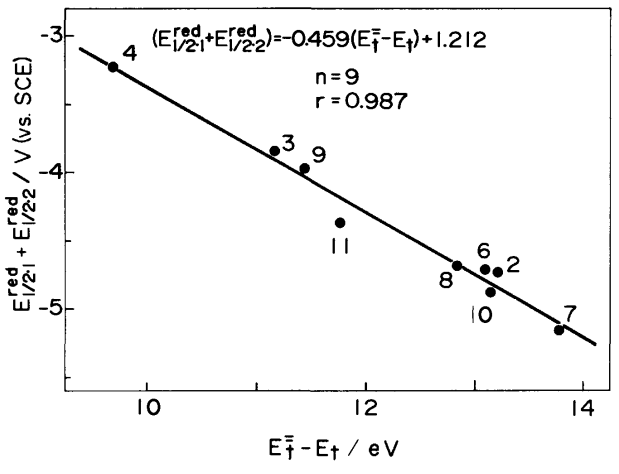

Fig. 3. Linear relation of $(E^{red}_{1/2\cdot1}+E^{red}_{1/2\cdot2})$ values to $(E^{=}_{t}-E_{t})$ calculated by ab initio STO-3G method for BAH's. Each sample number is the same as given in Table 1. See text for detail.

contribution to $(E^{red}_{1/2\cdot1}-E^{red}_{1/2\cdot2})$, as Hush and Blackledge[20] first pointed out, for if all the energy discussions are made for neutral molecules, $(\varepsilon^{-}_{so}-\varepsilon_{lu})=0$. Now it should be noted that the $\Delta G°$ term does not appear in Eq. 5, and the solvation energy term $(\Delta E^{=}_{solv}-\Delta E^{-}_{solv}$: negative value) cancels out the contribution from the orbital energy term $(\gamma^{-}_{ss}+\varepsilon^{-}_{so}-\varepsilon_{lu}$: positive value), so that, as may be seen in Fig. 4, the value of $(E^{red}_{1/2\cdot1}-E^{red}_{1/2\cdot2})$ becomes small and varies within a smaller range than in the structure change of $(\gamma^{-}_{ss}+\varepsilon^{-}_{so}-\varepsilon_{lu})$, in which γ^{-}_{ss} makes the largest contribution (see Table 1).[49,50] This fact seems to be the main reason why the slope of the $(E^{red}_{1/2\cdot1}-E^{red}_{1/2\cdot2})$ vs. $(\gamma^{-}_{ss}+\varepsilon^{-}_{so}-\varepsilon_{lu})$ plot becomes small.

Examination of the First and Second Oxidation Potentials of Benzenoid Alternant Hydrocarbons by Means of MO Calculations. Under the experimental conditions described above, the voltammetric study of the oxidation processes in AN using a platinum electrode shows that, although a reversible or quasireversible oxidation CV curve is recorded in the first oxidation process by selecting a suitable voltage-scan rate of 0.1—60 V s^{-1}, we could not succeed in obtaining a reversible or a quasireversible CV curve for the second oxidation process. An example is given in Fig. 5 for perylene. These experimental results show that the dications of BAH are more unstable than the dianions. However, note that if the strongly reactive 9- and 10-positions of anthracene are protected by CH_3 substitution, a reversible CV curve is safely recorded for both the first and second oxidation steps (see Table 2). The standard potential of the first oxidation step was evaluated by the use of $E^{oxd}_{1/2\cdot1}=(E'_{ap\cdot1}+E'_{cp\cdot1})/2$, where the superfix (′) of $E_{ap\cdot1}$ and $E_{cp\cdot1}$ indicates the first oxidation system. In the case of the second oxidation step, $E^{oxd}_{1/2\cdot2}$ was estimated by means of the $E^{oxd}_{1/2\cdot2}=E'_{ap\cdot2}-(E'_{ap\cdot1}-E^{oxd}_{1/2\cdot1})$ equation, which indicates that the $E^{oxd}_{1/2\cdot2}$ value occupies a position less positive than $E'_{ap\cdot2}$ by the same amount as $(E'_{ap\cdot1}-E^{oxd}_{1/2\cdot1})$ relative to the quasireversible first oxidation CV curve (see Fig. 5). For this treatment to get $E^{oxd}_{1/2\cdot2}$, we have employed the CV data at the sweep rate of v, where the $(E'_{ap\cdot2}-E'_{ap\cdot1})$ value becomes almost independent of an increasing v. At this scan rate, it appears reasonable to assume that an electron-transfer step at the electrode may play an important role in determining $E^{oxd}_{1/2\cdot2}$,[51] but the effect from succeeding chemical reactions may be diminished. All these experimental results are included in Table 2. As was reported by earlier workers,[14,15,17] the correlation of the $E^{oxd}_{1/2\cdot1}$ vs. ε_{ho} plot is quite good, as $E^{oxd}_{1/2\cdot1}=-0.770\varepsilon_{ho}-5.493$, with $r=0.963$ and $n=9$ (Compounds **2**, **3**, **6—12**). Only coronene deviates from the straight line, so when we delete it from the plotting the values of 0.989, −0.849, and −6.083 were obtained for the r, the slope, and the constant term respectively. If we use the vertical ionization potential (I_P) reported by Clar et al.[52] in lieu of the $-\varepsilon_{ho}$, the equation of $E^{oxd}_{1/2\cdot1}=0.853I_P-4.961$ is obtained, with $r=0.938$ and $n=9$. The slope is compatible with that of the $E^{oxd}_{1/2\cdot1}$ vs. ε_{ho} plot.[53] To examine Eq. 6, the mutual relation of $E^{oxd}_{1/2\cdot2}$ and $(\varepsilon^{+}_{so}-\gamma^{+}_{ss})$ was studied. The result is $E^{oxd}_{1/2\cdot2}=-0.528(\varepsilon^{+}_{so}-\gamma^{+}_{ss})-5.636$, with $r=0.875$ and $n=6$ (Compounds **3**, **6—9**, **11**), but if ε^{++}_{lu} is employed in place of $(\varepsilon^{+}_{so}-\gamma^{+}_{ss})$, we obtain the results illustrated in Fig. 6. Here, anthracene is excluded from the plotting because of its

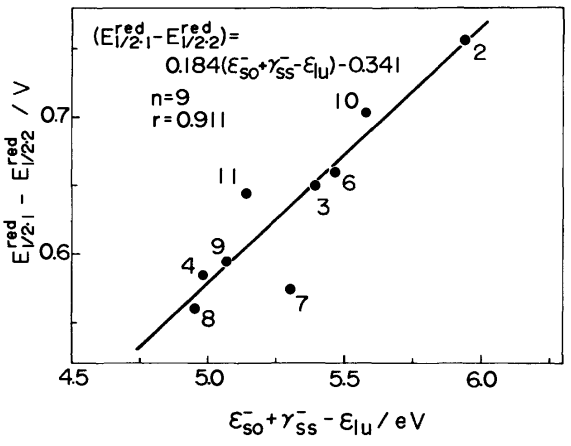

Fig. 4. Linear relation of $(E^{red}_{1/2\cdot1}-E^{red}_{1/2\cdot2})$ values to $(\varepsilon^{-}_{so}+\gamma^{-}_{ss}-\varepsilon_{lu})$ for BAH's. Each sample number is the same as given in Table 1. When $\varepsilon^{=}_{ho}$ is adopted instead of $(\varepsilon^{-}_{so}+\gamma^{-}_{ss})$, the correlation is: $(E^{red}_{1/2\cdot1}-E^{red}_{1/2\cdot2})=0.235(\varepsilon^{=}_{ho}-\varepsilon_{lu})-0.147$ with $r=0.925$.

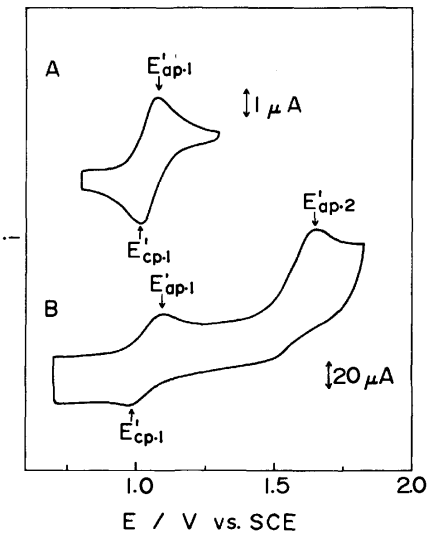

Fig. 5. Cyclic voltammograms of perylene in oxidation process at a Pt electrode. Solvent is AN containing 0.1 mol dm^{-3} TPAP and ca. 10 g of neutral alumina, the sample concentration being 1.0×10^{-3} mol dm^{-3}. The voltammograms were recorded at $v=0.2$ V s^{-1} for A and 22.4 V s^{-1} for B at 25 °C. $E'_{ap\cdot1}$, $E'_{cp\cdot1}$, and $E'_{ap\cdot2}$ indicate the peak potentials of the first anodic, cathodic, and the second anodic waves, respctively (see text).

large deviation from the linear relation. This deviation should be ascribed to the large reactivity of the 9- and 10-positions of the anthracene dications, so the $E^{oxd}_{1/2\cdot2}$ value is not so accurate as the other values.[54] Just as in the aforementioned $E^{red}_{1/2\cdot2}$ vs. $(\varepsilon^{-}_{so}+\gamma^{-}_{ss})$ correlation, the relation of $E^{oxd}_{1/2\cdot2}$ to $(\varepsilon^{+}_{so}-\gamma^{+}_{ss})$ indicates that, in comparison with the case of the $E^{oxd}_{1/2\cdot1}$ vs. ε_{ho} plot, the correlation coefficient is not so good and the slope value is small. The same discussion as has been made for interpreting Eq. 3 can also be applied to the present case. In addition, the problem that the reversibility of the second oxidation wave is not sufficient is not neglected here.

Our next discussion will be focused on Eq. 7. The relations of $(E^{oxd}_{1/2\cdot1}+E^{oxd}_{1/2\cdot2})$ to $(\varepsilon_{ho}+\varepsilon^{+}_{so}-\gamma^{+}_{ss})$ or $(\varepsilon_{ho}+\varepsilon^{++}_{lu})$ or $(E_t-E_t^{++})$ are as follows: $(E^{oxd}_{1/2\cdot1}+E^{oxd}_{1/2\cdot2})=-0.714(\varepsilon_{ho}+\varepsilon^{+}_{so}-\gamma^{+}_{ss})-13.229$ with $r=0.957$, $n=6$; $(E^{oxd}_{1/2\cdot1}+E^{oxd}_{1/2\cdot2})=-0.794(\varepsilon_{ho}+\varepsilon^{++}_{lu})-13.477$, with $r=0.979$ and $n=6$; $(E^{oxd}_{1/2\cdot1}+E^{oxd}_{1/2\cdot2})=-0.360(E_t-E_t^{++})-5.246$, with $r=0.999$ and $n=6$ for the CNDO/2 calculation; $(E^{oxd}_{1/2\cdot1}+E^{oxd}_{1/2\cdot2})=-0.492(E_t-E_t^{++})-3.697$, with $r=0.998$ and $n=6$ for the STO-3G calculation. Compounds **3**, **6—9**, **11** were employed for the correlation study. Again, anthracene was omitted from the plotting for the aforementioned reason. An example is shown in Fig. 7. The theoretical Eq. 7 seems to be well satisfied. However, quite a large difference between the total-energy-calculation models and the orbital-energy approximation is found for the slope values of the linear-regression equations. This is the same phenomenon as was observed and discussed in the correlations of $(E^{red}_{1/2\cdot1}+E^{red}_{1/2\cdot2})$ against $(\varepsilon^{-}_{so}+\varepsilon_{lu}+\gamma^{-}_{ss})$ or $(\varepsilon^{=}_{ho}+\varepsilon_{lu})$ or $(E^{=}_{t}-E_t)$ values (vide supra).

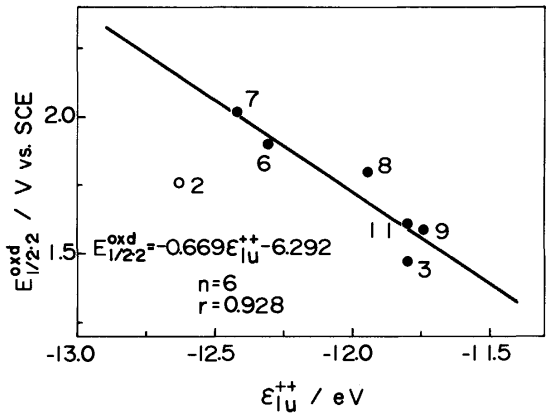

Fig. 6. Linear relation of $E^{oxd}_{1/2\cdot2}$ values to ε^{++}_{lu} for BAH's. Each sample number is the same as given in Table 1. See text for detail.

Next, let us consider the physical meaning of $(E^{oxd}_{1/2\cdot2}-E^{oxd}_{1/2\cdot1})$ given by Eq. 8, whose form is closely similar to Eq. 5 pertinent to $(E^{red}_{1/2\cdot1}-E^{red}_{1/2\cdot2})$, so that the same discussion as was made for Eq. 5 would be possible. It is well-known that the so-called "pairing property"[45,55] of the MO's obtained by the PPP method holds between occupied and unoccupied MO's of neutral BAH molecules and also between the SOMO or unoccupied MO's of the anion radicals and the SOMO or occupied MO's of the cation radicals. Our present calculations verified this, so the values of γ^{+}_{ss} and $(\varepsilon_{ho}-\varepsilon^{+}_{so})$ are equal to γ^{-}_{ss} and $(\varepsilon^{-}_{so}-\varepsilon_{lu})$ respectively. As a result, $(\varepsilon_{ho}-\varepsilon^{+}_{so}+\gamma^{+}_{ss})$ and $(\varepsilon^{-}_{so}-\varepsilon_{lu}+\gamma^{-}_{ss})$ are the same value. Also, the present calculations suggest that the values of $(\varepsilon^{=}_{ho}-\varepsilon_{lu})$ and $(\varepsilon_{ho}-\varepsilon^{++}_{lu})$ are equal to each other, because the pairing property found between the anion and cation radicals of BAH again holds between the MO's of the dianion and dication species as well as between the $\varepsilon^{=}_{ho}$ and ε^{++}_{lu}. This can also be inferred from the relations of Eqs. 9 and 11. Keeping in mind the above fact, we can expect that, judging from the comparison of Eqs. 5 and 8, the values of $(E^{oxd}_{1/2\cdot2}-E^{oxd}_{1/2\cdot1})$ should be the same as those of $(E^{red}_{1/2\cdot1}-E^{red}_{1/2\cdot2})$ if (i) the solvation effect on reversible redox potentials is not so different between DMF and

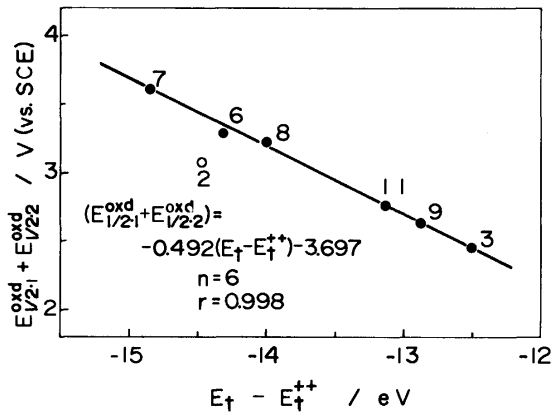

Fig. 7. Linear relation of $(E^{oxd}_{1/2\cdot1}+E^{oxd}_{1/2\cdot2})$ values to $(E_t-E_t^{++})$ calculated by ab initio STO-3G method for BAH's. Each sample number is the same as given in Table 1. See text for detail.

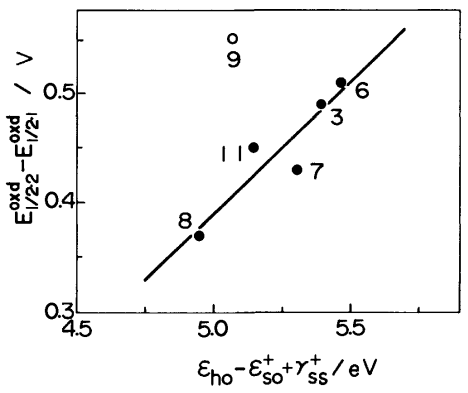

Fig. 8. Linear relation of $(E^{oxd}_{1/2\cdot2}-E^{oxd}_{1/2\cdot1})$ values to $(\varepsilon_{ho}-\varepsilon^{+}_{so}+\gamma^{+}_{ss})$ for BAH's with the slope=0.243, the constant term=−0.826, and $r=0.918$. Each sample number is the same as given in Table 1. See text for detail.

AN[56] and (ii) the solvation energies coming from mono- and dianions are the same as those of the mono- and dications (vide infra). In the present experiments, $E^{red}_{1/2\cdot1}$, $E^{red}_{1/2\cdot2}$, and $E^{oxd}_{1/2\cdot1}$ are for the reversible or quasireversible CV curves, but $E^{oxd}_{1/2\cdot2}$ is not and it is, therefore, less positive than the value in a reversible curve. The one exception is perylene, whose $(E^{oxd}_{1/2\cdot2}-E^{oxd}_{1/2\cdot1})$ value is quite close to the value of $(E^{red}_{1/2\cdot1}-E^{red}_{1/2\cdot2})$, as Table 2 shows, so we suppose that the $E^{oxd}_{1/2\cdot2}$ value of perylene in Table 2 may be near that of a reversible monocation and dication redox system. The correlation of Eq. 8 is: $(E^{oxd}_{1/2\cdot2}-E^{oxd}_{1/2\cdot1})=0.243(\varepsilon_{ho}-\varepsilon^{+}_{so}+\gamma^{+}_{ss})-0.826$, with $r=0.918$ and $n=5$; also, $(E^{oxd}_{1/2\cdot2}-E^{oxd}_{1/2\cdot1})=0.304(\varepsilon_{ho}-\varepsilon^{++}_{lu})-0.543$, with $r=0.922$ and $n=5$. The compounds employed for the correlation are **3**, **6—8**, **11**. Perylene deviates greatly from the above equations, so we have excluded it from the linear plotting, as is shown in Fig. 8. The reason is clear from the discussion above. In turn, for the same reason as was discussed in detail in connection with Eq. 5, the value of $(E^{oxd}_{1/2\cdot2}-E^{oxd}_{1/2\cdot1})$ comes out small and varies in a smaller range than in the case of $(\varepsilon_{ho}-\varepsilon^{+}_{so}+\gamma^{+}_{ss})$, where γ^{+}_{ss} makes the largest contribution (see Table 1).[49,50] Therefore, the slope of the $(E^{oxd}_{1/2\cdot2}-E^{oxd}_{1/2\cdot1})$ vs.$(\varepsilon_{ho}-\varepsilon^{+}_{so}+\gamma^{+}_{ss})$ plotting turns out to be small, as was seen in the discussion of Eq. 5.

Mutual Relation between Standard Reduction and Oxidation Potentials. In a series of alternant hydrocarbons, it is well-known[45,57] and has been experimentally verified that the sum of I_P and E_A is almost constant. The data shown in Table 2 support this relation, and Mulliken's electro-negativity $((I_P+E_A)/2)$[58] is constant in BAH and is 4.06 eV for the data in Table 2. This kind of property can be well described using just the PPP-SCFMO employed here; i. e., the pairing property of MO is well satisfied. In terms of the MO language employing Koopmans' theorem,[39] $(I_P+E_A)/2$ corresponds to $-(\varepsilon_{ho}+\varepsilon_{lu})/2$ for neutral molecules. The present calculations led to -5.92 eV for $(\varepsilon_{ho}+\varepsilon_{lu})/2$ and for the pairing orbitals between anion and cation radicals (e. g., $(\varepsilon^{+}_{so}+\varepsilon^{-}_{so})/2$) and also for those between dianion and dication species (e. g., $(\varepsilon^{++}_{lu}+\varepsilon^{=}_{ho})/2$). When we use Eqs. 1 and 2, the value of $(E^{oxd}_{1/2\cdot1}+E^{red}_{1/2\cdot1})/2$ is written by Eq. 13:

$$(E^{oxd}_{1/2\cdot1}+E^{red}_{1/2\cdot1})/2 = \Delta G^{\circ}-(\varepsilon_{1u}+\varepsilon_{ho})/2+(\Delta E^{+}_{solv}-\Delta E^{-}_{solv})/2 \quad (13)$$

where the eV unit is used for the energies. Taking into consideration the fact that Eqs. 1 and 2 are well fulfilled experimentally, the ΔE^{+}_{solv} term can be expected to cancel out the ΔE^{-}_{solv} term, so the term $(E^{oxd}_{1/2\cdot1}+E^{red}_{1/2\cdot1})$ turns out to be constant.[59] The values are listed in Table 2; the average potential is -0.342 ± 0.030 V. Now, we can estimate the ΔG° from Eq. 13 by putting $\Delta E^{+}_{solv}=\Delta E^{-}_{solv}$ (vide infra). Using the value of 5.92 eV for $-(\varepsilon_{lu}+\varepsilon_{ho})/2$, we obtain $\Delta G^{\circ}=-6.26$ eV.[60] However, when we use $(I_P+E_A)/2$ in place of $-(\varepsilon_{lu}+\varepsilon_{ho})/2$, $\Delta G^{\circ}=-4.40$ eV where we employ 4.056 ± 0.061 eV for the average value of the former (see Table 2). This ΔG° value is reasonable in view of the literature values.[11,61,62] Hereafter, therefore, we will use $\Delta G^{\circ}=-6.26$ eV for PPP orbital treatment, but

Table 3. Calculated Values of Second Oxidation Potential and Solvation Energies of Benzenoid Alternant Hydrocarbons

No.	Compound	$E^{oxd}_{1/2\cdot2}$(cal)[a]	E^{-}_{solv}[b] (eV)		E^{+}_{solv}[c] (eV)		$E^{=}_{solv}$[d] (eV)		E^{++}_{solv}[e] (eV)	
		V vs. SCE	[A]	[B]	[C]	[D]	[E]	[F]	[G]	[H]
1	Naphthalene	—	−1.35	−1.69	—	—	—	—	—	—
2	Anthracene	2.076	−1.26	−1.86	−1.24	−1.75	−7.71	−5.58	−7.99	−5.86
3	Naphthacene	1.630	−1.24	—	−1.17	−1.66	−7.23	−5.22	−7.25	−5.24
4	Pentacene	—	−1.24	—	—	—	−6.89	−4.98	—	—
5	Phenanthrene	—	−1.33	−1.61	—	—	—	—	—	—
6	Benz[*a*]anthracene	2.047	−1.31	−1.67	−1.27	−1.68	−7.43	−5.36	−7.49	−5.42
7	Chrysene	2.162	−1.23	−1.68	−1.25	−1.62	−7.19	−5.20	−7.37	−5.39
8	Dibenz[*a*,*h*]anthracene	1.985	−1.31	—	−1.27	−1.56	−7.01	−5.05	−7.11	−5.15
9	Perylene	1.635	−1.25	—	−1.22	−1.56	−6.98	−5.14	−6.95	−5.10
10	Pyrene	1.986	−1.16	−1.73	−1.28	−1.73	−7.20	−5.23	—	—
11	Benzo[*a*]pyrene	1.805	−1.13	—	−1.15	−1.56	−6.75	−4.84	−6.99	−5.07
12	Coronene	1.967	−1.37	—	−1.41	−1.61	—	—	—	—

a) Second oxidation potential calculated by means of this equation: $E^{oxd}_{1/2\cdot2}=E^{oxd}_{1/2\cdot1}+E^{red}_{1/2\cdot1}-E^{red}_{1/2\cdot2}$. See text for the details. b) Solvation energy of monoanion species. Calculations were made using Eq. 1; $E^{-}_{solv}\simeq(E^{-}_{solv}-E_{solv})=-FE^{red}_{1/2\cdot1}-\varepsilon_{1u}-6.26$ for [A], but $-FE^{red}_{1/2\cdot1}+E_A-4.40$ for [B]. c) Solvation energy of monocation species. Calculations were made using Eq. 2; $E^{+}_{solv}\simeq(E^{+}_{solv}-E_{solv})=FE^{oxd}_{1/2\cdot1}+\varepsilon_{ho}+6.26$ for [C], but $FE^{oxd}_{1/2\cdot1}-I_P+4.40$ for [D]. d) Solvation energy of dianion species. Calculatations were made using Eq. 4; $E^{=}_{solv}\simeq(E^{=}_{solv}-E_{solv})=-F(E^{red}_{1/2\cdot1}+E^{red}_{1/2\cdot2})-(\varepsilon^{-}_{so}+\gamma^{-}_{ss}+\varepsilon_{1u})-12.52$ for [E], but $-F(E^{red}_{1/2\cdot1}+E^{red}_{1/2\cdot2})-(\varepsilon^{=}_{ho}+\varepsilon_{1u})-12.52$ for [F]. e) Solvation energy of dication species. Calculations were made using Eq. 7; $E^{++}_{solv}\simeq(E^{++}_{solv}-E_{solv})=F(E^{oxd}_{1/2\cdot1}+E^{oxd}_{1/2\cdot2})+(\varepsilon^{+}_{so}-\gamma^{+}_{ss}+\varepsilon_{ho})+12.52$ for [G], but $F(E^{oxd}_{1/2\cdot1}+E^{oxd}_{1/2\cdot2})+(\varepsilon^{++}_{lu}+\varepsilon_{ho})+12.52$ for [H].

−4.40 eV in the consideration of the experimental I_P and E_A values.

Now we would like to discuss the mutual relation between $E^{oxd}_{1/2\cdot2}$ and $E^{red}_{1/2\cdot2}$. Taking the summation of Eqs. 3 and 6, and by dividing it by two, we obtain Eq. 14 (in eV units):

$$(E^{red}_{1/2\cdot2}+E^{oxd}_{1/2\cdot2})/2 = \Delta G^\circ - (\varepsilon^-_{so}+\varepsilon^+_{so})/2 + (\gamma^+_{ss}-\gamma^-_{ss})/2 + (\Delta E^{++}_{solv}-\Delta E^{=}_{solv})/2 \quad (14)$$

The MO-pairing property of the anion and cation PPP-SCFMO for BAH shows that $\gamma^+_{ss}-\gamma^-_{ss}=0$, and $(\varepsilon^+_{so}+\varepsilon^-_{so})/2=(\varepsilon_{ho}+\varepsilon_{lu})/2=-5.92$ eV. Provided that $\Delta E^{++}_{solv}-\Delta E^{=}_{solv}\simeq0$ just like $\Delta E^{+}_{solv}\simeq\Delta E^{-}_{solv}$ in Eq. 13, Eq. 14 comes out to be equal to Eq. 13, -i. e., $(E^{oxd}_{1/2\cdot1}+E^{red}_{1/2\cdot1})=(E^{oxd}_{1/2\cdot2}+E^{red}_{1/2\cdot2})$. Note that $E^{red}_{1/2\cdot1}$, $E^{red}_{1/2\cdot2}$, and $E^{oxd}_{1/2\cdot1}$ were experimentally determined from the reversible or quasireversible CV curves; therefore, we can calculate $E^{oxd}_{1/2\cdot2}$ by employing this equation: $E^{oxd}_{1/2\cdot2}=E^{oxd}_{1/2\cdot1}+E^{red}_{1/2\cdot1}-E^{red}_{1/2\cdot2}$. The calculated values are given in Table 3, while the correlation of the observed $E^{oxd}_{1/2\cdot2}$ values with the calculated values is illustrated in Fig. 9. We can see there that the observed and calculated $E^{oxd}_{1/2\cdot2}$ values, except for perylene and anthracene, fall as a good linear-least-squares correlation line. The observed values are positive-shifted by ≈0.2 V from the calculated values. This is reasonable, since the experimental values were determined from irreversible CV curves. Therefore, the effect of the succeeding chemical reaction on them could not be neglected, but the effect is in the same order in the above five substances. Anthracene deviated largely to the positive side from the regression line, showing that the effect of the following chemical reaction on it is very large; this tendency of anthracene was always found in the present correlation study of the oxidation processes. In turn, Fig. 9 indicates that perylene is in a position close to, but a little positive-shifted from, the theoretical line. Its $E^{oxd}_{1/2\cdot2}$ value should be near to that of the reversible equilibrium; this conclusion is the same as that derived from the foregoing discussion of the $(E^{oxd}_{1/2\cdot2}-E^{oxd}_{1/2\cdot1})$ value.

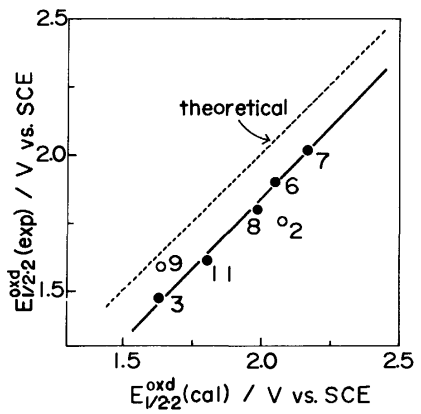

Fig. 9. Linear relation of the experimental $E^{oxd}_{1/2\cdot2}$ values to the calculated $E^{oxd}_{1/2\cdot2}$ ones given in Table 3 for BAH's. Each sample number is the same as given in Table 1. Regression equation is $E^{oxd}_{1/2\cdot2}(exp)=1.049E^{oxd}_{1/2\cdot2}(cal)-0.260$ with $r=0.995$, $n=5$ (full circles). See text for detail.

Evaluation of Solvation Energies of Ion Species. Now, let us discuss the solvation energies of anions or cations of BAH by applying Eqs. 1, 2, 4, and 7. From the former two equations, we can estimate the $(E^-_{solv}-E_{solv})\simeq E^-_{solv}$ and $(E^+_{solv}-E_{solv})\simeq E^+_{solv}$ values, and the latter two give the estimated values of $(E^{=}_{solv}-E_{solv})\simeq E^{=}_{solv}$ and $(E^{++}_{solv}-E_{solv})\simeq E^{++}_{solv}$, although the CV reversibility pertinent to the $E^{oxd}_{1/2\cdot2}$ value is not very good. Of course, ΔG° should be −6.26 eV for the PPP-orbital approximation,[60] but −4.40 eV for I_P and E_A. The calculated results are listed in Table 3, from which one can conjecture that, in the case of E^-_{solv} and E^+_{solv}, the values evaluated from the PPP calculations and the I_P or E_A value are both of almost the same order of magnitude, though the absolute values calculated from the experimental I_P and E_A values are a little larger than in the orbital approximation, and that their structure dependence is small, as is to be expected from the regression equations of the $E^{red}_{1/2\cdot1}$ vs. ε_{lu} (or E_A) and $E^{oxd}_{1/2\cdot1}$ vs. ε_{ho} (or I_P) relationships. On the other hand, the absolute values of $E^{=}_{solv}$ and E^{++}_{solv}, as estimated using $\varepsilon^{=}_{ho}$ and ε^{++}_{lu} in lieu of $(\varepsilon^-_{so}+\gamma^-_{ss})$ and $(\varepsilon^+_{so}-\gamma^+_{ss})$ (see Eqs. 4 and 7), are about 2 eV smaller than those obtained employing $(\varepsilon^-_{so}+\gamma^-_{ss})$ and $(\varepsilon^+_{so}-\gamma^+_{ss})$ directly. This is understandable when we take into consideration the correlation of Eqs. 9 and 11. However, the solvation energies themselves of the dianion or dication calculated using $\varepsilon^{=}_{ho}$ or ε^{++}_{lu} are more accurate than those obtained from $(\varepsilon^-_{so}+\gamma^-_{ss})$ or $(\varepsilon^+_{so}-\gamma^+_{ss})$, because the latter values are for the orbital approximation to the former values, derived from the overall MO calculation, just like the ε_{lu} or ε_{ho} in Eqs. 1 and 2. Now, in comparing the solvation energies of the dianion and dication with those of the monoanion and monocation under the same calculation models, we can see in Table 3 that $|E^{=}_{solv}|=4.2(\pm0.2)|E^-_{solv}|$ for Columns F and A and $|E^{++}_{solv}|=4.3(\pm0.2)|E^+_{solv}|$ for Columns H and C. In addition, the change in $|E^{=}_{solv}|$ with the ring size seems to be in a reasonable direction; e. g., $|E^{=}_{solv}|$ decreases gradually with the structure change of **2**→**3**→**4**, as would be inferred from the discussion of Eq. 3 (vide supra). These results can be understood on the basis of the Born-type equation pertaining to solvation energies, whose generalized form may be written as:[63]

$$E_{solv} = -\frac{1}{2}\left(1-\frac{1}{\varepsilon}\right)\sum_{A,B}\frac{Q_A\cdot Q_B}{R_{AB}} \quad (15)$$

where ε, Q_A and Q_B, and R_{AB} indicate a solvent's dielectric constant, the atomic charges on the A and B

atoms, and the atomic distance between A and B respectively. When A=B, R_{AB} stands for atomic radius. If we put $\sum_{A,B}(Q_A \cdot Q_B)/R_{AB} \equiv (Ze)^2/r$ (r is the cavity radius), according to original Born's equation,[64] then the solvation energies on the dianion or dication come out about four times as large as those of the monoanion or monocation. Also, with an increase in the r, i. e., with an increase in the molecular size, the solvation energies may decrease. Of course, this tendency is made prominant in doubly charged species than in singly charged ones, as can actually be found in Table 3. In the case of neutral molecules of BAH, the π-formal charge at each carbon atom is zero in the PPP calculations; their molecular dipole moments are also zero in a good approximation. Our CNDO/2 calculations gave similar results. These circumstances suggest that the solute-solvent interactions and the solvation energies of neutral BAH's turn out to be the same order for any BAH and very small[45] in comparison with those of the ionic species. Thus, we believe that the solvation energies here evaluated are quite close to those of the ion species themselves, although the values are obtained as the difference between the ion species and the neutral species. Finally, we can say that the standard reduction and oxidation potentials of BAH attributable to the formation of mono- and dianions and mono- and dications, and their mutual relations, can both be well-understood by applying the theories of the PPP-type semiempirical molecular orbitals and the Born-type solvation energies. The present quantitative discussion, pertinent to dianions and dications throughout the monoanions and monocations and to their mutual correlations, seems to be the first to treat BAH.

Appendix

Let us consider Eq. A-1, written as a linear combination of two variables, x_1 and x_2:

$$y = a_0 + a_1x_1 + a_2x_2 \qquad \text{(A-1)}$$

The condition necessary to satisfy simultaneously both equations, $y=a_0'+a_1x_1$ and $y=a_0''+a_2x_2$, is that the correlation coefficient, r_{12}, between x_1 and x_2 be perfectly zero. However, when the linear relation $y=b_0+b_1x_1$ is experimentally or theoretically assumed, then it can easily be verified that the x_2 should fulfill either one of the conditions, that x_2 be constant or be in a linear relation to the y values, i. e., $y=b_0'+b_2x_2$. Multiple regression analysis[65] shows, that if the above r_{12} is not zero, the a_2 value in Eq. A-1 is equal to the regression coefficient relevant to the single regression equation of y to the "residual," which is obtained by removing the x_1 effect from x_2. The same situation also holds for the physical meaning of the a_1 value in Eq. A-1, so that the a_1 and a_2 values in Eq. A-1 are theoretically somewhat complex, especially in the case of a large r_{12} value.

The authors wish to express their thanks to Professor Kōsuke Izutsu of the Faculty of Science, Shinshu University, for his encouragement and his helpful discussions on the problem of the mutual relation between reduction and oxidation potentials throughout the first and second steps.

References

1) Presented at the Symposia on the Structure Chemistry and Electronic State of Molecules (Tokyo, Sept., 1985, Abstract, p. 166) and Polarography and Electroanalytical Chemistry (Tokyo, Nov., 1986, Abstract, p. 1).

2) G. J Hoijtink, J. van Schooten, E. de Boer, and W. Y. Aalbersberg, *Rec. Trav. Chim.*, **73**, 355 (1954); B. I. Shapiro, V. M. Kazakova, and Y. K. Syrkin, *J. Structural Chem. (USSR)*, **6**, 516, 540 (1965).

3) P. H. Given and M. E. Peover, *J. Chem. Soc.*, **1960**, 385.

4) T. Kubota, Y. Ōishi, K. Nishikida, and H. Miyazaki, *Bull. Chem. Soc. Jpn.*, **43**, 1622 (1970).

5) R. F. Michielli and P. J. Elving, *J. Am. Chem. Soc.*, **90**, 1989 (1968).

6) G. J. Hoytink, "Advances in Electrochemistry and Electrochemical Engineering," John Wiley & Sons, New York (1970), Vol. 7, pp. 221—281.

7) A. J. Bard, A. Ledwith, and H. J. Shine, *Adv. Phys. Org. Chem.*, **13**, 155 (1976).

8) V. D. Parker, *Adv. Phys. Org. Chem.*, Academic Press, **19**, 131 (1983).

9) M. E. Peover, "Electroanalytical Chemistry," ed by A. J. Bard, Marcel Dekker, New York (1967), Vol. 2, Chap. 1.

10) Rafik O. Loutfy and Raouf O. Loutfy, *J. Phys. Chem.*, **77**, 336 (1973).

11) Rafik O. Loutfy and Raouf O. Loutfy, *Can. J. Chem.*, **54**, 1454 (1976); Rafic O. Loutfy and Raouf O. Lautfy, *J. Phys. Chem.*, **76**, 1650 (1972).

12) T. Kubota, H. Miyazaki, M. Yamakawa, K. Ezumi, and Y. Yamamoto, *Bull. Chem. Soc. Jpn.*, **52**, 1588 (1979) and the others of our papers cited therein.

13) J. Koutecký, *Z. Phys. Chem. (N. F.)*, **52**, 8 (1967).

14) M. J. S. Dewar, J. A. Hashmall, and N. Trinajstrić, *J. Am. Chem. Soc.*, **92**, 5555 (1970).

15) V. D. Parker, *J. Am. Chem. Soc.*, **98**, 98 (1976).

16) B. Case, N. S. Hush, R. Parsons, and M. E. Peover, *J. Electroanal. Chem.*, **10**, 360 (1965).

17) A. Streitwieser Jr., "Molecular Orbital Theory for Organic Chemists," John Wiley & Sons, New York (1961), p. 173.

18) T. Kubota, K. Nishikida, H. Miyazaki, K. Iwatani, and Y. Ōishi, *J. Am. Chem. Soc.*, **90**, 5080 (1968).

19) B. Uno, Y. Matsuhisa, K. Kano, and T. Kubota, *Chem. Pharm. Bull.*, **32**, 1 (1984), and the other references given therein.

20) N. S. Hush and J. Blackledge, *J. Chem Phys.*, **23**, 514 (1955).

21) S. Hünig, D. Scheutzow, P. Čársky, and R. Zahradnik, *J. Phys. Chem.*, **75**, 335 (1971); P. Čársky, S. Hünig, D. Scheutzow, and R. Zahradnik, *Tetrahedron*, **25**, 4781 (1969).

22) M. Senda and R. Takahashi, *Rev. Polarogr. (Kyoto)*, **20**, 56 (1974).

23) T. Kakutani, Y. Morihiro, M. Senda, R. Takahashi, and K. Matsumoto, *Bull. Chem. Soc. Jpn.*, **51**, 2847 (1978).

24) O. Hammerich and V. D. Parker, *Electrochim. Acta*, **18**, 537 (1973).
25) K. Kano, T. Konse, N. Nishimura, and T. Kubota, *Bull. Chem. Soc. Jpn.*, **57**, 2383 (1984).
26) T. Kubota, B. Uno, Y. Matsuhisa, H. Miyazaki, and K. Kano, *Chem. Pharm. Bull.*, **31**, 373 (1983).
27) In the case of reduction-CV measurements, a Metrohm EA 290 hanging-mercury-drop electrode was also used, but the reduction potentials concurred within a several mV with those obtained using the Pt electrode for all the samples employed. All the discussion in this text was, therfore, carried out using the data obtained by the use of the Pt electrode.
28) T. Kubota, H. Miyazaki, K. Ezumi, and M. Yamakawa, *Bull. Chem. Soc. Jpn.*, **47**, 491 (1974).
29) J. Juillard, "Recommended Methods for Purification of Solvents and Tests for Impurities," ed by J. F. Coetzee, (IUPAC), Pergamon Press, Oxford (1982), p. 32; J. F. Coetzee, *ibid.* (1982), p. 1.
30) The Merck Index was referred to in choosing the solvents. "The Merck Index," 9th, ed., ed by M. Windholz, S. Budavari, L. Y. Stroumtsos, and M. N. Fertig, Merck & Co., New Jersey (1976).
31) That the dianion of BAH may exist in either a singlet or triplet state is well known.[32] The present calculation was performed for the singlet closed system, since, if LUMO does not degenerate, the singlet species is usually more stable than in the triplet state, though the energy difference is not very large for common BAH dianions.
32) A. Minsky, A. Y. Meyer, R. Poupko, and M. Rabinovitz, *J. Am. Chem. Soc.*, **105**, 2164 (1983).
33) The ground state of LP-SCFMO calculation is not completely in the so-called SCF state,[34] so excited configurations are slightly mixed in the ground state. Neglecting this effect, the MO's were employed in this discussion.
34) H. C. Longuet-Higgins and J. A. Pople, *Proc. Phys. Soc. London Sec. A*, **68**, 591 (1955); A. Ishitani and S. Nagakura, *Theor. Chim. Acta (Berlin)*, **4**, 236 (1966); R. Zahradnik and P. Čársky, *J. Phys. Chem.*, **74**, 1235, 1240, 1249 (1970); K. Ezumi, T. Kubota, H. Miyazaki, and M. Yamakawa, *J. Phys. Chem.*, **80**, 980 (1976).
35) K. Nishimoto and L. S. Forster, *Theor. Chim. Acta (Berlin)*, **4**, 155 (1966).
36) Although the molecular dimensions seem to be somewhat different among the neutral, monoanion and monocation, and dianion and dication species, this was neglected since the effect seems to be small for the present rigid molecule.
37) N. Mataga and K. Nishimoto, *Z. Physik. Chem. (N. F.)*, **13**, 140 (1957).
38) Here, E_{solv}, E^{-}_{solv}, and $E^{=}_{solv}$ are the solvation energies for the neutral molecule, the monoanion radical, and the dianion respectively.
39) T. Koopmans, *Physica*, **1**, 104 (1933).
40) B. S. Jensen and V. D. Parker, *J. Am. Chem. Soc.*, **97**, 5211 (1975).
41) A rather large difference is found in the $E^{red}_{1/2\cdot2}$ value of **7** (chrysene), −2.730 V having been reported by Jensen and Parker.[40]
42) Also, we would expect a linear $E^{red}_{1/2\cdot1}$ vs. E_A (electron affinity) relation for the present BAH series, since E_A is parallel with ε_{lu}. The results are $E^{red}_{1/2\cdot1}=1.154E_A-2.759$, with $r=0.946$ and $n=6$ (Compounds **1**, **2**, **5**—**7**, **10**), the E_A values being cited from Ref. 43 and given in Table 2.
43) W. E. Wentworth, E. Chen, and J. E. Lovelock, *J. Phys. Chem.*, **70**, 445 (1966).
44) As may be understood from Fig. 2, if we choose such polyacenes as Compounds **2**—**4**, the $E^{red}_{1/2\cdot2}$ vs. $\varepsilon^{=}_{ho}$ plot of Eq. 3 gives a very good linear correlation. This kind of result was also found on the other plottings. The topological MO and molecular features of polyacenes may play an important role in this result.
45) N. Mataga and T. Kubota, "Molecular Interactions and Electronic Spectra," Marcel Dekker, New York (1970).
46) A. Carrington and A. D. McLachlan, "Introduction to Magnetic Resonance," Harper & Row, New York and London (1967).
47) Also, the Boltzmann distribution equilibrium between singlet and triplet states has been pointed out for the ground states of BAH dianions;[32] this fact may somewhat complicate the nature of the dianion in solution.
48) R. O. Loutfy, *J. Chem. Phys.*, **66**, 4781 (1977).
49) That the two-electron-repulsion-integrals (γ_{ll}, γ^{-}_{ss}, γ^{+}_{ss}) will have quite a large molecular-size dependence can easily be understood from, for example, the electron's angular correlation effect.[50].
50) C. Sandorfy, "Electronic Spectra and Quantum Chemistry," Prentice-Hall, New Jersey (1964).
51) R. J. Klingler and J. K. Kochi, *J. Am. Chem. Soc.*, **102**, 4790 (1980); J. O. Howell, J. M. Goncalves, C. Amatore, L. Klasinc, L. R. M. Wightman, and J. K. Kochi, *ibid.*, **106**, 3968 (1984).
52) R. Boschi, E. Clar, and W. Schmidt, *J. Chem Phys.*, **60**, 4406 (1974).
53) Dewar et al. reported this equation;[14] $E^{oxd}_{1/2\cdot1}=0.996I^{cal}_{P}-6.607$, with $r=0.987$ and $n=9$, and where I^{cal}_{P} is the I_P calculated by them.
54) It is well known that the dications of 9,10-dimethyl- (see Table 2) and 9,10-diphenylanthracenes[24] are cyclic voltammetrically stable.
55) a) A. D. McLachlan, *Mol. Phys.*, **4**, 49 (1961). b) A. D. McLachlan, *Mol. Phys.*, **2**, 271 (1959). c) T. Shida and S. Iwata, *J. Am. Chem. Soc.*, **95**, 3473 (1973).
56) In the case of the $E^{red}_{1/2\cdot1}$ and $E^{red}_{1/2\cdot2}$ measurements, DMF and AN gave almost the same values for perylene when a Pt electrode was used (see Table 2). This fact is reasonable judging from the Born equation, because the dielectric constants[29] of DMF (37.0) and AN (36.0) are almost equal to each other.
57) N. S. Hush and A. J. Pople, *Trans. Faraday Soc.*, **59**, 600 (1955); R. M. Hedges and F. A. Matsen, *J. Chem. Phys.*, **28**, 950 (1958); R. S. Becker and W. E. Wentworth, *J. Am. Chem. Soc.*, **85**, 2210 (1963); J. R. Hoyland and L. Goodman, *J. Chem. Phys.*, **36**, 21 (1962).
58) R. S. Mulliken, *J. Chem. Phys.*, **2**, 782 (1934); **3**, 537 (1935).
59) a) This relation was employed by Senda and Takahashi[22,23] to determine the standard electrode potential in nonaqueous solvents. b) Our data in Table 2 were obtained in DMF for reduction, but in AN for oxidation; thus, we can not omit the error due to the solvation-energy difference brought about by DMF and AN, though the difference is quite small.[56] Parker[15] reported the values of

$(E^{oxd}_{1/2\cdot1}+E^{red}_{1/2\cdot1})/2$ for BAH in AN; they are -0.313 ± 0.022 V (n=10) and $\Delta E^{+}_{solv}=\Delta E^{-}_{solv}$ within the limits of experiment error, though they adopted irreversible CV data for $E^{oxd}_{1/2\cdot1}$.

60) The coefficient of ε_{lu} or ε_{ho} in Eqs. 1 and 2 is constrained to unity on the assumption that, if the MO evaluation of the energies is correct, the coefficient becomes 1.

61) Parker[15] reported $\Delta G°=-4.4$ eV vs. SCE on the basis of the same treatment as was used here. Peover et. al.[16] reported $\Delta G°=-4.70$ eV in the case of the (Ag/Ag^{+}) electrode in AN. Alternatively, $\Delta G°$ values of -4.36 to -4.41 eV have also been reported for SCE.[62]

62) R. C. Larson, R. T. Iwamoto, and R. N. Adams, *Anal. Chim. Acta*, **25**, 371 (1961); J. E. Kuder, D. Wychick, R. L. Miller, and M. S. Walker, *J. Phys. Chem.*, **78**, 1714 (1974).

63) I. Jano, *C. R. Acad. Sci. (Paris)*, **261**, 103 (1963); O. Kikuchi, T. Kozaki, and K. Morihashi, *Nippon Kagaku Kaishi*, **1986**, 1409.

64) M. Born, *Z. Phys*, **1**, 45 (1920).

65) T. Okuno, H. Kume, T. Haga, and T. Yoshizawa, "Multivariate Analysis," (in Japanese), Nikkagiren Press, Tokyo (1978), Chapter II; N. R. Draper and H. Smith, "Applied Regression Analysis," John Wiley & Sons, New York (1968).

 © 1987 The Chemical Society of Japan Bull. Chem. Soc. Jpn., 60, 3879—3885 (1987)

The Phase Transition of 1-Alkyl-4-aza-1-azoniabicyclo[2.2.2]octane Bromides, C_n-DABCO-Br ($11 \leqq n \leqq 22$)

Kengo IMAMURA, Takashi NOGAMI,* Yasuhiko SHIROTA, Tsutomu ISHIOKA,† and Masamichi KOBAYASHI*,†

Department of Applied Chemistry, Faculty of Engineering, Osaka University, Yamadaoka, Suita, Osaka 565

†Department of Macromolecular Science, Faculty of Science, Osaka University, Toyonaka, Osaka 560

(Received May 25, 1987)

The phase transitions of a series of 1-alkyl-4-aza-1-azoniabicyclo[2.2.2]octane bromides were studied on the basis of DSC, measurements of the ionic conductivities of the bromide anion, and Raman spectroscopy. Two endothermic signals were observed at the temperatures of T_{c1} and T_{c2} ($T_{c1}<T_{c2}$) for most of the materials. The transition enthalpies and transition entropies were not very different for the transitions at T_{c1}, irrespective of the alkyl-chain lengths attached to DABCO nitrogens. On the other hand, these values tended to increase with an increase in the alkyl-chain lengths for the transitions at T_{c2}. The temperature dependences of the ionic conductivities of the bromide anion showed abrupt increases in the conductivities by a factor of 2—10. The conductivity jumps were observed around T_{c2}. The temperature dependences of the Raman spectra gave detailed information on the phase transition; (1) the change in the subcell structure took place at T_{c1}, with the concomitant occurrence of a conformational change in the alkyl group; (2) above T_{c2}, the alkyl chain takes a liquid-like disordered form, and a rotational motion of the DABCO portion sets in.

The solid-solid phase transitions of a series of bis(quaternary alkyl halides) of 1,4-diazabicyclo[2.2.2]-octane (DABCO) have been studied on the basis of DSC, IR absorption spectroscopy, and measurements of the ionic conductivities of the halide anion.[1-5] The phase transitions of quaternary alkyl bromide salts of 1-azabicyclo[2.2.2]octane were also studied.[6] Symmetric bis(quaternary alkyl halide) salts of DABCO showed endothermic signals at the transition temperatures (T_c) when the samples were heated from room temperature.[1,2] They showed exothermic signals around T_c when the samples were cooled after they had been heated above T_c. The absolute values of the endothermic and exothermic heats were equal, within the limits of experimental error. Abrupt increases in the ionic conductivity of the halide anion by a factor of 630—3600 were observed around at T_c. As the temperature was increased, the IR absorption spectra of the symmetric salts showed a sudden disappearance of the band progressions due to the CH_2 rocking-twisting branch at T_c. This fact shows that the trans-zigzag conformation of the long alkyl chains in the low temperature phase is destroyed and changes to a disordered form above T_c. The concomitant formation of voids facilitates the halide-anion transport above the transition temperature, giving rise to the conductivity jump.

The unsymmetric bis(quaternary alkyl bromides) of DABCO showed phenomena different from those of the symmetric salts.[3-5] Endothermic signals were also observed at the transition temperatures (T_c) when the virgin samples[7] were heated from room temperature. However, the exothermic signals were observed at much lower temperatures (T_c') than T_c when the samples were cooled after they had been heated above T_c. The temperature dependence of the IR absorption spectra of the unsymmetric salts revealed that a metastable phase was produced first when the samples had been cooled from a temperature above T_c. For some unsymmetric salts, the metastable phase was converted to the stable phase within a week when the salts were kept at room temperature. The thermodynamic properties of the unsymmetric salts could be explained on the basis of the free energy-temperature relation. Conductivity jumps of the bromide anion by a factor of 100—6000 were also observed around T_c for the virgin samples and around T_c' for the annealed samples.[7]

All of the previous studies were made on the phase transitions of bis(quaternary alkyl halides) of DABCO; it seems that it also be interesting to compare the phase transitions of mono(quaternary alkyl bromides) of DABCO with those of the bis(quaternary salts). Mono(quaternary alkyl bromide salt) of DABCO possesses both a hydrophilic DABCO cation and a hydrophobic alkyl group. Thus, it has a possibility of forming a Langmuir-Blodgett membrane[8] and may be useful in a molecular device by using abrupt changes in the ionic conductivities of the bromide anion and/or the disappearance of the birefringence above the transition temperatures.[2] We have studied the phase transitions of mono(quaternary alkyl bromides) of DABCO on the basis of DSC, the

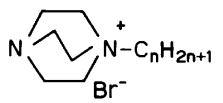

n= 11,12,13,14,15,16,17,18,22

Fig. 1. Mono(quaternary alkyl bromide) salts of DABCO.

measurements of the ionic conductivities of the bromide anion, and Raman spectroscopy. The materials studied are shown in Fig. 1. The names of the materials are abbreviated by the numbers of the alkyl carbons attached to DABCO nitrogens. For example, 4-dodecyl-1-aza-4-azoniabicyclo[2.2.2]octane bromide is abbreviated as C_{12}-DABCO-Br. Thus, the names of the materials in Fig. 1 are generally abbreviated as C_n-DABCO-Br ($11 \leqq n \leqq 22$). The names of the symmetric bis(quaternary alkyl bromide salts) of DABCO are similarly abbreviated as C_n-DABCO-C_n-Br_2.

Experimental

Syntheses of Mono(quaternary alkyl bromides) of DABCO. The mono(quaternary alkyl bromides) of DABCO were synthesized by the method reported previously.[3]

Measurements. The DSC and the measurements of the ionic conductivities of the bromide anion and the IR spectra were made by the methods reported previously.[1,2] The Raman spectra were measured on a JASCO CT-1000D double monochromator, using the 514.5 nm line (Ar ion laser) as the excitation source. The temperature of the sample was regulated by means of a Thermal Controller E5D (Omron Co., Ltd). In order to quench the fluorescence caused by unknown impurities, the sample held above T_{c2} was irradiated with the excitation beam for several h before the measurement.

Results and Discussion

DSC Measurements. The DSC measurements were made at the heating (or cooling) rate of 5 °C min^{-1}. Figure 2 shows the DSC thermogram of C_{17}-DABCO-Br as a typical example. Most of the samples gave two endothermic signals at the T_{c1} and T_{c2} temperatures ($T_{c1}<T_{c2}$) on heating. As will be shown later, abrupt increases in the ionic conductivities of the bromide anion occurred around T_{c2}. Thus, the phase transitions at T_{c1} and T_{c2} seem to be different in origin. The absolute values of the transition enthalpies at T_{c1} and T_{c2} are denoted as $\Delta H_{en,1}$ and $\Delta H_{en,2}$ respectively. However, C_{13}-DABCO-Br showed three transitions (assigned tentatively as one at T_{c1} and two at T_{c2}).[9] When the samples were cooled after they had once been heated above T_{c2}, exothermic signals were observed. However, the temperatures of the exothermic transitions were usually much lower than the corresponding endothermic temperatures, T_{c1} and T_{c2}. The thermal histories of the samples seem to influence the exothermic transition temperatures and the shapes of the DSC curves. On the other hand, the endothermic transition temperatures (T_{c1} and T_{c2}) were reproducible when the samples were heated after several heating/cooling cycles. $\Delta H_{en,1}$ and $\Delta H_{en,2}$ tend to decrease slightly when the cycles are repeated. Part of Table 1 shows the materials, T_{c1}, $\Delta H_{en,1}$, T_{c2}, $\Delta H_{en,2}$, and the transition entropies ΔS_1 ($=\Delta H_{en,1}/T_{c1}$) and ΔS_2 ($=\Delta H_{en,2}/T_{c2}$).

Figure 3 plots the transition temperatures (T_{c1} and T_{c2}) against the carbon numbers of the alkyl chains. This figure also shows the transition temperatures of the symmetric bis(quaternary alkyl bromide) salts of

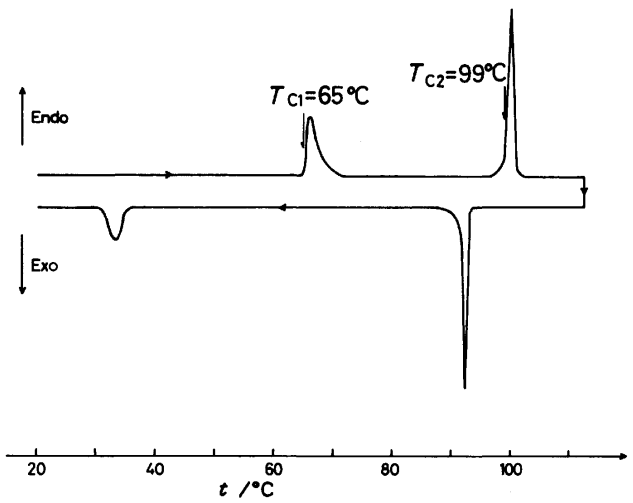

Fig. 2. DSC thermogram of C_{17}-DABCO-Br; scan rate=5 °C min^{-1}.

Table 1. Transition Temperatures (T_{c1} and T_{c2}), Transition Enthalpies ($\Delta H_{en,1}$ and $\Delta H_{en,2}$), Transition Entropies (ΔS_1 and ΔS_2), and Ratios of Ionic Conductivities of Bromide Anion Below (σ_l) and Above (σ_h) Transition Temperatures

Material	T_{c1} / °C	$\Delta H_{en,1}$ / kJ mol^{-1}	ΔS_1 / J mol^{-1} K^{-1}	T_{c2} / °C	$\Delta H_{en,2}$ / kJ mol^{-1}	ΔS_2 / J mol^{-1} K^{-1}	σ_h/σ_l
C_{11}-DABCO-Br	56	32.7	99	64	11.9	35	2
C_{12}-DABCO-Br	55	48.7	148	71	2.3	7	5
C_{13}-DABCO-Br	53	25.4	78	78, 86	3.8, 16.8	11, 47	3
C_{14}-DABCO-Br	60	29.8	89	73	26.4	76	10
C_{15}-DABCO-Br	62	31.1	93	79	31.5	90	5
C_{16}-DABCO-Br	67	31.7	93	85	34.5	96	6
C_{17}-DABCO-Br	65	31.6	93	99	40.6	109	7
C_{18}-DABCO-Br	67	30.4	89	85	25.9	72	3
C_{22}-DABCO-Br	76	33.0	95	107	50.9	134	4

DABCO (C_n-DABCO-C_n-Br_2)[2] for the sake of comparison. T_{c1} tends to increase with the increase in the alkyl-chain lengths for C_n-DABCO-Br ($n \geqq 13$). The variations in T_{c2} with the change in the alkyl-chain lengths were larger than those in T_{c1}. The transition temperatures of most of the symmetric bis(quaternary alkyl bromide) salts of DABCO were higher than T_{c1} and T_{c2}. This is reasonable because the molecular interaction arises mainly from the Coulomb force between N^+ and Br^-. Thus, the molecular interaction between the bis(quaternary salts) is stronger than that between the mono(quaternary salts); this gives rise to the higher transition temperatures for the former materials.

Figure 4 plots the transition enthalpies ($\Delta H_{en,1}$ and $\Delta H_{en,2}$) against the carbon numbers of the alkyl chains. This figure also shows the transition enthalpies of the symmetric bis(quaternary alkyl bromide) salts of DABCO (C_n-DABCO-C_n-Br_2)[2] for the sake of comparison. It is noteworthy that the $\Delta H_{en,1}$'s are close to 30 kJ mol^{-1}, irrespective of the alkyl-chain lengths.[10] On the other hand, the variations in the $\Delta H_{en,2}$'s with the alkyl-chain length are much larger than those in the $\Delta H_{en,1}$'s. These facts suggest that the origin of the phase transition at T_{c1} is common for all of the mono(quaternary salts) of DABCO. This point will be clarified by Raman spectroscopy later in this paper. Both the $\Delta H_{en,1}$ and $\Delta H_{en,2}$ values and their sum are smaller than the transition enthalpies of the symmetric bis(quaternary salts) with the same alkyl chain. This also comes from the fact that the intermolecular interaction of the bis(quaternary salts) is stronger than that of the mono(quaternary salts). No even-odd number effect of the alkyl carbons on the transition enthalpies was observed, unlike the cases of the bis(quaternary salts).[2,3] Similar characteristics described for the transition enthalpies were also applicable to the transition entropies (ΔS_1 and ΔS_2). It is especially noteworthy that the variations in ΔS_1 (78—99 J mol^{-1} K^{-1}) with the change in the alkyl-chain length are much smaller than those in ΔS_2.

Ionic Conductivities of the Bromide Anion. All of the samples were confirmed to be ionic conductors of the bromide anion by the method described previously.[1] The ionic conductivities were measured for sample pellets which had been dried overnight under a dynamic vacuum above T_{c2}. The conductivities less than 10^{-10} S cm^{-1} were below the lower limit of our

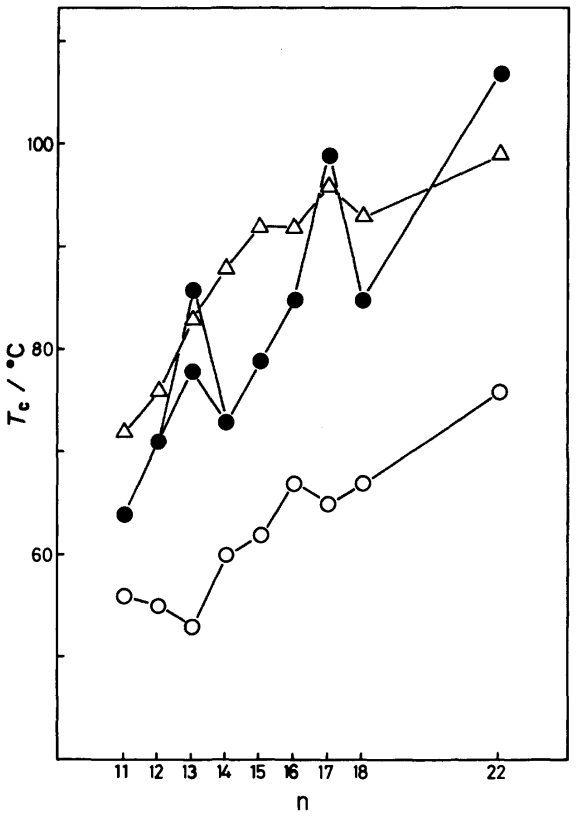

Fig. 3. The plots of the transition temperatures against the carbon numbers of alkyl grops.
○ T_{c1} of C_n-DABCO-Br; ● T_{c2} of C_n-DABCO-Br; △ T_c of C_n-DABCO-C_n-Br_2.

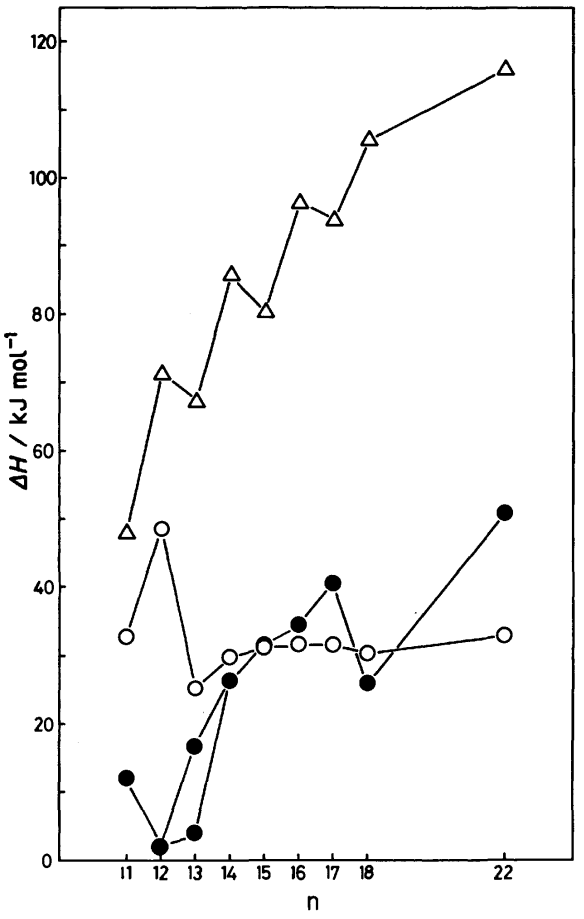

Fig. 4. The plots of the transition enthalpies against the carbon numbers of alkyl group.
○ $\Delta H_{en.1}$ of C_n-DABCO-Br; ● ΔH_{en2} of C_n-DABCO-Br; $\Delta\Delta H$ of C_n-DABCO-C_n-Br_2.

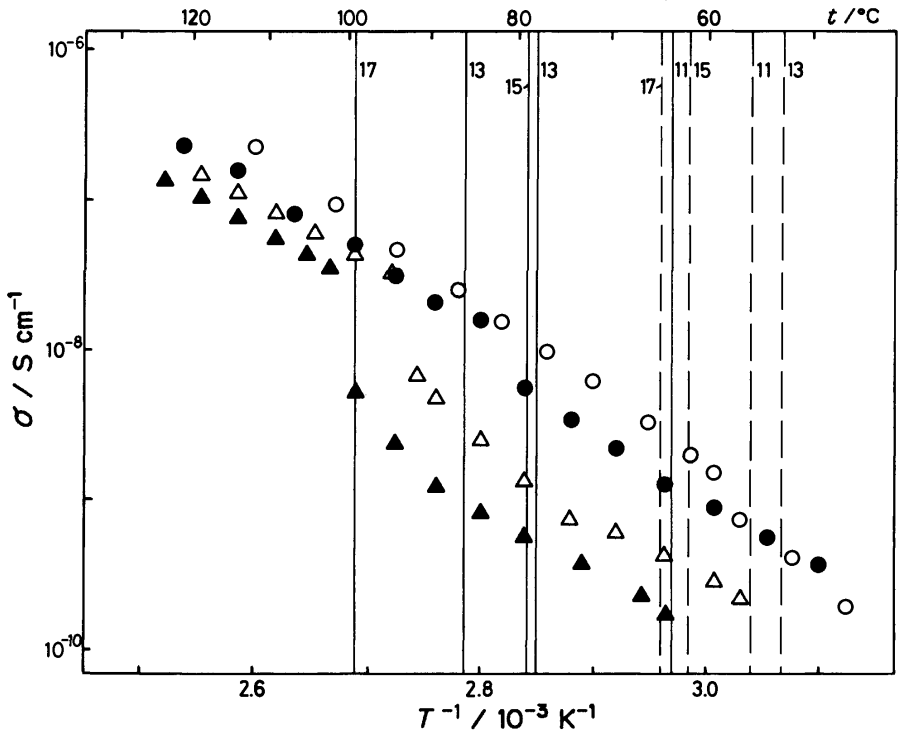

Fig. 5. Temperature dependences of ionic conductivities of bromide anion of monoquaternary DABCO bromide salts possessing odd numbers of alkyl carbons. The broken and solid lines represent T_{c1} and T_{c2} respectively. The numbers near these lines denote the numbers of alkyl carbons attached to DABCO nitrogens.
○ C_{11}-DABCO-Br; ● C_{13}-DABCO-Br; △ C_{15}-DABCO-Br; ▲ C_{17}-DABCO-Br.

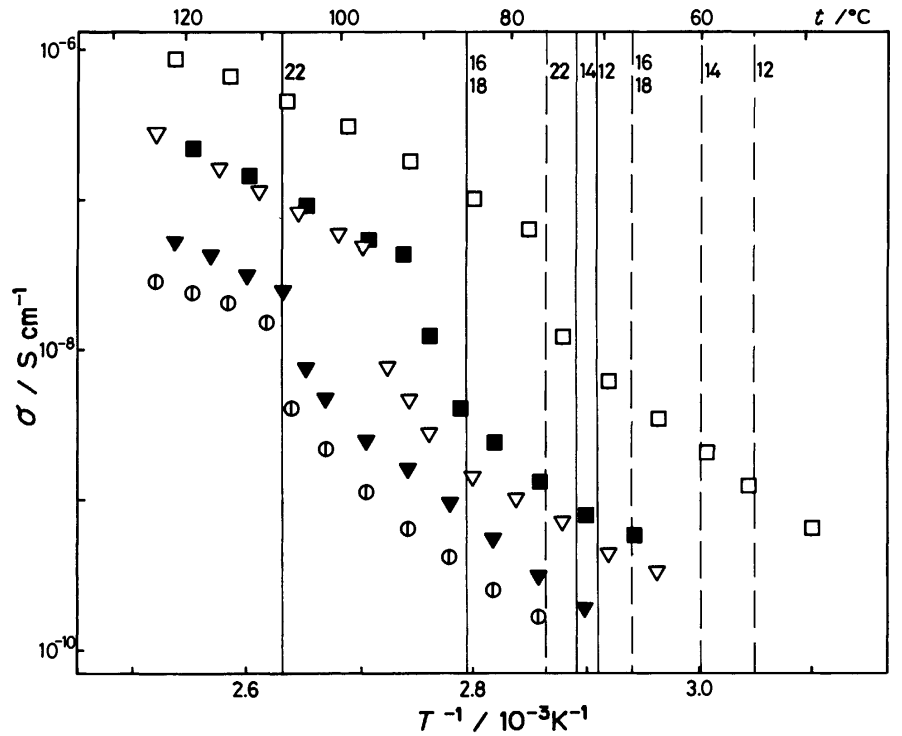

Fig. 6. Temperature dependences of ionic conductivities of bromide anion of monoquaternary DABCO bromide salts possessing even numbers of alkyl carbons. The broken and solid lines represent T_{c1} and T_{c2} respectively. The numbers near these lines denote the numbers of the alkyl carbons attached to DABCO nitrogens.
□ C_{12}-DABCO-Br; ■ C_{14}-DABCO-Br; ▽ C_{16}-DABCO-Br; ▼ C_{18}-DABCO-Br; Φ C_{22}-DABCO-Br.

measurement. Figures 5 and 6 show the temperature dependences of the ionic conductivities of the bromide anion of the mono(quaternary alkyl bromide salts) of DABCO, possessing odd and even numbers of alkyl carbons respectively. The broken and solid lines in these figures represent T_{c1} and T_{c2} respectively. The numbers near these lines represent the numbers of the alkyl carbons attached to the DABCO nitrogens.

All of the samples exhibited conductivity jumps. Table 1 shows the ratios of the conductivities below (σ_l) and above (σ_h) the temperature of the conductivity jumps. The σ_h/σ_l values (2—10) were two to three orders of magnitude smaller than those of the bis-(quaternary alkyl bromide salts) of DABCO; the latter salts gave σ_h/σ_l values of about 100—6000.[1-5] Figures 5 and 6 show that the temperatures of the conductivity jumps are much higher than T_{c1}. On the other hand, they are close to T_{c2} for C_n-DABCO-Br (n=12, 13, 16, 17, 22) and are about 10—20 °C higher than T_{c2} for C_n-DABCO-Br (n=14, 15, 18). From the above experimental results, it can be said that the conductivity jump is not caused by the transition at T_{c1}, but is more closely related to the transition at T_{c2}.[10] It can be said that the conductivities become lower with the increase in the alkyl-chain length. It is also noteworthy that the plots of the conductivities against the temperature are nearly parallel with each other for the DABCO salts, possessing even numbers of alkyl carbons both below and above the conductivity jumps (Fig. 6). On the other hand, the conductivities above the conductivity jumps are much closer to each other than are those below the conductivity jumps in the cases of the quaternary DABCO salts possessing odd numbers of alkyl carbons (Fig. 5). In this connection, a series of the bis(quaternary alkyl bromide salts) of DABCO exhibited somewhat different phenomena; their ionic conductivities of the bromide anion above the transition temperatures were very close, irrespective of the alkyl-chain lengths while they were very different below the transition temperatures.[1-5] The reasons for these different phenomena remain to be clarified.

Raman Spectroscopy. The DSC measurements showed that the $\Delta H_{en,1}$'s were close to each other (≈30 kJ mol^{-1}), irrespective of the alkyl-chain length attached to the DABCO nitrogens. The measurements of the ionic conductivities of the bromide anion revealed that the conductivity jump is not caused by the transition at T_{c1}, but is more closely related with the transition at T_{c2}. These results suggest that the transitions at T_{c1} and T_{c2} are different in origin. In order to clarify these two transitions, the temperature dependences of the Raman spectra of C_{17}-DABCO-Br and C_{22}-DABCO-Br were measured for powder samples as typical examples. Since similar changes in the Raman spectra were observed for these materials, only the Raman spectra of C_{17}-DABCO-Br are shown in Fig. 7.

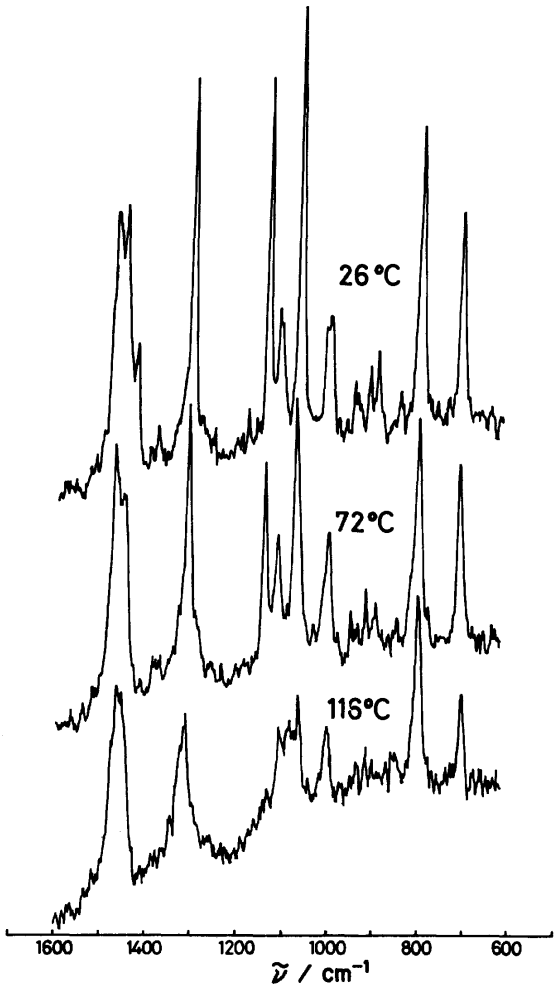

Fig. 7. Temperature dependence of the Raman spectra of C_{17}-DABCO-Br. T_{c1}=65°C, T_{c2}=99°C.

The most conspicuous spectral change at T_{c1} is the disappearance of the 1415 cm^{-1} band above T_{c1}. This band is associated with the A_g split component of the CH_2 scissoring $\delta(CH_2)$ mode,[11-13] and is characteristic of the $O_\perp$-type subcell, where the zigzag planes of the nearest neighboring alkyl chains are packed nearly perpendicular to each other. Therefore, the disappearance of this band means that, at the transition, the subcell structure changes to another type. This is consistent with the change observed in the IR spectrum, i.e., the split pairs due to the $\delta(CH_2)$ [at 1476 and 1463 cm^{-1}] and the CH_2 rocking $r(CH_2)$ modes [at 731 and 720 cm^{-1}] change to the singlets in the temperature range of $T_{c1}<T<T_{c2}$.

As for the subcell structure in the $T_{c1}<T<T_{c2}$ range, there are two possibilities, judging from the infrared and Raman spectra. One is the $T_{//}$-type packing, where the zigzag planes are all parallel to each other, and the other is the hexagonal type with a rotationally disordered orientation of the zigzag planes.[14-17]

When the spectra are measured on powder samples, as in the present case, these two subcells give rise to quite similar spectra and can hardly be distinguished from each other. Judging from the very large value of $\Delta H_{cn,1}$, the hexagonal packing may be the more plausible.

The strong Raman bands at 1295 cm^{-1} [the CH_2 twisting $t(CH_2)$ mode], 1131 cm^{-1} [the symmetric CC stretch $\nu_s(CC)$ mode], and 1062 cm^{-1} [the antisymmetric CC stretch $\nu_a(CC)$ mode], which appear in the lowest-temperature phase below T_{c1}, are characteristic of the all-trans conformation of the alkyl chain.[18-20] They decrease in intensity as the amount of conformational disorder accommodated in the chain increases, and smear into very broad bands when the chain takes a disordered form, as in the liquid alkanes.[18-20] In the $T_{c1}<T<T_{c2}$ temperature range, although these bands still exist with a strong intensity and with a narrow band width, the intensities decrease with an increase in the temperature. This indicates that, in this phase, a partial conformational disordering takes place in the alkyl chain. Above T_{c2}, all of these conformational-sensitive Raman bands change to those of the liquid alkanes, indicating that the alkyl chain may be assumed to take a liquid-like disordered form in the highest-temperature phase.

There are sharp Raman bands at 793 and 704 cm^{-1} in the present series of compounds, the positions being independent of the alkyl-chain length. They are associated with the C-C and C-N stretch modes of the bicyclic system.[21] Before and after the T_{c1} transition, these bands show no changes in either intensity or band width. Above T_{c2}, the 704 cm^{-1} band appreciably decreases in intensity. In the case of the bis(quaternary alkyl halides) of DABCO, a strong Raman band [due to the totally symmetric (NC_4) stretch mode] appears in the frequency region of 700—730 cm^{-1}; this band is broadened above the transition point, suggesting the onset of a rotational motion of the bicyclic system in the high temperature phase.[21] The spectral features of the present monosubstituted compounds are somewhat different from those of the disubstituted compounds.[22] The intensity depression of one of the ring bands indicates the occurrence of some disordering, either statically or dynamically, in the ionized bicyclic system above T_{c2}; it may be related to the abrupt increase in the ionic conductivity.

Summary

The phase transitions of a series of mono(quaternary alkyl bromides) of DABCO were studied on the basis of the DSC, the measurements of the ionic conductivities of the bromide anion, and Raman spectroscopy. The comparison of the phase transitions of the present materials with those of the bis(quaternary alkyl bromides) of DABCO will be discussed below. The present materials exhibited two transitions, at T_{c1} and T_{c2}, whereas the bis(quaternary alkyl bromides) or DABCO showed only one transition.[1-5] This comes from the difference in the crystal structure to be described below. The mono(quaternary salts) seem to possess an $O_\perp$-type subcell, judging from the presence of the crystal-field splitting in the Raman and IR spectra. On the other hand, no crystal-field splitting was observed for the bis(quaternary salts); they seem to possess either hexagonal packing or a $T_{/\!/}$-type packing.[23] The mono(quaternary salts) exhibited phase transitions at T_{c1}, probably arising from the conversion from the $O_\perp$-type subcell to hexagonal packing. On the other hand, the bis(quaternary salts) did not show such transitions; this was because of the different packing structures of the alkyl chain from those of the mono(quaternary salts). These facts demonstrate the difference in the number of transitions. As to the thermodynamic properties, no metastable phase was observed for C_n-DABCO-Br and C_n-DABCO-C_n-Br_2. On the other hand, a series of C_m-DABCO-C_n-Br_2 ($m \neq n$) gave rise to the metastable phase when they had been heated above the transition temperature and then cooled. Abrupt increases in the ionic conductivity by a factor of 2—10 were observed for the present materials around T_{c2}. These values were two to three orders of magnitude smaller than those of the bis(quaternary salts). This difference in values arises from the fact that the molecular motion of the bis(quaternary salts) seems to be more vigorous than that of the mono(quaternary salts) above the transition temperature.[22]

We are grateful to Professor Shigekazu Kusabayashi and Dr. Shunsuke Takenaka, Faculty of Engineering, Osaka University, for the use of the DSC apparatus.

References

1) J. Shimizu, T. Nogami, and H. Mikawa, *Solid State Commun.*, **54**, 1009 (1985).

2) J. Shimizu, K. Imamura, T. Nogami, and H. Mikawa, *Bull. Chem. Soc. Jpn.*, **59**, 1443 (1986).

3) K. Imamura, J. Shimizu, and T. Nogami, *Bull. Chem. Soc. Jpn.*, **59**, 2699 (1986).

4) J. Shimizu, K. Imamura, T. Nogami, and H. Mikawa, *Bull. Chem. Soc. Jpn.*, **59**, 3367 (1986).

5) K. Imamura, T. Nogami, and Y. Shirota, *Bull. Chem. Soc. Jpn.*, **60**, 111 (1987).

6) K. Imamura, T. Nogami, and Y. Shirota, *Bull. Chem. Soc. Jpn.*, **60**, 3499 (1987).

7) The virgin sample and the annealed sample indicate the synthesized sample and the sample heated at least once above T_{c2} respectively.

8) The monolayer of C_{18}-DABCO-Br was found to be formed by the Langmuir method, and its surface pressure became larger than 30 mN m^{-1}. We are grateful to Dr. Masahiro Irie, Institute of Scientific and Industrial Research, Osaka University, for the measurement of the π-A curve.

9) The transitions at 78 and 86 °C of C_{13}-DABCO-Br (Table 1) are tentatively assigned to T_{c2}, because the change in the Raman spectra at these temperatures are similar to those of C_{17}-DABCO-Br at T_{c2} (see the description of the Raman spectra).

10) In the case of C_{11}-DABCO-Br, the temperature of the conductivity jump is, exceptionally, close to T_{c1}. However, the separation between T_{c1} and T_{c2} is small (≈8 °C). Thus, the conclusion that the conductivity jump is related to the transition at T_{c2} can not be drawn for this material.

11) V. B. Carter, *J. Mol. Spectroscopy*, **34**, 356 (1970).

12) E. J. Boerio and J. L. Koenig, *J. Chem. Phys.*, **52**, 3425 (1970).

13) M. Kobayashi, H. Tadokoro, and R. S. Porter, *J. Chem. Phys.*, **73**, 3635 (1980).

14) K. Larsson, *Nature (London)*, **213**, 383 (1967).

15) W. Piesczek, G. R. Strobl, and K. Malzahn, *Acta Crystallogr., Sect. B*, **30**, 1278 (1974).

16) J. D. Barnes and B. Fanconi, *J. Chem. Phys.*, **56**, 5190 (1972).

17) G. Zerbi, R. Magni, M. Gussoni, K. H. Moritz, A. Bigotto, and S. Dirlikov, *J. Chem. Phys.*, **75**, 3175 (1981).

18) R. G. Strobl and W. Hagedorn, *J. Polym. Sci., Polym. Phys. Ed.*, **16**, 1181 (1978).

19) M. Kobayashi, *J. Mol. Struct.*, **126**, 193 (1985).

20) Y. Cho, Doctoral Thesis, Osaka University (1987).

21) T. Ishioka, M. Kobayashi, T. Nogami, and J. Shimizu, Prep. Mol. Struct. Symp., 398, Osaka (1986).

22) The temperature dependence of the Raman spectra of the symmetric bis(quaternary salts) of DABCO exhibited an almost complete disappearance of the signal ascribable to the C-C skeltal mode above the transition temperature (unpublished data). This is in sharp contrast to Fig. 7, which shows the presence of this signal even above T_{c2}.

23) In order to determine which of the two possibilities is true, the polarized Raman spectra must be measured for a single crystal. Since the hexagonal packing rarely exists over a wide temperature range, the low temperature phase probably possesses $T_{//}$-type packing.

The Molecular Structure of Thioxanthone as Studied by Gas Phase Electron Diffraction

Kinya IIJIMA,* Isao OONISHI,† Shoji FUJISAWA,† and Shuzo SHIBATA
Department of Chemistry, Faculty of Science, Shizuoka University, Oya, Shizuoka 422
†Department of Chemistry, Faculty of Science, Toho University, Miyama, Funabashi 274
(Received May 27, 1987)

The molecular structure of thioxanthone has been determined from gas electron-diffraction data. The molecular parameter values and their uncertainties are r_g(C-C)=1.401±0.001 Å, r_g(C-H)=1.099±0.007 Å, r_g(C-S)=1.751±0.002 Å, r_g(C-C_c)=1.498±0.004 Å, r_g(C_c-O)=1.232±0.006 Å, ∠CSC=103.4±0.3°, ∠CC_cC=119.4±0.6°, and θ(dihedral angle)=169.0±1.6°, where the angle parameters are r_α parameters. The dihedral angle of thioxanthone is much larger than those of related molecules.

The crystal structure studies of heterocyclic molecules such as type **1** have revealed that the dihedral angle between the two benzene rings changes in the wide range.[1-5] For example, the dihedral angles of thianthrene (X,Y=S),[1] thioxanthene (X=S, Y=CH_2),[4] and thioxanthone 10-oxide (X=SO, Y=CO)[5] are 128.1°, 135.3°, and 155.7°, respectively. On the other hand, the gas-phase electron diffraction study of thianthrene[6] has shown that this molecule vibrates with large amplitude by folding on the X-Y line, and that the minimum of the potential energy is at 128—130° of the dihedral angle.[6]

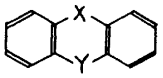

1

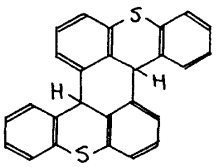

2

The compound **2** was synthesized from thioxanthone (X=S,Y=CO), but it was not obtained from condensation of thioxanthene which was the half of the object compound.[7] The difference in the molecular structures between thioxanthone and thioxanthene might be one of the factors proceeding the reaction. Thus we undertook the molecular structure determination of thioxanthone by means of a gas electron-diffraction method.

Experimental

O-Mercaptobenzoic acid was allowed to react with sulfuric acid in benzene by heating on a water bath. The crude product was purified by recrystallization from acetic acid solution, and then by sublimation in vacuum.

Electron diffraction photographs were taken by the use of an r^3-sector on Kodak Electron-Image plates at camera distances of 293.70 and 143.98 mm. The sample was sublimed at 455 K by a high-temperature nozzle. The accelerating voltage was 40 kV and the wavelength was determined from the diffraction patterns of thallium(I) chloride.[8] The exposure times were about 60 and 130 s for the long and the short camera-distance photographs, respectively, with an electron-beam current of 0.7 μA. The pressure in the diffraction chamber was 6.7×10^{-4} Pa during the experiment. Four and three plates were selected for the long and the short camera-distance photographs, respectively, and their optical densities were measured at 0.4 mm intervals by the use of a digital microphotometer. The electron diffraction unit and the digital microphotometer used in the present study have been described elsewhere.[9]

Analysis and Results

The scattering intensities in the range of q=9.0—52.5 $Å^{-1}$ were obtained from the long camera-distance

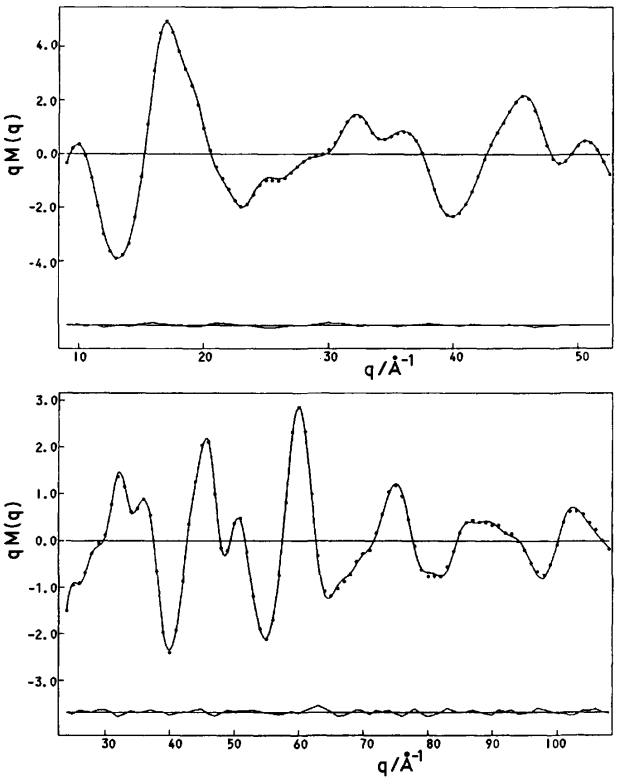

Fig. 1. Molecular intensities for thioxanthone. The upper figure shows the long camera-distance data and the lower figure the short camera-distance data. Dots represent the observed ones and solid curves the calculated ones. The residuals are shown at the lower parts of the figures.

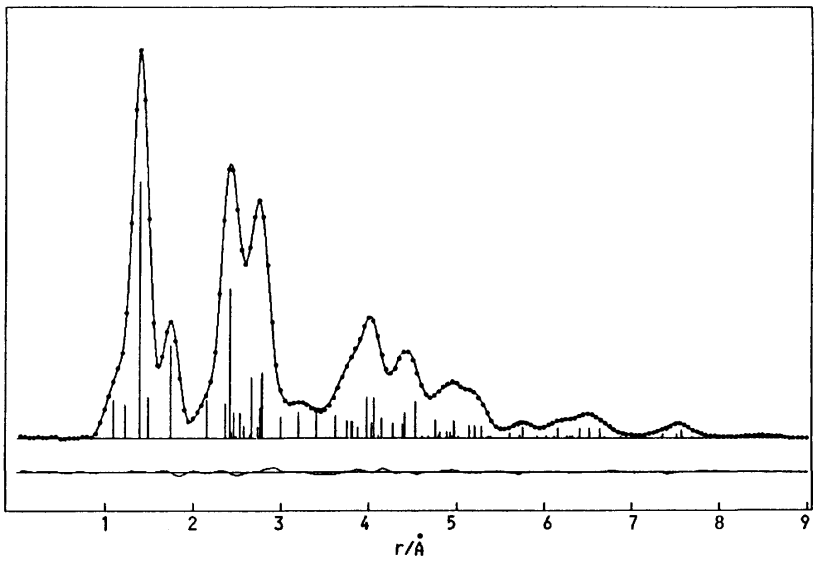

Fig. 2. Radial distribution curve for thioxanthone. Dots represent the experimental one, solid curve the theoretical one, and the difference is shown below. The vertical bars represent bond distances and the scattering powers.

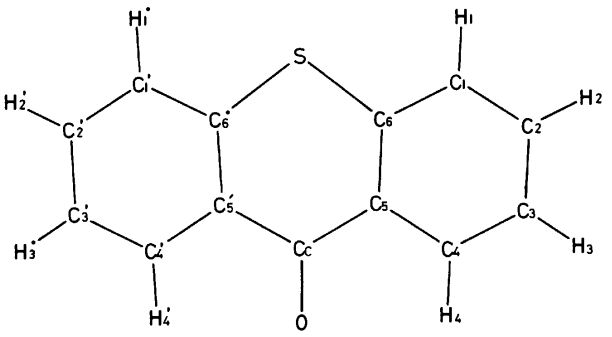

Fig. 3. Numbering of atoms in thioxanthone.

Table 1. Urey-Bradley Force Field for Thioxanthone

K(C-C)	5.46	H(CC(O)C)	0.15
K(C-H)	4.56	H(CCO)	0.40
K(C-S)	2.00	π(H)	0.30
K(C-C(O))	3.70	π(O)	0.62
K(C-O)	10.5	π(S)	0.50
Y(C-C)	0.20	π(C(O))	0.50
Y(C-S)	0.15	F(CC)	0.37
Y(C-C(O))	0.15	F(CH)	0.54
H(CCC)	0.33	F(CS)	0.50
H(CCH)	0.20	F(CC(O))	0.30
H(CCS)	0.15	F(CO)	0.40
H(CSC)	0.15	F(C(S)C)	0.20
H(CCC(O))	0.15	F(C(CO)C)	0.30

The potential function was defined as $V=1/2\sum K\Delta r^2 + 1/2\sum H(r\Delta\theta)^2 + 1/2\sum F\Delta q^2 + 1/2\sum Y\Delta\tau^2 + 1/2\sum \pi\Delta\sigma^2$, where the force constants of bond stretching, K, angle deformation, H, and repulsion between nonbonded atoms, F, are in 10^2 N m^{-1}, while those of torsion, Y, and out-of-plane, π, are in 10^{-18} N m.

plates and those in the range of q=24.0—108.0 Å^{-1} from the short camera-distance plates. Here q represents $(40/\lambda)\sin(\theta/2)$, where λ is the wavelength and θ is the scattering angle. They were leveled by using theoretical backgrounds, and the intensities for each camera distance were averaged. The elastic and inelastic scattering factors were taken from the tables prepared by Schäfer et al.[10] and by Cromer,[11] respectively. The inelastic scattering factor for hydrogen atom was taken from the table by Tavard et al.[12] The experimental molecular intensities obtained are shown in Fig. 1. Figure 2 shows the experimental radial distribution function, which is the Fourier transform of the modified molecular intensities, $qM(q)\exp(-bq^2)$, where the damping factor b was 0.0002 in the present study. The molecular model of thioxanthone and the numbering of the atoms are shown in Fig. 3.

The molecular parameters were obtained from least-squares analysis of the molecular intensities on the basis of the following assumption: 1) The molecule has C_s symmetry. 2) The benzene ring is a regular hexagon. 3) The sulfur and carbonyl carbon atoms are on the plane of the benzene ring. 4) The oxygen atom is on the $C_5C_cC_5'$ plane. With these assumption,the geometrical papameters, r_α,[13] refined by least-squares analysis were as follow; $r(C_1-C_2)$, $r(C_1-H_1)$, $r(C_6-S)$, $r(C_5-C_c)$, $r(C_c-O)$, $\angle SC_cC_5$, $\angle C_cC_5C_6$, and θ(dihedral angle).

The vibrational mean amplitudes and the shrinkage corrections, r_a-r_α,[13] were calculated from a Urey-Bradley force field. Since the normal vibration analysis of this molecule has not been performed, the force constants were refered from thianthrene[6] and acetone,[14] as listed in Table 1. The calculated mean

Table 2. Root-Mean-Square Amplitudes and Shrinkage Corrections for Thioxanthone (in 10^{-4} Å)

Atomic pair	l	r_a-r_α	Atomic pair	l	r_a-r_α
C_1-C_2	456	103	$C_4\cdots S$	697	50
$C_1\cdots C_3$	602	123	$C_4\cdots C_c$	739	74
$C_1\cdots C_4$	676	98	$C_4\cdots O$	1112	120
C_1-H_1	768	181	$C_5\cdots C_5'$	676	20
$C_1\cdots H_2$	971	218	$C_5\cdots C_6'$	774	8
$C_1\cdots H_3$	967	231	$C_5\cdots S$	655	24
$C_1\cdots S$	734	84	$C_5\cdots C_c$	500	35
$C_1\cdots C_c$	681	41	$C_5\cdots O$	654	90
$C_1\cdots O$	817	59	$C_6\cdots C_6'$	753	17
$C_2\cdots S$	745	100	C_6-S	557	43
$C_2\cdots C_c$	750	73	$C_6\cdots C_c$	638	14
$C_2\cdots O$	1016	92	$C_6\cdots O$	710	47
$C_3\cdots S$	755	82	$S\cdots C_c$	773	2
$C_3\cdots C_c$	752	91	$S\cdots O$	860	16
$C_3\cdots O$	1137	121	C_c-O	386	94

The numbering of the atoms is shown in Fig. 3.

Table 3. Molecular Parameters Obtained from Least-Squares Analysis for Thioxanthone

	r_α	r_g	ε[a]
$r(C_1-C_2)$/Å	1.389	1.401	0.001
$r(C_1-H_1)$/Å	1.077	1.099	0.007
$r(C_6-S)$/Å	1.745	1.751	0.002
$r(C_5-C_c)$/Å	1.491	1.498	0.004
$r(C_c-O)$/Å	1.220	1.232	0.006
$\angle SC_cC_5$/°	60.2		0.3
$\angle C_cC_5C_6$/°	123.2		0.3
θ/° [b]	169.0		1.6
$\angle C_6SC_6'$/° [c]	103.4		0.3
$\angle C_5C_cC_5'$/° [c]	119.4		0.6

a) Limits of error (see text). b) Dihedral angle. c) Dependent parameter.

amplitudes and the shrinkage corrections of some atomic pairs which give a large contribution to the electron diffraction intensities are listed in Table 2. The mean amplitudes of $l(C_1-C_2)$, $l(C_1\cdots C_3)$, $l(C_1-H_1)$, $l(C_6-S)$, $l(C_5-C_c)$, and $l(C_c-O)$ were refined by the least-squares calculations, and other mean amplitudes and the shrinkage corrections were fixed to the calculated values throughout the analysis. All the asymmetry parameters, κ,[13] were ignored.

The r_g parameters were calculated from the r_a paremeters obtained in the least-squares calculations,[13] and they are listed in Table 3 with dependent parameters and their limits of error. The observed mean amplitudes are listed in Table 4. The limits of error in the distances are the square root of the sum of the squares of the random and systematic errors, and those in the angles are the random errors. The random errors were 2.6 times as large as the errors

Table 4. Root-Mean-Square Amplitudes of Thioxanthone Obtained from Least-Squares Analysis

Atomic pair	l_{obsd}/Å[a]	ε/Å[b]	l_{calcd}/Å[c]
C_1-C_2	0.052	0.002	0.046
$C_1\cdots C_3$	0.064	0.002	0.060
C_1-H_1	0.071	0.009	0.077
C_6-S	0.056	0.003	0.056
C_5-C_c	0.067	0.008	0.050
C_c-O	0.049	0.010	0.039

a) Values obtained by least-squares calculations. b) Limits of error (see text). c) Values calculated from the force constants in Table 1.

estimated by the least-squares calculations. The systematic errors were estimated from the errors in both the measurements of camera distance (0.03%) and wavelength (0.09%). The best-fit molecular intensities and the theoretical radial distribution function are shown in Figs. 1 and 2, respectively. The experimental intensities, the experimental smooth backgrounds, and the correlation matrix for the molecular parameters are deposited in Document No. 8765 at the Office of the Editor of the Bulletin of the Chemical Society of Japan. The least-squares calculations were carried out on a HITAC M-280H computer in the Computer Center of the University of Tokyo.

Discussion

The value of the C_1-C_2 distance in Table 3 represents the average of all the C-C bond distances of the benzene rings in thioxanthone because of the assumption of a regular hexagon. The lower symmetry of the benzene ring of C_{2v} with the equal C-C bond distances, where the two fold axis lies along the $C_1\cdots C_4$ bond, was assumed in the analysis, but the structure of the benzene ring converged to a regular hexagon and the other molecular parameters agreed with the values in Table 3 within the limits of error. The observed mean amplitude of the C_1-C_2 bond is a little larger than the calculated value, but we did not try the further analysis, because the force constants used to calculate the mean amplitudes were tentative ones transfered from the related molecules.

The molecular parameters of thioxanthone and related molecules are listed in Table 5. The C-C and C-H distances of the benzene ring in thioxanthone are in good agreement with those of benzene.[15] The C-O distance of the central ring is much longer than that of acetone,[16] and the mean amplitude of this bond is larger than the calculated value. These facts seem to indicate that the double bond character of carbonyl group decreases in a cyclic molecule. Infrared absorption spectra showed similarly that the wave number of the C-O stretching in thioxanthone,

Table 5. Comparison of Molecular Parameters

	Thioxanthone	Thioxanthone 10-oxide	Thioxanthene	Thianthrene	Benzene	Acetone	Dimethyl sulfide
r(C-C)/Å	1.401(1)	1.386(12)[a]	1.386(6)[a]	1.400(2)	1.399(1)		
r(C-H)/Å	1.099(7)			1.082(22)	1.101(5)		
r(C-S)/Å	1.751(2)	1.788(3)	1.77(1)	1.770(3)			1.807(2)
r(C-C_c)/Å	1.498(4)	1.483(5)	1.50(1)			1.520(3)	
r(C_c-O)/Å	1.232(6)	1.223(5)				1.213(4)	
∠CSC/°	103.4(3)	99.0(2)	99.2(3)	104.1			99.05(4)
Dihedral angle/°	169.0(16)	155.7	135.3	131.4(3)			
Reference	This work	5	4	6	15	16	17

Distance parameters of gas molecules are r_g parameters.
a) Average value of C-C distances in the benzene rings.

1645 cm^{-1}, was much lower than that in acetone, 1738 cm^{-1}.[14]

Gillean et al. have shown that the C-S and C-C distances in the central ring of a heterocyclic molecule are in the range of 1.77—1.78 Å and 1.50—1.53 Å, respectively, and that they are insensitive to the oxidation state of sulfur atom and substitutions on the central carbon atom.[4] The C-S distance of gaseous thioxanthone, however, is 0.02 Å short out of the above range. The CSC angle is about 4° larger than the corresponding values of the other related molecules, though it is in agreement with that of gaseous thianthrene.[6]

The dihedral angle between the two benzene rings in thioxanthone is notably larger than those of thianthrene[6] and thioxanthene.[4] The flatness of the molecular plane of thioxanthone may be due to the sp^2 hybridization of the carbonyl carbon. Gallaher and Bauer have pointed out in the electron diffraction study[6] that thianthrene vibrates with large amplitude. However, we could not detect such a large amplitude motion in the analysis of thioxanthone. The inversion motion of thioxanthone may be also fixed by the carbonyl group of the central ring.

References

1) I. Rowe and B. Post, *Acta Crystallogr.*, **11**, 372 (1958).
2) A. L. Ternay, Jr., D. W. Chasar, and M. Sax, *J. Org. Chem.*, **32**, 2465 (1967).
3) J. Jackobs and M. Sundaralingam, *Acta Crystallogr., Sect. B*, **25**, 2487 (1969).
4) J. A. Gillean III, D. W. Phelps, and A. W. Cordes, *Acta Crystallogr., Sect. B*, **29**, 2296 (1973).
5) S. S. C. Chu, *Acta Crystallogr., Sect. B*, **32**, 1583 (1976).
6) K. L. Gallaher and S. H. Bauer, *J. Chem. Soc., Faraday Trans. 2*, **71**, 1173 (1975).
7) S. Fujisawa, I. Oonishi, and J. Aoki, 49th National Meeting of the Chemical Society of Japan, Tokyo, April 1984, 1H36.
8) W. Witt, *Z. Naturforsh., Teil A*, **19**, 1263 (1964).
9) S. Shibata, K. Iijima, R. Tani, and I. Nakamura, *Rep. Fac. Sci. Shizuoka Univ.*, **9**, 33 (1974).
10) L. Schäfer, A. C. Yates, and R. A. Bonham, *J. Chem. Phys.*, **55**, 3055 (1971).
11) D. T. Cromer, *J. Chem. Phys.*, **50**, 4857 (1969).
12) C. Tavard, D. Nicolas, and M. Rouault, *J. Chim. Phys.*, **64**, 540 (1967).
13) K. Kuchitsu and S. J. Cyvin, "Molecular Structures and Vibrations," ed by S. J. Cyvin, Elsevier, Amsterdam (1972), Chap. 12.
14) S. Mizushima and T. Shimanouchi, "Infrared Absorption and Raman Effect," Kyoritsu-Shuppan, Tokyo (1963).
15) K. Tamagawa, T. Iijima, and M. Kimura, *J. Mol. Struct.*, **30**, 243 (1976).
16) T. Iijima, *Bull. Chem. Soc. Jpn.*, **45** 3526 (1972).
17) T. Iijima, S. Tsuchiya, and M. Kimura, *Bull. Chem. Soc. Jpn.*, **50**, 2564 (1977).

 © 1987 The Chemical Society of Japan Bull. Chem. Soc. Jpn., 60, 3891—3894 (1987)

Entropy Changes in the Inclusion Complex Formation of α-Cyclodextrin with Alcohols as Studied by the Titration Calorimetry†

Hideaki FUJIWARA,* Haruyuki ARAKAWA, Saburo MURATA, and Yoshio SASAKI
Faculty of Pharmaceutical Sciences, Osaka University, 1-6 Yamada-Oka, Suita, Osaka 565
(Received June 5, 1987)

The inclusion complex formation of α-cyclodextrin(α-CD) with various alcohols has been studied by means of titration calorimetry. The titration curve was analyzed successfully by the formation of a 1:1 host-guest complex, and the thermodynamic parameters were determined. The entropies of reaction are estimated from the statistical thermodynamics of molecules. However, the estimated values are found to deviate by an order of magnitude from the experimental ones. To resolve such a discrepancy, α-CD in solution is assumed to include a definite number(n) of water molecules which are replaced by a guest molecule with the progress of reaction. The entropies thus estimated depend extensively on the value of n, and a value of n is determined for each alcohol so that it reproduces just the experimental entropy. The resulting n values are nearly constant for various alcohols studied and are within a reasonable range expected from the data reported in crystal, supporting the model of interpretation.

In a previous report of this series,[1] we have studied with especially the entropy term of reactions of dichlorodimethylstannane with pyridine measured by the titration calorimetry: A solvation model was presented to interpret discrepancy between the entropies observed and those estimated by statistical thermodynamics. To investigate further the validity of such a simple treatment of the entropy term for an elucidation of the role of solvent in reactions, the model is extended to the inclusion complex formation of α-cyclodextrin with alcohols in the present study.

Cyclodextrins are well-known in their ability to form inclusion complexes with various kinds of compounds. They are applied widely in industry,[2] such as for the pharmaceutics and food chemistry as well as for the analytical chemistry. They are also interested as an enzyme model in biochemistry.[3-5] All these applications make use of the "hydrophobic" cavity in cyclodextrin which can "include" different kinds of organic molecules, leading to the inclusion complexes. The inclusion complex formation has been studied quantitatively by not a few investigators and equilibrium constants and enthalpies and entropies have been discussed in relation to the driving forces for the inclusion phenomena.[2,3,5-9] Hitherto, hydrophobic, van der Waals, and hydrogen-bonding interactions between the host and guest molecules, conformational changes in cyclodextrin, and solvation of species in water are pointed out to be responsible to this phenomenon. Here, a release of less hydrogen-bonded water molecules in the cavity to the fully hydrogen-bonded bulk water surely contributes *enthalpically* much to the stabilization of the complex. This effect is pronounced in α-cyclodextrin (α-CD), where smaller number of water molecules are located in the cavity before inclusion occurs and hence hydrogen bonding between these water molecules is less extensive.

† Solvation Effect on the Reactions in Solution. II. See Ref. 1 for I.

In the present study, the entropy changes observed in the inclusion complex formation of α-CD with several alcohols in aqueous solution are interpreted on the basis of the statistical thermodynamics, from which the number of water molecules included in a free state of α-CD *in solution* can be estimated.

Experimental

Alcohols were all distilled in a glass vessel and α-CD from Tokyo Kasei Co. was recrystallized from water. Calorimetric titration was performed on a Tronac 558 isothermal/isoperibol calorimeter equipped with a CCP930 Programmer under an isothermal mode.[10a] α-CD was dissolved in the reaction vessel at a constant molarity, and alcohol was dissolved in the titrant solution. A total of 2 ml titrant was added in 20 steps to 50 ml solution in a stainless steel reaction vessel. Also a 20 ml titration buret was used for 1-hexanol and cyclohexanol, for which solubility in water is not so high as the other alcohols. The heat of reaction was measured within an error of ±0.04 J at 25.0 °C (±0.2 m°C).

Analysis of the titration data was made in a similar way as stated in Ref. 10.b. All these calculations and the calculation of the entropy terms discribed below were done on a NEAC ACOS-1000 computer at the Computation Center in Osaka University. Personal computers NEC PC-9800 were also used for the treatment of experimental data.

Results

The titration experiments were done several times for each alcohol. A typical run is shown in Fig. 1. The titration data were analyzed by the program CONDEP modified to the calorimetric experiments[10b] on the basis of a 1:1 complex formation. Standard deviation σ between the observed and the recalculated heats was smaller than 0.04 J, and systematic deviations were not observed between them. In the program CONDEP, integrated heat Q_i was dealt with originally under the incremental addition of titrant. In the present study, data were also processed with the differential heat q_i. These two calculations were confirmed to afford consistent results.[11]

The equilibrium constants determined are 9.7, 29.1, 81.4, 326, 801, and 56.4 $dm^3 mol^{-1}$ for ethanol, 1-propanol, 1-butanol, 1-pentanol, 1-hexanol, and cyclohexanol, respectively, at 25 °C. The enthalpies and entropies are summarized in Table 1 together with those hitherto published by other investigators. Reproducibility of these parameters was better than 95, 90, and 90% for K, ΔH^0, and ΔS^0, respectively, in the repeated experiments in the present study. The unit of concentration adopted is mol dm^{-3} (M) in the present study, and thermodynamic parameters also correspond to this unit. In Table 1, values cited from other sources are converted to correspond to the same unit when necessary.[14] In the Table, ΔH^0's for the same alcohol are rather in good agreement although method and experimental conditions differ among different investigators. As this contrast, ΔS^0 changes more or less depending on the sources of data. This would be inevitable because of the small contribution of ΔS^0 as judged by comparing $T\Delta S^0$ with ΔH^0.

Table 1. Enthalpies and Entopies for the Inclusion Complex Formation of α-Cyclodextrin with Several Alcohols[a)]

Alcohol	ΔH^0			ΔS^0		
	This work	Ref. 12	Ref. 13	This work	Ref. 12	Ref. 13
Ethanol	−2.4			11.2		
1-Propanol	−6.1	−6.8		7.7	4.6	
2-Propanol		−0.55			30.1	
1-Butanol	−10.2		−12	2.2	2.0	−2
1-Pentanol	−14.8	−14.1	−16	−1.4		−5
1-Hexanol	−17.2		−19	−2.1		−8
Neopentyl alcohol			−12			−12
Cyclo-hexanol	−12.2	−8.1	−14	−7.3	2.0	−14

a) ΔH^0 and ΔS^0 are given in units of kJ mol^{-1} and J K^{-1} mol^{-1}, respectively, the unit of concentration corresponding to mol dm^{-3}.

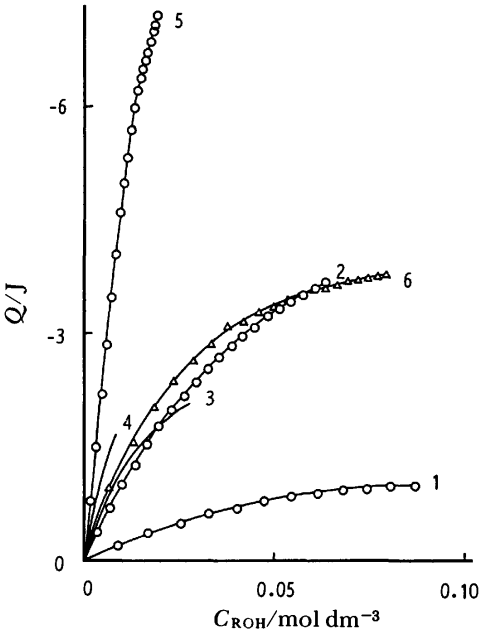

Fig. 1. The calorimetric titration curves for the α-CD plus alcohol systems.
The molarity of alcohol is plotted in abscissa and in ordinate plotted is the integrated heat of reaction.
1; Ethanol, 2; 1-propanol, 3; 1-butanol, 4; 1-pentanol, 5; 1-hexanol, 6; cyclohexanol.
The molarity of α-CD changes:
1; 0.014—0.012 M, 2; 0.0194—0.0187 M, 3; 0.0067—0.0064 M, 4; 0.0042—.0.0040 M, 5; 0.015—0.009 M, 6; 0.012—0.007 M. A half of C_{ROH} is plotted in curve 1 to save a space in the Figure.

Discussion

A thermochemical cycle is given in Fig. 2 for the entropies, where α-CD is assumed to include n molecules of water in solution that will be released with the progress of reaction. Following equations hold for this cycle:

$$\Delta S^0_{gas} = S^0_{CD\cdot B} + nS^0_{H_2O} - S^0_{CD\cdot nH_2O} - S^0_B \quad (1)$$

$$\Delta S^0_{soln} = \Delta S^0_{gas} + (\Delta S^s_{CD\cdot B} + n\Delta S^s_{H_2O} - \Delta S^s_{CD\cdot nH_2O} - \Delta S^s_B) \quad (2)$$

Note that nH_2O is attached to α-CD in the left-hand side of the formula in Fig. 2 to allow for the inclusion of water molecules in the cavity. These water molecules are considered to "solvate" strongly (or bind) to α-CD. That is to say, n molecules of water in the cavity are assumed to behave as if they constitute a rigid part of a whole molecule.[15] As this contrast, normal and weak "solvation" of each species is considered to be compensated for by the entropy of solution.

Estimation of ΔS^0_{gas} in Eq. 1 is not straightforward since calculation of $S^0_{CD,B}$ and S^0_{CD,nH_2O} needs detailed data on the vibrations in CD·B and CD·nH_2O which are lacking. However, most of the vibrational parts

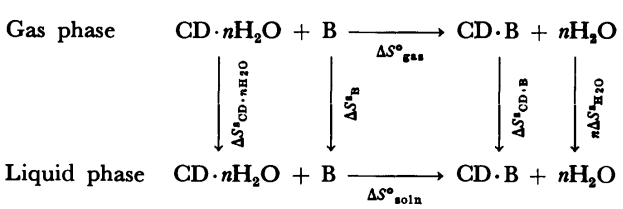

Fig. 2. A reaction scheme for the entropy changes in the inclusion complex formation of cyclodextrin(CD) with alcohols(B).
ΔS^s's are the entropies of solution of the components. In a free state, CD is assumed to include n molecules of water, which are released with the progress of reaction.

are expected to be cancelled out between those for the reactants and those for the products. The translational and the rotational parts of entropy can be estimated according to following Eqs.:[16]

$$S_{tr} = R(1.5\ln M + 2.5\ln T - \ln P - 1.1650) \quad (3)$$

$$S_{rot} = R(0.5\ln I_A I_B I_C + 1.5\ln T - \ln\sigma - 2.7106) \quad (4)$$

where the symbols have usual meanings. Such calculations afforded $\Delta S^0_{gas,calcd}$ as listed in Table 2, when n was set equal to two, a typical value reported first for a single crystal of α-CD hexahydrate.[17]

The value of $\Delta S^0_{gas,calcd}$ can be converted to that of $\Delta S^0_{soln,calcd}$ by means of Eq. 2 if the entropy of solution is predictable for each component. The experimental values are available for different compounds including water and alcohols, and the value is known to be linearly correlated with the thermodynamic third-law entropy of solute x in gas phase, $S^0_{298,x}(g)$. For example, Eq. 5 is reached in aqueous solution.[18] It is later reported that the coefficients in Eq. 5 may change depending on the types of compounds treated.[19]

$$\Delta S^s_x = -0.46\, S^0_{298,x}(g) + 27.5 \quad (5)$$

However, Eq. 5 is considered to be valid for the present case, since in Eq. 2 ΔS^s appears as the difference between that of water and that of alcohol and also as the difference between that of the cyclodextrin hydrate and that of its inclusion complex. Then Eq. 6 is reached from Eqs. 1, 2, and 5.

$$\Delta S^0_{soln} = 0.54\,\Delta S^0_{gas} + (n-1)\cdot 27.5 \quad (6)$$

Next, a correction is necessary for the difference in standard states. The thermodynamic third-law entropy $S^0_{298}(g)$ corresponds to a standard state of 1 atm, whereas the entropy of reaction is given against a standard state of 1 mol dm^{-3} in the present study. Therefore, following relation holds:

$$S^0_{298,x}(g) = S^0_x + R\cdot\ln 24.5 \quad (7)$$

where S^0_x is the standard entropy of x in gas phase corresponding to 1 mol dm^{-3} (1/24.5 atm) at 25 °C and an ideal gas behavior is assumed. The values of ΔS^0_{soln} thus estimated are also listed in Table 2.

The entropies calculated are all positive and very large compared to the experimental ones. If the vibrational and internal-rotational entropies are included into the calculation, the resulting $\Delta S^0_{gas,calcd}$ will be increased more or less. In fact, $\Delta S^0_{gas,calcd}$ was increased by 16% in the previous case of Me_2SnCl_2 plus pyridine.[1] Therefore, it is quite clear that above calculation fails to explain the experimental values of ΔS^0_{soln}. As a cause of this discrepancy, an error in n can be pointed out. Hitherto, two different values have been reported other than two stated above for the number of water molecules included in the α-CD cavity in crystal, i.e., n=1[20] and n=2.57[21] for different crystal modifications. In fact, the values of ΔS^0_{gas} and ΔS^0_{soln} calculated were found to depend highly on the value of n. Therefore, n was determined according to Eq. 8 so as to reproduce just the experimental value of ΔS^0_{soln}. Equation 8 was derived from Eqs. 1, 2, 5, and 7.

$$n = \frac{\Delta S^0_{soln} - 0.54(S^0_{CD\cdot B} - S^0_{CD\cdot nH_2O} - S^0_B) + 27.5 - 0.46R\cdot\ln 24.5}{0.54\, S^0_{H_2O} + 27.5 - 0.46R\cdot\ln 24.5} \quad (8)$$

The results are summarized in Table 3.[22] It is seen that n is nearly constant throughout the alcohols studied, although the experimental entropies do change depending on the alcohol. Such a constancy in n indicates that a same number of water molecules are released from the cavity when alcohols with a small size (ethanol) to a relatively large size (1-hexanol) are included, and supports that all of the water included in the cavity are expelled from the cavity on forming the complexes with these alcohols. This trend in solution is consistent with the results in crystal.[23] Also, the constancy in n means that ΔS^0_{soln} depends only on ΔS^0_{gas} (Eq. 6). This, in turn, means that ΔS^0_{soln} changes linearly with S^0_B on changing the alcohol studied, since in Eq. 1 $S^0_{H_2O}$ and S^0_{CD,nH_2O} are

Table 2. ΔS^0_{gas} Estimated from the Translational and the Rotational Entropies for the Reaction of α-CD·2H$_2$O+B→α-CD·B+2H$_2$O[a]

B(alcohol)	$\Delta S^0_{gas,calcd}$	$\Delta S^0_{soln,calcd}$
Ethanol	115.1	89.7
1-Propanol	103.2	83.2
2-Propanol	103.6	83.4
1-Butanol	100.1	81.6
1-Pentanol	92.6	77.5
1-Hexanol	86.2	74.0
Neopentyl alcohol	94.1	78.3
Cyclohexanol	88.9	75.5

a) In unit of J K^{-1} mol^{-1}

Table 3. The Number of Water Molecules (n) Released on the Complex Formation Reactions of α-CD·nH$_2$O+B→α-CD·B+nH$_2$O Determined from the Entropy of Reaction

B(alcohol)	n[a]		
	a	*b*	*c*
Ethanol	1.37		
1-Propanol	1.40	1.38	
2-Propanol		1.58	
1-Butanol	1.37		1.34
1-Pentanol	1.38	1.40	1.35
1-Hexanol	1.43		1.35
Neopentyl alcohol			1.29
Cyclohexanol	1.37	1.56	1.30

a) Calculated from data in this work(*a*), in Ref. 12(*b*), and in Ref. 13(*c*).

constant and $S^0_{CD,B}$ is almost constant for different alcohols because of an overwhelming size of cyclodextrin. In fact, ΔS^0_{soln} was observed to change linearly with the thermodynamic third-law entropy of alcohol in the present study. These correlations are under further study including various kinds of guest molecules. In this way n is said to be 1.4 on average for the alcohols studied here. Such a non-round number may result from a dynamic equilibrium of water in between the cavity and the bulk water. That is, the non-round number reflects only a statistical average of the number of water molecules included in the cavity in solution.

In conclusion, calculation of the entropy of reactions is expected to be valuable for the elucidation of the state and the role of water in the host-guest molecular interactions in solution.

References

1) H. Fujiwara, H. Arakawa, S. Murata, I. Ohtaku, M. Ishii, and Y. Sasaki, *Bull. Chem. Soc. Jpn*, **60**, 457 (1987).

2) J. Szejtli, "Cyclodextrins and Their Inclusion Complexes," Akademiai Kiado, Budapest (1982).

3) M. L. Bender and M. Komiyama, "Cyclodextrin Chemistry," Springer, Berlin (1978).

4) R. Breslow, *Adv. Chem. Ser.*, **191**, 1 (1981).

5) I. Tabushi, *Acc. Chem. Res.*, **15**, 66 (1982).

6) Y. Matsui, T. Nishioka, and T. Fujita, *Top. Curr. Chem.*, **128**, 61 (1985).

7) I. Tabushi, Y. Kiyosuke, T. Sugimoto, and K. Yamamura, *J. Am. Chem. Soc.*, **100**, 916 (1978).

8) J. F. Wojcik, *Bioorg. Chem.*, **12**, 130 (1984).

9) W. C. Cromwell, K. Bystroem, and M. R. Eftink, *J. Phys. Chem.*, **89**, 326 (1985).

10) a) H. Fujiwara and Y. Sasaki, *Bunseki*, **1987**, 225. b) H. Fujiwara, F. Sakai, A. Kawamura, N. Shimizu, and Y. Sasaki, *Bull. Chem. Soc. Jpn*, **58**, 2331 (1985).

11) If an unexpectedly large error occurs in an incremental step of k in titration, the error will be included to all the integrated heat Q_i later than $i=k$, although it is included to only q_k when differential heat is treated. On this contrary, random errors which occur in every step of titration will be reduced for the integrated heat Q_k by a partial cancellation in the summation of the differential heats q_i between $i=1$ to k. The consistent results reached from the analysis of Q_i and from than of q_i may be interpreted to indicate sufficiently small errors in the present experiment.

12) S. Takagi and M. Maeda, *J. Incl. Phenomena*, **2**, 775 (1984).

13) Y. Matsui and K. Mochida, *Bull. Chem. Soc. Jpn*, **52**, 2808 (1979).

14) Following equations were utillized for the conversion from mole fraction to mol dm^{-3}, the primed symbols corresponding to the unit of mole fraction.

$$\ln K = \ln K' - \ln(1000/MV)$$
$$\Delta H = \Delta H' + \alpha R \cdot T^2$$
$$\Delta S = \Delta S' + R\{\ln(1000/MV) - \alpha T\}$$

Here, MV is the molar volume of solute and α is the thermal expansion coefficient of solution.

15) A fraction of the water molecules may still be included in the cavity of α-CD in CD·B. However, this is not assumed in Fig. 2 for simplicity. When this is the case, say m molecules of water "bind" strongly to CD·B, the value of n discussed below needs be replaced by that of $n-m$ which is equal to a number of water molecules released in the reaction. However, as stated in the Discussion section, all of the water molecules included within the cavity are considered to be expelled from the cavity after the reaction.

16) G. Herzberg, "Molecular Spectra and Molecular Structure. II. Infrared and Raman Spectra of Polyatomic Molecules, Van Nostrand," New York (1945).

17) P. C. Manor and W. Saenger, *J. Am. Chem. Soc.*, **96**, 3630 (1974).

18) D. H. Wertz, *J. Am. Chem. Soc.*, **102**, 5316 (1980).

19) M. H. Abraham, *J. Am. Chem. Soc.*, **103**, 6742 (1981).

20) K. Lindner, Ph. D. Thesis, Universitat Gottingen (1980).

21) K. K. Chacko and W. Saenger, *J. Am. Chem. Soc.*, **103**, 3630 (1981).

22) The vibrational part of entropy is not included in the calculation of $S^0_{CD,B} - S^0_{CD,nH_2O} - S^0_B$ because of the lack of full vibrational data. This part is actually equal to that of the reaction of $CD \cdot nH_2O + B \rightarrow CD \cdot B + nH_2O$ because of a negligible amount of the vibrational part in H_2O. Accordingly, this part is expected to be small since the vibrational entropies for the latter reaction will be cancelled out between those for the reactants and those for the products. If the vibrational entropy of this kind is assumed to amount to 16% of $\Delta S^0_{gas,calcd}$ likely to the previous case,[1] $\Delta S^0_{CD,B} - \Delta S^0_{CD,nH_2O} - S^0_B$ in Eq. 8 is increased by 16 J K^{-1} mol^{-1} and the resulting n will be decreased by about 16%.

23) a) W. Saenger, R. K. McMullan, J. Fayos, and D. Mootz, *Acta Crystallogr., Sect. B*, **30**, 2019 (1974). b) B. Hingerty and W. Saenger, *J. Am. Chem. Soc.*, **98**, 3357 (1976).

 © 1987 The Chemical Society of Japan Bull. Chem. Soc. Jpn., 60, 3895—3901 (1987)

A Simple Model for the Kinetics of Beta Meander Formation of Homopolypeptide Chains

Hiroshi MAEDA
Department of Chemistry, Faculty of Science, Nagoya University, Nagoya 464
(Received June 5, 1987)

A simple kinetic theory is presented concerning the irreversible formation of intramolecularly folded β-structure of homopolypeptide chains through a bend formation. To reduce the number of parameters, the number of strands is limited to be less than five and the growth rate of the third and fourth strands is assumed to be so fast that the final strand length is attained immediately after the bend formation. Numerical calculations were carried out on relevant ranges of rate costants for relatively short chains. It was shown that experimentally found diverse kinetic patterns were all explicable based on the present model.

Folding of single homopolypeptide chains into the β-structure occurs, in principle, at any site on the chain and hence it is a stochastic process. Therefore, it differs from that of globular proteins, where the folding pathway is determined nearly uniquely by the amino acid sequence.[1-3] It is interesting and also important to know the difference between the folding of homopolypeptide chains and proteins containing the β-structure.

Several experimental studies have been done on the kinetics of intramolecular β-structures of poly(L-lysine) (PLL)[4-8] and its side-chain homolog,[9] poly(L-tyrosine) (PLT),[10,11] and poly(*S*-carboxymethyl-L-cysteine) (poly[Cys(CH_2COOH)]).[12] Thermally induced α-helix-to-β-structure conversion of PLL showed single exponential behavior,[5,6,8] while its pH-induced coil-to-β-structure conversion at high temperatures showed a lag phase when followed with light scattering or fluorescence.[7] In the case of poly(L-tyrosine), pH-induced coil-to-β-structure change was successfully described with two exponential terms and no lag phase was observed.[10] Time domains in these studies for the formation of the β-structure were about 10—10^2 min for PLL and poly[Cys(CH_2COOH)][12] but 10—10^2 s for PLT. Different behaviors of PLT from those of PLL were noticable as pointed out.[10] Fast changes in 10^{-2}—0.1 s region were observed in a recent study on PLT; the results were approximately fitted with two exponential terms but multi-relaxation time character was also observed.[11] Thermal coil-β-structure conversion of poly[Cys(CH_2COOH)] showed multi-relaxation time behavior.[12]

Since intramolecular folding of single polypeptide chain certainly consists of several steps, rate constants of these steps should be related to the time constants observed in experiments. However, such an attempt has been scarcely reported.

In view of the complex nature of the whole process of chain folding and also to reduce the number of parameters, we wish to present a highly approximate model in the present report. The model is of phenomenological nature and quantitative analyses of experimental data based on the present model are not intended. However, various kinetic behaviors such as single exponential, tow exponential terms, or lag phase, are all predicted from this simple model. Therefore, all the experimental data on homopolypeptides to data can be consistently interpreted according to this model.

Model. A symmetric polymer chain consisting of L units is considered. Directional nature of polypeptide chain is tentatively neglected. Each unit can assume three states: disordered state with no hydrogen bonds, β-conformation with one and two hydrogen bonds. Three basic assumptions of the model are:

1) Only the formation of the β-conformation is considered. No reversible reaction is considered.
2) Initiation of β-strand formation is thoroughly due to bend formation. Initiation by collision of two units distant apart on the chain is excluded.
3) Multiple initiation is inhibited.

Other assumptions are introduced below in the course of the description of the present model depicted in Fig. 1.

First bend occurs with a rate constant k_i between the η-th and $(\eta+1)$-th units of a random coil chain. Units are counted from one end of a symmetric chain. No units are incorporated in the bend portion (assumption 4). It is simple to modify the present theory to take into account any (fixed) number of units in the bend portion. We make assumption 4 only for the sake of simplicity. Two β-strands thus initiated grow with a rate constant k_+. At any stage of the growth, second bend can be formed with a rate constant k_b at either of the two junctions between random coil region and the growing β-strands. Growth of the third strand is assumed to be very fast compared with k_+ and k_b and hence final strand length is attained immediately after the second bend is formed (assumption 5). Third bend is restricted to take place, in our model, at the remaining junction between random coil region and the first two β-strands. Formation of the fourth strand is assumed to take place instantly, just as the third strand. No further bend formation is

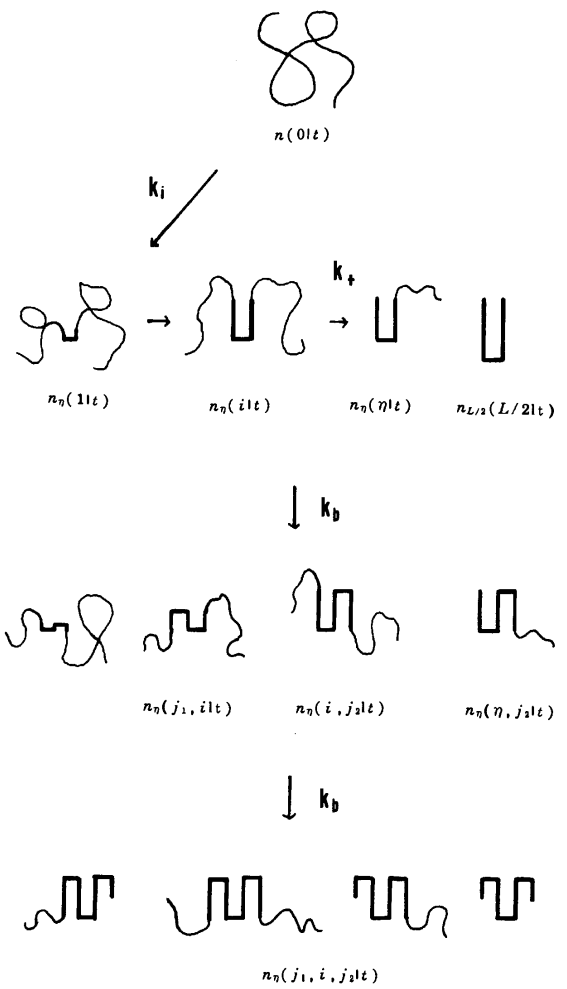

Fig. 1. Schematic representation of the model. Thick lines and thin curves represent the β-strands and random coil portions, respectively.

allowed (assumption 6). Some of these assumptions will be discussed later.

In this way, only those species consisting of two, three and four strands are considered in this model. We hope this simple model contains essentials of a general model where any number of strands is allowed. It is to be noted that three-strand species known as β-meander,[13] which are frequently found in proteins, are major products in this model.

At this stage, it is pertinent to consider the nature of the unit in the model. The unit does not necessarily correspond to a peptide unit nor an amino acid residue. Instead, it may correspond to p peptide groups together. Hence, chain length L of the model does not necessarily represent the degree of polymerization of actual polypeptide chain (DP). By virtue of this extension of the definition of unit, we need not calculate these cases with large L, say more than 100. If p is taken to 10, L=10 is sufficient to describe a chain of DP=100. With this definition of unit, the present model is also applicable to random and sequential copolypeptides, if p is taken to the repeating unit (or greater) in the latter case. Initiation rate constant k_i is not taken as position-dependent. Actually, however, an initiation near chain end is not effective, because two unstable short strands thus formed are dissociated and other initiation at the site much distant from chain ends will occur subsequently. If we take a value of p as such that formation of the β-conformation at p-th site from the chain end is stable enough, then in the present model we can assign the same value of k_i to the units near chain end as well as to other units in the interior of the chain. On the other hand, this extention of the definition of unit invalidates quantitative analyses of experimental data based on this model, unless p is evaluated reasonably. This is the reason why present model is of phenomenological nature.

Rate Equations and Solutions. All number concentrations n's are normalized to give unity at any time when they all are summed up. Time course of the concentration of random coil species, $n(0|t)$, is governed by Eq. 1.

$$dn(0|t)/dt = -Lk_i n(0|t) = -k_0 n(0|t) \tag{1}$$

where k_0 is defined as Lk_i. Let $n_\eta(i|t)$ denotes the concentration of a species at time t with two β-strands of length i starting from the first bend between η- and $(\eta+1)$-th units. Since the chain is symmetric, only those species of $\eta \leqq L/2$ are considered explicitly. Final results will be doubled in due course.

Rate equations for $n_\eta(i|t)$'s are as follows. For $\eta \leqq L/2-1$,

$$dn_\eta(1|t)/dt = k_i n(0|t) - (k_+ + 2k_b) n_\eta(1|t) \tag{2}$$

$$dn_\eta(i|t)/dt = k_+ n_\eta(i-1|t) - (k_+ + 2k_b) n_\eta(i|t) \quad (2 \leqq i \leqq \eta - 1) \tag{3}$$

$$dn_\eta(\eta|t)/dt = k_+ n_\eta(\eta-1|t) - k_b n_\eta(\eta|t) \tag{4}$$

$$dn_{L/2}(L/2|t)/dt = k_+ n_{L/2}(L/2-1|t) \quad (\eta = L/2) \tag{5}$$

For three strand species, $n_\eta(j_1,i|t)$ and $n_\eta(i,j_2|t)$ and four strand species, $n_\eta(j_1,i,j_2|t)$, their concentration changes are described by the following equations.

$$dn_\eta(j_1,i|t)/dt = k_b n_\eta(i|t) - k_b n_\eta(j_1,i|t) \tag{6}$$

$$dn_\eta(i,j_2|t)/dt = k_b n_\eta(i|t) - k_b' n_\eta(i,j_2|t) \tag{7}$$

$$dn_\eta(j_1,i,j_2|t)/dt = k_b n_\eta(j_1,i|t) + k_b n_\eta(i,j_2|t) \tag{8}$$

Here, j_1, j_2, and k_b' are defined as follows: j_1=Min(i, η–i), j_2=Min(i, $L-\eta$–i) and $k_b'=k_b (i \leqq \eta-1)$ or 0 $(i=\eta)$.

Initial conditions at t=0 are: concentrations of all species except random coil are zero and $n(0|0)$=1. Solutions of rate equations consistent with the initial conditions are given below.

$$n(0|t) = \exp(-k_0 t) \tag{9}$$

$$n_\eta(i|t) = (k_i/k_+)(k_+/k)^i \exp(-k_0 t)\gamma(i,kt)/(i-1)! \tag{10}$$

$$n_\eta(\eta|t) = (k_+/k_b) n_\eta(j_1, i=\eta-1|t) \quad (n \leqq L/2-1) \tag{11}$$

$$n_{L/2}(L/2|t) = k_i(k_+/k)^{L/2-1}\left[\frac{(1-\exp(-k_0t))}{k_0} - \sum_{r=0}^{L/2-2}\frac{k^r}{(k_++2k_b)^{r+1}}\gamma[r+1,(k_++2k_b)t]/r!\right] \quad (12)$$

For $1 \leqq i \leqq \eta$,

$$n_\eta(j_1,i|t) = k_i(k_+/k)^{i-1}(k_b/k)\left[\frac{(\exp(-k_0t)-\exp(-k_bt))}{k_b-k_0} - \frac{\exp(-k_bt)}{k_++k_b}\sum_{r=0}^{i-1}\left(\frac{k}{k_++k_b}\right)^r\gamma[r+1,(k_++k_b)t]/r!\right] \quad (13)$$

$$n_\eta(i,j_2|t) = n_\eta(j_1,i|t) \quad (i \leqq \eta-1) \quad (14a)$$

$$n_\eta(\eta,j_2|t) = (k_+/2k_b)n_\eta(j_1,i=\eta-1,j_2|t) \quad (14b)$$

$$n_\eta(j_1,i,j_2|t) = \frac{2k_ik_b^2}{k(k_0-k_b)}(k_+/k)^{i-1}\times\left[\frac{(1-\exp(-k_bt))}{k_b}\left(\frac{k}{k_++k_b}\right)^i-\frac{(1-\exp(-k_0t))}{k_0}\right] + \frac{2k_ik_b^2}{k(k_++k_b)}(k_+/k)^{i-1}\sum_{r=0}^{i-1}\left(\frac{k}{k_++k_b}\right)^r\times\left[\sum_{l=0}^{r}\frac{(k_++k_b)^l}{(k_++2k_b)^{l+1}}\gamma[l+1,(k_++2k_b)t]/l!\right] \quad (15)$$

In the above equations, k is defined as $k_++2k_b-k_0$ and $\gamma(i,x)$ is the incomplete gamma function defined below.

$$\gamma(i,x) = \int_0^x e^{-y}y^{i-1}dy = (i-1)![1-e^{-x}\sum_{r=0}^{i-1}\frac{x^r}{r!}] \quad (16)$$

From the concentrations given above, fraction f of the β-conformation or hydrogen-bonded units can be readilly calculated. Contributions from two-, three-, and four-strand species are denoted as f_1, f_2, and f_3, respectively. Calculations and the results are given in Appendix.

The extent of reaction Δf is defined as follows.

$$\Delta f(t) = [f(\infty)-f(t)]/f(\infty) \quad (17)$$

Here, $f(t)=f_1+f_2+f_3$ and $f(\infty)$ represents the final amount at $t=\infty$. The final amounts are also given in Appendix. After substituting these results in Appendix into the above three terms, the extent of reaction is explicitly represented in the below as a function of time. In the case of the fraction of the β-conformation f_β,

$$\Delta f_\beta(t) = a_1\exp(-k_0t)+a_2\exp(-k_bt) + \left[\sum_{r=0}^{L/2-2}a_{3,r}\frac{(kt)^r}{r!}\right]\exp\{-(k_++2k_b)t\} + \left[\sum_{r=0}^{L/2-2}a_{4,r}\sum_{l=0}^{r}(k_++k_b)^lt^l/l!\right]\exp\{-(k_++2k_b)t\} + \left[\sum_{r=0}^{L/2-2}a_{5,r}\sum_{l=0}^{r}(k_++2k_b)^lt^l/l!\right]\exp\{-(k_++2k_b)t\} \quad (18)$$

Here, $a_{i,r}$'s are complex functions of k_b/k_+, k_i/k_+, and L.

We confine ourselves for the moment to the case $k_+ \gg k_b$. Under this condition, strands can grow up to a considerable length before the next bend is formed. Since number of strands is limited to be smaller than five, fraction of the β-conformation will be very small in otherwise case $k_+ < k_b$. Under the limiting case considered here, the last three terms of Eq. 18 become functions of k_+t and Eq. 18 is reduced to a simple form. For a small t ($k_+t \ll 1$), first two terms can be approximated to be constant and the last three terms are expanded in power series of k_+t. After truncation of higher order terms in k_+t, Eq. 19 results.

$$\Delta f_\beta(k_+t \ll 1) = 1 - (a_{3,0}-a_{3,1}-a_{4,0}-a_{5,0})k_+t + O(k_+^2t^2) \quad (19)$$

Here, the following obvious relation is used.

$$\Delta f_\beta(0) = a_1 + a_2 + a_{3,0} + \sum_{r=0}^{L/2-3}a_{4,r} + \sum_{r=0}^{L/2-2}a_{5,r} = 1 \quad (20)$$

Since,

$$a_{3,1} - a_{3,0} = -(1-2/L)2k_+k_b/k^2 \approx O(k_i/k_+)$$

and

$$a_{4,0} \approx a_{5,0} \approx O(k_ik_b/k_+^2),$$

the coefficient of k_+t term in Eq. 19 is much smaller than unity under the limiting case considered. This means the presence of a lag phase. However, whether or not a lag phase is significant depends on the ratio t_0/τ_1, where t_0 and τ_1 denote a lag time and the time constant of the reaction, respectively.

Results of Numerical Calculations. Numerical calculations were carried out on the following sets of rate constants for chains of L=12, 24, and 48. (For simplicity, L is taken to be a multiple of 12)

$k_b/k_+ = 1\times10^{-1}$, 1×10^{-2}, and 1×10^{-3}

$k_b/k_i = 1$, 10, and 10^2.

One of the most complex behavior obtained is shown in Fig. 2 which was obtained for L=24, k_b/k_+=

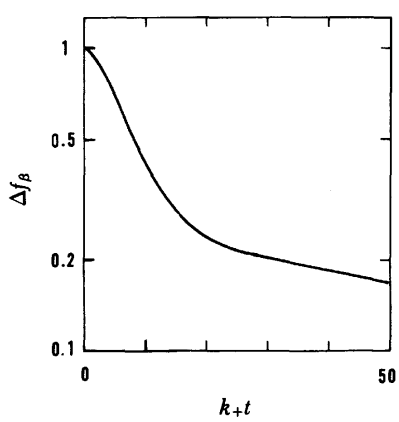

Fig. 2. A general kinetic pattern where log Δf_β is given as a function of reduced time k_+t.
L=24, $k_b/k_+=k_i/k_+=1\times10^{-2}$, $k_0/k_+=0.24$.

$k_i/k_+=1\times10^{-2}$. The time course is well approximated with the following formula of four parameters for a time range $t>t_0$.

$$\Delta f_\beta(t) = A_1 \exp[-(t-t_0)/\tau_1] + (1-A_1)\exp[-(t/\tau_2)] \quad (21)$$

In Table 1, values for the parameters are given for 26 cases. As seen from Table 1, many kinetics examined show simpler behavior than that shown in Fig. 2 or represented by Eq. 21. For about 9 examples, the time course can be approximated with single exponential term. About 6 examples show single exponential behavior accompanying a lag time t_0. Time course with two exponential terms without a lag time is found on 6 examples. A lag phase is discriminated when t_0/τ_1 exceeds 0.03.

At $k_b/k_+=1\times10^{-3}$ ($k_+\gg k_0$ or k_b), a general trend is seen which is valid irrespective of chain length. Two exponential character $0.7\exp(-k_0t)+0.3\exp(-k_bt)$ prevails if $k_0\gg k_b$ but single exponential dependence $\exp(-k_0t)$ is dominant if $k_b\gg k_0$. Examples of time course of various species are shown in Fig. 3 for a chain of $L=24$. In Fig. 3(a) where $k_0\gg k_b$ the contribution from two-strand species first reaches about 65% of the final fraction of the β-conformation, which is close to $A_1(0.73)$, with a rate constant close to k_0. The rest amount (35%) comes out as two-strand species are converted into three-strand species with a rate constant k_b. When k_0/k_b is reduced, as shown in Figs. 3(b) and (c), three-strand species are formed before two-strand species fully grow up, which is seen by a decrease of amplitude A_1 in Table 1. The rate of the formation of three-strand species is given by k_0 (which is now smaller than k_b).

This behavior resembles what is predicted from a following simple Scheme 1.

$$\text{Random coil} \xrightarrow{k_0} \text{Two-strand species} \xrightarrow{k_b} \text{Three-strand species}$$

Scheme 1.

At two other values of k_b/k_+, transition from two exponential character to single exponential one similarly takes place, as k_0/k_b is reduced. The following features are further noticed. In initiation-controlled regime ($k_b>k_0$), single exponential character prevails but the presence of a lag phase becomes significant, as k_+ approaches k_b, i.e., $k_b/k_+=1\times10^{-2}$ and 0.1. In bend-formation-controlled regime ($k_0>k_b$), on the other hand, two exponential character remains but the contribution of a lag phase becomes vanishing, as k_b/k_+ increases.

According to Scheme 1, a lag phase is expected if $k_0\sim k_b$. Some lag phases in Table 1 can be understood based on Scheme 1. However, lag phase in two exponential regime as well as in the initiation-controlled regime cannot be interpreted based on simple Scheme 1. In this case, recourse should be made to Eq. 18 to understand the origin and nature of the lag phase.

Table 1. Summary of Kinetic Patterns

$k_b/k_+=1\times10^{-3}$			
k_b/k_i	1	10	10^2
$L=12$	$0.71\ e^{-1.08\,k_0t}+0.29\ e^{-1.10\,k_bt}$	$e^{-0.94\,k_bt}$	$e^{-0.92\,k_0t}$
$L=24$	$0.73\ e^{-1.08\,k_0(t-t_0)}+0.21\ e^{-1.0\,k_bt}$ ($k_+t_0=4$; 3%)	$0.24\ e^{-1.42\,k_0t}+0.76\ e^{-1.3\,k_bt}$	$e^{-0.96\,k_0t}$
$L=48$	$0.73\ e^{-0.96\,k_0(t-t_0)}+0.27\ e^{-1.3\,k_bt}$ ($k_+t_0=5$; 5%)	$0.64\ e^{-1.08\,k_0t}+0.36\ e^{-1.1\,k_bt}$	$e^{-0.86\,k_0t}$
$k_b/k_+=1\times10^{-2}$			
k_b/k_i	1	10	10^2
$L=12$	$0.69\ e^{-1.08\,k_0t}+0.31\ e^{-1.1\,k_bt}$	$e^{-0.94\,k_bt}=e^{-0.78\,k_0t}$	$e^{-1.0\,k_0t}$
$L=24$	$0.73\ e^{-0.73\,k_0(t-t_0)}+0.27\ ^{-0.97\,k_bt}$ ($k_+t_0=1.3$; 6%)	$e^{-0.71\,k_0t}=e^{-1.7\,k_bt}$	$e^{-0.96\,k_0t}$
$L=48$	$0.71\ e^{-0.29\,k_0(t-t_0)}+0.29\ e^{-1.0\,k_bt}$ ($k_+t_0=1$; 3%)	$0.52\ e^{-1.15\,k_0(t-t_0)}+0.48\ e^{-1.2\,k_bt}$ ($k_+t_0=5$; 6%)	$e^{-0.86\,k_0t}$
$k_b/k_+=1\times10^{-1}$			
k_b/k_i	1	10	10^2
$L=12$	$0.73\ e^{-0.43\,k_0t}+0.28\ e^{-0.87\,k_bt}$	$e^{-0.92\,k_b(t-t_0)}=e^{-0.77\,k_0(t-t_0)}$ ($k_+t_0=1.3$; 5%)	$e^{-1.0\,k_0(t-t_0)}$ ($k_+t_0=6$; 3%)
$L=24$	$0.54\ e^{-0.17\,k_0t}+0.46\ e^{-1.20\,k_bt}$	$e^{-1.3\,k_b(t-t_0)}$ ($k_+t_0=1.2$; 7%)	$e^{-0.96\,k_0(t-t_0)}$ ($k_+t_0=4$; 4%)
$L=48$		$e^{-1.3\,k_b(t-t)}$ ($k_+t_0=0.6$; 3%)	$e^{-0.92\,k_0(t-t_0)}$ ($k_+t_0=5.5$; 10%)

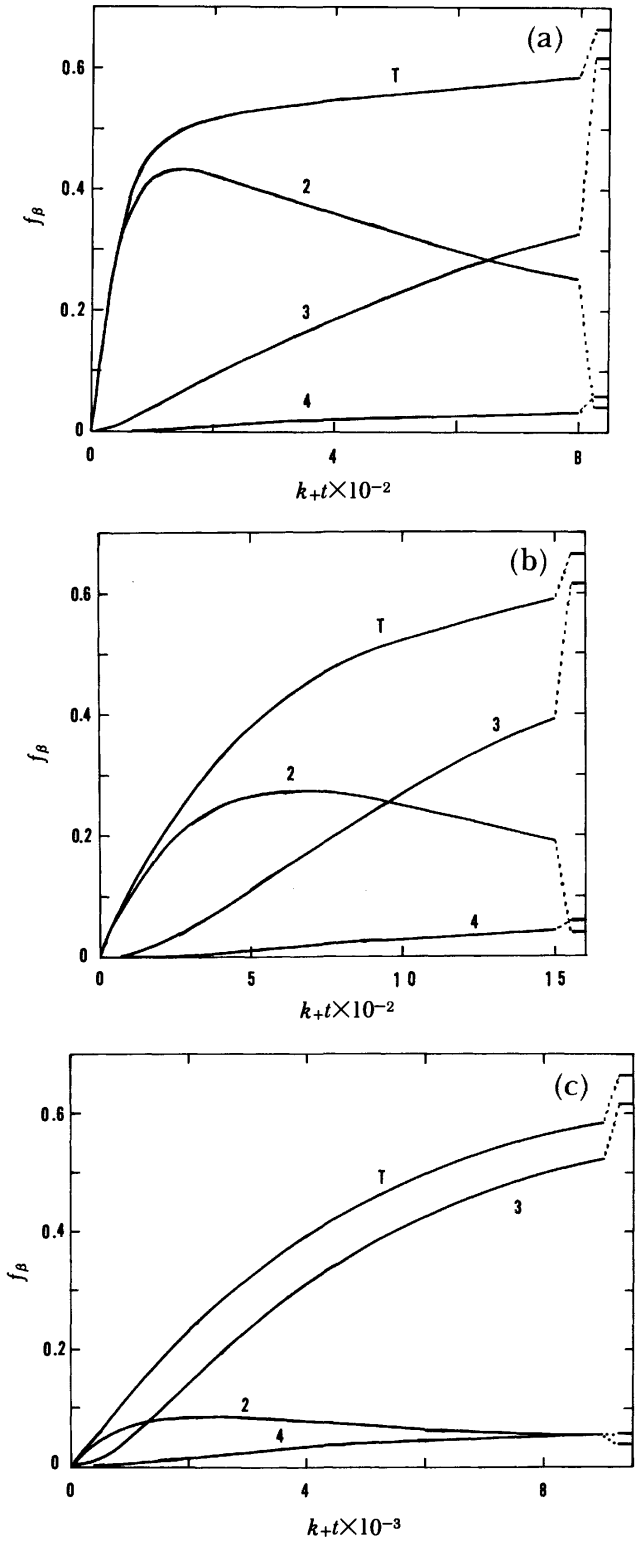

Fig. 3. Time course of various species under the condition where Scheme 1 holds approximately L=24, $k_b/k_+=1\times10^{-3}$. k_i/k_b: (a) 1, (b) 0.10, and (c) 1×10^{-2}.
In each figure (a)—(c), curves labelled as 2, 3, 4, and T represent the contributions from two- three-, four-strand species and their sum. Final values at $t=\infty$ are indicated by horizontal bars.

It is to be noted in Fig. 3 that final products are mostly three- strand species (β-meander). The population of four-strand species is significant under the situation $k_b/k_+=0.1$ in the case of L=24.

Experimental data on homopolypeptides published to date are systematically interpreted in terms of the present model. Their kinetics are not different from each other in essence but they all are explicable with the present model. The time constants obtained are expected to be related not to k_+ but rather to k_0 in the case of PLL[6-8] or to k_b and k_0 in the case of PLT.[10]

Recently, a progress has been made on the equilibrium theory of coil-β-structure conversion.[14-17] However, no attempt was made to evaluate various parameters from the comparison with experimental data. This indicates the difficult situation in the study of the β-structure to obtain proper experimental results consistent with the requirements of theories. The situation is worse in kinetic aspects than equilibrium ones. Hence, in the present study, no attempt is made to evaluate various rate constants from the comparison with published kinetic data.

Discussion

Some assumptions introduced in the present study are discussed briefly here.

(1) **Irreversibility.** It is desirable to take the reverse reaction into account. However, most experimental data were obtained under the condition that β-structure was nearly completely formed. Reverse reaction can be neglected under this condition. Furthermore, even under the condition where the fraction of the β-conformation is appreciably smaller than unity, there are several indications suggesting two processes; the first fast process followed by a slow annealing process.[12] It is likely that the fast growth step occurs irreversibly in a practical sense. Reversible nature of the reaction is partly taken into account even in the present model, for example, in the definition of unit or in the following discussion on (5).

(2) **Initiation through Bend Formation.** Formation of the β-structure was much slower in buffers than in unbuffered solutions under otherwise identical conditions in the case of PLL[7] and poly[Cys-(CH_2COOH)] (unpublished result). The findings indicate that collision of two random coil chains is much less effective than bend formation to initiate the β-structure. Since reaction between two random coil portions within a chain does not differ much from that between two random coil chains, the assumption is pertinent.

(3) **Multiple Initiation is not Considered.** For long chains, the fraction of the β-conformation reaches a limit, which is far below completion, even the limitation on the number of strands is removed. Therefore, initiation occurs at a unit outside of the

first β-sheet region and hence multiple initiation is a generally expected event. When all these locally formed β-sheets encounter each other, the first irreversible growth step terminates. Then, second annealing step follows where reversible nature of the reaction plays an essential role. The net increase in the fraction of the β-conformation is not big, however, accompanying this second step, although stability of the β-structure increases. Hence, the second step can be tentatively ignored. Then, present model can be applied to the case of multiple initiation, only by modifying the original chain length L_0 to L, the latter being roughly given by $L_0 f_\beta(\infty; L_0)$.

(4) **Calculations are Restricted under the Condition $k_+ > k_b$.** In the reverse situation of $k_b > k_+$, major products will be such that chains consisting of many bends connected by short strands. We are not interested in these species in the present study. Further, to examine the kinetics of the formation of such species, limitation on the number of strands (assumption 6) should be removed.

(5) **Propagation Rate.** Propagation rate of the first two strands is taken to be much smaller than that of the following strands. This partly takes reversible nature of strand growth into account in the present model. Since the first two strands are not as stable as the following ones, their propagation step proceeds in a more stochastic way.

(6) **Comparison with Helix-Coil Conversion.** Present analysis suggests that information about k_+ is not obtained from published experimental data. Consequently, it is misleading to compare slow formation rate of the β-structure with results on the fast propagation rate of helix formation.[18]

Since β-bend type III is equivalent to 3_{10} helix,[19] elementary processes in the α-helix initiation and bend formation are expected to be rather similar. However, there is at least one difference. For strand growth to occur significantly in the case of the β-structure, sufficient length will be required for both sides of an initiation site. Therefore, a given β-bend formation is not always valid for subsequent strand growth. For a helix to develop, on the other hand, it is required that either side of initiation site has a sufficient length. This different situation certainly makes considerable difference with respect to effective initiation rate constants between the α-helix and the intramolecular β-structure.

Appendix

Calculations of the Fraction of the β-Conformation. From the expressions on the concentrations given in the text, fraction f of the β-conformation or hydrogen-bonded units can be readilly calculated.

The contribution from two-strand species f_1 is explicitly written as follows.

$$f_1 = f_{11} + f_{12} + f_{13} \tag{A1}$$

$$f_{11} = (2m_1/L) \sum_{i=1}^{L/2-1} \sum_{\eta=i+1}^{L/2} i n_\eta(i|t)$$
$$= (2m_1/L) \sum_{i=1}^{L/2-1} i(L/2-i) n_\eta(i|t) \tag{A2}$$

$$f_{12} = (2m_1/L) \sum_{i=1}^{L/2-1} i\, n_i(i|t) \tag{A3}$$

$$f_{13} = (m_1/2) n_{L/2}(L/2|t) \tag{A4}$$

Similarly, contributions from three-strand species f_2 and four-strand species f_3 are given as follows.

$$f_2 = f_{21} + f_{22} + f_{23} \tag{A5}$$

$$f_{21} = (2m_2/L)[\sum_{i=1}^{L/4} \sum_{\eta=2i}^{L/2} i\, n_\eta(j_1=i,i|t)$$
$$+ \sum_{i=1}^{L/4} \sum_{\eta=i+1}^{L/2} i\, n_\eta(i,j_2=i|t)$$
$$+ \sum_{i=L/4+1}^{L/3-1} \sum_{\eta=i+1}^{L-2i} i\, n_\eta(i,j_2=i|t)]$$
$$= (2m_2/L)[\sum_{i=1}^{L/4} i(L/2-2i+1) n_\eta(j_1=i,i|t)$$
$$+ \sum_{i=1}^{L/4} i(L/2-i) n_\eta(i,j_2=i|t)$$
$$+ \sum_{i=L/4+1}^{L/3-1} i(L-3i) n_\eta(i,j_2=i|t)] \tag{A6}$$

$$f_{22} = (2/L)[\sum_{i=2}^{L/4} \sum_{\eta=i+1}^{2i-1} (\eta+m_3 i) n_\eta(j_1=\eta-i,i|t)$$
$$+ \sum_{i=L/4+1}^{L/2-1} \sum_{\eta=i+1}^{L/2} (\eta+m_3 i) n_\eta(j_1=\eta-i,i|t)$$
$$+ \sum_{i=L/4+1}^{L/3} \sum_{\eta=L-2i+1}^{L/2} (L-\eta+m_3 i) n_\eta(i,j_2=L-\eta-i|t)$$
$$+ \sum_{i=L/3+1}^{L/2-1} \sum_{\eta=i+1}^{L/2} (L-\eta+m_3 i) n_\eta(i,j_2=L-\eta-i|t)]$$
$$= (2/L)[\sum_{i=2}^{L/4} i(i-1)(3/2+m_3) n_\eta(j_1=\eta-i,i|t)$$
$$+ \sum_{i=L/4+1}^{L/2-1} (L/2-i)\left(m_3 i + \frac{L+2i+2}{4}\right) n_\eta(j_1=\eta-i,i|t)$$
$$+ \sum_{i=L/4+1}^{L/3} (i-L/4)(2i+L/2+2m_3 i-1)$$
$$n_\eta(i,j_2=L-i-\eta|t)$$
$$+ \sum_{i=L/3+1}^{L/2-1} \left(\frac{L-2i}{4}\right)(2m_2 i-1-i+3L/2)$$
$$n_\eta(i,j_2=L-i-\eta|t)] \tag{A7}$$

$$f_{23} = (2/L)[\sum_{i=1}^{L/3} m_2 i\, n_i(i,j_2=i|t)$$
$$+ \sum_{i=L/3+1}^{L/2-1} (L-i+m_3 i)\, n_i(i,j_2=i|t)] \tag{A8}$$

$$f_3 = f_{31} + f_{32} + f_{33} \tag{A9}$$

$$f_{31} = (2m_4/L) \sum_{i=1}^{L/4} \sum_{\eta=2i}^{L/2} i n_\eta(j_1=i,i,j_2=i|t)$$
$$= (2m_4/L) \sum_{i=1}^{L/4} (L/2-2i+1) i\, n_\eta(j_1=i,i,j_2=i|t) \tag{A10}$$

$$f_{32} = (2/L)[\sum_{i=2}^{L/4} \sum_{\eta=i+1}^{2i-1} (\eta+m_1 i)\, n_\eta(j_1=\eta-i,i,j_2=i|t)$$

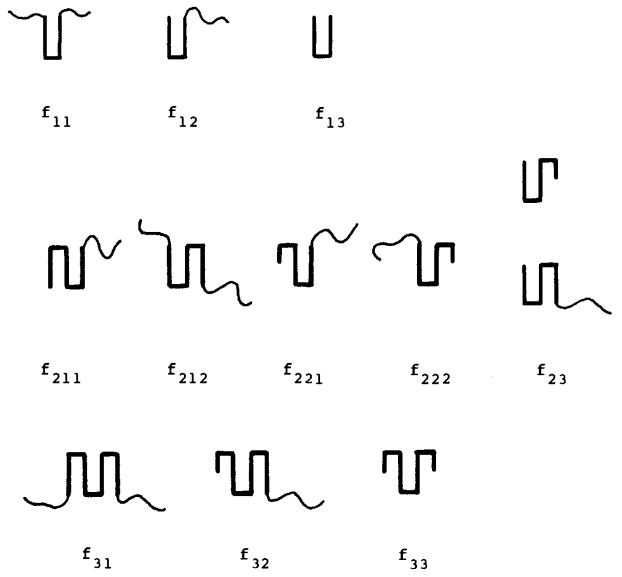

Fig. 4. Schematic representation of various species corresponding to respective contributions given in Eqs. A1—A12. Thick lines and thin curves represent the β-strands and random coil portions, respectively.

$$+\sum_{i=L/4+1}^{L/3}\sum_{\eta=i+1}^{L-2i}(\eta+m_1 i)\,n_\eta(j_1=\eta-i,i,j_2=i|t)$$
$$=(2/L)[\sum_{i=2}^{L/4} i(i-1)(3/2+m_1)\,n_\eta(j_1=\eta-i,i,j_2=i|t)$$
$$+\sum_{i=L/4+1}^{L/3}(L+2m_1 i-i+1)\left(\frac{L-3i}{2}\right)$$
$$n_\eta(j_1=\eta-i,i,j_2=i|t)] \quad \text{(A11)}$$

$$f_{33}=(2/L)[\sum_{i=L/4+1}^{L/3}\sum_{\eta=L-2i+1}^{L/2}(L-i+m_3 i)$$
$$n_\eta(j_1=\eta-i,i,j_2=L-\eta-i|t)$$
$$+\sum_{i=L/3+1}^{L/2-1}\sum_{\eta=i+1}^{L/2}(L-i+m_3 i)$$
$$n_\eta(j_1=\eta-i,i,j_2=L-\eta-i|t)]$$
$$=(2/L)[\sum_{i=L/4+1}^{L/3}(2i-L/2)(L-i+m_3 i)$$
$$n_\eta(j_1=\eta-i,i,j_2=L-\eta-i|t)$$
$$+\sum_{i=L/3+1}^{L/2-1}(L+m_3 i-i)(L/2-i)$$
$$n_\eta(j_1=\eta-i,i,j_2=L-\eta-i|t)] \quad \text{(A12)}$$

In the above equations except Eq. A4, a factor of 2 appears in order to take species with η greater than $L/2$ into account. In the above, (m_1, m_2, m_3, m_4) is (2, 3, 1, 4) for f_β (fraction of the β-conformation) or (1, 2, 0, 3) for f_{hb} (fraction of hydrogen bonded units). In Fig. 4, various species corresponding to each f_{ij} term are schematically represented.

Final Amounts of the β-Conformation or Hydrogen-Bonded Units. As the reaction proceeds, f reaches the final value $f(\infty)$ at $t=\infty$.

$$f(\infty)=f_{13}(\infty)+f_{23}(\infty)+f_{31}(\infty)+f_{32}(\infty)+f_{33}(\infty) \quad \text{(A13)}$$

These final values are functions of k_i/k_0 and k_b/k_+. Since $k_i/k_0=1/L$, the final values are solely determined by the ratio k_+/k_b for a given chain length L. Introducing $\xi=k_+/(k_++2k_b)$, they are written as follows.

$$f_{13}(\infty)=(m_1 k_i/2k_0)\xi^{L/2-1}$$
$$f_{23}(\infty)=(2k_i/Lk_0)[m_2\sum_{i=1}^{L/3} i\xi^{i-1}+\sum_{i=L/3+1}^{L/2-1}(L-i+m_3 i)\xi^{i-1}]$$
$$f_{31}(\infty)=\frac{4m_4 k_i k_b}{Lk_0 k_+}\sum_{i=1}^{L/4} i(L/2-2i+1)\xi^i$$
$$f_{32}(\infty)=\frac{4k_i k_b}{Lk_0 k_+}[(3/2+m_1)\sum_{i=2}^{L/4}(i^2-i)\xi^i$$
$$+(1/2)\sum_{i=L/4+1}^{L/3}(L-3i)(L-i+2m_1+1)\xi^i]$$
$$f_{33}(\infty)=\frac{4k_i k_b}{Lk_0 k_+}[\sum_{i=L/4+1}^{L/3}(2i-L/2)(L-i+m_3 i)\xi^i$$
$$+\sum_{i=L/3+1}^{L/2-1}(L/2-i)(L-i+m_3 i)\xi^i] \quad \text{(A14)}$$

References

1) Ch. Ghelis and J. Yon, "Protein Folding," Academic Press, New York (1982).
2) P. S. Kim and R. L. Baldwin, *Ann. Rev. Biochem.*, **51**, 459 (1982).
3) Th. E. Creighton, "Proteins," W. H. Freeman & Co., New York (1983).
4) B. Davidson and G. D. Fasman, *Biochemistry*, **6**, 1616 (1967).
5) S.-Y. C. Wooley and G. Holzwarth, *Biochemistry*, **9**, 3604 (1970).
6) C. R. Snell and G. D. Fasman, *Biochemistry*, **12**, 1017 (1973).
7) R. Hartman, R. C. Schwaner, and J. Hermans, Jr., *J. Mol. Biol.*, **90**, 415 (1974).
8) H.-A. Arfmann, R. Labitzke, and K. G. Wagner, *Biopolymers*, **16**, 1815 (1977).
9) H. Yamamoto and J. T. Yang, *Biopolymers*, **13**, 1109 (1974).
10) H. E. Auer and E. Patton, *Biophys. Chem.*, **4**, 15 (1976).
11) H. E. Auer and H. Miller-Auer, *Biopolymers*, **25**, 1607 (1986).
12) K. Fukada, H. Maeda, and S. Ikeda, *Polymers*, **28**, 1887 (1987).
13) W. L. Mattice, *Macromolecules*, **17**, 407 (1984).
14) W. L. Mattice and H. A. Scheraga, *Biopolymers*, **23**, 1701 (1984).
15) W. L. Mattice and H. A. Scheraga, *Macromolecules*, **17**, 2690 (1984).
16) W. L. Mattice and H. A. Scheraga, *Biopolymers*, **24**, 565 (1985).
17) W. L. Mattice, E. Lee, and H. A. Scheraga, *Can. J. Chem.*, **63**, 140 (1985).
18) J. Janin and S. J. Wodak, *Prog. Biophys. Mol. Biol.*, **42**, 21 (1983).
19) C. M. Venkatachalam, *Biochim. Biophys. Acta*, **303**, 211 (1973).

 © 1987 The Chemical Society of Japan Bull. Chem. Soc. Jpn., 60, 3903—3909 (1987)

The Microwave Spectra, Dipole Moments, and Two Isomers of Cyclopentadiene-1-carbonitrile

Takeshi SAKAIZUMI,* Hiromi KIKUCHI, Osamu OHASHI, and Ichiro YAMAGUCHI
Department of Chemistry, Faculty of Science and Technology, Sophia University,
Kioi-cho, Chiyoda-ku, Tokyo 102
(Received June 8, 1987)

The microwave spectra of two isomers of cyclopentadiene-1-carbonitrile generated by the pyrolysis of 1*H*-benzotriazole have been observed in the frequency range from 8.0 to 40.0 GHz. The rotational constants (MHz) have been determined as A=8353.7(9), B=1904.24(1), and C=1565.38(1) for 1,3-cyclopentadiene-1-carbonitrile, and A=8235.0(13), B=1902.07(2), and C=1559.67(2) for 1,4-cyclopentadiene-1-carbonitrile. The dipole moments (Debye) obtained are μ_a=4.15(15), μ_b=0.27(3), and μ_{total}=4.16(17) for 1,3-cyclopentadiene-1-carbonitrile and μ_a=4.36(25), μ_b=0.77(10), and μ_{total}=4.42(35) for 1,4-cyclopentadiene-1-carbonitrile.

Since 6-iminofulvene (**2**) is important as an intermediate molecular species[1] in organic chemical reactions, as shown in Scheme 1, we have tried to generate **2** by pyrolysis of 1*H*-benzotriazole (**1**) and to observe its spectrum by microwave spectroscopy.

Although the spectrum of **2** could not be assigned, we have observed the spectra of two isomers of cyclopentadiene-1-carbonitrile (1,3-cyclopentadiene-1-carbonitrile (**3**) and 1,4-cyclopentadiene-1-carbonitrile (**4**)).

Wentrup and Crow[2] have reported the formation of **3** from the pyrolysis of **1** by their NMR spectroscopic study. They have assigned the product isolated to the structure **3**, which is the thermodynamically stable isomer. Furthermore, they have indicated the presence of another isomer, which must be the structure **4**.

Ford and Seitzman,[3] using microwave spectroscopy, have reported the rotational constants (A, B, and C) and the a-component of the dipole moment of **3**.

In this study we observed the spectra of two isomers in the ground and excited vibrational states and of one deuterated species in the ground vibrational state. Beside the rotational constants and the a-component of the dipole moment of **3**, we determined the centrifugal distortion constants, the b-component of the dipole moment of **3**, which were not reported by Ford and Seitzman,[3] the rotational and centrifugal distortion constants and the dipole moment for **4**, and the ratio of formation for two isomers. The molecules **3** and **4** could not be differentiated immediately from only the comparison of the observed and calculated rotational constants. Therefore, we have identified one of the observed species as **3** from the r_s coordinate of the hydrogen atom in the methylene group, and the other species was identified as **4** from comparison of the observed and calculated dipole moments.

We will discuss the molecular structure and dipole moments of the pyrolysis products and the possible pyrolysis mechanism of 1*H*-benzotriazole (**1**).

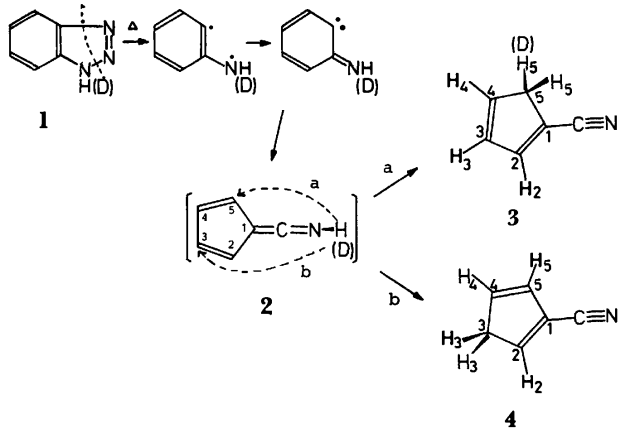

Scheme 1.

Experimental

The sample of 1*H*-benzotriazole obtained from Aldrich Co. was used without further purification. The deuterated precursor (-ND-) was prepared by refluxing the mixture of 1*H*-benzotriazole and CH_3OD (99.5% D) in D_2O (99.75% D). The deuterated precursor was confirmed by ^1H NMR and mass spectroscopy.

The pyrolysis mass spectrum of 1*H*-benzotriazole was observed by using a quadrupole mass spectrometer (ANELVA AQA-360). The molecular ion peak generated at 800 °C was m/z 91.

The pyrolysis apparatus consisted of an unpacked horizontal quartz tube (300 mm length and 5 or 20 mm i.d.) heated in a handmade electric furnace. The precursor was warmed at 90 °C with a pipe-type heater. The temperature of the electric furnace was monitored with a thermocouple fitted on the external wall of the quartz tube. The tube was connected to an inlet port on the side of a Stark waveguide cell (3m long X-band). The cell had large inlet and outlet ports at the ends to allow a rapid flow of vapour through the cell. The pressure at the exit end of the cell was 0.02 to 0.04 Torr (1 Torr=133.322 Pa). A pyrolytic temperature of 800 °C was chosen to generate **3** and **4** because the strongest spectral lines of the two isomers appeared at this temperature.

The microwave spectrometer employed was a conventional 100 kHz Stark modulated instrument. The microwave sources employed were a signal generator (HP 8672A) in the frequency range from 8 to 18 GHz and YIG-tuned GaAs oscillators (WJ 5600-301F and WJ 5610-302FD) from 18.0 to 26.5 GHz and from 26.5 to 40 GHz, respectively.

Results and Discussion

The spectrum of the pyrolysates at 800 °C consisted of four equidistantly spaced groups of spectrum lines between 26.5 and 40.0 GHz which were readily assigned to a-type R-branch transitions with J=8←7 to J=11←10 ($B+C\approx3450$ MHz). The spectrum lines of each group were dense, presumably due to the presence of two isomers and their vibrationally-excited states.

The typical spectra of two isomers observed by using the quartz tubes of 5 and 20 mm inner diameter at 800 °C are shown in Figs. 1(a) and (b), respectively. Although the spectra of Figs. 1(a) and (b) were observed under the same condition for the sample pressure, Stark voltage, and output power of microwave, the intensities of the spectrum lines in the ground and first excited state of set II in 10(0,10)←9(0,9) transition, as shown in Fig. 1(a), are weaker by about one falf than those in Fig. 1(b). Such a difference for set II was also observed in other transitions. The difference of the relative intensities of Figs. 1(a) and (b) is attributed to the differences of formation. This means that the observed spectrum lines can be assigned to two different molecules by using quartz tubes of two different inner diameters.

The spectrum lines of each K_{-1} value were assigned by their Stark effects. The stronger and weaker spectrum lines in each set were assigned to $v=0$ and $v=1$, respectively, as listed in Tables 1 to 4. The rotational and centrifugal constants were obtained by the least-squares method; they are listed in Table 5. The observed and calculated transition frequencies are in good agreement.

The values of $\Delta I(I_c-I_a-I_b)$ obtained for the stronger lines ($v=0$) of set I and set II are −3.040 and −3.047 uÅ^2, respectively. These values are almost the same as −3.102 uÅ^2 observed for cyclopentadiene.[4] The value suggests that the skeleton of the heavy atoms is planar and that two hydrogen atoms are located out of the molecular skeletal plane.

In order to identify the molecules of set I and set II, the rotational constants were calculated for the molecular models of fourteen candidates with unsaturated 3-, 4-, and 5-membered rings, under the

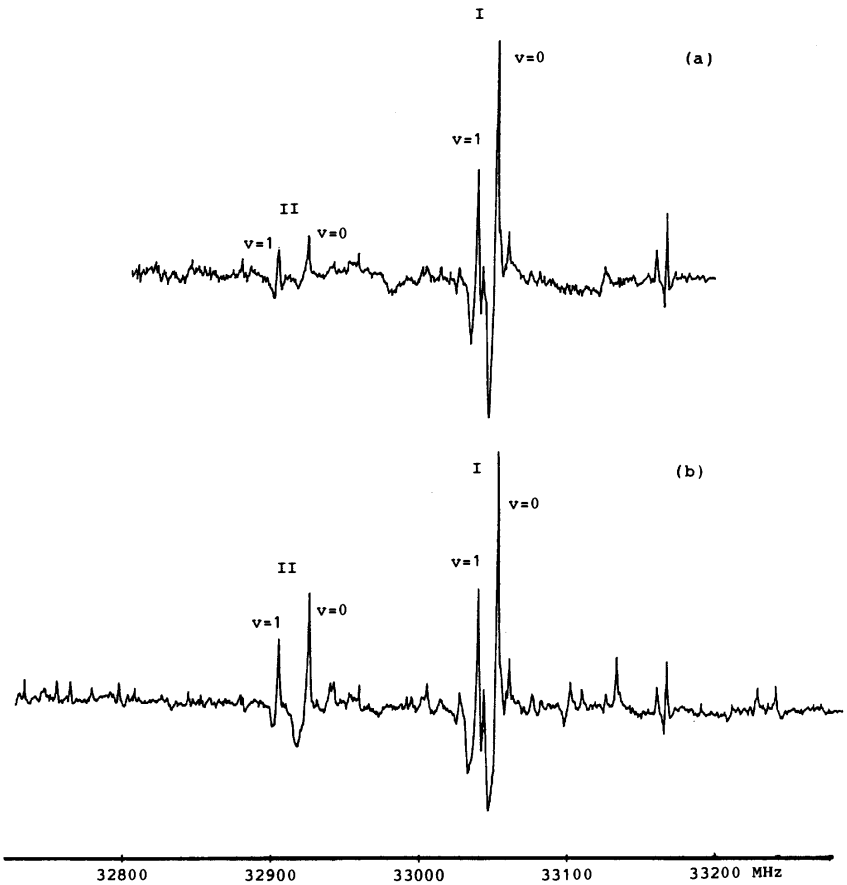

Fig. 1. Microwave spectra observed by using quartz tubes of two different inner diameters(ϕ) for two isomers (I and II) of cyclopentadiene-1-carbonitrile in 10(0,10)←9(0,9) transition at 800 °C. [(a): ϕ_{id}=5 mm, (b): ϕ_{id}=20 mm.
I: 1,3-Cyclopentadiene-1-carbonitrile (**3**), II: 1,4-Cyclopentadiene-1-carbonitrile (**4**).]

Table 1. Observed Rotational Transitions (MHz) of 1,3-Cyclopentadiene-1-carbonitrile (Set I) in the Ground Vibrational State

Transition	ν_{obsd}	$\Delta\nu$[a]	Transition	ν_{obsd}	$\Delta\nu$[a]
$3_{13}-2_{12}$	9892.84	0.26	$9_{18}-8_{17}$	32302.90	0.13
$3_{03}-2_{02}$	10356.70	−0.27	$10_{110}-9_{19}$	32592.24	0.01
$3_{12}-2_{11}$	10908.82	−0.04	$10_{010}-9_{09}$	33050.44	−0.16
$4_{14}-3_{13}$	13175.57	−0.07	$10_{29}-9_{28}$	34371.27	0.07
$4_{04}-3_{03}$	13749.82	0.25	$10_{9}-9_{9}$	34740.88	0.08
$4_{13}-3_{12}$	14529.16	−0.06	$10_{8}-9_{8}$	34748.83	−0.11
$5_{15}-4_{14}$	16447.47	0.28	$10_{7}-9_{7}$	34760.56	0.13
$5_{05}-4_{04}$	17093.48	−0.10	$10_{6}-9_{6}$	34777.87	−0.00
$5_{24}-4_{23}$	17319.28	0.19	$10_{5}-9_{5}$	34806.95	0.15
$5_{23}-4_{22}$	17573.64	0.09	$10_{47}-9_{46}$	34857.00	0.03
$5_{14}-4_{13}$	18134.86	−0.11	$10_{46}-9_{45}$	34867.37	−0.10
$8_{18}-7_{17}$	26178.04	−0.10	$10_{38}-9_{37}$	34876.97	−0.06
$8_{08}-7_{07}$	26795.44	−0.03	$10_{37}-9_{36}$	35110.85	0.03
$8_{27}-7_{26}$	27598.47	−0.02	$10_{19}-9_{18}$	35746.95	0.09
$8_{6}-7_{6}$	27804.48	−0.04	$11_{111}-10_{110}$	35779.36	0.03
$8_{5}-7_{5}$	27819.64	0.14	$10_{28}-9_{27}$	36006.06	0.04
$8_{36}-7_{35}$	27875.58	0.02	$11_{011}-10_{010}$	36150.71	−0.05
$8_{35}-7_{34}$	27952.50	−0.03	$11_{210}-10_{29}$	37728.60	−0.00
$8_{26}-7_{25}$	28557.70	−0.12	$11_{9}-10_{9}$	38221.06	−0.01
$8_{17}-7_{16}$	28812.07	0.01	$11_{8}-10_{8}$	38231.70	−0.02
$9_{19}-8_{18}$	29392.24	0.01	$11_{7}-10_{7}$	38246.75	−0.10
$9_{09}-8_{08}$	29936.26	−0.12	$11_{6}-10_{6}$	38270.00	0.08
$9_{28}-8_{27}$	30994.19	0.15	$11_{48}-10_{47}$	38372.23	0.14
$9_{8}-8_{8}$	31268.25	0.04	$11_{39}-10_{38}$	38374.11	0.02
$9_{7}-8_{7}$	31276.72	0.01	$11_{47}-10_{46}$	38392.90	−0.02
$9_{6}-8_{6}$	31289.44	−0.09	$11_{38}-10_{37}$	38743.60	0.08
$9_{5}-8_{5}$	31310.63	−0.17	$12_{112}-11_{111}$	38955.04	0.08
$9_{37}-8_{36}$	31376.44	−0.16	$11_{110}-10_{19}$	39136.89	0.05
$9_{36}-8_{35}$	31515.67	−0.07	$12_{012}-11_{011}$	39246.40	−0.02
$9_{27}-8_{26}$	32279.07	−0.10	$11_{29}-10_{28}$	39722.38	−0.06

a) $\Delta\nu=\nu_{obsd}-\nu_{calcd}$.

condition that the value of m/z is 91 (C_6H_5N), as evidenced from the pyrolysis mass spectrum. The structural parameters used were taken from fulvene,[5] methanimine,[6] cyclopentadiene,[4] diazoacetonitrile,[7] and 1,3-cyclopentadiene-1-carbonitrile,[3] as shown in Table 6. Among fourteen candidates, the rotational constants calculated for **2**, **3**, and **4** were very close to those observed, as shown in Table 7. Although the rotational constants observed for set I and set II are similar to those predicted for **2**, neither set I or set II can be assigned to **2** because the values of ΔI observed are quite different from those predicted for **2**, in which only one hydrogen atom of NH group is located out of the molecular skeletal plane. Both the rotational constants and ΔI predicted for **3** and **4** are very close to those observed. However, the estimated rotational constants for **3** and **4** are quite similar and can not distinguish clearly between set I and set II.

The model calculation for **3** and **4** suggests that the a-coordinates of their methylenic hydrogen atoms are quite different. We observed spectra of their deuterated species to identify the carrier of the spectra of set I and set II. The spectrum of the pyrolysates of a deuterated precursor was very complicated because of the appearance of the mixture of a deuterated and normal species. The spectrum lines of the deuterated species were distinguished from the comparison with those of the normal species. The spectrum lines were assigned by their Stark effects. The assigned transition frequencies of the monodeuterated species are listed in Table 8. The observed rotational and centrifugal distortion constants are shown in Table 9. The observed value of ΔI, −4.489 uÅ^2, is consistent with that of −4.543 uÅ^2 obtained for monodeuterated species of cyclopentadiene[4] in which the hydrogen atom of methylene group is replaced by a deuterium atom. The rotational constants and ΔI observed were compared with those calculated for the deuterated species, as shown in Table 9. The rotational constants observed are close to those calculated for *3*-H_5-*d*. Furthermore, from the moments of inertia obtained for the monodeuterated species and set I of the normal species, the r_s coordinate of the hydrogen atom was calculated by using Kraitchman's equation.[8] The

observed and calculated coordinates of the hydrogen atom in the methylene group are shown in Table 10. The r_s coordinate obtained for the hydrogen atom is consistent with that calculated from the model of **3**, as shown in Table 10. Therefore, the set I was concluded to be 1,3-cyclopentadiene-1-carbonitrile(**3**). This is consistent with the result reported by Ford and Seitzman.[3]

The spectrum of **4**-H_3-*d* species could not be observed because of very weak absorption intensities. However, the set II was assigned to 1,4-cyclopentadiene-1-carbonitrile (**4**) because the a- and b-components of the dipole moment observed for set II are in good agreement with those of **4** calculated from the group moments, as discussed in the following paragraph.

Table 2. Observed Rotational Transitions (MHz) of 1,3-Cyclopentadiene-1-carbonitrile (Set I) in the First Excited Vibrational State

Transition	ν_{obsd}	$\Delta\nu$[a]
8_{18} - 7_{17}	26213.18	−0.09
8_{08} - 7_{07}	26785.71	−0.04
8_{27} - 7_{26}	27630.90	0.19
8_{26} - 7_{25}	28643.41	0.05
8_{17} - 7_{16}	28825.23	−0.05
9_{19} - 8_{18}	29429.17	0.07
9_{09} - 8_{08}	29923.39	0.22
9_{28} - 8_{27}	31026.37	0.03
9_{27} - 8_{26}	32372.93	−0.12
9_{18} - 8_{17}	32307.07	−0.11
10_{110}- 9_{19}	32630.66	−0.05
10_{010}- 9_{09}	33037.55	−0.17
10_{29} - 9_{28}	34402.35	−0.04
11_{111}-10_{110}	35819.40	−0.08
10_{28} - 9_{27}	36102.64	0.12
11_{011}-10_{010}	36141.95	0.01
11_{210}-10_{29}	37757.33	−0.17
12_{112}-11_{111}	38997.13	0.07
11_{110}-10_{19}	39110.30	0.07
12_{012}-11_{011}	39244.59	0.07

a) $\Delta\nu=\nu_{obsd}-\nu_{calcd}$.

Table 4. Observed Rotational Transitions (MHz) of 1,4-Cyclopentadiene-1-carbonitrile (Set II) in the First Excited Vibrational State

Transition	ν_{obsd}	$\Delta\nu$[a]
8_{18} - 7_{17}	26126.27	0.02
8_{08} - 7_{07}	26684.07	−0.14
8_{27} - 7_{26}	27558.93	0.14
8_{17} - 7_{16}	28758.00	−0.08
9_{19} - 8_{18}	29329.47	0.17
9_{18} - 8_{17}	32224.79	−0.11
10_{110}- 9_{19}	32517.84	−0.11
10_{010}- 9_{09}	32906.29	−0.03
11_{111}-10_{110}	35693.70	0.01
10_{28} - 9_{27}	36056.95	0.06
11_{011}-10_{010}	35998.33	0.16
11_{210}-10_{29}	37648.32	−0.18
12_{112}-11_{111}	38858.22	−0.08
11_{110}-10_{19}	38989.52	0.15
12_{012}-11_{011}	39089.39	0.01

a) $\Delta\nu=\nu_{obsd}-\nu_{calcd}$.

Table 3. Observed Rotational Transitions (MHz) of 1,4-Cyclopentadiene-1-carbonitrile (Set II) in the Ground Vibrational State

Transition	ν_{obsd}	$\Delta\nu$[a]	Transition	ν_{obsd}	$\Delta\nu$[a]
3_{03} -2_{02}	10331.31	0.01	10_{7} - 9_{7}	34684.00	−0.06
5_{24} -4_{23}	17278.67	0.13	10_{6} - 9_{6}	34702.36	0.16
8_{18} -7_{17}	26093.37	0.12	10_{37} - 9_{36}	35051.44	0.10
8_{08} -7_{07}	26701.21	−0.08	10_{19} - 9_{18}	35657.31	−0.12
8_{27} -7_{26}	27529.42	0.11	11_{111}-10_{110}	35657.31	0.20
8_{7} -7_{7}	27734.00	0.19	10_{28} - 9_{27}	35958.44	−0.02
8_{6} -7_{6}	27743.46	0.18	11_{011}-10_{010}	36014.35	−0.03
8_{36} -7_{35}	27816.10	−0.01	11_{210}-10_{29}	37625.45	0.06
8_{26} -7_{25}	28519.42	−0.13	11_{10} -10_{10}	38128.00	−0.13
8_{17} -7_{16}	28750.22	−0.06	11_{9} -10_{9}	38136.60	0.18
9_{09} -8_{08}	29826.96	−0.05	11_{8} -10_{8}	38147.41	−0.10
9_{5} -8_{5}	31242.88	−0.15	11_{7} -10_{7}	38163.44	0.18
9_{36} -8_{35}	31458.00	−0.07	11_{6} -10_{6}	38187.22	−0.04
9_{27} -8_{26}	32237.21	−0.03	11_{38} -10_{37}	38684.00	0.11
9_{18} -8_{17}	32228.25	0.01	12_{112}-11_{111}	38819.84	−0.27
10_{110}-9_{19}	32482.41	−0.20	11_{110}-10_{19}	39030.36	0.15
10_{010}-9_{09}	32926.87	−0.24	12_{012}-11_{011}	39098.48	0.27
10_{9} -9_{9}	34663.46	−0.16	11_{29} -10_{28}	39666.73	−0.17

a) $\Delta\nu=\nu_{obsd}-\nu_{calcd}$.

Table 5. Observed Rotational (MHz) and Centrifugal Distortion (kHz) Constants and ΔI(uÅ^2) of 1,3-Cyclopentadiene-1-carbonitrile (Set I) and 1,4-Cyclopentadiene-1-carbonitrile (Set II)[a]

	Set I (3)		Set II (4)	
	$v=0$	$v=1$	$v=0$	$v=1$
A	8353.7(9)	7848.6(11)	8235.0(13)	7690.0(15)
B	1904.24(1)	1906.39(2)	1902.07(2)	1904.10(3)
C	1565.38(1)	1568.77(2)	1559.67(2)	1563.07(3)
Δ_J	0.08(3)	0.15(7)	0.07(7)	0.07(10)
Δ_{JK}	2.43(7)	4.7(35)	2.59(8)	9.4(53)
ΔI[b]	−3.047(10)	−7.338(15)	−3.040(16)	−7.811(18)

a) Figures in parentheses indicate the uncertainty attached to the last figures, estimated from 2.5 times the standard deviations. Conversion factor: 505376 uÅ^2 MHz. b) $\Delta I=I_c-I_a-I_b$.

Table 6. Structural Parameters Used to Calculate the Rotational Constants of Three Isomers (Bond Lengths in Å and Angles in Degree). [CP: Cyclopentadiene, CN: Carbonitrile]

6-Iminofulvene (2)		1,3-CP-1-CN (3)		1,4-CP-1-CN (4)	
$r(C_1-C_2)$, $r(C_1-C_5)$	1.470[a]	$r(C_1-C_5)$, $r(C_4-C_5)$	1.506[c]	$r(C_2-C_3)$, $r(C_3-C_4)$	1.506[b]
$r(C_2=C_3)$, $r(C_4=C_5)$	1.355[a]	$r(C_1=C_2)$, $r(C_3=C_4)$	1.345[c]	$r(C_1=C_2)$, $r(C_4=C_5)$	1.345[c]
$r(C_3-C_4)$	1.476[a]	$r(C_2-C_3)$	1.468[c]	$r(C_1-C_5)$	1.468[c]
$r(C_1=C)$	1.349[a]	$r(C_1-C)$	1.424[d]	$r(C_1-C)$	1.424[d]
$r(C=N)$	1.273[b]	$r(C\equiv N)$	1.165[d]	$r(C\equiv N)$	1.165[d]
$r(N-H)$	1.021[b]	$r(C_5-H_5)$	1.099[c]	$r(C_3-H_3)$	1.099[c]
$r(C_2-H_2)$, $r(C_5-H_5)$	1.078[a]	$r(C_4-H_4)$	1.078[c]	$r(C_2-H_2)$, $r(C_4-H_4)$	1.078[c]
$r(C_3-H_3)$, $r(C_4-H_4)$	1.080[a]	$r(C_2-H_2)$, $r(C_3-H_3)$	1.080[c]	$r(C_5-H_5)$	1.080[c]
$C_5-C_1-C_2$	106.6[a]	$C_1-C_5-C_4$	103.0[c]	$C_2-C_3-C_4$	103.0[c]
$C_1-C_2-C_3$, $C_1-C_5-C_4$	107.7[a]	$C_5-C_1-C_2$, $C_5-C_4-C_3$	109.2[c]	$C_3-C_2-C_1$, $C_3-C_4-C_5$	109.2[c]
$C_2-C_3-C_4$, $C_5-C_4-C_1$	109.0[a]	$C_1-C_2-C_3$, $C_4-C_3-C_2$	109.3[c]	$C_2-C_1-C_5$, $C_4-C_5-C_1$	109.3[c]
C_2-C_1-C	126.7[a]	C_2-C_1-C	136.1[e]	C_2-C_1-C	136.1[e]
$C_3-C_2-H_2$, $C_4-C_5-H_5$	127.6[a]	$C_3-C_4-H_4$	127.1[c]	$C_1-C_2-H_2$, $C_5-C_4-H_4$	127.1[c]
$C_2-C_3-H_3$, $C_5-C_4-H_4$	126.4[a]	$C_1-C_2-H_2$, $C_4-C_3-H_3$	126.0[c]	$C_4-C_5-H_5$	126.0[c]
$C=N-H$	110.4[b]	$C_1-C_5-H_5$	128.5[c]	$C_2-C_3-H_3$	128.5[c]
		$H_5-C_5-H_5$	106.3[c]	$H_3-C_3-H_3$	106.3[c]

a) Ref. 5, b) Ref. 6, c) Ref. 4, d) Ref. 7, e) Ref. 3.

Table 7. Observed and Calculated Rotational Constants (MHz) and ΔI(uÅ^2) of Sets I and II in the Ground Vibrational State

	Obsd		Calcd		
	Set I	Set II	2[a]	3[b]	4[c]
A	8353.7(9)	8235.0(13)	8317.54	8439.93	8297.46
B	1904.24(1)	1902.07(2)	1862.93	1908.60	1908.50
C	1565.38(1)	1559.67(3)	1530.11	1571.69	1566.61
ΔI[d]	−3.047(10)	−3.040(16)	−1.753	−3.117	−3.117

a) 6-Iminofulvene, b) 1,3-Cyclopentadiene-1-carbonitrile, c) 1,4-Cyclopentadiene-1-carbonitrile, d) $\Delta I=I_c-I_a-I_b$.

Table 8. Observed Rotational Transitions (MHz) of 1,3-Cyclopentadiene-1-carbonitrile-*d*

Transition	ν_{obsd}	$\Delta\nu$[a]	Transition	ν_{obsd}	$\Delta\nu$[a]
$8_{27}-7_{26}$	27392.85	−0.01	$11_{111}-10_{110}$	35411.69	0.05
$8_{5}-7_{5}$	27647.34	−0.05	$10_{28}-9_{27}$	35887.65	−0.19
$8_{36}-7_{35}$	27707.21	−0.01	$11_{011}-10_{010}$	35723.93	−0.01
$8_{26}-7_{25}$	28467.82	−0.00	$11_{210}-10_{29}$	37414.75	0.10
$8_{17}-7_{16}$	28621.27	0.04	$11_{9}-10_{9}$	37980.53	0.01
$9_{19}-8_{18}$	29101.49	−0.01	$11_{8}-10_{8}$	37992.69	0.12
$9_{28}-8_{27}$	30754.85	0.08	$11_{7}-10_{7}$	38009.77	−0.04
$9_{54}-8_{53}$	31119.43	0.10	$11_{6}-10_{6}$	38036.11	−0.13
$10_{110}-9_{19}$	32263.00	−0.17	$11_{57}-10_{56}$	38080.08	−0.12
$10_{29}-9_{28}$	34095.95	0.12	$11_{39}-10_{38}$	38136.61	0.02
$10_{7}-9_{7}$	34543.57	0.08	$11_{47}-10_{46}$	38181.17	0.17
$10_{6}-9_{6}$	34563.25	−0.18	$11_{38}-10_{37}$	38601.63	0.09
$10_{56}-9_{55}$	34596.58	−0.03	$11_{110}-10_{19}$	38788.32	−0.18
$10_{37}-9_{36}$	34961.12	0.12	$11_{29}-10_{28}$	39576.26	−0.05
$10_{19}-9_{18}$	35459.90	0.18			

a) $\Delta\nu=\nu_{obsd}-\nu_{calcd}$.

Table 9. Observed and Calculated Rotational (MHz) and Centrifugal Distortion (kHz) Constants and ΔI(uÅ^2) of Monodeuterated Species

	Obsd[a]	Calcd[b]	
		3-H_5-*d*	**4**-H_3-*d*
A	7830.1(8)	7932.89	8089.47
B	1898.11(2)	1903.11	1857.07
C	1548.78(2)	1556.53	1531.39
Δ_J	0.07(6)		
Δ_{JK}	2.21(11)		
ΔI[c]	−4.489(12)	−4.577	−4.598

a) Figures in parentheses indicate the uncertainty attached to the last figures, estimated from 2.5 times the standard deviations. b) The numbering of the hydrogen atoms of structures **3** and **4** is shown in Scheme 1. c) $\Delta I=I_c-I_a-I_b$.

Table 10. r_s Coordinates(Å) of Hydrogen Atom in Methylene Group

		|a|	|b|	|c|
Obsd		0.366(14)	1.817(3)	0.876(6)
Calcd[a]	**3**-H_5	0.185	1.753	0.879
	4-H_3	2.565	0.920	0.879

a) The numbering of the hydrogen atoms of structures **3** and **4** is shown in Scheme 1.

Table 11. Observed Stark Coefficients[a] and Dipole Moments(D)[b] of 1,3-Cyclopentadiene-(**3**) and 1,4-Cyclopentadiene-1-carbonitrile(**4**)

Transition	$\|M\|$	Set I (**3**)		Set II (**4**)	
		Obsd	Calcd	Obsd	Calcd
$3_{03}\leftarrow 2_{02}$	0	−0.360	−0.342	−0.504	−0.505
	1	−0.074	−0.105	—	
	2	0.699	0.605	0.764	0.718
$5_{24}\leftarrow 4_{23}$	0	−0.092	−0.128	—	
	1	1.659	1.692	2.087	2.103
μ_a		4.15(15)	3.87[c]	4.36(25)	4.34[c]
μ_b		0.27(3)	0.06[c]	0.77(10)	0.56[c]
μ_c		0.0[d]	0.0[d]	0.0[d]	0.0[d]
μ_{total}		4.16(17)	3.87[c]	4.42(35)	4.37[c]

a) [MHz/(V/cm)^2]$\times 10^{-4}$. b) Figures in parentheses indicate the uncertainty attached to the last figures, estimated from 2.5 times the standard deviations. c) The dipole moments were calculated from the group moments of cyclopentadiene (0.420 D)[4] and benzonitrile (4.14 D).[10] d) Assumed to be zero by symmetry.

Dipole Moment. The dipole moments in the ground vibrational state were determined from the Stark coefficients of M=0, 1, and 2 in 3(0,3)←2(0,2) and M=0 and 1 in 5(2,4)←4(2,3) transition for **3**, and of M=0 and 1 in 3(0,3)←2(0,2) and M=1 in 5(2,4)←4(2,3) transition for **4**, as shown in Table 11. The electric field strength in the absorption cell was calibrated using the dipole moment of the OCS molecule, 0.71521 D.[9] The c-components of the dipole moments for two isomers were assumed to be zero because of the plane of symmetry. The a-component of the dipole moment of **3** is the same as that of **4** within the limits of error. On the other hand, the b-component of the dipole moment of **3** is much smaller than that of **4**. The a- and b-components of the dipole moments observed for two isomers are consistent with those calculated from the group moments of cyclopentadiene (0.42 D)[4] and benzonitrile (4.14 D),[10] as shown in Table 11. This leads to the conclusion that set I and set II should be assigned to **3** and **4**, respectively. The a-component of the dipole moment observed for **3** is in

good agreement with that reported by Ford and Seitzman.[3]

Vibrationally-Excited State. The spectrum lines of the first excited vibrational state could be easily assigned by their Stark behaviour. The values of ΔI obtained for set I and set II are -7.338 and -7.811 uÅ^2, as listed in Table 5. The absolute values of ΔI are much larger than those in the ground vibrational state. This suggests that the assigned spectrum lines come from the first excited vibrational state of the out-of-plane vibrational mode.[11] The vibrational frequencies of set I and set II (v=1) were found to be 150±50 cm^{-1} and 110±50 cm^{-1}, respectively, from the relative intensity measurement. The vibrational mode may be of ring twisting or of ring bending. However, the lines due to the second excited state could not be found. If the vibrational mode were harmonic, the spectrum lines of the second excited state could be found easily at the frequencies which are predicted from the rotational constants linearly extrapolated to v=2 from v=0 and v=1. But the spectrum lines of this state could not be found at the predicted frequencies. This means that the separation of the vibrational levels for the out-of-plane vibrational mode is not equidistant.

Ratio of Formation for Two Isomers. In order to obtain the ratio of formation for two isomers, the relative intensities were observed directly from the peak intensities at higher Stark voltage, because the a-component of the dipole moment of **3** is the same as that of **4**, within the limits of error. The transitions observed by using the quartz tube of 20 mm i.d. for two isomers are 8(0,8)←7(0,7), 8(2,6)←7(2,5), 9(2,8)←8(2,7), 9(2,7)←8(2,6), 9(1,8)←8(1,7), 10(1,10)←9(1,9), 10(0,10)←9(0,9), and 10(2,8)←9(2,7), because these are not disturbed by other lines. The ratio of **3** to **4** were determined to be 2:1.

Pyrolysis Mechanism. On the possible pyrolysis mechanism of 1H-benzotriazole (**1**), the ring contraction into 6-iminofulvene (**2**) obviously proceeds through a 1,3-biradical via the carbene species,[12,13] and it is reasonable to assume that the new molecules of **3** and **4** shown in scheme 1 are generated according to paths(a) and (b) of the hydrogen atom of the imino group in **2**. The pyrolysis mechanism of path(a) may be explained by using a deuterium atom as tracer. The findings of the monodeuterated species (**3**-H_5-*d*) suggest that the deuterium atom in the ND group of **2** migrates to the position of C_5 according to path (a) to form the molecule of **3**-H_5-*d*.

Recently, Rodler et al.[14] have observed ketenimine (H_2C=C=NH) which has a structure similar to that of **2**, by microwave spectroscopy. Ketenimine, whose lifetime is less than 1 s, turns immediately into acetonitrile (H_3C–C≡N), which is the more stable species. The behaviour of the hydrogen atom in the imino group of **2** is supposed to be quite similar to that in ketenimine. Thus the hydrogen of NH group in 6-iminofulvene (**2**) probably migrates immediately to form 1,3-cyclopentadiene-1-carbonitrile (**3**) or 1,4-cyclopentadiene-1-carbonitrile (**4**).

References

1) W. D. Crow and C. Wentrup, *J. Chem. Soc., Chem. Commun.*, **1968**, 1026; C. Thetaz and C. Wentrup, *J. Am. Chem. Soc.*, **98**, 1258 (1976).

2) C. Wentrup and W. D. Crow, *Tetrahedron*, **26**, 4375 (1970).

3) R. G. Ford and H. A. Seitzman, *J. Mol. Spectrosc.*, **69**, 326 (1978).

4) D. Damiani, L. Ferretti, and E. Gallinella, *Chem. Phys. Lett.*, **37**, 265 (1976); L. H. Scharpen and V. W. Laurie, *J. Chem. Phys.*, **43**, 2765 (1965); V. W. Laurie, *J. Chem. Phys.*, **24**, 635 (1956).

5) P. A. Baron, R. D. Brown, F. R. Burden, P. J. Domaille, and J. E. Kent, *J. Mol. Spectrosc.*, **43**, 401 (1972).

6) R. Pearson, Jr. and F. J. Lovas, *J. Chem. Phys.*, **66**, 4149 (1977).

7) C. C. Costain and J. Yarwood, *J. Chem. Phys.*, **45**, 1961 (1966).

8) J. Kraitchman, *Am. J. Phys.*, **21**, 17 (1953).

9) J. S. Muenter, *J. Chem. Phys.*, **48**, 4544 (1968).

10) B. Bak, D. Christensen, W. B. Dixon, L. Hansen-Nygaard, and J. Rastrup-Andersen, *J. Chem. Phys.*, **37**, 2027 (1962); D. R. Lide, Jr., *J. Chem. Phys.*, **22**, 1577 (1954).

11) D. R. Herschbach and V. W. Laurie, *J. Chem. Phys.*, **40**, 3142 (1964).

12) C. Wentrup and W. D. Crow, *Tetrahedron*, **26**, 3965 (1970).

13) U. E. Wiersun and T. Nieuwenhuis, *Tetrahedron Lett*, **1973**, 2581.

14) M. Rodler, R. D. Brown, P. D. Godfrey, and L. M. Tack, *Chem. Phys. Lett.*, **110**, 447 (1984).

 © 1987 The Chemical Society of Japan Bull. Chem. Soc. Jpn., 60, 3911—3915 (1987)

Crystal Structures of the Configurationally Isomeric Dimers of 4(*e*)-Bromo-8-oxa-6-azabicyclo[3.2.1]octan-7-one

Takashi YAMANE,* Mitsuharu HONDA, Tamaichi ASHIDA, Kazuhiko HASHIMOTO,† and Hiroshi SUMITOMO†

Department of Applied Chemisty, Faculty of Engineering, Nagoya University, Chikusa-ku, Nagoya 464

†Faculty of Agriculture, Nagoya University, Chikusa-ku, Nagoya 464

(Received July 2, 1987)

The crystal structures of the major(Major) and minor(Minor) components of the dimer obtained from the anionic reaction of the racemates of 4(*e*)-bromo-8-oxa-6-azabicyclo[3.2.1]octan-7-one (Br-BOL) have been determined by X-ray method. Crystal data are: (Major) $P2_1/c$, a=10.852(3), b=5.207(3), c=22.146(5) Å, β=92.75(2)°, Z=4, R=0.083 for 1744 reflections; (Minor) $P2_1/c$, a=16.825(5), b=7.844(3), c=11.483(3) Å, β=121.40(2)°, Z=4, R=0.038 for 2026 reflections. The structure of each dimer is constructed of an original Br-BOL skeleton at a terminus and an rearranged bicyclic skeleton at another terminus. The configuration of the chiral C atom contained in the rearranged skeleton of Major is different from that of Minor, when the chirarity of a terminal Br-BOL skeleton in Major is coincided with that in Minor.

A bicyclic epoxy lactam, 8-oxa-6-azabicyclo[3.2.1]-octan-7-one (abbreviated as BOL), is an interesting starting material for new functional polymers with water permeability and ion selectivity.[1-4] The anionic polymerization of BOL in solution leads to a high-molecular-weight polyamide (poly(BOL)) through the N^6–C^7 scission of the amide group.[1,3] The conformation of the optically active poly(BOL) was revealed to be a double-stranded 10_3 helix by the X-ray diffraction method.[5] While the oligomers are obtained in the cationic reaction of BOL, suggesting that the reaction mechanism differs from that of the anionic polymerization.[6] In order to make the reaction mechanism clear the X-ray analysis of the resulting dimer (abbreviated as $(BOL)_2$) was carried out, and supports the mechanism that the cationic oligomerization proceeds through the C^5–N^6 scission of BOL.[7] In $(BOL)_2$ the BOL skeleton is conserved at a terminus and the tetrahydropyran ring occurs by the ring-opening in the second residue.[7]

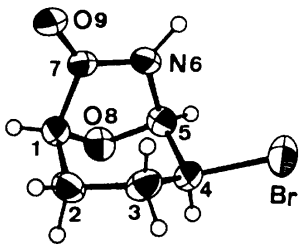

Br-BOL

Recently the 4-bromo-substituted derivative, 4(*e*)-bromo-8-oxa-6-azabicyclo[3.2.1]octan-7-one (abbreviated as Br-BOL), was synthesized in order to obtain an information upon the reactivity of the BOL skeleton.[8] The equatorial location of the Br atom with respect to the 6-membered ring was confirmed by the X-ray analysis of Br-BOL.[9] The anionic reaction of the racemates of Br-BOL forms an oligomer mixture containing mainly the dimer and the trimer.[8] By the IR and NMR studies of the oligomers the original Br-BOL skeleton was assigned at a terminus, though the remaining structure could not be confirmed. Furthermore the dimer was separated into two components, the major and minor component respectively, during the purification. The yielding ratio of the two components is about 6:1. The structural difference between the major and the minor components was conjectured to be a configurational difference of the chiral atom in each component. Therefore in order to determine the molecular structures of the dimers and to elucidate the oligomerization mechanism of Br-BOL, the crystal structure analyses of the dimers were undertaken.

Experimental

The crystals of the major component (abbr. as Major) obtained from an ethyl acetate–chloroform solution were colorless needles, and the crystals of the minor component (abbr. as Minor) grown from an ethyl acetate solution were colorless plates. The density of each component was measured by the flotation method in a 1,2-dibromoethane–CCl_4 solution. The X-ray intensity data were collected on a Rigaku four-circle diffractometer, using graphite monochromated radiation; Cu $K\alpha$(λ=1.5418 Å) for Major and Mo $K\alpha$(λ=0.71073 Å) for Minor. The intensity data were corrected for Lorentz and polarization effects, but the absorption correction was not carried out. Unit cell dimensions were obtained by the least-squares fit using 11 reflections with $55°<2\theta<70°$ for Major and 15 reflections with $20°<2\theta<32°$ for Minor. Crystal data and experimental conditions are shown in Table 1.

Both structures were solved by the heavy atom method. The refinement was carried out by the block-diagonal least-squares method (*HBLS* VI).[10] The function minimized was $\Sigma w(|F_o|-|F_c|)^2$. The weighting scheme adapted was $w=(\sigma^2(F_o)+a|F_o|^2)^{-1}$ for the observed reflections, where σ(F) is the standard deviation based on counting statistics. The isotropic temperature factors of the H atoms are fixed to the equivalent temperature factors(B_{eq})[11] of the corresponding atoms to which they are bound. At final stages of the

Table 1. Crystal Data and Experimental Conditions

	Major	Minor
Chemical formula	$C_{12}H_{15}N_2O_4Br$	$C_{12}H_{15}N_2O_4Br$
Mr	331.17	331.17
Space group	$P2_1/c$	$P2_1/c$
a/Å	10.852(3)	16.825(5)
b/Å	5.207(3)	7.844(3)
c/Å	22.146(5)	11.483(3)
β/°	92.75(2)	121.40(2)
V/Å^3	1249.9(8)	1293.4(8)
Z	4	4
d_{calcd}/g cm^{-3}	1.766	1.701
d_{obsd}/g cm^{-3}	1.71	1.69
μ/cm^{-1}	51.0(Cu $K\alpha$)	33.9(Mo $K\alpha$)
Crystal size/mm	0.5×0.05×0.05	0.5×0.5×0.2
Scan method	ω—2θ	ω—2θ
$\Delta\omega$/°	1.5+0.15 tan θ	2.0+0.35 tan θ
ω scan rate/(°min^{-1})	6—2[a]	3—1.5[a]
Background counting time/s	3—9[b]	4—8[b]
$2\theta_{max}$/°	125	55
No. of reflections		
measured	1983	2984
observed ($\|F_o\| > 3\sigma(F_o)$)	1744	2026

a) The scan rate was varied as a function of 2θ angle. b) The background counting time was changed correlated with the scan rate.

refinement, for Major a=0.017 and for Minor a=0.001 were applied. The final R values were 0.083 (R_w=0.111) for Major, and 0.038 (R_w=0.048) for Minor, respectively. All the scattering factors were taken from the International Tables for X-Ray Crystallography, Vol. IV.[12] The atomic parameters of the non-hydrogen atoms with B_{eq}'s are given in Table 2.[††] All the calculations were carried out on a FACOM M382 at Nagoya University Computation Center.

Results and Discussion

The bond distances and angles of Major and Minor are given in Fig. 1, together with the numbering of atoms. The corresponding bond distances and angles between the two components are in good agreements with each other, except for the N16–C22–C21 angle. The ∠N16–C22–C21 of Minor, 116.2(6)° is significantly larger than that of Major, 109.8(3)°. The fairly short contact of the Br···O28, 3.210(5) Å is observed in Minor. Therefore the widening of the ∠N16–C22–C21 of Minor may be to reduce the steric repulsion between the Br and O28 atoms. The bond distances and angles of the BOL skeleton within the two components are also quite normal when they are compared with those of BOL,[9] Br-BOL,[9] and $(BOL)_2$,[7] with the exception of the N16–C17 distance. The N16–C17 distances of 1.365(5) Å(Major) and 1.36(1) Å(Minor) are slightly longer than those of 1.329(4) Å(BOL[9]), 1.342(6) Å(Br-BOL[9]), and 1.341(5) and 1.330(5) Å($(BOL)_2$[7] in which two molecules are included in an asymmetric unit).

Stereoscopic views of Major and Minor drawn by *ORTEP* II[13] are shown in Fig. 2. At a terminus the original Br-BOL skeleton is conserved in both the

Table 2. Fractional Coordinates (×10^4) and Equivalent Isotropic Temperature Parameters (B_{eq}, ×10), with Their Estimated Standard Deviations in Parentheses

(a) Major

Atom	x	y	z	B_{eq}/Å^2
Br	−82(1)	1383(1)	1582(1)	39(1)
C11	3621(3)	5248(9)	1986(2)	34(2)
C12	3080(4)	4232(9)	2555(2)	35(2)
C13	1966(3)	2531(9)	2387(2)	29(2)
C14	1172(3)	3819(7)	1887(2)	25(1)
C15	1939(3)	4793(7)	1376(2)	23(1)
N16	2819(2)	2887(6)	1175(1)	21(1)
C17	3868(3)	3069(8)	1537(2)	28(2)
O18	2703(3)	6735(5)	1652(1)	34(1)
O19	4798(2)	1803(8)	1504(1)	43(1)
C21	3656(3)	3135(7)	167(2)	23(1)
C22	2829(3)	1632(7)	581(1)	20(1)
N23	1594(2)	1507(6)	302(1)	22(1)
C24	1200(3)	2942(7)	−170(2)	22(1)
C25	2135(3)	4787(7)	−416(2)	26(1)
C26	2890(4)	3341(9)	−870(2)	35(2)
C27	3804(4)	1879(8)	−449(2)	31(2)
O28	3034(2)	5531(5)	44(1)	24(9)
O29	180(2)	2676(5)	−428(1)	28(1)

(b) Minor

Atom	x	y	z	B_{eq}/Å^2
Br	961(1)	6088(1)	4599(1)	36(1)
C11	2020(5)	569(9)	5184(7)	28(2)
C12	972(5)	691(11)	4424(9)	36(3)
C13	652(5)	2550(10)	4022(8)	31(3)
C14	1273(5)	3708(8)	5221(7)	24(2)
C15	2301(4)	3324(8)	5840(6)	20(2)
N16	2578(4)	3067(6)	4835(5)	21(2)
C17	2422(5)	1423(7)	4408(6)	22(2)
O18	2387(3)	1644(6)	6378(5)	26(2)
O19	2564(5)	762(6)	3588(6)	36(2)
C21	2870(5)	5839(8)	3993(7)	22(2)
C22	3231(4)	4116(7)	4677(6)	20(2)
N23	4080(4)	4349(6)	6011(6)	23(2)
C24	4448(4)	5887(8)	6577(7)	23(2)
C25	3912(5)	7406(8)	5723(7)	23(2)
C26	4163(5)	7750(10)	4639(8)	31(3)
C27	3452(6)	6613(10)	3457(7)	32(3)
O28	2946(3)	7011(5)	4992(5)	22(1)
O29	5174(4)	6024(6)	7672(5)	35(2)

[††] The anisotropic thermal parameters of non-hydrogen atoms, the parameters of hydrogen atoms, the equations of best-planes, and the tables of the observed and the calculated structure factors were kept at the Chemical Society of Japan (as Document No. 8766).

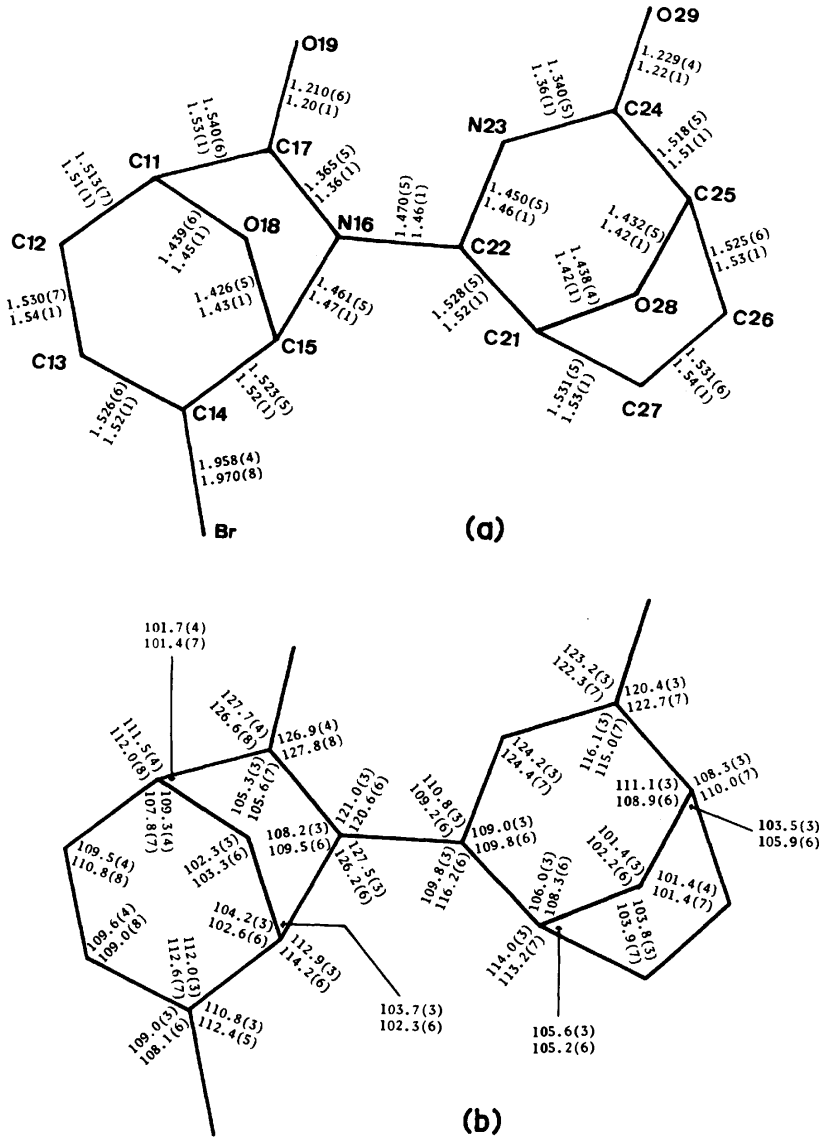

Fig. 1. (a) Bond distances(l/Å) and (b) bond angles(φ/°) for Major(upper) and Minor(lower).

components, as indicated by the spectral data.[8] A ring-opened skeleton was expected at the other terminus as similar to the structure of $(BOL)_2$.[7] The bicyclic skeleton (rearranged skeleton), however, is also kept at the other terminus in Major and Minor, though the skeletal rearrangement occurs via a transfer reaction. This may be a main reason why the structure of the oligomer could not be confirmed by the spectral data. A conformational difference around the N16–C22 bond is clearly observed between Major and Minor. For the molecules having the Br-BOL skeleton of the same configuration in Fig. 2, the torsion angles of C15–N16–C22–C21 and C15–N16–C22–N23 are 93.1(4) and −27.4(5)° for Major, and −75.5(9) and 49.4(9)° for Minor. BOL contains two asymmetric C atoms, C1 and C5, respectively. Each structure of the Br-BOL skeleton drawn in Fig. 2 is an enantiomer with C1 S and C5 R. The two components are, furthermore, essentially different in the configuration of the C25 atom contained in the rearranged skeleton, where the C25 atom corresponds to C1 in BOL. The configurations of the C11 (correspond to C1) and C25 atoms are the same in Major, and those are different in Minor. Thus it is shown that the oligomerization of Br-BOL prefers between the molecules with the same configuration of the BOL skeleton to between the molecules with the different configuration, taking the yielding ratio of the major and minor components into consideration. Therefore the configuration of the C1 and the corresponding C atoms in the trimer of Br-BOL was expected to be the same, and the expectation was confirmed by the structure analysis of the trimer.[14] A following mechanism for the oligomeric reaction is

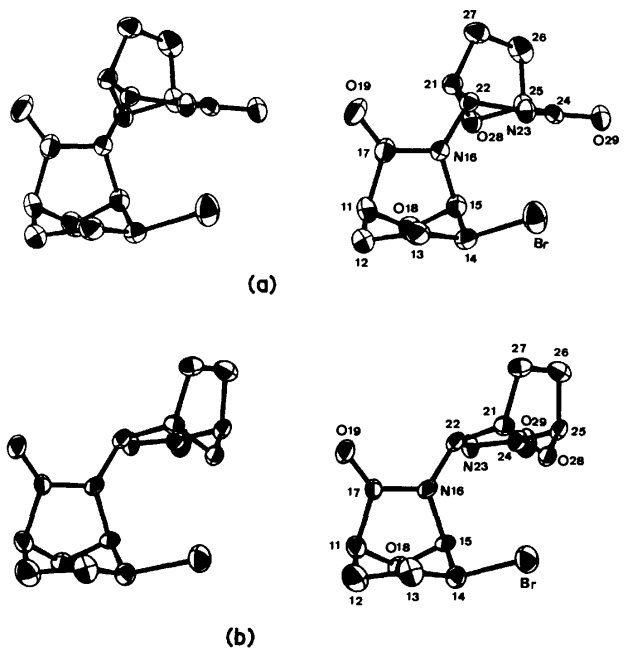

Fig. 2. Stereodrawings of (a) Major and (b) Minor. Atoms are drawn with 50% probability thermal ellipsoids. Both Br-BOL skeletons have the same configuration.

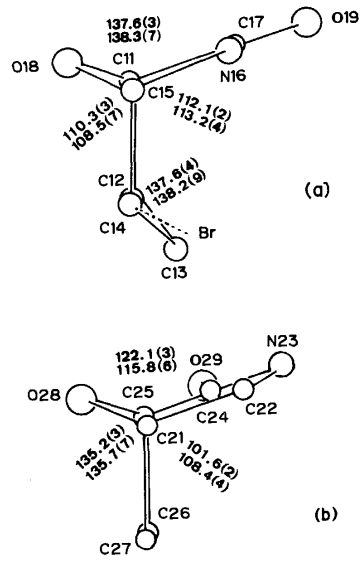

Fig. 3. Selected diheddral angles(φ/°) among the best-planes. Definitions are: (a) Br-BOL skeleton, plane I C11, C15, N16, C17, O19; plane II C11, C15 O18; plane III C11, C12, C14, C15; plane IV C12 C13, C14, (b) rearranged skeleton, plane V C22, N23, C24, C25, O29; plane VI C21, C25, O28; plane VII C21, C25, C26, C27. Major upper and Minor lower.

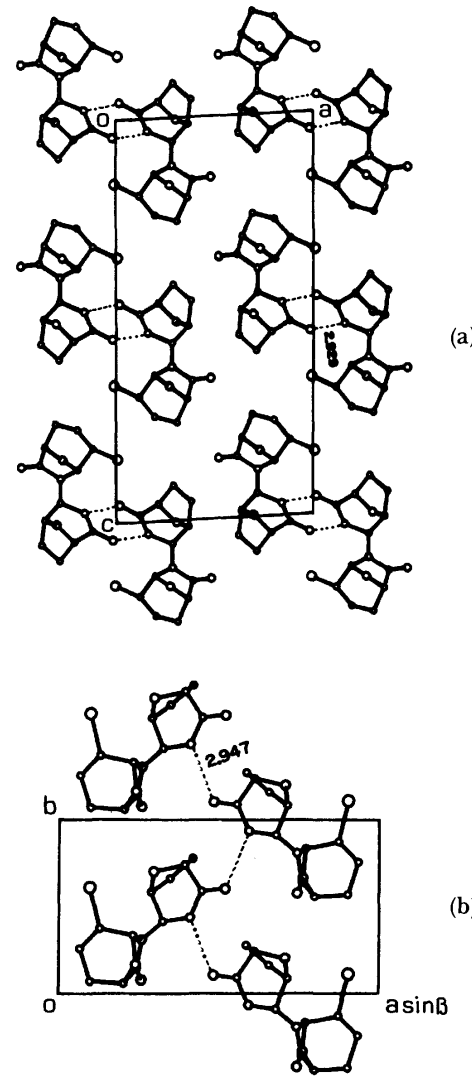

Fig. 4. Crystal Structures of (a) Major projected along the b axis, and (b) Minor projected along the c axis(Molecules on the equvalent positions (x, y, z) and ($-x$, 1/2+y, 1/2−z) only are drawn for clarity). Hydrogen bonds are shown with broken lines, and the distances are given in Å unit.

suggested; (i) The N6 atom of the amide group of a Br-BOL moiety at a terminus attacks at first the C5 atom of another Br-BOL molecule, (ii) the scission of the C5–O8 bond of the attacked part occurs, leading to the collapse of the bicyclic skeleton, (iii) the O8 atom approaches the C4 to which the Br bonds, and (iv) the formation of the C4–O8 bond generates the rearranged bicyclic skeleton, together with the elimination of the Br atom.

The dimer consists of seven planes: (a) BOL skeleton, plane I defined by C11, C15, N16, C17, and O19; plane II C11, C15, and O18; plane III C11, C12, C14, and C15; plane IV C12, C13, and C14, (b) rearranged skeleton, plane V C22, N23, C24, C25, and O29; plane VI C21, C25, and O28; plane VII C21, C25, C26, and C27. The C21 atom deviates by 0.38 Å in Major, and by 0.13 Å in Minor, from the plane V. The selected dihedral angles among the planes are given in Fig. 3. The dihedral angles in the BOL skeleton show good agreements with those found in the other

BOL skeleton.[7,9] The dihedral angles are, however, significantly different between the planes V and VI and between the planes V and VII, as compared with those in Major and Minor. This may reflect the configurational difference of the C25 atoms of Major and Minor.

The packing schemes of molecules in Major and Minor are shown in Figs. 4(a) and (b), respectively. The hydrogen bond of 2.929(4) Å occurs between N23 and O29$^{(i)}$ in Major, and that of 2.947(9) Å occurs between N23 and O29$^{(ii)}$ in Minor. [Symmetry code: (*i*) $(-x,-y,-z)$, (*ii*) $(1-x,-1/2+y,3/2-z)$] The H···O and ∠N-H···O are 2.29(5) Å and 160(6)° for Major, and 2.21(11) Å and 163(11)° for Minor. In Major a dimer structure is formed by hydrogen bonds related with an inversion center. On the other hand molecules are linked by hydrogen bonds around a two-fold screw axis, giving rise to infinite helical chains extended along the b axis in Minor.

References

1) H. Sumitomo and K. Hashimoto, *Macromolecules*, **10**, 1327 (1977).

2) K. Hashimoto and H. Sumitomo, *Macromolecules*, **13**, 786 (1980).

3) K. Hashimoto and H. Sumitomo, *J. Polym. Sci., Polym. Chem. Ed.*, **21**, 397 (1983).

4) H. Sumitomo and K. Hashimoto, "Contempory Topics in Polymer Sciences" Vol. 4, ed by W. J. Bailey and T. Tsuruta, Plenum Publishing (1984), p. 779.

5) Z. Zheng, T. Yamane, T. Ashida, K. Hashimoto, and H. Sumitomo, *Polym. J.*, **18**, 973 (1986).

6) K. Hashimoto and H. Sumitomo, *J. Polym. Sci., Polym. Chem. Ed.*, **22**, 1733 (1984).

7) T. Yamane, H. Nanayama, T. Ashida, K. Hashimoto, and H. Sumitomo, *Bull. Chem. Soc. Jpn.*, **58**, 2304 (1985).

8) K. Hashimoto, H. Sumitomo, and M. Suzuki, *Chem. Lett.*, **1986**, 767.

9) Y. Gu, T. Yamane, T. Ashida, K. Hashimoto and H. Sumitomo, *Bull. Chem. Soc. Jpn.*, **59**, 2085 (1986).

10) T. Ashida, "*UNICS-NAGOYA*," Nagoya University, Nagoya, Japan, 65 (1981).

11) W. C. Hamilton, *Acta Crystallogr.*, **12**, 609 (1959).

12) "International Tables for X-Ray Crystallography," Kynoch Press, Birmingham, England (1974), Vol. IV, p. 71.

13) C. K. Johnson, "*ORTEP* II," *Report ORNL*-5138, Oak Ridge National Laboratory, Tennessee, USA (1976).

14) T. Yamane, M. Honda, T. Ashida, K. Hashimoto, and H. Sumitomo, *Acta Crystallogr.*, to be published.

Orientation-Dependent ^{1}H and ^{13}C Isotropic Shifts of Low-Spin Tetracyano(1,2-diamine)ferrates(III)

Yoshitaka KURODA, Masafumi GOTO,* and Tomoya SAKAI
Faculty of Pharmaceutical Sciences, Nagoya City University, Mizuho-ku, Nagoya 467
(Received February 5, 1987)

Paramagnetic ^{1}H and ^{13}C NMR signals of low-spin tetracyanodiamineferrates(III), $[Fe^{III}(CN)_4(diamine)]^-$, containing ethylenediamine, (*R*)-1,2-propanediamine, (1*R*,2*R*)-*trans*-cyclohexanediamine, and *N*,*N*′-dimethylethylenediamine, were assigned by the use of rapid electron exchange between the Fe^{III} complex and the diamagnetic Fe^{II} complex with an identical set of ligands. The C–H on the five-membered chelate ring showed isotropic shifts with different signs depending on their orientations: 14—18 ppm downfield and ca. 16—23 ppm upfield for axial and equatorial protons respectively. The isotropic shifts for the ^{13}C nuclei were attenuated, their signs alternating with each separation by one carbon–carbon bond from the metal ion. The isotropic shift is compared with that of the Ni^{II} complex qualitatively in terms of the dipolar and Fermi contact shifts.

The paramagnetic NMR spectra of Fe^{III} complexes are widely used to assign their spin states and stereochemistry for rather complex molecules, such as those with porphyrins[1] and heme proteins.[2-4] There have, however, been few studies on the paramagnetic NMR spectroscopy for the Fe^{III} complexes with simple structures. The analysis of the simple Fe^{III} complexes will provide some insights into the mechanism of the paramagnetic shift.

The Fe^{III} complexes, tetracyano(diamine)ferrates(III) $[Fe^{III}(CN)_4(diamine)]^-$,[5-8] are low spin,[7,8] and their structures are so simple that all the paramagnetic signals can be identified.

The stereochemistry of the five-membered chelate rings formed with various diamines has been investigated by means of a wide range of experimental methods.[9] The present Fe^{III} complexes offer a good opportunity to study their NMR spectra because: 1) They are kinetically inert, and so there is no need to consider complex formation equilibrium; 2) the corresponding Fe^{II} complexes, tetracyano(diamine)ferrates(II) are diamagnetic, and their NMR spectra have been analyzed by conventional methods; 3) the rapid electron exchange between low-spin Fe^{II} and Fe^{III} complexes affords the time-averaged spectra of each complex, depending on the compositions for mixtures of them, and 4) the stereochemistry of the five-membered chelate rings formed with 1,2-diamines has been extensively studied, and so the existing information about them can be utilized for reference.

Reports on the paramagnetic NMR spectra of transition metal complexes with saturated ligands such as 1,2-diamines are relatively few in number. Ni^{II} complexes with diamines have been reported by Reilley and his colleagues,[10,11] while Ni^{II} and Co^{II} complexes with monoamines have been reported by Morishima et al.[12] The former studies have revealed the usefulness of paramagnetic NMR for the analysis of the structures of metal complexes in solution and their dynamics. The latter treated the origin of the paramagnetic shift and the orientation-dependence of spin propagation by considering spin-polarization and direct-spin-delocalization mechanisms. However, the NMR signals of the Ni^{II} complexes are relatively broad, and there is a problem that the chemical species responsible for NMR is really a mixture formed by an equilibrium among several species.

We have now investigated the paramagnetic NMR of these Fe^{III} complexes in order to elucidate the mechanism of the paramagnetic shift. In this paper, the assignments of all the C–H of some 1,2-diamines coordinated to the Fe^{III} center and a qualitative conclusion about the use of the isotropic shift for the analysis of the stereochemistry of chelate rings will be described.

Experimental

Materials. Sodium tetracyano(diamine)ferrates(III), and their corresponding Fe^{II} complexes were isolated according to the methods reported previously, using ethylenediamine (en),[5,13] (*R*)-1,2-propanediamine(*R*-pn),[6,7] (1*R*,2*R*)-*trans*-cyclohexanediamine(*R*-chxn),[6,7] and *N*,*N*′-dimethylethylenediamine(s-Me_2en)[5,13] as diamines.

^{1}H and ^{13}C NMR Measurements. A weighed sample (40—50 mg) in a sample tube 5 mm in diameter was dissolved in pD 2.0 DCl–D_2O (0.3 cm^3) to prevent a disproportionation reaction with concomitant diamine dehydrogenation[14] in a neutral or basic aqueous solution, from occurring. Sodium 3-trimethylsilylpropionate-2,2,3,3-d_4 (TSP; 0.00 ppm) and 1,4-dioxane (67.44 ppm) were used as the internal stadards for the ^{1}H and ^{13}C NMR measurements respectively. The chemical shift, δ, is positive for a downfield shift from the standards. The spectra were recorded with JEOL MH-100 and FX-100 spectrometers.

The ^{1}H and ^{13}C NMR spectra of the Fe^{II} complexes were measured in a manner similar to that described above except that D_2O was used as the solvent.

Changes in Chemical Shift by the Variation in the Mixing Ratio of the Fe^{III} and the Corresponding Fe^{II} Complexes (Variation Experiment). In a 5 cm^3 flask, ca. 300 mg (10^{-3} mol) of the Fe^{II} complex was dissolved in pD 2.0 DCl–D_2O containing 0.4% sodium 2,2-dimethyl-2-silapentane-5-sulfonate (DSS; 0.00 ppm) and 1,4-dioxane. Weighed amounts of the corresponding Fe^{III} complex were mixed

with this solution (0.5 cm^3) to make mixtures in various compositions. The ^1H and ^{13}C NMR spectra were measured at 300 K with JEOL MH-100 and FX-100 spectrometers.

Direct Preparation of the Sample Solution of the Fe^{III} s-Me_2en Complex. The isolated Fe^{II} s-Me_2en complex (50.2 mg) was dissolved in 0.5 cm^3 of D_2O. After standing at room temperature for more than 5 min, the solution was acidified by the addition of 45.1 mg of 37% DCl; $Na_2S_2O_8$ (104.0 mg) was then added at 0 °C. The mixture was allowed to stand at 0 °C for 2 h, and the resulting solution was used for the ^1H NMR measurement.

Results and Discussion

^1H and ^{13}C NMR Spectra of Fe^{III} Complexes and Assignments of Their Signals. Tetracyano(1,2-diamine)ferrate(III) and tetracyano(1,2-diamine)ferrate(II) complexes are both low-spin;[7,8] their electronic configurations are $(t_{2g})^5$ and $(t_{2g})^6$. The large variation in the chemical shifts and the diminution of the ^1H-^1H couplings precludes the assignments of the paramagnetic NMR signals by conventional methods. Since no previous examples of this class of Fe^{III} complex are known, we could not use any previously reported information about the chemical shift. The signals have been assigned by the use of the rapid electron exchange between the pair of low-spin Fe^{II} and Fe^{III} complexes (variation experiment). At first, the signals of the Fe^{II} complexes were assigned by conventional methods. Then the signals of the Fe^{III} complexes were correlated with those of the Fe^{II} complexes on the basis of the spectral changes induced by the variation in the ratio of the Fe^{III} complexes to the corresponding Fe^{II} complexes.

The values of the chemical shifts, δ, for the Fe^{III} and Fe^{II} complexes described below are summarized in Table 1. The numbering of the nuclei for each complex is denoted in Fig. 1 and is used throughout this paper.

(*R*)-1,2-Propanediamine Complex. The *R*-pn chelates are well known to have λ *gauche* conformations in the solid state,[15-18] in which the methyl groups are equatorial to the chelate ring. The conformations in solution have been investigated by means of ^1H NMR spectroscopy.[19-22] For example, the *R*-pn chelate ring of $[Co^{III}(CN)_4(R\text{-pn})]^-$ is predominantly in a λ *gauche* form in solution.[20,21] The ^1H NMR spectrum of $[Fe^{II}(CN)_4(R\text{-pn})]^{2-}$, has been shown to be similar to that of this Co^{III} complex.[6]

Figure 2 shows the ^1H NMR spectrum of $[Fe^{III}(CN)_4(R\text{-pn})]^-$. Three signals were observed — at 17.40, 9.31, and −20.05 ppm — with an area ratio of 2:3:1. The signal at 9.31 ppm was assigned to the methyl protons because of its area ratio. Because of an unpaired electron, the signals are distributed over the wide range of ca. 37 ppm.

Figure 3 shows the ^1H NMR spectra of the mixtures of Fe^{II} and Fe^{III} complexes obtained by varying the mole fraction of the latter, *f*, at 300 K. The spectrum

Table 1. ^1H and ^{13}C NMR Chemical Shifts[a] of $[Fe^{II,III}(CN)_4(diamine)]^{2-,-}$

Diamine	Nucleus	Chemical shift/ppm Fe^{II}	Chemical shift/ppm Fe^{III}	Isotropic shift/ppm	Contact shift of Ni^{II}/ppm[b]
en	H	2.50	−0.91	−3.41	93.8
	C	45.2	251.6	206.4	−328
R-pn	H^{1a}	2.74	17.40	14.66	21.0
	H^{2a}	2.16	17.40	15.24	21.0
	H^{2e}	2.61	−20.05	−22.66	148.3
	H^3	1.22	9.31	8.09	18.0
	C^1	52.7	241.5	188.8	−330
	C^2	50.9	248.0	197.1	−282
	C^3	19.6	−49.2	−68.8	471
R-chxn	H^{1a}	2.04	15.98	13.94	
	H^{2a}	1.16	10.86	9.70	
	H^{2e}	2.04	10.86	8.82	
	H^{3a}	1.16	6.61	5.45	
	H^{3e}	1.65	1.49	−0.16	
	C^1	60.6	258.3	197.7	
	C^2	35.6	−18.9	−54.5	
	C^3	25.3	30.0	4.7	
s-Me_2en	H^a	2.12	19.84	17.72	40.0[c]
	H^e	2.78	−12.84	−15.62	156.3[c]
	H^2	2.52	−17.59	−20.11	133.8[c]
	C^1	54.2	301.1	246.9	
	C^2	41.8	156.1	114.3	

a) The positive values indicate downfield shifts. b) Refs. 19 and 28. c) Racemic form.

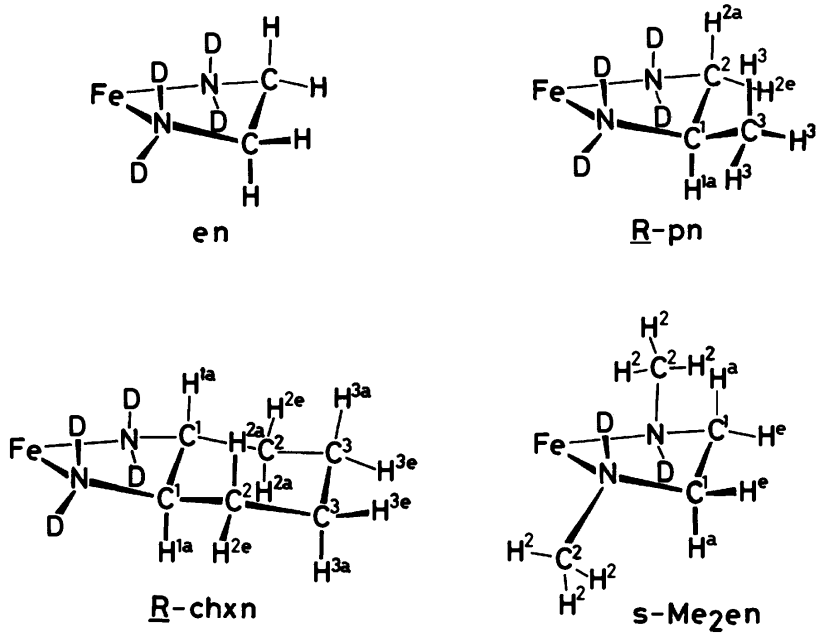

Fig. 1. Schematic structures of the chelates and the numbering of protons and carbons. Fe=Fe(CN)$_4$

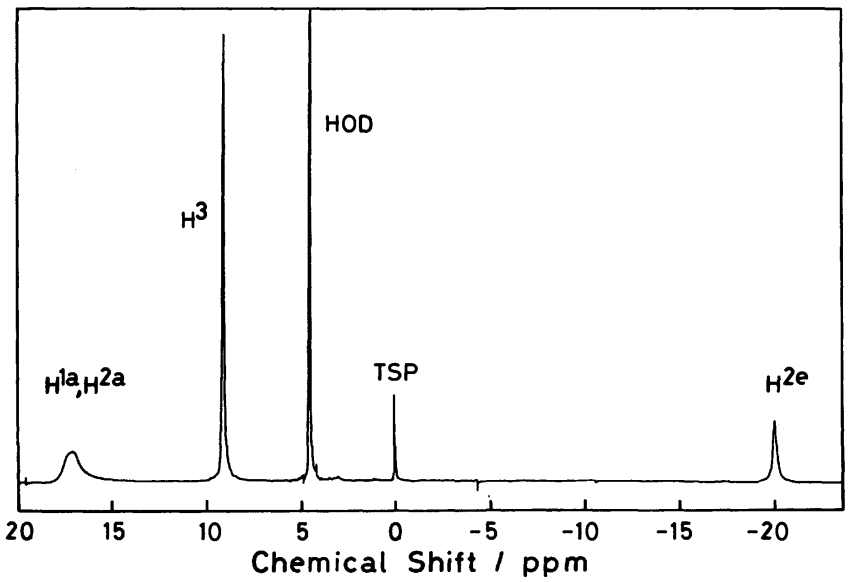

Fig. 2. ^{1}H NMR spectrum of $[Fe(CN)_4(R\text{-pn})]^-$ in 10^{-2} mol dm^{-3} DCl.

shown at the top is that of $[Fe^{II}(CN)_4(R\text{-pn})]^{2-}$; the signals at 2.74, 2.61, 2.16, and 1.22 ppm have been assigned to H^{1a}, H^{2e}, H^{2a}, and H^3 respectively.[6] When small amounts of the Fe^{III} complex were added to the Fe^{II} complex, the ^{1}H NMR spectra changed in shape depending on f: The signal of H^{2e} shifted to an upper field, but the other proton signals shifted downfield. The ^{1}H-^{1}H couplings ($^{3}J_{HCCH}$) could be observed in the region of small f values: the apparent doublet and triplet of H^{2e} and H^{2a} were observed clearly until f reached 0.055.

The δ values vary in proportion to f, as is shown in Fig. 4. This linear relationship shows that the signals for the mixtures are averaged by the rapid electron exchange between the Fe^{II} and Fe^{III} complexes.[23-25] The rate is in the region of fast-limit on the NMR time scale. By the extrapolation of f to 1.0, the Fe^{III} complex signals are assigned as listed in Table 1.

The ^{13}C NMR spectra of both $[Fe^{II}(CN)_4(R\text{-pn})]^{2-}$ and $[Fe^{III}(CN)_4(R\text{-pn})]^-$ showed three signals coupled with adjacent protons in off-resonance measurements. The signals at 241.5, 248.0, and −49.2 ppm for the Fe^{III} complex and those at 52.7, 50.9, and 19.6 ppm for the Fe^{II} complex are assigned to C^1, C^2, and C^3

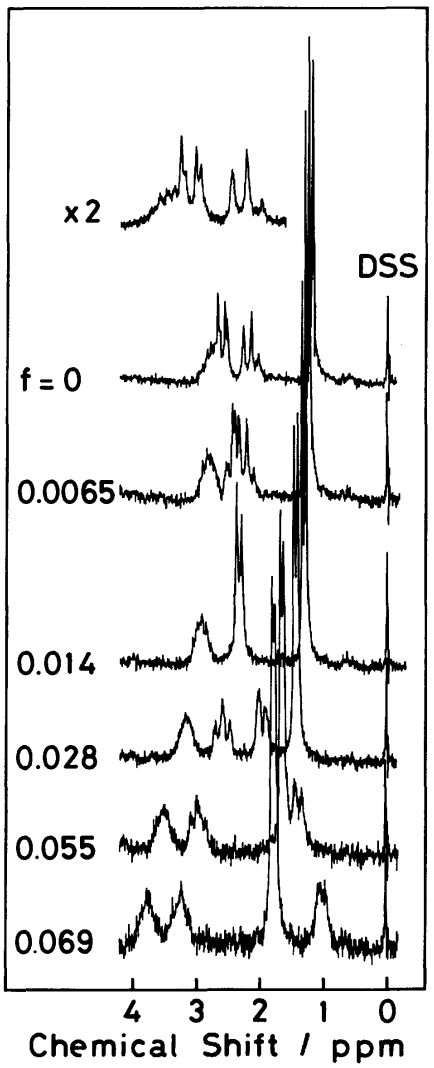

Fig. 3. ^{1}H NMR spectral changes of $[Fe(CN)_4(R\text{-pn})]^{2-}$ on addition of $[Fe(CN)_4(R\text{-pn})]^-$ in 10^{-2} mol dm^{-3} DCl. *f*: Mole fraction of the Fe^{III} chelate.

respectively.

Ethylenediamine Complex. As is shown in Table 1, only one signal is observed for each of the Fe^{III} and Fe^{II} complexes. The methylene proton signals appeared at 2.50 and −0.91 ppm for the Fe^{II} and Fe^{III} complexes respectively. Each value is in good agreement with the mean of the δ's for H^{2a} and H^{2e} of the *R*-pn chelate: 2.39 and −1.33 ppm for the Fe^{II} and Fe^{III} complexes respectively. This agreement indicates that the axial and equatorial methylene protons are averaged by the rapid interconversion of the chelate ring between δ and λ conformations.[11,19]

(1*R*,2*R*)-*trans*-Cyclohexanediamine Complex. The Fe^{II} complex, $[Fe(CN)_4(R\text{-chxn})]^{2-}$, shows three ^{13}C signals in the usual region: C^1, 60.6; C^2, 35.6; C^3, 25.3 ppm. This assignment is based on the multiplicity in the off-resonance experiment (a doublet, a triplet, and a triplet) and the electron withdrawing effect of the amino groups.

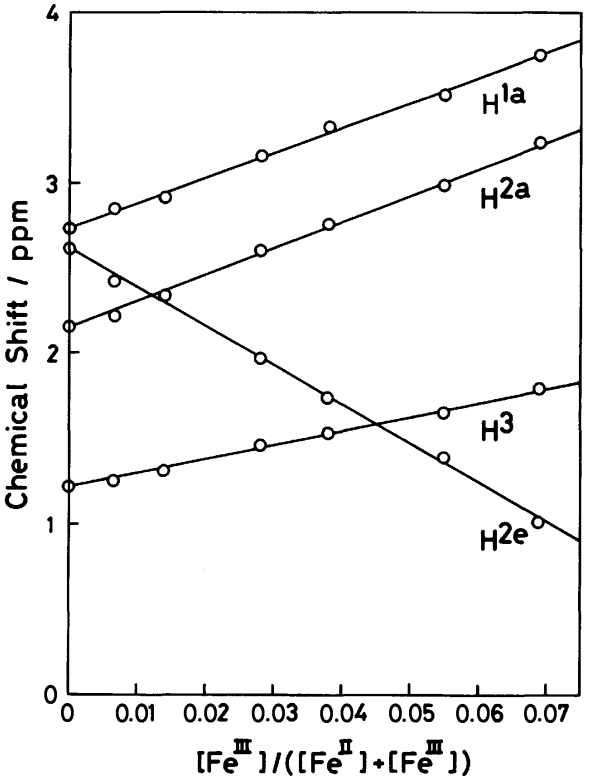

Fig. 4. Plots of chemical shifts of ^{1}H resonances of the mixture of $[Fe(CN)_4(R\text{-pn})]^{2-}$ and $[Fe(CN)_4(R\text{-pn})]^-$ vs. mole fractions of the Fe^{III} chelate.

The ^{13}C NMR spectrum of the corresponding Fe^{III} complex, shown in Fig. 5A, exhibited three signals — at 258.3, −18.9, and 30.0 ppm. These signals were correlated to those of the Fe^{II} complex as follows by means of the variation experiments: 258.3→60.6; −18.9→35.6; 30.0→25.3 ppm. They were thus assigned to C^1, C^2, and C^3 respectively.

The ^{1}H NMR spectrum of the Fe^{II} complex, shown at the top of Fig. 6, exhibited only three peaks — at 2.04, 1.65, and 1.16 ppm, with an area ratio of 2:1:2. These peaks have previously been assigned to a composite of H^{1a} and H^{2e}, H^{3e}, and a composite of H^{2a} and H^{3a} respectively.[6]

The Fe^{III} complex showed four ^{1}H NMR signals, with an area ratio of 1:2:1:1, at 15.98, 10.86, 6.61, and 1.49 ppm. These signals were correlated to those of the Fe^{II} complex by means of the variation experiments (Fig. 6). The results of the signal correlation are shown in Fig. 7.

The ^{1}H signals of the Fe^{III} complex were assigned in the following way. The signal at 1.49 ppm was correlated to the signal at 1.65 ppm attributable to H^{3e} for the Fe^{II} complex, and so it was assigned to H^{3e}. The ^{1}H selective irradiation at 6.61 or 1.49 ppm changed the Fe^{III} C^3 signal from a double-doublet (Fig. 5B) to a doublet, as is shown in Figs. 5C and D. Thus, the signal at 6.61 ppm was assigned to H^{3a}. Since the H^{1a} and H^{2a} in the Fe^{III} *R*-pn complex

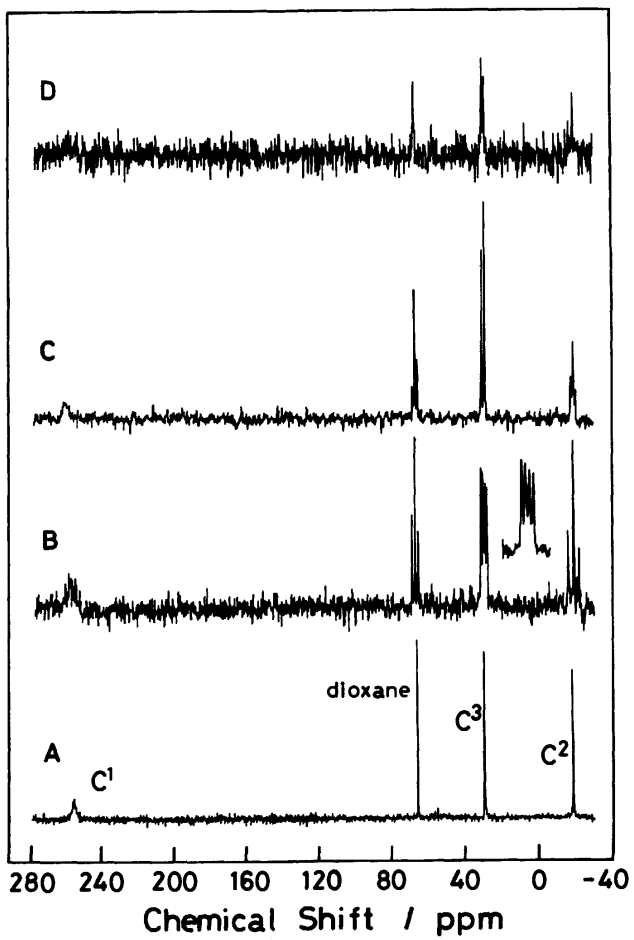

Fig. 5. ^{13}C NMR spectra of $[Fe(CN)_4(R\text{-chxn})]^-$. A. complete decoupling for ^{1}H; B. off-resonance for ^{1}H; C and D. selective irradiation at H^{3a} and H^{3e}.

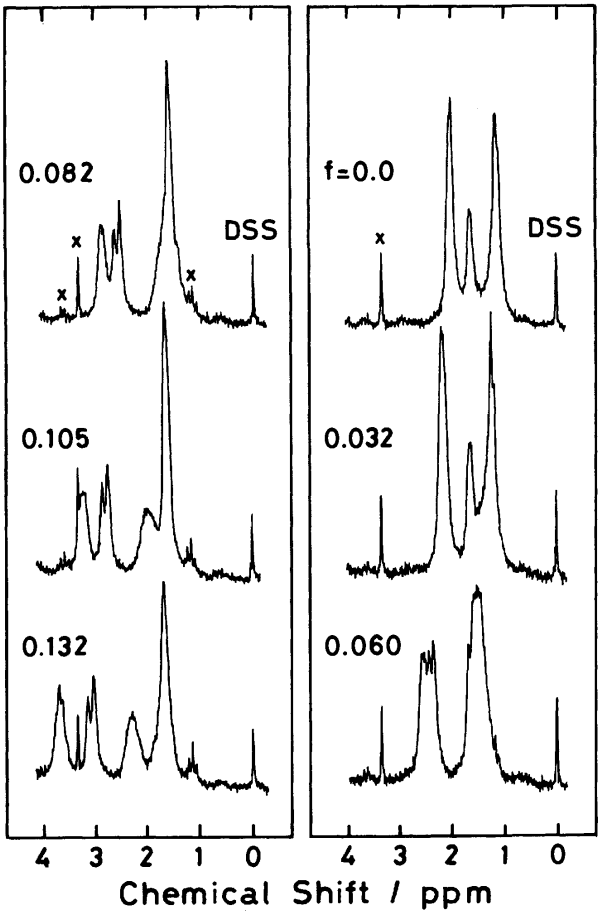

Fig. 6. ^{1}H NMR spectral changes of $[Fe(CN)_4(R\text{-chxn})]^{2-}$ on addition of $[Fe(CN)_4(R\text{-chxn})]^-$ in 10^{-2} mol dm^{-3} DCl. f: Mole fraction of the Fe^{III} chelate. X indicates signals due to methyl and ethyl alcohols.

resonated at the most downfield position, the signal at 15.98 ppm was assigned to H^{1a}. The remaining peak at 10.86 ppm corresponds to the two peaks at 1.16 and 2.04 ppm for the Fe^{II} complex and consists of H^{2a} and H^{2e} signals, with, incidentally, the same chemical shift.

***N,N'*-Dimethylethylenediamine Complex.** The s-Me_2en complex is able to adopt two kinds of geometrical isomers on coordination to a metal ion. A pair of the racemic form with two pseudoequatorial methyl groups is known to be more stable than the meso form with a pseudoaxial and a pseudoequatorial methyl group.[11,19]

The isolated $[Fe^{III}(CN)_4(s\text{-}Me_2en)]^-$ showed three ^{1}H NMR signals — at 19.84, −12.84, and −17.59 ppm with an area ratio of 1:1:3. The last signal was assigned to the methyl protons, H^2, on the basis of the area ratio. Since the Fe^{III} R-pn complex showed H^{2a} and H^{2e} signals at 17.40 and −20.05 ppm, the former two signals of the Fe^{III} s-Me_2en complex were assigned to H^a and H^e respectively. The separation of the H^a and H^e shifts by ca. 33 ppm shows that the Fe^{III} complex is the racemic form. The ^{13}C NMR spectrum

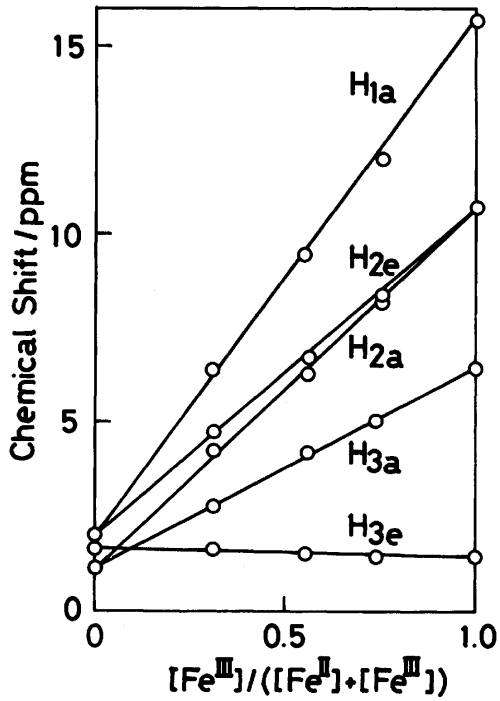

Fig. 7. Plots of chemical shifts of the mixture of $[Fe(CN)_4(R\text{-chxn})]^{2-}$ and $[Fe(CN)_4(R\text{-chxn})]^-$ vs. mole fraction of the Fe^{III} chelate.

of the Fe^{III} complex showed the methyl(C^2) and methylene(C^1) carbon signals at 156.1 and 301.1 ppm respectively.

The isolated Fe^{II} s-Me_2en complex showed the methyl signal at 2.52 ppm as a singlet and the methylene signals as an A_2B_2 multiplet, the apparent doublets of which at 2.12 and 2.78 ppm were assigned to H^a and H^e respectively, according to the results of Tiethof and Cooke.[26] However, the ^{13}C NMR spectrum of the isolated Fe^{II} complex exhibited two signals for the methylene carbon — at 54.2 and 52.8 ppm, with an intensity ratio of ca. 2:1, along with a single methyl signal at 41.8 ppm.[13] The cobalt complex isostructural to the Fe^{II} complex, $[Co^{III}(CN)_4$(s-Me_2en)]$^-$, also exhibited two methylene-carbon signals in a ratio of ca. 2:1.[27]

The results presented above suggest that the isolated Fe^{II} complex contained the racemic and meso isomers, while the isolated Fe^{III} complex consisted of only the racemic isomer. Since the meso isomer of the Fe^{III} complex was expected to have been eliminated during the procedures for isolation, the Fe^{II} complex was oxidized under acidic conditions and the resulting mixture was employed for NMR measurement without undertaking any procedure for separation. The two methylene and one methyl ^1H signals expected for the meso Fe^{III} complex were found at 6.40, 0.36, and −16.75 ppm, with an intensity ratio of 1:1:3, in addition to those for the racemic form. The chemical-shift difference of ca. 6 ppm between the two methylene singals is quite small compared with that of ca. 33 ppm for the racemic form. The s-Me_2en chelate in the meso isomer exists as an equilibrium mixture of the δ and λ forms shown in Fig. 8. Although the four methylene protons in each form are in a different magnetic environment because of the two unsymmetrical methyl groups, the conformational interconversion of the chelate ring between the two forms magnetically replace H^{1a} and H^{1e} with H^{2e} and H^{2a} respectively. Since the interconversion is very rapid in the NMR time scale at room temperature, each couple of the protons shows a mean signal. However, the difference in the chemical shift between the two mean signals can be expected to be much smaller than that for the racemic isomer, firstly because each mean signal is the average of an axial and an equatorial proton signal, and secondly because the difference in chemical shift between them arises only from the difference in position relative to the two methyl groups. Thus, the observation of the two mean signals of the methylene protons with a small separation from each other confirms the assignment of these signals to the meso isomer. The population of these isomers was obtained as racemic:meso=1.7:1 based on the signal intensities. Since the intensity ratio observed for the ^{13}C NMR spectrum of the isolated Fe^{II} complex is almost the same as this population, the signals at 54.2 and 52.8 ppm were assigned to the methylene carbon of the racemic and meso isomers respectively.

The variation experiment using the isolated Fe^{II} and Fe^{III} complexes showed the two sets of methylene and methyl signals. The intensity ratio between them was ca. 2:1. However, the changes in chemical shift observed in the variation experiment were not proportional to the mole fraction of the Fe^{III} complex, for there are electron exchange reactions among the racemic Fe^{II}, meso Fe^{II}, racemic Fe^{III}, and meso Fe^{III} complexes. The major and minor sets of signals, however, were correlated to the signals of the racemic and meso Fe^{III} complexes respectively. The analysis of this system will be described elsewhere.

The following arguments will be restricted to the racemic form.

Isotropic Shifts of the Fe^{III} Complexes and Comparison with Those of Ni^{II} Complexes. Isotropic shift for the Fe^{III} complex, δ^{iso}, is defined as the difference in chemical shift between the Fe^{III} and the corresponding Fe^{II} complexes: $\delta^{iso}=\delta_{Fe^{III}}-\delta_{Fe^{II}}$. The isotropic shifts are summarized in the third column of Table 1. The isotropic shifts of several $[Ni^{II}(H_2O)_{6-2x}$(diamine)$_x]^{2+}$,[19,28] defined as $\delta^{iso}=\delta_{Ni^{II}}-\delta_{free\ amine}$, are also incorporated in Table 1 for the sake of comparison.

The isotropic shift is the sum of two contributions: the Fermi contact shift (δ^{con}) and the dipolar shift (δ^{dip}). Since the distribution of the two unpaired spins in the $t_{2g}^6e_g^2$ configuration is spherical, δ^{dip} has been regarded as near zero for Ni^{II} complexes. Thus, the δ^{iso}'s for Ni^{II} complexes have been regarded as δ^{con}'s.[29]

A low-spin Fe^{III} complex has, on the other hand, a large magnetic anisotropy, and both terms contribute

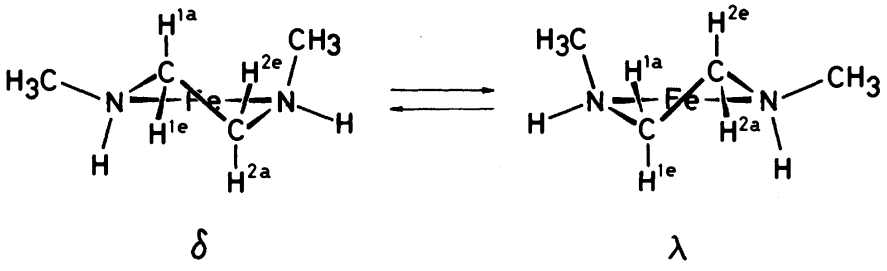

Fig. 8. Schematic structures of the meso s-Me_2en chelate. Fe=Fe(CN)$_4$

to δ^{iso}. If the δ^{iso} for the Fe^{III} complex arises from the Fermi contact interaction, the difference in spin transfer mechanism between low-spin Fe^{III} (L→vacant e_g) and Ni^{II} (L→singly occupied e_g) predicts that the sign of δ^{iso} for Fe^{III} is the opposite of that of Ni^{II}.[30] The observed sign of δ^{iso} is not, however, always opposite to that of the Ni^{II} complex, as represented by protons axial to the chelate ring. This confirms that both contributions operate in the Fe^{III} complexes. Qualitatively, however, the δ^{con} for Fe^{III} complex can reasonably be assumed to have the sign opposite to that of the Ni^{II} complex, but the magnitude is not necessarily the same.

Location Dependence of ^{13}C Isotropic Shifts. Carbon atoms bonded to the nitrogen have large positive δ^{iso}'s: 190—250 ppm for members of the chelate ring and 114 ppm for *N*-methyl carbon. The carbon atoms separated by one C–C bond from them, such as C^2 in *R*-chxn and C^3 in *R*-pn, have the smaller negative δ^{iso}'s of −54.5 and −68.8 ppm. The third carbon atom in *R*-chxn, C^3, has, in turn, the small positive δ^{iso} value of 4.7 ppm. ^{13}C δ^{iso} thus alternates in sign with each separation by one C–C bond and attenuates repidly as the number of bonds between the carbon and the Fe^{III} ion increases. This characteristic of ^{13}C δ^{iso} suggests that the Fermi contact shift, δ^{con}, predominates in ^{13}C δ^{iso} for the present Fe^{III} complexes; i.e., the unpaired electron spin is propagated through N–C and/or C–C bonds, mainly by the spin polarization effect.[31–33]

The δ^{iso} of the *N*-methyl carbon of the s-Me_2en complex is about half the δ^{iso} of the methylene carbon. However, the small difference in δ^{iso} between the methyl C^3 of *R*-pn and the methylene C^2 of *R*-chxn indicates that the spin is propagated more easily to the chelate ring than to the *N*-alkyl groups in the present Fe^{III} complexes.

The isotropic shifts of the relevant Ni^{II} complexes have been reported only for en and pn complexes.[28] The ratios of δ^{iso} for the Ni^{II} complexes to δ^{iso} for the Fe^{III} complexes are between −1.4 and −1.8 for the carbons on the chelate rings. This invariance of the ratio shows that Fermi-contact interaction makes the main contribution to the ^{13}C paramagnetic shifts of the Fe^{III} complexes as well as those of the Ni^{II} complexes.

Orientation Dependence of ^1H Isotropic Shifts. The axial protons on the five-membered chelate ring have shown positive δ^{iso}'s: 14.66 and 15.24, 13.94, and 17.72 ppm for the *R*-pn, *R*-chxn, and s-Me_2en complexes respectively. On the other hand, the equatorial protons have shown negative δ^{iso}'s: −22.66 and −15.62 ppm for the *R*-pn and s-Me_2en complexes. The results show that the axial and equatorial protons on the five-membered chelate ring show δ^{iso} values opposite in sign, whereas significant δ^{iso} values have been observed in Ni^{II} complexes only for equatorial protons.[11,19]

In the *R*-chxn complex, both protons bound to the carbon atom next to the chelate ring have positive δ^{iso}'s: H^{2a}, 9.70; H^{2e}, 8.82 ppm, but the δ^{iso}'s for protons bonded to the third carbon atom are different in sign and magnitude from each other: H^{3a}, 5.45; H^{3e}, −0.16 ppm. Thus ^1H δ^{iso} depends strongly upon the location and orientation of each nucleus within the molecule.

All axial protons have positive δ^{iso} values, which attenuate monotonously with the distance between the axial proton and the paramagnetic center, the Fe^{III} ion. However, the δ^{iso} value for the equatorial proton varies its sign with each separation by one C–C bond and attenuates more rapidly than that for the axial proton. Furthermore, the sign of δ^{iso} for each equatorial proton is opposite to that for the carbon atom to which the proton is bonded. These observations form a striking contrast to the results for the axial protons, which always show positive δ^{iso} values, and suggest the predominance of δ^{con} in δ^{iso} for the equatorial protons, i.e., the predominance of the spin-polarization effect in contributing to the spin propagation from the carbon atom to the equatorial proton. The monotonous behavior of δ^{iso} for the axial protons, on the other hand, seems to be attributable to the dominance of the dipolar shift, δ^{dip}. Thus, the δ^{iso}'s for the axial and equatorial protons are different in magnitude and sign from each other, though they are bonded to the same carbon atom in the present Fe^{III} complexes.

The present work was partially supported by a Grant-in-Aid for Scientific Research (No. 61540452) from the Ministry of Education, Science and Culture.

References

1) I. Morishima and T. Inubushi, *J. Am. Chem. Soc.*, **100**, 3568 (1978).
2) G. Williams, G. R. Moore, R. Porteous, M. N. Robinson, N. Soffe, and R. J. P. Williams, *J. Mol. Biol.*, **183**, 409 (1985).
3) G. R. Moore, M. N. Robinson, G. Williams, and R. J. P. Williams, *J. Mol. Biol.*, **183**, 429 (1985).
4) G. Williams, N. J. Clayden, G. R. Moore, and R. J. P. Williams, *J. Mol. Biol.*, **183**, 447 (1985).
5) V. L. Goedken, *J. Chem. Soc., Chem. Commun.*, **1972**, 207.
6) M. Goto, M. Takeshita, and T. Sakai, *Inorg. Chem.*, **17**, 314 (1978).
7) M. Goto, M. Takeshita, and T. Sakai, *Bull. Chem. Soc. Jpn.*, **54**, 2491 (1981).
8) M. Goto, M. Takeshita, and T. Sakai, *Chem. Lett.*, **1980**, 1081.
9) C. J. Hawkins and J. A. Palmer, *Coord. Chem. Rev.*, **44**, 1 (1982).
10) R. F. Evilia, D. C. Young, and C. N. Reilley, *Inorg. Chem.*, **10**, 433 (1971).
11) F. F. L. Ho and C. N. Reilley, *Anal. Chem.*, **42**, 600 (1970); **41**, 1835 (1969).

12) I. Morishima, K. Yoshikawa, and K. Okada, *J. Am. Chem. Soc.*, **98**, 3787 (1976) and the references cited therein.
13) M. Goto and V. L. Goedken, to be published.
14) M. Goto, M. Takeshita, N. Kanda, T. Sakai, and V. L. Goedken, *Inorg. Chem.*, **24**, 582 (1985).
15) R. Kuroda and Y. Saito, *Acta Crystallogr., Sect. B*, **30**, 2126 (1974).
16) Y. Saito and H. Iwasaki, *Bull. Chem. Soc. Jpn.*, **35**, 1311 (1962).
17) G. A. Barclay, E. Goldschmied, and N. C. Stephenson, *Acta Crystallogr., Sect. B*, **26**, 1559 (1970).
18) Y Saito, "Absolute Stereochemistry of Chelate Complexes," in "Topics in Stereochemistry," ed by E. L. Eliel and N. L. Allinger, Wiley, New York (1978), Vol. 10, p. 95.
19) C. J. Hawkins and R. M. Peachey, *Acta Chem. Scand.*, **A32**, 815 (1978).
20) S. Yano, H. Ito, Y. Koike, J. Fujita, and K. Saito, *Bull. Chem. Soc. Jpn.*, **42**, 3184 (1969).
21) C. J. Hawkins and R. M. Peachey, *Aust. J. Chem.*, **29**, 33 (1976).
22) L. E. Erickson, J. E. Sarneski, and C. N. Reilley, *Inorg. Chem.*, **14**, 3007 (1975).
23) M. W. Dietrich and A. C. Wahl, *J. Chem. Phys.*, **38**, 1591 (1963).
24) M. Shporer, G. Ron, A. Loewenstein, and G. Navor, *Inorg. Chem.*, **4**, 361 (1965).
25) M.-S. Chan, J. B. DeRoos, and A. C. Wahl, *J. Chem. Phys.*, **77**, 2163 (1973).
26) J. A. Tiethof and D. W. Cooke, *Inorg. Chem.*, **11**, 315 (1972).
27) M. Goto and Y. Kuroda, unpublished results.
28) C. E. Strouse and N. A. Matwiyoff, *J. Chem. Soc., Chem. Commun.*, **1970**, 439.
29) J. P. Jesson, *J. Chem. Phys.*, **47**, 582 (1967).
30) G. N. La Mar, "NMR of Paramagnetic Molecules," ed by G. N. La Mar, W. Dew. Horrocks, Jr., and R. H. Holm, Academic Press, New York (1973), Chap. 3, p. 105.
31) Z. Luz, *J. Chem. Phys.*, **48**, 4186 (1968).
32) W. D. Horrocks, Jr. and D. L. Johnston, *Inorg. Chem.*, **10**, 1835 (1971).
33) M. J. Scarlett, A. T. Casey, and R. A. Craig, *Aust. J. Chem.*, **23**, 1333 (1970); **24**, 31 (1971).

 © 1987 The Chemical Society of Japan Bull. Chem. Soc. Jpn., 60, 3925—3929 (1987)

Potentiometric Study of Equilibria in H^+-MoO_4^{2-}-$RAsO_3H^-$ (R=OH, C_6H_5, CH_3) Systems

Atsushi YAGASAKI, Hironobu TAKAHAMA, and Yukiyoshi SASAKI*
Department of Chemistry, Faculty of Science, The University of Tokyo,
Hongo, Bunkyo-ku, Tokyo 113
(Received March 7, 1987)

The equilibria $pH^+ + qMoO_4^{2-} + rRAsO_3H^- \rightleftharpoons (H^+)_p(MoO_4^{2-})_q(RAsO_3H^-)_r$ have been studied in 1 M Na(Cl) (1 M=1 mol dm^{-3}) at 25 °C by potentiometry. Heteropoly species which have q/r ratios higher than 5 have been found in the R=CH_3 and R=C_6H_5 systems besides the well known species of q/r=3. The species, denoted by (p,q,r) according to the equation above, (10, 7, 1), (11, 7, 1), and (11, 6, 1) are proposed as those high ratio species. The formation constant of each species has been determined. The result showed an apparent correlation with pK_a's of arsenic acid and its organic derivatives. Solution structures of the heteropoly species are also discussed.

Our preliminary investigations of the molybdate-methylarsonate and molybdate-phenylarsonate equilibria[1,2] indicated the existence of heteropolyanions of high (≥4) Mo/As ratios, which were supposed to have novel structures, in addition to the As_2Mo_6 species. Some evidence of the correlation between the formation constants of heteropolyanions and the pK_a's of arsonic acids was also obtained.

We have carried out a thorough investigation of those systems. This paper reports the results of the investigation.

Method of Analysis

The equilibria for various heteropolymolybdates can be represented by the generalized equation

$$pH^+ + qMoO_4^{2-} + rC \rightleftharpoons (H^+)_p(MoO_4^{2-})_qC_r \quad (1)$$

where C stands for the heteroatom source. For brevity the complex $(H^+)_p(MoO_4^{2-})_qC_r$ will be referred as (p,q,r). The symbol β_{pqr} will be used to represent the formation constant for the (p,q,r). Hence,

$$\beta_{pqr} = \frac{[(p,q,r)]}{h^p b^q c^r} \quad (2)$$

where h=[H^+], b=[MoO_4^{2-}], and c=[C], and the units are molarity. The condition for mass balance requires

$$H = h + \Sigma p\beta_{pqr}h^p b^q c^r \quad (3)$$

$$B = b + \Sigma q\beta_{pqr}h^p b^q c^r \quad (4)$$

and

$$C = c + \Sigma r\beta_{pqr}h^p b^q c^r. \quad (5)$$

H, B, and C stand for the formal stoichiometric concentrations of the reactants H^+, MoO_4^{2-}, and C, repectively. If the constants β_{pqr}'s are given, it is possible to calculate H, b, c, and $[(p,q,r)]$ for a solution of known h, B, and C by solving Eqs. 3—5. A set of (p,q,r)'s and β_{pqr}'s, that minimizes the difference between those calculated values and the observed values, was obtained using the least-squares method.

Experimental

Chemicals. NaCl (Matsunaga, JIS primary standard) was used after heating at 150 °C for 8 h. Molybdate stock solutions were prepared by using twice recrystallized $Na_2MoO_4 \cdot 2H_2O$ (Wako, S). $Na_2HAsO_4 \cdot 7H_2O$ (Wako, S) was used without further purification. $C_6H_5AsO_3HNa$ was obtained by reacting $C_6H_5AsO_3H_2$ (Wako) with an equivalent amount of NaOH (Wako, S). The crude product was recrystallized twice from water. $CH_3AsO_3Na_2 \cdot 6H_2O$ was prepared according to Quick.[3] The product was purified by dissolving in a small amount of water and reprecipitating with ethanol.

Apparatus and emf Measurements. All the emf measurements were performed at 25.0±0.1 °C in 1 M Na (Cl) medium. The cell assembly was immersed in an oil thermostat, which was placed in a thermostatted room. During the experiments a stream of N_2 gas was bubbled through the solution for removing dissolved O_2. N_2 gas from a cylinder was bubbled through solution of 10% NaOH, 10% H_2SO_4, and pure ionic medium before it came into contact with the equilibrium solution.

Potentiometric titrations were performed with an automated titrator equipped with Dosimat E 415 burettes.[4] The hydrogen ion concentration, h, was determined by measuring the emf of the cell,
−Ag, AgCl/1M NaCl/equilibrium solution/glass electrode +.
The Ag, AgCl reference electrode was prepared according to Brown.[5] TOA Electronics HGS-2005 glass electrodes were employed. The salt bridge was of the "Kawai" type.[6] In each titration, h was varied by addition of dilute hydrochloric acid.

The reading of the emf reached a stationary value within a few minutes. For each titration point the emf was checked and found to be stable within 0.1 mV over a period of 20 min. No precipitation was observed during the series of titrations.

The mathematical analysis of the emf data was performed with the least-squares program LETAGROPVRID version ETITR.[7] The computation was performed on the HITAC M-280H/M-200H and M682H systems of the Computer Centre of the University of Tokyo. The function $U=\Sigma(H_{calc}-H)^2$ was minimized. Separate determinations of the equilibrium constants were performed for the

Table 1. Acid Dissociation Constants of Arsenic Acid and Its Organic Derivatives

	H_2AsO_4	$C_6H_5AsO_3H_2$	$CH_3AsO_3H_2$
pK_1	2.01±0.02	3.35±0.01	3.78±0.02
pK_2	6.26±0.01	7.45±0.26	8.14±0.08

Table 2. Formation Constants of H^+-MoO_4^{2-}-$C_6H_5AsO_3H^-$ System

(p, q, r)	$\log \beta_{pqr}$		
	Model a	Model b	Model c
(9, 6, 2)	63.71±0.02	63.72±0.03	63.72±0.02
(10, 6, 2)	68.99±0.04	69.02±0.03	68.97±0.04
(11, 6, 1)	64.41±0.08	64.67±0.01	64.08±0.08
(10, 7, 1)	67.23±0.01		
(11, 7, 1)	70.80±0.01		
(13, 9, 1)		86.68±0.01	
(14, 9, 1)		90.08±0.13	
(9, 6, 1)			59.97±0.01
(10, 6, 1)			62.83±0.01
U/mM²	45.8	48.6	44.2

binary equilibria, H^+-$HAsO_4^{2-}$, H^+-$C_6H_5AsO_3^{2-}$, and H^+-MoO_4^{2-}.[1,8]

Results

H^+-MoO_4^{2-}-$C_6H_5AsO_3H^-$ System. Eight titrations were performed and 322 experimental points were obtained. The titrations covered the ranges $5.8 \geqq -\log h \geqq 2.0$, $39.0 \geqq B/\text{mM} \geqq 21.0$, $50.0 \geqq C/\text{mM} \geqq 4.7$, and $6.4 \geqq B/C \geqq 0.71$.

When only the known binary equilibria, H^+-MoO_4^{2-} and H^+-$C_6H_5AsO_3H^-$, are assumed to be present, the residuals $\Delta H = H_{calc} - H$ are very large and show systematic deviations, suggesting the existence of ternary equilibria, H^+-MoO_4^{2-}-$C_6H_5AsO_3H^-$.

Although the complexes (9,6,2) and (10,6,2) explained the data of low ($\leqq 3$) B/C ratios satisfactorily, speciation for the solutions of higher B/C ratios was less unambiguous. Three models, which are partly different in the choice of polyanions formed, explained the data equally well. The U values differ from one another only slightly, and this fact makes a simple selection based on the error-squares sum alone unrealistic. The numerical values of the formation constants are given in Table 2.

H^+-MoO_4^{2-}-$CH_3AsO_3H^-$ System. Twelve titrations were performed and 306 experimental points were obtained. The titrations covered the ranges $6.1 \geqq -\log h \geqq 2.0$, $48.0 \geqq B/\text{mM} \geqq 18.0$, $11.0 \geqq C/\text{mM} \geqq 3.6$, and $9.1 \geqq B/C \geqq 3.4$. The analysis was based on a preliminary report on the equilibria in this system.[1] The result is given in Table 3. As was the case in the H^+-MoO_4^{2-}-$C_6H_5AsO_3H^-$ system, it was not possible to choose the best model out of a number of the candidates by potentiometry alone.

Table 3. Formation Constants of H^+-MoO_4^{2-}-$CH_3AsO_3H^-$ System

(p, q, r)	$\log \beta_{pqr}$		
	Model a	Model b	Model c
(9, 6, 2)	64.38±0.02	64.37±0.02	64.39±0.02
(10, 6, 2)	69.16±0.05	69.31±0.04	68.95±0.04
(11, 6, 1)	66.27±0.03	66.19±0.03	66.23±0.01
(10, 7, 1)	67.83±0.03		
(11, 7, 1)	71.79±0.01		
(12, 9, 1)		82.17±0.14	
(13, 9, 1)		87.08±0.06	
(14, 9, 1)		90.53±0.04	
(9, 6, 1)			60.60±0.02
(10, 6, 1)			63.49±0.01
U/mM²	21.1	34.3	26.0

Table 4. Formation Constants of H^+-MoO_4^{2-}-$H_2AsO_4^-$ System

(p, q, r)	$\log \beta_{pqr}$	
	Model a	Model b
(8, 6, 2)	57.89±0.04	57.91±0.04
(9, 6, 2)	63.42±0.03	63.41±0.01
(10, 6, 2)	66.91±0.01	66.89±0.10
(13, 9, 1)	87.53±0.01	87.55±0.03
(14, 9, 1)	91.14±0.08	90.66±0.03
(15, 9, 1)	93.64±0.01	93.36±0.19
(16, 9, 1)	94.93±0.02	95.29±0.05
(16, 11, 1)		105.22±0.90
(17, 11, 1)		110.45±0.07
(18, 11, 1)		112.83±0.24
U/mM²	53.2	51.9

H^+-MoO_4^{2-}-$H_2AsO_4^-$ System. Ten titrations were performed and 448 experimental points were obtained. The titrations covered the ranges $6.8 \geqq -\log h \geqq 2.0$, $39.0 > B/\text{mM} \geqq 18.0$, $13.0 \geqq C/\text{mM} \geqq 2.5$, and $12.0 \geqq B/C \geqq 2.0$. The best fit was obtained with the formation of (16, 9, 1), (15, 9, 1), (14, 9, 1), (13, 9, 1), (10, 6, 2), (9, 6, 2), and (8, 6, 2). The species (6, 5, 2), which was reported to exist in the 3M $Na(ClO_4)$ medium as a minor species,[9] was not needed to explain our data. Although a slightly better fit was obtained with the introduction of (p, 11, 1)'s to the system, it was not possible to explain the data without (p, 9, 1)'s. The formation constants obtained are given in Table 4.

Discussion

The existence of heteropolyanions of high ($\geqq 4$) Mo/As ratios in molybdoarsonate systems has been reconfirmed in the present research. However, our potentiometric investigation failed to determine the

composition of those species. The reason will become clear if we consider the proton consumption factor $z_{q+r}=p/(q+r)$ of those high ratio species. The proton consumption factors of (10, 7, 1), (11, 7, 1), and (10, 6, 1), the high ratio species of model a, are 1.25, 1.38, and 1.43, respectively, while (9, 6, 1), one of the species of model b, has z_{q+r} of 1.29. The high ratio species of model c, namely (12, 9, 1), (13, 9, 1), and (14, 9, 1), have z_{q+r} of 1.20, 1.30, and 1.40. As a result, each of the three models for the molybdoarsonate systems would consume about the same amounts of proton as a whole. This means that potentiometry connot make a clear distinction among the three models, since in potentiometry we measure the proton concentration from which the average proton consumption $Z_{B+C}=(H-h)/(B+C)$ is calculated.

It is true that species other than those listed in Tables 2 and 3 cannot be totally excluded. In fact the combination of (6, 4, 1) and (7, 4, 1) gives a fairly good fit so far as B/C is not larger than 5.[1] In spite of this, we have selected the three models listed in Tables 2 and 3 from numerous possible combinations

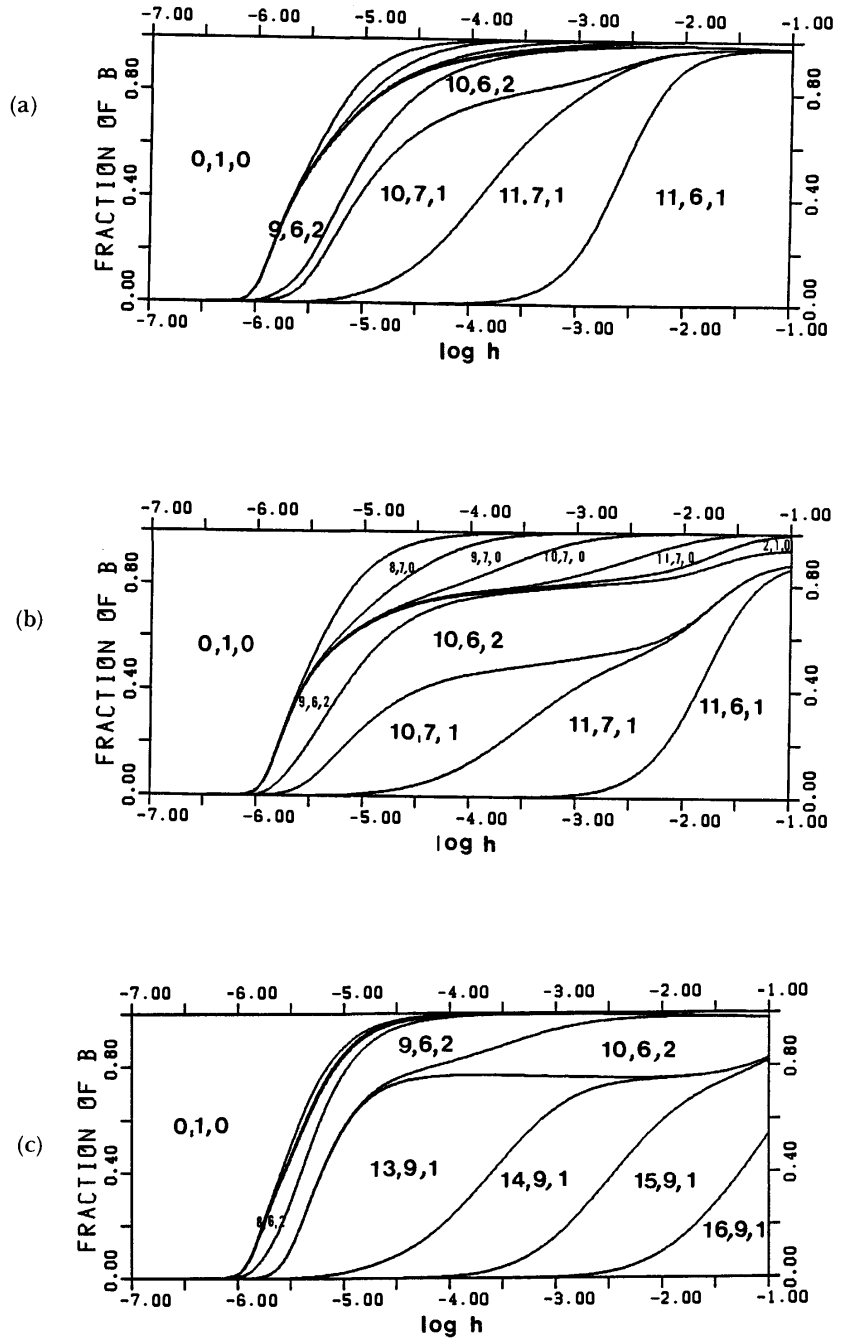

Fig. 1. Distribution of Mo among different species in H^+-MoO_4^{2-}-$RAsO_3H^-$ systems at B=30 mM and C=5 mM. (a) R=CH_3. (b) R=C_6H_5. (c) R=Oh.

as the final candidates for the molybdoarsonate systems, since the essence of least-squares analysis is to find the simplest possible model for a given system.

Among the three possible models for the molybdoarsonate system, we select model a in Tables 2 and 3, the combination of (p, 7, 1) and (11, 6, 1), as the most plausible one. Those are the species found in the molybdate-phenylphosphonate system, which have been studied by a combined emf-NMR method.[10] It is not likely that the molybdate-arsonate equilibria are totally different from the molybdate-phosphonate equilibria, since the molybdate-arsenate systems and molybdate-phosphate systems exhibit a nature similar to each other.

In the case of the H^+-MoO_4^{2-}-$H_2AsO_4^-$ system, it was possible to explain the data either with or without the $AsMo_{11}$ species. Considering the results of recent reports on the molybdate-phosphate system,[11,12] it is highly plausible that the $AsMo_6$ and $AsMo_{11}$ species co-exist in solution, in which case it is virtually impossible to determine the formation constants of them from potentiometric data alone.

The high ratio ($q/r \geqslant 6$) species of the molybdate-arsonate systems, except (11, 6, 1) of the H^+-MoO_4^{2-}-$CH_3AsO_3H^-$ system, are weak complexes. Whenever a notable amount of those species are formed, isopolymolybdates appear in a condiberable amount. This is the marked difference between the molybdate-arsonate system and molybdate-arsenate system. In the latter, isopolymolybdates hardly exist when $B/C \leqslant 9$.

The formation constants for the three systems are compared in Table 5. There exists a correlation between the formation constants of heteropolyanions and the pK_a's of arsenic and arsonic acids. The formation constants of the corresponding species increase as the pK_a increases, i.e. a certain heteropolyanion forms at a higher pH if a substance which has a greater pK_a is used to introduce heteroatoms. This tendency is clearly illustrated in Fig. 1, especially for the $AsMo_6$ species. While only 30% of the molybdenum in solution is bound in (11,6,1) at $-\log h = 2$, more than 90% is consumed to form the anion (11, 6, 1) in the molybdate-methylarsonate system at the same $-\log h$. It would be possible to obtain the As_4Mo_{12} species, which has been isolated from solution of pH<1,[13] from a less acidic solution if an arsonate which has still larger pK_a's is prepared without altering the basic tetrahedral structure very much.

Table 5. Comparison of the Formation Constants

(p, q, r)	$\log \beta_{pqr}$		
	R=CH_3	R=C_6H_5	R=OH
(9, 6, 2)	64.38	63.71	63.42
(10, 6, 2)	69.16	68.99	66.91
(11, 6, 1)	66.27	64.41	
(10, 7, 1)	67.83	67.23	
(11, 7, 1)	71.79	70.80	

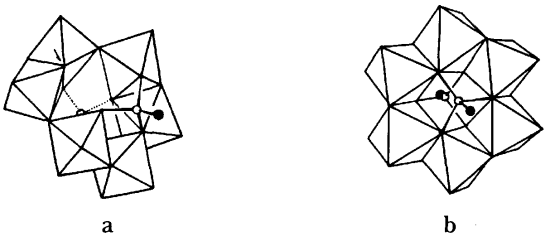

Fig. 2. Polyhedral model of (10, 6, 2). Each octahedron represents an MoO_6 unit. Open circles represent As atoms. R groups are represented by filled circles. An arrow indicates the position of the water molecule.

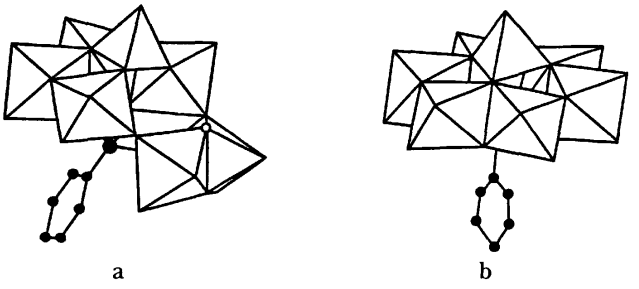

Fig. 3. Polyhedral model of (11, 7, 1). Large and small filled circles represent As and C atoms respectively. The water molecule is represented by an open circle. A tetrahedron represents an MoO_4 unit.

The species (10, 6, 2) is supposed to have the structure shown in Fig. 2a. The anion $[(C_6H_5As)_2Mo_6O_{24}(H_2O)]^{4-}$, which has the same composition as (10, 6, 2) of the H^+-MoO_4^{2-}-$C_6H_5AsO_3H^-$ system, is known to have this structure in crystals.[14] The structure shown in Fig. 2b is also possible for (10, 6, 2), and the anions $[(CH_3As)_2Mo_6O_{24}]^{4-}$ and $[H_2As_2Mo_6O_{24}]^{4-}$ have this structure in crystals.[15,16] However, IR, Raman, and ^1H NMR measurements have revealed that those anions are hydrated in aqueous solutions and have the structure shown in Fig. 2a.[16,17,18] Large-angle X-ray scattering was consistent with the structure shown in a and not with b.[19]

Both structures shown in Fig. 3 are possible for (11,7,1), and b is the one proposed for $[C_6H_5AsMo_7O_{25}]^{4-}$ by Klempere and co-workers from ^{17}O NMR measurements in anhydrous CH_3CN solutions.[20] Considering the fact mentioned above, the anions are likely to be hydrated in aqueous solution and have a structure like a. (10,7,1) can then be explained by dissociation of a proton from the water molecule. The same explanation would apply to (9,6,2) of the H^+-MoO_4^{2-}-$C_6H_5AsO_3H^-$ and H^+-MoO_4^{2-}-$CH_3AsO_3H^-$ systems.

The removal of the tetrahedral MoO_4^{2-} group from

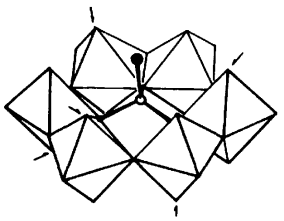

Fig. 4. Polyhedral model of (11, 6, 1). Arrows indicate the position of water molecules. Open and filled circles represent As atom and the organic group, respectively.

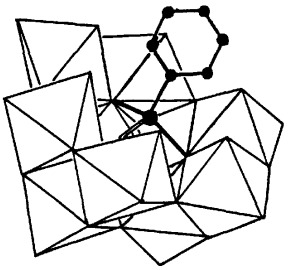

Fig. 5. Possible structure for (p, 9, 1) of the molybdate-arsonate system. Large and small filled circles represent As and C atoms respectively.

the structure shown in Fig. 3a and a slight rearrangement of the atoms yield the structure for the $RAsMo_6$ species, which is shown in Fig. 4. The anion $[CH_3AsMo_6O_{21}(H_2O)_6]^{2-}$, which has the same composition as (11,6,1) found in the H^+-MoO_4^{2-}-$CH_3AsO_3H^-$ system, has been reported to have this structure[21].

If it is (p,9,1) and not (p,7,1) that is formed in the molybdate-arsonate systems, the structure would be something like the one shown in Fig. 5.

All the structures shown in Figs. 3—5 are also possible in the inorganic molybdate-arsenate system. Those species might exist in the H^+-MoO_4^{2-}-$H_2AsO_4^-$ system as minor species.

References

1) H. Takahama, A. Yagasaki, and Y. Sasaki, *Chem. Lett.*, **1982**, 1953.
2) Y. Sasaki, Proceedings of the U. S.-Japan Seminar on the Catalytic Activity of Polyoxoanions, Shimoda, Japan (1985), p. 146.
3) A. J. Quick, *J. Am. Chem. Soc.*, **44**, 805 (1922).
4) O. Ginstrup, *Chem. Instrum.*, **4**, 141 (1973).
5) A. S. Brown, *J. Am. Chem. Soc.*, **56**, 645 (1934).
6) H. Ohtaki, *Denki Kagaku*, **44**, 326 (1976).
7) P. Brauner, L. G. Sillen, and R. Whiteker, *Arkiv Kemi*, **31**, 365 (1969).
8) A. Yagasaki and Y. Sasaki, *Bull. Chem. Soc. Jpn.*, **60**, 763 (1987).
9) L. Pettersson, *Acta Chem. Scand.*, **A29**, 677 (1975).
10) A. Yagasaki, I. Andersson, and L. Pettersson, *Inorg. Chem.*, in press.
11) L. Pettersson, I. Andersson, and L.-O. Ohman, *Inorg. Chem.*, **25**, 4726 (1987).
12) J. A. Rob van Veen, O. Sudmeijer, C. A. Emeis, and H. de Wit, *J. Chem. Soc., Dalton Trans.*, **1986**, 1825.
13) K. Nishikawa and Y. Sasaki, *Chem. Lett.*, **1975**, 1185.
14) K. Y. Matsumoto, *Bull. Chem. Soc. Jpn.*, **51**, 492 (1978).
15) W. Kwak, M. T. Pope, and T. F. Scully, *J. Am. Chem. Soc.*, **97**, 5753 (1975).
16) Y. Takeuchi, A. Kobayashi, Y. Sasaki, and N. Ingri, 41st National Meeting of the Chemical Society of Japan, Osaka, April 1980, Abstr. No. 3L13.
17) W. Kwak, L. M. Rajkovic, M. T. Pope, C. O. Quicksall, K. Y. Matsumoto, and Y. Sasaki, *J. Am. Chem. Soc.*, **99**, 6463 (1977).
18) S. H. Wasfi, W. Kwak, M. T. Pope, K. M. Barkigia, R. J. Butcher, and C. O. Quicksall, *J. Am. Chem. Soc.*, **100**, 7786 (1978).
19) G. Johansson, L. Pettersson, and N. Ingri, *Acta Chem. Scand.*, **A35**, 181 (1981).
20) W. G. Klemperer, C. Schwarts, and D. A. Wright, *J. Am.Chem. Soc.*, **107**, 6941 (1985).
21) K. Y. Matsumoto, *Bull. Chem. Soc. Jpn.*, **52**, 3284 (1979).

 © 1987 The Chemical Society of Japan Bull. Chem. Soc. Jpn., 60, 3931—3934 (1987)

The Formation of β-$LiFe_5O_8$ from Aqueous Suspensions and Its Properties

Masao KIYAMA,* Tokihiro KURATA,† and Toshio TAKADA††
Institute for Chemical Research, Kyoto University, Uji, Kyoto 611
(Received March 18, 1987)

Alkaline suspensions containing iron(III) hydroxide and excess LiOH were subjected to aging at temperatures between 40 and 90 °C or to autoclaving at 120 °C or above. The resulting products, identified by X-ray analysis as a spinel phase, were further subjected to magnetic examination at 300 K, BET surface-area measurements, and electron-microscopic observation. The ferromagnetic precipitates of β-$LiFe_5O_8$ were formed at lower temperatures and less excess LiOH concentrations than those at which the nonferromagnetic precipitates of α-$LiFeO_2$ were formed. Their saturation magnetization increased near 60 emu g^{-1} (1 emu $g^{-1}=4\pi\rho10^{-4}$ T, where ρ=specific gravity) with the increase in their mean particle size, D, their coercive force depending on the D. With a rise in the temperature of the suspension, superparamagnetic particles with vacancies of the Li ion, intermingled with the ferromagnetic cubic particles, slowly grew to ferromagnetic particles and the composition approached $LiFe_5O_8$.

The ferromagnetic compounds of $LiFe_5O_8$, which has a cubic inverse spinel structure at room temperature, are obtained below 1000 °C in air by the use of a ceramic method. This compound is known to have two modifications, the ordered and disordered phases. The Li and Fe(III) ions in the octahedral(B) sites are distributed in an ordered ratio of 1:3 below 735 °C, while they are randomly disordered above 755 °C.[1] The Curie temperature and saturation magnetization are not affected by the ordering.[2]

The synthesis of $LiFe_5O_8$ from an aqueous suspension was achieved for the first time in 1980,[3] in this laboratory. In the present study, it has been found that iron(III) hydroxide can react with the Li ion in an alkaline suspension to form $LiFe_5O_8$ if we choose appropriate concentrations of the iron(III) and Li ions and a suitable reaction temperature: a nonferromagnetic precipitate of α-$LiFeO_2$ with a cubic, disordered structure[4] is also obtained.

This paper will deal with the conditions needed for the formation of $LiFe_5O_8$ and its properties.

Experimental

The starting suspensions of a gelatinous precipitate of iron(III) hydroxide were prepared by adding an excess LiOH solution to an acidic solution of iron(III) nitrate (each of an analytical grade). A number of alkaline suspensions, varying in their excess LiOH concentrations, were also prepared. Each suspension was diluted with conductivity water to 1 dm^3 in a 1.3-dm^3 flask equipped with five inlet necks. The construction of the flask was similar to what has previously been described,[5] except that an electrode for a self-recording pH meter was not inserted. The individual 1-dm^3 suspensions, containing 0.2 M (1 M=1 mol dm^{-3}) Fe(III) and different excess LiOH concentrations in the 0.03—3.0 M range, were heated and kept at desired temperatures ranging from 40 to 90 °C, and nitrogen gas was bubbled into for 5 h at a constant rate of 250 dm^3 h^{-1} for effervescent aging.

A number of alkaline suspensions (0.2 dm^3), each containing 0.2 M Fe(III), were also prepared in a 0.3-dm^3 stainless steel autoclave by varying the excess LiOH concentration in the 0.03—3.0 M range. They were then heated at the rate of 4 °C min^{-1} to the desired temperature. They were kept at temperatures ranging from 120 to 280 °C with mechanical stirring at 100 rpm for 5 h and then allowed to cool to room temperature.

The resulting products were separated by filtration, washed several times with water, treated with acetone, and then dried at 30 °C in air. The products, which were found, by means of an X-ray diffraction examination using Co $K\alpha$ radiation, to consist of the spinel phase, were then subjected to BET surface-area measurements using nitrogen and to an electron-microscopic examination. Each weighing 100 mg, they were then packed in a brass cylinder 0.6 cm in diameter and 0.2 cm in height, and magnetic measurements were carried out at room temperature in a magnetic field up to 10 kOe (1 kOe=$10^6/4\pi$ A m^{-1}), using a vibrating-sample magnetometer.

The mean particle size, D, of the $LiFe_5O_8$ samples was estimated from the BET surface area, S (m^2 g^{-1}), by assuming that the sample consisted of cubic particles with a specific gravity of 5.0. The average particle size, d, for the samples with $D<50$ nm was further estimated from the line broadening of the X-ray diffraction peak for the (311) plane of the $LiFe_5O_8$ crystal structure.

Results and Discussion

The formation at 0.2 M Fe(III) of the products by aging or by autoclaving is shown in Fig. 1 in terms of the concentration of the excess LiOH and the reaction temperature. Dark brown, ferromagnetic precipitates with the spinel structure are formed in the presence of an excess of LiOH of at least 0.3 M by selecting an appropriate concentration and temperature. Apparently, the range of the excess LiOH concentration needed for the formation of the ferromagnetic precipitate becomes narrower with an increase in the

† Present address; Toda Kogyo Corp., 4, 1-2 Funairiminami, Hiroshima 733

†† Present address; Okayama University of Science, Ridai-cho, Okayama 700

temperature beyond 120 °C. Nonferromagnetic precipitates, each consisting of spherical α-$LiFeO_2$ particles, are formed in the ranges of excess LiOH concentrations and of autoclaving temperatures higher than those at which the ferromagnetic precipitates are formed.

The properties of five typical samples with the spinel structure, A through E, are given in Table 1. Electron-microscopic examination indicates that the growth of some of the extremely fine particles with the spinel structure begins at 120 °C and is promoted by a rise in the temperature (Fig. 2). The elevation of the temperature causes a significant increase in *d*, but only a slight increase in the *D* because of the extremely fine particles remaining in each sample. An increase in the difference between the *D* and *d* values for the sample shows that the particle-size distribution becomes wider. The magnetization, *M*, at 10 kOe and the coercive force, *Hc*, depend on the *d* and *D*.

The Mössbauer spectra of several $LiFe_5O_8$ samples with different *D* values, all taken at room temperature, are shown in Fig. 3. The sample with 4.7 nm in *D* consists only of superparamagnetic particles (Fig. 3(a)), and as the *D* value increases, the superparamagnetic particles coexist with the ferromagnetic

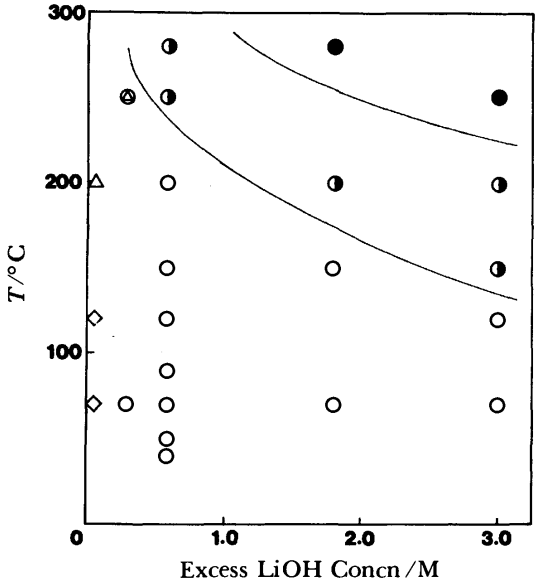

Fig. 1. Conditions for the formation at different temperatures, *T*, of $LiFe_5O_8$ from alkaline suspensions containing 0.2 M Fe(III) and various concentrations of excess LiOH.
○: $LiFe_5O_8$, ●: $LiFeO_2$, ◑: a mixture of $LiFe_5O_8$ and $LiFeO_2$, △: α-Fe_2O_3, ⊜: a mixture of α-Fe_2O_3 and $LiFe_5O_8$, ◇: α-FeO(OH).

Table 1. Typical $LiFe_5O_8$ Samples Prepared by the Aging or Autoclaving, at Various Temperatures (*T*), of Aqueous Suspensions, Each Containing 0.2 M Fe(III) and a 0.6 M Excess of LiOH

Sample	*T*/°C	*D*/nm	*d*/nm	*Hc*/Oe	*M*/emu g^{-1}
A	40	4.7	4	8	12
B	70	5.0	8	55	22
C	90	5.0	11	72	23
D	120	7.4	27	83	42
E	200	15.0	50	76	50
F[a)]	250	31.0	94	75	54

a) Prepared by the use of iron(III) sulfate in place of nitrate.

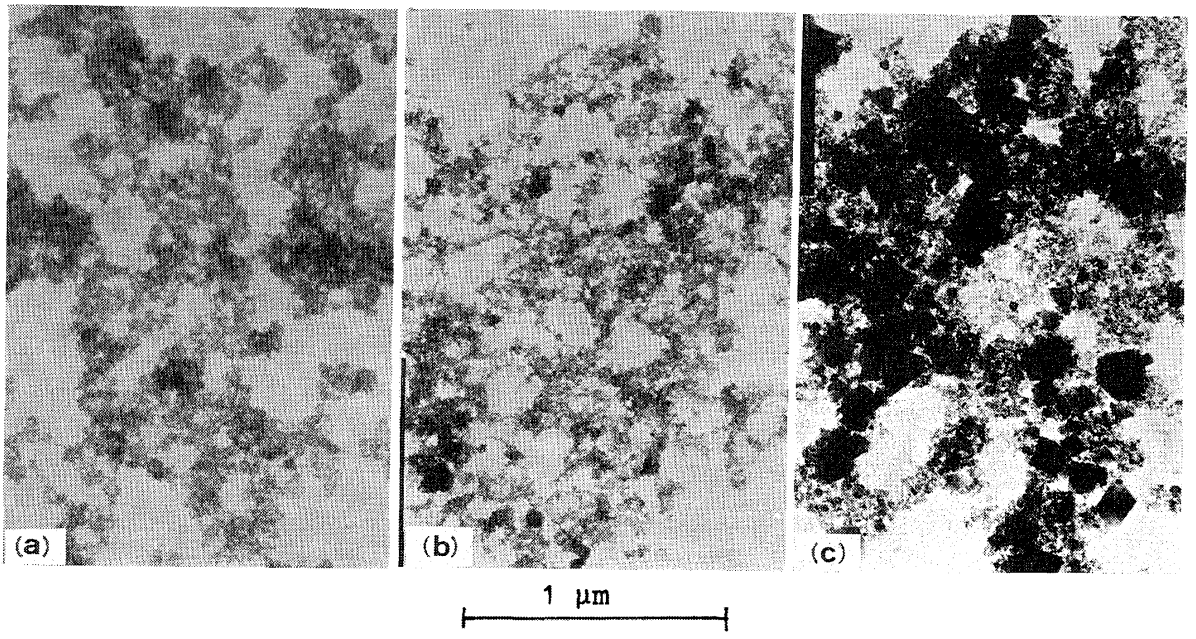

Fig. 2. Transmission electron micrographs of samples B(a), D(b), and E(c).

particles, until the former decrease (b and c). It is possible to prepare the samples with $D>15$ nm at 200 °C, as will be described later, by increasing the concentration of the Fe(III) in the starting suspension or by prolonging the reaction time. Such samples contained no superparamagnetic particles (Fig. 3(d)), and their hyperfine fields (49.4 T) were almost the same as that of $LiFe_5O_8$ prepared by a ceramic method.[6]

An increase in the Fe(III) concentration in the starting suspension under the conditions where the ferromagnetic precipitate was formed was found to cause an increase in D, as will be described below. The suspensions containing a 0.6 M excess of LiOH and either 0.1, 0.5, or 1.0 M Fe(III) were also prepared and subjected to autoclaving at 200 °C. The ferromagnetic precipitates thus obtained consisted of extremely fine particles, the cubic ones being 80—140 nm in size. As the Fe(III) concentration was increased, their D values increased from 14 to 23 nm without any appreciable change in the d (50—53 nm).

In order to examine the effect of the reaction time on the particle growth, suspensions, each containing 0.2 M Fe(III) and a 0.6 M excess of LiOH, were subjected to aging at 70 °C or autoclaving at 150 and 200 °C for different times (t). The t-dependence of the d and D values at 200 °C becomes significant after 10 h (Fig. 4). The extremely fine particles were found, by the use of an electron microscope, to coexist with cubic particles 100 nm in size, even in the sample prepared by autoclaving at 200 °C for 50 h.

Similar experiments were also conducted using Fe(III) chloride or sulfate in place of the nitrate. No particular difference could be found in the conditions for the formation of the ferromagnetic precipitate and for the particle growth. The temperature for the formation of the ferromagnetic precipitate in the presence of sulfates may be raised slightly, as is evidenced by Sample F in the Table.

The M values of the ferromagnetic samples prepared under various conditions are plotted against their D values in Fig. 5. The M value increases with the D, reaching near 60 emu g^{-1}. When the M values were plotted against the d, they irregularly and

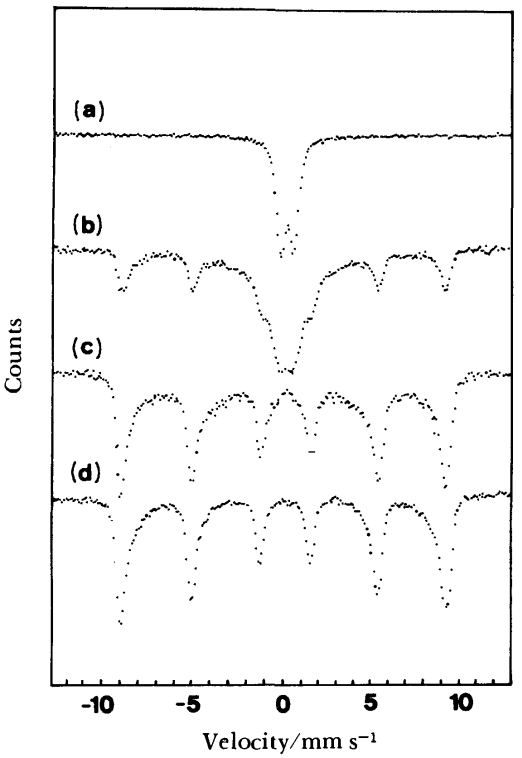

Fig. 3. Mössbauer spectra at 300 K of $LiFe_5O_8$ samples A(a), B(b), E(c), and 2E(d). Sample 2E prepared at 200 °C for 20 h (Fig. 4) and its hyperfine field is 49.4 T.

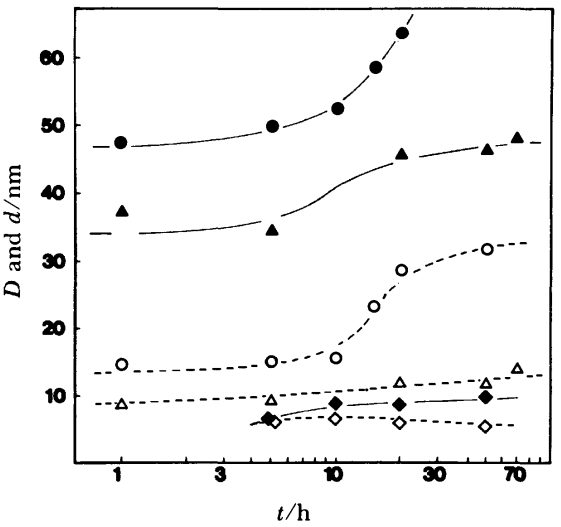

Fig. 4. Changes in the D(white) and d(black) of the samples prepared at 200 (circles), 150 (triangles), and 70 °C (tetragons) with time, t.

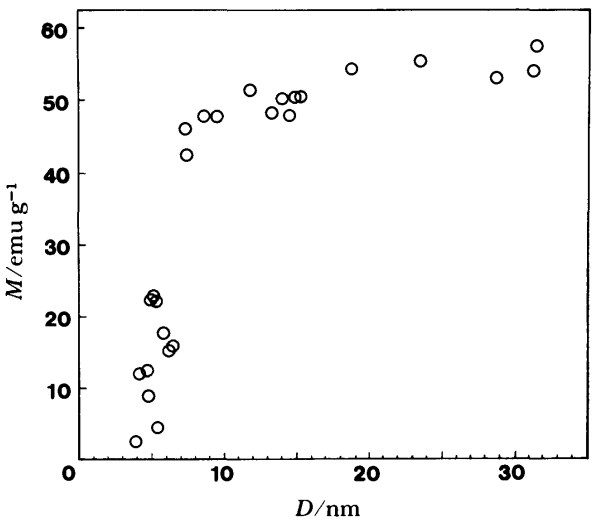

Fig. 5. Magnetization, M, at 10 kOe of $LiFe_5O_8$ samples plotted against their D values.

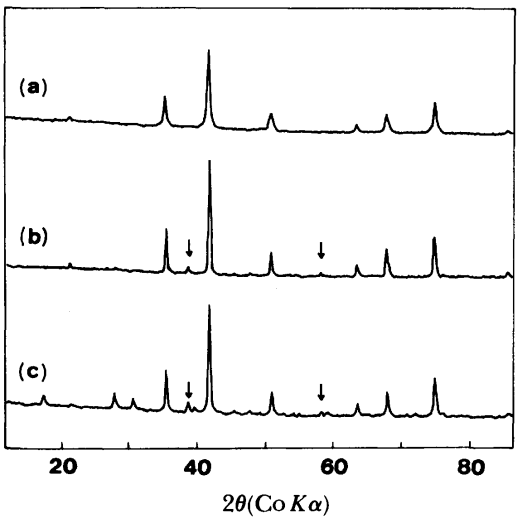

Fig. 6. X-Ray diffraction patterns of the β-$LiFe_5O_8$ sample E(a), and heat-treated samples by rapid cooling from 900 °C (b) and by slow cooling from 750 °C (c). Arrows in (b) and (c) indicate the peaks caused by the presence of α-Fe_2O_3.

remarkably increased to 40 emu g^{-1} with the increase in the d to 10 nm, while a further increase in d to 90 nm resulted in only a slight increase in M to near 60 emu g^{-1}. Presumably, an increase in the specific surface area causes an increase in the nonferromagnetic portion, which is reported to be the subsurface of the ferromagnetic particle, such as a γ-Fe_2O_3, $NiFe_2O_4$, CrO_2,[7] or $BaFe_{12}O_{19}$ particle.[8] Increasing the d values to 15 nm or the D values to 7 nm caused an increase in Hc to about 0.1 kOe as a result of the decrease in the number of superparamagnetic particles. A further increase in D or d resulted in a slight decrease in the Hc, probably because of the decrease in the number of single-domain ferromagnetic particles.

An X-ray diffraction examination showed that the ferromagnetic samples consisted of crystalline particles with a disordered spinel structure(β-$LiFe_5O_8$).[9] This indicates that the formation of β-$LiFe_5O_8$ proceeded at the temperatures where the β phase was unstable. The transformation between the α and β phases of the samples as a result of heat treatment in air was confirmed from the experimental results, where their structure remained unchanged upon rapid cooling from 900 °C, whereas it was transformed into an ordered spinel structure (α-$LiFe_5O_8$) by slow cooling from 750 °C (Fig. 6). Such heat-treated samples consisted of the spinel phase with or without the α-Fe_2O_3 phase; the content of α-Fe_2O_3 varied with the sample. Decreasing the D of the original samples from 15 to 8 nm caused a slight increase (to several %) in the content of α-Fe_2O_3, while a further decrease in the D to 4.7 nm resulted in an increase to 50% in its content. The formation of α-Fe_2O_3 by heat treatment indicates that the Li-ion content in the original sample was less than that in $LiFe_5O_8$. According to the chemical analysis by the use of inductively coupled plasma/atomic emission spectroscopy, the β-$LiFe_5O_8$ samples with $D>15$ nm contained Li and Fe ions in the atomic ratio (Li/Fe) of 0.2. This ratio decreased to 0.10 with the decrease in the D to 4.7 nm (Sample A).

In conclusion, the extremely fine particles, intermingled with ferromagnetic cubic particles, consisted of superparamagnetic and ferromagnetic particles. The superparamagnetic particles with vacancies of the Li ion slowly grew to ferromagnetic particles, and the composition approached $LiFe_5O_8$ when the D increased.

References

1) P. B. Braun, *Nature (London)*, **170**, 1123 (1952).
2) G. O. White and C. E. Patton, *J. Magn. Magn. Mater.*, **9**, 299 (1978).
3) M. Kiyama and T. Takada, *Bull. Inst. Chem. Res. Kyoto Univ.*, **58**, 193 (1980).
4) J. C. Anderson and M. Schieber, *J. Phys. Chem. Solids*, **25**, 961 (1964).
5) M. Kiyama, *Bull. Chem. Soc. Jpn.*, **47**, 1646 (1974).
6) W. H. Kelly, V. J. Folen, M. Hass, W. N. Schreiner, and C. B. Bead, *Phys. Rev.*, **124**, 80 (1961).
7) A. H. Morrish and K. Haneda, *J. Magn. Magn. Mater.*, **35**, 105 (1983).
8) H. Yamada, M. Takano, M. Kiyama, T. Takada, T. Shinjo, and K. Watanabe, "Advances in Ceramics," Vol. 16, 4th Intern. Conf. Ferrites, Am. Cerm. Soc. (1986), p. 169.
9) M. Schieber, *J. Inorg. Nucl. Chem.*, **26**, 1363 (1964).

 © 1987 The Chemical Society of Japan Bull. Chem. Soc. Jpn., 60, 3935—3939 (1987)

The Vapor Saturation Method for Preparing Aqueous Solutions of Solid Aromatic Hydrocarbons

Mayumi Akiyoshi, Toshio Deguchi, and Isao Sanemasa*
Department of Chemistry, Faculty of Science, Kumamoto University,
Kurokami 2-39-1, Kumamoto 860
(Received March 26, 1987)

A new method to prepare aqueous solutions saturated with solid aromatic hydrocarbons by making use of solute vapor is presented. Air is bubbled through an organic solvent in which an excess quantity of a solid hydrocarbon to be studied has been added, and the resulting vapor is introduced into water and circulated in a closed system. An aqueous solution saturated with a solid solute can thus be prepared in a short time without any need to remove solute microcrystals. Of benzene, cyclohexane, and 1-octanol used as organic solvents, 1-octanol is most promising for this purpose. Solubilities in water at 25.0 °C of nine aromatic hydrocarbons have been measured: Naphthalene, biphenyl, anthracene, phenanthrene, fluoranthene, (*o*-, *m*-, *p*-)terphenyl, and triphenylene. This method can be used for these solutes except phenanthrene.

The aqueous solubility of aromatic hydrocarbons is a fundamental physicochemical property important in both applied and theoretical chemistry. In recent years, partition studies on hydrophobic substances between 1-octanol and water have become of interest, which require convenient techniques to provide accurate solubility data.

For the preparation of aqueous solutions saturated with liquid or solid solutes, the most widely used technique is the "shake-flask" method.[1-14] This technique usually consists of two steps: (1) A mixture of water and an excess quantity of a solute is mechanically shaken for at least 24 h; (2) to ensure the removal of the excess solute phase, the mixture is allowed to stand for at least 24 h, centrifuged, or filtered. The second step is important in solubility measurements since hydrocarbons can exist in colloidal, micellar, or microparticulate form in appreciable quantities.

In order to speed up these time-consuming steps, the "generator column" method has recently been proposed.[15-19] This method adopts continuous pumping of water through a column filled with an inert support material, such as glass or quartz beads, coated with the solute of interest. When this method is combined with a second column packed with a hydrophobic support, the dissolved solute can be easily concentrated, and, moreover, in conjunction with the chromatographic technique, impurities in the solute material, when present, can be separated.

The aqueous solubility of various volatile nonelectrolytes has been observed to obey Henry's law.[20-24] This means that liquid or solid solute itself is not necessarily in contact with water to prepare aqueous solutions saturated with the solute, instead, the saturated vapor of solute at a constant temperature can be used. Based on this idea, we have proposed a method which involves a circulation of solute vapor in a closed system through water.[25] This technique has proved useful for saturating water with benzene or alkylbenzenes.[26-28] This technique, however, cannot be applied to such solutes as are present in solid state, probably due to the lack of effective vaporization of solid solute.

This study is concerned with the development of a new method to prepare aqueous solutions saturated with solid aromatic compounds. To a suitable organic solvent a solid solute to be studied is added in excess so that a part of the solute is always present in solid state in the solvent. Then, air is bubbled through the organic solvent, and the resulting vapor is introduced into water and circulated in a closed system. Our objects are (1) to compare solubility results with those reported in literatures, (2) to see the effect of organic solvents used to dissolve solid solutes on the solute aqueous solubility, and (3) to search such a possibility that the present method might offer some information about binary systems consisting of an aromatic hydrocarbon and an organic solvent.

Experimental

Materials. Distilled deionized water was used throughout this work. Naphthalene, biphenyl (98%), fluoranthene (98%), (*o*-, *m*-, *p*-)terphenyls, and triphenylene (97%), each of analytical reagent grade, and anthracene and phenanthrene, each of authentic (guaranteed) sample, were used as solutes without further purification; the minimum purities specified by the manufacturers (Wako Pure Chemical and Nakarai Chemicals Co.) are given in the parentheses. Benzene (99.5%), cyclohexane (99.5%), and 1-octanol (95%) were used as organic solvents to dissolve solid solutes. Amberlite XAD-2 resin (Rohm and Hass) of 80—100 mesh was used, when necessary, to concentrate solutes dissolved in water.

Apparatus and Procedures. The apparatus used for preparing aqueous solution saturated with solute vapor is essentially the same as that previously used,[25] except some minor modifications. The apparatus was composed of two main glass parts: a pear-shaped vessel of 30 cm^3 capacity in which a solid solute was placed together with an organic solvent (we call this vessel the "solute reservoir") and a pear-shaped vessel of 80 cm^3 capacity with a narrow orifice in the bottom in which up to 50 cm^3 water was placed (we

call this vessel the "solubility flask"). A Viton diaphragm airpump (Iwaki Type AP-32 Z) was incorporated into the assembly. The apparatus was fixed on a board and immersed, except the airpump part, in a water bath thermostated at 25.0±0.1 °C; the temperature of the airpump part was kept a few degrees higher than 25 °C.

An excess quantity of a solid aromatic hydrocarbon was added to an Erlenmeyer's flask and dispersed in an organic solvent by applying ultrasonic vibrations (Kaijo Denki "Sono Cleaner Mini") for ca. 1 h, and a 5—10 cm^3 portion with some solute crystals was pipetted out of the flask and transferred into the solute reservoir. By means of the pump, air was bubbled at a flow rate of ca. 0.5 or 1 $dm^3\ min^{-1}$ through the solute reservoir via a sintered glass ball, and the resulting vapor of the organic solvent and solid aromatic hydrocarbon was introduced through a trap into water in the solubility flask to disperse via a sintered glass ball, and circulated in a closed system.

After solubility equilibrium was attained, the apparatus was withdrawn out of the bath. A glass plug attached to the bottom of the solubility flask through a Teflon tube was removed, and a suitable portion of the aqueous phase was transferred to a 50 cm^3 cylindrical separatory funnel, in which 5 cm^3 of $CHCl_3$ had previously been placed; the funnel had been calibrated so that the volume of a water sample taken in can be read out to 0.1 cm^3. The extract, after dehydrated with anhydrous sodium sulfate, was analyzed with a Hitachi 100-50 spectrophotometer. In handling three solutes, anthracene, *p*-terphenyl, and triphenylene, 100 cm^3 of water sample (2×50 cm^3) was passed through an XAD-column and the solute adsorbed on the resin was eluted out with 5 cm^3 of $CHCl_3$.

Measurements were repeated on at least four water samples separately prepared, and the avarage was taken as the solubility.

Results

Factors Affecting Aqueous Solubility. The time required for saturating water with solute vapor will depend highly on the vapor circulation rate. In order to speed up the process, high circulation rates are desired. In practice, however, the rate was set at ca. 0.5 $dm^3\ min^{-1}$ for 1-octanol and at ca. 1 $dm^3\ min^{-1}$ for benzene and cyclohexane. With higher rates, the dead volume of the solute reservoir was so small that the organic solvent was caused to splash to a considerable degree into the adjacent trap. When 1-octanol, more viscous than the other two, was used, the circulation rate needed to be suppressed, otherwise part of the solvent was carried away into the trap.

At the prescribed circulation rate, the aqueous phase was found to become saturated with a solute in 30 min when benzene or cyclohexane was used as organic solvent and in 90 min in the case of 1-octanol. The results observed for naphthalene are shown in Fig. 1. The concentration of solute in the "saturated" aqueous solution was found to depend upon the organic solvent used to dissolve solid aromatic hydrocarbons. For three different solutes

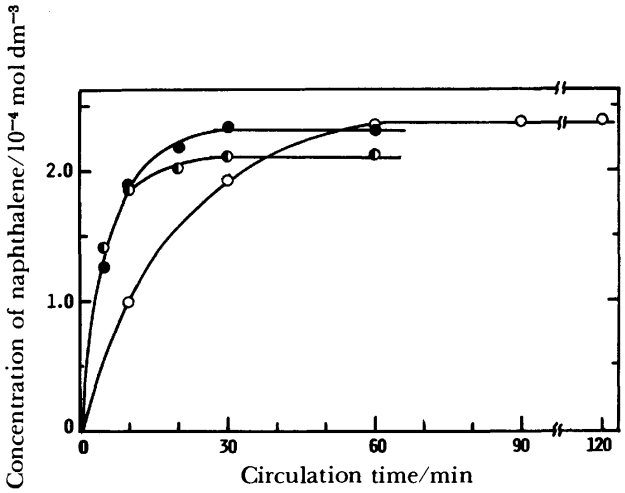

Fig. 1. Concentration of naphthalene in water at 25 °C vs. vapor circulation time. Vaporized from benzene(◐), cyclohexane(●), and 1-octanol(○) solutions.

Table 1. Dependence of Aqueous "Solubilities" of Naphthalene, Biphenyl, and *p*-Terphenyl on Organic Solvents Used to Dissolve the Solutes

Solute	Organic solvent used to dissolve the solute	Aqueous solubility measured/mol dm^{-3}
Naphthalene	Benzene	2.10×10^{-4}
	Cyclohexane	2.30×10^{-4}
	1-Octanol	2.35×10^{-4}
Biphenyl	Cyclohexane	3.92×10^{-5}
	1-Octanol	4.57×10^{-5}
p-Terphenyl	Benzene	3.8×10^{-8}
	1-Octanol	7.8×10^{-8}

the effect of organic solvents on their aqueous solubilities were studied (Table 1). The highest "solubility" was observed when the solid solute was dissolved in 1-octanol, while the lowest was observed with benzene.

Solubility of Solid Aromatic Hydrocarbons in Water. With 1-octanol as organic solvent, aqueous solutions saturated with solid aromatic hydrocarbons with two or three benzene rings were prepared, and each solubility at 25.0 °C was determined. The results are given in Table 2 together with literature values. There have been published a large number of data for naphthalene, biphenyl, anthracene, and phenanthrene and a less number for fluoranthene and triphenylene, but no data, to our knowledge, on terphenyls.

The present vapor saturation method was found inapplicable to phenanthrene; no reproducible results were obtained for this solute, and, moreover, the estimated "solubility" was far lower than the lowest literature value. Cyclohexane was used instead of 1-

Table 2. Solubilities of Solid Aromatic Hydrocarbons in Water at 25 °C

Solute	Solubility/mol dm^{-3}	
	This work	Literature value
Naphthalene	$(2.35\pm0.06)\times10^{-4}$	{2.34,[7] 2.36,[8] 2.39,[17] 2.43,[5,6,14] 2.45,[10] 2.46,[1] 2.47,[9,19] 2.472,[15] 2.53,[13] 2.54,[11] 2.62,[4] 2.68,[3]}$\times10^{-4}$
Biphenyl	$(4.57\pm0.05)\times10^{-5}$	{3.85,[1] 3.91,[12] 4.35,[18] 4.5,[9] 4.57,[10] 4.59,[5] 4.80,[6] 4.85,[3] 4.86,[13] 4.9[19]}$\times10^{-5}$
Anthracene	$(2.5\pm0.1)\times10^{-7}$	{2.30,[8] 2.50,[15,17] 2.6,[19] 4.1,[9] 4.17,[10] 4.2,[5,19] 4.47[2]}$\times10^{-7}$
Phenanthrene		{5.58,[1] 5.61,[17] 5.62,[15] 6.0,[6] 6.46,[8] 6.62,[5,19] 7.08,[10] 7.24,[9] 9.0[2]}$\times10^{-6}$
Fluoranthene	$(1.4\pm0.1)\times10^{-6}$	{1.02,[15] 1.26,[10] 1.3,[9,19] 1.32[2]}$\times10^{-6}$
o-Terphenyl	$(5.38\pm0.02)\times10^{-6}$	
m-Terphenyl	$(6.56\pm0.02)\times10^{-6}$	
p-Terphenyl	$(7.8\pm0.6)\times10^{-8}$	
Triphenylene	$(1.8\pm0.2)\times10^{-7}$	{0.29,[16] 1.86,[10] 1.88,[2] 1.9[9]}$\times10^{-7}$

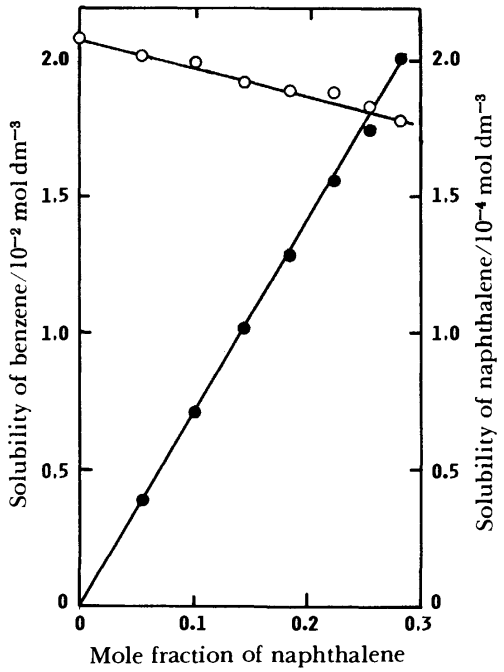

Fig. 2. Naphthalene-benzene binary system. Aqueous solubility of naphthalene(●) and benzene(○) at 25 °C.

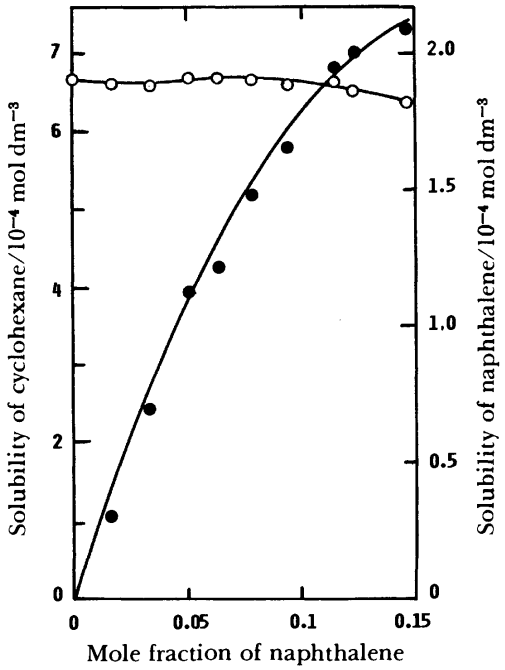

Fig. 3. Naphthalene-cyclohexane binary system. Aqueous solubility of naphthalene(●) and cyclohexane(○) at 25 °C.

octanol only to produce almost the same unsatisfactory results.

Naphthalene-Benzene and Naphthalene-Cyclohexane Binary Systems. A known quantity of naphthalene was added to a known amount of benzene or cyclohexane up to near saturation, and the vapor phase was circulated to saturate water. The concentration of each component in the water was measured after solubility equilibrium was attained.[29] The results are shown in Figs. 2 and 3 as a function of the mole fraction of naphthalene.

Discussion

Evaluation of the Present Method and Interpretation of Solubility Results. Although there are no available data on terphenyls, their solubility values estimated in this work seem to be reliable judging from their good reproducibility; the extremely low solubility observed for *p*-isomer may be ascribed to its relatively high melting point compared to the other two isomers. The generator column method gives an extremely low solubility for triphenylene,[16] but our value is in good agreement with the results obtained by the shake-flask method.

For anthracene, the solubility values reported to data are grouped into two well-defined values: 2.5 and 4.2×10^{-7} mol dm^{-3}. May et al.,[15] whose value belongs to the lower, attributed the higher value to the structural isomer, phenanthrene, present as an impurity. It is, however, still difficult to explain why one group is almost constantly 1.7 times as high as the other. When we consider that, as they insist, anthracene is contaminated with phenanthrene in at least 2% in most commercial products (the quantity sufficiently large for saturating water), that phenanthrene is ca. 20 times as water-soluble as anthracene, and that the molar absorptivity of phenanthrene is ca. 0.4 times that of anthracene at the same measuring wavelength in the same extractant, the "apparent" solubility of anthracene in water amounts to ca. 9 times the "true" solubility. Is there such a possibility that phenanthrene molecules once dissolved in water would come out to be held on the solid anthracene surface and that adsorption equilibrium would be realized between phenanthrene molecules in water and those in the solid surface to yield constantly the 1.7 times overestimated solubility of anthracene? Is there not such a possibility that anthracene molecules would dimerize in water in contact with solid anthracene? In any event, the present vapor saturation approach supports the lower value for this solute solubility.

The present method failed to saturate water with phenanthrene. At present we cannot provide satisfactory explanations to this failure. It is probable that the solid phenanthrene phase is to include 1-octanol molecules to form a complexed phase, presumably, with a changeable composition depending upon certain variables such as the ratio of solvent to solute and the size and surface state of solid particles. Since literature values themselves are scattered over a relatively wide range compared to the other solutes, we further speculate that water molecules also are more or less liable to be incorporated in the solid phenanthrene phase. There is, however, no evidence to support this.

Applicability of the Present Method. There are two potential applications of the method proposed here. One is to study the solubilizing effect of coexisting solutes such as surfactant on the aqueous solubility of solid aromatic hydrocarbons. Such studied should be conducted in the absence of solute phase of interest in excess, otherwise coexisting solute molecules will be adsorbed on the solid solute surface to change solution properties. The present method meets this requirement.

The other application of this method is to study the aqueous solubility of solid hydrocarbon as a function of its composition in an organic solvent used to dissolve the solid solute. Here, we have studied systems naphthalene-benzene and naphthalene-cyclohexane as examples. As can be seen from Figs. 2 and 3, the solubility of naphthalene increases almost linearly with its mole fraction in benzene, but this is not the case with cyclohexane. This seems to reflect the situation that the former system is nearly an ideal solution, whereas the latter system is far from being ideal.[30,31]

A question should naturally arise that the organic solvent phase is to get saturated with water vapor so as never to be made up by any "pure" binary system. We nevertheless approximate it a "binary" system, because the solubility of water in organic solvents such as benzene and cyclohexane is sufficiently low (in the case of 1-octanol this approximation is not valid because of high water solubility in this solvent).

The aqueous phase is to be saturated not only with the solid solute of interest but also with the organic solvent used to dissolve the solid solute, so that another question should arise as to whether any interaction between both the solutes takes place in the aqueous phase. Chiou et al.[32] have suggested a solubilization effect of 1-octanol; the solubility of a solute in water which has been saturated with 1-octanol is larger than that in 1-octanol-free water. This effect probably present itself only when there is an appreciable 1-octanol-solute interaction in the aqueous phase. Miller et al.,[19] on the other hand, have demonstrated, by using polynuclear aromatic hydrocarbons, biphenyl, and polychlorinated biphenyls as solutes, that 1-octanol saturated in water has little effect on the solubility of the substances in water. If any interaction does occur between solutes in water, benzene would have a stronger effect than 1-octanol and cyclohexane, because the concentration of benzene saturated in water is larger than those of 1-octanol and cyclohexane by one and two orders of magnitude, respectively.

It seems reasonable to interpret the dependence of the aqueous solubility of the solid hydrocarbon solutes on the organic solvents used to dissolve them (Table 1) in terms of the solute vapor pressure. We cannot discuss this point since no solute vapor pressures in the solute-organic solvent systems were measured in this study.

References

1) L. J. Andrews and R. M. Keefer, *J. Am. Chem. Soc.*, **71**, 3645 (1949).

2) H. B. Klevens, *J. Phys. Colloid Chem.*, **54**, 283 (1950).

3) R. L. Bohon and W. F. Claussen, *J. Am. Chem. Soc.*, **73**, 1571 (1951).

4) J. E. Gordon and R. L. Thorne, *J. Phys. Chem.*, **71**, 4390 (1967).

5) R. Wauchope and F. Getzen, *J. Chem. Eng. Data*, **17**, 38 (1972).

6) R. P. Eganhouse and J. A. Calder, *Geochim. Cosmochim. Acta*, **40**, 555 (1976).

7) F. M. van Meter and H. M. Neumann, *J. Am. Chem. Soc.*, **98**, 1382 (1976).
8) F. P. Schwarz, *J. Chem. Eng. Data*, **22**, 273 (1977).
9) D. Mackay and W. Y. Shiu, *J. Chem. Eng. Data*, **22**, 399 (1977).
10) S. H. Yalkowsky and S. C. Valvani, *J. Pharm. Sci.*, **69**, 912 (1980).
11) A. Vesala and H. Lönnberg, *Acta Chem. Scand., Ser. A*, **34**, 187 (1980).
12) S. Banerjee, S. H. Yalkowsky, and S. C. Valvani, *Environ. Sci. Technol.*, **14**, 1227 (1980).
13) M. Janado, Y. Yano, Y. Doi, and H. Sakamoto, *J. Solution Chem.*, **12**, 741 (1983).
14) D. Bennett and W. J. Canady, *J. Am. Chem. Soc.*, **106**, 910 (1984).
15) W. E. May, S. P. Wasik, and D. H. Freeman, *Anal. Chem.*, **50**, 175, 997 (1978).
16) W. E. May, *Adv. Chem. Ser.*, **185**, 143 (1980).
17) S. P. Wasik, M. M. Miller, Y. B. Tewari, W. E. May, W. J. Sonnefeld, H. DeVoe, and W. H. Zoller, *Residue Reviews*, **85**, 29 (1983).
18) M. M. Miller, S. Ghodbane, S. P. Wasik, Y. B. Tewari, and D. E. Martire, *J. Chem. Eng. Data*, **29**, 184 (1984).
19) M. M. Miller, S. P. Wasil, G. L. Huang, W. Y. Shiu, and D. Mackay, *Environ. Sci. Technol.*, **19**, 522 (1985).
20) R. L. Brown and S. P. Wasik, *J. Res. Natl. Bur. Stand., Sec. A*, **78**, 453 (1974).
21) C. Sutton and J. A. Calder, *J. Chem. Eng. Data*, **20**, 320 (1975).
22) I. Sanemasa, *Bull. Chem. Soc. Jpn.*, **48**, 1795 (1975).
23) D. Mackay, W. Y. Shiu, and R. P. Sutherland, *Environ. Sci. Technol.*, **13**, 333 (1979).
24) I. Sanemasa, T. Kobayashi, C. Y. Piao, and T. Deguchi, *Bull. Chem. Soc. Jpn.*, **57**, 1352 (1984).
25) I. Sanemasa, M. Araki, T. Deguchi, and H. Nagai, *Bull. Chem. Soc. Jpn.*, **55**, 1054 (1982).
26) I. Sanemasa, S. Arakawa, M. Araki, and T. Deguchi, *Bull. Chem. Soc. Jpn.*, **57**, 1539 (1984).
27) I. Sanemasa, S. Arakawa, C. Y. Piao, and T. Deguchi, *Bull. Chem. Soc. Jpn.*, **58**, 3033 (1985).
28) I. Sanemasa, Y. Miyazaki, S. Arakawa, M. Kumamaru, and T. Deguchi, *Bull. Chem. Soc. Jpn.*, **60**, 517 (1987).
29) Benzene was determined by UV spectroscopy after correcting the naphthalene absorption, and cyclohexane was analyzed by gas chromatography in the same way as described in Ref. 28.
30) E. McLaughlin and H. A. Zainal, *J. Chem. Soc.*, **1959**, 863.
31) E. McLaughlin and H. A. Zainal, *J. Chem. Soc.*, **1960**, 3854.
32) C. T. Chiou, D. W. Schmedding, and M. Manes, *Environ. Sci. Technol.*, **16**, 4 (1982).

 © 1987 The Chemical Society of Japan Bull. Chem. Soc. Jpn., 60, 3941—3946 (1987)

The Condensation and Decomposition of Alkaline Earth and Phenyl Phosphoramidates with Acids

Shoji SATO, Takao TAKAYANAGI, and Makoto WATANABE*
Department of Industrial Chemistry, Chubu University, Matsumoto-cho, Kasugai, Aichi 487
(Received April 21, 1987)

Alkaline earth and phenyl phosphoramidates were reacted with dried hydrogen chloride, acetic acid, and oxalic acid. The alkaline earth phosphoramidates other than the magnesium salt reacted with the acids to produce ortho- and polyphosphates, but did not react with them to make polyphosphates containing imino groups. The hydrolysis of the phosphoramidates to orthophosphate has been considered to be the initiation of the production of polyphosphates:

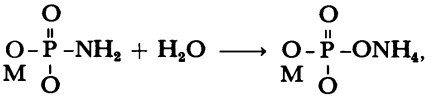

where M stands for an alkaline earth metal ion. The formation of polyphosphates can be explained, for example, by this equation:

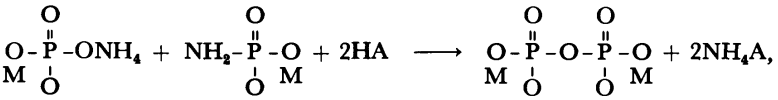

where HA stands for acid. Magnesium phosphoramidate reacted with acetic acid and oxalic acid to produce orthophosphate, polyphosphates, and imidodiphosphate. The production of the imidodiphosphate can be indicated by the following equation:

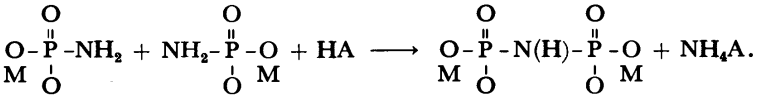

There are many types of phosphorus-nitrogen compounds. Phosphazenes are the best-known and the most intensively investigated compounds because they can be used as inorganic rubber and have been thought to have widely varying applications in industry. Other phosphorus-nitrogen compounds have not yet been well-studied, however. Phosphoramidates can be used as a new type of chemical fertilizer, for they have a P-N covalent bond, and as flame-proof materials. They can also be used as starting materials for the preparation of many organic and inorganic phosphorus compounds. The present authors have previously reported the syntheses and thermal behavior of some phosphoramidates.[1-6] The phosphoramidates produced ortho- and polyphosphates and did not make polyphosphates containing imino groups when they were heated in air at a moderately high temperature (100—1000 °C). An amino group on phosphoramidates was, accordingly, thermally unstable in air, and it was impossible to make imidodiphosphate from phosphoramidates by thermal condensation. Therefore, in this work, the chemical reactions of alkaline earth and phenyl phosphoramidates with hydrogen chloride, acetic acid, and oxalic acid have been done in order to study the condensation and decomposition of the amino groups in the phosphoramidates.

Experimental

Preparation of Phosphoramidates. The phenyl phosphoramidate and potassium hydrogenphosphoramidate were prepared by the method described in Ref. 7. The alkaline earth phosphoramidates other than strontium phosphoramidate were prepared by wet processes.[3,4,6] The strontium phosphoramidate dihydrate, $SrPO_3NH_2 \cdot 2H_2O$, was prepared by this method: Strontium dichloride hexahydrate (5.4 g) was dissolved in 120 cm^3 of water, and the pH of the solution was adjusted to 10.5 with aqueous ammonia. Potassium hydrogenphosphoramidate (5.4 g) was dissolved in 400 cm^3 of water. The solutions were mixed by stirring at 5 °C, and a precipitate was filtered off. Acetone was added to the filtrate, and a white precipitate was filtered off, washed with 50 vol% aqueous ethanol and acetone, and then dried in air at room temperature (15—25 °C).

Reaction of Phosphoramidates with Hydrogen Chloride. About 3—5 g of a phosphoramidate sample was put in a reaction glass tube. Dried hydrogen chloride, which had been prepared by adding concentrated hydrochloric acid to concentrated sulfuric acid and by then passing the resulting gas through concentrated sulfuric acid, was introduced into the reaction tube. The reaction product was washed quickly with ethanol to remove the HCl gas adsorbed on the product.

Reaction of Phosphoramidates with Acetic Acid. About 2 g of a phosphoramidate sample was placed in a mixed

solution of 5 cm^3 of acetic acid and 20 cm^3 of chloroform. The resulting mixture was heated at 25 and 60 °C while being stirred. The solid product was filtered off and washed with ethanol. The phenyl phosphoramidate dissolved in a solution of acetic acid. After the reaction, water was added to the reaction mixture; a white precipitate was filtered off and subjected to further analysis.

Reaction of Phosphoramidates with Oxalic Acid. Oxalic acid (3 g) was dissolved in 100 cm^3 of ethanol, after which about 2 g of phosphoramidate was added to the solution. The mixture was heated at 25 and 60 °C while being stirred. The product was treated in the same way as in the reaction with acetic acid.

Quantitative Analysis of Nitrogen. The amount of total nitrogen and that of ammonium ions in a sample were measured by the Kjeldahl technique.

Paper Chromatography and Colorimetry of Phosphates. A sample (0.1 g) was dissolved in a 6% EDTA (disodium dihydrogen ethylenediaminetetraacetate dihydrate) solution by adjusting the pH of the solution to 9—10. The paper-chromatographic separation and the colorimetric determination of the phosphate species in the solution were performed by the method described in our previous paper.[1]

HPLC Technique. The HPLC system which was developed by Yoza was employed to achieve the separation and determination of phosphate species in a sample.[8] A separation column (2.6 mm×500 mm) with TSK-GEL (SAX-F0011), a Shimadzu spectrophotometer (UV-110-02), and the KCl eluents of 0.20 and 0.40 mol dm^{-3} were used to separate and determine the phosphate species in the sample solution. About 10 mg of the reaction product was dissolved in water or a 6% EDTA solution, and 200 mm^3 of the solution was injected into the column.

X-Ray Diffractometry. An X-ray diffraction diagram of a sample was taken with nickel-filtered Cu $K\alpha$ radiation using a Rigaku X-ray diffractometer, RAD-1B.

IR Spectrophotometry. An IR spectrum of a sample was recorded on a JASCO IR spectrophotometer, A-3, using the KBr disc method.

^{31}P NMR Measurement. The reaction products of alkaline earth phosphoramidates and that of phenyl phosphoramidate were dissolved in a 6% EDTA solution and ethanol respectively. The ^{31}P NMR spectra of the sample solutions were taken by means of a JNM-GX270 spectrograph. The chemical shifts are reported relative to external 85%-orthophosphoric acid, with the positive shifts being downfield.

Results and Discussion

Reaction with Hydrogen Chloride. The contents of nitrogen and phosphate species in the reaction products are presented in Table 1, along with the X-ray-diffraction data. The paper-chromatographic separation between phosphoramidate and orthophosphate could not be achieved with the developing solvents employed in this experiment. According to the results shown in Table 1, alkaline earth phosphoramidate reacted with HCl gas to produce ortho- and polyphosphates. The amino groups of the phosphoramidates were converted to ammonia at the same time. The IR spectra of the products in Fig. 1 indicate the absorption of NH_4^+ at 1400 cm^{-1} and those of the P-O-P and/or P-N(H)-P linkages at about 900 and 700 cm^{-1} respectively. The IR data agree well with those in Table 1. The polyphosphates formed by the reaction of strontium phosphoramidate with HCl gas degraded to phosphates with shorter chain lengths with the passage of the reaction time. The data in Table 1 and Fig. 1 do not provide any information about the formation of a P-N(H)-P linkage in the products. The ^{31}P NMR spectra of the products of alkaline earth phosphoramidates gave peaks due to phosphoramidate, orthophosphate, and polyphosphates; they are shown

Table 1. Compositions of the Reaction Products of Phosphoramidates with HCl Gas

Phosphoramidate	Reaction time/min	Total N/%	N/% as NH_4^+	X-Ray dif.	Phosphate (P%)			
					Amido and Ortho	Di	Tri	Higher
$MgPO_3NH_2 \cdot 7H_2O$	60	5.5	4.0	NH_4Cl, UK	41.5	31.1	20.1	7.3
	180	5.1	4.5	NH_4Cl, UK	44.3	49.4	6.2	
	300	4.9	4.8	NH_4Cl, UK	41.3	47.5	5.5	5.7
$CaPO_3NH_2 \cdot H_2O$	60	6.6	3.3	NH_4Cl, UK	59.3	19.5	8.8	12.4
	180	5.9	4.3	NH_4Cl, UK	57.3	18.0	12.6	12.1
	300	5.7	5.4	NH_4Cl, UK	57.1	18.3	13.5	11.1
$SrPO_3NH_2 \cdot 2H_2O$	60	3.9	3.1	NH_4Cl, UK	45.3	23.5	18.2	13.0
	180	3.4	3.3	NH_4Cl, UK	68.4	15.5	9.8	6.3
	300	4.0	4.0	NH_4Cl, UK	93.9	6.1	—	—
$BaPO_3NH_2 \cdot H_2O$	60	4.6	1.8	SM, UK	50.9	38.6	10.5	
	180	4.5	3.8	UK	63.8	26.6	9.6	
	300	4.0	3.0	UK	47.6	34.3	18.1	
$PONH_2(OC_6H_5)_2$	60	5.6	—	SM	100	—	—	—
	180	5.6	—	SM	100	—	—	—
	300	5.6	—	SM	100	—	—	—

SM and UK stand for the starting material and an unknown substance respectively.

in Fig. 2. The peaks of phosphoramidate (−3—−6 ppm) and an end-PO_4 group (−9—−11 ppm) in an acidic solution shifted to +7—+9 ppm and −4—−6 ppm respectively in a basic solution. The NMR

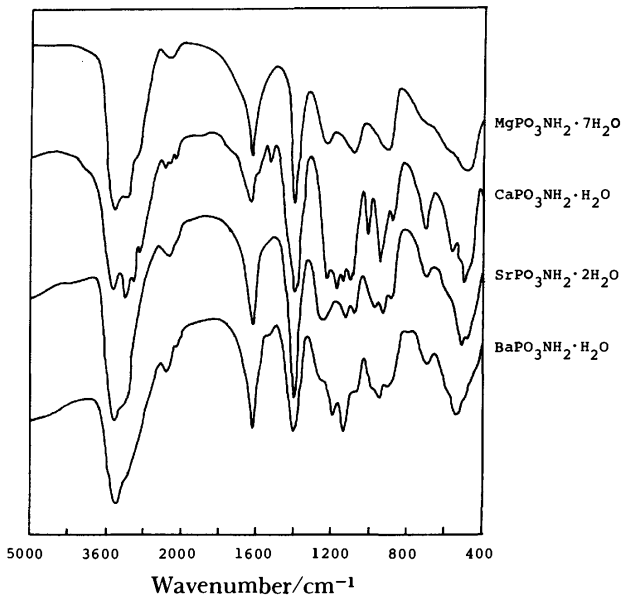

Fig. 1. IR spectra of the reaction products of phosphoramidates with HCl gas for 1 h.

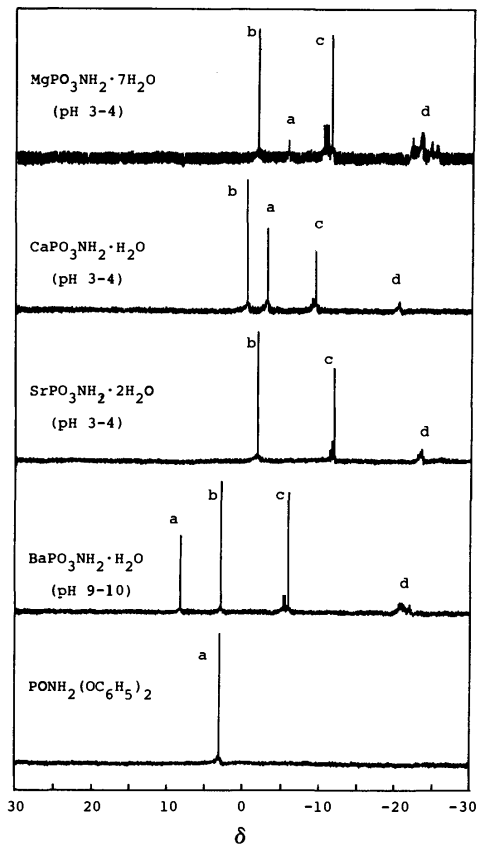

Fig. 2. ^{31}P NMR spectra of the reaction products of phosphoramidates with HCl.
a: Phosphoramidate, b: orthophosphate, c: end-PO_4 group, d: middle-PO_4 group.

data did not give any peak of a compound with a P-N(H)-P linkage. The reaction of alkaline earth phosphoramidates with HCl did not exhibit the following process:

$$-\overset{|}{\underset{|}{P}}-NH_2 + NH_2-\overset{|}{\underset{|}{P}}- + HCl \longrightarrow -\overset{|}{\underset{|}{P}}-N(H)-\overset{|}{\underset{|}{P}}- + NH_4Cl \quad (1)$$

Instead, the processes can be written thus for these reaction systems:

$$\begin{matrix} & & O & & & & O & \\ & & \| & & & & \| & \\ O & - & P & - & NH_2 & + H_2O \longrightarrow & O & - & P & - & ONH_4 \\ M & & | & & & & M & & | & & \\ & & O & & & & O & & & & \end{matrix} \quad (2)$$

$$\begin{matrix} O & & & & O & & \\ \| & & & & \| & & \\ O & - & P & - & ONH_4 + NH_2 & - & P \\ | & & & & & & | \\ M & & O & & & & O \end{matrix} \begin{matrix} - & O & \\ & \| & \\ & P & \\ & | & \\ & O & M \end{matrix} + 2HCl \longrightarrow$$

$$\begin{matrix} & & O & & O & & \\ & & \| & & \| & & \\ O & - & P & - & O & - & P \\ | & & & & & & | \\ M & & O & & O & & M \end{matrix} \begin{matrix} - & O & \\ & \| & \\ & P & \\ & | & \\ & O & M \end{matrix} + 2NH_4Cl \quad (3)$$

$$\begin{matrix} O & & O & & & & O & \\ \| & & \| & & & & \| & \\ O & - & P & - & O & + NH_2 - & P & - & O \\ | & & & & & & | & & \\ M & & O & & M & & O & & M \end{matrix} + 2HCl \longrightarrow$$

$$\begin{matrix} & & O & & O & & O & \\ & & \| & & \| & & \| & \\ O & - & P & - & O & - & P & - & O \\ | & & & & & & & & \\ M & & O & & O & & O & & M \\ & & & & M_{1/2} & & & & \end{matrix} + M_{1/2}Cl + NH_4Cl \quad (4)$$

The phosphoramidate with an OH group was considered to form a zwitterion:[9]

$$\begin{matrix} & & O & & & & \\ & & \| & & & & \\ O & - & P & - & NH_2 & + H_2O(HCl) \longrightarrow \\ M & & | & & & & \\ & & O & & & & \end{matrix}$$

$$\begin{matrix} & & O & & & & \\ & & \| & & & & \\ HO & - & P & - & NH_2 & + M_{1/2}OH(M_{1/2}Cl) \\ & & | & & & & \\ & & O & & & & \\ & & M_{1/2} & & & & \end{matrix} \quad (5)$$

$$\begin{matrix} & & O & & & & O & & \\ & & \| & & & & \| & & \\ HO & - & P & - & NH_2 & \longrightarrow & ^-O & - & P & - & NH_3^+ \\ & & | & & & & | & & & & \\ & & O & & & & O & & & & \\ & & M_{1/2} & & & & M_{1/2} & & & & \end{matrix} \quad (6)$$

This zwitterion is active and can react with water and phosphates to form ortho- and polyphosphates respectively:

$$\begin{matrix} & & O & & & & O & \\ & & \| & & & & \| & \\ ^-O & - & P & - & NH_3^+ + H_2O \longrightarrow & HO & - & P & - & ONH_4 \\ & & | & & & & | & & & \\ & & O & & & & O & & & \\ & & M_{1/2} & & & & M_{1/2} & & & \end{matrix} \quad (7)$$

$$\begin{matrix} & & O & & & & O & \\ & & \| & & & & \| & \\ ^-O & - & P & - & NH_3^+ + HO & - & P & - & ONH_4 + HCl \longrightarrow \\ & & | & & & & | & & \\ & & O & & & & O & & \\ & & M_{1/2} & & & & M_{1/2} & & \end{matrix}$$

$$\begin{matrix} & & O & & O & & \\ & & \| & & \| & & \\ HO & - & P & - & O & - & P & - & ONH_4 + NH_4Cl \\ & & | & & & & | & & \\ & & O & & & & O & & \\ & & & & M & & & & \end{matrix} \quad (8)$$

It is difficult to get information about the presence of the zwitterion, so it is impossible to determine which process is most reasonable for the reaction system. The water in the reaction is, however, thought to come from the crystal water and/or the adsorbed water of the phosphoramidates and from the slight amount of water in the gas in the reaction systems. It was difficult to remove the adsorbed water and the water in the gas completely. In the reactions of magnesium and strontium phosphoramidates, a degradation of polyphosphates to phosphates with shorter chain lengths was observed. Usually this reaction does not occur in a solid state at room temperature. The water contained in the products may be strongly acidic as a result of the dissolution of the HCl gas. The degradation can be caused by the acidic water. Phenyl phosphoramidate did not react with HCl gas at all.

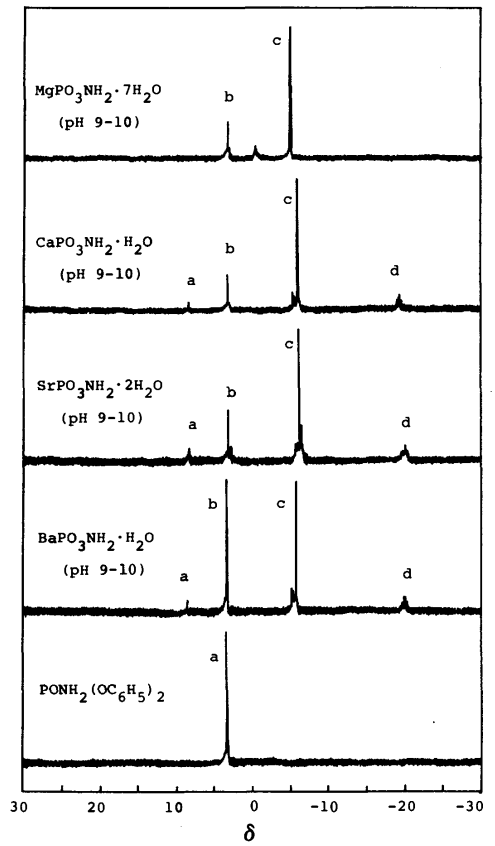

Fig. 3. ^{31}P NMR spectra of the reaction products of phosphoramidates with acetic acid.
a: Phosphoramidate, b: orthophosphate, c: end-PO_4 group, d: middle-PO_4 group.

Reaction with Acetic Acid. The chemical compositions and X-ray diffraction data of the products at 60 °C are shown in Table 2. (The data of the reaction products at 25 °C are not listed because the processes at 25 °C are almost the same as those at 60 °C except for the reaction rates.) Alkaline earth phosphoramidates reacted with acetic acid to produce ortho- and polyphosphates. The amino groups in the phosphoramidates seemed to be converted to ammonia at the same time. The total content of nitrogen in the products was small. Phenyl phosphoramidate did not react with acetic acid at all. The ^{31}P NMR spectral data in Fig. 3 indicate that the products of the alkaline earth phosphoramidates give peaks due to phosphoramidate, orthophosphate, and polyphosphates. Accordingly, the following several reaction processes can be written for the reaction systems:

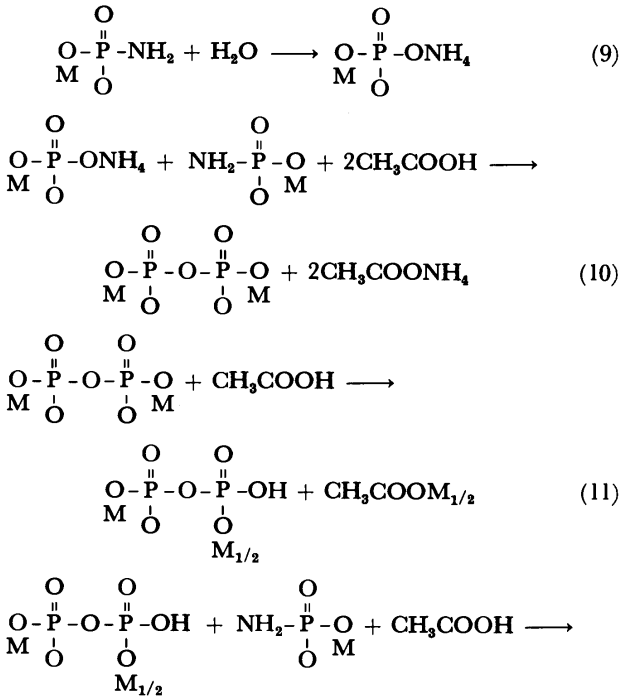

Table 2. Compositions of the Reaction Products of Phosphoramidates with Acetic Acid at 60 °C for 25 h

Phosphoramidate	Total N/%	N/% as NH_4^+	X-Ray dif.	Phosphate (P%)			
				Amido and Ortho	Di	Tri	Higher
$MgPO_3NH_2 \cdot 7H_2O$	2.9	2.5	AM	10.2	81.8	5.5	2.5
$CaPO_3NH_2 \cdot H_2O$	2.2	2.1	AM	18.0	64.6	17.4	
$SrPO_3NH_2 \cdot 2H_2O$	1.6	1.4	AM	23.0	60.3	15.9	0.8
$BaPO_3NH_2 \cdot H_2O$	1.9	0.5	UK	34.6	44.5	13.3	7.6
$PONH_2(OC_6H_5)_2$	5.6	—	SM	100	—	—	—

AM stands for an amorphous substance.

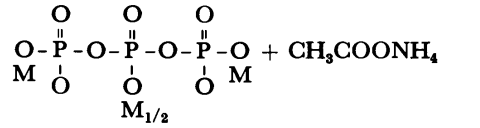

(12)

or

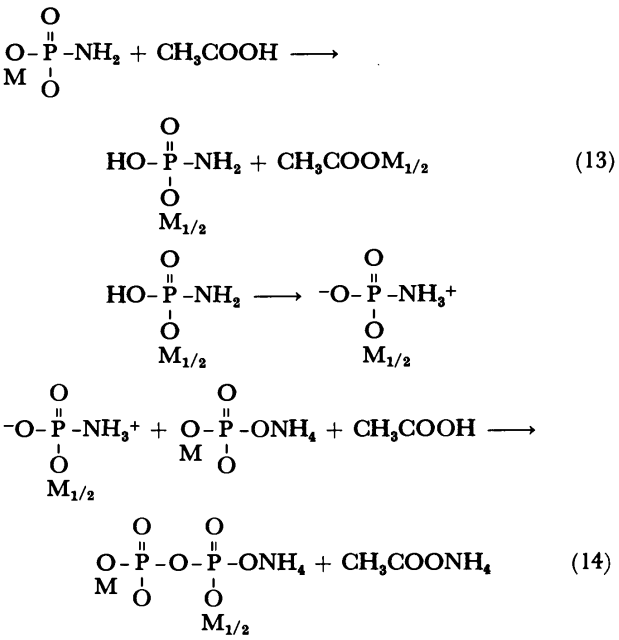

(13)

(14)

The water in the above equation can come from the crystal water and the adsorbed water of the phosphoramidates. The reaction product of magnesium phosphoramidate showed a small unknown ^{31}P NMR peak at about −0.3 ppm. An HPLC analysis of the product was performed in order to get information about the unknown substance. As Fig. 4 shows, the peak at 10.1 min was identified as that of imidodiphosphate. It was, therefore, concluded that magnesium phosphoramidate reacted with HCl to form orthophosphate, polyphosphates, and also imidodiphosphate according to this reaction:

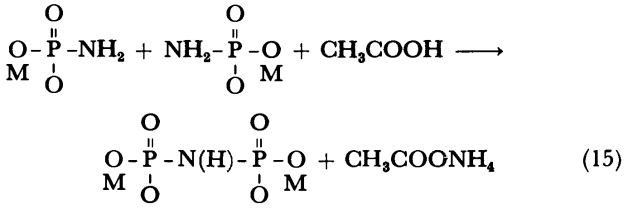

(15)

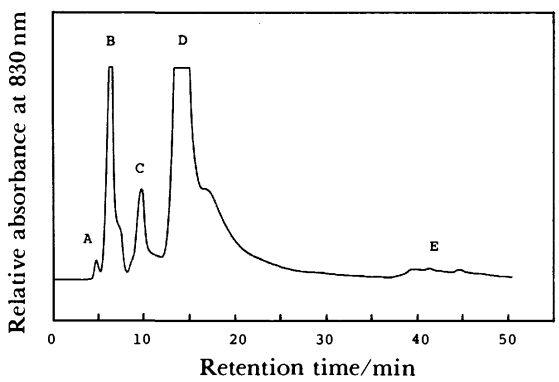

Fig. 4. HPLC profile of the reaction product of magnesium phosphoramidate with acetic acid at 60 °C for 25 h.
A: Phosphoramidate, B: orthophosphate, C: imidodiphosphate, D: diphosphate, E: higher polyphosphates.

Reaction with Oxalic Acid. The chemical compositions and X-ray diffraction data of the products are shown in Table 3, while the ^{31}P NMR spectra of the products are presented in Fig. 5. All the products except for that of the reaction of magnesium phosphoramidate were ortho- and polyphosphates. The ^{31}P NMR spectrum of the reaction product of magnesium phosphoramidate showed unknown peaks at about −0.3 and 2—4 ppm. The HPLC profile in Fig. 6 indicates that the product contains imidodiphosphate (10.3 min). Therefore, the unknown NMR peak at −0.3 ppm was concluded to be due to imidodiphosphate. The other NMR peaks at 2—4 ppm were thought to be caused by the polyphosphates containing a P-N(H)-P linkage, for the phosphates having a structure associated with a PO_4 group exhibit ^{31}P NMR peaks in a magnetic field higher than that of orthophosphate. Accordingly, one can write the following equation, for example, for the reaction of the phosphoramidates with oxalic acid:

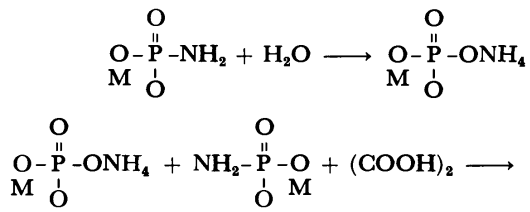

Table 3. Compositions of the Reaction Products of Phosphoramidates with Oxalic Acid at 60 °C for 25 h

Phosphoramidate	Total N/%	N/% as NH_4^+	X-Ray dif.	Phosphate (P%)			
				Amido and Ortho	Di	Tri	Higher
$MgPO_3NH_2 \cdot 7H_2O$	4.1	2.5	UK	42.8	36.8	11.8	8.6
$CaPO_3NH_2 \cdot H_2O$	4.4	3.3	SM, UK	45.2	30.3	24.5	
$SrPO_3NH_2 \cdot 2H_2O$	3.0	2.7	UK	28.2	30.8	41.0	
$BaPO_3NH_2 \cdot H_2O$	4.9	0.3	SM	85.7	10.4	3.9	
$PONH_2(OC_6H_5)_2$	5.6	—	SM	100	—	—	—

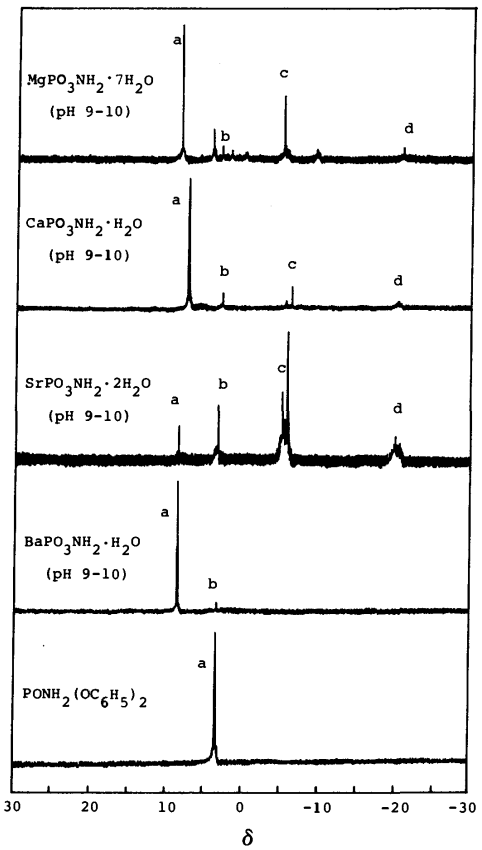

Fig. 5. ^{31}P NMR spectra of the reaction products of phosphoramidates with oxalic acid.
a: Phosphoramidate, b: orthophosphate, c: end-PO_4 group, d: middle-PO_4 group.

(16)

This condensation can also be written for magnesium phosphoramidate as:

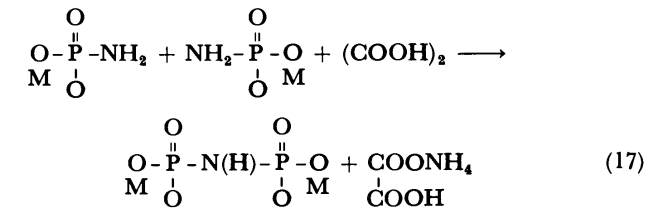

(17)

The reaction rate of the phosphoramidates with oxalic acid seemed to be slower than that with acetic acid, because the amounts of unreacted phosphoramidates in the reaction products with oxalic acid were larger than those with acetic acid.

Conclusion

Alkaline earth phosphoramidates other than magnesium salt reacted with hydrogen chloride, acetic acid, and oxalic acid to produce ortho- and polyphosphates. Magnesium phosphoramidate also produced ortho- and polyphosphates when it was reacted with hydrogen chloride, while the magnesium phosphoramidate reacted with acetic acid and oxalic acid to make orthophosphate, polyphosphates, and imidodiphosphate. The amount of the imidophosphate was small. Therefore, an amino group on alkaline earth phosphoramidates was unstable in these reaction systems and was decomposed to an ammonium ion. It seemed to be difficult to make imidodiphosphate by the chemical condensation of the phosphoramidates with the acids. Phenyl phosphoramidate was very stable and did not react with these acids at all.

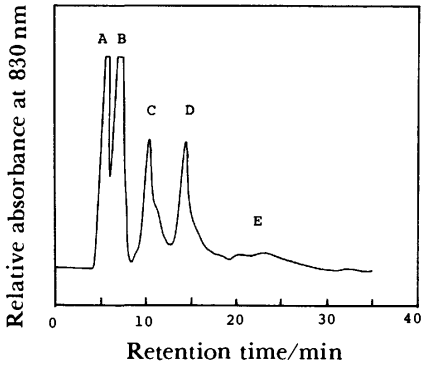

Fig. 6. HPLC profile of the reaction product of magnesium phosphoramidate with oxalic acid at 60 °C for 25 h.
A: Phosphoramidate, B: orthophosphate, C: imidodiphosphate D: diphosphate, E: higher polyphosphates.

References

1) M. Watanabe, T. Inagaki, and S. Sato, *Bull. Chem. Soc. Jpn.*, **56**, 458 (1983).
2) M. Watanabe, T. Inagaki, Y. Morii, and T. Yamada, *Setsuko To Setsukai*, **184**, 111 (1983).
3) M. Watanabe, Y. Morii, and S. Sato, *Bull. Chem. Soc. Jpn.*, **57**, 2087 (1984).
4) M. Watanabe, Y. Morii, and S. Sato, *Bull. Chem. Soc. Jpn.*, **57**, 2914 (1984).
5) S. Sato, M. Watanabe, and T. Yamada, *Setsuko To Setsukai*, **199**, 357 (1985).
6) S. Sato and M. Watanabe, *Bull. Chem. Soc. Jpn.*, **58**, 3513 (1985).
7) A. H. Herzog and M. L. Nielsen, *Anal. Chem.*, **30**, 1490 (1958), and the references cited therein.
8) Presented at the 4th symposium of Inorganic Phosphorus Chemistry, Nagoya, November 1983.
9) D. E. C. Corbridge, "Phosphorus," Elsevier, Amsterdam (1980), p. 222.

 © 1987 The Chemical Society of Japan Bull. Chem. Soc. Jpn., 60, 3947—3952 (1987)

Studies on Mixed Chelates. XV. An ESR Investigation of Solvatochromic Copper(II) Complexes with Various *N*-Alkylated Ethylenediamines and β-Diketonates

Naomi HOSHINO,† Naoko KODAMA, Yutaka FUKUDA, and Kozo SONE*
Department of Chemistry, Faculty of Science, Ochanomizu University,
Otsuka, Bunkyo-ku, Tokyo 112
(Received May 5, 1987)

ESR spectra were obtained for frozen solutions of copper(II) mixed chelate complexes, [Cu(diam)(dike)]-ClO_4, having various *N*-alkylated ethylenediamines (diam) and β-diketonate ligands (dike). The ESR *g*-factor ($g_{//}$) determined from apparently axial signals may be correlated by a decreasing function to pK_a of dikeH or diam ligand for the series of [Cu(tmen)(dike)]$^+$ or [Cu(diam)(acac)]$^+$, respectively. On the other hand, the $g_{//}$ values gradually increased when the former series of complexes were dissolved in more strongly coordinating solvents, and a relationship was found between $g_{//}$ and Donor Number of the solvent. These trends are regarded as ligand substituent effect and solvent effect on the $g_{//}$ factor, and are analyzed using a crystal field model of a C_{2v} symmetry.

Previous studies from this laboratory showed that a series of mixed chelate complexes of copper(II), [Cu(diam)(dike)]$^+$, in which diam and dike designate *N*-alkylated ethylenediamines and β-diketonates, respectively (Structure I), possesses an interesting coloring behavior in organic solutions.[1] Namely, in the case of [Cu(tmen)(acac)]ClO_4 (R^1—R^6=CH_3), for instance, the color of the solutions ranges from reddish violet (in nitrobenzene) through azure (in formamide) to green (in piperidine) and it follows the donor ability of the solvent. This has been quantitatively revealed by the linear relationship between the wavenumber of the visible absorption maximum and Donor Number (DN) of the solvent.[2-4]

Demonstration of such a remarkable solvatochromism has exemplified an application of this complex as a teaching tool or a color indicator for solvent parameters.[4] On the other hand, interpretation of this solvent effect on the electronic spectra of [Cu(diam)(dike)]$^+$ in solution has been limited to rather qualitative terms. Information on the structure of the complexes and the nature of solvent interaction is essential for full understanding of the chemistry of these mixed chelate complexes. We therefore conducted a new study on the electronic structure of [Cu(diam)(dike)]$^+$ complexes in solution by means of the ESR spectroscopy and attempted to find a correlation between the previously obtained absorption spectral data and the ESR parameters for the mixed chelate complexes. The ESR *g*-factors are under electronic effects of both diam and dike substituents and also of ligated solvent molecules. Both effects were interpreted using a simple crystal field model of C_{2v} symmetry, which is described in this paper.

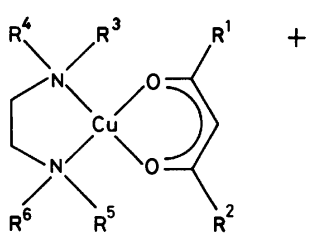

Structure I

† Present address: Department of Molecular Assemblies, Institute for Molecular Science, Myodaiji, Okazaki 444.

Experimental

Materials. Preparation of the complexes, [Cu(diam)-(dike)]ClO_4, used in this study has been reported elsewhere.[2] Our choice of the perchlorate salts is based on the fact that perchlorate ion does not coordinate to the mixed chelate cation in the solvents used in this study.[5] Table 1 provides a list of two series of complexes prepared, [Cu(tmen)(dike)]- and [Cu(diam)(acac)]ClO_4, and organic solvents used.

Measurements. Solvents used for ESR measurements were dried and purified by conventional methods. All of the solvents were added with tetrabutylammonium tetrafluoroborate (TBAB, 0.1 mol dm^{-3}) for the purpose of improving ESR resolution. ESR spectra were obtained for frozen solutions containing 5×10^{-3} mol dm^{-3} of complexes at 123 K in the X-band region using a JEOL JES-FE2XG spectrometer equipped with a 100 kHz magnetic field modulation. The ESR parameters were determined directly from the spectra, with the magnetic field calibrated using a standard Mn^{2+} sample (supplied by JEOL together with a computer program, GVALUE, for calculating *g*-values). Reported values involve errors within ±0.003 for $g_{//}$ values and $\pm3\times10^{-4}$ cm^{-1} for $A_{//}$ values. The $g_{//}$ was positioned at the center of four hyperfine peaks due to the Cu nucleus, three of which from lower magnetic field were well resolved.

Results and Discussion

ESR Data for [Cu(diam)(dike)]$^+$. The X-band ESR spectra obtained for the series of [Cu(diam)-(dike)]$^+$ complexes are typically of nearly axial type. An example is shown in Fig. 1. The apparent $g_{//}$

Table 1. List of Complexes and Solvents Used in This Study

Complex	[Cu(tmen)(dike)]ClO_4			
	dike[a]	R^1	R^2	pK_a of dikeH[b]
1	hfac	CF_3	CF_3	6.0
2	tfac	CF_3	CH_3	8.8
3	acac	CH_3	CH_3	12.7
4	dipm	$C(CH_3)_3$	$C(CH_3)_3$	15.9

Complex	[Cu(diam)(acac)]ClO_4					
	diam[a]	R^3	R^4	R^5	R^6	pK_a of diam[c]
3	tmen	CH_3	CH_3	CH_3	CH_3	14.7
5	asym-dmen	CH_3	CH_3	H	H	15.7
6	asym-deen	C_2H_5	C_2H_5	H	H	16.4
7	sym-deen	C_2H_5	H	C_2H_5	H	17.1
8	teen	C_2H_5	C_2H_5	C_2H_5	C_2H_5	—

Solvent	Abbreviation	Mark (in Figs. 2 and 3)	DN[d]
1,2-Dichloroethane	DCE	○	0
Nitromethane	NM	△	2.7
Acetonitrile	AN	□	14.1
Acetone	AC	●	17.0
Methanol	MeOH	▲	19
N,*N*-Dimethylformamide	DMF	■	26.6
Dimethyl sulfoxide	DMSO	▽	29.8

a) The following abbreviations were used for the ligands: hfac=1,1,1,5,5,5-hexafluoroacetylacetonate, tfac=1,1,1-trifluoroacetylacetonate, acac=acetylacetonate, dipm=dipivaloylmethanate, tmen=*N*,*N*,*N'*,*N'*-tetramethylethylenediamine, asym-dmen=*N*,*N*-dimethylethylenediamine, asym-deen=*N*,*N*-diethylethylenediamine, sym-deen=*N*,*N'*-diethylethylenediamine, teen=*N*,*N*,*N'*,*N'*-tetraethylethylenediamine. b) Reference 6. c) "Stability Constants Supplement No. 1," The Chemical Society, London (1971). d) DN: Donor Number of the solvent (see text and Reference 1).

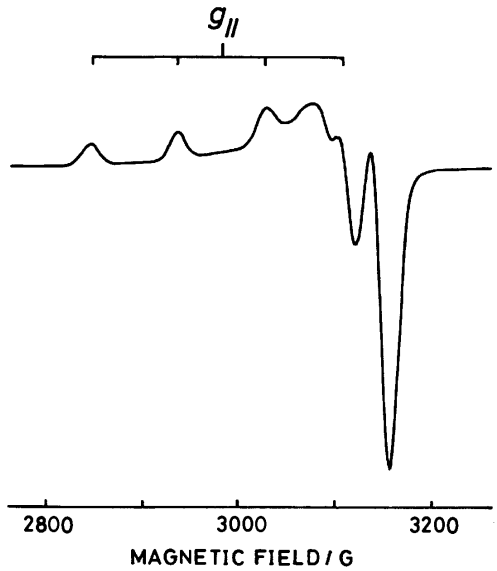

Fig. 1. ESR spectrum of $[Cu(tmen)(acac)]^+$ in acetonitrile containing 0.1 mol dm^{-3} of TBAB (ESR recorded at 123 K).

values can be determined from the spectra and fall in the range between 2.21 and 2.27, while the apparent $g_\perp$ values are found around g=2.0. As discussed below, theory predicts a slightly rhombic spectrum rather than an axial spectrum and simulation might yield two g-values resolved for the $g_\perp$ region. However, we focus our attention to the $g_{//}$ values alone in this paper. Table 2 lists the observed $g_{//}$ and $A_{//}$ values for all of the complexes studied in seven different solvents.

In analyzing the trend in g-values, two correlations are noted: (1) $g_{//}$ vs. ligand basicity (in the same solvent) and (2) $g_{//}$ vs. solvent basicity (for the same ligand pair). With regard to the first relationship, Fig. 2 compiles plots of $g_{//}$ values against pK_a of β-diketones and *N*-alkylated ethylenediamines. The pK_a of β-diketone varies widely upon substitution of R^1 and R^2 groups and is known to represent ligand basicity of β-diketonate.[6] The general trend noted in Fig. 2 is that, for each of the solvents, $g_{//}$ value of the complex decreases as the β-diketonate ligand becomes more basic or more strongly coordinating. In addition, it appears that curvature of the fitted lines increases across DCE→DMSO in the order of increasing donor ability of the solvent. Substitution on the diam ligands has little effect on the $g_{//}$ factor. Perhaps substitution of R^3—R^6 groups, which are not as remote as R^1 and R^2 groups, involves more than just electronic effect.

Table 2. ESR Parameters Determined for Various Solutions of Cu(II) Mixed Chelate Complexes

Complex	$g_{//}$ ($\lvert A_{//}\rvert/10^{-4}$ cm^{-1})						
	DCE	NM	AN	AC	MeOH	DMF	DMSO
1	2.231	2.237	2.239	2.246	2.242	2.260	2.264
	(190)	(185)	(183)	(182)	(183)	(188)	(180)
2	2.226	2.224	2.228	2.237	2.236	2.238	2.240
	(190)	(187)	(187)	(187)	(189)	(191)	(191)
3	2.219	2.218	2.220	2.228	2.226	2.225	2.233
	(192)	(192)	(188)	(190)	(189)	(190)	(190)
4	2.214	2.215	2.216	2.223	2.223	2.224	2.226
	(193)	(193)	(189)	(190)	(190)	(190)	(192)
5	2.220	2.221	2.225	2.228	2.227	2.230	2.233
	(195)	(192)	(191)	(190)	(190)	(185)	(188)
6	2.217	2.223	2.225	2.229	2.230	2.228	2.236
	(189)	(184)	(186)	(185)	(186)	(179)	(181)
7	2.220	2.222	2.227	2.228	2.230	2.232	2.232
	(191)	(191)	(189)	(190)	(189)	(183)	(188)
8	2.210	2.216	2.227	2.224	2.226	2.234	2.242
	(196)	(186)	(182)	(186)	(186)	(175)	(178)

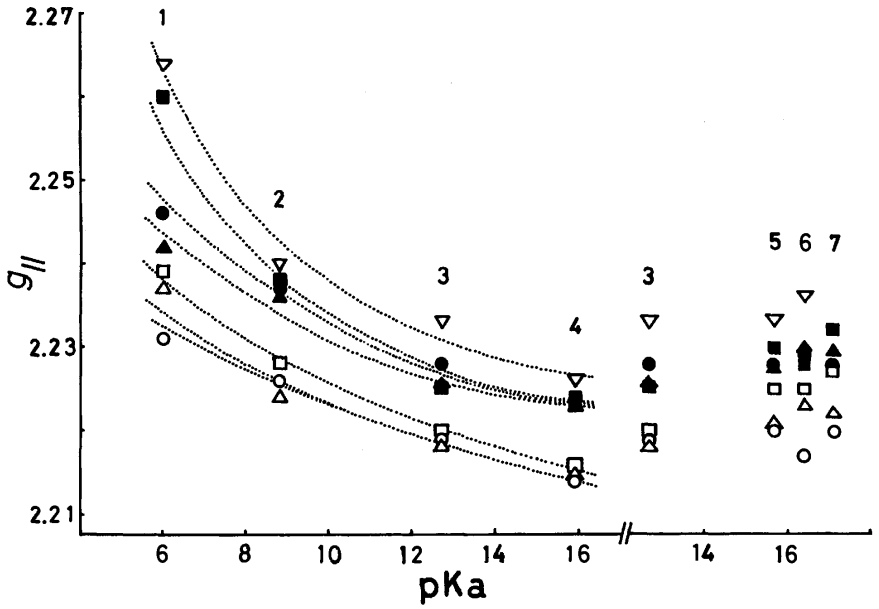

Fig. 2. Plots of $g_{//}$ values against pK_a of dikeH or diam for the series of [Cu(tmen)-(dike)]$^+$ (left) or [Cu(diam)(acac)]$^+$ (right) dissolved in different solvents.

On the other hand, Fig. 3 plots $g_{//}$ values for the series of four complexes, [Cu(tmen)(dike)]$^+$, against solvent Donor Number (DN). A general trend can be seen; for the same complex, the $g_{//}$ value increases as the solvent property changes from noncoordinating to strongly coordinating (increase in DN). Again the curvature of the fitted lines becomes greater across dipm→hfac, here in the order of decreasing in-plane ligand basicity.

Symmetry of [Cu(diam)(dike)]$^+$ and Copper d-Orbital Sequence. The molecular structure of [Cu-(diam)(dike)]$^+$ is shown schematically in Fig. 4, together with the coordinate system. It is safely assumed that the complex belongs to the point group C_{2v}. It should be noted that with this choice of coordinate system z axis remains as the unique symmetry axis so that a standard character table can be used, although the geometrical chelate plane is now in xz plane rather than more conventional xy plane. Thus each of the d-orbital wave functions is labelled as shown in Fig. 4.

Other workers have discussed the structure of Schiff base complexes of copper(II) as belonging to $C_{2v}(x)$ point group,[7,8] in which the coordinate system

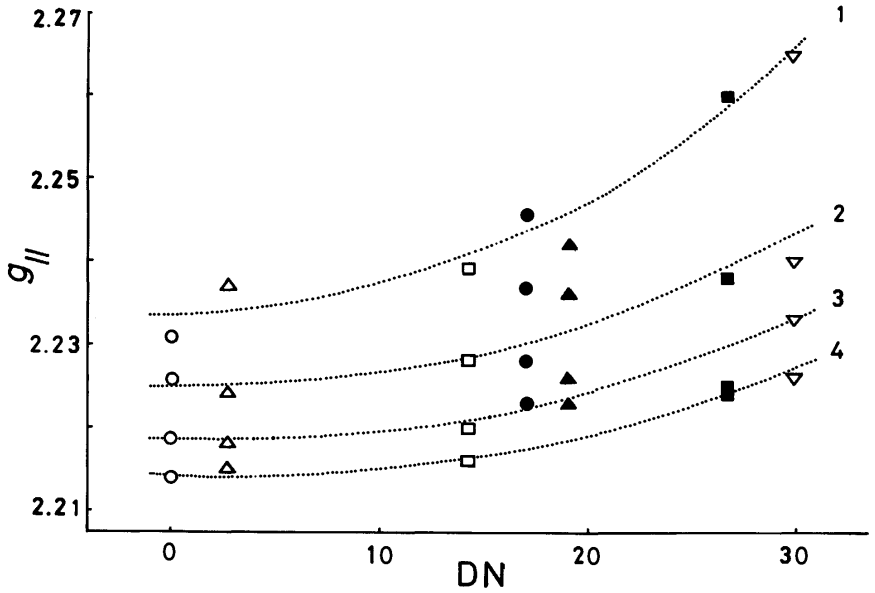

Fig. 3. Plots of $g_{//}$ values against solvent Donor Number (DN) for the series of [Cu(tmen)(dike)]$^+$ complexes.

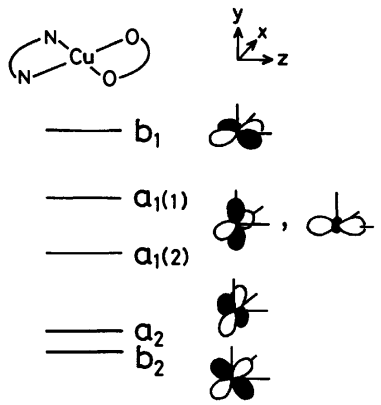

Fig. 4. Structure, coordinate system, and expected d-orbital pattern for [Cu(diam)(dike)]$^+$.

appears more familiar, with z axis perpendicular to the geometrical chelate plane but no longer being the twofold axis. The mixed chelate complex [Cu(diam)-(dike)]$^+$ used to be approximated, for convenience, to have D_{4h} symmetry indistinguishing N–N and O–O donor sets.[1] In the present paper, we use the strict C_{2v} representations particularly for the purpose of explaining the solvent effect observed in this study.

Work is in progress towards acquiring single crystal electronic spectral data on [Cu(diam)(dike)]$^+$ that we can use for sequencing the d-orbitals split under the C_{2v} crystal field. As yet, we have to make the most reasonable estimates for the orbital energies. The ground state is undoubtedly B_1 with d_{xz} orbital singly occupied. The d_{xy} (a_2) and d_{yz} (b_2) orbitals would have similar energies; they correspond to the e_g orbitals in the D_{4h} approximation. The remaining d_{z^2} and $d_{x^2-y^2}$ (a_1) should mix with each other under the crystal field;

$$a_1(1) = a \cdot d_{z^2} + b \cdot d_{x^2-y^2} \quad (1)$$

$$a_1(2) = b \cdot d_{z^2} - a \cdot d_{x^2-y^2} \quad (2)$$

in which a and b are the mixing coefficients. Then the g-values are related to the excited state energies via the orbital reduction parameters k_x, k_y, and k_z by the equations;

$$g_y = 2.0023 - 2\lambda k_y^2 \left[\frac{(\sqrt{3}a-b)^2}{E(a_1(1))} + \frac{(a+\sqrt{3}b)^2}{E(a_1(2))} \right] \quad (3)$$

$$g_x = 2.0023 - \frac{2\lambda k_x^2}{E(d_{xy})}. \quad (4)$$

$$g_z = 2.0023 - \frac{2\lambda k_z^2}{E(d_{yz})} \quad (5)$$

where λ is the spin-orbit coupling constant (-828 cm^{-1}). For the present purpose, however, it suffices to note that the spin-orbit coupling between the ground B_1 term and excited A_1 terms should include contributions from both d_{z^2} and $d_{x^2-y^2}$ orbitals. This is the major consequence of lowering the symmetry from approximate D_{4h} to the more precise C_{2v} (z axis in chelate plane). Under a condition that $\sqrt{3}a=b$ or $a=-\sqrt{3}b$, the expression for g_y is reduced to the one involving the energy of "$d_{z^2-x^2}$" orbital, which is equivalent to the results of $C_{2v}(x)$ treatment.[7,8] Since the precise symmetry of the crystal field in [Cu-(diam)(dike)]$^+$ is unknown, we leave the mixing coefficients a and b as undetermined parameters.

According to the above model, the most likely energy sequence of the d-orbitals in [Cu(diam)-(dike)]$^+$ is $d_{xz} > a_1(1)$, $a_1(2) \geqslant d_{yz} \approx d_{xy}$ and the three g-values are expected to follow the order; $g_y > g_x \approx g_z$. Comparison with actual ESR signals, which are

nearly of axial type, indicates that $g_y=g_{//}$. The dependences of $g_{//}$ values on ligand basicity and on solvent can now be explained in terms of changes in $E(a_1(1))$ and/or $E(a_1(2))$ in the expression for g_y.

Interpretation of Substituent and Solvent Effects on the $g_{//}$ Values. Figure 5(A) illustrates how the d-orbital energies of [Cu(tmen)(dike)]$^+$ complexes are affected by increasing the basicity of dike ligand. Most notable change is a rise in b_1 orbital (d_{xz}) energy since the orbital lobes are directed towards the ligand. This should bring about an increase in both $E(a_1(1))$ and $E(a_1(2))$ and consequently a decrease in the $g_{//}$ value, following Eq. 3. If pK_a of the β-diketones are linearly related to the energy terms as in the case of [Cu(dike)$_2$] complexes,[6] the $g_{//}$ values would be inversely proportional to the pK_a as long as crystal field model is appropriate. The relationships demonstrated in Fig. 2 can be reasonably taken as the inverse proportionality and lend support to the above model.

Figure 5(B) illustrates how the d-orbital energies of [Cu(diam)(dike)]$^+$ are affected upon coordination of solvent molecules (S) along the y axis, bringing about the solvent effect on the $g_{//}$ values. To simplify the discussion, the mixing coefficients a and b in Eqs. 1 and 2 are assumed to be 1 and 0, respectively (mixing is negligibly small). Then the expression for g_y is reduced to the following.

$$g_y = 2.0023 - 2\lambda k_y^2\left[\frac{3}{E(d_{z^2})} + \frac{1}{E(d_{x^2-y^2})}\right] \quad (6)$$

The d_{z^2} orbital is placed above $d_{x^2-y^2}$ in the Figure since it has some "in-plane" lobal character, though not directed to the donor atoms. At any rate, it should be noted that the primary effect of coordination of the solvent is to increase the energy of $d_{x^2-y^2}$ orbital. The d_{z^2} orbital would also rise and, as an overall effect, the decreased $E(a_1)$ terms should yield larger $g_{//}$ values. Degree of the changes in energy is dependent on coordinating ability of the solvent, for which DN can be a reasonable measure. Thus the plots of $g_{//}$ values vs. DN of solvents, shown in Fig. 3, follow the relationship in Eq. 3.

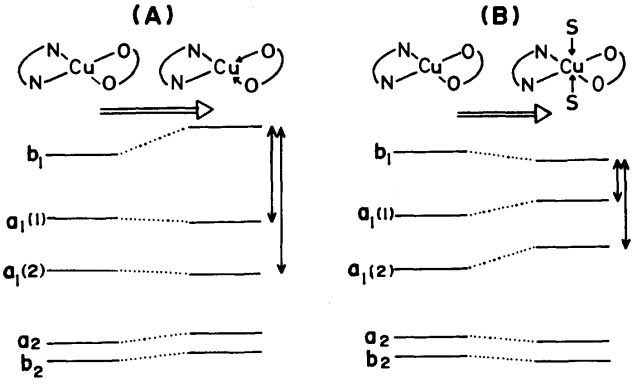

Fig. 5. The efffects of varying the substituents of dike ligand (A) and of changing the solvent (B) on the relative energies of d-orbritals in [Cu(diam)-(dike)]$^+$. Horizontal arrow shows increase in the ligand basicity (O→ in A) or the degree of solvation (S→ in B), i.e., the coordination power of dike ligand or the solvent molecules increases from left to right. Vertical arrows indicate the energy terms which appear in the $g_{//}$ expression.

ESR parameters of [Cu(dike)$_2$] have been extensively investigated by other workers.[6,9,10] In most of these studies, an MO scheme has been favorably employed. Solvent-dependency of the ESR parameters of these complexes was particularly difficult to explain, since under D_{4h} symmetry the spin-orbit coupling relates $g_{//}$ to the energy difference between $d_{x^2-y^2}$ and d_{xy}, both of which have only the in-plane lobal component. Effect of axial coordination was interpreted as an indirect effect on the energy of the highest $d_{x^2-y^2}$ orbital and/or on bonding characters in the complexes.

In contrast, the present model explains the solvent effect as a direct consequence of coordination. There may seem to be little inadequacy in D_{4h} approximation for the present CuN_2O_2 chelate complexes at first, but recognizing the fact that the lowering symmetry results in mixing of in-plane and axial d-orbitals along x, y, and z axes is important in the explanation of the remarkable solvent effect, both on the ESR parameters and on electronic spectra.

Comparison with Absorption Spectral Data. Finally, the information from the ESR spectroscopy is to be compared to the electronic spectral data obtained previously. The energies for solution absorption

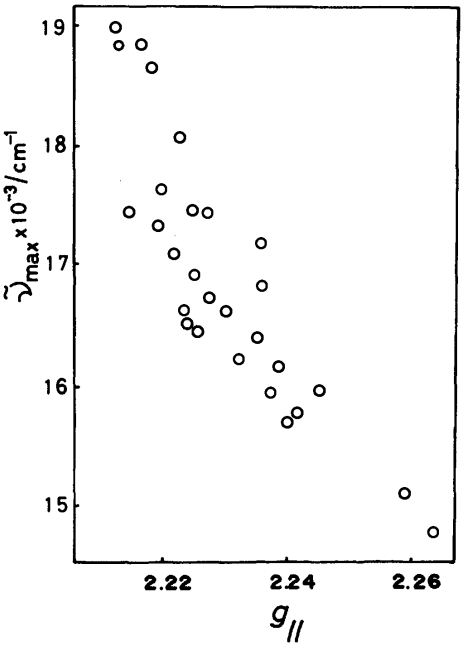

Fig. 6. Correlation between the energies of absorption spectral maxima ($\tilde{\nu}_{max}$) and ESR $g_{//}$ values for the series of [Cu(tmen)(dike)]$^+$ complexes in solution.

spectral maxima are plotted against $g_{//}$ values in Fig. 6. The 28 data points (the series of four complexes [Cu(tmen)(dike)]$^+$ in seven solvents) fall in a region on the plot that suggests the overall linear relationship between $\tilde{\nu}_{max}$ and $g_{//}$. It is clear at least that the d–d band observed in the visible region for solutions consists of $B_1 \rightarrow A_1$ transition(s). Due to the remarkable solvatochromism, the visible band at around 550 nm used to be arbitrarily assigned to $B_{1g} \rightarrow E_g$ transition under D_{4h} symmetry, which appeared to be most affected by changing degrees in solvation, despite the fact that the energy of this transition may well extend into the ultraviolet region.[11] Precise band assignment is not possible until absorption spectrum of a single crystal has been analyzed but in the meantime the C_{2v} crystal field model seems to adequately explain both absorption spectral and ESR spectral properties of [Cu(diam)-(dike)]$^+$ series.

This work was partially supported by a Grant-in-Aid for Scientific Research No. 59430009 from the Ministry of Education, Science and Culture. The authors would like to thank Dr. Makoto Chikira of Chuo University for helpful discussion.

References

1) K. Sone and Y. Fukuda, "Studies in Physical and Theoretical Chemistry," **27**, 251 (1983).

2) Y. Fukuda and K. Sone, *Bull. Chem. Soc. Jpn.*, **45**, 465 (1972).

3) Y. Fukuda, A. Shimura, M. Mukaida, E. Fujita, and K. Sone, *J. Inorg. Nucl. Chem.*, **36**, 1265 (1974).

4) R. W. Soukup and R. Schmid, *J. Chem. Educ.*, **62**, 459 (1985).

5) DCE may be an exception, since ion-pair formation seems to take place in it (cf. Refs. 1 and 3, and also R. W. Soukup and K. Sone, *Bull. Chem. Soc. Jpn.*, **60**, 2286 (1987)). New analogues, [Cu(diam)(dike)]X (X=B(C_6H_5)$_4$ or PF_6), have been synthesized, and the anion effect on their ESR parameters will be reported elsewhere.

6) H. Yokoi and T. Kishi, *Chem. Lett.*, **1973**, 749.

7) M. A. Hitchman, *Inorg. Chem.*, **16**, 1985 (1977).

8) R. L. Lancione, H. C. Allen, Jr., and D. R. Sydor, *J. Coord. Chem.*, **4**, 153 (1975).

9) T. Ogata, T. Fujisawa, N. Tanaka, H. Yokoi, *Bull. Chem. Soc. Jpn.*, **49**, 2759 (1976).

10) J. I. Zink and R. S. Drago, *J. Am. Chem. Soc.*, **94**, 4550 (1972).

11) The electronic absorption spectra of [Cu(diam)-(dike)]ClO_4 in organic solvents typically contain one visible band and a noticeable shoulder (390—400 nm) at the foot of intense ultraviolet absorption. If an estimated value for g_x of 2.03 and one for k_x^2 of 0.5[7] are used to calculate the energy of d_{xy} orbital, it follows that the corresponding transition should appear around 340 nm.

The Base-Catalyzed Isomerization of the Bis(ethylenediamine-*N*-acetato)cobalt(III) Complex

Hiroshi KAWAGUCHI,* Ryuichi NIIYAMA, Tomoharu AMA, and Takaji YASUI
Department of Chemistry, Faculty of Science, Kochi University, Akebono-cho, Kochi 780
(Received May 22, 1987)

The isomerization reaction among six geometrical isomers of $[Co(edma)_2]^+$, which were all resolved into optically active isomers except for the achiral C_i-trans(O) isomer, has been studied in a basic aqueous solution. It has been found that the reaction is stereoselective and that the main reaction schemes may be described as follows: (1) $\Lambda\Delta\Lambda$(S,S)-C_2-trans(O) $\rightleftharpoons$ $\Delta\Lambda\Delta$(R*,S)-C_1-cis(O) $\rightleftharpoons$ $\Delta\Lambda$(R,R)-cis(O)trans(NH) $\rightleftharpoons$ meso(R,S)-C_i-trans(O)$\rightarrow\Lambda\Delta\Lambda$(R,R)[or $\Delta\Lambda\Delta$(S,S)]-cis(O)trans(NH_2) and (2) meso(R,S)-C_i-trans(O)$\leftarrow(+)^{CD}_{504}$-mer$\rightarrow\Lambda\Delta\Lambda$(S,S)-$C_2$-trans(O). In each of the isomerization steps of (1), the inversion occurs at one of two secondary-N centers of the coordinated edma ligands. The rate of deuteration at the secondary-NH was also measured for all geometrical isomers; a linear relationship between the rates of the deuteration and isomerization was found. It was suggested that the isomerization of the $[Co(edma)_2]^+$ system proceeded through the deprotonated five-coordinated intermediates formed by Co–O bond-rupture in the conjugate-base forms.

Numerous data of intramolecular rearrangement (isomerization and inversion) reactions have been reported, and two major pathways of twist and bond-rupture mechanisms have been proposed.[1,2] Complexes with multidentate ligands[3,4] can be used for mechanistic studies of rearrangement reactions, because (1) the coupled chelate rings restrict the number of different possible interconversions and (2) such molecules possess more distinguishable points of reference by which the paths of specific rearrangements can be traced. Recently it has been found that an interesting rearrangement (inversion-isomerization) occurs in the chiral complexes containing multidentate ligands.[5–7] Also, in the substitution reactions of the chiral complexes containing tetradentate ligands, some examples of inversion-isomerization have been reported.[8–10] Examples concerning structure-reactivity patterns in octahedral complexes have been reviewed by House[11] and by Radanovic.[12]

The bis(ethylenediamine-*N*-acetato)cobalt(III) ion, $[Co(edma)_2]^+$, provides six geometrical isomers, as is shown in Fig. 1. When the edma ligand coordinates to a cobalt(III) ion, the secondary nitrogen (-C-NH-C-) becomes asymmetric (R or S). Although each isomer of $[Co(edma)_2]^+$ may be expected to provide several diastereomers, some of them (except for the mer isomer, E-3) do not exist because of structural restrictions. The possible configurations[13] for the geometrical isomers containing facially coordinated edma are listed in Table 1. In previous papers,[14,15] we reported the preparation and characterization of the six geometrical isomers and also the determination of the absolute configurations of the chiral isomers, except for the mer isomer (E-3).

Recently we have found that the isomers of $[Co(edma)_2]^+$ isomerized to other one with inversion at one of the secondary nitrogen (sec-N) centers of the coordinated edma ligands.[16] In this paper the details of these isomerization reactions will be reported. The deuteration reactions at the sec-N centers will also be described.

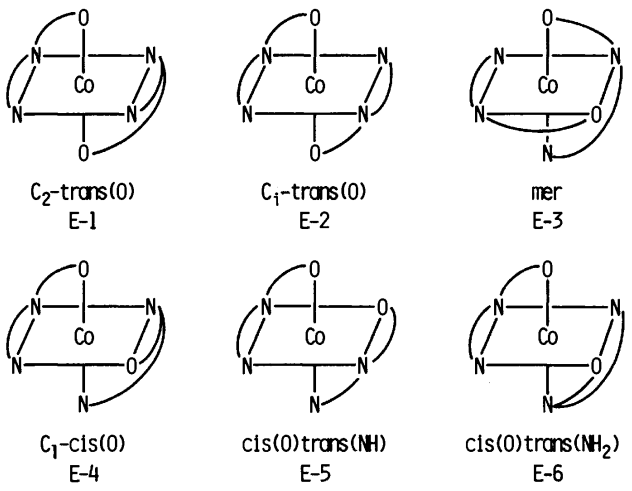

Fig. 1. The six geometrical isomers of the $[Co(edma)_2]^+$ ion.

Experimental

Complexes. The complexes examined here were prepared and resolved according to the methods described in our previous papers.[14,15] They are $(+)^{CD}_{543}$-C_2-*trans*(O)-

Table 1. Possible Configurations and CD Signs of the $[Co(edma)_2]^+$ Ion

Isomer	Possible configuration and CD sign	
E-1	$(-)^{CD}_{548}$-$\Delta\Lambda\Delta$(R,R)	$(+)^{CD}_{548}$-$\Lambda\Delta\Lambda$(S,S)
E-2	(R,S)	(achiral isomer)
E-4	$(+)^{CD}_{534}$-$\Lambda\Delta\Lambda$(S*,R)	$(-)^{CD}_{534}$-$\Delta\Lambda\Delta$(R*,S)
E-5	$(-)^{CD}_{521}$-Δ(GG)Λ(EE)(R,R)	$(+)^{CD}_{521}$-Λ(GG)Δ(EE)(S,S)
E-6	$(-)^{CD}_{509}$-$\Delta\Lambda\Delta$(R*,R*)	$(+)^{CD}_{509}$-$\Delta\Lambda\Delta$(S*,S*)

R or S: Chirality around the asymmetric nitrogen. R* or S*: Chirality around the asymmetric nitrogen being present at the position trans to ligating oxygen atom. G and E represent the glycinate-ring and ethylenediamine-ring of the edma ligand respectively.

$[Co(edma)_2]Cl\cdot 2H_2O$ (E-1), C_i-*trans*(O)-$[Co(edma)_2]Cl\cdot 2H_2O$ (E-2), $(+)^{CD}_{504}$-*mer*-$[Co(edma)_2]Br$ (E-3), $(-)^{CD}_{534}$-C_1-*cis*(O)-$[Co(edma)_2]Cl\cdot 2H_2O$ (E-4), $(-)^{CD}_{521}$-*cis*(O)*trans*(NH)-$[Co(edma)_2]Br$ (E-5), $(-)^{CD}_{509}$-*cis*(O)*trans*(NH_2)-$[Co(edma)_2]Cl\cdot 1.5H_2O$ (E-6).

Spectral Change in the Isomerization Reaction Solution. The time-course changes in the absorption and CD spectra of each isomer in a basic aqueous solution were followed by the use of a Hitachi 557 spectrophotometer and a JASCO J-22 spectropolarimeter. All the chemicals used were of a reagent grade, and the deionized water was degassed before use. The reaction was started by stirring a buffer solution into the complex solution in a reaction vessel kept in a thermostat. About 3 cm^3 of the reaction solution was then quickly transferred into the cell with a stopper in order to record the absorption and CD spectra. The following conditions were set: Complex concentration, 2.68 or 4.66×10^{-3} M (M=mol dm^{-3}); pH, 10.24—10.37 (Na_2CO_3–$NaHCO_3$ buffer); temperature, 40.1 or 30.1 °C.

Isomerization. $(-)^{CD}_{534}$-E-4 Isomer: This isomer (0.150 g) was dissolved in 200 cm^3 of water in a reaction vessel kept in a thermostated bath at 40.0 °C. The reaction was started by stirring 300 cm^3 of a buffer solution [Na_2CO_3(0.1165 M)–$NaHCO_3$(0.03887 M)] previously kept at 40.0 °C into the reaction vessel. The temperature and the pH of the reaction solution were checked with a thermister thermometer (Takara D221) and a pH meter (Toa TSC-10A) respectively. During the experiment (160 h), the reaction solution was kept at 40.0±0.1 °C, with the pH 10.35±0.02.

At prescribed time intervals, a constant volume (40.0 or 30.0 cm^3) of the reaction solution was taken out and acidified to pH 6 in order to stop the reaction. The acidified solution was poured onto an SP-Sephadex C-25 column (3.0 cm×60 cm, Na^+ form). The adsorbed band was developed with a 0.2 M NaCl aqueous solution and separated into two bands, el-1 and el-2 in order of elution. The el-1 eluate contained $(+)^{CD}_{543}$-E-1 (major) and E-2 (minor), while the el-2 eluate contained $(-)^{CD}_{534}$-E-4 and $(-)^{CD}_{521}$-E-5. Each of the el-1 and el-2 eluates was concentrated to a constant volume (10.0 or 5.0 cm^3) and used for the measurements of the absorption and CD spectra. From the binary-curve analysis of the absorption spectrum of the concentrated el-1 eluate (on the basis of the known absorption data of authentic E-1 and E-2), the amounts of E-1 and E-2 formed were calculated. The optical purity of $(+)^{CD}_{543}$-E-1 in the el-1 eluate was obtained from the CD intensity of the el-1 eluate and the concentration of E-1 estimated from the absorption data. The amounts and optical purities of $(-)^{CD}_{534}$-E-4 and $(-)^{CD}_{521}$-E-5 were also estimated from the binary-curve analyses of the absorption and CD spectra of the el-2 eluate. In these curve-analyses, the spectral data at 20—25 points in the visible region were used; the analyses were carried out on an NEC PC-9801F computer using the least-squares method.

The isomerization reactions of the other isomers were carried out by a procedure similar to that used for $(+)^{CD}_{534}$-E-4. The reaction conditions were the same as those in the case of $(+)^{CD}_{534}$-E-4.

Deuteration. The deuteration reactions were carried out for the six geometrical isomers of the $[Co(edma)_2]^+$ complex in a DCl(0.096 M)-D_2O solution and followed with a ^1H NMR spectrometer (JEOL MH-100). The solutions were 0.15—0.25 M in complex concentration. The reactions were started by dissolving the complex in DCl-D_2O solution in a thermostat at 80 °C. About 0.5 cm^3 aliquots of the reaction solutions were rapidly quenched in an ice bath, and then the ^1H NMR spectra were measured.

Results and Discussion

The Absorption and CD Spectral Changes in a Basic Aqueous Solution. $(-)^{CD}_{534}$-E-4 Isomer: Figure 2 shows the changes in the absorption and CD spectra of $(-)^{CD}_{534}$-E-4 in a basic solution (pH 10.37) at 40.1 °C. The absorption maximum in the 1st d-d band region shifts gradually to a longer wavelength (from 502 to 525 nm), and the final spectral pattern is similar to that of E-1 (λ_{max} 530 nm). The initial isosbestic points at 527 and 450 nm, which are lost at longer times, are close to the cross points (522 and 449 nm) between the absorption curve of the E-1 and that of E-4. On the other hand, the CD spectrum of $(-)^{CD}_{534}$-E-4 in a basic aqueous solution changes drastically, as is shown in Fig. 2; that is, the CD patterns in the 1st band region are almost inverted with the passage of time. In the initial stage of the reaction, isoextinct points are observed at 497 and 400 nm, which are near in position to the cross points (494 and 399 nm) between the CD curve of $(+)^{CD}_{543}$-E-1 and that of $(-)^{CD}_{534}$-E-4. Further, the final CD curve in Fig. 2 resembles that of

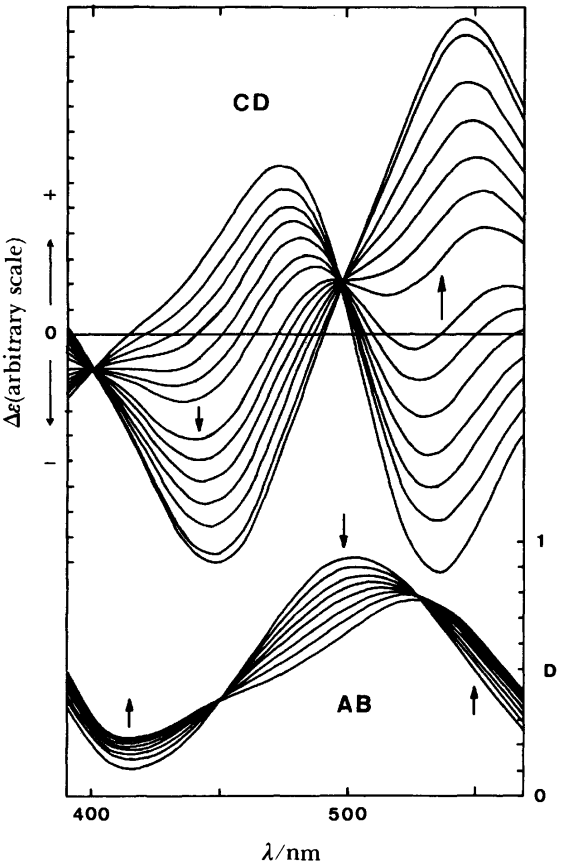

Fig. 2. The absorption (AB) and CD spectral changes of $(-)^{CD}_{534}$-E-4 in a basic aqueous solution (pH 10.37) at 40.1 °C. The final AB and CD curves were recorded after 95 h.

$(+)^{CD}_{543}$-E-1. These results indicate that optically active $(+)^{CD}_{543}$-E-1 was formed in a considerable amount from $(-)^{CD}_{534}$-E-4. No minor products in this reaction were identified by the present experimental procedure.

$(+)^{CD}_{521}$-E-5 and Other Isomers: Figure 3 shows the absorption and CD spectral changes (till 61 days) of $(+)^{CD}_{521}$-E-5, which were measured under the same conditions as those used for $(-)^{CD}_{534}$-E-4. The change in the absorption curve, in which the absorption maximum shifts to the lower energy side (from 478 to 516 nm), suggests that the trans(O) type isomers are formed in considerable concentrations at the final equilibrium stage of the reaction. It is apparent from the CD spectral change that optically active products are formed. However, the products could not be identified on the basis of those CD data.

The same measurements were performed for other isomers of $[Co(edma)_2]^+$. These absorption and CD spectral changes were complicated, indicating that some kinds of isomers were formed in the reactions. The spectral changes in the basic aqueous solutions were relatively faster in E-4, E-3, and E-6 than in the others.

The Identification and Quantification of the Isomerization Reaction Products. The band adsorbed on an SP-Sephadex C-25 column, which contains six geometrical isomers of $[Co(edma)_2]^+$ (E-1—E-6), separated into 3 bands—el-1 (E-1 and E-2), el-2 (E-3, E-4, and E-5), and el-3 (E-6) in order of elution, when developed with 0.2 M NaCl as the eluent. In order to estimate the amounts of the starting material and products in the isomerization reaction solution at an arbitrary time, this chromatographic separation technique was used. Constant volumes of the reaction solution were taken out from the reaction vessel at prescribed time intervals. The solution was acidified to pH 6 to stop the reaction and then poured onto an SP-Sephadex column. The adsorbed band was separated into 3 bands (el-1, el-2, and el-3) by development with 0.2 M NaCl. The eluate from each band was concentrated to a constant volume, and the absorption spectra of the concentrated solution were measured. The amount of the E-6 isomer was estimated from the absorption data of the el-3 eluate. This el-3 band was detected only in a case of the isomerization reaction used E-6 as the starting material. The amounts of E-1 and E-2 were estimated from the binary-curve analysis of the absorption spectrum of the concentrated el-1 solution. If the three isomers of E-3, E-4, and E-5 are present in the reaction solution, all these isomers should be included in the el-2 solution. In the preliminary isomerization reaction of each isomer (except for the E-3 isomer), the ^1H NMR spectrum of the residue obtained from the el-2 eluate was measured to check the formation of E-3 on the basis of the difference in the glycinate-ring $-CH_2-$ signal pattern of E-3 from those of the others.[14,15] In the cases of the isomers except E-3, the formation of E-3 was not detected throughout the isomerization reaction. Therefore, the absorption curve of the el-2 solution was analyzed as the curve of a mixture of E-4 and E-5. While in the isomerization reaction using E-3 as a starting material, the absorption spectrum of the el-2 eluate was identical to that of pure E-3, indicating no formation of either E-4 or E-5. (However, at longer reaction times, the absorption and CD curves of the el-2 eluate was better fitted by those of a mixture of E-3 and a very small amount of E-4.)

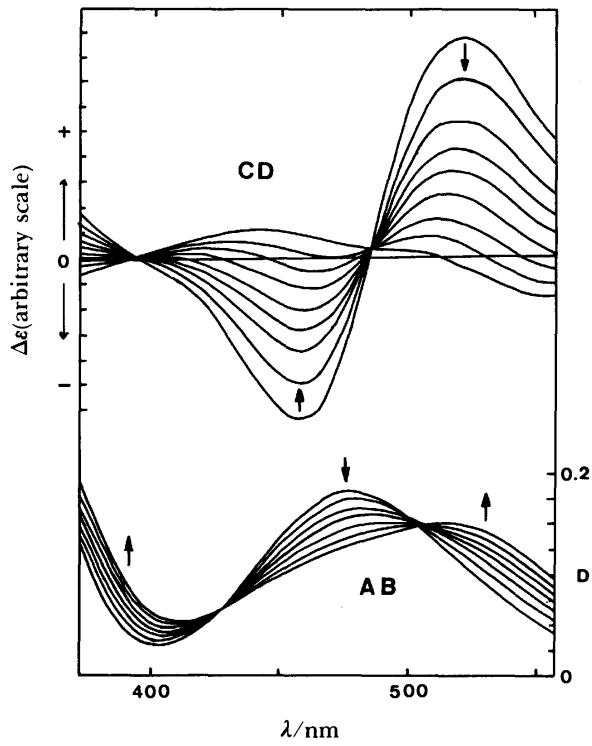

Fig. 3. The absorption (AB) and CD spectral changes of $(+)^{CD}_{521}$-E-5 in a basic aqueous solution (pH 10.25) at 40.1 °C. The final AB and CD curves were recorded after 61 days.

When the optically active isomers were used as starting materials (except for achiral E-2), the CD spectra of the el-1—el-3 eluates were also measured. The CD spectra of the el-1 and el-3 solutions are due to the optical activities of E-1 and E-6 respectively. From the binary-curve analyses of the CD and absorption spectra of the el-2 solution, the optical purities of E-4 and E-5 were estimated.

In a weak acidic or neutral solution at room temperature, the isomerization of each isomer was not observed, at least not for several days. Therefore, the progress of the isomerization reaction during such procedures as chromatographic separation and concentration under reduced pressure should be negligible. In this experiment, the solutions (el-1—el-3) used for the measurements of the absorption and CD

spectra contained a considerable amount of NaCl. As the absorption and CD spectra, especially the CD spectrum, of the $[Co(edma)_2]^+$ complex are affected by the amount of coexisting NaCl, the absorption and CD data of the isomers of $[Co(edma)_2]^+$, which were obtained in an NaCl aqueous solution, were used for the absorption and CD curve analyses of the el-1—el-3 eluates.

Base-Catalyzed Isomerization Reaction. $(-)^{CD}_{534}$-E-4 Isomer: The isomerization reaction of $(-)^{CD}_{534}$-E-4 was carried out in a carbonate buffer solution (pH 10.35) at 40.0 °C. Figure 4 shows the concentration changes in $(-)^{CD}_{534}$-E-4 and the reaction products. A part of the numerical data (five data points) are listed in Table 2, together with the enantiomer excess percentage of each product. In the isomerization reaction of E-4 over a period of 150 h, three products — E-1 (major), E-5, and E-2 — were formed. The formation of E-2 was not detected during the first ca. 50 h; after that time, its amount increased very slowly. The E-2 isomer is likely to be produced from the E-5 or E-1 isomer. Therefore, the reaction paths in this isomerization may be expected to be as follows:

$$\text{E-4} \longrightarrow \text{E-5} \xrightarrow{?} \text{E-2}$$
$$\text{E-4} \longrightarrow \text{E-1} \xrightarrow{?} \text{E-2}$$

Throughout the reaction (150 h), no racemization of the starting material occurred: The recovered $(-)^{CD}_{534}$-E-4 retained 100% optical purity. As is shown in Table 2, $(+)^{CD}_{543}$-E-1 and $(-)^{CD}_{521}$-E-5, which were formed from $(-)^{CD}_{534}$-E-4 in a basic aqueous solution, showed optical purities of ca. 100% and ca. 60% respectively: These two isomerization paths are thus stereoselective.

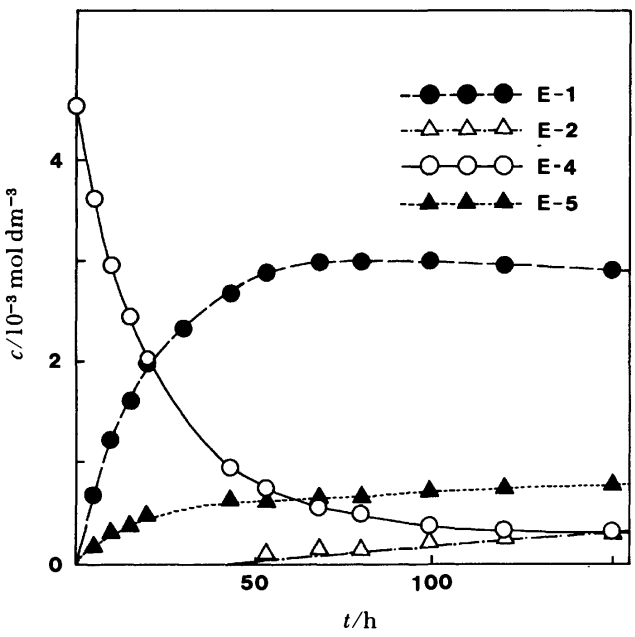

Fig. 4. The isomerization reaction of $(-)^{CD}_{534}$-E-4 in a basic aqueous solution (pH 10.35) at 40.0 °C.

$(+)^{CD}_{543}$-E-1 Isomer: In the isomerization reaction using $(+)^{CD}_{543}$-E-1 as the starting material, E-4 was formed first (Fig. 5 and Table 2). The amount of E-4

Table 2. The Concentration Changes and Optical Purities of the Starting Materials and Products in the Isomerization Reaction (40.0 °C, pH 10.35)

(i) $(+)^{CD}_{543}$-E-1

t/h	Concn/10^{-3} mol dm^{-3} (optical purity/%)			
	$(+)^{CD}_{543}$-E-1	E-2	$(-)^{CD}_{534}$-E-4	$(-)^{CD}_{521}$-E-5
10	4.41 (100)		0.16 (90)	
25	4.20 (100)		0.32 (80)	0.10 (20)
50	3.99 (100)	0.08	0.41 (80)	0.24 (20)
100	3.67 (100)	0.20	0.43 (80)	0.34 (20)
150	3.48 (100)	0.24	0.41 (80)	0.45 (20)

(ii) E-2

t/h	Concn/10^{-3} mol dm^{-3}		
	E-1	E-2	E-5
10		4.46	0.08
34		4.53	0.26
66		4.31	0.38
100		4.15	0.48
150	0.07	3.97	0.57

(iii) $(+)^{CD}_{504}$-E-3

t/h	Concn/10^{-3} mol dm^{-3} (optical purity/%)		
	$(+)^{CD}_{543}$-E-1	E-2	$(+)^{CD}_{504}$-E-3
3	0.06 (100)	0.05	4.49 (95)
6	0.13 (100)	0.11	4.32 (95)
26	0.53 (100)	0.49	3.46 (90)
53	0.93 (100)	0.92	2.72 (90)

(iv) $(-)^{CD}_{534}$-E-4

t/h	Concn/10^{-3} mol dm^{-3} (optical purity/%)			
	$(+)^{CD}_{543}$-E-1	E-2	$(-)^{CD}_{534}$-E-4	$(-)^{CD}_{521}$-E-5
10	1.22 (100)		2.96 (100)	0.31 (60)
20	1.96 (100)		2.02 (100)	0.48 (60)
43	2.69 (100)		0.95 (100)	0.63 (60)
68	2.99 (100)	0.15	0.56 (100)	0.65 (60)
99	3.01 (100)	0.21	0.38 (100)	0.71 (60)

(v) $(-)^{CD}_{521}$-E-5

t/h	Concn/10^{-3} mol dm^{-3} (optical purity/%)			
	$(+)^{CD}_{543}$-E-1	E-2	$(-)^{CD}_{534}$-E-4*	$(-)^{CD}_{521}$-E-5
30		0.05	0.12	4.37 (100)
68	0.23 (80)	0.11	0.12	4.13 (100)
100	0.35 (80)	0.17	0.12	3.96 (100)
164	0.59 (80)	0.26	0.13	3.66 (100)

* The optical purity is unreliable.

(vi) $(-)^{CD}_{509}$-E-6

t/h	Concn/10^{-3} mol dm^{-3} (optical purity/%)		
	E-2	E-5	$(-)^{CD}_{509}$-E-6
0.5	0.20		4.45 (100)
2	0.87	0.17	3.37 (100)
5	1.89	0.27	2.15 (100)
9	2.84	0.34	1.10 (100)
18	3.70	0.42	0.32 (100)

increased until ca. 50 h, but after that it was almost constant throughout the reaction examined here (150 h). The formation of E-5 was first observed ca. 20 h after the start of the reaction. The amount of E-5 increased with the passage of time and exceeded the amount of E-4 after ca. 140 h. The formation of E-2, in a very small amount, was observed later than that of E-5. From the results of the isomerization reactions of both E-1 and E-4, the following reaction path may be presumed:

$$\text{E-1} \longrightarrow \text{E-4} \longrightarrow \text{E-5} \longrightarrow \text{E-2}$$

As is shown in Table 2, $(-)^{CD}_{534}$-E-4, which was obtained by the isomerization reaction of $(+)^{CD}_{543}$-E-1, retained an optical purity of 80—90%, showing a high stereoselectivity in the E-1→E-4 change. On the other hand, the $(-)^{CD}_{521}$-E-5 produced in the same reaction retained an optical purity of only ca. 20%. This value is a little lower than the value to be expected from the presumed reaction path of $(+)^{CD}_{543}$-E-1→$(-)^{CD}_{534}$-E-4→$(-)^{CD}_{521}$-E-5, because pure $(+)^{CD}_{543}$-E-1 produced $(-)^{CD}_{534}$-E-4 with an optical purity of 80—90% and pure $(-)^{CD}_{534}$-E-4 produced $(-)^{CD}_{521}$-E-5 with an optical purity of ca. 60%. However, the successive reactions of $(+)^{CD}_{543}$-E-1→$(-)^{CD}_{534}$-E-4→$(-)^{CD}_{521}$-E-5 can also be supported by the following consideration. The absolute configurations of $(+)^{CD}_{543}$-E-1 and $(-)^{CD}_{521}$-E-5 are ΛΔΛ(S,S) and Δ(GG)Λ(EE)(R,R) respectively, as is shown in Table 1. If E-5 is formed directly from E-1, the inversions at the two asymmetric N centers must occur simultaneously. However, such inversions are very difficult judging from the consideration using molecular models. (If a direct $(+)^{CD}_{543}$-E-1→$(+)^{CD}_{521}$-E-5 change with a retention of the sec-N configuration by twist mechanism is slightly involved, the optical purity of $(-)^{CD}_{521}$-E-5 may be lowered.) The isomerization of E-1 was slower than that of E-4.

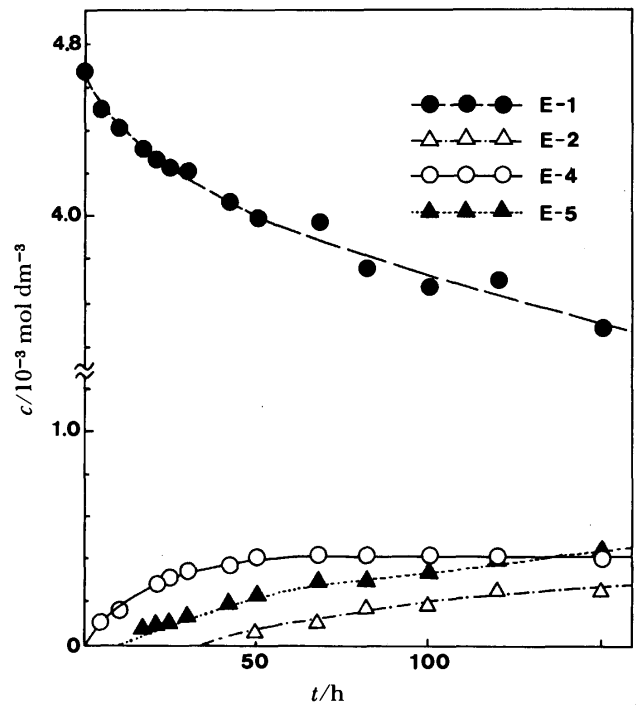

Fig. 5. The isomerization reaction of $(+)^{CD}_{543}$-E-1 in a basic aqueous solution (pH 10.35) at 40.0 °C.

$(-)^{CD}_{521}$-E-5 Isomer: The isomerization of $(-)^{CD}_{521}$-E-5 was also slow under the conditions of pH 10.35 and 40.0 °C. In this reaction, the formations of E-4 and E-2 first occurred, and then E-1 was formed. Early in the reaction (10—20 h) the amounts of the products were in the order of E-4>E-2>E-1. After ca. 30 h, the concentration of E-4 reached its maximum and thereafter did not increase, while the concentrations of E-1 and E-2 increased with the passage of time (Table 2), E-1 (after ca. 40 h) and E-2 (after ca. 70 h) exceeding E-4 in the amount formed. Thus, the following reaction paths may be presumed by considering the reaction paths of E-4:

$$\text{E-5} \longrightarrow \text{E-4} \longrightarrow \text{E-1}$$
$$\text{E-5} \longrightarrow \text{E-2}$$

We could not calculate the optical purity of the E-4 produced in the isomerization reaction of $(-)^{CD}_{521}$-E-5, because too little of it was formed for us to estimate the optical purity from the curve analyses of the absorption and CD spectra of the el-2 eluate [a mixture of E-5 (major) and E-4 (minor)]. The E-1 isomer obtained by the isomerization of $(-)^{CD}_{521}$-E-5 was of the $(+)^{CD}_{543}$ form, with an optical purity of ca. 80% (Table 2). Judging from the results of the isomerization of $(-)^{CD}_{534}$-E-4, the isomerization reaction of $(-)^{CD}_{521}$-E-5 can be expected to produce $(-)^{CD}_{534}$-E-4 selectively. This reaction path is the reverse of the isomerization path of $(+)^{CD}_{543}$-E-1 (E-1→E-4→E-5).

E-2 and $(-)^{CD}_{509}$-E-6 Isomers: The isomerization reaction of achiral E-2 is slow, and the major product is E-5, as is shown in Table 2. At longer times (>ca. 100 h), a small amount of E-1 was formed. (After 215 h, the E-1 constitutes ca. 30% of the reaction products.) It is thought that the E-1 is formed by the path of E-2→E-5→E-4→E-1. However, the formation of E-4 could not be observed. This is probably because the E-4→E-1 change is faster than the E-5→E-4 change.

The isomerization of $(-)^{CD}_{509}$-E-6 is the fastest among the reactions of this series (Table 2). The half-lives (with regard to the decrease in E-6) is ca. 4—5 h under the conditions of pH 10.35 and 40.0 °C. The isomerization reaction of $(-)^{CD}_{509}$-E-6 produced E-2 (major), E-5, and by-products. The E-5 formed in this reaction was racemate; this fact is favorable to the reaction path of E-6→E-2(achiral)→E-5. However, the observed formation rate of E-5 is a little faster than that to be expected from the path of E-6→E-2→E-5, where the E-2→E-5 change is very slow. Another reaction path passing through an achiral intermediate

(or transition state) may, therefore, be thought to exist.

In the initial stage of the isomerization reaction of $(-)^{CD}_{509}$-E-6, a violet by-product was formed in a small amount. The amount of the violet by-product, which was a noncharged and optically active complex, was maximal ca. 3 h after the reaction start, and thereafter it gradually decreased. The violet complex could not be isolated, because it was unstable and was formed in only a small amount. During the concentration of the solution containing the violet complex under reduced pressure at 40 °C, the complex changed to E-2. In the isomerization reaction of E-6, the decomposition product, which was a species with a charge of more than +2, was observed after ca. 7 h; its amount increased slowly with the passage of time. The isomerization studies of E-6 and E-3 (to be discussed in the next section) were not sufficient, for the preparation of these isomers was very difficult.

$(+)^{CD}_{504}$-E-3 Isomer: The isomerization reaction of $(+)^{CD}_{504}$-E-3 was followed over a period of 53 h under the conditions of pH 10.35 and 40.0 °C. E-3 is thought to be thermodynamically less stable because of its meridional chelate form; however, the isomerization rate was slower than that of E-4 or E-6 (Table 2). The products were $(+)^{CD}_{543}$-E-1, with an optical purity of ca. 100%, and E-2; the formation ratio of these two isomers was ca. 1:1. The racemization of $(+)^{CD}_{504}$-E-3 was almost negligible throughout the reaction. The other products were in the limit of the accuracy of the experimental method. (However, it was presumed that a small amount of $(-)^{CD}_{534}$-E-4 was formed through the path of E-3→E-1→E-4 at longer times.) The E-3 ion provides six possible diastereomers, arising from three chiral centers (cobalt and two sec-N of coordinated two edma ligands): $\Lambda(C_2)$(R,R), $\Lambda(C_2)$-(R,S), and $\Lambda(C_2)$(S,S) and the $\Delta(C_2)$ series.[17] Judging from the racemization rate of *mer*-[Co(edma)(dien)],[18] it is presumed that the inversion of the sec-N configuration in E-3 occurs rapidly under the present reaction conditions; that is, the equilibration of the RR⇄RS⇄SS is rapidly attained. Therefore, the configuration at the cobalt center in E-3 is the main factor in determining the configuration of the E-1 formed, even though the shift of the RR⇄RS⇄SS equilibrium must also be taken into consideration. As the absolute configuration of the isolated $(+)^{CD}_{504}$- or $(-)^{CD}_{504}$-E-3 has not yet been determined, the reaction scheme of E-3 can not be discussed in detail. However, the formation of E-2 excludes the possibility of a twist mechanism for the isomerization of E-3.

The Main Isomerization Paths of the $[Co(edma)_2]^+$ Series. From the isomerization data examined here, the main paths of the isomerization of the $[Co(edma)_2]^+$ series are represented in Scheme 1.

(The "fast" in the scheme indicates qualitatively the relative rate of each path.) This isomerization scheme is different from that of the $[Co(ida)_2]^-$ system,[4] in which the isomerization proceeds through the mer isomer. In the present scheme, it is noteworthy that the inversion at one of two sec-N centers in $[Co(edma)_2]^+$ occurs in each isomerization step, except for the E-3→E-1 and E-3→E-2 changes. These experimental results can not be explained by the twist mechanism. The reasons are as follows: In all the isomers containing facially coordinated edma ligands (1) the twisting about the pseudo-C_3 axis passing through the triangle faces of the chelated edma ligands does not result in the inversion at the asymmetric sec-N of the edma ligand and (2) the possible twistings about other pseudo-C_3 axes provide E-3 (mer). (In the *fac*-$[Co(edma)_2]^+$ isomers, some of the twisting about the pseudo-C_3 axes is not possible because of the limits of the ligating manner of the linear terdentate edma ligand.) Thus, the isomerization reaction of the $[Co(edma)_2]^+$ series should be explained by the Co-O bond-rupture mechanism. (Recently, Baraniak et al. have revealed that the Co-O bond fission occurs in the $[Co(\beta\text{-ala})(en)_2]^+$ ion under alkaline conditions.[19])

When the coordination sites of the O and sec-N atoms of one edma ligand in the *fac*-$[Co(edma)_2]^+$ ion are exchanged for one another, the isomerization of the complex and the inversion at the sec-N center occur simultaneously. Such an exchange in *ΔΔΛ*(*S,S*)-E-1 leads to *ΔΔΔ*(*R*,S*)-E-4, corresponding to the $(+)^{CD}_{543}$-E-1→$(-)^{CD}_{534}$-E-4 change in Scheme 1. As E-4 is

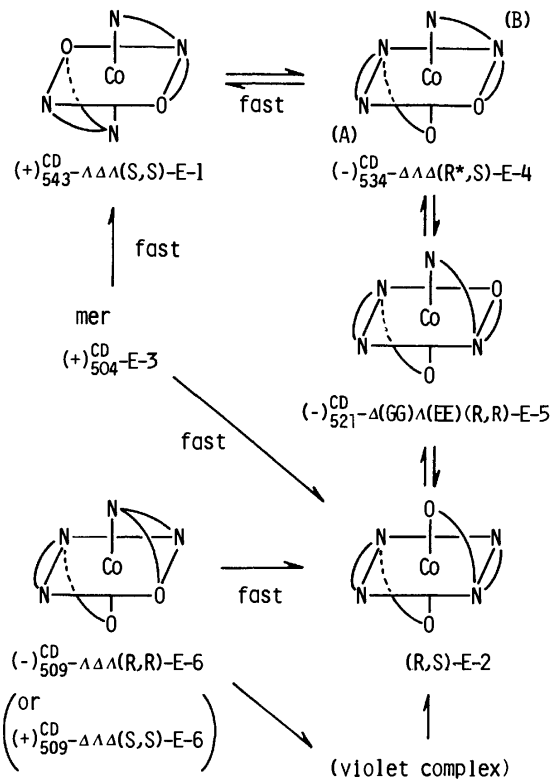

Scheme 1.

the C_1 symmetry, the two edma ligands [(A) and (B) in Scheme 1] of E-4 are not equivalent: The sec-N of the (A) edma is in the trans position to the O atom of another edma ligand, while the sec-N of the (B) edma is in the trans position to the terminal N atom of the (A) edma ligand. The exchange of the coordination sites of the ligating sec-N and O atoms in the (A) edma ligand leads to the $(-)^{CD}_{534}$-E-4→$(+)^{CD}_{543}$-E-1 change, while the similar exchange in the (B) edma ligand leads to the $(-)^{CD}_{534}$-E-4→$(-)^{CD}_{521}$-E-5 change. Similarly, the exchange between the coordination sites of the sec-N and O atoms in one edma ligand of the $[Co(edma)_2]^+$ ion is found in the isomerization steps of $(-)^{CD}_{509}$[or $(+)^{CD}_{509}$]-E-6→E-2 and $(-)^{CD}_{521}$-E-5→$(-)^{CD}_{534}$-E-4 (Scheme 1). In the slow isomerization step of E-2⇄$(-)^{CD}_{521}$[or $(+)^{CD}_{521}$]-E-5, an exchange between the coordination sites of the terminal-N and O atoms in one edma ligand can be found. This exchange also results in the inversion at the asymmetric sec-N center.

Deuteration of the sec-NH Proton. The H–D exchange reaction of the two sec-NH protons in $[Co(edma)_2]^+$ was carried out in DCl–D_2O at 80 °C. In the ^1H NMR spectra for all isomers of $[Co(edma)_2]^+$, the two protons of the glycinate-ring (G-ring) $-CH_2-$ of the edma ligand are not equivalent, and the resulting AB system is further coupled to the proton on the adjacent sec-N atom to give an eight-line ABX spectrum. The kinetic data for the *fac*-$[Co(edma)_2]^+$ isomers were obtained by following the collapse of the ABX signal to an AB signal as the sec-NH protons exchange with D^+. The E-4 isomer has two kinds of sec-NH protons depending on the geometrical situation: Sec-NH of (A) and (B) edma in Scheme 1. The signals due to the G-ring $-CH_2-$ of (A) and (B) edma have been assigned in our previous paper.[15] However, this method was not suitable for the H–D exchange reaction of E-3, because the ABX spectrum was observed in a narrow chemical shift region. The rate data of the H–D exchange for E-3 was calculated from the decrease in the sec-NH peak area relative to the total G-ring $-CH_2-$ peak area. The H–D exchange results are collected in Table 3. The rate of the H–D exchange is fast in E-6 and in one of the edma ligands [(A) edma in Scheme 1] of E-4. These sec-NH lie in the position trans to the ligating oxygen atom (trans(O)-sec-NH). In E-3, the H–D exchange rate of sec-NH, which lies in the position trans to the ligating nitrogen atom (trans(N)-sec-NH), is comparable to those of the trans(N)-sec-NH in the fac isomers (Table 3). These results indicate that the H–D exchange rate of sec-NH is affected by the nature of the atom ligating in the trans coordination site rather than by the chelation form of the edma ligand (mer or fac).

Table 3. The H-D Exchange Rates of the Sec-NH Protons of the $[Co(edma)_2]^+$ Ion at 80 °C

Isomer	k' / 10^{-3} s^{-1}	Isomer	k' / 10^{-3} s^{-1}	Isomer	k' / 10^{-3} s^{-1}
E-1	0.048	E-2	0.050	E-3	0.17
E-4 (A)	1.2	E-5	0.075	E-6	1.4
(B)	0.18				

(A): The position trans to the ligating O atom.
(B): The position trans to the ligating N atom.
Solvent: DCl(0.096 M)–D_2O.

In Scheme 1, each isomerization step (except for E-3→E-1 and E-3→E-2) is shown to be accompanying the inversion at one of two asymmetric sec-N centers. In the slow isomerization paths, such as the E-4⇄E-5 change, the inversion occurs at the trans(N)-sec-N center, accompanied by a slow H–D exchange of the trans(N)-sec-NH proton. On the other hand, in the fast isomerization paths, such as E-4→E-1 and E-6→E-2, the inversion occurs at the trans(O)-sec-N center, accompanied by the fast H-D exchange of the trans(O)-sec-NH proton; a linear relationship can been seen between the rates of the isomerization and the H–D exchange. The isomerization reaction of the $[Co(edma)_2]^+$ complex is base-catalyzed and probably involves a conjugate base intermediate. Even though the $[Co(edma)_2]^+$ complex has more than one potentially acidic amine protons, the reactive conjugate base intermediate should be produced by the deprotonation at the secondary amine, for that deprotonation is essential for the inversion of the configuration about the sec-N center. (In this case, the isomerization rate constant (k_{obsd}) is represented, by using the pre-equilibrium constant (K_{CB}) and the isomerization rate constant of the conjugate base (k_0), as $k_{obsd}=K_{CB}k_0$.) If the H–D exchange rate is taken as a criterion for the degree of the deprotonation of the sec-NH proton (acidity),[20] it is probable that the acidity of the sec-NH is reflected in the difference in the isomerization rate for this series of complexes.

All the experimental data for the reactions of the $[Co(edma)_2]^+$ series are most satisfactorily accommodated by the proposal of transient five-coordinated intermediates formed by Co–O bond rupture. In the Co–O bond-ruptured state, the inversion at the sec-N of "bidentate edma" can be expected to occur easily under the present experimental conditions (40 °C, pH 10.35), judging from the inversion data of the cobalt(III) complexes containing *N*-methylethylenediamine or sarcosine as a ligand.[21–24] For the isomerization of E-4, the mechanism shown in Scheme 2 may be proposed. A similar reaction scheme may be presumed for the other isomerization process in Scheme 1. However, the postulated intermediate in the E-2⇄E-5 path may be pictured as Scheme 3, because, in this isomerization, an exchange between the coordination sites of the terminal-N and O atoms in one edma ligand occurs.

For E-3, which contains meridionaly coordinated edma, the rate of the H–D exchange at the sec-N

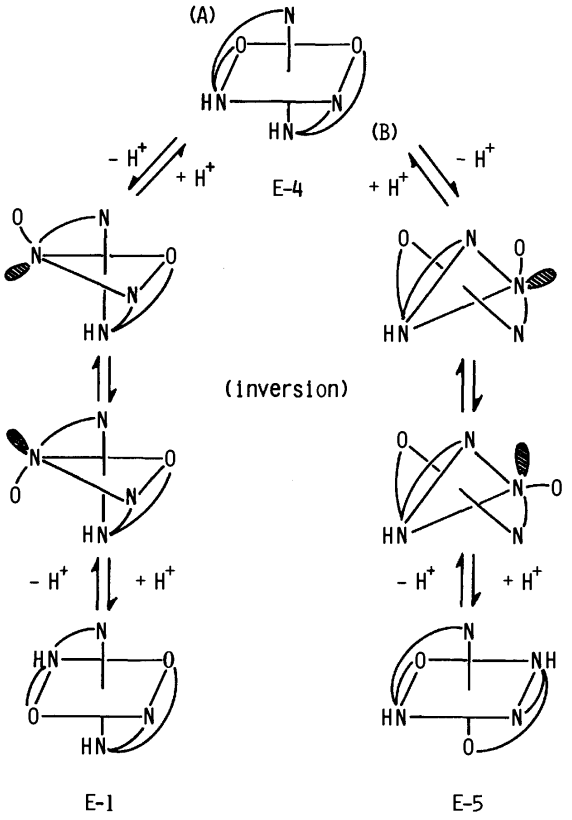

Scheme 2.

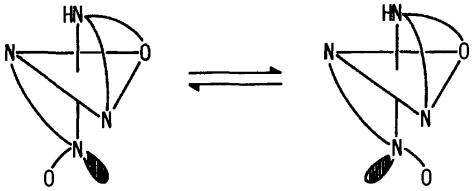

Scheme 3.

position is relatively slow, but the rate of the isomerization is relatively fast compared with those of the fac isomers (Tables 2 and 3); the result found for E-3 is different from those obtained in the fac isomers, in which "linear relationships" between the rates of the H-D exchange and isomerization reactions are observed. This may be attributed to the fact that the mer structure of an coordinated edma is thermodynamically less stable as a result of the strain on its mer chelate ring form. This unstability may be one of the reasons for the relatively rapid isomerization of E-3.

References

1) F. Basolo and R. G. Pearson, "Mechanism of Inorganic Reactions," 2nd ed., Wiley, New York (1967).
2) A. Sault, F. Fry, and J. C. Bailar, Jr., *J. Inorg. Nucl. Chem.*, **42**, 201 (1980), and the refs. cited therein.
3) G. H. Searle, F. R. Keene, and S. F. Lincoln, *Inorg. Chem.*, **17**, 2362 (1978).
4) H. Kawaguchi, T. Ama, and T. Yasui, *Bull. Chem. Soc. Jpn.*, **57**, 2422 (1984).
5) M. A. Cox, R. H. Griffiths, P. A. Williams, and R. S. Vagg, *Inorg. Chim. Acta*, **103**, 155 (1985), and the refs. cited therein.
6) T. J. Goodwin, P. A. Williams, and R. S. Vagg, *Inorg. Chim. Acta*, **86**, L73 (1984).
7) Y. Fujii, K. Shiono, K. Ezuka, and T. Isago, *Bull. Chem. Soc. Jpn.*, **53**, 3537 (1980).
8) J. A. Chambers, T. J. Goodwin, M. W. Mulqi, P. A. Williams, and R. S. Vagg, *Inorg. Chim. Acta*, **75**, 241 (1983), and the refs. cited therein.
9) D. A. House and V. McKee, *Inorg. Chem.*, **23**, 4237 (1984).
10) D. A. House, *Aust. J. Chem.*, **35**, 659 (1982).
11) D. A. House, *Coord. Chem. Revs.*, **23**, 223 (1977).
12) D. J. Radanovic, *Coord. Chem. Revs.*, **54**, 159 (1984).
13) Modifying the conventional nomenclature designated by the IUPAC tentative rule: *Inorg. Chem.*, **9**, 1 (1970).
14) T. Yasui, H. Kawaguchi, and T. Ama, *Chem. Lett.*, **1983**, 1277.
15) T. Ama, H. Kawaguchi, T. Yasui, K. Matsumoto, and S. Ooi, *Bull. Chem. Soc. Jpn.*, **58**, 2561 (1985).
16) R. Niiyama, Y. Matsunami, T. Ama, H. Kawaguchi, and T. Yasui, presented at the Symposium by the Chemical Society of Japan, Kochi, October 1984, Abstr., No. 1E07.
17) $\Delta(C_2)$ and $\Lambda(C_2)$ in the *mer*-$[Co(edma)_2]^+$ ion represent the right-hand and left-hand helix respectively about the C_2 (or pseudo-C_2) axis of the complex.
18) H. Kawaguchi, unpublished research.
19) E. Baraniak, D. A. Buckingham, C. R. Clark, and A. M. Sargeson, *Inorg. Chem.*, **25**, 1952 (1986).
20) In general, the deprotonation of the NH proton is characterized by its own acidity constant (K_{CB}) and not by the exchange rate. D. A. Buckingham, B. M. Foxman, and A. M. Sargeson, *Inorg. Chem.*, **9**, 1790 (1970); E. Ahmed and M. L. Tobe, *ibid.*, **15**, 2635 (1976); S. Balt, W. E. Renkema, and P. C. M. Van Zijl, *Inorg. Chim. Acta*, **45**, L241 (1980).
21) H. Kawaguchi, M. Matsuki, T. Ama, and T. Yasui, *Bull. Chem. Soc. Jpn.*, **59**, 31 (1986).
22) B. Halpern, A. M. Sargeson, and K. R. Turnbull, *J. Am. Chem. Soc.*, **88**, 4630 (1966).
23) M. Fujita, Y. Yoshikawa, and H. Yamatera, *Bull. Chem. Soc. Jpn.*, **50**, 3209 (1977).
24) D. A. Buckingham, L. G. Marzilli, and A. M. Sargeson, *J. Am. Chem. Soc.*, **89**, 825 (1967); *ibid.*, **89**, 3429 (1967); *ibid.*, **90**, 6028 (1968).

 © 1987 The Chemical Society of Japan Bull. Chem. Soc. Jpn., 60, 3961—3966 (1987)

Kinetic Study of the Polymerization of Styrene in the Presence of Various Organic Hydroperoxides

Takeshi KOMAI* and Kazuo MATSUYAMA
Chemicals & Explosives Research Laboratory, Nippon Oil & Fats Co., Ltd.,
Taketoyo-Cho, Chita-Gun, Aichi 470-23
(Received January 5, 1987)

The polymerizations of styrene initiated by 2,2′-azobisisobutyronitrile have been carried out in the presence of various organic hydroperoxides, scuh as 1,1-dimethylethyl ($\mathbf{I}_a$), 1,1-dimethylbutyl ($\mathbf{I}_b$), and 1-methyl-1-phenylethyl hydroperoxides ($\mathbf{I}_c$) at 60 °C. The polymerization rate increased with the concentration of $\mathbf{I}_c$, but became rather retarded with that of $\mathbf{I}_a$ and $\mathbf{I}_b$. This phenomenon can be explained by the difference in the radical induced decomposition for the hydroperoxides. The hydroperoxide ($\mathbf{I}_c$) decomposes with a radical displacement on the peroxide bond; however, $\mathbf{I}_a$, and $\mathbf{I}_b$, in addition to this reaction, decompose with the radical hydrogen abstraction of the hydroperoxyl group. The peroxyl radical formed (ROO·) subsequently gave rise to a primary radical termination.

So far, many investigators have been interested in the decomposition of hydroperoxides (ROOH) which are significant substances as initiators for radical polymerization and intermediates in autoxidation processes[1] and biological systems.[2] However, the decomposition of hydroperoxides has not yet been made sufficiently clear. The decomposition mechanism of hydroperoxides is much more complicated than those of the other types of peroxides, i.e., dialkyl peroxide, diacyl peroxide and peroxyester.[3] For instance, the apparent rate constants for the decomposition reaction are considerably influenced by the structure and concentration of hydroperoxides, and on solvents.[4] This phenomenon has been attributed to the possibility that different types of decompositions occur simultaneously in the reaction. In addition to two types of homolytic radical decompositions, i.e., uni- (Eq. 1) and bimolecular decompositions (Eq. 2),

$$\mathrm{ROOH} \longrightarrow \mathrm{RO}\cdot + \cdot\mathrm{OH} \quad (1)$$

$$2\mathrm{ROOH} \longrightarrow \mathrm{RO}\cdot + \mathrm{H_2O} + \cdot\mathrm{OOR} \quad (2)$$

hydroperoxide decomposes with the following molecularly assisted homolysis (Eq. 3) and epoxidation (Eq. 4) in the presence of styrene (M). Furthermore,

$$\mathrm{ROOH} + \mathrm{M} \longrightarrow (\mathrm{MOH})\cdot + \mathrm{RO}\cdot \quad (3)$$

$$\mathrm{ROOH} + \mathrm{M} \longrightarrow \mathrm{C_6H_5CH(O)CH_2} + \mathrm{ROH} \quad (4)$$

two types of radical-induced decompositions (direct attack on the peroxide bond (Eq. 5) and hydrogen abstraction of the hydroperoxyl hydrogen atom (Eq. 6)), have also been postulated regarding the polymerization of styrene (N is polystyryl radical.).[3,5,6]

$$\mathrm{N} + \mathrm{ROOH} \longrightarrow \mathrm{NON\ (polymer)} + \mathrm{RO}\cdot \quad (5)$$

$$\mathrm{N} + \mathrm{ROOH} \longrightarrow \mathrm{NH\ (polymer)} + \mathrm{ROO}\cdot \quad (6)$$

For these reasons, the behavior of hydroperoxides in the polymerization process has not been fully understood.

Quantitative information concerning the decomposition of hydroperoxides was obtained by several kinetic studies on the polymerization. Johnson and Tobolsky[7] reported apparent chain-transfer constants of 1,1-dimethylethyl ($\mathbf{I}_a$) and 1-methyl-1-phenylethyl hydroperoxides ($\mathbf{I}_c$), 0.035 and 0.063, respectively. They did not recognize any difference of polymerization activity with the structure of hydroperoxide. A retardation of the polymerization rate has been observed for a high concentration of $\mathbf{I}_a$. Walling and Heaton explained this phenomenon kinetically by assuming a chain transfer of polystyryl radical with an $\mathbf{I}_a$ dimer to yield an unreactive species.[5] In this work, we studied kinetically polymerization in the presence of hydroperoxide using 2,2′-azobisisobutyronitrile (AIBN) as an initiator at 60 °C. The homolytic and ionic decompositions of Eqs. 1—4 are minimized under this experimental condition; the hydroperoxide may be mainly consumed with radical induced decompositions of Eqs. 5 and 6, i.e., chain-transfer reactions.

Results and Discussion

Kinetic Scheme. The bulk polymerization of styrene initiated by AIBN at 60 °C has been achieved in the presence of three hydroperoxides (**I**); the kinetic data are shown in Table 1. The overall scheme for the polymerization can be given as follows.

$$\mathrm{ROOH} = \mathrm{R_aR_bR_cCOOH} \quad (\mathbf{I})$$

$\mathbf{I}_a$: 1,1-dimethylethyl hydroperoxide ($\mathrm{R_a}=\mathrm{R_b}=\mathrm{R_c}=\mathrm{CH_3}$)

$\mathbf{I}_b$: 1,1-dimethylbutyl hydroperoxide ($\mathrm{R_a}=\mathrm{R_b}=\mathrm{CH_3}$, $\mathrm{R_c}=n\text{-}\mathrm{C_3H_7}$)

$\mathbf{I}_c$: 1-methyl-1-phenylethyl hydroperoxide ($\mathrm{R_a}=\mathrm{R_b}=\mathrm{CH_3}$, $\mathrm{R_c}=\mathrm{C_6H_5}$)

Decomposition of the initiators:

$$\mathrm{AIBN} \longrightarrow 2\mathrm{R}_1 + \mathrm{nitrogen} \quad 2f_1k_{d1}[\mathrm{AIBN}], \quad (7)$$

where R_1 is $(\mathrm{CH_3})_2\dot{\mathrm{C}}\text{-}\mathrm{CN}$, f_1, fraction of primary radical (R_1) escaping from solvent cage, k_{d1}, decomposition constant of AIBN. Chain initiation by the hydroperoxide is based on the reaction of Eqs. 1—3; however, only the bimolecular reaction between the

hydroperoxide and styrene (Eq. 3) becomes important in bulk polymerization at lower temperatures. Tobolsky and Matlack found that the rate of chain initiation (R_i) from hydroperoxide could be interpreted as bimolecular reactions of several types as shown in Eq. 8:[8]

$$R_i = k_{d2}[\mathrm{ROOH}][\mathrm{M}] + k'_{d2}[\mathrm{ROOH}][\mathrm{X}] \quad (8)$$

Here, X is a specific solvent, and k_{d2} and k'_{d2} are rate constants of bimolecular reactions, respectively. In bulk polymerization of styrene, the second term of the right-hand side in Eq. 8 can be neglected.

Chain initiation:

Table 1. Polymerization of Styrene at 60 °C

	[ROOH] mol l^{-1}	[AIBN] mol l^{-1}	[M] mol l^{-1}	$10^5 R_p$ mol l^{-1} s^{-1}	$\bar{n}$
None	0	0.0239	8.31	9.48	588
	0	0.01194	8.33	7.35	787
	0	0.00478	8.34	4.02	1332
	0	0.00239	8.34	2.70	2011
$\mathbf{I_a}$	0.240	0.0239	8.10	7.58	274
	0.192	0.0239	8.14	7.04	309
	0.192	0.0239	8.14	7.07	315
	0.0973	0.0239	8.22	7.90	412
	0.0502	0.0239	8.26	8.85	502
	0.0235	0.0239	8.29	8.86	593
	0.240	0.00478	8.13	4.38	361
	0.191	0.00478	8.17	4.36	430
	0.0957	0.00478	8.25	3.96	681
	0.0497	0.00478	8.29	4.00	942
	0.0249	0.00478	8.32	4.31	1130
	0.193	0	8.18	2.92	595
$\mathbf{I_b}$	0.193	0.0239	8.09	7.04	281
	0.1446	0.0239	8.14	8.08	327
	0.0965	0.0239	8.20	8.04	401
	0.0484	0.0239	8.25	8.58	471
	0.0239	0.0239	8.28	9.07	548
	0.239	0.00481	8.07	4.38	318
	0.191	0.00481	8.12	4.28	385
	0.1431	0.00481	8.17	4.36	446
	0.0960	0.00481	8.23	4.38	606
	0.0475	0.00481	8.28	4.71	831
	0.0241	0.00481	8.31	4.22	1081
	0.191	0	8.13	3.16	455
	0.0960	0	8.24	2.27	916
	0.0480	0	8.29	1.69	1592
$\mathbf{I_c}$	0.192	0.0239	8.03	10.00	222
	0.0962	0.0239	8.17	9.89	327
	0.0490	0.0239	8.24	9.33	424
	0.0243	0.0239	8.27	9.33	506
	0.192	0.00478	8.06	6.60	250
	0.0956	0.00478	8.20	5.51	433
	0.0499	0.00478	8.26	4.45	652
	0.192	0	8.06	5.74	260

$$R_1 + M \longrightarrow N_1 \qquad k_{pr1}[R_1][M] \quad (9)$$

$$R_2 + M \longrightarrow N_2 \qquad k_{pr2}[R_2][M] \quad (10)$$

$$R_3 + M \longrightarrow R_5 \qquad k_{pr3}[R_3][M] \quad (11)$$

$$R_4 + M \longrightarrow N_2 \qquad k_{pr4}[R_4][M] \quad (12)$$

$$R_5 + M \longrightarrow N_2 \qquad k_{pr5}[R_5][M] \quad (13)$$

where k_{prj} is rate constant for the addition of primary radical, R_j (R_2=RO·, R_3=ROO·, R_4=(MOH)·, and R_5=ROOCH$_2$ĊHC$_6$H$_5$) to styrene and N_j is the polystyryl radical of j monomeric units. Walling and Heaton suggested that 60% of the 1-phenyl-2-*t*-alkylperoxyl ethyl radical (R_5) arising from Eq. 11 should yield styrene oxide in pure styrene at 70 °C.[5] The γ-scission of R_5 in Eq. 15 competes with the addition to styrene (Eq. 13):

$$R_5 \longrightarrow RO\cdot + \underset{\diagdown\,O\,\diagup}{CH_2\text{-}CHC_6H_5} \qquad k_\gamma[R_5] \quad (15)$$

Here, k_γ is rate constant of the γ-scission. The 2-cyano-2-propyl[9] and alkoxyl radicals[10] of R_1 and R_2 are very reactive against styrene, and R_4 and R_5 have the similar reactivity as polystyryl radical. The peroxyl radical of R_3 is most stable compared with the other radicals.

Propagation:

$$N_n + M \longrightarrow N_{n+1} \qquad k_p[N][M], \quad (16)$$

where k_p is propagation rate constant.

Chain transfer:

$$N_n + M \longrightarrow N_1 + \text{polymer} \qquad k_{trM}[N][M], \quad (17)$$

where k_{trM} is rate constant of transfer to styrene. Equations 5 and 6 are chain transfer to the hydroperoxide and the rates may be written respectively as:

$$\text{Rate of attack on the peroxide bond} = k_{trP}[N][\mathrm{ROOH}] \quad (18)$$

$$\text{Rate of hydrogen abstraction} = k_{trH}[N][\mathrm{ROOH}], \quad (19)$$

where k_{trP} and k_{trH} are the rate constants, respectively.

Termination:

$$N_n + N_s \longrightarrow \text{polymer} \qquad \bar{k}_t[N] \quad (20)$$

$$N_n + R_3 \longrightarrow \text{polymer} \qquad \bar{k}_{tpr3}[N][R_3] \quad (21)$$

where $\bar{k}_t$ is the rate constant of termination between polymer radicals, and k_{tpr3} is the rate constant of a primary radical termination between polymer and peroxyl redicals. Here, only the most stable peroxyl radical is considered to participates in a primary radical termination under these polymerization conditions.[11]

The polymerization rate is written:

$$R_p = k_p[N][M] + k_{pr1}[R_1][M] + k_{pr2}[R_2][M] + k_{pr3}[R_3][M] + k_{pr4}[R_4][M] + k_{pr5}[R_5][M] \simeq k_p[N][M] \quad (22)$$

The average chain length, $\bar{n}$, is written:

$$\bar{n} = \frac{k_p[N][M]}{\bar{k}_t[N]^2 + k_{trH}[N][M] + k_{trP}[N][M] + k_{tpr3}[N][R_3] + k_{trM}[N][M]} \quad (23)$$

Material balances under steady state condition give:

$$\frac{d[R_1]}{dt} = 2f_1k_{d1}[AIBN] - k_{pr1}[R_1][M] = 0 \quad (24)$$

$$\frac{d[R_2]}{dt} = k_{d2}[ROOH][M] + k_r[R_5] + k_{trP}[N][ROOH] - k_{pr2}[R_2][M] = 0 \quad (25)$$

$$\frac{d[R_3]}{dt} = k_{trH}[N][ROOH] - k_{tpr3}[R_3][N] - k_{pr3}[R_3][M] = 0 \quad (26)$$

$$\frac{d[R_4]}{dt} = k_{d2}[ROOH][M] - k_{pr4}[R_4][M] = 0 \quad (27)$$

$$\frac{d[R_5]}{dt} = k_{pr3}[R_3][M] - k_r[R_5] - k_{pr5}[R_5][M] = 0 \quad (28)$$

$$\frac{d[N]}{dt} = k_{pr1}[R_1][M] + k_{pr2}[R_2][M] + k_{pr4}[R_4][M] + k_{pr5}[R_5][M] - k_{trH}[N][ROOH] - k_{trP}[N][ROOH] - k_{tpr3}[N][R_3] - \bar{k}_t[N]^2 \quad (29)$$

Polymerization Initiated by AIBN. Data on a polymerization initiated by AIBN in the absence of hydroperoxide are analyzed by the conventional relationship between $\bar{n}$ and R_p.[7]

$$\frac{1}{\bar{n}} = \frac{k_{trM}}{k_p} + \frac{\bar{k}_tR_p}{k_p^2[M]^2} \quad (30)$$

Now, we obtained $k_{trM}/k_p = 6\times10^{-5}$ and $\bar{k}_t/k_p^2 = 1130$ mol s l^{-1}; the former is the same value as that of Johnson and Tobolsky, the later is between 840 and 1350 mol s l^{-1} in Ref. 12. The value of f_1k_{d1} for AIBN was found to be 3.1×10^{-6} s^{-1} from the usual polymerization rate equation.[7]

Polymerization Initiated by Hydroperoxide. The relationship among R_p, [M], and [ROOH] involving primary radical termination in the polymerization initiatedy a hydroperoxide is given by the following equation:

$$\frac{\bar{k}_tR_p^2}{k_p^2[M]^3[ROOH]} = 2k_{d2} - \frac{2(k_{tpr3}k_{trH}/k_p^2k_{pr3})(R_p/[M]^2)^2}{1+(k_{tpr3}/k_pk_{pr3})(R_p/[M]^2)} \quad (31)$$

The second term of the right-hand side in Eq. 31 shows the retardation of the rate based on a primary radical termination of the peroxyl radical. The value of the left-hand side in the equation approaches $2k_{d2}$ when $(R_p/[M]^2)^2$ is sufficiently close to zero. Figure 1 shows plots of ln $(\bar{k}_tR_p^2/k_p^2[M]^3[ROOH])$ vs. $(R_p/[M]^2)^2$ using the data from this work, the references[5,13] and the k_{d2} values obtained from the intercept of the plot (Table 2). The values of k_{d2} for $\mathbf{I}_a$ were found to be 6.1×10^{-9} s^{-1} at 60 °C and 8.4×10^{-9} s^{-1} at 70 °C, respectively.

The apparent chain transfer constant, k_{trC}/k_p, can be obtained from the conventional relationship between $\bar{n}$, R_p, [M], and [ROOH]:[5]

$$\frac{k_{trC}}{k_p} = \frac{[M]}{[ROOH]}\left(\frac{1}{\bar{n}} - \frac{k_{trM}}{k_p} - \frac{\bar{k}_tR_p}{k_p^2[M]^2}\right) \quad (32)$$

The values of k_{trC}/k_p were found to be 0.048 for $\mathbf{I}_a$, 0.065 for $\mathbf{I}_b$ and 0.117 for $\mathbf{I}_c$, respectively, from the data in Table 1. The value for $\mathbf{I}_a$ is between 0.035 at 60 °C[7] and 0.064 at 70 °C.[5]

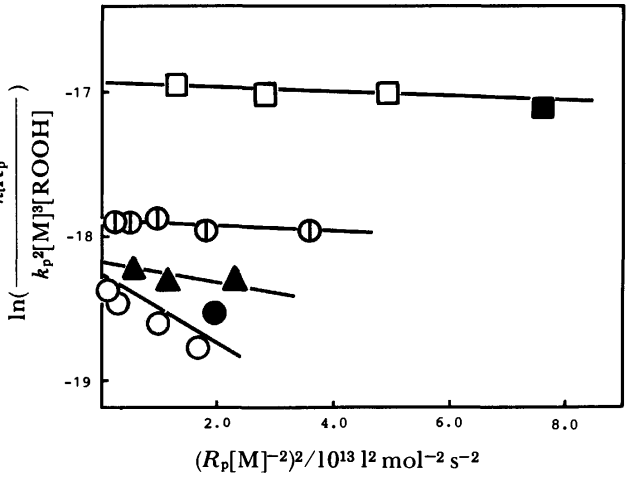

Fig. 1. Determination for chain initiation rate constants of some hydroperoxides: ○, $\mathbf{I}_a$ at 60 °C; ⊙, $\mathbf{I}_a$ at 70 °C; △, $\mathbf{I}_b$ at 60 °C; □, $\mathbf{I}_c$ at 60 °C; Closed circles, this work; Open circles, the data of references.[5,12]

Table 2. Various Rate Constants in the Polymerization of Styrene Initiated by AIBN in the Presence of Some Hydroperoxides at 60 °C

ROOH	$10^6f_1k_{d1}$ / s^{-1}	10^9k_{d2} / s^{-1}	k_{trH}/k_p	$(k_{trP}\cdot 2k_{trH})/k_p$	k_{trP}/k_p	$10^8\,k_{pr3}k_{trH}/k_{tpr3}$ / l s mol^{-1}	
						From Eq. 34.	From Eq. 36.
$\mathbf{I}_a$	2.3	6.1	0.025	0.09	0.040	1.2	1.7
$\mathbf{I}_b$	2.3	6.4	0.028	0.11	0.054	1.4	1.8
$\mathbf{I}_c$	2.3	22	0	0.117	0.117	—	—

Polymerization Initiated by AIBN in the Presence of Hydroperoxide. The relationship among R_p, [M], [AIBN], and [ROOH] in the polymerization initiated by AIBN in the presence of ROOH is

$$\frac{\bar{k}_t R_p^2}{k_p^2[M]^2[AIBN]} = 2f_1k_{d1} + 2\left(k_{d2}[M] - \frac{k_{trH}[N]}{1+k_{pr3}[M]/k_{tpr3}[N]}\right) \times \frac{[ROOH]}{[AIBN]} \quad (33)$$

When the value of $k_{tpr3}[N][R_3]$ is larger than that of $k_{pr3}[R_3][M]$, because $1/(1+k_{pr3}[M]/k_{tpr3}[N]) \simeq (1-k_{pr3}[M]/k_{tpr3}[N])$, Eq. 33 becomes:

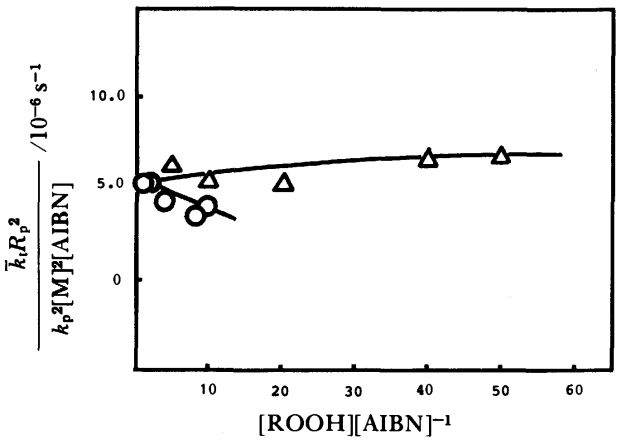

Fig. 2. Application of Eq. 34 to the data in the polymerization of styrene initiated by AIBN in the presence of I_a at 60 °C: Δ, [AIBN]=0.0048; O, [AIBN]=0.0239 mol l^{-1}; ——, Curves calculated by Lagrange's interpolation method, using the values of Table 2.

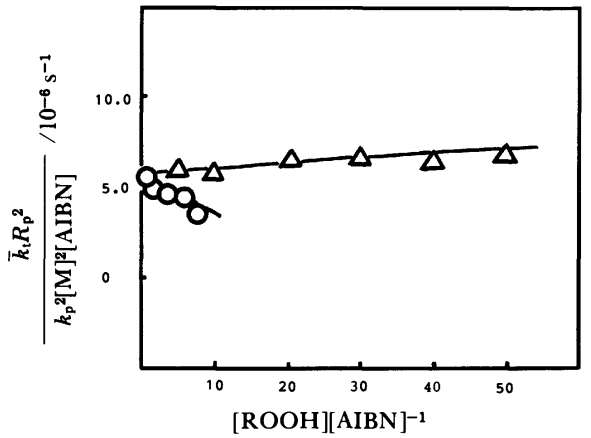

Fig. 3. Application of Eq. 34 to the data in the polymerization of styrene initiated by AIBN in the presence of I_b at 60 °C: Δ, [AIBN]=0.0048; O, [AIBN]=0.0239 mol l^{-1}; ——, Curves calculated by Lagrange's interpolation method, using the values of Table 2.

$$\frac{\bar{k}_t R_p^2}{k_p^2[M]^2[AIBN]} = 2f_1k_{d1} + 2\left(k_{d2}[M] - \frac{k_{trH}R_p}{k_p[M]} + \frac{k_{pr3}k_{trH}[M]}{k_{tpr3}}\right) \times \frac{[ROOH]}{[AIBN]} \quad (34)$$

The second term of the right-hand side in Eq. 34 shows chain initiation by hydroperoxide which depends on the polymerization rate (R_p). Figures 2—4 show plots of the values of the left-hand side in Eq. 34 against [ROOH]/[AIBN] at two concentrations of AIBN. The plots give a linear line for I_c, but two linear-like curves for I_a and I_b, respectively. The former increases linearly with [ROOH]/[AIBN]. However, the later remarkably decreases with [ROOH]/[AIBN] at a higher concentration of AIBN (higher polymerization rate) and distinctly shows a retardation owing to the hydroperoxide. The value of f_1k_{d1} was obtained from the intercept of the curves (shown in Table 2). Furthermore, the values of k_{trH}/k_p and $k_{pr3}k_{trH}/k_{tpr3}$ for I_a and I_b were estimated from Eq. 34 by a least-squares method using values of f_1k_{d1} and k_{d2} (also shown in Table 2). Using these values, the solid curves in Figs. 2 and 3 could be simulated using Lagrange's interpolation method. The value of k_{d2} for I_c obtained from the slope of the staight line in Fig. 4 was found to be 1.6×10^{-8} s^{-1}.

The relationship among $\bar{n}$, R_p, [M], and [ROOH] is

$$\frac{1}{\bar{n}} = \frac{k_{trM}}{k_p} + \left[\frac{k_{trP}}{k_p} + \left(\frac{2k_{tpr3}[N]+k_{pr3}[M]}{k_{tpr3}[N]+k_{pr3}[M]}\right)\frac{k_{trH}}{k_p}\right]\frac{[ROOH]}{[M]} + \frac{\bar{k}_t R_p}{k_p^2[M]^2} \quad (35)$$

The second term of the right-hand side in Eq. 35 exhibits a dependence on the chain length for chain transfers to hydroperoxide and the primary radical termination of the peroxyl radical. This term changes

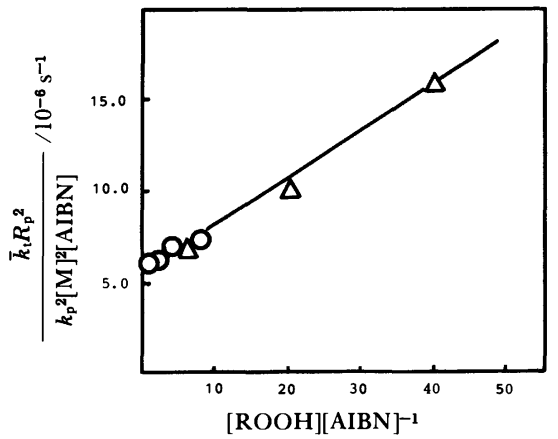

Fig. 4 A plot of $\bar{k}_tR_p^2/k_p^2[M]^2[AIBN]$ vs. [ROOH]/[AIBN] for the polymerization of styrene initiated by AIBN in the presence of I_c at 60 °C: Δ, [AIBN]=0.0048: O, [AIBN]=0.0239 mol l^{-1}.

largely with the relationship between $k_{tpr3}[N][R_3]$ and $k_{pr3}[M][R_3]$. When the value of $k_{tpr3}[N][R_3]$ is larger than that of $k_{pr3}[M][R_3]$, because $(2k_{tpr3}[N]+k_{pr3}[M]/(k_{tpr3}[N]+k_{pr3}[M])\simeq(2-k_{pr3}[M]/k_{tpr3}[N])$, Eq. 35 becomes:

$$\frac{1}{\bar{n}} = \frac{k_{trM}}{k_p} + \left(\frac{k_{trP}+2k_{trH}}{k_p} - \frac{k_{pr3}k_{trH}[M]^2}{k_{tpr3}R_p}\right)\frac{[ROOH]}{[M]} + \frac{\bar{k}_tR_p}{k_p^2[M]^2} \quad (36)$$

When $k_{tpr3}[N][R_3] \ll k_{pr3}[R_3][M]$, the value of $(2k_{tpr3}[N]+k_{pr3}[M])/(k_{tpr3}[N]+k_{pr3}[M])$ changes slightly with the value of $k_{pr3}[M]/k_{tpr3}[N]$: For example, it is 1.5 when $k_{pr3}[M]=k_{tpr3}[N]$, and 1.0 when $k_{pr3}[M] \gg k_{tpr3}[N]$. The values of $(1/\bar{n}-k_{trM}/k_p-\bar{k}_tR_p/k_p^2[M]^2)[M]/[ROOH]$ rearranged from Eq. 36 are plotted against $1/R_p$ for $\mathbf{I}_a$ and $\mathbf{I}_b$ in Figs. 5. and 6, respectively. The figures show that the value of $(1/\bar{n}-k_{trM}/k_p-\bar{k}_tR_p/k_p^2[M]^2)[M]/[ROOH]$ decreases with increasing $1/R_p$ and aproaches to a nearly constant value near the value of 3.0×10^4 l s mol^{-1} where $k_{tpr3}[N]\simeq k_{pr3}[M]$. The values of $(k_{trP}+2k_{trH})/k_p$ and $k_{pr3}k_{trH}/k_{tpr3}$ are estimated from the intercept and slop of Figs. 5 and 6 (Table 2). The value of $(1/\bar{n}-k_{trH}/k_p-\bar{k}_tR_p/k_p^2[M]^2)[M]/[ROOH]$ for $\mathbf{I}_c$ is constant against $1/R_p$ and the value of $(k_{trP}+2k_{trH})/k_p$ was found to be 0.117. The values of k_{trP}/k_p were calculated using the data in Table 2.

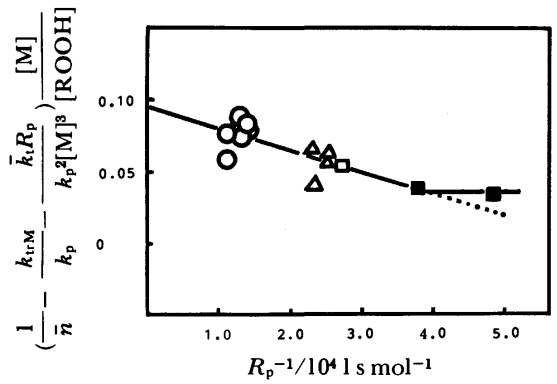

Fig. 5. Application of Eq. 36 to the data in the polymerization of styrene initiated by AIBN in the presence of $\mathbf{I}_a$ at 60 °C: □, [AIBN]=0; ■, [AIBN]=0 (the data of Baysal and Tobolsky[13]); △, [AIBN]=0.0048; ○, [AIBN]=0.0239 mol l^{-1}.

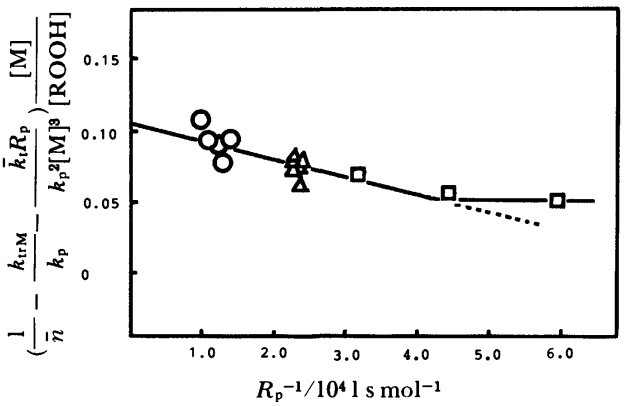

Fig. 6. Application of Eq. 36 to the data in the polymerization of styrene initiated by AIBN in the presence of $\mathbf{I}_b$ at 60 °C: □, [AIBN]=0; △, [AIBN]=0.0048; ○, [AIBN]=0.0239 mol l^{-1}.

Table 2 summarizes the rate constants in the polymerization of styrene initiated by AIBN in the presence of hydroperoxide at 60 °C. The same values of f_1k_{d1} for three hydroperoxides agree with those for a polymerization initiated only by AIBN. The values of k_{d2} and k_{trP}/k_p for $\mathbf{I}_c$ are larger than those of $\mathbf{I}_a$ and $\mathbf{I}_b$. The value of k_{trP}/k_p for $\mathbf{I}_a$ agrees reasonably well with 0.39 of k_{trC}/k_p for 1,1-dimethylethyl deuterioperoxide,[5] which hardly seemed to undergo a deuterium abstraction reaction of the deuterioperoxyl group. The value of k_{trH}/k_p for $\mathbf{I}_a$ is almost similar to that of $\mathbf{I}_b$, but is very different with that of $\mathbf{I}_c$. The values of $k_{pr3}k_{trH}/k_{tpr3}$ for $\mathbf{I}_a$ are almost similar to those of $\mathbf{I}_b$ in the cases in Eqs. 34 and 36; the values obtained from Eq. 34 are approximately equal to those from of Eq. 36. The values of $k_{pr3}k_p/k_{tpr3}$ calculated from the data in Table 2 were found to be in the range 5 to 7×10^{-7} l s mol^{-1}. These values are hardly influenced by the structure of the hydroperoxides and are much smaller than those of benzoyl peroxide and AIBN at 60 °C.[14] The bimolecular reaction between radicals is diffusion controlled; this result indicates that the rate constant (k_{pr3}) for the addition of the *t*-alkylperoxyl radical to styrene is one to six-hundredth as large as those of the primary radicals from benzoyl peroxide and AIBN. In fact, a rate constant of 1.3 l mol^{-1} s^{-1} for the addition of the 1,1-dimethylethylperoxyl radical to styrene at 30 °C was reported[15] to be much smaller than 55 mol^{-1} s^{-1} of the polystyryl radical. The ratio of the addition to styrene against the primary radical termination for *t*-alkylperoxyl radical was found to be in the range 0.3 to 1.2 in this work. Thus, the unexpected behavior of $\mathbf{I}_a$ and $\mathbf{I}_b$ may be sufficiently explained by the usual primary radical termination between polymer and peroxyl radicals[14] without assuming a chain transfer with the hydroperoxide dimer to yield unreactive species.[5] The phenomenon of inhibition and retardation in polymerization by traces of molecular oxygen may also be explained by the termination between the polymer radical and the peroxyl radical formed.[16]

In conclusion, the rates of the styrene-assisted homolysis and the radical displacement reaction on the peroxide bond of the hydroperoxides are considerably influenced by the structure of hydroperoxides, and the oders in the both reactions: $\mathbf{I}_c \gg \mathbf{I}_b > \mathbf{I}_a$.[17] A radical hydrogen abstraction reaction by polystyryl radical was observed for *t*-alkyl hydroperoxides ($\mathbf{I}_a$ and $\mathbf{I}_b$), but not for α-aryl-substituted *s*-alkyl hydroperoxides ($\mathbf{I}_c$).

Experimental

Materials. The commercial products of I_a and I_b from Nippon Oil & Fats Co., Ltd. were distilled under reduced pressure. The commercial product of I_c from Nippon Oil & Fats Co., Ltd. was purified by isolation of the sodium salt, regeneration of the hydroperoxide by carbon dioxide and vacuum distillation. The distilled materials were shown to be 97—99% pure by iodometric titration. The commercial product of AIBN was purified by recrystallization. Styrene was fractionated under reduced pressure, stored at −20 °C and used within 24 h.

Procedure. Styrene and initiators were put in a glass ampoule and degassed under reduced pressure by the freeze-thaw technique. The polymerization of styrene was carried out at 60.0±0.2 °C. The conversions were estimated by gel permeation chromatography (GPC). Ultimate conversions were less than 10%. The average molecular weight of polymer was estimated by GPC.

References

1) L. F. Martin, "Organic Peroxide Technology," Noyes Data Corporation, New Jersey (1973).

2) W. A. Pryor, "Free Radicals in Biology Vol. I," ed by W. A. Pryor, Academic Press, New York (1976), Chap. 1.

3) R. Hiatt, "Organic Peroxides Vol. II," ed by D. Swern, John Wiley & Sons, Inc., New York (1971), Chap. 1.

4) R. Hiatt and K. C. Irwin, *J. Org. Chem.*, **33**, 1436 (1968).

5) C. Walling and L. Heaton, *J. Am. Chem. Soc.*, **87**, 38 (1965).

6) C. Walling and Y. Chang, *J. Am. Chem. Soc.*, **76**, 4878 (1954).

7) D. H. Johnson and A. V. Tobolsky, *J. Am. Chem. Soc.*, **74**, 938 (1952).

8) A. V. Tobolsky and L. R. Matlack, *J. Polym. Sci.*, **55**, 49 (1961).

9) K. Ito, *J. Polym. Sci.*, **15**, 1759 (1977).

10) (a) M. V. Encina, M. Rivera, and E. A. Lisi, *J. Polym. Sci., Polym. Chem. Ed.*, **16**, 1709 (1978); (b) P. C. Wong, D. Griller, and J. C. Scaiano, *J. Am. Chem. Soc.*, **104**, 5106 (1982).

11) K. Matsuyama, T. Komai, and K. Ito, *J. Polym. Sci., Polym. Chem. Ed.*, **24**, 2425 (1986).

12) G. R. Ham, "Vinyl Polymerization Vol. I, Part I," ed by G. E. Ham, Marcel Kekker, Inc., New York (1967), p. 15.

13) B. Baysal and A. V. Tobolsky, *J. Polym. Sci.*, **8**, 529 (1952).

14) P. C. Deb and G. Meyerhoff, *Eur. Polym. J.*, **10**, 709 (1974); The values of $k_{pr3}k_p/k_{tpr3}$ for benzoyl peroxide and AIBN at 60 °C were reported in this reference to be 1.1×10^{-5} and 4.9×10^{-5} l s mol^{-1}, respectively.

15) J. A. Howard, *Can. J. Chem.*, **50**, 2298 (1972).

16) Ref. 12, p. 186.

17) The orders in the reactions may be explained by considering the following structures at transition state containing a nonclassical bridged component; [M (or N) HO· ·O-$CR_aR_bR_c$⟷M (or N) HO$^-$ O⟹CR_aR_b ⟷M$^+$ (or N$^+$) HO$^-$ ·O-$CR_aR_bR_c$].

 © 1987 The Chemical Society of Japan Bull. Chem. Soc. Jpn., 60, 3967—3972 (1987)

Preparation and Reaction of Optically Active Organotransition Metal Complexes. II.[1] Preparation and Photoracemization of Optically Active (1-Cyanoethyl)cobaloxime Complexes Coordinated with Various Axial Ligands

Shoe BABA,† Yoshiaki OHGO,* and Seiji TAKEUCHI
Niigata College of Pharmacy, 5-13-2 Kamishin'ei-cho, Niigata 950-21
†Niigata Academy of Medical Technology, 5-13-3 Kamishin'ei-cho, Niigata 950-21
(Received March 16, 1987)

Optically active (1-cyanoethyl)cobaloxime complexes coordinated with various pyridines, phosphines and amines etc. as axial ligands were prepared and their photoracemization rates were measured in a solution state. It was found that the steric factor, rather than the electronic, of the axial ligand controlled, predominantly, the rate of Co–C bond homolysis in these alkylcobaloximes.

Syntheses and reactions of chiral alkyl transition metal complexes can provide a clearer description of the elementary process of catalytic reactions involving alkyl transition metal intermediates. We have shown various useful properties of optically active alkyl cobalt complexes for an elucidation of solution-state and solid-state reactions of the Co–C bond formation and cleavage.[1-4,7]

In relation to coenzyme B_{12} chemistry, extensive investigations on the reactions of alkyl cobalt complexes, including thermal and photochemical decompositions, have been made by UV-VIS and NMR spectroscopies using achiral complexes. However, spectroscopic methods involving achiral complexes include, in general, possibilities for underestimating or overestimating the rate of Co–C bond cleavage unless an elaborated kinetic treatment is made.[4] A chiroptical measurement using optically active alkyl metal complexes provides a more simple, precise evaluation of the forward rate, since alkyl radicals formed by bond homolysis are "planar or rapidly inverting pyramid".[5] Thus, recombinations of these species with Co(II) and all other subsequent reactions such as radical coupling, beta-elimination etc., will give substantially racemic or achiral products (Eqs. 1 and 2).[4]

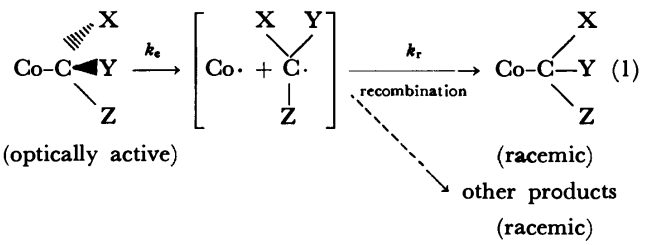

(1)

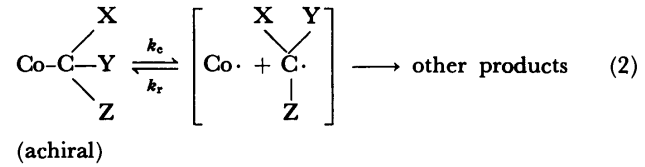

(2)

Consequently, Eqs. 3 and 4 were established for the Co–C bond homolysis of the optically active alkyl complexes:

$$-\mathrm{d[R]}/\mathrm{d}t = k_c[\mathrm{R}] \quad (3)$$

and

$$-\mathrm{d}\alpha/\mathrm{d}t = k_c\alpha. \quad (4)$$

Here, k_c is the rate constant for the Co–C bond cleavage, k_r the rate constant for the recombination, [R] the concentration of the reactant and α the optical rotation.

We wish to describe here the preparation of optically active (1-cyanoethyl)bis(dimethylglyoximato)-cobalt(III) complexes which have chirality at the carbon bound directly to the cobalt atom (Fig. 1) as well as the influence of the axial ligand on the rate of the photochemical Co–C bond homolysis.

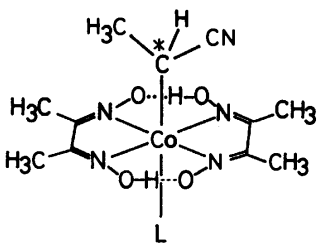

L: pyridines
phosphines
amines
etc.

Fig. 1. Chiral (1-cyanoethyl)cobaloximes coordinated with various axial ligands.

Results and Discussion

Preparation of Optically Active (1-Cyanoethyl)-cobaloximes. Optically active (1-cyanoethyl)cobaloximes which are coordinated with various axial ligands were prepared according to the method described in a previous paper.[1] The newly prepared

Table 1. ^{1}H NMR Chemical Shifts of Chiral (1-Cyanoethyl)cobaloximes Coordinated with Various Axial Ligands

Cobaloxime	Axial ligand	^{1}H NMR chemical shift δ/ppm[a]		
		CH_3CHCo	CH_3CHCo	CH_3(DMG)
2	4-Cyanopyridine (4-CN-Py)	0.545 (d, 3H)	nc[b]	2.221 2.247 (12H)
3	4-Chloropyridine (4-Cl-Py)	0.550 (d, 3H)	nc	2.233 2.259 (12H)
4	4-Methylpyridine (4-Me-Py)	0.564 (d, 3H)	nc	2.22 2.25 (12H)
5	Triethylphosphine (PEt_3)	0.663 (q, 3H)	2.089 (m, 1H)	2.286, 2.301 2.315 (12H)
6	Tributylphosphine ($P(n\text{-}Bu)_3$)	0.656 (q, 3H)	2.043 (m, 1H)	2.271, 2.286 2.301 (12H)
7	Diethyl(phenyl)phosphine (PEt_2Ph)	0.645 (q, 3H)	2.1 (m, 1H)	2.002, 2.017 (12H)
8	Diphenylmethylphosphine ($PMePh_2$)	0.654 (t, 3H)	2.314 (m, 1H)	1.830, 1.842 1.864, 1.880 (12H)
9	Diphenylethylphosphine ($PEtPh_2$)	0.617 (q, 3H)	2.28 (m, 1H)	1.893, 1.908 1.915, 1.930 (12H)
10	Triphenylphosphine (PPh_3)	0.539 (t, 3H)	2.40 (m, 1H)	1.875, 1.890 1.912, 1.956 (12H)
11	Tris(*p*-chlorophenyl)phosphine ($P(p\text{-}ClC_6H_4)_3$)	0.526 (t, 3H)	2.30 (m, 1H)	1.917, 1.932 1.950, 1.964 (12H)
12	Triethyl phosphite ($P(OEt)_3$)	0.688 (q, 3H)	2.14 (m, 1H)	2.258, 2.277 2.296 (12H)
13	Piperidine	0.459 (d, 3H)	nc	2.373, 2.386 (12H)
14	Pyrrolidine	0.505 (d, 3H)	nc	2.345, 2.355 (12H)
15	H_2O	0.205 (3H)	nc	2.246, 2.27 2.315, 2.325 (12H)

a) Solvent: $CDCl_3$; Internal standard: TMS. b) nc: The chemical shift is not clear because of overlapping with the signals of methyl protons of dimethylglyoximes.

complexes were characterized by elemental analyses as well as IR and NMR spectra. The ^{1}H NMR spectra and main bands of the IR spectra are shown in Tables 1 and 2. Their configurations and specific rotations are given in Table 3.

Photoracemization Reaction for (4-Substituted Pyridine)-Coordinated Cobaloximes. The optical rotations of a methanol solution of the optically active (1-cyanoethyl)cobaloxime complexes coordinated with various 4-substituted pyridines gradually decreased owing to Co–C bond cleavage upon visible-light irradiation. ln α vs. time were approximately linear. The k_c values obtained from the slopes of these first-order rate plots decreased only slightly with increasing pK_a value of the axial ligand (Table 4). This trend coincides with that in a thermal reaction,[4] and shows that the electron-donation ability of 4-substituted pyridine ligand influences, to some degree, the rate of the Co–C bond photolysis. However, the effect is very small in this series.

Photoracemization Reaction of Phosphine-Coordinated Cobaloximes. A photoracemization reaction of the optically active (1-cyanoethyl)cobaloxime complexes coordinated with various phosphines was carried out under the same conditions as that of (4-substituted pyridine)-coordinated complexes, except for the use of chloroform as the solvent.

The ^{1}H NMR spectrum of the PPh_3-coordinated complex solution suggested that the equilibrium accompanying an axial ligand dissociation existed in this system (Eq. 5).

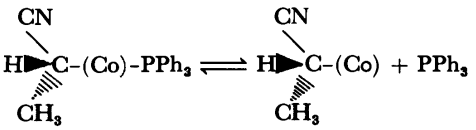

(5)

Table 2. Main IR Absorption Data of (1-Cyanoethyl)cobaloximes

Cobaloxime	IR absorption data/cm^{-1} a)			
	Cyanoethyl ν(C=N)	Glyoxime ν(C=N)	Glyoxime ν(O-H)	Others
2	2202	1555	3440	pyridine ν(C=C): 1606
3	2198	1555	3440	pyridine ν(C=C): 1592
4	2205	1550	3410	pyridine ν(C=C): 1620
5	2189	1580	3440	
6	2194	1553	3440	
7	2193	1575	3450	
8	2197	1540	3440	
9	2200	1580	3450	
10	2195	1555	3440, 3530	

a) KBr disk.

Table 3. Configurations and Specific Optical Rotations of Chiral (1-Cyanoethyl)cobaloximes Coordinated with Various Axial Ligands

Cobaloxime	Configuration	$[\alpha]^{RT}_{578}$	
		CH_3OH soln	$CHCl_3$ soln
2	*R*	+61.8	
3	*R*	+53.4	
4	*R*	+48.6	
5	*S*	−44.8	−53.3
6	*R*	+37.6	+46.6
7	*R*	+52.3	+54.0
8	*R*	+44.1	+24.1
9	*R*	+46.4	+50.0
10	*R*	+52.5	+73.1
11	*R*		+57.0
12	*R*	+47.8	+57.6
13	*R*	+50.5	+61.1
14	*R*		+70.2

In order to obtain the rate for the "ligand-on" form, free phosphine was added to the cobaloxime solution and photoracemization experiments were carried out. The value of k_c increased with increasing added free PPh_3 and reached a maximum in the case of the PPh_3 complex **10** (Fig. 2). This phenomenon shows that the rate of racemization is faster in "ligand-on" form than in "ligand-off" form, because addition of PPh_3 will promote the formation of "ligand-on" complex. A similar phenomenon was also observed in the P(*p*-$ClC_6H_4)_3$-coordinated complex **11** (Fig. 2). On the contrary, the addition of free phosphine did not substantially affect the photoracemization rate in the case of complexes coordinated with PEt_3, P(*n*-Bu)$_3$, $PMePh_2$, and $PEtPh_2$ (**5**, **6**, **8**, and **9**) (Fig. 3). These

Table 4. k_c Values for Photoracemization of (4-Substituted Pyridine)-Coordinated Cobaloximes

Cobaloxime	**2**	**3**	**4**
$k_c \times 10^5/s^{-1}$	6.1	5.7	5.1
Axial ligand	4-CN-Py	4-Cl-Py	4-Me-Py
pK_a(at 25 °C)a)	1.86	3.83	6.03

a) A. Fischer, W. J. Galloway, and J. Vaughan, *J. Chem. Soc.*, **1964**, 3591.

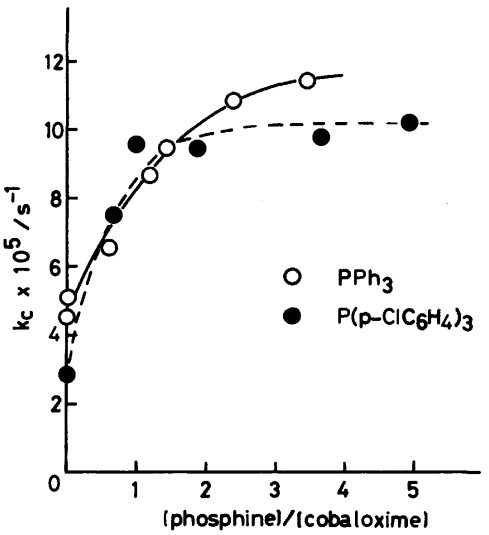

Fig. 2. Increase of k_c with addition of free phosphine to the PPh_3 and P(*p*-$ClC_6H_4)_3$-coordinated cobaloximes.

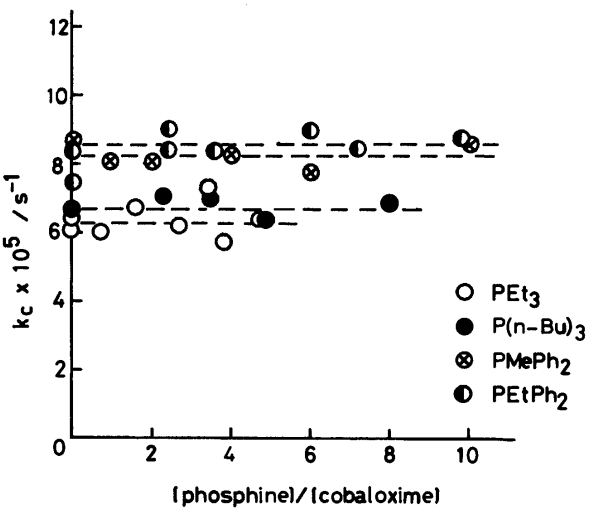

Fig. 3. Relationship between k_c and the mole ratio of added free phosphine to the cobaloximes coordinated with PEt_3, P(*n*-Bu)$_3$, $PMePh_2$, and $PEtPh_2$.

results show that the degree of ligand dissociation is negligibly small in the latter complexes, even without the addition of free phosphine since these phosphines have both stronger basicities and smaller steric

Table 5. $k_{c,max}$ Values for Photoracemization of Phosphine-Coordinated Cobaloximes

Cobaloxime	5	6	8	9	11	10
$k_{c,max} \times 10^5/s^{-1}$	6.2	6.7	8.3	8.6	10	11
Axial ligand	PEt_3	$P(n\text{-}Bu)_3$	$PMePh_2$	$PEtPh_2$	$P(p\text{-}ClC_6H_4)_3$	PPh_3
Cone angle/°	132[a]	132[a]	136[a]	140[a]	145[b]	145[a]
pK_a[c]	8.65	8.43	4.65	4.91	2.86	2.73

a) Ref. 6. b) Estimated value. c) Ref. 9.

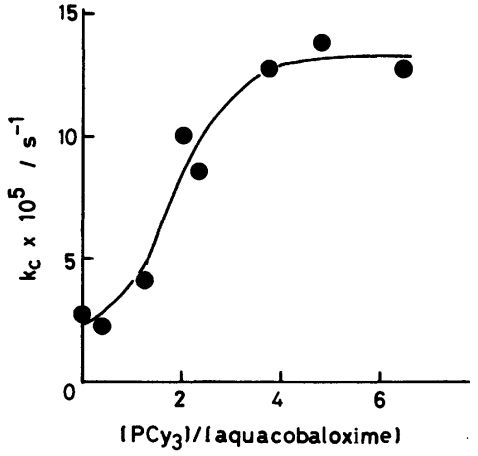

Fig. 4. Increase of k_c with addition of free PCy_3 to the aquacobaloxime.

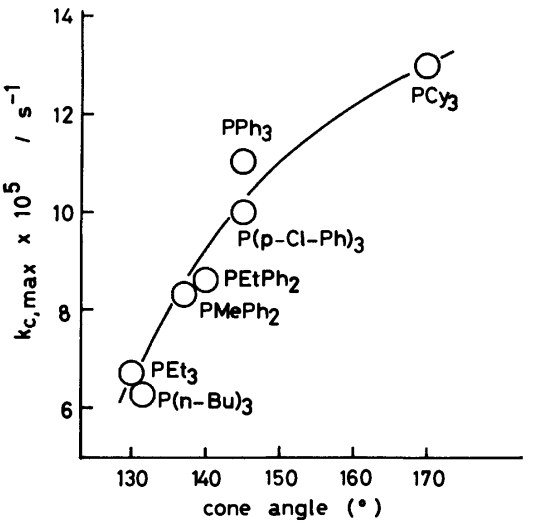

Fig. 5. Relationship between $k_{c,max}$ and the cone angle for phosphine-coordinated cobaloximes.

hindrances than PPh_3 and $P(p\text{-}ClC_6H_4)_3$. This can be seen from Table 5, which shows the large pK_a values of the conjugated acids and the small Tolman's cone angles[6] on these phosphines. On the other hand, the Co–P bonds in the former complexes (**10** and **11**) are weakened owing to the weak basicity and steric bulkiness of the triarylphosphines; therefore, ligand dissociation will be promoted.

Steric Influence of the Axial Phosphine on the Co–C Bond Photocleavage. Table 5 gives $k_{c,max}$, the maximum value of photoracemization rate constant obtained for the "ligand-on" form whose formation was promoted by the addition of free phosphine. The value of $k_{c,max}$ increased in the following order: $PEt_3 \lesssim P(n\text{-}Bu)_3 < PMePh_2 \lesssim PEtPh_2 < P(p\text{-}ClC_6H_4)_3 < PPh_3$. Either the electronic or steric factor of the phosphine ligand is responsible for this order. As can be seen from Table 5, the value of $k_{c,max}$ increased with an increase in the cone angle as well as a decrease in the pK_a value. Therefore, it cannot be determined whether the electronic or the steric effect acts as a dominant factor in influencing the value of $k_{c,max}$.

Tricyclohexylphosphine (PCy_3) has maximum values with respect to both the cone angle (170° [6]) and pK_a (9.70[9]), compared with preceding phosphines. Therefore, if the electronic factor is dominant in the case of the PCy_3-coordinated complex, the photoracemization rate will be minimum. On the contrary, if the steric factor is dominant, the maximum photoracemization rate will be obtained. Unfortunately, a PCy_3-coordinated complex could not be isolated, perhaps owing to its instability. However, the PCy_3-coordinated complex was formed in situ by the addition of PCy_3 to a chloroform solution of the aqua-coordinated complex **15**. This was confirmed by the ^1H NMR spectrum. The photoracemization experiment on this solution revealed that $k_{c,max}$ is $13 \times 10^{-5}\ s^{-1}$ (Fig. 4); this is the largest value obtained for all the cobaloxime complexes coordinated with pyridines and phosphines.

Consequently, as revealed by Fig. 5, these experimental data clearly demonstrate that the cone angle of a phosphine ligand is a dominant factor influencing the value of $k_{c,max}$ (the rate of Co–C bond photocleavage).††

In Table 6, the structural parameters around the Co atom based on the X-ray crystallographic analyses[7] are summarized for the complexes coordinated with $P(n\text{-}Bu)_3$, $PEtPh_2$, and PPh_3 (**6**, **9**, and **10**). The values of θ (the acute dihedral angle between the planes of the two glyoximato groups), d (the displacement of the Co

†† Recently Halpern et al. have reported a similar result in thermal reaction for the alkylcobaloximes.[8]

Table 6. Comparisons of Crystallographic Data[a] for **6**, **9**, and **10**

Complex	**6**	**9**	**10**
Axial ligand	$P(n\text{-}Bu)_3$	$PEtPh_2$	PPh_3
θ/°[b]	1.5	4.8	9.4
d/Å[c]	0.026	0.048	0.078
Co-P/Å	2.316	2.370	2.410
Co-C/Å	2.089	2.098	2.08

a) Ref. 7. b) The acute dihedral angle between the planes of the two glyoximato groups. The bending is toward the 1-cyanoethyl group. c) The displacement of the Co atom toward the P atom from the mean plane composed of four nitrogen atoms in the equatorial ligand.

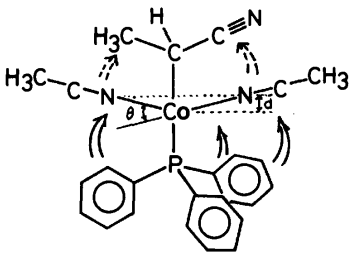

Fig. 6. Repulsive interaction in the PPh_3-coordinated cobaloxime.

atom toward the P atom from the mean plane composed of four nitrogen atoms in the equatorial ligand), and the Co-P distances increased with an increase in the cone angle of the phosphine ligand, probably in order to avoid the shortest contacts between the substituents of the phosphine ligand and the cobaloxime moiety. On the other hand, the Co-C bond length varied little. Therefore, with increasing steric bulkiness of the phosphine ligand, the 1-cyanoethyl group and the cobaloxime moiety come so close together that their mutual repulsion increases and the Co-C bond becomes strongly strained. This situation is depicted in Fig. 6 using, as an example, the PPh_3-coordinated cobaloxime.

In a solution state, the steric effect of the phosphine ligand on the Co-C bond may operate in a similar manner as that of the above description regarding a crystalline state. Thus, it is concluded that the acceleration of the photocleavage of the Co-C bond is responsible for the increase of the strain on this bond, arising from an increase in the steric bulkiness of the phosphine ligand. The electronic effect of the axial ligand on the Co-C bond photocleavage is found to be much smaller than the steric effect and, therefore, to be masked by the steric factor within this series.

Experimental

Apparatus. The IR spectra were recorded on a JASCO A-3 spectrometer using KBr disks. The ^1H NMR spectra were obtained on a JEOL FX-200 spectrophotometer, using TMS as the internal standard.

The optical rotations were measured on a Perkin-Elmer 241 polarimeter.

Photoracemization. The sample for photoracemization was dissolved under dim light at ca. 2×10^{-3} mol dm^{-3} in chloroform which was freed from dissolved oxygen by bubbling with a stream of argon for about 30 min. The sample solution was placed in a glass (Pyrex) cell for a measurement of the optical rotation; photoreactions were carried out under the conditions of visible-light irradiation using four 40-W fluorecent lamps "white" (Matsushita Elec. Ind. Co.) at 25±2 °C. The cell was placed at the distance of ca. 3.0 m from the light source; at that distance the radiation intensity was 0.008 mW cm^{-2}. The optical rotations (α), which gradually decreased upon irradiation, were measured at regular time intervals. In the dark conditions, the optical rotation didn't vary while standing overnight.

Materials. All chemicals were reagent grade commercial materials and used without further purification.

All chiral (1-cyanoethyl)cobaloximes coordinated with various pyridines, phosphines, amines etc. were prepared by a ligand exchange reaction for [(*R*) or (*S*)-1-cyanoethyl]bis-(dimethylglyoximato)[(*S*)-1-phenylethylamine]cobalt(III) (**1**(*R*) or **1**(*S*)) prepared according to a preceding paper.[1] All the preparative operations were performed in the dark.

[(*R*)-1-Cyanoethyl](4-cyanopyridine)bis(dimethylglyoximato)cobalt(III) (2): To a methanol solution (10 cm^3) of 0.50 g of **1**(*R*) were added 0.8 cm^3 of 2 mol dm^{-3} hydrochloric acid and 0.17 g of 4-cyanopyridine. After standing for 4 h at 30 °C, water (10 cm^3) was added to the reaction mixture; the solution was then cooled overnight. Deposited dark brown crystals were collected by filtration; 0.44 g (91%). The crude product was recrystallized several times from acetone-water to give plates. Found: C, 45.34; H, 5.10; N, 22.14%. Calcd for $C_{17}H_{22}N_7O_4Co$: C, 45.64; H, 4.96; N, 21.92%.

(4-Chloropyridine)[(*R*)-1-cyanoethyl]bis(dimethylglyoximato)cobalt(III) (3) and [(*R*)-1-Cyanoethyl]bis(dimethylglyoximato)(4-methylpyridine)cobalt(III) (4): These were similarly prepared for **2** by using 4-chloropyridine and 4-methylpyridine, respectively, in place of 4-cyanopyridine. For **3**: Crude yield, 71%. Brown needles (acetone-water). Found: C, 42.14; H, 5.08, N, 18.71%. Calcd for $C_{16}H_{22}N_6O_4ClCo$: C, 42.07; H, 4.85; N, 18.40%. For **4**: Crude yield, 74%. Brown needles (acetone-water). Found: C, 46.37; H, 5.82; N, 19.34%. Calcd for $C_{17}H_{25}N_6O_4Co$: C, 46.79; H, 5.77; N, 19.26%.

[(*S*)-1-Cyanoethyl]bis(dimethylglyoximato)(triethylphosphine)cobalt(III) (5): To a acetone (30 cm^3) solution of a 1.5 g of **1**(*S*) were added 1.62 cm^3 of 2 mol dm^{-3} hydrochloric acid and 0.72 cm^3 of PEt_3. After having been stirred for 20 h under a nitrogen atmosphere at room temperature, a 10 cm^3 of water was added to the solution. The resulting solution was concentrated under reduced pressure. Deposited orange crystals were collected by filtration; 1.25 g (84%). The crude product was recrystallized from methanol-water to give columns. Found: C, 44.09; H, 7.53; N, 15.07%. Calcd for $C_{17}H_{33}N_5O_4CoP$: C, 44.25; H, 7.21; N, 15.18%.

[(*R*)-1-Cyanoethyl]bis(dimethylglyoximato)(triphenylphosphine)cobalt(III) (10): A 0.50 g of **1**(*R*) was dissolved in methanol (20 cm^3) and then 0.42 g of PPh_3 and 0.54 cm^3 of

2 mol dm^{-3} hydrochloric acid were added. The reaction mixture was stirred overnight under an argon atmosphere at room temperature. Then, 10 cm^3 of water was added and the resulting solution was cooled. Deposited dark brown crystals were collected by filtration; 0.57 g (87%). The crude product was recrystallized several times from methanol–water to give flakes. Found: C, 56.66; H, 5.79; N, 11.26%. Calcd for $C_{29}H_{33}N_4O_5CoP$: C, 57.52; H, 5.49; N, 11.57%.

[(*R*)-1-Cyanoethyl]bis(dimethylglyoximato)(tributylphosphine)cobalt(III) (6) and [(*R*)-1-Cyanoethyl]bis(dimethylglyoximato)(diphenylmethylphosphine)cobalt(III) (8): These complexes were similarly prepared for **10** by using P(*n*-Bu)$_3$ and PMePh$_2$ respectively in place of PPh$_3$. For **6**: Crude yield, 56%. Orange columns (methanol–water). Found: C, 50.85; H, 8.85; N, 12.85%. Calcd for $C_{23}H_{45}N_5O_4CoP$: C, 50.64; H, 8.31; N, 12.84%. For **8**: Crude yield, 68%. Brown plates (acetone–water). Found: C, 52.97; H, 5.82; N, 12.97%. Calcd for $C_{24}H_{31}N_5O_4CoP$: C, 53.04; H, 5.75; N, 12.89%.

[(*R*)-1-Cyanoethyl][diethyl(phenyl)phosphine]bis(dimethylglyoximato)cobalt(III) (7): 1.0 g of **1**(*R*) was dissolved in methanol (30 cm^3) and then 0.6 cm^3 of PEt$_2$Ph and 1.08 cm^3 of 2 mol dm^{-3} hydrochloric acid were added. The solution was stirred for 46 h under a nitrogen atmosphere at room temperature and then concentrated under reduced pressure. 10 cm^3 of acetone was added to the residual syrup. After the deposited white needles were removed by filtration, water was added to the filtrate and the resulting solution was cooled. Deposited brown crystals were collected by filtration; 0.70 g (64%). The crude product was recrystallized several times from acetone–water. Found: C, 49.34; H, 6.72; N, 13.67%. Calcd for $C_{21}H_{33}N_5O_4CoP$: C, 49.51; H, 6.53; N, 13.75%.

[(*R*)-1-Cyanoethyl]bis(dimethylglyoximato)(diphenylethylphosphine)cobalt(III) (9): 1.0 g of **1**(*R*) was dissolved in acetone (20 cm^3) and then 0.77 cm^3 of PEtPh$_2$ and 1.08 cm^3 of 2 mol dm^{-3} hydrochloric acid were added. The solution was stirred for 23 h under a nitrogen atmosphere at room temperature and then dried under reduced pressure. To the acetone solution of the residue was added water. Deposited brown crystals were collected by filtration; 0.76 g (63%). The crude product was recrystallized twice from acetone–water to give plates. Found: C, 53.74; H, 6.09; N, 12.55%. Calcd for $C_{25}H_{33}N_5O_4CoP$: C, 53.86; H, 5.97; N, 12.56%.

Aqua[(*R*)-1-cyanoethyl]bis(dimethylglyoximato)cobalt(III) (15): To a methanol (20 cm^3) solution of 4.0 g of **1**(*R*) was added 8.6 cm^3 of 2 mol dm^{-3} hydrochloric acid and the solution was stirred for 16 h under a nitrogen atmosphere at room temperature. A 17 cm^3 of 6 mol dm^{-3} hydrochloric acid was added. The resulting aqua complex was extracted with three 60 cm^3 portions of dichloromethane. The extract was neutralized by adding solid potassium carbonate. After standing overnight, the dichloromethane was dried under reduced pressure to give a crystalline mass of **15**; 2.2 g (87%). This complex was satisfactorily used for further syntheses of **11**, **13**, and **14**. The structure of **15** was confirmed by the ^{1}H NMR spectrum.

[(*R*)-1-Cyanoethyl]bis(dimethylglyoximato)[tris(*p*-chlorophenyl)phosphine]cobalt(III) (11): A 0.65 g of **15** was dissolved in dichloromethane and 0.70 g of P(*p*-ClC$_6$H$_4$)$_3$ was added. The solution was stirred for 7 h under a nitrogen atmosphere at room temperature and then the solvent was removed under reduced pressure. To the resulting syrup acetone (20 cm^3) and a small amount of water were added. After the white precipitate had been removed by filtration, the filtrate was cooled. The deposited brown crystals were collected by filtration. The crude product was recrystallized from acetone–water. The structure of **11** was confirmed by the ^{1}H NMR spectrum. The pattern of spectrum was analogous to that of **10**.

[(*R*)-1-Cyanoethyl]bis(dimethylglyoximato)(piperidine)cobalt(III) (13): A 0.80 g of **15** was dissolved in methanol (5 cm^3) and 0.38 cm^3 of piperidine was added. The solution was allowed to stand overnight at room temperature. A 5 cm^3 of water was added and the resulting solution was cooled overnight to give dark brown flakes; 0.55 g (58%). The crude product was recrystallized several times from methanol–water. The structure of **13** was confirmed by the ^{1}H NMR spectrum.

[(*R*)-1-Cyanoethyl]bis(dimethylglyoximato)(pyrrolidine)cobalt(III) (14): This complex was similarly prepared for **13** by using pyrrolidine in place of piperidine. Crude yield, 0.25 g (45%). Dark brown plates (methanol–water). The structure of **14** was confirmed by the ^{1}H NMR spectrum.

[(*R*)-1-Cyanoethyl]bis(dimethylglyoximato)(triethylphosphite)cobalt(III) (12): A 0.35 g of **2** was dissolved in dichloromethane (3 cm^3) and 0.15 cm^3 of P(OEt)$_3$ was added. After having been stood for 1 h at room temperature, the solution was dried under reduced pressure. To the residual syrup were added 0.5 cm^3 of methanol and successively 2 cm^3 of water and then the solution was cooled overnight to give yellow leaflets; 0.12 g (30%). The crude product was recrystallized from methanol–water. The structure of **12** was confirmed by the ^{1}H NMR spectrum.

References

1) For the preceding report of this series, Part I, see Y. Ohgo, S. Takeuchi, Y. Natori, J. Yoshimura, Y. Ohashi, and Y. Sasada, *Bull. Chem. Soc. Jpn.*, **54**, 3095 (1981).

2) Y. Ohgo, S. Baba, H. Wada, and S. Takeuchi, 46th National Meeting of the Chemical Society of Japan, Niigata, October 1982, Abstr., No. 2D12; Y. Ohgo and S. Takeuchi, *Chem. Lett.*, **1985**, 407; Y. Ohgo and S. Takeuchi, *J. Chem. Soc., Chem. Commun.*, **1985**, 21.

3) Y. Ohashi, Y. Sasada, and Y. Ohgo, *Chem. Lett.*, **1978**, 743; Y. Ohashi, K. Yanagi, T. Kurihara, Y. Sasada, and Y. Ohgo, *J. Am. Chem. Soc.*, **103**, 5805 (1981); Y. Ohashi, K. Yanagi, T. Kurihara, Y. Sasada, and Y. Ohgo, *ibid.*, **104**, 6353 (1982); Y. Ohashi, A. Uchida, Y. Sasada, and Y. Ohgo, *Acta Crystallogr., Sect. B*, **39**, 54 (1983); T. Kurihara, Y. Ohashi, Y. Sasada, and Y. Ohgo, *ibid.*, **39**, 243 (1983).

4) Y. Ohgo, K. Orisaku, E. Hasegawa, and S. Takeuchi, *Chem. Lett.*, **1986**, 27.

5) F. D. Greene, M. A. Berwick, and J. C. Stowell, *J. Am. Chem. Soc.*, **92**, 867 (1970).

6) C. A. Tolman, *Chem. Rev.*, **77**, 313 (1977).

7) T. Kurihara, A. Uchida, Y. Ohashi, Y. Sasada, Y. Ohgo, and S. Baba, *Acta Crystallogr., Sect. B*, **39**, 431 (1983); Y. Tomotake, A. Uchida, Y. Ohashi, Y. Sasada, Y. Ohgo, and S. Baba, *Acta Crystallogr., Sect. C*, **40**, 1684 (1984); Y. Ohashi, private communication.

8) F. T. T. Ng, G. L. Rempel, and J. Halpern, *Inorg. Chim. Acta*, **77**, L165 (1983).

9) G. M. Kosolapoff and L. Maier, "Organic Phosphorus Compounds," Wiley-Interscience, New York (1972), Vol. 1, Chap. 1, pp. 124—168.

 © 1987 The Chemical Society of Japan Bull. Chem. Soc. Jpn., 60, 3973—3978 (1987)

The Effect of Intramolecular Hydrogen Bonding on the Rotational Barriers about the C-N Bonds of *o*-Hydroxyarenecarboxamides

Hiroko SUEZAWA,* Kin-ya TSUCHIYA, Eiji TAHARA, and Minoru HIROTA
Department of Applied Chemistry, Faculty of Engineering, Yokohama National University, Hodogaya-ku, Yokohama 240
(Received April 2, 1987)

Rotational barriers about the C-N bonds of several *o*-hydroxyarenecarboxamides were determined in four solvents (namely, chloroform, pyridine, methanol, and dimethyl sulfoxide) by DNMR spectroscopy and compared with those of arenecarboxamides void of ortho-hydroxyl group. The height of the rotational barrier is correlated with the strength of the intramolecular O-H···O=C hydrogen bond. The unusual solvent effect on the rotational barriers of these hydroxy-amides are ascribed to the cleavage of the intramolecularly hydrogen bonded chelate ring which occurs in both hydrogen-donating and -accepting solvents.

Rather extensive studies have been reported on the dynamic NMR spectroscopic behaviors of amides,[1-7] and rotational barriers about the C-N bonds of unsaturated and aromatic amides have been shown to be strongly affected by the conjugative properties of their hydrocarbon moiety with the carbonyl group, as revealed by the rotational barriers of *N,N*-dimethylacrylamide[1] and *N,N*-dimethylbenzamide[2] (69.8 and 64.9 kJ mol^{-1}, respectively) which are considerably lower than that of *N,N*-dimethylformamide (87.4 kJ mol^{-1}).[3] Several *o*-substituted benzamides have higher rotational barriers than those of the unsubstituted and the high barrier has been ascribed to the steric inhibition, at least partly, of the conjugation between the aryl and the carboxamide groups.[2,7] Several years ago, we reported on the effect of intramolecular hydrogen bonding on the rotational barrier of *N,N*-dimethylsalicylamide.[8] The report showed that the rotational barrier of the *o*-hydroxy amide is significantly lower than those of usual *N,N*-dimethylbenzamides. Similar lowering in the rotational barrier due to the effect of hydrogen bonding was also illustrated with *o*-aminobenzamide by Jackman in his book.[9]

In this research, the rotational barriers of several other *N,N*-dimethyl-*o*-hydroxyarenecarboxamides were determined in order to further clarify the effect of intramolecular hydrogen bonding. Solvent effect on the rotational barriers of several benzamides were also studied systematically and the peculiar solvent effect on the rotational barriers of *o*-hydroxyarenecarboxamides was disclosed and interpreted.

Experimental

N,N-Dimethyl- and *N,N*-dibenzylarenecarboxamides were prepared as usual by the reaction of the corresponding aroyl chlorides with dimethyl- and dibenzylamines, respectively.

^{1}H and ^{13}C NMR spectra were recorded on a JEOL FX-90Q spectrometer using 10-mm probe. The samples for the measurements were prepared by dissolving ca. 100 mg of the amide in ca. 1.5 ml of the solvent, the concentrations of the solutions being adjusted to be ca. 0.5 mol dm^{-3}. Chloroform-*d*, methanol-d_4, pyridine-d_5, and dimethyl-d_6 sulfoxide (DMSO-d_6) were used as solvents throughout this work. The ^{1}H and ^{13}C spectra were obtained at 89.56 and 22.50 MHz, respectively. Temperature-dependent NMR in order to obtain ΔG^* were measured with an aid of JES-VT-3 variable temperature apparatus. The ΔG^* values were determined at the coalescence temperatures. In order to evaluate the ΔG^* values very accurately, the rates of exchange between the two sites were computed by the simulation of line shapes near the coalescence temperature and used supplementally.

Results and Discussion

Variable temperature measurements on the methyl ^{1}H signals of various *N,N*-dimethyl- and *N,N*-dibenzyl-*o*-hydroxyarenecarboxamides were carried out in four perdeuterated solvents, namely, chloroform, methanol, pyridine, and dimethyl sulfoxide (DMSO) and the free energies for of activation of the internal rotation about the C-N partial double bonds (hereafter named "rotational barrier(s)" and noted as ΔG^*) were determined.[10] The rotational barriers of the amides hereby measured in these solvents are given in Table 1a together with some from the similar measurements on methyl ^{13}C signals. The rotational barriers from the both nuclei agree with each other excellently, showing the reliability of the ΔG^* values.

The rotational barriers about the C-N partial double bonds of amides were shown to become higher as the solvents become more polar. This trend was ascribed to the effect of polar solvents which favor the polar mesomeric structure **II** and stabilize the ground state rather than the transition state of the internal rotation.[7] In this investigation, the solvent effect was reexamined with the aim of elucidating the effect of hydrogen-donating and hydrogen-accepting abilities of solvents on the rotational barriers of the amides.

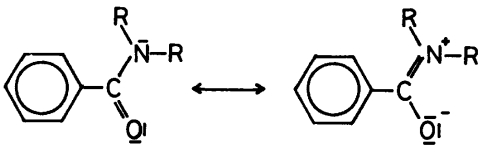

(I) (II)

Table 1a. Rotational Barriers about the C-N Bonds (ΔG^*) and Coalescence Temperatures (T_c) of *N,N*-Dialkylarenecarboxamides from ^{1}H DNMR in Several Solvents

No.	X	ΔG^*/kJ mol^{-1} (T_c/K)[a]				$\Delta\Delta G^*_{solv}$/kJ mol^{-1} [b]		
		Chloroform	Methanol	Pyridine	DMSO	CD_3OD	C_5D_5N	DMSO
(a)	*N,N*-Dimethylbenzamides $XC_6H_4CON(CH_3)_2$							
1	H	65.5(302.0)	67.8(308.6)	63.2(299.7)	—	+2.3	−2.3	—
2	*p*-Cl	64.6(296.2)	67.2(304.5)	63.3(297.8)	65.1(295.3)	+2.6	−1.3	+0.5
3	*p*-CH_3O	61.4(274.7)	63.3(278.0)	58.8(274.7)	—	+1.9	−2.6	—
4	*p*-CH_3	64.0(292.2)	66.5(300.3)	62.0(291.0)	—	+2.5	−2.0	—
5	*p*-OH	63.2(283.5)	61.4(263.6)	57.6(265.8)	—	−1.8	−3.6	—
6	*o*-Cl	—	—	78.5(373.0)	80.4(375.5)			
7	*o*-CH_3O	—	—	75.7(358.0)	77.5(361.2)			
8	*o*-CH_3	74.1(349.2)	—	72.6(347.0)	74.6(350.2)	—	−1.5	+0.5
9	*o*-OH	51.1(236.8)	59.6(275.7)	57.1(265.3)	—	+8.5	+6.0	—
10	2-OH 5-Cl	51.3(239.0)	61.1(282.5)	59.2(274.6)	63.1(291.3)	+9.8	+7.9	+11.8
11	2-OH 5-NO_2	51.6(241.0)	61.6(286.6)	61.0(284.8)	64.1(298.3)	+10.0	+9.4	+12.5
12	2-OH 5-CH_3O	51.3(231.8)	59.7(275.0)	56.8(259.8)	—	+8.4	+5.5	—
13	2-OH 3,5-Me_2	50.9(234.0)	55.4(255.0)	53.6(239.6)	—	+4.5	+2.7	—
14	2-CH_3O 3,5-Me_2	—	—	77.6(357.4)	79.2(359.4)			
(b)	*N,N*-Dibenzylbenzamides $XC_6H_4CON(CH_2C_6H_5)_2$							
15	H	64.3(304.3)	65.0(305.0)	62.6(302.0)	63.5(297.0)	+0.7	−1.7	−0.8
16	*p*-Cl	63.1(300.8)	63.3(299.5)	62.8(301.0)	63.6(297.0)	+0.2	−0.3	+0.5
17	*p*-CH_3O	60.3(284.8)	59.9(279.0)	59.0(281.0)	—	−0.4	−0.7	—
18	*p*-CH_3	63.3(299.4)	63.8(299.8)	62.0(296.3)	—	+0.5	−1.3	—
19	*o*-OH	54.1(240.5)	62.1(294.7)	61.8(295.5)	65.9(311.2)	+8.0	+7.7	+11.8
20	*o*-Cl	68.3(306.3)	—	67.0(295.0)	—	—	−1.3	—
21	*o*-CH_3O	67.0(299.0)	68.2(306.2)	67.7(304.5)	68.4(305.2)	+1.2	+0.7	+1.4
(c)	*N,N*-Dimethylnaphthamides $XC_{10}H_6CON(CH_3)_2$							
22	1-$CONMe_2$	—	—	74.6(351.6)	76.4(355.8)			
				*74.4(367.2)	*75.4(372.0)			
23	2-$CONMe_2$	65.9(298.1)	68.6(307.2)	64.2(296.8)	63.9(290.0)	+2.7	−1.7	−2.0
				*64.8(321.8)	*64.6(321.2)			
24	1-$CONMe_2$ 2-OH	55.9(258.4)	66.9(317.6)	65.4(302.8)	69.0(319.3)	+11.0	+9.5	+13.1
25	2-$CONMe_2$ 1-OH	49.0(220.8)	52.0(233.7)	—	—	+3.0	—	—
26	2-$CONMe_2$ 3-OH	55.6(246.9)	66.3(301.8)	63.6(291.0)	67.4(307.6)	+10.7	+8.0	+11.8
27	1-$CONMe_2$ 2-CH_3O	—	—	90.5(419.5)	91.9(424.0)			
28	2-$CONMe_2$ 1-CH_3O	—	—	78.2(360.5)	79.8(362.7)			
				*77.6(380.9)	*79.5(390.7)			
29	2-$CONMe_2$ 3-CH_3O	—	—	78.9(365.3)	81.7(372.0)			
				*78.8(385.4)	*79.9(388.2)			

a) The asterisks in the table denote the rotational barriers (and T_c) from ^{13}C DNMR. b) $\Delta\Delta G^*_{solv} = \Delta G^*$(solvent) $- \Delta G^*(CDCl_3)$.

Strong intramolecular C=O···H-O hydrogen bond in *o*-hydroxyarenecarboxamides is expected to be kept intact in chloroform which is known as a less polar solvent. The persistence of the intramolecular hydrogen bond was proved by the appearance of the chelated O-H absorption in their infrared spectra (Table 3).[11] Methanol is a protic solvent and may interact with the amides as a hydrogen donor. Thus, its hydroxyl group can form a hydrogen bond very probably with the carbonyl oxygen atom of the amide.

Table 1b. Chemical Shifts for of *N*-Methyl (CH_3) and *N*-Methylene (CH_2) Protons of the *N,N*-Dialkyl Amides in Table 1a

No. of Compd.	Chemical shift δ/ppm			
	$CDCl_3$	CD_3OD	C_5D_5N	$(CD_3)_2SO$
(a) CH_3 proton chemical shifts				
1	3.05	3.03	2.99	2.93
2	3.07	3.03	2.89	2.96
3	3.06	3.04	2.96	2.96
4	3.05	3.03	2.92	2.93
5	3.06	3.04	2.97	2.96
6	2.99	—	2.88	2.88
7	2.98	2.97	2.89	2.85
8	2.98	—	2.89	2.87
9	3.17	3.01	3.02	2.88
10	3.17	3.01	3.00	2.88
11	3.24	3.02	3.03	2.91
12	3.16	3.01	3.02	2.88
13	3.15	3.02	2.92	2.91
14	2.99	—	2.92	2.87
22	2.98	2.99	2.89	2.92
23	3.04	3.07	2.97	3.02
24	3.04	3.04	3.02	2.90
25	3.19	3.08	2.91	3.00
26	3.23	3.03	3.03	2.90
27	3.03	3.00	2.95	2.90
28	3.06	3.05	2.94	2.97
29	3.01	3.00	2.92	2.90
(b) CH_2 proton chemical shifts				
15	4.55	4.54	4.67	4.49
16	4.53	4.55	4.68	4.51
17	4.58	4.56	4.73	4.51
18	4.56	4.54	4.67	4.49
19	4.69	4.48	4.45	4.45
20	4.22	4.15	4.34	4.27
21	4.24	4.23	4.36	4.22

Since the oxygen atom can behave as a biligated ligand, the intermolecular hydrogen bond itself may not induce directly the destruction of the intramolecular hydrogen bond but should, at least, weaken the bond considerably. Both pyridine and DMSO are known as strong hydrogen acceptors and expected to cleave the intramolecular hydrogen bond. Of these two, the hydrogen accepting power of DMSO is particularly strong and the intramolecular hydrogen bond in the *o*-hydroxy amides should be destroyed almost completely in this solvent.

Though it is not the main purpose of this paper, it may be useful to survey briefly the general tendency of the perturbation caused by the solvent on the rotational barriers of the amides void of *o*-hydroxyl group. As easily deduced from the $\Delta\Delta G^{\ddagger}$ solv values defined as the difference in $\Delta G^{\ddagger}$ between the respective solvent and chloroform ($\Delta\Delta G^{\ddagger}_{solv}=\Delta G^{\ddagger}(solvent)-\Delta G^{\ddagger}(CDCl_3)$) and given in Table 1, the rotational barrier icreases in the following order of the solvent: pyridine chloroform DMSO methanol. This sequence does not agree with the increasing order of dielectric constants[10] but coincides with the order of increasing acidity of C-H or O-H group in the solvent molecule, suggesting the participation of the hydrogen-bond-like interaction **III** of the solvent X-H group with the carbonyl oxygen of the amide, which stabilizes the mesomeric structure II. However, the effect is not very significant and perturbs the rotational barrier at most by 3 or 4 kJ mol^{-1}.

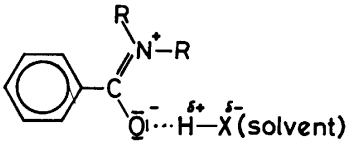

(III)

In contrasts, the rotational barriers of *o*-hydroxy amides **9**—**13**, **19**, and **24**—**26** suffer a very large solvent effect. The increases in the rotational barriers by about 10 kJ mol^{-1} were observed both in hydrogen-donating and in hydrogen-accepting solvents. In order to rationalize the large increase in $\Delta G^{\ddagger}$ by the influence of the solvent, the effect of *o*-hydroxyl group on the rotational barrier was reinvestigated. Ortho-substituent effect can be evaluated separately by the increment $\Delta\Delta G^{\ddagger}_{ortho}$ which is defined as the difference in $\Delta G^{\ddagger}$ between the ortho-substituted and the unsubstituted (para-substituted) amides.

The $\Delta\Delta G^{\ddagger}_{ortho}$ values for several ortho-substituted arene-carboxamides are given in Table 2. Considerably large positive $\Delta\Delta G^{\ddagger}_{ortho}$ values (more than 10 kJ mol^{-1} in many cases) for *o*-substituted *N,N*-dimethylarenecarboxamides **6**—**8**, **14**, **27**—**29** can be attributed to the steric inhibition of resonance pointed out by Jackman et al.[2] In *N,N*-dibenzyl amides **20** and **21**, the ortho effect is apparently diminished, probably due to the destabilization of planar (or nearly planar) ground state caused by the bulkier benzyl group.

On the contrary, *o*-hydroxyarenecarboxamides **9**—**13**, **19**, and **24**—**26** have negative $\Delta\Delta G^{\ddagger}_{ortho}$ values. The decrease in the rotational barrier comes to as large as ca. 17 kJ mol^{-1} in chloroform in which the dissolved amide is supposed to maintain the chelation by intramolecular hydrogen bonding. When the solvent is capable of forming hydrogen bond with the *o*-hydroxy amide either as a hydrogen acceptor or a hydrogen donor, the difference ($\Delta\Delta G^{\ddagger}_{ortho}$) tends to be less negative. The $\Delta\Delta G^{\ddagger}_{ortho}$ becomes even positive in DMSO which is known to act as a very strong hydrogen acceptor in forming hydrogen bond. Negative $\Delta\Delta G^{\ddagger}_{ortho}$ value corresponds to the fact that the rotational barrier is lower than that of the unsubstituted or para-substituted amide used as the reference. On the basis of MO calculations, the lowering of the rotational barrier is attributed to the

decreased C–N bond order in chelated *o*-hydroxyarenecarboxamide in our previous report.[8]

If the chelation is responsible for the low rotational barrier, the barrier is expected to gain the normal height when the intramolecular hydrogen bond is cleaved. As observed with **19** and **26**, this was realized by dissolving the *o*-hydroxy amides in DMSO. Small positive $\Delta\Delta G^{\ddagger}_{ortho}$ might arise from the normal ortho effect due to steric hindrance caused by the solvated hydroxyl group at the ortho-position. In sharp contrast to the *o*-hydroxy amides, the corresponding *o*-methoxyarenecarboxamides **7**, **14**, **21**, and **27—29** showed normal ortho effect due to steric hindrance to the aryl-carbonyl conjugation. Therefore, the lowering of the rotational barrier observed with the *o*-hydroxyamides is ascribable to the effect of intramolecular hydrogen bonding.

The strength of the intramolecular hydrogen bond in the six-membered chelate ring of this type has been correlated with the bond order (or bond length) of the bond joining the ring carbon atoms holding the hydroxyl and carbonyl substituents.[12,13] The chelate rings of *o*-hydroxyarenecarbaldehydes and *o*-hydroxyaryl ketones have been shown to be more stable when the double bond character of the respective C–C bond is higher and, hence, its bond length is shorter. From this point of view, the rotational barriers of three *o*-hydroxyamides **9**, **25**, and **26** were compared

Table 2. The Increase of Rotational Barrier Due to the Ortho Effect[a]
$\Delta\Delta G^{\ddagger}_{ortho}=\Delta G^{\ddagger}_{ortho}-\Delta G^{\ddagger}_{unsubst.}$

No. of compd.	$\Delta\Delta G^{\ddagger}_{ortho}$//kJ mol^{-1}			
	Chloroform	Methanol	Pyridine	DMSO
6	+15.3(+15.2)	—	—	—(+15.3)
7	—	—	+12.5(+16.9)	—
8	+8.6(+10.1)	—	+9.4(+10.6)	—
9	−14.4(−12.1)	−8.2(−2.3)	−6.1(−2.5)	—
10	−14.2	−6.7	−4.0	—
11	−13.9	−6.2	−2.2	—
12	−14.2	−8.1	−6.4	—
13	−14.6	−12.4	−9.6	—
16	+4.0(+5.2)	—	+4.4(+4.2)	—
17	+2.7(+6.7)	+3.2(+8.3)	+5.1(+8.7)	+4.9
19	−10.2	−3.0	−0.8	+2.4
24	—	—	−9.2	−7.4
25	−16.9	−16.6	—	—
26	−10.3	−2.3	−0.6	+3.5
27	—	—	+15.9	+14.5
28	—	—	+14.0	+15.9
29	—	—	+14.7	+17.8

a) $\Delta\Delta G^{\ddagger}_{ortho}'(=\Delta G^{\ddagger}_{ortho}-\Delta G^{\ddagger}_{para})$ are given in parentheses.

Table 3. Effect of the Strength of Intramolecular Hydrogen Bonding in the Chelate Ring upon the Rotational Barriers of *o*-Hydroxyarenecarboxamides

Chelated structure	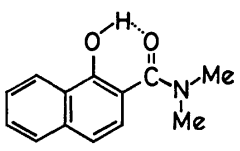 (**25**)	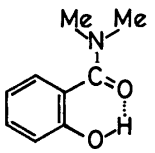 (**9**)	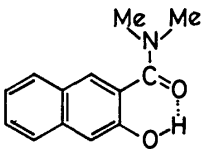 (**26**)
$\Delta G^{\ddagger}(CDCl_3)$/kJ mol^{-1}	49.0	51.1	55.6
d_{C-O}/Å[14]	1.371	1.397	1.412
$\delta_{OH}(CDCl_3)$/ppm[a]	11.55	9.99	9.37
$\nu_{C=O}$/cm^{-1} [b]	1634	1638	1648
ν_{O-H}/cm^{-1} [b]	3158(shoulder)[c]	3228	3245

a) Chemical shifts at infinite dilution in chloroform-*d*. b) Infrared absorption spectra both in the hydroxyl and carbonyl stretching regions were measured with the dilute carbon tetrachloride solutions using a 1 cm cell. c) Overlapped with C–H absorption bands.

(Table 3). As discussed previously, the partial double bond character of the amide C-N bond is expected to be reduced as the endocyclic C-C bond order increases and, hence, the chelation becomes favorable. Thus the higher bond order of the C-C bond holding the hydroxyl and carboxamide groups should result in the lower rotational barrier. Strengths of the intramolecular hydrogen bond of this type can be evaluated by the chemical shift of hydroxyl proton at infinite dilution, since the chemical shift in a very dilute solution of an inert solvent is affected predominantly by the intramolecular circumstances and tends to shift towards lower field as the hydrogen bond becomes stronger.[12,13] The infrared carbonyl spectra also help us to estimate the strength of the chelation by the low frequency shift which reflects the lowering of the carbonyl bond order. As shown in Table 3, the lowest OH chemical shift and the lowest carbonyl frequency of **25** provide experimental supports to the theoretical consequence that its chelation should be the strongest of the three hydroxyamides in Table 3. As a whole, the evidence from the spectra supports the conclusion from the bond order, and the chelation becomes gradually strong in the order of **26**, **9**, and **25**. In accord with this conclusion and the above deduction, the rotational barrier in chloroform is the lowest with **25** and the highest with **26**.

The rotational barrier of *N,N*-dimethylsalicylamide **9** seems insensitive to the electronic effect by the substituent para to the hydroxyl group. The ΔG^* values for a series of 5-substituted salicylamides **9**—**13** are identical with each other within the limit of experimental error (Table 1). *N,N*,3-Trimethylsalicylamide **13** is less susceptible to the solvent effect than other salicylamides **9**—**12** investigated. 3-Methyl group might prevent the hydroxyl group from taking the conformation anti to the carbonyl group in one hand and hinder the access of the solvent molecule to the hydroxyl group on the other hand. In this way, the intramolecular hydrogen bond of salicyl moiety is protected towards the attack of the solvent by the neighboring methyl group. Peri-hydrogen atom in 1-hydroxy-2-naphthamide **25** may also play a similar role in protecting its intramolecular hydrogen bond. Therefore, these amides are less sensitive to the effect of solvents capable of forming hydrogen bonds.

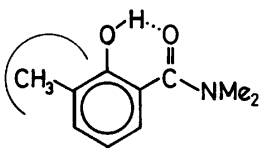

(IV)

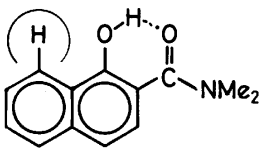

(V)

Chemical shifts of the CH_3 signals of *N,N*-dimethyl amides and the CH_2 signals of *N,N*-dibenzyl amides at temperatures higher than their coalescence temperatures (T_c) are given in Table 1b. Methyl and benzyl CH_2 signals should move towards down-field in the increasing order of ΔG^* due to increasing positive charge by the mesomeric contribution of **II**. As the solvent induced shift of the ^1H chemical shift is quite small, it seemed rather difficult to derive a definite conclusion from the solvent shift of the signal of individual amide. However, a general survey on the data in Table 1 allowed the conclusion that the expected trend is partly observed with the CH_3 signals of substituted benzamides **1**—**8** and naphthamides **23**, **24**, **27**—**29** void of an *o*-hydroxyl group, which showed up-field shifts of CH_3 signals and the lowering of ΔG^* in pyridine compared to those in chloroform. Apparently inverse solvent shift was observed with *o*-hydroxy amides **9**—**14**, **24**—**26**. This might be caused by the magnetic anisotropy effect by the hydrogen-bonded chelate ring. However, further study on the solvent effect is needed before we conclude the nature of the effect undoubtedly.

In conclusion, significantly low rotational barriers about the C-N partial double bonds of *N,N*-dialkylsalicylamides were shown very confidently to be originated from the chelation by intramolecular hydrogen bonding by examining the effects of solvents and structural changes on the barrier.

The authors wish to express their hearty thanks to Professor Masatsune Kainosho, Tokyo Metropolitan University, for his very valuable advice throughout this work. We are also very grateful to Professor L. M. Jackman, Pennsylvania State University, for his valuable discussion and encouragement which we received from him when he visited our university. This research is partly supported by a Grant-in-Aid for Scientific Research from the Ministry of Education, Science and Culture,

References

1) R. F. Hobson and L. W. Reeves, *J. Magn. Reson.*, **10**, 243 (1974).

2) L. M. Jackman, T. E. Kavanagh, and R. C. Haddon, *Org. Magn. Reson.*, **1**, 109 (1969).

3) M. Ravinovitz and A. Pines, *J. Am. Chem. Soc.*, **91**, 1585 (1969).

4) M. T. Rogers and J. C. Woodbrey, *J. Phys. Chem.*, **66**, 540 (1962); R. H. Garner and T. H. Siddall, III, *Tetrahedron Lett.*, **1966**, 3513; R. C. Neuman, Jr. and V. Jonas, *J. Am. Chem. Soc.*, **90**, 1970 (1968); G. P. Schiemenz and G. Stein, *Tetrahedron*, **26**, 2007 (1970); L. W. Reeves, R. C. Shaddick, and K. N. Shaw, *Can. J. Chem.*, **49**, 3684 (1971). T. Drakenberg, *Tetrahedron Lett.*, **1972**, 1743. C. H. Yoder and R. D. Gardner, *J. Org. Chem.*, **46**, 64 (1981).

5) P. K. Korver, K. Spaargaren, P. J. van der Haak, and Th. J. de Boer, *Org. Magn. Reson.*, **2**, 295 (1970); **3**, 605, 615 (1971).

6) K. Spaargaren, C. Kruk, T. A. Molenaar-Langeveld, P. K. Korver, P. J. van der Haak, and Th. J. de Boer, *Spectrochim. Acta, Part A*, **28**, 965 (1972).

7) L. M. Jackman, "Dynamic Nuclear Magnetic Resonance Spectroscopy," ed by L. M. Jackman and F. A. Cotton, Academic Press, N. Y. (1975), p. 208.
8) M. Hirota and K. Todokoro, *Chem. Lett.*, **1974**, 777.
9) L. M. Jackman, p. 222 of Ref. 7.
10) Dielectric constants of the solvents are 4.80 for $CHCl_3$, 12.3 for C_5H_5N(pyridine), 32.6 for CH_3OH, and 40.0 for CH_3SOCH_3. Hereafter, the deuterated solvents will be denoted without indicating the labelling by deuterium.
11) These hydroxy amides have very broad absorption bands (of which half widths are ca. 500 cm^{-1}) characteristic of chelated hydroxyl group in the OH stretching region (See Table 3).
12) I. M. Hunsberger, *J. Am. Chem. Soc.*, **72**, 5626 (1950).
13) A. L. Porte, H. S. Gutowsky, and I. M. Hunsberger, *J. Am. Chem. Soc.*, **82**, 5057 (1960).
14) Bond lengths in the corresponding bonds of parent hydrocarbons are given. The data are cited from "Kagaku Benran," 2nd ed, ed by Chemical Society of Japan, Maruzen Book Publ. Ltd., Tokyo (1975), p. 1386.

 © 1987 The Chemical Society of Japan Bull. Chem. Soc. Jpn., 60, 3979—3983 (1987)

Fe_3O_4-Catalyzed Halogen-Exchange Reactions of Polyhalomethanes

Masahiro NAKADA,* Sei-ichi TOKUMOTO, and Minoru HIROTA†,*
Chemical Laboratory, Chiba Institute of Technology, Tsudanuma, Narashino 275
†Department of Applied Chemistry, Faculty of Engineering, Yokohama National University, Hodogaya-ku, Yokohama 240
(Received June 5, 1987)

Triiron tetraoxide pretreated by polyhalomethane was shown to catalyze the halgen-exchange reactions of polyhalomethanes $CH_lBr_mCl_n$(l=1 or 2). The exchange proceeds consecutively giving, for example, $CHBrCl_2$, $CHBr_2Cl$, and $CHBr_3$ as the main products from $CHCl_3$. The mechanism of the reaction is discussed briefly.

In recent decades, the contamination of environment with polyhalogenated compounds have induced serious problems in several countries.[1] Thus, thermal and photochemical behaviors of polyhalogenated hydrocarbons have been investigated rather extensively aiming the potential applications for their detoxication.[2–5] We have also studied the acid-catalyzed and the photochemical dehalogenation and rearrangement of polyhalobenzenes in this point of view.[6–8] One of our studies concerned with the dechlorination of polychlorobenzenes over Fe_3O_4.[9] This modification of iron oxide was shown to catalyze the cleavage of carbon–halogen bonds of polyhalobenzenes effectively and gave the dehalogenated products in the presence of hydrogen donor such as hexane and decahydronaphthalene.

In this paper, we wish to report on the halogen-exchange reactions of polyhalomethanes over Fe_3O_4 in order to clarify further the behaviors of Fe_3O_4 towards halogenated hydrocarbons.

Experimental

Materials. The polyhalomethanes were commercially available. Their purities were certified by gas chromatography. Triiron tetraoxide (magnetite, Fe_3O_4) was prepared according to the method described by Kiyama.[10] Firstly, 6 M†† aqueous solution of sodium hydroxide was added gradually to an aqueous solution containing iron(II) and iron(III) chlorides in a 1:2 molar ratio so as to regulate the final pH of the solution to be ca. 11. The suspension of colloidal iron hydroxides was then filtered, washed with several portions of water, and calcinated at 623 K. Active Fe_3O_4 thus obtained is very fine and its specific surface area was determined to be 92.6 $m^2 g^{-1}$ by the BET adsorption measurement. Thus prepared Fe_3O_4 was employed as the catalyst for the halogen-exchange reactions. In each run of the halogen-exchange reaction, a 300 mg portion of the Fe_3O_4 catalyst was pretreated at 623 K with 50 microliter of chloroform or bromoform in the stream of helium. In order to maintain the catalytic activity uniform throughout a series of the experiments, the catalyst was heated further at the same temperature for about 2 h until the evolution of hydrogen halide ceased completely.

Procedures for the Pulse Thermolysis and the Analyses of the Products. The reaction was carried out at temperatures ranging from 393 to 593 K using a pulse micro-reactor connected directly to a gas chromatograph. The sample was introduced in portions of 1 microliter to the thermostatic inlet connected to the reaction chamber containing 300 mg of Fe_3O_4 and carried to the reactor by a stream of helium. The products of the reaction were analyzed by a Shimadzu GC-4C PTF gas chromatograph using a 2 m stainless steel column containing DNP (20 wt%). Peaks on the chromatogram were identified by comparing them with those of authentic samples and by GC/MS measurements. GC/MS were recorded on a Shimadzu GC/MS QP 1000 mass spectrometer. Details of the apparatus for the reaction were described in one of our previous papers.[11]

Results and Discussion

Role of the Pretreatment with Polyhalomethane and the Mechanism of Halogen Exchange. When polyhalomethanes were treated with freshly prepared Fe_3O_4 at 623 K without prior treatment with trihalomethanes, the oxidative decomposition took place giving carbon dioxide and water. Thus the reaction is potentially applicable to the detoxication of polyhaloalkanes. Hydrogen halide (HCl or HBr) was not detected as a gaseous product in the process of these reactions when the catalyst is new. The oxidative decomposition reaction seemed to proceed irreversibly, and repeated feeds of polyhalomethane gradually reduce the catalytic activity of Fe_3O_4 for the oxidative decomposition. Deactivation of the catalyst is undesirable from the view point of applying the reaction to the detoxication. Thus the reactions over polyhalomethane-poisoned Fe_3O_4 were further studied. The peak for the unreacted starting material becomes observable in the chromatogram after several repetition of the pulse reaction with polyhalomethanes (dichloromethane (**1**), trichloromethane (**3**), dibromomethane (**6**), and tribromomethane (**7**)). At the same time, evolution of hydrogen halide became observable after repeated dose of polyhalomethane. When a mixed halomethane $CH_lCl_mBr_n$ was fed under similar conditions or when polybromomethane was introduced over polychloromethane-pretreated Fe_3O_4 (or vice versa), there appeared several other peaks ascribable to the products of halogen-exchange reactions in the gas chromatogram. An example

†† 1 M=1 mol dm^{-3}.

which shows the formation of $CHCl_3$, $CHBrCl_2$, and $CHBr_2Cl$ from $CHBr_3$ is illustrated in Fig. 1. This reveals the fact that the pretreated catalyst promotes the halogen exchange of polyhalomethanes. The activity of the Fe_3O_4 catalyst for the oxidative decomposition tends to be a constant stationary value when the total dose of **1** or **3** exceeds ca. 0.2 mmol (ca. 20 microliter) (Fig. 2).[12] At this stage, the formation of iron(II) chloride on the surface of the catalyst was evidenced by detecting iron(II) ion from the aqueous extract obtained by washing the pretreated catalyst with water. Chloride ion, and/or bromide ion in cases when bromo-substituted methane was subjected to the reaction, was also present, but iron(III) ion was detected in neither cases. Thus the oxidative decomposition should proceed via the reductive chlorination of Fe(III) oxide. As a result, the surface of Fe_3O_4 is expected to become covered partly by iron(II) chloride in the process of pretreatment by polychloromethanes, and similarly covered by iron(II) bromide when treated with polybromomethanes. The pretreated catalysts were used for the halogen-exchange reactions throughout this series of experiments. The catalyst regains its reactivity for oxidative

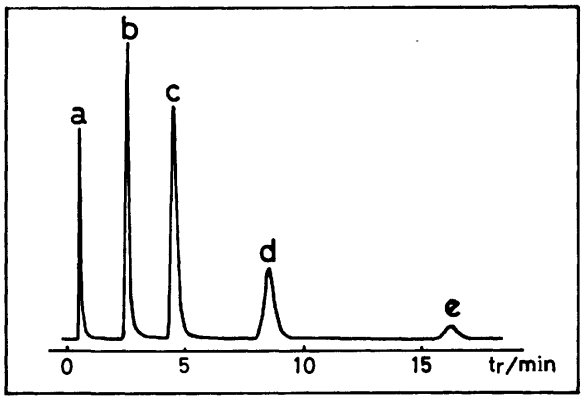

Fig. 1. Gas chromatogram of the reaction products obtained by introducing $CHBr_3$ over Fe_3O_4 (pretreated by $CHCl_3$) at 433 K. Peaks **a**—**e** are assigned to CO_2, $CHCl_3$, $CHBrCl_2$, $CHBr_2Cl$, and unreacted $CHBr_3$, respectively.

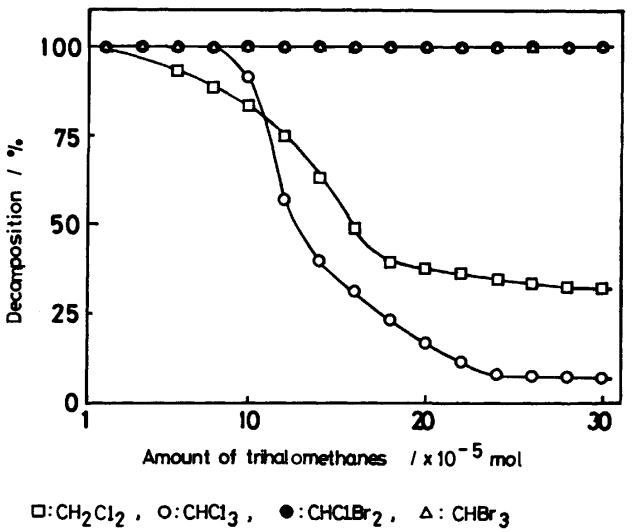

Fig. 2. Effect of the repeated doses of polyhalomethanes on the activity of Fe_3O_4 for the oxidative decomposition producing CO_2 at 623 K.

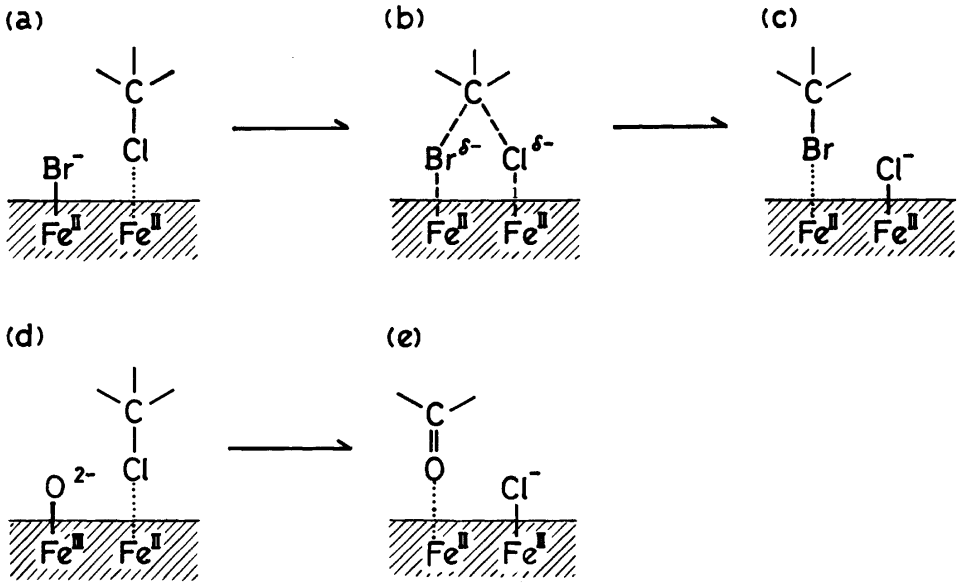

Fig. 3. Schematic description of the proposed mechanism of the halogen-exchange reactions over Fe_3O_4 pretreated by polyhalomethane.[14] Schema **a** to **c** shows the process of replacement of chlorine to bromine on the surface of $CHBr_3$-pretreated Fe_3O_4 catalyst. During the process of pretreatment, oxide ion (O^{2-}) bound to Fe(III) is assumed to be replaced reductively by halide ion as illustrated by schema **d** and **e**.

decomposition after being washed with water.

In a run in which a well-blended and annealed mixture of newly prepared Fe_3O_4 and a small amount of iron(II) chloride was used as catalyst, the oxidative decomposition took place as usual but the halogen exchange did not proceed to a measurable extent. This fact suggests that nonhalogenated iron sites (probably Fe(II)) on the suface of the catalyst should play a critical role in the pathway of the halogen-exchange reaction. The mere contact of polyhalomethane with chloride ion does not seem to induce the exchange of halogen measurably, since the chlorine atoms of chlorinated methanes were shown to exchange very slowly with chloride ion even in a homogeneous liquid phase.[13] On the other hand, neither oxidative decomposition nor halogen exchange proceeds to give considerable amounts of the products when Fe_2O_3 (hematite) was employed instead of Fe_3O_4 as the catalyst. These facts imply that Fe(II) species should play a crucial role in the reaction. By all accounts, Fe(II) species linked to halogen is assumed to behave as a halogen donor and Fe(II) species adjacent to the Fe(II)-halogen linkage to act as a halogen acceptor in the reaction.

A mechanism which involves a bridged transition state (shown in Fig. 3b) might be one of the most probable pathways which explains the exchange reaction. The reaction is supposed to proceed through the following three steps in this mechanism. The mechanism is illustrated by the example of dechlorination-bromination in Fig. 3. (i) In the first step, the chlorine atom of a chlorinated methane molecule (ClCXYZ) forms a coordinative bond to the free iron(II) site located adjacent to the brominated iron(II) species. (ii) A bridged structure like illustrated in Fig. 3b is formed on the surface of the catalyst. Bromide transfer from an Fe(II) site to carbon and chloride transfer from carbon to an adjacent free Fe(II) site proceeds simultaneously through this bridge. (iii) Newly formed brominated methane (BrCXYZ) leaves from the surface. Halogen ligated Fe(II) group on the surface is expected to be

Table 1. Products of the Reactions over Fe_3O_4 Pretreated with $CHBr_3$[a)]

Substrate	Reaction temp/K	Reaction product/mol% (Reactant=100%)							
		CH_2Cl_2	CH_2BrCl	CH_2Br_2	$CHCl_3$	$CHBrCl_2$	$CHBr_2Cl$	$CHBr_3$	CO_2
CH_2Cl_2	393	**98.5**	1.5						
(1)	433	**87.5**	12.0						
	473	**62.0**	32.6	4.9					0.5
	513	**34.1**	47.1	17.8					1.0
	553	**25.6**	48.2	23.5					2.7
	593	**21.1**	48.8	24.9					5.2
CH_2BrCl	393		**100.0**						
(2)	433		**97.7**	1.2					1.1
	473		**91.8**	6.3					1.9
	513		**78.4**	18.2					3.4
	553		**61.3**	33.1					5.6
	593		**49.2**	44.2					6.6
$CHCl_3$	393				**80.2**	16.2	3.6		
(3)	433				**53.6**	32.7	11.3	2.1	0.3
	473				**39.1**	43.4	14.9	2.0	0.6
	513				**28.4**	46.4	15.8	2.1	7.3
	553				**19.4**	32.6	13.3	2.6	32.1
	593				**12.9**	17.5	9.2	3.2	57.2
$CHBrCl_2$	393					**94.7**	5.1		0.2
(4)	433					**70.8**	18.9	3.4	6.9
	473					**53.1**	27.5	8.6	10.8
	513					**45.2**	30.1	10.4	14.3
	553					**34.5**	28.2	11.0	26.3
	593					**21.9**	22.7	10.8	44.6
$CHBr_2Cl$	393					0.5	**93.4**	6.1	
(5)	433					8.4	**70.9**	20.2	0.5
	473					11.2	**57.9**	29.4	1.5
	513					12.1	**47.6**	36.1	4.2
	553					9.7	**36.8**	35.1	18.4
	593					8.9	**20.2**	25.1	45.8

a) Bold figures in the Tables 1 and 2 represent the percentages of the remaining reactant.

formed by the reductive chlorination–deoxygenation of Fe(III)–O group by a polyhalomethane during the process of pretreatment (as illustrated by the process from (d) to (e) of Fig. 3). The scheme includes a bridged structure which has not been supported by direct experimental evidence and, therefore, is rather speculative. However this explains the overall process of the halogen-exchange reaction if we assume that C–Cl bonds are considerably more difficult to cleave than C–Br bonds. Especially, the fact that the well-blended mixture of Fe_3O_4 and $FeCl_2$ does not activate the exchange reaction supports the participation of the neighboring Fe(II)–Cl and nonligated Fe(II) sites of the surface.

Quantitative Survey on the Halogen-Exchange Reactions. Dichloromethane (**1**), bromochloromethane (**2**), trichloromethane (**3**), bromodichloromethane (**4**), and dibromochloromethane (**5**) were vaporized in the stream of helium at various temperatures and introduced to the reactor filled with fine particles of the Fe_3O_4 catalyst pretreated with bromoform. The products of the pulse reactions are given as a function of temperature in Table 1. The results of the similar reactions of dibromomethane (**6**), **2**, tribromomethane (**7**), and **4** over the Fe_3O_4 catalyst pretreated with chloroform are also shown in Table 2.

Both dechlorination–bromination and debromination–chlorination reactions proceed predominantly in the runs carried out at lower temperatures. Multiple exchange also occurs giving, for example, bromodichloro-, dibromochloro-, and tribromomethanes starting from chloroform. Since the singly exchanged product is the most predominant and the triply exchanged one the least predominant, only one halogen atom must be exchanged by a single contact of the substrate (polyhalomethane) on the surface of the pretreated Fe_3O_4. The halogen atoms are exchanged consecutively, giveing a multiply exchanged product after multiple contacts to the active site of the catalyst. The oxidative decomposition producing carbon dioxide becomes significant in the runs at elevated temperatures. Trihalomethanes are more susceptible to the decomposition, producing carbon dioxide and water as the most predominant product at higher temperatures. In contrasts, dihalomethanes (**1**, **2**, and **6**) produce carbon dioxide only subsidiarily in the range of temperature investigated.

The dechlorination–bromination reactions in Table 1 behave remarkably different from the debromination–chlorination reactions in Table 2 in some respects. The dechlorination–bromination seems to be a kinetically controlled reaction of which rate-determining step is the cleavage of C–Cl bond. The

Table 2. Products of the Reactions over Fe_3O_4 Pretreated with $CHCl_3$[a)]

Substrate	Reaction temp/K	Reaction product/mol% (Reactant=100%)							
		CH_2Cl_2	CH_2BrCl	CH_2Br_2	$CHCl_3$	$CHBrCl_2$	$CHBr_2Cl$	$CHBr_3$	CO_2
CH_2BrCl	393	34.4	**62.5**			3.0			0.1
(**2**)	433	48.1	**42.1**			8.1			1.7
	473	43.9	**43.1**			10.9			2.1
	513	39.1	**45.3**			12.6			3.0
	553	36.8	**45.2**			12.9			5.1
	593	37.0	**42.4**			6.3			14.3
CH_2Br_2	393	29.5	21.1	**48.4**					
(**6**)	433	67.2	17.6	**14.8**					0.4
	473	63.2	25.7	**9.7**					1.4
	513	34.5	44.5	**18.8**					2.2
	553	22.1	42.6	**29.5**					5.8
$CHBrCl_2$	393				82.6	**11.2**			6.2
(**4**)	433				80.8	**11.9**	0.2		7.1
	473				70.7	**13.8**	1.1		14.4
	513				55.2	**18.6**	2.1		24.1
	553				29.9	**17.1**	2.5		50.5
	593				20.1	**8.7**			71.2
$CHBr_3$	393				15.0	27.3	28.1	**16.7**	12.9
(**7**)	433				11.8	24.4	28.9	**14.3**	20.6
	473				4.8	11.8	23.5	**23.4**	36.5
	513				0.3	2.7	18.4	**38.8**	39.8
	553						16.3	**13.8**	69.9
	593						11.9	**8.2**	78.9

a) See the footnote of Table 1.

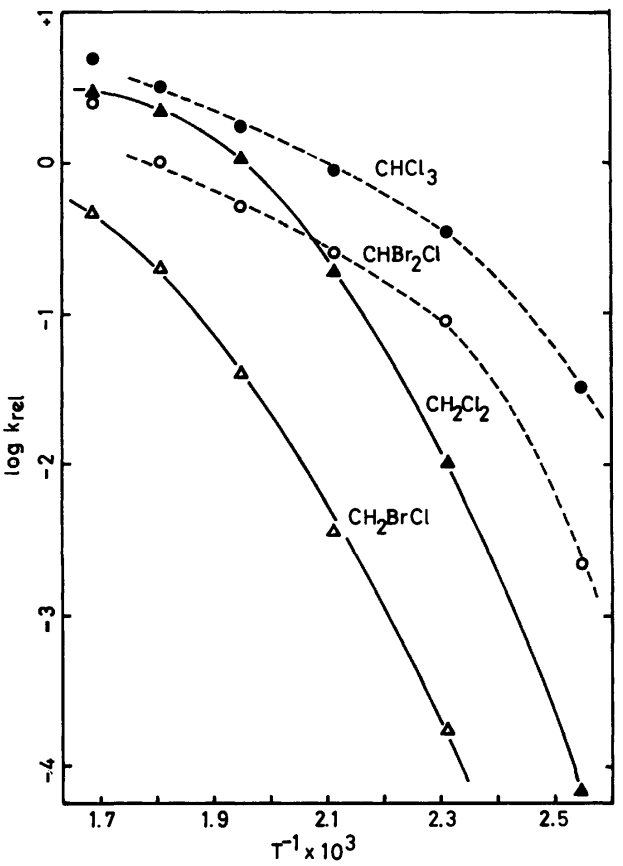

Fig. 4. The Arrhenius plots for the consumption of chlorinated methanes over Fe_3O_4 pretreated by $CHBr_3$.

plots of logarithm of the relative rate[15] (k_{rel}) versus the inverse of reaction temperature ($1/T$), illustrated in Fig. 4, gave the activation energies for the decay of (poly)chloromethanes. The apparent activation energies (E_a) at 427 K for **1**, **2**, **3**, and **5** are 47.2, 54.0, 16.1, and 18.3 kJ mol^{-1}, respectively. The E_a values for trihalomethanes **3** and **5** are considerably lower than those for dihalomethanes **1** and **2**. The lower E_a for trihalomethanes can partly be accounted for the contribution of the steric and electrostatic repulsion among three halogen atoms of trihalomethanes, which facilitates the release of halogen atom.

On the contrary, debromination-chlorination reactions were more complicated. It produced a mixture of a significant amounts of multiply exchanged, further-chlorinated, and oxidized products in addition to the singly exchanged product. The decrease of the starting material was irregularly dependent on the reaction temperature, suggesting that the initial cleavage of C-Br bond is not rate-determining at least at elevated temperatures and that multiple exchange and retro-exchange(dechlorination-bromination) proceed rather extensively. Some bond-forming steps in these secondary processes must determine the rate of the reaction. Since the C-Br bond energy is considerably lower than that of C-Cl bond and, therefore, chlorinated methanes are more stable than the corresponding brominated methanes, the above interpretation is reasonable.

The authors are grateful to Professor S. Fukushi, Chiba Institute of Technology, for his valuable advice and encouragement throughout this work. They also thank heartily to Dr. Tetsuo Ishii, Yokohama Research Institute for Environmental Protection, for his discussion from the view of environmental science and for the measurement of GC/MS spectra.

References

1) D. B. Pealal, *CRC Crit. Rev. Environ. Control*, **5**, 469 (1975); A. K. Ahmed, *Environment*, **18**, 6 (1976); W. Klein and I. Weisgerber, *Environ. Qual. Saf.*, **5**, 237 (1976).

2) L. Vollner, H. Rohleder, W. Klein, and F. Korte, *GSF-Ber.*, **205**, 71 (1975).

3) L. J. Bailin, B. L. Hertzler, and D. A. Oberacker, *Environ. Sci. Technol.*, **12**, 673 (1978).

4) T. Nishiwaki, A. Ninomiya, K. Anda, and S. Nakayama, *Nippon Kagaku Kaishi*, **1972**, 2225; **1973**, 2326.

5) H. H. Vogt, *Chem. Labor Betr.*, **29**, 136; 139 (1978).

6) M. Nakada, K. Ishibashi, S. Fukushi, and M. Hirota, *Bull. Chem. Soc. Jpn.*, **52**, 3761 (1979).

7) M. Nakada, S. Fukushi, H. Nishiyama, K. Okubo, K. Kume, M. Hirota, and T. Ishii, *Bull. Chem. Soc. Jpn.*, **56**, 2447 (1983).

8) K. Morisaki, Y. Miura, K. Abe M. Hirota, and M. Nakada, *Chem. Lett.*, **1987**, 1589.

9) Cui Xiang Hao, M. Nakada, T. Yamaguchi, S. Fukushi, and M. Hirota, *Bull. Chem. Soc. Jpn.*, **58**, 1707 (1985).

10) M. Kiyama, *Bull. Chem. Soc. Jpn.*, **47**, 1646 (1974).

11) M. Nakada, A. Uzawa, S. Fukushi, H. Tomita, and M. Hirota, *Nippon Kagaku Kaishi*, **1984**, 843.

12) When polybromomethanes (**6** and **7**) were treated at lower temperatures, the extent of the decomposition was shown to decrease gradually as the amount of dose increased, giving dose vs. percentage of decomposition curves which are similar to those for **1** and **3**.

13) K. Tanabe, *Nippon Kagaku Zasshi*, **87**, 629 (1966) and references cited therein.

14) As triiron tetraoxide (magnetite) is known to be composed of $Fe^{II}Fe^{III}[Fe^{III}O_4]$, one of Fe(III) is coordinated tetrahedrally by four oxide (O^{2-}) ions and located in the neighborhood of a free Fe(II) species in the inverse spinnel type lattice. This arrangement is illustrated schematically in Fig. 3d depicting only one Fe(III)-oxide-ion linkage which is oriented outward from the surface of the catalyst.

15) Relative rate constants (k_{rel}) were estimated from the percentages of residual reactants by assuming the decay of polyhalomethanes to obey the first-order rate law.

 © 1987 The Chemical Society of Japan Bull. Chem. Soc. Jpn., 60, 3985—3990 (1987)

Racemic Structure and Optical Resolution by Preferential Crystallization of DL-Cysteine Salts of Substituted Benzenesulfonic Acids

Tadashi SHIRAIWA,* Hirohide TAZOH, Michio SUNAMI, Yujin SADO, and Hidemoto KUROKAWA
Faculty of Engineering, Kansai University, Yamate-cho, Suita, Osaka 564
(Received April 9, 1987)

Infrared absorption spectrum, solubility, and thermodynamic analysis indicated that DL-cysteine salts of benzenesulfonic acid (DL-BA salt) and 4-ethylbenzenesulfonic acid (DL-4-EB salt) are conglomerates at room temperature, but DL-BA salt forms a racemic compound at the melting point. These DL-salts were optically resolved by the preferential crystallization. As for DL-4-EB salt, suitable conditions were estimated by the free energy of critical nucleation in supersaturated solutions. The successive preferential crystallization in ethanol at 20 °C was found to give D- and L-4-EB salts with optical purity of 97—100% in the resolution yield of 83—90%. Purification and following treatment with triethylamine gave optically pure D- and L-Cys's.

L-Cysteine (abbreviated as L-Cys) is a useful material for medicines, food additives, and cosmetics, and D-Cys is also noted to be useful for medicines.[1] Since L-Cys has been obtained from hair, optical resolution by preferential crystallization of DL-Cys has been reported only for DL-cysteine hydrochloride monohydrate[1] and DL-4-thiazolidinecarboxylic acid.[2,3] This paper describes a possibility of optical resolution by the preferential crystallization of DL-cysteine salts of substituted benzenesulfonic acids. These DL-salts include benzenesulfonate (DL-BA salt), 4-methylbenzenesulfonate (DL-4-MB salt), 4-ethylbenzenesulfonate (DL-4-EB salt), 3-aminobenzenesulfonate, 4-amino-3-methylbenzenesulfonate, and 2-hydroxy-5-sulfobenzoate.

Since only DL-BA salt has the melting point, its racemic structure was examined by the thermodynamic analysis.[4,5] As for other DL-salts that decompose on heating, the racemic structures were estimated by comparing infrared absorption spectra or solubility values of the DL-salts with those of the corresponding L-salts. The DL-BA and -4-EB salts seemed to be conglomerate at room temperature, but DL-BA salt appeared to form a racemic compound at the melting point. These DL-salts were subjected to optical resolution by preferential crystallization. As for DL-4-EB salt, suitable conditions were examined by the free energy of critical nucleation in supersaturated solutions,[3,6-8] and the successive preferential crystallization was tried in ethanol at 20 °C.

Experimental

Materials. DL- and L-Cysteines were purchased from Sigma Chemicals Co. and Wako Pure Chemicals Ind., respectively, and substituted benzenesulfonic acids and triethylamine from Wako Pure Chemicals Ind. and Kanto Chemical Co. Ltd., respectively.

Preparation of Salts. A mixture of 0.005 mol of DL- or L-Cys and equimolar substituted benzenesulfonic acid in 15 cm^3 of methanol was stirred for 30 min at 40 °C. After addition of 30 cm^3 of diethyl ether, the solution was stirred for 30 min in an ice bath. The salt formed was filtered and recrystallized from ethanol. In the cases of DL- and L-BA salts, the initial mixture was allowed to stand for 1 d at 5 °C, and the salts formed were recrystallized from 1-propanol.

DL-BA salt: Mp 179 °C; Found: C, 38.62; H, 4.66; N, 5.04% (Calcd for $C_9H_{13}O_5NS_2$: C, 38.70; H, 4.69; N, 5.01%). L-BA salt: Mp 205 °C; Found: C, 38.63; H, 4.69; N, 5.03%; $[\alpha]_{436}^{20}$ +9.23° (*c* 1.00, 5 mol dm^{-3} HCl).

DL-4-MB salt: Mp 212—215 °C (decomp); Found: C, 40.76; H, 5.10; N, 4.66% (Calcd for $C_{10}H_{15}O_5NS_2$: C, 40.94; H, 5.15; N, 4.77%). L-4-MB salt: Mp 225—227 °C (decomp); Found: C, 40.91; H, 5.11; N, 4.74%; $[\alpha]_{436}^{20}$ +8.08° (*c* 1.00, 5 mol dm^{-3} HCl).

DL-4-EB salt: Mp 176—179 °C (decomp); Found: C, 42.83; H, 5.58; N, 4.59% (Calcd for $C_{11}H_{17}O_5NS_2$: C, 42.98; H, 5.58; N, 4.59%). L-4-EB salt: Mp 199—200 °C (decomp); Found: C, 42.87; H, 5.56; N, 4.55%; $[\alpha]_{436}^{20}$ +7.15° (*c* 1.00, 5 mol dm^{-3} HCl).

D-4-EB salt with 89% optical purity was obtained from the mother liquor in the optical resolution of the corresponding DL-salt. After refluxing a mixture of 1.76 g of the D-salt and 5 cm^3 of ethanol for 20 min, the mixture was stirred for 30 min at 20 °C. The precipitated salt was collected by filtration to give optically pure D-salt in 1.43 g yield; mp 199—201 °C (decomp); $[\alpha]_{436}^{20}$ −7.15° (*c* 1.00, 5 mol dm^{-3} HCl).

Table 1. Preparation of Supersaturated Solutions

DL-Salt	Solvent[a]	Degree of supersaturation[b]	Mass of DL-salt
		%	g
BA[c]	Ethanol	118	8.485
	1-Propanol	149	2.887
	1-Butanol	215	1.534
4-EB[d]	Ethanol	143	3.084
		153	3.299
		160	3.450
		165	3.558
		170	3.666
		188	4.054

a) Solvent: 50 cm^3. b) Temperature: 20 °C. c) BA: Benzenesulfonate. d) 4-EB: 4-Ethylbenzenesulfonate.

Optical Resolution. Preferential Crystallization: DL-BA or -4-EB salt was dissolved in 50 cm^3 of ethanol, 1-propanol, or 1-butanol at 40 °C to give racemic solutions with the degree of supersaturation of 118—215% at 20 °C; results of preparation of these supersaturated solutions were summarized in Table 1. The solution was slowly cooled to 20 °C and seeded with 0.050 g of the L-salt. After the solution was stirred at 120 rpm by a 1.5 cm×4.0 cm stirrer at 20 °C, the precipitated salt was collected by filtration, washed with diethyl ether, and dried. The optical purity, yield of optically pure modification (YOPM), and degree of resolution of the L-salt were determined by the equations described in a previous paper.[9]

Successive Preferential Crystallization: The DL-4-EB salt (3.450 g) was dissolved in 50 cm^3 of ethanol at 40 °C. After cooling to 20 °C, the solution was seeded with 0.050 g of the L-salt and stirred for 62 min at 120 rpm and 20 °C. The precipitated salt was collected by filtration, and 0.465 g of the DL-4-EB salt was dissolved in the filtrate at 40 °C. After being seeded with 0.050 g of D-salt at 20 °C, the procedure was followed in a similar way. The optical resolution was performed for the initial solution containing 3.450 g of the DL-4-EB salt and 0.100 g of the L-salt in the same manner as in the single-step resolution. The degree of resolution of the D- and L-4-EB salts was calculated by

Degree of resolution/%=[YOPM×100/g]/[(Operation amount of D- or L-salt/g)−1.078].

Preparation of Optically Active Cysteine. Optically pure D- or L-4-EB salt (1.363 g) was dissolved in 25 cm^3 of methanol. After the solution was adjusted at pH 5—6 with triethylamine and stirred for 30 min in an ice bath, the precipitated Cys was collected by filtration to give about 0.51 g each of optically pure D- and L-Cys's. D-Cys: $[\alpha]_D^{20}$ +16.5° (*c* 1.00, water). L-Cys: $[\alpha]_D^{20}$ −16.5° (*c* 1.00, water) (lit,[10] $[\alpha]_D^{20}$ −16.5° (water)).

Measurements. The specific rotation was measured by a Union Giken PM-101 digital polarimeter with a quartz cell of 1.0 dm path length. Infrared spectra were obtained in the range 4000—400 cm^{-1} by a JASCO A-102 infrared spectrophotometer by the KBr disk method. The enthalpy of fusion was determined by a Rigaku Denki differential scanning calorimeter DSC-8230.

The mixture of the DL- or L-salt (BA, 4-MB, and 4-EB salts) and solvent (ethanol, 1-propanol, and 1-butanol for the BA salt; ethanol for the 4-MB and 4-EB salts) was stirred at 20 °C, in the presence of the solid salt. A constant volume of the solution was withdrawn from the mixture, avoiding contamination of the solid salt, diluted in an appropriate concentration, and the absorbance was measured at 263 nm by a Shimadzu double-beam spectrophotometer UV-150-02 with a quartz cell of 0.1 dm path length. After stirring the mixture until the absorbance showed a constant value, the solubility was determined on the basis of the absorbance calibration curves prepared previously.

Results and Discussion

Racemic Structure. In the salts that decompose on heating, infrared spectra of the DL-salts were compared with those of the corresponding L-salt. DL-4-MB and -4-EB salts showed infrared spectra identical with those of L-salts. The solubility of DL-4-EB salt was 2.21 times as large as that of the L-salt. However, the solubility of DL- and L-4-MB salts was approximately equal to each other, as listed in Table 2; the value of α is 1.19 (α=solubility of DL-salt/solubility of L-salt). DL-4-EB salt was optically resolved by preferential crystallization, as will be described in a later section, whereas DL-4-MB salt was unable to resolve by this procedure.

The above results suggest that the DL-4-EB salt is a conglomerate at room temperature, and that the DL-4-MB salt forms a racemic solid solution.[11-14]

Other DL-salts form racemic compounds because their infrared spectra are different from those of the corresponding L-salts.[11]

Racemic Structure of DL-Benzenesulfonate. Only the DL- and L-BA salts show melting points. The mole fraction of the L-salt at the eutectic point was calculated to be 0.61 from the melting point and the

Table 2. Solubility of Cysteine Salt of Substituted Benzenesulfonic Acids[a]

Salt	Solvent	Solubility/g/(100 cm^3 solvent)		
		DL-Salt	L-Salt	α[b]
BA[c]	Ethanol	14.381	9.305	1.55
	1-Propanol	3.875	2.725	1.42
	1-Butanol	1.427	0.980	1.46
4-MB[d]	Ethanol	2.296	1.932	1.19
4-EB[c]	Ethanol	4.313	1.952	2.21

a) Temperature: 20 °C. b) α=solubility of DL-salt/solubility of L-salt. c) See notes in Table 1. d) 4-MB: 4-Methylbenzenesulfonate.

Table 3. Thermodynamic Data of Cysteine Salt of Benzenesulfonic Acid

Salt	Mp θ_m/K	ΔH^f[a] / kJ mol^{-1}	ΔG_T^f[b]/kJ mol^{-1}		Eutectic point		
			ΔG_{453}^f	ΔG_{293}^f	Mole fraction[c]	Temperature/K Found	Calcd[c]
DL-BA[d]	452	31.8	−0.91	+0.12	0.61	451	451
L-BA[d]	478	33.9	—	—			

a) ΔH^f: Enthalpy of fusion. b) ΔG_T^f: Gibbs energy of formation of racemate at *T* K. The ΔG_T^f's at the melting point (ΔG_{453}^f) and at 293 K (ΔG_{293}^f) were calculated from the equations in Refs. 4 and 5. c) These values were calculated from the Schröder-Van Laar and Prigogine-Defay equations. d) See note in Table 1.

enthalpy of fusion (ΔH^f),[4] and the observed melting point of mixture with the composition agreed with the calculated eutectic temperature (451 K);[4] these values are listed in Table 3 and the binary melting point diagram is shown in Fig. 1. These results indicated that DL-BA salt forms a racemic compound at the melting point.[4]

The Gibbs energy of formation of the racemate from its antipode at melting point (ΔG^F_{452}/kJ mol^{-1}) and 293 K (ΔG^F_{293}) was calculated from the melting temperature and ΔH^f,[4,5] and listed in Table 3. The negative ΔG^F_{452} value supports the above result. However, the positive ΔG^F_{293} suggests that DL-BA salt does not form a racemic compound at 293 K, although the absolute value is small (+0.12 kJ mol^{-1}). The DL-BA salt shows infrared spectrum identical with that of the L-salt and is more soluble than the L-salt, as listed in Table 2; the values of α are 1.42—1.55 in ethanol, 1-propanol, and 1-butanol.[11-14]

The above results indicate that DL-BA salt is a conglomerate at room temperature though the DL-salt forms a racemic compound at the melting point.

Preferential Crystallization. Optical resolution of the DL-BA and -4-EB salts was attempted by preferential crystallization at 20 °C with the L-salt as seed crystals, and the results are given in Tables 4 and 5, respectively.

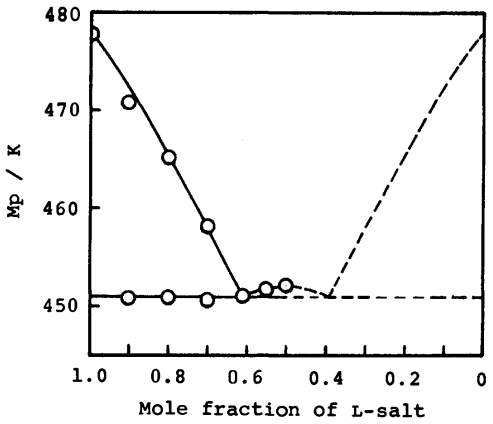

Fig. 1. Binary melting point diagram of cysteine salt of benzenesulfonic acid.

Since it was possible to resolve these DL-salts by preferential crystallization, it was confirmed that the DL-BA and -4-EB salts are conglomerates at room temperature. Although the L-BA salt with approximately 90% optical purity is obtained from 1-propanol and 1-butanol solutions, the yield of optically pure modification (about 0.05 g) and degree of resolution (about 12%) are extremely low. The small absolute value of ΔG^F_{293} of DL-BA salt may be the reason why the optical resolution by preferential crystallization is poor.

On the other hand, the optical resolution of the DL-4-EB salt gave better result than that of the DL-BA salt. This result indicates that the use of the DL-4-EB salt is more favorable for obtaining optically pure Cys in a high yield.

Estimation of Suitable Conditions for Optical Resolution. Relationship between Factors for Crystallization and Free Energy of Critical Nucleation: Suitable conditions for optical resolution of the DL-4-EB salt were estimated by free energy of critical nucleation (Δg_{max}/J nucleus^{-1}) and factors of crystallization of the D- and L-salts for different degrees of supersaturation of 143, 153, and 188%;[3,8] the values of Δg_{max} were calculated by the equations described in the previous papers.[8,15] The amounts of crystallization of the D- and L-salts were calculated from the data in Table 5.[16] The relationship between the amount of crystallization and resolution time is shown in Fig. 2. The speed of crystallization of the L-salt (R_L/g min^{-1}) was calculated from linear plots of Fig. 2; the straight lines had the correlation coefficient of 0.97—0.99. The retardation time for crystallization of the D-salt (θ_D/min) was defined as the time that elapsed before the D-4-EB salt begins to crystallize rapidly and was estimated from Fig. 2. The values of Δg_{max}, R_L, and θ_D are listed in Table 6.

Table 4. Preferential Crystallization of DL-Cysteine Salt of Benzenesulfonic Acid[a]

Solvent	Degree of supersaturation / %	Resolution time / min	Yield / g	Optical purity / %	YOPM[b] / g	Degree of resolution / %
Ethanol	118	5	0.256	32.7	0.034	5.3
		20	1.281	5.4	0.020	3.1
1-Propanol	149	10	0.120	87.6	0.055	11.6
		20	0.479	30.8	0.098	20.7
1-Butanol	215	10	0.109	93.3	0.052	12.7
		20	0.161	82.5	0.083	20.2
		30	0.195	60.6	0.068	16.6
		40	0.286	34.0	0.047	11.5

a) Solvent: 50 cm^3. Seed crystals: 0.050 g of L-salt. Temperature: 20 °C. b) YOPM: Yield of optically pure modification.

Table 5. Preferential Crystallization of DL-Cysteine Salt of 4-Ethylbenzenesulfonic Acid[a)]

Degree of supersaturation / %	Resolution time / min	Yield / g	Optical purity / %	YOPM[b)] / g	Degree of resolution / %
143	30	0.074	100	0.024	5.2
	90	0.241	100	0.191	41.2
	120	0.270	100	0.220	47.4
	150	0.393	100	0.343	73.9
	170	0.426	95.8	0.358	77.2
	180	0.467	88.9	0.365	78.8
	190	0.582	59.8	0.298	64.2
	210	0.730	41.8	0.255	55.0
153	60	0.319	99.0	0.266	46.6
	90	0.477	100	0.427	74.8
	100	0.560	83.6	0.418	73.2
	110	0.589	76.5	0.401	70.2
	120	0.882	31.9	0.231	40.5
160	62	0.515	98.2	0.456	70.5
	70	0.601	82.7	0.447	69.1
165	50	0.524	92.5	0.435	62.1
	60	0.656	77.0	0.455	64.9
170	40	0.485	96.1	0.416	55.1
	50	0.684	71.2	0.437	57.9
188	5	0.111	100	0.061	6.4
	15	0.245	92.2	0.176	18.5
	18	0.325	94.2	0.256	27.0
	20	0.412	91.7	0.328	34.6
	25	0.653	79.2	0.467	49.2
	35	1.241	12.5	0.105	11.1

a) Solvent: 50 cm³ of ethanol. Seed crystals: 0.050 g of L-salt. Temperature: 20 °C. b) YOPM: See note in Table 4.

The relationship between R_L and Δg_{max} for the degree of supersaturation of 143, 153, and 188% and that between θ_D and Δg_{max} are then obtained as

$$\ln R_L = -1.660 \ln \Delta g_{max} - 70.92, \quad (1)$$

$$\ln \theta_D = 1.526 \ln \Delta g_{max} + 64.76, \quad (2)$$

where the correlation coefficients are higher than 0.999.

Suitable Conditions for Optical Resolution: The optical resolution at θ_D-5 min seems to be a better criterion for evaluating the results of optical resolution than that at θ_D min, because the unseeded D-salt begins to crystallize rapidly after θ_D min. The amount of crystallization of L-salt at θ_D-5 min ($W^c_{(-5)}/g=R_L(\theta_D-5)$) is derived from Eqs. 1 and 2 and expressed by

$$W^c_{(-5)} = 2.120 \times 10^{-3} \Delta g_{max}^{-0.1344} - 7.950 \times 10^{-31} \Delta g_{max}^{-1.660}. \quad (3)$$

Since the values of R_L for the degree of supersaturation of 143, 153, and 188% are calculated by the least-squares method from linear plots in Fig. 2,

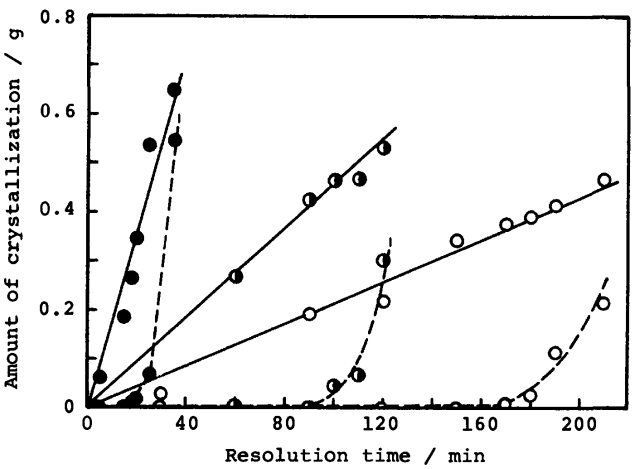

Fig. 2. Relationship between amounts of crystallization of D- and L-cysteine salts of 4-ethylbenzenesulfonic acid and resolution time.
Conditions: Solvent 50 cm³ of ethanol; seed crystals 0.050 g of L-salt; temperature 20 °C. Degree of supersaturation: ○ 143%; ◑ 153%; ● 188%. ——: L-Salt. ——: D-Salt.

Table 6. Free Energy of Critical Nucleation and Factors for Preferential Crystallization of Cysteine Salt of 4-Ethylbenzenesulfonic Acid[a)]

Degree of supersaturation %	Δg_{max}[b)] $\times 10^{-18}$ J nucleus^{-1}	R_L[c)] $\times 10^{-3}$ g min^{-1}	θ_D[d)] min	$W_{(-5)}$[e)]/g Found	Calcd I[f)]	Calcd II[g)]
143	10.95	2.387	175	0.367	0.391	0.361
153	7.393	4.242	95	0.427	0.402	0.430
160	5.868	6.512[h)]	66	0.461	0.405	0.449
165	5.059	8.331[h)]	55	0.455	0.405	0.447
170	4.412	10.46[h)]	45	0.426	0.403	0.433
188	2.901	21.25	23	0.266	0.377	0.269

a) Conditions of crystallization: Solvent 50 cm^3 of ethanol; seed crystals 0.050 g of L-salt; temperature 20 °C. b) Δg_{max}: Free energy of critical nucleation at 20 °C in ethanol. c) R_L: Speed of crystallization of L-salt. d) θ_D: Retardation time for crystallization of D-salt. e) $W_{(-5)}$: Amount of crystallization of L-salt at θ_D-5 min. f) These values of $W_{(-5)}$ were calculated from Eq. 3. g) These values of $W_{(-5)}$ were calculated from Eq. 5. h) These values of R_L were calculated from Eq. 1.

the straight lines obtained do not always pass through the origin. Therefore, the calculated values of $W^c_{(-5)}$ from Eq. 3 show relatively large deviation from experimental values at θ_D-5 min ($W_{(-5)}$/g); the values of $W^c_{(-5)}$ are listed under "Calcd I" in Table 6 and those of $W_{(-5)}$ are also listed under "Found" in Table 6. On the other hand, the linear relationship between $W^c_{(-5)}$ and $W_{(-5)}$ for the degree of supersaturation of 143, 153, and 188% is expressed by

$$W_{(-5)} = 6.249W^c_{(-5)} - 2.084, \quad (4)$$

where the correlation coefficient is 0.998. Eliminating $W^c_{(-5)}$ in Eqs. 3 and 4, we have

$$W_{(-5)} = 1.325 \times 10^{-2}\Delta g_{max}{}^{-0.1344} - 4.969 \times 10^{-30}\Delta g_{max}{}^{-1.660} - 2.084. \quad (5)$$

In order to test Eq. 5, the values of $W_{(-5)}$ for the degree of supersaturation of 160, 165, and 170% calculated from Eq. 5 are listed in Table 6 as Calcd II. The optical resolution for these degrees of supersaturation was carried out at the resolution time approximately equal to the calculated value of θ_D-5 from Eq. 2. The resulting data are listed in Table 5. The amounts of crystallization of the L-salt obtained from the data agree well with the calculated values of $W_{(-5)}$ from Eq. 5, as shown in Table 6. The values of $W_{(-5)}$ for other degree of supersaturation were also calculated from Eq. 5, and the relationship between $W_{(-5)}$ and degree of supersaturation is shown in Fig. 3.

Figure 3 suggests that the maximum amount of the L-4-EB salt with high optical purity can be obtained with degree of supersaturation of 160—165%. When $W_{(-5)}$ in Eq. 5 or $W^c_{(-5)}$ in Eq. 4 is differentiated with respect to Δg_{max} and the differential coefficient is put equal to zero, the value of Δg_{max} that gives the maximum $W_{(-5)}$ or $W^c_{(-5)}$ was calculated to be 5.55×10^{-18} J nucleus^{-1}. This value is approximately equal to the value for an ethanol solution with 160% degree of supersaturation (5.87×10^{-18} J nucleus^{-1}); the

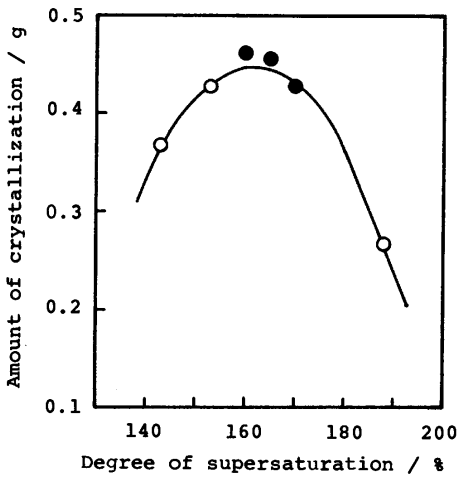

Fig. 3. Crystallization of L-cysteine salt of 4-ethylbenzenesulfonic acid at θ_D-5 min.
Conditions: Solvent 50 cm^3 of ethanol; seed crystals 0.050 g of L-salt; temperature 20 °C. ——: Calculated amount of crystallization of L-salt at θ_D-5 min from the data for degree of supersaturation of 143, 153, and 188% (○). ●: Experimental amount for degree of supersaturation of 160, 165, and 170%.

value of Δg_{max} for 165% degree of supersaturation is 5.06×10^{-18} J nucleus^{-1}.

The above result suggests that the optical resolution with 160% degree of supersaturaiton at resolution time of 62 min is the most favorable for obtaining the L-4-EB salt with high optical purity in high yield; θ_D calculated from Eq. 2 is 67 min. The results in Table 5 indicate that the optical resolution under these conditions gives the L-4-EB salt with 98.2% optical purity in 70.5% degree of resolution and the yield of optically pure modification (0.456 g) is maximum at θ_D-5 min. This result supports the above suggestion.

Successive Preferential Crystallization of DL-4-Ethylbenzenesulfonate. In order to obtain the D- and L-4-EB salts with high optical purity, the successive

Table 7. Successive Preferential Crystallization of DL-Cysteine Salt of 4-Ethylbenzenesulfonic Acid[a)]

Run	Added amount of DL-salt	Operation amount[b)]/g		Resolution time	Salt obtained				
					Yield	Optical purity	YOPM[c)]	Degree of resolution	
	g	D-Salt	L-Salt	min	g	%	g	%	
1[d)]	3.450	1.725	1.725	62	L 0.515	98.2	0.456	70.5	
2	0.465	1.953	1.497	52	D 0.578	93.0	0.486	55.7	
1[e)]	3.450	1.725	1.825	30	L 0.736	98.5	0.675	90.3	
2	0.686	2.062	1.488	30	D 0.912	97.3	0.837	85.0	
3	0.862	1.643	1.905	40	L 0.782	100	0.732	88.4	
4	0.732	2.009	1.539	40	D 0.828	100	0.778	83.4	

a) Solvent: 50 cm^3 of ethanol. Seed crystals: 0.050 g of D- or L-salt. Temperature: 20 °C. b) The operation amounts of D- and L-salts in solution were calculated on the basis of analyses of the salt obtained in Run 1 or 1—3. c) YOPM: See note in Table 4. d) Degree of supersaturation of the initial solution: 160%. e) DL-Salt (3.450 g) and 0.100 g of L-salt were dissolved in the initial solution.

preferential crystallization was attempted with an initial solution with 160% degree of supersaturation; the result is listed in Table 7. Although it was also possible to obtain the D-4-EB salt with 93.0% optical purity, the degree of resolution (55.7%) was not so high as expected.

The L-4-EB salt (0.100 g) was dissolved in the initial solution to induce more rapid crystallization of the L-salt with high optical purity. This optical resolution was found to give the D- and L-4-EB salts with optical purity of 97—100% in degree of resolution of 83—90%, as shown in Table 7. The yields of optically pure modification of the D- and L-salts obtained also increased to 19—24% of the amounts of the DL- and L-salts contained in the initial solution. The purified D- and L-4-EB salts were treated with triethylamine to give optically pure D- and L-Cys's in 93—94% yield, respectively.

The above results show that suitable conditions are predictable by Δg_{max} and that the optical resolution by preferential crystallization of DL-4-EB salt efficiently gives the optically active Cys.

References

1) C. Inoue, Y. Kurima, and S. Moriguchi, Jpn. Patent, 70859 (1982); *Chem. Abstr.*, **97**, 163490 (1982).

2) T. Shiraiwa, Y. Sado, M. Komure, and H. Kurokawa, *Chem. Lett.*, **1987**, 621.

3) T. Shiraiwa, Y. Sado, M. Komure, and H. Kurokawa, *Bull. Chem. Soc. Jpn.*, **60**, 3277 (1987).

4) M. Leclercq, A. Collet, and J. Jacques, *Tetrahedron*, **32**, 821 (1976).

5) T. Shiraiwa, H. Yoshida, M. Tsuda, and H. Kurokawa, *Bull. Chem. Soc. Jpn.*, **60**, 947 (1987).

6) T. Nakai, *Bull. Chem. Soc. Jpn.*, **42**, 2143 (1969).

7) T. Nakai, "Shoseki Kogaku," Baifukan, Tokyo (1986), Chap. 2.

8) T. Shiraiwa, H. Miyazaki, T. Imai, M. Sunami, and H. Kurokawa, *Bull. Chem. Soc. Jpn.*, **60**, 661 (1987).

9) T. Shiraiwa, Y. Ohmichi, K. Iwafuji, and H. Kurokawa, *Nippon Kagaku Kaishi*, **1983**, 1070.

10) J. S. Davies, "Amino Acids and Peptides," Chapman and Hall, London, New York (1985), p. 130.

11) H. Nohira, "Shizen Bunsho no Joken to Jitsuyo Rei," ed by S. Ohtsuka and T. Mukaiyama, Kagaku Dojin, Kyoto (1982), p. 165.

12) J. Jacques, A. Collet, and S. H. Wilen, "Enantiomers, Racemates, and Resolutions," John Wiley and Sons, New York, Chichester, Brisbane, Tronto (1981), pp. 178—192.

13) K. Yamanari, J. Hidaka, and Y. Shimura, *Bull. Chem. Soc. Jpn.*, **46**, 3724 (1974).

14) T. Watanabe, *Noguchi Kenkyusho Jiho*, **16**, 46 (1969).

15) In order to calculate Δg_{max}, the value of molecular volume of 4-EB salt (3.811×10^{-28} m^3) was measured at 20 °C in ethanol. The molecular radius was calculated to be 4.498×10^{-10} m on the assumption of spherical molecule. The values of the radius (5.734×10^{-10} m) and interfacial energy (8.889×10^{-3} J m^{-2}) of embryo in the saturated ethanol solution at 20 °C were calculated on the basis of the solubility of DL-4-EB salt according to the procedure reported in Refs. 6—8; the average number of 4-EB salt molecule forming the embryo in the saturated solution is 2.072.

16) T. Shiraiwa, Y. Ohmichi, and H. Kurokawa, *Nippon Kagaku Kaishi*, **1983**, 1102.

 © 1987 The Chemical Society of Japan Bull. Chem. Soc. Jpn., 60, 3991—3998 (1987)

Mathematical Analysis of Noncatalytic Coal Dissolution Using Tetralin and the Prediction of Coal Conversion, SRC Yield and Aromaticity of SRC

Hideyuki TAGAYA,* Masayuki SUGAI, Kazuo ITO, Hisako ANDO, and Koji CHIBA*

Department of Chemical Engineering, Faculty of Engineering, Yamagata University, Johnan, Yonezawa 992

(Received April 10, 1987)

Mathematical analyses of noncatalytic coal dissolution using tetralin at 350—460 °C were carried out. Coal conversion, SRC yield and aromaticity of SRC could be predicted fairly well by regression equations using liquefaction conditions as explanation variables. The equation derived from coal conversions in 67 experiments using the C% and volatile matter of 6 coals and liquefaction conditions could predict coal conversions fairly well (R=0.972). The conversions predicted by the proposed equation were also compared with those reported by previous investigators. Although it was suggested that long heating-up period was detrimental to coal conversion, the equation was a good indication of the conversion in solvent extract liquefaction.

There are three alternative processes for direct coal liquefaction (solvent extraction, catalytic hydrogenation and carbonization). In the solvent extraction process coal may be extracted and dissolved at temperatures of 350—450 °C by the action of hydrogen donor solvents with and without catalyst or molecular hydrogen being present.[1] Several solvent extraction process using different modes have been developed. The Pott-Broche process was developed in Germany in 1920s and the process was a prototype of the SCF process in 1950s, the SRC process in the early 1960s and the EDS process in 1960s. It has been well-understood that in noncatalytic coal dissolution, hydrogen from the donor solvents reacts directly with coal molecules to produce hydrocarbon liquids.[2] Therefore, many researchers have attempted to evaluate the hydrogen-donor ability of coal-liquefaction solvents[3] and hydroaromatic compounds such as tetralin are known as donors.[4] In the Pott-Broche and the SCF processes tetralin was used as a solvent. Recently, many laboratory-scale liquefaction processes using tetralin have been intensively investigated.[5-20] Coal conversion has proved to be largely dependant not only on the rank of coal but also on the liquefaction conditions. However, most of the previous studies using tetralin were investigations concerning specific liquefaction conditions[5,7-18] and those using specific coal.[6,19,20] A quantitative evaluation of coal conversion by suitable variables is required for the effective dissolution by establishment of optimal conditions. The object of the present study is to obtain the relationship between explanation variables (coal properties, liquefaction conditions) and observed variables (coal conversion, SRC yield and aromaticity of SRC) and to compare the coal conversions predicted by the proposed relation with the actual conversions obtained in this study and in the previous investigators.[5-16]

Experimental

Coal Sample and Solvent. Seven coals were used in this study. Analyses of these coals are given in Table 1. They were ground to a size that could pass through a 100-mesh (149 μm) screen and were dried at 107 °C in a nitrogen atmosphere. Six types of coal, except Wandoan coal, were used in the study in order to obtain regression equations. Reagent-grade tetralin was used after distillation under reduced pressure.

Coal Liquefaction Procedure. Coal (6—18 g) and tetralin (6—18 g) were placed in a magnetically stirred autoclave and pressurized to ≈5.1 MPa with hydrogen or nitrogen. The autoclave was heated to the reaction temperature and maintained for the nominal reaction time. At the completion of a run, the autoclave was cooled by an electric fan to room temperature. Materials remaining in the autoclave after the liquefaction were extracted with benzene. Conversion to a benzene-soluble material was calculated according to the following equation:

Conversion (wt%, daf coal basis)=
100(coal charged−benzene insoluble material)/daf coal.

Tetralin was recovered from the benzene extract by vacuum distillation at 240 °C and 933 Pa and was analyzed by GC to calculate the transferred hydrogen from tetralin to

Table 1. Analyses of Coals (wt%)

Coal	Ultimate analysis (daf)				Proximate analysis (coal)			
	C	H	N	Odiff	Mois	FC	VM	Ash
Yallourn	69.8	4.0	0.8	25.4	13.3	51.9	32.8	2.0
Wandoan	77.6	6.2	0.8	15.4	9.2	38.6	44.9	7.3
Taiheiyo	77.9	5.8	0.7	15.6	4.8	35.8	47.5	11.9
Horonai	79.4	6.0	1.1	13.4	3.1	44.6	45.4	6.9
Miike-1	80.9	6.4	0.9	11.8	2.1	36.7	37.6	23.6
Minamiohyubari	83.5	6.1	1.3	9.3	1.3	40.8	52.2	5.7
Miike-2	85.9	6.1	1.3	6.7	2.3	46.9	43.9	6.9

coal. The distillation residue was weighed as a solvent refined coal (SRC).

Calculation of Aromaticity of SRC. The aromaticity of SRC was calculated using the Brown-Ladner method.[21] The ^{1}H NMR data required for the calculation were obtained using a Hitachi R 22 apparatus (90 MHz). The distribution of hydrogen was estimated from the intensities of the three different ^{1}H NMR bands (hydrogen on aromatic carbon atoms; δ=6—9, hydrogen on α carbon atoms; δ=2—4.5, hydrogen on other nonaromatic carbons; δ=0.3—2).

Statistical Method. To obtain the relationship between explanation variables (coal properties, liquefaction conditions) and observed variables (coal conversion, SRC yield and aromaticity of SRC), a factorial experimental design was used.[20,22] Thus, the variables of interest were identified and a set of 10 experiments (at least) was performed in which the reaction conditions were changed in a systematic way.[23] The conversion, SRC yield, and aromaticity of SRC were measured under various conditions.

Results and Discussion

Yallourn (a set of 11 experiments), Taiheiyo (15), Horonai (10), Miike-1 (10), Minamiohyubari (11), and Miike-2 (10) coals were liquefied in a hydrogen atmosphere (0—5.1 MPa) using tetralin at 350—460 °C. Under these liquefaction conditions, coal conversion increased linearly with the amounts of transferred hydrogen from tetralin to coal. This indicated that the undesirable regression reaction was minor in these conditions. The observed Yallourn coal conversion, SRC yield and aromaticity of SRC are shown in Table 2. The reproducibility of the data is indicated by the values for duplicate runs at 440 °C under 5.1 MPa for 20 min and at 410 °C under 2.5 MPa for 40 min. This reproducibility shows that application of the data to a regression analysis is possible.[23] Least-squares regression analyses were performed using these data and the resulting equations allowed for a calculation of the conversion, SRC yield and aromaticity of SRC (f_a). The equations derived from the data in Table 2 are given in Eqs. 1—3, where T is the temperature (°C), P the pressure (MPa), and t the time (min):

$$\text{Conversion} = -164.18 + 0.513T - 0.0369P + 0.136t, \quad (1)$$

$$\text{SRC yield} = -59.82 + 0.191T + 0.0221P + 0.0691t, \quad (2)$$

and

$$f_a \times 1000 = -138 + 1.77T - 1.53P + 0.500t. \quad (3)$$

Coefficients of correlation for Eqs. 1—3 were as large as 0.996, 0.936, and 0.934, respectively. Predicted values using the Eqs. 1—3 are also shown in Table 2 (in parentheses). It is clear that the predicted values are close to the observed values.

For other coals, satisfactory results, as well as for Yallourn coal, were obtained. The resulting coefficients for 6 coals for the factors (temperature, pressure, solvent/coal ratio, and time) and correlation coefficients are listed in Table 3. Needless to say, the temperature was main factor for predicting coal conversion and SRC yield. In liquefaction using a catalyst, it was reported that the reaction-rate constant for the liquefaction increased linearly with the reaction pressure.[24] Even in a non-donor solvent like decalin without a catalyst, participation of hydrogen molecules in the liquefaction was suggested.[25] However, it was understood that a donor solvent like tetralin fulfilled the main role of hydrogen donation in the solvent-extraction process.[26] For the equations of conversion, the coefficients in pressure for Yallourn and Taiheiyo coals were negative. However, their absolute values were small. The effect of hydrogen pressure on coal conversion was small under these conditions. Positive values of coefficients in pressure

Table 2. Observed (Obs.) and Predicted (Pred.) Yallourn Coal Conversion, SRC Yield and Aromaticity of SRC Using Tetralin in a Hydrogen Atmosphere

Temp °C	Press MPa[a]	Time min	Conversion		SRC yield		Aromaticity	
			obs.	(pred.)	obs.	(pred.)	obs.	(pred.)
440	5.1	20	65.9	(64.2)	24.6	(25.7)	0.665	(0.646)
440	5.1	20	62.3	(64.2)	23.9	(25.7)	0.646	(0.646)
440	5.1	60	68.2	(69.7)	32.7	(28.5)	0.634	(0.666)
440	0.0	20	64.4	(64.4)	27.6	(25.6)	0.644	(0.653)
440	0.0	60	70.3	(69.9)	25.5	(28.3)	0.707	(0.673)
380	5.1	20	33.0	(33.4)	13.3	(14.3)	0.556	(0.540)
380	5.1	60	39.8	(38.9)	17.1	(17.0)	0.568	(0.560)
380	0.0	20	33.0	(33.6)	16.4	(14.1)	0.532	(0.546)
380	0.0	60	37.9	(39.1)	15.9	(16.9)	0.568	(0.566)
410	2.5	40	53.9	(51.7)	20.9	(21.3)	0.585	(0.606)
410	2.5	40	52.2	(51.7)	21.1	(21.3)	0.604	(0.606)

a) Total pressure was 5.1 MPa (2.5 MPa and 0 MPa mean 2.5 MPa of hydrogen+2.5 MPa of nitrogen and 5.1 MPa of nitrogen, respectively).

were obtained for the equations of SRC yields, except for Taiheiyo coal. This indicated that increasing pressure suppressed the formation of gaseous products.[19]

The aromaticity of SRC tended to increase with the reaction temperature, except for Miike coal-2 in which negative coefficient (−0.167) was obtained although its absolute value was small. From the increasing aromaticity of SRC, two reaction mechanisms were considered: In one mechanism, the value of aromaticity increased owing to a further reaction of the liquefaction products. In the other mechanism, compounds having higher values of aromaticity were liquefied proceeding liquefaction. The aromaticity of SRC scarcely changed upon a thermal treatment.[27] This indicated that the latter mechanism in which, as the liquefaction proceeded, compounds having more condensed-ring were cleaved and liquefied, was reasonable.

If the coefficients were well correlated with the coal properties, the meaning of the coefficients might be clear; however, we could find no good correlations between the coefficients for the factors and the coal properties. Figure 1 is a plot of the conversion predicted from the regression equation against the actual conversion for the 6 coals. The predicted conversions are in fair agreement with the observed conversions over the wide conversion range (5—90%). Figure 1 also shows the conversions under a nitrogen atmosphere (12 experiments) as a closed key. They were also in good agreement with the predicted values. It is evident that the role of molecular hydrogen to increase coal conversion is minor under these mild liquefaction conditions with no catalyst.[19]

Similar satisfactory relationships between predicted and observed SRC yield were also attained. However, a smaller coefficient of correlation than that for conversion was observed in the case of the relationship between predicted and observed aromaticity of SRC. As shown in Table 2, the difference of aromaticity in repeated runs at 440 and at 410 °C were 0.19 and 0.19 (not small). The smaller coefficient of correlation is partly due to an experimental error in determining the aromaticity of SRC.

A useful way for attaining an effective solvent extraction of coals is to obtain an equation which can describe the change in coal conversion by using the properties of the coals. Regression analyses using coal properties (C%, H%, N%, H/C, volatile matter, fixed carbon, and ash) and liquefaction conditions as explanation variables were carried out in various combinations. We choose C%, volatile matter and liquefaction conditions since the coefficient of correlation was largest when they were used. The equations derived from the 67 experiments using 5 explanation variables (2 coal properties and 3 liquefaction conditions) are given in Eqs. 4—6, where C is the C% of coal (wt%), VM the volatile matter based on dry coal (wt%), T the temperature (°C), P the pressure (MPa), and t the time (min):

Table 3. Results of Multiple Regression Analyses

Coal	Observed variable[a]	Factor				Constant	R[c]
		Temp °C	Press MPa	S/C[b]	Time min		
Yallourn	Conv	0.513	−0.0369		0.136	−164.18	0.996
	SRC	0.191	0.0221		0.0691	−59.82	0.936
	f_a	1.77	−1.53		0.500	−138	0.934
Taiheiyo	Conv	0.606	−1.26			−197.67	0.993
	SRC	0.376	−0.193			−117.37	0.986
	f_a	1.44	−7.00			−6	0.939
Horonai	Conv	0.768	0.610		0.280	−279.64	0.994
	SRC	0.462	0.0659		0.187	−164.54	0.992
	f_a	1.45	0.549		0.494	−58	0.979
Miike-1	Conv	0.722	1.44	−1.63		−233.24	0.980
	SRC	0.449	2.36	2.34		−150.31	0.927
	f_a	0.781	6.78	−22.6		409	0.810
Minamiohyubari	Conv	0.831	0.274		0.148	−308.80	0.993
	SRC	0.538	0.514		0.0565	−197.17	0.975
	f_a	1.03	−1.98		8.07	167	0.747
Miike-2	Conv	0.713	0.835	0.625		−245.94	0.994
	SRC	0.479	1.06	3.61		−168.25	0.982
	f_a	−0.167	2.25	−5.86		673	0.987

a) Conv=Conversion, SRC=SRC yield, f_a=Aromaticity of SRC×10^3. b) Solvent/Coal ratio. c) Correlation coefficient.

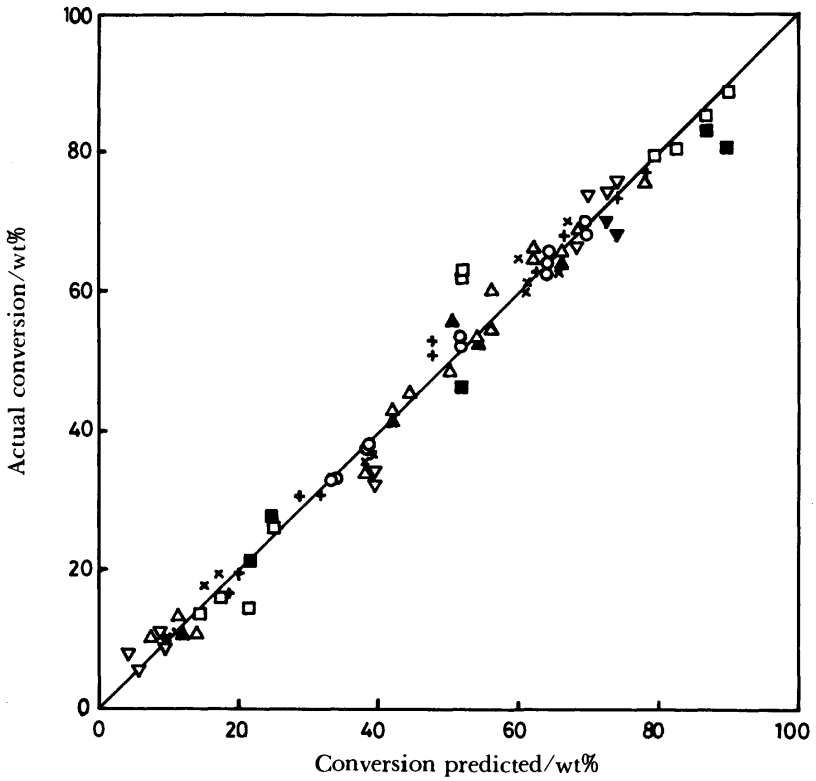

Fig. 1. Comparision of conversions predicted by the six regression equations for each coal and actual conversions obtained: ○, Yallourn (H_2); △, Taiheiyo (H_2); ▲, Taiheiyo (N_2); +, Horonai (H_2); □, Miike-1 (H_2); ■, Miike-1 (N_2); ×, Minamiohyubari (H_2); ▽, Miike-2 (H_2); ▼, Miike-2 (N_2).

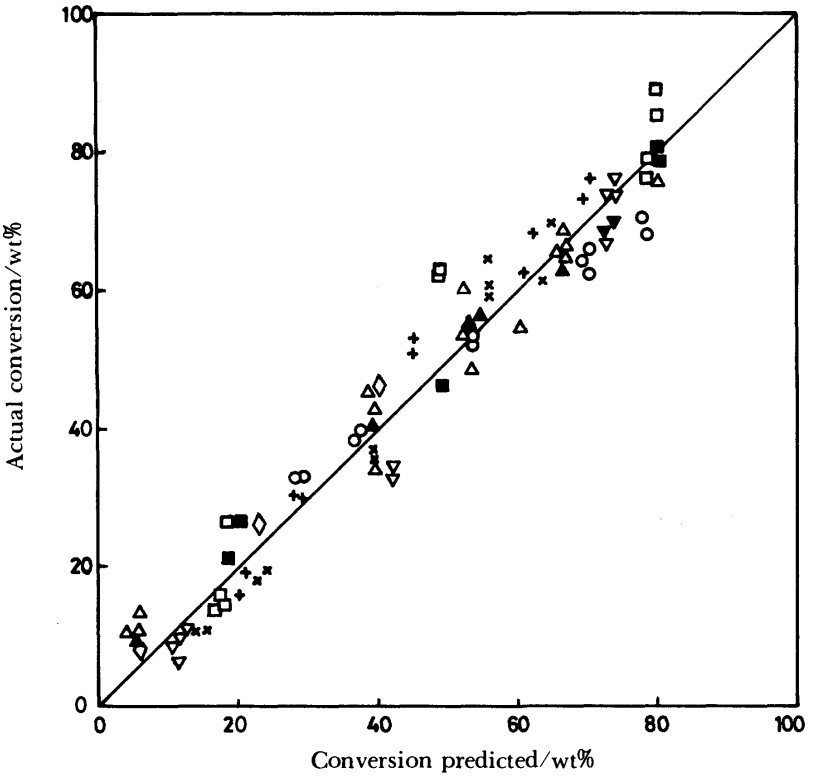

Fig. 2. Comparision of conversions predicted by the regression equation and actual conversions obtained: The key is as in Fig. 1; ◇, Wandoan (N_2).

$$\text{Conversion} = -208.01 + 0.188C - 1.08VM + 0.684T + 0.210P + 0.212t, \quad (4)$$

$$\text{SRC yield} = -203.93 + 0.868C - 0.367VM + 0.417T + 0.571P + 0.242t, \quad (5)$$

and

$$f_a \times 100 = -9.523 + 0.708C - 0.685VM + 0.108T - 0.220P + 0.0332t. \quad (6)$$

Coefficients of correlation for Eqs. 4—6 were 0.972, 0.900, and 0.795, respectively. A smaller coefficient of correlation (0.948) was obtained when the regression equation was derived using C, T, P, t as explanation variables (except for VM). Volatile matter is known to decrease with an increase in the coal rank;[28] however, volatile matters of higher-rank coals in this study (Miike coal-1 and -2) are smaller than those of lower-rank coals (Taiheiyo and Horonai coals). The present study, in which volatile matter and coal rank are two important variables, indicates the possibility that they are significant independant properties of coal. The possibility that volatile matter concerned well with the amounts of linkages which were easily cleaved and the resulted radical consumed hydrogen was not excluded. Comparision of predicted values and actual values using the Eqs. 4—6 are shown in Fig. 2—4. Figure 2 shows that the conversions obtained with wide-range conditions and coal ranks can be well predicted only from one Eq. 4. We also added to Fig. 2 the conversions obtained in the liquefaction of Wandoan coal (a set of 3 experiments). The difference between observed and predicted conversions of Wandoan coal were only 3—6%. Although there are small scatter in Figs. 3 and 4, especially in Fig. 4, the equations are sufficient for predicting SRC yield and aromaticity of SRC.

We compared the conversion predicted by the proposed Eq. 4 with the results obtained by previous investigators,[5-16] as shown in Fig. 5. There is considerable scatter. Actual conversions by investigators 4, 8, and 10 were fairly larger than predicted; however, those by investigators 2, 3, and 5 were smaller than predicted. Here, we must note the difference of liquefaction apparatus among investigators as shown in Table 4. Investigators 4, 8, and 10 used tubing bomb as the reactor which did not require so long heating up period (0.5—1.5 min). Investigator 5 used 4l autoclave and required 120 minutes to reach reaction temperature (400 °C). In addition, investigators 2, 3, and 6 used 300 ml and investigator 12 used 500 ml autoclave. We used 100 ml magnetically stirred autoclave and required 60 minutes to 400 °C. These facts indicate that in a prediction using Eq. 4, the conversion is overestimated for a larger reactor which requires a long heating-up period and is underestimated for a smaller reactor like tubing bomb. It is well-known that coal liquefaction is proceeded even in the course of heating-up period.[29] However, our results suggest that extending the heating-up period

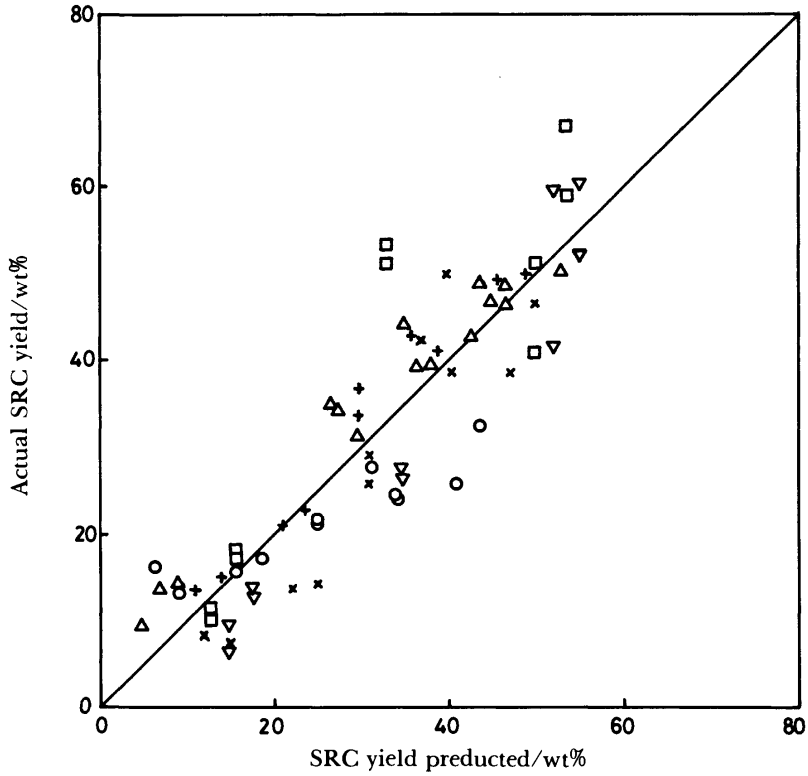

Fig. 3. Comparision of SRC yield predicted and actual SRC yields. The key is as in Fig. 1.

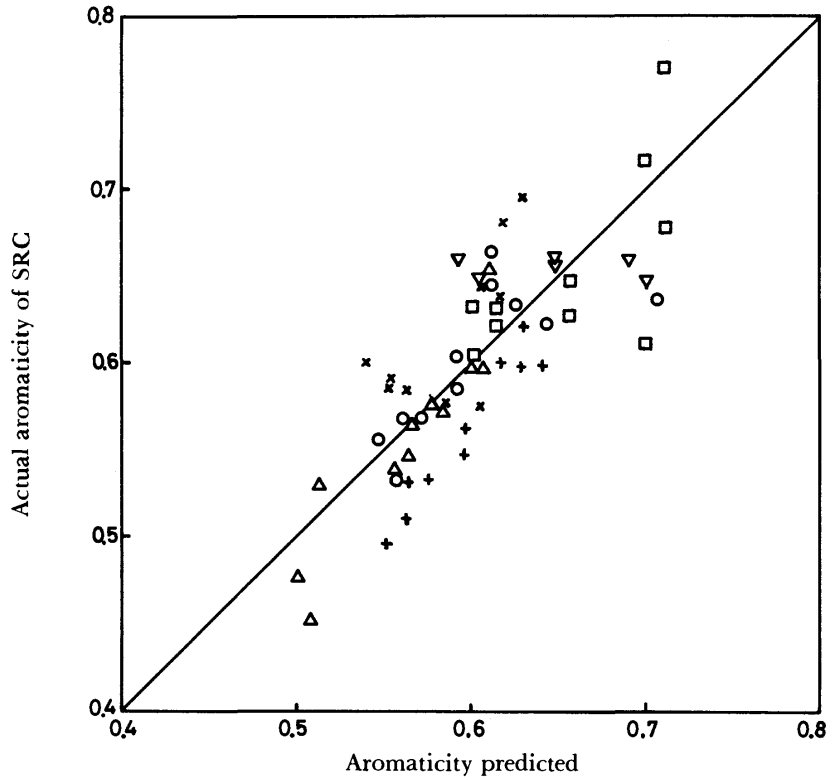

Fig. 4. Comparision of aromaticity of SRC predicted and actual aromaticity of SRC. The key is as in Fig. 1.

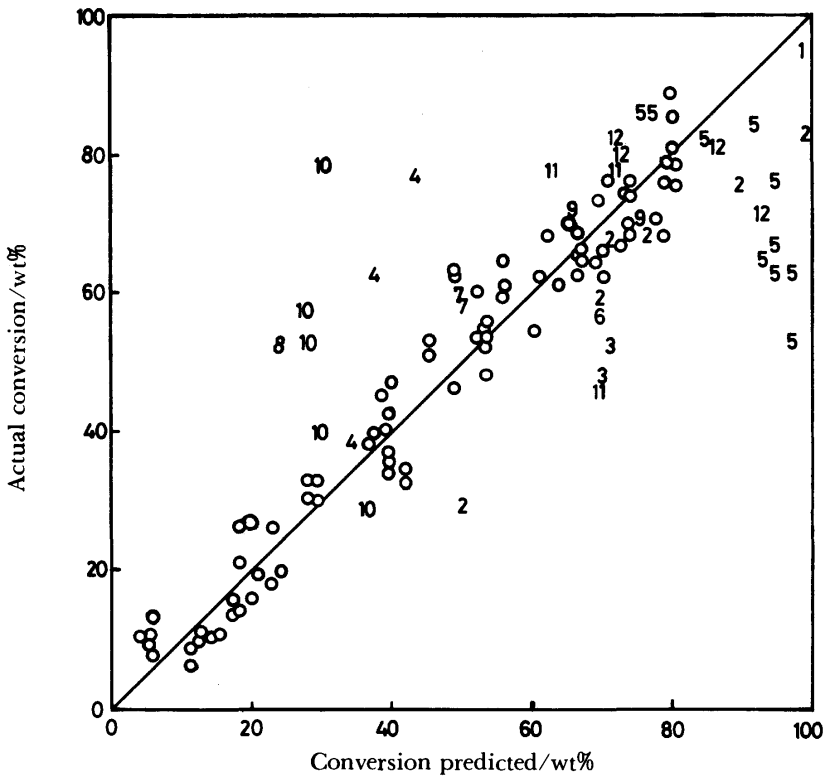

Fig. 5. Comparision of conversions predicted and actual conversions in this study (O) and conversions obtained by other investigators. The key is as in Table 4.

Table 4. Liquefaction Conditions Employed for the Present Study and Previous Investigations

Key	Investigator	Temperature °C	Reactor ml	Heating-up period/min
○	Present authors	350—460	100	60 to 400 °C
1	Angelovich et al.[5]	440	2000	≈140
2	Kamiya and Sato[6]	378—465	300	45 to 436 °C
3	Sato et al.[7]	436	300	45
4	Neavel[8]	400	8.1	0.5
5	Cudmore[9]	400	4000	120
6	Sato and Kamiya[10]	435	300	45
7	Awadalla and Smith[11]	400	50	90
8	Kawai et al.[12]	400	14.5	1.5
9	Moritomi et al.[13]	450	27	≈3
10	Kawai et al.[14]	400	14.5	1.5
11	Miyamoto et al.[15]	450	Micro-flow reactor	
12	Nakada et al.[16]	450	500	≈110

does not contribute to an increase in coal conversion. The influence of the heating-up period on brown coal carbonization was reported by Mochida et al.[30] They found that the occurrence of some fusion of the coal was evident at rapid heating rates (600 °C/3 min and 2 s) whereas that did not occur at low heating rates (600 °C/1 h). They also concluded that the rapid heating rates and high liquefaction temperatures might allow the rapid transfer of reactive, and relatively inert, hydrogen in the solvent to the thermal decomposition fragments of the coal to stabilize them. A detrimental effect, involving pretreatment at low temperatures, on the conversion was confirmed during the liquefaction of Miike coal-2. Conversion of pretreatment coal (pretreatment at 200 °C for 60 min in tetralin) at 400 °C for 60 min (35.9%) was almost similar to 35.4% of no pretreatment coal. However, the conversion of pretreatment coal at 250 °C for 60 min in tetralin was 29.0%, about 6% lower than that of no pretreatment coal. This is directly related to the bad influence of the long heating-up period on coal conversion. In the conversion prediction using Eq. 4, the influence of the heating-up period was not considered. Including the influence of the heating-up period into the prediction is difficult, however, qualitative discussion as long heating up period is detrimental is possible. It is clear that the Eq. 4 is a good indication of the conversion in solvent extract liquefaction.

Conclusion

Conversion, SRC yield and aromaticity of SRC of six kinds of coals (Yallourn, Taiheiyo, Horonai, Miike-1, Minamiohyubari and Miike-2) at 350—460 °C under hydrogen atmosphere were fairly predicted by 18 regression equations (coefficients of correlation were 0.747—0.996) using liquefaction conditions as explanation variables. Conversions under nitrogen atmosphere were also in good agreement with the predicted. Following equation was derived from coal conversions in 67 experiments using 2 coal properties (C% and Volatile matter) and 3 liquefaction conditions having a high coefficient of correlation (0.972):

$$\text{Conversion} = -208.01 + 0.188C\% - 1.08\ \text{Volatile matter} + 0.684\ \text{Temperature} + 0.210\ \text{Pressure} + 0.212\ \text{Time}$$

Coal conversions of previous investigators using small reactor as tubing bomb were underestimated by the above equation and those using large reactor were overestimated. It was suggested that a long heating up period was detrimental. Above equation is a good indication of the conversion in solvent extract liquefaction. Sufficient prediction of SRC yield and aromaticity of SRC were attained by regression equations using same 2 coal properties and 3 liquefaction conditions as explanation variables.

References

1) Y. T. Shah, "Reaction Engineering in Direct Coal Liquefaction," Addison-Wesley Publishing Company (1981).
2) G. P. Curran, R. T. Struck, and E. Gorin, *Ind. Eng. Chem. Process Des. Dev.*, **6**, 166 (1967).
3) a) B. C. Bockrath, E. Bittner, and J. McGrew, *J. Am. Chem. Soc.*, **106**, 135 (1981). b) B. C. Bockrath and R. P. Noceti, *Am. Chem. Soc. Div. Fuel Chem. Preprints*, **26**, 94 (1981). c) C. W. Curtis, J. A. Guin, M. A. Hale, and N. L. Smith, *Fuel*, **64**, 461 (1985). d) J. W. Clarke, T. D. Rantell, and C. E. Snape, *Fuel*, **61**, 707 (1982). e) D. C. Cronauer, D. M. Jewell, Y. T. Shah, and K. A. Keuser, *Ind. Eng. Chem. Fundam.*, **17**, 291 (1978). f) K. Chiba, H. Tagaya, T. Kobayashi, and Y. Shibuya, *Ind. Eng. Chem. Research*, **26**, 1329 (1987). g) K. Chiba, H. Tagaya, and N. Saito, *Energy & Fuels*, **1**, 338 (1987).
4) T. Obara, T. Yokono, and Y. Sanada, *Fuel*, **62**, 813 (1983).
5) J. M. Angelovich, G. R. Pastor, and H. F. Silver, *Ind. Eng. Chem. Process Des. Dev.*, **9**, 106 (1970).
6) Y. Kamiya and Y. Sato, *Sekitan Kagaku Kaigi*, **12**, 53 (1975).
7) Y. Sato, T. Yao, and Y. Kamiya, *Sekitan Kagaku Kaigi*, **13**, 25 (1976).
8) R. C. Neavel, *Fuel*, **55**, 237 (1976).
9) J. F. Cudmore, *Fuel Processing Technology*, **1**, 227 (1977).
10) Y. Sato and Y. Kamiya, *Nenryou Kyoukai Shi*, **57**, 21 (1978).
11) A. A. Awadalla and B. E. Smith, *Fuel*, **61**, 631 (1982).
12) T. Kawai, A. Yokouchi, K. Esumi, K. Meguro, H. Honda, and Y. Yamada, *Nenryou Kyoukai Shi*, **61**, 746 (1982).
13) H. Moritomi, H. Nagaishi, M. Naruse, Y. Sanada,

and T. Chiba, *Nenryou Kyoukai Shi*, **62**, 254 (1983).
14) a) T. Kawai, K. Esumi, K. Meguro, H. Honda, *Fuel*, **63**, 1615 (1984). b) T. Kawai, K. Esumi, K. Meguro, H. Honda, and Y. Yamada, *Nenryou Kyokai Shi*, **61**, 390 (1982).
15) Y. Miyamoto, J. Miyazaki, and Y. Ogo, *Sekitan Kagaku Kaigi*, **23**, 37 (1986).
16) Y. Nakada, S. Ueda, T. Yoshida, and Y. Maekawa, *Sekitan Kagaku Kaigi*, **18**, 163 (1981).
17) M. B. Abdel-Baset, R. F. Yarzab, and P. H. Given, *Fuel*, **57**, 89 (1978).
18) a) Y. Naruse, T. Miyakawa, and S. Ito, *Sekitan Kagaku Kaigi*, **19**, 213 (1982). b) idem, ibid, **20**, 112 (1983).
19) H. Tagaya, K. Chiba, S. Sato, K. Ito, and M. Sakurai, *Nippon Kagaku Kaishi*, **1983**, 1172.
20) H. Tagaya, K. Chiba, S. Sato, K. Miyashita, and M. Sagawa, *Nippon Kagaku Kaishi*, **1983**, 1181.
21) J. K. Brown and W. R. Ladner, *Fuel*, **39**, 87 (1960).
22) J. W. Larsen, T. L. Sams, and B. R. Rodgers, *Fuel*, **60**, 335 (1981).
23) N. R. Draper and H. Smith, "Applied Regression Analysis," John Wiley and Sons Inc., New York (1966).
24) a) Y. Maekawa, T. Ishii, and G. Takeya, *J. Chem. Eng. Japan*, **10**, 101 (1977). b) M. G. Pelipetz, J. R. Solmmon, J. Bayer, and E. L. Clark, *Ind. Eng. Chem.*, **45**, 806 (1953).
25) K. Chiba, H. Tagaya, S. Sato, and S. Ohgi, *Bull. Chem. Soc. Jpn.*, **60**, 653 (1987).
26) Y. Sato and Y. Kamiya, *Nenryou Kyoukai Shi*, **56**, 103 (1986).
27) K. Chiba, H. Tagaya, S. Sato, and S. Ohgi, *Yamagata Daigaku Kiyo*, **19**, 61 (1986).
28) H. Kimura and S. Fujii, "Sekitan Kagaku to Kogyo," Sankyo Shuppan, Tokyo (1977), p. 90.
29) a) Y. Kitaoka, M. Ueda, K. Murata, H. Ito, and K. Mikami, *Fuel*, **61**, 919 (1982). b) M. Morita, S. Sato, T. Hashimoto, and S. Hara, *Nenryou Kyoukai Shi*, **59**, 314 (1980).
30) I. Mochida, Y. Moriguchi, T. Shimohara, Y. Korai, H. Fujitsu, and K. Takeshita, *Fuel*, **61**, 1014 (1982).

 © 1987 The Chemical Society of Japan Bull. Chem. Soc. Jpn., 60, 3999—4003 (1987)

Optical Resolution of Alcohols as Carbamates by HPLC on Cellulose Tris(phenylcarbamate) Derivatives[1)]

Yoshio Okamoto,* Zun-Kui Cao,† Ryo Aburatani, and Koichi Hatada
Department of Chemistry, Faculty of Engineering Science, Osaka University, Toyonaka, Osaka 560
(Received April 17, 1987)

The optical resolutions of various alcohols as phenylcarbamates were examined by HPLC on chiral stationary phases derived from sixteen cellulose tris(phenylcarbamate) derivatives. The optical resolving power of chiral stationary phases was greatly influenced by substituents on the phenyl groups of the cellulose derivatives. Also, cellulose tris(3,5-dimethylphenylcarbamate) could very efficiently resolve many racemic phenylcarbamates, including the carbamates of 2-butanol, 3-buten-2-ol, and 1-phenylethanol. Racemic phenylcarbamates having electron-donating substituents on the phenyl group were better resolved than those having electron-withdrawing substituents. The benzoates of most alcohlos were not resolved as efficiently as the carbamates.

Optical resolution by chiral high-performance liquid chromatogaphy (HPLC) has been attracting much attention as a procedure for obtaining optical isomers and determining their purity; many chiral stationary phases (CSP) have been reported over the past several years.[2)] We recently reported that phenylcarbamate derivatives of polysaccharides,[3)] particularly cellulose,[4-10)] show characteristic optical resolving abilities to a variety of enantiomers. The optical resolving power of nineteen cellulose tris(phenylcarbamate) (CTPC) derivatives depended greatly on the inductive effect of substituents on the phenyl group and either 3,5-dimethyl or 3,5-dichloro derivatives (CTPC-3,5-Me_2 or -3,5-Cl_2) showed the best resolution to many of the racemic compounds examined.[4)] CTPC-3,5-Me_2, which has the most electron-donating substituent, seemed to effectively resolve polar compounds that could interact with the carbonyl group of the urethane bond of the carbamate. However, CTPC-3,5-Cl_2 seemed to possess a higher resolving power for compounds that can be adsorbed on the NH group of the urethane bond.

The optical resolution of alcohols is laborious and usually they are resolved as diastereomeric salts of acid phthalates. A direct resolution of alcohols by chiral HPLC has been attained only for several aromatic alcohols.[4,11,12)] However, many alcohols, including aliphatic alcohols, have been successfully resolved by chiral HPLC as proper derivatives, such as esters[12,13)] or urethanes.[14,15)] Racemic 3,5-dinitrophenylcarbamates of racemic alcohols have been utilized for effective chiral discrimination through a π–π interaction.[14,15)] In this work, in order to attain an efficient resolution of alcohols by HPLC, the urethanes of various racemic alcohols were prepared by reactions with twelve substituted phenyl isocyanates; they were subjected to optical resolution on 16 CTPC derivatives **1**—**16**.

† Present address: Department of Chemistry, Jilin University, Changchun, Jilin, People's Republic of China.

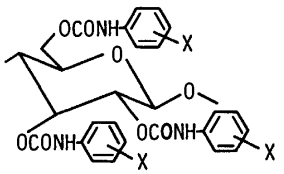

X=

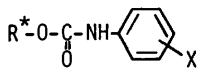

X=

1: 4-CH_3O	**9**: 4-NO_2	3,4-$(CH_3)_2$, 3,5-$(CH_3)_2$,
2: 4-C_2H_5	**10**: 3-CH_3	2,6-$(CH_3)_2$, 4-CH_3, 3-CH_3,
3: 4-CH_3	**11**: 3,5-$(CH_3)_2$	2-CH_3, H, 4-F, 4-Cl,
4: H	**12**: 3,4-$(CH_3)_2$	4-Br, 3,5-Cl_2, 4-NO_2
5: 4-F	**13**: 2,6-$(CH_3)_2$	
6: 4-Cl	**14**: 3-Cl	
7: 4-Br	**15**: 3,5-Cl_2	
8: 4-CF_3	**16**: 2,6-Cl_2	

Experimental

Materials. Details on the preparation of CSPs were described previously.[4)] CTPC derivatives (25wt% of silica gel) were adsorbed on macroporous silica gel (diameter 10 μm, pour size 400 nm), and used as CSPs. Racemic alcohols were allowed to react with substituted phenyl isocyanates in the presence of a small amount of pyridine to give racemic carbamates. The carbamates were purified by either distillation or recrystallization.

Chromatographic Analyses. CSPs were packed in a stainless-steel tube (25 cm×0.46(id) cm) by a slurry method. Chromatographic analyses were carried out on a JASCO TRIROTAR-II chromatograph equipped with UV (JASCO UVIDEC-100-III) and polarimetric (JASCO DIP-181C) detectors. The optical resolution was monitored in a flow cell (50 mm×2(id) mm) at full lamp (mercury) intensity without a filter. Optical resolution was performed with a hexane-2-propanol mixture at a flow rate of 0.5 or 1.0 ml min^{-1} at 25 °C. Dead time (t_0) of the chromatograph system was estimated with 1,3,5-tri-*t*-butylbenzene as a non-retained compounds.[16)]

Results and Discussion

2-Butanol was completely resolved into enantiomers as phenylcarbamate on cellulose tris(4-ethylphenylcarbamate) (**2**) as shown in Fig. 1. Capacity

factors (k_1' and k_2') for the first- and second-eluting isomers, which were estimated as $(t_1-t_0)/t_0$ and $(t_2-t_0)/t_0$, were obtained as 0.88 and 1.61, respectively, and separation factor ($\alpha=k_2'/k_1'$), which represents the chiral recognition ability of CSP, was determined to be 1.83. The resolution factor (R_s), which stands for the efficiency of a column, can be estimated by $2(t_2-t_1)/(W_1+W_2)$, where W_1 and W_2 are bandwidths of the peaks. Here, R_s was 3.84. Such an effective optical resolution of simple aliphatic alcohol derivatives by HPLC does not seem to have been reported before.[4,11-15]

Phenylcarbamates of 2-butanol and 1-phenylethanol were subjected to resolution on CTPC derivative columns (Table 1). Chiral recognition abilities of CSPs depended greatly on the substituents of CTPCs. Among nine para-substituted CTPCs **1**—**9**, methyl and ethyl derivatives exhibited better resolving powers for both racemic carbamates, suggesting that an electron-donating group would be preferable to an electron-withdrawing group. However, a more electron-donating substituent, methoxyl, was not better than alkyl. This may be attributed to the adsorption of the solute on the methoxyl group.[4] Since the methoxyl group is far from a chiral glucose

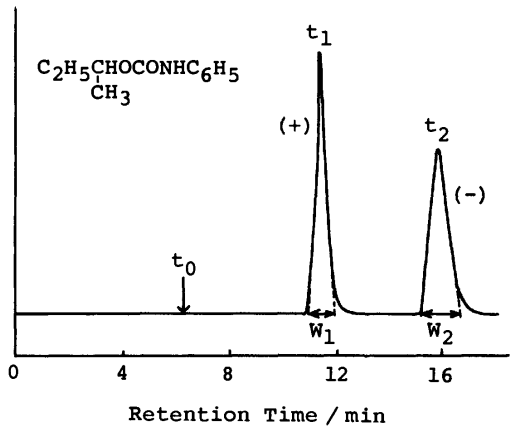

Fig. 1. Resolution of *s*-butyl phenylcarbamate on cellulose tris(4-ethylphenylcarbamate) (hexane–2-propanol(90:10), 0.5 ml min^{-1}, 25 °C).

Table 2. Resolution of *s*-Butyl Phenylcarbamate (*s*-$C_4H_9OCONHC_6H_4X$) on Cellulose Tris(phenylcarbamate) (**4**) and Tris(3,5-dimethylphenylcarbamate) (**11**)

X	**4**[a]			**11**[b]		
	k_1'	α	R_s	k_1'	α	R_s
3,4-$(CH_3)_2$	4.17	1.54	2.63	3.05	2.84	8.74
3,5-$(CH_3)_2$	2.71	1.45	2.35	2.14	2.50	7.53
2,6-$(CH_3)_2$	3.13	1.05		1.99	1.0	
4-CH_3	3.85	1.33	2.49	1.63	2.67	7.98
2-CH_3	3.39	1.43	2.96	2.15	3.01	9.24
3-CH_3	2.61	1.08	0.70	2.09[c]	1.32	2.60
H	3.72	1.34	1.81	1.85	2.78	8.57
4-F	3.01	1.11	1.17	0.67	1.42	2.10
4-Cl	2.81	1.10	0.86	0.63	1.22	1.11
4-Br	3.03	1.09	0.88	2.45[c]	1.19	1.49
3,5-Cl_2	1.65	1.11	0.78	0.54	1.19	0.88
4-NO_2	13.75	1.05		1.00	1.00	

a) Eluent: hexane–2-propanol (98:2), 0.5 ml min^{-1}, 25 °C. b) Eluent: hexane–2-propanol (90:10), 1.0 ml min^{-1}, 25 °C. c) Eluent: hexane–2-propanol (98:2), 1.0 ml min^{-1}, 25 °C.

Table 1. Resolution of *s*-Butyl and 1-Phenylethyl Phenylcarbamates on CTPC Derivative Columns[a]

No.	CTPC's substituent	Hammett σ value	$C_2H_5(CH_3)CHOCONHC_6H_5$[b]			$C_6H_5(CH_3)CHOCONHC_6H_5$[c]		
			k_1'	α	R_s	k_1'	α	R_s
1	4-CH_3O	−0.27	0.76	1.22	0.57	1.96	1.94	2.28
2	4-C_2H_5	−0.15	0.88	1.83	3.84	1.38	4.35	10.43
3	4-CH_3	−0.17	1.00	1.46	2.06	2.02	2.90	7.67
4	H	0	1.00	1.29	1.47	2.16	2.09	4.48
5	4-F	0.06	0.84	1.20	0.90	1.91	1.48	2.43
6	4-Cl	0.23	0.67	1.0		1.63	1.0	
7	4-Br	0.23	0.80	1.18	1.09	1.88	1.20	1.17
8	4-CF_3	0.54	1.00	1.0		1.56[d]	1.24	1.85
9	4-NO_2	0.78	0.88	1.0		2.35	1.0	
10	3-CH_3	−0.07	0.52	1.29	1.00	0.80	1.95	2.70
11	3,5-$(CH_3)_2$		1.83	2.79	10.02	2.34[e]	4.52	12.41
12	3,4-$(CH_3)_2$		0.91	1.92	3.36	1.58	3.18	7.65
13	2,6-$(CH_3)_2$		0.93	1.0		1.87	1.0	
14	3-Cl	0.37	0.73	1.15	0.67	1.59	1.27	1.79
15	3,5-Cl_2		0.88	1.16	0.77	1.28	1.73	3.80
16	2,6-Cl_2		0.97	1.0		2.52	1.0	

a) Eluent: hexane–2-propanol (90:10), 0.5 ml min^{-1}, 25 °C. b) (*S*)-(+)-Isomer eluted first. c) (*S*)-(−)-Isomer eluted first. d) (*R*)-(+)-Isomer eluted first. e) 1.0 ml min^{-1}.

unit, such an adsorption must lower the optical resolving power of CSP. To attain an effective chiral recognition, solutes must be adsorbed on the urethane bond of CSP.

Dimethyl-substituted derivatives **11** and **12**, particularly the former, possessed a better resolving power over monosubstituted derivatives. However, 2,6-dimethyl-substituted derivative **13** showed no chiral recognition, as observed in the previous work.[4] 2,6-Dichloro derivative **16** also exhibited no resolving power. In almost all cases, (±)-1-phenylethyl phenylcarbamate was better resolved than (±)-*s*-butyl phenylcarbamate and both (*S*) isomers were eluted first. Reversed elution order of enantiomers was observed only in the resolution of (±)-1-phenylethyl phenylcarbamate on **8**. The reason for this is not clear.

s-Butyl phenylcarbamates (*s*-$C_4H_9OCONHC_6H_4X$) having various substituents were resolved on **4** and **11** (Table 2). The latter column always showed better resolving power than the former, and good resolution was attained on racemic unsubstituted phenylcarbamate (X=H) and methyl-substituted phenylcarbamates except for 2,6-dimethyl and 3-methyl derivatives. In all runs, (+)-isomers were eluted first. These results suggest that simple unsubstituted phenylcabamates of racemic alcohols may be one of the most suitable carbamates for resolution. Electron-withdrawing substituents were not suitable.

The resolution of phenylcarbamates of various aliphatic alcohols, including an allyl alcohol, were examined on columns packed with **4** and **11** (Fig. 2 and Table 3). All alcohols having a hydroxy group on the asymmetric carbon were sufficiently resolved as carbamates particularly on **11**, probably eluting (*S*)-(+)-isomers first. However, the carbamates of alcohols carrying a methylene group between hydroxy group and asymmetric carbon were not resolved as efficiently as the above alcohols. It can be expected that chiral discrimination will become more difficult as the distance between the urethane group and asymmetric center of racemic carbamates increases, since the urethane group must be adsorbed on CTPCs.

Table 4 shows the comparison data of the resolution of phenylcarbamates and benzoates of racemic alcohols on an **11** column. Most alcohols were better

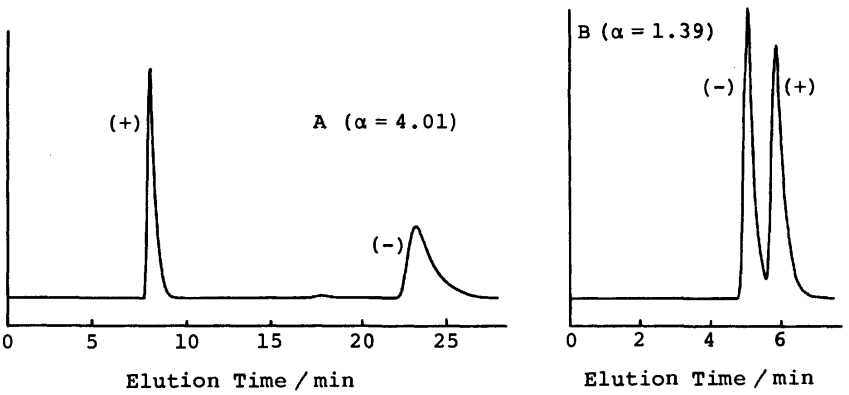

Fig. 2. Resolution of phenylcarbamates of 3-buten-2-ol (A) and 3-octanol (B) on cellulose tris(3,5-dimethylphenylcarbamate) (hexane–2-propanol(90:10), 1.0 ml min^{-1}, 25 °C).

Table 3. Resolution of Aliphatic Alcohols as Phenylcarbamate ($ROCONHC_6H_5$) on Cellulose Tris(phenylcarbamate) (**4**) and Tris(3,5-dimethylphenylcarbamate) (**11**)

R	**4**[a]			**11**[b]		
	k_1'	α	R_s	k_1'	α	R_s
$CH(CH_3)C_2H_5$	3.72(+)	1.34	1.81	1.85(+)	2.78	8.57
$CH(CH_3)C_3H_7$	2.93(+)	1.43	2.64	1.47(+)	3.26	7.80
$CH(CH_3)C_6H_{13}$	1.94(+)	1.47	2.81	1.19(+)	3.90	9.57
$CH(CH_3)CH{=}CH_2$	4.90(+)	1.59	3.32	1.68(+)	4.01	8.61
$CH(CH_3)CH(CH_3)_2$	2.52(+)	1.41	2.21	0.84(+)	3.16	5.85
$CH(C_2H_5)C_5H_{11}$	1.54(−)	1.08	0.30	0.67(−)	1.39	1.42
$CH_2CH(CH_3)C_2H_5$	5.33(+)	1.05		4.00[c]	1.00	
$CH_2CH(CH_3)C_3H_7$	5.27	1.00		6.42	1·00	
$CH_2CH(CH_3)C_6H_5$	3.13(−)[b]	1.11	0.39	9.42(+)	1.06	

a) Eluent: hexane-2-propanol (98:2), 0.5 ml min^{-1}, 25 °C. b) Eluent: hexane-2-propanol (90:10), 1.0 ml min^{-1}, 25 °C. c) Eluent: hexane-2-propanol (80:20), 1.0 ml min^{-1}, 25 °C.

Table 4. Resolution of Racemic Alcohols as Phenylcarbamates ($ROCONHC_6H_5$) and Benzoates ($ROCOC_6H_5$) on Cellulose Tris(3,5-dimethylphenylcarbamate)[a]

R	Phenylcarbamate				Benzoate			
	Eluent[b]	k_1'	α	R_s	Eluent[c]	k_1'	α	R_s
$CH(CH_3)C_2H_5$	B	1.85(+)	2.78	8.57	A	0.33	1.00	
$CH(CH_3)C_3H_7$	B	1.47(+)	3.26	7.80	A	0.31	1.00	
$CH(CH_3)C_6H_{13}$	B	1.19(+)	3.90	9.57	A	0.23	1.00	
$CH(CH_3)C_6H_5$	B	2.34(−)	4.52	12.41	A	0.74(−)	1.18	1.20
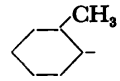	A	3.60(+)	1.82	5.87	A	0.33	1.00	
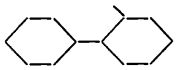	A	2.20(+)	2.06	5.95	A	0.24	1.00	
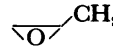	C	2.43(−)	1.17	0.89	A	3.86(+)	1.18	1.70
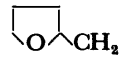	C	4.32(+)	1.76	4.08	A	2.14	1.00	
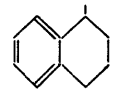	B	3.51(−)	1.05		A	0.74(+)	1.08	0.45
$CH(CH_3)C_2H_5$	B	0.54(+)[d]	1.19	0.88	A	0.17[e]	1.00	

a) Eluent: A, hexane–2-propanol(98:2) B: hexane–2-propanol (90:10) C: hexane–2-propanol(80:20). b) 1.0 ml min^{-1}. c) 0.5 ml min^{-1}. d) As 3,5-dichlorophenylcarbamate. e) As 3,5-dichlorobenzoate.

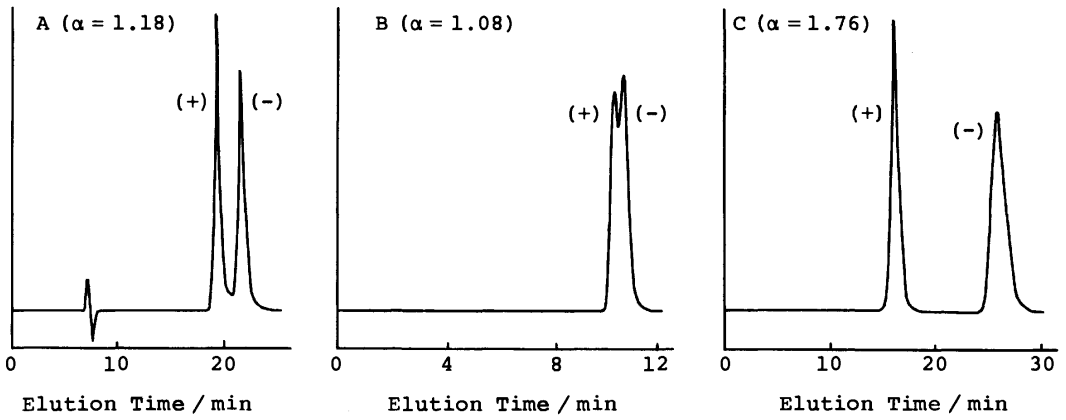

Fig. 3. Resolution of benzoates of glycidol (A) and 1,2,3,4-tetrahydro-1-naphthol (B), and carbamate of tetrahydrofurfuryl alcohol (C) on cellulose tris(3,5-dimethylphenylcarbamate) (A, B: hexane–2-propanol(98:2), 0.5 ml min^{-1}, 25 °C, C: hexane–2-propanol(80:20), 1.0 ml min^{-1}, 25 °C).

resolved as phenylcarbamates than benzoates. The benzoates of glycidol and 1,2,3,4-tetrahydro-1-naphthol were exceptionally better resolved than the carbamates (Fig. 3). The carbamate of tetrahydrofurfuryl alcohol was much better resolved than the benzoate (Fig. 3). Although glycidol and tetrahydrofurfuryl alcohol possess a methylene group between asymmetric center and hydroxyl group, these were resolved as phenylcarbamates. Adsorption on ether groups may contribute effective chiral discrimination.

Several 1,2- and 1,3-diols were also separated into enantiomers as phenylcarbamates (Table 5). The separation of diastereomers and the resolution of enantiomers were attained on 2,4-pentanediol.

One of possible space-filling structure (CPK) of CTPC is shown in Fig. 4. The carbamate and phenyl groups are aligned without any difficulty so that hydrogen bonds are formed between 2-3 carbamate groups and 2-6 carbamate groups.[17] These hydrogen bonds must contribute to the fixation of the adjacent glucose units which may lead to the formation of a liquid crystal phase.[18] The regularly arranged -NHCOO- groups of CTPC must be the most attractive adsorbing sites. Since the racemic esters were not well resolved, the hydrogen bonding and dipole interactions between the urethane bond of CTPC and the ester group of the solutes do not seem to strong enough to attain effective chiral discrimina-

Table 5. Resolution of Diols as Phenylcarbamates on Cellulose Tris(3,5-dimethylphenylcarbamate)[a]

Racemate	k_1'	α	R_s
$CH_3CHOCONHC_6H_5$ $CH_2OCONHC_6H_5$	4.24(−)	1.90	3.42
$CH_3CHOCONHC_6H_5$ CH_2 $CH_3CHOCONHC_6H_5$	0.52(+)[b]	8.76	2.94
$CH_3CH_2CH_2CHOCONHC_6H_5$ $CH_3CH_2CHOCONHC_6H_5$	2.01(+)[c]	1.25	0.89
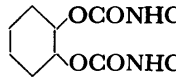	0.71(−)	1.31	0.97

a) Eluent: hexane–2-propanol (80:20), 0.5 ml min^{-1}, 25 °C. b) Capacity factor of meso-isomer was 1.92. c) Only one enantiomeric pair was found.

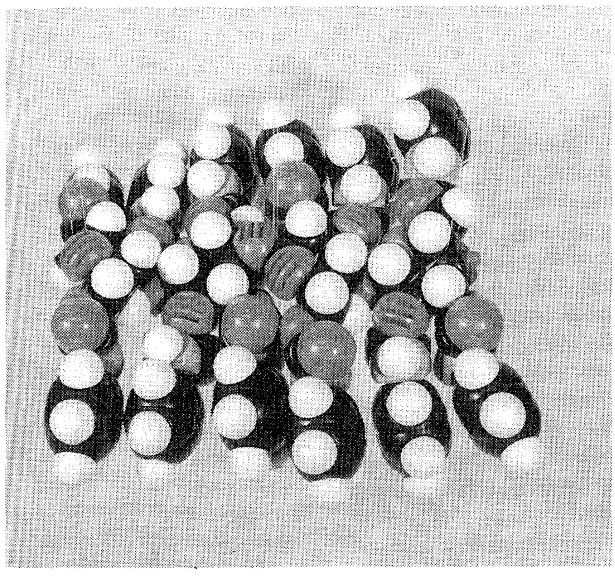

Fig. 4. CPK model of cellulose tris(phenylcarbamate).

tion. A stronger interaction between the two urethane groups of CTPC and solutes may be responsible for the effective chiral discrimination of the racemic carbamates.

The authors wish to thank Mr. Mitsunobu Kawashima for his support in the experiment. This work was partially supported by a Grant-in-Aid for Scientific Research No. 61470108 from the Ministry of Education, Science and Culture and the Mitsubishi Foundation.

References

1) Chromatographic Resolution XVI. XV: Y. Okamoto, R. Aburatani, S. Miura, and K. Hatada, *J. Liq. Chromatogr.*, **10**, 1613 (1987).

2) "Special Issue on Optical Resolution by Liquid Chromatography," ed by S. Hara and J. Cazes, *J. Liq. Chromatogr.*, **9**, 283 (1986).

3) Y. Okamoto, M. Kawashima, and K. Hatada, *J. Am. Chem. Soc.*, **106**, 5357 (1984).

4) Y. Okamoto, M. Kawashima, and K. Hatada, *J. Chromatogr.*, **363**, 173 (1986).

5) J. Daub, L. Jacob, J. Salback, and Y. Okamoto, *Chimia*, **39**, 393 (1985).

6) Y. Okamoto, H. Sakamoto, K. Hatada, and M. Irie, *Chem. Lett.*, **1986**, 983.

7) Y. Okamoto, M. Kawashima, R. Aburatani, K. Hatada, T. Nishiyama, and M. Masuda, *Chem. Lett.*, **1986**, 1237.

8) Y. Okamoto, R. Aburatani, M. Kawashima, K. Hatada, and N. Okamura, *Chem. Lett.*, **1986**, 1767.

9) Y. Okamoto, D. Dirnberger, T. Burgemester, G. Dannhardt, and W. Wiegrebe, *Arch. Pharm. (Weiheim)*, **319**, 1122 (1986).

10) H. Ogoshi, K. Saito, K. Sakurai, T. Watanabe, H. Toi, Y. Aoyama, and Y. Okamoto, *Tetrahedron Lett.*, **27**, 6365 (1986).

11) W. H. Pirkle and J. M. Finn, *J. Org. Chem.*, **46**, 2935 (1981).

12) T. Shibata, I. Okamoto, and K. Ishii, *J. Liq. Chromatogr.*, **9**, 313 (1986).

13) Y. Okamoto, S. Honda, K. Hatada, and H. Yuki, *Bull. Chem. Soc. Jpn.*, **58**, 3053 (1985).

14) N. Oi and H. Kitahara, *J. Chromatogr.*, **265**, 117 (1983).

15) W. H. Pirkle and T. C. Pochapsky, *J. Am. Chem. Soc.*, **108**, 352 (1986).

16) H. Koller, K.-H. Rimböck, and A. Mannschreck, *J. Chromatogr.*, **282**, 89 (1983).

17) H. Bittiger and G. Keilich, *Biopolymer*, **7**, 539 (1959).

18) A. K. Gupta, E. Marchal, and W. Burchard, *Macromolecules*, **8**, 843 (1975).

 © 1987 The Chemical Society of Japan Bull. Chem. Soc. Jpn., 60, 4005—4014 (1987)

Synthetic Studies of Amphotericin B. II.[1] A Facile Synthesis of the C-1—C-12 Segments of the Amphotericin B Aglycon†

Mitsuhiro KINOSHITA,* Masahiko MORIOKA, Masato TANIGUCHI, and Jun SHIMIZU
Department of Applied Chemistry, Faculty of Science and Technology, Keio University, Hiyoshi, Kohoku-ku, Yokohama 223
(Received April 23, 1987)

3-Deoxy-1,2-*O*-isopropylidene-α-D-*glycero*-D-*erythro*-pentofuranose (**11**) was stereoselectively converted into the Witting salt **8** corresponding to the C-1—C-6 portion of amphotericin B aglycon (**1**) in 57% overall yield in 8 steps. The aldehydic segment **9** or **10** corresponding to the C-7—C-12 portion of **1** was also derived in 6 steps from **11** in 53 or 38% overall yield, respectively. Wittig condensation of **8** with **9** or **10** followed by four-step conversion afforded the C-1—C-12 segment, (3*S*,5*R*,8*R*,9*R*,11*S*)-1-*O*-*t*-butyldimethylsilyl-12-iodo-3,5:8,9-di-*O*-isopropylidene-11-*O*-[(2-methoxyethoxy)methyl]-1,3,5,8,9,11-dodecanehexol (**4**) or (2*S*,4*R*,5*R*,8*R*,10*S*)-1,2-anhydro-12-*O*-*t*-butyldimethylsilyl-4,5:8,10-di-*O*-isopropylidene-1,2,4,5,8,10,12-dodecaneheptol (**5**) in 26 or 15% overall yield from **11**, respectively.

In our studies directed toward the total synthesis of amphotericin B,[2] a clinically valuable important member of the polyene macrolide antibiotics, our general synthetic plan[1] of its free aglycon **1** required two major segments, **2** and **3** corresponding to the C-1—C-19 and C-21—C-37 portions of **1**, respectively. The enantiospecific synthesis of the latter **3** from carbohydrate has already been accomplished in our laboratories.[1] The retrosynthetic examination of **2** revealed that a disconnection of the C-12—C-13 bond devided **2** into the C-1—C-12 segment **4** or **5** and the C-13—C-19 segment **6** (Scheme 1). The asymmetric synthesis of other kinds of C-1—C-12 segments, **7a**[3] and **7b**[4] have been reported. Recent synthetic efforts

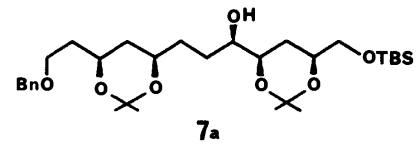

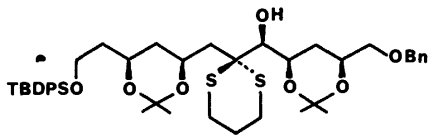

of **1** and its chiral building blocks have been announced.[5] In this paper, we wish to describe a facile syntheses of **4** and **5** from D-glucose. As shown in the synthetic plan of **4** and **5** (Scheme 2), both the C-1—C-6 segment **8** and the C-7—C-12 segment **9** or

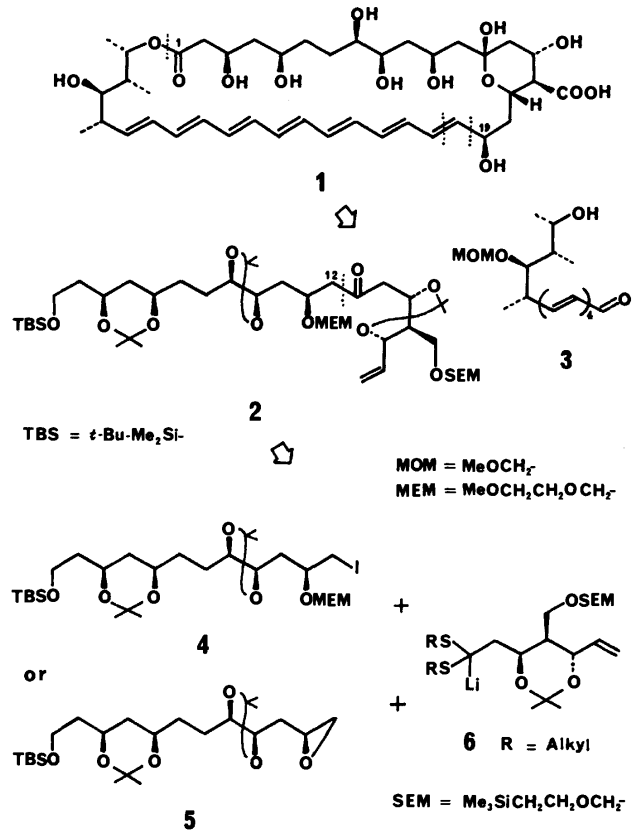

Scheme 1.

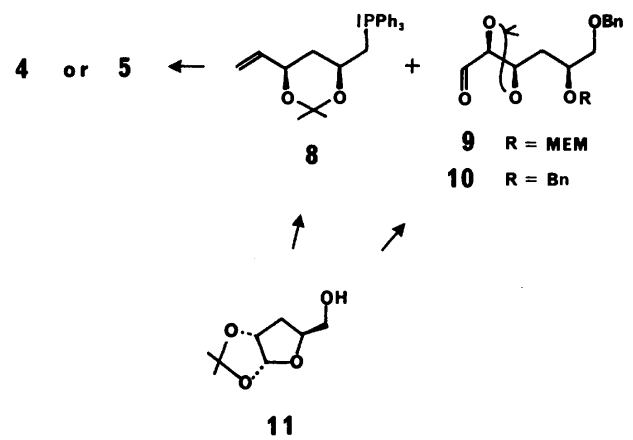

Scheme 2.

† A part of this paper was read at the 52nd National Meeting of the Chemical Society of Japan, Kyoto, April 1986, Abstr., No. 4N05.

10 would be derived from the common 3-deoxy-1,2-*O*-isopropylidene-α-D-*glycero*-D-*erythro*-pentofuranose (**11**)[6] which is obtainable from D-glucose. Wittig coupling of **8** with **9** or **10** followed by a sequence of reactions involving hydroboration and catalytic hydrogenation would give **4** or **5**.

Preparation of 8. Dithioacetalization of **11** with ethanthiol and boron trifluoride etherate afforded **12** which was regioselectively *t*-butyldiphenylsilylated[7] to give **13** in 92% overall yield from **11**. 2,4-*O*-Isopropylidenation of **13** with 2,2-dimethoxypropane (DMP) and a catalytic amount of H_2SO_4 in acetone afforded **14**, which was treated with 1:1 $HgCl_2$–HgO (red) in 80% aqueous acetone to give the aldehyde **15** in 94% overall yield from **13**. Wittig methylenation[8] of **15** with methylenetriphenylphosphorane in ether afforded **16** in 90% yield. Desilylation of **16** with tetrabutylammonium fluoride (TBAF) in THF gave **17** in 99% yield. Treatment[9] of **17** with triphenyl-

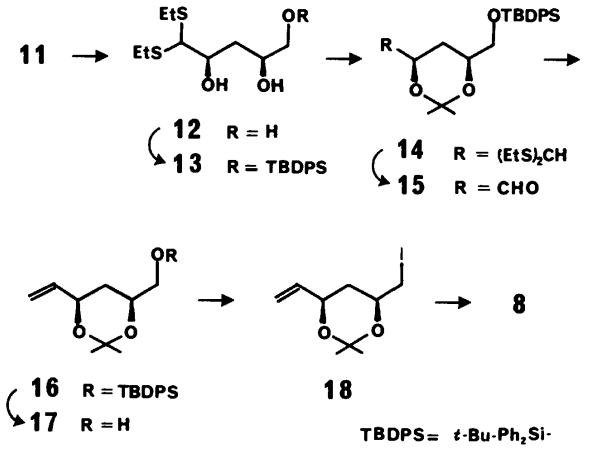

Scheme 3.

phosphine, imidazole, and iodine in benzene afforded the iodide **18** in 88% yield, which was allowed to react with triphenylphosphine in refluxed benzene to provide **8** in 88% yield. The overall yield of **8** from **11** was 57% in 8 steps.

Preparation of 9 and 10. 5-*O*-Benzylation of **11** with sodium hydride and benzyl bromide in DMF afforded **19** in 97% yield. Hydrolysis of **19** with a 1:1 mixture of 3.2 M†† hydrochloric acid and dioxane gave **20** in 92% yield. Grignard reaction of **20** with large excess of vinylmagnesium bromide in THF afforded a ca. 3.5:1[10] syn/anti diastereomeric mixture **21** in 95% yield. Regioselective 4,5-*O*-isopropylidenation[11] of **21** with a catalytic amount of iodine in acetone gave a 54% yield of the major product **22** and a 24% yield of a mixture of **22** and its 3-epimer **22′** after chromatography. The chromatography also afforded a third fraction which consisted of **22**, **22′**, and a small amount of inseparable mixture of two epimeric 2,4-*O*-isopropylidene derivatives of **21**. Methoxyethoxy-

†† 1 M=1 mol dm^{-3}.

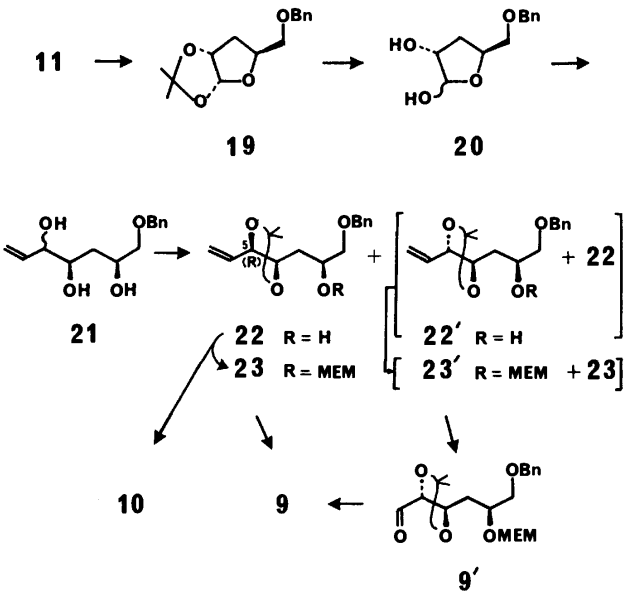

Scheme 4.

methylation of **22** with (2-methoxyethoxy)methyl chloride (MEM-Cl) and *N*,*N*-diisopropylethylamine gave **23** in 98% yield, which was oxidized with OsO_4–$NaIO_4$[12] to afford **9** in 92% yield. The mixture of **22** and **22′** was methoxyethoxymethylated to give in 94% yield a mixture of **23** and **23′**, which was oxidized with OsO_4–$NaIO_4$ to afford **9** and its epimer **9′** in 38 and 26% yields, respectively after chromatography. An isomerically pure sample of **22′** obtained by chromatographic separation of the aforesaid epimeric mixture was methoxyethoxymethylated and then oxidized to yield a mixture of **9** (20%) and **9′** (50%). Exposure of **9′** to methanolic K_2CO_3 at 23 °C for 4.5 h gave **9** in 68% yield. No starting **9′** was detected by ^{13}C NMR of the unpurified product. The total yield of the major product **9** from **11** amounted to 53%. The complete epimerization of **9** to **9′** indicated that the aldehyde **9** had presumably the desired 2,3-syn structure which would be thermodynamically more stable than the anti structure (in the basic conditions of epimerization). The structures of **22** and **22′** were thus presumed as depicted in Scheme 4. The (5R)-configuration of **22** was confirmed by the transformation of **22** into the (2*S*)-2-hydroxy ester **30** as shown in Scheme 5. Oxidation of **22** with OsO_4–$NaIO_4$ afforded the free aldehyde **24**. No hemiacetal structure was detected by ^1H NMR of the reaction product. This observation also supported the 2,3-syn structure of **24**. Oxidation of **24** with the periodite reagent (K_2CO_3, I_2, KI)[13] followed by treatment of the resulting carboxylic acid **25** with diazomethane gave **26** which was hydrogenolyzed over Pd-black to yield **27**. Periodate-oxidation of **27** followed by $NaBH_4$(0.5 molar) reduction of the resulting **28** afforded **29**. Finally, **29** was de-*O*-isopropylidenated to give **30**. Since the CD spectrum of **30** showed the (+)-CD Cotton effect which reflected

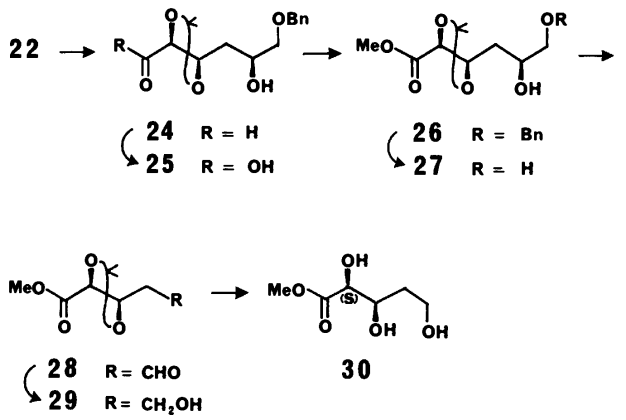

Scheme 5.

the (S)-configuration at the C-2 carbon atom,[14] the (5R)-configuration of **22** as depicted was confirmed. On the other hand, benzylation of **22** followed by OsO_4–$NaIO_4$ oxidation provided another C-7—C-12 segment **10** in 82% yield.

Preparation of 4 and 5. Wittig coupling between **8** and **9** or **10** was best achieved under the modified Secruist and Wu's conditions.[15] Treatment of 1 equivalent of **8** with 1 equivalent of butyllithium in 2:1 THF–HMPA at −70 °C under argon generated an orange-colored ylide which condensed with 0.9 equivalents of **9** or **10** at −50 °C to afford a single product **31** or **32** in 70 or 52% yield, respectively. The ^1H NMR examination showed both **31** and **32** to be the

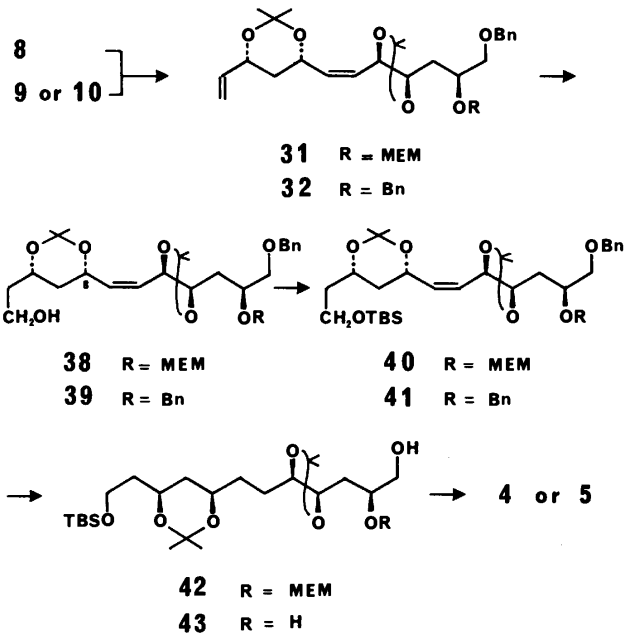

Scheme 6.

isomerically pure (6Z)-olefines. The configurational integrity[15] of left half of the condensation product **31** or **32** was confirmed by the following experimental results (Scheme 7). The aforesaid aldehyde **15** was converted in 3 steps into its homologous aldehyde dimethyl acetal **33** according to the procedure developed in our laboratories.[16] The acetal **33** was transformed via the intermediate **34** into the Wittig salt **35**. Wittig reaction of **35** with heptanal was carried out by the same procedure as described for the reaction of **8** with **9** to afford only the condensation product **36** of (Z)-configuration. OsO_4–$NaIO_4$ oxidation of **36** followed by $NaBH_4$ reduction of the product **37** gave **34** which proved to be identical in all respects with a sample of the intermediate **34** derived from **15**, cleanly indicating that the (2S)-configuration of **35** was retained during the Wittig reaction.

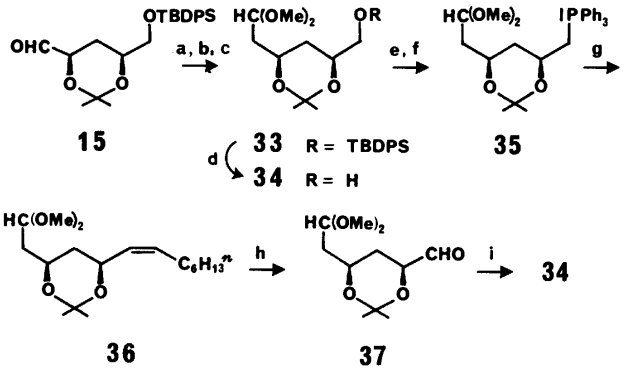

(a) $MeOCH_2PPh_3Cl$, $NaCH_2SOMe$, ether; (b) NBS, MeOH; (c) *n*-Bu_3SnH, AIBN, PhMe; (d) TBAF, THF; (e) Ph_3P, DEAD, MeI; (f) Ph_3P, PhH, 84 °C, 4 d; (g) *n*-BuLi, 2:1 THF–HMPA; *n*-$C_6H_{13}CHO$; (h) OsO_4, $NaIO_4$, 3:1 dioxane–H_2O; (i) $NaBH_4$, MeOH.

Scheme 7.

The regioselective hydroboration of **31** or **32** with 1.8 equivalents of dicyclohexylborane in THF at 25 °C followed by treatment with alkaline hydrogen peroxide at 50 °C afforded **38** or **39** in 90 or 85% yield, respectively. The *t*-butyldimethylsilylation (TBS-Cl, Py, 23 °C) of **38** or **39** gave the silyl ether **40** or **41** in 95 or 90% yield, respectively. Simultaneous catalytic reduction of the double bond and benzyloxy group in **40** proceeded effectively with Raney Ni W-4 in ethanol to give **42** in 84% yield. Whereas the reduction of **40** with Pd-black in *t*-butyl alcohol provided a complex mixture involving the partially desilylated and de-*O*-isopropylidenated products. On the contrary, the catalytic reduction of **41** with Pd-black in *t*-butyl alcohol proceeded cleanly to afford the diol **43** in 98% yield. Iodination[17] of **42** with triphenylphosphine, diethyl azodicarboxylate (DEAD), and methyl iodide in benzene provided the segment **4** in 92% yield. One stage epoxidation[18] of **43** with triphenylphosphine, DEAD, and 3A molecular sieves in benzene afforded another segment **5** in 70% yield.

Experimental

Melting points were determined on a micro hot stage Yanaco MP-S3 and were uncorrected. Optical rotations

were measured on a Carl Zeiss photoelectric polarimeter and a JASCO DIP-360 photoerectric polarimeter in chloroform, and ^{1}H NMR spectra in $CDCl_3$ using TMS on either a Varian EM-390 or a Bruker WM 250 spectrometer. ^{13}C NMR spectra were measured on a JEOL FX 90A in $CDCl_3$, and IR spectra on a Hitachi Perkin-Elmer spectropotometer. High-performance liquid chromatography (HPLC) was carried out on a Waters 208 Compact Liquid Chromatograph, and TLC on Merck TLC plates (60F-254, 0.25 mm) and on Merck HPTLC plates (60F-254) for "HPTLC." Column chromatography was performed on silica gel, Wakogel C-200 and Merck Kieselgel 60 (230—400 mesh) for "Flash Chromatography." In general, organic solvents were purified and dried by the appropriate procedure, and evaporation and concentration were carried out under reduced pressure below 30 °C, unless otherwise noted.

(2*S*,4*R*)-5,5-Bis(ethylthio)-1,2,4-pentanetriol (12). To an ice-cooled solution of **11**[6] (8.05 g, 46.2 mmol) in ethanethiol (240 ml) was added boron trifluoride etherate (2.40 ml) and the mixture was stirred at room temperature for 2 h. The reaction mixture was neutralized (pH=7) with triethylamine and evaporated. The residue was chromatographed on silica gel (220 g) with 10:1 chloroform–methanol to afford **12** (10.5 g, 95%): colorless syrup, R_f=0.41 (10:1 chloroform–methanol); $[\alpha]_D^{35}$ +61.5° (*c* 1.05); IR ($CHCl_3$) 3440 cm^{-1}; ^{1}H NMR (90 MHz) δ=1.27 (6H, t, 2×MeCH$_2$S, *J*=7.0 Hz), 1.50—2.10 (2H, m, 2×H-3), 2.70 (4H, q, 2×MeCH$_2$S), and 3.40—4.10 (8H, m, 3×OH, 2×H-1, H-2, H-4, H-5).

Found: C, 45.04; H, 8.14%. Calcd for $C_9H_{20}O_3S_2$: C, 44.97; H, 8.39%.

(2*S*,4*R*)-1-*O*-(*t*-Butyldiphenylsilyl-5,5-bis(ethylthio)-1,2,4-pentanetriol (13). To an ice-cooled solution of **12** (2.02 g, 8.4 mmol) in DMF (20.2 ml) was added dropwise imidazole (744 mg, 10.9 mmol) and *t*-butyldiphenylsilyl chloride (2.62 ml, 10.8 mmol), and the mixture was stirred at 25 °C for 0.5 h. The reaction mixture was then poured into cold water (40 ml) and extracted with chloroform (3×40 ml). The extracts were washed with saturated aqueous NaCl, dried, and evaporated to a syrup which was chromatographed on silica gel (200 g) with 7:1 benzene–ethyl acetate to give a pure sample of **13** (3.69 g, 92%): coloreless syrup; R_f=0.60 (3:1 toluene–ethyl acetate); $[\alpha]_D^{25}$ +14.6° (*c* 1.64); IR($CHCl_3$) 3480, 1110 cm^{-1}; ^{1}H NMR (90 MHz) δ=1.13 (9H, s, *t*-Bu), 1.27 (6H, t, 2×MeCH$_2$S, *J*=7.0 Hz), 1.41—2.00 (2H, m, 2×H-3), 2.70 (4H, dd, 2×MeCH$_2$S), 2.85—3.20 (2H, brs, 2×OH), 3.63 (2H, d, 2×H-1, *J*=6.6 Hz), 3.76—4.13 (3H, m, H-2, H-4, H-5), and 7.20—7.81 (10H, m, 2×Ph).

Found: C, 62.80; H, 7.89%. Calcd for $C_{25}H_{38}O_3S_2Si$: C, 62.72; H, 8.00%.

(2*S*,4*R*)-1-*O*-(*t*-Butyldiphenylsilyl)-5,5-bis(ethylthio)-2,4-*O*-isopropylidene-1,2,4-pentanetriol (14). To an ice-cooled solution of **13** (11.9 g, 37.4 mmol) and 2,2-dimethoxypropane (9.2 ml, 74.8 mmol) in dry acetone (360 ml) was added 1.0% H_2SO_4 in acetone (1.8 ml). After being stirred at room temperature for 20 min, the mixture was neutralized with $NaHCO_3$ (pH=7) under ice cooling, and evaporated. The residue was partitioned between ethyl acetate and water. The organic layer was separated, and washed with water and saturated aqueous NaCl, dried, and evaporated to afford an essentially pure sample of **14** (19.4 g, 100%) as a pale yellow syrup. An analytical sample was obtained after silica gel column chromatography with 10:1 hexane–ethyl acetate: R_f=0.80 (3:1 hexane–ethyl acetate); $[\alpha]_D^{32}$ −14.2° (*c* 1.00); IR ($CHCl_3$) 1110 cm^{-1}; ^{1}H NMR (90 MHz) δ=1.08 (9H, s, *t*-Bu), 1.28 (6H, t, 2×MeCH$_2$S, *J*=7.5 Hz), 1.40 (6H, s, CMe$_2$), 1.58—1.88 (2H, m, 2×H-3), 2.73 (4H, q, 2×SCH$_2$), 3.42—4.25 (5H, m, 2×H-1, H-2, H-4, H-5), and 7.21—7.90 (10H, m, 2×Ph).

(2*R*,4*S*)-6-*O*-(*t*-Butyldiphenylsilyl)-2,4-*O*-isopropylidene-2,4,5-trihydroxypentanal (15). A mixture of the aforesaid sample of **14** (19.1 g, ca. 36.8 mmol), aqueous 80% acetone, $HgCl_2$ (43.0 g, 162 mmol), and HgO(red)(35.1 g, 162 mmol) was stirred vigorously at room temperature for 20 min. The resulting mixture was filtered through a Celite and the filter cake was washed with acetone. The combined filtrate and washings were concentrated to remove acetone. The aqueous residue was extracted with chloroform (3×40 ml) and extracts were washed with aqueous 10% KI (2×30 ml) and saturated aqueous NaCl, dried, and evaporated. The residue was chromatographed on silica gel (760 g) with 3:1 hexane–ethyl acetate to afford **15** (14.3 g, 94% from **13**): colorless syrup, R_f=0.34 (3:1 hexane–ethyl acetate); $[\alpha]_D^{26}$ +16.6° (*c* 1.06); IR($CHCl_3$) 1735, 1110 cm^{-1}; ^{1}H NMR (90 MHz) δ=1.10 (9H, s, *t*-Bu), 1.45 (6H, s, CMe$_2$), 1.66—2.00 (2H, m, 2×H-3), 3.43—4.57 (4H, m, H-2, H-4, 2×H-5), 7.10—7.91 (10H, m, 2×Ph), and 9.63 (1H, d-like, CHO).

(2*S*,4*R*)-1-*O*-(*t*-Butyldiphenylsilyl)-2,4-*O*-isopropylidene-5-hexene-1,2,4-triol (16). A 4 M solution of methylsulfinylmethanide anion in DMSO (5.0 ml, 20 mmol) prepared from sodium hydride and DMSO was added dropwise to a stirred suspension of methyltriphenylphosphonium bromide (7.1 g, 19.9 mmol) in dry ether (82 ml) under argon at 25 °C. The mixture was stirred at 25 °C for 25 min, and to the resulting yellow suspension of ylide, a solution of **15** (2.05 g, 4.97 mmol) in dry ether (41 ml) was added dropwise over a 5-min period. After being stirred at 25 °C for 20 min, the reaction mixture was poured into an ice–water (100 ml) and the mixture was extracted with ether(3×50 ml). The extracts were washed with saturated aqueous NaCl, dried, and evaporated. The residue was chromatographed on silica gel (100 g) with 15:1 hexane–ethyl acetate to afford **16** (1.84 g, 90%): colorless syrup, R_f=0.79 (4:1 hexane–ethyl acetate); IR($CHCl_3$) 1105 cm^{-1}; $[\alpha]_D^{25}$ +2.0°, $[\alpha]_{365}^{25}$ +10.0° (*c* 1.00); ^{1}H NMR (90 MHz) δ=1.04 (9H, s, *t*-Bu), 1.38 (6H, s, CMe$_2$), 1.50—1.90 (2H, m, H-3), 3.33—3.65 (2H, m, 2×H-1), 3.80—4.15 (1H, m, H-2), 4.20—4.50 (1H, m, H-4), 5.07 (1H, ddd, H-6*Z*, J_{gem}=$J_{6Z,4}$=ca. 1.2, $J_{6Z,5}$=9.3 Hz), 5.21 (1H, ddd, H-6*E*, $J_{6E,4}$=ca. 1.2, $J_{6E,5}$=15.9 Hz), 5.82 (1H, ddd, H-5, $J_{5,4}$=5.7 Hz), and 7.0—7.9 (10H, m, 2×Ph).

Found: C, 73.16; H, 8.25%. Calcd for $C_{25}H_{34}O_3Si$; C, 73.13; H, 8.35%.

(2*S*,4*R*)-1-Iodo-2,4-*O*-isopropylidene-5-hexene-2,4-diol (18). To a solution of **16** (10.9 g, 26.5 mmol) in THF (100 ml) was added dropwise a 1M solution of TBAF in THF (53 ml). After being stirred at 24 °C for 15 min, the mixture was poured into cold water (150 ml) and extracted with ethyl acetate (3×150 ml). The combined extracts were washed with saturated aqueous NaCl, dried, and evaporated to afford a syrup which was chromatographed on silica gel (230 g) with 1:1 hexane–ethyl acetate to give **17** (4.54 g, 99%) as a colorless syrup. A mixture of the alcohol **17** (4.33 g, 25.1 mmol), triphenylphosphine (13.2 g, 50.3 mmol), imidazole (3.46 g, 50.3 mmol), iodine (9.6 g, 37.7 mmol), and benzene (65 ml) was stirred at 60 °C for 45 min. The resulting mixture was then cooled to 0 °C and aqueous $Na_2S_2O_3$ and $NaHCO_3$ were added in sequence. After

vigorous stirring at 0 °C for 10 min, the reaction mixture was extracted with ethyl acetate (3×50 ml) and the extracts were washed with saturated aqueous NaCl, dried, and evaporated. The residue was chromatographed on silica gel (350 g) with 12:1 hexane–ether to give **18** (5.93 g, 84%) and a mixture of **18** and triphenylphosphine (2.3 g) which was separated by chromatography to afford an additional sample of **18** (0.28 g, 4%). The total yield of **18** was 6.21 g (88%): colorless syrup, R_f=0.84 (3:1 hexane–ethyl acetate); $[\alpha]_D^{33}$ +19.4° (*c* 1.04); ^{1}H NMR (90 MHz) δ=1.25 (1H, ddd, H-3, $J_{3,2}=J_{3,4}$=10.5, J_{gem}=12.0 Hz), 1.47 (6H, s, CMe_2), 1.90 (1H, ddd, H-3, $J_{3,2}=J_{3,4}$=3.3 Hz), 3.07—3.30 (2H, m, 2×H-1), 3.83—4.13 (1H, m, H-2), 4.27—4.57 (1H, m, H-4), 5.07 (1H, ddd, H-6Z, $J_{gem}=J_{6Z,4}$=ca. 1.5, $J_{6Z,5}$=9.3 Hz), 5.20 (1H, ddd, H-6E, $J_{6E,4}$=ca. 1.5, $J_{6E,5}$=15.9 Hz), and 5.86 (1H, ddd, H-5, $J_{5,4}$=5.7 Hz)

Found: C, 38.32; H, 5.24%. Calcd for $C_9H_{15}O_2I$: C, 38.32; H, 5.36%.

[[(4*S*,6*R*)-2,2-Dimethyl-6-vinyl-1,3-dioxan-4-yl]methyl]triphenylphosphonium Iodide (8). A mixture of **18** (5.57 g, 19.7 mmol), triphenylphosphine (13.0 g, 49.3 mmol), and benzene (30 ml) was stirred at 80 °C for 5 d. The resulting insoluble matter was collected by filtration and washed with hexane (100 ml) and benzene (200 ml), then dried over NaOH pellets under reduced pressure for 10 h to afford **8** (9.5 g, 88%) as a white powder. An analytical sample was obtained by column chromatography with 10:1 chloroform–methanol: mp 194—196 °C; R_f=0.52 (10:1 chloroform–methanol); $[\alpha]_D^{33}$ +32.0° (*c* 1.02); IR (KBr) 1435, 1108 cm^{-1}; ^{1}H NMR (90 MHz) δ=0.83, 1.13 (each 3H, each s, CMe_2), 1.21—2.10 (4H, m, 2×H-5, CH_2P), 3.50—4.00 (1H, m, H-4), 4.07—4.53 (1H, m, H-6), 5.08 (1H, ddd, CH=C$\underline{H}_2$ (*Z*), $J_{gem}=J_{Z,6}$=ca. 1.2, J_Z=10.2 Hz), 5.24 (1H, ddd, CH=C$\underline{H}_2$ (*E*), $J_{E,6}$=ca. 1.2, J_E=15.6 Hz), 5.79 (1H, ddd, C$\underline{H}$=CH_2, *J*=6.0 Hz), and 7.46—8.07 (15H, m, 3×Ph).

Found: C, 59.88; H, 5.63%. Calcd for $C_{27}H_{30}O_2PI$: C, 59.57; H, 5.55%.

5-*O*-Benzyl-3-deoxy-1,2-*O*-isopropylidene-α-D-*glycero*-D-*glycero*-pentofuranose (19). To a solution of **11**[6] (5.0 g, 28.7 mmol) in DMF (50 ml) was added 55% NaH (2.5 g, 57.4 mmol) at 0 °C. The mixture was stirred at 25 °C for 0.5 h, and benzyl bromide (5.12 ml, 43.0 mmol) was added dropwise at 0 °C. After being stirred at 25 °C for 0.5 h, the reaction mixture was poured into cold water (300 ml) which was extracted with ethyl acetate (3×150 ml). The extracts were washed with saturated aqueous NaCl, dried, and evaporated. The residue was chromatographed on silica gel (400 g) with 4:1 hexane–ethyl acetate to afford **19** (7.42 g, 97%): pale yellow syrup, R_f=4:1 (hexane–ethyl acetate); $[\alpha]_D^{28}$ −15° (*c* 1.00); ^{1}H NMR (90 MHz) δ=1.31, 1.50 (each 3H, each s, CMe_2), 1.70—2.25 (2H, m, 2×H-3), 3.50—3.80 (2H, m, 2×H-5), 4.20—4.55 (1H, m, H-4), 4.60 (2H, s, C$\underline{H}_2$Ph), 4.71 (1H, dd, H-2, $J_{2,1}=J_{2,3}$=4.0 Hz), 5.82 (1H, d, H-1), and 7.33 (5H, s, Ph).

Found: C, 68.43; H, 7.55%. Calcd for $C_{15}H_{20}O_4$: C, 68.16; H, 7.63%.

5-*O*-Benzyl-3-deoxy-D-*glycero*-D-*glycero*-pentofuranose (20). To an ice-cooled solution of **19** (7.39 g, 28.0 mmol) in dioxane (74 ml) was added dropwise 3.2M aqueous HCl (74 ml) over a 15-min period. After being stirred at 25 °C for 1.25 h, the reaction mixture was neutralized (pH=7) with solid $NaHCO_3$ (3.0 g). The insoluble matter was filtered and washed with dioxane. The combined filtrate and washings were evaporated. The residue was taken up in dioxane and the resulting precipitates were filtered and washed with dioxane (5×8 ml). The filtrate and washings were evaporated, and the residue was chromatographed on silica gel (63 g) with 1:4 toluene–ethyl acetate to give a pure sample of **20** (5.78 g, 92%): colorless syrup, R_f=0.21 (1:1 toluene–ethyl acetate); $[\alpha]_D^{26}$ −14° (*c* 1.03, EtOH after 2d); ^{1}H NMR (90 MHz, after addition of D_2O) δ=1.70—2.20 (2H, m, 2×H-3), 3.30—3.75 (2H, m, 2×H-5), 4.10—4.30 (1H, m, H-4), 4.30—4.70 (1H, m, H-2), 4.58 (2H, s, C$\underline{H}_2$Ph), 5.22 (ca. 0.6H, s, β-H-1), 5.32 (ca. 0.4H, α-H-1, *J*=4.0 Hz), and 7.34 (5H, s, Ph).

Found: C, 63.98; H, 7.21%. Calcd for $C_{12}H_{16}O_4$: C, 64.27; H, 7.19%.

(2*S*,4*R*,5*R*)-1-*O*-Benzyl-6-heptene-1,2,4,5-tetrol (21) and Its (5*S*)-Epimer (21′). To a solution of vinylmagnesium bromide in THF which was prepared from vinyl bromide (18.2 ml, 258 mmol) and magnesium (6.27 g, 258 mmol) in THF (125 ml), was added dropwise a solution of **20** (5.78 g, 25.8 mmol) in THF (52 ml) over a 7-min period. After being stirred at 25 °C for 3.5 h, the reaction was quenched by addition of $Na_2SO_4\cdot 10H_2O$ (solid), and the resulting mixture was filtered through a Celite. The filter cake was washed with acetone (5×50 ml) and the combined filtrate and washings were evaporated. The residue was charged together with silica gel (15 g) on a column of silica gel (325 g) by using 15:1 chloroform–methanol and then eluted with the same solvent system to afford a mixture of **21** and its epimer **21′** (6.19 g, 95%): colorless syrup, R_f=0.36 (1:4 toluene–ethyl acetate); ^{1}H NMR (90 MHz) δ=1.50—1.80 (2H, m, 2×H-3), 3.17 (3H, s, 3×OH), 3.30—3.55 (2H, m, 2×H-1), 3.60—4.25 (3H, m, H-2, 4, 5), 4.55 (2H, s, C$\underline{H}_2$Ph), 5.10—5.45 (2H, m, 2×H-7), 5.65—6.10 (1H, m, H-6), and 7.33 (5H, s, Ph).

Found: C, 66.59; H, 8.06%. Calcd for $C_{14}H_{20}O_4$: C, 66.65; H, 7.99%.

(2*S*,4*R*,5*R*)-1-*O*-Benzyl-4,5-*O*-isopropylidene-6-heptene-1,2,4,5-tetrol (22) and Its (5S)-Epimer (22′). A mixture of **21** (1.57 g, 6.24 mmol), acetone (78.7 ml), and iodine (475 mg, 1.87 mmol) was stirred at 25 °C for 2 h. To the reaction mixture was added saturated aqueous $Na_2S_2O_3$ (30 ml), and the mixture was extracted with chloroform (3×100 ml). The extracts were washed with saturated aqueous NaCl, dried, and evaporated. The residue (2.18 g) was flushchromatographed on silica gel (270 g) with 7:1 chloroform–ethyl acetate to afford a pure sample of **22** (622 mg), a mixture of **22** and **22′** (799 mg), and a mixture of **22**, **22′**, and two epimeric 2,4-acetonides (288 mg). The fraction containing **22** and **22′** (799 mg) was again flushchromatographed on silica gel (80 g) with 4:1 hexane–ethyl acetate to give a pure sample of **22** (363 mg) and a mixture of **22** and **22′** (435 mg). A total yield of **22** amounted to 985 mg (54%). **22**: colorless syrup, R_f=0.59 (6:1 chloroform–ethyl acetate, HPTLC); $[\alpha]_D^{27}$ −5.13°, $[\alpha]_{365}^{27}$ −27.4° (*c* 1.44); ^{1}H NMR (90 MHz) δ=1.35 (6H, s, CMe_2), 1.78 (2H, dd, 2×H-3, $J_{3,2}=J_{3,4}$=4.5 Hz), 2.77 (1H, br-s, OH), 3.45 (2H, d, H-1, $J_{1,2}$=5.4 Hz), 3.66—4.27 (3H, m, H-2, 4, 5), 4.56 (2H, s, C$\underline{H}_2$Ph), 5.23 (1H, ddd-like, H-7Z, J_{gem}=2.4, $J_{7Z,5}$<1.0, $J_{7Z,6}$=10.0 Hz), 5.37 (1H, ddd-like, H-7E, $J_{7E,5}$<1.0, $J_{7E,6}$=15.6 Hz), 5.82 (1H, ddd, H-6, $J_{6,5}$=6.9 Hz), and 7.35 (5H, s, Ph).

Found: C, 70.10; H, 8.22%. Calcd for $C_{17}H_{24}O_4$: C, 69.84; H, 8.27%.

A pure sample of **22′** was obtained by flashchromatog-

raphy of a sample of ca. 1:1 mixture of **22** and **22′** in other experiment. **22′**: colorless syrup, R_f=0.48 (6:1 chloroform–ethyl acetate, HPTLC); $[\alpha]_D^{24}$ +4.0°, $[\alpha]_{365}^{24}$ +14.4° (*c* 0.96); ^{1}H NMR (90 MHz) δ=1.38, 1.51 (each 3H, each s, CMe_2), 1.65 (2H, dd, 2×H-3, *J*=6.0, 6.0 Hz), 3.03 (1H, br-s, OH), 3.46 (2H, d, 2×H-1, *J*=5.4 Hz), 3.80—4.20 (1H, m, H-2), 4.20—4.70 (2H, m, H-4, 5), 4.59 (2H, s, $C\underline{H}_2Ph$), 5.26 (1H, ddd-like H-7Z, J_{gem}=2.1, $J_{7Z,5}$<1.0, $J_{7Z,6}$=9.6 Hz), 5.31 (1H, ddd-like, H-7*E*, $J_{7E,5}$<1.0, $J_{7E,6}$=18.0 Hz), 5.82 (1H, ddd, H-6, $J_{6,5}$=8.1 Hz), and 7.38 (5H, s, Ph).

Found: C, 69.54; H, 8.24%. Calcd for $C_{17}H_{24}O_4$: C, 69.84; H, 8.27%.

(2*S*,4*R*,5*R*)-1-*O*-Benzyl-4,5-*O*-isopropylidene-2-*O*-[(2-methoxyethoxy)methyl]-6-heptene-1,2,4,5-tetrol (23). To a cold solution of **22** (1.61 g, 5.50 mmol) in CH_2Cl_2 (16.1 ml) was added *N*,*N*-diisopropylethylamine(4.79 ml, 27.5 mmol) and then (2-methoxyethoxy)methyl chloride (MEM-Cl)(1.85 ml, 16.5 mmol). After being stirred at 40 °C for 1.5 h, the mixture was poured into cold water which was extracted with ethyl acetate (3×30 ml). The extracts were washed with saturated aqueous NaCl, dried, and evaporated. The residue was chromatographed on silica gel (105 g) with 4:1 hexane–acetone to give a pure sample of **23** (2.06 g, 98%): colorless syrup, R_f=0.40 (4:1 hexane–acetone); $[\alpha]_D^{27}$ +3.8°, $[\alpha]_{546}^{27}$ +4.3°, $[\alpha]_{437}^{27}$ +4.9° (*c* 1.27); ^{1}H NMR (90 MHz) δ=1.35, 1.40 (each 3H, each s, CMe_2), 1.56—2.07 (2H, m, 2×H-3), 3.37 (3H, s, OMe), 3.43—4.17 (9H, m, 2×H-1, H-2, 4, 5, $-OCH_2CH_2O-$), 4.57 (2H, s, $C\underline{H}_2Ph$), 4.83 (2H, s, $-OCH_2O-$), 5.24 (1H, ddd-like, H-7Z, J_{gem}=2.1, $J_{7Z,5}$<1.0, $J_{7Z,6}$=10.5 Hz), 5.39 (1H, ddd-like, H-7E, $J_{7E,5}$<1.0, $J_{7E,6}$=16.5 Hz), 5.83 (1H, ddd, H-6, $J_{6,5}$=6.0 Hz).

Found: C, 66.08; H, 8.32%. Calcd for $C_{21}H_{32}O_6$: C, 66.29; H, 8.48%.

(2*S*,3*R*,5*S*)-6-*O*-Benzyl-2,3-*O*-isopropylidene-5-*O*-[(2-methoxyethoxy)methyl]-2,3,5,6-tetrahydroxyhexanal (9). To a stirred solution of **23** (477 mg, 1.25 mmol) in 75% aqueous dioxane (19.1 ml) was added OsO_4. (15.9 mg, 0.063 mmol) at 23 °C. After 15 min to this mixture was added sodium periodate (powder, 802 mg, 3.75 mmol). After being stirred at 23 °C for 2.5 h, the mixture was filtered through a Celite and the filter cake was washed with dioxane. The filtrate and washings were concentrated and diluted with chloroform (20 ml). The mixture was washed with saturated aqueous $Na_2S_2O_3$ and NaCl, dried, and evaporated. The residue was chromatographed on silica gel (24 g) with 6:1 chloroform–acetone to afford **9** (439 mg, 91.5%): colorless syrup, R_f=0.41 (6:1 chloroform–acetone), $[\alpha]_D^{27}$ −3.3°, $[\alpha]_{365}^{27}$ −26.9° (*c* 1.04); IR($CHCl_3$) 1730 cm^{-1}; ^{1}H NMR (90 MHz) δ=1.34, 1.77 (each 3H, each s, CMe_2), 1.98 (2H, dd, 2×H-4, *J*=6.0, 6.0 Hz), 3.34 (3H, s, OMe), 3.34—3.83 (6H, m, $-OCH_2CH_2O-$, 2×H-6), 3.83-4.30 (3H, m, H-2, 3, 5), 4.52 (2H, s, CH_2Ph), 4.77 (2H, s, $-OCH_2O-$), 7.30 (5H, s, Ph), and 9.72 (ca. 0.6H, CHO, *J*=1.8 Hz); ^{13}C NMR (22.50 MHz) δ=25.99, 26.99 (each q, $C\underline{M}e_2$), 35.44 (t, C-4), 58.74 (q, OMe), 66.97, 71.57, 73.12, 73.44 (each t, $\underline{C}H_2Ph$, $-OCH_2O-$, $-OCH_2CH_2O-$), 71.82, 73.63 (each d, C-3, 5), 84.77 (dd, C-2), 94.82 (t, C-6), 110.77 (s, $\underline{C}Me_2$), 127.48, 127.54, 128.19 (each d, Ph), 138.05 (s, Ph), and 200.35 (d, CHO).

(2*R*)-Epimer 9′ of 9. By the method described in the preparation of **23**, the aforesaid mixture of **22** and **22′** (416 mg) was methoxyethoxymethylated to afford a mixture of **23** and **23′** (508 mg, 94%). This mixture was oxidized with OsO_4–$NaIO_4$ by the same procedure as described in the preparation of **9** to give a crude mixture of **9** and **9′** which was flashchromatographed on silica gel (51 g) with 7:1 chloroform–ethyl acetate to afford **9** (193 mg, 38%) and **9′** (182 mg, 36%). **9′**: colorless syrup, R_f=0.66 (6:1 chloroform–acetone); $[\alpha]_D^{24}$ −7.6°, $[\alpha]_{365}^{24}$ −47.2° (*c* 1.02); IR($CHCl_3$) 1730 cm^{-1}; ^{1}H NMR (90 MHz) δ=1.37, 1.57 (each 3H, each s, CMe_2), 1.73—2.10 (2H, m, 2×H-4), 3.36 (3H, s, OMe), 3.40—3.80 (6H, m , $-OCH_2CH_2O-$, 2×H-6), 3.80—4.20 (1H, m, H-5), 4.20—4.80 (2H, m, H-2, 3), 4.54 (2H, s, CH_2Ph), 4.79 (2H, s, $-OCH_2O-$), 7.30 (5H, s, Ph), and 9.63 (1H, d, CHO, *J*=3.0 Hz); ^{13}C NMR (22.50 MHz) δ=25.13, 27.48 (each q, $C\underline{M}e_2$), 31.57 (t, C-4), 58.74 (q, OMe), 67.01, 71.53, 73.05, 73.56 (each t, $\underline{C}H_2Ph$, $-OCH_2O-$, $-OCH_2CH_2O-$), 71.53, 75.05 (each d, C-3, 5), 81.69 (dd, C-2), 94.80 (t, C-6), 110.26 (s, $\underline{C}Me_2$), 127.49, 128.27 (each d, Ph), 138.00 (s, Ph), and 201.87 (d, CHO).

Epimerization of 9′ to 9. To a sample of **9′** (182 mg, 0.475 mmol) was added a solution of K_2CO_3 (20 mg, 0.143 mmol) in methanol (3.63 ml). After being stirred at 23 °C for 4.5 h, the reaction mixture was evaporated. The residue was partitioned between chloroform (10 ml) and water. The chloroform layer was separated and washed with saturated aqueous NaCl, dried, and evaporated. The residue was flushchromatographed on silica gel (18.2 g) with 7:1 chloroform–ethyl acetate to afford **9** (123 mg, 68%) whose TLC, ^{1}H and ^{13}C NMR spectra were identical with those of the aforesaid sample of **9** derived from **23**.

Methyl (2*S*,3*R*,5*R*)-6-*O*-Benzyl-2,3-*O*-isopropylidene-2,3,5-trihydroxyhexanoate (26). By the procedure described in the preparation of **9**, **22** (197 mg, 0.673 mmol) was oxidized with OsO_4–$NaIO_4$ to afford crude aldehyde **24** (192 mg, 97%). To a solution of this aldehyde in 70% aqueous dioxane (6.70 ml) was added a solution of K_2CO_3 (568 mg, 4.11 mmol) and $KHCO_3$ (411 mg, 4.11 mmol) in water (7.70 ml) and then added a solution of KI (649 mg, 3.91 mmol) and I_2 (248 mg, 0.978 mmol) in water (0.96 ml) dropwise under stirring. The mixture was stirred at 23 °C for 1.75 h, after which period $Na_2S_2O_3$ (960 mg) was added to the reaction mixture at 0 °C. This mixture was washed with ether (10 ml) and the aqueous layer was acidified (pH =2—3) with 10% aqueous H_2SO_4 at 0 °C. The mixture was immediately extracted with chloroform (3×10 ml). The extracts were washed with saturated aqueous NaCl, dried, and evaporated to give the crude acid **25** (161 mg, 77% from **22**) as white crystals. The crystalline **25** was dissolved in a solution of diazomethane in ether and then evaporated to afford a syrup which was flushchromatographed on silica gel (5.1 g) with 3:1 chloroform–ethyl acetate to give **26** (163 mg, 74% from **22**): colorless syrup, R_f=0.49 (1:1 toluene–ethyl acetate); IR ($CHCl_3$) 1750 cm^{-1}; $[\alpha]_D^{26}$ +9.3°, $[\alpha]_{365}^{26}$ +21.8° (*c* 1.23); ^{1}H NMR (90 MHz) δ=1.44 (6H, s, CMe_2), 1.70—2.15 (2H, m, 2×H-4), 2.3—2.90 (1H, br-s, OH), 3.47 (2H, d, 2×H-6, *J*=3.0 Hz), 3.78 (3H, s, COOMe), 3.90—4.40 (3H, m. H-2, 3, 5), 4.58 (2H, s, CH_2Ph), and 7.35 (5H, s, Ph).

Found: C, 62.95; H, 7.41%. Calcd for $C_{17}H_{24}O_6$: C, 62.95; H, 7.46%.

Methyl (2*S*,3*R*)-2,3,5-Trihydroxypentanoate (30). A mixture of **26** (289 mg, 0.89 mmol), Pd-black, and methanol (5.8 ml) was vigorously stirred at room temperature for 10 min under bubbling with H_2 gas, and then filtered. The filtrate was evaporated to a colorless syrup of **27** (209 mg,

100%). To a solution of this syrup in acetone (2.10 ml) was added a solution of $NaIO_4$ (381 mg, 1.78 mmol) in water (3.8 ml) under ice-cooling. After being stirred for 15 min, the precipitate was filtered and washed with acetone. The combined filtrate and washings were concentrated. The aqueous residue was extracted with dichloromethane 6 times. The extracts were dried and evaporated to afford a syrup of **28** (180 mg). To an ice-cold solution of this syrup (33 mg, 0.163 mmol) in methanol (0.33 ml) was added $NaBH_4$ (31 mg, 0.082 mmol). After being stirred at 0 °C for 10 min, the mixture was neutralized with CO_2 and then evaporated. The residue was pertitioned between ethyl acetate and saturated aqueous NaCl, and the aqueous layer was extracted with ethyl acetate three times. The organic layers were dried and evaporated to give a syrup which was chromatographed on silica gel (2.3 g) with 1:1 hexane–ethyl acetate to afford **29** (23.5 mg, 70% yield from **26**) as a syrup. A solution of **29** (23.5 mg) and *p*-toluenesulfonic acid (2.2 mg, 0.015 mmol) in methanol (0.23 ml) was stirred at 33 °C for 19 h. The reaction mixture was neutralized with Amberlite IR-45 (OH type) at 0 °C, and then filtered. The resin was washed with methanol, and the combined filtrate and washings were evaporated to afford a syrup (21 mg). This syrup was chromatographed on silica gel (1.0 g) with 5:1 chloroform–methanol to give **30** (16 mg, 84% yield from **29**): colorless syrup, R_f=0.42 (5:1 chloroform–methanol); IR ($CHCl_3$) 3370, 1735 cm^{-1}; $[\alpha]_D^{30}$ +17.9° (*c* 0.47); CD $[\theta]_{210}$ +4105 (*c* 0.10, H_2O); ^1H NMR (90 MHz) δ=1.77—2.17 (2H, m, 2×H-4), 2.57—2.93 (1H, br-s, OH), 3.17—4.47 (6H, m, 2×OH, H-2, 3, 2×H-5), and 3.87 (3H, s, COOMe).

(2*S*,3*R*,5*S*)-5,6-Di-*O*-benzyl-2,3-*O*-isopropylidene-2,3,5,6-tetrahydroxyhexanal (10). To an ice-cold solution of **22** (570 mg, 1.95 mmol) in DMF (3.3 ml) was added 55% NaH (255 mg, 5.85 mmol), and the mixture was stirred at 24 °C for 0.5 h, after which period TBAF (72 mg, 0.195 mmol) was added, and after 5 min, to the stirred mixture was added benzyl bromide (464 µl, 3.90 mmol) dropwise under ice-cooling. After being stirred at 24 °C for 3 h, the reaction mixture was poured into cold water (8.0 ml) and the mixture was extracted with ethyl acetate (3×8.0 ml). The extracts were washed with saturated aqueous NaCl, dried, and evaporated. The residue (1.12 g) was chromatographed on silica gel (75 g) with 8:1 hexane–acetone to afford a colorless syrup of the 2-*O*-benzyl derivative of **22** (710 mg, 95%). A sample (1.59 g, 4.17 mmol) of this benzyl derivative was oxidized with OsO_4–$NaIO_4$ by the procedure described in the preparation of **9**. The crude product was chromatographed on silica gel (80 g) with 2:1 hexane–ethyl acetate to give **10** (1.38 g, 86%): colorless syrup, R_f=0.21 (2:1 hexane–ethyl acetate); IR($CHCl_3$) 1730 cm^{-1}; $[\alpha]_D^{27}$ −3.6°, $[\alpha]_{365}^{27}$ −29.7° (*c* 0.99); ^1H NMR (90 MHz) δ=1.41, 1.45 (each 3H, each s, CMe_2), 2.00 (2H, dd, 2×H-4, $J_{4,3}$=$J_{4,5}$=5.4 Hz), 3.40—4.40 (ca. 5.5H, m, H-2, 3, 5, 2×H-6, H-1), 4.55 (2H, s, CH_2Ph), 4.52, 4.66 (2H, ABq, CH_2Ph, *J*=9.6 Hz), 7.37 (10H, s, 2×Ph), and 9.66 (ca. 0.5H, CHO, *J*=ca. 1.5 Hz).

(2*S*,4*R*,5*R*,8*S*,10*R*)-(6*Z*)-1-*O*-Benzyl-4,5:8,10-di-*O*-isopropylidene-2-*O*-[(2-methoxyethoxy)methyl]-6,11-dodecadiene-1,2,4,5,8,10-hexol (31). To a suspension of **8** (77.8 mg, 0.143 mmol) in 2:1 THF–HMPA (477 µl) was added a 1.56M butyllithium in hexane (92 µl, 0.143 mmol) at −70 °C under Ar, and the mixture was stirred at −70 °C for 22 min. To the yellow colored mixture was added a solution of **9** (48.4 mg, 0.127 mmol) in THF (149 µl), and the mixture was stirred at −70 °C for 0.5 h. The reaction mixture was allowed to warm to −50 °C and diluted with THF (1.2 ml). The reaction was quenched by addition of aqueous NH_4Cl at room temperature. This mixture was extracted with ethyl acetate (3×1.0 ml), and the extracts were washed with saturated aqueous NaCl, dried, and evaporated. The residue was chromatographed on silica gel (3.5 g) with 3:1 hexane–ethyl acetate to afford a pure sample of **31** (46.0 mg, 70%): colorless syrup, R_f=0.45 (3:1 hexane–ethyl acetate); $[\alpha]_D^{32}$ −8.5°, $[\alpha]_{365}^{32}$ −38.5° (*c* 1.20); ^1H NMR (250 MHz) δ=1.34, 1.40, 1.49, 1.53 (12H, each s, 2×CMe_2), 1.70—1.86, 1.92—2.05 (4H, each m, 2×H-3, 2×H-9), 3.36 (3H, s, OMe), 3.46—4.04 (8H, m, 2×H-1, H-2, 4, -OCH_2CH_2O-), 4.33—4.43 (1H, m, H-10), 4.38 (1H, dd, H-5, $J_{5,4}$=$J_{5,6}$=8.8 Hz), 4.47 and 4.59 (2H, ABq, CH_2Ph, *J*=11.25 Hz), 4.69—4.85 (1H, m, H-8), 4.80 (2H, s, -OCH_2O-), 5.13 (1H, ddd, H-12*Z*, J_{gem}=$J_{12Z,10}$=ca. 1.2, $J_{12Z,11}$=10.5 Hz), 5.25 (1H, ddd, H-12*E*, $J_{12E,10}$=ca. 1.2, $J_{12E,11}$=17.8 Hz), 5.45 (1H, dd, H-6, $J_{6,7}$=11.2 Hz), 5.62 (1H, dd, H-7, $J_{7,8}$=7.5 Hz), and 5.81 (1H, ddd, H-11, $J_{11,10}$=4.8 Hz).

Found: C, 66.95; H, 8.29%. Calcd for $C_{29}H_{44}O_8$: C, 66.90; H, 8.52%.

(2*S*,4*R*,5*R*,8*S*,10*R*)-(6*Z*)-1,2-Di-*O*-benzyl-4,5:8,10-di-*O*-isopropylidene-6,11-dodecadiene-1,2,4,5,8,10-hexol (32). By the procedure described in the preparation of **31**, the ylide generated from **8** (66.0 mg, 0.121 mmol) was allowed to react with **10** (42.4 mg, 0.110 mmol) to afford, after silica gel chromatography with 4:1 hexane–ethyl acetate, the coupling product **32** (30.1 mg, 52%): colorless syrup; R_f=0.75 (2:1 hexane–ethyl acetate $[\alpha]_D^{30}$ −19.4° (*c* 1.80), ^1H NMR (250 MHz) δ=1.37, 1.39, 1.44, 1.45 (each 3H, each s, 2×CMe_2), 1.50—1.60, 1.79—2.04 (each 2H, each m, 2×H-3, 2×H-9), 3.50—3.62 (2H, m, 2×H-1), 3.75—3.92 (2H, m, H-2, 4), 4.19—4.32 (1H, m, H-10), 4.53 (2H, s, CH_2Ph), 4.52 and 4.70 (2H, ABq, CH_2Ph, *J*=11.3 Hz), 4.42—4.79 (2H, m, H-5, 8), 5.12 (1H, ddd, H-12Z, J_{gem}=$J_{12Z,10}$=ca. 1.2, $J_{12Z,11}$=11.2 Hz), 5.23 (1H, ddd, H-12E, $J_{12E,11}$=17.5, $J_{12E,10}$=ca. 1.2 Hz), 5.41 (1H, dd, H-6, $J_{6,5}$=9.5, $J_{6,7}$=10.5 Hz), 5.58 (1H, dd, H-7, $J_{7,8}$=7.5 Hz), 5.78 (1H, ddd, H-11, $J_{11,10}$=5.0 Hz), and 7.20—7.45 (10H, m, 2×Ph).

Found: C, 73.36; H, 8.02%. Calcd for $C_{32}H_{42}O_6$: C, 73.53; H, 8.10%.

(2*S*,4*R*)-2,4-*O*-Isopropylidene-6,6-dimethoxy-1,2,4-hexanetriol (34). A 4M methylsulfinylmethanide anion in DMSO[8] (1.25 ml, 4.98 mmol) was added dropwise to a stirred suspension of (methoxymethyl)triphenylphosphonium chloride (1.71 g, 4.98 mmol) in ether under Ar at room temperature. The mixture was sirred for 20 min and then, to the resulting red suspension of the ylide, a solution of **15** (1.03 g, 2.49 mmol) in ether (20 ml) was added dropwise. After being stirred at room temperature for 10 min, the resulting suspension was poured into an ice–water, and the mixture was extracted with ethyl acetate (3×80 ml). The extracts were washed with saturated aqueous NaCl, dried, and evaporated. The residue was chromatographed on silica gel (100 g) with 6:1 hexane–ethyl acetate to a syrup (1.10 g, 96.5%) of methyl enol ether of the homologus aldehyde of **15**. To an ice-cold solution of the methyl enol ether (0.91 g, 2.07 mmol) in methanol (9.0 ml) were added solid $NaHCO_3$ (0.21 g, 2.48 mmol) and NBS (0.44 g, 0.248 mmol) successively. After being stirred at 0 °C for 0.5 h, the mixture was evaporated and the residue was extracted with ethyl acetate (20 ml). The extract was washed with water and saturated

aqueous NaCl, dried, and evaporated to a syrup which was chromatographed on silica gel (80 g) with 6:1 hexane–ethyl acetate to afford a syrup (1.10 g, 96.5%) of the bromo dimethyl acetal. A solution of this bromo acetal (1.10 g), tributylstannane (0.8 ml) and AIBN (66 mg) in toluene (17 ml) was stirred at 60 °C for 2 h and then evaporated. The residue was chromatographed on Kieselgel (50 g) with 10:1 toluene–ethyl acetate to give a syrup of **33** (0.78 g, 83%). A mixture of **33** (228 mg), THF (2.3 ml), and 1M TBAF in THF (0.96 ml) was stirred at 0 °C for 1.5 h and then poured into cold water (10 ml). The mixture was extracted with ethyl acetate (3×15 ml). The extracts were washed with saturated aqueous NaCl, dried, and evaporated. The residue was chromatographed on silica gel (4.5 g) with 1:2 hexane–ethyl acetate to afford **34** (88 mg, 78%): colorless syrup, R_f=0.52 (3:1 hexane–ethyl acetate); $[\alpha]_D^{26}$ −11°(*c* 0.97); ^{1}H NMR (90 MHz) δ=1.38, 1.45 (each 3H, each s, CMe_2), 1.03—1.60 (2H, m, 2×H-3), 1.73 (2H, dd-like 2×H-5, $J_{5,4}=J_{5,6}$=5.4 Hz), 1.96—2.26 (1H, br-s, OH), 3.36, 3.39 (each 3H, each s, 2×OMe), 3.41—3.66 (2H, m, 2×H-1), 3.76—4.22 (2H, m, H-2, 4), and 4.53 (1H, t, H-6).

Found: C, 56.14; H, 9.26%. Calcd for $C_{11}H_{22}O_5$: C, 56.39; H, 9.46%.

[[(4*R*,6*R*)-2,2-Dimethyl-6-(2,2-dimethoxyethyl)-1,3-dioxan-4-yl]methyl]triphenylphosphonium Iodide (35). A solution of **34** (265 mg, 1.13 mmol), triphenylphosphine (889 mg, 3.39 mmol), and DEAD (0.53 ml, 3.39 mmol) in benzene (5.0 ml) was stirred at 0 °C and then methyl iodide (0.21 ml, 3.39 mmol) was added. The mixture was stirred at room temperature for 1 h and then evaporated. The residue was taken up in ethyl acetate (10 ml) which was washed successively with saturated aqueous $NaHCO_3$ (7.5 ml), $Na_2S_2O_3$ (7.5 ml), and NaCl, dried, and evaporated. The residue was chromatographed on silica gel (12 g) with 5:1 hexane–ethyl acetate to afford a syrup of iodide (276 mg, 71%). A solution of this syrup (235 mg) and triphenylphosphine (386 mg) in benzene (0.76 ml) was stirred at 84 °C for 5 d. The reaction mixture was evaporated and the residual solid was triturated with hexane (10×7.0 ml) to give the Wittig salt **35** (348 mg, 78%): colorless crystals, mp 200—201 °C (MeOH–ether); $[\alpha]_D^{15}$+14.6° (*c* 1.03); ^{1}H NMR (90 MHz) δ=0.77,1.09 (each 3H, each s, CMe_2), 3.28, 3.31 (each 3H, each s, 2×OMe), and 4.51 (1H, *t*, C<u>H</u>$(OMe)_2$, *J*=6.0 Hz).

Found: C, 57.08; H, 6.02; I, 20.62%. Calcd for $C_{29}H_{36}O_4PI$: C, 57.43; H, 5.98; I, 20.92%.

(3*R*,5*S*)-(6*Z*)-1,1-Dimethoxy-3,4-*O*-isopropylidene-5-tridecene-3,4-diol (36). By the procedure described in the preparation of **31**, the ylide generated from **35** (109 mg, 0.179 mmol) was condensed with heptanal (36.1 μl, 0.269 mmol) to afford, after silica-gel chromatography with 8:1 hexane–ethyl acetate and with 16:1 hexane–acetone, the condensation product **36** (18.2 mg, 32%): colorless syrup, R_f=0.35 (8:1 hexane–ethyl acetate); ^{1}H NMR (250 MHz) δ=0.89 (3H, t, 3×H-13, *J*=7.0 Hz), 1.20—1.85 (12H, m, 2×H-2, 2×H-4, -C<u>H</u>$_2$C<u>H</u>$_2$C<u>H</u>$_2$C<u>H</u>$_2$Me), 1.40, 1.50 (each 3H, each s, CMe_2), 2.0—2.2 (2H, m, 2×H-8), 3.34, 3.38 (each 3H, each s, 2×OMe), 4.0—4.1 (1H, m, H-3), 4.57 (1H, dd, H-1, $J_{1,2}$=4.5, 7.0 Hz), 4.69 (1H, ddd, H-5, $J_{5,4}$=2.8, 11.8 Hz, $J_{5,6}$=8.0 Hz), 5.35 (1H, approximately dd, dd after decoupled with 2×H-8 protons, H-6, $J_{6,7}$=11.8 Hz), and 5.4—5.6 (1H, m, d after decoupled with 2×H-8 protons, H-7).

Preparation of 34 from 36 via 37. By the procedure described in the preparation of **9**, a sample of **36** (103 mg) was oxidized with OsO_4–$NaIO_4$ to afford a crude syrup of the aldehyde **37** (30.4 mg, 40%): ^{1}H NMR (90 MHz) δ=1.45 (6H, s, CMe_2), 3.34, 3.35 (each 3H, each s, 2×OMe), and 9.61 (0.5H, s, CHO). To an ice-cold solution of the syrup (30 mg) in methanol (0.3 ml) was added $NaBH_4$ (10.0 mg). After being stirred at 0 °C for 2 h, the mixture was neutralized with CO_2 and treated successively with IR-45 and CG-50 resin. The resulting methanol solution was evaporated to a syrup which was purified by silica-gel chromatography with 1:1 hexane–ethyl acetate to afford **34** (19 mg) in 24% overall yield from **36**. This sample proved to be identical with the sample of **34** obtained from **15** by TLC, $[\alpha]_D$ and ^{1}H NMR.

(2*S*,4*R*,5*R*,8*S*,10*S*)-(6*Z*)-1-*O*-Benzyl-4,5:8,10-di-*O*-isopropylidene-2-*O*-[(2-methoxyethoxy)methyl]-6-dodecene-1,2,4,5,8,10,12-heptol (38). To a solution of dicyclohexylborane (0.854 mmol) in THF (0.48 ml) was added a solution of **31** (247 mg, 0.475 mmol) in THF (0.74 ml) at 0 °C under Ar, and the mixture was stirred at 25 °C for 25 min. The reaction was quenched by addition of water (1.22 ml). To this mixture was added 3M aqueous NaOH (0.284 ml) and 30% H_2O_2 (0.256 ml) at 0 °C. After being stirred at 5 °C for 1 h, the reaction mixture was extracted with chloroform (3×2.0 ml). The extracts were washed with saturated aqueous NaCl, dried, and evaporated. The residue was chromatographed on silica gel (13 g) with 1:3 hexane–ethyl acetate to afford a pure sample of **38** (229 mg, 90%): colorless syrup, R_f=0.48 (1:3 hexane–ethyl acetate); $[\alpha]_D^{30}$ −6.7°, $[\alpha]_{365}^{30}$−24.1° (*c* 1.77); ^{1}H NMR (250 MHz) δ=1.34, 1.37, 1.39, 1.48 (each 3H, each s, 2×CMe_2), 1.20—2.07 (7H, m, 2×H-3 2×H-9, 2×H-11, OH), 3.36 (3H, s, OMe), 3.43-3.63 (4H, m, -OCH_2CH_2O-), 3.63—4.21 (7H, m, 2×H-1, H-2, 4, 10, 2×H-12), 4.36 (1H, ddd-like, H-5, $J_{5,7}$<1.0, $J_{5,4}=J_{5,6}$=8.8 Hz), 4.46 and 4.61 (2H, ABq, CH_2Ph, *J*=12.5 Hz), 4.65-4.80 (1H, m, H-8), 4.80 (2H, s, -OCH_2O-), 5.45 (1H, dd, H-6, $J_{6,7}$=10.5 Hz), 5.62 (1H, dd, H-7, $J_{7,8}$=7.5 Hz), and 7.20—7.54 (5H, m, Ph).

Found: C, 64.65; H, 8.57%. Calcd for $C_{29}H_{46}O_9$: C, 64.66; H, 8.61%.

(2*S*,4*R*,5*R*,8*S*,10*S*)-(6*Z*)-1,2-Di-*O*-benzyl-4,5:8,10-di-*O*-isopropylidene-6-dodecene-1,2,4,5,8,10,12-heptol (39). By the procedure described in the preparation of **38**, the title compound **39** (24.9 mg, 85%) was obtained from **32** (28.2 mg) after silica-gel chromatography with 1:2 hexane–ethyl acetate: colorless syrup, R_f=0.55 (1:2 hexane–ethyl acetate); $[\alpha]_D^{29}$ −19.6° (*c* 1.43); ^{1}H NMR (90 MHz) δ=1.40, 1.46 (each 6H, each s, 2×CMe_2), 1.60—2.20 (6H, m, 2×H-3, 2×H-9, 2×H-11), 2.44 (1H, br-s, OH), 3.40—4.20 (7H, m, 2×H-1, H-2, 4, 10, 2×H-12), 4.30—4.93 (4H, m, H-5, 8, CH_2Ph), 4.55 (2H, s, CH_2Ph), 5.20—5.75 (2H, m, H-6, 7), and 7.36 (10H, s, 2×Ph).

Found: C, 71.08; H, 8.14%. Calcd for $C_{32}H_{44}O_7$: C, 71.08; H, 8.20%.

(2*S*,4*R*,5*R*,8*S*,10*S*)-(6*Z*)-1-*O*-Benzyl-12-*O*-*t*-butyldimethylsilyl-4,5:8,10-di-*O*-isopropylidene-2-*O*-[(2-methoxyethoxy)methyl]-6-dodecene-1,2,4,5,8,10,12-heptol (40). To an ice-cold solution of **38** (40 mg, 0.0613 mmol) in pyridine (0.33 ml) was added TBS-Cl (13.9 mg, 0.092 mmol). After being stirred at 23 °C for 2 h, the mixture was poured into cold water (1.0 ml) and the resulting mixture was extracted with ethyl acetate (3×1.0 ml). The extracts were washed with saturated aqueous NaCl, dried and evaporated. The residue was chromatographed on silica gel (2.0 g) with 4:1

hexane–ethyl acetate to afford **40** (38.1 mg, 95%): colorless syrup, R_f=0.74 (1:2 hexane–ethyl acetate); $[\alpha]_D^{31}$ −10.9° (*c* 1.43); ^{1}H NMR (250 MHz) δ=0.89 (9H, s, *t*-Bu), 1.34, 1.35, 1.40, 1.45 (each 3H, each s, 2×CMe$_2$), 1.49—2.05 (6H, m, 2×H-3, 2×H-9, 2×H-11), 3.36 (3H, s, OMe), 3.47—3.58 (4H, m, -OCH$_2$CH$_2$O-), 3.59—4.13 (7H, m, 2×H-1, H-2, 4, 10, 2×H-12) 4.38 (1H, ddd-like, H-5, $J_{5,7}$<1.0, $J_{5,6}$=$J_{5,4}$=9.3 Hz), 4.46 and 4.60 (2H, ABq, CH$_2$Ph, *J*=11.8 Hz), 4.63—4.77 (1H, m, H-8), 4.80 (2H, s, -OCH$_2$O-), 5.44 (1H, dd, H-6, $J_{6,7}$=10.5 Hz), 5.62 (1H, dd, H-7, $J_{7,8}$=7.5 Hz), and 7.31 (5H, s, Ph).

Found: C, 64.64; H, 9.14%. Calcd for $C_{35}H_{60}O_9Si$: C, 64.38; H, 9.26%.

(2*S*,4*R*,5*R*,8*S*,10*S*)-(6*Z*)-1,2-Di-*O*-benzyl-12-*O*-*t*-butyldimethylsilyl-4,5:8,10-di-*O*-isopropylidene-6-dodecene-1,2,4,5,8,10,12-heptol (41). By the procedure described in the preparation of **40**, a sample of **39** (76.0 mg) was silylated to afford, after silica-gel chromatography with 6:1 hexane–ethyl acetate, **41** (82.6 mg, 90%): colorless syrup R_f=0.47 (5:1 hexane–ethyl acetate); $[\alpha]_D^{31}$ −18.7° (*c* 1.43); ^{1}H NMR (90 MHz) δ=0.94 (9H, s, *t*-Bu), 1.40 and 1.46 (each 6H, each s, 2×CMe$_2$), 1.40—2.20 (6H, m, 2×H-3, 2×H-9, 2×H-11), 3.40-4.20 (7H, m, 2×H-1, H-2, 4, 10, 2×H-12), 4.30—4.90 (6H, m, H-5, 8, 2×CH$_2$Ph), 5.20—5.80 (2H, m, H-6, 7), and 7.37 (10H, s, 2×Ph).

Found: C, 69.35; H, 8.75%. Calcd for $C_{38}H_{58}O_7Si$: C, 69.69; H, 8.93%.

(2*S*,4*R*,5*R*,8*R*,10*S*)-12-*O*-*t*-Butyldimethylsilyl-4,5:8,10-di-*O*-isopropylidene-2-*O*-[(2-methoxyethoxy)methyl]-1,2,4,5,8,10,12-dodecaneheptol (42). A solution of **40** (28.1 mg) in ethanol (0.56 ml) was stirred with a catalytic amount of Raney Ni W-4 for 2 h under bubbling with H_2 gas. The reaction mixture was filtered through a sintered-glass funnel and the catalyst was washed with ethanol. The combined filtrate and washings were evaporated, and the residue was chromatographed on silica gel (1.0 g) with hexane–ethyl acetate to afford **42** (20.5 mg, 84%): colorless syrup, R_f=0.34 (1:1 hexane–ethyl acetate); $[\alpha]_D^{33}$ +35.7° (*c* 0.74); ^{1}H NMR (90 MHz) δ=0.90 (9H, s, *t*-Bu), 1.38, 1.42 (each 6H, each s, 2×CMe$_2$), 1.17—2.10 (10H, m, 2×H-3, 2×H-6, 2×H-7, 2×H-9, 2×H-11), 2.90 (1H, br-s, OH), 3.40 (3H, s, OMe), 3.43—4.30 (13H, m, 2×H-1, H-2, 4, 5, 8, 10, 2×H-12, -OCH$_2$CH$_2$O-), and 4.81 (2H, s, -OCH$_2$O-).

Found: C, 59.84; H, 9.81%. Calcd for $C_{28}H_{56}O_9Si$: C, 59.54; H, 9.99%.

(2*S*,4*R*,5*R*,8*R*,10*S*)-12-*O*-*t*-Butyldimethylsilyl-4,5:8,10-di-*O*-isopropylidene-1,2,4,5,8,10,12-dodecaneheptol (43). A mixture of **41** (138 mg), Pd-black, and *t*-BuOH was vigorously stirred at 30 °C for 1 h under bubbling with H_2 gas, and then the suspension was filtered. The filtrate was evaporated to a syrup which was chromatographed on silica gel (5.0 g) with 1:2 hexane–ethyl acetate to afford **43** (99 mg, 98%): colorless syrup, R_f=0.52 (1:2 hexane–ethyl acetate); $[\alpha]_D^{28}$ +10.3° (*c* 0.66); ^{1}H NMR (90 MHz) δ=0.87 (9H, s, *t*-Bu), 1.32, 1.36, 1.38 (12H, each s, 2×CMe$_2$), 1.10—1.90 (10H, m, 2×H-3, 2×H-6, 2×H-7, 2×H-9, 2×H-11), and 2.70—4.20 (11H, m, 2×H-1, H-2, 4, 5, 8, 10, 2×H-12, 2×OH).

Found: C, 60.51; H, 9.69%. Calcd for $C_{24}H_{48}O_7Si$: C, 60.47; H, 10.15%.

(3*S*,5*R*,8*R*,9*R*,11*S*)-1-*O*-*t*-Butyldimethylsilyl-12-iodo-3,5:8,9-di-*O*-isopropylidene-11-*O*-[(2-methoxyethoxy)methyl]-1,3,5,8,9,11-dodecanehexol (4). To a cold (10 °C) solution of **42** (41.3 mg, 0.073 mmol) and triphenylphosphine (57.5 mg, 0.219 mmol) in benzene (0.83 ml) was added DEAD (0.045 ml, 0.219 mmol). After being stirred at 24 °C for 10 min, methyl iodide (0.0136 ml, 0.219 mmol) was added to the mixture at 10 °C. The mixture was stirred at 24 °C for 3 h and then water (1.5 ml) was added. The mixture was extracted with benzene (3×1.0 ml), and extracts were washed with saturated aqueous NaCl, dried, and evaporated. The residue was chromatographed on silica gel (2.4 g) with 4:1 hexane-ethyl acetate to afford **4** (45.1 mg, 92%): colorless syrup, R_f=0.43 (4:1 hexane–ethyl acetate); $[\alpha]_D^{26}$ +11.3° (*c* 1.28); ^{1}H NMR (250 MHz) δ=0.89 (9H, s, *t*-Bu), 1.36, 1.37 (each 6H each s, 2×CMe$_2$), 1.43—1.93 (10H, m, 2×H-2, 2×H-4, 2×H-6, 2×H-7, 2×H-10), 3.39 (3H, s, OMe), 3.30—4.22 (13H, m, 2×H-1, H-3, 5, 8, 9, 11, 2×H-12, -OCH$_2$CH$_2$O-), and 4.80 (2H, s, -OCH$_2$O-).

Found: C, 50.20; 8.04%. Calcd for $C_{28}H_{55}O_8SiI$: C, 49.84; H, 8.22%.

(2*S*,4*R*,5*R*,8*R*,10*S*)-1,2-Anhydro-12-*O*-*t*-butyldimethylsilyl-4,5:8,10-di-*O*-isopropylidene-1,2,4,5,8,10,12-dodecaneheptol (5). A mixture of **43** (24.2 mg, 0.051 mmol), triphenylphosphine (29.3 mg, 0.112 mmol), molecular sieves 3A powder (242 mg) and benzene (1.21 ml) was vigorously stirred at 85 °C for 10 min, and DEAD (17.6 μl, 0.112 mmol) was added dropwise to the mixture. After being stirred at 85 °C for 4 d, the cold reaction mixture was filtered through a sintered-glass funnel and filter cake was washed with benzene (5×1.0 ml). The combined filtrate and washings were evaporated. The residue was flushchromatographed on silica gel (2.3 g) with 4:1 hexane–ethyl acetate to give **5** (16.3 mg, 70%): colorless syrup, R_f=0.50 (4:1 hexane-ethyl acetate) $[\alpha]_D^{30}$ +8.4°, $[\alpha]_{365}^{30}$ +21.5° (*c* 1.05); ^{1}H NMR (90 MHz) δ=0.89 (9H, s, *t*-Bu), 1.36, 1.39 (each 6H, each s, 2×CMe$_2$), 1.20—2.00 (10H, m, 2×H-3, 2×H-6, 2×H-7, 2×H-9, 2×H-11), 2.53 (1H, dd, H-1, $J_{1,2}$=2.7 Hz, J_{gem}=5.1 Hz), 2.77 (1H, dd, H-1), 3.0—3.3 (1H, m, H-2), and 3.40—4.20 (6H, m, H-4,5,8,10).

Found: C, 62.89; H, 9.63%. Calcd for $C_{24}H_{46}O_6Si$: C, 62.84; H, 10.11%.

We are grateful to the Institute of Microbial Chemistry for the generous support of our program. The present work was partially supported by a Grant-in-Aid for Scientific Research No. 60470091 from the Ministry of Education, Science and Culture. We would like to thank Miss Yoshiko Koyama of the Institute for 250 MHz ^{1}H NMR spectral analyses, and Dr. Morio Yashiro for ^{13}C NMR spectral analyses. We are also thank Messers Saburo Nakada and Akio Takahashi of Keio University for elemental analyses.

References

1) Part I: M. Kinoshita, H. Takami, M. Taniguchi, and T. Tamai, *Bull. Chem. Soc. Jpn.*, **60**, 2151 (1987).

2) J. Vandeputte, J. L. Wachtel, and E. T. Stiller, *Antibiot. Annu.*, **1956**, 587.

3) S. Masamune, P. Ma, H. Okumoto, J. W. Ellingboe, and Y. Ito, *J. Org. Chem.*, **49**, 2837 (1984).

4) G. Solladie and J. Hutt, *Tetrahedron Lett.*, **28**, 797 (1987).

5) J. Abiko, T. Takemasa, and S. Masamune, 54th National Meeting of the Chemical Society of Japan, Tokyo,

April 1987, Abstr. No. 3III L 28; J. Abiko, T. Masamune, R. Kennedy, and S. Masamune, *ibid.*, No. 3III L 29; S. Hanessian, S. P. Sahoo, and M. Botta, *Tetrahedron Lett.*, **28**, 1143, 1147 (1987); D. Liang, H. Pauls, and B. Fraser-Reid, M. Georges, A. M. Mubarak, and S. Jarosz, *Can. J. Chem.* **64**, 1800 (1986).

6) H. Redlich and B. Schneider, *Liebigs Ann. Chem.*, **1983**, 412.

7) S. Hanessian and P. Lavullee, *Can. J. Chem.*, **53**, 2975 (1975).

8) E. J. Corey and M. Chaykovsky, *J. Am. Chem. Soc.*, **84**, 866 (1962), see also Ref. 16.

9) P. J. Garegg and B. Samuelsson, *J. Chem. Soc., Chem. Commun.*, **1979**, 978.

10) The isomeric ratio was determined by the HPLC analysis.

11) K. P. R. Kartha, *Tetrahedron Lett.*, **27**, 3415 (1986).

12) P. Pappo, D. S. Allen, Jr., R. U. Lemieux, and W. S. Johnson, *J. Org. Chem.*, **21**, 478 (1956).

13) E. Zissis, R. K. Ness, and H. G. Fletcher, Jr., *Carbohydr. Res.*, **20**, 9 (1971); M. Kinoshita, H. Hamazaki, and M. Awamura, *Bull. Chem. Soc. Jpn.*, **51**, 3595 (1978).

14) I. P. Dirkx and F. L. J. Sixma, *Rec. Trv. Chim.*, **83**, 522 (1964); J. C. Craig and S. K. Roy, *Tetrahedron*, **21**, 1847 (1965).

15) J. A. Secrist III and S.-R. Wu, *J. Org. Chem.*, **44**, 1434 (1979).

16) M. Nakata, Y. Ikeyama, H. Takao, and M. Kinoshita, *Bull. Chem. Soc. Jpn.*, **53**, 3252 (1980).

17) H. Loibner and E. Zbiral, *Helv. Chim. Acta*, **59**, 2100 (1976).

18) S. Achab and B. C. Das, *Synth. Commun.*, **12**, 931 (1982).

 © 1987 The Chemical Society of Japan Bull. Chem. Soc. Jpn., 60, 4015—4018 (1987)

Preparation of Methyl 2-Arylpropanoates by the Reaction of 2-Hydroxypropiophenone Dimethyl Acetals with Sulfuryl Chloride in the Presence of an Amide or a Weak Base

Takayoshi YAMAUCHI,* Kaneaki HATTORI, Kenji NAKAO, and Kentaro TAMAKI
Sakai Research Laboratories, Sakai Plant, Kyowa Hakko Kogyo Co. Ltd.,
1-1-53, Takasu-cho, Sakai-shi, Osaka 590
(Received May 2, 1987)

Treatment of 2-hydroxypropiophenone dimethyl acetals [*p*-$RC_6H_4C(OMe)_2CH(OH)Me$] (**1**; R=H, *i*-Bu, OMe, Ph, Br) with sulfuryl chloride in the presence of an amide or a weak base affords methyl 2-arylpropanoates (**2**) in good to excellent yields via 1,2-aryl migration of **1**. The hydrolysis of **2** leads to the corresponding acids, some of which are pharmaceutically important compounds having nonsteroidal anti-inflammatory and analgesic activities. The aryl migration proceeds stereospecifically with complete inversion of configuration at the β-carbon atom.

It has been known that 2-arylpropanoic acids are useful medical drugs having antipyretic action or nonsteroidal antiinflammatory activity[1,2] Some of these acids are required to be optically active. Many preparative methods for optically active or inactive 2-arylpropanoic acids have so far been developed. Among them, methods using 1,2-aryl migration in alkyl aryl ketones and their derivatives have proven to be very useful;[3] alkyl esters of 2-arylpropanoic acids were obtained by direct oxidation of alkyl aryl ketones in alcohols with thallium(III) nitrate trihydrate,[4-7] (diacetoxyiodo) benzene,[8] iodine-silver nitrate[7] and also by treatment of enamines with diphenyl phosphorazidate.[9] Further, the same compounds were produced as well from aryl 1-haloalkyl ketones or their acetals either by treating them with silver salts[10,11] or Lewis acids,[12,13] or by heating them in protic polar solvents in the absence of metal catalysts.[14] Recently, we also disclosed several new methods for the synthesis of 2-arylpropanoic acid alkyl esters from aryl 1-haloalkyl ketones and related substances.[15-18]

Tsuchihashi et al.[19-21] reported that a base-promoted rearrangement of chiral acetals of 1-aryl-2-sulfonyloxy-1-alkanones proceeds with a complete inversion of the configuration to afford optically active 2-arylalkanoic acids.

We report here a new and facile one-pot preparative method of methyl 2-arylpropanoates from 2-hydroxypropiophenone dimethyl acetals by using sulfuryl chloride in the presence of an amide or a weak base.

Results and Discussion

The reaction was generally carried out by adding sulfuryl chloride to a mixture of 1-aryl-1,1-dimethoxy-2-propanol (**1**) and weak bases or amides in dichloromethane at −50—0 °C. The resulting mixture was stirred for 1—3 h at the same temperature. The main product was methyl 2-arylpropanoate (**2**) and its alkaline hydrolysis afforded the corresponding acid **3** (Scheme 1). Typical results are summarized in Table 1. In these reactions pyridine, diisopropylamine or potassium acetate was found to be effective as a base. *N,N*-Dimethylformamide (DMF) worked as solvent as well as a base and, thus, the treatment of **1** with sulfuryl chloride in this solvent resulted in a high yield formation of **2**. The yield of the rearranged product is satisfactory at lower

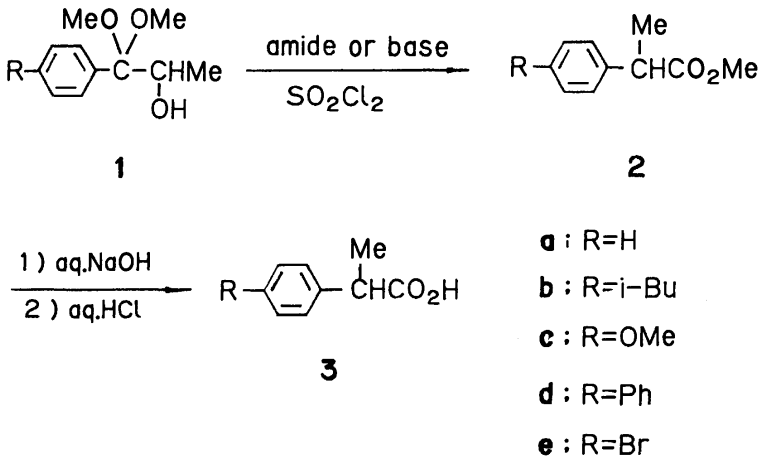

Scheme 1.

reaction temperatures, and generally high when the substituent R is an electron-releasing group such as isobutyl, methoxyl, or phenyl. This tendency is similar to that observed in thallium(III) nitrate-mediated[16] and silver salt-mediated[11] synthesis of alkyl 2-arylpropanoates from aryl 1-haloethyl ketones. The treatment of **1b** in DMF with thionyl chloride instead of sulfuryl chloride at 20 °C for 3 h afforded the expected **2b** in only 17% yield, 2-chloro-4'-isobutylpropiophenone being the main product (47%). The rearrangement did not occur with thionyl bromide or seleninyl chloride ($SeOCl_2$) in pyridine. From the viewpoint of industrial applications of this preparative method, experiments involving the combinational use of sulfur dioxide and halogen gas instead of sulfuryl chloride were also carried out. The reaction proceeded using SO_2–Cl_2, which was revealed to be more economical. Typical results are shown in Table 2. When sulfur dioxide and bromine were used, the yield of **2b** was low, while the rearrangement hardly occurred with a combination of sulfur dioxide and iodine.

Next, the stereochemistry of this rearrangement was investigated using optically active (*R*)-(−)-1-(4-isobutylphenyl)-1,1-dimethoxy-2-propanol [(*R*)-(−)-**1b**] derived from (*S*)-(−)-**1**-(4-isobutylphenyl)-2-methylsulfonyloxy-1-propanone [(*S*)-(−)-**5b**] which in turn was synthesized from L-(+)-lactic acid (**4**) via 5 steps by the known methods[21] (Scheme 2, see Experimental section). Compound (*R*)-(−)-**1b** was obtained in 91% chemical yield by treating optical pure (*S*)-(−)-**5b** with sodium methoxide in methanol at room temperature for 1 h. This procedure is known to proceed with an inversion of the configuration at asymmetric carbon.[22,23] Thus, the stereochemistry of (*R*)-(−)-**1b** should be that shown in Scheme 2. The optical purity of (*R*)-(−)-**1b** was estimated to be 74% ee by NMR measurement using a chiral shift reagent, Eu(hfc)$_3$, indicating the occurrence of a slight racemization under this acetalization condition. A treatment of (*R*)-(−)-**1b**, thus obtained, with sulfuryl chloride in pyridine at −50 °C afforded (*S*)-(−)-**2b** of 74% ee. The result clearly shows that the rearrangement of (*R*)-(−)-

Table 1. Preparation of **2** from **1**[a]

Compound	Base or amide	Reaction condition		Yield of **2**[b]
		Temp/°C	Time/h	%
1a	Pyridine	−50	3	55
1b	Pyridine	−50	3	86
1b	Pyridine	0	1	73
1b	(*i*-Pr)$_2$NH[d]	0	3	72[c]
1b	*i*-PrNH$_2$[d]	0	3	61[c]
1b	AcOK[d]	0	3	64
1b	DMF[e]	−50	3	84
1b	DMF[e]	0	3	86[c]
1c	Pyridine	−50	3	85
1d	Pyridine	−50	3	87
1e	Pyridine	−50	3	54

a) Carried out using **1** (5 mmol), SO_2Cl_2 (7.5 mmol), and a base or an amide (12.5 ml) in dichloromethane (12.5 ml). b) Isolated yield by column chromatography. c) Determined by GLC analysis. d) 10 mmol. e) DMF was used as the solvent (12.5 ml).

Table 2. Preparation of **2b** from **1b** Using Halogen, Sulfur Dioxide, and Base[a]

Base	Halogen	Yield of **2b**[b]
		%
Et_3N	Cl_2	95 (88)[d]
Et_3N	Cl_2[c]	93
Pyridine	Cl_2	94
Pyridine	Br_2	48
Pyridine	I_2	Trace
i-PrNH$_2$	Cl_2	75
Et_2NH	Cl_2	52

a) Carried out using **1b** (10 mmol), base (15 mmol), sulfur dioxide (15 mmol), halogen (15 mmol), and dichloromethane (61 ml) at −50 °C for 3 h. b) Determined by GLC analysis. c) 10 mmol. d) Isolated yield.

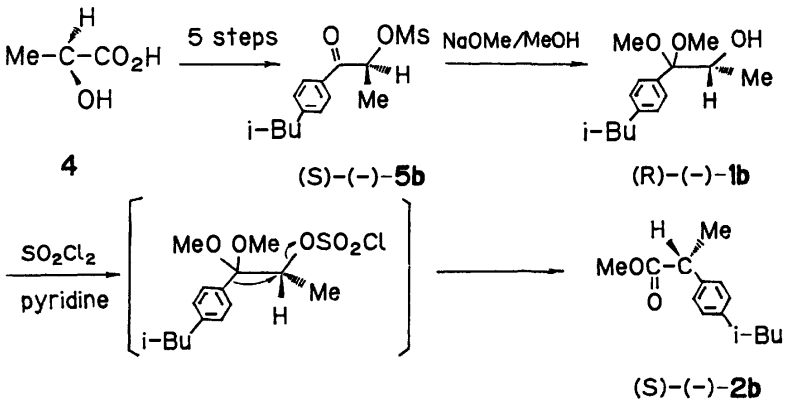

Scheme 2.

1b to (*S*)-(−)-**2b** proceeded with a complete inversion of the configuration at the β-carbon atom (Scheme 2). This new and economical method for the preparation of an optically active 2-arylalkanoic acid is industrially important.

Experimental

^{1}H NMR spectra were recorded with a JEOL FX-90Q (90 MHz) instrument on solutions in $CDCl_3$ with Me_4Si as an internal standard. GLC analyses were carried out with a Shimadzu 4CMPF apparatus by using DEGS (2%) on Gas Chrom Q (3 mm×1.5 m) and OV-101 (0.24 mm×30 m) columns (N_2 as carrier gas). IR spectra were recorded with a Shimadzu IR-435 spectrometer. Melting points were determined with Yanagimoto MP micro melting-point determination apparatus and were uncorrected. Optical rotations were measured on a Union PM-201 automatic polarimeter.

All organic and inorganic materials were commercial products of the purest grade. 1-Aryl-1,1-dimethoxy-2-propanols (**1**) were prepared by the literature method[19] from methanol, sodium methoxide, and 2-halopropiophenone.

Rearrangement of 1 to Methyl 2-Arylpropanoates (2). A typical example is as follows. To the solution of **1b** (1.26 g, 5 mmol) in pyridine (12.5 ml) and dichloromethane (12.5 ml) was added sulfuryl chloride (1.01 g, 7.5 mmol) at −50 °C under stirring. After the mixture was stirred for 3 h at the same temperature, saturated aqueous $NaHCO_3$ (25 ml) was added and then an aqueous layer was extracted with chloroform (3×75 ml). The extract was dried over $MgSO_4$ and the solvent was removed by evaporation under reduced pressure. The resulting oily residue was purified by column chromatography on SiO_2 [hexane–ethyl acetate (30:1) as eluent] to give **2b** (0.95 g, yield 86%) as a pale yellow oil.

An experiment using isopropylamine, diisopropylamine or potassium acetate as a base was carried out in a 1/5-fold scale and **2b** was analyzed by GLC using triphenylmethane as an internal standard [2% DEGS on Gas Chrom Q, (3 mm×1.5 m) column at 100→200 °C (5 °C min^{-1})]. The yield of **2a**, **2c**, **2d**, and **2e** was determined by GLC on OV-101 (0.24 mm×30 m) column [at 120→260 °C (4 °C min^{-1})] using an internal standard: pentamethylbenzene for **2a** and **2c**, and biphenyl for **2d** and **2e**.

Experiments using $SOCl_2$/DMF, $SOBr_2$/pyridine, and $SeOCl_2$/pyridine were similarly carried out.

Alkaline hydrolysis of **2** to **3** was carried out as previously reported.[15–17]

Rearrangement of 1b with Sulfur Dioxide and Halogen. To a solution of **1b** (10 mmol) in dichloromethane (40 ml) were added an amine (15 mmol) and a solution of sulfur dioxide (0.96 g, 15 mmol) in dichloromethane (7 ml) successively, and the resulting mixture was cooled down to −50 °C. To the mixture was added dropwise a solution of halogen (15 mmol) in dichloromethane (14 ml) and the mixture was stirred at −50 °C for 3 h. After a similar treatment as above, **2b** in the extract was analyzed by GLC and isolated by column chromatography in a pure form (as described above).

Synthesis of (*R*)-(−)-1-(4-Isobutylphenyl)-1,1-dimethoxy-2-propanol [(*R*)-(−)-1b]. **(a) (−)-Ethyl L-Lactate (6).** A solution of L-(+)-lactic acid (**4**, 89.2 g, 0.99 mol) and concentrated sulfuric acid (8.93 g, 91 mmol) in ethanol (893 ml) was refluxed for 2 h. After it had been cooled down, the mixture was neutralized to pH 5.2 with saturated aqueous $NaHCO_3$. Evaporation of the solvent left an oily residue which was distilled to give **6**; bp 78.5 °C/43 Torr (1 Torr=133.322 Pa) (67.3 g, 57 mmol, 57.5% yield); $[\alpha]_D^{19}$ −10.7° (neat) [lit,[24] $[\alpha]_D^{19}$ −11.26° (neat)]; Found: C, 76.05; H, 9.13%. Calcd for $C_{14}H_{20}O_2$: C, 76.32; H, 9.15%. ^{1}H NMR ($CDCl_3$) δ=1.30 (3H, t), 1.42 (3H, d), 3.32 (1H, s), 4.1—4.4 (3H, m).

(b) (−)-Ethyl (*S*)-2-(Methylsulfonyloxy) propanoate (7). To a solution of **6** (64.7 g, 548 mmol) in dichloromethane (110 ml) was added methylsulfonyl chloride (81.6 g, 712 mmol) at −20 °C, then pyridine (52.0 g, 657 mmol) was added dropwise at −15—−20 °C for 1 h. After the mixture was stirred at −15 °C for 3 h, it was quenched with water (137 ml), neutralized to pH 4.7 with 3 mol dm^{-3} sodium hydroxide (190 ml), and extracted with dichloromethane (356 ml). The organic layer was washed with brine (685 ml) and dried ($MgSO_4$). The solvent was evaporated under reduced pressure and an only residue was distilled in vacuo to give **7**; bp 106 °C/2.5 Torr (74.1 g, 378 mmol, 68.9% yield, lit,[21] bp 97—102 °C/2 Torr); $[\alpha]_D^{22}$ −52.3 °C (*c* 1.00, $CHCl_3$) [lit,[21] $[\alpha]_D^{19}$ −50.55 (*c* 1.00, $CHCl_3$)]; ^{1}H NMR ($CDCl_3$) δ=1.29 (3H, t), 1.58 (3H, d), 3.11 (3H, s), 4.22 (2H, q), 5.06 (1H, q).

(c) (*S*)-(−)-2-(Methylsulfonyloxy)propionic Acid (8). A solution of potassium hydroxide (25 g, 446 mmol) in water (250 ml) was slowly added to **7** (72.8 g, 371 mmol) at 5—10 °C during 1 h. The mixture was stirred at 10—15 °C for 3 h, then acidified to pH 1.0 with concentrated hydrochloric acid (35 ml), and extracted with ethyl acetate (3×450 ml). The organic layer was dried ($MgSO_4$) and evaporated under reduced pressure. The crystalline residue was suspended with hexane (180 ml) and filtered to give crude **8**; mp 69 °C (55.1 g, 328 mmol, 88.4% yield, lit,[21] mp 65—72 °C); $[\alpha]_D^{22}$ −53.9° (*c* 1.00, $CHCl_3$) [lit, [21] $[\alpha]_D^{22}$ −49.8° (*c* 1.00, $CHCl_3$)]; ^{1}H NMR ($CDCl_3$) δ=1.68 (3H, d), 3.12 (3H, s), 5.15 (1H, q), 9.10 (1H, br s).

(d) (*S*)-(−)-2-(Methylsulfonyloxy)propionyl Chloride (9). A mixture of **8** (55.1 g, 328 mmol) and thionyl chloride (78 g, 656 mmol) was refluxed for 4 h. The mixture was distilled in vacuo to give **9**; bp 91—93 °C/2 Torr (52.9 g, 283 mmol, 86.4% yield, lit,[21] bp 70—74 °C/1.5 Torr); ^{1}H NMR ($CDCl_3$) δ=1.75 (3H, d), 3.17 (3H, s), 5.28 (1H, q).

(e) (*S*)-(−)-1-(4-Isobutylphenyl)-2-methylsulfonyloxy-1-propanone [(*S*)-(−)-5b]. To a solution of isobutylbenzene (20.1 g, 150 mmol) and **9** (18.7 g, 100 mmol) in nitromethane (100 ml) was added iron(III) chloride (17.8 g, 110 mmol) at 5—10 °C. The mixture was stirred at room temperature for 4 h, then quenched with water (200 ml), and extracted with ethyl acetate (2×100 ml). The organic layer was washed with brine (200 ml) and dried ($MgSO_4$). The solvent was evaporated under reduced pressure to leave an oily residue which was purified by column chromatography on SiO_2 [hexane–ethyl acetate (30:1—4:1) as eluent] to give (*S*)-(−)-**5b**; mp 82.5 °C (15.0 g, 52.9 mmol) 52.9% yield, lit,[21] mp 81—82 °C), $[\alpha]_D^{24}$ −52.53° (*c* 1.00, $CHCl_3$) [lit,[21] $[\alpha]_D^{24}$ −52.48° (*c* 1.00, $CHCl_3$)], IR (KBr disk) 2960, 1697, 1609, 1240, 1180, 1023, and 745 cm^{-1}, ^{1}H NMR ($CDCl_3$) δ=0.90 (6H, d), 1.63 (3H, d) 1.6—2.1 (1H, m), 2.53 (2H, d), 3.10 (3H, s), 6.00 (1H, q), 7.23 (2H, d), 7.83 (2H, d).

(f) (*R*)-(−)-1b. To a solution of (*S*)-(−)-**5b** (10.0 g,

35 mmol) in methanol (70 ml) was added a solution of sodium methoxide (3.78 g, 70 mmol) in methanol (47 ml) at room temperature and the mixture was stirred for 1 h. After water (300 ml) and ethyl acetate (100 ml) were added to the mixture, two layers were separated and the aqueous layer was then extracted with ethyl acetate (100 ml). The combined organic layers were dried ($MgSO_4$). Evaporation of the solvent under reduced pressure left an oily residue which was distilled in vacuo to give (*R*)-(−)-**1b**; bp 97—100 °C/0.2 Torr (8.07 g, 32 mmol, 91.4% yield); $[\alpha]_D^{21}$ −1.64 °C (*c* 1.00, $CHCl_3$); ^1H NMR ($CDCl_3$) δ=0.89 (6H, d), 0.97 (3H, d), 1.6—2.1 (1H, m), 2.35 (1H, br. s), 2.45 (2H, d), 3.20 (3H, s), 3.36 (3H, s), 3.95—4.20 (1H, m), 7.08 (2H, d), 7.34 (2H, d); when the signal at δ=3.36 of methoxy group was determined in the presence of 5 mol% of tris[3-(heptafluoropropylhydroxymethylene)-*d*-camphorato] europium(III) [Eu(hfc)$_3$], this signal was separated into two signals at δ=3.93 and 4.03. From the integration value of these signals, the ratio of (−)-form/(+)-form was determined to be 87/13 (74±2% ee).

(−)-Methyl (*S*)-2-(4-Isobutylphenyl) propanoate [(*S*)-(−)-2b]. To a solution of (*R*)-(−)-**1b** (5.0 g. 19.8 mmol), pyridine (3.13 g, 39.6 mmol), and dichloromethane (3.96 ml) was added sulfuryl chloride (4.01 g, 29.7 mmol) at −50 °C for 10 min. The mixture was stirred at the same temperature for 3 h and then quenched with saturated aqueous $NaHCO_3$ (50 ml). The resulting mixture was added with water (100 ml) and chloroform (100 ml). The two layers were separated and the aqueous layer was extracted with chloroform (100 ml). The combined organic layers were washed with brine (100 ml) and dried ($MgSO_4$). Evaporation of the solvent left a light-yellow oil which was subjected to column chromatography on SiO_2 [hexane–ethyl acetate (10:1—5:1) as eluent] to give (*S*)-(−)-**2b**; bp 85—86 °C/0.3 Torr (3.46 g, 15.7 mmol, 79.3% yield); $[\alpha]_D^{23}$ −48.4° (*c* 1.00, $CHCl_3$) lit,[21] $[\alpha]_D^{23}$ −56.2° (*c* 1.00, $CHCl_3$); ^1H NMR ($CDCl_3$) δ=0.09 (6H, d), 1.47 (3H, d), 1.6—2.1 (1H, m), 2.44 (2H, d), 3.63 (3H, s), 3.68 (1H, q), 7.05 (2H, d), 7.18 (2H, d); when the signal at δ=3.63 of ester methyl group was determined in the presence of 80 mol% of Eu(hfc)$_3$, this signal was separated into two signals at δ=5.68 and 5.74. From the integration value of these signals, the ratio of (−)-form/(+)-form was determined to be 87/13 (74±2% ee).

We thank Dr. Sakae Uemura of Kyoto University for useful discussions.

References

1) See, for example; T. Y. Shen, *Angew. Chem., Int. Ed. Engl.*, **11**, 460 (1972).
2) J.-P. Rieu, A. Boucherle, H. Cousse, and G. Mouzin, *Tetrahedron*, **42**, 4095 (1986).
3) For a recent review, see, C. Giordano, G. Castaldi, and F. Uggeri, *Angew. Chem., Int. Ed. Engl.*, **23**, 413 (1984).
4) A. McKillop, B. P. Swann, and E. C. Taylor, *J. Am. Chem. Soc.*, **95**, 3340 (1973).
5) E. C. Taylor, R. L. Robey, K.-T. Liu, B. Favre, H. T. Bozimo, R. A. Conley, C.-S. Chiang, A. McKillop, and M. E. Ford, *J. Am. Chem. Soc.*, **98**, 3037 (1976).
6) E. C. Taylor, C.-S. Chiang, A. McKillop, and J. F. White, *J. Am. Chem. Soc.*, **98**, 6750 (1976).
7) S. D. Higgins and C. B. Thomas, *J. Chem. Soc., Perkin Trans. 1*, **1982**, 235.
8) Y. Tamura, Y. Shirouchi, and J. Haruta, *Synthesis*, **1984**, 231.
9) T. Shioiri and N. Kawai, *J. Org. Chem.*, **43**, 2936 (1978).
10) C. Giordano, G. Castaldi, F. Casagrande, and L. Abis, *Tetrahedron Lett.*, **23**, 1385 (1982).
11) C. Giordano, G. Castaldi, F. Casagrande, and A. Belli, *J. Chem. Soc., Perkin Trans. 1*, **1982**, 2575.
12) G. Castaldi, A. Belli, F. Uggeri, and C. Giordano, *J. Org. Chem.*, **48**, 4658 (1983).
13) C. Giordano, G. Castaldi, F. Uggeri, and F. Gurzoni, *Synthesis*, **1985**, 436.
14) G. Castaldi, C. Giordano, and F. Uggeri, *Synthesis*, **1985**, 505.
15) K. Fujii, K. Nakao, and T. Yamauchi, *Synthesis*, **1982**, 456; *idem, J. Chem. Soc., Perkin Trans. 1*, **1987**, 1433.
16) K. Fujii, K. Nakao, and T. Yamauchi, *Synthesis*, **1983**, 444; *idem, J. Chem. Soc., Perkin Trans. 1*, **1987**, 1255.
17) S. Uemura, S. Fukuzawa, T. Yamauchi, K. Hattori, S, Mizutaki, and K. Tamaki, *J. Chem. Soc., Chem. Commun.*, **1984**, 426; *idem, J. Chem. Soc., Perkin Trans. 1*, **1986**, 1983.
18) Preliminary communication of this paper, T. Yamauchi, K. Hattori, K. Nakao, and K. Tamaki, *Synthesis*, **1986**, 1044.
19) G. Tsuchihashi, K. Kitajima, and S. Mitamura, *Tetrahedron Lett.*, **22**, 4305 (1981).
20) G. Tsuchihashi, S. Mitamura, K. Kitajima, and K. Kobayashi, *Tetrahedron Lett.*, **23**, 5427 (1982).
21) G. Tsuchihashi, K. Kitajima, and S. Mitamura, Jpn. Kokai Tokkyo Koho, JP, 10525/1983 [*Chem. Abstr.*, **98**, 178945y (1983)].
22) N. D. Kimpe, L. D. Buyck, R. Verhe, and N. Schamp, *Chem. Ber.*, **116**, 3631 (1983).
23) G. Tsuchihashi, S. Mitamura, A. Kitajima, and K. Kobayashi, 47th Annual Meeting of the Chemical Society of Japan, Kyoto, March 1983, Abstr. II, No. 1F06.
24) C. E. Wood, J. E. Such, and F. Scarf, *J. Chem. Soc.*, **1926**, 1928.

 © 1987 The Chemical Society of Japan Bull. Chem. Soc. Jpn., 60, 4019—4026 (1987)

NAD(P)$^+$-NAD(P)H Models. 64. The Quantitative Elucidation of the Mechanistic Aspects in the Silica Gel-Catalyzed Reduction of α,β-Unsaturated Carbonyl Compounds by a Model of NAD(P)H

Shinro YASUI,* Masayuki FUJII,† and Atsuyoshi OHNO†
Tezukayama College, Gakuen-Minami, Nara 631
†Institute for Chemical Research, Kyoto University, Uji, Kyoto 611
(Received May 9, 1987)

Eight α,β-unsaturated carbonyl compounds, 1-(2′- or 4′-substituted phenyl)-3-phenyl-2-propen-1-ones (2′- or 4′-substituted chalcones), were subjected to the reduction by an NAD(P)H model in the presence of silica gel in benzene. All of these afforded quantitatively the corresponding saturated carbonyl compounds, whereas no 1,2-reduction took place. For 2′-methoxy, 4′-methyl, 4′-bromo, and 4′-nitro derivatives as well as the unsubstituted carbonyl compound, the apparent reactivity of the substrate increases with the increase in electron-withdrawing ability of the substituent, whereas the degree of the adsorption onto the surface of silica gel decreases. It is also apparent that the 4′-hydroxy derivative exerts lower reactivity than the 2′-hydroxy derivative in spite of much more efficient adsorption of the former. In order to uniformly interpret the apparent results, the data obtained were quantitatively analyzed in terms of kinetics as well as equilibrium constants for the adsorption of the substrates onto the surface of silica gel. It has been revealed that the silanol group on the surface of silica gel acts as a general-acid catalyst in the reduction.

Attentions have been paid recently upon the selective reductions by an NAD(P)H model with its advantage in mildness of reducing ability.[1-6] A certain catalyst sometimes plays a crucial role in such reductions, and there is no doubt that the success for highly selective reduction by an NAD(P)H model depends on a novel catalytic system. For example, we presented the rhodium complex-catalyzed reductive dehalogenation by an NAD(P)H model as a selective reaction applicable to organic halides of several types.[4] Recently, we found that silica gel acts as a catalyst in the selective hydrogenations of carbon-carbon multi-bonds in 1,2-bis(ethoxycarbonyl)alkenes and -alkynes with an NAD(P)H model although the yield of the reduction product was not satisfactory.[5] Semiquantitative analyses of the reduction have suggested that silanol groups on the surface of silica gel contribute to the reaction through general acid catalysis. The analysis was based on the comparisons of the reactivity and the equilibrium constant for the adsorption of these substrates onto the surface of silica gel. We also suggested a possibility that a hydride-equivalent transfers from the NAD(P)H model adsorbed on the surface of silica gel to the substrate in the bulk phase. Nevertheless, the role of silica gel could not be definitively clarified, because the structures of the substrates subjected to the reduction were largely different from each other and quantitative argument on the structure-reactivity relationship was little possible.[5]

More striking catalysis by silica gel was found in the 1,4-reduction of α,β-unsaturated carbonyl compound by an NAD(P)H model; the reduction brings about the corresponding saturated carbonyl compound in quantitative amount whereas no 1,2-reduction takes place.[6] Moreover, functional groups such as carbonyl and ester groups as well as isolated carbon-carbon double bond are inert under the conditions. Then, we intended to examine the reduction of a series of α,β-unsaturated carbonyl compounds by an NAD(P)H model in details to elucidate the role of silica gel.

In this article, we wish to report the results for the reduction of α,β-unsaturated carbonyl compounds, 1-(2′- or 4′-substituted phenyl)-3-phenyl-2-propen-1-ones (2′- or 4′-substituted chalcones) (**1a—h**), by an NAD(P)H model, 3,5-bis(ethoxycarbonyl)-1,4-dihydro-2,6-dimethylpyridine (Hantzsch ester: HEH), in the presence of silica gel in benzene. The reduction of **1a—h** afforded the corresponding saturated carbonyl compounds, 1-(2′- or 4′-substituted phenyl)-3-phenyl-1-propanone (**2a—h**), respectively. No 1,2-reduction was detected. Detailed discussion on the mechanism will be presented based on kinetics and thermodynamics.

Results

In order to obtain reliable results in the product analyses, the kinetics, and equilibrium constants for the adsorption onto the surface of silica gel, silica gel of relatively large mesh, silica gel 60 with 35—70 mesh (Nakarai Chem. Co.), was employed as a catalyst.[5] As an NAD(P)H model, HEH was used because of its higher tolerance against self-decomposition in the presence of silica gel during the reaction.[6] It has been confirmed that water contained in commercial silica gel affects little both the reactivity and the equilibrium,[7] and then neither dryness nor purification of the silica gel is necessary prior to use. Benzene has been found to be the best in this reaction among the solvents examined.

Reduction with HEH. The reaction of 1.0×10^{-1}

mmol of **1** with 1.5×10^{-1} mmol of HEH in the presence of 0.2 g of the silica gel in 1 ml of benzene was carried out under the nitrogen atomosphere at 70 °C in the dark with mechanical stirring. After appropriate period, the reaction mixture was analyzed on VPC according to the procedure described previously.[5] The results are summarized in Table 1. From the viewpoint of amounts of the starting material and the product, it is obvious that the 1,4-reduction is almost exclusive process. The order of apparent reactivity is **1d<1e≃1c≤1f<1a<1g<1b<1h**.

Table 1. Reduction of **1** by HEH in the Presence of the Silica Gel[a]

Substrate	Reaction time/h	Yield[b]/% Recov.[c]	Redn.[d]	
1a	1	65	26	
	1.5	54	38	
	2.5	34	51	
	18	Trace	87	(56)
1b	0.5	74	21	
	1	49	51	
	1.5	32	68	
	2.5	20	80	
	4	ND[e]	95	(85)
	16[f]	81	13	
1c	1	85	15	
	2.5	58	42	
	18	ND[e]	100	(80)
1d	1	87	13	
	2.5	70	30	
	4	58	42	
	18	<8	92	(69)
1e	1	80	20	
	2.5	59	41	
	4	41	59	
	18	ND[e]	99	(93)
1f	1	76	24	
	2.5	51	47	
	4	35	61	
	5.5	23	77	
	18	ND[e]	96	(95)
1g	1	69	29	
	2.5	35	63	
	4	21	76	
	18	ND[e]	98	(88)
1h	0.5	57	43	
	1	25	74	
	2	8	92	
	4	ND[e]	100	(97)

a) 1.0×10^{-1} mmol of **1** and 1.5×10^{-1} mmol of HEH were used. The reaction was carried out in 1 ml of benzene at 70 °C in the dark under N_2 atmosphere in the presence of 0.2 g of the silica gel. b) The yield determined by VPC analysis based on the amount of the substrate used. The values in parentheses indicate the isolated yield from the reaction of 5.0×10^{-1} mmol of **1** and 7.5×10^{-1} mmol of HEH in the presence of 1.0 g of the silica gel in 5 ml of benzene. c) The yield of the recovered starting material. d) The yield of the reduction product, corresponding saturated carbonyl compound. e) Not detected. f) Without the silica gel.

Reduction products isolated from the run in larger scale after enough reaction period were analyzed on NMR and IR spectrometers. Importantly, all substrates examined afforded the corresponding saturated carbonyl compounds **2a—h** in quantitative yields along with 3,5-bis(ethoxycarbonyl)-2,6-dimethylpyridine (HE_{ox}), the oxidized form of HEH, in slightly more than theoretical amount, whereas no 1,2-reduction products were recognized.[8] Small portion of HE_{ox} may be resulted from autoxidation of HEH on the surface of silica gel although the details are not clear.

Adsorption onto the Surface of Silica Gel. As described previously,[5] the degree of the adsorption of **1** onto the surface of silica gel can be evaluated by an equilibrium constant K_{Ad} ($=S_{Ad}/(S_{Bulk}\cdot Q_{free})$) (Eq. 1)

$$S_{Bulk} + Q_{free} \overset{K_{Ad}}{\rightleftarrows} S_{Ad} \quad (1a)$$

$$Q_{free} = Q_0 - S_{Ad} \quad (1b)$$

where S_{Bulk} and S_{Ad} are the amounts (mmol) of **1** in bulk phase and adsorbed one, respectively. Q_0 is the "effective" amount (mmol) of adsorbing centers for **1** on the 0.2 g of silica gel, which can be counted as the maximum amount (mmol) of **1** to be adsorbed. The equilibrium constant K_{Ad} was obtained from the slope and the intercept of the plot of $1/S_{Ad}$ vs. $1/S_{Bulk}$ with the amount of **1** being variable, based on Eq. 2 derived from Eq. 1. Excellent linear correlations (correlation coefficients; $r>0.999$) were seen in the double-reciprocal plots for all substrates.

$$\frac{1}{S_{Ad}} = \frac{1}{K_{Ad}\cdot Q_0}\cdot\frac{1}{S_{Bulk}} + \frac{1}{Q_0} \quad (2)$$

Since the experiment was performed in 1 ml of benzene, each term with the dimension of mmol is equivalent to molarity (M (M=mol dm^{-3})) and the equilibrium constant K_{Ad} thus obtained has a

Table 2. Equilibrium Constants K_{Ad} for Adsorption of the Substrates into the Surface of the Silica Gel[a]

Substrate	K_{Ad}/M^{-1}	Substrate	K_{Ad}/M^{-1}
1a	693	**2f**	1.90
1b	3.33	HEH	51.1
1c	9.51	HE_{ox}	44.5
1d	9.64	**3**	21.3
1e	9.11	**4**	12.2
1f	6.81		
1g	5.49		
1h	4.25		

a) At 70 °C.

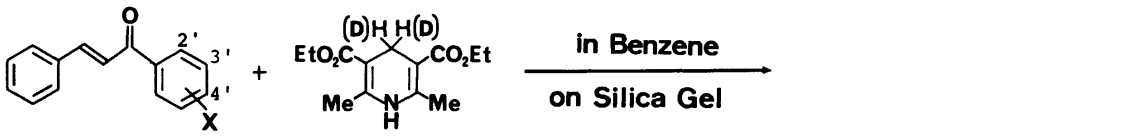

1a; X = 4'-OH
b; X = 2'-OH
c; X = 4'-OMe
d; X = 2'-OMe
e; X = 4'-Me
f; X = H
g; X = 4'-Br
h; X = 4'-NO_2

HEH

2

HE_{ox}

dimension of M^{-1}. The values of K_{Ad} for **1a—h** are summarized in Table 2 together with that for HEH reported previously.[5] Table 2 also involves the values for 4-phenyl-3-buten-2-one (**3**), 4-phenyl-2-butanone (**4**), and **2f** as well as HE_{ox}. It should be emphasized that, as expected from the Eq. 2, each plot gave the identical value for the intercept within experimental error. Since the substrates have wide range of K_{Ad} values (from 3.33 M^{-1} for **1b** to 693 M^{-1} for **1a**), Q_0 of $(7.25\pm0.25)\times10^{-2}$ mmol was obtained with an excellent accuracy. The value of Q_0 elucidated here is well coincident with that previously calculated-($(7.37\pm0.28)\times10^{-2}$ mmol) based on the same method for diethyl maleate, fumarate, and acetylenedicarboxylate as well as for HEH.[5] Recently, the amount of acidic active sites on a silica gel as well as its B.E.T. surface area was reported based on a measurement by means of titration with pyridine.[9] From the values reported, the amount of acidic active sites on the 0.2 g of silica gel is calculated to be 7.0×10^{-2} mmol, which excellently agrees with Q_0 elucidated in the present study, suggesting that the "adsorbing center" defined above corresponds to the "acidic active site" in the literature.

Kinetics. The data listed in Table 1 were kinetically investigated. Since no reduction of **1** with HEH takes place in the absence of silica gel, there remains no doubt that the reaction proceeds according to any one of Eqs. 3—5:

$$\mathbf{1}_{Ad} + HEH_{Ad} \xrightarrow{k_{AA}} \text{Products} \quad (3)$$

$$\mathbf{1}_{Bulk} + HEH_{Ad} \xrightarrow{k_{BA}} \text{Products} \quad (4)$$

$$\mathbf{1}_{Ad} + HEH_{Bulk} \xrightarrow{k_{AB}} \text{Products} \quad (5)$$

The corresponding rate expressions are those shown in Eqs. 6—8, respectively.

$$\text{rate} = k_{AA}[\mathbf{1}]_{Ad}[HEH]_{Ad} \quad (6)$$

$$\text{rate} = k_{BA}[\mathbf{1}]_{Bulk}[HEH]_{Ad} \quad (7)$$

$$\text{rate} = k_{AB}[\mathbf{1}]_{Ad}[HEH]_{Bulk} \quad (8)$$

It is not straightforward to obtain second-order rate constants k_{AA}, k_{BA}, and k_{AB} because each concentration term is governed by complex functions of either equilibrium constants K_{Ad} for coexisting components, **1**, **2**, HEH, and HE_{ox}, or their stoichiometric concentrations, which change complicatedly during the reaction. Here, it may be profitable to simulate the change of $[\mathbf{1}]_{Ad}$, $[\mathbf{1}]_{Bulk}$, $[HEH]_{Ad}$, and $[HEH]_{Bulk}$ as a function of stoichiometric concentration of **1**, $[\mathbf{1}]_{Total}$ ($=[\mathbf{1}]_{Ad}+[\mathbf{1}]_{Bulk}$). The computer-assisted simulation was performed by using the K_{Ad} values for **1**, **2**, HEH, and HE_{ox}.[10] The K_{Ad} values for the reduction products **2** were not obtained experimentally except for that for **2f**. However, arbitrary change in K_{Ad} for **2** from one-fifth to twice of that for the corresponding **1** scarcely affected the simulations.[11] The simulation curves for the reactions of 1.0×10^{-1} mmol of the substrate with 1.5×10^{-1} mmol of HEH in 1 ml of the solvent (the reaction conditions in the present study) are depicted in Figs. 1 and 2.

The simulations for **1b—h** afforded the results with a similar propensity as exemplified in Fig. 1 for **1f**, where $[\mathbf{1}]_{Ad}$, $[\mathbf{1}]_{Bulk}$, $[HEH]_{Ad}$, and $[HEH]_{Bulk}$ are linearly correlated with $[\mathbf{1}]_{Total}$ approximately. Then, for **1b—h** Eqs. 6—8 can be analyzed in terms of second-order rate equations with respect to $[\mathbf{1}]_{total}$.[12] The second-order rate equations thus derived from Eqs. 6—8, respectively, are mathematically equivalent. Accordingly, the data in Table 1 afforded kineticaly indistinguishable three sets of second-order rate constants for the reactions of **1b—h**. The data after long reaction period in Table 1 were, unfortunately, not available for the kinetic analyses, because the reaction gives rise to the decomposition of HEH and/or the change in the activity of the silica gel after long period. However, that the rate constant were obtained with moderate reliability (correlation

coefficients; $r>0.99$) demonstrates the validity of the treatment at least at an early stage of the reaction. Table 3 summarizes the second-order rate constants k_{AA}, k_{BA}, and k_{AB} corresponding to Eqs. 6—8, respectively, for **1b—h**.

On the other hand, Fig. 2 shows that during the decrease in $[\mathbf{1a}]_{Total}$ from 1.0×10^{-1} M to ca. 0.4×10^{-1} M, $[HEH]_{Ad}$ was kept almost constant (1.34×10^{-2} M$\simeq$ 1.40×10^{-2} M under the assumption that K_{Ad} for **2a** is 139 M^{-1}), whereas $[HEH]_{Bulk}$ dramatically decreased. In fact, it was found that the observed rate for the reduction of **1a** obeys a first-order rate equation with respect to $\mathbf{1a}_{Ad}$ or $\mathbf{1a}_{Bulk}$ with an excellent linear correlation at least before ca. 50% of **1a** was consumed

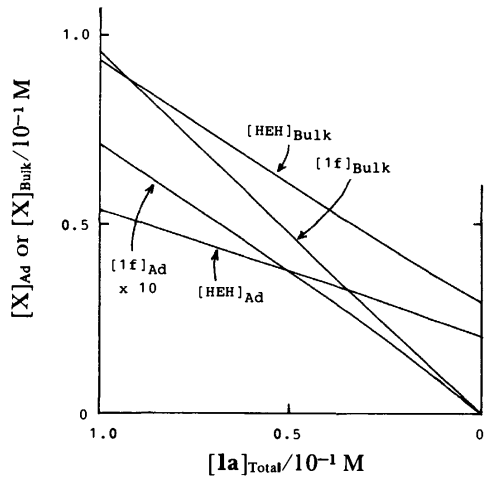

Fig. 1. The simulation curves of $[\mathbf{1f}]_{Ad}$, $[\mathbf{1f}]_{Bulk}$, $[HEH]_{Ad}$, and $[HEH]_{Bulk}$ as a function of $[\mathbf{1f}]_{Total}$.

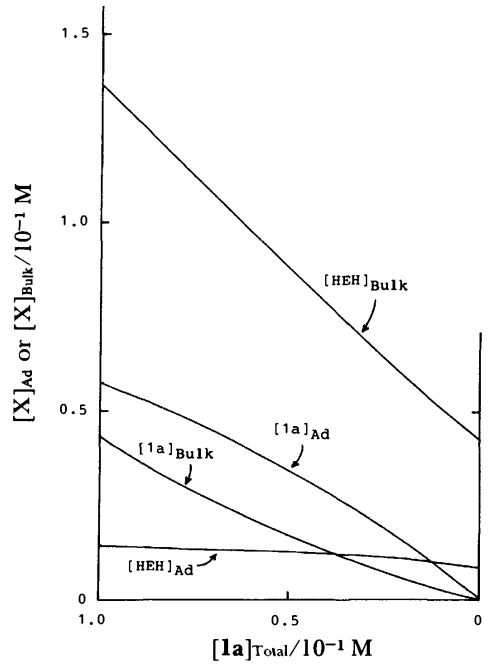

Fig. 2. The simulation curves of $[\mathbf{1a}]_{Ad}$, $[\mathbf{1a}]_{Bulk}$, $[HEH]_{Ad}$, and $[HEH]_{Bulk}$ as a function of $[\mathbf{1a}]_{Total}$.

(correlation coefficients; $r>0.999$). The finding manifests invalidity of Eq. 8 composed of two varying terms ($[\mathbf{1a}]_{Ad}$ and $[HEH]_{Bulk}$), and in turn excludes Eq. 5 as a possible reaction path. Therefore, we obtained second-order rate constants k_{AA} and k_{BA} for the reaction of **1a** by dividing the observed first-order rate constants by 1.3×10^{-2} M (=$[HEH]_{Ad}$ in Fig. 2). The results are listed in Table 3.

Deuterium Isotope Effect. In the reduction of **1f** by 3,5-bis(ethoxycarbonyl)-1,4-dihydro-2,6-dimethylpyridine-4,4-d_2 (HEH-4,4-d_2), the NMR spectrum of the product **2f** confirmed the incorporation of quantitative amount of a deuterium into the β-position. Thus, Michael-type migration of a hydride-equivalent occurs in this reaction. Interestingly, it has been confirmed that the hydrogen at the 4-position of 1-benzyl-1,4-dihydronicotinamide, an NAD(P)H model, also migrates onto the β-position of 4-(unsubstituted or *p*-bromo- and *p*-nitrocinnamoyl)-pyridines in the presence of magnesium perchlorate in acetonitrile.[13]

Reductions of **1a**, **b**, **f**, and **g** by HEH-4,4-d_2 were kinetically followed, and primary kinetic deuterium isotope effects calculated for k_{AA} are listed in Table 4. The values indicate that a hydride-equivalent transfers from HEH to **1** in the rate-determining step.

Discussion

In Fig. 3, $\log(K^X_{Ad}/K^H_{Ad})$ derived from the values in Table 2 are plotted against the substituent σ-values. The σ-values for the 4′-substituents are tentatively

Table 3. Second-Order Rate Constants for the Reduction of **1** by HEH[a]

Substrate	k_{AA}[b] min^{-1} M^{-1}	k_{BA}[b] $\times10^{-1}$ min^{-1} M^{-1}	k_{AB}[b] min^{-1} M^{-1}
1a	0.526±0.083	6.02 ±1.55	—
1b	0.06 ±0.92	3.20 ±0.37	5.06 ±0.75
1c	0.910±0.143	0.599±0.037	0.496±0.066
1d	0.555±0.034	0.965±0.097	0.304±0.011
1e	1.03 ±0.11	1.00 ±0.11	0.568±0.037
1f	1.71 ±0.09	1.29 ±0.07	0.790±0.004
1g	3.17 ±0.33	2.08 ±0.22	1.67 ±0.18
1h	15.1 ±2.1	7.50 ±1.04	9.23 ±1.18

a) Derived from the data in Table 2. b) Errors contain those originated from uncertainty of K_{Ad} for **2** along with standard deviation; see text for details.

Table 4. Primary Kinetic Deuterium Isotope Effect

Substrate	k^H_{AA}/k^D_{AA}
1a	5.2±0.6
1b	5.5±0.9
1f	5.1±0.7
1g	5.4±1.0

used for the corresponding 2′-substituents, because the electronic effects of substituents at the 2′- and 4′-positions upon a side chain are reasonably assumed to be equivalent. The plot for **1a** locates far above the area, so it is omitted. For **1c—g**, a linear correlation (correlation coefficient; r=0.990) is seen with ρ=−0.50, indicating that, for these substrates, the more electron-releasing the substituent, the larger the K_{Ad} value. That **1c** and **1d** has almost identical K_{Ad} suggests that an ortho-substituent exerts no steric effect on the adsorption. The K_{Ad} value for **1b** is much smaller than expected from its σ-value. The finding supports the importance of carbonyl oxygen for the adsorption. That is, the adsorption through the carbonyl oxygen would be prevented in **1b** by its strong coordination with the 2′-hydroxyl group through a hydrogen-bonding to form a stable six-membered ring, which can be recognized by anomalously low chemical shift (δ from TMS=12.8 in $CDCl_3$) of the 2′-hydroxyl proton in the NMR spectrum of **1b**. The absence of appreciable absorption in the 3500—3600 cm^{-1} range in the IR spectrum also supports the proposal. The K_{Ad} for **1a** is unexpectedly large, which seems to be mainly attributed to the extremely low solubility of **1a** in benzene. Interestingly, the nitro group in **1h** is likely to result in an additional contribution to the adsorption. Smaller K_{Ad} values for the saturated carbonyl compounds **2f** and **4** than those for the corresponding α,β-unsaturated carbonyl compounds **1f** and **3**, respectively, may be due to thermodynamically less stable coordination of the former compounds than those of the latter compounds, respectively. That is, the induced small positive charge on the carbonyl group is not mesomerically stabilized by the phenyl ring on the β-position in saturated compounds. Alternatively, the π-bond in the carbon-carbon double bond of an α,β-unsaturated carbonyl compound may contribute to the adsorption.

All data listed in Table 2 reveals that electrostatic interaction between the carbonyl oxygen of **1** and the silanol group on the surface of silica gel is a predominant factor in the adsorption of **1**, as proposed previously for diethyl maleate, fumarate, and acetylenedicarboxylate.[5]

Figure 4 shows an excellent linear correlation between $\log(k^X_{AA}/k^H_{AA})$ derived from the data in Table 3 and the Hammett σ-value (ρ=1.22: correlation coefficient; r=0.998) except for **1b** and **1d**, where points for 2′-substituted derivatives are plotted against σ-values of the corresponding 4′-substituents (vide supra). As will be described later, there are convincing reasons against the deviations of plots for **1b** and **1d**. On the other hand, rather a U-shaped correlation between $\log(k^X_{BA}/k^H_{BA})$ and the σ-values can be seen in Fig. 5, with the plot for **1a** being largely deviated positively. There is no reason for the reaction between **1** in the solution and HEH on the surface of silica gel to exert a U-shaped Hammett relationship. The Hammett plot for k^X_{AB}/k^H_{AB} shows slightly positive deviations for **1c** and **1e** as seen in Fig. 6. Thus, the correlation in k^X_{AB}/k^H_{AB} is poorer than that in k^X_{AA}/k^H_{AA}. Note that the definition of k_{AB} is impossible for the reaction of **1a** as mentioned above. Finally, we infer that the reactions in the present study are most reasonably interpreted in terms of the kinetics represented by Eq. 6 instead of those in Eqs. 7 and 8.

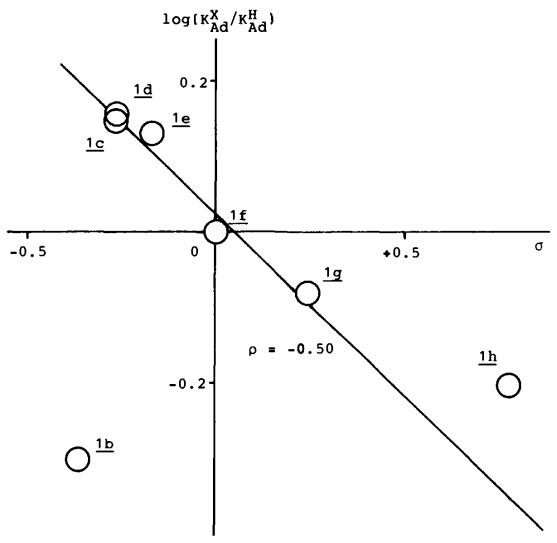

Fig. 3. The Hammett plot of $\log(K^X_{Ad}/K^H_{Ad})$ vs. σ-value.

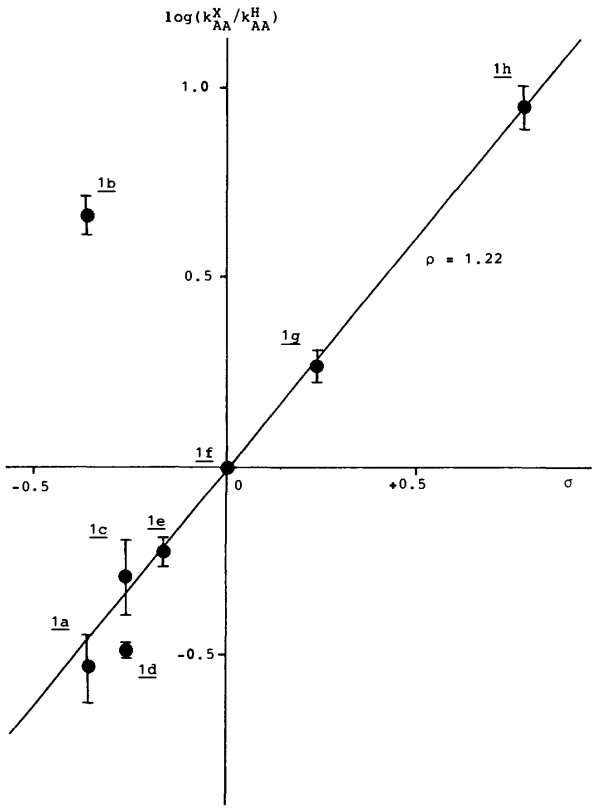

Fig. 4. The Hammett plot of $\log(k^X_{AA}/k^H_{AA})$ vs. σ-value.

Namely, since the equilibration is much faster process than the reduction,[5] the transfer of a hydride-equivalent appears to take place between HEH and **1**, both adsorbed on the surface of silica gel.

Nevertheless, our previous study on the reductions of diethyl maleate, fumarate, and acetylenedicarboxylate by HEH in the presence of silica gel has postulated that the transfer of a hydride-equivalent takes place from the HEH adsorbed on the surface of silica gel to the substrate in bulk phase.[5] First-order dependency of the reaction rate on both $[\mathbf{1}]_{Ad}$ and $[HEH]_{Ad}$ in the present reaction (Eq. 6) does not necessarily require the transfer of a hydride-equivalent between HEH and **1**, both adsorbed on the surface of silica gel, at the rate-determining step. Alternatively, we can take into account the local concentration(s) of **1** and/or HEH in the outer sphere of the silica gel. Since adsorption and desorption of the materials are in rapid equilibrium at the interface of the silica gel and the bulk phase, the local concentrations of HEH and **1** in the outer sphere would be approximately proportional to $[HEH]_{Ad}$ and $[\mathbf{1}]_{Ad}$, respectively. If this is the case, kinetic results obtained from the present study might accommodate the transfer of a hydride-equivalent from HEH to **1** in the outer sphere of the silica gel. As proposed previously, it is also possible that one of the two components, perhaps HEH counterpart, exists on the surface of silica gel during the transfer of a hydride-equivalent.[5]

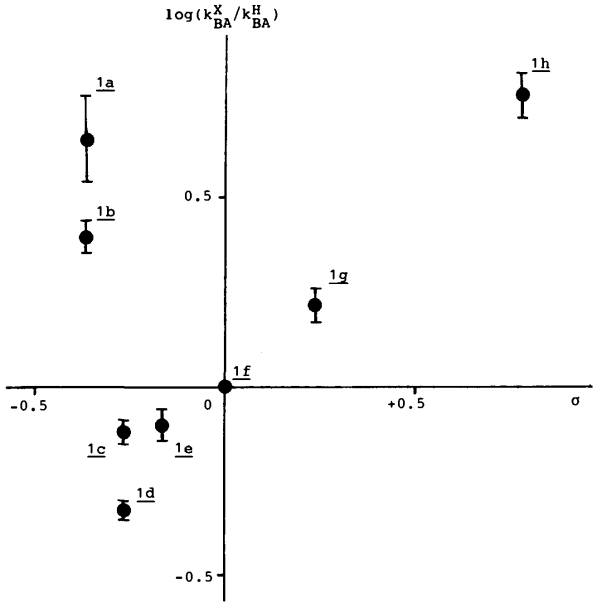

Fig. 5. The Hammett plot of $\log(k^X_{BA}/k^H_{BA})$ vs. σ-value.

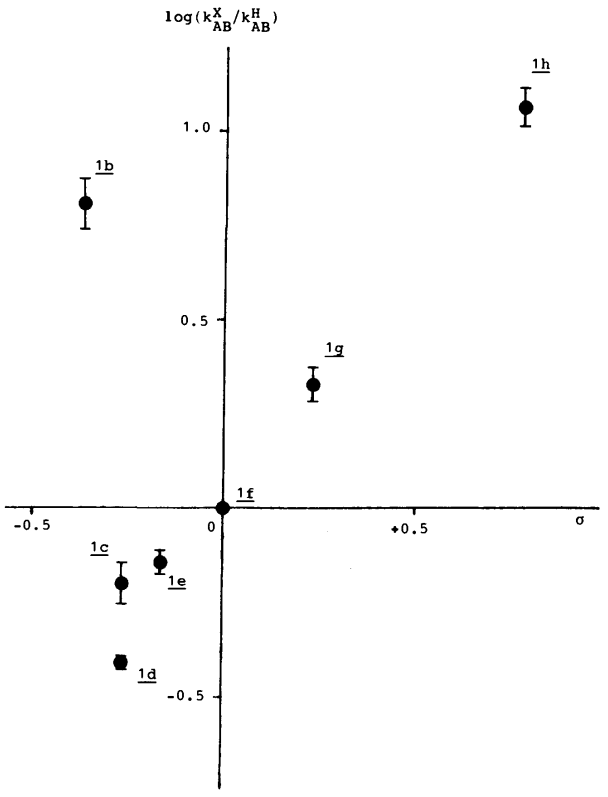

Fig. 6. The Hammett plot of $\log(k^X_{AB}/k^H_{AB})$ vs. σ-value.

The values of primary kinetic deuterium isotope effects listed in Table 4 clearly indicate that a hydrogen is migrating more or less in the rate-determining step.[14] It is also evident that these are approximately identical in magnitude irrespective of the reactivity of the substrate, which would postulate that the same mechanism persists for a hydride-equivalent transfer steps for **1a**, **f**, and **g**, as that for **1b**.[15] Unexpectedly high reactivity of **1b** is reasonably attributable to the intramolecular acid catalysis by the 2′-phenolic hydrogen in **1b**. Indeed, **1b** is reduced to **2b** by HEH in benzene without silica gel although the yield is low (Table 1). The transition state for the other substrates may stabilized as well by a hydroxylic proton of silanol group on the surface of silica gel. Considering that **1** is absorbed onto the surface of silica gel through the interaction of its carbonyl oxygen with a proton of a silanol group, a participation of the silanol group to the carbonyl oxygen of **1** in the outer sphere would be reasonably anticipated. Such a participation of the acidic silanol group may be not specific- but general-acid catalysis in view of extremely low basicity of the carbonyl oxygen of **1**[16] and moderate acidity of the silanol group,[17] although it cannot be demonstrated at present that the protonation is partially rate-determining. The positive ρ-value in this reaction shows the predominance of the hydride-equivalent transfer from HEH compared with the proton transfer from the silanol group at the transition state. Interestingly, in the reduction of *p*-methoxybenzaldehyde by NADH-dependent yeast alcohol dehydrogenase, the transfer of a proton from a water molecule onto the carbonyl oxygen does not participate in the rate-determining step, whereas the

transfer of a hydride equivalent onto the carbonyl carbon constitutes the sole rate-determining step.[18]

The present simulation has predicted that a large amount of silanol groups remain free during the reaction. It should be noted that the value of Q_0 does not represent the amount of all silanol groups on the surface, but it merely designates the "effective" amount of adsorbing centers on the surface for the materials used in the present study. A previous report has shown that only "free" silanol groups on the convex outer surface, the amount of which is calculated from the reported data to be 0.64 mmol per 0.2 g of silica gel, is ethoxylated by treating silica gel with ethanol. 2-Propoxylation and 2-methyl-2-propoxylation of silanol groups takes place, to the extents of two-third and one-third of that of ethoxylation, respectively, when silica gel is treated with 2-propanol and 2-methyl-2-propanol under the same conditions.[19] In addition, note that benzene molecule as a solvent in the present study does not perturb the silanol group because of its nonpolarity. Thus, during the present reaction, quite numerous silanol groups on the surface of silica gel possibly act as general-acid catalysts.

The mechanism is partly supported by the fact that k_{AA} for **1d** is smaller than that for **1c** even though these compounds have practically identical K_{Ad}. The ortho-substituent in **1d** may intervene an assistance by a silanol group during the process for the transfer of a hydride-equivalent.

Our previous study has revealed that active aluminas give rise to no reduction in spite of comparable adsorption of both a substrate and HEH onto their surfaces as those onto silica gel.[5] This fact indicates that silica gel not only adsorbs the materials but also plays a crucial role such as general-acid catalysis by the silanol group on the surface, as shown schematically in Fig. 7. Interestingly, an infrared spectroscopic study has revealed that when ethanol is adsorbed through hydrogen bonding, the silanol groups of silica gel act as proton donors, whereas on alumina the surface oxygen atoms play a dominant role as proton acceptors.[20]

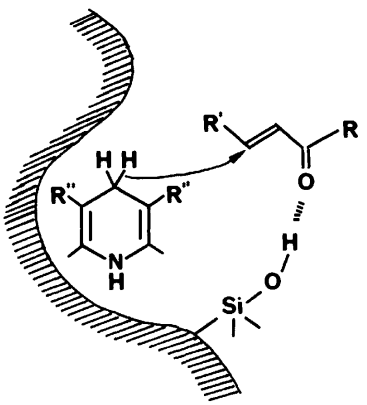

Fig. 7. Schematic representation of the reaction of **1** with HEH in the presence of silica gel.

In conclusion, we believe that the quantitative analysis in the present study has proven general-acid catalysis by silanol groups on the surface of silica gel in the reduction of α,β-unsaturated carbonyl compounds by an NAD(P)H model. Moreover, the silica gel unambiguously withdraws the materials subjected to the reduction closer to its surface. The dual roles of silica gel may be claimed as "enzyme-like." There are several examples for enzymatic hydrogenation of carbon–carbon double bond with a coenzyme NADH or NADPH, a redox potential of which is known to be equivalent to that of NAD(P)H models so far studied.[21] Thus, in a mimetic system an enzyme-like catalyst which exerts the dual ability, binding and catalysis, is required.

Finally, we wish to emphasize that the reduction system composed of HEH and silica gel is an excellent tool for chemo- and regio-selective reduction of α,β-unsaturated carbonyl compound due to its simplicity relative to other systems described in the recent reports.[22]

Experimental

Apparatus. VPC analyses and elemental analyses were performed on a Yanaco G-180 gas chromatograph and a Yanaco MT-3 elemental analyzer, respectively. ^{1}H NMR and IR spectra were recorded on a JEOL GX 400 FT NMR spectrometer and a Hitachi 260-10 infrared spectrophotometer, respectively. Computer-assisted simulations were run on an NEC PC-9801 VM2 personal computer with an N_{88} BASIC program.

Materials. 3,5-Bis(ethoxycarbonyl)-1,4-dihydro-2,6-dimethylpyridine (HEH) was prepared as reported previously.[23] HEH-4,4-d_2 was synthesized according to the same procedure as described for HEH using paraformaldehyde-d_6 in place of formaldehyde. 400 MHz ^{1}H NMR spectrum confirmed deuterium content at the 4-position to be 98%. 2′- or 4′-Substituted chalcones **1a**—**h** were obtained by condensation of benzaldehyde with the corresponding 2′- or 4′-substituted acetophenone followed by recrystalization from ethanol.[24] Spectral data as well as the results of elemental analyses of these compounds were satisfactory. Silica gel 60 (35—70 mesh) (Nakarai Chem. Co.) was commercially available.

Procedures. Measurements of adsorption onto the surface of the silica gel and product analyses were succeeded according to the procedures described previously.[5]

References

1) K. Nakamura, S. Yasui, A. Ohno, and S. Oka, *Tetrahedron Lett.*, **24**, 2001 (1983).

2) K. Nakamura, M. Fujii, A. Ohno, and S. Oka, *Chem. Lett.*, **1984**, 925; K. Nakamura, A. Ohno, and S. Oka, *Tetrahedron Lett.*, **24**, 3335 (1983).

3) S. H. Mashraqui and R. M. Kellogg, *J. Am. Chem. Soc.*, **105**, 7792 (1983).

4) S. Yasui, K. Nakamura, and A. Ohno, *Chem. Lett.*, **1984**, 1984; S. Yasui, K. Nakamura, M. Fujii, and A. Ohno, *J. Org. Chem.*, **50**, 3283 (1985).

5) S. Yasui, M. Fujii, K. Nakamura, and A. Ohno, *Bull. Chem. Soc. Jpn.*, **60**, 963 (1987).

6) K. Nakamura, M. Fujii, A. Ohno, and S. Oka, *Tetrahedron Lett.*, **25**, 3983 (1984).

7) The content of water in the silica gel 60 has been measured to be 4.6±0.2 mmol g^{-1} on a Kirl-Fisher moisture content meter. See Ref. 5.

8) No reduction of nitro group was detected.

9) J. V. Sinisterra and J. M. Marinas, *Tetrahedron Lett.*, **27**, 4971 (1986).

10) Each concentration term is simulated by resolving the following equations simultaneously without any approximation,

$$K^{1}_{Ad} = [\mathbf{1}]_{Ad}/(([\mathbf{1}]_{Total}-[\mathbf{1}]_{Ad})\cdot[Q]_{free})$$
$$K^{2}_{Ad} = [\mathbf{2}]_{Ad}/(([\mathbf{2}]_{Total}-[\mathbf{2}]_{Ad})\cdot[Q]_{free})$$
$$K^{HEH}_{Ad} = [HEH]_{Ad}/(([HEH]_{Total}-[HEH]_{Ad})\cdot[Q]_{free})$$
$$K^{HE\text{-}ox}_{Ad} = [HE_{ox}]_{Ad}/(([HE_{ox}]_{Total}-[HE_{ox}]_{Ad})\cdot[Q]_{free})$$
$$[Q]_{free} = [Q^{0,\cdot 2}_{0}]-[\mathbf{1}]_{Ad}-[\mathbf{2}]_{Ad}-[HEH]_{Ad}-[HE_{ox}]_{Ad}$$

and

$$[\mathbf{1}]_{Total}+[\mathbf{2}]_{Total} = 1.0\times10^{-1}\ M$$
$$[HEH]_{Total}+[HE_{ox}]_{Total} = 1.5\times10^{-1}\ M$$
$$[\mathbf{1}]_{Total}-[\mathbf{2}]_{Total} = [HEH]_{Total}-[HE_{ox}]_{Total}$$

where superscripts **1**, **2**, HEH, and HEox denote the values referred to **1**, **2**, HEH, and HE_{ox}, respectively.

11) The approximations may be reasonable considering that the observed K_{Ad} values for saturated carbonyl compounds **2f** and **4** are 1/3.57 and 1/1.75 of those for the corresponding α,β-unsaturated carbonyl compounds **1f** and **3**, respectively (Table 2).

12) The simulation allows the following approximations:

$$[\mathbf{1}]_{Ad} = A[\mathbf{1}]_{Total}$$
$$[\mathbf{1}]_{Bulk} = A'[\mathbf{1}]_{Total}$$
$$[HEH]_{Ad} = B[\mathbf{1}]_{Total}+C$$
$$[HEH]_{Bulk} = B'[\mathbf{1}]_{Total}+C'$$

where the parameters A, A', B, B', C, and C' are constants directly given by the correlation plotted in Fig. 1. Discrepancy between concentrations simulated and thus approximated is ca. 4×10^{-4} M (<1%) in maximum (for **1d**; when $[\mathbf{1d}]_{Total}=0.5\times10^{-1}$ M under the assumption of K_{Ad} (for **2d**)=1.93 M^{-1}.) Based on these approximations, Eqs. 6—8 afford a second-order rate equation with respect to $[\mathbf{1}]_{Total}$ as a following formula:

$$kt = c_1\cdot\ln\{(c_2\cdot(c_3[\mathbf{1}]_{Total}+c_4))/([\mathbf{1}]_{Total}\cdot(c_2\cdot c_3+c_4))\}$$

where c_1, c_2, c_3, and c_4 are constants, and in the equation derived from Eq. 6 where $k=k_{AA}$, for example, they are put as $c_1=1/(A\times C)$, $c_2=0.1$ (an initial concentration of **1**), $c_3=B$, and $c_4=C$, respectively.

13) S. Yasui and A. Ohno, unpublished result.

14) The mechanism of the transfer of a hydride-equivalent in the present study may be investigated in terms of successive transfers of an electron and a hydrogen atom (or an electron, a proton, and an electron) as proposed in NAD(P)H model-mediated reductions of several types of the substrates. Unfortunately, the present data in our hands provide no informations in this respect. Note that since **1** is supposed to be a strongly electron-deficient substrate under the silica gel catalysis, the step of an initial electron transfer would not be experimentally appreciable. See: S. Yasui and A. Ohno, *Bioorganic Chem.*, **14**, 70 (1986).

15) The theory demands, of course, identical values of kinetic primary deuterium isotope effect only when the position of the transition state along the reaction coordinate are exactly the same. There is no reason at all that the values of k^{H}_{AA}/k^{D}_{AA} obtained here must be identical. We only note that the values are roughly identical in the magnitude, which would certify the consideration in this place at least qualitatively.

16) For a review see: V. A. Palm, Ü. L. Haldna, and A. J. Talvic, "Chemistry of the Carbonyl Group," ed by S. Patai, Interscience, New York (1966), p.421.

17) C. Walling, *J. Am. Chem. Soc.*, **72**, 1164 (1950); H. A. Benesi, *ibid.*, **78**, 5490 (1956).

18) K. M. Welsh, D. J. Creighton, and J. P. Klinman, *Biochemistry*, **19**, 2005 (1980).

19) S. Kondo, H. Fujiwara, E. Okazaki, and T. Ichii, *J. Colloid Interface Sci.*, **75**, 328 (1980).

20) H. Jeziorowski, H. Knözinger, W. Meye, and H. D. J. Müller, *J. Chem. Soc., Faraday Trans. 1*, **69**, 1744 (1973).

21) R. M. Kellogg and O. Piepers, *J. Chem. Soc., Chem. Commun.*, **1982**, 402.

22) A. Alba, A. Aramendia, V. Borau, A. Gabcia-Raso, C. Jimenez, and J. M. Marinas, *Can. J. Chem.*, **62**, 917 (1984); E. Keinan and N. Greenspoon, *J. Am. Chem. Soc.*, **108**, 7314 (1986); H. Stamm, A. Sommer, A. Onistschenko, and A. Woderer, *J. Org. Chem.*, **51**, 4979 (1986); H. Chikashita and K. Itoh, *Bull. Chem. Soc. Jpn.*, **59**, 1747 (1986).

23) A. Singer and S. M. McElvain, *Org. Synth.*, Coll. Vol., 2, 214 (1966).

24) For details see: E. P. Kohler and H. M. Chadwell, *Org. Synth.*, Coll. Vol., 1, 78 (1967); T. Asahina, *Bull. Chem. Soc. Jpn.*, **9**, 131 (1934).

 © 1987 The Chemical Society of Japan Bull. Chem. Soc. Jpn., 60, 4027—4036 (1987)

New Synthetic Method of [2.2]Cyclophanes via Diselena[3.3]cyclophanes

Hiroyuki HIGUCHI, Keita TANI, Tetsuo OTSUBO,† Yoshiteru SAKATA, and Soichi MISUMI*

The Institute of Scientific and Industrial Research, Osaka University, Ibaraki, Osaka 567
†Department of Applied Chemistry, Faculty of Engineering, Hiroshima University, Higashihiroshima, Hiroshima 724

(Received May 25, 1987)

Syntheses of cyclic diselenides through diselenolates and the following deselenation reactions by means of three ways were studied. The preparation of the cyclic diselenides in the presence of excess sodium borohydride gave thirty-eight diselenides containing diselena[3.3]cyclophanes and alicyclic diseleno compounds in high yields in addition to two triple-bridged selenacyclophanes. Photodeselenation of the diselenides in tris(dimethylamino)phosphine afforded series of [2.2]cyclophanes in much higher yields than those of the other two methods, i.e. benzyne-Stevens rearrangement/Raney nickel hydrogenolysis and pyrolytic deselenation at ca. 650 °C. The present study demonstrates that the photodeselenation method, combined with the synthesis of their precursor diselenides, is much superior to the conventional dechalcogenation methods.

The chemistry of cyclophanes has been drastically developed by the emergence of the synthetic methods via various types of desulfurizations of dithia cyclophanes.[1] Especially, pyrolysis of disulfones has been appreciated to be very useful for the preparation of [2.2]cyclophanes.[2] Organoseleniums are also

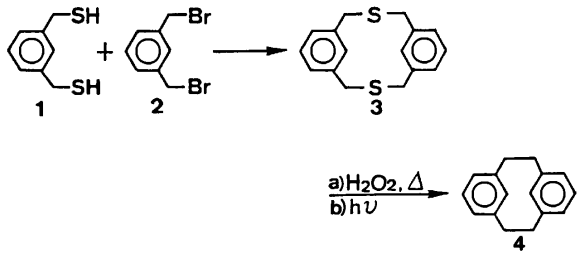

expected to be applicable to the synthesis of cyclophanes in place of the corresponding organosulfur compounds because C–Se bonds undergo more easily bond fission both thermally and photochemically than the corresponding C–S bonds.

In fact, bis(arylmethyl) selenide and diselenide thermally decomposed with extrusion of elemental selenium to give 1,2-diarylethane.[3] Recently, we reported flash vacuum pyrolysis of a series of dibenzyl selenides and diselenides at 600 °C to give bibenzyl derivatives in high yields[4,5] and the formation (23% yield) of [2.2]paracyclophane by a similar pyrolytic way of 1,4-bis(phenylselenomethyl)benzene.[5,6] An attempt to synthesize cyclophanes via diselenacyclophanes was carried out first by Mitchell but it gave a low yield of [2.2]metacyclophane derivative.[7]

The bibenzyl formation by thermal selenium extrusion stimulated us to develop general synthetic methods for [2.2]cyclophanes via diselena[3.3]cyclophanes.

After various examinations on reaction conditions, we found a general synthesis of diselenacyclophanes in high yields by reductive coupling of bisselenocyanate and dihalide.[8] Here we report general synthetic methods of a variety of [2.2]cyclophanes from diselena[3.3]cyclophanes by a few deselenation ways, i.e. (a) benzyne-Stevens rearrangement/hydrogenolysis, (b) photodeselenation with tris(dimethylamino)phosphine, and (c) flash pyrolysis under reduced pressure.

Results and Discussion

Selenacyclophanes: Synthesis and Properties. Dithia[3.3]cyclophane, a good precursor of [2.2]cyclophane, is generally prepared by coupling of appropriate dithiol and dihalide with potassium hydroxide. On the other hand, diselenol or diselenolate anion is unsuitable to synthesize diselena[3.3]cyclophane **6**,

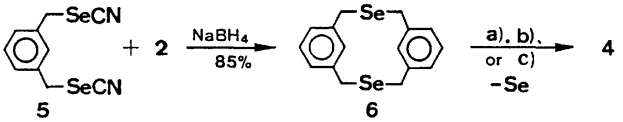

because it is highly air-sensitive under alkaline conditions to give hardly separable diselenide polymer. The first synthesis of **6** was achieved by coupling of dihalide with sodium selenide and by deselenation of tetraselena[4.4]cyclophane with $P(NEt_2)_3$ both in low yield.[7,9]

After many examinations of reaction conditions, we found an improved synthesis of **6** by coupling of bisselenocyanate **5** and dibromide **2** under reductive environment: A mixture of **2** and **5** (1:1 ratio) in EtOH–THF is dropwise added to a large excess of $NaBH_4$ in EtOH–THF using high dilution technique.

A wide range of mixing ratio of EtOH–THF is usable as the reaction solvent according to solubilities of reactant and a ratio of 5:95 (EtOH–THF) is convenient for the coupling in good yield. A suspension of excess $NaBH_4$ is also effective for high yield of coupling product, by holding the reaction system in reductive condition for suppression of oxidative polymerization.

Table 1. Yields, Melting Points, Crystal Forms, and ^{1}H NMR and Analytical Data of Selenacyclophanes

Compound	Yield/%	Mp θ_m/°C	Crystal form (solvent)	^{1}H NMR/δ ($CDCl_3$)	Found/% (Calcd) C	Found/% (Calcd) H	MS
6	85	120—122 121—122[c]	Prism (hex.[a])	3.78(s, 8H, CH_2), 6.46(s, 2H, inner ArH), 7.04(m, 6H, ArH)	52.31 (52.46)	4.23 (4.37)	368 (M^+)
7	83	201—202 201—202[d]	Needle (CH_2Cl_2-C_6H_6)	3.66(s, 8H, CH_2), 7.25—7.50(m, 8H, ArH)	52.74 (52.46)	4.37 (4.37)	368 (M^+)
8	78	129—130	Needle (C_6H_6-hex.[a])	3.31(s, 4H, CH_2), 3.66(s, 4H, CH_2), 6.00(bs, 1H, inner ArH), 7.14—7.82(m, 7H, ArH)	52.21 (52.46)	4.41 (4.37)	368 (M^+)
9	81	168—170	Needle (C_6H_6)	3.57(s, 4H, CH_2), 3.94(s, 4H, CH_2), 5.61(bs, 1H, inner ArH), 6.98(s, 4H, ArH), 6.87—7.16 (m, 3H, ArH)	52.35 (52.46)	4.62 (4.37)	368 (M^+)
10	73	214—215	Prism (CH_2Cl_2-C_6H_6)	3.89(s, 8H, CH_2), 6.84(s, 8H, ArH)	52.16 (52.46)	4.70 (4.37)	368 (M^+)
11	78	183—189	Prism (CH_2Cl_2-C_6H_6)	2.98(bs, 8H, CH_2), 3.36, 3.67 (ABq, 4H, $SeCH_2$), 3.71(bs, 4H, $SeCH_2$), 5.25(br, 1H, ArH), 6.23(s, 2H, ArH), 6.41, 6.62 ($A_2'B_2'$m, 4H, ArH), 6.65—6.95 (m, 3H, ArH)	63.18 (62.90)	5.18 (5.24)	498 (M^+)
12	68	182—184	Pale yellow Prism (C_6H_6)	2.34—3.44(m, 8H, CH_2), 3.29 (s, 4H, $SeCH_2$), 3.52, 3.83(ABq, 4H, $SeCH_2$), 5.37(bs, 1H, ArH), 5.87(s, 2H, ArH , 6.32, 6.49 ($A_2'B_2'$m, 4H, ArH), 6.75—6.98 (m, 3H, ArH)	63.08 (62.90)	5.11 (5.24)	498 (M^+)
13	74	177—179	Prism (C_6H_6-hex,[a])	2.42—3.38(m, 8H, CH_2), 3.59, 3.82(ABq, 4H, $SeCH_2$), 3.76(bs, 4H, $SeCH_2$), 5.75(s, 2H, ArH), 6.22, 6.44($A_2'B_2'$m, 4H, ArH), 6.63, 6.67($A_2'B_2'$m, 4H, ArH)	63.23 (62.90)	5.31 (5.24)	498 (M^+)
14[b]	30	>212 (decomp)	Needle (CH_2Cl_2-C_6H_6)	2.24—3.26(m, 16H, CH_2), 3.47, 3.72(ABq, 8H, $SeCH_2$), 5.53(s, 4H, ArH), 6.16, 6.37($A_2'B_2'$m, 8H, ArH)	68.77 (69.01)	5.67 (5.75)	628 (M^+)
15[b]	34	>204 (decomp)	Column (CH_2Cl_2-C_6H_6)	2.29—3.37(m, CH_2, 16H), 3.45, 3.82(ABq, 8H, $SeCH_2$), 5.58(s, 4H, ArH), 6.18, 6.36($A_2'B_2'$m, 8H, ArH)	68.59 (69.01)	5.65 (5.75)	628 (M^+)
16[b]	27	194—198 >190 (decomp)[e]	Powder (C_6H_6-hex.[a])	2.56—3.18(m, 16H, CH_2), 3.42, 3.92(ABq, 8H, $SeCH_2$), 5.78(s, 4H, ArH), 6.24, 6.47($A_2'B_2'$m, 8H, ArH)	68.89 (69.01)	5.58 (5.75)	628 (M^+)
17[b]	36	235—241 (decomp) >235 (decomp)[e]	Needle (CH_2Cl_2-C_6H_6)	2.08—2.82(m, 8H, CH_2), 2.90 (bs, 8H, CH_2), 3.36(s, 8H, $SeCH_2$), 6.15(s, 4H, ArH), 6.29, 6.46($A_2'B_2'$m, 8H, ArH)	68.75 (69.01)	5.38 (5.75)	628 (M^+)
18	80	204—208	Needle (THF)	4.06, 4.74(ABq, 8H, CH_2), 6.30 (s, 4H, NapH), 7.58—7.63(m, 4H, NapH), 8.08—8.14(m, 4H NapH)	61.60 (61.81)	4.61 (4.32)	468 (M^+)
19	41	203.5—204.5	Prism (C_6H_6)	4.01(s, 8H, CH_2), 7.00(s, 4H, NapH), 7.16(bs, 8H, NapH)	61.66 (61.81)	4.23 (4.32)	468 (M^+)

Table 1. (Continued)

Compound	Yield/%	Mp θ_m/°C	Crystal form (solvent)	^{1}H NMR/δ ($CDCl_3$)	Found/% (Calcd) C	Found/% (Calcd) H	MS
20	77	139—144	Prism (C_6H_6)	3.83, 4.01(ABq, 4H, CH_2), 4.21, 4.36(ABq, 4H, CH_2), 6.36(m, 2H, ArH), 6.70(s, 2H, NapH), 6.86(m, 2H, ArH), 7.47—7.57 (m, 2H, NapH), 8.00—8.10 (m, 2H, NapH)	57.61 (57.71)	4.29 (4.36)	418 (M^+)
21	98	207—209.5	Prism (C_6H_6)	3.46, 3.69(ABq, 4H, CH_2), 4.35 (s, 4H, CH_2), 5.57(bs, 1H, inner ArH), 6.48(t, 1H, ArH, 6.65(d, 2H, ArH), 7.22(s, 2H, NapH), 7.33—7.37(m, 2H, NapH), 8.01—8.04(m, 2H, NapH)	57.66 (57.71)	4.37 (4.36)	418 (M^+)
22	79	162.5—163.5	Prism (C_6H_6-hex.[a])	3.74(s, 2H, CH_2), 4.00(s, 6H, CH_2), 5.75(d, 1H, NapH), 7.09 (s, 4H, ArH), 7.35—7.47(m, 3H, NapH), 7.63—7.75(m, 2H, NapH)	57.53 (57.71)	4.51 (4.36)	418 (M^+)
23	81	126—127.5	Column (C_6H_6-hex.[a])	3.79(bs, 2H, CH_2), 3.84(bs, 2H, CH_2), 3.88(bs, 2H, CH_2), 4.17 (bs, 2H, CH_2), 6.21(bs, 1H, inner ArH), 6.64(bs, 1H, inner NapH), 7.06—8.04(m, 8H, ArH and NapH)	57.71 (57.71)	4.39 (4.36)	418 (M^+)
24	67	>256 (decomp)	Column (C_6H_6)	3.91(s, 12H, CH_2), 6.90(s, 6H, ArH)	46.10 (45.88)	3.90 (3.85)	474 (M^+)
25	55	>230 (decomp)	Column (C_6H_6-hex.[a])	3.41—4.04(m, 12H, CH_2), 5.92 (bs, 1H, ArH), 6.91(d, 1H, ArH), 7.07(bs, 1H, ArH), 7.08 (d, 1H, ArH), 7.22(bs, 2H, ArH)	45.75 (45.88)	3.73 (3.85)	474 (M^+)
64[b]	(anti) 10	219—221.5 (decomp)	Prism ($CHCl_3$)	3.30(s, 6H, Me), 3.51, 3.87 (ABq, 8H, CH_2), 7.01(t, 2H, ArH), 7.31(d, 4H, ArH)	50.42 (50.72)	4.73 (4.73)	428 (M^+)
	(syn) 51	212—214 (decomp)	Prism ($CHCl_3$)	3.42, 4.57(AMq, 8H, CH_2), 3.55(s, 6H, Me), 6.61(t, 2H, ArH), 6.99(d, 4H, ArH)	50.70 (50.72)	4.96 (4.73)	428 (M^+)
66[b]	24	173.5—175	Needle (C_6H_6-hex.[a])	3.77(s, 4H, CH_2), 3.81(s, 6H, Me), 3.82(s, 4H, CH_2), 6.48 (d, 2H, inner ArH), 6.66(d, 2H, ArH), 7.01(dd, 2H, ArH) ^{77}Se NMR −2.76(s)	50.48 (50.72)	4.94 (4.73)	428 (M^+)
68[b]	18	151.5—152.5	Prism (C_6H_6-hex.[a])	3.71(s, 4H, CH_2), 3.80(s, 4H, CH_2), 3.81(s, 6H, Me), 6.38 (d, 2H, inner ArH), 6.72(d, 2H, ArH), 7.12(dd, 2H, ArH) ^{77}Se NMR 15.7(s), −33.5(s)	50.73 (50.72)	4.49 (4.73)	428 (M^+)

a) Hexane. b) Pairs of selenacyclophanes (**14** and **15**, **16** and **17**, syn and anti **64**, **66** and **68**) were obtained at the same time by appropriate coupling reaction. The structure of **66** and **68** was determined by ^{77}Se NMR measurement. c) Ref. 7. d) Ref. 5. e) Ref. 11.

Table 1 shows yields of a variety of selena[3^n]cyclophanes including triple-bridged compounds. This method is convenient to prepare unsymmetrical diselenacyclophanes as well as symmetrical ones and easy to purify the product because tedious polymer is not formed. The yields of such selenacyclophanes are much higher than those of the corresponding thiacyclophanes,[10] just as multilayered ones and triple-bridged ones. For example, triselena[3^3](1,3,5)-cyclophane **24** is afforded in a good yield by more than 10 times that (5.3% yield) of the corresponding trithiacyclophane.[10m] Two pairs of isomeric quadru-

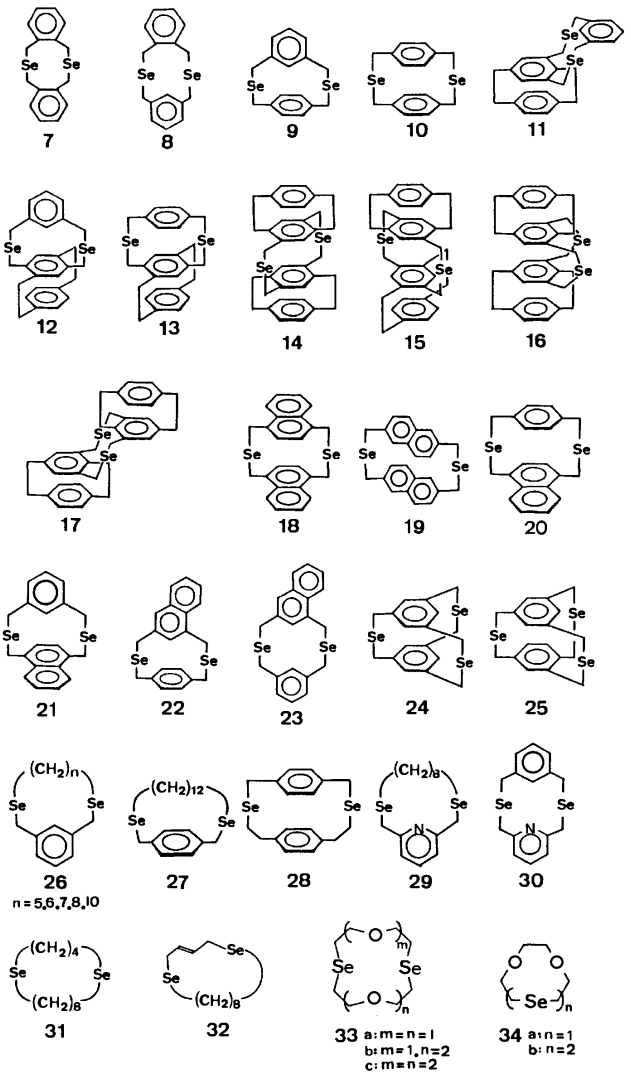

ple-layered selenacyclophanes (**14** and **15**; **16**[11] and **17**[11]) are obtained as a mixture of about 1:1 isomeric ratio and separated by silica-gel column chromatography.

It is not clear whether 2,11-diselena[3.3]metacyclophane **6** consists of an equilibrating mixture of syn- and anti-conformers in solution at room temperature,[12] whereas the corresponding dithiacyclophane **3** exists only in syn-conformer in both solid state and solution.[13] A conformational equilibrium is expected from molecular model examination also for triple-layered diselenacyclophane **11** and diselenanaphthalenometacyclophane **23**, both of which contain the partial structure, diselena[3.3]metacyclophane. On the basis of ^{1}H NMR data, that is, the chemical shifts of the inner aromatic protons and the coupling pattern of bridge methylene protons, cyclophane **23** is in similar equilibrium, while cyclophane **11**, on the contrary, exists as anti-conformer only.[14] A reasonable explanation for the predominance of anti-conformer is steric repulsion among vicinal three methylenes attached to the inner benzene ring. Both of symmetrical naphthalenophanes, **18** and **19**, exist only in one of two conformers, and the structure of **18** is confirmed to be antiform by comparison of its ^{1}H NMR spectrum with that of the corresponding dithia[3.3]naphthalenophane.[10g]

Diselena[*m*]cyclophanes (**26** and **27**), diselenapyridinophanes (**29** and **30**), alicyclic diselenides (**31** and **32**), and diselenocrown ethers (**33** and **34**) are similarly prepared in good yields as shown in Table 2. 2,13-Diselena[4.4]paracyclophane **28** is prepared by two ways, i.e. couplings of 1,4-bis(bromoethyl)benzene with 1,4-bis(cyanoselenatomethyl)benzene in 38% yield and of 1,4-bis(2-cyanoselenatoethyl)benzene with 1,4-bis(bromomethyl)benzene in 77% both in the presence of $NaBH_4$. The difference in the yields suggests a preferable S_N2 substitution of bromine at benzyl position by selenolate anion. On the other hand, coupling reactions of two pairs of dibromides and diselenocyanates, i.e. **35**+**36** and **37**+**38**, unexpectedly give different selenocrown compounds, **34b** and **34a**, respectively. The formation of unusual ring-contracted compound **34a** seems reasonable to assume a template effect of sodium ion in an intermediate **39**. Similar ring contractions were observed in cyclizations of polythioethers.[15]

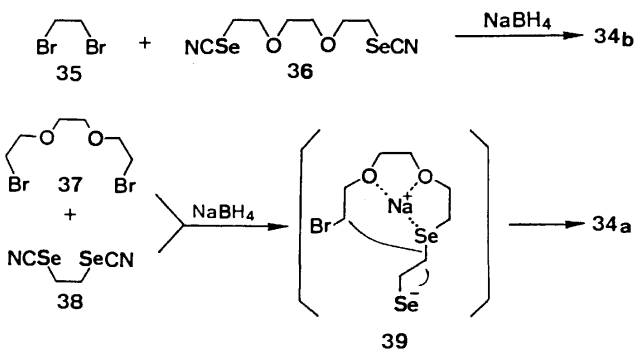

The structures of all selenacyclophanes were determined by MS and ^{1}H NMR spectra and elemental analyses as shown in Table 1.

Syntheses of Cyclophanes by Deselenation: Desulfurization of polythia[3^n]cyclophanes to [2^n]cyclophanes has usually been carried out by i) Stevens or Wittig rearrangement and the following Raney Ni hydrogenolysis, ii) irradiation in the presence of $P(OR)_3$, and iii) oxidation to the corresponding sulfone and the following pyrolytic desulfonation. Selenium extrusion reactions are carried out by modifying the above-stated desulfurization methods. A series of [2^n]cyclophanes are obtained from polyselena[3^n]cyclophanes by three methods, (A)—(C), as follows:

(A) Benzyne-Stevens rearrangement/hydrogenolysis,

(B) Photodeselenation with tris(dimethylamino)phosphine $P(NMe_2)_3$,

Table 2. Yields, Mp's, Crystal Forms, and ^{1}H NMR and Analytical Data of Cyclic Selenides

Compound	Yield/%	Mp θ_m/°C	Crystal form (solvent)	^{1}H NMR/δ ($CDCl_3$)	Found/% (Calcd) C	H	N	MS
26 $n=5$	48	>135	Solid (hex.[a])	1.21—1.25(m, 6H, CH_2), 2.28 (t, 4H, $SeCH_2$), 3.78(s, 4H, $SeCH_2$), 7.14—7.31(m, 4H, ArH)	46.94 (46.99)	5.75 (5.47)		334 (M^+)
$n=6$	Quant.	80—83.7	Solid (pentane)	1.20—1.56(m, 8H, CH_2), 2.44 (t, 4H, $SeCH_2$), 3.74(s, 4H, $SeCH_2$), 7.16—7.23(m, 4H, ArH)	48.46 (48.56)	5.92 (5.83)		348 (M^+)
$n=7$	Quant.	66.5—72.5	Solid (pentane)	1.10—1.60(m, 10H, CH_2), 2.46 (t, 4H, $SeCH_2$), 3.72(s, 4H, $SeCH_2$), 7.04—7.29(m, 4H, ArH)	49.88 (50.00)	6.45 (6.17)		362 (M^+)
$n=8$	87	38—43	Semisolid	1.13—1.57(m, 12H, CH_2), 2.46 (t, 4H, $SeCH_2$), 3.69(s, 4H, $SeCH_2$), 7.16(bs, 4H, ArH)	51.49 (51.34)	6.73 (6.48)		376 (M^+)
$n=10$	53	Colorless oil		1.28—1.73(m, 16H, CH_2), 2.46 (t, 4H, $SeCH_2$), 3.73(s, 4H, $SeCH_2$), 7.14—7.25(m, 4H, ArH)	53.79 (53.74)	6.91 (6.48)		404 (M^+)
27	79	104—108	Needle (C_6H_6-hex.[a])	0.95—1.76(m, 20H, CH_2), 2.48 (t, 4H, $SeCH_2$), 3.74(s, 4H, $SeCH_2$), 7.19(s, 4H, ArH)	55.62 (55.81)	7.28 (7.44)		432 (M^+)
28	77 (38)	152—155	Needle (C_6H_6)	2.63—3.01(A_2B_2m, 8H, CH_2), 3.46(s, 4H, $SeCH_2$), 6.78(s, 4H, ArH), 6.83(s, 4H, ArH)	55.06 (54.82)	5.22 (5.08)		396 (M^+)
29	78	101—102	Needle (hex.[a])	1.27—1.75(m, 12H, CH_2), 2.63 (t, 4H, $SeCH_2$), 3.81(s, 4H, $SeCH_2$), 7.15—7.64(m, 3H, PyH)	47.96 (48.00)	6.33 (6.13)	3.81 (3.73)	377 (M^+)
30	93	168—168.5	Prism (C_6H_6-hex.[a])	3.91(s, 4H, CH_2), 3.99(s, 4H, CH_2), 6.89—7.35(m, 6H, ArH and PyH), 7.06(bs, 1H, inner ArH)	48.88 (49.05)	4.07 (4.09)	3.88 (3.81)	369 (M^+)
31	70	47—48	Solid (hex.[a])	1.40—1.87(m, 16H, CH_2) 2.54—2.68(dt, 8H, $SeCH_2$)	43.92 (44.17)	7.18 (7.33)		328 (M^+)
32	80	48—53	Solid (pentane)	1.24—1.68(m, 12H, CH_2), 2.57 (t, 4H, $SeCH_2$), 3.13—3.19(m, 4H, allylic H), 5.52—5.64(m, 2H, olefinic H)	44.22 (44.44)	6.61 (6.78)		326 (M^+)
33 a: $m=n=1$	60	Colorless oil		2.87(t, 8H, $SeCH_2CH_2O$), 3.85(t, 8H, $SeCH_2CH_2O$)	31.80 (31.78)	5.50 (5.30)		304 (M^+)
b: $m=1$ $n=2$	78	Colorless oil		2.74—2.93(m, 8H, $SeCH_2$), 3.64(s, 4H, OCH_2CH_2O), 3.72—3.90(m, 8H, OCH_2)	34.61 (34.68)	5.85 (5.78)		348 (M^+)
c: $m=n=2$	85	98—99.5	Prism (C_6H_6-hex.[a])	2.85(t, 8H, $SeCH_2CH_2O$), 3.63(s, 8H, OCH_2CH_2O), 3.79(t, 8H, $SeCH_2CH_2O$)	37.10 (36.93)	6.19 (6.15)		392 (M^+)
34 a: $n=1$	40	Colorless oil		2.90(t, 4H, $SeCH_2CH_2O$), 3.65(s, 4H, OCH_2CH_2O), 4.10(t, 4H, $SeCH_2CH_2O$)	37.36 (36.93)	6.46 (6.15)		196 (M^+)
b: $n=2$	76	Colorless oil		2.76(t, 4H, $SeCH_2CH_2O$), 3.17(s, 4H, $SeCH_2CH_2Se$), 3.61(s, 4H, OCH_2CH_2O), 3.96(t, 4H, $SeCH_2CH_2O$)	31.77 (31.78)	5.57 (5.30)		304 (M^+)

a) Hexane.

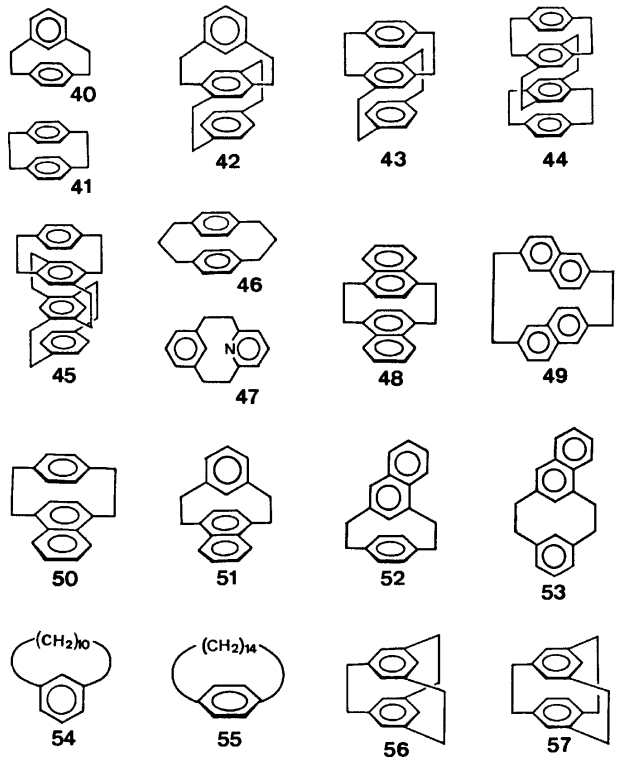

(C) Flash pyrolysis under reduced pressure.
The yields of [2.2]cyclophanes as well as multilayered, naphthaleno-, and pyridino-cyclophanes are shown in Table 3. The table reveals that the benzyne-hydrogenolysis method (A) is obviously superior to the direct extrusion by flash pyrolysis (C) and the yields are comparable to those of the transformation of the corresponding dithiacyclophanes into cyclophanes by benzyne-hydrogenolysis method. Pyrolysis of **28** gives 1,4-divinylbenzene (73% yield) as main product and [2.2]paracyclophane **41**[16] (6%) as a by-product without the desired [3.3]paracyclophane **46**. The reaction seems to proceed via a biradical intermediate **59** which was presumed to generate by pyrolysis of diselenide **58**.[5]

The second method, photodeselenation (B) generally gives higher yield of [2.2]cyclophane than those of the two methods, (A) and (C), as seen in Table 3. Tris(dimethylamino)phosphine is an effective reagent of many well-known reagents for dechalcogenation.[17] The photodeselenation by this reagent proceeds more rapidly than desulfurization with trialkyl phosphite $P(OR)_3$ from the corresponding dithiacyclophane and gives easily separable products. In the case of diselena[3.3]orthometacyclophane, the desired [2.2]-orthometacyclophane is not afforded even by the use of all methods, probably due to highly severe strain predicted in the product. Also, diselena[3.3]ortho-cyclophane **7**[5] affords quantitative yield of benzo-selenophene **61**[5] which may be formed by favorable

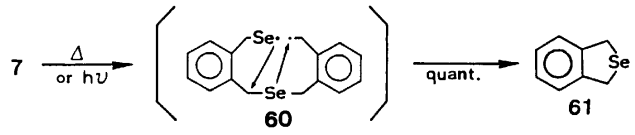

intramolecular cyclization of intermediary biradical species **60** into two of the five-membered ring. Both triple-bridged cyclophanes, **56** and **57**, are given in low yield because of more severe strain. Compound **57**, which polymerizes easily at room temperature,[10k,l] is obtained in fairly good yield (11%) at lower temperature in spite of severe strain. On irradiation of triselenacyclophane **24**, an unexpected 2,7-dimethyl-tetrahydropyrene **62**[10n] is afforded in higher yield (10%) than the normal product **56**[10n] (4%). The formation of **62** is explainable in terms of 1,5-hydrogen shift of transannularly bridged intermediate **63**.

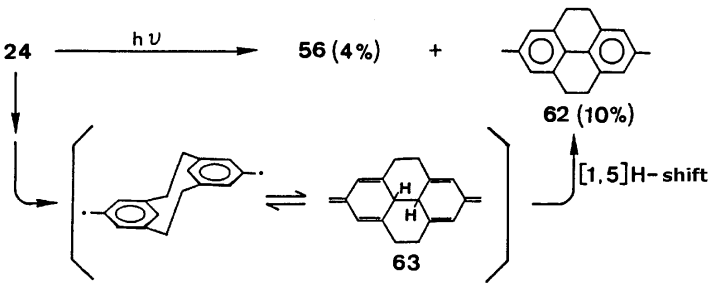

Consequently, Table 3 shows the photodeselenative synthesis of [2.2]cyclophane to be the most useful method compared to the other ones, (A) and (C). This method is particularly convenient for synthesis of para-para series [2.2]cyclophanes such as **41**,[16] **43**,[18] **44**,[18] **45**,[18] **48**,[19] and **50**,[16a] compared to those of meta-para and meta-meta series. Firstly we assume from this finding that the yield of cyclophane may increase with the increase in rigidity of starting diselena[3.3]cyclophane. In order to confirm such an assumption, three isomeric diselena[3.3]metacyclophane derivatives, **64**, **66**, and **68**, were synthesized and subjected to the photodeselenation reaction. The

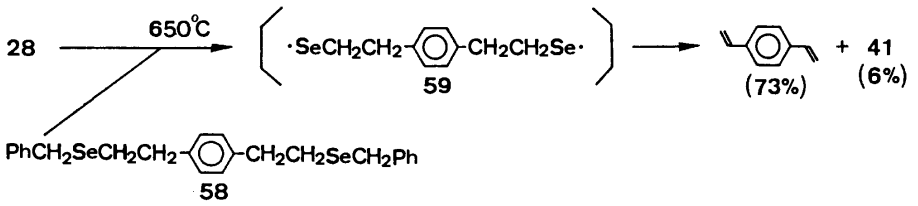

Table 3. Yields by Three Methods, Mp's, Crystal Forms, and ^{1}H NMR, MS, and/or Analytical Data

Compound	Yield/% Method (A) (B) (C)	Mp θ_m/°C	Crystal form (solvent)	^{1}H NMR/δ ($CDCl_3$)	MS and/or analysis
4	49 48 8	 133—134 134.5—135[b]	Prism (hex.[a])	2.08, 2.95(m, 8H, CH_2), 4.16(bs, 2H, inner ArH), 6.90—7.39(m, 6H, ArH)	MS 208 (M^+)
40	42 53 13	 80—81 81—81.5[c]	Plate (hex.[a])	1.96—3.16(m, 8H, CH_2), 5.28(s, 1H, inner ArH), 6.42—6.92(m, 7H, ArH)	MS 208 (M^+)
41	28 93 11	 286—289 285—287[d]	Prism (C_6H_6)	3.06(s, 8H, CH_2), 6.48(s, 8H, ArH)	MS 208 (M^+)
42	37 51 17	 145—146 144—145[e]	Prism (C_6H_6)	1.52—3.62(m, 16H, CH_2) 4.90(s, 1H, ArH of inner benzene), 5.12(bs, 1H, meta inner ArH), 6.17(s, 1H, ArH of inner benzene), 6.24—6.86(m, 7H, ArH)	MS 338 (M^+)
43	26 80 Trace	 >229 (decomp) 230 (decomp)[f]	Plate (C_6H_6-hex.[a])	2.23—3.16(m, 16H, CH_2), 5.40(s, 2H, ArH), 6.07(s, 8H, ArH)	MS 338 (M^+)
44	— 87 —	 >247 (decomp) >250 (decomp)[f]	Prism (C_6H_6)	2.07—3.21(m, 24H, CH_2), 5.12(s, 4H, ArH), 6.01(s, 8H, ArH)	MS 468 (M^+)
45	— 90 —	 >241 (decomp) >240 (decomp)[f]	Needle (hex.[a])	2.08—3.24(m, 24H, CH_2), 5.15(s, 4H, ArH), 5.99(s, 8H, ArH)	MS 468 (M^+)
46	12 None None[g]	 102—103 104.3—105.3[h]	Needle (MeOH)	2.03(m, 4H, CH_2), 2.72(t, 8H, CH_2), 6.66(s, 8H, ArH)	MS 236 (M^+)
47[i]	37 25 17	 >158 (decomp)	Column (hex.[a])	2.23—2.46, 3.08—3.46(m, 8H, CH_2), 4.38(s, 1H, inner ArH), 7.03—7.66(m, 6H, ArH and PyH)	MS 209 (M^+)
48	 — 75 anti:syn =9:1 —	(anti) 295—297 299—301[j] (syn) 245—245.5 243—245[k]	 Prism (C_6H_6) Prism (C_6H_6)	3.00—3.75(m, 8H, CH_2), 5.73(s, 4H, NapH), 7.33(m, 4H, NapH), 7.65(m, 4H, NapH) 3.56(m, 8H, CH_2), 6.72(s, 4H, NapH), 7.15(m, 8H, NapH)	MS 308 (M^+) MS 308 (M^+)
49	— 43 —	 365—368 368—369[i]	Needle (C_6H_6-hex.[a])	2.63—3.30(m, 8H, CH_2), 6.44(bs, 4H, NapH), 6.88(dd, 4H, NapH), 7.11(d, 4H, NapH)	MS 308 (M^+)
50	— 78 —	 113—114 114—115[j]	Needle (C_6H_6-hex.[a])	3.03—3.70(m, 8H, CH_2), 5.50(s, 2H, ArH), 6.35(s, 2H, NapH), 6.63(s, 2H, ArH), 7.30(m, 2H, NapH), 7.58(m, 2H, NapH)	MS 258 (M^+)
51	— 78 —	 155.5—156.5	Prism (hex.[a])	2.14—2.34(m, 6H, CH_2), 2.50— 2.82(m, 2H, CH_2), 3.96(d, 1H, inner ArH), 6.05(s, 2H, NapH), 6.69—7.12(m, 3H, ArH), 7.50— 7.63(m, 2H, NapH), 8.01—8.14 (m, 2H, NapH)	C(%) H(%) Found 93.01 7.13 Calcd 92.98 7.02 MS 258 (M^+)

Table 3. (Continued)

Compound	Yield/% Method (A) (B) (C)	Mp θ_m/°C	Crystal form (solvent)	^{1}H NMR/δ ($CDCl_3$)	MS and/or analysis
52	— 75 —	132—133	Prism (hex.[a])	2.25—2.35(m, 2H, CH_2), 2.47—2.55(m, 1H, CH_2), 2.73—2.81(m, 1H, CH_2), 2.91—2.97(m, 1H, CH_2), 3.17—3.23(m, 2H, CH_2), 3.48—3.53(m, 1H, CH_2), 5.29—5.62(m, 2H, ArH), 5.61(d, 1H, inner NapH), 7.21—7.33(m, 2H, ArH), 7.38—7.45(m, 3H, NapH), 7.72—7.75(m, 1H, NapH), 7.88—7.91(m, 1H, NapH)	C(%) H(%) Found 92.88 6.85 Calcd 92.98 7.02 MS 258 (M^+)
53	— 52 —	171—172	Prism (hex.[a])	2.05—2.33(m, 4H, CH_2), 3.12—3.30(m, 3H, CH_2), 3.97—4.00(m, 1H, CH_2), 4.19(bs, 1H, inner ArH), 4.50(bs, 1H, inner NapH), 7.10—7.17(m, 2H, ArH), 7.30—7.34(m, 1H, ArH), 7.45—7.50(m, 2H, NapH), 7.60(bs, 1H, NapH), 7.86—7.88(m, 1H, NapH), 8.09—8.13(m, 1H, NapH)	C(%) H(%) Found 93.02 7.20 Calcd 92.98 7.02 MS 258 (M^+)
54	22 — Trace	Colorless oil[m]		0.76—1.38(m, 12H, CH_2), 1.55—1.83(m, 4H, CH_2), 2.65(t, 4H, CH_2), 6.82—7.21(m, 4H, ArH)	MS 216 (M^+)
55	11 None Trace	40.5—42 41—42[m]	Powder (pentane)	0.62—1.87(m, 24H, CH_2), 2.55—2.69(m, 4H, CH_2), 7.04(bs, 4H, ArH)	MS 272 (M^+)
56	Trace 4 —	202—204 204—206[n]	Prism (C_6H_6-CH_2Cl_2)	2.74(s, 12H, CH_2), 5.71(s, 6H, ArH)	MS 234 (M^+)
57	— Trace 11 (−78°C) —	86—88 87—88[o]	Prism (hex.[a])	1.65—3.51(m, 12H, CH_2), 5.04(t, 1H, ArH), 5.85(d, 1H, ArH), 6.32 (t, 1H, ArH), 6.61, 6.83(ABq, 2H, ArH), 6.82(d, 1H, ArH)	MS 234 (M^+)
65	— 99[p] 89[q] —		Column (hex.[a])	2.59—2.73(m, 8H, CH_2), 2.93(s, 6H, Me), 6.87(t, 2H, ArH), 7.05(d, 4H. ArH)	C(%) H(%) Found 80.34 7.45 Calcd 80.56 7.51 MS 268 (M^+)
67	— 16 —	193—194 182[r]	Column (hex.[a])	1.66—1.74(m, 2H, CH_2), 2.02—2.10(m, 2H, CH_2), 2.94—2.99(m, 2H, CH_2), 3.52—3.58(m, 2H, CH_2), 3.85(s, 6H, Me), 4.30(d, 2H, inner ArH), 6.84(d, 2H, ArH), 7.04(dd, 2H, ArH)	C(%) H(%) Found 80.84 7.63 Calcd 80.56 7.51 MS 268 (M^+)
69	— 14 —	145—146 132—134[r]	Column (MeOH)	1.68, 3.52(AX, 4H, CH_2), 2.06, 2.99(AX, 4H, CH_2), 3.86(s, 6H, Me), 4.29(d, 2H, inner ArH), 6.83 (d, 2H, ArH), 7.02(dd, 2H, ArH)	C(%) H(%) Found 80.47 7.36 Calcd 80.56 7.51 MS 268 (M^+)

a) Hexane. b) K. Burri and W. Jenny, *Helv. Chim. Acta*, **50**, 1978 (1967). c) D. J. Cram, R. C, Helgeson, D. Lock, and L. A. Singer, *J. Am. Chem. Soc.*, **88**, 1324 (1966). d) Ref. 16b. e) Ref. 1d. f) Ref. 18. g) [2.2]-paracyclophane **41** was obtained about 6% yield. h) D. J. Cram, N. L. Allinger, and H. Steinberg, *J. Am. Chem. Soc.*, **76**, 6132(1954). i) J. R. Fletcher and I. O. Sutherland, *J. Chem. Soc., Chem. Commun.*, **1969**, 1504. j) Ref. 16a. k) Ref. 19. l) Ref. 10i. m) T. Otsubo and S. Misumi, *Synth. Commun.*, **8**, 285 (1978); S. Hirano, H. Hara, T. Hiyama, S. Fujita, and H. Nozaki, *Tetrahedron*, **31**, 2219 (1975). n) Ref. 10n. o) Ref. 10k, l. p) From anti **64**. q) From syn **64**. r) Ref. 20.

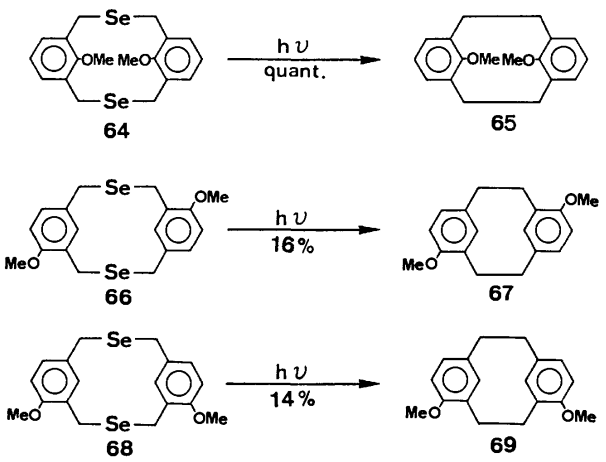

most rigid isomer **64** (syn and anti) gives similarly rigid anti-dimethoxy[2.2]metacyclophane **65** in quantitative yield, whereas isoelectronically substituted, but flexible isomers, **66** and **68**, afford the corresponding dimethoxymetacyclophanes, **67**[20] and **69**,[20] both in low yield.

Furthermore a typical example for our assumption is deselenation of diselena[3.3]biphenylophane **70** to

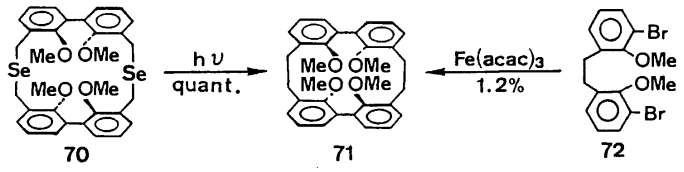

spherand-like macrocyclic compound **71** which is a rigidly constructed molecule and has a cavity suited to encapsulate selectively lithium ion.[21] In fact, the photodeselenation of **70** proceeds with quantitative yield of **71**, compared to low yield (1.2%) by the previous method. Unfortunately, this photodeselenation method is not suitable for cyclic selenides other than dibenzyl selenide form, e.g. diselenides **27**, **28**, and **32**. Consequently, the present synthetic method of [2.2]cyclophanes by means of the photodeselenation of diselenides demonstrates that this method is much more superior to any other conventional dechalcogenation method reported so far.

Experimental

All melting points are uncorrected. ^{1}H NMR spectra were recorded on a JEOL FX-100 (100 MHz) and Bruker WM360 (360 MHz) spectrometers using chloroform-*d* as a solvent and tetramethylsilane as an internal standard. Phenyl selenocyanate (PhSeCN)[22] was employed as the external standard for ^{77}Se measurement of **66** and **68**. Mass spectra were recorded on a Hitachi RMU-7 spectrometer (70 eV) using the direct injection technique and described here for organoselenium compounds.

General Synthetic Method of Selenides, 6—34, 64, 66, and 68. All selenium compounds were prepared by coupling of di- or tri-halides with bis- or tris-selenocyanates,[4] which were easily obtained by treatment of the corresponding halides with potassium selenocyanate, in the presence of large excess of sodium borohydride. The general procedure will be illustrated below by using the synthesis of 2,11-diselena[3.3]paracyclophane **10** as an example.[8]

A solution of 1,4-bis(selenocyanatomethyl)benzene (1.60 g, 5.1 mmol) and 1,4-bis(bromomethyl)benzene (1.32 g, 5.0 mmol) in 100 ml of ethanol and peroxide-free THF (1:1 v/v) was added to a suspension of an excess of $NaBH_4$ (commercial grade, ca. 2 g) in a mixture (1l) of ethanol and peroxide-free THF (1:19 v/v) under bubbling Ar with vigorous stirring at 40—50 °C for 13 h. After adding a small amount of ice, the reaction mixture was concentrated to ca. 100 ml. Dichloromethane and water were added to the concentrate and the organic layer was separated, washed with sat. NaCl aq, and dried over anhyd magnesium sulfate. The crude colorless residue obtained by evaporation of the solvent was recrystallized from benzene-dichloromethane to give colorless prisms of diselenaparacyclophane **10** (1.35 g, 73% yield).

In the case of oily products, **26** (n=10), **33a—b**, **34**, pale yellow oil obtained by solvent evaporation was purified by gel-permeation liquid chromatography with chloroform.

General Procedures of Deselenation. (A) Benzyne-Stevens Rearrangement/Raney Nickel Hydrogenolysis. To a solution of selenacyclophane (1 mmol) and isopentyl nitrite (2 g) in 1,2-dichloroethane (20 ml) was dropwise added a solution of anthranilic acid (4 mmol, 2 equiv.) in dichloromethane (20 ml) with vigorous stirring at reflux for more than 4 h under a nitrogen atmosphere. After removal of the solvent, the residue was chromatographed on silica gel with carbon tetrachloride or benzene to give a pale yellow solid or semisolid. A suspension of this rearranged product and Raney Ni (W-2, ca. 1 g) in ethanol (50 ml) was stirred at gentle reflux for 17—23 h under hydrogen. Worked up the mixture, a semisolid residue was chromatographed on silica gel with benzene-hexane to give cyclophane in a yield shown in Table 3.

(B) Photodeselenation with Tris(dimethylamino)phosphine. A solution of selenacyclophane (50—100 mg) and excess tris(dimethylamino)phosphine (1—1.5 g) in peroxide-free THF (30—80 ml) was irradiated with a 400 W high-pressure mercury lamp at room temperature under bubbling nitrogen until the starting material consumed completely. The residue obtained by solvent evaporation was chromatographed on silica gel with benzene-hexane or purified by gel permeation liquid chromatography to give cyclophane as shown also in Table 3. All of the cyclophanes described in Table 3 were identified by comparison of their ^{1}H NMR spectra, other physical properties and/or elemental analyses.

(C) Flash Pyrolysis under Reduced Pressure. A pyrex tube closed at one end, 45 cm long and 1 cm diameter, was used for pyrolysis. A sample (ca. 100 mg) of selenacyclophane was placed at the closed end of the tube. The other end was connected to a vacuum system (1—5 mmHg (1 mmHg=133.322 Pa)) and cooled with Dry Ice or liq. nitrogen. The middle part was placed in an electric furnace (25 cm long) preheated at 650 °C. After heating for ca. 3 min, the sample part was slidden within the furnace. Pyrolysis immediately occurred and the pyrolysate condensed at the cooled part. The organic products were

extracted with dichloromethane and purified by gel permeation liquid chromatography (Nihon Bunseki Kogyo LC-08) with chloroform or column chromatography on silica gel with benzene–hexane to give cyclophane as shown also in Table 3.

The authors wish to express their deep thanks to the Material Analytical Center, ISIR, Osaka University, for measurements of NMR and MS spectra and microanalyses. They also wish to thank the Ministry of Education of Japan for their finacial support.

References

1) a) J. Bruhin, W. Kneubühler, and W. Jenny, *Chimia*, **27**, 277 (1973); b) V. Boekelheide, I. D. Reingold, and M. Tuttle, *J. Chem. Soc., Chem. Commun.*, **1973**, 406; c) F. Vögtle and P. Neumann, *Synthesis*, **1973**, 85; d) N. Kannen, T. Otsubo, Y. Sakata, and S. Misumi, *Bull. Chem. Soc. Jpn.*, **49**, 3307 (1976); e) R. H. Mitchell and V. Boekelheide, *J. Am. Chem. Soc.*, **96**, 1547 (1974); f) T. Otsubo and V. Boekelheide, *Tetrahedron Lett.*, **1975**, 3881; g) V. Boekelheide, *Acc. Chem. Res.*, **13**, 65 (1980) and references cited therein.

2) F. Vögtle and L. Rossa, *Angew. Chem., Int. Ed. Engl.*, **18**, 515 (1979).

3) A. Couture, A. Lablache-Combier, R. Lapouyade, and G. Felix, *J. Chem. Res.*, (S), **1979**, 258.

4) T. Otsubo, F. Ogura, H. Yamaguchi, H. Higuchi, and S. Misumi, *Synth. Commun.*, **10**, 595 (1980).

5) H. Higuchi, T. Otsubo, F. Ogura, H. Yamaguchi, Y. Sakata, and S. Misumi, *Bull. Chem. Soc. Jpn.*, **55**, 182 (1982).

6) H. Higuchi, Y. Sakata, S. Misumi, T. Otsubo, F. Ogura, and H. Yamaguchi, *Chem. Lett.*, **1981**, 627.

7) R. H. Mitchell, *Can. J. Chem.*, **58**, 1398 (1980).

8) H. Higuchi and S. Misumi, *Tetrahedron Lett.*, **23**, 5571 (1982).

9) R. H. Mitchell, *Can. J. Chem.*, **54**, 238 (1976); R. H. Mitchell, *Tetrahedron Lett.*, **1975**, 1363.

10) a) R. S. Givens, R. J. Olsen, and P. L. Wylie, *J. Org. Chem.*, **44**, 1608 (1979); b) R. H. Mitchell, T. Otsubo, and V. Boekelheide, *Tetrahedron Lett.*, **1975**, 219; c) F. Vögtle, *Chem. Ber.*, **102**, 3077 (1969); d) V. Boekelheide and P. H. Andereson, *Tetrahedron Lett.*, **1970**, 1207; e) V. Boekelheide, P. H. Anderson, and T. A. Hylton, *J. Am. Chem. Soc.*, **96**, 1558 (1974); f) T. Otsubo, H. Horita, and S. Misumi, *Synth. Commun.*, **6**, 591 (1976); g) T. Otsubo and V. Boekelheide, *J. Org. Chem.*, **42**, 1085 (1977); h) R. H. Mitchell, R. J. Carruthers, L. Mazuch, and T. W. Dingle, *J. Am. Chem. Soc.*, **104**, 2544 (1982); i) M. Haenel and H. A. Staab, *Chem. Ber.*, **106**, 2203 (1973); j) F. Vögtle and L. Schunder, *Chem. Ber.*, **102**, 2677 (1969); k) M. Nakazaki, K. Yamamoto, and Y. Miura, *J. Chem. Soc., Chem. Commun.*, **1977**, 206; l) *idem*, *J. Org. Chem.*, **43**, 1041 (1978); m) F. Vögtle, *Justus Liebigs Ann. Chem.*, **735**, 193 (1970); n) V. Boekelheide and R. A. Hollins, *J. Am. Chem. Soc.*, **95**, 3201 (1973).

11) H. Higuchi, E. Kobayashi, Y. Sakata, and S. Misumi, *Tetrahedron*, **42**, 1731 (1986).

12) G. W. Bushnell and R. H. Mitchell, *Can. J. Chem.*, **60**, 362 (1982).

13) W. Anker, G. W. Bushnell, and R. H. Mitchell, *Can. J. Chem.*, **57**, 3080 (1979).

14) Further discussion will be reported elsewhere.

15) L. A. Ochrymowycz, C.-P. Mak, and J. D. Michna, *J. Org. Chem.*, **39**, 2079 (1974); E. Weber and F. Vögtle, *Liebigs Ann. Chem.*, **1976**, 891.

16) a) D. J. Cram, C. K. Dalton, and G. R. Knox, *J. Am. Chem. Soc.*, **85**, 1088 (1963); b) D. J. Cram and H. Steinberg, *J. Am. Chem. Soc.*, **73**, 5691 (1951).

17) E. J. Corey and E. Block, *J. Org. Chem.*, **34**, 1233 (1969).

18) T. Otsubo, S. Mizogami, I. Otsubo, Z. Tozuka, A. Sakagami, Y. Sakata, and S. Misumi, *Bull. Chem. Soc. Jpn.*, **46**, 3519 (1973).

19) H. H. Wasserman and P. M. Keehn, *J. Am. Chem. Soc.*, **91**, 2374 (1969).

20) S. Akabori, T. Sato, and K. Hata, *J. Org. Chem.*, **33**, 3277 (1968); T. Sato, S. Akabori, M. Kainosho, and K. Hata., *Bull. Chem. Soc. Jpn.*, **39**, 856 (1966).

21) T. Kaneda, S. Umeda, H. Tanigawa, S. Misumi, Y. Kai, H. Morii, K. Miki, and N. Kasai, *J. Am. Chem. Soc.*, **107**, 4802 (1985).

22) S. Tomoda, Y. Takeuchi, and Y. Nomura, *Chem. Lett.*, **1981**, 1069.

 © 1987 The Chemical Society of Japan Bull. Chem. Soc. Jpn., 60, 4037—4049 (1987)

Chemical Studies on Products Obtained from Verdohemochrome IXα Dimethyl Ester by Treatment with Ammonia under Air

Setsuo SAITO* and Norihiro TAMURA†

Faculty of Pharmaceutical Sciences, Josai University, Keyakidai 1-1, Sakado, Saitama 350-02

†Department of Chemistry, Josai Dental University, Keyakidai 1-1, Sakado, Saitama 350-02

(Received May 25, 1987)

Verdohemochrome IXα dimethyl ester [bis(pyridine)iron(II) 5-oxaprotoporphyrin IX dimethyl ester] gave 5-azaprotohemin IX dimethyl ester (**2**) and six tripyrrin derivatives upon treatment with ammonia under air, followed by methylation. The reaction of **2** with concd HCl in acetic acid in the presence of ferrous sulfate, followed by methylation gave demetallated product, 5-azaprotoporphyrin IX dimethyl ester (**8**), accompanied by products obtained by the hydration and reduction of both or one of the vinyl groups of **8**. 8,12-Bis[2-(methoxycarbonyl)ethyl]-3,7,13-trimethyl-1-oxo-2-vinyltripyrrin-14-carbaldehyde, obtained as a major tripyrrin product by an oxidative degradation of **1**, gave a pyrromethene derivative, 3,7-bis[2-(methoxycarbonyl)ethyl]-2,8-dimethyl-1-methoxy-5-pyrromethene-9-carbaldehyde by the reaction with $Tl(OAc)_3$ under air. The structures of all products obtained in the present study were determined by spectral measurements.

In human beings and many animals, endogenous heme (protoheme IX) is oxidized by heme oxygenase at the α-position to eliminate the α-carbon bridge, resulting in cleavage of the porphyrin ring and formation of an open chain tetrapyrrolic compound, biliverdin IXα.[1] The latter is subsequently reduced to bilirubin IXα by biliverdin reductase.[2] Verdohemochrome IXα was postulated as being an intermediate in the reaction process.[3,4] Biliverdins are the final products in coupled oxidation, a term used by Lemberg et al.[3b] to describe an analogous reaction of heme in a pyridine solution in the presence of ascorbic acid under air.[5] Jackson et al.[6] and Bonnett et al.[7] observed the formation of the verdohemochromes by

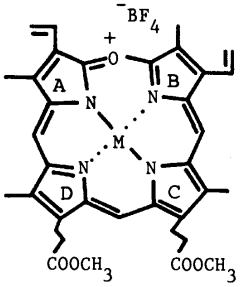

(1) M = Fe(II)·Py_2

(13) M = Zn

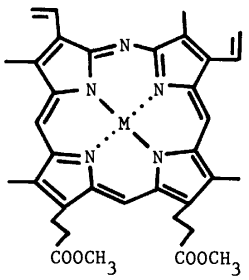

(2) M = Fe(III)·Cl

(3) M = Fe(II)·Py_2

(4) M = Fe(II)·Py·CO

(5) M = Fe(II)·$(TsCH_2NC)_2$

(14) M = Zn

Py = pyridine

$TsCH_2NC$ = p-$CH_3C_6H_4SO_2CH_2NC$

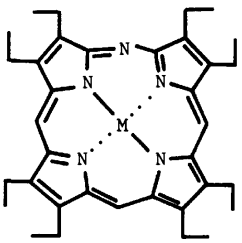

(6) M = Fe(III)·Cl

(7) M = 2H

Scheme 1.

oxygenation of the corresponding oxyporphyrins; their results, thus, supported Lemberg's proposal[5a] for the formation of verdohemochromes. Lagarias[8] and Hirota and Itano[9] elucidated the structure of octaethylhemochrome, which was obtained by the coupled oxidation of octaethylheme in pyridine, as bis(pyridine)iron(II) octaethyloxaporphyrin.

We previously prepared verdohemochrome IXα by the coupled oxidation of hemoglobin and myoglobin.[4] We recently synthesized verdohemochromes by ring closure of the corresponding biliverdins.[10] Verdohemochromes are particularly susceptible to oxidative attack at the *meso*-carbons[11] at which four pyrrole rings are linked to constitute the oxaporphyrin macrocycle. Furthermore, the oxonium bridge of verdohemochromes are easily subjected to hydrolysis to open the porphyrin ring, resulting in the formation of biliverdins.[12] On successive treatment with KOH–MeOH and excess mineral acid, verdohemochrome IXα undergoes hydrolysis and demetallation to give biliverdin IXα. This reaction is accompanied by autoxidation of the chromophore to give a small amount of pink compounds. It was thought that verdohemochrome IXα gave many degradation products because of its asymmetric structure. We previously reported the oxidative degradation of octaethylverdohemochrome, a symmetric molecule, as a model compound to obtain various tripyrrins.[13]

In this paper, the detailed spectral studies of 5-azaprotohemin IX dimethyl ester (**2**) are reported. Furthermore, the isolation and structural investigations of demetallation products obtained by the reaction of **2** with concd HCl in acetic acid in the presence of iron(II) sulfate, and those of tripyrrin derivatives obtained by oxidative degradation of verdohemochrome IXα dimethyl ester (**1**) in ammonia under air are reported. The degradation of tripyrrin (**21**) with thallium(III) acetate under air is also reported.

Results and Discussion

We previously reported the formation of 5-azaprotohemin IX dimethyl ester (**2**) in good yield by treatment of verdohemochrome IXα dimethyl ester (**1**) with ammonia under argon.[10] This reaction was accompanied by the formation of a small amount of impurities that appeared as pink spots on thin layer chromotography (TLC). In an attempt to increase the yield of the pink compounds, **1** was treated with ammonia under air. The reaction mixture showed, after methylation, six pink spots (products I—VI) and a greenish brown spot (product VII) on TLC (CH_2Cl_2–MeOH, 98:2, v/v). The all products were isolated by column chromatography and preparative high performance liquid chromatography (HPLC).

Product VII was identified as authentic 5-azaprotohemin IX dimethyl ester (**2**) by mixed TLC, HPLC, and electronic absorption spectrophotometry, and by the ^{1}H NMR spectrum of iron(II) 5-azaprotoporphyrin IX dimethyl ester obtained by reduction of **2** with $Na_2S_2O_4$.

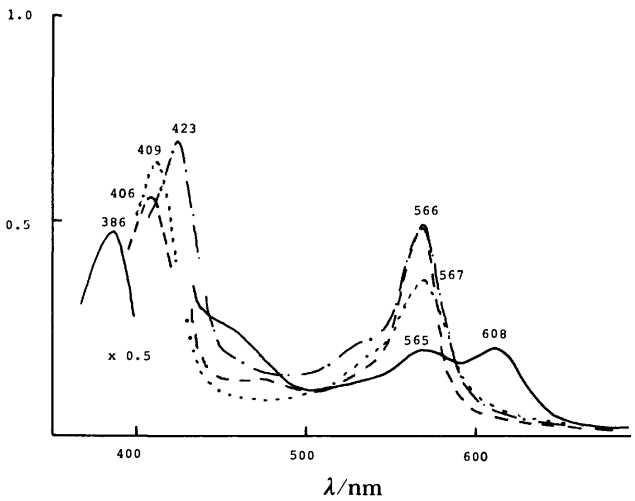

Fig. 1. Electronic absorption spectra. Spectra (1% pyridine–CH_2Cl_2, v/v) of 5-azaprotohemin IX dimethyl ester (**2**) (2.5×10^{-5} M), ——; bis(pyridine)iron(II) 5-azaprotoporphyrin IX dimethyl ester (**3**), – – –; carbon monoxide co-ordination complex (**4**), ····; bis(tosylmethyl isocyanide) complex (**5**), —·—·.

The electronic absorption spectrum of compound **2** in 1% pyridine–CH_2Cl_2 showed peaks at 386, 565, and 608 nm (Fig. 1). This spectrum was not changed by the addition of excess tosylmethyl isocyanide ($TsCH_2NC$) or by the introduction of carbon monoxide. The ^{1}H NMR spectrum of **2** in $CDCl_3$ showed broadened signals (Fig. 2a). These results indicate that the oxidation state of the central metal atom of **2** is Fe(III). This was also suggested from that the addition of sodium azide resulted in the spectrum of bis(azide)-iron(III) 5-azaprotoporphyrin IX dimethyl ester with maxima at 408 and 565 nm (the data was not shown). The addition of sodium dithionite resulted in the spectrum of iron(II) 5-azaprotoporphyrin IX dimethyl ester bis(pyridine) complex **3** with maxima at 406 and 566 nm (Fig. 1). Introduction of carbon monoxide into the solution of complex **3** produced iron(II) 5-azaprotoporphyrin IX dimethyl ester carbon monoxide complex **4**. Addition of excess $TsCH_2NC$ to the solutions of **3** and **4** resulted in the electronic spectrum of iron(II) 5-azaprotoporphyrin IX dimethyl ester bis($TsCH_2NC$) complex **5**, which was identified by FAB-mass spectrum data and elemental analysis as well as the ^{1}H NMR spectral data (Fig. 2b).

Demetallation of Compound 2. Various methods for the removal of iron from hemins are known.[13] Lemberg et al.[14] and Morell et al.[15] recommended the use of the iron(II) sulfate method as the mildest and most convenient method for the preparation of

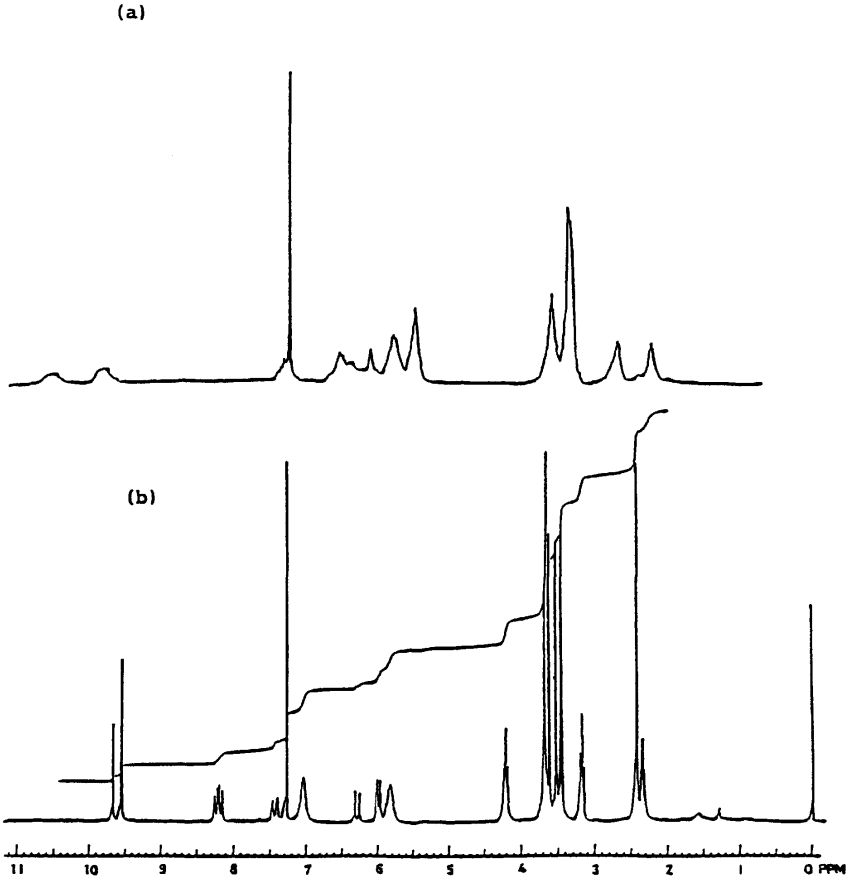

Fig. 2. 270 MHz FT ^{1}H NMR ($CDCl_3$). (a) 5-Azaprotohemin IX dimethyl ester (**2**), (b) Bis(tosylmethyl isocyanide)iron(II) 5-azaprotoporphrin IX dimethyl ester (**5**).

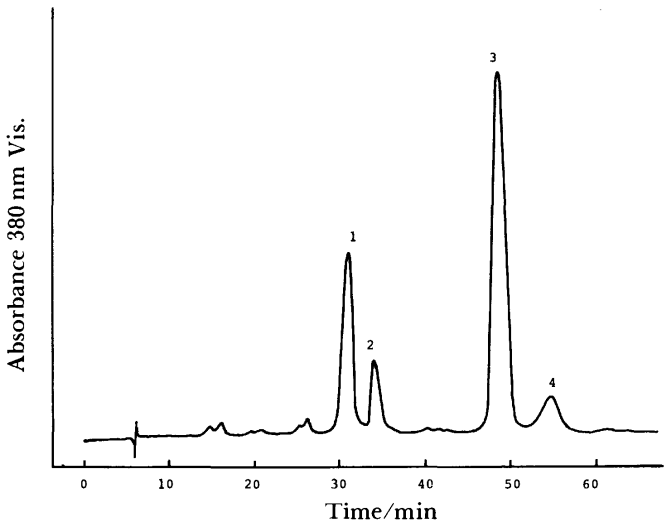

Fig. 3. High-performance liquid chromatogram of a reaction mixture obtained by the reaction of **1** with concd HCl in acetic acid in the presence of $FeSO_4$. Condition: column, SSC-ODS-H-4251, 10ϕX250 mm; mobile phase, benzene-MeOH (1:99, v/v); visible 380 nm; flow rate, 1.0 ml min^{-1}; chart speed, 0.5 cm min^{-1}.

protoporphyrin having a labile vinyl side chain. We previously reported that the removal of iron from octaethylazahemin **6** by treatment with concd HCl in acetic acid in the presence of iron(II) sulfate gave a single product, octaethylazaprophyrin (**7**), in good yield.[10] However, compound **2** gave a mixture composed for the most part of four azaporphyrin derivatives, **8**—**11**, by the same method. Figure 3 illustrates the separation of the four products by analytical HPLC with use of isocratic elution. The products were isolated by preparative HPLC.

All products **8**—**11** showed the proton signals of three *meso*-methine groups and two imino groups in their ^{1}H NMR spectra (Table 1). In addition, the major product **8** showed the proton signals of two vinyl groups. The FAB-mass spectrum of compound **8** showed a molecular ion peak at *m/z* 591. These results suggest that compound **8** is 13,17-bis[2-(methoxycarbonyl)ethyl]-3,8-divinyl-2,7,12,18-tetramethyl-5-azaporphyrin.

Product **9** showed the proton signals of two ethyl groups as well as those of three *meso*-methine groups and two imino groups, but no vinyl protons in its ^{1}H NMR spectrum. These results indicate that

Table 1. ^{1}H NMR Data (δ in $CDCl_3$, Multiplicity and J/Hz in Parentheses)

	8	9	10	11
meso-H	9.57, 9.57, 9.40	10.01, 9.85, 9.84	9.96, 9.90, 9.76	10.06, 9.97, 9.86
H_A	7.45 (dd, 17.6, 2.6)	—	—	—
H_B	6.15 (dd, 11.7, 2.6)	—	—	—
H_C	8.17 (dd, 17.6, 11.7)	—	—	—
H_D	6.35 (dd, 18.0, 1.5)	—	6.40 (dd, 18.0, 1.4)	—
H_E	6.13 (dd, 11.4, 1.5)	—	6.18 (dd, 12.0, 1.4)	—
H_F	8.07 (dd, 18.0, 11.4)	—	8.15 (dd, 18.0, 12.0)	—
CH_3 on Pyrrole	3.61, 3.45, 3.38, 3.34	3.36, 3.56, 3.54, 3.52	3.61, 3.49, 3.48, 3.46	3.69, 3.57, 3.56, 3.52
>-CH_2	4.17 (4H, m)	4.31 (4H, t, 7.5)	4.27 (4H, t, 6.2)	4.35 (2H, t, 7.8), 4.30 (2H, t, 7.8)
-CH_2CO-	3.07 (4H, m)	3.22 (4H, t, 7.5)	3.18 (4H, t, 6.2)	3.23 (4H, t, 7.8)
OCH_3	3.61, 3.61	3.64, 3.64	3.63, 3.62	3.65, 3.63
NH	−3.81 (2H)	−2.73 (2H)	−3.08 (2H)	−2.73 (2H)
Others	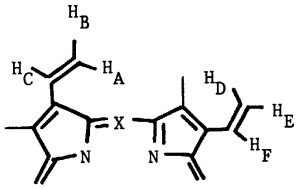 X=O^+, N, CH	3.97 (4H, q, 7.6, -$C\underline{H}_2CH_3$×2), 1.81 (6H, t, 7.6, -$CH_2C\underline{H}_3$×2)	8.34 (1H, d, 8.8, OH, exchangeable with D_2O), 6.13 (1H, m, changed to q, after addition of D_2O, -$C\underline{H}$(OH)CH_3) 2.16 (3H, d, 6.6, -CH(OH)$C\underline{H}_3$)	6.46 (1H, q, 6.6, -$C\underline{H}$(OH)CH_3) 3.39 (2H, q, 7.3, -$C\underline{H}_2CH_3$) 2.18 (3H, d, 6.6, -CH(CH)$C\underline{H}_3$) 1.83 (3H, t, 7.3, -$CH_2C\underline{H}_3$)

	5	12	13	14
meso-H	9.96, 9.54, 9.54	9.98, 9.98, 9.85, 9.85	9.28, 9.05, 8.97	9.04, 8.74, 8.73
H_A	7.42 (dd, 17.5, 2.6)	6.31 (dd, 18.0, 2.5)	6.69 (d, 17)	7.40 (dd, 17.8, 2.0)
H_B	5.99 (dd, 10.4, 2.6)	6.14 (dd, 11.4, 2.5)	6.00 (d, 9)	6.12 (dd, 11.9, 2.0)
H_C	8.20 (dd, 17.5, 10.4)	8.18 (dd, 18.0, 11.4)	7.35 (dd, 17, 9)	8.08 (dd, 17.8, 11.9)
H_D	6.28 (dd, 17.6, 1.5)	6.30 (dd, 17.6, 2.5)	6.17 (d, 17)	6.34 (dd, 17.8, 1.3)
H_E	6.00 (dd, 11.9, 1.5)	6.13 (dd, 11.4, 2.5)	6.10 (d, 9)	6.11 (dd, 11.5, 1.3)
H_F	8.22 (dd, 17.6, 11.9)	8.16 (dd, 17.6, 11.4)	7.58 (dd, 17, 9)	8.00 (dd, 17.8, 11.5)
CH_3 on Pyrrole	3.61, 3.52, 3.45, 3.45	3.59, 3.58, 3.53, 3.52	3.64, 3.09, 3.06, 3.03	3.53, 3.33, 3.24, 3.15
>-CH_2	4.21 (4H, t, 7.5)	4.31 (4H, t, 7.7)	3.85 (4H, t, 6.5)	3.98 (2H, t, 7.7) 3.95 (2H, t, 7.7)
-CH_2CO-	3.18 (4H, t, 7.5)	3.21 (4H, t, 7.7)	3.02 (4H, t, 6.5)	2.87 (2H, t, 7.7), 2.86 (2H, t, 7.7)
OCH_3	3.68, 3.68	3.65, 3.65	3.65, 3.65	3.57, 3.56
NH	—	−4.09 (2H)	—	—
Others	7.05 (4H, broad s, *ortho*-H on $TsCH_2NC$) 5.38 (4H, broad s, *meta*-H on $TsCH_2NC$) 2.42 (CH_3 on $TsCH_2NC$) 2.34 (CH_2 on $TsCH_2NC$)			

compound **9** is 3,8-diethyl-13,17-di[2-(methoxycarbonyl)ethyl]-2,7,12,18-tetramethyl-5-azaporphyrin. This conclusion was supported by the FAB-mass spectrum, which showed a molecular ion peak at m/z 611.

Product **10** showed the proton signals of one vinyl group and one 1-hydroxyethyl group (-CH(OH)CH_3) as well as those of three *meso*-methine groups and two imino groups. The FAB-mass spectrum of **10** showed a molecular ion peak at m/z 609. These results indicate that one of two vinyl groups of compound **8** is hydrated to obtain compound **10a** or **10b** during demetallation. For an elucidation of the structure of compound **10**, chemical shifts of vinyl protons in

compound **10** were compared with those of porphyrin derivatives **5**, **8**, **12**, and **13** in the ^{1}H NMR spectra. In this discussion, all vinyl protons on both vinyl groups at C-3 and C-8 are lettered A—F (Table 1).

The porphyrin derivatives **5**, **8**, **12**, and **13** had two vinyl groups at C-3 and C-8. In the partial structure (Table 1), when the bridge-head atom X was nitrogen (N) or oxonium (O^+), the H_A protons (δ 7.42 in **5**, 7.45 in **8**, and 6.69 in **13**) had lower chemical shifts than the other terminal vinyl protons, H_B, H_D, and H_E (δ 6.0—6.4) (Table 1). When X was the methine group (CH), as in compound **12**, all terminal vinyl protons (H_A, H_B, H_D, and H_E) in **12** appeared at δ 6.1—6.3, close to the chemical shifts of H_B, H_D, and H_E protons of compounds **5**, **8**, and **13**. These results suggest that the H_A-proton on the vinyl group at C-3 in compounds **5**, **8**, or **13** is favorably located close to the adjacent hetero atom and appears at lower field in the ^{1}H NMR spectra. Compound **12** had no bridge-head hetero atom on the porphyrin ring, therefore all terminal vinyl protons (H_A, H_B, H_D, and H_E) of compound **12** resulted in similar shifts (δ 6.1—6.3). H_D and H_E protons of the vinyl group at C-8 of compounds **5**, **8**, and **13** were located too far from the bridge-head hetero atoms and the chemical shifts of those protons (δ 6.0—6.4) were close to those to the terminal vinyl protons (H_A, H_B, H_D, and H_E) (δ 6.1—6.3) of compound **12**. In the ^{1}H NMR spectrum of compound **10** which had one vinyl group, two terminal vinyl protons appeared at δ 6.40 and 6.18, close to the chemical shifts of the terminal vinyl protons (H_D, δ 6.35 and H_E, 6.13) on the vinyl group at C-8 of compound **8**. Therefore the terminal vinyl protons appeared at δ 6.40 and 6.18 were assignable to H_D and H_E proton, respectively, on the vinyl group at C-8 of compound **10a**. These results suggest that compound **10** is 13,17-bis[2-(methoxycarbonyl)ethyl]-3-(1-hydroxyethyl)-2,7,12,18-tetramethyl-8-vinyl-5-azaporphyrin (**10a**).

Product **11** showed the proton signals of the 1-hydroxyethyl group and the ethyl group, but not those of the vinyl group. Either structure **11a** or structure **11b** was assignable to compound **11**. Though the exact structure of compound **11** was not determined, structure **11a** seems more likely because the vinyl group at C-3 in compound **8** would be more readily hydrated than that at C-8.

Electronic absorption spectra of compounds **8**—**11**

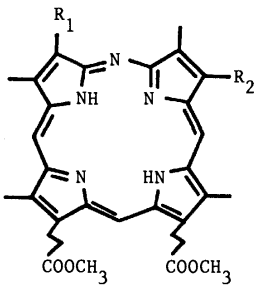

(8) $R_1 = R_2 = -CH=CH_2$

(9) $R_1 = R_2 = -CH_2CH_3$

(10a) $R_1 = -CH(OH)CH_3$, $R_2 = -CH=CH_2$

(10b) $R_1 = -CH=CH_2$, $R_2 = -CH(OH)CH_3$

(11a) $R_1 = -CH(OH)CH_3$, $R_2 = -CH_2CH_3$

(11b) $R_1 = -CH_2CH_3$, $R_2 = -CH(OH)CH_3$

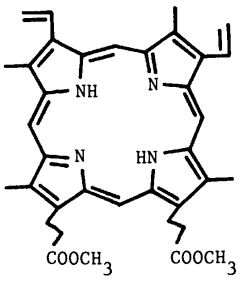

(12)

Scheme 2.

Table 2. Electronic Absorption Spectra of 5-Azaporphyrins in CH_2Cl_2

Compound	λ_{max}/nm (ε_{mM})					
	Soret band	V	IV	III	II	I
8	389(138.0)	517(11.5)	548(25.7)	570(12.5)	625(26.8)	670(10.8)
9	381(151.5)	509(9.7)	540(24.4)	562(10.6)	616(25.4)	661(11.1)
10	375(145.2)	500(8.4)	534(25.7)	560(10.3)	610(25.2)	651(3.3)
11	376(142.6)	502(9.1)	535(26.4)	559(9.3)	611(25.9)	650(1.2)

in CH_2Cl_2 are listed in Table 2. All spectra showed five satellite bands, numbered I to V, as well as Soret band, respectively. The molar extinction of each band decreased with decrease in number of vinyl groups. Hypochromic shifts in the Soret bands (389→381→375 and 376 nm) corresponded to the number of vinyl groups, two in **8**, one in **10**, and none in **9** and **11**. Similar hypochromic shifts were observed in bands I—V. The extinction coefficients of band II and IV were greater than those of bands I, III, and V in all spectra. The extinction coefficients of band I of compounds **9** and **11**, which had no vinyl group, were especially small.

Preparation of Zinc Azaporphyrin (14). Iron azaprotoporphyrin complex **2** was easily obtained from the corresponding verdohemochrome **1** by treatment with ammonia. However, the reaction of zinc 5-oxaprotoporphyrin dimethyl ester **13** with ammonia, followed by methylation, gave only an open chain tetrapyrrole compounds, biliverdin IXα dimethyl ester **15**,[10,16,17] by hydrolysis but not zinc azaporphyrin complex **14**. Zinc 5-azaprotoporphyrin IX dimethyl ester **14** was prepared by the reaction of azaprotoporphyrin IX dimethyl ester **8** with $Zn(OAc)_2$ in methanol. The ^1H NMR spectra (Table 1) of the zinc complex **14** was similar to that of **8**; the H_A-proton (δ 7.40) was shifted to lower field than the other terminal vinyl protons (H_B, H_D, and H_E) (δ 6.11—6.34). The FAB-mass spectrum showed fragment ion peaks at *m/z* 653, 655, and 657, which correspond to the cations $C_{35}H_{35}N_5O_4{}^{64}Zn^+$, $C_{35}H_{35}N_5O_4{}^{66}Zn^+$, and $C_{35}H_{35}N_5O_4{}^{68}Zn^+$, respectively.

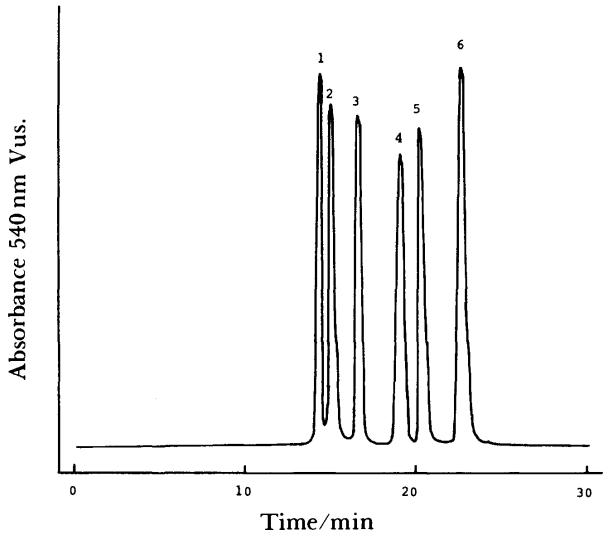

Fig. 4. High-performance liquid chromatogram of the degradation products. Condition: column, LiChrosorb SI-60, 4.6ϕ×250 nm; mobile phase, CH_2Cl_2-MeOH, 97.5:2.5 (v/v); visible, 540 m,; flow rate, 1.0 ml min^{-1}; chart speed, 0.5 cm min^{-1}. Injection was at time zero. Peak 1, **16**; 2, **17**; 3, **18**; 4, **20**; 5, **19**; 6, **21**.

Structures of Tripyrrins 16—21. Products (I—VI) were isolated by column chromatography and preparative HPLC. Figure 4 shows HPLC chromatogram for the isolated products (I—VI). The products (I—VI) showed the proton signals of two methine groups, three methyl groups, two 2-(methoxycarbonyl)ethyl groups, and one vinyl group in their ^1H NMR spectra (Table 3). These results indicate that the products (I—VI) are tripyrrin derivatives which are derived by the loss of one of the terminal pyrrole rings from the tetrapyrrole derivatives, verdohemochromes and biliverdins by oxidative degradation.[18,19] In addition to these signals, products I and II showed the singlet of the methoxycarbonyl group (δ 3.98 in I and 3.98 in II, respectively). The EI mass spectra of both I and II showed molecular ion peaks at *m/z* 535 (relative intensity: 38.4% in I and 92.7% in II, respectively). These results suggest that products I or II is either of the two tripyrrins (**16** or **17**).

Products III and V showed the proton signals of the dimethyl acetal group [δ 5.61 (-C<u>H</u>$(OCH_3)_2$) and 3.38 (-CH$(OC\underline{H}_3)_2$) in III, and 5.61 (-C<u>H</u>$(OCH_3)_2$ and 3.38 (-CH$(OC\underline{H}_3)_2$) in V, respectively] as well as those of

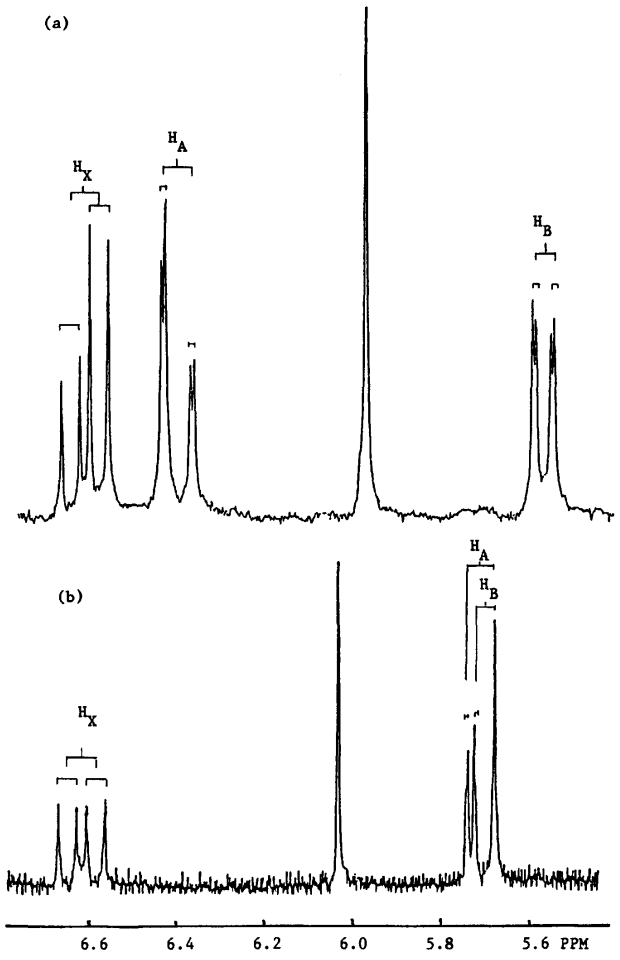

Fig. 5. Partial ^1H NMR spectra (downfield) of compounds **16** and **17**. (a), **16**; (b), **17**.

two *meso*-methine groups, two 2-(methoxycarbonyl)-ethyl groups, and one vinyl group in their ^{1}H NMR spectra. These results suggest that product III or V is either of the two tripyrrins **18** or **19**. This conclusion was also suggested by the EI mass spectra of III and V, which showed molecular ion peak at *m/z* 551.

The ^{1}H NMR spectra of products IV and VI showed the proton signals of the aldehyde group (δ 9.83 in IV and 9.82 in VI, respectively) as well as those of two *meso*-methine groups, two 2-(methoxycarbonyl)ethyl groups, and one vinyl group. The EI mass spectra of IV and VI showed molecular ion peak at *m/z* 505. These results suggest that product IV or VI is either of two tripyrrins **20** or **21**.

The exact structures of these products **16—21** were elucidated by comparing the chemical shifts of the vinyl protons of the products **16—21** with those of porphyrin derivatives **5**, **8**, and **13**, and those of biliverdin derivatives **15**, and **22—24** in the ^{1}H NMR spectra (Tables 3 and 4, and Fig. 5). As mentioned

Table 3. ^{1}H NMR Data for Tripyrrins (δ in $CDCl_3$, Multiplicity and *J*/Hz in Parentheses)

	16	**17**	**18**	**19**
meso-H	6.85, 5.96	6.85, 6.05	6.87, 5.99	6.84, 6.06
H_A	6.39 (dd, 17.7, 2.4)	5.71 (dd, 16.9, 1.1)	6.35 (dd, 17.6, 2.2)	5.69 (dd, 17.6, 0.5)
H_B	5.56 (dd, 11.6, 2.4)	5.70 (dd, 11.7, 1.1)	5.52 (dd, 11.0, 2.2)	5.68 (dd, 11.5, 0.5)
H_X	6.60 (dd, 17.7, 11.6)	6.66 (dd, 16.9, 11.7)	6.60 (dd, 17.6, 11.0)	6.65 (dd, 17.6, 11.5)
CH_3 on pyrrole	2.34, 2.21, 2.09	2.34, 2.10, 2.08	2.20, 2.09, 2.04	2.08, 2.07, 2.04
>-CH_2-	2.94 (4H, m)	2.94 (4H, m)	2.96 (2H, t, 7.1) 2.92 (2H, t, 7.1)	2.96 (2H, t, 7.1) 2.92 (2H, t, 7.1)
-CH_2CO-	2.55 (4H, m)	2.55 (4H, m)	2.54 (4H, t, 7.1)	2.55 (4H, t, 7.1)
/\\/$COOCH_3$	3.69, 3.65	3.67, 3.65	3.67, 3.65	3.67, 3.65
NH	11.20, 9.36	11.25, 9.56	10.90, 9.33	11.20, 9.45
Others	3.98 (3H, s, >-$COOCH_3$)	3.98 (3H, s, >-$COOCH_3$)	5.61 (1H, s, -C<u>H</u>$(OCH_3)_2$) 3.38 (6H, s, -CH$(OCH_3)_2$)	5.61 (1H, s, -C<u>H</u>$(OCH_3)_2$) 3.38 (6H, s, -CH$(OC\underline{H}_3)_2$)

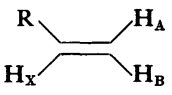

	20	**21**
meso-H	6.83, 5.95	6.84, 6.01
H_A	6.54 (dd, 17.7, 3.1)	5.70 (dd, 18.3, 0.5)
H_B	5.49 (dd, 10.4, 3.1)	5.69 (dd, 12.2, 0.5)
H_X	6.60 (dd, 17.7, 10.4)	6.63 (dd, 18.3, 12.2)
CH_3 on pyrrole	2.34, 2.19, 2.09	2.33, 2.09, 2.07
>-CH_2-	2.96 (2H, t, 7.4) 2.91 (2H, t, 7.4)	2.96 (2H, t, 7.3) 2.93 (2H, t, 7.3)
-CH_2CO-	2.57 (4H, t, 7.4)	2.57 (4H, t, 7.3)
/\\/$COOCH_3$	3.67, 3.65	3.67, 3.59
NH	11.25, 9.39	11.23, 9.59
Others	9.83 (1H, s, -CHO)	9.82 (1H, s, -CHO)

Table 4. Chemical Shifts (δ in $CDCl_3$) for Vinyl Protons of Compounds **15** and **22—24**[a)]

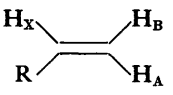

	15	**22**	**23**	**24**
Vinyl				
δ_A	6.12, 5.66	5.45, 6.12	5.49, 5.40	5.66, 5.50
δ_B	5.43, 5.64	5.44, 5.31	5.44, 5.38	5.64, 5.44
δ_X	6.50, 6.62	6.68, 6.49	6.73, 6.60	6.61, 6.76

a) These data were obtained by Rasmussen et al.[20)]

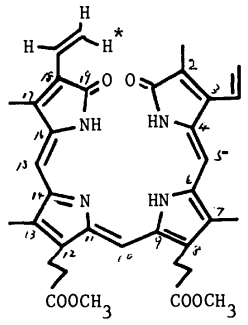

(15)

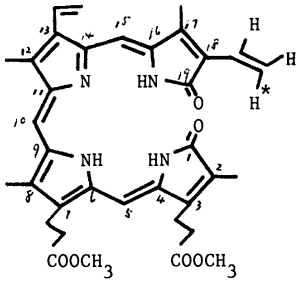

(22)

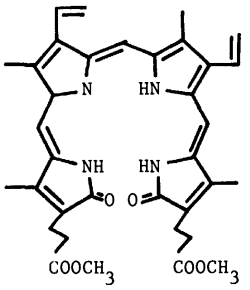

(23)

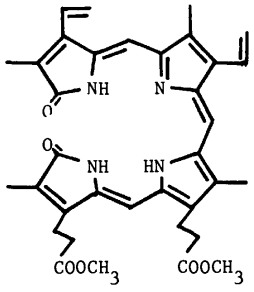

(24)

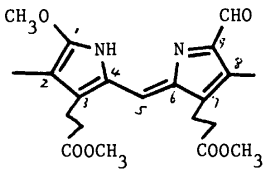

(27)

Scheme 3.

above, porphyrins **5**, **8**, and **13** have two vinyl groups at C-3 and C-8. The H_A-protons on the vinyl groups at C-3 in compounds **5**, **8**, and **13** appeared at lower field than the other terminal vinyl protons (H_B on vinyl group at C-3, and H_D and H_E on vinyl group at C-8). This conclusion will be applied to the assignment of the vinyl groups of biliverdins **15** and **22**—**24**.

Rasmussen et al.[17] reported the ^{1}H NMR spectra of four biliverdin dimethyl ester isomers **15** and **22**—**24**, of the IX series, but did not report detailed assignment of the vinyl protons. All vinyl groups of compounds **23** and **24**, and the vinyl groups at C-3 of **15** and at C-13 of **22** were located apart from the carbonyl groups of the terminally located pyrrole rings; all terminal vinyl protons (H_A and H_B in Table 4) of these vinyl groups appeared at δ 5.38—5.66. On the other hand, the protons marked with an asterisk (*) on the vinyl group at C-18 of **15** and that at C-18 of **22** were located close to the carbonyl groups (at C-19). These protons (H*) of **15** and **22**, therefore, appeared at lower fields (δ 6.12) in the ^{1}H NMR spectra of these compounds (Table 4).

Six tripyrrin derivatives **16**—**21** were divided into two groups (A and B) (Table 5) by comparison of the chemical shifts of the terminal vinyl protons (H_A and H_B) in their ^{1}H NMR spectra (Table 3). Figure 6 showed the partial ^{1}H NMR spectra (downfield) of compounds **16** and **17**. A comparison of the spectra shows the H_A-proton at a lower field (δ 6.39) than the H_B-proton (δ 5.56) in compound **16**. On the other hand, both the H_A and H_B protons of **17** showed nearly the same chemical shift at δ 5.71 and 5.70, respectively. The results indicate that the vinyl group of compound **16** is located close to the carbonyl group at C-1, and that the vinyl group of compound **17** is located at C-3 at a greater distance from the carbonyl group. Therefore, products I and II are identified as 14-methoxycarbonyl-8,12-bis[2-(methoxycarbonyl)-ethyl]-3,7,13-trimethyl-2-vinyltripyrrin-1-one (**16**) and 14-methoxycarbonyl-8,12-bis[2-(methoxycarbonyl)ethyl]-2,7,13-trimethyl-3-vinyltripyrrin-1-one (**17**), respec-

tively.

The same comparisons were done between products III and V, and also between IV and VI. The H_A-protons of products III and V appeared at lower fields (δ 6.35 in III and 6.54 in V, respectively). H_A-protons of V and VI were observed at δ 5.69 in IV and 5.70 in VI, respectively; these chemical shift values were close to those of the H_B-protons (δ 5.68 in IV and 5.69 in VI). Thus, products III—VI were identified as 8,12-bis[2-(methoxycarbonyl)ethyl]-3,7,13-trimethyl-1-oxo-2-vinyltripyrrin-14-carbaldehyde dimethyl acetal (**18**), 8,12-bis[2-(methoxycarbonyl)ethyl]-3,7,13-trimethyl-1-oxo-2-vinyltripyrrin-14-carbaldehyde (**20**), 8,12-bis[2-(methoxycarbonyl)ethyl]-2,7,13-trimethyl-1-oxo-3-vinyltripyrrin-14-carbaldehyde dimethyl acetal (**19**), and 8,12-bis[2-(methoxycarbonyl)-ethyl]-2,7,13-trimethyl-1-oxo-3-vinyltripyrrin-14-carbaldehyde (**21**), respectively. Compounds **16**, **18**, and **20** in group A (Table 5) accordingly were products of the loss of pyrrole ring B from compound **1** by oxidation degradation, and compound **17**, **19**, and **21** were products of the loss of ring A from **1**.

The electronic absorption spectra of compounds **16**—**21** are listed in Table 6. In comparisons of the spectra of compounds in group A with those of compounds in group B (Tables 5 and 6), individual bands of compound **16** had higher wavelength by 5—6 nm than the corresponding bands of compound **17**, 543, 509, 475sh, and 327 nm in **16** and 537, 504, 470sh, and 322 nm in **17**. The same results were obtained

Table 5. Structures of Tripyrrins

Group A	Group B
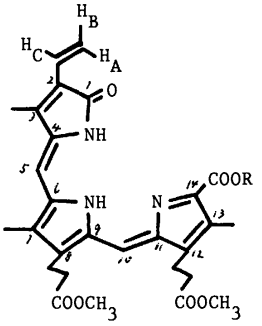 (16) R = CH_3 (25) R = H	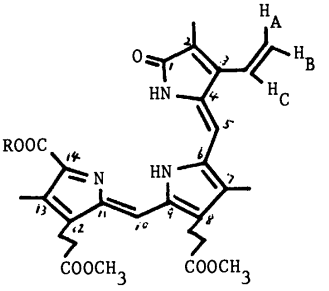 (17) R = CH_3 (26) R = H
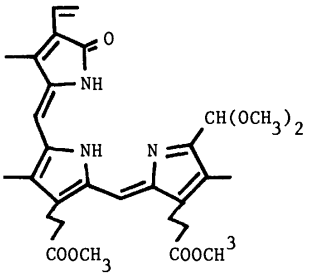 (18)	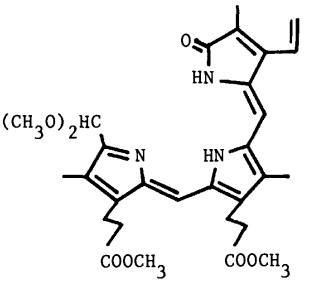 (19)
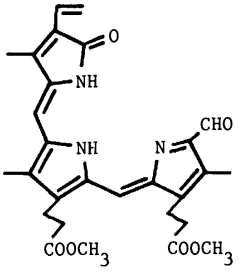 (20)	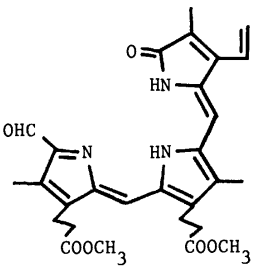 (21)

Table 6. Electronic Absorption Spectra of Degradation Products in CH_2Cl_2

	Group A							
	Free base λ_{max}/nm (ε_{mM})				Zinc complex[a] λ_{max}/nm (ε_{mM})			
16	543 (16.2)	509 (14.8)	475 sh[b] (7.8)	327 (25.9)	629 (22.2)	583 (12.0)	545 sh (5.6)	351 (28.7)
18	549 (14.4)	515 (14.5)	480 sh (8.4)	330 (32.2)	634 (13.4)	588 (10.0)	550 sh (5.2)	352 (31.7)
20	548 (15.6)	515 (15.7)	480 sh (9.2)	330 (37.0)	635 (14.9)	558 (10.6)	550 sh (5.3)	351 (35.5)

	Group B							
	Free base λ_{max}/nm (ε_{mM})				Zinc complex λ_{max}/nm (ε_{mM})			
17	537 (15.9)	504 (15.1)	470 sh (8.4)	322 (21.4)	624 (22.7)	578 (13.4)	540 sh (5.8)	345 (20.6)
19	543 (16.4)	510 (17.2)	475 sh (10.2)	325 (32.4)	630 (15.9)	585 (12.3)	547 sh (6.1)	345 (32.8)
21	543 (14.7)	510 (15.1)	475 sh (10.1)	325 (34.5)	630 (16.5)	585 (14.0)	547 sh (7.1)	341 (38.8)

a) 50 μl of zinc acetate (0.85 M) in MeOH was added to each sample cuvette. b) sh=shoulder.

Table 7. ^{13}C Chemical Shifts ($CDCl_3$) for Compounds **20** and **21** at 67.8 Mz (Downfield from Me_4Si)

	meso-C (C-5, 10)	CH_2=$\underline{C}$H-	$\underline{C}H_2$=CH-	$\underline{C}H_2CH_2CO$	$CH_2\underline{C}H_2CO$	$COO\underline{C}H_3$	$\underline{C}OOCH_3$	CH_3	CHO	C-1	Ring carbon atoms except C-1
20	96.1	122.5	125.4	19.7	34.9	51.6	172.8	9.8	177.7	169.8	145.6, 143.4, 139.7, 134.9,
	114.3			19.2			172.7	9.4			133.3, 133.2, 130.2, 128.7,
								8.5			128.3
21	96.8	123.0	126.1	19.8	35.0	51.7	173.0	9.8	178.0	169.1	153.3, 144.6, 143.5, 139.9,
	114.3			19.2			171.1	8.6			135.1, 133.3, 133.2, 130.9, 130.3, 128.7

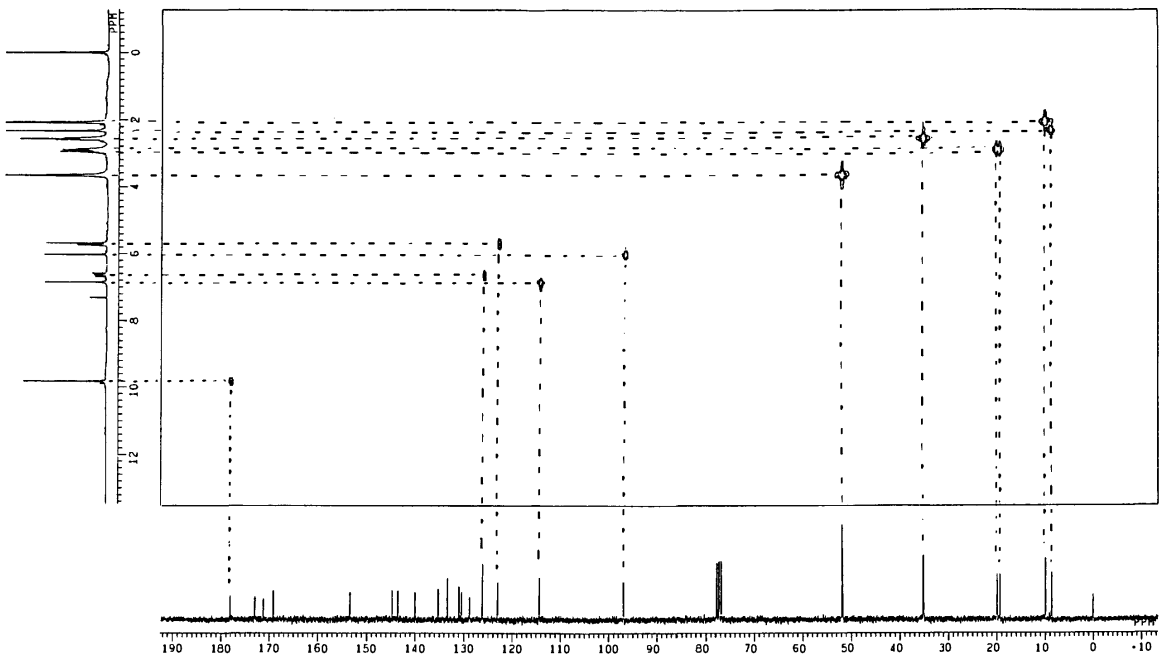

Fig. 6. Two dimensional (^1H-^{13}C) NMR spectrum of **21**.

between **18** and **19**, and between **20** and **21**.

The ^{13}C NMR spectra of compounds **20** and **21**, which were major products by oxidative degradation of **1**, are given in Table 7. The carbon signals were assigned by the single pulse hetero decoupling method (with NOE) and by the two dimentional (^1H-^{13}C) NMR spectra (the 2D NMR spectrum of **21** is shown in Fig. 6).

Degradation of Compound 1 on TLC under Air. Verdohemochrome IXα dimethyl ester **1** showed a single band at R_f 0.53 on preparative TLC (CH_2Cl_2–MeOH, 9:1, v/v). When the TLC plate was allowed to stand for a week under air, the color of the green band changed to pink. The band was scraped off and extracted. The extracts showed two major spots (R_f 0.36 and 0.32) and two minor spots (R_f 0.06 and 0.04) on TLC (CH_2Cl_2–MeOH, 98:2, v/v). The major products with R_f 0.36 and 0.32 were identified as compounds **20** and **21**, respectively, by mixed TLC, HPLC, and ^1H NMR spectra. The minor products with R_f 0.06 and 0.04 were unstable. The products showed the ^1H NMR spectra similar to those of **20** and **21**, respectively, except for absence of the signal of the methoxyl methyl proton. After methylation, the product with R_f 0.06 gave compound **20**, and that with R_f 0.04 gave compound **21**. These results suggest that the minor products with R_f 0.06 and 0.04 on TLC are compounds **25** and **26**, respectively.

Oxidative Degradation of 8 with Tl(OAc)$_3$. We previously reported the oxidative degradation of octaethylbiliverdin with thallium(III) acetate under air.[18] Further oxidation of the major tripyrrin derivative **21** was studied. The mixture obtained by the reaction of **21** with $Tl(OAc)_3$ in CH_2Cl_2–MeOH (9:1) under air showed two yellow spots (R_f 0.42 and 0.31) on TLC (benzene–acetone, 9:1, v/v). The compound with R_f 0.42 was isolated by column chromatography, but the compound with R_f 0.31 was so unstable that its isolation was unsuccessful. The ^1H NMR spectrum of the compound with R_f 0.42 on TLC showed the proton signals of an aldehydo group (δ 9.68) and a metoxyl group (δ 4.13) as well as those of two 2-(methoxycarbonyl)ethyl groups and two methyl groups but no vinyl group. The EI mass spectrum showed a molecular ion peak at m/z 402 and fragment ion peaks at m/z 387 (M^+-CH_3), 371 (M^+-OCH_3), and 343 ($M^+-COOCH_3$). These results suggest that the product is 3,7-bis[2-(methoxycarbonyl)ethyl]-2,8-dimethyl-1-methoxy-5-pyrromethene-9-carbaldehyde (**27**).

Thus, tripyrrin derivatives **16**—**21** were easily obtained from verdohemochrome IXα dimethyl ester **1** by oxidative degradation. Tripyrrin **21** was also oxidatively degraded to produce pyrromethene derivative **27**. Schaefer et al.[20] reported that cytochrome P-450 and free ferriprotoporphyrin IX were destroyed to obtain propentdyopents (dipyrrole derivatives) by NADPH-P-450 reductase in the presence of NADPH and O_2. In the present study, though the product **27** obtained by the reaction of tripyrrin **21** with $Tl(OAc)_3$ under air is different from those obtained by Shaefer et al. because of the difference of the reaction methods, the possibility of the presence of new metabolic path way for heme, heme→verdohemochrome→tripyrrins→dipyrrole derivatives, is offered.

Experimental

Materials. Verdohemochrome IXα dimethyl ester (**1**) was obtained by the method of Saito and Itano.[4] All chemicals and solvents were of reagent grade and were obtained from commercial sources.

Measurements. Electronic absorption spectra were recorded with a Hitachi Model 100-50 spectrophotometer. EI and FAB mass spectra were obtained with JEOL JMS-DX 300 mass spectrometer. High resolution mass spectra were obtained with JEOL OISG-2 mass spectrometer. ^1H NMR spectra at 270 MHz and ^{13}C NMR spectra at 67.8 MHz of samples in $CDCl_3$ solution containing Me_4Si were recorded with a JEOL JNM-GX 270 FT NMR spectrometer. The Shimadzu LC-6A liquid chromatograph, equipped with a Shimadzu system controller SCL-6A, a Shimadzu SPD-6AV UV-VIS spectrophotometric detector, and a Shimadzu C-R3A Chromatopac, were used for analytical high-performance liquid chromatography (HPLC), and were further equipped with an SSC autoinjector 6310 and an SSC fraction collector 6320 (Senshu Scientific Co. LTD.) for preparative HPLC. Analytical thin layer chromatography (TLC) and preparative TLC were performed on DC-Alufolien Kieselgel 60 HF_{254} (Merck) and Kieselgel 60 HF_{254} (Merck), respectively. Wacogel C-200 was used for column chromatography. Melting points were determined with a Yanako micro melting apparatus.

Reaction of 1 with Ammonia. Verdohemochrome IXα dimethyl ester (**1**) (460 mg, 502 μmol) was dissolved in the solution of pyridine (5 ml) and concd ammonia (50 ml) and allowed to stand under air overnight. The reaction mixture was poured into ice water (100 ml) and extracted with CH_2Cl_2 (150 ml×3). The combined organic extracts were washed with H_2O, dried over Na_2SO_4, and filtered. The filtrate was dissolved in 5% H_2SO_4–MeOH (150 ml) and allowed to stand overnight. The reaction mixture was poured into ice water (200 ml) and extracted with CH_2Cl_2 (200 ml×3). The combined organic extracts were washed with H_2O, dried over Na_2SO_4, and filtered. The filtrate was evaporated to give a residue which showed six pink spots (I, R_f 0.49; II, 0.44; III, 0.41; IV, 0.38; V, 0.34; and VI, 0.30) and a greenish brown spot (VII, 0.07) on TLC (CH_2Cl_2–MeOH, 98:2, v/v). The residue was dissolved in CH_2Cl_2 (5 ml) and subjected to column chromatography (CH_2Cl_2–MeOH, gradient up to 10%, v/v). Product VII was isolated, and products I—VI were partially purified. The partially purified products were subjected to preparative HPLC (LiChrosorb SI-60, 10φ, 250 mm, solvent system: CH_2Cl_2–MeOH, 97.5:2.5, v/v).

Product VII, yield 93.3 mg, 27.3%, was identified as 5-azaprotohemin IX dimethyl ester (**2**) by mixed TLC and electronic absorption spectrum, and the ^1H NMR spectrum of iron(II) bis(tosylmethyl isocyanide)-5-azaprotoheme IX dimethyl ester derived from **2** by the method of Saito and Itano.[10]

Product I: Yield 8 mg (3.0%), EI MS (70 eV) *m/z* (rel intensity) 535 (M^+, 38.4), 504 (M^+-OCH_3, 9.5), 503 (M^+-HOCH_3, 11.3), 462 (12.0), 448 (5.4), 444 (11.3), 430 (15.5), 416 (10.8), 388 (6.0), 239 (13.3), 237 (9.5), 234 (8.4), 235 (7.1), 183 (10.0), 178 (19.6), 85 (13.1), 83 (11.1), 71 (16.2), 69 (13.4), 57 (32.5), 44 (41.1), 43 (26.9), 32 (24.2), 28 (100). Found: *m/z* 535.2326. Calcd for $C_{29}H_{33}N_3O_7$: M, 535.2316.

Product II: Yield 15 mg (5.6%), EI MS (70 eV) *m/z* (rel intensity) 535 (M^+, 92.7), 504 (M^+-OCH_3, 22.5), 503 (M^+-HOCH_3, 9.5), 476 ($M^+-COOCH_3$, 6.6), 462 (13.9), 449 (10.0), 448 (33.8), 444 (20.0), 430 (19.9), 416 (28.0), 388 (14.8), 375 (11.0), 165 (8.9), 57 (11.4), 43 (9.6), 32 (18.5), 28 (100). Found: *m/z* 535.2303. Calcd for $C_{29}H_{33}N_3O_7$: M, 535.2316.

Product III: Yield 16 mg (5.8%), EI MS spectrum *m/z* (rel intensity) 551 (M^+, trace), 368 (5.1), 279 (5.6), 149 (22.8), 127 (6.4), 125 (7.2), 114 (6.7), 111 (12.9), 99 (11.9), 97 (22.5), 86 (62.0), 84 (79.9), 44 (100). Found: *m/z* 551.2631. Calcd for $C_{30}H_{37}N_3O_7$: M, 551.2629.

Product V: Yield 26 mg (9,4%), EI MS (70 eV) *m/z* (rel intensity) 551 (M^+, 5.5), 491 (5.0), 368 (6.0), 300 (9.0), 124 (5.1), 115 (12.3), 124 (17.4), 100 (41.9), 96 (35.9), 86 (17.3), 84 (22.3), 72 (96.4), 44 (48.1), 43 (100). Found: *m/z* 551.2625. Calcd for $C_{30}H_{37}N_3O_7$: M, 551.2629.

Product IV: Yield 32 mg (12.6%), EI MS (70 eV) *m/z* (rel intensity) 505 (M^+, 5.5), 418 (10.5), 358 (6.3), 181 (7.2), 148 (11.0), 136 (5.2), 122 (6.8), 108 (11.7), 94 (9.7), 57 (5.0), 44 (22.9), 43 (5.6), 32 (23.0), 28 (100). Found: *m/z* 505.2209. Calcd for $C_{28}H_{31}N_3O_6$: M, 505.2211.

Product VI: Yield 75 mg (29.6%), EI MS (70 eV) *m/z* (rel intensity) 505 (M^+, 60.4), 474 (10.0), 446 (5.3), 432 (22.5), 418 (26.1), 358 (10.8), 345 (6.6), 330 (8.9), 313 (5.5), 300 (5.0), 225 (6.1), 57 (13.6), 44 (14.0), 43 (8.9), 32 (20.6), 28 (100). Found: *m/z* 505.2215. Calcd for $C_{28}H_{31}N_3O_6$: M, 505.2211.

Demetallation of 2. To a solution of compound **2** (85 mg) in pyridine (1 ml) and acetic acid (30 ml), a solution of $FeSO_4$ (80 mg) in concd HCl (1 ml) was added under argon, and the reaction mixture was allowed to stand for 30 min. The reaction mixture was poured into ice water (50 ml) and extracted with CH_2Cl_2 (50 ml×3). The combined organic extracts were washed with water, dried over Na_2SO_4, and filtered. The filtrate was evaporated to give a residue which was dissolved in 5% H_2SO_4–MeOH (200 ml) and allowed to stand overnight. The mixture was poured into ice water (300 ml) and extracted with CH_2Cl_2 (150 ml×3). The combined organic extracts were washed with water, dried over Na_2SO_4, and filtered. The filtrate was evaporated to give a residue which was subjected to preparative HPLC (column: SSC-ODS-H-4251, 10ϕ, 250 mm; solvent system: 1% benzene–MeOH) to isolate compounds **8**—**11**. All products **8**—**11** had melting points over 300 °C.

Compound **8**: yield 33.5 mg (47.3%), FAB MS *m/z* 591 (100%). Found: C, 70.93; H, 6.31; N, 11.59%. Calcd for $C_{35}H_{37}N_5O_4$: C, 71.05; H, 6.30; N, 11.84%.

Compound **9**: yield 6.1 mg (8.6%), FAB MS *m/z* 595 (100%). Found: C, 70.47; H, 6.96; N, 11.69%. Calcd for $C_{35}H_{41}N_5O_4$: C, 70.56; H, 6.94; N, 11.76%.

Compound **10**: yield 3.4 mg (4.8%), FAB MS *m/z* 609 (100%). Found: C, 69.02; H, 6.41; N, 11.38%. Calcd for $C_{35}H_{39}N_5O_5$: C, 68.95; H, 6.45; N, 11.49%.

Compound **11**: yield 7.9 mg (10.7%), FAB MS *m/z* 611 (100%). Found: C, 68.85; H, 6.75; N, 11.22%. Calcd for $C_{35}H_{41}N_5O_5$: C, 68.72; H, 6.76; N, 11.45%.

Reaction of 13 with Ammonia. Compound **13** (20 mg) was dissolved in pyridine (1 ml) and concd aqueous ammonia (30 ml) under argon. The mixture was allowed to stand overnight, poured into ice water (150 ml), and extracted with CH_2Cl_2 (150 ml×3). The combined organic extracts were washed with water, dried over Na_2SO_4, and filtered. The filtrate was evaporated to give a residue which was dissolved in 5% H_2SO_4–MeOH (100 ml) and allowed to stand overnight. The reaction mixture was poured into ice water (200 ml) and extracted with water, dried over Na_2SO_4, and filtered. The filtrate was evaporated to give a residue which was subjected to column chromatography (benzene–acetone, gradient up to 5%) to obtain biliverdin IXα dimethyl ester (**15**), which was identified by TLC, mass spectrum, and ^1H NMR spectrum. No azaporphrin derivative was obtained by this reaction.

Preparation of 14. To a solution of compound **8** (12 mg) in CH_2Cl_2 (5 ml), a solution of zinc acetate (20 mg) in MeOH (10 ml) was added and warmed at 60 °C for 30 min. The solvent was evaporated, and the resulting residue was dissolved in CH_2Cl_2 (10 ml) and filtered and washed with CH_2Cl_2 (10 ml×3). The combined filtrates were evaporated to obtain a residue which was subjected to column chromatography (CH_2Cl_2–MeOH, gradient up to 5%) to isolate compound **14**. Found: C, 63.99; H, 5.41; N, 10.43%. Calcd for $C_{35}H_{35}N_5O_4Zn$: C, 64.13; H, 5.38; N, 10.68%. λ_{max} (CH_2Cl_2) nm (ε_{mM}) 588 (31.7), 547 (8.4), and 406 (87.1).

Iron(II) Bis(tosylmethyl isocyanide)-5-azaprotoporphyrin IX Dimethyl Ester (5). To a solution of **2** (17 mg) in pyridine (5 ml) and CH_2Cl_2 (20 ml), a solution of sodium dithionite (30 mg) in H_2O (1 ml) was added. The solution was vigorously shaken, and the mixture was washed with H_2O (20 ml×2), dried over Na_2SO_4, and filtered. The filtrate was added with pure $TsCH_2NC$ (25 mg) and subjected to column chromatography (CH_2Cl_2) to obtain compound **5**. Yield 17.5 mg (60.6%). Found: C, 61.05; H, 5.27; N, 9.14%. Calcd for $C_{53}H_{53}N_7O_8S_2Fe$: C, 61.44; H, 5.16; N, 9.46%.

Autoxidation of 1 on TLC. Compound **1** (150 mg) was dissolved in CH_2Cl_2 (1 ml) and chromatographed by prep. TLC (CH_2Cl_2–MeOH, 9:1, v/v). After development, the TLC plate was allowed to stand for a week under air at room temperature. The colored band was scraped off and extracted with CH_2Cl_2–MeOH (9:1, v/v). The extract was evaporated to give a residue, which was subjected to column chromatography (CH_2Cl_2–MeOH, gradient up to 10%) to obtain major product **20** (15.2 mg, 18.4%) and **21** (23.1 mg, 27.9%), and two minor products **25** (4.0 mg, 5.0%) and **26** (7.3 mg, 9.1%). The major porducts were identified with compounds **20** and **21**, respectively, by mixed TLC, HPLC, and ^1H NMR spectra. Though the minor products **25** and **26** were unstable, their ^1H NMR spectra were obtained. ^1H NMR ($CDCl_3$) of **25** δ=11.23—10.50 (2H, exchangeable with D_2O), 9.40 (1H, NH, exchangeable with D_2O), 6.84 (1H, s, *meso*-H), 6.59 (1H, dd, J=17.8 and 11.1 Hz, H_X), 6.38 (1H, dd, J=17.8 and 2.1 Hz, H_A), 5.96 (1H, s, *meso*-H), 5.55 (1H, dd, J=11.6 and 2.1 Hz, H_B), 3.67 and 3.65 (each 3H, s, $COOCH_3$), 2.96 (4H, >-CH_2-×2), 2.55 (4H, -CH_2CO-×2), 2.32, 2.18, and 2.07 (each 3H, s, CH_3). ^1H NMR ($CDCl_3$) of **26** δ=11.20—10.00 (2H, exchangeable with D_2O), 9.45 (1H, exchangeable with D_2O), 6.84 (1H, s, *meso*-H), 6.65 (1H, dd, J=17.8 and 11.0 Hz, H_X), 6.05 (1H, s, *meso*-H), 5.66 (1H, dd, J=17.8 and 1.4 Hz, H_A), 5.67 (1H, dd, J=11.0 and 1.4 Hz, H_B), 3.67 and 3.65 (each 3H, s, $COOCH_3$), 2.95 (4H,

$\gtrless$-CH_2-×2), 2.56 (4H, -CH_2CO-×2), 2.28, 2.07, and 2.04 (each 3H, s, CH_3).

Reaction 21 with Tl(OAc)$_3$. To a solution of **21** (50 mg) in CH_2Cl_2 (45 ml), a solution of thallium(III) acetate sesquihydrate (41 mg) in MeOH (5 ml) was added under air. The reaction mixture was poured into ice water (100 ml) and extracted with CH_2Cl_2 (100 ml×3). The combined organic extracts were washed with H_2O, dried over Na_2SO_4, and filtered. The filtrate was evaporated to obtain a residue which showed two yellow spots (R_f 0.42 and 0.31, benzene–acetone, 9:1, v/v). The residue was subjected to column chromatography to isolate the product **27** (22.7 mg, 57.0%) with R_f 0.42. The product with R_f 0.31 was so unstable that it could not be isolated. EI MS (70 eV) *m/z* (rel intensity) 402 (M^+, 100), 387 (14.7), 371 (17.3), 343 (16.5), 330 (8.6), 329 (38.8), 316 (10.1), 315 (47.4), 314 (25.7), 313 (61.8), 287 (8.0), 285 (8.8), 281 (7.3), 225 (11.9). λ_{max} (CH_2Cl_2) (ε_{mM}) 421 (30.1), 401 (27.8), and 380sh (16.0). ^{1}H NMR ($CDCl_3$) δ=11.75 (1H, NH, exchangeable with D_2O), 9.68 (1H, CHO), 6.45 (1H, s, *meso*-H), 4.13 (3H, s, $\gtrless$-OCH_3), 3.68 and 3.65 (each 3H, s, $COOCH_3$), 2.90 and 2.85 (each 2H, t, J=7.7 Hz, $\gtrless$-CH_2–), 2.55 and 2.52 (each 2H, t, J=7.7 Hz, -CH_2CO–), 2.31 and 1.91 (each 3H, s, CH_3). Found: *m/z* 402.1777. Calcd for $C_{21}H_{26}N_2O_6$: M, 402.1790.

References

1) A. H. Jackson, "Iron in Biochemistry and Medicine," ed by A. Jacobs and M. Morwood, Academic Press, London (1975), p. 145; P. O'Carra, "Porphyrins and Metalloporphyrins," ed by K. M. Smith, Elsevier, Amsterdam (1975), P. 123.

2) R. Schmid and A. F. McDonagh, "The Porphyrins," ed by D. Dolphin, Academic Press, New York (1979), Vol. VI, p. 257; R. Tenhunen, H. S. Marver, and R. Schmid, *J. Biol. Chem.*, **244**, 6388 (1969); R. Tenhunen, H. S. Marver, N. R. Pimstone, W. F. Trager, D. Y. Cooper, and R. Schmid, *Biochemistry*, **11**, 1716 (1972).

3) a) E. C. Foulkes, R. Lemberg, and P. Purdom, *Proc. R. Soc. London, Ser. B*, **138**, 368 (1951); b) R. Lemberg, B. Cortis-Jones, and M. Norrie, *Biochem. J.*, **32**, 149 (1938).

4) S. Saito and H. A. Itano, *Proc. Natl. Acad. Sci. U.S.A.*, **79**, 1393 (1982).

5) a) R. Lemberg, *Biochem. J.*, **29**, 2322 (1935); b) E. Y. Levin, *Biochemistry*, **5**, 2845 (1966).

6) A. H. Jackson, G. W. Kenner, and K. M. Smith, *J. Chem. Soc. C*, **1968**, 320.

7) R. Bonnett and M. J. Dimsdale, *J. Chem. Soc., Perkin Trans. 1*, **1972**, 2540.

8) J. C. Lagarias, *Biochim. Biophys. Acta*, **717**, 12 (1982).

9) T. Hirota and H. A. Itano, *Tetrahedron Lett.*, **24**, 995 (1983).

10) S. Saito and H. A. Itano, *J. Chem. Soc., Perkin Trans. 1*, **1986**, 1.

11) R. Lemberg and J. W. Legge, "Hematin Compounds and Bile Pigments," Interscience, New York (1949), p. 130; T. K. With, "Bile Pigments," Academic Press, New York (1968), p. 56.

12) P. O'Carra and E. Colleran, *J. Chromatogr.*, **50**, 458 (1970).

13) J.-H. Fuhrhop and K. M. Smith, "Porphyrins and Metalloporphyrins," ed by K. M. Smith, Elsevier, Amsterdam (1975), p. 800.

14) R. Lemberg, B. Bloomfield, P. Caiger, and W. Lockwood, *Aust. J. Exp. Biol. Med. Sci.*, **33**, 435 (1955).

15) D. B. Morell and M. Stewart, *Aust. J. Exp. Biol. Med. Sci.*, **34**, 211 (1956); D. B. Morell, J. Barrett, and P. S. Clezy, *Biochem. J.*, **78**, 793 (1961).

16) P. O'Carra and E. Colleran, *FEBS Lett.*, **5**, 295 (1969).

17) R. D. Rasmussen, W. H. Yokoyama, S. G. Blumenthal, D. E. Bergstorm, and B. H. Ruebner, *Anal. Biochem.*, **101**, 66 (1980).

18) S. Saito and H. A. Itano, *J. Chem. Soc., Perkin Trans. 1*, **1987**, 1183.

19) F. Eivazi, M. F. Hudson, and K. M. Smith, *Tetrahedron Lett.*, **1976**, 3837.

20) W. H. Schaefer, T. M. Harris, and F. P. Guengerich, *Biochemistry*, **24**, 3254 (1985).

 © 1987 The Chemical Society of Japan Bull. Chem. Soc. Jpn., 60, 4051—4060 (1987)

Utilization of Sulfide, Sulfoxide, and Sulfone Groups as Regiochemical Control Elements in the Diels-Alder Reaction of Naphthoquinones

Masatomo Iwao* and Tsukasa Kuraishi
Department of Chemistry, Faculty of Liberal Arts, Nagasaki University,
1-14 Bunkyo-machi, Nagasaki 852
(Received May 27, 1987)

The Diels-Alder reactions of 2-phenylthio-, 2-phenylsulfinyl-, and 2-phenylsulfonyl-1,4-naphthoquinones, which were unsymmetrically substituted by methoxyl group on the benzenoid ring, with some vinylketene acetals were studied. The regioselectivity of the reactions was cleanly controlled by each of these sulfur substituents. In addition, the reactivity of the naphthoquinones were greatly enhanced by introduction of the sulfone or sulfoxide group. As a result of this study, several anthraquinones including natural products, such as pachybasin and phomarin 6-methyl ether, and 11-deoxyanthracyclinones were efficiently synthesized.

The Diels-Alder reaction of naphthoquinone derivatives with a variety of polarized dienes has been regarded as one of the most efficient methods for the synthesis of highly substituted anthraquinones[1] and tetracyclic anthracyclinone systems.[2] The regioselectivity of this reaction has been proved to be controlled by several factors in the naphthoquinone moiety, such as intramolecular hydrogen bonding between peri hydroxyl group and quinone carbonyl,[3] resonance effect of oxygen functionalities on the benzenoid ring,[3,4] and inductive effect of halo substituents (Cl, Br) on the quinonoid ring.[1,2] Of these, the directing priority of the halo substituents seems to be the highest and consequently they have been employed most widely as regiochemical control elements of the reactions. However, it is sometimes difficult[5] to synthesize pure halonaphthoquinones regiospecifically in a few steps, except by the Diels-Alder approaches developed independently by Brassard[1c,f] and Cameron[1b,g,h]. Therefore, it is desirable to devise new directing groups which may be readily and regiospecifically introduced into the quinonoid ring.

Recently, we have developed[6] a regiospecific one-pot synthesis of 2-phenylthionaphthoquinones from substituted tertiary benzamides using directed lithiation strategy (Scheme 1). We expected that the phenylthio group in these quinones could excert a powerful regiochemical controlling effect for the Diels-Alder reaction by its conversion into the corresponding electron-withdrawing sulfoxide or sulfone groups. Boeckman et al.[3,7] were the first to examine the Diels-Alder reaction of this type of quinone, namely, tolylsulfinyljuglones, with isoprene or the diene derived from 7,7-dimethoxybicyclo-[4.2.0]oct-1(6)-en-2-one, and observed modest regioselectivities. In addition, Kraus and Woo[8] reported recently on a similar reaction using several different types of dienes but did not pursue regiochemical studies. In this paper, we describe the regioselective Diels-Alder reaction of naphthoquinone sulfoxides **2a—c**, sulfones **3a—c**, and sulfides **1a—c** with the vinylketene acetals **5**, **6**, **26**, and isoprene (**33**).

Results and Discussion

The sulfoxides **2a—c** were easily prepared in good yields from the corresponding sulfides **1a—c** by treatment with 1 equivalent of *m*-chloroperbenzoic acid (MCPBA)[3] in chloroform at 0 °C. However, the corresponding sulfone could not be obtained by MCPBA oxidation. Thus, TLC indicated that treatment of **1a** with 2 equivalents of MCPBA did not produce the sulfone **3a**, but a mixture of **1a**, **2a**, **4**, and another unidentified product. The epoxy sulfone **4** was obtained in good yield by treatment of **3a** with 3 equivalents of MCPBA. On the other hand, oxidation of **1a** with 4 equivalents of hydrogen peroxide[9] in refluxing acetic acid for 15 minutes gave the desired sulfone **3a** in 84% yield. In a similar manner, **3b** was obtained in 83% yield from **1b**. Oxidation of **1c** under similar conditions gave tarry material. However, at a lower temperature (80 °C), the sulfone **3c** was obtained in 66% yield.

We examined initially the Diels-Alder reaction of the quinones **2a**, **3a**, and **1a**, unsubstituted on the benzenoid ring, with mixed vinylketene acetal **5**[1d] readily prepared from methyl 3-methyl-2-butenoate. The sulfoxide **2a** was treated with 2 equivalents of **5** in

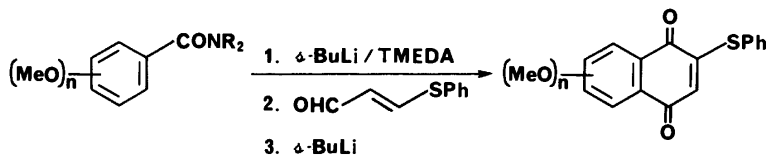

Scheme 1.

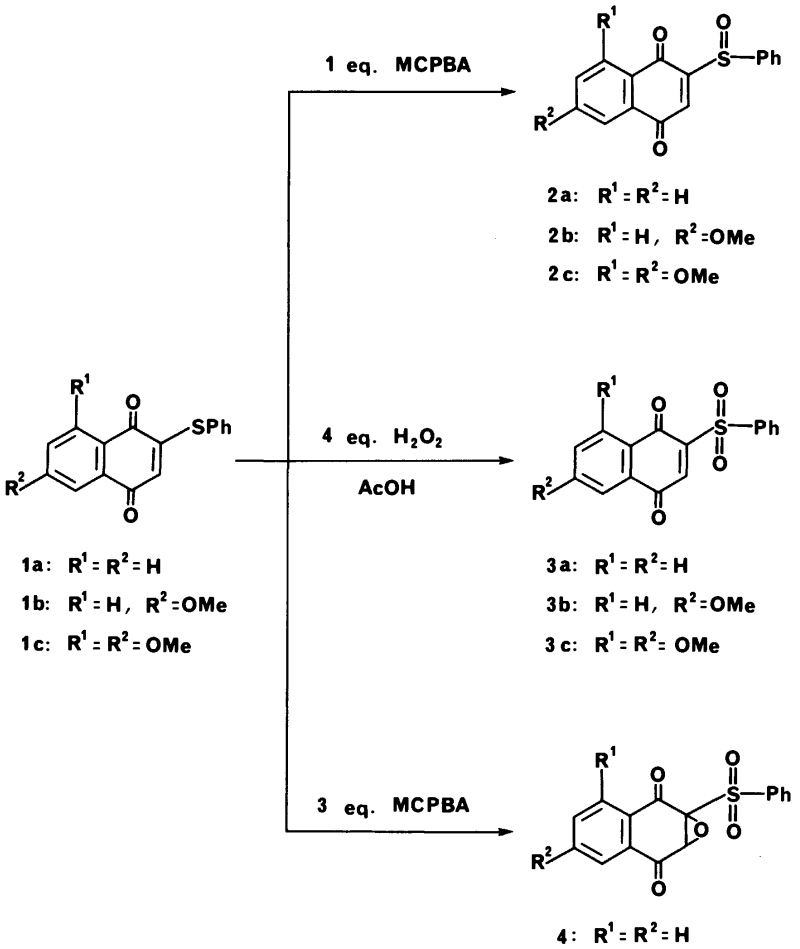

Scheme 2.

toluene at 0 °C. After 1 hour, TLC indicated the disappearance of starting quinone **2a**. However, the yellow color of the quinone did not disappear during this period which may indicate that the elimination of benzenesulfenic acid from the Diels-Alder adduct **7** (n=1, R^1=R^2=H, R^3=Me) is spontaneous under these conditions to regenerate the quinonoid structure. After evaporation of toluene, the residual oil was treated with aqueous methanolic HCl to effect aromatization to give 1-hydroxy-3-methylnaphthoquinone (pachybasin) (**8**) and its *O*-methyl derivative **9** in low yields and poor selectivity (**8**: 28%; **9**: 14%). On the other hand, the base-catalyzed aromatization using triethylamine which was employed at first by Rapoport[2g] in their aklavinone synthesis provided **8** almost exclusively although the yield again was low (Table 1: Entry 1). We used this mild and highly selective aromatization method as a standard procedure for other cases described below. The Diels-Alder reaction of the sulfone **3a** with **5** is very rapid. When **5** was added to a toluene solution of **3a** at 0 °C, the yellow color of **3a** disappeared almost instantaneously and TLC indicated the absence of starting quinone **3a**. On treatment with triethylamine, smooth elimination of benzenesulfinic acid and methanol from the adduct **7** (n=2, R^1=R^2=H, R^3=Me) took place and **8** was obtained in 86% yield accompanying with a trace amount of **9** (Entry 2). The sulfide **1a** is much less reactive toward **5** compared with **2a** and **3a**. It took 12 hours to complete the Diels-Alder reaction in refluxing benzene and additional 2 days for the triethylamine-catalyzed aromatization. In this reaction, the selectivity of **8** to **9** is somewhat low, but the total yield of the quinonoid products is excellent (Entry 3).

Next, we examined the Diels-Alder reaction of 6-methoxynaphthoquinones **2b**, **3b**, and **1b** with vinylketene acetal **5** to see the regiochemical controlling effect of the sulfoxide, sulfone, and sulfide groups (Entries 4—6). In every case, the reaction proceeded regiospecifically to give 1-hydroxy-6-methoxy-3-methylanthraquinone (phomarin 6-methyl ether) (**10**) as a major product in addition to a minor amount of its *O*-methyl derivative **11**.

In order to confirm the regiospecificity of these reactions, we have synthesized the regioisomer of **10**, 1-hydroxy-7-methoxy-3-methylanthraquinone (**24**), using the directed lithiation strategy developed by

Table 1. Diels-Alder Reaction of Sulfur-Substituted Naphthoquinones with Vinylketene Acetals

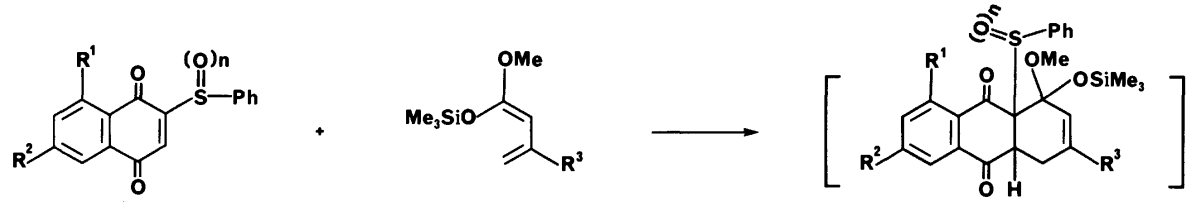

1a-c: n=0
2a-c: n=1
3a-c: n=2

5: R^3 = Me
6: R^3 = OMe

7

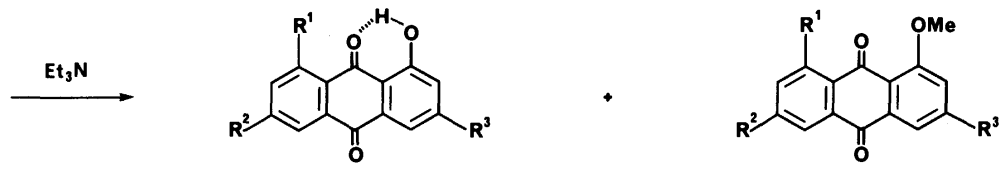

8: R^1 = R^2 = H, R^3 = Me
10: R^1 = H, R^2 = OMe, R^3 = Me
12: R^1 = R^2 = OMe, R^3 = Me
14: R^1 = R^2 = H, R^3 = OMe
16: R^1 = H, R^2 = R^3 = OMe
18: R^1 = R^2 = R^3 = OMe

9: R^1 = R^2 = H, R^3 = Me
11: R^1 = H, R^2 = OMe, R^3 = Me
13: R^1 = R^2 = OMe, R^3 = Me
15: R^1 = R^2 = H, R^3 = OMe
17: R^1 = H, R^2 = R^3 = OMe
19: R^1 = R^2 = R^3 = OMe

Entry	Naphthoquinone	Vinylketene acetal	Solvent[a]	Condition[b]		Anthraquinone(yield/%)[c]	
				Diels-Alder	Aromatization		
1	**2a**	**5**	T	A (1 h)	A (4 h)	**8**(41)	**9**(<1)
2	**3a**	**5**	T	A (1 h)	A (4 h)	**8**(86)	**9**(<1)
3	**1a**	**5**	B	D (12 h)	D (48 h)	**8**(81)	**9** (11)
4	**2b**	**5**	T	A (1 h)	A (4 h)	**10**(43)	**11**(<1)
5	**3b**	**5**	T	A (1 h)	A (4 h)	**10**(84)	**11** (1)
6	**1b**	**5**	B	D (30 h)	D (24 h)	**10**(81)	**11** (9)
7	**2c**	**5**	T	C (5 h)	B (18 h)	**12**(42)	**13** (5)
8	**3c**	**5**	T	C (1 h)	B (18 h)	**12**(81)	**13** (8)
9	**1c**	**5**	B	D (68 h)	D (24 h)	**12**(50)	**13** (11)
10	**2a**	**6**	T	A (0.5 h)	A (6 h)	**14**(73)	**15**(<1)
11	**3a**	**6**	T	A (0.5 h)	A (6 h)	**14**(66)	**15**(<1)
12	**1a**	**6**	B	C (120 h)	D (40 h)	**14**(77)	**15** (1)
13	**2b**	**6**	T	A (1 h)	A (3 h)	**16**(81)	**17** (6)
14	**2c**	**6**	T	C (1 h)	B (18 h)	**18**(65)	**19** (19)

a) T: Toluene; B: benzene. b) A: 0 °C; B: 0°C→room temperature; C: room temperature; D: reflux. c) Isolated yield after chromatography.

Snieckus[10] (Scheme 3). Thus *N,N*-diethyl-2-methoxy-4-methylbenzamide (**20**) was sequentially ortho-lithiated (*s*-BuLi-TMEDA-ether/−78 °C) and treated with *p*-anisaldehyde. The crude condensation product was treated with *p*-toluenesulfonic acid in refluxing benzene to give the phthalide **21** in 45% yield. Compound **21** was hydrogenated over palladium on charcoal to give the benzylbenzoic acid **22**. Without purification, crude **22** was treated with trifluoroacetic anhydride (TFAA) in dichloromethane followed by chromium trioxide to give the anthraquinone **23** in 29% overall yield from **21**. Selective demethylation of **23** with boron tribromide afforded the desired isomer **24** in 86% yield. The most characteristic difference between **10** and **24** was observed in their ^{1}H NMR spectra. Thus, the

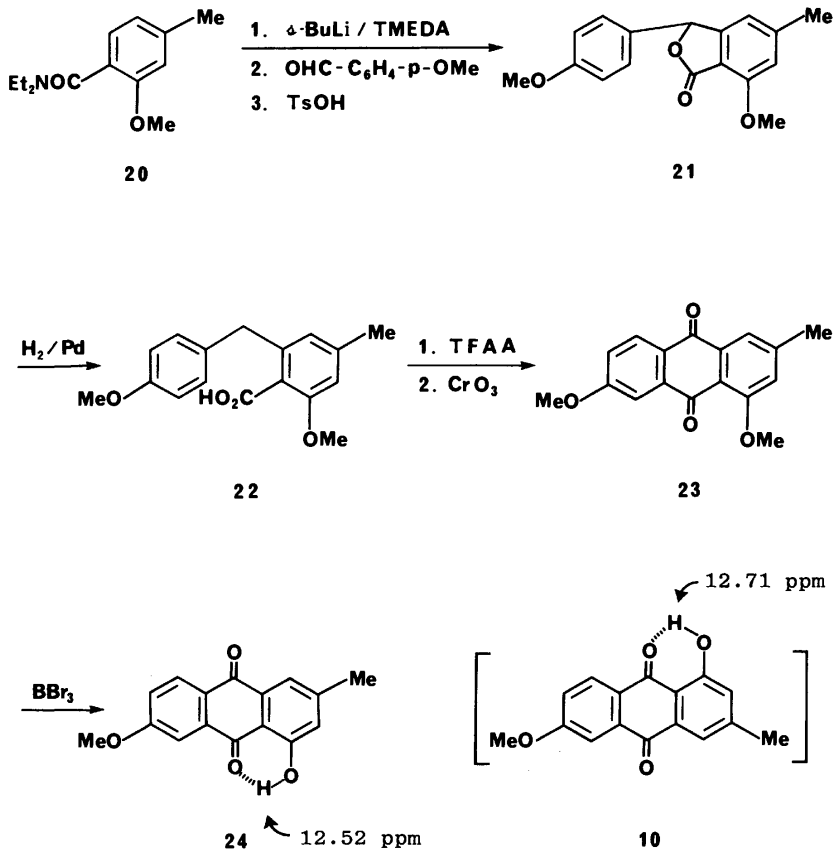

Scheme 3.

absorptions of the strongly hydrogen-bonded peri hydroxyl protons for these compounds appeared at considerably different chemical shifts (**10**: δ 12.71, **24**: δ 12.52). This is apparently due to the difference of the resonance effect[2b,g] of the methoxyl group in the hydrogen-bonded quinone carbonyl in each isomer. This result suggests that the regioselectivity of the Diels–Alder reaction of mixed vinylketene acetals of type **5** with methoxy-substituted naphthoquinones could be generally established by ^{1}H NMR spectroscopy.

Next, we carried out the Diels–Alder reaction of 6-methoxy-1,4-naphthoquinone (**25**) with **5** to confirm the necessity of the sulfur substituents for the regiospecific Diels–Alder reactions (Scheme 4). When **25** was treated with **5** in refluxing benzene for 20 hours, and the crude Diels–Alder adduct was oxygenated under alkaline conditions, a 3.1 : 1 mixture of **24** and **10** was obtained in 78% yield. The ratio of **24** to **10** was determined by integration of the hydroxyl proton NMR absorptions of each isomer in the mixture. This result could be rationalized[4,23] as follows. The electron-donating effect of the methoxyl group at the 6 position weakens the electron-withdrawing effect of the C-1 carbonyl compared with C-4 which causes the electron-rich center of **5** to react preferentially at the C-2 position of the quinone **25** to give the anthraquinone **24** as a major product after

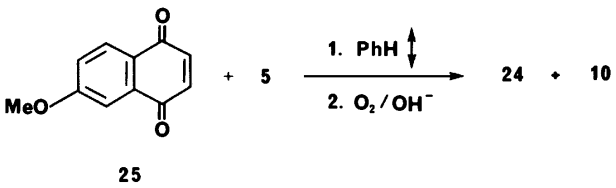

Scheme 4.

oxidative and hydrolytic work-up. This experiment revealed that the sulfur substituents on the quinonoid ring of **2b**, **3b**, and **1b** can overcome the electronic effect of 6-methoxyl group, and are essential for the regiospecific Diels–Alder reactions.

It is of interest to determine the effect of an additional methoxyl group in 5,7-dimethoxynaphthoquinone derivatives **2c**, **3c**, and **1c** on the regioselectivity of the Diels–Alder reaction. In these compounds, the electron-releasing effect of two methoxyl groups at 5 and 7 positions should result in considerable increase of electron density of the quinonoid ring and decrease of the electron-withdrawing effect of C-4 carbonyl rather than C-1. These effects should reduce both reactivity and regioselectivity of these compounds compared with monomethoxylated quinones described above.

The sulfoxide **2c** was actually much less reactive

toward **5** compared with unsubstituted sulfoxide **2a** or mono-methoxylated compound **2b**. However, the Diels-Alder reaction was completed within 5 hours at room temperature and, after triethylamine-catalyzed aromatization, 1-hydroxy-6,8-dimethoxy-3-methylanthraquinone (emodin 6,8-dimethyl ether) (**12**) and its *O*-methyl derivative **13** were obtained in 42% and 5% yields, respectively (Table 1: Entry 7). The regioselectivity of this reaction was proved by careful examination of the hydroxyl proton region of ^{1}H NMR spectrum of the crude product, which showed only a sharp singlet at δ 13.09 which was identical with a reported value[1e] for emodin 6,8-dimethyl ether. In addition, structure of **13** was identified by direct spectroscopic and TLC comparisons with an authentic sample.[11] The sulfone **3c** was more reactive than the sulfoxide **2c**, and the Diels-Alder reaction with **5** was completed within 1 hour at room temperature. After triethylamine-catalyzed aromatization, **12** was obtained in good yield (81%) in addition to a small amount of **13** (8%) (Entry 8). The sulfide **1c** was much less reactive toward **5**. It took 68 hours in refluxing benzene to complete the reaction. However, the reaction was again regiospecific, and emodin derivatives were obtained in modest yields after triethylamine-catalyzed aromatization (Entry 9). Therefore, it was revealed from these experiments that the directing and activating effects of the sulfur substituents attached directly on the quinonoid ring were quite strong to outweigh the electronic effect of two methoxyl groups on the benzenoid ring. It appears that the effects of the sulfur substituents are stronger than those of the halo substituents since Brassard has reported[1d] that 3-chloro-5,7-dimethoxynaphthoquinone was almost unreactive toward the vinylketene acetals of type **5**.

The vinylketene acetal **6**[1d] was also allowed to react with some sulfur-substituted naphthoquinones, and the expected anthraquinone products were obtained regiospecifically in good yields (Table 1: Entries 10—14).

The synthesis of anthracyclinone aglycone is of current interest due to the potent antitumor activity of anthracycline antibiotics.[12] Based on the studies described above, some 11-deoxyanthracyclinones were easily synthesized regiospecifically by cycloaddition of

Table 2. Synthesis of 11-Deoxyanthracyclinones

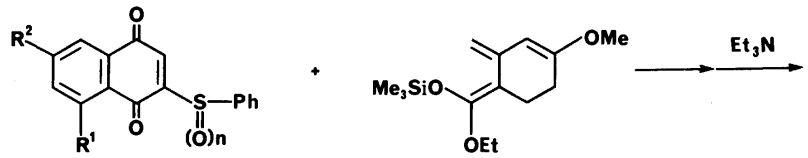

2a-c: n=1
3a-c: n=2

26

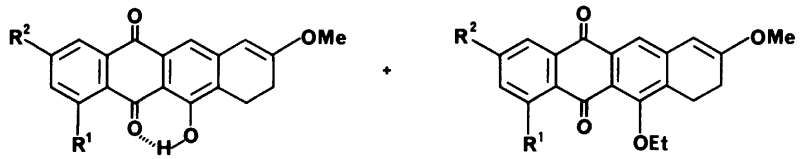

27: $R^1 = R^2 = H$
29: $R^1 = H$, $R^2 = OMe$
31: $R^1 = R^2 = OMe$

28: $R^1 = R^2 = H$
30: $R^1 = H$, $R^2 = OMe$
32: $R^1 = R^2 = OMe$

Entry	Naphthoquinone	Condition[a]	Anthracyclinone (yield/%)[b]	
1	**2a**	A	**27** (56)	**28** (34)
2	**3a**	A	**27** (57)	**28** (4)
3	**2b**	A	**29** (44)	**30** (47)
4	**3b**	A	**29** (69)	**30** (10)
5	**2c**	B	**31** (27)	**32** (32)
6	**3c**	B	**31** (37)	**32** (3)

a) A: Diels-Alder(0 °C, 1 h), aromatization(0 °C→room temperature, 18 h); B: Diels-Alder(room temperature, 1 h), aromatization(0 °C→room temperature, 18 h). All reactions were carried out in toluene. b) Isolated yield after chromatography.

Gesson's vinylketene acetal **26**,[2d] prepared in two steps from commercially available Hageman's ester, with the naphthoquinone sulfoxides **2a—c** and sulfones **3a—c**. The results are summarized in Table 2. In general, the sulfoxides reacted with **26** in good yields to give, after triethylamine-catalyzed aromatization, mixtures of 5-hydroxyanthracyclinones and their *O*-ethyl derivatives. However, the selectivity of the former compounds to the latter was very poor (Entries 1,3,5). On the other hand, the total yields of anthracyclinone products from the sulfones were somewhat lower, but the hydroxy compounds were obtained in good selectivity (Entries 2,4,6).

Finally, the regiochemical outcome of the Diels–Alder reactions of the sulfoxide **2b** and the sulfone **3b** with isoprene (**33**) was briefly examined (Scheme 5). Although the sulfoxide **2b** reacted smoothly with **33** in refluxing benzene, the reaction was not regiospecific and, after oxidation, a mixture of the anthraquinone products **34** and **35** was obtained in the ratio of 7:3, as determined by gas chromatography using nematic liquid crystals[4,13] as stationary phase. From the sulfone **3b**, a mixture of **34** and **35** was obtained in a somewhat improved ratio (8:2). It therefore appears that both sulfoxide and sulfone groups are insufficiently strong directing group for the regiospecific Diels–Alder reaction with relatively unpolarized diene **33**. Therefore, use of the polarized dienes such as vinylketene acetals is essential[14] for the regiospecific Diels–Alder reaction of the sulfur-substituted naphthoquinones.

In conclusion, we have shown that the sulfone, sulfoxide and sulfide groups, especially the former two, offer effective regiochemical control and activating elements in the Diels–Alder reaction of naphthoquinones. Since the regiospecific synthesis of 2-phenylthionaphthoquinones has been established,[6] the sulfur-directed Diels–Alder reaction described herein provides easy access to a wide range of highly substituted anthraquinones and anthracyclinones under mild conditions.

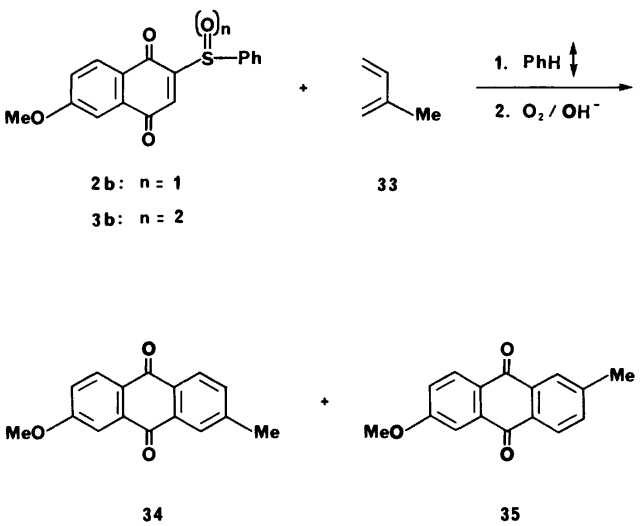

Scheme 5.

Experimental

General. All melting points are uncorrected. Mass spectra (MS) were determined on JEOL JMS-DX303 spectrometer. IR spectra were obtained in Nujol mulls with JASCO A-100 spectrometer. UV spectra were recorded in 95% ethanol on Hitachi 323 spectrometer. High field ^{1}H NMR spectra (400 MHz) were obtained with JEOL JNM-GX400 spectrometer using $CDCl_3$ as a solvent and TMS as an internal standard. Routine ^{1}H NMR spectra (60 MHz) were recorded on Hitachi R-600 machine. Elemental analyses were performed at microanalytical laboratory in Nagasaki University. Gas chromatography was performed on a Shimadzu GC-8A apparatus using flame ionization detector. Thin-layer chromatography was performed on Merck 0.2 mm precoated aluminum sheets of silica gel 60 F_{254} (Art 5554). For column chromatography, Merck silica gel 60 (230—400 mesh) (Art 9385) was employed.

2-Phenylsulfinyl-1,4-naphthoquinone (2a): Under ice-cooling, 2.16 g (10 mmol) of 80% MCPBA was added portionwise to a solution of 2.66 g (10 mmol) of **1a** in 150 ml of chloroform, and stirred for 4 h. The chloroform solution was washed with sodium hydrogencarbonate solution, dried over sodium sulfate, and evaporated. The residue was recrystallized from dichloromethane–hexane to give 2.64 g (94%) of **2a** as orange needles. An analytical sample was purified by recrystallization from methanol; mp 158.5—160 °C. IR: 1655, 1580, 1055, and 1050 cm^{-1}. ^{1}H NMR (400 MHz) δ=7.49 (m, 3H, H-3′, H-4′, H-5′), 7.65 (s, 1H, H-3), 7.76 (m, 2H, H-6, H-7), 7.85 (m, 2H, H-2′, H-6′), 8.00 (near d, 1H, H-5 or H-8, J=ca. 8 Hz), and 8.10 (near d, 1H, H-8 or H-5, J=ca. 8 Hz). Found: C, 68.10; H, 3.48; S, 11.50%. Calcd for $C_{16}H_{10}O_3S$: C, 68.07; H, 3.57; S, 11.36%.

6-Methoxy-2-phenylsulfinyl-1,4-naphthoquinone (2b): This compound was obtained from **1b** in a similar manner as described above in 89% yield; yellow needles from methanol; mp 181—181.5 °C. IR: 1670, 1650, 1585, and 1045 cm^{-1}. ^{1}H NMR (400 MHz) δ=3.94 (s, 3H, OMe), 7.18 (dd, 1H, H-7, J=8.8 and 2.6 Hz), 7.49 (m, 3H, H-3′, H-4′, H-5′), 7.52 (d, 1H, H-5, J=2.9 Hz), 7.60 (s, 1H, H-3), 7.85 (m, 2H, H-2′, H-6′), and 7.94 (d, 1H, H-8, J=8.8 Hz). Found: C, 65.23; H, 3.78; S, 10.31%. Calcd for $C_{17}H_{12}O_4S$: C, 65.37; H, 3.87; S, 10.27%.

5,7-Dimethoxy-3-phenylsulfinyl-1,4-naphthoquinone (2c): This compound was prepared from **1c** in a similar manner as described for **2a** in 98% yield; yellow needles from dichloromethane–methanol; mp 231.5—233.5 °C (decomp). IR: 1650, 1635, 1595, and 1045 cm^{-1}. ^{1}H NMR (400 MHz) δ=3.93 (s, 3H, OMe), 3.94 (s, 3H, OMe), 6.69 (d, 1H, H-6, J=2.2 Hz), 7.25 (d, 1H, H-8, J=2.2 Hz), 7.46 (m, 3H, H-3′, H-4′, H-5′), 7.53 (s, 1H, H-3), and 7.87 (m, 2H, H-2′, H-6′). Found: C, 63.29; H, 4.03; S. 9.37%. Calcd for $C_{18}H_{14}O_5S$: C, 63.15; H, 4.12; S, 9.37%.

2-Phenylsulfonyl-1,4-naphthoquinone (3a): To a hot solution of 1133 mg (4.25 mmol) of **1a** in 100 ml of acetic acid was added 2.0 ml (17.6 mmol) of 30% hydrogen peroxide solution, and the mixture was refluxed for 15 min. The solution was concentrated under reduced pressure to several

ml to precipitate yellow fine crystals, which were collected by filtration and washed with methanol giving 1061 mg (84%) of practically pure sulfone **3a**. Recrystallization from methanol afforded yellow fine plates; mp 190—191.5 °C (lit,[15] mp 192 °C). IR: 1665, 1585, 1330, and 1165 cm^{-1}. ^1H NMR (400 MHz) δ=7.59 (near t, 2H, H-3′, H-5′, J=ca. 7.5 Hz), 7.68 (near t, 1H, H-4′, J=ca. 7.5 Hz), 7.78 (m, 2H, H-6, H-7), 7.85 (s, 1H, H-3), 8.03 (m, 1H, H-5 or H-8), 8.08 (m, 1H, H-8 or H-5), and 8.15 (d, 2H, H-2′, H-6, J=7.7 Hz). Found: C, 64.20; H, 3.33; S, 10.86%. Calcd for $C_{16}H_{10}O_4S$: C, 64.42; H, 3.38; S, 10.75%.

6-Methoxy-2-phenylsulfonyl-1,4-naphthoquinone (3b): This compound was obtained from **1b** in a similar manner as described for **3a**; Yellow needles from methanol, mp 201—203 °C (decomp). IR: 1670, 1660, 1595, 1340, and 1155 cm^{-1}. ^1H NMR (400 MHz) δ=3.95 (s, 3H, OMe), 7.22 (dd, 1H, H-7, J=8.8 and 2.6 Hz), 7.48 (d, 1H, H-5, J=2.6 Hz), 7.59 (near t, 2H, H-3′, H-5′, J=ca. 7.5 Hz), 7.68 (near t, 1H, H-4′, J=ca. 7.5 Hz), 7.80 (s, 1H, H-3), 7.97 (d, 1H, H-8, J=8.8 Hz), and 8.15 (d, 2H, H-2′, J=7.7 Hz). Found: C, 62.20; H, 3.68; S, 9.82%. Calcd for $C_{17}H_{12}O_5S$: C, 62.19; H, 3.68; S, 9.77%.

5,7-Dimethoxy-3-phenylsulfonyl-1,4-naphthoquinone (3c): To a warm solution of 326 mg (1.00 mmol) of **3a** in 30 ml of acetic acid was added 0.45 ml (4.0 mmol) of 30% hydrogen peroxide solution. The mixture was kept at 80 °C for 4 h, and evaporated to dryness. The residue was recrystallized from dichloromethane-ethanol giving 235 mg (66%) of orange needles of **3c**. Mp 230—234.5 °C (decomp) was measured in a sealed capillary. IR: 1690, 1660, 1595, 1550, 1340, 1325, and 1160 cm^{-1}. ^1H NMR (400 MHz) δ=3.92 (s, 3H, OMe), 3.95 (s, 3H, OMe), 6.73 (d, 1H, H-6, J=2.2 Hz), 7.20 (d, 1H, H-8, J=2.2 Hz), 7.56 (near t, 2H, H-3′, H-5′, J=ca. 7.5 Hz), 7.64 (near t, 1H, H-4′, J=ca. 7.5 Hz), 7.76 (s, 1H, H-2), and 8.15 (d, 2H, H-2′, H-6′, J=7.7 Hz). Found: C, 60.17; H, 3.78; S, 9.16%. Calcd for $C_{18}H_{14}O_6S$: C, 60.33; H, 3.94; S, 8.95%.

2,3-Epoxy-2-phenylsulfonyl-1,4-naphthoquinone (4): Under ice-cooling, 4.50 g (21 mmol) of 80% MCPBA was added all at once to a stirred solution of 1.85 g (7.0 mmol) of **1a** in 170 ml of chloroform. The mixture was stirred for 2 h at 0 °C and left overnight at room temperature. An additional 0.20 g (0.9 mmol) of 80% MCPBA was added, and the mixture was stirred for further 8 h. The chloroform solution was washed with sodium hydrogencarbonate solution, dried over sodium sulfate and evaporated. The residual oil was crystallized by trituration with ether and the crystals were collected by filtration to give 2.01 g (92%) of **4**. Recrystallization from dichloromethane-ether (charcoal) afforded colorless prisms, mp 151.5—153.5 °C. MS m/z=314 (M^+). IR: 1695, 1585, 1575, 1345, 1335, 1165, and 1145 cm^{-1}. ^1H NMR (400 MHz) δ=4.80 (s, 1H, H-3), 7.64 (near t, 2H, H-3′, H-5′, J=ca. 7.5 Hz), 7.75 (near t, 1H, H-4′, J=ca. 7.5 Hz), 7.78 (m, 2H, H-6, H-7), 7.94 (dd, 1H, H-5 or H-8, J=7.0 and 1.8 Hz), 8.02 (dd, 1H, H-8 or H-5, J=7.5 and 1.5 Hz), and 8.19 (d, 2H, H-2′, H-6′, J=7.3 Hz). Found: C, 61.38; H, 3.07; S, 10.33%. Calcd for $C_{16}H_{10}O_5S$: C, 61.14; H, 3.21; S, 10.20%.

Diels-Alder Reaction of the Naphthoquinones 1a—c, 2a—c, and 3a—c with the Vinylketene Acetals 5, 6, and 26; General Procedure: Under nitrogen atmosphere, 2.0 mmol of the vinylketene acetal was added to a solution or suspension of 1.0 mmol of the naphthoquinone in 50 ml of dry toluene or benzene. After completion of the Diels-Alder reaction, 1.0 ml of triethylamine was added and the aromatization reaction was conducted. The reaction conditions for both the Diels-Alder and aromatization reactions were shown in Table 1 or 2 for each cases. When the Diels-Alder reaction was slow (Table 1: Entries 6,9,12), small portions of additional vinylketene acetal were added until the starting quinone had disappeared (TLC analysis) (Entry 6: 2 equiv of the vinylketene acetal for the quinone; Entry 9: 25 equiv; Entry 12: 3 equiv). When the reaction was completed, the reaction mixture was evaporated to dryness under reduced pressure. The residue was washed with methanol and filtered giving the quinonoid products, which were chromatographed on silica gel using dichloromethane or a mixture of dichloromethane and acetone (20:1) as eluents. From the first yellow band, the hydroxy quinone was obtained, and its *O*-alkylated derivative was obtained from the next yellow band. The yield of each compound is shown in Table 1 or 2. The following quinones were obtained in this manner.

1-Hydroxy-3-methylanthraquinone (Pachybasin) (8): Yellow needles from ethanol; mp 176.5—177.5 °C (lit,[16,17] mp 176—177 °C; lit,[1j] mp 179—180 °C). IR: 1670, 1635, 1585, and 1570 cm^{-1}. ^1H NMR (400 MHz) δ=2.47 (s, 3H, Me), 7.11 (s, 1H, H-2), 7.64 (s, 1H, H-4), 7.80 (m, 2H, H-6, H-7), 8.29 (m, 2H, H-5, H-8), and 12.57 (s, 1H, OH). Found: C, 75.70; H, 4.16%. Calcd for $C_{15}H_{10}O_3$: C, 75.62; H, 4.23%.

1-Methoxy-3-methylanthraquinone (9): Yellow needles from methanol; mp 190—191 °C (lit,[16] mp 187—188 °C; lit,[17] mp 185—187 °C. IR: 1670, 1655, 1595, and 1590 cm^{-1}. ^1H NMR (400 MHz) δ=2.50 (s, 3H, Me), 4.04 (s, 3H, OMe), 7.14 (s, 1H, H-2), 7.7—7.8 (m, 2H, H-6, H-7), 7.77 (s, 1H, H-4), 8.21 (dd, 1H, H-8 or H-5, J=7.6 and 1.4 Hz), and 8.27 (dd, 1H, H-5 or H-8, J=7.5 and 1.4 Hz). Found: C, 76.04; H, 4.67%. Calcd for $C_{16}H_{12}O_3$: C, 76.18; H, 4.79%.

1-Hydroxy-6-methoxy-3-methylanthraquinone (Phomarin 6-Methyl Ether) (10): Yellow needles from ethanol; mp 188.5—189 °C (lit,[1f] mp 187.0—187.5 °C; lit,[18] mp 193 °C). R_f (TLC-benzene)=0.41. IR: 1670, 1630, and 1590 cm^{-1}. UV: 267.5 (log ε 4.61), 292sh (4.25), and 411 nm (3.93). ^1H NMR (400 MHz) δ=2.46 (s, 3H, Me), 3.99 (s, 3H, OMe), 7.10 (s, 1H, H-2), 7.26 (dd, 1H, H-7, J=8.4 and 2.8 Hz), 7.63 (s, 1H, H-4), 7.71 (d, 1H, H-5, J=2.8 Hz), 8.24 (d, 1H, H-8, J=8.8 Hz), and 12.71 (s, 1H, OH). Found: C, 71.85; H, 4.39%. Calcd for $C_{16}H_{12}O_4$: C, 71.64; H, 4.51%.

1,6-Dimethoxy-3-methylanthraquinone (11): Yellow needles from methanol; mp 189.5—190 °C. IR: 1665, 1650, 1600, 1575, and 1560 cm^{-1}. ^1H NMR (400 MHz) δ=2.50 (s, 3H, Me), 3.96 (s, 3H, OMe), 4.03 (s, 3H, OMe), 7.13 (s, 1H, H-2), 7.25 (dd, 1H, J=8.4 and 2.6 Hz), 7.63 (d, 1H, H-5, J=2.6 Hz), 7.76 (s, 1H, H-4), and 8.21 (d, 1H, H-8, J=8.4 Hz). Found: C, 72.36; H, 5.04%. Calcd for $C_{17}H_{14}O_4$: C, 72.33; H, 5.00%.

1-Hydroxy-6,8-dimethoxy-3-methylanthraquinone (Emodin 6,8-Dimethyl Ether) (12): Orange needles from ethanol; mp 211.5—213 °C (lit,[19] mp 211.0 °C; lit,[1e] mp 204—205 °C). IR: 1665, 1625, 1590, and 1550 cm^{-1}. ^1H NMR (400 MHz) δ=2.43 (s, 3H, Me), 3.99 (s, 3H, OMe), 4.02 (s, 3H, OMe), 6.78 (d, 1H, H-7, J=2.3 Hz), 7.07 (s, 1H, H-2), 7.45 (d, 1H, H-5, J=2.8 Hz), 7.56 (s, 1H, H-4), and 13.09 (s, 1H, OH). Found: C, 68.55; H, 4.64%. Calcd for $C_{17}H_{14}O_5$: C, 68.45; H, 4.73%.

1,3,8-Trimethoxy-6-methylanthraquinone (13): Hygroscopic yellow needles from methanol; mp 228.5—229.5 °C (lit,[20] mp 227—228 °C; lit,[11] mp 229 °C). IR: 1650, 1600,

and 1555 cm^{-1}. ^{1}H NMR (400 MHz) δ=2.47 (s, 3H, Me), 3.95 (s, 3H, OMe), 3.96 (s, 3H, OMe), 3.99 (s, 3H, OMe), 6.77 (d, 1H, H-2, J=2.6 Hz), 7.10 (s, 1H, H-7), 7.32 (d, 1H, H-4, J=2.6 Hz), and 7.64 (s, 1H, H-5). This compound was shown to be identical with an authentic sample[11] by spectroscopic and TLC comparisons.

1-Hydroxy-3-methoxyanthraquinone (Xanthopurprine 3-Methyl Ether) (14): Yellow needles from ethanol; mp 195—196.5 °C (lit,[21] mp 193—194 °C; lit,[1d] mp 193.5—194.5 °C). IR: 1675, 1630, 1590, and 1565 cm^{-1}. ^{1}H NMR (400 MHz) δ=3.93 (s, 3H, OMe), 6.68 (d, 1H, H-2, J=2.3 Hz), 7.34 (d, 1H, H-4, J=2.3 Hz), 7.77 (m, 2H, H-6, H-7), 8.26 (m, 2H, H-5, H-8), and 12.86 (s, 1H, OH). Found: C, 70.75; H, 3.85%. Calcd for $C_{15}H_{10}O_4$: C, 70.86; H, 3.96%.

1,3-Dimethoxyanthraquinone (15): Yellow needles from methanol; mp 163.5—164 °C (lit,[22] mp 163 °C; lit,[21] mp 154—155 °C). IR: 1665, 1655, 1590, 1580, and 1555 cm^{-1}. ^{1}H NMR (400 MHz) δ=3.99 (s, 3H, OMe), 4.02 (s, 3H, OMe), 6.79 (d, 1H, H-2, J=2.3 Hz), 7.46 (d, 1H, H-4, J=2.3 Hz), 7.71 (dt, 1H, H-6 or H-7, J=7.8 and 1.4 Hz), 7.77 (dt, 1H, H-7 or H-6, J=7.3 and 1.4 Hz), 8.21 (dd, 1H, H-8 or H-5, J=7.8 and 0.9 Hz), and 8.27 (dd, 1H, H-5 or H-8, J=7.8 and 0.9 Hz). Found: C, 71.50; H, 4.52%. Calcd for $C_{16}H_{12}O_4$: C, 71.64; H, 4.51%.

1-Hydroxy-3,6-dimethoxyanthraquinone (16): Orange needles from ethanol; mp 220—221 °C. IR: 1675, 1620, and 1585 cm^{-1}. ^{1}H NMR (400 MHz) δ=3.94 (s, 3H, OMe), 3.98 (s, 3H, OMe), 6.71 (d, 1H, H-2, J=2.3 Hz), 7.27 (dd, 1H, H-7, J=8.8 and 2.8 Hz), 7.36 (d, 1H, H-4, J=2.8 Hz), 7.70 (d, 1H, H-5, J=2.3 Hz), 8.23 (d, 1H, H-8, J=8.8 Hz), and 13.01 (s, 1H, OH). Found: C, 67.63; H, 4.21%. Calcd for $C_{16}H_{12}O_5$: C, 67.60; H, 4.25%.

1,3,6-Trimethoxyanthraquinone (17): Yellow microcrystals from ethanol; mp 242—243 °C (lit,[23] mp 240—241.5 °C). IR: 1655, 1645, 1595, 1575, and 1560 cm^{-1}. ^{1}H NMR (400 MHz) δ=3.96 (s, 3H, OMe), 3.98 (s, 3H, OMe), 4.01 (s, 3H, OMe), 6.79 (d, 1H, H-2, J=2.6 Hz), 7.25 (dd, 1H, H-7, J=8.8 and 2.6 Hz), 7.45 (d, 1H, H-4, J=2.6 Hz), 7.63 (d, 1H, H-5, J=2.6 Hz), and 8.22 (d, 1H, H-8, J=8.8 Hz). Found: C, 68.54; H, 4.70%. Calcd for $C_{17}H_{14}O_5$: C, 68.45; H, 4.73%.

1-Hydroxy-3,6,8-trimethoxyanthraquinone (18): Orange microcrystals from chloroform-ethanol; mp 257—258 °C. IR: 1620, 1590, and 1550 cm^{-1}. ^{1}H NMR (400 MHz) δ=3.92 (s, 3H, OMe), 3.99 (s, 3H, OMe), 4.03 (s, 3H, OMe), 6.71 (d, 1H, H-2, J=2.3 Hz), 6.80 (d, 1H, H-7, J=2.3 Hz), 7.30 (d, 1H, H-4, J=2.8 Hz), 7.47 (d, 1H, H-5, J=2.3 Hz), and 13.40 (s, 1H, OH). Found: C, 65.12; H, 4.44%. Calcd for $C_{17}H_{14}O_6$: C, 64.97; H, 4.49%.

1,3,6,8-Tetramethoxyanthraquinone (19): Hygroscopic yellow microcrystals from ethanol, mp 222—223 °C (lit,[22] mp 220—221 °C, lit,[24] mp 224—225 °C). IR: 1655, 1600, and 1560 cm^{-1}. ^{1}H NMR (400 MHz) δ=3.96 (s, 6H, OMe), 3.99 (s, 6H, OMe), 6.76 (d, 2H, H-2, H-7, J=2.6 Hz), and 7.31 (d, 2H, H-4, H-5, J=2.6 Hz). An analytical sample was obtained by sublimation at 150—180 °C/0.15 mmHg (1 mmHg=133.322 Pa). Found: C, 65.66; H, 4.88%. Calcd for $C_{18}H_{16}O_6$: C, 65.85; H, 4.91%.

6-Hydroxy-9-methoxy-7,8-dihydro-5,12-naphthacenedione (27): Orange needles from dichloromethane; mp 243—244 °C. MS m/z=306 (M$^+$). IR: 1665, 1615, 1590, 1570, and 1550 cm^{-1}. ^{1}H NMR (400 MHz) δ=2.49 (near t, 2H, H-8, J=ca. 8.5 Hz), 3.03 (near t, 2H, H-7, J=ca. 8.5 Hz), 3.78 (s, 3H, OMe), 5.65 (s, 1H, H-10), 7.45 (s, 1H, H-11), 7.77 (m, 2H, H-2, H-3), 8.27 (m, H-1, H-4), and 12.99 (s, 1H, OH). Found: C, 74.42; H, 4.52%. Calcd for $C_{19}H_{14}O_4$: C, 74.45; H, 4.60%.

6-Ethoxy-9-methoxy-7,8-dihydro-5,12-naphthacenedione (28): Yellow needles from dichloromethane–hexane, mp 203.5—204.5 °C. MS m/z=334 (M$^+$). IR: 1670, 1630, 1575, and 1540 cm^{-1}. ^{1}H NMR (400 MHz) δ=1.53 (t, 3H, CH_3 of OEt, J=7.0 Hz), 2.46 (near t, 2H, H-8, J=ca. 8 Hz), 3.08 (near t, 2H, H-7, J=ca. 8 Hz), 3.78 (s, 3H, OMe), 4.03 (q, 2H, CH_2 of OEt, J=7.0 Hz), 5.71 (s, 1H, H-10), 7.72 (s, 1H, H-11), 7.7—7.8 (m, 2H, H-2, H-3), 8.21 (dd, 1H, H-4 or H-1, J=7.3 and 1.5 Hz), and 8.26 (dd, 1H, H-1 or H-4, J=7.7 and 1.5 Hz). Found: C, 75.37; H, 5.42%. Calcd for $C_{21}H_{18}O_4$: C, 75.43; H, 5.43%.

6-Hydroxy-2,9-dimethoxy-7,8-dihydro-5,12-naphthacenedione (29): Orange needles from dichloromethane–hexane; mp 232—233 °C. MS m/z=336 (M$^+$). IR: 1670, 1630, 1615, 1595, 1560, and 1550 cm^{-1}. ^{1}H NMR (400 MHz) δ=2.49 (near t, 2H, H-8, J=ca. 8.5 Hz), 3.02 (near t, 2H, H-7, J=ca. 8.5 Hz), 3.78 (s, 3H, OMe), 3.98 (s, 3H, OMe), 5.64 (s, 1H, H-10), 7.23 (dd, 1H, H-3, J=8.8 and 2.9 Hz), 7.43 (s, 1H, H-11), 7.68 (d, 1H, H-1, J=2.9 Hz), 8.21 (d, 1H, H-4, J=8.8 Hz), and 13.10 (s, 1H, OH). Found: C, 71.36; H, 4.75%. Calcd for $C_{20}H_{16}O_5$: C, 71.42; H, 4,79%.

6-Ethoxy-2,9-dimethoxy-7,8-dihydro-5,12-naphthacenedione (30): Yellow needles from dichloromethane–ether–hexane; mp 224—225 °C. MS m/z=364 (M$^+$). IR: 1670, 1630, 1600, 1570, and 1540 cm^{-1}. ^{1}H NMR (400 MHz) δ=1.52 (t, 3H, CH_3 of OEt, J=7.0 Hz), 2.45 (near t, 2H, H-8, J=ca. 8 Hz), 3.07 (near t, 2H, H-7, J=ca. 8 Hz), 3.77 (s, 3H, OMe), 3.96 (s, 3H, OMe), 4.02 (q, 2H, CH_2 of OEt, J=7.0 Hz), 5.69 (s, 1H, H-10), 7.23 (dd, 1H, H-3, J=8.8 and 2.6 Hz), 7.63 (d, 1H, H-1, J=2.6 Hz), 7.69 (s, 1H, H-11), and 8.20 (d, 1H, H-4, J=8.8 Hz). Found: C, 72.61; H, 5.50%. Calcd for $C_{22}H_{20}O_5$: C, 72.51; H, 5.53%.

6-Hydroxy-2,4,9-trimethoxy-7,8-dihydro-5,12-naphthacenedione (31): Orange needles from dichloromethane–ether–hexane; mp 257—259 °C (decomp). MS m/z=366 (M$^+$). IR: 1670, 1630, 1615, 1595, and 1550 cm^{-1}. ^{1}H NMR (400 MHz) δ=2.47 (near t, 2H, H-8, J=ca. 8.5 Hz), 3.02 (near t, 2H, H-7, J=ca. 8.5 Hz), 3.77 (s, 3H, OMe), 3.98 (s, 3H, OMe), 4.03 (s, 3H, OMe), 5.62 (s, 1H, H-10), 6.78 (d, 1H, H-3, J=2.3 Hz), 7.39 (s, 1H, H-11), 7.46 (d, 1H, H-1, J=2.3 Hz), and 13.48 (s, 1H, OH). Found: C, 68.57; H, 4.92%. Calcd for $C_{21}H_{18}O_6$: C, 68.85; H, 4.95%.

6-Ethoxy-2,4,9-trimethoxy-7,8-dihydro-5,12-naphthacenedione (32): Yellow needles from dichloromethane–ether; mp 207.5—209.5 °C. MS m/z=394 (M$^+$). IR: 1665, 1635, 1595, 1580, and 1565 cm^{-1}. ^{1}H NMR (400 MHz) δ=1.50 (t, 3H, CH_3 of OEt, J=7.0 Hz), 2.43 (near t, 2H, H-8, J=ca. 8 Hz), 3.06 (near t, 2H, H-7, J=ca. 8 Hz), 3.76 (s, 3H, OMe), 3.95 (s, 3H, OMe), 3.97 (s, 3H, OMe), 4.07 (q, 2H, CH_2 of OEt, J=7.0 Hz), 5.67 (s, 1H, H-10), 6.76 (d, 1H, H-3, J=2.2 Hz), 7.34 (d, 1H, H-1, J=2.6 Hz), and 7.60 (s, 1H, H-11). Found: C, 69.89; H, 5.64%. Calcd for $C_{23}H_{22}O_6$: C, 70.04; H, 5.62%.

***N,N*-Diethyl-2-methoxy-4-methylbenzamide (20):** This amide was prepared under standard conditions[10] from the corresponding acid via the acid chloride and purified by Kugelrohr distillation, bp 130 °C/0.1 mmHg. Colorless solid, mp 60—62 °C. IR: 1610, 1575, and 1510 cm^{-1}. ^{1}H NMR (400 MHz) δ=1.02 (near t, 3H, CH_3 of NEt_2, J=ca. 7 Hz), 1.23 (near t, 3H, CH_3 of NEt_2, J=ca. 7 Hz), 2.35 (s, 3H,

Me), 3.15 (q, 2H, CH_2 of NEt_2, J=ca. 7 Hz), 3.56 (br s, 2H, CH_2 of NEt_2), 3.79 (s, 3H, OMe), 6.71 (s, 1H, H-3), 6.77 (d, 1H, H-5, J=7.3 Hz), and 7.06 (d, 1H, H-6, J=7.7 Hz). Found: C, 70.66; H, 8.69; N, 6.15%. Calcd for $C_{13}H_{19}NO_2$: C, 70.56; H, 8.65; N, 6.33%.

7-Methoxy-3-(4-methoxyphenyl)-5-methyl-1(3*H*)-isobenzofuranone (21): A solution of 13.8 ml (16.5 mmol) of *s*-BuLi (1.20 M in cyclohexane (1 M=1 mol dm^{-3})) was slowly injected into a stirred solution of 3320 mg (15 mmol) of **20** and 2.5 ml of TMEDA in 250 ml of anhydrous ether at −78 °C under nitrogen atmosphere. After stirring for 1 h, a solution of 2246 mg (16.5 mmol) of *p*-anisaldehyde in ether was injected. After 1 h, Dry Ice-acetone bath was removed and the solution was stirred overnight. The reaction mixture was quenched by saturated ammonium chloride solution, washed successively with water and brine solution, dried over sodium sulfate and evaporated to give an oily residue. A solution of this material and 1 g of *p*-toluenesulfonic acid in 200 ml of benzene was refluxed for 6 h. The reaction mixture was washed twice with sodium hydrogencarbonate solution, dried over sodium sulfate and evaporated. The residual oil was dissolved in ether and the mixture was left overnight. The precipitate was collected by filtration giving 1167 mg of **21**. An additional 765 mg of **21** was obtained from the mother liquor after silica-gel chromatography using dichloromethane as eluent. The total yield was 1932 mg (45%). An analytical sample was obtained by recrystallization from dichloromethane-ether-hexane to give colorless needles; mp 118—118.5 °C. IR: 1750 and 1605 cm^{-1}. ^1H NMR (400 MHz) δ=2.40 (s, 3H, Me), 3.80 (s, 3H, OMe), 4.00 (s, 3H, OMe), 6.21 (s, 1H, H-3), 6.62 (s, 1H, H-6), 6.73 (s, 1H, H-4), 6.89 (d, 2H, H-3′, H-5′, J=8.4 Hz), and 7.18 (d, H-2′, H-6′, J=8.8 Hz). Found: C, 72.10; H, 5.55%. Calcd for $C_{17}H_{16}O_4$: C, 71.82; H, 5.67%.

1,7-Dimethoxy-3-methylanthraquinone (23): A mixture of 1008 mg (3.55 mmol) of **21** and 370 mg of 5% palladium on charcoal in 100 ml of glacial acetic acid was stirred at 80 °C overnight under an atmosphere of hydrogen. The catalyst was removed by filtration, and the filtrate was evaporated under reduced pressure giving an oily residue. In order to remove acetic acid contaminant, toluene was added and the whole was evaporated. The residual crude acid **22** was dissolved in 150 ml of dry dichloromethane, and 3 ml of trifluoroacetic anhydride was added at 0 °C. The mixture was stirred at room temperature for 5 h and evaporated. Methanol was added to the residue and the whole was evaporated. The residue was dissolved in dichloromethane and the solution was washed with sodium hydrogencarbonate solution, dried over sodium sulfate and evaporated to give a dark oil. A mixture of this oil, 0.4 g of chromium trioxide and a few drops of water in 90 ml of acetic acid was stirred at room temperature for 3.5 h. The mixture was evaporated to dryness, and the residue was dissolved in dichloromethane. The solution was washed with sodium hydrogencarbonate solution, filtered through celite, dried over sodium sulfate and evaporated. The residue was chromatographed over silica gel using a mixture of dichloromethane and ether (20:1) giving 294 mg (29%) of **23**. An analytical sample was obtained by recrystallization from methanol to give yellow needles; mp 181—182 °C (lit,[25] mp 183—184 °C). IR: 1665, 1650, 1595, and 1555 cm^{-1}. ^1H NMR δ=2.50 (s, 3H, Me), 3.97 (s, 3H, OMe), 4.04 (s, 3H, OMe), 7.11 (s, 1H, H-2), 7.20 (dd, 1H, H-6, J=8.8 and 2.6 Hz), 7.70 (d, 1H, H-8, J=2.6 Hz), 7.77 (s, 1H, H-4), and 8.17 (d, 1H, H-5, J=8.8 Hz). Found: C, 72.61; 4.85%. Calcd for $C_{17}H_{14}O_4$: C, 72.33; H, 5.00%.

1-Hydroxy-7-methoxy-3-methylanthraquinone (24): A solution of 85 mg (0.34 mmol) of boron tribromide in 5 ml of dichloromethane was added to a stirred solution of 80 mg (0.28 mmol) of **23** in 40 ml of dry dichloromethane at −78 °C. After 1 h, Dry Ice-acetone bath was removed and the mixture was stirred for 1.5 h. The mixture was washed with 5% sodium carbonate solution, dried over sodium sulfate and evaporated. The residue was purified by silica-gel chromatography using benzene as eluent giving 65 mg (86%) of **24**. An analytical sample was obtained by recrystallization from ethanol to give yellow needles; mp 191—192 °C and 201—201.5 °C (double melting point) (lit,[25] mp 198—199 °C). R_f (TLC-benzene)=0.37. IR: 1670, 1630, 1590, and 1565 cm^{-1}. UV: 272.5 (log ε 4.59), 295 (4.29), and 390 nm (3.90). ^1H NMR (400 MHz) δ=2.46 (s, 3H, Me), 3.99 (s, 3H, OMe), 7.08 (s, 1H, H-2), 7.26 (dd, 1H, H-6, J=8.7 and 2.8 Hz), 7.64 (s, 1H, H-4), 7.72 (d, 1H, H-8, J=2.8 Hz), 8.23 (d, 1H, H-5, J=8.7 Hz), and 12.52 (s, 1H, OH). Found: C, 71.41: H, 4.37%. Calcd for $C_{16}H_{12}O_4$: C, 71.64; H, 4.51%.

Diels-Alder Reaction of 6-Methoxynaphthoquinone (25) and the Vinylketene Acetal 5: A solution of 188 mg (1.0 mmol) of **25**[4,26] and 373 mg (2.0 mmol) of **5** in 50 ml of benzene was refluxed for 20 h, and evaporated to dryness. The residual oil was dissolved in a mixture of 10 ml each of THF and ethanol, 10 ml of 5% aqueous sodium hydroxide was added, and oxygen was bubbled through the resulting solution for 3 h. The mixture was acidified with hydrochloric acid and diluted with water. The yellow precipitate was collected by filtration and washed with water. Chromatography of the precipitate over silica gel using dichloromethane as eluent afforded 210 mg (78%) of a 3.1:1 mixture of the hydroxy quinones **24** and **10**, and 39 mg (14%) of a mixture of the methoxy quinones **23** and **11**. The ratio of **24** to **10** was determined by integration of the absorptions of the hydroxyl proton of each isomer by 400 MHz NMR. The ratio of **23** to **11** could not be estimated correctly by 400 MHz NMR because of the similarity of the spectra of the two isomers. However, it was apparent that **23** was a major product (**23**/**11**>5) from the comparison of the spectrum (aromatic region) of the mixture with those of authentic samples. Attempts to separate the mixture of **23** and **11** by GC or analytical HPLC were not successful.

Diels-Alder Reaction of 2b or 3b with Isoprene (33): A mixture of 156 mg (0.5 mmol) of **2b** and 1.0 ml (10 mmol) of isoprene in 20 ml of benzene was refluxed for 4 h, and evaporated to dryness. The residue was dissolved in a mixture of 5 ml each of THF and ethanol, and 5 ml of 5% aqueous sodium hydroxide was added. Oxygen was bubbled through this solution for 2 h. The mixture was diluted with water, and the precipitate was collected by filtration giving 77 mg (61%) of slightly colored fine needles of a 7:3 mixture of 2-methoxy-7-methylanthraquinone (**34**) and 2-methoxy-6-methylanthraquinone (**35**). The ratio was estimated by gas chromatography (2.5% BBBT/2 m×2.6 mm I.D./230 °C). Spectral data of the mixture were as follows. MS m/z=252 (M^+). ^1H NMR (400 MHz) δ=2.53 (s, Me of **34** and **35**), 3.99 (s, OMe of **34** and **35**), 7.25 (partially overlapped dd, H-3 of **34** and **35**), 7.56 (d, H-7 of **35**, J=8.1 Hz), 7.58 (d, H-6 of **34**, J=8.1 Hz), 7.72 (d, H-1 of **34** and **35**, J=2.6 Hz), 8.08 (s, H-8 of **34** and H-5 of **35**), 8.18 (d, H-8 of **35**, J=8.1 Hz), 8.19 (d,

H-5 of **34**, J=7.7 Hz), and 8.24 (d, H-4 of **34** and **35**, J=8.8 Hz). These values of the chemical shifts and coupling constants are almost identical with the reported values[4] for **34** and **35**. In a similar manner **2b** was treated with isoprene giving a 8:2 mixture of **34** and **35** in 84% combined yield.

References

1) a) J. Banville and P. Brassard, *J. Org. Chem.*, **41**, 3018 (1976); b) D. W. Cameron, G. I. Feutrill, P. G. Griffiths, and D. J. Hodder, *J. Chem. Soc., Chem. Commun.*, **1978**, 688; c) G. Roberge and P. Brassard, *J. Chem. Soc., Perkin Trans. 1*, **1978**, 1041; d) J. Savard and P. Brassard, *Tetrahedron Lett.*, **1979**, 4911; e) K. Krohn, *ibid.*, **21**, 3557 (1980); f) C. Brisson and P. Brassard, *J. Org. Chem.*, **46**, 1810 (1981); g) D. W. Cameron, G. I. Feutrill, and P. Perlmutter, *Tetrahedron Lett.*, **22**, 3273 (1981); h) D. W. Cameron, C. Conn, and G. I. Feutrill, *Aust. J. Chem.*, **34**, 1945 (1981); i) V. Guay and P. Brassard, *J. Org. Chem.*, **49**, 1853 (1984); j) N. Benfaremo and M. P. Cava, *ibid.*, **50**, 139 (1985); k) B. Simoneau, J. Savard, and P. Brassard, *ibid.*, **50**, 5433 (1985).

2) a) J. P. Gesson, J. C. Jacquesy, and M. Mondon, *Tetrahedron Lett.*, **22**, 3351 (1981); b) J. G. Bauman, R. B. Barber, R. D. Gless, and H. Rapoport, *ibid.*, **22**, 4777 (1981); c) B. A. Pearlman, J. M. Mcnamara, H. Hasan, S. Hatakeyama, H. Sekizaki, and Y. Kishi, *J. Am. Chem. Soc.*, **103**, 4248 (1981); d) J. P. Gesson, J. C. Jaquesy, and M. Mondon, *Nouv. J. Chim.*, **7**, 205 (1983); We thank Professor Gesson for a reprint.; e) J. P. Gesson, J. C. Jaquesy, and B. Renoux, *Tetrahedron Lett.*, **24**, 2557, 2761 (1983); f) *Idem. Tetrahedron*, **40**, 4743 (1984); g) J. G. Bauman, R. C. Hawley, and H. Rapoport, *J. Org. Chem.*, **50**, 1569 (1985).

3) R. K. Boeckman, Jr., T. M. Dolak, and K. O. Culos, *J. Am. Chem. Soc.*, **100**, 7098 (1978) and references cited therein.

4) T. R. Kelly, N. D. Parekh, and E. N. Trachtenberg, *J. Org. Chem.*, **47**, 5009 (1982).

5) R. L. Hannan, R. B. Barber, and H. Rapoport, *J. Org. Chem.*, **44**, 2153 (1979).

6) M. Iwao and T. Kuraishi, *Tetrahedron Lett.*, **26**, 6213 (1985).

7) R. K. Boeckman, Jr., M. H. Delton, T. M. Dolack, T. Watanabe, and M. D. Glick, *J. Org. Chem.*, **44**, 4396 (1979).

8) G. A. Kraus and S. H. Woo, *J. Org. Chem.*, **51**, 114 (1986).

9) B. Eistert, H. Fink, and A. Müller, *Ber.*, **95**, 2403 (1962).

10) S. O. de Silva, M. Watanabe, and V. Snieckus, *J. Org. Chem.*, **44**, 4802 (1979).

11) M. Watanabe, T. Fukuda, T. Miyashita, and S. Furukawa, *Yakugaku Zasshi*, **105**, 11 (1985); We thank Dr. Watanabe for an authentic sample of emodin trimethyl ether.

12) For leading references and a recent review of anthracyclinone chemistry, see: T. R. Kelly, Ed. *Tetrahedron*, **40**, 4539—4793 (1984); Tetrahedron Symposia-in-Print No. 17.

13) G. M. Muschik, T. Kelly, and W. B. Manning, *J. Chromatogr.*, **202**, 75 (1980).

14) Significance of diene polarization in the Diels-Alder reaction of naphthoquinones has been examined by Boeckman, et al.: see, Refs. 3 and 7.

15) D. B. Bruce and R. H. Thomson, *J. Chem. Soc.*, **1954**, 1428.

16) S. Shibata and M. Takido, *Pharm. Bull. (Tokyo)*, **3**, 156 (1955).

17) G. P. Slater, R. H. Haskins, L. R. Hogge, and L. R. Nesbitt, *Can. J. Chem.*, **45**, 92 (1967).

18) E. J. C. Brew and R. H. Thomson, *J. Chem. Soc. C*, **1971**, 2007.

19) J. Banville, J. L. Grandmaison, G. Lang, and P. Brassard, *Can. J. Chem.*, **52**, 80 (1974).

20) J. Banville and P. Brassard, *J. Chem. Soc., Perkin Trans. 1*, **1976**, 613.

21) A. R. Burnett and R. H. Thomson, *J. Chem. Soc. C*, **1968**, 2437.

22) T. F. Low, R. J. Park, M. D. Sutherland, and I. Vessey, *Aust. J. Chem.*, **18**, 182 (1965).

23) D. W. Cameron, M. J. Crossley, G. I. Feutrill, and P. G. Griffiths, *Aust. J. Chem.*, **31**, 1335 (1978).

24) G. M. Holmwood and J. C. Roberts, *J. Chem. Soc. C*, **1971**, 3899.

25) A. R. Mehendale, *Ind. J. Chem.*, **14B**, 953 (1976).

26) J. F. Garden and R. H. Thomson, *J. Chem. Soc.*, **1957**, 2483.

 © 1987 The Chemical Society of Japan Bull. Chem. Soc. Jpn., 60, 4061—4065 (1987)

The Mechanism of the Reaction of (Arylthio)trimethylgermanes with Benzyl Bromides Giving Aryl Benzyl Sulfides. A Kinetic Study

Seizi KOZUKA,* Shoji TAMURA, Satoshi ISHIBASHI, Sadamu OHYA, and Waichiro TAGAKI

Department of Applied Chemistry, Faculty of Engineering, Osaka City University, Sugimoto 3-Chome, Sumiyoshi, Osaka 558

(Received May 29, 1987)

A kinetic study has been conducted on the reaction of (arylthio)trimethylgermanes with benzyl bromides. The reaction was found to be second order and the rate was largely accelerated in polar solvents. Both ρ values due to substituents on arylthio and benzyl groups revealed nucleophilic attack of the sulfur atom on benzylic carbon atom as the reaction mechanism. Rates of the reactions of trimethyl(*p*-tolylthio)stannane with substituted benzyl chlorides were also examined to compare the substituent effects. Steric crowd around the sulfur atom has been found as an important factor to control the reaction mechanism.

Different kinetic aspects have been observed for the reactions of aroyl chlorides with a series of organometallic sulfur compounds. Individually different mechanisms have been suggested for the reactions of (arylthio)trimethylstannanes,[1] germanes,[2] and silanes,[3] regardless of quite similar outcomes of the reaction products. The difference has also been observed between the reactions of haloalkanes with (arylthio)trimethylstannanes[4] and analogous silanes.[5] Namely, a negative ρ value due to the substituents on the arylthio group and inversion of the carbon atom of the haloalkane were observed for the reaction of the arylthiostannanes. Accordingly, a nucleophilic attack of the sulfur atom has been suggested for the reaction. Relative reactivity of the haloalkanes also supported the mechanism.[4] On the other hand, a large positive ρ value was observed for the reaction of (arylthio)trimethylsilanes with a reactive haloalkane of phenacyl bromide.[5] Initial formation of a 5-coordinated intermediate followed by rate-determining cleavage of the silicon–sulfur bond has been claimed for the reaction (Scheme 1). In this connection, a kinetic study is of interest on the reaction of germanium analogue with haloalkanes.

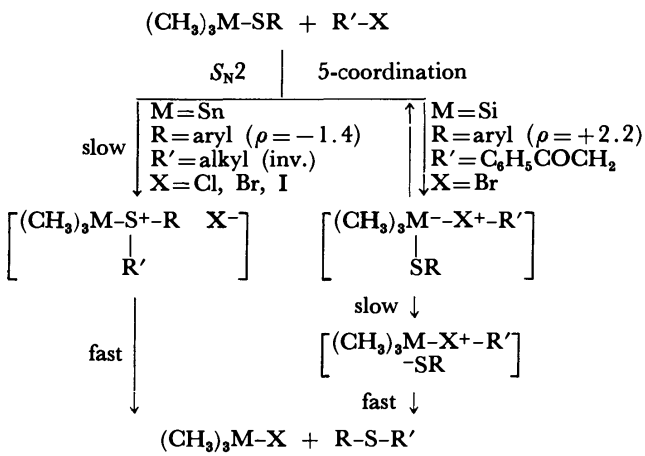

Scheme 1.

We have conducted a kinetic study on the reaction of (arylthio)trimethylgermanes with benzyl bromides.

Results and Discussion

The reaction of trimethyl(phenylthio)germane with benzyl bromide was found to give bromotrimethylgermane and benzyl phenyl sulfide in quantitative yields. No other product was found in the reaction mixture. Products were isolated and characterized.

$$(CH_3)_3Ge\text{-}SC_6H_5 + C_6H_5CH_2\text{-}Br \xrightarrow{100\,^\circ C,\ 30\ h} (CH_3)_3Ge\text{-}Br + C_6H_5S\text{-}CH_2C_6H_5$$

The reaction was monitored by observing ^1H NMR trimethyl signals of the starting germane (δ=0.47) and the product (δ=0.85). The rate constant, k_2, was obtained by least-squares calculation of relative intensities of the trimethyl signal at time intervals. The reaction was found to obey second order rate equation. Kinetic experiments were done at various temperatures in several solvents to observe activation parameters and solvent effect. The results are given in Table 1.

Dichloromethane used as a solvent was observed to react with the arylthiogermane. However, the rate of this reaction was found to be much smaller than that of the reaction with benzyl bromide under the same reaction conditions and the solvent reaction can be neglected. No reaction was found with the other solvents.

Activation parameters given in Table 1 are quite similar to those of the analogous reactions which proceed by ionic processes.[4,5] Solvent effect on the rate of the reaction also supports ionic mechanism for the present reaction since large acceleration in polar solvent was observed.

Effects of the substituents both in the arylthio (X) and the benzyl (Y) moieties were examined to clarify the reaction mechanism. The results are shown in Tables 2 and 3. A clear negative ρ value due to the substituents of the arylthio moiety (ρ_X=−1.41) was

Table 1. Activation Parameters and Solvent Effects on the Rates of the Reactions of $(CH_3)_3GeSC_6H_5$ (0.262 mol dm^{-3}) with $C_6H_5CH_2Br$ (0.318 mol dm^{-3})

Solvent(ε)[a]	Temp/°C	$k_2\times10^4$/dm^3 mol^{-1} s^{-1}	$\Delta H^{\ddagger}_{400}$/kJ mol^{-1}	$\Delta S^{\ddagger}_{400}$/JK^{-1} mol^{-1}	k_{rel} at 140 °C
C_6H_6(2.28)	130	0.0870±0.0031	65.8	−181	1.00
C_6H_6	140	0.151±0.022	γ=0.996[b]		
C_6H_6	150	0.225±0.017			
$C_6H_5OCH_3$(4.33)	130	0.446±0.021	70.6	−155	5.0
$C_6H_5OCH_3$	140	0.757±0.024	γ=0.999		
$C_6H_5OCH_3$	150	1.23 ±0.02			
CH_2Cl_2(8.9)	130	3.48 ±0.20	67.2	−147	41
CH_2Cl_2	140	6.17 ±0.56	γ=0.995		
CH_2Cl_2	150	9.24 ±0.89			
C_6H_5CN(25.2)	110	2.19 ±0.16	80.8	−106	110
C_6H_5CN	120	4.61 ±0.45	γ=0.998		
C_6H_5CN	130	7.72 ±0.43			

a) Dielectric constants. b) Correlation coefficient.

Table 2. Rate Constants for the Reactions of $(CH_3)_3GeSC_6H_4X$ (0.262 mol dm^{-3}) with $C_6H_5CH_2Br$ (0.318 mol dm^{-3})

Solvent	Temp/°C	X	k_2/dm^3 mol^{-1} s^{-1}	ρ_X (γ)[a]
C_6H_6	150	*p*-OCH_3	6.29±0.37×10^{-5}	
C_6H_6	150	*p*-CH_3	3.66±0.43×10^{-5}	
C_6H_6	150	H	2.25±0.17×10^{-5}	−1.41
C_6H_6	150	*p*-Cl	1.02±0.19×10^{-5}	(0.994)
C_6H_6	150	*m*-Cl	7.66±0.76×10^{-6}	
C_6H_5CN	130	*p*-OCH_3	1.33±0.07×10^{-3}	
C_6H_5CN	130	*p*-CH_3	1.07±0.07×10^{-3}	
C_6H_5CN	130	H	7.72±0.43×10^{-4}	−0.76
C_6H_5CN	130	*p*-Cl	5.32±0.67×10^{-4}	(0.998)
C_6H_5CN	130	*m*-Cl	4.28±0.18×10^{-4}	

a) Correlation coefficient.

Table 3. Rate Constants for the Reactions of $(CH_3)_3GeSC_6H_5$ (0.262 mol dm^{-3}) with $YC_6H_4CH_2Br$ (0.318 mol dm^{-3})

Solvent	Temp/°C	Y	k_2/dm^3 mol^{-1} s^{-1}
C_6H_6	150	*p*-CH_3	3.97±0.37×10^{-5}
C_6H_6	150	H	2.25±0.17×10^{-5}
C_6H_6	150	*p*-Cl	2.37±0.28×10^{-5}
C_6H_6	150	*p*-Br	2.22±0.14×10^{-5}
C_6H_5CN	130	*p*-CH_3	1.36±0.12×10^{-3}
C_6H_5CN	130	H	7.72±0.43×10^{-4}
C_6H_5CN	130	*p*-Cl	7.20±0.38×10^{-4}
C_6H_5CN	130	*p*-Br	6.53±0.32×10^{-4}

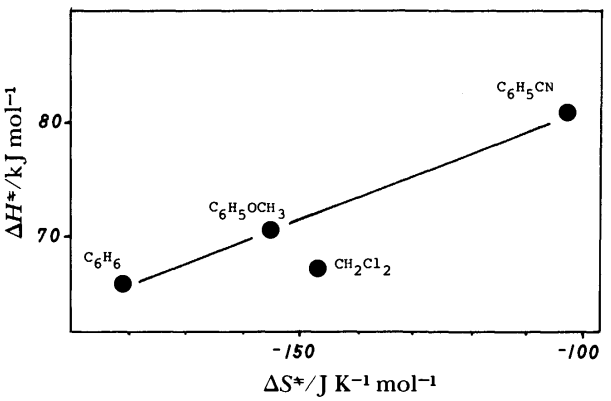

Fig. 1. Plot of $\Delta H^{\ddagger}$ vs. $\Delta S^{\ddagger}$ in various solvents.

observed in benzene solution. This result together with the large solvent effect supports a nucleophilic attack of the sulfur atom as the mechanism for the reaction carried out even in a nonpolar solvent. The effect, on the other hand, appeared substantially smaller in a polar solvent like benzonitrile (ρ_X= −0.76). However, it does not necessarily suggest another mechanism for the reaction in benzonitrile. Rather, the observed linear isokinetic relationship shown in Fig. 1 suggests similarity in the mechanism for the reactions in these solvents, although the plot for the reaction in dichloromethane appeared somewhat deviated. One possible explanation for the small absolute ρ value observed in benzonitrile is to consider the greater stabilization of the polar transition state in the polar solvent and hence stabilization or destabilization by the substituent becomes less important. This interpretation, however, contradicts with the results observed for the analogous reaction in which an enhanced substituent effect was observed in a polar solvent.[6] Thus, the smaller negative ρ value observed in benzonitrile is difficult to explain but it is clearly negative anyway in accordance with the nucleophilic mechanism.

The substituent (Y) effect due to the benzyl group (ρ_Y) appeared somewhat obscure. Rate acceleration by electron donating substituent was observed in all the solvents examined. Almost no effect, on the other

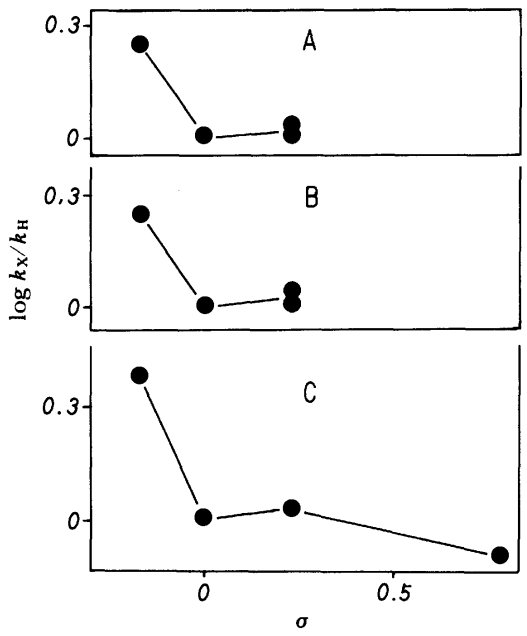

Fig. 2. Hammett plots for the reactions of $(CH_3)_3GeSC_6H_5$+$YC_6H_4CH_2Br$: A, in C_6H_6; B, in C_6H_5CN and $(CH_3)_3SnSC_6H_4CH_3$-*p*+$YC_6H_4CH_2Cl$: C, in $CHCl_3$.

hand, was observed by electron-withdrawing substituents. Thus, bent or curved Hammett plots were obtained as shown in Fig. 2. The bent plots do not contradict with the nucleophilic mechanism. Indeed, a quite similar bent plot has also been reported for the nucleophilic reaction of benzenethiol with substituted benzyl bromides.[7]

Moreover, rate of the reaction of trimethyl(*p*-tolylthio)stannane with substituted benzyl chlorides was measured in order to make sure the mechanism, since a nucleophilic mechanism has been accepted conclusively for such reaction by many evidences.[4] The plot is shown in Fig. 2. A similar bent plot was obtained. The observed bent or curved plot is quite common for the nucleophilic reactions with the substituted benzyl halides.

Thus, all the results obtained by the present study support a mechanism involving nucleophilic attack of the sulfur atom on the benzylic carbon atom (Scheme 2). The formation of the sulfonium intermediate would be the rate-determining step and the salt would decompose rapidly. Neither any precipitation was formed even in a nonpolar solvent nor signals corresponding to the salt were observed during the reaction. A stannylsulfonium salt of this type had once been reported as an isolable product[8] but we later found that the structure of the isolated product was wrong and concluded that the salt cannot be isolated.[9]

The mechanism for the present reaction which has thus been suggested, is quite different from that of the reaction of the same arylthiogermanes with benzoyl

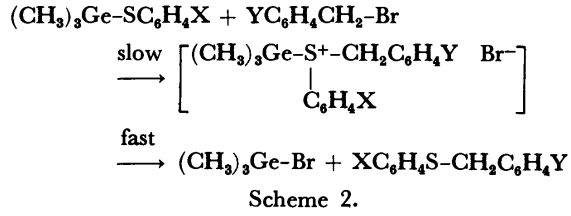

Scheme 2.

chloride.[2] The kinetic aspects observed in the present study are quite similar with those of the reaction of the arylthiostannanes with haloalkanes[4] and different from those of the reaction of the arylthiosilanes with phenacyl bromide.[5]

There are several factors which may control the course of the reaction. Nucleophilicity of the sulfur atom and 5-coordination ability of the germanium atom might be important factors. However, the difference in the mechanisms of the present reaction and that of the reaction with benzoyl chloride[2] cannot be explained in terms of those factors since the same arylthiogermanes were used.

On inspection of the present results and those of the previously reported, the reactivity of benzoyl chloride[2] is appeared smaller than expected.[10] In other words the reactivity of the arylthiogermanes seems to be restricted toward aroyl chlorides and the restriction may change the mechanism. Namely, the reaction of the arylthiogermanes with benzoyl chloride proceeds only slightly faster than the reaction with benzyl bromide and these two reactions proceed by different mechanisms. Aroyl chlorides would be expected to have much higher reactivity than benzyl bromides for the reaction with nucleophiles. In fact, much faster reaction of benzoyl chloride was observed than that of benzyl bromide with the arylthiostannanes and the reactions have been known to proceed by a common mechanism i.e., nucleophilic attack of the sulfur atom.[11]

The restricted reactivity of the arylthiogermanes toward benzoyl chloride can also be recognized by comparing the rates of the reactions of the arylthiogermanes and the stannanes with these two halides.[1,2,4] The arylthiogermanes are substantially less reactive than the arylthiostannanes for the reactions with benzoyl chloride. On the other hand, no such substantial difference in their reactivities was observed for the reactions with benzyl bromide.[12] Only the reaction of the arylthiogermanes with benzoyl chloride, among these four reactions, has been known to involve a 5-coordinated intermediate.[2]

There should be a special factor to restrict the reactivity of the arylthiogermanes toward aroyl chlorides. The mechanism of the reaction seems to be closely related to the reactivity as has hither been discussed. The facile reaction involves a nucleophilic attack of the sulfur atom, while 5-coordinated intermediate is formed when the nucleophilic reaction

was disturbed. The factor to control the reactivity together with the mechanism would be a steric effect. The aroyl halides may have more steric requirements than that of benzyl halides upon nucleophilic attacks. Thus, benzyl bromide accepts a facile nucleophilic attack even by a bulky nucleophile like the arylthiogermanes. On the other hand, benzoyl chloride cannot be attacked by a bulky nucleophile and the reaction proceeds by forming a 5-coordinated intermediate when forced to proceed.[2]

The same concept can also be applied to the other reactions of this type. The loger metal–sulfur bond would reduce the steric crowd around the sulfur atom and hence allows the sulfur atom to act as a nucleophile. The reaction of the arylthiostannanes of the longer metal–sulfur bond, with aroyl chlorides has been known to proceed by the nucleophilic process.[1] On the other hand, the shorter metal–sulfur bond increases the steric crowd and restricts the nucleophilic attack. The reaction of the arylthiogermanes with benzoyl chloride proceeds via 5-coordinated intermediate as mentioned above.[2] In this connection, it is quite natural that the reaction of the arylthiosilanes having the shortest metal–sulfur bond with benzoyl chloride involves 5-coordinated intermediate.[3] The borderline bond length lies between the tin–sulfur and the germanium–sulfur bonds for the reaction with aroyl chlorides in changing the mechanism from nucleophilic reaction to the 5-coordination process.

The difference in the mechanisms of the reactions of a series of metal–sulfur compounds with benzyl bromide can also be rationalized by their different bond lengthes. The reaction of the arylthiostannanes with benzyl bromide undergoes by a nucleophilic attack of the sulfur atom on the benzylic carbon.[4] In the present study, the shorter metal–sulfur bond like the arylthiogermanes has been found to attack on the benzyl bromide in a similar way due to less steric requirements of the halide. The 5-coordination process suggested for the reaction of the arylthiosilanes with phenacyl bromide[5] can be understood in terms of the steric crowd due to the shortest metal–sulfur bond length. Among the reactions with primary haloalkanes, only the reaction of the arylthiosilanes would involve a 5-coordinated intermediate although any kinetic evidence with a common haloalkane like benzyl bromide has not been obtained yet.[13]

The steric effect has thus been found to be an important factor to control the course of the reaction. Other factors such as the nucleophilicity and the 5-coordination ability dependent on the individual metals cannot be ruled out but seem to be not important at least for the reactions discussed here.

Experimental

Materials. Solvents were dried and distilled. Substituted benzyl bromides and chlorides were purified by distillation or recrystallization before use. The preparations of (arylthio)trimethylgermanes were reported previously.[2]

Product Analysis. Trimethyl(phenylthio)germane (1.10 g, 5.6×10^{-3} mol) was heated with an equimolar amount of benzyl bromide (0.94 g) in a sealed tube at 100 °C for 30 h. ^{1}H NMR analysis of the reaction mixture showed only signals due to bromotrimethylgermane and benzyl phenyl sulfide. Bromotrimethylgermane was isolated by distillation (bp 113—114 °C, 65%). Benzyl phenyl sulfide was obtained from the residue and was purified by recrystallization, mp 41—43 °C (from hexane, 98%, lit,[14] 41—43.5 °C).

Kinetics. The rates of the reactions of the arylthiogermanes (0.262 mol dm^{-3}) with benzyl bromides (0.318 mol dm^{-3}) were measured by the procedure reported recently.[2] The rates of the reactions of trimethyl(*p*-tolylthio)stannane (0.06 mol dm^{-3}) with benzyl chlorides (0.6 mol dm^{-3}) were measured by the previous method.[4] Pseudo-first-order rate constants k_1 for the reactions of $(CH_3)_3SnSC_6H_4CH_3$-*p* with $ClCH_2C_6H_4Y$-*p* in chloroform at 130 °C are as follows: Y=CH_3, 2.36×10^{-5} s^{-1}; H, 9.96×10^{-6} s^{-1}; Cl, 1.05×10^{-5} s^{-1}; NO_2, 7.86×10^{-6} s^{-1}.

The Reaction of (Arylthio)trimethylgermanes with the Solvents. Dichloromethane solution of trimethyl(phenylthio)germane (0.262 mol dm^{-3}) was heated at 150 °C for 110 min. The reaction conditions correspond to more than 75% completion of the reaction of the germane with benzyl bromide. Small amount of chlorotrimethylgermane was found in the mixture by ^{1}H NMR analysis (δ=0.72). Pseudo-first-order rate constant was estimated based on the conversion: $k_1=1.2\times1.0^{-5}$ s^{-1}. Thus, the reaction with the solvent was negligible under the conditions used for the kinetics. No reaction was found with the other solvents.

References

1) S. Kozuka and I. Naribayashi, *Bull. Chem. Soc. Jpn.*, **52**, 3639 (1979).

2) S. Kozuka, S. Tamura, T. Yamazaki, S. Yamaguchi, and W. Tagaki, *Bull. Chem. Soc. Jpn.*, **58**, 3277 (1985).

3) S. Kozuka and I. Naribayashi, *Mem. Fac. Engin. Osaka City Univ.*, **22**, 115 (1981).

4) S. Kozuka and S. Ohya, *Bull. Chem. Soc. Jpn.*, **51**, 2651 (1978).

5) S. Kozuka, T. Higashino, and T. Kitamura, *Bull. Chem. Soc. Jpn.*, **54**, 1420 (1981).

6) A more enhanced substituent effect, ρ_X=+2.32, was observed in benzonitrile than in tetrachloromethane (ρ_X=+1.46) although the signs are opposite and hence a different machanism has been suggested.[2]

7) R. F. Hudson and G. Klopman, *J. Chem. Soc.*, **1962**, 1062.

8) E. W. Abel and D. B. Brady, *J. Chem. Soc.*, **1965**, 1192.

9) S. Kozuka and S. Ohya, *J. Organomet. Chem.*, **149**, 191 (1978).

10) For instance, extrapolation of the present result and comparing with that reported[2] gives $k_2(C_6H_5COCl)/k_2(C_6H_5CH_2Br)$ is only 9 in CH_2Cl_2 at 100 °C.

11) The reaction of $(CH_3)_3SnSC_6H_4CH_3$-*p* with benzyl

bromide in nonpolar solvent proceeds only at elevated temperatures (k_1=2.65×10^{-4} s^{-1} at 115 °C in $CHCl_3$)[4] while that with benzoyl chloride proceeds at around room temperature (k_2=4.5×10^{-5} mol^{-1} dm^{3}s^{-1} at 34 °C in CCl_4).[1] These reactions proceed by nucleophilic mechanisms.

12) The retes of the reactions are as follows: $(CH_3)_3GeSC_6H_5+C_6H_5COCl$; k_2=3.45×10^{-4} dm^3 s^{-1} at 130 °C in CCl_4,[2] and $(CH_3)_3SnSC_6H_5+C_6H_5COCl$; k_2=5.2×10^{-5} dm^3 mol^{-1} s^{-1} at 43 °C in CCl_4.[1] Extraporations of their Arrhenius plots gave relative reactivity of the phenylthiogermane and the phenylthiostannane with benzoyl chloride: k_2(GeS)/k_2(SnS)=ca. 0.025 at 100 °C in CCl_4. On the other hand, direct comparison of their reactivity toward benzyl bromide is difficult due to difference in their reaction conditions. However the rate of the reaction of $(CH_3)_3SnSC_6H_4CH_3$-*p* + $C_6H_5CH_2Br$[4,11] is only slightly faster than that in nonpolar solvents as shown in Table 1.

13) Kinetic study on the reaction of the arylthiosilanes with benzyl halides was failed due to facile decomposition of the reactant.[5] However, the reaction with phenacyl bromide has been found to proceed via 5-coordinated intermediate.[5]

14) "Beilstein Handbuch der Organischen Chemie," **6**, p. 454.

 © 1987 The Chemical Society of Japan Bull. Chem. Soc. Jpn., 60, 4067—4078 (1987)

Simple Generation of Ester-Stabilized Azomethine Ylides from 2-Amino Esters and Carbonyl Compounds. Stereochemistry of Their Cycloadditions

Otohiko Tsuge,* Shuji Kanemasa, Masayuki Ohe, Kiyotaka Yorozu, Shigeori Takenaka, and Kazunori Ueno

Institute of Advanced Material Study, and Department of Molecular Science and Technology, Interdisciplinary Graduate School of Engineering Sciences, Kyushu University, Kasugakoen, Kasuga 816

(Received May 30, 1987)

Condensation of 2-amino esters with carbonyl compounds leads to simple generation of ester-stabilized azomethine ylides which are trapped by olefinic dipolarophiles as cycloadducts. Anti ylides are exclusively involved in the cycloadditions when *N*-substituted 2-amino esters are employed for the ylide generation, while syn ylides from *N*-unsubstituted 2-amino esters. Relative stability among all possible ylide isomers has been inspected and the selective involvement of particular ylidic forms has been explained on the ground of 1,5-dipole interaction or hydrogen bonding stabilization. Endo- and exo-selectivity of the cycloadditions is also discussed.

Cycloaddition of azomethine ylides with olefinic and acetylenic dipolarophiles affords pyrrolidines, pyrrolines, and pyrroles. The importance of azomethine ylide chemistry is being increased more than ever as a tool for constructing the nitrogen-containing five-membered heterocycles which are often central ring systems of numerous natural products. Its synthetic application was encouraged by the recent discovery of new generation methods of azomethine ylides, including wide range of stabilized to nonstabilized azomethine ylides. Two typical methods involve the desilylation route[1] discovered by Vedejs; the imine route[2] by Grigg, Joucla, and Tsuge, separatedly.

Griggs' method of generating azomethine ylides is based upon a thermal tautomerization of imine (Eq. 1). The acidic hydrogen adjacent to both the imine

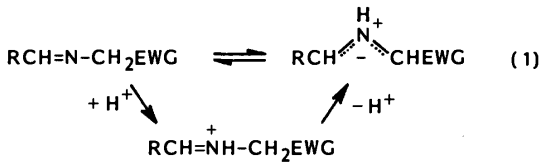

(1)

nitrogen and ester moiety migrates onto the nitrogen (1,2-proton migration). This imine–azomethine ylide tautomerization is known to be catalyzed by an acid which facilitates the reaction by the rapid formation of an iminium intermediate.[3] It is therefore envisaged that the iminium compounds which will be produced from the condensation of *N*-substituted 2-amino esters with carbonyl compounds would allow ready deprotonation to lead to the generation of ester-stabilized azomethine ylides (Eq. 2). This process has been

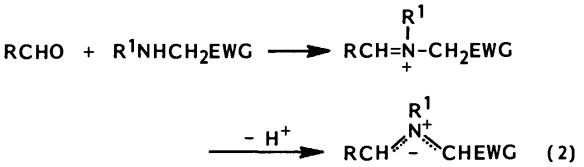

(2)

recently realized by several groups,[4-6] while the reaction examples were quite limited so that no details of this promising azomethine ylide generation are known.

The present article describes full details of the 2-amino ester route as a simple and general generation method of ester-stabilized azomethine ylides. Stereochemical features of the cycloaddition of ester-stabilized azomethine ylides with olefins have been figured out. The origin of anti- and syn-selectivity with respect to the ylides as well as the endo-, exo, and regioselectivity of the cycloaddition is discussed.[7]

Results and Discussion

Generation and Cycloaddition of *N*-Substituted Azomethine Ylides of Ester-Stabilized Types. According to the Eq. 2, benzaldehyde and ethyl *N*-methylaminoacetate (**1**) were heated under reflux in toluene. The water eliminated was removed by the aid of a Dien-Stark trap and the azomethine ylide **A** (R=Ph, R^1=Me, EWG=COOEt) generated was captured by *N*-(*p*-tolyl)maleimide to give three stereoisomers of **1**:**1** cycloadducts **4a**, **5a**, and **6a** in 93% of total yield (Scheme 1 and Table 1).

Their structures are readily assigned as 3a,4-trans-6,6a-cis- (**4a**, 69%), 3a,4-cis-6,6a-trans- (**5a**, 20%), and 3a,4-cis-6,6a-cis-isomer (**6a**, 4%) on the basis of the vicinal coupling constants as well as other spectral and analytical data: **4a**: $J_{3a,4}$=0.8 and $J_{6,6a}$=9.4 Hz; **5a**: $J_{3a,4}$=8.8 and $J_{6,6a}$=5.7 Hz; **6a**: $J_{3,3a}$=8.8 and $J_{6,6a}$=7.0 Hz. Thus, **4a** and **5a** are cycloadducts to the anti form of ylide **A** and **6a** to the syn ylide.

Aliphatic aldehydes can be used as carbonyl compounds albeit low yield formation of the cycloadducts. The azomethine ylide **A** (R=Et, R^1=Me, EWG=COOEt) derived from propanal reacted with the maleimide to produce 48% yield of two stereoisomeric cycloadducts **4b** and **5b** to the anti

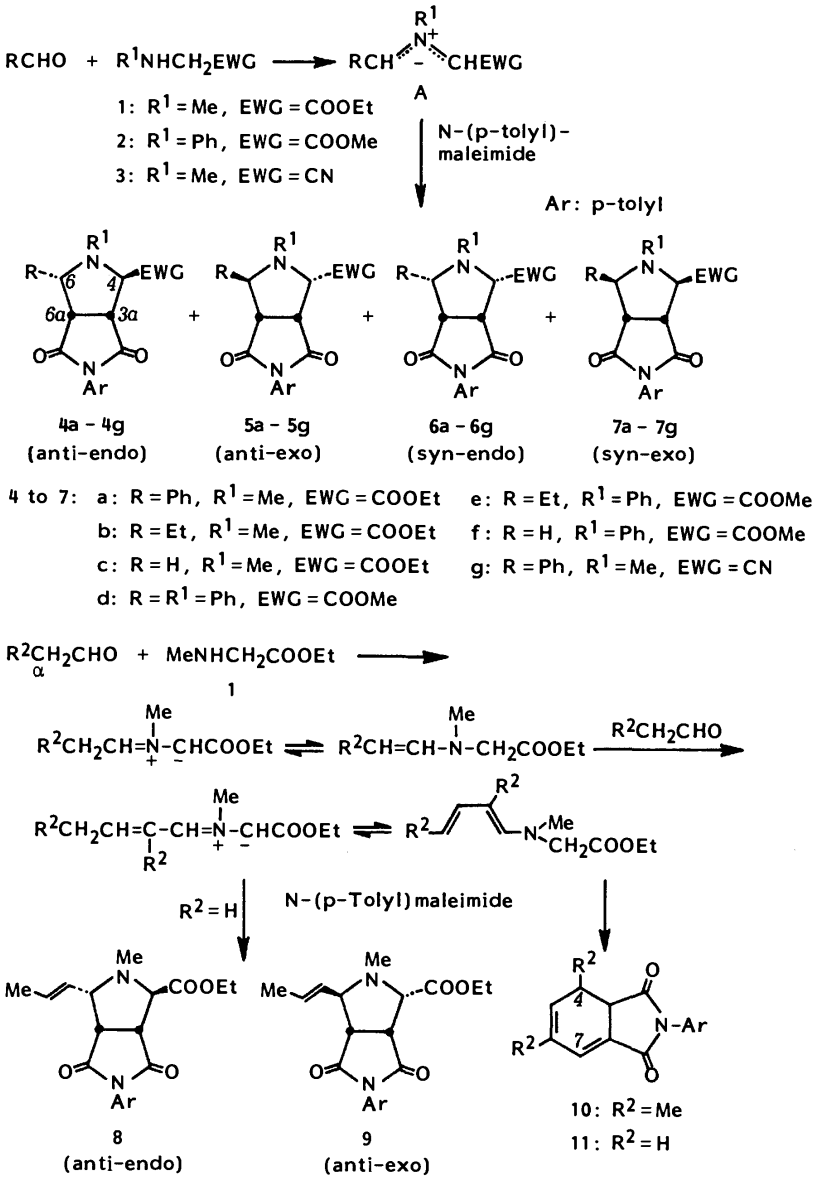

Scheme 1.

Table 1. Cycloaddition of *N*-(*p*-Tolyl)maleimide with Ester- or Cyano-Stabilized Azomethine Ylides **A** Generated from 2-Amino Esters **1**, **2** or Nitrile **3** and Aldehydes

Entry	Amine	Aldehyde	Product	R	R^1	R^2	EWG	Yield[a] %	Isomer ratio[b]	anti : syn	endo : exo
1	**1**	PhCHO	**4a**+**5a**+**6a**	Ph	Me	—	COOEt	93	69 : 20 : 4	96 : 4	78 : 22
2	**1**	EtCHO	**4b**+**5b**+**10**	Et	Me	Me	COOEt	66	37 : 11 : 18	anti only	77 : 23
3	**1**	MeCHO	**8**+**9**+**11**	—	—	H	—	87	58 : 18 : 11	anti only	76 : 24
4	**1**	$(CH_2O)_n$	**4c**+**5c**	H	Me	—	COOEt	93	58 : 35	—	62 : 38
5	**2**	PhCHO	**4d**+**5d**	Ph	Ph	—	COOMe	77	35 : 42	anti only	45 : 55
6	**2**	EtCHO	**4e**+**5e**	Et	Ph	—	COOMe	64	30 : 34	anti only	47 : 53
7	**2**	$(CH_2O)_n$	**4f**+**5f**	H	Ph	—	COOMe	78	1 : 1[c]	—	50 : 50
8	**3**	PhCHO	**4g**+**5g**+**6g**+**7g**	Ph	Me	—	CN	49	12 : 12 : 16 : 9	49 : 51	57 : 43

a) Total yield. b) Yield of separated products. c) Determined by ^{1}H NMR.

ylide together with the third product **10** which was assigned as 4,6-dimethyl-2-(*p*-tolyl)-1,3,3a,4-tetrahydro-2*H*-isoindole-1,3-dione. When ethanal was employed, no trace of the cycloadducts of methyl-substituted azomethine ylide **A** (R=Me) was even detected but two stereoisomeric cycloadducts **8**+**9** to 1-propenyl-substituted ylide were obtained. Isoindoledione **11** was again accompanied.

Formation of **8** to **11** was not surprising since we have already experienced a similar reaction pattern in the reaction of aminoacetonitrile with aliphatic aldehydes.[3b] As illustrated in Scheme 1, an aliphatic aldehyde undergoes condensation with ethyl *N*-methylaminoacetate **1** to generate the expected azomethine ylide which is in equilibrium with an enamine isomer. The enamine then adds to the second molecule of the aldehyde to form 1-alkenyl-substituted azomethine ylide which is also equilibrating with the dienamine. 1,3-Dipolar cycloaddition of the ylide leads to **8** and **9**, while Diels–Alder reaction of the latter gives **10** and **11** after the elimination of amino ester **1**.

The condensation of **1** with paraformaldehyde generated the azomethine ylide **A** (R=H, R[1]=Me, EWG=COOEt) bearing an ester as the only *C*-substituent. It was captured by *N*-(*p*-tolyl)maleimide to give two stereoisomeric cycloadducts **4c** and **5c** in an excellent combined yield.

Reactions of methyl *N*-phenylaminoacetate (**2**) with benzaldehyde, propanal, and paraformaldehyde generated azomethine ylides **A** (R[1]=Ph, EWG=COOMe) whose cycloadditions with *N*-(*p*-tolyl)maleimide afforded mixtures of endo- and exo-cycloadducts to the anti forms of ylides **A** (**4d**+**5d** to **4f**+**5f**, Scheme 1 and Table 1).

The exclusive involvement of the anti form of *N*-substituted azomethine ylides **A** (EWG=COOR[2]) bearing a ylide-stabilizing ester in their cycloadditions contrasts with the extremely poor selectivity of cyano-stabilized azomethine ylide **A** (EWG=CN), with respect to both the ylide configuration and cycloaddition approach. For instance, reaction of *N*-methylaminoacetonitrile (**3**) with benzaldehyde in the presence of *N*-(*p*-tolyl)maleimide gave a mixture of four stereoisomeric cycloadducts **4g**, **5g**, **6g**, and **7g**, all possible stereoisomers, in a comparable ratio (Table 1).

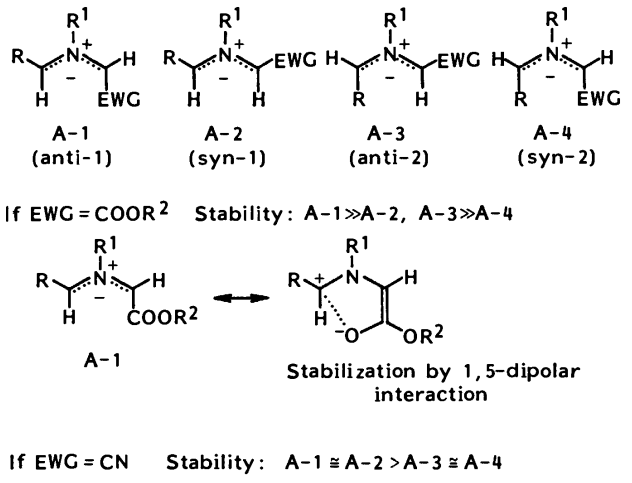

Fig. .1. Stable configuration of *N*-substituted azomethine ylides of ester- and cyano-stabilized types.

Each two anti (**A-1** and **A-3**) and syn configurations (**A-2** and **A-4**) are possible for the *N*-substituted azomethine ylide **A** with an ester or a cyano stabilizing substituent (Fig. 1). Their relative stability may be estimated on the ground of steric and electronic interactions among the substituents.

The U-shaped syn ylide **A-4** of ester-stabilized type is first discarded as the concerned species because it is too congested to exist as a stable form. Although the other three ylides seem equally stable from a sterical standpoint, only the S-shaped anti ylide **A-1** with the ester group opposite to the *N*-substituent R[1] has an additional stabilization by 1,5-dipole interaction.[8,9] In the end the relative stability of ester-stabilized ylides (EWG=COOR[2]) becomes as follows: **A-1**≫**A-2**≅**A-3**≫**A-4**. Accordingly the anti ylide **A-1** must have been selectively involved in its cycloaddition.

On the other hand such stabilization by an extended dipole is impossible in the case of cyano-stabilized azomethine ylide **A** (EWG=CN). Cyano moiety is only slightly bulkier than hydrogen so that the difference of steric stability between **A-1** and **A-2**, and also **A-3** and **A-4**, is negligible. Thus the relative stability becomes in the following order: **A-1**≅**A-2**>**A-3**≅**A-4**. Poor stereoselectivity will be unavoidable in the cycloadditions of *N*-substituted azomethine ylides **A** of cyano-stabilized types.

Exclusively stereospecific cycloadditions of the azomethine ylide **A** (R=Ph, R[1]=Me, EWG=COOEt) derived from **1** and benzaldehyde is shown in Scheme 2 and Table 2. Contrary to the poor stereoselectivity observed in the cycloaddition to *N*-(*p*-tolyl)maleimide

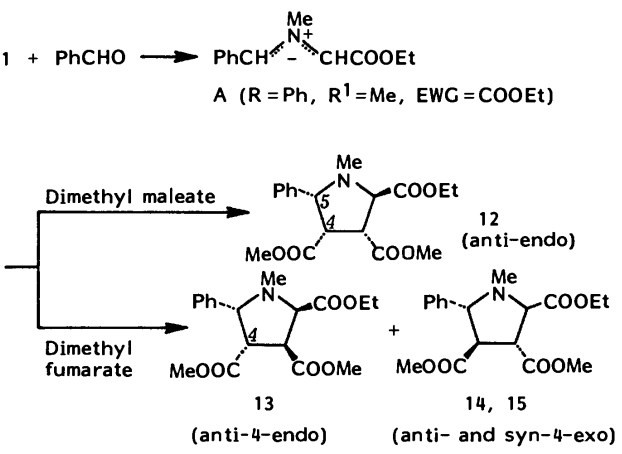

Scheme 2.

(Entry 1 of Table 1), the reaction with dimethyl maleate was highly endo-selective leading to **12**. With dimethyl fumarate, three stereoisomeric cycloadducts **13**—**15** were produced. Similar dramatic change of stereoselectivity has been recently reported by Joucla.[5] 4,5-Cis structure of **12** and **13** was assigned on the basis of the intense shielding of 4-ester moiety by the adjacent phenyl (5-Ph).

With unsymmetrically substituted olefins such as methyl acrylate and (*E*)-β-nitrostyrene, the above ylide **A** (R=Ph, R^1=Me, EWG=COOEt) as well as its *N*-phenyl analog **A** (R=R^1=Ph, EWG=COOMe) underwent highly endo- and regioselective cycloadditions giving 2,3-cis-3,4-trans-4,5-cis-cycloadducts **16a**—**16d** as single isomers (Scheme 3 and Table 2). As will be realized soon, these high regio- and stereoselectivities can not be achieved without the phenyl substituent.

The azomethine ylide bearing an ester moiety as the only *C*-substituent was previously generated by thermolysis of aziridine-2-carboxylates,[6a,b] deprotonation of *N*-(phenylthiomethyl)aminoacetates,[6c] or desilylation of *N*-(trimethylsilylmethyl)iminoacetates.[6d] This ylide **A** (R=H, R^1=Me, EWG=COOEt) which was more simply generated from **1** and paraformaldehyde under reflux in toluene undergoes cycloadditions to unsymmetrically substituted olefins, but both the regio- and stereoselectivities are very poor like the precedents. Thus a mixture of two regioisomeric cycloadducts **17a** or **17b** was produced with methyl acrylate or phenyl vinyl sulfone, respectively (Scheme 3). It is noteworthy that this ylide showed high reactivity toward styrene as an aryl-substituted olefin to give the regioselective cycloadduct **17c**. This is the first example for the cycloaddition of ester-stabilized azomethine ylide to such an aryl-substituted olefin as styrene.[10,11]

As some incorrect structural assignments are contained in the previous work,[13] our structural

Table 2. Cycloaddition of Ester-Stabilized Azomethine Ylides **A** and **B**

Entry	2-Amino ester	Aldehyde	Olefin	Condition[a]	Product (yield/%)[b]	Isomer ratio[c]	anti : syn	endo : exo
1	**1**	Benzaldehyde	Dimethyl maleate	A, 1 h	**12** (62)		anti only	endo only
2	**1**	Benzaldehyde	Dimethyl fumarate	A, 1 h	**13**+**14**+**15** (87)[d]	3 : 3 : 2		
3	**1**	Benzaldehyde	Methyl acrylate	A, 1 h	**16a** (73)		anti only	endo only
4	**1**	Benzaldehyde	β-Nitro-styrene	A, 1 h	**16b** (72)		anti only	endo only
5	**2**·HCl	Benzaldehyde	Methyl acrylate	B, 24 h	**16c** (31)		anti only	endo only
6	**2**·HCl	Benzaldehyde	β-Nitro-styrene	B, 24 h	**16d** (39)		anti only	endo only
7	**1**	Paraform-aldehyde	Methyl acrylate	C, 12 h	**17a** (100)[e]	6 : 5[f]	—	g)
8	**1**	Paraform-aldehyde	Phenyl vinyl sulfone	A, 1 h	**17b** (82)[e]	1 : 4[h]	—	g)
9	**1**	Paraform-aldehyde	Styrene	C, 12 h	**17c** (61)[i]	1 : 1[j]	—	50 : 50
10	**18**	Benzaldehyde	*N*-Methyl-maleimide	A, 24 h	**19a** (100)		syn only	endo only
11	**18**	Benzaldehyde	*N*-Methyl-maleimide	D, 13 h	**19a**+**20** (100)		67 : 33	endo only
12	**18**	Phenylglyoxal	*N*-Methyl-maleimide	E, 16 h	**19b** (100)		syn only	endo only
13	**18**	2-Methyl-propanal	*N*-Methyl-maleimide	A, 20 h	**19c** (58)		syn only	endo only
14	**18**	Cyclohexa-none	*N*-Methyl-maleimide	A, 19 h	**21** (85)		—	endo only

a) A: Under reflux in toluene, B: Uuder reflux in toluene together with *N*,*N*-diisopropylethylamine, C: At 180 °C in a sealed tube together with anhydrous potassium carbonate, D: At room temperature in acetonitrile in the presence of acetic acid (10 mol%), E: Under reflux in chloroform. b) Yield of isolated products. c) Determined by ^{1}H NMR. d) Only **15** was separated from the other two. e) Inseparable mixture of two regioisomers. f) 2,3-Isomer : 2,4-isomer=6 : 5 (^{1}H NMR). g) Stereostructure remains unsolved. h) 2,3-Isomer : 2,4-isomer=1 : 4 (^{1}H NMR). i) Inseparable mixture of two stereoisomers. j) Both 2,3-isomers.

analysis on **17a—17c** based upon the ^{13}C NMR is summarized in Table 3. Adjacent substitution with an ester brings about a downfield ^{13}C shift by 3—5 ppm, and with a phenyl by 7—10 ppm. Substitution with a sulfonyl makes no significant shift to the adjacent carbon. Thus **17a** and **17b** were assigned as mixtures of two regioisomers, while their stereostructures could not be determined. Also apparent is the 2,3-disubstituted structure of **17c**. A 6:5 ratio of 2,3- to 2,4-substitution of **17a** is opposite to the reported one (1:3),[6c] indicating that regioselectivity in the azomethine ylide cycloadditions strongly depends upon the generation method or reaction medium.

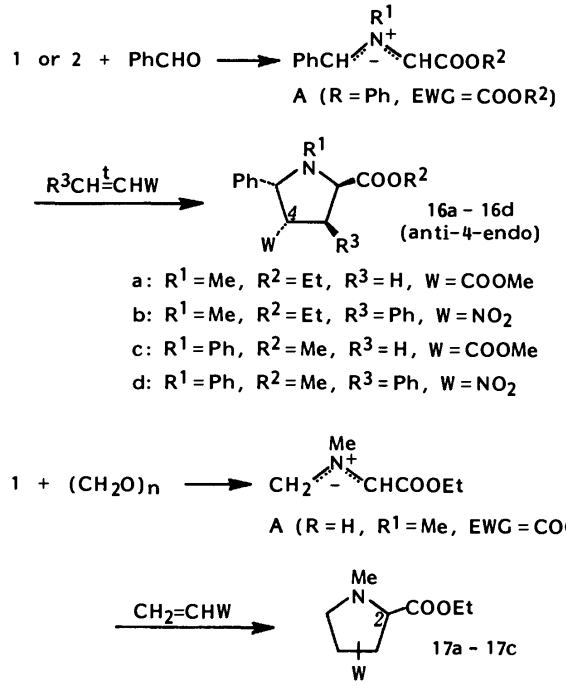

Scheme 3.

Generation and Cycloaddition of *N*-Unsubstituted (or *N*-Protonated) Azomethine Ylides of Ester-Stabilized Types. As shown with Eq. 1 *N*-(alkoxycarbonylmethyl)imines undergo a ready thermal tautomerization and this reaction is one of the most useful generation methods of *N*-unsubstituted azomethine ylides of ester-stabilized types.[2] This procedure may be simplified by omitting the isolation step of the imines and this modified method would be especially useful when imine esters as ylide precursors are labile.[3b] Our procedure consists of heating a mixture of 2-amino ester and carbonyl compound under continuous removal of water (Eq. 3).[14]

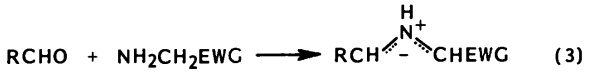

(3)

N-Unsubstituted azomethine ylides **B** of ester-stabilized types were directly generated by similar reactions of methyl aminoacetate (**18**) with carbonyl compounds and trapped with *N*-methylmaleimide to provide the exclusive formation of endo-cycloadducts **19a—19c** and **21** to the syn form of **B** (Scheme 4 and

Table 3. ^{13}C NMR Chemical Shifts for the Ring Carbons of **17a—17c**[a]

	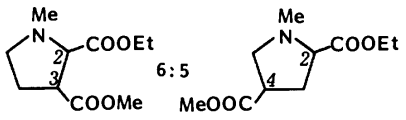 17a (2,3-isomer)	17a (2,4-isomer)	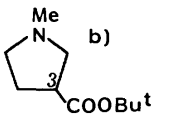	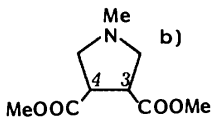
	6:5		b)	b)
				3,4-cis 3,4-trans
2-C	70.24 (d)	66.83 (d)	58.24 (t)	58.35 (t) 59.06 (t)
3-C	47.12 (d)	32.77 (t)	41.94 (d)	45.85 (d) 45.94 (d)
4-C	27.83 (t)	41.47 (d)	27.47 (t)	
5-C	55.77 (t)	58.83 (t)	55.30 (t)	

	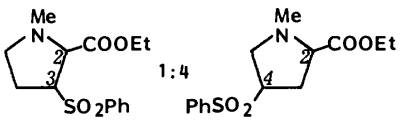 17b (2,3-isomer)	17b (2,4-isomer)	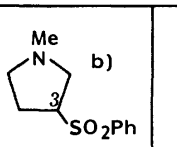	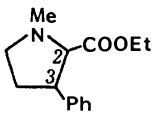 17c (1:1 mixture)
	1:4		b)	2,3-trans 2,3-cis
2-C	66.95 (d)	65.36 (d)	55.47 (t)	76.01 (d) 73.01 (d)
3-C	65.71 (d)	29.59 (t)	62.48 (d)	49.65 (d) 47.94 (d)
4-C	24.71 (t)	60.30 (d)	25.94 (t)	31.94, 32.71 (each t)
5-C	54.94 (t)	54.24 (t)	55.30 (t)	55.83, 56.12 (each t)

a) All recorded in $CDCl_3$. b) See Ref. 12.

Table 2). Benzaldehyde and cyclohexanone form relatively stable imines so that the thermal tautomerization method could be also applied to these imines. Although the imines of **18** with phenylglyoxal and 2-methylpropanal are too unstable to be isolated, our method worked well in both cases. However a serious limitation appeared when such aldehydes as propanal and cinnamaldehyde were employed. No corresponding azomethine ylides were trapped by a maleimide dipolarophile.

As shown above the imine derived from **18** and benzaldehyde tautomerized into a syn form of azomethine ylide **B** (R=Ph) on heating in toluene. To our surprise the stereoselectivity with respect to the ylide was extremely decreased when the same imine was heated in acetonitrile in the presence of acetic acid (10 mol%). Thus a 1:2 mixture of the syn and anti ylide cycloadducts **19a**+**20** was obtained. This will be discussed later.

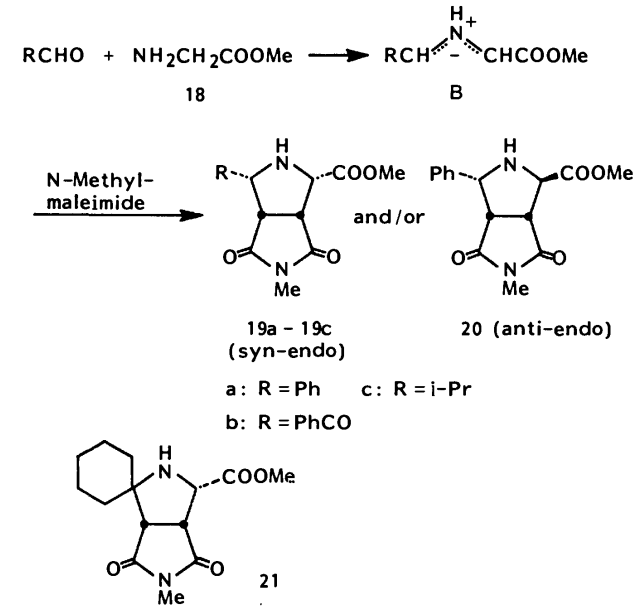

Scheme 4.

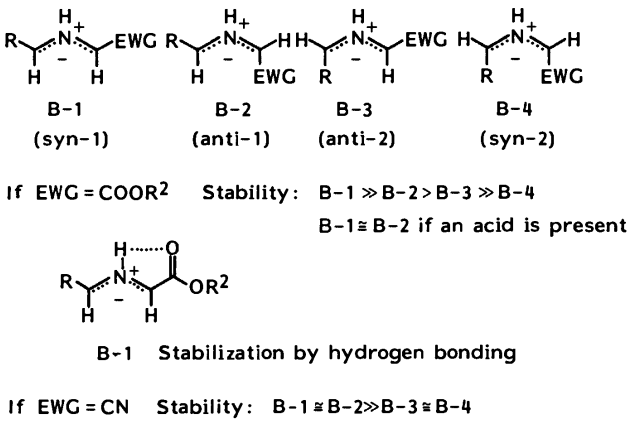

Fig. 2. Stable configuration of *N*-protonated azomethine ylides of ester- and cyano-stabilized types.

Four configurations including each two syn (**B-1** and **B-4**) and anti ylidic forms (**B-2** and **B-3**) are also possible for the *N*-unsubstituted azomethine ylide **B** of ester- or cyano-stabilized type (Fig. 2). In all the cycloaddition examples described in Scheme 4 with an exception the syn form of ester-stabilized ylide **B** (EWG=COOMe) was exclusively incorporated in the cycloadducts, indicating higher stability of the syn ylide. This makes a striking contrast to the case of *N*-substituted ylide **A** where anti form has predominated. It is quite easy to understand that ylide **B-1** is much more stabilized than the other syn ylide **B-4** on the basis of both steric consideration and the hydrogen bonding between the ester carbonyl and NH hydrogen. In a polar or protic solvent this hydrogen bonding becomes fragile, and the positively charged ylide nitrogen is stabilized through the coordination of the solvent molecules nearby. In this case syn configuration **B-1** is no longer the most stable.

In the case of *N*-protonated azomethine ylide **B** (EWG=CN) of cyano-stabilized type, syn ylide **B-1** and anti ylide **B-2** would have an identical stability. Poor stereoselectivity with respect to the ylidic carbon bearing a CN substituent has been previously demonstrated.[3b]

Stereochemical Aspects of Cycloaddition of Ester-Stabilized Azomethine Ylides. The predominant participation in cycloaddition of the anti ylide **A-1** of *N*-substituted azomethine ylide (Fig. 1) and of the syn ylide **B-1** of *N*-unsubstituted ylide has been discussed above (Fig. 2). Table 1 summarizes the endo–exo ratios of cycloadducts derived from *N*-substituted azomethine ylides **A** (EWG=COOEt or COOMe) bearing a variety of *C*-substituents and *N*-(*p*-tolyl)-maleimide, and Entries 10—14 of Table 2 show the exclusive formation of endo cycloadducts from *N*-unsubstituted azomethine ylides **B** and the maleimide. Apparently the endo–exo selectivity depends upon the *N*-substituents.

Endo and exo approaches of maleimide to an azomethine ylide 1,3-dipole is illustrated in Fig. 3 with Approach I and II, respectively (either A or B is an ester moiety). In Approach II (exo) there exist four sets of near-eclipsed repulsion (H/CO, A/CO, R/H, B/H), and in Approach I (endo) steric repulsion

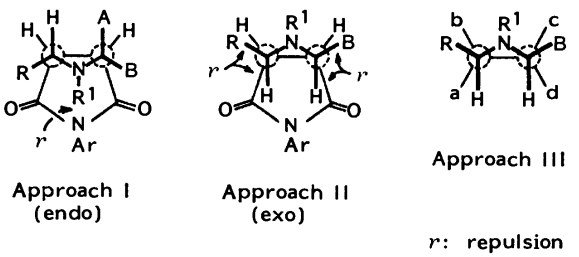

Fig. 3. Approaches between azomethine ylide $RCH{=}\overset{+}{N}(R^1)\text{-}\underline{C}AB$ and olefinic dipolarophiles.

between both the *N*-substituents (R^1 and Ar) is the only barrier. Accordingly it is readily understood that cycloaddition becomes highly endo-selective if the *N*-substituent R^1 is small in size, for instance a hydrogen. On the other hand this steric repulsion is critical when R^1 is bulky, the endo selectivity becoming lowered.

The small bond angle of CO–CH=CH and the planer geometry make maleimides a very special dipolarophile. The *N*-substituent repulsion of Approach I and the eclipsed repulsion of Approach II are both amplified compared with other acyclic dipolarophiles whose approach is illustrated with Approach III (Fig. 3). Now the substituents a and d are not bonded so that the steric repulsion toward the *N*-substituent R^1 is reduced. This may be the main reason why the cycloaddition of ylide **A** (R=Ph, R^1=Me, EWG=COOEt) to dimethyl maleate was absolutely endo-selective to lead to **12** (Entry 1 of Table 2). Attractive interaction working between the phenyl substituent and the ester group, each is on either the ylide or olefin, is also responsible for the high endo selection as shown with Entries 3—6 of Table 2.

The present generation method of ester-stabilized azomethine ylides is valuable because of 1) simple procedure using readily available 2-amino esters and carbonyl compounds, 2) high yield formation of a variety of ylides, 3) no need of the isolation of ylide precursors, 4) mild generation conditions. As the aziridine route leading to ester-stabilized azomethine ylides with no other ylide-stabilizing substituent requires the pyrolysis at an elevated temperature,[6a] the ylide trapping with olefins are not so effective as the present case.

Experimental

General. Melting points were determined on a Yanagimoto melting point apparatus and are uncorrected. IR spectra were taken with a JASCO IRA-1 or a JASCO A-702 spectrometer. ^{1}H NMR spectra were recorded on a Hitachi R-40 (90 MHz) or a JEOL FX-100 instrument (100 MHz) and ^{13}C NMR on a JEOL FX-100 spectrometer at 25.05 MHz. Chemical shifts are expressed in parts per million downfield from tetramethylsilane as an internal standard. Mass spectra were measured with a JEOL-01SG-2 spectrometer at 70 eV of ionization energy. High resolution mass spectra were also obtained on the same instrument. Elemental analyses were performed on a Hitachi 026 CHN analyzer. Thin-layer chromatography (TLC) was accomplished on 0.2 mm precoated plates of silica gel 60 F-254 (Merck). Visualization was made with ultraviolet light (254 and 365 nm), iodine, molybdophosphoric acid (5% in ethanol), or *p*-anisaldehyde (5% in ethanol containing 5% of sulfuric acid). For preparative column chromatography, Wakogel C-200, C-300 (Wako), and Silicagel 60 (Merck) were employed. Flash chromatography was carried out on an EYELA EF-10 apparatus using a column (20×180 mm) packed with Silicagel 60 (Merck, size: 0.04—0.063 mm). Gas liquid chromatography (GLC) was accomplished on a Yanaco G-2800 gas chromatograph with an ionization flame detector using a glass column (SE-30, 3×2000 mm) or a glass capillary column (Silicone GE, SE-30, 0.25×50000 mm). Micro vacuum distillation was carried out on a Sibata GTO-250R Kugelrohr distilling apparatus. Solvents were evaporated with a Tokyo Rikakikai rotary evaporator type-V at about 50 °C unless otherwise stated.

General Procedure for the Azomethine Ylide Generation from the Condensation of 1—3 with Carbonyl Compounds. An amine (**1**, **2**, or **3**) and an aldehyde were heated under reflux in dry toluene (5 ml for 1 mmol of the amine) in the presence of *N*-(*p*-tolyl)maleimide. The water formed was continuously removed by the aid of a Dean-Stark trap. Equimolar amounts of the amine and *N*-(*p*-tolyl)maleimide were used, while the aldehydes were employed in excess: Benzaldehyde and propanal: 1.5 equivalent. Acetaldehyde and paraformaldehyde: 5 equivalents. The reaction conditions as well as the results are all summarized in Table 1.

4a+5a+6a: This mixture was chromatographed over silica gel with hexane–ethyl acetate (10:1 vol/vol) to give **4a** (63%), **5a** (21%), and then **6a** (7%). **4a**: Colorless needles (benzene–hexane); mp 151—152 °C; IR (KBr) 1720 and 1700 cm^{-1}; ^{1}H NMR ($CDCl_3$) δ=1.35 (3H, t, COOEt), 2.28 2.32 (each 3H, s, NMe and *p*-Me), 3.47 (1H, dd, J=8.0 and 0.8 Hz, 3a-H), 3.75 (1H, dd, J=9.4 and 8.0 Hz, 6a-H), 4.25 (2H, q, COOEt), 4.40 (1H, br s, 4-H), 4.49 (1H, d, J=9.4 Hz, 6-H), and 6.8—7.4 (9H, m, Ar); ^{13}C NMR ($CDCl_3$) δ=14.47 (q, COOEt), 21.18 (q, *p*-Me), 35.56 (q, NMe), 48.65 (d, 3a-C), 50.42 (d, 6a-C), 61.00 (t, COOEt), 67.53 (d, 4-C), 69.06 (d, 6-C), 128.00 128.10, 128.54, 128.77, 129.83 (each d), 129.48, 137.19, 138.54 (each s), 171.01 (s, COOEt), 174.84, and 176.54 (each s, CON); MS *m/z* (rel intensity, %) 393 (M^+, 1), 320 (25), 319 (base peak), and 158 (42). Found: C, 70.42; H, 6.20; N, 7.03%. Calcd for $C_{23}H_{24}N_2O_4$: C, 70.37; H, 6.17; N, 7.13%. **5a**: Pale yellow liquid; IR (neat) 1780 and 1700 cm^{-1}; ^{1}H NMR ($CDCl_3$) δ=1.27 (3H, t, COOEt), 2.16, 2.26 (each 3H, s, NMe and *p*-Me), 3.41 (1H, dd, J=9.7 and 5.7 Hz, 6a-H), 3.85 (1H, dd, J=9.7 and 8.8 Hz, 3a-H), 4.17 (2H, q, COOEt), 4.27 (1H, d, J=8.8 Hz, 4-H), 4.37 (1H, d, J=5.7 Hz, 6-H), and 7.0—7.4 (9H, m, Ar); ^{13}C NMR ($CDCl_3$) δ=14.30 (q, COOEt), 21.24 (q, *p*-Me), 35.06 (q, NMe), 46.94 (d, 3a-C), 53.47 (d, 6a-C), 61.29 (t, COOEt), 67.48 (d, 4-C), 69.12 (d, 6-C), 126.69, 127.90, 128.38, 129.01, 129.95 (each d), 129.60, 138.89, 139.89 (each s), 174.01, 175.59, and 176.36 (each s, COOEt and CON); MS *m/z* (rel intensity, %) 393 (M^+, 1), 320 (23), 319 (base peak), 158 (21), 143 (6), and 42 (5). Found: C, 70.57; H, 6.24; N, 7.12%. Calcd for $C_{23}H_{24}N_2O_4$: C, 70.39; H, 6.16; N, 7.14%. **6a**: Colorless needles (benzene–hexane); mp 179—180.5 °C; IR (KBr) 1730 and 1700 cm^{-1}; ^{1}H NMR ($CDCl_3$) δ=1.34 (3H, t, COOEt), 2.25, 2.31 (each 3H, s, NMe and *p*-Me), 3.42 (1H, d, J=7.0 Hz, 4-H), 3.52 (1H, dd, J=8.8 and 7.5 Hz, 6a-H), 3.68 (1H, dd, J=7.5 and 7.0 Hz, 3a-H), 3.74 (1H, d, J=8.8 Hz, 6-H), 4.32 (2H, dq, COOEt), and 6.9—7.4 (9H, m, Ar); MS *m/z* (rel intensity, %) 393 (M^+, 1), 320 (25), 319 (base peak), 160 (6), 158 (23), 143 (7), and 42 (5). Found: C, 70.12; H, 6.16; N, 7.04%. Calcd for $C_{23}H_{24}N_2O_4$: C, 70.37; H, 6.17; N, 7.13%.

4b+5b+10: This mixture was separated into **4b** (37%), **5b** (11%), and **10** (18%) through column chromatography over silica gel by using hexane–ethyl acetate (10:1 vol/vol). **4b**: Pale yellow liquid; IR (neat) 1780, 1730, and 1710 cm^{-1}; ^{1}H NMR ($CDCl_3$) δ=1.03 (3H, t, Et), 1.26 (3H, t, COOEt), 1.4—1.8 (2H, m, Et), 2.34 (6H, s, NMe and *p*-Me), 3.20 (1H,

m, 6-H), 3.38 (1H, dd, J=8.0 and 0.5 Hz, 3a-H), 3.42 (1H, dd, J=8.0 and 6.5 Hz, 6a-H), 3.99 (1H, d, J=0.5 Hz, 4-H), 4.15 (2H, q, COOEt), 7.04, and 7.25 (each 2H, d, J=8.0 Hz, Ar); ^{13}C NMR ($CDCl_3$) δ=10.59 (q, Et), 14.41 (q, COOEt), 21.18 (q, p-Me), 22.18 (t, Et), 35.41 (q, NMe), 47.18, 47.36 (each d, 3a- and 6a-C), 60.89 (t, COOEt), 65.83 (d, 4-C), 68.30 (d, 6-C), 126.42, 129.90 (each d), 129.60, 138.77 (each s), 170.66 (s, COOEt), 176.01, and 177.01 (each s, CON); MS m/z (rel intensity, %) 344 (M^+, 5), 272 (20), and 271 (base peak). Found: C, 66.15; H, 6.95; N, 8.04%. Calcd for $C_{19}H_{24}N_2O_4$: C, 66.24; H, 7.04; N, 8.13%. **5b**: Pale yellow liquid; IR (neat) 1755 and 1715 cm^{-1}; ^{1}H NMR ($CDCl_3$) δ=1.15 (3H, t, Et), 1.30 (3H, t, COOEt), 1.6—1.8 (2H, m, Et), 2.28, 2.32 (each 3H, s, NMe and p-Me), 3.1—3.6, 3.9—4.2 (3H+1H, m, 3a-, 4-, 6-, and 6a-H), 4.25 (2H, q, COOEt), and 7.0—7.3 (4H, m, Ar); MS m/z (rel intensity, %) 344 (M^+, 2) and 271 (base peak). HRMS Found: m/z 344.1721. Calcd for $C_{19}H_{24}N_2O_4$: M, 344.1734. **10**: Pale yellow grains (benzene–hexane) mp 109—110 °C; IR (KBr) 1763 and 1700 cm^{-1}; ^{1}H NMR ($CDCl_3$) δ=0.88 (3H, d, J=6.9 Hz, 7-Me), 1.91 (3H, s, 5-Me), 2.36 (3H, s, p-Me), 3.8—4.1 (1H, m, 7-H), 4.69 (1H, dd, J=8.7 and 3.0 Hz, 7a-H), 5.8—6.0 (1H, m, 6-H), 6.8—6.9 (1H, m, 4-H), and 7.1—7.3 (4H, m, Ar); MS m/z (rel intensity, %) 267 (M^+, base peak), 134 (77), 133 (26) 119 (59), 106 (36), and 91 (49). Found: C, 76.42; H, 6.43; N, 5.28%. Calcd for $C_{17}H_{17}NO_2$: C, 76.38; H, 6.41; N, 5.24%.

8+9+11: This mixture was separated into **8** (58%), **9** (18%), and **11** (11%) through column chromatography over silica gel with hexane–ethyl acetate (10:1 vol/vol). **8**: Pale yellow liquid; IR (neat)1780, 1732, and 1712 cm^{-1}; ^{1}H NMR ($CDCl_3$) δ=1.26 (3H, t, COOEt), 1.70 (3H, d, 1-propenyl), 2.24, 2.35 (each 3H, s, NMe and p-Me), 3.3—3.6, 3.6—3.9 (2H+1H, m, 3a-, 6-, and 6a-H), 4.03 (1H, s, 4-H), 4.16 (2H, q, COOEt), 4.9—5.3, 5.6—5.9 (each 1H, m, 1-propenyl), 7.04, and 7.26 (each 2H, d, Ar); ^{13}C NMR ($CDCl_3$) δ=13.94 (q, COOEt), 17.30 (q, 1-propenyl), 20.65 (q, p-Me), 34.59 (q, NMe), 47.53, 48.42 (each d, 3a- and 6a-C), 60.24 (t, COOEt), 66.42, 67.01 (each d, 4- and 6-C), 125.94, 128.07, 129.30, 130.54 (each d), 129.30, 137.95 (each s), 170.13 (s, COOEt), 174.83, and 176.25 (each s, CON); MS m/z (rel intensity, %) 356 (M^+, 11), 284 (20), 283 (base peak), and 122 (47). HRMS Found: m/z 356.1743. Calcd for $C_{20}H_{24}N_2O_4$: M, 356.1735. **9**: Pale yellow liquid; IR (neat) 1780, 1740, and 1714 cm^{-1}; ^{1}H NMR ($CDCl_3$) δ=1.24 (3H, t, COOEt), 1.74 (3H, d, 1-propenyl), 2.23, 2.32 (each 3H, s, NMe and p-Me), 3.1—4.0 (4H, m, 3a-, 4-, 6-, and 6a-H), 4.16 (2H, q, COOEt), 5.2—5.6, 5.6—6.0 (each 1H, m, 1-propenyl), and 7.1—7.3 (4H, m, Ar); ^{13}C NMR ($CDCl_3$) δ=14.18 (q, COOEt), 17.82 (q, 1-propenyl), 21.18 (q, p-Me), 35.00 (q, NMe), 46.89, 50.71 (each d, 3a- and 6a-C), 61.18 (t, COOEt), 67.01, 67.89 (each d, 4-and 6-C), 126.48, 126.60, 128.48, 129.83 (each d), 129.60, 138.66 (each s), 170.48 (s, COOEt), 175.71, and 176.48 (each s, CON); MS m/z (rel intensity, %) 356 (M^+, 6), 284 (20), 283 (base peak), and 122 (26). HRMS Found: m/z 356.1733. Calcd for $C_{20}H_{24}N_2O_4$: M, 356.1734. **11**: Colorless prisms (benzene–hexane); mp 158—160 °C; IR (KBr) 1765 and 1710 cm^{-1}; ^{1}H NMR ($CDCl_3$) δ=2.36 (3H, s, p-Me), 2.2—2.6, 2.6—3.1, 3.4—3.8 (each 1H, m, 7- and 7a-H), 6.2—6.4, 6.9—7.1 (2H+1H, m, 4-, 5-, and 6-H), and 7.22 (4H, m, Ar); MS m/z (rel intensity, %) 239 (M^+, 19), 132 (22), 106 (77), 105 (95), 78 (base peak), 77 (74), 52 (30), and 51 (35). HRMS Found: m/z 239.0951. Calcd for $C_{15}H_{13}NO_2$: M, 239.0946.

4c+5c: This mixture was separated into **4c** (58%) and **5c** (35%) through column chromatography over silica gel with hexane–ethyl acetate (5:1 vol/vol). **4c**: Colorless needles (benzene–hexane); mp 120—121 °C; IR (KBr) 1724 and 1711 cm^{-1}; ^{1}H NMR ($CDCl_3$) δ=1.29 (3H, t, COOEt), 2.35, 2.39 (each 3H, s, NMe and p-Me), 3.1—3.3, 3.4—3.6 (each 2H, m, 3a-, 6-, and 6a-H), 3.97 (1H, s, 4-H), 4.20 (2H, q, COOEt), and 7.0—7.3 (4H, m, Ar); ^{13}C NMR ($CDCl_3$) δ=14.35 (q, COOEt), 21.06 (q, p-Me), 36.89 (q, NMe), 44.71 (d, 6a-C), 49.00 (d, 3a-C), 55.65 (t, 6-C), 60.83 (t, COOEt), 67.77 (d, 4-C), 126.36, 129.77 (each d), 129.77, 138.60 (each s), 170.19 (s, COOEt), 176.83, and 178.30 (each s, CON); MS m/z (rel intensity, %) 316 (M^+, 3), 243 (base peak), and 82 (43). Found: C, 64.54; H, 6.46; N, 8.76%. Calcd for $C_{17}H_{20}N_2O_4$: C, 64.54; H, 6.37; N, 8.86%. **5c**: Colorless needles (benzene–hexane); mp 106—108 °C; IR (KBr) 1776, 1747, and 1707 cm^{-1}; ^{1}H NMR ($CDCl_3$) δ=1.30 (3H, t, COOEt), 2.34 (6H, s, NMe and p-Me), 2.58 (1H, dd, J=9.5 and 7.5 Hz, one of 6-H), 3.21 (1H, d, J=8.0 Hz, 4-H), 3.33 (1H, ddd, J=8.0, 7.5, and 1.0 Hz, 6a-H), 3.54 (1H, dd, J=9.5 and 1.0 Hz, the other of 6-H), 3.61 (1H, t, J=8.0 Hz, 3a-H), 4.24 (2H, q, COOEt), and 7.1—7.3 (4H, m, Ar); ^{13}C NMR ($CDCl_3$) δ=14.06 (q, COOEt), 21.06 (q, p-Me), 39.83 (q, NMe), 43.83 (d, 6a-C), 47.83 (d, 3a-C), 57.83 (t, 6-C), 61.24 (t, COOEt), 70.18 (d, 4-C), 126.54, 129.60 (each d), 129.71, 138.66 (each s), 169.42 (s, COOEt), 175.48, and 177.66 (each s, CON); MS m/z (rel intensity, %) 316 (M^+, 2), 243 (base peak), and 82 (59). Found: C, 64.39; H, 6.43; N, 8.78%. Calcd for $C_{17}H_{24}N_2O_4$: C, 64.54; H, 6.37; N, 8.86%.

4d+5d: This mixture was chromatographed over silica gel with hexane–ethyl acetate (5:1 vol/vol) to afford **4d** (35%) and then **5d** (42%). **4d**: Colorless prisms (benzene–hexane); mp 203—205 °C; IR (KBr) 1780, 1730, and 1715 cm^{-1}; ^{1}H NMR ($CDCl_3$) δ=2.28 (3H, s, p-Me), 3.61 (1H, dd, J=8.1 and 0.8 Hz, 3a-H), 3.68 (3H, s, COOMe), 4.04 (1H, dd, J=10.0 and 8.1 Hz, 6a-H), 5.43 (1H, d, J=0.8 Hz, 4-H), 5.48 (1H, d, J=10.0 Hz, 6-H), 6.5—6.8 (5H, m, Ar), and 7.0—7.3 (9H, m, Ar); ^{13}C NMR ($CDCl_3$) δ=20.53 (q, p-Me), 49.42 (d, 3a- and 6a-C), 52.24 (q, COOMe), 63.18 (d, 4-C), 64.48 (d, 6-C), 116.08, 118.82, 126.06, 127.78, 128.60, 128.87, 129.23 (each d), 137.91, 138.17, 145.02 (each s), 172.03 (s, COOMe), 173.47, and 175.71 (each s, CON); MS m/z (rel intensity, %) 440 (M^+, 28), 382 (27), 381 (base peak), and 220 (31). Found: C, 73.87; H, 5.64; N, 6.29%. Calcd for $C_{27}H_{24}N_2O_4$: C, 73.62, H, 5.49; N, 6.36%. **5d**: Colorless needles (benzene–hexane); mp 189—190 °C; IR (KBr) 1730 and 1710 cm^{-1}; ^{1}H NMR ($CDCl_3$) δ=2.36 (3H, s, p-Me), 3.54 (1H, dd, J=9.9 and 3.7 Hz, 6a-H), 3.56 (3H, s, COOMe), 4.06 (1H, t, J=9.9 Hz, 3a-H), 5.26 (1H, d, J=9.9 Hz, 4-H), 5.53 (1H, d, J=3.7 Hz, 6-H), 6.5—6.8, and 7.0—7.4 (14H, m, Ar); ^{13}C NMR ($CDCl_3$) δ=20.71 (q, p-Me), 46.30 (d, 3a-C), 52.12 (q, COOMe), 54.53 (d, 6a-C), 64.36 (d, 4- and 6-C), 116.01, 118.89, 126.48, 126.65, 127.60, 129.01, 129.66 (each d), 138.36, 142.36, 144.77 (each s), 171.95 (s, COOMe), 174.77, and 176.42 (each d, CON); MS m/z (rel intensity, %) 440 (M^+, 22), 382 (29), 381 (base peak), and 220 (28). Found: C, 73.39; H, 5.61; N, 6.31%. Calcd for $C_{27}H_{24}N_2O_4$: C, 73.62; H, 5.49; N, 6.36%.

4e+5e: This mixture was separated into **4e** (30%) and **5e** (34%) through column chromatography over silica gel by using hexane–ethyl acetate (10:1 vol/vol). **4e**: Colorless needles (benzene–hexane); mp 150—152 °C; IR (KBr) 1790, 1741, and 1713 cm^{-1}; ^{1}H NMR ($CDCl_3$) δ=1.02 (3H, t, 6-Et), 1.2—1.5, 1.7—2.1 (each 1H, m, 6-Et), 2.36 (3H, s, p-Me), 3.50 (3H, s, COOMe), 3.52 (1H, dd, J=8.2 and 0.9 Hz, 3a-H), 3.79

(1H, dd, J=9.1 and 8.2 Hz, 6a-H), 4.26 (1H, dt, J=9.1, 9.1, and 1.7 Hz, 6-H), 4.96 (1H, d, J=0.9 Hz, 4-H), and 6.8—7.4 (9H, m, Ar); ^{13}C NMR ($CDCl_3$) δ=10.29 (q, 6-Et), 21.24 (q, p-Me), 22.53 (t, 6-Et), 47.12, 48.47 (each d, 3a- and 6a-C), 51.83 (q, COOMe), 61.77 (d, 4-C), 67.48 (d, 6-C), 121.12, 122.60, 126.36, 129.19, 130.01 (each d), 128.54, 139.01, 145.24 (each s), 171.48 (s, COOMe), 175.54, and 176.13 (each s, CON); MS m/z (rel intensity, %) 392 (M^+, 24), 334 (24), 333 (base peak), and 172 (26). Found: C, 70.47; H, 6.14; N, 7.12%. Calcd for $C_{23}H_{24}N_2O_4$: C, 70.39; H, 6.16; N, 7.14%. **5e**: Colorless prisms (benzene–hexane); mp 161.5—162.5 °C; IR (KBr) 1778, 1743, and 1714 cm^{-1}; ^{1}H NMR ($CDCl_3$) δ=0.95 (3H, t, 6-Et), 1.2—1.9 (2H, m, 6-Et), 2.36 (3H, s, p-Me), 3.37 (1H, dd, J=8.8 and 1.9 Hz, 6a-H), 3.61 (3H, s, COOMe), 3.88 (1H, dd, J=9.5 and 8.8 Hz, 3a-H), 4.56 (1H, ddd, J=9.0, 3.0, and 1.9 Hz, 6-H), 4.69 (1H, d, J=9.5 Hz, 4-H), and 6.6—7.3 (9H, m, Ar); ^{13}C NMR ($CDCl_3$) δ=9.79 (q, 6-Et), 21.12 (q, p-Me), 23.30 (t, 6-Et), 46.89, 49.24 (each d, 3a- and 6a-C), 52.47 (q, COOMe), 63.83, 63.95 (each d, 4- and 6-C), 117.01, 120.07, 126.60, 129.48, 129.95 (each d), 138.89, 145.07 (each s), 171.07 (s, COOMe), 175.54, and 177.07 (each s, CON); MS m/z (rel intensity, %) 392 (M^+, 16), 334 (25), 333 (base peak), 172 (56), 144 (21), 143 (22), and 76 (22). Found: C, 70.31; H, 6.22; N, 7.00%. Calcd for $C_{20}H_{24}N_2O_4$: C, 70.39; H, 6.10; N, 7.14%.

4f+5f: (a 1:1 mixture (^{1}H NMR)): Chromatographic separation of this mixture (silica gel, hexane–ethyl acetate (5:1 vol/vol)) was unsuccessful. **4f+5f**: Colorless solid; IR (KBr) 1780, 1741, and 1714 cm^{-1}; ^{1}H NMR ($CDCl_3$) δ=2.35 (3H, s, p-Me), 3.64, 3.68 (each 1/2×3H, s, COOMe), 3.7—4.2 (4H, m, 3a-, 6-, and 6a-H), 4.74 (1/2H, d, J=9.0 Hz, 4-H), 5.00 (1/2H, s, 4-H), and 6.6—7.4 (18H, m, Ar); ^{13}C NMR ($CDCl_3$) δ=21.18 (q, p-Me), 43.47, 44.24 (d, 6a-C), 47.77, 49.12 (d, 3a-C), 50.65, 50.83 (each t, 6-C), 52.53, 52.36 (each q, COOMe), 62.95, 63.36 (each d, 4-C), 114.48, 119.54, 119.66, 126.30, 126.48, 129.19, 129.30, 129.56, 129.95 (each d), 139.13, 145.78, 146.07 (each s), 171.60, 175.01, 176.01, 176.83, and 177.60 (each s, COOMe and CON); MS m/z (rel intensity, %) 364 (M^+, 18), 306 (18), 305 (80), 144 (base peak), and 77 (26). Only **5f** was separated by crystallization from benzene–hexane. **5f**: Colorless needles (benzene–hexane); mp 170—172 °C; IR (KBr) 1785, 1738, and 1714 cm^{-1}; ^{1}H NMR ($CDCl_3$) δ=2.36 (3H, s, p-Me), 3.64 (3H, s, COOMe), 3.7—4.2 (4H, m, 3a-, 6-, and 6a-H), 4.74 (1H, d, J=9.0 Hz, 4-H), and 6.6—7.4 (9H, m, Ar); MS m/z (rel intensity, %) 364 (M^+, 25), 306 (21), 305 (base peak), 144 (44), 85 (24), 83 (32), and 43 (26). Found: C, 68.97; H, 5.55; N, 7.68%. Calcd for $C_{21}H_{20}N_2O_4$: C, 69.21; H, 5.53; N, 7.69%.

4g+5g+6g+7g: This mixture was chromatographed over silica gel with hexane–ethyl acetate whose ratio was gradually changed from 10:1 vol/vol to 1:1 to afford **4g** (12%), **5g** (12%), **6g** (16%), and then **7g** (9%). **4g**: Colorless needles (benzene–hexane); mp 194—195 °C; IR (KBr) 1700 cm^{-1}; ^{1}H NMR ($CDCl_3$) δ=2.31, 2.32 (each 3H, s, NMe and p-Me), 3.4—3.6, 4.0—4.1 (2H+1H, 3a-, 6-, and 6a-H), 4.60 (1H, s, 4-H), and (9H, m, Ar); ^{13}C NMR ($CDCl_3$) δ=21.18 (q, p-Me), 36.24 (q, NMe), 48.83, 49.08 (each d, 3a- and 6a-C), 57.83 (d, 4-C), 69.95 (d, 6-C), 115.12 (s, CN), 125.20, 127.95, 128.95, 129.94 (each d), 135.07, 138.89 (each s), 173.43, and 174.71 (each s, CON); MS m/z (rel intensity, %) 345 (M^+, 63), 158 (83), 157 (base peak), and 118 (22). Found: C, 72.95; H, 5.56; N, 12.20%. Calcd for $C_{21}H_{19}N_3O_2$: C, 73.02; H, 5.56; N, 12.17%. **5g**: Pale yellow liquid; IR (neat) 1780 and 1710 cm^{-1}; ^{1}H NMR ($CDCl_3$) δ=2.30, 2.36 (each 3H, NMe and p-Me), 3.41 (1H, dd, J=9.4 and 6.7 Hz, 6a-H), 3.85 (1H, dd, J=6.7 and 1.0 Hz, 6-H), 3.88 (1H, dd, J=9.4 and 8.3 Hz, 3a-H), 4.58 (1H, dd, J=8.3 and 1.0 Hz, 4-H), and 7.0—7.4 (9H, m, Ar); ^{13}C NMR ($CDCl_3$) δ=21.17 (q, p-Me), 35.94 (q, NMe), 47.00 (d, 3a-C), 53.06 (d, 6a-C), 58.06 (d, 4-C), 69.78 (d, 6-C), 114.00 (s, CN), 126.65, 127.72, 128.73, 129.19, 130.07 (each d), 128.89, 138.48, 139.24 (each s), 173.25, and 175.13 (each s, CON); MS m/z (rel intensity, %) 345 (M^+, 84), 160 (76), 158 (91), 157 (base peak), and 107 (48). Found: C, 72.80; H, 5.96; N, 11.29%. Calcd for $C_{21}H_{19}N_3O_2$: C, 73.02; H, 5.56; N, 12.17%. **6g**: Colorless needles (benzene–hexane); mp 189—190 °C; IR (KBr) 1700 cm^{-1}; ^{1}H NMR ($CDCl_3$) δ=2.32, 2.37 (each 3H, s, NMe and p-Me), 3.4—3.8 (4H, m, 3a-, 4-, 6-, and 6a-H), and 7.0—7.4 (9H, m, Ar); MS m/z (rel intensity, %) 345 (M^+, 68), 158 (base peak), and 157 (90). Found: C, 72.79; H, 5.56; N, 12.14%. Calcd for $C_{21}H_{19}N_3O_2$: C, 73.02; H, 5.56; N, 12.17%. **7g**: Colorless needles (benzene–hexane); mp 195—196.5 °C; IR (KBr) 1700 cm^{-1}; ^{1}H NMR ($CDCl_3$) δ=2.33, 2.38 (each 3H, s, NMe and p-Me), 3.47 (1H, dd, J=9.0 and 6.9 Hz, 6a-H), 3.68 (1H, d, J=6.9 Hz, 6-H), 3.70 (1H, d, J=6.2 Hz, 4-H), 3.90 (1H, dd, J=9.0 and 6.2 Hz, 3a-H), and 7.0—7.4 (9H, m, Ar); MS m/z (rel intensity, %) 345 (M^+, 30), 158 (52), 157 (base peak), 116 (53), 115 (60), and 107 (88). Found: C, 73.26; H, 5.61; N, 12.03%. Calcd for $C_{21}H_{19}N_3O_2$: C, 73.02; H, 5.56; N, 12.17%.

Generation of Azomethine Ylide A (R=Ph, R^1=Me, EWG=COOEt) from 1 and Benzaldehyde, and Ylide Trapping with Dimethyl Maleate or Fumarate Leading to 12—15. A mixture of **1** (0.22 g, 1.66 mmol), benzaldehyde (0.24 g, 2.26 mmol), and dimethyl maleate or fumarate (0.24 g, 1.66 mmol) in dry toluene (15 ml) was heated under reflux under the reaction conditions listed in Table 2. The water formed was removed by the aid of a Dean–Stark trap. The solvent was evaporated in vacuo and the residue was chromatographed over silica gel. Elution of the maleate mixture with hexane–ethyl acetate (10:1 vol/vol) afforded **12** (0.368 g, 62%). Elution of the fumarate mixture (**13**:**14**:**15**= 3:3:2 (^{1}H NMR)) with hexane–ethyl acetate (20:1 vol/vol) gave **15** (0.194 g, 33%) and then **13+14** (0.323 g, 54%, **13**:**14**=1:1 (^{1}H NMR)).

12: Colorless needles (benzene–hexane); mp 93—94 °C; IR (KBr) 1740 and 1722 cm^{-1}; ^{1}H NMR ($CDCl_3$) δ=1.31 (3H, t, COOEt), 2.20 (3H, s, NMe), 3.17 (3H, s, 4-COOMe), 3.64 (3H, s, 3-COOMe), 3.5—3.7, 4.1—4.5 (2H+3H, m, 2-, 3-, 4-H, and COOEt), 4.60 (1H, d, J=6.5 Hz, 5-H), and 7.24 (5H, s, Ph); ^{13}C NMR ($CDCl_3$) δ=14.35 (q, COOEt), 34.53 (q, NMe), 48.77 (d, 3-C), 51.24, 53.18 (each q, COOMe), 52.12 (d, 4-C), 61.00 (t, COOEt), 65.71 (d, 2-C), 70.83 (d, 5-C), 127.83, 128.18, 128.42, 128.72 (each d), 137.71 (s), 171.31, and 173.43 (each s, COOMe and COOEt); MS m/z (rel intensity, %) 349 (M^+, 11) and 276 (base peak). Found: C, 61.81; H, 6.63; N, 4.13%. Calcd for $C_{18}H_{23}NO_6$: C, 61.88; H, 6.64; N, 4.01%.

13+14: Colorless viscous liquid; IR (neat) 1725 cm^{-1}; ^{1}H NMR ($CDCl_3$) δ=1.30, 1.31 (each 1/2×3H, t, COOEt), 2.16, 2.20 (each 1/2×3H, s, NMe), 3.03 (1/2×3H, s, 4-COOMe of **13**), 3.4—3.7 (1H, m, CH), 3.65 (3H, s, COOMe), 3.77 (1/2×3H, s, COOMe), 3.9—4.4 (3H, m, CH), 4.24, 4.25 (each 1/2×2H, COOEt), and 7.2—7.4 (5H, m, Ph); ^{13}C NMR ($CDCl_3$) δ=14.41 (q, COOEt), 34.88, 35.71 (each q, NMe), 47.77, 48.77 (each d, 3-C), 51.18, 51.47, 52.24, 52.77 (each q, COOMe), 54.65 (d, 4-C), 60.65, 60.89 (each t, COOEt), 67.65, 68.42 (each d, 2-C), 69.18, 70.01 (each d, 5-C), 128.18, 128.72

(each d), 141.24 (s), 171.48, 171.78, 172.36, and 172.95 (each s, COOMe and COOEt); MS *m/z* (rel intensity, %) 349 (M^+, 16), 276 (base peak), 244 (63), 216 (54), and 184 (22). HRMS Found: *m/z* 349.1593. Calcd for $C_{18}H_{23}NO_6$: M, 349.1524.

15: Colorless liquid; IR (neat) 1725 cm^{-1}; ^1H NMR ($CDCl_3$) δ=1.29 (3H, t, COOEt), 2.24 (3H, s, NMe), 3.3—4.0 (4H, m, 2-, 3-, 4-, and 5-H), 3.59, 3.66 (each 3H, s, COOMe), 4.20 (2H, q, COOEt), and 7.2—7.4 (5H, m, Ph); ^{13}C NMR ($CDCl_3$) δ=14.24 (q, COOEt), 39.36 (q, NMe), 48.53 (d, 3-C), 52.18, 52.18 (each q, COOMe), 54.12 (d, 4-C), 61.12 (t, COOEt), 68.71 (d, 2-C), 74.01 (d, 5-C), 128.01, 128.36, 128.72 (each d), 139.83 (s), 171.01, 171.36, and 172.95 (each s, COOEt and COOMe); MS *m/z* (rel intensity, %) 349 (M^+, 9), 276 (base peak), 244 (65), 216 (73), 184 (30), and 158 (25). HRMS Found: *m/z* 349.1519. Calcd for $C_{18}H_{23}NO_6$: M, 349.1524.

Capture of the Ester-Stabilized Azomethine Ylides A (R=Ph, EWG=COOR[2]) with Methyl Acrylate or (*E*)-β-Nitrostyrene Leading to 16. An identical procedure was applied to a mixture of **1** or **2** (0.93 mmol), benzaldehyde (1.32 mmol, 1.5 equiv), and methyl acrylate (4.67 mmol, 5 equiv) in dry toluene (10 ml) or a mixture of **1** or **2** (0.94 mmol), benzaldehyde (0.94 mmol), and (*E*)-β-nitrostyrene (0.87 mmol) in toluene (8 ml). When **2**·HCl was used, and equimolar amount of *N,N*-diisopropylethylamine was added to the mixture. The reaction conditions as well as the results are summarized in Table 2. Products were purified through column chromatography over silica gel with hexane–ethyl acetate (10:1 vol/vol).

16a: Colorless liquid; IR (neat) 1730 cm^{-1}; ^1H NMR ($CDCl_3$) δ=1.30 (3H, t, COOEt), 2.04 (1H, ddd, *J*=13.1, 8.7, and 1.7 Hz, one of 3-H), 2.26 (3H, s, NMe), 2.72 (1H, ddd, *J*=13.1, 9.0, and 8.0 Hz, the other of 3-H), 3.04 (3H, s, COOMe), 3.62 (1H, ddd, *J*=10.0, 9.0, and 8.7 Hz, 4-H), 3.97 (1H, dd, *J*=8.0 and 1.7 Hz, 2-H), 4.18 (2H, q, COOEt), 4.38 (1H, d, *J*=10.0 Hz, 5-H), and 7.22 (5H, s, Ph); ^{13}C NMR ($CDCl_3$) δ=14.47 (q, COOEt), 30.59 (t, 3-C), 35.47 (q, NMe), 48.89 (d, 4-C), 51.06 (q, COOMe), 60.30 (t, COOEt), 65.77 (d, 2-C), 69.36 (d, 5-C), 127.66, 128.01, 128.54 (each d), 139.89 (s), 173.01, and 173.71 (each s, COOEt and COOMe); MS *m/z* (rel intensity, %) 291 (M^+, 5), 219 (15), 218 (base peak), and 158 (15). Found: C, 66.16; H, 7.26; N, 4.96%. Calcd for $C_{16}H_{21}NO_4$: C. 65.94; H, 7.28; N, 4.81%.

16b: Colorless viscous liquid; IR (neat) 1720, 1540, and 1365 cm^{-1}; ^1H NMR ($CDCl_3$) δ=0.94 (3H, t, COOEt), 2.30 (3H, s, NMe), 3.92 (2H, q, COOEt), 4.30 (1H, d, *J*=7.3 Hz, 2-H), 4.70 (1H, dd, *J*=10.0 and 7.3 Hz, 3-H), 4.88 (1H, d, *J*=10.0 Hz, 5-H), 6.03 (1H, t, *J*=10.0 Hz, 4-H), and 7.2—7.4 (10H, m, Ph); ^{13}C NMR ($CDCl_3$) δ=13.88 (q, COOEt), 35.77 (q, NMe), 49.53 (d, 2-C), 60.48 (t, COOEt), 69.95 (d, 3-C), 70.95 (d, 5-C), 91.95 (d, 4-C), 127.66, 128.06, 128.36, 128.65, 128.89 (each d), 134.36, 139.89 (s), 171.31 (s, COOEt); MS *m/z* (rel intensity, %) 354 (M^+, 1), 308 (14), 281 (38), 235 (22), 234 (base peak), 115 (17), and 91 (20). Found: C, 67.89; H, 6.30; N, 7.98%. Calcd for $C_{20}H_{22}N_2O_4$: C, 67.78; H, 6.27; N, 7.91%.

16c: Colorless needles (benzene–hexane); mp 174—176 °C; IR (KBr) 1730 cm^{-1}; ^1H NMR ($CDCl_3$) δ=2.16 (1H, ddd, *J*=13.5, 6.8, and 0.8 Hz, one of 3-H), 2.88 (1H, dt, *J*=13.5, 13.5, and 9.0 Hz, the other of 3-H), 3.36 (3H, s, 4-COOMe), 3.72 (3H, s, 2-COOMe), 3.90 (1H, ddd, *J*=13.5, 9.0, and 6.8 Hz, 4-H), 4.73 (1H, dd, *J*=9.0 and 0.8 Hz, 2-H), 5.26 (1H, d, *J*=9.0 Hz, 5-H), and 6.3—7.2 (10H, m, Ph); MS *m/z* (rel intensity, %) 339 (M^+, 28), 281 (17), 280 (base peak), 220 (16), and 77 (15). Found: C, 70.77; H, 6.26; N, 4.29%. Calcd for $C_{20}H_{21}NO_4$: C, 70.78; H, 6.24; N, 4.13%.

16d: Colorless needles (benzene–hexane); mp 205—207 °C; IR (KBr) 1730, 1550, and 1360 cm^{-1}; ^1H NMR ($CDCl_3$) δ=3.33 (3H, s, COOMe), 4.70 (1H, dd, *J*=11.8 and 8.6 Hz, 3-H), 5.04 (1H, d, *J*=8.6 Hz, 2-H), 5.64 (1H, d, *J*=9.2 Hz, 5-H), 6.28 (1H, dd, *J*=11.8 and 9.2 Hz, 4-H), and 6.4—7.3 (15H, m, Ph); MS *m/z* (rel intensity, %) 402 (M^+, 44), 356 (23), 343 (29), 297 (25), 296 (base peak), 115 (15), 104 (21), and 77 (23). Found: C, 71.52; H, 5.60; N, 7.06%. Calcd for $C_{24}H_{22}N_2O_4$: C, 71.62; H, 5.51; N, 6.96%.

Capture of the Ester-Stabilized Azomethine Ylide A (R=H, R[1]=Me, EWG=COOEt) with Unsymmetrically Substituted Olefins Leading to 17. A similar procedure employing **1** (2 mmol), paraformaldehyde (10 mmol, 5 equiv), and an olefin (methyl acrylate and styrene: 3 mmol, 1.5 equiv phenyl vinyl sulfone: 2 mmol, 1 equiv) afforded **17**. The reaction conditions and results are listed in Table 2. Purification of the products was carried out through column chromatography over silica gel with the following eluents: **17a** and **17c**: hexane–ethyl acetate (10:1 vol/vol), **17b**: hexane–ethyl acetate (1:1 vol/vol).

17a (a 6:5 mixture of 2,3- and 2,4-diesters (^1H NMR)): Pale yellow liquid; IR (neat) 1740 cm^{-1}; ^1H NMR ($CDCl_3$) δ=1.27 (3H, t, COOEt), 2.40 (5/11×3H, s, NMe), 2.42 (6/11×3H, s, NMe), 2.0—2.7, 3.0—3.5 (each 3H, m, CH_2 and CH), 3.68, 3.70 (3H, each s, COOMe), 4.20, and 4.22 (2H, each, q, COOEt); ^{13}C NMR ($CDCl_3$) 2,3-isomer: δ=14.30 (q, COOEt), 27.83 (t, 4-C), 40.36 (q, NMe), 47.12 (d, 3-C), 51.88 (q, COOMe), 55.77 (t, 5-C), 60.65 (t, COOEt), 70.24 (d, 2-C), 172.07, and 174.19 (each s, COOEt and COOMe). 2,4-isomer: δ=14.30 (q, COOEt), 32.77 (t, 3-C), 40.71 (q, NMe), 41.47 (d, 4-C), 52.06 (q, COOMe), 58.83 (t, 5-C), 60.89 (t, COOEt), 66.83 (d, 2-C), 172.65, and 174.37 (each s, COOEt and COOMe); MS *m/z* (rel intensity, %) 215 (M^+, 4), 156 (11), 142 (base peak), 83 (13), and 82 (42). HRMS Found: *m/z* 215.1146. Calcd for $C_{10}H_{17}NO_4$: M, 215.1157.

17b (a 1:4 mixture of 2,3- and 2,4-isomers (^1H NMR)): Pale yellow liquid; IR (neat) 1741, 1308, and 1149 cm^{-1}; ^1H NMR ($CDCl_3$) δ=1.25 (3H, t, COOEt), 2.39 (3H, s, NMe), 2.0—3.5, 3.6—4.1 (5H+1H, m, CH_2 and CH), 4.16 (2H, q, COOEt), 7.4—7.7, and 7.8—8.0 (3H+2H, m, Ph); ^{13}C NMR ($CDCl_3$) 2,3-isomer: δ=13.29 (q, COOEt), 24.71 (t, 4-C), 38.94 (q, NMe), 54.94 (t, 5-C), 59.89 (t, COOEt), 65.71 (d, 3-C), 66.95 (d, 2-C), 127.89, 128.72, 133.24 (each d), 137.36 (s), and 169.66 (s, COOEt). 2,4-isomer: δ=13.29 (q, COOEt), 29.59 (t, 3-C), 38.94 (q, NMe), 54.24 (t, 5-C), 59.89 (t, COOEt), 60.30 (d, 4-C), 65.36 (d, 2-C), 127.60, 128.72, 133.24 (each d), 137.66 (s), and 170.84 (s, COOEt). MS *m/z* (rel intensity, %) 297 (M^+, 3), 224 (84), 82 (41), and 81 (base peak). HRMS Found: *m/z* 297.1034. Calcd for $C_{14}H_{19}NO_4S$: M, 297.1034.

17c (a 1:1 mixture of 2,3-cis and 2,3-trans isomers (GLC)): Pale yellow liquid; IR (neat) 1745 and 1730 cm^{-1}; ^1H NMR ($CDCl_3$) δ=0.78 (3H, t, COOEt), 2.40 (3H, s, NMe), 2.0—2.7, 3.1—4.2 (2H+5H, m, CH_2 and CH), and 7.15 (5H, m, Ph); ^{13}C NMR ($CDCl_3$) δ=13.65, 14.24 (each q, COOEt), 31.94, 32.71 (each t, 4-C), 40.71, 40.83 (each q, NMe), 47.94, 49.65 (each d, 3-C (cis, trans)), 56.12, 55.83 (each t, 5-C), 60.24, 60.77 (each t, COOEt), 73.01, 76.01 (each d, 2-C (cis, trans)), 126.65, 126.95, 127.66, 128.25, 128.65 (each d), 141.48, 143.13 (each s), 171.13, and 172.72 (each s, COOEt); MS *m/z* (rel intensity, %) 233 (M^+, 2), 161 (12), 160 (base peak), and 43

(12). HRMS Found: m/z 233.1395. Calcd for $C_{14}H_{19}NO_2$: M, 233.1415.

Generation of Azomethine Ylides B from Methyl Aminoacetate (18) and Carbonyl Compounds, and Ylide Trapping with *N*-Methylmaleimide Leading to 19—21. A mixture of methyl aminoacetate (**18**) (0.178 g, 2 mmol), *N*-methylmaleimide (0.222 g, 2 mmol), and a carbonyl compound (benzaldehyde, cyclohexanone: 2 mmol in toluene (20 ml); phenylglyoxal: 2 mmol in chloroform (20 ml); 2-methylpropanal: 6 mmol in toluene (20 ml)) was heated under reflux. The reaction time is summarized in Table 2. The solvent was evaporated in vacuo. The residue was chromatographed over silica gel with diethyl ether to give **19—21**.

19a: Colorless prisms (benzene–hexane); mp 215—216 °C; IR (KBr) 3300, 1740, and 1690 cm^{-1}; ^1H NMR ($CDCl_3$) δ=2.41 (1H, br t, NH), 2.85 (3H, s, NMe), 3.40 (1H, dd, J=8.0 and 7.5 Hz, 6a-H), 3.66 (1H, dd, J=7.5 and 6.8 Hz, 3a-H), 3.85 (3H, s, COOMe), 4.04 (1H, dd, J=6.8 and 5.5 Hz, 4-H), 4.47 (1H, dd, J=8.0 and 5.5 Hz, 6-H), 7.30 (5H, br s, Ph); MS m/z (rel intensity, %) 288 (M^+, 23), 229 (86), 177 (79), 144 (59), 117 (base peak), and 115 (21). Found: C, 62.37; H, 5.53; N, 9.54%. Calcd for $C_{15}H_{16}N_2O_4$: C, 62.49; H, 5.59; N, 9.72%.

19b: Colorless prisms (acetonitrile); mp 228—230 °C; IR (KBr) 3310, 1775, 1740, and 1695 cm^{-1}; ^1H NMR ($CDCl_3$) δ=2.67 (3H, s, NMe), 2.92 (1H, t, J=11.0 Hz, NH), 3.68 (1H, dd, J=8.1 and 7.7 Hz, 3a-H), 3.70 (3H, s, COOMe), 3.91 (1H, t, J=7.7 Hz, 6a-H), 4.04 (1H, dd, J=11.0 and 8.1 Hz, 4-H), 4.98 (1H, dd, J=11.0 and 7.7 Hz, 6-H), 7.4—7.8 (3H, m, Ph), and 7.9—8.1 (2H, m, Ph); MS m/z (rel intensity, %) 257 (M^+−59, 8), 211 (base peak), 179 (32), 151 (56), 105 (36), 97 (15), 95 (18), 94 (94), 91 (31), and 76 (50). Found: C, 60.82; H, 5.09; N, 8.87. Calcd for $C_{16}H_{16}N_2O_5$: C, 60.75; H, 5.10; N, 8.86%.

19c: Colorless needles (benzene–hexane); mp 166—167 °C; IR (KBr) 3360, 1750, and 1680 cm^{-1}; ^1H NMR ($CDCl_3$) δ=1.03, 1.20 (each 3H, d, J=6.9 Hz, *i*-Pr), 1.6—2.2 (2H, m, NH and *i*-Pr), 2.80 (1H, dd, J=10.1 and 7.2 Hz, 6a-H), 2.94 (3H, s, NMe), 3.29 (1H, t, J=7.2 Hz, 3a-H), 3.50 (1H, t, J=7.2 Hz, 6-H), 3.81 (3H, s, COOMe), and 3.88 (1H, d, J=7.2 Hz, 4-H); ^{13}C NMR ($CDCl_3$) δ=20.94, 21.06 (each q, *i*-Pr), 25.12 (q, NMe), 29.36 (d, *i*-Pr), 47.47, 49.18 (each d, 3a- and 6a-C), 52.42 (q, COOMe), 62.59 (d, 6-C), 69.18 (d, 4-C), 170.71 (s, COOMe), 175.78, and 176.13 (each s, CON); MS m/z (rel intensity, %) 254 (M^+, 3), 211 (base peak), 195 (45), 179 (32), 151 (55), 110 (31), 94 (60), 68 (32), 67 (36), 40 (36), and 38 (28). Found: C, 56.65; H, 7.07; N, 10.87%. Calcd for $C_{12}H_{18}N_2O_4$: C, 56.68; H, 7.13; N, 11.02%.

20: A mixture of **18** (0.178 g, 2 mmol) and benzaldehyde (0.212 g, 2 mmol) in dry dichloromethane (20 ml) was heated under reflux for 2 h. The dichloromethane was dried over magnesium sulfate and evaporated in vacuo. The residue was dissolved in acetonitrile (10 ml) containing acetic acid (0.024 g, 10 mol%). After *N*-methylmaleimide (0.222 g, 2 mmol) was added the mixture was stirred at room temperature for 13 h. A similar separation procedure gave **19a** and **20**. **20**: Colorless prisms (benzene–hexane); mp 141—142 °C; IR (KBr) 3300, 1740, and 1690 cm^{-1}; ^1H NMR ($CDCl_3$) δ=2.59 (1H, br, NH), 2.88 (3H, s, NMe), 3.35 (1H, dd, J=8.5 and 7.8 Hz, 6a-H), 3.66 (1H, d, J=7.8 Hz, 3a-H), 3.78 (3H, s, COOMe), 4.39 (1H, s, 4-H), 4.59 (1H, dd, J=8.5 and 4.0 Hz, 6-H), and 7.30 (5H, br s, Ph); MS m/z (rel intensity, %) 288 (M^+, 21), 229 (96), 228 (21), 144 (base peak), 143 (28), 117 (76), and 115 (30). Found: C, 62.64; H, 5.62; N, 9.58%. Calcd for $C_{15}H_{16}N_2O_4$: C, 62.49; H, 5.59; N, 9.72%.

21: Colorless prisms (benzene–hexane); mp 120.5—121 °C; IR (KBr) 3400, 2990, 1755, 1725, and 1680 cm^{-1}; ^1H NMR ($CDCl_3$) δ=1.1—2.2 (10H, m, *c*-Hex), 1.96 (1H, br, NH), 2.91 (3H, s, NMe), 2.96 (1H, d, J=7.8 Hz, 6a-H), 3.52 (1H, t, J=7.8 Hz, 3a-H), 3.80 (3H, s, COOMe), and 4.02 (1H, d, J=7.8 Hz, 4-H); ^{13}C NMR ($CDCl_3$) δ=22.41, 23.18, 25.94, 34.93, 37.12 (each t, *c*-Hex), 24.94 (q, NMe), 50.53 (d, 6a-C), 52.42 (q, COOMe), 55.18 (d, 3a-C), 60.42 (d, 4-C), 65.36 (s, 6-C), 171.24 (s, COOMe), 176.13, and 176.42 (each s, CON); MS m/z (rel intensity, %) 280 (M^+, 20), 237 (66), 221 (54), 177 (72), 165 (25), 136 (40), 93 (22), 80 (base peak), 79 (21), 53 (26), 41 (33), and 39 (21). Found: C, 59.79; H, 7.15; H, 9.75%. Calcd for $C_{14}H_{20}N_2O_4$: C, 59.99; H, 7.19; N, 9.99%.

References

1) E. Vedejs and G. R. Martinez, *J. Am. Chem. Soc.*, **101**, 6452 (1979); Reviews: N, Imai, Y. Terao, and K. Achiwa, *Yuki Gosei Kagaku Kyokai Shi*, **43**, 862 (1985); E. Vedejs and F. G. West, *Chem. Rev.*, **86**, 941 (1986) and references cited therein.

2) R. Grigg, J. Kemp, G. Sheldrick, and J. Trotter, *J. Chem. Soc., Chem. Commun.*, **1978**, 109; M. Joucla and J. Hamelin, *Tetrahedron Lett.*, **1978**, 2885; O. Tsuge, K. Ueno, and K. Oe, *Chem. Lett.*, **1979**, 1407; Review: R. Grigg, *Bull. Soc. Chim. Belg.*, **93**, 593 (1984) and references cited therein.

3) a) R. Grigg and H. Q. N. Gunaratne, *J. Chem. Soc., Chem. Commun.*, **1982**, 384 (1982); b) O. Tsuge, K. Ueno, S. Kanemasa, and K. Yorozu, *Bull. Chem. Soc. Jpn.*, **59**, 1809 (1986).

4) P. N. Confalone and E. M. Huie, *J. Org. Chem.*, **48**, 2994 (1983); *J. Am. Chem. Soc.*, **106**, 7175 (1984).

5) M. Joucla, J. Mortier, and J. Hamelin, *Tetrahedron Lett.*, **26**, 2775 (1985).

6) Other methods to ester-stabilized azomethine ylides: a) P. Deshong, D. A. Kell, and D. R. Sidler, *J. Org. Chem.*, **50**, 2309 (1985); b) P. Deshong, D. R. Sidler, D. A. Kell, and N. N. Aronson Jr., *Tetrahedron Lett.*, **26**, 3747 (1985); c) N. Imai, Y. Terao, K. Achiwa, and M. Sekiya, *ibid.*, **25**, 1579 (1984); d) N. Imai, Y. Terao, and K. Achiwa, *Heterocycles*, **23**, 1107 (1985).

7) Part of the present work has been presented as a communication letter (O. Tsuge, S. Kanemasa, M. Ohe, K. Yorozu, S. Takenaka, and K. Ueno, *Chem. Lett.*, **1986**, 1271).

8) O. Tsuge, S. Kanemasa, and S. Takenaka, *Heterocycles*, **20**, 1907 (1983); *Chem. Lett.*, **1985**, 355; *Bull. Chem. Soc. Jpn.*, **58**, 3137, 3320 (1985).

9) H. Ardill, R. Grigg, V. Sridharan, S. Surendrakumar, S. Thianpatanagul, and S. Kanajun, *J. Chem. Soc., Chem. Commun.*, **1986**, 602.

10) The ester-stabilized azomethine ylides derived from pyrolysis of aziridinecarboxylates failed to react with styrene (Ref. 6a).

11) It is known that azomethine ylides generated by dehydration of trialkylamine *N*-oxides are highly reactive to nonactivated alkenes as well as aryl-substituted olefins (R. Beugelmans, G. Negron, and G. Roussi, *J. Chem. Soc., Chem. Commun.*, **1983**, 31; L. B.-Iguertsira, J. Chastanet, G. Negron, and G. Roussi, *Can. J. Chem.*, **63**, 725 (1985); J. Chastanet and G. Roussi, *J. Org. Chem.*, **50**, 2910 (1985)).

12) Our unpublished data which will be published as a following article in this journal.

13) It has been reported that the reactions of A (R=H, R^1=*p*-$MeOC_6H_4$ or $PhCH_2$, EWG=COOMe) with *t*-butyl acrylate or phenyl vinyl sulfone lead to a mixture of stereoisomers of 2,4-substituted pyrrolidines (Ref. 6a).

14) It is not clear whether the *N*-protonated azomethine ylide is formed directly by the 1,3-elimination of an intermediary hemiacetal (or iminium salt) or via an imine.

Simple Generation of Nonstabilized Azomethine Ylides through Decarboxylative Condensation of α-Amino Acids with Carbonyl Compounds via 5-Oxazolidinone Intermediates

Otohiko TSUGE,* Shuji KANEMASA, Masayuki OHE, and Shigeori TAKENAKA
Institute of Advanced Material Study, and Department of Molecular Science and Technology, Interdisciplinary Graduate School of Engineering Sciences, Kyushu University, Kasugakoen, Kasuga 816
(Received May 30, 1987)

Heating α-amino acids with a variety of carbonyl compounds generates *N*-unsubstituted or *N*-substituted azomethine ylides of nonstabilized types through the elimination of water and carbon dioxide. The ylides are captured by olefinic, acetylenic, and carbonyl dipolarophiles producing pyrrolidines, pyrrolines, and oxazolidines. The reaction involves intermediary 5-oxazolidinones which can be sometimes isolated. Some synthetic equivalents of parent azomethine ylide, methaniminium methylide, are accessible by this route.

In the previous paper a simple generation method of ester- or cyano-stabilized azomethine ylides was reported.[1a] This method is a modification of imine-azomethine ylide tautomerism[2] and involves the condensation of α-amino esters or nitriles with aldehydes leading to iminium compounds, which spontaneously deprotonate at the position adjacent to the electron-withdrawing group (EWG) to generate the ylides (Eq. 1).

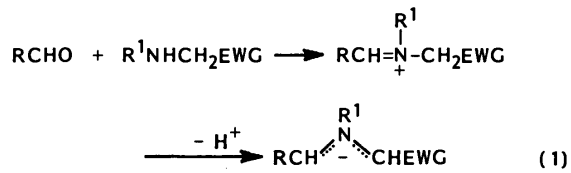

During this investigation we noticed that the condensation of α-amino acids with carbonyl compounds would afford a general route to azomethine ylides bearing no stabilizing substituent.[3] As shown in Eq. 2 the intermediates expected to be formed in this condensation are iminium acids which will then undergo ready decarboxylation leading to azomethine ylides.[4]

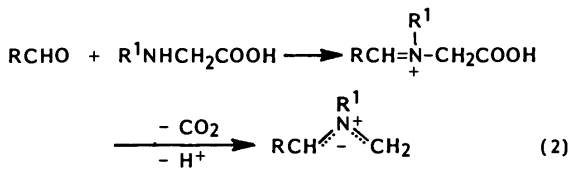

In the present article, we will present a general and practical generation method of nonstabilized azomethine ylides via the decarboxylative condensation route and the scope and limitation of the method will be discussed.[1b]

Results and Discussion

Benzaldehyde and a slightly excess of *N*-methylaminoacetic acid (sarcosine, **1**) were heated to reflux in toluene in the presence of electron-deficient olefins to give cycloadducts **2a—2d** (Scheme 1 and Table 1), indicating the formation of azomethine ylide **AY-A** (R=Ph, R′=H). poor endo- and exo-selectivity of these reactions is consistent with the reported results on the related ylides derived from *N*-benzylidene-(trimethylsilyl)methylamine.[5,6] The reaction with dimethyl maleate gave two cycloadducts, 3,4-cis-adduct **2c** in a poorer yield (11%) and 3,4-trans-adduct

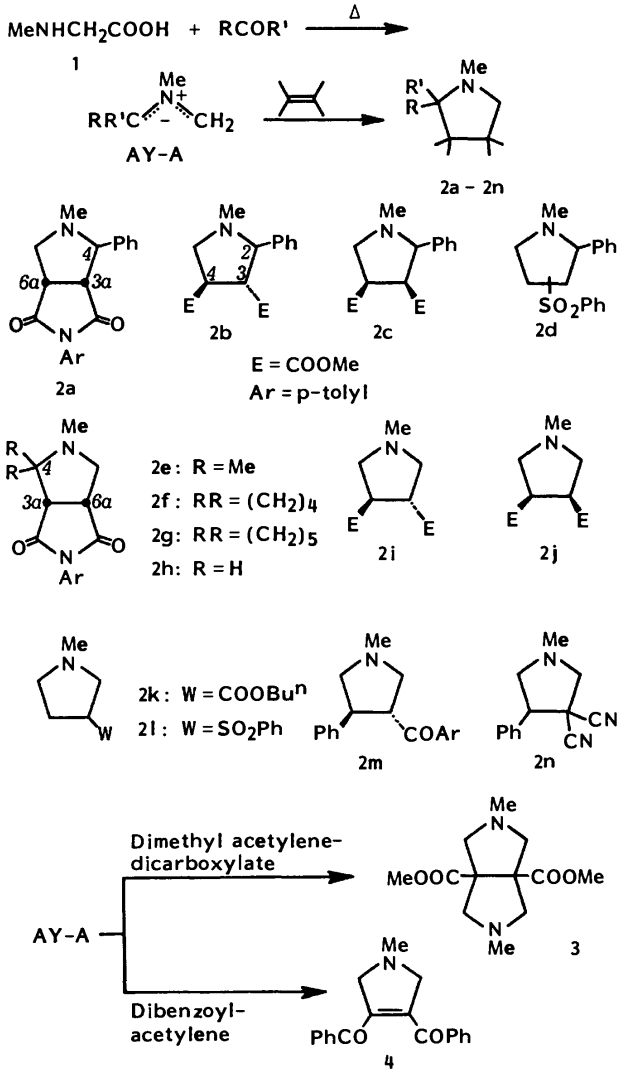

Scheme 1.

2b (71%) as a major product. Under the reaction conditions, the 3,4-cis-adduct **2c** does not epimerize into the 3,4-trans-adduct **2b**, and the isomerization of dimethyl maleate into fumarate does not proceed at an appreciable rate. Catalysis of benzaldehyde in the isomerization was not observed.

The poor stereospecificity is not due to the isomerization of dimethyl maleate into fumarate prior to its cycloaddition trapping, consequently.[7] A stepwise mechanism is responsible for the nonstereospecific cycloaddition of ylide **AY-A** (R=Ph, R′=H).

Azomethine ylides **AY-A** (R, R′=alkyl) with two substituents at the same carbon are available by similar reactions of **1** with ketones. The cycloadducts **2e—2g** to *N*-(*p*-tolyl)maleimide were obtained in high yields (Scheme 1 and Table 1).

Azomethine ylide **AY-A** (R=R′=H) carrying no *C*-substituent is also accessible by the condensation of **1** with paraformaldehyde under reflux in toluene. 2,5-Unsubstituted pyrrolidines **2h—2l** were produced by trapping ylide **AY-A** with a variety of olefinic dipolarophiles. Both the cycloadditions to dimethyl fumarate and maleate were exclusively stereospecific to give **2i** and **2j**, respectively. This high stereospecificity makes a striking contrast to the previous cycloadditions of **AY-A** (R=Ph, R′=H) leading to **2b** and **2c**. With dimethyl acetylenedicarboxylate two molecules of the ylide **AY-A** (R=R′=H) were incorporated in the reaction to give perhydropyrrolo-[3,4-*c*]pyrrole-3a,6a-dicarboxylate **3**.

Azomethine ylides **AY-A** (R=R′=H) bearing no *C*-substituent have been previously generated by several routes, all of which have utilized *N*-silylmethyl amine reagents.[8] Our method has some advantages over these precedents: 1) Our ylide generation starts with readily available chemicals, paraformaldehyde and sarcosine (**1**). 2) Reaction can be performed by a simple operation under almost neutral conditions. 3) Cycloaddition takes place with a variety of dipolarophiles producing high yields of cycloadducts.

The above decarboxylative ylide generation utilizing paraformaldehyde was further applied to cyclic α-amino acids such as 2-pyrrolidinecarboxylic acid (proline, **5**) and 4-thiazolidinecarboxylic acid (**7**). Cyclic azomethine ylides **AY-B** and **AY-C** generated were captured with *N*-(*p*-tolyl)maleimide or dimethyl maleate to give **6**, **8**, and **9**, all as mixtures of stereoisomers (Scheme 2 and Table 2). Each two stereoisomers of the maleimide cycloadducts **6** and **8** could be separated through column chromatography, while **9** was a 5:4 mixture (GLC) of two inseparable stereoisomers.

It was surprising to know that 3-phenyl-5-oxazolidinone (**11**) was isolated in a quantitative yield in the reaction of *N*-phenylaminoacetic acid (**10**) with paraformaldehyde under reflux in toluene for 15 min. The azalactone **11** readily eliminated carbon dioxide by heating to generate azomethine ylide **AY-D**, which was in situ trapped with olefinic dipolarophiles to give **12a—12c** (Scheme 3 and Table 2).

Table 1. Generation and Cycloaddition of Azomethine Ylides **AY-A** Generated from Sarcosine **1** and Carbonyl Compounds

Entry	Carbonyl compound	Type of ylide[a]	Dipolarophile	Condition[b]	Product (yield/%)[c]	Isomer ratio[d]
1	Benzaldehyde	A1	*N*-(*p*-Tolyl)maleimide	A, 1 h	**2a** (86)	5 : 2
2	Benzaldehyde	A1	Dimethyl fumarate	A, 1 h	**2b** (86)	1 : 1
3	Benzaldehyde	A1	Dimethyl maleate	A, 2 h	**2b** (71) + **2c** (11)	**2b**: 1 : 1 **2c**: 2 : 1
4	Benzaldehyde	A1	Phenyl vinyl sulfone	A, 2 h	**2d** (29)[e,f]	
5	Acetone	A2	*N*-(*p*-Tolyl)maleimide	A, 9 h	**2e** (85)	
6	Cyclopentanone	A3	*N*-(*p*-Tolyl)maleimide	A, 5 h	**2f** (79)	
7	Cyclohexanone	A4	*N*-(*p*-Tolyl)maleimide	A, 3 h	**2g** (91)	
8	Paraformaldehyde	A5	*N*-(*p*-Tolyl)maleimide	B, 15 min	**2h** (89)	
9	Paraformaldehyde	A5	Dimethyl fumarate	B, 15 min	**2i** (80)	
10	Paraformaldehyde	A5	Dimethyl maleate	B, 15 min	**2j** (84)	
11	Paraformaldehyde	A5	Butyl acrylate	B, 15 min	**2k** (79)	
12	Paraformaldehyde	A5	Phenyl vinyl sulfone	B, 15 min	**2l** (84)	
13	Paraformaldehyde	A5	2-Benzylidene-4′-methylacetophenone	A, 1 h	**2m** (93)	
14	Paraformaldehyde	A5	Benzylidenemalononitrile	A, 1 h	**2n** (94)	
15	Paraformaldehyde	A5	Dimethyl acetylenedicarboxylate	B, 15 min	**3** (68)	
16	Paraformaldehyde	A5	Dibenzoylacetylene	B, 15 min	**4** (36)	

a) A1: R=Ph, R′=H, A2: R=R′=Me, A3: RR′=$(CH_2)_4$, A4: RR′=$(CH_2)_5$, A5: R=R′=H. b) A: Under reflux in toluene with *N*,*N*-diisopropylethylamine (1.5 equiv), B: Under reflux in toluene. c) Yield of isolated products. d) Mixture of stereoisomers whose ratio was based on ^{1}H NMR. e) 2-(Dimethylamino)ethyl phenyl sulfone was obtained in 55% yield. f) Mixture of two regioisomers.

Successful isolation of the azomethine ylide precursor **11** enabled the use of some activated aldehydes as dipolarophiles. Thus heating **11** with *p*-nitrobenzaldehyde or phenylglyoxal gave the oxazolidine cycloadduct **13a** or **13b**, respectively. Pyruvaldehyde was incorporated into 5-oxazolidinone skeleton through an acetal-exchange reaction of **11**. The resulting acetyl-substituted 5-oxazolidinone **A** underwent the decarboxylative generation of azomethine ylide **AY-E**, which was captured by the same aldehyde to give cycloadduct **13c** (Scheme 3).

It is now apparent that the condensation of *N*-substituted α-amino acids with carbonyl compounds offers a simple and versatile generation route to a variety of nonstabilized azomethine ylides **AY-A** to **AY-D**, presumably via 5-oxazolidinone intermediates.[9] Extension of this method to the generation of *N*-unsubstituted azomethine ylides of nonstabilized types is worthy to be tested. This may be achieved by the reaction of *N*-unsubstituted α-amino acids with carbonyl compounds (Eq. 3).

$$RCHO + NH_2CH_2COOH \longrightarrow RCH^{\overset{H}{N^+}}{}^{-}CH_2 \qquad (3)$$

According to Eq. 3, glycine (**14**) was allowed to react with carbonyl compounds under reflux in toluene to

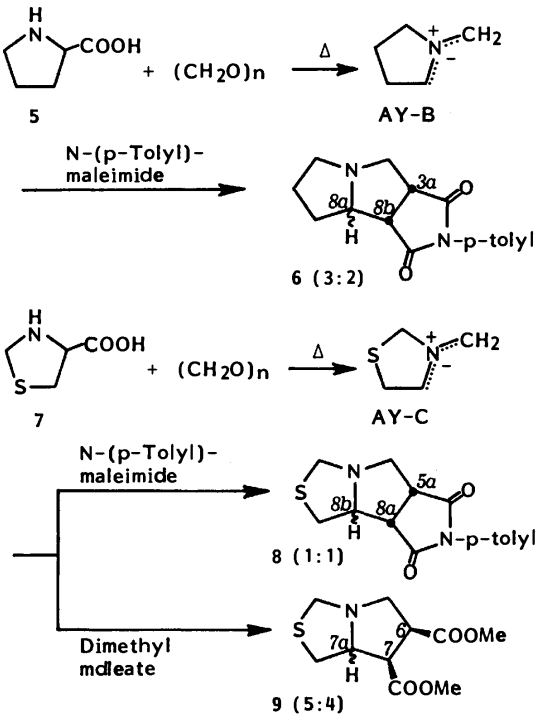

Scheme 2.

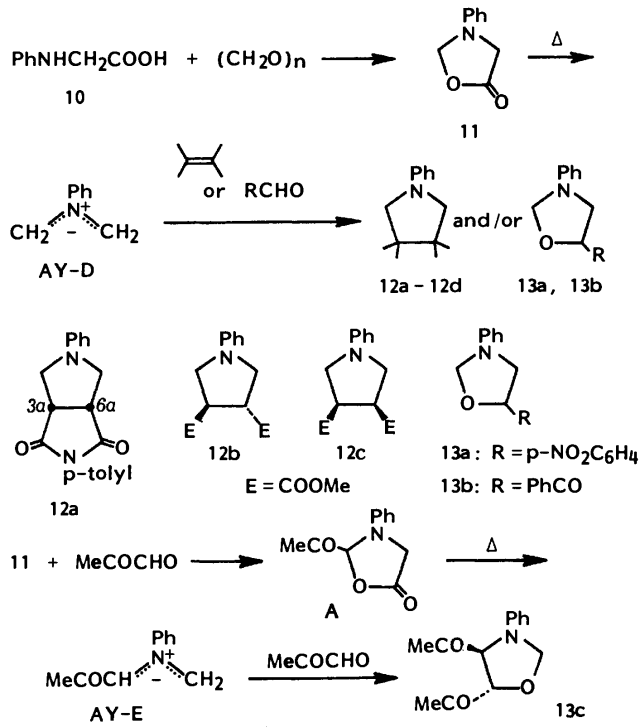

Scheme 3.

Table 2. Generation of Azomethine Ylides **AY-B** to **AY-E** from *N*-Substituted 2-Amino Acids and Carbonyl Compounds

Entry	2-Amino acid	Carbonyl compound	Type of ylide	Dipolarophile	Condition[a]	Product (yield/%)[b]	Isomer ratio[c]
1	**5**	Paraformaldehyde	B	*N*-(*p*-Tolyl)maleimide	A, 15 min	**6** (100)	3 : 2[d]
2	**7**	Paraformaldehyde	C	*N*-(*p*-Tolyl)maleimide	A, 30 min	**8** (81)	41%+40%[e]
3	**7**	Paraformaldehyde	C	Dimethyl maleate	A, 30 min	**9** (77)	5 : 4[f]
4	**10**	Paraformaldehyde	D	*N*-(*p*-Tolyl)maleimide	B, 8 h	**12a** (92)	
5	**10**	Paraformaldehyde	D	Dimethyl fumarate	B, 8 h	**12b** (97)	
6	**10**	Paraformaldehyde	D	Dimethyl maleate	B, 8 h	**12c** (65)	
7	**10**	Paraformaldehyde	D	*p*-Nitrobenzaldehyde	B, 4 h	**13a** (51)	
8	**10**	Paraformaldehyde	D	Phenylglyoxal	B, 8 h	**13b** (39)	
9	**10**	Paraformaldehyde	E	Pyruvaldehyde	B, 3 h	**13c** (26)	

a) A: Under reflux in toluene, B: 3-Phenyl-1,3-oxazolidin-5-one (**11**) was first prepared by heating **10** with paraformaldehyde (0.5 h in toluene), and its decarboxylation was conducted in the presence of a dipolarophile under reflux in toluene. b) Yield of isolated products. c) Mixture of stereoisomers. d) Determined by ^{1}H NMR. e) Yield of isolated isomers. f) Determined by GLC.

generate *N*-unsubstituted azomethine ylides **AY-F**. The use of acetone and cyclopentanone as carbonyl compounds afforded the maleimide cycloadducts **15a** and **15b**, but the yields were unsatisfactory (Scheme 4 and Table 3).

The decarboxylative condensation of **14** with formaldehyde was expected to offer a direct generation method of parent azomethine ylide **AY-F** (R=H), methaniminium methylide, whose preparation is so far unknown. The ylide generation from **14** and paraformaldehyde under reflux in toluene was followed by the cycloaddition trapping with *N*-(*p*-tolyl)maleimide, benzylidenemalononitrile, or dimethyl fumarate. The cycloadducts obtained were not the expected 1,2,5-unsubstituted pyrrolidines but their *N*-methylene-bridged dimers **16a—16c**.[10] Use of less than one equivalent of paraformaldehyde was not effective, and the identical products **16** were only afforded in poorer yields.

Similar reactions of paraformaldehyde with 2-aminopropanoic acid (alanine) or 2-amino-3-hydroxypropanoic acid (serine) in the presence of *N*-(*p*-tolyl)maleimide under reflux in toluene led to the formation of complex mixture of products.

Two routes are possible for the formation of *N*-methylene-bridged pyrrolidines **16a—16c**: participation of either the parent azomethine ylide **AY-F** (R=H) or *N*,*N*′-methylenebis(azomethine ylide) **AY-**

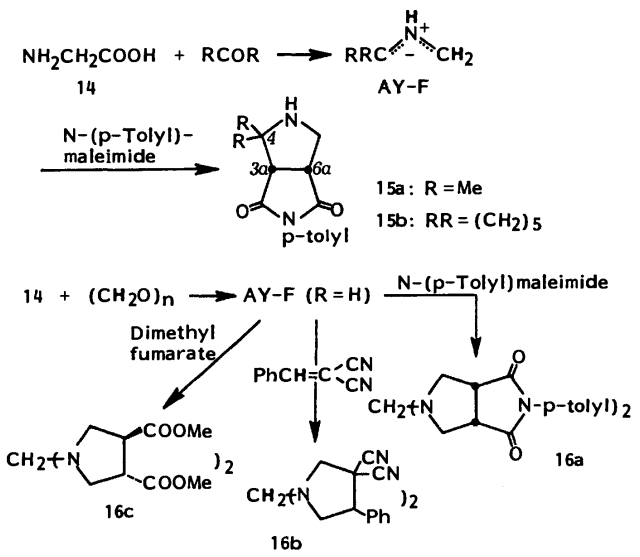

Scheme 4.

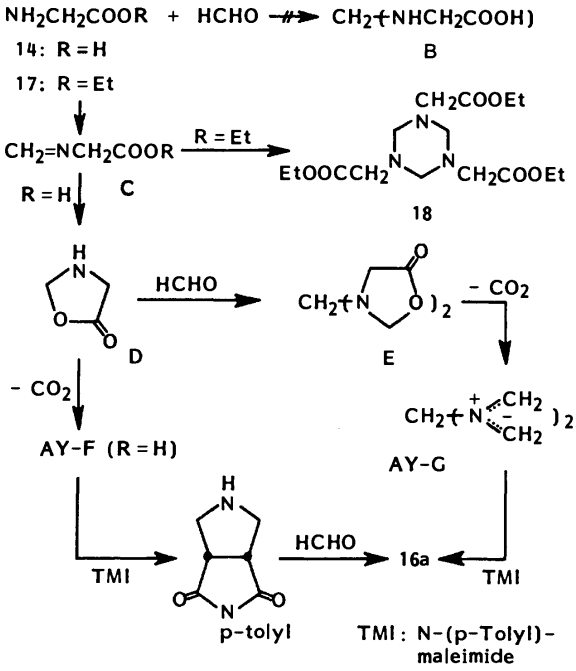

Fig. 1. Two possible routes to **16a**.

Table 3. Generation of Azomethine Ylides **AY-F**, **AY-H**, and **AY-I** from Aminoacetic Acid or Its Equivalents **20** and **26**

Entry	2-Amino acid	Carbonyl compound	Type of ylide[a]	Dipolarophile	Condition[b]	Product (yield/%)[c]
1	**14**	Acetone	F1	*N*-(*p*-Tolyl)maleimide	A, 48 h	**15a** (29)
2	**14**	Cyclohexanone	F2	*N*-(*p*-Tolyl)maleimide	A, 8 h	**15b** (30)
3	**14**	Paraformaldehyde	F3	*N*-(*p*-Tolyl)maleimide	A, 1 h	**16a** (65)
4	**14**	Paraformaldehyde	F3	*N*-(*p*-Tolyl)maleimide	B, 15 min	**16a** (74)
5	**14**	Paraformaldehyde	F3	Benzylidenemalononitrile	C, 12 h	**16b** (71)
6	**14**	Paraformaldehyde	F3	Dimethyl fumarate	A, 3 h	**16c** (52)
7	**20**		H	*N*-(*p*-Tolyl)maleimide	D, 48 h	**21a** (74)
8	**20**		H	Dimethyl fumarate	D, 48 h	**21b** (73)
9	**20**		H	Dimethyl maleate	D, 48 h	**21c** (63)
10	**26**	Paraformaldehyde	I	Dimethyl fumarate	A, 15 min	**27a** (100)
11	**26**	Paraformaldehyde	I	Dimethyl maleate	A, 15 min	**27b** (91)
12	**26**	Paraformaldehyde	I	*N*-(*p*-Tolyl)maleimide	A, 15 min	**27c** (93)
13	**26**	Paraformaldehyde	I	Butyl acrylate	A, 15 min	**27d** (38)

a) F1: **AY-F** (R=Me), F2: **AY-F** (RR=$(CH_2)_5$), F3: **AY-F** (R=H). b) A: Under reflux in toluene, B: Under reflux in DMF, C: Under reflux in toluene with potassium carbonate (excess), D: Under reflux in toluene using **20**. c) Yield of isolated product.

G. The initial methylene bridging of glycine (**14**) leading to methylenediamine-*N*,*N*′-diacetic acid (**B**) is unlikely to happen since the reaction of ethyl aminoacetate (**16**) with paraformaldehyde forms 1,3,5-tris(ethoxycarbonylmethyl)-1,3,5-triazine **18**, a trimer of ethyl *N*-methyleneaminoacetate **C** (R=Et) (Fig. 1). *N*-Methyleneaminoacetic acid **C** (R=H) cyclizes into labile 5-oxazolidinone (**D**).[11] This heterocycle **D** loses carbon dioxide generating the parent azomethine ylide **AY-F** (R=H) whose cycloaddition to *N*-(*p*-tolyl)maleimide and subsequent reaction with formaldehyde gives **16a**.[12] Another route to **16a** is the initial bridging of **D** forming *N*,*N*′-methylenebis(5-oxazolidinone) (**E**), elimination of carbon dioxide generating *N*,*N*′-methylenebis(azomethine ylide) **AY-G**, and the final cycloaddition. Discrimination of the both routes depends upon the stability of intermediary 5-oxazolidinone **D**.

One of the synthetic equivalents of the parent azomethine ylide **AY-F** (R=H) will be *N*-triphenylmethyl azomethine ylide **AY-H**. Reaction of *N*-(triphenylmethyl)aminoacetic acid (**19**) with aqueous formaldehyde in ethanol or with paraformaldehyde under reflux in toluene gave 3-(triphenylmethyl)-5-oxazolidinone (**20**) as a stable compound, both in quantitative yields (Scheme 5). When heated under reflux in toluene, **20** gradually eliminated carbon dioxide to generate the parent ylide equivalent **AY-H**, which was captured by *N*-(*p*-tolyl)maleimide, dimethyl fumarate, or maleate leading to cycloadducts **21a—21c** (Scheme 5 and Table 3). The triphenylmethyl moiety of **21a** and **21b** was readily removed on treatment with hydrochloric acid in dichloromethane at room temperature to give **22a—22c**.

In contrast with the ready formation of 5-oxazolidinone **20** from **19** and paraformaldehyde, similar reactions of **19** with acetaldehyde or benzaldehyde all resulted in the quantitative recovery of **19**. The bulky triphenylmethyl group of **19** may have inhibited its attack to these aldehydes. On the other hand, 3-triphenylmethyl-4-methyl-5-oxazolidinone (**24**) was obtained in a high yield from *N*-(triphenylmethyl)-2-aminopropanoic acid (**23**) and paraformaldehyde. However heating **24** in the presence of a variety of dipolarophiles yielded no cycloadducts. *N*-(Methyl)triphenylmethylamine **25** was the only product.[13]

There are some problems in the employment of 3-(triphenylmethyl)-5-oxazolidinone **20** as a synthetic equivalent of parent azomethine ylide **AY-F** (R=H). Table 3 indicates that 1) the decarboxylative ylide generation takes many hours (48 h), 2) the yields of cycloadducts **21** remain to be improved (63—74%), and 3) removal of the triphenylmethyl moiety is not a high-yield reaction. Since the thermal stability of 5-oxazolidinones seems to decrease with the decreased steric size of the 3-substituent, a 5-oxazolidinone bearing a smaller 3-substituent, which should be readily removable after the cycloaddition, is needed.

We chose *N*-benzylaminoacetic acid (**26**) as the parent ylide equivalent. Although all attempts to isolate the corresponding 5-oxazolidinone failed, the reaction of **26** with paraformaldehyde was completed in 15 min under reflux in toluene. The azomethine ylide **AY-I** generated was captured by *N*-(*p*-tolyl)-maleimide, dimethyl maleate, fumarate, and butyl acrylate to give excellent yields of cycloadducts **27a—**

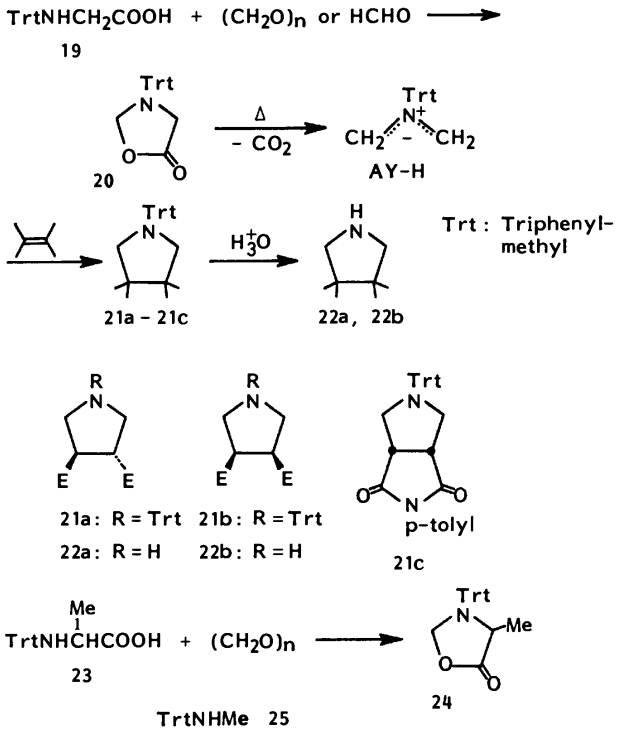

Scheme 5.

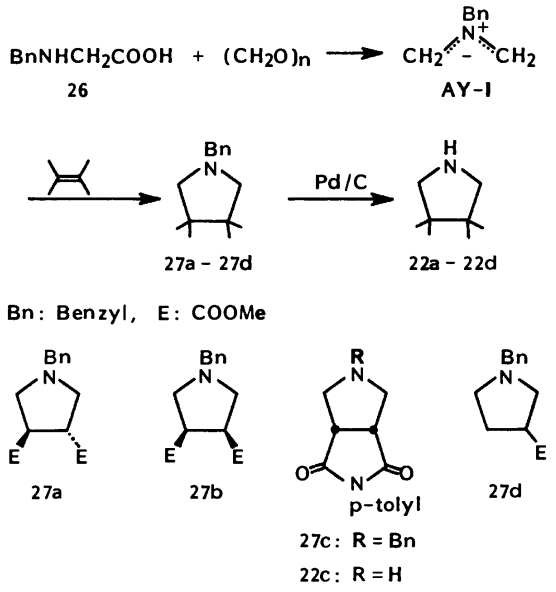

Scheme 6.

27d (Scheme 6 and Table 3). Debenzylation of **27c** by Pd/C proceeded smoothly under reflux in xylene to produce a quantitative yield of **22c**. However, similar debenzylation of ester-substituted pyrrolidines **27a—27b** and **27d** led to a complex mixture of many products. In these cases also the debenzylation was completed, but subsequent condensation of the resulting secondary amine moiety with the esters would be a main reason for the complex results.

Experimental

General. Melting points were determined on a Yanagimoto melting point apparatus and are uncorrected. IR spectra were taken with a JASCO IRA-1 or a JASCO A-702 spectrometer. ^{1}H NMR spectra were recorded on a Hitachi R-40 (90 MHz) or a JEOL FX-100 instrument (100 MHz) and ^{13}C NMR on a JEOL FX-100 spectrometer at 25.05 MHz. Chemical shifts are expressed in parts per million downfield from tetramethylsilane as an internal standard. Mass spectra as well as high resolution mass spectra were measured with a JEOL-01SG-2 spectrometer at 70 eV of ionization energy. Elemental analyses were performed on a Hitachi 026 CHN analyzer. Thin-layer chromatography (TLC) was accomplished on 0.2 mm precoated plates of silica gel 60 F-254 (Merck) or of aluminum oxide 60 F-254 type-E (Merck). Visualization was made with ultraviolet light (254 and 365 nm), iodine, molybdophosphoric acid (5% in ethanol), or *p*-anisaldehyde (5% in ethanol containing 5% of sulfuric acid). For preparative column chromatography, Wakogel C-200, C-300 (Wako), and Silicagel 60 (Merck) were employed. Flash chromatography was carried out on an EYELA EF-10 apparatus using a column (20×180 mm) packed with Silicagel 60 (Merck, size: 0.04—0.063 mm). Micro vacuum distillation was carried out on a Sibata GTO-250R Kugelrohr distilling apparatus. Solvents were evaporated with a Tokyo Rikakikai rotary evaporator type-V at about 50 °C unless otherwise stated.

General Procedure for the Generation of Azomethine Ylide AY-A from Sarcosine (1) and Carbonyl Compounds, and Subsequent Ylide Trapping with Olefins Leading to 2—4. A mixture of sarcosine **1**, carbonyl compound, and olefin was heated under reflux in toluene (10—15 ml for 1 mmol of the dipolarophile). A mixture of sarcosine hydrochloride and *N,N*-diisopropylethylamine (1.5 equiv of the hydrochloride) may be employed instead of **1**. The water formed was removed by the aid of a Dean-Stark trap. The reaction conditions are listed in Table 1. The molar equivalents of **1** and carbonyl compounds are based on dipolarophiles as follows: **1** (2 equiv)+benzaldehyde (1.5 equiv); **1** (2 equiv)+acetone (10 equiv); **1** (2 equiv)+cycloalkanones (1.5 equiv); **1** (2 equiv)+paraformaldehyde (5 equiv). After the completion of reaction the solvent was evaporated in vacuo. The residue was chromatographed over silica gel by using hexane–ethyl acetate (3:1 to 1:1 vol/vol) to give **2—4**. All the results are summarized in Table 1 in which yields are based on the dipolarophiles.

2a: This cycloadduct **2a** consists of two stereoisomers (3a,4-trans:3a,4-cis=2:5 (^{1}H NMR)). The 3a,4-trans isomer could be separated from the 3a,4-cis isomer by washing the mixture with diethyl ether (3a,4-trans isomer is less soluble) and through column chromatography over silica gel (hexane–diethyl ether=3:1 vol/vol). 3a,4-*trans*-**2a**: Colorless prisms (diethyl ether); mp 153—154 °C; IR (KBr) 1765 and 1695 cm^{-1}; ^{1}H NMR ($CDCl_3$) δ=2.15 (3H, s, *p*-Me), 2.36 (3H, s, NMe), 2.70 (1H, ddd, J=9.6, 8.2, and 5.8 Hz, 6a-H), 3.3—3.8 (2H, m, 3a-H and 6-H), and 7.0-7.4 (9H, m, Ar); ^{13}C NMR ($CDCl_3$) δ=21.00 (q, *p*-Me), 38.53 (q, NMe), 44.06 (d, 6a-C), 53.42 (d, 3a-C), 57.18 (t, 6-C), 72.42 (d, 4-C), 126.24, 127.83, 127.95, 128.65, 129.30, 129.66 (each d), 138.42, 139.07 (each s), 176.54, and 177.12 (each s, CON); MS *m/z* (rel intensity, %) 320 (M^+, 21), 158 (28), 132 (100), 118 (26), 115 (28), 91 (46), 82 (62), 77 (35), and 43 (28). Found: C, 74.70; H, 6.30; N, 8.62%. Calcd for $C_{20}H_{20}N_2O_2$: C, 74.97; H, 6.29; N, 8.74%. 3a,4-*cis*-**2a**: Colorless needles (benzene–hexane); mp 121—122.5 °C; IR (KBr) 1765 and 1695 cm^{-1}; ^{1}H NMR ($CDCl_3$) δ=2.18 (3H, s, *p*-Me), 2.33 (3H, s, NMe), 2.62 (1H, dd, J=9.4 and 6.5 Hz, 6a-H), 3.2—3.8 (4H, m, 3a-H, 4-H, and 6-H), and 7.0—7.4 (9H, m, Ar); ^{13}C NMR ($CDCl_3$) δ=21.12 (q, *p*-Me), 39.71 (q, NMe), 44.53 (d, 6a-C), 50.59 (d, 3a-C), 58.24 (t, 6-C), 73.30 (d, 4-C), 126.13, 128.07, 128.18, 128.54, 128.77, 129.71 (each d), 137.01, 138.36 (each s), 175.07, and 178.54 (each s, CON) MS *m/z* (rel intensity, %) 320 (M^+, 22), 158 (22), 133 (39), 132 (base peak), 118 (25), 91 (44), 82 (37), and 77 (24). Found: C, 75.24; H, 6.40; N, 8.64%. Calcd for $C_{20}H_{20}N_2O_2$: C, 74.97; H, 6.29; N, 8.74%.

2b: (An inseparable mixture of 2,3-cis and 2,3-trans isomers (1:1)): Colorless liquid; IR (neat) 1725 cm^{-1}; ^{1}H NMR ($CDCl_3$) δ=2.08, 2.17 (each 1/2×3H, s, NMe), 2.50, 2.67 (each 1H, dd, J=9.4 and 8.2 Hz, 5-H), 3.06, 3.60, 3.68, 3.74 (each 1/2×3H, s, COOMe), 3.2—3.7 (3H, m, 3-, 4-, and 5-H), and 7.2—7.4 (5H, m, Ph); ^{13}C NMR ($CDCl_3$) δ=39.26, 39.60 (each q, NMe), 43.99, 44.73 (each d, 4-C), 50.93, 51.66, 51.95, 52.44 (each q, COOMe), 54.69 (d, 3-C), 58.30, 58.50 (each t, 5-C), 72.75, 74.46 (each d, 2-C), 127.59, 127.78, 127.88, 128.12, 128.32 (each d), 138.37, 140.33 (each s), 171.97, 173.09, 173.29, and 173.63 (each s, COOMe); MS *m/z* (rel intensity, %) 277 (M^+, 14), 262 (42), 216 (33), 202 (25), 184 (33), 158 (base peak), 143 (35), 140 (40), 118 (42), 117 (20), 116 (31), 115 (95), 91 (73), 82 (40), 81 (23), 77 (51), 59 (68), 52 (23), 45 (23), and 43 (64). HRMS Found: *m/z* 277.1318. Calcd for $C_{15}H_{19}NO_4$: M, 277.1318.

2c: (An inseparable mixture of 2,3-cis and 2,3-trans isomers (1:2)): Colorless liquid; IR (neat) 1745 cm^{-1}; ^{1}H NMR ($CDCl_3$) δ=2.18 (2/3×3H, s, NMe), 2.23 (1/3×3H, s, NMe), 2.5—4.1 (5H, m, 2-, 3-, 4-, and 5-H), 3.20, 3.65 (each 1/3×3H, s, COOMe of 2,3-cis isomer), 3.60, 3.67 (each 2/3×3H, s, COOMe of 2,3-trans isomer), and 7.2—7.4 (5H, m, Ph); MS *m/z* (rel intensity, %) 277 (M^+, 30), 262 (44), 246 (21), 218 (21), 158 (37), 133 (31), 132 (95), 115 (base peak), 91 (22), 82 (28), and 42 (23). HRMS Found: *m/z* 277.1329. Calcd for $C_{15}H_{19}NO_4$: M, 277.1313.

2d: (An inseparable mixture of two regioisomers): Colorless liquid; IR (neat) 1295 and 1135 cm^{-1}; ^{1}H NMR ($CDCl_3$) δ=2.14 (3H, s, NMe), 2.3—2.9 (3H, 3- and 4-H), 3.1—3.8 (3H, m, 2- and 5-H), and 7.0—7.8 (10H, m, Ar); ^{13}C NMR ($CDCl_3$) δ=25.88 (t, 4-C of 2,3-isomer), 36.00 (t, 3-C of 2,4-isomer), 39.77 (q, NMe), 55.53, 56.24 (each t, 5-C), 61.00 (d, 4-C of 2,4-isomer), 70.24 (d, 3-C of 2,3-isomer), 70.83 (each d, 2-C), 127.36, 127.54, 127.89, 128.07, 128.48, 128.65, 128.95, 129.24, 129.36, 129.53 (each d), 133.71, 134.01, 140.60, and 141.01 (each s); MS *m/z* (rel intensity, %) 301 (M^+, 3), 159 (base peak), 158 (32), and 91 (22). HRMS Found: *m/z* 301.1136. Calcd for $C_{17}H_{19}NO_2S$: M, 301.1142.

This compound **2d** was accompanied by 2-(dimethyl-

amino)ethyl phenyl sulfone: Pale yellow liquid; IR (neat) 1319, 1306, and 1149 cm^{-1}; ^1H NMR ($CDCl_3$) δ=2.16 (6H, s, NMe_2), 2.5—2.8 (2H, m, NCH_2), 3.1—3.4 (2H, m, CH_2), 7.4—7.7 (3H, m, Ph), and 7.8—8.0 (2H, m, Ph); ^{13}C NMR ($CDCl_3$) δ=44.89 (q, NMe_2), 52.24, 53.83 (each t, CH_2), 128.01, 129.36, 133.83 (each d), and 139.66 (s); MS *m/z* (rel intensity, %) 213 (M^+, 4), 77 (64), 71 (98), 58 (base peak), 56 (28), 51 (29), and 42 (55). Found: C, 56.50; H, 7.05; N, 6.57%. Calcd for $C_{10}H_{15}NO_2S$: C, 56.31; H, 7.10; N, 6.57%.

2e: Colorless needles (benzene–hexane); mp 153—154 °C; IR (KBr) 1770 and 1710 cm^{-1}; ^1H NMR ($CDCl_3$) δ=1.06, 1.24 (each 3H, s, 4-Me), 2.20 (3H, s, *p*-Me), 2.35 (3H, s, NMe), 2.90 (1H, dd, *J*=9.9 and 8.0 Hz, one of 6-H (exo)), 2.94 (1H, d, *J*=7.3 Hz, 3a-H), 3.26 (1H, ddd, *J*=8.0, 7.3, and 1.7 Hz, 6a-H), 3.30 (1H, dd, *J*=9.9 and 1.7 Hz, the other of 6-H (endo)), and 7.0—7.3 (4H, m, Ar); ^{13}C NMR ($CDCl_3$) δ=18.77, 20.65 (each q, 4-Me), 22.41 (*p*-Me), 32.77 (q, NMe), 42.77 (d, 6a-C), 54.42 (d, 3a-C), 54.42 (t, 6-C), 62.30 (s, 4-C), 126.01, 129.24 (each d), 129.42, 137.89 (each s), 176.01, and 178.42 (each s, CON); MS *m/z* (rel intensity, %) 272 (M^+, 2), 257 (33), and 96 (base peak). Found: C, 70.53; H, 7.33; N, 9.96%. Calcd for $C_{16}H_{20}N_2O_2$: C, 70.56; H, 7.40; N, 10.29%.

2f: Colorless needles (diethyl ether); mp 145.5—147 °C; IR (KBr) 1770 and 1705 cm^{-1}; ^1H NMR ($CDCl_3$) δ=1.2—2.2 (8H, m, *c*-Pen), 2.22 (3H, s, *p*-Me), 2.35 (3H, s, NMe), 2.75 (1H, dd, *J*=10.2 and 8.2 Hz, one of 6-H (exo)), 2.97 (1H, d, *J*=7.9 Hz, 3a-H), 3.25 (1H, ddd, *J*=8.2, 7.9, and 1.2 Hz, 6a-H), 3.28 (1H, dd, *J*=10.2 and 1.2 Hz, the other of 6-H (endo)), and 7.0—7.3 (4H, m, Ar); ^{13}C NMR ($CDCl_3$) δ=20.82 (q, *p*-Me), 23.12, 23.35, 27.24, 29.83 (each t, *c*-Pen), 33.30 (q, NMe), 42.89 (d, 6a-C), 53.47 (d, 3a-C), 56.00 (t, 6-C), 74.71 (s, 4-C), 126.13, 129.30 (each d), 129.66, 137.95 (each s), 176.42, and 178.66 (each s, CON); MS m/z (rel intensity, %) 298 (M^+, 14), 269 (70), 256 (base peak), 108 (31), and 94 (29). Found: C, 72.54; H, 7.46; N, 9.08%. Calcd for $C_{18}H_{22}N_2O_2$: C, 72.45; H, 7.43; N, 9.39%.

2g: Colorless grains (benzene–hexane); mp 119—120 °C; IR (KBr) 1770 and 1710 cm^{-1}; ^1H NMR ($CDCl_3$) δ=1.1—1.9 (10H, m, *c*-Hex), 2.24 (3H, s, *p*-Me), 2.35 (3H, s, NMe), 2.8—3.4 (4H, m, 3a-, 6-, and 6a-H), and 7.0—7.3 (4H, m, Ar); ^{13}C NMR ($CDCl_3$) δ=21.12 (q, *p*-Me), 23.30, 23.71, 25.30, 26.00, 32.36 (each t, *c*-Hex), 33.12 (q, NMe), 43.00 (d, 6a-C), 50.42 (d, 3a-C), 54.77 (t, 6-C), 66.83 (s, 4-C), 126.48, 129.71 (each d), 129.83, 138.42 (each s), 176.72, and 179.07 (each s, CON); MS *m/z* (rel intensity, %) 312 (M^+, 34), 270 (22), 269 (base peak), and 256 (28). Found: C, 73.12; H, 7.69; N, 8.89%. Calcd for $C_{19}H_{24}N_2O_2$: C, 73.04; H, 7.74; N, 8.97%.

2h: Colorless prisms (benzene–hexane); mp 138—139 °C; IR (KBr) 1770 and 1708 cm^{-1}; ^1H NMR ($CDCl_3$) δ=2.24 (3H, s, *p*-Me), 2.35 (3H, s, NMe), 2.2—2.4, 3.1—3.4 (2H+4H, m, 3a-, 4-, 6-, and 6a-H), 7.04 (2H, d, Ar), and 7.26 (2H, d, Ar); ^{13}C NMR ($CDCl_3$) δ=21.00 (q, *p*-Me), 40.71 (q, NMe), 44.94 (d, 3a- and 6a-C), 58.83 (t, 4- and 6-C), 126.36, 129.66 (each d), 129.83, 138.36 (each s), and 178.66 (CON); MS *m/z* (rel intensity, %) 244 (M^+, 40), 82 (55), 57 (base peak), and 41 (24). Found: C, 68.93; H, 6.61; N, 11.33%. Calcd for $C_{14}H_{16}N_2O_2$: C, 68.83; H, 6.60; N, 11.47%.

2i: Colorless liquid; IR (neat) 1736 cm^{-1}; ^1H NMR ($CDCl_3$) δ=2.31 (3H, s, NMe), 2.6—3.0, 3.3—3.6 (4H+2H, m, 2-, 3-, 4-, and 5-H), and 3.70 (6H, s, COOMe); ^{13}C NMR ($CDCl_3$) δ=41.53 (q, NMe), 45.94 (d, 3- and 4-C), 59.06 (t, 2- and 5-C), 52.24 (q, COOMe), and 174.01 (s, COOMe); MS *m/z* (rel intensity, %) 201 (M^+, 7), 142 (13), 140 (27), 82 (base peak), 59 (21), 58 (33), and 42 (57). HRMS Found: *m/z* 201.0991. Calcd for $C_9H_{15}NO_4$: M, 201.1000.

2j: Colorless liquid; IR (neat) 1741 cm^{-1}; ^1H NMR ($CDCl_3$) δ=2.37 (3H, s, NMe), 2.6—2.8, 2.9—3.2, 3.2—3.4 (each 2H, m, 2-, 3-, 4-, and 5-H), and 3.65 (6H, s, COOMe); ^{13}C NMR ($CDCl_3$) δ=41.85 (q, NMe), 45.85 (d, 3- and 4-C), 51.81 (q, COOMe), 58.35 (d, 2- and 5-C), and 172.99 (s, COOMe); MS *m/z* (rel intensity, %) 201 (M^+, 7), 81 (base peak), 59 (25), 57 (27), and 41 (54); HRMS Found: *m/z* 201.1003. Calcd for $C_9H_{15}NO_4$: M, 201.1000.

2k: Colorless liquid; IR (neat) 2960, 2939, 2875 2779, and 1736 cm^{-1}; ^1H NMR ($CDCl_3$) δ=0.93 (3H, t, *n*-Bu), 1.2—1.8 (4H, m, *n*-Bu), 2.0—3.2 (7H, m, 2-, 3-, 4-, and 5-H), 2.35 (3H, s, NMe), and 4.08 (2H, t, *n*-Bu); ^{13}C NMR ($CDCl_3$) δ=12.94 (q, *n*-Bu), 18.41, 30.06 (each t, *n*-Bu), 27.47 (t, 4-C), 41.06 (q, NMe), 41.94 (d, 3-C), 55.30 (t, 5-C), 58.24 (t, 2-C), 63.65 (t, *n*-Bu), and 174.19 (s, COOBu-*n*); MS *m/z* (rel intensity, %) 185 (M^+, 7), 128 (56), 84 (24), 83 (28), 82 (57), 58 (42), 43 (base peak), 42 (67), and 40 (30). HRMS Found: *m/z* 185.1455. Calcd for $C_{10}H_{19}NO_2$: M, 185.1415.

2l: Pale yellow liquid; IR (neat) 1308 and 1147 cm^{-1}; ^1H NMR ($CDCl_3$) δ=2.0—2.9 (6H, m, 2-, 4-, and 5-H), 2.31 (3H, s, NMe), 3.5—3.9 (1H, m, 3-H), 7.4—7.7 (3H, m, Ph) and 7.8—8.0 (2H, m, Ph); ^{13}C NMR ($CDCl_3$) δ=25.94 (t, 4-C), 41.30 (q, NMe), 55.30, 55.47 (each t, 2- and 5-C), 62.48 (d, 3-C), 128.13, 129.13 (each d), 133.60, and 138.36 (each s); MS *m/z* (rel intensity, %) 225 (M^+, 3), 83 (base peak), 82 (45), and 41 (37). Found: C, 58.36; H, 6.76; N, 6.21%. Calcd for $C_{11}H_{15}NO_2S$: C, 58.63; H, 6.72; N, 6.22%.

2m: Colorless liquid; IR (neat) 1675 and 1605 cm^{-1}; ^1H NMR ($CDCl_3$) δ=2.34, 2.40 (each 3H, s, NMe and *p*-Me), 2.6—3.2, 3.7—4.1 (4H+2H, m, 2-, 3-, 4-, and 5-H), 7.12 (2H, d, COPh), 7.25 (5H, s, Ph), and 7.66 (2H, d, COPh); ^{13}C NMR ($CDCl_3$) δ=21.47 (q, *p*-Me), 42.00 (q, NMe), 46.65 (d, 4-C), 55.30 (d, 3-C), 60.36 (t, 2-C), 64.36 (t, 5-C), 126.60, 127.71, 128.72, 128.89. 129.30 (each d), 134.07, 143.83, 144.60 (each d), and 199.13 (s, CO); MS *m/z* (rel intensity, %) 279 (M^+, 42), 175 (51), 174 (base peak), 133 (59), 119 (20), 117 (26), 91 (28), 58 (32), 44 (22), and 43 (23). Found: C, 81.58; H, 7.58; N, 5.15%. Calcd for $C_{19}H_{21}NO$: C, 81.68; H, 7.58; N, 5.01%.

2n: Colorless needles (hexane); mp 78—80 °C; IR (KBr) 2250 cm^{-1}; ^1H NMR ($CDCl_3$) δ=2.49 (3H, s, NMe), 3.13 (2H, d, *J*=8.0 Hz, 5-H), 3.35 (2H, s, 2-H), 3.97 (1H, t, *J*=8.0 Hz, 4-H), and 7.37 (5H, s, Ph); ^{13}C NMR ($CDCl_3$) δ=40.48 (q, NMe), 40.67 (s, 3-C), 54.35 (d, 4-C), 58.79 (t, 2-C), 64.89 (t, 5-C), 113.87, 115.62 (each s, CN), 128.17, 128.76 (each d), and 135.01 (s); MS *m/z* (rel intensity, %) 211 (M^+, 3), 57 (88), and 41 (base peak). Found: C, 73.66; H, 6.20; N, 19.64%. Calcd for $C_{13}H_{13}N_3$: C, 73.90; H, 6.20; N, 19.89%.

3: Colorless prisms (benzene–hexane); mp 72—74 °C; IR (KBr) 1735 cm^{-1}; ^1H NMR ($CDCl_3$) δ=2.34 (6H, s, NMe), 2.71, 3.04 (each 4H, d, *J*=9.5 Hz, 2-, 3-, 5-, and 6-H), and 3.65 (6H, s, COOMe); ^{13}C NMR ($CDCl_3$) δ=41.75 (q, NMe), 52.29 (q, COOMe), 63.87 (s, 3a- and 6a-C), 65.62 (t, 1-, 3-, 4-, and 6-C), and 173.92 (s, COOMe); MS *m/z* (rel intensity, %) 256 (M^+, 32), 180 (34), 94 (22), 58 (base peak), and 43 (25). Found: C, 56.30; H, 7.76; N, 10.70%. Calcd for $C_{12}H_{20}N_2O_4$: C, 56.23; H, 7.87; N, 10.93%.

4: Pale yellow grains (benzene–hexane); mp 157—158 °C; IR (KBr) 1640 cm^{-1}; ^1H NMR ($CDCl_3$) δ=2.55 (3H, s, NMe), 4.03 (4H, s, 2- and 5-H), and 7.0—7.5 (10H, m, Ph); ^{13}C NMR ($CDCl_3$) δ=42.30 (q, NMe), 64.48 (t, 2- and 5-C), 128.24, 128.54, 128.65 (each d), 133.24 (d), 137.66 (s), 143.95

(s, 3- and 4-C), and 193.12 (s, CO); MS *m/z* (rel intensity, %) 291 (M^+, 5), 105 (52), 77 (base peak), and 51 (25). HRMS Found: *m/z* 291.1204. Calcd for $C_{19}H_{17}NO_2$: M, 291.1258.

Generation of Azomethine Ylide AY-B or AY-C by the Reaction of Proline (5) or 4-Thiazolidinecarboxylic Acid (7) with Paraformaldehyde and Subsequent Ylide Trapping with Olefins Leading to 6, 8, and 9. As a typical procedure, the reaction of **5** with paraformaldehyde in the presence of a maleimide is described: A mixture of **5** (0.3 g, 2.61 mmol), paraformaldehyde (0.2 g, 6.7 mmol), and *N*-(*p*-tolyl)maleimide (0.25 g, 1.32 mmol) was heated under reflux in toluene (15 ml) for 15 min. The water formed was removed by an azeotropic distillation. The mixture was evaporated in vacuo and the residue (0.36 g, 100%, 3:2 by ^{1}H NMR) was chromatographed over silica gel by using hexane–ethyl acetate (1:1 vol/vol) to give two stereoisomers of **6**. The results are summarized in Table 2.

8a,8b-*trans*-6: Colorless prisms (benzene–hexane); mp 150—152 °C; IR (KBr) 1775 and 1710 cm^{-1}; ^{1}H NMR ($CDCl_3$) δ=1.5—2.2 (4H, m, 7- and 8-H), 2.36 (3H, s, *p*-Me), 2.7—3.1, 3.2—3.8 (3H+4H, m, 3a-, 4-, 6-, 8a-, and 8b-H), and 7.0—7.3 (4H, m, Ar); ^{13}C NMR ($CDCl_3$) δ=21.12 (q, *p*-Me), 23.59 (t, 7-C), 29.65 (t, 8-C), 45.94 (d, 3a-C), 50.06 (d, 8b-C), 51.95 (t, 6-C), 55.00 (t, 4-C), 69.12 (d, 8a-C), 126.48, 129.77 (each d), 129.77, 138.60 (each s), 177.83, and 178.37 (each s, CON); MS *m/z* (rel intensity, %) 270 (M^+, 15), 133 (31), 132 (28), 108 (27), 104 (26), 83 (base peak), 82 (23), 81 (59), 80 (54), 78 (21), and 77 (31). Found: C, 71.15; H, 6.72; N, 10.22%. Calcd for $C_{16}H_{18}N_2O_2$: C, 71.09; H, 6.71; N, 10.36%. **8a,8b-*cis*-6:** Colorless solid; mp 138—140 °C; IR (KBr) 1770 and 1710 cm^{-1}; ^{1}H NMR ($CDCl_3$) δ=1.6—3.9 (11H, m, CH_2 and CH), 2.16 (3H, s, *p*-Me), and 7.0—7.3 (4H, m, Ar); ^{13}C NMR ($CDCl_3$) δ=21.06 (q, *p*-Me), 24.83 (t, 7-C), 25.18 (t, 8-C), 48.24 (d, 3a-C), 48.42 (d, 8b-C), 52.95 (t, 6-C), 54.65 (t, 4-C), 68.42 (d, 8a-C), 125.95, 129.66 (each d), 129.83 (s), 177.12, and 179.01 (each s, CON); MS *m/z* (rel intensity, %) 270 (M^+, 13), 108 (21), 83 (base peak), 81 (39), 80 (35), 77 (21), 68 (21), 56 (49), 42 (23), and 40 (24). Anal. Found: C, 70.65; H, 6.75; N, 10.18%. Calcd for $C_{16}H_{18}N_2O_2$: C, 71. 09; H, 6.71; N, 10.36%.

8: A similar procedure employing **7** (0.2 g, 1.5 mmol), paraformaldehyde (0.2 g, 6.7 mmol), and *N*-(*p*-tolyl)maleimide (0.25 g, 1.32 mmol) in toluene (18 ml) followed by silica-gel chromatography gave **8a,8b-*trans*-8** (0.156 g, 41%, from the elution with hexane–ethyl acetate (2:1 vol/vol)) and **8a,8b-*cis*-8** (0.153 g, 40%, from the elution with ethyl acetate). **8a,8b-*trans*-8:** Colorless needles (benzene–hexane); mp 213-215 °C; IR (KBr) 1700 cm^{-1}; ^{1}H NMR ($CDCl_3$) δ=2.34 (3H, s, *p*-Me), 2.62 (1H, t, *J*=10.0 Hz, one of 1-H (exo)), 2.8—3.5 (5H, m), 3.78 (1H, dd, *J*=10.0 and 7.5 Hz, 8b-H), 4.10, 4.26 (each d, *J*=9.8 Hz, 3-H), and 7.0—7.3 (4H, m, Ar); MS *m/z* (rel intensity, %) 288 (M^+, 53), 242 (74), 101 (26), 81 (base peak), and 80 (24). Found: C, 62.53; H, 5.62; N, 9.53%. Calcd for $C_{15}H_{16}N_2O_2S$: C, 62.48; H, 5.59; N, 9.71%. **8a,8b-*cis*-8:** Colorless prisms (benzene–hexane); mp 162—164 °C; IR (KBr) 1775 and 1700 cm^{-1}; ^{1}H NMR ($CDCl_3$) δ=2.34 (3H, s, *p*-Me), 2.5—3.9 (7H, m), 4.04, 4.20 (each 1H, d, *J*=9.8 Hz, 3-H), 7.07 (2H, d, Ar), and 7.23 (2H, d, Ar); ^{13}C NMR ($CDCl_3$) δ=21.18 (q, *p*-Me), 30.71 (t, 1-C), 46.12 (d, 5a-C), 47.89 (d, 8a-C), 52.06 (t, 5-C), 57.18 (t, 3-C), 70.48 (d, 8b-C), 126.36, 129.19 (each d), 130.01, 139.07 (each s), 175.36, and 177.07 (each s, CON); MS *m/z* (rel intensity, %) 288 (M^+, 73), 242 (53), 101 (22), 100 (46), 81 (base peak), 80 (23), and 55 (22). Found: C, 62.72; H, 5.63; N, 9.70%. Calcd for $C_{15}H_{16}N_2O_2S$: C, 62.48; H, 5.59; N, 9.71%.

9: A similar procedure using **7** (0.2 g, 1.5 mmol), paraformaldehyde (0.2 g, 6.7 mmol), and dimethyl maleate (0.2 g, 1.39 mmol) in toluene (15 ml) followed by silica-gel chromatography gave **9** as a mixture of **7,7a-*trans*-9** and **7,7a-*cis*-9** (5:4 by GLC, 0.207 g, 77%, eluent: hexane–ethyl acetate (5:1 vol/vol)). The separation of either isomer was unsuccessful. **9:** Colorless liquid; IR (neat) 1735 cm^{-1}; ^{1}H NMR ($CDCl_3$) δ=2.6—4.3 (9H, m), 3.65, and 3.68 (each 3H, s, COOMe); ^{13}C NMR ($CDCl_3$) δ=32.65, 39.71 (each t, 4:5, 1-C), 44.71, 45.83 (each d, 4:5, 6-C), 48.60, 51.36 (each d, 4:5, 7-C), 51.89, 52.06, 52.18 (each q, COOMe), 53.30, .56.18 (each t, 4:5, 5-C), 58.00, 61.42 (each t, 4:5, 3-C), 68.48, 70.65 (each d, 5:4, 7a-C), 171.01, 171.66, 172.96, and 173.36 (each s, COOMe); MS *m/z* (rel intensity, %) 245 (M^+, 57), 214 (38), 212 (25), 199 (38), 140 (base peak), 101 (26), 81 (25), 80 (46), 59 (26), 55 (27), 41 (40), and 40 (24). HRMS Found: *m/z* 245.0731. Calcd for $C_{10}H_{15}NO_4S$: M, 245.0721.

General Procedure for the Generation of Azomethine Ylide AY-D by Thermolysis of 5-Oxazolidinone 11 and Subsequent Ylide Trapping with Olefins or Aldehydes Leading to 12 or 13. A mixture of *N*-phenylglycine (10, 0.2 g, 1.32 mmol) and paraformaldehyde (0.207 g, 6.9 mmol) was heated under reflux in toluene (10 ml). The water formed was removed by the aid of Dean-Stark trap. After 20 min the toluene was evaporated to dryness in vacuo to give almost pure **11** (0.215 g, 100%) as a labile solid: ^{1}H NMR ($CDCl_3$) δ=3.83 (2H, s, 4-H), 5.24 (2H, s, 2-H), 6.3—6.5 (2H, m, Ph), 6.7—6.9 (1H, m, Ph), and 7.0—7.3 (2H, m, Ph); ^{13}C NMR ($CDCl_3$) δ=46.18 (t, 4-C), 81.54 (t, 2-C), 112.60, 119.89, 129.42 (each d), 144.07 (s), and 171.42 (s, COO). The generation of ylide **AY-D** was conducted without isolation of the precursor **11** as follows: A mixture of **10** (0.2 g, 1.32 mmol) and paraformaldehyde (0.207 g, 6.9 mmol) was heated under reflux in toluene (10 ml) for 30 min under continuous removal of the water formed and then an olefin or an aldehyde (1.32 mmol) was added. The resulting mixture was heated under reflux. The residue obtained by evaporation of the solvent in vacuo was chromatographed over silica gel by using hexane–ethyl acetate to give **12** or **13**. The reaction conditions as well as the results are all summarized in Table 2.

12a: Colorless needles (ethyl acetate–hexane); mp 214—216 °C; IR (KBr) 1700 cm^{-1}; ^{1}H NMR ($CDCl_3$) δ=2.35 (3H, s, *p*-Me), 3.1—3.4, 3.4—3.7 (each 2H, m), 4.07 (2H, d, *J*=8.9 Hz, 4- and 6-H), 6.6—6.9 (3H, m, Ar), and 7.0—7.4 (6H, m, Ar); MS *m/z* (rel intensity, %) 306 (M^+, base peak), 144 (74), 119 (37), 105 (26), 104 (36), 91 (62), and 77 (46). Found: C, 74.61; H, 5.89; N, 8.90%. Calcd for $C_{19}H_{18}N_2O_2$: C, 74.49; H, 5.92; N, 9.14%.

12b: Colorless needles (hexane); mp 104—106 °C; IR (KBr) 1725 cm^{-1}; ^{1}H NMR ($CDCl_3$) δ=3.4—3.7 (6H, m, 2-, 3-, 4-, and 5-H), 3.72 (6H, s, COOMe), 6.4—6.8 (3H, m, Ph), and 7.1—7.3 (2H, m, Ph); ^{13}C NMR ($CDCl_3$) δ=45.53 (d, 3- and 4-C), 50.30 (t, 2- and 5-C), 52.36 (q, COOMe), 112.42, 117.12, 129.36 (each d), 147.31 (s), and 172.83 (s, COOMe); MS *m/z* (rel intensity, %) 263 (M^+, base peak), 202 (31), 145 (37), 144 (74), 119 (21), 104 (32), 91 (42), and 77 (41). Found: C, 64.17; H, 6.60; N, 5.39%. Calcd for $C_{14}H_{17}NO_4$: C, 63.87; H, 6.51; N, 5.32%.

12c: Colorless needles (hexane); mp 78—80 °C; IR (KBr) 1725 cm^{-1}; ^{1}H NMR ($CDCl_3$) δ=3.2—3.7 (6H, m, 2-, 3-, 4-, and 5-H), H), 3.65 (6H, s, COOMe), 6.4—6.8 (3H, m, Ph),

and 7.0—7.3 (2H, m, Ph); ^{13}C NMR ($CDCl_3$) δ=45.06 (d, 3- and 4-C), 49.06 (t, 2- and 5-C), 52.12 (q, COOMe), 111.95, 116.65, 129.36 (each d), 147.24 (s), and 172.31 (s, COOMe); MS *m/z* (rel intensity, %) 263 (M^+, 77), 204 (21), 145 (56), 144 (base peak), 104 (32), 91 (38), and 77 (49). Found: C, 63.94; H, 6.50; N, 5.58%. Calcd for $C_{14}H_{17}NO_4$: C, 63.87; H, 6.51; N, 5.32%.

13a: Yellow prisms (benzene–hexane); mp 118—120 °C; IR (KBr) 1595 and 1345 cm^{-1}; ^{1}H NMR ($CDCl_3$) δ=3.27 (1H, dd, *J*=8.6 and 7.5 Hz, one of 4-H), 3.86 (1H, dd, *J*=8.6 and 6.5 Hz, the other of 4-H), 5.05, 5.17 (each 1H, d, *J*=2.3 Hz, 2-H), 5.33 (1H, dd, *J*=7.5 and 6.5 Hz, 5-H), 6.4—6.6 (2H, m, Ph), 6.7—6.9 (1H, m, Ph), 7.1—7.3 (2H, m, Ph), 7.55 (1H, d, *J*=8.8 Hz, Ar), and 8.20 (1H, d, *J*=8.8 Hz, Ar); ^{13}C NMR ($CDCl_3$) δ=53.59 (t, 4-C), 78.88 (d, 5-C), 82.18 (t, 2-C), 113.07, 118.54, 123.95, 126.89, 129.60 (each d), 145.48, 147.31, and 147.89 (each s); MS *m/z* (rel intensity, %) 270 (M^+, 32), 119 (92), 91 (base peak), and 77 (35). Found: C, 67.00; H, 5.30; N, 10.17%. Calcd for $C_{15}H_{14}N_2O_3$: C, 66.66; H, 5.22; N, 10.36%.

13b: Pale yellow liquid; IR (neat) 1690 cm^{-1}; ^{1}H NMR ($CDCl_3$) δ=3.6—3.8 (2H, m, 4-H), 5.01, 5.04 (each 1H, d, *J*=2.1 Hz, 2-H), 5.50 (1H, dd, *J*=6.8 and 6.1 Hz, 5-H), 6.4—6.6 (2H, m, Ph), 6.7—6.9 (1H, m, Ph), 7.1—7.3 (2H, m, Ph), 7.3—7.6 (3H, m, PhCO), and 7.9—8.1 (2H, m, PhCO); ^{13}C NMR ($CDCl_3$) δ=48.36 (t, 4-C), 79.24 (d, 5-C), 82.06 (t, 2-C), 113.30, 118.42, 128.83, 128.95, 129.42 (each d), 133.83, 134.72, 145.42 (each s), 196.31 (s, CO); MS *m/z* (rel intensity, %) 253 (M^+, 39), 222 (23), 149 (30), 122 (49), 121 (56), 120 (34), 106 (40), 105 (base peak), 93 (26), 91 (29), 77 (77), 58 (29), 51 (25), and 43 (76). HRMS Found: *m/z* 253.1099. Calcd for $C_{16}H_{15}NO_2$: M, 253.1102.

13c: Pale yellow liquid; IR (neat) 1715 cm^{-1}; ^{1}H NMR ($CDCl_3$) δ=2.20, 2.23, (each 3H, s, COMe), 4.40 (1H, d, *J*=3.2 Hz, 4-H), 4.61 (1H, d, *J*=3.2 Hz, 5-H), 5.07, 5.18 (each 1H, d, *J*=2.5 Hz, 2-H), 6.4—6.5 (2H, m, Ph), 6.7—6.9 (1H, m, Ph), and 7.1—7.3 (2H, m, Ph); ^{13}C NMR ($CDCl_3$) δ=25.94, 26.41 (each q, COMe), 67.36 (d, 4-C), 82.71 (t, 2-C), 84.77 (d, 5-C), 113.19, 119.60, 129.89 (each d), 144.19 (s), 206.25, and 208.72 (each s, COMe); MS *m/z* (rel intensity, %) 233 (M^+, 21), 190 (base peak), 162 (25), 149 (50), 146 (32), 91 (22), 77 (25), and 43 (40). HRMS Found: *m/z* 233.1055. Calcd for $C_{13}H_{15}NO_3$: M, 233.1051.

General Procedure for the Generation of Azomethine Ylides AY-F from Glycine (14) and Carbonyl Compounds and Subsequent Ylide Trapping with Olefins Leading to 15 and 16. A mixture of **14** (0.2 g, 2.66 mmol), paraformaldehyde (0.2 g, 6.67 mmol), and an olefin (1.32 mmol) was heated under reflux in toluene or DMF (15 ml). The solvent as well as the reaction conditions is listed in Table 3 (Entries 1—6). After the completion of reaction the solvent was evaporated in vacuo and the residue was chromatographed over silica gel with ethyl acetate as an eluent to give **15** or **16**. The results are summarized in Table 3. Elemental analyses for **16a—16c** were not available because of the absence of parent ion peaks in their mass spectra.

15a: Colorless grains (benzene–hexane); mp 159—161 °C; IR (KBr) 3330 and 1700 cm^{-1}; ^{1}H NMR ($CDCl_3$) δ=1.31, 1.36 (each 3H, s, Me), 1.99 (1H, br s, NH), 2.35 (3H, s, *p*-Me), 2.9—3.1, 3.3—3.6 (1H+3H, m, 3a-, 6-, and 6a-H), and 7.0—7.3 (4H, m, Ar); ^{13}C NMR ($CDCl_3$) δ=21.12 (q, *p*-Me), 25.12, 28.83 (each q, Me), 47.94 (t, 6-C), 48.47 (d, 6a-C), 54.89 (d, 3a-C), 63.12 (s, 4-C), 126.30, 129.48 (each d), 129.83, 138.66 (each s), 176.36, and 178.66 (each s, CON); MS *m/z* (rel intensity, %) 258 (M^+, 2), 82 (base peak), and 67 (19). Found: C, 69.56; H, 7.03; N, 10.53%. Calcd for $C_{15}H_{18}N_2O_2$: C, 69.73; H, 7.04; N, 10.85%.

15b: Colorless grains (benzene–hexane); mp 148—150 °C; IR (KBr) 3300 and 1700 cm^{-1}; ^{1}H NMR ($CDCl_3$) δ=1.2—2.0 (10H, m, *c*-Hex), 2.35 (3H, s, *p*-Me), 2.96 (1H, br, NH), 3.1—3.6 (4H, m, 3a-, 6-, and 6a-H), and 7.0—7.3 (4H, m, Ar); ^{13}C NMR ($CDCl_3$) δ=22.71, 23.24, 25.59, 34.71, 36.36 (each t, *c*-Hex), 21.24 (q, *p*-Me), 47.53 (d, 6a-C), 47.83 (t, 6-C), 54.65 (d, 3a-C), 126.42, 129.54, 129.95 (each d), 138.77 (s), 176.36, and 179.01 (each s, CON); MS *m/z* (rel intensity, %) 258 (M^+, 2), 82 (base peak), and 67 (19). Found: C, 69.56; H, 7.03; N, 10.53%. Calcd for $C_{15}H_{18}N_2O_2$: C, 69.73; H, 7.04; N, 10.85%.

16a: Colorless needles (benzene–hexane); mp 102—104 °C; IR (KBr) 1705 cm^{-1}; ^{1}H NMR ($CDCl_3$) δ=2.32 (6H, s, *p*-Me), 2.3—2.6 (4H, m, CH), 3.1—3.5 (10H, m, CH_2), and 7.0—7.3 (8H, m, Ar); ^{13}C NMR ($CDCl_3$) δ=21.18 (q, *p*-Me), 44.24 (d, CH), 55.24 (t, CH_2), 72.01 (t, NCH_2N), 126.42, 129.95 (each d), 138.77 (s), and 178.66 (s, CON); MS *m/z* (rel intensity, %) 244 (M^+—228, 18), 243 (base peak) 96 (24), 81 (43), 80 (20), 68 (88), 55 (37), 43 (42), 42 (29), and 41 (25).

16b: Pale yellow liquid; IR (neat) 2250 cm^{-1}; ^{1}H NMR ($CDCl_3$) δ=3.2—4.1 (12H, m, CH_2 and CH) and 7.40 (10H, s, Ph); ^{13}C NMR ($CDCl_3$) δ=40.59 (s, q-C), 53.95 (d, CH), 54.89, 61.42 (each t, CH_2), 73.18 (t, NCH_2N), 114.01, 115.42 (each s, CN), 128.42, 129.30 (each d), and 134.36 (s); MS *m/z* (rel intensity, %) 211 (M^+—195, 17), 210 (base peak), 132 (36), 105 (32), 103 (23), 91 (34), and 42 (77).

16c: Colorless liquid; IR (neat) 1735 cm^{-1}; ^{1}H NMR ($CDCl_3$) δ=2.8—3.7 (14H, m, CH_2 and CH) and 3.68 (12H, s, COOMe); ^{13}C NMR ($CDCl_3$) δ=45.24 (d, CH), 52.24 (q, COOMe), 55.06 (t, CH_2), 74.36 (t, NCH_2N), and 174.07 (s, COOMe); MS *m/z* (rel intensity, %) 343 (M^+—43, 12), 312 (15), 200 (93), 140 (33), 82 (27), 68 (21), 59 (base peak), 41 (27), and 33 (44).

Triethyl Perhydro-1,3,5-triazine-1,3,5-triacetate (18): To a solution of aqueous formaldehyde (37%, 0.39 g, 4.85 mmol) in ethanol (0.5 ml) was added at 0 °C ethyl aminoacetate (**17**) (0.35 g, 3.39 mmol). The mixture was stirred at 0 °C for 10 h, diluted with dichloromethane (30 ml), and then dried over magnesium sulfate. The residue obtained by evaporating the solvent in vacuo was chromatographed over silica gel with hexane–ethyl acetate (1:1 vol/vol) to give **18** (0.208 g, 53%): Colorless liquid; IR (neat) 1735 cm^{-1}; ^{1}H NMR ($CDCl_3$) δ=1.24 (9H, t, COOEt), 3.39 (6H, NCH_2), 3.67 (6H, NCH_2N), and 4.13 (6H, q, COOEt); ^{13}C NMR ($CDCl_3$) δ=14.24 (q, COOEt), 54.06 (t, NCH_2), 60.71 (t, NCH_2N), 73.18 (t, COOEt), and 170.84 (s, COOEt).

3-(Triphenylmethyl)-5-oxazolidinone (20). This compound was prepared according to either of the following two methods: (1) A mixture of *N*-(triphenylmethyl)aminoacetic acid (**19**) (0.203 g, 0.64 mmol) and paraformaldehyde (0.1 g, 3.3 mmol) was heated under reflux in toluene (10 ml) for 15 min during which time the water formed was removed by the aid of a Dean-Stark trap. The residue, obtained by evaporation of the solvent, was dissolved in dichloromethane (30 ml). The dichloromethane was washed with water, dried over magnesium sulfate, and evaporated in vacuo to give colorless solid of **20** (0.189 g, 90%). (2) To a solution of **19** (0.205 g, 0.65 mmol) in ethanol (15 ml) was added at room temperature aqueous formaldehyde (37%, 0.3 ml). The mixture was stirred at room temperature for 2 h

and evaporated in vacuo. The residue was dissolved in dichloromethane (30 ml). This solution was dried over magnesium sulfate and evaporated in vacuo to give **20** (0.211 g, 99%). **20**: Colorless needles (benzene-hexane); mp 153—155 °C; IR (KBr) 1775 cm^{-1}; ^1H NMR ($CDCl_3$) δ=3.55 (2H, s, 4-H), 5.09 (2H, s, 2-H), and 7.0—7.5 (15H, m, Trt); ^{13}C NMR ($CDCl_3$) δ=48.77 (t, 4-C), 76.01 (s, Trt), 83.54 (t, 2-C), 127.42, 128.48, 128.89 (each d), and 142.66 (s); MS *m/z* (rel intensity, %) 244 (M^+−86, 24), 243 (base peak), and 165 (27). Found: C, 80.01; H, 5.87; N, 4.40%. Calcd for $C_{22}H_{19}NO_2$: C, 80.22; H, 5.81; N, 4.25%.

Generation of Azomethine Ylide AY-H by Thermolysis of 20 and Subsequent Ylide Trapping with Olefins Leading to 21. A mixture of **20** (0.396 g, 1.2 mmol) and an olefin (1 mmol) in dry toluene (20 ml) was heated under reflux for the period shown in Table 3 (Entries 7—9). The mixture was evaporated in vacuo and the residue was chromatographed over silica gel by using hexane-ethyl acetate (1:1 vol/vol) to give **21**. The results are listed in Table 3.

21a: Colorless prisms (benzene-hexane); mp 137—138.5 °C; IR (KBr) 1735 cm^{-1}; ^1H NMR ($CDCl_3$) δ=2.4—2.8, 3.2—3.4 (4H+2H, m, 2-, 3-, 4-, and 5-H), 3.65 (6H, s, COOMe), and 7.0—7.5 (15H, m, Trt); ^{13}C NMR ($CDCl_3$) δ=44.07 (d, 3- and 4-C), 49.83 (t, 2- and 5-C), 52.12 (q, COOMe), 73.95 (s, Trt), 126.48, 127.71, 129.30 (each d), 142.13 (s), 174.24 (s, COOMe); MS (at 40 eV) *m/z* (rel intensity, %) 429 (M^+, 1), 244 (21), 243 (base peak), and 165 (37). Found: C, 75.31; H, 6.43; N, 3.49%. Calcd for $C_{27}H_{27}NO_4$: C, 75.50; H, 6.34; N, 3.26%.

21b: Colorless needles (benzene-hexane); mp 140—141 °C; IR (KBr) 1735 cm^{-1}; ^1H NMR ($CDCl_3$) δ=2.5—2.8, 2.9—3.1 (2H+4H, m, 2-, 3-, 4-, and 5-H), 3.60 (6H, s, COOMe), and 7.0—7.6 (15H, m, Trt); ^{13}C NMR ($CDCl_3$) δ=44.18 (d, 3- and 4-C), 48.94 (t, 2- and 5-C), 51.71 (q, COOMe), 74.48 (s, Trt), 126.42, 127.66, 129.36 (each d), 142.42 (s), and 173.07 (s, COOMe); MS *m/z* (rel intensity, %) 429 (M^+, 1), 244 (33), 243 (base peak), and 165 (23). Found: C, 75.52; H, 6.43; N, 3.50%. Calcd for $C_{27}H_{27}NO_4$: C, 75.50; H, 6.34; N, 3.26%.

21c: Colorless prisms (benzene-hexane); mp 276—279 °C; IR (KBr) 1700 cm^{-1}; ^1H NMR ($CDCl_3$) δ=1.7—2.0 (2H, m, 3a- and 6a-H), 2.41 (3H, s, *p*-Me), 3.0—3.2, 3.5—3.7 (each 2H, m, 4- and 6-H), and 7.1—7.4 (19H, m, Ar); MS *m/z* (rel intensity, %) 473 (M^+, 1), 243 (base peak), 244 (22), and 165 (39). HRMS Found: *m/z* 472.2144. Calcd for $C_{32}H_{28}N_2O_2$: M, 472.2149.

General Procedure for the Elimination of Trityl Group of 21 Leading to 22. To a solution of **21a** or **21b** (0.1 g, 0.232 mmol) in dichloromethane (1 ml) was added concd HCl (0.05 ml). The mixture was stirred at room temperature for 0.5 h. Another portion of dichloromethane (30 ml) and then saturated aqueous sodium carbonate (30 ml) were added. The dichloromethane was dried over magnesium sulfate and evaporated in vacuo to give **22a** (0.023 g, 53%) or **22b** (0.022 g, 50%).

22a: Colorless liquid; IR (neat) 3330 and 1725 cm^{-1}; ^1H NMR ($CDCl_3$) δ=2.17 (1H, s, NH, D_2O exchangeable), 3.0—3.5 (6H, m, 2-, 3-, 4-, and 5-H), and 3.67 (6H, s, COOMe); ^{13}C NMR ($CDCl_3$) δ=48.18 (d, 3- and 4-C), 52.12 (t, 2- and 5-C), 52.30 (q, COOMe), and 174.54 (s, COOMe); MS *m/z* (rel intensity, %) 187 (M^+, 3), 68 (base peak), 59 (21), 43 (44), 42 (22), 41 (35), and 39 (31). HRMS Found: *m/z* 187.0861. Calcd for $C_8H_{13}NO_4$: M, 187.0844.

22b: Colorless liquid; IR (neat) 3300 and 1725 cm^{-1}; ^1H NMR ($CDCl_3$) δ=2.47 (1H, s, NH, D_2O exchangeable), 3.1—3.4 (6H, m, 2-, 3-, 4-, and 5-H), and 3.63 (6H, s, COOMe); ^{13}C NMR ($CDCl_3$) δ=47.71 (d, 3- and 4-C), 50.65 (t, 2- and 5-C), 52.00 (q, COOMe), and 173.54 (s, COOMe); MS *m/z* (rel intensity, %) 187 (M^+, 2), 68 (base peak), 59 (25), 43 (27), 42 (22), 41 (39), and 39 (33). HRMS Found: *m/z* 187.0843. Calcd for $C_8H_{13}NO_4$: M, 187.0844.

4-Methyl-3-triphenylmethyl-5-oxazolidinone (24): A mixture of *N*-triphenylmethyl-2-aminopropanoic acid (**23**) (1.12 g, 3.37 mmol) and paraformaldehyde (0.5 g, 16.7 mmol) was heated in toluene (30 ml) for 0.5 h. The water formed was removed by the aid of a Dean-Stark trap. The toluene was removed by evaporation in vacuo, the residue was dissolved in dichloromethane (30 ml). The dichloromethane was washed with water, dried over magnesium sulfate, and then evaporated to give **24** (1.01 g, 91%): Colorless needles (benzene-hexane); mp 174—177 °C; IR (KBr) 1775 cm^{-1}; ^1H NMR ($CDCl_3$) δ=1.52 (3H, d, *J*=7.2 Hz, 4-Me), 3.72 (q, 1H, *J*=7.2 Hz, 4-H), 5.15, 5.32 (each 1H, d, *J*=8.0 Hz, 2-H), and 7.1—7.5. (15H, m, Trt); ^{13}C NMR ($CDCl_3$) δ=15.41 (q, 4-Me), 55.42 (d, 4-C), 77.24 (s, Trt), 82.36 (t, 2-C), 127.24, 128.42, 128.77 (each d), 143.31 (s), and 177.01 (5-C); Ms *m/z* (rel intensity, %) 343 (M^+, 1), 266 (3), 244 (27), 243 (base peak), 241 (5), 239 (5), 166 (base peak), 165 (32), 91 (3), 78 (4), and 77 (4). Found: C, 80.43; H, 6.18; N, 4.20%. Calcd for $C_{23}H_{21}NO_2$: C, 80.44; H, 6.16; N, 4.08%.

***N*-(Triphenylmethyl)methylamine (25):** Colorless liquid; IR (neat) 3330, 1598, 1485, 1450, 900, and 700 cm^{-1}; ^1H NMR ($CDCl_3$) δ=1.5—1.7 (1H, br, NH), 2.03 (3H, s, NMe), and 7.0—7.5 (15H, m, Ph); ^{13}C NMR ($CDCl_3$) δ=30.59 (q, NMe), 71.42 (s, q-C), 126.36, 127.89 128.91 (each d), and 146.01 (s); MS *m/z* (rel intensity, %) 273 (M^+, 13), 243 (33), 196 (base peak), 165 (28), and 77 (22). HRMS Found: *m/z* 273.1515. Calcd for $C_{20}H_{19}N$: M, 273.1517.

Generation of Azomethine Ylide AY-I and Ylide Trapping with Olefins Leading to 27. A mixture of *N*-benzylaminoacetic acid (**26**) (0.33 g, 2 mmol), paraformaldehyde (0.18 g, 6 mmol), and an olefin (1 mmol) in dry toluene (10 ml) was refluxed for 15 min. The water formed was continuously removed. The toluene was evaporated in vacuo and the residue was chromatographed over silica gel with hexane-ethyl acetate (3:1 to 1:1 vl/vol) to give **27a**—**27d**. The results are summarized in Table 3. Cycloadducts **27a** and **27b** are known and their structures were confirmed by comparison of the spectral data with the reported ones.[8]

27c: Colorless plates (benzene-hexane); mp 129—130 °C; IR (KBr) 1770 and 1695 cm^{-1}; ^1H NMR ($CDCl_3$) δ=2.2—2.5 (2H, m, 3a- and 6a-H), 2.31 (3H, s, *p*-Me), 3.0—3.4 (4H, m, 4- and 6-H), 3.51 (2H, s, $PhCH_2$), and 7.0—7.2 (9H, m, Ar); ^{13}C NMR ($CDCl_3$) δ=21.12 (q, *p*-Me), 44.24 (d, 3a- and 6a-C), 56.47 (t, 4- and 6-C), 58.12 (t, $PhCH_2$), 126.36, 127.24, 128.30, 128.48, 129.83 (each d), 138.01, 138.60 (each s), and 178.66 (s, CON); MS *m/z* (rel intensity, %) 320 (M^+, 80), 319 (25), 243 (23), 229 (73), 133 (22), 92 (28), 91 (base peak), 42 (30), and 32 (28). Found: C, 74.95; H, 6.29; N, 8.75%. Calcd for $C_{20}H_{20}N_2O_2$: C, 74.98; H, 6.29; N, 8.74%.

27d: Colorless liquid; IR (neat) 1730 cm^{-1}; ^1H NMR ($CDCl_3$) δ=0.92 (3H, t, *n*-Bu), 1.2—1.8, 1.9—2.2, 2.3—3.1 (4H+2H+5H, m, *n*-Bu and CH_2), 3.60 (2H, s, $PhCH_2$), 4.06 (2H, t, *n*-Bu), and 7.1—7.4 (5H, m, Ph); ^{13}C NMR ($CDCl_3$) δ=13.71 (q, *n*-Bu), 19.12, 27.71, 30.71 (each t, *n*-Bu and 4-C), 42.24 (d, 3-C), 53.77, 56.77, 60.12, 64.48 (each t, *n*-Bu, 2-, and

5-C), 127.07, 128.36, 128.83 each d), 139.13 (s), and 175.19 (s, COOBu-*n*); MS *m/z* (rel intensity, %) 261 (M^+, 6), 170 (30), 91 (base peak), 72 (30), and 42 (39). HRMS Found: *m/z* 261.1751. Calcd for $C_{16}H_{23}NO_2$: M, 261.1728.

Debenzylation of 27c by Pd/C Leading to 22c. A mixture of **27c** (0.16 g, 0.5 mmol) and palladium on charcoal (5%, 0.15 g) in dry xylene (1.5 ml) was refluxed under an atmosphere of hydrogen (ca. 1 atm) for 3 h. The catalyst was filtered off and washed with dichloromethane (5 ml). The filtrate and washing were combined and evaporated in vacuo to give **22c** (0.11g, 96%): Colorless viscous liquid; IR (neat) 3300, 1770, and 1700 cm^{-1}; ^1H NMR ($CDCl_3$) δ=1.7—2.0 (1H, m, D_2O exchangeable, NH), 2.38 (3H, s, *p*-Me), 2.9—3.7 (4H, m, 3a-, 4-, 6, and 6a-H), and 7.0—7.4 (4H, m, Ar); MS *m/z* (rel intensity, %) 230 (M^+, 70), 188 (24), 107 (18), 96 (31), 91 (19), 68 (base peak), and 43 (78). HRMS Found: *m/z* 230.1050. Calcd for $C_{13}H_{14}N_2O_2$: M, 230.1054.

References

1) a) O. Tsuge, S. Kanemasa, M. Ohe, K. Yorozu, S. Takenaka, and K. Ueno, the preceding article in this bulletin. b) Part of the present work has been already reported as a communication letter (O. Tsuge, S. Kanemasa, M. Ohe, and S. Takenaka, *Chem. Lett.*, **1986**, 973).

2) R. Grigg, J. Kemp, G. Sheldrick, and J. Trotter, *J. Chem. Soc., Chem. Commun.*, **1978**, 109; M. Joucla and J. Hamelin, *Tetrahedron Lett.*, **1978**, 2885; O. Tsuge, K. Ueno, and K. Oe, *Chem. Lett.*, **1979**, 1407; Review: R. Grigg, *Bull. Soc. Chim. Belg.*, **93**, 593 (1984) and references cited therein.

3) Some decarboxylative ylide generation from α-amino acids is known: R. Grigg and S. Thianpatanagul, *J. Chem. Soc., Chem. Commun.*, **1984**, 180; C.-L. J. Wang, W. C. Ripka, and P. N. Confalone, *Tetrahedron Lett.*, **25**, 4613 (1984); R. Grigg, M. F. Aly, V. Sridharan, and S. Thianpatanagul, *J. Chem. Soc., Chem. Commun.*, **1986**, 182; M. Joucla and J. Mortier, *ibid.*, **1985**, 1566.

4) As ready decarboxylation of iminium acids: W. G. Phillips and K. W. Ratts, *Tetrahedron Lett.*, **1969**, 1383; K. W. Ratts, R. K. Howe, and W. G. Phillips, *J. Am. Chem. Soc.*, **91**, 6115 (1969); G. P. Rizzi, *J. Org. Chem.*, **35**, 2069 (1970).

5) Stereostructures of **2a—2c** were confirmed on the basis of the vicinal coupling J_{6-6a} (**3a,4-*trans*-2a**: 8.2 and 5.8 Hz; **3a,4-*cis*-2a**: 6.5 and 0 Hz), the magnetic shielding of the 3-COOMe by the 2-Ph (3-COOMe: **2,3-*cis*-2b**: δ=3.06; **2,3-*cis*-2c**: δ=3.20), and other spectral data given in Experimental section.

6) a) K. Achiwa, N. Imai, T. Inaoka, and M. Sekiya, *Chem. Pharm. Bull.*, **32**, 2878 (1984). b) O. Tsuge, S. Kanemasa, A. Hatada, and K. Matsuda, *Chem. Lett.*, **1984**, 801.

7) The formation of fumarate cycloadduct from an azomethine ylide cycloaddition to dimethyl maleate has been reported: M. Joucla, J. Mortier, and J. Hamelin, *Tetrahedron Lett.*, **26**, 2775 (1985). They have suggested a possibility of isomerization of dimethyl maleate into dimethyl fumarate in the presence of an amine.

8) A. Padwa and Y.-Y. Chen, *Tetrahedron Lett.*, **24**, 3447 (1983); A. Hosomi, Y. Sakata, and H. Sakurai, *Chem. Lett.*, **1984**, 1117; Y. Terao, H. Kotani, N. Imai, and K. Achiwa, *Chem. Pharm. Bull.*, **33**, 2762 (1985); A. Padwa, Y.-Y. Chen, U. Chiacchio, and W. Dent, *Tetrahedron*, **41**, 3529 (1985); A. Padwa, Y.-Y. Chen, W. Dent, and H. Nimmesgern, *J. Org. Chem.*, **50**, 4006 (1985).

9) An intermediacy of 5-oxazolidinones has been reported: A. Eschenmoser, *Chem. Soc. Rev.*, **5**, 377 (1976).

10) In the previous communication incorrect structures have been presented to **16a** and **16b** (See Ref. 1). They are correctly reassigned in this article.

11) 5-Oxazolidinone **D** is unknown. Thermal stability of its 3-substituted derivatives seems to depend upon the size of 3-substituent (See compounds **11** and **20**), indicating the thermal instability of the parent 5-oxazolidinone **D**.

12) In fact the reaction of *N*-unsubstituted cycloadduct **22c** with paraformaldehyde under reflux in toluene for 0.5 h led to a quantitative formation of **16a**.

13) *N*-(Methyl)triphenylmethylamine corresponds to the product derived through the hydrolysis of the expected azomethine ylide.

 © 1987 The Chemical Society of Japan Bull. Chem. Soc. Jpn., 60, 4091—4098 (1987)

Horner-Emmons Olefination of 4-Hydroxy-2-oxoalkylphosphonates and Related Compounds: Applications to the Syntheses of (±)-Gingerol, (±)-Yashabushiketol, and (±)-Dihydroyashabushiketol

Otohiko Tsuge,* Shuji Kanemasa, Norihiko Nakagawa, and Hiroyuki Suga
Institute of Advanced Material Study, and Department of Molecular Science and Technology, Interdisciplinary Graduate School of Engineering Sciences, Kyushu University, Kasugakoen, Kasuga 816
(Received June 19, 1987)

Horner–Emmons olefination of 4-hydroxy-2-oxoalkylphosphonates, readily available by hydrogenation of 5-substituted 3-phosphinylmethyl-2-isoxazolines, gives mainly E-isomers of 1-hydroxy-4-alken-3-ones bearing a variety of substituents at the 1-position. Use of the combination of triethylamine (or DBU)+lithium bromide as a weak base on the *O*-unprotected phosphonates is favored. Similar olefinations on the isoxazolines, 2-oxo-3-alkenylphosphonates, and 4-alkoxy-2-oxoalkylphosphonates have been also examined. Their synthetic applications to (±)-Gingerol, (±)-Yashabushiketol, and (±)-Dihydroyashabushiketol are described.

Regioselective 1,3-dipolar cycloaddition reactions of α-(diethoxyphosphinyl)acetonitrile oxide, a phosphorus-functionalized nitrile oxide, with unsymmetrically substituted olefins lead to 5-substituted 3-[(diethoxyphosphinyl)methyl]-2-isoxazolines (**1**).[1] Deprotonation occurs regioselectively at the side chain of **1** to form phosphorus-stabilized carbanions, which can be effectively utilized for the subsequent olefination, alkylation, or acylation to produce 3-substituted 2-isoxazolines. Hydrogenation of **1** on Raney Ni provides 4-hydroxy-2-oxoalkylphosphonates which are further dehydrated into 2-oxo-3-alkenylphosphonates.[1b]

The 4-hydroxy-2-oxoalkylphosphonates must be important as synthetic building blocks since they correspond to phosphorus-functionalized aldols. Their Horner–Emmons olefination leading to 1-hydroxy-4-alken-3-ones is therefore attractive. However 4-hydroxy-2-oxoalkylphosphonates and their *O*-protected derivatives are both base-sensitive so that the olefination may be only achieved under extremely mild and less basic conditions.[2]

With an aim of examining the synthetic utility of our phosphorus-functionalized nitrile oxide, α-(diethoxyphosphinyl)acetonitrile oxide,[1a] Horner–Emmons olefinations have been applied to 4-hydroxy-2-oxoalkylphosphonates and the related derivatives. The present article describes the details of these intractable olefinations which finally succeeded by the use of triethylamine (or 1,8-diazabicyclo[5.4.0]undec-7-ene (DBU)) + lithium bromide. Furthermore it should be noted that protection of the hydroxyl group has to be avoided. These olefination conditions were applied to the syntheses of some natural products such as (±)-Gingerol, (±)-Yashabushiketol, and (±)-Dihydroyashabushiketol.

Results and Discussion

4-Hydroxy-2-oxoalkylphosphonates **2a—e** are readily prepared by the cycloadditions of α-(diethoxyphosphinyl)acetonitrile oxide with monosubstituted olefins followed by hydrogenation of the cycloadducts **1a—e** on Raney Ni (Scheme 1).[1b] Initially two derivatives **2a,b** were protected as tetrahydropyranyl ethers **3a,b** and then subjected to the olefination reactions with benzaldehyde under various conditions. Deprotonation of **3a,b** with butyllithium or lithium diisopropylamide (LDA) in tetrahydrofuran (THF) at −78 °C and subsequent trapping with benzaldehyde, the usual reaction conditions frequently employed for the olefination of phosphoryl-stabilized carbanions,[3] resulted in the complex mixture of many products. After some efforts had been made to improve the reaction, a satisfactory result was obtained when a mixture of triethylamine (1.2 equiv) and lithium bromide (1.5 equiv) was used for the carbanion

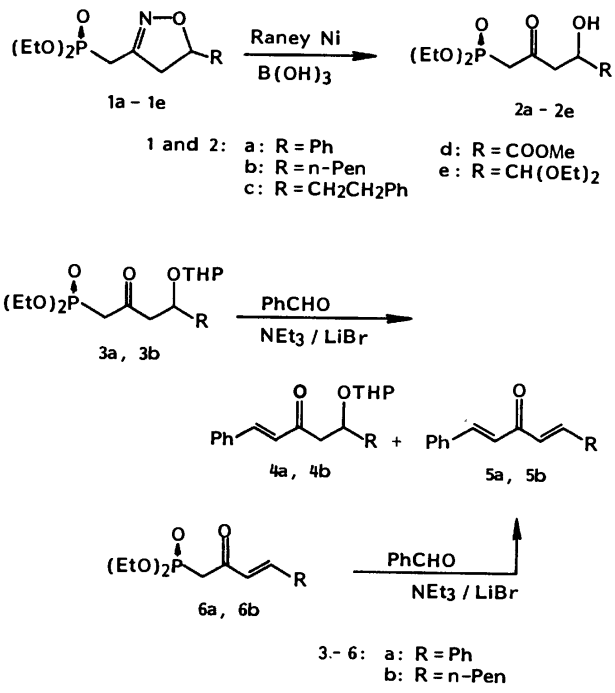

Scheme 1.

generation[4] and when the condensation with benzaldehyde was carried out at 0 °C in THF. However the desired olefins **4a,b** (**4a**: 64%, E only; **4b**: 54%, E only)[5] were accompanied by dienones **5a,b** (**5a**: 20%, E,E:E,Z=6:1; **5b**: 13%, 1E,4E:1Z,4E=8:1) as the elimination products of **4**. Several attempts to exclude the formation of dienones **5a,b** were not successful.

The dienones **5a,b** could be prepared, but in unsatisfactory yields (**5a**: 54%, E,E only; **5b**: 31%, 1E,4E:1Z,4E=9:1 as our best results[6]), by olefinations of 2-oxo-3-alkenylphosphonates **6a,b** (both E isomers) with benzaldehyde in the presence of lithium bromide and triethylamine, which were quantitatively and stereoselectively available by dehydration of **2a,b**.[1b]

Thus olefinations of either 4-alkoxy-2-oxoalkylphosphonates **3** or 2-oxo-3-alkenylphosphonates **6** could not provide a fruitful synthetic conversion.

To our surprise, not *O*-benzylated but *C*-benzylated product **7** was obtained (73% as a mixture of two diastereomers) when 4-hydroxy-2-oxononylphosphonate (**2b**) was treated with one equivalent of butyllithium followed by benzyl bromide (Scheme 2). In this reaction no elimination product **6b** was detected. The selective deprotonation adjacent to the phosphinyl moiety, not at the hydroxyl moiety, would be a result from high stabilization of the anionic center by the lithium chelation. These results indicate that *O*-unprotected 4-hydroxy-2-oxoalkylphosphonates **2** may undergo a successful olefination by the use of one equivalent of base and that the elimination as a major side reaction may be sufficiently suppressed when *O*-unprotected **2** is employed.[7]

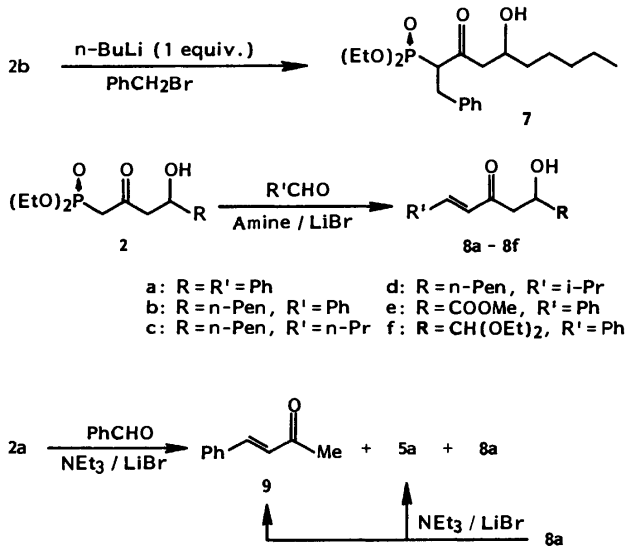

Scheme 2.

O-Unprotected 4-hydroxy-2-oxoalkylphosphonates **2** underwent smooth and E-selective olefinations with both aromatic and aliphatic aldehydes to give 1-hydroxy-4-alken-3-ones **8** (Scheme 2 and Table 1). Olefination of **2b** bearing an alkyl substituent (R=*n*-Pen) was effected by NEt_3+LiBr producing high yields of **8b—d** (Entries 3—5), while phenyl-substituted **2a** gave only very poor yield (21%) of **8a** under identical conditions (Entry 1). Beside the elimination reaction leading to **5a** (9%), the major side reaction in this case was retro aldol condensation giving **9** (31%). Formation of both **5a** and **9** was apparently due to the instability of **8a** under the reaction conditions: A 1:2 mixture of **5a** and **9** was yielded on treatment of **8a** with NEt_3+LiBr in THF at room temperature, while **8a** was inert without LiBr.

When DBU was used instead of triethylamine, the olefination reaction was significantly accelerated. The olefination reaction could be carried out at a lower temperature (0 °C) so that the side reactions were relatively suppressed. Thus the reaction of **2a** with benzaldehyde in the presence of DBU+LiBr (both 1 equiv) was very clean to give **8a** in 56% yield.[8,9] The unsatisfactory yield of **8a** was fully complemented by the recovery of the starting phosphonate **2a** (29%) and no formation of the side products **5a** and **9** (Entry 2).

It should be emphasized that 1-hydroxy-4-alken-3-ones **8e,f** bearing an ester or an acetal functionality

Table 1. Horner-Emmons Olefination of 4-Hydroxy-2-oxoalkylphosphonates **2a—e** Leading to 1-Hydroxy-4-alken-3-ones **8a—g**[a]

Entry		Aldehyde	Amine (equiv)	Temp/°C	Time/h	Product (yield/%)[b]
1	**2a** (R=Ph)	PhCHO	NEt_3 (1.2)	rt	24	**5a** (9), **8a** (21), **9** (31)
2	**2a**	PhCHO	DBU (1)[c]	0	24	**8a** (56)[d]
3	**2b** (R=*n*-Pen)	PhCHO	NEt_3 (1.2)	rt	24	**8b** (91)
4	**2b**	*n*-PrCHO	NEt_3 (1.2)	rt	24	**8c** (74)
5	**2b**	*i*-PrCHO	NEt_3 (1.2)	rt	24	**8d** (85)
6	**2d** (R=COOMe)	PhCHO	NEt_3 (1)	rt	15	**8e** (39)
7	**2d**	PhCHO	DBU (1)[c]	0	24	**8e** (52)[e]
8	**2e** (R=$CH(OEt)_2$)	PhCHO	NEt_3 (1.2)	rt	24	**8f** (64)[f]
9	**2c** (R=CH_2CH_2Ph)	PhCHO	DBU (1)[c]	0	24	**8g** (60)[g]

a) All reactions were carried out in dry THF in the presence of LiBr (1.5 equivalent). b) Yield of isolated products. c) One equivalent of LiBr was used. d) Recovered **2a**: 29%. e) Recovered **2d**: 21%. f) Recovered **2e**: 13%. g) Recovered **2c**: 18%.

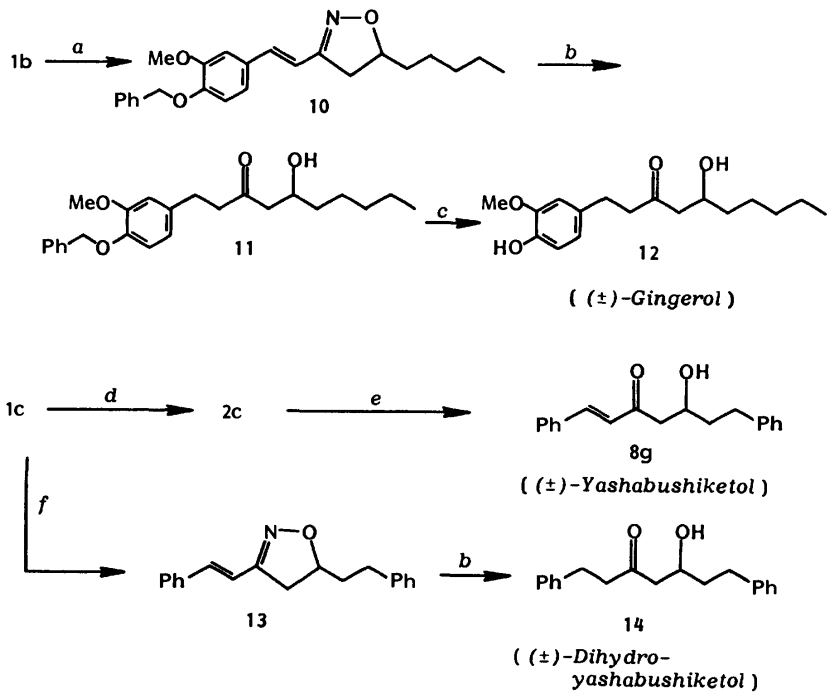

a: 1) *n*-BuLi in THF, −78 °C, 2) 4-benzyloxy-3-methoxybenzaldehyde, rt. *b*: Raney Ni/$B(OH)_3$ in aqueous EtOH/dichloromethane, rt. *c*: H_2/5% Pd–C in MeOH, rt. *d*: Raney Ni/$B(OH)_3$ in aqueous EtOH, rt. *e*: 1) DBU/LiBr in THF, 0 °C, 2) benzaldehyde, 0 °C. *f*: 1) *n*-BuLi in THF, −78 °C, 2) benzaldehyde, rt.

Scheme 3.

could be available by these olefinations (Entries 6—8).

Synthetic applications of the diethoxyphosphinyl moieties of **1** and **2** were next examined (Scheme 3). 3-[(Diethoxyphosphinyl)-methyl]-5-pentyl-2-isoxazoline (**1b**) was condensed with 4-benzyloxy-3-methoxybenzaldehyde (*n*-BuLi, in THF at −78 °C) giving **10** (only E-isomer) in 79% yield. The N–O bond cleavage as well as the C–C double bond hydrogenation was carried out with Raney Ni (W-2) producing **11** (68%). Dichloromethane was employed as a co-solvent which increased the solubility of **10** in ethanol.[10] Debenzylation of **11** with palladium on charcoal gave a quantitative yield of (±)-Gingerol (**12**).

The Raney Ni reduction of 3-[(diethoxyphosphinyl)methyl]-5-(2-phenylethyl)-2-isoxazoline (**1c**) gave diethyl 4-hydroxy-2-oxo-6-phenylhexylphosphonate (**2c**) in 74% yield. The Horner–Emmons olefination of **2c** with benzaldehyde in the presence of DBU-LiBr at 0 °C led to (±)-Yashabushiketol (**8g**) as a single E-isomer. Reverse operation of the above procedure on **1c** gave (±)-Dihydroyashabushiketol (**14**) via 3-styryl-2-isoxazoline **13** (only E-isomer).

Experimental

General. Melting points were determined on a Yanagimoto melting point apparatus and are not corrected. IR spectra were taken with a JASCO IRA-1 or a JASCO A-702 spectrometer. ^1H NMR spectra were recorded on a Hitachi R-40 (90 MHz) or a JEOL FX-100 instrument (100 MHz) and ^{13}C NMR on a JEOL FX-100 spectrometer at 25.05 MHz. Chemical shifts are expressed in parts per million downfield from tetramethylsilane as an internal standard. Mass spectra as well as high resolution mass spectra were measured with a JEOL-01SG-2 spectrometer at 70 eV of ionization energy. Elemental analyses were performed on a Hitachi 026 CHN analyzer. Thin-layer chromatography (TLC) was accomplished on 0.2 mm precoated plates of silica gel 60F-254 (Merck). Visualization was made with ultraviolet light (254 and 365 nm), iodine, molybdophosphoric acid (5% in ethanol), or *p*-anisaldehyde (5% in ethanol containing 5% of sulfuric acid). For preparative column chromatography, Wakogel C-200, C-300 (Wako), and Silicagel 60 (Merck) were employed. Micro vacuum distillation was carried out on a Sibata GTO-250R Kugelrohr distilling apparatus. Solvents were evaporated at about 50 °C unless otherwise stated.

Materials. 3-[(Diethoxyphosphinyl)methyl]-2-isoxazolines **1a,b** and **1d,e** were prepared by the cycloaddition reactions of α-(diethoxyphosphinyl)acetonitrile oxide to the corresponding olefins.[1b] Diethyl 4-hydroxy-2-oxoalkylphosphonates **2a,b** and **2d,e** were obtained by the Raney Ni reduction of **1** in the presence of boric acid.[1b] The preparation of **1c** and **2c** is presented in the synthetic procedure of Yashabushiketol **8g** and Dihydroyashabushiketol **14**.

Diethyl 2-Oxo-4-phenyl-4-(2-tetrahydropyranyloxy)butylphosphonate (3a). To a solution of **1a** (0.977 g, 3.25 mmol) in dry dichloromethane (10 ml) was added 3,4-dihydro-2*H*-

pyran (0.821 g, 9.76 mmol) and then pyridinium *p*-toluenesulfonate (PPTS, 0.245 g, 0.976 mmol). The mixture was stirred under nitrogen at room temperature for 17 h and poured into water. The products were extracted with diethyl ether (15 ml×2). The combined ether was washed with brine, dried over anhydrous magnesium sulfate, and evaporated in vacuo. The residue was chromatographed over silica gel by using ethyl acetate to give **3a** (1.092 g, 87%): Colorless liquid (a mixture of two diastereomers); IR (neat) 1710, 1240, 1020, and 790 cm^{-1}; ^1H NMR ($CDCl_3$) δ=1.28, 1.30 (6H, each t, J=7.0 Hz, OEt), 1.1—1.9 (6H, m, THP), 2.8—3.4 (2H, m, $COCH_2$), 3.0—4.0 (2H, m, THP), 3.04, 3.18 (2H, each d, $^2J_{HP}$=22.0 Hz, PCH_2), 4.07, 4.09 (4H, each dq, $^3J_{HP}$=9.0 and J=7.0 Hz, OEt), 4.36, 4.85 (1H, each br, THP), 5.04, 5.20 (1H, each dd, J=8.5 and 4.5 Hz, CHOTHP), and 7.1—7.4 (5H, m, Ph); ^{13}C NMR ($CDCl_3$) δ=16.32 (qd, $^3J_{CP}$=7.4 Hz, OEt), 19.18, 19.35, 25.35, 30.59 (each t, THP), 43.34 (td, $^1J_{CP}$=126,5 Hz, PCH_2), 51.95 (t, $COCH_2$), 62.12 (t, THP), 62.62 (td, $^2J_{CP}$=7.4 Hz, OEt), 73.42, 75.42 (each d, CHOTHP), 95.30, 99.18 (each d, THP), 126.60, 127.13, 127.66, 128.18, 128.48, 128.77 (each d), 140.89, 142.60 (each s), and 200.19 (d, $^2J_{CP}$=5.9 Hz, CO); MS *m/z* (rel intensity, %) 299 (8, M^+ − 85), 283 (11), 194 (18), 179 (50), 167 (15), 152 (50), 151 (42), 131 (36), 125 (39), 123 (89), 109 (75), 105 (61), 104 (base peak), 103 (70), 97 (35), 91 (41), 85 (84), 81 (76), 78 (51), and 77 (90). This compound **3a** was used for the following reaction without further purification.

Diethyl 2-Oxo-4-(2-tetrahydropyranyloxy)nonylphosphonate (3b). A similar procedure using **2b** (0.806 g, 2.74 mmol), 3,4-dihydro-2*H*-pyran (0.691 g, 0.75 mmol), and PPTS (0.206 g, 0.82 mmol) in dichloromethane (15 ml) for 15 h at room temperature gave **3b** (0.869 g, 84%) after column chromatography over silica gel with diethyl ether: Colorless liquid (a mixture of two diastereomers); IR (neat) 1710, 1250, 1020, and 780 cm^{-1}; ^1H NMR ($CDCl_3$) δ=0.7—1.8 (17H, m, *n*-Pen and THP), 1.32 (6H, t, J=7.0 Hz, OEt), 2.6—3.0 (2H, m, $COCH_2$), 3.10, 3.16 (2H, each d, $^2J_{HP}$=22.5 Hz PCH_2), 3.3—4.3 (3H, m, THP), 4.12 (4H, dq, $^3J_{HP}$=8.0 and J=7.0 Hz, OEt), and 4.4—4.7 (1H, m, CHOTHP); ^{13}C NMR ($CDCl_3$) δ=13.65 (q, *n*-Pen), 16.00 (qd, $^3J_{CP}$=5.9 Hz, OEt), 19.59, 20.06, 22.24, 24.47, 24.71, 25.18, 30.77, 30.88, 31.47, 34.12, 35.30 (each t, THP and *n*-Pen), 42.83, 43.00 (each td, $^1J_{CP}$=126.5 Hz, PCH_2), 48.30, 49.59 (each t, $COCH_2$), 62.18 (td, $^2J_{CP}$=5.9 Hz, OEt), 62.42, 63.00 (each t, THP), 73.36, 73.71 (each d, CHOTHP), 98.30, 98.89 (each d, THP), 200.72, and 200.84 (each d, $^2J_{CP}$=5.9 Hz, CO); MS *m/z* (rel intensity, %) 293 (M^+ −85, 16), 278 (39), 277 (base peak), 223 (77), 195 (27), 194 (45), 179 (26), and 85 (27). This compound **3b** was used for the following reaction without further purification.

General Procedure for the Horner–Emmons Olefinations of 3 Leading to 4 and 5. As a typical procedure the olefination of **4a** with benzaldehyde is described as follows: To a solution of lithium bromide (0.109 g, 1.25 mmol) in dry THF (1 ml) was added **3a** (0.402 g, 1.05 mmol in THF (4 ml)). The mixture was stirred under nitrogen at room temperature for 10 min and triethylamine (0.16 ml, 1.15 mmol) was added at 0 °C. The resulting mixture was stirred at 0 °C for 30 min. Addition of benzaldehyde (0.133 g, 1.25 mmol) was followed by the stirring at 0 °C for 18 h. The mixture was poured into ice water and extracted with dichloromethane (20 ml×2). The combined extracts were dried over magnesium sulfate and evaporated in vacuo. The residue was chromatographed over silica gel by using hexane–ethyl acetate (7:1 vol/vol) to give **4a** (0.226 g, 64%) and **5a** (0.049 g, 20%).

A similar procedure employing lithium bromide (0.102 g, 1.18 mmol) in dry THF (1 ml), **3b** (0.372 g, 0.983 mmol) in THF (4 ml), triethylamine (0.109g, 1.08 mmol), and benzaldehyde (0.125 g, 1.18 mmol) at 0 °C for 20 h gave **4b** (0.174 g, 54%) and **5b** (0.029 g, 13%) after the same chromatographic separation as shown above.

4a: (only E-isomer by ^1H NMR): Pale yellow liquid; IR (neat) 1660, 1610, 1580, and 1500 cm^{-1}; ^1H NMR ($CDCl_3$) δ=1.2—1.9 (6H, m, THP), 2.83 (1H, dd, J=16.0 and 4.5 Hz, one of $COCH_2$), 3.1—4.0 (2H, m, THP), 3.32 (1H, dd, J=16.0 and 9.5 Hz, the other of $COCH_2$), 4.3—4.4, 4.8—5.0 (1H, each m, THP), 5.16, 5.28 (1H, each dd, J=9.5 and 4.5 Hz, CHOTHP), 6.67, 6.76 (1H, each d, J=16.0 Hz, COCH=), 7.0—7.7 (10H, m, Ph), and 7.48, 7.52 (1H, each d, J=16.0 Hz, PhCH=); ^{13}C NMR ($CDCl_3$) δ=19.18, 25.35, 30.53 (each t, THP), 49.12 (t, $COCH_2$), 61.71, 62.06 (each t, THP), 73.48, 76.01 (each d, CHOTHP), 94.71, 99.24 (each d, THP), 126.48, 126.83, 127.07, 127.48, 128.01, 128.42, 128.72, 129.07 (each d), 130.65, 134.60 (each s), 141.42, 143.19 (each d), and 197.95 (s, CO); MS *m/z* (rel intensity, %) 336 (M^+, 3), 252 (15), 251 (24), 131 (base peak), 104 (16), 103 (23), and 85 (92). HRMS Found: *m/z* 336.1722. Calcd for $C_{22}H_{24}O_3$: M, 336.1724.

4b: (only E-isomer by ^1H NMR): Pale yellow liquid; IR (neat) 1650, 1610, 1580, and 1490 cm^{-1}; ^1H NMR ($CDCl_3$) δ=0.7—2.0 (17H, m, *n*-Pen and THP), 2.65, 2.71 (1H, each dd, J=15.5, 5.2 and J=15.5, 5.8 Hz, one of $COCH_2$), 2.97, 3.13 (1H, each dd, J=15.5, 7.3 and J=15.5, 6.2 Hz, the other of $COCH_2$), 3.3—4.3 (3H, m, THP and CHOTHP), 4.5—4.7 (1H, m, THP), 6.72, 6.74 (1H, each d, J=16.4 Hz, COCH=), and 7.2—7.6 (6H, Ph and =CH); ^{13}C NMR ($CDCl_3$) δ=14.06 (q, *n*-Pen), 20.00, 20.24, 22.59, 24.94, 25.18, 25.41, 31.24, 31.88, 34.65, 36.06, 45.89, 47.18, 62.95, 63.12 (each t, THP and *n*-Pen), 74.65, 76.01 (each d, CHOTHP), 98.83, 99.24 (each d, THP), 127.01, 127.24, 128.42, 129.07, 130.48, 130.65 (each d), 134.77, 134.95 (each s), 142.66, 143.01 (each d), 199.01, and 199.24 (each s, CO); MS *m/z* (rel intensity, %) 330 (M^+, 5), 131 (73), 103 (17), and 85 (base peak). HRMS Found: *m/z* 330.2171. Calcd for $C_{21}H_{30}O_3$: M, 330.2193.

5a: (a 6:1 mixture of E,E- and E,Z-isomers by ^1H NMR): Colorless solid; ^1H NMR ($CDCl_3$) E,E-isomer δ=7.00 (2H, d, J=15.6 Hz, COCH=), 7.1—7.7 (10H, m, Ph), and 7.65 (2H, d, J=15.6 Hz, PhCH=). E,Z-isomer δ=6.28 (1H, d, J=12.0 Hz, COCH=(Z)), 6.61 (1H, d, J=15.6 Hz, COCH=(E)), 6.90 (1H, d, J=12.0 Hz, PhCH=(Z)), and 7.1—7.7 (11H, m, Ph and PhCH= (E)). The major isomer of **5a** was identified to be (*E,E*)-1,5-diphenyl-1,4-pentadien-3-one by comparison with the authentic sample prepared from acetone and benzaldehyde.[11]

5b: (an 8:1 mixture of 1E,4E- and 1Z,4E-isomers by ^1H NMR): Pale yellow liquid; IR (neat) 1670, 1630, 1610, 1580, and 1500 cm^{-1}; ^1H NMR ($CDCl_3$) 1E,4E-isomer δ= 0.90 (3H, t, *n*-Pen), 1.0—1.8 (6H, m, *n*-Pen), 2.26 (2H, q, J=7.0 Hz, =$CHCH_2$), 6.40 (1H, dt, J=16.0 and 1.3 Hz, $COCH$=$CHCH_2$), 6.97 (1H, dt, J=16.0 and 7.0 Hz, =$CHCH_2$), 7.2—7.7 (5H, m, Ph), and 7.62 (1H, d, J=16.0 Hz, =CHPh); 1Z,4E-isomer δ=2.09 (2H, qd, J=7.0 and 1.5 Hz, =$CHCH_2$), 6.05 (1H, dt, J=16.0 and 1.5 Hz, $COCH$=$CHCH_2$), 6.20 (1H, d, J=12.8 Hz, PhCH=), 6.84 (1H, dt, J=16.0 and 7.0 Hz, =$CHCH_2$), 6.86 (1H, d, J=16.0 Hz, $COCH$=CHPh), and

7.2—7.7 (5H, m, Ph); ^{13}C NMR ($CDCl_3$) δ=14.00 (q, *n*-Pen), 22.53, 27.65, 27.94, 31.30, 31.47, 32.47, 32.77 (each t, *n*-Pen), 125.07, 128.48, 129.13, 129.54, 129.71, 130.54, 130.89 (each d), 135.13, 135.71 (each s), 138.89, 143.13, 148.60, 149.95 (each d), and 222.72 (s, CO); MS *m/z* (rel intensity, %) 228 (M^+, 20), 227 (34), 131 (25), 128 (37), 127 (20), 103 (59), 102 (22), 91 (22), 76 (66), 57 (32), 55 (37), 53 (22), 51 (27), 42 (25), and 40 (base peak). Found: C, 83.93; H, 8.76%. Calcd for $C_{16}H_{20}O$: C, 84.16; H, 8.83%.

A 2:1 mixture of 1E,4E- and 1Z,4E-isomers of **5b** was obtained in 30% yield when the reaction of **6b** with benzaldehyde was carried out at room temperature for 16 h in the presence of LiBr +NEt_3 (See Ref. 6). Their structures were clearly assigned on the basis of the ^{1}H NMR of this mixture, which was shown above.

General Procedure for the Olefination of 6 Leading to 5. As a typical procedure the olefination of **6b** with benzaldehyde is described below: To a solution of E-isomer of **6b** (0.197 g, 0.713 mmol) in dry THF (2 ml) was added lithium bromide (0.074 g, 0.856 mmol) under nitrogen. After 10 min at room temperature, the mixture was cooled to −20 °C. Benzaldehyde (0.076 g, 0.713 mmol) and then triethylamine (0.081 g, 0.11 ml, 0.799 mmol) were added. The resulting mixture was stirred for 2 h at −20 °C and then for 3 h at room temperature, poured into ice water, and extracted with diethyl ether (20 ml). The extract was washed with aqueous HCl, saturated aqueous sodium carbonate, and finally water. The organic layer was dried over magnesium sulfate and evaporated in vacuo. The residue was chromatographed over silica gel to give **5b** (0.052 g, 31%, a 9:1 mixture of E- and Z-isomers by ^{1}H NMR) and recovered **6b** (13%).

A similar procedure using **6a** (0.223 g, 0.79 mmol), lithium bromide (0.082 g, 0.948 mmol), triethylamine (0.088 g, 0.12 ml, 0.869 mmol), and benzaldehyde (0.168 g, 1.58 mmol) at room temperature for 21 h gave **5a** (0.097 g, 52%, a 6:1 mixture of E- and Z-isomers by ^{1}H NMR).

Diethyl 1-Benzyl-4-hydroxy-2-oxononylphosphonate (7). To a solution of **2b** (0.326 g, 1.11 mmol) in dry THF (2 ml) was added dropwise, at −78 °C under nitrogen, butyllithium (15% solution in hexane, 0.69 ml, 1.11 mmol). After 10 min, benzyl bromide (0.379 g, 2.22 mmol) and then dry hexamethylphosphoric triamide (HMPA, 2 ml) were added slowly. The resulting mixture was warmed to room temperature, stirred for 6 h, and then poured into ice water. The products were extracted in diethyl ether (20 ml×3), the combined extracts were washed with water (50 ml×5), dried over magnesium sulfate, and finally evaporated in vacuo. The residue was chromatographed over silica gel by using hexane-ethyl acetate (3:2 vol/vol) to give **7** (0.312 g, 73%): Pale yellow liquid; IR (neat) 3400, 1700, 1600, 1490, 1240, 1020, and 790 cm^{-1}; ^{1}H NMR ($CDCl_3$) δ=0.7—1.6 (11H, m, *n*-Pen), 1.32 (6H, t, *J*=7.0 Hz, OEt), 2.2—3.5 (6H, m, CH_2, PCH, and OH), 3.5—4.3 (1H, m, CHOH), 4.12 (4H, dq, $^3J_{HP}$=8.0 and *J*=7.0 Hz, OEt), and 7.0—7.4 (5H, m, Ph); ^{13}C NMR ($CDCl_3$) δ=14.06 (q, *n*-Pen), 16.41 (qd, $^3J_{CP}$=5.9 Hz, OEt), 22.65, 25.12, 31.77 (each t, *n*-Pen), 32.48 (td, $^2J_{CP}$=3.0 Hz, $PhCH_2$), 36.59 (t, *n*-Pen), 52.18, 52.30 (each t, $COCH_2$), 55.00, 55.42 (each dd, $^1J_{CP}$=123.5 Hz, PCH), 62.77 (td, $^2J_{CP}$=5.9 Hz, OEt), 63.12, 63.42 (each d, CHOH), 126.95, 128.83 (each d), and 206.22 (d, $^2J_{CP}$=4.4 Hz, CO); MS *m/z* (rel intensity, %) 384 (M^+, 8), 313 (28), 241 (base peak), and 91 (25). HRMS Found: *m/z* 384.2066. Calcd for $C_{20}H_{33}O_5P$: M, 384.2064.

General Procedure for the Horner-Emmons Olefination of 2a—e Leading to 8a—g. As a typical procedure the reaction of **2a** with benzaldehyde leading to **8a** is described as follows: To a solution of lithium bromide (0.044 g, 0.503 mmol) in dry THF was added **2a** (0.151 g, 0.503 mmol). This mixture was stirred at room temperature under nitrogen for 10 min and cooled down to 0 °C. After DBU (0.076 g, 0.503 mmol) was added the stirring was continued for 30 min. Benzaldehyde (0.107 g, 1.01 mmol) was added dropwise. The mixture was stirred at 0 °C for 24 h, poured into ice water, and then extracted with dichloromethane (20 ml×2). The combined extracts were dried over magnesium sulfate and evaporated in vacuo. The residue was chromatographed over silica gel with hexane-ethyl acetate (5:1 vol/vol) to give **8a** (0.071 g, 56%). The continued elution with ethyl acetate afforded **2a** (0.044 g, 29%).

The reactions of other phosphonates **2** with aldehydes were similarly carried out under the reaction conditions shown in Table 1 which also summarizes the results of the reactions.

8a: (a 20:1 mixture of E- and Z-isomers by ^{1}H NMR): Pale yellow liquid; IR (neat) 3400, 1650, 1600, 1580, and 1490 cm^{-1}; ^{1}H NMR ($CDCl_3$) δ=3.01, (1H, d, *J*=5.0 Hz, one of $COCH_2$), 3.02 (1H, d, *J*=7.0 Hz, the other of $COCH_2$), 3.74 (1H, br s, OH), 5.21 (1H, dd, *J*=7.0 and 5.5 Hz, CHOH), 6.65, 7.49 (each 1H, d, *J*=16.5 Hz, PhC<u>H</u>=C<u>H</u>), and 7.0—7.6 (10H, m, Ph); ^{13}C NMR ($CDCl_3$) δ=49.12 (t, $COCH_2$), 70.18 (d, CHOH), 125.89, 126.48, 127.71, 128.60, 129.13, 130.89 (each d), 134.36, 143.42 (each s), 143.95 (d), and 200.18 (s, CO); MS *m/z* (rel intensity, %) 252 (M^+, 59), 146 (31), 145 (34), 131 (95), 120 (68), 106 (23), 105 (base peak), 104 (33), 103 (77), 91 (21), 79 (33), and 78 (21). HRMS Found: *m/z* 252.1143. Calcd for $C_{17}H_{16}O_2$: M, 252.1149. Z-Isomer of **8a**: ^{1}H NMR ($CDCl_3$) δ=6.10 (d, *J*=12.7 Hz, COCH=(Z)).

8b: (a 23:1 mixture of E- and Z-isomers by ^{1}H NMR): Colorless prisms (hexane); mp 38—39 °C; IR (KBr) 3350 and 1630 cm^{-1}; ^{1}H NMR ($CDCl_3$) δ=0.6—1.7 (11H, m, *n*-Pen), 2.77 (2H, d, *J*=8.0 Hz, one of $COCH_2$), 2.80 (1H, d, *J*=4.0 Hz, the other of $COCH_2$), 3.24 (1H, br s, OH), 3.8—4.3 (1H, m, CHOH), 6.68, 7.53 (each 1H, d, *J*=16.0 Hz, PhC<u>H</u>=C<u>H</u>), and 7.0—7.6 (5H, m, Ph); ^{13}C NMR ($CDCl_3$) δ=14.06 (q, *n*-Pen), 22.65, 25.30, 31.83, 36.77 (each t, *n*-Pen), 47.24 (t, $COCH_2$), 68.01 (d, CHOH), 126.65, 128.60, 129.13, 130.83 (each d), 134.48 (s), 143.54 (d), and 201.01 (s, CO); MS *m/z* (rel intensity, %) 246 (M^+, 7), 146 (22), 131 (base peak), and 103 (29). Found: C, 78.10; H, 8.99%. Calcd for $C_{16}H_{22}O_2$: C, 78.01; H, 9.00%. Z-Isomer of **8b**: ^{1}H NMR ($CDCl_3$) δ=6.14 (d, *J*=12.6 Hz, COCH=(Z)).

8c: (Only E-isomer by ^{1}H NMR): Colorless liquid; IR (neat) 3400, 1650, and 1620 cm^{-1}; ^{1}H NMR ($CDCl_3$) δ=0.7—1.8 (16H, m, *n*-Pen and *n*-Pr), 2.20 (2H, dt, *J*=8.0 and 7.0 Hz, *n*-Pr), 2.64 (1H, d, *J*=8.0 Hz, one of $COCH_2$), 2.68 (1H, d, *J*=4.0 Hz, the other of $COCH_2$), 3.20 (1H, br s, OH), 3.8—4.2 (1H, m, CHOH), 6.04 (1H, dt, *J*=16.0 and 1.5 Hz, COCH=), and 6.84 (1H, dt, *J*=16.0 and 7.0 Hz, CH_2C<u>H</u>=); ^{13}C NMR ($CDCl_3$) δ=13.71, 14.06 (each q, *n*-Pen and *n*-Pr), 21.41, 22.71, 25.35, 31.94, 34.59, 36.77 (each t, *n*-Pen and *n*-Pr), 46.42 (t, $COCH_2$), 68.01 (d, CHOH), 131.13, 148.66 (each d, CH=CH), and 201.36 (s, CO); MS *m/z* (rel intensity, %) 212 (M^+, 1), 141 (55), 97 (base peak), 55 (89), 43 (35), and 41 (59). HRMS Found: *m/z* 212.1750. Calcd for $C_{13}H_{24}O_2$: M, 212.1775.

8d: (Only E-isomer by ^{1}H NMR): Colorless liquid; IR (neat) 3400, 1660, and 1625 cm^{-1}; ^{1}H NMR ($CDCl_3$) δ=0.7—1.8 (11H, m, *n*-Pen), 1.07 (6H, d, J=7.0 Hz, *i*-Pr), 2.1—2.7 (1H, m, *i*-Pr), 2.66 (1H, d, J=8.0 Hz, one of $COCH_2$), 2.70 (1H, d, J=4.0 Hz, $COCH_2$), 3.28 (1H, br s, OH), 3.9—4.2 (1H, m, CHOH), 6.03 (1H, dd, J=16.0 and 1.0 Hz, COCH=), and 6.83 (1H, dd, J=16.0 and 6.5 Hz, *i*-PrCH=); ^{13}C NMR ($CDCl_3$) δ=14.06 (q, *n*-Pen), 21.30 (q, *i*-Pr), 22.65, 25.30 (each t, *n*-Pen), 31.24 (d, *i*-Pr), 31.88, 36.71 (each t, *n*-Pen), 46.42 (t, $COCH_2$), 67.89 (d, CHOH), 128.13, 154.84 (each d), and 201.72 (s, CO); MS *m/z* (rel intensity, %) 212 (M^+, 3), 141 (31), 97 (base peak), 69 (21), 56 (24), 43 (44), and 41 (80). HRMS Found: *m/z* 212.1765. Calcd for $C_{13}H_{24}O_2$: M, 212.1775.

8e: (only E-isomer by ^{1}H NMR): Pale yellow liquid; IR (neat) 3500, 1730, 1660, and 1620 cm^{-1}; ^{1}H NMR ($CDCl_3$) δ=3.20 (2H, d, J=5.0 Hz, $COCH_2$), 3.5—3.8 (1H, m, OH), 3.76 (3H, s, COOMe), 4.64 (1H, q, J=5.5 Hz, CHOH), 6.71, 7.56 (each 1H, d, J=16.0 Hz, PhCH=CH), and 7.2—7.7 (5H, m, Ph); ^{13}C NMR ($CDCl_3$) δ=43.94 (t, $COCH_2$), 52.59 (q, COOMe), 67.30 (d, CHOH), 126.07, 128.60, 129.13, 130.95 (each d), 134.36 (s), 144.13 (d), 174.37 (s, COOMe), and 197.72 (s, CO); MS *m/z* (rel intensity, %) 234 (M^+, 11), 131 (base peak), 103 (76), 102 (21), 77 (63), and 52 (23); HRMS Found: *m/z* 234.0886. Calcd for $C_{13}H_{14}O_4$: M, 234.0891.

8f: (only E-isomer by ^{1}H NMR): Pale yellow liquid; IR (neat) 3450, 1650, 1610, 1580, and 1490 cm^{-1}; ^{1}H NMR ($CDCl_3$) δ=1.22 (6H, t, J=7.0 Hz, OEt), 2.8—3.0 (3H, m, $COCH_2$ and OH), 3.4—3.9 (4H, m, OEt), 4.20 (1H, ddd, J=9.0, 7.0, and 4.5 Hz, CHOH), 6.72, 7.57 (each 1H, d, J=16.5 Hz, PhCH=CH), and 7.2—7.7 (5H, m, Ph); ^{13}C NMR ($CDCl_3$) δ=15.06 (q, OEt), 41.77 (t, $COCH_2$), 63.12, 63.65 (each t, OEt), 68.71 (d, CHOH), 104.01 (d, $CH(OEt)_2$), 126.54, 128.18, 128.77, 130.36 (each d), 134.30 (s), 142.95 (d), and 199.60 (s, CO); MS *m/z* (rel intensity, %) 233 (M^+—45, 4), 131 (42), 103 (base peak), 77 (30), 75 (40), and 48 (45). Found: C, 68.88; H, 7.95%. Calcd for $C_{16}H_{22}O_4$: C, 69.04; H, 7.97%.

8g: All data will be presented below (in the synthesis of Yashabushiketol **8g**).

Synthesis of (±)-Gingerol 12. Butyllithium (15% in hexane, 3.69 ml, 6 mmol) was added at −78 °C to a solution of **1b** (1.748 g, 6 mmol) in dry THF (12 ml) and stirred under nitrogen for 30 min. After 4-benzyloxy-3-methoxybenzaldehyde (1.599 g, 6.6 mmol) was added, the resulting mixture was stirred at −78 °C for 1 h, at room temperature for 4 h, poured into cold aqueous ammonium chloride solution, and extracted with diethyl ether (30 ml×2). The combined extracts were dried over magnesium sulfate and evaporated in vacuo. The residue was chromatographed over silica gel by using dichloromethane to give **10** (1.802 g, 79%) as a single E-isomer (^{1}H NMR): Colorless prisms (diethyl ether-hexane); mp 112—113 °C; IR (KBr) 1600, 1580, and 1500 cm^{-1}; ^{1}H NMR ($CDCl_3$) δ=0.8—2.0 (11H, m, *n*-Pen), 2.74 (1H, d, J=16.0 and 8.5 Hz, one of 4-H), 3.19 (1H, d, J=16.0 and 10.0 Hz, the other of 4-H), 3.86 (3H, s, OMe), 4.4—4.8 (1H, m, 5-H), 5.12 (2H, s, CH_2Ph), 6.59, 6.94 (each 1H, J=16.0 Hz, ArCH=CH), 6.8—7.1 (3H, m, Ar), and 7.2—7.5 (5H, m, Ph); ^{13}C NMR ($CDCl_3$) δ=13.98 (q, *n*-Pen), 22.52, 25.18, 31.60, 35.23 (each t, *n*-Pen), 38.50 (t, 4-C), 55.90 (q, OMe), 70.92 (t, OCH_2Ph), 81.49 (d, 5-C), 109.49, 113.79, 116.47, 120.63, 127.24, 127.89, 128.51 (each d), 129.46 (s), 135.72 (d), 136.81, 149.04, 149.87 (each s), and 157.66 (s, 3-C); MS *m/z* (rel intensity, %) 379 (M^+, 3), 288 (7), 92 (8), 91 (base peak), and 66 (14). Found: C, 75.96; H, 7.67; N, 3.74%. Calcd for $C_{24}H_{29}NO_3$: C, 75.96; H, 7.70; N, 3.69%. The mixture of **10** (0.38 g, 1 mmol), Raney Ni (W-2, suspension in ethanol, 0.14 ml), and boric acid (0.135 g, 2.1 mmol) in ethanol (5 ml, containing dichloromethane (2 ml) and water (1 ml)) was stirred at room temperature at an ordinary atmospheric pressure of hydrogen for 48 h. Insoluble materials were filtered off by the aid of celite. The filtrate was mixed with dichloromethane (30 ml), the dichloromethane was washed with water, dried over magnesium sulfate, and evaporated in vacuo. The residue was chromatographed over silica gel with hexane-ethyl acetate (3:1 vol/vol) to give **11** (0.261 g, 68%): Colorless prisms (diethyl ether-hexane); mp 52—53 °C (lit,[12] mp 53—54 °C); IR (KBr) 3400, 1700, and 1590 cm^{-1}; ^{1}H NMR ($CDCl_3$) δ=0.9—1.6 (11H, m, *n*-Pen), 2.4—2.6, 2.6—3.0 (2H+5H, m, CH_2 and OH), 3.84 (3H, s, OMe), 3.8—4.1 (1H, m, CHOH), 5.08 (2H, s, CH_2Ph), 6.5—6.9 (3H, m, Ar), and 7.1—7.5 (5H, m, Ph); ^{13}C NMR ($CDCl_3$) δ=14.06 (q, *n*-Pr), 22.59, 25.18, 29.18, 31.77, 36.65, 45.24, 49.53 (each t, CH_2), 56.00 (q, OMe), 62.77 (d, CHOH), 71.30 (t, OCH_2Ph), 112.60, 114.65, 120.30, 127.48, 127.89, 128.65 (each d), 134.36, 137.54, 146.83, 149.95 (each s), and 211.31 (s, CO); MS *m/z* (rel intensity, %) 384 (M^+, 14), 151 (15), 149 (19), 137 (19), and 91 (base peak). Found: C, 75.15; H, 8.43%. Calcd for $C_{24}H_{32}O_4$: C, 74.97; H, 8.39%. A mixture of **11** (0.038 g, 0.1 mmol) and palladium on charcoal (5%, 0.07 g) in methanol (3 ml) was stirred at room temperature at an ordinary atmospheric pressure of hydrogen for 7 h and then filtered by the aid of celite. The filtrate was evaporated in vacuo. The residue was purified through column chromatography over silica gel with hexane-ethyl acetate (3:1 vol/vol) to give (±)-Gingerol **12** (0.029 g, 100%): Colorless liquid; IR (neat) 3420, 1710, and 1600 cm^{-1}; ^{1}H NMR ($CDCl_3$) δ=0.88 (3H, t, J=5.5 Hz, *n*-Pen), 1.0—1.8 (8H, m, *n*-Pen), 2.4—2.6, 2.6—3.2 (2H+5H, m, CH_2), 3.83 (3H, s, OMe), 3.7—4.2 (2H, m, CHOH and OH), and 6.4—6.9 (3H, m, Ar); MS *m/z* (rel intensity, %) 294 (M^+), 151 (16), 150 (55), 138 (13), and 137 (base peak). HRMS Found: *m/z* 294.1835. Calcd for $C_{17}H_{26}O_4$: M, 294.1830.

Synthesis of (±)-Yashabushiketol 8g. To a solution of *N*-2-(diethoxyphosphinyl)ethylidene hydroxylamine (0.625 g, 3.2 mmol) in dry *N*,*N*-dimethylformamide (DMF, 7 ml) was added at −20 °C *N*-bromosuccinimide (NBS, 1.139 g, 6.4 mmol in DMF (6.4 ml)). After 1 h at −20 °C and 30 min at 0 °C, dry diethyl ether (7 ml) was added. A mixture of triethylamine (0.324 g, 0.45 ml, 3.2 mmol) and 4-phenyl-1-butene (0.846 g, 6.4 mmol) in diethyl ether (7 ml) was added dropwise. The mixture was stirred at room temperaure for 18 h, poured into ice water, and extracted with dichloromethane (20 ml×2). The combined extracts were washed with water three times, dried over magnesium sulfate, and evaporated in vacuo. The residue was chromatographed over silica gel by using ethyl acetate to give **1c** (0.6 g, 58%): Pale yellow liquid; IR (neat) 1620, 1600, 1500, 1260, and 1025 cm^{-1}; ^{1}H NMR ($CDCl_3$) δ=1.32 (6H, t, J=7.0 Hz, OEt), 1.7—2.2, 2.4—3.3 (2H+4H, m, CH_2 and 4-H), 2.93 (2H, d, $^2J_{HP}$=22.0 Hz, PCH_2), 4.11 (4H, qd, J=7.0 and $^3J_{HP}$=8.0 Hz, OEt), 4.4—4.8 (1H, m, 5-H), and 7.0—7.4 (5H, m, Ph); ^{13}C NMR ($CDCl_3$) δ=16.00 (q, $^3J_{CP}$=5.9 Hz, OEt), 26.00 (td, $^1J_{CP}$=141.2 Hz, PCH_2), 31.30, 36.53 (each t, CH_2), 42.00 (t, 4-C), 62.27 (td, $^2J_{CP}$=7.4 Hz, OEt), 80.01 (d, 5-C), 125.83, 128.25, 141.01 (each d), and 151.16 (d, $^2J_{CP}$=10.3 Hz, 3-C); MS *m/z* (rel intensity, %) 325 (M^+, 21), 220 (base peak), 192 (22),

164 (39), and 91 (40). HRMS Found: *m/z* 325.1443. Calcd for $C_{16}H_{24}NO_4P$: M, 325.1442. The mixture of **1c** (0.461 g, 1.42 mmol), boric acid (0.191 g, 2.976 mmol), and Raney Ni (W-2, 0.2 ml) in ethanol (7.8 ml, containing water (1.3 ml) was stirred at room temperature at an ordinary pressure of hydrogen for 13 h. The reaction mixture was filtered through celite and the filtrate was treated with dichloromethane (25 ml). The dichloromethane was dried over magnesium sulfate and evaporated in vacuo. The residue was chromatographed over silica gel by using ethyl acetate to give **2c** (0.343 g, 74%): Colorless liquid; IR (neat) 3400, 1700, 1600, 1490, 1240, 1020, and 790 cm^{-1}; ^1H NMR ($CDCl_3$) δ=1.30 (6H, t, J=7.0 Hz, OEt), 1.6—2.0, 2.5—3.2 (2H+6H, m, CH_2), 3.52 (1H, br s, OH), 4.12 (4H, qd, J=7.0 and $^3J_{HP}$=8.0 Hz, OEt), and 3.9—4.2 (1H, m, CHOH); ^{13}C NMR ($CDCl_3$) δ=16.29 (qd, $^3J_{CP}$=5.9 Hz, OEt), 31.83, 38.59 (CH_2), 43.03 (td, $^1J_{CP}$=128.0 Hz, PCH_2), 51.36 (CH_2), 62.77 (td, $^2J_{CP}$=5.9 Hz, OEt), 67.01 (d, CHOH), 125.95, 128.54, 128.65 (each d), 142.13 (s), and 202.72 (d, $^2J_{CP}$=5.9 Hz, CO); MS *m/z* (rel intensity, %) 328 (M^+, 16), 310(43), 277 (22), 223 (47), 220 (29), 195 (34), 194 (23), 179 (34), 172 (20), 167 (26), 152 (50), 151 (25), 139 (39), 125 (37), 123 (45), 109 (21), 105 (21), 97 (30), and 91 (base peak). HRMS Found: *m/z* 328.1446. Calcd for $C_{16}H_{25}O_5P$: M, 328.1438. To a solution of lithium bromide (0.065 g, 0.75 mmol) in dry THF (0.5 ml) was added **2c** (0.165 g, 0.5 mmol, in THF (1.5 ml)) and stirred at room temperature for 10 min. After addition of DBU (0.076 g, 0.5 mmol, in THF (0.5 ml)) at 0 °C the stirring was continued for 1 h. Benzaldehyde (0.107 g, 1 mmol) was added and the mixture was stirred at 0 °C for 24 h. It was then poured into ice water and extracted with dichloromethane (20 ml×2). The combined extracts were dried over magnesium sulfate and evaporated in vacuo. The residue was chromatographed over silica gel with hexane-ethyl acetate (5:1 vol/vol) to give (±)-Yashabushiketol **8g** (0.084 g, 60%) as a single E-isomer (^1H NMR). Further eluent with ethyl acetate gave **2c** (0.029 g, 18%). **8g**: Colorless needles (hexane); mp 82—83 °C (lit,[13] mp 59.5—60.5 °C); IR (KBr) 3300, 1650, 1610, 1580, and 1490 cm^{-1}; ^1H NMR ($CDCl_3$) δ=1.6—1.9 (2H, m, $C\underline{H}_2CH_2Ph$), 2.4—2.9 (4H, m, $COCH_2$ and $CH_2C\underline{H}_2Ph$), 3.45 (1H, br s, OH), 3.9—4.3 (1H, m, CHOH), 6.65, 7.50 (each 1H, J=16.5 Hz, $PhC\underline{H}$=$C\underline{H}$), and 6.9—7.6 (5H, m, Ph); ^{13}C NMR ($CDCl_3$) δ=31.83, 38.30 (each t, CH_2CH_2Ph), 47.00 (t, $COCH_2$), 67.30 (d, CHOH), 126.01, 126.48, 128.54, 129.13, 130.89 (each d), 134.36, 142.13 (each s), 143.71 (d), and 200.89 (s, CO); MS *m/z* (rel intensity, %) 280 (M^+, 32), 175 (22), 131 (base peak), 103(38), 91 (41), 77 (20), and 32 (21). Found: C, 81.52; H, 7.12%. Calcd for $C_{19}H_{20}O_2$: C, 81.40; H, 7.19%.

Synthesis of (±)-Dihydroyashabushiketol 14. To a solution of **1c** (0.16 g, 0.492 mmol) in dry THF (1 ml) was added at −78 °C butyllithium (15% in hexane, 0.37 ml, 0.59 mmol) and stirred for 1 h under nitrogen. Benzaldehyde (0.104 g, 0.984 mmol) was added, the mixture was stirred at room temperature for 24 h, poured into aqueous ammonium chloride, and finally extracted with dichloromethane (20 ml×2). The combined extracts were washed with water, dried over magnesium sulfate, and evaporated in vacuo. The residue was chromatographed over silica gel by using hexane-ethyl acetate (5:1 vol/vol) to give **13** (0.102 g, 75%) as a single E-isomer (^1H NMR): Colorless needles (diethyl ether-hexane); mp 104—105 °C; IR (KBr) 1600 and 1490 cm^{-1}; ^1H NMR ($CDCl_3$) δ=1.6—2.3, 2.6—3.4 (2H+4H, m, CH_2 and 4-H), 4.5—4.9 (1H, m, 5-H), 6.64, 7.07 (each 1H, d, J=17.0 Hz, $PhC\underline{H}$=$C\underline{H}$), and 7.0—7.6 (5H, m, Ph); ^{13}C NMR ($CDCl_3$) δ=31.77, 37.00, 38.53 (each t, CH_2 and 4-C), 80.65 (d, 5-C), 118.36, 126.18, 127.07, 128.69, 129.01 (each d), 136.01 (s), 136.25 (d), 141.30 (s), and 157.77 (s, 3-C); MS *m/z* (rel intensity, %) 277 (M^+, 65), 276 (base peak), 143 (26), 115 (23), 103 (39), 91 (72), and 77 (44). Found: C, 82.35; H, 6.91; N, 5.05%. Calcd for $C_{19}H_{19}NO$: C, 82.28; H, 6.90; N, 5.05%. The mixture of **13** (0.166 g, 0.6 mmol) and Raney Ni (W-2, suspension in ethanol, 0.16 ml) in ethanol (6 ml, containing dichloromethane (2.4 ml) and water (1.2 ml)) was stirred at room temperature under hydrogen for 14 h. All insoluble materials were filtered off and the filtrate was treated with dichloromethane (30 ml). The mixture was washed with water, dried over magnesium sulfate, and evaporated in vacuo. The residue was chromatographed over silica gel with hexane-ethyl acetate (5:1 vol/vol) to give (±)-Dihydroyashabushiketol **14** (0.136 g, 80%): Colorless needles (hexane); mp 71—72 °C (lit,[14] mp 69—70.5 °C); IR (KBr) 3350, 1700, 1600, and 1500 cm^{-1}; ^1H NMR ($CDCl_3$) δ=1.4—1.9, 2.3—3.0 (2H+9H, m, CH_2 and OH), 3.8—4.2 (1H, m, CHOH), and 6.9—7.2 (10H, m, Ph); ^{13}C NMR ($CDCl_3$) δ=29.41, 31.71, 38.24, 44.89, 49.42 (each t), 66.89 (d, CHOH), 125.95, 126.24, 128.54 (each d), 140.95, 142.01 (each s), and 210.77 (s, CO); MS *m/z* (rel intensity, %) 282 (M^+, 6), 264 (19), 133 (19), 105 (48), 104 (base peak), 92 (15), 91 (base peak), and 77 (19). Found: C, 81.02; H, 7.95%. Calcd for $C_{19}H_{22}O_2$: C, 80.82; H, 7.85%.

References

1) a) O. Tsuge, S. Kanemasa, and H. Suga, *Chem. Lett.*, **1986**, 183; b) O. Tsuge, S. Kanemasa, H. Suga, and N. Nakagawa, *Bull. Chem. Soc. Jpn.*, **60**, 2463 (1987).

2) Under basic conditions, they suffer from ready elimination of the hydroxyl moiety, a carbon-carbon bond cleavage through the retro aldol reaction, or some other decompositions. See Ref. 4a.

3) W. S. Wadsworth, Jr., *Org. React.*, **25**, 73 (1977).

4) a) M. A. Blanchette, W. Choy, J. T. Davis, A. P. Essenfeld, S. Masamune, W. R. Roush, and T. Sakai, *Tetrahedron Lett.*, **25**, 2183 (1984); b) M. W. Rathke and M. Nowak, *J. Org. Chem.*, **50**, 2624 (1985); c) T. Rosen and C. H. Heathcock, *J. Am. Chem. Soc.*, **107**, 3731 (1985).

5) The isomer ratio was determined on the basis of ^1H NMR spectra of the crude reaction mixture unless otherwise stated.

6) The olefination of **6b** with benzaldehyde was investigated under a variety of conditions: 1) NaH in 1,2-dimethoxyethane (DME), 0 °C, 1 h; benzaldehyde, room temp, 0.5 h: complex mixture×recovered **6b** (9%). 2) *n*-BuLi in THF, −78 °C, 0.5 h; benzaldehyde, −78 °C room temp, 44 h: **5b** (6%, 1E,4E:1Z,4E=7:1). 3) LDA in THF, −78 °C, 0.5 h; benzaldehyde, −78 °C room temp, 16 h: **5b** (12%, 1E,4E:1Z,4E=6:1)+recovered **6b** (12%). 4) $MgBr_2 \cdot OEt_2$+NEt_3+benzaldehyde in acetonitrile, room temp, 19 h: complex mixture. 5) LiCl+*N*,*N*-diisopropylethylamine+benzaldehyde in acetonitrile, room temp, 19 h: **5b** (5%, 1E,4E:1Z,4E=3:1). 6) LiBr+NEt_3+benzaldehyde in THF, room temp, 16 h: **5b** (30%, 1E,4E:1Z,4E=2:1).

7) From the viewpoint of pK_a value, the leaving ability of a hydroxyl group is slightly inferior to that of an alkoxy

group (A. Streitwieser Jr. and S. P. Ewig, *J. Am. Chem. Soc.*, **97**, 190 (1975)).

8) When this reaction was performed at 0 °C for 24 h in the presence of NEt_3 (1.2 equiv)+LiBr (1.5 equiv), no trace of **5a** was formed (**8a**: 38%; **9**: 3%; recovered **2a**: 36%).

9) DBU and LiBr were used both in one equivalent in order to avoid the retro aldol condensation.

10) Raney Ni reduction of **10** in aqueous ethanol was too slow because of its poor solubility.

11) C. R. Conard and M. A. Dolliver, *Org. Synth.*, Coll. Vol. 2, 167 (1966).

12) A. Barco, S. Benetti, P. G. Baraldi, M. Guaruneri, G. P. Pollini, and D. Simoni, *J. Chem. Soc., Chem. Commun.*, **1981**, 599.

13) Y. Asakawa, F. Genjida, S. Hayashi, and T. Matsuura, *Tetrahedron Lett.*, **1969**, 3235; Y. Asakawa, *Bull. Chem. Soc. Jpn.*, **43**, 2223 (1970).

14) Y. Asakawa, *Bull. Chem. Soc. Jpn.*, **45**, 1794 (1972).

 © 1987 The Chemical Society of Japan Bull. Chem. Soc. Jpn., 60, 4099—4105 (1987)

Mechanism of the Pyrene-Sensitized Photolysis of *N*-(1-Naphthoyl)-*O*-(*p*-toluoyl)-*N*-phenylhydroxylamine

Tadamitsu SAKURAI,* Kensuke INOMATA, Takayoshi ISHIKAWA, Hiroyasu INOUE, Toshihiko HOSHI,† and Jun OKUBO†

Department of Applied Chemistry, Faculty of Technology, Kanagawa University, Kanagawa-ku, Yokohama 221

†Department of Chemistry, College of Science and Engineering, Aoyama Gakuin University, Setagaya-ku, Tokyo 157

(Received June 5, 1987)

The title hydroxylamine (NT) undergoes pyrene-sensitized photodecomposition to give rearrangement and fragmentation products. An analysis of linear Stern-Volmer plots, both for the sensitized photolysis of NT and for the fluorescence quenching of pyrene by NT, indicates the involvement of singlet pyrene in this photolysis. The observation of negligible effects of 1,3-cyclohexadiene and *trans*-stilbene as a triplet quencher on the reaction provides further supporting evidence for a singlet-pathway mechanism. A comparison of the relative state energies of NT and the sensitizer suggests the existence of a reactive singlet-exciplex intermediate formed between the singlet-state sensitizer and the ground-state NT. The results of solvent and micellar effects on the sensitized photolysis establish that electron transfer in the exciplex predominates in a polar solvent, and that in a nonpolar solvent energy transfer in this exciplex plays a major role in the reaction.

Our recent observation that the triplet-sensitized photolysis of *N*-(1-naphthoyl)-*O*-(*p*-toluoyl)-*N*-phenylhydroxylamine (NT) and related *N,O*-diacylhydroxylamines gives no rearranged products provided additional supporting evidence for the suggestion that "photoacyloxyl" migration proceeds mainly through the excited singlet state.[1,2] Furthermore, the results of micellar and solvent viscosity effects on the quantum yields for the direct photolysis of NT allowed us to conclude that the "in-cage" products are not derived from the reaction that occurs within the identical solvent cage but from recombination of two distinct spin-correlated radical pairs.[2] On the other hand, diaroyl peroxides have been known to undergo aromatic hydrocarbon-sensitized decompositions whose mechanism involves a reactive and nonemissive singlet-exciplex intermediate.[3-5] These works of Tokumaru and his co-workers on the mechanism of sensitized photolyses of the peroxides stimulated mechanistic investigation of the singlet-sensitized photolysis of our *N,O*-diacylhydroxylamines. NT was selected for the present study because we have already obtained detailed information regarding the mechanism of the direct and triplet-sensitized photolysis of this hydroxylamine.[2] We chose pyrene as a singlet sensitizer and investigated solvent and micellar effects on the pyrene-sensitized photolysis of NT in order to gain more definitive evidence for the reactive state (singlet or triplet state) from which "photoacyloxyl" migration takes place. We also hoped to clarify the mechanism of this sensitized photolysis.

Results

Pyrene-Sensitized Photolysis of NT (1). Irradiation of a N_2-purged benzene solution of NT (2.50—10.0×10^{-3} M, 1 M=1 mol dm^{-3}) in the presence of pyrene (3.00×10^{-3} M) with 366-nm light resulted in the sensitized decomposition of NT giving rearrangement (**2** and **3**) and fragmentation (**4** and **5**) products along with small amounts of unknown products.[6] These photoproducts undergo no sensitized decomposition under the same conditions as above. Pyrene

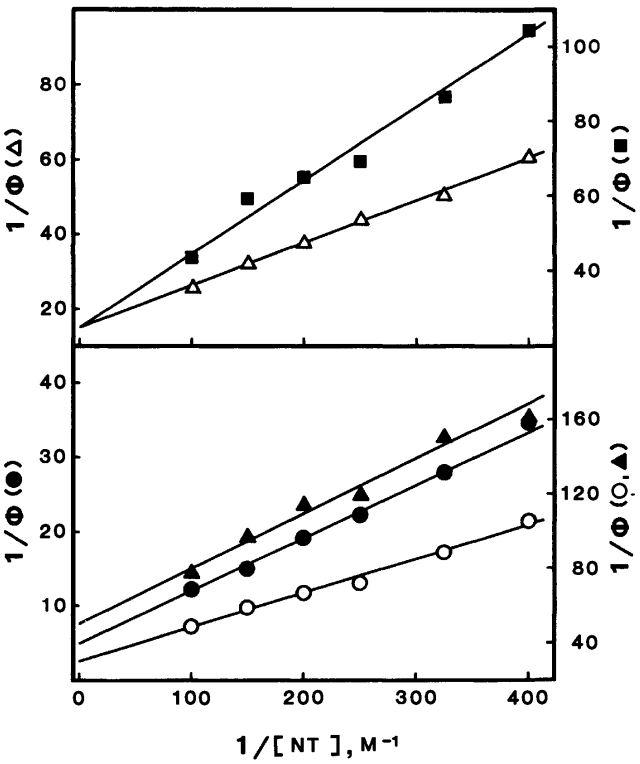

Fig. 1. Stern-Volmer plots of $1/\Phi_{-NT}$ (●), $1/\Phi_2$ (○), $1/\Phi_3$ (▲), $1/\Phi_4$ (△), and $1/\Phi_5$ (■) vs. 1/[NT] for pyrene (3.00×10^{-3} M)-sensitized photolysis of NT with 366-nm light in benzene under nitrogen at room temperature (25±3 °C).

was found to decompose to a negligible extent during the irradiation within the experimental errors of HPLC analysis. In addition, no NT was photolyzed to yield these products without the sensitizer. On the other hand, NT is not subjected to the sensitized decomposition to a measurable extent in the presence of relatively low concentrations of pyrene (less than 10^{-4} M).

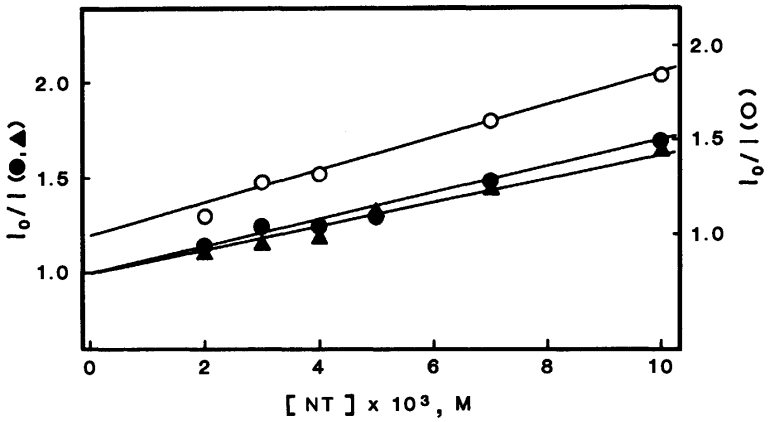

Fig. 2. Stern-Volmer plots for monomer-fluorescence quenching of pyrene (3.00×10^{-3} M) by NT in benzene (●), 1,2-dichloroethane (▲), and acetonitrile (○) under nitrogen at room temperature (23±1 °C). Excitation wavelength=366 nm. I and I_0 refer to fluorescence intensity at 390 nm of pyrene with and without NT, respectively.

Table 1. Solvent Effects on the Pyrene-Sensitized Photolysis of NT with 366-nm Light at 25±3 °C

Solvent (ε)[a]	$\Phi_{-NT,11m}$	$\Phi_{2,11m}$	$\Phi_{3,11m}$	$\Phi_{4,11m}$	$\Phi_{5,11m}$	(k_d/k_r+C^{b})	$\frac{k_t\tau_S^{c}}{M^{-1}}$	$\frac{k_t\tau_S^{d}}{M^{-1}}$	$\frac{\tau_S^{e}}{ns}$
Benzene	0.233	0.034	0.019	0.068	0.038	3.3	136	70	67
(2.275)								(88)[f]	(90)[g]
CH_2ClCH_2Cl	0.196	0.029	0.007[h]	0.066	0.064	4.1	94	62	75
(10.36)								(66)[f]	(98)[g]
CH_3CN	0.211	0.004[h]	0.003[h]	0.009[h,i]	0.147	3.8	93	86	52
(37.5)								(90)[f]	(64)[g]
CH_3CN	0.150[j]	0.044[j]	0.032[j]	0.012[i,j]	0.041[j]	—	—	—	—

a) Dielectric constant. Ref. 17, p. 108 (benzene), p. 356 (CH_2ClCH_2Cl), and p. 400 (CH_3CN). b) $C=k_R(1+k_d/k_r)/(k_s+k_2)$. c) Average of the $k_t\tau_S$ values determined from quantum yield (Φ_{-NT} and Φ_{2-5}) measurements. d) From quenching of pyrene-monomer fluorescence. e) Pyrene-monomer fluorescence lifetime. f) From quenching of pyrene-excimer fluorescence. g) Pyrene-excimer fluorescence lifetime. h) Because of fairly small quantum yield which gives less accurate intercept and intercept/slope ratio we could only determine approximate value. i) Due to side reactions of the amido radical taking place in competition with its hydrogen abstraction to form **4**.[1] j) Quantum yield for the direct photolysis with 313-nm light.[2]

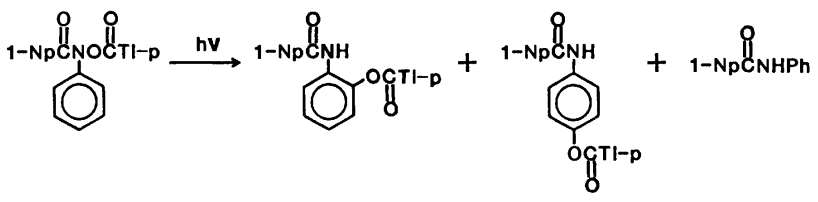

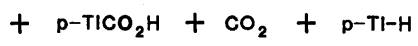

5 **6**

1-Np = 1-naphthyl, p-Tl = p-tolyl

A potassium trioxalatoferrate(III) actinometry was applied to determine quantum yields for the disappearance of NT (Φ_{-NT}) and for the appearance of photoproducts (Φ_{2-5}) at low conversions (5—10%) of starting NT.[7] Stern-Volmer plots of the reciprocal of NT concentration against the reciprocal of quantum yields for the sensitized photolysis measured in the presence of a constant concentration of pyrene (3.00×10^{-3} M) gave a straight line for any plot from which we are able to obtain the limiting quantum yields (Φ_{lim}), i.e., the quantum yields extrapolated to the infinite concentration of NT. Typical double reciprocal plots are shown in Fig. 1. Similar linear plots are observed also in 1,2-dichloroethane and acetonitrile.

Quenching of the Fluorescence of Pyrene by NT. Pyrene (3.00×10^{-3} M) in any solvent employed for the sensitization experiments exhibits a monomer fluorescence at 390 nm and an excimer one at 470 nm under nitrogen at room temperature (23±1 °C). The intensity ratio of monomer- to excimer-fluorescence is in the range of 0.6 to 0.9. These fluorescences were quenched by NT following linear Stern-Volmer relationships, as shown in Fig. 2. The quenching constants ($k_t\tau_S$ where k_t and τ_S refer to the rate constant for singlet energy transfer and the lifetime of singlet pyrene without NT, respectively) for the monomer and excimer fluorescences of this sensitizer have not much different values as seen from Table 1, indicating that the monomer and excimer species are in dynamic equilibrium with each other at photostationary state. A consideration of the relative state energies of pyrene-monomer (77 kcal mol^{-1}) and -excimer (≈60 kcal mol^{-1}) species responsible for the dual fluorescence allows us to assume that NT quenches the monomer fluorescence under our experimental conditions.[8] Measurements of monomer-fluorescence lifetimes under the same conditions as those for the sensitized photolysis permit estimations of the k_t values as 1.0×10^9, 0.8×10^9, and 1.7×10^9 M^{-1} s^{-1} in benzene, 1,2-dichloroethane, and acetonitrile, respectively (Table 1). These k_t values reveal that the pyrene fluorescence is quenched by NT at a rate which is close to the diffusion-controlled one.

Discussion

Solvent Effects on the Pyrene-Sensitization. Much higher singlet and triplet states of NT (the first singlet excitation energy, E_{S_1}=90; the first triplet excitation energy, E_{T_1}=59 kcal mol^{-1}; 1 kcal=4.184 kJ) in comparison with those of pyrene (E_{S_1}=77, E_{T_1}=48 kcal mol^{-1})[9] make singlet-singlet energy transfer from pyrene to NT endothermic and, hence, it very unlikely. It is known that dibenzoyl peroxide, whose structure is similar to that of NT, quenches the

		Process (rate constant)
$Py(S_0) \xrightarrow{h\nu} Py(S_1)$		Absorption of light
$Py(S_1) \xrightarrow{k_d'=1/\tau_s} Py(S_0)$		Deactivation of pyrene (k_d')
$Py(S_1) + NT(S_0) \xrightarrow{k_t} Py\cdot NT(S_1)$		Exciplex formation and energy transfer (k_t)
$Py\cdot NT(S_1) \xrightarrow{k_r} {}^1\overline{N\cdot\ \ \cdot T} + Py(S_0)$		Formation of primary cage (k_r)
$Py\cdot NT(S_1) \xrightarrow{k_d} Py(S_0) + NT(S_0)$		Deactivation of exciplex (k_d)
${}^1\overline{N\cdot\ \ \cdot T} \xrightarrow{k_s} {}^1\overline{N\cdot\,||\,\cdot T}$		Formation of secondary cage (k_s)
${}^1\overline{N\cdot\ \ \cdot T} \xrightarrow{k_2} \mathbf{2}$		Primary cage reaction (k_2)
${}^1\overline{N\cdot\ \ \cdot T} \xrightarrow{k_R} NT(S_0)$		Recombination (k_R)
${}^1\overline{N\cdot\,||\,\cdot T} \xrightarrow{k_3} \mathbf{3}$		Secondary cage reaction (k_3)
${}^1\overline{N\cdot\,||\,\cdot T} \xrightarrow{k_{-s}} {}^1\overline{N\cdot\ \ \cdot T}$		Regeneration of primary cage (k_{-s})
${}^1\overline{N\cdot\,||\,\cdot T} \xrightarrow{k_D} N\cdot + T\cdot$		Cage escape (k_D)
$N\cdot \xrightarrow{k_4} \mathbf{4}$		Hydrogen abstraction (k_4)
$N\cdot \xrightarrow{k_u^N}$	Unknown product(s)	Side reaction(s) (k_u^N)
$T\cdot \xrightarrow{k_5} \mathbf{5}$		Hydrogen abstraction (k_5)
$T\cdot \xrightarrow{k_6} \mathbf{6}$		Decarboxylation and hydrogen abstraction (k_6)
$T\cdot \xrightarrow{k_u^T}$	Unknown product(s)	Side reaction(s) (k_u^T)

N· = 1-NpC(=O)N(·)Ph T· = *p*-TlC(=O)O· Py = pyrene

Scheme 1.

fluorescence of pyrene through the formation of an nonemissive exciplex with a charge-transfer character.[4] This fact suggests the existence of a similar exciplex produced between the singlet-state pyrene monomer and the ground-state NT. The fluorescence from such an exciplex intermediate could not be detected under the present experimental conditions.

If the pyrene-sensitized decomposition of NT proceeds according to Scheme 1, then the following linear Stern-Volmer relationships can be derived between the reciprocals of quantum yields ($1/\Phi_{-NT}$ and $1/\Phi_{2-5}$) and the reciprocals of varying concentrations of NT (1/[NT]) under the steady-state approximation:

$$1/\Phi_{-NT} = C_1(1+k_R/(k_s+k_2))(1+1/k_t\tau_S[NT]), \quad (1)$$

$$1/\Phi_2 = C_1(1+(k_s+k_R)/k_2)(1+1/k_t\tau_S[NT]), \quad (2)$$

$$1/\Phi_3 = C_1C_2(1+(k_{-s}+k_D)/k_3)(1+1/k_t\tau_S[NT]), \quad (3)$$

$$1/\Phi_4 = C_1C_2C_3(1+k_u^N/k_4)(1+1/k_t\tau_S[NT]), \quad (4)$$

and

$$1/\Phi_5 = C_1C_2C_3(1+(k_6+k_u^T)/k_5)(1+1/k_t\tau_S[NT]), \quad (5)$$

where $C_1=1+k_d/k_r$, $C_2=1+(k_2+k_R)/k_s$, and $C_3=1+(k_3+k_{-s})/k_D$. In this Scheme processes for the formation and deactivation of the pyrene excimer were omitted because we presumed no participation of this excimer in the sensitized photolysis. As shown typically in Fig. 2 the observation of linear plots of $1/\Phi$ against 1/[NT] provides a supporting evidence for the mechanism given in Scheme 1. These linear plots allow for the estimation of the values of Φ_{lim}, $k_t\tau_S$, and $k_d/k_r+k_R(1+k_d/k_r)/(k_s+k_2)$ summarized in Table 1. The $k_t\tau_S$ values, thus evaluated, correspond well to those determined from the fluorescence quenching in any solvent employed, giving an additional evidence in support of Scheme 1.

To confirm that the pyrene-sensitized photolysis of NT occurs undoubtedly from the excited singlet state, we tried to quench the reaction by 1,3-cyclohexadiene (E_{S_i}=97, E_{T_i}=52.4 kcal mol^{-1})[9] and *trans*-stilbene (E_{S_i}=94, E_{T_i}<50 kcal mol^{-1})[9]. 1,3-Cyclohexadiene has previously been found to quench the NT phosphorescence efficiently,[1] while triplet pyrene sensitizes the isomerization of *trans*-stilbene.[10] These facts indicate that 1,3-cyclohexadiene and *trans*-stilbene become good quenchers for the NT and pyrene triplets, respectively. We assume here that intersystem crossing of the singlet exciplex Py·NT(S_1) produces these two triplets, NT(T_1) and Py(T_1), but not the triplet exciplex Py·NT(T_1). Triplet pyrene is also formed by intersystem crossing of the singlet pyrene-monomer and -excimer.[8] This assumption allows us to predict that both the compounds quench the triplet-derived reaction. Figure 3 clearly shows that neither 1,3-cyclohexadiene nor *trans*-stilbene exerts their quenching effects on the disappearance of NT and the appearance of any product **2**—**5**.[11] This finding provides a strong piece of evidence for a singlet-pathway mechanism depicted in Scheme 1. The fact that "photoacyloxyl" migration is also observed by the singlet sensitization, therefore, demonstrates that the rearrangement products **2** and **3** come from the singlet-state reaction but not from the triplet-state one.

As evident from Table 1, the singlet-sensitized photolysis gives the same product distribution as that derived from direct photolysis. Interestingly, the quantum yields for the formation of **2** and **3** (Φ_2 and Φ_3) are fairly small, especially in acetonitrile, compared with those for the direct photolysis. On the contrary, the quantum yield for the formation of **5** (Φ_5) in acetonitrile becomes larger in the sensitized photolysis than in the direct photolysis. In addition, Φ_5 decreases with decreasing the polarity of solvents. Although the sum of Φ_2 and Φ_5 for the direct photolysis undergoes negligible solvent polarity effects,[2] the decreased polarity of solvents increases this sum for the sensitized photolysis. Quantum yields Φ_2, Φ_3, and Φ_5 in benzene are comparable to Φ_2,

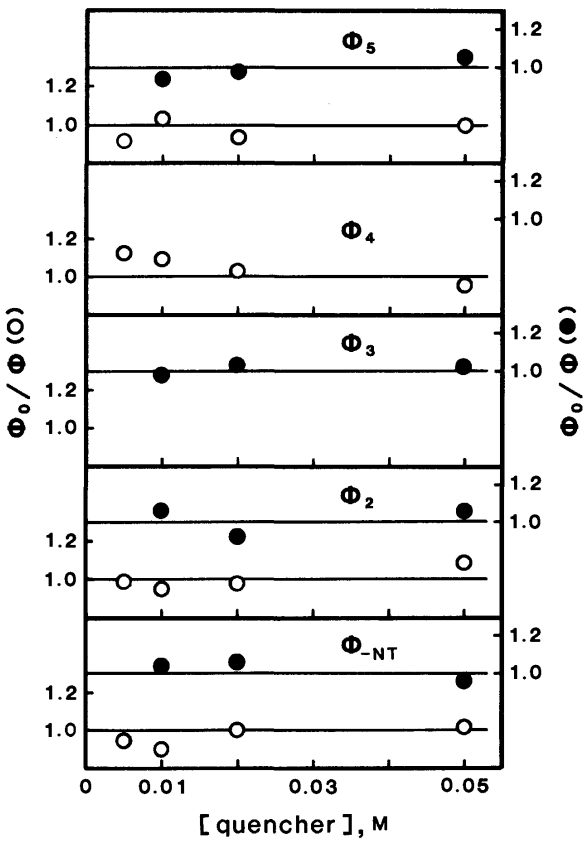

Fig. 3. Stern-Volmer plots for quenching of pyrene (3.00×10^{-3} M)-sensitized reaction of NT (6.67×10^{-3} M) with 366-nm light by 1,3-cyclohexadiene (●) and *trans*-stilbene (○) in 1,2-dichloroethane under nitrogen at room temperature (25±3 °C). Φ and Φ_0 are quantum yield for the reaction of NT with and without the quencher, respectively.

$$Py(S_1) + NT(S_0) \longrightarrow Py\cdot NT(S_1)$$

$$Py\cdot NT(S_1) \begin{cases} \xrightarrow{\text{path a}} Py(S_0) + {}^1\overline{N\cdot \quad \cdot T} \longrightarrow \mathbf{2}\text{—}\mathbf{5} + NT(S_0) \\ \xrightarrow{\text{path b}} NT^{\cdot-} + Py^{\cdot+} \end{cases}$$

$$NT^{\cdot-} \longrightarrow N\cdot + T^-$$

$$N\cdot \longrightarrow \mathbf{4}$$

$$T^- + Py^{\cdot+} \longrightarrow T\cdot + Py(S_0)$$

$$T\cdot \longrightarrow \mathbf{5}$$

N·=1-NpCONPh T·=*p*-TlCO(=O)·· Py=pyrene

Scheme 2.

Φ_3, and Φ_5 for the direct photolysis, respectively. As previously discussed we used here Φ_5 as a measure of the extent of an "out-of-cage" reaction, owing both to a complicated fragmentation of the amido radical and to a minor decarboxylation process of the toluoyloxyl radical.[2]

As shown in Scheme 1, an energy transfer in the singlet exciplex intermediate causes a homolytic cleavage of the N-O bond in a NT molecule and the reactivities of the resulting geminate-radical pair should be affected to a lesser extent by the polarity of solvents based on our previous results.[1,2] Accordingly, Scheme 1 cannot explain the observed solvent polarity effects on $\Phi_2+\Phi_3$ and Φ_5 for the sensitized reaction. Because exciplexes with a charge-transfer character are well known to have a tendency to dissociate into radical ion pairs in polar solvents,[5,12] solvent polarity effects on the quantum yields ($\Phi_2+\Phi_3$ and Φ_5) for the reaction can be accounted for in terms of Scheme 2. In this Scheme an energy transfer in the singlet exciplex (path a) competes with electron transfer in this exciplex (path b). Path a gives the singlet geminate-radical pair from which the products **2**—**5** and starting NT are derived as already indicated in Scheme 1. On the other hand, electron transfer from pyrene to NT in the exciplex intermediate (path b) generates a NT anion radical and a pyrene cation radical. Polar solvents stabilize this radical ion pair but nonpolar solvents do not.[12] A NT anion radical, thus formed, may readily decompose to afford the amido radical and *p*-methylbenzoate which is oxidized by a pyrene cation radical to give the toluoyloxyl radical and pyrene. The amido and toluoyloxyl radicals abstract hydrogen atom from solvent molecules to yield the fragmentation products **4** and **5**. The exclusive participation of path b in the reaction makes the value of $\Phi_2+\Phi_3$ negligibly small. If path a predominates, then the quantum yields for the sensitized photolysis are expected to be comparable to those for the direct photolysis. Therefore the polar solvent, acetonitrile, prefers electron transfer to energy transfer in the exciplex intermediate to reduce $\Phi_2+\Phi_3$ accompanied by an increase in Φ_5, whereas energy transfer predominates in the nonpolar solvent, benzene. Both energy- and electron-transfer pathways may be important in 1,2-dichloroethane.

In order to examine whether or not electron transfer in the exciplex intermediate is thermodynamically possible, the free energy change ΔG in electron transfer was calculated by using the simplified Weller equation[13]

$$\Delta G \text{ (kcal mol}^{-1}\text{)} = 23.06[E(Py^{\cdot+}/Py) - E(NT/NT^{\cdot-})] - E_{S_1},$$

where $E(Py^{\cdot+}/Py)$ is the oxidation potential of pyrene (1.16 V vs. SCE in acetonitrile),[14] $E(NT/NT^{\cdot-})$ is the reduction potential of NT (−1.86 V vs. SCE in acetonitrile), and E_{S_1} is the first singlet excitation energy of pyrene (77 kcal mol^{-1}). The calculation of the free energy change gives ΔG=−7.4 kcal mol^{-1}, strongly indicating electron transfer from the singlet-state pyrene to the ground-state NT to be thermodynamically very favorable process. Although the participation of both energy- and electron-transfer mechanisms in the singlet-sensitized photolysis modifies Eqs. 1—5 slightly, a linear relationship between $1/\Phi$ and 1/[NT] remains unaltered and the intercept/slope ratio of double reciprocal plots still give the same $k_t\tau_S$ values.

Micellar Effects on the Singlet Sensitization. Our previous study of micellar effects on the direct photolysis of NT provided us two interesting findings.[2] One is that diffusive separation of the singlet radical pair generated in hexadecyltrimethylammonium chloride (HTAC) micelles must be slow enough to allow efficient micellar cage reaction to yield exclusively **2**, **3**, and starting NT accompanying negligible formation of **4** and **5**. The other is that the appearance of the secondary cage-reaction product **3** is suppressed within the micelles owing to the high intramicellar viscosity. Based on these findings we expect that the micelle cage of HTAC can be used to distinguish between an energy- and an electron-transfer mechanisms both of which work in the pyrene-sensitized photolysis of NT depending on the polarity of solvents employed.

If the singlet-sensitized photolysis in HTAC micelles proceeds by an energy-transfer mechanism to result in the homolytic cleavage of the N-O bond in a NT molecule, then we expect negligibly small quantum yields for the formation of **4** and **5** compared to those of **2** and **3**. Thus the appearance of **4** and **5** in the micelles can be taken as indication for an electron-transfer mechanism. The sensitized decomposition of NT (3.00×10^{-3} M) by pyrene (1.00×10^{-3} M) in HTAC micelles (1.30×10^{-3} M) under nitrogen at room temperature (23±1 °C) gave the following results: Φ_{-NT}=0.051, Φ_2=0.005, Φ_3<0.001, Φ_4=0.012, and Φ_5=0.045. These results strongly suggest a dominant

electron-transfer mechanism for the reaction in HTAC micelles. Since hydrophobic nature of the amido and toluoyloxyl radicals should retard escape of these radicals from the micelle cage into the water phase,[15] we cannot offer a clear answer to the question of whether the rearranged products **2** is derived from recombination of the singlet geminate-radical pair or from recombination of the radical pair reencountered within the micelles after a NT anion radical decomposed to give the amido and toluoyloxyl radicals. The fact that the micelle surface has a polarity corresponding to that of alcohols seems to indicate minor contribution of an energy-transfer mechanism.[16,17]

Experimental

General Methods. Hitachi 638-50 HPLC apparatus with a 2.6×500-mm ODS (Hitachi gel #3050) column was used to accurately determine the concentrations of the starting materials that disappeared and of the photoproducts that appeared from linear calibration curves for each compound. Fluorescence spectra of pyrene with and without a quencher were taken under nitrogen on a Shimadzu RF-500 spectrophotofluorimeter. UV spectra were obtained with a Shimadzu UV-210A spectrophotometer. Fluorescence lifetimes of pyrene were measured under nitrogen on a Horiba NAES-1100 time-resolved spectrophotofluorimeter.

Materials and Solvents. *N*-(1-Naphthoyl)-*O*-(*p*-toluoyl)-*N*-phenylhydroxylamine (NT) and independently prepared authentic compounds **2**—**5** were the same as in previous studies.[2] Benzene and 1,2-dichloroethane (spectrograde from Dojin Chemical Co.) were used as received. Highly-purified acetonitrile was obtained by the modified procedure of Walden and Birr.[18] 1,3-Cyclohexadiene (Aldrich) was fractionally distilled just before its use and stored under nitrogen in a refrigerator. *trans*-Stilbene (reagent grade, Wako) was recrystallized twice from ethanol. Pyrene (reagent grade, Wako) was purified by repeated recrystallization from ethanol followed by sublimation at reduced pressure. Mobile phase for HPLC analysis consisted of acetonitrile (62 vol%) and water (38 vol%) (HPLC grade from Wako). Hexadecyltrimethylammonium chloride (HTAC, Wako) was recrystallized twice from acetone–methanol and sodium dodecyl sulfate (SDS, specially pure from Wako) was used as supplied.

Quantum Yields. The same methods as before was applied to determine the quantum yields for the pyrene-sensitized photolysis of NT.[2] The 366-nm light from a 450W high-pressure Hg lamp was isolated with Corning 0-52, Corning 7-37, and Toshiba IRA-25S glass filters (Transmittance=19% at 366 nm). Molar absorption coefficients of pyrene were determined to be 220, 190, and 130 ($M^{-1}\,cm^{-1}$) in benzene, 1,2-dichloroethane, and acetonitrile, respectively, so that more than 95% of the incident light is absorbed by pyrene in the sensitized decomposition of NT. All the quantum yields are average of more than three determinations. Quantum yields for the sensitized photolysis in HTAC micelles were measured at a pyrene concentration such that the [pyrene]/[micelle] ratio nearly equals unity. The micelle concentration was estimated based on the equation [micelle]=([HTAC surfactant] $-$cmc)/N, where [HTAC surfactant]=0.15 M, critical micelle concentration, cmc=1.3×10^{-3} M, and aggregation number, N=113.[19]

Fluorescence Lifetimes and Reduction Potential. Prior to fluorescence lifetime measurements, solutions were purged with oxygen-free nitrogen for about 10 min for deoxygenation. Fluorescence decay was traced by the use of a single photon counting technique for deconvolution of the data obtained with a computer attached to the apparatus. The reduction potential of NT was measured by cyclic voltametry in acetonitrile. For this purpose we used saturated calomel electrode (SCE) as a reference electrode and tetrabutylammonium bromide (0.1 M) as a supporting electrolyte.

We thank Dr. Kazuo Ohta, Faculty of Engineering, Tokyo Institute of Polytechnics, for determining fluorescence lifetimes.

References

1) T. Sakurai, S. Yamada, and H. Inoue, *Chem. Lett.*, **1983**, 975; T. Sakurai, H. Yamamoto, S. Yamada, and H. Inoue, *Bull. Chem. Soc. Jpn.*, **58**, 1174 (1985).

2) T. Sakurai, H. Sukegawa, and H. Inoue, *Bull. Chem. Soc. Jpn.*, **58**, 2875 (1985).

3) T. Nakata and K. Tokumaru, *Bull. Chem. Soc. Jpn.*, **43**, 3315 (1970); A. Kitamura, H. Sakuragi, M. Yoshida, and K. Tokumaru, *ibid.*, **53**, 1393 (1980); A. Kitamura, H. Tanikawa, K. Oohashi, H. Sakuragi, and K. Tokumaru, *ibid.*, **56**, 3786 (1983).

4) T. Urano, A. Kitamura, H. Sakuragi, and K. Tokumaru, *J. Photochem.*, **26**, 69 (1984).

5) T. Urano, H. Sakuragi, and K. Tokumaru, *Chem. Lett.*, **1985**, 735.

6) In the sensitized photolysis of NT in benzene there is a possibility of the formation of biphenyl whose chemical yield may be comparable to that of **4** and **5**. But it was impossible to check this possibility because we could not detect HPLC peak of biphenyl whose concentration was adjusted so as to become the same as that of **4** and **5** obtained by the photolysis under our analytical conditions. Additionally HPLC peak of any unknown product observed was not consistent with that of biphenyl.

7) C. G. Hatchard and C. A. Parker, *Proc. R. Soc. London, Ser. A*, **235**, 518 (1956).

8) J. B. Birks, "Photophysics of Aromatic Molecules," Wiley-Interscience, London (1970), pp. 301—316.

9) S. L. Murov, "Handbook of Photochemistry," Marcel Dekker, New York, N. Y. (1973), pp. 3—5.

10) G. S. Hammond, J. Saltiel, A. A. Lamola, N. J. Turro, J. S. Bradshaw, D. O. Cowan, R. C. Counsell, V. Vogt, and C. Dalton, *J. Am. Chem. Soc.*, **86**, 3197 (1964).

11) The fact that the HPLC peaks of *trans*-stilbene and 1,3-cyclohexadiene overlap with those of **3** and **4**, respectively, made it impossible to obtain Stern-Volmer plot for these products.

12) H. Masuhara and N. Mataga, *Acc. Chem. Res.*, **14**, 312 (1981); G. J. Kavarnos and N. J. Turro, *Chem. Rev.*, **86**, 401 (1986).

13) D. Rehm and A. Weller, *Isr. J. Chem.*, **8**, 259 (1970); idem, *Z. Phys. Chem.*, **69**, 183 (1970).

14) E. S. Pysh and N. C. Yang, *J. Am. Chem. Soc.*, **85**, 2124

(1963).

15) I. R. Gould, M. B. Zimmt, N. J. Turro, B. H. Baretz, and G. F. Lehr, *J. Am. Chem. Soc.*, **107**, 4607 (1985) and reference 6 cited therein.

16) K. Kalyanasundaram and J. K. Thomas, *J. Am. Chem. Soc.*, **99**, 2039 (1977); idem, *J. Phys. Chem.*, **81**, 2176 (1977).

17) Recent studies on the solubilization of pyrene in cationic HTAC micelles suggest a micelle surface as the solubilization site of pyrene in this micelle.[19,20] An interaction between the surfactant head group and pyrene has been shown to be major driving force for the solubilization. This interaction also seems to be responsible for the solubilization of NT in HTAC micelles since the solubility of NT in anionic SDS micelles was found to be much low compared to that in cationic HTAC micelles. Thus it is likely that both pyrene and NT are preferentially solubilized at the surface of HTAC micelles.

18) J. A. Riddick and W. B. Bunger, "Organic Solvents," in "Techniques of Chemistry," 3rd ed, ed by A. Weissberger, Wiley-Interscience, New York, N. Y. (1970), Vol. 2, p. 798.

19) A. Malliaris, J. Le Moigne, J. Sturm, and R. Zana, *J. Phys. Chem.*, **89**, 2709 (1985).

20) M. Almgren, F. Grieser, and J. K. Thomas, *J. Am. Chem. Soc.*, **101**, 279 (1979).

 © 1987 The Chemical Society of Japan Bull. Chem. Soc. Jpn., 60, 4107—4113 (1987)

Total Syntheses of Indicine *N*-Oxide, Intermedine *N*-Oxide, and Their Enantiomers Using Carbohydrate as a Chiral Educt

Yoshio NISHIMURA,* Shinichi KONDO, Tomio TAKEUCHI, and (the late) Hamao UMEZAWA
Institute of Microbial Chemistry, 3-14-23 Kamiosaki, Shinagawa-ku, Tokyo 141
(Received June 10, 1987)

The first completely enantioselective syntheses of indicine *N*-oxide, intermedine *N*-oxide, and their enantiomers have been achieved stereospecifically. A synthetic analogue modeled on indicine *N*-oxide showed the superior activity to indicine *N*-oxide itself against cancer cell in vitro test.

The pyrrolizidine alkaloids constitute an exceptionally large class of naturally occurring materials which possess in common the 1-azabicyclo[3.3.0]-octane skelton often functionalized by hydroxyl or stereochemically complex carboxylic ester moieties at a variety of structural sites. The pyrrolizidine alkaloids containing $\Delta^{1,2}$-unsaturated subgroup are associated with wide range of potent biological effects.[1] Indicine *N*-oxide (**1**)[2] shows marked antitumor effects without the hepatotoxicity normally associated with this class of compounds, while the very similar heliotrine (**2**)[1a,3] is an established carcinogen. Due to their intriguing chemical structures and their pharmacological activities, the $\Delta^{1,2}$-unsaturated pyrrolizidine alkaloids have attracted the synthetic attention in recent years.[4]

In order to investigate the relationships between structure and antitumor activity, we undertook the syntheses of **1** and three possible diastereomer (**3**—**5**)[5] of **1** by coupling of (+) and (−)-retronecine (**18** and **19**) with (+) and (−)-trachelanthic acid (**13** and **16**). Although the formal and relay syntheses of indicine (**23**)[6] and intermedine (**21**),[6,7] and the synthesis of inseparable four diastereomeric mixture of **22** by the combination of racemic retronecine and racemic trachelanthic acid[8] have been reported, little is known about the completely enantioselective syntheses of **21**, **22** and their enantiomers. Recently, we succeeded in the enantioselective synthesis of retronecine and its enantiomer.[9] In this paper we wish to report the first enantioselective syntheses of **1**, **3**, **4**, and **5** in a totally stereospecific fashion via the enantioselective synthesis of (+) and (−)-trachelanthic acid. Compounds **1** and **4** are enantiomers of compounds **3** and **5**, respectively. Here we also wish to present the synthesis of active analogue **26** of **1** against cancer cells in vitro test by the regioselective esterification of retronecine with (*S*)-(−)-α-methoxy-α-(trifluoromethyl)-phenylacetic acid (**24**).

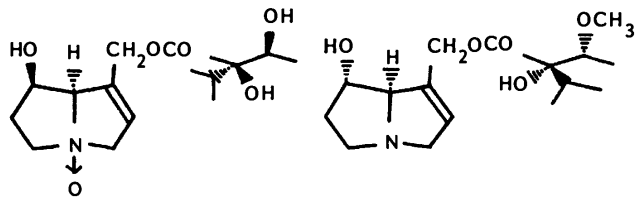

1: Indicine N-oxide 2: Heliotrine

Fig. 1.

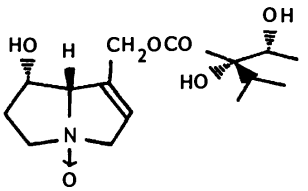

3: (-)-Indicine N-oxide

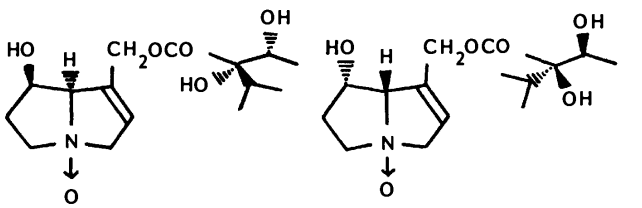

4: Intermedine N-oxide 5: (-)-Intermedine N-oxide

Fig. 2.

Results and Discussion

Synthesis of (+) and (−)-Trachelanthic Acid. The hitherto-known syntheses of trachelanthic acid are all of racemic form,[10] and **13** and **16** have been prepared via its optical resolution. Our approach to **13** and **16** involves, as the key step, the synthesis of a specific branched-chain sugar having a hydroxyl group and a isopropyl group at the branched position. Recently, a route to a branched-chain sugar having such asymmetric center by several steps have been described by Redlich.[11] The simple construction of such asymmetric center by one step sequence has been examined by Grignard reaction using isopropylmagnesium halide with a ulose having the desired stereochemistry.

Grignard reaction of **6** with 3 equiv of isopropylmagnesium bromide occurred stereospecifically to afford 1,2-*O*-isopropylidene-5-deoxy-3-*C*-isopropyl-β-D-lyxofuranose (**7**) and 1,2-*O*-isopropylidene-5-deoxy-β-D-lyxofuranose (**8**) in a yield of 52 and 35%, respectively. Stereospecific addition and reduction were caused by the attack of the bulky Grignard reagent to the carbonyl group from less sterically

hindered side. The configuration of branched chain at C-3 is assigned on the observation of NOE between 3-C-isopropyl and the protons at C-2 and C-4, and between 3-OH and the methyl groups of 1,2-*O*-isopropylidene and C-4. This is also confirmed by successful transformation to natural (+)-trachelanthic acid (**13**). Swern oxidation[12] of by-product **8** was effectively recycled to **6**. Benzylation of tertiary alcohol of **7** gave a corresponding benzyl ether **9** in a yield of 94%. Acid hydrolysis of **9** followed by acetylation produced an anomeric mixture **10** (α: 84%, β: 6% yield). Borohydride reduction of **10** afforded the tetrol **11** in a yield of 72%. Lemieux-von Rudloff oxidation[13] of **11** yielded the carboxylic acid **12** in a yield of 81%. Removal of protected group of **12** by hydrogenolysis afforded (+)-trachelanthic acid (**13**), whose structure was also supported by ^{1}H NMR and ^{13}C NMR spectra. The resulting acid **13** was converted to the acetonide **14** by treatment of 20 equiv of 2,2-dimethoxypropane and a trace amount of concd hydrochloric acid in a yield of 90%. (−)-Trachelanthic acid (**16**) was synthesized from **15** by the same sequence used for the synthesis of (+)-trachelanthic acid. Compound **16** was identical in all respects with **13** except for the sign of the specific rotation. The acid **16** was transformed into the acetonide **17** by a similar treatment mentioned above. The first enantioselective syntheses of **13** and **16** have thus been achieved by the convergent method employing D- and L-arabinose as a chiral source.

Total Syntheses of Indicine *N*-Oxide, Intermedine *N*-Oxide, Their Enantiomers, and Their Analogues. The first synthesis of hepatotoxic pyrrolizidine alkaloid was reported in the reconstruction of intermedine (**22**) by coupling 1-(chloromethyl)-1,2-dehydro-7β-hydroxy-8α-pyrrolizidine and (+)-trachelanthic acid sodium salt obtained from natural source in a low yield.[7]

For syntheses of **1**, **3**, **4**, and **5**, the coupling each of **18** and **19** with each of **14** and **17** was examined by regioselective esterification. The synthetic approaches to monoester pyrrolizidine alkaloids have been described by use of combinations of 1,1′-carbonyldiimidazole (CDI) and imidazoylsodium in tetrahydrofuran,[14] dicyclohexylcarbodiimide (DCC) and catalytic amount of 4-(dimethylamino)pyridine (DMAP) in toluene,[15] and CDI and a catalytic amount of imdiazoylsodium in *N*,*N*-dimethylformamide.[6] These studies suggested that the combination of DCC and DMAP was most suitable for our synthesis.

Treatment of **14** and **19** with DCC and DMAP in toluene followed by hydrolysis with 0.6 M hydrochloric acid afforded foamy (−)-indicine (**20**) (71% yield), identical in all respects with natural indicine[16] except for the sign of the specific rotation. Oxidation of **20** with *m*-chloroperbenzoic acid (MCPBA) in dry acetone gave **3** (84% yield), whose spectral properties were superimposable with those of natural indicine

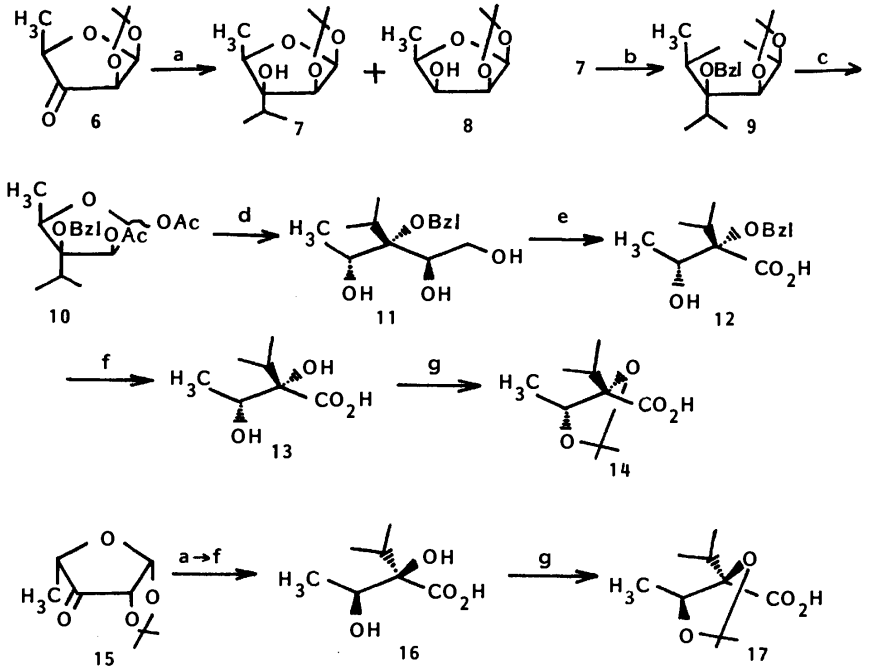

a) $(CH_3)_2CHMgBr/Et_2O$ (52%); b) NaH/DMF, then BzlCl (94%); c) i) 6 M HCl–AcOH (1:3); ii) Ac_2O/Py (90%); d) $NaBH_4$/EtOH, Δ (72%); e) $NaIO_4/KMnO_4/Na_2CO_3$/*t*-BuOH–H_2O (81%); f) H_2/10% Pd-C/MeOH (90%); g) $(CH_3)_2C(OCH_3)_2$/trace concd HCl (90%)

Scheme 1.

N-oxide.[16]

The synthesis of intermedine *N*-oxide (**4**) was achieved through the same sequence used for the synthesis of (−)-indicine *N*-oxide. Esterification of **18** with **14** followed by acid hydrolysis produced intermedine (**21**) (76% yield), identical in all respects with natural intermedine.[17] Oxidation of **21** with MCPBA in dry acetone afforded hygroscopic **4** quantitatively, whose structure was confirmed by ^{1}H NMR, ^{13}C NMR, IR, and mass spectra.

The synthesis of indicine *N*-oxide (**1**) from **18** and **17**, and the synthesis of (−)-intermedine *N*-oxide (**5**) from **19** and **17** were accomplished via indicine (**22**) and (−)-intermedine (**23**) by the same sequence used for the syntheses of **3** and **4**, respectively. The spectral properties of all of synthesized compounds were superimposable with those of natural specimens.[16,17] Thus, the diastereomeric set, which is composed of

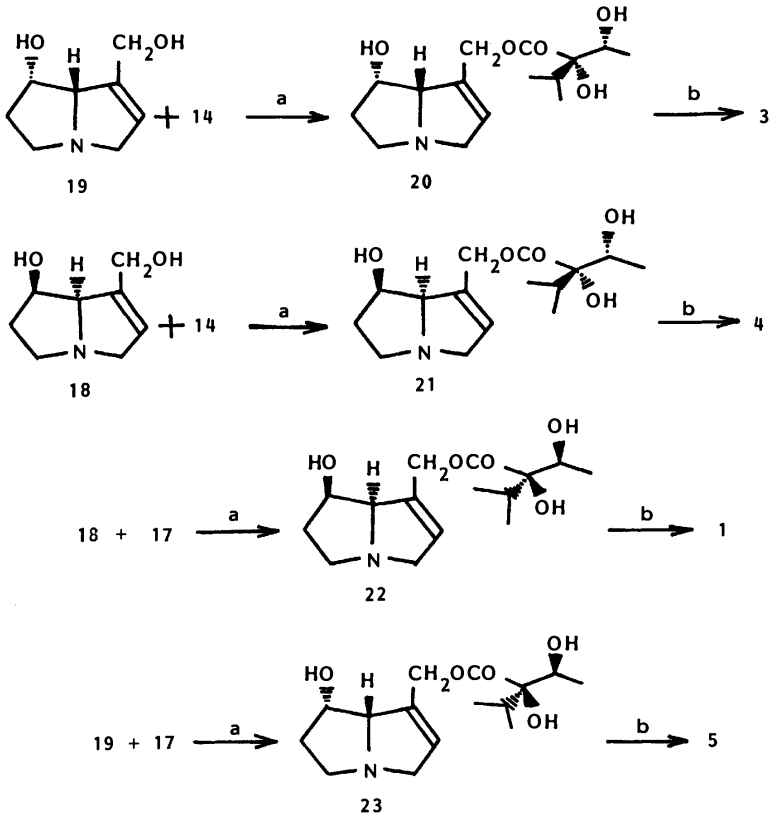

a) DCC/DMAP/PhCH$_3$, then 0.6 M HCl (71%);
b) mCPBA/CH$_3$COCH$_3$ (84%)

Scheme 2.

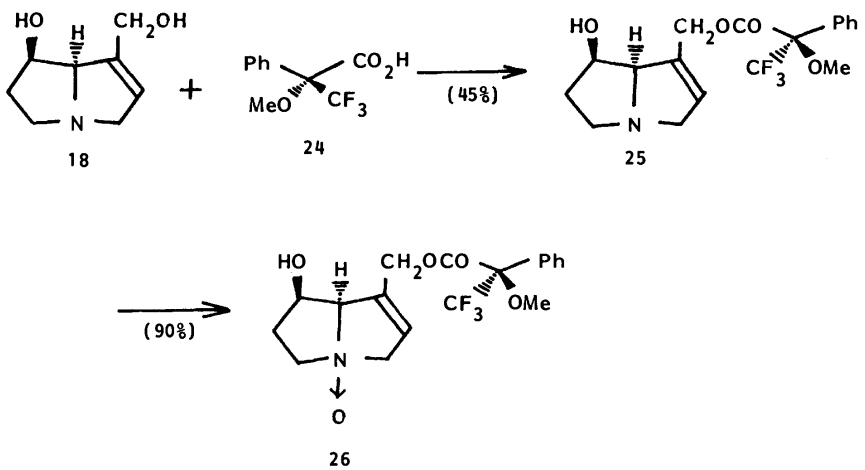

Scheme 3.

Table 1. The Antitumor Activity in Vitro Test (Inhibition/%)

Compound	Dose / μg ml^{-1}	IMC[a] / carcinoma	Tumor cell		
			P388	P388/ADR[b]	L1210
Indicine *N*-oxide (**1**)	100	42	77	57	10
	25	14	45	15	6
(−)-Indicine *N*-oxide (**3**)	100	42	0	0	0
	25	18	0	0	0
Intermedine *N*-oxide (**4**)	100	42	0	0	0
	25	22	0	0	0
(−)-Intermedine *N*-oxide (**5**)	100	42	0	0	0
	25	15	0	0	0
Compound **26**	100	82	75	33	76
	25	74	51	0	61

a) Mouse mammary carcinoma cells. b) Adriamycin-resistant P388 cells.

two enantiomeric pairs related to **1**, has successfully been synthesized.

In relation to these syntheses, we were interested in the synthesis of new analogue modeled on **1**. The antitumor activity of four diastereomers and indicine *N*-oxide derivatives[3b,18] suggested that the electronic and steric factor around α-carbon of necic acid esterified to (+)-retronecine played an important role in increasing antitumor activity. In view of these facts, we undertook to synthesize **26**. Treatment of **18** and **24** with DCC and DMAP in toluene gave 9-*O*-[(*S*)-(−)-2-methoxy-2-phenyl-3,3,3-trifluoropropionyl]retronecine (**25**) in a yield of 68%. Oxidation of **25** resulted in **26** (90% yield).

The antitumor activity of synthesized compounds is shown in Table 1. Among four diastereomers synthesized, **1** showed the best antitumor activity. Interestingly, the synthesized analogue **26** was found to have the superior activity to **1**.

Experimental

General Methods. Melting points were determined with a Yamato apparatus and were uncorrected. IR spectra were determined on a Hitachi Model 260-10 spectrophotometer. Optical rotations were measured with a Parkin-Elmer Model 241 polarimeter. The ^{1}H NMR spectra were recorded with Varian XL-100, Varian EM-390, Bruker WM250, and Jeol GX-400 spectrometers. Chemical shifts were expressed in values (ppm) with tetramethylsilane as an internal standard. Proton noise decoupled FT ^{13}C NMR spectra were taken at 100.4 MHz on a Jeol GX-400 spectrometer using tetramethylsilane as a reference. The mass spectra were taken by a Hitachi RMU-6M mass spectrometer for electron-impact ionization or RMU-7M for field-desorption and for secondary ionization.

1,2-*O*-Isopropylidene-5-deoxy-3-*C*-isopropyl-β-D-lyxofuranose (7). To a solution of **6** (1.3 g) in diethyl ether (26 ml) was added isopropylmagnesium bromide in ether (1 mol dm^{-3}, 13 ml) at −78 °C, and the mixture was stirred from −78 °C to room temperature, and then the mixture was stirred at room temp overnight. After addition of water, the reaction mixture was extracted with ether. The extract was washed with NaCl-saturated aqueous solution, dried over $MgSO_4$, and filtered. Evaporation of the filtrate to give a solid, which was subjected to the column chromatography on silic gel. Elution with toluene–acetone (10:1) gave solids of **7** (849 mg, 52%) and **8** (572 mg, 35%). **7**: mp 37.5—38.5 °C; $[\alpha]_D^{20}$ +9.8° (*c* 1.0, $CHCl_3$); IR ($CHCl_3$) 3540, 3000, 2970, 2940, 2880, 1470, 1460, 1390, 1380 cm^{-1}; ^{1}H NMR ($CDCl_3$, 400 MHz) δ=0.96 (6H, d, *J*=6.7 Hz, CH_3 of 3-C-isopropyl), 1.31 (3H d, *J*=6.7 Hz, 4-CH_3), 1.40 and 1.62 (3H each S, isopropylidene), 1.77 (1H heptet, *J*=6.7 Hz, CH of 3-C-isopropyl), 2.92 (1H, s, 3-OH), 4.08 (1H q, *J*=6.7 Hz, H-4), 4.32 (1H d, *J*=4.0 Hz, H-2) and 5.65 (1H d, *J*=4.0 Hz, H-1); MS (EI) *m/z* 217 (M^++1), 261, 215, 183.

1,2-*O*-Isopropylidene-3-*O*-benzyl-5-deoxy-3-*C*-isopropyl-β-D-lyxofuranose (9). To a solution of **7** (680 mg) in dry *N*,*N*-dimethylformamide (6.8 ml) was added NaH (50% in oil, 375 mg) at 0 °C. After the mixture was stirred at room temperature for 30 min, benzyl chloride (1.08 ml) was added to the mixture. Then the resulting mixture was stirred at room temperature overnight. After being quenched with water, evaporation of the solvent gave an oil. The oil was dissolved in chloroform, and the chloroform solution was washed with water, dried over $MgSO_4$, and filtered. Evaporation of the solvent gave an oil, which was subjected to the column chromatography on silica gel. Elution with toluene–acetone (10:1) gave an oil of **9** (906 mg, 94%): $[\alpha]_D^{25}$ +15.9° (*c* 0.79, $CHCl_3$); IR ($CHCl_3$) 3000, 2960, 1460, 1390, 1380 cm^{-1}; ^{1}H NMR ($CDCl_3$, 90 MHz) δ=0.90 and 0.93 (3H each d, *J*=6.7 Hz, CH_3 of 3-C-isopropyl), 1.27 and 1.57 (3H each s, isopropylidene), 1.37 (3H d, *J*=6.7 Hz, 4-CH_3), 2.27 (1H heptet, *J*=6.7 Hz, CH of 3-C-isopropyl), 4.17 (1H q, *J*=6.7 Hz, H-4), 4.43 (1H, d, *J*=4.4 Hz, H-2), 4.43 and 4.67 (2H ABq, CH_2-φ), 5.68 (1H, d, *J*=4.4 Hz, H-1) and 7.2—7.6 (5H m, phenyl); MS (SIMS) *m/z* 329 (M^++Na), 249, 143, 59, 43; (EI) *m/z* 305 (M^+−1), 291, 261, 248.

1,2-Di-*O*-acetyl-3-*O*-benzyl-5-deoxy-3-*C*-isopropyl-D-lyxofuranose (10). Compound **9** (840 mg) was dissolved in a mixture of 70% acetic acid–6 M† hydrochloric acid (4:1, 10 ml), and the mixture was allowed to stand at room temp for 2 h. After being neutralized with solid Na_2CO_3, the mixture was filtered, and the residue was washed with

† 1 M=1 mol dm^{-3}.

acetone. The filtrate and washings were combined, and evaporated to dryness to give an oil. To a solution of the oil in pyridine (12 ml) was added acetic anhydride (4 ml), and the mixture was allowed to stand at room temperature overnight. After being quenched with water, evaporation of the solvent gave a solid, which was dissolved in chloroform. The solution was washed with water, and dried over $MgSO_4$. Evaporation of the solvent gave an oil. The oil was subjected to the column chromatography on silica gel. Elution with toluene–acetone (10:1) gave the α-acetate of **10** (807 mg, 84%) and the β-acetate of **10** (58 mg, 6%). α-Acetate of **10**: $[\alpha]_D^{27}$ +62.7° (*c* 0.73, $CHCl_3$); IR ($CHCl_3$) 3030, 2980, 2950, 2880, 1750, 1375, 1250 (sh) cm^{-1}; ^1H NMR ($CDCl_3$, 90 MHz) δ=1.00 and 1.03 (3H each d, *J*=6.7 Hz, CH_3 of 3-C-isopropyl), 1.38 (3H d, *J*=6.7 Hz, 4-CH_3), 1.97 and 2.10 (3H each s, isopropylidene), 4.38 (1H q, *J*=6.7 Hz, H-4), 4.73 and 4.90 (2H ABq, *J*=12 Hz, CH_2-ϕ), 5.53 (1H d, *J*=3 Hz, H-2), 6.18 (1H d, *J*=3 Hz, H-1) and 7.2—7.6 (5H m, phenyl), MS (SIMS) *m/z* 373 (M^++Na), 291, 185, 142, 91, 84, 43.

β-Acetate of **10**: $[\alpha]_D^{27}$ +3.9° (*c* 0.55, $CHCl_3$); IR ($CHCl_3$) 3030, 2975, 2950, 2880, 1750, 1380, 1250 (sh) cm^{-1}; ^1H NMR ($CDCl_3$, 90 MHz) δ=1.00 and 1.05 (3H each d, *J*=7.0 Hz, CH_3 of 3-C-isopropyl), 1.40 (3H d, *J*=6.7 Hz, 4-CH_3), 1.97 and 2.0 (3H each s, -$COCH_3$), 2.37 (1H heptet, *J*=7.0 Hz, CH of 3-C-isopropyl), 4.23 (1H q, *J*=6.7 Hz, H-4), 4.62 and 4.83 (2H ABq, CH_2-ϕ), 5.42 (1H d, *J*=5.1 Hz, H-2), 6.26 (1H d, *J*=5.1 Hz, H-1) and 7.1—7.6 (5H m, phenyl), MS (SIMS) *m/z* 373 (M^++Na), 291, 185, 142, 91, 84.

(2*R*,3*S*,4*R*)-3-Benzyloxy-3-isopropyl-1,2,3,4-pentanetetrol (11). To a solution of **10** (816 mg) in ethanol (15 ml) was added $NaBH_4$ (2.64 g), and the mixture was stirred at room temperature overnight, and then refluxed under stirring for 20 h. After being quenched with acetic acid, evaporation of the solvent gave a solid. The solid was extracted with warm ethyl acetate, and the extract was evaporated to give an oil. The oil was subjected to the column chromatography on silica gel to give an oil of **11** (450 mg, 72%): $[\alpha]_D^{25}$ +6.8° (*c* 0.8, $CHCl_3$); IR ($CHCl_3$) 3560, 3420, 2970, 2940, 2880, 1460, 1380 (sh) cm^{-1}; ^1H NMR ($CDCl_3$, 400 MHz) δ=1.08 and 1.17 (3H each d, *J*=7.2 Hz, CH_3 of isopropyl), 1.39 (3H d, *J*=6.8 Hz, H-5), 2.25 (3H heptet, *J*=7.2 Hz, CH of isopropyl), 3.78 (1H dd, *J*=7.0 and 12 Hz, H-1), 3.91 (1H dd, *J*=3.6 and 12 Hz, H-1′), 4.13 (1H dd, *J*=3.6 and 7.0 Hz, H-2), 4.16 (1H q, *J*=6.8 Hz, H-4), 4.67 and 4.81 (2H ABq, *J*=11.2 Hz, CH_2-ϕ); MS (FD) *m/z* 268 (M^+), 223, 207, 149, 91, 61, 58, 32.

2-*O*-Benzyl-(+)-trachelanthic Acid (12). To a solution of **11** (330 mg) in *t*-butyl alcohol (5 ml) was added a solution of mixture of $NaIO_4$ (610 mg) and $KMnO_4$ (41 mg) in water (14 ml) and K_2CO_3, and the mixture was stirred at room temperature for 1 h. After being acidified with 1 M sulfuric acid, the mixture was extracted with dichloromethane. The extract was dried over $MgSO_4$, and filtered. The filtrate was evaporated to give an oil. The oil was subjected to the preparative thin-layer chromatography on silica gel developed with chloroform–methanol (9:1) to give an oil of **12** (252 mg, 81%): $[\alpha]_D^{25}$ −16.47° (*c* 0.87, $CHCl_3$); IR ($CHCl_3$) 3350, 2980, 2940, 2880, 1600, 1460, 1400 (sh) cm^{-1}; ^1H NMR ($CDCl_3$, 400 MHz) δ=0.96 and 1.02 (3H each d, *J*=7 Hz, CH_3 of isopropyl), 1.15 (3H d, *J*=7.0 Hz, H-4), 2.0—2.2 (1H broad m, CH of isopropyl), 4.17 (1H q, *J*=7.0 Hz, H-3), 4.59 and 4.74 (2H ABq, *J*=11.6 Hz, CH_2-ϕ); ^{13}C NMR ($CDCl_3$) δ=18.112, 18.629, 18.825 (3×CH_3), 31.903 (CH of isopropyl), 67.195 (CH_2-ϕ), 69.517 (C-3), 88.176 (C-2) and 178.509 (C-1); MS (FD) *m/z* 253 (M^+), 159, 58, 23.

(+)-Trachelanthic Acid (13). Compound **12** (173 mg) in methanol (17 ml) was stirred with 10% Pd/C (50 mg) under bubbling hydrogen gas at room temperature for 3 h. The catalyst was filtered off, and the filtrate was evaporated to give an oil. The oil was dissolved in 1 M hydrochloric acid, and the solution was extracted with ether. The extract was washed with NaCl-saturated aqueous solution, dried over $MgSO_4$, and filtered. The filtrate was evaporated to give a solid. The solid was crystallized from benzene–hexane to yield a crystal of **13** (100 mg, 90%): mp 89.5—90 °C; $[\alpha]_D^{25}$ +4.0° (*c* 0.85, EtOH); IR ($CHCl_3$) 3500, 3040, 2980, 2950, 2890, 1720, 1475, 1460 cm^{-1}; ^1H NMR ($CDCl_3$, 400 MHz) δ=0.96 and 0.99 (3H each d, *J*=7 Hz, CH_3 of isopropyl), 1.26 (3H d, *J*=6.5 Hz, CH_3), 2.01 (1H heptet, *J*=7 Hz, CH of isopropyl) and 2.24 (1H q, *J*=6.5 Hz, H-3); ^{13}C NMR ($CDCl_3$) δ=16.741, 16.825 and 16.881 (3×CH_3), 32.771 (CH of isopropyl), 69.656 (C-3), 82.567 (C-2) and 177.348 (C-1); MS (SIMS) *m/z* 163 (M^++1), 75, 57, 45.

2,3-*O*-Isopropylidene-(+)-trachelanthic Acid (14). To a solution of **13** (89 mg) in 2,2-dimethoxypropane (1.78 ml) was added concd hydrochloric acid (14 μl), and the mixture was allowed to stand at room temperature ovenight. Evaporation of the solvent gave an oil, which was solidified with ether. The solid was subjected to the preparative thin-layer chromatography developed with chloroform–methanol (3:1) to give a solid. The sublimation of the solid gave a crystal of **14** (100 mg, 90%): mp 54.5—55.5 °C; $[\alpha]_D^{25}$ −34.2° (*c* 0.35, EtOH); IR ($CHCl_3$) 2980, 2940, 2875, 1770, 1720, 1460, 1390, 1380, 1260 cm^{-1}; ^1H NMR ($CDCl_3$, 400 MHz) δ=0.91 and 1.02 (3H each d, *J*=6.7 Hz, CH_3 of isopropyl), 1.50 (3H d, *J*=6.5 Hz, CH_3), 2.20 (1H heptet, *J*=6.7 Hz, CH of isopropyl) and 4.36 (1H q, *J*=6.5 Hz, H-3); MS (SIMS) *m/z* 203 (M^++1) 162, 75, 57, 45.

(−)-Trachelanthic Acid (16). Procedures used for the synthesis from **15** were similar to those used for the preparation of **13** from **6**; the yield 93%: mp 89.5—90 °C; $[\alpha]_D^{25}$ −4.8° (*c* 0.51, EtOH).

2,3-*O*-Isopropylidene-(+)-trachelanthic Acid (17). Procedure employed was similar to that used for the preparation of **14** from **13** described above; the yield 88%: mp 55—56 °C; $[\alpha]_D^{25}$ +36° (*c* 0.31, EtOH).

(−)-Indicine (20). To a solution of mixture of (+)-retronecine (**18**, 21.5 mg) and **14** (46 mg) in toluene (3 ml) was added DCC (46.6 mg) and DMAP (3.35 mg), and the mixture was stirred at room temperature for 3 d. The precipitate was filtered off, and the residue was washed with a small amount of toluene. The filtrate was extracted with 0.6 M hydrochloric acid. The extract was allowed to stand at room temperature for 8 h. After being made basic by treatment with 28% NH_4OH solution, the mixture was treated with solid NaCl until saturation, and then the mixture was extracted with ether. The extract was dried over $MgSO_4$, and filtered. The filtrate was evaporated to give a foamy glass, which was subjected to the preparative thin-layer chromatography on silica gel developed with chloroform–methanol–concd aqueous ammonia (10:3:0.1) to give a foamy glass of **20** (29.4 mg, 71%): $[\alpha]_D^{23}$ −19° (*c* 2.6, EtOH); IR ($CHCl_3$) 3500 (br), 2975, 2950, 2875, 1730, 1475, 1460, 1390, 1380, 1325, 1305, 1230 (sho), 1180, 1160, 1110, 1080, 1035, 1005, 975, 890, 840 cm^{-1}; ^1H NMR ($CDCl_3$, 400 MHz) δ=0.92 and 0.97 (3H each d, *J*=7 Hz, CH_3 of isopropyl), 1.17 (3H d, *J*=6.7 Hz, H-13), 1.85—2.05 (2H m,

H-6,6'), 2.15 (1H heptet, J=7 Hz, CH of isopropyl), 2.65—2.85 (1H m, H-5), 3.2—3.35 (1H m, H-5'), 3.42 (1H dd, J=5.2 and 15.6 Hz, H-3), 3.96 (1H d, J=15.6 Hz, H-3'), 4.04 (1H q, J=6.7 Hz, H-12), 4.16 (1H broad s, H-8), 4.28 (1H broad s, H-7), 4.59 and 5.09 (2H ABq, J=12.4 Hz, H-9) and 5.91 (1H s, H-2); ^{13}C NMR ($CDCl_3$) δ=16.564, 17.166, 17.543 (3×CH_3), 32.345 (CH of isopropyl), 36.248 (C-6), 53.777 (C-5), 62.885 (C-3), 63.011 (C-9), 69.194 (C-12(?)), 71.321 (C-8), 78,679 (C-7(?)), 82.764 (C-11), 130.428 (C-2), 132.806 (C-1) and 175.364 (C-10); MS (SIMS) m/z 300 (M^++1), 138, 94, 80, 43: (FD) 299 (M^+), 262, 220, 186, 99, 58.

(−)-Indicine *N*-Oxide (3). To a solution of **20** (25 mg) in dry acetone (1.5 ml) was added MCPBA (18 mg), and the mixture was stirred at room temperature for 1 h. The mixture was directly subjected to the preparative thin-layer chromatography on silica gel to give a solid. The solid was crystallized from a mixture of acetone-methanol to yield a crystal of **3** (22.2 mg, 84%): mp 119—121 °C; $[\alpha]_D^{21}$ −34.7° (c 1.44, EtOH); IR ($CHCl_3$) 3300 (br), 2980, 2950 (sh), 1740, 1460 (sh), 1380, 1310 (sh), 1230 (br), 1185, 1165, 1145, 1100, 1060, 1025, 1010, 990, 950, 890, 835 cm^{-1}; ^{1}H NMR ($CDCl_3$, 400 MHz) δ=0.90 and 0.94 (3H each d, J=7 Hz, CH_3 of isopropyl), 1.15 (3H d, J=6.7 Hz, H-13), 1.88 (1H heptet, J=7 Hz, CH of isopropyl), 2.00 (1H broad m, H-6), 2.59 (1H m, H-6'), 3.65—3.80 (2H m, H-5,5'), 4.08 (1H q, J=6.7 Hz, H-12), 4.42 (1H s, H-3,3'), 4.62 (1H broad s, H-8 (?)), 4.68 (1H s, H-7(?)), 4.70 and 5.05 (2H ABq, J=12.4 Hz, H-9) and 5.81 (1H s, H-2); MS (SIMS) m/z 316 (M^++1), 136, 93, 75, 57, 45.

Intermedine (21). Procedure used was similar to that used for the preparation of **20** from **14** and **19**; the yield 76%: mp 140—141 °C; $[\alpha]_D^{23}$ +6.3 (c 1.2, EtOH); IR ($CHCl_3$) 3500, 2970, 2930, 2850, 1720, 1460 (sh), 1370 (sh), 1320 (sh), 1220 (broad), 1160, 1110, 1080, 1030, 1000, 970, 950, 910, 890, 840 cm^{-1}; ^{1}H NMR ($CDCl_3$, 400 MHz) δ=0.93 and 0.94 (3H each d, J=7 Hz, CH_3 of isopropyl), 1.21 (3H d, J=6.7 Hz, H-13), 1.9—2.1 (3H m, H-6,6' and CH of isopropyl), 2.65—2.85 (1H m, H-5), 3.30 (1H t, J=8.4 Hz, H-5'), 3.44 (1H dd, J=6 and 15.4 Hz, H-3), 3.96 (1H d, J=15.4 Hz, H-3'), 4.11 (1H q, J=6.7 Hz, H-12), 4.20 (1H broad s, H-8(?)), 4.27 (1H broad s, H-7(?)), 4.76 and 4.86 (2H ABq, J=12 Hz, H-9) and 5.96 (1H s, H-2); ^{13}C NMR ($CDCl_3$) δ=16.881, 17.118 and 17.244 (3×CH_3), 33.008 (CH of isopropyl), 36.254 (C-6), 53.822 (C-5), 62.537 (C-9), 62.872 (C-3), 69.293 (C-12), 70.901 (C-8), 78.734 (C-7), 83.015 (C-11), 131.203 (C-2), 132.531 (C-1) and 175.278 (C-10).

Intermedine *N*-Oxide (4). Procedure used was similar to that used for the preparation of **3** from **20**: the yield is 98%; $[\alpha]_D^{20}$ +8.6° (c 0.98, EtOH); IR ($CHCl_3$) 3200, 2980 (sh), 1740, 1460 (sh), 1380 (sh), 1310 (sh), 1230 (broad), 1185, 1170, 1145, 1100, 1060, 1025, 1010 cm^{-1}; ^{1}H NMR ($CDCl_3$, 400 MHz) δ=0.91 and 0.97 (3H each d, J=7 Hz, CH_3 of isopropyl), 1.16 (3H d, J=7 Hz, H-13), 1.85 (1H q, J=6.7 Hz, CH of isopropyl), 2.01 (1H broad d, J=11 Hz, H-6), 2.45—2.65 (1H m, H-6'), 3.75—3.85 (2H m, H-5,5'), 4.11 (1H q, J=6.7 Hz, H-12), 4.44 (2H broad t, J=18 Hz, H-3,3'(?)), 4.67 (1H broad s, H-8(?)), 4.75 (1H broad s, H-7(?)), 4.85 (2H broad t, J=14 Hz, H-9,9'(?)) and 5.81 (1H s, H-2); ^{13}C NMR ($CDCl_3$) δ=16.741, 17.174 and 17.636 (3×CH_3), 33.722 (CH of isopropyl), 34.701 (C-6), 61.292 (C-5), 69.223 (C-9(?)), 69.559 (C-12(?)), 69.908 (C-8(?)), 77.993 (C-3), 84.064 (C-11), 95.883 (C-7), 122.125 (C-2), 132.811 (C-1) and 174.802 (C-10).

Indicine (22) and Indicine *N*-Oxide (1). Procedures used were similar to those used for the preparations of **3** via **20** from **14** and **19**. **22**: $[\alpha]_D^{22}$ +19.5° (c 1.2, EtOH) [natural indicine[16]: $[\alpha]_D^{22}$ +20° (EtOH)]. **1**: mp 118—119 °C, $[\alpha]_D^{22}$ +35° (c 0.9, EtOH) [natural indicine *N*-oxide:[16] mp 119—120 °C, $[\alpha]_D^{21}$ +34.8° (EtOH)]. Synthetic **22** and **1** were identical in all respects with natural specimens.

(−)-Intermedine (23) and (−)-Intermedine *N*-Oxide (5). Procedures used were similar to those used for the preparation of **4** via **21** from **14** and **18**. **23**: mp 138—139 °C, $[\alpha]_D^{23}$ −7.1° (c 1.1, EtOH). **5**: $[\alpha]_D^{22}$ −9.1° (c 0.88, EtOH).

9-*O*-[(*S*)-(−)-2-Methoxy-2-phenyl-3,3,3-trifluoropropionyl]retronecine (25). To a solution of mixture of (+)-retronecine (**18**, 100 mg) and (*S*)-(−)-α-methoxy-α-(trifluoromethyl)phenylacetic acid (**24**, Aldrich Chem. Co., 302 mg) in dry toluene (10 ml) was added DCC (240 mg) and DMAP (18 mg), and the mixture was stirred at room temprature overnight. The precipitate was filtered off, and the filtrate was quenched with water. Evaporation of the solvent gave a solid, which was dissolved in dichloromethane. The solution was washed with NaCl-saturated aqueous solution, dried over $MgSO_4$, and filtered. The filtrate was evaporated to give a foamy glass, which was subjected to the preparative thin-layer chromatography on silica gel to give a foamy glass of **25** (169 mg, 68%): $[\alpha]_D^{21}$ −1.9° (c 0.95, $CHCl_3$); IR ($CHCl_3$) 3000, 2950, 2850, 1750, 1460, 1440, 1280, 1250, 1210, 1175 (sh), 1115 (sh), 1085, 1000 (sh), 840 cm^{-1}; ^{1}H NMR ($CDCl_3$, 90 MHz) δ=1.6—2.1 (2H m, H-6,6'), 2.4—3.0 (1H m, H-5), 3.1—3.4 (1H m, H-5'), 3.40 (1H dd, J=5.2 and 15.6 Hz, H-3), 3.53 (3H s, OCH_3), 3.93 (1H d, J=15.6 Hz, H-3'), 4.17 (1H broad s, H-7 and H-8), 4.93 (2H broad t, J=14.3 Hz, H-9,9'), 5.85 (1H s, H-2) and 7.2—7.7 (5H m, phenyl); MS (SIMS) m/z 386 (M^++1), 189, 136, 93, 80, 43.

9-*O*-[(*S*)-(−)-2-Methoxy-2-phenyl-3,3,3-trifluoropropionyl]retronecine *N*-Oxide (26). Procedure used was similar to that used for the preparation of **3** from **20**; the yield 90%: $[\alpha]_D^{20}$ +6.0° (c 1.45, $CHCl_3$); IR ($CHCl_3$) 2975 (sh), 1760, 1460, 1280, 1250, 1180 (sh), 1130 (sh), 1020, 1010, 840 cm^{-1}; ^{1}H NMR ($CDCl_3$, 90 MHz) δ=2.0 (1H broad d with a small coupling, J=12.6 Hz, H-6), 2.3—2.8 (1H m, H-6'), 3.53 (3H s, OCH_3), 3.5—3.9 (2H m, H-5,5'), 4.42 (2H broad s, H-3,3'), 4.53 (2H broad s, H-7 and H-8), 5.00 (2H broad s, H-9,9'), 5.70 (1H s, H-2) and 7.3—7.7 (5H m, phenyl); MS (SIMS) m/z 388 (M^++1), 189, 136, 93, 80.

We are very grateful to Dr. Mathew Suffness, National Cancer Institute and Dr. Leslie W. Smith, CSIRO for generous gifts of the authentic samples. We wish also thank to Mrs. Mieko Nagasawa, Pharmaceutical Research Laboratories, Meiji Seika Kaisha Ltd. for antitumor tests. This work was supported in part by a Contract NO1-CM-47593 with the Division of Cancer Treatment, National Cancer Institute, U.S.A., and by a Grant-in-Aid for Cancer Research from the Ministry of Education, Science and Culture, Japan (No. 62010013), and from the Ministry of Health and Welfare, Japan (No. 61-21).

References

1) a) C. K. Atal, *J. Nat. Prod.*, **42**, 603 (1979); b) A. R. Matlocks, "Phytochemical Ecology," ed by Harborne, J. B., Academic Press, London (1972), p. 179; c) L. W. Smith and C. C. Culvenor, *J. Nat. Prod.*, **44**, 129 (1981); d) J. Hartwell, *J.*

Cancer Treat. Rep., **60**, 1031 (1976); e) L. Leterndre, W. A. Smithson, G. S. Gilchrist, E. U. Bergert, C. H. Hoagland, M. M. Ames, G. Powis, and J. S. Korach, *Cancer (Philadelphia)*, **47**, 437 (1981).

2) M. Kugelman, W. C. Liu, M. Axelrod, J. J. McBride, and K. V. Rao, *J. Nat. Prod.*, **39**, 125 (1976); J. S. Kovach, M. M. Ames, G. Dowis, C. G. Moertel, R. G. Hahn, and E. T. Cregan, *Cancer Res.*, **39**, 4540 (1979).

3) a) G. P. Men'Shikov, *Ber. Dtsch. Chem. Ges. B*, **65**, 974 (1932); b) L. H. Zalkow, S. Bonett, L. Gelbaum, M. M. Gordon, B. B. Patil, A. Shani, and D. Van Derveer, *J. Nat. Prod.*, **42**, 603 (1979).

4) D. J. Robins, *Prog. Chem. Org. Nat. Prod.*, **1982**, 115; J. T. Wróbel, "The Alkaloids," Academic Press, London (1985), p. 327.

5) The synthesis of (−)-indicine *N*-oxide and intermedine *N*-oxide has been reported preliminarily: Y. Nishimura, S. Kondo, and H. Umezawa, *Tetrahedron Lett.*, **27**, 4323 (1986).

6) L. H. Zalkow, J. A. Glinski, L. T. Gelbaum, T. J. Fleischmann, L. S. McGowan, and M. M. Gordon, *J. Med. Chem.*, **28**, 687 (1985).

7) C. C. J. Culvenor and L. W. Smith, *Aust. J. Chem.*, **19**, 1955 (1966).

8) E. Vedejs, S. Larsen, and F. G. West, *J. Org. Chem.*, **50**, 2170 (1985).

9) Y. Nishimura, S. Kondo, and H. Umezawa, *J. Org. Chem.*, **50**, 5210 (1985).

10) R. Adams and B. L. Van Duuren, *J. Am. Chem. Soc.*, **74**, 5349 (1952); L. J. Dry and F. L. Warren, *J. Chem. Soc.*, **1952**, 3445; V. N. Kulakov, A. M. Likhosherstov, and N. K. Kochetkov, *Zh. Obsch. Khim.*, **37**, 146 (1967).

11) H. Redlich, J. Xiang-jun, H. Paulsen, and W. Francke, *Tetrahedron Lett.*, **22**, 5043 (1981).

12) A. J. Mancuso, S-L, Huang, and D. Swern, *J. Org. Chem.*, **43**, 2480 (1978).

13) R. U. Lemieux and E. Von Rudloff, *Can. J. Chem.*, **33**, 1701 (1955); *ibid.*, **33**, 1710 (1955); J-M. Bernassan and M. Fetizon, *Synthesis*, **1975**, 795.

14) W. M. Hoskins and D. H. G. Crout, *J. Chem. Soc., Perkin Trans. 1*, **1977**, 538.

15) J. R. Piper, K. Prasad, and Y-F. Shealy, *J. Labelled Compds. and Radiopharm.*, **18**, 1579 (1980).

16) The authentic samples of natural indicine and indicine *N*-oxide were provided by Dr. M. Suffness, National Cancer Institute, U.S.A.

17) The authentic sample of natural intermedine was provided by Dr. L. W. Smith, CSIRO, Australia.

18) L. T. Gelbaum, M. M. Gordon, M. Miles, and L. H. Zalkow, *J. Org. Chem.*, **47**, 2501 (1982).

2-Amino-1-methyl-1*H*-imidazole-4,5-dione: Synthesis and the Dimroth Type Rearrangement to Creatone (2-Methylamino-1*H*-imidazole-4,5-dione)

Hiroshi YAMAMOTO,* Chikara OHIRA, Toshiaki ASO, and Wolfgang PFLEIDERER*,†
Department of Chemistry, Faculty of Science, Okayama University, Tsushima, Okayama 700
†Universität Konstanz, Fakultät für Chemie, D-7750 Konstanz, F. R. Germany
(Received June 15, 1987)

Treatment of creatinine with BOC-ON gave 2-*t*-butoxycarbonylamino-1-methyl-1,5-dihydro-4*H*-imidazol-4-one, which was oxidized with mercury(II) acetate to the corresponding 1*H*-imidazole-4,5-dione. Deprotection of the amino group of this dione afforded the title compound **4**, which in turn was shown to undergo a facile, Dimroth-type rearrangement under weakly acidic conditions to give creatone, thus proving **4** to be the key intermediate in the formation of creatone from various starting materials. The equilibria among these compounds are discussed.

Creatine (**1**) and its dehydrated form creatinine (**2**) are present in the muscular tissue of many vertebrates and play important roles in energy transfer and storage.[1,2] We reported[3] that the oxidation product (creatone) of **1** and **2** with mercury(II) acetate possessed the structure **3** (2-methylamino-1*H*-imidazole-4,5-dione) rather than the previously presented ring-open formula **5**[4,5] (Scheme 1). Furthermore, it was suggested[3] that the previous structures **4** and **6** which had been respectively presented for the condensation product[6] of methylguanidine with diethyl oxalate and for the peroxyacid oxidation product[7] of 2,6-diamino-3-methyl-4(3*H*)-pyrimidones **7** or 2,6-diamino-1-methyl-4(1*H*)-pyrimidone (**8**) ought to be replaced by the revised formulation **3**, because all of these products were found to be identical with creatone (Scheme 1). It was also confirmed[8] that the acyclic compound **6** prepared from **3** reverted to **3** without producing any other isomers **4** and **5**. We have now prepared **4** (2-amino-1-methyl-1*H*-imidazole-4,5-dione) and confirmed a facile, Dimroth-type rearrangement of **4** to **3**, thus proving that **4** is the key intermediate in the formation of **3** from various precursors.

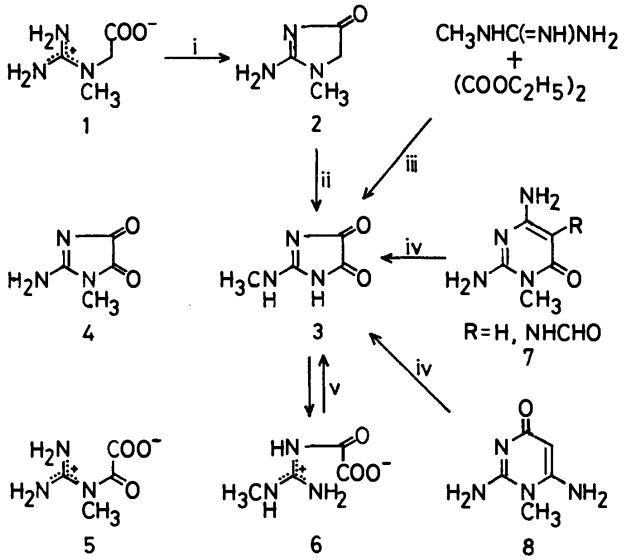

Scheme 1. Formation of creatone **3** from various starting materials, i. H^+, Ref. 21. ii. $Hg(OAc)_2$, Refs. 3—5. iii. reflux in EtOH, Ref. 6. iv. H_2O_2–HCOOH, Ref. 7. v. H_2O, Ref. 8.

Results and Discussion

As the oxidation of **1** and **2** with mercury(II) acetate resulted[3,8] in the exclusive formation of **3** without affording any of the postulated intermediates such as **4** and **5**, we had to devise a new scheme for preparing **4** by an alternative route: namely, the protection of the 2-amino group of creatinine (**2**), followed by the oxidation and then deprotection of the amino group of the resulting imidazoledione. Thus, in order to find a suitable protecting group, **2** was led to various kinds of NH(2)-substituted derivatives (see Scheme 2): 2-acetamido- (**9a**,[9] with acetic anhydride, 74% yield), 2-methoxycarbonylamino- (**9b**, with 1-methoxycarbonyl-3-methylimidazolium chloride, 71%), 2-*t*-butoxycarbonylamino- (**9c**, with 2-(*t*-butoxycarbonyloxyimino)-2-phenylacetonitrile (BOC-ON),[10] 75%), and 2-[2-(*p*-nitrophenyl)ethoxycarbonylamino]-1-methyl-1,5-dihydro-4*H*-imidazol-4-one (**9d**, with 1-methyl-3-[2-(*p*-nitrophenyl)ethoxycarbonyl]imidazolium chloride,[11] 95%).

The structures of these compounds were readily verified by the spectral data and the elemental analyses

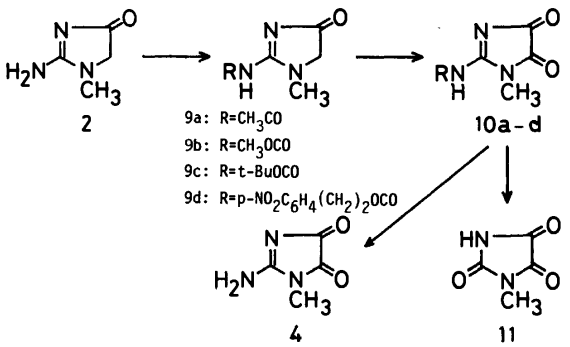

Scheme 2. Preparation of **4**.

Table 1. Physical Properties of Some Imidazole Derivatives

Compd.	^{1}H NMR parameter[a]				Ionization and UV spectra in water			
	CH_3-1	RNH-2	H_2-5	b)	h)	pK_a	λ_{max}/nm(log ε)	pH
2	3.05 s	7.3 brm	3.92 s	C[c]	+	4.85[l]		
	3.11 s	4.78 brs	4.22 s	D[c]	0		235(3.88)[j]	
	3.37 s	8.03 brm	4.66 s	T[d]				
3		2.98 d[e]	—	C	+	0.62[d]	212(3.97)[d]	−0.05
		2.96 s	—	D	0		204(4.13)[d]	4
		3.31 d[e]	—	T[d]	−	7.87[d]	234(4.00)[d]	10
4	3.22 s	7.4 brm	—	C	+	1.89±0.19	223, 270 sh (4.03, 3.06)[k]	0
	3.21 s		—	D	0		232, 296(4.05, 3.15)[k]	4
	3.57 s		—	T	−[l]	8.0±0.2	237(3.97)[k]	10
9a	3.13 s	2.19 s	3.93 s	C	+	3.37±0.01	232(3.935)	1
		8.5 brm			0		220, 252(4.13, 4.15)	6
	3.08 s	2.17 s	4.11 s	D	−	8.76±0.01	249(4.295)	12
9b	3.11 s	3.76 s	3.93 s	C	+	2.09±0.02	238(3.895)	0
		6.5 brm			0		212, 242(4.29, 4.125)	6
					−	9.13±0.01	236(4.43)	12
9c	3.12 s	1.50 s	3.91 s	C	+	2.22±0.06	227(3.84)	0
		7.6 brm			0		240(3.99)	7
					−	8.79±0.05	238(4.11)	12
9d	3.09 s	3.10 t[f]	3.92 s	C[c]	+	1.97±0.01	210, 230 sh, 278	0
		4.34 t[f]					(4.12, 4.02, 4.00)	
		7.40 brd[g]			0		214, 244, 279	5
		8.14 brd[g]					(4.45, 4.22, 4.00)	
		10.26 brm			−	9.18±0.03	237, 280 sh(4.47, 4.04)	12

a) δ values (at 60 MHz unless otherwise specified): s, singlet; d, doublet; t, triplet; m, multiplet; br, broad. b) Solvent: C, $CDCl_3$; D, D_2O; T, TFA. c) At 250 MHz. d) From Ref. 3. e) J=5 Hz. f) J=7 Hz, $ArCH_2$-CH_2OOC. g) J=9 Hz, O_2N-C_6H_4C. h) Species: monocation (+), neutral species (0), monoanion (−). i) From Ref. 22. j) From Ref. 23. k) Extrapolated value since the species gradually decomposes during the measurement. l) Likely for the ring-open species **6a**.

(see Table 1 for ^{1}H NMR and UV spectra as well as pK_a values, and the Experimental section for other data). The presence of a singlet (2H) at δ 3.9—4.0 (due to H_2-5) in the ^{1}H NMR spectra of **9a—d** eliminated the possibility of the enolated O(4)-substituted structure **12** for these compounds. Also the rather low, basic pK_a values (3.4—2.0) of **9a—d** were in agreement with the 2-amino-4-oxo form rather than the 2-imino-3-substituted form **13** which would be expected to have much higher pK_a values by analogy with those of related compounds (e.g. acetylguanidine, pK_a 8.26).[2b,12,13]

The 2-carbonyamino derivatives **9a—d** were then subjected to the oxidation with mercury(II) acetate. However, the oxidation conducted in water (as in the case of **1** and **2**)[3-5] gave no satisfactory results in general but appeared to cause decomposition into smaller fragments. After various attempts, the oxidation of **9b** and **9c** was accomplished by employing a two-layer system ($CHCl_3$–water), thus giving the 4,5-dioxo compounds **10b** (80% yield) and **10c** (50%), respectively (Scheme 2). Compound **9a**, however, did not give the expected product **10a** but yielded creatone (**3**) and a low yield of 1-methylparabanic acid (**11**)[14] under these conditions, whereas the

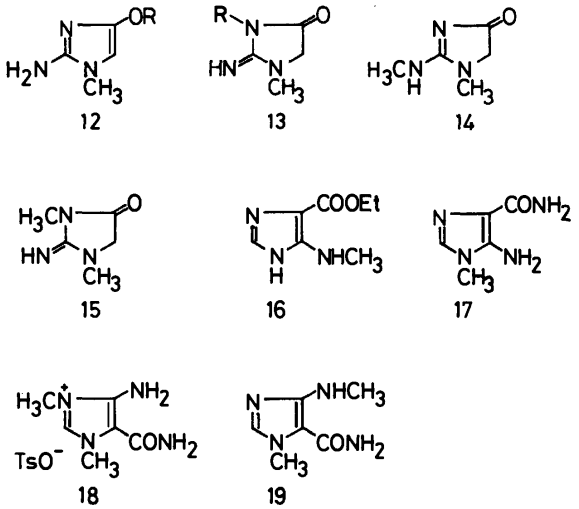

oxidation of **9d** gave only a low yield of unstable **10d** which was contaminated by a small amount of the inseparable starting material. The structures of these 4,5-dioxo compounds **10b—d** were established on the evidences of the spectral data (see Experimental section).

Deprotection of the 2-amino group of **10b—d** was

then examined under various conditions. Acid hydrolysis of **10b** (in 2 M†† HCl) resulted in the formation of a 60% yield of **11**, whereas treatment of **10b** with sodium benzenethiolate in HMPA caused profound decomposition. The desired compound **4** was, however, obtained in a 67% yield on heating **10c** in anhydrous trifluoroacetic acid (TFA) at 60 °C. A less satisfactory deprotection to obtain **4** was also accomplished by the treatment of **10d** with 1,8-diazabicyclo[5.4.0]undec-7-ene (DBU) in pyridine.[11]

The IR spectrum of **4** showed absorptions due to NH and C=O groups (3200, 3000, 1793, 1720, and 1700 cm^{-1}) but apparently differed from that[3] of **3** particularly in the fingerprint regions. Compound **4** showed a singlet at δ 3.22 due to N-Me and a broad multiplet at 7.4 due to NH_2 groups in $CDCl_3$; the N-Me singlet signal appeared at δ 3.57 and 3.21 in TFA and in D_2O, respectively. As the high-resolution MS confirmed the molecular formula $C_4H_5N_3O_2$, the 2-amino-1-methyl-1*H*-imidazole-4,5-dione structure was unequivocally assigned to **4**. It should be noted that the Me-1 signal of **4** appears at a slightly down-field when compared with the N-Me signals of **2** and **3** in the same solvent system; the conclusive N-Me parameters of **2** and **3** for the additional structural proof have been obtained for the first time in the present study in $CDCl_3$ (and D_2O) (see Table 1).

The UV spectra of the neutral and monocationic species of **4** are shown in Fig. 1; for their absorption maxima, see Table 1. It was found that **4** possessed a low, basic pK_a value (1.89) similar to that of **3** (0.6).[3] These figures indicate that the neutral species of **4** exists exclusively in the 2-amino-1*H*-imidazol-4-one form rather than in the 2-imino-2,3-dihydro-1*H*-imidazol-4-one form **4a** (Scheme 3) in water, taking into account the notable difference of the known pK_a values between the 2-amino-4-oxo and the 2-imino-4-oxo forms of such related compounds as **14** (4.55) and **15** (8.07),[2b] respectively.

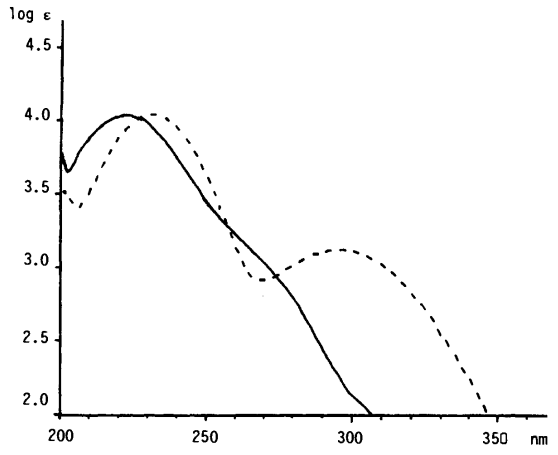

Fig. 1. UV Spectra of **4**: ——, pH 0; ------, pH 4.

†† 1 M=1 mol dm^{-3}.

Although **4** remained stable as solid or in anhydrous aprotic solvents, it was found to undergo rearrangement rapidly in aqueous acid ($t_{1/2}$ ca. 5 min at pH 4) and more slowly even at pH 7 ($t_{1/2}$ ca. 30 min), giving creatone **3** exclusively; it was possible to follow this rearrangement either by ^1H NMR in D_2O or by UV spectrometry in various pH buffer solns.[15] Thus, the protonation of an equilibrium mixture of the neutral species **4** and **4a** affords the resonance-stabilized monocation **4b** in acid, which in turn is readily transformed into an equilibrium with the ring-open forms **5** and **6**. Recyclization of the latter provides apparently the thermodynamically more stable product **3** in a manner similar to the Dimroth rearrangement[16] as illustrated in Scheme 3.

Even in weak alkaline regions, **4** was found to change into a transient species which showed a UV absorption maximum at 237 nm (at pH 10, with an apparent pK_a value of 8.0) but underwent a gradual decomposition into smaller fragments exhibiting virtually no UV absorptions ($t_{1/2}$=ca. 60 min). On the grounds of these spectral data and the pK_a value, the short-lived intermediate is presumed to be a ring-open, anionic species such as **6a** rather than the equilibrated 2,5-dihydro-2-imino-5-oxo-1*H*-imidazol-4-olate form **4c** which is expected normally to have a much higher pK_a value.

It has now become obvious that compound **4** is the initially formed key intermediate by the oxidation of creatine (**1**) and creatinine (**2**) to give creatone (**3**), the reaction of which proceeds at ca. pH 3.[3] The oxidized pyrimidone intermediates **20**—**23a** (Scheme 4) and then the seven-membered ring intermediate **24** derived by a Baeyer–Villiger reaction were previously suggested[3] for the possible reaction pathways for the

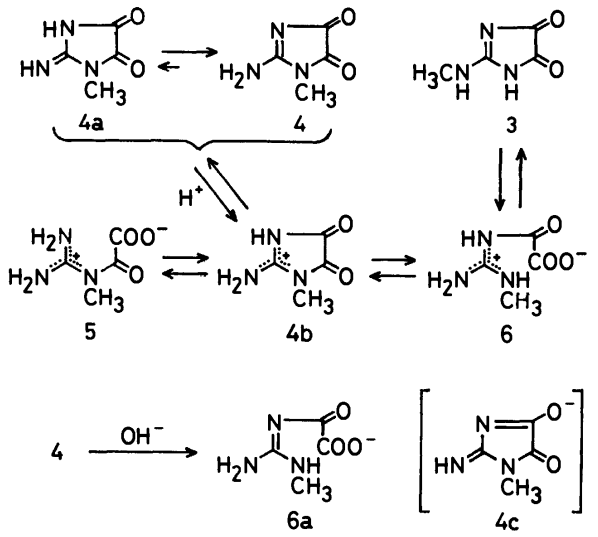

Scheme 3. Tautomeric forms and equilibria of **4** and the rearrangement to **3**.

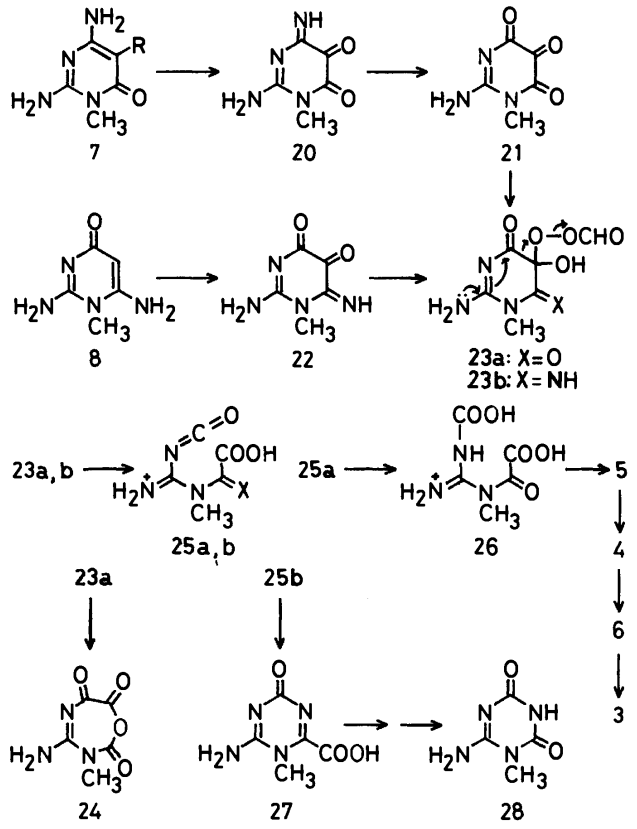

Scheme 4. Revised reaction pathways for the formation of **3** from 2,6-diamino-3-methyl-4(3*H*)-pyrimidones **7** and the 1-methyl-4(1*H*) isomer **8**.

oxidative ring-contraction of **7** and **8** to **3**. We now present here a slightly modified common, ring-open intermediates **25a** (instead of **24**) and **26** as illustrated in Scheme 4. Decarboxylation from **26** would afford **5** which subsequently is converted into **3** through the equilibrium shown in Scheme 3, while in the case of the peroxyacid oxidation of **8** the major product 1,3,5-triazine **28** is produced by the oxidative rearrangement through the previously presented intermediates[3] **22**, **23b**, **25b**, and then **27** (Scheme 4).

Many rearrangements have been known[17] involving the fission of a heterocyclic ring and ring closure in the alternate direction catalyzed by acid, base, heat, light, or miscellaneous reagents. As for the imidazole ring system, only a few examples of such rearrangements have been reported, to the best of our knowledge: i.e. **15**→**14** (in boiling methanol),[2b] **16**→**17** (in aq ammonia at 120 °C),[18] and **18**→**19** (with a basic ion-exchange resin).[19] The present rearrangement which takes place extremely fast under such mild conditions is certainly a unique example of the thermodynamically controlled ring transformation. Moreover, as creatone **3** has been isolated[20] from beef and regarded as a constituent of muscle tissue, the present findings are believed to be of value in connection with a biological implication, particularly in clarifying the possibility and mechanism of the reversible reaction between creatine and creatone (or an intermediate shown above), participating in an oxido-reductive process of organism.

Experimental

Melting points were determined with a Yanagimoto MP-S3 instrument and are uncorrected. All reactions were monitored by TLC (Merck silica gel 60F, 0.25 mm) with 2-propanol–AcOEt–water (5:3:1) or MeOH–$CHCl_3$ (1:9) as eluant. Column chromatography was performed with Wako C-200 silica gel. The IR spectra were taken with a Hitachi 215 spectrometer (as KBr disk). The ^1H NMR spectra were measured in $CDCl_3$ (unless otherwise stated) with a Hitachi R-600 (60 MHz, FT) or Bruker AM-250 cryospectrometer (250 MHz) at 27 °C. Chemical shifts (at 60 MHz unless otherwise specified) are recorded as δ values relative to tetramethylsilane [or sodium 3-(trimethylsilyl)-1-propanesulfonate in D_2O] as internal standard. The mass spectra were taken on a Shimadzu LKB-9000 low resolution or a JEOL JMX-HX100 high-resolution instrument, and are given in terms of *m/z* (rel intensity) compared with the base peak. The microanalyses were performed at University of Konstanz. The measurements of the ionization constants were carried out spectrophotometrically at 25 °C in 0.01 M buffers by the usual method.[12]

2-Acetamido-1-methyl-1,5-dihydro-4*H*-imidazol-4-one (9a). A better yield of **9a** was obtained by employing a slightly modified procedure of Ing.[9] Thus, a mixture of **2**[21] (0.50 g) and acetic anhydride (1 cm^3) was heated at 70 °C (oil bath) with swirling until the white suspension became a pale yellow soln (ca. 5 min), and then, after cooling with water, diluted with diethyl ether (10 cm^3). The mixture was allowed to stand overnight at 5 °C. The ppt was filtered and recrystd from EtOH/ether, giving **9a** as colorless needles (0.51 g, 74%): mp 124—125 °C (Ref. 9, 124—125 °C); IR 3170 (NH), 1770, 1740, and 1615 cm^{-1} (C=O, C=N); MS *m/z* 155 (M^+; 4.4), 154 (37.8), 140 (75.3), 113 (27.0), and 44 (100).

2-Methoxycarbonylamino-1-methyl-1,5-dihydro-4*H*-imidazol-4-one (9b). To a soln of 1-methylimidazole (0.44 cm^3) in dry ether (8 cm^3) was added methyl chloroformate (0.43 cm^3, 1.0 equiv) at 0 °C under nitrogen. After 5 min, the solvent was evaporated in vacuo and the white viscous tar (1-methoxycarbonyl-3-methylimidazolium chloride) was dissolved in dry DMF (7 cm^3) with stirring at 0 °C under nitrogen. To this soln was added **2** (0.50 g, 1.0 equiv) and the mixture was stirred at 20 °C under nitrogen. After 2 h, water (1 cm^3) was added. The solvent was evaporated in vacuo and the residue was triturated with AcOEt. The combined organic layers were dried (Na_2SO_4) and evaporated in vacuo. The residue was recrystd from AcOEt–ether, giving **9b** as pale yellow crystals (0.53 g, 71%): mp 132—133 °C; IR 3230 (NH), 1780, 1750, 1660, and 1620 cm^{-1} (C=O, C=N); MS *m/z* 171 (M^+; 45.9), 140 (63.8), 112 (24.7), 69 (33.9), 44 (100), and 42 (52.9).

Found: C, 42.07; H, 5.35; N, 24.25%. Calcd for $C_6H_9N_3O_3$: C, 42.10; H, 5.30; N, 24.55%.

2-*t*-Butoxycarbonylamino-1-methyl-1,5-dihydro-4*H*-imidazol-4-one (9c). A soln of **2** (240 mg), triethylamine (0.45 cm^3, 1.6 equiv), and BOC-ON (260 mg, 0.5 equiv) in dry DMF (16 cm^3) was heated at 60 °C for 4 d with stirring

under argon; more BOC-ON (3×260 mg) was added every 1 d. The solvent was evaporated in vacuo and the residue was triturated with $CHCl_3$. The combined organic layers were dried (Na_2SO_4) and evaporated in vacuo. The residue was chromatographed in a column of silica gel with AcOEt–hexane, giving **9c** as a pale yellow syrup (338 mg, 75%), which became colorless needles on recrystallization from ether-light petroleum: mp 33—34 °C; IR 3230 (NH), 1760, and 1655 cm^{-1} (C=O); MS *m/z* 213 (M^+; 0.7), 158 (100), 140 (57.1), 57 (57.0), 44 (20.7), and 18 (51.9).

Found: *m/z* 158.0562. Calcd for $C_5H_8N_3O_3$: M−C_4H_7, 158.0566.

1-Methyl-2-[2-(*p*-nitrophenyl)ethoxycarbonylamino]-1,5-dihydro-4*H*-imidazol-4-one (9d). To a suspension of **2** (23 mg) in dry DMF (0.5 cm^3) was added 1-methyl-3-[2-(*p*-nitrophenyl)ethoxycarbonyl]imidazolium chloride[11] (69 mg, 1.1 equiv) in one portion at 20 °C with stirring. After 45 min, cold water (3 cm^3) was added to the mixture at 5 °C. The resultant suspension was extracted with $CHCl_3$. The combined organic layers were dried (Na_2SO_4) and evaporated in vacuo and the residue was recrystd from AcOEt to give **9d** as almost colorless needles (60 mg, 95%): mp 146—147 °C; IR 3220 (NH), 1755, 1710, 1650, and 1620 cm^{-1} (C=O); MS *m/z* 307 (M+1; 4.53), 306 (M^+; 2.39), 260 (2.87), 167 (4.07), 157 (42.7), 149 (19.3), 140 (83.7), 139 (13.7), 137 (11.3), 112 (20.6), 91 (7.7), 69 (18), 44 (100), 43 (43.7), 42 (52.2), 31 (40.2), 30 (43.8), and 18 (28).

Found: C, 50.87; H, 5.02; N, 18.16%. Calcd for $C_{13}H_{14}N_4O_5$: C, 50.98; H, 4.61; N, 18.29%.

Oxidation of 9a. To a soln of **9a** (31 mg) in water (2 cm^3) was added mercury(II) acetate (128 mg, 2.0 equiv). The resultant mixture was set aside at 20—25 °C for 3 d. The ppt was filtered off and washed with a small amount of water. The combined filtrate and washings were saturated with H_2S (gas). The ppt was filtered off and washed with water. The combined filtrate and washings were once more filtered (with gravity) and evaporated in vacuo to give a white solid, which was triturated with $CHCl_3$ to give crude **11**; the solid which remained undissolved in $CHCl_3$ was identified by chromatography and spectroscopy (NMR, IR, and MS) to be mostly creatone **3** (10 mg, 39%). The former product **11** was chromatographed in a column of silica gel with 2% MeOH–$CHCl_3$, giving pure **11** as colorless needles (2 mg, 8%): mp 151—152 °C (from AcOEt–hexane, Ref. 14, 150—152 °C); pK_a 5.99±0.1; UV λ_{max} (pH 2) 213 nm (log ε 3.88), (pH 8) 221 and 285 nm (log ε 3.95 and 2.50); IR 3220, 1790, 1745, 1715, and 1660 cm^{-1}; ^1H NMR (250-MHz) δ=3.21 (3H, s, Me-1) and 7.98 (1H, brm, NH), (in D_2O) 3.11 (s, Me-1); MS *m/z* 128 (M^+; 48.6), 100 (44.3), 72 (21.9), 57 (83.6), 56 (100), 44 (25.0), 43 (26.6), 29 (51.1), and 28 (69.6). (Found: *m/z* 128.0235).

Even by employing the two-layer system (see below), oxidation of **9a** with $Hg(OAc)_2$ resulted in the formation of **3** and **11** only; no desired compound **10a** was obtained.

2-Methoxycarbonylamino-1-methyl-1*H*-imidazole-4,5-dione (10b). To a soln of **9b** (105 mg) in water (10 cm^3) was added $CHCl_3$ (20 cm^3) and then mercury(II) acetate (395 mg, 2.0 equiv). The mixture was stirred at 20 °C under the protection of light. After 90 min, it was separated and the aq layer was extracted with $CHCl_3$. The combined organic layers were dried (Na_2SO_4) and evaporated in vacuo. The residue was chromatographed in a column of silica gel with 5% MeOH–CH_2Cl_2, giving crude **10b** as a pale yellow solid. This was dissolved in CH_2Cl_2 (50 cm^3), washed with cold 0.5 M HCl (20 cm^3), dried (Na_2SO_4), and evaporated in vacuo. The residue was recrystd from CH_2Cl_2–hexane to give pure **10b** as colorless needles (89 mg, 80%): mp 192—193 °C; IR 3280, 1790, 1690, and 1650 cm^{-1}; ^1H NMR 3.26 (s, Me-1) and 3.84 (s, MeO); MS *m/z* 185 (M^+; 50.0), 157 (85.4), 155 (36.5), 126 (100), 99 (26.5), 83 (81.0), 69 (45.5), and 59 (19.6).

Found: *m/z* 185.0464. Calcd for $C_6H_7N_3O_4$: M, 185.0446.

2-*t*-Butoxycarbonylamino-1-methyl-1*H*-imidazole-4,5-dione (10c). A mixture of **9c** (68 mg) and mercury(II) acetate (225 mg, 2.2 equiv) in $CHCl_3$ (15 cm^3) and water (15 cm^3) was stirred at 20 °C for 6 h in the dark. After separation the aq layer was extracted with $CHCl_3$. The combined organic layers were washed with aq $NaHCO_3$, dried (Na_2SO_4), and evaporated in vacuo. The residue was chromatographed in a column of silica gel with AcOEt–hexane, giving **10c** as pale yellow needles (37 mg, 50%): mp 157—159 °C (from AcOEt–hexane); IR 3290, 1800, 1790, 1770, 1690, 1670, and 1650 cm^{-1}; ^1H NMR 1.55 (s, *t*-BuO) and 3.27 (s, Me-1); MS *m/z* 227 (M^+; ≃0), 212 (1.5), 172 (47.8), 154 (50.4), and 57 (100).

Found: *m/z* 172.0388. Calcd for $C_5H_6N_3O_4$: M−C_4H_7, 172.0357.

1-Methyl-2-[2-(*p*-nitrophenyl)ethoxycarbonylamino]-1*H*-imidazole-4,5-dione (10d). To a suspension of **9d** (32 mg) in water (30 cm^3) was added mercury(II) acetate (90 mg, 2.5 equiv), and the mixture was stirred at 20 °C for 3 d. Then more mercury(II) acetate (50 mg, 1.5 equiv) and water (10 cm^3) were added, and stirring was continued for 7 d (total). The pale yellow precipitate was filtered off and triturated with 5% MeOH–$CHCl_3$; the above filtrate was extracted with $CHCl_3$. The combined organic layers were evaporated in vacuo and the residue was chromatographed in a column of silica gel with $CHCl_3$→5% MeOH–$CHCl_3$, giving **10d** as pale yellow crystals (10 mg, 30%) (which, however, contained a small amount of inseparable **9d**): mp 182—184 °C (from $CHCl_3$–hexane); IR 3300, 1789, 1740, 1685, 1635 cm^{-1}; ^1H NMR (250-MHz) 3.17 (2H, t, *J*=6.8 Hz, $ArCH_2$), 3.27 (3H, s, Me-1), 4.49 (2H, t, *J*=6.8 Hz, CH_2OOC), 7.44 (2H, brd, *J*=8.9 Hz, H-2′,6′), 8.20 (2H, brd, *J*=8.9 Hz, H-3′,5′), and 10.29 (1H, brm, NH-2); MS *m/z* 320 (M^+; ≃0), 167 (4.0), 154 (47.3), 149 (100), 137 (17.7), 126 (27.8), 103 (17.0), 83 (67.3), and 28 (100). Compound **10d** was liable to decompose (presumably by hydrolysis or methanolysis) during the purification.

Found: C, 49.16; H, 4.12; N, 17.76%. Calcd for $C_{13}H_{12}N_4O_6$: C, 48.75; H, 3.78; N, 17.50%.

Attempted Deprotection of 10b. A soln of **10b** (22 mg) in 2 M HCl (10 cm^3) was stirred at 20 °C for 10 min, and then extracted with CH_2Cl_2. The organic layers were combined, dried (Na_2SO_4), and evaporated in vacuo. The residue was chromatographed in a column of silica gel with 10% ether–CH_2Cl_2, giving **11** (by IR, ^1H NMR, and TLC) as colorless plates (10 mg, 66%), mp 153—154 °C (Ref. 14, 150—152 °C).

2-Amino-1-methyl-1*H*-imidazole-4,5-dione (4). A. A soln of **10c** (4.5 mg) in anhyd TFA (1 cm^3) was heated at 60 °C for 1 h with stirring under argon. The mixture was diluted with dry $CHCl_3$ and then evaporated in vacuo to remove TFA, which was repeated several times. The residue

was washed with dry $CHCl_3$ and then with a small amount of dry AcOEt, giving **4** as a colorless crystalline powder (2.0 mg, 67%): mp 208—209 °C decomp; IR 3200, 3000, 1793, 1720, and 1700 cm^{-1}; MS *m/z* 127 (M^+; 88.0), 99 (M−CO, 87,7), 71 (M−2CO, 44.8), 56 (61.0), 42 (59.8), and 28 (100).

Found: *m/z* 127.0418. Calcd for $C_4H_5N_3O_2$: M, 127.0382.

B. A soln of **10d** (9 mg) and DBU (15 mg) in dry pyridine was stirred at 20 °C for 12 h under argon. The solvent was evaporated in vacuo below 20 °C (pump) and the residue was washed with dry cyclohexane, and then with a small amount of dry $CHCl_3$, giving crude **4** (by IR, ^1H NMR, and TLC) as a colorless powder (1 mg, ca. 25%), mp 205—208 °C decomp.

Rearrangement of 4 to 3. A soln of **4** (2.6 mg) in 1 M acetic acid (0.15 cm^3) was allowed to stand at 20 °C for 20 h. The ppt was filtered off and washed with cold water, giving colorless crystals which were identified by IR and ^1H NMR to be **3** (1.6 mg, 62%), mp 198—201 °C decomp (Ref. 3, 197—199 °C decomp).

The rearrangement of **4** (0.8 mg) in D_2O (0.6 cm^3) was pursued by ^1H NMR measurement (following a gradual decrease of the singlet signal of **4** at δ 3.21 with a simulaneous increase of the singlet of **3** at δ 2.98; $t_{1/2}$ ca. 14 min at pH 5).

On of us (H. Y.) is very grateful to the Alxander von Humboldt Foundation (F. R. Germany) for providing a research scholarship to him (in 1984). We are greatly indebted to Ms. Margarette Bischler (Univ. Konstanz) for the measurements of some of the pK_a values and UV spectra and to Mr. Shin-ichi Takekuma (Kinki University) for the mass spectra.

References

1) For reviews of the chemistry and biology of creatine, see S. Schipper and A. R. Day, "Heterocyclic Compounds," ed by R. C. Elderfield, Wiley, New York (1957), Vol. 5, p. 263; M. Cohn, *Quart. Rev. Biophys.*, **3**, 61 (1970).

2) For creatinine, see a) A. H. Ennor and J. F. Morrison, *Phys. Rev.*, **38**, 631 (1958); b) G. L. Kenyon and G. L. Rowley, *J. Am. Chem. Soc.*, **93**, 5552 (1971) and references cited therein.

3) H. Yamamoto and W. Pfleiderer, *Bull. Chem. Soc. Jpn.*, **55**, 1912 (1982).

4) L. Baumann and T. Ingvaldsen, *J. Biol. Chem.*, **35**, 277 (1918).

5) I. Greenwald, *J. Am. Chem. Soc.*, **41**, 1109 (1919).

6) W. Traube and K. Gorniak, *Z. Angew. Chem.*, **42**, 379 (1929).

7) H. Yamamoto and W. Pfleiderer, *Chem. Ber.*, **106**, 3194 (1973).

8) H. Yamamoto, T. Takahashi, and S. Inokawa, *Heterocycles*, **20**, 1067 (1983).

9) H. R. Ing, *J. Chem. Soc.*, **1932**, 2047.

10) M. Itoh, D. Hagiwara, and T. Kamiya, *Tetrahedron Lett.*, **1975**, 4393; *idem*, *Bull. Chem. Soc. Jpn.*, **50**, 718 (1977).

11) This amino-protecting group has been effectively employed for various nucleosides and nucleotides: F. Himmelsbach and W. Pfleiderer, *Tetrahedron Lett.*, **24**, 3583 (1983).

12) A. Albert and E. P. Serjeant, "Ionization Constants of Acid and Base," Methuen, London (1962).

13) J. Elguero, C. Marzin, A. R. Katritzky, and P. Linda, "The Tautomerism of Heterocycles," (Adv. Heterocyclic Chem. Supplement 1), Academic Press, New York (1976), p. 479.

14) 1-Methylparabanic acid (**11**) was obtained by treatment of 1-methylhydantoin 5-oxime with conc HCl [E. Schmidt, *Apoth. Ztg.*, **27**, 157 (1912)] or creatinine 5-oxime with 0.5 M HCl [G. Scagliarini and P. Pratesi, *Atti. Accad. Lincei*, **10**, 261 (1929)].

15) A closer kinetic study with regard to this rearrangement is to be conducted.

16) See D. J. Brown, "Mechanism of Molecular Migrations," ed by B. S. Thyagarajan, Interscience-Wiley, New York (1968), Vol. 1, p. 202; M. Wahren, *Z. Chem.*, **9**, 241 (1969).

17) H. C. van der Plas, "Ring Transformation of Heterocycles," Academic Press, New York (1973).

18) T. Brown, K. Kadir, G. Mackenzie, and G. Shaw, *J. Chem. Soc., Perkin Trans. 1*, **1979**, 3107.

19) A. K. Sen and A. K. Mukhopadhyay, *Indian J. Chem., Sect. B*, **23B**, 870 (1984).

20) T. Mann, *Biochem. Z.*, **268**, 339 (1934).

21) G. Edgar and W. S. Hinegardner, *Org. Synth.*, Coll. Vol. I, 172 (1932) and references cited therein.

22) A. K. Grzybowski and S. P. Datta, *J. Chem. Soc.*, **1964**, 187.

23) K. Matsumoto and H. Rapoport, *J. Org. Chem.*, **35**, 552 (1968).

 © 1987 The Chemical Society of Japan Bull. Chem. Soc. Jpn., 60, 4121—4126 (1987)

Asymmetric Induction in the Base-Catalyzed Reactions Using Polymer-Supported Quinines with Spacer Groups

Minoru INAGAKI, Jun HIRATAKE, Yukio YAMAMOTO, and Jun'ichi ODA*
Institute for Chemical Research, Kyoto University, Uji, Kyoto 611
(Received June 23, 1987)

New polymer-supported quinines having the spacer groups were synthesized and utilized for three types of base-catalyzed asymmetric reactions. Insertion of the spacer groups leads to improve the stereoselectivity in comparison with the polymer-catalyst with no spacer groups.

Cinchona alkaloid and its derivertives have been used as chiral catalysts in asymmetric reactions because of their unique stereochemical properties.[1-3] We also investigated the methanolysis of cyclic anhydrides using cinchona alkaloids as catalysts.[4] In order to obtain more easy-to-handle catalysts, many workers[5-9] have prepared polymer-supported cinchona alkaloids. In particular, Kobayashi et al. synthesized chiral functionalized polymers having relatively higher stereoselectivity by copolymerization with acrylonitrile and the vinyl group of the alkaloids.[7] But the utilization of a Kobayashi's polymers for the methanolysis of *cis*-2,4-dimethylglutaric anhydride resulted in low steroselectivity.

It has been found that the reactivity of catalyst or reagent is often reduced by being polymer-supported. One approach to overcome this drawback is introduction of spacer group between catalytic center and polymer matrix. By inserting a spacer group, the reactivity[10-13] and/or selectivity[14] can be improved. This also holds the case with immobilized enzymes.[15] Thus we prepared the polymer-supported quinine derivatives with spacer groups of various length, and applied them for three types of asymmetric base-catalyzed reactions.

Results and Discussion

Preparation of Polymer-Supported Quinines with Spacer Groups. The synthetic strategy is shown in Schemes 1—3. Our first attempt to submit methyl 3-mercaptopropionate to the reaction with quinine (**1**) was unsuccessful. But 3-mercaptopropionic acid easily reacted with **1** in the presence of 2,2′-azobisisobutyronitrile (AIBN) as a radical initiator to give the carboxylic acid derivative **2** as a colorless powder in 91% yield. In order to introduce a polymerizable double bond, esterification of **2** with allyl alcohol by the use of thionyl chloride afforded **3** having a spacer group as long as 8-atoms from the quinuclidine ring of quinine in 72% chemical yield. The carboxylic acid **2** was also esterified by the Mitsunobu reaction with the alcohol **4** derived from 6-chloro-1-hexanol to give the ester **5** having a spacer group of 15-atoms length in 94% yield. Copolymerization of quinine derivatives **3** and **5** with acrylonitrile in dry DMF afforded the polymers **6** and **7**, respectively. The crude polymers were reprecipitated and Soxhlet-extracted to remove unreacted monomers. The alkaloid content of **6** and **7** were determined by elemental analyses to be 1.10 and 1.24 mol%, respectively. These values were lower than

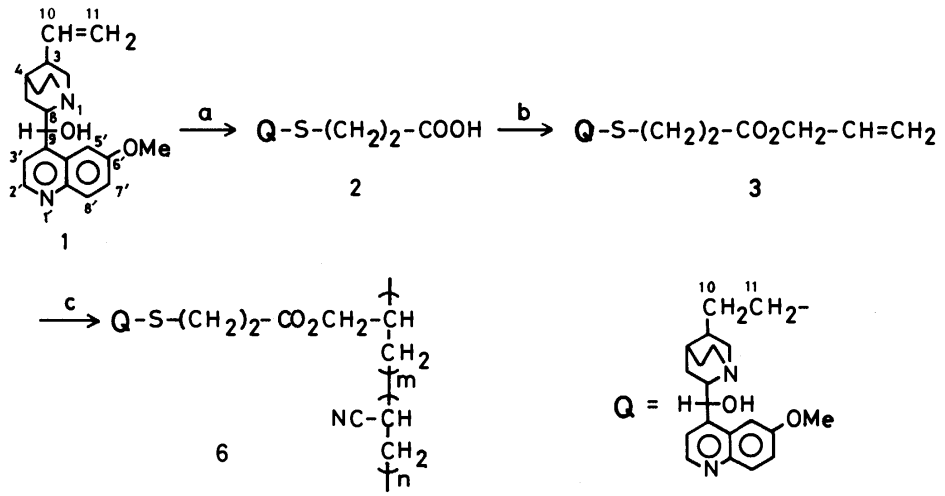

Scheme 1. (a): $HSCH_2CH_2COOH$, AIBN; 91%, (b): $HOCH_2CH{=}CH_2$, $SOCl_2$; 72%, (c): $CH_2{=}CHCN$. AIBN; 57%.

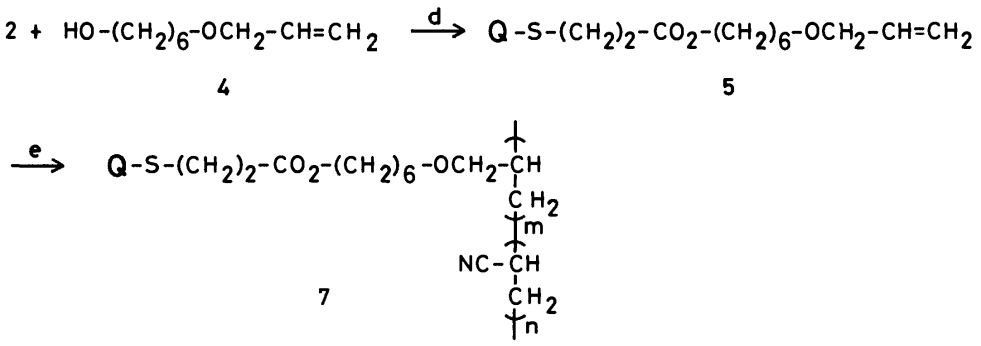

Scheme 2. (d): Diethyl azodicarboxylate, PPh_3; 94%, (e): CH_2=CHCN, AIBN; 43%.

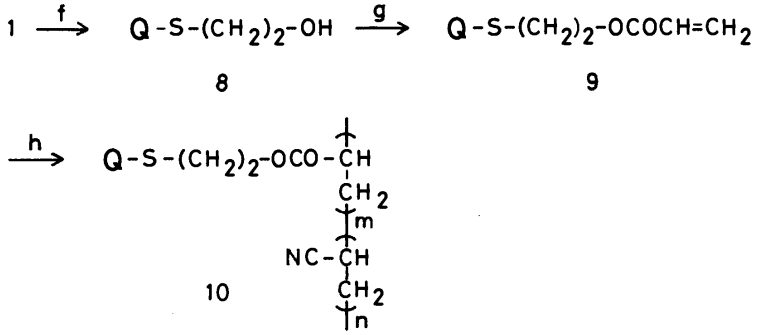

Scheme 3. (f): $HSCH_2CH_2OH$, AIBN; 77%, (g): diethyl azodicarboxylate, CH_2=CHCOOH, PPh_3; 67%, (h): CH_2=CHCN, AIBN; 57%.

Table 1. Physical Properties of Polymer-Supported Quinines with Spacer Groups

Polymer-catalyst	Spacer length	Initial molar ratio[a]	$[\alpha]_D$[b]/°	Elemental analysis/%			Alkaloid content/mol%
				C	H	N	
6	8	1 : 19	−5.6[c]	67.41	5.78	24.44	1.10
7	15	1 : 19	−6.5	67.62	5.95	23.81	1.24
10	7	1 : 9	−26.0	65.82	6.15	17.69	8.04
11	0	1 : 19	−10.4[d]	68.33	5.93	24.39	1.99

a) Initial molar ratio of monomer **1**, **3**, **5**, and **9** vs. acrylonitrile. b) Measured in DMF at 25 °C. c) At 27 °C. d) At 28 °C.

that expected from the initial alkaloid concentration (5 mol%) in the reaction mixture. Therefore we synthesized another copolymer with higher alkaloid content. The monomer having an acryloyl group was prepared which can polymerize with acrylonitrile more easily than simple terminal double bond.[16] Then, **1** was allowed to react with 2-mercaptoethanol to give **8**.[17] The compound **8** was converted to the acrylic ester **9** by the selective esterification of the primary hydroxyl group by the Mitsunobu reaction. It is worth noting that the secondary hydroxyl group of quinine moiety was exclusively esterified when **8** was treated with acryloyl chloride. Copolymerization of **9** with acrylonitrile (1:9 molar ratio) afforded the copolymer **10** having an alkaloid content of 8.04 mol%, which agreed with the initial molar ratio in the reaction mixture. To evaluate the spacer effect, we also synthesized the polymer **11** having no spacer group according to the Kobayashi's method.[18] The

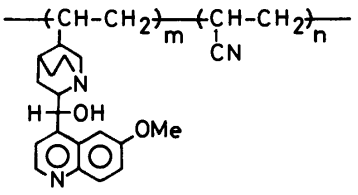

11

conditions employed in polymerizations and some properties of the polymers **6**, **7**, **10**, and **11** are compiled in Table 1.

Asymmetric Reactions Catalyzed by Polymer-Supported Quinine with Spacer Groups. Polymers **6**, **7**, **10**, and **11** were used as catalysts for three types of

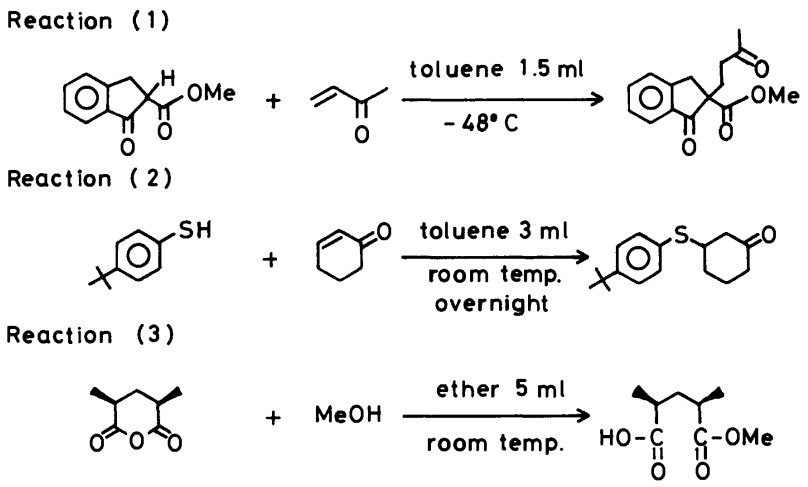

Scheme 4.

Table 2. Asymmetric Addition of Methyl 1-Oxo-2-indancaboxylate to 3-Buten-2-one Catalyzed by Polymers **6**, **7**, **10**, and **11**; the Reaction (1)[a]

Entry	Catalyst	Spacer length	Reaction period/h	Isolated yield/%	$[\alpha]_{578}^{25}$/°	e.e.[b] /%	Abs. config.
1	**7**	15	28	88	−50.4	65	*S*
2	**6**	8	28	96	−47.4	62	*S*
3	**10**	7	6.6 d	2[c]	—[d]	—	—
4	**11**	0	28	99	−37.8	49	*S*
5	**5**	—	14	quant.	−58.1	75	*S*
6	**3**	—	14	quant.	−58.7	76	*S*
7	**9**	—	27	quant.	−57.9	75	*S*
8	**1**	—	28	quant.	−58.7	76	*S*
9	**10**	7	3.9 d	92	−34.4	45	*S*

a) The reaction temperature was −48 °C for Entries 1—8 and room temperature for the Entry 9. b) Based on $[\alpha]_{578}^{25}=-77°$ (*c* 2, benzene) for the optically pure product. c) Determined by HPLC. d) Not measured.

base-catalyzed reactions including the Michael addition of methyl 1-oxo-2-indancarboxylate to 3-buten-2-one (Reaction (1)),[1] the conjugated addition of *p-t*-butylbenzenethiol to 2-cyclohexenone (Reaction (2)),[2] and the methanolysis of *cis*-2,4-dimethylglutaric anhydride (Reaction (3)).[4]

The results of the Reaction (1) catalyzed by polymers **6**, **7**, **10**, and **11** are shown in Table 2. The reaction was also effected using monomeric alkaloids **1**, **3**, **5**, and **9** for comparison. The monomers **3**, **5**, and **9**, as well as **1**, promoted the reaction to give the adduct quantitatively with 75—76% optical purity. Elongation of spacer arms from the (C)-3 vinyl group of quinine did not reduce the stereoselectivity (Table 2, Entries 5—8). In other words, the conformation of the catalytic center of quinine, around the hydroxyl group and nitrogen atom of quinuclidine moiety, was kept unaltered. Polymer-catalysts **6**, **7**, and **11** on the other hand, gave the product with 88—99% yield, and somewhat lower asymmetric yields than the corresponding monomers. The polymers **6** and **7** with spacer groups showed higher stereoselectivity 62 and 65% than **11** with no spacer 49% (Table 2, Entries **1**, 2 vs. 4).

The results of the Reaction (2) are shown in Table 3. The monomers **1**, **3**, **5**, and **9**, gave the addition product in high chemical yield with 25—45% e.e. Polymers **6**, **7**, and **11** also catalyzed the reaction with 89—98% chemical yield. But the optical purities were extremely reduced in comparison with their monomeric counterparts **1**, **3**, **5**, and **9**, respectively. The reason for this phenomena is unclear at present, but at least the result can not be attributed to spontaneous reaction in the presence of polymer matrix, since poly(acrylonitrile) itself has no catalytic activity (Table 3, Entry 5). Thus the polymer-catalysts, with or without spacer group, were found to be unsuitable so far as this asymmetric reaction.

On the other hand, polymers **6**, **7**, **10**, and **11** were good catalysts for the Reaction (3) as shown in Table 4. Although they showed lower stereoselectivity than the corresponding monomers **1**, **3**, **5**, and **9**,

Table 3. Asymmetric Addition of Thiol Catalyzed by Polymers **6**, **7**, **10**, and **11**; the Reaction (2)

Entry	Catalyst	Spacer length	Isolated yield/%	$[\alpha]_{578}^{35}$/°	e.e.[a] /%	Abs. config.
1	**7**	15	89	+ 5.8	8	*R*
2	**6**	8	90	+ 4.8	6	*R*
3	**10**	7	7[b]	—[c]	—	—
4	**11**	0	98	+ 4.2	5	*R*
5	poly(AN)[d]	—	7[b]	—[c]	—	—
6	**5**	—	83	+19.4	25	*R*
7	**3**	—	96	+27.1	35	*R*
8	**9**	—	87	+23.1	30	*R*
9	**1**	—	97	+31.5	41	*R*

a) Based on $[\alpha]_{578}^{21}=+77°$ (*c* 1, CCl_4) for optically pure product. b) Determined by HPLC. c) Not measured. d) Poly(acrylonitrile) containing no quinine moiety.

Table 4. Asymmetric Methanolysis of an Acid Anhydride Catalyzed by Polymers **6**, **7**, **10**, and **11**; the Reaction (3)

Entry	Catalyst	Spacer length	Reaction period[a] /day	e.e.[b] /%	Selectivity[c]
1	**7**	15	4.0	32	*R*-side
2	**6**	8	3.8	22	*R*-side
3	**10**	7	8.6[d]	20	*R*-side
4	**11**	0	2.6	14	*R*-side
5	**5**	—	1.5	12	*R*-side
6	**3**	—	2.0	57	*R*-side
7	**9**	—	2.0	29	*R*-side
8	**1**	—	3.8	50	*R*-side
9[e]	**7**	15	9.0	28	*R*-side
10[e]	**6**	8	12.2	33	*R*-side

a) Conversion = >95%. b) Determined by HPLC after converting the product to the diastereometric amide ester. c) We define the selectivity as *R*-side when the caboxyl group next to the asymmetric center with *R*-configuration was attacked preferentially by the nucleophile. d) The reaction was worked up at a conversion of ca. 40% and the e.e. was determined. e) Reuse of catalyst.

respectively, the effect of the spacer group was also observed clearly. The stereoselectivity of the reaction was improved from 14 to 22% e.e. by inserting a spacer group with 8-atoms length, moreover by inserting a 15-atoms-spacer the steroselectivity was raised up to 32% (Table 4, Entries 1, 2, and 4).

The polymer **10**, having another type of spacer group containing acryloyl moiety had a lower activity as to all the three Reactions (1)—(3). However, when the reaction was carried out at room temperature, the polymer **10** slowly catalyzed the Reaction (1) to give the *S* enantiomer of methyl 2-(3-oxobutyl)-1-oxo-2-indancarboxylate with 45% e.e. (Table 2, Entry 9). The similar feature was also observed for the Reaction (3) (Table 4, Entry 3). This indicates that configurational environment of the alkaloid moieties in polymer **10** was retained after the copolymerization in spite of their low catalytic activity.

One of the advantage of polymer-catalysts is that they can be recovered by filtration and reused. Thus the recovered polymers **6** and **7** were reused as the catalysts in the Reaction (3). As shown in Table 4, although the recovered **6** and **7** exhibited lower catalytic activity, the stereoselectivities were comparable with the first usages. (Table 4, Entries 9 and 10 vs. 1 and 2).

In summary, polymer-supported quinines were prepared in which the spacer arms was elongated to remote the catalytic center from polymer chain. Those polymers were found to be good catalysts for the three types of asymmetric reactions as well, and by inserting spacer groups, enantioselectivities were approached to those of the corresponding non-immobilized catalysts.

Experimental

General Procedure. The spectroscopic and analytical instruments were: ^1H NMR, Varian EM-360 (60 MHz), VXR-200 (200 MHz), and JEOL GX-400 (400 MHz); ^{13}C NMR, Varian VXR-200 (50 MHz) and JEOL GX-400 (100 MHz); IR, Hitachi 215; Elemental Analysis, Yanaco MT-3; MS, JEOL JMS-DX-300; Optical Rotation, Perkin-Elmer 241; GLC, Shimadzu GC-4B; HPLC, JASCO BIP-I. NMR spectra were measured in $CDCl_3$ with TMS as internal standard throughout unless otherwise specified. Toluene and methanol were distilled over CaH_2. Diethyl ether and THF were distilled from benzophenone ketyl before use. Acrylonitrile was distilled and immediately used for polymerization.

11-(2-Carboxyethylthio)-10,11-dihydroquinine (2): A mixture of **1** (9.73 g, 30 mmol), 3-mercaptopropionic acid (31.67 g, 300 mmol), and 2,2′-azobisisobutyronitrile (AIBN) (0.99 g, 6 mmol) in benzene (80 ml) was heated at 70 °C for 17 h under Ar atmosphere. The reaction mixture was extracted with 2 M† HCl (3×50 ml). The combined extracts were washed with ether (2×50 ml) and made alkaline (pH 8)

† 1 M=1 mol dm^{-3}.

with Na_2CO_3 powder to afford **2** as viscous semisolid. It became powder by cooling at 4 °C overnight. The powder was collected and dried, and used for the next step without further purification; 10.55 g (82%): $[\alpha]_D^{25}$ 211° (*c* 1.022, 0.1 M HCl); ^{1}H NMR (200 MHz, DMSO-d_6) δ=1.30—3.55 (19H, m, H of quinuclidine ring and spacer arms), 3.91 (3H, s, CH_3O), 5.54 (1H, d, *J*=4.4 Hz, H-9), 6.15 (3H, br s, OH and COOH), 7.37 (1H, dd, *J*=9.2 and 2.5 Hz, H-7′), 7.50 (1H, d, *J*=2.5 Hz, H-5′), 7.54 (1H, d, *J*=4.7 Hz, H-3′), 7.92 (1H, d, *J*=9.2 Hz, H-8′), 8.68 (1H, d, *J*=4.7 Hz, H-2′); ^{13}C NMR (50 MHz, DMSO-d_6) δ=21.427, 24.991, 26.705, 26.972, 28.969, 33.537, 33.592, 35.724, 41.844, 55.652, 56.051, 59.605, 68.936, 102,143, 118.958, 121.119, 126.501, 131.106, 143.768, 147.363, 148.007, 157.073, 174.080; MS (30 eV) *m/z* (rel intensity) 430 (M^+; 6), 242 (8), 44 (100); Found: *m/z* 430.1927. Calcd for $C_{23}H_{30}N_2O_4S$: M, 430.1927; IR (KBr) 3410 (OH), 1620 cm^{-1} (C=O).

11-[2-(Allyloxycarbonyl)ethylthio]-10,11-dihydroquinine (3): To a suspension of **2** (2.50 g, 5.81 mmol) in allyl alcohol (40 ml), was added thionyl chloride (1.45 g, 12.16 mmol) at 0 °C with stirring. Then the mixture was stirred at room temperature for 3 h. The resulting mixture was evaporated and quenched with 1 M NaOH at 0 °C, followed by extraction with CH_2Cl_2 (4×25 ml). The extracts were washed with brine and dried (Na_2SO_4). Evaporation followed by column chromatography on silica gel (eluent, $CHCl_3$(70)–MeOH(2)–NEt_3(1)) and concentration gave **3** as a syrup; 1.96 g (72%): $[\alpha]_D^{28}$ −122° (*c* 0.968, EtOH); ^{1}H NMR (400 MHz) δ=1.35—1.82, 2.32, 2.58, 2.99—3.05, and 3.47 (13H, m, H of quinuclidine ring and H-10), 2.41 (2H, m, H-11), 2.57 (2H, m, $C\underline{H}_2CO_2$), 2.71 (2H, m, $SC\underline{H}_2CH_2CO_2$), 3.90 (3H, s, CH_3O), 4.56 (2H, m, *J*=5.9 and 1.5 Hz, allyl H), 5.21 (1H, m, *J*=10.3, 2.5, and 1.5 Hz, (*Z*)-vinyl H), 5.29 (1H, m, *J*=17.1, 3.2, and 1.5 Hz, (*E*)-vinyl H), 5.36 (1H, br s, OH), 5.50 (1H, d, *J*=3.4 Hz, H-9), 5.88 (1H, m, *J*=17.1, 10.3, and 5.9 Hz, =CH), 7.21 (1H, d, *J*=2.4 Hz, H-3′), 7.25 (1H, dd, *J*=9.3, and 2.9 Hz, H-7′), 7.44 (1H, d, *J*=4.4 Hz, H-5′), 7.87 (1H, d, *J*=9.3 Hz, H-8′), 8.43 (1H, d, *J*=4.9 Hz, H-2′); ^{13}C NMR (100 MHz) δ=20.959, 25.512, 26.987, 27.483, 30.022, 34.182, 34.255, 34.678, 43.144, 55.681, 57.739, 59.695, 65.036, 70.670, 100.839, 117.798, 117.973, 120.980, 125.899, 130.905, 131.416, 143.530, 146.493, 146.741, 157.162, 170.662; MS (30 eV) *m/z* (rel intensity) 470 (M^+; 27), 282 (42), 32 (100); Found: *m/z* 470.2235. Calcd for $C_{26}H_{34}N_2O_4S$: M, 470.2239; IR (liquid) 3080 (OH), 1735 cm^{-1} (C=O).

6-Allyloxy-1-hexanol (4): The allyl ether **4** was prepared from 6-chloro-1-hexanol and allyl alcohol through its THP ether; 2.20 g (37% from 6-chloro-1-hexanol): bp (bath) 142—148 °C/13 mmHg††; ^{1}H NMR (200 MHz) δ=1.20—1.60 (8H, m, CH_2×4), 2.65 (1H, s, OH), 3.22—3.68 (4H, m, OCH_2×2), 4.83—4.92 (2H, m, allyl H), 5.05—5.26 (2H, m, CH_2=), 5.70—5.95 (1H, m, =CH).

11-[2-[6-(Allyloxy)hexyloxycarbonyl]ethylthio]-10,11-dihydroquinine (5): The carboxylic acid **2** (2.50 g, 5.81 mmol), **4** (1.10 g, 6.98 mmol), and triphenylphosphine (1.83 g, 6.98 mmol) were suspended in dry THF (60 ml), and diethyl azodicarboxylate (1.21 g, 6.98 mmol) was added dropwise to the mixture at 0 °C with stirring over a period of 15 min. The mixture was stirred overnight at room temperature and evaporated to dryness, and extracted with 2 M HCl (4×25 ml). The combined acid extract was washed with ether (6×35 ml) and made alkaline with NaOH pellet, and extracted with CH_2Cl_2 (4×25 ml). The extract was washed with brine and dried (Na_2SO_4). Evaporation gave **5**; 3.12 g (94%): $[\alpha]_D^{24}$ −101° (*c* 1.156, EtOH); ^{1}H NMR (400 MHz) δ=1.30—1.85, 2.35, 2.61, 3.02—3.08, and 3.47 (21H, m, H of quinuclidine ring, H-10, and CH_2×4), 2.42 (2H, t, *J*=7.3 Hz, H-11), 2.53 (2H, t, *J*=7.3 Hz, $C\underline{H}_2CO_2$), 2.70 (2H, t, *J*=7.3 Hz, $SC\underline{H}_2CH_2CO_2$), 3.40 (2H, t, *J*=6.4 Hz, $C\underline{H}_2OCH_2$–CH=), 3.87 (3H, s, CH_3O), 3.94 (2H, m, *J*=5.4 and 1.5 Hz, allyl H), 4.05 (2H, t, *J*=6.8 Hz, $CO_2OC\underline{H}_2$), 4.88 (1H, br s, OH), 5.16 (1H, m, *J*=10.3 and 1.5 Hz, (*Z*)-vinyl H), 5.25 (1H, m, *J*=17.1, 3.4, and 1.5 Hz, (*E*)-vinyl H), 5.52 (1H, m, H-9), 5.90 (1H, m, *J*=17.1, 10.3, and 5.4 Hz, =CH), 7.22 (1H, d, *J*=2.4 Hz, H-5′), 7.27 (1H, dd, *J*=9.3, and 2.4 Hz, H-7′), 7.46 (1H, d, *J*=4.4 Hz, H-3′), 7.90 (1H, d, *J*=9.3 Hz, H-8′), 8.51 (1H, d, *J*=4.4 Hz, H-2′); ^{13}C NMR (50 MHz) δ=21.404, 25.688, 25.835, 25.908, 27.157, 28.013, 28.586, 29.683, 30.196, 34.452, 34.631, 34.882, 43.627, 55.805, 58.202, 59.876, 64.770, 70.242, 71.580, 71.811, 101.370, 116.688, 118.423, 121.382, 126.527, 131.343, 134.941, 144.029, 147.326, 147.725, 157.657, 171.846; MS (70 eV) *m/z* (rel intensity) 570 (M^+; 4), 382 (5), 32 (100); Found: *m/z* 570.31328. Calcd for $C_{32}H_{46}N_2O_5S$: M, 570.31278; IR (liquid) 3150 (OH), 1740 cm^{-1} (C=O).

Alkaloid 3–Acrylonitrile Copolymer (6): The alkaloid **3** (1.91 g, 4.06 mmol), acrylonitrile (4.09 g, 77.14 mmol), and AIBN (0.018 g, 0.11 mmol) in dry DMF (14.8 ml) were heated at 60 °C for 21 h under Ar atmosphere. The reaction mixture was poured into boiling MeOH (1000 ml). Precipitated polymer was filtered, reprecipitated twice and Soxhlet-extracted with MeOH (5 h) to remove unreacted monomers. The residue was dried (over P_2O_5 in vacuo at 70 °C (4 h)), to give the polymer **6**; 3.39 g (57%): $[\alpha]_D^{27}$ −5.6° (*c* 1.022, DMF); Elemental analysis. Found: C, 67.41; H, 5.78; N, 24.44%; Alkaloid content 1.10 mol%.

Alkaloid 5–Acrylonitrile Copolymer (7): The alkaloid **5** (2.58 g, 4.52 mmol), acrylonitrile (4.56 g, 85.89 mmol), and AIBN (0.021 g, 0.13 mmol) in dry DMF (17.5 ml) were heated at 60 °C for 22 h under Ar atmosphere. The same purification process described above afforded the polymer **7**; 3.08 g (43%): $[\alpha]_D^{25}$ −6.5° (*c* 1.086, DMF); Elemental analysis. Found: C, 67.62; H, 5.95; N, 23.81%; Alkaloid content 1.24 mol%.

11-(2-Hydroxyethylthio)-10,11-dihydroquinine (8): Quinine (**1**) (9.73 g, 30 mmol), 2-mercaptoethanol (18.75 g, 240 mmol), and AIBN (0.99 g, 6 mmol) in benzene (80 ml) were heated at 70 °C for 28 h under Ar atmosphere. The reaction mixture was extracted with 2 M HCl (2×50 ml). The extracts were washed with ether (2×50 ml), and made alkaline with NaOH pellet. The liberated oil was taken up with CH_2Cl_2 (3×50 ml). The combined extracts were washed with brine and dried (Na_2SO_4). Evaporation and chromatography on silica gel (eluent $CHCl_3$(70)–MeOH-(2)–NEt_3(1)) afforded **8** as a syrup; 9.25 g (77%): $[\alpha]_D^{25}$ −108° (*c* 1.030, EtOH), (Ref. 17 $[\alpha]_D^{25}$ −140.6° (EtOH)); ^{1}H NMR (400 MHz) δ=1.22—1.80, 2.26, 2.52, 2.90—3.00, and 3.48 (13H, m, H of quinuclidine ring and H-10), 2.37 (2H, m, H-11), 2.59 (2H, t, *J*=6.4 Hz, SCH_2), 3.63 (2H, t, *J*=6.4 Hz, CH_2O), 3.83 (3H, s, CH_3O), 4.36 (1H, br s, OH), 5.49 (1H, m, H-9), 5.59 (1H, br s, OH), 7.13—7.26, 7.43, 8.79, and 8.42 (5H, m, H of quinoline ring); ^{13}C NMR (50 MHz) δ=20.880,

†† 1 mmHg=133.322 Pa.

25.633, 27.945, 29.956, 34.586, 35.154, 43.189, 55.742, 58.157, 59.681, 60.700, 68.403, 71.322, 101.509, 118.476, 121.377, 126.532, 130.996, 143.709, 147.110, 148.461, 157.733; MS (70 eV) *m/z* (rel intensity) 402 (M^+; 57), 357 (49), 214 (100).

11-[2-(Acryloyloxy)ethylthio]-10,11-dihydroquinine (9): To a suspension of **8** (4.00 g, 9.94 mmol), acrylic acid (0.745 g, 10.33 mmol), and triphenylphosphine (2.71 g, 10.33 mmol) in dry THF (100 ml), was added dropwise a solution of diethyl azodicarboxylate (1.80 g, 10.33 mmol) in dry THF (5 ml) with stirring at 0 °C over a period of 15 min. The mixture was stirred at 0 °C for 30 min and then at room temperature overnight. The reaction mixture was evaporated to dryness. The residue was dissolved in 2 M HCl (80 ml). Aqueous layer was washed with ether (6×30 ml), made alkaline with Na_2CO_3 powder and extracted with CH_2Cl_2 (2×50 ml). The extracts were washed with brine and dried (Na_2SO_4), and the solvent was evaporated. The residue was flush chromatographed on silica gel (eluent $CHCl_3$-(50)-MeOH(2)-NEt_3(1)) to afford **9**; 3.02 g (67%): $[\alpha]_D^{25}$ −105° (*c* 1.044, EtOH); ^1H NMR (400 MHz) δ=1.34—1.83, 2.38, 2.61, 3.02—3.08, and 3.53 (13H, m, H of quinuclidine ring and H-10), 2.45 (2H, t, *J*=7.3 Hz, H-11), 2.70 (2H, t, *J*=6.8 Hz, SCH_2), 3.84 (3H, s, CH_3O), 4.23 (2H, a, *J*=6.8 Hz, CH_2O), 5.56 (2H, m, H-9 and OH), 5.80 (1H, m, *J*=10.3, 2.4, and 1.5 Hz, (*Z*)-vinyl H), 6.07 (1H, m, *J*=17.1 and 10.3 Hz, =CH), 6.34 (1H, m, *J*=17.1 and 1.5 Hz, (*E*)-vinyl H), 7.21 (1H, d, *J*=2.9 Hz, H-5′), 7.23 (1H, dd, *J*=9.3 and 2.4 Hz, H-7′), 7.46 (1H, d, *J*=4.4 Hz, H-3′), 7.86 (1H, d, *J*=9.3 Hz, H-8′), 8.45 (1H, d, *J*=4.4 Hz, H-2′); ^{13}C NMR (50 MHz), δ=20.931, 25.543, 27.738, 30.221, 30.403, 33.723, 34.431, 43.182, 55.699, 58.008, 59.781, 63.433, 71.111, 101.338, 118.456, 121.338, 126.457, 128.059, 131.142, 131.142, 143.832, 147.202, 148.059, 157.676, 165.846; MS (70 eV) *m/z* (rel intensity) 456 (M^+; 87), 357 (99), 268 (100); Found: *m/z* 456.20527. Calcd for $C_{25}H_{32}N_2O_4S$: M, 456.20817; IR (liquid) 3160 (OH), 1725 cm^{-1} (C=O).

Alkaloid 9-Acrylonitrile Copolymer (10): A solution of the alkaloid **9** (1.95 g, 4.27 mmol), acrylonitrile (2.04 g, 38.40 mmol), and AIBN (0.012 g, 0.07 mmol) in dry DMF (10.0 ml) was heated at 65 °C for 42 h under Ar atmosphere. The same purification process described for the polymer **5** gave the polymer **10**; 2.29 g (57%): $[\alpha]_D^{25}$ −26.0° (*c* 1.008, DMF); Elemental analysis. Found: C, 65.82; H, 6.15; N, 17.69%; Alkaloid content 8.04 mol%.

Quinine-Acrylonitrile Copolymer (11): According to reported procedure,[18] a mixture of **1** and acrylonitrile (1:19) was copolymerized in dry DMF. The crude polymer was purified as above to give the polymer **11** having no spacer; 8.09 g (29%): $[\alpha]_D^{28}$ −10.4° (*c* 1.00, DMF); Elemental analysis. Found: C, 68.33; H, 5.93; N, 24.39%; Alkaloid content 1.99 mol%.

Asymmetric Addition of Methyl 1-Oxo-2-indancarboxylate Catalyzed by 7. Typical Procedure for the Reaction (1): A mixture of the polymer-catalyst **7** (59.0 mg, 0.0125 mmol of alkaloid), methyl 1-oxo-2-indancarboxylate (47.5 mg, 0.25 mmol), and freshly distilled 3-buten-2-one (35.0 mg, 0.50 mmol) in dry toluene (1.5 ml) was stirred at −48 °C. The conversion was monitored by HPLC (hexane(100)-*i*-PrOH(5), detect at 280 nm). Evaporation of the filtrate afforded the pure adduct and its optical rotation was measured at 578 nm (25 °C) in benzene. The purity and structural integrity were certified by ^1H NMR and TLC.

Asymmetric Addition of the Thiol Catalyzed by 6. Typical Procedure for the Reaction (2): A mixture of the polymer catalyst **6** (80.0 mg, 0.015 mmol), *p-t*-butylbenzenethiol (301 mg, 1.81 mmol), and 2-cyclohexenone (150 mg, 1.56 mmol) in dry toluene (3 ml) was stirred overnight at room temperature. The reaction mixture was washed successively with 2 M HCl (2×10 ml), 2 M KOH (2×10 ml), and brine (1×10 ml) followed by drying over Na_2SO_4. Then the optical rotation was measured at 578 nm (25 °C) in CCl_4.

Asymmetric Methanolysis of the Acid Anhydride Catalyzed by 6. Typical Procedure for the Reaction (3): The polymer-catalyst **6** (52.6 mg, 0.01 mmol of alkaloid), *cis*-2,4-dimethylglutaric anhydride (14.2 mg, 1.0 mmol), and dry methanol (32.0 mg, 1.0 mmol) in dry ether (5 ml) were allowed to react at room temperature. The conversion was monitored by GLC (2% XE-60, 2 m, 160 °C). After removing polymer-catalyst by filtration, the half-ester obtained was converted to the diastereomeric amide ester using (*R*)-1-(1-naphthyl)ethylamine.[4] The diastereomeric ratio of the amide ester was determined by HPLC (hexane(100)-*i*-PrOH(6), detection at 280 nm).

References

1) H. Wynberg and R. Helder, *Tetrahedron Lett.*, **1975**, 4057.
2) H. Hiemstra and H. Wynberg, *J. Am. Chem. Soc.*, **103**, 417, (1981).
3) Ulf-H. Dolling, P. Davis, and E. J. J. Grabowski, *J. Am. Chem. Soc.*, **106**, 446 (1984).
4) J. Hiratake, Y. Yamamoto, and J. Oda, *J. Chem. Soc., Chem. Commun.*, **1985**, 1717; J. Hiratake, M. Inagaki, Y. Yamamoto, and J. Oda, *J. Chem. Soc., Perkin Trans. 1*, **1987**, 1053.
5) K. Hermann and H. Wynberg, *Helv. Chim. Acta*, **60**, 2208 (1977).
6) P. Hodge, E. Khoshdel, and J. Waterhouse, *J. Chem. Soc., Perkin Trans. 1*, **1983**, 2205.
7) N. Kobayashi and K. Iwai, *J. Am. Chem. Soc.*, **100**, 7071 (1978).
8) N. Kobayashi and K. Iwai, *J. Polym. Sci., Polym. Chem. Ed.*, **18**, 923 (1980).
9) N. Kobayashi and K. Iwai, *Macromolecules*, **13**, 31 (1980).
10) J. M. Brown and J. A. Jenkins, *J. Chem. Soc., Chem. Commun.*, **1976**, 458.
11) H. Molinari and F. Montanari, *J. Chem. Soc., Chem. Commun.*, **1977**, 639.
12) H. Molinari, F. Montanari, S. Quici, and P. Tundo, *J. Am. Chem. Soc.*, **101**, 3920 (1979).
13) M. Tomoi, M. Goto, and H. Kakiuchi, *J. Polym. Sci., Polym. Chem. Ed.*, **25**, 77 (1987).
14) N. Kobayashi and K. Iwai, *Macromol. Chem., Rapid Commun.*, **2**, 105 (1981).
15) Hyun Pyo Kim, Si Myung Byun, Young Il Yeom, and Sung Wan Kim, *J. Pharm. Sci.*, **72**, 225 (1983).
16) T. Tamikado and Y. Iwakura, *J. Polym. Sci.*, **36**, 529 (1959). Y. Tsuda, *Kogyo Kagaku Zasshi*, **62**, 1112 (1959).
17) N. Kobayashi and K. Iwai, *J. Polym. Sci., Polym. Lett. Ed.*, **20**, 85 (1982).
18) N. Kobayashi and K. Iwai, *J. Polym. Sci., Polym. Chem. Ed.*, **18**, 223 (1980).

 © 1987 The Chemical Society of Japan Bull. Chem. Soc. Jpn., 60, 4127—4131 (1987)

The Study on Peptide and Protein Syntheses. Infrared Spectroscopic Conformational Analysis of Oligo-L-leucines Containing Only One D-Amino Acid Residue[1)]

Mitsuaki NARITA,* Shinya HONDA, and Hiroshi UMEYAMA
Department of Industrial Chemistry, Faculty of Technology, Tokyo University of Agriculture and Technology, Koganei 184
(Received July 1, 1987)

In order to investigate the influence of a D-amino acid residue on the conformational behavior of peptides and proteins, IR spectroscopic conformational analysis of oligo-L-Leus containing only one D-Ala or D-Val residue was performed in the solid state. For the estimation of their structures, a CPK model and Ramachandran map were very helpful. The D-amino acid residue is clearly inhibited to take the values of the backbone dihedral angles ϕ and ψ for β-sheet structures formed by L-amino acid residues, while it is allowed for the D-amino acid residue to take the values ϕ and ψ for helical structures formed by L-amino acid residues. The IR absorption spectroscopic analysis of samples after application of strong shear stress was also useful for the investigation. The effect of shear stress on β-sheet-like structure→helix conformational change is larger for oligo-L-Leus containing a D-Ala residue than those containing a D-Val residue, indicating that the D-Ala residue is more favorable in a helical structure than the D-Val residue. This tendency can be also easily confirmed using CPK model. The significance of this study was discussed in relation to protein synthesis and design of three-dimensional structures of peptides using D-amino acid residues.

In our recent papers,[2-8)] we have demonstrated that a β-sheet aggregation plays an important role in the insolubility of oligopeptides larger than octa- or nonapeptide levels and that replacement of an L-amino acid residue with an Aib residue promotes helical folding in an oligopeptide to improve its solubility to a remarkable extent. The solubility improvement was clearly explained by the fact that the values of the backbone dihedral angles ϕ and ψ of the Aib residue were restricted to helical regions.[4)] The Aid residue in an oligopeptide is inhibited to take the values of ϕ and ψ corresponding to a β-sheet region, and a β-sheet structure of the oligopeptide containing the Aib residue is destroyed due to steric hindrance of the Aib residue. A D-Ala residue has the structure that the C_L^β methyl group in the Aib residue is replaced by a hydrogen atom, and the D-Ala residue in oligo-L-Leus is also inhibited to take the values of ϕ and ψ corresponding to a β-sheet structure formed by oligo-L-Leus. Therefore, it is interesting to investigate the conformational behavior of oligo-L-Leus containing only one D-Ala residue.

The concern in this paper is to investigate the influence of a D-amino acid residue on the conformational behavior of oligo-L-Leus containing only one D-Ala or D-Val residue in the solid state. The investigation is significant in the study on peptide and protein syntheses since racemization during coupling reaction is inevitable. It also gives information for the design of three-dimensional structures, especially β-turn structures, of peptides using D-amino acid residues.

Experimental

Materials. The peptides used in this study are in the following: Boc-L-Leu$_3$-D-X-L-Leu$_3$-OBzl: X=Ala **1a**, X=Val **1b**; Boc-L-Leu$_4$-D-X-L-Leu$_4$-OBzl: X=Ala **2a**, X=Val **2b**; Boc-L-Leu$_5$-D-X-L-Leu$_3$-OBzl: X=Ala **3a**, X=Val **3b**; Boc-L-Leu$_4$-L-X-L-Leu$_4$-OBzl: X=Ala **4a**, X=Val **4b**. Preparation and solubility properties of the peptides **1**—**4** will be reported elsewhere.[9)] The peptides **1a** and **3a** are soluble in dichloromethane, tetrahydrofuran, and highly polar solvents such as *N*,*N*-dimethylformamide and dimethyl sulfoxide. The peptides **1b** and **3b** are less soluble in dichloromethane and tetrahydrofuran and soluble in the highly polar solvents. The peptides **2** and **4** are insoluble even in the highly polar solvents. The solid samples of the peptides **1a** and **3a** were obtained by repeated recrystallization from aqueous ethanol and the solid sample of the peptide **1b**, from methanol. Those of the peptides **2**, **3b**, and **4** were obtained by repeated washing with hot methanol. The purity of the peptides was confirmed by elemental and amino acid analyses. The peptides soluble in *N*,*N*-dimethylformamide gave a single peak on high-performance liquid chromatography.

IR Measurements. The IR absorption spectra of the solid samples were recorded with a JEOL Model JIR-100 FT-IR spectrometer in a Nujol mull. The IR absorption spectra (Fig. 1) of the peptides **1**—**4** under slight shear stress were obtained after the solid samples were pulverized with Nujol by weak shear stress.[8,13)] The IR absorption spectra (Fig. 2) of the peptides **1**—**4** after application of shear stress were also obtained in a Nujol mull after the solid samples were pulverized without Nujol by strong shear stress.[8,13)]

Results

IR Absorption Spectra of the Peptides 1—4 in the Solid State. Figure 1 shows the IR absorption spectra of the peptides **1**—**4** in the most significant spectral regions for the conformational assignments (3500—3100 cm^{-1}, amide A; 1800—1600 cm^{-1}, amide I). All of the peptides show a strong band at 3280—3270 cm^{-1} and a negligible small band around 3425 cm^{-1} in the amide A region, suggesting that the Boc-urethane

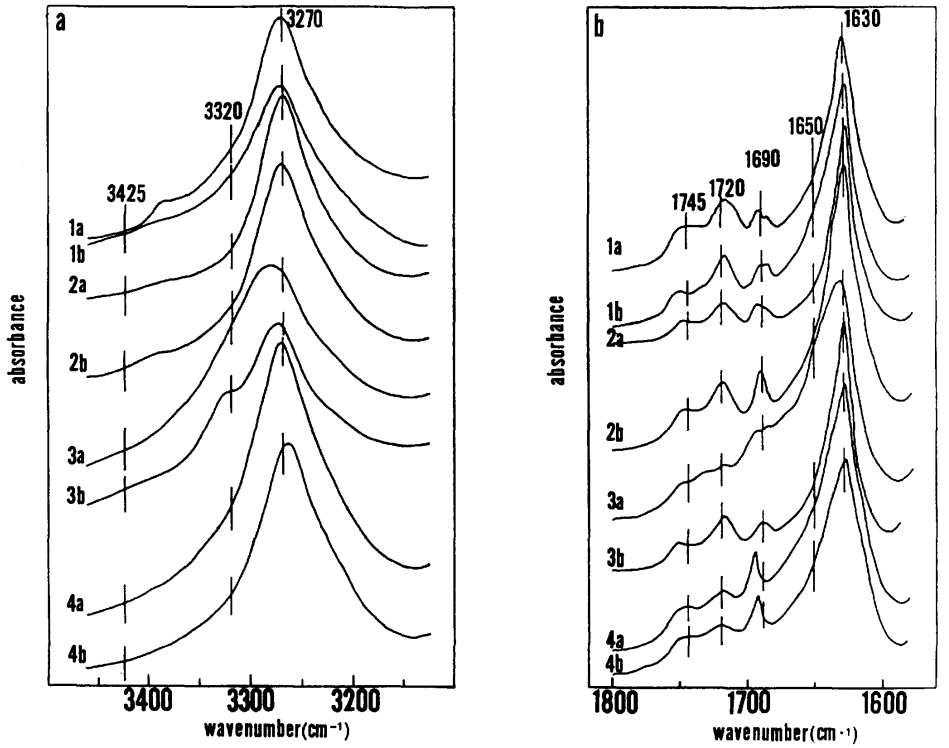

Fig. 1. IR absorption spectra of the peptides **1**—**4** in the solid state under slight shear stress. a: The amide A region; b: the amide I region.

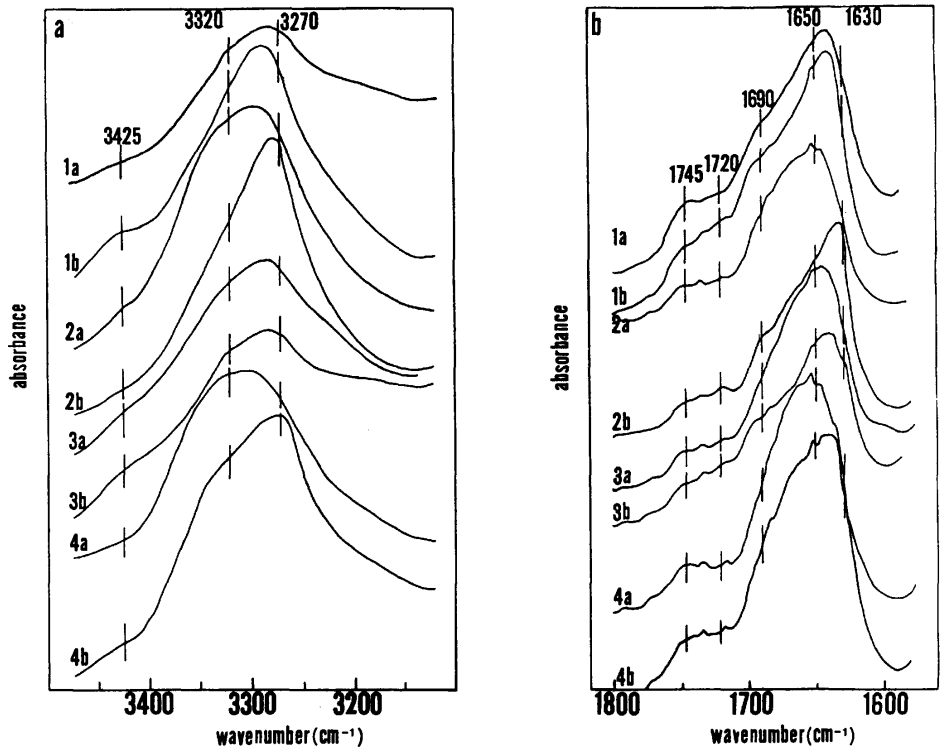

Fig. 2. IR absorption spectra of the peptides **1**—**4** in the solid state after application of strong shear stress. a: The amide A region. b: the amide I region.

N-H bond and peptide N-H bonds are mostly subjected to hydrogen bonding in the solid state. The bands around 1745 cm^{-1} and 1720 cm^{-1} are assigned to the Bzl-ester carbonyl group and the Boc-urethane carbonyl group, respectively, and the bands at 1690—1625 cm^{-1}, mainly to hydrogen-bonded amide-carbonyl groups. The strong bands at 3280—3270 cm^{-1} in the amide A region and at 1635—1625 cm^{-1} in the amide I region and the weak band at 1690 cm^{-1} in the amide I region suggest that the peptides **1—3** have an antiparallel β-sheet-like structure, while those of the peptides **4a** and **4b** containing only L-amino acid residues are indicative of an antiparallel β-sheet (β_A-sheet) structure.[10-12] The peptides **3a** and **3b** are accompanied by a shoulder band around 3320 cm^{-1}, indicating a contribution of other conformations.

The Influence of Shear Stress on Peptide Conformations in the Solid State. It has been reported that β-sheet→helix conformational change in the solid state brings about by application of shear stress.[8,13] Figure 2 shows the IR absorption spectra of the peptides **1—4** after application of strong shear stress. These spectra indicate the influence of shear stress on peptide conformations to a small or considerable extent. The increase in intensities of 3320-cm^{-1} and 1655-cm^{-1} shoulder bands of the peptides strongly suggests the onset of a helical structure although the increase in intensity of a 3425-cm^{-1} shoulder band is not negligible, which is assigned to N-H bonds free from hydrogen bonding.

Discussion

The IR absorption spectra (Fig. 1) of the peptides **1—4** under a slight influence of shear stress are reproducibly obtained when solid samples are pulverized with Nujol by weak shear stress, indicating that the peptides **1—3** have a β_A-sheet-like structure, while the peptides **4a** and **4b** have a β_A-sheet structure. The solubility of the nonapeptides **2a** and **2b** is as low as that of Boc-(L-Leu)$_9$-OBzl and the nonapeptides **4a** and **4b**, also suggesting that they have successive-strong intermolecular hydrogen bonds like β-sheet aggregation. The solubility of peptides forming successive-intermolecular hydrogen bonds is strongly dependent on peptide chain length,[2-7] and the heptapeptides **1a** and **1b** is actually more soluble than the nonapeptides **2a** and **2b**.

For the estimation of the structures of the peptides **1—3**, a CPK model and Ramachandran map[14] are quite helpful. The values of the backbone dihedral angles ϕ and ψ of an L-amino acid residue are allowed in the regions outlined by solid lines in Fig. 3a, and those of a D-amino acid residue, in the regions outlined by solid lines in Fig. 3b. The restriction of the values ϕ and ψ in Fig. 3 results entirely from the steric repulsion of $C^{\beta}_{L,i}$ and $C^{\beta}_{D,i}$ with O_{i-1}, N_{i+1}, and H_{i+1} (Fig. 4). Therefore, the D-Ala and D-Val residues in the peptides **1** and **2** clearly can not exist in β_A-sheet and parallel β-sheet (β_P-sheet) structures formed by L-amino acid residues. Furthermore, Fig. 3 suggests three possibilities of the conformation of the peptides **1** and **2**. The first one is the right handed helical (H_R) structure, where the L-Leu, D-Ala, and D-Val residues should have the values of ϕ and ψ corresponding to the H_R region. The second one is the segment-separated structure, where β-sheet structures are separated by the D-Ala or D-Val residue into two peptide segments as proposed previously for tertiary peptide bond-containing polypeptides.[2,15] The last one is the β_P- or β_A-sheet-like structure as shown in Fig. 5. In the β_P-sheet-like structure shown in Fig. 5a, the L-Leu residues have the values of ϕ and ψ corresponding to the β_P region in the L-configuration:

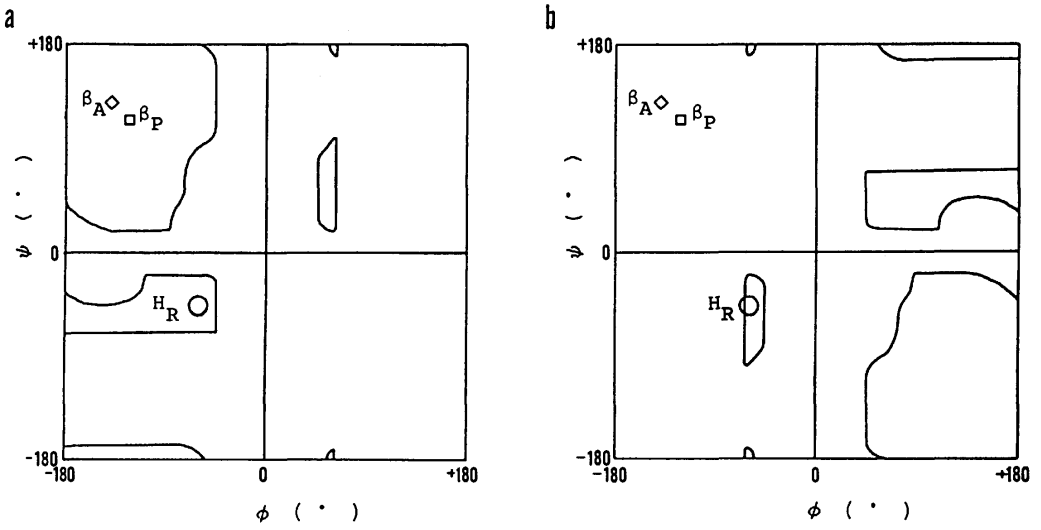

Fig. 3. Ramachandran map of amino acid residues except for glycine and proline residues. a: L-Amino acid residues; b: D-amino acid residues.

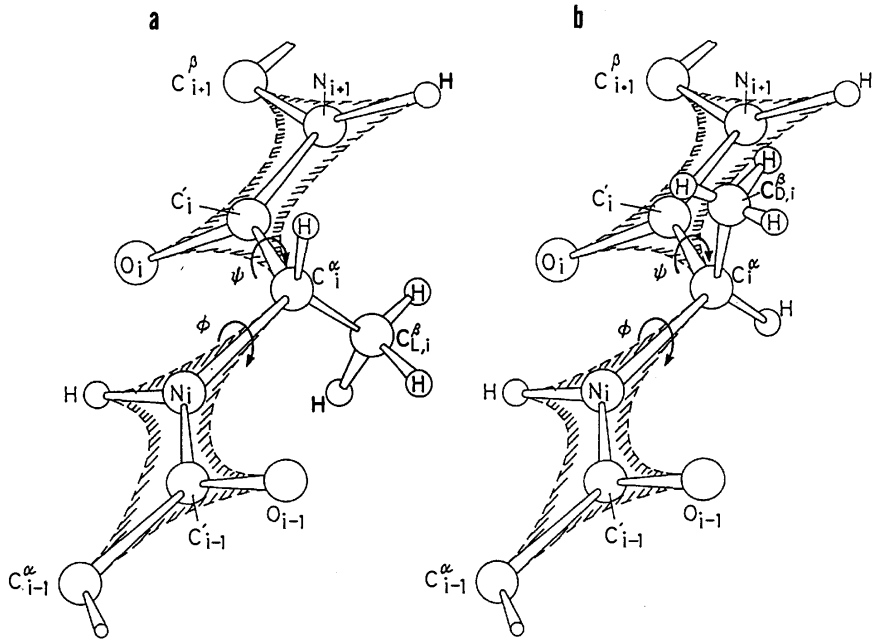

Fig. 4. The structure of peptide backbone and the backbone dihedral angles ϕ and ψ. a: L-Amino acid residues; b: D-amino acid residues.

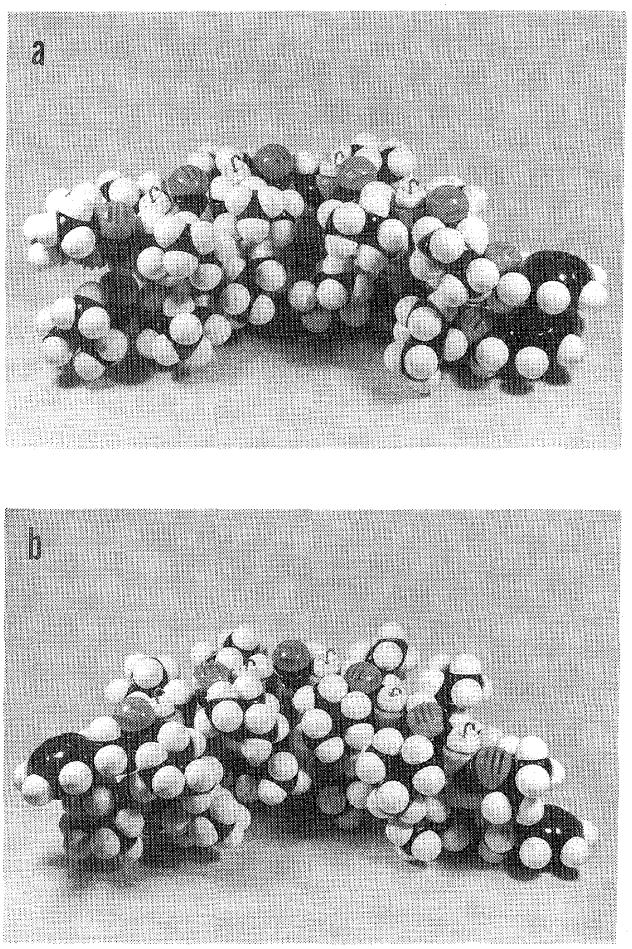

Fig. 5. The CPK model of theβ_P- and β_A-sheet-like structures of the peptide **2a**. a: The β_P-sheep-like structure; b: the β_A-sheet-like structure.

ϕ=−119° and ψ=+120°, while the D-Ala and D-Val residue have the other values in the regions outlined by solid lines in Fig. 3b. In the β_A-sheet-like structure shown in Fig. 5b, the L-Leu residues have the values of ϕ and ψ corresponding to the β_A region in the L-configuration: ϕ=−139° and ψ=+135°, and the D-Ala and D-Val residue have the other values in Fig. 3b. The solubility of peptides having the helical or segment-separated structure is expected to be easily soluble in organic solvents.[2,4,15] In addition to the above consideration, the IR absorption spectra (Fig. 1) and solubility properties of the peptides **1** and **2** strongly suggest that they have the β_A-sheet-like structure shown in Fig. 5b although an L-Leu residue is favorable in both β_A- and β_P-sheet structures.[16] The β_A-sheet-like structure of the peptides **1** and **2** is also supported by the solubility behavior and IR absorption spectrum (Fig. 1) of the peptide **3a**. When the peptide **3a** is favorable in a β_P-sheet-like structure having successive-intermolecular hydrogen bonds, it will be insoluble in highly polar solvents. However, the peptide **3a** is easily soluble even in medium-polar solvents such as dichloromethane and tetrahydrofuran, and its IR absorption spectrum (Fig. 1) rather suggestes the β_A-sheet-like structure containing other conformational contribution.

The IR absorption spectra (Fig. 2) of the peptides **1**—**4** after application of shear stress are also useful for investigating the influence of a D-amino acid residue on the conformational behavior of oligo-L-Leus containing only one D-amino acid residue. They are reproducibly obtained when solid samples are pulverized without Nujol by strong shear stress. The

effect of shear stress on β-sheet-like structure→helix conformational change is larger for oligo-L-Leus containing a D-Ala residue, **1a—3a**, than those containing a D-Val residue, **1b—3b**. This result indicates that the D-Ala residue is more favorable in a helical structure than the D-Val residue. In fact, this tendency can be easily confirmed using a CPK model. The difference of conformational preference in the D-Ala and D-Val residues subsequently brings about the solubility difference of the peptides **3a** and **3b**. The peptide **3a** is easily soluble in dichloromethane, while the peptide **3b** is nearly insoluble. The peptide **3a** is indeed estimated to have a helical structure in dichloromethane solution as well as Boc-(L-Leu)$_4$-Aib- (L-Leu)$_4$-OBzl and the peptide **1a**.[4,17] The same tendency of conformational transformation is observed in the peptides **4a** and **4b** having a typical β_A-sheet structure. The effect of shear stress on β-sheet→helix conformational change is also larger for the peptide **4a** having an L-Ala residue than the peptide **4b** having an L-Val residue (Fig. 2), but both peptides are insoluble even in highly polar solvents such as *N*,*N*-dimethylformamide and dimethyl sulfoxide. The conformational behavior and solubility properties of the peptides **3** and **4** clearly suggest that, in the case of oligopeptides containing a D-Ala residue, the inhibition of the values ϕ and ψ in the β-sheet region and the allowance of the values ϕ and ψ in the helical region promote helical folding to improve their solubility as pointed out for oligopeptides containing an Aib residue.[4]

The conformational behavior of the peptides **1—3** is significant in the study on peptide and protein syntheses. The results obtained indicate that a D-amino acid residue resulted in inevitable racemization in coupling reactions can not exist in β_A- and β_P-sheet structures of peptides and proteins and brings about remarkable conformational change shown in Fig. 5 at least in the β-sheet regions. On the other hand, Fig. 3 suggests that, due to steric hindrance, β-turn structures can be kept stable using a D-amino acid residue in the position $i+1$ or $i+2$ of β-turn structures. We are now working on the design of β-turn structures using a D-amino acid residue.

The authors wish to thank Ajinomoto Co., Ltd., for the generous gift of various amino acids. We also wish to thank Mitsubishi Kasei Co., Ltd., for the generous gift of Boc-S reagents.

References

1) This paper forms Part VIII of "Designs of Three-dimensional Structures of Peptides and Proteins and the Synthetic Route for Peptides and Proteins" series. This series follows "Design of the Synthetic Route for Peptides and Proteins Based on the Solubility Prediction Method Part VII," see M. Narita, M. Doi, and T. Nakai, *Bull. Chem. Soc. Jpn.*, **60**, 3255 (1987). Abbreviaions used are in the following: IR, infrared; Leu, leucine residue; Ala, alanine residue; Val, valine residue; Aib, α-aminoisobutyric acid residue; Boc, *t*-butoxycarbonyl; OBzl, benzyl ester.

2) M. Narita, T. Fukunaga, A. Wakabayashi, K. Ishikawa, and H. Nakano, *Int. J. Peptide Protein Res.*, **23**, 306 (1984).

3) M. Narita, K. Ishikawa, H. Nakano, and S. Isokawa, *Int. J. Peptide Protein Res.*, **24**, 14 (1984); M. Narita, K. Ishikawa, J.-Y. Chen, and Y. Kim, *ibid.*, **24**, 580 (1984).

4) M. Narita, M. Doi, H. Sugasawa, and K. Ishikawa, *Bull. Chem. Soc. Jpn.*, **58**, 1473 (1985); M. Narita, K. Ishikawa, H. Sugasawa, and M. Doi, *ibid.*, **58**, 1731 (1985); M. Narita, J.-Y. Chen, H. Sato, and Y. Kim, *ibid.*, **58**, 2494 (1985).

5) M. Narita, T. Ogura, K. Sato, and S. Honda, *Bull. Chem. Soc. Jpn.*, **59**, 2433, 2439, 2445 (1986).

6) M. Narita, M. Doi, K. Kudo, and Y. Terauchi, *Bull. Chem. Soc. Jpn.*, **59**, 3553 (1986).

7) M. Narita, M. Doi, and T. Nakai, *Bull. Chem. Soc. Jpn.*, in press.

8) M. Narita, M. Doi, and H. Takegahara, *Bull. Chem. Soc. Jpn.*, in press.

9) M. Narita, S. Honda, and H. Umeyama, in preparation.

10) T. Miyazawa and E. J. Blout, *J. Am. Chem. Soc.*, **83**, 712 (1961); Yu. N. Chirgadze and N. A. Nevskaya, *Biopolymers*, **15**, 627 (1976).

11) K.-H. Altmann, A. Florsheimer, and M. Mutter, *Int. J. Peptide Protein Res.*, **27**, 314 (1986), and references cited therein.

12) M. Narita, S. Isokawa, Y. Tomotake, and S. Nagasawa, *Polym. J.*, **15**, 25 (1983), and references cited therein.

13) R. Katakai and Y. Nakayama, *J. Chem. Soc., Chem. Commun.*, **1977**, 924; R. Katakai, *J. Chem. Soc., Perkin Trans. 1*, **1979**, 905.

14) G. N. Ramachandran and V. Sasisekharan, *Adv. Protein Chem.*, **23**, 283 (1968).

15) M. Narita, S. Nagasawa, J.-Y. Chen, H. Sato, and Y. Tanaka, *Makromol. Chem.*, **185**, 1069 (1984); M. Narita, N. Ohkawa, S. Nagasawa, and S. Isokawa, *Int. J. Peptide Protein Res.*, **24**, 129 (1984); S. Isokawa, T. Asakura, and M. Narita, *Macromolecules*, **18**, 871 (1985); S. Isokawa, I. Tominaga, T. Asakura, and M. Narita, *ibid.*, **18**, 878 (1985).

16) S. Lifson and C. Sander, *Nature (London)*, **282**, 109 (1979).

17) M. Narita, S. Honda, and H. Umeyama, in preparation.

 © 1987 The Chemical Society of Japan Bull. Chem. Soc. Jpn., 60, 4133—4137 (1987)

Enzyme Sensors Based on Coated-Wire Electrode. Use of Carboxyl-Substituted Poly(vinyl chloride) as a Support for Immobilizing Penicillinase

Jun-ichi Anzai, Masahiko Shimada, Tetsuo Osa,* and Chien-wu Chen†
Pharmaceutical Institute, Tohoku University, Aobayama, Sendai 980
†Department of Pharmacy, Kao-Hsiung Medical College, Kao-Hsiung, Taiwan, Republic of China
(Received April 23, 1987)

A poly(vinyl chloride) derivative which contained 1.8% carboxyl residue was used to prepare a potentiometric sensor sensitive to penicillin G. A pH-sensitive base electrode was fabricated by covering an Ag wire electrode with the membrane composed of the carboxyl-substituted poly(vinyl chloride), *o*-nitrophenyl octyl ether, and tridodecylamine. The sensitive layer of the pH-sensitive electrode was modified with penicillinase to make a penicillin-sensitive electrode. Penicillinase was adsorbed to the surface of the polymer membrane by immersing the sensitive layer of the electrode in the penicillinase solution. Treatment of the pH-sensitive electrode with ca. 0.3% penicillinase solution at pH 6.7 (1 mM†† phosphate buffer) resulted in favorable performance of the penicillin sensor. The long-term stability of the penicillin sensor thus prepared was satisfactorily good.

Enzyme sensors have been considered to have great potential as analytical tools for sensing precursors and metabolites in biological fluids, some kinds of drugs, and other biologically important compounds. To data, many kinds of electric and optical devices, including ion- and gas-sensitive conventional types of electrodes, semiconductor electrodes, thermistors, and optical fibers, coupled with enzymes have been employed for developing enzyme sensors.[1-10]

Many researchers have used potentiometric pH-sensitive devices as base electrodes on which enzyme is immobilized. Mosbach et al. reported that a pH glass electrode can be used as a base electrode to construct enzyme sensors sensitive to glucose, urea, and penicillin by covering the electrode surface with glucose oxidase, urease, and penicillinase membranes, respectively.[11] The principle of operation of the sensors was that the changes in H^+ concentration arising from the enzymatic reaction in the enzyme membrane were detected as local pH change by the pH glass electrode.

Recently, metal electrodes coated with metal oxide layer (IrO_2 or RuO_2), which can serve as pH sensors, have been utilized as base electrodes for preparing potentiometric enzyme sensors.[12-15] The metal oxide electrodes are of considerable interest due to their mechanical strength as well as ease of miniaturization as compared with the conventional type of glass electrode.

We have used an ion-sensitive field effect transistor (ISFET) as a pH-sensitive base electrode for developing micro enzyme sensors.[16-19] In the course of our study on the ISFET-based enzyme sensors, it has become obvious that high-performance enzyme sensors can be prepared by covering the ISFET gate with the enzymes which catalyze the reactions resulting in pH changes of the medium. Another interesting device for preparing potentiometric enzyme sensors is a pH-sensitive metal electrode coated with solvent polymeric membrane containing neutral carrier sensitive to H^+. The membrane-coated Ag electrode has a merit in miniaturizing the sensor body due to the absence of internal reference solution. We have already reported that urea and penicillin sensors can be prepared based on the Ag electrode which is coated with poly(vinyl chloride)–tridodecylamine composite membrane coupled with the enzyme–albumin crosslinked membrane.[20,21] However, the life time of the enzyme–albumin crosslinked membrane was not long. A poor surface adhesion between the polymer membrane and the enzyme membrane was also a drawback.

In this paper, we report that the poly(vinyl chloride) derivative which contains 1.8 wt% carboxyl residue can be used as a polymer matrix of pH-sensitive coated-wire electrode and that, using the coated-wire electrode, penicillin-sensitive electrode can be prepared by immobilizing penicillinase on the polymer surface mainly through electrostatic interaction. The present technique would provide a facile method to make enzyme sensors by the use of polymer-coated electrode.

Experimental

Materials. The carboxyl-substituted poly(vinyl chloride) (PVC-COOH), nominally 1.8 wt% carboxyl residue, was used as received from Aldrich Chemical Co. Poly(vinyl chloride) (PVC) was purchased from Wako Chemical Co. Sodium tetraphenylborate (NaTPB), tridodecylamine (TDA), and *o*-nitrophenyl octyl ether (NPOE) were of extra pure reagent grade. Penicillinase was purchased from Miles Chemical Co. Penicillin G potassium salt was obtained from Wako Chemical Co.

Electrode Preparation. Figure 1 shows the schematic representation of the electrode. The top of Ag wire (0.5 mm

†† (M=mol·dm^{-3}).

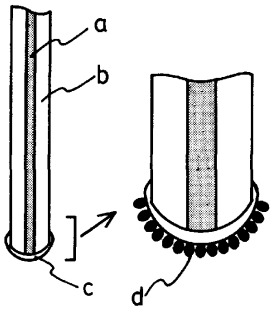

Fig. 1. Schematic representation of the penicillin-sensitive electrode.
a: Ag wire; b: Teflon rod; c: PVC-COOH-TDA membrane; d: penicillinase.

diameter) mounted in a Teflon rod was coated with a pH-sensitive solvent polymeric membrane composed of PVC-COOH (31%), NPOE (63%), TDA (5.5%), and NaTPB (0.5%). The polymer membrane was prepared by dip-coating method using tetrahydrofuran solution of the materials. The thickness of the polymer membrane thus prepared was about 0.2 mm. Prior to enzyme immobilization, the pH response of the coated-wire electrode was checked. Then, the polymer layer of the electrode was further modified with penicillinase by immersing the top of the electrode in the penicillinase solution. After treatment for about 15 h at 5—10 °C, the probe was rinsed adequately with the working buffer.

Measurements. All potentiometric measurements were carried out at 23 °C, using a digital multimeter (TR 6843, Takeda Riken Co.) and a saturated calomel electrode (SCE). Solutions were not stirred during the measurements, and the probe was rinsed with the working buffer after each measurement. The electrode was stored in a refrigerator at about 4 °C when not in use.

Results and Discussion

PVC-TDA-Coated Electrode. It has been demonstrated previously that the PVC-TDA composite membrane can serve as a pH sensor.[22,23] A metal electrode coated with the PVC-TDA membrane was also examined.[24] The use of PVC-COOH for preparing coated-wire electrode has been first reported by Satchwill and Harrison.[25] They have demonstrated that the potentiometric response of K^+-sensitive electrode coated with the PVC-COOH-valinomycin membrane is comparable to that of the parent PVC-based device.

The pH response of the PVC-COOH-TDA-coated electrode was checked using 50 mM KH_2PO_4 solutions containing varying amounts of NaOH (Fig. 2). The electrode potential depended linearly on the solution pH over the range of pH 4.3—10.2. The pH sensitivity was about 50 mV/decade, and the response was satisfactorily fast (20—30 s). The pH response of the electrode is almost the same as that of the PVC-TDA-based electrode.[22-24] These results suggest that the PVC-COOH can be used as a polymer matrix

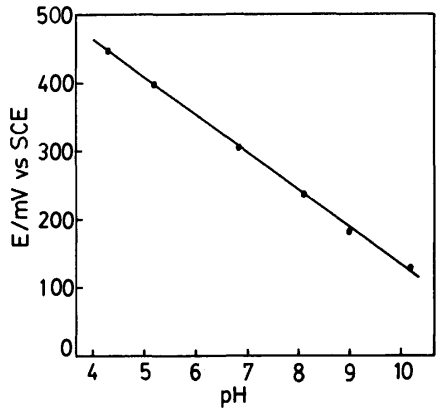

Fig. 2. pH response of the PVC-COOH-TDA-coated electrode. The pH values of the solutions were adjusted by adding varying amounts of NaOH to 50 mM KH_2PO_4.

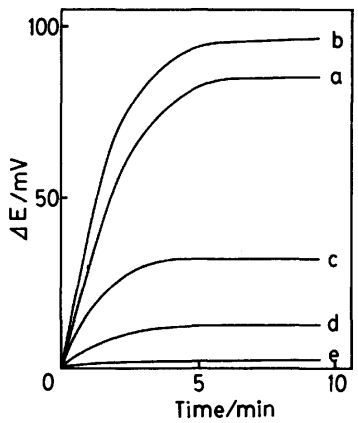

Fig. 3. Typical response curves of the penicillin sensor for penicillin G solutions in 5 mM phosphate buffer at pH 7.0.
Penicillin G concentration: a: 30; b: 10; c: 3; d: 1; e: 0.1 mM.

of the pH-sensitive membrane for constructing enzyme sensors.

Penicillin-Sensitive Electrode. The PVC-COOH-TDA-coated electrode was modified with penicillinase for making penicillin-sensitive electrode, by treating the sensitive layer with 0.3% penicillinase solution which was prepared in 1 mM phosphate buffer at pH 7.0. The potentiometric response of the penicillin sensor thus prepared was examined for 0.1—30 mM penicillin G in 5 mM phosphate buffer of pH 7.0 (Figs. 3 and 4). When the electrode was immersed in the penicillin G solution, the electrode potential shifted in the positive direction and reached steady-state value after 4—6 min. The positive shift of the potential means that the pH value around the PVC-COOH-TDA membrane decreased (cf. Fig. 2). This is reasonably explained based on the enzymatic reaction of penicillinase (1), where H^+ is liberated from

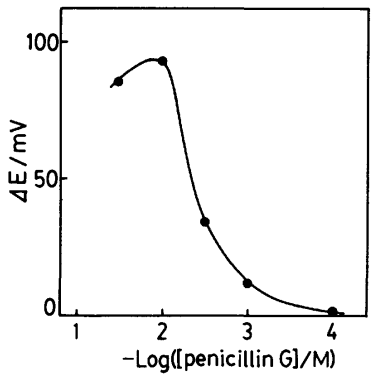

Fig. 4. Calibration graph of the penicillin sensor in 5 mM phosphate buffer at pH 7.0.

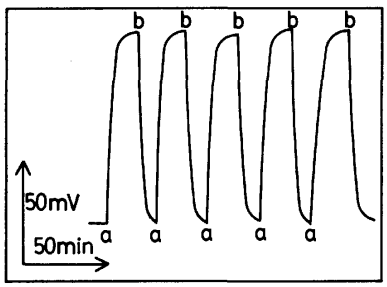

Fig. 5. Reproducibility of the penicillin sensor. Sample solution was 10 mM penicillin G in 5 mM phosphate buffer at pH 7.0. The sensor was immersed in the sample solution (a) and rinsed with the working buffer (b).

penicilloic acid produced. The value of the potential shift, ΔE, depended on the concentration of penicillin G in the solution. It is clear that penicillinase was adsorbed irreversibly to the surface of the PVC-COOH-TDA membrane without inactivation. The reduced response of the sensor for 30 mM penicillin G solution may be explained based on the fact that, as a result of the progress of the enzymatic reaction, the pH value around the polymer surface shifted down to ca. pH 5 at which penicillinase lost its catalytic activity to some degree.[26]

The reproducibility of response of the penicillin sensor was checked by repeatedly immersing the probe in 10 mM penicillin G in 5 mM phosphate buffer at pH 7.0 (Fig. 5). The reproducibility of the sensor was satisfactorily good. After the electrode potential had reached a steady-state value in the sample solution, the original potential was recovered in 10—15 min by immersing the probe in the working buffer. Potential drift during the series of measurements was small.

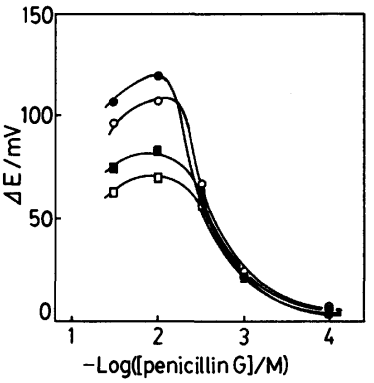

Fig. 6. Effects of pH of penicillinase solution on the response of the sensor.
The pH values of the penicillinase solutions were 5.2 (—□—), 6.0 (—○—), 6.7 (—●—), and 7.8 (—■—). The penicillin G solutions were prepared in 5 mM phosphate buffer at pH 7.0.

We also tried to immobilize penicillinase to the pH-sensitive electrode prepared by the use of parent PVC-TDA membrane under the same conditions. After treatment with penicillinase solution, the PVC-TDA-coated electrode responded to penicillin G to some extent, but the response disappeared after repeated measurements of the sample. This is presumably due to the desorption of penicillinase from the surface of PVC-TDA membrane. These results suggest that the carboxyl groups in PVC-COOH serve as ionic sites for binding penicillinase by the electrostatic force of attraction.

In order to establish the optimum conditions of enzyme solution in which the pH-sensitive electrode is treated, the effects of pH and ionic concentration of the enzyme solution, as well as the enzyme concentration, on the potentiometric response were examined. Figure 6 illustrates the calibration graphs for the enzyme sensors prepared by treating the probe in 0.3% penicillinase solutions at pH 5.2, 6.0, 6.7, and 7.8. At all pH tested, penicillinase was adsorbed to the membrane surface. The penicillin G sensors prepared at pH 6.0 and 6.7 showed relatively higher response as compared with those prepared at pH 5.2 and 7.8. These results imply that the electrode surface binds penicillinase efficiently in the pH region where PVC-COOH and penicillinase are charged negatively and positively, respectively.

Figure 7 shows the effects of buffer strength of the penicillinase solutions in which the PVC-COOH-TDA-coated electrode was treated for immobilizing penicillinase. The concentration of penicillinase was

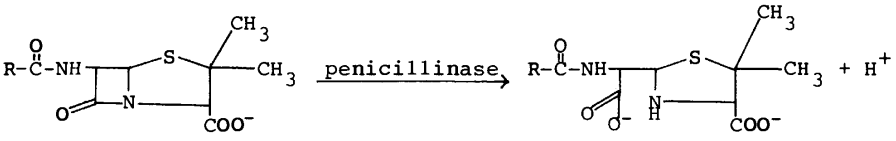

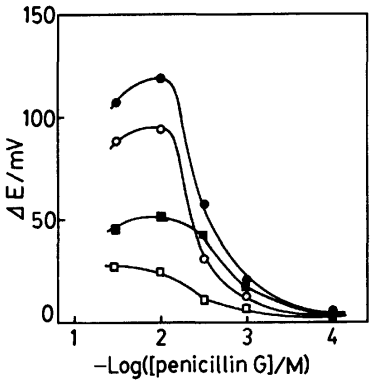

Fig. 7. Effects of buffer strength of penicillinase solution on the response of the sensor.
The buffer concentrations of penicillinase solutions were 1 (—●—), 5 (—○—), 20 (—■—), and 50 mM (—□—).
The penicillin G solutions were the same as used for Fig. 6.

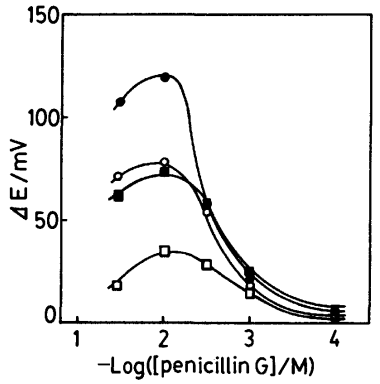

Fig. 8. Effects of penicillinase concentration on the response of the sensor.
The penicillinase concentrations were 0.07% (—■—), 0.3% (—●—), 0.7% (—○—), and 1.3% (—□—).
The penicillinase solutions were prepared in 1 mM phosphate buffer at pH 6.7.
The penicillin G solutions were the same as used for Fig. 6.

0.3% and the pH of the solutions was adjusted at 6.7. The results clearly demonstrate that the penicillin sensors prepared in the lower strength buffers exhibit higher response. This should arise from the difference in the enzyme load on the electrode. In other words, the penicillinase solution of lower buffer concentration favors the binding of penicillinase to the membrane, which situation agrees with the fact that the main force of attraction between penicillinase and PVC-COOH-TDA membrane is electrostatic one. Mitz et al. reported a similar effect of salt concentration, which was observed in immobilizing enzymes onto some cellulose ion exchangers.[27]

In Fig. 8 are shown the effects of penicillinase

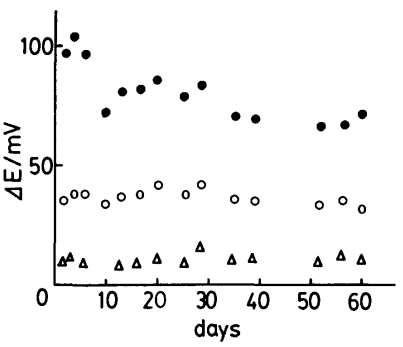

Fig. 9. The long-term stability of the penicillin sensor. The ΔE values were recorded for 10 (—●—), 3 (—○—), and 1 mM (—Δ—) penicillin G in 5 mM phosphate buffer at pH 7.0.

concentration in the solutions from which penicillinase was adsorbed to the electrode. The pH values of the solutions were kept constant at 6.7 by 1 mM phosphate buffer. The penicillin sensor prepared in 0.3% penicillinase solution exhibited the highest response. Unexpectedly, the sensor prepared in 1.3% penicillinase solution showed a decreased response, which may result from the enhanced ionic strength in the 1.3% penicillinase solution. From the results shown in Figs. 6, 7, and 8, it is recommended that, to construct high-performance penicillin sensor, the PVC-COOH-TDA-coated electrode is treated with 0.3% penicillinase solution prepared in 1 mM phosphate buffer at pH 6.7.

The long-term stability of the sensor was examined. The ΔE values of the sensor for 0.1, 3, and 10 mM penicillin G solutions were plotted in Fig. 9. Though the response of the sensor for 10 mM penicillin G solution slightly reduced after 10 days, the sensor can be used for more than 2 months.

Thus, it has been demonstrated that PVC-COOH membrane can be used for immobilizing penicillinase on its surface, as well as for the polymer matrix for making a pH-sensitive base electrode.

The present work was supported in part by a Grant-in-Aid for Special Project Research (No. 61127003) from Ministry of Education, Science and Culture.

References

1) S. J. Updike and G. P. Hicks, *Nature (London)*, **214**, 986 (1967).
2) S. J. Updike and G. P. Hicks, *Science*, **158**, 270 (1967).
3) G. G. Guilbault and F. Shu, *Anal. Chem.*, **44**, 2161 (1972).
4) B. Danielsson, B. Mattiasson, R. Karlsson, and F. Winquist, *Biotechnol. Bioeng.*, **21**, 1749 (1979).
5) K. Mosback and B. Danielsson, *Anal. Chem.*, **53**, 83A (1981).
6) S. Caras and J. Janata, *Anal. Chem.*, **52**, 1935 (1980).
7) S. Caras and J. Janata, *Anal. Chem.*, **57**, 1924 (1985).

8) Y. Ikariyama, M. Aizawa, and S. Suzuki, *J. Solid-State Biochem.*, **5**, 223 (1980).
9) M. Gotoh, E. Tamiya, I. Karube, and Y. Kagawa, *Anal. Chim. Acta*, **187**, 287 (1986).
10) S. Shiono, Y. Hanazato, and M. Nakato, *Anal. Sci.*, **2**, 517 (1986).
11) H. Nilsson, A. Akerlund, and K. Mosback, *Biochem. Biophys. Acta*, **320**, 529 (1973).
12) P. W. Alexander and J. P. Joseph, *Anal. Chim. Acta*, **131**, 103 (1981).
13) R. M. Ianniello and A. M. Yacynych, *Anal. Chim. Acta*, **146**, 249 (1983).
14) N. J. Szuminisky, A. K. Chen, and C. C. Liu, *Biotechnol. Bioeng.*, **2**, 642 (1984).
15) D. C. Roberts, J. A. Osborn, and A. M. Yacynych, *Anal. Chem.*, **58**, 140 (1986).
16) J. Anzai, T. Kusano, T. Osa, H. Nakajima, and T. Matsuo, *Bunseki Kagaku*, **33**, E131 (1984).
17) J. Anzai, Y. Ohki, T. Osa, H. Nakajima, and T. Matsuo, *Chem. Pharm. Bull.*, **33**, 2556 (1985).
18) J. Anzai, S. Tezuka, T. Osa, H. Nakajima, and T. Matsuo, *Chem. Pharm. Bull.*, **34**, 4373 (1986).
19) J. Anzai, S. Tezuka, T. Osa, H. Nakajima, and T. Matsuo, *Chem. Pharm. Bull.*, **35**, 693 (1987).
20) J. Anzai and T. Osa, *Chem. Pharm. Bull.*, **34**, 3522 (1986).
21) J. Anzai, M. Shimada, H. Fu, and T. Osa, *Chem. Pharm. Bull.*, **35**, 4568 (1987).
22) P. Schulthess, Y. Shijo, H. V. Pharm, E. Pretsch, D. Amman, and W. Simon, *Anal. Chim. Acta*, **131**, 111 (1981).
23) D. Amman, F. Lanter, R. A. Steiner, P. Schulthess, Y. Shijo, and W. Simon, *Anal. Chem.*, **53**, 2267 (1981).
24) H. Abe and S. Takizawa, Abst. 4th Sensor Symp., (Yokohama), 1985, 1.
25) T. Satchwill and D. J. Harrison, *J. Electroanal. Chem.*, **202**, 75 (1986).
26) "Koso Handbook," ed by N. Tamiya and B. Maruo, Asakura Shoten, Tokyo (1982), p. 598.
27) M. A. Mitz and R. J. Schlueter, *J. Am. Chem. Soc.*, **81**, 4024 (1959).

A New Method for the Determination of Optical Purity of Norleucine Based on Enthalpy of Transition in Solid-Solid Phase Transition

Masayuki MATSUMOTO,* Hirofumi YAJIMA,† and Ryuichi ENDO†
M & A Laboratory, 428-12 Kami-asao, Asao-ku, Kawasaki 215
†Department of Applied Chemistry, Faculty of Science, Science University of Tokyo, 1-3 Kagurazaka, Shinjuku-ku, Tokyo 162
(Received May 20, 1987)

Synopsis. A new method for determining the optical purity based on enthalpy of transition in solid-solid phase transition was introduced. The enthalpy of transition of norleucine recovered by an optical resolution procedure was measured by means of DSC. The magnitude of optical purity based on enthalpy of transition was in agreement with that based on specific rotation.

For the products obtained by optical resolution procedure or asymmetric synthesis, it is necessary to determine the magnitude of optical purity. The method for the determination of optical purity based on specific rotation has frequently been used.[1] A large amount of sample (about 0.1 g) is required to measure its specific rotation with dissolution procedure, whereas only small amount of sample (a few mg) is required to measure its enthalpy of transition by DSC without dissolution procedure.

In the course of thermoanalytical and calorimetric studies on polymorphic behaviors of crystalline modification for aliphatic α-amino acids with normal alkyl chains, we have found that the α-form DL-norleucine (DL-NL) is transformed into the γ-form DL-NL at 390 K with the enthalpy of transition of 4.4 kJ mol^{-1} by DSC[3] and that the α-γ transition of DL-NL is of the first order.[4]

In this report, a new method for the determination of optical purity based on enthalpy of transition is introduced. The enthalpy of transition of norleucine recovered by optical resolution procedure was measured by means of DSC. The magnitude of optical purity based on enthalpy of transition was compared with that based on specific rotation.

Experimental

L-Phenylalanine (L-Phe) and L-tryptophan (L-Try) were purchased from Tokyo Kasei Co., and DL-norleucine (DL-NL) and D-norleucine (D-NL) from Sigma Chemical Co. All the samples used were the purest reagents commercially available: The purity of the compounds was guaranteed by each manufacturers to be more than 98%. These samples were further purified by recrystallization from aqueous solution. Active carbon, which was purchased from Wako Chemical Co., was G. R. grade. The procedure of optical resolution was based on the method described by Shiraiwa et al.[5] The measurement of enthalpy of transition was carried out by means of DSC. The apparatus and procedure were tha same as described in the previous works.[3,4] The specific rotation was determined by Japan Spectroscopic Co. Model J-20 for 5 mol dm^{-3} HCl solution by using a 0.1 dm path-length quartz cell.

DL-NL (0.02 mol) and L-Phe (0.01 mol) were dissolved in 35 cm^3 of 1 mol dm^{-3} sodium hydroxide solution and to the alkaline solution containing DL-NL was added 70 cm^3 of water. By adding 1 mol dm^{-3} HCl to the above solution, the pH was adjusted to 5—6 (isoelectric point). Precipitates obtained by stirring the solution for 10 min at 0 °C were collected by filtration. The similar procedure was performed in the case of DL-NL and L-Try. The precipitates were then dissolved in 50 cm^3 of water and active carbon (ten times of samples by weight) was added to the solution. The mixture was shaken at room temperature for 3 h and carbon powders were filtered off. The filtrate was evaporated to dryness at 40 °C under reduced pressure and then the residure was collected. The samples obtained by this procedure were dried in a desiccator and used (denoted as samples NL-A and NL-B) Other procedure for evaporating water from aqueous solution containing DL-NL was also performed. For example, a solution containing equimolar amounts (0.02 mol) of DL-NL and L-Phe in 350 cm^3 of water was concentrated to 180 cm^3 at 60 °C and the precipitates formed were collected by filtration (sample NL-C). A filtrate was again concentrated to 90 cm^3 at 60 °C and the resulting precipitates were collected by filtration (sample NL-D). Separation of free NL from the adduct was based on the adsorption difference between NL and Phe on active carbon.[6]

Results and Discussion

The DSC method for determining optical purity, which is equal to enantiomeric purity is based on phase diagrams.[7] Since α-amino acids, in general have no melting point and enthalpy of fusion, this method is not applicable to the amino acid samples.

In this study, we assume that crystalline amino acid that is racemic compound shows a solid-solid phase transition and that there is no interaction between DL- and D- or L-isomer in crystalline state. The magnitude of optical purity by thermal method, p_{th}, is defined as

$$p_{th} = \frac{\Delta H_t^{DL} - \Delta H_t^{obs}}{\Delta H_t^{DL}}, \quad (1)$$

where ΔH_t^{DL} and ΔH_t^{obs} are the enthalpy of transition of racemic compound and the observed enthalpy of transition of mixture of DL-and D- or L-isomer in amino acids, respectively. The observed enthalpy of transition of amino acid recovered by optical resolution procedure, ΔH_t^{obs}, is expressed as

$$\Delta H_t^{obs} = (1-y)\Delta H_t^{DL}, \quad (2)$$

where y is enantiomer excess.
Equation 2 can be rewritten as

$$\Delta H_t^{obs} = 2x\,\Delta H_t^{DL} \text{ for } 0 \leqslant x \leqslant 0.5, \quad (3)$$

$$\Delta H_t^{obs} = 2(1-x)\Delta H_t^{DL} \text{ for } 0.5 \leqslant x \leqslant 1.0, \quad (4)$$

where x is mole fraction of D- or L-isomer of the amino acid. The correlation between ΔH_t^{obs} and x is schematically shown in Fig. 1.

In fact there is an example of racemic compound

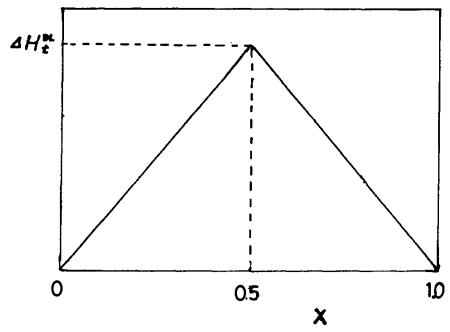

Fig. 1. The correlation between enthalpy of transition, ΔH_t^{obs} and mole fraction of D- or L-isomer, x.

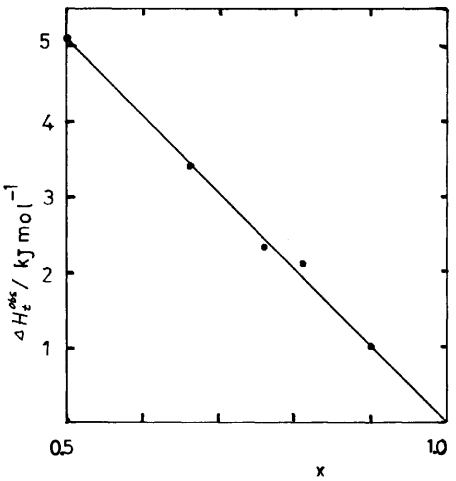

Fig. 2 A plot of enthalpy of transition, ΔH_t^{obs} against mole fraction of D-isomer.

with a solid-solid phase transition.[2,3] The α-form DL-NL is transformed into the γ- form DL-NL at 390 K with the enthalpy of transition of 4.4 kJ mol^{-1} at null heating rate by DSC.[4] To confirm whether Eq. 4 holds in the case of NL, the enthalpy of transition by DSC was determined in the range of mole fraction of D-isomer between 0.5 and 1.0 at a heating rate of 5 K min^{-1}. The results obtained are summarized in Table 1. As is shown in Fig. 2, a plot of ΔH_t^{obs} against mole fraction of D-isomer was found to be linear. We can accordingly calculate the magnitude of optical purity of NL recovered by optical resolution from the enthalpy data obtained for mixtures of known mole fractions without dissolution procedure.

An attempt to resolve aliphatic amino acids by using L-phenylalanine as resolving agent has been introduced by Shiraiwa et al.[5] The results of optical resolution by their method are summarized in Table 2, in which the magnitudes of optical purity by DSC are compared with those by specific rotation. The samples of NL-A and NL-B in Table 2 were recovered by using L-Phe and L-Try as resolving agents, respectively. The samples of NL-C and NL-D were obtained by evaporating water from aqueous solution. The optical purity in Table 2 is the percent optical

Table 1. The Experimental Values of ΔH_t^{obs} at Enantiomer Excess of D-Norleucine by Arbitrary Mixing of DL- and D-Isomer

Enantiomer excess of D-isomer	Mole fraction of D-isomer	Peak temperature	Enthalpy of transition[a]
y	x	T/K	ΔH_t^{obs} /kJ mol^{-1}
0.32	0.66	392.5	3.4
0.52	0.76	392.4	2.3
0.61	0.81	392.4	2.1
0.80	0.90	392.5	1.0
0.00	0.50	392.2	5.1

a) The values of enthalpy of transition at heating rate, 5 K min^{-1}.

Table 2. The Comparison of Optical Purity Values Determined by DSC with Those by Specific Rotation

Sample	Enthalpy of transition ΔH_t^{obs} /kJ mol^{-1}	Optical purity by DSC %	Optical purity by specific rotation[a] %	Configuration[b]
NL-A	4.7±0.0	7.8	8.2	L
NL-B	4.6±0.0	9.8	10	L
NL-C	1.6±0.0	69	84	D
NL-D	3.5±0.1	31	28	D

a) Ratio of $[\alpha]_D^{20}$ (c=0.5, 5 mol dm^{-3} HCl solution). b) Configuration obtained from specific rotation.

purity. As is shown in Table 2, the values of optical purity by DSC agree fairly well with those by specific rotation. Therefore, it is concluded that the method for determining the optical purity based on enthalpy of transition is applicable to the sample of norleucine.

We are grateful to Dr. Kazuko S. Kunihisa of National Chemical Laboratory for Industry for advice in DSC measurements and to Dr. Tadashi Shiraiwa of Kansai University for useful suggestion on optical resolution by adduct formation between aliphatic and aromatic amino acid.

References

1) M. Raban and K. Mislow, "Modern method for the determination of optical purity" in "Topics in Stereochemistry," ed by N. L. Allinger and E. L. Eliel, Wiley-Interscience, New York (1967), Vol. 2, p. 199.

2) A. Grunenberg, D. Bougeard, and B. Schroder, *Thermochim. Acta*, **77**, 59 (1984).

3) M. Matsumoto and K. S. Kunihisa, *Chem. Lett.*, **1984**, 1279.

4) M. Matsumoto, H. Yajima, and T. Handa, *Bull. Chem. Soc. Jpn.*, **59**, 3803 (1986).

5) T. Shiraiwa, Y. Sado, K. Sakaguchi, A. Ikawa, and H. Kurokawa, *Nippon Kagaku Kaishi*, **1985**, 1734.

6) S. M. Partridge, *Biochem. J.*, **44**, 521 (1949).

7) "Enantiomers, Racemates, and Resolutions," ed by J. Jacques, A. Collet, and S. H. Wilen, John Wiley & Sons, New York (1981), p. 151.

[2π+2σ] and [4π+2σ] Type Cycloaddition Reactions of Furan and Benzofurans with Benzocyclopropene

Katsuhiro SAITO,* Hiraku ISHIHARA, and Shinzo KAGABU†
Department of Chemistry, Nagoya Institute of Technology, Gokiso-cho, Showa-ku, Nagoya 466
†Department of Chemistry, Faculty of Education, Gifu University, Yanagido, Gifu 501-11
(Received May 15, 1987)

Synopsis. Reactions of benzocyclopropene with furan and benzofuran afforded [2π+2σ]-type cycloaddition products, where the furans act as 2π-components and benzocyclopropene acts as a 2σ-component. A similar reaction with 1,3-diphenylisobenzofuran gave a [4π+2σ]-type cycloaddition product using the furan as a 4π-component.

It is known that benzocyclopropene (**1**) is a highly strained and reactive species, which is likely to behave as a 6π-donator in [6π+4π]-type cycloaddition reactions,[1] except a reaction with butadiene, where **1** reacts as a 2σ-donator affording a [2π+2σ]-type cycloadduct among many product mixtures.[1b]

While the addition reactions of **1** with various kinds of olefins have been extensively investigated,[1,2] only a few reactions with heterocyclic partners are known. As one part of our research on the cycloaddition reactions of heterocyclic compounds, we investigated cycloaddition reactions of furan derivatives with **1**.[3] Here, the results of these reactions will be reported.

A chloroform solution of furan **2** and an equimolar amount of **1** was allowed to stand at room temperature for 6 days. The separation and purification of the reaction mixture by thin-layer chromatography on silica gel afforded a [2π+2σ]-type cycloadduct **3** in a 39% yield. The reaction of **1** with benzofuran **4**, also gave [2π+2σ]-type cycloadducts **5** in a yield of 25%. On the other hand, the reaction of **1** with 1,3-diphenylisobenzofuran **6** gave a [4π+2σ]-type cycloadduct **7** in a 71% yield.

The structure of **3** was determined on the basis of its spectral, especially ^{1}H NMR spectral properties. The good resemblance of the ^{1}H NMR spectral properties of **3** to those of the analogous compound such as **8** supports the structure of **3**.[4] The orientation of the dihydrofuran moiety in **3** was determined on the basis of the coupling constants in its ^{1}H NMR spectrum as follows. The coupling pattern of the signal of the methine proton H_e shows that the neighbouring protons of H_e are only two methylene protons (H_a and H_b) and a methine proton (H_c). The structure which satisfies the above terms is **3**. Another possible structure such as **9** can not explain the NMR spectral properties. The stereochemistry of **3** was deduced on the basis of the coupling constants in the ^{1}H NMR spectrum as shown in the figure. The structure of **5** was also determined on the basis of its spectral properties, comparing them to those of **3**.

The molecular ion peak in the high-resolution Mass spectrum indicates that **7** is a 1:1 adduct of **1** and **6**. The NMR spectrum shows that **7** is an unsymmetrical compound that has geminal protons. The IR spectrum designates that **7** has no carbonyl or hydroxyl groups, showing that the oxygen atom of **7** is an ether oxygen. These considerations lead to the structure shown in the figure.

The reaction is most likely initiated by the cleavage of a cyclopropene bond in a homolytic fashion to give a diradical intermediate **10**, which attacks the furans to produce the cycloadducts via a diradical inter-

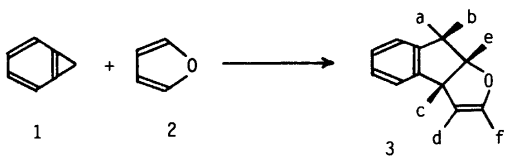

1 2 3

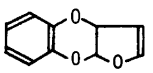

8

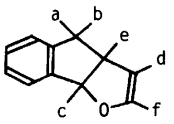

9

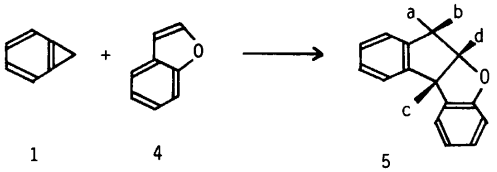

1 4 5

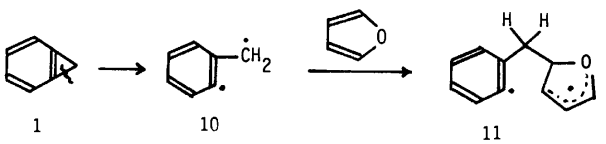

1 10 11

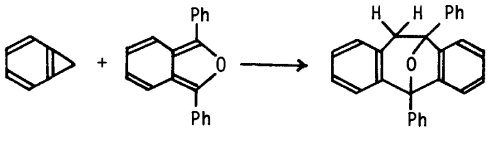

1 6 7

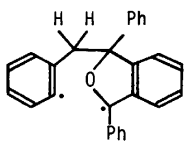

13

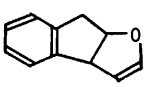

12

mediate **11**.[1b] The stabilization of **11** by the delocalization of the radical electron is considered to determine the orientation of the dihydrofuran moiety in the final cycloadduct **12**. The reaction of **1** with **6** is also considered to proceed via the diradical intermediate **10**, which attacks the 1-position of **6** to produce the benzyl radical-type intermediate **13**. The cyclization of **13** keeping the benzene structure in the isobenzofuran moiety, affords **7**.

The same type of reactions of **1** with pyrrole derivatives such as 1-methyl-, 1-phenyl-, and 1-(methoxycarbonyl)pyrrole resulted in a recovery of the starting materials. The difference between the reactivities of furans and pyrroles are considered to be attributable to the difference in the degree of the aromaticity of these two kinds of compounds. It is known that furans are less aromatic than pyrroles because of a strong electronegativity of oxygen atom comparing to that of nitrogen atom.[5] Thus, it is cocluded that less aromatic compounds, furans, react with **1**; on the other hand, the more aromatic compounds, pyrroles, are electronically too stable to react with **1**.

Experimental

NMR spectra were measured with Varian XL 200 or Hitachi R-20B spectrometers with tetramethylsilane as an internal standard. IR spectra were measured with DS-701G spectrometer. Mass spectra were measured with Hitachi M-52 or JMS-DX300 spectrometers. Wako gel B5F was used for thin-layer chromatography.

Reaction of 1 with 2. A mixture of **1** (90 mg, 1 mmol) and **2** (70 mg, 1 mmol) in chloroform (0.3 ml) was allowed to stand at room temperature for 6 days. The reaction mixture was separated by thin-layer chromatography on silica gel using benzene as a developing solvent to give an oil **3** (65 mg, 39%, R_f=0.70).

3: Found: *m/z* 158.0711. Calcd for $C_{11}H_{10}O$: M, 158.0732. MS *m/z* (rel intensity) 158 (M^+, 87), 129 (100), 83 (87). IR (neat) 3050, 2920, 1615, 1480 cm^{-1}. ^1H NMR ($CDCl_3$) δ=3.16 (dd, H_a), 3.37 (dd, H_b), 4.36 (ddd, H_c), 5.09 (dd, H_d), 5.31 (ddd, H_e), 6.24 (dd, H_f), 7.2 (m, 4H). Coupling constants in Hz: J_{ab}=18, J_{ae}=2, J_{be}=7, J_{cd}=3, J_{ce}=10, J_{cf}=2, J_{df}=3.

Reaction of 1 with 4. A mixture of **1** (50 mg, 0.6 mmol) and **4** (71 mg, 0.6 mmol) in chloroform (0.3 ml) was heated at 50 °C for 40 h. The reaction mixture was separated by thin-layer chromatography on silica gel using petroleum ether (bp 35—60 °C)-chloroform 1:4 as a developing solvent to give an oil **5** (30 mg, 25%, R_f=0.75).

5: Found: *m/z* 208.0873. Calcd for $C_{15}H_{12}O$: M, 208.0888. MS *m/z* (rel intensity) 208 (M^+, 100), 189 (10), 179 (17), 115 (10). IR (neat) 3050, 2920, 1593, 1480 cm^{-1}. ^1H NMR ($CDCl_3$) δ=3.34 (dd, H_a), 3.49 (dd, H_b), 4.82 (d, H_c), 5.61 (ddd, H_d), 6.8—7.6 (m, 8H). Coupling constants in Hz: J_{ab}=18, J_{ad}=2, J_{bd}=6, J_{cd}=9.

Reaction of 1 with 6. A mixture of **1** (45 mg, 0.5 mmol) and **6** (130 mg, 0.5 mmol) in chloroform (0.3 ml) was allowed to stand at room temperature for 7 days. The reaction mixture was separated by thin-layer chromatography on silica gel using petroleum ether (bp 35—60 °C)-benzene 1:4 as a developing solvent to give an oil **7** (120 mg, 71%, R_f=0.70).

7: Found: *m/z* 360.1502. Calcd for $C_{27}H_{20}O$: M, 360.1514. MS *m/z* (rel intensity) 360 (M^+, 1), 120 (2), 83 (100). IR (neat): 3050, 2920, 1593, 1480 cm^{-1}. ^1H NMR ($CDCl_3$) δ=3.17 (d, 1H, J=17 Hz), 3.75 (d, 1H, J=17 Hz), 7.0—7.8 (m, 18H).

References

1) a) E. Vogel, W. Grimme, and H. Gunther, *Angew. Chem.*, **80**, 279 (1968); b) Korte, Ph. D. Thesis, University of Koln, 1968; c) B. Halton, *Chem. Rev.*, **73**, 113 (1973); d) W. E. Billups, *Acc. Chem. Res.*, **11**, 245 (1978); e) H. Kato and S. Toda, *J. Chem. Soc., Chem. Commun.*, **1982**, 510; f) J. C. Martin and J. M. Muchowski, *J. Org. Chem.*, **49**, 1040 (1984).

2) R. Anet and F. A. L. Anet, *J. Am. Chem. Soc.*, **86**, 525 (1964); E. Vogel, W. Grimme, and S. Karte, *Tetrahedron Lett.*, **1965**, 3625; W. E. Billups, A. J. Blakeny, and W. Y. Chow, *J. Chem. Soc., Chem. Commun.*, **1971**, 1461; *idem., Org. Synth.*, **55**, 12 (1976).

3) K. Saito and K. Takahashi, *Heterocycles*, **12**, 263 (1979); K. Saito, S. Iida, and T. Mukai, *ibid.*, **19**, 1197 (1982); K. Saito, H. Kojima, T. Okudaira, and K. Takahashi, *Bull. Chem. Soc. Jpn.*, **56**, 175 (1983); K. Saito, S. Iida, and T. Mukai, *ibid.*, **57**, 3483 (1984); K. Saito and Y. Horie, *Heterocycles*, **24**, 579 (1986); K. Saito, T. Mukai, and S. Iida, *Bull. Chem. Soc. Jpn.*, **59**, 2485 (1986).

4) W. M. Horspool, J. M. Tedder, and Z. U. Din, *J. Chem. Soc. C*, **1969**, 1694.

5) D. S. Sappenfeld and M. Kreevoy, *Tetrahedron*, **19**, 1957 (1963); D. T. Klark, *ibid.*, **24**, 3285, 4689 (1968); G. M. Marino, *J. Heterocycl. Chem.*, **9**, 817 (1972); T. J. Thomas, R. W. Roth, and J. G. Verkade, *J. Am. Chem. Soc.*, **94**, 8854 (1972); R. M. Acheson, "An Introduction to the Heterocyclic Compounds," John Willey and Sons, Inc. (1976), Chap. 3.

Oxidation of Aliphatic Secondary and Benzylic Alcohols to Carbonyl Compounds by Peracetic Acid in the Presence of Sodium Bromide in Acetic Acid

Takashi MORIMOTO,* Masao HIRANO, Hiroyuki ASHIYA, Hidetaka EGASHIRA, and Xiumin ZHUANG
Department of Industrial Chemistry, Faculty of Technology, Tokyo University of Agriculture and Technology, Koganei, Tokyo 184
(Received June 10, 1987)

Synopsis. Alcohols were smoothly oxidized by peracetic acid in the presence of sodium bromide to give the corresponding carbonyl compounds in good yields.

The conversion of hydroxyl groups to the corresponding carbonyl groups is one of the most important methods for synthetic chemistry and many procedures have been developed. Many of them are the oxidation using metallic oxidants in amounts ranging from stoichiometric to large excess. However, these oxidants are environmentally hazardous and rather expensive. Thus, a number of catalytic systems including [$RuCl_2(PPh_3)_3$]-*t*-BuOOH,[1] pyridinium dichromate-$Me_3SiOOSiMe_3$,[2] $R_4N^+Br_4MoO^-$-*t*-BuOOH,[3] 2,4-dimethyl-2,4-pentanediol-CrO_3-peracetic acid,[4] and sodium bromate-hydrogen bromide[5] have recently been reported for this purpose. In this paper we report that aliphatic secondary and benzylic alcohols can be smoothly converted to carbonyl compounds in good yields by peracetic acid in the presence of sodium bromide.

Results and Discussion

The reaction of peracetic acid with alcohols was conducted in acetic acid in the presence of sodium bromide. GLC analysis showed that only carbonyl compound and starting material were involved in the product mixture under suitable conditions. Thus, a small excess of the oxidant was used for the completion of the reaction. The results were summarized in Table 1.

$$\text{CHOH} + \text{AcOOH} \xrightarrow[\text{AcOH}]{\text{NaBr}} \text{C=O} + \text{AcOH} + H_2O$$

Benzylic and aliphatic secondary alcohols (Entries 1—8) were converted smoothly to the corresponding carbonyl compounds in good yields by using 10—20% excess of peracetic acid and 0.5—1 equivalent of sodium bromide. The oxidation of hindered aliphatic secondary alcohols was slow and thus the oxidation of terpenoid alcohols (Entries 9—11) required 1.5 equivalent of sodium bromide as promoter and 50% excess of peracetic acid as an oxidant in order to get good yields of the products. Aliphatic primary alcohols were much slowly oxidized to give aldehydes in poor yields. The oxidation in raised temperature was unsuccessful, perhaps due to the self-decomposition of peracetic acid.

In order to clarify a real active species and reaction path of the present reaction, the independent oxidations of benzyl alcohol with peracetic acid, with bromine and also with the combination of these two reagents were carried out, since peracetic acid is a strong oxidant and bromine, which may be formed during the reaction, is also an oxidant. Peracetic acid, itself, could not oxidize the alcohol to benzaldehyde but converted it to benzyl acetate in the absence of sodium bromide. Indeed bromine itself also oxidized the alcohol, but the reaction was considerably slow and resulted in lower yield of benzaldehyde. The combination of peracetic acid with bromine gave the better results (60—70% yield by GLC analysis) but the

Table 1. The Oxidation of Alcohols by Peracetic Acid-Sodium Bromide in Acetic Acid

Entry No.	Alcohol[a]	AcOOH/Sub. mole ratio	NaBr/Sub. mole ratio	Temp °C	Time h	Yield[b] mol%
1	$PhCH_2OH$	1.1	1.0	60	2	91
2	$PhCH(OH)CH_3$	1.1	0.1	60	2	86
3	$Ph_2CH(OH)$	1.1	0.5	60	2	75
4	2-Heptanol	1.2	0.5	30	1	79
5	2-Octanol	1.1	0.5	30	1	81
6	2-Methylcyclohexanol	1.2	0.7	30	1	89
7	4-*t*-Butylcyclohexanol	1.2	1.0	30	1	88
8	Cyclododecanol	1.2	0.7	40	1	93
9	*l*-Menthol	1.5	1.5	60	2	91
10	Borneol	1.5	1.5	30	2	88
11	Isoborneol	1.5	1.5	30	2	94

a) Ca. 0.5 g of substrates were used in every run. b) Isolated yields.

yield was inferior to those by the combination of peracetic acid and sodium bromide. These results may show that the true oxidant for alcohol is acetyl hypobromite which comes from the reaction of peracetic acid with bromide ion or bromine. Acetyl hypobromite has been suggested to be a reacting species for the bromination[6] of aromatic compounds and bromoacetoxylation[7] of olefins by peracetic acid–bromine or bromide ion. Thus, the acetyl hypobromite might be a real active oxidant.

$$AcOOH + AcOH + NaBr \longrightarrow AcOBr + AcONa + H_2O$$

$$AcOBr + \begin{array}{c}\diagdown\\ CHOH\\ \diagup\end{array} \longrightarrow AcOH + HBr + \begin{array}{c}\diagdown\\ C{=}O\\ \diagup\end{array}$$

$$AcONa + HBr \longrightarrow AcOH + NaBr$$

The present reaction may be a useful process of synthesizing simple ketones from the economical and environmental points of view, since the reagents used are cheap, the yields are good and nothing except water and acetic acid is formed.

Experimental

^{1}H NMR spectra were measured for solutions in CCl_4 on a JEOL model PMX-60 spectrometer. IR spectra were recorded for thin film or KBr disk on a JASCO DS-403G spectrophotometer. GLC was carried out on a Shimadzu GC-6A instrument with a 2-m glass column packed with 5% PEG-20M on Chromosorb WAW-DMCS or on a Shimadzu GC-4C instrument with a 2-m glass column packed with 1.5% Silicone OV-17 on Chromosorb WAW-DMCS, with temperature programming.

All reagents were commercially available and were used without purification. Peracetic acid was prepared from 60% hydrogen peroxide and acetic anhydride[7] and the concentration was determined by the iodometry.

Oxidation Procedures. A typical procedure is as follows. Sodium bromide (ca. 0.5 g), alcohol (0.5 g), and acetic acid (3 ml) were placed in a two naked round-bottomed flask, equipped with a dropping funnel and a condenser, the top of which was connected to the argon-filled balloon. After flashing with argon, peracetic acid (2—3 mol dm^{-3}) was added dropwise to the magnetically stirred mixture for a given period and the stirring was continued for an another hour. The reaction mixture was poured into brine (30 ml) and the product was extracted with ether (15 ml×3). Combined ethereal solution was washed with brine, 10% aq Na_2CO_3, and brine and then dried (Na_2SO_4). After filtration, the ether was removed on a rotary evaporator under a reduced pressure to give colorless to pale-yellow oil or solid, which was purified by flash chromatography (silica GLC and hexane–ethyl acetate). Products were identified by ^{1}H NMR and IR spectra. GLC analyses showed that the purities of products were satisfactory.

References

1) S. Murahashi, K. Ito, T. Naota, and Y. Maeda, *Tetrahedron Lett.*, **22**, 5327 (1981): S. Murahashi, T. Naota, and N. Nakajima, *ibid.*, **26**, 925 (1985).

2) S. Kanemoto, K. Oshima, S. Matsubara, K. Takai, and H. Nozaki, *Tetrahedron Lett.*, **24**, 2185 (1983).

3) Y. Masuyama, M. Takahashi, and Y. Kurusu, *Tetrahedron Lett.*, **25**, 4417 (1984): B. M. Trost and Y. Masuyama, *ibid.*, **25**, 173 (1984).

4) E. J. Corey, E-P. Barrett, and P. A. Magriotis, *Tetrahedron Lett.*, **26**, 5855 (1985).

5) S. Kajigaeshi, T. Nakagawa, N. Nagasaki, H. Yamasaki, and S. Fujisaka, *Bull. Chem. Soc. Jpn.*, **59**, 747 (1986).

6) Y. Ogata and K. Aoki, *J. Org. Chem.*, **31**, 1625 (1966).

7) Y. Ogata and K. Aoki, *J. Org. Chem.*, **31**, 4181 (1966).

8) D. Swern "Organic Reactions," John Wiley & Sons, Inc. (1953), Vol. 7, p. 378.

Modified Solubility Parameter as an Index to Correlate the Solubility in Supercritical Fluids

Yutaka IKUSHIMA,* Tomio GOTO, and Masahiko ARAI†
Government Industrial Research Institute, Tohoku, Nigatake 4-Chome, Sendai 983
†Chemical Research Institute of Non-Aqueous Solutions, Tohoku University, Katahira, Sendai 980
(Received April 1, 1987)

Synopsis. The conventional solubility parameter was modified so that it could be applied to supercritical fluids. It was found that the parameters could correlate the experimental solubility data of some hydrophobic solutes in carbon dioxide, ethylene, and carbon dioxide-entrainer systems.

Supercritical fluids have the capacity to dissolve nonvolatile and thermolabile materials without denaturalization by several orders of magnitude greater than gases in the standard state.[1-4] However, since the dissolving power is widely variable from one supercritical solvent to another, a supercritical fluid (SCF) method has been a considerable trial-and-error process and, consequently, has required much expenses and time. With the addition of a proper entrainer to supercritical solvents, the extraction efficiency can be enhanced compared to SCF alone in many extraction processes;[5-9] particular attention has been drawn to the effect of entrainer. However, the solubility significantly varies with the entrainer. Therefore, recently a parameter for representing the effect of the entrainer has been desired. The solubility parameter concept[10] has widely been used for many years for interpreting and predicting the thermodynamic behavior of a solution. In recent years, the SCF extraction method has been remarkably noted; for supercritical fluids a similar solubility parameter is expected to be presented.[11]

The purpose of this paper is to extend the conventional solubility parameter concept to SCF with an assumption of random mixing of the spieces present in the mixture and to examine its usefulness in selecting a suitable supercritical solvent and entrainer in the SCF extraction process.

Solubility Parameter for Supercritical State. The basic assumption in the solubility parameter concept is that there is a correlattion between the cohesive energy and mutual solubility. The definition of the solubility parameter δ is in terms of the square root of the molecular cohesive energy, $(-E)$, per unit volume.

$$\delta = (-E/V)^{1/2} \tag{1}$$

$-E$ is the energy of a liquid relative to its ideal vapor at the same temperature. It can, therefore, be considered that $-E$ consists of the energy required to vaporize the liquid to its saturated vapor and, then, to isothermally expand it to infinite volume.

$$-E = \Delta U_v + \int_{v=v}^{v=\infty} (\partial U/\partial V)_T dV, \tag{2}$$

where ΔU_v is the energy to vaparize liquid to saturated vapor. At the critical temperature, the first term in Eq. 2 is zero, and $-E$ can be represented as

$$-E = \int_{v=v}^{v=\infty} (\partial U/\partial V)_T dV. \tag{3}$$

Equation 3 can be modified to express δ more conveniently:

$$-E = (H^*-H) - RT(1-z) = \Delta H - RT(1-z) \tag{4}$$

and

$$\delta = [(\Delta H - RT(1-z))/V]^{1/2}, \tag{5}$$

where H^*, H, z, and R are the standard enthalpy, molar enthalpy, compressibility factor, and gas constant, respectively. ΔH is represented from the thermodynamic relations as follows:

$$\Delta H = RT_c T_r^2 \int_0^{P_r} (\partial z/\partial T_r)_{P_r} dP_r/P_r. \tag{6}$$

ΔH can be also determined using:

$$\Delta E/T_c = \Delta H/T_c - (1-z)RT_r, \tag{7}$$

where T_c, T_r, and P_r are the critical temperature, reduced temperature, and reduced pressure, respectively. Here, the function $\Delta E/T_c$ is available in the literature as functions of T_r and P_r.[12] In addition, to make δ applicable to any solvent, the solubility parameter is expressed in terms of reduced parameters. Thus,

$$\delta_r = [P_r/z(T_r \int_0^{P_r} (\partial z/\partial T_r)_{P_r} dP_r/P_r - 1 + z)]^{1/2}, \tag{8}$$

where δ_r is the modified solubility parameter, $(\delta/P_c^{1/2})$.

Application of Solubility Parameter. Next, we turn to the application of δ_r and examine how δ_r values fit experimental data well. Kurnik[13] has

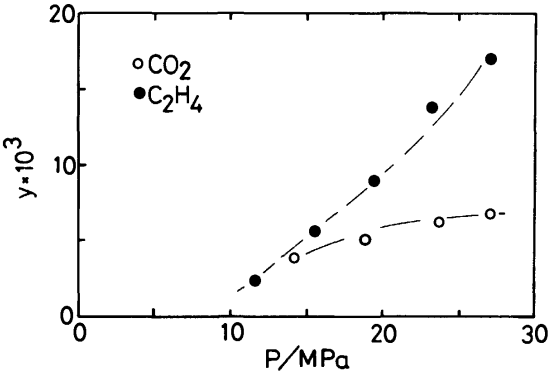

Fig. 1. Experimental solubilities for 2,6-dimethylnaphthalene in supercritical carbon dioxide and ethylene at 318 K.[13]

studied the solubility of 2,6-dimethylnaphthalene in different kinds of supercritical fluids at the same temperature. Figure 1 shows its solubility in supercritical carbon dioxide and ethylene at pressures of 11.6—27.0 MPa and 318 K. This reveals a great difference between carbon dioxide and ethylene in the power of dissolving the solute. The solubility curves for carbon dioxide and ethylene are separated over the range of the pressures examined. The solubility for ethylene increases more rapidly with the pressure than does that for carbon dioxide. These two curves scarcely imply a similarlity to each other.

Figure 2 shows the same solubility data using the modified solubility parameter (δ_r). The data for these two solvents fall on a single line. We have obtained a good correlation between the experimental data and the δ_r. The δ_r was found to be a good parameter for the solubility of 2,6-dimethylnaphthalene.

Recently, higher fatty acids have been noted in terms of their medicinal purposes and their utility as precursors of prostaglandins.[14,15] Therefore, we have examined the extration efficiency of *dl*-α-tocopherol,[16] triolein,[7,8] mixtures of triglycerides,[7,8] higher fatty acid methyl esters[17] on the addition of entrainers to the CO_2. Further, Sako et al. reported[9] the extraction of lipid, which contained γ-linolenic acid(γ-C_{18-3}), from fungi using hexane as an entrainer. Table 1 indicates the enhancement factors in the solubility on the extraction of *dl*-α-tocopherol, triolein, lipid in fungi, mixtures of tristearin and triolein, and stearic-(C_{18-0}), oleic-(C_{18-1}), linoleic-(C_{18-2}), and linolenic (C_{18-3}) acid methyl esters with the addition of several entrainers to the CO_2 at 19.6 MPa. The enhancement factor α is definited as

$$\alpha = C_2/C_2^*, \tag{9}$$

where C_2 and C_2^* are the solubility on the extraction with and without entrainer, respectively. The concentrations of each entrainer in CO_2 are 4 or 10 per cent by weight. As entrainers, ethyl acetate, ethanol, aceone, ether, dichloromethane, and hexane were sued. On the extraction of lipid such as glycerides and fatty acid methyl esters with supercritical carbon dioxide (SC-CO_2), the addition of ethanol and ether decrease the extraction efficiency, but ethyl acetate, hexane, and dichloromethane enhance it.

We think that these effects of the entrainer could be due to a difference in the cohesive energy before and after mixing the CO_2 with the entrainer. The difference is given as energy of dissolution, ΔE_M, using the solubility parameter:

$$\Delta E_M = n_1V_1n_2V_2(\delta_1-\delta_2)^2/(n_1V_1+n_2V), \tag{10}$$

where subscripts of 1 and 2 indicate the solvent and entrainer, respectively, and n is the amount of them fed into the extractor. Furthermore, we modify ΔE_M to make it applicable to any entrainer in the following way. Thus,

$$\Delta E_M' = [n_1V_1n_2V_2/(n_1V_1+n_2V_2)][(\delta_1-\delta_2)^2/(P_{1c}P_{2c})^{1/2}]. \tag{11}$$

The energy per mole of an entrainer is given as $\Delta E_2'$.

$$(\partial\Delta E_M'/\partial n_2) = \Delta E_2' = V_2\phi_1^2(\delta_1-\delta_2)^2/(P_{1c}P_{2c})^{1/2}, \tag{12}$$

where ϕ_1 stands for the volume fraction of solvent. The concentration of an entrainer in the CO_2 is low, and $\phi_1 \simeq 1$.

We use the $\Delta E_2'$ as a parameter for expressing the effect of the entrainer. Figure 3 shows the relation between the enhancement factor α and the $\Delta E_2'$. The values of the α and $\Delta E_2'$ are indicated in Tables 1 and 2, respectively. The $\Delta E_2'$ of these entrainers is found to conveniently express the solubility data under conditions examined. The less $\Delta E_2'$ an entrainer has, the more it can enhance the extraction efficiency. Namely, when the solubility parameter of an entrainer is closed to that of the CO_2, the $\Delta E_2'$ is decreased and the solubility is increased.

On the extraction of lipid such as glycerides or fatty acids with SC-CO_2 under constant experimental

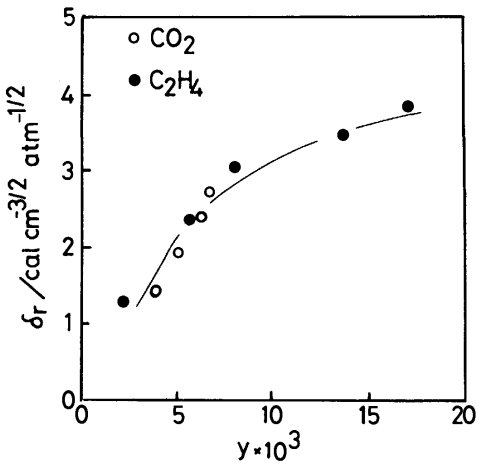

Fig. 2. Correlation of modified solubility parameters of supercritical carbon dioxide and ethylene with solubility of 2,6-dimethylnaphthalene.

Table 1. Effects of Entrainers on Extraction Efficiency

Solute	Enhancement factor α					
	$CH_3COOC_2H_5$	CH_2Cl_2	$(CH_3)_2CO$	C_2H_5OH	$C_2H_5OC_2H_5$	C_6H_{14}
Triolein[7,8]	1.83	1.43	0.75	0.54	0.71	
Tristearin and triolein[7,8]	2.17					
Lipid containing γ-C_{18-3}[9]						4.0, 2.3
C_{18-0}, C_{18-1}, C_{18-2}, and C_{18-3}[17]	1.85	1.40	1.06			
dl-α-Tocopherol[16]	1.89	1.38				

Table 2. Values of $\Delta E_2'$

	$\Delta E_2'$/cal mol^{-1} atm^{-1}
C_6H_{14}	1.6
$CH_3COOC_2H_5$	10.5
CH_2Cl_2	16.9
$(CH_3)_2CO$	20.1
C_2H_5OH	30.1
$C_2H_5OC_2H_5$	3.7

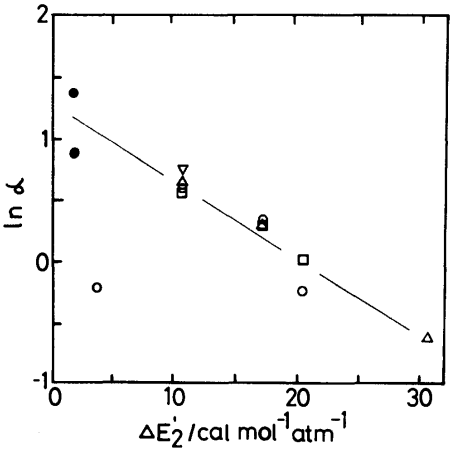

Fig. 3. Relationship between $\Delta E_2'$ and solubilities of lipids and *dl*-α-tocopherol with carbon dioxide-entrainer.[7-9,16,17] (□): A mixture of C_{18-0}, C_{18-1}, C_{18-2}, and C_{18-3} acid methyl esters, (●): lipid containing γ-C_{18-3} acid, (○): triolein, (▽): a mixture of tristearin and triolein, (△): *dl*-α-tocopherol.

conditions, if only we calculate the $\Delta E_2'$ value of the entrainer used, we can determine how much entrainer can enhance the extraction efficiency compared to the CO_2 alone. Furthermore, as shown in Table 1, in such a case that *dl*-α-tocopherol is extracted with the CO_2-ethyl acetate or CO_2-dichloromethane, the extraction efficiency is increased similarly to that of the lipid; a plot of the α against the $\Delta E_2'$ of ethyl acetate or dichloromethane is in agreement with that of the lipid. Therefore, parameter $\Delta E_2'$ might be applicable to the solubility data of not only the lipid but, also other hydrophobic materials. However, at present, the number of the solubility data using entrainers is few; we do not have any distinct evidence whether $\Delta E_2'$ could represent the solubility data using other materials as solutes or in the ranges of other pressures and temperatures. Further, on using ether as an entrainer for the extraction of triolein (Fig. 3), the $\Delta E_2'$ of ether can not represent the solubility data well. A possible reason for this is that there may be some association between ethyl ether and methyl ester molecules, causing the random-mixing assumption to be invalid in this case. We are further examining the adaptability of the parameters for the other extraction systems.

References

1) C. A. Irani and E. W. Funk, "Recent Development in Separation Science," CRC Press, Cleaveland (1977), ed by N. N. Li, Vol. 3, Part A, p. 171.
2) L. G. Randall, *Sep, Sci, Tech.*, **17**, 1 (1982).
3) B. Subrananian and M. A. Hchugh, *Ind. Eng. Process Des, Dev.*, **25**, 1 (1986).
4) Y. Ikushima, N. Saito, K. Hatakeda, S. Ito, T. Asano, and T. Goto, *Bull. Chem. Soc. Jpn.*, **59**, 3709 (1986).
5) G. Brunner, *Fluid Phase Equilibria*, **10**, 289 (1983).
6) G. Brunner, S. Peter, B. Retzlaff, and R. Riha, High Pressure Scienec and Technolgy, 6th AIRART Conf., **1**, 565 (1979).
7) Y. Ikushima, N. Saito, K. Hatakeda, S. Ito, T. Asano, and T. Goto, *Chem. Lett.*, **1985**, 1789.
8) Y. Ikushima, N. Saito, K. Hatakeda, S. Ito, T. Asano, and T. Goto, Proc. of World Congress the 3 rd of Chem. Eng., **2**, 766 (1986).
9) T. Sako, T. Yokochi, T. Sugeta, N. Nakazawa, T. Hakuta, O. Suzuki, S. Sato, and H. Yoshitome, *Yukagaku*, **35**, 463 (1986).
10) J. H. Hildebrand, J. M. Prausnitz, and R. L. Scott, "Regular and Related Solutions," Van Nostrand-Reinhold, Princeton, N. J., (1979).
11) S. R. Allada, *Ind. End. Chem. Process Des. Dev.*, **23**, 344 (1984).
12) O. H. Hougen, K. M. Watoson, and R. A. Ragatz, "Chemical Process Principles," 2nd ed, Part 2, Thermodynamics, Asia Publishing Home, Bombay, India (1960).
13) R. T. Kurnik, J. H. Samuel, and R. C. Reid, *J. Chem. Eng. Data*, **26**, 47 (1981).
14) T. O. Lossonczy, *Am. J. Clin. Nutr.*, **31**, 1340 (1978).
15) T. A. B, Sanders and K. M. Younger, *Br. J. Nutr.*, **45**, 613 (1981).
16) To be submitted.
17) To be submitted.

The Influence of Ureas on the Phase-Transition Behavior of the Dipalmitoylphosphatidylcholine Vesicle Membrane

Tohru INOUE,* Kenji MIYAKAWA,† and Ryosuke SHIMOZAWA
Department of Chemistry, Faculty of Science, Fukuoka University, Nanakuma, Jonan-ku, Fukuoka 814-01
†Department of Applied Physics, Faculty of Science, Fukuoka University, Nanakuma, Jonan-ku, Fukuoka 814-01
(Received April 13, 1987)

Synopsis. The gel-to-liquid-crystalline phase transition of the dipalmitoylphosphatidylcholine vesicle membrane was observed in the presence of urea, ethylurea, and butylurea by monitoring the scattered light intensity of the vesicle suspension. Urea showed no significant effect on either the transition temperature, T_m, or the transition width, W, whereas ethylurea and butylurea depressed T_m without affecting W.

In a previous work,[1] we studied the gel-to-liquid-crystalline phase transition of the dipalmitoylphosphatidylcholine (DPPC) vesicle membrane in the presence of surfactants with several types of head group and different hydrocarbon chain lengths. It was found that all the surfactants examined induced the depression of the phase-transition temperature, depending on the surfactant concentration. This depression of the transition temperature was interpreted in terms of the partitioning of the surfactant molecule into the lipid membrane.

In addition to the transition temperature, the transition width was also affected by the addition of surfactants. It was observed that surfactants other than the series of alkanoyl-*N*-methylglucamides (MEGA)[††] increased the transition width and that the extent of the widening depended on the type of head group, but not on the hydrocarbon-chain length in a homologous series of surfactants.

The transition width is a measure of the cooperativity of the phase transition. The widening of the transition width induced by the addition of surfactants was interpreted as resulting from the fact that the surfactant molecules incorporated in the membrane tend to disrupt the interaction between lipid molecules responsible for the cooperativity. The origin of the cooperativity in the phase transition of the lipid bilayer has been attributed to the excluded volume interaction between hydrocarbon chains of lipid molecules.[2] However, the strong dependence of the transition width on the type of hydrophilic group of surfactants added suggests that the inter-head group interaction between lipid molecules also contributes to the cooperativity. Along the lines of this interpretation, it is of interest that MEGA's retain the transition width unaltered; i.e., MEGA's do not perturb the cooperativity. This feature may be attributed not to the electrical neutrality, but to the unique structure of the hydrophilic head group of these surfactants, because hexaethylene glycol monododecyl ether (nonionic surfactant),[1] 1-alkanols,[3,4] and uncharged anesthetic molecules[5,6] also exhibit a broadening effect on the phase transition. The hydrophilic group of MEGA contains both hydrogen-bond-donating and -accepting groups, which are lacking in other additives affecting the transition width. This led to the speculation that the hydrogen bond may play some role in the interaction associated with the cooperativity of the transition.

In order to test the above hypothesis, we have now studied the effects of urea and alkylurea on the phase-transition behavior of the DPPC vesicle membrane. These compounds are typical protein denaturants and have a strong tendency to form hydrogen bonds.

Experimental

The synthetic dipalmitoylphosphatidylcholine (DPPC) was obtained from Sigma. The ultrapure urea and reagent-grade ethylurea (Wako Pure Chemical Industries) and butylurea (99%, Aldrich) were used without further purification. The water was deionized and doubly distilled, once from an alkaline potassium permanganate solution.

The vesicle suspension of DPPC in water was prepared by sonication in the cup-horn of a Branson Sonifier, Model 185, at 45 °C (above the gel-to-liquid-crystalline phase-transition temperature) for about 30 min. The size of the vesicles thus prepared was estimated from the quasielastic light-scattering measurements to be about 160 nm in diameter; considering the size and the phase-transition pattern, these vesicles may be regarded as multilamellar. The sample suspension was prepared by mixing the stock DPPC suspension with the additive solution to give the desired additive concentration and by then sonicating it again at 45 °C for about 5 min. The DPPC concentration was kept at about 5×10^{-4} M[†††] throughout the experiments.

The gel-to-liquid-crystalline phase transition of the DPPC vesicle membrane was followed by means of the scattered light intensity. The details of the procedure were described elsewhere.[1] The measurements were repeated at least three times with a given sample; a good reproducibility was obtained for the transition temperature and the transition width.

Results and Discussion

The transition temperature, T_m, and the transition width, W, of the gel-to-liquid-crystalline phase transition of the DPPC vesicle membrane were measured as functions of the additive concentration. The transition temperature was expressed in terms of

†† 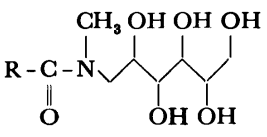

††† 1 M=1 mol dm^{-3}.

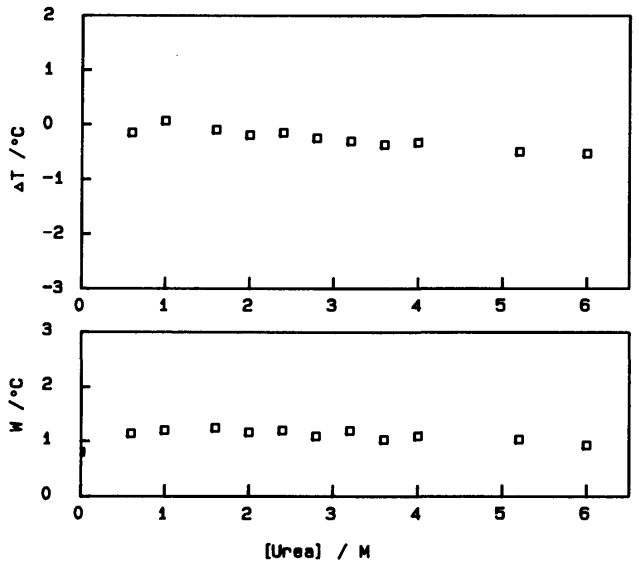

Fig. 1. Effect of urea on the transition temperature, ΔT, and transition width, W, of the gel to liquid-crystalline phase transition of DPPC vesicle membrane. $\Delta T=T_m-T_{m,0}$ where T_m and $T_{m,0}$ are the transition temperatures with and without additives, respectively.

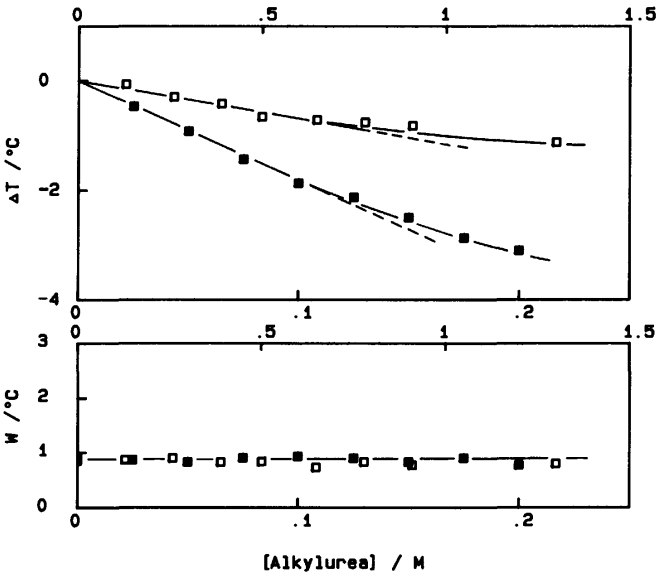

Fig. 2. Effect of alkylureas on ΔT and W of the gel to liquid-crystalline phase transition of DPPC vesicle membrane. □; ethylurea (upper scale) and ■; butylurea (lower scale).

the difference between $T_{m,0}$ (without additives) and T_m (with additives); i.e., $\Delta T=T_m-T_{m,0}$. The results obtained with urea are shown in Fig. 1. Neither T_m nor W is significantly affected by the presence of urea over a wide range of concentrations up to 6 M, although a slight decrease in T_m and a slight increase in W are seen. It is well-known that T_m is generally depressed by the dissolution of small molecular additives in the membrane as a result of an effect analogous to the freezing-point depression. The unaltered T_m suggests that urea is not incorporated into the lipid membrane.

It is believed that urea induces the breakdown of the water structure because of its strong tendency to form hydrogen bonds. Hammes and Schimmel[7] have demonstrated, on the basis of the ultrasonic absorption data in an aqueous urea solution, that the bulk water structure is broken down continuously with an increase in the urea concentration. The almost constant T_m and W values observed in DPPC-urea system indicate that the nature of the vesicle membrane is insensitive to the structure of bulk water with regard to the gel-to-liquid-crystalline phase transition.

The effects of ethylurea and butylurea on the phase-transition behavior are shown in Fig. 2. ΔT decreases linearly with an increase in the concentrations of the additives with the deviation from the linearity in the high-concentration region. On the other hand, W is unchanged by the presence of the additives. This behavior is just the same as that observed in studying the effects of the MEGA-series surfactants.[1]

Previously,[1] we have studied the effects of various surfactant molecules on the phase-transition behavior of the DPPC vesicle membrane; it was found that the transition width was dependent on the type of head group rather than on the hydrocarbon-chain length of the added surfactant. On the basis of this observation, and taking into account the fact that the head groups of surfactants may be located between head groups of DPPC when incorporated in the membrane, it was suggested that, in addition to the excluded volume interaction between hydrocarbon chains,[2] some other interaction between lipid head groups may participate in the cooperativity of the transition. MEGA series surfactants (Ref. 1) and alkylurea (this work) do not affect the transition width (or perturb the cooperativity). The common feature of both types of additives is that the hydrophilic group has a hydrogen-bond-donating group and -accepting group, which is lacking in other types of additives broadening the transition width (or weakening the cooperativity). If we assume that lipid head groups are connected throughout the membrane by the intermolecular hydrogen-bond-donating-accepting system, and that this system is responsible for the cooperativity of the transition, then it is plausible that the connection is broken and, hence, the cooperativity is weakened by introducing additives other than MEGA's or alkylureas. MEGA's and alkylureas may retain the hydrogen-bond system because of their hydrogen-bond-donating and -accepting nature. This may imply that the interaction between lipid head groups in the membrane is not disturbed by the presence of these additives and that, hence, the cooperativity is unaffected by the addition. A hydrogen bond associated with phosphatidylcholine has been reported recently,[8] where it was shown that hydrogen-bonding long-chain compounds form 2:1 complexes with DPPC when both hydrogen-bond-donating and -accepting groups are present.

The direct hydrogen bond between lipid head

groups is unlikely, considering the structure of phosphatidylcholine. It may be speculated that the hydrogen-bond interaction is mediated by water molecules present at the membrane surface. Indeed, it is regarded that the lipid head group in the bilayer dispersed in an aqueous media is fairly strongly hydrated:[9,10] 10—20 water molecules per lecithin molecule.

This work was supported in part by funds from the Central Research Institute of Fukuoka University.

References

1) T. Inoue, K. Miyakawa, and R. Shimozawa, *Chem. Phys. Lipids*, **42**, 261 (1986).
2) J. F. Nagle, *Ann. Rev. Phys. Chem.*, **31**, 157 (1980).
3) A. G. Lee, *Biochemistry*, **15**, 2448 (1976).
4) M. J. Pringle and K. W. Miller, *Biochemistry*, **18**, 3314 (1979).
5) D. M. Mountcastle, R. L. Biltonen, and M. J. Halsey, *Proc. Natl. Acad. Sci. U.S.A.*, **75**, 4906 (1978).
6) A. G. Macdonald, *Biochim. Biophys. Acta*, **507**, 26 (1978).
7) G. G. Hammes and P. R. Schimmel, *J. Am. Chem. Soc.*, **89**, 442 (1967).
8) J. M. Boggs, G. Rangaraj, and K. M. Koshy, *Chem. Phys. Lipids*, **40**, 23 (1986).
9) P. L. Yeagle, *Acc. Chem. Res.*, **11**, 321 (1978).
10) J. N. Israelachvili, S. Marcelja, and R. G. Horn, *Q. Rev. Biophys.*, **13**, 121 (1980).

Surface Tensions of Molten Binary $PrCl_3$-NaCl, $PrCl_3$-KCl, and $PrCl_3$-$CaCl_2$ Systems

Kazuo IGARASHI* and Junichi MOCHINAGA
Department of Synthetic Chemistry, Faculty of Engineering, Chiba University, Chiba-shi, Chiba 260
(Received April 23, 1987)

Synopsis. The surface tensions of molten binary $PrCl_3$-NaCl, $PrCl_3$-KCl, and $PrCl_3$-$CaCl_2$ systems were measured by a maximum bubble pressure method, and the results were expressed as linear functions of the temperature. The isotherms of surface tension of the $PrCl_3$-MCl (M=Na and K) systems had minimum; however, such behavior was not observed in the isotherm of the $PrCl_3$-$CaCl_2$ system.

An investigation of the surface tension of molten salts is of interest in understanding the characteristics of the melts. The surface tensions of some molten binary RCl_3-MCl (M=alkali metal) mixtures containing rare earth chlorides RCl_3 have been measured by Smirnov and Stepanov,[1] Kurmaev et al.,[2] and Igarashi et al.,[3] but those of molten binary systems containing $PrCl_3$ have not yet been reported. We have already measured the densities,[4] refractive indexes,[5] and electrical conductivities[6] of molten $PrCl_3$-alkali and -alkaline earth chloride mixtures in order to elucidate the physical properties of charge-asymmetric melts. In the present study the surface tensions of molten binary $PrCl_3$-NaCl, $PrCl_3$-KCl, and $PrCl_3$-$CaCl_2$ mixtures were measured.

Experimental

Chemicals. $PrCl_3$ was prepared and purified in the same way as that previously reported.[5] Impurities in the purified $PrCl_3$ were analyzed, their contents being less than 100 ppm.[6] The chemicals NaCl, KCl, and $CaCl_2$ were of analytical reagent grade, and dried with conventional techniques.[7] The prepared mole ratios of mixtures were checked by chelate titration.

Measurement Procedure. In the present study the maximum bubble pressure method was applied for determining the surface tension of melts because of the precision of the measurement at the elevated temperature. As working gas argon was used, which was purified by passing through chemical traps filled with molecular sieves 4A and titanium sponges at 900 °C to remove possible H_2O, N_2, and O_2 contaminations. A manometer filled with *n*-butyl phthalate colored red by a dyestuff was used to measure the pressure of the working gas bubble, which was kept at 30.4±0.1 °C by a circulation of thermostatted water. The temperature of a furnace was raised above the liquidus temperature of the sample according to the phase diagrams[8,9] and kept constant. The temperature of the melts was maintained within ±1 °C with a temperature controller, and measured with a C.A. thermocouple sheathed with a fused silica tube. Pt-10%Rh alloy capillary was used for a creation of bubble. The accurate inside diameter of the capillary tip was determined by the surface tension of distilled water at room temperature. The diameter of the capillary at elevated temperature was corrected by use of the coefficient of thermal expansion for the alloy.[10] The surface tensions of the melts were calculated using Schrödinger's equation[11] giving the relation between bubble pressure and surface tension.

Results and Discussion

The surface tensions of molten pure NaCl, KCl, and $CaCl_2$ obtained were compared with the values recommended by Janz et al.[12,13] Our results yield smaller values than the recommended ones, but the departures are within 1%. There are no data on the surface tension of molten $PrCl_3$ except our data.[3]

The surface tensions of these binary systems in the liquid state were represented as linear functions of temperature, $\gamma=a-bt$, (t/°C). The parameters a and b obtained by the method of least squares are summarized in Table 1. The isotherms of surface tension for the molten $PrCl_3$-NaCl, $PrCl_3$-KCl, and $PrCl_3$-$CaCl_2$ systems at 850, 900, and 950 °C are shown in Figs. 1, 2, and 3, respectively. The isotherm at each temperature of the $PrCl_3$-NaCl system had a minimum at about 60 mol% $PrCl_3$. The minimum was also observed in the isotherm of the $PrCl_3$-KCl system, but the composition in the minimum was recognized to shift to low concentration of $PrCl_3$, i.e., about 30 mol% $PrCl_3$. On the other hand, as can be seen in Fig. 3, the isotherms of the $PrCl_3$-$CaCl_2$ system showed quite different behavior, i.e., the surface tension decreased curvilinearly with a increase of

Table 1. Surface Tensions of Molten Binary $PrCl_3$-NaCl, $PrCl_3$-KCl, and $PrCl_3$-$CaCl_2$ Systems

	$\gamma=a-bt$	γ/10^{-3} N m^{-1}, t/°C			
System	$PrCl_3$ mol%	a	$b\times10^{-2}$	σ	Temp range/°C
$PrCl_3$-NaCl	0.0	173.07	7.47	0.18	830—950
	29.0	149.35	5.58	0.23	820—929
	43.1	164.29	7.47	0.06	890—930
	57.1	151.79	6.25	0.19	878—940
	71.0	153.90	6.40	0.11	815—925
	86.2	158.90	6.74	0.09	875—910
	100.0	135.96	3.73	0.03	830—926
$PrCl_3$-KCl	0.0	157.07	7.52	0.23	854—936
	20.0	147.93	6.69	0.27	818—939
	43.1	139.77	5.59	0.26	820—940
	57.1	134.59	4.82	0.10	842—942
	70.9	131.22	4.04	0.10	820—949
	86.0	130.67	3.70	0.19	881—952
$PrCl_3$-$CaCl_2$	0.0	178.18	3.95	0.29	800—946
	20.0	193.58	6.99	0.23	880—930
	29.9	171.07	5.21	0.24	850—940
	43.0	180.39	6.63	0.08	865—930
	55.6	163.41	5.55	0.22	870—940
	71.0	141.94	3.94	0.33	870—940
	86.0	138.03	3.87	0.10	840—940

σ is the standard error of estimate in 10^{-3} N m^{-1}.

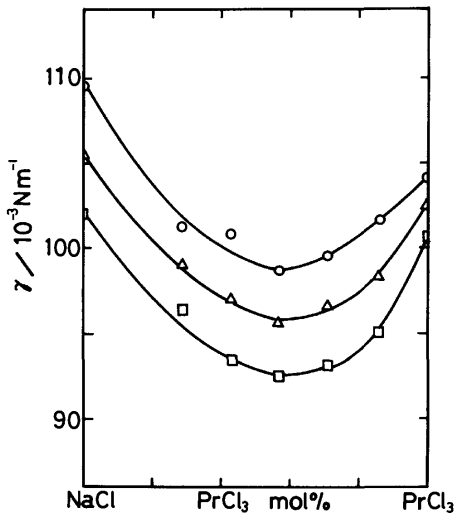

Fig. 1. Isotherms of surface tension of molten $PrCl_3$–NaCl system at 850(○), 900(△), and 950(□)°C.

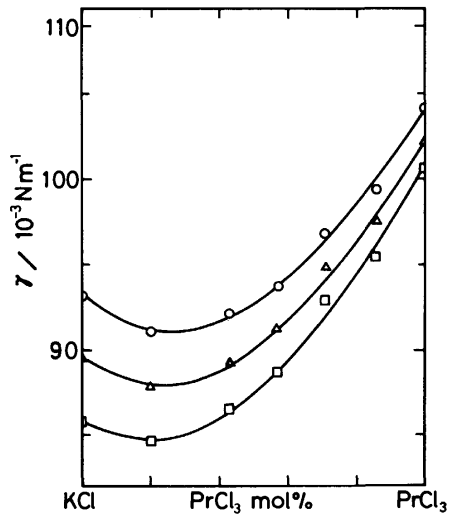

Fig. 2. Isotherms of surface tension of molten $PrCl_3$–KCl system at 850(○), 900(△), and 950(□)°C.

$PrCl_3$ concentration without the minimum. We have measured the surface tensions of molten $LaCl_3$–MCl (M=Na[14] and K[15]) and –$CaCl_2$[14] systems. A similar behavior to the isotherms of surface tension of the $PrCl_3$ systems observed in this work has also been found in the corresponding three $LaCl_3$ mixtures. There are no data available on the structure of molten chloride mixtures containing $PrCl_3$. Fortunately, the structure of molten $LaCl_3$–MCl(M=Na[16] and K[16–18]) and –$CaCl_2$[16] systems has been investigated by Raman spectroscopy. The ionic radius of Pr^{3+} ion is 0.099 nm, which is almost equal to that of La^{3+} ion, viz., 0.1032 nm.[19] From the similarity of the density in valence and the very small difference in ionic radii, 0.004 nm, the structures of the molten $PrCl_3$ systems are expected to be extremely close to those of the corresponding molten $LaCl_3$ systems. In the alkali chloride-rich $PrCl_3$–NaCl and $PrCl_3$–KCl melts, a $PrCl_6^{3-}$ octahedron is thought to be a predominant

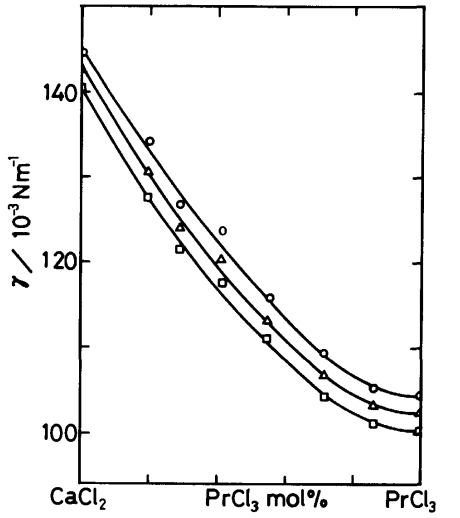

Fig. 3. Isotherms of surface tension of molten $PrCl_3$–$CaCl_2$ system at 850(○), 900(△), and 950(□)°C.

configuration since a similar species is found in the alkali chloride-rich $LaCl_3$–NaCl and $LaCl_3$–KCl melts.[16–18] The complex behavior of the isotherms of the surface tension in both systems seems to be due to such complex species formed in the melts. It has been reported that there exists little such octahedral complex species in the $LaCl_3$–$CaCl_2$ system.[16] The fact implies that the $PrCl_3$–$CaCl_2$ system does not deviate significantly from a cation random mixture. A simple composition change of the surface tension in this system seems to be attributable to such mixing of the melt.

The authors would like to express their sincere gratitude to Mr. Yasuo Saito for assistance in measuring the surface tensions.

References

1) M. V. Smirnov and V. P. Stepanov, *Tr, Inst. Elektrokhim., Akad. Nauk SSSR, Ural Filial*, **12**, 3 (1969); M. V. Smirnov and V. P. Stepanov, *ibid.*, **12**, 9 (1969); M. V. Smirnov and V. P. Stepanov, *ibid.*, **14**, 58 (1970); V. P. Stepanov and M. V. Smirnov, *ibid.*, **14**, 62 (1970).

2) R. Kh. Kurmaev, L. A. Kupriyanova, N. A. Maltsev, and V. A. Krokhim, *Izv. Vyssh. Ucheb. Zaved., Tsvet. Met.*, **17**, 28 (1974).

3) K. Igarashi, J. Mochinaga, and S. Ueda, *Bull. Chem. Soc. Jpn.*, **51**, 1551 (1978).

4) J. Mochinaga and K. Igarashi, *Bull. Chem. Soc. Jpn.*, **48**, 713 (1975).

5) Y. Iwadate, K. Kikuchi, K. Igarashi, and J. Mochinaga, *Z. Naturforsch.*, **37a**, 1284 (1982).

6) Y. Iwadate, K. Igarashi, J. Mochinaga, and T. Adachi, *J. Electrochem. Soc.*, **133**, 1162 (1986).

7) K. Igarashi, Y. Iwadate, H. Ohno, and J. Mochinaga, *Z. Naturforsch.*, **40a**, 520 (1985).

8) T. Hattroi, H. Ikezawa. R. Hirano, and J. Mochinaga, *Nippon Kagaku Kaishi*, **1982**, 952.

9) J. Kutscher and A. Schneider, *Z. Anorg. Allg. Chem.*, **408**, 135 (1974).

10) B. Barter and A. S. Darling, *Platinum Metals Rev.*, **4**, 138 (1960).

11) E. Schrödinger, *Ann. Phys.*, **46**, 413 (1917).

12) G. J. Janz, Proc. 3th International Symposium on Molten Salts(Electrochem. Soc. USA), Proc. Vol. **81—9**, 52 (1981).
13) G. J. Janz, R. P. T. Tomkins, C. B. Allen, J. R. Downey, Jr., G. L. Gardner, U. Krebs, and S. K. Singer, *J. Phys. Chem. Ref. Data*, **4**, 958, 971 (1975).
14) K. Igarashi, Y. Iwadate, and J. Mochinaga, *Z. Naturforsch. a*, in press (1987).
15) K. Igarashi and J. Mochinaga, *Z. Naturforsch.*, **42a**, 690 (1987).
16) K. Ohno, K. Igarashi, J. Mochinaga, N. Umesaki, and N. Iwamoto, "Proceeding of the 5th Symposium on Rare Earths, Tokyo, March 30—31, 1987," p. 140.
17) V. A. Maroni, E. J. Hathaway, and G. N. Papatheodorou, *J. Phys. Chem.*, **78**, 1134 (1974).
18) G. N. Papatheodorou, *Inorg. Nucl. Chem. Lett.*, **11**, 483 (1975).
19) R. D. Shannon, *Acta Crystallogr., Set. A*, **32**, 751 (1976).

First ESR Spectrum of a Selenoaminyl Radical[1)]

Yozo MIURA* and Osamu TSUMORI
Department of Applied Chemistry, Faculty of Engineering, Osaka City University, Sumiyoshi-ku, Osaka 558
(Received May 11, 1987)

Synopsis. *N*-(*o*-Nitrophenylseleno)-3,5-di-*t*-butylphenylaminyl radical, generated by photolysis of *N*-(3,5-di-*t*-butylphenyl)-*o*-nitrobenzeneselenenamide in the presence of di-*t*-butyl peroxide, has been studied by ESR spectroscopy. The ESR parameters are compared with those for the corresponding sulfur analogue.

Thioaminyl radicals (RNSR′) have an interesting structure in which a divalent sulfur attaches directly to the radical center. Our ESR spectroscopic studies on a variety of thioaminyls have shown that they are electronically substantially stabilized by conjugative delocalization of the unpaired electron from the nitrogen to the sulfur,[2)] and that some thioaminyls can be isolated as pure radical crystals or bydrazine-like dimers.[3–5)]

In the extension of these ESR studies our interest was focused on electronically related selenoaminyls (RNSeR′). However, in contrast to a wide ESR study on thioaminyls, there has appeared no ESR report on selenoaminyls in the literature. In this paper we report the first ESR spectrum of a selenoaminyl.

Results and Discussion

Selenenamides are known to be relatively labile owing to the weak N–Se bonds sensitive to hydrolysis;[6)] in particular, the compounds of the type RNHSeR′ are much more labile. This was shown by the repeated failures in obtaining the desired RNHSePh compounds from benzeneselenenyl chloride and RNH_2 (R: alkyl or aryl). However, *o*-nitrobenzeneselenenamide derivatives ($RNHSeC_6H_4NO_2$-*o*) exhibited high stabilities.[6)] That is, the reactions of *o*-nitrobenzeneselenenyl chloride with RNH_2 gave the desired *N*-alkyl- and *N*-aryl-*o*-nitrobenzeneselenenamides (**1**) in 53—67% yields.[7)]

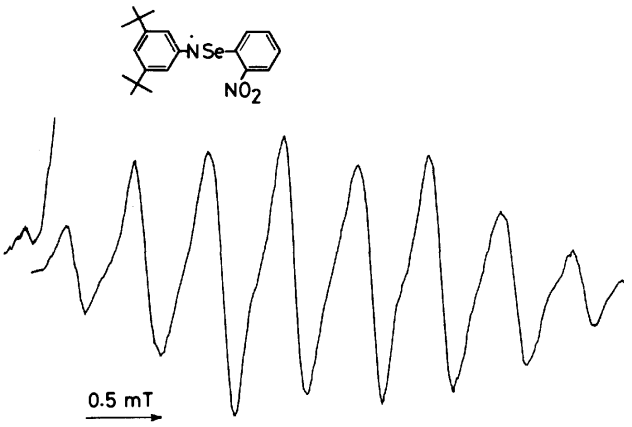

Fig. 1. ESR spectrum of **2a** recorded during photolysis of a solution of **1a** in 1:4 (v/v) di-*t*-butyl peroxide–benzene at 20 °C. The left wing is shown at high gain (5 times), and a satellite line due to ^{77}Se is seen.

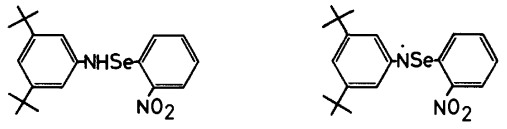

1a **2a**

The generation of selenoaminyl radicals was performed by the photolysis of solutions of **1** in the presence of di-*t*-butyl peroxide. When being irradiated in the cavity of an ESR instrument using a 1 kW xenon lamp, a solution of **1a** gave a 1:3:4:4:4:4:3:1 octet ESR spectrum with a relatively broad line width (peak-to-peak width, ca. 0.14 mT) as illustrated in Fig. 1. This signal, upon interruption of the UV-irradiation, disappeared immediately. In cases of other *o*-nitrobenzeneselenenamides,[7)] no ESR spectra attributable to the corresponding selenoaminyls were found for the solutions in the temperature range −50—20 °C.

The hyperfine splitting (hfs) constants for **2a**, determined by computer simulation, are a_N: 0.972 (1N), a_H: 0.453 (2H) and 0.525 mT (1H). On the basis of the numbers of the equivalent protons we could readily assign these three protons to the anilino ortho (2H) and para (1H) benzene ring protons. Interestingly, upon recording at higher gain a satellite line due to ^{77}Se (I=1/2, natural abundance 7.6%) was found in the left (low field) wing of the parent spectrum (see, Fig. 1). The assignment of this satellite line was made by its intensity ratio to the parent spectrum (experimental value ca. 3%, theoretical 3.8%). The ESR parameters are listed in Table 1.

For a comparison of the ESR parameters, we also prepared *N*-(*o*-nitrophenylthio)-3,5-di-*t*-butylphenylaminyl (**4**), the corresponding sulfur analogue, by oxidation of *N*-(3,5-di-*t*-butylphenyl)-*o*-nitrobenzenesulfenamide (**3**) with PbO_2. The ESR spectrum is illustrated in Fig. 2. This aminyl, in contrast to the very short-lived **2a** radical, persisted over a long period (> a day) in benzene at room temperature and the radical solution showed a green color [λ_{max} (benzene) 590 nm].[3)]

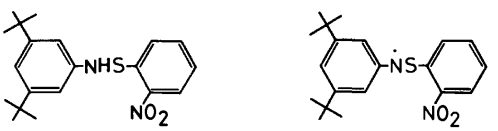

3 **4**

As found in Fig. 1, there is no splitting due to the phenylseleno benzene ring protons. However, the

Table 1. ESR Parameters for **2a** and Related Aminyls[a,b]

Radical	a_N	$a_{o\text{-}H}$[c]	$a_{p\text{-}H}$[c]	a_{other}	g
2a[d,e]	0.972	0.453	0.525	0.61 (^{77}Se)	2.011
4[e,f]	0.958	0.406	0.480	0.074 ($a_{o\text{-}H}$)[g] 0.088 ($a_{p\text{-}H}$)[g]	2.0054
5[h]	0.944	0.565	0.713		

a) Hyperfine splitting constants are given in mT. b) Temperature, 20±2 °C. c) Anilino benzene ring protons. d) Solvent, 1 : 4 (v/v) di-*t*-butyl peroxide–benzene. e) The hyperfine splitting constants are determined by computer simulation. f) Solvent, benzene. g) Phenylthio benzene ring protons. h) Taken from Ref. 11.

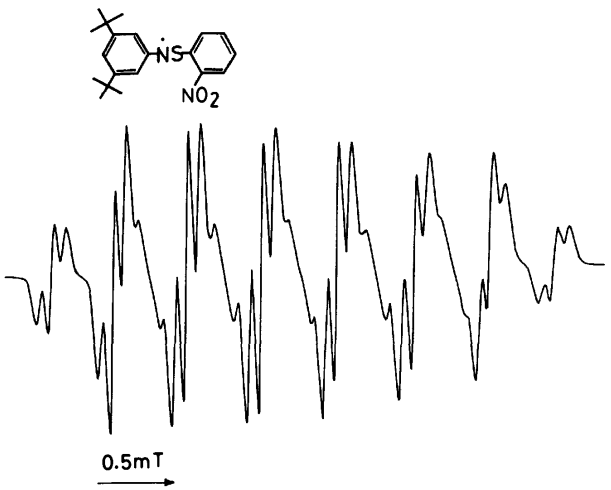

Fig. 2. ESR spectrum of **4** in benzene at 20 °C, generated by oxidation of **3** with PbO_2.

unusually high g value (2.011), as well as the relatively high $a_{^{77}Se}$ value (0.61 mT), is strongly suggestive of a considerable delocalization of the unpaired electron onto the selenium. Because of the large spin-orbit coupling parameter for selenium (1688 cm^{-1}; 382 cm^{-1} for sulfur),[8,9] the delocalization will cause the ESR lines to be considerably broadened.[10] Accordingly, small hfs's will have no effect on the spectrum other than to broaden the ESR lines.

When comparing the ESR parameters for **2a** with those for **4**, one will find some interesting differences in the ESR parameters between them. First, in the spectrum of **4** the hfs's of 0.074 and 0.088 mT due to the phenylthio benzene ring protons are found. On the other hand, in that of **2a** no splitting due to the phenylseleno benzene ring protons was detected. Second, the hfs constants for the anilino benzene ring protons of **2a** are 0.045—0.047 mT higher than those for **4**. These differences in hfs constants strongly suggest the lower ability of the selenium to delocalize the unpaired electron. That is, the dipolar canonical structure **B** seems to contribute less to the resonance hybride of **2a** than does the corresponding dipolar canonical structure **D** to the hybrid of **4**.

A B

C D

On the other hand, when comparing the ESR parameters for **2a** with those for 3,5,*N*-tri-*t*-butylphenylaminyl (**5**)[11] which is substituted at the nitrogen by a *t*-butyl group that has a negligibly small ability to delocalize the unpaired electron, one will note that the anilino benzene ring proton hfs constants for **2a** are substantially lower (0.112—0.188 mT) than those for **5** (see: Table 1). The sums of the spin densities on the ortho and para carbons of each anilino benzene ring ($\sum\rho_{o\text{-and }p\text{-}C}$) of **2a**, **4**, and **5**, derived from Table 1 using Q_H^{CH}=−2.7 mT, are 0.530 (**2a**), 0.479 (**4**), and 0.683 (**5**), these magnitudes being strongly suggestive

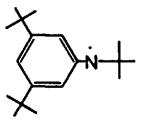

5

of the order: sulfur>selenium>*t*-Bu for the ability to delocalize the unpaired electron. This order, however, is not in agreement with the report of Gilbert et al.,[8,10] in which they showed the opposite order: ρ_{Se}^{π} (0.085)>ρ_S^{π} (0.076) based on the Hückel MO calculations with McLachlan's perturbation treatment on phenothiazine and phenoselenazine neutral radicals. The discrepancy seemed to come from the choice of parameters used in their calculations. To confirm this point calculations were performed using the same set of parameters as in the literature[8,10] ($\alpha_N=\alpha+0.8\beta$, $\alpha_S=\alpha+1.25\beta$, $\alpha_{Se}=\alpha+1.21\beta$, $\alpha_{NO_2\text{-}C}=\alpha+0.1\beta$, $\beta_{CN}=1.0\beta$, $\beta_{NS}=\beta_{CS}=\beta_{NSe}=\beta_{CSe}=0.57\beta$, and λ=0.7). In the present calculations the molecules are assumed to be planar. The results of the calculations certainly showed the same order as that of Gilbert, et al.: ρ_{Se}^{π} (0.138)>ρ_S^{π} (0.127). Although, in the above calculations the magnitude of β_{NS} is taken to be the same as that β_{NSe} and the magnitude of β_{CS} is taken to be the same as that of β_{CSe}, these are not physically realistic because of the loss of overlap due to extension of orbitals in the selenium. We think that k_{NS} and k_{CS} (for $\beta_x=k_x\beta$) should be larger than k_{NSe} and k_{CSe}, respectively. From this viewpoint, the magnitudes of β_{NS} and β_{CS} were changed from 0.57β to 0.65β.[12] Recalculations using these modified parameters afforded the order ρ_S^{π} (0.158)>ρ_{Se}^{π} (0.138), which is in agreement with the experimental results. Consequently, we wish to

conclude that the ability of selenium to delocalize the unaired electron is lower than sulfur.

Experimental

Melting points were determined on a Yanagimoto micro melting point apparatus and are uncorrected. IR spectra were run on a JASCO A-202 spectrophotometer. ^{1}H NMR spectra were recorded on a JEOL JNM-PS-100 spectrometer and chemical shifts (δ) are expressed in ppm relative to internal tetramethylsilane.

3,5-Di-*t*-butylaniline[13] and *o*-nitrobenzeneselenenyl chloride[14] were prepared by the reported procedures.

***N*-(3,5-Di-*t*-butylphenyl)-*o*-nitrobenzeneselenenamide (1a).** To a stirred solution of 1.00 g (4.87 mmol) of 3,5-di-*t*-butylaniline and 0.73 g (7.2 mmol) of triethylamine in 200 ml of dry ether was added dropwise at 0 °C a solution of 1.00 g (4.23 mmol) of *o*-nitrobenzeneselenenyl chloride in 50 ml of dry ether. After being stirred at the same temperature for 2 h, the reaction mixture was filtered and evaporated under reduced pressure. The residual red solid mass was crystallized from hexane to afford red prisms: mp 160—162 °C; yield 1.11 g (65%); IR (KBr) 3360 cm^{-1} (NH); ^{1}H NMR ($CDCl_3$) δ=1.25 (s, *t*-Bu, 18H), 5.10 (s, NH, 1H), 6.73—8.40 (m, aromatic, 7H). Found: C, 59.44; H, 6.66; N, 6.92%. Calcd for $C_{20}H_{26}N_2O_2Se$: C, 59.25; H, 6.47; N, 6.91%.

***N*-(3,5-Di-*t*-butylphenyl)-*o*-nitrobenzenesulfenamide (3).** To a stirred solution of 2.00 g (9.74 mmol) of 3,5-di-*t*-butylaniline and 1.5 g (15 mmol) of triethylamine in 100 ml of dry ether was added dropwise at 0 °C a solution of 2.2 g (12 mmol) of *o*-nitrobenzenesulfenyl chloride in 100 ml of dry ether. After being stirred at the same temperature for 2 h, the reaction mixture was filtered and evaporated under reduced pressure. The residual orange powdery solid was subjected to column chromatography (alumina, Merck art 1097) using benzene as eluant, and crystallization from benzene–hexane gave yellow prisms: mp 138—140 °C; yield 2.61 g (75%); IR (KBr) 3400 cm^{-1} (NH); ^{1}H NMR ($CDCl_3$) δ=1.26 (s, *t*-Bu, 18H), 5.09 (s, NH, 1H), 6.78—8.37 (m, aromatic, 7H). Found: C, 66.96; H, 7.28; N, 7.54%. Calcd for $C_{20}H_{26}N_2O_2S$: C, 67.01; H, 7.31; N, 7.81%.

ESR Measurements. Radicals **2** were generated by the photolysis of solutions of 10—25 mg of **1** in 0.20 ml of 1:4 (v/v) di-*t*-butyl peroxide–benzene (or toluene) using a 1 kW xenon lamp. Aminyl **4** was generated by treating 50 mg of **3** in 3 ml of benzene with 2 g of PbO_2. All the solutions were degassed by three freeze-pump-thaw cycles using a high vacuum system. ESR spectra were recorded on a JEOL JES-FE-2XG spectrometer equipped with an X-band microwave unit and 100 kHz field modulation. Hyperfine splitting constants and g values were determined by a comparison with Fremy's salt in an aqueous K_2CO_3 solution (a_N=1.309 mT, g=2.0057). Estimated accuracy for the hfs constants, ±0.01 mT.

We thank Prof. Tadatoshi Ohta and Dr. Hitoshi Tanaka of Tokushima University for making it possible to use the JEOL JES-FE-2XG ESR spectrometer at Tokushima University and for valuable suggestions on the ESR spectra.

References

1) ESR studies of nitrogen-centered free radicals. 30. Part 29: Y. Miura, M. Isogai, and M. Kinoshita, *Bull. Chem. Soc. Jpn.*, **60**, 3065 (1987).

2) Y. Miura, H. Asada, M. Kinoshita, and K. Ohta, *J. Phys. Chem.*, **87**, 3450 (1983).

3) Y. Miura, A. Yamamoto, Y. Katsura, and M. Kinoshita, *J. Org. Chem.*, **45**, 3875 (1980).

4) Y. Miura, A. Yamamoto, Y. Katsura, M. Kinoshita, S. Sato, and C. Tamura, *J. Org. Chem.*, **47**, 2618 (1982).

5) Y. Miura, T. Kunishi, M. Isogai, and M. Kinoshita, *J. Org. Chem.*, **50**, 1627 (1985).

6) T. Kobayashi and T. Hiraoka, *Bull. Chem. Soc. Jpn.*, **52**, 3366 (1979) and references cited therein.

7) We also prepared, besides **1a**, *N*-(*p*-*t*-butylphenyl)-(**1b**), *N*-*t*-butyl-(**1c**), and *N*-(1-adamantyl)-*o*-nitrobenzeneselenenamides (**1d**) in a similar manner. The melting points, yields, IR (KBr) and ^{1}H NMR ($CDCl_3$) data of these compounds are as follows: **1b**: red plates with mp 131—133 °C (crystallized from hexane); yield 53%; IR 3330 cm^{-1} (NH); ^{1}H NMR δ=1.27 (s, *t*-Bu, 9H), 5.05 (s, NH, 1H), 6.77—8.41 (m, aromatic, 8H). **1c**: orange prisms with mp 42—43 °C (crystallized from hexane); yield 67%; IR 3320 cm^{-1} (NH); ^{1}H NMR δ=1.24 (s, *t*-Bu, 9H), 2.91 (s, NH, 1H), 7.16—8.51 (m, aromatic, 4H). **1d**: orange needles with mp 74—76 °C (crystallized from hexane); yield 59%; IR 3290 cm^{-1} (NH); ^{1}H NMR δ=1.61—2.04 (m, adamantyl, 15H), 2.86 (s, NH, 1H), 7.18—8.60 (m, aromatic, 4H).

8) M. F. Chiu, B. C. Gilbert, and P. Hanson, *J. Chem. Soc., B*, **1970**, 1700.

9) J. C. Scaiano and K. U. Ingold, *J. Phys. Chem.*, **80**, 1901 (1976).

10) M. F. Chiu and B. C. Gilbert, *J. Chem. Soc., Perkin Trans. 2*, **1973**, 258.

11) S. F. Nelsen and R. T. Landis, *J. Am. Chem. Soc.*, **95**, 8707 (1973).

12) N. M. Atherton and J. N. Ockwell, *J. Chem. Soc., A*, **1967**, 771.

13) N. L. Allinger, H. M. Blatter, L. A. Freiberg, and F. M. Markowski, *J. Am. Chem. Soc.*, **88**, 2999 (1966).

14) K. B. Sharpless and M. W. Young, *J. Org. Chem.*, **40**, 947 (1975); Houben-Weyl, "Methoden der Organischen Chemie," Band IX. Georg Thieme Verlag, Stuttgart (1955), pp. 1096, 1162.

Prediction of Mutual Solubility Curve for *t*-Butyl Alcohol-Water System Utilizing Salting Out Phenomenon

Zhang QING-ZHI,* Wang JIAN-JI, Lu YAN, Lu JIN-SUO, and Tadashi KATO†
Department of Chemistry, Henan Teacher's University, Henan, China
†Department of Chemistry, Faculty of Science, Tokyo Metropolitan University, Setagaya-ku, Tokyo 158
(Received May 22, 1987)

Synopsis. The consolute temperatures (T_s) for ternary solutions of water-tetrahydrofuran-salt and water-*t*-butyl alcohol (TBA)-salt (salt: ammonium chloride or potassium chloride) were measured. From a plot of T_s against the salt concentration, the mutual solubility curve for the water-TBA system was predicted. The critical solution temperature and the critical composition were estimated to be about 200 °C and 0.15—0.2 (mole fraction of TBA), respectively.

Although *t*-butyl alcohol (TBA) is completely miscible with water, some experimental results suggest the existence of the lower critical solution temperature (LCST) above the boiling pont.[1-4] As is well-known, one of the criteria for an LCST is the relation $T|\Delta S^E| > |\Delta H^E|$, where ΔS^E and ΔH^E are the excess entropy and excess enthalpy, respectively. This relation holds for the TBA-water system.[1,5] Iwasaki and Fujiyama[2] have shown that the concentration fluctuations obtained from light scattering intensities increase rapidly with increasing temperature. This indicates that the system approaches the critical point as the temperature increases. However, the mutual solubility curve itself has not yet been predicted. In the present work, we have attempted to obtain a mutual solubility curve indirectly by utilizing the salting-out phenomenon for the water-TBA system. For a comparison, we have also studied a water-tetrahydrofuran (THF) system whose solubility curve can be measured directly under ordinary conditions.

Experimental

All the reagents used in this work were analytically pure reagent grade and were purified by the conventional method. Water was triply distilled in an all-Pyrex still.

The experimental procedures are summerized as follows.[6,7] Weighed ammounts of water, organic reagent (TBA or THF), and salt were sealed in ampoules. These ampoules were then put into a temperature-controlled water bath whose temperature was increased at a constant rate (about 0.2 °C per minute). The consolute temperature was determined by visual observation.

Results and Discussion

Figures 1—3 show semilogarithmic plots of the consolute temperature (T_s) against the mole fraction of salt (x_3) for ternary solutions of water-THF-ammonium chloride, water-THF-potassium chloride, and water-TBA-potassium chloride, respectively. In each series of measurements, the mole fraction of nonelctrolyte before adding salt,

$$x_2' = \frac{n_2}{n_1+n_2}, \quad (1)$$

was kept constant. Here, n_1 and n_2 are the number of moles of water and nonelectrolyte (THF or TBA), respectively. It can be seen from the figure that T_s^0 decreases with an increase in the salt concentration.

In the water-THF system, the consolute temperature for the salt-free system, T_s^0, can be observed directly under an atmosphere, as is illustrated in Fig. 1. Although the water-TBA system does not have the

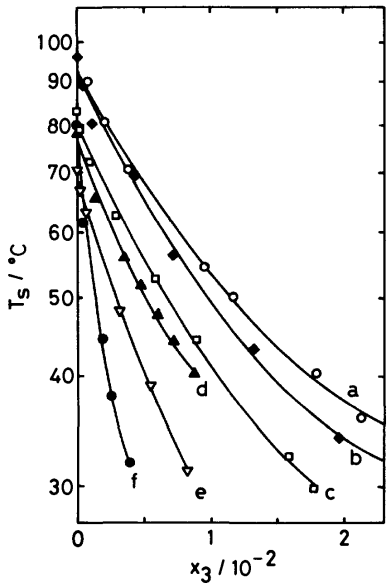

Fig. 1. A semilogarithmic plot of the consolute temperature against the mole fraction of salt for water-THF-ammonium chloride system. a: x_2'= 0.082, b: 0.095, c: 0.116, d: 0.136, e: 0.195, f: 0.364.

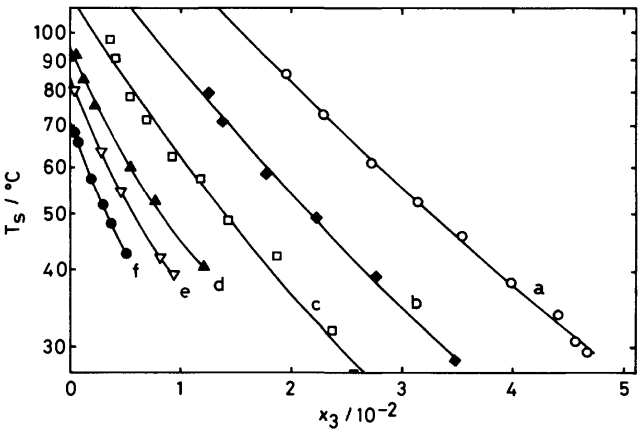

Fig. 2. A semilogarithmic plot of the consolute temperature against the mole fraction of salt for water-THF-potassium chloride system. a: x_2'= 0.035, b: 0.047, c: 0.065 d: 0.087, e: 0.097, f: 0.141.

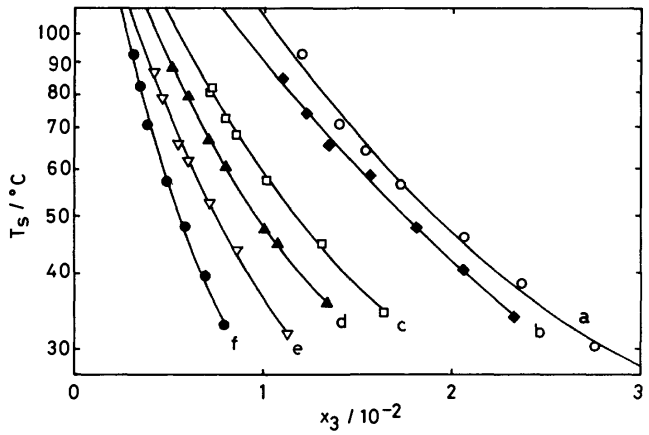

Fig. 3. A semilogarithmic plot of the consolute temperature against the mole fraction of salt for water-TBA-potassium chloride system. a: x_2'= 0.049, b: 0.055, c: 0.097, d: 0.135, e: 0.190, f: 0.267.

LCST under ordinary conditions, the limiting value of T_s as $x_3 \to 0$ may be regarded as the consolute temperature for the salt-free system. As can be seen from Fig. 3, however, it seems difficult to obtain the limiting value uniquely. We therefore have tried to determine an empirical formula for describing the relation between T_s and X_s. It has been found that all the present data can be fitted to the equation

$$\log T_s = a + bx_3 + cx_3^2, \quad (2)$$

where a, b, and c are the fitting parameters. The solid lines in Figs. 1—3 represent the best-fit curves obtained by the least-squares method. The T_s^0 values for the water-THF and water-TBA systems have been calculated from the parameter a (=log T_s^0). It should be noted that the validity of this procedure depends on the applicability of Eq. 2 in the low x_3 region.

In Figs. 4 and 5, the T_s^0 values, thus obtained, are plotted against the mole fraction of THF and TBA (x_2), respectively.[8] The closed circles in Fig. 4 represent T_s^0 values directly observed. It can be seen from the figure that the T_s^0 values obtained from the fitting procedure coinside with the observed values, at least in the range $0.08 < x_2 < 0.4$. This indicates that Eq. 2 can be applied to the THF system at least in the range $x_3 < 0.02$ (see Figs. 1 and 2). We have assumed that the same holds true for the TBA system.[9]

Figure 5 suggests the existence of a minimum in the solubility curve. The LCST and the critical composition are thus estimated to be 200 °C and 0.15—0.2, respectively. Bender and Pecora[10] have obtained concentration dependence of the correlation length by means of dynamic light scattering. They have shown that the correlation length takes a maximum at x_2=0.15 in the temperature range 10—40 °C. The Kirkwood-Buff integral G_{ij} (i, j=1 or 2 for a binary solution composed of 1 and 2) for the water-TBA system have been reported by several authors.[3,11,12] According to these data, G_{12} also takes a minimum at x_2=0.15. These x_2 values are closed to the critical composition estimated in the present work.

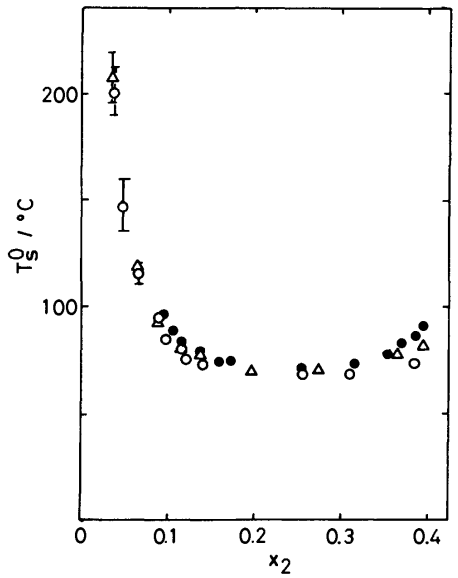

Fig. 4. Mutual solubility curve for water-THF system calculated from log T_s—x_3 plots for water-THF-potassium chloride(○) and water-THF-ammonium chloride(△) systems. Closed circles represent observed values.

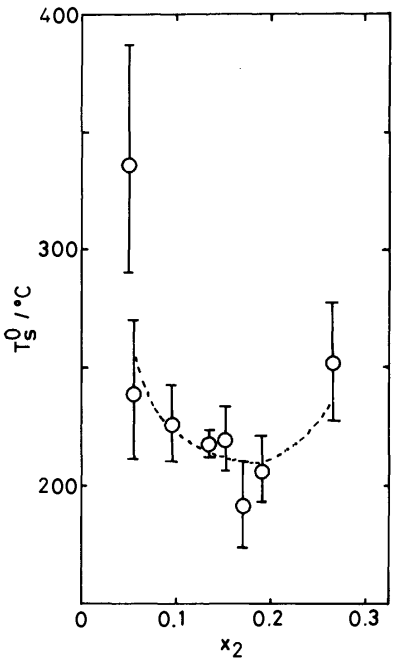

Fig. 5. Mutual solubility curve for water-TBA system calculated from log T_s—x_3 plots for water-TBA-potassium chloride system.

This suggests that the critical phenomenon of demixing dominates the mixing states, even at temperatures some 150—200 °C below the critical consolute temperature.

References

1) For example, F. Franks and D. S. Reid, "Water," ed

by F. Franks, Plenum Press, New York (1973), Vol. 2, Chap. 5.

2) K. Iwasaki and T. Fujiyama, *J. Phys. Chem.*, **81**, 1908 (1977); **83**, 463 (1979).

3) H. D. Bale, R. E. Shepler, and D. K. Sorgen, *Phys. Chem. Liq.*, **1**, 181 (1968).

4) T. Kato, M. Yudasaka, and T. Fujiyama, *Bull. Chem. Soc. Jpn.*, **55**, 1284 (1982).

5) J. Kenttamaa, E. Tmmila, and M. Martti, *Ann. Acad. Sci. Fenn. A*, **93**, 1 (1959).

6) Li Jun Fu, *J. Xinxiang Normal College*, **6**, 9 (1965).

7) Li Jun Fu, *J. Xinxiang Normal College*, **2**, 31 (1983).

8) Measurements of T_s were made also at compositions other than those shown in Figs. 1—3.

9) The slight difference between calculated and observed T_s^0 values for the potassium chloride system arises from the lack of data in the low x_3 region. This may cause serious error in the estimation of T_s^0 for the water-TBA system because T_s cannot be observed up to much higher concentration of salt than the THF system. At present, however, it seems difficult to confirm the validity of Eq. 2 for the TBA system.

10) T. M. Bender and R. Pecora, *J. Phys. Chem.*, **90**, 1700 (1986).

11) E. Matteoli and L. Lepori, *J. Chem. Phys.*, **80**, 2856 (1984).

12) K. Nishikawa, *Chem. Phys. Lett.*, **132**, 50 (1986).

Re-extraction Behavior of Nitrosyl Ruthenium Complex in Tributyl Phosphate-Dodecane Solvent System

Akira SASAHIRA,* Tatsuo IZUMIDA,* and Fumio KAWAMURA*
Energy Research Laboratory, Hitachi, Ltd., Moriyama-cho, Hitachi, Ibaraki 316
(Received February 10, 1987)

Synopsis. A re-extraction of the nitrosyl ruthenium complex from a tributyl phosphate-dodecane solvent system to a nitric acid solution was carried out. A longer aging of the organic phase before re-extraction lowered the re-extraction yield, while nitric acid extracted into the organic phase increased it. These results could be explained using a model with two organic species.

The extraction behavior of nitrosyl ruthenium has been studied for the past few years[1-7] owing to its presence in spent nuclear fuel. Ruthenium is distributed between the organic and aqueous phases and is a contamination during fuel reprocessing. Tributyl phosphate (TBP) is a common extraction reagent in nuclear fuel reprocessing. The extraction reaction in the system, nitrosyl ruthenium–nitric acid–TBP, was originally proposed as [8]

$$RuNO^{3+}(w.) + mNO_3^-(w.) + nTBP(w.) \rightleftarrows RuNO(NO_3)_m^{(3-m)+}\cdot(TBP)_n(o.), \quad (1)$$

where (w.) and (o.) denote aqueous and organic phases. However, since it was pointed out that complex formation and deformation are very slow,[9] studies concerning the partition coefficients and formation-deformation reaction rate of each complex were necessary. The extraction reaction can be described in the following reaction scheme:

$$RuNO(NO_3)_m^{(3-m)+}(w.) + (m-x)NO_3^-(w.) \rightleftarrows RuNO(NO_3)_x^{(3-x)+}(w.), \quad (2)$$

$$RuNO(NO_3)_x^{(3-x)+}(w.) + yTBP(w.) \rightleftarrows RuNO(NO_3)_x(TBP)_y^{(3-x)+}(w.), \quad (3)$$

and

$$RuNO(NO_3)_x(TBP)_y^{(3-x)+}(w.) \rightleftarrows RuNO(NO_3)_x(TBP)_y^{(3-x)+}(o.). \quad (4)$$

However the only important species is RuNO $(NO_3)_3$, since other anionic or cationic species are less extractable. Further, Prurtt[1] examined the extraction rate of mixtures of nitrosyl ruthenium nitrate complexes and found that the extraction was not completed within 4 hours. It was suggested that the slow extraction is due to a slow conversion of ruthenium complexes in the organic phase, but not the conversion of ruthenium species in the aqueous phase.[2] On the other hand, re-extraction behavior of nitrosyl ruthenium was not examined except for Maya's report.[2] In this paper we report on the effects of the re-extraction period, aging period of the organic phase before re-extraction, and acid concentration of the aqueous phase on the re-extraction rate.

Experimental

Preparation. An acid solution of nitrosyl ruthenium complexes was prepared by dissolving RuNO $(NO_3)_3$ (α-products) in a 3 mol·dm^{-3} nitric acid solution. The acid solution was aged in a dark box for 6 months in order to equilibrate the reactions between the ruthenium complexes, such as in Eq. 2.[4] The acid solution contained 15.7×10^{-3} mol·dm^{-3} of the complexes. A solvent containing TBP was prepared by mixing 3:7 volume of reagent grade TBP and reagent grade dodecane (both Wako Chemical Co.).

Re-extraction. An organic phase containing ruthenium was obtained by the extraction of ruthenium from 20 cm^3 of the aged acid solution using 200 cm^3 of TBP solvent. The extraction was carried out for 5 min in a separatory funnel. The concentration of extracted ruthenium was about 1×10^{-3} mol·dm^{-3}. Then, the organic phase was aged from 5 min to 7 d before re-extraction. Ruthenium was re-extracted from 5 cm^3 of aged organic phase using 5 to 20 cm^3 of fresh aqueous phase containing 1 to 6 mol·dm^{-3} of nitric acid.

Analytical Method. Ruthenium concentration in the aqueous phase was measured by colorimetry.[10] The ruthenium in the organic phase was re-extracted into Na_2SO_3 solution (0.5 mol·dm^{-3}) and measured by colorimetry.

Results and Discussion

First of all, the prepared organic phase was aged from 5 min to 24 h before a 2 min re-extraction into nitric acid solution. Since the nitric acid concentration in the aqueous phase after the extraction was 1 mol·dm^{-3}, ruthenium was re-extracted into nitric acid of the same concentration to avoid changing the acid concentration in the organic phase. The concentration ratio of ruthenium in the organic phase to the aqueous phase is plotted against the aging period before re-extraction in Fig. 1. The ratio increased with the aging period and depended on the volume ratio of organic and aqueous phases. However, a residual factor, R, defined as

$$R = \frac{\text{Organic Ru concentration after re-extraction}}{\text{Organic Ru concentration before re-extraction}}, \quad (5)$$

did not depend on the volume ratio (Fig. 2). This behavior was expected from the two species model.[2] The reaction is written as

$$Ru(s) \underset{k_2}{\overset{k_1}{\rightleftarrows}} Ru(r), \quad (6)$$

where Ru(s) and Ru(r) denote strippable and retained ruthenium species in the organic phase; k_1 and k_2 are rate constants. If the re-extraction period was

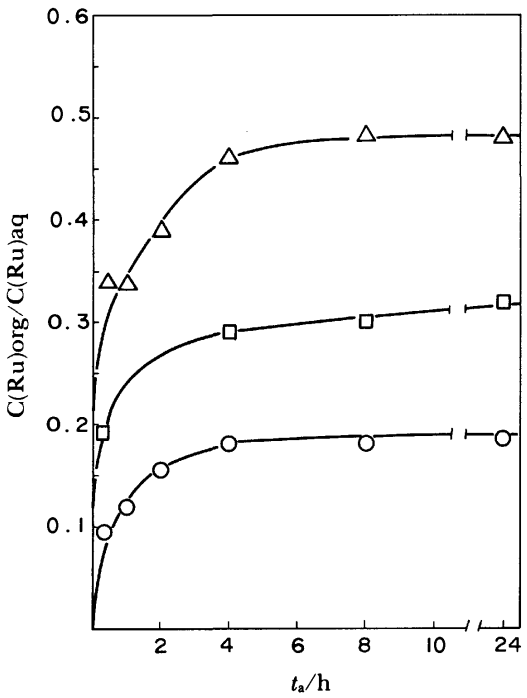

Fig. 1. Variation of ruthenium concentration ratio with organic phase aging period after 5 min extraction denoted as ta.
Aqueous volume/organic volume; △: 1, □: 2, ○: 4. Concentration of aqueous nitric acid was 1 mol·dm^{-3} and re-extraction period was 2 min.

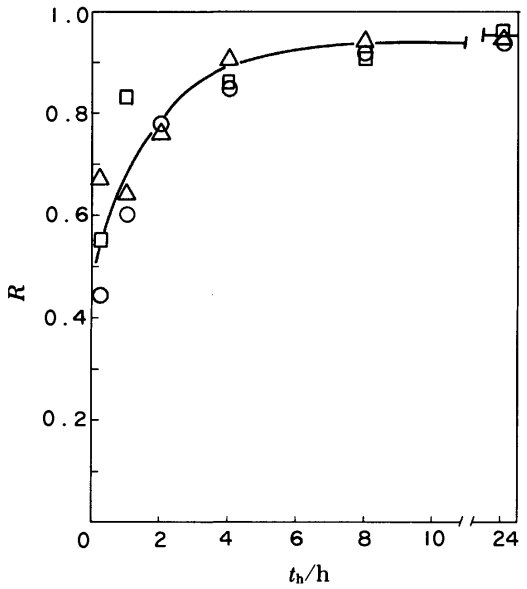

Fig. 2. Variation of ruthenium residual factor in organic phase with organic phase aging period.
Aqueous volume/organic volume; △: 1, □: 2, ○: 4. Concentration of aqueous nitric acid was 1 mol·dm^{-3} and re-extraction period was 2 min.

sufficiently short to avoid conversion between Ru(r) and Ru(s) during re-extraction, the residual factor was equal to the mole ratio of Ru(r) to Ru(s) at the end of

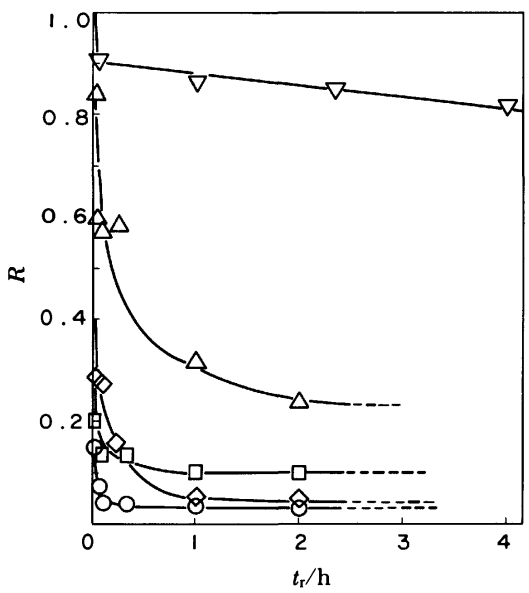

Fig. 3. Variation of ruthenium residual factor in organic phase, aged for 7 d, with re-extraction period denoted as t_r. Concentrations of aqueous nitric acid were ▽: 1, △: 2, □: 3, ◇: 4, ○: 6 mol·dm^{-3}, respectively.

aging. Then, the residual factor was expected to be independent of the volume ratio. On the other hand, the Ru concentration in the aqueous phase was expected to decrease with increasing aqueous phase volume upon dilution. These predictions from this model agreed with the experimental results given in Figs. 1 and 2. Rate constants k_1 and k_2 were calculated from the dependency of residual factor on the aging period by using the rate equation of an "Opposing Reaction."[11] The estimated values of k_1 and k_2 were 5×10^{-1} and 4×10^{-2} h^{-1}, respectively.

Next, the effect of the re-extraction period on the residual factor was measured. The used organic phase was aged for 7 d to equilibrate reaction 6. For a 2 min re-extraction into 1 mol·dm^{-3} nitric acid, the residual factor was equal to that of the organic phase aged 24 h, within the experimental error. The residual factor for re-extraction into 1 to 6 mol·dm^{-3} nitric acid is plotted against the re-extraction period in Fig. 3. For re-extraction into 1 mol·dm^{-3} nitric acid, it was observed that a rapid transfer of ruthenium into the aqueous phase was followed by a slow transfer. The former must be a stripping of species Ru(s) initially existing in the aged organic phase. The latter must be a stripping of Ru(s) formed from Ru(r) during re-extraction. The formation rate constant of Ru(s) calculated from the slope of slow transfer is shown in Table 1 as k(obs.). The calculated value agreed well with the value of k_2. For re-extraction into 2 mol·dm^{-3} nitric acid, ruthenium was transferred much more rapidly. For re-extraction into 3—6 mol·dm^{-3}, the partition equilibrium of ruthenium seemed to be established quickly. The nitric acid, extracted into the organic phase, would enhance the formation reaction of Ru(s) from Ru(r). The rate

Table 1. Rate Constant of Ru(s) Formation Reaction, k(obs.), Estimated from Re-extraction Rate

HNO_3 / mol·dm^{-3}	k(obs.) / h^{-1}
1.0	4×10^{-2}
2.0	9×10^{0}
3.0	$\geqq9\times10^{1}$
4.0	$\geqq8\times10^{1}$
6.0	$\geqq1\times10^{2}$

constants of the formation reaction of Ru(s) on the re-extraction into 2—6 mol·dm^{-3} nitric acid were calculated from the initial slopes of the residual factor versus the re-extraction period, and are shown in Table 1.

The two species model seemed to be a reasonable mechanism for the re-extraction of nitrosyl ruthenium complexes. However, further experiments would be required to clarify the mechanism of the conversion reaction between the two species of ruthenium in the organic phase.

References

1) D. J. Pruett, *Radiochim. Acta*, **27**, 115 (1980).
2) L. Maya, *J. Inorg. Nucl. Chem.*, **43**, 385 (1981).
3) L. Maya, *J. Inorg. Nucl. Chem.*, **41**, 67 (1979).
4) G. G. Boswell and S. Soentono, *J. Inorg. Nucl. Chem.*, **43**, 1625 (1981).
5) J. Blasius, J. P. Glatz, and W. Neumann, *Radiochim. Acta*, **29**, 159 (1981).
6) J. Blasius, H. J. Luxenburger, and W. Neumann, *Radiochim. Acta*, **36**, 149 (1984).
7) J. Blasius and K. Muller, *Radiochim. Acta*, **37**, 217 (1984).
8) E. Hallaba, R. Azzam, *Z. Phys. Chem.*, **237**, 177 (1966).
9) J. J. Diana, DP-TR-37 (1977).
10) G. R. Belew, *Anal. Chem.*, **33**, 886 (1961).
11) S. W. Benson, "The Foundations of Chemical Kinetics," McGraw Hill, New York (1960), p. 29.

The Magnetic Field Effects on Electrolysis. II.[1] The Anodic Surface Oxidation of Gold

Takeshi WATANABE,† Yoshifumi TANIMOTO,*,†† Ryoichi NAKAGAKI, Mitsuo HIRAMATSU,†††
Tadayoshi SAKATA, and Saburo NAGAKURA
Institute for Molecular Science, Myodaiji, Okazaki 444
(Received April 2, 1987)

Synopsis. In the anodic oxidation of gold in an acidic solution, the electrode surface is covered with a black deposit. It dissolves immediately after the application of an external magnetic field (1 T). The results are discussed in terms of a magnetohydrodynamic mechanism.

In previous work,[1] the magnetic field effects on the electrochemical reduction of hexacyanoferrate(II) and oxidation of hexacyanoferrate(III) were studied by means of potentiometry. It was shown that the magnetic field effects on these redox reactions can be interpreted in terms of a magnetohydrodynamic (MHD) mechanism in which an electrolyte flow near the electrode is affected by an external magnetic field.

In the present paper we report on magnetic field effects on the anodic surface oxidation of gold in an acidic solution.

Experimental

The experimental set-up was essentially the same as that described previously.[1] An electrolytic cell and electrodes were placed between the pole pieces of an electromagnet (Tokin SEE-15). A magnetic field did not affect the potential of a saturated calomel electrode (SCE) used as a reference. One side of a gold plate electrode (5×10 mm) was covered with an epoxide glue. The electrode plate was always kept parallel to the magnetic flux.

Electrolysis was carried out by using a potentio/galvano stat (Hokuto Denko, HA-102). The purest grade sulfuric acid, sodium sulfate, and sodium chloride were used as received. Water was distilled twice before use.

Results and Discussion

Figure 1 shows the potential–current curves of a gold electrode in an acidic solution observed in the absence and the presence of a magnetic field (1 T). An electric current increases with the increasing electric potential and reaches a maximum at 1.2 V, a sudden drop of the current appearing at 1.23 V. By increasing the potential, however, the current again increases. Gas (probably O_2) evolves at higher potentials (>1.4 V).

The anodic behavior of Au in chloride solutions has been reported by several research groups.[2-5] Concerning anodic oxidation of gold in NaCl–H_2SO_4 and KCl–$HClO_4$ solutions,[4,5] the current increase with increasing potential in the range of 1.0—1.4 V was reported to be due to the dissolution of Au:

$$Au + 4Cl^- \longrightarrow AuCl_4^- + 3e^-. \quad (1)$$

Thus, the current increase in the range of 1.0—1.2 V shown in Fig. 1, can be attributable to the Reaction 1 mentioned above. A sudden drop at 1.23 V is due to the formation of a passive oxide and/or adsorbed oxygen film on the Au electrode. In the presence of a magnetic field, the electrolytic current at 1.1—1.2 V increases by about 300% compared with the one in the zero field, as shown in Fig. 1. Judging from the results in a previous paper,[1] this current increase is attributable to the MHD mechanism, since the MHD force is expected to affect the mass transfer near the electrode surface.

Upon electrolysis at an electric potential of about 1.2 V, the surface is covered with a black deposit in the absence of a magnetic field, as reported in the literature.[4] By applying a magnetic field, the black deposit on the surface was found to dissolve, suggesting that the MHD mechanism is operative in the present reaction. In order to make this point clearer, the influence of the orientation of electrode

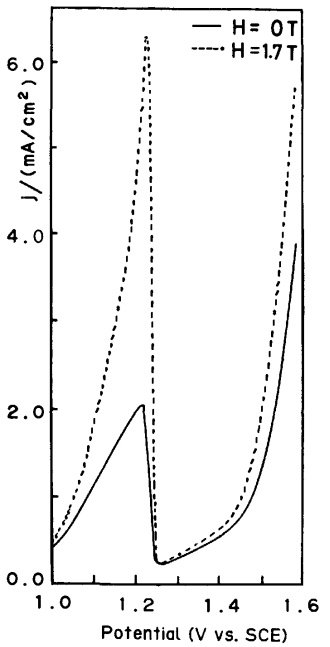

Fig.1 Mangetic field effects on the potential–current curves of the anodic surface oxidation of gold. Concentrations of Na_2SO_4, H_2SO_4, and NaCl are 0.1, 0.05, and 0.01 mol dm^{-3}, respectively.

† Present address: Toray Research Center, INC, Sonoyama, Otsu 520.

†† Adjunct associate professor of Institute for Molecular Science (1983—85). Faculty of Pharmaceutical Sciences, Kanazawa University, Takara-machi, Kanazawa 920.

††† Visiting research fellow from Hamamatsu Photonics K. K. (1983—85). Hamamatsu Photonics K. K., Ichino-cho, Hamamatsu 435.

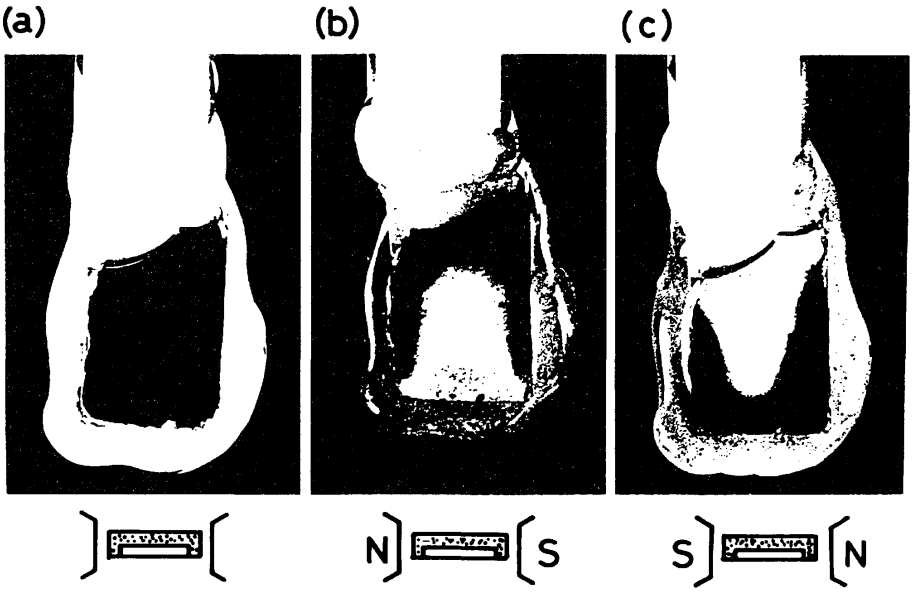

Fig. 2. Magnetic field effects on the deposit on a gold electrode in the absence (a) and in the presence ((b) and (c)) of a magnetic field (1 T). Electrolysis is carried out at 1.2 V vs SCE. Concentrations of Na_2SO_4, H_2SO_4, and NaCl are 0.1, 0.05, and 0.2 mol dm^{-3}, respectively. Top views of two magnetic field orientations with respect to the electrode are also illustrated in the figure. Dotted area indicates the epoxide glue and the rest is the gold electrode.

with respect to a magnetic field on the dissolution of the black deposit was examined.

Figure 2 shows the effects of a magnetic field (1 T) on the black deposit on the Au electrode. In the absence of a magnetic field, the surface of the Au electrode is covered with a black deposit 2—3 min after the start of electrolysis (a). Then, a magnetic field is applied in the direction shown in (b). The deposit immediately starts to dissolve from the bottom of the electrode. On the other hand, when a magnetic field is applied in the opposite direction, as shown in (c), after the electrolysis at zero field, dissolution of the deposit occurs from the top of the electrode.

Electrochemical corrosion and passivation of metal electrodes are affected by various experimental factors such as composition and concentration of electrolyte, current density, pH, and temperature. Taking into account the reports on the deposit on an Au electrode[2,4,6] and others,[7] the black deposit observed in the present study may be a hydrated oxide of Au, though its chemical composition has not yet been determined. According to the literature,[8-10] halogen ions, such as Cl^- and Br^-, attack the oxide film on metal electrodes, resulting in a dissolution of the oxide film. Therefore, the magnetic field effects on the dissolution of the black deposit can be interpreted in terms of the MHD mechanism as described below.

The MHD force $\boldsymbol{F}$ to the electrolytic current $\boldsymbol{j}$ in the magnetic field $\boldsymbol{H}$ can be given by

$$\boldsymbol{F} = \boldsymbol{j} \times (\mu \boldsymbol{H}), \quad (2)$$

where μ is the magnetic permeability. In the orientation of the electrode with respect to the magnetic field shown in Fig. 2 (b), the MHD flow of the electrolyte occurs upward. This means an increasing supply of Cl^- from the bulk solution to the electrode surface, leading to an upward dissolution of the hydrated oxide deposit on the electrode. Similarly, in the orientation shown in (c), the electrolyte flows downward, resulting in a downward dissolution of the deposit.

In the absence of a magnetic field, Cl^- ions are supplied from a bulk solution to the electrode surface by such mass-transport processes as diffusion, convection, and electrophoretic migration. In the presence of a magnetic field, they are further supplied by the MHD flow. This efficient and orientation-dependent mass-transport process is observed as a dissolution of the black deposit (Fig. 2). Furthermore, an enhanced dissolution of the deposit by the MHD flow was also observed as an increase in the electrolytic current in the potential–current curve (Fig. 1).

It is noteworthy that the MHD flow of the electrolyte has no influence on the electrolytic current in the passive state around 1.35 V (Fig. 1). This fact suggests that bonding of the passive oxide film to the metal surface is probably strong, as the passive film might be quite thin.[11,12] On the other hand, the black (hydrated oxide) deposit appearing arround 1.2 V may loosely cover the electrode surface. Therefore, we may conclude that the external magnetic field significantly affects the mass-transport processes near the electrode surface, while it seldom influences those inside the surface. Thus, the present results *visually* demonstrate the importance of the MHD-induced flow for the mass-transport process near the electrode, though quite a few are reported for the magnetic field effects on the electrolytic current.[13]

References

1) Part I of this series: T. Watanabe, Y. Tanimoto, T. Sakata, R. Nakagaki, M. Hiramatsu, and S. Nagakura, *Bull. Chem. Soc. Jpn.*, **58**, 1251 (1985).
2) F. P. A. Robinson and F. A. Frost, *Corrosion*, **19**, 115t (1963).
3) G. Just and R. Landsberg, *Electrochim. Acta*, **9**, 817 (1964).
4) T. Heumann and H. S. Panesar, *Z. Phys. Chem. (Leipzig)*, **229**, 84 (1965).
5) J. N. Gaur and G. M. Schmid, *J. Electroanal. Chem.*, **24**, 279 (1970).
6) S. Barnartt, *J. Electrochem. Soc.*, **106**, 722 (1959).
7) N. Sato, *Denki Kagaku*, **46**, 584 (1978).
8) S. C. Britton and U. R. Evans, *J. Chem. Soc.*, **1930**, 1773.
9) M. Maeda, *Naturwiss.*, **44**, 557 (1957).
10) A. Kozawa, *Denki Kagaku*, **31**, 682 (1963).
11) A. Hickling, *Trans. Faraday Soc.*, **42**, 518 (1946).
12) S. B. Brummer and A. C. Makrides, *J. Electrochem. Soc.*, **111**, 1122 (1964); S. B. Brummer, *ibid.*, **112**, 633 (1965).
13) See Ref. 1 and references therein.

The Magnetic Field Effects on Electrolysis. III.[1] The Anodic Oxidation of Phenylacetate Ion

Takeshi WATANABE,† Yoshifumi TANIMOTO,*,†† Ryoichi NAKAGAKI, Mitsuo HIRAMATSU,††† and Saburo NAGAKURA

Institute for Molecular Science, Myodaiji, Okazaki 444

(Received April 2, 1987)

Synopsis. In anodic oxidation of the phenylacetate ion, the formation yield of benzaldehyde increases by about 40% in the presence of a magnetic field (0.67 T), while 1,2-diphenylethane is insensitive to the field. The results are interpreted in terms of the magnetohydrodynamic mechanism.

In previous studies,[1,2] we have investigated external magnetic field effects on inorganic electrochemical processes and demonstrated that the magnetohydrodynamic (MHD) effect plays an important role in redox reactions. In the MHD mechanism, a flow of electrons and ions is affected by an external magnetic field, resulting in the perturbation on the mass-transport process near the electrode. As an extention of the above-mentioned investigation, we have studied the magnetic field effects on organic electrochemical processes.

In the present paper, we report on the magnetic field effects on the electrolysis of the phenylacetate ion, as an example of the Kolbe reaction, which may be preparatively useful.

Experimental

Phenylacetic acid was prepared by the hydrolysis of ethyl phenylacetate,[3] and was purified by recrystallization. Solvents for high-performance liquid chromatography (HPLC) grade, methanol, dioxane and water, were used as received.

The electrolysis was carried out using a potentio/galvano stat (Hokuto Denko, HA-102). An aerated methanol-dioxane solution (50 ml), containing phenylacetic acid (0.05 mol dm^{-3}) and its potassium salt (0.05 mol dm^{-3}), was electrolyzed between two platinum plate electrodes (5 mm×10 mm) at a constant density of 9 mA cm^{-2} for about 90 min (0.1 F mol^{-1}). Argon or oxygen gas was bubbled through the solution during the electrolysis, when necessary. A magnetic field was applied with an electromagnet (Tokin SEE-10).

The reaction products were analyzed on an HPLC apparatus (Waters model 590 liquid chromatograph) and a UV detector (Waters 481 LC-spectrophotometer). The products were identified from the agreement of their UV absorption spectra and retention times with those of authentic samples, by monitoring the absorbance at 260 nm.

Results and Discussion

Figure 1a shows a typical chromatogram of the reaction mixture obtained by electrolysis in the absence of a magnetic field. The five peaks in the chromatogram have been identified as benzaldehyde (PhCHO), benzyl methyl ether ($PhCH_2OCH_3$), toluene ($PhCH_3$), benzyl phenylacetate ($PhCH_2COOCH_2Ph$), and 1,2-diphenylethane ($PhCH_2CH_2Ph$), though the other two peaks with retention times of 10.2 and 16.8 min remain unidentified. Figure 1b shows the effects of a magnetic field (0.67 T) on the product yields. In the presence of a magnetic field, the yield of benzaldehyde increases by about 40%, while those of 1,2-diphenylethane and others are insensitive to the magnetic field (summarized in Table 1).

The electrolysis of substituted phenylacetate ions in methanol was studied in detail by Coleman et al.[4] According to their proposed mechanism, the plausible

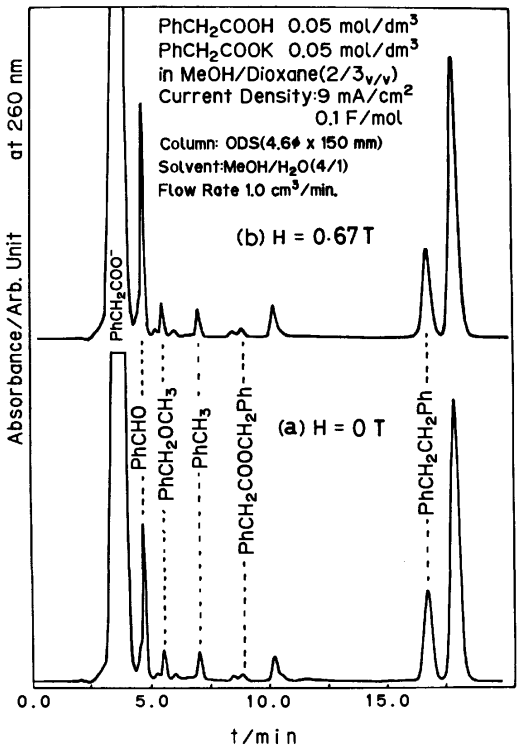

Fig. 1. Typical chromatograms of the reaction mixture after the electrolysis of an aerated solution of phenylacetic acid and its potassium salt in the absence (a) and in the presence (b) of a magnetic field (0.67 T).

† Present address: Toray Research Center, INC, Sonoyama, Otsu 520.

†† Adjunct associate professor of Institute for Molecular Science (1983—85). Faculty of Pharmaceutical Sciences, Kanazawa University, Takara-machi, Kanazawa 920.

††† Visiting research fellow from Hamamatsu Photonics K. K. (1983—85). Hamamatsu Photonics K. K., Ichino-cho, Hamamatsu 435.

Table 1. The External Magnetic Field Effects on the Product Yields for the Electrolysis of an Aerated Phenylacetate Ion Solution[a)]

	PhCHO	$PhCH_2OCH_3$	$PhCH_3$	$PhCH_2COOCH_2Ph$	$PhCH_2CH_2Ph$
$\phi(H)/\phi(O)$[b)]	1.39	1.06	0.95	1.01	0.97
	(0.19)	(0.23)	(0.13)	(0.11)	(0.04)

a) Values in parentheses denote experimental errors. b) $\phi(H)$ and $\phi(O)$ are the relative yield in the presence and the absence of a magnetic field (0.67 T).

pathways of the present reaction could be summarized as follows:

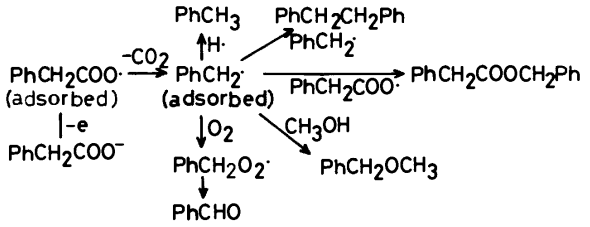

The benzyl radical generated via the phenylacetoxy radical by the one-electron oxidation of phenylacetate ion, undergoes the following reactions: coupling of radicals and an addition of molecular oxygen. Benzaldehyde could result from the addition of oxygen to the benzyl radical.[5)] The oxygen involved in the reaction could be either dissolved oxygen or oxygen produced electrochemically from the hydroxide ion.

In order to clarify the role of molecular oxygen in the benzaldehyde formation, electrolysis was carried out under two extreme conditions. In the electrolysis under the argon bubbling, the yield of benzaldehyde slightly decreased (≈15%), while that of 1,2-diphenylethane remained unchanged on the removal of dissolved oxygen by argon. On the other hand, in a reaction under oxygen bubbling, a significant increase (≈20 times) in the yield of benzaldehyde was observed in a concomitant decrease (70—80%) in that of 1,2-diphenylethane. These observations indicate that the dissolved molecular oxygen is responsible for the formation of benzaldehyde in aerated solutions. In argon-bubbled solutions, the molecular oxygen produced electrochemically from the hydroxide ion could be a major source of molecular oxygen in benzaldehyde formation.

In a previous study,[1)] the external magnetic field effects on electrolytic currents in hexacyanoferrate(II) and hexacyanoferrate(III) solutions were investigated under various conditions by means of potentiometry. All the results were interpreted in terms of the MHD mechanism, in which a flow of electrolyte is affected by a MHD force $\boldsymbol{F}$ with the relation $\boldsymbol{F}=j\times(\mu\boldsymbol{H})$, j, μ, and $\boldsymbol{H}$ being the electrolytic current density, the magnetic permeability, and the magnetic field, respectively. Furthermore, it was demonstrated that, in electrochemical oxidation of gold, a MHD-induced flow even causes a visual change in the color of the electrode surface, in addition to that in the potential-current curve.[2)] Taking the above-mentioned observations into account, the magnetic field effects on the present oxidation reaction can mostly be interpreted in terms of the MHD mechanism. The mass-transport from the bulk solution to the electrode surface occurs via diffusion, convection, and electrophoretic migration in the absence of a magnetic field. In the presence of a magnetic field, a MHD-induced flow of electrolyte opens a new and efficient process of mass-transport from the bulk solution to the electrode. In the present electrolysis of phenylacetate ion, the reaction between benzyl radical and dissolved molecular oxygen is responsible for the formation of benzaldehyde. Thus, in a presence of a magnetic field, the supply of molecular oxygen from the bulk solution to the electrode surface can be improved because of the MHD flow. This results in the acceleration on the reaction of benzyl radical and molecular oxygen to yield benzaldehyde on the electrode surface. An effort to measure the magnetic field effects on the potential-current curve of the present solution was failed because of its high impedance (typically ≈20 V cm^{-1}).

An external magnetic field is expected to decrease the yields of the coupling products, which are formed via the competing paths with the benzaldehyde formation. However, no effects were detected concerning the yield of 1,2-diphenylethane and other coupling products, as shown in Table 1. In the present current conditions (9 mA cm^{-2}), benzaldehyde could be a minor product, since the relative yields of 1,2-diphenylethane, benzyl methyl ether, and benzaldehyde were reported to be 1:0.48:0.12 at the current density of about 7 mA cm^{-2}.[4)] Therefore, magnetic-field-induced change of benzaldehyde yield does not influence appreciably those of the coupling products because of the material balance.

The external magnetic field effects on photochemical and thermal reactions have been interpreted in terms of the radical pair model, in which triplet and singlet intersystem crossing of a radical pair, a short-lived intermediate, is affected by a magnetic field.[6)] Magnetic field effects due to a radical pair mechanism might be effective in the present reaction, since the coupling reaction of radicals, such as benzyl radicals, on the electrode could proceed via the radical-pair intermediate. However, we could not observe any appreciable magnetic field effects on the yield of 1,2-diphenylethane. The rate-determining step for the present coupling of radicals adsorbed on the electrode might not be the intersystem crossing in the radical pair, since the diffusion of adsorbed radicals on the electrode could be quite slow. Otherwise, the intersystem crossing might be accelerated by a magnetic-field-independent path, i.e., the spin-orbit interaction,[7,8)] since the radical pairs (radicals) are strongly adsorbed on the platinum electrode.

To our knowledge, this is the first report of the

magnetic field effect in organic electrochemistry, though a large number of papars have been concerned with inorganic electrochemistry.[1,2,9-11] We believe that the present finding demonstrates the applicability of an external magnetic field effect to the mechanistic study of organic electrochemistry.

References

1) Part II of this series: T. Watanabe, Y. Tanimoto, R. Nakagaki, M. Hiramatsu, T. Sakata, and S. Nagakura, *Bull. Chem. Soc. Jpn.*, **60**, 4163 (1987).

2) T. Watanabe, Y. Tanimoto, T. Sakata, R. Nakagaki, M. Hiramatsu, and S. Nagakura, *Bull. Chem. Soc. Jpn.*, **58**, 1251 (1985).

3) R. Adams and A. F. Thal, *Org. Synth.*, Coll. Vol. 2, 63 (1922).

4) J. P. Coleman, J. H. P. Utley, and B. C. L. Weedon, *J. Chem. Soc., Chem. Commun.*, **1971**, 438; J. P. Coleman, R. Lines, J. H. P. Utley, and B. C. L. Weedon, *J. Chem. Soc., Perkin Trans. 2*, **1974**, 1064.

5) Y. Takegami, Y. Fujimura, H. Ishii, and T. Iwamoto, *Kogyo Kagaku Zasshi*, **68**, 196 (1965).

6) For example, see: Y. Tanimoto, H. Hayashi, S. Nagakura, H. Sakuragi, and K. Tokumaru, *Chem. Phys. Lett.*, **41**, 267 (1976); Y. Tanimoto, T. Watanabe, R. Nakagaki, M. Hiramatsu, and S. Nagakura, *ibid.*, **116**, 341 (1985); R. Nakagaki, M. Hiramatsu, T. Watanabe, Y. Tanimoto, and S. Nagakura, *J. Phys. Chem.*, **89**, 3222 (1985); Y. Tanimoto, M. Takayama, M. Itoh, R. Nakagaki, and S. Nagakura, *Chem. Phys. Lett.*, **129**, 414 (1986); Y. Tanimoto, N. Okada, M. Itoh, K. Iwai, K. Sugioka, F. Takemura, R. Nakagaki, and S. Nagakura, *ibid.*, **136**, 42 (1987).

7) F. J. J. de Kanter, J. A. den Hollander, A. H. Huizer, and R. Kaptein, *Mol. Phys.*, **34**, 857 (1985).

8) G. L. Closs and O. D. Redwine, *J. Am. Chem. Soc.*, **107**, 6131 (1985).

9) S. Mohanta and T. Z. Fahidy, *Can. J. Chem. Eng.*, **50**, 248 (1972).

10) F. Takahashi, Y. Sakai, and T. Tamura, *Electrochim. Acta*, **28**, 1147 (1983).

11) R. Aogaki and K. Fueki, *J. Electrochem. Soc.*, **131**, 1295 (1984).

Stoichiometry Determination of Cation-Macrocyclic Complexes Based on the ^{1}H NMR Chemical Shift of the Cation-Coordinated Water Molecules

Tadashi Iwachido,* Koichi Shibuya,† Naoki Nakamura,† and Shoji Motomizu†
College of Liberal Arts, Okayama University, Tsushima, Okayama 700
†Department of Chemistry, Faculty of Science, Okayama University, Tsushima, Okayama 700
(Received May 23, 1987)

Synopsis. The stoichiometries of alkali and alkaline earth metal complexes with macrocyclic ligands were determined in a water-containing nitrobenzene solution by means of ^{1}H NMR. The chemical shift of the water protons was more sensitive to the complexation than that of the methylene protons of the ligands.

In early papers,[1-5] we showed that alkali and alkaline earth metal cations exist as hydrated state in a water-containing nitrobenzene solution and, when these cations undergo complexation with macrocyclic ligands, the water molecules attached to the cations are partially or almost fully released. These findings suggest that the equivalence point of the complexation may be detected by observing the chemical shift of the water protons as a function of the ligand concentration. The stoichiometries of unsubstituted 12- to 18-membered crown ether complexes with the alkali and alkaline earth metal cations have been determined by means of ^{1}H NMR.[6] In this paper, the usefulness of the method was confirmed with macrocyclic ligands, such as 21-crown-7 (21C7), 24-crown-8 (24C8), 4,7,13,16-tetraoxa-1,10-diazacyclooctadecane (C22) and 4,7,13,16,21,24-hexaoxa-1,10-diazabicyclo[8.8.8]hexacosane (C222).

Experimental

Materials. 21C7 was synthesized according to the method of Dale and Kristiansen.[7] The crude product was adsorbed on a cation-exchange column (Amberlite CG 120) connected to an anion-exchange column (Amberlite IRA-400, Rohm & Haas) and then eluted by water. Colored impurities were also removed by the deionization process. Evaporation of the solvent under reduced pressure left a viscous residue. The substance was dissolved in a small quantity of acetonitrile and then cooled in a refrigerator. The resulting crystalline 21C7-acetonitrile complex was decomposed under vacuum for at least 12 h at room temperature. The 21C7 thus obtained was ^{1}H NMR spectroscopically pure. 24C8 was synthesized in the same way. C22 and C222 (Merck) were used without further purification.

The alkali and alkaline earth metal salts with 2,2′,4,4′,6,6′-hexanitrodiphenylamine (HND) were prepared as described previously.[6] The Li, Sr, and Ba salts contained 4 molecules of water of crystallization, the Ca salt 11, and the K, Rb, and Cs salts contained none.

For ^{1}H NMR measurements, solutions were prepared by dissolving weighed ligands and salts into deuterated nitrobenzene (99%, Merck), the water content being adjusted by adding a certain amount of water-saturated nitrobenzene. The K, Rb, and Cs salts were made $(2.5—4.0)\times10^{-2}$ mol dm^{-3} solutions and the others $(1.5—5.0)\times10^{-3}$ mol dm^{-3} solutions. The ligands were made about 0.8 or 0.04 mol dm^{-3} solutions; the concentrated solutions were used for the titration of the concentrated salt solution.

NMR Measurements. To an NMR tube, 400 μl of the salt solution was transferred and the chemical shift of the water proton was measured on a Hitachi FT-NMR R600 (60 MHz) spectrometer. A 5 μl-aliquot of a ligand solution was added to the solution and mixed well on a vibrator-type mixer. The chemical shifts of both the water proton and the ligand protons were measured. The measurements were repeated until the ligand/cation mole ratio increased to about 2 or 3. Tetramethylsilane was used as internal standard. The chemical shifts were reproduceced within 0.4 Hz. All the measurements were carried out at 25 °C.

Results and Discussion

^{1}H NMR Spectra. The chemical shift spectra for Ca^{2+}–C222 at different ligand/cation mole ratios are shown in Fig. 1. The spectrum of the free ligand (**0**) consisted of a triplet due to $-OCH_2-$ (about δ 3.6), a triplet for $-NCH_2-$ (about δ 2.6), and a singlet for $-OCH_2CH_2O-$ (δ 3.7). A peak at δ 2.5 may be due to residual water in the solvent. Resonance signals centered at about δ 8 are due to the aromatic protons of undeuterated nitrobenzene. The spectrum of a water-containing ligand-free $Ca(HND)_2$ solution (**1**) consisted of two singlets (water and aromatic protons of HND at δ 3.2 and 8.8, respectively). Addition of the ligand to this solution resulted in a strong upfield shift of the water protons (from δ 3.2 in **1** to 3.0 in **2**

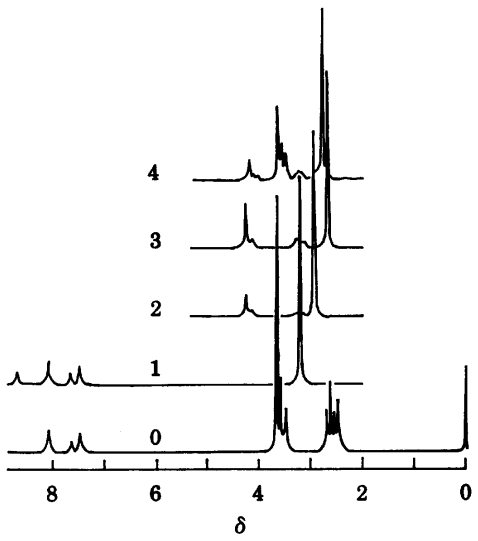

Fig. 1. ^{1}H NMR spectra of the water and ligand protons for Ca^{2+}–C222.
Initial concn of Ca^{2+}: 0.0048 M (1 M=1 mol dm^{-3}).
0: C222, **1**: [L]/[M]=0, **2**: [L]/[M]=0.5, **3**: [L]/[M]=1, **4**: [L]/[M]=2.0.

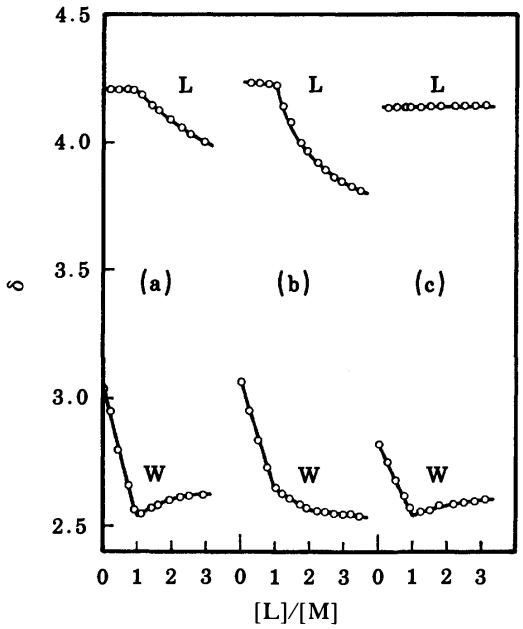

Fig. 2. Signal shifts of the ligand and water protons as a function of [L]/[M].
W: water signal, L: ligand signal.
(a): Ca^{2+}(0.0048 M)-C222, (b): Ca^{2+}(0.0024 M)-21C7, (c): Ca^{2+}(0.0022 M)-C22.

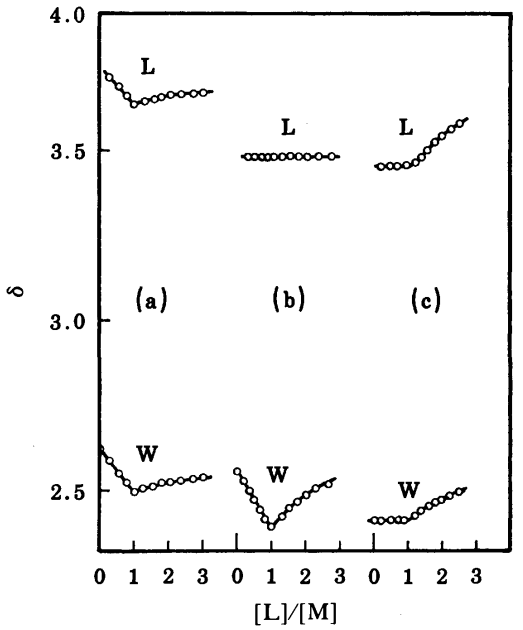

Fig. 3. Signal shifts of the ligand and water protons as a function of [L]/[M].
W: water signal, L: ligand signal.
(a): Li^{+}(0.034 M)-C222, (b): K^{+}(0.034 M)-C222, (c): Cs^{+}(0.031 M)-C222.

([C222]/[Ca^{2+}]=0.5)) and a strong downfield shift of the methylene signals due to complexation (from δ 2.6 and 3.6 in **0** to δ 3.2 (weak) and 4.2 in **2**, respectively). As the titration proceeded, the water signal continued to shift upfield until the equivalence point (**3**, [C222]/[Ca^{2+}]=1) was reached, but the signals of the complexed ligand showed virtually no shift. The further addition of the ligand caused a downfield shift of the water signal and a slight upfield shift of the signals of the complexed ligand (**4**, [C222]/[Ca^{2+}]=2). It was noted that, in spectrum **4**, the free ligand signals reappeared at δ 2.6 (not clear) and 3.6; the reappearance of the free ligand signals in the presence of excess ligand, however, was observed only with Sr^{2+}- and Ba^{2+}-15C5.

The spectral changes for C22 complexes were quite similar to those of C222. Uncomplexed 21C7 and 24C8 each gave a sharp singlet at δ 3.7 and their signal-shift patterns due to complexation were almost identical with those of 12- to 18-membered crown ethers.[6] Concerning the shift patterns, we found no fundamental difference between the 12- to 24-membered crown ethers and the nitrogen-containing macrocycles.

The magnitude and direction of the signal shifts for Ca^{2+}–C222 can clearly be seen from Fig. 2a, where curve W denotes the shift of the water signal and curve L, that of the ligand signal (-OCH_2CH_2O-). Hereafter, the signal shift measurements for C22 and C222 were made on this signal because of the ease of the measurements. Some typical shift patterns are shown in Figs. 2 (b,c) and 3 (a,b,c).

Curves W always exhibited a single break point at [L]/[M]=1, indicating the formation of 1:1 (M:L) complexes in the solution. There were, however, a few cases in which curves L lacked a break point. The curve W for Ca^{2+}–21C7 exhibited two break points at [L]/[M]=1 and 2 (Fig. 2b); the curve L, however, showed no break point at [L]/[M]=2. The curve L for Rb^{+}–C22 (Fig. 2c) lacked a break point. The same observation was true for K^{+}–C222 (Fig. 3b). The C222 signal (Fig. 3a) shifted upfield as the titration proceeded. The upfield shift was characteristic of all the complexes formed between small cations and ligands having a relatively large cavity. The water signal in Fig. 3c exhibited no shift until the equivalence point was reached; this was the case with Cs^{+}–C222 alone.

Chemical Shift of Water Protons. The complexation between hydrated cations and macrocyclic ligands can simply be represented as follows:

$$M(H_2O)_i + L \rightleftharpoons M(H_2O)_jL + (i-j)H_2O \quad (1)$$

$$kH_2O + L \rightleftharpoons L(H_2O)_k \quad (2)$$

where $i>j$. Two types of water molecules, i.e., cation- or ligand-bound and free, are present during the course of the titration. Based on the fast proton exchange between the bound and free water molecules, the water signal gave only one population-averaged peak. The population of the free water increases with the ligand concentration (Eq. 1). The characteristic upfield shift of water protons before the equivalence point can be explained by taking into account that the free water resonates at a higher field than the bound water. The downfield shift beyond the equivalence point can likewise be accounted for by a decrease in the free water (Eq. 2).

Table 1. [L]/[M] Values at the Break Points for the Alkali Metal Complexes

Ligand	Signal	Li^+	Na^+		K^+	Rb^+	Cs^+
12C4[a]	L[b]	1.00	0.88	2.02	0.96	0.97	1.03
	W[c]	0.98	0.99	1.99	0.97	0.99	1.00
15C5[a]	L	1.04	1.02		0.99	0.96	1.00
	W	0.98	1.00		0.99	0.98	0.96
18C6[a]	L	0.97	1.00		—	—	—
	W	1.05	0.95		1.00	0.98	1.01
21C7	L	1.00	—[d]		1.03	0.97	1.00
	W	1.00	1.02		1.00	1.00	1.00
24C8	L	1.00	1.00		1.00	0.96	1.02
	W	1.00	0.98		0.99	0.99	0.95
C22	L	0.99	1.00		1.06	1.02	1.00
	W	0.99	1.00		1.01	1.00	0.99
C222	L	1.03	—		—	—	0.99
	W	0.96	0.99		1.00	1.00	0.99

a) Revised from the data in Ref. 7; a few were redetermined. b) Ligand signal. c) Water signal. d) The symbol "—" indicates the lack of a break point.

Table 2. [L]/[M] Values at the Break Points for the Alkaline Earth Metal Complexes

Ligand	Signal	Ca^{2+}		Sr^{2+}		Ba^{2+}	
12C4[a]	L[b]	—[d]	2.00	—	2.00	1.00	2.00
	W[c]	—	1.96	0.94	1.97	1.02	2.00
15C5[a]	L	0.99	2.00	1.02		—	—
	W	0.98	2.07	0.98	1.92	1.00	1.96
18C6[a]	L	1.04		0.99		1.00	
	W	0.98		1.01		1.04	
21C7	L	1.01		1.02		0.98	
	W	1.00	2.00	0.97		0.98	
24C8	L	1.05		1.00		0.97	
	W	0.98		0.99		0.96	
C22	L	—		1.09		0.97	
	W	0.99		0.99		0.98	
C222	L	1.02		0.99		1.05	
	W	1.00		1.00		0.99	

a) Revised from the data in Ref. 7; a few were redetermined. b) Ligand signal. c) Water signal. d) The symbol "—" indicates the lack of a break point.

It follows from the above discussion that the [L]/[M] ratio at the break point represents the stoichiometry of the complex in solution.

Usefulness of the Water Signal. The curves W were always V-shaped, exhibiting at least one break point; this has enabled sensitive and accurate stoichiometry determination. On the other hand, the curves L were mostly less sensitive and, for some complexes, completely insensitive to the complexation. It can, therefore, be concluded that the water signal is used to advantage in determining the stoichiometries of macrocyclic complexes.

Stoichiometries of the Complexes. The [L]/[M] ratios at the break points are summarized in Tables 1 and 2, together with the revised ones for 12C4, 15C5, and 18C6. The data obtained were all consistent with those reported by others.[8] As regards the present experiments, 1:1 complexes were found for all complexation systems. 1:2 complex was found only for Ca^{2+}–21C7.

References

1) S. Motomizu, K. Tôei, and T. Iwachido, *Bull. Chem. Soc. Jpn.*, **22**, 1006 (1969).
2) M. Kawasaki, K. Tôei, and T. Iwachido, *Chem. Lett.*, **1972**, 417.
3) T. Iwachido, M. Kimura, and K. Tôei, *Chem. Lett.*, **1976**, 1101.
4) T. Iwachido, M. Minami, A. Sadakane, and K. Tôei, *Chem. Lett.*, **1977**, 1151.
5) T. Iwachido, M. Minami, M. Kimura, A. Sadakane, M. Kawasaki, and K. Tôei, *Bull. Chem. Soc. Jpn.*, **53**, 703 (1980).
6) T. Iwachido, K. Shibuya, and K. Tôei, *Chem. Lett.*, **1985**, 307.
7) J. Dale and P. O. Kristiansen, *Acta Chem. Scand.*, **26**, 1471 (1972).
8) "Coordination Chemistry of Macrocyclic Compounds," ed by G. A. Melson, Plenum Press, New York (1979), p. 180, and the references cited therein.

Crystal and Molecular Structure of Bis(benzylamine)bis(thiocyanato)-cadmium(II), $[Cd(SCN)_2(C_6H_5CH_2NH_2)_2]$

Masahiro TANIGUCHI* and Akira OUCHI
Department of Chemistry, College of Arts and Sciences, The University of Tokyo, Komaba, Meguro-ku, Tokyo 153
(Received May 23, 1987)

Synopsis. The crystal and molecular structure of the title complex was determined by means of a single-crystal X-ray diffraction method. A crystal of $CdC_{16}H_{18}N_4S_2$, F. W. 442.8, is monoclinic, with the space group of $P2_1/n$, a=27.390(19), b=5.7709(8), c=5.8733(9) Å, β=90.35(3)°, U=928.3(7) Å^3, Z=2, D_m=1.57(3), D_x=1.58 Mg m^{-3}, and μ(Mo $K\alpha$)=1.59 mm^{-1}. The cadmium(II) atom is hexa-coordinated being ligated with two thiocyanato (SCN) sulfur atoms, as well as with two SCN and two benzylamine nitrogen atoms, where the respective pairs of the same kinds of atoms are all in trans-configuration. Each cadmium atom is at the center of symmetry, and the coordination structure around the atom is symmetric. The metal atoms are lined along c-axis, and the pair of the neighboring metal atoms are doubly bridged by SCN ions, although the bridges are a little weaker than the other same type adducts.

There are already several structural reports about the Lewis-base (L) adducts of cadmium(II) thiocyanate, $Cd(SCN)_2L_2$, where L is 1-, 2-, or 3-methylpyridine,[1,2] dibenzylamine,[3] 2-imidazolidinethione,[4] or 1*H*-1,2,4-triazole.[5] In all of them, the octahedrally coordinated cadmium(II) complex cores are laid linearly, and each pair of the neighboring metal atoms are doubly bridged by the thiocyanate (SCN) ions.

This time, we could obtain the same type adduct of benzylamine (bza), $Cd(SCN)_2(bza)_2$, and it was thought to be interesting to clarify its structure due to the reasons as follows. First, how is the direction of the benzene rings of the ligands in the crystal? Although their benzene rings can rotate around the methylene-carbon atom, even in the complex molecule, they must be laid regularly in the crystal to attain the closest packing in it. Therefore, what kind of the arrangement of the rings is adopted there, or whether the π-electron interaction due to the overlapping of the benzene rings exists or not, are interesting problems. Secondly, a preliminary test has shown that the crystal has a unit cell in which only the a-axis is very long, while the other two axes are short; why such long and short periodicities in the crystal take place? Thirdly, to better clarify the character of this type of the double SCN bridging, it is necessary to add more data about the complexes with the bridge.

From these points of view, we determined its crystal and molecular structures by the single-crystal X-ray diffraction method.

Experimental

Synthesis of Bis(benzylamine)bis(thiocyanato)cadmium-(II). Cadmium(II) thiocyanate (0.57 g, 2.5 mmol) was dissolved into 20 cm^3 of methanol; benzylamine (0.53 g, 5 mmol) dissolved into 10 cm^3 of methanol was added to it, and mixed. The mixed solution gradually became turbid and precipitation started soon. After being left standing about 30 min at ambient temperature, the deposited crystals were filtered off, washed with acetone, and dried in open air. Yield, 1.0 g (90%). Found; Cd, 25.37; C, 43.07; H, 4.03; N, 12.57%. Calcd for ($CdC_{16}H_{18}N_4S_2$) Cd, 25.38; C, 43.39; H, 4.10; N, 12.65%.

Single Crystal X-Ray Structure Analysis. The colorless crystal used for the structure determination was 0.3×0.3×0.15 mm^3 in size, and was used without shaping. The intensities in the range of $3<2\theta<60°$ (2θ) were collected on a Rigaku AFC-6A automated four-circle X-ray diffractometer using graphite monochromated Mo $K\alpha$ radiation (λ=0.71073 Å), by means of ω-scan technique (scan speed 4° min^{-1}; scan width 1.08° (θ)). The intensities were corrected for Lorentz and polarization factors, but no corrections were made for absorption and extinction. Of 3667 independent intensities collected, 2273 with $|F_o|>3\sigma(|F_o|)$ were used for the structure determination.

All the calculations were carried out on a HITAC M-680H computer at the Computer Center of the University of Tokyo, using UNICS III.[6] The scattering factors were taken from Ref. 7.

The structure was solved by the heavy-atom method. The positions of the metal and some sulfur atoms were deduced from a three dimensional Patterson map: other non-hydrogen atoms were succesively located by means of the Fourier syntheses. The positional, isotropic and then anisotropic thermal parameters were refined by a block-diagonal least-squares method. At the final step, all hydrogen atoms were added in the refinement, fixing at the calculated positions (C–H=1.08 Å for the benzene-ring hydrogen atoms, and 1.09 Å for the methylene ones, β_{iso}=8.0 Å^2 being given). The final R and R_w values[8] thus obtained were 0.042 and 0.052, respectively.

Results and Discussion

The selected bond lengths and bond angles are shown in Table 1. A perspective drawing of the complex together with the numbering scheme of the atoms, except the benzene rings of the ligands, is shown in Fig. 1.[9] The projections of the unit cell along b- and c-axes are shown in Figs. 2 and 3, respectively.[10]

The cadmium atoms are lined along c-axis and the respective pair of the side-by-side metal atoms are bridged by two SCN ions as in the case of the other $Cd(SCN)_2L_2$ type adducts.[1-5]

As shown in Fig. 1, around one cadmium(II) atom, two SCN sulfur, two SCN nitrogen, and two bza nitrogen atoms are coordinated, where each pair of the same kinds of the ligating atoms are in trans-configurations. The bond lengths are; Cd–S is 2.7540(15), Cd–N(SCN) is 2.372(3), and Cd–N(bza) is 2.294(3) Å, respectively. The Cd–N(bza) bond length is shorter than, and the Cd–N(SCN) length is longer than, the corresponding bonds of the other Cd-

Table 1. Bond Lengths and Bond Angles of the Title Complex with Estimated Standard Deviations in Parentheses

Bond length	(l/Å)	Bond length	(l/Å)	Bond length	(l/Å)
Cd-S	2.7540(15)	Cd-N(1^{ii})	2.372(3)	Cd-N(2)	2.294(3)
S-C(1)	1.652(4)	N(1)-C(1)	1.143(5)	N(2)-C(2)	1.482(6)
C(2)-C(3)	1.496(6)				
Bond angle	**(ϕ/°)**	**Bond angle**	**(ϕ)/°**	**Bond angle**	**(ϕ/°)**
S-Cd-N(1^{ii})	90.52(9)	S-Cd-N(2)	87.69(9)	N(1^{ii})-Cd-N(2)	88.17(12)
Cd-S-C(1)	99.15(14)	Cd-N(1^{ii})-C(1^{ii})	145.2(3)	S(1)-C(1)-N(1)	177.3(4)
Cd-N(2)-C(2)	118.7(3)	N(2)-C(2)-C(3)	112.8(4)	C(2)-C(3)-C(4)	120.4(4)
C(2)-C(3)-C(8)	120.8(4)	C(4)-C(3)-C(8)	118.8(4)		

Key to the symmetry operation: ii, $-x$, $-y$, $1-z$.

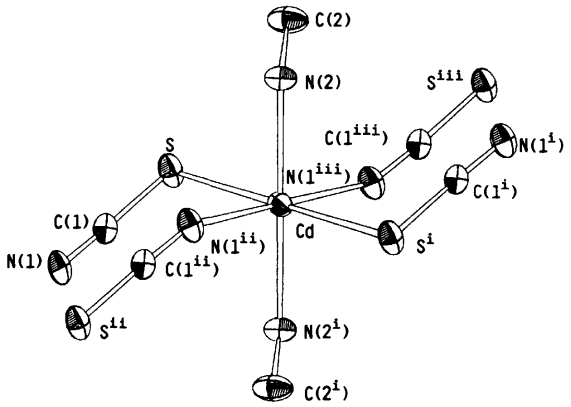

Fig. 1 A perspective drawing of the title complex around the central metal atom with the numbering scheme of the ligating atoms. The key to the symmetry operation: i, $-x$, $-y$, $-z$; ii, $-x$, $-y$, $1-z$; iii, x, y, $-1+z$.

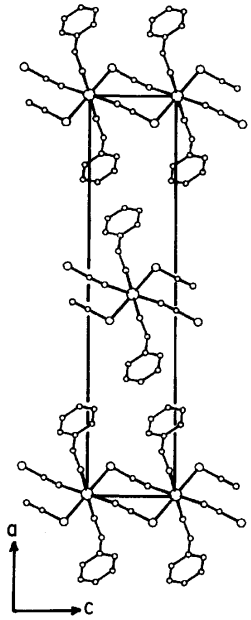

Fig. 2. The projection of the unit cell along b-axis.

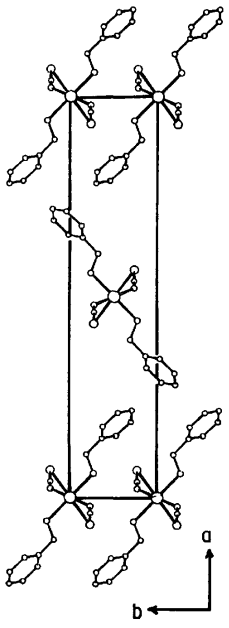

Fig. 3. The projection of the unit cell along c-axis.

$(SCN)_2L_2$ type Lewis base adducts, although their Cd-S(SCN) bond lengths are not much different from each other.[1-5] It is noteworthy that the Cd-N(base) bonds are stronger than the Cd-N(SCN) bonds in this complex; reverse to the other base adducts.

The Cd-N-C(SCN) angle, 145.2(3)°, is much smaller than the other thiocyanato complexes: commonly in the range of 180—160°.[11] However, S-C-N angle, 177.3(4)°, as well as Cd-S-C, 99.15(14)°, are not much different from the corresponding values of the type of cadmium(II) thiocyanate adducts ($Cd(SCN)_2L_2$).[1-5]

An eight-membered ring consisting of the two metal atoms and two SCN ions bridging them is in the chair form. The metal atom deviates 1.063 Å from the least-squares plane by six atoms of the two SCN ions (the average deviation of the six atoms are 0.010 Å); the deviation is much larger than the other adducts of this type.[1-5]

From these data, we deduce that the ring is quite deformed and the bridging of the double SCN chains in this complex is weaker than those in the other complexes of this type: The Cd···Cd distance, 5.8733(9) Å (the same as the c-axis length) is longer than the corresponding distances of the latters.[1-5]

As shown in Figs. 2 and 3, no bridgings are found between the complex chains. Respective chains are parallel to the bc-plane. They are intercalated by the parallel hydrophobic layers consisting of the ligand benzene-rings of both side complexes; the rings from both side complexes are not interposed with each other, and the rings from one side metal complexes are not parallel with those of the other side metal complexes. There is no overlapping between the neighboring parallel benzene-ring planes,[12] and no π-electron interaction between the benzene rings are expected. However, such short structural periodicities found in the directions of the b- and c-axes are probably due to the quite regular and closely packed arrangement of the benzene rings in the crystal as above mentioned.

References

1) M. Taniguchi, M. Shimoi, and A. Ouchi, *Bull. Chem. Soc. Jpn.*, **59**, 2299 (1986).

2) M. Taniguchi, Y. Sugita, and A. Ouchi, *Bull. Chem. Soc. Jpn.*, **60**, 1321 (1987).

3) M. Taniguchi and A. Ouchi, *Bull. Chem. Soc. Jpn.*, **60**, 1192 (1987).

4) L. Cavalca, M. Nardelli, and G. Fava, *Acta Crystallogr.*, **13**, 125 (1960).

5) J. G. Haasnoot, G. C. M. de Keyzer, and G. C. Verschoor, *Acta Crystallogr., Sect. C*, **39**, 1207 (1983).

6) T. Sakurai and K. Kobayashi, *Rikagaku Kenkyusho Hokoku*, **55**, 69 (1979).

7) "International Tables for X-Ray Crystallography," Kynoch Press, Birmingham (1974), Vol. IV, pp. 72, 150.

8) $R=\Sigma||F_o|-|F_c||/\Sigma|F_o|$;
$R_w=\{\Sigma w(|F_o|-|F_c|)^2/\Sigma w|F_o|^2\}^{1/2}$ where
$w=1/[\{\sigma(|F_o|)\}^2+(0.0006|F_o|)^2]$

9) The numbering of the benzene-ring carbon atoms are as follows. The stem methylene carbon atom, C(2), is bonded with the ring carbon atom C(3), and the ring carbon atoms are numbered successively from C(3) to C(8) where the C(3) and C(8) atoms are bonded.

10) The positions of the hydrogen atoms, the final anisotropic temperature factors of non-hydrogen atoms, the final F_o-F_c table, and some additional data of bond lengths and bond angles are deposited as Document No. 8762, at the Office of the Editor of Bull. Chem. Soc. Jpn.

11) A. F. Wells, "Structural Inorganic Chemistry," fifth ed, Clarendon, Oxford, U. K. (1984), p. 935.

12) It was examined that when one ring is projected to the other ring plane, whether the projection and the latter ring was overlapping or not.

Terpenoids. IX.[1] Permanganate Oxidation of Thujopsene. 2.[2] Neutral Products

Shizuo NAGAHAMA* and Masato TAZAKI
The Kumamoto Institute of Technology, Ikeda 4-22-1, Kumamoto 860
(Received April 10, 1987)

Synopsis. Permanganate oxidation of thujopsene **1** in dry and aqueous acetone was reexamined with a careful separation of the neutral part of the products. In dry acetone, the major products were Δ^9-thujopsen-8β- and 8α-ols (**2** and **3**) which easily decomposed to thujopsadiene **6**. In aqueous acetone, **1** gave 8β-hydroxythujopsan-9-one **8** and thujopsane-8α,9α-diol **11** as main products, besides 8β,9β-diol **10**, 8α-hydroxythujopsan-9-one **9**, and epimeric allyl alcohols **2** and **3**. The hydroxy ketone **8** was isomerized to a ring contracted compound, 4α-acetyl-4β-hydroxy-6α,10,10-trimethyltricyclo[4.4.0.0^{1,3}]decane **4** during alumina chromatography. 8β,9-Epoxy-10-thujopsanone **5** was isolated as a minor product. Kawamura's glycol was an eutectic mixture of **10** and **11**.

For the structural elucidation of thujopsene **1**, permanganate oxidation of this compound in dry acetone has been studied.[2,3] From the neutral part of the products, a considerable amount of "isomerized hydrocarbon" was isolated by distillation[2] and identified later as thujopsadiene **6** by the author.[4] The formation of such a diene **6** by permanganate oxidation is interesting and a reexamination was undertaken.

Kawamura[5] obtained a glycol, mp 92—3 °C, from thujopsene by permanganate oxidation in aqueous acetone. Later Traas et al.[6] obtained thujopsane-8β,9β-diol **10** (mp was not announced) and 8α,9α-diol **11**, mp 79—80 °C, from thujopsene by osmium tetraoxide oxidation. To clarify the relation of these products, permanganate oxidation in aqueous acetone (Kawamura's conditions) has also been carried out.

Results and Discussion

Oxidation in Dry Acetone: The neutral products showed two main peaks on GLC analysis (PEG-HT), in a ratio of about 2:1, accompanying at least 8 minor peaks, besides unchanged hydrocarbon **1**. The mixture was chromatographed on an alumina column and the main product isolated as an oil. The IR spectrum of the oil showed the presence of an OH group. The NMR spectrum showed four tertiary methyl groups, two vinyl protons and some protons on a cyclopropane ring. The structure was considered to be Δ^9-thujopsen-8β-ol **2**.

The second main product **3** (produced in about half the amount of **2**) crystallized and was identified as Δ^9-thujopsen-8α-ol, mp 110—2 °C (lit, mp 110—2 °C).[7] It was unstable and decomposed, on standing, to a liquid from which thujopsadiene **6** and mayurone **7** could be separated. The amount of **6** in the neutral product was estimated as about 1% from the analysis of the hydrocarbon fraction separated by column chromatography. Therefore most of **6** previously obtained[2] was considered to be a secondary product from these allyl alcohols by dehydration during distillation.

Two major by-products were separated as crystals. One was previously described as "oxyketone," $C_{15}H_{24}O_2$, mp 68—70.5 °C.[3] The NMR data showed one acetyl group at 2.31 ppm as well as three tertiary methyl groups and some protons on the cyclopropane ring. Thus a ring contracted structure, 4α-acetyl-4β-hydroxy-6α,10,10-trimethyltricyclo[4.4.0.0^{1,3}]-decane **4** was proposed for this compound. The β-hydroxy configuration was based on a high field shift of Hα-C(2) upon $NaBH_4$ reduction of **4** to the corresponding glycols. The NMR analysis of the initial mixture showed the absence of **4** and the presence of 8β-hydroxy-9-thujopsanone **8** (see below). Thus **4** was formed from **8** by α-ketol rearrangement during separation on the alumina column. Another by-product mp 75—7 °C possessed an IR band at 1690 cm^{-1} which is characteristic of a C=O group adjacent to a three membered ring. NMR data showed one singlet proton on an epoxy ring at δ 3.14, four tertiary methyl groups and cyclopropane protons. Thus, the 8β,9-epoxy-10-thujopsanone **5** structure was assigned to this compound. The β-configuration of the epoxy ring was proposed, based on the high magnetic field shift of Hα-C(6).

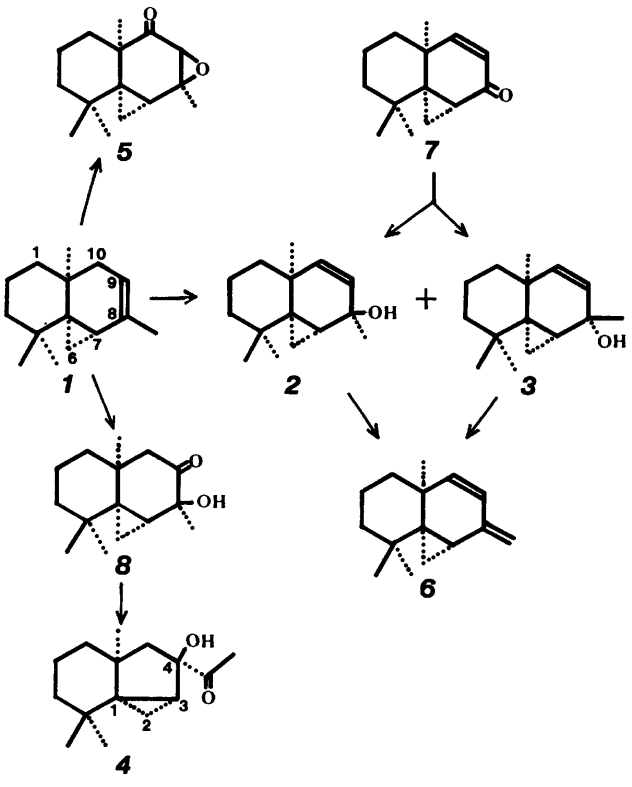

Since the formation of allyl alcohols on permanganate oxidation of alkenes is unfamiliar to our knowledge, further study of the structure of **2** and **3** was required. Grignard methylation of mayurone **7** gave **2** and **3** in a ratio of 1:9. Relative values of the lanthanoide-induced shift (LIS) using $Eu(fod)_3$ and $Pr(fod)_3$ are summarized in Table 1. The data show that the OH group of **3** is closer to the cyclopropane ring than that of **2**. Thus, the OH group in **3** must be in an α-configuration, and that in **2** in a β-configuration. Interestingly, all of the three tertiary methyl groups remote from the OH group in the epimers **2** and **3** showed the same chemical shifts. The difference in the LIS values of the bridge head proton, H-C(7), in **2** and **3** is small. These results show that the epimers have the same ring conformation in which the cyclohexene ring has a boat form with a flag pole of a C(1) atom. The LIS data observed for two vinyl protons and two methylene protons on the cyclopropane ring are consistent with this conformation.

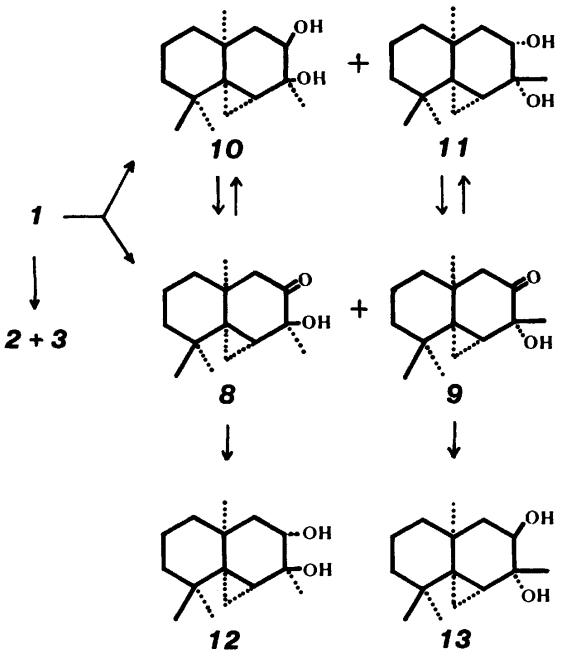

Table 1. Lanthanoide-Induced Shift (LIS) of **2** and **3**

Proton	Chemical shift δ/ppm		Relative LIS	
	2	**3**	**2**	**3**
(Cyclopropane)				
Hα on C(6)	0.02	0.22	0.449	0.754
Hβ on C(6)	0.44	0.39	0.321	0.465
H on C(7)	1.55	1.48	0.990	0.916
(Vinylic)				
H on C(9)	5.24	5.10	0.786	0.983
H on C(10)	5.15	4.92	0.368	0.340
(Methyl)				
Me on C(8)	1.28	1.40	1.00	1.00
Me	0.66	0.65	0.152	0.207
Me	1.07	1.06	0.143	0.156
Me	1.17	1.15	0.216	0.216

Oxidation in Aqueous Acetone: Gas chromatographic analysis of the neutral product obtained under Kawamura's conditions showed two main peaks besides more than 12 minor peaks. Chromatographic separation with silica gel gave a mixture of *cis*-8,9-diols **10** and **11** as one of the main products. The mixture of **10** and **11** showed a single peak on gas chromatography. The ratio of **10** to **11** was about 1:4 by NMR analysis. Further chromatography of the mixture on neutral alumina gave 8β,9β-diol **10**, mp 68—71 °C and 8α,9α-diol **11**, mp 71—3 °C. Repeated recrystallization of a mixture of **10** and **11** from hexane gave binary eutectic crystals of mp 92 °C corresponding to Kawamura's glycol.

Another main product **8** was separated as an oil. IR showed the presence of OH and C=O groups. NMR showed an isolated CH_2-(C=O) group, four tertiary methyl groups and a cyclopropane ring. $NaBH_4$ reduction of **8** gave **10** and a *trans*-diol **12**, mp 62—3 °C in a ratio of 2:1. CrO_3 oxidation of **10** in pyridine gave **8**. Thus **8** was 8β-hydroxythujopsan-9-one. Semicarbazone, mp 230 °C.

The epimeric 8α-hydroxythujopsan-9-one **9** was obtained as a crystalline minor product, mp 97—8 °C. $NaBH_4$ reduction of **9** gave **11** and a *trans*-diol **13**, mp 76—8 °C in a ratio of about 2:3. CrO_3 oxidation of **11** gave **9**. α-Ketol rearrangement of **8** was easy as described above. However, the rearrangement of **9** was found to be slow.

Δ^9-Thujopsen-8β-ol (**2**) and -8α-ol (**3**), the main products under nonaqueous conditions, became minor products.

Experimental

The ^1H NMR spectra were measured with JEOL JNM-PMX 60si in $CDCl_3$ solution. GLC analyses were performed on a Shimadzu GC-5A gas chromatograph with PEG-HT glass column 1.0 or 1.5 m. The column temperature was elevated from 100 to 220 °C at a rate of 5 °C min^{-1}.

Thujopsene **1** was separated from Hiba wood neutral oil perchased from Soda Aromatic Co., by a spinning band distillation with Tokyo Kagaku Seiki Co., Model SB 818 (1.8 m height) and the fraction of bp 124—6 °C/10 mmHg† (purity 95% up) was used immediately after passing through a silica-gel column to eliminate some autoxidation products.

Oxidation in Dry Acetone: Thujopsene **1** 30.4 g (0.149 mol) was dissolved in 250 ml of dry acetone and 47 g (0.30 mol) of $KMnO_4$ was added portionwise below 6 °C under nitrogen atmosphere. The mixture was stirred for 12 h and MnO_2 was filtered off. Evaporation of the acetone left 11.8 g of residue. The MnO_2 was washed twice with acetone and additional 7.7 g of extract was obtained. The combined residue was dissolved in hexane and shaken with aqueous Na_2CO_3 solution and NaOH solution successively, giving 14 g of neutral products. Gas chromatography showed unreacted hydrocarbon **1** 33.5%, thujopsadiene **6** 2%, **2** 28.5%, **3** 14.5%, **8** 6.5% and **5** 5%. Extraction of MnO_2 with hot water gave neutral product 1.1 g. Gas chromatography showed 67% of thujopsane-8,9-diol.

† 1 mmHg=133.322 Pa.

Separation by Column Chromatography: The separation was accomplished by passage through an alumina column (320 g). Hexane eluted hydrocarbons and **5** successively. Hexane-CH_2Cl_2 (4:1) eluted **2**, hexane-CH_2Cl_2 (1:1) eluted **3** and CH_2Cl_2 eluted **4**. Δ^9-Thujopsen-8β-ol (**2**): Oil. IR (neat) 3400 (OH), 3060, 1665, 1100, 910, and 760 cm^{-1}. ^1H NMR ($CDCl_3$) δ=0.02 (1H, dd, J=5 and 4 Hz), 0.44 (1H, dd, J=9 and 4 Hz), 0.66 (3H, s), 1.07 (3H, s), 1.17 (3H, s), 1.28 (3H, s), 1.0—1.7 (6H, m), 1.55 (1H, ddd, J=9, 5 and 2 Hz), 5.15 (1H, d, J=10 Hz), and 5.24 (1H, dd, J=10 and 2 Hz). Δ^9-Thujopsen-8α-ol (**3**): mp 110—2 °C. IR (KBr) 3300 (OH), 3060, 1660, 1125, 1090, 940, 750, and 738 cm^{-1}. ^1H NMR ($CDCl_3$) δ=0.29 (1H, dd, J=5 and 4 Hz), 0.39 (1H, dd, J=9 and 4 Hz), 0.65 (3H, s), 1.0—1.7 (6H, m), 1.06 (3H, s), 1.15 (3H, s), 1.40 (3H, s), 1.48 (1H, ddd, J=9, 5 and 2 Hz), 4.92 (1H, d, J=10 Hz), and 5.10 (1H, dd, J=10 and 2 Hz). Ring contracted hydroxy ketone **4**: mp 69—70 °C. IR (KBr) 3450, 3370, 3200, 1698, 1350, 1235, and 1048 cm^{-1}. ^1H NMR ($CDCl_3$) δ=0.35—0.82 (2H, m), 0.60 (3H, s), 1.03 (3H, s), 1.13 (3H, s), 1.3—2.3 (7H, m, broad), 1.33 (1H, d, J=14 Hz), 1.72 (1H, d, J=14 Hz), 2.31 (3H, s), and 3.75 (1H, broad). 8β,9-Epoxy-10-thujopsanone (**5**): mp 75—7 °C. IR (KBr) 3050, 3025, 1690 (C=O), 1372, 1250, 1090, 850, and 818 cm^{-1}. ^1H NMR ($CDCl_3$) δ=0.00 (1H, dd, J=6 and 5.5 Hz), 0.78 (1H, dd, J=8.5 and 6 Hz), 0.67 (3H, s), 1.05 (3H, s), 1.33 (3H, s), 1.52 (3H, s), 1.3—2.3 (6H, m), 1.77 (1H, dd, J=8.5 and 5.5 Hz) and 3.14 (1H, s).

Isomerization of 8-Hydroxy-9-thujopsanone 8 to 4 by Alumina: Eighty three mg of **8** was dissolved in hexane and loaded on a column containing 10.5 g alumina deactivated with 1.05 ml of water. After one day, 82 mg of **4** was eluted with ether as the sole product.

Synthesis of 2 and 3 from Mayurone (7): To a Grignard reagent from 0.080 ml of methyl iodide in 3 ml ether was added dropwise 21 mg of mayurone in 1 ml ether. After 15 min at 0 °C, the mixture was cooled on a Dry Ice methanol bath, hydrolyzed with aqueous ammonium acetate, and extracted with hexane-ether (1:1). The extract was washed twice with saturated sodium chloride, dried over sodium sulfate and evaporated to give 21 mg of residue. GLC of the residue showed 7% of **2**, and 63% of **3** besides 11% of **6** and 12% of an unidentifiable product.

Lanthanoide-Induced Shift (LIS) of 2 and 3: ^1H NMR spectra were measured for ca. 20 mg of **2** and **3** in 0.35 ml $CDCl_3$ by adding stepwise $Eu(fod)_3$ and $Pr(fod)_3$ (3—5 mg for each measurement). The LIS values of CH_3-C(8) were from +2.4 to −8.0 ppm for **2** and from +3.4 to −5.5 ppm for **3**. A good straight line was obtained when the chemical shift values of each proton at various concentrations of the shift reagents were plotted against the corresponding values of CH_3-C(8). The relative value of LIS (1.00 for CH_3-C(8)) was obtained from the slope. The chemical shift values of cyclopropane ring protons were also obtained by extrapolating the concentration of the shift reagents to zero. The results are summarized in Table 1.

Oxidation in Aqueous Acetone: Potassium permanganate 14.0 g (88.6 mmol) was added portionwise to a mixture of thujopsene 14.0 g (68.5 mmol) in 140 ml of acetone and 14 ml of water under ice water cooling. The mixture was stirred overnight and filtered. The filtrate was evaporated under reduced pressure, and the residue was dissolved in hexane. The MnO_2 was extracted with hot water several times. The oil which separated from the water layer was extracted with hexane. The hexane solutions were combined and extracted with aqueous sodium carbonate solution. They afforded 13.4 g of neutral product and 1.7 g of acidic product. Gas chromatography of the neutral product yielded unreacted hydrocarbon **1** 26%, thujopsadiene **6** 0.4%, **2** 8.0%, **3** 4.0%, **8** 22.1%, **9** 4.5% and cis-diols (**10** and **11**) 25.1%.

Separation: The neutral product 27 g was chromatographed on a column (45 mm i.d. ×49 cm) packed with 350 g of Fuji gel CQ-3 silica gel. The eluent was fed with a Chemco Low Prep Pump Model 81-M-2. Hexane eluted hydrocarbons. Most of **2** and **3** were dehydrated to **6** on a SiO_2 column. Hydroxy ketone **8**, 5.86 g was eluted with hexane -CH_2Cl_2 (4:1). Hydroxy ketone **9**, 0.95 g was eluted with hexane-CH_2Cl_2 (1:1). Then, a mixture of *cis*-diols, **10** and **11**, 6.95 g was eluted with CH_2Cl_2. A similar oxidation product was chromatographed on alumina containing 10% H_2O gave **4** instead of **8**. **8**: oil. IR(neat) 3480, 3050, 1715, 1140, 1090, and 958 cm^{-1}. ^1H NMR ($CDCl_3$) δ=0.43—0.86 (2H, m), 0.62 (3H, s), 1.06 (3H, s), 1.1—1.66 (7H, m), 1.20 (3H, s), 1.28 (3H, s), 1.66 (1H, d, J=14 Hz), 2.35 (1H, d, J=14 Hz), and 3.37 (1H, broad). **9**: mp 97—8 °C. IR(KBr) 3480, 3070, 3050, 1704, 1168, and 1106 cm^{-1}. ^1H NMR ($CDCl_3$) δ=0.44—0.80 (2H, m), 0.70 (3H, s), 1.06 (3H, s), 1.18 (3H, s), 1.4—1.75 (7H, m), 1.52 (3H, s), 2.10 (1H, d, J=16.5 Hz), 2.31 (1H, d, J=16.5 Hz) and 2.92 (1H, broad).

Reduction of 8 and 9: **8** (385 mg) was dissolved in methanol (20 ml) and reduced with excess $NaBH_4$. The product (319 mg) was chromatographed on a silica-gel column (10 g). Methylene chloride eluted 175 mg of **10**, mp 68—71 °C. Ether eluted 85 mg of 8β,9α-diol **12**. **12**: mp 61—3 °C (recrystallized from hexane). IR (Nujol) 3440, 3150, 1170, 1140, 1103, 1080, and 1035 cm^{-1}. ^1H NMR ($CDCl_3$) δ=−0.01—0.57 (2H, m), 0.55 (3H, s), 0.9—1.9 (9H, m), 0.96 (3H, s), 1.07 (3H, s), 1.18 (3H, s), 2.47 (2H, broad), and 3.75 (1H, X part of ABX, $J_{AX}+J_{BX}$=16.5 Hz).

Hydroxy ketone **9**, 387 mg was reduced similarly, to give 53 mg of **11**, mp 72—3 °C and 82 mg of 8α,9β-diol **13**. **13**: mp 76—8 °C (from hexane). IR (Nujol) 3300, 1145, 1106, and 1082 cm^{-1}. ^1H NMR ($CDCl_3$) δ=0.29—0.66 (2H, m), 0.79 (6H, s), 1.09 (3H, s), 1.1—1.7 (9H, m), 1.33 (3H, s), 2.25—2.57 (3H, m, broad), and 3.51 (1H, X part of ABX, $J_{AX}+J_{BX}$=16.5 Hz).

References

1) Part VIII of this series: S. Nagahama, *Bull. Chem. Soc. Jpn.*, **37**, 1029 (1964).

2) Part 1: S. Akiyoshi and S. Nagahama, *Bull. Chem. Soc. Jpn.*, **30**, 886 (1957).

3) S. Nagahama, H. Kobayashi, and S. Akiyoshi, *Bull. Chem. Soc. Jpn.*, **35**, 1140 (1962).

4) Unpublished. The authors are indebted to professor S. Ito, Tohoku University for the IR and NMR spectra.

5) J. Kawamura, *Bull. Govt. Forest Expt. Station*, **30**, 59 (1930).

6) P. C. Traas, L. M. van der Linde, and H. J. Takken, *Recueil Trav. Chim. Pays-Bas*, **93**, 264 (1974).

7) This is corresponding to Ohloff's[8] Δ^3-thujopsen-2α-ol.

8) G. Ohloff, H. Strickler, B. Willhalm, C. Borer, and M. Hinder, *Helv. Chim. Acta*, **53**, 623 (1970).

The Thermally-Controlled Chemoselective Reduction of 5*H*-Pyrrolo[3,4-*b*]pyridine-5,7(6*H*)-dione with Sodium Borohydride

Takehiko GOTO,* Minoru SAITO, and Ryu SATO
Department of Resource Chemistry, Faculty of Engineering, University of Iwate, Ueda, Morioka 020
(Received April 22, 1987)

Synopsis. The title reaction produced either 2-(hydroxymethyl)nicotinamide or 6,7-dihydro-7-hydroxy-5*H*-pyrrolo[3,4-*b*]pyridin-5-one as the major product at room temperature or −20 °C, respectively, along with the corresponding regioisomers as minor products. These novel compounds were converted to known compounds in order to establish their isomeric structures.

Although the reduction of phthalimide with metal borohydride to 2-(hydroxymethyl)benzamide or 2,3-dihydro-3-hydroxy-1*H*-isoindol-1-one has been well-known,[1] there has been few studies on the application of this reduction to the aza-analogs, for instance 5*H*-pyrrolo[3,4-*b*]pyridine-5,7(6*H*)-dione(quinolinimide **1**). Recently, Cotrel et al.[2] have reported in a patent the reduction of 6-substituted quinolinimides with potassium borohydride to 6-substituted 6,7-dihydro-7-hydroxy-5*H*-pyrrolo[3,4-*b*]pyridin-5-one and the corresponding 5-hydroxy-7-oxo isomer in low yields, which were transformed to pharmacologically active compounds. The isomeric structures and the spectroscopic characterizations of these isomers, however, have not been established. In conjunction with our ongoing studies on the synthesis of 2,3-dihydro-3-(substituted amino)-1*H*-isoindol-1-ones[3a] and their 2-alkyl derivatives[3b] of which the anti-inflammatory activity has been observed,[4] our attention has been focused on the synthesis of their aza-analogs. First, we envisioned the synthesis of 6,7-dihydro-7-hydroxy-5*H*-pyrrolo[3,4-*b*]pyridin-5-one (**2**) by the reduction of quinolinimide (**1**) with sodium borohydride ($NaBH_4$) because of the easy availability of both the substrate and the reducing agent, and the feasibility of converting the hydroxyl group to various functional groups. Surprisingly, there has been no report on **2** and the corresponding regioisomer **3** in the literature to our knowledges. We wish to report in this paper the temperature-controlled chemoselective reduction of quinolinimide (**1**) with $NaBH_4$ to give the mixture either of **2** and **3** at −20 °C, or of 2-(hydroxymethyl)nicotinamide (**4**) and 3-hydroxymethyl-2-pyridinecarboxamide (**5**) at ambient temperature. The present reaction provides a convenient method for the synthesis of the novel heterocycle **2** or **4**, both of which can be easily separated from the corresponding minor regioisomer **3** or **5**.

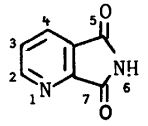

1

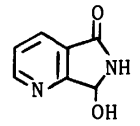

2

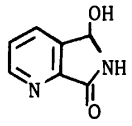

3

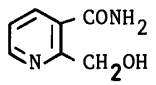

4

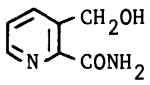

5

Results and Discussion

Reduction at Room Temperature. Quinolinimide (**1**) was smoothly reduced with an excess amount of $NaBH_4$ in methanol–chloroform (1 : 1 v/v) to yield two products which exhibited much different chromatographic behaviors on TLC. After the usual work-up, these components were easily separated on a silica-gel column. The analytical data of these materials indicated either chemical structure **4** or **5**; however, we could not assign the isomeric structure of each hydroxymethylcarbamoylpyridine because of their very similar spectral character. Although a description of **5** could not be found in the literature, there was only one report as to the formation of **4** from furo[3,4-

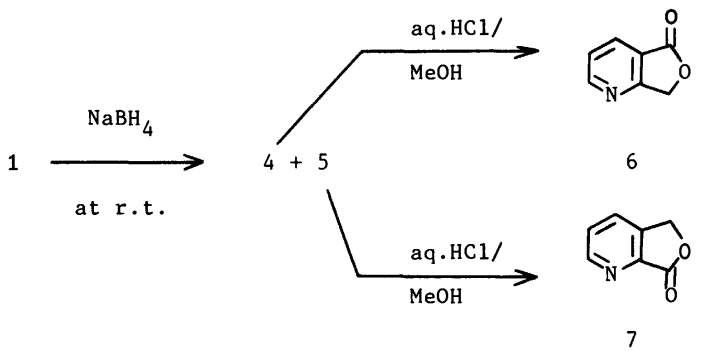

Scheme 1.

b]pyridin-5(7*H*)-one (**6**) with ammonia by Sato et al.[5] The melting point and IR spectra reported by them were identical with those of our sample of **4**. In order to obtain a further confirmation of the assignment, we achieved the transformations of **4** and **5** to the known azaphthalide **6** and **7**,[6] respectively (Scheme 1). Thus, **4** and **5** were smoothly hydrolyzed and cyclized in hot acidic methanol to produce **6** and **7** in 74 and 78% yield, respectively. Consequently, it was revealed that the yields of **4** and **5** were 50 and 23%, respectively, from quinolinimide (**1**). The moderate yield of **4** might be synthetically acceptable in view of the availability of the substrate **1** and reducing agent, and the simple, one-step procedure starting from **1**.

Reduction at −20 °C. The reduction of **1** with $NaBH_4$ also proceeded smoothly at −20 °C to lead a mixture involving two components, **2** and **3**, quantitatively. The ^1H NMR of the mixture showed that the ratio of **2** and **3** was 3:1; the cleanly chemoselective formation of **2** and **3** without the contamination of **4** and **5** was achieved. Fortunately, isomerically pure **2** was obtained by recrystallization of the mixture two times in a moderate yield (53%), in spite of the very similar chromatographic property of **2** and **3**. Isomerically pure **3** was obtained from the mother liquor after recrystallization only in very low yield. Since **2** and **3** were novel compounds, as far as we know, their chemical structures were determined by elemental analysis and spectral data. Isomeric assignments were easily achieved by the transformation of **2** and **3** to **4** and **5**, respectively, with $NaBH_4$ at room temperature in good yields (Scheme 2).

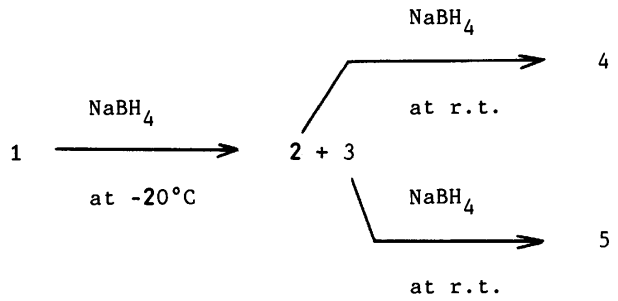

Scheme 2.

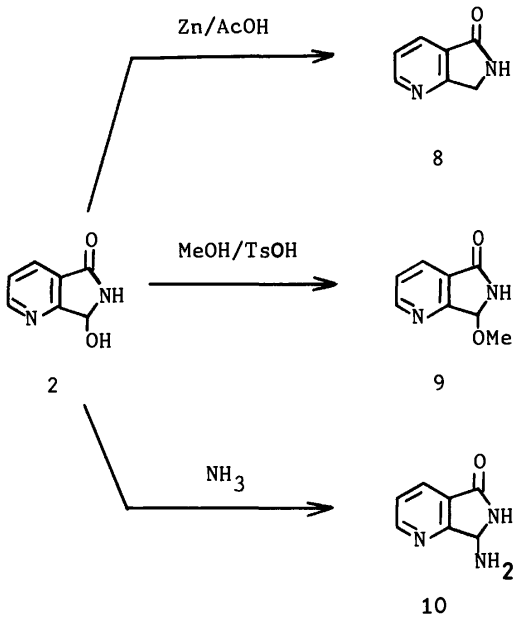

Scheme 3.

Since the hydroxy lactam **2** has been available in multigram scale through the procedure described above, we preliminarily tried to convert the hydroxyl group to other functional groups, as shown in Scheme 3. Thus, the reduction of **2** with zinc powder in acetic acid gave 6,7-dihydro-5*H*-pyrrolo[3,4-*b*]pyridin-5-one (**8**)[7] in good yield (71%). The treatment of **2** with methanol in the presence of a catalytic amount of *p*-toluenesulfonic acid[8] afforded **9** in excellent yield (94%). Finally, the desired 7-amino derivative **10** was obtained by the amination of **2** with liquid ammonia in high yield (83%). The chemical structures of these novel compounds, **9** and **10**, were confirmed by elemental analysis and spectral data.

In summary, we achieved the chemoselective synthesis of either **2** or **4**, along with **3** or **5**, which are interesting intermediates for the synthesis of some biologically active compounds, and some of their fundamental derivations. Further applications of these compounds will soon be reported elsewhere.

Experimental

Melting points were uncorrected. NMR, IR, and mass spectra were recorded with HITACH R-22, HITACH 295, and HITACH RUM-6M, respectively. Elemental analyses were determined with YANAGIMOTO MT-3.

5*H*-Pyrrolo[3,4-*b*]pyridine-5,7(6*H*)-dione (1) was prepared from commercially available 2,3-pyridinedicarboxylic acid and acetamide according to a procedure in a literature.[7]

6,7-Dihydro-7-hydroxy-5*H*-pyrrolo[3,4-*b*]pyridin-5-one (2) and 5,6-Dihydro-5-hydroxy-7*H*-pyrrolo[3,4-*b*]pyridin-7-one (3) by the Reduction of 1 with $NaBH_4$. Into a solution of **1** (2.96 g, 20 mmol) in 200 ml of methanol–chloroform (1:1 v/v) cooled at −20 °C under agron was added $NaBH_4$-powder (1.13 g, 30 mmol). After 30 min, the reaction mixture was acidified with aqueous HCl approximately to pH 3. The resulting mixture was stirred for 10 min and basified with aqueous NaOH approximately to pH 9. Throughout the procedure the reaction mixture was kept at about −20 °C. After being warmed up to room temperature, the mixture was concentrated in vacuo to give a solid. This material was purified over a short silica-gel column (methanol–chloroform, 1:5 v/v) to give the mixture of **2** and **3** (2.9 g, 96%). The mixture was recrystallized from ethanol two times to give isomerically pure **2** as white crystals (1.59 g, 53%): mp 201 °C (decomp); ^1H NMR (DMSO-d_6) δ=5.82 (1H, d, J=9 Hz, H-7), 6.49 (1H, d, J=9 Hz, OH), 7.50 (1H, dd, J=7 and 5 Hz, H-3), 8.03 (1H, dd, J=7 and 2 Hz, H-4), 8.75 (1H, dd, J=5 and 2 Hz, H-2), and 9.04 (1H, br s, NH); IR (KBr) 1740 (C=O), 3000 and 3270 (NH and OH) cm^{-1}; MS (70 eV) m/z 150 (M^+); Found: C, 56.39; H, 4.08; N, 18.72%. Calcd for $C_7H_6N_2O_2$: C, 56.00; H, 4.03; N, 18.66%.

The solid residue (1.05 g) from the mother liquor was triturated in hot methanol–chloroform (1:5 v/v, 30 ml) for 1 h. Then, the unsoluble material was filtered, washed with the same solvent, and recrystallized from methanol–ether to give isomerically pure **3** as white crystals (0.23 g). Decomp

185 °C; ^{1}H NMR (DMSO-d_6) δ=5.94 (1H, d, J=9 Hz, H-5), 6.53 (1H, d, J=9 Hz, OH), 7.57 (1H, dd, J=9 and 6 Hz, H-3), 8.01 (1H, dd, J=9 and 2 Hz, H-4), 8.74 (1H, dd, J=6 and 2 Hz, H-2), and 9.24 (1H, br s, NH); IR (KBr) 1710 (C=O), 3230 (NH and OH) cm^{-1}; MS (70 eV) m/z 150 (M^+); Found: C, 56.35; H, 4.02; N, 18.41%. Calcd for $C_7H_6N_2O_2$: C, 56.00; H, 4.03; N, 18.66%.

2-(Hydroxymethyl)nicotinamide (4) and 3-Hydroxymethyl-2-pyridinecarboxamide (5) by the Reduction of 1. Compound **1** (1.48 g, 10 mmol) in 100 ml of methanol–chloroform (1 : 1 v/v) was reduced with $NaBH_4$ (0.76 g, 20 mmol) at room temperature (about 20 °C) for 1 h by a procedure similar to that described above. When the crude product was chromatographed (silica gel, MeOH–$CHCl_3$ (1 : 5 v/v)), **5** was obtained from the first fraction as white crystals (0.36 g, 23%): mp 154 °C (from ethanol); ^{1}H NMR (DMSO-d_6) δ=4.89 (2H, d, J=6 Hz, CH_2), 5.31 (1H, t, J=5 Hz, OH), 7.50 (1H, br s, NH), 7.54 (1H, dd, J=9 and 5 Hz, H-5), 8.02 (1H, br s, NH), 8.10 (1H, dd, J=9 and 1 Hz, H-4), and 8.46 (1H, dd, J=5 and 2 Hz, H-6); IR (KBr) 1710 (C=O), 3100 and 3350 (NH and OH) cm^{-1}; MS (70 eV) m/z 152 (M^+); Found: C, 55.54; H, 5.28; N, 18.45%. Calcd for $C_7H_8N_2O_2$: C, 55.26; H, 5.30; N, 18.41%.

The second fraction gave **4** (0.76 g, 50%) as white crystals: mp 148 °C (from ethanol, lit,[5] 146—147 °C); ^{1}H NMR (DMSO-d_6) δ=4.68 (2H, d, J=5 Hz, CH_2), 5.22 (1H, t, J=5 Hz, OH), 7.35 (1H, dd, J=8 and 5 Hz, H-5), 7.58 (1H, br s, NH), 7.89 (1H, dd, J=8 and 2 Hz, H-4), 8.00 (1H, br s, NH), and 8.54 (1H, dd, J=5 and 2 Hz, H-6); IR (KBr) 1640, 1680 (C=O), 3150 and 3340 (NH and OH) cm^{-1}; MS (70 eV) m/z 152 (M^+); Found: C, 55.04; H, 5.26; N, 18.49%. Calcd for $C_7H_8N_2O_2$: C, 55.26; H, 5.30; N, 18.41%.

Starting with **2** or **3** (0.15 g, 1 mmol), a similar reduction gave the same products, **4** or **5**, in 78 or 99% yield, respectively.

Furo[3,4-*b*]pyridin-5(7*H*)-one (6). Into a solution of **4** (0.46 g, 3 mmol) in 15 ml of methanol was added 6 ml of concd HCl and the mixture was heated at 80 °C for 1.5 h. The reaction mixture was neutralized with aqueous NaOH, and concentrated in vacuo. After the residue was extracted with chloroform (10 ml×3), the combined extracts were washed with water, dried with sodium sulfate, and concentrated in vacuo to afford spectroscopically pure **6** (0.30 g, 74%) as white crystals (mp 144 °C, from chloroform–hexane, lit,[6] 142 °C; Found: C, 62.46; H, 3.71; N, 10.39%. Calcd for $C_7H_5NO_2$: C, 62.22, H, 3.73, N, 10.37%).

Furo[3,4-*b*]pyridin-7(5*H*)-one (7) was obtained from **5** with the same procedure for **6** in 72% yield as white crystals (mp 164 °C, from chloroform–ether, lit,[6b] 162 °C; Found: C, 62.40; H, 3.69; N, 10.37%. Calcd for $C_7H_5NO_2$: C, 62.22, H, 3.73, N, 10.37%).

6,7-Dihydro-5*H*-pyrrolo[3,4-*b*]pyridin-5-one (8) was obtained from **2** with zinc powder in acetic acid according to von Dobeneck's procedure[7] in 71% yield as white crystals (mp 204 °C, from ethanol, lit,[7] 204—206 °C; ^{1}H NMR (DMSO-d_6) δ=4.44 (2H, s, H-7), 7.50 (1H, dd, J=8 and 5 Hz, H-3), 8.10 (1H, dd, J=8 and 2 Hz, H-4), and 8.75 (2H, dd+br s, J=5 and 2 Hz, H-2+NH).

6,7-Dihydro-7-methoxy-5*H*-pyrrolo[3,4-*b*]pyridin-5-one (9). A solution of **2** (1.50 g, 10 mmol) and *p*-toluenesulfonic acid (0.04 g, 0.2 mmol) in 50 ml of methanol was refluxed for 24 h. After the reaction mixture was concentrated in vacuo, aqueous $NaHCO_3$ was added to the residue, and the resulting mixture was sufficiently extracted with chloroform. The combined organic layers were dried with sodium sulfate and concentrated in vacuo to give practically pure **9** (1.5 g, 94%) as white crystals: mp 150 °C (from chloroform–hexane); ^{1}H NMR (DMSO-d_6) δ=3.43 (3H, s, CH_3), 5.88 (1H, s, H-7), 7.46 (1H, dd, J=8 and 6 Hz, H-3), 8.10 (1H, br s, NH), 8.13 (1H, dd, J=8 and 2 Hz, H-4), and 8.79 (1H, dd, J=6 and 2 Hz, H-2); IR (KBr) 1720 (C=O), 3100 and 3180 (NH) cm^{-1}; MS (70 eV) m/z 164 (M^+); Found: C, 58.88; H, 4.91; N, 17.12%. Calcd for $C_8H_8N_2O_2$: C, 58.53; 4.91; N, 17.06%.

6,7-Dihydro-7-amino-5*H*-pyrrolo[3,4-*b*]pyridin-5-one (10). A solution of **2** (0.30 g, 2 mmol) in 20 ml of liquid ammonia was heated in an autoclave at 110 °C for 48 h. After the evaporation of ammonia at room temperature, the residue was chromatographed over silica gel (methanol–chloroform, 1 : 5 v/v) to afford **10** (0.25 g, 83%) as white crystals: decomp 160 °C (from methanol); ^{1}H NMR (DMSO-d_6) δ=2.44 (2H, br s, NH_2), 5.32 (1H, s, H-7), 7.47 (1H, dd, J=8 and 5 Hz, H-3), 7.99 (1H, dd, J=8 and 2 Hz, H-4), and 8.72 (2H, dd+br s, J=5 and 2 Hz, H-2+NH); IR (KBr) 1720 (C=O) and 3160 (NH and NH_2) cm^{-1}; Found: C, 56.40; H, 4.74; N, 27.84%. Calcd for $C_7H_7N_3O$: C, 56.37; H, 4.73; N, 28.17%.

The present work was partially supported by a Grant-in-Aid for Scientific Research No. 60740263 from the Ministry of Education, Science and Culture.

References

1) For examples, Z. Horii, C. Iwata, and Y. Tamura, *J. Org. Chem.*, **26**, 2273 (1961); F. C. Uhle, *ibid.*, **26**, 2998 (1961); Y. Kondo and B. Witkop, *ibid*, **33**, 206 (1968).

2) C. Cotrel, C. Crisan, C. Jeanmart, and M. N. Messer, Ger. Offen., 2423650 (1974); *Chem. Abstr.*, **82**, 112103k (1975); C. Cotrel, C. Crisan, C. Jeanmart, and M. N. Messer, Fr. Demande, 2263752 (1975); *Chem. Abstr.*, **84**, 121901n (1976); C. Cotrel, C. Crisan, C. Jeanmart, and A. Leger, Ger. Offen., 2615067 (1976); *Chem. Abstr.*, **86**, 43743n (1977).

3) a) R. Sato, T. Senzaki, T. Goto, and M. Saito, *Chem. Lett.*, **1984**, 1599; b) R. Sato, T. Senzaki, T. Goto, and M. Saito, *Bull. Chem. Soc. Jpn.*, **59**, 2950 (1986).

4) S. Ogata, Jpn. Patent, 80127389; *Chem. Abstr.*, **95**, 25058z (1981); M. H. Sherlock, U. S. Patent, 3296276 (1967); *Chem. Abstr.*, **67**, 73519u (1967).

5) Y. Sato, T. Iwashige, and T. Miyadera, *Chem. Pharm. Bull.*, **8**, 427 (1960).

6) a) W. R. Ashcroft, M. G. Beal, and J. A. Joule, *J. Chem. Soc., Perkin Trans. 1*, **1981**, 3012; b) G. Queguiner and A. Godard, *Compt. Rend., Sec. C*, **1969**, 1646.

7) H. von Dobeneck and B. Hansen, *Chem. Ber.*, **105**, 3611 (1972).

8) D. A. Burnett, J.-K. Choi, D. J. Hart, and Y.-M. Tsai, *J. Am. Chem. Soc.*, **106**, 8201 (1984).

Synthesis of Novel Bis-Crown and Double-Armed Crown Ethers Having the 18-Crown-6 Residue

Koichiro NAEMURA,* Hiroshi IWASAKA, and Hiroaki CHIKAMATSU
Department of Chemistry, Faculty of Engineering Science, Osaka University, Toyonaka, Osaka 560
(Received May 8, 1987)

Synopsis. The 18-crown-6 derivative possessing two hydroxyl groups was prepared from the Diels–Alder adduct of 1,7-(1,2-ethanediylidene)-18-crown-6 with dimethyl 2-butynedioate. By using the crown ether as the key intermediate, novel bis-crown and double-armed crown ethers having the 18-crown-6 residue were synthesized, and their abilities to extract metal picrates were investigated.

Since Smid and co-workers first prepared the bis-crown ether,[1] a variety of bis-crown ethers have been synthesized and their complexing properties have been investigated, because of interests in their unique binding properties. Here we report the syntheses of novel bis-crown and double-armed crown ethers having the 18-crown-6 residue and the solvent extraction of metal picrates with these crown ethers. Bis-crown ethers are divided into several groups according to a variation of the linkage holding two macrorings[2] together and bis-crown ethers described in this paper may be classified into a group which is referred to as a "hinged" bis-crown ether.[2,3]

We chose the crown ether **8** possessing two hydroxyl groups as well as the 18-crown-6 residue as the key intermediate for the preparation of bis-crown and double-armed crown ethers having the 18-crown-6 residue. Treatment of **1**[4] with dimethyl 2-butynedioate in refluxing toluene gave the adduct **4** in 71% yield. Catalytic hydrogenation of **4** over 10% Pd/C in methanol afforded the diester **7** in 79% yield. The diester **9** containing the 15-crown-5 residue was obtained from **2**[5] in 52% overall yield via the adduct **5**.

Assignment of the configuration of **7** and **9** was based on their ^{1}H NMR spectra with those of **11** and **12** with known configurations.[6] Chemical shifts on endo- and exo-protons on the ethano bridge in **7**, **9**, **11**, and **12** are summarized in Table 1. The endo-protons in **11** are shifted considerably downfield due to a deshieding effect of the endo-carbonyl groups on C2 and C3, and the endo-protons in **7** and **9** are also shifted to downfield. From the data described above, we assigned the endo-configuration to **7** and **9** as shown in their structural formulas.

Table 1. Chemical Shifts of Endo- and Exo-Protons on the Ethano Bridge

	endo-proton	exo-proton
7	1.9—2.2	1.4—1.7
9	1.9—2.2	1.4—1.7
11	1.9—2.1	1.6—1.8
12	1.4—1.6	1.7—1.9

Reduction of **7** and **9** with $LiAlH_4$ in tetrahydrofuran (THF) gave **8** (81%) and **10** (78%), respectively. High dilution condensation of **8** with triethylene glycol, tetraethylene glycol, and pentaethylene glycol ditosylate in dimethyl sulfoxide (DMSO)–1,2-dimethoxyethane (DME) in the presence of NaH gave **15** (22%), **16** (26%), and **17** (45%), respectively. Treatment of **10** with pentaethylene glycol ditosylate in high dilution conditions afforded **18** in 42% yield. The structures of these crown ethers were confirmed on the basis of their ^{1}H NMR and mass spectra as well as elemental analyses.

Double-armed crown ethers **19** and **20** containing the 18-crown-6 residue were also prepared from **8**. Treatment of **8** with 3,6-dioxaheptyl and 3,6,9-trioxadecyl *p*-toluenesulfonate in *N*,*N*-dimethylformamide (DMF) in the presence of NaH provided **19** (68%) and **20** (20%), respectively. Our attempts to prepare directly **19** from **1** by the Diels–Alder reaction of **1** with 2,5,8,13,16,19-hexaoxa-10-icosyne, prepared by condensation of 2-butyne-1,4-diol with 3,6-dioxaheptyl *p*-toluenesulfonate and KOBu^t in THF,

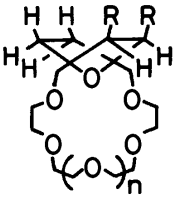

7 n=1 R=CO_2CH_3
8 n=1 R=CH_2OH
9 n=0 R=CO_2CH_3
10 n=0 R=CH_2OH

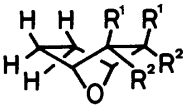

11 R^1=CO_2CH_3 R^2=H
12 R^1=H R^2=CO_2CH_3

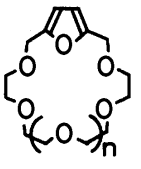

1 n=1
2 n=0

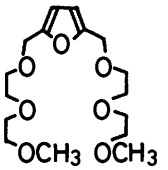

3

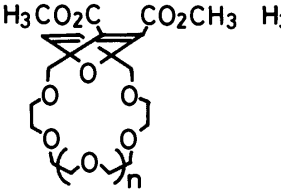

4 n=1
5 n=0

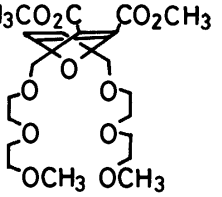

6

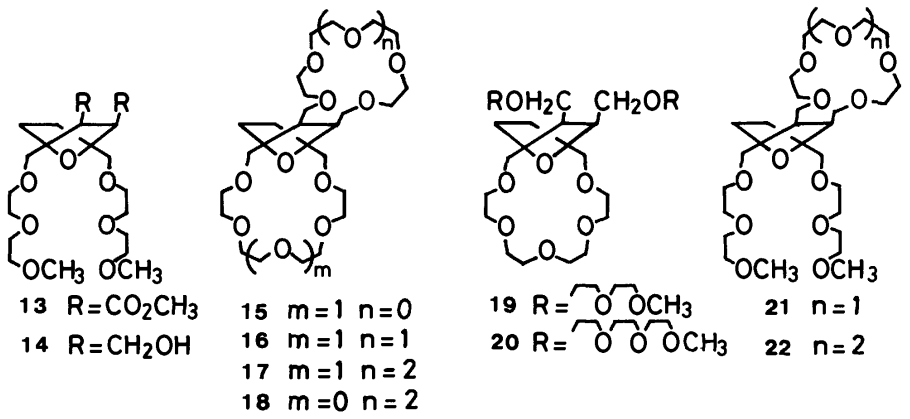

were unsuccessful, because the reaction did not give any Diels-Alder adduct.

We next turned our attention to the preparation of the other type of polyether that is O_7-monopodand[7] bound to a crown ether framework by two single bonds. A similar set of reactions described for **8** transformed the monopodand **3** into the key intermediate **14** (25% overall yield) via **6** and **13**. The structure of **13** was confirmed by its ^{1}H NMR spectrum exhibiting signals of the endo-protons at C5 and C6 at δ 2.0—2.2 and the exo-protons at δ 1.5—1.7. High dilution condensation of **14** with tetraethylene glycol and pentaethylene glycol ditosylate gave **21** (47%) and **22** (37%), respectively.

The cation-binding ability of these crown ethers was estimated by solvent extraction of aqueous solution of metal picrate with a chloroform solution containing crown ether, and the results are given in Table 2.

Among crown ethers described here, the bis-crown ether **16** containing the 18-crown-6 and the 17-crown-5 residue possesses the highest extractability towards all cations examined in this study, and both double-armed crown ethers **19** and **20** also exhibit higher extractabilities towards all cations than the parent 18-crown-6. However, in the case of the bis-crown ethers **15** and **17**, both of which contain also the 18-crown-6 residue, the additional crown ether framework contributes hardly to raise the extractability of the bis-crown ether.

Table 2. Extraction of Metal Picrates[a]

Host	Extractability/%					
	Li^+	Na^+	K^+	Rb^+	Cs^+	Ag^+
15	3.0	9.5	66.5	56.0	34.8	43.0
16	4.3	21.2	76.5	68.3	41.4	56.6
17	1.2	13.3	66.3	57.8	35.0	44.0
18	1.0	5.3	9.2	9.1	8.3	28.9
19	3.0	16.2	77.1	68.3	40.5	51.4
20	5.8	14.0	71.0	57.2	37.8	50.5
21	2.2	1.1	1.5	0	0	7.0
22	0	3.0	3.8	7.3	1.5	3.2
18-Crown-6	3.1	6.0	66.3	55.2	34.7	29.2

a) The solvent extraction was carried out according to the procedure reported in our preceding paper.[8]

Experimental

2,5-Bis(2,5,8-trioxanonyl)furan (3). To a suspension of potassium *t*-butoxide (11.2 g, 0.100 mol) in dry THF (300 mL) was added 2,5-bis(hydroxymethyl)furan[4] (3.84 g, 0.0300 mol) and then a solution of 3,6-dioxaheptyl *p*-toluenesulfonate (27.4 g, 0.100 mol) in dry THF (100 mL) was added to the reaction mixture. After the mixture was refluxed for 12 h, a solid was filtered off and the filtrate was condensed in vacuo. The residue was chromatographed on alumina (benzene eluent) to give **3** (4.06 g, 41% yield): bp 160—162 °C (0.02 mmHg (1 mmHg=133.322 Pa)). Found: C, 57.50; H, 8.41%. Calcd for $C_{16}H_{28}O_7$: C, 57.81; H, 8.49%.

18,19-Bis(methoxycarbonyl)-3,6,9,12,15,22-hexaoxatricyclo-[15.2.2.1^{1,17}]docosa-18,20-diene (4). A solution of **1**[4] (1.00 g, 3.50 mmol) and dimethyl 2-butynedioate (5.82 g, 41.0 mmol) in toluene (20 mL) was refluxed for 15 h. After evaporation of volatile materials, the residue was chromatographed on alumina ($CHCl_3$) to give **4** (1.06 g, 71%): mp 84—86 °C (lit,[4] mp 55—60 °C); ^{1}H NMR ($CDCl_3$) δ=3.5—3.9 (16H, m), 3.75 (6H, s), 4.15 (2H, d J=12 Hz), 4.31 (2H, d J=12 Hz), 6.99 (2H, s). Found: C, 55.88; H, 6.50%. Calcd for $C_{20}H_{28}O_{10}$: C, 56.07; H, 6.59%.

15,16-Bis(methoxycarbonyl)-3,6,9,12,19-pentaoxatricyclo-[12.2.2.1^{1,14}]nonadeca-15,17-diene (5). The diester **5** (1.31 g, 69%) was prepared from **2**[5] (1.20 g, 4.95 mmol) and dimethyl 2-butynedioate (7.10 g, 50.0 mmol) as an oil: ^{1}H NMR ($CDCl_3$) δ=3.5—3.9 (12H, m), 3.82 (6H, s), 4.08 (2H, d J=12 Hz), 4.42 (2H, d J=12 Hz), 7.03 (2H, s). Found: C, 55.92; H, 5.97%. Calcd for $C_{18}H_{24}O_9$: C, 56.24; H, 6.29%.

2,3-Bis(methoxycarbonyl)-1,4-bis(2,5,8-trioxanonyl)-7-oxabicyclo[2.2.1]hepta-2,5-diene (6). The diester **6** (1.68 g, 41%) was prepared from **3** (2.86 g, 8.61 mmol) and dimethyl 2-butynedioate (12.2 g, 86.1 mmol) as an oil: ^{1}H NMR ($CDCl_3$) δ=3.35 (6H, s), 3.5—3.7 (16H, m), 3.75 (6H, s), 4.20 (4H, s), 7.03 (2H, s). Found: C, 55.05; H, 7.30%. Calcd for $C_{22}H_{34}O_{11}$: C, 55.68; H, 7.22%.

***cis*-18,19-Bis(methoxycarbonyl)-3,6,9,12,15,22-hexaoxatricyclo[15.2.2.1^{1,17}]docosane (7).** A mixture of **4** (2.85 g, 6.65 mmol) and methanol (70 mL) was shaken at room temperature with 10% Pd/C (390 mg) at 1 atm of hydrogen. After a usual workup, chromatography (Al_2O_3, benzene-$CHCl_3$ 1:1) gave **7** (2.27 g, 79%): mp 62—63 °C (hexane-benzene) ^{1}H NMR ($CDCl_3$) δ=1.4—1.7 (2H, m), 1.9—2.2 (2H, m), 3.5—3.7 (22H, m), 3.62 (6H, s). Found: C, 55.08; H, 7.44%. Calcd for $C_{20}H_{32}O_{10}$: C, 55.54; H, 7.46%.

***cis*-15,16-Bis(methoxycarbonyl)-3,6,9,12,19-pentaoxatricyclo[12.2.2.1^{1,14}]nonadecane (9).** The diester **9** (992 mg, 75%) was obtained from **5** (1.31 g, 3.41 mmol): mp 58—60 °C (hexane-benzene); ^{1}H NMR ($CDCl_3$) δ=1.4—1.7 (2H, m), 1.9—2.2 (2H, m), 3.66 (6H, s), 3.6—3.9 (18H, m). Found: C,

55.42; H, 7.24%; Calcd for $C_{18}H_{28}O_9$: C, 55.66; H, 7.27%.

***cis*-2,3-Bis(methoxycarbonyl)-1,4-bis(2,5,8-trioxanonyl)-7-oxabicyclo[2.2.1]heptane (13).** The diester **13** (1.20 g, 71%) was obtained from **6** (1.68 g, 3.54 mmol) as an oil after chromatography (Al_2O_3, benzene): ^1H NMR ($CDCl_3$) δ= 1.5—1.7 (2H, m), 2.0—2.2 (2H, m), 3.36 (6H, s), 3.37 (2H, s), 3.64 (6H, s), 3.5—3.8 (20H, m). Found: C, 55.03; H, 7.94%; Calcd for $C_{22}H_{38}O_{11}$: C, 55.24; H, 8.01%.

***cis*-18,19-Bis(hydroxymethyl)-3,6,9,12,15,22-hexaoxatricyclo[15.2.2.$1^{1,17}$]docosane (8).** A solution of **7** (800 mg, 1.85 mmol) in dry THF (40 mL) was added to a suspension of $LiAlH_4$ (220 mg, 5.80 mmol) in dry THF (40 mL) and the mixture was refluxed for 12 h. After a usual workup, chromatography on alumina ($CHCl_3$–methanol 20:1) gave **8** (563 mg, 81%) as a hygroscopic oil: ^1H NMR ($CDCl_3$) δ=1.54 (4H, s), 2.60 (2H, br s), 3.67 (2H, s), 3.5—3.9 (24H, m); MS *m/z* 376 (M^+).

***cis*-15,16-Bis(hydroxymethyl)-3,6,9,12,19-pentaoxatricyclo-[12.2.2.$1^{1,14}$]nonadecane (10).** The diol **10** (300 mg, 78%) was obtained from **9** (450 mg, 1.16 mmol) as a hygroscopic oil after chromatography on alumina ($CHCl_3$–methanol 100:1): ^1H NMR ($CDCl_3$) δ=1.51 (4H, s), 2.64 (2H, br s), 3.5—3.9 (20H, m), 3.88 (2H, s); MS *m/z* 332 (M^+).

***cis*-2,3-Bis(hydroxymethyl)-1,4-bis(2,5,8-trioxanonyl)-7-oxabicyclo[2.2.1]heptane (14).** The diol **14** (585 mg, 60%) was obtained from **13** (1.10 g, 2.30 mmol) as an oil after chromatography (Al_2O_3, $CHCl_3$): ^1H NMR ($CDCl_3$) δ=1.6—1.8 (4H, m), 2.58 (2H, br s), 3.37 (6H, s), 3.49 (2H, s), 3.5—3.8 (24H, m). Found: C, 56.38; H, 9.30%. Calcd for $C_{20}H_{38}O_9$: C, 56.85; H, 9.07%.

2,5,8,11,14,19,22,25,28,33-Decaoxatetracyclo[15.14.2.$1^{1,16}$.$0^{17,30}$]-tritriacontane (15). To a suspension of NaH (96 mg, 4.0 mmol) in 30 mL of DMSO–DME (1:3) was added **8** (486 mg, 1.30 mmol) and then the mixture was heated at 50 °C for 1 h. A solution of triethylene glycol ditosylate (595 mg, 1.30 mmol) in 60 mL of DMSO–DME (1:3) was added to the mixture at 50±5 °C over a 10 h period and the reaction mixture was heated at this temperature for an additional 30 h. After a small amount of water was added to the chilled reaction mixture, the solvent was evaporated in vacuo. The residue was extracted with $CHCl_3$. After a usual workup, chromatography on alumina ($CHCl_3$) gave **15** (140 mg, 22%) as an oil: ^1H NMR ($CDCl_3$) δ=1.68 (4H, br s), 2.50 (2H, br s), 3.4—3.8 (36H, m); MS *m/z* 490 (M^+). Found: C, 58.25; H, 8.49%. Calcd for $C_{24}H_{42}O_{10}$: C, 58.75; H, 8.63%.

4,7,10,13,16,21,24,27,30,33,37-Undecaoxatetracyclo-[17.15.2.$1^{1,19}$.$0^{2,18}$]heptatriacontane (16). Compound **16** (144 mg, 26%) was prepared from **8** (400 mg, 1.06 mmol) and tetraethylene glycol ditosylate (530 mg, 1.06 mmol) as an oil after chromatography (Al_2O_3, $CHCl_3$–methanol 50:1): ^1H NMR ($CDCl_3$) δ=1.73 (4H, br s), 2.23 (2H, br s), 3.3—3.9 (40H, m); MS *m/z* 534 (M^+). Found: C, 58.02; H, 8.60%. Calcd for $C_{26}H_{46}O_{11}$: C, 58.41; H, 8.67%.

4,7,10,13,16,19,24,27,30,33,36,40-Dodecaoxatetracyclo[20.15.2.$1^{1,22}$.$0^{2,21}$]tetracontane (17). Compound **17** (230 mg, 45%) was obtained from **8** (330 mg, 0.877 mmol) and pentaethylene glycol ditosylate (480 mg, 0.877 mmol) as an oil: ^1H NMR ($CDCl_3$) δ=1.67 (4H, br s), 2.44 (2H, br s), 3.3—3.9 (44H, m); MS *m/z* 578 (M^+). Found: C, 57.58; H, 8.65%. Calcd for $C_{28}H_{50}O_{12}$: C, 58.11; H, 8.71%.

4,7,10,13,16,19,24,27,30,33,37-Undecaoxatetracyclo[20.12.2.$1^{1,22}$.$0^{2,21}$]heptatriacontane (18). Compound **18** (204 mg, 42%) was obtained from **10** (300 mg, 0.903 mmol) and pentaethylene glycol ditosylate (500 mg, 0.914 mmol) as an oil: ^1H NMR ($CDCl_3$) δ 1.72 (4H, br s), 2.50 (2H, br s), 3.4—3.8 (40H, m); MS *m/z* 534 (M^+). Found: C, 57.72; H, 8.79%. Calcd for $C_{26}H_{46}O_{11}$: C, 58.41; H, 8.67%.

18,19-Bis(2,5,8-trioxanonyl)-3,6,9,12,15,22-hexaoxatricyclo[15.2.2.$1^{1,17}$]docosane (19). To a suspension of NaH (40 mg, 1.7 mmol) in dry DMF (10 mL) was added a solution of **8** (200 mg, 0.532 mmol) in dry DMF (10 mL). After the mixture was heated at 50±5 °C for 1 h, a solution of 3,6-dioxaheptyl *p*-toluenesulfonate (320 mg, 1.17 mmol) in DMF (10 mL) was added to the mixture and then it was heated at 50±5 °C for an additional 30 h. After a similar workup described for the preparation of **15**, chromatography (Al_2O_3, benzene–$CHCl_3$) provided **19** (210 mg, 68%) as an oil: ^1H NMR ($CDCl_3$) δ=1.70 (4H, br s), 2.48 (2H, br s), 3.36 (6H, s), 3.4-3.8 (40H, m); MS *m/z* 580 (M^+). Found: C, 57.47; H, 9.09%. Calcd for $C_{28}H_{52}O_{12}$: C, 57.91 H, 9.03%.

18,19-Bis(2,5,8,11-tetraoxadodecyl)-3,6,9,12,15,22-hexaoxatricyclo[15.2.2.$1^{1,17}$]docosane (20). Compound **20** (135 mg, 20%) was obtained from **8** (376 mg, 1.00 mmol) and 3,6,9-trioxadecyl *p*-toluenesulfonate (795 mg, 2.50 mmol) as an oil: ^1H NMR ($CDCl_3$) δ=1.68 (4H, br s), 2.45 (2H, br s), 3.32 (6H, s), 3.4—3.8 (48H, m); MS *m/z* 668 (M^+). Found: C, 56.72; H, 9.08%. Calcd for $C_{32}H_{60}O_{14}$: C, 57.46; H, 9.04%.

1,19-Bis(2,5,8-trioxanonyl)-4,7,10,13,16,22-hexaoxatricyclo-[17.2.1.$0^{2,18}$]docosane (21). Compound **21** (160 mg, 47%) was prepared from **14** (250 mg, 0.592 mmol) and tetraethylene glycol ditosylate (300 mg, 0.597 mmol) as an oil: ^1H NMR ($CDCl_3$) δ=1.70 (4H, br s), 2.50 (2H, br s), 3.38 (6H, s), 3.5—3.9 (40H, m); MS *m/z* 580 (M^+). Found: C, 57.06; H, 9.10%. Calcd for $C_{28}H_{52}O_{12}$: C, 57.91; H, 9.03%.

1,22-Bis(2,5,8-trioxanonyl)-4,7,10,13,16,19,25-heptaoxatricyclo[20.2.1.$0^{2,22}$]pentacosane (22). Compound **22** (164 mg, 37%) was obtained from **14** (300 mg, 0.710 mmol) and pentaethylene glycol ditosylate (390 mg, 0.710 mmol) as an oil: ^1H NMR ($CDCl_3$) δ=1.69 (4H, br s), 2.50 (2H, br s), 3.37 (6H, s), 3.5—3.9 (44H, m); MS *m/z* 624 (M^+). Found: C, 57.08; H, 8.97%. Calcd for $C_{30}H_{56}O_{13}$: C, 57.67; H, 9.04%.

References

1) K. H. Wong, M. Bourgoin, and J. Smid, *J. Chem. Soc., Chem. Commun.*, **1974**, 715.

2) G. W. Gokel and S. H. Korezeniowski, "Macrocyclic Polyether Syntheses," Springer-Verlag, Berlin, Heidelberg, and New York (1982), p. 34.

3) R. C. Helgeson, T. L. Tarnowski, and D. J. Cram, *J. Org. Chem.*, **44**, 2538 (1979); R. C. Helgeson, G. R. Weisman, J. L. Toner, T. L. Tarnowski, Y. Chao, J. M. Mayer, and D. J. Cram, *J. Am. Chem. Soc.*, **101**, 4928 (1979).

4) J. M. Timko and D. J. Cram, *J. Am. Chem. Soc.*, **96**, 7159 (1974); J. M. Timko, S. S. More, D. M. Walba, P. C. Hiberty, and D. J. Cram, *ibid.*, **99**, 4207 (1977).

5) D. N. Reinhoudt and R. T. Gray, *Tetrahedron Lett.*, **1975**, 2105.

6) T. A. Eggelete, H. de Koning, and H. O. Huisman, *Tetrahedron*, **29**, 2491 (1973).

7) E. Weber and F. Vögtle, *Inorg. Chim. Acta*, **45**, L65 (1980).

8) K. Naemura, I. Ebashi, and M. Nakazaki, *Bull. Chem. Soc. Jpn.*, **58**, 767 (1985).

Ortho-Selective Alkylation of Phenols with Symmetric Sulfides and Sulfuryl Chloride

Kikumasa SATO,* Seiichi INOUE, Osamu MIYAMOTO, Hiroshi IKEDA, and Tomomi OTA
Department of Applied Chemistry, Faculty of Engineering, Yokohama National University, Tokiwadai, Hodogaya-ku, Yokohama 240
(Received May 18, 1987)

Synopsis. Sulfuryl chloride has been shown to be useful activator for sulfides in the selective preparation of ortho-alkylated phenols via [2,3]sigmatropic rearrangement. By this process, ortho-alkylated phenols have been prepared with various symmetric sulfides in good yields. The rearrangement products having 3-chloropropyl or 3-methyl-3-butenyl moiety have been converted into 2*H*-1-benzopyran derivatives.

We reported previously ortho-selective alkylation of phenols with sulfoxides and thionyl chloride via a [2,3]sigmatropic rearrangement.[1-3] However, in general, sulfoxides are hygroscopic and accessible by the oxidation of the corresponding sulfides. Therefore, we hoped that phenoxysulfonium salts **3** could be prepared from sulfides,[4] which are easier to handle than sulfoxides. Since the intermediates in the formation of phenoxysulfonium salts **3** with sulfoxides and thionyl chloride seem to be chlorosulfonium salts, we anticipated that the same sulfonium salts could be generated when sulfuryl chloride was used as an activator of sulfides. In this paper, we report a new method of selective ortho-alkylation of phenols using dialkyl sulfides and sulfuryl chloride, and also the facile preparation of 2*H*-1-benzopyrans by the cyclization of the resulting *o*-alkylphenols.

When sulfide was used, the operation of the alkylation of phenol could be simplified compared to the use of sulfoxides. Namely, sulfuryl chloride was added to a mixture of phenol **2** and sulfide **1** in dichloromethane at low temperature, followed by addition of triethylamine and then the reaction mixture was warmed to room temperature before work-up. We found that both the temperature and the period of the reaction of a sulfide with sulfuryl chloride affected the yield of **5**. The yield of *o*-alkylated phenol **5** decreased when the reaction time was prolonged at the same temperature. This tendency is enhanced at higher temperature, because of the thermolability of phenoxysulfonium salts **3**.

We investigated the alkylation of phenol **2** with various symmetric dialkyl sulfides **1** (Scheme 1). These results are summarized in the Table 1. Reaction of phenol (**2**; X=H) and sulfides **1** afforded the corresponding *o*-alkylated phenols **5** in good yields. Also, we investigated the reaction of para-substituted phenols **2** (X=Me, Cl, Ph, CO_2Et) with bis(2-acetoxyethyl) sulfide (**1**; R=CH_2OAc). In these cases, the expected products **5f—i** were obtained in good yields, except in the case of **5i**.

Next we studied the conversion of the rearrangement products **5j** and **5m** into 2*H*-1-benzopyran derivatives. We reported previously a facile synthesis of coumarin

Table 1. Ortho-Selective Alkylation of Phenols with Symmetric Sulfides and Sulfuryl Chloride

Product	R	X	Yield/%[a]
5a	H	H	72 (78)
5b	Me	H	67 (69)
5c	Ph	H	56 (68)
5d	CH_2CO_2Me	H	70 (80)
5e	CH_2OAc	H	77
5f	CH_2OAc	Me	73
5g	CH_2OAc	Cl	61
5h	CH_2OAc	Ph	76[b]
5i	CH_2OAc	CO_2Et	31[b]
5j	CH_2CH_2Cl	H	83 (61)
5k	CH_2CMe_2Cl	H	67
5l	CH_2CMe_2OAc	H	77
5m	$CH_2CMe{=}CH_2$	H	63

a) Yields from the corresponding sulfoxides are given in parentheses. see Ref. 2. b) Dichloromethane-*N*,*N*-dimethylformamide (10:1) was used as a solvent.

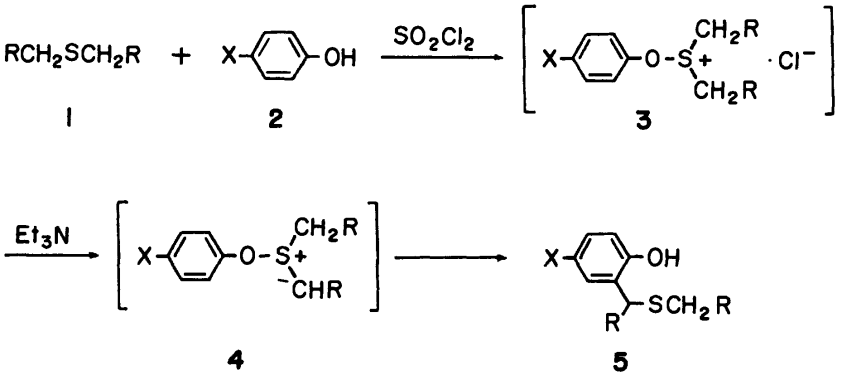

Scheme 1.

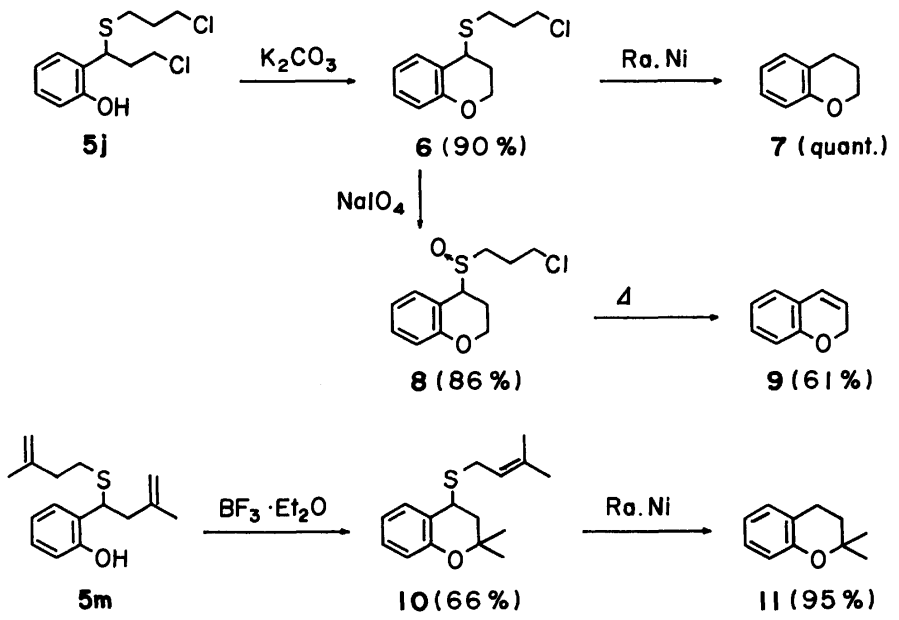

Scheme 2.

from **5d**.[2] Herein, we report the preparation of chromene and chromane derivatives. The results are illustrated in Scheme 2. Thus, the treatment of **5j** with potassium carbonate followed by Raney nickel afforded chromane (**7**). Also, chromene (**9**) was prepared by sodium periodate oxidation of **6**, followed by β-elimination of sulfoxide **8**. Cyclization of **5m** with boron trifluoride etherate gave chromane derivative **10**, which possessed a 3-methyl-2-butenylthio group as the result of migration of carbon-carbon double bond. Then desulfurization of **10** with Raney nickel gave 2,2-dimethylchromane (**11**) in 95% yield. These results demonstrate that the terminally functionalized *o*-alkylphenols **5d**, **5j**, and **5m**, which are readily obtained by the present [2,3]sigmatropic rearrangement, are very useful for the synthesis of 2*H*-1-benzopyran derivatives.

Experimental

Melting points are uncorrected. IR spectra were measured on either a Hitachi 215 or a Hitachi 260-50 spectrometer. ^{1}H NMR spectra were obtained with a JEOL JNM-C-60M or a JEOL FT-90Q with tetramethylsilane as an internal standard. The known compounds were established on the basis of spectroscopic properties of itself and of the description of literature. Column chromatography was normally effected with Wakogel C-200 (Wako Pure Chemical Industries).

General Procedure. Sulfuryl chloride (2.2 ml, 22 mmol) was added dropwise to the mixture of sulfide **1** (22 mmol) and phenol **2** (66 mmol) in dry dichloromethane (200 ml) at −40 °C. After the reaction mixture was stirred for 20 min at −40 °C, triethylamine (20 ml) was added to the reaction mixture at −30 °C. The solution was allowed to warm to room temperature, and it was then poured into dilute hydrochloric acid. The organic layer was separated and the aqueous solution was extracted with ether. The combined organic layers were washed with water and brine, dried ($MgSO_4$), and then evaporated. The residue was chromatographed on a column to give the ortho-alkylated phenol **5**.

The following new compounds were prepared using the above procedure. The other compounds were established on the basis of spectroscopic properties of itself and of the products prepared from phenol and the corresponding sulfoxides.[2]

2-[2-Acetoxy-1-(2-acetoxyethylthio)ethyl]phenol (5e): Yield 77%. IR (neat) 3370, 2940, 1730, 1710, 1240, and 1220 cm^{-1}. ^{1}H NMR ($CDCl_3$) δ=2.03 (6H, s), 2.71 (2H, t, J=6), 4.18 (2H, t, J=6), 4.3—4.7 (3H, m), and 6.7—7.5 (5H, m). Found: C, 56.58; H, 6.03%. Calcd for $C_{14}H_{18}O_5S$: C, 56.36; H, 6.08%.

2-[2-Acetoxy-1-(2-acetoxyethylthio)ethyl]-4-methylphenol (5f): Yield 73%. Mp 64—65 °C. IR (KBr) 3280, 2920, 1730, 1700, 1270, and 1240 cm^{-1}. ^{1}H NMR ($CDCl_3$) δ=2.03 (6H, s), 2.23 (3H, s), 2.68 (2H, t, J=6), 4.15 (2H, t, J=6), 4.42 (3H, s), and 6.5—7.1 (4H, m). Found: C, 57.59; H, 6.43%. Calcd for $C_{15}H_{20}O_5S$: C, 57.68; H, 6.45%.

2-[2-Acetoxy-1-(2-acetoxyethylthio)ethyl]-4-chlorophenol (5g): Yield 61%. Mp 95—96.5 °C. IR (KBr) 3230, 2930, 1730, 1695, 1270, and 1245 cm^{-1}. ^{1}H NMR ($CDCl_3$) δ=2.07 (6H, s), 2.6—2.8 (2H, m), 4.20 (2H, t, J=6), 4.2—4.3 (3H, m), and 6.7—7.3 (4H, m). Found: C, 50.66; H, 5.11%. Calcd for $C_{14}H_{17}ClO_5S$: C, 50.53; H, 5.15%.

2-[2-Acetoxy-1-(2-acetoxyethylthio)ethyl]-4-phenylphenol (5h): Yield 76%. IR (neat) 3400, 2950, 1735, 1710, and 1230 cm^{-1}. ^{1}H NMR ($CDCl_3$) δ=2.05 (6H, s), 2.7—2.9 (2H, m), 4.22 (2H, t, J=6), 4.5—4.7 (3H, m), and 6.8—7.6 (9H, m). Found: C, 64.30; H, 5.90%. Calcd for $C_{20}H_{22}O_5S$: C, 64.15; H, 5.92%.

Ethyl 3-[2-Acetoxy-1-(2-acetoxyethylthio)ethyl]-4-hydroxybenzoate (5i): Yield 31%. IR (neat) 3230, 2970, 1740, 1710, 1270, and 1230 cm^{-1}. ^{1}H NMR ($CDCl_3$) δ=1.39 (3H, t, J=7), 2.06 (6H, s), 2.77 (2H, t, J=7), 4.1—4.7 (7H, m), 6.92 (1H, d, J=8), 7.92 (1H, dd, J=2, 8), 8.04 (1H, d, J=2), and 8.34 (1H, bs). Found: C, 55.54; H, 6.02%. Calcd for $C_{17}H_{22}O_7S$: C, 55.12; H, 5.99%.

2-[3-Chloro-1-(3-chloro-3-methylbutylthio)-3-methylbutyl]phenol (5k): Yield 67%. IR (neat) 3350, 1580, 1490, 1450, 1370, and 1230 cm^{-1}. ^{1}H NMR ($CDCl_3$) δ=1.43, 1.57 (12H, each s), 1.7—2.0 (4H, m), 2.2—2.6 (2H, m), 4.42 (1H, t, J=7), 6.20 (1H, bs), and 6.6—7.3 (4H, m). Found: C, 57.53; H,

7.21%. Calcd for $C_{16}H_{24}Cl_2OS$: C, 57.31; H, 7.21%.

2-[3-Acetoxy-1-(3-acetoxy-3-methylbutylthio)-3-methylbutyl]phenol (5l): Yield 77%. IR (neat) 3300, 2970, 1720, and 1250 cm^{-1}. ^1H NMR ($CDCl_3$) δ=1.32 (6H, s), 1.42, 1.46 (6H, each s), 1.67 (3H, s), 1.88 (3H, s), 2.0—3.2 (6H, m), 4.50 (1H, dd, J=4, 8), 6.7—7.3 (4H, m), and 7.87 (1H, bs). Found: C, 62.50; H, 7.77%. Calcd for $C_{20}H_{30}O_5S$: C, 62.80; H, 7.90%.

2-[3-Methyl-1-(3-methyl-3-butenylthio)-3-butenyl]phenol (5m): Yield 63%. IR (neat) 3320, 3075, 2925, 1645, and 750 cm^{-1}. ^1H NMR ($CDCl_3$) δ=1.60, 1.67 (6H, each s), 2.2—2.4 (4H, m), 2.57 (2H, d, J=8), 4.17 (1H, t, J=8), 4.67 (4H, bs), and 6.6—7.3 (5H, m). Found: C, 73.53; H, 8.44%. Calcd for $C_{16}H_{22}OS$: C, 73.24; H, 8.45%.

4-(3-Chloropropylthio)-3,4-dihydro-2*H*-1-benzopyran (6). Potassium carbonate (2.76 g, 20 mmol) was added to a solution of **5j** (0.51 g, 1.83 mmol) in acetone (30 ml). After the mixture was refluxed for 3 h, it was filtered. The filtrate was concentrated. The residue was chromatographed on a column (benzene) to give **6** (0.40 g, 90%). IR (neat) 1580, 1480, 1260, and 750 cm^{-1}. ^1H NMR (CCl_4) δ=1.8—2.3 (4H, m), 2.57 (2H, t, J=7), 3.55 (2H, t, J=6), 3.95 (1H, t, J=4), 4.1—4.6 (2H, m), and 6.6—7.3 (4H, m). Found: C, 59.07; H, 6.17%. Calcd for $C_{12}H_{15}ClOS$: C, 59.37; H, 6.23%.

3,4-Dihydro-2*H*-1-benzopyran (7). The mixture of **6** (60 mg, 0.25 mmol) and Raney nickel (W4) (ca. 4 g) in ethanol (5 ml) was refluxed for 1 h. After the mixture was filtered, the filtrate was concentrated. The residual oil was chromatographed on a column (5% AcOEt–hexane) to give **7** (33 mg, quant.)

4-(3-Chloropropylsulfinyl)-3,4-dihydro-2*H*-1-benzopyran (8). A solution of sodium periodate (0.396 g, 1.85 mmol) in water (2 ml) was added dropwise to a solution of **6** (0.383 g, 1.58 mmol) in ethanol (6 ml) at 0 °C. The solution was stirred for 24 h at 0 °C. After the precipitate was filtered, the filtrate was poured into water. The aqueous solution was extracted with chloroform. The organic layer was washed with brine, dried ($MgSO_4$), and then evaporated. The residue was chromatographed on a column (13% AcOEt–benzene) to afford **8** (0.354 g, 86%). IR (neat) 3400, 1580, 1485, 1220, and 1030 cm^{-1}. ^1H NMR (CCl_4) δ=1.6—2.5 (4H, m), 2.5—3.0 (2H, m), 3.60 (2H, t, J=7), 3.8—3.9 (1H, m), 4.0—4.4 (2H, m), and 6.7—7.2 (4H, m). Found: C, 55.61; H, 5.83%. Calcd for $C_{12}H_{15}ClO_2S$: C, 55.70; H, 5.84%.

2*H*-1-Benzopyran (9). A solution of **8** (0.20 g, 0.774 mmol) in toluene (100 ml) was refluxed for 3 h and then concentrated. The residual oil was chromatographed on a column (30% benzene–hexane) to give **9** (0.062 g, 61%).

3,4-Dihydro-2,2-dimethyl-4-(3-methyl-2-butenylthio)-2*H*-1-benzopyran (10). Boron trifluoride etherate (0.1 ml, 0.8 mmol) was added to a solution of **5m** (100 mg, 0.8 mmol) in dichloromethane (3 ml) at room temperature under nitrogen atmosphere. After the mixture was stirred for 90 min, it was washed with water. The organic layer was dried and then evaporated. The residual oil was chromatographed on a column (2% AcOEt–hexane) to afford **10** (66 mg, 66%). IR (neat) 2980, 1605, and 760 cm^{-1}. ^1H NMR (CCl_4) δ=1.23, 1.43 (6H, each s), 2.07 (2H, d, J=8.2), 5.20 (1H, t, J=8). Found: C, 73.60; H, 8.53%. Calcd for $C_{16}H_{22}OS$: C, 73.24; H, 8.45%.

3,4-Dihydro-2,2-dimethyl-2*H*-1-benzopyran (11). The mixture of **10** (60 mg, 0.23 mmol) and Raney nickel (W4) (ca. 4 g) in ethanol (5 ml) was refluxed for 1.5 h. After the mixture was filtered, the filtrate was concentrated. The residual oil was chromatographed on a column (5% AcOEt–hexane) to give **11** (35 mg, 95%).

We are indebted to Mr. Shuichi Sato and Mr. Norimichi Iwase for valuable technical help and to Mrs. Hiroko Suesawa for measuring some of the NMR spectra.

References

1) K. Sato, S. Inoue, K. Ozawa, and M. Tazaki, *J. Chem. Soc., Perkin Trans. 1*, **1984**, 2715.

2) Reaction of phenol with dialkyl sulfoxides and synthesis of coumarins; K. Sato, S. Inoue, K. Ozawa, T. Kobayashi, T. Ota, and M. Tazaki, *J. Chem. Soc., Perkin Trans. 1*, **1987**, 1753.

3) The reactions of phenol with dimethyl sulfoxide and other activators have been reported; M. G. Burden and J. G. Moffat, *J. Am. Chem. Soc.*, **87**, 4656 (1965); K. E. Pfitzner and J. P. Marino, *ibid.*, **87**, 4658 (1965); Y. Hayashi and R. Oda, *J. Org. Chem.*, **32**, 457 (1967); G. R. Pettit and T. H. Brown, *Can. J. Chem.*, **45**, 1306 (1967). Y. Hiraki, M. Kamiya, R. Tanikaga, N. Ono, and A. Kaji, *Bull. Chem. Soc. Jpn.*, **50**, 447 (1977); P. Claus, *Monatsh. Chem.*, **102**, 913 (1971).

4) *o*-Methylthiomethylation of phenol was reported using dimethyl sulfide and *N*-chlorosuccinimide or chlorine as an activator of the sulfide; P. G. Gassman and D. R. Amick, *J. Am. Chem. Soc.*, **100**, 7611 (1978).

Halogenation Using Quaternary Ammonium Polyhalides. IV.[1] Selective Bromination of Phenols by Use of Tetraalkylammonium Tribromides

Shoji KAJIGAESHI,* Takaaki KAKINAMI,† Tsuyoshi OKAMOTO,†
Hiroko NAKAMURA,† and Masahiro FUJIKAWA†
Department of Industrial Chemistry, Faculty of Engineering, Yamaguchi University, Tokiwadai, Ube 755
†Department of Industrial Chemistry, Ube Technical College, Tokiwadai, Ube 755
(Received May 18, 1987)

Synopsis. Reaction of phenols with calculated amounts of benzyltrimethylammonium tribromide or tetrabutylammonium tribromide in dichloromethane–methanol for 0.5—1 h under mild conditions gave, selectively, the objective mono-, di-, or tribromophenols in good yields.

Previous work in this series[2] has shown that the reaction of phenols (**1**) with benzyltrimethylammonium tribromide (BTMA Br_3) (**2a**) in dichloromethane–methanol at room temperature readily gave bromophenols (**3**). In this paper, we wish to report a selective bromination of **1** by use of tetraalkylammonium tribromides (**2**), such as **2a** or tetrabutylammonium tribromide (TBA Br_3) (**2b**).

Results and Discussion

In general, it is difficult to carry out a step-by-step bromination of **1** with bromine since **1** reacts very rapidly with the reagent and leads to the polybromo-substituted phenols. For the purpose of the syntheses of monobromophenols from **1**, some technique in which the position of the substrate is blocked by an appropriate substituent group has frequently been employed.[3,4]

The well-known method for preparing pure monobromophenols is a diazotization of the corresponding aromatic amines and a subsequent heating with water. However, sometimes this method requires a tediously long synthetic pathway to obtain the bromophenols.

We have recently found that the reaction of **1** with calculated amounts of **2a** or **2b** in dichloromethane–methanol at room temperature gives the desirable mono-, di-, or tribromophenols in good yields. For instance, reactions of phenol (**1a**) with 1.0 equiv of **2b** gave *p*-bromophenol (**3a-1**), and with 2.0 equiv of **2a** gave 2,4-dibromophenol (**3a-2**); furthermore, reactions with 3.0 equiv of **2a** gave 2,4,6-tribromophenol[2] in good yields, respectively. Especially, we emphasize that our procedure is a highly useful method for synthesizing monobromophenols. The results are summarized in the Table 1. (The results for an exhaustive bromination of several **1** with sufficient amounts of **2a** are already shown by us[2]).

Compounds 2,4-dibromophenol[6] (**3a-2**), 2-bromo-4-*t*-butylphenol[12] (**3e-1**) and 2,4,6-tribromo-1,3-benzenediol[24] (**3m-2**) have been prepared by special methods. Our method easily gave these compounds in good yields, respectively. However, as a limitation of this method, attempts at the monobromination of less reactive **1**, such as nitrophenols, were unsuccessful.[28]

Experimental

4-Bromo-3,5-dimethylphenol (3i-1): Typical Procedure (1). To a solution of 3,5-dimethylphenol (**1i**) (0.50 g, 4.09 mmol) in dichloromethane (30 ml)–methanol (20 ml) was added dropwise **2b** (2.0 g, 4.13 mmol) under stirring at room temperature. The mixture was stirred for 30 min until a decoloration of the orange solution took place. The solvent was distilled and to the obtained residue was added water (30 ml). The mixture was extracted with ether (40 ml×4). The ether layer was then dried with magnesium sulfate and evaporated in vacuo to give a residue which was recrystallized from methanol–water (1:3) affording **3i-1** as colorless crystals; yield 0.77 g (93%); mp 115—116 °C (lit,[18] mp 115—116 °C).

2,4-Dibromo-3,5-dimethylphenol (3i-2): Typical Procedure (2). To a solution of **1i** (0.50 g, 4.09 mmol) in dichloromethane (30 ml)–methanol (20 ml) was added dropwise **2a** (3.2 g, 8.23 mmol) under stirring at room temperature. The mixture was stirred for 30 min until a decoloration of the orange solution took place. A subsequent same work-up as above gave **3i-2** as colorless crystals; yield 1.07 g (93%); mp 72—73 °C (lit,[18] mp 72—73 °C).

2,4,6-Tribromo-3,5-dimethylphenol (3i-3): Typical Procedure (3). A mixture of **1i** (0.50 g, 4.09 mmol) and **2a** (4.95 g, 12.70 mmol) in dichloromethane (50 ml)–methanol (20 ml) was stirred for 1 h at room temperature until a discoloration of the orange solution took place. A subsequent same work-up as above gave **3i-3** as colorless crystals; yield 1.63 g (90%); mp 166—169 °C (lit,[19] mp 166 °C).

References

1) Part III, S. Kajigaeshi, T. Kakinami, H. Tokiyama, T. Hirakawa, and T. Okamoto, *Bull. Chem. Soc. Jpn.*, **60**, 2667 (1987).
2) Part II, S. Kajigaeshi, T. Kakinami, H. Tokiyama, T. Hirakawa, and T. Okamoto, *Chem. Lett.*, **1987**, 627.
3) D. C. Huston and M. M. Ballard, *Org. Synth.*, Coll. Vol. II, 97 (1943).
4) C. F. Koelsch, *Org. Synth.*, Coll. Vol. III, 132 (1955).
5) R. Adams and C. S. Marvel, *Org. Synth.*, Coll. Vol. I, 128 (1941).
6) F. G. Pope and A. S. Wood, *J. Chem. Soc.*, **101**, 1824 (1912).
7) K. Auwers, *Justus Liebigs Ann. Chem.*, **415**, 157 (1918).
8) W. Werner, *Bull. Soc. Chim. Fr.*, [2] **46**, 278 (1886).
9) R. Walther and W. Zipper, *J. Prakt. Chem.*, [2] **91**, 376 (1915).
10) E. Werner, *Bull. Soc. Chim. Fr.*, [2] **46**, 276 (1886).
11) H. E. Ungande and E. F. Orwoll, *Org. Synth.*, Coll.

Table 1. Bromophenols(**3**) from Phenols(**1**) Using Tetraalkylammonium Tribromides(**2**)

Phenols(**1**)		Product(**3**)		**2** used	Molar ratio (**2**/**1**)	Yield[a] %	Mp(θ_m/°C) or Bp(θ_b/°C) Found	Reported
	(**1a**)	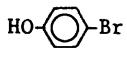	(**3a-1**)	**2b**	1.0	93	61—63	63[5]
		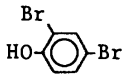	(**3a-2**)	**2a**	2.0	87	38—39	40[6]
	(**1b**)	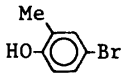	(**3b-1**)	**2b**	1.0	93	62—63	64[7]
		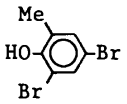	(**3b-2**)	**2a**	2.1	91	56.5	57[8]
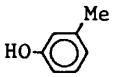	(**1c**)	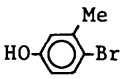	(**3c-1**)	**2b**	1.0	93	59—61	62[9]
		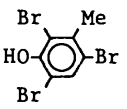	(**3c-2**)	**2a**	3.1	93	81	81—82[10]
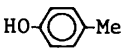	(**1d**)	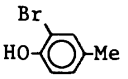	(**3d-1**)	**2b**	1.0	90	218—219/ 760 mmHg	218—219/[11] 760 mmHg
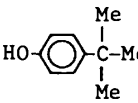	(**1e**)	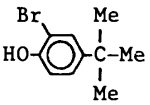	(**3e-1**)	**2a**	1.0	89	49—52	52[12]
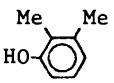	(**1f**)	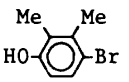	(**3f-1**)	**2b**	1.0	93	89—91	92[13]
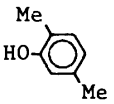	(**1g**)	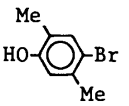	(**3g-1**)	**2b**	1.0	93	86—87	87[14]
		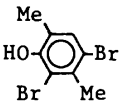	(**3g-2**)	**2a**	2.1	93	79	79—80[15]
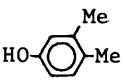	(**1h**)	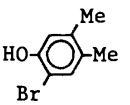	(**3h-1**)	**2b**	1.0	93	78—79	80[16]
		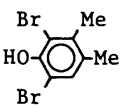	(**3h-2**)	**2a**	2.1	93	38—40	39—40[17]
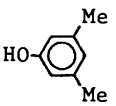	(**1i**)	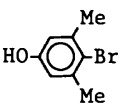	(**3i-1**)	**2b**	1.0	93	115—116	115—116[18]
		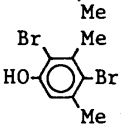	(**3i-2**)	**2a**	2.0	93	72—72	72—73[18]
		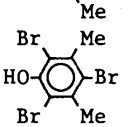	(**3i-3**)	**2a**	3.1	90	166—169	166[19]

Table 1. (Continued)

Phenols(**1**)		Product(**3**)		**2** used	Molar ratio (**2**/**1**)	Yield[a] %	Mp(θ_m/°C) or Bp(θ_b/°C) Found	Reported
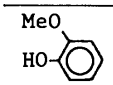	(**1j**)	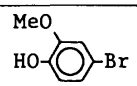	(**3j-1**)	**2b**	1.0	90	35—39	46[20]
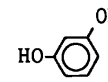	(**1k**)	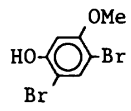	(**3k-1**)	**2a**	2.0	93	65—66	73—75[21]
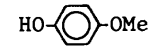	(**1l**)	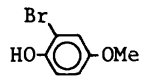	(**3l-1**)	**2b**	1.0	90	42—43	45[22]
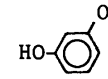	(**1m**)	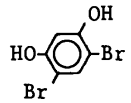	(**3m-1**)	**2a**	2.0	92	109—110	110—112[23]
		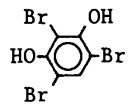	(**3m-2**)	**2a**	3.1	93	111.5—113.5	112[24]
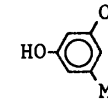	(**1n**)	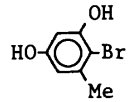	(**3n-1**)	**2b**	1.0	93	132—135	135[25]
		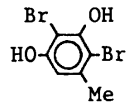	(**3n-2**)	**2a**	2.0	93	125—126	124—125[26]
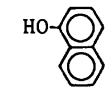	(**1o**)	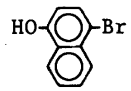	(**3o-1**)	**2b**	1.0	93	127	127—128[27]
		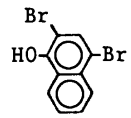	(**3o-2**)	**2a**	2.0	93	107—108	105.5[27]
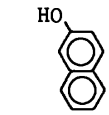	(**1p**)	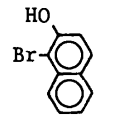	(**3p-1**)	**2b**	1.0	93	84	84—85[27]

a) Yield of isolated product. 1 mmHg = 133.322 Pa.

Vol. III, 130 (1955).
12) E. W. Lewis, *J. Chem. Soc.*, **83**, 330 (1903).
13) W. F. Short, H. Stromberg, and A. E. Wiles, *J. Chem. Soc.*, **1936**, 319.
14) K. Auwers and H. Ercklentz, *Justus Liebigs Ann. Chem.*, **302**, 113 (1898).
15) K. Auwers, *Justus Liebigs Ann. Chem.*, **302**, 114 (1898).
16) A. W. Crossley and D. J. Bartlett, *J. Chem. Soc.*, **103**, 1299 (1913).
17) K. Auwers, *Justus Liebigs Ann. Chem.*, **344**, 172 (1906).
18) K. Auwers and E. Borsche, *Ber.*, **48**, 1715 (1915).
19) E. Knoevenagel, *Ber.*, **26**, 1952 (1893).
20) K. W. Rosenmund and W. Kuhnhenn, *Ber.*, **56**, 1262 (1923).
21) M. Kohn, *J. Am. Chem. Soc.*, **74**, 1601 (1952).
22) S. Nametkin, K. S. Bokarav, and N. N. Mel'nikov, *Doklady Akad. Nauk SSSR*, **77**, 293 (1951); *Chem. Abstr.*, **45**, 10213 (1951).
23) J. Zehenter, *Monatsh. Chem.*, **8**, 296 (1887).
24) R. Benedikt, *Ber.*, **11**, 2168 (1878).
25) L. A. Yanovskaya, A. P. Terent'ev, and L. I. Belen'kii, *Zhur. Obshchei Khim.*, **22**, 1954 (1952). *Chem. Abstr.*, **47**, 8033 (1953).
26) H. J. Lylance, *J. Chem. Soc.*, **1963**, 5580.
27) F. Reverdin and H. Kauffmann, *Ber.*, **28**, 3054 (1895).
28) For instance, the reaction of 4-nitrophenol with 1.0 equiv of **2a** in dichloromethane–methanol for 1 h at room temperature gave a mixture of 2,6-dibromo-4-nitrophenol and 4-nitrophenol recovered in the ratio of 1:1 on ^{1}H NMR spectra.

Asymmetric Diels-Alder Reaction of Acrylamides Having *trans*-2,5-Disubstituted Pyrrolidines as Chiral Auxiliaries

Yasuhiro KAWANAMI,* Tsutomu KATSUKI,† and Masaru YAMAGUCHI†
Department of Chemistry, Faculty of Education, Kagawa University, Takamatsu, Kagawa 760
†Department of Chemistry, Faculty of Science, Kyushu University 33,
Higashi-ku, Fukuoka 812
(Received June 2, 1987)

Synopsis. The asymmetric Diels-lder reaction between chiral acrylamides derived from (2R,5R)-2,5-disubstituted pyrrolidines and cyclopentadiene gave (1*R*,2*R*,4*R*)-5-norbornene-2-carboxylic acid amides **3a—c** with excellent diastereoface selectivity. The amides **3a—c** were converted into the corresponding carboxylic acid by an iodolactonization-reduction sequence and 2,5-disubstituted pyrrolidines were recovered intact.

The Diels-Alder reaction[1] provides one of the useful methods of creating new chiral centers and some highly diastereoselective examples employing different types of optically active dienophiles have been reported in the last few years.[2-4] Recently, we have developed chiral auxiliaries, *trans*-2,5-disubstituted pyrrolidines,[5] which were quite effective for asymmetric α-alkylations,[5] α-acylation,[6] aldol reaction,[7] and [2,3]-Wittig rearrangement[8] of carboxylic acids through their amides. In this note, we wish to describe the asymmetric Diels-Alder reaction of acrylamides **1a—c** bearing the same chiral auxiliaries with cyclopentadiene under Lewis acid catalyzed and uncatalyzed conditions.

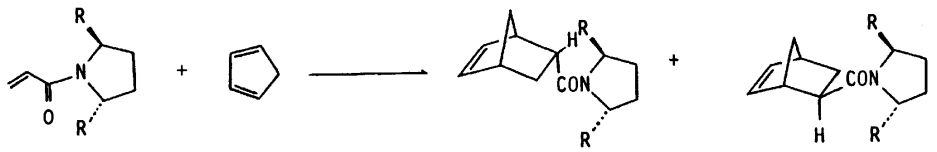

1a; R=COOMe
1b; R=CH_2OMe
1c; R=CH_2OCH_2OMe

2

The dienophiles **1a—c** were prepared by the acylation of the corresponding (2R,5R)-2,5-disubstituted pyrrolidines[5] with acryloyl chloride and Et_3N in CH_2Cl_2 at 0 °C. Then, **1a—c** were submitted to Diels-Alder reaction with cyclopentadiene in toluene under various conditions. The reaction proceeded smoothly to give (1*R*,2*R*,4*R*)-5-norbornene-2-carboxylic acid amides **3a—c** as major isomers. The results obtained were summarized in Table 1. Aluminum trichloride among Lewis acids examined afforded the highest *endo*- and almost quantitative diastereoface selectivity (Entries 5 and 8). Diethylaluminum chloride also gave the same degree of diastereomeric excess as aluminum trichloride but the *endo*

Table 1. Asymmetric Diels-Alder Reaction of **1a—d** with **2**[a]

Entry	Dienophile R	Catalyst	Temp °C	Time h	Yield[b] %	endo : exo[c] (**3** : **4**)	%de of *endo*-**3**[d,e]
1	**1a**(R=COOMe)	none	rt	48	81	68 : 32	67
2	**1a**	BF_3-OEt_2	−10	4	65	87 : 13	90
3	**1a**	$AlCl_3$	0	2	85	87 : 13	94
4	**1b**(R=CH_2OMe)	none	rt	24	80	68 : 32	85
5	**1b**	$AlCl_3$	0	1	71	89 : 11	98
6	**1c**(R=CH_2OMOM)[f]	none	rt	42	75	69 : 31	90
7	**1c**	BF_3-OEt_2	−10	1	76	92 : 8	94
8	**1c**	$AlCl_3$	0	1	76	95 : 5	98
9	**1c**	Et_2AlCl	0	1	73	86 : 14	98
10	**1d**[g]	$AlCl_3$	0	1	76	91 : 9	73[h]

a) Reactions were carried out in 0.2—0.5 mol dm^{-3} toluene solution of **1**. b) Isolated yield. c) Ratios were determined after column chromatography separation. Each compound gave satisfactory ^1H NMR analysis. d) Determined by ^1H NMR spectra in the presence of Eu(fod)$_3$ and/or ^{13}C NMR spectra. e) Configurations of the adducts were deduced to be 2'R from the configuration of (+)-(1*R*,2*R*,4*R*)-5-norbornene-2-carboxylic acid. f) MOM=CH_2OMe. g) Acrylamide derived from (*S*)-*O*-methoxymethylprolinol. h) Absolute configuration was determined to be 2'S.

selectivity suffered a small loss (Entry 9). In the reactions in the absence of catalyst, the diastereoface selectivity depended on the substituent on the pyrrolidine ring and the best result (90% de) was obtained when the amide **1c** was used (Entry 6). This result is noteworthy because highly diastereoselective Diels-Alder reactions with one exception[2] have usually been attained in the presence of Lewis acid catalysts.[1] An acrylamide **1d** derived from (*S*)-*O*-methoxymethylprolinol, was examined for comparison and only moderate diastereoface selectivity (73% de) was obtained under aluminum trichloride-catalyzed conditions, though high *endo* selectivity was also observed (Entry 10).

The major *endo*-adducts **3** were converted to (+)-(1*R*,2*R*,4*R*)-5-norbornene-2-carboxylic acid[2,9] by the sequence, i) iodolactonization to a iodo lactone using iodine in H_2O-DME[10] and ii) reduction of the iodo lactone by zinc in methanol. Chiral auxiliaries were also recovered by this iodolactonization process.

Although the exact steric cource of the reaction is not clear at present, absolute configurations of cycloaddition products and a CPK-model examination suggest that the acrylamide exists as a cisoid conformer due to the severe repulsion between the *cis*-vinylic hydrogen on the β-carbon atom and one of the C_2-symmetrically placed substituents on the pyrrolidine ring and that the amide is attacked by cyclopentadiene on its less hindered side (*si*-face). Further work on the reaction of other combinations of dienophiles and dienes is under way.

Experimental

Melting points were uncorrected. ^{1}H NMR and ^{13}C NMR spectra were obtained at 90 MHz in $CDCl_3$ with TMS as an internal standard.

(2*R*,5*R*)-*N*-Acryloyl-*trans*-2,5-bis(methoxycarbonyl)pyrrolidine (1a). Acryloyl chloride (0.21 ml, 2.58 mmol) was added to a solution of (2*R*,5*R*)-*trans*-2,5-bis(methoxycarbonyl)pyrrolidine (242 mg, 1.29 mmol) and triethylamine (0.36 ml, 2.58 mmol) in dichloromethane (4 ml) at 0 °C and the mixture was stirred for 1 h. The reaction mixture was diluted with ether and filtered through Celite. The filtrate was concentrated and chromatographed on silica gel (hexane-acetone, 10:3) to give **1a** (172 mg, 58%): $[\alpha]_D^{23}$ +118° (*c* 1.14, EtOH); UV (EtOH) 206 nm (ε 4065); IR (neat) 1740, 1650, and 1615 cm^{-1}; ^{1}H NMR δ=1.92—2.63 (4H, m), 3.73 (3H, s), 3.75 (3H, s), 4.6—4.8 (2H, m), 5.70 (1H, dd, *J*=9.5 and 4.0 Hz), 6.06—6.55 (2H, m); Found: C, 54.98; H, 6.16; N, 5.54%. Calcd for $C_{11}H_{15}NO_5$: C, 54.77; H, 6.27; N, 5.81%.

(2*R*,5*R*)-*N*-Acryloyl-*trans*-2,5-bis(methoxymethyl)pyrrolidine (1b): Yield, 72%; $[\alpha]_D^{23}$ +70.6° (*c* 1.36, EtOH); UV (EtOH) 206 nm (ε 7890); IR (neat) 1640 and 1610 cm^{-1}, ^{1}H NMR δ=1.8—2.2 (4H, m), 3.06—3.08 (4H, m), 3.30 (6H, s), 3.9—4.4 (2H, m), 5.66 (1H, dd, *J*=8.4 and 4.2 Hz), 6.25—6.68 (2H, m); Found: C, 61.70; H, 9.26; N, 6.39%. Calcd for $C_{11}H_{19}NO_3$: C, 61.95; H, 8.98; N, 6.57%.

(2*R*,5*R*)-*N*-Acryloyl-*trans*-2,5-bis(methoxymethoxymethyl)-pyrrolidine (1c): Yield, 79%; $[\alpha]_D^{23}$ +50.0° (*c* 0.72, EtOH); UV (EtOH) 206 nm (ε 7500); IR (neat) 1640 and 1608 cm^{-1}; ^{1}H NMR δ=1.8—2.4 (4H, m), 3.25—3.86 (4H, m), 3.35 (6H, s), 4.12 (1H, m), 4.30 (1H, m), 4.59 (4H, s), 5.66 (1H, dd, *J*=4.2 and 8.4 Hz), 6.26—6.70 (2H, m); Found: C, 56.86; H, 8.75; N, 5.27%. Calcd for $C_{13}H_{23}NO_5$; C, 57.13; H, 8.48; N, 5.12%.

Representative Procedure for Diels-Alder Reaction of Acrylamides with Cyclopentadiene. Aluminum trichloride (122 mg, 0.904 mmol) was added to a solution of **1c** (206 mg, 0.753 mmol) in toluene (3.7 ml) at 0 °C. After 5 min, freshly distilled cyclopentadiene (0.5 ml, 6 mmol) was added to the solution. The mixture was stirred for 1 h, quenched with saturated aqueous $NaHCO_3$ solution, and extracted with ethyl acetate. The organic layer was washed with brine, dried over $MgSO_4$, and concentrated in vacuo. The concentrate was chromatographed on silica gel (hexane-acetone, 5:2) to give the less polar *exo*-isomer (**4c**, 10 mg, 4%) and the more polar *endo*-isomer (**3c**, 185 mg, 72%).

4c: IR (neat) 1635 cm^{-1}; ^{1}H NMR δ=1.1—1.4 (2H, m), 1.78—2.50 (7H, m), 2.75 (1H, m), 2.92 (1H, m), 3.32 (3H, s), 3.35 (3H, s), 3.2—3.8 (4H, m), 3.93—4.32 (2H, m), 4.56 (2H, s), 4.60 (2H, s), 6.15 (2H, m).

3c: $[\alpha]_D^{23}$ +161.8° (*c* 1.23, EtOH); IR (neat) 1640 cm^{-1}; ^{1}H NMR δ=1.15—2.40 (8H, m), 2.82—3.72 (7H, m), 3.35 (6H, s), 4.20 (2H, m), 4.60 (4H, s), 5.76 (1H, dd, *J*=2.6 and 5.6 Hz), 6.25 (1H, dd, *J*=3.1 and 5.6 Hz); ^{13}C NMR δ=25.1, 27.5, 29.2, 42.0, 43.2, 46.6, 50.2, 55.1, 55.2, 56.8, 57.3, 67.0, 69.4, 96.5, 96.6, 130.3, 137.3, 173.0; Found: C, 63.49; H, 8.79; N, 4.17%. Calcd for $C_{18}H_{29}NO_5$: C, 63.69; H, 8.61; N, 4.13%.

(2*R*,5*R*)-*N*-[(1*R*,2*R*,4*R*)-5-Norbornene-2-carbonyl]-*trans*-2,5-bis(methoxycarbonyl)pyrrolidine (3a): $[\alpha]_D^{23}$ +212.6° (*c* 1.98, EtOH); IR (neat) 1735 and 1650 cm^{-1}; ^{1}H NMR δ=1.16—2.98 (10H, m), 3.17 (1H, m), 3.70 (3H, s), 3.77 (3H, s), 4.61 (1H, m) 4.79 (1H, d, *J*=7.4 Hz), 5.89 (1H, dd, *J*=6.0 and 3.0 Hz), 6.19 (1H, dd, *J*=6.0 and 3.0 Hz); ^{13}C NMR δ=26.9, 29.6, 30.1, 42.3, 42.8, 45.9, 49.8, 52.0, 52.6, 59.3, 131.5, 136.7, 172.3, 172.5, 173.0; Found: C, 62.52; H, 6.93; N, 4.58%. Calcd for $C_{16}H_{21}NO_5$: C, 62.53; H, 6.89; N, 4.56%.

(2*R*,5*R*)-*N*-[(1*R*,2*R*,4*R*)-5-Norbornene-2-carbonyl]-*trans*-2,5-bis(methoxymethyl)pyrrolidine (3b): $[\alpha]_D^{23}$ +213° (*c* 1.0, EtOH); IR (neat) 1640 cm^{-1}; ^{1}H NMR δ=1.15—2.55 (9H, m), 2.82—3.68 (6H, m), 3.32 (3H, s), 3.35 (3H, s), 4.15 (2H, m), 5.74 (1H, m), 6.24 (1H, m); ^{13}C NMR δ=25.0, 27.3, 29.0, 42.0, 43.0, 46.6, 50.2, 56.5, 57.1, 58.6, 59.0, 71.4, 74.5, 130.3, 137.4, 173.0; Found: C, 68.54; H, 9.27; N, 5.00%. Calcd for $C_{16}H_{25}NO_3$: C, 68.79; H, 9.02; N, 5.01%.

Conversion of (+)-3c to (+)-(1*R*,2*R*,4*R*)-5-Norbornene-2-carboxylic Acid. Iodine (57.8 mg, 0.228 mmol) was added to a solution of **3c** (70.3 mg, 0.207 mmol) in H_2O-DME (1:1, 0.6 ml) at room temperature and the mixture was stirred for 1 day. The resultant solution was diluted with ethyl acetate and washed with saturated $Na_2S_2O_3$ and with 0.5 mol dm^{-3} HCl. The organic layer was further washed with saturated $NaHCO_3$ and with brine, dried over $MgSO_4$, and concentrated. The residue was subjected to preparative TLC (hexane-acetone, 10:3) to give the iodo lactone (**5**, 34.6 mg, 63%): ^{1}H NMR δ=1.59—2.80 (6H, m), 3.20 (1H, m), 3.89 (1H, d, *J*=2.6 Hz), 5.13 (1H, d, *J*=5.3 Hz). The whole aqueous solution was made basic with $NaHCO_3$ and extracted with chloroform-ethanol (3:1). The extract was dried over $MgSO_4$ and concentrated to recover (2*R*,5*R*)-2,5-bis(methoxymethoxymethyl)pyrrolidine (63%). The iodo lactone **5** was then treated with zinc (120 mg, 1.84 mmol) and CuBr (40 mg, 0.279 mmol) in methanol at room temperature for 2 h. The mixture was filtered through Celite and concentrated. The residue was submitted to bulb-to-bulb distillation (130—140 °C/2133 Pa, bath temperature) to give (+)-5-norbornene-2-carboxylic acid (12.3 mg, 68%); $[\alpha]_D^{23}$ +146° (*c* 0.615, EtOH) [lit,[2] $[\alpha]_D^{23}$ −147.14° (*c* 0.49, EtOH) for (*S*)-acid].

The compounds [(+)-**3a** and (+)-**3b**] were also converted into the same (+)-norbornene-2-carboxylic acid in a similar manner.

The present work was partially supported by a Grant-in-Aid for Scientific Research No. 61740306 from the Ministry of Education, Science and Culture.

References

1) For a review, see; L. A. Paquette, "Asymmetric Synthesis" ed by J. D. Morrison, Vol. 3, Academic Press, New York (1984), p. 455. See, also; K. Narasaka, M. Inoue, and N. Okada, *Chem. Lett.*, **1986**, 1109; K. Narasaka, M. Inoue, and T. Yamada, *ibid.*, **1986**, 1967.

2) W. Choy, L. A. Reed, III, and S. Masamune, *J. Org. Chem.*, **48**, 1137 (1983); S. Masamune, L. A. Reed, III, J. T. Davis, and W. Choy, *ibid*, **48**, 4441 (1983).

3) W. Oppolzer, C. Chapuis, G. M. Dao, D. Reichlin, and T. Godel, *Tetrahedron Lett.*, **23**, 4781 (1982).

4) D. A. Evans, K. T. Chapman, and J. Bisaha, *J. Am. Chem. Soc.*, **106**, 4261 (1984).

5) Y. Kawanami, Y. Ito, T. Kitagawa, Y. Taniguchi, T. Katsuki, and M. Yamaguchi, *Tetrahedron Lett.*, **25**, 857 (1984); M. Enomoto, Y. Ito, T. Katsuki, and M. Yamaguchi, *ibid.*, **26**, 1343 (1985); S. Ikegami, T. Hayama, T. Katsuki, M. Yamaguchi, *ibid.*, **27**, 3403 (1986); T. Hanamoto, T. Katsuki, and M. Yamaguchi, *ibid.*, **27**, 2463 (1986).

6) Y. Ito, T. Katsuki, and M. Yamaguchi, *Tetrahedron Lett.*, **25**, 6015 (1984); **26**, 4643 (1985).

7) T. Katsuki and M. Yamaguchi, *Tetrahedron Lett.*, **26**, 5807 (1985).

8) M. Uchikawa, T. Hanamoto, T. Katsuki, and M. Yamaguchi, *Tetrahedron Lett.*, **27**, 4577 (1986).

9) The acid could not be obtained by ordinary hydrolysis of **3** (1 mol dm^{-3} HCl, reflux) because of the lability of the acid under the conditions.

10) Y. Tamaru, M. Mizutani, Y. Furukawa, S. Kawamura, Z. Yoshida, K. Yanagi, and M. Minobe, *J. Am. Chem. Soc.*, **106**, 1079 (1984).

Electroreduction of *m*-Hydroxybenzoic Acid.[1] Preparation of *m*-Phenoxybenzyl Alcohol for the New Insecticide Ethofenprox

Ryu Oi, Chitoshi Shimakawa, Yasushi Shimokawa, and Shinji Takenaka*
Research Dept. Omuta Factory, Mitsui Toatsu Chemicals, Inc., Omuta, Fukuoka 836
(Received June 5, 1987)

Synopsis. The electroreduction of *m*-hydroxybenzoic acid was examined from both mechanistic and technical points of view, and a practical route to *m*-phenoxybenzyl alcohol has been developed.

Recently, various kinds of artificial pyrethroids having *m*-phenoxybenzyloxy group have been developed and their characteristic features have received much attention in the insecticide chemistry. Among these pyrethroids, due to low toxicity to fish as well as to mammals and excellent pesticidal activity, the exceptional potency of ethofenprox (**4**)[2] has opened up an important market, especially in agriculture for pest control. In our research project on the development of a commercially feasible procedure for the synthesis of **4**, we needed an efficient procedure for producing *m*-phenoxybenzyl alcohol (**3**) (Scheme 1).

Many attempts have been made to prepare **3**; majority of the hitherto disclosed procedures relies upon partial oxidation of *m*-phenoxytoluene (**5**). For example, the halogenation of **5** followed by hydrolysis[3] has been intensively investigated, but the product selectivity is not necessarily satisfactory. On the other hand, alternative route to **3** has been performed by the air-oxidation of **5** followed by the electroreduction.[4] However, there still remain some difficulties in operating in the industrial practice, since the air-oxidation requires vigorous conditions, e.g., high temperature and high pressure, and the substrate concentration in the electrolysis is impractically low.

Herewith, we describe a new efficient procedure for the synthesis of **3** (Scheme 1) involving electroreduction of *m*-hydroxybenzoic acid (**1**), which is easily available on a commercial basis, and subsequent condensation of hydroxybenzyl alcohol **2** with bromobenzene.[5]

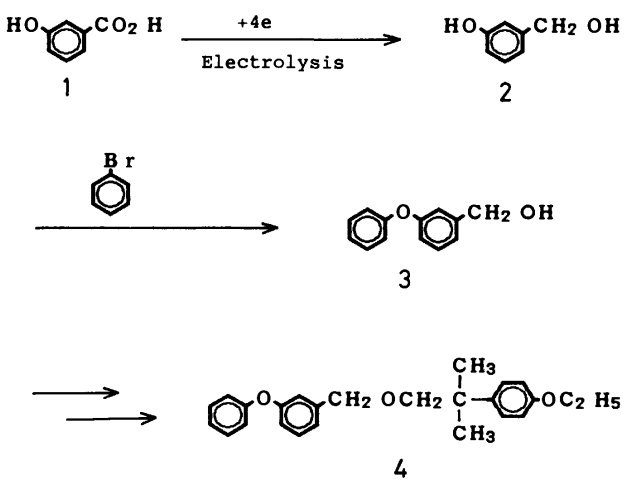

Scheme 1.

The merit of this approach strongly depends upon ease of the operation and high yield of the electrochemical reduction step (**1**→**2**). Reduction of the carboxylic acid **1** to alcohol **2** has been performed by the chemical reduction with borane–dimethyl sulfide,[6] but the use of a stoichiometric amount of the expensive reduction agent is impractical. As a potential tool for the catalytic hydrogenation of **1**, electroreduction has received some attention.[7] The yield of **2** reported so far, however, is insufficient (44%), and the commercial application of the electrolysis procedure has been out of consideration.

In order to improve the yield of **2** sufficient for practical use, we reinvestigated the electrochemical reduction of **1** from both mechanistic and technical points of view.

Electroreduction was carried out with two lead electrodes using an H-shaped two compartment cell divided by ion-exchange membrane in aqueous H_2SO_4 solution. The results under various electrolysis conditions are summarized in Table 1. Satisfactory current efficiency was attained in the aqueous acidic media (Entries 1—4), while in neutral conditions (Entry 8), the reduction was very slow, and no appreciable amount of **2** was detected in basic conditions (Entry 9). A lead cathode gave better results than mercury one (Entries 3 and 6). Attempts were made to assess the relative importance of acids in this reduction by influences of current efficiency upon several different H_2SO_4 concentrations (Table 1, Entries 1—4). Better results were obtained at higher H^+ concentrations, but decomposition of product **2** was promoted at the same time.

Next, we studied this phenomenon from voltammetric viewpoint. In the acidic electrolysis systems, reduction of **1** competes with the hydrogen evolution reaction. Therefore, particular attention should be paid to the relative reduction potential of **1** against hydrogen overvoltage. It is of interest to note that in spite of the fact that no appreciable shifts of hydrogen overvoltage of lead electrode were observed with the variation of H_2SO_4 concentration (−1.73—1.75 V vs. Hg/Hg_2SO_4), reduction wave of **1** appeared more clearly at higher H_2SO_4 concentrations. The reduction wave shifts to ca. −1.66 V from −1.71 V by increasing the H_2SO_4 concentration from 5% up to 17.5%, while no appreciable change of the potential was observed over 17.5% (Table 1, Entries 1—4). These results are good in accordance with the variation of the current efficiency. These remarkable effects of the concentration of H_2SO_4 are well understood by assuming the four electron reduction mechanism[8] involving protonated aromatic carboxylic acid as a

Table 1. Electroreduction of *m*-Hydroxybenzoic Acid (**1**)[a]

Entry	Solvent electrolyte	Conversion of **1**[b,c] %	Current efficiency[c] %	Yield of **2**[c] %	Reduction potential of **1**[d]
1	5% aq H_2SO_4	10.5	4.2	8.7	−1.71
2	10% aq H_2SO_4	51.0	20.4	48.1	−1.69
3	17.5% aq H_2SO_4	99.9	40.0	91.5(90)[h]	−1.66
4	25% aq H_2SO_4	100.0	40.0	86.4(85)[h]	−1.66
5[e]	17.5% aq H_2SO_4	25.1	10.0	21.4	
6[f]	17.5% aq H_2SO_4	81.2	32.5	75.1	
7[g]	17.5% aq H_2SO_4	99.9	40.0	31.6	
8	15% aq Et_4NOTs	3.3	1.3	2.9	
9	15% aq NaOH	—	—	—	

a) The electroreduction was curried out under constant current of 16 A dm^{-2} with an H-shaped devided cell fitted with two lead electrodes at 50 °C. The amount of each 15% of **1**(vs. solvent) was added portionwise. b) Electricity was passed up to 10 F mol^{-1}. c) Analyzed by HPLC based on **1**. d) V vs. Hg/Hg_2SO_4. e) **1** was added all at once at the beginning. f) A Hg pool cathode was used. g) Carried out at 80 °C. h) Isolated yield based on **1**.

reactive species. Thus, in more acidic solutions, a greater proportion of activated **1** by protonation may contribute to move the reduction potential in positive direction and to improve the current efficiency.

In a practical sense, it is important to operate the electrolysis at a high substrate concentration, since the concentration is directly related to the production efficiency and economy. Unfortunately, carboxylic acid **1** has a low solubility in the water, and when **1** was added beyond its solubility, deposits of insoluble parts of **1** covered the surface of the cathode to disturb the desired reduction (Table 1, Entry 5). In order to obtain a 10% homogeneous solubility of **1**, reaction temperature must be raised above 80 °C. However, product **2** is easily decomposed in the acidic solution, and the decomposition rate undesirably increases as the temperature rises. Lower yield of **2** at 80 °C (Table 1, Entry 7) compared with that at 50 °C (Entry 3) seems to be ascribed to thermal decomposition of **2**.

The contradictory problems can be solved by portionwise addition of **1**. When the electrolysis was carried out at 50 °C by adding **1** little by little during the course of electrolysis with a gradual generation of the product, reduction of significant amount of the carboxylic acid could be achieved and finally concentration of the product reached to 15%. This can be ascribed to the fact that in contrast to the poor solubility of starting **1**, product **2** is very soluble in the water, and the presence of **2** improves the solubility of **1** significantly. Due to these investigations, this electrochemical reduction has successfully gone through pilot plant test and is being studied for the commercial production.

Experimental

Melting points are uncorrected and were determined in open-ended capillaries. IR spectra were recorded on a Hitachi 285 grating spectrometer, and ^1H NMR spectra were measured at 90 MHz with a Nippon Denshi FX-90Q spectrometer. Chemical shifts are quoted in parts par million downfield from Me_4Si used as an internal reference. Cyclic voltammetric experiments were performed by using Hokuto Denko Ltd. Model HA-303 potentio-galvanostat, HB-104 function generator and Riken Denshi Co., Ltd. Model F-3 X-Y plotter.

Consumption of the starting material and purity of products were checked on a Shimazu HPLC system (Model LC-5A pump, SPD-2A spectrophotometric detector) using *p*-nitrophenol as an internal standard. For reverse-phase chromatography, Dupont Zorvax ODS column (a 4.6 mm diameter, 25 cm length stainless steel) was used. An eluent solvent of 40/60 MeCN–H_2O was buffered with 0.3 mmol dm^{-3} AcOH and 3 mmol dm^{-3} AcONa. The flow rate was 0.5 ml min^{-1} and fixed-wavelength detection (266 nm) was used.

Materials. *m*-Hydroxybenzoic acid (**1**) was available as a commercial product of our company. *m*-Hydroxybenzyl alcohol (**2**) was purchased from Aldrich Chemicals Co. as authentic sample.

Apparatus. An H-shaped cell divided with ion-exchange membrane (Asahi Glass Co., Ltd. Selemion CMV) was used, which was equipped with two lead plate electrodes (50 cm^2, 12 cm apart), stirring bars, and a thermometer. A vessel was immersed in a hot water bath at 50 °C and regulated dc power was supplied by Kikusui Electronics Co. Model PAD 35—60L.LP.

General Procedures. Electrochemical Reduction of *m*-Hydroxybenzoic Acid (1). Into both the anode and cathode compartments was placed a 17.5% water solution of H_2SO_4 (200 g each). After regulated dc power (16 A dm^{-2}) was supplied at 50 °C, to the catholytes was portionwise added *m*-hydroxybenzoic acid (**1**; 6.85 g h^{-1}, total 35.0 g, 0.253 mol) during the first 6 F mol^{-1} (5.1 h). After being electrolyzed (10 F mol^{-1}, 8.5 h) at 50 °C, the catholytes were extracted with diethyl ether. The extract was washed with brine, dried (Na_2SO_4) and concentrated in vacuo, giving a brown oil (29.3 g). The rapidly crystallized at room temperature, giving tan crystals, mp 68—70 °C (lit,[7] mp 73 °C), with IR and ^1H NMR spectrums identical with that reported for the authentic material.[9] The crystals were checked on HPLC and purity of *m*-hydroxybenzyl alcohol (**2**) was 96.5% (90.0% yield based on **1**), along with 0.1% of starting material **1** by using an internal standard.

We thank Prof. Sigeru Torii, Dr. Hideo Tanaka (Okayama University, Jpn.), and Dr. Akihiro Tamaki (General Manager of Research Dept., Omuta Factory, Mitsui Toatsu Chemicals, Inc., Jpn.) for many helpful

discussions as this work progressed. We thank Morihiko Hoshioka (Director of Omuta Factory, Mitsui Toatsu Chemicals, Inc., Jpn.) for giving us an opportunity to present this work.

References

1) S. Takenaka, R. Oi, C. Shimakawa, and Y. Shimokawa, 7th Electroorganic Chemistry Symposium, Kyoto, June 1986, Abstr., No. 25, p. 53; *idem*, International Symposium on Electroorganic Synthesis, Kurashiki, Oct. 1986, Abstr., No. PI04.

2) S. Numata, "Seibutsu Kassei Bussitsu no Bunshi Sekkei," ed by H. Yoshioka and K. Shutoh, Soft Science Co., Tokyo (1986), Chap. 9, p. 338.

3) For example, Nippon Oils and Fats Co., Ltd. Jpn. Patent Kokai 81-166142 (1981); *Chem. Abstr.*, **96**, 162334w (1982).

4) A. Chaintreau, G. Adrian, and Couturier, *Synth. Commun.*, **11**, 439 (1981).

5) S. Takenaka and R. Oi, Jpn. Patent Kokai 86-186339 (1986); *Chem. Abstr.*, **105**, 226022g (1986).

6) C. F. Lane, H. Mayatt, J. Daniels, and H. B. J. Hopps, *J. Org. Chem.*, **39**, 3052 (1974).

7) C. Mettler, *Ber.*, **38**, 1743 (1905).

8) M. Brikett and A. T. Kuhn, *Electrochim. Acta*, **21**, 991 (1976).

9) "Standard Proton NMR Spectra Collection," Sadter Research Laboratories, a division of Bio-Rad Laboratories, Inc., (1980), IR: No. 18817, ^{1}H NMR: No. 13297.

 © 1987 The Chemical Society of Japan Bull. Chem. Soc. Jpn., 60, 4197—4201 (1987)

$AlBr_3$ Group Reorientation in $NaAl_2Br_7$ and KAl_2Br_7 Studied by Means of ^{81}Br, ^{27}Al NQR and ^{27}Al NMR

Koji YAMADA,* Tsutomu OKUDA, and Sumio ICHIBA
Department of Chemistry, Faculty of Science, Hiroshima University, Naka-ku, Hiroshima 730
(Received February 27, 1987)

^{81}Br NQR spin-lattice relaxation times for MAl_2Br_7 (M=Na and K) were measured from 77 to 373 K and the reorientational activation energies of the $AlBr_3$ groups about Al-Br(bridge) axes were determined. In the case of $NaAl_2Br_7$, the reorientation of the $AlBr_3$ group was also confirmed by a motional narrowing effect of the ^{27}Al NMR using a single crystal. In order to examine the effect of the reorientation on the Al site, ^{27}Al NQR frequencies in $NaAl_2Br_7$ were observed as a function of temperature by a SEDOR technique. The asymmetry parameter (η) of the electric field gradient (efg) tensor was found to increase at one of the two Al sites with the onset of the reorientation.

NQR spin-lattice relaxation times (T_1) have been measured in order to study reorientation of molecules or molecular fragments[1,2] and also molecular motions in the vicinity of phase transitions.[3] This is due to the fact that the NQR relaxation rate increases because of the large fluctuation of its efg tensor induced by molecular motions. The dynamical properties of the compounds containing reorientationable groups such as $-CCl_3$, $-PCl_3$, and $=PCl_3$ have been studied by ^{35}Cl NQR T_1.[4-9] In contrast to proton NMR experiment in the solid state, the measurements of the NQR relaxation times give dynamical information at each crystallographically different site. This advantage was clearly shown for p-$CCl_3C_6H_4Cl$[4] and $AlBr_3 \cdot 2CH_3CN$ which has the ionic structure $AlBr(CH_3CN)_5^{2+} \cdot 2AlBr_4^- \cdot CH_3CN$.[10]

According to the crystal structures of KAl_2Br_7 and $NH_4Al_2Br_7$, the $Al_2Br_7^-$ anion consists of two $AlBr_4$ tetrahedra sharing one Br atom. The Al-Br-Al bridge angle is close to regular tetrahedral one and the two $AlBr_3$ groups are arranged in a staggered configuration to minimize halogen-halogen repulsions.[11,12] In our previous paper it was shown from the ^{27}Al NMR experiments, using a single crystal of KAl_2Br_7, that the angle between efg z-axes of the ^{27}Al was by about 9 degrees larger than that of ∠Al-Br-Al.[13] Similarly the angle between approximate C_3 axes of $AlBr_3$ groups, which were determined as a geometrical means of the three efg z-axes of the terminal Br atoms, is larger than ∠Al-Br-Al and almost consistent with the angle deduced from the ^{27}Al NMR. Accordingly, the approximate C_3 axis of the $AlBr_3$ group is not parallel to the Al-Br(bridge) direction and hence the bridging bond forms a "bent bond" or "banana bond" similar to the Al-Br-Al bond that occurs in the dimeric Al_2Br_6 molecule.[14,15] The steric hindrance of the two $AlBr_3$ groups seems to be the reason for the "bent bond." Therefore, these two $AlBr_3$ groups may affect each other in the activation process of their reorientations. In this paper we report the dynamical property of the two $AlBr_3$ groups in the $Al_2Br_7^-$ anion by means of ^{81}Br NQR and ^{27}Al NMR. Furthermore, the effect of the $AlBr_3$ reorientation on the ^{27}Al NQR parameters was investigated as a function of temperature.

Experimental

The compounds $NaAl_2Br_7$ and KAl_2Br_7 were obtained by crystallizing the molten mixture containing $AlBr_3$ and relevant alkali bromides by the Bridgman method. About 5% excess of $AlBr_3$ was added above the stoichiometric ratio because of the incongruent melting property of the compounds.[11,16]

The ^{81}Br NQR relaxation time T_1 was measured by the 90°-90° pulse method using a Matec pulse spectrometer. A typical pulse length for the 90° pulse was about 5 μs with a coil diameter of 12 mm. ^{27}Al and ^{23}Na NQR signals were detected by the ^{81}Br-^{27}Al and ^{81}Br-^{23}Na spin echo double resonance (SEDOR) method respectively, where a strong ^{81}Br NQR echo signal was monitored. The relative positions of the Br atoms within the anion were also determined, because the sensitivity of the SEDOR method depends upon the dipole-dipole interaction under study.[17] The experimental procedure has been described elsewhere.[18]

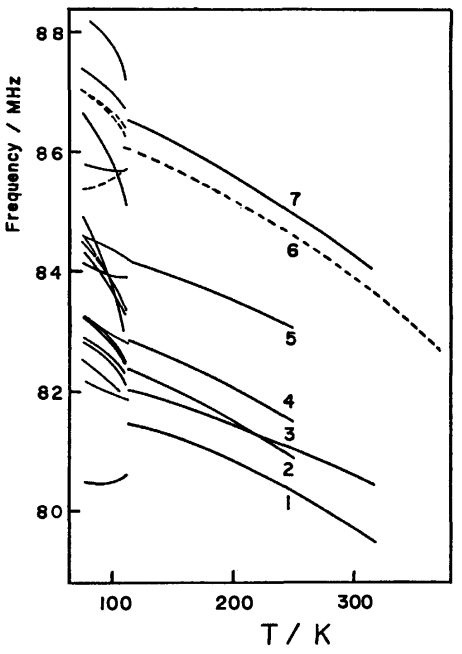

Fig. 1. Temperature dependence of the ^{81}Br NQR frequency in $NaAl_2Br_7$. The dotted curve Br(6) was assigned to the bridging atom.

Table 1. ^{27}Al and ^{23}Na NQR Parameters in $NaAl_2Br_7$ at Selected Temperature[a)]

Nucleus	Temp/K	Assignment[b)]	ν_1/MHz	ν_2/MHz	η	e^2Qqh^{-1}/MHz
^{27}Al	90	Al(1)′	1.306	2.561	0.039	8.692
		Al(1)′	1.356	2.696	0.068	8.995
		Al(1)′	1.370	2.735	0.037	9.120
		Al(2)′	1.460	2.767	0.213	9.285
		Al(2)′	1.482	2.869	0.161	9.611
		Al(2)′	1.522	2.982	0.127	9.972
	292	Al(1)	1.317	2.606	0.091	8.702
		Al(2)	1.456	2.873	0.102	9.598
^{23}Na	78		0.613, 0.493, 0.483			
	129		0.542			

a) Estimated error in ν is ±0.003 MHz. b) Below 113±1 K, Al(1) and Al(2) lines split into three lines Al(1)′ and Al(2)′ respectively.

Results and Discussion

$NaAl_2Br_7$. Figure 1 shows the temperature dependence of the ^{81}Br NQR frequencies. Above the phase transition temperature (T_c=113±1K) seven ^{81}Br NQR lines were observed as reported previously.[13] Below T_c, however, the spectrum was very complicated and totally 21 ^{81}Br NQR lines could be detected suggesting three nonequivalent $NaAl_2Br_7$ units in the low temperature phase. This ^{81}Br NQR spectrum is consistent with ^{27}Al and ^{23}Na NQR spectra which have the six pairs of ν_1 (1/2↔3/2) and ν_2 (3/2↔5/2) and three lines respectively, as shown in Table 1. Above T_c two sets of three ^{81}Br NQR lines disappeared at about 250K and 320K respectively, but the remaining single line could be detected up to near the decomposition temperature of 370K. The relative positions of all the Br atoms in the $Al_2Br_7^-$ anion were determined by the SEDOR technique as described above. Then, the sets of three resonance lines which disappeared at almost the same temperatures could be assigned to the same $AlBr_3$ group and the remaining line to the bridging atom. There was no significant difference in the T_1 vs. temperature behavior among the three lines assigned to the same $AlBr_3$ group. Therefore, the temperature dependence of the ^{81}Br NQR spin-lattice relaxation times (T_1) were measured precisely only for three Br(1), Br (2), and Br (6) sites as shown in Fig. 2 together with their assignment. A small dip was observed near T_c for each line. The feature above 160 K is similar to that found in the compounds containing such reorientational groups as CCl_3 or PCl_3. The drastic decrease of the T_1 for Br (1) and Br (2) at high temperature may come from the $AlBr_3$ group reorientation about its approximate C_3 axis for the following reasons; (1) there was no significant difference in the T_1 vs. temperature curves which were assigned to the same $AlBr_3$ group, (2) the bridging atom Br (6) showed no drastic decrease of T_1 with temperature and (3) a line width transition of the ^{27}Al NMR was observed as described later. In this case the ^{81}Br NQR relaxation rate $(1/T_1)_{obs}$ may be described as a sum of the two mechanisms, lattice vibration $(1/T_1)_{vib}$ and reorientation of

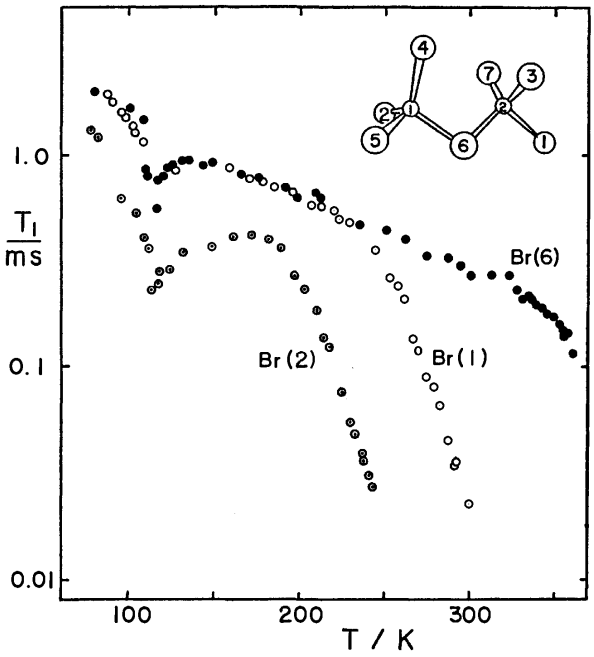

Fig. 2. Temperature dependence of the ^{81}Br NQR spin-lattice relaxation times T_1 in $NaAl_2Br_7$.

the $AlBr_3$ group $(1/T_1)_{reo}$ as follows,

$$(1/T_1)_{obs} = (1/T_1)_{vib} + (1/T_1)_{reo} = a\,T^n + b\exp(-V/RT), \quad (1)$$

where V is the activation energy of the reorientation motion of the $AlBr_3$ group and the parameters a, n, and b are determined experimentally. Table 2 shows these parameters determined by a non-linear least squares method. Joes et al. showed that if the librational fluctuation governs the relaxation, n is equal to 2 for I=3/2 nuclei.[19] The value of n obtained for the Br (1) is smaller than the theoretical one. This is probably due to the additional contribution to T_1 near the phase transition point, because the parameter n for the bridging Br (6) shows a value close to the theoretical one in the temperature range from 180 to 350K as shown in Table 2.

The $AlBr_3$ group reorientation could also be detected as a motional narrowing phenomena of the

Table 2. Best Fit Parameters of Eq. 1

Compound	Assignment	$a/10^{-2}$ s	n	$b/10^{12}$ s	V/kJ mol^{-1}	Temp/K
$NaAl_2Br_7$	Br(1), Al(2)Br_3	140.0	1.3	1.55	43.5	$171<T<300$
	Br(5), Al(1)Br_3			0.105	30.2	$182<T<243$
	Br(6), Brridge	2.9	2.1			$180<T<350$
KAl_2Br_7	Br(1), Al(1)Br_3	0.23	2.3	3470	81.4	$80<T<345$
	Br(2), Al(2)Br_3	0.26	2.2	5530	75.1	$80<T<368$

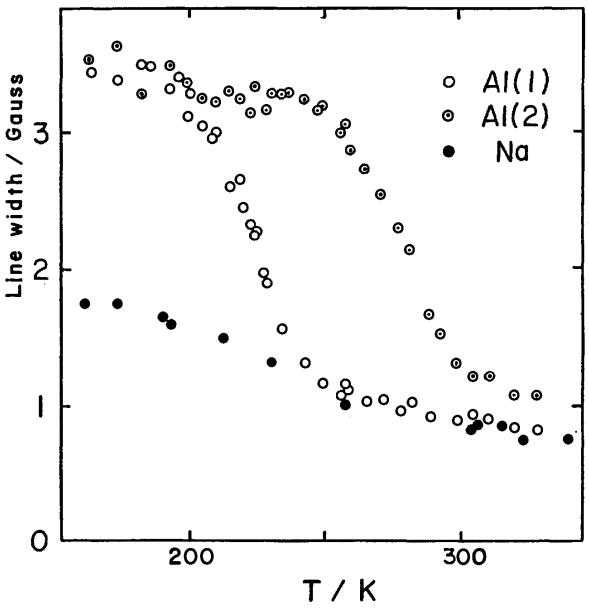

Fig. 3. ^{27}Al and ^{23}Na NMR line widths are plotted against temperature for $NaAl_2Br_7$ using single crystal.

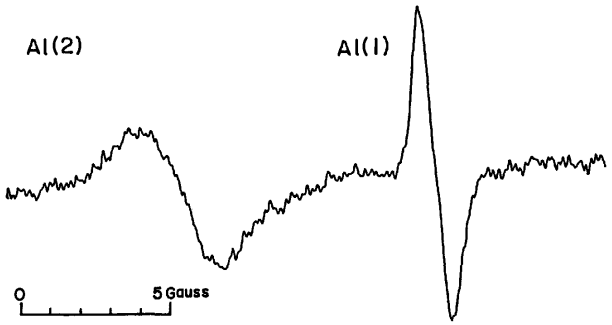

Fig. 4. Typical ^{27}Al NMR spectra for $(1/2\leftrightarrow -1/2)$ transitions at 271 K. A motional narrowing is completed for the Al(1) site at this temperature. The modulation width was chosen to be about 1/3 of each absorption line.

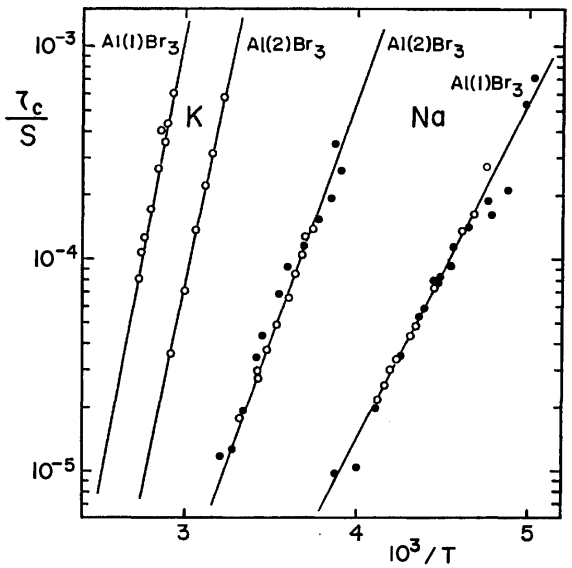

Fig. 5. Temperature dependence of the correlation times, τ_c, of the $AlBr_3$ reorientation for $NaAl_2Br_7$ and KAl_2Br_7. The lines were calculated from the second term of the Eq. 1 using the parameters in Table 1. O: from ^{81}Br NQR T_1 data, ●: from ^{27}Al NMR line width data.

^{27}Al NMR using a single crystal at 16 MHz. Figure 3 plots the line width against temperature together with that of the ^{23}Na NMR, where the line width is defined as the separation between the maximum and the minimum of the derivative curve. Because of the large quadrupole coupling constant at the Al site, central transitions $(-1/2\leftrightarrow 1/2)$ were shifted as a function of the crystal orientation with respect to the external magnetic field in terms of the second order quadrupole effect. Thus, the line width of the ^{27}Al NMR was observed at each site separately as a function of temperature. A precise analysis and assignment of the quadrupole splitting lines was reported previously.[13] Figure 4 shows a typical ^{27}Al NMR spectrum recorded at 271 K at a certain crystal orientation with respect to the external magnetic field, where Al (1) and Al (2) sites are in a motional narrowing and a rigid state in the NMR time scale, respectively. In general at the temperature where a line width transition takes places the following relation holds between the reorientational correlation time, τ_c, and the line width.

$$\tau_c=(1/H\alpha\gamma)\tan[\pi(H^2-B^2)/2(C^2-B^2)], \quad (2)$$

where B, H, and C are the line width above, within and below the transition region respectively, γ is the gyromagnetic ratio and α is a numerical constant. On the other hand, the correlation time of the $AlBr_3$ reorientation is calculated from the $(T_1)_{reo}$ data using a simple relation, $(T_1)_{reo}=(3/4)\tau_c$.[20] The correlation times from the ^{81}Br NQR data are plotted against temperature in Fig. 5. If $\alpha=3.1\pm0.1$ is adopted as a numerical constant in Eq. 2 the correlation times from the ^{27}Al NMR agree well with those of the ^{81}Br NQR as shown in Fig. 5. This finding suggests that both the abrupt decrease in the NQR T_1 and the motional nar-

rowing of the ^{27}Al NMR are governed by the same mechanism, i.e., $AlBr_3$ reorientation about the C_3 axis.

In view of the low potential barrier of the $AlBr_3$ reorientation, the diffusion of the Na^+ cation was suspected to occur in the same manner as a Li^+ in $LiAlCl_4$.[21] The ^{23}Na line width was also measured as a function of temperature as shown in Fig. 3. Two central transitions ($-1/2 \leftrightarrow 1/2$) resulted from the monoclinic system were shifted by the second order quadrupole effect because of the large quadrupole coupling constant. The line width was observed at a certain orientation of the crystal where two central transitions separated from each other. The line width decreases from 1.8 to 0.8 Gauss. However, the narrowing limit of 0.8 Gauss is too large as a result of the diffusion and the narrowing temperature range is almost the same as that of the ^{27}Al NMR. Therefore, the ^{23}Na NMR narrowing probably results from the $AlBr_3$ groups reorientation and not from the diffusion of the Na^+ cation.

Figure 6 shows the temperature dependence of the ^{27}Al and ^{23}Na NQR frequencies above 113 K. The quadrupole coupling constants (e^2Qq/h) and asymmetry parameters (η) for the ^{27}Al are calculated using an exact formula for nuclear spin $I=5/2$[22] as is shown in Fig 7. If the reorientational frequency is much higher than that of NQR, the asymmetry parameter of the ^{27}Al reduces to zero due to the motional averaging of the

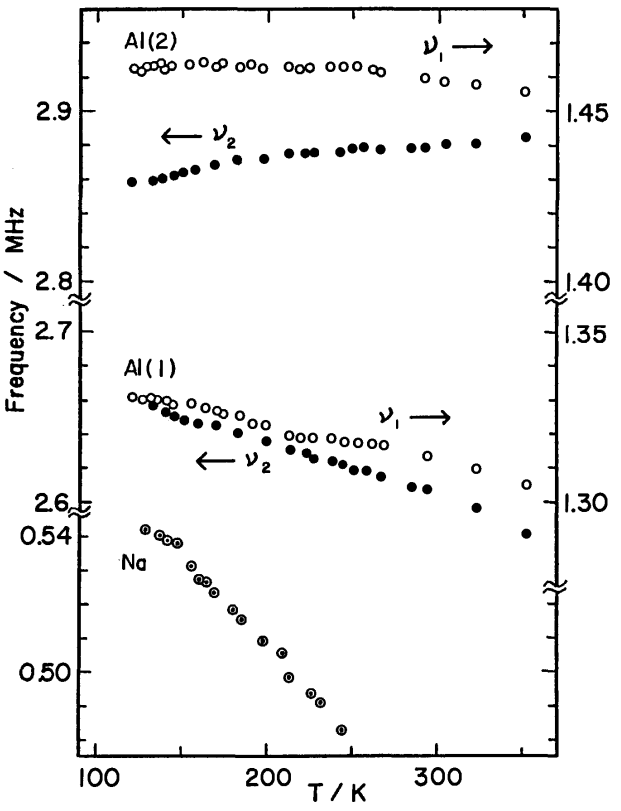

Fig. 6. Temperature dependence of the ^{27}Al and ^{23}Na NQR frequencies for $NaAl_2Br_7$. In the case of the ^{27}Al ν_1 and ν_2 correspond to ($1/2 \leftrightarrow 3/2$) and ($3/2 \leftrightarrow 5/2$) transitions, respectively.

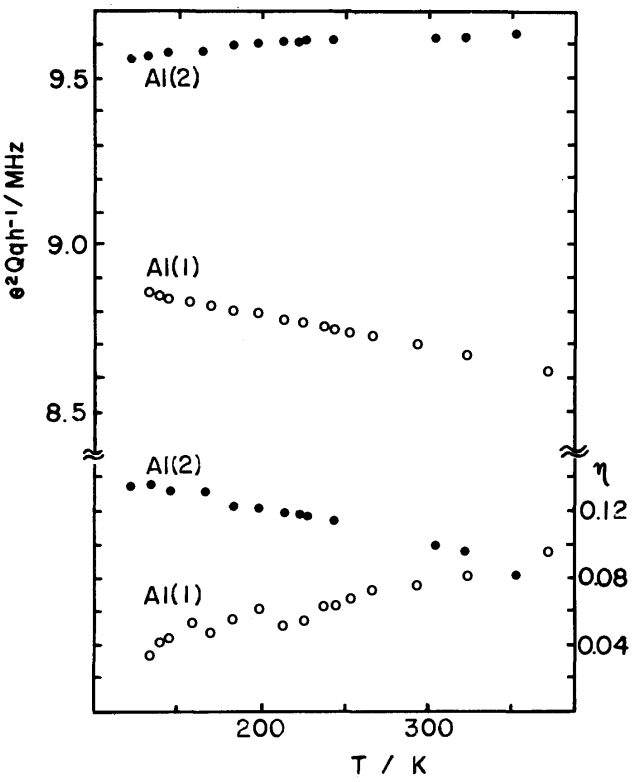

Fig. 7. Quadrupole coupling constant (e^2Qq/h) and asymmetry parameter (η) for the ^{27}Al NQR are plotted against temperature for $NaAl_2Br_7$.

$AlBr_3$ group. This is not the case, as is also expected from the temperature dependence of the correlation time in Fig. 5. However, it is interesting to note that at the Al (1) site the value of η increases with the onset of the $AlBr_3$ group reorientation. If the asymmetry parameter of the Al site is assumed to increase with the extent of the "bend bond" for the Al-Br (bridge) bond, the increase of the asymmetry parameter with the onset of the reorientation would be understandable because the activation energy for the reorientation is expected to decrease with the extent of the "bent bond."

KAl_2Br_7. The temperature dependence of the seven ^{81}Br NQR lines and their assignment for KAl_2Br_7 have been reported previously;[13,23] three lines belonging to the same $AlBr_3$ group disappeared at a temperature about 30 degrees below the decomposition temperature. Accordingly the reorientation of the $AlBr_3$ group was predicted from the fade out phenomena. Figure 8 shows the temperature dependence of the spin-lattice relaxation times for the ^{81}Br NQR lines which were assigned to the different $AlBr_3$ groups. Because of the overlapping of the NQR lines over the wide temperature range, the T_1 vs. temperature curve for the bridging Br could not be obtained. Table 1 shows the best fit parameters to Eq. 1. The values of b for these two sites are much larger than the values expected from the classical rotator approximation. A possible reason is the temperature dependency of the activation energy as suggested by the NMR experiment for ammonium sul-

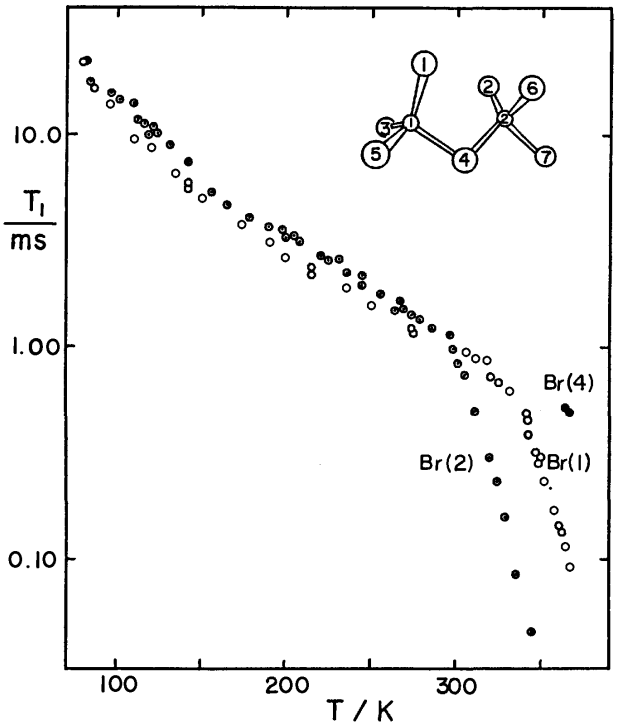

Fig. 8. Temperature dependence of the ^{81}Br NQR spin-lattice relaxation times T_1 in KAl_2Br_7.

fate.[24] For simplicity we assume that the activation energy V decreases linearly with increasing temperature as

$$V = V_0 - CT, \tag{3}$$

where V_0 is an activation energy extrapolated to 0 K and where C is a temperature coefficient. The Eq. 1 then becomes

$$1/T_1 = a\,T^n + 10^{12} \exp(-(V_0 - CT)/RT), \tag{4}$$

$$= a\,T^n + b_0 \exp(-V_0/RT), \tag{5}$$

where $b_0 = 10^{12} \exp(C/R)$. In these equations $b = 10^{12}$ s was assumed as a pre-exponent factor from the classical rotator model. Eq. 5 is the same as that of Eq. 1. Therefore, only from the measurements in the narrow temperature range is it impossible to deduce whether the activation energy has a temperature dependence or not. Using the values of Table 2 the temperature coefficient C were calculated to be 0.068 and 0.072 kJ mol^{-1} K^{-1} for the Br (1) and Br (2) sites, respectively. Accordingly activation energies fall down to about 70% of the values listed in Table 1, at the temperature where the NQR signals disappear. At present we have no other experimental evidence for the temperature dependence of the activation energy. However it may be reasonable because the two $AlBr_3$ groups have large steric repulsions and affect each other in the activation process of the reorientation.

References

1) H. Chihara and N. Nakamura, *Adv. Nucle. Quadrupole Reson.*, **4**, 1 (1981).
2) R. S. Lotfullin and G. K. Semin, *Adv. Nucle. Quadrupole Reson.*, **2**, 1 (1975).
3) R. L. Armstrong, *J. Magn. Reson.*, **20**, 214 (1975).
4) T. Kiichi, N. Nakamura, and H. Chihara, *J. Magn. Reson.*, **30**, 603 (1978).
5) Y. Yoshioka, N. Nakamura, and H. Chihara, *J. Mol. Struc.*, **111**, 195 (1983).
6) M. MaCkowski and M. Zdanowska, *Acta Phys. Pol.*, **A48**, 723 (1975).
7) I. V. Izmestyev, *Opt. Spectrosc.*, **30**, 557 (1971).
8) I. A. Kjunzel, V. A. Mokeeva, and G. B. Soifer, *Spectroscopy Lett.*, **8**, 113 (1975).
9) I. A. Kjunzel, V. A. Mokeeva, G. B. Soifer, and I. G. Shaposhinikov, *J. Magn. Reson.*, **20**, 394 (1975).
10) K. Yamada, T. Okuda, and H. Negita, *Z. Naturforsch.*, **41a**, 230 (1986).
11) E. Rytter, B. E. D. Rytter, H. A. ϕye, and J. Krogh-Moe, *Acta Crystallogr., Sect., B*, **29**, 1541 (1973).
12) E. Rytter, B. E. D. Rytter, H. A. ϕye, and J. Krogh-Moe, *Acta Crystallogr., Sect., B*, **31**, 2177 (1975).
13) K. Yamada, *J. Sci. Hiroshima Univ.*, **A41**, 77 (1977).
14) P. A. Casabella, P. J. Bray, and R. G. Barnes, *J. Chem. Phys.*, **30**, 1393 (1959).
15) T. Okuda, H. Terao, O. Ege, and H. Negita, *J. Chem. Phys.*, **52**, 5480 (1970).
16) C. T. H. M. Cronenberg and J. W. van Spronsen, *Z. Anorg. Allg. Chem.*, **354**, 103 (1967).
17) M. Emshwiller, E. L. Hahn, and D. Kaplan, *Phys. Rev.*, **118**, 414 (1960).
18) K. Yamada and T. Okuda, *J. Phys. Chem.*, **89**, 4269 (1985).
19) L. V. Jones, M. Sabir, and J. A. S. Smith, *J. Phys.*, **C11**, 4077 (1978).
20) S. Alexander and A. Tzalmona, *Phys. Rev.*, **A138**, 845 (1965).
21) W. Weppner and R. A. Huggins, *Phys. Lett.*, **58A**, 4, 245 (1976).
22) R. B. Creel, H. R. Brooker, and R. G. Barnes, *J. Magn. Reson.*, **41**, 146 (1980).
23) N. Weiden and A. Weiss, *J. Magn. Reson.*, **20**, 403 (1978).
24) D. E. O'Reilly and T. Tsang, *J. Chem. Phys.*, **46**, 1291 (1976).

^{81}Br NQR and ^{119}Sn Mössbauer Spectra for $SnBr_3^-$ Anions

Koji YAMADA,* Tomoko HAYASHI, Takako UMEHARA, Tsutomu OKUDA, and Sumio ICHIBA
Department of Chemistry, Faculty of Science, Hiroshima University, Higashisenda-machi, Naka-ku, Hiroshima 730
(Received April 30, 1987)

The structures of the $SnBr_3^-$ anions in $MSnBr_3$ (M=$(CH_3)_2NH_2$, $(CH_3)_3NH$) and $MSnBr_3 \cdot H_2O$ (M=K, NH_4) were deduced by means of ^{81}Br NQR spectroscopy. The former compounds have three ^{81}Br NQR lines in the frequency range 73—80 MHz at 77 K, indicating the presence of pyramidal $SnBr_3^-$ anions. The anion structure of the latter hydrate, on the other hand, was presumed to be square-pyramid with one terminal and two bridging Br atoms, because two of the ^{81}Br NQR frequencies were considerably low compared with that of the terminal atom. Phase transitions were observed for the latter hydrates. Associated with these, drastic increases of the NQR frequencies were observed only for the bridging atoms, suggesting significant changes in the bridging network.

The trihalostannate(II) anion, SnX_3^- (X=Cl and Br), in the solid state still provides us with interesting structural subjects. Two quite different structures for the SnX_3^- anions have been reported for $CsSnCl_3$[1] and $CsSnBr_3$:[2] The former contains a discrete anion with bond angles ∠XSnX, close to 90°, like an isoelectronic $SbCl_3$; however the latter contains a regular octahedron with six bridging bromines. The latter is a typical example of a hypervalent state of Sn(II). In this case the available orbitals of the tin atom are mainly 5p orbitals, since both the participation of the outer 5d orbitals to the bond may be small and the 5s orbital is full. On account of the orbital deficiency of the Sn(II) state, the trans Br-Sn-Br bond is regarded as being a three-center four-electrons bond (abbreviated as a 3c-4e bond) and each Sn-Br bond is weaker than that of a normal two-center two-electron bond (2c-2e). Some interesting phenomena associated with the 3c-4e bond have been observed for anions such as $SbBr_4^-$,[3] $SbBr_6^{3-}$,[4] and I_3^-.[5] For these structural and bonding subjects, halogen NQR is a useful technique owing to the high sensitivity of the NQR frequency to the bond nature.

Halogen NQR studies for trihalostannate(II) anions were only reported for $CsSnX_3$ (X=Cl, Br, and I).[6] In this paper the structure and bonding of $SnBr_3^-$ anions are discussed on the basis of ^{81}Br NQR and ^{119}Sn Mössbauer data. Furthermore, a possible model of a structural change accompanied by a phase transition is proposed for $MSnBr_3 \cdot H_2O$ (M=K, NH_4) utilizing the 3c-4e bond.

Experimental

All compounds, except for $NH_4SnBr_3 \cdot H_2O$, were crystallized from aqueous solutions containing stoichiometric amounts of $SnBr_2$ and relevant alkali bromide or alkylammonium bromide. $NH_4SnBr_3 \cdot H_2O$ was obtained from an aqueous solution containing about twice the stoichiometric amount of NH_4Br. H_2O and Br were analyzed by means of TG and potentiometric titration with $AgNO_3$, respectively. Anal. for $(CH_3)_3NHSnBr_3$. Found: C, 8.23; H, 2.42; N, 3.051; Br, 57.31%. Calcd for $C_3H_{10}NSnBr_3$: C, 8.61; H, 2.41; N, 3.35; Br, 57.28%. Anal. for $(CH_3)_2NH_2SnBr_3$. Found: C, 5.73; H, 2.07; N, 3.27; Br, 59.34%. Calcd for $C_2H_8NSnBr_3$: C, 5.94; H, 1.99; N, 3.46; Br, 59.26%. Anal. for $KSnBr_3 \cdot H_2O$. Found: Br, 56.4; H_2O, 4.22%. Calcd for $KSnBr_3 \cdot H_2O$: Br, 57.7; H_2O, 4.34%. Anal. for $NH_4SnBr_3 \cdot H_2O$. Found: H, 1.24; N, 3.72; Br, 60.77; H_2O, 4.18%. Calcd for $NH_4SnBr_3 \cdot H_2O$; H, 1.53; N, 3.55; Br, 60.77; H_2O, 4.31%.

^{81,79}Br NQR were searched in the frequency range from 20 to 100 MHz with a super-regenerative spectrometer or a pulsed spectrometer (Matec model 5100+525). The former was sensitive, even near the phase transition temperature (T_c) or at high temperature where the relaxation time (T_1) was short, T_1<100 μs. On the other hand, a pulse spectrometer was applied at low temperature where only the spin echo signal was detected due to its large line width. NQR lines were assigned with the aid of the quadrupole moment ratio, $(Q(^{79}Br)/(Q(^{81}Br)=1.1971)$.

^{119}Sn Mössbauer spectra were recorded by means of a constant acceleration-type spectrometer.

Results

^{81}Br NQR for $MSnBr_3$ (M=$(CH_3)_2NH_2$ and $(CH_3)_3NH$). Table 1 shows the ^{81}Br NQR frequencies for tribromostannate(II) anions. Three ^{81}Br NQR were detected in the frequency range of 73—80 MHz at 77 K for these two compounds. This frequency range is consistent with that expected from the ^{35}Cl NQR frequency for $CsSnCl_3$, where three NQR lines were observed at about 10.8 MHz for the pyramidal $SnCl_3^-$ anion.[6] Accordingly, it is thought that these compounds contain discrete $SnBr_3^-$ anions and, therefore, a frequency of about 73—80 MHz at 77 K corresponds to the normal 2c-2e bond for this anion.

^{81}Br NQR for $MSnBr_3 \cdot H_2O$ (M=K and NH_4). Although there has been no crystal structure determination for both compounds, it was suggested by means of IR spectra that the water molecule associates with the cation for the chloride analog.[7] As Table 1 shows, ^{81}Br NQR lines were detected over the wide frequency region 35—83 MHz, suggesting the existence of both terminal and bridging Br atoms. Figure 1 shows the temperature dependence of the ^{81}Br NQR frequencies. The disappearance of NQR signals was observed just below and above the phase-transition temperature (T_c). The highest NQR signal is exceptional and shows a small dip in the corresponding temperature range (Fig. 2). From this figure the phase-transition temperature was determined to be T_c=273±0.5 K.

Table 1. ^{81}Br NQR Frequencies for $MSnBr_3$ and $MSnBr_3 \cdot H_2O$

Compound	Temperature/K	Frequency/MHz
$(CH_3)_2NH_2SnBr_3$	77	78.06, 77.76, 72.92
	293	74.90, 74.28, 71.65
$(CH_3)_3NHSnBr_3$	77	80.11, 79.77, 79.29
$KSnBr_3 \cdot H_2O$	77	78.25, 78.07, 58.25, 56.33, 55.09, 52.23
	298	75.96, 40.45, 37.25
$NH_4SnBr_3 \cdot H_2O$	77	84.40, 79.79, 59.09, 58.12, 53.18, 51.62
	300	79.89, 38.56, 37.63

Estimated error ±0.01 MHz.

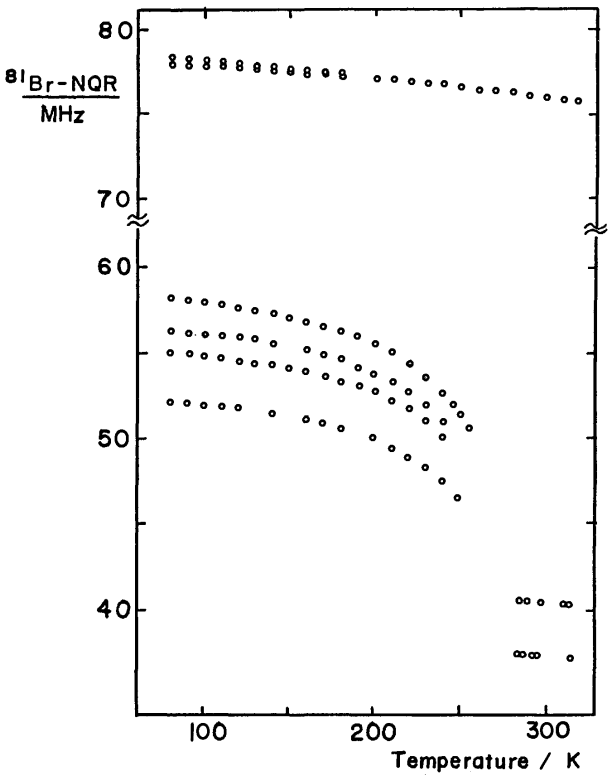

Fig. 1. Temperature dependence of the ^{81}Br NQR frequencies for $KSnBr_3 \cdot H_2O$.

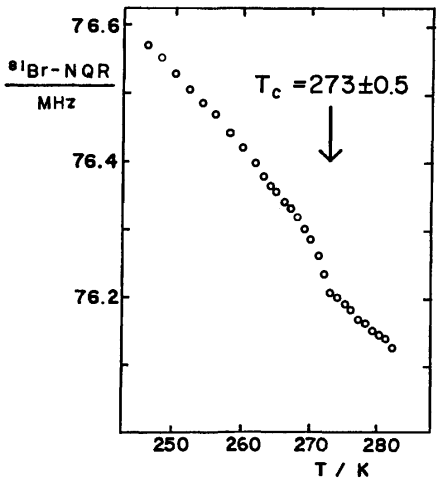

Fig. 2. Temperature dependence of the highest ^{81}Br NQR frequency in $KSnBr_3 \cdot H_2O$ near phase transition temperature.

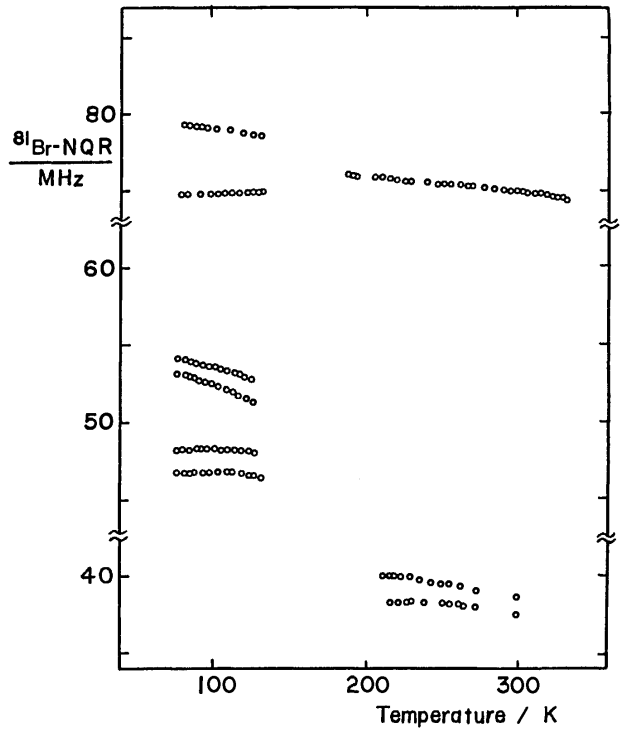

Fig. 3. Temperature dependence of the ^{81}Br NQR frequencies for $NH_4SnBr_3 \cdot H_2O$.

Because of the continuity of the highest ^{81}Br NQR frequency, this phase transition was supposed to be second-order type. Below T_c each line split into two, but the highest frequency line could not be resolved into two until about 90 degrees below T_c. This is due to its very small splitting compared with the line width. A phase transition was also observed for M=NH_4 (Fig. 3); unfortunately, the transition temperature was not determined owing to the disappearance of the NQR signals between 130 and 190 K. According to our preliminary T_1 measurements for both compounds, these disappearances of the NQR signals arise from their very short relaxation times (T_1) and also from the large line width ($1/T_2^*$) near T_c to detect NQR signals. Below T_c three NQR lines split into six lines for both compounds, suggesting at least two Sn sites. In connection with these phase transitions the most interesting feature is that the drastic increases of the NQR frequencies for the lower four lines with decreasing temperature. At 77 K the NQR frequencies

Table 2. ^{119}Sn Mössbauer Parameters for $MSnBr_3$ and $MSnBr_3 \cdot H_2O$ at 93 K[a)]

Compound	Line width	Isomer shift	Quadrupole splitting
		mms^{-1}	
$(CH_3)_3NHSnBr_3$	0.83	3.89	0.88
$(CH_3)_2NH_2SnBr_3$	0.86	3.55	0.82
$KSnBr_3 \cdot H_2O$	0.89	3.73	0.74
	0.89	3.60	1.02
$NH_4SnBr_3 \cdot H_2O$	0.93	3.67	0.98
$CsSnBr_3$[b)]	0.84	3.96	0

a) Estimated error $\pm 0.05\ mms^{-1}$. b) Ref. 2.

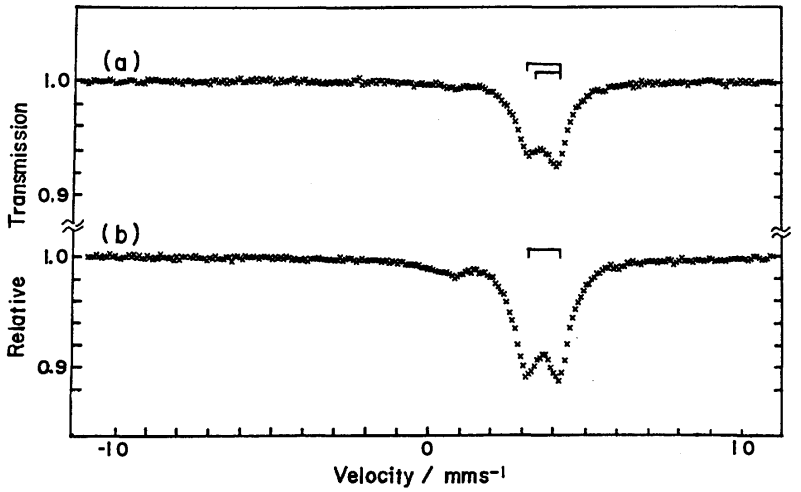

Fig. 4. ^{119}Sn Mössbauer spectra for $KSnBr_3 \cdot H_2O$ (a) and $(NH_4)SnBr_3 \cdot H_2O$ (b) at 93 K.

increased about 40% more than those of the high-temperature phase. These finding were not understandable only from the change of the crystal fields. No anomalous peak associated with these phase transitions was detected for $MSnBr_3 \cdot H_2O$ from the DTA measurements in the corresponding temperature.

^{119}Sn Mössbauer Effect. Table 2 shows the Mössbauer parameters of $MSnBr_3$(M=$(CH_3)_2NH_2$, $(CH_3)_3NH$) and $MSnBr_3 \cdot H_2O$ (M=K, NH_4). All these compounds showed quadrupole doublets. In the latter hydrates, however, the doublets are slightly asymmetric, even for powdered samples (Fig. 4). This is consistent with the NQR result; that is, there are at least two crystallographically different Sn sites at 93 K. In the potassium salt the spectrum was analyzed as two quadrupole doublets (Table 2).

Discussion

Structures of $SnBr_3^-$ Anions Based on the 3c-4e Bond Model. Figure 5 shows three structural models for the SnX_3^- anions based on the 3c-4e bonds. Model **A** exists in the perovskite $CsSnBr_3$, in which the Sn forms regular octahedron with six bridging Br atoms. In this case typical 3c-4e bonds are formed in the three orthogonal directions. While model **C** exists in $CsSnCl_3$,[1)] in which the Sn forms distorted octahedron with three short Sn-Cl bonds and three interanionic

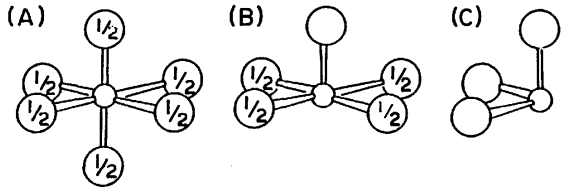

Fig. 5. Structural models for SnX_3^- anion, where 1/2 denotes bridging halogen.

interactions Sn··· Cl (not shown in this figure). In this structure it is also possible to consider that the Sn atom in $CsSnCl_3$ forms extremely unsymmetrical 3c-4e bonds along the three orthogonal directions. If one of the three 3c-4e bonds in the model **A** structure becomes asymmetric, it changes to model **B**. Several structural changes associated with the symmetric-asymmetric 3c-4e bond have been observed for Sb(III) compounds when the temperature or the counter cation was changed.[3,4)]

The anion structures in $MSnBr_3$(M=$(CH_3)_2NH_2$, $(CH_3)_3NH$) can be expressed as model **C**, since three ^{81}Br NQR lines were detected in a narrow frequency region of 73—80 MHz. On the other hand, $MSnBr_3 \cdot H_2O$ (M=K, NH_4) yielded only one NQR signal assigned to a terminal atom at room temperature. Two more signals were detected at about one half of the terminal NQR frequency. Therefore, model **B** is

most plausible for the anion structure in these hydrates from their NQR spectra. Then, the NQR frequency for the bridging Br was estimated as confirming this model on the basis of the Townes-Dailey method under following conditions: (1) The net charge on the Br atom does not change as the result of a structural change from model **A** to **C** and (2) the bridging bond angle is close to 90°; hence, the bond is formed using only p orbitals. The population of the p_z orbital, N_z, for the terminal atom could be estimated assuming $\eta=0$ using following equation:

$$(e^2Qq_{obs}/h)/(e^2Qq_p/h)=2\,\nu_{obs}/(e^2Qq_p/h)=(2-N_z), \quad (1)$$

where $(e^2Qq_p/h)=643$ MHz. Since ν_{obs} for the terminal atom is on average 78 MHz at 77 K, the populations were determined to be $N_z=1.76$ and $N_y=N_x=2$ for p_z, p_y and p_x orbitals, respectively. On the other hand, in the case of symmetrical bridge using the p_z and p_x orbitals, the p electron populations change to $N_z=N_x=1.88$ and $N_y=2$, since the net charge on the Br atom is assumed to be constant. Between these two extremes the populations can be expressed using parameter b as

$$N_z=1.76+b,$$
$$N_y=2, \quad (2)$$

and

$$N_x=2-b.$$

Then, the NQR frequency for the bridging atom is calculated as a function of b using following equations:

$$(e^2Qq_{obs}/h)/(e^2Qq_p/h)=|N_z-(N_x+N_y)/2| \quad (3)$$

$$\eta=3(N_y-N_x)/(2N_z-N_y-N_x), \quad \text{for } 0<b<0.08 \quad (4)$$

$$\eta=3(N_z-N_x)/(2N_y-N_z-N_x), \quad \text{for } 0.08<b<0.12 \quad (5)$$

$$\nu_{obs}=(1/4)(e^2Qq_{obs}/h)(1+\eta^2/3)^{-2/1} \quad (6)$$

Figure 6 shows the calculated NQR frequency as a function of b. This figure shows that the NQR frequency decreases drastically in forming a bridging bond and that the principal z- and y-axes of the efg tensor change their orientations with each other in the range $0.08<b<0.12$. The observed NQR frequencies, ν_{obs}, for two hydrates are about 38.5 MHz, which are in good agreement with that obtained with this model in the range $b=0.07$—0.12. One NQR line was observed for the perovskite $CsSnBr_3$ near 63 MHz,[6] which is about 50% higher than that expected from this model. This is probably due to the fact that the bridging bond Sn-Br-Sn in the perovskite structure is linear in contrast to this model.

According to the recent crystal structure analysis for $CsSnI_3$, the SnI_3^- anion was proved to exist in the form of model **B**.[8] The SnI_3^- anion forms a distorted octahedron in which one pair of short and long Sn-I bonds at the trans position and four Sn-I bonds with intermediate lengths exist.

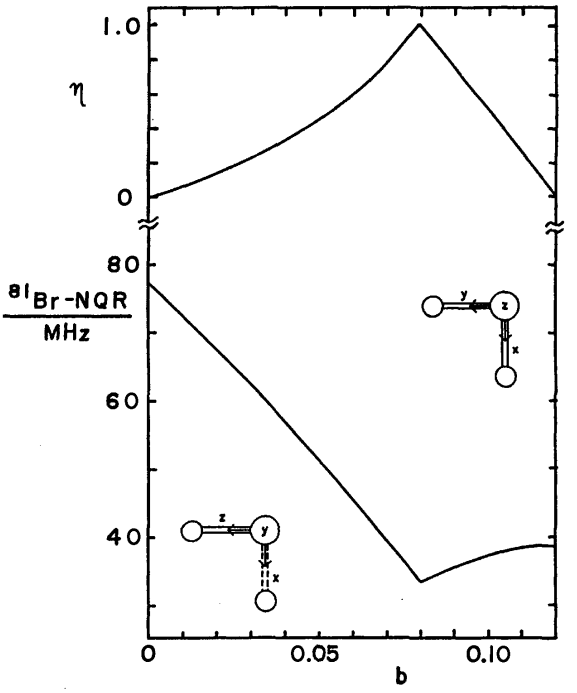

Fig. 6. Calculated ^{81}Br NQR frequencies for the bridging Br atom are plotted as a function of parameter b, where $b=0$ and $b=0.12$ correspond to terminal and symmetric bridge Br, respectively. At $b=0.08$ the efg z and y axes change their orientations each other.

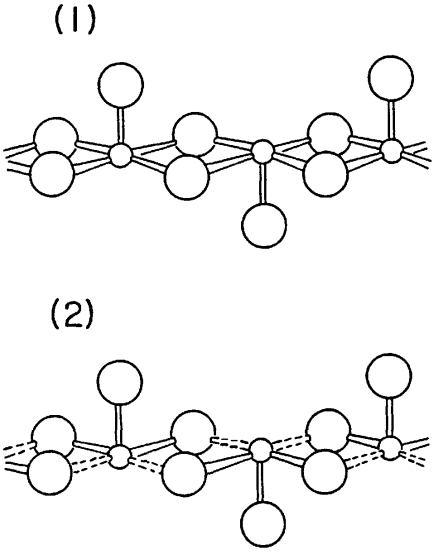

Fig. 7. Proposed structural models for high (1) and low (2) temperature phases.

Proposed Structural Changes for $MSnBr_3\cdot H_2O$ (M=K, NH_4) below Phase Transition Temperatures. The temperature dependence of the ^{81}Br NQR for these compounds differs from each other, especially near T_c. However, the spectra at 77 K and room temperature resemble each other, suggesting similar changes take place around the Sn environments associated with the phase transitions. The drastic increases of NQR

frequencies can be easily explained in terms of the slight change in the bridging Sn-Br-Sn bond, as shown in Fig. 6. That is, at high temperature the bridging Sn-Br-Sn bond is formed almost symmetrically, whereas at lower temperature one side of the bridging bond becomes weaker than the other. This change is more understandable by applying a 3c-4e bond model for the trans Br-Sn-Br as shown in Fig. 7. At temperatures above T_c the trans Br-Sn-Br bond is regarded as being a symmetrical 3c-4e bond. Below T_c, however, it becomes asymmetric Br-Sn$\cdots$Br and increases its NQR frequency (Fig. 6) owing to a decrease in parameter b. This type of structural change was also observed for $(C_5H_5NH)SbBr_4$, where the axial Br-Sb-Br bond is symmetric or asymmetric above and below T_c and, finally, the anion structure is more reasonably expressed as $SbBr_3 \cdot Br^-$ at 77 K.[3]

Correlation between ^{119}Sn Mössbauer Parameters and Structure. As Table 2 shows, the change of the isomer shifts is considerably large compared with that of $Sn^{IV}Cl_6^{2-}$ anions.[9] This is probably due to the fact that the SnX_3^- anion changes drastically its structure with a change in the counter cation as well as with temperature (as described above). In spite of their quit different ^{81}Br NQR spectra, the ^{119}Sn quadrupole coupling constant changes only slightly. However, the observed feature was consistent with structural models of the anion which were proposed by the ^{81}Br NQR. That is, the magnitude of the quadrupole coupling constant is expected from the point charge model as **B>C>A**. For a more satisfactory interpretation of these Mössbauer parameters, an X-ray structural determination may be required for each compound.

References

1) F. R. Poulsen and S. E. Rasmussen, *Acta Chem. Scand.*, **1970**, 24, 150.

2) J. Barrett, S. R. A. Bird, J. D. Donaldson, and J. Silver, *J. Chem. Soc. A*, **1971**, 3105. J. D. Donaldson, J. Silver, S. Hadjiminolis, and S. D. Poss, *J. Chem. Soc., Dalton Trans.*, **1974**, 1500.

3) T. Okuda, K. Yamada, H. Ishihara, M. Hiura, S. Gima, and H. Negita, *J. Chem. Soc., Chem. Commun.*, **1981**, 979.

4) T. Okuda, M. Hiura, E. Koshimizu, H. Ishihara, Y. Kushi, and H. Negita, *Chem. Lett.*, **1982**, 1321.

5) A. Sasane, D. Nakamura, and M. Kubo, *J. Phys. Chem.*, **71**, 3249 (1967); Y. Kume and D. Nakamura, *J. Mag. Reson.*, **21**, 235 (1976).

6) D. E. Scaife, P. F. Weller, and W. G. Fisher, *J. Solid State Chem.*, **1974**, 9, 308.

7) M. Falk, C. H. Haung, and O. Knop, *Can. J. Chem.*, **1974**, 52, 2928.

8) P. Mauersberger and F. Huber, *Acta Crystallogr., Sect. B*, **36**, 683 (1980).

9) J. D. Donaldson, D. C. Puxley, and M. J. Tricker, *J. Inorg. Nucl. Chem.*, **37**, 655 (1975).

The Influence of Molecular Conformation on the Electronic Relaxation Processes. Complex Formation in the Ground State and Triple Fluorescences of 6-Acetoxyspiro[aceanthyrylene-2(1*H*),9′(10′*H*)-anthracene]-10′-one

Tsuneo Fujii,* Masahiro Hirano,† Yoshihiro Uno,†† Satoshi Suzuki, and (the late) Kiyoichi Hirakawa§
Department of Industrial Chemistry, Faculty of Engineering, Shinshu University, Wakasato, Nagano 380
§Department of Chemistry, Faculty of Textile Science and Technology, Shinshu University, Ueda, Nagano 386
(Received March 26, 1987)

The absorption spectra of 6-acetoxyspiro[aceanthyrylene-2(1*H*),9′(10′*H*)-anthracene]-10′-one(**2**) in cyclohexane, dichloromethane, and chloroform have been observed. The absorption spectra have been also observed as a function of concentration of chlorinated methanes in mixtures with cyclohexane. It was revealed that **2** forms a ground state complex with chlorinated methanes. The equilibrium constants for the ground-state complex formation with dichloromethane and chloroform were determined to be 0.14 and 0.17 $mol^{-1}dm^3$, respectively. The fluorescence and fluorescence excitation spectra of **2** have been obtained as a function of excitation wavelengths and emission wavelengths in cyclohexane and chlorinated methanes. The spiro compound emits structured fluorescence(FM) in cyclohexane. On the other hand, three types of fluorescence bands (FM, FC, and FE) were observed in chlorinated methanes. The FC and FE bands are both structureless and their peak wavenumbers are 20800 and 18700 cm^{-1}. The quenching of fluorescence quantum yield and lifetime were treated by Stern-Volmer kinetics considering the complex formation in both the ground and the excited states of the system. Based on the experimental findings, the origins of FM, FC, and FE bands are explained by the complex formation between **2** and chlorinated methanes in the ground state and exciplex formation in the excited state.

The emission spectra of molecules which have somewhat specific molecular geometry in the ground and excited states are interesting problem from the stand point of the relation between the electronic structure and the geometrical specificity of the molecules. In previous papers the authors presented the influence of molecular conformation on the electronic relaxation processes of biphenyl[1] and *m*-terphenyl[2] which have conformational flexibility. Becker and Sandross[3] found dual fluorescences for 1′2′-dihydrospiro[anthracene-9(10*H*),3′-[3*H*]benz[*de*]anthracene]-10-one(**1**, Diagram 1) in various solvents. **1** has a six-membered ring containing a spiro carbon atom and has two possible conformations. The anthracene ring is not perpendicular to the anthrone ring in **1**. Photoexcitation of the anthracene chromophore in **1** in chloroform and other solvents gives rise to two types of fluorescences. One is an anthracene-like fluorescence and its assigned to the anthracene moiety. The other fluorescence is a structureless emission (σ_{max}=18700 cm^{-1}). They attributed this fluorescence band to radiative deactivation of an excited intramolecular charge-transfer complex between the electron-donating anthracene moiety and the electron-withdrawing anthrone moiety.

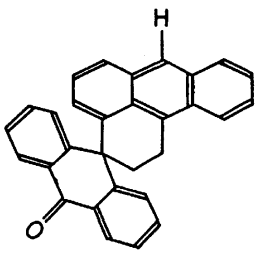

Diagram 1. 1′,2′-Dihydrospiro[anthracene-9(10*H*), 3′-[3*H*]benz[*de*]anthracene]-10-one.

In this paper, the absorption, fluorescence, and fluorescence excitation spectra of 6-acetoxyspiro[aceanthyrylene-2(1*H*), 9′(10′*H*)-anthracene]-10′-one(**2**, Diagram 2) in cyclohexane, dichloromethane, chloroform, and cyclohexane-chlorinated methane mixtures are reported. In contrast to the case of **1**, **2** has a five-membered ring containing a spiro carbon atom and has a rigid geometry. The anthracene position is connected to the anthrone ring though the five-membered ring. The two rings are precisely perpendicular.

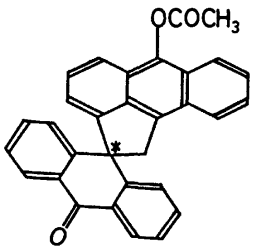

Diagram 2. 6-Acetoxyspiro[aceanthyrylene-2(1*H*), 9′(10′*H*)-anthracene]-10′-one.

The fluorescence spectrum of **2** has an anthracene-like structure in cyclohexane. In the mixtures of cyclohexane and chlorinated methanes shows a remarkable excitation-wavenumber dependence. In chlorinated-methanes, however, two broad fluorescence

†Present address: R & D. Center, Mitsumi Electric Co., Ltd., Sakai 1601, Atsugi-shi, Kanagawa.
††Present address: Central Research Institute, Taiyo Yuden Co., Ltd., Hongo, Haruna, Gunma, Gunma 370-33.

bands are observed and anthracene-like fluorescence spectrum is strongly quenched in the solvents. This remarkable fluorescence change of **2** suggests that **2** may specifically interact with chlorinated methanes in an energetically favourable conformation.

Fluorescence quenching is discussed based on the data of quantum yield and lifetime. It is shown that **2** forms a ground state complex with chlorinated methanes and emits three types of fluorescence. Fluorescence quenching by added chlorinated methanes is interpreted by Stern-Volmer kinetics. The origins of the triple fluorescences are explained by the complex formation between **2** and chlorinated methanes in the ground and excited states.

Experimental

2 was synthesized according to the method given in the literature.[4] Cyclohexane and dichloromethane (Wako Pure Chemical Industries Inc., Luminasol grade), chloroform (Wako, Spectrosol grade), ethanol (Wako, S. G. S. grade), and sulfuric acid (Wako, S grade) were used without further purification. The absorption and emission spectra were observed at room temperature using a Hitachi 220 recording spectrophotometer and a Hitachi MPF-2A fluorescence spectrophotometer. The data were transferred to an NEC PC-8001 microcomputer for processing. The fluorescence quantum yields were determined with reference to those of anthracene in cyclohexane,[5] 9,10-diphenylanthracene in ethanol,[6] and quinine sulfate in sulfuric acid.[7] Fluorescence lifetimes were determined with a single-photon fluorescence lifetime instrument arranged in this laboratory. The fluorescence lifetimes obtained by the instrument were found to agree well with the widely accepted literature values.[8] The sample solutions were prepared just prior to measurements and stored in the dark. The solutions were degassed when necessary.

Results and Discussion

Absorption Spectra and Complex Formation in the Ground State. The absorption spectra of **2** in cyclohexane and dichloromethane are shown in Fig. 1. Although the spectrum in dichloromethane shifts to the red compared with that in cyclohexane, the spectral difference between these spectra is small, except that a very weak absorption band appears between 23500 and 21500 cm^{-1} in chlorinated methanes (see next).

The absorption spectrum at high concentration of **2** in chloroform is shown in Fig. 2. It is seen from Fig. 2 that a very weak and broad band exists around 22700 cm^{-1}. This frequency region coincides with a new fluorescence excitation band for FC emission (see below). Almost the same spectral feature was obtained in **2** and dichloromethane system.

The spectrum observed in chloroform is similar to that observed in dichloromethane. These spectral features were unchanged after a week. The band with fine structure which appears between 23800 and 31200

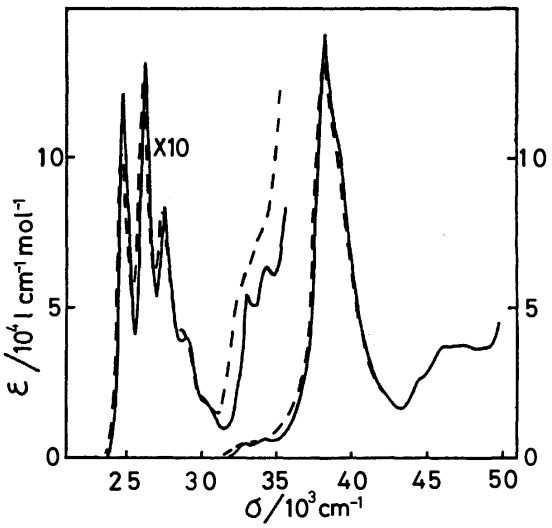

Fig. 1. The absorption spectra of **2** in cyclohexane (——) and dichloromethane (----). The spectrum observed in chloroform is almost the same as that observed in dichloromethane.

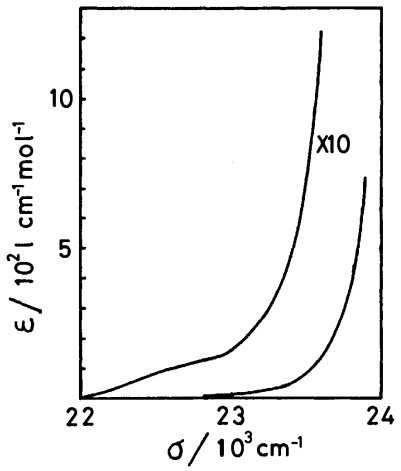

Fig. 2. The absorption spectrum of **2** in dichloromethane at higher concentration.

cm^{-1} and the intense band which appears between 35700 and 43500 cm^{-1} closely resemble the ^1L_a and ^1B_b transitions of anthracene. The band which appears between 31200 and 35700 cm^{-1} can be assigned to the local transition of the anthrone chromophore in **2**. Therefore the whole absorption spectrum of **2** is composed of the absorption spectrum of the anthracene chromophore and that of the anthrone chromophore except for an band in the lowest frequency region that appears in chlorinated methanes. Note that the strong ^1L_a transition due to the anthracene chromophore obscures the weak n-π^* transition of anthrone around 25000 cm^{-1}.[9]

To make clear the origin of the very weak absorption band which appears in chlorinated methanes, the absorption spectra of **2** in cyclohexane-dichloromethane and cyclohexane-chloroform mixed solvents are shown in Figs. 3 and 4 respectively as a function of the

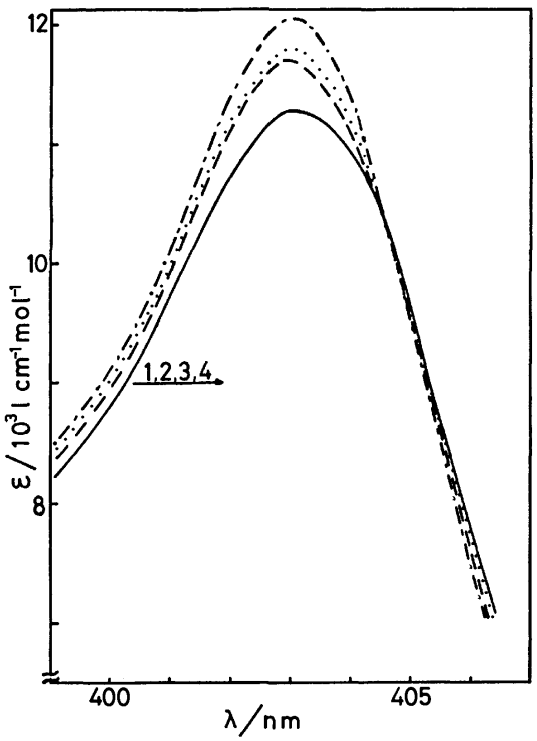

Fig. 3. The absorption spectra of **2** in cyclohexane-dichloromethane mixed solvent. Concentrations for dichloromethane are 1: 0, 2: 0.20, 3: 0.31, 4: 1.01 mol dm^{-3}.

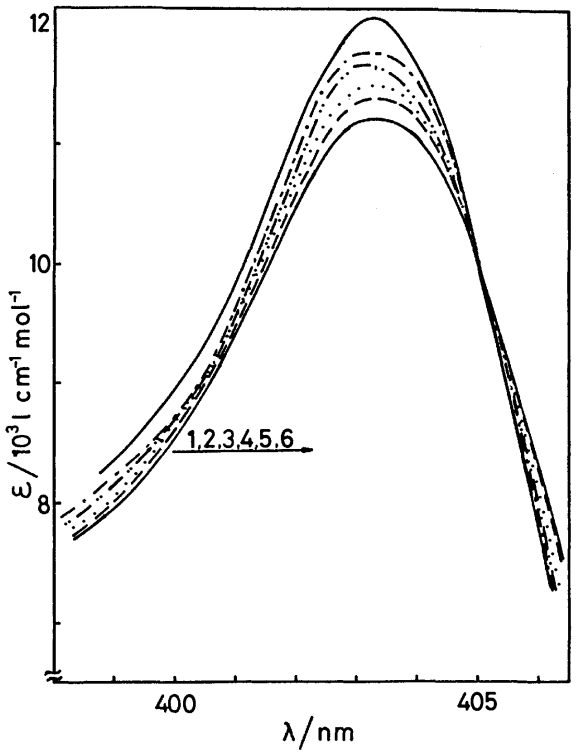

Fig. 4. The absorption spectra of **2** in cyclohexane-chloroform mixed solvent. Concentrations for chloroform are 1: 0, 2: 0.10, 3: 0.20, 4: 0.40, 5: 0.70, 6: 1.0 mol dm^{-3}.

concentration of chlorinated methanes. As the concentration of dichloromethane increases, the peak intensity of vibrational bands decreases (Fig. 3). An isosbestic point appears in the spectra. These observations indicate that an equilibrium between two species occurs in the ground state of this system. A similar spectral feature is also seen in the cyclohexane-chloroform mixed solvents (Fig. 4). The spectral feature was unchanged after a week unless the solutions were stored in the light. Therefore it is safely concluded that a complex is formed between chlorinated methanes and **2** in its ground state. The equilibrium constant of the ground state complex, K_C, can be determined by the usual procedure.[10] The K_C values were 0.14 and 0.17 mol dm^{-3} for the ground state complex between **2** and dichloromethane and between **2** and chloroform, respectively.

It is noted that the K_C value in **2** and chloroform system is larger than that in **2** and dichloromethane system. This difference between two K_C values may be attributable to the difference of the numbers of chlorine atoms in dichloromethane and chloroform.

The formation of ground-state complexes between aromatic molecules and halomethanes has been established for anthracene.[11,12] In the ground-state complexes of anthracene, halomethanes are located on the plane of anthracene ring. Ware and Lewis showed that there are higher complexes of carbon tetrachloride with anthracene and this higher complexes are responsible for the origin of wavelength effects in the fluorescence quenching of anthracene.[12]

There are two possible configurations for a complex between **2** and chlorinated methanes. One is the configuration in which chlorinated methanes are located on the anthracene ring, similar to complexes between anthracene and halomethanes. The other is the configuration in which chlorinated methanes are connected to the C=O group of **2** through hydrogen bonding between **2** and chlorinated methanes. Baba and Takemura found that anthrone forms a ground-state complex with triethylamine.[13] They also reported that a very weak n-π^* absorption band appears in the red edge side of a stronger absorption band due to the formation of a complex between anthrone and triethylamine in the ground state. This situation is similar to what we observe for **2** and chlorinated methanes. Therefore it is safely concluded that chlorinated methanes are either connected to the C=O group of **2** through a hydrogen bond or are located on the plane of **2** in the ground state.

This very weak absorption band is not obvious in cyclohexane solution. Taking into account the discussion in the previous section, one possible interpretation for the appearance of the band is an n-π^* band in anthrone, normally around 25000 cm^{-1}, shifted to the red due to a ground-state complex formation between **2** and chlorinated methanes. Another possible interpretation of this band is that the n-π^* band shifts to

the red due to the distortion of the anthrone ring system in **2**.

Fluorescence and Fluorescence Excitation Spectra. The fluorescence and fluorescence excitation spectra of **2** in cyclohexane are given in Fig. 5. Although it is not shown in Fig. 5, there are no excitation-wavenumber and no emission-wavenumber dependent changes in the fluorescence emission or fluorescence excitation spectra of **2** in cyclohexane. The fluorescence spectrum of **2** has an anthracene-like structure and the fluorescence excitation spectrum of **2** also has an anthracene-like structure. Hereafter the anthracene-like structured band is referred to as FM fluorescence band, meaning "molecular fluorescence." It is noted that the FM band is a similar emission band observed in cyclohexane for **1**.[3]

Figure 6 shows the excitation-wavenumber dependence of fluorescence spectra of **2** in dichloromethane. When **2** is excited at 33330 and 25000 cm^{-1}, it exhibits an anthracene-like fluorescence band on the higher wavenumber side and a broad band on the lower wavenumber side (σ_{max}=18700 cm^{-1}). On the other hand, when **2** is excited at 23800 cm^{-1}, it has only one broad and structureless fluorescence band (σ_{max}=20800 cm^{-1}). Similar characteristics are seen in the excitation-wavenumber dependence of fluorescence spectra of **2** in chloroform (Fig. 7). Hereafter the broad bands which show peaks at 20800 and 18700 cm^{-1} are referred to as FC and FE fluorescence bands, respectively. They will be assigned below to "complex fluorescence" and "exciplex fluorescence." It is noted that the FE band has seen in some solvents for **1** but the FE band was not seen in the fluorescence spectra of **1**.[3]

Figure 8 shows the observation-wavenumber dependence of the fluorescence spectra of **2** compound in dichloromethane. When the spectrum is observed at a wavenumber of 22730 cm^{-1}, which corresponds to a peak of the FM band, the spectrum is similar to the fluorescence excitation spectrum observed in cyclohexane. With decreasing the observation wavenumber below 22730 cm^{-1}, a shoulder appears on the red side of the anthracene-like band. When the spectrum is observed at 20830 cm^{-1}, which corresponds to the peak of the FC band, a new excitation band appears around 22700 cm^{-1}. A mirror symmetry relation is found

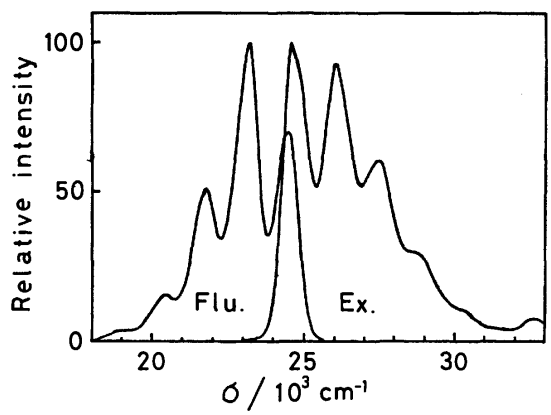

Fig. 5. The fluorescence and fluorescence excitation spectra of **2** in cyclohexane.

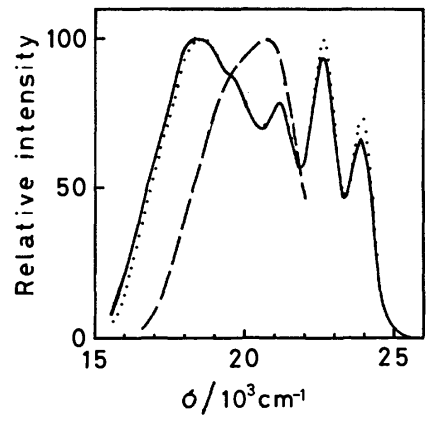

Fig. 7. The fluorescence spectra of **2** in chloroform. Excitation wavenumbers are as follows, 1(——): 31250, 2(·····): 27780, 3(----): 23810 cm^{-1}.

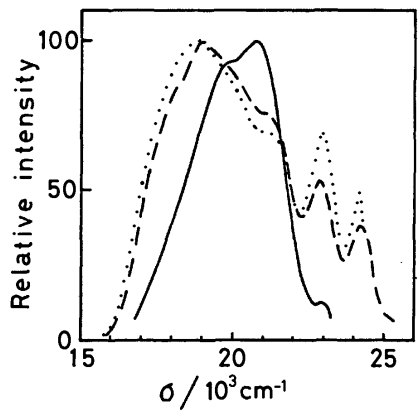

Fig. 6. The fluorescence spectra of **2** in dichloromethane. Excitation wavenumbers are as follows, 1(----): 33300, 2(·····): 25000, 3(——): 23800 cm^{-1}.

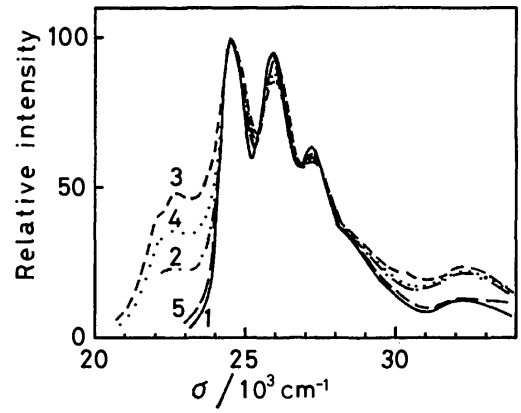

Fig. 8. The fluorescence excitation spectra of **2** in dichloromethane. Emission wavenumbers are as follows, 1(——): 22730, 2(-·-·-): 21740, 3(----): 20330, 4(·····): 20000, 5(——): 17860 cm^{-1}.

between this broad band and the FC band. When the spectrum is observed at around 18000 cm^{-1}, which corresponds to the peak of the FE band, the spectrum is similar to the fluorescence excitation spectrum observed in cyclohexane.

The observation-wavenumber dependence of fluorescence excitation spectra of the compound in chloroform is given in Fig. 9. It is seen from Fig. 9 that the spectral features in chloroform are almost the same as in dichloromethane, but the spectral characteristics in chloroform are not so obvious as in dichloromethane.

These results indicate that the FM and FE bands originate from the same ground-state species which show the anthracene-like fluorescence excitation spectra. On the other hand, the FC band originates from a ground state species which shows a broad fluorescence excitation spectrum around 22700 cm^{-1} in chlorinated methanes.

The data in Figs. 1 to 9 indicate the origins of the

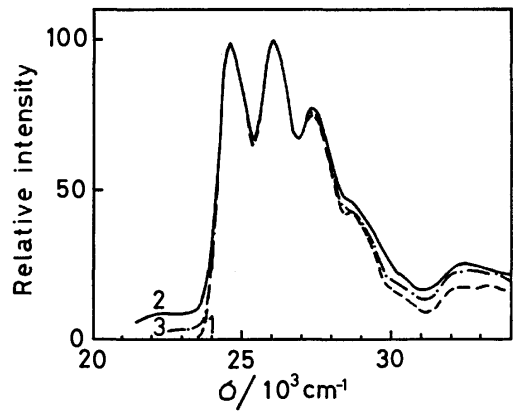

Fig. 9. The fluorescence excitation spectra of **2** in chloroform. Emission wavenumbers are as follows, 1(----): 22730, 2(——): 20830, 3(-·-·-): 18180 cm^{-1}.

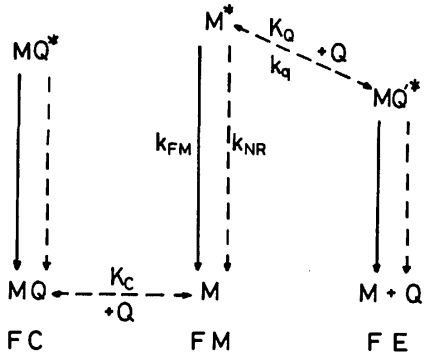

Fig. 10. Reaction scheme of **2**. M is **2**, Q is chlorinated methanes, MQ is a ground-state complex between **2** and chlorinated methanes, M* and MQ* are an excited-state species of M and MQ, MQ'* is an exciplex between M* and chlorinated methanes, K_C is equilibrium constant of complex formation in the ground state. K_Q is defined in the text and k's are rate constants. When the initial concentration of quencher, [C], is enough larger than that of **2**, then we can put [Q]=[C].

fluorescence bands, FM, FC, and FE may be summarized as follows: The FM band can be assigned to a fluorescence of the anthracene chromophore from the excited **2**. The FC band originates from excitation of a complex which is formed between **2** and chlorinated methanes in the ground state. The FE band is an emission from an exciplex which is formed between excited **2** and chlorinated methanes.

Kinetic Consideration. The reaction scheme for the interaction of **2** with chlorinated methanes discussed in the above section is illustrated in Fig. 10. If initial concentration of quencher, initial concentration of **2**, equilibrium concentration of **2**, equilibrium concentration of quencher, and equilibrium concentration of the complex are denoted by [C], [B], [M], [Q], and [MQ], respectively, then

$$[B] = [M] + [MQ], \tag{1}$$

$$[C] = [Q] + [MQ]. \tag{2}$$

Equilibrium constant of complex formation among M, Q, and MQ is

$$K_C = \frac{[MQ]}{[M][Q]} \tag{3}$$

Therefore [MQ] is represented as

$$[MQ] = K_C \times [M] \times [Q]. \tag{4}$$

The fraction of the incident light intensity absorbed by M is given by[5]

$$a = \frac{\varepsilon_M[M]}{\varepsilon_M[M] + \varepsilon_{MQ}[MQ]} \tag{5}$$

$$= \frac{1}{1 + a \times K_C \times [Q]}, \tag{6}$$

where ε_M and ε_{MQ} represent the molar absorption coefficients for M and MQ and a is equal to $\varepsilon_{MQ}/\varepsilon_M$.

The fluorescence intensity of the FM band in the absence of quenchers is written as

$$F_0 = \frac{k_{FM}}{k_{FM} + k_{NR}} \times [M^*]_{[Q]=0} \tag{7}$$

where $[M^*]_{[Q]=0}$ indicates excited concentration of **2** at equilibrium concentration ([Q]) of chlorinated methanes is equal to 0. When [Q] is not equal to 0, the fluorescence intensity of **2** can be written as

$$F_Q = \frac{k_{FM}}{k_{FM} + k_{NR} + k_q[Q]} \times [M^*]_{[Q]}, \tag{8}$$

where $[M^*]_{[Q]}$ represents excited concentration of **2** where equilibrium concentration of chlorinated methanes is [Q]. $[M^*]_{[Q]}$ can be rewritten as

$$[M^*]_{[Q]} = [M^*]_{[Q]=0} \times a. \tag{9}$$

Then Stern-Volmer equations for the ratio of the fluorescence intensity (RQY) and for the ratio of the

fluorescence lifetime (RTF) for the FM band can be rewritten as

$$\mathrm{RQY} = \frac{F_0}{F_Q} = \frac{k_{FM} + k_{NR} + k_q[Q]}{k_{FM} + k_{NR}} \times \frac{[M^*]_{[Q]=0}}{[M^*]_{[Q]}}$$

$$= (1 + a \times K_C \times [Q]) \times (1 + K_Q \times [Q]), \quad (10)$$

$$\mathrm{RTF} = \frac{k_{FM} + k_{NR} + k_q[Q]}{k_{FM} + k_{NR}} = 1 + K_Q \times [Q], \quad (11)$$

where

$$K_Q = \frac{k_q}{k_{FM} + k_{NR}}$$

Under the condition that the initial concentration of quencher, [C], is much larger than that of **2**, [B], Eqs. 10 and 11 can be written as

$$\mathrm{RQY} = (1 + a \times K_C \times [C]) \times (1 + K_Q \times [C]) \quad (10a)$$

$$\mathrm{RTF} = 1 + K_Q \times [C]. \quad (11a)$$

Figure 11 plots the RQY for the FM band of **2** as a function of [C], a concentration of dichloromethane or chloroform, in cyclohexane-dichloromethane or cyclohexane-chloroform mixed solvents. It is seen from Fig. 11 that the plots are nonlinear. This nonlinearity is attributed to the decrease of concentration of free **2** at higher concentration of chlorinated methanes due to the formation of the ground-state complex between **2** and chlorinated methanes. The nonlinearity is also attributed to exciplex formation between the excited **2** and chlorinated methanes. The experimental curves are well represented by Eq. 10a. The Stern-Volmer constant for deexcitation processes, K_Q, can be determined by Eq. 10a. The K_Q values of 0.20 and 0.09 $\mathrm{mol^{-1}\,dm^3}$ were obtained for the deexcitation processes between the excited compound and chloroform and between the compound and dichloromethane, respectively.

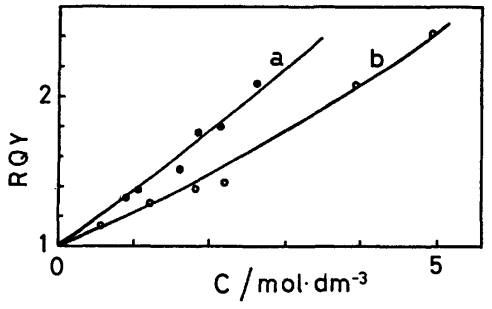

Fig. 11. Stern-Volmer plots of fluorescence quantum yield of **2** in cyclohexane-dichloromethane(a) and cyclohexane-chloroform(b). Since the excitation wavelength corresponds to an isosbestic point, a=1 in Eq. 10a. The solutions are not degassed.

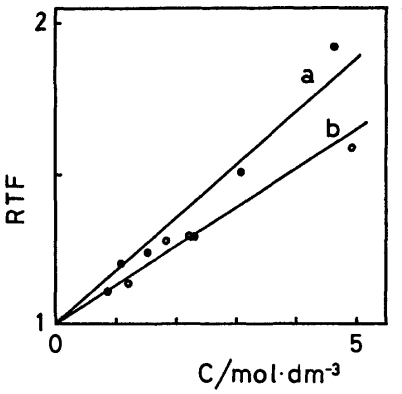

Fig. 12. Stern-Volmer plots of fluorescence lifetime of **2** in cyclohexane-dichloromethane(a) and cyclohexane-chloroform(b). The solutions are not degassed.

Figure 12 plots the RTF of **2** as a function of [C] in cyclohexane-dichloromethane and cyclohexane-chloroform mixed solvents. Figure 12 shows that the plots are linear within the experimental error and experimental results are well represented by Eq. 11a. The K_Q values obtained from the RTF plots are 0.18 and 0.12 $\mathrm{mol^{-1}\,dm^3}$ for chloroform and dichloromethane system, respectively.

The K_Q values obtained from the quenching of fluorescence quantum yields agree well with those obtained from the decrease in fluorescence lifetimes. These results confirm that the FM band originates from an excited **2**, the FC band originates from a complex formed in the ground state, and the FE band originates from an exciplex between excited **2** and chlorinated methanes.

Comparison of 2 with 1.[3] **1** and **2** are similar compounds. **1** emits only the FM and FE bands. Becker and Sandross has assigned the FM band to a fluorescence of the anthracene chromophore and the FE band to an exciplex fluorescence which originates from a solvent-assisted intramolecular charge-transfer interaction between the ground-state anthrone and excited-state anthracene. On the other hand, **2** emits the FM, FC, and FE fluorescences.

This difference may be attributable to the difference of molecular geometries between **1** and **2**. The geometry of **1** and that of **2** are similar but not identical. **1** has the six-membered ring containing a spiro carbon atom and has two possible conformations. Furthermore, the twisted angle between anthracene and anthrone rings are not perpendicular. **2**, however, has the five-membered ring containing a spiro carbon atom and has a rigid conformation. The anthracene ring is precisely perpendicular to the anthrone ring in **2**.

The assignment about the origin of the FM band by Becker and Sandross agrees with our conclusion. On the origin of the FE band, our conclusion is not in conflict with Becker and Sandross since the formation of an intermolecular complex may be responsible for an excited-intramolecular charge-transfer complex. Although it is difficult at present to presume what type geometry is acceptable for the exciplex geometry, there are possible geometries for the exciplex between **2** and chlorinated methanes. One is a similar conformation to the ground-state complex between anthracene and halogenated methanes where halogenated methanes are located on the plane of anthracene ring.[10] The other is a conformation where halogenated methanes are located surrounding the anthrone ring. In this case anthrone ring has geometrical distortion due to the connection through the five-membered ring with the anthracene ring. The electronic structure of the exciplex would resemble that of a σ-π complex suggested by Becker and Sandross for **1**.[3] The study of the more detailed kinetic consideration including similar compounds as **1** and **2** will be the object of further work.

The authors are much indebted to Professor Takeshi Takemura of Hokkaido University for his helpful suggestion about the possible structures of the ground-state complex between **2** and chlorinated methanes.

References

1) T. Fujii, S. Suzuki, and S. Komatsu, *Chem. Phys. Lett.*, **57**, 175 (1978); T. Fujii, S. Komatsu, and S. Suzuki, *Bull. Chem. Soc. Jpn.*, **55**, 2516 (1982).

2) T. Fujii, S. Suzuki, and H. Arita, *Chem. Phys. Lett.*, **111**, 350 (1984).

3) H.-D. Becker and K. Sandross, *Chem. Phys. Lett.*, **53**, 228 (1978); H.-D. Becker, *Pure Appl. Chem.*, **54**, 1589 (1982).

4) S. Nakazawa, K. Hirakawa, S. Fujimori, and K. Iwasaki, *J. Chem. Soc., Perkin Trans. 1*, **1979**, 2055.

5) J. B. Birks, "Photophysics of aromatic molecules," Wiley-Interscience, New York (1970).

6) W. W. Mantulin and J. R. Huber, *Photochem. Photobiol.*, **17**, 139 (1973); J. R. Huber, M. A. Mahaney, and W. W. Mantulin, *J. Photochem.*, **2**, 67 (1967/1968).

7) W. H. Melhuish, *J. Phys. Chem.*, **65**, 229 (1961).

8) R. A. Lampert, L. A. Chewter, D. Phillips, D. V. O'Connor, A. J. Robert, and S. R. Merch, *Anal. Chem.*, **55**, 68 (1983).

9) F. Doerr, *Z. Electrochem.*, **61**, 950 (1957).

10) J. A. A. Kelelaar, C. van de Stolpe, A. Goudsmit, and W. Dzcubzs, *Rec. Trav. Chim.*, **71**, 1104 (1952).

11) E. J. Bowen, F. R. S. and W. S. Metcalf, *Proc. R. Soc. London, Ser. A*, **206**, 437 (1951).

12) C. Lewis and W. R. Ware, *Chem. Phys. Lett.*, **15**, 290 (1972); W. R. Ware and C. Lewis, *J. Chem. Phys.*, **57**, 3546 (1972).

13) H. Baba and T. Takemura, *Tetrahedron*, **24**, 3779 (1968); T. Takemura and H. Baba, *ibid.*, **24**, 5311 (1968).

 © 1987 The Chemical Society of Japan Bull. Chem. Soc. Jpn., 60, 4217—4222 (1987)

Effects of NH_3 on ^{13}C-Selective Infrared Multiple Photon Decomposition of CF_2HCl by a CO_2 Laser

Kyoko SUGITA* and Shigeyoshi ARAI
The Institute of Physical and Chemical Research, Wako-shi, Saitama 351-01
(Received March 30, 1987)

The effects of NH_3 on product yields and ^{13}C enrichment factors have been examined for the IRMPD of CF_2HCl using a CO_2 TEA laser. The IRMPD of neat CF_2HCl yields only C_2F_4 and HCl as final products. The addition of NH_3 resulted in the formation of CF_3H and NH_4Cl in addition to C_2F_4, and enhanced significantly the decomposition of CF_2HCl. The enrichment factors of ^{13}C in C_2F_4 and CF_3H decreased with increasing NH_3, but the decreases were relatively small. The mechanism of the IRMPD in the presence of NH_3 is discussed on the basis of the observed results.

It has been well-established that four-atom or larger molecules absorb numerous photons and undergo unimolecular decomposition when their resonant vibration modes are irradiated with high-fluence radiation from infrared lasers.[1] The photochemical phenomenon is called infrared multiple photon decomposition (IRMPD in abbreviation). IRMPD frequently exhibits remarkable isotope effects, reflecting the relatively large isotope shifts on infrared absorption. A number of studies have been already published on isotope separation of elements from hydrogen to uranium.[1-3] However, it is not easy to obtain practical amounts of enriched products in laser isotope separation by use of IRMPD, although selectivities are high. Recently, Kamioka et al. have succeeded in producing silicon isotopes on a practical scale using the IRMPD of Si_2F_6.[4,5]

Natural carbon consists of two isotopes, i.e., 98.9% of ^{12}C and 1.1% of ^{13}C. The IRMPD of CF_2Cl_2, CF_3X (X=Cl, Br, or I), and CF_2HCl has been extensively studied with the intention of ^{13}C separation; most of the studies have been succinctly reviewed in the introductory section of the paper by Outhouse et al.[6] The IRMPD of CF_3Br was found to produce C_2F_6 with a ^{13}C content of 80%, and that of CF_2HCl to produce C_2F_4 with 90—96% under selected irradiation conditions.[7-9] However, the enrichment of ^{13}C above 70% is attainable only with a great sacrifice of the yield. Outhouse et al. have demonstrated production rates of 0.23 $g\,h^{-1}$ for 50% ^{13}C and of 0.011 $g\,h^{-1}$ for 72% ^{13}C using a high power CO_2 TEA laser (10 J, 10 Hz)[6]. Therefore, there is general agreement that practical ^{13}C separation requires a two-stage process. For example, the first process is intended to increase a ^{13}C content from 1.1% to 20—50% (enrichment factor, 23—90) and the following second process is the production of ^{13}C above 90% (enrichment factor, 9—36). Since a high selectivity is not needed in each step, one can obtain a relatively large production rate of ^{13}C by such a two-stage process.

Abdushelishvili et al. have proposed the IRMPD of CF_3Br or CF_3I in the presence of NO, where NO scavenged CF_3 radicals produced from the first ^{13}C-selective IRMPD.[10] The resulting product, i.e., CF_3NO was presumed to be converted into CF_3Br or CF_3I for the second IRMPD, where the chemical conversion could be easily achieved by heating CF_3NO in Br_2 or I_2 vapor. Arai and his coworkers found that the IRMPD of C_2F_6 in the presence of Br_2 formed CF_3Br with 20—30% ^{13}C.[11] The further IRMPD of the enriched CF_3Br resulted in the production of C_2F_6 with 90% ^{13}C. On the other hand, Hackett et al. showed that the production of C_2F_4 with 95—99% ^{13}C from equimolar mixtures of 50% $^{12}CF_2HCl$ and 50% $^{13}CF_2HCl$ was very efficient in energy expenditure.[6,12] They predicted the production rate of 1.7 $g\,h^{-1}$ for 99% ^{13}C, assuming that equimolar mixtures were irradiated in a flow system with 10 J pulses at a repetition rate of 10 Hz. However, enriched CF_2HCl must be provided from other enrichment process. Recently, Ma et al. proposed the two-stage IRMPD of CF_2Cl_2-HI or CF_2ClBr-HI mixtures, where the first process was the production of CF_2HCl with ^{13}C content of 30% and the second process was the further enrichment by the selective decomposition of the CF_2HCl.[13] In view of the efficient decomposition of CF_2ClBr at low fluences, the IRMPD of CF_2ClBr-HI mixtures could be one of the most effective two-stage processes to the practical enrichment of ^{13}C.

IRMPD of several fluorocarbons has been examined in our group for the development of a practical two-stage ^{13}C enrichment. In the course of the study we found that NH_3 significantly enhanced the decomposition yield in the IRMPD of CF_2HCl. The effect could be applied to an improvement of a ^{13}C yield in separation processes involving IRMPD of CF_2HCl. The present paper describes detailed experimental results and decomposition mechanisms.

Experimental

The experimental apparatus and procedures are essentially the same as were described elsewhere.[14,15]

Laser beams from a Lumonics 103-2 CO_2 TEA laser were focussed on the center of a reaction cell by a BaF_2 lens with a focal length of 60 cm, where the resulting focus area was about 0.045 cm^2. The laser was operated without nitrogen gas at a repetition rate of 0.7 Hz. A typical pulse had a half width of about 80 ns and a triangle profile without a tail.

Output energies were measured with a Scientech 362 energy power meter and a Scientech 360001 detector. The reaction cell was a 113 cm long and 2.0 cm diameter cylindrical Pyrex tube equipped with KBr windows at both ends. In addition, the cell has KBr side windows for infrared spectrophotometric analysis, where the optical path length was 5.0 cm. The total volume was 393 cm^3.

Formation amounts and isotopic compositions of products were determined by using a Shimadzu GC-7A gas chromatograph coupled with a NEVA quadrapole mass spectrometer, where a 3 mm ϕ and 3 m long VZ-10 column was mainly employed under programmed temperature variations. CF_2HCl purchased from Nitto Fluorochemical Co. was distilled repeatedly at low temperatures and the middle fractions were used as irradiation samples. We could not detect impurities such as C_2F_4 and CF_3H except for a trace amount of CF_2Cl_2. NH_3 from Suzuki Shokan Co. was also distilled repeatedly at low temperatures.

Results

The infrared absorption spectra of natural CF_2HCl and NH_3 are shown in Fig. 1. The bands centered at 1105 and 1120 cm^{-1} in CF_2HCl are assigned to CF_2 symmetric and antisymmetric stretching vibration modes, respectively. The bands at 932 and 968 cm^{-1} in NH_3 are due to degenerate symmetric deformation modes, where their R branches are extending on the higher wavenumber side. A ^{13}C isotope shift has been reported to be nearly 30 cm^{-1} for CF_2HCl.[16] In comparison to usual infrared absorption spectra, the band shapes become broader and the peaks shift to the red side in multiple-photon absorption spectra, depending on a laser fluence. The previous study of the IRMPD of CF_2HCl has shown that the decomposition probability of ^{13}C bearing molecules is considerably larger than that of ^{12}C bearing molecules in a wavenumber region from 1030 cm^{-1} to 1060 cm^{-1}.[9] Since this study was concerned with ^{13}C enrichment, we employed mainly the 9P (20) line at 1046.85 cm^{-1} and the 9P (22) line at 1045.02 cm^{-1} for irradiation of the mixtures. Although NH_3 also absorbed some of the laser radiation, neat NH_3 did not decompose at all under the present irradiation conditions, probably because of insufficient fluences for decomposition of a simple four-atom molecule.[17]

The IRMPD of neat CF_2HCl gives only C_2F_4 and HCl as stable final products; these are the same products as in homogeneous gas-phase thermolysis.[18,19] The addition of NH_3 causes the formation of a new product, which can be definitely identified as CF_3H on the basis of its retention time on gas chromatography, a peak wavenumber in infrared spectroscopy, and a cracking pattern in mass spectrometry. In addition, we observed thick deposition of a white solid on the cell walls. The element analysis of the solid showed C, 1.04; H, 7.39; N, 25.7% in weight; the composition was consistent with NH_4Cl. No fluorocarbons containing Cl, (for example, CFH_2Cl, $CFHCl_2$, $C_2F_2Cl_2$) were detected on gas chromatography.

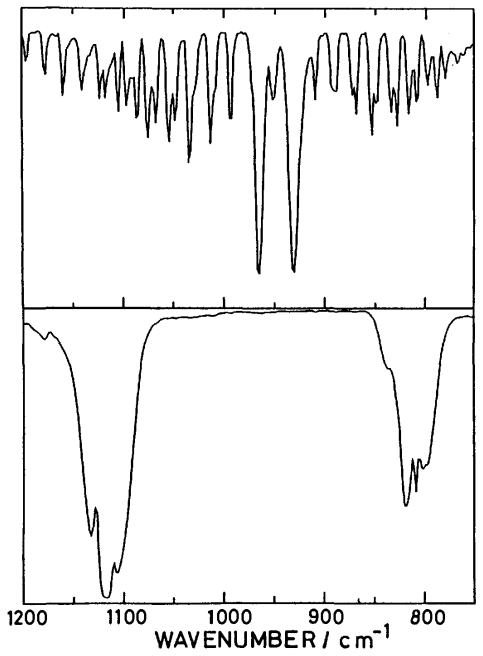

Fig. 1. Infrared absorption spectra of CF_2HCl (lower) and NH_3 (upper).

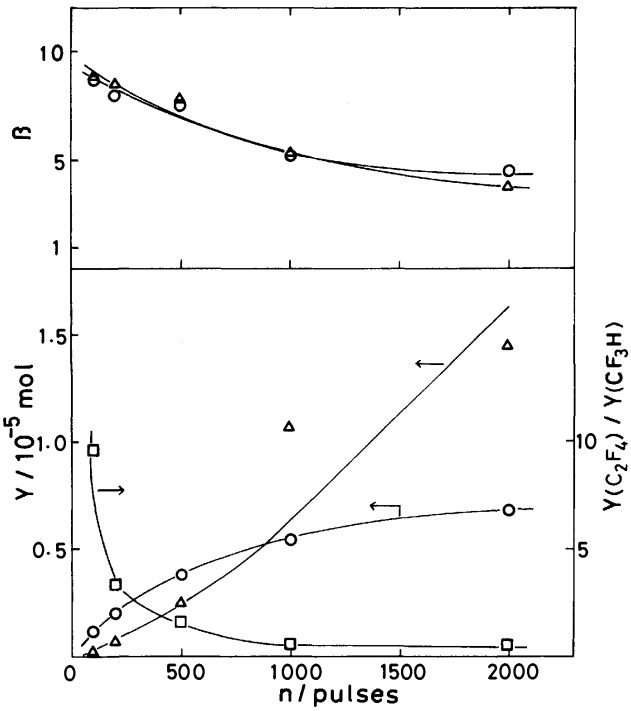

Fig. 2. Effects of pulse number n on yields Y (lower) and enrichment factors β (upper) for IRMPD of CF_2HCl-NH_3 mixtures at 5 Torr and 5 Torr.
○, $Y(C_2F_4)$ or $\beta(C_2F_4)$; △, $Y(CF_3H)$ or $\beta(CF_3H)$; □, $Y(C_2F_4)/Y(CF_3H)$. Laser wavenumber, 1046.85 cm^{-1}; laser fluence at focus, about 27 J cm^{-2}.

Figure 2 shows the effects of pulse number on yields and enrichment factors for the IRMPD of CF_2HCl-NH_3 mixtures at 5 Torr plus 5 Torr (1 Torr=133.322 Pa). The yield for C_2F_4, $Y(C_2F_4)$ is defined as a total amount of C_2F_4 produced, while that for CF_3H,

$Y(CF_3H)$ has a similar definition. The enrichment factors for C_2F_4 and CF_3H are as follows.

$\beta(C_2F_4)=\{[^{13}C]/[^{12}C]$ in $C_2F_4\}/\{[^{13}C]/[^{12}C]$ in natural$\}$

$\beta(CF_3H)=\{[^{13}C]/[^{12}C]$ in $CF_3H\}/\{[^{13}C]/[^{12}C]$ in natural$\}$

Ratios of $[^{13}C]$ to $[^{12}C]$ in C_2F_4 were determined from ion intensities of $^{12}CF_2^+$ at m/z=50 and those of $^{13}CF_2^+$ at m/z=51 for the C_2F_4 peak in GC-MS. On the other hand, we obtained similar ratios in CF_3H from ion intensities at m/z=50 ($^{12}CF_2^+$), m/z=51 ($^{12}CF_2H^+$ and $^{13}CF_2^+$), and m/z=52 ($^{13}CF_2H^+$), taking the cracking pattern of CF_3H into consideration. Figure 2 includes plots of $Y(C_2F_4)/Y(CF_3H)$ vs. number of pulses. $Y(C_2F_4)$ predominates over $Y(CF_3H)$ at small pulse numbers, but $Y(C_2F_4)$ decreases to about a half of $Y(CF_3H)$ at 2000 pulses. For pulse numbers less than 1000, logarithmic plots of $[CF_2HCl]_n/[CF_2HCl]_0$ vs. number of pulses give a good straight line, as shown in Fig. 3, where $[CF_2HCl]_0$ and $[CF_2HCl]_n$ are the amounts of CF_2HCl before and after n-pulse irradiation, respectively. The slope corresponds to a so-called specific decomposition rate in IRMPD, which is 2.1×10^{-4} pulse^{-1} in this case.

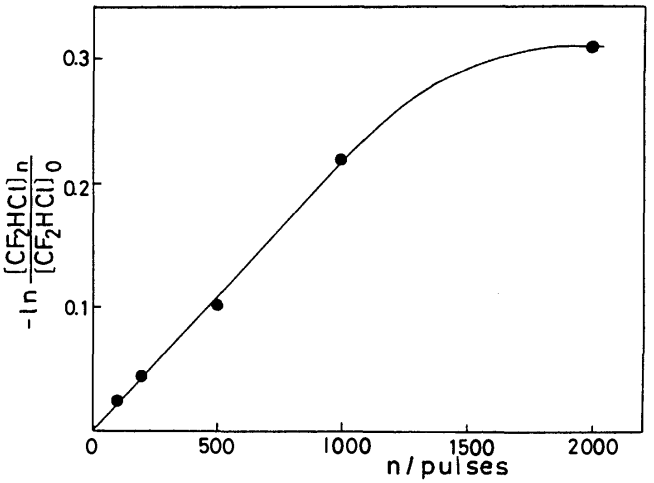

Fig. 3. Logarithmic plots of $[CF_2HCl]_n/[CF_2HCl]_0$ vs. number of pulses for IRMPD of CF_2HCl–NH_3 mixtures at 5 Torr and 5 Torr. $[CF_2HCl]_n$ and $[CF_2HCl]_0$, see text. Laser wavenumber, 1046.85 cm^{-1}; laser fluence at focus, about 27 J cm^{-2}.

Figure 4 shows the laser line dependences of yields and enrichment factors for the IRMPD of 10 Torr CF_2HCl and 10 Torr NH_3, where the number of laser pulses is 1000 at each line. In these irradiations, fluences at the focus were adjusted to fall within 20.8±2.8 J cm^{-2} by inserting polyethylene films into the beam path. However, that for the 9P(34) line at 1033.49 cm^{-1} was 12.5 J cm^{-2} at a maximum output. Although $Y(C_2F_4)$ and $Y(CF_3H)$ decrease with decreasing wavenumber, $\beta(C_2F_4)$ and $\beta(CF_3H)$ have maxima at the 9P (26) line, i.e., 1041.28 cm^{-1} and the 9P (30) line, i.e., 1037.43 cm^{-1}. In addition, the parallel relations between C_2F_4 and CF_3H in yield and enrichment factor suggest that both compounds have the same origin, which must be a CF_2 radical produced in the ^{13}C selective IRMPD of mixtures. There seems to be a structure in the wavenumber dependences of $\beta(C_2F_4)$ and $\beta(CF_3H)$. The structure may originate from the nar-

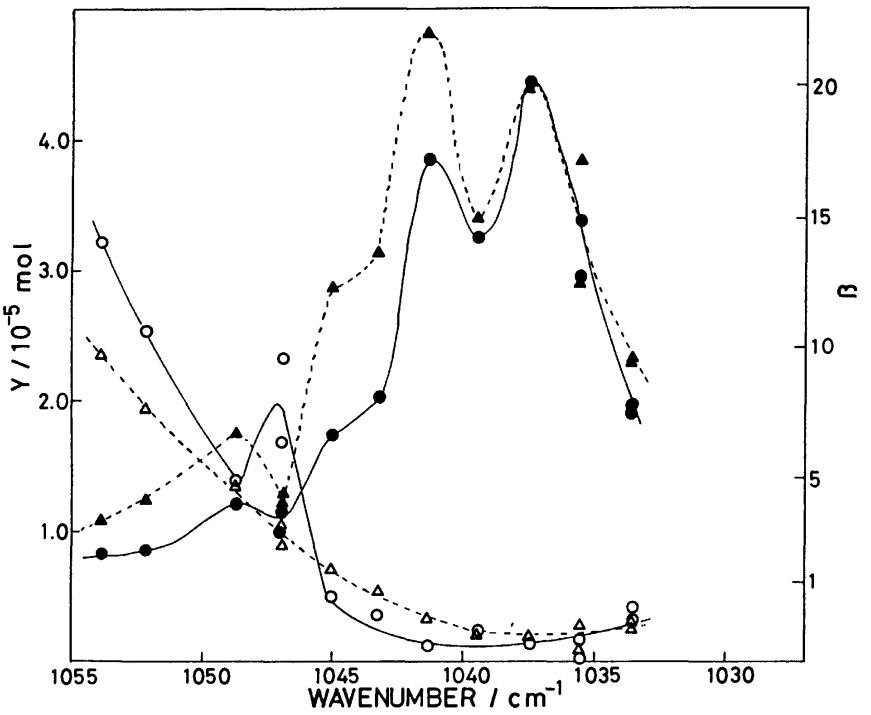

Fig. 4. Laser line dependences of yields Y and enrichment factors β for IRMPD of CF_2HCl–NH_3 mixtures at 10 Torr and 10 Torr. ○, $Y(C_2F_4)$; △, $Y(CF_3H)$; ●, $\beta(C_2F_4)$; ▲, $\beta(CF_3H)$; pulse number, 1000. Fluences, see text.

row resonance of the laser radiation with rotation-vibration transition energy in the discrete energy-level region.[1] In the IRMPD of neat CF_2HCl for different irradiation frequencies at 1053.92, 1046.85, 1041.28, and 1035.47 cm^{-1}, the enrichment factor increased rapidly with decreasing wavenumber. We consider that a non-selective thermal process may contributes to the formation of both C_2F_4 and CF_3H in mixtures of 10 Torr CF_2HCl and 10 Torr NH_3. The contribution becomes more significant with decreasing wavenumber, resulting in a rapid decrease in $\beta(C_2F_4)$ or $\beta(CF_3H)$ below 1035 cm^{-1}.

In order to obtain standard data for comparison, we examined briefly the IRMPD of neat CF_2HCl under the same experimental conditions as the CF_2HCl-NH_3 mixtures. Figure 5 shows the pressure dependences of $Y(C_2F_4)$ and $\beta(C_2F_4)$, where the laser was adjusted to the 9P (22) line and the fluences were set at about 30 J cm^{-2}. As NH_3 is added to 1.0 Torr CF_2HCl, $Y(C_2F_4)$ decreases rapidly and, after passing through a minimum, increases gradually with increasing NH_3 (see Fig. 6). $Y(CF_3H)$ increases simply with increasing NH_3, while both $\beta(C_2F_4)$ and $\beta(CF_3H)$ decrease. Hereafter, we define a total carbon yield, $Y(C)$ as 2 $Y(C_2F_4)$ for neat CF_2HCl or $Y(CF_3H)+2\ Y(C_2F_4)$ for

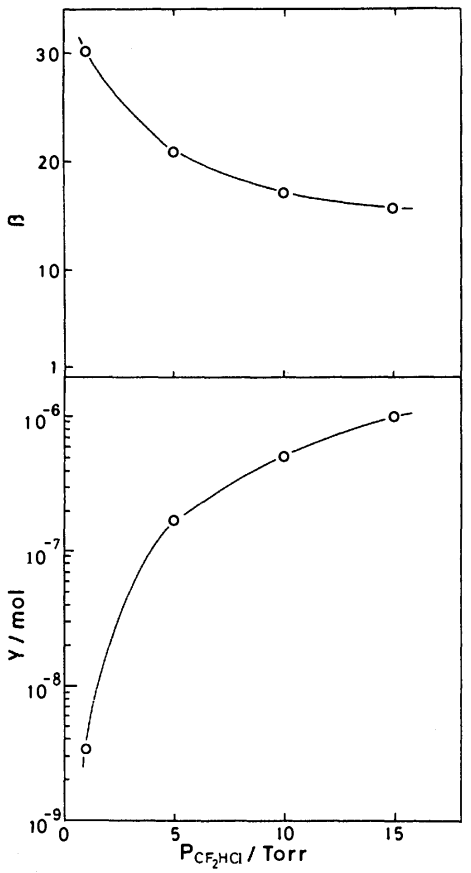

Fig. 5. Pressure dependences of $Y(C_2F_4)$ and $\beta(C_2F_4)$ for IRMPD of neat CF_2HCl. Laser wavenumber, 1045.02 cm^{-1}; laser fluence at focus, about 29 J cm^{-2}; pulse number, 1000.

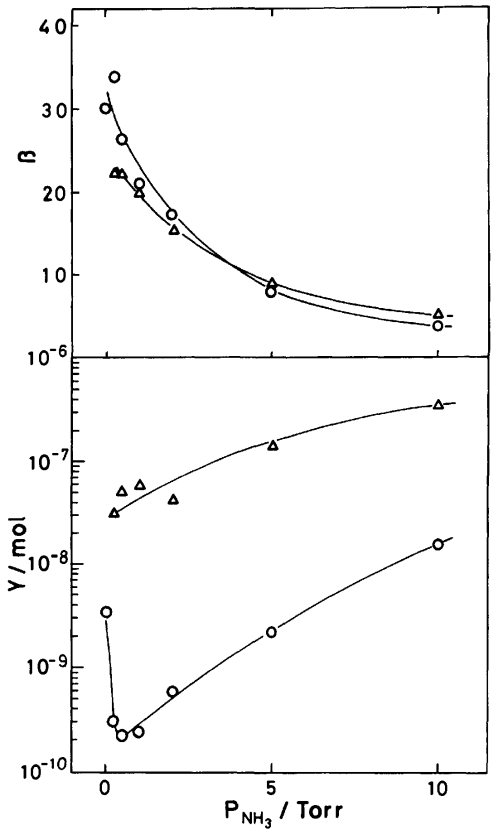

Fig. 6. Effects of NH_3 pressure on yields Y and enrichment factors β for IRMPD of CF_2HCl (1.0 Torr)-NH_3 mixtures. O, $Y(C_2F_4)$ or $\beta(C_2F_4)$; Δ, $Y(CF_3H)$ or $\beta(CF_3H)$. Laser wavenumber, 1045.02 cm^{-1}; laser fluence at focus, about 29 J cm^{-2}; pulse number, 1000.

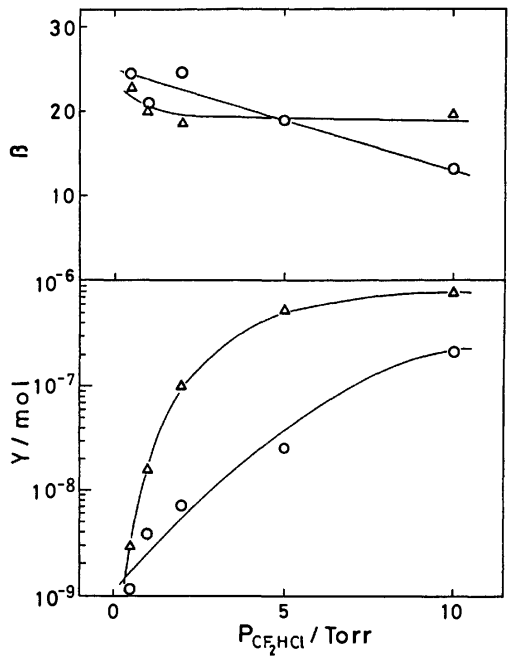

Fig. 7. Effects of CF_2HCl pressure on yields Y and enrichment factors β for IRMPD of CF_2HCl-NH_3 (1.0 Torr) mixtures. O, $Y(C_2F_4)$ or $\beta(C_2F_4)$; Δ, $Y(CF_3H)$ or $\beta(CF_3H)$. Laser wavenumber, 1045.02 cm^{-1}; laser fluence at focus, about 29 J cm^{-2}; pulse number, 1000.

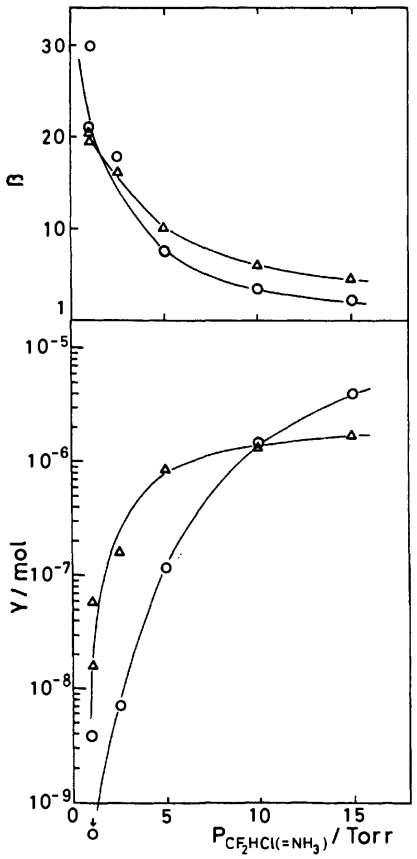

Fig. 8. Effects of total pressure on yields Y and enrichment factors β for IRMPD of equimolar CF_2HCl–NH_3 mixtures. ○, $Y(C_2F_4)$ or $\beta(C_2F_4)$; △, $Y(CF_3H)$ or $\beta(CF_3H)$. Laser wavenumber, 1045.02 cm^{-1}; laser fluence at focus, about 28 J cm^{-2}; pulse number, 1000.

mixtures. $Y(C)$ for the mixture of 1.0 Torr CF_2HCl and 1.0 Torr NH_3 was found to be 5.8×10^{-7} mol, while $Y(C)$ for 1.0 Torr neat CF_2HCl was only 6.8×10^{-8} mol; the former yield is about 8 times as large as the latter. The corresponding enrichment factors were $\beta(CF_3H)$= 20 for the mixture and $\beta(C_2F_4)$=30 for the neat CF_2HCl.

Fluence effects on yields and enrichment factors were examined for mixtures of 1.0 Torr CF_2HCl and 5.0 Torr NH_3 in the range from 12 to 30 J cm^{-2}. For examples, $Y(CF_3H)$ and β (CF_3H) at 12 J cm^{-2} were 1.96×10^{-7} mol and 26, respectively, while those at 30 J cm^{-2} were 1.40×10^{-6} mol and 9.0, respectively. $Y(C_2F_4)$ was much less than $Y(CF_3H)$ at either fluence. An increase in fluence enhances product yields and reduces enrichment factors. When CF_2HCl was added to 1.0 Torr NH_3, we observed an increase in $Y(C_2F_4)$ or $Y(CF_3H)$ and a decrease in $\beta(C_2F_4)$ or $\beta(CF_3H)$ with increasing CF_2HCl, as shown in Fig. 7. Similar results were also obtained with total pressure effects on equimolar mixtures of CF_2HCl and NH_3, as shown in Fig. 8.

Discussion

The IRMPD of neat CF_2HCl has been explained satisfactorily in terms of the initial photochemical decomposition of CF_2HCl into CF_2 and HCl, and the subsequent combination between two carbene radicals.[9,18]

$$CF_2HCl + nh\nu \rightarrow CF_2 + HCl \quad (1)$$

$$2\,CF_2 \rightarrow C_2F_4 \quad (2)$$

The same products, i.e., C_2F_4 and HCl have been obtained with the thermal decomposition of CF_2HCl, and the activation energy for the initial decomposition has been found to be 56 kcal mol^{-1} (1 cal=4.184 J) at pressures above 100 Torr.[19] Since the addition of HCl results in a decrease in decomposition rate, the following back reaction is considered to occur in thermolysis.

$$HCl + CF_2 \rightarrow CF_2HCl \quad (3)$$

The heat of formation for CF_2, $\Delta H_f(CF_2)$ show large divergence among several determinations.[19,20] The enthalpy change of the initial decomposition is calculated to be 41 kcal mol^{-1} on the basis of $\Delta H_f(CF_2)$= −49.5 kcal mol^{-1}.[19]

In the presence of NH_3, one can consider the following bimolecular decomposition with an enthalpy change much less than that of Reaction 1.

$$CF_2HCl + nh\nu \rightarrow CF_2HCl^* \quad (4)$$

$$CF_2HCl^* + NH_3 \rightarrow CF_2 + NH_4Cl \quad \Delta H = -1 \text{ kcal mol}^{-1} \quad (5)$$

Therefore, the activation energy of Reaction 5 may be considerably smaller than the 56 kcal mol^{-1} observed for Reaction 1. The reduction in activation energy means that a certain fraction of the excited molecules, which cannot decompose without NH_3, undergo Reaction 5 in the IRMPD of mixtures, where excited CF_2HCl originates from ^{13}C-selective multiple-photon absorption. We conclude that the observed large increases in product yields are caused by the contribution of such excited parent molecules into laser-induced decomposition via Reaction 5.

The formation of C_2F_4 is explained simply by dimerization of two CF_2 radicals in mixtures. However, the rapid decrease of $Y(C_2F_4)$ by adding NH_3 suggests that CF_2 radicals react directly with NH_3 to form a key product, which is responsible for the formation of CF_3H via some subsequent process. The reaction and subsequent process may be as follows.

$$CF_2 + NH_3 \rightarrow HCF_2NH_2 \quad (6)$$

$$CF_2 + HCF_2NH_2 \rightarrow CF_3H + HCFNH \quad (7)$$

A further reaction of CF_2 with HCFNH will give CF_3H and HCN.

$$CF_2 + HCFNH \rightarrow CF_3H + HCN$$

The relative yield of CF_3H to the yield of C_2F_4 tends to increase with increasing pulse number, as shown in

Table 1. IRMPD of CF_2HCl-NH_3 Mixtures

CF_2HCl Torr	NH_3 torr	Pulse number	Fluence[a] J cm^{-2}	$Y(C_2F_4)$	$Y(CF_3H)$	$\beta(C_2F_4)$	$\beta(CF_3H)$	Y(C) per pulse
1.0	0	1000	31	3.4×10^{-8}	0	30	—	6.8×10^{-11}
1.0	1.0	200	25	4.2×10^{-8}	Small	19	b)	4.2×10^{-10}
5.0	0	1000	30	1.7×10^{-6}	0	21	—	3.4×10^{-9}
5.0	5.0	100	28	4.0×10^{-7}	3.5×10^{-8}	18	b)	8.4×10^{-9}
10.0	0	1000	26	5.0×10^{-6}	0	17	—	1.0×10^{-8}
10.0	10.0	30	19	4.9×10^{-7}	2.6×10^{-7}	12	9	4.2×10^{-8}
10.0	10.0	100	26	2.1×10^{-6}	9.8×10^{-7}	8	8	5.1×10^{-8}
10.0	10.0	200	27	3.9×10^{-6}	2.1×10^{-6}	7	8	5.0×10^{-8}

a) Fluence at focus. b) Selectivity could not be determined because of a small yield of CF_3H.

Fig. 2. This fact seems to indicate that the accumulation of a certain compound during pulse irradiation causes the observed preferential formation of CF_3H in a late period. However, we failed to detect directly HCF_2NH_2 by gas chromatography.

CF_2HCl is one of the most promising working molecules in ^{13}C separation by IRMPD. Gauthier et al. have reported that the irradiation of 100 Torr natural CF_2HCl with the CO_2 laser radiation at 1046.9 cm^{-1} and 3.5 J cm^{-2} yields C_2F_4 containing 50% ^{13}C at the efficiency that an absorption of 140 photons produces one carbon atom.[9] Therefore, a 100-watt CO_2 TEA laser can produce carbon at rate of 1.3 g h^{-1}, if 50% of the laser radiation is absorbed by CF_2HCl. Although the production rate is sufficiently high in their experiment, the ^{13}C content must be increased to 90% or higher for practical purposes. In the previous paper we have proposed the two-stage IRMPD separation of ^{13}C using CF_2Cl_2-HI and CF_2ClBr-HI mixtures, where the first IRMPD gives CF_2HCl with a ^{13}C content of about 30% and the second IRMPD of the CF_2HCl is expected to result in the production of highly enriched ^{13}C. Since CF_2ClBr decomposes at low laser fluences, one can obtain a relatively high yield of CF_2HCl in the CF_2ClBr-HI mixture. The production of 90% ^{13}C from the CF_2HCl with a ^{13}C content of about 30% corresponds to a separation process with an enrichment factor of only 21.

Table 1 tabulates yields and enrichment factors for the IRMPD of CF_2HCl in the presence of NH_3. The results clearly demonstrate that a total carbon yield per pulse increases significantly by adding NH_3 without a large loss of selectivity. The effect may be useful for the second stage in the IRMPD separation of ^{13}C using a CF_2ClBr-HI mixture.

References

1) V. S. Letokhov, "Nonlinear Laser Chemistry," Springer-Verlag, New York (1983), Chaps. 5 and 6.

2) T. Ooyama and S. Arai, *Rev. Laser Eng.*, **10**, 173 (1982).

3) S. Arai, Y. Ishikawa, and T. Ooyama, *Rev. Laser Eng.*, **13**, 707 (1985).

4) M. Kamioka, S. Arai, Y. Ishikawa, S. Isomura, and N. Takamiya, *Chem. Phys. Lett.*, **119**, 357 (1985).

5) M. Kamioka, Y. Ishikawa, H. Kaetsu, S. Isomura, and S. Arai, *J. Phys. Chem.*, **90**, 5727 (1986).

6) A. Outhouse, P. Lawrence, M. Gauthier, and P. A. Hackett, *Appl. Phys., B*, **36**, 63 (1985).

7) M. Drouin, M. Gauthier, R. Pilon, P. A. Hackett, and C. Willis, *Chem. Phys. Lett.*, **60**, 16 (1978).

8) T. Watanabe, T. Ooyama, O. Hayashi, Y. Ishikawa, T. Ishii, and S. Arai, *Nippon Kagaku Kaishi*, **1984**, 1517.

9) M. Gauthier, C. G. Cureton, P. A. Hackett, and C. Willis, *Appl. Phys. B*, **28**, 43 (1982).

10) G. I. Abdushelishvili, O. N. Avatkov, V. N. Bagratashvili, V. Yu. Baranov, A. B. Bakhtadze, E. P. Velikhov, V. M. Vetsko, I. G. Gverdtsiteli, V. S. Dolzhikov, G. G. Esadze, S. A. Kazakov, Yu. R. Kolomiiskii, V. S. Letokhov, S. V. Pigul'skii, V. D. Pis'mennyi, E. A. Ryabov, and G. I. Tkeshelashvili, *Sov. J. Quantum Electron*, **12**, 459 (1982).

11) S. Arai, T. Watanabe, Y. Ishikawa, T. Ooyama, O. Hayashi, and T. Ishii, *Chem. Phys. Lett.*, **112**, 224 (1984).

12) M. Gauthier, A. Outhouse, Y. Ishikawa, K. O. Kutschke, and P. A. Hackett, *Appl. Phys., B*, **35**, 173 (1984).

13) P. Ma, K. Sugita, and S. Arai, *Chem. Phys. Lett.*, **137**, 590 (1987).

14) K. Sugita, Y. Ishikawa, and S. Arai, *J. Phys. Chem.*, **87**, 3469 (1983).

15) K. Sugita, Y. Ishikawa, and S. Arai, *Appl. Phys. B*, **36**, 111 (1985).

16) A. V. Evseeu, V. S. Letokhov, and A. A. Puretzky, *Appl. Phys., B*, **36**, 93 (1985).

17) N. Bloembergen and A. H. Zewail, *J. Phys. Chem.*, **88**, 5459 (1984).

18) E. Grunwald, K. J. Olszyna, D. F. Dever, and B. Knishkowy, *J. Am. Chem. Soc.*, **99**, 6515 (1977).

19) G. R. Barnes, R. A. Cox, and R. F. Simmons, *J. Chem. Soc. B*, **1971**, 176.

20) J. L. Franklin, J. G. Dillard, H. M. Rosenstock, J. T. Herron, and K. Drax, NSRDS-NBS26, Nat. Bur. Stand. (U.S.), 1969.

 © 1987 The Chemical Society of Japan Bull. Chem. Soc. Jpn., 60, 4223—4228 (1987)

Monolayer Formation of Dilauroylphosphatidylcholine at the Polarized Nitrobenzene-Water Interface

Takashi KAKIUCHI, Masataka YAMANE, Toshiyuki OSAKAI, and Mitsugi SENDA*
Department of Agricultural Chemistry, Faculty of Agriculture, Kyoto University, Sakyo-ku, Kyoto 606
(Received April 27, 1987)

Double layer capacitance of the polarized nitrobenzene-water interface has been measured in the presence of the adsorption of L-α-dilauroylphosphatidylcholine (DLPC). The double layer capacitance was lowered with the increase of the DLPC concentration in the negative branch of the potential range where the aqueous phase was in negative potential with respect to the nitrobenzene phase. A saturated monolayer of DLPC was formed at a concentration of DLPC above 20 $\mu mol\,dm^{-3}$. The area occupied by a DLPC molecule at the saturated monolayer was 0.73 nm^2 which was estimated by comparing the capacitance data with those obtained from a spread monolayer of DLPC at the interface. In the negative branch the monolayer was stable over 100 mV of the applied potential across the monolayer. The adsorption was described by the Frumkin adsorption isotherm. The interaction between the adsorbed DLPC molecule was weak, corresponding to the penetration of nitrobenzene molecules and, possibly, ions between the hydrocarbon chains of DLPC. This penetration also explains the high capacitance value of 11 $\mu F\,cm^{-2}$ for the saturation monolayer. In the potential range where the aqueous phase is positive, the capacitance increased with the DLPC concentration.

Recent advances in electrochemistry of the oil-water interface have established the basic experimental methods and the relevant theories for studying the ion-transfer processes taking place at the interface.[1-4] Based on this recent achievement a quantitative study of the effect of an adsorbed monolayer of phospholipids and related compounds on ion transfer processes across the oil-water interface has now become possible. It is expected to provide fundamental information for a better understanding of the mass-transfer processes occurring at biological as well as artificial membranes. Koryta et al.[5] have reported that the ion-transfer reaction at the nitrobenzene-water interface became irreversible in the presence of lecithin in the nitrobenzene phase. Similar retardation of ion-transfer reaction has also been found for the tetraethylammonium ion transfer across the 1,2-dichloroethane-water interface in the presence of egg yolk lecithin.[6] However, in these studies the state of the adsorbed lecithins at the interface was not characterized enough to investigate in depth the mechanism of the retardation of the ion-transfer rate. Even the formation of a monolayer at the interface has not been confirmed. The purpose of the present communication is to establish the condition of the monolayer formation of phosphatidylcholine at the nitrobenzene-water interface, which is essential to the detailed study of the double layer structure and ion-transfer processes across lipid monolayers. We have studied the monolayer formation using L-α-dilauroylphosphatidylcholine (DLPC). This phospholipid monolayer is also expected to serve as a model particularly useful for studying ion-phospholipid interactions, since at polarized oil-water interfaces the structure of the electrical double layer can be studied in detail by electrocapillary measurements. Watanabe et al. have studied the adsorption of phospholipids at the methyl isobutyl ketone-water interface and have elucidated interesting qualitative features of phospholipid adsorption including the effect of pH on the aqueous solution side.[7-9] Their studies are mainly concerned with the effect of foreign substances as well as solution pH rather than the adsorption properties of the phospholipid monolayer itself. Recently, Girault and Schiffrin[10] have reported the adsorption behavior of phosphatidylcholine and phosphatidylethanolamine at the polarized 1,2-dichloroethane-water interface by measuring electrocapillary curves. In the present study, we have measured the differential capacitance of the polarized nitrobenzene-water interface in the presence of phosphatidylcholine monolayers formed by the two methods: i.e. adsorbed monolayer and spread monolayer.

Experimental

DLPC was obtained from Sigma Ltd. and was used without further purification. Tetrapentylammonium tetraphenylborate (TPnATPB) was prepared from tetrapentylammonium iodide and sodium tetraphenylborate and was twice recrystallized from acetone-ethanol mixture. Aqueous solution of reagent grade tetrapentylammonium chloride (TPnACl) was treated with silver chloride to remove trace iodide ion. Lithium chloride monohydrate (a Merck's Spurapur grade) was dissolved in water to prepare the stock solution. The concentration of TPnACl and LiCl solutions were determined by potentiometric titration with a standard silver nitrate solution. Nitrobenzene was distilled under reduced pressure. The middle 60% of the distillate was shaken with active alumina and then equilibrated with water after filtrating off the precipitates. Triply distilled water was used throughout the measurements. All other chemicals used were of reagent grade.

The electrochemical cell is represented by:

I	II	III	IV	V	VI	VII
		50 mmol dm^{-3}	0.1 mol dm^{-3}	0.1 mol dm^{-3}		(I)
Ag	AgCl	TPnACl	TPnATPB	LiCl	AgCl	Ag
		(W)	(NB)	(W)		

The interface between Phases IV and V is the polarized nitrobenzene-water interface. The potential of the right-hand side of the cell with respect to the left is denoted as E_{O+}^{W-}, where super- and subscripts, W− and O+, indicate that the right-hand and left-hand side reference electrodes are reversible to an anion, Cl^- ion in Phase V, and a cation, $TPnA^+$ ion in Phase IV, respectively.

A flat polarized nitrobenzene-water interface was formed at the orifice of a glass tube of 0.548 cm inner diameter. Other details of the measuring cell have been described elsewhere.[11] The double layer capacitance was measured by phase-selective ac polarography. The principle of the method and the type of measuring cell have been described previously.[11] An ac voltage of 50.0 Hz and 5 mV^{p-p} was superimposed on the dc voltage. In the adsorption method ac polarograms were usually recorded with a scan rate of 5 $mV\,s^{-1}$ from E_{O+}^{W-}=0.15 to 0.48 V. No change was observed in the shape of the polarogram if recorded with a scan rate of 0.5 $mV\,s^{-1}$ or if the sweep direction was reversed. In the spread method, the impedance was measured at a fixed potential as a function of time. All measurements were made at 25.0±0.5 °C.

A monolayer of DLPC at the interface between Phases IV and V was made in two ways: The formation of the monolayer by adsorption of DLPC from nitrobenzene phase (the adsorption method) and by placing a known amount of DLPC as a toluene-chloroform solution on the interface (the spread method). In the adsorption method a nitrobenzene solution of DLPC was prepared by adding a needed amount of 10 $mmol\,dm^{-3}$ chloroform solution of DLPC to 0.1 $mol\,dm^{-3}$ TPnATPB nitrobenzene solution with a micro syringe. The mixture was then sonicated at 27 °C to dissolve the added DLPC completely. Without this sonication treatment small particles persisted in the solution and sometimes gave rise to a characteristic peak in the far positive potential range in a capacitance vs. potential curve. In the spread method phosphatidylcholine was first dissolved in 3:2 (v/v) toluene-chloroform mixture to prepare the stock solutions of various concentrations. The 3:2 toluene-chloroform mixture has a density of 1.1, which is smaller than that of the nitrobenzene solution, 1.18, and larger than that of the aqueous solution, 1.0, and was used as a spreading solvent to avoid undesirable mixing due to density difference. This mixed solvent itself introduced no detectable change in the double layer capacitance. The DLPC solutions for the spreading method were stored in a decicator containing the solvent of the same composition in the bottom compartment. On spreading DLPC at the interface the solution of 1×10^{-6} dm^3 was applied through an L-shaped fine glass capillary of 0.55 mm inner diameter which was connected to a 1×10^{-5} dm^3 micro syringe mounted on a micro manipulator. The tip of the capillary was drawn out to a sharp conical shape with an orifice of 0.15 mm inner diameter. First the capillary was inserted in the nitrobenzene solution beneath the interface. Then the tip was brought up through the interface into the aqueous solution side just above the interface and a few tenths of 1×10^{-6} dm^3 DLPC solution were squeezed out of the tip of a micro syringe to form a small "bubble" at the tip. The tip was then brought down slowly to a position just beneath the interface. The "bubble" spontaneously spread away over the interface while the tip was passing through the interface. This procedure was repeated several times to complete the spreading of 1×10^{-6} dm^3 DLPC solution. The time needed for the spreading procedure was typically 30 s. The time at the completion of the final spreading was taken as t=0 for the later analysis of the data. After the spreading, the interface was brought down in close proximity to the glass frit of the reference electrode compartment. The shape of the interface was then readjusted to obtain a flat interface. The solution resistance was then measured promptly. This resistance measurement was made every time before an impedance measurement. Usually it took 0.5—1.5 min from the completion of the spreading to the start of the impedance measurement.

Results and Discussion

Adsorbed Monolayer. The double layer capacitance of the interface was measured in the potential range between E_{O+}^{W-}=0.15 and 0.48 V for ten different concentrations of DLPC from c=0.1 to 100 $\mu mol\,dm^{-3}$. The time required to attain adsorption equilibrium was checked by measuring the capacitance as a function of time. Figure 1 illustrates the time dependence of the capacitance at c=5 $\mu mol\,dm^{-3}$ and at E_{O+}^{W-}=0.20 V after the formation of a new nitrobenzene-water interface at the orifice of the glass tube. In this case, Fig. 1 shows that at least 60 min was needed to reach a time invariant value. We recorded ac polarograms to obtain the capacitance (C) vs. potential (E_{O+}^{W-}) curves after a sufficiently long time, usually 60 min, had elapsed. Some of the results are shown in Fig. 2. The vertical bars in the figure show the standard errors for the triplicate measurements. The capacitance decreased with the concentration of DLPC in the range of E_{O+}^{W-} between 0.15 and 0.35 V as shown in Fig. 2, indicating the strong adsorption of DLPC at the interface. At a concentration higher than 20 $\mu mol\,dm^{-3}$, the capacitance showed no further decrease. This probably corresponds to the formation of a saturated monolayer in this potential range. The minimum capacitance value for this saturated monolyer was 11 $\mu F\,cm^{-2}$ at E_{O+}^{W-}=0.24 V. This is significantly higher than the value, ca. 1 $\mu F\,cm^{-2}$ found in bilayer lipid membrane.[12] If the monolayer is only a half of a bilayer lipid membrane, the capacitance would be at least one fifth of the measured value. The observed high capac-

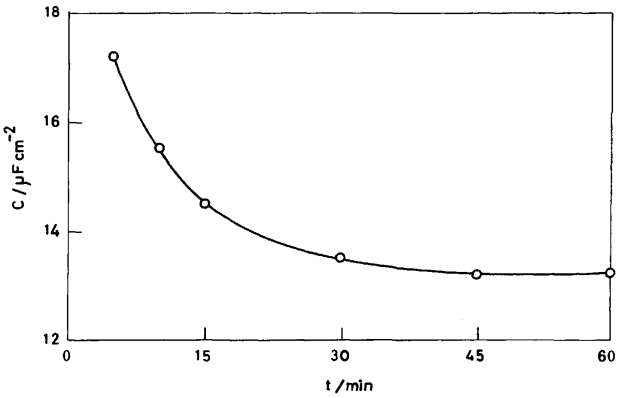

Fig. 1. Change of the double layer capacitance with time for 5 $\mu mol\,dm^{-3}$ DLPC at E_{O+}^{W-}=0.20 V.

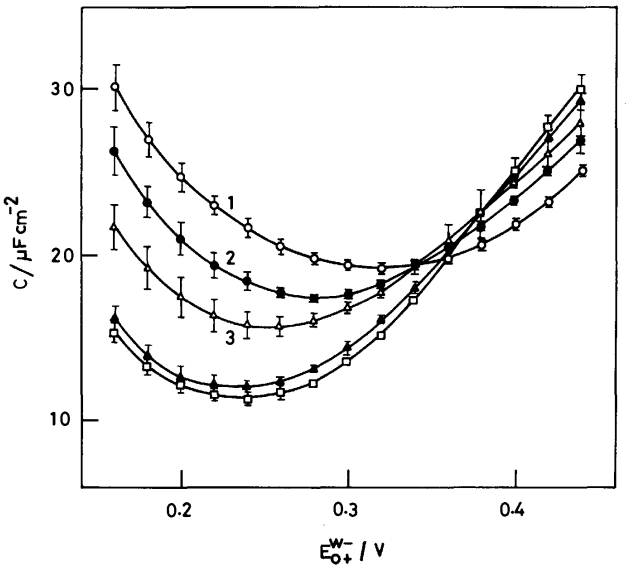

Fig. 2. Equilibrium double layer capacitance vs. applied potential curves recorded by the adsorption method for a given concentration of DLPC: 0(○), 1(●), 2(△), 10(▲), and 50(□) μmol dm^{-3} in nitrobenzene.

itance presumably reflects the penetration of solvent nitrobenzene molecules and, possibly, $TPnA^+$ and TPB^- ions into the hydrocarbon chain part of the monolayer, resulting in the higher effective dielectric constant of the monolayer.

At potentials positive to 0.35 V, the capacitance increased with the DLPC concentration. Since the potential of zero charge for the base solutions, $E^{W-}_{O+,pzc}$, is 0.34 V,[13] the results in Fig. 2 indicate that DLPC exhibits asymmetrical adsorption behavior with respect to the potential drop across the interface. There is a decrease of the capacitance with increasing concentration of DLPC in the negative branch, that is, at $E^{W-}_{O+} < E^{W-}_{O+,pzc}$, but an increase of the capacitance with DLPC concentration in the positive branch, that is at $E^{W-}_{O+} > E^{W-}_{O+,pzc}$ Such a dependence of the adsorption of phospholipid at the oil-water interface may be of importance in relevance to the dependence of physicochemical properties of biological and artificial membranes on the trans-membrane potential. Change of the adsorbed state of phosphatidylcholines with the applied voltage has also been observed at the mercury-solution interface.[14,15]

Spread Monolayer. To confirm the formation of a DLPC monolayer at the interface, we have measured the double layer capacitance after spreading a known amount of DLPC at the interface. After the spreading of the DLPC solution, the capacitance in the negative branch continuously increased with time owing to the desorption of DLPC molecules from the interface to the nitrobenzene phase. The capacitance value at E^{W-}_{O+}=0.24 V is plotted against the square root of time in Fig. 3. The straight line in Fig. 3 up to 900 s indicates that the desorption of DLPC is diffusion

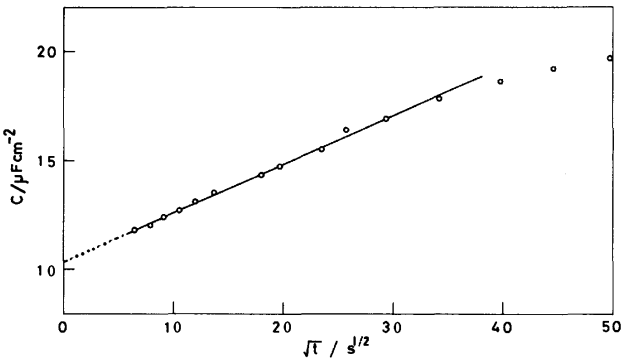

Fig. 3. Change of the double layer capacitance with time at E^{W-}_{O+}=0.240 V after spreading 1×10^{-6} dm^3 of 80 μmol dm^{-3} DLPC in 3:2 toluene-chloroform mixture.

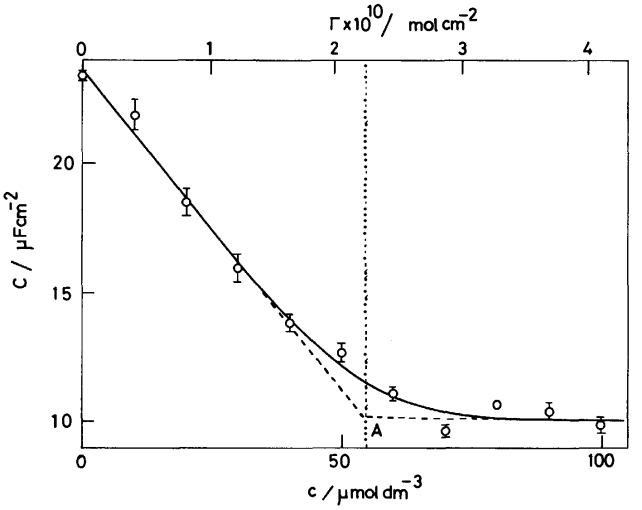

Fig. 4. Extrapolated double layer capacitance at t=0 and at E^{W-}_{O+}=0.240 V as a function of the concentration of DLPC in spreading solution at the interface. Upper scale indicates the calculated amount of DLPC to be present at the interface.

limited.[16] By extrapolating the initial straight line in Fig. 3 to t=0 we obtained the capacitance value at which a known amount of DLPC was supposed to be spread at the interface. The capacitance at t=0 thus obtained at E^{W-}_{O+}=0.24 V is plotted in Fig. 4 as a function of the DLPC concentration in the spreading solution. The upper scale in Fig. 4 indicates the spread amount of DLPC, Γ, in mol cm^{-2} unit calculated by assuming that the whole DLPC molecules contained in the spreading solution participated in the monolayer formation. The vertical bars show the standard errors for the triplicate measurements. The capacitance first decreased linearly with Γ and then reached a saturation value of 10.5 μF cm^{-2} at c=80 μmol dm^{-3} of the spreading solution. This linear change of the capacitance is in accord with Eq. 1,[17] which is based on the Frumkin's parallel plate condenser model:

$$C = C'\theta + (1-\theta)C^0 \quad (1)$$

where C^0 and C' are the C values at θ=0 and 1, respec-

tively, and θ is the surface coverage. At the concentrations of DLPC in the spreading solution above 80 μmol dm^{-3} there was no further decrease in the capacitance, indicating the formation of a saturated DLPC monolayer at the interface. If Eq. 1 holds at any value of θ, the two straight parts of the curve in Fig. 4 should cross each other at Point A. The deviation of the experimental curve from Point A indicates that at higher coverage certain portion of the spread DLPC molecules escaped from the interface and did not take part in the monolayer formation. Only after an excess of DLPC was applied, did the surface seem fully covered with the DLPC molecules as envisaged by the saturation of the capacitance value in Fig. 4. Hence, it would be reasonable to adopt a value of Γ at Point A in Fig. 4 for estimating the packing density of the saturated monolayer. The Γ value at Point A is 2.3×10^{-10} mol cm^{-2}, which corresponds to the area occupied by a DLPC molecule being 0.73 nm^2. This value is close to that for a lecithin bilayer in a liquid crystal phase. In the case of a bilayer composed of dipalmitoylphosphatidylcholine in the presence of excess water, the area was found to be 0.7 nm^2 at temperatures above the critical temparature, T_c=41 °C, whereas the area becomes 0.48 nm^2 at temperatures below T_c.[18] On the other hand, when the area per molecule in the monolayer at the air-water interface is 0.70 nm^2/molecule, didecanoyl- and dimyristoylphosphatidylcholines take on a liquid-expanded state at 25 °C.[19] The present result, therefore, indicates that the saturated DLPC monolayer formed at the nitrobenzene-water interface is in the liquid-expanded state and the DLPC molecules in the monolayer are as dense as the packing of the phosphatidylcholine molecules in the bilayer above T_c. It has been established that in a mesomorphic lamellar phase above T_c, the hydrocarbon chains are in a melted and liquid-like state.[20] This is in harmony with the interpretation for the high capacitance value of DLPC monolayer described above. In the liquid-expanded monolayer the hydrocarbon chains are melted and in a highly fluid and mobile state.[20] In contrast, a more dense liquid-condensed or solid monolayer would give a much lower capacitance value, since in such a membrane the solvent molecules and ions can not be accommodated in the hydrocarbon part which is in a crystaline state. Phillips[21] has recommended the phosphatidylcholine monolayer at the air-water interface occuping 0.70 nm^2/molecule as the most appropriate for membrane-oriented experiments using the monolayer. In this respect, the DLPC monolayer at the polarized nitrobenzene water interface can be used to study the properties, e.g., transfer of ions across the lipid-water interface, of biological as well as artificial lipid membranes.

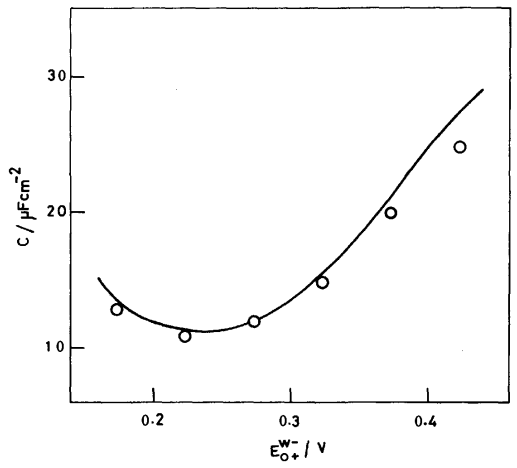

Fig. 5. Comparison of the capacitance data obtained from the adsorption method (—) at 20 μmol dm^{-3} DLPC and the spread method (O). For the spread method, 1×10^{-6} dm^3 of 100 μmol dm^{-3} DLPC was applied to the interface.

In order to check if the monolayer formed by the spread method is the same as that formed in the adsorption method at the higher concentration of DLPC, we compared in Fig. 5 the C vs. E^{W-}_{O+} curve at c=20 μmol dm^{-3} recorded by the adsorption method with the C values at several E^{W-}_{O+} obtained by extrapolating C values to t=0 for the spread monolayer when a DLPC molecule has an area of 0.73 nm^2. The agreement between the values from the two methods is excellent except at the positive extreme of E^{W-}_{O+}. It is clear from this figure that the saturated monolayer formed in the adsorption method is essentially the same as that formed in the spread method. Consequently, a condensed monolayer of DLPC whose occupied area is 0.73 nm^2 can be formed also by the adsorption method, provided that the concentration of DLPC in nitrobenzene is sufficiently high.

Adsorption Isotherm in the Negative Branch. The surface coverage can be estimated using Eq. 1, though this equation is strictly valid only when the change of θ with the electrical potential is negligible,[22] which we assume in the present analysis. This assumption would become inadequate in the positive branch where $d\theta/dE^{W-}_{O+}$ is relatively large. The adsorption isotherm obtained at E^{W-}_{O+}=0.24 V is shown with error bars in Fig. 6. In the calculation of θ we took the C values

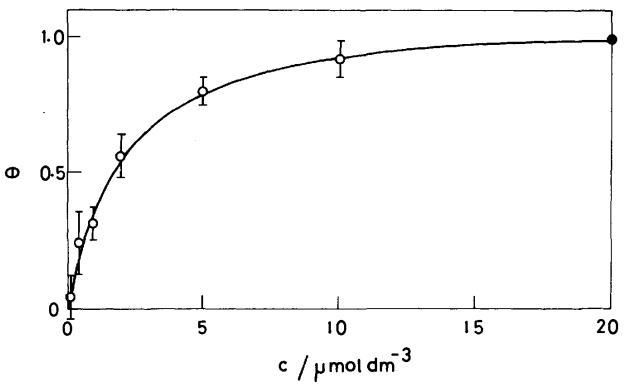

Fig. 6. Adsorption isotherm for DLPC at E^{W-}_{O+}= 0.24 V.

for c=20 mol dm^{-3} as C' in Eq. 1. Similarly, isotherms were obtained at the potentials between E^{W-}_{O+}=0.18 and 0.26 V. These isotherms were analyzed by using the Frumkin isotherm of the form:[17]

$$\beta c = \frac{\theta}{1-\theta}\exp(-2a\theta) \qquad (2)$$

where β is the adsorption coefficient, c is the concentration of phosphatidylcholine, and a is the interaction parameter. Figure 7 illustrates $\ln[\theta/\{c(1-\theta)\}]$ vs. θ plot at E^{W-}_{O+}=0.24 V to test this isotherm. Vertical bars in the figure show the standard error which was calculated from the experimental error in the capacitance measurements taking account of the error propagation. The solid line in Fig. 7 is the curve calculated through the weighted linear regression. The experimental isotherm can thus be fitted well to the Frumkin isotherm. From the intercept and the slope of this regression curve, $\ln\beta$ and the interaction parameter were found to be -1.1 ± 0.3 and -0.28 ± 0.05, respectively, where the intervals designate standard errors. Similar fittings were obtained for the data between E^{W-}_{O+}=0.18 and 0.26 V. The $\ln\beta$ and a values are plotted in Fig. 8 as a function of E^{W-}_{O+}. The vertical bars in the figure indicate the standard errors. In the potential range examined, neither $\ln\beta$ nor a depend strongly on the potential. In other words, DLPC forms a stable monolayer in the potential range of about 100 mV between E^{W-}_{O+}=0.18 and 0.26 V, irrespective of the change of the electrical potential difference across the interface. This greatly simplifies the interpretation of the data when studying the ion-transfer reaction across the DLPC monolayer in this potential range. The average value of $\ln\beta$, -1.1, is equivalent to the standard adsorption energy of 37 kJ mol^{-1}, if we choose 1 mol dm^{-3} and θ=1 for the standard states in the nitrobenzene and in the adsorption layer, respectively. This value of the standard adsorption energy is approximately four times greater than that for the adsorption of hexadecyltrimethylammonium ion at the nitrobenzene-water interface in similar polarization potential range.[23] The small α value, 0.25 on average, means a weak attractive interaction between the adsorbed DLPC molecules. The observed weak interaction is probably due to the penetration of nitrobenzen molecules between the hydrocarbon chains of the phosphatidylcholine molecules resulting in reduced cohesion between the chains. The reduced interaction between hydrocarbon chain is manifested by the behavior of phosphatidylcholines at the oil-water interface: Mingins et. al.[24] have found that diacylphosphatidylcholines having hydrocarbon chains shorter than C_{14} do not show a characteristic phase transition at the heptane-water interface between 5 and 20 °C.

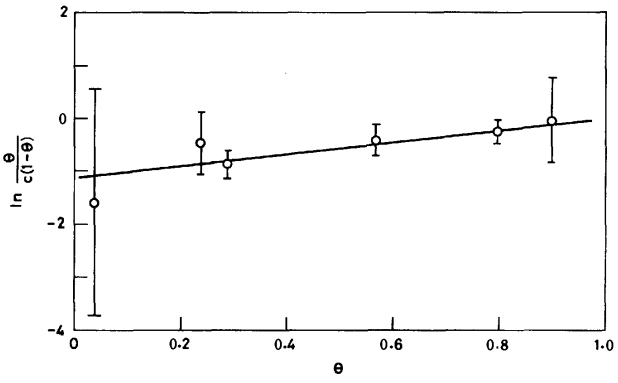

Fig. 7. Test of the Frumkin isotherm for the adsorption of DLPC at E^{W-}_{O+}=0.24 V.

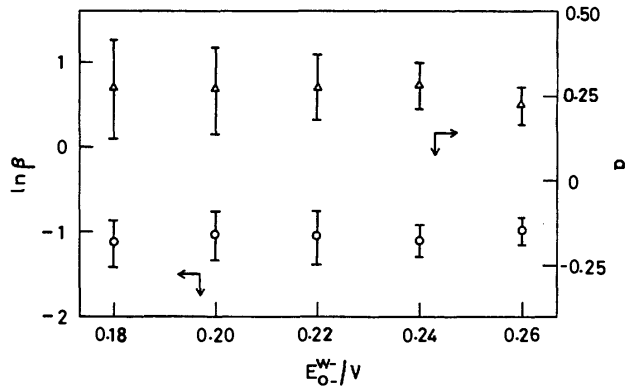

Fig. 8. Logarithm of the adsorption coefficient (○) and the interaction parameter (△) of the Frumkin isotherm for the adsorption of DLPC as a function of the electrical potential.

Adsorption in the Positive Branch. According to our prelimimary results of the interfacial tension measurements, the interfacial tension in this potential region showed a tendency to recover from the extremely low value in the more negative potential range, but still remains lower than the interfacial tension for the base solution. A similar change of the interfacial tension with the applied potential has been observed by Girault and Schiffrin[6,10] at the 1,2-dichloroethane-water interface. Consequently, the observed increase of the capacitance in Fig. 2 may be ascribed to the change of the orientation of adsorbed DLPC molecules, possibly accompanied by a partial desorption with the change of the electrical potential difference across the interface. The concomitant increase of the real part of the addmittance was observed in the positive branch, suggesting the presence of non-equilibrium processes at the interface.

The authors thank Masatoshi Nakanishi for his assistance in part of the capacitance measurements.

This work was supported by Grant-in-Aid for Scientific Research No. 60211017 from the Ministry of Education, Science and Culture.

References

1) M. Senda and T. Kakutani, *Hyomen*, **18**, 535 (1980).

2) J. Koryta, *Electrochim. Acta*, **24**, 293 (1979); **29**, 445 (1984).

3) See for review up to 1980, J. Koryta and P. Vanysek,

"Advances in Electrochemistry and Electrochemical Engineering," ed by H. Gerischer and C. W. Tobias, John Wiley and Sons, New York (1981), Vol. 12, p. 113.

4) H. H. J. Girault and D. J. Schiffrin, "Electroanalytical Chemistry," ed by A. J. Bard, Marcel Dekker, Submitted.

5) J. Koryta, Le Q. Hung, and A. Hofmanova, *Studia Biophysica*, **90**, 25 (1982).

6) H. H. J. Girault and D. J. Schiffrin, "Charge and Field Effect in Biosystems," ed by M. J. Allen and P. N. R. Usherwood, Abacus Press, England (1984).

7) A. Watanabe, M. Matsumoto, H. Tamai, and R. Gotoh, *Kolloid Z. Z. Polym.*, **228**, 58 (1968).

8) A. Watanabe, A. Fujii, Y. Sakamori, K. Higashitsuji, and H. Tamai, *Kolloid Z. Z. Polym.*, **243**, 42 (1971).

9) A. Watanabe, H. Tamai, and K. Higashitsuji, *J. Colloid Interface Sci.*, **43**, 548 (1973).

10) H. H. J. Girault and D. J. Schiffrin, *J. Electroanal. Chem. Interfacial Electrochem.*, **179**, 277 (1984).

11) T. Osakai, T. Kakutani, and M. Senda, *Bull. Chem. Soc. Jpn.*, **57**, 370 (1984).

12) H. T. Tien, "The Chemistry of Biosurfaces," ed by M. L. Hair, Vol. 1, Chap. 6, p. 239, Marcel Dekker, New York (1972).

13) T. Kakiuchi, M. Nakanishi, and M. Senda, Submitted to Bull. Chem. Soc. Jpn.

14) L. Pospisil, E. Muller, and H. D. Dorfler, *Electrochim. Acta*, **29**, 773 (1984).

15) L. Pospisil, E. Muller, H. Emons, and H. D. Dorfler, *J. Electroanal. Chem. Interfacial Electrochem.*, **170**, 319 (1984).

16) T. Kakiuchi and M. Senda, to be published.

17) B. B. Damaskin, O. A. Petrii, and V. V. Batrakov, "Adsorption of Organic Compounds on Electrodes," Plenum Press, New York (1971), Chap. 3.

18) M. C. Phillips, "Progress in Surface and Membrane Science," ed by J. F. Danielli, M. D. Rosenberg, and D. A. Cardenhead, Vol. 5, p. 139, Academic Press, New York (1972).

19) M. C. Phillips and D. Chapman, *Biochim. Biophys. Acta*, **163**, 301 (1968).

20) D. Chapman, R. W. Williams, and B. D. Ladbrooke, *Chem. Phys. Lipids*, **1**, 445 (1967).

21) Ref. 18, p. 165.

22) M. Senda and I. Tachi, *Rev. Polarography (Kyoto)*, **10**, 89 (1962).

23) T. Kakiuchi, M. Kobayashi, and M. Senda, *Bull. Chem. Soc. Jpn.*, **60**, 3109 (1987).

24) J. Mingins, J. A. G. Taylor, B. A. Pethica, C. M. Jackson, and B. Y. Yue, *J. Chem. Soc., Faraday Trans. 1*, **78**, 323 (1982).

 © 1987 The Chemical Society of Japan Bull. Chem. Soc. Jpn., 60, 4229—4232 (1987)

Shock Tube Studies of the Oxidation of Acetylene in Fuel-Rich Mixtures

Tohru KOIKE* and Kihei MORINAGA
Department of Chemistry, National Defense Academy, Hashirimizu, Yokosuka 239
(Received May 16, 1987)

The oxidation of C_2H_2 in fuel-rich mixtures was studied in the temperature range 1600—2500 K by a shock-tube technique combined with UV absorption spectroscopy. The absorption profile, attributed to both an increase of C_4H_2 and a decrease of C_2H_2, could be modeled with a reaction mechanism comprising 38 elementary reactions. The progress of the oxidation was found to be greatly influenced by the pyrolysis steps of C_2H_2.

The kinetics of C_2H_2 oxidation at high temperatures above 1000 K has been studied in shock waves and flames. The progress of the oxidation was monitored by various measuring techniques and the obtained results have been subjected to discussion concerning the reaction mechanism.

White and Gardiner[1] did a literature survey for C_2H_2 oxidation in shock waves and carried out extensive computer modeling for a reaction employing the reported experimental results. The reaction mechanism adopted was one devised by Olson and Gardiner[2,3] to model CH_4 oxidation in shock waves. The reaction mechanism includes various reaction steps involving the primary products of C_2H_2, C_2H_4, C_2H_6 and CH_2O appearing in CH_4 oxidation. Therefore, it was considered that the reaction mechanism devised for CH_4 oxidation could be applicable to C_2H_2 oxidation. The consequences were not satisfactory for C_2H_2 oxidation nor for other three species oxidations. A completely different reaction mechanism appropriate to each oxidation had to be devised.

Such a conclusion has also been derived from modeling studies of C_2H_2 oxidation in flames by Levy,[4] in which a modified reaction mechanism based on that by Olson and Gardiner[2] was used. One of difficulties in using their reaction mechanism is that the concentration of CH_4 is modeled too large in comparison with the measured value. To improve on these difficulties, he included ketene as an intermediate species produced by a reaction between C_2H_2 and OH,

$$C_2H_2 + OH = C_2H_2O + H \quad (7)$$

$$C_2H_2O + OH = CH_2O + CHO$$

instead of

$$C_2H_2 + OH = CH_3 + CO,$$

where the elementary reactions with numbers exhibit the reactions adopted in the present reaction mechanism of Table 1. His intention is that the two-step decay of C_2H_2 by OH does not give a CH_n group directly and the concentration of CH_4 given by computer modeling does not become as large as modeled above.

Recently, Gardiner's group[5] further studied C_2H_2 oxidation in shock waves by computer modeling for the reported data concerning the ignition delay, including their own data for a laser-schlieren experiment, and the exponential growth. In the derived reaction mechanism, ketene as well as the ketene radical were taken into account:

$$C_2H_2O + OH = C_2HO + H_2O. \quad (9)$$

The assumed product of this reaction is different from the above, i.e., the formyl groups are not produced.

All of the experimental results concerning C_2H_2 oxidation in shock waves reported so far are for fuel-lean mixtures. The role of pyrolysis steps in C_2H_2 oxidation must be small in these experiments. We carried out oxidation in rich mixtures and measured the concentration of C_4H_2 through UV absorption spectroscopy at 216 nm. The obtained absorption profile was subjected to computer modeling using the above-mentioned reaction mechanism. The applicability of the mechanism to the present case was examined.

Experimental

The rectangular shock-tube and optical set-up used were fully described in a previous paper.[6]

Briefly, the light from a D_2-lamp (Hanau, D200F) was detected by a photomultiplier (Hamamatsu, R208) with a monochromator (Jarrell-Ash, JE25) after passing through two shock-tube windows. The test gas compositions used were $C_2H_2/O_2/Ar$=3/1/96 and 5/1/94 prepared from 99.6% pure C_2H_2, 99.99% pure O_2 and 99.999% pure Ar. Hereafter, and in the figure captions, the former mixture is abbreviated as a 3/1 mixture and the latter as a 5/1 mixture. The shock velocity was measured with a universal counter (Takeda-Riken, TR5002) by detecting signals from 4 piezo-gauges (International Transducer, PK16-13) mounted on the shock-tube with a 10-cm spacing. The shock temperature was calculated from the measured shock velocity by assuming a full relaxation and no chemical reaction.

Results and Discussion

Figure 1 shows a representative oscillogram obtained in this study. It can be seen that absorption increases to a maximum value after showing shock front absorption by C_2H_2, and then decreases. The decrease was not observed for C_2H_2/Ar mixtures without O_2.[6] We estimated the absorption A from the oscillogram according to the equation $A=\ln(I_o/(I_o-\Delta I_t))$, where I_o is the incident light intensity and ΔI_t the absorbed

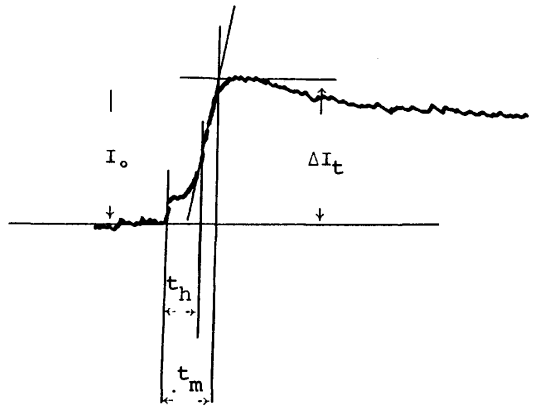

Fig. 1. A sample oscillogram for the 3/1 mixture. P_1=10 Torr and T_2=2114 K. Parameters t_h and t_m used in computer modeling are shown schematically.

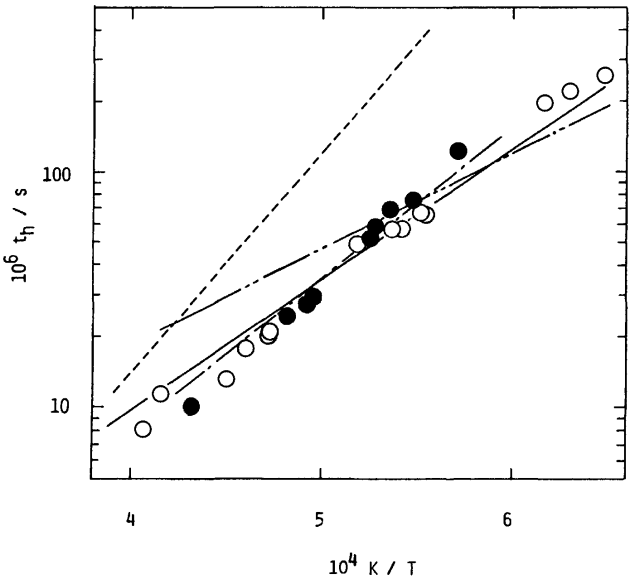

Fig. 2. Relation between t_h and $10^4/T$. Symbols used are: ○ for the 3/1 mixture. ● for the 5/1 mixture. Lines are by computer modeling: (——) for the 3/1 mixture, (–·–·–) for the 5/1 mixture, (– – – –) for the C_2H_2/Ar mixture without O_2.[6] These three lines are modeled using Table 1 reaction mechanism. (–·–··–) for the 3/1 mixture. Ref. 5 reaction mechanism is used.

intensity at reaction time t (laboratory time). The parameter t_h used for computer modeling was derived from this A and defined to be the time when A reaches half of its maximum value. The maximum A are further divided by $[C_2H_2]_0$, the shock front concentration of C_2H_2, so as to be able to compare the values of A directly in different test gas mixtures. These values of t_h and A are plotted vs. $10^4/T$ in Figs. 2 and 3, respectively. In the figures, the values of t_h and A evaluated for the C_2H_2 mixture without O_2 (C_2H_2/Ar= 3.2/96.8) are shown for a comparison.[6] It can be seen that the A for a 3/1 mixture is smaller than that for a 5/1 mixture. This tendency can also be seen in the t_h value. The values for a C_2H_2 mixture without O_2 are

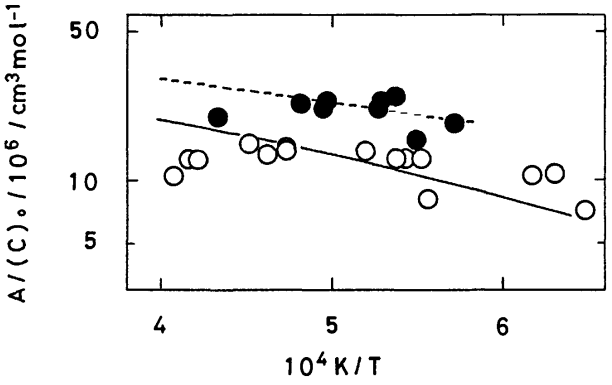

Fig. 3. Relation between A and $10^4/T$. Symbols and lines are the same as in Fig. 2. For the 5/1 mixture, the values are almost the same as those for the C_2H_2/Ar mixture.[6]

much larger than those for 3/1 and 5/1 mixtures.

We adopted computer modeling in order to interpret the measured profile of the absorption more quantitatively and to obtain a reasonable reaction mechanism. We tried it first using the reaction mechanism of Gardiner's group,[5] since the experiments were done under similar conditions to the present. Their mechanism is composed of 23 elementary reactions (Reactions 1—23 in Table 1); the only exception is that k_2 is 1/5 of that in Table 1.[8,9]

It is well-known that absorption is an aggregate by the species present in the reaction region. As for the species in C_2H_2 oxidation. C_2H_2, C_4H_2, CO_2, O_2, C_6H_2, and C_2H_2O are expected to absorb 216-nm light. The absorptions by C_6H_2 and C_2H_2O were, however, neglected in the computer modeling, since absorption data at such high temperatures as the present were not available for these two species. From a former study of C_2H_2 pyrolysis,[6] it is expected that $[C_6H_2]$ only reaches a value less than 1/10 of $[C_4H_2]$. As for the growth of C_2H_2O, it is expected to be small due to the rich mixtures investigated. Thus, ignoring absorptions by these two species does not seem to greatly influence the computer modeling results. The absorptivities of the first 4 species obtained by several workers[6,7] are shown vs. $10^4/T$ in Fig. 4. These absorptivities were incorporated into the present computer program[6] and computations were carried out. The absorption given by $A=\sum a_i[C_i]d$ was evaluated, where a_i and $[C_i]$ are the absorptivity and the concentration of species i, respectively,and d is the light-path length. From the absorption modeling, the two parameters corresponding to the above t_h and A were evaluated. Only the t_h values are plotted in Fig. 2, since the values of A are not very much dependent on the kinetic parameters. It was found that the t_h values by computer modeling are not in accordance with the experimental results.

It is important to determine whether a proposed reaction mechanism can reproduce other experimental results. We carried this out further using one mechanism by Levy[4] and another one by Miller et al.[10] in

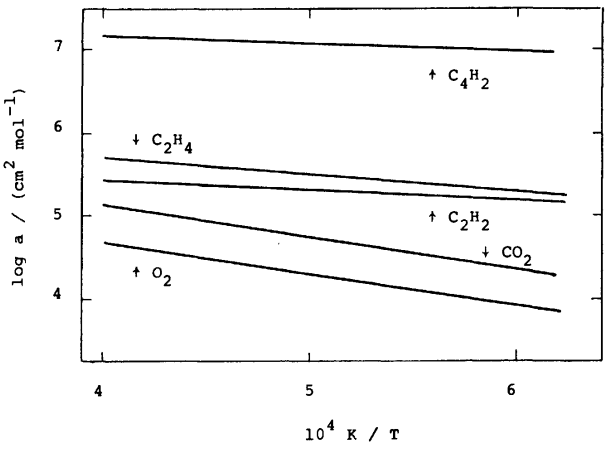

Fig. 4. Absorptivities used in computer modeling.

addition to that by Gardiner's group as above. All of the reaction mechanisms by these three groups include the chemistry of ketene groups. As for the case by Miller et al., they derived the reaction mechanism so as to be able to reproduce both of the experimental results by shock waves and flames. The shock-tube data investigated by them were, however, not adopted in the work by Gardiner's group. Thus, the present modeling plays roles in making up for such a deficiency. As for the modeling results, these two mechanisms by Levy and by Miller et al. were not appropriate for reproducing the present results. The t_h values by Levy's mechanism is larger, like the results by Gardiner's group, whereas the values by the mechanism by Miller et al. is smaller than that from the experiment.

There are two other mechanisms proposed by Jachimowski[11] and by Shaub and Bauer,[12] in which the chemistry of ketene groups is not included. These mechanisms were found not to be appropriate for reproducing the present experimental results.

One of the reasons of such failures in computer modeling could be given as follows. Acetylene in rich mixtures as in the present is expected to decay primarily through pyrolysis steps. Therefore, the k values of the reactions concerning such steps must be adopted with care. We showed in a previous paper[6] that the k_3 value largely depends on the absorption profile and proposed a smaller value than those previously reported. The k_3 value adopted in the three mechanisms by Jachimowski, by Shaub and Bauer and by Miller et al.[10] is the same as proposed by Browne et al.[14] This k_3 value is almost one order larger than the value accepted in the previous paper.[6]

As for the mechanisms by Gardiner's group and by Levy, a reasonable k_3 value is adopted. Therefore, the failure in computer modeling seems to be due to the absence of any important decaying processes of C_2H_2 necessary for rich mixtures. We added Reactions 24—38 to the reaction mechanism by Gardiner's group[5] so as to be appropriate to the present mixtures. This

Table 1. Reaction Mechanism and Rate Constants $k=A\exp(-E/RT)$ (mol, cm, s, and kcal units)

No.	Reaction	log A	E
1	$C_2H_2+M=C_2H+H+M$	16.62	107.00
2	$C_2H_2+C_2H_2=C_4H_3+H$	13.0	45.9
3	$C_2H+H_2=H+C_2H_2$	12.9	2.63
4	$C_2H_2+C_2H=C_4H_2+H$	13.6	0.0
5	$C_2H_2+O=CH_2+CO$	8.61+1.5 log T	1.7
6	$C_2H_2+O=C_2HO+H$	14.63	12.1
7	$C_2H_2+OH=C_2H_2O+H$	14.60	18.6
8	$C_2H_2O+M=CO+CH_2+M$	15.56	57.3
9	$C_2H_2O+OH=C_2HO+H_2O$	13.0	2.7
10	$C_2H_2O+H=C_2HO+H_2$	13.48	8.5
11	$C_2H+O_2=C_2HO+O$	13.0	0.0
12	$C_2HO+H=CH_2+CO$	13.48	0.0
13	$CH_2+O_2=CO_2+H+H$	13.48	1.5
14	$O+H_2=OH+H$	14.34	13.7
15	$OH+H_2=H_2O+H$	13.72	6.5
16	$H+O_2=OH+O$	17.08−0.9 log T	16.63
17	$H_2+M=H+H+M$	12.34+0.5 log T	92.6
18	$H+O_2+M=HO_2+M$	15.4	0.0
19	$HO_2+H=OH+OH$	14.4	1.9
20	$OH+OH=H_2O+O$	13.53	5.0
21	$HO_2+H=H_2+O_2$	13.4	0.7
22	$HO_2+OH=H_2O+O_2$	13.7	1.0
23	$CO+OH=CO_2+H$	12.6	8.0
24	$C_4H_2+O=C_3H_2+CO$	13.43	1.72
25	$C_4H_2+OH=C_3H_2+CHO$	13.48	0.0
26	$C_3H_2+O=C_2H+CHO$	13.83	0.0
27	$C_3H_2+OH=C_2H_2+CHO$	13.83	0.0
28	$C_4H_3+M=C_4H_2+H+M$	16.0	60.0
29	$C_4H_2+M=C_4H+H+M$	17.53	80.0
30	$C_2H_2+C_4H=C_6H_2+H$	13.6	0.0
31	$C_4H_2+C_2H=C_6H_2+H$	13.6	0.0
32	$C_6H_2+M=C_6H+H+M$	16.7	80.0
33	$H+C_4H_2=H_2+C_4H$	13.3	0.0
34	$H+C_6H_2=H_2+C_6H$	13.3	0.0
35	$C_2H_2+OH=C_2H+H_2O$	12.78	7.0
36	$C_2H_2+O=C_2H+OH$	15.5−0.6 log T	15.0
37	$C_4H_2+O=C_4H+OH$	13.0	0.0
38	$C_4H_2+OH=C_4H+H_2O$	13.0	0.0

extended mechanism is the final one determined in this study. By computer modeling with this reaction mechanism, we could reproduce the experimental t_h data shown in Fig. 2.

From the obtained oscillograms, parameters t_m, corresponding to the time when the absorption A reaches a maximum value, were also evaluated and are plotted in Fig. 5 vs. $10^4/T$. The t_m values found by modeling are also shown in the figure for a comparison. This value for t_m has been used as a parameter in previous modeling studies.[6,13] A good agreement between experiment and modeling could be obtained for a 3/1 mixture. For a 5/1 mixture, however, the values by modeling are larger than those by experiment. This incompatibility could not be diminished without greatly disordering the mechanism by Gardiner's group;[5] thus, the k_3 value had to be increased by more than two times. In this case, however, we could not reproduce the other parameter t_h and the t_m in the 3/1 mixture. Therefore, it can be said that the t_m in the 5/1 mixture does not accord with the reaction mechanism

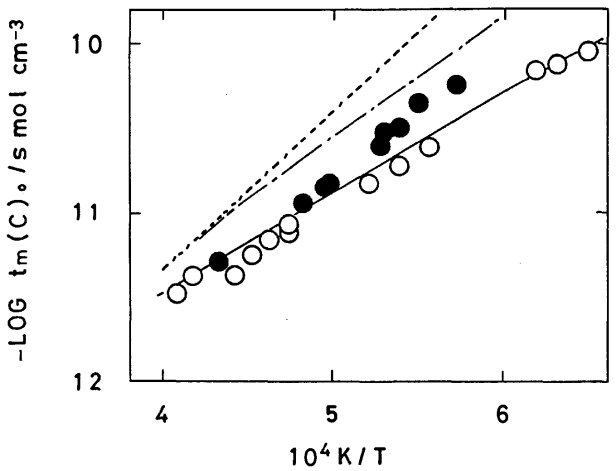

Fig. 5. Relation between t_m and $10^4/T$. Symbols and lines are the same as in Fig. 2.

in Table 1 and remains uninterpretable.

The features of the mechanism shown in Table 1, except for Reactions 1—23, can be described as follows. Reactions 24—27 show the degradation process of C_4H_2 by oxides to smaller hydrocarbons.[15] These reactions, as well as Reactions 37 and 38, seem to be concerned with a decrease in the absorption after exhibiting a maximum value. This can be an evidence to support the idea that the absorption measured in the C_2H_2 mixtures without O_2 did not show a decrease. There have been, however, only a few studies in which the oxidation of C_4H_2 were measured directly. We did not go into this point further and only adopted Reactions 24—27, 37, and 38 as such reactions for the decay of C_4H_2. Reactions 28—34 are concerned with polyacetylenes and polyacetylene radicals. Since the concentrations of these species are modeled to be large, these reactions must be important under the present fuel-rich conditions, as in the pyrolysis of C_2H_2. Abstraction reactions of H atom, 35—38, by an O atom and an OH radical produce acetylene radicals. The number of reaction channels to produce acetylene radicals is larger in the present experiment than that in C_2H_2 pyrolysis. Since the acetylene radicals play roles as chain carriers, the overall reaction rate is expected to become larger in the present experiment. This is in accordance with the measured results of the overall reaction rate given by the reciprocals of t_h and t_m in Figs. 2 and 5. Gardiner's group ignored these reactions as not being important.

As for the reaction mechanism of the oxidation of C_2H_2, Shaub and Bauer[12] referred to two important points differring from the present treatment. One is that the ketene and the ketene radical produced as intermediates were presumed to decompose via unimolecular steps very rapidly. Reactions of the ketene groups were not considered explicitely in their reaction mechanism. The mechanism shown in Table 1 includes not only such steps but also the H atom abstraction reactions by an O atom and an OH radical. The other different point is that they considered reactions involving the CH_2 radical to be unimportant. In Table 1, however, the reaction between CH_2 radical and O_2 was assumed to be the main route to produce CO_2.[5] Reaction 23 has been known as a primary step in producing CO_2 in hydrocarbon oxidation.

In conclusion, the present experimental results could be explained with an extended reaction mechanism based upon that by Gardiner's group.[5] All of the rate constants used were obtained from the existing literature.

References

1) J. N. White and W. C. Gardiner, Jr., *J. Phys. Chem.*, **83**, 562 (1979).
2) D. B. Olson and W. C. Gardiner, Jr., *Combust. Flame*, **39**, 241 (1980).
3) D. B. Olson W. C. Gardiner, Jr., *J. Phys. Chem.*, **81**, 2414 (1977).
4) J. M. Levy, *Combust. Flame*, **46**, 7 (1982).
5) Y. Hidaka, C. S. Eubank, W. C. Gardiner, Jr., and S. M. Hwang, *J. Phys. Chem.*, **88**, 1006 (1984).
6) T. Koike and K. Morinaga, *Bull. Chem. Soc. Jpn.*, **54**, 530 (1981).
7) T. Tsuboi, *Jpn. J. Appl. Phys.*, **14**, 1371 (1975), and references therein.
8) T. Tanzawa and W. C. Gardiner, Jr., 17th Int. Combust. Symp., The Combustion Institute, Pittsburgh (1979), p. 563.
9) T. Koike and K. Morinaga, in preparation.
10) J. A. Miller, R. E. Mitchell, M. D. Smooke, and R. J. Kee, 19th Int. Combust. Symp., The Combustion Institute, Pittsburgh (1982), p. 181.
11) C. J. Jachimowski, *Combust. Flame*, **29**, 55 (1977).
12) W. M. Shaub and S. H. Bauer, *Combust. Flame*, **32**, 35 (1978).
13) W. Gardiner, T. Tanzawa, T. Koike, and K. Morinaga, *Bull. Chem. Soc. Jpn.*, **58**, 1851 (1985).
14) W. G. Browne, R. P. Porter, J. D. Verlin, and A. H. Clark, 11th Int. Combust. Symp., The Combustion Institute, Pittsburgh (1967), p. 1035.
15) J. Warnatz, "Combustion Chemistry," ed by W. C. Gardiner, Jr., Springer-Verlag, New York (1984), p. 197.

Application of the SPE Method to Organic Electrochemistry. VIII. The Incorporation of an Iron Redox Couple into Pt-Nafion and Its Behavior as a Mediator

Zempachi OGUMI,* Toshiyuki MIZOE, Naoki YOSHIDA, and Zen-ichiro TAKEHARA
Department of Industrial Chemistry, Faculty of Engineering, Kyoto University, Sakyo-ku, Kyoto 606
(Received 26 May, 1987)

Fe^{2+} and Fe^{3+} were incorporated into Pt-Nafion. The full incorporation of Fe^{2+} into H^+-type Nafion was attained beyond 0.3 M† $FeSO_4$. The ion-exchange selectivity of Fe^{2+} was estimated to about 2 to H^+. The incorporated ions exhibited diffusional behavior inside the composite electrode. The formal potential of the incorporated iron(III/II) redox couple was dependent on both the H_2SO_4 and the Fe^{3+} and Fe^{2+} concentrations. The potential shift was, however, not so large as that reported on some redox systems on polymer-coated electrodes. The incorporated redox couple was revealed to behave as a mediator in the oxidation of L-ascorbic acid.

The present authors have investigated the application of the SPE method to organic electrochemistry[1,2] using Nafion as an SPE material. Electroorganic syntheses mediated by a redox system are very attractive and have been investigated by many workers. The present authors also attempted to utilize some redox mediators in an SPE electrolyzer, though only mediators dissolved in a solution were used.[3,4] The fixing of a mediator system into an SPE composite electrode would facilitate the separation process after an electrolysis and would demand only a small amount of the mediator. These advantages enable one to use an expensive mediator. In this work, the use of a redox mediator fixed in an SPE composite electrode prepared by the electroless deposition of Pt on Nafion (Pt-Nafion) was preliminarily examined using an iron-redox system.

Pt-Nafion has inherently the structure of a Nafion-coated electrode. Many workers have investigated Nafion-coated electrodes prepared by the casting of a Nafion solution.[5,6] A solution-cast Nafion film does not, however, have the well-known structure of Nafion without curing above 120 °C.[7] On the other hand, nobody would hesitate to accept the reported structure model of Nafion on Pt-Nafion prepared by the electroless plating method under the mild conditions adopted in this work. Pt-Nafion, therefore, may serve as a typical model of an electrode coated with Nafion with a better defined structure. The electrochemical behavior of an iron-redox couple in Pt-Nafion will also be briefly examined.

Experimental

Chemicals. Commercially available chemicals of a reagent grade were used without further purification.

Pt-Nafion Composite Electrodes. Nafion 125, a perfluorinated cation-exchange membrane, was used as an SPE material. Platinum was deposited on one side of the Nafion from chloroplatinic(VI) acid employing an electroless plating method described peviously,[8] using $NaBH_4$ as a reductant. After electroless plating, platinum was further electrolytically deposited in order to decrease the surface ohmic resistivity to less than 0.7 Ω between the two ends of the deposit (3 cm in diameter).

Electrolysis Cell. The SPE composite electrode, with an effective geometric surface area of 3.1 cm^2, was placed in a glass cell described elsewhere.[2] The electrode potential was set vs. the Ag/AgCl reference electrode via a Luggin capillary inserted in a counter-electrode compartment using a potentiostat (Hokuto Denko HA-301). During experiments, argon was introduced into the working-electrode compartment. In all cases, the set potential contained a junction potential at the interface between Nafion and the contacting solution and a fairly large ohmic drop through the Nafion.

Incorporation of Fe^{2+} and Fe^{3+} into Pt-Nafion. After platinum deposition, the Pt-Nafion was immersed in 1M H_2SO_4 for more than 2h in order to change the counter ion into H^+. This H^+-type Pt-Nafion was then immersed in a $FeSO_4$ or $Fe_2(SO_4)_3$ solution of different concentrations under argon purging into the solution.

Amounts of Fe^{3+} and Fe^{2+} Incorporated in Pt-Nafion. A chronoamperometry technique was first used to measure the amount of iron ions in the Pt-Nafion. The decaying current after potential stepping with and without incorporation was integrated. The difference in values with and without the incorporation gave the amount of Fe^{2+} or Fe^{3+} in Pt-Nafion.

Pt-Nafion incorporated with Fe^{2+} or Fe^{3+} was immersed in 2M H_2SO_4 or 0.3M EDTA so that the incorporated Fe^{2+} or Fe^{3+} could be extracted into the solution. The amount of iron ions in the extract was measured by a fluorescent X-ray analysis method using Kelex Ultra-Trace 0600. In some experiments, iron(II) or iron(III) ion was oxidized by H_2O_2 or reduced by L-ascorbic acid[AH_2] respectively during immersion in order to fix the ionic form at Fe^{3+} or Fe^{2+}.

Mediation by Iron-Redox Couple Incorporated in Pt-Nafion. Using a 25 mM AH_2 aqueous solution, the capability of mediation by the iron-redox couple was examined by means of the cyclic voltammetry and potential pulse electrolysis techniques. An AH_2 solution was introduced into either the working or counter-electrode compartment.

Results and Discussion

The Incorporation of Iron Ions into Pt-Nafion. The amounts of Fe^{2+} incorporated into Pt-Nafion from aqueous $FeSO_4$ in various concentrations were

† 1M=1 mol dm^{-3}.

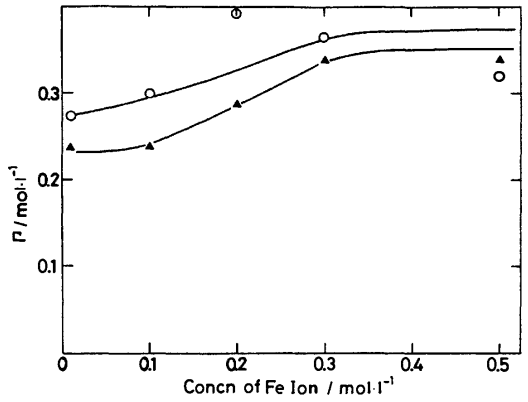

Fig. 1. The amount of Fe^{2+} up-taken into Nafion 125, Γ, by X-ray fluorescence (○) and chronoamperometric (▲) measurements.

measured by means of a chronoamperometry technique and fluorescent X-ray analysis. The incorporated Fe^{3+}/Fe^{2+} showed diffusional behavior, which allowed us to use a chronoamperometry technique in order to estimate the amount of Fe^{2+} in Pt-Nafion. As Fig. 1 shows, the results obtained by the two methods agreed fairly well. The amount reached the ceiling value of about 0.34—0.37 mol dm^{-3}-whole wet resin in a 0.30 M $FeSO_4$ soaking solution. The exchange site concentration of Nafion 125 after standard boiling-water treatment in the H^+ form was estimated as ca. 1 equivalent dm^{-3}-whole wet resin, ca. 3 equivalent dm^{-3}-dry resin. The results obtained here correspond to ca. 0.7 equivalent dm^{-3}-whole wet resin, which is about 70% of the estimated value of a full exchange.

Redox Behavior of Incorporated Fe^{3+} and Fe^{2+} Ions. Incorporated iron ions showed redox behavior on cyclic voltammetry measurements. After a decrease in the current during several initial sweeps, steady voltammograms were obtained. Changing a potential sweep rate, the peak currents were examined on Pt-Nafion placed in contact with 0.025 M H_2SO_4, which had precedingly been equilibrated with 0.25 M $Fe_2(SO_4)_3$. The anodic and cathodic peak currents exhibited a linear dependence on the square root of the sweep rate, suggesting the usual diffusional properties of the redox species existing in the Pt-Nafion and a negligible contribution from a migration effect. On the other hand, a linear dependence of the peak currents on the sweep rate has been reported on many polymer-coated electrodes, including a Nafion coated electrode, and an electron-hopping conduction process has been reported to take place in a Nafion-coating film on electrodes.[6,10] In the present case, however, we need not consider this process, because the Nafion keeps its structure as an ion-exchange membrane in which the conduction is exclusively sustained by the diffusional and migrational movements of ionic species, and so electronic conduction must be insignificant.

The Exchange Selectivity of Fe^{2+}. The increase in the H_2SO_4 concentration at 0.05 M $FeSO_4$ caused a decrease in the anodic peak current on Pt-Nafion incorporated with iron ions. This decrease implies the exchange of H^+ with Fe^{2+} or Fe^{3+} in Pt-Nafion. The exchange selectivity, K, of ion exchange membranes was calculated. Assuming the activity coefficient of Fe^{2+} $\gamma_{Fe}=1$ and using a mean activity coefficient of H_2SO_4 for γ_H, the molar fraction of Fe^{2+} in Pt-Nafion, $\bar{x}$, was calculated. $\bar{x}$ is shown in Fig. 2. Since the $\bar{x}$ calculated assuming $K=2.0$ agrees well with the experimental results, we obtained the selectivity constant of 2.0 for Fe^{2+} in Nafion. The value of $K=2.0$ is acceptable in view of the reported values of 0.97, 1.24, 3.60, and 2.30 for Zn^{2+}, Co^{2+}, Cu^{2+}, and Mg^{2+} respectively.[11]

Formal Potential of the Iron-Redox Couple Incorporated in Pt-Nafion. The formal potential of the iron-redox couple incorporated in Pt-Nafion, E_p^f, was obtained by means of cyclic voltammetry measure-

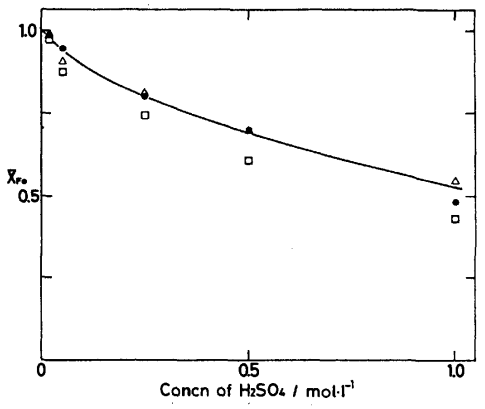

Fig. 2. The dependence of Fe^{2+} molar fraction inside Pt-Nafion, $\bar{x}$, on H_2SO_4 concentration at 0.05 M $FeSO_4$. Solid line; experimental result, Calculated values assuming $K=2.0$ (△) and $K=1.4$ (□).

Table 1. Dependences of the Formal Potential, E^f, on the H_2SO_4 Concentration at 0.05 M $FeSO_4$ on Pt-Nafion and Pt Plate Electrodes

H_2SO_4/M	E^f/mV Pt-Nafion	E^f/mV Pt-plate	ΔE^f/mV
0.005	446	465	−14
0.025	462	468	−6
0.05	460	465	−5
0.25	468	465	+3
0.5	467	461	+6
1.0	486	466	+20

Table 2. Dependences of the Formal Potential, E^f, on the $FeSO_4$ Concentration at 0.025 M H_2SO_4 on Pt-Nafion and Pt Plate Electrodes

$FeSO_4$/M	E^f/mV Pt-Nafion	E^f/mV Pt-plate	ΔE^f/mV
0.005	430	466	−36
0.01	435	464	−29
0.05	453	456	−3
0.1	463	456	+3
0.3	470	450	+20

ments; a set of values are listed in Tables 1 and 2, together with the values in an aqueous solution on a conventional bare Pt electrode, E_s^f. The values were calculated as a middle point between the anodic and cathodic peak potentials. As shown in the tables, the potential difference, $\Delta E^f = E_p^f - E_s^f$, changes from a negative to a positive value with an increase in the H_2SO_4 or Fe_2SO_4 concentration. Some authors have previously noticed a systematic shift of the formal potential of some redox couples incorporated in the polymer coating on electrodes. Braun et al.,[12] for instance, reported a very big potential shift of $[Fe(CN)_6]^{3-/4-}$ (over 200 mV) incorporated in an anion-exchange layer on glassy carbon. Tsou and Anson[13] examined the shift of the formal potential of some redox couples using pyrolytic graphite electrodes covered with Nafion or a polymerized perfluorinated calboxylic acid type cation exchanger. They observed a negative ΔE^f for the more hydrophobic redox couples, $[Ru(NH_3)_6]^{3+/2+}$ and positive ΔE^f for the more hydrophobic redox couple, $[Os(bpy)_3]^{3+/2+}$. They explained this as follows. In the case of hydrophilic redox couples, the oxidized redox half is stabilized more by the electrostatic interaction with a coating polyelectrolyte than is the reduced redox half. In the case of hydrophobic redox couples, on the other hand, the reduced redox half is stabilized more by the hydrophobic interaction with the coating polyelectrolyte than is the oxidized redox half. They also explained the dependence of the potential shift on the ionic strength as the result of a combination of two interactions in the opposite direction, increased electrostatic interactions at a lower ionic strength, and stronger hydrophobic interactions at a higher ionic strength.

In the present results shown in Tables 1 and 2, however, neither the potential shift nor the change in ΔE^f with the concentration of the outer solution were so large as the value observed by Tsou and Anson. Iron(III) and iron(II) ions are so hydrophilic that the contribution of the hydrophobic interaction with Nafion is insignificant. The change in E^f with the concentration could be ascribed to the change in the Donnan potential, which was not estimated here. The characteristic ionomer structure of Nafion,[11] which is widely accepted, can be directly adopted in the case of Pt-Nafion, while the structure of Nafion on a polymer-coated electrode prepared from liquid Nafion should be dependent on the treatment after coating and might be different from the structure of the membrane Nafion. The ionomer structure of Nafion renders the behavior of the hydrophilic species inside the Nafion similar to that in the homogeneous aqueous phase. This leads to the smaller ΔE^f value on Pt-Nafion than on polymer-coated electrodes prepared from the liquid Nafion.

The redox potential of Fe(III)/Fe(II) is well-known to be affected by an anion in solution. In the present case, some direct effects of a $-SO_3^-$ group of Nafion, such as coordinating to and ion-pairing with redox cations, must be taken into consideration in any further discussion.

Indirect Oxidation of AH_2. From the above results, it seems that the redox potential of Fe(III)/Fe(II) in Nafion dose not differ much from the value in a usual aqueous system; the Fe(III) ion in Nafion can, therefore, be expected to oxidize AH_2 to dehydroascorbic acid.[14]

In the use of SPE composite electrodes incorporated with a redox mediator, two different configurations in the electrolysis system are possible, as is shown in Fig. 3. Case a is a distinguishing configuration for an SPE electrolyzer. In this case, a substrate solution is not required to contain any electrolyte; even neat substrate fluid can be used. Case b is the same configuration as in a usual polymer-coated electrode, though the coating polymer layer is much thicker than on the latter. In Case a, the substrate must be transferred to the reaction site through a thin, porous metal electrode layer. In Case b, the mediator or substrate must pass through a coating Nafion layer.

In the configuration of Case b, the electrode poten-

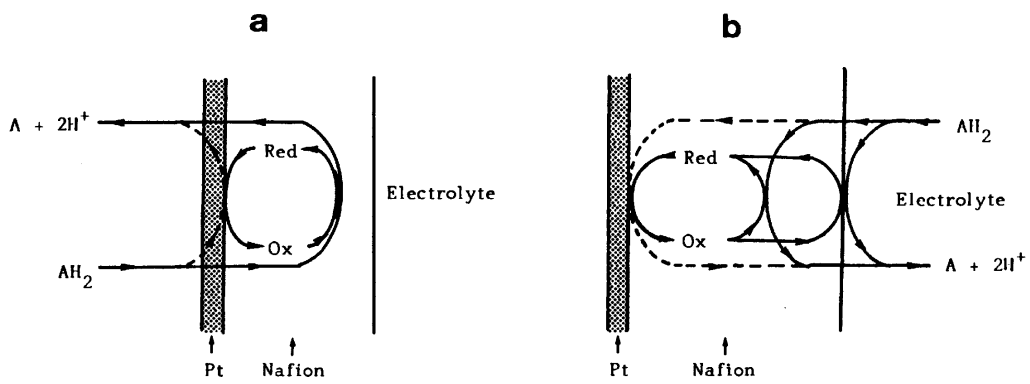

AH_2 : L-ascorbic acid, A : dehydroascorbic acid, Red : Fe^{2+}, Ox : Fe^{3+}

Fig. 3. Schematic diagrams of a mediation reaction by a redox couple incorporated in an SPE composite electrode. a: a substrate is introduced in a working electrode compartment, b: a substrate is introduced in a counter electrode compartment.

tial was stepped from 0.4 to 0.75 V, where the Fe(II) ion was oxidized to the Fe(III) ion. As is shown in Fig. 3 (b), AH_2 can be oxidized by two different courses: The direct oxidation of AH_2 on the Pt electrode bound to Nafion and indirect oxidation by the Fe(III) ion produced by the oxidation of the Fe(II) ion on the Pt electrode at the surface or inside the layer of the Nafion film. In the former, AH_2 has to penetrate through the Nafion layer and so reach the Pt electrode (the broken line in Fig. 3 (b)). In the latter, the Fe(III) ion has to move from the Pt electrode to the Nafion surface and so come in contact with the solution containing AH_2. If the Fe(III) ion meets with AH_2, which comes into the Nafion layer from the solution on the way to the Pt surface, it will oxidize the AH_2 there (the solid line in Fig. 3 (b)). The current due to the direct oxidation was estimated from measurements of the current after the potential stepping described above, without any incorporation of the iron-redox couple. Line a in Fig. 4 shows the direct oxidation current, the values of which increase linearly with the increase in the concentration of AH_2 in the counter-electrode compartment, as can be predicted from its simple diffusional mass-transfer through the Nafion layer. The incorporation of the iron-redox couple enhances the oxidation current after the potential stepping. The oxidation current should contain the oxidation of the Fe(II) ion incorporated in the Nafion layer. The latter would, however, fall off to zero after the consumption of the whole Fe(II) ion if Fe(II) was not regenerated by the reaction with AH_2. Therefore, the increase in the current should be ascribed to the indirect oxidation mediated by the iron redox couple, because the current was measured under steady-state conditions. The increase in current upon the incorporation of the iron-redox couple is shown by line b in Fig. 4. The increment was calculated by subtracting the values shown by line a from the values

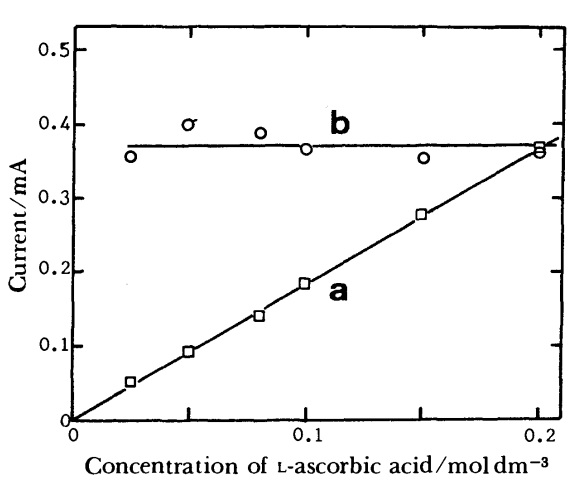

Fig. 4. Oxidation current of AH_2 in 25 mM H_2SO_4 in a counter electrode compartment of Pt-Nafion without incorporation of the redox couple (a), and with incorporation of Fe^{3+} and Fe^{2+} after subtraction of the direct oxidation current of AH_2 (b).

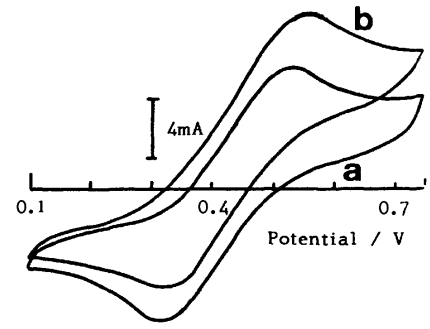

Fig. 5. Cyclic voltammograms on Pt-Nafion incorporated with Fe^{3+} and Fe^{2+} containing with water (a), and 25 mM AH_2 (b) in a working electrode compartment.

obtained with the incorporation. The subtraction does not give the correct value of the indirect oxidation in an exact sense, because the simple diffusional mass-transfer is no longer valid when diffusing AH_2 reacts with the Fe(III) ion on the way. However, the increment still gives evidence of the contribution of the indirect oxidation process. Details of the rate of the indirect oxidation relative to the direct oxidation will be discussed in successive papers, together with problems in the mass-transfer and reaction zone in the Nafion layer.

Figure 5 shows cyclic voltammograms obtained in the configuration of Case a in Fig. 3. Curves a and b were obtained without and with 25 mM AH_2 respectively in the working-electrode compartment. The current increases to the positive direction throughout the potential range of the potential sweep. It has been reported that AH_2 is oxidized directly at the potential examined here in the low pH region.[14] Therefore, it seems that the increase observed here was caused by both the direct oxidation of AH_2 on Pt and its indirect oxidation mediated by the iron-redox couple. The increase is more remarkable at the positive potential, where the Fe(II) ion is oxidized to the Fe(III) ion, than at the negative potential where the Fe(II) ion is stable. These phenomena suggest qualitatively that the indirect oxidation process takes place in the configuration of a in Fig.3. It is difficult to separate the contributions to the current-increase from the two courses of oxidation in this configuration. The increase in the current upon a mediatory action of the redox couple was, however, larger in the configuration of Case a than in that of Case b (cf. Fig. 3. This means that the former configuration is preferable. The results in Figs. 4 and 5 show the applicability of the redox couples incorporated in an SPE composite electrode as mediators for the electrochemical reactions of organic substances.

We wish to thank Dr. Masanobu Kitamura for his help in the fluorescent X-ray measurement.

References

1) Z. Ogumi, K. Nishio, and S. Yoshizawa, *Denki Kagaku*, **49**, 212 (1981).
2) Z. Ogumi, H. Yamashita, K. Nishio, Z. Takehara, and S. Yoshizawa, *Electrochim. Acta*, **28**, 1687 (1983).
3) Z. Ogumi, S. Ohashi, and Z. Takehara, *Nippon Kagaku Kaishi*, **1984**, 1788.
4) Z. Ogumi, S. Ohashi, and Z. Takehara, *Electochim. Acta*, **30**, 121 (1985).
5) I. Rubinstein and A. J. Bard, *J. Am. Chem. Soc.*, **102**, 6641 (1980).
6) D. A. Buttry and F. C. Anson, *J. Am. Chem. Soc.*, **104**, 4824 (1982).
7) W. G. Grot, "Nafion As A Separator In Electrolytic Cells," Extended Abstract of Electrochemical Society of Japan Spring Meeting, Tokyo, April 5—7, 1986, p. 35.
8) Z. Ogumi, Z. Takehara, and S. Yoshizawa, *J. Electrochem. Soc.*, **131**, 769 (1984).
9) E. I. du pont de Nemours & Co., Inc., E-05569, 2/76 (catalog).
10) I. Rubinstein and A. J. Bard, *J. Am. Chem. Soc.*, **103**, 5007 (1981).
11) A. Steck and H. L. Yeager, *Anal. Chem.*, **52**, 1215 (1980).
12) H. Braun, W. Storck, and K. Doblhofer, *J. Electrochem. Soc.*, **130**, 807 (1983).
13) Y. M. Tsou and F. Anson, *J. Electrochem. Soc.*, **131**, 595 (1984).
14) M. M. Taqui Khan and A. E. Martell, *J. Am. Chem. Soc.*, **86**, 4176 (1967).

Thermal and Ferroelectric Properties of (*S*)-2-Methylbutyl Esters of α-Substituted 4-(4-Alkoxybenzoyloxy)cinnamic Acid

Jun NAKAUCHI,* Yoshitaka KAGEYAMA, Mioko UEMATU, and Shunsuke MINAMI
Tokyo Research Laboratory, Mitsubishi Rayon Co. Ltd., Noborito, Tama-ku, Kawasaki, Kanagawa 214
(Received May 26, 1987)

Three homologous series of (*S*)-2-methylbutyl esters of α-substituted 4-(4-alkoxybenzoyloxy)cinnamic acid **Ia** (α-H), **Ib** (α-CH_3), and **Ic** (α-CN) have been synthesized and their thermal and ferroelectric properties have been investigated. The mesomorphic transition temperatures for the homologous series (**Ia**, **Ib**, and **Ic**) depend on the α-substituents as well as the terminal alkoxyl chain length. In comparison with Schiff base analogues, the transition temperatures from the isotropic phase to smectic A for all the homologous series are a little lower; however, their transition temperatures from the smectic A phase to chiral smectic C show significantly different features. The thermal stability of the chiral smectic C phase has been discussed from the view point of the local intermolecular dipole-dipole interaction in the homologous series (**Ia**, **Ib**, and **Ic**) and the Schiff base analogues. The spontaneous polarization for the homologous series is in the order of the homologues: **Ib** > **Ia** > **Ic** and their polarity is negative for **Ia** and **Ib** and positive for **Ic** homologues, respectively. These results have also been discussed in terms of the α-substituent effect on the spontaneous polarization.

Since the discovery of ferroelectricity in smectic liquid crystals containing a chiral group in the molecular structure (Sm*C phase),[1] extensive studies have been carried out not only from a fundamental point of view, but for practical applications as well. However, the relation between the ferroelectricity in the Sm*C phase and the molecular structure has not been well understood so far. Two plausible reasons are the limited number of compounds which have been investigated regarding their physical properties and the drastic change of the thermal stability in the mesophase frequently caused by altering the molecular structure slightly. Thererofe, the synthesis of various novel compounds with the Sm*C phase and the measurement of their fundamental physical propertries are necessary in order to elucidate the relationship between the ferroelectricity and the molecular structure.

From this point of view, the following homologous series (**Ia**, **Ib**, and **Ic**) of general formula:

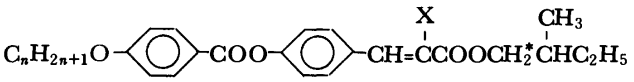

(**Ia** : X = -H, $n = 5—16$; **Ib** : X = -CH_3, $n = 5—16$; **Ic** : X = -CN, $n = 7—12$)

have been synthesized and their thermal and ferroelectric properties have been investigated. These compounds have a characteristic molecular structure in the sense that the -CH=N- linkage of well-known Schiff base analogues ((*S*)-2-methylbuthyl 4-(4-alkoxybenzylideneamino)cinnamate)

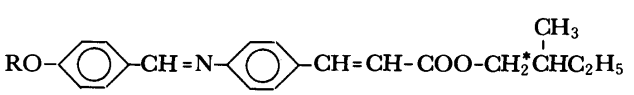

is replaced with a -COO- linkage. Such a mesogen unit was reported to be a suitable structure for the Sm*C phase,[2] and some compounds shown in the above formula (**Ia** : n=5—14, **Ic** : n=5—12) have already been synthesized; their thermal porperties and polarity were reported by Goodby et al.[3-5] However, the effect of the α-substituents on the mesomorphic thermal stability and other ferroelectric properties have not been discussed so far.

In the present paper, we compare the physical properties of the homologous series (**Ia**, **Ib**, and **Ic**) with those of the Schiff base analogues reported by P. Keller et al.[6] and Ph. Martinot-Lagarde et al.,[7,8] and discuss the effect of the molecular structure on the thermal stabilty in the mesophase and the ferroelectricity in the Sm*C phase.

Experimental

Preparation of Materials. All the reagents purchased from Tokyo Kasei Co. Ltd. were used without further purification. *p*-Hydroxy-α-methylcinnamic acid was prepared by a Perkin reaction according to the literature.[9] (*S*)-2-Methylbutyl esters of α-substituted *p*-hydroxycinnamic acid were synthesized by an esterification reaction of *p*-hydroxy-α-substituted cinnamic acid with (*S*)-2-methyl-1-butanol using a Soxhlet extractor. Their specific rotations ($[\alpha]_D$) measured in diethyl ether at 23 °C were +5.35°, +3.59°, and +8.16° for α-H, α-CH_3, and α-CN derivatives, respectively. (*S*)-2-Methylbutyl esters of α-substituted 4-(4-alkoxybenzoyloxy)cinnamic acid were synthesized by a reaction of (*S*)-2-methylbutyl esters of α-substituted *p*-hydroxycinnamic acid with *p*-alkoxybenzoyl chloride and triethylamine in the diethyl ether solution. The crude products obtained were purified twice by recrystallization from their solution with diethyl ether and pentane. Their elementary analysis data are listed in Table 1.

Measurements of Physical Properties. An identification of the mesophase was carried out using a Nikon polarizing microscope equipped with a Mettler FP-52 heating stage. Transition temperatures were measured using a Daini Seikosha SSC-560 differential scanning calorimeter (DSC) at a scanning rate of 2.5 °C min^{-1} under an N_2 atomsphere.

The spontaneous polarization (*P*s) was determined by a triangular-wave method reported by Miyasato et al.[10] The frequency, the maximum amplitude and the cell thickness were 1.0 Hz, ±70 V and 50 μm, respectively.

The tilt angle (θ/°) and the polarity (the direction of *P*s)

Table 1. Elemental Analyses for Homologous Series **Ia**, **Ib**, and **Ic**

(**Ia** Homologues)				
Carbon No.	Calcd (%)		Found (%)	
n	C	H	C	H
5	73.56	7.60	73.73	7.83
6	73.95	7.81	74.13	8.07
7	74.31	8.02	74.40	8.29
8	74.65	8.21	74.65	8.44
9	74.97	8.39	75.10	8.45
10	75.27	8.56	75.34	8.79
11	75.56	8.72	75.61	8.96
12	75.83	8.87	75.77	9.14
14	76.33	9.15	76.19	9.27
16	76.78	9.40	76.85	9.62

(**Ib** Homologues)				
Carbon No.	Calcd (%)		Found (%)	
n	C	H	C	H
5	73.95	7.81	74.28	7.93
6	74.31	8.02	74.35	8.19
7	74.65	8.21	74.60	8.41
8	74.97	8.39	75.08	8.56
9	75.27	8.56	75.55	8.79
10	75.56	8.72	75.55	8.80
11	75.83	8.87	75.86	8.90
12	76.08	9.01	76.22	9.14
14	76.56	9.28	76.54	9.38
16	76.99	9.52	77.19	9.78

(**Ic** Homologues)						
Carbon No.	Calcd (%)			Found (%)		
n	C	H	N	C	H	N
7	72.93	7.39	2.93	72.96	7.53	2.89
8	73.29	7.59	2.85	73.27	7.79	2.84
9	73.64	7.77	2.77	73.58	7.98	2.69
10	73.96	7.95	2.70	73.90	8.17	2.64
11	74.27	8.12	2.62	74.16	8.36	2.49
12	74.55	8.28	2.56	74.34	8.57	2.49

were determined by applying a *D.C.* field to a specimen placed between crossed polarizers and by observing the direction of extinction by rotating the stage. The polarity is defined by the direction that the molecules are tilted with respect to the layer normal, as shown in following picture.

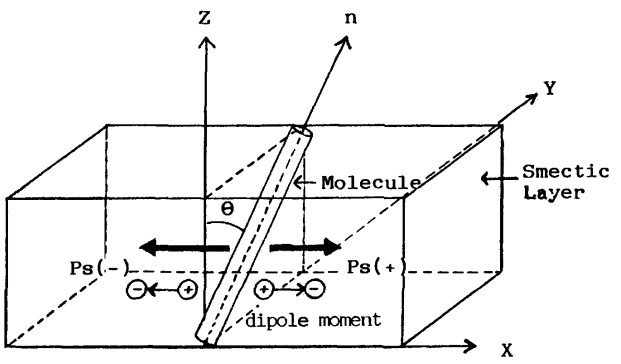

Results and Discussion

Figures 1, 2, and 3 show the mesomorphic trends of each homologous series (**Ia**, **Ib**, and **Ic**). A normal

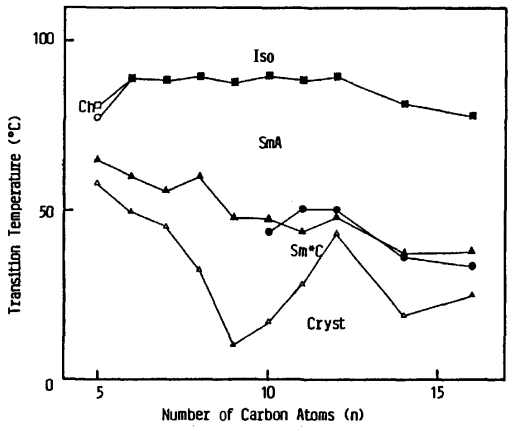

Fig. 1. Plots of the transition temperatures against the number of carbon atoms (n) in the n-alkoxyl chain of (*S*)-2-methylbutyl 4-(4-alkoxybenzoyloxy)-cinnamates (**Ia** homologues): Iso-Ch (-□-); Iso-SmA (-■-); Ch-SmA (-○-); SmA-Sm*C (-●-); SmA-Cryst or Sm*C-Cryst (-△-); melting point (-▲-).

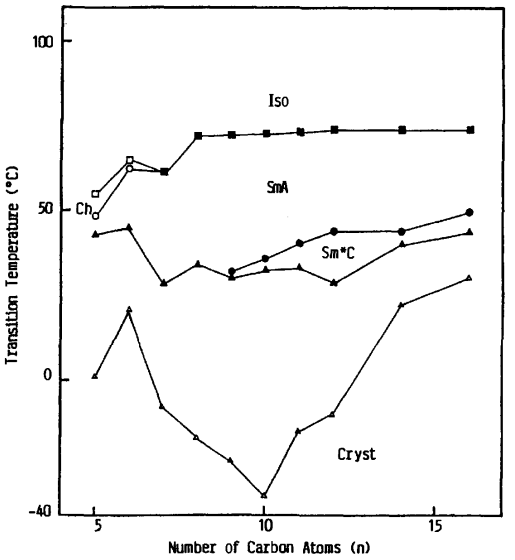

Fig. 2. Plots of the transition temperatures against the number of carbon atoms (n) in the n-alkoxyl chain of (*S*)-2-methylbutyl 4-(4-n-alkoxybenzoyloxy)-α-methylcinnamates (**Ib** homologues): Iso-Ch (-□-); Iso-SmA (-■-); Ch-SmA (-○-); SmA-Sm*C (-●-); SmA-Cryst or Sm*C-Cryst (-△-); melting point (-▲-).

odd-even alternation for the isotropic (Iso) to smectic A (SmA) and for SmA to chiral smectic C (Sm*C) can clearly be seen in **Ia** homologues, though it is ambiguous in **Ib** and **Ic** homologues. In all the homologous series investigated, cholesteric (Ch) appears in the lower alkoxyl chain homologues, whose number of the carbon in terminal alkoxyl chain are n=5, n=6, and n=9 for **Ia**, **Ib**, and **Ic** homologues, respectively. The Sm*C phase of **Ia** and **Ic** homologues injected at decyloxy and heptyloxy derivatives appears as a monotropic transition from SmA, except for enantiotropic undecyloxy and dodecyloxy derivatives of **Ia** homologues. On the other hand, the Sm*C phase of **Ib** homologues

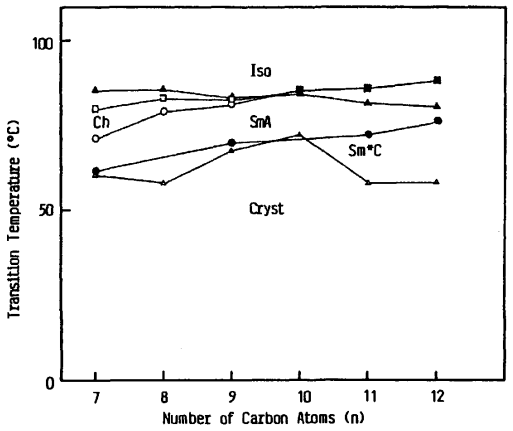

Fig. 3. Plots of the transition temperatures against the number of carbon atoms (n) in the n-alkoxyl chain of (S)-2-methylbutyl 4-(4-n-alkoxybenzoyloxy)-α-cyanocinnamates (**Ic** homologues): Iso-Ch (-□-); Iso-SmA (-■-); Ch-SmA (-○-); SmA-Sm*C (-●-); SmA-Cryst or Sm*C-Cryst (-△-); melting point (-▲-).

injected at nonyloxy derivative appears as an enantiotropic one from SmA with a wider temperature range than those of **Ia** and **Ic** homologues. Plots of the transition temperatures from SmA to Sm*C against the number of carbon atoms in the alkoxyl chain in **Ia** homologues are "parabolic" as Goodby et al. referred to;[11] however, this trend was not seen in **Ib** and **Ic** homologues.

In order to compare the thermal stability of SmA and Sm*C phase for homologous series (**Ia**, **Ib**, and **Ic**) with those for the Schiff base analogues reported by Keller et al.,[6] the transition temperatures from Iso to SmA and from SmA to Sm*C against the carbon number of the terminal alkoxyl chain are plotted in Figs. 4a and 4b, respectively. As is evident from Fig. 4a, the transition temperatures from the Iso phase to SmA for each homologues with different α-substituents are a little lower than those for the Schiff base analogues. This trend is attributed to the effect of replacing the -CH=N- linkage in the core with the -COO- linkage on the thermal stability for SmA phase.[12]

On the other hand, the thermal stability of the Sm*C phase for the homologous series (**Ia**, **Ib**, and **Ic**) is significantly different from those for the Schiff base analogues. That is, the transiton temperatures from SmA phase to Sm*C for the Schiff base analogues decrease in the order of the analogues: α-H > α-CN > α-CH_3. However, those for the homologous series decrease in the order of the homologues (α-CN > α-H ≈ α-CH_3 (**Ic** > **Ia** ≈ **Ib**)), respectively.

According to McMillan's theory,[13] if a molecule has both central and out-board dipole moments, the transition temperature from SmA to Sm*C depends on the local intermolecular dipole-dipole interaction among these dipole moments.

In the homologous series (**Ia**, **Ib**, and **Ic**), the central dipole corresponds to the dipole of the ester linkage of

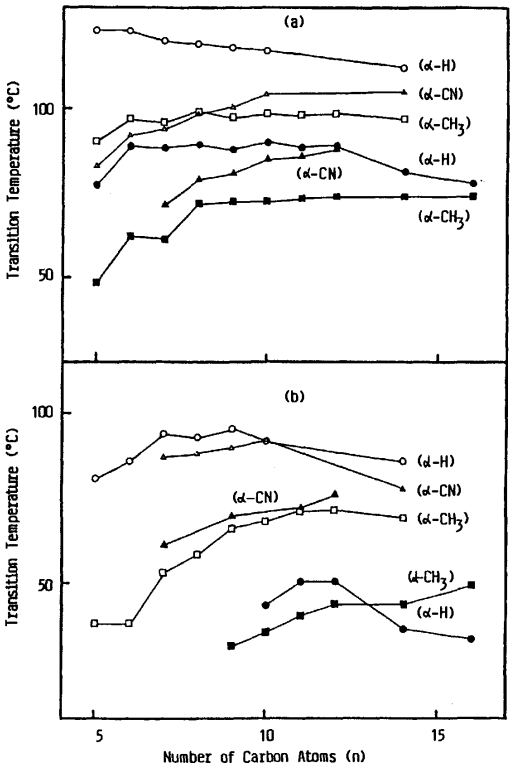

Figs. 4a and 4b. Plots of the transition temperatures from Iso phase to SmA (4a) and from SmA phase to Sm*C (4b) against the number of carbon atoms in the n-alkoxyl chain of the homologous series **Ia** (-●-), **Ib** (-■-), and **Ic** (-▲-), and those of the Schiff base analogues α-H (-○-), α-CH_3 (-□-), and α-CN (-△-).

the core (6.34×10^{-30} C m)[14] and the out-board dipoles correspond to dipoles of the ether linkage (4.27×10^{-30} C m)[14] and the ester linkage of the cinnamoyl moiety including the α-substituent. It is noteworthy that the direction of the dipole moment of the homologous series (-COO-: 6.34×10^{-30} C m) to the molecular axis is quite defferent from that of the Schiff base analogues (-CH=N-: 5.24×10^{-30} C m),[14] if the molecule has the all trans configulation, as shown in the following schemes

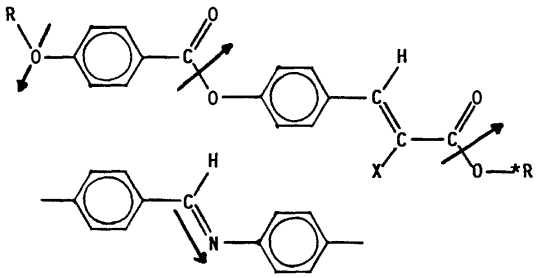

These facts indicate that the different dependence of the SmA-Sm*C transition temperature on the α-substitution between the homologous series (**Ia**, **Ib**, and **Ic**) and the Schiff base analogues can be attributed to a difference in the local intermolecular dipole-dipole interaction caused by replacing the central link-

age -CH=N- with -COO-.

The temperature dependence of the spontaneous polarization in the Sm*C of the homologous series **Ia**, **Ib**, and **Ic** are shown in Figs. 5, 6, and 7, respectively. As is evident from the figures, the spontaneous polarization of the homologous series is in the order of the homologues (**Ib**>**Ia**>**Ic**) and shows a maximum at certain alkoxyl chain length in each homologues. The maximum value was observed in the **Ib** homologue with a terminal dodecyloxyl chain (60 $\mu C\,m^{-2}$). These facts show that spontaneous polarization strongly depends on the α-substituents in the cinnamoyl moiety as well as the terminal alkoxyl chain length.

The polarities of the spontaneous polarization in the homologous series are negative for **Ia** and **Ib** homologues and positive for **Ic** homologues, respectively. The alternation of polarity between **Ia**, **Ib**, and **Ic**, which was observed in the Schiff base analogues,[8] has already been reported and interpreted as tilt variations between the core and the terminal chain by Goodby et al.[5] To confirm the tilt variations among the homologous series, the tilt angles for the dodecyloxy homologues for **Ia**, **Ib**, and **Ic** were measured. Figure 8 shows the temperature dependence of the tilt angle in the Sm*C phase for **Ia**, **Ib**, and **Ic** homologues. The tilt angle measured by the optical method corresponds to the angle of the core in the molecule tilted to the smectic layer. Therefore, the core of the **Ic** homologue has the most tilted structure among three homologues. This result seems to be in conflict with the speculation of Goodby et al. However, in the present study, the thickness of the smectic layer has not been measured yet; hence, the tilt variations between the core and the terminal chain are not clear at this stage.

According to Meyer et al.,[1] the spontaneous polari-

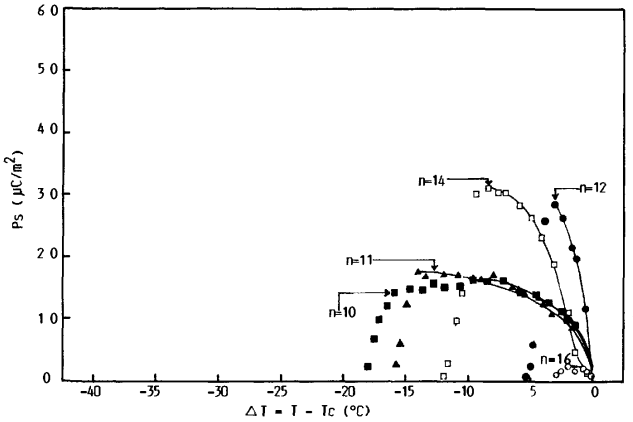

Fig. 5. Temperature dependence of the spontaneous polarization of **Ia** homologues. The cell thickness, the frequency and the maximum amplitude of applied voltage are 50 μm, 1.0 Hz, and ±70 V, respectively.

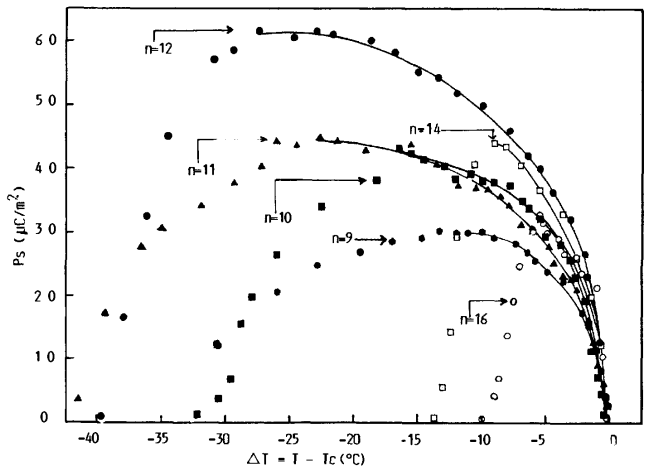

Fig. 6. Temperature dependence of the spontaneous polarization of **Ib** homologues. The cell thickness, the frequency and the maximum amplitude of applied voltage are 50 μm, 1.0 Hz, and ±70 V, respectively. The deviation of the plots from the curve satisfied the relation: $Ps \propto (\Delta T)^{\beta}$ at the lower temperature side is probably due to the applied voltage not enough to reverse the spontaneous polarization completely.

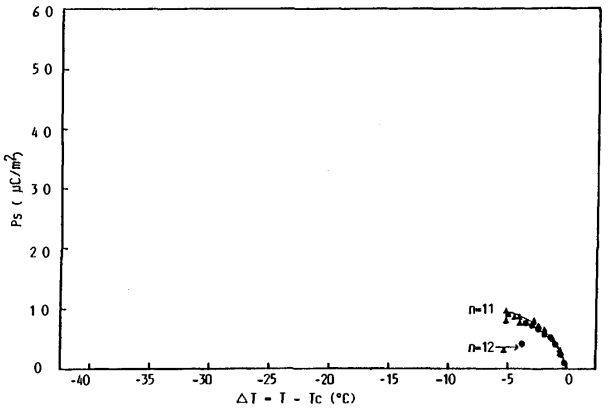

Fig. 7. Temperature dependence of the spontaneous polarization of **Ic** homologues. The cell thickness, the frequency and the maximum amplitude of applied voltage are 50 μm, 1.0 Hz, and ±70 V, respectively.

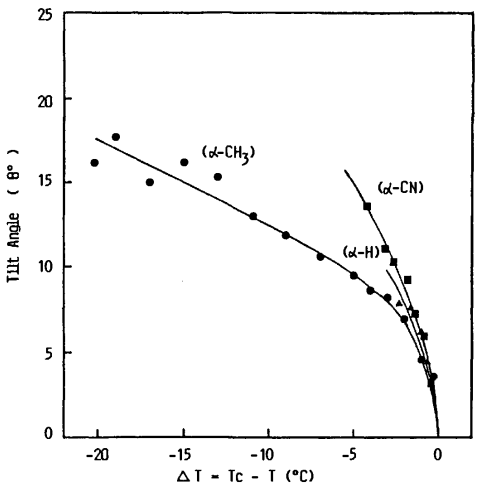

Fig. 8. Temperature dependence of the tilt angle for the homologous series **Ia** (-▲-), **Ib** (-●-), and **Ic** (-■-).

zation originates from the perpendicular component of the dipole moment in the polar group attached to the asymmetric carbon atom. The structure of the cinnamoyl moiety adjecent to the asymmetric carbon for the homologous series (**Ia**, **Ib**, and **Ic**) are schematically pictured as follows.

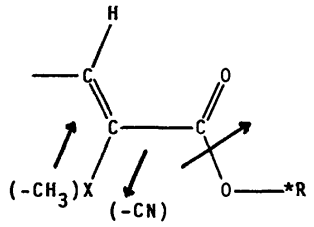

The contribution of the α-substituent to the dipole moment or the 2-methylbutoxycarbonyl group is inverse between **Ib** and **Ic** homologues. In comparison with the unsubstituted homologues **Ia**, **Ib** homologues have an electron-releasing methyl group so that the dipole moment of the ester group in the cinnamoyl moiety is enhanced, thus leading to the increase of spontaneous polarization. On the other hand, **Ic** homologues have a strong electron-withdrawing cyano group (13.01×10^{-30} Cm)[15] with the opposite direction of the dipole moment to that of the dipole moment of the ester group in the cinnamoyl moiety (6.34×10^{-30} Cm); hence the perpendicular component of the net dipole moment to the molecular axis decreases and has the opposite direction to those of **Ia** and **Ib** homologues. The **Ic** homologues have a smaller spontaneous polarization with opposite polarity.

The authors thank Dr. Toshio Yoshihara for his helpful discussion.

References

1) R. B. Meyer, L. Liebelt, L. Strzelecki, and P. Keller, *J. de Physique*, **36**, L-69 (1975).
2) J. W. Goodby and T. M. Leslie, "Liquid Crystals and Ordered Fluids," Plenum, New York (1984), Vol. 4, p. 1.
3) J. W. Goodby, *Science*, **231**, 350 (1986).
4) J. W. Goodby, E. Chin, T. M. Leslie, J. M. Geary, and J. S. Patel, *J. Am. Chem. Soc.*, **108**, 4729 (1986).
5) J. W. Goodby and E. Chin, *J. Am. Chem. Soc.*, **108**, 4736 (1986).
6) P. Keller, L. Liebert, and L. Strzelecki, *J. de Physique*, **37**, C3-27 (1976).
7) Ph. Martinot-Lagarde, *J. de Physique*, **37**, C3-129 (1976).
8) Ph. Martinot-Lagarde, R. Duke, and G. Durand, *Mol. Cryst. Liq. Cryst.*, **75**, 249 (1981).
9) J. R. Johnson, "Organic Reaction," ed by R. Adams, W. E. Bachman, J. R. Johnson, L. F. Fieser, and H. R. Snyder, Robert E. Krieger Pub., Huntington, New York (1978), Vol. 1, p. 210.
10) K. Miyasato, S. Abe, H. Takezoe, A. Fukuda, and E. Kuze, *Jpn. J. Appl. Phys.*, **22**, L661 (1983).
11) J. W. Goodby and G. W. Gray, *Mol. Cryst. Liq. Cryst.*, **48**, 127 (1978).
12) G. W. Gray, "The Molecular Physics of Liquid Crystals," ed by G. R. Luckhurst and G. W. Gray, Academic Press., London, New York, San Francisco (1979), Chap. 1.
13) W. L. McMillan, *Phys. Rev. A*, **8**, 1921 (1973).
14) R. T. Klingbiel, D. J. Genova, T. R. Criswell, and J. P. Van Meter, *J. Am. Chem. Soc.*, **96**, 7651 (1974).
15) V. I. Minkin, O. A. Osipov, and Yu. A. Zhdanov, "Dipole Moments in Organic Chemistry," Plenum Press., New York, London (1970), p. 226.

Spectroscopic Investigations on 9-(4-Dimethylaminophenyl)-10-cyanoanthracene

Wolfram Baumann,* Beate Schwager, Norbert Detzer, Tadashi Okada,† and Noboru Mataga,*,†
Institute of Physical Chemistry, University of Mainz, D65 Mainz, West Germany
†Department of Chemistry, Faculty of Engineering Science, Osaka University, Toyonaka, Osaka 560, Japan
(Received June 4, 1987)

Excited state dipole moments of 9-(4-dimethylaminophenyl)-10-cyanoanthracene determined from the electric field effect on solutions in several solvents as well as fluorescence spectra, ground state absorption and S_n-S_1 transient absorption spectra show that this molecule most probably fluoresces from two excited states in nonpolar and medium polar solvents, whereas only one highly polar excited state emits in polar solvents.

The spectroscopic and kinetic behaviour of 4-(9-anthryl)-*N*,*N*-dimethylaniline (ADMA) and some derivatives has been investigated in several papers.[1-15] In particular, the fluorescence at least in sufficiently polar solvents originates from a polar state which is stabilized in polar solvents through solvent-solute interaction and/or formation of a twisted conformer so that its energy, originally higher than the less polar first Frank-Condon (FC) excited singlet state, becomes the energetically lowest. From electro-optical absorption and emission measurements[7,12] it has been shown that polarizability effects due to mere solvent solute interaction can describe the observed effects, but also a description of the experimental material assuming mere twisting to a so-called "twisted intramolecular charge-transfer (TICT) state" was shown to be possible.[9,12] A crucial point is the interpretation of the electro-optical absorption measurement in the long wavelength shoulder. Here, Herzberg-Teller coupling between two nearby electronic states as discussed with the related compound *p*-dimethylaminobenzonitril (DMABN) and some of its derivatives[16] could cause problems in the interpretation of the measured quantities. Hence, the molecule 9-(4-dimethylaminophenyl)-10-cyanoanthracene (10-CN-ADMA) was synthesized[17] in order to study the effect of a larger charge transfer present already in the ground state on the solvent dependence of the fluorescence. Also there was some hope that the long wavelength shoulder in the absorption spectrum would be broader at least in polar solvents than this is the case with ADMA. Then, electro-optical absorption measurements could be performed with less inherent systematic error than with ADMA.[7]

Experimental

Outline of Electro Optical Absorption (EOAM) and Integral Electro Optical Emission (IEOEM) Measurements. With EOAM, the effect of an external electric field E_a on the absorption $A^E(\tilde{\nu}, \chi)$ of solute molecules is measured dependent on the wavenumber $\tilde{\nu}$ and the angle χ between the direction of E_a and the polarization direction of the linearly polarized light used to measure $A^E(\tilde{\nu}, \chi)$. The method has been worked out extensively by Liptay and co-workers.[18] From a suitable experiment,[19] the experimental quantity $L(\tilde{\nu}, \chi)$ is determined as defined by the following Eq. 1,

$$A^E(\tilde{\nu}, \chi) = A(\tilde{\nu}, \chi)[1 + L(\tilde{\nu}, \chi) E_a^2] \quad (1)$$

From the measured wavenumber and angular dependence of $L(\tilde{\nu}, \chi)$ the terms ${}^aE$ to ${}^aI$ can be determined as shown in Ref. 18. With the transitions considered in this paper, they are related to the molecular dipole moments through the following Eqs. 2 to 4, if only explicit dipole terms have to be taken into account

$${}^aE = 2\beta^2 f_e^2 \mu_g^2 \quad (2)$$

$${}^aF = {}^aG = \beta f_e^2 \mu_g \Delta^a\mu \quad (3)$$

$${}^aH = {}^aI = f_e^2 (\Delta^a\mu)^2 \quad (4)$$

For further definitions see below. Integral electro optical emission measurement (IEOEM)[12,20] are a modified (an integral) version of spectrally resolved electro optical emission measurements (EOEM).[21] With IEOEM the effect of E_a on the fluorescence photon flux $p_1^E(\phi)$ from the whole fluorescence band is measured without spectral resolution in an optical broad band experiment, dependent on the angle ϕ between the direction of E_a and the polarization direction given by an analyzing polarizer in the fluorescence light beam. The method has been described and checked with various systems in refs.[20-23] Equation 5 defines the experimental quantity $\chi_1(\phi)$

$$p_1^E(\phi) = p_1[1 + \chi_1(\phi) E_a^2] \quad (5)$$

From the angular dependence of χ_1, two experimental terms ${}^iD$ and ${}^iE$ can be derived. As is shown elsewhere,[20,22] a linear combination of these quantities is related to the dipole moment of the fluorescent state

$${}^eE = {}^iE - 4{}^iD = 2\beta^2 f_e^2 \mu_e^2 \quad (6)$$

$$\beta = (kT)^{-1} \quad (7)$$

with Boltzmann's constant k and the temperature T.

$$\Delta^a\mu = (1 - f'\alpha_e^{oFC})^{-1} (1 - f\alpha_e^{oFC}) (1 - f\alpha_g^{o})^{-1} (1 - f'\alpha_g^{o}) (\mu_e^{FC} - \mu_g) \quad (8)$$

$$\mu_g = (1 - f\alpha_g^{o})^{-1} \mu_g^{o} \quad (9)$$

$$\mu_e^{FC} = (1 - f\alpha_e^{oFC})^{-1} \mu_e^{oFC} \quad (10)$$

$$\mu_e = (1 - f\alpha_e^{o})^{-1} \mu_e^{o} \quad (11)$$

$$\mu_g^{FC} = (1 - f\alpha_g^{oFC})^{-1} \mu_g^{oFC} \quad (12)$$

μ^o are the dipole moments of the considered equilibrium and Frank-Condon (FC) states of the free solute and α^o their polarizabilities. Subscripts e and g indicate excited state and ground state properties, respectively.

$$f_e = 3\varepsilon/(2\varepsilon + 1) \cdot 1 \quad (13)$$

$$f = [(\varepsilon - 1)/(2\varepsilon + 1)]/(2\pi\varepsilon_o a^3) \cdot 1 \quad (14)$$

$$f' = [(n^2 - 1)/(2n^2 + 1)]/(2\pi\varepsilon_o a^3) \cdot 1 \quad (15)$$

In the used model,[18,21] the solute dipole is approximated by a point dipole in the center of a sphere with radius a, determined by the solute's size. f_e then connects the field in the empty sphere to the externally applied field E_a and f and f' describe the effect of the reaction field due to polarization of the solvent shell around the solute dipole ε_0 is the permittivity of the vacuum. Equation 8 reduces to

$$\Delta^a\mu = \mu_e^{FC} - \mu_g \qquad (16)$$

in nonpolar solvents are used.

Conventional Absorption and Fluorescence Spectra. Ground-state absorption spectra have been measured using a Perkin Elmer-Hitachi model 340 spectral photometer with data handler, connected to a Digital Equipment LSI 13/2 computer with Watanabe WX4671 plotter. Spectral bandwidth was 0.4 nm. The quanta-corrected fluorescence spectra have been recorded using a Farrand MK II fluorometer connected to the mentioned computer system. Quanta calibration of the emission channel was performed using an EG&G 1000 Watts quartz-halogen lamp, calibrated to an NBS-standard. Spectral bandwidth was 2 nm, excitation wavelength was 400 nm.

Transient Absorption Spectra. Picosecond time-resolved transient absorption spectra were measured by means of a microcomputer-controlled, mode-locked Nd^{3+}: YAG laser photolysis system described elsewhere.[24] The third harmonic of a single picosecond pulse was used for excitation.

Compounds. 10-CN-ADMA has been prepared and carefully purified as described else where.[17] All solvents have been purified using standard procedures[25] and were dried under reflux conditions over Na-K-alloy or where this was impossible by chromatography over alumina, immediately before preparing the solutions, undre Ar protective overpressure.

Results and Discussion

Results from EOAM. The long wavelength shoulder of the absorption spectrum of 10-CN-ADMA[17] in dioxane is represented in Fig. 1 and is compared with 9-cyanoanthracene. EOAM investigations have been performed at 298 K in cyclohexane and dioxane solutions. The results are given in Table 1 together with the calculated dipole moments.

The effective ground state dipole moment μ_g does not show a solvent dependence that could be due to a

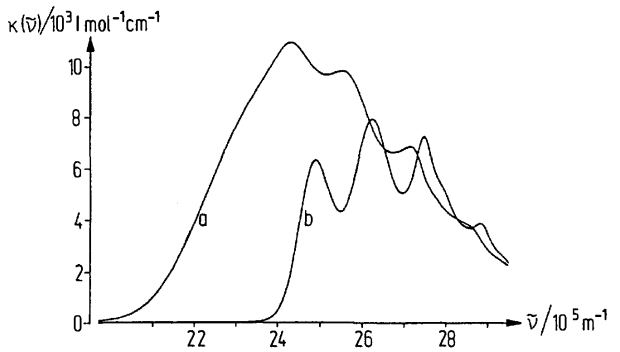

Fig. 1. Absorption coefficient $\kappa(\tilde{\nu})$ within the first absorption band of 10-CN-ADMA (a), compared to that of 9-cyanoanthracene (b), in dioxane at 298 K.

Table 1. Results from EOAM on 10-CN-ADMA

	Cyclohexane	Dioxane
Range	438—455 nm	439—470 nm
${}^aD/10^{-20}V^{-2}m^2$	−420	−720
${}^aE/10^{-20}V^{-2}m^2$	8100±1000	7500±1400
${}^aF={}^aG/10^{-40}CV^{-1}m^2$	3600± 400	5100±400
f_e	1.202	1.223
$\mu_g/10^{-30}Cm$	21.8±1.3	20.6± 1.8
$\Delta^a\mu/10^{-30}Cm$	56.5±10	83.3±15
$\mu_e^{FC}/10^{-30}Cm$	78.3±10	103.9±15

Table 2. Results from IEOEM on 10-CN-ADMA at 298 K in Various Solvents Errors Amount to about 10%

	${}^iD/10^{-20}V^{-2}m^2$	${}^iE/10^{-20}V^{-2}m^2$
Heptane	174	38300
Cyclohexane	0	41700
Dipentyl ether	2200	76800
Dibutyl ether	2340	87100
Dipropyl ether	2200	98800
Diisopropyl ether	2560	113500
Dioxane	186	110200
Fluorobenzene	−1940	111700
Benzotrifluoride	−3910	117400

reaction field induced part and what could be separated using Eq. 9. Hence, $\mu_g=(21\pm2)10^{-30}$ Cm is used as an upper limit for μ_g°. This value agrees well with the sum of μ_g° of *N,N*-dimethylaniline and of 9-cyanoanthracene[26] which amounts to $19.1\cdot10^{-30}$ Cm.

The change of the effective dipole moment with excitation is found to be solvent dependent, even if the very large experimental error of $\Delta^a\mu$ is taken into account. This is due to the fact that the measurement is done in a slope which is a small part only of the whole absorption to the polar FC-state. Nevertheless, the effective dipole moment μ_e^{FC} is found to be very large in both solvents, although the value of μ_e^{FC} found in dioxane must be discussed as an approximation, since Eq. 16 is not valid in dioxane where reaction field induced terms cannot be neglected. Referring to Eq. 10, obviously μ_e^{FC} in cyclohexane is an upper limit for μ_e^{oFC}.

The values found for $\Delta^a\mu$ are larger than those reported in Table 5 of Ref. 7, which would be in agreement with the model of an intramolecular charge-transfer excited state where the charge centers would be further apart in 10-CN-ADMA than in ADMA itself.

Results from IEOEM. Table 2 represents the experimental quantities ${}^iD$ and ${}^iE$.

Discussion Assuming One Emitting Species or State. If one emitting species or state is assumed, μ_e can be calculated using Eq. 6. The values are given in Table 3. They show a strong solvent dependence which might be interpreted as reaction field induced amounts to the total effective dipole moment μ_e. Then with Eq. 17 from a regression analysis of μ_e^{-1} on $(\varepsilon-1)/(2\varepsilon+1)$, μ_e° as well as the polarizability density

Table 3. Some Results from IEOEM on 10-CN-ADMA Assuming a One State System. Errors of μ_e Are about 5%, Those of μ_e^0 and α_e^0/a^3 Are Derived from the Standard Error of the Regression Coefficients

	$\mu_e/10^{-30}$C m
Heptane	47.4
Cyclohexane	49.4
Dipentyl ether	59.7
Dibutyl ether	62.9
Dipropyl ether	66.9
Diisopropyl ether	70.4
Dioxane	78.7
Fluorobenzene	73.3
Benzotrifluoride	74.7
$\mu_e^0/10^{-30}$C m	37.1±1.8
$(\alpha_e^0/a^3)/10^{-10}$C V^{-1}m^{-1}	0.74±0.13

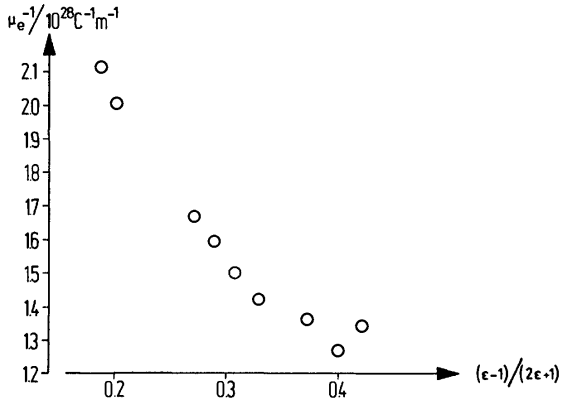

Fig. 2. Plot of μ_e^{-1} of 10-CN-ADMA versus $(\varepsilon-1)/(2\varepsilon+1)$.

α_e^0/a^3 can be derived.

$$\mu_e^{-1}=(\mu_e^0)^{-1}-(\alpha_e^0/(\mu_e^0 2\pi\varepsilon_0 a^3))(\varepsilon-1)/(2\varepsilon+1) \quad (17)$$

Fig. 2 shows a plot according to Eq. 17, which hardly could be interpreted as a straight line. A better interpretation seems to be a curve that levels off to a horizontal line at μ_e around $80\cdot10^{-30}$ C m, at high solvent polarity. Table 3 displays the results from a respective linear regression analysis, too. The permanent dipole moment μ_e^0 seems to be pretty small. Contrasting this, the polarizability density α_e^0/a^3 is pretty large, in the order of what had been reported in Ref. 7 with ADMA. This unusual finding is based on the assumption that only one state or species emits. On the other hand, from investigations on ADMA and some other derivatives[6] as well as from the bent curve of Fig. 2 and from the disagreement between μ_e determined in cyclohexane and μ_e^{FC}, it might follow that perhaps two emitting species or states determine the spectroscopic behavior of 10-CN-ADMA. This idea is also supported by the change of the spectral shape of the fluorescence of 10-CN-ADMA, when going from nonpolar to polar solvents, as shown in Fig. 3.

Discussion Assuming Two Emitting Species or States. For the considerations in this section, terms like $f\alpha_e^0$ are assumed to be much smaller than 1, in all

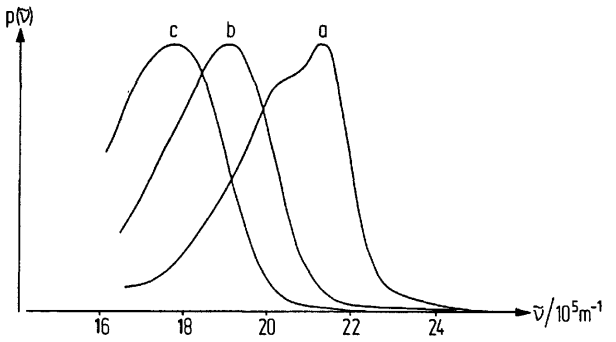

Fig. 3. Fluorescence spectrum of 10-CN-ADMA, a: in methylcyclopentane; b: in diisopropyl ether; c: in fluorobenzene, at 298 K, Excitation wavelength was 400 nm, sample concentration $1\cdot10^{-5}$ mol dm^{-3}.

solvents, that is induced amounts to μ_e are assumed to be negligible, and hence $\mu_e=\mu_e^0$, with the two-state model. Also it is assumed as the working hypothesis in this section, that there are a polar fluorescent species or state A and a less polar fluorescent species or state B which emit simultaneously to give the observed broad fluorescence band. State A may be the intramolecular charge transfer state just discussed and state B probably a locally excited 9-cyanoanthracene like state with some admixture of the dimethylaniline→cyanoanthracene charge transfer character. No assumption is made with respect to the conformation of 10-CN-ADMA in these two states, as to whether the two states are to be considered as conformers. With this model, the solvent dependence of the dipole moment μ_e shown in Table 3 and in Fig. 3 is due to a change of the ratio q of the fluorecence intensities of B and A

$$q=p_{1B}/p_{1A} \quad (18)$$

Consequently, the value of μ_e in polar solvents that gets constant around $\mu_e^0=80\cdot10^{-30}$ C m would be due to almost only the A state emission and $\mu_e^0=47.4\cdot10^{-30}$ C m in heptane might be assumed as due to almost pure B-state emission. Then q can be calculated according to Eq. 19, which is taken from[20]

$${}^cE_A={}^cE_M(1+q)-{}^cE_B q. \quad (19)$$

The values of q are given in Table 4. They are founded on the assumed values for $\mu_e^0(A)=80\cdot10^{-30}$ C m and $\mu_e^0(B)=47\cdot10^{-30}$ C m or alternatively $\mu_e^0(B)=35\cdot10^{-30}$ C m, by which ${}^cE_A$ and ${}^cE_B$ have been calculated according to Eq. 6. In principle, q can be used for the kinetic interpretation of the activation barrier between the two states. A quantitative discussion will be given together with respective data of other related molecules in a forthcoming communication.[27]

S_n-S_1 Absorption Spectra. S_n-S_1 absorption spectra have been measured at 298K in cyclohexame, fluorobenzene, tetrahydrofuran, 1-butanol, and acetonitrile. The measurements suffered from the very low solubility of 10-CN-ADMA in all solvents-which is the reason for the noisy spectra. Figure 4 shows these spectra at

Table 4. The Ratio q as Determined from IEOEM on a Two State Model Basis, Founding on $\mu_e^0(A)=80\cdot10^{-30}$C m and $\mu_e^0(B)=47\cdot10^{-30}$C m*, and $\mu_e^0(B)=35\cdot10^{-30}$C m**

	q*	q**
Heptane	110	4.06
Cyclohexane	17.1	3.26
Dipentyl ether	2.09	1.21
Dibutyl ether	1.40	0.89
Dipropyl ether	0.85	0.59
Diisopropyl ether	0.53	0.39
Dioxane	0.05	0.04
Fluorobenzene	0.32	0.25
Benzotrifluoride	0.24	0.19

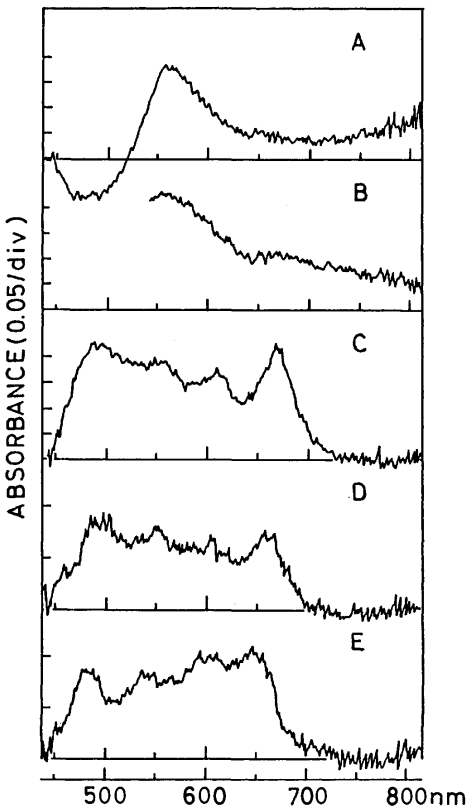

Fig. 4. S_n–S_1 transient absorption spectra of 10-CN-ADMA in some solvents, taken at 298 K, A: in cyclohexane, 100 ps after the 355 nm excitation pulse; B: in fluorobenzene, after 100 ps; C: in tetrahydrofuran, after 200 ps; D: in 1-butanol, after 200 ps; E: in acetonitrile, after 100 ps.

100 ps delay time after the excitation with the laser pulse of about 25 ps duration. The spectral band shape has not indicated any change depending on the delay time except in 1-butanol. Even in 1-butanol the spectral shape has reached its steady state within this time interval. The spectra change considerably when passing from nonpolar to polar solutions. In cyclohexane, an absorption band with peak around 570 nm and broad absorption without distinct peak in 600—800 nm region are observed. This transient absorption spectrum is somewhat similar to that of 9-cyanoanthracene (9-CA) (Fig. 5) as well as that of ADMA

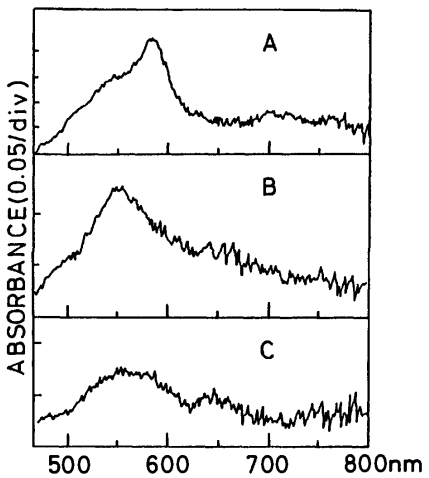

Fig. 5. S_n–S_1 transient absorption spectra, taken at 298 K, of A: 9-CA in cyclohexane, 100 ps after the 355 nm excitation pulse; B: 9-CA+DMA(ca. 0.1 M) in acetonitrile, after 66 ps; C: 9-CA+DMA(ca. 0.1 M) in acetonitrile, after 300 ps.

in cyclohexane solutions.

In tetrahydrofuran, 1-butanol and acetonitrile (Fig. 4), the spectra are very similar to each other, but quite different from that in cyclohexane. The spectral shape in these polar solvents with peaks at 550, 610, and 660 nm is very similar to those of some derivatives of and compounds related to ADMA,[28] where the anthryl moiety is quite isolated from the other part of these compounds, except that the spectra of 10-CN—ADMA are ca. 70—80 nm bule-shifted compared with those of ADMA. It had been emphasized there that the S_n-S_1 spectra of the latter compounds in polar solvents resemble the anthracene anion.[28] In Fig. 5, the transient absorption spectra of 9-CA in cyclohexane (A, at 100 ps delay time) and 9-CA+*N*,*N*-dimethylaniline (DMA) in acetonitrile (B and C, at 66 and 300 ps delay times, respectively) are indicated. The spectrum B is mainly due to the S_1 state of 9-CA because of the relative low concentration of DMA (ca. 0.1 M), while the spectrum C is mainly due to the $(9\text{-CA})^-\cdots DMA^+$ ion pair which shows decay due to back electron transfer within 1 ns. Although this absorption spectrum of the $(9\text{-CA})^-\cdots DMA^+$ ion pair is much broader compared with the spectra of 10-CN-ADMA in polar solvents given in Fig. 4, its wavelength region agrees very well with those of 10-CN-ADMA in polar solvents, which suggests strongly that the excited 10-CN-AMDA in polar solvents should be characterized by a large intramolecular charge separation between the 9-CA and DMA moieties. The broadening of the spectrum in Fig. 5C compared to those of Fig. 4C, D, E, could be ascribed to the difference in the ion-pair structures. Namely, the π-electronic systems of 9-CN^- and DMA^+ of the ion pair in the case of Fig. 5C might be in a closer contact (presumably face to face?) than in the case of the intramolecular charge-transfer state of 10-CN-ADMA in polar solvents. This is exactly what was

derived experimentally from IEOEM, where a dipole moment in between 70 and $80 \cdot 10^{-30}$ C m has been found, which is equivalent to a charge transfer over 0.5 nm.

The band at 660 nm which is quite intense in the polar solvents, tetrahydrofuran, 1-butanol, and acetonitrile, is also contained in the spectra in cyclohexane and fluorobenzene solutions, although quite weakly. Hence, these spectra might be considered as a superposition of a 9-CA anion spectrum from a locally excited 9-CA like state. In this case, the dipole moment of the excited 10-CN-ADMA determined in cyclohexane ought to be represented very roughly by the sum of the first singlet excited state dipole moment of 9-CA[22] and of the ground state dipole moment of dimethylaniline,[26] which would amount to about $35 \cdot 10^{-30}$ C m. This value was used as an alternative value for calculating q in Table 4. It is considerably less than the experimental value reported for heptane solutions (Table 3). The difference could either be ascribed to the fact that the two molecular subunits cannot be considered isolated, or that even in heptane there is some amount of A-state emission.

The large value for μ_e in Table 3 found for fluorobenzene indicates that there is almost a full charge transfer in fluorobenzene although the S_n-S_1 spectrum is not yet the one of the ion-pair like state, as revealed in the polar solvents tetrahydrofuran, 1-butanol and acetonitrile. This means that such an ion pair like state is not yet reached in fluorobenzene, i.e. the electronic structure of the excited state is still slightly less polar.

The two state interpretation of the S_n-S_1 spectra is also in agreement with the ground state absorption spectrum, which shows a long wavelength shoulder fronting the 9-CA like first absorption band. From EOAM in this shoulder, the highyl polar ICT character of the respective FC-state was derived as described already. Figure 6 shows the ground state absorption spectrum in cyclohexane between 20 and $40 \cdot 10^5$ m^{-1}. The absorption bands around 32 and $38 \cdot 10^5$ m^{-1} might be due to transitions to the same excited states as those reached by the S_n-S_1 absorption processes in cyclohexane at 570 nm ($17.5 \cdot 10^5$ m^{-1}) and 870 nm ($11.5 \cdot 10^5$ m^{-1}), which can be seen if a small stabilization of about 1 to $1.5 \cdot 10^5$ m^{-1} of the equilibrium excited state with respect to the first FC-excited state at $22.5 \cdot 10^5$ m^{-1} is taken into account.

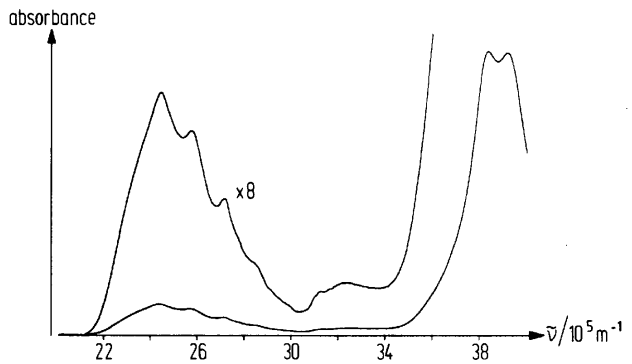

Fig. 6. Ground state absorption spectrum of 10-CN-ADMA in cyclohexane at 298 K. Concentration was 1.2 10^{-5} mol dm^{-3}.

Concluding Remarks. The absorption and fluorescence behavior of 10-CN-ADMA can be well-understood assuming two nearby electronic states, a very polar state A and a less polar state B. From the electric field dependence of these spectra, equilibrium excited state dipole moments μ_e as well as Franck-Condon excited state dipole moments μ_e^{FC} could be determined. The values from these measurements fit well to the results from solvent shift measurements of the fluorescence[17] and to those from the solvent dependent S_n-S_1 spectra. The very solvent dependent S_n-S_1 spectra as well as the levelling off of the μ_e^{-1} values discussed above (Discussion Assuming Two Emitting Species or States) make the two state model strongly favoured.

The observed dipole moment μ_e°(A) of about $80 \cdot 10^{-30}$ C m is in agreement with the picture of about one-electron charge transfer between the 9-cyanoanthracene and the dimethylaniline moieties.

The agreement between μ_e° and μ_e^{oFC} although within large errors, shows that there does not occur any dramatic change of the dipole moment after excitation, as had been one of the working hypotheses at the beginning of the application of the TICT model[29,30] to various compounds. Hence, no decision can be made whether there is a conformational change of 10-CN—ADMA after excitation to a TICT state, or whether there is simply an intramolecular charge transfer state.

The Mainz group gratefully acknowledges financial support by the Fonds der Chemischen Industrie and the Deutsche Forschungsgemeinschaft. The present work was also partly supported by Grants-in-Aid (Nos. 5843003, 60040059, 61040046, and 61123008) from the Japanese Ministry of Education, Science and Culture to N.M.

References

1) R. Ide, Y. Sakata, S. Misumi, T. Okada, and N. Mataga, *J. Chem. Soc., Chem. Commun.*, **1972**, 1009.

2) T. Okada, T. Fujita, M. Kubota, S. Masaki, N. Mataga, R. Ide, Y. Sakata, and S. Misumi, *Chem. Phys. Lett.*, **14**, 563 (1972).

3) N. Nakashima, N. Mataga, C. Yamanaka, R. Ide, and S. Misumi, *Chem. Phys. Lett.*, **18**, 386 (1973).

4) E. A. Chandross in "The Exciplex," ed by M. Gordon and W. R. Ware, Academic Press, New York (1975).

5) T. Okada, T. Fujita, and N. Mataga, *Z. Physik. Chem.*, **NF 101**, 57 (1976).

6) A. Siemiarczuk, Z. R. Grabowski, A. Krówczynski, M. Asher, and M. Ottolenghi, *Chem. Phys. Lett.*, **51**, 315 (1977).

7) W. Baumann, F. Petzke, and K.-D. Loosen, *Z. Naturforsch.*, **34a**, 1070 (1979).

8) Z. R. Grabowski, K. Rotkiewicz, and A. Siemiarczuk, *J. Luminescence*, **18/19**, 420 (1979).
9) Z. R. Grabowski, K. Rotkiewicz, A. Siemiarczuk, D. J. Cowley, and W. Baumann, *Nouv. J. Chim.*, **3**, 443 (1979).
10) M. Migita, T. Okada, N. Mataga, Y. Sakata, S. Misumi, N. Nakashima, and K. Yoshihara, *Bull. Chem. Soc. Jpn.*, **54**, 3304 (1981).
11) A. Siemiarczuk, J. Koput, and A. Pohorille, *Z. Naturforsch.*, **37a**, 598 (1982).
12) W. Baumann and H. Bischof, *J. Mol. Struct.*, **84**, 181 (1982).
13) T. Okada, M. Kawai, T. Ikemachi, N. Mataga, Y. Sakata, S. Misumi, and S. Shionoya, *J. Phys. Chem.*, **88**, 1976 (1984).
14) A. Siemiarczuk, *Chem Phys. Lett*, **110**, 437 (1984).
15) T. Okada, Y. Kobayashi, H. Yamasa, and N. Mataga, *Chem. Phys. Lett.*, **128**, 583 (1986).
16) G. Wermuth, *Z. Naturforsch.*, **38a**, 368 (1983).
17) N. Detzer, W. Baumann, B. Schwager, J.-C. Fröhling, and C. Brittinger, *Z. Naturforsch.*, **42a**, 395 (1987).
18) W. Liptay in "Excited States," ed by E. C. Lim, Academic Press, New York (1974), Vol. 1.
19) W. Baumann, *Ber. Bunsenges. Phys. Chem.*, **80**, 231 (1976).
20) W. Baumann and H. Bischof, *J. Mol. Struct.*, **129**, 125 (1985).
21) W. Baumann and H. Deckers, *Ber. Bunsenges. Phys. Chem.*, **81**, 786 (1977).
22) H. Bischof, W. Baumann, N. Detzer, and K. Rotkiewicz, *Chem. Phys. Lett.*, **116**, 180 (1985).
23) H. Bischof and W. Baumann, *Z. Naturforsch.*, **40a**, 874 (1985).
24) a) H. Masuhara, N. Ikeda, H. Miyasaka, and N. Mataga, *J. Spectrosc. Soc. Jpn.*, **31**, 19 (1982). b) H. Miyasaka, H. Masuhara, and N. Mataga, *Laser Chem.*, **1**, 359 (1983).
25) "Technique of Organic Chemistry Vol. VII, Organic Solvents," ed by A. Weissberger, Interscience Publ., New York (1967).
26) A. L. McClellan, "Tables of Experimental Dipole Moments," Vol. 1, ed by W. H. Freeman, San Francisco (1963) and Vol. 2, Rahara Enterprises, El Cerrito (1974).
27) W. Baumann, to be published.
28) T. Okada, N. Mataga, W. Baumann, and A. Siemiarczuk, *J. Phys. Chem.*, **91**, 4490 (1987).
29) K. Rotkiewicz, K.-H. Grellmann, and Z. R. Grabowski, *Chem. Phys. Lett.*, **19**, 315 (1973).
30) W. Rettig, *Angew. Chem.*, **98**, 969 (1986).

 © 1987 The Chemical Society of Japan Bull. Chem. Soc. Jpn., 60, 4251—4257 (1987)

Temperature Dependence of the Reflectance Spectra of the Single Crystals of Bis(ethylenedithio)tetrathiafulvalenium Salts. α-(BEDT-TTF)$_3$(ReO$_4$)$_2$ and α-(BEDT-TTF)$_2$I$_3$

Kyuya YAKUSHI,* Hirohisa KANBARA, Hiroyuki TAJIMA, Haruo KURODA, Gunzi SAITO,† and Takehiko MORI††
Department of Chemistry, Faculty of Science, The University of Tokyo, Hongo, Tokyo 113
†Institute for Solid State Physics, the University of Tokyo, Roppongi, Tokyo 106
††Institute for Molecular Science, Okazaki, Aichi 444
(Received June 15, 1987)

Polarized reflectance spectra were measured on the single crystals of α-(BEDT-TTF)$_3$(ReO$_4$)$_2$ and α-(BEDT-TTF)$_2$I$_3$. The optical spectra of these materials were interpreted on the basis of a simple semimetallic band model, and the anisotropic character of the intermolecular interaction in these crystals was quantitatively examined by analyzing the observed spectra. The observed temperature dependence of reflectance spectrum reflects the change of the electronic structure accompanying the metal-insulator phase transition, and is consistent with our interpretation of the spectra.

In the charge-transfer salts of BEDT-TTF(bis(ethylenedithio)tetrathiafulvalene), the Peierls instability is expected to be suppressed by the introduction of a relatively strong interchain interaction through sulfur atoms.[1,2] In fact studies on the crystal structures of BEDT-TTF salts revealed a presence of the two-dimensional network of short S-S contacts.[3] The optical experiment on (BEDT-TTF)$_4$(ClO$_4$)$_2$(TCE)$_{1.0}$ proved that a strong charge-transfer interaction between donor molecules takes place through these S-S contacts.[4] Some of the trihalide salts of BEDT-TTF remain metallic down to low temperature and exhibit a superconducting transition at ambient pressure.[5-8] However. a large majority of BEDT-TTF salts undergo a metal-insulator transition at low temperature. The nature of this metal-insulator transition has not been well characterized so far. α-(BEDT-TTF)$_3$(ReO$_4$)$_2$[9,10] and α-(BEDT-TTF)$_2$I$_3$[11-13] belong to this kind of BEDT-TTF salt, showing the metal-insulator transition at 88 and 135 K, respectively. The phase transitions of these materials have been studied by means of the electrical[9,11] and magnetic[10,12,13] experiments. These experiments are sensitive to a small change near a Fermi surface, whereas the optical experiment probes the overall band structure. Furthermore, the optical experiment is a powerful tool to inspect the effect of an electron-electron correlation. We have conducted a systematic study on the metallic BEDT-TTF salts and analyzed the optical spectra on the basis of a simple one-electron band model.[14-18] In this paper we present the experimental results of the temperature dependence of the reflectance spectra of α-(BEDT-TTF)$_3$(ReO$_4$)$_2$ and α-(BEDT-TTF)$_2$I$_3$, and discuss the change of the electronic structure accompanying the metal-insulator phase transition.

Experimental

Single crystals of α-(BEDT-TTF)$_3$(ReO$_4$)$_2$ and α-(BEDT-TTF)$_2$I$_3$ were prepared by using an electrochemical method from the tetrahydrofuran and benzonitrile solutions, respectively. The dimensions of the crystal used in this experiment were 1×2 mm^2 for α-(BEDT-TTF)$_2$I$_3$ and 1.5×1.5 mm^2 for α-(BEDT-TTF)$_2$I$_3$. Polarized reflectance spectra were measured from 720 cm^{-1} to 25000 cm^{-1} by using the two types of microspectrophotometers, the one for the visible and near-infrared regions and the other for the infrared region, both of which were designed in our laboratory (Department of Chemistry, the University of Tokyo) to measure the reflectivity of a tiny crystal.[13,19] A polarized reflectance spectrum was measured for the two polarization directions parallel to the optical axes projected onto the crystal face. These axes were searched by using the light of 3330 cm^{-1}, because the dispersion of reflectivity around this wavenumber was strongest in the spectral region concerned with the present experiment. The optical axes are mutually perpendicular and give the maximum and minimum reflectivities. The crystallographic axes which correspond to these directions were identified by means of X-ray diffraction. As cryostats to cool the sample crystal, Oxford CF104A was used for the infrared spectrometer and CTi SPECTRIM^{tm} for the visible spectrometer. The sample crystal was fixed with vacuum grease on a Si single crystal plate, the surface of which was painted by carbon paint to remove a stray light, and was transferred from one cryostat to another. The Si plate was glued with silver paint onto the goniometer head which was fixed to the cold stage of the cryostat. A thermocouple, Au(Fe)/Chromel, was attached near the sample on the goniometer head. The electrical resistivity of α-(BEDT-TTF)$_3$(ReO$_4$)$_2$ were measured along the c-axis by using a low-frequency four-probe method. The electrical contacts to the 10 μm gold wires were made by carbon paint.

Results and Discussion

α-(BEDT-TTF)$_3$(ReO$_4$)$_2$. The crystal of α-(BEDT-TTF)$_3$(ReO$_4$)$_2$ belongs to the monoclinic system, six BEDT-TTF molecules being contained in the unit cell.[20] Figure 1 shows the polarized reflectance spectrum measured on the (010) crystal face, the arrangement of BEDT-TTF molecules in one of the two crystallographically equivalent molecular sheets being also shown there. The maximum dispersion was found for the light polarization parallel to the [102] axis. This axis coincides with the direction of the maximum overlap integral between the neighboring

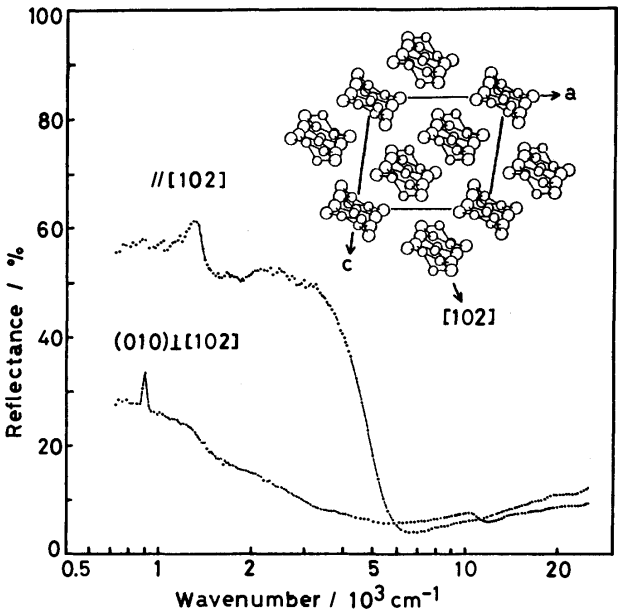

Fig. 1. Reflectance spectrum of α-(BEDT-TTF)$_3$(ReO$_4$)$_2$. The inset shows the crystal structure viewed nearly along the long axis of BEDT-TTF molecule.

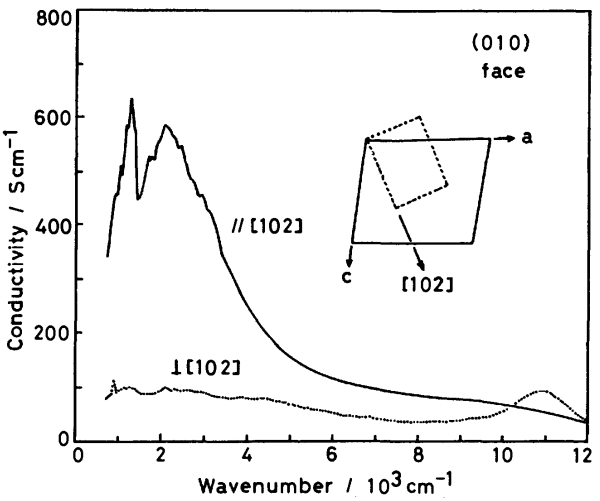

Fig. 2. Conductivity spectrum of α-(BEDT-TTF)$_3$(ReO$_4$)$_2$. The inset shows the relation between the unit cell (solid line) and the reduced cell (dotted line).

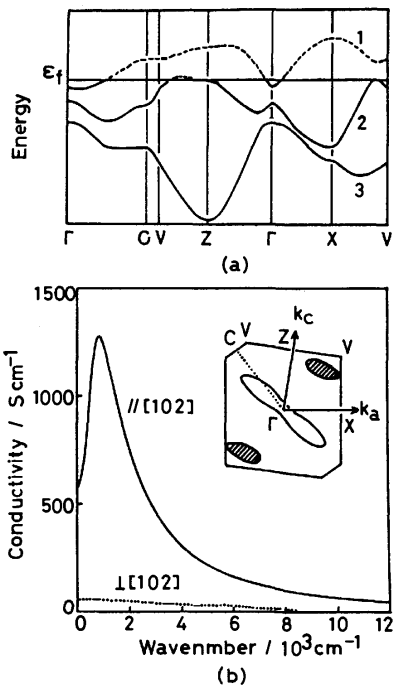

Fig. 3. (a) Band structure of α-(BEDT-TTF)$_3$(ReO$_4$)$_2$. (b) Conductivity spectrum of α-(BEDT-TTF)$_3$(ReO$_4$)$_2$ calculated by assuming the point charge approximation. The inset shows the names of special points and the Fermi surface in the Brillouin zone.

BEDT-TTF molecules. Therefore, this material is essentially composed of the molecular chains along the [102] axis, although the molecules are stacking along the [$\bar{1}$01] axis. However, a weak dispersion was also observed in the low-wavenumber region of the ⊥[102] spectrum. This dispersion clearly indicates the existence of a significant magnitude of interchain interaction. Figure 2 shows the optical conductivity spectrum obtained through the Kramers-Kronig transformation of the reflectance spectrum illustrated in Fig. 1. The integrated intensity of the electronic transition in the infrared region is related to the magnitude of the intermolecular interaction along the polarization direction. In order to obtain a quantitative measure for the anisotropy of the intermolecular interaction, we calculated the average transfer integrals in the hypothetical reduced unit cell drawn in the inset of Fig. 2. The method of calculation is the same as the one used by Jacobsen in the analysis of β-(BEDT-TTF)$_2$I$_3$.[21] We calculated the plasma frequency by the following equation,

$$\omega_p^2 = 8\int_0^{10\times10^3\,\mathrm{cm}^{-1}} \sigma(\omega)\,\mathrm{d}\omega$$

and obtained $\omega_{p//}$=9.5×10^3 cm^{-1} and $\omega_{p\perp}$=4.8×10^3 cm^{-1}. Then, the transfer integrals were calculated to be $t_{//}$=0.10 eV and $t_\perp$=0.07 eV by using $d_{//}$=6.0 Å (//[102]) and $d_\perp$=4.4 Å (⊥[102]). The ratio, $t_{//}/t_\perp$=1.4, is much smaller than the corresponding value, 10, found for (TMTSF)$_2$PF$_6$.[22] This fact indicates the strong two dimensionality of α-(BEDT-TTF)$_3$(ReO$_4$)$_2$.

The conductivity spectrum of the //[102] polarization exhibits a broad peak around 2000 cm^{-1} and a sharp peak at 1250 cm^{-1}. The feature that the conductivity falls down at low wavenumber showing a peak around 2000 cm^{-1} is not dependent on the method of extrapolation of the reflectivity which has to be assumed in the Kramers-Kronig transformation. This spectral shape inevitably comes from the low reflectivity in the low-wavenumber region. The presence of the peak is also supported by the comparison with the DC electrical conductivity which corresponds to the

optical conductivity at zero wavenumber. The DC conductivity measured at room temperature along the c-axis is about 20 $S\,cm^{-1}$, which is much smaller than the maximum conductivity, 600 $\Omega^{-1}\,cm^{-1}$ at 2000 cm^{-1}. The observed shape of the conductivity spectrum is significantly different from that predicted from a Drude model. For organic conductors, the deviation from the Drude-like line shape in conductivity spectrum has been often interpreted as the one associated with a strong Coulomb interaction between conduction electrons. This kind of interpretation was given for the spectrum of $(TMTTF)_2X$ salts.[23,24] If this is the case, the optical transition across a Hubbard gap or equivalently the charge-transfer transition between the BEDT-TTF cations should be observed around 5×10^3 cm^{-1}[25] in the //[102] spectrum, since two of the three BEDT-TTF molecules are formally cations, and in this situation the probability for the neighboring BEDT-TTF molecules to be the cation state is quite large. In fact, the corresponding charge-transfer band was observed in the case of the radical salts of TTF halides[26] which have a similar situation. However, we could not find any dispersion corresponding to the charge-transfer between neighboring cations in the near infrared region of the //[102] spectrum. Therefore, we adopted another standpoint, that is to consider the effect of the interband transition on the basis of one-electron model. For example, the optical spectrum of graphite is considerably deviated from a Drude model due to the presence of the interband transition

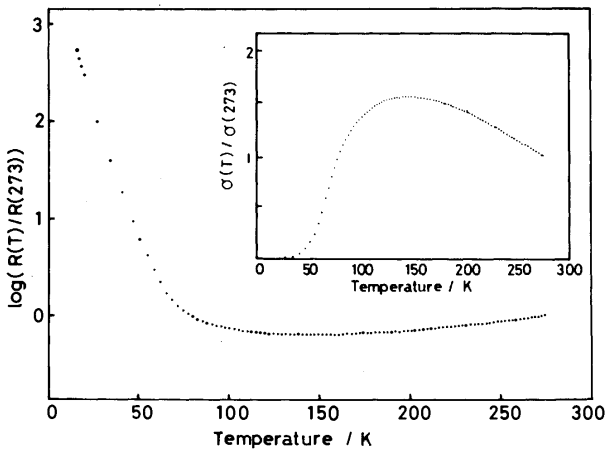

Fig. 4. Temperature dependence of the electrical resistivity and conductivity (inset) of α-(BEDT-TTF)$_3$(ReO$_4$)$_2$.

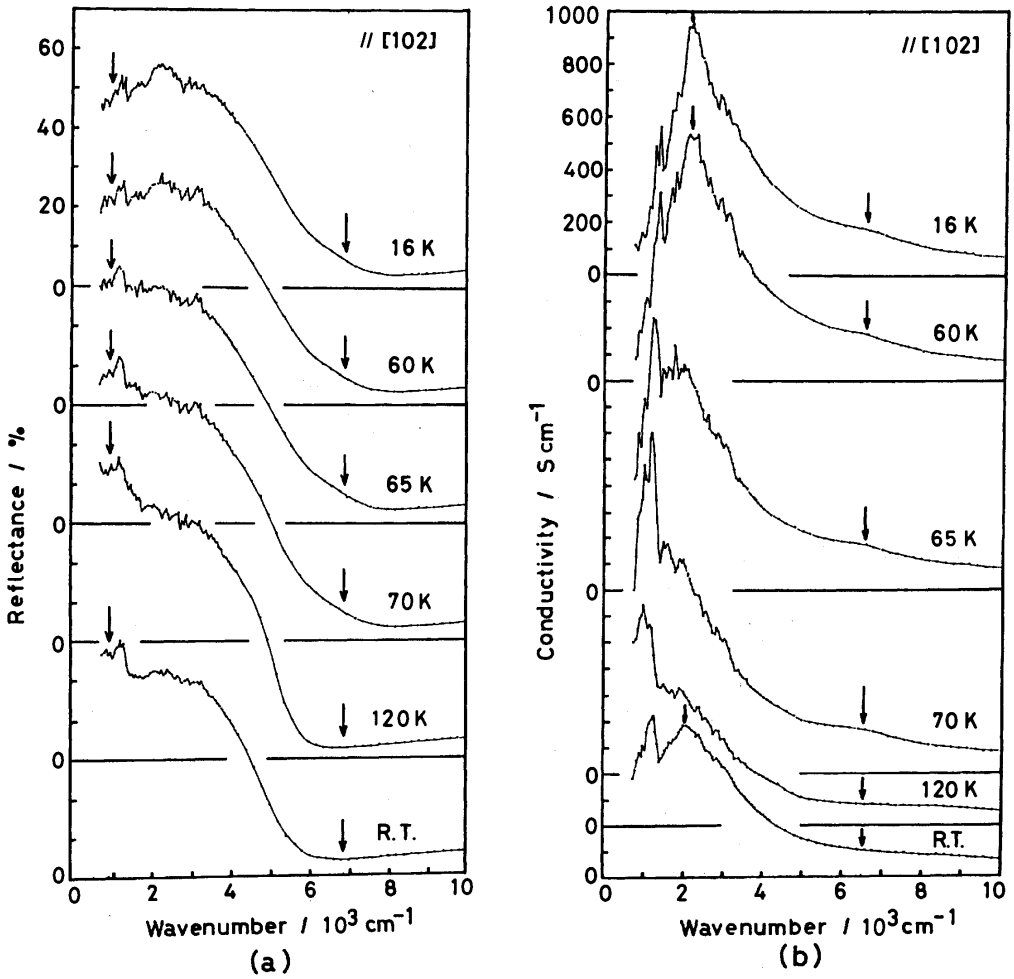

Fig. 5. Temperature dependence of (a) reflectance spectrum and (b) conductivity spectrum of α-(BEDT-TTF)$_3$(ReO$_4$)$_2$.

near the plasma edge.[27] To examine the effect of the interband transition we calculated the two-dimensional band structure in the (010) plane using the tight binding approximation within the framework of the extended Huckel method. The π-band produced from the HOMO's of BEDT-TTF splits into three, among which the lower two bands were nearly filled as shown in Fig. 3a, since the two-dimensional unit cell contains three BEDT-TTF molecules and two of them is oxidized. Therefore, this material is predicted to have a semimetallic small Fermi surface. Figure 3b shows the conductivity spectrum calculated by the point charge approximation on the basis of this band structure.[16] This spectrum contains the contribution of the intraband transition associated with the conduction electrons at the small Fermi surface, and the contribution of the interband transition from the bands 2 and 3 to the band 1. The agreement with the observed spectrum shown in Fig. 2 is qualitatively good.

Parkin et al. found a metal-insulator transition in the experiment on the electrical resistivity of α-$(BEDT\text{-}TTF)_3(ReO_4)_2$: The resistivity showed a shallow minimum at about 150 K and steeply increased at about 115 K.[9] On the other hand, Carneiro et al. reported a gentle phase transition at about 88 K in the ESR expriment.[10] Our result of the electrical resistivity measured along the c-axis was illustrated in Fig. 4. The shallow minimum appeared at almost the same temperature as that of Parkin et al., but this sample showed a steeper slope at about 85 K. No hysteresis was observed in the cooling and heating cycle. This metal-insulator transition is very gentle and is similar to the temperature dependence of the magnetic susceptibility. Figure 5a shows the temperature dependence of the //[102] reflectance spectrum. On lowering temperature, salient changes were observed typically around 900 and 6800 cm^{-1} as shown by arrows in Fig. 5a. Let us first discuss the change observed in the low-wavenumber region. The temperature dependence of the reflectivity at 900 cm^{-1} were plotted in Fig. 6a. A gentle but remarkable change of reflectivity takes place around the phase-transition temperature. The increase of the reflectivity from room temperature to 120 K is probably related to the increase of the relaxation time of the conduction electrons, and the decrease below 70 K corresponds to the disappearance of the conduction electrons probably due to the some structural change. The temperature dependence of the optical conductivity spectra were shown in Fig. 5b. The peak of the interband transition shifts to the low-wavenumber side on lowering the temperature from room temperature to 120 K, then shifts to the high wavenumber side from 70 K to 60 K, and remains at the same position below 60 K down to 16 K. The reason for the gradual shift of the interband transition below 70 K is not clear at present. Since the peak position of the interband transition at 16 K is almost the same as that of room temperature spectrum, we consider that the metal-insulator transition brings about a minor change to the overall structure of the energy band, although it gradually introduces a small band gap at low temperature. In contrast to the temperature dependence of reflectivity around 900 cm^{-1}, the reflectivity change at 6800 cm^{-1} abruptly increases on going

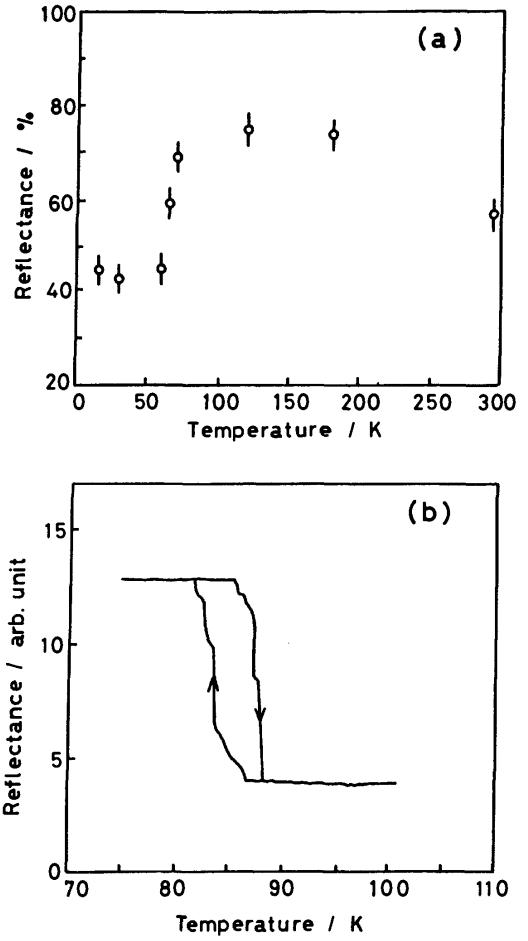

Fig. 6. Temperature dependence of the reflectivity of α-$(BEDT\text{-}TTF)_3(ReO_4)_2$ at (a) 900 cm^{-1} and (b) 6800 cm^{-1}.

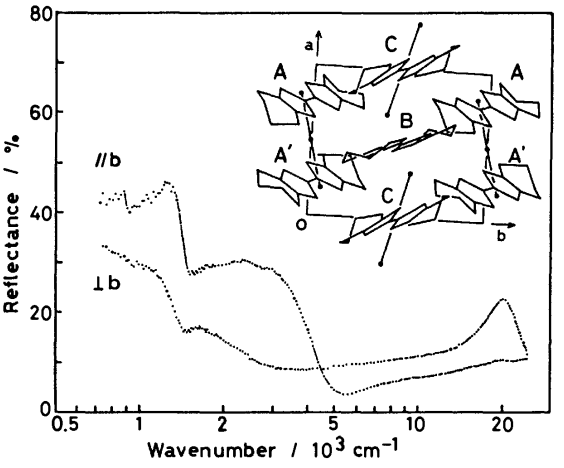

Fig. 7. Reflectance spectrum of α-$(BEDT\text{-}TTF)_2I_3$. The inset shows the crystal structure projected onto the (001) plane.

from the metallic phase to the semiconductive phase, as shown in Fig. 5a. The details of the temperature dependence were examined at 6000 cm^{-1} by changing the sample temperature at the rate of 2° min^{-1}. The results are shown in Fig. 6b, which clearly indicates the abrupt reflectivity change around the phase transition temperature reported by Carneiro et al. The increase of the reflectivity is reflected on appearance of a hump at about 6500 cm^{-1} in the conductivity spectrum as shown in Fig. 5b. This new hump may be associated with the transition from the band 3 to the band 1 which is introduced by a small structural change on the phase transition. Another possible assignment is that this weak hump corresponds to the charge-transfer band between BEDT-TTF^{+} which appears as the result of the reduction of the screening effect in the semiconductive phase.

α-(BEDT-TTF)$_2I_3$. The crystal of α-(BEDT-TTF)$_2I_3$ belongs to triclinic system and the unit cell contains four BEDT-TTF molecules as shown in Fig. 7.[10] The structure is composed of two crystallographically independent stacks along the a-axis. However, the maximum reflectivity at 3330 cm^{-1} was found in the polarization direction parallel to the b-axis. Figure 7 shows the polarized reflectance spectra measured on the (001) crystal face. The reflectivity and the anisotropy of the reflectance spectrum are much smaller

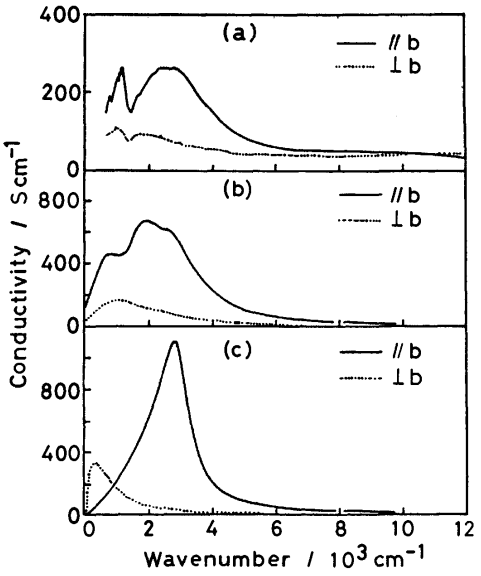

Fig. 8. Conductivity spectrum of α-(BEDT-TTF)$_2I_3$. (a) The observed spectrum (b) calculated spectrum based on the two-dimensional model (c) calculated spectrum based on the one-dimensional model.

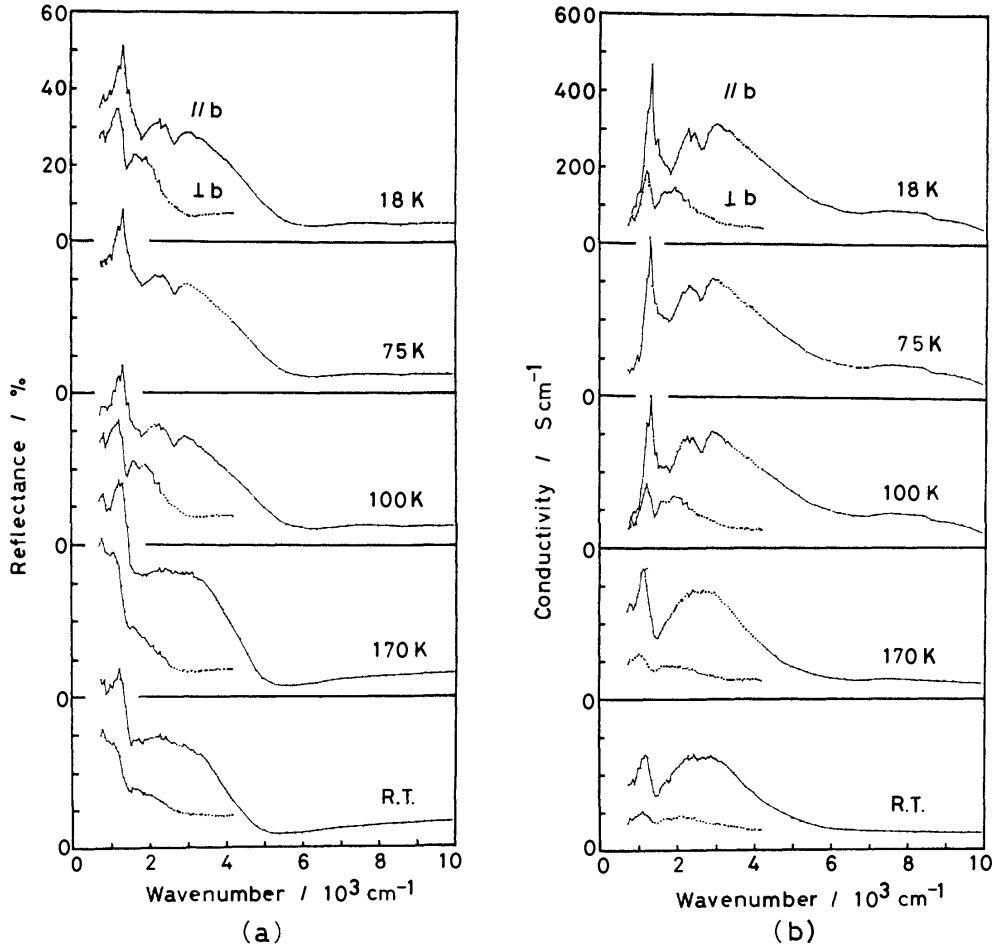

Fig. 9. Temperature dependence of (a) reflectance spectrum and (b) conductivity spectrum of α-(BEDT-TTF)$_2I_3$.

than those of α-(BEDT-TTF)$_3$(ReO$_4$)$_2$. The conductivity spectrum was shown in Fig. 8a. The average transfer integrals obtained by the same method mentioned in the previous section were $t_{//}$=0.07 eV and $t_{\perp}$=0.06 eV, the ratio being 1.2, where we used the anisotropic plasma frequencies $\omega_{p//}$=6.5×10^3 cm^{-1} and $\omega_{p\perp}$=4.6×10^3 cm^{-1} and the reduced unit cell parameters, $d_{//}$=5.4 Å (//b) and $d_{\perp}$=4.6 Å ($\perp$b). The small anisotropy of transfer integrals is in accord with the almost isotropic electrical resistivity.[10] We calculated the conductivity spectra of the intraband and interband transitions based on the semi-metallic band structure reported by Mori et al.[28] The calculated result shown in Fig. 8b coincides qualitatively with the observed spectra: The transition probability for the //b polarization is larger than that for the $\perp$b polarization, and the //b transition appears at the higher wavenumber region than the $\perp$b transition. According to the overlap integral calculated by Mori et al., the largest two integrals which are those between C and A′ and between A′and B are markedly larger as compared with the remaining integrals. If we neglect the latters, the electronic structure becomes one-dimensional along the zigzag chain through C-A′-B-A-C. The conductivity spectra calculated by this model are shown in Fig. 8c. We wish to emphasize that the interchain interaction is quite important to reproduce the line shape of the observed spectrumm.

α-(BEDT-TTF)$_2$I$_3$ is metallic at room temperature and exhibits a metal-insulator transition at 135 K, according to the experiment of the electrical resistivity.[10] It was also reported that the intensity and the line width of ESR signal suddenly decreased at about 135 K.[11,12] The study by X-ray diffraction elucidated the structural change that the inversion symmetry, which exists in the high-temperature phase, is lost in the low-temperature phase.[29] The change of the infrared spectrum also indicated the symmetry breaking at low temperature.[30] All these experiment suggest that the phase change is of the first order. Figures 9a and 9b show the temperature dependence of the reflectance spectrum and the conductivity spectrum. The spectra at different temperatures in the metallic phase are essentially the same with each other, and those in the semiconductive phase are also the same with each other. To examine the temperature dependence in detail, we conducted the same experiment as that we have done on α-(BEDT-TTF)$_3$(ReO$_4$)$_2$, at the wavenumber of 5600 cm^{-1}. The reflectivity change took place abruptly and no hysteresis was observed as shown in Fig. 10. These optical results are consistent with the results of other experiments. The remarkable features found for the spectrum of the semiconductive phase are (1) the decrease of the reflectivity and therefore the decrease of the conductivity in the low-wavenumber region, (2) the splitting (2350 and 2950 cm^{-1}) of the broad interband transition at 2600 cm^{-1}, and (3) the increase of the reflectivity around the tail of

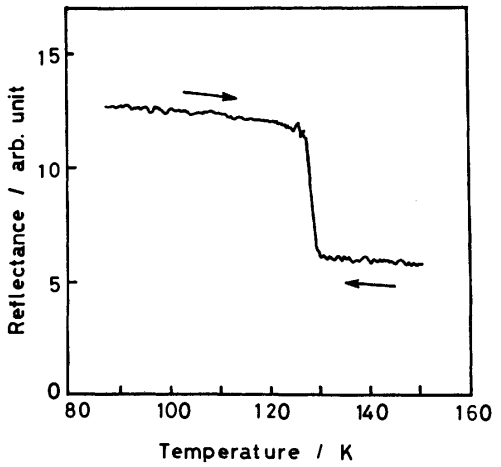

Fig. 10. Temperature dependence of the reflectivity of α-(BEDT-TTF)$_2$I$_3$ at 5600 cm^{-1}.

the interband transition at about 5000 cm^{-1}. The first one corresponds to the disappearance of the conduction electrons. The second and the third are probably related to a small change of the band structure arising from the slight structural change. Incidentally, it is worth to be noted that the spectral change observed at 5000 cm^{-1} on α-(BEDT-TTF)$_2$I$_3$ is very much similar to that observed for the semiconductive phase of α-(BEDT-TTF)$_3$(ReO$_4$)$_2$.

Summary and Conclusion

The anisotropic character of intermolecular interaction was examined by determining the average transfer integrals from the observed reflectance data. We conclude that the two-dimensional interaction of α-(BEDT-TTF)$_3$(ReO$_4$)$_2$ is weaker than that of α-(BEDT-TTF)$_2$I$_3$ but significantly stronger than that of Bechgaard salts. The observed electronic transition of the BEDT-TTF salts in the infrared region was interpreted to be an overlap between the strong interband transition and the weak intraband transition. We found two common features on the temperature dependence of the reflectance spectra of the two salts. The one is the decrease of the reflectance at low wavenumber on lowering temperature in the semiconductive phase due to the decrease of the density of conduction electrons, the other is the appearance of a new hump at high-wavenumber region. A curious phenomenon was found in the temperature dependence of the hump of α-(BEDT-TTF)$_3$(ReO$_4$)$_2$: This hump appeared abruptly near the phase transition temperature although the phase transition takes place rather gradually. Finally it should be noted that the optical conductivity spectra did not change drastically between the metallic and semiconductive phases. This fact further support that the electronic transition of the infrared region is attributable mainly to the interband transition.

References

1) G. Saito, T. Enoki, K. Toriumi, and H. Inokuchi, *Solid State Commun.*, **42**, 557 (1982).

2) G. Saito, T. Enoki, and H. Inokuchi, *Chem. Lett.*, **1982**, 1395.

3) H. Kobayashi, R. Kato, T. Mori, A. Kobayashi, Y. Sasaki, G. Saito, T. Enoki, and H. Inokuchi, *Mol. Cryst. Liq. Cryst.*, **107**, 33 (1984).

4) H. Tajima, K. Yakushi, H. Kuroda, G. Saito, and H. Inokuchi, *Solid State Commun.*, **49**, 769 (1984).

5) E. B. Yagubskii, I. F. Shchegolev, V. N. Laukhin, P. A. Kononovich. M. V. Kartsovnik. A. V. Zvarykina, and L. Z. Buravov, *JETP Lett.*, **39**, 12 (1984).

6) K. Murata, M. Tokumoto, H. Anzai, H. Bando, G. Saito, K. Kajimura, and T. Ishiguro, *J. Phys. Soc. Jpn.*, **54**, 1236 (1985).

7) J. M. Williams, H. H. Wang, M. A. Beno, T. J. Emge, L. M. Sowa, P. T. Copps, F. Behroozi, L. N. Hall, K. D. Carlson, and G. W. Crabtree, *Inorg. Chem.*, **23**, 3839 (1984).

8) J. M. Williams, M. A. Beno, U. Geiser, M. A. Firestone, K. S. Webb. L. Nunez, G. W. Crabtree, and K. D. Carlson, *Physica B+C (Amsterdam)*, **29** (1985).

9) S. S. P. Parkin, E. M. Engler, V. Y. Lee, and R. R, Schumaker, *Mol. Cryst. Liq. Cryst.*, **119**, 375 (1985).

10) K. Carneiro, J. C. Scott, and E. M. Engler, *Solid State Commun.*, **50**, 477 (1984).

11) K. Bender, K. Dietz, H. Endres, H. W. Helberg, I. Hennig, H. J. Keller, H. W. Schafer, and D. Schweitzer, *Mol. Cryst. Liq. Cryst.*, **107**, 45 (1984).

12) E. L. Venturini, L. J. Azevedo, J. E. Shirber, J. M. Williams, and H. H. Wang, *Phys. Rev., B*, **32**, 2819 (1985).

13) T. Sugano, G. Saito, and M. Kinoshita, *Phys. Rev. B*, **34**, 117 (1986).

14) H. Kuroda, K. Yakushi, H. Tajima, and G. Saito, *Mol. Cryst. Liq. Cryst.*, **125**, 135 (1985).

15) H. Tajima, K. Yakushi, H. Kuroda, and G. Saito, *Solid State Commun.*, **56**, 159 (1985).

16) H. Tajima, K. Yakushi, H. Kuroda, and G. Saito, *Solid State Commun.*, **56**, 251 (1985).

17) H. Tajima. H. Kanbara, K. Yakushi, H. Kuroda, and G. Saito, *Solid State Commun.*, **57**, 911 (1986).

18) K. Yakushi, H. Tajima, H. Kanbara, M. Tamura, H. Kuroda, G. Saito, H. Kobayashi, R. Kato, and A. Kobayashi, *Physica*, **143B**, 463 (1986).

19) Y. Iyechika, K. Yakushi, and H. Kuroda, *Solid State Commun.*, **49**, 769 (1980).

20) H. Kanbara, H. Tajima, S. Aratani, K. Yakushi, H. Kuroda, G. Saito, A. Kawamoto, and J. Tanaka, *Chem. Lett.*, **1986**, 437.

21) C. S. Jacobsen, J. M. Williams, and H. H. Wang, *Solid State Commun.*, **54**, 937 (1985).

22) C. S. Jacobsen, D. B. Tanner, and K. Bechgaard, *Phys. Rev. B*, **28**, 7019 (1983).

23) C. S. Jacobsen, I. Johannsen, and K. Bechgaard, *Phys. Rev. Lett.*, **53**, 194 (1984).

24) K. Yakushi, S. Aratani, K. Kikuchi, H. Tajima, and H. Kuroda, *Bull. Chem. Soc. Jpn.*, **59**, 363 (1986).

25) We studied the optical spectrum of the 1 : 1 salts of BMDT-TTF which has the same conjugated moiety as BEDT-TTF, in order to estimate the on-site Coulomb energy. We found a charge-transfer band between BMDT-TTF's at about 5×10^3 cm^{-1} which is polarized parallel to the S-S direction. M. Yoshitake, K. Yakushi, H. Kuroda, H. Kobayashi, R. Kato, and A. Kobayashi, *Bull. Chem. Soc. Jpn.*, to be published.

26) H. Kuroda, K. Yakushi, and Y. Cao, *Mol. Cryst. Liq. Cryst.*, **85**, 325 (1982).

27) D. M. Hoffman, R. E. Heinz, G. L. Doll, and P. C. Eklund, *Phys. Rev. B*, **32**, 1278 (1985).

28) T. Mori, A. Kobayashi, Y. Sasaki, H. Kobayashi, G. Saito, and H. Inokuchi, *Chem. Lett.*, **1984**, 957.

29) Y. Nogami, S. Kagoshima, T. Sugano, and G. Saito, *Synthetic Metals.* **16**, 367 (1986).

30) M. Meneghetti, R. Bozio, and C. Pecile, *J. Phys. (Paris).* **47**, 1377 (1986).

 © 1987 The Chemical Society of Japan Bull. Chem. Soc. Jpn., 60, 4259—4266 (1987)

A High-Resolution Solid-State ^{13}C NMR Study of the Secondary Structure of Linear (1→3)-β-D-Glucans: A Conformational Elucidation of Noncrystalline and Crystalline Forms by Means of Conformation-Dependent ^{13}C Chemical Shifts

Hazime SAITÔ,* Ryoko TABETA, Motoko YOKOI, and Tomoki ERATA†
Biophysics Division, National Cancer Center Research Institute, Tsukiji 5-chome, Chuo-ku, Tokyo 104
†Bruker Japan Co., Ltd., 21-5, Ninomiya, Yatabe, Tsukuba, Ibaraki 305
(Received June 19, 1987)

The high-resolution solid-state ^{13}C NMR spectra of annealed curdlan, a (1→3)-β-D-glucan, were recorded in order to obtain reference data on the ^{13}C chemical shifts of the triple helix form, which would be useful for the conformational elucidation of two distinct noncrystalline forms, curdlan- and laminaran-types. It was found that the C-3 peak of crystalline annealed glucan is substantially displaced from that of noncrystalline starting powder, reflecting the conformational change. The laminaran-type conformation, which is found in either laminaran or a number of fungal branched glucans, was identical with the triple helix, judging from the similarity in the ^{13}C NMR spectra, although the linewidths of the former are much larger than those of the latter. The curdlan-type form, on the other hand, was ascribed to the single helix form on the basis of the previous data on high-resolution ^{13}C NMR. In addition, the ^{13}C NMR spectra of crystalline paramylon showed a number of additional signals other than the peaks of triple-helical annealed curdlan, in spite of the similarity in the X-ray diffraction patterns.

It has been previously shown that the solution properties, including the gelation behavior, of a number of (1→3)-β-D-glucans vary greatly with various parameters, such as the degree of branching, the molecular weight, and the manner of annealing.[1,2] Undoubtedly, such properties might be closely related to the secondary or tertiary structures of these polysaccharides in the solid, fully or partially hydrated, and unhydrated portions of gels, and a (fully hydrated) aqueous solution.

A fully hydrated aqueous solution of a linear (1→3)-β-D-glucan (Fig. 1) is achieved either at a higher alkaline solution (>0.2 M NaOH (1 M=1 mol dm^{-3})) or at neutral pH for lower molecular-weight glucan[3,4] and the relevant molecular conformation of this state is effectively random-coiled, as may be seen from the displacements of the ^{13}C chemical shifts as well as the relaxation parameters. The molecular architecture of the gel state formed by a linear (1→3)-β-D-glucan (curdlan) (Fig. 1) is , however, very complicated. It is considered to consist of the following two or three regions: fully or partially hydrated and unhydrated portions. In particular, the former, which is not detected by X-ray diffraction, gives rise to well-resolved isotropic ^{13}C NMR signals.[2-5] The rest of the immobilized unhydrated region, which is not detected by means of high-resolution NMR, can be characterized by the triple[7-10] or single helices[11] and their dehydrated aggregates by means of X-ray diffraction.

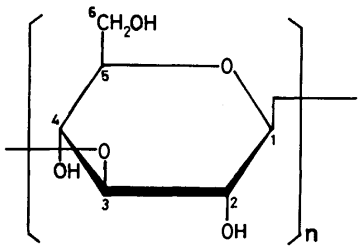

Fig. 1. Primary structure of a linear (1→3)-β-D-glucan. Curdlan (from *Alcaligenes faecalis*), n=540; laminaran (from *Porio cocos*), n=38; paramylon (from *Euglena gracila*).

The conformational feature of curdlan powder used as the starting material of gel formation or of the lyophilized sample from the gel cannot, however, be analyzed by the use of the X-ray diffraction method because of its extremely poor crystallinity: alternative means must be utilized. In fact, only 30% of the former is crystalline.[12] Nevertheless, our previous finding, based on the ^{13}C NMR data, showed that spray-dried or lyophilized (1→3)-β-D-glucans from various sources in the solid state do not necessarily take a disordered conformation,[13,14] but two kinds of distinct, regular secondary structures, curdlan-type and laminaran-type forms, as revealed by the conformation-dependent ^{13}C chemical shifts.[15,16] This finding is based on the fact that the ^{13}C chemical shifts of the C-1 and C-X carbons at the glycosidic linkage of various types of glucans are closely related to the torsion angles of C-1-O$_{gly}$ (ϕ) and C-X-O$_{gly}$ (ψ), respectively.[17-19] Hence, the conformation of the noncrystalline region can be as well characterized by this NMR technique as that of the crystalline portion.

In the present paper, we recorded the ^{13}C NMR spectra of several types of curdlan samples annealed at various temperatures, together with two additional linear (1→3)-β-D-glucans, laminaran and paramylon (Fig. 1), in order to clarify these conformations further. As a result, we were able to ascribe the curdlan- and laminaran-type conformations[14] of a variety of noncrystalline (1→3)-β-D-glucans to the single- and triple-helical conformations, respectively. It was further

shown, on the basis of the ^{13}C spin-lattice relaxation data, that the molecular organization of the noncrystalline portion was not dynamically disordered as compared with that of the crystalline samples.

Experimental

Materials. Curdlan powder was provided by Takeda Chemical Industries Co., Ltd., Osaka. Laminaran was purchased from Nutritional Biochemistry Corporation, Ohio, USA. Paramylon was a generous gift from Professor B. A. Stone of La Trobe University, Australia. The annealed curdlan samples were prepared by a manner similar to that described previously.[7] That is, an aqueous suspension of curdlan powder was heated at various temperatures (80—180 °C) in a sealed bomb. The resulting gel samples were cooled either slowly or rapidly, together with dehydration by means of air-drying or immersion in a methanol solution. The densities of the resultant samples were measured by means of floatation in a xylene-carbon tetrachloride. The crystallinities were estimated from the X-ray powder patterns at room humidity (40% r. h.) by the use of a Rigaku Geigerflex X-ray diffractometer RAD IIIA, employing Ni-filtered Cu $K\alpha$ radiation generated at 40 kV and 30 mA.

Method. The high-resolution solid state ^{13}C NMR spectra at 75.46 MHz were recorded on a Bruker CXP-300 spectrometer by means of the cross polarization-magic angle spinning (CP-MAS) method. Powdered samples were placed in an alumina rotor used for the double air-bearing-type MAS system and spun as fast as 3—3.5 kHz. The duration of the 90° pulse was 4 μs. The contact, sampling and repetition times were 1 ms, 20—30 ms, and 4 s, respectively. The ^{13}C chemical shifts were referred to TMS through the peak position of the glycine carboxyl group (176.0 ppm). The ^{13}C spin-lattice relaxation times (T_{1C}'s) were measured by the method of cross polarization enhancement, with an inversion of the proton-spin temperature.[20]

Results

Figures 2 and 3 show the ^{13}C CP-MAS NMR spectra of annealed curdlan at various temperatures, together with those of laminaran, curdlan powder, and paramylon. Figures 4A and B illustrate some X-ray powder diffraction patterns of annealed curdlan under different conditions (Table 1) and of laminaran, respectively. The powder X-ray diffraction patterns of Samples 1 and 2 and of paramylon[9] (data not shown) exhibit high crystallinity and coincide with that of the triple-helical conformation, previously analyzed.[7-9] On the other hand, the diffraction patterns of Samples 3, 5, and 6 and also of laminaran were very diffusive because of their lower crystallinity. The extent of crystallinity from the X-ray diffraction is parallel with the magnitude of the density, as is summarized in Table 1.

It is noteworthy that Samples 1 and 2 gave the narrowest NMR signals (about 1 ppm linewidths) among all the samples examined herein except for paramylon. In parallel with this observation, the crystallinity of these two samples is found to be significantly improved by the annealing, as is shown by the X-ray powder diffraction (Fig. 4A) and density data (Table 1). The ^{13}C NMR peaks of C-3 and C-2/C-5 carbons are also displaced from those of the starting curdlan powder (Table 2).

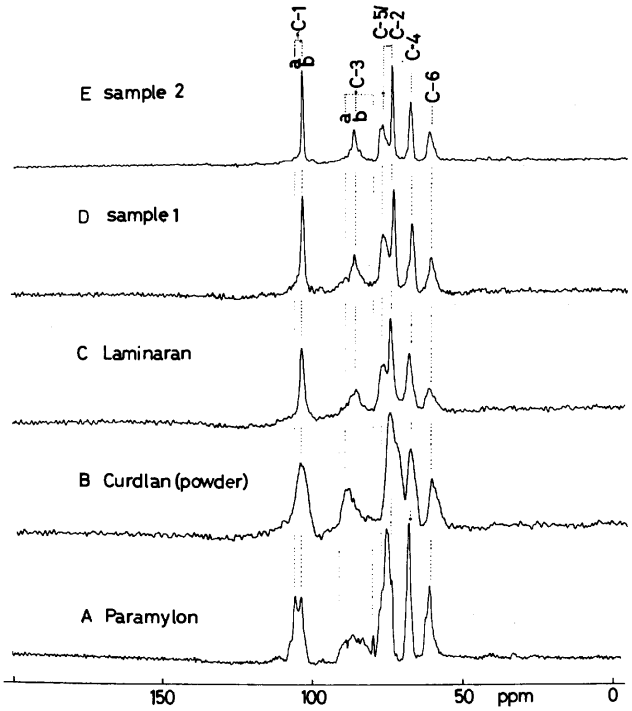

Fig. 2. 75.46 MHz ^{13}C CP-MAS NMR spectra of some linear (1→3)-β-D-glucans in the solid state.
A: Paramylon, B: curdlan powder, C: laminaran, D: Sample 1 (annealed curdlan at 180°C, followed by slow cooling), and E: Sample 2 (annealed curdlan at 150°C, followed by slow cooling).

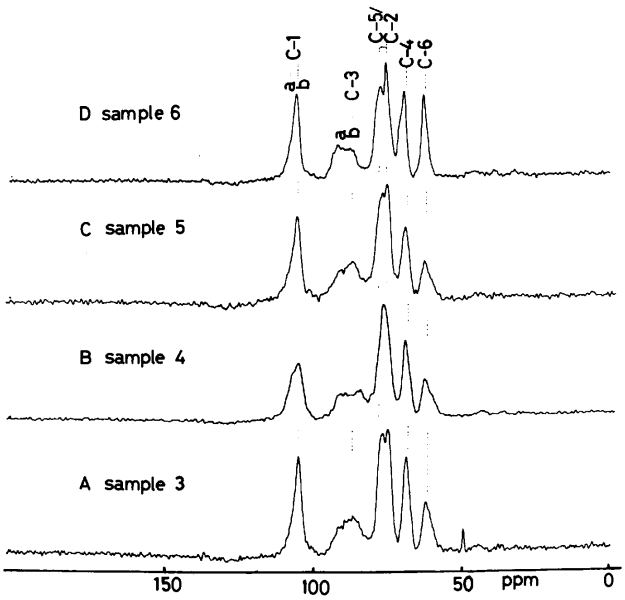

Fig. 3. 75.46 MHz ^{13}C CP-MAS NMR spectra of annealed curdlan, followed by rapid cooling (A—C).
A: Sample 3 (annealing at 180°C), B: Sample 4 (annealing at 150°C), C: Sample 5 (annealing at 120°C), and D: Sample 6 (annealing at 80°C, followed by slow cooling).

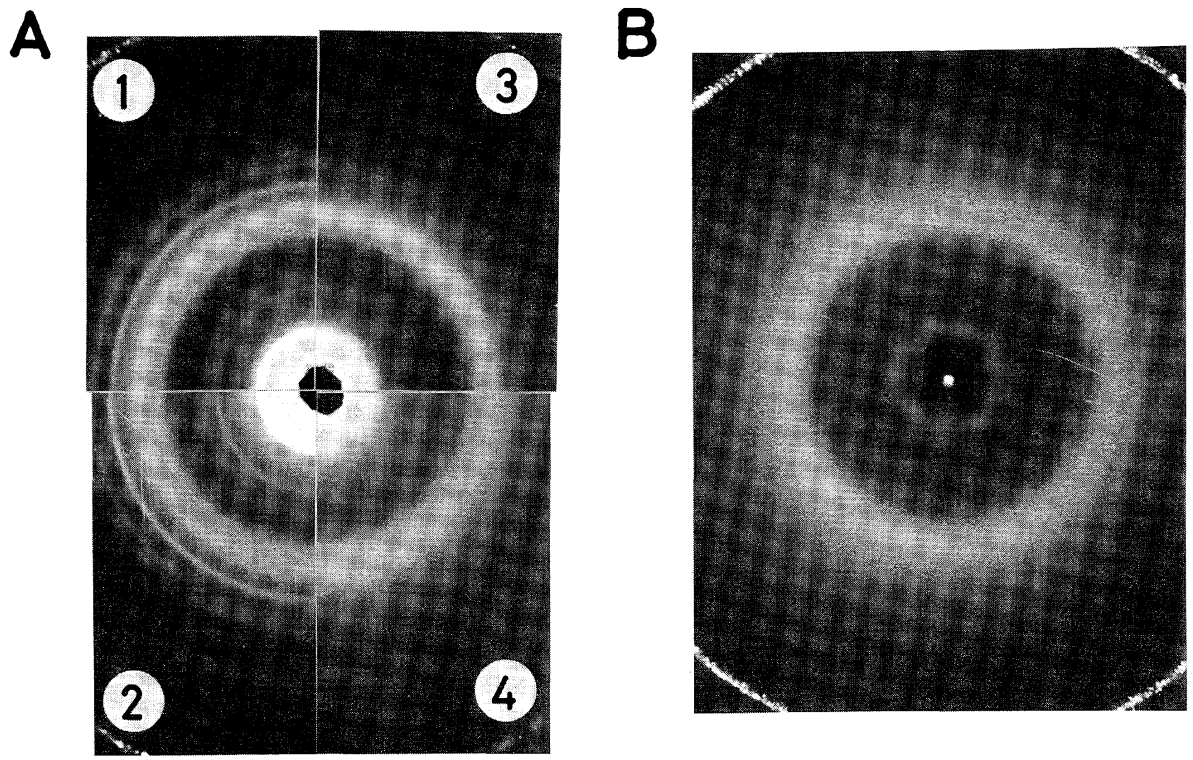

Fig. 4. X-Ray powder diffraction patterns of some (1→3)-β-D-glucans in the solid state. A: Annealed curdlan: 1; Sample 1, 2; Sample 2, 3; Sample 3, and 4; Sample 5. B: Laminaran.

Table 1. Characteristics of Annealed Curdlan together with Paramylon

Sample	Condition for sample preparation		Density	Crystallinity (by X-ray diffraction)
	Annealing temp/°C	After annealing	g cm^{-3}	
1	180	Slowly cooled/air-dried	1.49	High[a]
2	150	Slowly cooled/MeOH-dehydrated	1.49	High
3	180	Rapidly cooled/MeOH-dehydrated	1.45	Low
4	150	Rapidly cooled/air-dried	1.49	High
5	120	Rapidly cooled/MeOH-dehydrated	1.48	Low
6	80	Slowly cooled/MeOH-dehydrated	1.46	Very low
Curdlan powder			1.44[b]	Very low
Paramylon			1.53[b]	High

a) Slightly lower than that of Samples 2 and 4. b) Ref. 12.

Table 2. ^{13}C Chemical Shifts (ppm from TMS) of Annealed (1→3)-β-D-Glucans and Related Polysaccharides

		Annealed sample						Untreated sample		
		Sample 1	Sample 2	Sample 3	Sample 4	Sample 5	Sample 6	Laminaran	Curdlan	Paramylon
C-1	a				105.6					105.7
	b	103.7	103.6	103.5	103.5	103.7	103.7	103.4	104.1	103.8
C-2		74.3	74.3	74.5	76.0[a]	74.6[a]	74.3[a]	74.3	74.0	76.2
C-3	a			90.4	89.8	89.7	90.1		89.7	89.5
	b	87.1	86.9	85.9		86.6	85.0	86.9		
					83.8					80.4
C-4		68.6	68.4	68.7	69.2	68.6	68.4	68.4	69.3	68.9
C-5		78.0	78.4	78.4	76.0[a]	76.0[a]	76.3[a]	76.7	76.1	76.2
			77.5							
C-6		62.2	61.8	62.2	62.5	62.7	61.9	62.1	62.3	61.7
										63.0

a) The peak assignment may be interchangeable.

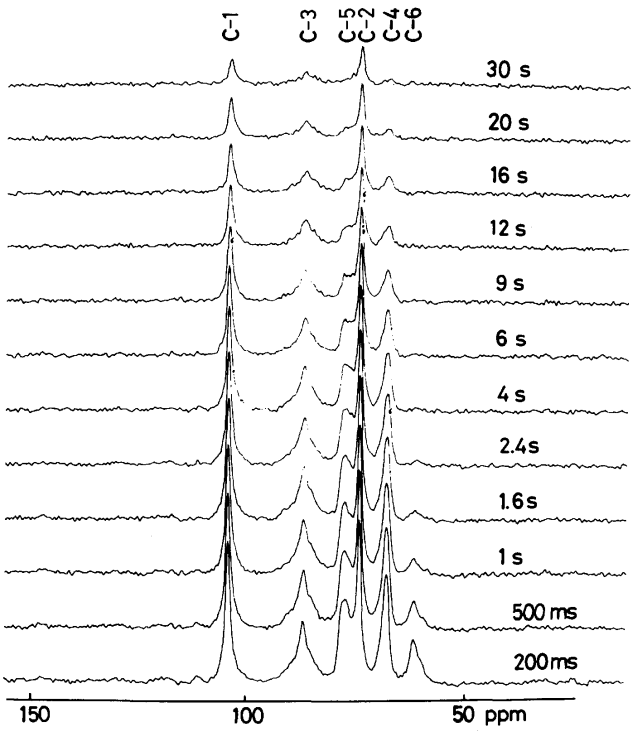

Fig. 5. Stacked plot of ^{13}C NMR peak intensities of annealed curdlan obtained by cross polarization for the T_{1C} measurements. Delay times between two 90° pulses are indicated in the right-hand side. Number of transients is 100.

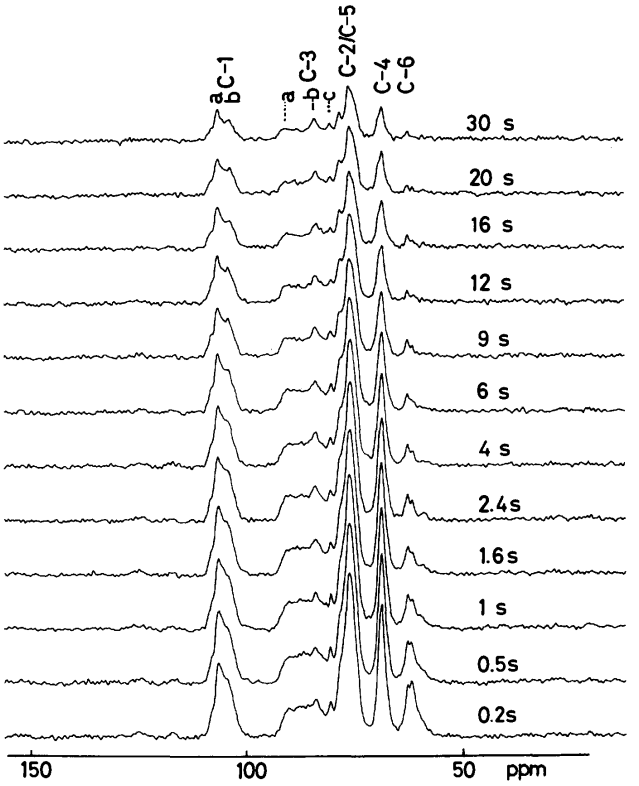

Fig. 6. Stacked plot of ^{13}C NMR peak intensities of paramylon obtained by cross polarization for the T_{1C} measurements. Delay times between two 90° pulses are indicated in the right-hand side. Number of transients is 100.

Surprisingly, the ^{13}C NMR pattern of laminaran is very similar to that of the annealed curdlan (Samples 1 and 2) in spite of its poor crystallinity, as may be seen from the X-ray diffraction data (Fig. 4B). The conformational change in curdlan from the noncrystalline to the crystalline form, however, is not complete when annealed samples at 150 and 120 °C were cooled rapidly (Samples 3 and 5). As a result, the C-3 NMR peak consists of two kinds of contributions: the peak from unconverted noncrystalline powder (C-3a) and that from converted crystalline species (C-3b). Further, it is interesting to note that the high-field shoulder of the C-3 peak in Sample 4 is resonated at 83.8 ppm, much higher than that of most annealed samples (86—87 ppm). In addition, the C-1 peaks appear to be split into doublet, 105.6 and 103.5 ppm. These data show that the ^{13}C NMR spectral pattern of Sample 4 resembles that of paramylon. Crystallinity and density of Sample 4 are found to be very high in spite of the broadened linewidths of its ^{13}C NMR pattern.

Figures 5 and 6 illustrate some typical examples of a stacked plot of the ^{13}C NMR spectra of annealed curdlan and paramylon, respectively, for measurements of the ^{13}C spin-lattice relaxation times (T_{1C}'s) by cross-polarization.[20] In this pulse sequence, the peak intensity at the delay time t after turning off the ^{13}C H_1 field, $M_{net}(t)$, decays exponentially from its initial value, $2M_{cp}(0)$, as is shown by Eq. 1,

Table 3. ^{13}C Spin-Lattice Relaxation Times of Some (1→3)-β-Glucans (s)[a]

	Curdlan		Laminaran	Paramylon
	Powder	Annealed[b]		
C-1	14	16	26	31(a),[c] 30(b)[c]
C-2	10[d]	18	24	22[d]
C-3	11	16	20	26(a),[c] 34(b),[c] 32(c)[c]
C-4	7.8	8.2	13	12
C-5	10[d]	9.3	10	22[d]
C-6	1.0	1.2	1.7	6.3

a) Estimated error ±15%. b) Sample 2 (see Table 1). c) Letters in parentheses denote the peak indicated in Fig. 6. d) Not distinguishable.

$$M_{net}(t) = 2M_{cp}(0)\exp(-t/T_{1C}) \quad (1)$$

Thus, the T_{1C} values were obtained from a plot of log $M_{net}(t)$ vs. t, as is summarized in Table 3. Interestingly, it appears that the T_{1C} values of the annealed curdlan and laminaran can be classified into the following three groups: peaks with short (1.2—1.7 s for C-6), intermediate (8—13 s for C-4 and C-5), and long (16—26 s for C-1, C-2, and C-3) relaxation times. The existence of such a step in the relaxation times could be related to the ease of spin diffusion process with the hydroxymethyl group which undergoes rapid internal reorientation process. There appears to be no signifi-

cant differences in the T_{1C} values of curdlan between the noncrystalline and crystalline forms. The T_{1C} values of laminaran and paramylon are, however, significantly longer than those of curdlan. In particular, the C-6 T_{1C} of paramylon is 5—6 times as long as those of the curdlan samples (Table 3). Further, we found that the T_{1C} values differ among the three peaks, C-3a, b and c (see Fig. 6 and Table 3).

Discussion

Triple Helix: Laminaran-Type Form. The sharp ^{13}C NMR pattern of annealed curdlan at 150—180 °C (Figs. 2D and E) is straightforwardly ascribed to the triple-helical conformation,[7-9] in view of its characteristic X-ray powder-diffraction patterns (Fig. 4A). The above-mentioned pronounced peak narrowing (ca. 1 ppm) is obviously caused by the improved crystallinity of samples due to annealing in the presence of water, as is consistent with our previous observation of annealed chitosan.[21] The achievement of peak-narrowing as well as conformational change is not sufficient when annealed samples at 120—180 °C are cooled rapidly (Samples 3 and 5, see Fig. 3). In fact, the magnitude of the conformational change to the triple helix is, at most, 50% at the time of annealing (150—180 °C); additonal conversion was achieved by a slow crystallization process, together with concomitant dehydration during the course of the slow cooling.

Subsequently, we found that the laminaran-type conformation[14] found in laminaran and fungal branched glucans is identified with the same triple-helical conformation in view of the similarity in ^{13}C NMR patterns between laminaran and annealed curdlan (Samples 1 and 2) (Fig. 2C—E). This finding is in contrast to the observation by means of X-ray diffraction: laminaran exhibits a poor crystallinity, judging from the X-ray diffraction (Fig. 4B), whereas annealed curdlan (Samples 1 and 2) exhibits a high crystallinity and its diffraction pattern is obviously different from that of laminaran (Fig. 3A). Nevertheless, the present ^{13}C NMR data show that the overall conformation of noncrystalline laminaran is the same as that of the triple-helix form of annealed curdlan, but the presence of conformations whose torsion angles are slightly deviated from those of the most stable triple-helical conformation results in line-broadening. In addition, it is pointed out that a number of fungal branched (1→3)-β-D-glucans take a triple-helical conformation similar to that of laminaran, judging from the similarity of the ^{13}C NMR spectra, as discussed in the previous[14] and subsequent papers.[22]

Single Helix: Curdlan-Type Form. No information is available from X-ray diffraction as to the conformation of the curdlan-type form arising from the noncrystalline portion of the powder sample. In fact, curdlan powder accounts for only about 30% crystalline portion as estimated from density-measurements.[12] Nevertheless, the conformation of the remaining major portion (about 70%) is not always completely disordered, because the C-3 ^{13}C NMR peaks of this form from various samples are always resonated at the same position (89.6±0.5 ppm), which is clearly distinguishable from that of the above-mentioned triple-helix conformation (86.4±0.5 ppm). It should be emphasized that this form corresponds to the *native* conformation of curdlan, directly isolated from solid cultures of *Alcaligenes faecalis*.[13] In a similar manner, we previously showed, on the basis of the ^{13}C chemical shifts, that the molecular conformation of the disordered or random-coiled form, as judged by the X-ray diffraction, of silk fibroin is very similar to that of the crystalline silk I form.[23,24] This discrepancy may arise from the fact that conformational analysis by means of X-ray diffraction requires regular arrangement of the molecules under consideration with the neighboring molecules or interstrands, whereas the present ^{13}C NMR approach is able to afford the conformational characterization of individual molecules, irrespective of the manner of the arrangement of the neighboring molecules.

As has been demonstrated previously, intense high-resolution ^{13}C NMR signals of curdlan gel are visible (70—80%)[5] at the temperature of swelling (54 °C; low-set gel), but the peak-intensities are substantially decreased by annealing at temperatures higher than 54 °C, together with the development of the turbidity. Obviously, the portion which gives rise to the high-resolution NMR signals corresponds with the fully hydrated region, so as to give freedom of isotropic molecular motion with the correlation times of an order of 10^{-9} s.[2-4] This portion turned out to be an ordered conformation by the characteristic displacement of the C-3 ^{13}C chemical shifts[3,4] as well as by optical rotatary dispersion, intrinsic viscosity, flow birefringence, and shift of absorption maximum with Congo Red.[25-27] We previously ascribed this ordered conformation to a single helix, in view of the ease of swelling in aqueous media, resulting in the formation of a fully hydrated region able to give high-resolution ^{13}C NMR signals.[2-4,28] The relative proportion of such a fully hydrated portion (65—80%),[2] as observed by high-resolution ^{13}C NMR, at the temperature of swelling, is very close to the estimated proportion of the noncrystalline region (about 70% by density measurement[12]). Thus, it is natural to consider that the conformation of the noncrystalline portion of curdlan powder arises from this single helix. This view is based on premise that the conformation achieved in aqueous media could be preserved in lyophilized samples, because no further heat treatment required for conformational transition is given. In supporting this view, we previously found that the conformations of silk I and (L-Ala-Gly)$_n$ II achieved in an aqueous solution are also retained in lyophilized solids, judging

from the ^{13}C NMR data.[23] In addition, we showed previously that lyophilized (1→3)-β-D-glucans gave the same peak positions, depending on their molecular weight or on the solvents used.[36] In this connection, it should be taken into account that the single helix form, which is an energetically favored conformation in the fully hydrated state, is not always favored in the solid. For this reason, the conformation achieved in a lyophilized or spray-dried sample should not be considered to be the most stable conformation, as established by the calculation of the conformational energy.[12]

Interestingly, the ^{13}C NMR spectra of Samples 3, 5, and 6 (Figs. 3A, C, and D, respectively) are very similar to those of the acid-degraded lower-molecular-weight fraction (DP_n 14—131) of curdlan (see Fig. 4 of Ref. 14). Obviously, in these samples the relative proportion of the triple-helix form is increased to about 50%, as compared with that (about 10% from the peak area) of the starting curdlan powder.[12] These samples do not any longer possess gel-forming ability, because there are very few portions left able to swell because of the increased proportion of the triple helix. These results clearly show that gel-forming ability of (1→3)-β-D-glucan is simply related to the relative proportion of the triple helix. As for the gelation behavior of branched (1→3)-β-D-glulcans, however, we will discuss it in more detail in the subsequent paper.[22]

Paramylon. It has been shown that the X-ray powder diffraction pattern of paramylon is very similar to that of the hydrate triple helix of curdlan.[9] Unexpectedly, however, the ^{13}C NMR spectrum of paramylon can not be explained simply by the peak profile of the triple-helical curdlan alone, although the presence of the ^{13}C NMR peaks from the latter can easily be recognized. Instead, the presence of the conformational heterogeneity of this paramylon is well demonstrated by the spreads of several C-3 carbon signals, ranging from 89.5 to 80.4 ppm, their maximum separation being 9.1 ppm, in addition to the observation of the doublet C-1 peaks. This view is also confirmed by the observation of the differential behavior of the ^{13}C spin-lattice relaxation times among the peaks ascribed to the same carbons (C-3 or C-5/C-2 peaks) of paramylon (see Fig. 6 and Table 3). Further, it appears that the C-2/C-5 peaks consist of the superposition of several kinds of peaks, indicating the presence of a conformational heterogeneity. It is obvious that Fig. 2 also contains peaks from the curdlan-type form. Therefore, it is conceivable that highly crystalline paramylon (see the density data in Table 1) contains conformers which are essential for relaxing conformational strain, in addition to the usual triple helix. In this connection, it is interesting that a paramylon-like conformation was produced by annealing at 150 °C, followed by rapid cooling (Sample 4; Table 1 and Fig. 3B), although the crystalline packing of paramylon which is produced at the time of biosynthesis can not be well reproduced by a simple annealing procedure.

^{13}C Spin-Lattice Relaxation Data. The observed relaxation times, ranging from 8 to 34 s, indicate that these polysaccharides lack molecular motion whose correlation time of an order of 10^{-8} s effective in shortening the T_{1C} values. Instead, the spin-lattice relaxation of this magnitude may be mainly affected by the ^{13}C spin diffusion.[37] The presence of the fast rotational motion of the hydroxymethyl group leads to the effective ^{13}C T_{1C} relaxation pathways coupled with spin exchange. Then, it is expected that the ^{13}C T_{1C}'s of the C-4 and C-5 carbons are subsequently reduced as a result of the spin exchange with the C-6 hydroxylmethyl group, because the rate of the spin exchange is proportional to r^{-6} where r is the interatomic distance. On the contrary, longer T_{1C} values observed in paramylon could be interpreted in terms of lack of efficient relaxation pathways due to plausible restricted rotation of the hydroxymethyl group. This is an additional piece of evidence which suggests that the conformation of paramylon is different from that of the triple-helical curdlan.

Therefore, it appears that these ^{13}C T_{1C} values reflect the manner of crystalline packing, effective in the spin diffusion process. In fact, the present ^{13}C T_{1C} values of (1→3)-β-D-glucans are much shorter than those of the crystalline component of cellulose[38,39] but longer than those of the noncrystalline component.[38] No such a distinction can, however, be observed in the present cases. In fact, noncrystalline samples characterized by X-ray diffraction are not necessarily motionally disordered. On the contrary, it has been shown that the T_{1C}'s of the amorphous portion of polyethylene or polyoxymethylene (50—200 ms) are much shorter than those of crystalline portion (20—2000 s).[40-42] The observed reduction of the former can be explained mainly in terms of the presence of segmental motions in the solid.

Concluding Remarks. The molecular conformations of noncrystalline polysaccharides do not necessarily take a disordered form, although this view cannot be clarified by X-ray diffraction study. Nevertheless, we previously showed that two distinct types of conformations of (1→3)-β-D-glucans, the curdlan- and laminaran-type forms, are distinguishable for a number of noncrystalline solid samples by an examination of the characteristic displacements of the C-3 ^{13}C chemical shifts. As an illustrative example, we attempted to reveal the conformations of these two forms with the aid of a high-resolution NMR study of curdlan gel and a high-resolution solid-state ^{13}C NMR study of annealed curdlan. Thus, the curdlan- and laminaran-type forms were ascribed to single and triple helix conformations, respectively. Finally, we pointed out that the conformation of paramylon can not be accounted for simply by the presence of the triple helix of annealed curdlan alone, in view of the

spreads of the ^{13}C chemical shifts and differences in the spin-lattice relaxation times.

The authors wish to thank Dr. Kozo Ogawa, Radiation Center of Osaka Prefecture, for his preparation of the annealed samples, and measurements of the density and the X-ray diffraction, and for his stimulating discussion. The authors are also grateful to Professor B. A. Stone for a generous gift of paramylon.

References

1) T. Harada, "Extracellular Microbial Polysaccharides," ed by P. A. Sandford and A. Laskin, ACS Symp. Ser. No. 45, American Chemical Society, Washington D. C. (1977), pp. 265—283.

2) H. Saitô, "Solution Properties of Polysaccharides," ed by D. A. Brant, ACS Symp. Ser. No. 150, American Chemical Society, Washington D. C. (1981), pp. 125—147.

3) H. Saitô, T. Ohki, and T. Sasaki, *Biochemistry*, **16**, 908 (1977).

4) H. Saitô, E. Miyata, and T. Sasaki, *Macromolecules*, **11**, 1244 (1978).

5) In the gel state, ^{13}C NMR peaks are usually suppressed to some extent because of the restricted molecular motions caused by the presence of cross links. The observed maximum peak intensities of swollen gels were 65—80% as referred to the peak intensities of fully hydrated 0.22M NaOH solution (Ref. 2). Further heating of the gel sample (80 °C) resulted in the subsequent reduction of the peak intensities to about 20% in parallel with the development of turbidity and a shrinkage of the gel sample. A similar extent of peak intensities (20—50%) was noted at an ambient temperature. In this connection, it is worthwhile to recall that the introduction of 0.1 and 1 mol% cross links in a chemically cross-linked synthetic polymer resulted in the reduction of peak intensities to 55 and 35%, respectively (Ref. 6).

6) K. Yokota, A. Abe, S. Hosaka, I. Sakai, and H. Saitô, *Macromolecules*, **11**, 97 (1978).

7) R. H. Marchessault, Y. Deslandes, K. Ogawa, and P. R. Sundararajan, *Can. J. Chem.*, **55**, 300 (1977).

8) Y. Deslandes, R. H. Marchessault, and A. Sarko, *Macromolecules*, **13**, 1466 (1980).

9) C. T. Chuah, A. Sarko, Y. Deslandes, and R. H. Marchessault, *Macromolecules*, **16**, 1375 (1983).

10) W. S. Fulton and E. D. T. Atkins, "Fiber Diffraction Methods," ed by A. D. French and K. H. Gardner, ACS Symp. Ser. No. 141, American Chemical Society, Washington, D. C. (1980) pp. 385—410.

11) H. Takeda, N. Yasuoka, N. Kasai, and T. Harada, *Polym. J.*, **10**, 365 (1978).

12) R. H. Marchessault and Y. Deslandes, *Carbohydr. Res.*, **75**, 231 (1979).

13) H. Saitô, R. Tabeta, and T. Harada, *Chem. Lett.*, **1981**, 571.

14) H. Saitô, R. Tabeta, T. Sasaki, and Y. Yoshioka, *Bull. Chem. Soc. Jpn.*, **59**, 2093 (1986).

15) H. Saitô, *Magn. Reson. Chem.*, **24**, 835 (1986).

16) H. Saitô, R. Tabeta, A. Shoji, T. Ozaki, I. Ando, and T. Asakura, "Magnetic Resonance in Biology and Medicine," ed by G. Govil, C. L. Kheterapal, and A. Saran, Tata McGraw-Hill, New Delhi (1985), pp. 195—215.

17) H. Saitô, G. Izumi, T. Mamizuka, S. Suzuki, and R. Tabeta, *J. Chem. Soc., Chem. Commun.*, **1982**, 1386.

18) F. Horii, A. Hirai, and R. Kitamaru, "Polymers for Fibers and Elastomers," ACS Symp. Ser. No. 260, American Chemical Society, Washington, D. C. (1982) pp. 27—42.

19) R. L. Dudley, C. A. Fyfe, P. J. Stephenson, Y. Deslandes, G. K. Hammer, and R. H. Marchessault, *J. Am. Chem. Soc.*, **105**, 2469 (1983).

20) D. A. Torchia, *J. Magn. Res.*, **30**, 613 (1978).

21) H. Saitô, R. Tabeta, and K. Ogawa, *Macromolecules*, **20**, 2424 (1987).

22) H. Saitô, R. Tabeta, Y. Yoshioka, C. Hara, T. Kiho, and S. Ukai, *Bull. Chem. Soc. Jpn.*, **60**, 4267 (1987).

23) H. Saitô, R. Tabeta, T. Asakura, Y. Iwanaga, A. Shoji, T. Ozaki, and I. Ando, *Macromolecules*, **17**, 1405 (1984).

24) T. Asakura, A. Kuzuhara, R. Tabeta, and H. Saitô, *Macromolecules*, **18**, 1841 (1985).

25) K. Ogawa, T. Watanabe, J. Tsurugi, and S. Ono, *Carbohydr. Res.*, **23**, 399 (1972).

26) K. Ogawa, J. Tsurugi, and T. Watanabe, *Carbohydr. Res.*, **29**, 397 (1973).

27) K. Ogawa, J. Tsurugi, and T. Watanabe, *Chem. Lett.*, **1973**, 95.

28) A decade ago,[3,4] we proposed that the ^{13}C NMR observation in gels is solely limited to the rather flexible *single* helical portion (the correlation time being in the order of 10^{-8} s) where molecular chains are fully exposed to the diluent and the peak areas of the triple-helical portion are lost under high-resolution NMR conditions. In fact, it is very difficult to account for the presence of the peak arising from the triple helix (86.4±0.4 ppm) in the ^{13}C NMR signal of elastic gel (88.7 ppm). Furthermore, we found that all of peak-areas were suppressed[29,30] when high-resolution ^{13}C NMR spectra of branched (1→3)-β-D-glucans taking the triple-helix conformation[31-33] were recorded in aqeuous media. Undoubtedly, such a suppression of peaks arose from an insufficient averaging of the C-H dipolar and/or chemical shift anisotropy interactions due to the presence of a slow tumbling motion of the stiff, rod-like molecules of the triple helix. In this connection, Yanaki et al. showed that the triple helix of schizophyllan, a branched (1→3)-β-D-glucan, is stiffer than that of native collagen, for the persistent chain length of the former (200±30 nm) is larger than that of the collagen triple helix (130 nm).[32,33] The preservation of chemical shift anisotropy as large as 50—140 ppm in native collagen[34,35] makes impossible the observation of the ^{13}C NMR spectra by means of high-resolution spectrometer. It may also be pointed out that the ease of the aggregation of the rod-like triple helix of curdlan, as manifested by syneris or dehydration, which are not seen in the triple helices of branched glucans, leads to an additional suppression of the NMR peaks.

29) H. Saitô, T. Ohki, N. Takasuka, and T. Sasaki, *Carbohydr. Res.*, **58**, 293 (1977).

30) H. Saitô, T. Ohki, and T. Sasaki, *Carbohydr. Res.*, **74**, 227 (1979).

31) T. Norisuye, T. Yanaki, and H. Fujita, *J. Polym. Sci., Polym. Phys. Ed.*, **18**, 547 (1980).

32) T. Yanaki, T. Norisuye, and H. Fujita, *Macromolecules*, **13**, 1462 (1980).

33) Y. Kashiwagi, T. Norisuye, and H. Fujita, *Macromolecules*. **14**, 1220 (1981).

34) S. K. Sarkar, C. E. Sullivan, and D. A. Torchia, *J. Biol.*

Chem., **258**, 9762 (1983).
35) S. K. Sarkar, C. E. Sullivan, and D. A. Torchia, *Biochemistry*, **24**, 2348 (1985).
36) This finding shows that the density of the triple-helical cross links is less than 10% in the low-set gel (Ref. 1). The observation of such a low density of cross links accounts well for the presence of high-resolution ^{13}C NMR signals in the gel state by taking into account of our previous data on chemically cross-linked gels.[5,6]
37) N. M. Szeverenyi, M. J. Sullivan, and G. E. Maciel, *J. Magn. Reson.*, **47**, 462 (1982).
38) F. Horii, A. Hirai, and R. Kitamaru, *J. Carbohydr. Chem.*, **3**, 641 (1984).
39) D. L. VanderHart, *J. Magn. Reson.*, **72**, 13 (1987).
40) W. L. Earl and D. L. VanderHart, *Macromolecules*, **12**, 762 (1972).
41) E. M. Menger, W. S. Veeman, and E. de Boer, *Macromolecules*, **10**, 384 (1977).
42) "High Resolution NMR Spectroscopy of Synthetic Polymers in Bulk," ed by R. A. Komoroski, VCH Publishers, Deerfield, Florida (1986).

 © 1987 The Chemical Society of Japan Bull. Chem. Soc. Jpn., 60, 4267—4272 (1987)

A High-Resolution Solid-State ^{13}C NMR Study of the Secondary Structure of Branched (1→3)-β-D-Glucans from Fungi: Evidence of Two Kinds of Conformers, Curdlan-Type Single-Helix and Laminaran-Type Triple-Helix Forms, as Manifested from the Conformation-Dependent ^{13}C Chemical Shifts

Hazime Saitô,* Ryoko Tabeta, Yûko Yoshioka,† Chihiro Hara,†† Tadashi Kiho,††† and Shigeo Ukai†††
Biophysics Division, and †Chemotherapy Division, National Cancer Center Research Institute, Tsukiji 5-chome, Chuo-ku, Tokyo 104
††Shotoku Gakuen Women's Junior College, Nakauzura, Gifu 500
†††Gifu Pharmaceutical University, Mitahora-higashi, Gifu 502
(Received June 19, 1987)

The high-resolution ^{13}C NMR spectra of a variety of fungal branched (1→3)-β-D-glucans were recorded in a DMSO solution and a lyophilized solid in order to gain an insight into the primary and secondary structures in relation to their gel-forming property. We found that all the five lyophilized branched (1→3)-β-D-glucans examined so far, except lentinan, exhibit the laminaran-type triple-helix form, as established by the close resemblance of the ^{13}C NMR spectra among them. On the contrary, lentinan taking the curdlan-type single-helix conformation was readily converted to the triple-helix form by lyophilization after having been dissolved in a 8M urea solution (1M=1 mol dm^{-3}) and dialysis against distilled water. This finding should be compared with the similar conformational change of curdlan: the conversion by this procedure was at most 50%; annealing at 150°C, followed by slow cooling, was essential for a complete conversion. This treatment did not induce the reverse conformational change from the triple helix to the single helix. The differential behavior of gel-formation between the linear and branched (1→3)-β-D-glucans was explained in terms of the molecular conformations in the solid and gel states.

The molecular conformation or polymorphs of crystalline polysaccharides have previously been analyzed by means of X-ray diffraction studies.[1] No information, however, is provided by this diffraction method as to the conformational feature of noncrystalline polymers or such region in crystalline samples. Nevertheless, the conformations of such portions are not necessarily the completely randomly coiled form. Instead, we have previously shown that a variety of biological macromolecules, such as polypeptides, fibrous proteins,[2-6] and polysaccharides,[7-10] obtained by lyophilization take regular conformation, as is shown by the characteristic displacements of ^{13}C chemical shifts. Thus, high-resolution solid-state ^{13}C NMR spectroscopy offers an excellent means for the conformational characterization of noncrystalline as well as crystalline samples. In particular, the ^{13}C chemical shifts vary significantly (up to 8 ppm) with the respective conformation as characterized by the glycosidic torsion angles (ϕ, ψ).[11-13] Thus, this approach has been used for the conformational characterization of a number of polysaccharides, including cellulose[12-19] chitin, chitosan,[9,20,21] amylose,[7,11] starch,[22-25] and (1→3)-β-D-glucans.[8,10,26-32]

The crystallinity of (1→3)-β-D-glucans is, in many instances, low so as to give a halo X-ray diffraction pattern, unless otherwise examined samples are extensively annealed. However, this treatment could severely alter the molecular conformation. Therefore, the development of a method for the in situ conformational characterization of a starting material is essential for better understanding of the conformational feature of these glucans in relation to their physical properties. For this purpose, we previously demonstrated[10] that at least four kinds of secondary structures could be distinguished by means of solid-state ^{13}C NMR spectra. In particular, two major forms, the curdlan- or laminaran-type forms, can readily be distinguished by means of the conformation-dependent ^{13}C chemical shifts when these samples are obtained either by lyophilization or spray-drying.[10] In the preceding paper, these curdlan- and laminaran-type forms were identified as having the single- and triple-helix conformation, respectively.[33]

Previously, we found that the gel-forming ability of linear (1→3)-β-D-glucans is related to the presence of a single helix as the major conformer, and swelling does not occur from samples taking the triple helix as the major conformation. In this connection, it is surprising to note that the two kinds of branched glucans previously studied, HA-β-glucan and lentinan, take the two different above-mentioned conformations, in spite of exhibiting a similar gel-forming property.[10] Therefore, it seems to be very important to clarify the stability and ease of conformational changes in branched (1→3)-β-D-glucans.

In the present paper, we will examine the ^{13}C NMR spectra of four additional branched (1→3)-β-D-glucans in order to clarify their conformations in the solid state. We noted that all five (1→3)-β-D-glucans assume the laminaran-type triple-helix. The curdlan-type single-helical conformation of lentinan was converted to the laminaran-type triple-helix when dialyzed after dissolving in 8M urea solution.

Table 1. Characteristics of Branched (1→3)-β-D-Glucans Used

Trivial name	Physical property	Chemical analysis		Source	Ref.
		m-(m'-)res./ b-res.[a]	1.6-linkage		
T-5-N	Soft gel	2.5(1.4)[b]	0.06	*Dictyophora industiata*	36
T-4-N	Highly viscous soln.	1.5	0	*Dictyophora industiata*	35
Schizophyllan	Extremely viscous	2	0	*Schizophyllum commune*	38
Scleroglucan		2	0	*Sclerotium rolfsii*	39
HA-β-Glucan	Non-elastic gel	3	0	*Pleurotus ostreatus*	34
Lentinan	Non-elastic gel	3.4—1.5	0.2	*Lentinus edodes*	37

a) m- and m'-residues stand for 3-mono-*O*-substituted glucosyl residues, while b-residue stands for the 3,6-di-*O*-substituted glucosyl residue. b) Data in parentheses are from enzymatic analysis (C. Hara, T. Kiho, and S. Ukai, *Carbohydr. Res.*, **117**, 201 (1983)).

Experimental

Table 1 summarizes the trivial names, physical properties, degrees of branching, and sources of isolation for the variety of fungal branched (1→3)-β-D-glucans used in this study. The isolation of HA-β-glucan[34] (from *P. ostreatus* (Fr.) Quél), T-4-N[35] and T-5-N[36] (from *Dictyophora indusiata* FISH.) was described previously. Lentinan[37] (from *Lentinus edodes*) was a generous gift from Dr. G. Chihara of the National Cancer Center Research Institute. Schizophyllan[38] and its partially depolymerized sample by sonication (from *Schizophyllum commune*) were donated by Kaken Pharmaceutical Co. Ltd., Tokyo, Japan. Scleroglucan[39] (from *Sclerotium rolfsii*) was provided by Taito Co. Ltd., Tokyo, Japan. These samples were first used as received, for the measurements of the high-resolution solid-state ^{13}C NMR spectra. Then, they (200 mg) were dissolved in an 8M urea solution (5 ml), dialyzed against distilled water, and lyophilized for use for further measurements of the solid-state-NMR. Curdlan (Takeda Chemical Industries, Osaka, Japan) and GE-3[40] (by courtesy of Dr. Y. Nishikawa of Kanazawa University) were used as reference compounds for the ^{13}C NMR spectra of (1→3)-β-D- and (1→6)-β-D-glucans, respectively.

The high resolution ^{13}C NMR spectra were recorded on a Bruker CXP-300 spectrometer operated at 75.46 MHz. These samples (30 mg) were dissolved in DMSO-d_6 (1.5 ml) and contained in a 10 mm NMR tube. Single-contact 75.46 MHz ^{13}C cross polarization-magic angle spinning (CP-MAS) NMR spectra were recorded on a Bruker CXP-300 spectrometer equipped with a CP-MAS accessory. Solid lyophilized samples were placed in an Andrew-Beams type rotor machined from perdeuterated poly(methyl methacrylate), and then spun as fast as 3 kHz. 90° Pulse width was 5 μs and repetition time was 4 s. Spectra were usually accumulated 1000—2000 times. Chemical shifts were calibrated indirectly from the signal of liquid benzene (118.5 ppm) and then converted to the value from tetramethylsilane.

Results and Discussion

Primary Structure. Figure 1 illustrates the ^{13}C NMR spectra of a variety of (1→3)-β-D-glucans with different degrees of branching (see Table 1) in a DMSO-d_6 solution. As has previously been described,[31] the ^{13}C NMR spectra recorded in a DMSO solution can be ascribed to glucans taking the random-coil form and the displacements of the peaks can be considered to arise mainly from the primary sequence of the glucans. Obviously, none of these branched

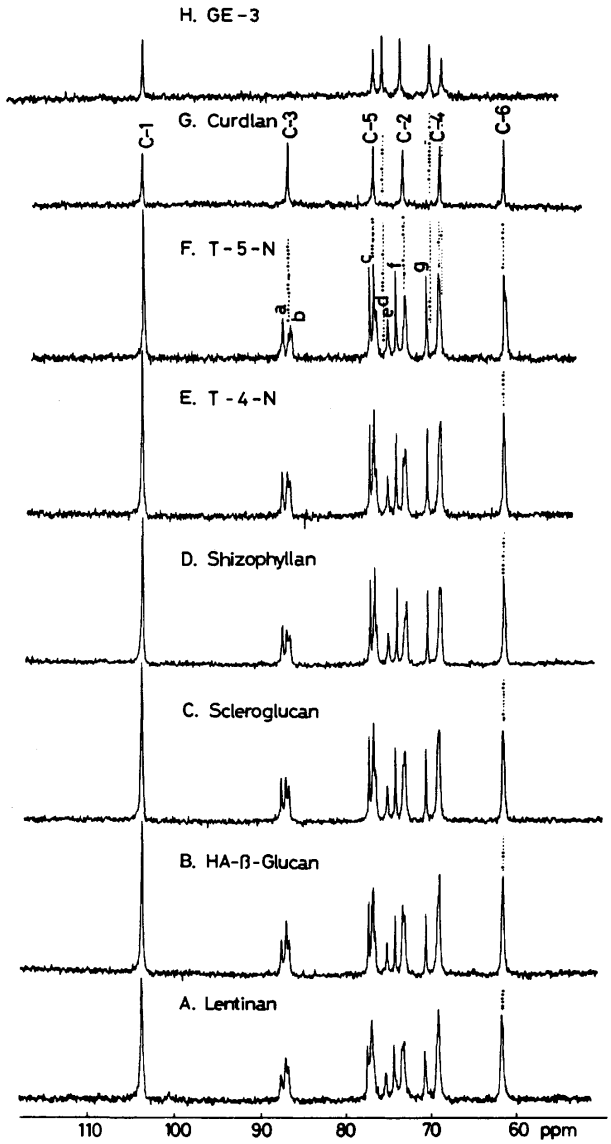

Fig. 1. High-resolution ^{13}C NMR spectra of a variety of branched (1→3)-β-D-glucans together with curdlan and GE-3 ((1→6)-β-D-glucans) in DMSO-d_6 solution (30 mg/1.5 ml DMSO-d_6).

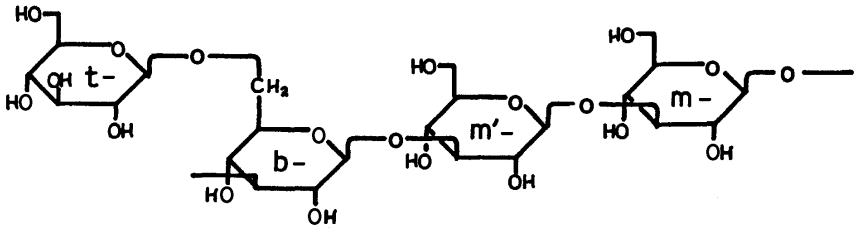

Fig. 2. Branching portion of branched (1→3)-β-D-glucans.

Table 2. The Assignment of the Peaks in the ^{13}C NMR Spectra of Various Branched (1→3)-β-D-Glucans

Peak	Chemical shift ppm	m- (or m'-) Residue	b-Residue	t-Residue
C-1	103.7	C-1	C-1′	C-1″
a	87.7	C-3 m′		
C-3	87.0	C-3 m		
b	86.4		C-3′	
c	77.4			C-3″
C-5	77.0	C-5		
d	76.7	C-5		C-5″
e	75.4		C-5′	
f	74.5			C-2″
C-2	73.8	C-2		
	73.6	C-2	C-2′	
g	70.9			C-4″
C-4	69.3	C-4	C-4′, C-6′	
C-6	61.8	C-6		C-6″

Table 3. Relative Peak Intensities of the ^{13}C NMR Spectra of Branched (1→3)-β-D-Glucans in a DMSO Solution

	Relative-peak intensity		
	C-4[a])/g	C-2[b])/f	C-3[c])/c
T-5-N	2.4	1.5	1.5
Schizophyllan	3.1	2.6	2.2
Scleroglucan	2.9	2.1	2.2
T-4-N	2.9	2.1	2.0
Lentinan	2.7	1.9	2.3
HA-β-glucan	3.2	3.1	2.6

a) The C-4 and g peaks contain C-4, C-4′, and C-6′, and C-4″, respectively. b) The C-2 and f peaks contain C-2 and C-2′, and C-2″, respectively. c) The C-3 and c peaks contain C-3 and C-3′, and C-3″, respectively.

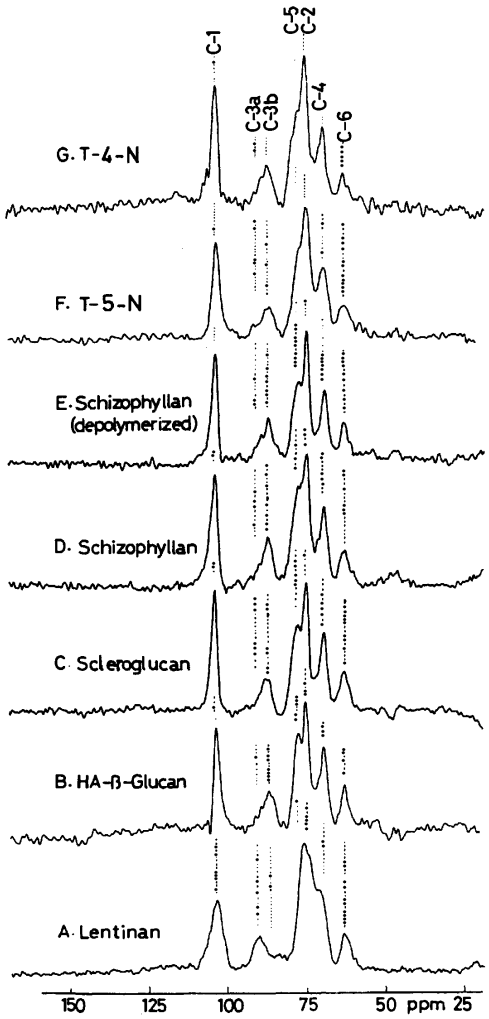

Fig. 3. 75.46 MHz High-resolution solid-state ^{13}C NMR spectra of a variety of branched (1→3)-β-D-glucans.

(1→3)-β-D-glucans possesses longer β-1,6 sequence, because no such signals can be seen as inferred from the peak-position of (1→6)-β-D-glucan (GE-3). The individual ^{13}C NMR signals were assigned to the carbons of the b-, m-(m'-), and t-residues (Fig. 2 and Table 2) on the basis of our previous assignment of the peaks for HA-β-glucan.[34] Further, it appears that two kinds of signals can be distinguished in the m- and m'-residues, as manifested by the C-3, C-5, and C-2 peaks. Further, the distinction of the peaks between m- and m'-residues is based on the data of Takeo and Tei[41] who synthesized some repeating units of branched (1→3)-β-D-glucans. The inspection of the ^{13}C NMR spectral profile leads to the classification of these polysaccharides into the following three regions: (1) HA-β-glucan, lentinan, and T-4-N, (2) scleroglucan and schizophyllan, and (3) T-5-N. In fact, the relative intensities of C-4, C-2, and C-3 with respect to those of the g, f, and c peaks (C-4″, C-2″, and C-3″, respectively, of the t-residue (side-group)), respectively, decrease in this order (Table 3). Undoubtedly, this is consistent with the degree of branching determined by the previous chemical analysis, as is summarized in Table 1.

Secondary Structure in the Solid State. Figure 3 summarizes the ^{13}C CP-MAS NMR spectra of a variety

Table 4. ^{13}C Chemical Shifts of Branched (1→3)-β-D-Glucans in the Solid State (ppm from TMS)

	Branched glucan							Linear glucan	
	Lentinan[c]		HA-β-D-glucan	Sclero-glucan	Schizo-phyllan	T-4-N	T-5-N	Curdlan[a] (triple helix)	Laminaran[b]
	Before	After							
C-1	103.2	103.5	102.9	103.3	103.5	103.3	103.2	103.6	102.9
C-2	73.3	74.0	73.6	73.8	74.2	74.0	74.1	74.3	73.9
C-3	89.3								
		86.1	85.7	86.7	86.3	85.9	85.7	86.9	85.5
C-4	69.1	68.9	67.9	67.9	68.1	68.1	68.4	68.4	67.8
C-5	75.0	76.0	76.0	76.6	76.8	76.4	76.4	77.5	76.6
C-6	61.8	62.3	61.5	61.3	61.5	61.7	61.9	61.8	61.7
		59.4							

a) Ref. 33. b) Ref. 10. c) The ^{13}C NMR spectra were recorded before and after treatment with 8M of urea.

of (1→3)-β-D-glucans in the solid state. Interestingly, all of the branched glucans, except for lentinan, give rise to a spectral pattern similar to that of laminaran and annealed curdlan adopting the triple helix (see Fig. 2 of Ref. 33), in spite of the differences in the degree of branching. This finding indicates that the manner of side-chain orientation does not affect the resulting back-bone conformation. The characteristic feature of the ^{13}C NMR pattern arising from the triple helix is that the C-3 peak is resonated at 86.4±0.5 ppm (C-3b). On the contrary, the C-3 peak of lentinan is resonated at 89.6±0.5 ppm (C-3a), characteristic of the presence of the single-helical curdlan-type form. This observation is in contrast to that of the previous X-ray diffraction study of lentinan, which suggests the presence of the triple helix.[42] This discrepancy might be, however, ascribed to the difference in the manner of sample preparation: the specimen for X-ray diffraction was obtained by fiber prepared from gel, whereas a spray-dried powder sample was used for the NMR study. In this connection, it is important to examine a plausible conformational change between spray-dried powder and lyophilized solid.

To confirm this point, we examined the conditions of the conformational change of branched (1→3)-β-D-glucans. We first dissolved these glucans in an 8M urea solution and then dialyzed it against distilled water and lyophilized to obtain solid samples. It was essential to utilize 8M urea to achieve a clear aqueous solution of branched glucans, corresponding to the completely random- coiled state, because these glucans take an ordered conformation (see Table 4). Figures 4 and 5 illustrate how the ^{13}C NMR spectra of (1→3)-β-D-glucans, taking the curdlan-type (single-helix) and laminaran-type (triple-helix) forms, respectively, are changed by treatment with 8M urea.

Interestingly, the lyophilization of lentinan resulted in a significant conformational change from the single helix to the triple-helix forms, as manifested by the displacements of the peaks from the C-3a to C-3b peak, as is indicated by the arrows, together with the characteristic change in the relative peak intensities in the C-2/C-5 peaks (Figs. 4A and B). On the contrary, the

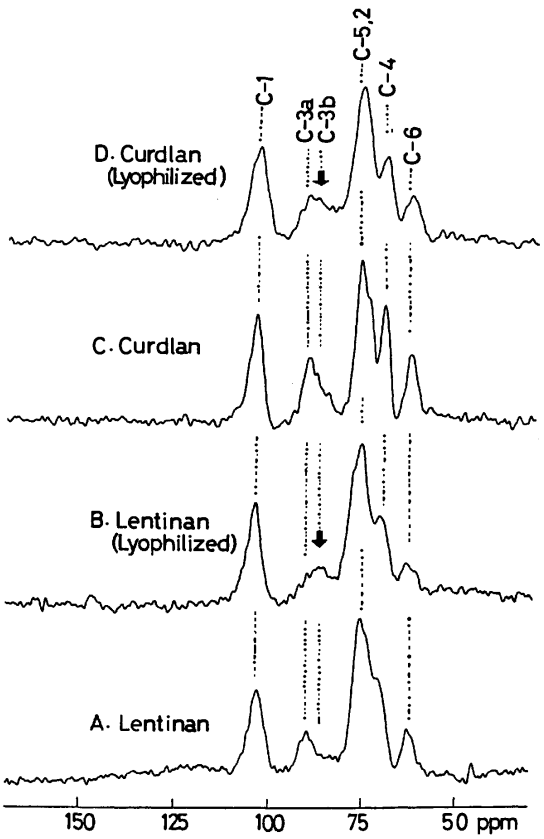

Fig. 4. Variation of high-resolution solid-state ^{13}C NMR spectra of lentinan (A and B) and curdlan (C and D) before and after treatment with 8 M urea and lyophilization. The peaks indicated by the arrows denote the peaks whose peak-intensities are varied.

extent of the conversion of curdlan is 50% at most, as judged from the relative peak-intensities between the C-3a and C-3b peaks. In fact, annealing of the sample at 150 °C, followed by slow cooling, is required for a complete conversion from the single to the triple helix, in the case of curdlan, a linear (1→3)-β-D-glucan.[33] Therefore, this distinction implies that the potential barrier to the converison from the single to the triple helix form in the linear glucan is much higher than that in the branched glucans. Accordingly, it may be

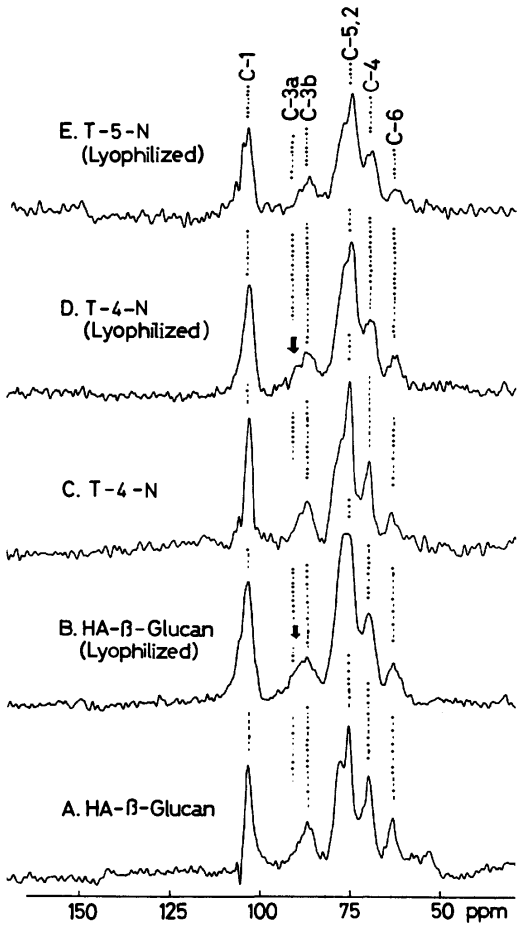

Fig. 5. Variation of high-resolution solid-state ^{13}CNMR spectra of HA-β-glucan (A and B), T-4-N (C and D) and T-5-N by treatment with 8 M urea.

concluded that the branched glucans obtained by lyophilization from the gel state take the triple-helix conformation. This result is reasonable, for branched glucans such as schizophyllan and scleroglucan take the triple helix in aqueous media[43-47] and any conformation achieved in aqueous media is usually preserved in a lyophilized solid, as has been discussed in the preceding paper.[33]

The two types of the above-mentioned conformations were also observed by Yadomae et al.[41] for branched (1→3)-β-D-glucans from *Grifora frodosa* and from *Sclerotinia sclerotiorum* IFO 9395.[48,49] Their terms of the two forms, "helix" and "native," correspond to the single and triple helix conformations, respectively, in view of the characteristic ^{13}CNMR peak-positions. They showed that milder and drastic conditions for isolation resulted in the conformations of the triple helix and single helix forms, respectively. This view seems generally to be correct in view of the presence of the triple helix in aqueous media. However, they also showed a conversion from the triple-helix conformations to the single-helix conformation by treatment with 8M urea. This finding was supported by the observation of an increased proportion of Congo Red bound to the glucans.[49] As pointed out previously, Congo Red is bound to the single-helical portion.[50]

It is now clear that the triple-helix form is the major form for lyophilized solid of the branched (1→3)-β-D-glucans, reflecting their major conformations in the gel state. On the contrary, curdlan powder contains the triple-helical region of less than 10%, as estimated from the ^{13}C NMR peak-intensity of the C-3 region.[33] This contradiction may be ascribed to apparent differences in the organization of the gel network between the linear and branched (1→3)-β-D-glucans. In the former, the major form is the single helix; the triple helix and its aggregates serve as portions of the cross-links.[28-30,33] Molecular chains other than the cross-links are sufficiently flexible, for high-resolution ^{13}C NMR signals are visible from the gel sample. In fact, the amount of the triple helix in lyophilized curdlan is less than 50%, even if the elastic gel has been annealed at 150 °C.[33]

On the contrary, gel from the branched glucan is not elastic and forms a viscous solution when the concentration is low. In addition, the ^{13}C NMR signals from the gel network are completely suppressed: the rate of molecular tumbling is longer than 10^{-6} s, for rod-like chains of the triple helix are stiffer than the native collagen fibril.[43,45] We previously pointed out that high-resolution ^{13}C NMR signals were made visible by a partial disruption of the triple helix to the single helix by adding NaOH (0.06—0.2 M).[27,28] Thus, the gel network of the branched (1→3)-β-D-glucans at a neutral pH arises mainly from the triple helix.

Concluding Remark. We have analyzed the two kinds of conformations of noncrystalline branched (1→3)-β-D-glucans in the solid state by means of the high-resolution solid-state ^{13}CNMR spectroscopy. The major conformation of the branched (1→3)-β-D-glucans is found to be the laminaran-type triple-helix on the basis of an examination of the conformation-dependent displacements of the ^{13}C chemical shifts. This obsevation is in contrast to that for the linear (1→3)-β-D-glucans, reported previously.[33] The curdlan-type single-helix conformation of spray-dried lentinan was easily converted to the laminaran-type triple helix, by the treatment with 8 M urea, followed by dialysis and lyophilization.

The authors wish to thank Dr. Goro Chihara and Dr. Takuma Sasaki of National Cancer Center Research Institute for their donation of samples and helpful discussion. They are also grateful to Kaken Pharmaceutical Co., Ltd. and Taito Co., Ltd. for their generous gifts of schizophyllan and scleroglucan, respectively.

References

1) H. Marchessault and A. Sarko, *Adv. Carbohydr. Chem.*, **22**, 421 (1967).

2) H. Saitô, R. Tabeta, A. Shoji, T. Ozaki, I. Ando, and T. Asakura, "Magnetic Resonance in Biology and Medicine," ed by G. Govil, C. L. Kheterapal, and A. Saran, Tata McGraw-Hill, New Delhi (1985), p. 195.
3) H. Saitô, *Magn. Reson. Chem.*, **24**, 835 (1986).
4) H. Saitô, R. Tabeta, A. Shoji, T. Ozaki, and I. Ando, *Macromolecules*, **16**, 1050 (1983).
5) H. Saitô, R. Tabeta, A. Shoji, T. Ozaki, I. Ando, and T. Miyata, *Biopolymers*, **23**, 2279 (1984).
6) T. Asakura, A. Kuzuhara, R. Tabeta, and H. Saitô, *Macromolecules*, **19**, 1841 (1985).
7) H. Saitô and R. Tabeta, *Chem. Lett.*, **1981**, 713.
8) H. Saitô, R. Tabeta, and T. Harada, *Chem. Lett.*, **1981**, 571.
9) H. Saitô, R. Tabeta, and S. Hirano, *Chem. Lett.*, **1981**, 1479.
10) H. Saitô, R. Tabeta, T. Sasaki, and Y. Yoshioka, *Bull. Chem. Soc. Jpn.*, **59**, 2093 (1986).
11) H. Saitô, G. Izumi, T. Mamizuka, S. Suzuki, and R. Tabeta, *J. Chem. Soc., Chem. Commun.*, **1982**, 1386.
12) F. Horii, A. Hirai, and R. Kitamaru, *ACS Symp. Ser.*, No. **260**, 27 (1982).
13) R. L. Dudley, C. A. Fyfe, P. J. Stephenson, Y. Deslandes, G. K. Hammer, and R. H. Marchessault, *J. Am. Chem. Soc.*, **105**, 2469 (1983).
14) R. Atalla, J. G. Gast, D. W. Sindorf, V. Bartuska, and G. E. Maciel, *J. Am. Chem. Soc.*, **102**, 3249 (1980).
15) W. L. Earl and D. L. VanderHart, *J. Am. Chem. Soc.*, **102**, 2351 (1980).
16) W. L. Earl and D. L. VanderHart, *Macromolecules*, **14**, 570 (1981).
17) G. E. Maciel, W. L. Kolodziejski, M. S. Bertran, and B. E. Dale, *Macromolecules*, **15**, 686 (1982).
18) R. H. Atalla and D. L. VanderHart, *Science*, **223**, 283 (1984).
19) C. A. Fyfe, R. L. Dudley, P. J. Stephenson, Y. Deslandes, G. K. Hammer, and R. H. Marchessault, *J. Macromol. Sci. Rev. Macromol. Chem. Phys.*, **C23**, 187 (1983).
20) H. Saitô, R. Tabeta, and S. Hirano, "Chitin and Chitosan. Proceeding of the Second International Conference on Chitin and Chitosan," ed by S. Hirano and S. Tokura, Japanese Society of Chitin and Chitosan (1982), pp. 71—76.
21) H. Saitô, R. Tabeta, and K. Ogawa, *Macromolecules*, **20**, 2424 (1987).
22) R. H. Marchessault, M. G. Taylor, C. A. Fyfe, and R. P. Veregin, *Carbohydr. Res.*, **144**, C1 (1985).
23) M. J. Gidley and S. M. Bociek, *J. Am. Chem. Soc.*, **107**, 7040 (1985).
24) B. P. Veregin, C. A. Fyfe, R. H. Marchessault, and M. G. Taylor, *Macromolecules*, **19**, 1030 (1986).
25) F. Horii, A. Hirai, and R. Kitamaru, *Macromolecules*, **19**, 930 (1986).
26) C. A. Fyfe, P. J. Stephenson, M. G. Taylor, T. L. Bluhm, Y. Deslandes, and R. H. Marchessault, *Macromolecules*, **17**, 501 (1984).
27) H. Saitô, T. Ohki, and T. Sasaki, *Carbohydr. Res.*, **74**, 227 (1979).
28) H. Saitô, *ACS Symp. Ser.*, No. **150**, 1125 (1981).
29) H. Saitô, T. Ohki, and T. Sasaki, *Biochemistry*, **16**, 908 (1977).
30) H. Saitô, E. Miyata, and T. Sasaki, *Macromolecules*, **11**, 1244 (1978).
31) H. Saitô, T. Ohki, N. Takasuka, and T. Sasaki, *Carbohydr. Res.*, **58**, 293 (1977).
32) H. Saitô, T. Ohki, Y. Yoshioka, and F. Fukuoka, *FEBS Lett.*, **68**, 15 (1976).
33) H. Saitô, R. Tabeta, M. Yokoi, and T. Erata, *Bull. Chem. Soc. Jpn.*, **60**, 4259 (1987).
34) Y. Yoshioka, R. Tabeta, H. Saitô, N. Uehara, and F. Fukuoka, *Carbohydr. Res.*, **140**, 93 (1985).
35) C. Hara, T. Kiho, and S. Ukai, *Carbohydr. Res.*, **117**, 201 (1983).
36) S. Ukai, C. Hara, and T. Kiho, *Chem. Pharm. Bull.*, **30**, 2147 (1982).
37) T. Sasaki and N. Takasuka, *Carbohydr. Res.*, **47**, 99 (1976).
38) S. Kikumoto, T. Miyajima, S. Ohkubo, and N. Komatsu, *Nippon Nogei Kagaku Kaishi*, **45**, 162 (1971).
39) T. L. Bluhm, Y. Deslandes, R. H. Marchessault, S. Perez, and M. Rinaudo, *Carbohydr. Res.*, **100**, 117 (1982).
40) Y. Nishikawa, T. Takeda, S. Shibata, and F. Fukuoka, *Chem. Pharm. Bull.*, **17**, 1910 (1969).
41) K. Takeo and S. Tei, *Carbohydr. Res.*, **145**, 293 (1986).
42) T. L. Bluhm and A. Sarko, *Can. J. Chem.*, **55**, 293 (1977).
43) T. Yanaki, T. Norisuye, and H. Fujita, *Macromolecules*, **13**, 1462 (1980).
44) T. Norisuye and H. Fujita, *J. Polym. Sci., Polym. Phys. Ed.*, **18**, 547 (1980).
45) Y. Kashiwagi, T. Norisuye, and H. Fujita, *Macromolecules*, **14**, 1220 (1981).
46) T. Yanaki, T. Kojima, and T. Norisuye, *Polym. J.*, **13**, 1135 (1981).
47) T. Yanaki and T. Norisuye, *Polym. J.*, **15**, 389 (1983).
48) N. Ohno, Y. Adachi, I. Suzuki, S. Oikawa, K. Sato, Y. Suzuki, M. Ohsawa, and T. Yadomae, *Chem. Pharm. Bull.*, **34**, 2555 (1986).
49) N. Ohno and T. Yadomae, *Carbohydr. Res.*, **159**, 293 (1987).

 © 1987 The Chemical Society of Japan Bull. Chem. Soc. Jpn., 60, 4273—4278 (1987)

Mutarotation of α-D-Glucose over Several Al_2O_3 Catalysts

Sentaro OZAWA, Jiro NAKATANI, Masanori SATO, and Yoshisada OGINO*
Department of Chemical Engineering, Faculty of Engineering, Tohoku University, Aramaki-Aoba, Sendai 980
(Received July 3, 1987)

The mutarotation of α-D-glucose to β-D-glucose has been studied at 25±0.1 °C using five kinds of alumina as catalysts. Two kinds of alumina with measurable surface basicities have exhibited high catalytic activities while the others with little surface basicities have exhibited low activities. Thus, the surface basic sites have been considered to be responsible for the catalytic activity observed. Any of crystal structures, surface areas, pore structures, and surface elemental compositions have no relation to the catalytic activity. It has also been revealed that the kinetics of the reaction is explained by a surface reaction mechanism

$$\alpha + 1 \underset{K_\alpha}{\rightleftharpoons} \alpha_{ad} \overset{k_1}{\underset{k_2}{\rightleftharpoons}} \beta_{ad} \underset{K_\beta}{\rightleftharpoons} \beta + 1,$$

where 1, K_α, K_β, k_1, and k_2 denote the active site, the adsorption equilibrium constant for α, the adsorption equilibrium constant for β, the rate constant for the surface forward reaction, and the rate constant for the surface backward reaction, respectively, and the subscript ad denotes an adsorbed state. The result of kinetic analysis has revealed that $K_\beta > K_\alpha$, indicating that the adsorption of β-glucose is stronger than that of α-glucose. This also supports the view that the surface basic sites are responsible for the catalytic activity.

Although abundant information about the mutarotation of α-D-glucose (an optical rotation change brought about by the rearrangement of α-D-glucose to β-D-glucose) catalyzed by acids and bases in homogeneous solutions is available in literature,[1-3] we have only scanty information[4,5] about this reaction over heterogeneous catalysts. The mutarotation of α-D-glucose has been regarded as one of fundamental reactions related to enzymic biochemical reactions,[2] and heterogeneous catalyses in this field have been lately calling the attention of world scientists. It appears worthwhile, therefore, to accumulate basic knowledge about the heterogeneous catalysis of the glucose mutarotation reaction.

The present paper reports the results of a catalysis study on the mutarotation of α-D-glucose over several alumina catalysts at 25 °C. The kinetics of the reaction has been established and the activities of the alumina catalysts are compared with respect to their properties.

Experimental

Catalyst. Five kinds of alumina used as catalysts in the present study have been commercially obtained, and their main properties are shown in Table 1. Each of these catalysts was pulverized in a mortar for 30 min, and then dried in an oven at 120 °C for 24 h before use.

Catalyst Characterization. The following characterization experiments were carried out for each catalyst; crystal structure (powder X-ray diffraction; Rigaku Geigerflex 2320 instrument; Cu $K\alpha$ radiation at 30 kV and 15 mA), surface elemental composition (XP spectra; Shimazu ESCA 750 instrument; Mg $K\alpha$ radiation), surface area and pore structure (nitrogen adsorption at 77 K), surface basicity (benzoic acid titration method[6]).

Catalytic Activity. Anhydrous α-D-glucose (Nakarai Kagaku) was dried for 24 h in a desiccator containing P_2O_5 under a pressure of ca. 1 Pa and at a temperature of 60 °C. Dimethyl sulfoxide used as a solvent was dried for 24 h using calcium hydride and then followed by a vacuum distillation (ca. 10^3 Pa at 72 °C). The middle distillate, thus obtained, was kept in a bottle flashed with dry nitrogen.

The reaction was carried out in the following manner using a three-neck flask (300 cm^3). Firstly, 100 cm^3 of the dry solvent and 0.005 mol of α-D-glucose were taken into the flask flashed with dry nitrogen, and the flask was immersed in a water bath kept at a constant temperature of 25±0.1 °C. Then, the reactant solution was stirred with a magnetic stirrer and the catalyst powder was added to initiate the reaction. At appropriate time intervals, ca. 3 cm^3 of the reacting solution was withdrawn from the flask using a syringe equipped with a catalyst filter. The sample solution was analyzed using an automatic digital polarimeter (Union Giken PM-101 instrument). Such measurements as mentioned above were continued until no change in the optical

Table 1. Properties of Alumina Catalysts

Catalyst	Crystal from	Surface area	Pore volume	Pore size	Surface composition/atom %				
		$m^2 g^{-1}$	$cm^3 g^{-1}$	Å	Al	O	C	Si	Na
Al-1[a]	γ	395	0.25	13	38.0	54.1	7.9	—	—
Al-2[b]	χ	243	0.36	31	34.3	52.7	11.0	2.0	—
Al-3[c]	χ	264	0.74	28	34.3	53.5	8.5	3.7	—
Al-4[d]	χ	200	0.75	75	33.9	51.0	11.1	4.0	—
Al-5[e]	χ	243	0.67	55	32.3	51.0	9.7	3.7	3.3

a) Activated alumina (Nakarai Kagaku), b) activated alumina (Nakarai Kagaku), c) Neobead-D (Mizusawa Kagaku), d) Neobread-DL (Mizusawa Kagaku), e) Neobead-P (Mizusawa Kagaku).

rotation (r) was observed (usually over 24 h).

Adsorption of Glucose. The amount of adsorption onto the catalyst was measured by a separate experiment. The experimental procedures were almost the same as those used in the activity measurement, except for the method of the glucose analysis. Namely, in this case, the sample solution taken out of the reaction system was analyzed to determine the total glucose using the anthrone colorimetric method;[7,8] an absorption intensity at 620 nm was measured using a Hitachi 330 spectrophotometer.

Results and Discussion

Mutarotation Activity. Part of the experimental results obtained in this work are shown in Fig. 1. The figure shows changes in the optical rotation (r) as a function of the reaction period (t). High activities of the catalysts Al-1 and Al-5 as well as low activities of the catalysts Al-2, Al-3, and Al-4 are evident in the figure. The dotted line in the figure represents the result of a repeated run over the Al-1 catalyst and demonstrates a good reproducibility of the measurement. The figure also contains part of the results of the adsorption measurements. It can be seen that the adsorption of glucose reaches equilibrium within 30 min while the mutarotation reaction is still continuing.

Kinetics. A homogeneous reaction model: As reported in literature,[1,2] the rearrangement of α-D-glucose to β-D-glucose accompanies a reduction of the optical rotation of the reacting solution until the reaction reaches equilibrium. In an homogeneous reaction, this change in the optical rotation obeys the first order reversible reaction kinetics.[1] Thus, the apparent rate

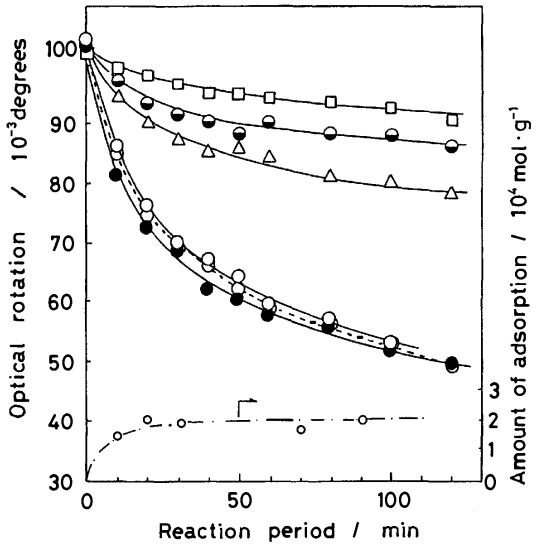

Fig. 1. Rates of mutarotation of α-D-glucose at 25 °C over alumina catalysts and the amount of glucose adsorption. ○: Al-1 (2.5 g), □: Al-2 (2.5 g), △: Al-3 (2.5 g), ◒: Al-4 (2.5 g), ●: Al-5 (2.5 g), ----: repeated run for Al-1 (2.5 g); initial concentration of glucose=0.05 mol·l^{-1} (every cases mentioned above). -·-○-·-: amount of adsorption onto Al-5 (3 g; initial glucose concentration=0.056 mol·l^{-1}).

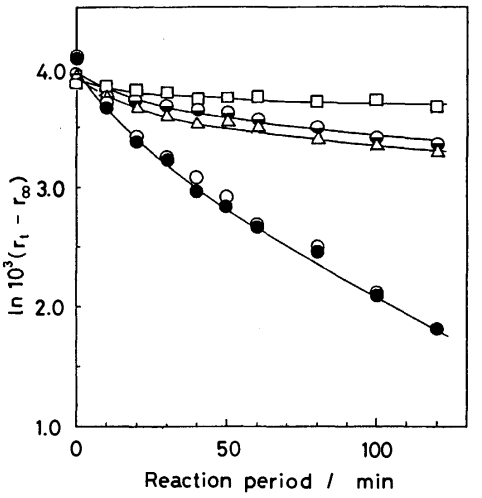

Fig. 2. The first order kinetic plots based on a homogeneous reaction model. ○: Al-1 (2.5 g), □: Al-2 (2.5 g), △: Al-3 (2.5 g), ◒: Al-4 (2.5 g), ●: Al-5 (2.5 g); initial concentration of glucose=0.05 mol·l^{-1}.

constant defined by

$$\alpha \underset{k_2}{\overset{k_1}{\rightleftharpoons}} \beta \qquad (1)$$

can be obtained from

$$k_1 + k_2 = -(1/t)\ln[(r_t - r_\infty)/(r_0 - r_\infty)], \qquad (2)$$

where r_t, r_0, and r_∞ denote the optical rotation r at a reaction period t, r at $t=0$ ($r_0=r_\alpha$), and r at equilibrium ($t=\infty$), respectively.

Although the rate equation, Eq. 2, is very simple and has been employed by Pincock et al.[4] in analyzing their catalysis data over alumina catalysts, it appears to be an oversimplification to assume that fine catalyst powder suspended in a reaction solution can be regarded as a homogeneous molecular or an ionic catalyst similar to H_3O^+ or OH^-. Indeed, as can be seen in Fig. 2, plots of $\ln[(r_t-r_\infty)/(r_0-r_\infty)]$ against the reaction period t have been nonlinear. Pincock et al.[4] have attributed the deviation of the first order plot from the linearity to a catalyst poisoning and have infered that the poisoning is due to glucose.

The present authors consider that the oversimplification adopted in applying Eq. 2 has caused the disagreement between the theory and experiments. It is more likely that α-glucose and β-glucose are competing in adsorption onto active sites. It is reasonable to consider that the β-glucose produced by the reaction would occupy part of the active sites and retard the reaction.

Heterogeneous reaction models: On the basis of the above-mentioned discussion, the present authors have adopted the following heterogeneous reaction model:

$$\alpha + 1 \rightleftharpoons \alpha_{ad} \rightleftharpoons \beta_{ad} \rightleftharpoons \beta + 1, \qquad (3)$$

where 1 denotes an active site on the catalyst surface.

Although Pincock et al.[4] have considered that the adsorption characteristics of α-glucose is identical with those of β-glucose, the present study assumes that the Langmuir type adsorption properties of α- and β-glucose are different from each other.

It must be pointed out that we have three different cases, even when the overall reaction is expressed by Eq. 3. Namely, there are three possible rate-determining steps, i.e. the surface reaction step, the adsorption step of α-glucose, and the desorption step of β-glucose. Each of these three cases yields its own rate equation, as can be seen below.

(1) When the surface reaction is the rate-determining step, the rate of decreasing of α-D-glucose concentration is expressed by

$$-\mathrm{d}[\alpha]/\mathrm{d}t = k_1[\alpha_{\mathrm{ad}}] - k_2[\beta_{\mathrm{ad}}], \tag{4}$$

where square bracket denotes the concentration, k_1 denotes the rate constant of the surface forward reaction, and k_2 denotes the rate constant of the surface backward reaction. If we define L_o, [G], K_α, and K_β as the total concentration of active sites, the total concentration of glucose $[\alpha]+[\beta]$, the adsorption equilibrium constants for α-glucose and β-glucose, respectively, Eq. 4 becomes

$$-\mathrm{d}X/\mathrm{d}t=[(1/(a+bX)][(\vec{k}_1+\overleftarrow{k}_2)/[\mathrm{G}]](X-k''), \tag{5}$$

where $X=[\alpha]/[\mathrm{G}]$, $a=(1/[\mathrm{G}])+K_\beta$, $b=K_\alpha-K_\beta$, $\vec{k}_1=k_1K_\alpha L_o$, $\overleftarrow{k}_2=k_2K_\beta L_o$, and $k''=\overleftarrow{k}_2/(\vec{k}_1+\overleftarrow{k}_2)$. An integration of Eq. 5 under the conditions that $X=1$ at $t=0$ and $X=X_\infty$ at $t=\infty$ gives

$$[1/(1-X)]\ln[(X-X_\infty)/(1-X_\infty)] = -At/(1-X)+B, \tag{6}$$

where $A=(\vec{k}_1+\overleftarrow{k}_2)/(a+bX_\infty)$, and $B=b/(a+bX_\infty)$. It must be noted here that the relation $X_\infty=\overleftarrow{k}_2/(\vec{k}_1+\overleftarrow{k}_2)$ also results from the integration process. Now we can convert the variable X into the optical rotations r_t, r_o, and r_∞, i.e. $X=(r_t-r_\beta)/(r_\alpha-r_\beta)=(r_t-r_\beta)/(r_o-r_\beta)$ and obtain a final expression of the integral rate equation:

$$[(r_o-r_\beta)/(r_o-r_t)]\ln[(r_t-r_\infty)/(r_o-r_\infty)] = -At[(r_o-r_\beta)/(r_o-r_t)]+B. \tag{7}$$

The rate equation, Eq. 7, can easily be compared with the experimental data. The value of the left hand side of Eq. 7 should have a linear relation with $(r_o-r_\beta)t/(r_o-r_t)$, and the straight line enables us to obtain the values of A and B. It must be pointed out that A should be positive because A has been defined by

$$A=(\vec{k}_1+\overleftarrow{k}_2)/[1+\{K_\alpha X_\infty+K_\beta(1-X_\infty)\}[\mathrm{G}]], \tag{8}$$

and $1-X_\infty>0$. On the other hand, B can be either positive or negative depending on the sign of $K_\alpha-K_\beta$, because B has been defined by

$$B=[\mathrm{G}](K_\alpha-K_\beta)/[1+\{K_\alpha X_\infty+K_\beta(1-X_\infty)\}[\mathrm{G}]]. \tag{9}$$

(2) When the adsorption of α-glucose is the rate-determining step, a rate equation with a form identical with that of Eq. 7 can easily be derived. In this case, however, the definition of A and B are different from those for the case (1), as we can see in Table 2.

(3) When the desorption of β-glucose is the rate-determining step, again a rate equation with the same form as Eq. 7 can be derived. The definition of A and B are, however, different from those for Eq. 7, as we can see in Table 2.

Comparison with experimental results: Plots of experimental values for $[(r_o-r_\beta)/(r_o-r_t)]\ln[(r_t-r_\infty)/(r_o-r_\infty)]$ against $(r_o-r_\beta)t/(r_o-r_t)$ values are exemplified in Figs. 3 and 4. Linear relations between the two quantities mentioned above are evident. This informs the validity of the heterogeneous reaction model discussed above. It must be pointed out that the linear plots shown in the figures reveal that $A>0$ and $B<0$. This implies that either the surface reaction mechanism (1) or the adsorption mechanism (2) is actually the case. The desorption mechanism (3) has to be excluded because this mechanism requires positive values of B (Table 2).

Although which of (1) and (2) is the true reaction mechanism can not be determined, from the kinetic treatments mentioned above, the adsorption data exemplified in Fig. 1 clearly indicate that the surface reaction mechanism is most probable. As already pointed out, the adsorption reaches equilibrium while the mutarotation reaction is still continuing (Fig. 1). If the adsorption of glucose controles the reaction rate,

Table 2. Properties of Kinetic Equations for Different Mechanisms

Rate-determining step	Definitions and properties of A and B	Notation
1. Surface reaction	$A=(\vec{k}_1+\overleftarrow{k}_2)/[1+\{K_\alpha X_\infty+K_\beta(1-X_\infty)\}[\mathrm{G}]]>0$ $B=[\mathrm{G}](K_\alpha-K_\beta)/[1+\{K_\alpha X_\infty+K_\beta(1-X_\infty)\}[\mathrm{G}]]>0$, or$<0$	$\vec{k}_1=L_oK_\alpha k_1$ and $\overleftarrow{k}_2=L_oK_\beta k_2$.
2. Adsorption of α-glucose[a]	$A=(\vec{k}_1+\overleftarrow{k}_2)/[1+\tilde{K}(1-X_\infty)[\mathrm{G}]]>0$ $B=-\tilde{K}[\mathrm{G}]/[1+\tilde{K}(1-X_\infty)[\mathrm{G}]]<0$	$\vec{k}_1=L_o\tilde{k}_1$, $\overleftarrow{k}_2=L_o(K_\beta/K)\tilde{k}_2$, and $\tilde{K}=[(K_\beta/K)+K_\beta]$.
3. Desorption of β-glucose[a]	$A=(\vec{k}_1+\overleftarrow{k}_2)/[1+\tilde{K}X_\infty[\mathrm{G}]]>0$ $B=[\mathrm{G}]\tilde{K}/[1+\tilde{K}X_\infty[\mathrm{G}]]>0$	$\vec{k}_1=L_oKK_\alpha\tilde{k}_1$, $\overleftarrow{k}_2=L_o\tilde{k}_2$, and $\tilde{K}=K_\alpha(1+K)$.

a) $\tilde{k}_1$ and $\tilde{k}_2$ denote the rate constants for the forward reaction and the backward reaction in the rate-determining step, respectively, and K denotes the equilibrium constant of the surface reaction $\alpha_{\mathrm{ad}} \rightleftarrows \beta_{\mathrm{ad}}$.

the reaction should reach equilibrium as soon as the adsorption reaches equilibrium. Thus, the mechanism (2) has to be discarded and we can conclude that the surface reaction mechanism (1) is most pertinent.

On the basis of the above-mentioned discussion, we can evaluate the kinetic parameters $\vec{k}_1$, $\vec{k}_2$, K_α, and K_β. For this purpose, linear relations between ($1/A$) and [G] and between ([G]/B) and [G] together with the relation $\vec{k}_2/(\vec{k}_1+\vec{k}_2)=X_\infty$ are available.[9] Part of the linear relationships mentioned above are shown in Fig. 5

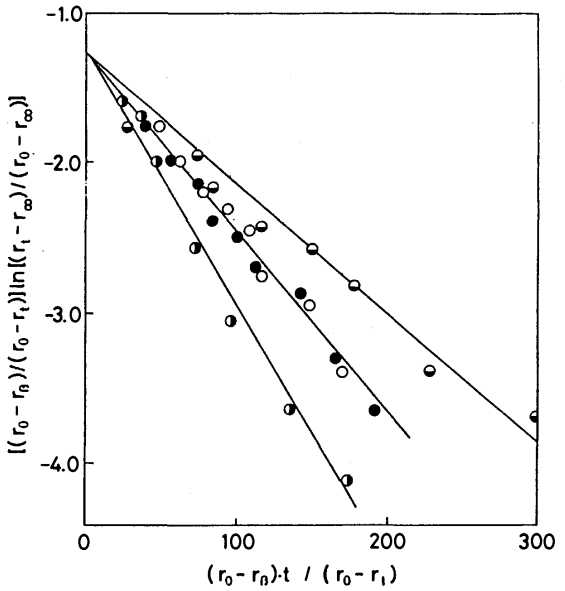

Fig. 3. Linear plots proving the applicability of the rate equation derived from a heterogeneous reaction model. ○: Al-1 (2.5 g), ◒: Al-5 (2.0 g), ●: Al-5 (2.5 g), ◑: Al-5 (4.0 g); initial concentration of glucose=0.05—0.056 mol·l^{-1}.

and kinetic parameters obtained are summarized in Table 3.

Activity and Property of Catalyst. As already pointed out, the Al-1 catalyst and the Al-5 catalyst exhibited approximately equal activities while crystal structures of these two catalysts were different from each other, i.e. γ-type for Al-1 and χ-type for Al-5 (Table 1). Furthermore, all of the less active Al-2, Al-3, and Al-4 catalysts were found to be the χ-type as the Al-5 catalyst while only the Al-5 catalyst exhibited a high catalytic activity. These facts inform that the crystal structures are not directly related to the catalytic activity. It has been reported by Pincock et al.[5] that α-alumina also exhibits a high catalytic activity for the glucose mutarotation.

Likewise, the surface areas, the pore sizes, and the surface elemental compositions shown in Table 1 did not influence the catalytic activities of the catalysts used in the present study. Insignificant relations between the catalytic activity and the pore structures shown in Table 1 and in Fig. 6 are particularly important, because this denies the pore diffusion controlling reaction mechanism. Pincock et al.[4] have also proven that the pore diffusion does not control the reaction rate by changing the size of the catalyst particle. An activation energy measurement would provide us with further support for the view mentioned above.

It appears most probable that the surface basic sites are responsible for the catalytic activity observed, though weak Brönsted acid sites have been postulated as the active sites over ordinary alumina catalysts.[4] As can be seen in Table 4, the Al-1 and Al-5 catalysts both exhibited high catalytic activities have been found to possess considerable amounts of surface basicity. On the other hand, the other catalysts (Al-2, Al-3, and Al-

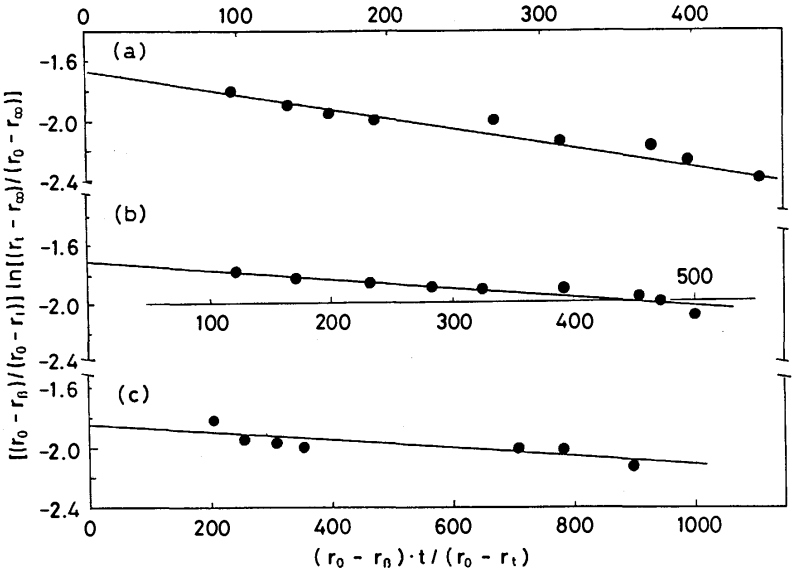

Fig. 4. Linear plots proving the applicability of the rate equation derived from a heterogeneous reaction model. (a) Al-3 (2.5 g), (b) Al-4 (2.5 g), (c) Al-2 (2.5 g); initial concentration of glucose=0.05 mol·l^{-1}.

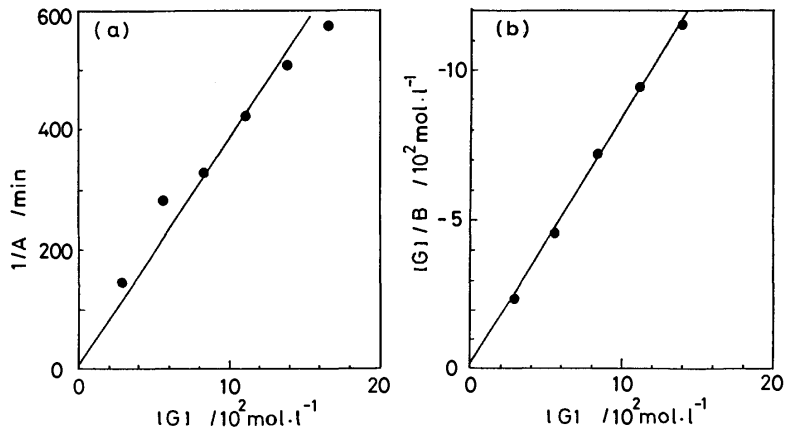

Fig. 5. Examples of linear plots between $1/A$ and [G] and between [G]/B and [G].

Table 3. Values for Kinetic Parameters[a] Obtained with Al-5 Catalyst

$\vec{k}_1$	$\overleftarrow{k}_2$	K_α	K_β	L_o[b]	k_1	k_2
min^{-1}	min^{-1}	$l \cdot mol^{-1}$	$l \cdot mol^{-1}$	mol-site·l^{-1}	mol·min^{-1}·mol-site^{-1}	mol·min^{-1}·mol-site^{-1}
7.84×10^{-2}	2.62×10^{-1}	3.15×10^{2}	1.84×10^{3}	5.0×10^{-4}	4.98×10^{-1}	2.86×10^{-1}

a) For surface reaction controlling mechanism. b) Total concentration of basic sites in 100 cm^3 of the reactant solution containing 1 g of catalyst.

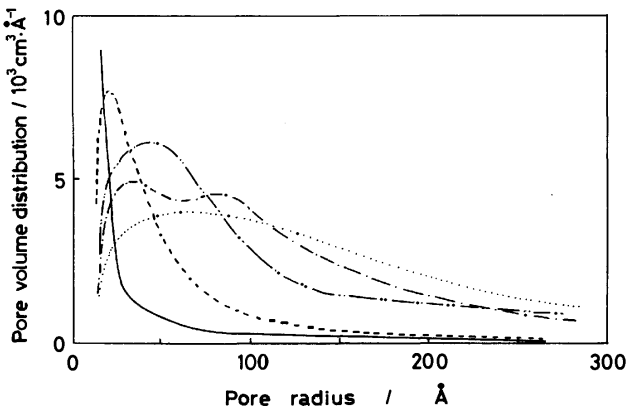

Fig. 6. Pore size distribution curves for the catalysts used. ——: Al-1, – – –: Al-2, –·–·–: Al-3, ·····: Al-4, ——·——: Al-5.

4) which have exhibited low catalytic activities possess little surface basicities. Adsorbed water or surface hydroxyl groups might have been weak catalytic sites over these three catalysts.

More important information suggested by the basicity data shown in Table 4 is that the total basic sites ($H_- \geqq 7.3$) are considered to catalyze the reaction. As we can see in the table, the total basicity of the Al-1 catalyst is approximately equal to that of the Al-5 catalyst. This corresponds well with the experimental result, i.e. almost identical activities of these catalysts. On the other hand, the contents of stronger basic sites with H_- values larger that 9.3 is larger for the Al-5 catalyst than for the Al-1 catalyst. If we assume that the strong basic sites are responsible for the catalytic

Table 4. Surface Basicities of Catalysts

Catalyst	Surface basicity/m mol g^{-1}		
	$9.3 > H_- > 7.3$	$H_- > 9.3$	Total
Al-1	0.036	0.009	0.045
Al-2	0	0	0
Al-3	0	0	0
Al-4	0	0	0
Al-5	0.025	0.025	0.05

activity, the activity of the Al-5 catalyst must be much larger than that of the Al-1 catalyst. This does not agree with the experimental result.

The surface reaction model coupled with the basic catalytic sites model is most probable in view of the different acidic properties of α- and β-glucose. Since the acid strength of β-glucose is about two times larger than that of α-glucose,[2] a stronger adsorption of β-glucose onto the basic sites can be expected, and the relation $K_\beta > K_\alpha$ obtained by the kinetic analysis is quite reasonable. Thus, the rate constants, k_1 and k_2, have been evaluated by assuming that L_o represents the basic sites concentration in the reaction system. The results are also included in Table 3.

References

1) W. Pigman and H. S. Isbell, *Adv. Carbohyd. Chem.*, **23**, 11 (1968).
2) H. S. Isbell and W. Pigman, *Adv. Carbohyd. Chem.*, **24**, 12 (1969).
3) B. Capon, *Chem. Rev.*, **69**, 407 (1969).
4) T. D. J. Dunstan and R. E. Pincock, *J. Phys. Chem.*, **88**, 5684 (1984).

5) T. D. J. Dunstan and R. E. Pincock, *J. Org. Chem.*, **50**, 863 (1985).
6) J. Take, N. Kikuchi, and Y. Yoneda, *J. Catal.*, **21**, 164 (1971).
7) D. L. Morris, *Science*, **107**, 254 (1948).
8) L. H. Koehler, *Anal. Chem.*, **24**, 2004 (1952).
9) Numerical calculations with Eqs. 8 and 9 as well as values of A, B, and [G] were also carried out in determining the magnitudes of kinetic parameters.

 © 1987 The Chemical Society of Japan Bull. Chem. Soc. Jpn., 60, 4279—4284 (1987)

Reaction of Allyl Phenyl Ether over Various Liquid Metal Catalysts

Sentaro Ozawa,* Yoshiki Sasaki, and Yoshisada Ogino
Department of Chemical Engineering, Faculty of Engineering, Tohoku University, Aramaki-Aoba, Sendai 980
(Received July 8, 1987)

Allyl phenyl ether has been reacted over various kinds of liquid metal catalysts (Sn, Ga, In, Tl, Pb, Cd, Bi, Zn) and without catalysts in the temperature range of 320—500 °C. Phenol (PN), 1,5-hexadiene (HD), benzofuran (BF), and *o*-allylphenol (*o*-AP) together with small amounts of unknown compounds have been found in the condensable products. The results of correlation among the conversion for PN, HD, and BF as well as the results of kinetic simulation of the products distribution have revealed that only the *o*-AP formation is catalyzed by the liquid metal. A clear compensation effect between the frequency factor and the activation energy has been found for the *o*-AP formation reaction, suggesting that a radicalic high energy and high entropy transition state is involved in the catalysis. A good correlation between the methyl group-catalyst metal bond energy and kinetic parameters of the *o*-AP formation reaction has also supported the radicalic transition state model.

Although much information about the catalysis of liquid metals has been accumulated by one of the present authors,[1,2] there remain many problems to be clarified. For instance, characteristics of reactions involving free radicals over liquid metals are not fully investigated. This kind of reaction is interesting not only from the scientific point of view but also from the practical point of view;[3-5] e.g. as model compounds reactions for coal liquefaction and heavy oils up grading reactions.

In the present study, the reaction of allyl phenyl ether which models ether linkages in coal structures has been examined using several liquid metals as catalysts. The experimental results have revealed that the reaction consists of noncatalytic decomposition reactions and a catalytic rearrangement reaction. This reaction scheme has been utilized to derive kinetic equations available for simulating the observed product distribution curves. The purpose of this paper is to report on details regarding the experimental results and to discuss the characteristic features of liquid metal catalysis.

Experimental

Materials. Tin (Sn), indium (In), gallium (Ga), thallium (Tl), cadmium (Cd), lead (Pb), bismuth (Bi), and zinc (Zn) were commercially obtained and used as catalysts in their molten states. Prior to the activity measurement, each catalyst metal was purified by the method reported earlier.[1] Ally phenyl ether (APE) was commercially obtained (reagent grade) and used as a reactant without further purification; benzene was used as a solvent of the reactant (2.5 wt% APE in benzene). Hydrogen was used as a carrier gas of the reactant and as a catalyst purification gas, after a deoxygenation with a Pd-catalyst at 250 °C and a drying with a liquid nitrogen trap.

Procedures. A bubbling type reactor[1,2] made from Pyrex glass was used in the activity measurements. Since details of the experimental method with a reactor of this type have already been reported elsewhere,[1,2] the precedures are only briefly described below.

After purification, the catalyst liquid metal was transferred from the catalyst preparatory tube to the reactor tube through a glass line connecting both tubes under a streaming of purified hydrogen which prevented the catalyst from contamination due to oxidation. Then the reactant solution and hydrogen were fed to the reaction system; the feed rate of the reactant solution was 5.25 $cm^3 h^{-1}$ and that of hydrogen was 82.5 $cm^3 min^{-1}$. The reactant solution was evaporated in a preheater and a gaseous mixture of allyl phenyl ether, benzene, and hydrogen was led to the bottom of the reactor. The mixture was then forced to bubble into the liquid metal catalyst (ca. 10 cm^3) kept at a predetermined reaction temperature. The effluents from the reactor were cooled and condensable materials were separated from gaseous materials. The products, thus obtained, were analyzed by means of a gaschromatography. The instrument used was a Hitachi-163 gaschromatographic apparatus equipped with a capillary column (Hewllet-Packard 19091A-105; 50 m) and a FI detector. The conditions of the analysis were as follows; sample size=1 μl for condensed samples, 1 cm^3 for gaseous samples; injection temperature=260 °C; flow rate=144 $cm^3 min^{-1}$; column temperature=keeping at 50 °C for 9 min followed by a raising at a rate of 10 °C min^{-1}. In addition to the above mentioned analysis, a gas chromatographic mass spectrometry was carried out in identifying important products (JEOL JMS-D300 instrument).

Results and Discussion

Products Distributions. The main products obtained were 1,5-hexadiene (HD), phenol (PN), benzofuran (BF), and *o*-allylphenol (*o*-AP). Methane and a small amount of propene were also found in the gaseous products. A few unknown products were observed. The amounts of these byproducts were estimated by gas chromatography using an averaged calibration curve obtained from the curves of known products. Part of the byproducts probably contain the C_3-group since the ratio of HD/PN was less than 1/2 (mole ratio). Another cause of the deficient HD formation would be polymerization of C_3-radicals; a contaminaion of the outlet of reactor suggested this. Uncertainties due to hydrogenation would be insignificant because the liquid metal little catalyzes the hydrogenation and the residence time is very short. This view is supported by the small amount of observed propene.

The temperature dependences of the above-men-

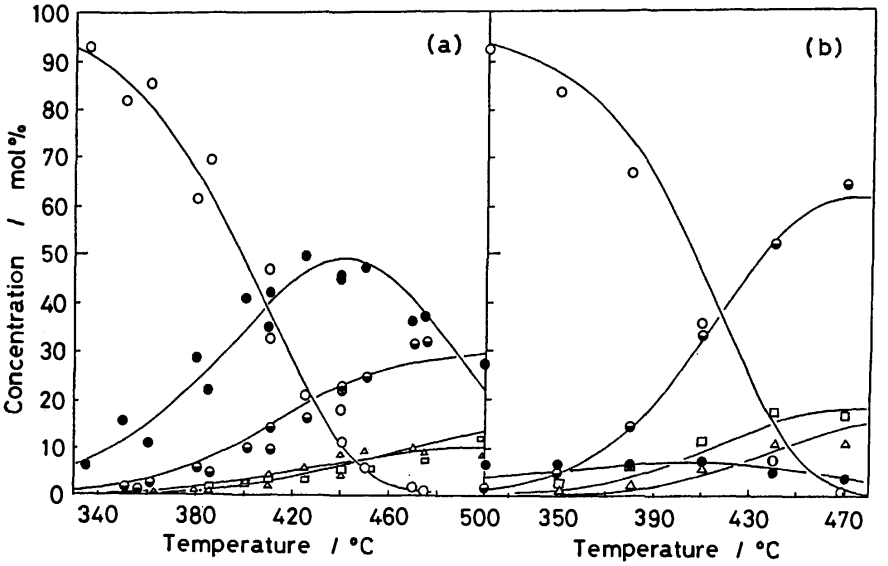

Fig. 1. Products distribution as a function of reaction temperature. (——) Simulation; (a) Sn catalyst; (b) without catalyst; ○: APE, ●: *o*-AP, ◒: PN, □: HD, △: BF.

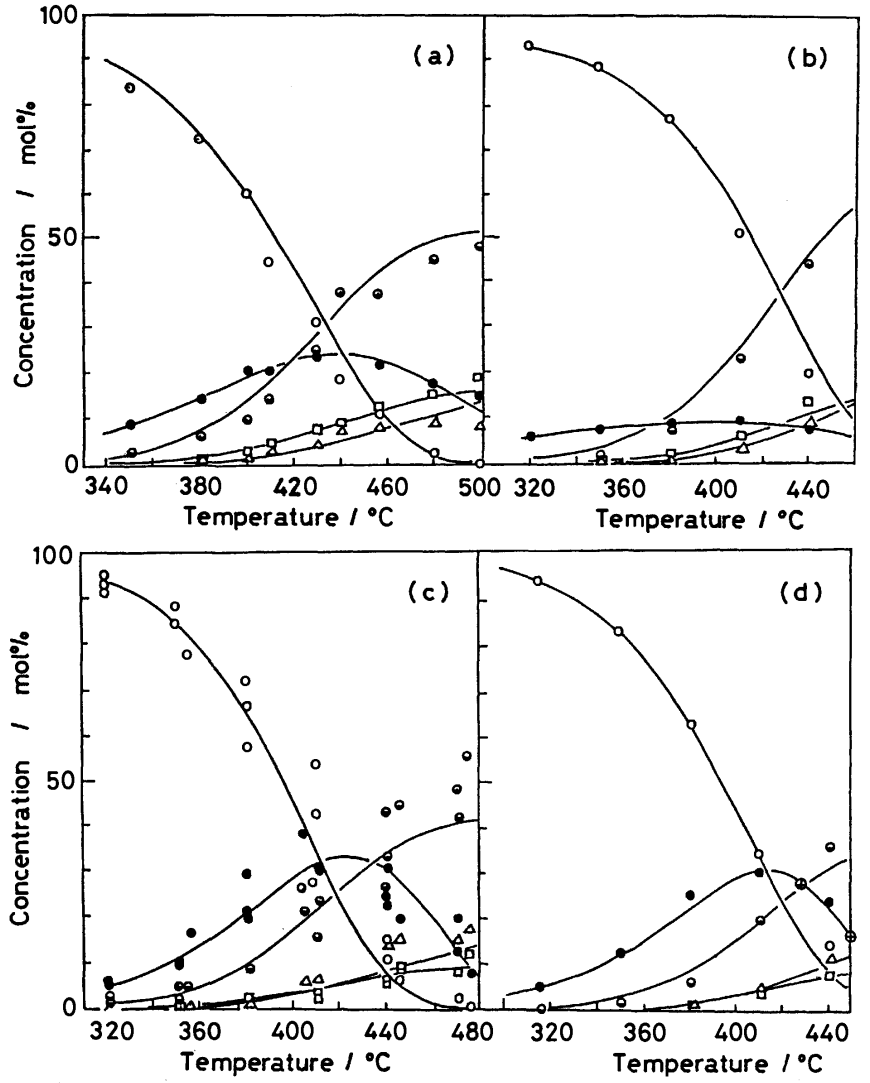

Fig. 2. Products distribution as a function of reaction temperature. (——) Simulation; (a) Pb catalyst, (b) Bi catalyst, (c) Ga catalyst, (d) In catalyst; ○: APE, ●: *o*-AP, ◒: PN, □: HD, △: BF; ⊕: *o*-AP formation activity of Zn catalyst.

tioned liquid products are shown in Figs. 1—3; data points representing concentrations estimated for unknown products were not shown, in order to avoid confusion. The first figure, Fig. 1, shows the two most typical cases observed in the present study. It is seen in Fig. 1 (a) that the reaction over the liquid tin (Sn) catalyst has produced a significant amount of *o*-AP. On the other hand Fig. 1 (b) shows that *o*-AP formation is insignificant and, instead, PN formation is significant in the noncatalytic reaction. This informs us of a difference between the catalytic reaction and the noncatalytic reaction, i.e. the former reaction favors the *o*-AP formation while the latter reaction favors the PN formation. The experimental results shown in Figs. 2 and 3 inform us of an existence of wide differences in the *o*-AP forming activity among the catalyst metals. Concentrations of other products (HD, PN, and BF) also vary upon changing the catalyst metal; however, the extent of variation is smaller compared with that observed for the *o*-AP concentration. This

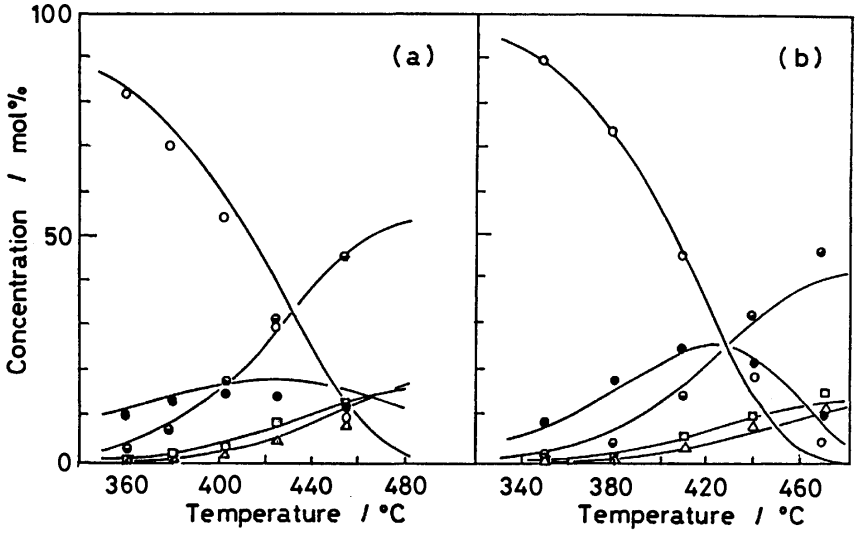

Fig. 3. Products distribution as a function of reaction temperature. (——) Simulation; (a) Cd catalyst, (b) Tl catalyst; ○: APE, ●: *o*-AP, ◒: PN, □: HD, △: BF.

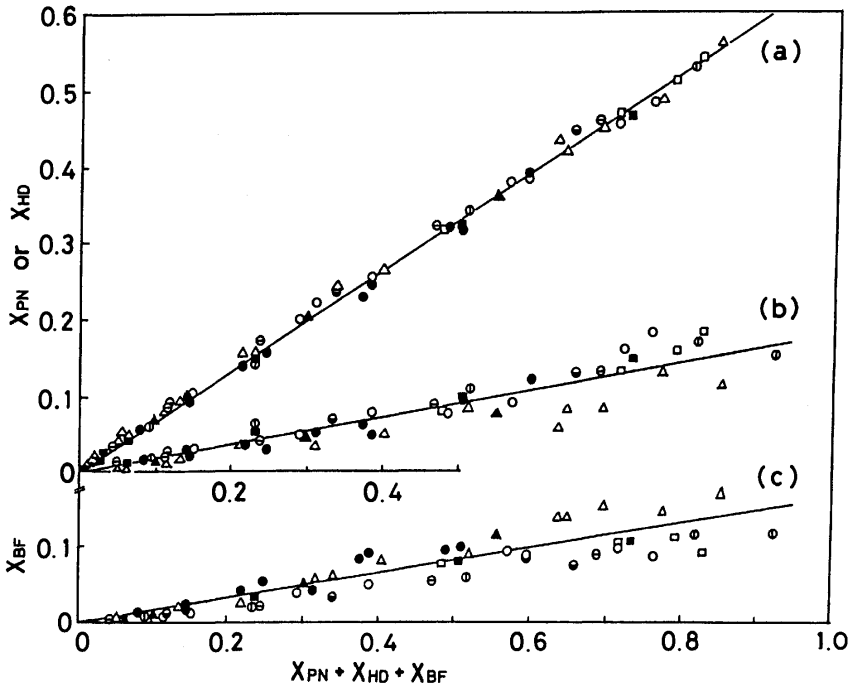

Fig. 4. Linear correlations between the sum of conversions for PN, HD, and BF and the individual conversion for PN, HD, or BF. (a) PN, (b) HD, (c) BF; ○: Pb, ◒: Bi, △: Ga, □: Zn, ●: Sn, ■: Tl, ⊖: Cd, ▲: In, ⊕: without catalyst.

suggests a mechanistic difference between the *o*-AP formation reaction and the other reactions forming HD, PN, and BF.

Relations among Conversions. The relations shown in Fig. 4 (a)—(c) reveal an important aspect of the reaction of allyl phenyl ether (APE). The abscissa of this figure represents the sum of conversions ($\sum X_j$; j=HD, PN, BF) and the ordinate represents the conversion for individual product, i.e. X_{HD}, X_{PN}, or X_{BF}. It can be seen in Fig. 4 (a) that a linear relation exists between $\sum X_j$ and X_{PN}. Furthermore, the straight line represents every data point, irrespective of the catalyst species and conditions used in taking the experimental data; data obtained with different catalysts, data obtained without catalysts, and the data obtained at different temperatures are represented by a single straight line. These facts indicate that the PN formation reaction is essentially noncatalytic, i.e. the catalysts have little affected the PN formation rate. Relations similar to that observed in Fig. 4 (a) can be seen both in Fig. 4 (b) and in Fig. 4 (c), though data points somewhat scatter around the correlation lines. It is possible, therefore, to consider that both the HD formation and BF formation are essentially noncatalytic. The temperature independences of the correlation lines mentioned above suggest that the temperature dependences of X_{HD}, X_{PN}, and X_{BF} are almost identical with each other.

Reaction Scheme and Kinetic Treatments. On the basis of the above-mentioned discussion, the reaction scheme shown in Fig. 5 has been assumed. The reaction scheme consists of five elementary steps. The steps forming HD, PN, and BF are noncatalytic while the step forming *o*-AP is catalytic. A noncatalytic step where *o*-AP decomposes to unknown product (UN) has been added in order to account for the decreasing of the *o*-AP concentration at high temperatures (Figs. 1—3). The symbols k_j (j=1—5) shown in the reaction scheme are the first-order rate constant of the j-th elementary step.

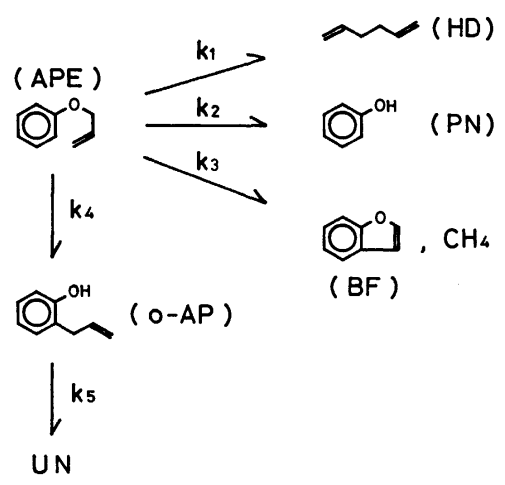

Fig. 5. Reaction scheme of allyl phenyl ether transformation.

If we assume that every step obeys irreversible first-order kinetics, the following relations can easily be derived:

$$1-X_{APE} = \exp(-kt), \quad (1)$$

$$X_{HD} = (k_1/k)[1-\exp(-kt)], \quad (2)$$

$$X_{PN} = (k_2/k)[1-\exp(-kt)], \quad (3)$$

$$X_{BF} = (k_3/k)[1-\exp(-kt)], \quad (4)$$

$$X_{o\text{-}AP} = \exp(-k_5 t)[k_4/(k-k_5)][1-\exp(k_5-k)t], \quad (5)$$

where $k=k_1+k_2+k_3+k_4$ and t denotes the reaction period (residence time).

From Eqs. 2—4 we can derive the following relations:

$$X_{HD}/(X_{HD}+X_{PN}+X_{BF}) = k_1/(k_1+k_2+k_3), \quad (6)$$

$$X_{PN}/(X_{HD}+X_{PN}+X_{BF}) = k_2/(k_1+k_2+k_3), \quad (7)$$

$$X_{BF}/(X_{HD}+X_{PN}+X_{BF}) = k_3/(k_1+k_2+k_3). \quad (8)$$

It is evident from these equations that, if activation energies for k_1, k_2, and k_3 are identical with each other, the right hand side of each equation becomes constant and the experimental results shown in Fig. 4 (a)—(c) can be explained. This result indicates that the kinetic treatment mentioned above is promissing. The extent of the constancy of the activation energies will be shown in the following section.

Simulation of Experimental Results. The validity of the reaction scheme and the kinetic treatment mentioned above has been proved by simulating experimentally observed products distribution curves. For this purpose, every rate constants (k_1—k_5) have been converted to the Arrhenius form, i.e. $k_j=a_j\exp(-E_j/RT)$; a_j is the frequecy factor, E_j is the activation energy, R is the gas constant, and T is the absolute temperature. With this expression and with Eqs. 1—5, the experimental results shown in Figs. 1—3 have been simulated and the most probable values for a_j and E_j have been determined; the residence time t has been estimated to be 0.1 s[6] from the reactant flow rate and the reactor volume, and a_j as well as E_j have been determined by trials. The results of simulation are shown in Figs. 1—3 by solid lines and the values of a_j and E_j are summarized in Table 1. The figures show that the experimental results have been well simulated by the calculated lines.

The values of kinetic parameters a_j and E_j (Table 1) deserve special comments. As can be seen in the table, the kinetic parameters (in particular the frequency factor) for the *o*-AP formation reaction, a_4, varies very widely upon changing the catalyst species. On the other hand, the extents of variation of kinetic parameters for other reactions are limited within small ranges compared with that of the *o*-AP formation step. These facts confirm that only the *o*-AP formation step has been catalyzed and the other steps have been little catalyzed by the liquid metal. It must also be pointed out that each value for E_1, E_2, and E_3 does not differ much from the average value of 142 kJ mol^{-1}. The deviations

Table 1. Values of Kinetic Parameters for Different Catalysts and for Noncatalytic Reaction

Catalyst	Frequency factor/s^{-1}					Activation energy/kJ mol^{-1}				
	$a_1/10^{10}$	$a_2/10^{10}$	$a_3/10^{12}$	a_4	$a_5/10^{12}$	E_1	E_2	E_3	E_4	E_5
Pb	1.3	0.8	1.8	2.7×10^5	0.5	135	124	167	65	163
Bi	1.5	1.0	2.0	8.5×10^1	—	135	124	165	24	—
Ga	1.5	6.0	3.0	9.5×10^7	4.0	135	134	165	95	163
Sn	1.3	0.9	2.0	1.8×10^8	0.7	135	126	165	98	162
In	1.5	2.0	2.5	2.2×10^7	0.5	135	128	163	86	146
Cd	1.5	1.1	2.0	5.0×10^3	—	135	126	165	43	—
Tl	1.5	4.5	2.0	3.5×10^7	3.0	134	134	165	91	159
Non	1.1	2.0	1.9	3.7×10^2	—	128	126	163	33	—

of every E_j values (j=1—3) from this average value inform us of the extent of approximation of the constant activation energy, i.e. E_j=constant, discussed in the preceding section.

Catalysis over Liquid Metals. As proved in the above mentioned discussion, only the *o*-AP formation step is regarded as a catalytic reaction. It must be pointed out here that this reaction is a well-known Claisen rearrangement reaction.[7,8] According to literature,[8] the rearrangement proceeds at low temperatures (190—220 °C) without catalysts, though a residence time of several hours is required to obtain a conversion of ca. 85%. Such a homogeneous noncatalytic Claisen rearrangement at low temperatures has been explained in terms of a [3,3]sigmatropic mechanism[8] which requires a highly ordered cyclic transition state. It is unlikely that this mechanism is applicable to explain the results obtained in the present study. The reaction temperature adopted in the present study is much higher and the residence time is much shorter than the respective values mentioned above. Furthermore, the experimental results have shown that the rearrangement is almost inhibited and decompositions prevail in the temperature range studied in this work, if the catalyst is not used. Thus, under the high-temperature conditions adopted in the present study, a homolytic cleavage of the allyl group-oxygen bond is considered to be predominant. It is not unlikely, therefore, that the rearrangement of APE to *o*-AP over the liquid metal proceeds through another mechanism similar to that proposed for the photo-Claisen rearrangement,[9,10] i.e. a radicals recombination mechanism.

In this connection, the relation shown in Fig. 6 reveals an important aspect of the catalysis. The figure shows the existence of a clear compensation effect between the frequency factor a_4 and the activation energy E_4. Qualitatively speaking, this relation indicates that the activation entropy increases with the increase in the activation enthalpy. Thus we can infer from Fig. 6 that a high activation entropy and a high activation enthalpy are associated with the rearrangement reaction over a high activity catalyst, e.g. Sn. In other words, the transition state over the catalyst is expected to have a loosened and unstable structure.

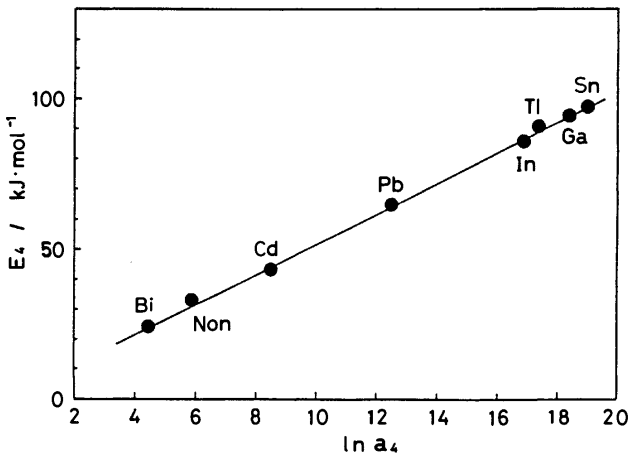

Fig. 6. A compensation effect between the frequency factor and activation energy for the rearrangement reaction.

Thus, a radicalic mechanism in which a phenoxyl radical and an allyl radical pair interaction is involved appears plausible. The cyclic transition state model proposed for the low-temperature homogeneous Claisen rearrangement is unprobable because this model should require a small activation entropy.[8]

If we assume the above-mentioned radicalic mechanism, the result shown in Fig. 6 suggests that the decreasing order of the radical-catalyst interaction energy would be Sn>Ga>Tl>In>Pb>Cd>Bi. This view is indirectly, but strongly, supported by the relation shown in Fig. 7. This figure informs us of that both a_4 and E_4 can be well correlated with the bond energy $Q_{C\text{-}Me}$, the bond energy per one carbon-metal linkage in $(CH_3)_n$-Me (Me=metal, n=an integer).[11-13] It is not unlikely that the $Q_{C\text{-}Me}$ value approximates the interaction energy between the reacting radical and the catalyst metal.

It appears worth reporting that the correlation shown in Fig. 7 enables us to discuss the catalytic activity of liquid zinc (Zn). Since this metal melts at ca. 420 °C, its activity can not be measured at low temperatures and, hence, kinetic parameters for this metal are unknown. It is possible, however, to expect that the activity of Zn would approximately be equal to that of In because $Q_{C\text{-}Zn}$ is 175.7 kJ mol^{-1} which lies

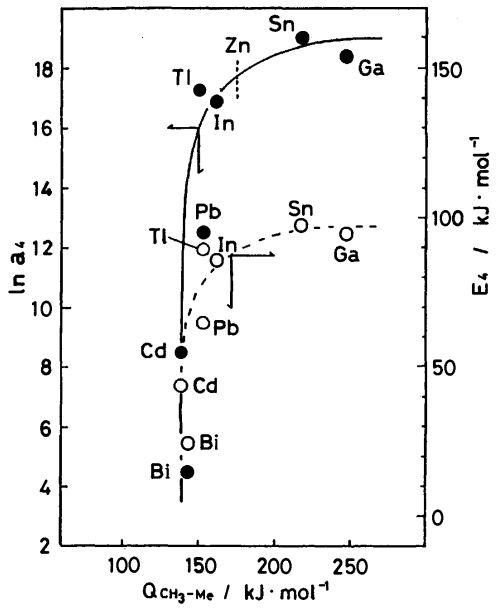

Fig. 7. Correlations between methyl group-metal bond energy and kinetic parameters for the rearrangement reaction. —●—: frequency factor, --○--: activation energy. The bond energy for Tl was taken from CRC "Handbook of Chemistry and Physics," 62nd ed, CRC Press Inc. (1981—1982, F-195. Other values were taken from H. A. Skinner, *Adv. Organomet. Chem.*, **2**, 49 (1964) and "Kagaku Binran; Kisohen II," ed by Chem. Soc. Jpn., Maruzen, Tokyo (1975), pp. 959—978.

close to the value of $Q_{C\text{-}In}$, as we can see in Fig. 7. Indeed, the experimental results shown in Fig. 2 (d; ⊕) inform that the catalytic activities observed for Zn at 430 and 455 °C are close to the line representing the *o*-AP formation activity of In.

References

1) Y. Ogino, *Catal. Rev.-Sci. Eng.*, **23**, 505 (1981).

2) Y. Ogino, "Catalysis and Surface Properties of Liquid Metals and Alloys," Marcel Dekker, Inc., New York (1987), pp. 9, 10.

3) D. D. Whitehurst, T. O. Michell, and M. Farcasiu, "Coal Liquefaction," Academic Press, New York (1980), pp. 274—342.

4) L. R. Rudnick and D. Tueting, *Fuel*, **63**, 153 (1984).

5) S. J. Hurff and M. T. Klein, *Ind. Eng. Chem. Fundam.*, **22**, 426 (1983).

6) The residence time t of 0.1 s is not so accurate but this never affects the value of the activation energy obtained. Instead, the error (Δt) in the residence time brings about a shift of logarithm of the frequency factor by $\ln(1+\Delta t/t)$ or ca. $\Delta t/t$ if $-1<\Delta t/t<1$. However the extent of this shift is expected to be almost identical for every catalysts used. Thus the relative magnitudes of frequency factors obtained would not vary. For the understanding of above mentioned description, it must be noted that the following relation has been used in evaluating, for instance, E_1 and a_1;

$$\ln(a_1 t)-E_1/RT= \ln(C_B/C_{A_o})+\ln[\ln(C_{A_o}/C_A)] -\ln[1-(C_A/C_{A_o})].$$

Methods similar to this were used in evaluating other E_j and a_j.

7) D. S. Tarbell, "Organic Reactions," ed by R. Adama, W. E. Bachmann, L. F. Fieser, J. R. Johnson, and H. R. Sryder, John Wiley & Sons, Inc., New York (1944), Vol. II, pp. 1—47.

8) S. A. Rhoads and N. R. Raulins," Organic Reactions," ed by J. E. Baldwin, R. B. Bittman, W. G. Duben, R. F. Heck, A. S. Kende, W. Leimgruber, J. A. Marshall, B. C. McKusick, J. Meinwald, B. M. Trost, and B. Weinstein, John Wiley & Sons., Inc., New York (1975), Vol. XXII, pp. 1—251.

9) G. Koga and N. Kikuchi, *Bull. Chem. Soc. Jpn.*, **41**, 745 (1968).

10) N. Shimamura and A. Sugimori, *Bull. Chem. Soc. Jpn.*, **44**, 281 (1971).

11) H. A. Skinner, *Adv. Organomet. Chem.*, **2**, 49 (1964).

12) "Kagaku Binran; Kiso-hen II," ed by Chem. Soc. Jpn., Maruzen, Tokyo (1975), pp. 959—978.

13) CRC "Handbook of Chemistry and Physics," 62nd ed, CRC Press Inc. (1981—1982), F-195.

Structural Retention of Decatungstates upon Photoreduction

Yoh SASAKI, Toshihiro YAMASE,* Yuji OHASHI,†,†† and Yoshio SASADA†
Research Laboratory of Resources Utilization, Tokyo Institute of Technology, Nagatsuta 4259, Midori-ku, Yokohama 227
†Department of Life Science, Tokyo Institute of Technology, Nagatsuta 4259, Midori-ku, Yokohama 227
(Received January 26, 1987)

The crystal structures of oxidized and photoreduced decatungstates are compared. Three specimens of decatungstate complexes were prepared in mixed solvents of H_2O-CH_3CN and were characterized by X-ray diffraction. Unit cell parameters are as follows: $(C_6H_{16}N)_4[W_{10}O_{32}]\cdot 2CH_3CN$; DECA M_r=2841.4, monoclinic, $P2_1/n$, a=14.617(2), b=17.783(3), c=11.755(2) Å, β=100.27(2)°, V=3006.5(9) Å^3, Z=2; $(C_6H_{16}N)_4[H_{1.5}W_{10}O_{32}]\cdot 8H_2O$; RED1 M_r=2905.4, monoclinic, $P2_1/n$, a=15.902(3), b=12.233(2), c=15.673(4) Å, β=93.76(2)°, V=3042(1) Å^3, Z=2; $Na_4[H_{1.8}W_{10}O_{32}]\cdot 14H_2O$; RED2 M_r=2696.7, monoclinic, $C2/m$, a=16.123(5), b=12.636(3), c=12.168(4) Å, β=117.40(2)°, V=2202(1) Å^3, Z=2; There is no obvious change in the anion frame among the three decatungstate complexes. Photoreduced decatungstates may coordinate protons which neutralize excess charge injected into anions. It is concluded that the structure of $W_{10}O_{32}$ is not largely altered up to two-electron reduction.

The photochemical properties of polyoxometalates in both solutions and solid states have been investigated.[1,2] To characterize the reduced polyoxometalates produced as a results of a photoredox reaction, it was decided to carry out a study of the crystal structure of photoreduced polyoxometalates. There have been only a few reports on the crystal structures of such reduced polyoxometalates as $(C_3H_{10}N)_4[Mo_{13}O_{40}]_{0.33}[H_4Mo_{12}O_{40}]_{0.67}$, $Rb_4H_8[H_2W_{12}O_{40}]\cdot 18H_2O$, and $Ca_{0.5}H_6PMo_{12}O_{40}\cdot 18H_2O$.[3-5] This paper describes the crystal structures of photoreduced decatungstates which are useful for catalytic H_2 production from water and organic substances.

The decatungstate anions, $[W_{10}O_{32}]^{4-}$[6] are stable in an acidic media and exhibit electrochemically reversible oxidation-reduction steps.[7] We prepared single crystals of two specimens of photoreduced decatungstates from H_2O-CH_3CN mixed solvents, and carried out X-ray diffraction studies.

Experimental

$(C_6H_{16}N)_4[W_{10}O_{32}]\cdot 2CH_3CN$; DECA. 3 g of $Na_2WO_4\cdot 2H_2O$ was dissolved in 40 cm^3 of water. The solution pH was adjusted to 1 using $HClO_4$. The solution was stirred at 80 °C for 30 min. Pale-yellow precipitates were obtained upon adding 20 cm^3 of a 2 mol dm^{-3} diisopropylammonium perchlorate aqueous solution and filtering. The precipitates were washed with water and diethyl ether and then recrystallized from a mixed solvent of H_2O-CH_3CN (1 : 4 v/v (pH 2)). Pale-yellow crystals were grown after 1—2 days.

$(C_6H_{16}N)_4[H_{1.5}W_{10}O_{32}]\cdot 8H_2O$; RED1. 1.8 g of the DECA powder was dissolved in 20 cm^3 mixed solvent of H_2O-CH_3CN (1 : 4 v/v (pH 2)). The solution was irradiated for 20 h by a use of a 500-W superhigh pressure mercury lamp in combination of a cut filter (λ>300 nm) under an argon atmosphere. Dark-blue crystals were grown from the photolyte at 5 °C within 2—3 days. The analysis of W^v in the blue crystals was achieved by $KMnO_4$ titration under an argon atmosphere and gave the composition of 1.5-electron reduction.

$Na_4[H_{1.8}W_{10}O_{32}]\cdot 14H_2O$; RED2. 5 g of $Na_2WO_4\cdot 2H_2O$ was dissolved in 20 cm^3 of H_2O. The solution pH was adjusted to 1 using $HClO_4$. The solution was stirred at 80 °C for 60 min and then 20 cm^3 of 2 mol dm^{-3} monoisopropylammonium perchlorate aqueous solution and 160 cm^3 of CH_3CN were added together. After cooling at room temperature, the solution was irradiated for 20 h in the same manner with RED1. Dark-blue platelike crystals were obtained from the solution at room temperature. The $KMnO_4$-titration analysis yielded a composition of 1.8 electron reduction per molecule.

X-Ray Structure Analysis. [DECA] The preliminary unit-cell dimensions and the space group were obtained from the oscillation and Weissenberg photographs. Systematic absences were $k=2n+1$ for $0k0$ and $h+l=2n+1$ for $h0l$. The cell parameters were refined by least-squares on the basis of 15 independent 2θ values in the range $22° < 2\theta < 29°$. Crystallographic data are summarized in Table 1.

A crystal of 0.2×0.2×0.3 mm, sealed in a glass capillary, was mounted on a Rigaku AFC-4 diffractometer. Intensity data were collected up to 2θ=55° using Mo $K\alpha$ radiation monochromated by graphite. The ω—2θ scan technique was applied with a scan rate of 8° (2θ) min^{-1}. Three standard reflections, measured every 50 reflections, showed a variation in intensity of less than 2%. A total of 6898 reflections were measured, of which 5776 with $|F_o| > 3\sigma(F_o)$ were used for the analysis. Correction was made for Lorentz and polarization factors, but neither for absorption nor extinction. The positions of the W atoms were obtained by a direct method using

Table 1. Crystallographic Data for Three Crystals

	DECA	RED1	RED2
M_r	2841.4	2905.4	2696.7
a/Å	14.617(2)	15.902(3)	16.123(5)
b/Å	17.783(3)	12.233(2)	12.636(3)
c/Å	11.755(2)	15.673(4)	12.168(4)
β/°	100.27(2)	93.76(2)	117.40(2)
V/Å^3	3006.5(9)	3042(1)	2202(1)
Space group	$P2_1/n$	$P2_1/n$	$C2/m$
Z	2	2	2
D_x/g cm^{-3}	3.14	3.17	4.07
D_m/g cm^{-3}	3.13	3.15	4.05
μ(Mo $K\alpha$)/cm^{-1}	183.5	181.4	280.9

††Present address: Department of Chemistry, Ochanomizu University, Otsuka, Bunkyo-ku, Tokyo 112.

MULTAN78.[8] Other C, N, and O atoms appeared on successive Fourier maps. The structure was refined by using a the block diagonal least-squares program called HBLS.[9] Anisotropic temperature factors were applied to all the atoms except O (15) and C (42), whose factors turned out to non-positive definite. No hydrogen atoms were found on the difference map and, thus, not included in the calculation. The weighting scheme was $w=\{\sigma^2(|F_o|)+(C|F_o|)^2\}^{-1}$, where C was 0.06. In the final difference map, maximum and minimum electron densities were 5.2 and 4.3 e Å^{-3} within 1.5 Å around a W atom. The final R and R_w values became 0.090 and 0.110 for 5776 reflections. Final positional and thermal parameters are given in Table 2. The atomic scattering factors, including anomalous dispersion terms, were taken from International Tables for X-Ray Crystallography.[10] Calculations were carried out on the FACOM-HITAC system M-180 and M-280 computer at this Institute.

[RED1]: Experimental details were similar to those for [DECA]. Systematic absences were $k=2n+1$ for $0k0$ and $h+l=2n+1$ for $h0l$. The cell parameters were refined using 18 independent 2θ values in the range $18°<2\theta<29°$. A crystal of 0.3×0.3×0.2 mm was used for data collection. A total of 6980 reflection were obtained, of which 6001 were $|F_o|>3\sigma(F_o)$. In a least-squares refinement with the program HBLS, the anisotropic temperature factors of 15 non-W atoms was shown to be non-positive definite. These atoms were refined with isotropic temperature factors. The C value in the weighting scheme was 0.08. A considerably high residual peak of 11.4 e Å^{-3} appeared near one of the W atoms (ca. 0.9 Å) and ±3.6 e Å^{-3} around the other W atoms. A refinement based on a disordered model was unsuccessful. The final R and R_w were 0.127 and 0.159 for 6001 reflections, respectively. Final positional and thermal parameters are shown in Table 3.

[RED 2]: Experimental detailes were similar to those for

Table 2. Atomic Coordinates with the Equivalent Isotropic and Isotropic Thermal Parameters (Å^2) for DECA

$B_{eq}=4/3\sum_i\sum_j B_{ij}a_ia_j$

Atom	x	y	z	B_{eq} or B/Å^2
W(1)	26752(6)	97320(5)	91268(8)	1.8
W(2)	7753(6)	107049(5)	81231(7)	1.8
W(3)	6635(6)	88798(5)	83663(8)	1.9
W(4)	15990(6)	90219(6)	111076(8)	2.1
W(5)	17128(6)	108438(5)	108345(8)	2.0
O(1)	377(1)	961(1)	876(1)	2.3
O(2)	61(1)	1131(1)	695(1)	2.9
O(3)	36(1)	815(1)	746(1)	3.2
O(4)	197(1)	839(1)	1220(2)	4.3
O(5)	232(1)	1152(1)	1165(2)	3.6
O(6)	209(1)	1041(1)	799(1)	1.9
O(7)	197(1)	895(1)	824(2)	2.8
O(8)	269(1)	907(1)	1041(1)	2.2
O(9)	287(1)	1052(1)	1019(1)	1.9
O(10)	43(1)	976(1)	743(1)	1.9
O(11)	103(1)	840(1)	984(1)	2.0
O(12)	195(1)	1000(1)	1181(1)	2.2
O(13)	135(1)	1134(1)	938(1)	2.2
O(14)	−55(1)	904(1)	879(1)	1.8
O(15)	37(1)	921(1)	1139(1)	1.9(3)*
O(16)	125(1)	989(1)	961(1)	1.5
N(1)	547(1)	873(1)	887(2)	2.0
C(10)	546(2)	853(2)	764(2)	3.7
C(11)	457(3)	814(2)	706(3)	4.2
C(12)	560(2)	931(2)	703(2)	2.6
C(20)	534(2)	804(2)	963(2)	2.6
C(21)	623(2)	759(2)	990(3)	2.9
C(22)	524(3)	838(2)	1079(3)	5.5
N(2)	255(1)	1083(1)	576(2)	2.4
C(30)	226(2)	1020(2)	491(2)	3.4
C(31)	122(2)	1008(2)	476(3)	4.2
C(32)	286(3)	955(2)	522(3)	5.1
C(40)	208(2)	1164(2)	550(2)	3.4
C(41)	252(2)	1210(2)	654(4)	4.9
C(42)	235(3)	1195(2)	436(3)	5.2(7)*
N(AN1)	457(2)	1116(2)	602(2)	4.7
C(AN1)	524(2)	1151(2)	622(3)	4.3
C(AN2)	601(2)	1201(2)	631(4)	5.4

Multiplied by 10^5 for W atoms, 10^3 for O, N, and C atoms. Atoms with asterisk were refined with the isotropic temperature factor.

Table 3. Atomic Coordinates with the Equivalent Isotropic and Isotropic Thermal Parameters (Å^2) for RED1

$B_{eq}=4/3\sum_i\sum_j B_{ij}a_ia_j$

Atom	x	y	z	B_{eq} or B/Å^2
W(1)	8147(7)	33066(9)	−3515(7)	1.4
W(2)	903(7)	12859(9)	−16074(7)	1.4
W(3)	−10737(7)	19818(9)	−436(7)	1.4
W(4)	5675(7)	16512(9)	13003(7)	1.4
W(5)	17534(7)	9154(9)	−2564(7)	1.4
O(1)	107(1)	471(2)	−52(1)	1.8(3)*
O(2)	1(1)	137(2)	−269(1)	2.0
O(3)	−203(1)	259(2)	−1(1)	2.4
O(4)	76(2)	202(2)	235(2)	2.8(4)*
O(5)	279(1)	72(2)	−35(1)	1.7
O(6)	52(1)	283(2)	−144(1)	1.5(3)*
O(7)	−48(1)	351(2)	−29(1)	1.4(3)*
O(8)	84(1)	319(2)	85(1)	1.3(3)*
O(9)	183(1)	260(2)	−41(1)	1.8(3)*
O(10)	−98(1)	182(2)	−119(2)	2.2
O(11)	−61(1)	207(2)	112(2)	2.7(4)*
O(12)	163(1)	114(2)	94(2)	2.1
O(13)	125(1)	96(2)	−144(1)	2.8
O(14)	−139(1)	51(2)	10(1)	1.5
O(15)	22(1)	17(2)	140(1)	1.9
O(16)	35(1)	155(1)	−14(1)	1.2(3)*
N(1)	144(2)	446(2)	235(2)	2.8
C(10)	79(2)	534(3)	247(2)	2.9
C(11)	−4(3)	477(4)	253(3)	4.0(8)*
C(12)	108(3)	597(4)	320(3)	5.1
C(20)	235(2)	468(3)	220(2)	3.1
C(21)	245(3)	554(4)	144(3)	4.7(9)*
C(22)	280(4)	378(6)	210(4)	7.0(14)*
N(2)	323(2)	361(2)	−124(2)	2.9
C(30)	408(2)	326(3)	−85(3)	3.9
C(31)	478(3)	398(5)	−102(4)	4.0(10)*
C(32)	392(4)	330(5)	18(4)	4.7(12)*
C(40)	319(2)	342(3)	−222(2)	3.1
C(41)	307(3)	220(4)	−244(3)	4.5(9)*
C(42)	238(4)	416(5)	−255(4)	6.9(14)*
O(W1)	−353(3)	182(3)	−107(2)	6.9
O(W2)	427(2)	−61(3)	−28(2)	5.9
O(W3)	−303(3)	427(4)	73(3)	7.1
O(W4)	101(3)	232(4)	−384(3)	9.4

Multiplied by 10^5 for W atoms, 10^3 for O, N, and C atoms. Atoms with asterisk were refined with the isotropic temperature factor.

Table 4. Atomic Coordinates with the Equivalent Isotropic and Isotropic Thermal Parameters ($Å^2$) for RED2

$B_{eq}=4/3\sum_i\sum_j B_{ij}a_ia_j$

Atom	x	y	z	B_{eq} or $B/Å^2$
W(1)	27866(8)	50000	29531(10)	1.6
W(2)	6687(8)	50000	27628(10)	1.6
W(3)	12315(5)	68234(6)	13073(7)	1.5
W(4)	18000(8)	50000	−1519(10)	1.5
O(1)	393(2)	500	413(2)	2.2
O(2)	40(2)	500	395(2)	2.5
O(3)	139(1)	818(1)	149(1)	2.7
O(4)	233(2)	500	−113(2)	2.1(4)*
O(5)	208(1)	500	385(2)	1.8
O(6)	250(1)	648(1)	262(1)	1.8
O(7)	299(1)	500	149(2)	1.5(3)*
O(8)	81(1)	648(1)	249(1)	1.7
O(9)	169(1)	651(1)	15(1)	1.8
O(10)	−56(1)	500	140(2)	1.4
O(11)	0	674(2)	0	1.8
O(12)	125(1)	500	133(2)	1.5
Na(1)	376(1)	500	−133(1)	2.8
Na(2)	0	653(2)	500	6.3
O(W1)	−94(2)	190(2)	173(2)	5.0
O(W2)	464(3)	500	96(7)	10.1
O(W3)	−52(2)	805(3)	582(3)	6.9
O(W4)	139(2)	652(3)	651(3)	7.7

Multiplied by 10^5 for W atoms, 10^3 for O, N, and C atoms. Atoms with asterisk were refined with the isotropic temperature factor.

[DECA]. Systematic absences were at $h+k=2n+1$. The space group was assigned to be $C2m$ or $C2/m$. The refinement of the structure on the latter gave a reasonable result. The cell parameters were refined with 15 reflections of $18°<2\theta<30°$. A crystal of 0.35×0.25×0.12 mm was used for data collection. The intensities were gradually decrease to 92% in the data collection. An absorption correction was made using the program DABEX.[11] The correction factors were from 1.421 to 1.817. The positions of W atoms were obtained by a direct method with MULTAN 78. The Na and O atoms appeared on the successive Fourier maps. The structure was refined by a full-matrix least-squares method with the SHELX 76 program.[12] Two oxygen atoms, O(4) and O(7), revealed non-positive definite and refined isotropically. The weighting scheme employed was $w=\{\sigma^2(|F_o|)+0.002869\times(|F_o|)^2\}^{-1}$. In the final difference map, a maximum and minimum height of 11.0 and −7.4 e $Å^{-3}$, respectively, appeared around one of the W atoms for distances of less than 1.4 Å. Final R and R_w became 0.084 and 0.098 for 2499 reflections, respectively. Final positional and thermal parameters are given in Table 4.†††

Results

Structure of Decatungstate. The approximate geometries of the decatungstate anions in the three crystals (DECA, RED1 and RED2) are similar to one another and to that found in the crystal of tributylammonium salts.[6] Figure 1 shows the numbering of the atoms.

It is composed of ten WO_6 octahedra sharing edges

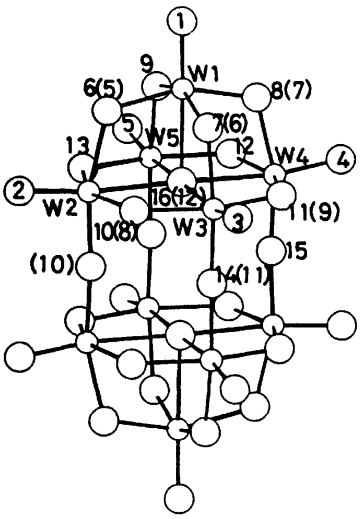

Fig. 1. The molecular structure of the decatungstate (DECA, RED1, and RED2) anions with the numbering on the atoms. Numbers in the bracket were given to RED2.

Table 5. Bond Distances (Å) in Decatungstate Anions (DECA, RED1, and RED2)

	DECA	RED1	RED2	
W(1)-O(1)	1.74(2)	1.78(2)	W(1)-O(1)	1.74(3)
W(2)-O(2)	1.74(2)	1.70(2)	W(2)-O(2)	1.69(3)
W(3)-O(3)	1.69(2)	1.70(3)	W(3)-O(3)	1.73(2)
W(4)-O(4)	1.72(2)	1.71(2)	W(4)-O(4)	1.75(3)
W(5)-O(5)	1.69(2)	1.68(2)		
W(1)-O(6)	1.89(2)	1.84(2)	W(1)-O(5)	1.91(2)
W(2)-O(6)	2.02(2)	2.02(2)	W(2)-O(5)	2.04(2)
W(1)-O(7)	1.92(2)	2.07(2)	W(1)-O(6)	1.92(2)
W(3)-O(7)	1.95(2)	2.14(2)	W(3)-O(6)	1.98(2)
W(1)-O(8)	1.91(2)	1.88(2)	W(1)-O(7)	1.96(2)
W(4)-O(8)	1.92(2)	2.06(2)	W(4)-O(7)	2.04(2)
W(1)-O(9)	1.87(2)	1.84(2)	W(2)-O(8)	1.93(2)
W(5)-O(9)	2.05(2)	2.07(2)	W(3)-O(8)	1.91(2)
W(2)-O(10)	1.90(2)	1.98(2)	W(3)-O(9)	1.91(2)
W(3)-O(10)	1.91(2)	1.82(2)	W(4)-O(9)	1.96(2)
W(3)-O(11)	1.92(2)	1.92(2)		
W(4)-O(11)	1.92(2)	1.95(2)		
W(4)-O(12)	1.95(2)	1.93(2)		
W(5)-O(12)	1.89(2)	1.92(2)		
W(5)-O(13)	1.91(2)	1.96(3)		
W(2)-O(13)	1.94(2)	1.90(3)		
W(3)-O(14)	1.94(2)	1.89(2)	W(2)-O(10)	1.91(2)
W(5)-O(14)	1.85(2)[a]	1.86(2)[b]	W(4)-O(10)	1.87(2)[c]
W(4)-O(15)	1.91(2)	1.90(2)	W(3)-O(11)	1.89(2)
W(2)-O(15)	1.88(2)[a]	1.89(2)[b]		
W(1)-O(16)	2.27(1)	2.30(2)	W(1)-O(12)	2.35(2)
W(2)-O(16)	2.28(1)	2.33(2)	W(2)-O(12)	2.33(2)
W(3)-O(16)	2.38(1)	2.34(2)	W(3)-O(12)	2.30(2)
W(4)-O(16)	2.33(1)	2.26(3)	W(4)-O(12)	2.34(2)
W(5)-O(16)	2.25(1)	2.38(2)		

a) Symmetry code (−x, 2−y, 2−z). b) Symmetry code (−x, −y, −z). c) Symmetry code (−x, y, −z).

†††The complete F_o-F_c data, anisotropic thermal parameters, bond distances of diisopropylammonium cations and acetonitrile in DECA and of the diisopropylammonium cations of RED1 and bond angles are deposited as Document No. 8756 at the Office of the Editor of Bull. Chem. Soc. Jpn.

and corners and has a pseudo point symmetry D_{4h}. Bond distances of the decatungstate in the three crystals are given in Table 5.

The corresponding bonds agreed with one another within the three crystals. There are three types of W-O bonds; terminal, bridging and central bonds. The terminal W-O bond, in which an oxygen atom has only one bond with a W atom, has a distance of 1.68—1.78 Å. The bridging W-O bond distance ranges from 1.84 to 2.07 Å, since the oxygen atom makes bonds with two W atoms. The central O atom has five bonds with the surrounding W atoms and the central W-O bond distances are 2.25—2.38 Å.

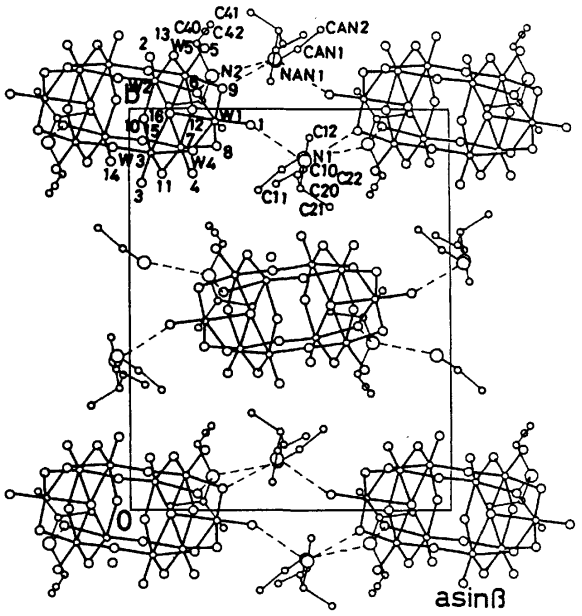

Fig. 2. The crystal structure of DECA viewed along the c axis. The hydrogen bonds are drawn with broken lines.

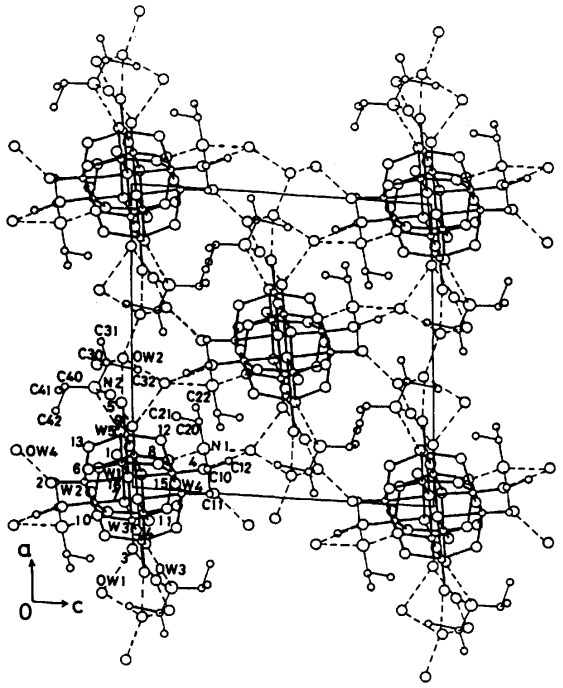

Fig. 3. The crystal structure of RED1 viewed along the b axis. The hydrogen bonds are drawn with broken lines.

Crystal Structure and Hydrogen-Bonding Scheme. The crystal structure of DECA viewed along the c axis is shown in Fig. 2.

The decatungstate anion in DECA is located at a center of symmetry. There are two diisopropylammonium cations and one CH_3CN solvent molecule per half an anion. One of the cations, N(1), makes two hydrogen bonds with O(1) and O(9) and links the anions along the *a*-axis. Another cation, N(2), has two hydrogen bonds with O(6) and the CH_3CN molecule. The distances of the hydrogen bonds are listed in Table 6. Figure 3 shows the crystal structure of RED1 viwed along the b-axis.

The decatungstate anion in RED1 also lies at a center of symmetry. Two cations and four water molecules take part in the three-dimensional hydrogen network; N(1) makes two hydrogen bonds with O(8) and O(W1), and N(2) has two bonds with O(9) and O(W3). Each water molecule has three or four hydrogen bonds with the anions and cations and with other water molecules.

Figure 4 shows the crystal structure of RED2 viewed along the b-axis. The decatungstate anion is at the position of symmetry 2/*m*.

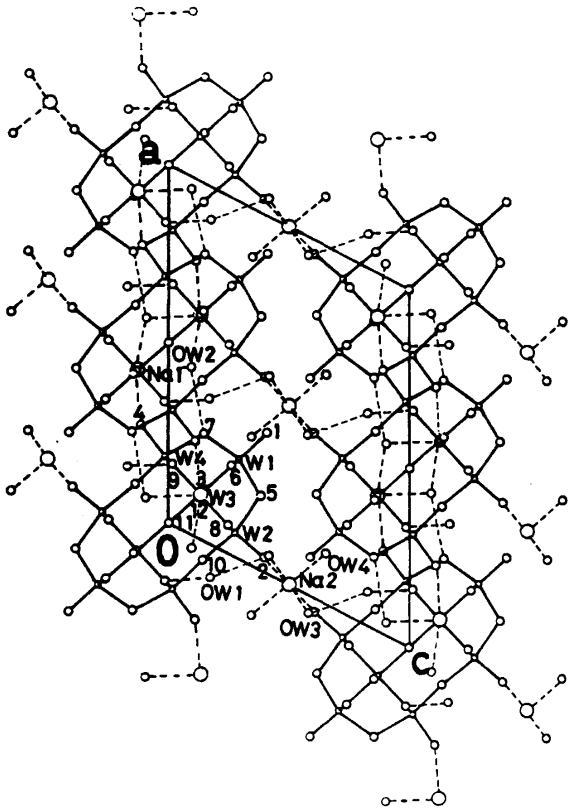

Fig. 4. The crystal structure of RED2 viewed along the b axis. Interactions among the oxygen atoms of the polyanions, water molecules and Na are shown with broken lines.

Table 6. Hydrogen Bond Distances (Å) in DECA and RED1, and Intermolecular Distances among the Oxygen Atoms of the Polyanions and Water Molecules, and Na in RED2

[DECA]		
N(1)-O(1)	2.93(3)	
N(1)-O(9)*	2.81(3)	*(1−x, 2−y, 2−z)
N(2)-O(6)	2.92(3)	
N(2)-O(AN1)	2.97(4)	
[RED1]		
N(1)-O(8)	2.94(4)	
N(1)-O(W1)*	2.93(5)	*(1/2+x, 1/2−y, 1/2+z)
N(2)-O(9)	2.93(4)	
N(2)-O(W3)*	2.73(5)	*(−x, 1−y, −z)
O(W1)-O(3)	2.96(5)	
O(W1)-O(4)*	3.02(5)	*(−1/2+x, 1/2−y, −1/2+z)
O(W1)-O(W2)*	2.90(6)	*(−x, −y, −z)
O(W2)-O(5)	2.85(4)	
O(W2)-O(W2)*	2.85(8)	*(1−x, −y, −z)
O(W2)-O(W4)*	2.90(7)	*(1/2−x, −1/2+y, −1/2−z)
O(W3)-O(3)	2.89(5)	
O(W3)-O(W4)*	2.58(7)	*(−1/2+x, 1/2−y, 1/2+z)
O(W4)-O(2)	2.75(6)	
[RED2]		
Na(1)-O(4)	2.44(3)	
Na(1)-O(W2)	2.48(8)	
Na(1)-O(W2)*	2.40(8)	*(1−x, 1−y, −z)
Na(2)-O(2)	2.56(4)	
Na(2)-O(W3)	2.49(5)	
Na(2)-O(W4)	2.14(5)	
O(W1)-O(9)*	2.87(3)	*(−x, 1−y, −z)
O(W1)-O(W3)*	2.82(5)	*(−x, 1−y, 1−z)
O(W2)-O(7)	3.01(9)	

The Na(1) cation interacts with O(3), O(4), and O(W2). The two Na(1) cations are bridged by the two O(W2) atoms and they make a tetragon. This tetragon unit connects the anion along the a- and b-axes. The Na(2) cation has octahedral interaction with O(2), O(W3), and O(W4). The two Na(2) cations are also bridged by two O(2) atoms of the neighboring anions. These octahedral units are stacked and make a column along the b-axis. This column connects the anions along the b- and c-axes. The intermolecular distances are given in Table 6.

Discussion

The structure of the decatungstate anion is not obviously changed by two-electron photoreduction. Electrochemical six-electron reduction of metatungstate $[H_2W_{12}O_{40}]^{6-}$ yields dark-brown crystals and the structural frame of the metatungstate anion is retained during the reduction.[4] However, the W-O bond distances are obviously changed by a six-electron reduction: each of the tungsten atoms in the WO_6 octahedra of a certain W_3O_{13} group is positioned with a shifting to a cavity center of the anion, resulting in a longer bond length between terminal oxygen and tungsten atoms compared to these of the WO_6 sites of other W_3O_{13} groups. Such a structural distortion induced by the six-electron reduction has been explained by a localization of six electrons within the specific edge-shared W_3O_{13} group of the metatungstate frame which consists of four W_3O_{13} groups with corner-shared bonding.

The photoreduced decatungstates of RED1 and RED2 consist of a mixture of protonated one- and two-electron reduced species, since flash photolysis of $[(C_4H_9)_4N]_4[W_{10}O_{32}]$ in CH_3CN, revealed that $[W_{10}O_{32}]^{5-}$ is produced by electron transfer from $[(C_4H_9)_4N]^+$ to $[W_{10}O_{32}]^{4-}$ and that upon protonation $[HW_{10}O_{32}]^{4-}$ (with $pK_a \approx 3.7$ in CH_3CN-H_2O of 9:1 v/v) suffers from the disproportionation to a protonated two-electron reduced species, $[H_2W_{10}O_{32}]^{4-}$, as summarized by Eqs. 1—3:[13,14]

$$[W_{10}O_{32}]^{4-} + [(C_4H_9)_4N]^+ \xrightarrow{h\nu} [W_{10}O_{32}]^{5-} + [N(C_4H_9)_3\cdot]^+ + H^+ + \text{1-butene}, \quad (1)$$

$$[W_{10}O_{32}]^{5-} + H^+ \rightleftarrows [HW_{10}O_{32}]^{4-}, \quad (2)$$

and

$$2[HW_{10}O_{32}]^{4-} \rightarrow [H_2W_{10}O_{32}]^{4-} + [W_{10}O_{32}]^{4-}. \quad (3)$$

Furthermore, it has been reported that the paramagnetic electron in the photoreduced decatungstate solid is delocalized over the anion by a large extent, compared with the six-electron reduced metatungstate.[2] The large degree of the electron-delocalization results in a decrease in the structural distortion due to a decrease in the formal electron density on a single WO_6 octahedron, leading to no obvious difference of the anion frame between the oxidized and photoreduced decatungstates (up to two-electron reduction). An X-ray structural analysis of the photoreduced decatungstates reveals the presence of four $[((CH_3)_2CH)_2NH_2]^+$ or Na^+ cations per decatungstate anion. This provides the compositions $(C_6H_{16}N)_4[H_xW_{10}O_{32}]\cdot 8H_2O$ and $Na_4[H_xW_{10}O_{32}]\cdot 14H_2O$. In conjunction with the result of the W^V analysis, in order to maintain electrical neutrality, therefore, the photoreduced species can be formulated as $(C_6H_{16}N)_4[H_{1.5}W_{10}O_{32}]\cdot 8H_2O$ and $Na_4[H_{1.8}W_{10}O_{32}]\cdot 14H_2O$, respectively. It must be recalled that the structure of $[(C_2H_5)_3NH]_3(H_3O)[Mo_8O_{26}]$ revealed the presence of one oxonium in addition to three $[(C_2H_5)_3NH]^+$, as cations.[15] The crystals of complexes of RED1 and RED2 incorporate several water molecules to form a complicated hydrogen-bonding network among the anions and water molecules. This enabled us to deduce the presence of aquahydrogen cations in the crystal; from the fact that the oxidized decatungstate has no water molecule in the crystal, it is inferred that the photoreduction of the decatungstates accompanies the incorporation of aquahydrogen cations for a conpensation of excess charges injected into the anion.

References

1) T. Yamase and R. Watanabe, *J. Chem. Soc., Dalton Trans.*, **1986**, 1669.

2) T. Yamase, *Polyhedron*, **5**, 79, (1986).
3) T. Yamase, T. Ikawa, Y. Ohashi, and Y. Sasada, *J. Chem. Soc., Chem. Commun.*, **1979**, 697.
4) Y. Jeannin, J. P. Launay, and M. A. Seid Sedjadi, *Inorg. Chem.*, **19**, 2933, (1980).
5) J. N. Barrows, G. B. Jameson, and M. T. Pope, *J. Am. Chem. Soc.*, **107**, 1771, (1985).
6) Von J. Fuchs, H. Hartl, W. Schiller, and U. Gerlach, *Acta Crystallogr., Sect. B*, **32**, 740, (1976).
7) T. Yamase, N. Takabayashi, and M. Kaji, *J. Chem. Soc., Dalton Trans.*, **1984**, 793.
8) P. Main, S. E. Hull, L. Lessinger, G. Germain, J. P. Declercq, and M. M. Woolfson, MULTAN 78, A System of Computer Programs for the Automatic Solution of Crystal Structures from X-Ray Diffraction Data. Univs. of York, England, and Louvain, Belgium.
9) Y. Ohashi, (1975). Unpublished version of an original program by T. Ashida.
10) "International Tables for X-Ray Crystallography," Kynoch Press, Birmingham (1974), Vol. IV, pp. 71—151.
11) K. Toriumi, (1977). DABEX, A System of Computer Programs for Absorption Correction and Calculation of Mean Path Lengths for the Secondary Extinction Correction.
12) G. H. Sheldric, "SHELX76, Program for Crystal Structure Determination," Univ. of Cambridge, England (1976).
13) T. Yamasé and T. Kurozumi, *J. Chem. Soc., Dalton Trans.*, **1983**. 2205.
14) T. Yamase, *Inorg. Chim. Acta*, **54**, L165, (1981); **64**, L155, (1982); **76**, L25, (1983).
15) P. K. Bharadwaj, Y. Ohashi, Y. Sasada, Y. Sasaki, and T. Yamase, *Acta Crystallogr., Sect. C*, **40**, 48, (1984).

Equilibrium Studies on the Species Formed in the Extraction of Divalent Transition Metal Ions with 8-Quinolinethiol and Its 2-Methyl Derivative

Akio YUCHI,* Kiminari SUGIURA, Hiroko WADA, and Genkichi NAKAGAWA
Department of Applied Chemistry, Nagoya Institute of Technology, Gokiso-cho, Showa-ku, Nagoya 466
(Received March 25, 1987)

The equilibria were studied in the extraction of divalent transition metal ions (M^{2+}: Co^{2+}, Ni^{2+}, Cu^{2+}, Zn^{2+}, Cd^{2+}) with 8-quinolinethiol(Hqt) and its 2-methyl derivative (Hmqt). Precipitates form in the Cd-Hqt and Cu-Hmqt systems. In other systems except the Co-Hqt, ML_2(L^-: qt^- or mqt^-) is responsible for the extraction. Effects of anions and solvents were examined in the Zn-Hqt system. The $Ni(qt)_2$, $Ni(mqt)_2$, and $Co(mqt)_2$ complexes hold the capacity to form the adduct with 1,10-phenanthroline. A mixture of diamagnetic Co(III) complexes is extracted in the Co-Hqt system. The main species was assigned as *mer(S)*-$Co(qt)_3$ by the ^{13}C NMR spectrum. The structures of other complexes are also discussed.

8-Quinolinethiol(Hqt), the sulfur-containing analogue of 8-quinolinol(Hq), has been used as a reagent having a preference for soft metal ions.[1] Several equilibrium studies on this reagent have been published.[2-9] The bis chelate, $M(qt)_2$ was assigned to the extracted species for common divalent transition metal ions (M^{2+}: Ni^{2+}, Cu^{2+}, Zn^{2+}, Cd^{2+}), whereas $Co(qt)_2(Hqt)$ or $Co(qt)_2(Hqt)_2$ to that for Co^{2+}.[5,9] The cobalt complex prepared, on the other hand, was characterized as $Co(qt)_2$ by IR and mass spectrometry,[10,11] or as $Co(qt)_3$ by polarography.[12]

Recently, we have made a systematic study on the extraction of divalent transition metal ions with 8-quinolinol.[13] Remarkable effects of solvents and anions (X^-) on the extraction were found, and were reasonably ascribed to the change in the contribution of three extracted species, $M_2q_3(Hq)_3X$, $Mq_2(Hq)$, and $M_2q_4(Hq)_2$.

In this work, we likewise studied the extraction equilibria of divalent transition metal ions with 8-quinolinethiol and its 2-methyl derivative (Hmqt) in detail. Complexes corresponding to the extracted species were prepared and their physicochemical properties as well as their capacities to form the adduct with 1,10-phenanthroline (phen) were investigated. Their structures are discussed through comparisons with the 8-quinolinol complexes.

Experimental

Reagents. 8-Quinolinethiol and its 2-methyl derivative were prepared as described in the literature,[14] and were stored as their disulfides or sodium salts.[15] Solutions of the thiols in organic solvents were prepared by extraction after the reduction of disulfides with phosphinic acid and neutralization with ammonia under a nitrogen atmosphere.

Metal(II) solutions were prepared from the sulfates and standardized against a Na_2H_2edta solution. Sodium perchlorate was recrystallized twice. Organic solvents were shaken, successively, three times with concd sulfuric acid, 4 mol dm^{-3} potassium hydroxide solution and distilled water.

Preparation of the Metal Complexes. The complexes of transition metal ions (Co, Ni, Cu, Zn, Cd) with Hqt and Hmqt were prepared by the reaction of a metal ion with a sodium salt of the thiols at the molar ratio of 1:2 in an aqueous solution. After being collected and washed with ethanol, these complexes were recrystallized from chloroform or benzene. The Cd-Hqt complex was not recrystallized because it is insoluble in common organic solvents. The precipitates obtained in the Co-Hqt and Cu-Hmqt systems were mixtures of chloroform-soluble and -insoluble species.

Determination of the metal content after decomposition of the complex with hydrogen peroxide and sulfuric acid showed the metal : ligand ratio of 1 : 2 except for the Co-Hqt and Cu-Hmqt complexes.[16] Chloroform-insoluble species in the Cu-Hmqt system has the ratio close to 1 : 1 (results for the Co-Hqt complexes are described below). Infrared spectra of Hqt complexes were in good agreement with those reported previously.[10]

Procedure. All the solutions used for the extraction were purged for 30 min with nitrogen gas. Details of the distribution measurement were the same as described previously.[13,17] A 1×10^{-4} mol dm^{-3} metal solution of the ionic strength 0.1 was shaken with an equal volume of an organic solvent containing 7.5×10^{-4} to 6.0×10^{-3} mol dm^{-3} thiol at 250 strokes min^{-1}. After phase separation, $-\log[H^+]$ higher than 2 was measured with a Radiometer pH METER 26. A solution containing 1.00×10^{-2} mol dm^{-3} perchloric acid and 9.00×10^{-2} mol dm^{-3} sodium perchlorate was used as a $-\log[H^+]$ standard. Below $-\log[H^+]$ 2, the analytical concentration of hydrogen ion was used as $-\log[H^+]$. Change in the activity coefficient is not so serious in the $-\log[H^+]$ range used.[18] Visible absorption spectra of the organic phase were recorded on a Union spectrophotometer SM-401 with a quartz cell of 10 mm. All the measurements were carried out with a thermoelectric circulating bath at 25±0.5 °C.

The adduct-formation constants were spectrophotometrically determined by adding various amounts of 1,10-phenanthroline to the complex solution (1×10^{-4} mol dm^{-3}) in the presence of excess ligand.

^{13}C NMR spectra were recorded on a Varian XL-200 Fourier transform spectrophotometer at a frequency of 50.3 MHz. The magnetic moment was measured by Faraday method with a torsion balance. JASCO chromatographic system MULTI-320 with a silica-ODS column was used for the separation of cobalt complexes.

Results and Discussion

Protonation Equilibria of 8-Quinolinethiolates. Protonation equilibria given by Eqs. 1 and 2 were spectrophotometrically studied (L^-: qt^- or mqt^-).

$$L^- + H^+ \overset{K_1}{\rightleftharpoons} HL \quad (1)$$

$$HL + H^+ \overset{K_2}{\rightleftharpoons} H_2L^+ \quad (2)$$

The protonation constants obtained and those in the literatures are as follows: log K_1=8.20 (8.38,[3] 8.36,[19] 8.39[20]) for Hqt and 9.03 (9.06[3]) for Hmqt, log K_2=2.08 (2.16,[3] 2.05[20]) for Hqt and 2.28 (2.28[3]) for Hmqt.

Partition of 8-Quinolinethiols. Distribution equilibria of 8-quinolinethiols between water and some organic solvents were studied at $-\log[H^+]$ around 5. The distribution constants obtained are as follows: K_D=325 (324[21]) for Hqt into chloroform, 166 (160[21]) for Hqt into benzene, 128 for Hqt into chlorobenzene, 353 for Hmqt into chloroform.

In neutral aqueous solutions, these thiols exist in both the molecular and the zwitter-ionic forms, which are related by

$$(\text{molecular}) \overset{K_t}{\rightleftharpoons} (\text{zwitter-ionic}), \quad (3)$$

where K_t is the tautomeric constant. The constants have been estimated for a series of substituted 8-quinolinethiols;[22] for example, $10^{1.43}$ for Hqt and $10^{1.79}$ for Hmqt. In nonpolar solvents, on the other hand, the equilibrium is shifted far to the left side, irrespective of the substituent. Thiols with tautomerism are expected to be distributed less into nonpolar solvents by a factor of $(1+K_t)$.

In a homologous series of organic extractants such as carboxylic acids and alkylamines, values of logK_D increase with increasing the carbon number. The increment of logK_D for an added methylene group, $\Delta\log K_D/CH_2$, ranges from 0.56 to 0.64.[23] The difference in logK_D between 8-quinolinol and its 2-methyl derivative is 0.64. The enhancement in partition must also operate on the molecular form of Hmqt, but may be compensated by the tautomeric effect. Thus, the K_D values for 8-quinolinethiol and its 2-methyl derivative do not differ so much (0.04 in logarithmic unit).

Extraction Time and Absorption Spectra of Extracted Species. Preliminary experiments showed the precipitate formation in the extraction systems of Cd-Hqt and Cu-Hmqt. In the other systems, approximate time required for equilibration was studied by measuring the absorbance of the organic phase during the extraction (Table 1). In the Ni-Hmqt system, the spectral change was very complicated. At $-\log[H^+]$ 4, the species with an absorption maximum at 472 nm, which agreed with that of $Ni(mqt)_2$ prepared, was first extracted within a day. It changed to the other species with a maximum at 390 nm over several days. At lower $-\log[H^+]$, the latter species was directly extracted in a shorter period. These reactions could not be identified at this stage. The slow extraction in the Ni-Hqt system is just expected from inert character of Ni^{2+}. The Co-Hqt system took an abnormally long time for equilibration in spite of labile character of Co^{2+}, which was actually exemplified by the Co-Hmqt system. In the other systems, equilibria were reached relatively fast. Shaking longer than 5 days caused the decrease in the absorbance together with the formation of precipitates, which did not contain metal ions. Quinolinethiols are supposed to be slowly decomposed under these conditions.

Spectral characteristics of the extracted species are summarized in Table 1. Absorption maxima of any system lie at longer wavelengths than those of 1:1 complexes, which have been previously reported.[2,3] Molar absorption coefficients range from 6000 to 9000, whereas that of the species in the Co-Hqt system is definitely large.

Treatment of Extraction Equilibria. Distribution

Table 1. Extraction of Divalent Transition Metal Ions with Hqt and Hmqt at 25 °C

System	Condition[a]	Shaking time	λ_{max} nm	ε	log K_{ex} Obtained	log K_{ex} Reported[b]
Co-Hqt	P-CF	48 h	467	12000	—	—
Ni-Hqt	P-CF	96 h	537	6200	4.52	3.4
Cu-Hqt[c]	P-CF	5 m	430	9000	—	—
Zn-Hqt	P-CF	10 m	403	7800	3.83	3.8
Zn-Hqt	S-CF	20 m	403	7800	3.27	—
Zn-Hqt	P-B	20 m	414	8100	3.21	—
Zn-Hqt	P-CB	15 m	413	7800	3.42	—
Cd-Hqt[d]	P-CF	—	—	—	—	—
Co-Hmqt	P-CF	100 m	454	7300	0.41	1.1
Ni-Hmqt[e]	P-CF	—	472	6200	—	0.6
			390	9900		
Cu-Hmqt[d]	P-CF	—	—	—	—	—
Zn-Hmqt	P-CF	10 m	403	7300	3.79	4.3
Cd-Hmqt	P-CF	5 h	390	9300	2.70	2.8

a) Anion: 0.1 mol dm^{-3} $NaClO_4$(P); 0.033 mol dm^{-3} Na_2SO_4(S). Solvent: chloroform (CF); benzene (B); chlorobenzene (CB). b) Ref. 5). c) 100% extraction. d) Precipitate formation. e) Two-step reaction.

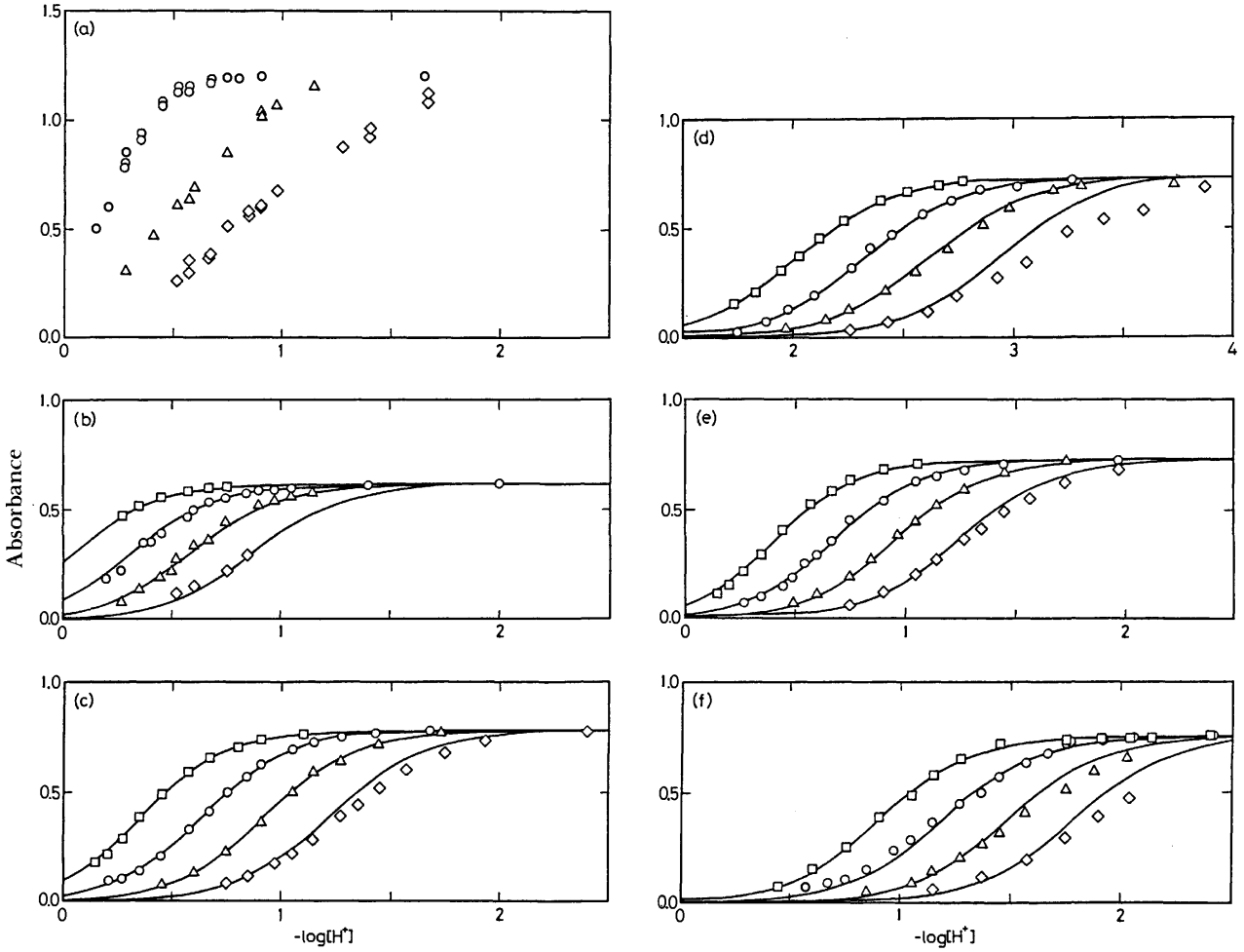

Fig. 1. Plot of absorbance vs. $-\log[H^+]$. Aqueous phase: $C_M=1\times10^{-4}$ mol dm^{-3}; 0.1 mol dm^{-3} $NaClO_4$. Organic phase: chloroform. C_{Hqt} or $C_{Hmqt}/10^{-3}$ mol dm^{-3}: (□) 6.0; (○) 3.0; (△) 1.5; (◇) 0.75. System, wavelength/nm: (a) Co^{2+}-Hqt, 467; (b) Ni^{2+}-Hqt, 537; (c) Zn^{2+}-Hqt, 403; (d) Co^{2+}-Hmqt, 454; (e) Zn^{2+}-Hmqt, 403; (f) Cd^{2+}-Hmqt, 410. Solid lines: calculated curves with constants in Table 1.

data were collected under various conditions in each system. Some of the results were shown as absorbance vs. $-\log[H^+]$ diagrams in Fig. 1.

With these extracting reagents, metal ions start to be extracted at low $-\log[H^+]$. As the concentration of H_2qt^+ or H_2mqt^+ in the aqueous phase is not negligible in this $-\log[H^+]$ range, the prominent equilibrium treatment assuming a general species $(M_jL_{2j}(HL)_m)_o$ could not be applied.[24] The composition of the solid complex prepared under the same conditions is taken into account, and the extracted species is assumed to be a neutral j-meric complex of the composition M_jL_{2j},[13]

$$jM^{2+}+2j(HL)_o \overset{K_{ex}}{\rightleftharpoons} (M_jL_{2j})_o+2jH^+, \quad (4)$$

where K_{ex} represents the extraction constant. The total concentration of metal(II) in the organic phase, $C_{M,o}$ is expressed as a logarithmic form by

$$\log C_{M,o}=j(\log C_{M,w}-2\log[H^+]+2\log[HL]_o)+\log jK_{ex}, \quad (5)$$

where $[HL]_o$ is calculated from the total concentration of the extracting reagent, C_{HL}, as follows:

$$[HL]_o=K_D\cdot C_{HL}/(K_D+1+[H^+]/K_2). \quad (6)$$

If the j-meric species is responsible for the extraction, the plot of $\log C_{M,o}$ vs. $(\log C_{M,w}-2\log[H^+]+2\log[HL]_o)$ would yield a straight line of slope j.

The results are shown in Fig. 2. Only a simple monomeric species, ML_2 is extracted except for the Co-Hqt system.

$$M^{2+}+2(HL)_o \rightleftharpoons (ML_2)_o+2H^+ \quad (7)$$

The extraction constants obtained are summarized in Table 1 together with literature values, which have been recalculated with the K_1 and K_D values used in the paper.[5]

Effects of Anions, Organic Solvents, and Central Metal Ions. In the extraction of divalent transition metal ions with 8-quinolinol, $M_2q_3(Hq)_3X$, $Mq_2(Hq)$, and $M_2q_4(Hq)_2$ are responsible for the extraction.[13] In the systems containing a hydrophobic anion and a polar solvent, metal ions start to be extracted at lower $-\log[H^+]$ because of the larger contribution of

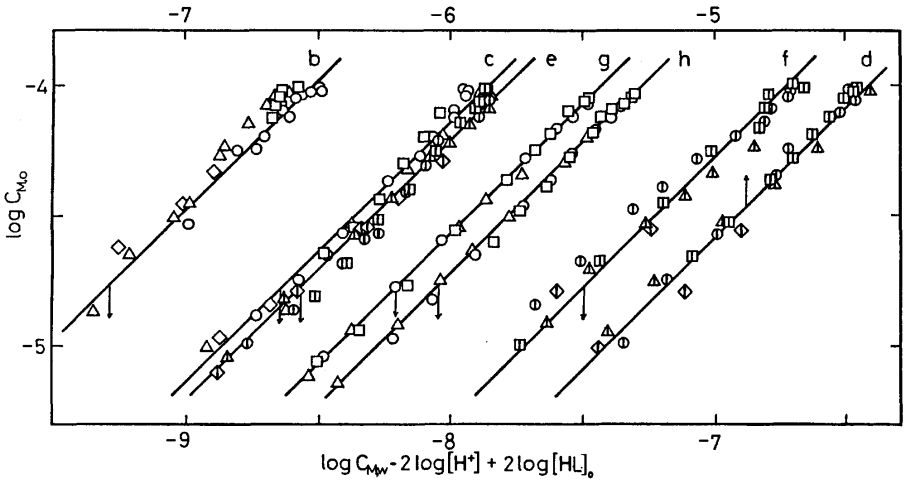

Fig. 2. Determination of the polymerization degree of metal(II) 8-quinolinethiolate according to Eq. 5. System: (b)—(f) same with Fig. 1; (g) Zn^{2+}-ClO_4^--Hqt-chlorobenzene; (h) Zn^{2+}-SO_4^{2-}-Hqt-chloroform. Solid lines: straight lines with a slope of unity.

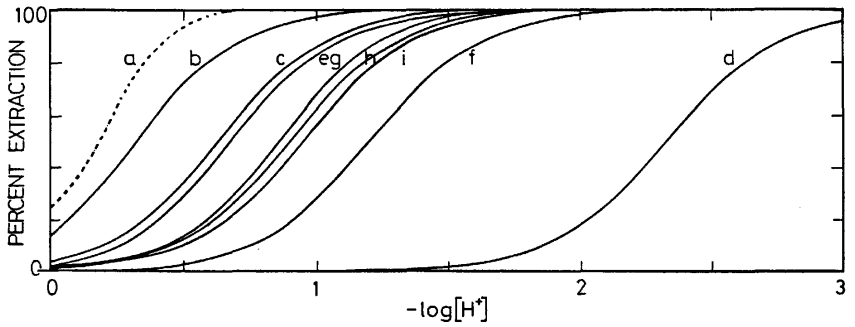

Fig. 3. Extraction curve for various systems. C_{Hqt} or C_{Hmqt}= 3.0×10^{-3} mol dm^{-3}. System: (a)—(h) same with Fig. 1 and 2; (i) Zn^{2+}-ClO_4^--Hqt-benzene. Curve (a) does not show the equilibrated state (see text for details).

$M_2q_3(Hq)_3X$. In the extraction with 8-quinolinethiol, on the other hand, the extraction curves do not change so much by solvents and anions (Fig. 3). This agrees with that only the neutral species $M(qt)_2$ is found as an extracted species.

Zinc ion has a stronger interaction with sulfate than with perchlorate in aqueous solutions.

$$Zn^{2+} + SO_4^{2-} \overset{K}{\rightleftharpoons} ZnSO_4 \qquad (8)$$

The constant, K at the ionic strength of 0.1 is estimated to be $10^{1.6}$ from the constant at infinite dilution ($10^{2.4}$) and the activity coefficient for divalent ions ($10^{-0.4}$). The side reaction coefficient of zinc with sulfate, $\alpha=1+K[SO_4^{2-}]$, is $10^{0.4}$, which is comparable to the difference in the extraction constant ($10^{0.56}$) between perchlorate and sulfate media.

The extraction constant for the Ni-Hqt system is larger than the literature value by 1.1 in logarithmic unit.[5] Care must be taken of slow equilibration in this system.

The data obtained in the Co-Hqt system (Fig. 1(a)) are not those expected for the equilibria expressed by Eq. 4. Moreover, species once extracted into chloroform could hardly be back-extracted. These, together with some findings mentioned above, indicate the formation of Co(III) complexes. This type of oxidation was suggested when abnormally large enthalpy change was found for the formation of the 1 : 1 complex with Hqt in 50v/v% aqueous dioxane.[4]

Adduct Formation. The complex solution (1×10^{-4} mol dm^{-3}) in chloroform was mixed with various amounts of 1,10-phenanthroline (4×10^{-5}—4×10^{-1} mol dm^{-3}) in the presence of excess thiol (3—6×10^{-3} mol dm^{-3}). Spectral change having isosbestic points was found with an absorption maximum shifted from 537 to 432 for $Ni(qt)_2$, and from 472 to 425 nm for $Ni(mqt)_2$. The $Co(mqt)_2$ complex also gave indication of the same reaction. This is ascribed to the formation of the 1 : 1 adduct,[25,26]

$$ML_2 + phen \overset{K_{add}}{\rightleftharpoons} ML_2(phen), \qquad (9)$$

where K_{add} denotes the adduct formation constant. From the absorbance change shown in Fig. 4, this constant was determined by the conventional method:

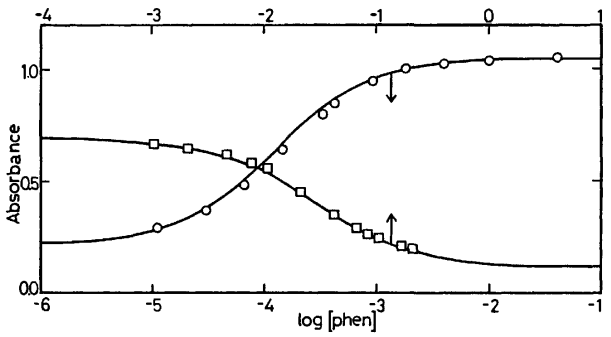

Fig. 4. Plot of absorbance vs. log[phen]. $C_{complex}$= 1×10^{-4} mol dm^{-3}; C_{Hqt} or C_{Hmqt}=3–6×10^{-3} mol dm^{-3}. Complex, wavelength/nm: (○) $Ni(qt)_2$, 432; (□) $Ni(mqt)_2$, 480. Solid lines: calculated curves with constants obtained.

Table 2. Analytical Data for the Co-Hqt Complexes Prepared under Various Conditions

Compound	Found (%)				
	Co	C	H	N	Cl
Prepared in aqueous ClO_4^- medium	9.47	53.5	3.0	6.7	6.0
Prepared in ethanol	10.66	55.0	3.1	7.8	
Extracted from SO_4^{2-} medium into benzene	10.70	60.3	3.2	7.6	
Calculated for $Co(qt)_2$	15.53	56.98	3.19	7.39	
Calculated for $Co(qt)_3$	10.92	60.10	3.37	7.79	

$\log K_{add}$=3.92 (3.97)[25] for $Ni(qt)_2$, 1.55 for $Ni(mqt)_2$, and <0 for $Co(mqt)_2$. On the other hand, no change was observed for $Cu(qt)_2$, $Zn(mqt)_2$, and $Cd(mqt)_2$ as well as $Zn(qt)_2$.[6,27] Some effects of phen on the extraction of Co^{2+} with Hqt have been reported,[26] but the Co-Hqt complex prepared does not show any spectral change. The Cd-Hqt and Cu-Hmqt complexes prepared are insoluble in chloroform. In the presence of phen, however, the adducts of these complexes are extracted without precipitate formation (see below).

Structures of Co-Hqt and Co-Hmqt Complexes. Analytical data for the Co-Hqt complexes prepared in aqueous perchlorate and ethanolic media are shown in Table 2. Neither gave a definite composition. Especially, the complex obtained from perchlorate medium contained chlorine, and consisted of at least 4 species as shown by chromatogram in Fig. 5(a). Since this mixture is diamagnetic in contrast to the Co-Hmqt, the cobalt in these complexes is oxidized to Co(III).

The extracts from a sulfate medium into benzene, on the other hand, had a composition close to $Co(qt)_3$. Although two geometrical isomers are possible for $Co(qt)_3$, only one species was practically found in chromatogram of Fig. 5(b). The ^{13}C NMR spectrum of this species given by Fig. 6 showed very complicated resonances (more than 19). Thus the complex is assigned as the *mer*(*S*) isomer, because only nine signals are expected for the *fac*(*S*) geometry.[28]

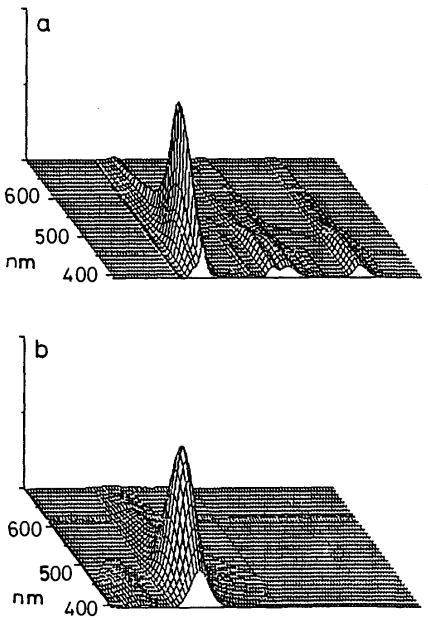

Fig. 5. Chromatograms of Co-Hqt complexes. (a) Complex prepared in perchlorate medium. (b) Complex extracted from sulfate medium into benzene. Column: CIG pre-packed column CPO-042-10 (200 mm×4-mm i.d.). Mobile phase: methanol-water (80:20 v/v).

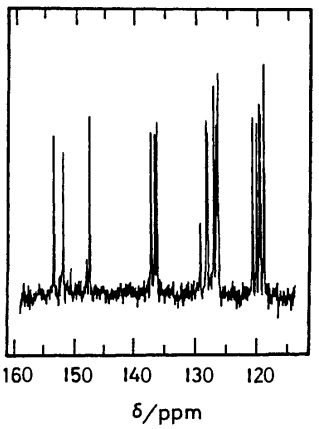

Fig. 6. ^{13}C NMR spectrum of $Co(qt)_3$ in $CDCl_3$ containing TMS as an internal standard.

The Co-Hmqt complex, on the other hand, is a simple 1 : 2 complex and is expected to have tetrahedral configuration judged from the magnetic moment (4.9 B.M.). The methyl group adjacent to the donor atom sometimes shows striking effect on the properties of the complex. In this case, steric hindrance in the formation of the tris chelate suppresses the oxidation of cobalt.

Structures of Other Complexes. The structure of $Cu(qt)_2$, which has the same composition with copper 8-quinolinolate, Cuq_2, was determined to be square-planar in solution by ESR spectra,[29,30] and in solid by X-ray crystallography.[31] This structure is stable and even phen cannot change the configuration to

octahedron. On the other hand, the Cu-Hmqt prepared, which is insoluble in organic solvents, has a metal : ligand ratio close to 1 : 1 and is expected to be a copper(I) complex. Coordinated water molecules, which are identified by the IR spectrum, can be replaced by phen to make the complex soluble in organic solvents. The 2-methyl substituent makes the planar structure unfavorable and increases the reducibility of the copper complex.

With 8-quinolinol, zinc is precipitated as $Znq_2 \cdot 2H_2O$ and is extracted as $Znq_2(Hq)$ or $Znq_2(phen)$. With thiols, on the other hand, $Zn(qt)_2$ or $Zn(mqt)_2$ is precipitated or extracted, and neither thiol nor phen can change the configuration to octahedron. By the change of the donor atom from O to S, tetrahedral structure is relatively stabilized for zinc. Since the 2-methyl group does not hinder the coordination of the second mqt^- with this configuration, $Zn(qt)_2$ and $Zn(mqt)_2$ have similar characteristics.

The structure of $Cd(mqt)_2$ was determined to be tetrahedral by X-ray crystallography.[32] Although $Cd(qt)_2$ prepared also has a metal : ligand ratio of 1 : 2 without coordinated waters, the behavior is fairly different from those of $Zn(qt)_2$ and $Cd(mqt)_2$; for example, $Zn(qt)_2$ has a solubility of 4.8×10^{-2} mol dm^{-3} in chloroform, whereas $Cd(qt)_2$ is insoluble but is solubilized in the presence of phen. Since cadmium ion has a larger ionic radius than zinc ion, $Cd(qt)_2$ may change the configuration to octahedron.

From the magnetic susceptibility measurements, $Ni(qt)_2$ (3.32 B.M.) was estimated to have a polymeric square planar structure,[33] whereas $Ni(mqt)_2$ (3.14 B.M.) a distorted tetrahedron.[34] These structures were confirmed by X-ray crystallographic studies.[35,36] In solution, on the other hand, a monomeric planar structure was proposed for $Ni(qt)_2$ from a kinetic study on its reaction with alkyl halide,[37] and from the equilibrium study on the adduct formation reaction.[25] $Ni(mqt)_2$ differs from $Ni(qt)_2$ in the absorption spectra and in the solubilities in chloroform,[34] and is believed to have the same structure in solution with that in the solid.

The planar $Ni(qt)_2$ keeps some capacity to be coordinated. A configurational change does not occur with weak ligands such as water as found in the precipitation of $Niq_2 \cdot 2H_2O$, but it does occur with stronger ligands such as phen. The 2-methyl substituent hinders the structural change to octahedron to make K_{add} of $Ni(mqt)_2$ small.

The authors wish to express their thanks to Dr. Tetsuo Asaji of Nagoya University for the measurement of magnetic susceptibility.

References

1) K. L. Cheng, K. Ueno, and T. Imamura, "Handbook of Organic Analytical Reagents," CRC Press (1982), pp. 377—388 and references therein.
2) A. Corsini, Q. Fernando, and H. Freiser, *Anal. Chem.*, **35**, 1424 (1963).
3) D. Kealey and H. Freiser, *Anal. Chem.*, **38**, 1577 (1966).
4) G. Gutnikov and H. Freiser, *Anal. Chem.*, **40**, 39 (1968).
5) J. Bankovskis, L. Cera, and A. Ievins, *Zh. Anal. Khim.*, **23**, 1284 (1968).
6) Yu. A. Zolotov, O. M. Petrukhin, and L. G. Gavrilova, *J. Inorg. Nucl. Chem.*, **32**, 1679 (1970).
7) N. A. Ulakhovich, H. C. Budnikov, T. S. Gorbunova, and A. P. Sturis, *Talanta*, **31**, 727 (1984).
8) Y. Nakabayashi, Y. Masuda, and E. Sekido, *Electrochim. Acta*, **30**. 347 (1985).
9) A. T. Rane and D. R. Nepali, *J. Radioanal. Chem.*, **90**, 39 (1985).
10) Y. Mido and E. Sekido, *Bull. Chem. Soc. Jpn.*, **44**, 2130 (1971).
11) Y. Kidani, S. Naga, and H. Koike, *Chem. Pharm. Bull.*, **23**, 1652 (1975).
12) G. K. Budnikov, T. S. Sharapova, A. P. Sturis, and V. F. Toropova, *Zh. Obshch. Khim.*, **49**, 1113 (1979); G. K. Budnikov, N. A. Ulakhovich, O. Yu. Kargina, and A. P. Sturis, *Zh. Obshch. Khim.*, **51**, 2588 (1981).
13) A. Yuchi, K. Imai, H. Wada, and G. Nakagawa, *Bull. Chem. Soc. Jpn.*, **59**, 3847 (1986).
14) D. Kealey and H. Freiser, *Talanta*, **13**, 1381 (1966).
15) J. A. W. Dalziel and D. Kealey, *Analyst*, **89**, 411 (1964).
16) E. Sekido, I. Fujiwara, and Y. Masuda, *Talanta*, **19**, 479 (1972).
17) A. Yuchi, S. Yamada, and M. Tanaka, *Anal. Chim. Acta*, **115**, 301 (1980).
18) R. A. Robinson and R. H. Stokes, "Electrolyte Solutions," 2nd ed, Butterworths (1959).
19) N. Nakamura and E. Sekido, *Talanta*, **17**, 515 (1970).
20) E. Sekido, T. Kobayashi, and Y. Masuda, *Bull. Chem. Soc. Jpn.*, **55**, 1321 (1982).
21) J. Bankovskis, L. Cera, and A. Ievins, *Zh. Analit. Khim.*, **18**, 555 (1963).
22) A. Kawase and H. Freiser, *Anal. Chem.*, **39**, 22 (1967).
23) M. Tanaka, Solvent Extr., *Proc. Int. Solvent Extr. Conf.*, **1971**, 16.
24) M. Tanaka and T. Niinomi, *J. Inorg. Nucl. Chem.*, **27**, 431 (1965).
25) K. S. Math and H. Freiser, *Anal. Chem.*, **41**, 1682 (1969).
26) K. Watanabe and K. Kawagaki, *Bunseki Kagaku*, **27**, 467 (1978).
27) E. Sekido and N. Fukui, *Bull. Inst. Chem. Res., Kyoto Univ.*, **53**, 139 (1975).
28) M. Kita, K. Yamanari, and Y. Shimura, *Chem. Lett.*, **1983**, 141.
29) A. Corsini, Q. Fernando, and H. Freiser, *Talanta*, **11**, 63 (1964).
30) N. Iordanov, M. Stankova, and D. Shopov, *Chem. Phys. Lett.*, **39**, 174 (1976).
31) O. G. Matyukhina, A. N. Sobolev, J. Lejejs, and Yu. A. Bankovskii, *Latv, PSR Zinat. Akad. Vestis, Kim. Ser.*, **1984**, 25; *Chem. Abstr.*, **100**, 201269b (1984).
32) L. Pecs, J. Ozols, A. Kemme, J. Bleidelis, and A. Sturis, *Latv. PSR Zinat. Akad. Vestis, Kim. Ser.*, **1979**, 259; *Chem. Abstr.*, **91**, 81809z (1979).
33) L. F. Lindoy, S. E. Livingstone, and T. N. Lockyer,

Aust. J. Chem., **19**, 1391 (1966).
34) J. C. Shoup and J. A. Burke, *Inorg. Chem.*, **12**, 1851 (1973).
35) L. Pecs and A. P. Sturis, *Latv. PSR Zinat. Akad. Vestis, Kim. Ser.*, **1978**, 493; *Chem. Abstr.*, **89**, 189358z (1978).
36) L. Pecs, J. Ozols, A. Kemme, J. Bleidelis, and A. Sturis, *Latv. PSR Zinat. Akad. Vestis, Kim. Ser.*, **1980**, 549; *Chem. Abstr.*, **93**, 248578d (1980).
37) J. A. Burke and E. C. Brink, *Inorg. Chem.*, **8**, 386 (1969).

The Thermal Decomposition of Ammonium *cyclo*-Hexaphosphate $(NH_4)_6P_6O_{18} \cdot 1.5H_2O$ and Ammonium *cyclo*-Tetraphosphate $(NH_4)_4P_4O_{12}$

Atsushi TAKENAKA,* Itaru MOTOOKA,† and Hiroyuki NARIAI
Department of Industrial Chemistry, Yonago National College of Technology, Ōtakazuna, Hikona-chō, Yonago, Tottori 683
†Department of Chemistry, Faculty of General Education, Kobe University, Tsurukabuto, Nada-ku, Kobe 657
(Received May 22, 1987)

Ammonium *cyclo*-hexaphosphate 1.5-hydrate $(NH_4)_6P_6O_{18} \cdot 1.5H_2O$ was prepared. Under conditions similar to those in the thermal analysis (TG-DTA), the hydrate was heated in an electric furnace. The atmospheres used then were streams of humid air, dried air and dry ammonia gas. The products were characterized by the X-ray diffraction method and by HPLC-flow injection analysis (HPLC-FIA). The thermal decomposition of anhydrous ammonium *cyclo*-tetraphosphate $(NH_4)_4P_4O_{12}$ was also investigated. From each ammonium *cyclo*-phosphate, very analogous ammonium polyphosphate was produced. Its formation was considered to result from the polymerization of some lower-condenced phosphate radicals, which were generated on the cleavage of the ring anions of the *cyclo*-phosphates. The radicals incorporated water molecules in the atmosphere, which causes less formation of the ammonium polyphosphate and exhibited a TG gain and an exothermal DTA break. The exotherm could be attributed theoretically to the incorporation in case of the *cyclo*-tetraphosphate. Moreover, the release of ammonia from the starting material was supposed to be a trigger for the cleavage of the ring anions.

The ammonium *cyclo*-tri- and *cyclo*-tetraphosphates have been studied in regard to several properties by many authors.[1-10] Especially Coates and Woodard summarized the preparations, stability, and X-ray diffraction data of ammonium lower-condenced phosphates containing ammonium *cyclo*-tetraphosphate, but the thermal stability of the *cyclo*-tetraphosphate was mentioned a little.[10] As with the *cyclo*-tetraphosphate, the thermal stability of the ammonium salt of *cyclo*-hexaphosphate with a twelve-membered ring anion has not been reported. Therefore, it seemed that it would be of interest to obtain detailed informations on the thermal stability of the ammonium salt of these *cyclo*-phosphates.

The purpose of the present work was to study the thermal decomposition of ammonium *cyclo*-hexaphosphate, mainly in connection with the effect of humidity in the atmosphere; its preparation was established. In addition, by comparison with that of the *cyclo*-hexaphosphate, the pyrolysis of ammonium *cyclo*-tetraphosphate was investigated more closely.

Experimental

Chemicals, and Analyses of Phosphorus and Nitrogen. Chemicals: Unless otherwise stated, guaranteed-grade reagents were used without further purification.

Analyses of Phosphorus and Nitrogen: With a HPLC-flow injection system, the total phosphorus was determined colorimetrically. The nitrogen content was obtained by means of an ammonia-distillation method.

X-Ray Diffraction Analysis. The X-ray powder diffraction patterns were measured with a Rigaku Denki diffractometer, using nickel-filtered Cu $K\alpha$ radiation.

Thermal Analysis. The thermal analyses (TG-DTA) were carried out at the rate of 2.5° min^{-1} by means of a Rigaku 8002 SD Thermal Analyser. The measurements were performed in stationary air or in a stream of dry N_2 gas at a rate of 100 $cm^3 min^{-1}$, which did not influence the temperatures assigned to DTA breaks. If required, an atmosphere of stationary N_2 gas was also used. It was attained by the evacuation of the furnace of the TG-DTA device, followed by the introduction of dry N_2 gas. This procedure was repeated three times.

HPLC-Flow Injection Analysis (HPLC-FIA). A JASCO TRIROTER V Liquid Chromatograph was used. The system was equipped with two injection ports called "loop-valve sampler." One loop-valve sampler, placed ahead of a column, is used for the separation and determination of phosphates. The other, for the total phosphorus analysis, is situated after the column. A polystyrene-based anion exchanger (TSK gel SAX, d_p=10 μm, Toyo Soda) was packed in the column.

The eluent was flowed through at 1.0 $cm^3 min^{-1}$. It was prepared from appropriate concentrations of an aq. potassium chloride soln. and an aq. 0.1% (w/v) EDTA-4Na soln. The Mo(V)-Mo(VI) reagent for the colorimetric analysis was the 10-fold-diluted aq. solution of the reagent prepared by Lucena-Conde and Prat.[11] At a flow rate of 0.8 $cm^3 min^{-1}$ it was introduced continuously into the stream of the effluent. Then the mixed solution was heated up to 140 °C by passing it through 10 m of 2.0×0.5 mm (O.D.×I.D.) PTFE tubing in an oil bath. The heteropoly blue thus formed was measured at 830 nm in a flow cell.

Thirty-mg portions of a sample were dissolved in water and diluted to 25 cm^3. When they were dissolved inadequately or not, 1—4 cm^3 of 10% (w/w) sodium chloride aq. soln. was then added. A two-cm^3 portion of this solution was transferred into a 50-cm^3 volumetric flask to be diluted. One hundred-μl portions of it were then analyzed.

When this solution contained many polyphosphates and/or their chain length became longer, the above-mentioned technique of analyzing the solution was not enough to produce the heteropoly blue completely. Consequently, the amount of the polyphosphates was estimated at less than the true value. To prevent this, a 2-cm^3 portion of 2-mol dm^{-3} hydrochloric acid was added to a 10-cm^3 portion of the preceding HPLC-FIA sample solution, and they were mixed well. It was allowed to stand at 70 °C for 1 h, cooled to room temperature, and then neutralized with ca. 2 cm^3 of

2-mol dm^{-3} sodium hydroxide aq. soln. This solution was subsequently diluted 5-fold and then injected into the loop-valve sampler located after the column in order to determine its total phosphorus content. The amount of the polyphosphates was calculated by subtracting the amount of phosphorus of all the phosphates (except for the polyphosphates) from the total phosphorus content.

Preparation of Ammonium *cyclo*-Hexa- and Ammonium *cyclo*-Tetraphosphates. Ammonium *cyclo*-Hexaphosphate $(NH_4)_6P_6O_{18} \cdot 1.5H_2O$: Ammonium *cyclo*-hexaphosphate could be prepared from sodium *cyclo*-hexaphosphate $Na_6P_6O_{18} \cdot 6H_2O$ by means of a cation exchanger. $Na_6P_6O_{18} \cdot 6H_2O$ was obtained in a way similar to the method reported by Griffith and Buxton.[12] A cation-exchange procedure was performed in accordance with the work by Coates and Woodard.[10]

The *cyclo*-hexaphosphate anion was contained at least 98.5% as phosphorus in the product. The impurities were mainly highly-condensed phosphates. The X-ray powder diffraction pattern did not agree with that of ammonium *cyclo*-hexaphosphate monohydrate prepared by Vol'fkovich et al.[13] (Table 1). Analyses of phosphorus and nitrogen: P, 30.55; N, 13.87%. The water content could be calculated based on the phosphorus value, as the molar ratio of phosphorus to nitrogen was 1.00:1.00. The formula was $(NH_4)_6P_6O_{18} \cdot 1.5H_2O$. Yield: about 11 g for 15 g of $Na_6P_6O_{18} \cdot 6H_2O$.

Ammonium *cyclo*-Tetraphosphate $(NH_4)_4P_4O_{12}$: Anhydrous ammonium *cyclo*-tetraphosphate was prepared by means of a cation-exchange method similar to that used for the *cyclo*-hexaphosphate. Sodium *cyclo*-tetraphosphate tetrahydrate[14] was used as the starting material. The ammonium *cyclo*-tetraphosphate was identified X-ray diffractometrically.[10]

Table 1. X-Ray Diffraction Data for Ammonium *cyclo*-Hexaphosphate

Present work		Vol'fkovich et al.	
d(A)[a]	Intensity[b]	d(A)	Intensity
6.55	VS	6.56	100
		4.99	10
4.44	S	4.46	80
4.19	S	4.20	10
3.81	M	3.86	60
3.62	M		
3.26	W	3.28	40
3.05	M	3.06	60
3.01	M	3.02	10
2.91	S	2.919	20
2.83	M	2.843	70
2.63	S	2.645	90
2.56	W	2.576	40
2.51	W	2.520	30
		2.503	10
		2.400	20
2.38	W	2.381	40
2.28	W		
2.22	VW	2.229	50
2.18	W	2.192	20
2.13	W	2.142	80
2.10	W	2.110	80
2.02	W	2.026	30

a) Cu $K\alpha$ radiation. b) VS: Very strong, S: strong, M: medium, W: weak, VW: very weak.

Thermal-Decomposition Processes. The ammonium *cyclo*-phosphate (0.2 g) was spread on a porcelain boat in a layer less than 1 mm thick, so as to get the desired atmosphere instantly. The boat was placed in a quartz tube, which had been set in a cylindrical electric furnace (I.D.×L: 35×350 mm) beforehand. The sample was heated at the same rate (2.5° min^{-1}) as in the TG-DTA measurements. As soon as it reached at the required temperature, it was taken out and cooled to room temperature in a desiccator.

The humidity of the air entering at 50 cm^3 min^{-1} into the quartz tube was controlled by means of a Heatless Air Drier HF 200-9-30 (Nippon Pure Gas Co., Ltd.) or an Ace Constant-humidity Generator Model AHC-1 (Ace Scientific Laboratory Co., Ltd.). The amounts of water vapor in the quartz tube were nearly 0 and 1.04 mg per minute respectively. These two atmospheres should be considered to show the effect of humidity on the thermal decomposition more obviously than in the corresponding TG-DTA measurements. In addition, a stream of NH_3 gas (purity: 99.9%) was also used by introducing it directly from the cylinder at 50 cm^3 min^{-1}.

Results and Discussion

Thermal Decomposition of Ammonium *cyclo*-Hexaphosphate 1.5-Hydrate $(NH_4)_6P_6O_{18} \cdot 1.5H_2O$. The results of the thermal analyses (TG-DTA) of ammonium *cyclo*-hexaphosphate 1.5-hydrate (P_{6m}) in stationary air and in a stream of dry N_2 gas are shown in Fig. 1, (a) and (b) respectively. Three endothermic breaks — at about 180, 195 and around 300 °C—are observed in both atmospheres. Exothermal breaks are shown at 205 °C. As P_{6m} has 1.5 moles of water of crystallization and is considered to bring humidity to the atmosphere on heating, it is supposed that hardly any difference in the DTA curves is recognized. The endothermic break at around 300 °C was apparently attributable to the melting of the product.

In the N_2 gas stream, no increase in weight is found in the temperature range measured, but in the stationary air there is an increase from 195 to 205 °C (Fig. 1, (b) and (a)).

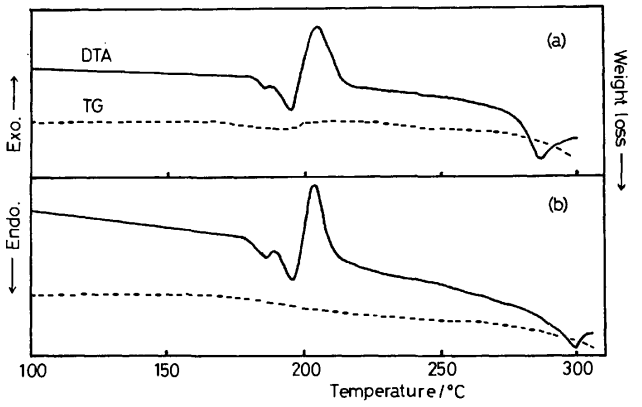

Fig. 1. TG-DTA analyses of ammonium *cyclo*-hexaphosphate in the two different atmospheres. (a): Performed in stationary air, (b): in a stream of N_2 gas.

In order to investigate the decomposition processes causing the DTA breaks in the range from 100 to 215 °C, many studies were carried out with a cylindrical electric furnace. The amount of P_{6m} and polyphosphates in the samples heated up to 100, 150, 180, 195, 205, and 215 °C are illustrated in Fig. 2.

Thilo and Grunze reported that the tetra- and octaphosphates were formed selectively in the course of the thermal decomposition of lithium *cyclo*-tetraphosphate tetrahydrate. They supposed that their formation was attributable to the polymerization of the "radicals," which had been produced thermally.[1] The same paper described that the radicals incorporated water molecules from the atmosphere. As the decomposition of P_{6m} is scarcely affected by the humidity (Fig. 2), the P_{6m} rings do not disappear upon hydrolysis, but decompose to "radicals." The TG-increase from 195 to 205 °C is probably due to the incorporation of water molecules. The polyphosphates form less in the presence of water vapor than in its absence (Fig. 2). Figure 3 shows that the total amount of oligophosphates is larger under the humid condition than under the dried condition. Thus, the incorporation of water molecules inhibits the polymerization of the radicals.

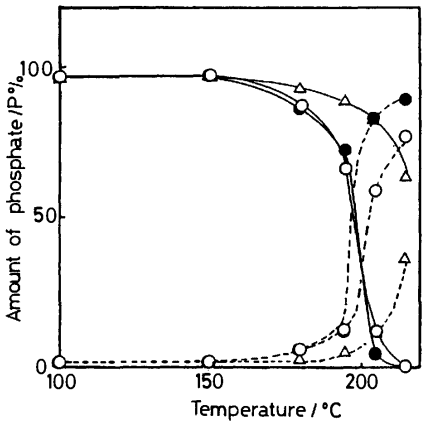

Fig. 2. Amounts of the *cyclo*-hexaphosphate and the polyphosphates in the products heated up to the required temperatures in the three different atmospheres. ——: *cyclo*-Hexaphosphate, ----: polyphosphates, ○: in a stream of humid air, ●: in a stream of dried air, △: in a stream of NH_3 gas.

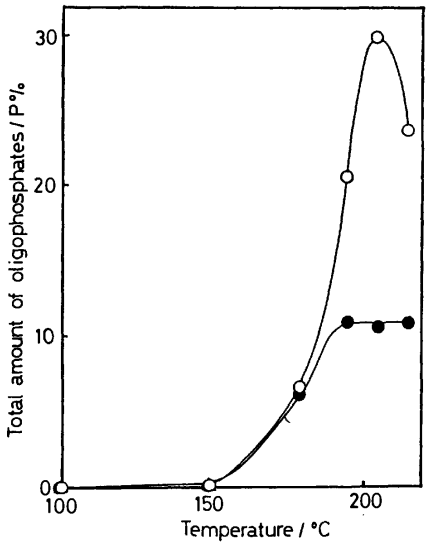

Fig. 3. Total amounts of oligophosphates in the humid and the dried atmospheres. ○: In a stream of humid air, ●: in a stream of dried air.

Among the oligophosphates contained in the samples, di-(P_2) and monophosphate(P_1) were more abundant than the others. This shows that the P_{6m} ring decomposed into three or six parts to produce the P_2 or the P_1 radicals.

At any rate, the endothermic break at 195 °C, regardless of humidity, probably corresponds to the cleavage of the P_{6m} rings. The following exothermal break at 205 °C must be caused by the bonding of the water molecules with the radicals (see the next subsection, for an analogous exothermal reaction is explained there thermodynamically).

In a stream of NH_3 gas, P_{6m} remained more abundantly than in the humid and dried atmospheres (Fig. 2). The departure of ammonia molecules from P_{6m} is thought to be the trigger for the cleavage of P_{6m} to the P_1 and the P_2 radicals.

Thermal Decomposition of Ammonium *cyclo*-Tetraphosphate $(NH_4)_4P_4O_{12}$. Since the ammonium *cyclo*-tetraphosphate (P_{4m}) used was an anhydrous salt, it was expected that the humidity effect on the thermal decomposition would be more obvious than in the case of *cyclo*-hexaphosphate(P_{6m}), which has 1.5 moles of water of crystallization.

Thermal analyses of P_{4m} were carried out in three atmospheres: in stationary air, in a stream of dry N_2 gas, and in stationary dry N_2 gas. Contrary to the case

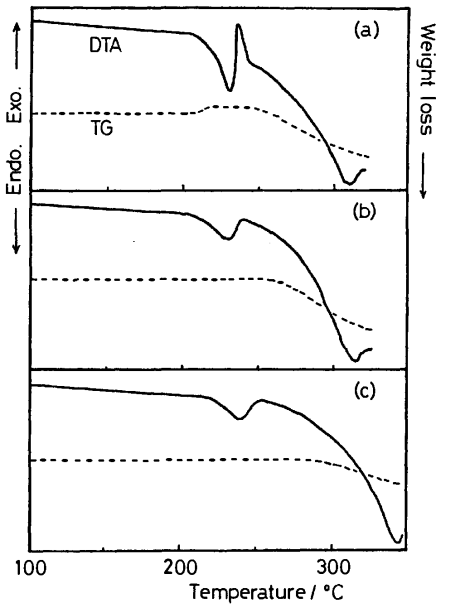

Fig. 4. TG-DTA analyses of ammonium *cyclo*-tetraphosphate in the three different atmospheres. (a): Performed in stationary air, (b): in a stream of N_2 gas, (c): in stationary N_2 gas.

of P_{6m}, the DTA curve in the humid atmosphere has an exothermal break at 238 °C (Fig. 4, (a)), while that in the dried atmosphere has no exotherm (Fig. 4, (b)). These DTA curves show endothermic processes at 233 and 230 °C respectively. On the DTA chart measured in the stationary dry N_2 gas, there is an endothermic break at the rather high temperature of 240 °C (Fig. 4, (c)).

P_{4m} was also heated up to 150, 200, 233, 238, and 244 °C (and sometimes 258 °C as well) in a cylindrical electric furnace. Figure 5 shows that the amount of P_{4m} in the products decreases rapidly between 200 and 238 °C in the humid and dried atmospheres. The decrease is independent of the humidity in the atmosphere. Therefore, the P_{4m} rings are not hydrolyzed.

If the polyphosphates are produced by the condensation of acidic ammonium oligophosphates, the thermogravimetric analysis will show a weight loss. However, in the dried atmosphere, the TG curve indicates no weight change (Fig. 4, (b)), and the amount of the polyphosphates increases rapidly in the range from 200 to 238 °C (Fig. 5). Consequently, the polyphosphates do not arise by the condensation, but are produced by the polymerization of the "radicals" which result from the cleavage of P_{4m}.

Only in the humid atmosphere is there an exothermal break, as is shown in Fig. 4, (a). Corresponding to this exotherm, a TG gain is observed. Therefore the exotherm at 238 °C may be attributed to the binding of the radicals with water molecules. The heat of the formation of the phosphate molecules brought about by the binding of the radicals with water molecules (ΔH; kJ mol^{-1}) can be calculated by means of the following scheme. In this scheme, ΔH should be

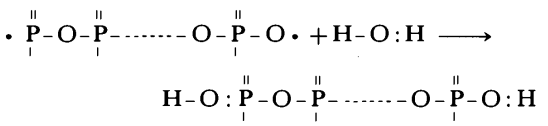

obtained by means of this equation; $\Delta H=(\text{O-H})_{H_2O}+[-\{(\text{O-H})+(\text{P-O})\}]\approx-(\text{P-O})$, where $(\text{O-H})_{H_2O}$ is the oxygen-hydrogen bond energy of water molecules, (O-H) is the oxygen-hydrogen bond energy of the phosphates produced, and (P-O) is the phosphorus-oxygen bond energy of the phosphates ca. 359.8 kJ mol^{-1}.[15] Consequently, the heat of the formation of the phosphates (ΔH) is the negative value of −359.8 kJ mol^{-1}. This value accounts for the exothermal reaction at 238 °C very well.

The radicals are considered to combine with water molecules in the atmosphere, so the water molecules can be expected to inhibit the radical polymerization. Practically, indeed, compared with the dried atmosphere, in the humid atmosphere the amount of the polyphosphates was poor, as is indicated in Fig. 5, while the total amount of the oligophosphates was rich.

Figure 6 represents the amount of the individual oligophosphate plotted against its chain length. Under the humid condition, mono-(P_1) and diphosphate (P_2) are present in larger quantities (Fig. 6, (a)). Only P_1 is detected in the dried atmosphere (Fig. 6, (b)). As a trace of water vapor may be found in the dried atmosphere, P_1 is thought to result from the P_1 radicals, trapping of the water molecules. Accordingly, it is concluded that the P_{4m} ring decomposes into four parts, thus producing the P_1 radicals, or perhaps into two parts, thus producing the P_2 radicals, as is revealed by the abundance of P_2 (Fig. 6, (a)). Moreover, the decomposition of the P_{4m} rings seems to cause the endothermic break at about 230 °C.

In a stream of ammonia gas, P_{4m} was very stable in the range from 150 to 244 °C (Fig. 5). The release of ammonia from the starting material of P_{4m}, must be a

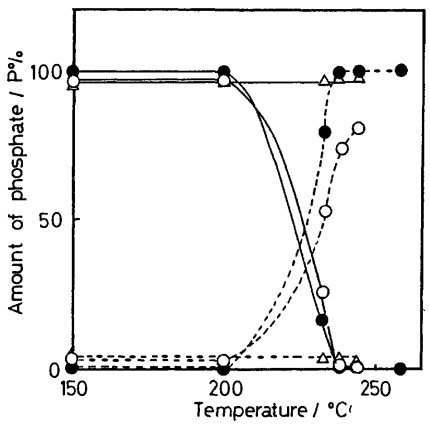

Fig. 5. Amounts of the *cyclo*-tetraphosphate and the polyphosphates in the products heated in the three different atmospheres. ——: *cyclo*-Tetraphosphate, ----: polyphosphates, ○: in a stream of humid air, ●: in a stream of dried air, △: in a stream of NH_3 gas.

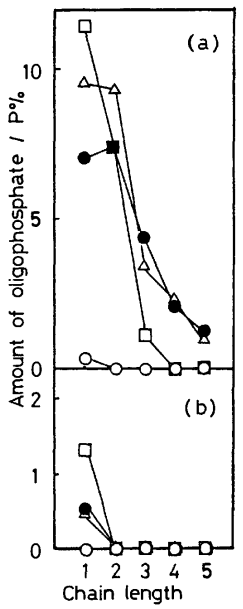

Fig. 6. Amount of the individual oligophosphate in the products. (a): In a stream of humid air, (b): in a stream of dried air, ○: 200 °C, ●: 233 °C, △: 238 °C, □: 244 °C.

Table 2. X-Ray Diffraction Data for Ammonium Polyphosphate Formed from Ammonium *cyclo*-Hexaphosphate $(NH_4)_6P_6O_{18}\cdot 1.5H_2O$ and Ammonium *cyclo*-Tetraphosphate $(NH_4)_4P_4O_{12}$

From $(NH_4)_6P_6O_{18}\cdot 1.5H_2O$		From $(NH_4)_4P_4O_{12}$	
d(A)[a]	Intensity[b]	d(A)[a]	Intensity[b]
6.86	W	6.92	W
		6.56	W
		6.24	W
5.99	VS	5.98	VS
		5.68	M
5.54	M	5.54	M
5.37	S	5.37	S
		5.16	W
		3.99	W
3.80	S	3.79	S
3.71	W	3.74	W
3.56	M	3.55	M
3.48	S	3.48	S
3.40	M	3.40	M
3.22	S	3.22	S
		3.12	W
3.09	W	3.07	M
3.02	VM	2.99	W
2.92	VW	2.91	M
2.88	M	2.88	VW
2.81	M	2.81	W
2.78	W	2.78	VW
2.74	W	2.74	W
2.70	W		

a) Cu $K\alpha$ radiation. b) VS: Very strong, S: strong, M: medium, W: very weak.

"trigger" for the cleavage of the P_{4m} anions, accompanied by the exotherm at about 230 °C. The shift of the exotherm to a higher temperature in the stationary N_2 gas (Fig. 5, (c)) is attributable to an enhanced partial pressure of ammonia by evacuation and may be thought to prove the "trigger reaction."

Characterization of the Polyphosphate. The X-ray diffraction data for the decomposition products of P_{6m} and P_{4m} are indicated in Table 2. The diffraction lines of the respective products are similar to each other, except for those of the starting materials. They also agree closely with the diffraction lines of ammonium polyphosphates reported by Shen et al.[16] and Frazier et al.[17] In addition, we observed that there was always a water-insoluble material, which must be ammonium polyphosphate,[16] in the product of P_{4m} heated above 233 °C.

References

1) V. H. Grunze and E. Thilo, *Z. Anorg., Allg. Chem.*, **281**, 284 (1955).
2) T. Iida, M. Sawada, T Yamada, and K. Itoh, *Bulletin of Nagoya Institute of Technology*, **27**, 205 (1975).
3) A. Menlibaev, D. Z. Sarazetdinov, M. Kh. Kim, and Zh. K. Shaidarbekova, *Izv. Akad. Nauk Kaz. SSR, Ser. Khim.*, **27**, 1 (1977).
4) Z. T. Wakefield, B. B. Luff, and R. C. Sheridan, *J. Chem. Eng. Data*, **16**, 195 (1971).
5) B. B. Luff, R. B. Reed, and Z. T. Wakefield, *J. Chem. Eng. Data*, **17**, 96 (1972).
6) B. M. Beglov, *Dokl. Akad. Nauk Uzb. SSR*, **1976**, 36.
7) C. Romers, J. A. A. Ketelaar, and C. H. MacGillavry, *Nature (London)*, **164**, 960 (1949).
8) C. Romers, J. A. A. Ketelaar, and C. H. MacGillavry, *Acta Cryst.*, **4**, 114 (1951).
9) D. A. Koster and A. J. Wagner, *J. Chem. Soc., Dalton Trans.*, **1970**, 435.
10) R. V. Coates and G. D. Woodard, *J. Chem. Soc.*, **1964**, 1780.
11) F. Lucena-Conde and L. Prat, *Anal. Chim. Acta*, **16**, 473 (1957).
12) E. J. Griffith and R. L. Buxton, *Inorg. Chem.*, **4**, 549 (1965)
13) S. I. Volf'kovich, L. V. Kuvasava, M. L. Koz'mina, and T. L. Roslaya, *Dokl. Akad. Nauk SSSR*, **220**, 844 (1975).
14) R. N. Bell, L. F. Audrieth, and F. Hill, *Ind. Eng. Chem.*, **44**, 568 (1952).
15) D. E. C. Corbridge, "Phosphorus: An Outline of its Chemistry, Biochemistry and Technology," 3rd ed., Elsevier Science Publishers, Amsterdam (1985), p. 35.
16) C. Y. Shen, N. E. Stahlheber, and D. R. Dyroff, *J. Am. Chem. Soc.*, **91**, 62 (1969).
17) A. W. Frazier, J. P. Smith, and J. R. Lehr, *J. Agr. Food Chem.*, **13**, 317 (1965).

Syntheses and Characterization of Dinuclear Manganese(II,II) and Manganese(II,III) Complexes with Phenolate and Two Carboxylate Bridges

Masatatsu SUZUKI, Masahiro MIKURIYA,† Shuji MURATA, Akira UEHARA,* Hiroki OSHIO,† Sigeo KIDA,† and Kazuo SAITO†

Department of Chemistry, Faculty of Science, Kanazawa University, Kanazawa 920
†Coordination Chemistry Laboratories, Institute for Molecular Science, Okazaki 444

(Received May 27, 1987)

Dinuclear manganese(II,II) and (II,III) complexes, $[Mn_2(L\text{-}py)(RCOO)_2]ClO_4 \cdot nH_2O$ and $[Mn_2(L\text{-}py)(RCOO)_2](ClO_4)_2 \cdot nH_2O$, were prepared, where L-py is 2,6-bis[bis(2-pyridylmethyl)aminomethyl]-4-methylphenolate(1−) and RCOO denotes CH_3COO or C_6H_5COO. X-Ray structure analysis of the mixed valence complex $[Mn_2(L\text{-}py)(C_6H_5COO)_2](ClO_4)_2 \cdot H_2O$ revealed that the complex cation involves octahedral manganese(II) and manganese(III) centers with N_3O_3 donor sets and that the two metal ions are linked by phenolato and two benzoato groups. Magnetic susceptibility measurements over temperature range 80—300 K indicated that both manganese(II,II) and (II,III) complexes exhibit weak antiferromagnetic interaction with spin-exchange coupling constant, J=−5—−7 cm^{-1}. Cyclic voltammograms of the mixed valence complexes showed two quasi-reversible redox couples at ca. 0.5 and ca. 1.0 V (vs. SCE), assignable to the redox reactions of Mn^{II}-Mn^{III}/Mn^{II}-Mn^{II} and Mn^{III}-Mn^{III}/Mn^{II}-Mn^{III}, respectively. The comproportionation constants for the reaction $(Mn^{III}\text{-}Mn^{III})+(Mn^{II}\text{-}Mn^{II}) \rightleftarrows 2(Mn^{II}\text{-}Mn^{III})$ at 20 °C were estimated as $2\text{—}3\times10^9$.

It has been pointed out that the manganese ions in the water oxidizing system of photosystem II in green plants are present as dinuclear or tetranulclear cluster, in which the di-, tri-, and/or tetravalent manganese ions are involved in the catalytic cycle of water oxidation.[1,2] Although many efforts have been devoted to understanding the role of the manganese ions operating in the cycle, little is known on the structure of the manganese site and the reaction mechanism of water oxidation.

It has been suggested that a mixed valence dinuclear manganese(II,III) center exists in chloroplasts in the dark.[3,4] For further elucidation of the above manganese site, it is needed to study in more detail the coordination chemistry of dinuclear mixed valence manganese(II,III) complexes with biologically relevant ligands such as 2- or 4-imidazolyl group, carboxylato and phenolato groups, etc. However, only a few suitable model complexes have been devised for this purpose.[5,6]

In the previous paper, we shortly communicated the synthesis and characterization of a mixed valence manganese(II, III) complex $[Mn_2(L\text{-}py)(CH_3COO)_2](ClO_4)_2 \cdot H_2O$, and proposed a dinuclear structure in which manganese(II) and manganese(III) ions are bridged by the phenolato and two acetato groups.[7] Reported herein are syntheses and the physicochemial properties of the dinuclear manganese(II, II) and (II, III) complexes with a dinucleating ligand (L-py) and a carboxylate ion, $[Mn_2(L\text{-}py)(RCOO)_2]ClO_4 \cdot nH_2O$ and $[Mn_2(L\text{-}py)(RCOO)_2](ClO_4)_2 \cdot nH_2O$ (RCOO=CH_3COO or C_6H_5COO), where L-py represents 2,6-bis[bis(2-pyridylmethyl)aminomethyl]-4-methylphenolate(1−) ion. The crystal structure of $[Mn_2(L\text{-}py)(C_6H_5COO)_2](ClO_4)_2 \cdot H_2O$ is also described, which is the first example of a mixed valence manganese(II, III) complex whose structure was determined by X-ray structure analysis.

Experimental

Materials. HL-py was synthesized as previously described.[8] $[Mn(dmso)_6](ClO_4)_3$ was prepared according to the method of literature.[9] The other chemicals were of reagent grade.

Preparation of Manganese(II, II) Complexes. $[Mn_2(L\text{-}py)(CH_3COO)_2]ClO_4 \cdot 0.5H_2O$ (**1a**): A solution of $Mn(CH_3COO)_2 \cdot 4H_2O$ (1 mmol) in 20 cm^3 of methanol was added with stirring to a solution of HL-py (0.5 mmol), triethylamine (1 mmol), and $NaClO_4$ (2 mmol) in 20 cm^3 of methanol. White crystals formed were filtered off, washed with ethanol and ether, and dried in vacuo.

$[Mn_2(L\text{-}py)(C_6H_5COO)_2]ClO_4 \cdot 2H_2O$ (**2a**): A solution of $Mn(ClO_4)_2 \cdot 6H_2O$ (1 mmol) in 20 cm^3 of methanol was added to a methanol solution (20 cm^3) of HL-py (0.5 mmol), C_6H_5COOH (1 mmol), and triethylamine (1.5 mmol) with stirring. White crystals obtained were filtered off, washed with ethanol and ether, and dried in vacuo.

Preparation of Manganese(II, III) Complexes. $[Mn_2(L\text{-}py)(CH_3COO)_2](ClO_4)_2 \cdot H_2O$ (**1b**): A solution of $Mn(CH_3COO)_3 \cdot 2H_2O$ (1 mmol) in 30 cm^3 of methanol was mixed with a solution of HL-py (0.5 mmol) in 20 cm^3 of methanol with stirring. To the resulting solution was added a methanol solution (20 cm^3) of $NaClO_4$ (4 mmol) to give dark green crystals, which were filtered off, washed with ethanol and ether, and dried in vacuo. Recrystallization was carried out from acetonitrile.

$[Mn_2(L\text{-}py)(C_6H_5COO)_2](ClO_4)_2 \cdot H_2O$ (**2b**): A solution of HL-py (0.5 mmol), C_6H_5COOH (1 mmol), and triethylamine (1.5 mmol) in 20 cm^3 of methanol was added to a suspension of $[Mn(dmso)_6](ClO_4)_3$ (1 mmol) in 30 cm^3 of acetone with stirring. The mixture was strirred for 30 min and filtered to remove the unreacted dmso complex. The filtrate was allowed to stand overnight to produce dark green crystals. They were recrystallized from acetonitrile.

Measurements. The electronic spectra in acetonitrile solution were measured on a Jasco UVIDEC 505 UV/VIS recording digital spectrophotometer and a Hitachi 323 recording spectrophotometer.

Infrared spectra were obtained by a KBr-disk method and a nujol mull method with a Jasco A-3 infrared spectrophotometer.

Magnetic susceptibilities were measured with a Shimazu torsion magnetometer MB-2 which was calibrated with $Hg[Co(NCS)_4]$. Diamagnetic correction was made by using Pascal's constants.

Cyclic voltammograms were obtained with a Yanagimoto P-900 in a cell containing a glassy carbon working electrode, a platinum-coil auxiliary electrode, and a saturated calomel electrode as reference electrode. Applied voltage was measured with a Takeda Riken TR-8651 electrometer. Acetonitrile was used as the solvent and tetrabutylammonium perchlorate as the supporting electrolyte. Ferrocene was added for an internal check on redox potential and reversibility. $E_{1/2}$ of ferrocene was 0.39 V (vs. SCE) with a peak-to-peak separation (ΔE) of 70 mV. For constant-potential electrolyses, Hokuto Denko HA-301 potentiostat/galvanostat was used to control the potentials. Current-time curves were recorded with a Rikenn Denshi SP-K1V recorder. Integration of current was carried out by integrating the area under the current vs. time curves. A two compartmental H-type cell with a glass frit containing a platinum gauze working electrode, platinum plate auxiliary electrode, and a saturated caromel electrode was used. For the reduction and oxidation of **1b**, applied potentials were +0.35 and +1.15 V (vs. SCE), respectively.

ESR spectra were measured on a JEOL JES-FE2XG ESR spectrometer (X-band microwave unit, 100 KHz field modulation) equipped with an Air Product LTD-3-110 liquid helium transfer system. The microwave frequency was monitored with a Takeda Riken TR5212 microwave counter, and the resonance magnetic field values of the signals were measured with an NMR field meter (ECHO Electronics Co., Ltd.)

Analyses of Manganese(II) and Manganese(III) Ions. Analysis of manganese(III) ion was carried out by iodometry and by the method described in the literature.[10] Total amount of manganese ion was determined colorimetrically.[11] The results are listed in Table 1.

X-Ray Crystal Structure Analysis of $[Mn_2(L\text{-}py)(C_6H_5COO)_2](ClO_4)_2 \cdot H_2O$. Crystal data: $[Mn_2(C_{33}H_{33}N_6O)(C_6H_5COO)_2](ClO_4)_2 \cdot H_2O$; $F.W.$=1098.69, monoclinic; $P2_1/c$; a=23.979 (4), b=11.357(1), and c=18.502(2) Å; β=97.29(1)°; V=4997.8(12) Å^3; Graphite monochromated Mo$K\alpha$ (λ=0.71073 Å); D_m=1.50, D_c=1.46 g cm^{-3}; Z=4; μ (Mo$K\alpha$)=6.60 cm^{-1}; A dark green crystal with dimensions of 0.10×0.18×0.37 mm.

Data Collection and Processing: The unit-cell parameters and intensities were measured on a Rigaku AFC-5 automated four-circle diffractometer by the 2θ-ω scan technique with a scan rate of 3° min^{-1}. A total of 9543 reflections with $2\theta < 50°$ was collected. Three standard reflections were monitored every 50 reflections. The intensities of two standard reflections showed a good stability, although one reflection underwent a significant decay: the intensities decreased to ca. 35% of initial intensity at the end of measurement. All attempts to obtain better single crystals were in vain, because the crystals were very fragile and not suitable for measurement. Therefore we used the above intensity data for analysis without correction for the intensity decay. The intensity data were corrected for the Lorentz-polarization effects and for absorption. Independent 3590 reflections with $|F_o| > 3\sigma(|F_o|)$ were considered as "observed" and were used for the structure analysis.

The structure was solved by the direct method. Refinement was carried out by the block-diagonal least-squares method. Oxygen atom of water molecule was found to be statistically distributed at two positions with occupancy factor of 0.5. All the non-hydrogen atoms were refined with isotropic thermal parameters. Hydrogen atoms were not included in the calculation. The weighting scheme $w=[\sigma^2_{count}+(0.015|F_o|)^2]^{-1}$ was employed. The final discrepancy factors were $R=\sum||F_o|-|F_c||/\sum|F_o|=0.116$ and $R_w=[\sum w(|F_o|-|F_c|)^2/\sum w|F_o|^2]^{1/2}=0.118$.

The atomic scattering factors and the anomalous dispersion corrections, $\Delta f'$ and $\Delta f''$, for Mn, Cl, O, N, and C, were taken from the International Tables for X-Ray Crystallography.[12] All the calculations were carried out on the HITAC M-680H computer at the Computer Center of the Institute for Molecular Science by the use of the UNICS-III,[13] MULTAN 78,[14] and ORTEP[15] programs. The final positional and thermal parameters of non-hydrogen atoms with their estimated standard deviations are given in Table 2. Observed and Calculated structure factors have been deposited as a Document No. 8773 at the office of the Editor.

Results and Discussion

Structure Description of $[Mn_2(L\text{-}py)(C_6H_5COO)_2](ClO_4)_2 \cdot H_2O$. Figure 1 shows a perspective view of the complex cation and the numbering system of

Table 1. Analytical Data and Effective Magnetic Moments of the Complexes

	Complex	Found (Calcd) (%)					μ_{eff} (Mn_2)/ B.M.[a]
		C	H	N	Mn(II)	Mn(III)	
1a	$[Mn_2(L\text{-}py)(CH_3COO)_2]ClO_4 \cdot 0.5H_2O$	51.30 (51.31)	4.34 (4.66)	9.33 (9.70)			7.8
2a	$[Mn_2(L\text{-}py)(C_6H_5COO)_2]ClO_4 \cdot 2H_2O$	54.80 (55.49)	4.23 (4.66)	8.20 (8.26)			7.7
1b	$[Mn_2(L\text{-}py)(CH_3COO)_2](ClO_4)_2 \cdot H_2O$	45.47 (45.60)	3.90 (4.23)	8.31 (8.62)	5.2 (5.64)	5.6 (5.64)	7.1
2b	$[Mn_2(L\text{-}py)(C_6H_5COO)_2](ClO_4)_2 \cdot H_2O$	51.26 (51.38)	3.79 (4.13)	7.73 (7.65)	5.0 (5.00)	5.0 (5.00)	7.1

a) At room temperature.

Table 2. Fractional Positional Parameters ($\times 10^4$) and Thermal Parameters of Non-Hydrogen Atoms with Their Estimated Standard Deviations in Parentheses

Atom	x	y	z	B/Å^3	Atom	x	y	z	B/Å^3
Mn(1)	2814(1)	−1794(2)	1662(1)	2.9(0.1)	C(12)	4290(8)	−4499(18)	1322(10)	6.0(0.5)
Mn(2)	1925(1)	446(2)	929(1)	3.0(0.1)	C(13)	3746(8)	−4813(18)	1062(10)	5.8(0.5)
Cl(1)	5543(2)	−2896(5)	3232(3)	5.7(0.1)	C(14)	3298(7)	−4051(15)	1152(9)	4.4(0.4)
Cl(2)	461(3)	6158(6)	2379(3)	8.2(0.2)	C(15)	3537(6)	−2025(15)	3125(8)	3.5(0.4)
O(1)	2375(4)	−465(9)	1866(5)	3.0(0.2)	C(16)	2968(6)	−2443(14)	3237(8)	3.4(0.4)
O(2)	3131(4)	−877(9)	785(5)	3.8(0.2)	C(17)	2847(7)	−2662(16)	3957(9)	5.0(0.5)
O(3)	2599(4)	587(9)	294(5)	3.9(0.2)	C(18)	2323(8)	−3154(18)	4037(10)	6.1(0.5)
O(4)	2230(4)	−2716(9)	1095(5)	3.6(0.2)	C(19)	1927(7)	−3428(16)	3427(9)	5.2(0.5)
O(5)	1648(4)	1293(10)	568(5)	4.1(0.3)	C(20)	2079(7)	−3120(15)	2730(8)	3.9(0.4)
OP(1)	5072(6)	−2191(14)	3381(8)	8.5(0.4)	C(21)	1327(7)	−67(15)	2346(8)	3.7(0.4)
OP(2)	5719(7)	−2551(15)	2564(9)	10.5(0.5)	C(22)	1231(6)	2035(15)	1907(8)	3.6(0.4)
OP(3)	5998(6)	−2773(14)	3784(8)	9.1(0.4)	C(23)	1799(6)	2565(14)	1962(6)	3.1(0.3)
OP(4)	5376(7)	−4065(16)	3178(9)	11.4(0.5)	C(24)	1961(7)	3485(15)	2462(9)	4.6(0.4)
OP(5)	751(7)	7027(15)	2025(9)	10.5(0.5)	C(25)	2497(8)	3944(17)	2504(10)	5.3(0.5)
OP(6)	498(8)	6406(18)	3154(10)	13.8(0.6)	C(26)	2858(8)	3491(17)	2060(9)	5.2(0.5)
OP(7)	−107(7)	6018(15)	2075(8)	10.0(0.5)	C(27)	2677(7)	2596(15)	1566(9)	4.0(0.4)
OP(8)	728(10)	5119(21)	2302(12)	16.5(0.8)	C(28)	704(7)	412(15)	1225(8)	4.1(0.4)
OW	4761(10)	2013(22)	4828(12)	5.7(0.6)[a]	C(29)	697(7)	1000(15)	476(9)	4.0(0.4)
OW′	4406(10)	604(22)	4476(12)	5.9(0.6)[a]	C(30)	186(7)	1410(16)	123(9)	5.0(0.4)
N(1)	3489(5)	−1261(11)	2437(6)	3.6(0.3)	C(31)	188(8)	1913(17)	−559(10)	5.4(0.5)
N(2)	3414(5)	−2978(12)	1494(7)	4.0(0.3)	C(32)	677(8)	1900(18)	−901(10)	5.9(0.5)
N(3)	2597(5)	−2655(11)	2665(6)	3.2(0.3)	C(33)	1161(7)	1466(16)	−482(9)	4.9(0.4)
N(4)	1245(5)	741(11)	1685(6)	3.1(0.3)	C(34)	3023(6)	−45(14)	339(8)	3.1(0.3)
N(5)	2158(5)	2154(11)	1533(6)	3.0(0.3)	C(35)	3441(6)	153(14)	−193(8)	3.1(0.3)
N(6)	1172(5)	1034(11)	191(6)	3.4(0.3)	C(36)	3925(7)	−556(15)	−171(9)	4.3(0.4)
C(1)	2383(6)	−20(14)	2551(8)	2.7(0.3)	C(37)	4293(7)	−411(16)	−693(9)	4.8(0.4)
C(2)	2893(6)	223(14)	2941(8)	3.2(0.3)	C(38)	4177(7)	467(16)	−1220(9)	4.9(0.4)
C(3)	2917(7)	653(15)	3669(9)	4.3(0.4)	C(39)	3713(8)	1201(17)	−1245(9)	5.2(0.5)
C(4)	2393(7)	820(15)	3942(8)	3.9(0.4)	C(40)	3326(7)	1056(15)	−705(9)	4.2(0.4)
C(5)	1882(7)	626(15)	3527(8)	4.1(0.4)	C(41)	1783(6)	−2351(14)	688(8)	3.6(0.4)
C(6)	1887(6)	190(14)	2814(8)	3.4(0.4)	C(42)	1391(6)	−3299(14)	330(8)	3.4(0.3)
C(7)	2406(7)	1260(16)	4772(9)	4.7(0.4)	C(43)	1370(7)	−4407(16)	635(9)	4.7(0.4)
C(8)	3431(7)	37(14)	2622(8)	3.6(0.4)	C(44)	975(8)	−5270(18)	304(10)	5.9(0.5)
C(9)	4003(6)	−1452(14)	2079(8)	3.4(0.4)	C(45)	662(8)	−4944(19)	−362(11)	6.7(0.5)
C(10)	3944(7)	−2653(15)	1742(8)	3.8(0.4)	C(46)	691(8)	−3851(16)	−687(9)	4.9(0.4)
C(11)	4413(8)	−3387(17)	1657(10)	5.5(0.5)	C(47)	1057(6)	−2974(15)	−323(8)	3.7(0.4)

a) Ocuppancy factor of 0.5.

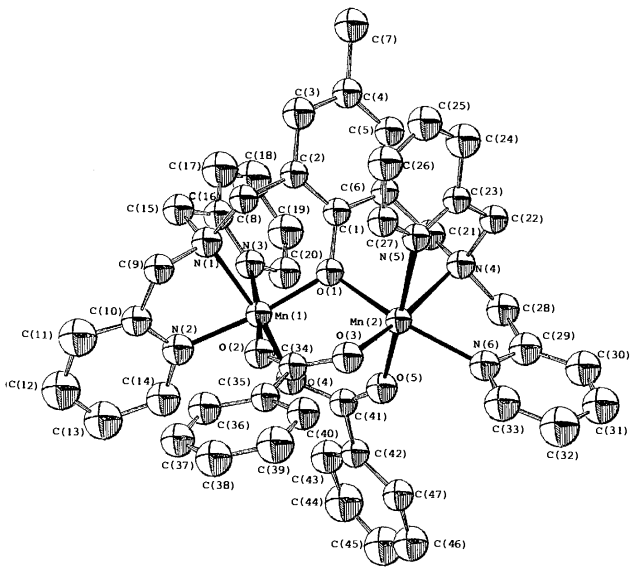

Fig. 1. Crystal structure of the complex cation $[Mn_2(L\text{-}py)(C_6H_5COO)_2]^{2+}$ showing the 50% probability thermal ellipsoids and the atom-labeling scheme.

atoms. The selected bond distances and anlges are listed in Table 3. The crystal structure consists of a discrete dinuclear cation $[Mn_2(L\text{-}py)(C_6H_5COO)_2]^{2+}$, two perchlorate anions, and a water molecule which is statistically distributed to the two positions. Each manganese atom is in a distorted octahedral coordination with a cis,cis-N_3O_3 configuration. The bond distances around the Mn(1) and Mn(2) moieties significantly differ from each other. The bond distances of Mn(1)-O and Mn(1)-N are in the ranges of 1.905(10)—2.147(11) Å and 2.022(14)—2.217(12) Å, respectively, while those of Mn(2)-O and Mn(2)-N are in the ranges of 2.123(11)—2.184(9) Å and 2.224(12)—2.304(13) Å, respectively. The Mn(1)-O and Mn(1)-N distances are comparable to those reported for manganese(III) complexes[16,17] and the Mn(2)-O and Mn(2)-N ones to those reported for manganese(II) complexes.[18] In the Mn(1) moiety, the Mn(1)-O(2) and Mn(1)-N(3) distances are much longer than Mn(1)-O(1), Mn(1)-O(4), Mn(1)-N(1), and Mn(1)-N(2) ones. The O(1), O(4), N(1), and N(2) atoms form an approximate square

Table 3. Selected Interatomic Distances (l/Å) and Angles (ϕ/°) of $[Mn_2(L\text{-py})(C_6H_5COO)_2](ClO_4)_2 \cdot H_2O$

(a) Manganese coordination spheres				(c) L-py moiety			
Mn(1)-Mn(2)	3.483(3)			O(1)-C(1)	1.363(17)		
(Mn(1) moiety)		(Mn(2) moiety)		(Mn(1) moiety)		(Mn(2) moiety)	
Mn(1)-O(1)	1.905(10)	Mn(2)-O(1)	2.184(9)	N(1)-C(8)	1.524(21)	N(4)-C(21)	1.521(20)
Mn(1)-O(2)	2.147(11)	Mn(2)-O(3)	2.123(11)	N(1)-C(9)	1.489(21)	N(4)-C(22)	1.527(21)
Mn(1)-O(4)	1.947(10)	Mn(2)-O(5)	2.162(11)	N(1)-C(15)	1.533(20)	N(4)-C(28)	1.504(19)
Mn(1)-N(1)	2.110(12)	Mn(2)-N(4)	2.304(13)	N(2)-C(10)	1.348(20)	N(5)-C(23)	1.327(20)
Mn(1)-N(2)	2.022(14)	Mn(2)-N(5)	2.273(12)	N(2)-C(14)	1.385(22)	N(5)-C(27)	1.335(20)
Mn(1)-N(3)	2.217(12)	Mn(2)-N(6)	2.224(12)	N(3)-C(16)	1.315(18)	N(6)-C(29)	1.316(21)
				N(3)-C(20)	1.370(20)	N(6)-C(33)	1.334(21)
Mn(1)-O(1)-Mn(2)	116.6(5)			C(1)-C(2)	1.367(20)	C(2)-C(3)	1.426(22)
O(1)-Mn(1)-O(2)	91.3(4)	O(1)-Mn(2)-O(3)	98.1(4)	C(2)-C(8)	1.501(23)	C(6)-C(21)	1.532(21)
O(1)-Mn(1)-O(4)	98.9(4)	O(1)-Mn(2)-O(5)	85.1(4)	C(9)-C(10)	1.499(23)	C(22)-C(23)	1.481(22)
O(1)-Mn(1)-N(1)	91.9(5)	O(1)-Mn(2)-N(4)	84.5(4)	C(15)-C(16)	1.484(22)	C(28)-C(29)	1.535(23)
O(1)-Mn(1)-N(2)	168.3(5)	O(1)-Mn(2)-N(5)	87.0(4)	Mn(1)-O(1)-C(1)	122.4(8)	Mn(2)-O(1)-C(1)	120.6(9)
O(1)-Mn(1)-N(3)	89.4(4)	O(1)-Mn(2)-N(6)	155.7(4)	Mn(1)-N(1)-C(8)	110.2(9)	Mn(2)-N(4)-C(21)	111.7(9)
O(2)-Mn(1)-O(4)	98.8(4)	O(3)-Mn(2)-O(5)	97.1(4)	Mn(1)-N(1)-C(9)	105.2(8)	Mn(2)-N(4)-C(22)	110.1(9)
O(2)-Mn(1)-N(1)	93.5(4)	O(3)-Mn(2)-N(4)	166.7(4)	Mn(1)-N(1)-C(15)	111.9(9)	Mn(2)-N(4)-C(28)	104.2(9)
O(2)-Mn(1)-N(2)	83.1(5)	O(3)-Mn(2)-N(5)	92.9(4)	Mn(1)-N(2)-C(10)	115.1(11)	Mn(2)-N(5)-C(23)	117.1(10)
O(2)-Mn(1)-N(3)	171.9(4)	O(3)-Mn(2)-N(6)	104.7(4)	Mn(1)-N(2)-C(14)	123.4(10)	Mn(2)-N(5)-C(27)	120.9(10)
O(4)-Mn(1)-N(1)	163.4(5)	O(5)-Mn(2)-N(4)	96.2(4)	Mn(1)-N(3)-C(16)	112.7(10)	Mn(2)-N(6)-C(29)	114.9(10)
O(4)-Mn(1)-N(2)	92.1(5)	O(5)-Mn(2)-N(5)	168.0(4)	Mn(1)-N(3)-C(20)	123.8(9)	Mn(2)-N(6)-C(33)	127.0(11)
O(4)-Mn(1)-N(3)	89.1(4)	O(5)-Mn(2)-N(6)	83.7(4)	C(20)-N(3)-C(16)	121.9(13)	C(33)-N(6)-C(29)	118.1(13)
N(1)-Mn(1)-N(2)	78.3(5)	N(4)-Mn(2)-N(5)	74.1(4)	O(1)-C(1)-C(2)	118.1(13)	O(1)-C(1)-C(6)	119.3(12)
N(1)-Mn(1)-N(3)	78.4(5)	N(4)-Mn(2)-N(6)	75.4(4)	C(2)-C(1)-C(6)	122.7(14)	C(1)-C(2)-C(3)	119.6(15)
N(2)-Mn(1)-N(3)	94.8(5)	N(5)-Mn(2)-N(6)	100.1(4)	C(1)-C(2)-C(8)	121.4(13)	C(1)-C(6)-C(21)	120.5(13)
				N(1)-C(8)-C(2)	109.4(13)	N(4)-C(21)-C(6)	110.8(13)
(b) Benzoate moiety				N(1)-C(9)-C(10)	106.1(13)	N(4)-C(22)-C(23)	111.1(13)
O(2)-C(34)	1.260(18)	O(4)-C(41)	1.297(17)	N(2)-C(10)-C(9)	115.3(14)	N(5)-C(23)-C(22)	118.5(13)
O(3)-C(34)	1.240(18)	O(5)-C(41)	1.258(20)	N(1)-C(15)-C(16)	108.8(12)	N(4)-C(28)-C(29)	108.3(13)
O(34)-C(35)	1.506(22)	O(41)-C(42)	1.525(22)	N(3)-C(16)-C(15)	119.1(13)	N(6)-C(29)-C(28)	117.6(13)
Mn(1)-O(2)-C(34)	142.9(10)	Mn(2)-O(3)-C(34)	126.6(10)				
Mn(1)-O(4)-C(41)	128.8(10)	Mn(2)-O(5)-C(41)	139.1(9)				
O(2)-C(34)-O(3)	125.1(14)	O(4)-C(41)-O(5)	125.8(14)				
O(2)-C(34)-O(35)	116.3(13)	O(4)-C(41)-C(42)	116.5(14)				
O(3)-C(34)-C(35)	118.5(13)	O(5)-C(41)-C(42)	117.8(13)				

plane involving Mn(1) atom at its center. The coordination geometry around Mn(1) is best described as an elongated octahedron, which is attributable to the Jahn-Teller effect of high spin d^4 ion (vide infra). Thus, the molecular structure clearly shows that the present complex consists of manganese(II) and manganese(III) ions whose valence states are firmly trapped.

The intramolecular Mn(1)-Mn(2) distance is 3.484 (3) Å. The manganese atoms are triply bridged by phenolate oxygen and two benzoate oxygens to form a cofacial bioctahedral structure. Such triply bridging structures have been found for some dinuclear manganese and iron complexes with bridging groups composed of two carboxylate and one oxide (hydroxide, or phenolate) ions.[19-22]

Two benzoato groups bridge the manganese atoms in syn-syn configuration. However, the bridging benzoato groups are not equivalent: one symmetrically bridges the manganese atoms, whereas the other does unsymmetrically. The Mn(1)-O(2) (2.147(11) Å) and Mn(2)-O(3) (2.123(11) Å) bonds of symmetrically bridging benzoato group are close to each other in length. However, the Mn(1)-O(4) (1.947(10) Å) and Mn(2)-O(5) (2.162(11) Å) bond lengths of unsymmetrically bridging benzoato group significantly differ from each other.

IR Spectra. The infrared spectrum of **2b** shows one $\nu_{asymm}(COO^-)$ at 1567 cm^{-1} and two $\nu_{symm}(COO^-)$ at 1407 and 1370 cm^{-1} (Fig. 2), indicating the presence of two types of benzoato groups, which is compatible with the result of X-ray structural analysis mentioned above. The $\Delta\nu$ value ($\nu_{asymm}(COO^-)-\nu_{symm}(COO^-)$) is useful for the diagnosis of coordination mode of carboxylato group, i.e., a symmetrically bridging carboxylato group gives $\Delta\nu$ value smaller than 200 cm^{-1}, whereas an unsymmetrically bridging one and monodentate one larger $\Delta\nu$ values.[23] Thus, the larger $\Delta\nu$ (197 cm^{-1}) of **2b** is assigned to that of the unsymmetrically bridging carboxylato group and the smaller value (160 cm^{-1}) to that of the symmetrically bridging one. On the other hand, the dinuclear manganese(II, II) complex **2a** shows one $\nu_{asymm}(COO^-)$ and one $\nu_{symm}(COO^-)$ at 1570 and 1400 cm^{-1} ($\Delta\nu$=170 cm^{-1}), respectively, indicating that the two carboxylato groups are equivalent and symmetrically bridge two manganese(II) ions. The complex **2a** seems to have a triply bridging structure similar to that of **2b**.

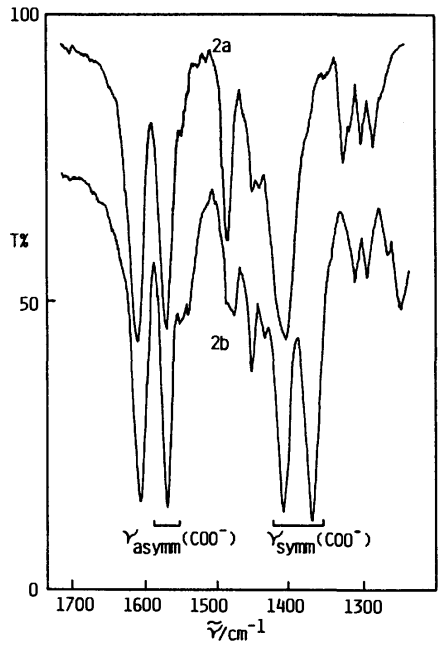

Fig. 2. Infrared spectra of $[Mn_2(L\text{-}py)(C_6H_5COO)_2]ClO_4\cdot 2H_2O$ (**2a**) and $[Mn_2(L\text{-}py)(C_6H_5COO)_2](ClO_4)_2\cdot H_2O$ (**2b**).

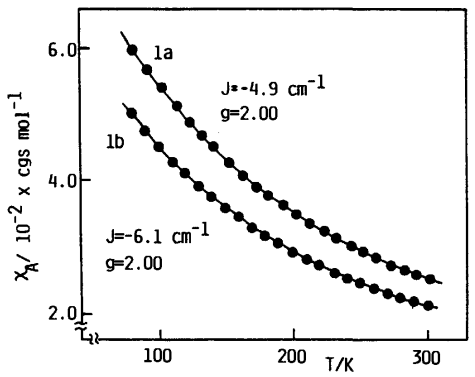

Fig. 3. Temperature dependence of magnetic susceptibilities of $[Mn_2(L\text{-}py)(CH_3COO)_2]ClO_4\cdot 0.5H_2O$ (**1a**) and $[Mn_2(L\text{-}py)(CH_3COO)_2](ClO_4)_2\cdot H_2O$ (**1b**).

Magnetic Susceptibilities. The effective magnetic moments of **1a** and **2a** at room temperature are 7.8 and 7.7 B.M./Mn_2, and those of **1b** and **2b** are 7.1 and 7.1 B.M./Mn_2, respectively, indicating that all the manganese(II) and (III) ions in the above complexes are of high spin. Magnetic susceptibilities of the complexes were measured in the temperature range from 80 to 300 K. The results were analyzed by the usual spin-spin interaction model based on exchange Hamiltonian $H=-2JS_1\cdot S_2$. The molar magnetic susceptibility of (χ_A) of an $S_1=5/2\cdot S_2=5/2$ spin exchange coupling dimer is given in Eq. 1, and that of an $S_1=2\cdot S_2=5/2$ spin exchange coupling dimer by Eq. 2,

$$\chi_A=\frac{2N\beta^2g^2}{\kappa T}\cdot\frac{x^{28}+5x^{24}+14x^{18}+30x^{10}+55}{x^{30}+3x^{28}+5x^{24}+7x^{18}+9x^{10}+11}+N\alpha \quad (1)$$

$$\chi_A=\frac{N\beta^2g^2}{4\kappa T}\cdot\frac{x^{24}+10x^{21}+35x^{16}+84x^{9}+165}{x^{24}+2x^{21}+3x^{16}+4x^{9}+5}+N\alpha \quad (2)$$

where $x=\exp(-J/\kappa T)$ and the symbols have their usual meanings. Figure 3 shows temperature dependence of the magnetic susceptibilities of **1a** and **1b**. The solid lines are the calculated curves by using the paremeters listed in Table 4. Both dinuclear manganese(II, II) and (II, III) complexes exhibit weak antiferromagnetic interaction (J=−4.9—−6.3 cm^{-1}: Table 4). The corresponding dinuclear mixed valence iron(II, III) complexes $[Fe_2(L\text{-}py)(RCOO)_2](BF_4)_2\cdot nH_2O$ and $[Fe_2(L\text{-}py)(CH_3COO)(OH)](BF_4)_2\cdot 2H_2O$ exhibited comparable magnitude of antiferromagnetic interaction (J=−3—−8 cm^{-1}).[24] These results suggest that the triply bridging unit consisting of phenolate and two carboxylate ions provides an weak antiferromagnetic interaction, regardless of the species (Fe or Mn ion) and oxidation state of metal ion.

Electronic Spectra. The aborption spectra of **1a** and **1b** are shown in Fig. 4. The complex **1a** shows no appreciable absorption in the region below 25000

Table 4. Magnetic Parameters of the Complexes

	Complex	J/cm^{-1}	g	Nα/10^{-6} cgs mol^{-1}
1a	$[Mn_2(L\text{-}py)(CH_3COO)_2]ClO_4\cdot 0.5H_2O$	−4.9	2.00	0
2a	$[Mn_2(L\text{-}py)(C_6H_5COO)_2]ClO_4\cdot 2H_2O$	−5.5	2.00	0
1b	$[Mn_2(L\text{-}py)(CH_3COO)_2](ClO_4)_2\cdot H_2O$	−6.1	2.00	0
2b	$[Mn_2(L\text{-}py)(C_6H_5COO)_2](ClO_4)_2\cdot H_2O$	−6.3	2.00	0

Table 5. Electronic Spectral Data of the Mixed Valence Complexes in Acetonitrile

	Complex	$\tilde{\nu}_{max}$ 10^3×cm^{-1}, (ε/mol^{-1} dm^3 cm^{-1})		
1b	$[Mn_2(L\text{-}py)(CH_3COO)_2](ClO_4)_2\cdot H_2O$	16.2(870)	17.8(820)	20.9(1230)
		21.7(1220)	23.4(1280)^s	26.0(1560)
2b	$[Mn_2(L\text{-}py)(C_6H_5COO)_2](ClO_4)_2\cdot H_2O$	15.8(830)	17.8(760)	20.8(1170)^s
		21.6(1180)^s	23.4(1290)^s	25.9(1490)

s: Shoulder.

cm^{-1}, indicating the electronic configuration of manganese(II) ion to be of high spin. The mixed valence complex **1b** exhibits six absorption bands including shoulders in the visible and near ultraviolet regions (Fig. 4 and Table 5). In general, six-coordinated manganese(III) complex displays one or two d-d bands (^5E_g to $^5T_{2g}$ electronic transitions in octahedral symmetry) in these regions.[17,25] The molar extinction coefficients of **1b** and **2b** are 800—1500 mol^{-1} dm^3cm^{-1}, which are considerably larger than those of d-d transitions of manganese(III) complexes. Judging from the numbers of absorption bands and their intensities, all the six bands can not be ascribed to the d-d transitions. Charge transfer transitions from $p\pi$ orbital of bridging phenolato group to half filled $d\pi^*$ orbitals of manganese(III) ion may appear in these regions as was observed for iron(III)-phenolato complexes.[26] It is also possible that intervalence charge transfer transition(IT) from Mn^{II} moiety to Mn^{III} moiety appears in these regions. More detailed assignment is not possible at the present stage.

It should be noted that the present mixed valence complexes exhibit no IT bands in the near infrared region, whereas the iron complexes $[Fe_2(L)(RCOO)_2]^{2+}$ (L=L-py or L-Bzim) (L-Bzim=2,6-bis[bis(2-benzimidazolylmethyl)aminomethyl]-4-methylphenolate-(1−) ion) showed an intense IT band at that region.[24,27] This fact might be due to a smaller extent of electron delocalization in the manganese complexes than that in the iron complexes.

Cyclic Voltammogram. Figure 5 illustrates the cyclic voltammogram of **1b** in acetonitrile at 20 °C. This complex shows two quasi-reversible redox couples at +1.02 and +0.47 V (vs. SCE). Controlled potential electrolysis of the complex **1b** was carried out in order to determine the number of electrons (n) transferred in the above two processes. The oxidation of the complex at +1.15 V and reduction at +0.35 V (vs. SCE) gave n values of 1.1±0.1 and 0.9±0.1, respectively, indicating that those two redox couples correspond to one-electron redox reactions assignable to $E_{1/2}{}^a$ (Mn^{III}-Mn^{III}/Mn^{II}-Mn^{III} (+1.02 V)) and $E_{1/2}{}^b$ (Mn^{II}-Mn^{III}/Mn^{II}-Mn^{II} (+0.47 V)). The complex **2b** also showed a similar cyclic voltammogram (Table 6).

From the separation of the redox potentials, $E_{1/2}{}^a$ and $E_{1/2}{}^b$, comproportionation constant (K at 20 °C) of the following reaction can be calculated by Eq. 3.

$$(Mn^{III}\text{-}Mn^{III})+(Mn^{II}\text{-}Mn^{II}) \rightleftarrows 2(Mn^{III}\text{-}Mn^{II})$$
$$E_{1/2}{}^a - E_{1/2}{}^b = RT/F \ln K \quad (3)$$

The values for **1b** and **2b** are 2.9×10^9 (ΔG=−53 kJ mol^{-1}) and 1.9×10^9 (ΔG=−52 kJ mol^{-1}), respectively, indicating that the mixed valence complexes are considerably stabilized. A dinuclear metal(II, II) complex must be more easily oxidized than a metal(II, III)

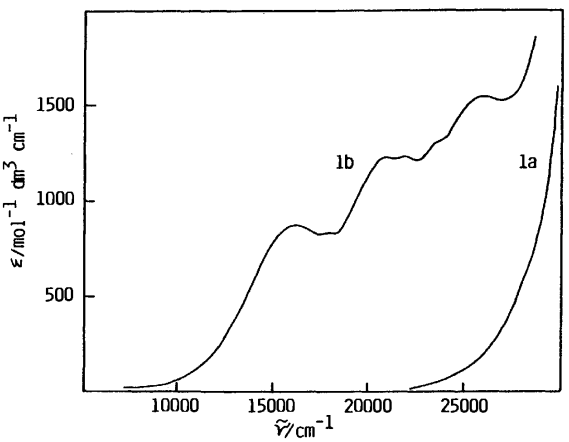

Fig. 4. Electronic spectra of $[Mn_2(L\text{-py})(CH_3COO)_2]$-$ClO_4\cdot0.5H_2O$ (**1a**) and $[Mn_2(L\text{-py})(CH_3COO)_2]$-$(ClO_4)_2\cdot H_2O$ (**1b**) in acetonitrile.

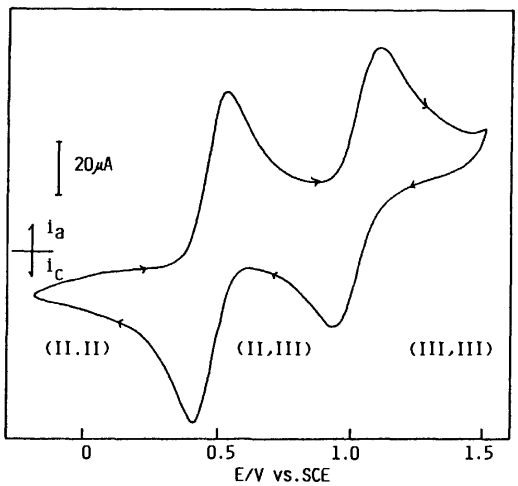

Fig. 5. Cyclic voltammogram of $[Mn_2(L\text{-py})$-$(CH_3COO)_2](ClO_4)_2\cdot H_2O$ (**1b**) in 0.1 mol dm^{-3} tetrabutylammonium perchlorate in acetonitrile at a glassy carbon electrode at a scan rate of 100 mV s^{-1}.

Table 6. Cyclic Voltammetric Data of the Mixed Valence Complexes

	Complex	$E_{1/2}{}^{a)}$ (E/V vs. SCE)	$E_{1/2}{}^{b)}$	$\Delta E^{a)}$ (ΔE/V)	$\Delta E^{b)}$	$R^{a)}$ ($i_{pa}{}^{d)}/i_{pc}{}^{e)}$)	$R^{b)}$	$K_c{}^{c)}$
1b	$[Mn_2(L\text{-py})(CH_3COO)_2](ClO_4)_2\cdot H_2O$	+0.47	+1.02	0.12	0.17	1.0	0.84	2.9×10^9
2b	$[Mn_2(L\text{-py})(C_6H_5COO)_2](ClO_4)_2\cdot H_2O$	+0.53	+1.07	0.10	0.12	1.0	0.84	1.9×10^9

(Experimental conditions: cf. Fig. 4) a) For Mn(II, III)/Mn(II, II) redox couple. b) For Mn(III, III)/Mn(II, III) redox couple. c) comproportionation constant at 20 °C. d) Anodic peak current. e) Cathodic peak current.

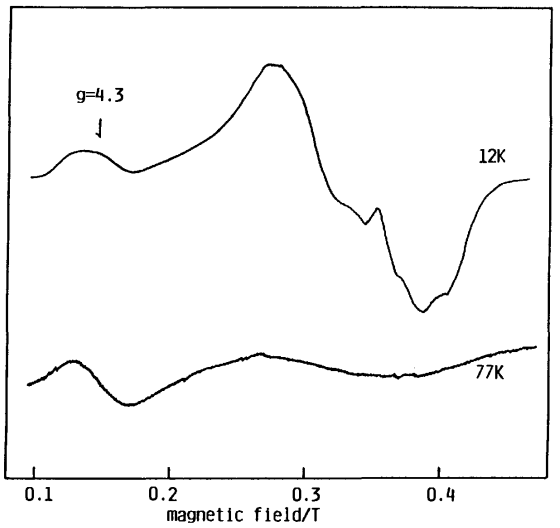

Fig. 6. ESR spectra of $[Mn_2(L\text{-}py)(CH_3COO)_2](ClO_4)_2 \cdot H_2O$ (**1b**) in acetonitrile at 12 and 77 K. Spectral conditions: microwave power, 1 mW at 12 K and 2 mW at 77 K; microwave frequency, 9.036 GHz at 12 K and 9.041 GHz at 77 K; modulation amplitude, 0.25 mT at 12 K and 0.32 mT at 77 K at 100 kHz; receiver gain, 6.5×100 at 12 K and 3×1000 at 77 K.

one from electrostatic point of view. The electrostatic effect seems to be important, but a steric requirement of dinucleating ligand L-py and two bridging carboxylate ions may also play an important role. Actually, the reaction of an equimolar mixture of Fe^{3+} and Mn^{2+} ions with L-py and carboxylate ions afforded a dinuclear heterometal (II, III) complex $[FeMn(L\text{-}py)(RCOO)_2]^{2+}$ with a slight contamination of homometal dinuclear complexes.[28] Thus, the present ligand system provides favorable coordination sites to M^{2+} and M^{3+} ions to form a mixed valence complex in the trapped valence state.

ESR Spectra. The ESR spectra of **1b** in acetonitrile were measured at 12 and 77 K. The spectrum at 12 K shows several resonances (Fig. 6). However, the signals almost disappear at 77K except for a signal at g=4.3. The g=4.3 signal may be ascribed to a distorted octahedral mononuclear manganese(II) complex with D and $E<0.1$ cm^{-1}, and $E/D \approx 1/3$[18] which is present as impurity formed by slight decomposition of the dinuclear complex. Such a temperature dependence of the signals suggests that the signals arise from the spin ground state of S=1/2. Mabad et al.[6] reported that the ESR of antiferromagnetically coupled dinuclear mixed valence manganese(II, III) complex shows a 16-hyperfine line ESR spectrum. As can be seen in Fig. 6, however, the present complexes show only broad signals.[29]

Finantial support from Ministry of Education, Science and Culture Grant-in-Aid for Scientific Research (No. 61540443) is gratefully acknowledged.

References

1) G. L. Lawrence and D. T. Sawyer, *Coord. Chem. Rev.*, **27**, 173 (1978).
2) K. Sauer, *Acc. Chem. Rev.*, **13**, 249 (1980).
3) T. Wydrzynski and K. Sauer, *Biochim. Biophys. Acta*, **589**, 56 (1980).
4) J. A. Kirby, D. B. Goodin, T. Wydrzynski, A. S. Robertson, and M. P. Klein, *J. Am. Chem. Soc.*, **103**, 5537 (1981).
5) H. Okawa, A. Honda, M. Nakamura, and S. Kida, *J. Chem. Soc., Dalton Trans.*, **1985**, 59.
6) B. Mabad, J. P. Tuchagues, Y. T. Hwang, and D. N. Hendrickson, *J. Am. Chem. Soc.*, **107**, 2801 (1985).
7) M. Suzuki, S. Murata, A. Uehara, and S. Kida, *Chem. Lett.*, **1987**, 281.
8) M. Suzuki, H. Kanatomi, and I. Murase, *Chem. Lett.*, **1981**, 1745.
9) C. P. Prabhakaran and C. C. Patel, *J. Inorg. Nucl. Chem.*, **30**, 867 (1968).
10) R. Blecher and T. S. West, *Anal. Chim. Acta*, **6**, 322 (1952).
11) E. B. Sandell, "Determination of Traces of Metals," 3rd ed, Interscience Publisher, New York (1959), p. 606.
12) "International Tables of X-Ray Crystallography," Kynoch Press, Birmingham (1974), Vol. 4.
13) T. Sakurai and K. Kobayashi, *Rikagaku Kenkyusho Hokoku*, **55**, 69 (1979).
14) P. Main, S. E. Hull, L. Lessinger, G. Germain, J. P. Declercq, and M. M. Woolfson, MULTAN 78, A System of Computor Programs for the automatic Solution of Crystal Structures from X-Ray Diffraction Data, University of York (1978).
15) C. K. Johnson, Report NO. ORNL3794, Oak Ridge National Laboratory, Oak Ridge, Tennessee (1965).
16) M. Mikuriya, N. Torihara, H. Okawa, and S. Kida, *Bull. Chem. Soc. Jpn.*, **54**, 1063 (1981) and references therein.
17) J. B. Vincent, K. Folting, J. C. Huffmann, and G. Christou, *Inorg. Chem.*, **25**, 996 (1986) and references therein.
18) B. Mabad, P. Cassoux, J. P. Tuchagues, and D. N. Hendrickson, *Inorg. Chem.*, **25**, 1420 (1986) and references therein.
19) a) K. Wieghardt, U. Bossek, D. Ventur, and J. Weiss, *J. Chem. Soc., Chemm. Commun.*, **1985**, 347; b) J. E. Sheats, R. S. Czernuszewicz, G. C. Dismukes, A. L. Rheingold, V. Petrouleas, J. Stubbe, W. H. Armstrong, R. H. Beer, and S. J. Lippard, *J. Am. Chem. Soc.*, **109**, 1435 (1987).
20) a) W. H. Armstrong, A. Spool, G. C. Papaefthymiou, R. B. Frankel, and S. J. Lippard, *J. Am. Chem. Soc.*, **106**, 3653 (1984) and references therein; b) K. Wieghardt, I. Tolksdorf, and W. Herrmann, *Inorg. Chem.*, **24**, 1230 (1985).
21) W. H. Armstrong and S. J. Lippard, *J. Am. Chem. Soc.*, **106**, 4632 (1984).
22) B. P. Murch, F. C. Bradley, and L. Que, Jr., *J. Am. Chem. Soc.*, **108**, 5027 (1986).
23) G. B. Deacon and R. J. Phillips, *Coord. Chem. Rev.*, **23**, 227 (1980).
24) M. Suzuki, A. Uehara, H. Oshio, K. Endo, M. Yanaga, S. Kida, and K. Saito, *Bull. Chem. Soc. Jpn.*, **60**, 3547 (1987).
25) a)J. I. Bullock, M. M. Patele, and J. E. Salmon, *J. Inorg. Nucl. Chem.*, **31**, 415 (1969); b) K. Yamaguchi and D. T. Sawyer, *Inorg. Chem.*, **24**, 971 (1985).

26) a) E. W. Aniscough, A. M. Brodie, J. E. Plowman, K. L. Brown, A. W. Addison, and A. R. Gainsford, *Inorg. Chem.*, **19**, 3655 (1980); b) J. W. Pyrz, A. L. Roe, L. J. Stern, and L. Que, Jr., *J. Am. Chem. Soc.*, **107**, 614 (1985).

27) M. Suzuki, A. Uehara, and K. Endo, *Inorg. Chim. Acta*, **123**, L9 (1986).

28) M. Suzuki, S. Murata, and A. Uehara, unpublished results.

29) Very recently, Diril et al. reported the crystal structure and ESR spectrum of **1b**. They observed a hyperfine structure (29 Mn hyperfine lines) at $g=2$ at 7.5 K. H. Diril, H. R. Chang, X. Zhang, S. K. Larsen, J. A. Potenza, C. G. Pierpont, H. J. Schugar, S. S. Isied, and D. N. Hendrickson, *J. Am. Chem. Soc.*, **109**, 6207 (1987).

 © 1987 The Chemical Society of Japan Bull. Chem. Soc. Jpn., 60, 4313—4316 (1987)

Treatment of Tetraalkoxysilanes with Amberlyst 15 Cation-Exchange Resin in Presence of Hexamethyldisiloxane

Isao HASEGAWA† and Sumio SAKKA*,†
Institute for Chemical Research, Kyoto University, Uji, Kyoto 611
†Division of Molecular Engineering, Graduate School of Engineering, Kyoto University, Sakyo-ku, Kyoto 606
(Received June 11, 1987)

Tetraalkoxysilanes were treated with Amberlyst 15 cation-exchange resin in hexamethyldisiloxane at 40 °C in order to substitute the trimethylsilyl group for the alkyl group in a tetraalkoxysilane partially. Tetramethoxy-, ethoxy-, propoxy-, and butoxysilanes were used for the experiments. After the treatment, $SiO_4R_{4-n}X_n$ ($1 \leqq n \leqq 4$, R=CH_3, C_2H_5, n-C_3H_7, and n-C_4H_9, X=$Si(CH_3)_3$) were detected by gas chromatography and were identified by combined gas chromatography-mass spectrometry. The degree of trimethylsilylation of tetraalkoxysilane changed with the molar ratio of hexamethyldisiloxane to tetraalkoxysilane and quantities of the reaction products in the system depended mainly on the ratio.

Tetraalkoxysilanes (TAOS) are promising materials as a source of silica for the synthesis of inorganic or organosilicon compounds. Hydrolysis and polycondensation of TAOS in the system of TAOS-ethanol-H_2O-HCl produce a variety of silicate species, however, even if the amount of added water for the hydrolysis is little.[1] This random polymerization would be caused by the tetra-functionality of TAOS. In other words, all four alkoxyl groups on a silicon atom have the same reactivity, making it difficult to control the reaction of a TAOS. In order to synthesize the compounds with controlled structures in their silicate skeletons from TAOS, it will be necessary to substitute functional groups of low reactivity, such as trimethylsilyl groups (-$Si(CH_3)_3$), for some of the functional groups of TAOS. Trimethylsilylation of silicates, originated by Lentz in 1964,[2] has been developed into several characteristic methods.[3] When the method of Götz and Masson[4] is applied to silicate minerals, such as hemimorphite, trimethylsilyl mono-, di-, and trialkoxy derivatives of silicate anions are formed by the side reaction of esterification of the silanol group with an alcohol used in the trimethylsilylating reagent.[5-8] On the basis of this esterification reaction, Kuroda et al. synthesized silicate-organic copolymer from hemimorphite and ethylene glycol in the reaction mixture for trimethylsilylation.[9] On the other hand, post-treatment with Amberlyst 15 cation-exchange resin in the presence of an excess of hexamethyldisiloxane ($(CH_3)_3Si$-O-$Si(CH_3)_3$) is necessary for the completion of trimethylsilylation. Such treatment would promote the exchange of the residual silanol groups or alcohol-esterified sites in the silicate skeleton with the trimethylsilyl groups, although there might be some other side reactions.[10-12]

It is expected that such partially trimethylsilylated alkoxysilanes might be more readily produced from TAOS as a silica source than silicate minerals. In this study, it is aimed to produce partially trimethylsilylated derivatives from 4 TAOS; tetramethoxy-, ethoxy-, propoxy-, and butoxysilanes (abbreviated to TMOS, TEOS, TPOS and TBOS, respectively) by treatment with Amberlyst 15 in hexamethyldisiloxane (HMDS). The effects of the molar ratio of HMDS to TAOS (abbreviated to the HMDS/TAOS ratio) and the time of the treatment on the distribution of the reaction products were studied by gas-liquid chromatography.

Experimental

Materials. Reagent grade tetramethoxy-, ethoxy-, propoxy-, and butoxysilanes were used. Hexamethyldisiloxane was used after a single distillation (bp 100—101 °C). Amberlyst 15 cation-exchange resin was used after heating in an oven at 80 °C for 4 h and cooling in a desiccator for standardization, as was suggested by Garzó et al.[12]

Preparation of Solutions. The solutions with the HMDS/TAOS ratios from 0.5 to 10.0 were prepared by mixing given amounts of TAOS and HMDS. After stirring for 5 min for homogeneity of the solution, ca. 0.5 g of Amberlyst 15 cation-exchange resin was added to the mixture (20 cm^3) and the vessel was sealed. After keeping standing the vessels in an oven at 40 °C for 85 h, the samples were analyzed by means of gas-liquid chromatography. The effect of the time of treatment was investigated by analyzing the sample with the HMDS/TEOS ratio of 4.0 at various time intervals.

Analytical Procedure. The solutions were analyzed by a Shimadzu GC-12A gas-liquid chromatograph equipped with a hydrogen flame-ionization detector and a CLH-702 split sample injection for capillary gas chromatography. The capillary column (length 25 m, i.d. 0.25 mm) of fused silica cross-linked immovable layer (ULBON HR-101, similar polarity to OV-101) as a stationary phase was used. The injection temperature was 330 °C. The column temperature was programmed to rise at 4 °C min^{-1} from 100 to 330 °C. The carrier gas was nitrogen and its flow rate was 0.34 cm^3 min^{-1} at the split rate of 1 : 104. Standard solutions of the mixed derivatives were not prepared, and so the results of gas-liquid chromatography are expressed in terms of percentages of total peak area. Although it is impossible to elucidate the distribution of the products quantitatively, the main product in the system can be determined from the peak area ratio.

Identification of the peaks on the gas chromatograms was made by conducting combined gas chromatograph-mass spectrometric analyses with a JEOL JMS-DX 300 gas chromatograph-mass spectrometer using an ionizing energy of 70 eV. The ion source block was maintained at 200 °C and the molecular separator at 230 °C. The column consisted of 1 m coiled glass packed with SE-30. The column was oper-

ated isothermally. The carrier gas was He (15 cm^3 min^{-1}).

Results and Discussion

Gas chromatograms of the products obtained by treating the TAOS-HMDS solutions at the HMDS/TAOS ratio of 4.0 with Amberlyst 15 for 85 h in an oven at 40 °C are shown in Fig. 1(a)—(d). Five peaks are seen in each gas chromatogram.

These peaks were identified by a combined gas chromatography-mass spectrometry. It is known from the mass spectra of trimethylsilylated derivatives of silicates[13] that the molecular ion is either of very low abundance or below detection limit and the most structurally informative ion is the one produced by the loss of a methyl radical from the molecular ion, $[M-15]^+$. Moreover, substitution of a trimethylsilyl group for an alkyl group is indicated by the difference in the mass numbers of $[M-15]^+$, in regard to neighboring peaks on the gas chromatogram. This difference corresponds to the difference between $-Si(CH_3)_3$ and $-C_nH_{2n+1}$ (n=1—4), an alkyl group in a TAOS.[5,6] These characteristics of the mass spectra were confirmed on four of the five peaks on the gas chromatogram. The mass number for the molecular ion corresponding to the other peak is that of TAOS used for preparation of the sample. Actually, the retention time of the peak corresponded to that of pure TAOS. Table 1 shows the assignments of peaks in each gas

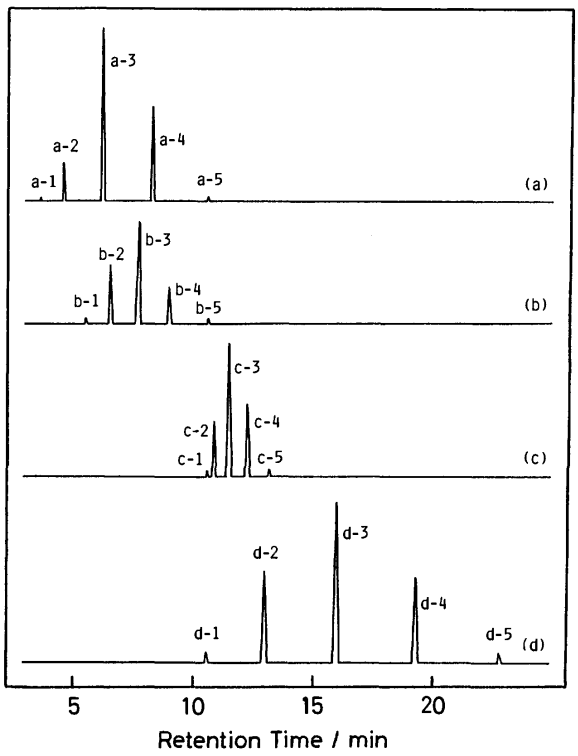

Fig. 1. Gas chromatograms of the products obtained by treating the TAOS-HMDS solutions at the HMDS/TAOS ratio of 4.0 with Amberlyst 15 at 40 °C for 85 h. TAOS: (a) TMOS, (b) TEOS, (c) TPOS, and (d) TBOS.

Table 1. Identification of the Peaks on the Gas Chromatograms in Fig. 1

TAOS	Peak	Formula
TMOS	a-1	$SiO_4(CH_3)_4$
	a-2	$SiO_4(CH_3)_3[Si(CH_3)_3]$
	a-3	$SiO_4(CH_3)_2[Si(CH_3)_3]_2$
	a-4	$SiO_4(CH_3)[Si(CH_3)_3]_3$
	a-5	$SiO_4[Si(CH_3)_3]_4$
TEOS	b-1	$SiO_4(C_2H_5)_4$
	b-2	$SiO_4(C_2H_5)_3[Si(CH_3)_3]$
	b-3	$SiO_4(C_2H_5)_2[Si(CH_3)_3]_2$
	b-4	$SiO_4(C_2H_5)[Si(CH_3)_3]_3$
	b-5	$SiO_4[Si(CH_3)_3]_4$
TPOS	c-1	$SiO_4[Si(CH_3)_3]_4$
	c-2	$SiO_4(C_3H_7)[Si(CH_3)_3]_3$
	c-3	$SiO_4(C_3H_7)_2[Si(CH_3)_3]_2$
	c-4	$SiO_4(C_3H_7)_3[Si(CH_3)_3]$
	c-5	$SiO_4(C_3H_7)_4$
TBOS	d-1	$SiO_4[Si(CH_3)_3]_4$
	d-2	$SiO_4(C_4H_9)[Si(CH_3)_3]_3$
	d-3	$SiO_4(C_4H_9)_2[Si(CH_3)_3]_2$
	d-4	$SiO_4(C_4H_9)_3[Si(CH_3)_3]$
	d-5	$SiO_4(C_4H_9)_4$

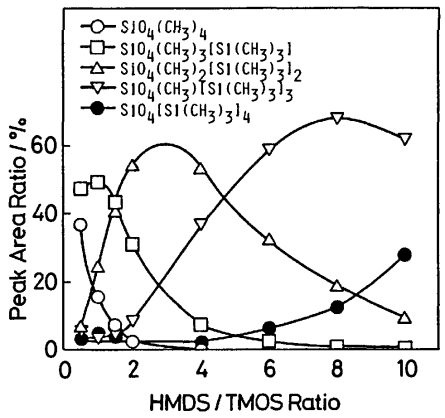

Fig. 2. Effect of the HMDS/TMOS ratio on the peak area ratios of the derivatives from TMOS ($SiO_4(CH_3)_4$) by Amberlyst treatment at 40 °C for 85 h.

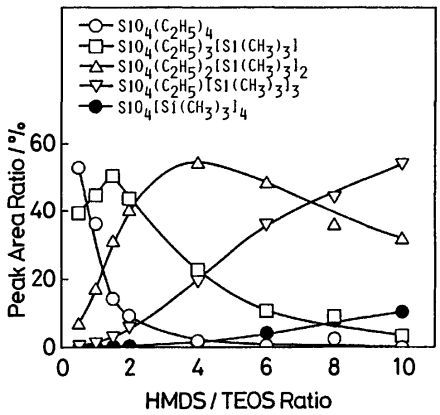

Fig. 3. Effect of the HMDS/TEOS ratio on the peak area ratios of the derivatives from TEOS ($SiO_4(C_2H_5)_4$) by Amberlyst treatment at 40 °C for 85 h.

chromatogram. It is seen that TAOS is partially or fully trimethylsilylated by Amberlyst treatment in HMDS.

Figures 2 and 3 show the effect of the HMDS/TAOS ratio on the distribution of the products in the TMOS- and TEOS- HMDS systems, respectively. The main product of the derivatives from TAOS varies with the HMDS/TAOS ratio, indicating that the degree of trimethylsilylation of TAOS is governed mainly by the HMDS/TAOS ratio. The tendencies of the variations in the distribution of products with the ratio in the TPOS- and TBOS-HMDS systems are almost the same as that in the TEOS-HMDS system. In the TEOS-, TPOS-, and TBOS-HMDS systems, the optimum conditions for partial trimethylsilylation are determined, regardless of the type of alkyl group, as follows; the HMDS/TAOS ratio of 1.5 for monosubstitution, the ratio of 4.0 for disubstitution and the ratio of 10.0 for trisubstitution. In the TMOS-HMDS system, however, the optimum ratios for the substitutions are slightly lower than those noted above.

On the other hand, a few peaks are slightly traced at longer retention time on the gas chromatograms. These peaks appear more clearly at lower HMDS/TAOS ratios or longer treating times. A typical gas chromatogram is shown in Fig. 4. This is the chromatogram for the sample at the HMDS/TEOS ratio of 1.0 treated with Amberlyst 15 for ca. 7 months at room temperature. Around the retention time from 14 to 17 min, three peaks (labeled a, b, and c in Fig. 4) appear, which can not be detected in such large peak areas when treated for 85 h at 40 °C.

In the combined gas chromatograph-mass spectrometric analyses, the peak a is assigned to $Si_2O_5(C_2H_5)_6$, which has the dimeric structure in the silicate skeleton. Also, from the rule on mass spectra of trimethylsilylated derivatives of silicates described above, it is considered that the peaks b and c are identified as $Si_2O_5(C_2H_5)_5[Si(CH_3)_3]$, whose molecular weight is 386 and $[M-15]^+$ is 371 (The mass spectrum of this compound is shown in Fig. 5.), and $Si_2O_5(C_2H_5)_4[Si(CH_3)_3]_2$, whose molecular weight is 430 and $[M-15]^+$ is 415. These compounds are also in the dimeric state of silicate structure. This dimerization might be caused by high TAOS concentrations in low HMDS/TAOS ratios. Moreover, these facts suggest that a long treatment time with Amberlyst 15 is not required for substitution of the trimethylsilyl group for the alkyl group in a TAOS, and makes the reactions between TAOS or partially trimethylsilylated alkoxysilanes proceed.

In order to clarify the effect of treatment time, the variation in the distribution of derivatives from TEOS at the HMDS/TEOS ratio of 4.0 with treatment time at 40 °C was investigated and the result is shown in Fig. 6. The main product at this ratio is $SiO_4(C_2H_5)_2[Si(CH_3)_3]_2$, as shown in Fig. 3. In initial ten hours, the less the degree of trimethylsilylation of the species is, the larger the peak area ratio is. However, $SiO_4(C_2H_5)_2[Si(CH_3)_3]_2$ becomes the main product after 14 h treatment. Although the peak area ratios of $SiO_4(C_2H_5)_3[Si(CH_3)_3]$ and $SiO_4(C_2H_5)[Si(CH_3)_3]_3$ vary further with the time of treatment, that of $SiO_4(C_2H_5)_2[Si(CH_3)_3]_2$ hardly varies on and after 48 h

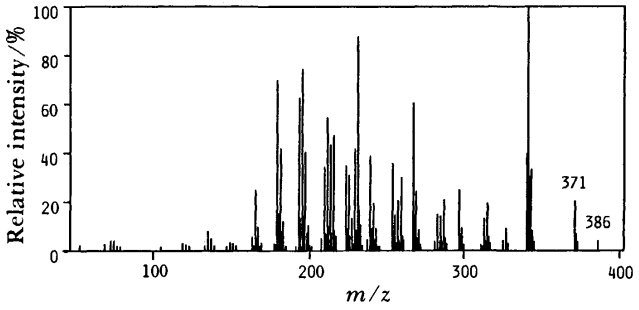

Fig. 5. Mass spectrum of $Si_2O_5(C_2H_5)_5[Si(CH_3)_3]$.

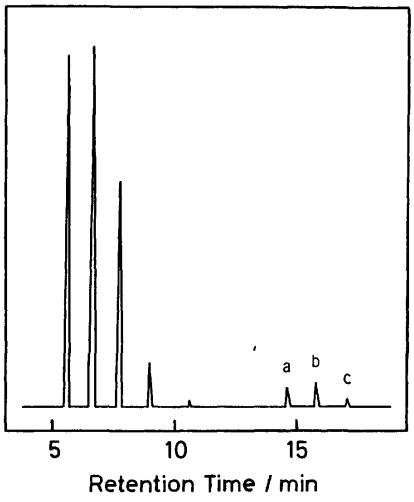

Fig. 4. Gas chromatogram of the TEOS-HMDS solution at the HMDS/TEOS ratio of 1.0 treated with Amberlyst 15 for ca. 7 months at room temperature.

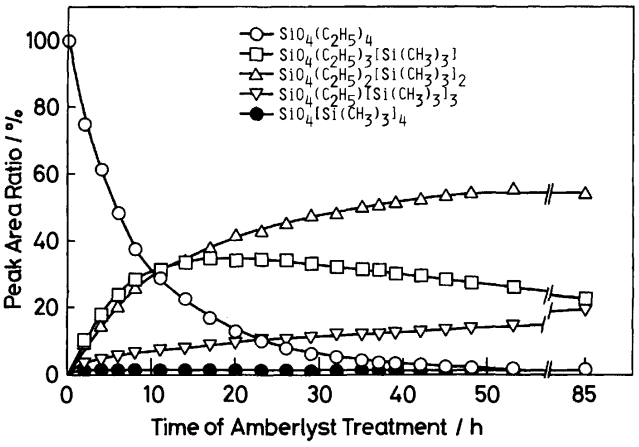

Fig. 6. Effect of the time of Amberlyst treatment on the peak area ratios of the derivatives formed in the TEOS-HMDS solution at the HMDS/TEOS ratio of 4.0 at 40 °C.

treatment at 40 °C. This indicates that the distribution of the derivatives varies with the time of treatment and the equilibrium relating to the formation of $SiO_4(C_2H_5)_2[Si(CH_3)_3]_2$ appears to be established on and after 48 h treatment at 40 °C.

In addition, the peaks at longer retention times on the gas chromatograms are traced in very small peak areas, indicating that the reactions between TEOS or partially trimethylsilylated ethoxysilanes hardly occur and only the substitution occurs in 85 h treatment.

From these results, it is concluded that TAOS is partially or fully trimethylsilylated by treating in HMDS with Amberlyst 15 cation-exchange resin. The degree of trimethylsilylation is governed by the HMDS/TAOS ratio. Within the treatment time of 85 h, reactions between TAOS or between partially trimethylsilylated alkoxysilanes scarcely occur and only substitution by the trimethylsilyl group proceeds. At lower HMDS/TAOS ratios, however, not only the substitution but also the dimerization occurs because of high concentrations of TAOS in the systems.

The present work was supported by a Grant-in-Aid for Scientific Research on Priority Areas, New Functionality Materials-Design, Preparation and Control, The Ministry of Education, Science and Culture, No. 62604011. The authors wish to express their sincere thanks to Dr. Kazuyuki Kuroda at Department of Applied Chemistry, Waseda University for useful discussions. Thanks are also due to Mr. Nakashi Nakamura at Science and Engineering Research Laboratory, Waseda University for measuring mass spectra.

References

1) I. Hasegawa and S. Sakka, *J. Non-Cryst. Solids*, in press.
2) C. W. Lentz, *Inorg. Chem.*, **3**, 574 (1964).
3) B. R. Currell and J. R. Parsonage, *J. Macromol. Sci., Chem.*, **A16**, 141 (1981).
4) J. Götz and C. R. Masson, *J. Chem. Soc., A*, **1970**, 2683.
5) K. Kuroda and C. Kato, *J. Inorg. Nucl. Chem.*, **41**, 947 (1979).
6) K. Kuroda and C. Kato, *J. Chem. Soc., Dalton Trans.*, **1979**, 1036.
7) H. P. Calhoun and C. R. Masson, *J. Chem. Soc., Dalton Trans.*, **1980**, 1282.
8) K. Kuroda, T. Koike, and C. Kato, *J. Chem. Soc., Dalton Trans.*, **1981**, 1957.
9) K. Kuroda and C. Kato, *Makromol. Chem.*, **179**, 2793 (1978).
10) H. P. Calhoun and C. R. Masson, *J. Chem. Soc., Dalton Trans.*, **1978**, 1342.
11) H. P. Calhoun and C. R. Masson, *J. Chem. Soc., Chem. Commun.*, **1978**, 560.
12) G. Garzó, A. Vargha, T. Székely, and D. Hoebbel, *J. Chem. Soc., Dalton Trans.*, **1980**, 2068.
13) F. F. H. Wu, J. Götz, W. D. Jamieson, and C. R. Masson, *J. Chromatogr.*, **48**, 515 (1970).

Stereospecific and Nucleophilic Additions of 2- and 3-Thienylmethylene. Reactions of 2- and 3-Thienylmethylene with *cis*- and *trans*-Stilbene, Dimethyl Maleate, Dimethyl Fumarate, and Styrene Derivatives

Katsuhiro SAITO,* Hiraku ISHIHARA, Toyonobu MURASE, Yoichi HORIE, and Etsuro MAEKAWA
Department of Chemistry, Nagoya Institute of Technology, Gokiso-cho, Showa-ku, Nagoya 466
(Received February 16, 1987)

The addition reactions of 2-thienylmethylene with *cis*- and *tarns*-stilbene afforded stereospecific adducts, respectively, indicating that the multiplicity of the carbene is singlet. The nucleophilicity of the carbenes was elucidated by an investigation of the relative rate ratio of the reactions of the carbene with various styrenes. An analogous result was afforded by reactions of 3-thienylmethylene with the same olefins mentioned above.

Much attention has been paid to the chemistry of carbenes from the view point of their electronic natures and chemical reactivities.[1] It is known that the reactivities of carbenes are influenced by substituents and especially by conjugation with olefinic groups.[1] However, the number of papers concerning the chemistry of carbenes conjugated with heterocyclic moieties seem to be few.[1,2]

Thiophene (**1**) is known to have an aromaticity due to the contribution of the ionic canonical formula (**1a**).[3] The reactivities of 2-thienylmeythylene (**2**) and 3-thienylmethylene (**3**) are considered to reflect conjugation with a thiophene ring. While Shechter has documented the chemical behaviors of **2** and **3**,[2] nothing is known concerning the addition reactions of these carbenes to olefins. As a part of our research on the reactivity of carbenes,[1] we investigated the addition reactions of **2** and **3** with olefins. Here we wish to report the results of these reactions.

Results and Discussion

The reaction of sodium salt of 2-thiophenecarbaldehyde tosylhydrazone (**4**) and 4 molar equivalents of *trans*-stilbene (**6**) in anhydrous diglyme gave the adduct (**7**) in a 12.1% yield. The same reaction using *cis*-stilbene (**8**) afforded adducts **9** and **10** in 4.4 and 2.2% yields, respectively. The reaction of **4** with dimethyl fumarate (**11**) and dimethyl maleate (**12**) yielded the same adduct **13** in the yields of 41.3 and 36.7%, respectively. Similar reactions of **5** with **6** and **8** gave adducts **14**, **15**, and **16** in the yields of 14.9, 11.3, and 5.5%, respectively. The reactions of **5** with **11** and **12** afforded the same adduct **17** in 38.5 and 31.0% yields, respectively.

The structures of the adducts were deduced on the basis of their spectral properties and were confirmed by comparisons of these spectral properties with those of analogous compounds.[4] The assignment of the structures of **9** and **10** are based on the chemical shifts of the cyclopropane proton H_b. Comparing the chemical shifts of the proton H_b of **9** and **10**, the chemical shift of the proton H_b of **9** should appear at lower field because of the paramagnetic anisotropic effect of the two phenyl groups located in the same side of the cyclopropane moiety as that of the proton H_b. The same consideration is applicable for **15** and **16**.

Reactions of the carbenes **2**, **3** with stilbenes **6**, **8** proceed in a strereospecific manner, indicating that the multiplicity of these carbenes are singlet.[1] On the

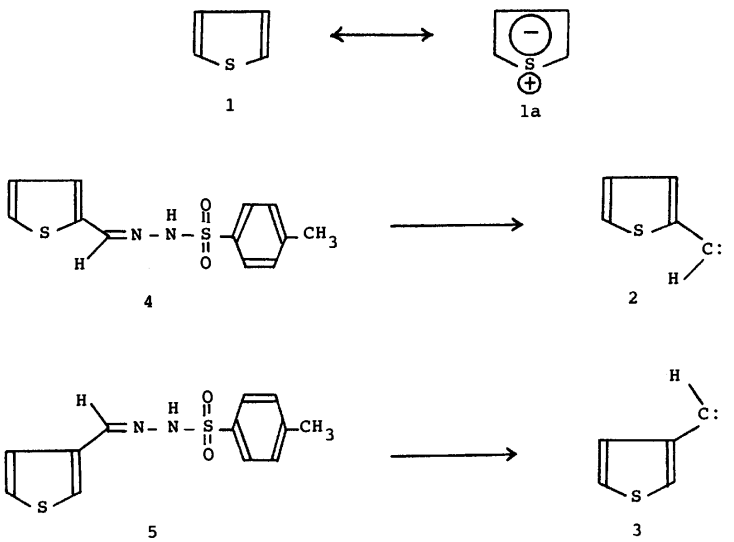

Fig. 1.

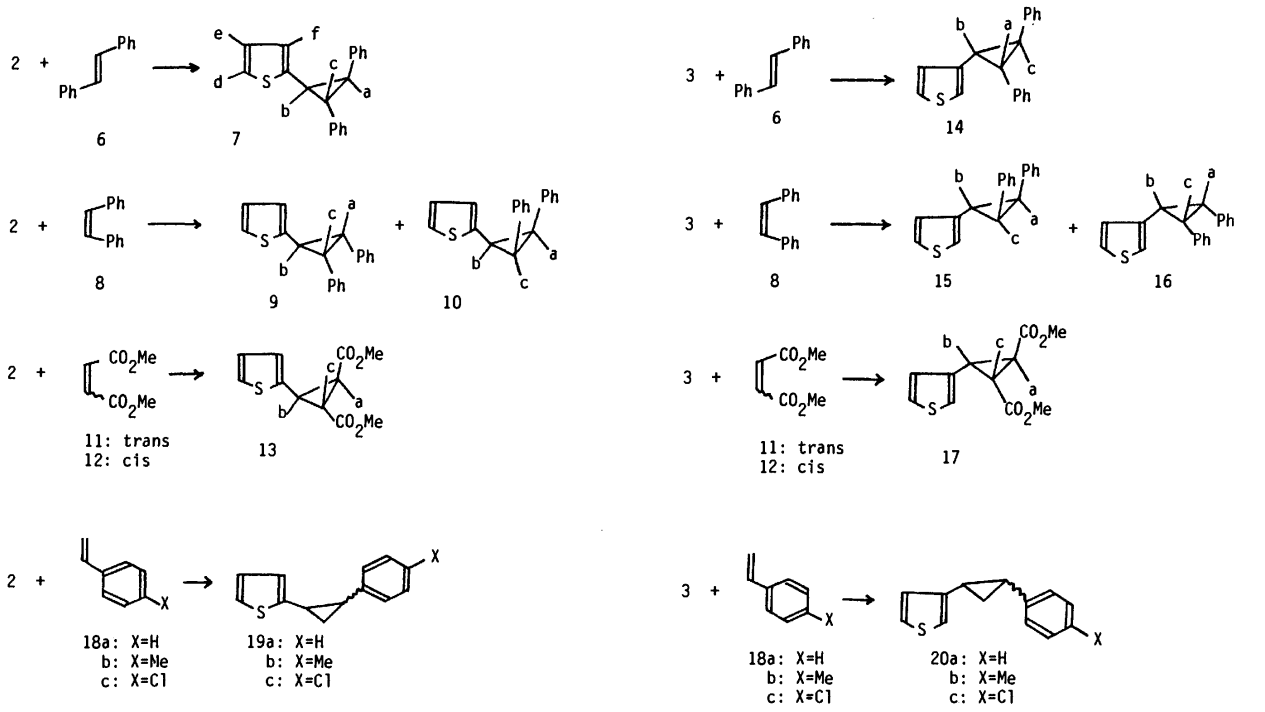

Fig. 2.

other hand, reactions of the carbenes **2**, **3** with the esters **11**, **12** do not seem to be stereospecific additions. It is known, however, that under the reaction conditions **12** isomerizes to **11**,[5] and that the reactivity of **11** to carbenes is higher than that of **12**.[6] Considering the above facts, the loss of stereospecificity of the present reactions is thought to be attributable to the isomerization of **12** to **11**.

There is a considerable difference in the product yields between reactions of the carbenes **2**, **3** with the stilbenes **6**, **8** and the esters **11**, **12**. Considering that the phenyl group of stilbenes is a very week electron-attracting group and, on the other hand, the ester group is a strong electron-attracting group, the above fact is thought to show the nucleophilicity of the carbenes.

In order to confirm the nucleophilicity of the carbenes, substituent effects on the addition reactions were investigated with styrene derivatives **18a**—c. Reactions of **2** with **18** gave the corresponding addition products **19a**—c in yields of 33.2, 38.0, and 48.5%, respectively. Similar reactions of **3** with **18** also afforded adducts **20a**—c in yields of 34.4, 32.7, and 33.0%, respectively. The relative rate ratios of **2** to the substituted styrenes was measured with the addition reactions of **2** to a mixture of **18a** and **18b** and a mixture of **18a** and **18c**[7] and found to be **18b** : **18a** : **18c** is 0.8 : 1.0 : 1.3. The relative rate ratios of **3** to the styrenes was also measured in the same manner to be **18b** : **18a** : **18c** is 0.8 : 1.0 : 1.6. This result is considered to demonstrate the nucleophilicity of **2** and **3**.

The electronic natures of **2** and **3** are considered to be as shown in **21** and **23**, respectively. The carbenic carbons have two carbenic electrons in the sp^2 orbital and leave a vacant 2p orbital, which delocalizes to the π-orbital system of the thienyl group. Consequently, the carbenic carbon atom shares the negative charge on the ring part of the thienyl group while forming a nucleophilic singlet carbenes, as shown in **22** and **24**, respectively.

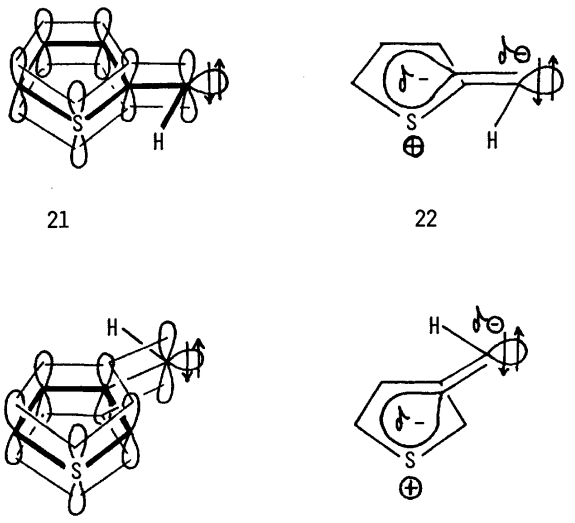

Fig. 3.

Experimental

Melting points were recorded on a Yanagimoto micro melting point apparatus and are uncorrected. NMR spectra were measured with a Varian XL 200 or Hitachi R-20B spec-

trometers with tetramethylsilane as an internal standard. IR sprectra were measured with a DS-701G spectrometer. Mass spectra were measured with a Hitachi M-52 or JMS-DX300 spectrometers. Wako gel C 200 and Wako gel B5F were used for column and thin-layer chromatography, respectively. Diglyme was dried over Molecular Sieves 3A 1/16. In all reactions, quantitative amounts of nitrogen gas and sodium *p*-toluenesulfinate were generated.

Reaction of 2 with 6. To a solution of **4** (2.52 g, 9 mmol) in diglyme (40 ml) was added sodium hydride (230 mg, 9 mmol), and **6** (6.48 g, 36 mmol); the reaction mixture was heated at 105 °C for 10 min to evolve a quantitative amount of nitrogen gas. After separating of a quantitative amount of sodium *p*-toluenesulfinate by filtration, the filtrate was poured into water, extracted with ether, washed with water and dried over anhydrous sodium sulfate. After removing of the solvent on a rotary evaporator, the oily residue was chromatographed on silica gel to give crystals **7** (300 mg, 12.1%) by the use of pet ether-benzene 9 : 1. The crystals were recrystallized from cyclohexane to give pure **7**. **7**: Mp 51—52 °C. Found: C, 82.46; H, 5.79%. Calcd for $C_{19}H_{16}S$: C, 82.60; H, 5.80%. MS *m/z* (rel intensity) 276 (M^+, 100), 192 (55), 185 (36). IR (oil): 3030, 2950, 1600, 1497 cm^{-1}. ^1H NMR (C_6D_6) δ=2.66 (dd, H_a), 2.74 (ddd, H_b), 2.89 (dd, H_c), 6.58 (d, H_d), 6.67 (dd, H_e), 6.75 (dd, H_f). Coupling constants in Hz: J_{ab}=8, J_{ac}=6, J_{bc}=6, J_{bf}=1, J_{de}=3, J_{ef}=5.

Reaction of 2 with 8. A mixture of **4** (2.52 g, 9 mmol), sodium hydride (230 mg, 9 mmol), and **8** (6.48 g, 36 mmol) in diglyme (40 ml) was reacted at 105 °C for 10 min. A column chromatographic separation of the reaction mixture gave an oil of 1 : 2 mixture of **9** and **10** (163 mg, **9**, 4.4%; **10**, 2.2%) by the use of pet. ether-benzene 9 : 1. Mixture of **9** and **10**: Found: *m/z* 276.0970. Calcd for $C_{19}H_{16}S$: M, 276.0967. MS *m/z* (rel intensity) 276 (M^+, 100), 192 (56), 185 (35). IR (oil): 3030, 2950, 1600, 1500 cm^{-1}. ^1H NMR (C_6D_6) δ=2.65 (bs, H_a, H_b, H_c of **10**), 2.75 (d, J=6 Hz, H_a, H_c of **9**), 3.01 (t, J=6 Hz, H_b of **9**), 6.4—7.4 (m).

Reaction of 2 with 11. A mixture of **4** (2.52 g, 9 mmol), sodium hydride (230 mg, 9 mmol), and **11** (5.18 g, 36 mmol) in diglyme (40 ml) was reacted at 140 °C for 30 min. Column chromatographic separation of the reaction mixture gave crystals **13** (893 mg, 41.3%) by the use of pet. ether-benzene 3 : 7. Recrystallization from ethyl acetate gave pure **13**. **13**: Mp 78—79 °C. Found: C, 54.80; H, 4.93%. Calcd for $C_{11}H_{12}O_4S$: C, 54.99; H, 5.03%. MS *m/z* (rel intensity) 240 (M^+, 65), 181 (95), 121 (100). IR (KBr): 3030, 2970, 1715, 1435 cm^{-1}. ^1H NMR (C_6D_6) δ=2.64 (dd, H_a), 2.85 (dd, H_b), 3.13 (dd, H_c), 6.96 (narrow m, 2H), 7.20 (narrow m, 1H). Coupling constants in Hz: J_{ab}=5, J_{ac}=10, J_{bc}=6.

Reaction of 2 with 12. A mixture of **4** (2.52 g, 9 mmol) sodium hydride (230 mg, 9 mmol), and **12** (5.18 g, 36 mmol) in diglyme (40 ml) was reacted at 140 °C for 30 min to give **13** (792 mg, 36.7%).

Reaction of 3 with 6. A mixture of **5** (2.52 g, 9 mmol), sodium hydride (230 mg, 9 mmol), and **6** (6.48 g, 36 mmol) in diglyme (40 ml) was reacted at 130 °C for 30 min. A column chromatogtraphic separation of the reaction mixture gave an oil **14** (370 mg, 14.9%) by the use of pet. ether-benzene 9 : 1. **14**: Found: *m/z* 276.0974. Calcd for $C_{19}H_{16}S$: M, 276.0972. MS *m/z* (rel intensity) 276 (M^+, 100), 192 (18), 185 (21). IR (oil): 3030, 2950, 1600 cm^{-1}. ^1H NMR (C_6H_6) δ=2.51 (m, H_a), 2.56 (m, H_b), 2.66 (m, H_c), 6.51 (narrow m, 2H), 6.73 (narrow m, 1H), 7.0—7.3 (m, 10H). Coupling constants in Hz: J_{ab}=8, J_{ac}=6, J_{bc}=6.

Reaction of 3 with 8. A mixture of **5** (2.52 g, 9 mmol), sodium hydride (230 mg, 9 mmol), and **8** (6.48 g, 36 mmol) in diglyme (40 ml) was reacted at 120 °C for 20 min. A column chromatographic separation of the reaction mixture gave an oil **15** (282 mg, 11.3%) and an oil **16** (137 mg, 5.5%) by the use of pet. ether-benzene 9 : 1 and 8 : 2, respectively. **15**: Found: *m/z* 276.0943. Calcd for $C_{19}H_{16}S$: M, 276.0973. MS *m/z* (rel intensity) 276 (M^+, 100), 192 (19), 185 (24). IR (oil): 3030, 2950, 1600, 1495 cm^{-1}. ^1H NMR (C_6H_6) δ=2.57 (d, J=6 Hz, H_a, H_b), 2.78 (t, J=6 Hz, H_c), 6.74 (narrow m, 1H), 6.81 (narrow m, 1H), 6.9—7.2 (m, 11H). **16**: Found: *m/z* 276.0952. Calcd for $C_{19}H_{16}S$: M, 276.0973. MS *m/z* (rel intensity) 276 (M^+, 100), 243 (14), 185 (24). IR (oil): 3030, 2950, 1600, 1497 cm^{-1}. ^1H NMR (C_6D_6) δ=2.54 (s, 3H, H_a, H_b, H_c), 6.64 (m, 3H), 7.0, (m, 10H).

Reaction of 3 with 11. A mixture of **5** (2.80 g, 10 mmol), sodium hydride (250 mg, 10 mmol), and **11** (5.76 g, 40 mmol) in diglyme (40 ml) was reacted at 130 °C for 30 min. A column chromatographic separation of the reaction mixture gave crystals **17** (924 mg, 38.5%) by the use of pet. ether-benzene 2 : 8. Recrystallization from cyclohexane gave pure **17**. **17**: Mp 72—73 °C. Found: C, 54.75; H, 4.99%. Calcd for $C_{11}H_{12}O_4S$: C, 54.99; H, 5.03%. MS *m/z* (rel intensity 240 (M^+, 52). 181 (100), 122 (91). IR (KBr): 3110, 3020, 2960, 1723 cm^{-1}. ^1H NMR ($CDCl_3$) δ=2.59 (m, H_a), 2.79 (m, H_b), 2.98 (m, H_c), 3.56 (s, 3H), 3.76 (s, 3H), 7.02 (m, 1H), 7.14 (m, 1H), 7.25 (m, 1H).

Reaction of 3 with 12. A mixture of **5** (2.80 g, 10 mmol), sodium hydride (250 mg, 10 mmol), and **12** (5.76 g, 40 mmol) in diglyme (40 ml) was reacted at 130 °C for 30 min to give **17** (744 mg, 31.0%).

Reaction of 2 with 18a. A mixture of **4** (2.52 g, 9 mmol), sodium hydride (230 mg, 9 mmol) and **18a** (3.75 g, 36 mmol) in diglyme (30 ml) was reacted at 105 °C for 10 min. A thin-layer chromatographic separation of the reaction mixture using pet. ether-benzene 4 : 1 as a developing solvent gave an oil **19a** (590 mg, 33.2 %, R_f=0.61).

19a: Found: C, 77.96; H, 5.97%. Calcd for $C_{13}H_{12}S$: C, 77.98; H, 6.04%. *m/z* (rel intensity) 200 (M^+, 100), 185 (13), 167 (14). IR (oil): 3100, 3050, 1600, 1500 cm^{-1}. ^1H NMR ($CDCl_3$) δ=1.36 (m, 2H), 2.28 (m, 2H), 6.5—7.5 (m, 8H).

Reaction of 2 with 18b. A mixture of **4** (2.52 g, 9 mmol), sodium hydride (230 mg, 9 mmol), and **18b** (4.25 g, 36 mmol) in diglyme (30 ml) was reacted at 105 °C for 10 min. A thin-layer chromatographic separation of the reaction mixture using pet. ether-ether 9 : 1 as a developing solvent gave **19b** (617 mg, 40.7%, R_f=0.60).

19b: Found: *m/z* 214.0826. Calcd for $C_{14}H_{14}S$: M, 214.0826. MS *m/z* (rel intensity): 214 (M^+, 100), 199 (43), 150 (30). IR (oil): 3100, 3030, 2930, 1520 cm^{-1}. ^1H NMR ($CDCl_3$) δ=1.26 (m, 2H), 2.23 (m, 2H), 2.24 (s, 3H), 6.5—7.2 (m, 7H).

Reaction of 2 with 18c. A mixture of **4** (2.52 g, 9 mmol), sodium hydride (230 mg, 9 mmol), and **18c** (4.99 g, 36 mmol) in diglyme (30 ml) was reacted at 105 °C for 10 min. A thin-layer chromatographic separation of the reaction mixture using cyclohexane-ethyl acetate 4 : 1 as a developing solvent gave an oil **19c** (802 mg, 38.1%, R_f=0.60).

19c: Found: *m/z* 234.0251. Calcd for $C_{13}H_{11}SCl$: M, 234.0270. MS *m/z* (rel intensity) 236 (M^+, 45), 234 (M^+, 100), 199 (55), 191 (41). IR (oil): 3080, 2920, 1493 cm^{-1}. ^1H NMR ($CDCl_3$) δ=1.30 (m, 2H), 2.18 (m, 2H), 6.4—7.3 (m, 7H).

Relative Rate Ratios of the Reaction of 2 to 18a—c.

Tosylhydrazone (**4**) was reacted with a 1 : 1 mixture of **18a** and **18b** as usual. The integrations of the signals of the cyclopropane carbons of **19a** and **19b** in ^{13}CNMR spectra show that the ratio of **19a** and **19b**, which indicates the relative rate ratios of **2** to **18a** and **18b** to be 1.0 and 0.8, respectively.[7] The same procedure as above using a 1 : 1 mixture of **18a** and **18c** gave the relative rate ratio of the reaction of **2** to **18a** and **18c** to be 1.0 and 1.3, respectively.

Reaction of 3 with 18a. A mixture of **5** (2.52 g, 9 mmol), sodium hydride (230 mg, 9 mmol), and **18a** (3.75 g, 36 mmol) in diglyme (30 ml) was reacted at 140 °C for 30 min. A thin-layer chromatographic separation of the reaction mixture using pet. ether-benzene 4 : 1 as a developing solvent gave **20a** (618 mg, 34.4%, R_f=0.50).

20a: Found: *m/z* 200.0667. Calcd for $C_{13}H_{12}S$: M, 200.0660. MS *m/z* (rel intensity): 200 (M^+, 100), 185 (25), 167 (25). IR (oil): 3030, 2930, 1603, 1500 cm^{-1} ^1H NMR ($CDCl_3$) δ=1.34 (m, 2H), 2.20 (m, 2H), 6.5—7.4 (m, 8H).

Reaction of 3 with 18b. A mixture of **5** (2.52 g, 9 mmol), sodium hydride (230 mg, 9 mmol), and **18b** (4.25 g, 36 mol), in diglyme (30 ml) was reacted at 140 °C for 60 min. A thin-layer chromatographic separation of the reaction mixture using pet. ether-benzene 4 : 1 as a developing solvent gave **20b** (630 mg, 32.7%, R_f=0.57).

20b: Found: *m/z* 214.0798. Calcd for $C_{14}H_{14}S$: M, 214.0817. MS *m/z* (rel intensity) 214 (M^+, 100), 200 (37), 181 (9). IR (oil): 3010, 2920, 1518 cm^{-1}. ^1H NMR ($CDCl_3$) δ=1.28 (m, 2H), 2.20 (m, 2H), 2.29 (s, 3H), 6.6—7.2 (m, 7H).

Reaction of 3 with 18c. A mixture of **5** (2.52 g, 9 mol), sodium hydride (230 mg, 9 mmol), and **18c** (4.25 g, 36 mmol) in diglyme (30 ml) was reacted at 140 °C for 60 min. A thin-layer chromatographic separation of the reaction mixture using pet. ether-benzene 4 : 1 as a developing solvent gave **20c** (697 mg, 33.0%, R_f=0.57).

20c: Found: *m/z* 234.0268. Calcd for $C_{13}H_{11}SCl$: M, 214.0270. MS *m/z* (rel intensity) 234 (M^+, 100), 199 (44), 183 (12). IR (oil): 3080, 2920, 1492 cm^{-1}. ^1H NMR ($CDCl_3$) δ=1.30 (m, 2H), 2.31 (m, 2H), 6.5—7.2 (m, 7H).

Relative Rate Ratios of the Reaction of 3 to 18a—c. Tosylhydrazone (**5**) was reacted with 1 : 1 mixtures of **18a** and **18b** or **18a** and **18c** as usual. The ratios of products **20a**, **20b**, and **20c** were measured by the same method as that employed in the case of reactions of **4** to be 1.0, 0.8, and 1.6, respectively.

References

1) W. Kirms, "Carbene Chemistry," Academic Press, (1964); R. Hoffmann, G. D. Zeiss, and G. W. V. Dine, *J. Am. Chem. Soc.*, **90**, 1485 (1968); R. Gleiter and R. Hoffmann, *ibid.*, **90**, 5457 (1968); G. L. Cross, *Top. Stereochem.*, **3**, 193 (1968); W. M. Jones and C. L. Ennis, *J. Am. Chem. Soc.*, **91**, 6391 (1969); H. Durr and G. Scheppers, *Chem. Ber.*, **103**, 380 (1970); T. T. Coburn and W. M. Jones, *J. Am. Chem. Soc.*, **96**, 5218 (1974); M. Oda, Y. Ito, and Y. Kitahara, *Tetrahedron Lett.*, **1975**, 2587; K. Saito, Y. Omura, and T. Mukai, *Chem. Lett.*, **1980**, 349; S. J. Chang, B. K. R. Shankar, and H. Shechter, *J. Org. Chem.*, **47**, 4226 (1982); R. H. Paker and W. M. Jones, *Tetrahedron Lett.*, **25**, 1245 (1984); K. Saito, Y. Omura, and T. Mukai, *Bull. Chem. Soc. Jpn.*, **58**, 1663 (1985); K. Saito and H. Ishihara, *ibid.*, **58**, 2664 (1985); **59**, 1095 (1986).

2) R. V. Hoffman and H. Shechter, *J. Am. Chem. Soc.*, **93**, 5940 (1971); R. V. Hoffman, G. G. Orphanides, and H. Shechter, *ibid.*, **100**, 7927 (1978); R. V. Hoffman and H. Shechter, *ibid.*, **100**, 7934 (1978).

3) D. S. Sappenfeld and M. Kreevoy, *Tetrahedron*, **19**, 1957 (1963); D. T. Klark, *ibid.*, **24**, 3285, 4689 (1968); G. M. Marino, *J. Heterocycl. Chem.*, **9**. 817 (1972); T. J. Thomas, R. W. Roth, and J. G. Verkade, *J. Am. Chem. Soc.*, **94**, 8854 (1972); R. M. Acheson, "An Introduction to the Heterocyclic Compounds," John Willey and Sons, Inc. (1976), Chap. 3; K. Saito and Y. Horie, *Heterocycles*, **24**, 579 (1986).

4) G. L. Cross, R. A. Moss, and J. J. Coyle, *J. Am. Chem. Soc.*, **84**, 4985 (1962); M. Jones Jr. and E. W. Petrillo, *Tetrahedron Lett.*, **1969**, 3953; C. J. Rostek and W. M. Jones, *ibid.*, **1969**, 3957; T. Toda, K. Saito, and T. Mukai, *Bull. Chem. Soc. Jpn.*, **52**, 151 (1979).

5) W. M. Jones and C. L. Ennis, *J. Am. Chem. Soc.*, **89**, 3069 (1967); T. Mukai, T. Nakazawa, and K. Isobe, *Tetrahedron Lett.*, **1968**, 565; W. M. Jones, B. N. Hamon, R. C. Joines, and C. L. Ennis, *ibid.*, **1969**, 3909.

6) L. Horner and E. Lignan, *Justus Liebigs Ann. Chem.* **591**, 21 (1955); R. Huisgen, *Angew. Chem., Int. Ed. Engl.*, **2**, 565 (1963).

7) L. W. Christensen, E. E. Waali, and W. M. Jones, *J. Am. Chem. Soc.*, **94**, 2118 (1972); Harmos, S. Tirakornpannarai, and E. E. Waali, *Tetrahedron Lett.*, **27**, 3701 (1986).

 © 1987 The Chemical Society of Japan Bull. Chem. Soc. Jpn., 60, 4321—4323 (1987)

A Facile Method for the Production of D-*p*-Hydroxyphenylglycine. Asymmetric Transformation of DL-*p*-Hydroxyphenylglycine Using (+)-1-Phenylethanesulfonic Acid

Ryuzo YOSHIOKA,* Masanori TOHYAMA,† Shigeki YAMADA,††
Osamu OHTSUKI, and Ichiro CHIBATA†††
Research Laboratory of Applied Biochemistry, Tanabe Seiyaku Co., Ltd., 16-89, Kashima 3-Chome, Yodogawa-ku, Osaka 532
(Received March 27, 1987)

A practical method for the production of D-*p*-hydroxyphenylglycine, useful as a starting material for preparing semisynthetic penicillins or cephalosporins, has been developed. The diastereomeric salts of DL-*p*-hydroxyphenylglycine with (+)-1-phenylethanesulfonic acid as a resolving agent, were efficiently resolved into less soluble D-*p*-hydroxyphenylglycine (+)-1-phenylethanesulfonate [D-HPG·(+)-PES] and soluble L-HPG·(+)-PES by the fractional crystallization of its salts in aqueous solution. The soluble L-HPG·(+)-PES could be easily epimerized into DL-HPG·(+)-PES by heating it with water containing a 0.1 molar equivalent of free DL-HPG in an autoclave. When the fractional crystallization of DL-HPG with (+)-PES was simultaneously carried out under the epimerizing conditions, the DL-HPG·(+)-PES was transformed into D-HPG·(+)-PES in up to 90% yield. The present asymmetric transformation should be a suitable method for preparing D-HPG in a large scale.

It is well-known that D-*p*-hydroxyphenylglycine is useful as a side chain of semisynthetic penicillins or cephalosporins.[1] Thus far, we have presented several methods for the production of D-*p*-hydroxyphenylglycine.[2-5] Our previous paper[5] showed that (+)-1-phenylethanesulfonic acid [(+)-PES] was a favorable resolving agent for the diastereomeric resolution of DL-*p*-hydroxyphenylglycine (DL-HPG) and, for the asymmetric transformation of DL-HPG: a combination of the fractional crystallization of the less soluble D-*p*-hydroxyphenylglycine (+)-1-phenylethanesulfonate [D-HPG·(+)-PES] and the epimerization of the soluble L-*p*-hydroxyphenylglycine (+)-1-phenylethanesulfonate [L-HPG·(+)-PES] in a system. In the previous work, the asymmetric transformation of DL-HPG·(+)-PES was performed in acetic acid in the presence of salicylaldehyde. In the course of our further studies, it has been found that the asymmetric transformation of DL-HPG·(+)-PES could be achieved merely by heating a mixture of DL-HPG, (+)-PES, and water in an autoclave. The present paper describes a simple method for the asymmetric transformation of DL-HPG by the use of (+)-PES as a resolving agent.

The advantages of asymmetric transformation have been described in our previous reports[4-6] and the literature.[7-9] An asymmetric transformation between two diastereomers by a combination of fractional crystallization of the less soluble diastereomer and the epimerization of the soluble diastereomer is known as a second-order asymmetric transformation. In order to perform such an asymmetric transformation, we must search for the conditions under which both fractional crystallization and epimerization can be carried out simultaneously, and for which the resolving agent is chemically and optically stable.

The solubility of L-HPG·(+)-PES in water at 20 °C is about 80 times greater than that of D-HPG·(+)-PES as was noted in our previous paper.[5] Consequently, the fractional crystallization of the less soluble D-HPG·(+)-PES from the solution consisting DL-HPG, (+)-PES, and water occurred efficiently. On the other hand, we previously reported that the salt of L-HPG with achiral sulfonic acid (*o*-toluenesulfonic acid) was readily racemized by heating it in water at 140 °C.[2] To combine this racemization method and the optical resolution method of DL-HPG with (+)-PES, we have studied the epimerization of the soluble L-HPG·(+)-PES in water; this study was carried out by using

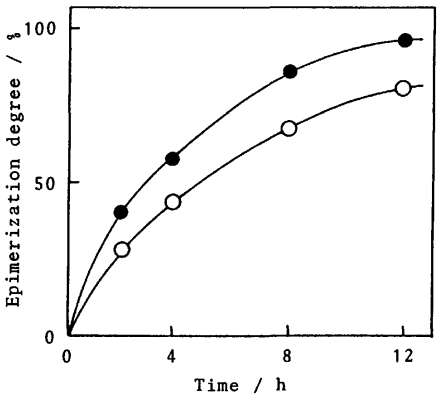

Fig. 1. Time course on epimerization of L-HPG·(±)-PES. The reactions were carried out at 140 °C in aqueous solution containing L-HPG·(±)-PES in a sealed tube. Additives: none (○), a 0.1 molar equivalent of DL-HPG (●).

†Present address: Chuoh Sellers Office Osaka Branch, Tanabe Seiyaku Co., Ltd., 5-37, Zuiko 2-Chome, Higashiyodogawa-ku, Osaka 533.
††Present address: Research Planning & Investigation Division Tanabe Seiyaku Co., Ltd., 16-89, Kashima 3-Chome, Yodogawa-ku, Osaka 532.
†††Present address: Research & Development Headquarters, Tanabe Seiyaku Co., Ltd., 16-89, Kashima 3-Chome, Yodogawa-ku, Osaka 532.

L-HPG·(±)-PES instead of L-HPG·(+)-PES to aim at accurately determining the racemization degree of the L-HPG moiety.

When L-HPG·(±)-PES was heated in water at 140 °C in a sealed tube, the epimerization of L-HPG·(±)-PES occurred as well as the racemization of L-HPG *o*-toluenesulfonate.[2] In Fig. 1, the time course of the epimerization of L-HPG·(±)-PES is shown together with that of adding a 0.1 molar equivalent of free DL-HPG. The presence of free DL-HPG considerably accelerated the rate of the epimerization. Under such epimerizing conditions, (+)-PES was confirmed to be chemically and optically stable in the manner described in our previous report.[5] Furthermore, the crystals of D-HPG·(+)-PES precipitated from the epimerizing solution were also detected to accumulate without redissolving into its solution. Thus the essential requirements for the intended asymmetric transformation were fulfilled.

In this kind of the asymmetric transformation (the second order), the composition of two diastereomers in the whole system is displaced to the one component by the crystallization. The yield of the desired diastereomer [D-HPG·(+)-PES] therefore is dependent on how much of the precipitate of the diastereomer crystallized in the reaction system. To increase the amount of the precipitate under the above conditions for epimerization, the amount of the solvent (in this case, water) must be minimized.

When the amount of water used as a solvent was almost equal to that of the ammonium (+)-1-phenylethanesulfonate [(+)-PES·NH_4, was used because it was easier to handle than (+)-PES (free acid: syrup or pasty crystals[5])], a good yield was obtained and the stirring state of the reaction mixture was satisfactory. A typical experiment of the resulting asymmetric transformation was performed by heating a slurry consisting of DL-HPG (35.3 g, 0.19 mol×1.1), (+)-PES·NH_4 (39.0 g, 0.19 mol), sulfuric acid (9.4 g, 0.19 mol×0.5), and water (40 ml) with stirring in a glass autoclave. This reaction proceeded in the slurry state of the solid-liquid heterogeneous system. In order to achieve a high yield in the above experiment, the optimal conditions of the reaction were examined in further detail. Figure 2 shows the yield of D-HPG·(+)-PES as a function of the reaction time for three different temperatures. The excessive heating resulted in a lowering of yield of D-HPG·(+)-PES owing to the decomposition of HPG although the (+)-PES was stable. The highest yield (91.2% based on the DL-HPG·(+)-PES) was obtained in the reaction at 125 °C for 20 h. The change in the composition of both diastereomeric salts during the period of the reaction is illustrated in Fig. 3.

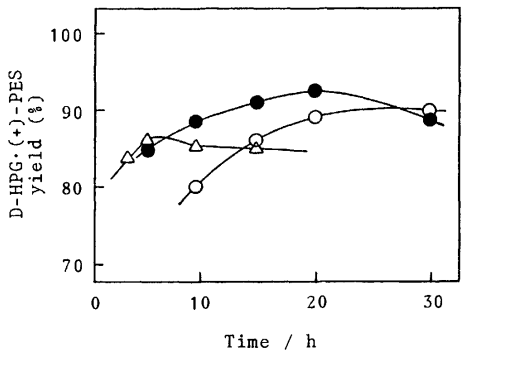

Fig. 2. Effect of temperature and time on asymmetric transformation of DL-HPG·(+)-PES. A mixture of DL-HPG (35.3 g), (+)-PES·NH_4 (39.0 g), sulfuric acid (9.4 g), and water (40 ml) was stirred at a temperature (○; 118 °C, ●; 125 °C, △; 135 °C) in an autoclave.

Since the D-HPG·(+)-PES obtained above was optically pure, it could be decomposed to optically pure D-HPG by neutralization with aqueous ammonia without further purification. The (+)-PES·NH_4 contained in the mother liquor after the separation of D-HPG could be reused as the resolving agent for the

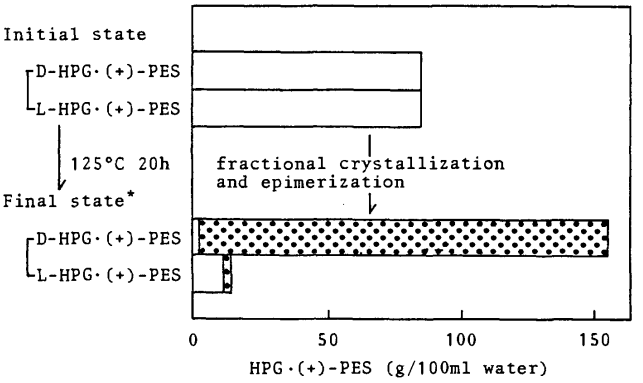

Fig. 3. The change in the composition of diastereomeric salts by asymmetric transformation. *: ▨, crystals of (+)-PES salt; □, (+)-PES salt in solution.

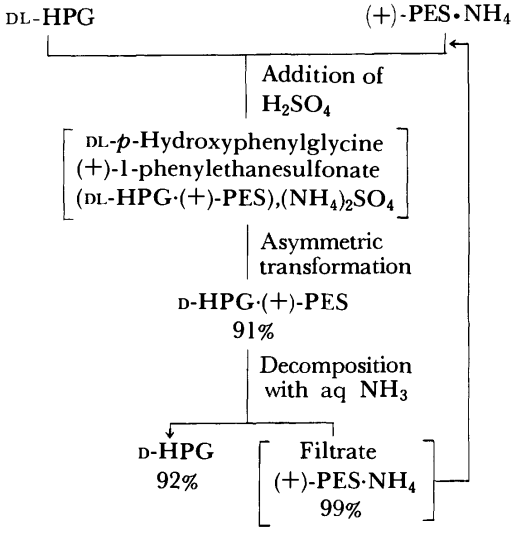

Scheme 1. Flowsheet for preparation of D-*p*-hydroxyphenylglycine by asymmetric transformation. [ ] were used in the next process without separation.

next asymmetric transformation without isolation. Our proposed repetitive process for preparing D-HPG is shown in Scheme 1. The asymmetric transformation presented here proceeds in a slurry state containing a large amount of solid and gives a high degree of transformation and a high yield of D-HPG·(+)-PES per a unit volume of water solvent (Fig. 3). This method for the preparation of D-HPG, therefore, has a definite advantage and is suitable for industrial application.

Experimental

Materials and Analyses. Optically active and racemic HPG manufactured by our company, Tanabe Seiyaku Co., Ltd., were used. (+)-1-Phenylethanesulfonic acid [(+)-PES] was prepared in a manner described in our previous report.[5] Optical rotations were measured with a Perkin-Elmer 141 automatic polarimeter. IR spectra were recorded on a Shimadzu IR-420 spectrophotometer. ^{1}H NMR spectra were measured with a Hitachi Perkin-Elmer R-40 spectrometer using tetramethylsilane as an internal standard. A glass autoclave TEM-U300 (Taiatsu Glass Industry Co., Ltd., Japan) was used. The temperature control for asymmetric transformation was carried out by a Thermo-mate oil bath BZ-21 (Yamato Scientific Co., Ltd., Japan).

Epimerization of L-HPG·(+)-PES. The experiments aimed at the epimerization of the diastereomeric salt were carried out using the 1 : 1 molar ratio salt of L-HPG with (±)-PES [L-HPG·(±)-PES]. The epimerization degree, i.e., the racemization degree of the L-HPG moiety was evaluated by measurement of the optical rotation. A mixture of L-HPG·(±)-PES (50 mg), DL-HPG (2.4 mg), and water (0.6 ml) was heated in a sealed tube at 140 °C. After heating for the prescribed time, the reaction mixture was diluted with water (10 ml), and the optical rotation was measured. The epimerization degree was evaluated from the change in the optical rotation. The results together with those without free DL-HPG are shown in Fig. 1.

Preparation of Ammonium (+)-1-Phenylethanesulfonate. A solution of (+)-PES [40.0 g; $[\alpha]_D^{25}$ +20.9 ° (*c* 3, DMSO)] in water was adjusted to pH 7 with 28% aqueous ammonia (14.5 ml). The aqueous solution was concentrated to dryness under reduced pressure. To the residue was added acetone (150 ml), and the resulting crystals were filtered, and dried at 90 °C to give (+)-PES·NH_4 (41.5 g; $[\alpha]_D^{25}$ +15.2 ° (*c* 1, MeOH); mp 208—209 °C; IR (Nujol) 3200, 1600, 1410, 1020, and 700 cm^{-1}; ^{1}H NMR (DMSO-d_6) δ=1.46 (3H, d, J=7 Hz, CH_3), 3.67 (1H, q, J=7Hz, CH), and 6.9—7.3 (5H, m, aromatic H).

Asymmetric Transformation of DL-HPG. A mixture of DL-HPG (35.3 g), (+)-PES·NH_4 (39.0 g), sulfuric acid (9.4 g), and water (40 ml) was heated at a prescribed temperature (118, 125, and 135 °C) in an autoclave fitted with a mechanical stirrer. The reaction system was a thick slurry during the reaction. After heating for a required time, into the heterogeneous reaction mixture were added water (40 ml) and sulfuric acid (0.9 g). The mixture was cooled to 5 °C and then stirred for 2 h. The crystals which precipitated were collected by filtration, washed with a small amount of cold water, and dried to give almost optically pure D-HPG·(+)-PES (yield, 54.4—61.9 g). The relationships between the yield of D-HPG·(+)-PES and the reaction time at each reaction temperature are shown in Fig. 2. The highest yield was obtained when the reaction mixture was treated at 125 °C for 20 h; yield of D-HPG·(+)-PES 61.9 g (91.2% based on the DL-HPG·(+)-PES); $[\alpha]_D^{25}$ −76.8° (*c* 1, MeOH); optical purity, 97.6%. The change in the composition of both diastereomeric salts during the reaction is shown in Fig. 3.

Preparation of D-HPG. A mixture of D-HPG·(+)-PES (60.0 g; optical purity, 97.6%) and water (60 ml) was heated at 60 °C with stirring. The suspended mixture was adjusted to pH 6.0 with 6 mol dm^{-3} aqueous ammonia. After stirring for 1 h at the same temperature, the mixture was stirred for 2 h at 5 °C. The reaction proceeded in a thick slurry. The crystals which precipitated were collected by filtration, washed with a small amount of cold water, and dried to give D-HPG (26.0 g) in a 91.6% yield; $[\alpha]_D^{25}$ −158.0° (*c* 1, 1 mol dm^{-3} HCl).

Found : C, 57.43 ; H, 5.40 ; N, 8.41%. Calcd for $C_8H_9NO_3$: C, 57.48 ; H, 5.43 ; N, 8.38%.

The mother liquor obtained after the separation of D-HPG was the aqueous solution containing (+)-PES·NH_4, which could be reused for the next asymmetric transformation in the form of the solution without isolating the (+)-PES·NH_4.

The authors wish to thank Dr. C. Hongo for his valuable advice during this work.

References

1) L. B. Crast, Jr., U.S. Patent, 3489750 (1970); *Chem. Abstr.*, **72**, 100725v (1970).

2) S. Yamada, C. Hongo, and I. Chibata, *Agric. Biol. Chem.*, **42**, 1521 (1978).

3) S. Yamada, C. Hongo, R. Yoshioka, and I. Chibata, *Agric. Biol. Chem.*, **43**, 395 (1979).

4) C. Hongo, M. Tohyama, R. Yoshioka, S. Yamada, and I. Chibata, *Bull. Chem. Soc. Jpn.*, **58**, 433 (1985).

5) R. Yoshioka, M. Tohyama, O. Ohtsuki, S. Yamada, and I. Chibata, *Bull. Chem. Soc. Jpn.*, **60**, 649 (1987).

6) C. Hongo, S. Yamada, and I. Chibata, *Bull. Chem. Soc. Jpn.*, **54**, 3286, 3291 (1981).

7) J. C. Clark, G. H. Phillipps, and M. R. Steer, *J. Chem. Soc., Perkin Trans. 1*, **1976**, 475.

8) M. M. Harris, "Progress in Stereochemistry," ed by W. Klyne and P. B. D. Mare, Butterworths Sientific Publications, London (1958), Vol. 2, p. 157.

9) J. Jacques, A. Collet, and S. H. Wilen, "Enantiomers, Racemates, and Resolutions," ed by John Wiley and Sons, Wiley-Interscience, New York (1981), p. 369.

 © 1987 The Chemical Society of Japan Bull. Chem. Soc. Jpn., 60, 4325—4333 (1987)

Preparation of Polyacetoxytropones and Polyhydroxytropolones by Acetolysis and Hydrolysis of Halotroponoids by Acetyl Trifluoroacetate with Exhaustive Displacement of Halogens on the Tropone Ring. Predominant Formation of Reductive Acetolysates from Fully-Substituted Tropones

Hitoshi TAKESHITA,* Akira MORI, Tomoyuki KUSABA,† and Hiroyasu WATANABE†
Research Institute of Industrial Science, 86, Kyushu University, Kasuga-koen, Kasuga, Fukuoka 816
†Graduate School of Engineering Sciences, 39, Kyushu University, Kasuga-koen, Kasuga, Fukuoka 816
(Received April 24, 1987)

Di-, tri-, and tetrahydroxytropolones were prepared in good yields by the acetolysis of corresponding halotropones or polyhalotropolones with acetyl trifluoroacetate followed by acetic acid hydrolysis. However, using the same treatment to obtain hexaacetoxytropone with fully substituted acetoxyhalotropones predominantly yielded fewer substituted acetoxytropones than expected; the mechanism of formation was shown to involve an acetic acid-mediated reduction of intermediary formed acetoxy-*p*-tropoquinone equivalents. A couple of 2,7-unsubstituted 3,4-diacetoxytropones were deduced to have cyclized 1,3-dioxole structures, 2-acetoxy-2-methyl-5*H*-cyclohepta-1,3-dioxol-5-ones. An acetolysis of the brominated 5-isopropyltropolones furnished an acetylated by-product, 2,3,7-triacetoxy-5-(1,1-dimethyl-2-oxopropyl)tropone, which might be formed by the acylation of an intermediate, 3,4,5,6-tetraacetoxy-8,8-dimethylheptafulvene.

It is well-known that polyhydroxytropolones are physiologically active; in the 1930's several carboxylic acid derivatives, stipitatic acid,[1] stipitatonic acid,[2] puberulic acid,[3] and puberulonic acid,[3] which all possessed additional hydroxyl groups, had already been isolated from microorganisms such as *Penicillium stipitatum Thom.* and *P. puberulum Bainier.* Even 3-hydroxytropolone (**1**) was recognized to be an antibiotic.[4]

Therefore, a systematic method for synthesizing polyhydroxylic tropolones is desirable; recently, we have demonstrated the facile preparation of **1** from 7-bromo-2-methoxytropone (**2**) by treatment with acetyl trifluoroacetate (ATA) prepared in situ from acetic anhydride and trifluoroacetic acid, with or without sodium acetate.[5]

In order to detemine its a versatility, we have extended this method to prepare 3- (**1**),[6] 4- (**3**),[7] and 5-hydroxytropolones (**4**),[8,9] along with several further hydroxylated tropolones, such as di-, tri-, tetra-, and pentahydroxytropolones. It is true that, to date, there has been no efficient method for the preparation of such fundamental derivatives, **1** and **3**; for the hydrochloric acid-hydrolysis of 3-bromotropolone (**5**) to **1** it was necessary to heat at 160—180 °C,[6] while an alkali fusion of **5** gave **3** instead of **1**. However, its yield was at most 17%.[7]

The attempted formation of pentaacetoxytropone (**6**) and hexaacetoxytropone (**7**) from corresponding halotroponoids by this method, however, yielded fewer substituted derivatives than predicted. After all, octachlorocycloheptatriene (**8**)[10] was converted to **7** in low yield together with some intermediary acetoxychlorotropones. Herein, we will show the results.

Results and Discussion

Acetolysis of Dihalotropones. First of all, in order to prepare fundamental hydroxytropolones, when 2,5-dichlorotropone (**9**)[11] and 2,7-dibromotropone (**10**)[12] were treated with ATA at 85 °C, a neat reaction occurred to form the halogen-free compounds, 2,5-diacetoxytropone (**11**)[8] and 2,7-diacetoxytropone (**12**),[8] 75 and 85%, respectively. Both **11** and **12** were identical with the authentic samples, as confirmed by direct comparisons. Under the conditions, **9** formed two intermediary chlorine-containing compounds, 5-acetoxy-2-chlorotropone (**13**)[13] and 2-acetoxy-5-chlorotropone (**14**), in 4 and 8% yields, respectively. Heating at a higher temperature, 100 °C, or for a prolonged period smoothly resulted in the replacement of all of the halogen atoms. In all cases, there was no ring-contracted benzene derivative. A mild hydrolysis of **11** and **12** with aqueous acetic acid gave, after evaporation of the solvent, **4** and **1** in nearly quantitative yields. Therefore, this may be applicable for preparing hydroxytropolones from corresponding halotropones.

Similarly, 4-chlorotropolone (**15**),[14] prepared from **9** via 2-amino-4-chlorotropone (**16**) by sequential reactions, was converted via 2,4-diacetoxytropone (**17**) and 3,4-diacetoxytropone (**18**) to 4-hydroxytropolone (**3**) as the sole product. An attempted hydrolysis of **15** with concentrated hydrochloric acid or acetolysis of **16** with the present reagent has been unsuccessful. Noteworthy was the structure of **18**. Namely, the ^{13}C NMR spectrum of **17** indicated an operating acetotropy[15,16] at room temperature, but that of **18** did not. In addition, its ^{1}H NMR showed another aspect of anomaly; the acetoxyl methyl signals on the troponoid rings generally appeared at δ=2.2 to 2.3; however, the acetoxyl signals of **18** were at a much higher region, i.e., one at 2.00, and the other at 2.08. These would not be ascribable to those on the aromatic ring. Moreover its ^{13}C NMR revealed a quarternary carbon signal at δ=124.3; this value has no analogy in any of the other

acetoxytropones that have been studied. Taking all these observations into account, **18** should be formulated as a cyclized 1,3-dioxole (**18a**) as depicted in Scheme 1. The formation of such a cyclized structure

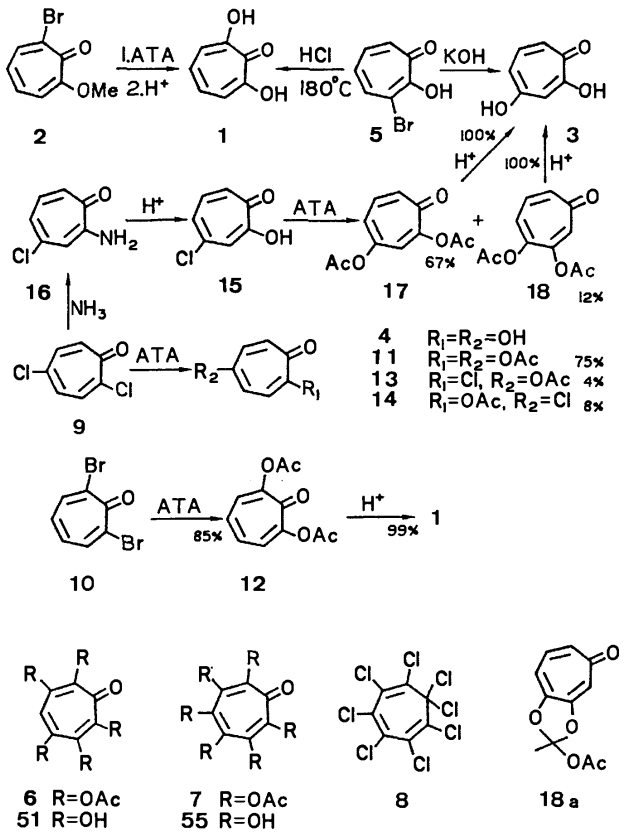

Scheme 1.

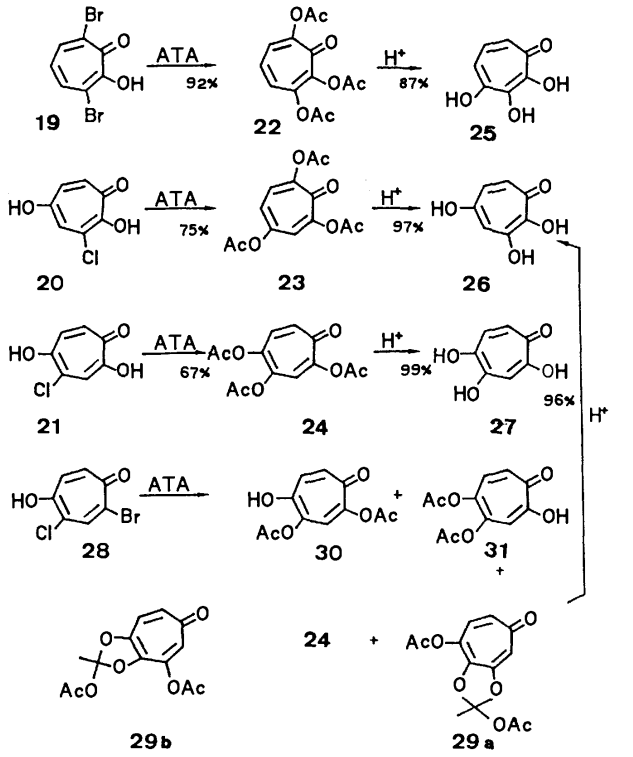

Scheme 2.

should be attributable to severe steric and repulsive non-bonding interactions of the *vic*-diacetoxyl groups on the seven-membered ring.[17]

Acetolysis of Dihalotropolones. By a similar acetolysis, 3,7-dibromotropolone (**19**),[18] 3-chloro-5-hydroxytropolone (**20**),[19] and 4-chloro-5-hydroxytropolone (**21**)[20] were respectively converted to triacetoxytropones, 2,3,7-triacetoxytropone (**22**), 2,4,7-triacetoxytropone (**23**),[21,22] and 2,4,5-triacetoxytropone (**24**), and further to dihydroxytropolones, 3,4-dihydroxytropolone (**25**),[3] 3,5-dihydroxytropolone (**26**),[19] and 4,5-dihydroxytropolone (**27**). From 2-bromo-4-chloro-5-hydroxytropone (**28**), four halogen-free products (**24**, **29**, **30**, and **31**) were isolated via silica-gel column chromatography; the major product obtained after elutions of **29** was the expected **24**. The ^{1}H NMR spectrum of **29** was identical with the "3,4,5-triacetoxytropone" already prepared by Itô et al., and its aqueous acetic acid hydrolysis indeed yielded **26**.[21,22] However, the ^{1}H NMR chemical shifts of the acetoxyl methyl signals again suggested a 1,3-dioxole derivative; the two methyl singlets at δ=2.01 and 2.08 were incompatible with the acetoxyl signals on the aromatic ring and were, therefore, tentatively assigned to be 2,8-diacetoxy-2-methyl-5*H*-cyclohepta-1,3-dioxol-5-one (**29a**), as depicted.[23,24] The formation of **29a** from **28** must involve a substitution at a remote position of the leaving group. More polar compounds, **30** and **31**, were partially-hydrolyzed diacetoxyhydroxytropones and the ^{1}H and ^{13}C NMR spectra distinguished the structures; **30**, showing a symmetry element, is therefore 2,4-diacetoxy-5-hydroxytropone.

Acetolysis of Bromo Derivatives Prepared from 4-, and 5-Isopropyltropolones. To extend the applicability of the reaction to alkyl derivatives, the acetolysis of dibromo derivatives of hinokitiol (**32**) and γ-

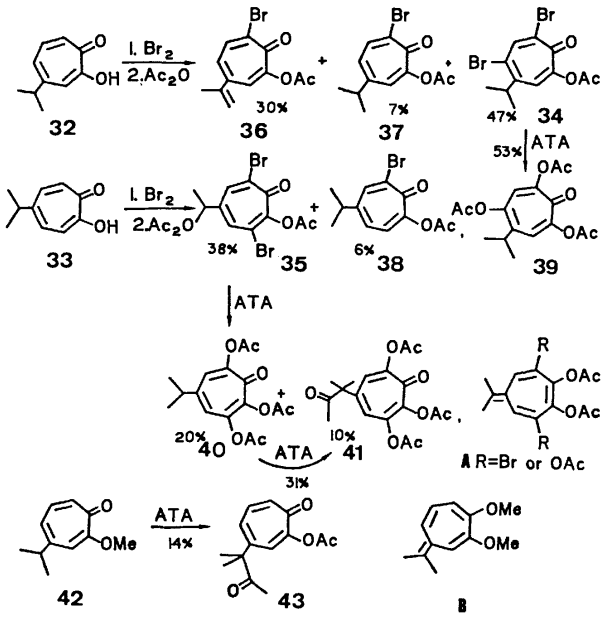

Scheme 3.

thujaplicin (**33**), 2-acetoxy-5,7-dibromo-4-isopropyltropone (**34**) and 2-acetoxy-3,7-dibromo-5-isopropyltropone (**35**),[25,26] was carried out. Through brominations, we have identified by-products, 2-acetoxy-7-bromo-4-isopropenyltropone (**36**) and 2-acetoxy-7-bromo-4-isopropyltropone (**37**) from **32** and 2-acetoxy-7-bromo-5-isopropyltropone (**38**) from **33**;[27] however, this is not further discussed.

The acetolysis of **34** and **35**, respectively, gave triacetoxytropones, 2,4,7-triacetoxy-5-isopropyltropone (**39**) and 2,3,7-triacetoxy-5-isopropyltropone (**40**) in good yields. A notable by-product in the acetolysis of **35** was the acylation product, 2,3,7-triacetoxy-5-(1,1-dimethyl-2-oxopropyl)tropone (**41**). An independent treatment of **40** gave **41** in a better yield, 31%. Evidently, **41** must be produced via a heptafulvene intermediate (**A**). The fact that such an acylated product from **34** did not appear might be due to the presence of an acetoxyl group at the vicinity of the isopropyl group, C-4. Indeed, acylation also occurred with a halogen-free heptafulvene (**B**) from 4-isopropyl-2-methoxytropone (**42**); a similar treatment of **42**, indeed, afforded 14% of the acylation product, 2-acetoxy-4-(1,1-dimethyl-2-oxopropyl)tropone (**43**). It has been emphasized that the Friedel-Crafts-type acylation and alkylation were not applicable to troponoids because of their insoluble metal chelate formation with the catalysts or easy protonation to form a delocalized stable cationic 6 π species by acid. The present example must constitute an overcoming of a deactivated reactivity towards the Friedel-Crafts acylation of the non-benzenoid aromatics. The electrophilic substitution of heptafulvenes has been successfully carried out only with some 8-monosubstituted heptafulvenes, such as 8-cyanoheptafulvene, showing that the reaction site is exclusively C-8.[28] The present examples are in that line.

Acetolysis of Polyhalo Troponoids: Occurrence of Reduction Process. Subsequently, when 4,6-dichloro-5-hydroxytropolone (**44**)[19] was treated with ATA, 2,4,5,7-tetraacetoxytropone (**45**) was obtained in 55% yield, and its mild hydrolysis gave 3,5,6-trihydroxytropolone (**46**) in 80% yield. On the other hand, 3,5,7-tribromotropolone (**47**) afforded 2,3,5,7-tetraacetoxytropone (**48**) and 3,4,6-trihydroxytropolone (**49**) in good yields.

However, the same treatment of 3,5,7-tribromo-4-hydroxytropolone (**50**), obtained from the bromination of **3**, afforded a small amount of pentaacetoxytropone (**6**). The hydrolysis of **6** gave tetrahydroxytropolone (**51**). Even more surprising was the predominant formation of **6** from 2,3,5,7-tetraacetoxy-4,6-dibromotropone (**52**), which was prepared together with 3,4,5,6-tetraacetoxy-2,7-dibromotropone (**53**) by a further bromination and acetylation of **48**;[29] the yield of the expected **7** was around 0.5%. Several other attempts to make **7** from fully-substituted acetoxyhalotropones always resulted in the formation of **6**. Although the yields for the acetolysis products in the polysubstituted derivatives could be improved by the addition of sodium acetate to the mixture, yields of the reduction products became more predominant. For example, **50** gave the expected **6** in 11% yield together with **45** in 60% yield, whose bromination and acetylation afforded 4,5,6-triacetoxy-3,7-dibromotropolone (**54**). On the other hand, **52** yielded **48** in 48% and **6** in 12% yield. Particularly, the formation of **48** from **52** indicates an occurrence of two-fold reduction.[30] Thus, in the acetolysis of the polyhalotropones, the yields of the substitution product could not be improved by the addition of sodium acetate. The results are summarized in Table 1. As a whole, in spite of intensive attempts, the formation of **7** from fully substituted polyacetoxyhalotropones was not reproducible. A mild hydrolysis of **7** gave pentahydroxytropolone (**55**) in 75% yield.

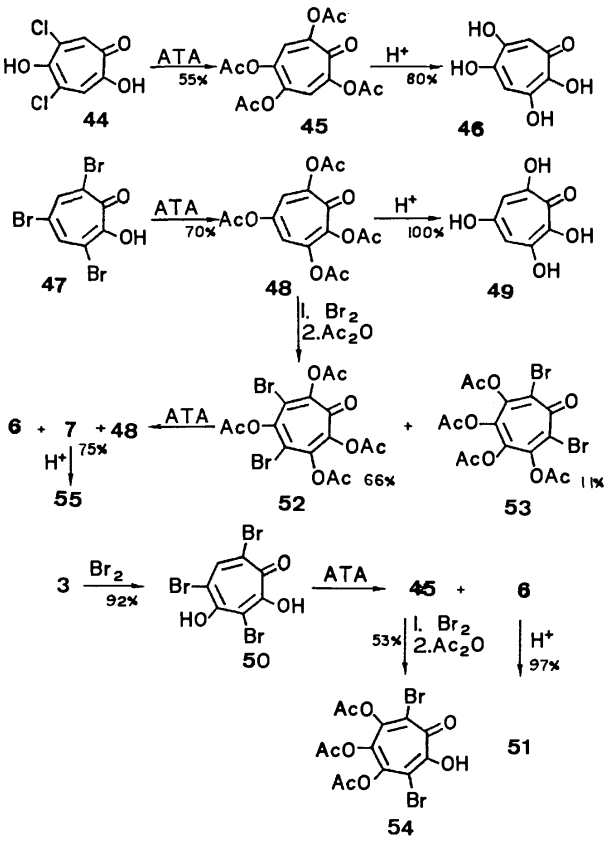

Scheme 4.

Table 1. Acetolysis of **50**, **52**, and **8** with ATA

Substrate	Condition	Addition	Yield/% of Product			
			6	**45**	**7**	**48**
50	85 °C, 9 h	—	11	—	—	—
50	125 °C, 2 d	NaOAc	11	60	—	—
52	110 °C, 5 d	—	2.6	—	0.5	—
52	110 °C, 5 d	NaOAc	12	—	—	48
8[a]	115 °C, 5 d[b]	NaOAc	3	—	0.6	—

a) Acetolyses of **8** under other conditions were cited in Experimental. b) These were followed by further heating at 160 °C for 2 d.

Nevertheless, ATA-acetolysis of **8** always gave **6** and **7** in low yields together with a mixture of intermediary trichloro and monochloro derivatives (**56** and **57**). The structure of an intermediate product, **56**, was of interest. Its elemental analysis was compatible to triacetoxytrichlorotropone, and the ^{1}H and ^{13}C NMR spectra suggested 1,3-dioxole, since two of the three acetoxymethyl signals appeared at δ=2.09 and 2.12 together with a signal at 124.1. This signal is ascribable to the ortho-acetate carbon, being parallel to "3,4-diacetoxytropone" (**18a**) and "3,4,5-triacetoxytropone" (**29a**), which exist as a cyclized 1,3-dioxole form. These observations, together with a low-field signal at 2.38, an acetoxyl group between two chlorine atoms, indicated the structure to be 2,7-diacetoxy-4,6,8-trichloro-2-methyl-5*H*-cyclohepta-1,3-dioxol-5-one, a cyclisate from 3,4,6-triacetoxy-2,5,7-trichlorotropone.

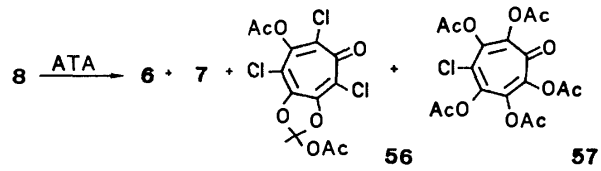

Scheme 5.

As far as we know, the previously known methods of hydrolyzing polyhalotropones have several limitations. Namely, an acid-hydrolysis of 2,7-dihalotropones to 3-halotropolones is rapid, but the second step of the substitution is very slow.[6] While 3,5,7-tribromotropolone (**47**) could be converted to 3,5,7-trialkoxytropolones together with several by-products, its hydrolysis to **49** was unsuccessful.[21] In addition to the above, a mechanistically-interesting elimination-addition reaction of 3- and 5-bromotropolones (**C** and **D**) with sodium methoxide is known to form, via benzyne-type intermediates, 3-, 4-, and 5-methoxytropolones (**E**, **F**, and **G**). However, this procedure should not be applicable to the displacement of *vic*-dihalo derivatives to alkoxyl groups.[31] Furthermore, the previously-studied sulfuric acid-hydrolysis of **8** gave structure-unidentified tetrachlorodihydroxytropones.[10] Thus, the utility of the present method for preparation of halogen-free derivatives is outstanding.

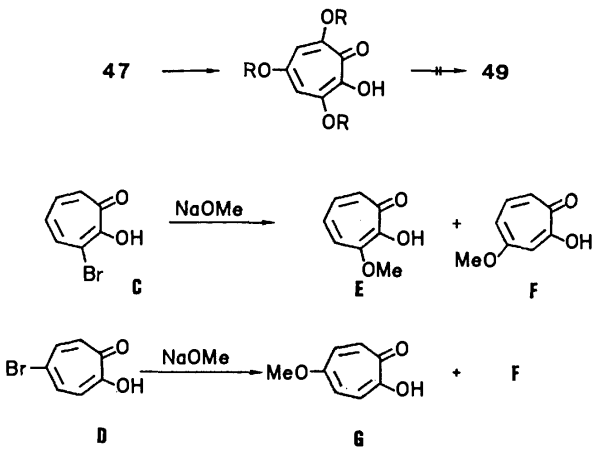

Scheme 6.

Since intermediates in the displacement of halogens, halogenated acetoxycycloheptatrienylium ions (**H**) should be formed, their further acetoxylation might be equally easy. To the contrary, the intermediate formed in the first step in an ordinary acid hydrolysis of polyhalotropones should be halogenated dihydroxycycloheptatrienylium salt (**L**), which can be deprotonated easily to tropolones (**K**). This is the reason why ordinary acid hydrolysis gives halogenated monohydroxylic tropones. In addition, this ATA acetolysis was inapplicable to the benzenoid compounds.[5] Therefore, this exhaustive displacement of acetoxyl group proceeded to the advantage of the formation of **H**.

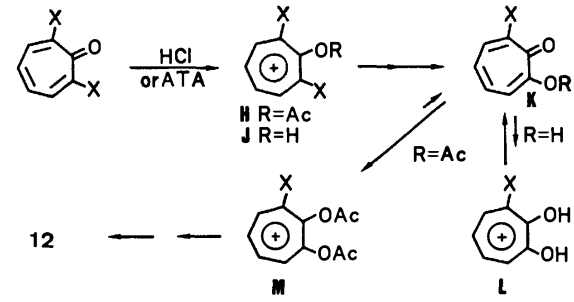

Scheme 7.

Mechanism of Formation of Reduction Products. Now, the reaction mechanism leading to reduced products should be explained. In the later steps of the acetolysis in polysubstituted troponoids (**P**), the acetolysates may become halogenated 2,5-diacetoxytropone derivatives (**Q**). In case of sterically hindered **Q**, the base, sodium acetate, may facilitate an elimination of acetyl halide (or hydrogen halide) rather than a substitution to form the *p*-tropoquinone (**R**) via an intermediate (**S**). Under these conditions, *p*-tropoquinones should be reduced by acetic acid to 2,5-diacetoxytropone derivative (**T**), being parallel to the previously described parent *p*-tropoquinone and other derivatives.[19,32]

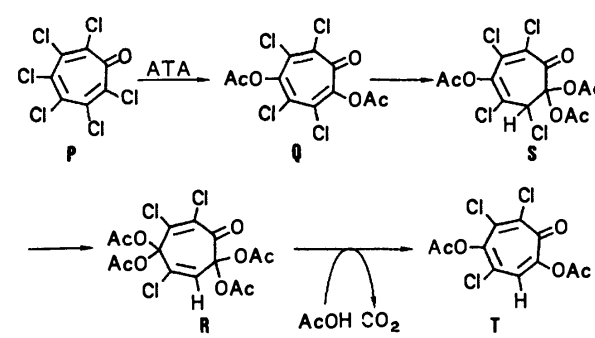

Scheme 8.

Conclusion

Before concluding, results of the bromination reac-

tion of polyhydroxytropolones must be mentioned. When **46** was treated with bromine in acetic acid at room temperature, a rapid decoloration of bromine was observed. The product after heating at 95 °C was, however, 2,5-dibromo-3,6-dihydroxy-*p*-benzoquinone (**58**);[33] evidently, a benzil-benzilic acid rearrangement product (**U**) of an intermediate, an *o*-tropoquinone hydrate derivative (**V**), was further decarboxylated to **58**, and a protection of free hydroxyl group must be essential to avoid the ring contraction.

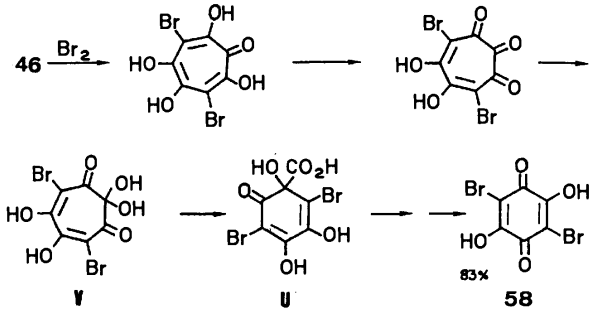

Scheme 9.

Finally, up to pentaacetoxytropone, the present procedure is satisfactory; but for fully oxygenated hexaacetoxytropone, the reduction process was predominant. Still, no ring-contraction to the benzenoid derivative occurred. This is the scope and limitation of this method. The ^{1}H- and ^{13}C NMR spectra of hexaacetoxytropone, a potential C_7-oxo carbon precursor, has disclosed a degenerated acetyl migration operative at room temperature, and the kinetic features of this rearrangement will be a subject of an independent publication.[16]

Experimental

Elemental analyses were carried out by Miss S. Hirashima, of the Research Institute of Industrial Science, Kyushu University. The NMR spectra were measured by a JEOL FX 100 Spectrometer in $CDCl_3$ solution, unless otherwise specified, and the chemical shifts expressed were in δ unit. The mass spectra were measured with a JEOL OISG-2 Spectrometer. The IR spectra were taken as KBr disks or as a liquid film inserted between NaCl plates using a Jasco IR-A 102 Spectrometer. The UV spectra were measured by a Hitachi U-3200 Spectrophotometer.

Preparation of Acetyl Trifluoroacetate (ATA). Ac_2O (50 cm^3) was mixed with CF_3COOH (5 cm^3) and AcOH (2.5 cm^3) at room temperature. The whole operation should be carefully undertaken in a good ventilated hood. Each time, a portion of the solution was taken out by pipette.

Acetolysis of 2,5-Dichlorotropone (9). An ATA solution[34] (5.6 cm^3) of **9** (100 mg) was sealed in an autoclave and heated at 85 °C for 10 h. After removal of the solvent in vacuo, the residue was chromatographed on a silica-gel column to give **14** [colorless crystals, mp 70.5—73.5 °C, 9 mg; 8%. Found: C, 54.17; H, 3.58%; *m/z* 198.0068 and 200.0023 (M^+). Calcd for $C_9H_7O_3Cl$: C, 54.41; H, 3.53%; M, 198.0081 and 200.0053. ^{1}H NMR δ=2.33 (3H, s), 7.05 (2H, dd, *J*=11, 1.5 Hz), and 7.24 (2H, dd, *J*=11, 1.5 Hz). ^{13}C NMR δ=20.6, 132.4, 132.8, 134.0 (2C), 140.2, and 168.0 (3C). IR ν: 1765, 1630, 1580, 1200, 1075, and 860 cm^{-1}], **13** [colorless crystals, mp 102—103 °C (lit,[12] 101.5—102 °C), 4 mg; 4%. ^{1}H NMR δ=2.29 (3H, s), 6.68 (1H, ddd, *J*=10.5, 2.5, 0.5 Hz), 6.97 (1H, dd, *J*=13, 2.5 Hz), 7.21 (1H, dd, *J*=13, 0.5 Hz), and 7.71 (1H, d, *J*=10.5 Hz). ^{13}C NMR δ=20.9, 122.2, 133.9, 134.2, 138.2, 147.4, 154.5, 168.9, and 179.4], and **11** [pale yellow needles, mp 93—95 °C (lit,[8] 91—92 °C), 95 mg; 75%. ^{1}H NMR δ=2.26 (3H, s), 2.31 (3H, s), 6.88 (2H, dd, *J*=10.5, 1.5 Hz), and 7.17 (2H, dd, *J*=10.5, 1.5 Hz). ^{13}C NMR δ=20.6, 20.9, 128.2 (2C), 133.0 (2C), 153.5, 167.9 (2C), and 168.7 (2C). IR ν: 1755, 1585, 1365, 1140, and 920 cm^{-1}].

Acetolysis of 2,7-Dibromotropone (10). An ATA solution (8 cm^3) of **10** (64.2 mg) and NaOAc (101 mg) was heated in a sealed tube at 100 °C for 24 h. The mixture was then heated in vacuo, and the residue was chromatographed on a silica-gel column to give **12** [a colorless crystals, mp 90—91 °C (lit,[5] 86—87 °C), 45.6 mg; 85%].

Hydrolysis of 12 to 1. An aqueous AcOH (50%, 10 cm^3) of **12** (490 mg) was heated at 100 °C for 16 h to give **1** [orange needles, mp 179—181 °C, 248 mg; 99%].

Attempted Acetolysis of 2-Amino-4-chlorotropone (16). An ATA solution (2 cm^3) of **16** (40 mg) was heated in a sealed tube at 100 °C for 6 h. After evaporation of the solvent in vacuo, the residue was chromatographed on a silica-gel column, but no identifiable compound was obtained.

Acetolysis of 4-Chlorotropolone (15). An ATA solution (50 cm^3) of **15** (1.197 g) was heated in an autoclave at 100 °C for 14 h. The mixture was then heated in vacuo to remove the solvent, and the residue was chromatographed on a silica-gel column to give **17** [colorless crystals, mp 101—102.5 °C, 1.138 g; 67%. Found: C, 59.72; H, 4.48%. Calcd for $C_{11}H_{10}O_5$: C, 59.46; H, 4.54%. ^{1}H NMR δ=2.22 (3H, s), 2.28 (3H, s), 6.79 (1H, ddd, *J*=9, 3, 2 Hz), 6.96 (1H, d, *J*=2 Hz), 7.00 (1H, dd, *J*=10, 9 Hz), and 7.13 (1H, dd, *J*=10, 3 Hz). ^{13}C NMR δ=20.5, 20.8, 129.5, 129.7, 130.0, 131.9, 156.0, 164.2, 167.8, 168.5, and 170.9. IR ν: 2940, 1740, 1580, 1515, 1365, 1185, 1100, 1005, and 915 cm^{-1}] and **18** [pale yellow crystals, mp 89—91 °C, 212 mg; 12%. Found: C, 59.39; H, 4.53%. ^{1}H NMR δ=2.00 (3H, s), 2.08 (3H, s), 6.44 (1H, dd, *J*=8, 2 Hz), and 6.65—7.05 (3H, m). ^{13}C NMR δ=21.5, 24.0, 107.0, 115.6, 124.3, 133.4, 136.7, 154.2, 157.0, 167.3, and 184.7. IR ν: 1775, 1680, 1400, 1110, 955, and 880 cm^{-1}. UV λ_{max}^{MeOH}: 239 nm (ε=23200), 246 (22600, sh), 257 (18900, sh), 271 (5400, sh), 301 (6200, sh), and 312 (7100)].

Hydrolysis of 2,4-Diacetoxytropone (17). An aqueous AcOH solution (50%, 20 cm^3) of **17** (1.22 g) was heated at 100 °C for 5 h. After removal of the solvent in vacuo, the residue was washed with AcOEt, and recrystallized from MeOH to give **3** [colorless crystals, mp 229—230 °C (lit,[1] 230—231 °C), 761 mg; 100%. ^{1}H NMR (CD_3OD) δ=6.72 (1H, ddd, *J*=10.7, 2.5, 1 Hz), 6.87 (1H, d, *J*=2.5 Hz), 6.92 (1H, dd, *J*=10.3, 1 Hz), and 7.24 (1H, dd, *J*=10.7, 10.3 Hz). ^{13}C NMR (CD_3OD) δ=114.7, 115.8, 121.5, 138.1, 168.4, 169.8, and 174.7. IR ν: 3210, 2930, 1590, 1420, 1210, and 730 cm^{-1}].

Hydrolysis of 18 to 3. An aqueous AcOH solution (3 cm^3) of **18** (100 mg) was heated at 100 °C for 5 h. The same work up as above yielded **3** [62 mg; 100%].

Acetolysis of 3,7-Dibromotropolone (19) to 2,3,7-Triacetoxytropone (22). An ATA solution (10 cm^3) of **19** (117.4 mg) and NaOAc (168 mg) was similarly heated in a sealed tube at 100 °C for 4 d. The mixture was then heated in vacuo to

remove the volatile material and the residue was chromatographed on a silica-gel column to give **22** [a pale yellow oil, 107.9 mg; 92%. Found: m/z[35] 280.0551 (M^+). Calcd for $C_{13}H_{12}O_7$: M, 280.0581. ^{1}H NMR δ=2.30 (6H, s), 2.32 (3H, s), and 6.9—7.2 (3H, m). ^{13}C NMR δ=20.3, 20.5 (2C), 128.8, 129.2 (2C), 154.4 (2C), 166.9 (2C), and 167.8 (3C). IR ν: 1770, 1740, 1600, 1370, 1150, 1010, and 875 cm^{-1}].

Acetolysis of 3-Chloro-5-hydroxytropolone (20) to 2,4,7-Triacetoxytropone (23). An ATA solution (10 cm^3) of **20** (50 mg) was similarly heated in a sealed tube at 90 °C for 7 h. The mixture was then heated to remove the solvent and the residue was chromatographed on a silica-gel column to give **23** [colorless crystals, mp 110—111 °C (lit,[21,22] 111—112 °C), 61 mg; 75%. ^{1}H NMR δ=2.26 (3H, s), 2.31 (6H, s), 6.84 (1H, dd, J=10.5, 2.5 Hz), 7.12 (1H, d, J=2.5 Hz), and 7.21 (1H, d, J=10.5 Hz). ^{13}C NMR δ=20.4 (2C), 20.6, 122.8, 127.6, 127.8, 151.9, 155.8, 158.5, 167.3, 167.6 (2C), and 168.3].

Acetolysis of 4-Chloro-5-hydroxytropolone (21) to 2,4,5-Triacetoxytropone (24). An ATA solution (2 cm^3) of **21** (120 mg) was heated in a sealed tube at 80 °C for 4 h. The mixture was then heated to remove the solvent and the residue was chromatographed on a silica-gel column to give **24** [colorless needles, mp 126.5—128 °C, 130 mg; 67%. Found: C, 55.69; H, 4.31%. Calcd for $C_{13}H_{12}O_7$: C, 55.72; H, 4.32%. ^{1}H NMR δ=2.26 (6H, s), 2.32 (3H, s), 6.89 (1H, d, J=11.5 Hz), 7.06 (1H, s), and 7.11 (1H, d, J=11.5 Hz). ^{13}C NMR δ=20.4, 20.6, 20.8, 121.9, 123.5, 129.9, 146.5, 153.6, 153.8, 166.1, 167.2, 167.5, and 167.8. IR ν: 3050, 1770, 1595, 1370, 1070 and 910 cm^{-1}. UV λ_{max}^{MeOH}: 235 nm (ε=24400), 280 (6800), 318 (8400), and 384 (2000, sh)].

Hydrolysis of 22 to 3,4-Dihydroxytropolone (25). An aqueous AcOH solution (50%, 2 cm^3) of **22** (40.7 mg) was heated at 100 °C for 7 h. After cooling the solution to room temperature, the separated crystals were collected by filtration to give **25** [colorless plates, mp 230 °C (decomp) (lit,[3] mp 237—238 °C), 19.4 mg; 87%. ^{1}H NMR (CD_3OD) δ=7.04 (3H, s). ^{13}C NMR (CD_3OD) δ=119.3 (2C), 129.4, 158.4 (2C), and 159.1 (2C)].

Hydrolysis of 23 to 3,5-Dihydroxytropolone (26). An aqueous AcOH solution (50%, 6 cm^3) of **23** (61 mg) was heated at 100 °C for 24 h. After cooling, the mixture was heated in vacuo to remove the volatile material, and the residue was recrystallized from MeOH and AcOEt to give **26** [colorless crystals, mp 219—222 °C (lit,[20] 223—224 °C, 30 mg; 97%. ^{1}H NMR (CD_3OD) δ=6.93 (1H, s), 6.99 (1H, d, J=12 Hz), and 7.31 (1H, d, J=12 Hz). ^{13}C NMR (CD_3OD) δ=116.4, 116.7 (2C), 126.5, 127.9, 156.4, and 167.7.].

Hydrolysis of 24 to 4,5-Dihydroxytropolone (27). An aqueous AcOH solution (50%, 6 cm^3) of **24** (130 mg) was heated at 100 °C for 24 h. After evaporation of the mixture in vacuo, the residue was washed with AcOEt and recrystallized from MeOH and AcOEt to give **27** [pale yellow needles, mp 285—289 °C. 70 mg; 99%. Found: C, 54.48; H, 3.93%. Calcd for $C_7H_6O_4$: C, 54.54; H, 3.93%. ^{1}H NMR (CD_3OD) δ=6.92 (2H, s) and 7.04 (1H, s). ^{13}C NMR (CD_3OD) δ=116.2 (2C), 126.3, 156.0 (2C), and 167.5 (2C). IR ν: 3250, 2950, 1405, 1210, and 1090 cm^{-1}].

Acetolysis of 2-Bromo-4-chloro-5-hydroxytropone (28). a) An ATA solution (50 cm^3) of **28** (703 mg) was heated in a sealed tube at 85 °C for 15 h. The mixture was then heated in vacuo to remove the volatile material, and the residue was chromatographed on a silica-gel column to give [29] [colorless prisms, mp 127—128.5 °C, 86 mg; 10%. Found: C, 55.87; H, 4.32%. Calcd for $C_{13}H_{12}O_7$: C, 55.72; H, 4.32%. ^{1}H NMR δ=2.01 (3H, s), 2.08 (3H, s), 2.29 (3H, s), 6.42 (1H, d, J=10 Hz), 6.82 (1H, s), and 6.96 (1H, d, J=10 Hz). ^{13}C NMR δ=20.6, 21.5, 24.0, 103.8, 115.0, 124.4, 124.8, 152.9, 153.6, 156.8, 167.3, 168.6, and 176.0. IR ν: 1765, 1595, 1440, 1200, 1115, and 945 cm^{-1}. UV λ_{max}^{MeOH}: 240 nm (ε=26600), 258 (18100, sh), 310 (7500, sh), and 320 (8150)], **24** [380 mg; 45%], and **30** [colorless crystals, mp 131.5—132.5 °C, 37 mg; 5%. Found: C, 55.31; H, 4.31%. Calcd for $C_{11}H_{10}O_6$: C, 55.46; H, 4.23%. ^{1}H NMR δ=2.23 (6H, s), 6.93 (1H, s), and 7.02 (2H, s). ^{13}C NMR δ=20.6 (2C), 122.3, 124.6 (2C), 155.0 (2C), and 166—172 (4C). IR ν: 3600—3300, 1765, 1750, 1555, 1535, 1155 and 910 cm^{-1}. UV λ_{max}^{MeOH}: 252 nm (ε=30400), 263 (27000, sh), 332 (8200), and 367 (6700, sh)].

b) A similar treatment of **28** (50 mg) in an ATA solution (5 cm^3) at 85 °C for 10 h gave **24** [23 mg; 39%] and **31** [colorless crystals, mp 131—132.5 °C, 11 mg; 22%. Found: C, 55.18; H, 4.17%. Calcd for $C_{11}H_{10}O_6$: C, 55.46; H, 4.23%. ^{1}H NMR δ=2.27 (3H, s), 2.29 (3H, s), 6.88 (1H, d, J=11.2 Hz), 6.91 (1H, s), and 7.10 (1H, d, J=11.2 Hz). IR ν: 3050, 1770, 1560, 1370, 1155, and 915 cm^{-1}. UV λ_{max}^{MeOH}: 252 nm (ε=29100), 337 (7200), 358 (6700, sh), and 371 (5500, sh)].

Hydrolysis of 29 to 26. Similarly, an aqueous AcOH solution (6 cm^3) of **29** (86 mg) was heated at 100 °C for 4 h to yield **26** [45 mg; 96%], whose identity with the authentic **26** was confirmed by direct comparisons.

Bromination of Hinokitiol (32).[25] An AcOH solution (50 cm^3) of **32** (1.20 g) was treated with Br_2 (3.2 g) dissolved in AcOH (32 cm^3) at 5 °C. The mixture was then heated at 95 °C for 3 h and kept for further 15 h at room temperature. After removal of the solvent in vacuo, the residue was acetylated with Ac_2O (2 cm^3) by heating at 100 °C for 4 h. After evaporation of the solvent, the residue was chromatographed on a silica-gel column to give **34** [a yellow oil, 1.25 g; 47%. Found: C, 39.40; H, 3.32%. Calcd for $C_{12}H_{12}O_3Br_2$: C, 39.59; H, 3.32%. ^{1}H NMR δ=1.21 (6H, d, J=7 Hz), 2.34 (3H, s), 3.53 (1H, sept, J=7 Hz), 7.13 (1H, s), and 8.59 (1H, s). ^{13}C NMR δ=20.6, 21.6 (2C), 38.4, 126.4, 137.0, 144.9 (2C), 150.8, 153.7, and 167.9 (2C). IR ν: 2980, 1780, 1630, 1470, 1370, 1175, 1115, and 755 cm^{-1}. UV λ_{max}^{MeOH}: 241 nm (ε=16600), 259 (24000), 264 (23400, sh), 340 (10600), and 416 (1450)], **36** [colorless crystals, mp 99—101.5 °C, 625 mg; 30%. Found: C, 50.94; H, 3.93%. Calcd for $C_{12}H_{11}O_3Br$: C, 50.91; H, 3.92%. ^{1}H NMR δ=2.13 (3H, dd, J=1.5, 0.5 Hz), 2.35 (3H, s), 5.33 (1H, q, J=1.5 Hz), 5.42 (1H, br s), 6.91 (1H, dd, J=10.5, 2 Hz), 7.45 (1H, d, J=2 Hz), and 8.12 (1H, d, J=10.5 Hz). ^{13}C NMR δ=20.6, 21.8, 118.7, 127.6, 128.0, 139.1, 139.9, 143.8, 146.0, 155.2, 168.3, and 171.7. IR ν: 3600—3300, 1770, 1610, 1500, 1375, 1200, 1090, 920, and 860 cm^{-1}. UV λ_{max}^{MeOH}: 241 nm (ε=12300), 247 (16300), 256 (15800, sh), 345 (12300), 358 (10500, sh), and 377 (4850, sh)], and **37** [a yellow oil, 149 mg; 7%. Found: m/z 284.0106 and 286.0071 (M^+). Calcd for $C_{12}H_{13}O_3Br$: M, 284.0048 and 286.0028. ^{1}H NMR δ=1.24 (6H, d, J=7 Hz), 2.36 (3H, s), 2.82 (1H, sept, J=7 Hz), 6.76 (1H, dd, J=10, 1.5 Hz), 7.19 (1H, d, J=1.5 Hz), 8.04 (1H, d, J=10 Hz). ^{13}C NMR δ=20.7, 22.9 (2C), 38.1, 128.2, 130.1, 138.3, 140.1, 154.4, 157.7, and 168.3 (2C). IR ν: 2930, 1775, 1605, 1365, 1190, 1160, and 1080 cm^{-1}. UV λ_{max}^{MeOH}: 226 nm (ε=14500), 248 (20200), 254 (18900, sh), and 331 (9100)].

Bromination of γ-Thujaplicin (33).[26] An AcOH solution (40 cm^3) of **33** (0.80 g) was similarly treated with Br_2 (2.2 g) in AcOH (22 cm^3) at 5 °C. The mixture was then heated at 95 °C for 3 h. After the removal of the volatile materials in

vacuo, the residue was treated with Ac_2O at 100 °C for 4 h. The mixture was then heated again in vacuo to remove the solvent, and the residue was chromatographed on a silica-gel column to give **35** [pale yellow crystals, mp 60—64 °C, 669 mg; 38%. Found: C, 39.80; H, 3.44%. Calcd for $C_{12}H_{12}O_3Br_2$: C, 39.59; H, 3.32%. ^{1}H NMR δ=1.25 (6H, d, J=7 Hz), 2.36 (3H, s), 2.79 (1H, sept, J=7 Hz), and 7.67 (2H, s). ^{13}C NMR δ=20.5, 22.9 (2C), 38.2, 135.2 (2C), 137.6 (2C), 149.9, and 167.0 (3C). IR ν: 3600—3300, 2960, 1770, 1610, 1590, 1175, 1130, 1090, and 810 cm^{-1}. UV λ_{max}^{MeOH}: 259 nm (ε=27000), 265 (26800), and 329 (7800)] and **38** [a yellow oil, 100 mg; 6%. Found: m/z 284.0137 and 286.0007 (M^+). Calcd for $C_{12}H_{13}O_3Br$: M, 284.0048 and 286.0028. ^{1}H NMR δ=1.25 (6H, d, J=7 Hz), 2.35 (3H, s), 2.83 (1H, sept, J=7 Hz), 6.92 (1H, d, J=10.5 Hz), 7.18 (1H, d, J=10.5 Hz), and 8.04 (1H, s). ^{13}C NMR δ=20.6, 23.1 (2C), 38.1, 129.1, 129.8, 135.8, 140.7, 152.8, and 168.4 (3C). IR ν: 2930, 1770, 1695, 1590, 1365, and 1175 cm^{-1}. UV λ_{max}^{MeOH}: 228 nm (ε=13000), 250 (21700), and 330 (8900)]. Several other products were detected on TLC, but no further fractionation was carried out.[27]

Acetolysis of 2-Acetoxy-5,7-dibromo-4-isopropyltropone (34). An ATA solution (50 cm^3) of **34** (1.157 g) was heated in an autoclave at 100 °C for 3 d. Then, the solvent was removed in vacuo, and the residue was chromatographed on a silica-gel column to give **39** [colorless crystals, mp 122—123 °C, 538 mg; 53%. Found: C, 59.71; H, 5.59%. Calcd for $C_{16}H_{18}O_7$: C, 59.62; H, 5.63%. ^{1}H NMR δ=1.18 (6H, d, J=7 Hz), 2.31 (6H, s), 2.33 (3H, s), 3.14 (1H, sept, J=7 Hz), 7.07 (1H, s), and 7.25 (1H, s). ^{13}C NMR δ=20.5 (3C), 22.0 (2C), 29.8, 127.7, 128.5, 142.3, 147.6, I55.1, 155.8, 167.9, 168.2, and 169.0 (2C). IR ν: 1765, 1630, 1600, 1510, 1370, 1200, 1125, 1050 and 940 cm^{-1}. UV λ_{max}^{MeOH}: 236 nm (ε=27100), 325 (9750), and 396 (390)].

Acetolysis of 2-Acetoxy-3,7-dibromo-5-isopropyltropone (35). An ATA solution (30 cm^3) of **35** (413 mg) was heated in an autoclave at 100 °C for 3 d. The mixture was then heated in vacuo to remove the solvent and the residue was chromatographed on a silica-gel column to give **40** [colorless crystals, mp 91—93 °C, 73 mg; 20%. Found: C, 59.36; H, 5.61%. Calcd for $C_{16}H_{18}O_7$: C, 59.62; H, 5.63%. MS m/z 322 (M^+). ^{1}H NMR δ=1.24 (6H, d, J=7 Hz), 2.30 (9H, s), 2.80 (1H, sept, J=7 Hz), and 6.97 (2H, s). ^{13}C NMR δ=20.4, 20.6 (2C), 22.8 (2C), 38.4, 128.0 (2C), 150.5, 154.1 (2C), 167.0 (2C), and 167.9 (3C). IR ν: 1780, 1610, 1375, 1200, 1165, and 1020 cm^{-1}. UV λ_{max}^{MeOH}: 238 nm (ε=26800), 322 (8400), and 391 (520, sh)] and **41** [colorless needles, mp 182—184 °C, 40 mg; 10%. Found: C, 59.35; H, 5.56%. Calcd for $C_{18}H_{20}O_8$: C, 59.33; H, 5.53%. ^{1}H NMR δ=1.45 (6H, s), 2.05 (3H, s), 2.31 (9H, s), and 6.92 (2H, s) ^{13}C NMR δ=20.4, 20.6 (2C), 24.7 (2C), 26.0, 55.5, 127.3 (2C), 145.5, 152.4, 153.5, 166.9 (2C), 167.8 (3C), and 208.8. IR ν: 3500—3300, 1775, 1710, 1605, 1365, 1200, 1160, and 1020 cm^{-1}. UV λ_{max}^{MeOH}: 240 nm (ε=26000), 321 (8000), and 400 (400)].

Acylation of 40 to 41. An ATA solution (3 cm^3) of **40** (50 mg) was heated at 100 °C for 3 d. After evaporation of the solvent in vacuo, the residue was chromatographed on a silica-gel column to give, after elution of the recovered **40** [19 mg; 38%], **41** [11 mg; 31%] whose identity with the authentic sample was confirmed by direct comparisons.

Acylation of 2-Methoxy-4-isopropyltropone (42). An ATA solution (7 cm^3) of **42** (57 mg) was heated in an autoclave at 95 °C for 2 d. A similar workup afforded **43** [a yellow oil, 11 mg; 14%. Found: m/z 248.1005 (M^+). Calcd for $C_{14}H_{16}O_4$: M, 248.1048. ^{1}H NMR δ=1.83 (6H, s), 2.01 (3H, s), 2.33 (3H, s), 6.7—7.2 (3H, m), and 7.13 (1H, d, J=0.5 Hz). ^{13}C NMR δ=20.7, 24.8 (2C), 25.9, 55.8, 131.7, 132.5 (2C), 133.4, 151.0, 168.4 (3C), and 209.5. IR ν: 2950, 1770, 1715, 1605, 1365, 1195, and 1145 cm^{-1}. UV λ_{max}^{MeOH}: 233 nm (ε=19000), 316 (6660), and 442 (790)].

Acetolysis of 4,6-Dichloro-5-hydroxytropolone (44) to 45 with ATA. An ATA solution (4 cm^3) of **44** (152 mg) was heated in a sealed tube at 80 °C for 2 d. After removal of the solvent in vacuo, the residue was chromatographed on a silica-gel column to give **45** [colorless needles, mp 166—167 °C, 136 mg; 55%. Found: C, 53.43; H, 4.11%. Calcd for $C_{15}H_{14}O_9$: C, 53.26; H, 4.17%. ^{1}H NMR δ=2.27 (6H, s), 2.32 (6H, s), and 7.16 (2H, s). ^{13}C NMR δ=20.5 (4C), 126.4 (2C), 142.5 (2C), 155.2 (2C), 167.1 (2C), and 167.3 (3C). IR ν: 1775, 1600, 1500, 1360, 1135, 1100, and 935 cm^{-1}].

Acid Hydrolysis of 45 to 46. An aqueous AcOH solution (33%, 9 cm^3) of **45** (150 mg) was heated at 100 °C for 4 h. The mixture was then heated in vacuo to remove the solvent, and the residue was washed with AcOEt to obtain insoluble product, **46** [pale yellow needles, mp 269—271 °C (decomp), 60 mg; 80%. Found: C, 49.12; H, 3.59%. Calcd for $C_7H_6O_5$: C, 49.42; H, 3.56%. ^{1}H NMR (CD_3OD) δ=6.98 (2H, s). ^{13}C NMR (CD_3OD) δ=112.0 (2C), 158.1 (2C), and 158.4 (3C). IR ν: 3600—3200, 1395, 1365, 1190, and 900 cm^{-1}. UV λ_{max}^{MeOH}: 256 nm (ε=25600), 281 (3700, sh), 332 (5400, sh), 353 (6500), and 329 (2900, sh)].

Acetolysis of 3,5,7-Tribromotropolone (47) to 48. a) An ATA solution (4 cm^3) of **47** (500 mg) was sealed in a pressure bottle and heated at 100 °C for 2 d. After cooling the mixture to room temperature, volatile materials were evaporated in vacuo, and the residue was chromatographed on a silica-gel column to give **48** [colorless needles, mp 133—134 °C, 326 mg; 70%. Found: C, 52.99; H, 4.13%. Calcd for $C_{15}H_{14}O_9$: C, 53.25; H, 4.18%. ^{1}H NMR δ=2.28 (3H, s), 2.31 (6H, s), 2.32 (3H, s), and 6.95 (2H, s). ^{13}C NMR δ=20.2, 20.5 (2C), 20.8, 124.0 (2C), 150.0, 153.4 (2C), 166.5, 167.2 (3C), and 168.2 (2C). IR ν: 3050, 1770, 1605, 1515, 1375, 1360, and 1020 cm^{-1}. UV λ_{max}^{MeOH}: 222 nm (ε=19500), 238 (29100), 280 (4600), and 322 (8500)].

b) Similarly, an ATA solution (16 cm^3) of **47** (500 mg) and NaOAc (330 mg) was heated at 110 °C for 2 d. The mixture was then heated in vacuo to remove the solvent and the residue was chromatographed on a silica-gel column to give **48** [356 mg; 76%].

Acid Hydrolysis of 2,3,5,7-Tetraacetoxytropone (48) to 49. An aqueous AcOH solution (50%, 5 cm^3) of **48** (326 mg) was heated at 100 °C for 24 h. After evaporation in vacuo, the mixture was washed with AcOEt, and the residue was collected by filtration to give **49** [pale yellow crystals, mp 263—266 °C (decomp), 164 mg; 100%. Found: C, 49.13; H, 3.55%. Calcd for $C_7H_6O_5$: C, 49.42; H, 3.56%. ^{1}H NMR (CD_3OD) δ=6.63 (2H, s). ^{13}C NMR (CD_3OD) δ=107.8 (2C), 151.5, 161.9 (2C), and 163.0 (2C). IR ν: 3370, 3300, 1580, 1480, 1400, 1010, and 850 cm^{-1}].

Bromination of 4-Hydroxytropolone (3) to 3,5,7-Tribromo-4-hydroxytropolone (50). An AcOH solution (13 cm^3) of **3** (440 mg), NaOAc (780 mg) was treated with bromine (1550 mg) in AcOH (15.5 cm^3) at 5 °C. The mixture was then heated at 95 °C for 1.5 h, and the mixture was heated in vacuo to remove the solvent. The residue was extracted with $CHCl_3$ and the organic extract was evaporated in vacuo to leave a crude product which was purified by recrystalliza-

tions from MeOH to yield **50** [pale green needles, mp 149—151 °C (lit,[7] 151 °C), 1.102 g; 92%. ^{1}H NMR (CD_3OD) δ=8.39 (1H, s). ^{13}C NMR (CD_3OD) δ=112.6, 113.8, 118.6, 142.9, 160.4, 161.5, and 167.3. IR ν: 3330, 1600, 1350, 1260, 1170, 1110, and 795 cm^{-1}].

Acetolysis of 3,5,7-Tribromo-4-hydroxytropolone (50) to 6. An ATA solution (50 cm^3) of **50** (343 mg) was heated in an autoclave at 85 °C for 9 h. The mixture was evaporated in vacuo to remove the solvent and the residue was chromatographed on a silica-gel column to give **6** [colorless crystals, mp 183.5—185 °C, 39 mg; 11%. Found: C, 51.28; H, 3.95%. Calcd for $C_{17}H_{16}O_{11}$: C, 51.52; H, 4.07%. ^{1}H NMR δ=2.28 (6H, s), 2.30 (9H, s), and 6.95 (1H, s). ^{13}C NMR (DMF-d_7) δ=20.1, 20.4, 123.5, 123.8, 147.4, 167.5, 167.7, and 168.6. IR ν: 1780, 1600, 1365, 1180, and 995 cm^{-1}. UV λ_{max}^{MeOH}: 218 nm (ε=18000), 240 (29900), 292 (6500), and 319 (7800)] together with a mixture of 2,4-diacetoxy-3,5,7-tribromotropone and a tetraacetoxybromotropone [283 mg].

Acetolysis of 50 to 45 and 6 in the Presence of NaOAc. An ATA solution (15 cm^3) of **50** (150 mg) and NaOAc (99 mg) was heated in an autoclave at 125 °C for 2 d. The solvent was then removed by heating the mixture in vacuo and the residue was chromatographed on a silica-gel column to give, from hexane-AcOEt (1 : 1), **45** [81 mg; 60%], identical with the authentic sample, and **6** [18 mg; 11%].

Acid Hydrolysis of 6. An aqueous AcOH solution (60%, 5 cm^3) of **6** (129 mg) was heated at 100 °C for 5 h. After removal of the solvent, the residue was recrystallized from MeOH-AcOEt to give **51** [brown crystals, mp>300 °C (decomp), 59 mg; 97%. Found: C, 44.78; H, 3.32%; m/z, 186.0158 (M$^+$). Calcd for $C_7H_6O_6$: C, 45.17; H, 3.25%; M, 186.0163. ^{1}H NMR (DMF-d_7) δ=6.77 (1H, s). ^{13}C NMR (DMF-d_7) δ=104.9, 142.0 (2C), 150.3 (2C), and 154.3 (2C). IR ν: 3510, 3400—3000, 1600, 1380, 1305, 1205, and 1030 cm^{-1}. UV λ_{max}^{MeOH}: 268 nm (ε=31500), 317 (2800, sh), 332 (3500, sh), 340 (3600, sh), and 360 (3000, sh)].

Bromination of 2,4,5,7-Tetraacetoxytropone (45) to 4,5,6-Triacetoxy-3,7-dibromotropolone (54). A $CHCl_3$ solution of **45** (90 mg) was treated with Br_2 (100 mg) in $CHCl_3$ (1 cm^3) at room temperature. Then, the mixture was heated at 60 °C for 4 h, and the mixture was heated in vacuo to remove the solvent, and the residue was acetylated with Ac_2O (2 cm^3) at 110 °C for 6 h. After removal of the solvent in vacuo, the residue was chromatographed on a silica-gel column to give **54** [a yellow oil, 28 mg; 53%. Found: C, 34.23; H, 2.34%; Calcd for $C_{13}H_{10}O_8Br_2$: C, 34.39; H, 2.22%. ^{1}H NMR δ=2.33 (9H, s). ^{13}C NMR δ=20.4 (2C), 166.0, and 166.2. IR ν: 3600—3300, 1790, 1610, 1375, 1165, 1010, and 960 cm^{-1}. UV λ_{max}^{MeOH}: 212 nm (ε=9900), 250 (20200, sh), 259 (23200, sh), 266 (22800, sh), 341 (6700), and 419 (800)] together with the recovered **45** [51 mg; 57%].

Bromination of 2,3,5,7-Tetraacetoxytropone (48) to 2,3,5,7-Tetraacetoxy-4,6-dibromotropone (52) and 3,4,5,6-Tetraacetoxy-2,7-dibromotropone (53). A $CHCl_3$ solution (25 cm^3) of **48** (356 mg) was treated with Br_2 (400 mg) in $CHCl_3$ (4 cm^3) at room temperature. The mixture was then heated to 60 °C for 4 h, and evaporated to remove the solvent. The residue was acetylated by Ac_2O (2 cm^3) at 95 °C for 6 h, and again evaporated in vacuo. The residue was chromatographed on a silica-gel column to give **52** [colorless needles, mp 140.5—142.5 °C, 342 mg; 66%. Found: C, 36.55; H, 2.55%. Calcd for $C_{15}H_{12}O_9Br_2$: C, 36.32; H, 2.44%. MS m/z 495 (M$^+$+1), 410, 368, 330, 328, 326 (1 : 2 : 1), 298. ^{1}H NMR δ=2.30 (3H, s), 2.32 (6H, s), and 2.37 (3H, s). ^{13}C NMR δ=20.2, 20.3 (2C), 20.7, 166.1, and 166.3. IR ν: 3600—3300, 1795, 1625, 1375, 1285, 1170, 1035, and 900 cm^{-1}. UV λ_{max}^{MeOH}: 257 nm (ε=25800) and 335 (7700)], and **53** [colorless crystals, mp 145—147 °C, 60 mg; 11%. Found: C, 36.18; H, 2.57%. ^{1}H NMR δ=2.27 (6H, s) and 2.33 (6H, s). ^{13}C NMR δ=20.0 (2C), 20.5 (2C), 130.6 (2C), 149.1 (4C), 165.8 (2C), and 166.1 (3C). IR ν: 1790, 1625, 1380, 1285, 1165, 1015, and 840 cm^{-1}. UV λ_{max}^{MeOH}: 232 nm (ε=16100), 268 (19300), and 332 (6900)].

Acetolysis of 2,3,5,7-Tetraacetoxy-4,6-dibromotropone (52). An ATA solution (15 cm^3) of **52** (311 mg) was sealed in an autoclave and heated at 100 °C for 5 d. After removal of the solvent in vacuo, the residue was chromatographed on a silica-gel column to give **6** [6.4 mg; 2.6%] and **7** [colorless crystals, mp 173—175 °C, 1.3 mg; 0.5%. Found: C, 50.16; H, 4.06%. Calcd for $C_{19}H_{18}O_{13}$: C, 50.23; H, 3.99%. (Calcd for $C_{17}H_{16}O_{12}$, as a pentaacetoxytropolone: C, 49.52; H, 3.91%). ^{1}H NMR δ=2.29 (18H, s). ^{13}C NMR δ=20.1 (6C) and 165.9 (6C). IR ν: 3600—3300, 1800, 1785, 1615, 1370, and 1175 cm^{-1}. MS m/z 412 (M$^+$−42), 370, 328, 286, 244, 202, and 176. UV λ_{max}^{MeOH}: 243 nm (ε=29700) and 320 (7300)].

Acetolysis of 52 in the Presence of NaOAc. Formation of 2,3,5,7-Tetraacetoxytropone (48) and Pentaacetoxytropone (6). An ATA solution (16 cm^3) of **52** (513 mg) and NaOAc (180 mg) was heated at 110 °C for 5 d. The mixture was then heated in vacuo to remove the solvent, and the residue was chromatographed on a silica-gel column to give **48** [168 mg; 48%] and **6** [49 mg; 12%].

Acetolysis of Octachlorocycloheptatriene (8). a) An ATA solution (15 cm^3) of NaOAc (200 mg) and **8** (200 mg) was sealed in a pressure bottle, and heated at 85 °C in an autoclave for 12 d. The solvent was then removed in vacuo, and the residue was chromatographed on a silica-gel column to give **56** [green needles, mp 128.5—130.5 °C, 20 mg; 10%. Found: C, 40.95; H, 2.64%. Calcd for $C_{13}H_9O_7Cl_3$: C, 40.71; H, 2.36%. ^{1}H NMR δ=2.09 (3H, s), 2.12 (3H, s), and 2.38 (3H, s). ^{13}C NMR δ=20.3, 21.6, 24.6, 111.9, 124.1 (2C), 134.8, 147.4, 148.9, 151.8, 166.1, 166.7, and 170.0. IR ν: 1780, 1595, 1360, 1170, 1120, and 995 cm^{-1}. UV λ_{max}^{MeOH}: 245 nm (ε=22100), 262 (31600), 271 (25500, sh), 328 (7200, sh), 340 (7800), 353 (6700, sh), and 372 (3500, sh)]. The rest of fractions were complex mixture of products, and no further fractionation was carried out.

b) An ATA solution (100 cm^3) of **8** (950 mg) and NaOAc (1.6 g) was sealed in a pressure bottle and heated in an autoclave at 130 °C for 5 d. The solvent was then removed in vacuo, and the residue was chromatographed on a silica-gel column to give **57** [20 mg; 2%. MS m/z 431 (M$^+$+1). ^{1}H NMR δ=2.31 (3H, s), 2.32 (6H, s), and 2.36 (6H, s). ^{13}C NMR δ=20.1 (5C) and 165.9 (5C). UV λ_{max}^{MeOH}: 248 nm (ε=22600), 278 (5400, sh), 295 (4900), and 325 (6100)], and a mixture consisted of pentaacetoxychlorotropone, triacetoxytrichlorotropones, and diacetoxytetrachlorotropones (ca. 70%).

c) An ATA solution (41 cm^3) of NaOAc (1.3 g) and **8** (750 mg) was heated similarly in an autoclave at 115 °C for 5 d, then 160 °C for 2 d. After removal of the solvent in vacuo, the residue was chromatographed on a silica-gel column to give **6** [23 mg; 3%], which was identical with the sample prepared from **50**, and **7** [colorless crystals, mp 173—175 °C, 6 mg; 0.6%.].

Acid Hydrolysis of Hexaacetoxytropone (7). An aqueous AcOH solution (50%, 4 cm^3) of **7** (3 mg) was heated at 95 °C

for 10 h. Removal of the volatile material left **55** [pale brown crystals, mp >300 °C, 1 mg; 75%. UV λ_{max}^{MeOH}: 226, 272, and 292 nm].

Bromination of 46 in AcOH. An AcOH solution (5 cm^3) of **46** (11 mg) and NaOAc (9 mg) was treated with Br_2 (20 mg) at room temperature. The mixture was then heated at 95 °C for 2 h, and evaporated the solvent in vacuo. The residue was extracted with $CHCl_3$, and again evaporated to give **58** [orange crystals, mp 222 °C (decomp) (lit,[33] mp 270 °C (decomp)), 16 mg; 83%. ^{13}C NMR (CD_3OD) δ=102.5 (2C) and 167.1 (4C). MS *m/z* 300, 298, 296 (M^+, 1:2:1)].

We wish to thank the Ministry of Education, Science and Culture for a financial assistance through the Grant-in-Aid for Scientific Research to A. M. (No. 60470025). We are also grateful to Mr. Kazushi Tomiyasu who prepared some of the starting materials.

References

1) J. H. Birkinshaw, A. R. Chambers, and H. Raistrick, *Biochem. J.*, **36**, 242 (1942); M. J. S. Dewar, *Nature (London)*, **155**, 50 (1945).

2) W. Segal, *Chem. Ind. (London)*, **1957**, 1040; K. Doi and Y. Kitahara, *Bull. Chem. Soc. Jpn.*, **31**, 794 (1958); G. L. Lange and P. de Mayo, *Chem. Commun.*, **1967**, 704.

3) J. H. Birkinshaw and H. Raistrick, *Biochem. J.*, **26**, 441 (1932); G. Barger and O. Dorrer, *ibid.*, **28**, 11 (1934); A. E. Oxford, H. Raistrick, and G. Smith, *Chem. Ind.*, **41**, 485 (1942); R. E. Corbett, C. H. Hassell, A. W. Johnson, and A. R. Todd, *J. Chem. Soc.*, **1950**, 1; R. E. Corbett, A. W. Johnson, and A. R. Todd, *ibid.*, **1950**, 6, 47; G. Aulin-Erdtman, *Acta Chem. Scand.*, **4**, 1031, 1325 (1950).

4) H. A. Kierst, G. G. Markoni, F. T. Counter, P. W. Ensminger, N. D. Jones, M. O. Chaney, J. E. Toth, and N. E. Allen, *J. Antibiotics*, **12**, 1651 (1982).

5) H. Takeshita, A. Mori, and T. Kusaba, *Synthesis*, **1986**, 578.

6) R. B. Johns, A. W. Johnson, and M. Tisler, *J. Chem. Soc.*, **1954**, 4605.

7) T. Nozoe and Y. Kitahara, *Proc. Jpn. Acad.*, **30**, 204 (1954); Y. Kitahara, *Sci. Repts. Tohoku Univ., Ser. I*, **39**, 258 (1956).

8) T. Nozoe, S. Seto, S. Itô, M. Sato, and T. Katono, *Sci. Repts. Tohoku Univ., Ser. I*, **37**, 191 (1953).

9) M. Oda and Y. Kitahara, *Tetrahedron Lett.*, **1969**, 3295.

10) K. Kusuda, N. Hara, and R. West, *Chem. Lett.*, **1982**, 1119.

11) T. Sato, *Nippon Kagaku Zasshi*, **80**, 1340 (1959); T. Nozoe, H. Takeshita, and K. Tajiri, *Bull. Chem. Soc. Jpn.*, **56**, 3679 (1983); H. Takeshita, A. Mori, H. Kondo, and K. Tajiri, *Kyushu Daigaku Seisan Kagaku Kenkyusho Hokoku*, **71**, 9 (1980).

12) S. Seto, *Sci. Repts. Tohoku Univ., Ser. I*, **37**, 275 (1953); T. Mukai, *Bull. Chem. Soc. Jpn.*, **31**, 846 (1958).

13) T. Nozoe, T. Asao, E. Takahashi, and K. Takahashi, *Bull. Chem. Soc. Jpn.*, **39**, 1310 (1966).

14) T. Sato, *Nippon Kagaku Kaishi*, **80**, 1171 (1959); K. Doi, *Bull. Chem. Soc. Jpn.*, **35**, 67 (1962); K. Takase, *ibid.*, **37**, 1298 (1964).

15) S. Masamune, A. V. Kemp-Jones, J. Green, D. L. Rabenstein, M. Yasunami, K. Takase, and T. Nozoe, *J. Chem. Soc., Chem. Commun.*, **1973**, 283.

16) H. Takeshita, A. Mori, H. Watanabe, T. Kusaba, S. Sugiyama, and M. Kodama, *Bull. Chem. Soc. Jpn.*, **60**, 4335 (1987).

17) During our kinetic studies on the acetoxytropones, we noticed that a thermal isomerization of *o*-diacetoxytropones to 1,3-dioxoles occurred gradually. The acetotropy was no longer operative in the latter molecule. This is also incompatible to the view that the 1,3-dioxole might be an intermediate of the acetoxyl migration.

18) T. Nozoe, S. Seto, Y. Kitahara, M. Kunori, and Y. Nakayama, *Proc. Jpn. Acad.*, **26** (7), 38 (1950); T. Nozoe, Y. Kitahara, K. Yamane, and Y. Yoshikoshi, *ibid.*, **27**, 18 (1951).

19) T. Kusaba, A. Mori, and H. Takeshita, *Bull. Chem. Soc. Jpn.*, **58**, 515 (1985)

20) M. Hirama and S. Itô, *Tetrahedron Lett.*, **1976**, 2339.

21) Y. Kitahara, *Sci. Repts. Tohoku Univ., Ser. I*, **39**, 275 (1956).

22) M. Hirama and S. Itô, *Chem. Lett.*, **1977**, 627.

23) Formations of these dioxoles, **18a** and **29a**, were supposed to be a secondary products due to a thermal elimination. Indeed, we frequently noticed an increasing of the peaks around δ=124 by heating. This means that the other vicinally diacetoxylated tropones may also form the dioxoles.

24) Between the two possibilities, **29a** is favored over **29b** on the basis of the chemical shift; the singlet signal ascribable to the C-2 proton at 6.82 was lower than estimated for that of 3-alkoxytropones.

25) S. Matsumoto, *Sci. Repts. Tohoku Univ., Ser. I*, **42**, 209 (1958).

26) T. Nozoe, S. Seto, K. Kikuchi, T. Mukai, S. Matsumoto, and M. Murase, *Proc. Jpn. Acad.*, **26**(7), 43 (1950).

27) In the latter case, 3,4-dibromo-5-isopropyltropolone was present among the product mixture. Its mechanism of formation may involve the heptafulvene intermediate of the acylation products.

28) M. Oda and Y. Kitahara, *Bull. Chem. Soc. Jpn.*, **44**, 296 (1970).

29) Chlorination of **48** gave 2,3,5,7-tetraacetoxy-4,6-dichlorotropone [^1H NMR δ=2.31 (3H, s), 2.34 (6H, s), and 2.39 (3H, s). ^{13}C NMR δ=20.2 (4C) and 166.3 (4C)], but its yield was only 14%.

30) Similar results were obtained in the acetolysis of **54**.

31) T. Yamatani, M. Yasunami, and K. Takase, *Tetrahedron Lett.*, **1970**, 1725.

32) H. Takeshita, T. Kusaba, and A. Mori, *Chem. Lett.*, **1982**, 701.

33) S. Kanda, *Nippon Kagaku Zasshi*, **83**, 635 (1962).

34) Sometimes, employment of a large quantity of ATA mixture with or without sodium acetate resulted in the improved acetolysate formation.

35) Some of hygroscopic compounds failed to obtain correct elemental analyses, but their homogeneity was ascertained by HPLC.

The Kinetic Evidence of the Concerted [1,9] Sigmatropy for the Acetyl Migration in the 2-Acetoxytropones. The NMR Spectral Analysis of the Seven-Fold Degenerated Acetotropy of Hexaacetoxytropone

Hitoshi TAKESHITA,* Akira MORI, Hiroyasu WATANABE,† Tomoyuki KUSABA,† Shigeru SUGIYAMA, and Mitsuaki KODAMA††

Institute of Advanced Material Study, 86, Kyushu University, Kasuga-koen, Kasuga, Fukuoka 816
†Graduate School of Engineering Sciences, 39, Kyushu University, Kasuga-koen, Kasuga, Fukuoka 816
††Pharmaceutical School of Tokushima Bunri University, Yamashirocho, Tokushima, 770

(Received May 11, 1987)

"The acetotropy" of 2-acetoxytropones was shown to be a concerted [1,9] sigmatropic process on the basis of a kinetic analysis. A little substituent effect for the activation free energy of the acetyl migration was recognized. Preferred tautomers of polyacetoxytropones were those having the carbonyl group at inner positions. As an extreme case, a "Merry-Go-Round"-type rearrangement was operative in hexaacetoxytropone.

Currently, we have developed a preparation method for polyacetoxytropones from polyhalotropones.[1] By this method, we have synthesized several polyacetoxytropones, including hexaacetoxytropone (**1**). The ^{1}H NMR of **1** revealed only one methyl signal in the ^{1}H NMR spectrum at room temperature, indicating the operation of a seven-fold symmetric degenerated [1,9] acetyl migration. This paper deals with a kinetic analysis with variable temperature ^{13}C NMR spectra of **1** and its related derivatives in order to ascertain the concerted nature of this rearrangement. The term, [1,9] sigmatropy, was first introduced in the literature by Harrison et al.[2] for a benzyl group migration in the isomerization of 2-benzyloxy-3-bromotropone to 2-benzyloxy-7-bromotropone.[3]

The acetyl migration in the 2-acetoxytropones was previously reported by Masamune et al.[4] and by Minkin et al.[5] Masamune et al. proposed an ionic mechanism which is assisted by the polarization of tropone carbonyl to form a delocalized 6π system in a seven-membered ring; however, at the same time, they inconsistently mentioned a small medium effect for the reaction rates. When we noticed a formation of the same thermolysates in the same product distribution[6] in the thermal homolytic rearrangement of 2-(2-furylmethoxy)-4-isopropyltropone and 2-(2-furylmethoxy)-6-isopropyltropone, we thought that prior to rearrangement, these ethers mutually isomerized via an electrocyclic process, a further example of the [1,9] alkyl shift process.[2] In view of the similarity, the acetotropy, the rearrangement of the acyl groups between two oxygens of C-1 and C-2 positions of tropolones, may well be concerted, too. Herein, we will show unequivocal evidence for the concerted mechanism of the acetotropy, that is the [1,9] sigmatropy.[7]

Chart 1.

Results and Discussion

Acetotropy of 2-Acetoxytropone and Its Acetoxy Derivatives. At first, the kinetics of the acetotropy of 2-acetoxytropone (**2**) were analyzed in order to make a comparison with the reported data.[4] Table 1 shows that both data were in accord within experimental error. Unexpectedly, 2,7-diacetoxytropone (**3**)[9] did not operate the acetotropy and its ^{1}H NMR signals retained their sharpness at a temperature between −50 and +100 °C, while 2,5-diacetoxytropone (**4**)[9] showed smooth acetotropy. Therefore, the acetyl migration is operative only between tautomers having the same degree of thermodynamic stability. In other words, in the case of **3**, a symmetrical 2,7-diacetoxy structure is much more stable than the unsymmetrical 2,3-diacetoxy structure. As will be shown in later, this applies to consecutively substituted polyacetoxytropones; the predominant tautomers in that category possess the carbonyl carbon as such having two adjacent acetoxyl groups (the "inner positions"). Further examples of acetotropy were obtained from 2-acetoxy-5-methoxytropone (**5**), 2-acetoxy-3,7-dibromo-5-isopropyltropone (**6**),[1] 2,3,7-triacetoxy-5-isopropyltropone (**7**),[1] 2,3,5,7-tetraacetoxytropone (**8**),[1] pentaacetoxytropone (**9**),[1] and 2,3,7-triacetoxy-5-(1,1-dimethyl-2-oxopropyl)tropone (**10**):[1] From the NMR spectros-

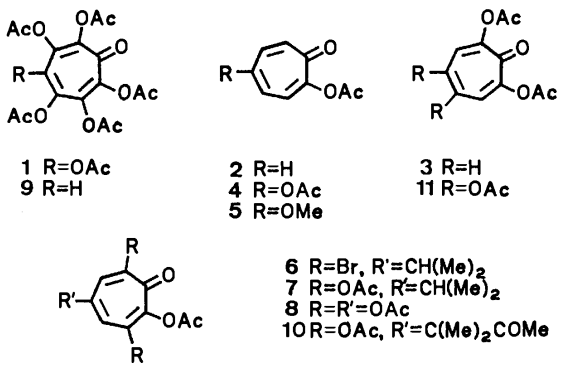

1 R=OAc
9 R=H

2 R=H
4 R=OAc
5 R=OMe

3 R=H
11 R=OAc

6 R=Br, R'=CH(Me)$_2$
7 R=OAc, R'=CH(Me)$_2$
8 R=R'=OAc
10 R=OAc, R'=C(Me)$_2$COMe

Chart 2.

copy, the acetotropy of **7** or **10** is operative only with an acetyl group between C-1 and C-2 oxygens, while **8** mainly exists as a tautomeric 1 : 1-mixture of **8b** and **8c**, and **9** was a mixture of **9b**, **9c**, **9d**, and **9e** (13 : 37 : 37 : 13). The absence of tautomers having the carbonyl carbon at the "outer position" in these polyacetoxytropones simplified the kinetic analyses. A notable case was that of 2,4,5,7-tetraacetoxytropone (**11**)[1] which showed no acetotropy at all.

Acetotropy of Hexaacetoxytropone. Now, it is noteworthy that **1**[1,10] exhibited a seven-fold symmetric, "Merry-Go-Round"-type degenerated acetotropy; at +50.2 °C, **1** exhibited only one methyl signal (20.05) and one carbonyl signal (167.47). However, the signals of tropone ring carbons were undetectable due to the broadenings by the chemical exchange. At −0.5 °C, these tropone ring signals were still undetectable, while the methyl signal (20.02) and the acetyl carbonyl signals (167.74 and 168.02) became broadened. At −15.4 °C, the spectrum changed to show three acetyl carbonyl signals (167.79, 168.03, and 168.35), three tropone ring signals (140.59, 145.61, and 149.17), and an unresolved methyl signal (20.14). At −60.1 °C, the exchange ceased; i.e., the methyls (20.13, 20.22, and 20.44), tropone ring signals (140.91, 146.17, and 149.45), the tropone carbonyl (169.00), and acetyl carbonyl signals (168.56, 168.82, and 169.18).

Kinetic Analyses of the Acetotropy. The kinetic data of these acetoxytropones are compiled in Table 1. In all cases, the activation free energies ($\Delta G^{\neq}$) were not much different, in spite of the different polarity and electronic effect of the substituents and different solvent polarity. Should an ionic intermediate be involved, the $\Delta G^{\neq}$ must become smaller to large extent by increasing the number of electron-releasing acetoxyl groups, and even by the polarity of the solvents. Consequently, the figures obtained by the present experiments were not consistent with an ionic mechanism. Previously, Harrison et al. proposed that the

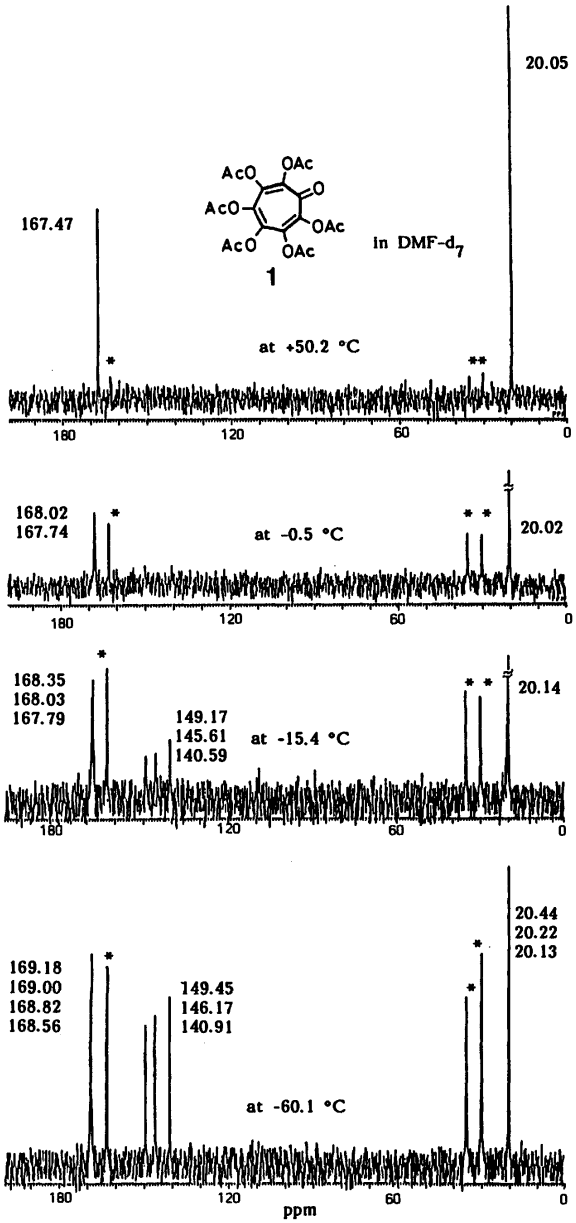

Fig. 1.

Table 1. Kinetic Data of Acetotropy of Several Acetoxytropones

Compd.		$\Delta H^{\neq}$/kJ mol^{-1}	$\Delta S^{\neq}$/J mol^{-1} K^{-1}	$\Delta G^{\neq}_{298}$/kJ mol^{-1}	r[a]
I: **2**	b)	42.6±2.5	−15.5±8.8	47.2±5.0	0.998
	c)	34.3±2.1	−42.2±7.5	46.4±4.2	0.997
	d)	(45.1)	(−8.3)	(47.7)	
6	b)	48.1±4.2	−8±16	50.2±8.8	0.994
7	b)	51.0±5.4	−11±20	54±12	0.991
10	b)	53.1±8.4	−4±31	54±18	0.981
	c)	40.5±5.0	−43±18	53±11	0.985
II: **1**	b)	41.0±6.3	−35±28	51±15	0.988
4	b)	39.3±2.5	−41.8±7.9	51.8±5.0	0.998
	c)	37.2±2.1	−43.5±7.1	50.2±4.2	0.998
5	b)	37.6±2.5	−54±11	53.5±5.4	0.996
	c)	40.1±1.7	−47.7±6.3	53.5±5.4	0.998
8	b)	39.3±3.8	−59±14	56.8±7.9	0.989
	c)	38.0±2.0	−57.3±7.9	54.8±4.2	0.995
9	b)	44.7±7.9	−35±28	55±16	0.975

a) Correlation coefficient of Eyring plot. b) Measured in DMF-d_7. c) Measured in $CDCl_3$. d) Ref. 4.

Equilibrium of Polyacetoxytropones

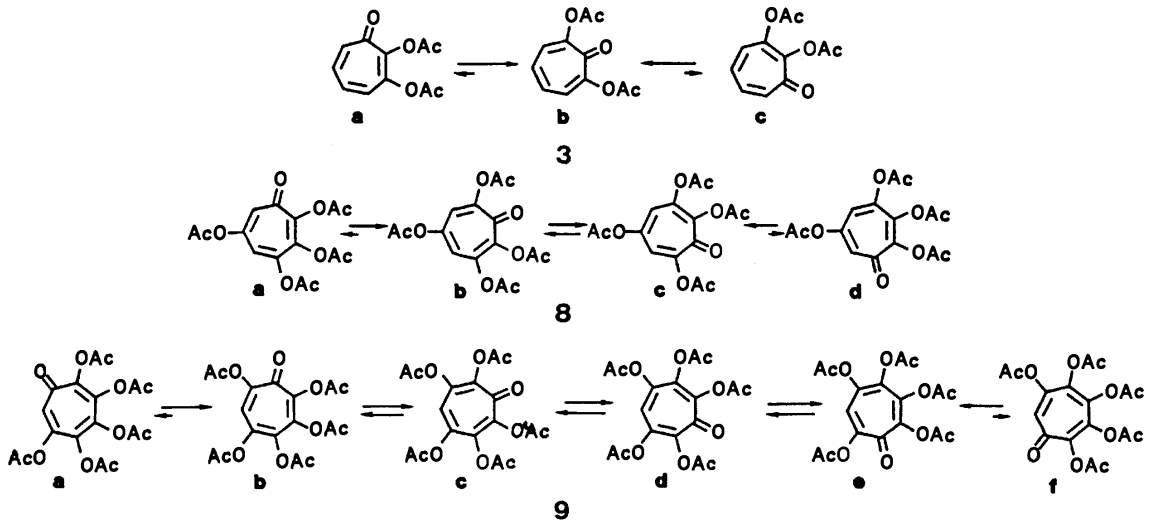

Scheme 1.

acetotropy of 2-acetoxytropones proceeds via an ionic intermediate in view of its small $\Delta G^{\neq}$;[2] however, their proposal seems to lack a sound basis. The figures of $\Delta G^{\neq}$ for [1,5] sigmatropies determined to date are in very wide range (27 to 210 kJ mol^{-1}),[11] and no definite conclusion should be drawn only from the $\Delta G^{\neq}$.

On the other hand, the activation entropies ($\Delta S^{\neq}$) should provide available information; the negative and small $\Delta S^{\neq}$ for the present acetotropies are in the range of many precedent figures of [1,5] sigmatropies;[11] also, the migration of the acetyl group must proceed via a concerted mechanism, i.e., [1,9] sigmatropy, but not via a radical mechanism which should show the positive $\Delta S^{\neq}$.

Further, an introduction of the oxygen functions into 5-position made the $\Delta S^{\neq}$ significantly larger negative in DMF (ε=36.7); if one looks at **2** and **4**, which showed most reliable parameters, $\Delta S^{\neq}$ are −16 J mol^{-1} K^{-1} for the former and −42 J mol^{-1} K^{-1} for the latter. Unfortunately, errors for other substrates are quite large, and it is not suitable for intensive discussions. However, if each compound could be classified as in Table 1, a very interesting tendency would be noticed. An average $\Delta S^{\neq}$ of **2**, **6**, **7**, and **10** (Group I) is −9 J mol^{-1} K^{-1}, the other hand, −45 J mol^{-1} K^{-1} in the case of other derivatives (Group II). All 2-acetoxytropones have the large negative $\Delta S^{\neq}$ (−42 to −57 J mol^{-1} K^{-1}) in chloroform (ε=4.70). This means that as far as the 2-acetoxytropones concern, the transition state of the acetotropy is less polar than the initial state. Particularly, the initial state of Group II compounds is less polar and less solvated than the initial state of Group I derivatives. The same classification might be true for $\Delta H^{\neq}$, owing to the results of compensation effect between $\Delta S^{\neq}$ and $\Delta H^{\neq}$.

Namely, polarized 6π contribution stabilizes the initial state in respect of tight solvation, but does not stabilize the transition state; therefore, polarized carbonyl oxygen does not assist but retard the rearrangement. This invalidates the Masamune's mechanism.

It will be interesting to compare these kinetic features to those of the isomerization of 2-benzyloxy-3-bromotropone to 2-benzyloxy-7-bromotropone, for which, we have recently established the concerted nature, the [1,9] sigmatropy, by an intensive high-pressure kinetic analysis.[3] Namely, in that rearrangement, the $\Delta S^{\neq}$, (−47 and −92 J mol^{-1} K^{-1} in isopropylbenzene (IP, ε=2.4) and 1-hexanol (ε=13.3), respectively), showed a weak, but not negligible, polarized contribution at the transition state. The value of $\Delta S^{\neq}$ of the present acetotropy in less polar chloroform is in the same range with the $\Delta S^{\neq}$ of that [1,9] sigmatropy in IP. These similarities did not contradict the view of a concerted mechanism for the acetotropy, i.e., the [1,9] sigmatropy. However, the $\Delta S^{\neq}$ in polar solvents were considerably different; $\Delta S^{\neq}$ of that benzyl migration (−92 J mol^{-1} K^{-1}) was more negative than the $\Delta S^{\neq}$ of the present acetotropy (−9 J mol^{-1} K^{-1}). The difference is surely attributable to a solvation effect in the transition states for the former and the initial states for the latter.[3]

All the findings supported the rearrangement of the acetyl group in the 2-acetoxytropones being the [1,9] sigmatropy, which could not be expected in benzenoid derivatives such as 2-acetoxybenzaldehyde.

Experimental

The compounds studied in this paper were prepared by means of reported procedures as indicated, except for 2-acetoxy-5-methoxytropone. Kinetic analysis of this process was performed by variable temperature ^{13}C NMR measurements at 100 MHz and 25 MHz in *N*,*N*-dimethylformamide-d_7 (DMF-d_7) or $CDCl_3$: Rate constants of the chemical exchange process were determined by broadened line-widths

of the exchangeable signals at the half height. Natural line widths were obtained from the signals of C-5 or the narrowest signal for each compound.[8] The ^{13}C NMR spectra were measured with JMN GX 400 Model and FX 100 Model Spectrometers, JEOL. The chemical shifts (δ unit) were from the internal Me_4Si.

Preparation of 2-Acetoxy-5-methoxytropone (5). A mixture of Ac_2O (10 cm^3) and 5-methoxytropolone (214 mg)[9] was heated at 90 °C for 3.5 h. The solvent was removed in vacuo and the residue was chromatographed on a silica-gel column to give **5** [colorless crystals, mp 90—91 °C, 269 mg; 99%. Found: *m/z* 194.0576 (M^+). Calcd for $C_{10}H_{10}O_4$: M, 194.0578. ^1H NMR δ=2.29 (3H, s), 3.77 (3H, s), 6.4—6.6 (2H, dm, J=12 Hz), and 7.0—7.2 (2H, dm, J=12 Hz). ^{13}C NMR δ=20.9, 56.1, 105.6, 129.5, 134.7, 140.1, 151.1, 163.7, 169.4, and 178.1].

The starting material, tropolone, was provided by Sankyo Co. Ltd., Tokyo, to whom our thanks are due. Also, we thank the Ministry of Education, Science and Culture for a financial support, a Grant-in-Aid for Scientific Research to A. M. (No. 60470025).

References

1) H. Takeshita, A. Mori, and T. Kusaba, *Synthesis*, **1986**, 578; H. Takeshita, A. Mori, T. Kusaba, and H. Watanabe, *Bull. Chem. Soc. Jpn.*, **60**, 4325 (1987). A part of study has been presented at the 80th Annual Meeting of the Chem. Soc. Jpn. (Abstract Papers, II, Tokyo, April, 1985, p. 1265).

2) R. M. Harrison, J. D. Hobson, and A. W. Midgley, *J. Chem. Soc., Perkin Trans. 1*, **1976**, 2403.

3) Recently, we have confirmed the concerted nature of the rearrangement by means of the high-pressure kinetic analysis. Discussion on the $\Delta S^{\neq}$ of this reaction was supported by activation volume and solvent effect. See S. Sugiyama, A. Mori, and H. Takeshita, *Chem. Lett.*, **1987**, 1247.

4) S. Masamune, A. V. Kemp-Jones, J. Green, D. L. Rabenstein, M. Yasunami, K. Takase, and T. Nozoe, *J. Chem. Soc., Chem. Commun.*, **1973**, 283.

5) V. I. Minkin, L. P. Olekhnovich, and Y. A. Zhdanov, *Acc. Chem. Res.*, **14**, 210 (1981).

6) H. Takeshita and H. Mametsuka, *Heterocycles*, **22**, 663 (1984).

7) R. B. Woodward and R. Hoffmann, "The Conservation of Orbital Symmetry" Verlag Chemie, GmbH, Weinheim/Bergstr., 1970, p. 117.

8) H. Gunther, J. Runsink, H. Schmickler, and P. Schmitt, *J. Org. Chem.*, **50**, 289 (1985).

9) T. Nozoe, S. Seto, S. Ito, M. Sato, and T. Katono, *Sci. Repts. Tohoku Univ., Ser. I*, **37**, 191 (1953).

10) It should be emphasized that the species involved in this acetotropy was not pentaacetoxytropolone (**A**), but **1**. Although, the difference for calculated carbon content, 0.71%, is larger than the experimental error, a discrimination of **A** and **1** on the basis of elemental analyses alone seems to be unconvincing. The ^{13}C NMR spectra at −60 °C firmly eliminated the possibility of **A**; three separated methyl signals were nearly 1:1:1 in peak heights.

11) C. W. Spangler, *Chem. Rev.*, **76**, 187 (1976).

The Solid-Phase ^{13}C NMR Spectra of Several Tropolone Derivatives

Akira MORI,* Shigeru SUGIYAMA, Hiroaki MAMETSUKA,† Kazushi TOMIYASU, and Hitoshi TAKESHITA*
Institute of Advanced Material Study, 86, Kyushu University, Kasuga-koen, Kasuga, Fukuoka 816
†Central Research Laboratories, Nippon Kokan Company, Ltd., Tsurumi-ku, Yokohama 210
(Received June 8, 1987)

The solid-phase ^{13}C NMR spectra of *o*-, *m*-, and *p*-hydroxytropolones were measured. In the solid state, the hydrogen shift between the C-1 and C-2 oxygens was frozen under the NMR time-scale; the major tautomer of the *o*-hydroxytropolone was shown to the 2,7-dihydroxytropone form, which was parallel to the previous assignment deduced from the IR spectroscopy. In addition, the solid-phase ^{13}C NMR of *o*-bromotropolone showed it to be 7-bromo-2-hydroxytropone.

It is well-known that the tropolones undergo rapid tautomerism in solution and their ^{13}C NMR spectra usually reveal averaged signals. However, in the solid state, this tautomerism is inhibited, e.g., parent tropolone exhibited six resolved lines.[1,2]

Recently, we have investigated the [1,9] sigmatropic acetoxyl migration of several polyacetoxytropones, including hexaacetoxytropone (**1**) and 2,3-diacetoxytropone (**2**), and elucidated the concerted nature of the process by means of a kinetic analysis.[3] In the case of **2**, apparently no acetotropic rearrangement has been detected in respect of high-temperature ^{13}C NMR; this was explained in terms of the thermodynamic stability of the symmetrical 2,7-diacetoxytropone structure (**2a**) over 2,3-diacetoxy isomer (**2b**). Even tri-, tetra-, and pentaacetoxytropones, the acetotropic equilibria were operative between tautomers having the carbonyl group at the inner positions. In this connection, the prototropy in the tropolone system seems to be worth investigating by means of solid-phase NMR measurement, since the NMR in solution represent the equilibrated structures by hydrogen exchange.

We wish to describe the investigations with *o*-hydroxytropolone (**3**), *m*-hydroxytropolone (**4**), and *p*-hydroxytropolone (**5**); these dihydroxytropones may constitute interesting tautomeric systems. Additionally included are the solid state and solution NMR behaviors of *o*-bromotropolone (**6**), being a point in dispute with its major tautomer in solution.

Experimental

The solid-phase ^{13}C NMR spectra were measured with a JEOL GX 270 spectrometer at 67.8 MHz, using the technique of high-power ^{1}H decoupling CP/MAS with a cross-polarization time of 2 ms. Chemical shifts were expressed by external reference to the Me_4Si. The actual reference compound was adamantame (methine carbon signal at δ=29.5). The samples, *o*-hydroxytropolone,[4] *m*-hydroxytropolone,[5] and *p*-hydroxytropolone,[6] *o*-bromotropolone[7] and their methyl ethers were prepared by known methods.

Results and Discussion

The ^{13}C NMR Spectra of *o*-, *m*-, and *p*-Hydroxytropolones. In the NMR of **3**, six lines appeared; its lowest signal at δ=168.1 was ascribable to a carbon having a pronounced carbonyl nature and the next two low-field signals, at δ=160.8 and 159.8, to carbons having the hydroxy nature. Superficially, the appearance of two separated hydroxy-bearing carbon signals together with exhibiting six lines favored the unsymmetrical 2,3-dihydroxytropone structure (**3a**), but the chemical shift of the lowest signal was considerably higher than that of tropolone (**7**), δ=177.5. If the magnetic non-equivalence arises from the arrangement in crystals, an alternative symmetrical 2,7-dihydroxytropone structure (**3b**) should be equally probable. This was the case from the ^{13}C NMR chemical shift comparisons between **3** and 2,3-dimethoxytropone (**8**) and 2,7-dimethoxytropone (**9**).[8] Thus, the solid-state ^{13}C NMR of **9** disclosed two separated methoxy carbon signals as well as six aromatic carbon signals, of which the magnetic non-equivalence should come from the molecular arrangement in the lattice. According to the X-ray crystallograhic analysis,[9] the tropolones are known to exist in the dimeric form with intermolecular hydrogen bondings between the α-hydroxyenone moiety; in the case of **3**, such a dimeric structure makes two kinds of hydroxyl groups, one is intermolecularly hydrogen-bonded and another isolated. The chemical shifts of **3** resembled those of **9** more closely than those of **8**. Therefore, the predominant tautomer of **3** must be 2,7-dihydroxytropone (**3b**), as being parallel to the previous result of the IR spec-

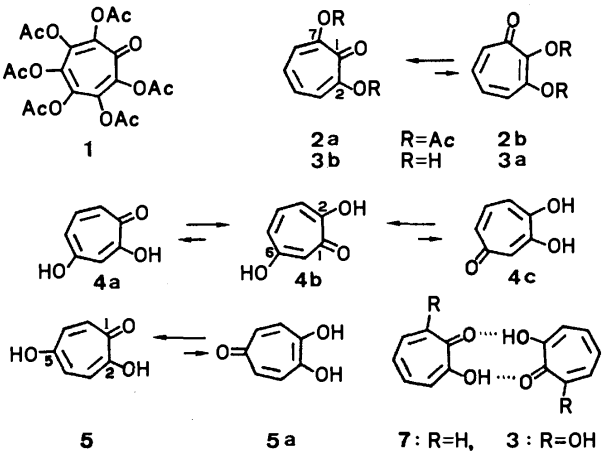

Scheme 1.

troscopy by Ikegami.[10] From these results, the signals of **3** were assigned as shown in Table 1 and the substituent effect of a hydroxyl group at C-7 was obtained to be +26.1. Furthermore, the solid-state NMR of its diacetate, *o*-diacetoxytropone (**2**),[3] exists as the symmetrical 2,7-diacetoxytropone (**2a**), which was also an exclusive tautomer in solution. Under similar conditions 2-acetoxytropones generally exist as equilibrated mixtures resulting from the [1,9] sigmatropic acetyl migration.[3]

In the case of **5**, separated seven line signals and the chemical shift of the carbonyl carbon, 173.5, eliminated the alternative 4,5-dihydroxytropone structure (**5a**).[11] From this result, the substituent effect of a hydroxyl group at C-5 was estimated to be 29.6, which was similar to the value (+26.1) obtained in **3** and that reported for a hydroxyl group of the benzenoid.[12]

On the other hand, the NMR spectrum of **4** showed considerably low-field shifted carbon signals for enolic carbons, at 164.6 and 170.3, together with a carbonyl carbon signal at 176.1. The appearance of a signal at 164.6, being appropriate for C-2 of the tropolone ring and the chemical shift of the carbonyl carbon, 176.1 eliminated the 3,4-dihydroxytropone structure (**4c**). While the substituent effect of a hydroxyl group was estimated to be +37.6 for **4a** and +28.6 for **4b**, the latter was in accord to those obtained for **3** and **5**. Thus, the major isomer of *m*-hydroxytropolone was assigned to be 6-hydroxytropolone (**4b**). The data were shown in Table 1. Consequently, α-hydroxy keto structures must be a more favorable contribution than others, and all of **3**, **4**, and **5** exist as frozen forms under the conditions for solid-phase NMR measurements.

The Tautomeric Form of *o*-Bromotropolone. According to the solid-state ^{13}C NMR spectra, the major tautomer of *o*-bromotropolone (**6**) in the solid state is indeed 7-bromo-2-hydroxytropone (**6b**). The spectrum of **6** disclosed five lines, among which, the

Table 1. Solid-Phase ^{13}C NMR of *o*-, *m*-, and *p*-Hydroxytropolones and Their Derivatives

Compd	Position							
	C-1	C-2	C-3	C-4	C-5	C-6	C-7	
7	177.5	165.4	113.0	133.7	128.1	141.7	133.7	
	(171.7)[a]	(171.7)	(123.9)	(137.5)	(128.2)	(137.5)	(123.9)	
$\Delta\delta$	−5.8	+6.3	+10.9	+3.8	+0.1	−4.2	−9.8	Σ=+1.3
3	168.1	160.8	123.2	130.1	130.1	121.5	159.8	
	(169.8)	(161.8)	(122.1)	(130.3)	(130.3)	(122.1)	(161.8)	
$\Delta\delta$	+1.7	+1.0	−1.1	+0.2	+0.2	+0.6	+2.0	Σ=+5.6
8	(180.7)	(154.5)	(158.6)	(127.8)	(129.7)	(140.5)	(133.2)	
9	162.9	173.0	161.7	112.0	127.0	127.0	115.4	
	(161.7)	(173.7)	(161.7)	(114.1)	(125.7)	(125.7)	(114.1)	
$\Delta\delta$	−1.2	+0.7	0	+2.1	−1.3	−1.3	−1.3	Σ=−2.3
4	176.1	164.6	112.0	136.2	123.4	170.3	113.9	
	(174.7)	(168.4)	(114.7)	(138.1)	(121.5)	(169.3)	(115.8)	
$\Delta\delta$	−1.4	+3.8	+2.7	+1.9	−1.0	−1.9	+1.9	Σ=+6.0
5	173.5	162.1	121.5	120.4	157.7	134.4	134.7	
	(169.4)	(169.4)	(127.5)	(126.4)	(160.9)	(126.4)	(127.5)	
$\Delta\delta$	−4.1	+7.3	+6.0	+6.0	+3.2	−8.0	+7.2	Σ=+17.6

a) The figures shown in the parentheses were those measured in $CDCl_3$ solutions.

Table 2. Solid-Phase ^{13}C NMR of *o*-Bromotropolones and Its Related Derivatives

Compd	Position							
	C-a	C-b	C-c	C-d	C-e	C-f	C-g	
7	177.5	165.4	113.0	133.7	128.1	141.7	133.7	
12	(180.1)[a]	(165.0)	(112.2)	(132.4)	(127.6)	(136.3)	(136.3)	
6	162.6	172.9	127.5	139.2	127.5	139.2	119.5	
	(165.7)	(170.9)	(129.8)	(142.7)	(126.4)	(137.4)	(120.1)	
$\Delta\delta$	+3.1	−2.0	+2.3	+3.5	−1.1	−1.8	+0.6	Σ=+4.6
11	162.8	171.7	136.7	136.7	126.0	136.7	114.3	
	(162.6)	(173.6)	(137.5)	(139.9)	(125.3)	(133.3)	(112.6)	
$\Delta\delta$	−0.2	+1.9	+0.8	+3.2	−0.7	−3.4	−1.7	Σ=−0.1
10	178.7	163.0	130.2	137.9	130.2	137.9	137.9	
	(179.6)	(163.3)	(128.4)	(138.4)	(128.6)	(135.1)	(138.2)	
$\Delta\delta$	+0.9	+0.3	−1.8	+0.5	−1.6	−2.8	+0.3	Σ=−4.2
$\Delta\delta$(**7**—**12**)	+2.6	−0.4	−0.8	−1.3	−0.5	−5.4	+2.6	$\lvert\Sigma\rvert$=13.6
$\Delta\delta$(**6**—**11**)	+0.2	−1.2	+9.2	−2.5	−0.5	−2.5	−5.2	$\lvert\Sigma\rvert$=21.3
$\Delta\delta$(**6**—**10**)	+5.8[b]	+0.4[b]	+2.7	−1.3	+2.7	−1.3	+18.4	$\lvert\Sigma\rvert$=32.5

a) The figures shown in the parentheses were those measured in $CDCl_3$ solutions. b) These values were differences between C-a of **6b** and C-b of **10** and between C-b of **6b** and C-a of **10**, respectively.

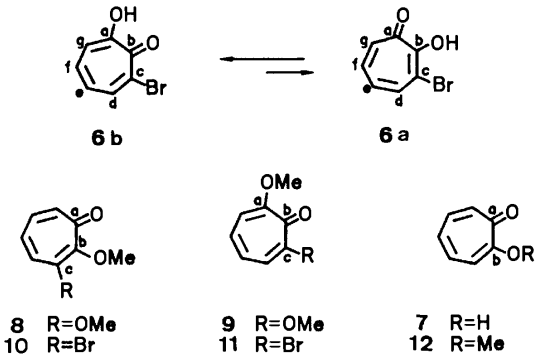

Scheme 2.

highest signal at δ=119.5 could be ascribable to the α-carbon of the hydroxyl group. This fact clarified its stable tautomer to be **6b** in the solid state.

To date, the major tautomer of **6** has been disputed; 3-bromo-2-hydroxytropone form (**6a**) was proposed by H. Sugiyama et al. on the basis of ^{1}H NMR chemical shift considerations in terms of the anisotropic effect from the bromine substituent in $CDCl_3$;[13] later, however, Bagli et al. claimed it to be **6b** on the basis of observing the triplet carbonyl carbon signal which spin-coupled to two β-protons in the ^{13}C NMR spectrum.[2] When the ^{1}H NMR spectrum of **6** was compared with isomeric 3-bromo-2-methoxytropone (**10**) and 7-bromo-2-methoxytropone (**11**), much better resemblance was observed between **6** and **10**, in favor of the H. Sugiyama's conclusion. However, the ^{13}C NMR of **6** in solution resembled **11** rather than **10**. This apparent contradiction called further careful investigation for the predominant tautomer of **6** in solution: Table 2 shows the solid-phase ^{13}C NMR of **6**, its two methyl ethers, **10** and **11**, together with reference compounds, unsubstituted tropolone, **7** and 2-methoxytropone (**12**). For the ^{13}C NMR spectra of **6**, **10**, and **11**, the chemical shifts measured in $CDCl_3$ solutions and as the solid state were parallel and showed agreement within 3.5 ppm in each other. In addition, the chemical shift of carbonyl carbon of **6** is closely related to that of **11**. By extending this to all carbons, the summations of the absolute values of the chemical shift differences for each carbon signals gave smaller $|\Delta\delta|$ in **6**—**11** (21.3) than **6**—**10** (32.5). The $|\Delta\delta|$ between **7** and **12** is 13.6. Furthermore, when we observed multiplicities of the carbonyl carbon signals, following the Bagli's procedure, **10** showed a doublet signal (J=11 Hz) while **11** showed a triplet signal (J=9.5 Hz). Consequently, **6** must predominantly exist as **6b**, 7-bromo-2-hydroxytropone form in solution and in the solid phase.

References

1) This information was obtained from the Ref. 2, which cited that C. Fyfe carried out the experiments.

2) D. Menard, M. St-Jacques, and J. F. Bagli, *Can. J. Chem.*, **60**, 231 (1982).

3) H. Takeshita, A. Mori, H. Watanabe, T. Kusaba, S. Sugiyama, and M. Kodama, *Bull. Chem. Soc. Jpn.*, **60**, 4335 (1987).

4) H. Takeshita, A. Mori, and T. Kusaba, *Synthesis*, **1986**, 578.

5) T. Nozoe and Y. Kitahara, *Proc. Jpn. Acad.*, **30**, 204 (1954).

6) M. Oda and Y. Kitahara, *Tetrahedron Lett.*, **1969**, 3285.

7) T. Nozoe, S. Seto, Y. Kitahara, M. Kunori, and Y. Nakayama, *Proc. Jpn. Acad.*, **26**, 38 (1950).

8) Substituent effect on ^{13}C NMR of troponoids has been reported. See J. F. Bagli and M. St-Jacques, *Can. J. Chem.*, **56**, 578 (1978); J. F. Bagli, T. Bogri, B. Palameta, and M. St-Jacques, *ibid.*, **57**, 1949 (1979).

9) H. Shimanouchi and Y. Sasada, *Tetrahedron Lett.*, **1970**, 242.

10) Y. Kitahara, *Sci. Repts. Tohoku Univ., Ser. I*, **39**, 258 (1956); Y. Ikegami, "IR Spectra" Vol. 8 of Zokan Kagaku no Ryoiki, Nankodo, Tokyo (1959), p. 33.

11) We observed the carbonyl carbon signal of 4,5-dimethoxytropone in $CDCl_3$ at δ=184.6. See H. Takeshita, A. Mori, Y. Goto, and T. Nagao, *Bull. Chem. Soc. Jpn.*, **60**, 1747 (1987).

12) J. B. Stothers, "Carbon-13 NMR Spectroscopy," Academic Press, New York (1972), Chap. 5.

13) H. Sugiyama, S. Itô, and T. Nozoe, *Tetrahedron Lett.*, **1965**, 179.

Peptide Synthesis in Aqueous Solution. II. Synthesis and Biological Activity of a Molluscan Neuropeptide, FMRFamide (Phe-Met-Arg-Phe-NH_2) Analogs for N-Terminal Moiety

Katsushige KOUGE, Haruko SOMA,† Yukari KATAKAI,† Hideo OKAI,*,†
Mayumi TAKEMOTO,†† and Yojiro MUNEOKA††
Sanshin Chemical Industrial Co. Ltd., 531, Nagahama, Hirao-cho, Kumage-gun, Yamaguchi 742-11
†Department of Fermentation Technology, Faculty of Engineering, Hiroshima University, Shitami, Saijo-cho, Higashihiroshima 724
††Physiological Laboratory, Faculty of Integrated Arts and Sciences, Hiroshima University, Higashisenda-machi, Naka-ku, Hiroshima 730
(Received May 14, 1987)

In order to elucidate the contribution of the N-terminal moiety (Phe[1] or Met[2]) of FMRFamide to the activity, 16 kinds of FMRFamide analogs were synthesized and their structure-activity relations are discussed. From the results, it was found that hydrophobic or bulky group in N-terminal contributes to the contractile effect, while the precise length of the side chain of amino acid at 2-position is due to a relaxing effect.

Previously, we reported that (*p*-hydroxyphenyl)dimethylsulfonium methyl sulfate(HODMSP · $MeSO_4^-$) active ester[1] enabled the formation of a peptide bond in aqueous solution and was applicable for the synthesis of a molluscan neuropeptide, FMRFamide (Phe-Met-Arg-Phe-NH_2),[2] which was isolated from the ganglia of the clam *Macrocallista nimbosa* by Price and Greenberg.[3] Particularly, this active ester method was recognized as an effective process for the coupling reaction with a peptide containing Arg, which has the free guanidine group. As a further utility of this method, we next tried to apply it to a synthetic study of the structure-activity relations of FMRFamide. FMRFamide is known to have diverse effects on molluscan muscles and neurons. In the anterior byssus retractor muscle of *Mytilus*, FMRFamide relaxes catch tension induced by acetylcholine at concentrations 10^{-8}—10^{-7} M[4] (1M=1 mol dm^{-3}) and elicits a contraction by a direct action on the muscle fibers at concentrations higher than 10^{-7} M,[5] as shown in Fig. 1.

With regard to the structure-activity relations of this peptide for these actions, Muneoka and Saitoh[6] tested a number of FMRFamide analogs and other peptide with biological actions in mammals, arthropods, and molluscans. From their report, we can draw an interesting conclusion that at least the structure of Arg^3-Phe^4-NH_2 moiety of FMRFamide is necessary for the production of both contraction and relaxation. Probably, this moiety will act as the binding unit to FMRFamide receptor. However, the role of the Phe^1 or Met^2 residue of N-terminal moiety in FMRFamide to these productions was not fully characterized.

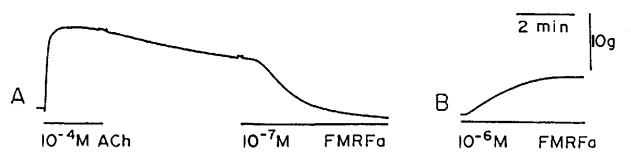

Fig. 1. Contractions and Relaxtations Produced by FMRFamide. A: Relaxing action of FMRFamide on ACh-induced catch tension. B: Contractile action of FMRFamide. ACH: Acetylcholine, FMRFa: FMRFamide.

In order to elucidate the contribution of Phe^1 or Met^2 to the activity, we synthesized 16 kinds of

Table 1. Contractile and Relaxing Effect of Analogs for N-Terminal Phe

Peptide		Contractile effect/M	Relaxing effect/M
Phe-Met-Arg-Phe-NH_2 (FMRFamide)	(**13a**)	10^{-7}	10^{-8}
Gly-Met-Arg-Phe-NH_2	(**13b**)	10^{-4}	—
Gly-Gly-Met-Arg-Phe-NH_2	(**13c**)	10^{-7}	—
Phe-Gly-Met-Arg-Phe-NH_2	(**13d**)	10^{-6}	—
Phe-Phe-Met-Arg-Phe-NH_2	(**17**)	10^{-7}	—
Phe-Phe-Gly-Met-Arg-Phe-NH_2	(**13e**)	10^{-6}	—
Ac-Phe-Met-Arg-Phe-NH_2	(**14**)	10^{-8}	—
Bz-Phe-Met-Arg-Phe-NH_2	(**15**)	10^{-8}	—

Table 2. Contractile and Relaxing Effect of Analogs for Met^2

Peptide	Contractile effect/M	Relaxing effect/M
Phe-Met-Arg-Phe-NH_2 (**13a**) (FMRFamide)	10^{-7}	10^{-8}
Phe-Gly-Arg-Phe-NH_2 (**23a**)	10^{-4}	—
Phe-Ala-Arg-Phe-NH_2 (**23b**)	10^{-5}	—
Phe-Abu-Arg-Phe-NH_2 (**23c**)	10^{-4}	—
Phe-Val-Arg-Phe-NH_2 (**23d**)	—	10^{-7}
Phe-Leu-Arg-Phe-NH_2 (**23e**)	10^{-6}	10^{-7}
Phe-Ile-Arg-Phe-NH_2 (**23f**)	10^{-5}	—
Phe-Nle-Arg-Phe-NH_2 (**23g**)	10^{-7}	10^{-8}
Phe-Phe-Arg-Phe-NH_2 (**23h**)	10^{-7} a)	—
Phe-Pro-Arg-Phe-NH_2 (**23i**)	10^{-5}	—

a) The contractile effect of this peptide was stronger than that of FMRFamide.

FMRFamide analogs shown in Table 1 and Table 2 and discussed their structure-activity relations of FMRFamide on a molluscan muscle.

The synthetic route for the FMRFamide analogs for Phe[1] is shown in Fig. 2. Z-Arg(NO_2)-OH was coupled with H-Phe-NH_2·HCl by means of mixed anhydride (MA) method to yield Z-Arg-(NO_2)-Phe-NH_2 (**5**). Removal of Z-group and NO_2-group from **5** by catalytic hydrogenation afforded the corresponding dipeptide amide (**6**). Boc-Met-OH was esterified by DCC and HODMSP·$MeSO_4^-$ to afford the water-soluble active ester (**7**). In aqueous solution, **7** was allowed to react with **6** in the presence of 1 M Na_2CO_3 at pH 7.2. To the reaction mixture containing the Boc-tripeptide amide (**8**), 1% picric acid was added and then the resulting Boc-tripeptide amide picrate (**9**) was isolated by extraction with ethyl acetate. The Boc-group was removed from **9** with trifluoroacetic acid and then hydrogen chloride in the presence of ethyl methyl sulfide to yield tripeptide amide (**10**). N-protected amino acid or peptide, which was prepared by the usual method, was esterified by DCC and HODMSP·$MeSO_4^-$ to afford the water-soluble active ester (**11**$_a$—**11**$_c$), which was allowed to react with **10** in the same manner as described for **8** to yield N-protected peptide amide (**12**$_a$—**12**$_c$). Finally the *p*-methoxybenzyloxycarbonyl group (pMZ-group) was removed with trifluoroacetic acid and then hydrogen chloride respectively, to yield desired peptides (**13**$_a$—**13**$_c$).

The synthetic route to **14**, **15**, and **17** is shown in Fig. 3. **14** or **15** was prepared by the coupling reaction of **10** and Ac-Phe-ODMSP·$MeSO_4^-$ or Bz-Phe-ODMSP·$MeSO_4^-$ in aqueous solution at pH 7.2, respectively. In the synthesis of **17**, pMZ-Phe-ODMSP·$MeSO_4^-$ was coupled with FMRFamide (**13**$_c$) in aqueous solution at pH 7.2 to yield **16**. The pMZ-group was removed from **16** with trifluoroacetic acid and then hydrogen chloride in the presence of ethyl methyl sulfide to yield **17**.

FMRFamide analogs for Met[2] were synthesized by the synthetic route, as shown in Fig. 4. The desired tetrapeptides (**23**$_a$—**23**$_i$) were prepared by stepwise

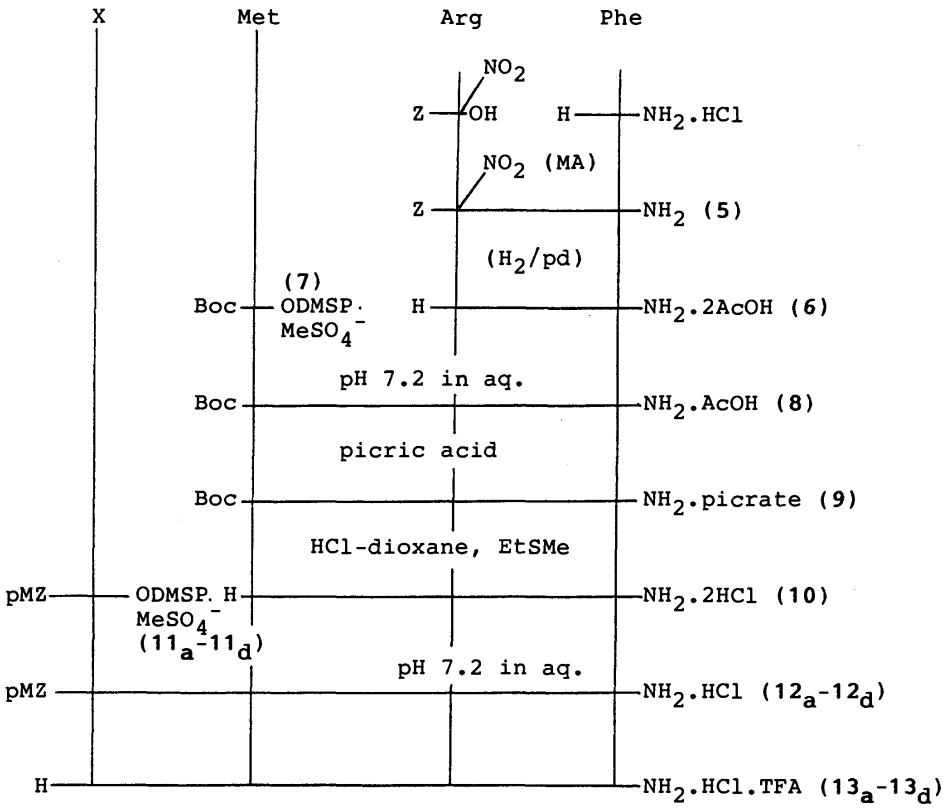

X: Phe(a), Gly(b), Gly-Gly(c), Phe-Gly(d), Phe-Phe-Gly(e).

-ODMSP.$MeSO_4^-$:

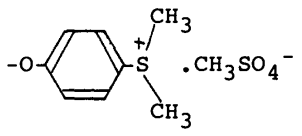

Fig. 2. Synthesis of FMRFamide Analogs for N-Terminal Phe.

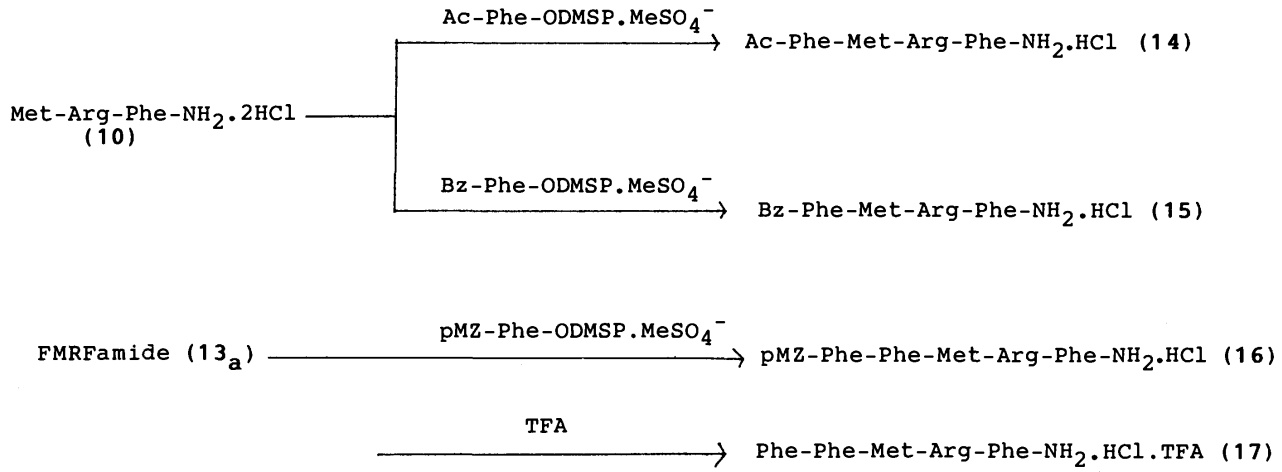

Fig. 3. Synthesis of FMRFamide Analogs for N-Terminal Phe.

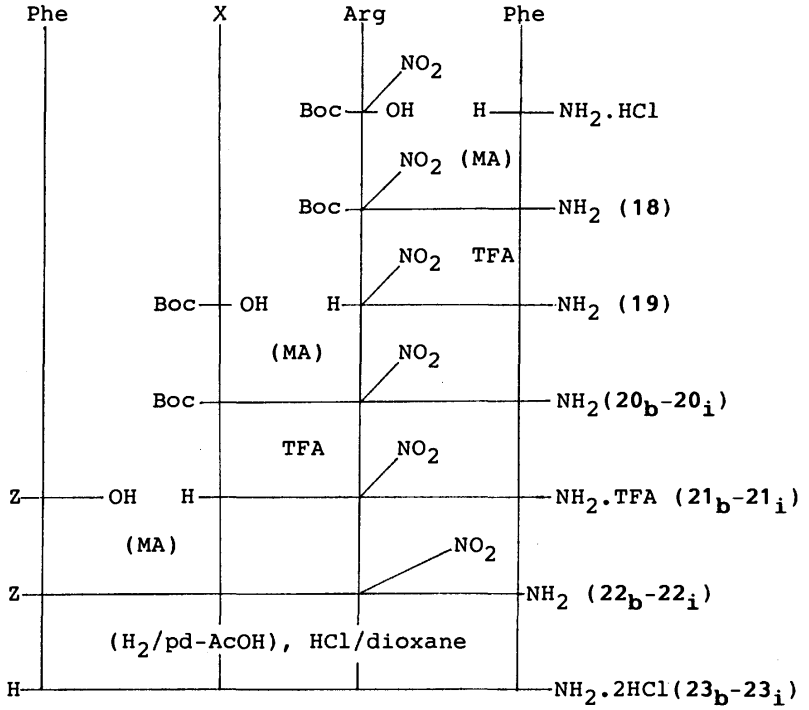

X: Ala(b), Abu(c), Val(d), Leu(e), Ile(f), Nle(g), Phe(h), Pro(i).

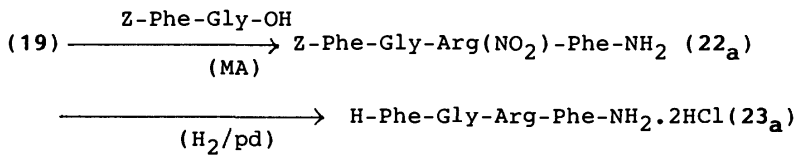

Fig. 4. Synthesis of FMRFamide Analogs for Met[2].

elongation from the C-terminal. Details of the synthetic route to those peptides is described in the experimental part.

In the synthesis of **23a**, Z-Phe-Gly-OH was coupled with **19** to yield **22a**. **22a** was then hydrogenated to give **23a**. The purity of synthetic peptides and their intermediates was confirmed by TLC with two solvent systems and by elemental analysis. The homogeneity of the final products was also confirmed by amino acid analysis.

Contractile effects and catch-relaxing effects of synthetic peptides on the anterior byssus retractor muscle of Mytilus were determined,[7] as shown in Tables 1 and 2. All the synthesized analogs of FMRFamide for Phe[1] producted only contraction and had no relaxing activity, as shown in Table 1. In the contractile activity, substitution of Gly for N-terminal Phe ($\mathbf{13_b}$) showed a decrease in contractile potency. But, extension of $\mathbf{13_b}$ by attaching Gly ($\mathbf{13_c}$) was almost equipotent to FMRFamide. When N-terminal Phe was separated from Met[2] by inserting a Gly residue and was replaced with Phe-Phe or Phe-Phe-Gly residue in FMRFamide, these peptides ($\mathbf{13_d}$, **17**, and $\mathbf{13_e}$) did not substantially change contractile activity. N-terminal acylation of FMRFamide with acetyl group or benzoyl group was slightly more active. These results indicate that hydrophobic or bulky group in N-terminal clearly contributes to the contractile effect of the peptide and the precise structure is not required for contractile activity.

In the analogs of FMRFamide for Met[2], Muneoka and Saitoh already reported that Nle can be substituted for Met[2].[6] We also recognized that this analog ($\mathbf{23_g}$) had both contractile and relaxing activity and each activity was comparable with that of FMRFamide, as shown in Table 2. Substitution of Leu for Met[2] showed a slight decrease in contractile and relaxing potency. In contrast, Gly, Ala, Abu, Ile, Phe, and Pro could not be substituted for Met[2]; these peptides had no relaxing activity. The most remarkable fact was that the peptide ($\mathbf{23_d}$), in which Val was substituted for Met[2], had only a relaxing activity. The results described above indicate that the precise length of the side chain of amino acid at 2-position, in addition to the hydrophobic group of N-terminal, contributes to the relaxing activity. In conclusion, we could biologicaly synthesize active peptides, which produced a contraction or a relaxation separately. From the viewpoint of pharmacology, we expect that these findings give an important clue to the designing effective relaxing peptides. For the structure-activity relations of FMRFamide, further studies are now in progress.

Experimental

All the melting points were uncorrected. The optical rotations were measured on a Union PM-101 polarimeter. TLC was carried out on Merck Silicagel G: R_{f_1}, 1-butanol-acetic acid-pyridine-water (4:1:1:2, v/v), R_{f_2}, $CHCl_3$-methanol (5:1, v/v), R_{f_3}, 1-butanol-acetic acid-water (3:3:2, v/v). Spots of materials possessing free amino group on TLC plate were detected by spraying with ninhydrin, and those of amino group blocked materials by spraying with 25% HBr in acetic acid and then ninhydrin. Amino acid analysis was performed by HPLC using JASCO TRI ROTAR-V and UVIDEC-100V apparatus.

Synthesis of Analogs for Phe[1]. Z-Arg(NO_2)-Phe-NH_2 (5): A solution of Z-Arg(NO_2)-OH (3.53g, 10 mmol) and NMM (1.1ml, 10 mmol) in THF (20 ml) was chilled to −5 °C, then ECF (1 ml, 10 mmol) was added to it. After 10 min, a precooled solution of H-Phe-NH_2·HCl (2.00 g, 10 mmol) and Et_3N (1.4 ml, 10 mmol) in $CHCl_3$ (20 ml) was added. The reaction mixture was refrigerated for 1 h and then allowed to stand overnight at room temperature. The mixture was concentrated in vacuo, and the solid was suspended in hot methanol (50 ml). The solid was filtered and washed with methanol; Yield 4.24g (85%); mp 218—221 °C; $[\alpha]_D^{20}$ −14° (*c* 0.5, DMF); R_{f_1} 0.91; R_{f_2} 0.41; Found: C, 55.56; H, 5.70; N, 19.38%; Calcd for $C_{23}H_{29}O_6N_7$: C, 55.34; H, 5.81; N, 19.63%.

H-Arg-Phe-NH_2·2AcOH (6): Compound **5** (2.5g, 5 mmol) in acetic acid (10 ml) was hydrogenated in the presence of palladium black. The filtrate was concentrated in vacuo and the residue was crystallized from ether as hygroscopic crystals; Yield 1.08 g (98%); $[\alpha]_D^{20}$ +9° (*c*1, H_2O); R_{f_1} 0.41; R_{f_3} 0.75.

Boc-Met-ODMSP·$MeSO_4^-$ (7) (Water-Soluble Active Ester): To a chilled solution of Boc-Met-OH (2.49g, 10 mmol) and HODMSP·$MeSO_4^-$ (2.66 g, 10 mmol) in CH_3CN (80 ml), DCC (2.06 g. 10 mmol) was added. The reaction mixture was held overnight at 0 °C and the DCurea which formed was filtered off. The filtrate was concentrated in vacuo, and the residual oil was washed with ether by decantation; Yield 3.93 g (80%); $[\alpha]_D^{20}$ −30° (*c*1, MeOH); R_{f_1} 0.82; R_{f_2} 0.34.

Boc-Met-Arg-Phe-$N\bar{H}_2$·Picrate (9): Compound **6** (0.88 g, 2 mmol) was dissolved in H_2O and the pH of the solution was adjusted to 7.2 by addition of Et_3N. Boc-Met-ODMSP·$MeSO_4^-$ (**7**) (0.99 g, 2 mmol) was added to the stirred solution below 20 °C, the pH being maintained automatically at 7.2 with Et_3N. After 12 h, 1% picric acid was added to the solution and the pH of the solution was adjusted to 5.6. A yellow precipitate was filtered off and it was dissolved in ethyl acetate (100 ml). The solution was washed successively with 4% sodium hydrogencarbonate, 4% citric acid and water, and then dried over anhydrous sodium sulfate. The solution was concentrated to an oily residue which was crystallized by addition of ether. It was recrystallized from $CHCl_3$; Yield 0.75 g (45%); mp 110 °C (decomp); $[\alpha]_D^{20}$ −14° (*c* 0.5, DMF); R_{f_1} 0.83; R_{f_2} 0.32; Found C, 46.84; H, 5.81; N, 17.95%; Calcd for $C_{25}H_{41}O_5N_7S \cdot C_6H_3N_3O_7 \cdot 1/2H_2O$; C, 47.17; H, 5.70; N, 17.74%; Amino acid ratios in acid hydrolyzate: Arg 0.94, Met 0.89, Phe 1.00.

H-Met-Arg-Phe-NH_2·2HCl (10): To a solution of **27** (0.78g, 1 mmol) and ethyl methyl sulfide, 4M HCl in dioxane (5 ml) was added. The solution was allowed to stand for 1 h at room temperature, and then concentrated in vacuo. The residue was crystallized with ether; Yield 0.47 g (90%); mp 140 °C (decomp); $[\alpha]_D^{20}$ +10° (*c* 0.5, H_2O); R_{f_1} 0.52; R_{f_3} 0.74; Found: C, 49.03; H, 6.87; N, 20.01%; Calcd for $C_{20}H_{33}O_3N_7S \cdot 2HCl$; C, 49.25; H, 6.97; N, 20.09%; Amino acid ratios in acid hydrolyzate: Arg 0.96, Met 0.84, Phe 1.00.

pMZ-X-ODMSP·$MeSO_4^-$ ($\mathbf{11_a}$—$\mathbf{11_d}$) (Water-Soluble Active Ester): pMZ-Phe-ODMSP·$MeSO_4^-$ ($\mathbf{11_a}$), pMZ-Gly-ODMSP·$MeSO_4^-$ ($\mathbf{11_b}$), pMZ-Gly-Gly-ODMSP·$MeSO_4^-$ ($\mathbf{11_c}$), pMZ-Phe-Gly-ODMSP·$MeSO_4^-$ ($\mathbf{11_d}$), pMZ-Phe-Phe-Gly-ODMSP·$MeSO_4^-$ ($\mathbf{11_e}$), Ac-Phe-ODMSP·$MeSO_4^-$, and Bz-Phe-ODMSP·$MeSO_4^-$ were also prepared from the corresponding carboxyl components and HODMSP·$MeSO_4^-$ by the same method as **7**.

$\mathbf{11_a}$: Yield 90%; R_{f_1} 0.85; R_{f_2} 0.51.

$\mathbf{11_b}$: Yield 85%; R_{f_1} 0.70; R_{f_2} 0.39.

$\mathbf{11_c}$: Yield 90%; R_{f_1} 0.72; R_{f_2} 0.38.

11_d : Yield 88%; R_{f_1} 0.82; R_{f_2} 0.45.

11_e : Yield 80%; R_{f_1} 0.85; R_{f_2} 0.51.

Ac-Phe-ODMSP · $MeSO_4^-$: Yield 82%; R_{f_1} 0.81; R_{f_2} 0.42.

Bz-Phe-ODMSP · $MeSO_4^-$: Yield 88%; R_{f_1} 0.88; R_{f_2} 0.55.

Since these compounds were obtained as the oily products, they were soon employed for the next reactions.

pMZ-X-Met-Arg-Phe-NH_2 · HCl (12_a—12_d and 14—16): The synthesis of pMZ-Gly-Met-Arg-Phe-NH_2 · HCl (**12_b**) is as follows. Compound **10** (0.52 g, 1 mmol) was dissolved in H_2O (10 ml) and the pH of the solution was adjusted to 7.2 by addition of 1M Na_2CO_3. pMZ-Gly-ODMSP · $MeSO_4^-$ (**11_b**) (0.59 g, 1.2 mmol) was added to the stirred solution below 20 °C, the pH being maintained automatically at 7.2 with 1M Na_2CO_3. After 12 h, the crude product was precipitated from the reaction mixture. It was filtered and then washed with 4% sodium hydrogencarbonate and water. It was recrystallized from methanol; Yield 0.23 g (32%); mp 146 °C (decomp); $[\alpha]_D^{20}$ −20° (*c* 0.5, DMF); R_{f_1} 0.75; R_{f_3} 0.81; Found: C, 50.72; H, 6.53; N, 15.21%; Calcd for $C_{31}H_{44}O_7N_8S$ · HCl · H_2O: C, 51.23; H, 6.47; N, 15.41%; Amino acid ratios in acid hydrolyzate: Arg 0.95, Gly 0.93, Met 0.87, Phe 1.00.

pMZ-Phe-Met-Arg-Phe-NH_2 (**12_a**), pMZ-Gly-Gly-Met-Arg-Phe-NH_2 · HCl (**12_c**), pMZ-Phe-Gly-Met-Arg-Phe-NH_2 · HCl (**12_d**), pMZ-Phe-Phe-Gly-Met-Arg-Phe-NH_2 · HCl (**12_e**), pMZ-Phe-Phe-Met-Arg-Phe-NH_2 · HCl (**16**), Ac-Phe-Met-Arg-Phe-NH_2 · HCl (**14**), Bz-Phe-Met-Arg-Phe-NH_2 · HCl (**15**) were prepared from the corresponding HODMSP.$MeSO_4^-$ active ester and **28** by the same method described for the preparation of **12_b**.

12_a: Yield 41%; mp 190 °C (decomp); $[\alpha]_D^{20}$ −20° (*c* 0.5, DMF); R_{f_1} 0.80; R_{f_3} 0.91; Found: C, 55.91; H, 6.31; N, 13.47%; Calcd for $C_{38}H_{50}O_7N_8S$ · HCl · H_2O: C, 55.87; H, 6.49; N, 13.71%; Amino acid ratios in acid hydrolyzate: Arg 0.95, Met 0.87, Phe 2.00.

12_c: Yield 31%; mp 136 °C (decomp); $[\alpha]_D^{20}$ −10° (*c* 0.5, DMF); R_{f_1} 0.74; R_{f_3} 0.80; Found: C, 49.87; H, 6.40; N, 15.61%; Calcd for $C_{33}H_{47}O_8N_9S$ · HCl · 3/2H_2O: C, 49.99; H, 6.43; N, 15.89%; Amino acid ratios in acid hydrolyzate: Arg 0.93, Gly 1.92, Met 0.89, Phe 1.00.

12_d: Yield 32%; mp 146°C (decomp); $[\alpha]_D^{20}$ −18° (*c* 0.5 DMF); R_{f_1} 0.74; R_{f_3} 0.82; Found: C, 54.76; H, 6.38; N, 14.21%; Calcd for $C_{40}H_{53}O_8N_9S$ · HCl · H_2O: C, 54.97; H, 6.41; N, 14.47%; Amino acid ratios in acid hydrolyzate: Arg 0.91, Gly 0.96, Met 0.87, Phe 2.00.

12_e: Yield 25%; mp 151 °C (decomp); $[\alpha]_D^{20}$ −30° (*c* 0.5, DMF); R_{f_1} 0.83; R_{f_3} 0.91; Found: C, 55.41; H, 6.39; N, 13.22%; Calcd for $C_{49}H_{62}O_9N_{10}S$ · HCl · 2H_2O: C, 55.65; H, 6.45; N, 13.48%; Amino acid ratios in acid hydrolyzate; Arg 0.95, Gly 0.93, Met 0.89, Phe 3.00.

14: Yield 30%; mp 72°C (decomp); $[\alpha]_D^{20}$ +35° (*c* 0.5, DMF); R_{f_1} 0.81; R_{f_3} 0.91; Found: C, 53.28; H, 6.72; N, 15.93%; Calcd for $C_{31}H_{44}O_5N_8S$ · HCl · H_2O: C, 53.93; H, 6.76; N, 16.12%; Amino acid ratios in acid hydrolyzate: Arg 0.93, Met 0.87, Phe 2.00.

15: Yield 35%; mp 118°C (decomp); $[\alpha]_D^{20}$ −16° (*c* 0.5, DMF); R_{f_1} 0.79; R_{f_3} 0.83; Found: C, 56.01; H, 6.36; N, 13.59%; Calcd for $C_{38}H_{50}O_7N_8S$ · HCl · 2/3H_2O: C, 56.29; H, 6.45; N, 13.81%; Amino acid ratios in acid hydrolyzate: Arg 0.95, Met 0.84, Phe 2.00.

16: Yield 33%; mp 146 °C (decomp); $[\alpha]_D^{20}$ −16° (*c* 0.5, DMF); R_{f_1} 0.80; R_{f_3} 0.85; Found: C, 57.21; H, 6.34; N, 12.67%; Calcd for $C_{47}H_{59}O_8N_9S$ · HCl · 2H_2O: C, 57.49; H, 6.52; N, 12.83%; Amino acid ratios in acid hydrolyzate: Arg 0.97, Met 0.88, Phe 3.00.

H-X-Met-Arg-Phe-NH_2 · HCl · TFA (13_a—13_d and 17): The synthesis of H-Gly-Met-Arg-Phe-NH_2 · HCl · TFA (**13_b**) is as follows. Compound **12_b** (0.36g, 0.5 mmol) and ethyl methyl sulfide (0.5 ml) were dissolved in TFA (5 ml). The reaction mixture was allowed to stand at room temperature. After 2 h, the solution was concentrated in vacuo. The residue was crystallized with ether; Yield 0.17 g (52%); mp 90 °C (decomp); $[\alpha]_D^{20}$ −6° (*c* 0.5, MeOH); R_{f_1} 0.76; R_{f_3} 0.85; Found: C, 42.87; H, 5.80; N, 16.65%; Calcd for $C_{22}H_{36}O_4N_8S$ · CF_3COOH · HCl · 1/2H_2O: C, 43.17; H, 5.84; N, 16.77%; Amino acid ratios in acid hydrolyzate: Arg 0.92, Gly 0.92, Met 0.88, Phe 1.00.

H-Phe-Met-Arg-Phe-NH_2 · HCl · TFA (**13_a**), H-Gly-Gly-Met-Arg-Phe-NH_2 · HCl · TFA (**13_c**), H-Phe-Gly-Met-Arg-Phe-NH_2 · HCl · TFA (**13_d**), H-Phe-Phe-Gly-Met-Phe-NH_2 · HCl · TFA (**13_e**), H-Phe-Phe-Met-Arg-Phe-NH_2 · HCl · TFA (**17**) were prepared from the corresponding pMZ-tetrapeptide amide by the same method described for the preparation of **13_b**.

13_a: Yield 92%; mp 164 °C (decomp); $[\alpha]_D^{20}$ +8° (*c* 0.5, H_2O); R_{f_1} 0.76; R_{f_3} 0.85; Found: C, 51.38; H, 5.94; N, 15.32%; Calcd for $C_{29}H_{42}O_4N_8S$ · CF_3COOH · HCl · 1/2H_2O: C, 51.62; H, 6.10; N, 15.53%; Amino acid ratios in acid hydrolyzate: Arg 0.92, Met 0.90, Phe 2.00.

13_c: Yield 90%; mp 175 °C (decomp); $[\alpha]_D^{20}$ −16° (*c* 0.5, MeOH); R_{f_1} 0.52; R_{f_3} 0.85; Found : C, 41.27; H, 5.82; N, 16.61%; Calcd for $C_{24}H_{39}O_5N_9S$ · CF_3COOH · HCl · 2H_2O: C, 41.54; H, 5.99; N, 16.76%; Amino acid ratios in acid hydrolyzate: Arg 0.91, Gly 1.95, Met 0.83, Phe 1.00.

13_d: Yield 100%; mp 110 °C (decomp); $[\alpha]_D^{20}$ +6° (*c* 0.5, MeOH); R_{f_1} 0.50; R_{f_3} 0.88; Found: C, 45.87; H, 6.09; N, 14.48%; Calcd for $C_{31}H_{45}O_5N_9S$ · CF_3COOH · HCl · 3H_2O: C, 46.10; H, 6.16; N, 14.66%; Amino acid ratios in acid hydrolyzate: Arg 0.95, Gly 0.92, Met 0.87, Phe 2.00.

13_e: Yield 87%; mp 121°C (decomp); $[\alpha]_D^{20}$ +4° (*c* 0.5, MeOH); R_{f_1} 0.83; R_{f_3} 0.91; Found: C, 51.19; H, 6.01; N, 14.01%; Calcd for $C_{40}H_{54}O_6N_{10}S$ · CF_3COOH · HCl · 3/2H_2O: C, 51.48; H, 6.02; N, 14.29%; Amino acid ratios in acid hydrolyzate: Arg 0.97, Gly 0.92, Met 0.84, Phe 3.00.

17: Yield 91%; mp 182 °C (decomp); $[\alpha]_D^{20}$ +2° (*c* 0.3, MeOH); R_{f_1} 0.77; R_{f_3} 0.90; Found: C, 51.32; H, 6.08; N, 13.38%; Calcd for $C_{38}H_{51}O_5N_9S$ · CF_3COOH · HCl · 2H_2O: C, 51.55; H, 6.12; N,13.52; Amino acid ratios in acid hydrolyzate: Arg 0.91, Met 0.83, Phe 3.00.

Synthesis of FMRFamide Analogs for Met^2. Boc-Arg(NO_2)-Phe-NH_2 (18): Boc-Arg(NO_2)-OH (1.58 g, 5 mmol) and H-Phe-NH_2 · HCl (1.00 g, 5 mmol) were coupled by the same method as described for the preparation of **5**. The reaction mixture was evaporated in vacuo and then poured into ice water. The resulting precipitate was filtered and washed with 4% sodium hydrogencarbonate, 4% citric acid and water successively. The purified product thus obtained was recrystallized from $CHCl_3$; Yield 1.97 g (84%); mp 115 °C (decomp); $[\alpha]_D^{20}$ −14° (*c* 0.5, DMF); R_{f_1} 0.86; R_{f_2} 0.56; Found: C, 51.37; H, 6.39; N, 20.96%; Calcd for $C_{20}H_{31}O_6N_7$: C, 51.56; H, 6.66; N, 21.05%.

H-Arg(NO_2)-Phe-NH_2 · TFA (19): This compound was prepared by the same method described for the preparation of **13_b**. Yield 1.49 g (89%); mp 103 °C (decomp); $[\alpha]_D^{20}$ +28° (*c* 0.5, DMF); R_{f_1} 0.66; R_{f_2} 0.00; Found: C, 41.54; H, 5.21; N, 19.71%; Calcd for $C_{15}H_{23}O_4N_7$ · CF_3COOH · 1/2H_2O: C, 41.83; H, 5.12; N, 20.08%.

Boc-X-Arg(NO_2)-Phe-NH_2 (20_b—20_i): Boc-Ala-Arg(NO_2)-Phe-NH_2 (20_b), Boc-Abu-Arg(NO_2)-Phe-NH_2 (20_c), Boc-Val-Arg(NO_2)-Phe-NH_2 (20_d), Boc-Leu-Arg(NO_2)-Phe-NH_2 (20_e), Boc-Ile-Arg(NO_2)-Phe-NH_2 (20_f), Boc-Nle-Arg(NO_2)-Phe-NH_2 (20_g), Boc-Phe-Arg(NO_2)-Phe-NH_2 (20_h), and Boc-Pro-Arg(NO_2)-Phe-NH_2 (20_i) were prepared from the corresponding Boc-amino acid and **19** by the same method described for the preparation of **18**.

20_b: Yield 63%; mp 115 °C (decomp); $[\alpha]_D^{20}$ −16° (*c* 0.5, DMF); R_{f_1} 0.81; R_{f_2} 0.64; Found: C, 50.32; H, 6.81; N, 20.21%; Calcd for $C_{23}H_{36}O_7N_8 \cdot 1/3H_2O$: C, 50.63; H, 6.78; N, 20.53%.

20_c: Yield 59% ; mp 120 °C (decomp); $[\alpha]_D^{20}$ −16° (*c* 0.5, DMF); R_{f_1} 0.92; R_{f_2} 0.39; Found: C, 51.09; H, 6.94; N, 19.74%; Calcd for $C_{24}H_{38}O_7N_8 \cdot 2/3H_2O$: C, 51.23; H, 6.99; N, 19.91%.

20_d: Yield 63%; mp 135 °C (decomp) $[\alpha]_D^{20}$ −12° (*c* 0.5, DMF); R_{f_1} 0.90; R_{f_2} 0.64; Found: C, 51.79; H, 7.03; N, 19.17%; Calcd for $C_{25}H_{40}O_7N_8 \cdot H_2O$: C, 51.53; H, 7.21; N, 9.22%.

20_e: Yield 70%; mp 122 °C (decomp); $[\alpha]_D^{20}$ −26° (*c* 0.5, DMF); R_{f_1} 0.88; R_{f_2} 0.64; Found: C, 52.83; H, 7.32; N, 19.16%; Calcd for $C_{26}H_{42}O_7N_8 \cdot 1/2H_2O$: C, 53.13; H, 7.32; N, 19.06%.

20_f: Yield 38%; mp 120 °C (decomp); $[\alpha]_D^{20}$ −20° (*c* 0.5, DMF); R_{f_1} 0.91; R_{f_2} 0.62; Found: C, 53.71; H, 7.34; N, 19.51%; Calcd for $C_{26}H_{42}O_7N_8$: C, 53.92; H, 7.26; N, 19.36%.

20_g: Yield 67%; mp 102 °C (decomp); $[\alpha]_D^{20}$ −26° (*c* 0.5, DMF); R_{f_1} 0.87; R_{f_2} 0.64; Found: C, 53.68; H, 7.26; N, 19.20%; Calcd for $C_{26}H_{42}O_7N_8$: C, 53.92; H, 7.26; N, 19.36%.

20_h: Yield 74%; mp 124 °C (decomp); $[\alpha]_D^{20}$ −8° (*c* 0.5, DMF); R_{f_1} 0.85; R_{f_2} 0.59; Found: C, 55.71; H, 6.53; N, 18.27%; Calcd for $C_{29}H_{40}O_7N_8$: C, 56.80; H, 6.53; N, 18.38%.

20_i: Yield 50%; mp 115 °C (decomp); $[\alpha]_D^{20}$ −24° (*c* 0.5, DMF); R_{f_1} 0.92; R_{f_2} 0.64; Found: C, 51.81; H, 6.76; N, 19.35%; Calcd for $C_{25}H_{38}O_7N_8 \cdot H_2O$: C, 51.71; H, 6.89; N, 19.29%.

H-Ala-Arg(NO_2)-Phe-NH_2 · TFA (21_b—21_i): H-Ala-Arg(NO_2)-Phe-NH_2 (21_b), H-Abu-Arg(NO_2)-Phe-NH_2 · TFA (21_c), H-Val-Arg(NO_2)-Phe-NH_2 · TFA (21_d), H-Leu-Arg(NO_2)-Phe-NH_2 · TFA (21_e), H-Ile-Arg(NO_2)-Phe-NH_2 · TFA (21_f), H-Nle-Arg(NO_2)-Phe-NH_2 · TFA (21_g), H-Phe-Arg(NO_2)-Phe-NH_2 · TFA (21_h), and H-Pro-Arg(NO_2)-Phe-NH_2 · TFA (21_i) were prepared by the same method described for the preparation of **19**.

21_b: Yield 91%; mp 117 °C (decomp); $[\alpha]_D^{20}$ +6° (*c* 0.5, DMF); R_{f_1} 0.68; R_{f_2} 0.21; Found: C, 54.78; H, 6.89; N, 25.30%; Calcd for $C_{18}H_{28}O_5N_8 \cdot CF_3COOH \cdot 2/3H_2O$: C, 54.65; H, 6.90; N, 25.48%.

21_c: Yield 96%; mp 116 °C (decomp); $[\alpha]_D^{20}$ +14° (*c* 0.5, DMF); R_{f_1} 0.86; R_{f_2} 0.20; Found: C, 43.08; H, 5.65; N, 18.98%; Calcd for $C_{19}H_{30}O_5N_8 \cdot CF_3COOH \cdot H_2O$: C, 43.33; H, 5.67; N, 19.24%.

21_d: Yield 96%; mp 140°C (decomp); $[\alpha]_D^{20}$ +22° (*c* 0.5, DMF); R_{f_1} 0.84; R_{f_2} 0.24; Found: C, 44.73; H, 5.77; N, 18.88%; Calcd for $C_{20}H_{32}O_5N_8 \cdot CF_3COOH \cdot 1/2H_2O$: C, 45.00; H, 5.79; N, 19.08%.

21_e: Yield 94%; mp 120°C (decomp); $[\alpha]_D^{20}$ +16° (*c* 0.5, DMF); R_{f_1} 0.80; R_{f_2} 0.15; Found: C, 45.68; H, 5.90; N, 18.38%; Calcd for $C_{21}H_{34}O_5N_8 \cdot CF_3COOH \cdot 1/2H_2O$: C, 45.95; H, 5.99; N, 18.63%

21_f: Yield 95%; mp 125 °C (decomp); $[\alpha]_D^{20}$ +24° (*c* 0.5, DMF); R_{f_1} 0.72; R_{f_2} 0.22; Found: C, 44.83; H, 6.01; N, 18.01%; Calcd for $C_{21}H_{34}O_5N_8 \cdot CF_3COOH \cdot H_2O$: C, 45.27; H, 6.06; N, 18.36%.

21_g: Yield 100%; mp 105 °C (decomp); $[\alpha]_D^{20}$ +16° (*c* 0.5, DMF); R_{f_1} 0.78; R_{f_2} 0.25; Found: C, 45.72; H, 5.83; N, 18.39%; Calcd for $C_{21}H_{34}O_5N_8 \cdot CF_3COOH \cdot 1/2H_2O$: C, 45.95; H, 5.99; N, 18.63%.

21_h: Yield 99%; mp 121 °C (decomp); $[\alpha]_D^{20}$ +4° (*c* 0.5, DMF); R_{f_1} 0.82; R_{f_2} 0.24; Found: C, 49.55; H, 5.21; N, 17.67%; Calcd for $C_{24}H_{32}O_5N_8 \cdot CF_3COOH$: C, 49.87; H, 5.27; N, 17.89%.

21_i: Yield 94%; mp 92 °C (decomp); $[\alpha]_D^{20}$ −8° (*c* 0.5, DMF); R_{f_1} 0.63; R_{f_2} 0.27; Found: C, 44.18; H, 5.50; N, 18.56%; Calcd for $C_{20}H_{30}O_5N_8 \cdot CF_3COOH \cdot H_2O$: C, 44.47; H, 5.55; N, 18.85%.

Z-Phe-X-Arg(NO_2)-Phe-NH_2 (22_b—22_i): Z-Phe-Ala-Arg(NO_2)-Phe-NH_2 (22_b), Z-Phe-Abu-Arg(NO_2)-Phe-NH_2 (22_c), Z-Phe-Val-Arg(NO_2)-Phe-NH_2 (22_d), Z-Phe-Leu-Arg(NO_2)-Phe-NH_2 (22_e), Z-Phe-Ile-Arg(NO_2)-Phe-NH_2 (22_f), Z-Phe-Nle-Arg(NO_2)-Phe-NH_2 (22_g), Z-Phe-Phe-Arg(NO_2)-Phe-NH_2 (22_h), and Z-Phe-Pro-Arg(NO_2)-Phe-NH_2 (22_i) were also prepared from the coupling reaction of the corresponding Z-amino acid and tripeptide amide by the same method described for the preparation of **18**. These protected peptides were recrystallized from ethyl acetate.

22_b: Yield 90%; mp 165 °C (decomp); $[\alpha]_D^{20}$ −6° (*c* 0.5, DMF); R_{f_1} 0.91; R_{f_2} 0.66; Found: C, 56.61; H, 6.10; N, 16.75%; Calcd for $C_{35}H_{43}O_8N_9 \cdot 3/2H_2O$: C, 56.44; H, 6.18; N, 16.92%.

22_c: Yield 85%; mp 174 °C (decomp); $[\alpha]_D^{20}$ −12° (*c* 0.5, DMF); R_{f_1} 0.90; R_{f_2} 0.53; Found: C, 57.59; H, 6.19; N, 16.63%; Calcd for $C_{36}H_{45}O_8N_9 \cdot H_2O$: C, 57.66; H, 6.27; N,16. 80%.

22_d: Yield 91%; mp 192 °C (decomp); $[\alpha]_D^{20}$ −6° (*c* 0.5, DMF); R_{f_1} 0.85; R_{f_2} 0.35; Found: C, 58.21; H, 6.48; N, 16.31%; Calcd for $C_{37}H_{47}O_8N_9 \cdot H_2O$: C, 58.17; H, 6.42; N, 16.50%.

22_e: Yield 79%; mp 196 °C (decomp); $[\alpha]_D^{20}$ −14° (*c* 0.5, DMF); R_{f_1} 0.88; R_{f_2} 0.47; Found: C, 58.87; H, 6.55; N, 16.37%; Calcd for $C_{38}H_{49}O_8N_9 \cdot H_2O$: C, 58.67; H, 6.56; N, 16.20%.

22_f: Yield 89%; mp 200 °C (decomp); $[\alpha]_D^{20}$ −10° (*c* 0.5, DMF); R_{f_1} 0.90; R_{f_2} 0.56; Found: C, 60.28; H, 6.57; N, 16.23%; Calcd for $C_{38}H_{49}O_8N_9$: C, 60.01; H, 6.45; N, 16.58%.

22_g: Yield 75%; mp 192 °C (decomp); $[\alpha]_D^{20}$ −12° (*c* 0.5, DMF); R_{f_1} 0.92; R_{f_2} 0.53. Found: C, 57.76; H, 6.32; N, 15.76%; Calcd for $C_{38}H_{49}O_8N_9 \cdot 3/2H_2O$: C, 58.00; H, 6.60; N, 16.01%.

22_h: Yield 95%; mp 186 °C (decomp); $[\alpha]_D^{20}$ −18° (*c* 0.5, DMF); R_{f_1} 0.93; R_{f_2} 0.62. Found: C, 60.99; H, 6.00; N, 15.74%; Calcd for $C_{41}H_{47}O_8N_9 \cdot 2/3H_2O$: C, 61.10; H, 5.92; N, 15.64%.

22_i: Yield 63%; mp 108 °C (decomp) $[\alpha]_D^{20}$ −24° (*c* 5.0, DMF); R_{f_1} 0.94; R_{f_1} 0.48; Found: C, 58.50; H, 6.06; N, 16.56%; Calcd for $C_{37}H_{45}O_8N_9 \cdot H_2O$: C, 58.33; H, 6.17; N, 16.54%.

Z-Phe-Gly-Arg(NO_2)-Phe-NH_2 (22_a): Z-Phe-Gly-OH (0.53 g, 1.5 mmol) and **19** (0.72 g, 1.5 mmol) were coupled by the same method as described for the preparation of **18**. It was recrystallized from ethyl acetate; Yield 0.85 g (80%); mp 183 °C (decomp); $[\alpha]_D^{20}$ −38° (*c* 0.5, DMF); R_{f_1} 0.88; R_{f_2} 0.66; Found: C, 56.82; H, 5.95; N, 17.21%; Calcd for $C_{34}H_{41}O_8N_9 \cdot H_2O$: C, 56.58; H, 5.96; N, 17.46%.

H-Phe-X-Arg-Phe-NH_2 · 2HCl (23_a—23_i): H-Phe-Gly-Arg-Phe-NH_2 · 2HCl (23_a), H-Phe-Ala-Arg-Phe-NH_2 · 2HCl (23_b), H-Phe-Abu-Arg-Phe-NH_2 · 2HCl (23_c), H-Phe-Val-Arg-Phe-NH_2 · 2HCl (23_d), H-Phe-Leu-Arg-Phe-NH_2 · 2HCl (23_e), H-Phe-Ile-Arg-Phe-NH_2 · 2HCl (23_f), H-Phe-Nle-Arg-Phe-NH_2 · 2HCl (23_g), H-Phe-Phe-Arg-Phe-NH_2 · 2HCl (23_h) and H-Phe-Pro-Arg-Phe-NH_2 · 2HCl (23_i) were also prepared from the corresponding protected tetrapeptides by the catalytic hydrogenation, according to the preparation of **6**. These peptides were obtained as hydrochlorides.

23_a: Yield 90%; mp 134 °C (decomp); $[\alpha]_D^{20}$ +16° (*c* 0.5,

MeOH); R_{f_1} 0.59; R_{f_2} 0.15; Found; C, 49.83; H, 6.55; N, 17.67%; Calcd for $C_{26}H_{36}O_4N_8 \cdot 2HCl \cdot 3/2H_2O$: C, 50.00; H, 6.57; N, 17.93%; Amino acid ratios in acid hydrolyzate: Arg 0.94, Gly 0.91, Phe 2.00.

23$_b$: Yield 99%; mp 129 °C (decomp); $[\alpha]_D^{20}$ −8° (*c* 0.5, MeOH); R_{f_1} 0.67; R_{f_2} 0.21; Found; C, 51.22; H, 6.65; N, 17.91%; Calcd for $C_{27}H_{38}O_4N_8 \cdot 2HCl \cdot H_2O$: C, 51.51; H, 6.67; N, 17.79%; Amino acid ratios in acid hydrolyzate: Arg 0.93, Ala 0.94, Phe 2.00.

23$_c$: Yield 96%; mp 140 °C (decomp); $[\alpha]_D^{20}$ −6° (*c* 0.5, MeOH); R_{f_1} 0.63; R_{f_2} 0.18; Found: C, 50.63; H, 6.86; N, 16.70%; Calcd for $C_{28}H_{40}O_4N_8 \cdot 2HCl \cdot 2H_2O$: C, 50.82; H, 6.95; N, 16.93%; Amino acid ratios in acid hydrolyzate: Arg 0.94, Phe 2.00.

23$_d$: Yield 93%; mp 174 °C (decomp); $[\alpha]_D^{20}$ −19° (*c* 0.5, MeOH); R_{f_1} 0.72; R_{f_2} 0.19; Found: C, 51.37; H, 6.80; N, 16.53%; Calcd for $C_{29}H_{42}O_4N_8 \cdot 2HCl \cdot 2H_2O$: C, 51.55; H, 7.10; N, 16.58%; Amino acid ratios in acid hydrolyzate: Arg 0.94, Val 0.91, Phe 2.00.

23$_e$: Yield 94%; mp 172 °C (decomp); $[\alpha]_D^{20}$ −14° (*c* 0.5, MeOH); R_{f_1} 0.76; R_{f_2} 0.21; Found: C, 54.30; H, 7.06; N, 16.67%; Calcd for $C_{30}H_{44}O_4N_8 \cdot 2HCl \cdot 2/3H_2O$: C, 54.13; H, 7.11; N, 16.83%; Amino acid ratios in acid hydrolyzate: Arg 0.90, Leu 0.93, Phe 2.00.

23$_f$: Yield 88%; mp 170 °C (decomp); $[\alpha]_D^{20}$ −16° (*c* 0.5, MeOH); R_{f_1} 0.77; R_{f_2} 0.22; Found: C, 51.96; H, 7.21; N, 16.31%; Calcd for $C_{30}H_{44}O_4N_8 \cdot 2HCl \cdot 2H_2O$: C, 52.25; H, 7.25; N, 16.24%; Amino acid ratios in acid hydrolyzate: Arg 0.92, Ile 0.88, Phe 2.00.

23$_g$: Yield 94%; mp 102 °C (decomp); $[\alpha]_D^{20}$ −6° (*c* 0.5, MeOH); R_{f_1} 0.71; R_{f_2} 0.21; Found: C, 52.01; H, 7.23; N, 16.01%; Calcd for $C_{30}H_{44}O_4N_8 \cdot 2HCl \cdot 2H_2O$: C, 52.25; H, 7.25; N, 16.24%; Amino acid ratios in acid hydrolyzate: Arg 0.99, Phe 2.00.

23$_h$: Yield 93%; mp 181 °C (decomp): $[\alpha]_D^{20}$ −2° (*c* 0.5, MeOH); R_{f_1} 0.69; R_{f_2} 0.22; Found: C, 55.21; H, 6.30; N, 15.51%; Calcd for $C_{33}H_{42}O_4N_8 \cdot 3/2H_2O$: C, 55.46; H, 6.30; N, 15.67%; Amino acid ratios in acid hydrolyzate: Arg 0.92, Phe 3.00.

23$_i$: Yield 98%; mp 92 °C (decomp); $[\alpha]_D^{20}$ −18° (*c* 0.5, MeOH); R_{f_1} 0.59; R_{f_2} 0.23; Found: C, 51.54; H, 6.95; N, 16.60%; Calcd for $C_{29}H_{41}O_4N_8 \cdot 2HCl \cdot 2H_2O$: C, 51.71; H, 6.98; N, 16.63%; Amino acid ratios in acid hydrolyzate: Arg 0.90, Pro 0.85, Phe 2.00.

We wish to thank Professor Yojiro Muneoka of Hiroshima University for biological assays and helpful discussions.

References

1) K. Kouge, T. Koizumi, H. Okai, and T. Kato, *Bull. Chem. Soc. Jpn.*, **60**, 2409 (1987).

2) Abbreviations used are according to IUPAC-IUB Commissions, *Eur, J. Biochem.*, **138**, 9 (1984). Other abbreviations: DCC, dicyclohexylcarbodiimide; DCurea, *N,N'*-dicyclohexylurea; ECF, ethyl chloroformate; NMM, *N*-methylmorpholine; TFA, trifluoroacetic acid; Bz-, benzoyl-.

3) A. D. Price and J. M. Greenberg, *Science*, **197**, 670 (1977).

4) Y. Muneoka and M. Matsuura, *Comp. Biochem. Physiol.*, **81c**, 61 (1985)

5) A. D. Price and J. M. Greenberg, *Am. Zool*, **19**, 163 (1979).

6) Y. Muneoka and H. Saitoh, *Comp. Biochem. Physiol.*, **85c**, 207 (1986).

7) We asked Professor Yojiro Muneoka of Hiroshima University to measure the biological assays. He measured these assays according to the Ref. 6.

Peptide Synthesis in Aqueous Solution. III. Synthesis and Biological Activity of Cyclohexylamide Derivatives of Peptides Related to a Molluscan Neuropeptide, FMRFamide (Phe-Met-Arg-Phe-NH_2)

Katsushige KOUGE, Yukari KATAKAI,† Haruko SOMA,† Miyuki KONDO,†
Hideo OKAI,*,† Mayumi TAKEMOTO,†† and Yojiro MUNEOKA††
Sanshin Chemical Industrial Co. Ltd., 531, Nagahama, Hirao-cho, Kumage-gun, Yamaguchi 742-11
†Department of Fermentation Technology, Faculty of Engineering, Hiroshima University, Shitami, Saijo-cho, Higashihiroshima 724
††Physiological Laboratory, Faculty of Integrated Arts and Sciences, Hiroshima University, Higashisenda-machi, Naka-ku, Hiroshima 730
(Received May 14, 1987)

In order to investigate the role of C-terminal Phe^4-NH_2 of FMRFamide (Phe-Met-Arg-Phe-NH_2) to the biological activity, 30 kinds of cyclohexylamide derivatives of peptides related to FMRFamide were synthesized and their FMRFamide-like activity was measured. From the results, it was found that the peptide which was placed at C-terminal Phe^4-NH_2 by D-Ala-CHA showed only a relaxing activity. Furthermore, it was recognized that Met-Arg-Asp-diCHA inhibited FMRFamide contraction selectively.

The molluscan neuropeptide FMRFamide(Phe-Met-Arg-Phe-NH_2)[1] which was isolated from the ganglia of the clam *Macrocallista nimbosa* by Price and Greenberg,[2] causes a relaxation or a contraction, depending on its concentration, in the anterior byssus retractor muscle of *Mytilus*. Low concentrations of this peptide(10^{-8}—10^{-7}M, 1M=1mol dm^{-3}) relax acetylcholine-induced catch-tension,[3] whereas high concentrations(higher than 10^{-7}M) cause contraction.[4] In a previous paper,[5] we reported the synthesis of FMRFamide analogs for N-terminal moiety and discussed their structure-activity relations. Consequently, it was found that the precise structure of the N-terminal moiety is indispensable for the FMRFamide-like activity. However, we did not deal with the structure-activity relations of the C-terminal moiety in that paper. Muneoka and Saitoh[6] already reported that the substitution of D-Arg or Lys for Arg,[3] the substitution of D-Phe for C-terminal Phe, and the removal of the C-terminal amide eliminated contractile activity and greatly reduced relaxing activity in the relations of the C-terminal moiety. From their report, it is assumed that the C-terminal moiety (Arg^3-Phe^4-NH_2) of this peptide serves as a binding unit to the FMRFamide receptor, so that it gives rise to a FMRFamide-like activity.

To learn more about the role of C-terminal Phe^4-NH_2 to the activity, we designed FMRFamide analogs and fragments, which possess the fundamental structure shown in Fig. 1. Since the substitution of cyclohexylamide of D-amino acid for C-terminal Phe^4-NH_2 seems to substantially keep the molecular structure of FMRFamide, we expected that these peptides were designed to exhibit the same activity as the FMRFamide one.

In this paper, for the first step of this study, about thirty kinds of cyclohexylamide derivatives of di-, tri-, and tetrapeptide were synthesized and the FMRFamide-like activity of these peptides were measured. Further, antagonistic effects of these peptides to FMRFamide- or acetylcholine-induced contractions were examined in order to determine the interaction of FMRFamide and its receptor.

The synthetic route to the cyclohexylamide deriva-

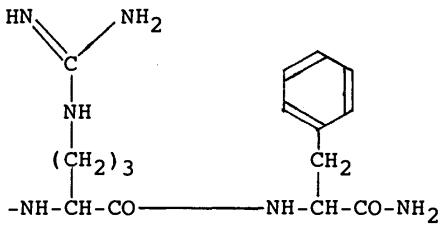

-Arg-Phe-NH_2(FMRFamide)

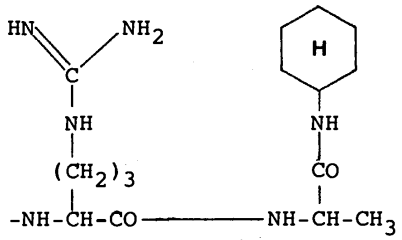

-Arg-D-Ala-CHA

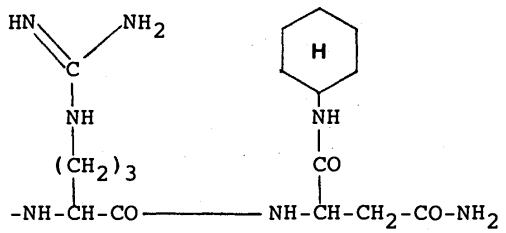

-Arg-D-Asn-CHA

Fig. 1. Cyclohexylamide derivatives of FMRFamide.

tives of di-, tri-, and tetrapeptide is shown in Fig. 2. For the synthesis of FMRFamide, the method of selective acylation to Arg residue in aqueous solution was employed.[7] Boc-X-OH(X; Gly, D/L-Ala, Abu, D/L-Asn, Gln, Asp, or Gln was coupled with cyclohexylamide by the mixed anhydride(MA) method to yield $\mathbf{2_a}$—$\mathbf{2_i}$. The N-terminal protecting group of $\mathbf{2_a}$—$\mathbf{2_i}$ was removed by the action of hydrogen chloride in dioxane to yield $\mathbf{3_a}$—$\mathbf{3_i}$, and then Z-Arg-(NO_2)-OH and $\mathbf{3_a}$—$\mathbf{3_i}$ were condensed to yield $\mathbf{4_a}$—$\mathbf{4_i}$. The removal of the Z-group and NO_2-group from $\mathbf{4_a}$—$\mathbf{4_i}$ by hydrogenation afforded the free dipeptide cyclohexylamide($\mathbf{5_a}$—$\mathbf{5_i}$). Boc-Met-OH was esterified by DCC and *p*-(hydroxyphenyl)dimethylsulfonium methyl sulfate (HODMSP·$MeSO_4^-$) to afford the water-soluble active ester (**6**). In an aqueous solution, compound **6** was allowed to react with $\mathbf{5_a}$—$\mathbf{5_i}$ in the presence of 1M Na_2CO_3 (1M=1 mol dm^{-3}) at pH 7.2. To the reaction

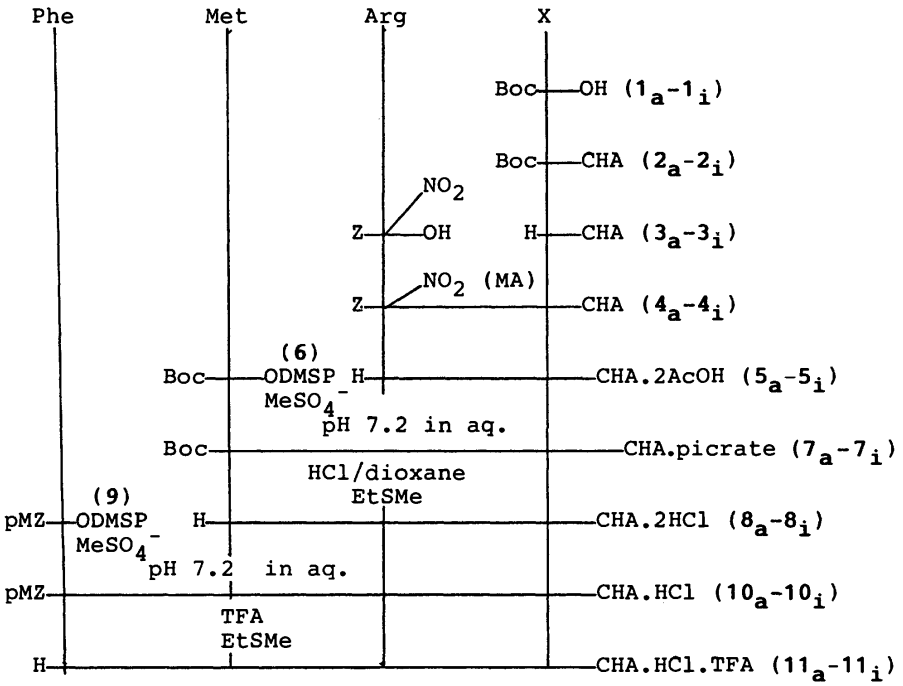

X: Gly(a),Ala(b),D-Ala(c), Abu(d), Asn(e),D-Asn(f),Gln(g),
Asp(h),Glu(i),

-ODMSP.$MeSO_4^-$:

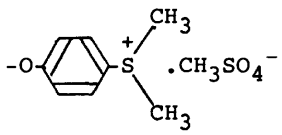

Fig. 2. Synthesis of cyclohexylamide derivatives of peptides.

Table 1. Contractile and Relaxing Effect of Synthesized Peptide

Peptide		Contractile effect/M				Relaxing effect/M				
		10^{-7}	10^{-6}	10^{-5}	10^{-4}	10^{-8}	10^{-7}	10^{-6}	10^{-5}	10^{-4}
Phe-Met-Arg-Phe-NH_2 (FMRFamide)		±	+	++		+				−
Phe-Met-Arg-Gly-CHA	(**11a**)				−					−
Phe-Met-Arg-Ala-CHA	(**11b**)				−					−
Phe-Met-Arg-D-Ala-CHA	(**11c**)				−		±	+	++	++
Phe-Met-Arg-Abu-CHA	(**11d**)				−					−
Phe-Met-Arg-Asn-CHA	(**11e**)				−					−
Phe-Met-Arg-D-Asn-CHA	(**11f**)				−					−
Phe-Met-Arg-Gln-CHA	(**11g**)				−					−
Phe-Met-Arg-Asp-diCHA	(**11h**)				−					−
Phe-Met-Arg-Glu-diCHA	(**11i**)				−					−

+: Effect, −: no effect.

Table 2. Antagonistic Action of Dipeptides

Peptide	Antagonistic action			
	Ach (10^{-4} M) contraction/M		FMRFa (10^{-6} M) contraction/M	
	10^{-5}	10^{-4}	10^{-5}	10^{-4}
Arg-Gly-CHA (**5a**)		*		*
Arg-Ala-CHA (**5b**)		−		−
Arg-D-Ala-CHA (**5c**)		*		*
Arg-Abu-CHA (**5d**)		*		*
Arg-Asn-CHA (**5e**)		−		−
Arg-D-Asn-CHA (**5f**)		−		−
Arg-Gln-CHA (**5g**)		−		−
Arg-Asp-diCHA (**5h**)		+	+	
Arg-Glu-diCHA (**5i**)		±		+

+: Effect, −: no effect, *: increasing contraction.

Table 3. Antagonistic Action of Tripeptides

Peptide	Antagonistic action			
	Ach (10^{-4} M) contraction/M		FMRFa (10^{-6} M) contraction/M	
	10^{-5}	10^{-4}	10^{-5}	10^{-4}
Met-Arg-Gly-CHA (**8a**)		−		−
Met-Arg-Ala-CHA (**8b**)		−		−
Met-Arg-D-Ala-CHA (**8c**)		−		−
Met-Arg-Abu-CHA (**8d**)		−		−
Met-Arg-Asn-CHA (**8e**)		−		±
Met-Arg-D-Asn-CHA (**8f**)		−		−
Met-Arg-Gln-CHA (**8g**)		−		±
Met-Arg-Asp-diCHA (**8h**)		±	+	++
Met-Arg-Glu-diCHA (**8i**)		+	+	++

+: Effect, −: no effect.

mixture containing the Boc-tripeptide cyclohexylamide acetate, 1% picric acid was added and then the resulting Boc-tripeptide cyclohexylamide picrate(**7a**—**7i**) was isolated by extraction with ethyl acetate. The Boc-group was removed from **7a**—**7i** with hydrogen chloride in the presence of ethyl methyl sulfide to yield tripeptide cyclohexylamide(**8a**—**8i**). pMZ-Phe-OH was esterified by DCC and HODMSP·$MeSO_4^-$ to afford the water-soluble active ester(**9**), which was allowed to react with **8a**—**8i** in the same manner as described for the preparation of Boc-tripeptide cyclohexylamide to yield pMZ-tetrapeptide cyclohexylamide(**10a**—**10i**). Finally, the pMZ-group was removed from **10a**—**10i** with trifluoroacetic acid to yield free tetrapeptide cyclohexylamide(**11a**—**11i**).

The purity of the synthetic peptides was confirmed by TLC in two solvent systems and by elemental analysis. The homogeneity of the tri- or tetrapeptides were confirmed by amino acid analysis.

The FMRFamide-like activity of these synthesized peptides on the anterior byssus retractor muscle was determined,[8] as shown in Table 1. All of the cyclohexylamide derivatives of di- or tripeptide synthesized showed neither contractile activity nor relaxing activity between 10^{-8} and 10^{-4} M. In the tetrapeptides, the

Table 4. Antagonistic Action of Tetrapeptides

Peptide	Antagonistic action			
	Ach (10^{-4} M) contraction/M		FMRFa (10^{-6} M) contraction/M	
	10^{-5}	10^{-4}	10^{-5}	10^{-4}
Phe-Met-Arg-Gly-CHA (**11a**)		−	−	+
Phe-Met-Arg-Ala-CHA (**11b**)		−	−	+
Phe-Met-Arg-D-Ala-CHA (**11c**)		+		+
Phe-Met-Arg-Abu-CHA (**11d**)	+	+		+
Phe-Met-Arg-Asn-CHA (**11e**)		+		++
Phe-Met-Arg-D-Asn-CHA (**11f**)		+		+
Phe-Met-Arg-Gln-CHA (**11g**)		+		++
Phe-Met-Arg-Asp-diCHA (**11h**)		++		++
Phe-Met-Arg-Glu-diCHA (**11i**)		++		++

+: Effect, −: no effect.

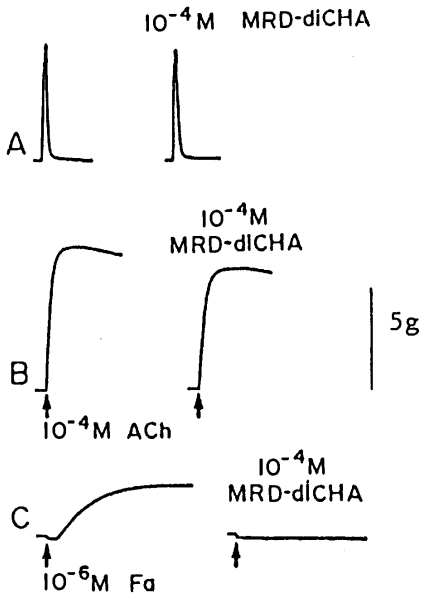

Fig. 3. Antagonistic action of Met-Arg-Asp-diCHA(MRD-diCHA) on contractions produced by electrical pulses (A), Acetylcholine (B), and FMRFamide (C). Fa: FMRFamide, Ach: Acetylcholine.

peptide which was replaced at C-terminal Phe^4-NH_2 by D-Ala-CHA showed only a relaxing activity. Its potency was one tenth as compared with that of FMRFamide, but the fact that this peptide had only a relaxing activity is noteworthy from the viewpoint of pharmacology.

Muneoka and Saitoh[6] reported that Phe-Met-Arg-D-Phe-NH_2 antagonized strongly FMRFamide contraction. It is very important to determine the antagonists

Table 5. Yields and Analytical Data of Protected and Free Dipeptides

Compound	Yield %	Mp θ_m/°C	$[\alpha]_D$/° (Solvent)	Formula	Found(Calcd)/% C	H	N	R_{f_1}	R_{f_2}
4a	74	124(decomp)	+8 (*c* 0.5, DMF)	$C_{22}H_{33}O_6N_7$	53.49 (53.75	6.70 6.71	19.81 19.94)	0.80	0.55
4b	70	149(decomp)	+6 (*c* 1, DMF)	$C_{23}H_{35}O_6N_7$	53.49 (54.64	6.88 6.92	19.30 19.38)	0.82	0.61
4c	68	151(decomp)	−4 (*c* 0.5, DMF)	$C_{23}H_{35}O_6N_7$	54.39 (54.64	6.90 6.92	19.42 19.38)	0.82	0.62
4d	72	181(decomp)	+6 (*c* 0.5, DMF)	$C_{24}H_{37}O_6N_7$	55.18 (55.47	7.11 7.12	18.59 18.86)	0.83	0.61
4e	60	216(decomp)	−3 (*c* 1, DMF)	$C_{24}H_{36}O_7N_8 \cdot 1/2H_2O$	50.01 (50.25	6.40 6.45	19.28 19.53)	0.87	0.48
4f	74	188(decomp)	+13 (*c* 1, DMF)	$C_{24}H_{36}O_7N_8 \cdot H_2O$	49.45 (49.48	6.51 6.52	18.99 19.22)	0.85	0.48
4g	84	195(decomp)	+5 (*c* 1, DMF)	$C_{25}H_{38}O_7N_8 \cdot 2/3H_2O$	52.20 (52.25	6.88 6.85	19.21 19.49)	0.91	0.79
4h	75	205(decomp)	+4 (*c* 0.5, DMF)	$C_{30}H_{45}O_7N_8$	56.98 (57.26	7.05 7.15	17.57 17.80)	0.91	0.79
4i	82	265(decomp)	−2 (*c* 1, DMF)	$C_{31}H_{47}O_7N_8$	57.58 (57.88	7.29 7.31	17.28 17.41)	0.93	0.76
5a	94	Hygroscopic	—	$C_{14}H_{28}O_2N_6 \cdot 2CH_3COOH$	—	—	—	0.54	0.21
5b	92	Hygroscopic	—	$C_{15}H_{30}O_2N_6 \cdot 2CH_3COOH$	—	—	—	0.55	0.20
5c	96	Hygroscopic	—	$C_{15}H_{30}O_2N_6 \cdot 2CH_3COOH$	—	—	—	0.60	0.23
5d	88	Hygroscopic	—	$C_{16}H_{32}O_2N_6 \cdot 2CH_3COOH$	—	—	—	0.58	0.30
5e	91	Hygroscopic	—	$C_{16}H_{31}O_3N_7 \cdot 2CH_3COOH$	—	—	—	0.60	0.39
5f	94	115—118	+22 (*c* 0.5, MeOH)	$C_{16}H_{31}O_3N_7 \cdot 2CH_3COOH \cdot H_2O$	47.11 (47.37	8.03 8.08	19.08 19.32)	0.60	0.40
5g	80	110—113	+22 (*c* 0.5, MeOH)	$C_{17}H_{33}O_3N_7 \cdot 2CH_3COOH \cdot 3/2H_2O$	47.29 (47.57	8.27 8.30	18.43 18.49)	0.63	0.38
5h	97	113—115	+4 (*c* 1, MeOH)	$C_{22}H_{40}O_3N_7 \cdot 2CH_3COOH \cdot 2H_2O$	51.28 (51.51	8.54 8.58	16.01 16.17)	0.72	0.43
5i	91	116—118	+12 (*c* 0.5, MeOH)	$C_{23}H_{42}O_3N_7 \cdot 2CH_3COOH \cdot 2H_2O$	52.02 (52.29	8.68 8.71	15.71 15.80)	0.71	0.42

of FMRFamide for the elucidation of the mechanism of its biological actions. Therefore, these synthesized peptides were tested regarding their abilities to block FMRFamide-induced contractions or the contractions produced by other actions.[8] The results of antagonistic activity tests are shown in Tables 2—4. As shown in Table 2, Arg-Asp-diCHA(**5h**) and Arg-Glu-diCHA(**5i**) antagonized FMRFamide contrations and acetylcholine contractions. From Table 3, it was found that Met-Arg-Asp-diCHA(**8h**) and Met-Arg-Glu-diCHA(**8i**) exhibit higher activities than the corresponding dipeptides to block FMRFamide-induced contractions, respectively. In particular, Met-Arg-Asp-diCHA(**8h**) inhibited FMRFamide contraction selectively and had no effects upon acetylcholine contractions, as shown in Fig. 3. Most of the synthesized tetrapeptides antagonized FMRFamide contraction and acetylcholine contraction. The ability of the inhibition generally enhanced with the increasing of the hydrophobicity of C-terminal, but the selective inhibition observed in Met-Arg-Asp-diCHA(**8h**) was not observed.

From the results described above, we could synthesize a relaxing peptide by the subsutitution of cyclohexylamide derivatives for C-terminal Phe^4-NH_2. This fact will lead us to design more useful relaxing peptide. Furthermore, the result that the synthesized peptide possessing high hydrophobicity at C-terminal antagonized FMRFamide contraction, was compatible with the hypothesis that the hydrophobic C-terminal of FMRFamide serves as a binding unit to the receptor.

Experimental

All the melting points were uncorrected. The optical rotations were measured on a Union PM-101 polarimeter. TLC was carried out on Merck Silicagel G: R_{f_1}, 1-butanol-acetic acid-pyridine-water(4 : 1 : 1 : 2, v/v), R_{f_2}, $CHCl_3$-methanol (5 : 1, v/v). Spots of material possessing free amino group on TLC plate were detected by spraying with ninhydrin, and those of amino group blocked materials by spraying with 25% HBr in acetic acid and then ninhydrin. Amino acid analysis was performed by HPLC using JASCO TRI ROTAR-V and UVIDEC-100 V apparatus.

Synthesis of Cyclohexylamide Derivatives of Peptides. Z-Arg(NO_2)-X-CHA(4a—4i): To a solution of Z-Arg(NO_2)-OH in THF and equimolar NMM, equimolar ECF was added at −5 °C. After 10 min, a solution of equimolar H-X-CHA·HCl(**3a—3i**) and NMM in $CHCl_3$ was added. The reaction mixture was stirred in an ice bath for 1 h and then at room temperature overnight. The mixture was evaporated in vacuo, and the oily residue was dissolved in ethyl acetate. The solution was washed with water, 4% sodium hydrogencarbonate, 0.5M hydrochloric acid, and water, successively, and then dried over anhydrous sodium

Table 6. Yields and Analytical Data of Protected and Free Tripeptides

Compound	Yield %	Mp θ_m/°C	$[\alpha]_D$/° (Solvent)	Formula	Found(Calcd)/% C	H	N	R_{f_1}	R_{f_2}
7a	65	130(decomp)	−6 (*c* 0.5, DMF)	$C_{24}H_{45}O_5N_7S\cdot C_6H_3O_7N_3$	46.49 (46.74	6.21 6.23	17.94 18.16)	0.80	0.20
7b	48	150(decomp)	−4 (*c* 0.5, DMF)	$C_{25}H_{47}O_5N_7S\cdot C_6H_3O_7N_3\cdot 1/2H_2O$	47.01 (47.25	6.38 6.47	17.51 17.77)	0.80	0.30
7c	54	152(decomp)	+10 (*c* 0.5, DMF)	$C_{25}H_{47}O_5N_7S\cdot C_6H_3O_7N_3\cdot H_2O$	46.58 (46.72	6.23 6.52	17.41 17.57)	0.81	0.31
7d	56	156(decomp)	−6 (*c* 0.5, DMF)	$C_{26}H_{49}O_5N_7S\cdot C_6H_3O_7N_3$	47.79 (48.02	6.47 6.50	17.31 17.49)	0.82	0.31
7e	70	154(decomp)	−8 (*c* 0.5, DMF)	$C_{26}H_{48}O_6N_8S\cdot C_6H_3O_7N_3\cdot H_2O$	45.69 (45.98	6.30 6.34	18.42 18.43)	0.82	0.31
7f	43	158(decomp)	+14 (*c* 0.5, DMF)	$C_{26}H_{48}O_6N_8S\cdot C_6H_3O_7N_3\cdot 2/3H_2O$	46.30 (46.31	6.11 6.31	18.28 18.56)	0.82	0.31
7g	47	164(decomp)	−12 (*c* 0.5, DMF)	$C_{27}H_{50}O_6N_8S\cdot C_6H_3O_7N_3\cdot 2H_2O$	45.39 (45.66	6.50 6.57	17.11 17.20)	0.81	0.30
7h	62	158(decomp)	−2 (*c* 1, DMF)	$C_{32}H_{57}O_6N_8S\cdot C_6H_3O_7N_3$	49.97 (50.13	6.57 6.59	16.67 16.92)	0.82	0.31
7i	71	182(decomp)	−14 (*c* 0.5, DMF)	$C_{33}H_{59}O_6N_8S\cdot C_6H_3O_7N_3$	51.38 (50.67	6.62 6.71	16.47 16.66)	0.80	0.28
8a	84	115(decomp)	−6 (*c* 0.5, MeOH)	$C_{19}H_{37}O_3N_7S\cdot 2HCl\cdot 2H_2O$	41.28 (41.33	7.75 7.78	17.48 17.74)	0.58	0.21
8b	91	121(decomp)	−12 (*c* 0.5, MeOH)	$C_{20}H_{39}O_3N_7S\cdot 2HCl\cdot 3/4H_2O$	43.82 (44.15	7.73 7.81	17.88 18.01)	0.59	0.25
8c	78	123(decomp)	+24 (*c* 0.5, MeOH)	$C_{20}H_{39}O_3N_7S\cdot 2HCl\cdot 3/2H_2O$	43.05 (43.08	7.54 7.89	17.44 17.58)	0.58	0.25
8d	80	105(decomp)	−8 (*c* 0.5, MeOH)	$C_{21}H_{41}O_3N_7S\cdot 2HCl\cdot H_2O$	44.69 (44.86	7.88 8.00	17.31 17.43)	0.58	0.24
8e	94	125(decomp)	−6 (*c* 0.5, MeOH)	$C_{21}H_{40}O_4N_8S\cdot 2HCl\cdot 3H_2O$	39.94 (40.19	7.62 7.65	17.59 17.85)	0.60	0.30
8f	85	127(decomp)	+10 (*c* 0.5, MeOH)	$C_{21}H_{40}O_4N_8S\cdot 2HCl\cdot 3/2H_2O$	41.78 (41.99	7.38 7.49	18.63 18.65)	0.61	0.31
8g	88	130(decomp)	−3 (*c* 0.5, MeOH)	$C_{22}H_{42}O_4N_8S\cdot 2HCl\cdot 2H_2O$	42.19 (42.37	7.64 7.70	17.78 17.96)	0.67	0.30
8h	84	129(decomp)	−10 (*c* 0.5, MeOH)	$C_{27}H_{49}O_4N_8S\cdot 2HCl\cdot H_2O$	48.01 (48.24	7.83 7.88	16.41 16.66)	0.70	0.32
8i	92	138(decomp)	−8 (*c* 0.5, MeOH)	$C_{28}H_{51}O_4N_8S\cdot 2HCl\cdot 2H_2O$	47.61 (47.75	8.02 8.09	15.69 15.90)	0.70	0.34

sulfate. The filtrate was evaporated in vacuo. The oily residue was crystallized with ether. In the case of peptides containing D/L-Asn, Gln, Asp, and Glu, the reaction mixture was evaporated in vacuo, and the resulting residue was poured into ice-water. The solid was filtered and the filter cake was washed with 4% sodium hydrogencarbonate, 0.5M hydrochloric acid, and water, successively. The product thus obtained was recrystallized from ethyl acetate. These results were summarized in Table 5.

H-Arg-X-CHA · 2AcOH(5_a—5_i): A solution of Z-Arg-(NO_2)-X-CHA(4_a—4_i) in acetic acid was hydrogenated in the presence of palladium black at room temperature for 21 h. The catalyst was removed by filtration, and the filtrate was evaporated in vacuo. The residue was crystallized with ether. These results are summarized in Table 5.

Boc-Met-ODMSP · $MeSO_4^-$(6)(Water-Soluble Active Ester): To a chilled solution of Boc-Met-OH (2.49g, 10 mmol) and HODMSP · $MeSO_4^-$(2.66g, 10 mmol) in CH_3CN (80 ml), DCC (2.06g, 10 mmol) was added. The reaction mixture was held overnight at 0 °C and the DCurea which formed was filtered off. The filtrate was concentrated in vacuo, and the residual oil was washed with ether by decantation; Yield 3.93g (80%); $[\alpha]_D^{20}$ −30° (*c* 1, MeOH); R_{f_1} 0.82; R_{f_2} 0.34.

Boc-Met-Arg-X-CHA(7_a—7_i): H-Arg-X-CHA · 2AcOH (5_a—5_i) was dissolved in H_2O and the pH of the solution was adjusted to 7.3 by addition of 1M Na_2CO_3. Equimolar Boc-Met-ODMSP · $MeSO_4^-$ was added to the stirred solution below 20 °C, the pH being maintained automatically at 7.2 with 1M Na_2CO_3. After 12 h, 1% picric acid was added to the solution and the pH of the solution was adjusted to 5.6. Yellow precipitate was filtered off and it was dissolved in ethyl acetate. The solution was washed successively with 4% sodium hydrogencarbonate, 4% citric acid and water, and then dried over anhydrous sodium sulfate. The solution was concentrated to an oily residue which was crystallized by addition of ether. It was recrystallized from $CHCl_3$. These results are summarized in Table 6.

H-Met-Arg-X-CHA · 2HCl(8_a—8_i): To a solution of Boc-Met-Arg-X-CHA(7_a—7_i), TFA and ethyl methyl sulfide was added. The reaction mixture was concentrated in vacuo. To a residue, 4M HCl in dioxane was added and then the resulting hydrochloride salt was solidified with acetone. These results are summarized in Table 6.

pMZ-Phe-ODMSP · $MeSO_4^-$(9)(Water-Soluble Active Ester): pMZ-Phe-OH (3.29g, 10 mmol) and HODMSP · $MeSO_4^-$ (2.66g, 10 mmol) were coupled by the same method as **6**. It was an oily product; Yield of the oily product 5.20 g

Table 7. Yields and Analytical Data of Protected and Free Tetrapeptides

Compound	Yield %	Mp θ_m/°C	$[\alpha]_D$/° (Solvent)	Formula	Found(Calcd)/% C	H	N	R_{f_1}	R_{f_2}
10a	74	101(decomp)	−4 (*c* 0.5, DMF)	$C_{37}H_{54}O_7N_8S\cdot HCl$	56.01 (56.19	6.85 6.95	14.02 14.16)	0.81	0.25
10b	68	96(decomp)	−8 (*c* 0.5, DMF)	$C_{38}H_{56}O_7N_8S\cdot HCl\cdot 1/2H_2O$	56.18 (56.07	7.10 7.13	13.48 13.76)	0.83	0.29
10c	65	98(decomp)	+4 (*c* 0.5, DMF)	$C_{38}H_{56}O_7N_8S\cdot HCl\cdot 1/2H_2O$	55.84 (56.07	6.98 7.13	13.53 13.76)	0.83	0.30
10d	58	132(decomp)	−5 (*c* 0.5, DMF)	$C_{39}H_{58}O_7N_8S\cdot HCl$	57.01 (57.20	7.16 7.21	13.48 13.68)	0.82	0.31
10e	71	178(decomp)	−8 (*c* 0.5, DMF)	$C_{39}H_{57}O_8N_9S\cdot HCl\cdot H_2O$	54.21 (54.10	6.48 6.93	14.43 14.55)	0.83	0.33
10f	70	182(decomp)	+10 (*c* 0.5, DMF)	$C_{39}H_{57}O_8N_9S\cdot HCl\cdot H_2O$	53.88 (54.10	6.77 6.93	14.31 14.55)	0.83	0.33
10g	63	163(decomp)	−20 (*c* 0.5, DMF)	$C_{40}H_{59}O_8N_9S\cdot HCl\cdot 1/2H_2O$	54.92 (55.17	6.81 7.00	14.29 14.47)	0.84	0.32
10h	43	175(decomp)	−10 (*c* 0.5, DMF)	$C_{45}H_{66}O_8N_9S\cdot HCl$	58.11 (58.18	6.99 7.11	13.24 13.56)	0.83	0.38
10i	67	181(decomp)	−10 (*c* 0.3, DMF)	$C_{46}H_{68}O_8N_9S\cdot HCl$	58.32 (58.59	7.18 7.21	13.18 13.36)	0.81	0.40
11a	84	98(decomp)	−6 (*c* 0.5, MeOH)	$C_{28}H_{46}O_4N_8S\cdot HCl\cdot CF_3COOH\cdot H_2O$	47.15 (47.45	6.58 6.59	14.58 14.75)	0.62	0.19
11b	89	115(decomp)	−8 (*c* 0.5, MeOH)	$C_{29}H_{48}O_4N_8S\cdot HCl\cdot CF_3COOH\cdot 3/2H_2O$	49.38 (49.66	7.03 7.07	14.80 14.94)	0.64	0.30
11c	87	117(decomp)	+6 (*c* 0.5, MeOH)	$C_{29}H_{48}O_4N_8S\cdot HCl\cdot CF_3COOH\cdot 2H_2O$	46.81 (47.05	6.80 6.82	14.00 14.15)	0.65	0.30
11d	90	110(decomp)	−8 (*c* 0.5, MeOH)	$C_{30}H_{50}O_4N_8S\cdot HCl\cdot CF_3COOH\cdot H_2O$	48.57 (48.85	6.80 6.86	14.17 14.24)	0.65	0.31
11e	91	121(decomp)	−8 (*c* 0.5, MeOH)	$C_{30}H_{49}O_5N_9S\cdot HCl\cdot CF_3COOH\cdot 3/2H_2O$	47.31 (47.43	6.45 6.46	15.21 15.55)	0.67	0.33
11f	85	120(decomp)	+7 (*c* 0.5, MeOH)	$C_{30}H_{49}O_5N_9S\cdot HCl\cdot CF_3COOH\cdot 2H_2O$	45.78 (46.06	6.47 6.59	15.01 15.10)	0.67	0.34
11g	94	115(decomp)	−10 (*c* 0.5, MeOH)	$C_{31}H_{51}O_5N_9S\cdot HCl\cdot CF_3COOH\cdot H_2O$	45.41 (47.73	6.60 6.62	15.01 15.17)	0.66	0.35
11h	80	134(decomp)	−10 (*c* 0.5, MeOH)	$C_{36}H_{58}O_5N_9S\cdot HCl\cdot CF_3COOH\cdot H_2O$	50.61 (50.89	6.83 6.91	13.81 14.05)	0.73	0.41
11i	83	142(decomp)	−30 (*c* 0.5, MeOH)	$C_{37}H_{60}O_5N_9S\cdot HCl\cdot CF_3COOH\cdot 1/2H_2O$	51.66 (51.94	6.81 6.99	13.81 13.97)	0.73	0.43

(90%); $[\alpha]_D^{20}$ −7° (*c* 1, MeOH); R_{f_1} 0.85; R_{f_2} 0.51.

pMZ-Phe-Met-Arg-X-CHA · HCl(10$_a$—10$_i$): H-Met-Arg-X-CHA (**8$_a$—8$_i$**) was dissolved in H_2O and the pH of the solution was adjusted to 7.2 by addition of 1M Na_2CO_3. A slight excess of pMZ-Phe-ODMSP · $MeSO_4^-$ was added to the stirred solution below 20 °C, the pH being maintained automatically at 7.2 with 1M Na_2CO_3. After 12 h, the crude product was precipitated from the reaction mixture. It was filtered and then washed with 4% sodium hydrogencarbonate and water. After removal of moisture by drying, it was recrystallized from methanol or ethyl acetate. These results are summarized in Table 7.

H-Phe-Met-Arg-X-CHA · HCl · TFA(11$_a$—11$_i$): pMZ-Phe-Met-Arg-X-CHA · HCl (**10$_a$—10$_i$**) and ethyl methyl sulfide were dissolved in TFA. The reaction mixture was allowed to stand at room temperature. After 2 h, the solution was concentrated in vacuo. The residue was crystallized with ether. These results were summarized in Table 7.

We wish to thank Professor Yojiro Muneoka of Hiroshima University for biological assays and helpful discussions.

References

1) Abbreviations used are according to IUPAC-IUB Commissions, *Eur, J. Biochem.*, **138**, 9 (1984). Other abbreviations: DCC, dicyclohexylcarbodiimide; DCurea, *N,N'*-dicyclohexylurea; ECF, ethyl chloroformate; NMM, *N*-methylmorpholine; TFA, trifluoroacetic acid; CHA, cyclohexylamide group.

2) A.D.Price and J.M.Greenberg, *Science*, **197**, 670 (1977).

3) Y. Muneoka and M. Matsuura, *Comp. Biochem. Physiol.*, **81c**, 61 (1985).

4) A. D. Price and J. M. Greenberg, *Am. Zool*, **19**, 163 (1979).

5) K. Kouge, H. Soma, Y. Katakai, H. Okai, *Bull. Chem. Soc. Jpn.*, submitted.

6) Y. Muneoka and H. Saitoh, *Comp. Biochem. Physiol.*, **85c**, 207 (1986).

7) K. Kouge, T. Koizumi, H. Okai, and T. Kato, *Bull. Chem. Soc. Jpn.*, **60**, 2409 (1987).

8) We asked Professor Yojiro Muneoka of Hiroshima University to measure the biological assays. He measured these assays according to the Ref. 6.

Quantitative Analysis of Partition Behavior of Substituted Phenols from Aqueous Phase into Liposomes Made of Lecithin and Various Lipids

Hideto MIYOSHI,* Hiroaki MAEDA, Nobuya TOKUTAKE, and Toshio FUJITA
Department of Agricultural Chemistry, Faculty of Agriculture, Kyoto University, Sakyo-ku, Kyoto 606
(Received May 25, 1987)

The partition coefficient of a series of substituted phenols in lecithin-liposome-water systems, P(L/W), was quantitatively analyzed by use of physicochemical molecular and substituent parameters. The effects on the P(L/W) value of the incorporation of cholesterol and charged lipids such as cardiolipin or stearylamine into the liposomal membranes were examined with the perturbation of the bilayered membrane structure induced by these lipids being taken into account. The partition behavior of phenols was primarily decided by the hydrophobicity, represented in terms of the 1-octanol-water partition coefficient, P(O/W). The partitioned phenols seemed to be in membrane close to the interface. The steric and electronic effects of substituents on the partitioning into liposomes varied significantly depending upon the type of lipids incorporated. The variations in these effects reflect differences in the structure of the interfacial region of the lecithin bilayer modified by the incorporation of various lipids.

The partition behavior of a variety of medicinal and agricultural chemicals has been studied extensively with the use of artificial lipid membranes as models of biomembranes.[1-5] In most of these studies, the effects of lipid composition,[1,2] temperature,[3,4] or the pH of the bulk aqueous phase[5] on the partition coefficient have been examined for a limited series of compounds. Only a few investigations have dealt with effects of physicochemical characteristics on the partition behavior of a series of systematically selected chemicals.[6,7]

We have quantitatively analyzed various physicochemical factors that decide the partition coefficient, P(L/W), of a series of substituted phenols in the nonionized form in a lecithin-liposome-water system.[8] The partition was governed most strongly by molecular hydrophobicity represented in terms of the partition coefficient in the 1-octanol-water system, P(O/W), as a reference. It was also affected by the acidity of phenols: The higher the electron-withdrawing ability of the substituent, the easier was the partitioning into the liposomal membrane. The basicity of the hydrogen-bond acceptor in the liposomal membrane seemed to be greater than that of the oxygen of 1-octanol used as the reference phase for the partitioning. The steric bulkiness of substituents was more unfavorable to partitioning into the liposomes than into 1-octanol. The 2,6-disubstitution showed the most unfavorable steric effect. The steric bulkiness of substituents at the meta or para position was less unfavorable. That of monoortho substitution was negligible. From these results, we assumed that the partitioned phenol molecules would be oriented with the benzene ring in the apolar interior and the phenolic OH group in the polar interfacial region of the membrane.

In this study, we measured the P(L/W) values for a number of substituted phenols including newly synthesized compounds to continue examinations of the partition behavior of phenols in artificial membranes. The substitution pattern was varied so that the steric effect of substituents specific for their positions could be analyzed in more detail than in our previous study. The effects of the incorporation of various kinds of lipids, such as cardiolipin (negatively charged), stearylamine (positively charged) and cholesterol, into bilayered lecithin liposomes on the partition behavior of substituted phenols were analyzed by comparison of quantitative structure-partitioning relationships derived with these partitioning systems.

Here, we report details of these analyses and discuss differences in physicochemical factors that govern the partitioning behavior of substituted phenols in various kinds of membranes.

Experimental

Materials. Lecithin was prepared from fresh egg yolk and purified by the method of Singleton et al.[9] Most of the phenols were the same as those studied before.[8,10] Additional phenols were purchased from Nakarai Chemicals, Ltd., except for 2-alkyl-4,6-dinitrophenols, which were synthesized by the nitration of 2-alkylphenols.[11] The structures of newly synthesized phenols were confirmed by elementary analysis and spectra. Phenols were purified by either distillation or silica-gel column chromatography before use. Reagent-grade stearylamine, cardiolipin, *N*-dansylhexadecylamine (DSHA), and anthroylstearic acid (AS) were obtained from the Sigma Chemical Co. Cholesterol was of reagent grade and was further purified by recrystallization from ethanol.

Preparation of Liposome. Lecithin bilayered liposome was prepared by a procedure slightly different from that reported previously.[8] Dry lecithin (100 mg) was suspended in 20 ml of an aspartate buffer (0.04 M† sodium aspartate, 0.25 M Na_2SO_4, and 0.2 mM EDTA), adjusted to pH 6.0 by the addition of NaOH, and sonicated in an ice-cooled bath under Ar gas. Bilayered liposome was separated from the undispersed lecithin by centrifugation and from multilayered liposome by gel filtration on Sepharose 4B at 4 °C. Cholesterol-lecithin liposome (1 : 10, m/m), cardiolipin-lecithin liposome (1 : 5, m/m), and stearylamine-lecithin

† 1 M=1 mol dm^{-3}.

liposome (1 : 5, m/m) were prepared from the corresponding dry lipid mixture in a similar way. The amount of lecithin in the liposome suspension was estimated from that of phosphorus by a modification of the Bartlett method.[12]

Measurement of Partition Coefficient. The partition coefficient, P(L/W), of each substituted phenol between the liposomal membrane and the external aqueous phase was measured by equilibrium dialysis at pH 6.0.[8] A solution of phenols, the concentration range of which is from 10^{-5} to 10^{-4} M, was prepared in the same pH 6.0 aspartate buffer as for the preparation of liposome. At this pH, all of these compounds except for 2,4,6-trichlorophenol and 2,4-dinitro derivatives exist almost completely as the nonionized form. In an equilibrium dialysis cell (ten 1-ml chambers, Sanko Plastic Co.), the liposome suspension (1 ml) was equilibrated with the phenol solution (1 ml) through a cellophane dialysis membrane at 25 °C for 12 h. The partition coefficient, P(L/W), was calculated by Eq. 1,

$$P(\mathrm{L/W}) = \frac{2(C_0 - C)}{C \times C_L} \quad \left[\frac{\text{mol phenols/kg lipids}}{\text{mol phenols/l buffer}}\right] \qquad (1)$$

where C is the concentration at equilibrium of the phenol in the liposome-free chamber, C_0 is that of the phenol in a control experiment without liposome, and C_L is the concentration of lecithin (kg l^{-1}) in the liposome suspension. The total amount of lecithin in 1 ml of the liposome suspension was about 1 mg. The concentration of the phenol was measured spectrophotometrically on a Shimadzu UV-360 spectrophotometer. For the 2,4-dinitro derivatives, the P(L/W) value was measured at pH 3.0. Since the dinitro derivatives exist as an equilibrated mixture of ionized and nonionized species even at this pH (3—8% ionized), this gave the apparent value. Using lecithin-liposome, we examined the effect of variations in the pH of the bulk aqueous phase on the apparent P(L/W) value for 2,4,6-trichloro- and 2,4-dinitrophenols.

Measurement of Polarity of Liposomal Membrane. Variations in the polarity of interfacial and interior regions of the liposome membrane were estimated from the change in λ_{max} of the emission spectrum of DSHA and AS, respectively, incorporated in liposomes.[13] DSHA or AS was mixed with lecithin at the molar ratio of 1 : 50 in chloroform. After removal of the chloroform, liposomes containing the fluorescent probe were prepared in a similar way. All fluorescent measurements were made on a Shimadzu RF-503A spectrophotometer equipped with a thermoregulated cell compartment at 25 °C. The emission λ_{max} of DSHA- and AS-liposome was observed at around 520 and 450 nm, respectively, with excitation at 330 nm and with the slit width of 5 nm for both excitation and emission sides. As an index of polarity, the emission λ_{max} value of DSHA and AS in various organic solvents was also measured.

Results

pH Dependence of Log P(L/W). For 2,4,6-trichloro- and 2,4-dinitrophenols, the effect of variations in pH on the apparent log P(L/W) was examined (Fig. 1). These phenols were partitioned into the liposome membrane even from the bulk aqueous phase, where they are invariably in the ionized form.[8]

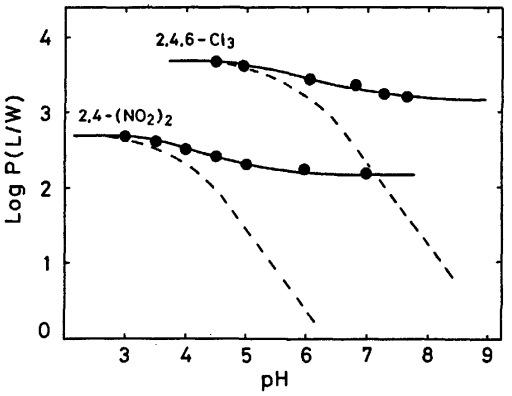

Fig. 1. Dependence on pH of the apparent log P(L/W) value for 2,4,6-trichloro- and 2,4-dinitrophenols. The dotted line is for the dependence of the log P(L/W) value according to the pH-partition model.[14]

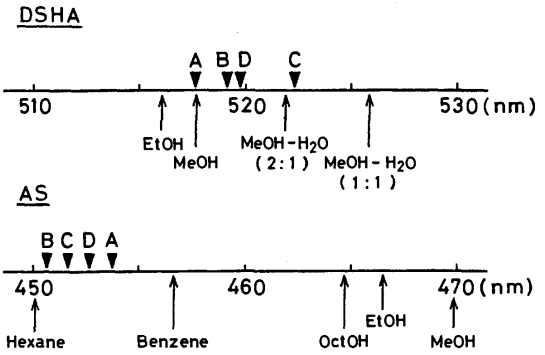

Fig. 2. Positions of the fluorescence emission maximum of DSHA and AS in lecithin liposome (A), cholesterol-lecithin liposome (B), cardiolipin-lecithin liposome (C), and stearyamine-lecithin liposome (D), together with those of various solvents.

Judging from the differences in the apparent log P(L/W) value in regions of lower to higher pH, the partition of the phenolate anions was lower than that of the neutral phenols, although the difference was not large. The partition behavior of 2,4,6-trichloro- and 2,4-dinitrophenols did not obey the pH-partition model,[14] in which the partition of ionized species from aqueous to organic phases such as 1-octanol can be neglected.

Polarity of Liposome Membrane. The emission λ_{max} values of DSHA and AS incorporated in various kinds of liposomes are shown in Fig. 2 together with those measured in various organic solvents. The fluorescent moieties of DSHA and AS have been said to be in the aqueous interface and the hydrophobic fattyacid regions of artificial membranes, respectively.[13] The λ_{max} of DSHA in the genuine lecithin bilayer was 518 nm, which corresponds to that in methanol. That of AS was between those in hexane and benzene. The λ_{max} of DSHA increased after the incorporation of cholesterol, stearylamine, or cardiolipin toward the λ_{max} in

Table 1. Partition Coefficient of Substituted Phenols and Physicochemical Parameters

Substituent	log P (O/W)[a]	Δlog K_A[a]	ΔV_w (m, p)[b]	ΔV_w (di-ortho)[b]	log P(L/W)		log P(L/W)[c]		log P(L/W)$^-$		log P(L/W)$^+$	
			$10\,cm^3\,mol^{-1}$	$10\,cm^3\,mol^{-1}$	Obsd	Calcd[c]	Obsd	Calcd[d]	Obsd	Calcd[e]	Obsd	Calcd[f]
H	1.46	0	0	0	1.97	2.04	1.93	1.95	2.10	2.06	1.96	1.96
2-Me	1.97	−0.30	0	0	2.45	2.42	2.27	2.31	2.48	2.41	2.38	2.34
3-Me	2.02	−0.10	1.12	0	2.34	2.43	2.21	2.36	2.32	2.45	2.25	2.38
4-Me	1.94	−0.16	1.12	0	2.42	2.36	2.33	2.30	2.43	2.39	2.40	2.32
2-Et	2.47[g]	−0.22[h]	0	0	2.81	2.82	2.69	2.69	2.69	2.77	2.72	2.72
4-Et	2.58	−0.23	2.14	0	2.88	2.82	2.78	2.77	2.73	2.85	2.83	2.80
2-*n*-Pr	2.93[g]	−0.36[h]	0	0	3.13	3.19	3.03	3.04	3.04	3.10	3.06	3.07
4-*n*-Pr	3.06	−0.23	3.07	0	3.09	3.17	3.18	3.13	3.09	3.19	3.13	3.17
2-*s*-Bu	3.27	−0.36	0	0	3.47	3.45	3.34	3.28	3.28	3.33	3.35	3.32
4-*s*-Bu	3.27[i]	−0.25[i]	4.09	0	3.43	3.29	3.45	3.29	3.32	3.34	3.43	3.32
2-*t*-Bu	3.31	−1.18	0	0	3.51	3.42	3.46	3.26	3.47	3.32	3.53	3.33
3-*t*-Bu	3.31	−0.14	4.09	0	3.25	3.33	3.18	3.33	3.27	3.37	3.26	3.36
4-*t*-Bu	3.31	−0.25	4.09	0	3.43	3.32	3.31	3.32	3.40	3.37	3.34	3.35
2-Ph	3.09	0.01	0	0	3.40	3.33	3.37	3.17	3.40	3.22	3.40	3.20
4-Ph	3.20	0.43	4.33	0	3.24	3.28	3.25	3.28	3.43	3.32	3.40	3.29
4-*t*-Pent	3.87	−0.25	5.20	0	3.64	3.72	3.55	3.74	3.66	3.76	3.57	3.78
2,6-$(Me)_2$	2.30	−0.64	0	2.24	2.47	2.39	2.37	2.26	2.39	2.45	2.38	2.45
2,6-$(Et)_2$	3.03	−0.59	0	4.28	2.73	2.73	2.60	2.57	3.02	2.82	2.91	2.89
2-Cl	2.15	1.50	0	0	2.73	2.70	2.43	2.56	2.51	2.63	2.47	2.53
3-Cl	2.50	0.96	0.95	0	2.78	2.90	2.81	2.79	2.80	2.85	2.75	2.78
4-Cl	2.39	0.60	0.95	0	2.89	2.79	2.73	2.68	2.88	2.75	2.76	2.68
3-Me-4-Cl	3.10	0.43	2.07	0	3.29	3.29	3.31	3.21	3.21	3.25	3.19	3.22
2,4-Cl_2	3.06	2.09	0.95	0	3.54	3.43	3.22	3.28	3.45	3.31	3.21	3.24
2,6-Cl_2	2.75	3.19	0	1.90	2.84	3.08	2.78	2.89	2.80	3.00	2.75	2.93
2,4,6-Cl_3	3.69	3.99	0.95	1.90	3.61	3.85	3.50	3.64	3.70	3.72	3.67	3.66
4-SO_2Me	0.58	2.15	3.80	0	1.27	1.35	1.30	1.43	1.41	1.54	1.32	1.36
4-CN	1.60[g]	2.03[k]	1.20	0	2.11	2.26	2.01	2.18	2.35	2.26	2.08	2.13
3-CF_3	2.95[g]	1.03[l]	1.90	0	3.25	3.22	3.05	3.13	3.17	3.18	3.00	3.12
3-NO_2	2.00	1.58	1.43	0	2.56	2.53	2.49	2.45	2.61	2.53	2.41	2.42
2,4-$(NO_2)_2$	1.54	5.89	1.43	0	2.70	2.50	2.63	2.39	2.60	2.42	2.24	2.21
2-Me-4,6-$(NO_2)_2$	2.13[m]	5.54[m]	1.43	2.60	2.66	2.63	2.60	2.49	2.59	2.63	2.67	2.49
2-Et-4,6-$(NO_2)_2$	2.67[m]	5.55[m]	1.43	3.50	3.02	2.95	2.90	2.78	2.91	2.95	2.85	2.85
2-*i*-Pr-4,6-$(NO_2)_2$	3.10[m]	5.51[m]	1.43	4.50	3.14	3.17	3.09	3.20	3.27	3.18	3.36	3.40
2-*s*-Bu-4,6-$(NO_2)_2$	3.56	5.47	1.43	5.52	3.50	3.41	2.98	2.98	3.34	3.43	3.15	3.12

a) Unless otherwise noted, from Ref. 8. b) From A. Bondi, *J. Phys. Chem.*, **68**, 441 (1964). c) By Eq. 4. d) By Eq. 5. e) By Eq. 6. f) By Eq. 7. g) From log P data bank compiled by Pomona College Medicinal Project, Claremont, California, U. S. A., 1983. h) From J. Epstein, *J. Am. Chem. Soc.*, **86**, 3075 (1964). i) Taken as the same as that of 2-*s*-butylphenol. j) Taken as the same as that of 4-*t*-butylphenol. k) From A. Albert and E. P. Serjeant, "Ionization Constants of Acids and Bases," Methuen, London (1962), p. 130. l) Estimated according to a procedure published by T. Fujita, *Prog. Phys. Org. Chem.*, **12**, 1 (1976). m) Newly measured.

aqueous alcohol, indicating that the polarity of the membrane surface region increased. The incorporation of cardiolipin had the strongest effect. The λ_{max} of AS decreased after the incorporation of one of these lipids, suggesting that the polarity was lowered in the membrane interior.

Analysis of Log *P*(L/W). The log P(L/W) values in four different liposome-water systems are listed in Table 1, where P(L/W), P(L/W)^C, P(L/W)$^+$, and P(L/W)$^-$ represent the partition coefficients measured with liposomes of genuine lecithin, cholesterol-lecithin, stearylamine-lecithin, and cardiolipin-lecithin, respectively. As shown in Fig. 1, the log P(L/W) of 2,4-dinitrophenol ionized by 7.5% at pH 3.0 did not seem to differ much from that of the nonionized form. Along with previous data on 2-*s*-butyl-4,6-dinitrophenol,[8] the log P(L/W) values measured at pH 3.0 for 2,4-dinitrophenol and its 6-substituted derivatives were used without further correction for the following analyses, as approximate values for their nonionized form.

We previously measured the log P(L/W) values of nonionized phenols in the lecithin-liposome-water system using Tris-HCl buffer (10 mM Tris, 50 mM NaCl, 0.2 mM EDTA).[8] The previous relationship between log P(L/W) and log P(O/W) was analyzed by regression analysis with the steric and electronic effects of substituents taken into account, as shown in Eq. 2:

$$\log P(\mathrm{L/W}) = \underset{(0.070)}{0.870}\log P(\mathrm{O/W}) + \underset{(0.029)}{0.064}\,\Delta\log K_A$$
$$\underset{(0.042)}{-0.111}\,\Delta V\mathrm{w(di\text{-}ortho)} \underset{(0.033)}{-0.074}\,\Delta V\mathrm{w(m,p)} + \underset{(0.182)}{0.629} \quad (2)$$
$$(n=26,\ s=0.117,\ r=0.986)$$

In this and the following equations, n is the number of phenols, s is the standard deviation, and r is the correlation coefficient. The figures in parentheses are the 95% confidence interval. As a steric parameter, the relative van der Waals volume of substituents, ΔVw, was used. The ΔVw is the Vw value of substituents relative to that of H and multiplied by 0.1 to make the magnitude similar to other parameters according to Eq. 3.[15]

$$\Delta V\mathrm{w} = [V\mathrm{w(X)} - V\mathrm{w(H)}] \times 0.1 \quad (3)$$

ΔVw(di-ortho) is the sum of the parameters of both ortho substituents for di-ortho substituted phenols. ΔVw(m,p) is such a sum for meta and para substituents. The $\Delta\log K_A$ value [$\log K_A$(substituted phenols)$-\log K_A$(unsubstituted phenol)] is used as the electron-withdrawing index of substituents. Here, the possible relationship between the newly measured log P(L/W) and log P(O/W) values was also analyzed in a similar way. Equations 4—7 gave the best correlation for the various liposome-water systems.

$$\log P(\mathrm{L/W}) = \underset{(0.064)}{0.820}\log P(\mathrm{O/W}) + \underset{(0.025)}{0.079}\,\Delta\log K_A$$
$$\underset{(0.037)}{-0.124}\,\Delta V\mathrm{w(di\text{-}ortho)} \underset{(0.029)}{-0.050}\,\Delta V\mathrm{w(m,p)} + \underset{(0.168)}{0.821} \quad (4)$$
$$(n=34,\ s=0.114,\ r=0.981)$$

$$\log P(\mathrm{L/W})^c = \underset{(0.063)}{0.750}\log P(\mathrm{O/W}) + \underset{(0.026)}{0.064}\,\Delta\log K_A$$
$$\underset{(0.037)}{-0.122}\,\Delta V\mathrm{w(di\text{-}ortho)} + \underset{(0.174)}{0.854} \quad (5)$$
$$(n=34,\ s=0.119,\ r=0.976)$$

$$\log P(\mathrm{L/W})^- = \underset{(0.059)}{0.714}\log P(\mathrm{O/W}) + \underset{(0.024)}{0.053}\,\Delta\log K_A$$
$$\underset{(0.034)}{-0.076}\,\Delta V\mathrm{w(di\text{-}ortho)} + \underset{(0.162)}{1.015} \quad (6)$$
$$(n=34,\ s=0.111,\ r=0.978)$$

$$\log P(\mathrm{L/W})^+ = \underset{(0.052)}{0.756}\log P(\mathrm{O/W}) + \underset{(0.021)}{0.031}\,\Delta\log K_A$$
$$\underset{(0.030)}{-0.057}\,\Delta V\mathrm{w(di\text{-}ortho)} + \underset{(0.144)}{0.859} \quad (7)$$
$$(n=34,\ s=0.099,\ r=0.985)$$

Each of the terms is significant at a level higher than 99.5% except for the $\Delta\log K_A$ in Eq. 7, which is significant at the 99% level. The addition of the ΔVw(m,p) term to Eqs. 5—7 was not justified over the 95% level. In each correlation, the regression coefficients of the $\Delta\log K_A$ and ΔVw terms were much lower than that for the log P(O/W) value. This does not mean that the steric and electronic effects of substituents were not important. In general, the variations in log P(O/W) values were much lower than those in $\Delta\log K_A$ and ΔVw values throughout the series of compounds. The lower regression coefficients for the $\Delta\log K_A$ and ΔVw terms were attributable to a range of variations much higher than that for the log P(O/W) term.

Discussion

Yeagle et al.[16] showed that the choline moiety of the lecithin head groups is oriented almost parallel to the surface plane of bilayered liposomes and that the positively charged trimethylammonio groups are associated electrostatically with the negatively charged phosphates of neighboring lipids. Here, we examined the polarity of the interfacial region of various kinds of liposomes in terms of the shift in the emission maximum of DSHA. The polarity increased with the incorporation of negatively as well as positively charged lipid, suggesting that the inter-head group interactions of the kind studied by Yeagle et al. were weakened and that the interfacial structure was loosened so that the binding of water molecules with the charged head groups on the membrane surface was enhanced. The effects of the cardiolipin molecule, with a large polar head group, were particularly strong. This molecule could perturb the membrane surface structure markedly, increasing the surface polarity very much.

According to Sunamoto et al.[17] the addition of cholesterol molecules to the lecithin bilayer allows closer molecular packing and reduces the mobility of the fatty acid chain of the lecithin above the phase transition temperature of lipids (that of the egg yolk lecithin is approx. -7 to -15 °C[18]). The emission maximum of AS was shifted toward a shorter wavelength. The polarity of the interior region of the liposome was decreased by the incorporation of cholesterol, consistent with the highly packed structure (Fig. 2). However, the addition of cholesterol caused an increase in the polarity around the fluorescent moiety of DSHA. This suggests that the inter-head group interactions were also weak in the cholesterol-lecithin liposome. Our result is consistent with the ^{31}P NMR studies[19] demonstrating that the inter-polar head interactions of phospholipid bilayered membranes are slightly weakened by the addition of cholesterol molecules.

Phenolate anions were partitioned into the liposome membrane, although the extent of partitioning is lower than that of neutral phenols.[8] Generally, the partitioning of charged species into the hydrophobic interior of a lipid membrane is energetically unfavorable.[3] Thus, the phenol molecules, regardless of their dissociation conditions, would be in a region close to the surface of the membrane holding the polar OH group toward the external aqueous phase. Colly and Metcalfe[20] studied the partition behavior of benzyl alcohol in liposomes using NMR spectroscopy and showed that the hydroxyl group projects toward the

aqueous phase. Their observation would be consistent with the model stated above for the orientation of phenols.

The coefficient of the log P(O/W) term in Eqs. 4—7 was from 0.71 to 0.82, which suggests that the partitioning of phenols occurs mainly into a phase less hydrophobic than 1-octanol.[3] Although the variations in the slope were not great, they seemed to correspond to those in the polarity of the membrane surface region; the slope decreased as the polarity increased. This would also suggest that the partitioned phenol molecules are mainly in the region of the membrane surface rather than the more hydrophobic interior.

The significance of the $\Delta \log K_A$ term would be that the basicity of the hydrogen-bond acceptor in the membrane surface region is higher than that of the oxygen of 1-octanol. We have suggested that the phenolic OH group interacts with the phosphate group of the neighboring lecithin.[8] This suggestion may need revision because this type of the interaction seems to be energetically unfavorable from the ^{31}P NMR studies of the lecithin-cholesterol interaction by Yeagle et al.[16] They have shown that the hydrogen bonding of the OH group of the incorporated cholesterol with the carbonyl group of the ester moiety of the lecithin molecule is energetically more favorable than that with the phosphate. If the hydrogen bonding occurs with the phosphate group, a part of nonpolar steroid ring should be exposed in the polar aqueous phase that is energetically less favorable. Thus, the interaction of the OH group of phenols with the carbonyl moiety of lecithin may also be more favorable although the acidity of the OH group in phenols is higher than that in cholesterol (Fig. 3-A). Incorporation of stearylamine (a positively charged lipid) to lecithin liposome reduced the coefficient of $\Delta \log K_A$ term, as shown by Eq. 7, suggesting a reduction in the hydrogen-bonding effect. It is probable that the positively charged amino groups compete with the phenols for the above kind of hydrogen-bonding interaction with hydrogen acceptors.

As shown in Eqs. 2 and 4, the bulkiness of meta and para substituents but not of the mono-ortho substituent was unfavorable to partition into the liposome. We have suggested[8] that the substituted phenols are incorporated from the side of the benzene ring, with the polar OH group projecting toward the external aqueous phase. In this situation, meta and para substituents would have an unfavorable effect on packing in the lecithin molecules, the effect depending upon their volume (Fig. 3-B). For ortho substituted derivatives, both the OH group and the single ortho substituent would be close to the outside of the membrane, with little steric effect on the packing structure of the membrane.[8] Such positional specificity in the steric effect was, however, not observed in Eqs. 5—7. Steric demands for the meta and para substituents were apparently made less strict in the partitioning into the mixed lipid liposomes. These findings are in accord with the partitioning model where the partitioned phenol molecules are close to the surface region of the membrane. With incorporation of lipids other than lecithin, the structure of the membrane surface was loosened even in regions corresponding to the meta and para positions of phenols.

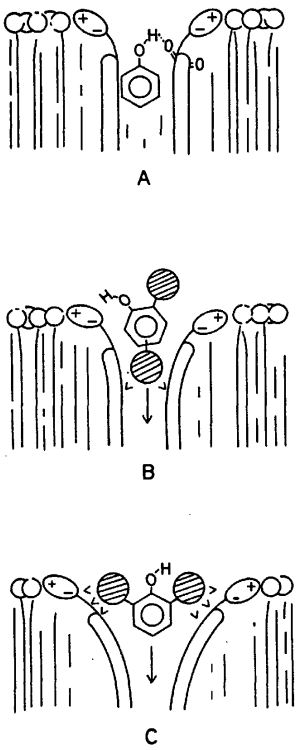

Fig. 3. Partition model of substituted phenols in liposome membrane. 3-A) The OH group of unsubstituted phenol interacts with the carbonyl moiety of lecithin. 3-B) Insertion of meta and para substituents into packed fatty acid chains is unfavorable, whereas that of the ortho substitution into phenols shows negligible effect. 3-C) Di-ortho substituents act as a wedge against the parallel arrangement of lecithin molecules and hinder the hydrogen bond of the OH group.

The steric bulkiness of di-ortho substituents lowered the partitioning into liposome in each of the liposome-water systems. Di-ortho substituents probably act as a wedge against the parallel arrangement of lecithin molecules and hinder the interaction of OH groups with hydrogen-acceptor groups (Fig. 3-C).[8] This kind of steric hindrance is somewhat reduced by the addition of charged lipids to liposome (Eqs. 6 and 7). The conformation of the head groups was more perturbed by the charged lipids more than by cholesterol, as observed by fluorescent probe studies, which is consistent with the above difference in the steric effect of di-ortho substituents.

Equation 4 for log P(L/W) measured in the genuine lecithin liposome was essentially equivalent to Eq. 2 published previously[8] except for the intercept. The higher intercept value for Eq. 4 is probably due to the

Table 2. Log P(L/W) of 2,6-Dialkyl-4-(2,2-dicyanovinyl)phenols

Alkyl	log P(O/W)[a]	Δlog K_A[b]	ΔV_w(m, p)[c]	ΔV_w(di-ortho)[c]	log P(L/W)	
			10 cm^3 mol^{-1}	10 cm^3 mol^{-1}	Obsd	Calcd[d]
H	2.23	2.94	4.04	0	2.80	2.68
Me	3.08	3.07	4.04	2.24	3.20	3.11
Et	4.12	3.00	4.04	4.28	3.61	3.70

a) Newly measured. b) From Ref. 10. c) From A. Bondi, *J. Phys. Chem.*, **68**, 441 (1964). d) By Eq. 4.

higher ionic strength in the aqueous phase used here. The higher the ionic strength, the higher would be the partitioning into the lipid phase. Although the ionic strength would affect the membrane structure, the perturbation may be not so significant since the other terms, which decide the partitioning behavior of phenols, in two equations are almost equal.

To confirm the validity of Eq. 4 for the partition coefficient in the lecithin-liposome-water system, we measured the log P(L/W) value for structurally complex 2,6-dialkyl-4-(2,2-dicyanovinyl)phenols, and compared the observed values with the ones calculated by Eq. 4 (Table 2). The fact that observed values for the three dicyanovinyl phenols agreed with those calculated by Eq. 4 indicates the applicability of the equation to a wide range of phenols to predict their partition coefficient in the lecithin-liposome-water system.

The accumulation of this kind of knowledge on partition behavior of series of systematically selected compounds into various artificial membrane systems from aqueous media should provide reliable means for explanation of their mode of interactions with various biomembranes.

The calculations were done with a FACOM M382 computer at the Data Processing Center of this university. We thank Dr. Takaaki Nishioka, Institute for Chemical Research, Kyoto University for invaluable discussion.

References

1) K. W. Miller, *Br. J. Pharmacol.*, **61**, 57 (1977).
2) M. Luxnat and H. J. Galla, *Biochim. Biophys. Acta*, **856**, 274 (1986).
3) Y. Katz and J. M. Diamond, *J. Membrane Biol.*, **17**, 69 (1974).
4) M. Ahmed, J. S. Burton, J. Hadgraft, and I. W. Kellaway, *J. Membrane Biol.*, **58**, 181 (1981).
5) M. R. Eftink, R. K. Puri, and M. D. Ghahramani, *Biochim. Biophys. Acta*, **813**, 137 (1985).
6) P. Seeman, W. O. Kwant, M. Goldberg, and M. Chan-Wang, *Biochim. Biophys. Acta*, **255**, 178 (1972).
7) N. P. Franks and W. R. Lieb, *Proc. Natl. Acad. Sci. U.S.A.*, **83**., 5116 (1986).
8) H. Miyoshi, T. Nishioka, and T. Fujita, *Bull. Chem. Soc. Jpn.*, **59**, 1099 (1986).
9) S. Singleton, M. S. Gray, M. L. Brown, and J. L. white, *J. Am. Oil. Chem. Soc.*, **42**, 53 (1965).
10) H. Miyoshi, T. Nishioka, and T. Fujita, *Biochim. Biophys. Acta*, **891**, 194 (1987).
11) W. Oettmeier and K. Masson, *Pestic. Biochem. Physiol.*, **141**, 86 (1980).
12) I. Shibuya, H. Honda, and B. Maruo, *Agr. Biol. Chem.*, **31**, 111 (1967).
13) A. S. Waggoner and L. Stryer, *Proc. Natl. Acad. Sci. U.S.A.*, **67**, 579 (1970).
14) H. Terada, K. Yoshikawa, Y. Yoshikawa, and F. Kametani, *Chem. Pharm. Bull.*, **29**, 7 (1981).
15) T. Fujita and H. Iwamura, *Top. Curr. Chem.*, **114**, 119 (1981).
16) P. L. Yeagle, W. C. Hutton, C. H. Huang, and R. B. Martin, *Proc. Natl. Acad. Sci. U.S.A.*, **72**, 3477 (1975).
17) J. Sunamoto, T. Hamada, and H. Murase, *Bull. Chem. Soc. Jpn.*, **53**, 2773 (1980).
18) D. Chapman, "Form and Function of Phospholipids," ed by G. B. Ansell, R. M. C. Dawson, and J. N. Hawthorne, Elsevier, Amsterdam (1973), p. 117.
19) M. F. Brown and J. Seeling, *Biochemistry*, **17**, 381 (1978).
20) C. M. Colley and J. C. Metcalfe, *FEBS Lett.*, **24**, 241 (1972).

Reactions of Aryl Ketones and Coumarins with Iodine(III) Tris(trifluoroacetate)

Norihiro FUKUYAMA, Hiroshi NISHINO, and Kazu KUROSAWA*
Department of Chemistry, Faculty of Science, Kumamoto University, Kurokami 2-39-1, Kumamoto 860
(Received June 15, 1987)

The reaction of acetophenones with iodine(III) tris(trifluoroacetate) yields 3′- and/or 2-iodo derivatives, depending upon the substituent on the aromatic ring and the reaction conditions. The reaction was examined by changing the molar ratio of acetophenone versus the reagent, reaction temperature, and solvent. In similar reactions flavanones and coumarins gave iodo derivatives in which iodine is incorporated at various positions orientated by the oxygen functions. 1,2-Diphenylethanone yields 2-hydroxy-2-(2-iodophenyl)-1-phenylethanone and 1-(2-iodophenyl)-2-phenylethanedione. The reactions of other aromatic ketones such as 9-xanthenone, 9-fluorenone, and anthrone also give iodo derivatives in moderate to good yields. The mechanisms for the iodination at the α-carbon to the carbonyl group have been discussed.

Although several iodination reactions of aromatic hydrocarbons and ketones have been investigated,[1,2] it is still desirable to seek a better method for iodination. The reaction of iodine(III) tris(trifluoroacetate) (ITT), which is readily prepared by the oxidation of iodine with fuming nitric acid in trifluoroacetic anhydride,[3] has been carried out only with a limited number of aromatic substrates such as benzene, toluene, and chlorobenzene by Maletina et al.[4] In Maletina's procedure, iodination products were obtained when a reaction intermediate, bis(trifluoroacetoxy) derivative, was treated with aqueous sodium iodide (Scheme 1).

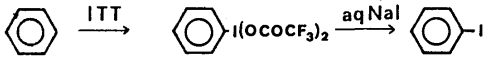

Scheme 1.

We have studied the reaction for its applicability to a wide variety of compounds. We chose acetophenones, 1,2-diphenylethanone, flavanones, coumarins, 9-xanthenone, 9-fluorenone, and anthrone as the substrate, because they were polyfunctionalized compounds, and some biological activity is expected for their iodination products.[5] At first, the iodination of several acetophenone derivatives **1a—e** was examined in order to understand the dependency of yields on the reaction time, reaction temperature, solvents and substituent effects.

Results

A mixture of acetophenone (**1a**) and ITT in a molar ratio of 1 : 1 was stirred in dichloromethane at 23 °C and the reaction mixture was treated with aqueous sodium iodide, giving 3′-iodoacetophenone (**2a**) in a 41% yield (Table 1, Entry 2). The reaction of **1a** with ITT in a molar ratio of 1 : 2 gave 92% yield of **2a** after 24h (Entry 4). At 0 °C or at the refluxing temperature of dichloromethane, yields of **2a** became lower (Entries 1 and 3). A remarkable change in the products was demonstrated by reaction media. In chloroform, in which ITT is readily soluble, the reaction yielded only 2-iodoacetophenone (**3a**) and 2-hydroxyacetophenone

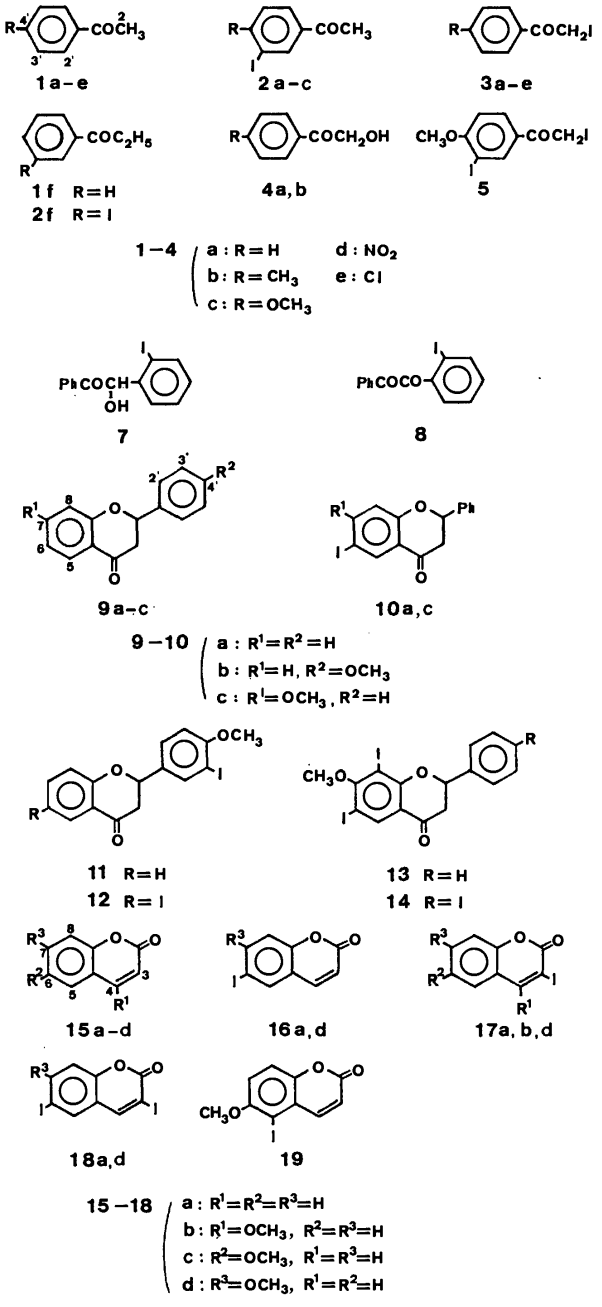

Fig. 1.

Table 1. Reactions of Acetophenones (**1a—e**), Propiophenone (**1f**), and 1,2-Diphenylethanone (**6**) with $I(OCOCF_3)_3$ at Room Temperature

Entry	Substrate	Molar ratio[a]	Solvent	Time h	Recovery %	Product (yield/%)[b]
1	**1a**	1:1	CH_2Cl_2	24[c]	70	**2a**[13](10)
2	**1a**	1:1	CH_2Cl_2	12	20	**2a**(41)
3	**1a**	1:1	CH_2Cl_2	6[d]		**2a**(22)
4	**1a**	1:2	CH_2Cl_2	24		**2a**(92)
5	**1a**	1:1	$CHCl_3$	6		**3a**[14](65) **4a**[15](14)
6	**1a**	1:1	CH_3CN	6	18	**3a**(14)
7	**1a**	1:1	CCl_4	8	27	**2a**(16)
8	**1a**	1:2	CCl_4	24		**2a**(32)
9	**1b**	1:1	CH_2Cl_2	7		**2b**[13](85)
10	**1b**	1:1	$CHCl_3$	6	22	**3b**[16](63) **4b**[17](15)
11	**1c**	1:1	CH_2Cl_2	0.5		**2c**[18](97)
12	**1c**	1:1	$CHCl_3$	3	27	**2c**(15) **3c**[19](39) **5**(8)
13	**1d**	1:1	CH_2Cl_2	48	41	**3d**[20](9)
14	**1d**	1:2	$CHCl_3$	7	62	**3d**(36)
15	**1e**	1:2	$CHCl_3$	6	20	**3e**[21](73)
16	**1f**	1:1	CH_2Cl_2	6		**2f**(92)
17	**6**	1:2	CH_2Cl_2	6		**7**(83) **8**(7)

a) Substrate: $I(OCOCF_3)_3$. b) Yields based on the substrate added. c) The reaction at 0 °C. d) The reaction at reflux temperature.

Table 2. Reactions of Flavanones (**9a—c**) and Coumarins (**15a—d**) with $I(OCOCF_3)_3$ in CH_2Cl_2 at Room Temperature

Entry	Substrate	Molar ratio[a]	Time h	Recovery %	Product (yield/%)[b]
18	**9a**	1:1	12	34	**10a**[22](43)
19	**9a**	1:1.5	12		**10a**(49)
20	**9b**	1:1.5	2		**11**[23](43) **12**(42)
21	**9c**	1:1.5	6		**10c**(67) **13**(7)
22	**10c**	1:2	12		**14**(93)
23	**15a**	1:1	24	39	**16a**[24](38) **17a**(7)
24	**15a**	1:1.5	24	21	**16a**(55) **17a**(5) **18a**(2)
25	**15a**	1:2	48		**16a**(38) **18a**(38)
26	**15b**	1:1	8		**17b**(88)
27	**15c**	1:1	24	15	**19**(68)
28	**15d**	1:1	24	25	**16d**(43) **17d**(35) **18d**(5)

a) Substrate: $I(OCOCF_3)_3$. b) Yields based on the substrate added.

(**4a**) in a shorter reaction time (Entry 5). In carbon tetrachloride **2a** was again found to be the main product, but in poor yields (Entries 7 and 8). 4′-Methylacetophenone (**1b**) or 4′-methoxyacetophenone (**1c**) in dichloromethane gave the corresponding 3′-iodo derivatives **2b** and **2c** in excellent yields (Entries 9 and 11). On the other hand, 4′-nitroacetophenone (**1d**) yielded 2-iodo-4′-nitroacetophenone (**3d**) in poor yield (Entry 13). Propiophenone (**1f**) gave 3′-iodo derivative **2f** (Entry 16). The reactions of **1b**, **1c**, **1d**, and 4′-chloroacetophenone (**1e**) in chloroform resulted in 2-iodo derivatives **3b**, **3c**, **3d**, and **3e** in moderate to good yields (Entries 10, 12, 14, and 15). In the case of **1c** diiodo compound **5** was also isolated (Entry 12). The reaction of 1,2-diphenylethanone (**6**) with ITT yielded two products, **7** and **8**. The structure of **7** was concluded to be 2-hydroxy-2-(2-iodophenyl)-1-phenylethanone since an AB spin system due to a methine proton and a hydroxy proton appeared at δ 4.50 and 5.20 with J value of 6.0 Hz in the ^{1}H NMR spectrum. One of the doublets at δ 4.50 disappeared upon deutration and the other collapsed to a singlet. The spectral data for **8** indicated that it is an iodine-substituted benzil. The ^{1}H NMR spectrum showed the presence of nine aromatic hydrogen atoms, three of which appeared at a slightly lower field. Therefore, the structure of **8** is assigned to be 1-(2-iodophenyl)-2-phenylethanedione. Benzoin **7** could be oxidized to **8** by iodine in a 73% yield.

Flavanones. The reaction of flavanone (**9a**) yielded 6-iodoflavanone (**10a**) (Table 2, Entry 18). With increasing the amount of the reagent (ITT) the yield of **10a** increased slightly (Entry 19). When 4′-methoxyflavanone (**9b**) was treated with ITT, it gave 3′-iodo (**11**) and 3′,6-diiodo derivative (**12**) (Entry 20). 7-Methoxyflavanone (**9c**) similarly yielded 6-iodo

Table 3. Physical, Spectral, and Analytical Data for the New Compounds

Compound	Mp (θ_m/°C) (solvent)	IR/cm^{-1}	^{1}H NMR (δ, J/Hz)	Formula M or C, H (%): Found (Calcd)
2f	Colorless liquid	1688 (>C=O)	1.17 (3H, t, J=7.2, CH_3), 2.91 (2H, q, J=7.2, CH_2), 7.10 (1H, m, H-5′), 7.73 (1H, m, H-4′), 7.88 (1H, m, H-6′), 8.20 1H, m, H-2′)	C_9H_9IO M: 259.9698 (259.9696)
5	115—116 (Ethanol)	1670 (>C=O)	3.93 (3H, s, OCH_3), 4.27 (2H, s, CH_2), 6.87 (1H, d, J=7.8, H-5′), 7.95 (1H, dd, J=7.8, 1.8, H-6′), 8.39 (1H, d, J=1.8, H-2′)	$C_9H_8I_2O_2$ C: 27.17 (26.89) H: 2.11 (2.01)
7	113.2—114.2 (Ethanol)	1678 (>C=O) 3460 (OH) 3620 (OH)	4.50 (1H, d, J=6.0, OH), 6.20 (1H, d, J=6.0, CH), 6.9—7.5 (6H, m, ar. H), 7.8—8.0 (3H, m, ar. H)	$C_{14}H_{11}IO_2$ C: 49.64 (49.73) H: 3.25 (3.28)
8	Yellow liquid	1679 (>C=O)	7.0—7.8 (6H, m, H-3′—H-5′, H-3″—H-5″), 7.8—8.3 (3H, m, H-6′, H-2″, H-6″)	$C_{14}H_9IO_2$ M: 335.9649 (335.9649)
10c	112—113 (Ethanol)	1676 (>C=O)	2.85 (1H, dd, J=16.2, 5.4, HCH), 2.98 (1H, dd, J=16.2, 11.4, HCH), 3.82 (3H, s, OCH_3), 5.46 (1H, dd, J=5.4, 11.4, CH), 6.36 (1H, s, H-8), 7.34 (5H, s, Ph), 8.19 (1H, s, H-5)	$C_{16}H_{13}IO_3$ C: 50.38 (50.55) H: 3.42 (3.45)
12	180—182 (Benzene-hexane)	1691 (>C=O)	2.84 (1H, dd, J=16.8, 6.0, HCH), 2.97 (1H, dd, J=16.8, 10.8, HCH), 3.90 (3H, s, OCH_3), 5.34 (1H, dd, J=6.0, 10.8, CH), 6.79 (1H, d, J=8.4, H-8 or H-5′), 6.82 (1H, d, J=8.4, H-5′ or H-8), 7.39 (1H, dd, J=8.4, 1.8, H-6′), 7.73 (1H, dd, J=8.4, 1.8, H-7), 7.87 (1H, d, J=1.8, H-2′), 8.16 (1H, d, J=1.8, H-5)	$C_{16}H_{12}I_2O_3$ C: 38.24 (37.95) H: 2.49 (2.39)
13	120—121 (Ethanol)	1690 (>C=O)	2.93 (1H, m, J=16.0, 4.0, HCH), 3.01 (1H, m, J=16.0, 12.0, HCH), 3.89 (3H, s, OCH_3), 5.52 (1H, q, CH), 8.20 (1H, s, H-8)	$C_{16}H_{12}I_2O_3$ C: 37.69 (37.97) H: 2.37 (2.39)
14	174.5—175.5 (Ethanol)	1705 (>C=O)	2.95 (2H, d, J=8, CH_2), 3.85 (3H, s, OCH_3), 5.50 (1H, t, J=8, CH), 7.1—7.9 (4H, m, ar. H), 8.20 (1H, s, H-5)	$C_{16}H_{11}I_3O_3$ C: 30.50 (30.41) H: 1.75 (1.80)
16d	194—195 (Ethanol)	1730 (>C=O)	3.95 (3H, s, OCH_3), 6.23 (1H, d, J=8.4, H-3), 6.72 (1H, s, H-8), 7.55 (1H, d, J=8.4, H-4), 7.85 (1H, s, H-5)	$C_{10}H_7IO_3$ M: 301.9453 (301.9439)
17a	88—89 (Ethanol)	1728 (>C=O)	7.1—7.7 (4H, m, ar. H), 8.31 (1H, s, H-4)	$C_9H_5IO_2$ C: 39.83 (39.73) H: 1.82 (1.85)
17b	89—90 (Ethanol)	1717 (>C=O)	4.14 (3H, s, OCH_3), 7.1—7.9 (4H, m, ar. H)	$C_{10}H_7IO_3$ C: 39.75 (39.76) H: 2.33 (2.34)
17d	153—154 (Ethanol)	1721 (>C=O)	3.90 (3H, s, OCH_3), 6.79 (1H, d, J=1.8, H-8), 6.87 (1H, dd, J=1.8, 8.4, H-6), 7.36 (1H, d, J=8.4, H-5), 8.28 (1H, s, H-4)	$C_{10}H_7IO_3$ C: 39.60 (39.76) H: 2.28 (2.34)
18a	151—152 (Ethanol)	1736 (>C=O)	7.01 (1H, m, H-8), 7.8—8.0 (2H, m, H-5, H-7), 8.34 (1H, s, H-4)	$C_9H_4I_2O_3$ C: 27.23 (27.16) H: 1.00 (1.01)
18d	251—252 (Ethanol)	1731 (>C=O)	3.94 (3H, s, OCH_3), 6.73 (1H, s, H-8), 7.77 (1H, s, H-5), 8.16 (1H, s, H-4)	$C_{10}H_6I_2O_3$ C: 28.22 (28.07) H: 1.43 (1.41)
19	140—141 (Ethanol)	1722 (>C=O)	3.93 (3H, m, OCH_3), 6.40 (1H, d, J=10.2, H-3), 7.05 (1H, d, J=9.6, H-8), 7.25 (1H, d, J=9.6, H-7), 7.96 (1H, d, J=10.2, H-4)	$C_{10}H_7IO_3$ C: 39.90 (39.76) H: 2.44 (2.34)

derivative **10c** and 6,8-diiodo derivative **13** (Entry 21). The repeated iodination of **10c** with ITT gave 4′,6,8-triiodo-7-methoxyflavanone (**14**) (Entry 22).

Coumarins. The reaction of coumarin (**15a**) with ITT yielded 6-iodo (**16a**) and 3-iodocoumarin (**17a**) (Entry 23). The ^{1}H NMR spectrum of **16a** showed an AB quartet with a J value of 9.6 Hz due to H-3 and H-4, and three aromatic hydrogen atoms. The

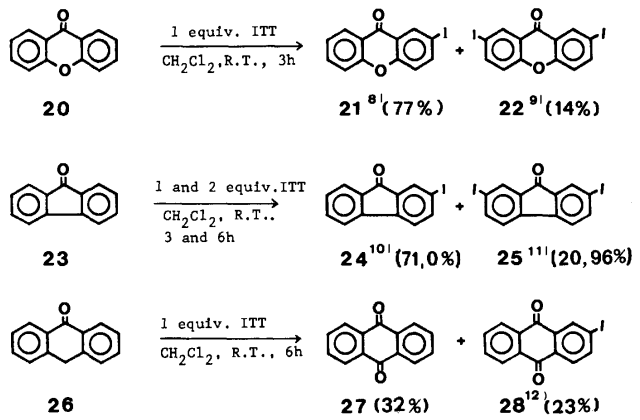

Fig. 2.

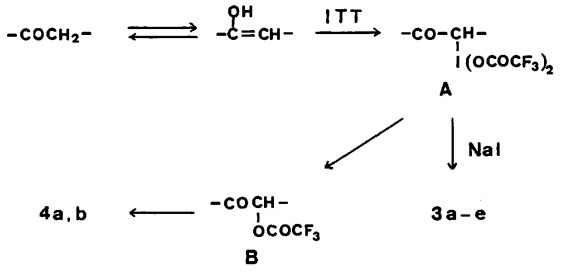

Scheme 2.

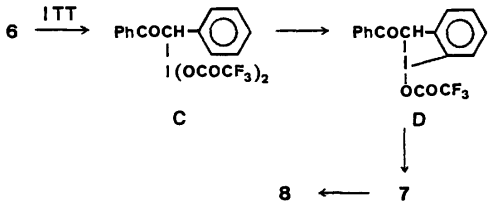

Scheme 3.

^{1}H NMR spectrum of **17a** exhibited a multiplet at the aromatic region corresponding to four hydrogen atoms, H-5—H-8, and a singlet at δ 8.31, indicating the presence of H-4. 3,6-Diiodocoumarin (**18a**) was obtained in a reaction at a molar ratio of 1 : 1.5 and the yield increased remarkably in the reaction at a molar ratio of 1 : 2 (Entries 24 and 25). Introduction of a methoxy group at the C-4 yielded 3-iodo derivative **17b** as the sole product in the reaction of **15b** (Entry 26), while that of a methoxy group at the C-6 in **15c** changes the site of the reaction to the C-5. A methoxy group at the C-7 in **15d** activated the C-3 as well as the C-6, giving **16d**, **17d**, and **18d** (Entry 28).

Other Aromatic Ketones. The reactions of 9-xanthenone (**20**), 9-fluorenone (**23**), and anthrone (**26**) with ITT in dichloromethane were examined and it was found that **20** and **23** gave monoiodo and diiodo derivatives, respectively, and **26** gave anthraquinone (**27**) and 2-iodoanthraquinone (**28**) in moderate yields (Fig. 2).

Discussion

The reaction of ITT with simple aromatic compounds has been reported by Maletina et al.[4] Our study revealed that the electron-donating groups, such as methyl and methoxy groups in acetophenones, enhance the reactivity as shown in Entries 9 and 11. The electron-withdrawing substituents, such as the nitro group, deactivate the aromatic ring and, thus, the reaction occurs at the α-carbon atom to the carbonyl group. The reaction at the aromatic ring can be interpreted as an electrophilic aromatic substitution[4] as shown in Scheme 1. The reaction of acetophenone (**1a**) with ITT in chloroform showed quite different products from those in dichloromethane. 2-Hydroxyacetophenone (**4a**) was obtained along with **3a** and the reaction took much shorter time. A mechanism for the iodination of acetophenone (**1a**) at the C-2 is depicted in Scheme 2. A keto-enol equilibrium and the subsequent addition of ITT to the double bond gave an alkyliodine(III) intermediate **A** which is then decomposed to **3a—e** and **4a,b** during work-up with aqueous sodium iodide. It may be also possible that in the reaction the intermediate **A** could partially be converted to 2-(trifluoroacetoxy)acetophenone (**B**), which may give rise to **4a** during the work-up. In fact, the analogue of **B** prepared from 2-bromoacetophenone with sodium trifluoroacetate was readily hydrolyzed on TLC to give **4a**. It should be noted that iodine is incorporated regiospecifically into the ortho-position in benzyl moiety and a hydroxyl group is introduced onto the methylene group in the reaction of **6** with ITT in dichloromethane. The formation of **7** could be accounted for by modifying the mechanism which has been described for the reaction of acetophenones with ITT in chloroform (as shown in Scheme 3). The reaction intermediate **C** may form an iodine(III)-containing cyclic compound **D** which could be decomposed during work-up to give **7**. The oxidation of benzoin to benzil has precedence.[6]

The orientation in the reaction of coumarins with ITT is quite similar to the orientation in the nitration and the sulfonation of coumarin (**15a**) in which the aromatic ring and the pyrone ring undergo the electrophilic aromatic substitution.[7] The reaction of 4-methoxycoumarin (**15b**) and 7-methoxycoumarin (**15d**) with ITT yielded 3-iodo derivatives **17b** and **17d** that are expected from the consideration of the electron-donating effect of the methoxy group. The reaction of 9-xanthenone (**20**) and 9-fluorenone (**23**) gave 2-iodo derivatives as the major product and diiodo derivatives. These iodo derivatives have been previously prepared by various methods.[8-12] However, the ease of operation in the iodination with ITT made the latter better for the preparation of these compounds. The formation of 2-iodoanthracene (**28**) deserves comments. Anthraquinone (**27**) could not give **28** on treatment with ITT. It therefore follows that anthrone (**26**) was iodinated at the 2-position and then oxidized to **28**.

Conclusion

The reaction of ITT proved to be useful for the iodination of aromatic ketones, particularly for those activated by oxygen functions. The fact that **10c** gave triiodo derivative **14** would also indicate the synthetic utility of the reaction for the preparation of periodinated aromatic compounds. The regiospecific iodination that was observed in the reaction of **6** may suggest that iodine could be incorporated at the ortho-position of a vinyl group in aromatic substrates.

Experimental

Measurements. All the ^{1}H NMR spectra were taken in deuteriochloroform solutions with a Hitachi Perkin-Elmer R-24 NMR spectrometer (60 MHz) with tetramethylsilane as the internal standard. The IR spectra were measured in chloroform solutions on a JASCO A-102 IR spectrometer. The MS sperctra were obtained with a JMS-O1SG-2 and a JMS DX300 instrument. The melting points were determined with a Yanagimoto micromelting point apparatus and were not corrected. The HPLC analysis were performed on an ALTEX model 330/110A/153 isocratic liquid chromatograph equipped with an UNSIL Pack 5C18 250A column, eluting with methanol or 80% aqueous methanol.

Materials. Iodine(III) tris(trifluoroacetate),[3] 4′-methoxyacetophenone[25](**1c**), 1,2-diphenylethanone[26] (**6**), flavanone[27] (**9a**), 4′-methoxyflavanone[28] (**9b**), 7-methoxyflavanone[29] (**9c**), 4-methoxycoumarin[30] (**15b**), 6-methoxycoumarin[31] (**15c**), and 7-methoxycoumarin[32] (**15d**) were prepared by the methods described in the literature. The other 4′-substituted acetophenones **1b**, **d**, and **e**, propiophenone (**1f**), coumarin (**15a**), 9-xanthenone (**20**), 9-fluorenone (**23**), and anthrone (**26**) were purchased from Wako Pure chemical Industries, Ltd. Acetophenone (**1a**) was commercially available from Katayama chemical Industries, Ltd.

Reaction of Iodine(III) Tris(trifluoroacetate). The general procedure for the reaction of ITT was follows. To a solution of a substrate (1 mmol) in a solvent (20 cm^3), iodine(III) tris(trifluoroacetate) (1—2 mmol as shown in Tables 1 and 2, and in Fig. 2) was added under an atmosphere of nitrogen. The solution was stirred with the undissolved ITT at 23 °C. A high-pressure liquid chromatographic analysis was performed on aliquots which were withdrawn periodically from the reaction mixture with the aid of a pipet. There appeared several peaks due to the substrate and products in the chromatogram. When one of the product peaks became maximum (the time is shown in the Tables 1 and 2, and in Fig. 2), the reaction mixture was treated with 20% aqueous sodium iodide solution (20 cm^3) with stirring for 30 min and extracted with dichloromethane or chloroform. The organic layer was washed with a saturated sodium hydrogencarbonate solution, 5% sodium thiosulfonate solution, and water. The solvent was removed under reduced pressure. The products were separated on TLC with benzene or chloroform as the developing solvent. The yields on reasonably pure products are summarized in Tables 1 and 2, and in Fig. 2. Analytical samples were further purified by distillation or recrystallization. The known compounds were identified by comparing them with spectral data and/or the melting points found in the literature. The physical, spectral, and analytical data for the new compounds are listed in Table 3.

A Typical Procedure for the Reaction of Acetophenone (1a) with ITT. To a solution of **1a** (1 mmol) in calcium chloride-dried chloroform (20 cm^3) was added iodine(III) tris(trifluoroacetate) (1 mmol) under an atmosphere of nitrogen. The solution was stirred for 6h at 23 °C. After adding 20% aqueous sodium iodide solution (20 cm^3), the mixture was stirred for 30 min. The chloroform layer was washed with a saturated sodium hydrogencarbonate solution, 5% aqueous sodium thiosulfonate solution, and water. After the removal of the chloroform, the resulting liquid was fractionated on a silica-gel plate eluting with benzene, giving **3a** and **4a** in yields shown in Table 1 (Entry 5). 2-Iodoacetophenone (**3a**): Light-brown liquid;[14] IR ($CHCl_3$) ν/cm^{-1}=3012, 1676, 1600, 1581, 1492, 1449, 1418, 1316, 1303, 1271, 1181, 1169, 1004, 983, 697; ^{1}H NMR ($CDCl_3$) δ=4.32 (2H, s), 7.3—7.6 (3H, m), 7.8—8.0 (2H, m); MS *m/z* (rel intensity) 246 (55, M$^+$), 141 (6), 127 (23), 105 (100), 77 (51). 2-Hydroxyacetophenone (**4a**): Colorless needles; mp 85—86 °C (sublimed) (lit,[15] mp 86—87 °C); IR ($CHCl_3$) ν/cm^{-1}=3484, 3012, 1597, 1448, 1285, 1202, 1091, 972, 661; ^{1}H NMR ($CDCl_3$) δ=3.7 (1H, br. s), 4.90 (2H, s), 7.3—7.7 (3H, m), 7.8—8.1 (2H, m); MS *m/z* (rel intensity) 136 (6, M$^+$), 105 (100), 77 (55).

2-(Trifluoroacetoxy)acetophenone (B). A mixture of 2-bromoacetophenone (2.0 g), sodium trifluoroacetate (1.36 g), and 2-butanone (20 cm^3) was heated under reflux for 24 h. After the removal of the 2-butanone under reduced pressure, the resulting semisolid was extracted with chloroform. The chloroform solution evaporated to give a light-brown liquid (2.1 g, 90%). IR ($CHCl_3$) ν/cm^{-1}=1685 (>C=O) and 1783 ($OCOCF_3$); ^{1}H NMR ($CDCl_3$) δ=4.88 (2H, s, -OCH_2-) and 7.3—8.0 (5H, m, Ph). **B** could not be purified and was hydrolyzed to give **4a** on a silica-gel plate eluting with benzene.

Oxidation of 2-Hydroxy-2-(2-iodophenyl)-1-phenylethanone (7) with Iodine. A mixture of **7** (100 mg), sodium methoxide which prepared by dissolving metallic sodium (13.6 mg) in methanol (5 cm^3), and iodine (150 mg) was heated under reflux for 30 min. After the removal of the methanol, the resulting mixture was triturated with water and then extracted with benzene. The benzene solution evaporated and the product was purified on a silica-gel plate with chloroform as developing solvent, giving light-yellow liquid (72.4 mg, 73%). The IR and ^{1}H NMR spectra were identical with those of **8** obtained by the ITT oxidation of **6**.

We wish to thank Professor Hitoshi Takeshita and Associate Professor Akira Mori of the Research Institute of Industrial Science, Kyushu University, and Dr. Teruyoshi Marunaka of Taiho Pharmaceutical Co. Ltd., Tokushima, for their kind assistance in obtaining the mass spectra.

References

1) R. O. Norman and R. Taylor, "Electrophilic Substitution in Benzenoid Compounds" Elsevier, Amsterdam (1965).

2) H. Suzuki, "Shin-Jikken Kagaku Kôza," ed by S. Nishida, Maruzen, Tokyo (1977), **14** [1], p. 307.

3) M. Schmeisser, K. Dahmen, and P. Sartori, *Chem. Ber.*, **100**, 1633 (1967).

4) I. I. Maletina, V. V. Orda, and L. M. Yagupolskii, *Zh. Org. Khim.*, **10**, 294 (1974); *Chem. Abstr.*, **80**, 120418v (1974).

5) A. Ito, H. Watanabe, M. Naito, H. Aoyama, Y. Nakagawa, and N. Fujimoto, *JNCI, J. Natl. Cancer Inst.*, **77**, 277 (1986); *Chem. Abstr.*, **105**, 132361q (1986).
6) B. B. Corson and R. W. McAllister, *J. Am. Chem. Soc.*, **51**, 2822 (1929).
7) R. Livingstone, "Rodd's Chemistry of Carbon Compounds," ed by S. Coffey, Elsevier North-Holland Inc., (1977), **IV** [E], p. 108.
8) R. Q. Brewster and F. Strain, *J. Am. Chem. Soc.*, **56**, 117 (1934).
9) J. Bertrand, *Bull. Soc. Chim. Fr.*, **1948**, 428.
10) M. D. Barnett, G. H. Daub, F. N. Hayes, and D. G. Ott, *J. Am. Chem. Soc.*, **81**, 4583 (1959).
11) V. T. Slyusarchuk, and A. N. Novikov, *Zh. Org. Khim.*, **3**, 1323 (1967); *Chem. Abstr.*, **69**, 43669g (1967).
12) F. Kaufler, *Ber.*, **37**, 59 (1904).
13) D. E. Pearson, H. W. Pope, W. W. Hargrove, and W. E. Stamper, *J. Org. Chem.*, **23**, 1412 (1958).
14) C. Paal and H. Stern, *Ber.*, **32**, 532 (1899).
15) H. Hunnius, *Ber.*, **10**, 2006 (1877).
16) M. A. Collet, *Compt. Rend. Acad. Sci.*, **128**, 312 (1899).
17) M. Tiffeneau, *Compt. Rend. Acad. Sci.*, **137**, 1260 (1903).
18) M. T. Bogert and L. P. Curtin, *J. Am. Chem. Soc.*, **45**, 2161 (1923).
19) J. W. Baker, *J. Chem. Soc.*, **1932**, 1148.
20) J. W. Baker, *J. Chem. Soc.*, **1931**, 2416.
21) M. A. Collet, *Bull. Soc. Chim. Fr.*, **23**, 829 (1875).
22) N. B. Mulchandani and N. H. Shah, *Chem. Ber.*, **98**, 1913 (1960).
23) K. P. Mathai and S. Sethna, *J. Indian Chem. Soc.*, **41**, 347 (1964).
24) B. B. Dey and K. K. Row, *J. Chem. Soc.*, **125**, 554 (1924).
25) M. A. Wahl and C. Silberaweig, *Compt. Rend. Acad. Sci.*, **150**, 538 (1910); *Chem. Abstr.*, **4**, 2092 (1910).
26) C. F. H. Allen and W. E. Barker, *Org. Synth.*, Coll. Vol. 2, 156 (1948).
27) A. Löwenbein, *Ber.*, **57**, 1515 (1924).
28) A. Edelstein and St. v. Kostanecki, *Ber.*, **38**, 1507 (1905).
29) St. v. Kostanecki and M. L. Stoppani, *Ber.*, **37**, 1180 (1904).
30) I. M. Heilbron and D. W. Hill, *J. Chem. Soc.*, **1927**, 1705.
31) F. Tieman and W. H. M. Müller, *Ber.*, **14**, 1985 (1881).
32) F. Tieman and C. L. Reimer, *Ber.*, **12**, 993 (1879).

Preparation of Bicyclo[3.3.1]nonane-2,4-dione Derivatives

Yoshinobu INOUYE, Tsutomu KOJIMA, Jun OWADA, and Hiroshi KAKISAWA*
Department of Chemistry, University of Tsukuba, Sakura-mura, Niihari-gun, Ibaraki 305
(Received June 17, 1987)

Bicyclo[3.3.1]nonane-2,4-dione and 7-*endo*-benzyloxy-9-methylenebicyclo[3.3.1]nonane-2,4-dione were prepared starting from bicyclo[3.3.1]nonan-2-one and 7-*endo*-benzyloxybicyclo[3.3.1]nonane-2,9-dione, respectively. The key reaction was the NCS oxidation of the 2,2-ethylenedioxy-4-phenylthiobicyclo[3.3.1]nonanes, derived from the corresponding bicyclo[3.3.1]non-3-en-2-ones.

In the course of our study on the synthesis of the taxane framework,[1] we investigated the preparation of bicyclo[3.3.1]nonane-2,4-dione derivatives. Such systems had been reported by several workers,[2] but methodologies had limited application to the preparation of poly functionalized bicyclic derivatives. We chose the transformation from a ketone(**i**) to a 1,3-diketone(**iii**) via an α,β-unsaturated ketone(**ii**) (Scheme 1) because carbonyl compounds are easy to prepare and several efficient methods to their transformation have recently been developed. However, as shown later, there exists clear differences in a bicyclic ring system as compared to an acyclic or a monocyclic one; especially, the conformation of the ring is frequently fixed in the former system and the methods applicable to the latter are not always suitable in the bicyclic system. In this report, we wish to describe our results concerning the preparation of bicyclo[3.3.1]nonane-2,4-dione (**1**) and 7-*endo*-benzyloxy-9-methylenebicyclo-[3.3.1]nonane-2,4-dione (**2**) starting from bicyclo[3.3.1]-nonan-2-ones via α,β-unsaturated carbonyl compounds. The bicyclic diketone **1** have been successfully converted to the 3β-trinortaxane derivative.[1]

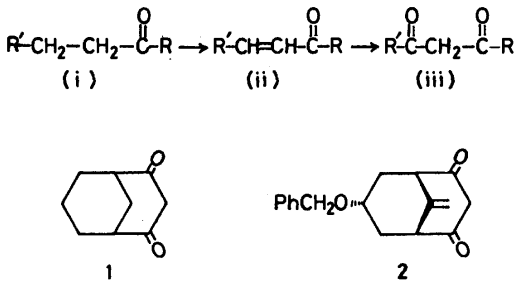

Scheme 1.

A. Bicyclo[3.3.1]nonane-2,4-dione (1). As the parent bicyclo[3.3.1]nonane-2,4-dione (**1**) had been unknown, our initial efforts were focused on the preparation of **1**. The reaction of a cyclohexanone enamine with acrylaldehyde[3] or acryloyl chloride[4] is one of the useful methods for constructing a bicyclo[3.3.1]-nonane framework. Schaefer and co-workers[5] prepared bicyclo[3.3.1]non-3-en-2-one (**5**) via **4** by starting from the amine **3** derived from the reaction of 1-morpholinocyclohexene and acrylaldehyde followed by Wolff-Kishner reduction. We followed the reaction and could improve the total yield up to 28% (lit,[5] 23%) by changing the oxidizing agent of the nitrogen from H_2O_2 to purified *m*-chloroperbenzoic acid (MCPBA). However, the yield was still low and a short-step synthesis of **5** was then examined. When **3** was oxidized with $Hg(OAc)_2$[6] in 5% acetic acid in water bicyclo-[3.3.1]nonan-2-one (**6**) was obtained in 61% yield after the hydrolysis of the iminium salt produced. A usual bromination-dehydrobromination[7] smoothly afforded the desired enone **5** in 88% yield.

A direct oxidation of the enone **5** with H_2O_2 or with *t*-butyl hydroperoxide catalyzed by Pd(II)[8] resulted in the recovery of the starting enone. The reaction of the epoxy ketone **7**, prepared by treating **5** with alkaline H_2O_2 in methanol, with tetrakis(triphenylphosphine)-palladium and 1,2-bis(trimethylphosphino)ethane[9] in

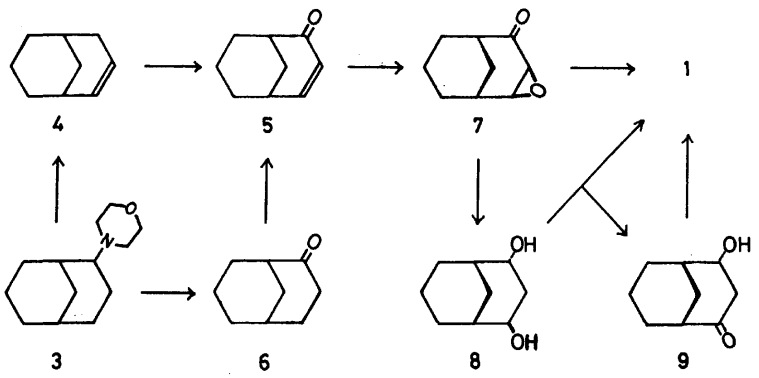

Scheme 2.

toluene gave a target diketone **1** but in only 20% yield with several concomitant. Although the above two procedures[8,9] have been found to be effective to acyclic or monocyclic analogues, the present results were considered to be due to a facile β-elimination of the axial hydroxyl (or corresponding oxygen) group. Lithium aluminium hydride reduction of **7** afforded a 2-*endo*,4-*exo*-diol **8**, one hydroxyl of which was equatorial and the other axial. As the axial hydroxyl group is known to be liable to oxidation with Cr(VI) and the equatorial hydroxyl is less eliminable, the oxidation of **8** would proceed via an equatorial hydroxy ketone **9**. Among various chromium reagents, chromium etherate[10] at low temperature was proved to be most suitable to afford **1**. Treatment of the diol **8** with an equimolar amount of $CrO_3 \cdot Et_2O$ in dichloromethane over Celite at −60—−40 °C gave **1** in 30% yield accompanied with **9** (34%) and the starting diol (20%). The equatorial hydroxy ketone **9** was also converted to **1** under the same conditions in 50% yield with 41% recovery.

The structure of **1** was confirmed to be β-diketones by the typical behavior of the absorption maximum in the UV spectra: λ_{max} at 255 nm (log ε=4.13) in ethanol shifted to 281 nm (4.31) with the addition of a base. The IR spectra of **1** in KBr (1625 and 1590 cm^{-1}) and in chloroform (1730sh, 1705, 1630sh, and 1600br cm^{-1}) suggest that the β-diketone **1** exists in a monoketo monoenol form when it is solid, but in a mixture of a monoketo monoenol and a diketo forms in solution.

Recently, Fetizon and co-workers[11] reported the preparation of bicyclo[3.3.1]nonane-2,4-dione derivatives under a similar reaction sequences in a comparable yield.

Although the target β-diketone **1** was obtained, the low overall yield and complexity at the last oxidation stage of the reaction sequences required us to search for other approaches. We utilized a sulfur group in place of the oxygen since the sulfur group is easy to introduce to an enone[12,13] and since the sulfur is less apt to eliminate that an alkoxyl group under acidic conditions. The sulfide may be converted into a ketone by the oxidation either to a corresponding sulfoxide followed by a Pummerer rearrangement[14] or to a chloro sulfide followed by hydrolysis.[15] Heating a mixture of the enone **5**, ethylene glycol, and thiophenol in benzene in the presence of a catalytic amount of *p*-toluenesulfonic acid (*p*-TsOH) afforded a 4-phenylthio acetal **10** in good yield. The treatment of **10** with 1.05 equimolar amount of *N*-chlorosuccinimide (NCS) in purified (dried) carbon tetrachloride[13] at room temperature gave a new spot on TLC in 3 h, but filtration of the mixture through a silica-gel column gave two spots. The R_f value of the second was identical with that of a vinyl sulfide **11**. It was suggested that the initially formed intermediate was hydrolyzed with the water present in the column. Thus, the NCS oxidation of **10** under the addition of water resulted in one-pot conversion of **10** into **11**. The subsequent hydrolysis of the vinyl sulfide **11** into **1** was quantitatively accomplished under either acidic or basic conditions (see Experimental).

In the present method, **1** was obtained in 40% overall yield from the amine **3**.

B. 7-Benzyloxy-9-methylenebicyclo[3.3.1]nonane-2,4-dione(2). The successful preparation of **1** prompted us next to examine whether this method is applicable to a more functionalized bicyclo[3.3.1]nonan-2-one. The starting ketone chosen was 7-substituted 2,9-dione (e.g., **15**), which has functional groups at both rings and the bridged carbon. **15** can be prepared by the reaction of 4-benzyloxy-1-morpholinocyclohexene with acryloyl chloride.[4] The stereochemistry of the 7-substituent had been proven only in the case of 4-*t*-butyl-6-methyl-1-morpholinocyclohexene(**12**); the major isomer (**13b**/**13a**=4/1) was subjected to X-ray crystal analysis to establish the syn relation between the *t*-butyl group and the bridge C=O group.[16] We used 4-benzyloxy-1-morpholinocyclohexene(**14**) as a starting material. After a reexamination of several reaction conditions,[6,18,19] we found that the addition of hydroquinone to the procedure reported by Aredova and co-workers[19] improved the yield up to 80%. From an ^1H NMR study, **15** was found to consist of two stereoisomers (**15a**/**15b**=2.2/1.0). The characteristic features of the two isomers in ^1H NMR spectra are the shape of the signal of C_7-H — a broad singlet at δ=3.72 in **15a** and a triplet of triplet at 3.89 (J=10.8 and 5.4 Hz) in **15b**, and that of the benzylic protons — an AB quartet at 4.20 and 4.50 with J=11.6 Hz in **15a** and a sharp singlet at 4.50 in **15b**. These properties suggested that the benzyloxyl group of the major isomer **15a** was anti to the bridged C=O group and existed in axial in contrast to the *t*-butyl group of **13b**. This was unequivocally confirmed by an X-ray crystal analysis[20] of **20a** (vide infra).

As the β-diketones **15** was unstable to alkali, the enolizable C_2-carbonyl group was protected by treating **15a** and **15b** with t-butyldimethylsilyl or trimethylsilyl triflate as silyl enol ether **16** (R′=$SiBu^tMe_2$; TBS) or **17**

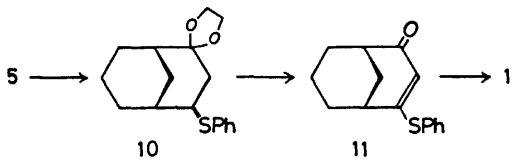

Scheme 3.

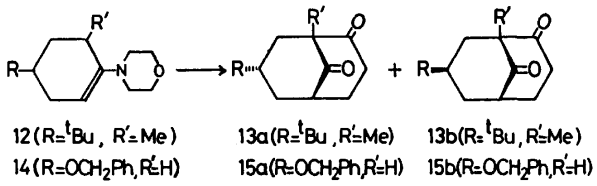

Scheme 4.

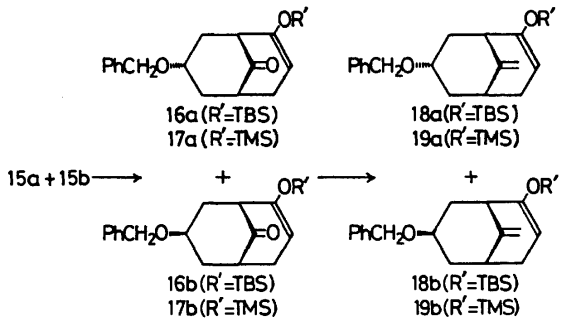

Scheme 5.

(R′=$SiMe_3$; TMS), respectively. These silyl enol ethers were then converted into 9-methylene derivatives **18** (R′=TBS) or **19** (R′=TMS), respectively, by treating with methylenetriphenylphosphorane. The ratio of **18a** to **18b** (or **19a** to **19b**) remained unchanged during these transformations.

The conversion of the silyl enol ether into an α,β-unsaturated carbonyl compound **20** was achieved either oxidation with palladium acetate or benzeneselenenylation followed by oxidation-elimination of the phenylseleno group. The stable TBS enolates (**18a**+**18b**) were treated with palladium acetate in acetonitrile.[21] Of interest, only **18a** was converted into an anticipated **20a** (99% based on the amount of **18a** in the mixture) but **18b** recovered almost quantitatively. The coordination of Pd(II) with both the oxygen of the benzyloxyl group and the olefin as shown in **A** may accelerate the reaction.

On the other hand, benzeneselenenylation[22,23] was successfully carried out with unstable TMS enolates (**19a**+**19b**). The reaction with one equivalent of benzeneselenenyl chloride in THF gave a mixture of phenylseleno ketones **21a** and **21b**, which without a further purification was oxidized with H_2O_2 in dichloromethane-pyridine[23] to give a mixture of **20a** and **20b** in 46% yield. In the large scale preparation of **20**, the TMS enolates (**17a** and **17b**) were successively treated with methylenetriphenylphosphorane, benzeneselenenyl chloride, and H_2O_2 to give **20** (**20a**/**20b**=9.6/1.0)[24] in 50% overall yield.

The benzeneselenenylation of 7-benzyloxy-9-methylenebicyclo[3.3.1]nonan-2-one (**22a**), obtained by the hydrolysis of **18a** or **19a**, gave a 2-phenylseleno ketone **21a** in 43% yield accompanied with 11% of a bridgehead seleno ketone **23a**; while the reaction of TMS enol ethers (**19a** and **19b**) with two equivalent benzeneselenenyl chloride afforded, besides **21a** (24%), an α-phenylseleno α,β-unsaturated ketone **24b** in 18% yield.

Conversion from the α,β-unsaturated ketone **20a** into β-dicarbonyl compound **2** was achieved under a similar process to that used in the preparation of **1**, except for a slight modification of the reaction conditions. A direct conversion of **20a** to an acetal **26a** was unsuccessful. The addition of thiophenol to **20a** in the presence of a catalytic amount of triethylamine

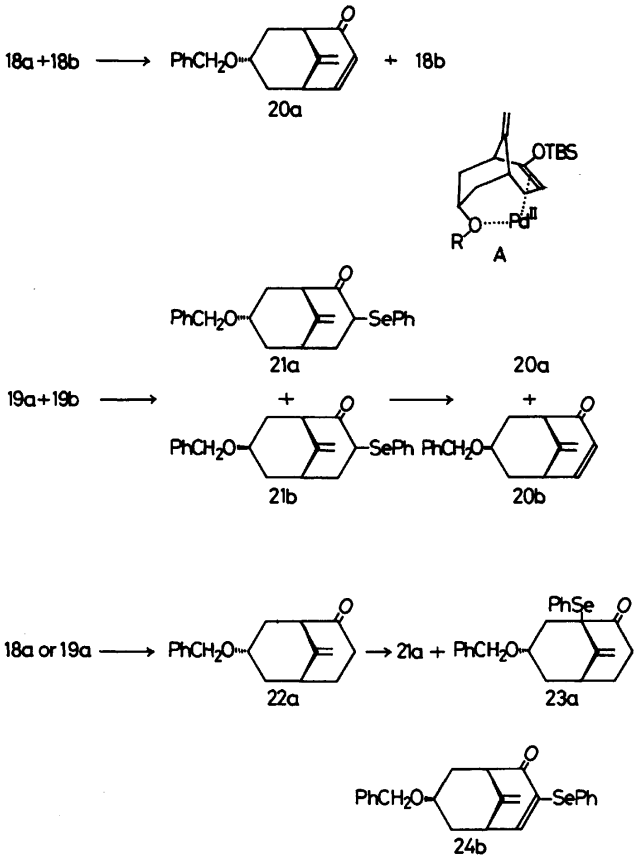

Scheme 6.

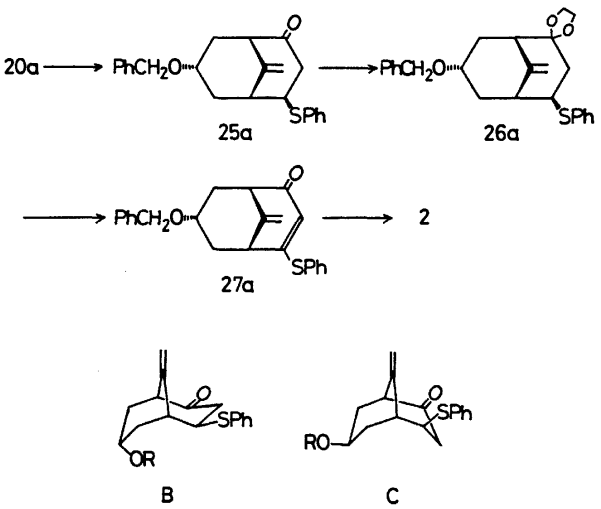

Scheme 7.

afforded a 4-phenylthio ketone **25a** in quantitative yield. On the other hand, **20b** did not react at all. Thus, when the mixture of **20a** and **20b** was subjected to the thiophenol addition, **25a** and unreacted **20b** were obtained; they were separable by chromatography. The difference in the reactivity of **20a** and **20b** toward thiophenol can be rationalized by comparing their conformations: In **20a** the axial benzyloxyl group distorts the other ring to the boat form resulting the phenylthio group being equatorial (**B**), while in **20b**,

the axial phenylthio group (**C**), if produced, is eliminated easily to revert to the starting **20b**.[25]

The acetalization of **25a** was employed by 1,2-bis(trimethylsiloxy)ethane to give **26a** in high yield.[26] The oxidation of **26a** with NCS in the presence of water gave a vinyl sulfide **27a**, which was hydrolyzed to the target β-diketone **2** in good yield. The diketone **2** exists almost in a ketonic form, even in solution (cf. **1**).

A successful preparation of **1** and **2** proved that the present method has wide applications to the preparation of a bicyclic β-diketone.

Experimental

Melting points are uncorrected. Column chromatography was performed with Wako C-300 silica gel unless otherwise stated. IR and UV spectra were recorded on a Hitachi 215 grating and a Hitachi 340 spectrophotometers, respectively. ^1H and ^{13}C NMR spectra were measured in $CDCl_3$ on a JEOL LMN-FX90Q spectrometer using TMS as the internal standard unless otherwise stated. High-resolution mass spectra were performed at Nippon Roche Research Center, Kamakura.

Bicyclo[3.3.1]non-2-ene (4). A solution of 825 mg of MCPBA (100% activity: washed three times with KH_2PO_4-NaH_2PO_4 buffer, pH=7.50, and dried under reduced pressure) in 40 ml of $CHCl_3$ was added gradually to an ice-cooled and stirred solution of 1.00 g of 2-morpholinobicyclo[3.3.1]-nonane (**3**)[5] in 20 ml of $CHCl_3$. Stirring was continued for 3 h, during which the mixture was allowed to come to room temperature. Removing of the solvent under reduced pressure and chromatography (alumina, $CHCl_3$) of the residue gave 1.02 g (95%) of an *N*-oxide. The flask containing 1.02 g of the *N*-oxide equipped with a distillation set and tandem Dry Ice traps, was heated slowly to 110 °C under reduced pressure. After 1 h, the temperature was raised to 145 °C and kept for 5 h. In the first trap, 370 mg (65%) of **4** was collected. Mp, 96—98 °C (purified by sublimation, lit,[5] 96.5—98.5 °C).

Bicyclo[3.3.1]non-3-en-2-one (5). A) From **4**. According to the known procedure,[5] **5** was obtained from **4** in a comparable yield. Mp 97—98 °C (from pentane) (lit,[5] 97.5—98.5 °C).

B) From **6**. To a solution of 22.8 g of phenyltrimethylammonium tribromide[27] in 400 ml of THF, was added a solution of 8.38 g of **6** in 40 ml of THF at a once at 0 °C. The mixture was stirred for 30 min at that temperature and then was poured into a solution of saturated aqueous NaCl and 0.1 M (1 M=1 mol dm^{-3}) aqueous $Na_2S_2O_3$ (1 : 1) through a filter paper. The solids were washed with ether, and the filtrate was extracted with CH_2Cl_2. The combined organic solution was washed with water, brine, and dried over $MgSO_4$. Evaporation of the solvent and recrystallization of the crude product from pentane gave 10.4 g of 3-bromobicyclo[3.3.1]nonan-2-one. Chromatography of the mother liquid with CH_2Cl_2 gave further 1.86 g of the product. The total yield was 12.3 g (93%). Mp 115—116 °C (from benzene); IR ($CHCl_3$) 2940, 2860, and 1715 cm^{-1}; ^1H NMR δ=1.00—3.32 (12H, m), and 4.87 (1H, dd, *J*=12 and 9 Hz).

Found: C, 49.76; H, 6.02%. Calcd for $C_9H_{13}OBr$: C, 49.79: H, 6.03%.

A mixture of 4.71 g of the bromo ketone, 14.2 g of freshly dried LiBr (heated at 120 °C for 20 h under reduced pressure), 8.70 g of anhyd Li_2CO_3 (dried under reduced pressure prior to use) and 80 ml of DMF was heated at 110 °C for 5 h. The cooled mixture was poured into 500 ml of ice-cooled 10% AcOH-H_2O by filtration and the solids were washed with CH_2Cl_2. The combined organic solution was shaken with saturated $NaHCO_3$, water, brine, and dried over $MgSO_4$. Distillation of the solvent at the ordinary pressure and chromatography of the residue with CH_2Cl_2-pentane (10 : 2) gave 2.82 g (95%) of **5**.

Bicyclo[3.3.1]nonan-2-one (6). A mixture of 10.0 g of **3** and 15.3 g of $Hg(OAc)_2$ in 100 ml of 5% AcOH-H_2O was heated at 90 °C for 2 h. After cooling to room temperature, 250 ml of brine was added to the mixture. The precipitates were filtered off and washed with ether. The filtrate was extracted with ether and the combined organic solution was washed with 1 M HCl, water, and dried over anhyd Na_2SO_4. Evaporation of the solvent at the ordinary pressure and sublimation of the residue gave 4.0 g (61%) of **6** as crystals; mp 131—134 °C (lit,[5] mp 134—137 °C); IR ($CHCl_3$) 2930, 2860, 1690, and 1450 cm^{-1}.

3,4-*exo*-Epoxybicyclo[3.3.1]nonan-2-one (7). To a solution of 243 mg of **5** in 50 ml of MeOH, was added 0.56 ml of 30% H_2O_2 and then was added drop by drop 0.88 ml of 6 M NaOH solution over a period of 2 h at 0 °C. The whole was allowed to warm and kept in the range of 15—20 °C for 4 h. The products were extracted with ether and the extract was washed with water, brine, and dried over $MgSO_4$. Careful concentration of the solution under 30 mmHg (1 mmHg= 133.32Pa) and filtration of the residue through a silica-gel layer with CH_2Cl_2-pentane (1 : 1) gave 248 mg (91%) of **7**; mp 94—96 °C (from pentane); IR ($CHCl_3$) 2950, 1700, 1080, and 1000 cm^{-1}; ^1H NMR δ=2.37—2.67 (2H, m), 3.26 (1H, d, *J*=3.5 Hz), and 3.37 (1H, t, *J*=3.5 Hz).

Found: C, 70.91; H, 7.96%. Calcd for $C_9H_{10}O_2$: C, 71.02; H, 7.94%.

Bicyclo[3.3.1]nonane-2-*endo*, 4-*exo*-diol (8). A mixture of 614 mg of **7**, 240 mg of $LiAlH_4$, and 100 ml of dry ether was refluxed for 5 h. Work up as usual and chromatography with ether gave 603 mg (97%) of **8** accompanied with 13 mg (2.1%) of a 1,2-diol.

8; Mp 205—206 °C (from hexane); IR ($CHCl_3$) 3600, 3400br, 2950, and 2905 cm^{-1}; ^1H NMR δ=1.20—2.30 (12H, m), 3.88 (1H, m, $W_{1/2}$=7 Hz), 4.00 (1H, m, $W_{1/2}$=12 Hz), and 4.66 (2H, s).

Found: C, 68.87; H, 10.28%. Calcd for $C_9H_{16}O_2$: C, 69.19; H,10.33%.

Bycyclo[3.3.1]nonane-2,4-dione (1). A) From **11**. Procedure (i). A mixture of 176 mg of **11**, 25 ml of 25% KOH solution and 25 ml of water was refluxed for 2 h. To the resulted solution, 90 ml of CH_2Cl_2 and 90 ml of 2M HCl solution were added. The layers were separated and the aqueous layer was extracted with CH_2Cl_2. The combined organic solution was washed with water, brine, and dried over anhyd Na_2SO_4. Evaporation of the solvent and recrystallization of the residue gave 109 mg (99%) of **1**.

1; Mp 136—138 °C (from benzene); UV (EtOH) 255 nm (log ε=4.13); UV (EtOH-OH^-) 281 nm (4.31); IR (KBr) 3400br, 1625, 1590, 1185, and 1145 cm^{-1}; IR ($CHCl_3$) 3200br, 1730sh, 1705, 1630sh, 1600br, 1185, and 1145 cm^{-1}; ^1H NMR δ=1.20—2.83 (10H, m), 3.37 (2H×1/3, br. AB, *J*=12 Hz), 5.62 (1H×2/3, s), and 6.82 (1H×2/3, br. s.).

Found: C, 70.74; H, 7.89%. Calcd for $C_9H_{12}O_2$: C, 71.02; H,

7.94%.

Procedure (ii). A mixture of 120 mg of **11**, 15 ml of concd HCl and 11 ml of dioxane was refluxed for 6 h. The resulting mixture was poured into 50 ml of water and was extracted with CH_2Cl_2. The extract was washed with 5% $NaHCO_3$ solution, water, brine, and dried over $MgSO_4$. Evaporation of the solvent and recrystallization of the residue gave 74 mg (99%) of **1**.

B) From **7**. A mixture of 249 mg of the epoxy ketone **7**, 7.7 mg of 1,2-bis(diphenylphosphino)ethane, and 24.8 mg of tetrakis(triphenylphosphine)palladium (prepared[28] prior to use) in 1 ml of degassed toluene was placed in a sealed tube under argon and heated at 80 °C for 24 h. Chromatography of the residue with CH_2Cl_2-ether (1 : 1) afforded 48 mg (20%) of **1** and 20 mg (10%) of the starting **7**.

C) From **8**. To a solution of 408 mg of **8** in CH_2Cl_2 (12.3 ml) and ether (4.1 ml), were added 523 mg of celite and 523 mg of CrO_3 successively at −60 °C. The temperature was kept in the range of −60—−40 °C for 6 h. To the mixture were added 82 ml of ether and 500 mg of Celite, and after 15 min, the suspension was filtered through a Celite pad. Removal of the solvent and chromatography on silica gel gave 118 mg (30%) of **1**, 139 mg (34%) of 4-*endo*-hydroxybicyclo-[3.3.1]nonan-2-one (**9**) and 81 mg (20%) of the starting diol **8**.

9; Oil; IR (CCl_4) 3600, 3460, 2940, 2855, and 1700 cm^{-1}; ^1H NMR δ=1.36—2.90 (12H, m), 3.25 (1H, br. s), and 4.17 (1H, br. t, J=4.5 Hz).

2,2-Ethylenedioxy-4-*exo*-phenylthiobicyclo[3.3.1]nonane (10). A mixture of 3.40 g of **5**, 3.30 g of thiophenol, 3.10 g of ethylene glycol, 70 mg of *p*-TsOH, and 300 ml of benzene was refluxed through a water separator for 10 h. After the solvent had been removed, the residue was dissolved in 100 ml of CH_2Cl_2. The solution was washed with a 1M NaOH solution, water, brine, and dried over anhyd Na_2SO_4. Evaporation of the solvent afforded 5.86 g (81%) of **10** as crystals; mp 107.5—108.5 °C (from hexane); IR (KBr) 1585, 1115, 1080, 1050, 1035, 745, and 690 cm^{-1}; ^1H NMR δ=1.25—2.04 (10H, m), 2.06 (1H, br. d, J=16.3 Hz), 2.39 (1H, dd, J=16.3 and 7.3 Hz), 3.62 (1H, br. d, J=7.3 Hz), 3.98 (4H, m), and 7.18—7.50 (5H, m).

Found: C, 70.32; H, 7.60%. Calcd for $C_{17}H_{22}O_2S$: C, 70.30; H, 7.63%.

4-Phenylthiobicyclo[3.3.1]non-3-en-2-one (11). To a solution of 4.56 g of **10** in 1 L of CCl_4, was added successively 2.36 g of NCS (98% activity) and 1 ml of water. After vigorous stirring for 5 h, the resulted white crystals were removed by filtration. Evaporation of the solvent and chromatography of the residue with benzene-AcOEt (92 : 8) gave 3.42 g (89%) of **11** as an oil; IR ($CHCl_3$) 1635, 1560, 1345, 1290, 1150, 1085, 1055, 980, and 875 cm^{-1}; ^1H NMR δ=1.40—2.00 (7H, m), 2.12—2.78 (3H, m), 5.61 (1H, s), and 7.43 (5H, br. s.)

Found: m/z 244.0920. Calcd for $C_{15}H_{16}OS$: M, 244.0921.

7-*endo*-Benzyloxybicyclo[3.3.1]nonane-2,9-dione(15a) and 7-*exo*-Benzyloxybicyclo[3.3.1]nonane-2,9-dione(15b). A mixture of 4-benzyloxycyclohexanone[17] (40 g), 17 g of morpholine, 400 mg of TsOH in 400 ml of benzene-toluene (1 : 1) was refluxed through a Dean-Stark trap until no more water separated (ca. 36 h). Evaporation of the solvent and excess morpholine gave a crystalline enamine (52 g). To a boiling mixture of 20 g of the crude enamine, 500 mg of hydroquinone, and 1 L of dry benzene, a solution of acryloyl chloride (16.7 g) in 250 ml of dry benzene was added drop by drop over a period of 2 h. The whole was vigorously stirred at that temperature for an additional 18 h. The precipitates were collected by filtration, washed with dry hexane and then dissolved in 500 ml of ice-cooled water. The solution was kept at 0 °C for 4 h and then was extracted with CH_2Cl_2 (100 ml×5). The combined extracts were dried over $MgSO_4$ and were evaporated. The residue was distilled (bath temp 180 °C/0.03 mmHg) to give 15.1 g (80%) of a bicyclic dione **15** as an epimeric mixture of the 7-benzyloxyl group (**15a**/**15b**=2.2/1.0). The each epimer could be separable by preparative TLC.

15a: Oil; IR (CCl_4) 1730, 1705, 1140, 1090, 1070, and 695 cm^{-1}; ^1H NMR δ=1.50—3.20 (10H, m), 3.72 (1H, br. s, $W_{1/2}$=8 Hz), 4.20 and 4.50 (2H, AB, J=11.6 Hz), and 7.30 (5H, s); ^{13}C NMR δ=22.7(t), 37.5(t), 38.2(t), 40.8(t), 43.2(d), 60.0(d), 70.0(t), 72.0(d), 127.6(d), 128.4(d), 137.7(s), 209.0(s), and 212.0(s).

Found: C, 73.82; H, 7.03%. Calcd for $C_{16}H_{18}O_3$: C, 74.39; H, 7.02%.

15b: Oil; IR (CCl_4) 1735, 1705, 1090br and 695 cm^{-1}; ^1H NMR δ=1.50—2.95 (9H, m), 3.18 (1H, m), 3.89 (1H, tt, J=10.4 and 5.8 Hz), 4.50 (2H, s), and 7.30 (5H, s); ^{13}C NMR δ=23.0(t), 38.1(t), 38.6(t), 40.0(t), 42.7(d), 62.3(d), 69.9(d), 71.0(t), 127.5(d), 127.8(d), 129.6(d), 137.9(s), 208.4(s), and 209.3(s).

7-Benzyloxy-1-(*t*-butyldimethylsiloxy)-9-methylenebicyclo-[3.3.1]non-2-ene (18). To an ice-cooled mixture of 30 g of **15** (**15a**/**15b**=2.2/1.0), 32.4 ml of triethylamine, and 1 L of carbon tetrachloride, was added 46 g of TBSOTf drop by drop, and the solution was stirred at room temperature for 6 h. The triethylammonium trifluoromethanesulfonate produced was removed through a short alumina column. Concentrating the filtrate gave a crude oily **16** (43 g, 100%), IR (CCl_4): 1720, 1660, 1190, 1175, and 1090 cm^{-1}, which was employed for the next reaction without a further purification.

To a suspension of 48.5 g of methyltriphenylphosphonium bromide in 300 ml of dry tetrahydrofuran at 0 °C under argon was added drop by drop 97.5 ml (1.50 mol) of butyllithium-hexane solution. The mixture was stirred for 1.5 h at room temperature. To the resulting Wittig reagent, a solution of 43 g of the TBS enol ethers **16** in 500 ml of THF was added at a once and the whole was stirred for 1.5 h. After most of the solvent had been evaporated below 40 °C, 30 ml of benzene was added and the solution was filtered through a short alumina column. Evaporating the solvent gave 43.7 g (100%) of a mixture of **18a** and **18b** (**18a**/**18b**=2.2/1.0); IR (CCl_4) 1660, 1190sh, 1175, 1095, and 890 cm^{-1}.

7-*endo*-Benzyloxy-9-methylenebicyclo[3.3.1]non-3-en-2-one (20a) and 7-*exo*-Benzyloxy-9-methylenebicyclo[3.3.1]non-3-en-2-one(20b). A) From **18**. To a vigorously stirred solution of **18** (512 mg) in 10 ml of dry acetonitrile, was added 273 mg of $Pd(OAc)_2$ under argon at 0 °C, and the whole was stirred at room temperature for 8 h. Chromatography of the mixture with benzene and $CHCl_3$ gave 271 mg (99% based on **18a**) of **20a** and 110 mg of the recovered **18b**.

20a: Mp 88.5—89.5 °C (from hexane); IR (KBr) 1670, 1650, 900, and 695 cm^{-1}; ^1H NMR δ=1.5—3.2 (6H, m), 3.77 (1H, br. s), 4.23 and 4.30 (2H, AB, J=11.6 Hz) 4.73 (1H, s) 4.77 (1H, s), 5.98 (1H, d, J=9.7 Hz), 7.14 (1H, dd, J=9.7 and 6.5 Hz), and 7.30 (5H, br. s); ^{13}C NMR δ=34.7(t), 36.7(t), 39.8(d), 52.2(d), 70.3(t), 72.9(d), 104.8(t), 127.3(d), 128.3(d), 130.0(d), 138.5(s), 150.2(s), 152.0(d), 153.1(d), and 202.1(s).

Found: C, 80.42; H, 7.23%. Calcd for $C_{17}H_{18}O_2$: C, 80.28; H, 7.13%.

B) From **19** via **21**. To an ice-cooled solution of 9.23 g of **15** (**15a**/**15b**=2.2/1.0) and 5.97 ml of triethylamine in 90 ml of CCl_4, 6.91 ml of TMSOTf was added drop by drop and the mixture was stirred at room temperature for 6 h. The whole was filtered through an anhyd K_2CO_3 column with CCl_4 and concentration of the solvent gave 11.8 g (100%) of **17**; ^{1}H NMR δ=0.1 (9H, s), 1.7—2.5 (8H, m), 3.4 (1H, m), 4.2 and 4.4 (2H, AB, J=13 Hz), 4.7 (1H, m), and 7.2 (5H, s).

To a suspension of 1.26 g of methyltriphenylphosphonium bromide in 20 ml of THF, 2.99 ml of 1.3 M butyllithium-hexane solution was added at 0 °C and the whole was stirred at room temperature for 30 min. A solution of 1.06 g of **17** in 20 ml of THF was added and the stirring was continued for 1 h. The TMS enol ethers **19** were unstable and were used immediately to a subsequent reaction without a further purification.

A solution of 615 mg (1 molar equivalent) of benzeneselenenyl chloride in 10 ml of THF was added to the mixture and the whole was stirred for 1 h when **19** disappeared (TLC check). After evaporating the solvent, the oily residue (1.28 g) containing a crude **21** was dissolved in 10 ml of CH_2Cl_2, 0.5 ml of pyridine was added and 1.9 ml of 15% aqueous H_2O_2 was added drop by drop under vigorous stirring at room temperature. After 25 min, 5 ml of CH_2Cl_2 and 6.2 ml of saturated $NaHCO_3$ were added and the mixture was stirred for 30 min. An organic layer was separated and the aqueous layer was extracted with CH_2Cl_2. The combined organic extract was washed with 3M HCl, water, saline, and dried over anhyd Na_2SO_4. After the solvent had been evaporated, the residue was chromatographed with hexane-AcOEt (5 : 1) to give 404 mg of **20a** and **20b** (**20a**/**20b**=9.6/1.0). **20b**: ^{1}H NMR δ=4.38 (2H, s) and 6.00 (1H, d, J=9.6 Hz).

When 2 molar equivalents of benzeneselenenyl chloride were used, 18% of **24b** was obtained accompanied with 24% of a mixture of **21a** and **21b**, and 30% of unknown materials.

24b; Oil; ^{1}H NMR δ=1.2—2.7 (4H, m), 3.0—3.35 (1H, m), 3.35—3.55 (1H, m), 3.67 (1H, tt, J=11.0 and 5.0 Hz), 4.48 (2H, br. s), 4.76 (2H, s), 6.50 (1H, d, J=6.6 Hz), and 7.2—7.8 (10H, m); ^{13}C NMR δ=34.4(t), 37.0(t), 42.4(d), 53.9(d), 70.7(t), 71.1(d), 106.6(t), 126.5(s), 127.5(d), 128.3(d), 128.8(d), 129.6(d), 136.6(d), 136.9(s), 138.4(s), 146.1(d), 147.5(s), and 196.8(s).

Found: m/z 410.0787. Calcd for $C_{23}H_{22}O_2Se$: M, 410.0783.

7-*endo*-Benzyloxy-9-methylenebicyclo[3.3.1]nonan-2-one (22a). The TMS (**18**) or TBS (**19**) enolates were hydrolyzed by a usual method to give a mixture of saturated ketones **22a** and **22b**. From those 7-*endo*-benzyloxy-9-methylenebicyclo-[3.3.1]nonan-2-one (**22a**) was obtained by chromatography with benzene.

22a; Oil; ^{1}H NMR δ=2.5—3.1 (10H, m), 3.65 (1H, quint, J=3.0 Hz), 4.13 and 4.41 (2H, AB, J=11.4), 4.70 and 4.78 (2H, AB, J=2.0 Hz), and 7.25 (5H, s).

Found: m/z 256.1458. Calcd for $C_{17}H_{20}O_2$: M, 256.1462.

Benzeneselenenylation of 22a. To a solution of 0.25 mmol of LDA in 4 ml of THF, was added a solution of 64 mg of **22a** in 5 ml of THF at −78 °C and the mixture was stirred at room temperature for 30 min. Benzeneselenenyl chloride (54 mg) was added to the cooled (−78 °C) solution and the mixture was stirred at that temperature for 5 h. After had been warmed to 0 °C, a piece of ice was added and the solution was acidified, extracted with ether. The ether layer was washed with water, saline, and dried over anhyd Na_2SO_4. Evaporating the solvent and the chromatography of the residue with benzene-AcOEt (7 : 1) gave 44 mg (43%) of **21a** and 11 mg (11%) of **23a**.

21a; Oil; IR ($CHCl_3$) 1685, 1650, 1080br, and 895 cm^{-1}; ^{1}H NMR δ=1.5—3.0 (7H, m), 3.25 (1H, m), 3.65 (1H, m), 3.79 (1H, dd, J=7.6 and 2.0 Hz), 4.05 and 4.39 (2H, AB, J=12.0 Hz), 4.79 and 4.90 (2H, AB, J=1.8 Hz), and 7.1—7.6 (10 H, m).

23a; Mp 85—86 °C (from hexane); IR ($CHCl_3$) 1715 and 900 cm^{-1}; ^{1}H NMR δ=1.5—3.2 (9H, m), 3.72 (1H, m), 4.05 and 4.45 (2H, AB, J=12.0 Hz), 5.15 and 5.61 (2H, AB, J=1.8 Hz), and 7.1—7.8 (10H, m); ^{13}C NMR δ=25.1(t), 37.9(d), 39.1(t), 40.4(t), 42.5(t), 61.4(s), 69.7(t), 74.7(d), 112.0(t), 127.3—138.5 (Ph-×2), 150.1(s), and 210.2(s).

Found: C, 67.33; H, 5.94%. Calcd for $C_{17}H_{24}O_2Se$: C, 67.14; H, 5.88%.

7-*endo*-Benzyloxy-9-methylene-4-*exo*-phenylthiobicyclo-[3.3.1]nonan-2-one (25a). A) From **20a**. To a solution of 825 mg of the enone **20a** and 358 mg of thiophenol in 5 ml of chloroform at 0 °C was added 0.02 µl of triethylamine. The solution was stirred at room temperature for 6 h and was filtered through a short silica-gel column. The solvent was removed and the residue was recrystallized from hexane to give 1.11 g (94%) of a sulfide **25a**, mp 82.5—83 °C; IR (KBr) 1710, 1075, 1040, 915, 750, 735, 730, 695, and 685 cm^{-1}; ^{1}H NMR δ=1.54—1.98 (2H, m), 2.20 (1H, dd, J=16 and 8 Hz), 2.50—3.00 (4H, m), 2.73 (1H, dd, J=16 and 6 Hz). 3.69 (1H, br. s), 4.06 (1H, ddd, J=8, 6, and 1 Hz), 4.13 and 4.45 (2H, AB, J=11.6 Hz), 4.84 and 4.89 (2H, AB J=1.8 Hz), and 7.30 (5H, br. s).

Found: C, 75.85; H, 6.63%. Calcd for $C_{23}H_{24}O_2S$: C, 75.78; H, 6.63%.

B) From the mixture of **20a** and **20b**. Triethylamine (0.0035 µl) was added to the solution of 144 mg of **20** (**20a**/**20b**=3.5/1.0) and 0.064 ml of thiophenol in 1 ml of $CHCl_3$ and the mixture was stirred at room temperature for 6 h. The solvent was removed and the residue was chromatographed with hexane-AcOEt (5 : 1) and recrystallized from hexane to give 200 mg (97%) of **25a**. **20b** was recovered from the mother liquid.

7-*endo*-Benzyloxy-2,2-ethylenedioxy-9-methylene-4-*exo*-phenylthiobicyclo[3.3.1]nonane(26a). To a solution of 80 mg of TBSOTf in 40 ml of dichloromethane was added at −78 °C 934 mg of 1,2-bis(trimethylsiloxy)ethane[26] and 1.04 g of the sulfide **25a** successively. The solution was stirred for 4 h at −10 °C, and filtered through a short silica-gel column. The solvent was removed and chromatography of the residue with hexane-AcOEt (6 : 1) gave 1.07 g (93%) of an acetal **26a** as an oil: IR ($CHCl_3$) 1655, 1580, 1355, and 900 cm^{-1}; ^{1}H NMR δ=1.4—2.7 (5H, m), 3.05 (1H, dd, J=14.8 and 6.8 Hz), 3.4—3.7 (2H, m), 3.53 (1H, d, J=6.8 Hz), 3.6 (1H, m), 3.94 (4H, m), 4.31 and 4.58 (2H, AB, J=11.6 Hz), 4.84 and 4.97 (2H, AB, J=2.2 Hz), and 7.32 (10H, br. s.)

Found: m/z 408.1763. Calcd for $C_{25}H_{28}O_3S$: M, 408.1758.

7-*endo*-Benzyloxy-9-methylene-4-phenylthiobicyclo[3.3.1]-non-3-en-2-one(27a). To a solution of 680 mg of **26a** in 30 ml of CCl_4 was added 234 mg of NCS and 0.5 ml of water at a once and the suspension was stirred for 3 h. Filtration of the precipitates at room tempertature, evaporation of the solvent and chromatography of the residue with hexane-AcOEt (7 : 1) gave 537 mg (89%) of a vinyl sulfide **27a** as an oil; IR (CCl_4) 1660sh, 1650, 1580, 1080, and 900 cm^{-1}; ^{1}H NMR δ=1.8—2.2 (2H, m), 2.4—2.8 (2H, m), 3.17 (2H, br. s), 3.89 (1H, br. s), 4.37 and 4.47 (2H, AB, J=10.8 Hz), 4.84 (1H, s), 5.45 (1H, s), and 7.3 (10H, br. s).

Found: *m/z* 362.1346. Calcd for $C_{23}H_{22}O_2S$: M, 362.1339.

7-*endo*-Benzyloxy-9-methylenebicyclo[3.3.1]nonane-2,4-dione(2). To a solution of 500 mg of **27a** in 15 ml of ethanol, was added 15 ml of 25% aqueous KOH solution under argon and the solution was heated to reflux for 12 h. After had been cooled to room temperature, the whole was poured into ice-water. The solution was acidified, extracted with ether (100 ml×3). The extracts were dried over anhyd Na_2SO_4 and was concentrated to give a crude diketone **2** as crystals. Recrystallization from hexane-benzene (10:1) gave 343 mg (92%) of pure **2**; mp 91—91.5 °C; IR (CCl_4) 1720sh, 1710, 1235, 1080, 905, and 690 cm^{-1}; ^1H NMR δ=1.94 (2H, br. d, J=16.1 Hz), 2.65 (2H, br. d, J=15.2 Hz), 3.12 and 3.28 (2H, AB, J=17.9 Hz), 3.69 (1H, quint, J=5.4 Hz), 4.27 (2H, s), 5.02 (2H, s), and 7.25 (5H, br. s); ^{13}C NMR δ=38.8(t), 51.7(d), 55.3(t), 69.8(t), 72.2(d), 111.3(t), 127.4(d), 127.6(d), 128.5(d), 137.5(s), 145.2(s), and 205.1(s).

Found: C, 75.48; H, 6.68%. Calcd for $C_{17}H_{18}O_3$: C, 75.53; H, 6.71%.

The authors are deeply indebted to Dr. Noboru Nakayama, Nippon Roche Research Center, for the measurement of the high-resolution mass spectra. The present work was supported in part by a Grant-in-Aid from university of Tsukuba Project Research (1986).

References

1) T. Kojima, Y. Inouye, and H. Kakisawa, *Chem. Lett.*, **1985**, 323.

2) T. A. Spencer, M. D. Newton, and S. W. Baldwin, *J. Org. Chem.*, **29**, 787 (1964); H.-M. Hutmacher, H. Kruger, and H. Musso, *Chem. Ber.*, **110**, 3118 (1977); F. Effenberger, K.-H. Schonwalder, and J. J. Stezowski, *Angew. Chem., Int. Ed. Engl.*, **21**, 871 (1982).

3) G. Stork and H. K. Landesman, *J. Am. Chem. Soc.*, **78**, 5129 (1956).

4) P. W. Hickmott and J. R. Hargreaves, *Tetrahedron*, **23**, 3151 (1967).

5) J. P. Schaefer, J. C. Lark, C. A. Flegal, and L. M. Honig, *J. Org. Chem.*, **32**, 1372 (1967).

6) N. J. Leonard, A. S. Hay, R. W. Fulmer, and V. W. Gash, *J. Am. Chem. Soc.*, **77**, 439 (1955); H. Mohrle and D. Schittenhelm, *Chem. Ber.*, **104**, 2475 (1971).

7) E. J. Corey and A. G. Hortmann, *J. Am. Chem. Soc.*, **87**, 5736 (1965); J. Grimshaw, J. T. Grimshaw, and H. R. Juneja, *J. Chem. Soc., Perkin Trans. 1*, **1972**, 50.

8) J. Tsuji, H. Nagashima, and K. Hori, *Chem. Lett.*, **1980**, 257.

9) M. Suzuki, A. Watanabe, and R. Noyori, *J. Am. Chem. Soc.*, **102**, 2095 (1980).

10) S. J. Flatt, G. W. J. Fleet, and B. J. Taylor, *Synthesis*, **1979**, 815.

11) M. Fetizon, I. Hanna, and R. Zeghdoudi, *Synth. Commun.*, **16**, 1 (1986).

12) I. Kuwajima, T. Murofushi, and E. Nakamura, *Synthesis*, **1976**, 602: D. A. Evans, L. K. Truesdale, K. G. Grimm, and S. L. Nesbitt, *J, Am. Chem. Soc.*, **99**, 5009 (1977).

13) P. Bakuzis and M. L. F. Bakuzis, *J. Org. Chem.*, **46**, 235 (1981).

14) J.-P. Corbet and C. Benezra, *Can. J. Chem.*, **57**, 213 (1979).

15) L. A. Paquette, W. D. Klobucar, and R. A. Snow, *Synth. Commun.*, **6**, 575 (1976): P. Bakuzis and M. L. F. Bakuzis, *J. Org. Chem.*, **42**, 2362 (1977) and references cited therein.

16) P. W. Hickmott, P. J. Cox, and G. A. Sim, *J. Chem. Soc., Perkin Trans. 1*, **1974**, 2544.

17) D. A. Prins, *Helv. Chim. Acta*, **40**, 1621 (1957); H. Plieninger and H. J. Grasshoff, *Chem. Ber.*, **90**, 1973 (1957).

18) P. W. Hickmott, G. J. Miles, G. Sheppard, R. Urbani, and C. T. Yoxall, *J. Chem. Soc., Perkin Trans. 1*, **1973**, 1514: D. Gravel and S. Rahal, *Can. J. Chem.*, **53**, 2671 (1975); K. E. Harding, B. A. Clement, L. Morono, and J. P.-Katalinic, *J. Org. Chem.*, **46**, 940 (1981).

19) E. N. Aredova, V. V. Sevost's Yanova, M. M. Krayuskin, S. S. Novikov, and F. Karpenko, *Izv. Akad. Nauk SSSR, Ser. Khim.*, **1976**, 1408.

20) Y. Inouye, T. Kojima, and H. Kakisawa, *Acta Crystallogr., Sect. C*, **43**, 1599 (1987).

21) Y. Ito, T. Hirao, and T. Saegusa, *J. Org. Chem.*, **43**, 1011 (1978).

22) S. Danishefsky and C. F. Yan, *Synth. Commun.*, **8**, 211 (1978).

23) H. J. Reich, J. M. Renga, and I. L. Reich, *J. Am. Chem. Soc.*, **97**, 5434 (1975).

24) The 7-*exo*-benzyloxy derivative **19b** seemed to be decomposed during the benzeneselenenylation process.

25) Another possibility due to the stereoelectronic accerelation of the axial benzyloxyl group in **20a** was suggested by one of the referees.

26) A somewhat lower (60%) yield was observed in ordinary acetalization conditions (ethylene glycol-TsOH).

27) W. S. Johnson, J. D. Bass, and K. L. Williamson, *Tetrahedron*, **19**, 861 (1963).

28) D. R. Coulson, *Inorg. Synth.*, **13**, 121 (1972).

 © 1987 The Chemical Society of Japan Bull. Chem. Soc. Jpn., 60, 4377—4384 (1987)

Efficient Carbonyl Addition of Polyfluorochloroethyl, -ethylidene, and -ethenyl Units by Means of 1,1,1-Trichloro-2,2,2-trifluoroethane and Zinc

Makoto FUJITA and Tamejiro HIYAMA*
Sagami Chemical Research Center, 4-4-1 Nishiohnuma, Sagamihara, Kanagawa 229
(Received July 22, 1987)

Thermally stable zinc carbenoid CF_3CCl_2ZnCl was prepared from 1,1,1-trichloro-2,2,2-trifluoroethane and zinc powder in *N,N*-dimethylformamide and was allowed to add to carbonyls of aldehydes and α-keto esters in excellent yields to give 1-substituted 2,2-dichloro-3,3,3-trifluoro-1-propanols. Employment of excess zinc induced further reductive β-elimination to afford 1-substituted 2-chloro-3,3,3-trifluoropropenes (**3**) and 1-substituted 2-chloro-3,3-difluoro-2-propen-1-ols (**4**). Exclusive formation of **3** was achieved by use of acetic anhydride as the co-reagent, whereas **4** was produced with an aluminium chloride catalyst highly selectively.

Introduction of fluorine to biologically active compounds often results in remarkable modification of their activity owing to increased stability and lipophilicity as well as to mimic and block effect of fluorine atom.[1] Therefore, various methods have been developed recently for the introduction of fluorinated groups to organic molecules.[2] Readily accessible fluorohalocarbons such as CF_2Br_2, $CFCl_3$, and HCF_2Cl are frequently utilized for this purpose as fluorine-containing building blocks.[3] However, 1,1,1-trifluoro-2,2,2-trihaloethanes (CF_3CX_3, X=Cl, Br) have scarecely been employed as the fluorine source,[4] though they are also commercially available. A carbenoid reagent of type CF_3CX_2-Mtl which might be derived from CF_3CX_3 attracted our interest, as it should provide us a facile way for the nucleophilic introduction of CF_3CX_2 group. In striking contrast to extensive studies on perfluoroalkylmetals,[5] the chemistry of the organo-metallics of the formula CF_3CX_2Mtl remained unexplored at the outset of our study. Only the Grignard reagent CF_3CX_2MgX[6] was recorded which, however, are labile and does not achieve carbonyl addition even at low temperatures. Thus, we searched for a practically stable reagent of this type and found that 1,1-dichloro-2,2,2-trifluoroethylzinc chloride fulfils our criteria.[7] Its preparation and carbonyl addition are described herein.

Results and Discussion

Preparation of CF_3CCl_2ZnCl. When 1,1,1-trichloro-2,2,2-trifluoroethane was added to a suspension of small excess of zinc powder in *N,N*-dimethylformamide (DMF) in the presence of copper(I) chloride catalyst[8] at room temperature, exothermic reaction took place, and most of the zinc was consumed within 1 h. At the expense of the peak of CCl_3CF_3(δ=−81.1), a new peak appeared at δ=−72.3, which was assigned as that of CF_3CCl_2ZnCl.[9] Upon hydrolysis CF_3CCl_2H was produced quantitatively. The reaction with carbon dioxide gave 2,2-dichloro-3,3,3-trifluoropropanoic acid (18% yield)[10] (Scheme 1). Thermal stability of the zinc carbenoid deserves particular attention: No decomposition was observed in DMF solution after several days at room temperature. The zinc reagent could be prepared in tetrahydrofuran (THF) solution also in a similar manner.

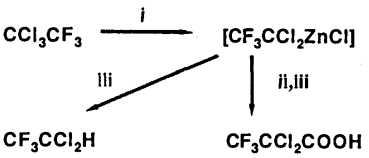

i: Zn, CuCl cat, DMF (or THF)
ii: CO_2
iii: H_3O^+

Scheme 1.

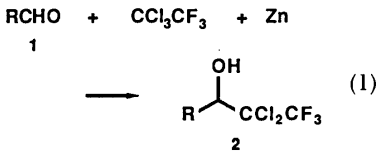

a: R = Ph
b: R = 3,4-(OCH_2O)-C_6H_3
c: R = 4-Cl-C_6H_4
d: R = 3,4-Cl_2-C_6H_3
e: R = PhCH=CH
f: R = Me_2C=CH
g: R = PhCH(Me)
h: R = c-C_6H_{11}

2a': PhCH(OH)CBrClCF$_3$
2a": PhCH(OH)CBr_2CF$_3$

Aldehyde Addition of CF_3CCl_2ZnCl. The synthetic utility of the zinc reagent is demonstrated by an aldehyde addition. Although the pre-prepared reagent does undergo addition to aldehyde carbonyl, the Barbier-type conditions were found more efficient. Treatment of aldehydes (**1**) with 1,1,1-trichloro-2,2,2-trifluoroethane (1.2—1.5 mol) and zinc powder (1.0—1.2 mol) in DMF afforded CF_3CCl_2 adducts **2** (Eq. 1). Results are summarized in Table 1. The reaction with aromatic aldehydes proceeded smoothly in good yields. Though the carbonyl addition to some aliphatic and α,β-unsaturated aldehydes were sluggish, the addition of copper(I) chloride, dichlorobis(triphenylphosphine)palladium(II), or dichlorobis(triphenylphosphine)nickel(II) catalyst or ultrasonic irradiation[5c] improved the yields significantly (Runs 9—12,

Table 1. Aldehyde Addition of CX_3CF_3/Zn Reagent[a]

Run	Aldehyde	CX_3CF_3[b]	Condition	Product	Yield[c] %
1	**1a**	CCl_3CF_3 (1.2)	r.t. 3 h; 50 °C, 2 h	**2a**	86
2	**1a**	CBr_2ClCF_3 (1.2)	0 °C, 0.5 h; 50 °C, 2 h	**2a′**	23[b]
3	**1a**	CBr_3CF_3 (1.5)	0 °C, 0.2 h	**2a″**	27
4	**1b**	CCl_3CF_3 (1.2)	0 °C, 0.2 h; 50 °C, 2 h	**2b**	80
5	**1c**	CCl_3CF_3 (1.5)	0 °C, 0.2 h; 50 °C, 2 h	**2c**	87
6	**1d**	CCl_3CF_3 (1.2)	r.t., 0.5 h; 50 °C, 4.5 h	**2d**	96
7	**1e**	CCl_3CF_3 (1.2)	r.t., 1 h; 50 °C, 17 h	**2e**	82
8	**1f**	CCl_3CF_3 (1.5)	60 °C, 12 h	**2f**	22
9	**1f**	CCl_3CF_3 (1.5)	50 °C, 8 h[e,f]	**2f**	60
10	**1f**	CCl_3CF_3 (1.5)	50 °C, 8 h[g]	**2f**	61[d]
11	**1f**	CCl_3CF_3 (1.5)	50 °C, 8 h[h]	**2f**	72[d]
12	**1f**	CCl_3CF_3 (1.5)	r.t.—50 °C, 8 h[i]	**2f**	83[d]
13	**1g**	CCl_3CF_3 (1.2)	0 °C, 0.3 h; 50 °C, 12 h	**2g**	60
14	**1h**	CCl_3CF_3 (1.2)	0 °C, 0.3 h; 50 °C, 23 h	**2h**	16
15	**1h**	CCl_3CF_3 (1.2)	50 °C, 5 h[f]	**2h**	61

a) The ratio of CX_3CF_3 to Zn was 1.0 to 1.2. All the reactions were carried out in DMF (1 ml $mmol^{-1}$) of **1**. b) Values in the parentheses are molar equivalents to **1**. c) Isolated yields unless otherwise noted. d) GLC yield. e) The aldehyde **1f** was added dropwise over 1 h after the carbenoid was prepared. f) Copper (I) chloride (5 mol%) was employed. g) A catalyst $PdCl_2(PPh_3)_2$ (1 mol%) was used. h) Carried out in the presence of $NiCl_2(PPh_3)_2$ (1 mol%). i) Ultrasonic irradiation was applied.

Table 2. Transformation of **1** to **3** with CCl_3CF_3, Zn, and Ac_2O[a]

Run	Aldehyde	CCl_3CF_3/Zn/Ac_2O[b]			Reaction condition	Product (yield/%)[c]
1	**1a**	1.5	3.0	—	50 °C, 16 h	**3a** (14) **4a** (57)[d]
2	**1a**	1.5	3.0	1.5	r.t., 5 h; 50 °C, 2 h	**3a** (53) [86 : 14]
3	**1a**	2.0	5.0	1.5	50 °C, 7 h	**3a** (75) [86 : 14]
4	**1a**	2.0	5.0	1.0[e]	50 °C, 7 h	**3a** (67) [86 : 14]
5	**1a**	1.5	3.0	0.3[f]	0 °C, 1 h	**3a** (42) [86 : 14]
6	**1a**	1.5	3.0	0.3[g]	50 °C, 18 h	**3a** (13) [86 : 14] **4a** (54)
7	**1a**	1.5	3.0	1.0[g]	50 °C, 7 h	**3a** (30) [86 : 14] **4a** (52)
8	**1a**	i) 1.2	1.1	—	50 °C, 24 h	**3a** (78)
		ii) —	2.0	1.6	50 °C, 4 h	[87 : 13]
9	**1b**	i) 1.2	1.1	—	50 °C, 24 h	**3b** (81)
		ii) —	2.0	1.6	50 °C, 4 h	[85 : 15]
10	**1b**	i) 1.2	1.1	—	50 °C, 12 h	**3b** (63)
		ii) —	2.0	1.6[h]	50 °C, 4 h	[86 : 14]
11	**1c**	2.0	5.0	1.5	50 °C, 4 h	**3c** (73) [88 : 12]
12	**1c**	i) 1.2	1.1	—	50 °C, 24 h	**3c** (76)
		ii) —	2.0	1.6	50 °C, 4 h	[88 : 12]
13	**1e**	i) 1.2	1.1	—	50 °C, 24 h	**3e** (72)
		ii) —	2.0	1.6	50 °C, 4 h	[89 : 11]
14	**1f**	i) 1.2	1.1	—	50 °C, 1 h[i]	**3f** (53)
		ii) —	2.0	1.6	50 °C, 4 h	[88 : 12]
15	**1h**	i) 1.2	1.1	—	50 °C, 24 h[i]	**3h** (50)
		ii) —	2.0	1.6	50 °C, 4 h	[85 : 15]

a) All the reactions were carried out in DMF (1 ml $mmol^{-1}$). b) Molar ratio of CCl_3CF_3, Zn, and Ac_2O. Single step procedure corresponds to Procedure A, whereas the two-step procedure means Procedure B. c) The values in the brackets are Z/E ratio of **3**. d) Accompanied by **2a** (17—19% yields). e) Titanium-(IV) chloride (0.12 ml, 1.0 mmol) was employed in lieu of acetic anhydride. f) Acetic anhydride was replaced by $SiCl_4$ (0.3 mmol). g) Boron trifluoride etherate (0.3 mmol) was used in place of acetic anhydride. h) Acetyl chloride (0.1 ml, 1.6 mmol) was employed instead of acetic anhydride. i) $NiCl_2(PPh_3)_2$ (2 mol%) was employed as the catalyst.

and 15). Other 1,1,1-trifluoro-2,2,2-trihaloethanes e.g. CBr_2ClCF_3 and CBr_3CF_3 also were applicable, thouth the yields were inferior (Runs 2 and 3). No ketone adducts were isolated under the reaction conditions. Lewis acids such as $AlCl_3$ and $TiCl_4$ were totally ineffective for the ketone addition. DMF solvent is essential to the carbonyl reaction, as in THF the aldehyde addition did not take place.

Attempted reaction of the zinc carbenoid with benzoyl chloride failed. Although benzoyl chloride was consumed immediately in DMF, benzoic acid was isolated after workup with trifluoroacetic acid. Possibly the zinc reagent promoted the reaction of PhCOCl with DMF to give rise to a Vilsmeier reagent $[Me_2N{=}CHOCOPh]^+Cl^-$ or $[Me_2N{=}CHCl]^+PhCOO^-$. Parallel experiment in THF induced ring-opening of the THF ring to yield 4-chlorobutyl benzoate. Thus, strong acid character as well as low nucleophilicity of the zinc carbenoid is now revealed.

Transformation of RCHO (1) into RCH=C(Cl)CF_3 (3). When excess zinc is applied to the aldehyde addition, further reductive β-elimination is expected to afford 2-chloro-1,1,1-trifluoro-2-alkene (**3**) and/or 2-chloro-1,1-difluoro-1-alken-3-ol (**4**) (Eq. 2). Actually, treatment of benzaldehyde with CCl_3CF_3 (1.5 mol) and

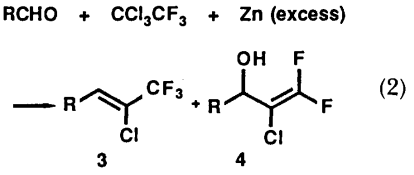

(2)

zinc (3.0 mol) afforded a mixture of **3a** (14%) and **4a** (57%) (Table 2, Run 1). In order to control the two pathways, the effect of various additives was studied.

By use of excess acetic anhydride (1.5—1.6 mol) as the additive, conversion of RCHO into **3** was achieved highly selectively. Various aldehydes including aromatic, aliphatic, and α,β-unsaturated ones were successfully converted into **3**, and the results are summarized in Table 2. Employment of 2 mol of CCl_3CF_3 and large excess of zinc (5 mol) was desirable for giving **3** in satisfactory yields (Procedure A). The amount of zinc could be reduced to 3.1 mol without decrease of the yield by a modified two-step but one-pot procedure (Procdure B): i) Formation of C-C bond with CCl_3CF_3 (1.2 mol) and zinc (1.1 mol) and ii) reduction with zinc (2 mol) and acetic anhydride (1.5 mol). Such Lewis acids as $TiCl_4$ and $SiCl_4$[11] were also effective for exclusive transformation of benzaldehyde into **3a**, whereas boron trifluoride etherate did not significantly affect the selectivity (Runs 6 and 7). Acetyl chloride also could be used in lieu of acetic anhydride for the Procedure B (Run 10).

The reaction pathway should involve formation of an acetate of **2** as the intermediate, since the acetate of **2a** was produced (79% yield) when zinc (1.2 mol), CCl_3CF_3 (1.2 mol), and acetic anhydride (1.2 mol) were employed. Actually, treatment of the acetate with zinc in DMF produced **3a** in good yields (Eq. 3).[14] In order to check an alternative route which goes through a *gem*-dimetallic species like $CF_3CCl(ZnBr)_2$, we allowed CBr_2ClCF_3 to react with zinc at 50 °C and observed a β-elimination to give $CF_2{=}CClBr$. This was successively converted into $CF_2{=}CClZnBr$ under the reaction conditions (Eq. 4). These results contrast sharply to the carbonyl methylenation with $CH_2X_2/Zn/TiCl_4$

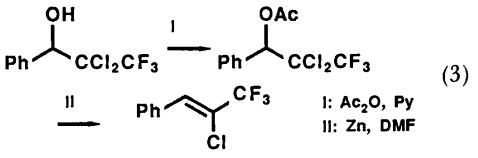

(3)

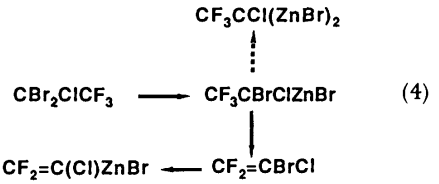

(4)

which involves $CH_2(ZnX)_2$ as the intermediate.[11a]

Synthetic utility of this reaction was demonstrated by a one-pot synthesis of 2-chloro-1,1,1-trifluoro-5-methyl-2,4-hexadiene (**3f**)[12b,c] which is one of key synthetic precursors for artificial pyrethroids containing $CH{=}C(Cl)CF_3$ moiety in common.[12,13] Although the same transformation can be effected with $CCl_3CF_3/PPh_3/Zn$ reagent,[4b] this Wittig type olefination method requires use of 2 mol of triphenylphosphine and tedious separation of triphenylphosphine oxide contaminated in the products and thus is apparently unpractical.

Transformation of RCHO (1) into RCH(OH)CCl=CF_2 (4). In striking contrast, aluminium chloride catalyst promoted highly selective transformation to **4**. For example, in the presence of 10 mol% of aluminium chloride, benzaldehyde was converted into **4a** in 86% yield accompanied by a trace amount of **3a** (<5%). With the increase of the proportion of $AlCl_3$ to 30 mol%, both yield and selectivity decreased considerably. **4a** was no longer produced on employment of 1 mol of $AlCl_3$: A mixture of 2,2-dichloro-3,3,3-trifluoro-1-phenyl-1-propanol (**2a**) (37%) and **3a** (11%) resulted. The effect of $AlCl_3$ may be explained as follows. Catalytic amount of $AlCl_3$ can interact with CF_3 group of the primary adduct and direct the reductive elimination to produce **4**, whereas an equimolar amount of $AlCl_3$ substitutes ZnCl of the primary adduct to weaken the C-O bond of the primary adduct. The $AlCl_3$-catalyzed method was applied to various aldehydes. Results summarized in Table 3 show that 1-substituted 2-chloro-3,3-difluoro-2-propen-1-ols of various kinds are readily accessible through the methodology disclosed herein.

The reaction was monitored by ^{19}F NMR which

Table 3. Transformation of **1** to **4**[a]

Run	Aldehyde	$AlCl_3$[b]	Reaction time	Product (yield/%)
1	**1a**	0.1	18 h	**4a** (86)
2	**1a**	0.3	18 h	**4a** (80)
3	**1a**	1.0	18 h	**2a** (37)
				3a (11)
				4a (0)
4	**1d**	0.3	3.5 h	**4d** (72)
5	**1g**	0.1	18 h	**4g** (86)[c]
6	**1g**	0.3	19 h	**4g** (39)[c]
7	**1h**	0.1	9 h	**4h** (52)
8	**1h**	0.3	9 h[d]	**4h** (36)
9	**1k**	0.3	18 h	**4k** (41)

a) All the reactions were carried out in DMF (1 ml $mmol^{-1}$) at 50 °C with **1**, CCl_3CF_3, and Zn in a molar ratio of 1 : 1.5 : 3.0. b) Molar equivalents to aldehyde. c) Roughly 1:1 diastereoisomeric mixture. d) Copper(I) chloride catalyst (5 mol%) was used.

showed formation of an aldehyde adduct of CF_3CCl_2ZnCl at the early stage of the reaction. The observation clearly eliminates the possibility of the intermediacy of CF_2=C(Cl)ZnCl.

The achievement of the practical transformation of aldehydes to **4** is of great value from synthetic viewpoint, as the aldehyde adducts of CX=CF_2 group (X=F, Cl) are key intermediates for a number of fluorine containing carbonyl compounds.[14] Whereas the carbonyl addition is usually carried out with labile LiCX=CF_2[15,16] below −100 °C, the $CX_3CF_3/Zn/AlCl_3$ (cat) reagent can do the same transformation at 50 °C.[17]

Addition of CF_3CCl_2ZnCl to α-Keto Esters and DMF. Although the zinc carbenoid did not add across ketone carbonyls, the reagent reacted with α-keto esters **5** (Eq. 5). The yields of the aducts **6** were moderate even in the presence of large excess of the reagent. The conversion-based yields were quantitative, though. Possibly the intermediate adduct is in equilibrium between **5** and the zinc reagent which gradually decomposes to shift the equilibrium to the starting material.

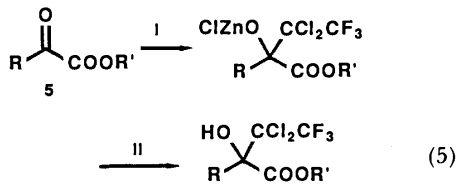

(5)

Attempted Reaction with Chlorosilanes. In the presence of chlorosilanes, the CF_3CCl_2ZnCl reagent reacted with DMF to give α-silyloxy *N,N*-dimethylamines **7** in good yields (Eq. 6). As CF_3CCl_2ZnCl alone does not interact with DMF, **7** may be derived from a Vilsmeier type reagent $[Me_2N^+=CHOSiR_3]Cl^-$ generated in situ from R_3SiCl and DMF.

$$HCONMe_2 + R_3SiCl + CCl_3CF_3 \longrightarrow CF_3CCl_2CH(NMe_2)OSiR_3 \quad (6)$$

7

a: $SiR_3 = SiMe_2t\text{-}Bu$
b: $SiR_3 = SiEt_3$

A new zinc carbenoid reagent CF_3CCl_2ZnCl is readily prepared from commercially available CCl_3CF_3 and zinc and is shown to undergo carbonyl addition. Although it did not exhibit enough reactivity to achieve coupling with a wide variety of electrophiles, the zinc reagent allowed us to introduce three kinds of C_2 units containing both chlorine and flourine atoms. Synthetic application to artificial pyrethroids is disclosed in following article.[18]

Experimental

Melting points and boiling points are uncorrected. Bulb-to-bulb distillation was carried out by use of Büchi Kugelrohr or Glass Tube Oven (Shibata GTO 250R). ^1H NMR spectra (tetramethylsilane as an internal standard) were obtained with a Varian EM-390, Varian XL-100A, Hitachi R-90H, or Bruker AM-400 spectrometer, chemical shifts being given in ppm units, ^{19}F NMR spectra (trichlorofluoromethane as an internal standard) with a Hitachi R-20B or Varian XL-100A spectrometer, ^{13}C NMR spectra with a Bruker AM-400. IR data of neat liquid film samples (unless otherwise noted) were recorded with a JASCO A-202. Mass spectra (70 eV unless otherwise noted) were recorded with a RMU-6MG, high mass with a Hitachi M-80A spectrometer. GLC analyses were performed with a Shimadzu GC-7A chromatograph (FID detector). Preparative GLC were carried out with a Shimadzu GC-3Bt chromatograph (TCD detector). TLC analyses were performed by means of Merck Silica Gel 60 F_{254} (0.25 mm thick). Preparative TLC plates were prepared with Merck Kiesel-Gel PF_{254}. Column chromatography was carried out with silica-gel (Wakogel C-200) at atmospheric pressure. Ultrasonic irradiation was performed with a Wakenyaku UW-10 (250 W, 28 KHz) cleaner. DMF was distilled over calcium hydride and stored over Molecular Sieve 4A. Zinc powder purchased from Wako Pure Chemical Industries, Ltd. was washed successively with dil hydrochloric acid, water, ethanol, diethyl ether and finally with absolute diethyl ether, and dried under reduced pressure. 1,1,1-Trichloro-2,2,2-trifluoroethane was purchased from Tokyo Kasei Kogyo Co. and used directly.

A Typical Procedure for Generation of CF_3CCl_2ZnCl and Its Aldehyde Addition. To a solution of benzaldehyde (**1a**) (2.12 g, 20.0 mmol) in DMF (20 ml) were added 1,1,1-trichloro-2,2,2-trifluoroethane (4.52 g, 24.1 mmol) and zinc powder (1.44 g, 22.1 mmol), and the resulting mixture was stirred for 3 h at room temperature and for 2 h at 50 °C before treatment with sat aq ammonium chloride solution (30 ml). Extraction with diethyl ether (2×30 ml), drying the ethereal extract over magnesium sulfate, concentration, followed by distillation, gave 2,2-dichloro-3,3,3-trifluoro-1-phenyl-1-propanol (**2a**) (4.49 g, 86% yield) as a colorless oil. Bp 100 °C (bath temp)/1 Torr;† ^1H NMR ($CDCl_3$) δ=2.90 (d, *J*=5 Hz, 1H), 5.20 (d, *J*=5 Hz, 1H), 7.25—7.55 (m 5 H); ^{19}F NMR

† 1 Torr=133.322 Pa.

($CDCl_3$-$CFCl_3$) δ=−74.4 (s); IR 3460, 1248, 1188, 1061, 874, 766, 712, 700, 666, 612 cm^{-1}; MS *m/z* (rel intensity) 260 (M^++2, trace), 258 (M^+, trace), 107 (100), 79 (55), 77 (30), and 51 (13).

Found: C, 41.44; H, 2.82%. Calcd for $C_9H_7Cl_2F_3O$: C, 41.73; H, 2.72%.

2-Bromo-2-chloro-3,3,3-trifluoro-1-phenyl-1-propanol (2a′): A colorles oil. ^1H NMR ($CDCl_3$) (a 1 : 1 mixture of two steteoisomers) δ=2.83 (d, *J*=5 Hz, 1 H), 5.20, 5.25 (d, *J*=5 Hz, 1 H), and 7.3—7.7 (m, 5 H); MS *m/z* (rel intensity) 304 (M^++2, trace), 302 (M^+, trace), 107 (100), 79 (43), 77 (20), 51 (8).

Found: *m/z* 301.9299. Calcd for $C_9H_7BrClF_3O$: M, 301.9320.

Formation of **4a** (12%) was shown by GLC assay of the crude reaction mixture.

2,2-Dibromo-3,3,3-trifluoro-1-phenyl-1-propanol (2a″): A colorless oil. ^1H NMR ($CDCl_3$) δ=2.86 (br s, 1 H), 5.11 (s, 1 H), and 7.25—7.65 (m, 5 H); ^{19}F NMR ($CDCl_3$-$CFCl_3$) δ=−70.1 (s); IR 3455, 1236, 1188, 1172, 698 cm^{-1}; MS *m/z* (rel intensity) 250 (2), 107 (100), 79 (39), 77 (21), and 51 (11).

Found: C, 31.33; H, 1.96%. Calcd for $C_9H_7Br_2F_3O$: C, 31.07; H, 2.03%.

2,2-Dichloro-3,3,3-trifluoro-(3,4-methylenedioxyphenyl)-1-propanol (2b): A colorless oil. ^1H NMR ($CDCl_3$) δ=3.12 (d, *J*=5 Hz, 1 H), 5.20 (d, *J*=5Hz, 1 H), 6.00 (s, 2 H), 6.75—7.55 (m, 3 H); ^{19}F NMR ($CDCl_3$-$CFCl_3$) δ=−75 (s); IR 3500, 1490, 1450, 1250, 1200, 1029 cm^{-1}; MS *m/z* (rel intensity) 306 (M^++4, trace), 304 (M^++2, 4,) 302 (M^+, 6), 151 (100), 149 (12), 123 (11), 93 (59), 65 (33), 63 (10), 39 (10).

Found: C, 39.86; H, 2.30%. Calcd for $C_{10}H_6Cl_2F_3O_3$: C, 39.63; H, 2.33%.

2,2-Dichloro-3,3,3-trifluoro-(4-chlorophenyl)-1-propanol (2c): Colorless crystals, mp 85 °C. ^1H NMR ($CDCl_3$) δ=2.93 (d, *J*=5 Hz, 1 H), 5.21 (d, *J*=5 Hz, 1 H), 7.25—7.60 (m, 4 H); ^{19}F NMR ($CDCl_3$-$CFCl_3$) δ=−75.0 (s); IR (KBr) 3480, 1241, 1209, 1185, 881, 831 cm^{-1}; MS *m/z* (rel intensity) 294 (M^++2, trace), 292 (M^+, trace), 143 (36), 141 (100), 113 (19), 77 (67).

Found: C, 36.65; H, 2.07%. Calcd for $C_9H_6Cl_3F_3O$: C, 36.83; H, 2.06%.

2,2-Dichloro-3,3,3-trifluoro-1-(3,4-dichlorophenyl)-1-propanol (2d): A colorless oil. ^1H NMR ($CDCl_3$) δ=2.97 (br d, *J*=4 Hz, 1 H), 5.17 (br d, *J*=4 Hz, 1H), 7.2—7.8 (m, 3 H); ^{19}F NMR ($CDCl_3$-$CFCl_3$) δ=−74.2 (s); IR 3480, 1473, 1253, 1188, 1033, 884, 866, 824, 713, 659 cm^{-1}; MS *m/z* (rel intensity) 330 (M^++4, trace), 328 (M^++2, trace), 326 (M^+, trace), 179 (11), 177 (66), 175 (100), 149 (12), 147 (22), 113 (17), 111 (54), 75 (14).

Found: C, 32.81; H, 1.41%. Calcd for $C_9H_5OCl_4F_3$: C, 32.96; H, 1.54%.

4,4-Dichloro-5,5,5-trifluoro-1-phenyl-1-penten-3-ol (2e): A colorless oil. ^1H NMR ($CDCl_3$) δ=2.53 (br s, 1 H), 4.80 (d, *J*=5 Hz, 1 H), 6.27 (dd, *J*=5 and 16 Hz, 1H), 6.82 (d, *J*=16 Hz, 1H), 7.20—7.50 (m, 5 H); ^{19}F NMR ($CDCl_3$-$CFCl_3$) δ=−73.9 (s); IR 3450, 1257, 1195, 969, 870, 751, 722, 694 cm^{-1}; MS *m/z* (rel intensity) 286 (M^++2, trace), 284 (M^+, 2), 134 (11), 133 (100), 115 (22), 103 (10), 77 (15), 55 (37).

Found: C, 46.35; H, 3.02%. Calcd for $C_{11}H_9Cl_2F_3O$: C, 46.34; H, 3.18%.

2,2-Dichloro-1,1,1-trifluoro-5-methyl-4-hexen-3-ol (2f). Zinc powder (1.50 g, 24 mmol) and copper(I) chloride (99 mg, 1.00 mmol) were suspended in DMF (20 ml) at room temperature. After 5 min, 1,1,1-trichlorotrifluoroethane (4.75 ml, 40 mmol) was added, and the whole was stirred for 20 min at room temperature. Exothermic reaction soon took place, and the vessel was occasionally cooled with ice-water bath. Then, 3-methyl-2-butenal (**1f**) (1.81 g, 21.5 mmol) was added over 10 min to this mixture at 60 °C. Workup and purification by column chromatography (CH_2Cl_2-hexane 1 : 2 to 2 : 1) gave **2f** (3.0 g, 60% yield) as a colorless oil, bp 65—67 °C/0.6 Torr. ^1H NMR ($CDCl_3$) δ=1.77(d, *J*=1.4 Hz, 3 H), 1.81 (d, *J*=1.4 Hz, 3 H), 2.08 (br s, 1 H), 4.80 (d, *J*=9.1 Hz, 1 H), 5.33 (d, *J*=9.1Hz, 1H); ^{19}F NMR ($CDCl_3$-$CFCl_3$) δ=−74.6 (s); IR 3420, 1258, 1204, 1052, 872, 724 cm^{-1}; MS *m/z* (rel intensity) 221 (trace), 219 (trace), 85 (100), 55 (10), 41 (29), 39 (12), 29 (15).

Found: C, 35.30; H, 3.83%. Calcd for $C_7H_9Cl_2F_3O$: C, 35.47; H, 3.83%.

A control experiment in the absence of copper(I) chloride catalyst gave **2f** in 16% yield.

An experiment which employed dichloro[bis(triphenylphosphine)]palladium was carried out by adding 1,1,1-trichloro-2,2,2-trifluoroethane (0.18 ml, 1.5 mmol), $PdCl_2(PPh_3)_2$ (7.5 mg, 0.011 mmol) and zinc powder (78 mg, 1.2 mmol) to a solution of **1f** (86 mg, 1.0 mmol) in DMF (1 ml) and by stirring the reaction mixture at room temperature for 1 h and at 50 °C for 8 h. The yield of **2f** was estimated to be 61% by GLC assay (internal standard: tridecane; column: 5% silicone SE-30 on Uniport HP, 2 m; carrier gas: N_2, 50 ml min^{-1}): R_t 2.97 min.

The adduct **2f** was alternatively prepared by ultrasonic irradiation. To a solution of **1f** (84 mg, 1.0 mmol) in DMF (1 ml) was added 1,1,1-trichloro-2,2,2-trifluoroethane (0.18 ml, 1.5 mmol) and zinc powder (78 mg, 1.2 mmol), and the mixture was allowed to warm gradually to 50 °C under ultrasoic irradiation which was continued for 2 h at 50 °C. The yield was estimated by GLC.

2,2-Dichloro-1,1,1-trifluoro-4-phenyl-3-pentanol (2g): A colorless oil. ^1H NMR ($CDCl_3$), δ=1.46 (d, *J*=7.0, Hz, 3 H), 2.37 (d, *J*=8.1 Hz, 1 H), 3.52 (dq, *J*=2.1 and 7.0 Hz, 1 H), 4.31 (dd, *J*=2.1 and 8.1 Hz, 1 H), 7.33 (s, 5 H); ^{19}F NMR ($CDCl_3$-$CFCl_3$) δ=−74.8 (s); IR 3550, 1250, 1194, 870, 704 cm^{-1}; MS *m/z* (rel intensity) 288 (M^++2, trace), 286 (M^+, trace), 106 (10), 105 (100), 103 (5), 79 (9), 77 (7).

Found: C, 46.02; H, 3.97%. Calcd for $C_{11}H_{11}Cl_2F_3O$: C, 46.02; H, 3.86%.

2,2-Dichloro-1-cyclohexyl-3,3,3-trifluoro-1-propanol (2h). Cyclohexanecarbaldehyde (**1h**) (112 mg, 1.00 mmol) and 1,1,1-trichloro-2,2,2-trifluoroethane (0.18 ml, 1.5 mmol) were added to a suspension of zinc powder (78 mg, 1.20 mmol) and copper(I) chloride (5 mg, 0.05 mmol) in DMF (1 ml), and then the reaction mixture was stirred for 5 h at 50 °C. Workup followed by preparative TLC (CH_2Cl_2) gave **2h** (156 mg, 61% yield) as a colorless oil. ^1H NMR ($CDCl_3$) δ=1.0—2.3 (m, 12H), 3.94 (br s, 1H); ^{19}F NMR ($CDCl_3$-$CFCl_3$): δ=−75.1 (s); IR 3490, 2950, 2875, 1252, 1200 cm^{-1}; MS *m/z* (rel intensity) 245 (M^+−19, trace), 113 (19), 95 (60), 83 (100), 82 (18), 67 (17), 55 (84), 41 (39).

Found: C, 40.90; H, 5.08%. Cacld for $C_9H_{13}Cl_2F_3O$: C, 40.78; H, 4.94%.

In the absence of the copper catalyst, the yield of **2h** was 16%.

2,2-Dichloro-3,3,3-trifluoro-1-phenylpropyl Acetate. A solution of 2,2-dichloro-3,3,3-trifluoro-1-phenyl-1-propanol (0.62 g, 2.4 mmol) in pyridine (1 ml) and acetic anhydride (1

ml) was allowed to react for 4 h at room temperature. Work-up and purification by preparative TLC (CH_2Cl_2-hexane 1:2) gave the desired acetate (0.69 g, 96% yield) as a colorless oil. ^1H NMR ($CDCl_3$) δ=2.15 (s, 3 H), 6.35 (s, 1 H), 7.3—7.6 (m, 5 H); ^{19}F NMR ($CDCl_3$-$CFCl_3$) δ=−74.7 (s); IR 1767, 1373, 1248, 1204, 1040,1028, 938, 840, and 699 cm^{-1}; MS *m/z* (rel intensity) 302 (M^++2, trace), 300 (M^+, trace), 149 (27), 107 (87), 79 (14), 77 (13), 43 (100).

Found: C, 43.79; H, 2.79%. Calcd for $C_{11}H_9Cl_2F_3O_2$: C, 43.88; H, 3.01%.

Zinc Reduction of 2,2-Dichloro-3,3,3-trifluoro-1-phenyl-1-propyl Acetate. Zinc powder (40 mg, 0.61 mmol) was added to a DMF (0.5 ml) solution of the acetate (0.150 g, 0.50 mmol), and the mixture was stirred for 2 h at 50 °C. GLC assay (dodecane as the internal standard; 5% SE-30, 2 m; 120 °C; N_2 50 ml min^{-1}, R_t 5.81 min for **3a** and 12.0 min for the standard) revealed **3a** was produced in 88% yield.

Transformation of 1c to 3c. A Typical Procedure A for the Preparation of 3. To a solution of 4-chlorobenzaldehyde (**1c**) (139 mg, 0.99 mmol) in DMF (1 ml) was added 1,1,1-trichloro-2,2,2-trifluoroethane (0.24 ml, 2.0 mmol) and zinc powder (0.33 g, 5.0 mmol), and the mixture was stirred for 10 min at 0 °C and for 4 h at 50 °C. Water (10 ml) was added, and the resulting mixture was extracted with diethyl ether (3×10 ml). The ethereal extract was dried over anhydrous magnesium sulfate and concentrated under reduced pressure. Purification by preparative TLC (CH_2Cl_2-hexane 1:2) afforded 2-chloro-1-(4-chlorophenyl)-3,3,3-trifluoropropene (**3c**) (175 mg, a mixture of (Z)- and (E)-isomers, 73% yield) as a colorless oil. Bp 75 °C (bath temp)/1 Torr. ^1H NMR ($CDCl_3$) δ=7.25 (s, 1 H), 7.40 (d, *J*=10 Hz, 2 H), 7.67 (d, *J*=10 Hz, 2 H) were attributed to the (Z) isomer. ^{19}F NMR ($CDCl_3$-$CFCl_3$) δ=−69.1 (s, for (Z)-isomer) and −61.7 (s, for (E)-isomer) with the intensity ratio of 88:12. IR 1495, 1307, 1288, 1173, 1140, 1106, 962 cm^{-1}; MS *m/z* (rel intensity) 244 (M^++4, 11), 242 (M^++2, 66), 241 (M^++1, 10), 240 (M^+, 100), 207 (10), 205 (28), 187 (13), 185 (38), 170 (14), 169 (23), 136 (15), 75 (16), 74 (10), 50 (12).

Procedure B Exemplified by the Preparation of 3a. To a solution of benzaldehyde (**1a**, 105 mg, 0.99 mmol) in DMF (1 ml) were added 1,1,1-trichlorotrifluoroethane (0.142 ml, 1.2 mmol) and zinc powder (72 mg, 1.1 mmol). The mixture was stirred for 1 h at room temperature and for 24 h at 50 °C before the addition of acetic anhydride (0.15 ml) and zinc powder (131 mg, 2.0 mmol). Stirring was continued for 4 h at 50 °C. Water (1 ml) and 5 drops of conc hydrochloric acid were added to quench the reaction. Extraction with diethyl ether (3×3 ml), concentration, followed by ^{19}F NMR assay ($CDCl_3$-$CFCl_3$, internal standard: 1,3,5-trichloro-2,4,6-trifluorobenzene), showed two doublets at δ=−69.9 (d, *J*=0.8 Hz) and −62.1 (s) attributed to (*Z*)- and (*E*)-**3a** respectively in a ratio of 87:13 and 87% yield. ^1H NMR ($CDCl_3$) δ=7.2—7.5 (m, 4 H), 7.5—7.8 (m, 2 H); IR 1287, 1216, 1176, 1140, 692 cm^{-1}; MS *m/z* (rel intensity) 208 (M^++2, 34), 207 (M^++1, 10), 206 (M^+, 100), 171 (39), 151 (59), 102 (16), 75 (11), 51 (15), 50 (10).

Found: C, 52.05; H, 2.89%. Calcd for $C_9H_6ClF_3$: C, 52.32; H, 2.93%.

Followings were synthesized by the Procedure B.

2-Chloro-3,3,3-trifluoro-1-(3,4-methylenedioxyphenyl)propene (3b): Z:E=85:15, a colorless oil, bp 70 °C (bath temp)/0.1 Torr. ^1H NMR ($CDCl_3$) (a Z/E mixture) δ=6.03 (s, 2 H), 6.7—7.4 (m, 3 H); ^{19}F NMR ($CDCl_3$-$CFCl_3$) δ=−68.4 (s) for the (Z)-isomer and δ=6.00 (s, 2 H); −61.2 (s) respectively for the (E)-isomer. IR 1507, 1496, 1450, 1291, 1262, 1251, 1174, 1133, 1040 cm^{-1}; MS *m/z* (rel intensity) 252 (M^++2, 34), 251 (M^++1, 39), 250 (M^+, 100), 249 (87), 157 (26), 137 (16), 107 (12), 87 (12), 63 (11), 62 (13).

Found: C, 47.81; H, 2.47%. Calcd for $C_{10}H_6ClF_3O_2$: C, 47.93; H, 2.41%.

4-Chloro-5,5,5-trifluoro-1-phenyl-1,3-pentadiene (3e): Z:E=89:11, a colorless oil, bp 60—70 °C (bath temp)/0.1 Torr. ^1H NMR ($CDCl_3$) δ=6.6—7.2 (m, 2 H), 7.2—7.6 (m, 6 H); ^{19}F NMR ($CDCl_3$-$CFCl_3$) δ=−68.5 (s) for the (Z)-isomer and δ=−61.8 (s) for the (E)-isomer. MS *m/z* (rel intensity) 234 (M^++2, 17), 232 (M^+, 50), 197 (31), 178 (14), 177 (100), 146 (10), 129 (14), 128 (61), 127 (16), 77 (10), 63 (11), 51 (15).

Found: C, 56.74; H, 3.25%. Calcd for $C_{11}H_8ClF_3$: C, 56.79; H, 3.47%.

1-Cyclohexyl-2-chloro-3,3,3-trifluoropropene (3h): Z:E=85:15, a colorless oil, bp 70 °C (bath temp)/12 Torr; ^1H NMR ($CDCl_3$) δ=1.1—2.0 (m, 10 H), 2.3—2.7 (m, 1 H), 6.32 (d, *J*=9.0 Hz, 1 H); ^{19}F NMR ($CDCl_3$-$CFCl_3$) δ=−69.2 (s) for the (Z)-isomer and δ=6.05 (d, *J*=9 Hz, 1 H); −62.2(s) respectively for the (E)-isomer.

Found: C, 50.82; H, 5.64%. Calcd for $C_9H_{12}ClF_3$: C, 50.84; H,5.69%

Transformation of 1 to 4. A Typical Procedure. Zinc powder (194 mg, 2.97 mmol) was added to a DMF (3 ml) solution of 3,4-dichlorobenzaldehyde (**1d**) (174 mg. 0.99 mmol), 1,1,1-trichloro-2,2,2-trifluoroethane (0.18 ml, 1.5 mmol), and aluminium chloride (39 mg, 0.3 mmol) at 0 °C. The reaction mixture was stirred for 1 h at 0 °C and for 3.5 h at 50 °C, treated with sat ammonium chloride aq solution (4 ml), and extracted with diethyl ether (3×10 ml). The ethereal extract was dried over anhydrous magnesium sulfate and concentrated in vacuo. Purification by preparative TLC gave 2-chloro-1-(3,4-dichlorophenyl)-3,3-difluoro-2-propen-1-ol (**4d**, 193 mg, 72% yield) as a colorless oil, bp 130 °C (bath temp)/1 Torr. ^1H NMR ($CDCl_3$) δ=2.48 (br s, 1 H), 5.70 (br s, 1 H), 7.1—7.6 (m, 3 H); ^{19}F NMR ($CDCl_3$-$CFCl_3$) δ=−85.1 (d, *J*=40 Hz, 1 F), −89.4 (d, *J*=40 Hz, 1 F); IR 3400, 1747, 1394, 1290, 1132, 1032, 1010, 885, 827, 717 cm^{-1}; MS *m/z* (rel intensity) 276 (M^++4; 14), 274 (M^++2, 43), 270 (M^+, 45), 239 (25), 237 (38), 219 (24), 217 (25), 177 (63), 175 (100), 149 (32), 147 (52), 127 (37), 125 (41), 113 (29), 111 (89), 91 (34), 75 (35), 74 (25).

Found: C, 39.32; H, 1.96%. Calcd for $C_9H_5Cl_3F_2$: C, 39.53; H, 1.84%.

2-Chloro-3,3-difluoro-1-phenyl-2-propen-1-ol (4a): ^1H NMR ($CDCl_3$) δ=2.88 (br s, 1 H), 5.67 (br s, 1 H), 7.36 (s, 5 H); ^{19}F NMR ($CDCl_3$-$CFCl_3$) δ=−86.6 (dd, *J*=2 and 20 Hz, 1F), −90.4 (dd, *J*=3 and 20 Hz, 1 F); IR 3400, 1744, 1292, 1008, 701 cm^{-1}; MS *m/z* (rel intensity) 206 (M^++2, 11), 204 (M^+, 34), 186 (12), 185 (11), 184 (31), 183 (22), 169 (29), 151 (16), 149 (10), 127 (10), 125 (17), 107 (99), 105 (26), 91 (32), 79 (100), 78 (30), 77 (59), 75 (10), 51 (42), 50 (19), 39 (12), 28 (17), 18 (27).

Found: *m/z* 204.0137. Calcd for $C_9H_7ClF_2O$: M^+, 204.0152.

2-Chloro-1,1-difluoro-4-phenyl-1-penten-3-ol (4g): A colorless oil. ^1H NMR ($CDCl_3$) δ=1.42 (d, *J*=7.2 Hz, 3 H), 2.25 (br s, 1 H), 2.97 and 3.08 (q, *J*=7.2 Hz, 1 H), 4.53 (dt, *J*=10 and 3 Hz, 1 H), 7.1—7.4 (m, 5H) for the Z/E isomer mixture. ^{19}F NMR ($CDCl_3$-$CFCl_3$) δ=−87.5 (dd, *J*=2 and 38 Hz, 1F), −90.5 (dd, *J*=3 and 38 Hz, 1 F); MS *m/z* (rel inten-

sity) 232 (M^+, trace), 106 (23), 105 (100), 103 (7), 79 (13), 77 (15), 51 (7).

Found: C, 57.01; H, 4.84%. Calcd for $C_{11}H_{11}OClF_2$: C, 56.79; H, 4.76%.

1-Cyclohexyl-2-chloro-3,3-difluoro-2-propen-1-ol (4h): A colorless oil. ^1H NMR ($CDCl_3$) δ=0.5—1.8 (m, 10 H), 2.03 (br d, J=10 Hz, 1 H), 4.07 (d, J=10 Hz, 1 H); ^{19}F NMR ($CDCl_3$-$CFCl_3$) δ=−82.1 (dd, J=2 and 40 Hz, 1 F), −91.8 (m of dd, J=3 and 40 Hz, 1 F); IR 2950, 1746, 1287, 996 cm^{-1}; MS m/z (rel intensity) 210 (M^+, trace), 127 (9), 84 (7), 83 (99), 82 (22), 67 (8), 56 (5), 55 (100), 53 (5), 41 (50), 39 (16), 29 (10), 27 (12).

Found: m/z 210.0612. Calcd for $C_9H_{13}OClF_2$: M, 210.0621.

2-Chloro-1,1-difluoro-1-tridecen-3-ol (4k): ^1H NMR ($CDCl_3$) δ=0.7—1.0 (m, 3 H), 1.25 (s, 16 H), 1.45—1.9 (m, 2H), 1.77 (br s, 1 H), 4.35—4.6 (m, 1H); ^{19}F NMR ($CDCl_3$-$CFCl_3$) δ=−87.0 (dd, J=39 and 2 Hz, 1 F), −91.0 (dd J=39 and 3 Hz, 1F); IR 3380, 2945, 2875, 1747, 1288 cm^{-1}; MS m/z (rel intensity) 250 (M^+, trace), 129 (34), 127 (100), 57 (22), 55 (14), 43 (39), 41 (25), 29 (15).

Found: m/z 250.1326. Calcd for $C_{13}H_{21}ClF_2O$: M, 250.1299.

Addition of CF_3CCl_2ZnCl to α-Keto Esters. A Typical Procedure. Zinc powder (125 mg, 2.0 mmol) and copper(I) iodide (5 mg, 0.05 mmol) were added to a DMF (1 ml) solution of methyl phenylglyoxylate (**5a**) (164 mg, 1.0 mmol). To this mixture was added 1,1,1-trichloro-2,2,2-trifluoroethane (0.18 ml, 1.5 mmol) drop by drop at room temperature. The reaction mixture was stirred for 10 min, treated with saturated ammonium chloride aq solution (10 ml), and then extracted with diethyl ether (2×10 ml). The ethereal extract was dried over anhydrous magnesium sulfate and concentrated under reduced pressure. Purification by preparative TLC (silica gel, CH_2Cl_2) afforded methyl 3,3-dichloro-4,4,4-trifluoro-2-hydroxy-2-phenylbutanoate (**6a**, 175 mg, 55% yield) as a colorless oil, bp 70 °C (bath temp)/0.2 Torr. ^1H NMR ($CDCl_3$) δ=4.00 (s, 3 H), 4.72 (s, 1 H), 7.3—7.5 (m, 3 H), 7.9—8.2 (m, 2 H); ^{19}F NMR ($CDCl_3$-$CFCl_3$) δ=−70.6 (s); IR 3490, 1732, 1272, 1240, 1206 cm^{-1}; MS m/z (rel intensity) 259 (M^++2−COOMe, 7), 257 (M^+−COOMe, 11), 193 (6), 165 (25), 153 (5), 151 (7), 106 (8), 105 (100), 78 (12), 77, (29), 59 (6), 51 (10), 15 (8).

Found: C, 41.55; H, 2.97%. Calcd for $C_{11}H_9Cl_2F_3O_3$: C, 41.67; H, 2.86%.

Ethyl 3,3-Dichloro-4,4,4-trifluoro-2-hydroxy-2-methylbutanoate (6b): A colorless oil. ^1H NMR ($CDCl_3$) δ=1.35 (t, J=7.0 Hz, 3H), 1.78 (s, 3 H), 4.11 (s, 1 H), 4.35 (q, J=7.0 Hz, 2 H); ^{19}F NMR ($CDCl_3$-$CFCl_3$) δ=−72.4 (s); IR 3500, 1734, 1241, 1200, 1187 cm^{-1}; MS m/z (rel intensity) 197 (M^++2−COOEt, 13), 195 (M^+−COOEt, 20), 160 (18), 142 (5), 140 (14), 131 (6), 117 (6), 67 (6), 45 (7), 43 (100), 29 (47), 27 (11), 18 (12).

Found: C, 31.37; H, 3.44%. Calcd for $C_7H_9Cl_2F_3O_3$: C, 31.25; H, 3.37%.

Reaction of CF_3CCl_2ZnCl with DMF and Chlorotrialkylsilanes. A Typical Procedure. Zinc powder (0.78 g, 12 mmol) and 1,1,1-trichloro-2,2,2-trifluoroethane (1.42 ml, 12 mmol) were added slowly to a solution of t-butylchlorodimethylsilane (1.52 ml, 10 mmol) in DMF (10 ml) under cooling with water bath. The mixture was stirred for 1 h at room temperature. The whole was charged on a short silica gel (20 g) column and eluted with hexane (ca. 100 ml). The eluate was concentrated and again subjected to colum chromatography (silica gel, 10 g, hexane). Concentration of the hexane eluate and distillation gave 1-(t-butyldimethylsiloxy)-2,2-dichloro-3,3,3-trifluoro-1-dimethyl-1-propanamine (**7a**, 2.02 g, 60% yield) as a colorless oil, bp 50 °C (bath temp)/0.15 Torr. ^1H NMR ($CDCl_3$) δ=0.16 (s, 6 H), 0.98 (s, 9 H), 2.53 (s, 6 H), 4.71 (s, 1 H); ^{19}F NMR ($CDCl_3$-$CFCl_3$) δ=−75.2 (s); IR 1257, 1198, 1184, 1088, 1061, 840, 783 cm^{-1}; MS m/z (rel intensity) 324 (M^+−Me, trace), 208 (29), 188 (68), 131 (45), 130 (23), 116 (26), 102 (39), 85 (37), 83 (54), 75 (32), 74 (22), 73 (100), 59 (28).

Found: C, 38.83; H, 6.52; N, 4.12%. Calcd for $C_{11}H_{22}Cl_2F_3NOSi$: C, 38.93; H, 6.58; N, 4.07%.

2,2-Dichloro-1-triethylsiloxy-3,3,3-trifluoro-*N*,*N*-dimethyl-1-propanamine (7b): Bp 95 °C (bath temp)/0.3 Torr. ^1H NMR ($CDCl_3$) δ=0.2—1.2 (m, 15 H), 2.50 (s, 6 H), 4.70 (s, 1 H); IR 2975, 2899, 1260, 1196, 1182, 1068, 1008, 942, 902, 812, 742 cm^{-1}.

This work was partially supported by a Grant-in-Aid for Special Research on Organochemical Resources (Nos. 61111001 and 62101001) from the Ministry of Education, Science and Culture. We thank Ms. Tomoe Morita and Mr. Masanori Ueno for their experimental assistance.

References

1) a) Ciba Foundation, "Carbon-Fluorine Compounds-Chemistry, Biochemistry, and Biological Activities," Elsevier, Amsterdam (1972). b) R. Filler, "Biochemistry Involving Carbon-Fluorine Bond," Am. Chem. Soc., Washington D.C. (1976). c) "Biomedical Aspects of Fluorine Chemistry," ed by R. Filler and Y. Kobayashi, Elsevier Biomedical Press, Amsterdam (1982). d) F. A. Smith, *Chemtech*, **1973**, 422. e) R. Filler, *ibid.*, **1974**, 752.

2) a) W. A. Sheppard and C. M. Sharts, "Organic Fluorine Chemistry," W. A. Benjamin (1969). b) R. D. Chambers, "Fluorine in Organic Chemistry," Wiley-Interscience, 1973. c) M. Hudlicky, "Chemistry of Organic Fluorine Compounds," Ellis Horwood (1976).

3) a) Wittig-type olefination with fluorohalocarbons: D. Naae and D. J. Burton, *Synth. Commun.*, **3**, 197 (1973); S. Hayashi, T. Nakai, N. Ishikawa, D. J. Burton, D. G. Naae, and H. S. Kesling, *Chem. Lett.*, **1979**, 983; M. Suda, *Tetrahedron Lett.*, **22**, 1421 (1981); W. A. Vinson, K. S. Prickeett, B. Spahic, and P. R. O. Mintellano, *J. Org. Chem.*, **48**, 4661 (1983); M. J. Van Hamme and D. J. Burton, *J. Organomet. Chem.*, **169**, 123 (1979); *idem*, *J. Organomet. Chem.*, **169**, 123 (1979); D. J. Burton and D. G. Cox, *J. Am. Chem. Soc.*, **105**, 650 (1983); D. J. Burton and P. E. Grenlimb, *J. Org. Chem.*, **40**, 2796 (1975). b) Reactions of Fluorohalocarbons with carbanions: T. Y. Shen, S. Lulcas, and L. H. Sarett, *Tetrahedron Lett.*, **1961**, 43; P. Bey and J. P. Vevert, *ibid.*, **1978**, 1215; P. Bey, J. P. Vevert, V. V. Dorsselaer, and M. Kolb, *J. Org. Chem.*, **44**, 2732 (1979); P. Bey, F. Gerhart, V. V. Dorsselaer, and C. Danzin, *J. Med. Chem.*, **26**, 1551 (1983); S. Kosuge, H. Nakai, and M. Kurono, *Prostaglandins*, **18**, 737 (1979); I. Rico, D. Cantacuzene, and C. Wakselman, *J. Chem. Soc., Perkin Trans. 1*, **1982**, 1063; S. T. Purrington, T. S. Everett, and C. L. Bumgardner, *Tetrahedron Lett.*, **25**, 1329 (1984).

4) a) Cu(I)-catalyzed addition of CCl_3CF_3 to olefins: P. Martin, J. Streith, G. Rihs, T. Winkler, and D. Bellus,

Tetrahedron Lett., **26**, 3947 (1985); D. Bellus, *Pure Appl. Chem.*, **57**, 1827 (1985). b) The Wittig type olefination with $CCl_3CF_3/PPh_3/Zn$ reagent was disclosed anonymously: *Res Discl.*, **219**, 239 (1982) [*Chem. Abstr.*, **98**, 16322r (1983)].

5) Carbonyl addition of R_f-Mtl compounds: a) Mtl=Li, O. R. Pierce, E. T. McBee, and G. F. Judd, *J. Am. Chem. Soc.*, **76**, 474 (1954); R. D. Chambers, W. K. R. Musgrave, and J. Savory, *J. Chem. Soc.*, **1962**, 1993; P. G. Gassman and N. J. O'Reilly, *Tetrahedron Lett.*, **26**, 5243 (1985). b) Mtl=Mg, R. N. Haszeldin, *J. Chem. Soc.*, **1952**, 3423; **1953**, 1748; **1954**, 1273; D. D. Denson, C. F. Smith, and C. Tamborski, *J. Fluorine Chem.*, **3**, 247 (1973/4); C. F. Smith, E. J. Soloski, and C. Tamborski, *ibid.*, **4**, 35 (1974); L. S. Chen, G. J. Chen, and C. Tamborski, *ibid.*, **26**, 341 (1984). c) Mtl=Zn, T. Kitazume and N. Ishikawa, *Chem. Lett.*, **1981**, 1679; N. Ishikawa, M. Takahashi, T. Sato, and T. Kitazume, *J. Fluorine Chem.*, **22**, 585 (1983); N. J. O'Reilly, M. Maruta, and N. Ishikawa, *Chem. Lett.*, **1984**, 517; T. Kitazume and N. Ishikawa, *J. Am. Chem. Soc.*, **107**, 5186 (1985); S. Benefice, H. Blancou, and A. Commeyras, *Tetrahedron*, **40**, 1541 (1984). d) Mtl=Ca, G. Santini, M. L. Blanc, and J. G. Riess, *J. Chem. Soc., Chem, Commun.*, **1975**, 678; G. Santini, M. L. Blanc, and J. G. Riess, *J. Organomet. Chem.*, **140**, 1 (1977). e) Mtl=Mn, T. Kitazume and N. Ishikawa, *Nippon Kagaku Kaishi*, **1984**, 1725.

6) I. Hemer, A. Posta, and V. Dedek, *J. Fluorine Chem.*, **26**, 467 (1984); I. Hemer, J. Havlicek, and V. Dedek, *ibid.*, **34**, 241 (1986).

7) Preliminary reports have appeared in: a) M. Fujita, T. Morita, and T. Hiyama, *Tetrahedron Lett.*, **27**, 2135 (1986). b) M. Fujita and T. Hiyama, *ibid.*, **27**, 3655 (1986). Later, Lang reported almost the same chemistry: R. W. Lang, *Helv. Chim. Acta*, **69**, 881 (1986). Torii et al. have achieved the $PbBr_2$/Al-promoted transformation recently: H. Tanaka, S. Yamashita, Y. Katayama, and S. Torii, *Chem. Lett.*, **1986**, 2043.

8) Zinc-copper couple: H. E. Simmon, T. L. Cairns, and S. A. Vladuchick, *Org. React.*, **20**, 1 (1973).

9) The true structure is unclear. It may exist as an aggregate or a disproportionated form $[(CF_3CCl_2)_2Zn \cdot ZnCl_2]$.

10) Ger. Offen. 1900758 [*Chem. Abstr.*, **73**, 87470g].

11) Similar deoxygenative behavior of Lewis acids is observed in the carbonyl methylenation with CH_2CX_2/Zn/Lewis acid reagent: a) K. Takai, Y. Hotta, K. Oshima, and H. Nozaki, *Bull. Chem. Soc. Jpn.*, **53**, 1698 (1980). b) J. Hibino, T. Okazoe, K. Takai, and H. Nozaki, *Tetrahedron Lett.*, **26**, 5579 (1985); **26**, 5581 (1985).

12) a) P. D. Bently, R. Cheetham, R. K. Huff, R. Pascoe, and J. D. Sayle, *Pestic. Sci.*, **11**, 156 (1980). b) D. Holland and D. A. Laidler, *J. Mol. Cat.*, **11**, 119 (1981). c) D. A. Laidler and D. J. Milner, *J. Organomet. Chem.*, **270**, 121 (1984). d) E. L. Plummer, R. P. Seuders, D. E. Seelye, and R. R. Start, *Pestic. Sci.*, **15**, 509 (1984). e) Japan Kokai Tokkyo Koho 53-95945; 54-112820; 54-130537; 55-59142; 55-89248; 55-111488; 59-92830.

13) M. Fujita, T. Hiyama, and K. Kondo, *Tetrahedron Lett.*, **27**, 2139 (1986).

14) a) J. F. Normant, J. P. Foulon, D. Masure, R. Sauvetre, and J. Villieras, *Synthesis*, **1975**, 122. b) C. Chuit, R. Sauvetre, D. Masure, M. Baudry, J. F. Normant, and J. Villieras, *J. Chem. Res. (S)*, **1977**, 104. c) R. Sauvetre, D. Masure, C. Chuit, and J. F. Normant, *Synthesis*, **1978**, 128.

15) Though silylation and addition of $LiCCl{=}CF_2$ to hexafluoroacetone were reported, we failed to get an undecanal adduct even at −130 °C.

16) Preparations and reactions of $LiCX{=}CF_2$ (X=F, Cl): a) D. Seyferth, T. Wada, and G. Raab, *Tetrahedron Lett.*, **1960**, 20. b) P. Tarrant, P. Johncock, and J. Savory, *J. Org. Chem.*, **28**, 839 (1963). c) F. G. Drakesmith, R. D. Richardson, O. J. Stewart, and P. Tarrant, *ibid.*, **32**, 286 (1967); **33**, 473 (1968). d) R. Sauvetre, D. Masure, C. Chuit, and J. F. Normant, *Compt. Rend. Serie C*, **1979**, 335. e) S. Martin, R. Sauvetre, and J. F. Normant, *Tetrahedron Lett.*, **24**, 5615 (1983). f) *idem.*, *J. Organomet. Chem.*, **264**, 155 (1984). g) J. P. Gillet, R. Sauvetre, and J. F. Normant, *Tetrahedron Lett.*, **26**, 3999 (1985). H) T. Hiyama, K. Nishide, and M. Obayashi, *Chem. Lett.*, **1984**, 1765.

17) Fluoride ion catalyzed aldehyde addition of polyhaloethenylsilanes proceeds also under mild conditions: M. Fujita and T. Hiyama, *J. Am. Chem. Soc.*, **107**, 4085 (1985).

18) M. Fujita, K. Kondo, and T. Hiyama, *Bull. Chem. Soc. Jpn.*, **60**, 4385 (1987).

Practical, Stereocontrolled Synthesis of Polyfluorinated Artificial Pyrethroids

Makoto FUJITA, Kiyosi KONDO, and Tamejiro HIYAMA*
Sagami Chemical Research Center, 4-4-1 Nishiohnuma, Sagamihara, Kanagawa 229
(Received July 22, 1987)

Practical and stereocontrolled approaches to polyfluorinated synthetic pyrethroids based on aldehyde addition of CF_3CCl_2ZnCl are described. The zinc reagent was allowed to react with 3-formyl-2,2-dimethylcyclopropanecarboxylates (**6**) to give the corresponding adducts. These were acetylated and then reduced again with zinc to afford (1*R**, 3*S**)-3-(2-chloro-3,3,3-trifluoro-1-propenyl)-2,2-dimethylcyclopropanecarboxylates (**12**). The (1R*, 3R*)-isomer was derived from 2,2-dichloro-1,1,1-trifluoro-5-methyl-4-hexen-3-ol by diazoacetylation, Cu(II)-catalyzed intramolecular carbene addition, and finally by the zinc reduction. An alternative access to **12** and its halogen homologues of the (*Z*)-pyrethroids involves addition of 1-halo-2,2-difluoroethenyl group across the CHO group of **6** and subsequent regio- and stereoselective halogenation.

In spite of high insecticidal activity and low mammalian toxicity, use of such natural pyrethroids as pyrethrin I and pyrethrin II has been limited owing to rapid biological degradation and poor photo-oxidative stability.[1] Since the discovery of a photo-stable and more potent analogue permethrin (**1a**), a great deal of effort has been made in search for new highly potent artificial pyrethroids, and a number of derivatives including cypermethrin (**1b**) and deltamethrin (**1c**) have been developed and used currently.

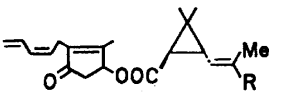

R = Me : Pyrethrin I

R = COOMe : Pyrethrin II

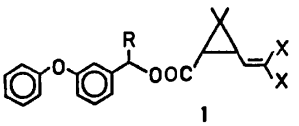

1

a : X = Cl, R = H (permethrin)

b : X = Cl, R = CN (cypermethrin)

c : X = Br, R = CN (deltamethrin)

New fluorinated analogues having a $CH=C(Cl)CF_3$ group commonly in place of $CH=CCl_2$ moiety are found recently to exhibit remarkably enhanced activity: Typical examples are cyhalothrin (**2a**)[2] and bifenthrin (**2b**),[3] which show, in addition to intensified insecticidal activity, 50 to 100 fold acaricidal activity as compared to **1**. Although several synthetic methods for **2** are reported to date,[2-4] the stereochemical control yet remained unsettled. Described herein is practical and stereocontrolled synthesis of **2** based on aldehyde-addition of CF_3CCl_2ZnCl reagent.[5]

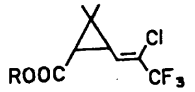

2

a: R = 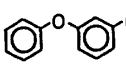 (cyhalothrin)

b: R = 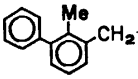 (bifenthrin)

Retrosynthetic analysis of **2** led us to a new strategy (Scheme 1) which is characterized by a new transformation of CHO group to $CH=C(Cl)CF_3$ moiety through two routes as summarized in Scheme 1. The one involves the addition of $^-CCl_2CF_3$ to an aldehyde carbonyl and subsequent reductive β-elimination (route *a*). The other will be realized by the addition of $^-CCl=CF_2$ followed by S_N'-type fluorination (route *b*).

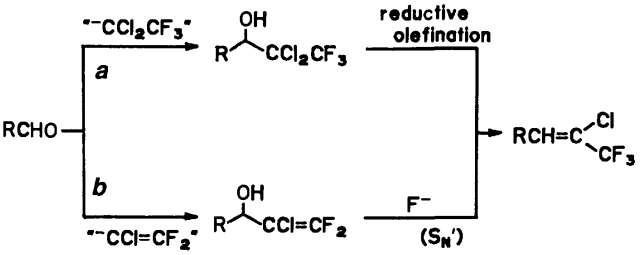

Scheme 1.

Results and Discussion

Stereocontrolled Synthesis of 2. The first step of the route *a* is now readily achieved by the recently found zinc carbenoid reagent CF_3CCl_2ZnCl.[6] The second step was studied benzaldehyde-CCl_2CF_3 adduct **3a** as the model. Reduction of **3a** under the standard conditions (zinc in acetic acid) gave the desired olefin **4a** in only 33% yield in contrast to the related reduction in permethrin synthesis.[1] The yield of **4a** was improved to 84% by the reduction of the acetate **5a** in *N*,*N*-dimethylformamide (DMF). The mesylate **5a'** equally underwent the reductive olefination to give **4a** in 65% yield. Similarly, the acetate **5b** derived from 3-methyl-2-butenal was reduced to a diene **4b**, another precursor of our target compound **2**.

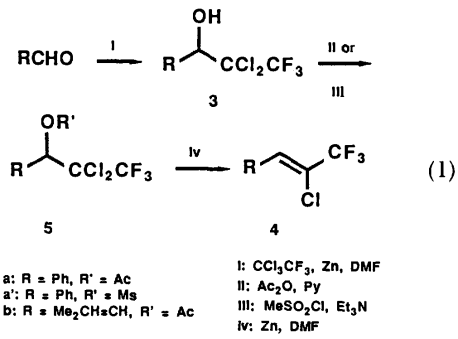

These findings were successfully applied to 3-formyl-2,2-dimethylcyclopropanecarboxylates **6**[7] which were readily prepared by ozonolysis[8] of the corresponding chrysanthemates (81—89% yield). The addition of CF_3CCl_2ZnCl to **6** took place in good yields (Scheme 2 and Table 1). The adducts **7** were acetylated, and the resulting acetates **8** were transformed to **12** whose stereochemistry was proved to be uniform (1R*, 3S*) with the Z/E ratio of 86 : 14 to 93 : 7. As the alcohols **7** consisted of ca. 1 : 1 mixture of two diastereomers, each isomer was separated by column chromatography. To check the stereochemical course of the reductive olefination, each diastereomer was converted into **12**, whose Z/E ratios were almost the same and thus totally independent of the configuration of the OH group in **7**. The mesylate (**9**), benzoate (**10**), and tosylate (**11**) of **7** also are potential precursors of **12**. Results are summarized in Table 1.

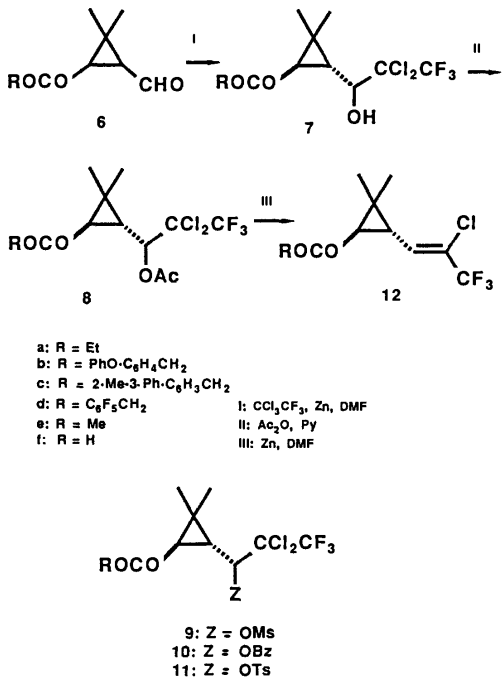

Scheme 2.

Table 1. Transformation of **6** to **12**

Aldehyde	**7** (yield/%)	**8** (yield/%)	**12** (yield/%)
6a[a]	58	93	86[d]
6b[b]	74	98	74[d]
6c[b]	86	100	95[e]
6d[b]	71	—	—
6e[c]	75	—	—

a) Trans/cis=4 : 1. b) Trans/cis=6 : 1. c) Trans/cis=100 : 0. d) Z/E=6 : 1. e) Z/E=8 : 1.

It should be noted that, though trans/cis isomeric mixture (4 to 6 : 1) of **6** was employed, only *trans*-**6** gave the adduct **7**. The CF_3CCl_2 adducts of the *cis*-**6** apparently underwent lactonization under the reaction conditions to give a bicyclic lactone **13** (<10% yield) which was isolated in some cases. The lactone **13** was not produced from pure *trans*-**6e**. Thus, the correlation of *trans*-**6**→**7** and *cis*-**6**→**13** is disclosed. Since *cis*-**6** is easily epimerized to the trans-isomer under the basic conditions,[9] a method is now established for control of the trans-configuration on the cyclopropane ring.

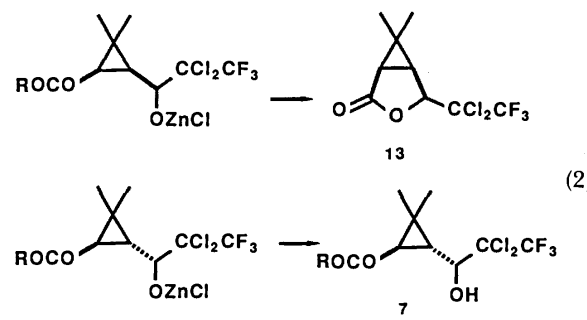

A one-step transformation of **6c** to **12c** (*trans*-bifenthrin) was effected with the $CF_3CCl_3/Zn/Ac_2O$ reagent (Eq. 3)[10] Although the same transformation was previously carried out by the Wittig type olefination using 1,1,1-trichloro-2,2,2-trifluoroethane, triphenylphosphine (2 mol), and zinc,[4c] the method disclosed herein is apparently more practical in view of low cost of reagents and much simpler separation technique.

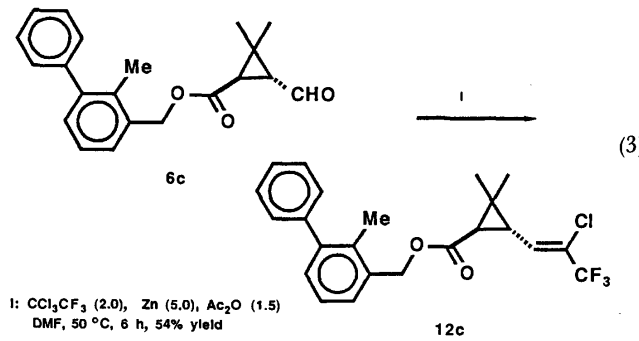

The (1R*,3R*)-isomer of **2** was synthesized stereospecifically according to Scheme 3.[11] The alcohol **14**[6] was treated with diketene in the presence of potassium carbonate to give the acetylacetate **15** (88% yield), which was converted into the diazoacetate **16** by treatment with a slight excess of *p*-toluenesulfonyl (tosyl) azide and triethylamine followed by alkaline hydrolysis (82% yield from **15**). Intramolecular cyclopropanation of **16** was successfully performed with copper(II) acetylacetonate catalyst to give the lactone **13** in 75%

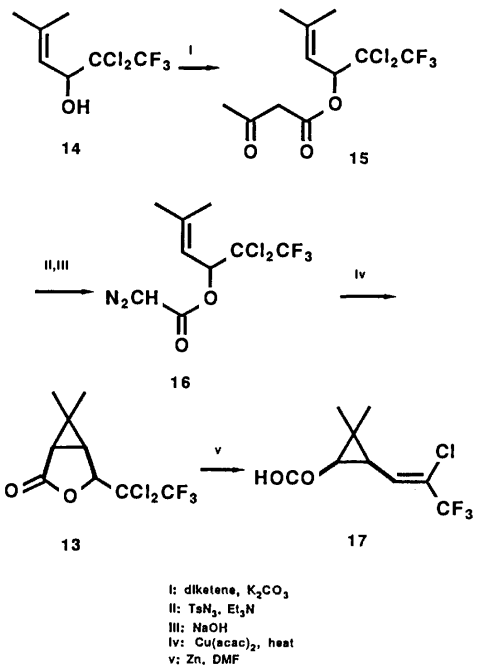

Scheme 3.

yield. Finally, reduction with zinc afforded the cis-acid **17** in 84% yield.

Regio- and Stereocontrolled Halogenation of 1-Substituted 2-Chloro-3,3-difluoro-2-propen-1-ols. In order to effect the transformation of route *b* in Scheme 1, we studied fluorination of the adducts **18** which are readily accessible by the reaction of aldehydes with $CCl_3CF_3/Zn/AlCl_3$ (cat) reagent[10] or by polyfluoroethenylsilane/F^- (catalyst) reagent.[12] Although several reagents for fluorinating alcohols have been developed,[13] the reaction applied to allylic alcohols is problematic due to side reactions like dehydration and lack of regioselectivity.[13a,14] In contrast, polyfluoroallylic alcohols **18** are found to be fluorinated with diethylaminosulfur trifluoride (DAST) under high regio- and stereocontrol (Eq. 4). When 1,1,2-trifluoro-1-tridecen-3-ol (**18a**) was treated with DAST, quantitative formation of 1,1,1,2-tetrafluoro-2-tridecene (**19a**) free of any stereo- or regioisomers was demonstrated by ^{19}F NMR. The configuration of **19a** was confirmed to be Z as judged by $^3J_{H-F}$ value (33 Hz).[15] The fluoride attack at the difluoromethylene carbon is particularly facilitated by highly electronegative fluorine substituent, and thus smooth and regioselective nucleophilic attack by fluoride ion is achieved under concomitant

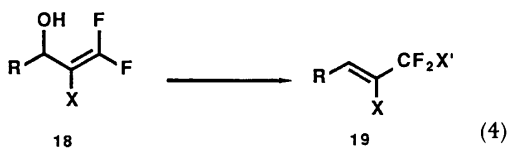

(4)

a: R = n-$C_{10}H_{21}$, X = F
b: R = n-$C_{10}H_{21}$, X = Cl
c: R = c-C_6H_{11}, X = Cl
d: R = Ph, X = Cl

no superscript : X' = F
': X' = Cl
'': X' = Br

Table 2. Halogenation of **18**

Alcohol	Reagent[a] Solvent	Condition	Product[b] (yield/%)[c]
18a	DAST (1.0)/CH_2Cl_2	−78 °C—r.t., 0.2 h	**19a** (90)
18a	$SOCl_2$ (1.0)/Et_2O[e]	r.t., 3 h	**19a'** (85)
18b	DAST (1.0)/CH_2Cl_2	−78 °C—r.t., 0.3 h	**19b** (70)
18b	$SOCl_2$ (1.4)/Et_2O	50 °C, 13 h[d]	**19b'** (90)
18b	$SOBr_2$ (1.2)/Et_2O	50 °C, 4 h[d]	**19b''** (84)
18b	PBr_3 (1.05)/Et_2O	r.t., 1.5 h; 35 °C, 13 h	**19b''** (67)
18c	$SOCl_2$ (1.0)/Et_2O	50 °C, 18 h[d]	**19c'** (75)
18d	$SOCl_2$ (1.1)/Et_2O	50 °C, 12 h[d]	**19d'** (79)

a) Values in the parentheses refer to molar ratio to **18**. b) Only (Z)-isomers were isolated. c) Isolated yields. d) Carried out in a sealed tube. e) Pyridine (2.0 mol) was added.

deoxygenation.[16] Chlorination and bromination of the allylic alcohols **18** also proceeded with high regio- and stereoselectivity to allord (Z)-2-alkenes **19'** and **19''**, which should have been yielded by a cyclic S_Ni'-mechanism. The stereochemistry was determined again by ^1H and/or ^{13}C NMR spectrometry.[17] Results are summarized in Table 2. Thus, halogen analogues of **3** grew readily accessible by the two-step strategy which involves the aldehyde addition of $^-CCl=CF_2$ group and subsequent regio- and stereoselective halogenation.

Halogen analogues of **2** such as **21** and **22** were also shown to have high insecticidal activity.[2a,4f] The regio- and stereocontrolled halogenation disclosed above was applied successfully to the synthesis of these halogen analogues as well. The $CX=CF_2$ adducts **20** were prepared from **6** by the addition of trifluoroethenyllithium[18] or by the fluoride ion mediated addition of polyfluoroethenylsilanes[12] followed by acid hydrolysis. Fluorination or chlorination of **20** afforded respectively **21** or **22** under high regiocontrol (Eq. 5).

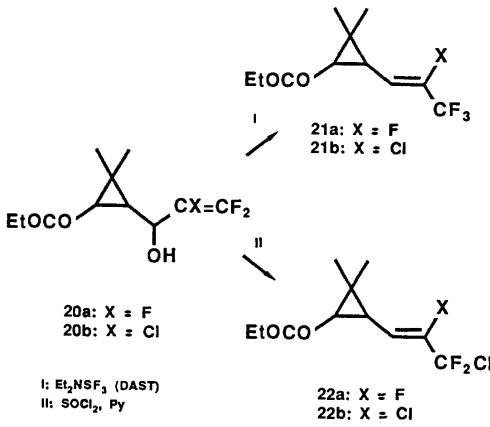

(5)

In summary, the method reported in this paper provides facile ways to polyfluorinated artificial pyrethroids under high stereocontrol. Practicability of these processes deserves particular emphasis: Most of reagents are commercially available, and the reaction conditions of each step are mild enough.

Experimental

Experimental apparatus and instrumental facilities are the same as those of the preceding paper.

2,2-Dichloro-3,3,3-trifluoro-1-phenylpropyl Methanesulfonate (5a′). Triethylamine (0.42 ml, 3 mmol) and methanesulfonyl chloride (0.155 ml, 2.0 mmol) were successively added to an ethereal solution (10 ml) of 2,2-dichloro-3,3,3-trifluoro-1-phenyl-1-propanol (**3a**, 0.26 g, 1.0 mmol) at 0 °C, and the resulting mixture was stirred for 2 h at 0 °C and for 1 h at room temperature. Workup and purification by preparative TLC (CH_2Cl_2-hexane 1 : 1) gave **5a′** (0.29 g, 85% yield) as a viscous colorless oil. ^{1}H NMR ($CDCl_3$) δ=2.65 (s, 3 H), 6.00 (s, 1 H), 7.2—7.9 (m, 5 H); ^{19}F NMR ($CDCl_3$-$CFCl_3$) δ=−75.0 (s); IR 1369, 1191, 962, 900, 819, 740, 701 cm^{-1}; MS *m/z* (rel intensity) 338 (M^++2, trace), 336 (M^+, 4), 185 (51), 107 (100), 79 (26), 77 (22), 51 (13).

Found: C, 35.56; H, 2.70%. Calcd for $C_{10}H_9Cl_2F_3O_3S$: C, 35.63; H, 2.69%.

4-Acetoxy-5,5-dichloro-6,6,6-trifluoro-2-methyl-2-hexene (5b). A mixture of 5,5-dichloro-6,6,6-trifluoro-2-methyl-2-hexen-4-ol (**3b**, 0.116 g, 0.49 mmol), acetic anhydride (0.2 ml), and pyridine (0.2 ml) was stirred for 8 h at room temperature. Concentration in vacuo followed by preparative TLC (CH_2Cl_2-hexane 1 : 1) gave **5b** (0.131 g, 96% yield) as a colorless oil. ^{1}H NMR ($CDCl_3$) δ=1.83 (s, 6 H), 2.10 (s, 3 H), 5.28 (d, *J*=9.3 Hz, 1 H), 6.08 (d, *J*=9.3 Hz, 1 H); ^{19}F NMR ($CDCl_3$-$CFCl_3$) δ=−75.1 (s); IR 1767, 1254, 1208, 1190, 1024 cm^{-1}; MS *m/z* (rel intensity) 280 (M^++2, trace), 278 (M^+, trace), 183 (10), 85 (100), 43 (88), 41 (10).

Found: C, 38.73; H, 3.94%. Calcd for $C_9H_{11}Cl_2F_3O_2$: C, 38.73; H, 3.97%.

2-Chloro-1,1,1-trifluoro-5-methyl-2,4-hexadiene (4b). Zinc powder (36 mg, 0.55 mmol) and copper(I) chloride (1 mg) were added to a solution of **5b** (0.142 g, 0.51 mmol), and the whole was stirred for 6 h at 50 °C before quenching with water (2 ml) and 3 drops of conc hydrochloric acid. Extraction with pentane (4×3 ml), drying over magnesium sulfate, followed by careful concentration at 0 °C under reduced pressure gave **4b** (77 mg, 82% yield) as a colorless oil which consisted of (Z)- and (E)-isomers in a ratio of 85 : 15. ^{1}H NMR ($CDCl_3$) δ=1.87 (s, 3 H), 1.96 (s, 3 H), 6.13 (d, *J*=11.1 Hz, 1 H), 7.01 (d, *J*=11.1 Hz, 1 H) for the (Z)-isomer, δ=6.83 (d, *J*=11.1 Hz, 1 H) for the (E)-isomer, ^{19}F NMR ($CDCl_3$-$CFCl_3$) δ=−69.0 (s) for the (Z)-isomer and −62.1 (s) for the (E)-isomer.

A Typical Procedure for the Preparation of 2,2-Dimethyl-3-(2-methyl-1-propenyl)cyclopropanecarboxylates. To an ethereal solution (10 ml) of 2,2-dimethyl-3-(2-methyl-1-propenyl)cyclopropanecarbonyl chloride[8] (2.80 g, 15.0 mmol) was added (2-methyl-3-phenylphenyl)methanol (2.97 g, 15.0 mmol) dissolved in pyridine (1.5 ml) and diethyl ether (10 ml), and the whole was stirred for 3 h at room temperature. Workup and purification by column chromatography (CH_2Cl_2-hexane 1 : 2) gave (2-methyl-3-phenylphenyl)methyl 2,2-dimethyl-3-(2-methyl-1-propenyl)cyclopropanecarboxylate (0.29 g, 85% yield) as a colorless viscous oil. ^{1}H NMR ($CDCl_3$) δ=1.14 (s, 3 H), 1.29 (s, 3 H), 1.54 (d, *J*=5 Hz, 1 H), 1.71 (s, 6 H), 2.17 (dd, *J*=5 and 8 Hz, 1 H), 2.22 (s, 3 H), 4.94 (d, *J*=8 Hz, 1 H), 5.20 (s, 3 H); IR 1733, 1160, 764, 707 cm^{-1}; MS *m/z* (rel intensity) 348 (trace, M^+), 182 (21), 181 (94), 166 (35), 165 (28), 123 (100), 81 (23).

Found: C, 82.52; H, 8.14%. Calcd for $C_{24}H_{28}O_2$: C, 82.72; H, 8.10%.

According to the similar procedure, following esters were prepared and characterized spectrometrically.

(3-Phenoxyphenyl)methyl 2,2-Dimethyl-3-(2-methyl-1-propenyl)cyclopropanecarboxylate: 98% yield as a trans/cis mixture. ^{1}H NMR ($CDCl_3$) δ=1.12 (s, 3 H), 1.24 (s, 3 H), 1.42 (d, *J*=5 Hz, 1 H), 1.69 (s, 6 H), 2.04 (dd, *J*=5 and 8 Hz, 1 H), 4.85 (d, *J*=8 Hz, 1H), 5.04 (s, 2 H), 6.8—7.4 (m, 9 H) for the trans isomer, δ=1.18 (s, 3 H), 1.23 (s, 3 H), 1.69 (s, 6 H), 5.03 (s, 2 H), 5.33 (d, *J*=8 Hz, 1 H), 6.8—7.4 (m, 9 H) for the cis isomer. IR 1732, 1591, 1492, 1260, 1219, 1160, 694 cm^{-1}.

(Pentafluorophenyl)methyl 2,2-Dimethyl-3-(2-methyl-1-propenyl)cyclopropanecarboxylate: 85% yield. ^{1}H NMR ($CDCl_3$) δ=1.13, 1.19, 1.25, 1.26 (s, totally 6 H), 1.37 (d, *J*=5 Hz, 1 H), 2.05 (dd, *J*=5 and 8 Hz, 1 H), 4.85 and 5.27 (br d, *J*=8 Hz, totally 1 H), 6.32 and 6.33 (s, totally 1 H); ^{19}F NMR ($CDCl_3$-$CFCl_3$) δ=−142 (m, 2 F), −153 (m, 1 F), −162 (m, 2 F); IR 1736, 1527, 1509, 1153, 1133 cm^{-1}.

A Typical Procedure for the Preparation of 3-Formyl-2,2-dimethylcyclopropanecarboxylates. Ozone was bubbled into an ethyl acetate (10 ml) solution of (2-methyl-3-phenylphenyl)methyl 2,2-dimethyl-3-(2-methyl-1-propenyl)-cyclopropanecarboxylate (0.70 g, 2.0 mmol) at −78 °C until the solution became pale blue. Excess ozone and the ozonide were reduced by addition of dimethyl sulfide (1 ml), and the reaction mixture was allowed to warm to room temperature. Concentration under reduced pressure followed by purification by column chromatography (CH_2Cl_2-hexane 1 : 1) afforded (2-methyl-3-phenylphenyl)methyl 3-formyl-2,2-dimethylcyclopropanecarboxylate **6c** (0.59 g, 92% yield) as a colorless viscous oil. The trans/cis ratio was estimated to be 6 : 1 by ^{1}H NMR analysis. ^{1}H NMR (400 MHz, $CDCl_3$) δ=1.31 (s, 3 H), 1.36 (s, 3 H), 2.22 (s, 3 H), 2.53 (d, *J*=1.5 Hz, 1 H), 2.53 (s, 1 H), 5.23 (s, 2 H), 7.23—7.44 (m, 8 H), 9.59 (dd, *J*=1.1 and 2.5 Hz, 1 H) for the trans-isomer. δ=1.27 (s, 3 H), 1.58 (s, 3 H), 1.88 (dd, *J*=6.5 and 8.6 Hz, 1 H), 2.20 (d, *J*=8.6 Hz, 1 H), 2.23 (s, 3 H), 5.28 (s, 3 H), 7.23—7.44 (m, 8 H), 9.79 (d, *J*=6.5 Hz, 1 H) for the cis-isomer. IR 1730, 1710, 1233, 1164, 1112, 763, 704 cm^{-1}; MS *m/z* (rel intensity) 322 (M^+, trace), 182 (18), 181 (100), 180 (74), 179 (16), 178 (12), 167 (11), 166 (56), 165 (67), 152 (10), 97 (61), 43 (12), 41 (36).

Found: C, 77.97; H,6.92%. Calcd for $C_{21}H_{22}O_3$: C, 78.23; H, 6.88%.

By the similar procedure, **6b** and **6d** were prepared.

(3-Phenoxyphenyl)methyl 3-Formyl-2,2-dimethylcyclopropanecarboxylate (6b): 82% yield. ^{1}H NMR ($CDCl_3$) δ=1.29 (s, 3 H), 1.32 (s, 3 H), 2.46 (ABq, 2 H), 5.06 (s, 2 H), 6.8—7.5 (m, 9 H), 9.56 (dd, *J*=1.8 and 1.8 Hz, 1 H) for the trans isomer, δ=1.8—2.3 (m, 2H), 9.73 (d, *J*=6.7 Hz, 1 H) for the cis isomer. IR 1732, 1711, 1588, 1492, 1258, 1215, 1167, 693 cm^{-1}; MS *m/z* (rel intensity) 325 (M^++1, 2), 324 (M^+, 21), 184 (20), 183 (100), 97 (40), 77 (10), 41 (10).

Found: C, 74.08; H, 6.31%. Calcd for $C_{20}H_{20}O_4$: C, 74.06; H, 6.21%.

(Pentafluorophenyl)methyl 3-Formyl-2,2-dimethylcyclopropanecarboxylate (6d): 89% yield. ^{1}H NMR ($CDCl_3$) δ=1.30 (s, 3 H), 1.36 (s, 3 H), 2.4—2.6 (m, 2 H), 5.15—5.25 (m, 2 H), 9.58 (d, *J*=3.0 Hz, 1 H) for the trans isomer, δ=1.55 (s, 3 H), 1.86 (dd, *J*=6.0 and 8.5 Hz, 1 H), 2.11 (d, *J*=8.5 Hz, 1H), 9.72 (d, *J*=6.0 Hz, 1 H) for the cis isomer. ^{19}F NMR ($CDCl_3$-$CFCl_3$) δ=−141.8 (m, 2 F), −152.2 (m, 1 F), −161.3 (m, 2 F); IR 1740, 1712, 1528, 1512, 1160, 1133, 1056, 946 cm^{-1}; MS *m/z* (rel intensity) 294 (M^++1, 2), 293 (M^+, 11), 181

(100), 113 (11), 97 (90), 69 (10), 67 (14), 43 (17), 41 (37).

Ethyl (1*R,3*S**)-3-(2,2-Dichloro-3,3,3-trifluoro-1-hydroxypropyl)-2,2-dimethylcyclopropanecarboxylate (7a). A Typical Procedure for the Reaction of 6 with a CCl_3CF_3/Zn Reagent.** To a DMF (1 ml) solution of **6a** (trans/cis 4 : 1 mixture, 0.174 g, 1.0 mmol) were added zinc powder (96 mg, 1.47 mmol) and 1,1,1-trichloro-2,2,2-trifluoroethane (0.36 ml, 3.0 mmol) at 0 °C. The solution was stirred for 2 h at 0 °C and for 10 h at 50 °C, then treated with sat ammonium chloride aq solution (2 ml), and extracted with diethyl ether (3×2 ml). The combined ethereal extract was dried over magnesium sulfate and concentrated under reduced pressure to give a crude product. Purification by preparative TLC (CH_2Cl_2–hexane 1 : 1) afforded **7a** (54: 46 diastereomeric mixture, 0.188 g, 58% yield) as a viscous colorless oil. ^1H NMR (400 MHz, $CDCl_3$) δ=1.22 (s, 3 H), 1.25 (s, 3 H), 1.29 (t, J=7.2 Hz, 3 H), 1.69 (d, J=5.8 Hz, 1 H), 1.94 (dd, J=5.8 and 8.9 Hz, 1H), 2.63 (br s, 1 H), 3.82 (br d, J=8.9 Hz, 1 H), 4.10—4.20 (m, 2 H) for the major isomer, δ=1.26 (t, J=7.2 Hz, 3 H), 1.30 (s, 3 H), 1.33 (s, 3 H), 1.70 (d, J=5.4 Hz, 1 H), 1.82 (dd, J=5.4 and 9.6 Hz, 1 H), 2.43 (br d, 1 H), 3.82 (br d, J=9.6 Hz, 1 H), 4.10—4.20 (m, 2 H) for the minor isomer; ^{19}F NMR ($CDCl_3$-$CFCl_3$) δ=−74.3 (s) for the major isomer, −74.7 (s) for the minor isomer. IR 3465, 1710, 1260, 1200 cm^{-1}; MS m/z (rel intensity) 277 (11), 197 (13), 142 (11), 141 (100), 125 (16), 113 (59), 98 (20), 97 (18), 95 (30), 69 (18), 67 (22), 59 (29), 55 (41), 53 (10), 43 (30).

Found: C, 41.02; H, 4.67%. Calcd for $C_{11}H_{15}Cl_2F_3O_3$: C, 40.89; H, 4.68%.

Adducts **7b—e** were prepared similarly.

(3-Phenoxyphenyl)methyl 3-(2,2-Dichloro-3,3,3-trifluoro-1-hydroxypropyl)-2,2-dimethylcyclopropanecarboxylate (7b): A colorless viscous oil. The two diastereomers were separated by preparative TLC (CH_2Cl_2). The less polar isomer (R_f 0.70) showed ^1H NMR ($CDCl_3$) δ=1.21 (s, 3 H) 1.24 (s, 3 H), 1.73 (d, J=5.8 Hz, 1 H), 1.94 (dd, J=5.8 and 9.0 Hz, 1 H), 2.44 (d, J=9.6 Hz, 1 H), 3.79 (dd, J=8.7 and 9.0 Hz, 1 H), 5.07 (s, 2 H), 6.8—7.4 (m, 8 H); ^{19}F NMR ($CDCl_3$-$CFCl_3$) δ=−75.0 (s); IR 3480, 1713, 1588, 1490, 1255, 1180, 870 cm^{-1}; MS m/z (rel intensity) 478 (M^++2, 3), 476 (M^+, 4), 200 (5), 184 (16), 183 (100), 77 (6).

Found: C, 55.39; H, 4.53%. Calcd for $C_{22}H_{21}Cl_2F_3O_4$: C, 55.36; H, 4.43%.

The more polar one: R_f 0.55 (CH_2Cl_2), ^1H NMR ($CDCl_3$) δ=1.28 (s, 3 H), 1.32 (s, 3 H), 1.7—1.9 (m, 2 H), 2.35 (d, J=8.4 Hz, 1 H), 3.78 (dd, J=8.4 and 8.0 Hz, 1 H), 5.06 (s, 2 H), 6.8—7.4 (m, 8 H); ^{19}F NMR ($CDCl_3$-$CFCl_3$) δ=−74.6 (s); IR 3470, 1728, 1713, 1583, 1491, 1254, 1200, 870, 692 cm^{-1}; MS m/z (rel intensity) 478 (M^++2), 476 (M^+, 2), 184 (16), 183 (100), 89 (6), 77 (9), 55 (10), 51 (6), 41 (6).

Found: C, 55.43; H, 4.52%. Calcd for $C_{22}H_{21}Cl_2F_3O_4$: C, 55.36; H, 4.43%.

(2-Methyl-3-phenylphenyl)methyl 3-(2,2-Dichloro-3,3,3-trifluoro-1-hydroxypropyl)-2,2-dimethylcyclopropanecarboxylate (7c): The two diastereomers were separated by preparative TLC (CH_2Cl_2). The less polar isomer, R_f 0.45: colorless solid, mp 155—156 °C. ^1H NMR ($CDCl_3$) δ=1.26 (s, 6 H), 1.76 (d, J=6.0 Hz, 1 H), 1.97 (dd, J=6.0 and 8.7 Hz, 1 H), 2.19 (s, 3 H), 2.59 (d, J=9.0 Hz, 1H), 3.81 (dd, J=8.7 and 9.0 Hz, 1 H), 5.18 (s, 2 H), 7.15—7.50 (m, 8 H); ^{19}F NMR ($CDCl_3$-$CFCl_3$) δ=−74.6 (s); IR (KBr) 3460 (br), 1728, 1711, 1257, 1220, 1200, 1180, 1113, 873, 760, 702 cm^{-1}; MS m/z (rel intensity) 476 (M^++2, trace), 474 (M^+, trace), 182 (16), 181 (100), 180 (91), 179 (10), 166 (38), 165 (40).

Found: C, 57.99; H, 5.04%. Calcd for $C_{23}H_{23}Cl_2F_3O_3$: C, 58.12; H, 4.88%.

The more polar isomer (R_f 0.33) was a colorless oil, ^1H NMR ($CDCl_3$) δ=1.31 (s, 3 H), 1.32 (s, 3 H), 1.79 (d, J=5 Hz, 1 H), 1.93 (dd, J=5 and 8 Hz, 1 H), 2.19 (s, 3 H), 2.35 (d, J=8 Hz, 1 H), 3.82 (t, J=8 Hz, 1 H), 5.20 (s, 2 H), 7.2—7.4 (m, 8 H): ^{19}F NMR ($CDCl_3$-$CFCl_3$) δ=−74.3 (s); IR 3425, 1711, 1260, 1227, 1200, 1184, 706 cm^{-1}; MS m/z (rel intensity) 277 (trace), 198 (14), 182 (15), 181 (100), 180 (90), 179 (17), 167 (10), 166 (40), 165 (63), 152 (10), 151 (10), 57 (22), 56 (11), 43 (17).

Found: C, 58.40; H, 4.96%. Calcd for $C_{23}H_{23}Cl_2F_3O_3$: C, 58.12; H, 4.88%.

(Pentafluorophenyl)methyl 3-(2,2-Dichloro-3,3,3-trifluoro-1-hydroxypropyl)-2,2-dimethylcyclopropanecarboxylate (7d): The two isomers were separated by preparative TLC (CH_2Cl_2). The less polar isomer showed R_f 0.65, mp 75 °C, and ^1H NMR ($CDCl_3$) δ=1.22 (s, 3 H), 1.24 (s, 3 H), 1.67 (d, 1 H), 1.95 (dd, 1 H), 2.43 (d, 1 H), 3.80 (dd, 1 H), 5.19 (t, 2 H); ^{19}F NMR ($CDCl_3$-$CFCl_3$) δ=−75.0 (s); IR (KBr) 1727, 1529, 1510, 1253, 1190, 1168, 1134, 1053, 940, 932, 868 cm^{-1}; MS m/z (rel intensity) 476 (M^++2, trace), 474 (M^+, trace), 293 (35), 181 (100), 59 (11), 55 (13).

Found: C, 40.60; H, 2.61%. Calcd for $C_{16}H_{12}Cl_2F_8O_3$: C, 40.44; H, 2.55%.

The more polar isomer (R_f 0.53, mp 103—104 °C): ^1H NMR ($CDCl_3$) δ=1.31 (s, 3 H), 1.33 (s, 3 H), 1.69 (d, 1 H), 1.81 (dd, 3 H), 2.33 (d, 1 H), 3.77 (dd, 1 H), 5.17 (t, 2 H); ^{19}F NMR ($CDCl_3$-$CFCl_3$) δ=−74.6 (s); IR (KBr) 3440, 1721, 1526, 1509, 1260, 1223, 1220, 1188, 1178 cm^{-1}; MS m/z (rel intensity) 293 (29), 181 (100), 55 (13).

Found: C, 40.55; H, 2.64%. Calcd for $C_{16}H_{12}Cl_2F_8O_3$: C, 40.44; H, 2.55%.

Methyl 3-(2,2-Dichloro-3,3,3-trifluoro-1-hydroxypropyl)-2,2-dimethylcyclopropanecarboxylate (7e): A colorless oil consisted of two diastereomers. ^1H NMR (400 MHz, $CDCl_3$) δ=1.23 (s, 3 H), 1.25 (s, 3 H), 1.71 (d, J=5.8 Hz, 1 H), 1.95 (dd, J=5.8 and 9.0 Hz, 1 H), 2.75 (d, J=9.0 Hz, 1 H), 3.71 (s, 3 H), 3.83 (t, J=5.8 Hz, 1 H) for the major isomer δ=1.29 (s, 3 H), 1.33 (s, 3 H), 1.72 (d, J=5.5 Hz, 1 H), 1.83 (dd, J=5.5 and 9.7 Hz, 1 H), 2.48 (d, J=7.8 Hz, 1 H), 3.70 (s, 3 H), 3.83 (dd, J=7.8 and 9.7 Hz, 1 H), 3.70 (s, 3 H), 3.83 (dd, J=7.8 and 9.7 Hz, 1 H); ^{19}F NMR ($CDCl_3$-$CFCl_3$) δ=−75.1 (s) for the major isomer, −75.5 (s) for the minor isomer. IR 3465, 1716, 1260, 1200, 1180, 872 cm^{-1}; MS m/z (rel intensity) 277 (5), 128 (11), 127 (100), 125 (15), 98 (14), 97 (16), 96 (10), 95 (49), 73 (18), 69 (15), 67 (27), 59 (24), 55 (30), 43 (20), 41 (32).

Found: C, 39.11; H, 4.30%. Calcd for $C_{10}H_{13}Cl_2F_3O_3$: C, 38.86; H, 4.24%.

Acetylation of 7a. A mixture of **7a** (0.31 g, 0.94 mmol), pyridine (1 ml) and acetic anhydride (1 ml) was stirred for 5 h at room temperature. Concentration in vacuo followed by purification by column chromatography (CH_2Cl_2–hexane 1 : 1) gave ethyl 3-(1-acetoxy-2,2-dichloro-3,3,3-trifluoropropyl)-2,2-dimethylcyclopropanecarboxylate (**8a**) as a mixture of two diastereomers in a ratio of 55 : 45 (0.32 g, 93% yield) as a colorless oil. ^1H NMR (400 MHz, $CDCl_3$) δ=1.24 (s, 3 H), 1.26 (t, J=7.1 Hz, 3 H), 1.32 (s, 3 H), 1.59 (d, J=5.7 Hz, 1 H), 2.06 (dd, J=5.7 and 9.8 Hz, 1 H), 2.13 (s, 3 H), 4.09—4.22 (m, 2 H), 5.35 (d, J=9.8 Hz, 1H) for the major isomer, δ=1.17 (s, 3 H), 1.26 (s, 3 H), 1.26 (t, J=7.1 Hz, 3 H), 1.77 (d, J=5.6 Hz, 1 H), 2.01 (dd, J=5.7 and 10.1 Hz, 1 H),

2.15 (s, 3 H), 4.09—4.22 (m, 2 H), 5.28 (d, J=10.1 Hz, 1 H); ^{19}F NMR ($CDCl_3$-$CFCl_3$) δ=−75.5 (s) for the major isomer, −74.6 (s) for the minor isomer; IR 1769, 1732, 1374, 1262, 1250, 1208, 1188, 1030 cm^{-1}; MS m/z (rel intensity) 331 (trace), 329 (3), 197 (11), 141 (37), 113 (18), 43 (100).

Found: C, 42.75; H, 4.59%. Calcd for $C_{13}H_{17}Cl_2F_3O_4$: C, 42.76; H, 4.69%.

(3-Phenoxyphenyl)methyl 3-(1-Acetoxy-2,2-dichloro-3,3,3-trifluoro-propyl)-2,2-dimethylcyclopropanecarboxylate (8b): A colorless oil composed of two diastereomers. ^{1}H NMR (400 MHz, $CDCl_3$) δ=1.22 (s, 3 H), 1.31 (s, 3 H), 1.66 (d, J=5.7 Hz, 1 H), 2.07 (s, 3 H), 2.08 (dd, J=5.7 and 9.9 Hz, 1 H), 5.11 (s, 2 H), 5.35 (d, J=9.9 Hz, 1 H), 6.90—7.15 (m, 5 H), 7.25—7.40 (m, 4 H) for the major isomer, δ=1.16 (s, 3 H), 1.24 (s, 3 H), 1.84 (d, J=5.6 Hz, 1 H), 2.03 (dd, J=5.6 and 10.1 Hz, 1 H), 2.13 (s, 3 H), 5.05—5.15 (m, 1 H), 5.12 (d, J=10.1 Hz, 1 H), 5.28 (d, 1 H), 6.09—7.15 (m, 5 H), 7.25—7.40 (m, 4 H); ^{19}F NMR ($CDCl_3$-$CFCl_3$) δ=−76.0 (s) for the major isomer, −75.2 (s) for the minor isomer; IR 1767, 1732, 1588, 1492, 1446, 1374, 1255, 1205, 1168, 1028, 692 cm^{-1}; MS m/z (rel intensity) 521 (M^++3, trace), 520 (M^++2, 2), 519 (M^++1, 1), 518 (M^+, 4), 184 (16), 183 (100), 43 (55).

Found: C, 55.52; H, 4.67%. Calcd for $C_{24}H_{23}Cl_2F_3O_5$: C, 55.51; H, 4.46%.

(2-Methyl-3-phenylphenyl)methyl 3-(1-Acetoxy-2,2-dichloro-3,3,3-trifluoropropyl)-2,2-dimethylcyclopropanecarboxylate (8c) Derived from the Less Polar Isomer of 7c: 98% yield, a colorless oil, R_f 0.46 (CH_2Cl_2-hexane 1 : 1). ^{1}H NMR ($CDCl_3$) δ=1.27 (s, 3 H), 1.33 (s, 3 H), 1.70 (d, J=6 Hz, 1 H), 2.09 (s, 3 H), 2.13 (dd, J=6 and 10 Hz, 1 H), 2.22 (s, 3 H), 5.25 (s, 2 H), 5.40 (d, J=10 Hz, 1 H), 7.2—7.5 (m, 8 H); ^{19}F NMR ($CDCl_3$-$CFCl_3$) δ=−75.5 (s); IR 1754, 1749, 1730, 1256, 1228, 1204, 1188, 1160, 1028, 758, 702 cm^{-1}; MS m/z (rel intensity) 518 (M^++2, trace), 516, (M^+, trace), 182 (15), 181 (100), 180 (86), 166 (28), 165 (30), 43 (38).

Found: C, 58.31; H, 4.91%. Calcd for $C_{25}H_{25}Cl_2F_3O_4$: C, 58.04; H, 4.87%.

The Diastereomeric Acetate Derived from the More Polar Isomer of 7c. This compound was obtained in 100% yield as a colorless oil, R_f 0.39 (CH_2Cl_2-hexane 1 : 1). ^{1}H NMR ($CDCl_3$) δ=1.18 (s, 3 H), 1.30 (s, 3 H), 1.85 (d, J=6 Hz, 1 H), 2.05 (dd, J=6 and 10 Hz, 1 H), 2.14 (s, 3 H), 2.20 (s, 3 H), 5.19 (s, 2 H), 5.24 (d, J=10 Hz, 1 H), 7.1—7.5 (m, 8 H); ^{19}F NMR ($CDCl_3$-$CFCl_3$) δ=−74.8 (s); IR 1770, 1730, 1260, 1230—1160 (br), 1031, 842, 762, 704 cm^{-1}; MS m/z (rel intensity) 518 (M^++2, trace), 516 (M^+, trace), 182 (15), 181 (100), 180 (74), 166 (24), 165 (25), 43 (31).

Found: C, 58.13; H, 4.90%. Calcd for $C_{25}H_{25}Cl_2F_3O_4$: C, 58.04; H, 4.87%.

Ethyl 3-[2,2-Dichloro-3,3,3-trifluoro-1-(methylsulfonyloxy)propyl]-2,2-dimethylcyclopropanecarboxylate (9a). Methanesulfonyl chloride (0.073 ml, 0.94 mmol) and triethylamine (0.133 ml, 0.95 mmol) were added to an ethereal solution (2 ml) of **7a** (0.135 g, 0.79 mmol) at 0 °C, and the mixture was stirred for 2 h at room temperature. Workup and TLC purification (CH_2Cl_2-hexane 1 : 1) gave **9a** (0.157 g, 80% yield) as a colorless oily diastereomeric mixture. ^{1}H NMR ($CDCl_3$) δ=1.2—1.4 (m, 9 H), 1.8—2.2 (m, 2 H), 3.12 and 3.16 (s, totally 3 H), 4.14 (q, J=7.2 Hz, 2 H), 4.89 and 4.90 (d, J=10 Hz, totally 1 H); ^{19}F NMR ($CDCl_3$-$CFCl_3$) δ=−74.8 (s) and −73.8 (s); IR 1730, 1368, 1257, 1232, 1180, 932, 896, 809 cm^{-1}; MS m/z (rel intensity) 357 (5), 355 (7), 269 (12), 233 (18), 232 (10), 231 (24), 199 (33), 198 (11), 197 (100), 195 (19), 175 (11), 161 (32), 159 (20), 141 (69), 137 (15), 113 (28), 97 (12), 95 (14), 80 (10), 79 (26), 69 (10), 67 (13), 59 (17), 43 (14), 41 (28).

Found: C, 35.86; H, 4.27%. Calcd for $C_{12}H_{17}Cl_2F_3O_5S$: C,35.92; H, 4.27%.

(2-Methyl-3-phenylphenyl)methyl 3-[2,2-Dichloro-3,3,3-trifluoro-1-(methylsulfonyloxy)propyl]-2,2-dimethylcyclopropanecarboxylate (9c): 97% yield a colorless oil of a 1 : 1 diastereomeric mixture. ^{1}H NMR ($CDCl_3$) δ=1.26, 1.31, 1.38 (s, totally 6 H), 1.9—2.3 (2 H), 2.18, 2.20 (s, totally 3 H), 3.03, 3.13 (s, totally 3 H), 4.88, 4.99 (d, J=10 Hz, totally 1 H), 5.19 (s, 2 H), and 7.1—7.5 (m, 8 H); ^{19}F NMR ($CDCl_3$-$CFCl_3$) δ=−73.7 (s), −74.8 (s); IR 1729, 1360, 1252, 1230—1160 (br), 928, 808, 761, 704 cm^{-1}; MS m/z (rel intensity) 554 (M^++2, trace), 552 (M^+, trace), 182 (17), 181 (100), 180 (45), 179 (11), 166 (32), 165 (33).

Found: C, 52.02; H, 4.68%. Calcd for $C_{24}H_{25}Cl_2F_3O_5S$: C, 52.09; H, 4.55%.

(2-Methyl-3-phenylphenyl)methyl 3-(1-Benzoyloxy-2,2-dichloro-3,3,3-trifluoropropyl)-2,2-dimethylcyclopropanecarboxylate (10c). Benzoyl chloride (0.114 ml, 0.98 mmol) and triethylamine (0.137 ml, 0.98 mmol) were added to an ethereal solution (2 ml) of **7c** (0.39 g, 0.82 mmol) at 0 °C, and the mixture was stirred for 12 h at room temperature. As TLC assay showed slow consumption of **7c**, benzoyl chloride (0.23 ml, 2.0 mmol) and triethylamine (0.28 ml, 2.0 mmol) were further added, and stirring was continued for 10 h at room temperature. Workup and preparative TLC (CH_2Cl_2-hexane 1 : 1) gave **10c** (0.175 g, 37% yield) as a colorless oil. ^{1}H NMR ($CDCl_3$) δ=1.32 (s, 3 H), 1.40 (s, 3 H), 1.81 (d, J=5 Hz, 1 H), 1.96 (s, 3 H), 2.21 (dd, J=5 and 10 Hz, 1 H), 5.07 (s, 2 H), 5.58 (d, J=10 Hz, 1 H), 7.0—7.6 (m, 11 H), 7.9—8.1 (m, 2 H); ^{19}F NMR ($CDCl_3$-$CFCl_3$) δ=−75.5 (s); IR 1732, 1450, 1068, 1028, 889, 836, 830, 799, 762, 706 cm^{-1}; MS m/z (rel intensity) 580 (M^++2, trace), 578 (M^+, trace), 182 (16), 181 (100), 180 (94), 179 (10), 166 (35), 165 (36), 105 (35), 77 (10).

Found: C, 62.26; H, 4.78%. Calcd for $C_{30}H_{27}Cl_2F_3O_4$: C, 62.19; H, 4.70%.

(2-Methyl-3-phenylphenyl)methyl 3-[2,2-Dichloro-3,3,3-trifluoro-1-(*p*-tolylsulfonyloxy)propyl]-2,2-dimethylcyclopropanecarboxylate (11c). Sodium hydride (50% in oil, 12 mg, 0.25 mmol) and *p*-toluenesulfonyl chloride (39 mg, 0.20 mmol) were added to **7c** (97 mg, 0.20 mmol) dissolved in diethyl ether (0.5 ml) and DMF (0.5 ml), and the mixture was stirred for 12 h at room temperature. Workup and purification by preparative TLC (CH_2Cl_2-hexane 1 : 1) gave **11c** (83 mg, 65% yield) as a viscous oil. ^{1}H NMR ($CDCl_3$) δ=1.23, 1.33, 1.37 (s, totally 3 H), 1.9—2.3 (m, 2 H), 2.19, 2.21 (s, totally 3 H), 2.37, 2.43 (s, totally 3 H), 4.85—5.05 (m, 1 H), 5.15, 5.16 (s, totally 2 H), 7.1—7.4 (m, 10 H), 7.6—7.9 (m, 2 H); ^{19}F NMR ($CDCl_3$-$CFCl_3$) δ=−74.6 (s) and −73.3 (s); IR 1730, 1600, 1360, 1387, 1114, 1096, 560 cm^{-1}; MS m/z (rel intensity) 630 (M^++2, trace), 628 (M^+, trace), 182 (15), 181 (100), 180 (74), 166 (30), 165 (28).

Found: C, 57.23; H, 4.70%. Calcd for $C_{30}H_{29}Cl_2F_3O_5S$: C, 57.24; H, 4.64%.

Reduction of 8a with Zinc. Zinc powder (35 mg, 0.54 mmol) was added to a DMF (0.5 ml) solution of **8a** (0.183 g, 0.50 mmol) and the mixture was stirred for 4 h at 50 °C before quenching by addition of sat ammonium chloride aq solution (1 ml). Extraction with diethyl ether (5×1 ml), drying the ethereal extract over magnesium sulfate, concentration in vacuo, followed by preparative TLC (CH_2Cl_2-hexane

1 : 1) gave ethyl (1*R**,3*S**)-3-(2-chloro-3,3,3-trifluoro-1-propenyl)-2,2-dimethylcyclopropanecarboxylate (**12a**) as a Z/E=6 : 1 mixture (0.116 g, 86% yield, a colorless oil). ^{1}H NMR (400 MHz, $CDCl_3$) δ=1.24 (s, 3 H), 1.28 (t, J=7.1 Hz, 3 H), 1.33 (s, 3 H), 1.77 (d, J=5.3 Hz, 1 H), 2.40 (ddq, J=5.3, 9.3, and 1.0 Hz, 1 H), 4.10—4.22 (m, 2 H), 6.15 (dq, J=9.3 and 1.0 Hz, 1 H) for the (Z)-isomer, δ=1.21 (s, 3 H), 1.27 (t, J=7.1 Hz, 3 H), 1.28 (s, 3 H), 1.69 (d, J=5.4 Hz, 1 H), 2.38—2.44 (m, 2 H), 4.10—4.22 (m, 2 H), 5.89 (d, J=9.4 Hz, 1 H) for the (E)-isomer; ^{19}F NMR ($CDCl_3$-$CFCl_3$) δ=−68.9 (s) for the (Z)-isomer, −62.5 (d, J=3.2 Hz) for the (E)-isomer; IR 1731, 1286, 1229, 1176, 1142 cm^{-1}.

(3-Phenoxyphenyl)methyl 3-(2-Chloro-3,3,3-trifluoro-1-propenyl)-2,2-dimethylcyclopropanecarboxylate (12b): A colorless oil. ^{1}H NMR ($CDCl_3$) δ=1.21 (s, 3 H), 1.30 (s, 3 H), 1.76 (d, J=5.4 Hz, 1 H), 2.37 (dd, J=5.4 and 9.0 Hz, 1 H), 5.06 (s, 2 H), 6.08 (d, J=9.0 Hz, 1 H), 6.8—7.4 (m, 8 H) for the (Z)-isomer, δ=1.22 (s, 3 H), 1.70 (d, J=5.4 Hz, 1 H), 5.82 (d, J=9.0 Hz, 1 H) for the (E)-isomer; ^{19}F NMR ($CDCl_3$-$CFCl_3$) δ=−69.2 (s), −62.9 (s) for the (E)-isomer; IR 1732, 1588, 1492, 1283, 1256, 1221, 1167, 1140, 1113, 693 cm^{-1}.

When **8b** (49 mg, 0.094 mmol) was treated with zinc (9 mg, 0.13 mmol) in THF (0.2 ml) for 23 h at 50 °C, **12b** was obtained in 88% isolation yield. Z/E=77 : 23.

(2-Methyl-3-phenylphenyl)methyl 3-(2-Chloro-3,3,3-trifluoro-1-propenyl)-2,2-dimethylcyclopropanecarboxylate (12c): A colorless oil, Z/E=89 : 11 from the less polar isomer of **8c**. ^{1}H NMR ($CDCl_3$) δ=1.23 (s, 3 H), 1.35 (s, 3 H), 1.82 (d, J=5 Hz, 1 H), 2.22 (s, 3 H), 2.42 (dd, J=5 and 9 Hz, 1 H), 5.20 (s, 2 H), 6.10 (dq, J=10 and 1 Hz, 1 H), 7.15—7.5 (m, 8 H) for the (Z)-isomer, δ=1.23 (s, 3 H), 1.29 (s, 3 H), 5.85 (d, J=9.1 Hz, 1 H); ^{19}F NMR ($CDCl_3$-$CFCl_3$) δ=−68.7 (s) for the (Z)-isomer, −62.5 (s) for the (E)-isomer.

The more polar isomer of **8c** gave **12c** of Z/E=93 : 7 in a similar yield.

One-Pot Conversion of 6c into 12c. To a DMF (1 ml) solution of **6c** (0.28 g, 0.87 mmol) were added 1,1,1-trichloro-2,2,2-trifluoroethane (0.21 ml, 1.7 mmol), zinc powder (0.29 g, 4.4 mmol) and acetic anhydride (0.12 ml), and the mixture was stirred for 6 h at 50 °C. After quenching with water (2 ml) and 2 drops of conc hydrochloric acid, the reaction mixture was extracted with diethyl ether (3×3 ml). The ethereal extract was dried over anhydrous magnesium sulfate and concentrated in vacuo. Purification by column chromatography (dichloromethane-hexane 1 : 3 to 1 : 2) gave **12c** (0.20 g, 54% yield) as a colorless oil which consisted of 6 : 1 (Z)- and (E)-isomers.

By applying **9c** and **10c** to the reduction with zinc, we obtained **12c** in 95% (Z/E=88 : 12) and 98% (Z/E=86 : 14) yield respectively.

4-(2,4-Dioxobutoxy)-5,5-dichloro-6,6,6-trifluoro-2-methyl-2-hexene (15). A mixture of **14** (0.95 g, 4.0 mmol), sodium acetate (50 ml), and diketene (0.5 ml) was heated at 80 °C for 4 h under stirring and then charged on a silica-gel column. Elution with dichloromethane-hexane 1 : 1 gave **15** (1.13 g, 88% yield) as a colorless oil. ^{1}H NMR ($CDCl_3$) δ=1.83 (s, 6 H), 2.26 (s, 3 H), 3.46 (s, 2 H), 5.28 (d, J=9.6 Hz, 1 H), 6.08 (d, J=9.6 Hz, 1 H) for the keto form, δ=1.97 (s, 3 H), 5.03 (s, 1 H), 6.17 (d, J=9.6 Hz, 1 H) for the enol tautomer; ^{19}F NMR ($CDCl_3$-$CFCl_3$) δ=−75.0 (s); IR 3480, 1756, 1728, 1255, 1210, 1188, 1149 cm^{-1}; MS m/z (rel intensity) 285 (2), 183 (9), 127 (5), 86 (6), 85 (100), 84 (5), 83 (5), 69 (6), 67 (7), 58 (5), 55 (9), 44 (12), 43 (48), 41 (24).

Found: C, 40.89; H, 3.96%. Calcd for $C_{11}H_{13}Cl_2F_3O_3$: C, 41.14; H, 4.08%.

4-Diazoacetoxy-5,5-dichloro-6,6,6-trifluoro-2-methyl-2-hexene (16). Triethylamine (0.060 ml, 0.43 mmol) and *p*-toluenesulfonyl azide (80 mg, 0.41 mmol) were added to an acetonitrile (1 ml) solution of **15** (0.128 g, 0.40 mmol), and the mixture was stirred for 0.5 h at room temperature. At this point, all of **15** was converted into the diazo compound as assayed by TLC. Sodium hydroxide (1,2 M† aq solution, 1 ml) was added, and stirring was continued for 1 h at room temperature. Extraction with diethyl ether (3×2 ml) and then with dichloromethane (2 ml), drying the combined organic extract over magnesium sulfate, concentration in vacuo, and finally purification by column chromatography (CH_2Cl_2-hexane 1 : 1) gave **16** (0.100 g, 82% yield) as a pale yellow oil. ^{1}H NMR ($CDCl_3$) δ=1.85 (s, 6 H), 4.77 (s, 1 H), 5.03 (d, J=9.6 Hz, 1 H), 6.13 (d. J=9.6 Hz, 1 H); ^{19}F NMR ($CDCl_3$-$CFCl_3$) δ=−75.0 (s); IR 2120, 1710, 1376, 1210, 1188, 1163 cm^{-1}; MS m/z (rel intensity) 278 (11), 221 (20), 219 (33), 213 (47), 185 (25), 184 (20), 183 (64), 147 (30), 143 (44), 127 (49), 125 (54), 97 (25), 79 (21), 77 (24), 70 (69), 53 (26), 51 (20), 43 (31), 42 (69), 41 (100).

Found: C, 35.45; H, 2.86; N, 9.21%. Calcd for $C_9H_9Cl_2F_3N_2O_2$: C, 35.43; H, 2.97; N, 9.18%.

4-(1,1-Dichloro-2,2,2-trifluoroethyl)-6,6-dimethyl-3-oxabicyclo[3.1.0]hexan-2-one (13). An dioxane (0.5 ml) solution of **12** (38 mg, 0.12 mmol) was added over 0.5 h to a refluxing suspension of copper(II) acetylacetonate (1 mg) in dioxane (3 ml), and the heating and stirring were continued for additional 2.5 h. The reaction mixture was treated with water (5 ml) and extracted with diethyl ether (2×10 ml). The extract was dried over magnesium sulfate and concentrated under reduced pressure to afford a crude product which was purified by column chromatography (CH_2Cl_2-hexane 1 : 2) to give **13** (26 mg, 75% yield) as colorless crystals, mp 49—60 °C. ^{1}H NMR ($CDCl_3$) δ=1.25 (s, 6 H), 2.11 (d, J=5.7 Hz, 1 H), 2.36 (d, J=5.7 Hz, 1 H), 4.61 (s, 1 H); ^{19}F NMR ($CDCl_3$-$CFCl_3$) δ=−75.2 (s); IR (KBr) 1802, 1260, 1212, 1194, 1070, 1012, 908 cm^{-1}. MS m/z (rel intensity) 278 (M^++2, 2), 276 (M^+, 3), 243 (32), 241 (92), 205 (10), 199 (23), 197 (64), 161 (34), 159 (11), 141 (47), 126 (11), 125 (100), 97 (86), 96 (16), 95 (12), 91 (14), 81 (63), 79 (35), 77 (12), 69 (31), 67 (39), 65 (14), 63 (11), 55 (12), 53 (48), 51 (16), 43 (51), 42 (13).

Found: C, 38.98; H, 3.20%. Calcd for $C_9H_9Cl_2F_3O_2$: C, 39.02; H, 3.27%.

(1*R,3*R**)-3-(2-Chloro-3,3,3-trifluoro-1-propenyl)-2,2-dimethylcyclopropanecarboxylic Acid (17).** Zinc powder (6 mg, 0.09 mmol) was added to a DMF (0.1 ml) solution of **13** (23 mg, 0.083 mmol), and the resulting mixture was stirred for 3 h at 60 °C before quenching by addition of water (1 ml) and conc hydrochloric acid (0.5 ml). Extraction with diethyl ether (4×3 ml), drying the ethereal extract over magensium suflate, and concentration in vacuo gave rise to **17** (17 mg, 84% yield, Z/E=93 : 7) as colorless crystals, mp 103—105 °C (sublime).[19] ^{1}H NMR ($CDCl_3$) δ=1.33 (s, 6 H), 1.96 (d, J=8 Hz, 1 H), 2.22 (dd, J=8 and 9 Hz, 1 H), 6.81 (d, J=9 Hz, 1 H) for the (Z)-isomer, 6.52 (d, J=9 Hz, 1 H) attributed to the (E)-isomer. ^{19}F NMR ($CDCl_3$-$CFCl_3$) δ=−68.8 (s) for the (Z)-isomer, −62.0 (s) for the (E)-isomer; IR 1708, 1437, 1293, 1272, 1194, 1146, 1128 cm^{-1}.

Ethyl 3-(2,3,3-Trifluoro-1-hydroxy-2-propenyl)-2,2-di-

†1 M=1 mol dm^{-3}.

methylcyclopropanecarboxylate (**20a**). Gaseous chlorotrifluoroethene (240 ml at room temperature, 10 mmol) was dissolved in a mixture of THF (10 ml), hexane (1 ml), and diethyl ether (1 ml) at −78 °C. The solution was cooled at −130 °C. Butyllithium (1.67 M hexane solution, 6.0 ml, 10 mmol) was added dropwise to the solution, and the mixture was stirred for 1 h at −130 °C. To this solution was added **6a** (2.0 g, 12 mmol) dissolved in the trap solvent mixture composed of THF (10 ml), hexane (1 ml) and diethyl ether (1 ml) at −130 °C drop by drop over a period of 5 min. The reaction mixture was allowed to warm gradually to −40 °C over 7 h. Workup and purification by column chromatography (CH_2Cl_2-AcOEt 1 : 0 to 1 : 1) gave **20a** (0.63 g, 25% yield) as a colorless viscous oil. ^{1}H NMR ($CDCl_3$) δ=1.1—1.4 (m, 9 H), 1.65 (d, J=6 Hz, 1 H), 1.84 (dd, J=6 and 10 Hz, 1 H), 3.76—4.1 (m, 2 H), 4.10 (q, J=7 Hz, 2 H); ^{19}F NMR ($CDCl_3$-$CFCl_3$) δ=−102 (ddd, J=6, 33, and 81 Hz, 1 F), −120 (ddd, J=1, 37, and 47 Hz, 1 F), −188 (m, 1 F); IR 3440, 2970, 1791, 1730, 1709, 1306, 1256, 1213, 1175, 1114, 1100, 1072, 1032, 1018 cm^{-1}; MS m/z (rel intensity) 207 (6), 142 (17), 141 (100), 114 (12), 113 (78), 111 (27), 109 (12), 96 (11), 95 (55), 69 (17), 67 (36), 59 (39), 55 (19), 53 (11), 43 (31), 41 (38).

Found: m/z 207.0673. Calcd for $C_{11}H_{15}F_3O_3$: M, 207.0632.

The adduct **20a** was alternatively prepared by the reaction of **6a** with triethyl(trifluoroethenyl)silane. A THF solution of tris(diethylamino)sulfonium difluorotrimethylsilicate (TASF) (1.0 M solution 0.1 ml, 0.1 mmol) was added to a mixture of **6a** (0.175 g, 1.0 mmol), triethyl(trifluoroethenyl)-silane (0.24 g, 1.2 mmol) and THF (2 ml) at 0 °C. The reaction mixture was stirred for 1 h at 0 °C and for 10 h at room temperature. Workup followed preparative TLC (hexane-dichloromethane 1 : 1) afforded ethyl (1*R**,3*R**)-3-(1-triethylsiloxy-2,3,3-trifluoro-2-propenyl)-2,2-dimethylcyclopropanecarboxylate (22 mg) and its (1R*,3R*)-isomer (75 mg). Total yield was 39%. The (1R*,3R*)-isomer exhibited ^{1}H NMR consistent to the structure (J=8.7 Hz for the coupling constant of the ring proton, 2.58: 1 diastereomeric mixture); IR 1795, 1730 cm^{-1}; Found: m/z 337.1415. Calcd for $C_{15}H_{24}F_3O_3Si$: M−Et, 337.1444. The (1R*,3R*)-isomer exhibited J=5.52 Hz for the coupling constant of the ring proton (ca. 1 : 1 diastereomeric mixture); IR 1790, 1735 cm^{-1}; Found: m/z 337.1431. Calcd for $C_{15}H_{24}F_3O_3Si$: M−Et, 337.1445.

Desilylation was effected by treating the silyl ether with 0.2 M hydrochloric acid (0.5 ml) and THF (0.5 ml) at room temperature for 0.5 h. Workup and TLC purification gave **20a** quantitatively.

Ethyl 3-(2-Chloro-3,3-difluoro-1-hydroxy-2-propenyl)-2,2-dimethylcyclopropanecarboxylate (20b). A THF solution (1.0 M, 0.1 ml) of TASF (0.1 mmol) was added to a mixture of **6a** (0.34 g, 2.0 mmol), (1-chloro-2,2-difluoroethenyl)-triethylsilane (0.21 g, 1.0 mmol) and THF (2 ml) at room temperature. The reaction mixture was stirred for 16 h, and then worked up. Preparative TLC (dichloromethane-hexane 1 : 1) afforded **20b** (27 mg), its triethylsilyl ether (49 mg) and the recovered **6a** (101 mg). The silyl ether (39 mg out of the 49 mg sample) was dissolved in 0.2 M hydrochloric acid-THF 1 : 1 mixture (1 ml), and the solution was stirred for 1 h at room temperature. Work-up and preparative TLC afforded **21b** (27 mg, 99% yield) as a colorless oil. ^{1}H NMR ($CDCl_3$) δ=1.1—1.4 (m, 9 H), 1.67 (d, J=5 Hz, 1 H). 1.87 (d, J=5 and 10 Hz, 1 H), 2.29 (br s, 1 H), 3.95—4.3 (m, 3 H); ^{19}F NMR ($CDCl_3$-$CFCl_3$) δ=−87 (dd, J=4 and 40 Hz, 1 F), −91 (dd, J=9 and 40 Hz, 1 F); MS m/z (rel intensity) 223 (5), 142 (24), 141 (100), 127 (32), 125 (12), 114 (19), 113 (92), 96 (14), 95 (53), 69 (19), 67 (38), 61 (14), 59 (37), 55 (14), 53 (13), 43 (33), 41 (39).

Found: m/z 223.0349. Calcd for $C_9H_{10}ClF_2O_2$: M−OEt, 223.0336.

2-Chloro-1,1-difluoro-1-tridecen-3-ol (18b). The silyl ether of **18b** was prepared by the similar procedure as above, starting from undecanal (0.93 ml, 4.5 mmol), 1-chloro-2,2-difluoroethenyltriethylsilane (0.53 g, 3.0 mmol), THF (6 ml), and TASF (0.3 mmol). TLC purification using dichloromethane-hexane 1 : 2 gave 2-chloro-1,1-difluoro-3-triethylsilyloxy-1-tridecene (0.33 g, 39% yield) as a colorless oil. ^{1}H NMR ($CDCl_3$) δ=0.45—0.8 (m, 6 H), 0.8—1.15 (m, 12 H), 1.30 (s, 16 H), 1.45—1.85 (m, 2 H), 4.35—4.65 (m, 1 H), ^{19}F NMR ($CDCl_3$-$CFCl_3$) δ=−88 (d, J=44 Hz, 1 F), −92 (d, J=44 Hz, 1 F); IR 2950, 1747, 1470, 1286, 1100, 1002, 750, 730 cm^{-1}; MS m/z (rel intensity) 355 (38), 354 (25), 353 (M$^+$−Et, 96), 241 (27), 115 (36), 109 (16), 105 (72), 104 (11), 103 (100), 97 (35), 95 (37), 91 (15), 89 (35), 87 (38), 83 (42), 81 (33), 77 (63), 75 (85), 71 (15), 69 (43), 67 (28), 59 (27), 57 (32), 55 (58), 47 (26), 43 (59), 41 (35).

Found: C, 60.02; H, 9.44%. Calcd for $C_{19}H_{37}ClF_2OSi$: C, 59.58; H, 9.74%.

Acid-catalyzed desilylation was effected in 0.2 M hydrochloric acid and THF in 83% yield to give **18b** as a colorless oil. ^{1}H NMR ($CDCl_3$) δ=0.7—1.0 (m, 3 H), 1.25 (s, 16 H), 1.45—1.9 (m, 2 H), 1.77 (br s, 1 H), 4.35—4.6 (m, 1 H); ^{19}F NMR ($CDCl_3$-$CFCl_3$) δ=−87 (dd, J=39 and 2 Hz, 1 F), −91 (dd, J=39 and 3 Hz, 1F); IR 3380, 2945, 2875, 1747, 1288 cm^{-1}; MS m/z (rel intensity) 250 (M$^+$−H_2O, trace), 129 (34), 127 (100), 57 (2), 55 (14), 43 (39), 41 (25).

Found: m/z 250.1326. Calcd for $C_{13}H_{21}ClF_2$: M−H_2O, 250.1299.

Fluorination of 18a. A Typical Fluorination Procedure. To a solution of DAST (82 mg, 0.50 mmol) dissolved in dichloromethane (5 ml) was added dropwise 1,1,2-trifluoro-1-tridecen-3-ol (**18a**, 0.123 g, 0.49 mmol) at −78 °C, and the solution was allowed to warm to room temperature over 10 min. The solution was concentrated under reduced pressure, and the residue was subjected to column chromatography (dichloromethane-haxane 1 : 9) to afford 1,1,1,2-tetrafluoro-2-tridecene (**19a**, 0.112 g, 90% yield) as a colorless oil. ^{1}H NMR ($CDCl_3$) δ=0.8—1.0 (m, 3 H), 1.1—1.6 (m, 16 H), 2.1—2.4 (m, 2 H), 5.53 (dt J=33 and 7.8 Hz, 1 H); ^{19}F NMR ($CDCl_3$-$CFCl_3$) δ=−72 (d, J=12 Hz, 3 F), −137 (dq, J=33 and 12 Hz, 1F); IR 2940, 2870, 1833, 1470, 1362, 1194, 1148, 1050 cm^{-1}; MS m/z (rel intensity) 254 (M$^+$, trace), 97 (12), 85 (12), 84 (16), 83 (15), 71 (23), 70 (31), 69 (30), 57 (54), 56 (47), 55 (34), 43 (100), 42 (16), 41 (46).

Found: m/z 254.1647. Calcd for $C_{13}H_{22}F_4$: M, 254.1659.

2-Chloro-1,1,1-trifluoro-2-tridecene (19b): ^{1}H NMR ($CDCl_3$) δ=0.7—1.0 (m, 3 H), 2.27 (s, 16 H), 2.1—2.4 (m, 2 H), 6.43 (tq, J=7 and 1 Hz, 1 H); ^{19}F NMR ($CDCl_3$-$CFCl_3$) δ=−69 (m), IR 2940, 2865, 1307, 1186, 1148 cm^{-1}; MS m/z (rel intensity) 270 (M$^+$, trace), 111 (10), 98 (12), 97 (18), 85 (14), 84 (28), 83 (25), 71 (32), 70 (64), 69 (56), 57 (77), 56 (97), 55(55), 43 (100), 42 (25), 41 (66).

Found: C, 57.95; H, 8.17%. Calcd for $C_{13}H_{22}ClF_3$: C, 57.67; H, 8.19%.

Ethyl 3-(2,3,3,3-Tetrafluoro-1-propenyl)-2,2-dimethylcyclopropanecarboxylate (21a): A colorless oil. ^{1}H NMR ($CDCl_3$) δ=1.21 (s, 3 H), 1.27 (t, J=7.1 Hz, 3 H), 1.30 (s, 3 H),

1.67 (d, J=5.3 Hz, 1 H), 2.32 (dd, J=5.3 and 9.8 Hz, 1 H), 4.15 (q, J=7.1 Hz, 1 H), 5.30 (dd, J=9.8 and 31.5 Hz, 1 H); ^{19}F NMR ($CDCl_3$-$CFCl_3$) δ=−72.8 (d, J=11.8 Hz, 3 F), −136.9 (dq, J=31.5 and 11.8 Hz, 1 F); MS m/z (rel intensity) 254 (M^+, 3), 209 (24), 182 (10), 181 (92), 141 (18), 115 (11), 97 (12), 77 (11), 59 (10), 47 (21), 41 (21).

Found: m/z 254.0936. Calcd for $C_{11}H_{14}F_4O_2$: M, 254.0929.

Ethyl 3-(2-Chloro-3,3,3-trifluoro-1-propenyl)-2,2-dimethylcyclopropanecarboxylate (21b): A colorless oil. ^{1}H NMR ($CDCl_3$) δ=1.22 (s, 3 H), 1.27 (t, J=7 Hz, 3 H), 1.33 (s, 3 H), 1.74 (d, J=5.1 Hz, 1 H), 2.37 (dd, J=5 and 10 Hz, 1 H), 4.13 (m, 2 H), 6.13 (d, J=10 Hz, 1 H); ^{19}F NMR ($CDCl_3$-$CFCl_3$) δ=−69 (s); IR 1733, 1724, 1304, 1286, 1228, 1176, 1144 cm^{-1}; MS m/z (rel intensity) 270 (M^+, 1), 225 (18), 119 (24), 197 (68), 161 (20), 141 (27), 41 (18).

Chlorination of 18a. A Typical Chlorination Procedure. Pyridine (0.081 ml, 1.0 mmol) and thionyl chloride (0.038 ml, 0.50 mmol) were added to an ethereal solution (1 ml) of **18a** (0.126 g, 0.50 mmol) at 0 °C, and the mixture was stirred for 3 h at room temperature. The precipitated material was filtered off, and the filtrate was concentrated under reduced pressure. Preparative TLC (dichloromethane-hexane 1 : 5) afforded 1-chloro-1,1,2-trifluoro-2-tridecene (**19a'**, 0.115 g, 85% yield) as a colorless oil. ^{1}H NMR ($CDCl_3$) δ=0.7—1.0 (m, 3 H), 1.1—1.6 (m, 16 H), 2.0—2.4 (m, 2 H), 5.47 (dt, J=33 and 8 Hz, 1 H); ^{19}F NMR ($CDCl_3$-$CFCl_3$) δ=−59 (dt, J=17 and 3 Hz, 2 F), −131 (ddt, J=33, 17, and 4 Hz, 1 F); IR 2940, 2870, 1470, 1146, 1052, 928 cm^{-1}; MS m/z (rel intensity) 243 (trace), 97 (14), 85 (12), 84 (18), 83 (20), 71 (24), 70 (36), 69 (34), 57 (57), 56 (52), 55 (38), 43 (100), 42 (16).

Found: C, 57.85; H, 8.06%. Calcd for $C_{13}H_{22}ClF_3$: C, 57.67; H, 8.19%.

1,2-Dichloro-1,1-difluoro-2-tridecene (19b'). Thionyl chloride (0.020 ml, 0.27 mmol) was added to **18b** (54 mg, 0.20 mmol) dissolved in diethyl ether (0.4 ml), and the solution was stirred for 2 h at room temperature and for 15 h at 50 °C. Workup and purification by preparative TLC (dichloromethane-hexane 1 : 10) afforded **19b'** (52 mg, 90% yield) as a colorless oil. ^{1}H NMR ($CDCl_3$) δ=0.7—1.0 (m, 3 H), 1.26 (s, 16 H), 2.1—2.4 (m, 2 H), 6.40 (t, J=7 Hz, 1 H); ^{19}F NMR ($CDCl_3$-$CFCl_3$) δ=−54.1 (s): IR 2950, 2880, 1244, 1142, 1128, 1008, 825 cm^{-1}; MS m/z (rel intensity) 288 (M^++2, 3), 286 (M^+, 4) 124 (12), 111 (11), 98 (13), 97 (20), 85 (14), 84 (28), 83 (26), 71 (28), 70 (55), 69 (50), 57 (66), 56 (72), 55 (49), 43 (100), 42 (18), 41 (64).

Found: C, 54.37; H, 7.82%. Calcd for $C_{13}H_{22}Cl_2F_2$: C, 54.36; H, 7.72%.

1-Cyclohexyl-2,3-dichloro-3,3-difluoropropene (19c'). This was prepared by the procedure applied to the synthesis of **19b'** and obtained as a colorless oil, bp 75—80 °C (bath temp)/12 Torr (1 Torr=133.322 Pa). ^{1}H NMR ($CDCl_3$) δ=0.8—2.0 (m, 10 H), 2.2—2.8 (m, 1 H), 6.26 (d, J=9.3 Hz, 1 H); ^{19}F NMR ($CDCl_3$-$CFCl_3$) δ=−54.0 (s); IR 2945, 2870, 1449, 1246, 1212, 1129, 1096, 996, 828 cm^{-1}; MS m/z (rel intensity) 228 (M^+, 1), 137 (13), 115 (5), 101 (5), 83 (8), 82 (100), 81 (21), 69 (9), 68 (5), 67 (69), 55 (10), 54 (16), 41 (25).

Found: C, 47.00; H, 5.36%. Calcd for $C_9H_{12}Cl_2F_2$: C, 47.19; H, 5.28%.

Ethyl 3-(3-Chloro-2,3,3-trifluoro-1-propenyl)-2,2-dimethylcyclopropanecarboxylate (22a). This was obtained as a colorless oil which consisted of ca. 1 : 1 stereoisomers. ^{1}H NMR ($CDCl_3$) δ=1.21 (s, 3 H), 1.27 (t, J=7.2 Hz, 3 H), 1.31 (s, 3 H), 1.67 (d, J=5.5 Hz, 1 H), 2.30 (ddd, J=5.5, 9.7, and 0.9 Hz, 1 H), 4.18 (m, 2 H), 5.26 (dd, J=9.7 and 31 Hz, 1 H) for the (1R*,3R*)-isomer, δ=1.27 (s, 3 H), 1.27 (t, J=7.2 Hz, 3 H), 1.89 (d, J=8.6 Hz, 1 H), 2.11 (dd, J=8.6 and 9.8 Hz, 1 H), 4.18 (m, 2 H), 6.10 (dd, J=9.8 and 33 Hz, 1H); ^{19}F NMR ($CDCl_3$-$CFCl_3$) δ=−58.5 (d, J=17 Hz, 2 F), −58.8 (d, J=17 Hz, 2 F), −131 (dt, J=31 and 17 Hz, 1 F); IR 1733, 1221, 1190, 1152, 1136, 1091, 1062, 1050, 934 cm^{-1}; MS m/z (rel intensity) 270 (M^+, 3), 225 (17), 199 (19), 197 (58), 162 (11), 161 (14), 141 (20), 97 (11), 65 (15), 59 (10), 41 (19).

Found: m/z 270.0643. Calcd for $C_{11}H_{14}F_3ClO_2$: M, 270.0633.

Ethyl 3-(2,3-Dichloro-3,3-difluoro-1-propenyl)-2,2-dimethylcyclopropanecarboxylate (22b): A colorless oil. ^{1}H NMR ($CDCl_3$) δ=1.23 (s, 3 H), 1.28 (t, J=7.2 Hz, 3 H), 1.33 (s, 3 H), 1.75 (d, J=5.3 Hz, 1 H), 2.39 (dd, J=5.3 and 9.2 Hz, 1 H), 4.14 (q, J=7.2 Hz, 1 H), 6.23 (d, J=9.2 Hz, 1 H); ^{19}F NMR ($CDCl_3$-$CFCl_3$) δ=−54 (s); MS m/z (rel intensity) 286 (M^+, trace), 241 (10), 215 (25), 213 (37), 177 (12), 141 (17), 77 (10), 61 (15), 41 (17).

Found: m/z 286.0358. Calcd for $C_{11}H_{14}Cl_2F_2O$: M, 286.0338.

1-Bromo-2-chloro-1,1-difluoro-2-tridecene (19b''). Thionyl bromide (33 mg, 0.16 mmol) was added to **18b** (24 mg, 0.13 mmol) dissolved in diethyl ether (0.5 ml), and the mixture was stirred for 4 h at 40 °C in a sealed tube. Workup and preparative TLC (dichloromethane-hexane 1 : 10) afforded **19b''** (36 mg, 84% yield) as a colorless oil. ^{1}H NMR ($CDCl_3$) δ=0.8—1.0 (m, 3 H), 1.1—1.7 (m, 16 H), 2.1—2.4 (m, 2 H), 6.40 (t, J=7.2 Hz, 1 H); ^{19}F NMR ($CDCl_3$-$CFCl_3$) δ=−48.8 (s); IR 2945, 2875, 1824, 1470, 1233, 1141, 1128, 990, 802 cm^{-1}; MS m/z (rel intensity) 330 (M^+, trace), 124 (11), 97 (7), 85 (11), 84 (6), 83 (10), 71 (21), 70 (11), 69 (15), 57 (53), 56 (16), 55 (27), 43 (100), 42 (11), 41 (57).

Found: m/z 330.0554. Calcd for $C_{13}H_{22}BrClF_2$: M, 330.0560.

The compound **19b''** was alternatively prepared in 67% yield by treatment of **18b** with an equimolar amount of phosphorus tribromide at 0 °C in ether and stirring the reaction mixture at room temperature for 1.5 h and at 35 °C for 13 h.

This work was partially supported by a Grant-in-Aid for Special Research on Organochemical Resources (Nos. 61111001 and 62101001) from the Ministry of Education, Science and Culture. We thank Ms. Tomoe Morita and Mr. Masanori Ueno for their experimental assistance. We also thank FMC Corporation and Kuraray Co. Ltd., for their generous gift of (2-methyl-3-phenylphenyl)methanol and 3-methyl-2-butenal respectively.

References

1) a) D. Arlt, M. Jautelat, and R. Lantzsch, *Angew. Chem., Int. Ed. Engl.*, **20**, 703 (1981). b) K. Matsui and K. Kondo, *Kagaku to Kogyo (Osaka)*, **60**, 293 (1986).

2) a) P. D. Bentley, R. Cheetham, R. K. Huff, R. Pascoe, and J. D. Sayle, *Pestic. Sci.*, **11**, 156 (1980). b) A. R. Jutsum, M. D. Collins, R. M. Perrin, D. D. Evans, R. A. H. Davies, and C. N. E. Ruscoe, Abstract of 1984 British Crop Protection Conference, 5A-4 (1984) [*Chem, Abstr.*, **103**, 137082t (1985)].

3) a) U.S. Patent, 4341796 [*Chem. Abstr.*, **97**, 194606y (1982)]. b) U.S. Patent, 4332815 [*Chem. Abstr.*, **98**, 72491g (1982)]. c) U.S. Patent, 4395567 [*Chem. Abstr.*, **99**, 195255m (1983)].

4) a) D. Holland and D. A. Laidler, *J. Mol. Catal.*, **11**, 119 (1981). b) D. A. Leidsler and D. J. Milner, *J. Organomet. Chem.*, **270**, 121 (1984). c) D. Bellus, *Pure Appl. Chem.*, **57**, 1827 (1985). d) E. L. Plummer, R. P. Seidlers, D. E. Seelye, E. Cavid, and R. R. Stewart, *Pestic. Sci.*, **15**, 509 (1984). e) Anon. (UK), *Res. Discl.*, **219**, 239 (1982). f) Japan Kokai Tokkyo Koho 53-95945; 54-112820; 54-130537; 55-59142; 55-89248; 55-111488; 59-92830.

5) Parts of the present article are disclosed in preliminary forms. a) M. Fujita, T. Hiyama, and K. Kondo, *Tetrahedron Lett.*, **27**, 2139 (1986). b) M. Fujita and T. Hiyama, *ibid.*, **27**, 3659 (1986).

6) a) M. Fujita, T. Morita, and T. Hiyama, *Tetrahedron Lett.*, **27**, 2135 (1986). b) M. Fujita and T. Hiyama, *ibid.*, **27**, 3655 (1986). c) R. W. Land, *Helv. Chim. Acta*, **69**, 881 (1986); Japan Kokai Tokkyo Koho 60-224648; 61-218555. d) Japan Kokai Tokkyo Koho 61-161225.

7) Dimethyl acetal of **6e** is available from Dynamit Nobel AG.

8) Ger. Offen., 1935386 [*Chem. Abstr.*, **72**, 100135c (1970)].

9) S. Julia, M. Julia, and G. Linstrumelle, *Bull. Soc. Chim. Fr.*, **1964**, 2693.

10) M. Fujita and T. Hiyama, *Bull. Chem. Soc. Jpn.*, **60**, 4377 (1987).

11) Similar strategy was applied to NRDC 182 synthesis: K. Kondo, T. Takashima, A. Negishi, K. Matsui, T. Fujimoto, K. Sugimoto, C. E. Hatch III, and J. S. Baum, *Pestic. Sci.*, **11**, 180 (1980); C. E. Hatch III, J. S. Baum, T. Takashima, and K. Kondo, *J. Org. Chem.* **45**, 3281 (1980). However, under the same conditions, **13** could not be converted into **17**.

12) M. Fujita and T. Hiyama, *J. Am. Chem. Soc.*, **106**, 4629 (1984).

13) Fluorination of alcohols with a) DAST: W. J. Middleton, *J. Org. Chem.*, **40**, 574 (1975); W. J. Middleton and E. M. Bingham, *Org. Synth.*, **57**, 50 (1977). b) Hexafluoropropene/diethyamine reagent: A. Takaoka, H. Iwakiri, and N. Ishikawa, *Bull. Chem. Soc. Jpn.*, **51**, 1267 (1978). c) HF/pyridine: G. A. Olah, M. Nojima, and I. Kerekes, *Synthesis*, **1973**, 786. d) SF_4: L. W. Tullock, F. S. Fawcett, W. C. Smith, and D. D. Coffam, *J. Am. Chem. Soc.*, **82**, 539 (1960). e) $PhSF_3$: W. A. Sheppard, *Org. Synth.*, Coll. Vol. V, 959 (1973). f) SeF_4: G. A. Olah, M. Nojima, and I. Kerekes, *J. Am. Chem. Soc.*, **96**, 925 (1974). g) Ph_3PF_2: Y. Kobayashi and C. Akashi, *Chem. Pharm. Bull.*, **16**, 1009 (1968). h) Et_2NCF_2CHClF: E. D. Bergmann and A. M. Cohen, *Isr. J. Chem.*, **8**, 925 (1970).

14) K. Bannai, T. Toru, T. Obi, T. Tanaka, N. Okamura, K. Watanabe, A. Azato, and S. Kurozumi, *Tetrahedron*, **39**, 3807 (1983).

15) Stereochemical assignment of fluoroalkenes: S. E. Banks, "Fluorocarbon and their derivatives," MacDonald Technical Scientific (1970), p. 233.

16) W. A. Sheppard and C. M. Sharts, "Organic Fluorine Chemistry," Benjamin, New York (1969), Chap. 3.

17) E. Pretsch, T. Clerc, J. Seible, and W. Smith, "Tabellen zur Strukturaufklarung Organische Verbindungen mit Spektroskopischen Methoden," Springer-Verlag, New York (1981), H-215.

18) a) D. Seyferth, T. Wada, and G. Raab, *Tetrahedron Lett.*, **1960**, 20. b) P. Tarrant, P. Jphncock, and J. Savory, *J. Org. Chem.*, **28**, 839 (1963). c) F. G. Drakesmith, R. D. Richardson, O. J. Stewart, and P. Tarrant, *ibid.*, **33**, 286 (1967). d) F. G. Drakesmith, O. J. Stewart, and P. Tarrant, *ibid.*, **33**, 473 (1968). e) R. Sauvetre, D. Masure, S. Chuit, and J. F. Normant, *Compt. Rend., Serie C*, **1979**, 335. f) T. Hiyama, K. Nishide, and M. Obayashi, *Chem. Lett.*, **1984**, 1765. g) S. Martin, R. Sauvetre, and J. F. Normant, *Tetrahedron Lett.*, **24**, 5615 (1983). h) S. Martin, R. Sauvetre, and J. F. Normant, *J. Organomet. Chem.*, **264**, 155 (1984). i) J. P. Gillet, R. Sauvetre, and J. F. Normant, *Tetrahedron Lett.*, **26**, 3999 (1985).

19) Although the cis-acid has been claimed in Ref 4f, its mp is not noted. Pure trans-acid **12f** has been reported to have mp 97—103 °C (Ref. 4f); cis/trans 1 : 1 mixture, mp 64—74 °C or oil.

 © 1987 The Chemical Society of Japan Bull. Chem. Soc. Jpn., 60, 4395—4399 (1987)

Kinetics of Oxidation of Pyridoxine by Chloramine-T in Acid Medium

Beby JAYARAM and Netkal M. MADE GOWDA*,†,††
Department of Chemistry, V. V. Pura College of Science, Bangalore 560004, India
†Department of Chemistry, Purdue University School of Science, Indiana University-Purdue University at Indianapolis, Indianapolis, Indiana 46223, U.S.A.
(Received September 26, 1986)

The kinetics of oxidation of pyridoxine (PRX) by chloramine-T (CAT) in the presence of hydrochloric acid (0.04—0.14 M) have been studied over the temperature range of 303—323 K. The rate of the reaction shows first-order dependence on each of CAT, PRX, and chloride ion concentrations. The reaction rate is independent of hydrogen ion concentration. Variations of ionic strength and dielectric constant of the medium have negligible effect on the rate. Addition of the reaction product, *p*-toluenesulfonamide, decreases the rate showing a negative first order dependence. The solvent isotope effect has been studied by using heavy water. The activation parameters, E_a, ΔH^*, and ΔS^* are computed from the reaction rates at various temperatures. The mechanism of PRX oxidation proposed and the rate law derived are consistent with the observed kinetics.

Considerable progress has been made on the chemistry of *N*-haloamines.[1] The diverse nature of the chemistry of these compounds is due to their ability to act as sources of halonium cations, hypohalite species, and nitrogen anions; as a result they interact with a wide range of functional groups, effecting an array of molecular transformations. Sodium *N*-chloro-*p*-toluenesulfonamide, p-$CH_3C_6H_4SO_2NClNa \cdot 3H_2O$, commonly known as chloramine-T (CAT), is a very prominent member of this series of organic *N*-haloamines. CAT behaves both as oxidizing and chlorinating agent in acidic and alkaline media. Normally, CAT undergoes a two-electron change in its reaction giving the products, *p*-toluenesulfonamide (RNH_2) and sodium chloride. The redox potential of a CAT-RNH_2 couple depends on the pH and decreases with increase in pH of the solution. CAT furnishes different types of reactive species, depending on the pH of the medium.[3] In the acid solution monochloramine-T (RNHCl, where R=p-$CH_3C_6H_4SO_2$), dichloramine-T ($RNCl_2$), HOCl, and H_2OCl^+ are the reactive species while $RNCl^-$ and OCl^- ions are formed in alkaline medium. CAT forms free chlorine in acid solutions containing chloride. An extensive review of the literature on the chemistry of CAT and its analogs has been reported.[1,5] Although, the oxidative capacity of CAT has been widely used in the assay of a large number of chemical compounds,[6-9] only a little information is available about the kinetics of reactions.[10-12]

Pyridoxine (PRX) finds applications in pharmaceutical industries. Pyridoxine, pyridoxal, and pyridoxamine are collectively known as vitamine B_6 complex. In the biological system they are converted into pyridoxal phosphate which is the coenzyme for amino acid decarboxylase and for transaminase. PRX has been oxidized[13] to pyridoxal by acidic MnO_2 and by alkaline $KMnO_4$ solutions.[14] Least information is available in literature on the kinetics of oxidation of pharmaceuticals with organic haloamines which may throw some light on the mechanisms of metabolic conversions of the former in the biological system. Therefore, as a part of our broad program on mechanistic studies of haloaminometric reactions in generel and medicinal compounds in particular, we have studied the kinetics and mechanism of oxidation of pyridoxine by chloramine-T in acid medium.

Experimental

Pyridoxine hydrochloride (Fluka Chemical Corp., Hauppauga, N.Y.) was assayed by a spectrophotometric[15] method before use and found to be 99.8% pure. An aqueous concentrated solution of the compound was prepared and used as a stock solution. CAT (E. Merck) was purified by the method of Morris et al.[16] Chlorine solution was prepared by passing chlorine into distilled water. Aqueous solutions of CAT and chlorine were standardized by the iodometric method and preserved in brown bottles. Heavy water (D_2O) was obtained from Bhabha Atomic Research Centre, Bombay, India. The ionic strength of the medium was maintained constant using a concentrated solution of sodium perchlorate. Doubly distilled water was used throughout the investigations. All other reagents used were of Analar grade.

Stoichiometry. Reaction mixtures containing varying ratios of CAT to PRX were kept at room temperature (300±2 K) in the presence of 0.1 M (1 M=1 mol dm^{-3}) HCl for 24 h. The determination of the unreacted CAT showed that one mole of PRX could consume one mole of CAT:

$$C_8H_{11}NO_3+RNClNa \rightarrow C_8H_9NO_3+RNH_2+Na^++Cl^-$$

where R=p-$CH_3C_6H_4SO_2$

This stoichiometry is in agreement with the one reported in the literature.[17]

Product Analysis. The reduction product of CAT, *p*-toluenesolfonamide (RNH_2) was detected by paper chromatography[18] with benzyl alcohol saturated with water as the solvent and 0.5% vanillin in 1% HCl (in ethanol) as spraying reagent (R_f=0.90). The oxidation product of PRX, pyridoxal ($C_8H_9NO_3$), was identified[19] as semicarbazone (melting point 509 K).

Kinetic Measurements. The reaction was carried out in glass stoppered Pyrex boiling tubes whose outer surface was coated black to eliminate photochemical effects. Requisite amounts of PRX, acid, sodium perchlorate, and water (to keep the total volume constant for all runs) were taken in the

††Present address: Department of Chemistry, Western Illinois University Macomb, Illinois 61455, U.S.A.

tube and thermostated at 313 K for 30 min for thermal equilibrium. A measured amount of CAT or chlorine solution, also thermostated at the same temperature, was rapidly added to the mixture in the boiling tube. The progress of the reaction was monitored by the iodometric estimation of the unreacted CAT or chlorine present in known aliquots of the mixture withdrawn at different intervals of time. The course of the reaction was studied for over two half-lives. The rate constants calculated were reproducible within ±3% error.

Results

The kinetic runs for the reaction between PRX and CAT were performed at 313 K in the presence of several initial concentrations of mineral acids. The reaction was found to be moderate only in acidic chloride solution. Hence, a detailed study was made on the kinetics of oxidation of PRX by CAT in HCl medium.

Effcet of Varying Reactant Concentrations. For varying concentrations of CAT with constant [HCl] (0.1M) and a known excess of the substrate, plots of log titre vs. time were linear with the same slope indicating a first order dependence of the reaction rate on [CAT]. Values of the pseudo-first order rate constants, k, are presented in Table 1. The kinetics performed with varying concentrations of chlorine (where the molar concentration range of chlorine was the same as that of CAT) under identical experimental conditions gave k values comparable to that of CAT; this showed a first order dependence of the rate on chlorine concentration also (Table 5).

Table 1. Effects of Reactant Concentrations on the Rate[a)]

$10^4\times$[CAT]/M	$10^3\times$[PRX]/M	$10^4\times k/s^{-1}$
3.0	5.0	5.08
4.0	5.0	5.10
5.0	5.0	5.12
6.0	5.0	5.12
7.0	5.0	5.14
5.0	2.0	2.25
5.0	4.0	4.41
5.0	6.0	6.32
5.0	8.0	8.13
5.0	10.0	10.03
5.0	5.0	5.21[b)]
5.0	5.0	5.14[c)]

a) [HCl]=0.1 M; temp: 313 K. b) 0.5 M $NaClO_4$. c) In D_2O medium.

Table 2. Dependence of Reaction Rate on Hydrogen Ion and Chloride Ion Concentrations[a)]

[HCl]/M	[NaCl]/M	$10^4\times k/s^{-1}$
0.06	0.08	7.98
0.08	0.06	7.99
0.10	0.04	7.98
0.12	0.02	7.97
0.14	—	7.97
0.08	—	4.52
0.08	0.02	5.83
0.08	0.04	6.92
0.08	0.06	7.99
0.08	0.08	8.93

a) [CAT]=5.0×10^{-4} M; [PRX]=5.0×10^{-3} M; temp: 313 K. When $[H^+]$ is varied, constant total $[Cl^-]$= 0.14 M; When $[Cl^-]$ is varied, constant $[H^+]$=0.08 M.

An increase in [PRX], at constant [CAT] and [HCl], increased the rate. A plot of log k vs. log [PRX] gave a straight line with unit slope, showing a first-order dependence of the rate on [PRX]. The values of k obtained for different [PRX] are presented in Table 1.

Effect of Varying $[Cl^-]$ and $[H^+]$. At constant concentrations of H^+ (0.08 M), PRX (5×10^{-3} M), and CAT (5×10^{-4} M), addition of NaCl increased the reaction rate (Table 2). A plot of log k vs. log $[Cl^-]$ was linear with unit slope showing a first-order dependence of rate on $[Cl^-]$. Similarly, the influence of H^+ was studied by varying suitably the concentrations of both HCl and NaCl (Table 2), keeping Cl^- (0.14 M), PRX (5×10^{-3} M), and CAT (5×10^{-4} M) concentrations constant. It is observed that the rate is independent of $[H^+]$ showing a zero-order.

Effects of Varying Ionic Strength and Addition of Toluenesulfonamide. The change in ionic strength of the medium affected by adding sodium perchlorate at constant concentrations of PRX (5×10^{-3} M), CAT (5×10^{-4}), and HCl (0.1 M) had no significant influence on the rate of reaction (Table 1). The influence of the reaction product on the rate was studied by carrying out the reaction in presence of various concentrations of the product, *p*-toluenesulfonamide. The reaction rate decreased (Table 3) with the increase in the product concentration. A plot of log k vs. log $[RNH_2]$ gave a straight line with unit negative slope indicating a first order retardation of rate by $[RNH_2]$.

Effect of Solvent Isotope. The reaction was also studied using D_2O, instead of H_2O, as the solvent keeping other factors constant (Table 1). The solvent isotope effect (k_{H_2O}/k_{D_2O}) was found to be 1.01, indicating a negligible effect of the solvent isotope on the reaction rate.

Effects of Dielectric Constant and Temperature. The reaction was studied at 313 K by adding methanol to the reaction mixture at constant concentrations of PRX (5×10^{-3} M), CAT (5×10^{-4} M), and HCl (0.1 M). The reaction rate increased with decrease in dielectric constant (D) or with increase in methanol content of the medium (Table 4). A plot of log k vs. $1/D$ gave a straight line with a positive slope. The effect of temperature on the rate was studied by performing the kinetics at various temperetures (303—323 K) (Table 4) keeping [PRX], [CAT], and [HCl] constant. From the

Table 3. Effect of *p*-Toluenesulfonamide (RNH_2) on the Reaction Rate[a)]

$10^4[RNH_2]$/M	2.0	4.0	6.0	8.0	10.0
$10^4k/s^{-1}$	4.94	2.82	2.03	1.47	1.10

a) [CAT]=5.0×10^{-4} M; [PRX]=5.0×10^{-3} M; [HCl]= 0.1 M; temp: 313 K.

Table 4. Effects of Temperature and Dielectric Constant (D) on the Rate[a)]

Temp/K	$10^4 \times k/s^{-1}$	Methanol weight %	D[b)]	$10^4 \times k/s^{-1}$[c)]
303	1.98	00.0	73.22	5.12
308	3.20	10.0	69.00	6.20
313	5.12	20.0	64.88	7.11
318	8.25	30.0	60.58	9.20
323	14.15	40.0	56.17	11.49

Thermodynamic Parameters[d)]

ΔH^*/kJ mol^{-1}	ΔS^*/JK^{-1} mol^{-1}
80.45	−44.37

a) [CAT]=5.0×10^{-4} M; [PRX]=5.0×10^{-3} M; [HCl]= 0.10 M. b) Ref. 24, average of D values at 308 and 318 K. c) Temp: 313 K. d) Calculation based on energy of activation equals 84.51 kJ mol^{-1}; ΔH^*: enthalpy of activation; ΔS^*: entropy of activation.

Arrhenius plot of log k vs. $1/T$, the energy of activation and then the thermodynamic parameters, enthalpy of activation (ΔH^*) and entropy of activation (ΔS^*), were evaluated in a standard manner (Table 4).[20)]

Discussion

The substrate pyridoxine exhibits several equilibria[21)] depending on the pH of the solution:

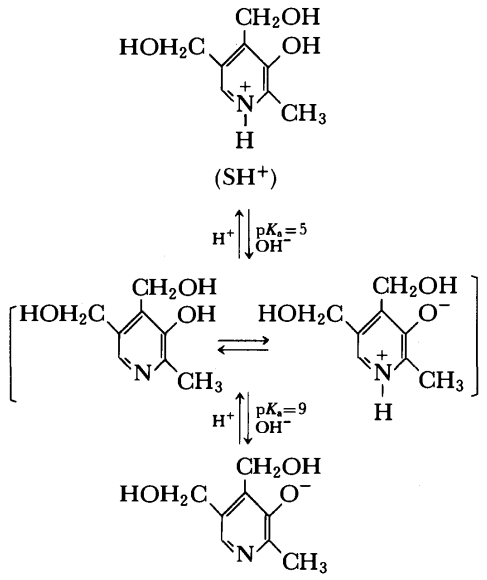

(1)

In the acidic conditions employed in the present investigations, the substrate (S) exists in the protonated form (SH^+).

Acidified CAT solutions contain RNHCl, $RNCl_2$, and HOCl as the oxidizing species.[3)] The observed first-order dependence of rate on [CAT] shows that $RNCl_2$ is not the oxidizing species in the reaction sequence. In acidic chloride solution, HOCl or monochloramine-T forms molecular chlorine. The formation of free chlorine[4)] from the acid form of CAT is presumed to occur through the following steps:

Table 5. Effect of Chlorine Concentration on the Rate[a)]

$10^4 \times$[Chlorine]/M	$10^3 \times$[PRX]/M	$10^4 \times k/s^{-1}$
3.0	5.0	5.20
4.0	5.0	5.20
4.8	5.0	5.11
5.6	5.0	5.13
6.6	5.0	5.15

a) [HCl]=0.10 m; temp: 313 K.

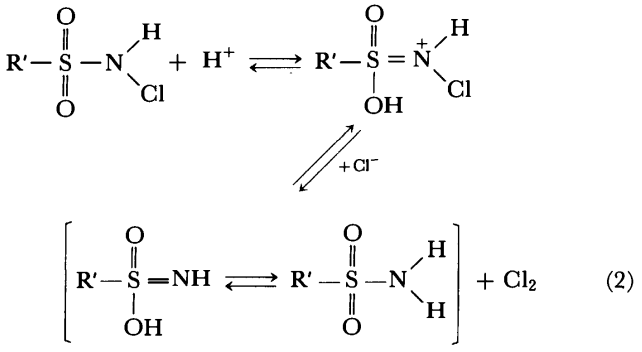

(2)

where R′=CH_3-C_6H_4.

Therefore, in the present system one can expect RNHCl or Cl_2 to be the effective oxidizing species. To verify this possibility, some experiments were carried out with chlorine water under identical experimental conditions. It is found that kinetic data with Cl_2 (Table 5) are almost identical with those with CAT (Table 1). The first order retardation of the rate by p-toluenesulfonamide ($R'SO_2NH_2$ or RNH_2) supports the involvement of Cl_2 in the oxidation sequence.

Based on these and other facts the reaction mechanism, Scheme 1, has been proposed. Scheme 1 involves the equilibrium reaction forming the protonated RNHCl species, RN^+H_2Cl, which on interaction with Cl^- forms Cl_2. The free chlorine formed interacts with the protonated substrate, SH^+, in a slowest and rate determining step to form an intermediate X. The intermediate then interacts with a solvent molecule, in a fast step, to form the end-products of the reaction.

$$RNHCl + H^+ \overset{K_1}{\rightleftharpoons} RN^+H_2Cl \quad (3)\ (\text{slow})$$

$$RN^+H_2Cl + Cl^- \overset{K_2}{\rightleftharpoons} RNH_2 + Cl_2 \quad (4)\ (\text{slow})$$

$$Cl_2 + SH^+ \xrightarrow{k_3} X \quad (5)$$

(slowest and rate determining)

$$X + H_2O \xrightarrow{k_4} \text{Products} \quad (6)\ (\text{fast})$$

Scheme 1.

Based on the above scheme, the total CAT concentration is given by

$$[CAT]_T=[RNHCl]+[RN^+H_2Cl]+[Cl_2] \quad (7)$$

By making the appropriate substitutions in Eq. 7

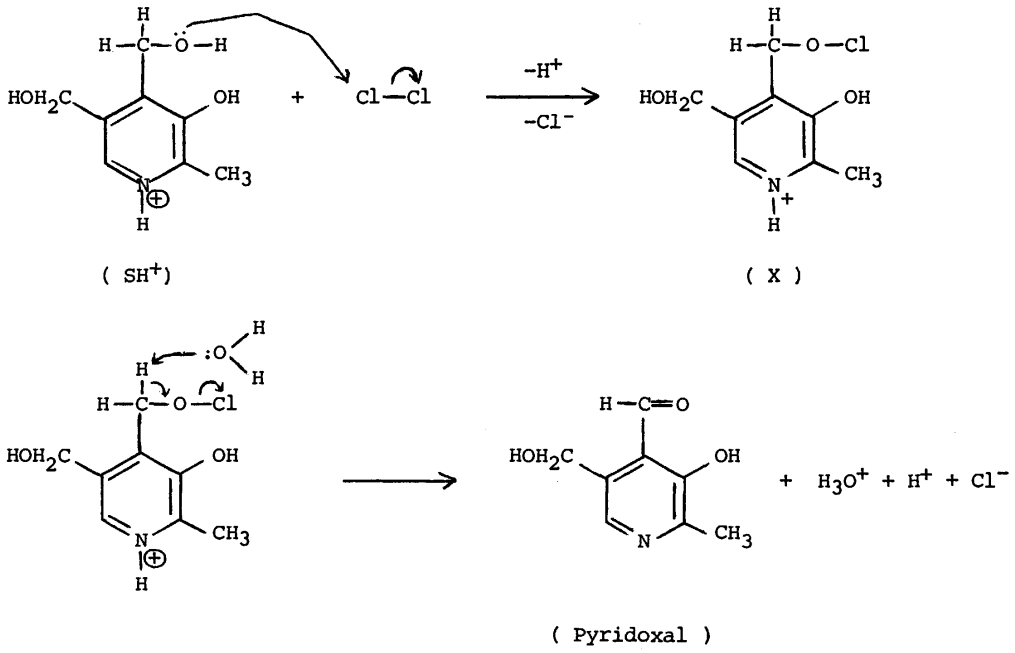

Scheme 2.

using the equilibria of Scheme 1, the Eq. 8 for $[Cl_2]$ can be obtained.

$$[Cl_2] = \frac{K_1K_2[CAT]_T[H^+][Cl^-]}{K_1[H^+][RNH_2] + [RNH_2] + K_1K_2[H^+][Cl^-]} \quad (8)$$

From Scheme 1, the reaction rate is

$$\text{Rate} = -d[CAT]_T/dt = k_3[Cl_2][SH^+] \quad (9)$$

The substitution for $[Cl_2]$ in the above equation leads to the rate expression as follows:

$$\frac{-d[CAT]_T}{dt} = \frac{K_1K_2k_3[CAT]_T[SH^+][H^+][Cl^-]}{K_1[H^+][RNH_2] + [RNH_2] + K_1K_2[H^+][Cl^-]} \quad (10)$$

If $K_1[H^+][RNH_2] \gg [RNH_2] + K_1K_2[H^+][Cl^-]$, the last two terms can be neglected.

$$\frac{-d[CAT]_T}{dt} = \frac{K_2k_3[CAT]_T[SH^+][Cl^-]}{[RNH_2]} \quad (11)$$

By rearranging the rate expression 11, we get

$$k_{obsd} = \frac{-d\ln[CAT]_T}{dt} = \frac{-d[CAT]_T}{[CAT]_T} \cdot \frac{1}{dt} = \frac{K_2k_3[SH^+][Cl^-]}{[RNH_2]} \quad (12)$$

This rate law 11 is in agreement with the experimentally observed unit orders in [CAT], $[SH^+]$, and $[Cl^-]$, zero order in $[H^+]$, and inverse first order in $[RNH_2]$ (Tables 1—3). The plots, k_{obsd} vs. $[SH^+]$ or $[Cl^-]$ or $1/[RNH_2]$, were all linear passing through the origin in conformity with the rate law 12.

A possible mechanistic pathway for the PRX oxidation is shown in Scheme 2. A mechanism involving the formation of the intermediate (X), hypochlorite ester of PRX, due to the electrophilic attack of Cl_2 on one of the primary alcohol groups of the protonated substrate (SH^+) in the important rate determining step has been suggested. In the mechanism of bromine oxidation of alcohols, hypobromite ester is considered to be a possible intermediate. Kruse et al.[21,22] have proposed that the primary or secondary alcohol forms a hypobromite ester as the intermediate which then readily loses hydrogen bromide to form the carbonyl product. Our proposed mechanism involving hypochlorite ester as the intermediate is in agreement with that of Kruse et al. The observed absence of solvent isotope effect (Table 1) does not rule out the possibility of the hydride transfer. It does, however, show that the proton transfer in the rate-determining step may be ruled out; this may not always be the case. The nucleophilic attack by the water molecule may facilitate the cleavage of the weak O-Cl bond of the hypochlorite to form the aldehyde, pyridoxal, as the oxidation product of PRX.

The proposed mechanism is supported by the observed thermodynamic parameters (Table 4). The negative entropy of activation indicates formation of the compact transition state, hypochlorite species.[20] The positive effect of dielectric constant of the medium on the rate (Table 4) supports the involvement of positive ion-dipole interaction in the rate determining step which is in agreement with the kinetic theories.[20,23,24] The negligible effect of ionic strength of the medium (Table 1) conforms to the ion-neutral molecule interaction in the rate determining step. The negligible solvent isotope effect and the negative effect of the reaction product, *p*-toluenesulfonamide, on the rate (Table 3) are also in conformity with the proposed mechanism.

References

1) M. M. Campbell and G. Johnson, *Chem. Rev.*, **78**, 65 (1978).
2) A. Berka, J. Vulterin, and J. Zyka, "Newer Redox Titrants," Pergamon, New York (1965), p. 37.
3) E. Bishop and V. J. Jennings, *Talanta*, **1**, 197 (1958).
4) V. R. S. Rao, D. Venkappayya, and G. Aravamudan, *Talanta*, **17**, 770 (1970).
5) B. T. Gowda and D. S. Mahadevappa, *J. Chem. Soc., Perkin Trans. 2*, **1983**, 323.
6) B. Jayaram and S. M. Mayanna, *Analyst*, **106**, 720 (1981).
7) B. Jayaram and S. M. Mayanna, *Talanta*, **30**, 798 (1983).
8) D. S. Mahadevappa and B. T. Gowda, *Talanta*, **30**, 359 (1983).
9) B. Jayaram and N. M. Made Gowda, *Analyst*, **110**, 985 (1985).
10) M. M. Natarajan and V. Thiagarajan, *J. Chem. Soc., Perkin Trans. 2*, **1975**, 1590.
11) D. S. Mahadevappa, K. S. Rangappa, B. T. Gowda, and N. M. Made Gowda, *J. Phys. Chem.*, **85**, 3651 (1981).
12) B. Jayaram and S. M. Mayanna, *Oxid. Commun.*, **7**, 21 (1984).
13) F. Yasuo, Jpn. Patent 7039260 (CL.C.07d, A.6.1K), 1970, *Chem. Abstr.*, **74**, 12547 p (1971).
14) S. A. Harris, D. Heyl, and K. Folkers, *J. Am. Chem. Soc.*, **66**, 2088 (1944).
15) R. C. Shah, P. V. Raman, and M. M. Mehta, *J. Pharm. Sci.*, **54**, 432 (1965).
16) J. C. Morris, J. A. Salazar, and M. A. Wineman, *J. Am. Chem. Soc.*, **70**, 2036 (1948).
17) B. Jayaram and N. M. Made Gowda, *J. Assoc. Off. Anal. Chem.*, **69**, 47 (1986).
18) D. S. Mahadevappa and N. M. Made Gowda, *Talanta*, **22**, 771 (1975).
19) "Dictionary of Organic Compounds," ed by J. R. A. Pollock and R. Stevens, Eyre and Spottilwood Publishers Ltd., London (1965), Vol. 5, p. 2820.
20) A. Frost and R. G. Pearson, "Kinetics and Mechanisms," 2nd ed, Wiley, New York (1961); K. J. Laidler and H. Eyring, *Am. New York Acad. Sci.*, **39**, 303 (1940); K. J. Laidler, "Reaction Kinetics," Pergamon, New York (1963).
21) P. F. Kruse, Jr., K. L. Grist, and T. A. McCoy, *Anal. Chem.*, **26**, 1319 (1954).
22) R. Filler, *Chem. Rev.*, **63**, 21 (1963).
23) E. S. Amis, "Solvent Effects on Reaction Rates and Mechanisms," Academic Press, New York (1966).
24) S. G. Entelis and R. P. Tiger, "Reaction Kinetics in the Liquid Phase," Wiley, New York (1976).
25) P. S. Albright and L. J. Gosting, *J. Am. Chem. Soc.*, **68**, 1061 (1946).

Excited-State and Ground-State Proton-Transfer Reactions in 5-Aminoindole

Hemant Kumar SINHA, Sneh Kumar DOGRA,* and Mannam KRISHNAMURTHY†
Department of Chemistry, Indian Institute of Technology, Kanpur 208016, India
†Department of Chemistry, A.U.P.G. Extension Centre, Nuzvid-521201, A.P., India
(Received October 16, 1986)

Dual fluorescence emissions are observed when the electron-donating group ($-NH_2$) is present at the position 5 of indole moiety. From the study of solvent effect and the large blue shift observed in the fluorescence spectra at 77 K, it is concluded that the long wavelength fluorescence band (480 nm) is assigned to the more polar state and the short wavelength band (350 nm) to the less polar state of 5-aminoindole (AI). Monocation is formed by protonating the amino group and no proton-induced fluorescence quenching of the neutral species is observed prior to its being protonated. This is mainly due to the shorter life of the conjugated acid-base pair. CNDO/S calculations indicate that dication is formed by protonating the C-3 position of the monocation of AI in the S_0 state but position 4 of monocation of AI in the S_1 state. Monoanion is formed by the deprotonation of >NH group in the S_0 state, but from the deprotonation of $-NH_2$ group in the S_1 state.

It is now well-established that the monocation of 5-hydroxy derivatives of indole fluoresces at ≈520 nm[1-5] and this band is used as an analytical tool for the diagonosis as well as for the estimation purposes. Unlike the other prototropic reactions of indole and indole derivatives,[6] the proton is added either at position 6 or at position 4[3-5] (the latter is preferred) of the 5-hydroxy derivatives, rather than at position 3 in the former compounds. The fluorescence band of the monocations of 5-hydroxy derivatives is very large red shifted (520 nm) as compared to that of the neutral molecules (≈360 nm) and no explanation is available in literature.

Recently, we have reinvestigated the spectral characteristics of some of the indole derivatives (mostly the carboxylic acids)[7-9] in different solvents and at various pH. It has been found that a new weak fluorescence band (≈460 nm) has been observed only in the compounds where 5-OH or 5-OCH_3 group is present in the indole moiety.[5] For example, in the fluorescence spectrum of 5-hydroxy-3-indoleacetic acid the ≈460 nm band is observed in the neutral species as well as in the case of monoanion formed by the deprotonation of -COOH group, but this band is absent if the deprotonation takes place from the -OH group. It has been further shown[4,5] that the charge densities in S_0 and S_1 states are maximum at position 6 or 4 in the case when -OH or -OMe group is present at position 5 of indole, and this leads to cannonical structure III or IV rather than II (Scheme 1) which is generally present in the other indole derivatives. If this phenomenon is due to the presence of electron-donating groups at position 5, the fluorescence band at ≈480 nm should also be observed in the case of amino group. The present study has been undertaken to see whether the observation of two fluorescence bands is due to the characteristic feature of the presence of electron-donating groups at position 5. The effects of solvents and pH on the spectral characteristics have also been studied. The ground state and excited-state pK_a values have been determined and discussed.

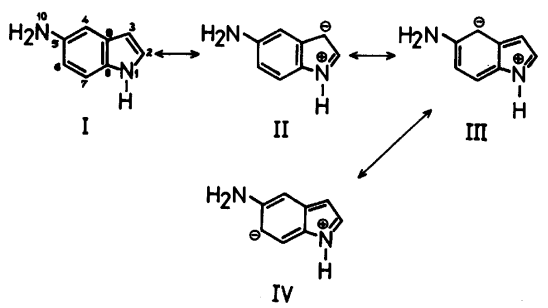

Scheme 1. Various cannonical forms of 5-aminoindole.

Method and Material

5-Aminoindole (AI) was obtained from Aldrich and was recrystallized from ethanol. The purity of the compound was checked by noting the sharp mp, absorption spectrum, and getting the similar fluorescence spectra when excited at different wavelengths. Spectrograde methanol, analytical grade sulfuric acid, sodium hydroxide, and phosphoric acid (BDH) were used. Analytical grade acetonitrile (E. Merck), cyclohexane (IDPL), ether, and ethanol were further purified by the procedures, as described in literature.[10] Triply distilled water was used for aqueous solutions. pH of the solutions in the range of 3—12 were adjusted by adding appropriate amount of sodium hydroxide and phosphoric acid, as phosphate buffers do not quench the fluorescence. A modified Hammett's acidity scale[11] for H_2SO_4-H_2O mixtures and Yagil's basicity scale[12] for NaOH-H_2O mixtures were used for aqueous solutions of pH less than 1 and pH greater than 13 respectively.

The absorption spectra were recorded on a Shimadzu spectrophotometer model UV 190, equipped with a chart recorder model U 135. The fluorescence measurements were carried out on the laboratory made scanning spectrofluorimeter, details were available elsewhere.[13] Both monochromators were calibrated with a low-pressure mercury lamp from time to time and the band width used for excitation was 8 nm. Fluorescence quantum yields were determined with the solutions having absorbance less than 0.1 and from the corrected fluorescence spectra, using quinine sulfate in 0.05 M (1 M=1 mol dm^{-3}) H_2SO_4 as a reference.[14] For absorptiometric and fluorimetric titrations, the solutions were prepared just before taking measurements. Isosbestic wavelengths were used as exciting wavelengths to measure the

Table 1. Absorption Maxima (λ^{ab}_{max}) and Molar Extinction Coefficients (ε) of 5-Aminoindole in Various Solvents and Its Prototropic Forms in Aqueous Solutions

Specie	Solvent	λ^{ab}_{max}/nm (log ε)[a]		
Neutral	Cyclohexane		270 sh	229 sh
		314	263	214
Neutral	Ether	316(3.32)	268(3.60)	214(4.26)
Neutral	Acetonitrile	315(3.26)	269(3.70)	219(4.42)
Neutral	Methanol	308(3.43)	270(3.76)	213(4.41)
Neutral	Ethanol	306(3.44)	270(3.76)	214(4.42)
Neutral	Water (pH=8)	305(3.43)	269(3.69)	199(4.51)
Anion	KOH (H_-=17)	312(3.69)	230(4.44)	
Cation	Water (pH=3)	286(3.70)	218(4.47)	200(4.17)
		280(3.75)		
Dication	H_2SO_4 (H_0=−7)	280(3.73)	236(3.62)	204(3.98)
			228(3.62)	191(4.05)

a) ε values are in $dm^3\,mol^{-1}\,cm^{-1}$.

fluorescence intensity. The concentrations of the solutions were of the order of 10^{-4}—10^{-5} mol dm^{-3}.

Both Pariser-Parr-Pople (PPP)[15,16] and CNDO/S[17] methods were employed to calculate the transitions energies, ground and excited state charge densities at various centres of the molecule and its prototropic species. All configurations obtained by single electron excitation from occupied molecular orbital to unoccupied molecular orbital were considered in all configuration interaction calculations. The species were assumed to be planar and the rings were taken as regular pentagon and hexagon. All ring C-C, C-N, and C-NH_2 bond lengths were taken as 1.40 Å.

Results and Discussion

Effect of Solvents. Table 1 lists the absorption maxima, log ε_{max} and Table 2 the fluorescence band maxima and quantum yields of AI in different solvents. The data in Table 1 clearly indicate that the absorption band maxima of AI are large red-shifted as compared to indole[6] or even 5-hydroxyindole (HI).[5] All band maxima are red-shifted as the polarity or the proton accepting nature of the solvents increases while a blue shift is noticed if the proton donor capacity of the solvents increases. Similar to 5-hydroxy derivatives, AI also exhibits dual fluorescence band systems, one at ≈350 nm and the other at ≈480 nm. The fluorescence intensity of the latter band system is much less than that of the former. The ratio of the band intensities remains the same value in different solvents as well as with the 100 fold change in the concentration of AI. The fluorescence maxima of both bands are red-shifted with change of solvents from cyclohexane to water, where the red shift observed in the shorter wavelength band is less than that in the longer wavelength band. In the measurements of fluorescence spectra at 77 K, the blue shift observed in the long wavelength fluorescence band (≈80 nm) is very large compared to that in the shorter wavelength band (≈30 nm). These data are compiled in Table 2 and the spectra are depicted in Fig. 2. The fluorescence quantum yield decreases under the above environments, such that we are unable to detect the long wavelength emission in water.

Table 2. Fluorescence Maxima (λ^{fl}_{max}) and Quantum Yield (ϕ_f) of 5-Aminoindole in Various Solvents and Its Prototropic Forms in Aqueous Solutions at 298 K

Specie	Solvent	λ^{fl}_{max}/nm (ϕ_f)		
Neutral	Cyclohexane	482	352	(0.27)
Neutral	Ether	495	362	(0.30)
Neutral	Acetonitrile	503	368	(0.39)
Neutral	Methanol	512	370	(0.30)
Neutral	Ethanol	519	372	(0.19)
Neutral	Water (pH=8)	—	374	(0.03)
		432	345	—
Anion	KOH (H_-=17)	460	365	
Cation	Water (pH=3)		357	(0.32)
			328	—
Dication	H_2SO_4 (H_0=−8)			
			—	—

a) Values underlined are at 77 K.

It is now well-established that the long wavelength absorption band of indole is a mixture of ^1L_b and ^1L_a bands[15-18] i.e., the absorption band near 285 nm is due to the transition from the ground state to the ^1L_b state, around 272 nm to the ^1L_a state, whereas the band maximum near 220 nm is due to the ^1B state. The larger red shift observed in the 285 nm band system of AI as compared to that in 272 nm band system, is consistent with the earlier results that the former transition is polarised along the longer axis and the latter along the shorter axis. The -NH_2 group situated along the longer axis may perturb the ^1L_b state more than the ^1L_a state. The larger red shift observed in the absorption maximum is because of the fact that the lone-pair electrons on the amino group perturb the π cloud of the aromatic moiety much better than those on the hydroxyl group.

The fluorescence spectrum of indole and its derivatives in polar solvents has been proposed as the combination of two emission bands[18-22] i.e., due to the emission from the two closed lying ^1L_a and ^1L_b states. The assignment of the fluorescence spectrum as a combination of two bands is based on the results of polarized fluorescence excitation, fluorescencspectra,

and the fluorescence decay times of indoles. The present study also suggests the presence of two closed lying excited electronic states, because the absorption spectrum and the excitation spectra recorded at both fluorescence maxima resemble each other. The large difference in the fluorescence band maxima is due to the increased polarity in one of the electronic states, that is, one of them is much more stablished. This phenomenon has been further confirmed from the study of fluorescence spectra recorded at 77 K. The blue shift observed in the case of long wavelength band is much larger (≈80 nm) than that in the shorter wavelength band (≈30 nm). Further, stability of the states depends upon the nature, orientation and position of the substituent in the parent molecule. Similar to 5-hydroxyindole,[4] spectral data and charge densities at various atomic centres have been carried out on AI by the semiemperical-SCF MO-CI method (PPP) and by CNDO/S methods. The data are listed in Table 3 and 4 respectively. The data in Table 3 indicate that values of λ_{max} predicted by the CNDO/s method agree nicely with those observed for various species and the result proves the validity of the method. The data in Table 4 have clearly indicated that, similar to those of 5-hydroxyindole, the charge densities increase at the positions 4 and 6 (preferably at latter center) in comparison to position 3, normally observed in the case of indole. This suggests that charge migration takes place from heterocyclic to homocyclic ring leading to polarize the indole molecule. Cannonical structures arising from this intramolecular charge transfer are given in Scheme 1. Thus 480 nm band represents the fluorescence band may be due to more polarized cannonical structure II or IV of AI. This band cannot be assigned to the excimer or exciplex emission as the I_{480}/I_{350} ratio remains the same even when the concentration of AI is varied by 100 fold or the solvent is changed. The long wavelength emission is due to the presence of electron-donating group because on protonation of $-NH_2$ group to produce $-NH_3^+$ (see later) the 480 nm band disappears. Lastly this 480 nm band also cannot be assigned to the phosphorescence spectra on the basis of no effect of dissolved oxygen on the emission intensity. Oxygen from the solutions was removed by bubbling nitrogen and no phosphorescence was observed at 298 K, using an Amino-Bowman

Table 3. Theoretical Values of Absorption Maxima (in nm) and Oscillator Strength(f) of Different Prototropic Forms of 5-Aminoindole

Method	PPP	(f)	CNDO/s	(f)	Experimental
Neutral	296.7	0.04	314.5	0.03	314
	263.0	0.19	266.9	0.10	263 270
	221.0	0.12	233.6	0.19	
	208.2	0.34	229.8	0.39	229
			214.9	0.25	214
Monocation ($-NH_3^+$)			312.7	0.01	
			283.9	0.10	286, 280
			236.1	0.23	
			221.8	0.44	218
			210.7	0.08	200
Monoanion (>N^-)			317.3	0.04	312
			244.0	0.68	
			237.1	0.08	230
					218
					200

Table 4. Ground and Excited State Charge Densities at Various Centers of the Different Prototropic Forms of 5-Aminoindole

		N_1	C_2	C_3	C_4	C_5	C_6	C_7	C_8	C_9	N_{10}
Neutral	PPP	1.689	1.070	1.087	1.040	0.996	1.037	1.034	1.070	1.034	1.941
		(1.645)	(1.122)	(0.991)	(1.037)	(0.994)	(1.048)	(1.039)	(1.058)	(1.052)	(1.935)
Neutral	CNDO	5.126	4.05	3.982	3.996	3.970	4.000	4.05	3.96	4.06	5.220
		(5.112)	(4.138)	(3.988)	(4.057)	(3.925)	(4.001)	(4.144)	(3.852)	(4.066)	(5.137)
Cation	CNDO	5.114	3.833	4.150	4.090	3.935	4.055	4.001	3.920	3.960	4.846
		(5.054)	(3.758)	(4.003)	(4.154)	(3.792)	(4.086)	(4.036)	(3.946)	(3.985)	(4.844)
Anion	CNDO	5.442	3.953	4.226	4.147	3.918	4.122	4.051	3.975	3.994	5.254
		(5.170)	(4.097)	(3.968)	(4.245)	(3.896)	(4.172)	(4.233)	(3.996)	(4.038)	(5.237)

The values in the parentheses are the excited state charge densities. The numbering of the atomic centers are shown in Scheme 1.

phosphorescope. The similar kind of behavior has been observed in the case of monocations of benzimidazole and methyl-substituted benzimidazoles.[23-25]

The dependence of the shifts of absorption and fluorescence band maxima of AI upon solvent polarity or hydrogen-bond-formation capacity of solvents is consistent with the earlier findings on the similar groups that proton-donating nature of solute leads to red shift and that proton-accepting nature of solute to blue shift. Thus ether and acetonitrile are acting as proton-accepting solvents, whereas methanol and water as proton-donating ones in the S_0 state. Since the intramolecular charge transfer from $-NH_2$ group to the ring is more effective in the S_1 state than in S_0, this group acts as a better proton donor in S_1 state. The decrease in the fluorescence quantum yield with increase in the solvent polarity or hydrogen-bonding power of solvents is due to interactions between the S_1 state and solvent molecules resulting in an increase of the rates of radiationless processes. This is further manifested by an increase in the Stokes shift under similar conditions.

Effect of pH. The absorption and fluorescence spectra of AI have been investigated in the H_0/pH/H_- range of −10 to 17. The relevant data are compiled in Tables 1 and 2 respectively. The absorption and fluorescence spectra of the various prototropic species are shown in Figs. 1 and 2. The spectral changes observed in the absorption spectrum of AI are consistent with the earlier results of the compounds containing amino groups. The neutral AI exists over the range of pH 14 to 3. With a decrease in pH, the absorption spectrum of AI is blue-shifted and the blue shift observed in the long wavelength band is so large that it is merged with the ^1L_a band system, resembling with that of indole molecule.[6] This clearly indicates that the monocation is formed by protonating the

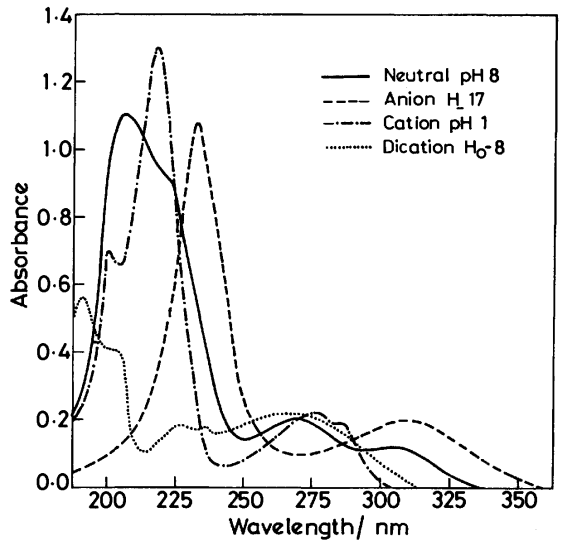

Fig. 1. Absorption spectra of various prototropic forms of AI at 298 K.

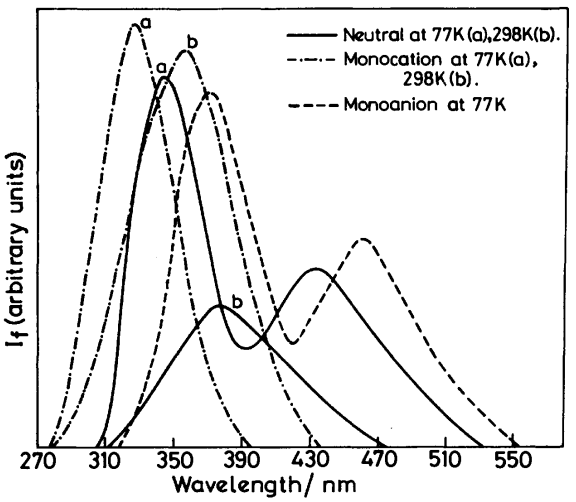

Fig. 2. Fluorescence spectra of AI in different solvents and at different pH at 298 K.

amino group in the S_0 state. Further increase in the acid strength, does not involve much change in the long wavelength band, except the vibrational structures, however, the intensity of 218 nm band system decreases and it is replaced by the two band systems, one at 236 and the other at 204 nm. This is a characteristic feature of the ring carbon atom of indole moiety.[6] Since there is already a presence of positive charge on the carbocyclic ring due to the presence of $-NH_3^+$ group, it is proposed that the protonation will take place at C-3 position normally observed for the indole molecule. This is further confirmed from calculated data of Table 4 that the charge density at position 3 is the maximum in the ground state of AI monocation (AI^+). With an increase in the basic strength, the absorption spectrum of AI is red-shifted and indicates the formation of monoanion. The monoanion can be formed by the deprotonation of either >NH group or $-NH_2$ group leading to the red shift. Further the pK_a values of both deprotonation reactions fall in the same range of basic strength.[12,26] The charge-density calculations, as shown in Table 4, have clearly indicated that the formal charge at the nitrogen atom of >NH group of indole molecule does not change due to the presence of amino group at position 5. Further the charge density at the nitrogen atom of >NH group is less than that at the nitrogen atom of $-NH_2$ group. This indicates that monoanion (AI^-) is formed by the deprotonation of imino group rather than amino group.

Thefluorescence spectrum of AI also follows the similar changes as observed in the absorption spectrum, within the same acidic and basic range i.e., the neutral species exists in the pH range of 7 to 14, monocation starts appearing below pH 6. Only one fluorescence band, similar to indole, has been observed for AI^+, indicating that the presence of electron-donating group is necessary at the position 5 for the emission of long wavelength fluorescence band. Dication of AI is nonfluorescent and this behaviour is similar to the

monocation of indole or other indole derivatives. Although the charge density is maximum at position 3 of AI^+ in the ground state, the charge density is maximum at position 4 of AI^+ in the first excited singlet state, similar to the neutral AI molecule and actually it decreases at position 3 in the S_1 state in comparison to S_0 (Table 4). The driving force behind this intramolecular charge migration from the heterocyclic to the carbocyclic ring is due to the presence of positive charge on the latter ring. On the basis of charge densities at the various atomic centers, it is concluded that the dication in the S_1 state is formed by protonating the carbon center at position 4 rather than at position 3. Similar to dication, the monoanion of AI is also nonfluorescent. Literature data show that monoanion formed by the deprotonation of >NH group of indole and some of its derivatives as well as the monoanions formed by the deprotonation of similar group in indazoles and benzimidazoles[2,13,27-29] are fluorescent, whereas that formed by the deprotonation of $-NH_2$ group is nonfluorescent,[30-32] with few exceptions.[33] Our data suggest that, though the ground state prototropic reaction is from the >NH group, but in the excited state, it is from the $-NH_2$ group.

Further charge density data at the two nitrogen centres do not point out clearly but the decrease in the formal charges at the nitrogen atom of $-NH_2$ (0.09) is larger than that at the nitrogen atom of >NH group (0.01). So the deprotonation in the excited singlet state, most probably is from the $-NH_2$ group. This is confirmed from the fluorescence spectral study at 77 K. Since at such a low temperature and in the frozen state, the species is present in the ground state environments, even when excited. The observation of two fluorescence bands at H_ 16 and at 77 K, clearly indicate that the electron-donating group at position 5 is not disturbed in the highly basic conditions and confirming that the deprotonation in the S_0 state takes place from the >NH group. Similar behavior has been observed in the case of 2-aminobenzimidazoles[34] and aminoindazoles.[35-37]

pK_a Values. The pK_a values for the different prototropic reactions have been determined absorptiometrically and are listed in Table 5. The values of pK_a's obtained for neutral-monoanion[12] and monocation-neutral[26] equilibria are in the range of pK_a's for similar reactions. The pK_a for the protonation of indole-ring carbon atom is less than that of indole (3.5)[6] and it is due to the presence of positive charge on the carbocyclic ring.

The pK_a^* values have been determined with the help of fluorimetric titration method (Fig. 3) and Förster cycle method,[37] using absorption and fluorescence data, wherever applicable. For example, pK_a^* for the neutral-monoanion equilibrium can not be calculated by the latter method as the equilibrium involved in S_0 and S_1 states are different. Similarly pK_a^* for dication-monocation equilibrium, because the protonation involves change in the structure of indole moiety as well as the dication is non-fluorescent. The

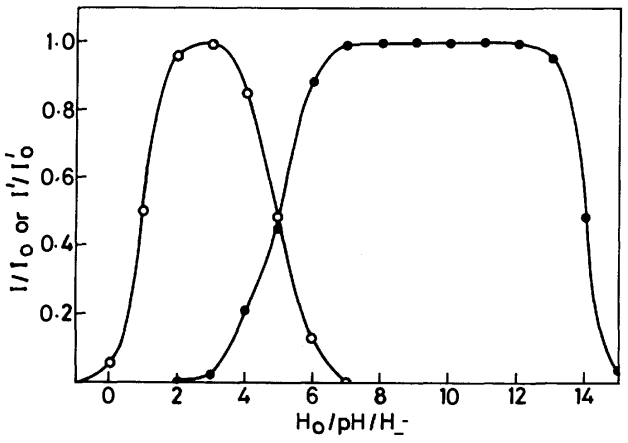

Fig. 3. Plot of I/I_0 vs. H_0/pH/H_ at 298 K.

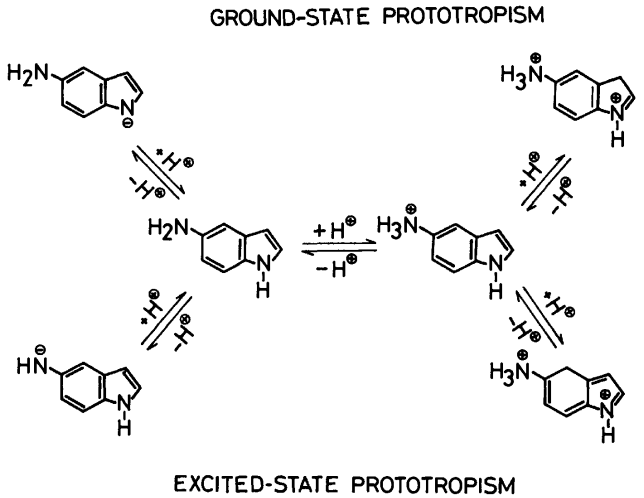

Scheme 2. Different prototropic reactions of 5-aminoindole.

Table 5. The pK_a Values of the Prototropic Equilibria of 5-Aminoindole in Aqueous Solutions

Equilibrium	p$K_a(S_0)$	p$K_a(S_1)$[a]	p$K_a(S_1)$[b]	p$K_a(S_1)$[c]
Neutral ⇌ Anion	16.1	14.0	14.5	12.8[d]
Cation ⇌ Neutral	5.0	5.0	0.4	0.3
Dication ⇌ Cation	−4.7	1.0	—	—

a) By fluorimetric titration. b, c) By Förster's method using absorption (b) and fluorescence (c) maxima. d) Using fluorescence maxima at 77 K.

results of fluorimetric titrations have indicated that the $-NH_2$ group becomes strong acid and carbon centre of indole more basic on excitation. These results are consistent with the earlier findings. Only ground state pK_a is obtained from the fluorimetric titrations for monocation-neutral equilibrium, which is little unusual for this kind of prototropic reaction, because in general, proton-induced fluorescence quenching[30,31,38] is observed before $-NH_2$ group gets protonated. Since the Förster cycle method has clearly indicated that $-NH_3^+$ group becomes stronger acid on excitation, it is concluded that the radiative lifetimes of the neutral and singly protonated species must be too short for proton exchange to occur appreciably within these lifetimes of conjugated species at pH≈5. Therefore, a prototropic equilibrium is not established within the lifetimes of the lowest excited singlet states of these molecules and thus fluorescence intensities measured at pH≈5 reflect the relative ground state concentrations of AI and AI^+. Hence, the ground-state pK_a is determined by fluorimetric titration in this case. Similar behavior has been observed in the prototropic reaction of 4-(9-anthryl)-*N*,*N*-dimethylaniline.[39] The difference between the pK_a^* values obtained by the Förster cycle method and absorption and fluorescence data is due to the different solvent relaxation for the conjugated species in S_0 and S_1 states. All the prototropic reactions are mentioned in Scheme 2.

Conclusion

The presence of electron-donor group at the position 5 of indole molecule, leads to the dual fluorescence, one nearly at≈360 nm and the other at≈480 nm. The latter one is because of more polar electronic state than that of the former. Monocation is formed by protonating the $-NH_2$ group and the dication further protonating the C-3 position in S_0 state but the position 4 of indole moiety in the S_1 state. The deprotonation of >NH group takes place in the S_0 state but of $-NH_2$ group in the S_1 state to form the monoanion. No proton-induced fluorescence quenching is observed before protonating amino group, and fluorimetric titrations have given the ground state pK_a value, indicating that the lifetimes of the conjugate species are very small to achieve the prototropic equilibrium in S_1 state.

The authors are grateful to the Department of Science and Technology for the financial support to the project entitled "Proton Transfer Reactions in the Excited States."

References

1) S. Udenfriend, D. F. Bogdanski, and H. Weisbach, *Science*, **122**, 972 (1955).
2) J. W. Bridges and R. T. Williams, *Biochem. J.*, **107**, 225 (1968).
3) R. F. Chen, *Proc. Natl. Acad. Sci., U.S.A.*, **60**, 598 (1968).
4) T. Kishi, M. Tanaka, and J. Tanaka, *Bull. Chem. Soc. Jpn.*, **50**, 1267 (1977).
5) M. Krishnamurthy, H. K. Sinha, and S. K. Dogra, unpublished results.
6) W. A. Remers, "The Chemistry of Heterocyclic Compounds" ed by W. J. Houlihan, Wiley Interscience, New York (1972), Vol. 25, pp. 11, 19, 24.
7) P. Phaniraj, H. K. Sinha, and S. K. Dogra, *J. Photochem.*, **34**, 209 (1986).
8) M. Krishnamurthy, A. K. Mishra, and S. K. Dogra, *Photochem Photobiol.*, **45**, 359 (1987).
9) M. Krishnamurthy, H. K. Sinha, and S. K. Dogra, *J. Lumin.*, **35**, 343 (1986).
10) J. A. Riddick and W. B. Bunger, "Organic Solvents," Wiley Interscience, New York (1970), pp. 502, 803.
11) M. J. Jorgenson and D. R. Hartter, *J. Am. Chem. Soc.*, **85**, 878 (1963).
12) G. Yagil, *J. Phys. Chem.*, **81**, 1034 (1967).
13) M. Swaminathan and S. K. Dogra, *Indian J. Chem.*, **22A**, 853 (1983).
14) S. R. Meach and D. Phillips, *J. Photochem.*, **23**, 193 (1983).
15) R. Pariser and R. G. Parr, *J. Chem. Phys.*, **21**, 767, 4660 (1953).
16) J. A. Pople, *Trans. Faraday Soc.*, **49**, 1315 (1953).
17) J. DelBene and H. H. Jaffe, *J. Chem. Phys.*, **48**, 1807, 4050 (1968).
18) M. Sun and P. S. Song, *Photochem. Photobiol.*, **25**, 3 (1977).
19) P. S. Song and W. E. Kurtin, *J. Am. Chem. Soc.*, **91**, 4892 (1969).
20) J. J. Aaron, A. Tine, M. E. Wojciechowska, and C. Parkanyi, *J. Lumin.*, **33**, 33 (1985).
21) J. J. Aaron, A. Tine, C. Villiers, C. Parkanyi, and D. Bouin, *Croat. Chem. Acta*, **56**, 157 (1983).
22) A. G. Szabo and D. M. Rayer, *J. Am. Chem. Soc.*, **102**, 554 (1980)
23) M. Kondo and H. Kuwano, *Bull. Chem. Soc. Jpn.*, **42**, 1433 (1969).
24) P. C. Tway and L. J. C. Love, *J. Phys. Chem.*, **86**, 5223, 5227 (1982).
25) M. Krishnamurthy, P. Phaniraj, and S. K. Dogra, *J. Chem. Soc., Perkin Trans. 2*, **1986**, 1917.
26) J. F. Ireland and P. A. H. Wyatt, *Adv. Phys. Org. Chem.*, **12**, 159 (1976).
27) M. Swaminathan and S. K. Dogra, *J. Photochem.*, **21**, 245 (1983).
28) A. K. Mishra, M. Swaminathan, and S. K. Dogra, *J. Photochem.*, **26**, 49 (1984).
29) M. Swaminathan and S. K. Dogra, *Indian J. Chem.*, **22A**, 278 (1983).
30) M. Swaminathan and S. K. Dogra, *Can. J. Chem.*, **61**, 1064 (1983).
31) A. K. Mishra and S. K. Dogra, *J. Photochem.*, **23**, 163 (1983).
32) A. K. Mishra and S. K. Dogra, *J. Chem. Soc., Perkin Trans. 2*, **1984**, 943.
33) U. Pandey, N. B. Joshi, and D. D. Pant, *Chem. Phys. Lett.*, **72**, 209 (1980); Th. Förster, *Z. Elecktrochem.*, **54**, 531 (1950).
34) A. K. Mishra and S. K. Dogra, *Indian J. Chem.*, **24A**,

384 (1985); *Bull. Chem. Soc. Jpn.*, **58**, 3587 (1985); *J. Photochem.*, **31**, 333 (1985); *Indian J. Chem.*, **24A**, 815 (1985).
35) M. Swaminathan and S. K. Dogra, *J. Am. Chem. Soc.*, **105**, 6223 (1983).
36) A. K. Mishra and S. K. Dogra, *Indian J. Chem.*, **24A**, 285 (1985).
37) P. Phaniraj, A. K. Mishra, and S. K. Dogra, *Indian J. Chem.*, **24A**, 913 (1985).
38) H. Shizuka, *Acc. Chem. Res.*, **18**, 141 (1985); H. Shizuka and S. Tobita, *J. Am. Chem. Soc.*, **104**, 6919 (1982).
39) H. Shizuka, T. Ogiwara, and E. Kimura, *J. Phys. Chem.*, **89**, 4302 (1985).

 © 1987 The Chemical Society of Japan Bull. Chem. Soc. Jpn., 60, 4409—4415 (1987)

Spectral Characteristics of Phenylenediamines and Their Various Protonated Species

R. MANOHARAN and Sneh Kumar DOGRA*
Department of Chemistry, Indian Institute of Technology, Kanpur 208016, India
(Received November 25, 1986)

Increase in the Stokes shift [$\bar{\nu}_{abs}(max)-\bar{\nu}_{flu}$ (max)] with an increase in the polarity and hydrogen-bonding capacity of the solvents is the maximum for *p*-phenylenediamine and the minimum for *m*-phenylenediamine. These studies have indicated that the two amino groups in *o*- and *p*-phenylenediamines are not in the same plane of the benzene ring. Spectral characteristics of monocations and dications resemble to those of aniline and benzene respectively. pK_a values for the dication-monocation and monocation-neutral equilibria have been determined, both in S_0 and S_1 states, and discussed.

If $\pi\rightarrow\pi^*$ is the lowest energy transition, the protonation at the tertiary nitrogen atom leads to the red shift in the absorption and fluorescence spectra of the molecule.[1] Schulman et al.[2] in their study of prototropic reactions of 1,10-phenanthroline have revealed that the spectral changes, observed in the absorption spectrum on protonation, followed the normal trend, but the emitting state of the monocation, formed by protonating one of the tertiary nitrogen atom is of lower energy than that of the dication, formed by protonating the second tertiary nitrogen atom i.e., red shift is followed by the blue shift in the above prototropic reactions. This anomalous behavior has been attributed to the very large solvent relaxation in the S_1 state of monocation and this has been further confirmed when the similar study was carried out in nonpolar medium, where the solvent relaxation is negligible. The similar behavior has been observed in our earlier study on 2,7-fluorenediamine,[3] where the two amino groups are symmetrical, like the two tertiary nitrogen atoms of 1,10-phenanthroline.

The aim of the present study is to see whether 1,2-, 1,3-, 1,4-phenylenediamines follow the similar trend or these molecules behave in a different fashion. Secondly, most of the prototropic studies carried out on the disubstituted benzenes are on the donor-acceptor substituents.[4-7] This kind of study, carried on the donor-donor substituents is very rare.[8-11] Since amino groups are electron donating, we have undertaken this study to see the effect of solvents and pH on the spectral changes of these three isomers of phenylenediamines.

Method and Material

o-Phenylenediamine (*o*PA) and *p*-phenylenediamine (*p*PA) were obtained from Aldrich Chemical Co. and *m*-phenylenediamine (*m*PA) was prepared by the reduction of *m*-nitroaniline as suggested in literature.[12] *o*PA was recrystallized from water, *m*PA from benzene, and *p*PA from diethyl ether repeatedly.[13] The purity of these compounds was checked by their sharp mp, absorption data and getting the similar fluorescence spectra when excited with different wavelengths. Spectrograde BDH methanol, analytical grade sulfuric acid, orthophosphoric acid, and sodium hydroxide (BDH) were used without further purification. Cyclohexane (IDPL), ether (BDH), and acetonitrile (E. Merck) were further purified by the procedures, as suggested in literature.[14] Triply distilled water was used for the aqueous study. Modified Hammett's acidity scale[15] for aqueous H_2SO_4 and Yagil's basicity scale[16] for aqueous NaOH were used for solutions below pH 1 and above pH 13 respectively. pH of the solutions in the range of 3 to 11 was adjusted by the addition of appropriate amount of NaOH and H_3PO_4.

Absorption spectra were recorded on a Shimadzu spectrophotometer, model UV 190, equipped with a chart recorder, model U 135. Fluorescence measurements were carried out on a scanning spectrofluorimeter, fabricated in our laboratory, the details of which were available elsewhere.[17] Both monochromators were calibrated from time to time with low-pressure mercury lamp and the band width of the excitation monochromator was 8 nm. pH of the solutions in the range of 1—13 was measured on a Toshniwal's pH meter, model CL-44A. Fluorescence quantum yields were measured on the solutions, having absorbance less than 0.1, fluorescence spectra were corrected and quinine sulfate in 0.05M H_2SO_4 (1M=1 mol dm^{-3}) was used as a standard.[18] The excitation wavelengths (λ_{exc}) used for *o*PA, *m*PA, and *p*PA were 275, 285, and 288 nm respectively. For absorptiometric and fluorimetric titrations, the solutions were prepared just before taking measurements and the concentrations of the solutions were of the order of 1×10^{-4} M (1M=1 mol dm^{-3}). To measure the fluorescence intensity at any analytical wavelength, isosbestic wavelengths were used for excitation. For dication-monocation equilibria of all diamines, a mercury-xenon lamp was used instead of a xenon lamp, normally used in the spectrofluorimeter. This is because of the low intensity of the xenon arc lamp below 270 nm.

Results and Discussion

Effect of Solvents. Table 1 depicts the absorption maxima, log ε_{max}, fluorescence maxima, and quantum yields of *o*PA, *m*PA, and *p*PA in the solvents of different polarity and hydrogen bond forming tendency, as well as at different proton concentrations. Figures 1—3 show the fluorescence spectra of these three diamines under the above environments. Data in Table 1 clearly indicate that the absorption spectra of all isomers are largely red shifted and the vibrational structure of the long wavelength band is completely lost in any one of the solvents compared to those of benzene. The intensity of each band of benzene is increased. The above results are quite consistent with

Table 1. Absorption and Fluorescence Spectral Data of Phenylenediamines in Different Solvents and at Various pH

Solvent (pH)	*o*-Phenylenediamine		*m*-Phenylenediamine		*p*-Phenylenediamine	
	λ_{abs} (log ε)	λ_{flu} (ϕ_f)	λ_{abs} (log ε)	λ_{flu} (ϕ_f)	λ_{abs} (log ε)	λ_{flu} (ϕ_f)
Cyclohexane	290.0(3.59) 234.0(3.85) 209.5(4.45)	330(0.020)	(sh)301.5(3.33) 293.3(3.42) 241.0(3.86) 214.0(4.46)	318(0.096)	316.5(3.23) 246.3(3.81) 207.5(3.69)	365(0.13)
Ether	294.0(3.55) 239.0(3.79) 212.0(4.35)	350(0.056)	296.3(3.5) 242.0(3.92) 218.5(4.47)	322(0.087)	320 (3.37) 247.5(3.96) 207.5(3.79)	381(0.17)
Acetonitrile	295.0(3.66) 240.0(3.90) 208.0(4.55)	352(0.02)	297.5(3.46) 243.0(3.89) 217.0(4.49)	326(0.015)	321.0(3.25) 247.5(3.84) 200.0(4.20)	388(0.065)
Methanol	293.5(3.52) 238.7(3.79) 210.0(4.48)	355(0.019)	292.5(3.36) 242.5(3.85) 213.5(4.48)	332(0.011)	307.5(3.27) 242.5(3.96) 204.0(4.05)	395(0.073)
Water	288 (3.53) 232.0(3.88) 205.0(4.57)	— —	289.0(3.30) 238.0(3.86) 210.0(4.51)	— —	302.5(3.28) 239.0(3.90) 197.5(4.33)	— —
Monocation (pH=3.5)	280 (3.24) 222.5(3.83) 194.0(4.16)	335(0.048)	282.5(3.24) 232.0(3.85) 205.0(4.08)	340(0.027)	283.5(3.08) 233.5(3.87) 201.3(4.01)	345(0.019)
Dication (H_0=−8)	261.0(2.16) 256.5(2.32) 251.5(2.36) 246.5(2.31) 237.0(2.10) 206.5(2.98)	275 —	262.0(2.0) 257.5(2.19) 252.5(2.22) 247.5(2.15) 237.5(1.92) 207.5(2.99)	275 —	262.5(2.27) 257.5(2.4) 252.5(2.39) 244.0(2.26) 236.0(2.13) 206.0(3.0)	275 —

ε values are in $dm^3 mol^{-1} cm^{-1}$.

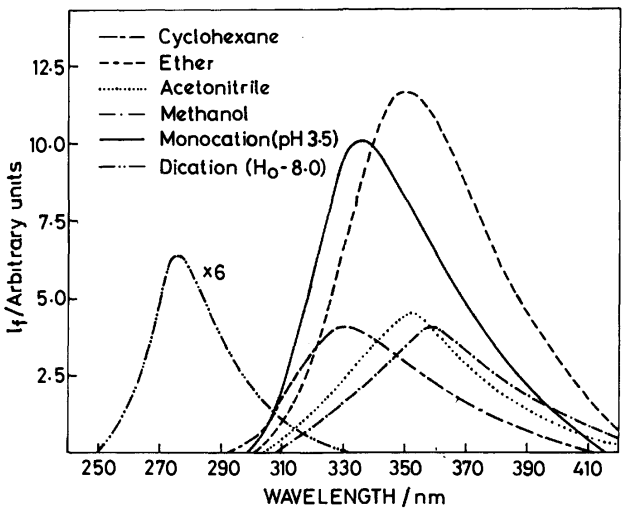

Fig. 1. Fluorescence spectra of *o*PA in different solvents and pH at 298 K. Concd = 5.0×10^{-4} M.

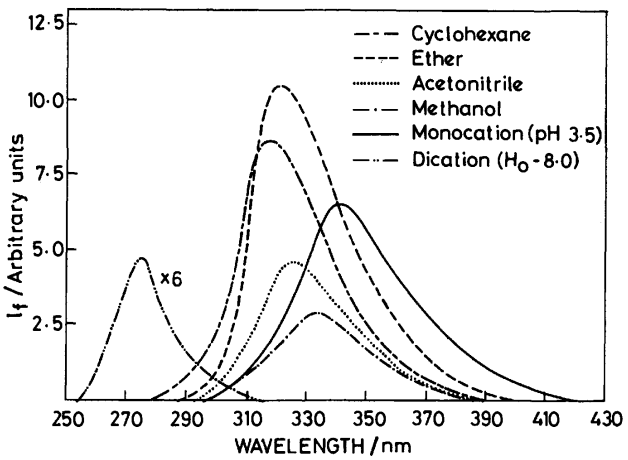

Fig. 2. Fluorescence spectra of *m*PA in different solvents and pH at 298 K. Concd = 5.0×10^{-4} M.

the presence of amino groups in the ring, because it completely destroys the hexagonal symmetry of the benzene ring. Therefore the symmetry forbidden selection rule is reduced resulting in an increase in the value of the transition dipole moment. The large red shift in λ_{max} and loss in the vibrational structure of the absorption spectrum are due to the strong interactions of the amino group with the π cloud of the benzene ring.

The absorption maxima of all bands of diamines are red-shifted with an increase in the polarity of aprotic solvents but are blue-shifted with an increase in the

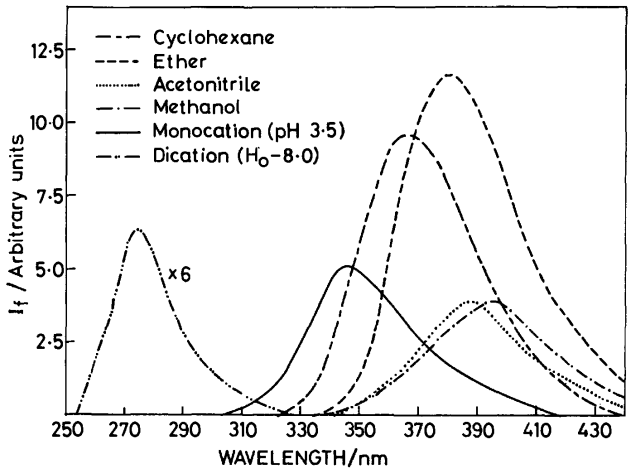

Fig. 3. Fluorescence spectra of *p*PA in different solvents and pH at 298 K. Concd $=5.0\times10^{-4}$ M.

proton-donor capacity of solvents. On the other hand, the fluorescence maxima of all diamines are regularly red-shifted under the above environments. The fluorescence quantum yield is quite small and further decreases in going from cyclohexane to water, where it is completely nonfluorescent at room temperature. The effect of solvents on the absorption and fluorescent maxima is agreeing with results observed earlier in the case of amino groups[19] i.e., the dispersive interactions and proton-donor nature of the solute lead to red shift and the proton-acceptor of solute leads to the blue shift in the absorption and fluorescence spectra of molecule if $\pi\rightarrow\pi^*$ is the lowest energy transition. Our data clearly indicate that in S_0 state, all diamines are acting as a proton donor in ether and acetonitrile, whereas a proton acceptor in methanol and water. The results of fluorescence spectra can be explained on the ground that charge migration from the amino group towards the benzene ring increases on excitation, thereby decreasing the charge density on the nitrogen atom and increasing the proton-donor capacity of the amino group. The decrease in the fluorescence quantum yield of all diamines, under the above environments is due to their strong interactions with the solvents and thus increasing the rates of radiationless processes. This is further manifested from the Stokes shift, which increases with the increase in the polarity of the solvents.

The Stokes shift $[\bar{\nu}_{abs}(max)-\bar{\nu}_{flu}(max)]$ observed for three amines is minimum for *m*PA (2630 cm^{-1}) and nearly same for *o*PA and *p*PA (4180, 4200 cm^{-1}) in cyclohexane. But an increase in the Stokes shift with an increase in the solvent polarity is the maximum for *p*PA and the minimum for *m*PA (See Table 2). Although no data is available for the polarity or dipole moment of these molecules in the excited states but it is quite clear from the data that the polarity and dipole moment of these molecules increase upon excitation. Our data further suggest that two amino groups present at the para position are not in the plane

Table 2. Stokes Shifts (cm^{-1}) Observed for Phenylenediamines in Different Solvents

Solvent	*o*PA	*m*PA	*p*PA
Cyclohexane	4180	2625	4200
Ether	5440	2730	5000
Acetonitrile	5480	2940	5380
Methanol	5902	4070	7200
Water (pH=8)	—	—	—
Monocation (pH=3.5)	5860	5990	6290
Dication ($H_0=-8$)	1950	1800	1800

of benzene ring. Had these groups been planar to the benzene ring, the dipole moment of *p*PA would have been zero, and thus the molecule would have been nonpolar in both S_0 and S_1 states. The dipole moment data of these molecules, available in the ground state,[20] do indicate that $-NH_2$ groups in the cases of *o*PA and *p*PA are not in the same plane of the benzene ring whereas in the case of *m*PA these groups are in the same plane of benzene. These conclusions are based on the fact that the calculated dipole moments of diamines (based on the vector addition of amino groups) do not agree with the observed ones. We, also, conclude from our data that the similar geometries of these molecules are present in the first excited singlet state.

Effect of Proton Concentration. The absorption and fluorescence spectra of all diamines have been studied in the H_0/pH/H_- range of -10 to 17. The relavent data are compiled in Table 1 and the fluorescence spectra of the various prototropic species of these amines are also shown in Fig. 1—3 respectively. The results observed are on the right track. With the decrease of pH (from≈8, depending on the particular diamine) the absorption spectra of all diamines are blue shifted and the absorption spectra so obtained resemble to that of aniline.[21] This clearly suggests that the species so formed is a monocation, obtained by protonating one of the amino groups. With the further increase of proton concentration, the absorption spectra are further blue-shifted and the long wavelength broad band is replaced by a structured spectrum, in each case. This spectrum resembles to that of benzene molecule.[22] This is further manifested from the similar vibrational frequencies as observed in the case of benzene coupled with the electronic transition, as well as from a decrease in the molecular extinction coefficient of the absorption bands of this species, resembling more closely to that of ^1L_b transition in benzene. The above results clearly indicate that the latter species is a dication, formed by protonating the second amino group. The above behavior clearly resembles to that of the aromatic compounds containing the amino group.[19,23-25]

The absorption spectra of ortho- and metadiamines do not change till pH 14 but after and at H_- 15, a small but a regular red shift is noticed and it continued even upto H_- 17, the highest basic conditions used and the

band maxima is observed at the same wavelength (295 nm). On the other hand, the absorption spectrum of *p*PA starts getting red shifted at pH $\geqslant$13 and is continuously red-shifted even at H_- 17, with a band peak at 313 nm. The above results are consistent with the results that deprotonation of the amino group leads to a red shift in the spectra.

The behavior of fluorescence spectra of the various species formed in these acid region is the same as observed in the ground state, i.e., around pH 4, the fluorescence spectrum of each amine is blue-shifted and resembles to the fluorescence spectrum of aniline ($\approx$340 nm in ethanol).[21] Around H_0 −8, the fluorescence spectrum is further largely blue-shifted in each case, with the band maximum at 275 nm and this resembles more closely to the fluorescence spectrum of benzene, without the band structure.[21] The above results clearly suggest that the former species is a monocation formed by the protonation of the amino group and the second species is a dication, formed by the protonation of the second amino group. The loss in the structure of the second species in the fluorescence spectrum, as compared to that in the ground state, is due to the stronger interactions in such a highly ionic medium. The assignment of the species is further confirmed by getting the fluorescence band maximum of the monocation nearly at the same wavelength and that of dication exactly at the same point in cases of the diamines studied. This is because, during these prototropic reactions, the species formed in the first case is close to aniline and in the second case, it is close to benzene, as the lone pairs are mopped by protons.

No fluorescence emission is observed from the neutral species as well as from the monoanions of these amines at room temperature and even upto H_- 17, the highest basic conditions used. This is consistent with the earlier results that monoanions formed by the deprotonation of aromatic amines, in general, are non-fluorescent, with few exceptions.[27,28]

Equilibrium Constants in the Ground and Excited States. pK_a values of dication-monocation and monocation-neutral equilibria have been calculated spectrophotometrically and are compiled in Table 3. The values of pK_a's obtained agree with literature values within experimental errors.[29] The pK_a for the neutral-monoanion cannot be determined because the absorption maxima in each case was constantly red-shifted even at the highest basic conditions used but one thing is certain that the pK_a value of neutral-monoanion equilibrium of *p*PA is smaller than that of *o*PA and *m*PA. The difference in the pK_a values of monocation-neutral equilibria between *o*PA and *m*PA is quite small but it is quite large in the case of *p*PA. Further the pK_a values for *o*PA (4.50) and *m*PA (4.80) are not very different from that of aniline (4.66).[30] Since the amino group is an electron donating group and it is ortho- and para-directing, it will not change the charge densities at the nitrogen atom of the other $-NH_2$ group in case of *m*PA. Thus the pK_a value for *m*PA will be close to that of aniline, as observed. For *o*PA, it was expected that its value should be greater than that of aniline. However the small decrease in the pK_a value of *o*PA was observed. This may be due to the steric hindrance of the two amino groups adjacent to each other. The high pK_a value for monocation-neutral equilibrium of *p*PA can be explained as follows: Because of the symmetry of the amino groups, the average charge densities at both nitrogen atoms will be same. But at any particular instant, if one of the nitrogen atom becomes more acidic, the other will

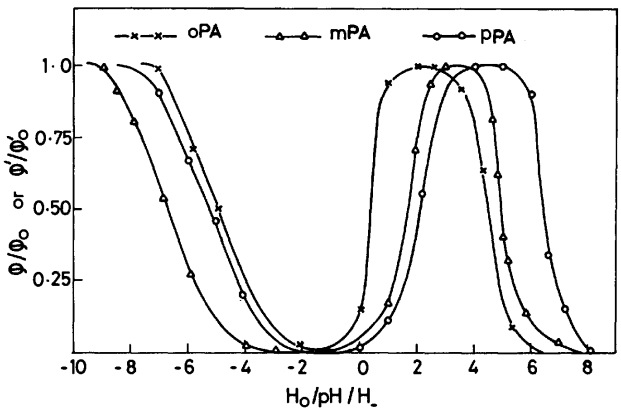

Fig. 4. Plot of relative intensities (ϕ/ϕ_0) vs. H_0/pH/H_- for different phenylenediamines.

Table 3. pK_a Values of Different Equilibria of Phenylenediamines in the S_0 and S_1 States

Equilibrium	pK_a[a]	pK_a[b]	p$K_a(S_1)$[c]	p$K_a(S_1)$[d]	p$K_a(S_1)$[e]
***o*PA**					
Dication-monocation	1.86	1.20	−5.2	−11.5	−5.2
Monocation-neutral	4.65	4.50	2.42	—	4.35[f]
***m*PA**					
Dication-monocation	1.89	2.0	−3.8	−12.6	−6.9
Monocation-neutral	4.86	4.8	3.1	—	4.9[f]
***p*PA**					
Dication-monocation	2.54	2.4	−5.9	−13.1	−5.1
Monocation-neutral	6.11	6.10	1.3	—	6.2[f]

a) Literature value. b) Present work. c, d) Calculated using the Förster cycle method with absorption and fluorescence data respectively. e) Fluorimetric method. f) Apparent pK_a* value.

become more basic and since the steric hindrance is minimum for *p*PA, the pK_a value for the monocation-neutral equilibrium would be the highest, whereas it would be the lowest for neutral-monoanion equilibrium among the diamines.

pK_a^* values for all equilibria have been calculated fluorimetrically (Fig. 4) as well as using the Förster cycle method[27] wherever it is applicable, except for the neutral-monoanion case where both species are nonfluorescent. All values have been compiled in Table 3. For the monocation-neutral equilibrium, the formation curves of the monocations are plotted only because the neutral species are nonfluorescent in aqueous medium. It is clear from Fig. 4 that the fluorimetric titration curves have given only the ground state pK_a values for the monocation-neutral equilibria. Whereas the Förster cycle method, using absorption data only, have shown that the amino group becomes stronger acid on excitation to the first excited singlet state. It is thus concluded that the radiative lifetimes of the neutral and singly protonated species must be too short for proton exchange to occur appreciably within these lifetimes at pH 4—6. Due to this reason the prototropic equilibrium is not established within the lifetimes of the lowest excited singlet states of these molecules. Thus the fluorescence intensities measured at pH ≈4—6 reflect the ground-state concentrations of neutral and monocation species. Consequently, the ground-state pK_a is determined by fluoremetric titrations in this case. Secondly, though the neutral molecules are nonfluorescent, the fluorimetric curves by giving the ground state pK_a values have clearly shown that the proton-induced fluorescence quenching is not observed for the neutral species, before forming the monocations. Otherwise one would have observed a different pK_a value from the formation curve of monocation, if the proton-induced fluorescence quenching of the neutral species had been observed. This behavior is very similar to that observed for 4-(9-anthryl)-*N*,*N*-dimethylaniline by Shizuka et al.[31] Shizuka et al. have clearly shown from their time dependence fluorescence study that the lifetimes of the conjugate acid-base pair is very short, even though the intramolecular charge-transfer state $^1A^*_{CT}$ is very rapidly produced via $^1A^*$. Similar explanation can be offered in the cases of all diamine derivatives of benzene.

In the dication-monocation equilibrium the fluorescence of monocation is quenched in the pH region where the dication is present in the ground state but not fluorescent in the S_1 state. The dications start emitting only below H_0 −4. This behavior is similar to the prototropic reactions of aromatic monoamines and decreases in the fluorescence intensity of monocations is attributed to the proton-induced fluorescence quenching. Thus the pK_a^* values have been calculated from the formation curves of the dications and the values are listed in Table 3. The data of Table 3 clearly indicate that the $-NH_3^+$ group is a stronger acid in the S_1 state than in the S_0 state, consistent with the earlier results.[19,23-26] The pK_a^* values calculated with the help of the Förster cycle method and using absorption and fluorescence data do not agree with each other. This is because: (i) The long wavelength absorption band of monocation is broad whereas that of dication is structured. On the other hand the fluorescence spectrum of both species are broad and structureless, (ii) the solvent relaxation for monocation in the S_1 state is very large in comparison to that observed for dication. This can be seen from the Stokes shift observed for the monocation (≈5960 cm^{-1}) and for the dication (≈1900 cm^{-1}). Thus it can be concluded that pK_a^* values determined by fluorimetric titrations will be more close to the actual values. The pK_a^* values for neutral-monoanion equilibrium cannot be calculated because neither neutral species nor monoanion is emitting.

Proton-Induced Fluorescence Quenching. As said earlier no correspondence is observed between the decrease in the fluorescence intensities of the monocations and the increase in the fluorescence intensities of the dications. This has been attributed to proton-induced fluorescence quenching in the pH range of 1 to 4. This is because the SO_4^{2-} ion concentration (produced by adding K_2SO_4) equivalent to that obtained by the addition of H_2SO_4, do not quench the fluorescence of monocations. The model suggested by Shizuka et al.[32-34] can be transformed to simple Stern-Volmer plot under the conditions that the lifetimes of the

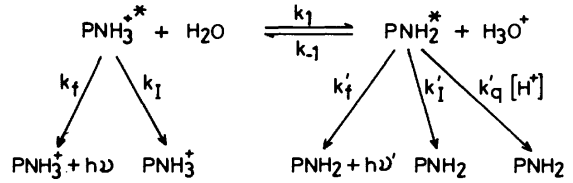

P=Monocations of phenylenediamines

Scheme 1.

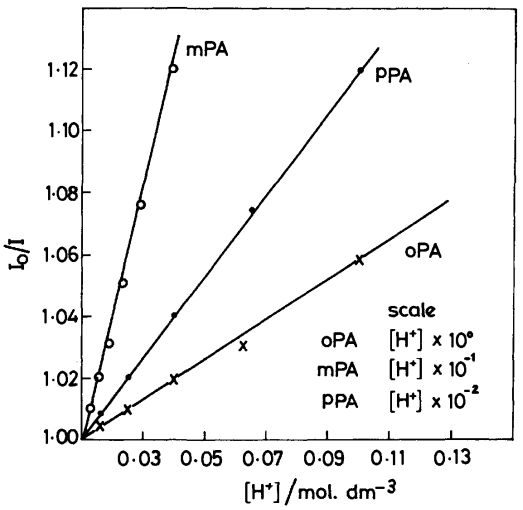

Fig. 5. Stern-Volmer plot for the monocations of different phenylenediamines.

Table 4. Proton Transfer Kinetic Data for Monocations of Different Phenylenediamines

Compd.	$\kappa_q\tau$	τ_{FM}	ϕ_f	τ	κ_q
	$dm^3\,mol^{-1}$	ns		ns	$dm^3\,mol^{-1}\,sec^{-1}$
oPA	0.63	35	0.048	1.68	3.8×10^8
mPA	45	39	0.027	1.1	4.1×10^{10}
pPA	128	45	0.019	0.86	1.5×10^{11}

monocations are short in comparison to those of dications and concentration of H^+ are small to have any backward reaction, dipicted in Scheme I. i.e.

$$\frac{I_0}{I} = 1 + k_q\tau[H^+]$$

where I and I_0 are the fluorescence intensities with and without the quencher respectively, k_q is the proton-induced fluorescence quenching constant and τ is the lifetime of the basic species. I_0/I vs. $[H^+]$ is plotted in Fig. 5 and the $k_q\tau$ values obtained for all three monocations are listed in Table 4. The natural radiative lifetimes of monocation of three diamines are estimated from the corrected fluorescence spectra, using Strickler and Berg's relations.[37] The actual lifetimes are determined from the relation $\tau=\tau_{FM}\,\phi$ where ϕ is the quantum yield of the respective monocation. These values for three species are listed in Table 4. To the first approximation, assuming that the monocations of the three diamines will behave like aniline, the results obtained about the τ_{FM} of monocations of *o*-, *m*-, and *p*- diamines [35, 39, 45 ns respectively] are not very far off from the experimentally determined τ_{FM} of aniline in ethanol (34 ns). The difference in τ is due to the difference in the quantum yields of these species. The smallest lifetime of the para species is due to the larger interactions with solvent molecules which is further manifested by the greater Stoke's shift observed for this species. From our study it is difficult to offer any exact explanation for the large increase in the $k_q\tau$ value in going from the monocation of *o*PA to *p*PA. It may be speculated that steric factor may be playing the major role in the proton-induced fluorescence quenching, although the Stokes shift observed for the monocation of *p*PA is the maximum but do not differ so much from those of other amines if energy of the state has to do anything for this quenching.

Conclusion

Large spectral changes, both in the absorption and fluorescence spectra of *o*PA and *p*PA have clearly indicated that the two amino groups in *p*PA are not in the same plane of the benzene ring. Larger pK_a value for the monocation-neutral equilibrium of *p*PA as compared to *o*PA and *m*PA, indicates that the charge density at the nitrogen atom of amino group is larger than that at the respective atom of other two compounds. In case of *o*PA, the steric hindrance plays the role in having the minimum pK_a value for this equilibrium. Fluorimetric titration curves have indicated that the lifetimes of the monocation-neutral conjugate acid-base pair are quite short to allow the acid-base equilibria in the excited singlet state.

The authors are thankful to the Department of Science and Technology, for the financial support to the project entitled "Proton Transfer reactions in the excited states."

References

1) J. F. Ireland and P. A. H. Wyatt, *Adv. Phys. Org. Chem.*, **12**, 132 (1976).
2) S. G. Schulman, P. T. Tidwell, J. J. Cetorelli, and J. D. Winefordner, *J. Am. Chem. Soc.*, **93**, 3179 (1971).
3) R. Manoharan and S. K. Dogra, *Can. J. Chem.*, in press.
4) W. Bartok, P. J. Lucchesi, and N. S. Snider, *J. Am. Chem. Soc.*, **84**, 1842 (1962).
5) E. L. Wehry and L. B. Rogers, *J. Am. Chem. Soc.*, **87**, 4234, 4237 (1965).
6) J. D. Winefordner, S. G. Schulman, and L. B. Sanders, *Photochem. Photobiol.*, **13**, 381 (1971).
7) E. L. Wehry, *J. Am. Chem. Soc.*, **89**, 41 (1967).
8) R. W. Cowgill, *Photochem. Photobiol.*, **13**, 183 (1971).
9) J. W. Bridges and R. T. Williams, *Biochem. J.*, **107**, 225 (1968).
10) D. V. S Jain, F. S. Nandel, and Prem Lata, *Indian J. Chem*, **21A**, 559 (1982).
11) R. S. Sarpal and S. K. Dogra, *J. Photochem.*, **38**, 263 (1987).
12) B. S. Furniss, A. J. Hannaford, V. Rogers, P. W. G. Smith, and A. R. Tatchett, "Vogel's Text Book of Practical Organic Chemistry," ELBS, London (1980), p. 660.
13) J. G. F. Druce, *J. Chem Soc.*, **113**, 715 (1918).
14) J. A. Riddick and W. B. Bunger, "Organic Solvents," Wiley Interscience, New York (1970), pp. 592—594, 798—805.
15) M. J. Jorgenson and D. R. Hartter, *J. Am. Chem. Soc.*, **85**, 878 (1963).
16) G. Yagil, *J. Phys. Chem.*, **71**, 1034 (1967)
17) M. Swaminathan and S. K. Dogra, *Indian J. Chem.*, **22A**, 853 (1983).
18) S. R. Meech and D. Phillips, *J. Photochem.*, **23**, 193 (1983).
19) A. K. Mishra and S. K. Dogra, *J. Photochem.*, **23**, 163 (1983); *J. Chem. Soc., Perkin Trans. 2* **1984**, 943.
20) C. P. Smyth, "Dielectric Behaviour and Structure," McGraw Hill, New York (1955), pp. 326—333.
21) I. B. Berlman, "Hand book of Fluorescence Spectra of Aromatic Molecules," Academic Press, New York (1965), pp. 59, 60.
22) F. A. Matsen, R. S. Becker, and D. R. Scott, "Techniques of Organic Chemistry," ed by W. West, Wiley Inter-

science, New York (1968), Vol. IX, p. 261.
23) A. K. Mishra and S. K. Dogra, *Indian J. Chem.*, **24A**, 285 (1985); **24A**, 364 (1985); *Bull. Chem. Soc. Jpn.*, **58**, 3587 (1985); *J. Photochem.*, **31**, 333 (1985).
24) M. Swaminathan and S. K. Dogra, *J. Am. Chem. Soc.*, **105**, 6223 (1983); *Can. J. Chem.*, **61**, 1064 (1983).
25) P. Phaniraj, A. K. Mishra, and S. K. Dogra, *Indian J. Chem.*, **24A**, 913 (1985).
26) R. V. Subba Rao, M. Krishnamurthy, and S. K. Dogra, *J. Photochem.*, **24**, 55 (1986); *Indian J. Chem.*, **25A**, 917 (1986).
27) Th. Förster, *Z. Elektrochem.*, **54**, 42 (1950).
28) U. K. Pandey, N. B. Joshi, and D. D. Pant, *Chem. Phys. Lett.*, **72**, 209 (1980).
29) "Dictionary of Organic Compounds," ed by J. Bukingham, 5th ed, Chapman and Hall (1982), pp. 1529, 1530.
30) D. D. Perrin, "Dissociation Constants of Organic bases in Aqueous Solutions," Butter Worths, London (1965), p. 58.
31) H. Shizuka, T. Ogiwara, and E. Kimura, *J. Phys. Chem.*, **89**, 4302 (1985).
32) K. Tsutsumi and H. Shizuka, *Chem. Phys. Lett.*, **52**, 485 (1977); *Z. Phys. Chem., N.F.*, **111**, 129 (1978); *J. Photochem.*, **9**, 334 (1978); *Z. Phys. Chem., N.F.*, **122**, 129 (1980).
33) H. Shizuka, K. Tsutsumi, H. Takeuchi, and I. Tanako, *Chem. Phys. Lett.*, **62**, 408 (1979).
34) K. Tsutsumi, S. Sekiguchi, and H. Shizuka, *J. Chem. Soc., Faraday Trans. 1*, **78**, 1087 (1982).
35) H. Shizuka and S. Tobika, *J. Am. Chem. Soc.*, **104**, 6919 (1982).
36) H. Shizuka, *Acc. Chem. Res.*, **18**, 141 (1985).
37) S. J. Strickler and R. A. Berg, *J. Chem. Phys.*, **37**, 814 (1962).

Mass Spectral and Pyrolytic Studies of Some 4,4-Disubstituted 1,4-Dihydro-2*H*-3,1-benzoxazin-2-ones

Baman Prasad ACHARYA, Bijaya Kumar MISRA, and Yerramalli Ramachandra RAO*
Regional Research Laboratory, Bhubaneswar-751013, India
(Received August 21, 1986)

Pyrolysis of 4,4-diaryl-1,4-dihydro-2*H*-3,1-benzoxazin-2-ones at 230—240 °C gives 9-arylacridines and (2-aminophenyl)diarylmethanes. Their formation correlates well with the mass fragmentation of the respective parent compounds.

Benzazetin-2(1*H*)-ones (**1**) have been postulated as reactive intermediates in the pyrolysis and photolysis of isatoic anhydride and 3-substituted 1,2,3-benzotriazin-

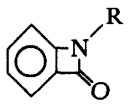

1

4(3*H*)-ones;[1,2] their formation during the mass fragmentation has also been observed. We had prepared some 4,4-diaryl-1,4-dihydro-2*H*-3,1-benzoxazin-2-ones (**2**) by Friedel-Crafts acylation of arenes with 2-isocyanatobenzoyl chlorides.[3,4] Their mass spectra show appearance of peaks at *m/z* M^+-44 and M^+-45 which are characteristic of these benzoxazinones **2**. In Table 1 are given prominent fragment ions with relative abundances and the fragmentation pattern is depicted in Chart 1.

It is observed that these benzoxazinones decompose at their melting points and in view of the known corre-

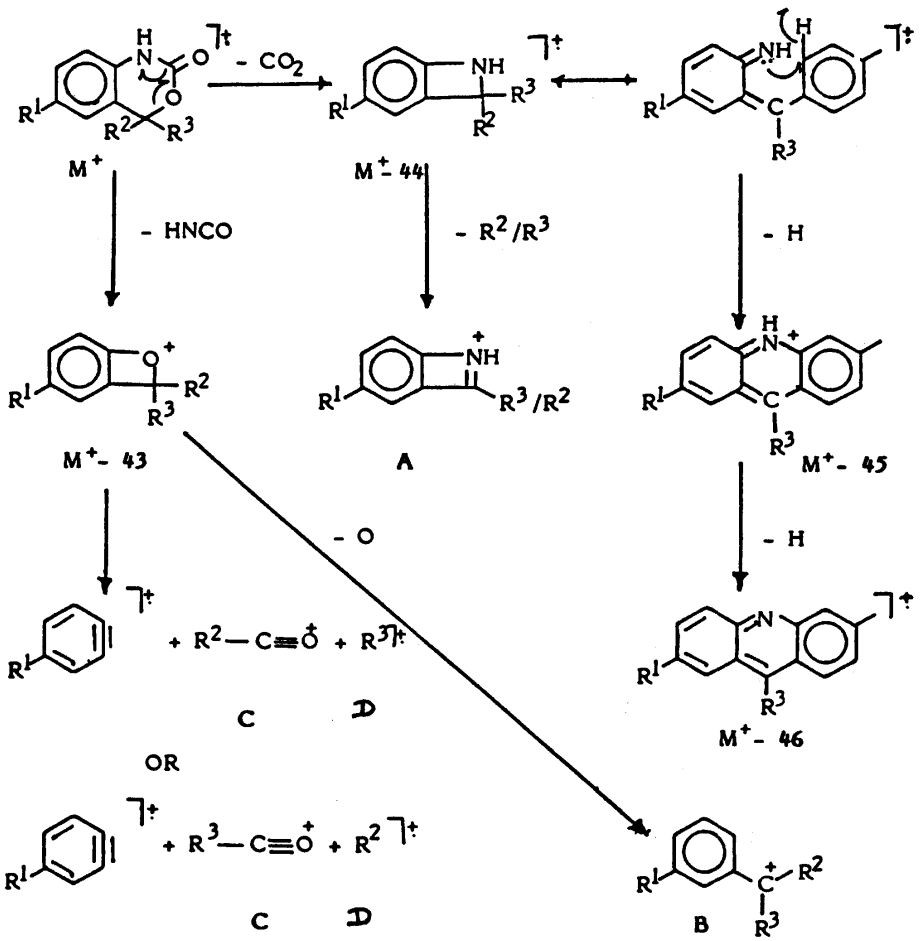

	R^1	R^2	R^3		R^1	R^2	R^3
a)	H	C_6H_5	C_6H_5	e)	H	C_6H_5	C_6H_4-OCH_3 (*p*)
b)	H	C_6H_4-CH_3 (*p*)	C_6H_4-CH_3 (*p*)	f)	Cl	C_6H_5	C_6H_5
c)	H	C_6H_4-OCH_3 (*p*)	C_6H_4-OCH_3 (*p*)	g)	H	C_6H_5	OCH_3
d)	H	C_6H_5	C_6H_4-CH_3 (*p*)	h)	H	C_6H_5	OC_2H_5

Chart 1.

Table 1. Prominent Ions Found in the Mass Spectra of 4,4-Disubstituted 1,4-Dihydro-2*H*-3,1-benzoxazin-2-ones. Percentage of Relative Abundances are Mentioned in Parentheses

	Compound **2**	M^+	M^+-43	M^+-44	M^+-45	M^+-46	Other fragment			
							A	B	C	D
a)	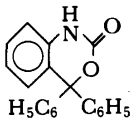	301 (2)	258 (10)	257 (47)	256 (100)	255 (14)	180 (30)	—	105 (5)	77 (10)
b)	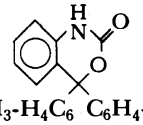	329 (2)	286 (10)	285 (45)	284 (95)	283 (15)	194 (55)	270 (100)	119 (11)	91 (18)
c)	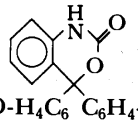	361 (2)	318 (15)	317 (50)	316 (100)	315 (62)	210 (65)	302 (47)	135 (11)	107 (15)
d)	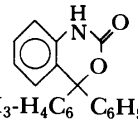	315 (4)	272 (10)	271 (46)	270 (100)	269 (20)	194(30) 180(28)	256 (70)	119(12) 105(10)	77 (12)
e)	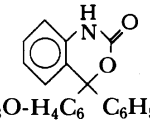	331 (2)	288 (10)	287 (40)	286 (100)	285 (30)	210(33) 180(26)	272 (40)	135(9) 105(11)	77(15) 107(5)
f)	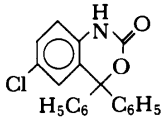	335 (7)	292 (40)	291 (42)	290 (100)	289 (10)	214 (3)	—	105 (13)	77 (24)
g)	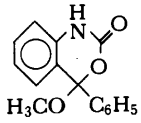	255 (4)	—	211 (59)	210 (100)	—	196 (37)	180 (35)	—	—
h)	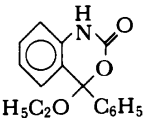	269 (2)	226 (6)	225 (37)	224 (52)	223 (5)	196 (100)	180 (39)	—	—

lation of pyrolytic and electron impact reactions of some of the closely related compounds viz isatoic anhydride and 3-substituted 1,2,3-benzotriazin-4(3*H*)-ones, it is of interest to study the pyrolysis and photolysis of these 4,4-disubstituted benzoxazinones **2**; we report here the results of these investigations.

When the benzoxazinones (**2a, b, f**) are pyrolyzed at 230—240 °C without solvent, 9-arylacridines (**3a, b,** f) are obtained in 45—60% yield along with (2-aminophenyl) diarylmethanes (**4a, b,** f†) in 10—25% yield. These are separated by column chromatography and identified through their spectral data and comparison with authentic samples[6,7] wherever possible. The formation of **3** and **4** from the above pyrolysis reaction is depicted in Scheme 1.

It is likely that the two hydrogen atoms lost in the final step of formation of **3** add to the intermediate **5**. In order to verify this, the benzoxazinone (**2a**) is pyrolyzed in presence of hydrogen donors such as sodium borohydride and hydroquinone; however, no improvement in the yield of **4** is observed and products with the same relative distribution are obtained. Pyrolysis carried out in the presence of nucleophile e.g. methyl anthranilate also did not produce any additional product.

When 4-methoxy-4-phenyl-1,4-dihydro-2*H*-3,1-benzoxazin-2-one (**2g**) is pyrolyzed at 230 °C, it afforded 2-aminobenzophenone (**6**, 49%) and 6,12-diphenyldibenzo(*b,f*)(1,5)diazocine (**7**, 8.5%). The formation of dibenzodiazocine **7** seems to be through the dimerization of the

† **4f** was not isolated, but observed on TLC only.

intermediate **5g** (Scheme 2) similar to the dimerization observed in the pyrolysis of isatoic anhydride and 1,2,3-benzotriazin-4(3*H*)-one reported earlier.[1,2]

Although these benzoxazinones **2** afforded the expected products on pyrolysis, they are found to be quite stable to photolysis and are recovered back unchanged after irradiation in a Hanovia reactor with a 400 W lamp for 24 h.

In the case of **2a, b, f**, no dimerization product is obtained, whereas dimerization products are invariably obtained in the reactions of isatoic anhydride and 3-substituted 1,2,3-benzotriazin-4(3*H*)-ones. This is probably due to the stabilization of the intermediate **5** by extended mesomeric interaction with the aromatic residue. No evidence for either the free radical or ionic mechanisms could be obtained as the product composition did not change when the pyrolysis is carried out in the presence of hydroquinone, a known free radical trap or sodium borohydride. However, in view of the correlation with the mass fragmentations, the free radical mechanism is preffered.[5] Formation of no other additional product in the presence of methylanthranilate supports this view. In the case of **2g** however, the intermediate **5g** dimerises to some extent and dibenzodiazocine **7** is obtained (Scheme 2).

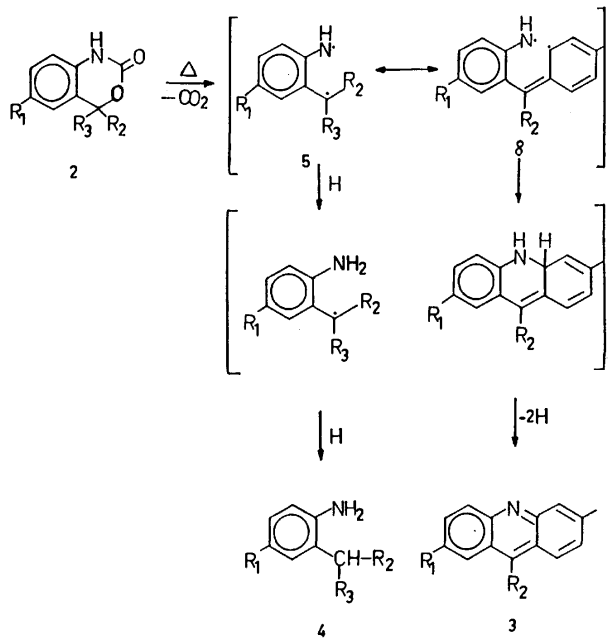

Scheme 1.

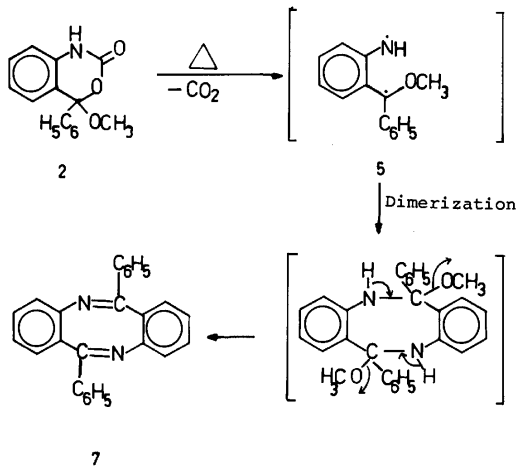

Scheme 2.

Experimental

4,4-Disubstituted 1,4-dihydro-2*H*-3,1-benzoxazin-2-ones (**2**) are prepared according to the known procedure.[3,4] Yields are given after crystallization. Melting points reported are not corrected.

General Procedure of the Pyrolysis of 4,4-Disubstituted 1,4-Dihydro-2*H*-3,1-benzoxazin-2-ones (2): 4,4-Disubstituted 1,4-dihydro-2*H*-3,1-benzoxazin-2-ones (**2**) were pyrolyzed without solvent in an open mouth round bottomed flask at 230—240 °C for 3 h. After cooling, the mass was taken up in benzene (10 ml), filtered to remove the unreacted **2**, which remained insoluble and the filtrate was subjected to column chromatography on silica gel by successively eluting with benzene-hexane (1 : 1), benzene, and benzene-ethyl acetate (9 : 1) when (2-aminophenyl)diarylmethanes (**4**), 9-arylacridines (**3**) and some unreacted **2** were obtained in the same order of elution. These compounds were further purified by recrystallization.

Pyrolysis of 4,4-Diphenyl-1,2-dihydro-2*H*-3,1-benzoxazin-2-one (2a): The captioned compound **2a** (750 mg) was pyrolyzed as above; the following compounds were obtained:

(i) (2-Aminophenyl)diphenylmethane (**4a**) (180 mg, 28%), mp 127 °C (benzene-hexane), lit,[6] 126—128 °C; IR (Nujol) ν_{max} 3470, 3375, and 1610 cm^{-1}; MS *m/z* (rel intensity) 259 (M^+, 100), 258 (19), 182 (37), 181 (8), 180 (28), 167 (9), 91 (3). Found: C, 88.096; H, 6.552; N, 5.13%. Calcd for $C_{19}H_{17}N$: C, 88.031; H, 6.564; N, 5.405%.

(ii) 9-Phenylacridine (**3a**) (280 mg, 44%), mp 184 °C (benzene-hexane), lit,[7] 185 °C; MS *m/z* (rel intensity) 255.3 (M^+, 100), 254.3 (86.6), 253.3 (17.7), 252.3 (11.5), 251.2 (6.4), 227.2 (6.8), 226.2 (11.1), 127.2 (20.8), 126.2 (20.2), 113.2 (12.4). Found: C, 89.412; H, 5.098; N, 5.49%. No absorptions in the NH and carbonyl region are observed in the IR spectrum.

(iii) Unreacted **2a**. (130 mg).

Pyrolysis of 4,4-Di-*p*-tolyl-1,4-dihydro-2*H*-3,1-benzoxazin-2-one (2b): Analogously, pyrolysis of **2b** (350 mg) yielded.

(i) (2-Aminophenyl)di-*p*-tolylmethane (**4b**) (20 mg, 7%), semisolid, purified by passing over a short column of silica gel; IR (Nujol) ν_{max} 3450, 3360, 1610 cm^{-1}; MS *m/z* 287 (M^+, 100), 286 (11), 196 (40), 195 (19), 194 (57), 91 (49). Found: C, 87.52; H, 7.262; N, 4.87%. Calcd for $C_{21}H_{21}N$: C, 88.05; H, 7.317; N, 4.88%.

(ii) 2-*p*-Tolyl-3-methylacridine (**3b**) (210 mg, 70%), mp 143 °C (methanol); MS *m/z* (rel intensity) 283.3 (M^+, 100), 282.3 (18.2), 281.3 (5), 280.3 (4), 279.3 (1.6), 254.2 (2.4), 141.2 (29), 140.2 (2.7), 127.1 (19). Found: C, 89.049; H, 6.06; N, 4.8%. Calcd for $C_{21}H_{17}N$: C, 89.049; H, 6.007; N, 4.94%. IR spectrum shows no absorptions in the NH or carbonyl regions.

(iii) Unreacted **2b** (80 mg).

Pyrolysis of 6-Chloro-4,4-diphenyl-1,4-dihydro-2*H*-3,1-benzoxazin-2-one (2f): From the pyrolysis of the captioned compound **2f** (400 mg), were obtained 2-chloro-9-phenylacridine (**3f**) (210 mg, 64.5%), mp 133 °C (methanol); MS *m/z*

(rel intensity) 289.3 (M^+, 100), 288.3 (18.7), 254.3 (52), 253.3 (23.2), 252.3 (11.7), 251.3 (10), 227.2 (5), 144.8 (2.6), 127.2 (16.6), 125.8 (20.8). Found : C, 78.78; H, 4.087; N, 4.79%. Calcd for $C_{19}H_{12}ClN$: C, 78.893; H; 4.152; N, 4.847%. Its IR spectrum has no absorptions in the carbonyl or NH regions.

Unreacted **2f** (130 mg) from the column was recovered.

Pyrolysis of 4-Methoxy-4-phenyl-1,4-dihydro-2*H*-3,1-benzoxazin-2-one (2g): The above compound **2g** (500 mg) when pyrolyzed at 235 °C yielded.

(i) 6,12-Diphenyldibenzo[*b,f*][1,5]diazocine (**7**) (30 mg, 8.5%), mp 188 °C (methanol). Lit,[3] 186—188 °C, found to be identical with an authentic sample by mixed mp and superimposable IR spectrum.

(ii) 2-Aminobenzophenone (**6**) (190 mg, 49%), mp and mixed mp 106 °C (methanol).

(iii) Unreacted **2g** (75 mg).

Pyrolysis of 2a in Presence of Hydroquinone or Sodium Borohydride: The compound **2a** (300 mg, 0.001 mol) was pyrolyzed in presence of hydroquinone (1.1 g, 0.01 mol) at 235 °C for 3 h. After usual work up, were isolated **4a** (75 mg, 27%), **3a** (110 mg, 43%) and unreacted **2a** (50 mg).

Similar result wes obtained when the reaction is carried out in the presence of sodium borohydride also.

Pyrolysis of 2a in Presence of Methyl Anthranilate: A mixture of **2a** (300 mg, 0.001 mol) and methyl anthranilate (1.51 g, 0.01 mol) was heated for 3 h at 235 °C. After usual workup, was obtained **3a** (120 mg, 47%). **4a** was observed on TLC but could not be separated from the unreacted methyl anthranilate.

Photochemical Reaction of 4,4-Diphenyl-1,4-dihydro-2*H*-3,1-benzoxazin-2-one (2a): A solution of **2a** (300 mg) in methanol (400 ml) was irradiated with 400 W ultraviolet lamp in s Hanovia photochemical reactor, with Pyrex filter for 6 h. After one hour, the color of the solution changed to yellow. However, TLC at the end of 6 h showed no change, it was further irradiated for additional 18 h. Even then, no change was observed and the parent compound **2a** (275 mg, 90%) was recovered back after removal of solvent by distillation.

Similar observation of stability to UV irradiation was observed in the case of **2g** also.

We thank Dr. M. Bapuji for his help in recording the mass spectra at the Technical University, West Berlin and Professor P. K. Jena, Director, Reginal Research Laboratory, Bhubaneswar for awarding a fellowship to BPA.

References

1) T. Kappe and W. Stadlbauer, "Advances in Heterocyclic Chemistry," ed by A. R. Katritzky and A. J. Boulton, Academic Press, New York (1981), Vol. 28, p. 140.

2) R. J. Kobylecki and A. McKillop, "Advances in Heterocyclic Chemistry," Vol. 19, 254 (1976) and references cited therein.

3) B. K. Misra, Y. R. Rao, and S. N. Mahapatra, *Indian J. Chem.*, **22B**, 1132 (1983).

4) B. P. Acharya and Y. R. Rao, *J. Chem. Res., (S)*, **1987**, 96; *J. Chem. Res. (M).*, **1987**, 1001.

5) We thank the referee for suggesting the free radical mechanism.

6) P. A. Petynuin and N. G. Panterova, *Zh. Obsch. Khim.*, **26**, 3191 (1956); *Chem. Abstr.*, **51**, 8745 (1957).

7) C. J. Bickelhaupt, P. D. Koe, R. Lourens, L. R. Mast, G. L. V. Mourin, H. Vermeer, and R. J. M. Weustink, *Tetrahedron*, **32**, 1921 (1976).

 © 1987 The Chemical Society of Japan Bull. Chem. Soc. Jpn., 60, 4421—4423 (1987)

Conformations of Some Monosubstituted *N*-Benzylideneanilines

Lalit N. PATNAIK* and Sarojini DAS
Department of Chemistry, Ravenshaw College, Cuttack 753003, India
(Received August 23, 1986)

Theoretical computations , using quantum mechanical PCILO method, have been carried out on the conformations of four monosubstituted *N*-benzylideneanilines—*N*-benzylidene-4-nitroaniline (**1a**), *N*-benzylidene-4-dimethylaminoaniline, *N*-(4-nitrobenzylidene)aniline, and *N*-(4-dimethylaminobenzylidene)-aniline. The aniline ring is found to be most twisted (60°) in **1a**, while in all other cases , the twist angle is 30°. The results have been compared with earlier experimental findings and rationalized in terms of two factors contributing to nonplanarity , namely , the overlapping of bridge nitrogen lone pair with the π-system of the aniline ring and a steric interaction between the azomethine hydrogen and one of the ortho hydrogens in the aniline ring.

Experimental and theoretical studies on the molecular conformation of *N*-benzylideneanilines have been reported by a number of workers.[1-5] These studies were initially meant to account for the marked dissimilarity in the electronic absorption spectra of *N*-benzylideneanilines (**BA**) and the isoelectronic molecules stilbene (**S**) and azobenzene (**AB**). It is now generally agreed that the difference arises on account of nonplanar conformation of *N*-benzylideneaniline in contrast to the nearly planar structure of azobenzene and stilbene.

We have reported earlier the results of theoretical (perturbative configuration interaction over localized orbitals, PCILO) computations on the conformation of *N*-(4-dimethylaminobenzylidene)-4-nitroaniline (**1e**), *N*-(4-nitrobenzylidene)-4-dimethylaminoaniline (**1f**), and the corresponding stilbene (**2**) and azobenzene (**3**) derivatives.[6] The computed conformations were rationalized in terms of two factors that facilitate the nonplanar structure: i) An interaction of the nitrogen lone pair and the aromatic system (CT-2)[7] and ii) repulsion between the hydrogen in -CH=N- and one of the ortho hydrogens of the aniling ring, which is released by the twisting of the *N*-phenyl bond. On the other hand there could also be intramolecular charge transfer between the substituents (CT-1). Smaller the twist angle, larger is the contribution of CT-1.[7]

Recently, Akaba et al. have reported the results of their NMR (Proton and ^{13}C) studies on mono- and di-(in the two aromatic rings) substituted *N*-benzylideneanilines.[4,5] The nonadditivity of substituent effect observed for **1** (X=NMe_2) and **1** (Y=NO_2) is interpreted in terms of substituent-substituent interactions (synonimous with CT-1, described earlier) accompanied by conformational changes with substituents in these *N*-benzylideneanilines. It was found that for *N*-benzylideneanilines carrying the variable substituent X on the anilinobenzene ring, the azomethine protons undergo upfield shifts with increasing electron-withdrawing property of X, whereas those for *N*-benzylideneanilines carrying the variable substituent Y on the benzylidene benzene ring exhibited the expected low field shifts with increasing electron-withdrawing property of Y. This anomalous upfield shift of the azomethine proton has been attributed to the increase in the twist angle of the aniline ring from the molecular plane containing -C=N- bond.

The theoretical and experimental facts accumulated so far indicate that the substitution in the rings is an important factor in determining the twist angles Φ and θ. Most spectroscopists, however, seem to emphasize that the origin of nonplanarity can be attributed to the

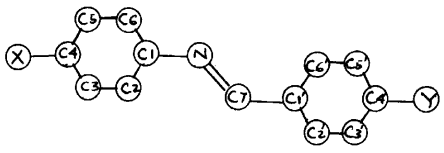

1a: X=NO_2; Y=H
1b: X=NMe_2; Y=H
1c: X=H; Y=NO_2

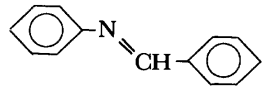

(**BA**)

1d:X=H; Y=NMe_2
1e: X=NO_2; Y=NMe_2
1f: X=NMe_2; Y=NO_2

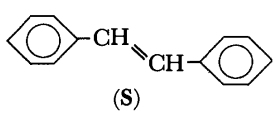

(**S**)

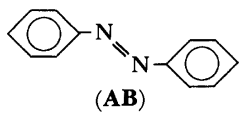

(**AB**)

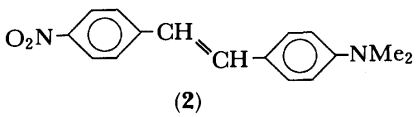

(**2**)

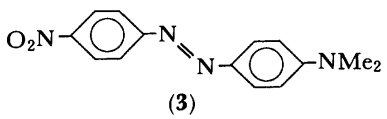

(**3**)

delocalization of the azomethine lone pair. We report here the theoretical computations of the conformations of four monosubstituted *N*-benzylideneanilines (**1a—d**). A preliminary communication of this work was made earlier[6] as corroborating evidence in favour of our contention that *N*-benzylideneaniline conformations depend both, on the delocalization of the bridge nitrogen lone pair and ortho hydrogen interactions. The present paper deals with a detailed report on the conformational energetics of these molecules and a comparison of the computed results with earlier findings that illustrates an interesting interplay between theory and experiment.

Procedure

Among the more recently developed theoretical methods for all-valence electrons, PCILO is extensively used in conformational studies, because of its proven success with quite diverse types of molecules.[8-14] This method was therefore chosen for present work. It may, however, be mentioned that the PCILO method requires the choice of definite pattern of localized chemical bonds. The investigation under report deals with molecules involving delocalized bonds. Difficulties, that may arise in the calculations on such molecules within the PCILO framework have been discussed in some detail in our earlier communications.[6,15]

The torsion angles have been indicated in the structures **1** and are defined as

$$\Phi = C_2\text{-}C_1\text{-}N\text{-}C_7$$
$$\theta = N\text{-}C_7\text{-}C_{1'}\text{-}C_{2'}$$

the clockwise direction being positive. The cis and trans dihedral angles have been taken as 0 and 180°, respectively.

Since it is considered that the theoretical equilibrium geometry in the gas phase is closer to the standard geometry rather than X-ray values, we have adopted the standard geometries from People and Beveridge.[16] All bond angles involving sp^2 and sp^3 hybrid orbitals, have been taken as 120 and 109.47°, respectively.

The PCILO energies have been computed as a function of Φ and θ at 30° intervals with preselected values of the other geometrical parameter.

Results and Discussion

***N*-Benzylidene-4-nitroaniline (1a):** There are four reports on the conformation of **1a**. Skrabal and collaborators[17] from a comparison of its electronic absorption spectra with *N*-benzylideneaniline, have proposed that the twist angle of the aniline ring (Φ) should be of the same order as that in case of *N*-benzylideneaniline, which is 55°. Theoretical calculations (CNDO/s) and UV spectral studies by Akaba et al. indicate Φ=70—85° and that the twist of the aniline ring in soln and gas phase is more than *N*-benzylideneaniline itself.[1] This contention was further confirmed from the photoelectron spectra.[2] From NMR measurements on substituted *N*-benzylideneanilines, it was proposed that the introduction of the electron-withdrawing nitro group at the 4-position of the aniline ring enhances the delocalization of nitrogen (of -N=CH-) lone pair electrons into the ring that leads to an increase in the value of Φ in solution which in turn changes the ring current effect by the aniline ring exerted on HC (7) resulting in an anomalous upfield shift.[5]

Results of the present computations show that the aniline ring in **1a** is twisted by 60° in either directions. The rotational energy barrier with respect to the planar conformation is 1.96 kcal mol^{-1} (1 cal=4.184J). It is seen from the results described in Table 1, Φ=30 to 90° through 60°, represents low energy regions indicating that the molecule has a good deal of conformational flexibility in this region. This situation is sim-

Table 1. Preferred Conformations of Monosubstituted *N*-Benzylideneanilines

Molecule	Energy of the planar conformation	Global minimum		Low-energy regions		
	kcal mol^{-1}	Φ/deg	θ/deg	Φ/deg	θ/deg	Energy kcal mol^{-1}
1a		60	0	30	0	0.28
	1.96	−60	0	−30	0	0.28
				90	0	0.53
				−90	0	0.53
1b	1.53	30	0	60	0	0.82
		−30	0	−60	0	0.82
1c	1.51	30	0	60	0	0.06
		−30	0	−60	0	0.06
				90	0	0.78
				−90	0	0.78
1d	1.54	30	0	60	0	0.16
		−30	0	−60	0	0.16

ilar to the value of Φ=70—85°, proposed by Akaba et al.[1] PCILO calculations on *N*-benzylideneaniline itself give value of 36° of Φ.[12] Thus, it is seen that theoretical computations and spectral measurements (UV, PES, and NMR) lead to the same conclusion that the aniline ring in **1a** is more twisted than *N*-benzylideneaniline.

***N*-Benzylidene-4-dimethylaminoaniline (1b)**: UV absorption spectra by Skrabal et al.[17] reveal only a small torsion angle for the aniline ring in **1b**. Although the NMR work is not very explicit about the conformational state of this particular molecule, it appears by implication that two opposite factors will operate here (a) in the absence of any electron-attracting substituent at the 4-position on the benzylidene ring, the through-conjugative interaction is obviously impaired leading to less planarity and (b) on the other hand, presence of the electron-donating dimethylamino group would lead to a smaller twist angle, Φ.

The present computational results indicate the aniline ring to be twisted out of plane by ±30°. This conformation is of 1.53 kcal mol^{-1} higher energy than the planar conformation. The low energy region is confined to ±60° with an energy barrier of 0.82 kcal mol^{-1}. These results clearly indicate that there must, at least, be one more factor contributing to nonplanarity, besides the delocalization of the nitrogen lone pair. As described in our earlier work,[6] we identify the factor as the interaction between HC(2) and HC(7).

***N*-(4-Nitrobenzylidene)aniline (1c)**: For **1c**, a torsion angle similar to BA is predicted from UV results,[17] which means $\Phi\approx$55°. HMO calculations by Minkin[18] give Φ=44°. We find the value of Φ=±30° from present calculations. The energy barrier with respect to the planar structure is 1.51 kcal mol^{-1}. However, it is seen from Table 1 that the region Φ=±60° is only of 0.06 kcal mol^{-1} higher energy. Since an energy barrier of this magnitude can easily be overcome in the solution or solid state, it may be concluded that the experimental (UV) and the theoretical conformations lead to the same result.

***N*-(4-Dimethylaminobenzylidene)aniline (1d)**: From the UV spectral study, **1d** is found to be more or less planar. The results are, however, not unambiguous. The present calculation shows that the aniline ring is twisted out of plane by ±30° with a rotational energy barrier of 1.54 kcal mol^{-1}. The low energy region is indicated by Φ=±60°, which is only of 0.16 kcal mol^{-1} higher energy.

It can be seen from Table 1 that the results with respect to **1b—d** are strikingly similar. This implies that perhaps there is a common mechanism that determines the conformational characteristics of these molecules and it appears most rational that this mechanism is the interaction between the ortho hydrogen HC(2) and HC(7), since in all the three cases, CT 1 (π-electron delocalization between the substituents) and CT 2 (delocalization of the nitrogen lone pair to the substituent in the aniline ring) will either be extremely weak or altogether absent. This hypothesis is supported by the results obtained with respect to **Ia**. In this molecule there can be a substantial overlapping of the *N*-lone pair with the aniline ring bearing the strongly electron-withdrawing NO_2 group (CT 2) which reinforces the nonplanar structure due to ortho hydrogen interaction leading to a greater twist angle Φ (=60°).

The authors are grateful to Dr. Anil Saran of the Tata Institute of Fundamental Research, Bombay, for many helpful discussions and to the Department of Atomic Energy, Government of India for the award of a research grant for computation and fellowship to one of them (S.D.).

References

1) R. Akaba, K. Tokumaru, and T. Kobayashi, *Bull. Chem. Soc. Jpn.*, **53**, 1993 (1980) and references therein.
2) R. Akaba, K. Tokumaru, T. Kobayashi, and C. Utsunomiya, *Bull. Chem. Soc. Jpn.*, **53**, 2002 (1980).
3) R. Akaba, H. Sakuragi, and K. Tokumaru, *Bull. Chem. Soc. Jpn.*, **58**, 301 (1985).
4) R. Akaba, H. Sakuragi, and K. Tokumaru, *Bull. Chem. Soc. Jpn.*, **58**, 1186.(1985).
5) R. Akaba, H. Sakuragi, and K. Tokumaru, *Bull. Chem. Soc. Jpn.*, **58**, 1711 (1985).
6) L. N. Patnaik and S. Das, *Int. J. Quantum Chem.*, **27**, 135 (1985).
7) H. Nakai, M. Shiro, K. Ezumi, S. Sakata, and T. Kubota, *Acta Crystallogr. Sect. B*, **32**, 1827 (1976).
8) S. Diner, J. P. Malrien, and P. Claverie, *Theor. Chim. Acta*, **13**, 1 (1969).
9) F. Jordan, M. Gilbert, J. P. Malrien, and U. Pincelli, *Theor, Chim. Acta*, **15**, 211 (1971).
10) D. Perahia and A. Pullman, *Chem. Phys. Lett.*, **19**, 73 (1973).
11) B. Pullman and A. Saran, *Prog. Nucl. Acid Res. Mol. Biol.*, **16**, 215 (1976).
12) P. Jacques and J. Faure, *Theor. Chim. Acta*, **46**, 307 (1977).
13) A. Goursot, P. Jacques, and J. Faure, *J. Chem. Phys.*, **20**, 319 (1977).
14) A. Saran, *Int. J. Quantum Chem.*, **20**, 439 (1981).
15) L. N. Patnaik and S. Das, *Tetrahedron*, **41**, 4961 (1985).
16) J. A. People and D. L. Beveridge, "Approximate Molecular Orbital Theory," McGraw-Hill, New York (1970), p. 111.
17) P. Skrabal, J. Steiger, and H. Zollinger, *Helv. Chim. Acta*, **58**, 800 (1975).
18) V. I. Minkin, Yu. A. Zhadanov, E. A. Medyantzeva, and Yu. A. Ostroumov, *Tetrahedron*, **23**, 3651 (1967).

Synthesis of Pyrano[4,3-*c*]pyrazol-4(1*H*)-ones and -4(2*H*)-ones from Dehydroacetic Acid. Homo- and Heteronuclear Selective NOE Measurements for Unambiguous Structure Assignment

Albert CANTOS, Pedro de MARCH, Marcial MORENO-MAÑAS,* Anna PLA, Francisco SANCHEZ-FERRANDO,* and Albert VIRGILI
Departament de Química. Universitat Autnoma de Barcelona, Campus de Bellaterra, 08193 Barcelona, Spain
(Received October 20, 1986)

Cyclization of dehydroacetic acid *N*-substituted hydrazones furnished 1-substituted 3,6-dimethylpyrano-[4,3-*c*]pyrazol-4(1*H*)-ones, together with varying amounts of *N*,*N*'-disubstituted 5-hydroxy-3-methyl-4-(3-methyl-1*H*-pyrazol-5-yl)-1*H*-pyrazoles. The same pyranopyrazolones were obtained regioselectively without side reactions from *N*-alkylhydrazines and 4-chloro-3-(1-chlorovinyl)-6-methyl-2*H*-pyran-2-one, ("Dehydroacetchlorid"), while *N*-arylhydrazines gave the 2-aryl-3,6-dimethylpyrano[4,3-*c*]pyrazol-4(2*H*)-ones. NMR NOE methods, including long-range selective heteronuclear $^{13}C\{^1H\}$ NOE enhancement measurements, allowed unambiguous distinction between -4(1*H*)-ones and -4(2*H*)-ones.

The reactions of dehydroacetic acid **1** and derivatives with hydroxylamine or hydrazines are a rich source of several types of heterocycles[1] (Scheme 1). Thus, the initially formed oxime **2** or hydrazones **3** have been converted into 3,6-dimethyl-4*H*-pyrano[3,4-*d*]isoxazol-4-one (**4**)[2] or into pyrano[4,3-*c*]pyrazol-4(1*H*)-ones (**5**),[3] 4-acetoacetyl-2,4-dihydro-5-methyl-3*H*-pyrazol-3-ones (**6**),[4] 2,4-dihydro-5-methyl-3*H*-pyrazol-3-ones (**7**)[5] or their formal condensation dimers 5-hydroxy-3-methyl-4-(3-methyl-1*H*-pyrazol-5-yl)-1*H*-pyrazoles (**8**),[3,4] pyrano[2,3-*c*]pyrazol-4(1*H*)-ones (**9**),[4] and 5-(2-oxopropyl)-1*H*-pyrazole-4-carboxylates (**10**).[3b,c] 4-(5-Isoxazolyl)isoxazole (**11**) has also been reported[6] from reaction of **1** with hydroxylamine. Even the formation of 5-anilino-1,5-dihydro-3,6-dimethyl-1-phenyl-4*H*-pyrazolo[4,3-*c*]pyridin-4-one from **1** and phenylhydrazine was once claimed,[7] although this reaction was later shown[4] to afford only **8b**. Depending upon the reaction conditions, most compounds **5**—**10** can be obtained directly from **1** and hydrazines, usually as mixtures with the corresponding hydrazones **3**.[3c] Furthermore, reaction of the methyl ether of dehydroacetic acid (**12**) with phenylhydrazine or hydroxylamine gives 3,6-dimethyl-2-phenylpyrano[4,3-*c*]pyrazol-4(2*H*)-one (**13b**)[3c,8] or 3,6-dimethyl-4*H*-pyrano[4,3-*c*]isoxazol-4-one (**14**)[3c,8] while Oppenheim's "Dehydroacetchlorid,"[9] of hitherto-unknown constitution, has long been known[9b] to react with phenylhydrazine giving an as yet unidentified isomer, mp 203 °C, of **5b**.

Clearly, some sort of control on regioselectivity is desirable for this manifold of reactions and in general in pyrazole and isoxazole syntheses. Thus, in the related case of β-substituted enones, the treatment with hydroxylamine under carefully controlled conditions has been reported to afford regioselectively the isomeric 3,5-disubstituted isoxazoles through pH control of the more nucleophilic center in hydroxylamine.[10a] Also, a regioselective synthesis of 3,5-disubstituted

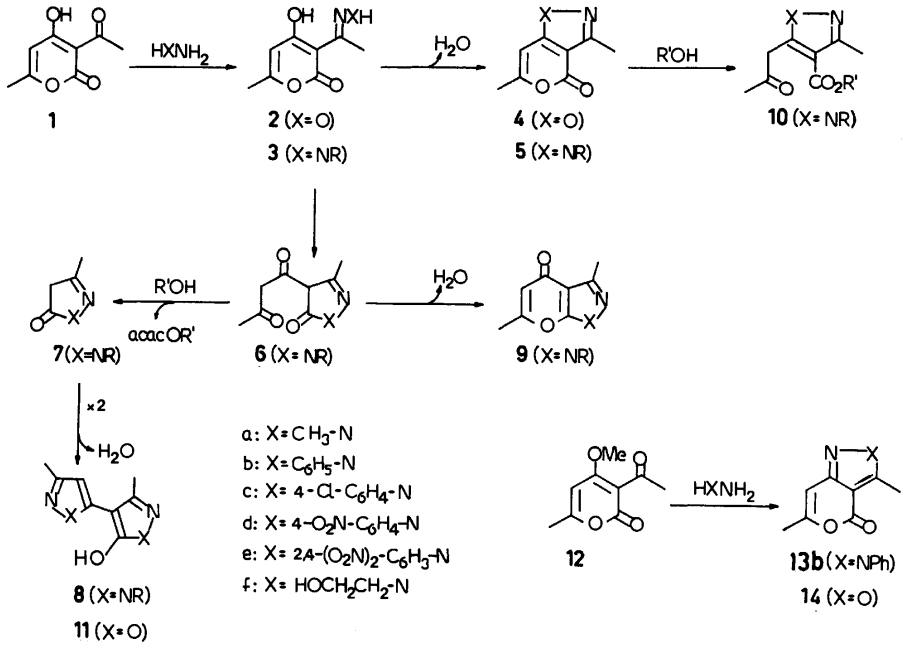

Scheme 1.

isoxazoles based on the reactivity of 3-methylthio-2-buten-1-ones has been recently reported.[10b]

We herein report on: i) The synthesis of several new hydrazones **3**, their cyclization to pyranopyrazolones **5**, and their conversion to pyrazolylpyrazoles **8**; ii) the identification of Oppenheim's "Dehydroacetchlorid" as 4-chloro-3-(1-chlorovinyl)-6-methyl-2*H*-pyran-2-one (**15**) and its regioselective conversion into pyranopyrazolones **5** or **13**; iii) an NMR study of some of these compounds, mainly based on NOE measurements, which allows unambiguous structure assignment between pairs of possible isomers.[11]

Results and Discussion

Reaction of **1** with hydrazines in methanol yielded the corresponding hydrazones **3a—e** in fair to good yields (Table 1). The configuration of the C=N double bond was not determined. Nevertheless, hydrazones **3a—c** were cyclized to the corresponding pyrano[4,3-*c*]pyrazol-4(1*H*)-ones **5a—c** (Table 2), although the very insoluble hydrazones **3d—e** could not be cyclized, due to the very low nucleophilicity of the aryl-bound nitrogen atom.

Formation of pyrazolylpyrazole **8c** upon treatment of hydrazone **3c** with aqueous HCl in DME under reflux has precedent in the known[3a] formation of **8b**, together with **5b**, when **1** is reacted with two equivalents of phenylhydrazine hydrochloride. Thus, a possible mechanism through **6c** can be envisaged (Scheme 2, path b). However, we have been unable to find the 3,4′-bipyrazoles **16**. (Scheme 2, path a). Therefore, an alternative mechanism through pyrazolone **7c** cannot be excluded, since its formation from **6c** involves a simple retro-Claisen condensation and the closely related compound **7b** (Ar=C_6H_5) is known[13] to yield **8b** upon heating.

In the present work, reaction or **1** with two equivalents of either methylhydrazine or (2-hydroxyethyl)-hydrazine also gave the corresponding pyrazolylpyrazoles **8a** and **8f** (Table 3).

NMR experiments, summarized below, showed convincingly, that the product from the first reaction of Table 3 was indeed **8a**, rather than **16a**. The 80 MHz ^{1}H NMR spectrum of **8a** in $CDCl_3$ showed the presence of several unresolved long range couplings, which were uncovered by resolution enhancement via gaussian multiplication and zero-filling of the FID prior to Fourier transformation.[14] In this way, the assignments shown in Table 4 were made. Double irradiation experiments, also shown in Table 4, confirmed these assignments.

In order to complete the characterization of **8a**, a homonuclear ^{1}H{^{1}H} NOE experiment was performed, using the NOE difference technique.[15] Irradiation of the $N_{1'}$-methyl at δ 3.51 gave about 1% increase in the signals of the C-methyl groups, a result which rules out constitution **16a**, for which a much more significant (≃15%) increase of the adjacent C-methyl group, at δ 2.06, was expected. The only clear increase from this NOE difference experiment was a 10% enhancement of the 5-hydroxyl proton, at δ 8.5—9.5, thus showing that the conformation of **8a** is *seqcis*, and not *seqtrans* (Scheme 3), possibly due to steric hindrance between both methyl groups in the latter.

A similar conclusion was drawn for compound **8c**,

Table 1. Preparation of Oxime **2** and Substituted Hydrazones **3** of Dehydroacetic Acid[a]

Product	X	Molar ratio $HXNH_2$/**1**	Condition	Yield %	Mp θ_m/°C
2	O	2.1[b]	R.t., 17 h	76	171—173[f]
3a	CH_3N	1.1[c]	R.t., 25 h[d]	50[e]	100—102
3b	C_6H_5N	1.1[c]	R.t., 1 h	91	211—212[g]
3c	4-ClC_6H_4N	1.1[b]	R.t., 15 h	95	188—190
3d	4-NO_2-C_6H_4N	1.2[c]	Refl., 16 h	93	220—223
3e	2,4-$(NO_2)_2C_6H_3N$	1.2[c]	Refl., 21 h	35	228—231

a) A 0.1 M (1 M=1 mol dm^{-3}) solution of **1** in MeOH was used, unless otherwise stated. b) A mixture of $HXNH_2$·HCl and 10% excess sodium acetate trihydrate was used. c) Free $HXNH_2$ was used. d) Solvent: DME. e) Pyrazolylpyrazole **8a** was detected in the mother liquor. f) Lit, 171—173°C (Ref. 6). g) Lit, 211—212°C (Ref. 12).

Table 2. Cyclization of Hydrazones **3**

Starting material	Reagent	Reaction condition	Product	Yield/%	Mp θ_m/°C
3a	1 equiv 1M HCl	DME, r.t., 23 h	**5a**	73	152—154
3b	Cat. TsOH	Xylene, reflux, 12 h	**5b**[a,b]	33	156—157[d]
3c	1.2 equiv 1M HCl	DME, reflux, 49 h	**5c**[c]	18	220—222

a) Neither Mitsunobu's reagent (EtO_2CN=NCO_2Et/PPh_3) nor $POCl_3$ under reflux achieved the desired increase in the yield of **5b** and/or decrease in by-product **9b**. b) Also obtained was a second product, in 30% yield, identified as 3,6-dimethyl-1-phenylpyrano[2,3-*c*]pyrazol-4(1*H*)-one, **9b**, mp 150°C (lit, 150°C (Ref. 4)). c) Also obtained was pyrazolylpyrazolone **8c**, mp 272—275°C, in 17% yield. See text for characterization. d) Lit, 156—157°C (Ref. 3b).

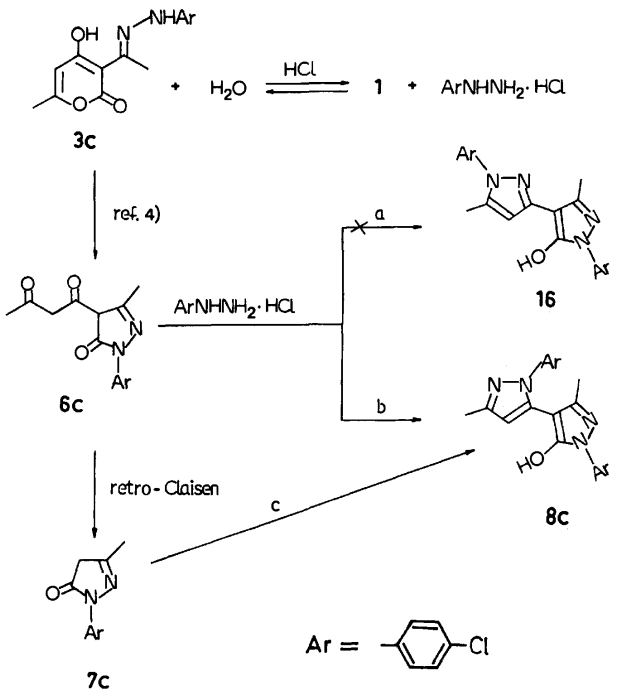

Scheme 2.

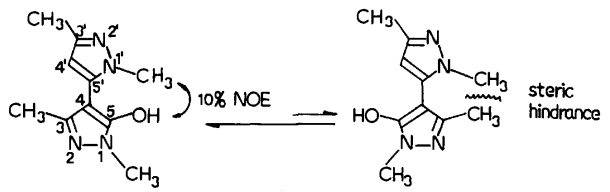

Scheme 3.

in which irradiation of the C_3-methyl protons at δ 2.72 gave no significant increase for any of the *p*-chlorophenyl singlets. The results are summarized in Scheme 4.

(2-Hydroxyethyl)hydrazine-derived pyrazolylpyrazole **8f** could not be structurally assigned by NOE measurements. However, the close similarity between its spectra and those of **8a** points to a common structural type for both compounds (See experimental). In particular, the UV spectrum of **8a** shows peaks at 210, 226, and 260 nm, while **8f** shows 207, 226, and 258 nm. Also, the aromatic carbons exhibit very similar chemical shifts in the ^{13}C NMR spectra of both compounds.

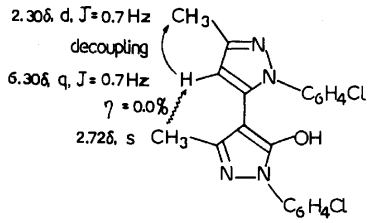

Scheme 4.

Identification and Reactions of Oppenheim's "Dehydroacetchlorid": Preparation of 1-Alkyl-3,6-dimethylpyrano[4,3-*c*]pyrazol-4(1*H*)-ones (5), and 2-Aryl-3,6-dimethylpyrano[4,3-*c*]pyrazol-4(2*H*)-ones (13). As early as 1876, Oppenheim and Precht reported[9a] that reaction of **1** with phosphoryl chloride and phosphorus pentachloride gave a compound, $C_8H_6O_2Cl_2$, mp 101 °C, which they named "Dehydroacetchlorid." We have now found, that reaction of **1** with phosphoryl chloride gives 4-chloro-3-(1-chlorovinyl)-6-methyl-2*H*-pyran-2-one (**15**), mp 100 °C, and therefore we propose this constitution for "Dehydroacetchlorid." Constitution **15** is clear from elemental analysis and spectral data (see Experimental). Furthermore, in 1890 Feist reported[9b] that reaction of **15** with phenylhydrazine gave an unidentified compound, mp 203 °C, isomeric with **5b**. We have repeated this reaction and, in our hands, the resulting compound showed mp 209—210 °C. This compound was identical with **13b**, previously obtained by a Russian group[3c,8] from reaction of 3-acetyl-4-methoxy-6-methyl-2*H*-pyran-2-one (**12**) with phenylhydrazine. A comparison between the

Table 3. Preparation of Pyrazolylpyrazoles **8**

Starting material	Reagent	Reaction condition	Product	Yield/%	Mp θ_m/°C
1	$MeNHNH_2$ (2 equiv)	DME, r.t., 47 h	**8a**	33	203—204
3c	1M aq HCl (1.2 equiv)	DME, reflux, 49 h	**8c**[a]	17	272—275
1	$HOCH_2CH_2NHNH_2$ (2.5 equiv)	DME, reflux, 91 h	**8f**	38	79—82

a) See also Table 2, entry 3.

Table 4. The Assigned 80 MHz ^1H NMR Spectrum of **8a**, 50 mM in $CDCl_3$[a]

Proton	δ/ppm	Mult.	J/Hz	Decouplin and NOE
N_1-Me	3.63	q	0.3	
C_3-Me	2.01	q	0.3	Note[b]
C_5-OH	8.5—9.5	broad	—	Note[c]
$N_{1'}$-Me	3.51	q	0.3	
$C_{3'}$-Me	2.06	dq	0.6; 0.3	Note[d,e]
$C_{4'}$-H	5.78	q	0.6	

a) See Scheme 3 for numbering. b) Upon irradiation at δ 3.63 collapses to a singlet. c) Upon low power presaturation at δ 3.51 under NOE difference conditions, this signal shows a 10% enhancement in its integrated area. d) Collapses to a quartet, J=0.3 Hz, when decoupling from $C_{4'}$-H at δ 5.78. e) Collapses to a doublet, J=0.6 Hz, when decoupling from $N_{1'}$-Me at δ 3.51.

reactions of **1**, **12**, and **15** with hydroxylamine or phenylhydrazine is worth here. Thus, **1** gives only products derived from initial attack on the side-chain carbonyl group, and therefore **1** can be converted into the fused heterocycles **4** and **5**, but not into the isomeric **13** and **14**. However, the increased electrophilicity of C-4 in both **12** and **15** opens up the way to **13** and **14** via initial attack of the nucleophile on the now more reactive C-4. This point was confirmed by reaction of **15** with several arylhydrazines (Scheme 5), which furnished the expected 3,6-dimethyl-2-arylpyrano[4,3-*c*]pyrazol-4(2*H*)-ones (**13**) in fair to good yields (Table 5). Furthermore, reaction of **15** with alkylhydrazines gave the 3,6-dimethyl-1-alkylpyrano[4,3-*c*]pyrazol-4(1*H*)-ones (**5**) (Table 5), i.e., the products also expected from initial attack of the now more nucleophilic, substituted nitrogen of the hydrazine on C-4 of the pyrone ring of **15**.

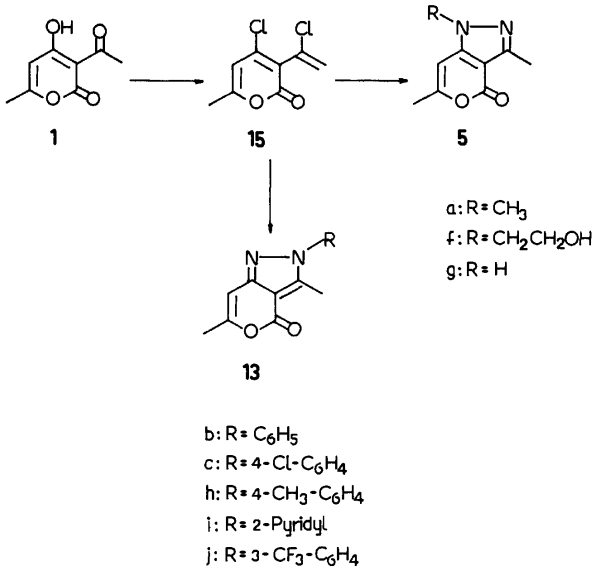

Scheme 5.

Distinguishing between 1-Substituted 5 and 2-Substituted Pyranopyrazoles 13: NOE Measurements. Throughout the present work, we felt the need for a quick and reliable method for ascertaining the constitution of new pyranopyrazolones as **5** or **13** in an unambiguous way. Since the new compounds were crystalline solids, X-ray diffraction analysis was one possibility, but we were seeking for a faster, more versatile method. The new 2-D NMR techniques[16] were also out of question, because usually they require large amounts of sample and long measuring times. Hopefully, homonuclear $^1H\{^1H\}$ NOE measurements[17] particularly in the useful NOE difference mode,[18] are very helpful for the constitutional assignment of simple fused heterocycles.[15] Thus, in 3,6-dimethylpyrano[4,3-*c*]pyrazol-4(1*H*)-ones (**5**), the group bound to N-1 has

Table 5. Reactions of **15** with Hydrazines, $RNHNH_2$

R	Equiv hydraz.	Reaction condition	Product	Yield/%	Mp θ_m/°C
H	4.1[a]	EtOH, reflux, 1.75 h	**5g**	21	192—194
CH_3	3.1[b]	DME, r.t., 20 h	**5a**	40	152—154
$HOCH_2CH_2$	3.6[b]	MeOH, r.t., 40 h	**5f**	81	144—146
H_2NCO	3.2[c]	EtOH, reflux, 21 h	**5g**[d]	49	192—194
C_6H_5	4.9[b]	DME, reflux, 54 h	**13b**	53	209—210[f]
4-ClC_6H_4	3.1[c]	MeOH, reflux, 91 h	**13c**	83	179—182
4-MeC_6H_4	3.2[c]	MeOH, reflux, 66 h	**13h**	58	172—173
2-Pyridyl	3.1[b]	MeOH, reflux, 39 h	**13i**	33	154—155
3-CF_3-C_6H_4	3.2[b]	MeOH, reflux, 66 h	**13j**	76	156—157
4-$NO_2C_6H_4$	3.1[b]	DME, reflux, 20 h	None[e]		

a) Hydrazine hydrate (98%) was used. b) The substituted hydrazine was used as the free base. c) A mixture of $RNHNH_2 \cdot HCl$ and 1.2 equiv $NaOAc \cdot 3H_2O$ in MeOH was used. d) A second solid, mp 248—250 °C, identified as 1,2-hydrazinedicarboxamide, was also obtained from this reaction. e) Starting materials were recovered unaltered due to the poor nucleophilicity of 4-nitrophenylhydrazine. f) Lit, 210 °C (Refs. 3c and 8).

Table 6. Homonuclear NOE Enhancements in Pyrano[4,3-*c*]pyrazol-4(1*H*)-ones **5** and **13**[a]

Compound	Irradiated proton		Enhanced proton		η/%
	Numbering	δ/ppm	Numbering	δ/ppm	
5a	N_1-Me	3.9	H_7	6.15	4.4
5c	H_{Ar}	7.6	H_7	6.3	10.0
5f	H_7	6.2	N_1-CH_2	4.1	1.7
			C_6-Me	2.3	1.0
13b	C_3-Me	2.8	H_{Ar}	7.5	5.3
13c	C_3-Me	2.8	H_{Ar}	7.5	5.0
13h	H_{Ar}	7.3	C_3-Me	2.75	2.5
13i	C_3-Me	3.1	·····None·····		
	H_7	6.25	C_6-Me	2.3	1.6
13j	C_3-Me	2.8	H_{Ar}	7.6—7.8	4.8

a) Determined on 10 mM solutions in $CDCl_3$, using the NOE difference technique.

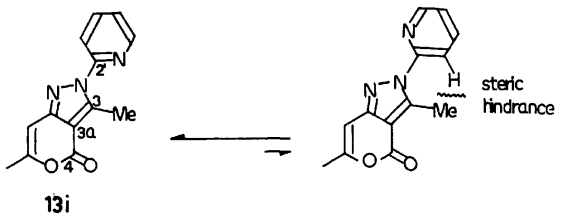

Scheme 6.

its protons close to H-7, while in the isomeric -4(2*H*)-ones the N-2 bound group is close to the C-3 methyl group. A series of homonuclear $^1H\{^1H\}$NOE difference experiments, summarized in Table 6, confirmed this expectations, and provided clear-cut proof for structures **5** and **13**. One exception was compound **13i**, for which no homonuclear NOE enhancements were found besides the trivial C_6-Me{H_7}. The lack of NOE on any pyridine proton upon irradiation at the C-3 methyl protons was taken as evidence for conformation *seqtrans*, rather than *seqcis* (Scheme 6).

Finally, proof for constitution **13i** rather than **5i** was obtained by means of the recently reported technique[19,20] of long range, selective heteronuclear $^{13}C\{^1H\}$NOE measurements. Thus, the assigned ^{13}C NMR spectrum of **13i** is given in Table 7. As shown in Scheme 6, the C-3 methyl protons are close to four quaternary carbons, namely C-3, C-3a, and C-4 of the pyranopyrazole nucleus, as well as, to the C-2′ carbon of the pyridine substituent. Therefore, low power preirradiation of the C-3 methyl protons should result in a NOE enhancement of these four quaternary carbons.[19,20]

As shown in Table 7, this was indeed the case. This result, which proves constitution **13i**, rules out the alternative constitution **5i**, in which the pyridine C-2′ carbon atom is too far apart from the C-3 methyl protons to undergo any NOE enhancement.

On the other hand, the doubt between constitutions **5g** or **13g** for the product obtained from reaction of **15** with unsubstituted hydrazine could not be solved by NOE methods. However, its constitution was unambiguously determined as **5g** by comparison of its UV spectrum (215 nm, log ε=4.33 and 255 nm, log ε=3.79) with those of **5a** (218 nm, log ε=4.40 and 258 nm, log ε=4.01) and **5g** (218 nm, log ε=4.38 and 259 nm, log ε=3.80).

Experimental

General. Mp's have been determined on a Kofler block (Reichert, Wien). UV spectra were run in a Perkin-Elmer 550 instrument. IR spectra were measured on a Perkin-Elmer 1310 instrument. 80 MHz ^{1}H and 20 MHz ^{13}C NMR spectra were recorded in the FT mode on a Bruker WP80SY instrument. MS were taken under EI (70 eV) using a Hewlett-Packard 5985-B instrument.

General preparation procedures, yields and melting points are given in Tables 1—3 and 5. Separations were carried out by column chromatography on silica gel Merck 7754. Special NMR procedures have been described in detail elsewhere: Gaussian resolution enhancement-zero filling,[14] measurement of $^1H\{^1H\}$NOEs by the NOE difference technique,[15] assignment of carbon spectra by selective proton decoupling[19] and measurement of long range, selective heteronuclear NOE enhancements.[20]

Dehydroacetic Acid Oxime (2). Prepared according to the described procedure.[6] IR (KBr) 3400—2500, 1660 cm^{-1}; ^{1}H NMR (d_6-DMSO) δ=2.15 (3H, s), 2.35 (3H, s), 4.7—6.2 (1H, broad absorption), 6.05 (1H, s); ^{13}C NMR (d_6-DMSO) δ=13.3, 19.2, 95.1, 102.0, 158.7, 161.9, 163.0, 173.4; MS *m/z* (%) 183 (M^+, 44), 166 (33), 139 (21), 126 (38), 85 (36), 69 (33), 67 (35), 43 (100).

Preparation of Substituted Dehydroacetic Acid Hydrazones 3. The reaction conditions are summarized in Table 1.

Dehydroacetic Acid Methylhydrazone (3a). IR (KBr) 3300, 1690, 1570 cm^{-1}; ^{1}H NMR ($CDCl_3$) δ=2.2 (3H, s), 2.7 (3H, s), 2.8 (3H, s), 5.7 (1H, s); ^{13}C NMR ($CDCl_3$) δ=15.9, 19.5, 38.3, 94.8, 106.6, 162.2, 163.6, 172.2, 182.8; MS *m/z* (%) 196 (M^+, 35), 181 (18), 154 (22), 139 (100), 111 (25), 85 (38), 69 (40), 43 (82). This compound did not give a correct elemen-

Table 7. The Assigned 20 MHz ^{13}C NMR Spectrum of 3,6-Dimethyl-2-(2-pyridyl)pyrano[4,3-*c*]pyrazol-4(2*H*)-one (**13i**) in $CDCl_3$

Carbon	δ_C/ppm	Selective decoupling[a]		Selective heteronuclear NOE[b]	
		Irradn. at δ_H/ppm	Collapses to a singlet	Presatn. at δ_H/ppm	η/%
C_3-Me	13.5	3.1	Yes		
C_6-Me	19.8	2.3	Yes		
C_7	96.5	6.3	Yes		
C_{3a}	106.6	—	—	3.1	+24
$C_{5'}$	117.3	7.35	Yes		
$C_{3'}$	122.6	7.85	Yes		
$C_{4'}$	138.5	7.85	Yes		
C_3	145.3	—	—	3.1	+66
$C_{6'}$	147.7	8.50	Yes		
C_{7a}	150.6	6.3	Yes		
$C_{2'}$	152.5	—	—	3.1	+11
C_6	157.6	2.3	Yes		
C_4	159.9	—	—	3.1	+16

a) CW irradiation, decoupling power DP=18H (i.e, 18dB attenuation below nominal 10W). b) CW presaturation, decoupling power DP=55L (i.e., $\gamma B_2 \simeq 2.5$ Hz) for 25s.

tal analysis.

Dehydroacetic Acid Phenylhydrazone (3b).[12] ^{1}H NMR (d_6-DMSO): δ=2.05 (3H, s), 2.5 (3H, s), 5.9 (1H, s), 6.8—7.05 (3H, m), 7.1—7.5 (2H, m), 9.05 (1H, s).

Dehydroacetic Acid (4-Chlorophenyl)hydrazone (3c). IR (KBr) 3300, 1680, 1590 cm^{-1}; ^{1}H NMR ($CDCl_3$+CF_3COOH) δ=2.4 (3H, s), 3.0 (3H, s), 6.4 (1H, s), 6.8, 6.9, 7.3, 7.4 (4H, AB system); ^{13}C NMR ($CDCl_3$+CF_3COOH) δ=18.3, 19.6, 94.6, 104.4, 115.8, 129.5, 130.1, 141.5, 165.9, 168.8, 175.1, 180.5; MS m/z (%) 294 (20), 292 (M^+, 58), 237 (86), 235 (80), 125 (41), 99 (53), 85 (60), 43 (100); Found: C, 57.64; H, 3.99; N, 9.53%. Calcd for $C_{14}H_{13}ClN_2O_3$: C, 57.45; H, 4.48; N, 9.57%.

Dehydroacetic Acid (4-Nitrophenyl)hydrazone (3d). IR (KBr) 3180, 1670, 1590 cm^{-1}; ^{1}H NMR ($CDCl_3$+CF_3COOH) δ=2.5 (3H, s), 3.1 (3H, s), 6.4 (1H, s), 7.1, 7.2, 8.4, 8.5 (4H, AB system); ^{13}C NMR ($CDCl_3$+CF_3COOH) δ=17.2, 19.5, 95.7, 105.3, 107.6, 121.8, 142.1, 149.4, 165.5, 166.4, 174.7, 181.8; MS m/z (%) 303 (M^+, 86), 261 (42), 246 (100), 85 (61), 43 (80), Found: C, 55.48; H, 4.23; N, 13.73%. Calcd for $C_{14}H_{13}N_3O_5$: C, 55.45; H, 4.32; N, 13.86%.

Dehydroacetic Acid (2,4-Dinitrophenyl)hydrazone (3e). IR (KBr) 3300, 1720, 1700, 1570 cm^{-1}; ^{1}H NMR ($CDCl_3$) δ=2.3 (3H, s), 2.7 (3H, s), 6.0 (1H, s), 7.4 (1H, d, J=14 Hz), 8.4 (1H, dd, J=14 Hz, J'=3 Hz), 9.2 (1H, d, J=3 Hz), 11.3 (1H, s), 14.7 (1H, s); ^{13}C NMR ($CDCl_3$+CF_3COOH) δ=17.7, 19.4, 96.7, 105.4, 115.0, 121.9, 131.6, 132.4, 140.6, 145.2, 166.8, 168.8, 177.0, 182.3; MS m/z (%) 348 (M^+, 36), 306 (20), 291 (28), 256 (26), 151 (43), 109 (44), 85 (54), 67 (90), 43 (100); Found: C, 48.52; H, 3.35; N, 15.93%. Calcd for $C_{14}H_{12}N_4O_7$: C, 48.28; H, 3.47; N, 16.09%.

Preparation of Pyrano[4,3-*c*]pyrazol-4(1*H*)-ones (5). The reaction conditions are summarized in Table 2.

1,3,6-Trimethylpyrano[4,3-*c*]pyrazol-4(1*H*)-one (5a). UV (EtOH) 218 (log ε=4.40), 258 (log ε=4.01) nm; IR (KBr) 3090, 1720 cm^{-1}; ^{1}H NMR ($CDCl_3$) δ=2.3 (3H, s), 2.5 (3H, s), 3.8 (3H, s), 6.1 (1H, s); ^{13}C NMR ($CDCl_3$) δ=12.4, 19.9, 35.4, 91.8, 103.4, 145.2, 148.7, 158.6, 159.1; MS m/z (%) 178 (M^+, 67), 163 (100), 43 (26); Found: C, 60.67; H, 5.62; N, 15.58%. Calcd for $C_9H_{10}N_2O_2$: C, 60.67; H, 5.66; N, 15.72%.

3,6-Dimethyl-1-phenylpyrano[4,3-*c*]pyrazol-4(1*H*)-one (5b).[3b] IR (KBr) 3070, 2950, 1725, 1620, 1590, 1500, 1325, 945, 760 cm^{-1}; ^{1}H NMR ($CDCl_3$) δ=2.2 (3H, s), 2.55 (3H, s), 6.3 (1H, s), 7.3 (5H, s); ^{13}C NMR ($CDCl_3$) δ=12.6, 20.1, 92.9, 105.0, 123.2, 128.0, 129.5, 138.4, 144.7, 150.2, 158.8, 160.0; MS m/z (%) 240 (M^+, 100), 239 (9), 226 (11), 225 (73), 77 (15), 51 (10), 43 (22).

1-(4-Chlorophenyl)-3,6-dimethylpyrano[4,3-*c*]pyrazol-4-(1*H*)-one (5c). IR (KBr) 3050, 1740 cm^{-1}; ^{1}H NMR ($CDCl_3$+CF_3COOH) δ=2.4 (3H, s), 2.7 (3H, s), 6.4 (1H, s), 7.4, 7.5, 7.6, 7.7 (4H, AB system); ^{13}C NMR ($CDCl_3$+CF_3COOH) δ=11.4, 19.7, 93.2, 104.9, 126.1, 130.7, 133.6, 137.3, 147.0, 152.0, 161.6, 164.3; MS m/z (%) 276 (34), 274 (M^+, 100), 261 (29), 259 (86), 75 (27), 43 (53); Found: C, 60.86; H, 3.88; N, 10.64%. Calcd for $C_{14}H_{11}ClN_2O_2$: C, 61.31; H, 4.01; N, 10.22%.

1-(4-Hydroxyethyl)-3,6-dimethylpyrano[4,3-*c*]pyrazol-4-(1*H*)-one (5f). UV (EtOH) 218 (log ε=4.38), 259 (log ε=3.80) nm; IR (KBr) 3360, 1710, 1080, 1030 cm^{-1}; ^{1}H NMR ($CDCl_3$) δ=2.3 (3H, s), 2.5 (3H, s), 3.1 (1H, br), 4.0—4.2 (4H, m), 6.3 (1H, s); ^{13}C NMR ($CDCl_3$) δ=12.4, 19.9, 51.3, 60.9, 92.5, 103.3, 146.0, 149.2, 159.0, 159.1; MS m/z (%) 209 (M^+, 100), 177 (60), 164 (39), 43 (47).

3,6-Dimethylpyrano[4,3-*c*]pyrazol-4(1*H*)-one (5g). Prepared following the conditions described in Table 5. UV (EtOH) 215 (log ε=4.33), 255 (log ε=3.79) nm; IR (KBr) 3180, 3120, 1690 cm^{-1}; ^{1}H NMR ($CDCl_3$+CF_3COOH) δ=2.4 (3H, s), 2.9 (3H, s), 6.7 (1H, s); ^{13}C NMR ($CDCl_3$+CF_3COOH) δ=11.2, 20.5, 93.7, 105.1, 147.0, 149.0, 159.3, 165.7; MS m/z (%) 164 (M^+, 80), 149 (100), 43 (14); Found: C, 58.26; H, 4.52; N, 17.22%. Calcd for $C_8H_8N_2O_2$: C. 58.53; H, 4.91; N,17.06%.

Preparation of 5-Hydroxy-3-methyl-4-(3-methyl-1*H*-pyrazol-5-yl)-1*H*-pyrazoles (8). The reaction conditions are summarized in Table 3.

1,3-Dimethyl-5-hydroxy-4-(1,3-dimethyl-1*H*-pyrazol-5-yl)-1*H*-pyrazole (8a). IR (KBr) 2920 cm^{-1}; ^{1}H NMR ($CDCl_3$) δ=2.0 (2H, s), 2.1 (3H, s), 3.5 (3H, s), 3.7 (3H, s), 5.8 (1H, s); ^{13}C NMR ($CDCl_3$) δ=11.2, 13.0, 30.7, 36.3, 93.6, 106.3, 135.3, 144.2, 147.1, 157.7; MS m/z (%) 206 (M^+, 100), 135 (42), 65 (20), 43 (33), Found: C, 58.05; H, 6.96; N, 27.09%. Calcd for $C_{10}H_{14}N_4O$: C, 58.24; H, 6.84; N, 27.16%.

1-(4-Chlorophenyl)-5-hydroxy-3-methyl-4-[1-(4-chlorophenyl)-3-methyl-1*H*-pyrazol-5-yl]-1*H*-pyrazole (8c). IR (KBr) 3450, 1610 cm^{-1}; ^{1}H NMR ($CDCl_3$+CF_3COOH) δ=2.3 (3H, s), 2.6 (3H, s), 6.8 (1H, s), 7.2—7.6 (8H); ^{13}C NMR ($CDCl_3$+CF_3COOH) δ=10.6, 93.2, 111.8, 125.8, 126.9, 130.4, 130.5, 131.1, 131.6, 137.6, 139.1, 139.5, 148.2, 149.0, 157.6; MS m/z (%) 402 (12), 400 (62), 398 (M^+, 96), 231 (24), 113 (100), 111 (34), 75 (32); Found: C, 60.26; H, 4.04; N, 13.81%. Calcd for $C_{20}H_{16}Cl_2N_4O$: C, 60.30; H, 4.02; N, 14.17%.

5-Hydroxy-1-(2-hydroxyethyl)-3-methyl-4-[3-methyl-1-(2-hydroxyethyl)-1*H*-pyrazol-5-yl)]-1*H*-pyrazole (8f). IR (KBr) 3280, 2940 cm^{-1}; ^{1}H NMR (D_2O) δ=2.1 (3H, s), 2.2 (3H, s), 3.8 (4H), 4.0 (4H), 6.1 (1H, s); ^{13}C NMR (D_2O) δ=11.1, 13.2, 47.0, 51.6, 60.2, 61.3, 95.7, 108.0, 136.5, 146.7, 150.0, 161.6; MS m/z (%) 266 (M^+, 100), 235 (74), 223 (20), 178 (29); No correct elemental analysis for this compound was achieved.

3,6-Dimethyl-1-phenylpyrano[2,3-*c*]pyrazol-4(1*H*)-one (9b).[4] This compound was obtained as by-product in the cyclization reaction of **3b** to **5b**. ^{1}H NMR ($CDCl_3$) δ=2.4 (3H, s), 2.6 (3H, s), 6.0 (1H, s), 7.3—7.9 (5H, s); ^{13}C NMR ($CDCl_3$) δ=13.7, 19.2, 106.7, 112.4, 120.8, 127.1, 129.2, 137.1, 146.5, 153.5, 161.4, 175.4; MS m/z (%) 240 (M^+, 100), 200 (70), 132 (20), 91 (58), 77 (15), 51 (10).

3,6-Dimethylpyrano[4,3-*c*]pyrazol-4(2*H*)-ones (13). The reaction conditions are summarized in Table 5.

3,6-Dimethyl-2-phenylpyrano[4,3-*c*]pyrazol-4(2*H*)-one (13b).[3c,8] IR (KBr) 3070, 2900, 1715, 1635, 1580, 1270, 1220, 1150, 1080, 1040, 960 cm^{-1}; ^{1}H NMR ($CDCl_3$) δ=2.2 (3H, s), 2.6 (3H, s), 6.25 (1H, s), 7.45 (5H, s); ^{13}C NMR ($CDCl_3$) δ=11.8, 19.9, 96.7, 105.8, 125.3, 129.0, 129.3, 138.6, 143.2, 151.0, 157.4, 160.1; MS m/z (%) 240 (M^+, 100), 239 (28), 225 (83), 77 (55), 51 (21), 43 (26).

2-(4-Chlorophenyl)-3,6-dimethylpyrano[4,3-*c*]pyrazol-4-(2*H*)-one (13c). IR (KBr) 3100, 1760 cm^{-1}; ^{1}H NMR ($CDCl_3$+CF_3COOH) δ=2.4 (3H, s), 2.7 (3H, s), 6.7 (1H, s), 7.3, 7.4, 7.6, 7.7 (4H, AB system); ^{13}C NMR ($CDCl_3$+CF_3COOH) δ=11.3, 19.6, 95.2, 105.3, 127.4, 130.7, 133.1, 138.5, 147.8, 150.2, 161.6, 163.0; MS m/z (%) 276 (34), 274 (M^+, 100), 261 (27), 259 (82), 152 (23), 111 (45), 75 (53), 43 (78); Found: C, 61.21; H, 3.88; N, 10.06%. Calcd for $C_{14}H_{11}ClN_2O_2$: C, 61.31; H, 4.01; N, 10.22.%

3,6-Dimethyl-2-(4-methylphenyl)pyrano[4,3-*c*]pyrazol-4-(2*H*)-one (13h). IR (KBr) 3100, 1725 cm^{-1}; ^{1}H NMR ($CDCl_3$) δ=2.3 (3H, d, J=1.5 Hz), 2.4 (3H, s), 2.6 (3H, s), 6.3 (1H, q, J=1.5 Hz), 7.3 (4H, s); ^{13}C NMR ($CDCl_3$) δ=11.8, 19.8, 21.0, 96.7, 106.0, 125.1, 129.8, 138.1, 139.1, 143.1, 150.8, 157.2, 160.0; MS m/z (%) 254 (M^+, 100), 239 (93), 132 (10), 91

(32); Found: C, 70.58; H, 5.33; N, 10.85%. Calcd for $C_{15}H_{14}N_2O_2$: C, 70.85; H. 5.55; N, 11.02%.

3,6-Dimethyl-2-(2-pyridyl)pyrano[4,3-*c*]pyrazol-4(2*H*)-one (13i). IR (KBr) 3080, 1720 cm^{-1}; ^1H NMR ($CDCl_3$) δ=2.3 (3H, s), 3.1 (3H, s), 6.3 (1H, s), 7.3 (1H, m), 7.8—7.9 (2H, m), 8.5 (1H, m); ^{13}C NMR ($CDCl_3$) δ=13.5, 19.8, 96.5, 106.6, 117.3, 122.6, 138.5, 145.3, 147.7, 150.6, 152.5, 157.6, 159.9; MS *m/z* (%) 241 (M^+, 95), 226 (100), 198 (38), 170 (33), 78 (77); Found: C, 64.60; H, 4.29; N, 17.47%. Calcd for $C_{13}H_{11}N_3O_2$: C, 64.72; H, 4.60: N, 17.42%.

3,6-Dimethyl-2-(3-trifluoromethylphenyl)pyrano[4,3-*c*]-pyrazol-4(2*H*)-one (13j). IR (KBr) 3100, 1730 cm^{-1}; ^1H NMR ($CDCl_3$) δ=2.3 (3H, d, *J*=1.7 Hz), 2.6 (3H, s), 6.3 (1H, q, *J*=1.7 Hz), 7.7 (4H, m); ^{13}C NMR ($CDCl_3$) δ=11.8, 19.8, 96.5, 106.2, 122.3 (q, *J*=4 Hz), 124.0 (q, *J*=273 Hz), 125.5 (q, *J*=4 Hz), 128.2, 130.0, 131.7 (q, *J*=33 Hz), 139.0, 143.5, 151.3, 157.8, 159.7; MS *m/z* (%) 308 (M^+, 100), 293 (89), 216 (26), 186 (32), 161 (37), 145 (79), 141 (26), 63 (52), 43 (97); Found: C, 58.39; H, 3.48; N, 9.05%. Calcd for $C_{15}H_{11}F_3N_2O_2$: C, 58.45; H, 3.60; N, 9.09%.

4-Chloro-3-(1-chlorovinyl)-6-methyl-2*H*-pyran-2-one (15). A solution of **1** (4.02 g, 24 mmol) in 30 ml of phosphoryl chloride was refluxed for 4.5 h. The cooled mixture was poured very slowly and with stirring over 200 g of ice. This water solution was extracted with chloroform and the organic phase was washed with sodium hydrogenocarbonate. This extract was dried over magnesium sulfate and removal of the solvent left 3.6 g of a black residue. This crude was purified by sublimation at 85 °C/0.2 mmHg (1 mmHg=133.322Pa) affording 1.827 g (33% yield) of a white solid identified as **15**: Mp 100 °C (lit: 101 °C (Ref. 9a)); IR (KBr) 3070, 1700 cm^{-1}; ^1H NMR ($CDCl_3$) δ=2.2 (3H, s), 5.55 (1H, d, *J*=2 Hz), 5.85 (1H, d, *J*=2 Hz), 6.2 (1H, s); ^{13}C NMR ($CDCl_3$) δ=19.6, 106.5, 121.0, 121.2, 130.0, 149.5, 158.9, 162.1; MS *m/z* (%) 208 (5), 206 (32), 204 (M^+, 46), 178 (20), 176 (33), 171 (24), 169 (72), 143 (32), 141 (100), 137 (3), 135 (21), 133 (33), 77 (25), 63 (53) ,43 (47); Found: C, 46.65; H, 2.98%. Calcd for $C_8H_6Cl_2O_2$: C, 46.87; H, 2.95%.

Financial support from "Comisión Asesora de Investigación Cientifica y Técnica" through project No. 2014/83 and a generous gift of dehydroacetic acid from LONZA A.G. (Basel) are gratefully acknowledged. We also thank generous funding from "Fundación María Francisca de Roviralta", which allowed the purchase of the NMR spectrometer and "Direcció General d'Ensenyament Universitari", Generalitat de Catalunya, for the NMR data system.

References

1) For recent examples involving dehydroacetic acid derivatives or coumarins see: a) B. Chantegrel and S. Gelin, *Synthesis*, **1985**, 548; b) B. Chantegrel, A. I. Nadi, and S. Gelin, *J. Heterocycl. Chem.*, **21**, 17 (1984); c) B. Chantegrel, A. I. Nadi, and S. Gelin, *J. Org. Chem.*, **49**, 4419 (1984); d) S. Gelin, B. Chantegrel, and C. Deshayes, *J. Heterocycl. Chem.*, **19**, 989 (1982); e) D. S. Rao, M. C. Ganorkar, C. S. Reddy, and V. T. John, *Curr. Sci.*, **49**, 511 (1980); f) R. Motokuni, M. Tanaka, S. Hashimoto, and T. Suzue, Jpn. Patent 7778895 (*Chem. Abstr.*, **87**, 168029m (1977)); g) A. S. Shawali, B. E. Elanadouli, and H. A. Albar, *Tetrahedron*, **41**, 1877 (1985); h) B. Chantegrel, A. Nadi, and S. Gelin, *Synthesis*, **1983**, 214; i) B. Chantegrel, A. Nadi, and S. Gelin, *Tetrahedron Lett.*, **24**, 38 (1983).

2) a) G. Minunni, *Gazz. Chim. Ital.*, **29II**, 456 (1899); b) E. Marcus, J. K. Chan, and J. L. Hughes, *J. Chem. Eng. Data*, **12**, 151 (1967).

3) a) R. Stollé, *Ber.*, **38**, 3023 (1905); b) E. Benary, *Ber.*, **43**, 1070 (1910); c) A. A. Akhrem, A. M. Moiseenkov, F. A. Lakhvich, and S. P. Smul'skii, *Izv. Akad. Nauk SSSR, Ser. Khim.*, **1971**, 1098.

4) S. Gelin, B. Chantegrel, and A. I. Nadi, *J. Org. Chem.*, **48**, 4078 (1983).

5) R. von Rothenburg, *Ber.*, **27**, 790 (1894).

6) A. Inoue and S. Iguchi, *Chem. Pharm. Bull.*, **12**, 381 (1964).

7) V. K. Makesh and R. S. Gupta, *Indian J. Chem.*, **12**, 570 (1974).

8) A. A. Akhrem, A. M. Moiseenkov, F. A. Lakhvich, V. I. Kadentsev, and O. S. Chizhov, *Izv. Akad. Nauk SSSR, Ser. Khim.*, **1970**, 1206.

9) a) A. Oppenheim and H. Precht, *Ber.*, **9**, 1099 (1876); b) F. Feist, *Liebigs Ann. Chem. Pharm.*, **257**, 253 (1890); c) F. Feist, *Ber.*, **25**, 335 (1892).

10) a) C. Kashima, N. Yoshiwara, S. Shirai, and Y. Omote, *Chem. Lett.*, **1982**, 1455; b) M. Yokoyama, K. Tsuji, and M. Kushida, *J. Chem. Soc., Perkin Trans. 1*, **1986**, 67.

11) Preliminary communication: A. Cantos, P. de March, M. Moreno-Mañas, A. Pla, F. Sánchez-Ferrando, and A. Virgili, *Chem. Lett.*, **1986**, 295.

12) W. H. Perkin, Jr. and C. Bernhart, *Ber.*, **17**, 1522 (1884).

13) V. Jonescu and V. Georgescu, *Bull. Soc. Chim. Fr.*, **41**, 1515 (1927).

14) P. de March and F. Sánchez-Ferrando, *Afinidad*, in the press.

15) M. R. Cuberes, M. Moreno-Mañas, and F. Sánchez-Ferrando, *Magn. Reson. Chem.*, **23**, 814 (1985).

16) A. Bax, "Two-Dimensional Nuclear Magnetic Resonance in Liquids," Delft University Press, Dordrecht, Holland (1982).

17) J. H. Noggle and R. E. Schirmer, "The Nuclear Overhauser Effect. Chemical Applications," Academic Press, New York (1971).

18) J. K. M. Sanders and J. D. Mersh, *Progress Nucl. Magn. Reson. Spectroscopy*, **15**, 353 (1982).

19) F. Sánchez-Ferrando, *Magn. Reson. Chem.*, **23**, 185 (1985).

20) C. Cativiela and F. Sánchez-Ferrando, *Magn. Reson. Chem.*, **23**, 1072 (1985).

Photochemical Reactions of the Natural Furocoumarin, Imperatorin

M. M. Abou-Elzahab,* M. A. Metwally, A. M. Dawidar, M. Abdel-Mogib, and E. A. Abu-Mustafa†
Chemistry Department, Faculty of Science, Mansoura University, Mansoura, A. R. Egypt
†Lab. of Natural Products, National Research Centre, Dokki, Cairo, Egypt
(Received November 17, 1986)

Photochemical behavior of imperatorin was investigated including photolysis and sigmatropic effects in different solvents and photodimerization. The structures of the photoproducts obtained were determined by chemical and spectral methods.

Natural and synthetic coumarins are important due to their biological activities, e.g. photosensitizing effect of xanthotoxin and trimethylpsorolene.[1] Behavior of coumarins and furocoumarins (xanthotoxin only) under irradiation with ultraviolet light has been studied previously.[2-9]

Imperatorin (**1**), known also as ammidin is a natural furocoumarin and occurs in the fruits of *Ammi majus* (Umbelliferea).[10] No previous studies on the photolysis of imperatorin are reported. This paper deals with the behaviour of imperatorin towards:

a) Photolysis and sigmatropic reactions in different solvents. b) Photodimerization.

Results and Discussion

Photolysis and Sigmatropic Reactions in Different Solvents. Irradiation of **1** in different solvents (cf. Experimental) at room temperature resulted in the formation of two furocoumarins (R_f 0.28 and 0.36) in all the tried solvents, but with different yields (Table 1). IR spectrum of the first product, R_f 0.28, $C_{11}H_6O_4$, M^+ 202, showed bands at 1720 and 3340 cm^{-1} characteristics for δ-lactone and associated OH groups (phenolic, from iron(III) chloride test) respectively. It was thought to be xanthotoxol (**2**) from MS (Chart 1). The ^1H NMR of its acetate derivative in $CDCl_3$ solution showed two singlet peaks at δ 2.50 and 7.53 for -OCOC<u>H</u>$_3$ and aromatic proton at C-5 respectively, two doublets at δ 6.35 and 7.76 (J=10 Hz) for two α-pyrone protons, and other two furan protons. The mass spectrum showed molecular ion at m/z 202, and only one mode of fragmentation (Chart 1). Final confirmation was obtained by mixed melting point with an authentic sample (mp and mixed mp 240 °C) and also by its transformation to xanthotoxin, a natural furocoumarin, mp and mixed mp 145 °C (cf. Experimental).

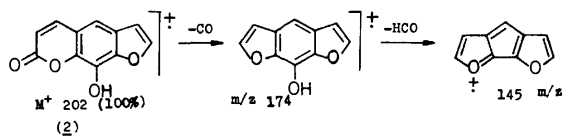

Chart 1.

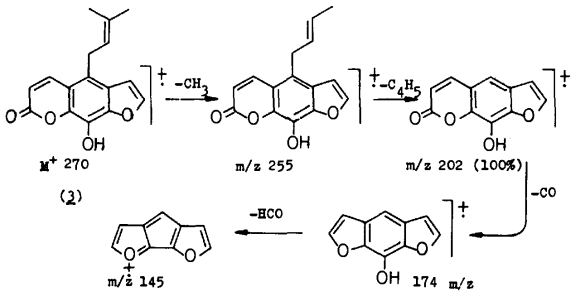

Chart 2.

IR spectrum of the second product, R_f 0.36, $C_{16}H_{14}O_4$, M^+ 270, mp 228 °C indicated the presence of a hydroxyl group and δ-lactone. It was thought to be *allo*-imperatorin (**3**) from its fragmentation behavior (Chart 2) in the mass spectrum.

The ^1H NMR spectrum of its acetate derivative supported the above identification as *allo*-imperatorin where it displayed a singlet at δ 2.5 for -OCOC<u>H</u>$_3$. The isoprenyl group attached at C-5 showed signals at δ 4.15 and 4.29 due to C<u>H</u>$_2$, H-9 (both doublet of doublets J=12.5) 4.22 due to H-10 (doublet of doublets J=5), and 2.2 singlet for 2C<u>H</u>$_3$. Final confirmation was achieved by preparing *allo*-imperatorin followed by mixed mp where no depression occurred. (cf. Experimental).

Table 1. Yields with Different Solvents

Solvent	Xanthotoxol (**2**)	*allo*-Imperatorin (**3**)	Imperatorin dimer (**4**)
	mg	mg	mg
Benzene	25	16	—
1,4-Dioxane	18	19	—
Tetrahydrofuran	13	16	—
Ethyl acetate	4	4	—
Acetone	26	25	—
Acetonitrile	15	5	—
Dimethyl sulfoxide	46	17	—
Acetic acid	246	23	—
Methanol	73	22	11

The mechanism of photolysis of imperatorin (**1**) to produce these products **2** and **3** may be illustrated as in Scheme 1 where xanthotoxol (**2**) is produced via antrafacial [1,5] hydrogen shift, whereas, *allo*-imperatorin (**3**) is most likely formed through aromatic Claisen rearrangement, where the isoprenyl group underwent one inversion to give an ortho-isomer and another to give the para-isomer via [3,3] sigmatropic rearrangement.

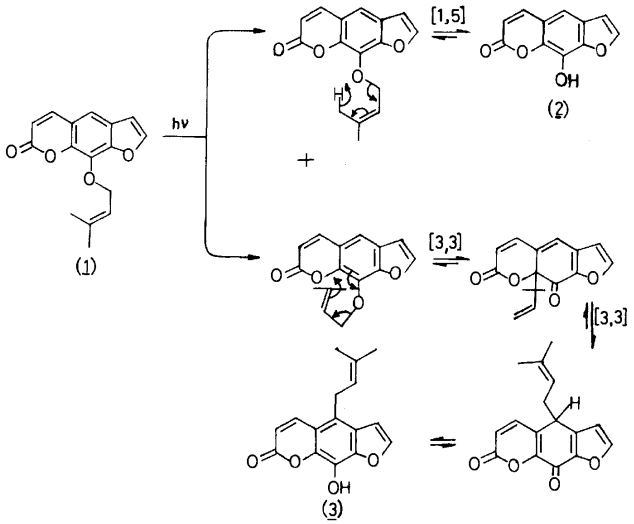

Scheme 1.

Photodimerization Reaction. Imperatorin (**1**) was irradiated in methanolic solution where the dimeric product head-to-head syn (**4**) was formed via [2+2] photo-cycloaddition in addition to xanthotoxol (**2**) and *allo*-imperatorin (**3**).

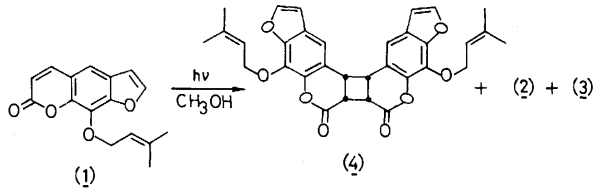

Formulation of the photo-dimer (**4**) was based on analytical and spectral data. IR spectrum showed a band at 1750 cm^{-1} characteristic of δ-lactone. The mass spectrum showed the expected molecular ion at

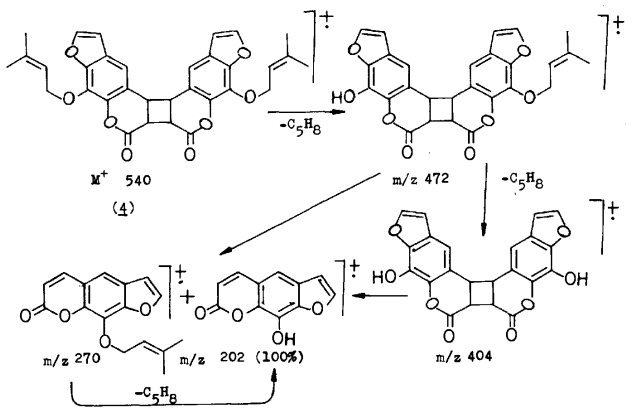

Chart 3.

m/z 540, and only one mode of fragmentation (Chart 3).

This result is in agreement with the work of Anet[8] who reported that photo-irradiation of coumarin in ethanol solution produced a dimer **5**, having the head-to-head syn structure. In contrast, Kruch and Farid[7] found that irradiation of xanthotoxin in non-polar solvents led to formation of the dimer **6**, having the head-to-head anti structure.

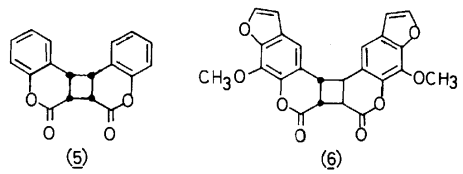

The weight loss due to the acid hydrolysis of the dimer **4** afforded other support to the structure, where it was found that the calculated value (12.6 mg) is in good agreement with the observed value (12.1 mg). The acid hydrolysis of the dimer **4** gave a gray dimer **7**, containing hydroxyl groups as shown from IR spectrum (3500 cm^{-1}). The dimer **7** was methylated with methyl iodide in the presence of anhydrous potassium carbonate to give the dimer **8**. The IR spectrum showed absence of any OH group.

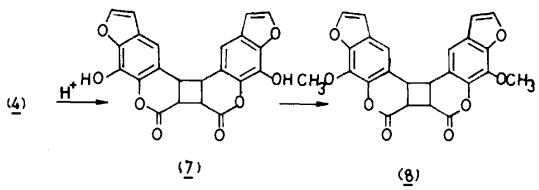

The difference in melting points and solubilities of xanthotoxin dimer (**8**) and that of Krauch and Farid[7] showed that the configuration of the two dimers is different, i.e. the dimer is not head-to-head anti **8**. The abnormally high melting point of the dimer **8** will not be surprising when we know that the melting point of the head-to-head syn coumarin dimer **5** is 100 °C higher than the head-to-head anti dimer.[11]

Experimental

Imperatorin was supplied by Memphis Chemical Co., Cairo, Egypt. All melting points (°C) are uncorrected and were taken in a Fischer electric melting point apparatus. Infrared spectra were recorded on a Unicam SP 2000 infrared Spectrophotometer using KBr pellet technique. ^1H NMR spectra were obtained in $CDCl_3$ on a Brucker 400 MHz apparatus. Mass spectra were measured on a Varian Mat 711, direct inlet at 70 eV. The photolysis apparatus used is a 500 W medium pressure wide spectrum mercury lamp (Hanovia TQ 718) supported in a water cooled quartz tube.

Irradiation of Imperatorin (1): A solution of imperatorin (**1**) (675 mg, 0.0025 mole) in different solvents (10 ml) (except methanol) (Table 1), was irradiated in the corning glass test tubes which were degassed, sealed in vacuo. The irradiation was carried out without filter at 25—30 °C, for 100 h. The tubes were opened and the solution was evaporated to dryness to give gummy material, which was further separated by

TLC (silica gel, benzene-ethyl acetate 9 : 1) to give xanthotoxol (**2**) (R_f 0.28, mp 240 °C) and *allo*-imperatorin (**3**) (R_f 0.36, mp 228 °C) (cf. Table 1).

Xanthotoxol (2): IR 3340 (OH), 3000 (CH, CH_2 str.), 1720 (δ-lactone), and 1600 (C=C) cm^{-1}. MS *m/z* (rel intensity) 202 (M^+, 100) ($C_{11}H_6O_4$), 174 (48, M-CO), 145 (10, $M-C_2HO_2$), 118 (10), 90 (16), 75 (22), and 61 (52).

***allo*-Imperatorin (3)** IR: 3330 (OH), 3000 (CH_2, CH_3 str.), 1720 (δ-lactone), and 1600 (C=C) cm^{-1}. MS *m/z* (rel intensity) 270 (M^+, 0.6, $C_{16}H_{14}O_4$), 255 (0.8, $M-CH_3$), 202 (100, $M-C_5H_8$), 174 (48, $M-C_6H_8O$), 144 (5, $M-C_7H_9O_2$), 118 (4), 90 (18), 75 (8), and 61 (52).

Acetylation of Xanthotoxol (2): A solution of xanthotoxol (**2**) (0.5 g) in acetic anhydride (10 ml) was refluxed for 2 h. The reaction mixture was diluted with water (10 ml). The solvent was evaporated under reduced pressure to dryness and the residue was washed with toluene, then petroleum ether 40—60 °C, to give a solid material which was recrystallized from ethanol to give *O*-acetylxanthotoxol as pale yellow crystals; mp 175 °C (lit,[12] 175 °C). IR 1750 ($OCOCH_3$), 1720 (δ-lactone), 1630 and 1600 (C=C) cm^{-1}. ^1H NMR δ=2.5 (s, 3H, $OCOCH_3$), 6.35 (d, 1H, H-3, *J*=10 Hz), 7.77 (d, 1H, H-4, *J*=10 Hz), 7.53 (s, 1H, H-5), 6.83 (d, 1H, H-6, *J*=2.5 Hz), and 7.67 (d, 1H, H-7, *J*=2.5 Hz).

Methylation of Xanthotoxol (2): A solution of xanthotoxol (**2**) (0.5 g), methyl iodide (1 ml) in acetone (10 ml) in the presence of potassium carbonate (2 g) as base catalyst was refluxed on water bath for 6 h. Potassium iodide was separated and filtered off. The acetone solution was evaporated under reduced pressure to give xanthotoxin which was recrystallized from ethanol to give colourless crystals; mp 145 °C (lit,[13] 146 °C). IR 3120 (CH_2, CH_3 str.), 1730 (δ-lactone), and 1600 (C=C) cm^{-1}. ^1H NMR δ=4.3 (s, 3H, OCH_3), 6.37 (d, 1H, H-3, *J*=10 Hz), 7.77 (d, 1H, H-4, *J*=10 Hz), 7.34 (s, 1H, H-5), 6.8 (d, 1H, H-6, *J*=2.5 Hz), and 7.69 (d, 1H, H-7, *J*=2.5 Hz). MS *m/z* (rel intensity) 216 (M^+, 100, $C_{12}H_8O_4$), 201 (23, $M-CH_3$), 173 (32, $M-C_2H_3O$), 145 (10, $M-C_3H_3O_2$), 117 (2), 89 (12) and 63 (10).

Acetylation of *allo*-Imperatorin (3): *allo*-Imperatorin (**3**) (0.5 g) was acetylated according to method used for xanthotoxol acetate to give *allo*-imperatorin acetate, colourless crystals, mp 126 °C. (lit,[15] 108 °C) IR 1750 ($OCOCH_3$), 1720 (δ-lactone), 1630, and 1600 (C=C) cm^{-1}. ^1H NMR δ=2.5 (s, 3H, $OCOCH_3$), 6.38 (d, 1H, H-3, *J*=10 Hz), 7.77 (d, 1H, H-4, *J*=10 Hz), 6.83 (d, 1H, H-6, *J*=2.5 Hz), 7.79 (d, 1H, H-7, *J*=2.5 Hz), 4.15 (d, 1H, CH_2, H-9, *J*=12.5 Hz), 4.29 (d, 1H, CH_2, H-9, *J*=12.5 Hz), 4.22 (dd, 1H, H-10, *J*=5 Hz), and 2.2 (s, 6H, $2CH_3$, H-12 and H-13).

Rearrangement of Imperatorin (1) to *allo*-Imperatorin (3): Imperatorin (**1**) (1 g) was fused at 200 °C, for 25 min. under reduced pressure. The melted product changes to solid. The solid product was washed with CH_2Cl_2, and then recrystallized from ethanol to give the colourless crystals of *allo*-imperatorin (**3**); mp 228 °C (lit,[14,15] 228 °C).

Irradiation of Imperatorin (1) in Methanol Solution: Irradiation of imperatorin (**1**) (675 mg, 0.0025 mol) in methanol for 100 h gave a solid material which was washed with hot methanol to give 11 mg of the dimeric product (**4**) (mp above 360 °C). Evaporation of the filtrate afforded a mixture of two compounds. Further separation with TLC (silica gel, benzene-ethyl acetate 9 : 1) afforded xanthotoxol (**2**) (R_f 0.28, mp 240 °C) and *allo*-imperatorin (**3**) (R_f 0.36, mp 228 °C).

Imperatorin Dimer (4): IR: 3000 (CH_2, CH_3 str.), 1750 (δ-lactone), and 1610 (C=C) cm^{-1}. MS *m/z* (rel intensity) 540 (M^+, 3, $C_{32}H_{24}O_8$), 472 (6, $M-C_5H_8$), 404 (0.8, $M-C_{10}H_{16}$), 270 (20, ½M), 202 (100, ½M−C_5H_8), 174 (20, ½M−C_6H_8O), 149 (20), 89 (10), and 69 (20).

Acid Hydrolysis of Imperatorin Dimer (4) into Xanthotoxol Dimer (7); A mixture of imperatorin dimer (**4**) (0.05 g), ethanol (10 ml) and a mixture of concentrated sulfuric acid and ethanol (1.5 ml: 12.5 ml), was refluxed with stirring for 6 h. The initial white precipitate was converted into a gray precipitate (0.0379 g) which was filtered off and washed with ethanol mp>360 °C. IR (Nujol) 3500 (OH), 1750 (α-pyrone) and 1610 (C=C) cm^{-1}.

Methylation of Xanthotoxol Dimer (7) into Xanthotoxin Dimer (8): A mixture of xanthotoxol dimer (**7**) (0.026 g), methyl iodide (1 ml), anhydrous potassium carbonate (2 g) and acetone (10 ml) was refluxed on a water bath for 6 h. The inorganic salt with the insoluble faint brown product were filtered off, washed with diluted hydrochloric acid, distilled water then methanol to give the methylated dimer (**8**), mp>360 °C. IR(Nujole) 3000 (CH_3 str.), 1730 (α-pyrone), and 1600 (C=C) cm^{-1}.

We are indebted to Professor Dr. F. Bohlmann, TU Berlin, West Germany for spectral measurements.

References

1) T. O. Seine, *J. Pharm. Sci.*, **53**, 231 (1964).
2) G. S. Hammond, C. A. Stout, and A. A. Lamola, *J. Am. Chem. Soc.*, **86**, 3103 (1964).
3) H. Morrison, H. Curtis, and T. McDowell, *J. Am. Chem. Soc.*, **88**, 5415 (1966).
4) K. Muthuramu and V. Ramamurthy, *J. Org. Chem.*, **47**, 3976 (1982).
5) N. Ramasubbu, T. N. GuruRow, K. Venkatesan, V. Ramamurthy, and C. N. Ramachanra Rao, *J. Chem. Soc., Chem. Commun.*, **1982**, 178.
6) F. D. Lewis, D. K. Howard, and J. D. Oxman, *J. Am. Chem. Soc.*, **105**, 3344 (1983).
7) C. H. Krauch and S. Farid, *Chem. Ber.*, **100**, 1685 (1967).
8) F. A. L. Anet, *Can. J. Chem.*, **40**, 1249 (1962).
9) G. O. Schenck, I. Von Wilucki, and C. H. Krauch, *Chem. Ber.*, **95**, 1409 (1962).
10) E. A. Abu-Mustafa, F. K. A. El-Bay, and M. B. E. Fayez, *Naturwissenschaften*, **62**, 40 (1975).
11) C. H. Krauch, S. Farid, and G. O. Schenck, *Chem. Ber.*, **99**, 625 (1966).
12) Yu. E. Orlov and A. P. Prokopenko, *Zh. Obshch. Khim.*, **40**, 1159 (1970).
13) E. A. Abu-Mustafa, B. A. H. El-Tawil, and M. B. E. Fayez, *Indian J. Chem.*, **5**, 283 (1967).
14) T. Noguti and M. Kawakami, *Yakugaku Zasshi*, **61**, 77 (1941).
15) M. A. Loutfy and H. A. Abu-Shady, *J. Pharm. Sci.*, **66**, 1623 (1977).

Protection of Functional Groups and Stannylation of Phenylalanine

S. A. METWALLY,*,† H. H. COENEN, and G. STÖCKLIN
Institut für Chemie 1 (Nuklearchemie), Kernforschungsanlage Jülich GmbH, D-5170 Jülich, Federal Republic of Germany
(Received December 8, 1986)

The protection of both amino and carboxylic acid groups in *p*-halogenated phenylalanine was done by using different reagents. The protected amino acid was stannylated by using hexamethyldistannane in the presence of tetrakis(triphenylphosphine)palladium as catalyst.

Substituted especially halogenated aromatic amino acids are generally prepared from appropriate, already substituted aryl derivatives, for example benzaldehydes.[1] Radiohalogenation with short lived isotopes, however, necessitates a fast introduction of the halogen, if possible in the last reaction step. *p*-Fluoro-L-phenylalanine labelled with the positron emitter fluorine-18 ($T_{1/2}$=110 min) was recently suggested as a potential tracer for measuring cerebral protein synthesis in vivo in man using positron emission tomography.[2] The direct electrophilic fluorination of L-phenylalanine leads to *p*-fluorophenylalanine, but only in low yields and the ortho- and meta-product which are also formed are difficult to separate.[2] Fluorodemetallation reactions on suitably metallated phenylalanine derivatives can provide a way to regioselective halogenation.

There are not many examples of complex biomolecules which were labelled by fluorodemetallation reactions.[3] However, a recent systematic study on simple aryltrimethyl compounds of group IVB showed that tin derivatives are most suitable for fluorodemetallation.[4] There are ample precedences in the literature for cleavage of aryl-tin bonds by halogens and interhalogens (I_2, Br_2, Cl_2, ICl, IBr). Given these facts, and the ease with which aromatic substrates can be metallated, and subsequently stannylated,[5,6] it occurred to us that such substances might be ideal substrates for fluorination using elemental fluorine.

The aim of this work is the preparation of a suitable stannylated phenylalanines to be used for ^{18}F-fluorination. The need of a variety of amino- and carboxyl protecting groups which can be cleaved under relatively mild conditions to the corresponding amino acids is well recognized. The protection groups have to meet the following requirements in our specific case: The condensation and cleavage reactions have to proceed without racemization and the cleavage has to be fast with respect to the half life of fluorine-18. The protecting groups should not hinder the stannylation and fluorination.

Results and Discussion

The need of a *p*-stannylated derivative of phenylalanine for the direct regiospecific radiofluorination stimulated a search for suitable halogenated precursors with appropriate protecting groups for the metallation. In view of the necessary regiospecific labelling with fluorine-18, *p*-iodo- and *p*-bromo-L-phenylalanine were found useful intermediates which were prepared according to Scheme 1.

p-Iodo-L-phenylalanine was prepared from the commercially available L-*p*-aminophenylalanine by chelating the α-amino and the carboxyl group using copper(II) ions to form a stable copper complex[7] in which the aromatic amino group is free to react with appropriate reagents. The latter was diazotized by sodium nitrite-hydrochloric acid mixture to form the corresponding diazotized phenylalanine copper complex. The diazonium salt was transformed into the corresponding *p*-iodo-L-phenylalanine.

A less expensive way is the *N*-acylation of *p*-bromo-DL-phenylalanine with subsequent enzymatic deacylation of the L-enantiomer. The stereochemical purity of the *p*-halo-L-phenylalanines was tested by chiral TLC

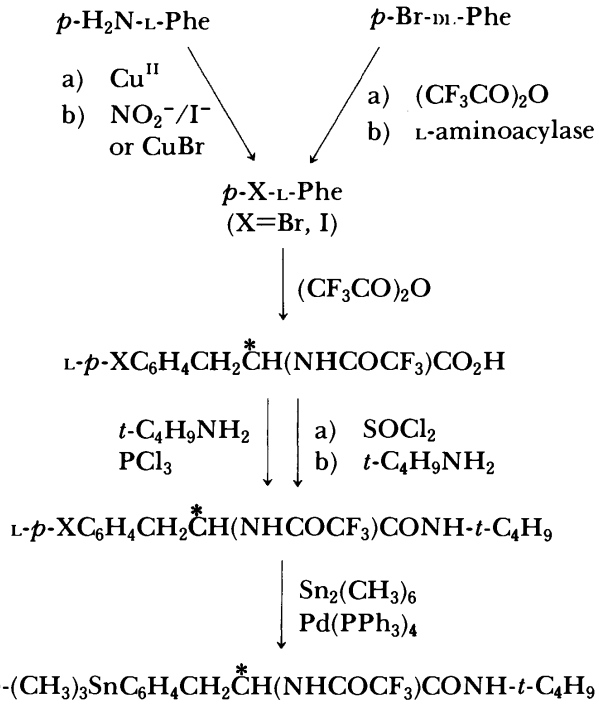

L-Phe is a notation for L-phenylalanine.

L indicates the configuration of $\overset{*}{C}$ atom.

Scheme 1.

†On leave from Chemistry Department, Faculty of Science, Assiut University, Assiut, Egypt.

plates and chiral HPLC (see Experimental).

We have protected both the two functional groups by different types of blocking moieties: the carboxyl group was blocked by *t*-butylamide[8] or *t*-butyl ester[9] while the protecting groups for the amino function were trifluoroacetyl,[10] acetyl,[11] trityl,[12] and *o*-nitrobenzenesulfenyl groups.[11] Under the reaction conditions used, trifluoroacetyl and acetyl for the amino group and the conversion into *t*-butylamide for the carboxyl group proved to be the best protecting groups with respect to the requirements stated above (cf. Scheme 1). Hydrolysis of the protected amino acids was tested under various conditions, where hydroiodic acid (56% super pure) was found to be very suitable since the reaction was completed in the course of 15 min. Hydrochloric acid at different concentrations and temperatures failed to achieve such hydrolysis. The effect of protection for L-phenylalanine functional groups and also of the succeeding stannylation step on racemisation were tested after hydrolysis to the corresponding free L-phenylalanine. In this way the hydrolysis conditions were also checked for racemisation. It was noted that the amidation with *t*-butyl amine and PCl_3, given as an alternative in Scheme 1, was not as stated in the literature[8] and up to 10% of D-isomer was formed in some preparations.

Stannylation of the protected *p*-halophenylalanine was tried using different routes: a) Grignard reaction: Stannylation via Grignard reaction, using the known technique[13] did not give rise to stannylated products. b) Stannylation using an aryllithium intermediate:[14] The interaction of protected *p*-halophenylalanine with butyllithium followed by the reaction with trimethylstannyl chloride resulted in the formation of *p*-butylphenylalanine derivatives. c) Stannylation with Pd(0) catalysts: The stannylation was successful using hexamethyldistannane and protected *p*-iodo- or *p*-bromophenylalanine in presence of tetrakis(triphenylphosphine)palladium(0) as catalyst. This method was tested according to the wide application of this palladium catalyst in stannylation of simple organic compounds.[15-17] No stannylation for complex molecules such as protected phenylalanine was found in the literature. The features of this reaction can be summarized as follows:

a) *p*-Iodo-DL-phenylalanine (protected at both amino and carboxy group) behaves like simple iodo aromatic compounds[16] and gave a distinctly better yield than the *p*-bromo derivative.

b) The cleavage of hexamethyldistannane by the *p*-chloro-DL-phenylalanine derivative did not proceed even at 135 °C and 35 bar to any significant extent, and more drastic conditions led to decomposition of the catalyst.[18]

c) The completion of the reaction is clearly visualized since the catalyst serves as an indicator; as soon as *p*-halogenated-DL-phenylalanine derivative is consumed, Pd metal precipitates and the brown solution turns colorless.

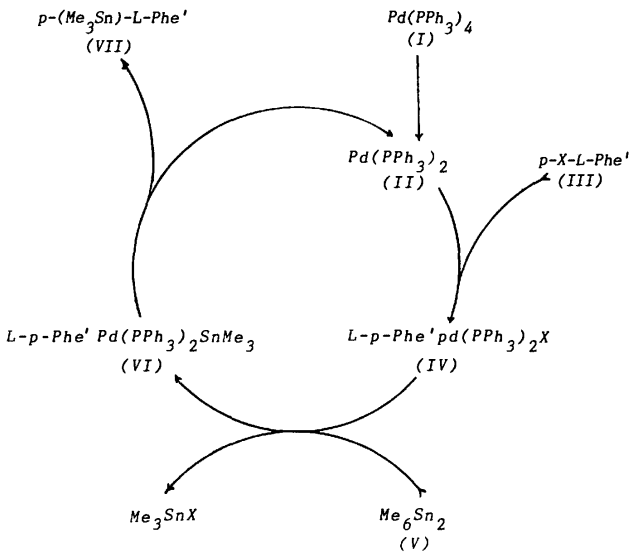

X=Br, I
Ph=phenyl
Phe'=protected phenylalanine

Scheme 2.

It can be assumed that the first step in the stannylation reaction is the dissociation of the catalyst (I) into bis(triphenylphosphine)palladium (II) possibly complexed with the solvent. Oxidative addition of (II) to the protected *p*-iodo- or *p*-bromo-DL-phenylalanine (III) gives iodo- or bromo-DL-phenylalanine bis(triphenylphosphine)palladium (IV). This complex interacts with hexamethyldistannane (V) under substitution of the halogen substituent by the trimethylstannyl group to yield Phe' $Pd(PPh_3)_2SnMe_3$ (VI) which dissociates to the *p*-stannylated phenylalanine derivative (VII) and the bis(triphenylphosphin)palladium (II). The reaction cycle is shown in Scheme 2 and is similar to the selective ketone synthesis from acid chlorides and tetraalkylstannane catalysed by $[PdCl(PhCH_2)(PPh_3)_2]$.[19]

Dichlorobis(triphenylphosphine)palladium also was found to initiate the reaction of hexamethyldistannane (V) with *p*-iodo- or *p*-bromo-DL-phenylalanine derivatives, but the catalyst was not active as Pd(0) complex. This is implied by the fact that with the divalent complex the reaction went to only 20% completion at 115 °C in 20 h. The present system thus may furnish the only convenient method for aromatic amino acid stannylation.

Experimental

Melting points are uncorrected. The ^1H NMR measurements were performed on an 80 MHz Brucker spectrometer (WP 80), using TMS as internal standard and $CDCl_3$ or D_2O as solvents. Mass spectra were recorded at 70 eV on an AEI MS 12 mass spectrometer using a direct insertion technique and a probe temperature ranging between 150 and 200 °C. IR spectra were recorded in KBr on a Perkin-Elmer model 20

spectrophotometer. Hexamethyldistannane was prepared according to published procedures.[20] The substituted phenylalanines and the palladium catalyst were from Aldrich (Steinheim, FRG). Other solvents and reagents were from Merck (Darmstadt, FRG), unless otherwise noted.

Synthesis of *p*-Iodo-L-phenylalanine: *p*-Amino-L-phenylalanine hydrochloride hydrate (0.5 g) was dissolved in water (15 ml) and boiled under reflux for 45 min with an excess (1 g) of black copper oxide. The excess copper oxide was filtered off and the solution was concentrated and cooled to give green crystals of the *p*-amino-L-phenylalanine copper complex (0.45 g). It was dissolved in dilute hydrochloric acid (20 ml) and cooled to 0 °C. Cold soldium nitrite solution (0.06 g in 5 ml of water) was added and the resulting diazonium salt was kept in ice for 30 min. The solution was boiled under reflux with potassium iodide (0.2 g) and the copper complex was decomposed by hydrogen sulphide and the precipitated copper sulphide was removed by filtration. *p*-Iodo-L-phenylalanine was isolated by the addition of sodium acetate and identified by TLC.

Synthesis of *p*-Bromo-L-phenylalanine: *N*-Trifluoroacetyl-*p*-bromo-DL-phenylalanine was prepared as described below and 0.5 g was dissolved in phosphate buffer (pH 7—7.2) and 12 mg $CaCl_2$ and 1 ml aminoacylase solution (*N*-acylamino acid amidohydrolase EC 3.5.1.14, 3.2 mol dm^{-3}, 25 U mg^{-1}) added. The solution was kept at 38 °C for 20 h then acidified (pH 3). The precipitated enzyme was separated by centrifugation. The supernatant is adjusted to pH 5.5—6 and concentrated until the free L-amino acid starts to crystalize. After cooling for several hours the *p*-bromo-L-phenylalanine is filtered off, washed with H_2O and ethanol, and identified by TLC.

Protection of *p*-Halo-DL-phenylalanines: *N*-Trifluoroacetyl-*p*-halo-DL-phenylalanine. The following is a representative and modified procedure to that known in the literature.[11] Dry *p*-bromo-DL-phenylalanine (0.96 g) was dissolved in a 10—15 fold amount of dry trifluoroacetic acid (warming if necessary). The solution was cooled in an ice-salt bath to −10 °C. Trifluoroacetic anhydride (1.2 mol) (0.929 g; 0.61 ml) was added gradually in the course of a few minutes. The temperature was increased to 10 °C and left for 30 min. The reaction mixture was dried under vacuum at a maximum temperature of 30 °C using a well cooled receiver. The nonreacted amino acid was removed by dissolving the residue in dry ether followed by filtration and evaporation of ether. The solid was recrystallized from benzene to give colorless needles of *N*-trifluoroacetyl-*p*-bromo-DL-phenylalanine, mp 152 °C yield 1.25g. IR 1680—1730 (-COOH, C=C) 3100 cm^{-1} (sec. amide), ^1H NMR ($CDCl_3$) δ=7.3—7.8 (q, 4 aromatic H); MS M^+: 329 and 331. Calcd for $C_{11}H_9NO_3BrF_3$: C, 38.82; H, 2.64; N, 4.11%. Found: C, 38.85; H, 2.71; N, 4.32%.

***N*-Trifluoroacetyl-*p*-chloro-DL-phenylalanine.** Colorless needles from benzene, mp 114 °C, yield 90%. Found: C, 44.82; H, 3.26; N, 4.64%. Calcd for $C_{11}H_9NO_3F_3Cl$: C, 44.74; H, 3.05; N, 4.74%.

***N*-Trifluoroacetyl-*p*-iodo-DL-phenylalanine.** Colorless needles from benzene, mp 148 °C, yield 83%. Found: C, 34.28; H, 2.64; N, 3.75%. Calcd for $C_{11}H_9NO_3F_3I$: C, 34.10; H, 2.32; N, 3.61%.

***N*-Trifluoroacetyl-*p*-bromo-DL-phenylalanine *t*-Butylamide:** The following are typical general procedures: a) *N*-Trifluoroacetyl-*p*-bromo-DL-phenylalanine (1 g) is dissolved in dry pyridine (10 ml) by warming if necessary. *t*-Butylamine (1.31 ml) is added and the mixture is cooled in an ice bath. Phosphorus trichloride (0.13 ml) in 5 ml dry pyridine is added gradually to the cold reaction mixture. The solution is heated under reflux for 3 h, followed by concentration to one third and poured on ice-cold water. The solid product was filtered, washed with water until pyridine free and dried. It was crystallized from ethanol into colorless needles of *N*-trifluoroacetyl-*p*-bromo-DL-phenylalanine *t*-butylamide, mp 127 °C, yield 0.5 g. b) Alternatively: 25 ml $SOCl_2$ were added to *N*-trifluoroacetyl-*p*-bromo-L-phenylalanine (4.75 g) and kept for 3 h at 40 °C. Subsequently, the excess of $SOCl_2$ was evaporated. The residual acid chloride was dissolved in 30 ml CH_2Cl_2 and *t*-butylamine added dropwise until alkaline reaction (2.2 ml). The CH_2Cl_2 solution was extracted 4 times with water and then dried over Na_2SO_4. After evaporation to dryness the residue was recrystallized from ethanol. Yield 1.4 g, 26%.

***N*-Trifluoroacetyl-*p*-chloro-DL-phenylalanine *t*-Butylamide:** Colorless needles from ethanol mp 132 °C, yield 55%. ^1H NMR ($CDCl_3$) δ=1.17 (s, 9H), 4.25 (d, 2H), 5.25 (t, 1H), 7.37—7.75 (q, 4 aromatic H). Found: C, 51.84; H, 4.66; N, 8.12%. Calcd for $C_{15}H_{16}ClN_2O_2F_3$: C, 51.72; H, 4.59; N, 8.04%.

***N*-Trifluoroacetyl-*p*-iodo-L-phenylalanine *t*-Butylamide:** Colorless needles from ethanol mp 129 °C, yield 50%. ^1H NMR ($CDCl_3$) δ=1.15 (s, 9H), 4.25 (d, 2H), 5.31 (t, 1H), 7.35—7.70 (q, 4 aromatic H). Found: C, 34.28; H, 2.68; N, 3.82%. Calcd for $C_{15}H_{16}IN_2O_2$: C, 34.10; H, 2.32; N, 3.61%.

***p*-Halogeno-DL-phenylalanine *t*-Butyl Ester:** The following is a typical procedure: A large amount of concentrated sulfuric acid (about 1 ml per 1 g of amino acid) is added to a suspension of the amino acid in diethylene glycol dimethyl ether (5 to 10 ml per 1 g of amino acid), an equal volume of liquid isobutene (liquified by passing the gaseous isobutene in a wide glass tube immersed in Dry Ice-acetone mixture) was added and the mixture was shaken overnight in a pressure gold-lined steal bottle. The solution was cautiously poured into excess 2 M (1 M=1 mol dm^{-3}) sodium hydroxide and the ester was extracted under vacuum to leave an oil (all of the three *p*-halogenophenylalanines). Addition of dilute hydrochloric acid resulted in the immediate precipitation of the ester hydrochloride. The nonreacted amino acid precipitates soon after extraction from the aqueous layer. The yield was almost quantitative and 5 g of *p*-chloro-DL-phenylalanine, for example, gave 5.9 g of the *t*-butyl ester hydrochloride and 0.7 g of *p*-chlorophenylalanine was isolated from the aqueous layer. Trials to carry the reaction in presence of concentrated sulfuric acid without solvent failed.

***p*-Chloro-DL-phenylalanine *t*-Butyl Ester Hydrochloride:** Colorless flakes from water mp 221 °C (decomp) ^1H NMR (D_2O) δ=1.38 (s, 9H), 4.5 (d, 2H), 5.25 (t, 1H), 7.25—7.8 (q, 4 aromatic H). Found: C, 53.74; H, 6.68; N, 4.88%. Calcd for $C_{13}H_{19}NCl_2O_2$: C, 53.60; H, 6.52; N, 4.81%.

***p*-Bromo-DL-phenylalanine *t*-Butyl Ester Hydrochloride:** Colorless flakes from dil ethanol mp 214 °C (decomp). ^1H NMR (D_2O) δ=1.35 (s, 9H), 4.57 (d, 2H), 5.3 (t, 1H), 7.25—7.75 (q, 4 aromatic H). Found: C, 46.64; H, 5.76; N, 4.22%. Calcd for $C_{13}H_{19}BrClNO_2$; C, 46.42; H, 5.65; N, 4.16%.

***p*-Iodo-DL-phenylalanine *t*-Butyl Ester Hydrochloride:** Colorless flakes from water mp 233 °C (decomp) ^1H NMR (D_2O) δ=1.38 (s, 9H), 4.55 (d, 2H), 5.3 (t, 1H), 7.3—7.8 (q, 4 aromatic H). Found: C, 40.86; H, 5.12; N, 3.78%. Calcd for

$C_{13}H_{19}NClIO_2$: C, 40.73; H, 4.96; N, 3.95%.

***t*-Butyl Esters of *N*-Acetyl-, *N*-Nitrobenzesulfenyl, and *N*-Trityl-*p*-halogeno-DL-phenylalanine**: The following is a general method: Either 0.01 mol of acetyl chloride, *o*-nitrobenzenesulfenyl chloride or trityl bromide was added to a solution of 0.01 mol of *p*-halogeno-DL-phenylalanine *t*-butyl ester hydrochloride in 25 ml of dry chloroform and 2.8 ml of triethylamine. After being left at room temperature for 6 h, the solution was successively washed with water, dilute acetic acid, aqueous potassium hydrogencarbonate solution, and again with water. It was dried over sodium sulfate and evaporated under vacuum to dryness. The crude products were usually crystallized from ethanol, methanol, or ethyl acetate-petroleum ether.

***N*-Acetyl-*p*-chloro-DL-phenylalanine *t*-Butyl Ester**: Colorless needles from toluene, mp 123 °C, yield 47%. ^{1}H NMR ($CDCl_3$) δ=1.38 (s, 9H), 2.1 (s, 3H), 4.87 (d, 2H), 5.18 (t, 1H), 7.25—7.75 (q, 4 aromatic H). Found: C, 60.58; H, 6.82; N, 4.64%. Calcd for $C_{15}H_{20}ClNO_3$: C, 60.6; H, 6.73; N, 4.71%.

***N*-Acetyl-*p*-bromo-DL-phenylalanine *t*-Butyl Ester**. Colorless needles from benzene, mp 138 °C, yield 55%. ^{1}H NMR ($CDCl_3$) δ=1.37 (s, 9H), 2.2 (s, 3H), 4.82 (d, 2H), 5.2 (t, 1H), 7.32—7.75 (q, 4 aromatic H). Found: C, 56.78; H, 6.36; N, 4.48%. Calcd for $C_{15}H_{20}BrNO_3$: C, 56.60; H, 6.28; N, 4.40%.

***N*-Acetyl-*p*-iodo-DL-phenylalanine *t*-Butyl Ester**: Colorless needles from benzene, mp 127 °C, yield 63%. ^{1}H NMR ($CDCl_3$) δ=1.38 (s, 9H), 2.3 (s, 3H), 4.86 (d, 2H), 5.2 (t, 1H), 7.32—7.8 (q, 4 aromatic H). Found: C, 46.52; H, 5.28; N, 3.64%. Calcd for $C_{15}H_{20}NO_3I$: C, 46.27; H, 5.14; N, 3.59%.

Stannylation of *p*-Halo-*N*-acetyl- or *N*-Trifluoroacetyl-L-phenylalanine *t*-Butylamide: The following is a general procedure for the stannylation of protected *p*-halophenylalanines: A mixture of hexamethyldistannane (39 mmol), *p*-bromo- or *p*-iodo-*N*-trifluoro- or *N*-acetyl-L-phenylalanine *t*-butylamide (2.5 mmol), tetrakis(triphenylphosphine)palladium(0) (1.3×10^{-4} mol) and dioxane (50 ml) was heated under reflux for 5 h whereby palladium metal was precipitated as fine black powder. The mixture was cooled and filtered, and the filtrate was evaporated under vacuum to a residue. This was taken up in ether or benzene and the solution was washed several times with water and dried over $MgSO_4$. The solvent was removed to leave the product which was crystallized from benzene.

***N*-Acetyl-*B*-[4-(trimethylstannyl)phenyl]-L-alaine *t*-Butylamide**. White crystals, yield 15—20%. ^{1}H NMR ($CDCl_3$) δ=7.6 (p, 4H, aryl H), 0.34 (s, with Sn satellites, 9H, $SnMe_3$), 1.18 (s, 9H, *t*-butyl H), 2.06 (s, 3H), 2.06 (s, 3H). The mass spectrum showed the expected parent ion at *m/z* 410. Found: C, 52.74; H, 7.54; N, 3.48; Sn, 28.94%. Calcd for $C_{18}H_{30}O_2N_2Sn$: C, 52.68; H, 7.31; N, 3.41; Sn, 28.78%.

***N*-Trifluoroacetyl-*B*-[4-(trimethylstannyl)phenyl]-L-alanine *t*-Butylamide**. White crystals, yield 15—20%. ^{1}H NMR ($CDCl_3$) δ=7.8 (q, 4H, aryl H), 0.32 (s, with Sn satellites, 9H, $SnMe_3$), 1.18 (s, 9H, *t*-butyl H), the mass spectrum indicated the expected parent ion at *m/z* 464. Found: C, 46.64; H, 5.88; N, 3.14; Sn, 25.86%. Calcd for $C_{18}H_{27}O_2NSnF_3$: C, 46.55; H, 5.81; N, 3.01; Sn, 25.43%.

Chromatographich Analysis of Enantiomeric Purity: The enantiomeric purity of all phenylalanine derivatives prepared were checked in form of the free amino acid on chiral TLC plates or by means of chiral HPLC. In the case of protected compounds blocking groups were previously hydrolised. Typically 5 to 10 mg of the compound were heated for 20 min in 2 ml 56% pure HI at 140 °C in a closed reaction vial. The chiral TLC plates from Macherey-Nagel (Düren, FRG) were developed with methanol-H_2O-acetonitrile 50 : 50 : 200 (v/v/v). For chiral HPLC a column from serva (Heidelberg, FRG) (Si-100 Polyol, Chrial Pro Cu, 5 µm, 4×250 mm) was used with a 1 mM $CuSO_4$ solution as eluant and a flow of 4 ml min^{-1}.

The authors thank Mr. M. Wutz for valuable experimental assistance and Dipl. Chem. K. Reisinger for the performance of mass spectra.

References

1) G. L. Barrett, "Chemistry and Biochemistry of the Amino Acids," Chapman and Hall, London and New York (1985).

2) W. Bodsch, H. H. Coenen, K. Takahashi, K-A. Hossman, and G. Stöcklin, *J. Neurochem.*, in press (1986).

3) M. J. Adam, *Appl. Radiat. Isot.*, **37**, 811 (1986).

4) H. H. Coenen and S. M. Moerlein, *J. Fluor. Chem.*, in press.

5) R. C. Larock, *Tetrahedron*, **38**, 1713 (1982).

6) H. H. Coenen, S. M. Moerlein, and G. Stöcklin, *Radiochim. Acta*, **34**, 47 (1983).

7) A. C. Kurtz, *J. Biol. Chem.*, **122**, 477 (1937).

8) S. Goldschmidt and H. Lautenschlager, *Justus Liebigs Ann. Chem.*, **580**, 68 (1953).

9) A. L. McClosky, G. S. Fonken, R. W. Kluiber, and W. S. Johnson, *Org. Synth.* Coll. Vol. 4, 261 (1963).

10) F. Weygand and E. Czendes, *Angew. Chem.*, **64**, 136 (1952).

11) M. Bergmann, F. Stern, and C. Witte, *Justus Liebigs Ann. Chem.*, **449**, 277 (1926).

12) A. Hilmann-Elies, G. Hilmann, and H. Jatzkewitz, *Z. Naturforschg.*, **8b**, 445 (1953).

13) Zervas, D. Borovas, and E. Gazis, *J. Am. Chem. Soc.*, **85**, 3660 (1963).

14) K. L. Jaura, L. K. Churmani, and K. K. Sharman, *Indian J. Chem.*, **4**, 329 (1966).

15) A. N. Kashin, I. G. Bumagina, N. A. Bumagin, V. N. Bakunin, and I. P. Beletskaya, *Zh. Org. Khim.*, **17**, 905 (1981).

16) M. Kosugi, T. Ohya, and T. Migita, *Bull. Chem. Soc. Jpn.*, **56**, 3855 (1983).

17) N. A. Bumagin, I. G. Bumagina, and I. P. Beletskaya, *Dokl. Akad. Nauk SSSR*, **274**, 1103 (1984).

18) H. Azizian, C. Eaborn, and A. Pidcock, *J. Organomet. Chem.*, **215**, 49 (1981).

19) D. Milstein and J. K. Stille, *J. Am. Chem. Soc.*, **100**, 3636 (1978).

20) G. F. Smith, H. G. Kuivila, R. Simon, and L. Sultan, *J. Am. Chem. Soc.*, **103**, 833 (1981).

The Control of the Particles of Magnetite

Keizo MATSUDA,* Masami SUMIDA, Kazumi FUJITA, and Shunmei MITSUZAWA
Department of Chemistry, Faculty of Science, Tokai University, Kitakaname Hiratsuka-shi 259-12
(Received March 24, 1987)

Synopsis. Fine particles of magnetite were prepared by the hydrolysis of urea.[1] The effects of the amount of urea on the particles were investigated. The expected particles were prepared in the range 0.8 to 2.2 μm in size by controlling the amount of urea. Fine particles of magnetite of 0.8 μm in size were prepared from a solution with R=60 (R=urea/iron(III) mol ratio).

For the synthesis of magnetite by the wet method, there are four methods: (1) The coprecipitation method adding a strong alkalline solution to a solution containing Fe^{2+} and Fe^{3+} ions;[2] (2) the air-oxidation method bubbling air into a suspension solution of green rust;[3] (3) the reaction of iron(III) hydroxide sol and Fe metal;[4] and (4) the method adding the non-ion surface active agent to mixed iron(III) hydroxide sol and Fe metal.[5]

In the first three methods, the obtained particles were ultrafine particles under 0.06 μm and the particles in the latter were 5 μm. It was clear that magnetite was prepared by the hydrolysis of urea from the solution containing Fe^{2+} and Fe^{3+} ions,[1] or from the aqueous suspension of β-FeOOH containing Fe^{2+} ions.[6] The fine particles of the crystalline magnetite were obtained by these methods. The pH of the solution dissolved Fe^{2+}, Fe^{3+}, ions and urea increased with the hydrolysis of urea. It increased rapidly by the hydrolysis of a great amount of urea; then, the particles of obtained magnetite became small. The change of the pH of each solution with various R values and the particle size of magnetite precipitated from each solution were measured. From these results, the relation between the distribution of particle sizes of magnetite and amount of urea (R=6—60) was discussed.

Experimental

Magnetite was synthesized by heating a solution containing urea, iron(II) chloride, and iron(III) chloride at 98 °C. A reaction apparatus, already described,[6] was used. Zero point zero five mol of iron(III) chloride and the prescribed amount of urea (the range of R=6 to 60) were dissolved in 0.3 dm^3 of distilled water; and the solution was transfered into three neck flask of 1 dm^3. Iron(II) chloride of 0.025 mol was dissolved with bubbling N_2 gas in the solution at the rate of 1 $dm^3\,min^{-1}$. The time required to raise the temperature up to 98 °C from temperature was 5 min and the reaction time was measured from the time when up to 98 °C was reached. After the programed reaction time, the products were filtered, washed with a large amount of boiling water until iron(II) ion could not be detected. They were then dried in a vacuum desiccator on P_2O_5 powder and were stored. In measurement of particle size of magnetite, centrifugal particles size analyzer (Shimazu CP-50) were used. Sodium hexametaphosphate (0.3%) was used as disparse medium.

Results and Discussion

The change of the pH of each solution with R=6, 10, 20, and 60 with reaction time are shown in Fig. 1. The rate of the pH rise increased rapidly with an increase in R and the final pH of the solution became high. The rate of the pH rise slowed down at pH 4—5 in the solution with R=6 and 10. These phenomena were not observed in the solutions with R=20 and 60.

On the other hand, the changes of the intensities of X-ray diffraction patterns of the products obtained from the solution with R=6 with reaction time are shown in Fig. 2. From the results of measurements of pH and X-ray diffraction patterns of products, β-FeOOH was produced at pH 1—2 and magnetite was produced at pH 4—5. α-FeOOH was recognized from the solutions with R=6 and 10. Magnetite and α-FeOOH were produced at the same time; after that, α-FeOOH gradually decreased and α-FeOOH was finally transformed into magnetite.[6] α-FeOOH was not observed from the solutions with R=20 and 60. The relation between the intensities of the X-ray diffraction (311) plane of magnetite produced from solutions R=6, 10, and 20 and the reaction time is shown in Fig. 2. Magnetite precipitated rapidly, since the rate of the rise of pH was quick with an increase in R.

The average particle sizes of magnetite produced from the solutions with R=6—60 were determined by a centrifugal particle size analyzer. The relation between the average particle sizes and R is shown in Fig. 3. The average particle sizes of magnetite became small with the increase in R. The average particle sizes

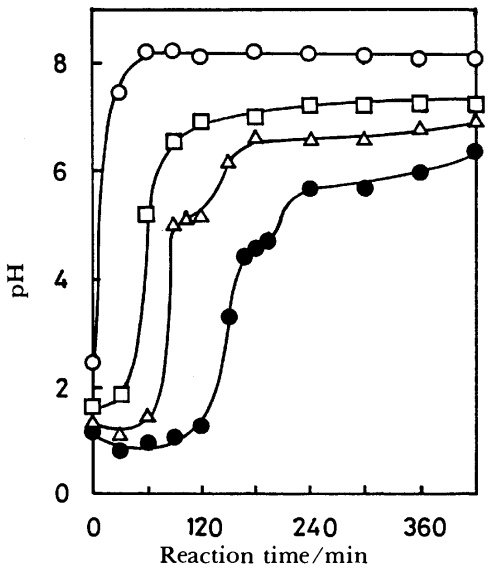

Fig. 1. Relation between change of pH and reaction time. Conditions: R=Urea/iron(III) ion mole ratio. ○—○: R=60, □—□: R=20, △—△: R=10, ●—●: R=6.

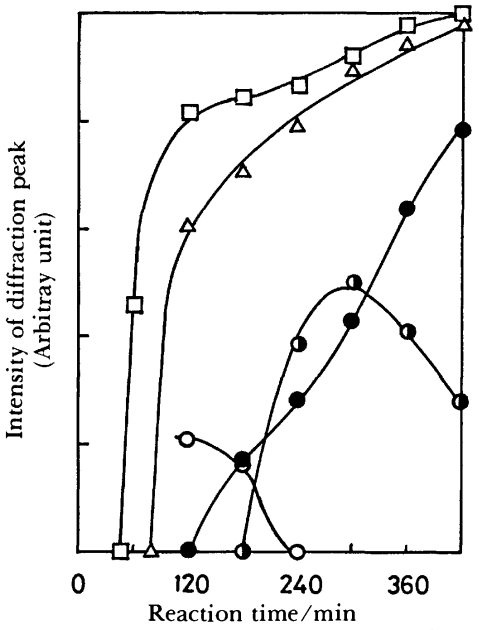

Fig. 2. The relative intensities of X-ray diffraction of magnetite, β-FeOOH and α-FeOOH vs. reaction time after the solution temperature of 98°C reached. Conditions: R=Urea/iron(III) ion mole ratio. □—□: Magnetite (311)plane, R=20. △—△: Magnetite (311)plane, R=10. ●—●: Magnetite (311)plane, R=6. ○—○: β-FeOOH (310)plane, R=6. ◑—◑: α-FeOOH (110)plane, R=6.

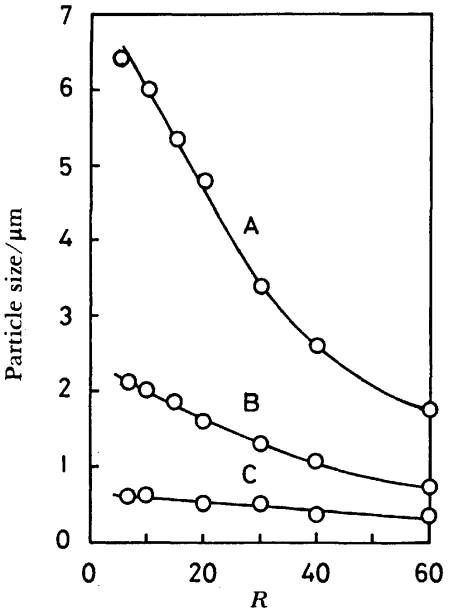

Fig. 3. Plots of average particle size of magnetite and width of distribution of particles. Conditions: A: Upper limit of distribution of particles. B: Average particles. C: Lower limit of distribution of particles.

of magnetite produced from the solutions R=6 and 60 were 2.2 and 0.8 μm, respectively. The widths of the distribution of particle size of magnetite prepared under the various conditions are shown in Fig. 3. The width of distribution was small with the increase of R.

When R value (as R=6) was small, the rate of the rise of pH was slow and the hydrolysis of urea was a rate-determining step in the formation of magnetite, and the pH of the solution was kept at constant of pH about 4.6 during precipitation magnetite. Therefore, nucleation of magnetite took place slightly compared with R=60; the particles precipitated in the first stage were aged for longer periods and the particles became large; however, the particles precipitated in the latter stage were small because of no aging. It was considered that the particle size of β-FeOOH formed in the initial stage of the reaction became large, when R value was small,[7] and that effected the particle size of magnetite. The average size, as a whole, was large. The distribution of particle size was widespread.

When the R value was large, the rate of the rise of pH was rapid and the pH value quickly reached 7—8. Therefore, a high nucleation of magnetite also quickly took place (at a breath). The particles of magnetite produced were small, the width of distribution in particle size narrowed.

It was clear that the R value was large, the average particle size was smaller and that the distribution of particle size was uniformed. When the R value was small, the particles of magnetite precipitated in the initial stage were aged and became large; however, the particles precipitated in the latter stage increased with increasing pH, and were small. Therefore, it was considered that this distribution was not normal; the large particles were a little but the distribution was widespread. When R value was large, the particles precipitated in the first stage were small and amount of particles was much. Therefore, it was considered that the particles were not aged and the particles were small, and that the distribution of particle size was uniformed.

On the ground of these facts, it was elucidated that the magnetite particles of the expected size in the range of 0.8 to 2.2 μm were prepared by hydrolysis of urea easily. The average particle size of 0.8 μm was obtained from the solution with R=60, and the particles were distribution in the range of 0.3—1.75 μm.

References

1) K. Matsuda and I. Kayama, *Nippon Kagaku Kaishi*, **1983**, 23.
2) T. Sugimoto and E. Matijevic, *J. Colloid Interface Sci.*, **74**, 227 (1980).
3) Y. Tamaura, T. Yosida, and T. Katsura, *Bull. Chem. Soc. Jpn.*, **57**, 2411 (1984).
4) K. Kandori, A. Kitahara, and K. Kon-no, *Nippon Kagaku Kaishi*, **1982**, 722.
5) K. Kandori, H. Arai, K. Kon-no, and A. Kitahara, *Nippon Kagaku Kaishi*, **1984**, 1357.
6) K. Matsuda, *Nippon Kagaku Kaishi*, **1983**, 1589.
7) A. Kato and Y. Morimitsu, *Nippon Kagaku Kaishi*, **1984**, 800.

Adsorption of Uranium from Nitric Acid Solutions Using Crystalline Hydrous Titanium Dioxide Fibers

Yū KOMATSU,* Yoshinori FUJIKI, and Takayoshi SASAKI
National Institute for Research in Inorganic Materials, 1-1 Namiki, Sakura-mura, Niihari-gun, Ibaraki 305
(Received May 2, 1987)

Synopsis. The adsorption of uranium on an ion exchanger of crystalline hydrous titanium dioxide fibers from nitric acid solutions has been studied. The rate of the adsorption of uranium was much higher than that of alkaline earth metal ions. The adsorption behavior of uranium was well explained by their ion exchange with hydrogen ions in the fibers.

Hydrous titanium dioxides have been mentioned for use in the extraction of uranium from seawater.[1,2] However, conventional hydrous titanium dioxide has been prepared of a fine particle powder and is not very suitable for column operations. Recently, Ohta and Fujiki have reported[3] a new type of hydrous titanium dioxide, crystalline hydrous titanium dioxide fibers, which is a derivative of potassium tetratitanate ($K_2Ti_4O_9$) fibers. The adsorption of alkali metal ions,[4,5] alkaline earth metal ions,[6-9] and bivalent transition metal ions[10] from weakly acidic solutions on the fibers has been studied by the authors. In the present work, the adsorption properties of crystalline hydrous titanium dioxide fibers for uranium are studied in order to obtain further information on the fibers.

Experimental

The titanium dioxide used was of 99.9% purity. Potassium tetratitanate fibers, $K_2Ti_4O_9$, were grown by the slow-cooling method in a K_2MoO_4 flux melt.[3] The fiber of about 10 g was filled in a glass column and converted to the protonated form, $H_2Ti_4O_9 \cdot nH_2O$, by passing 1 mol dm^{-3} hydrochloric acid until detection limit of potassium ion in the effluent by an atomic absorption method(Hitachi Polarized Zeeman Atomic Absorption Spectrophotometer 180-80). The weight of uranyl nitrate was measured as unhydrated state. All the other reagents used were of analytical grade. The measurements of the ion-exchange equilibria were made in a similar way to that in the previous study,[7] except that the fiber and the aqueous solution were agitated 50 times a day by hand.

The distribution coefficient K_d of uranium was obtained by mixing 0.1 g of the fiber with 10 cm^3 of the aqueous solution containing various concentrations of uranium and calculated as:

$$K_d = \frac{\text{(amount of uranium of sorbed per 1 g of the fiber)}}{\text{(amount of uranium per 1 cm}^3\text{ of solution)}} \quad (1)$$

Here, the weight of the solid was measured in the air-dried state.

The pH values of the solutions were controlled with nitric acid and were measured by a TOA pH meter(model HM-20E). The uranium contents in the supernatant solution was determined with a Daini Seikosha Inductively Coupled Plasma Optical Emission Spectrophotometer(model SPS-1100).

Results and Discussion

Figure 1 gives the percent adsorption values for uranium between fibers and aqueous solution as a function of the contact time. Although 10—14 days were required to attain equilibrium for alkaline earth metal ions[7] and bivalent transition metal ions,[10] the equilibrium of uranium was attained within three days.

Crystalline hydrous titanium dioxide fibers have two exchangeable protons in the chemical formula. When alkali metal ions are incorporated in the hydrated fibers, one of these protons may be replaced with an alkali metal ion by ion exchange. An alkaline earth metal ion or a bivalent transition metal ion can replace the two protons in the fiber. As can be seen in Fig. 2, the distribution coefficient of uranium is first-

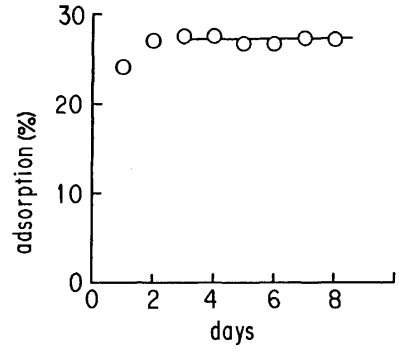

Fig. 1. The percent absorption of the uranium as a function of contact time at 298 K. Ion exchanger: $H_2Ti_4O_9 \cdot nH_2O$ (0.1 g). Aqueous phase: nitric acid containing 1×10^{-4} mol dm^{-3} uranyl nitrate at initial time (10 cm^3).

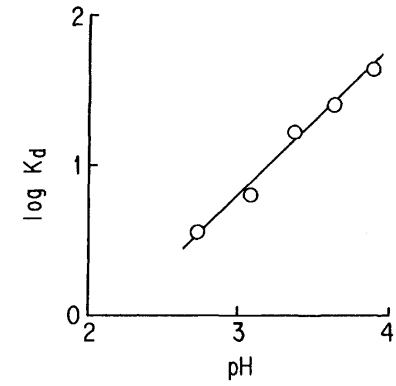

Fig. 2. The distribution coefficient of the uranium as a function of pH in the aqueous solution at 298 K. Ion exchanger: $H_2Ti_4O_9 \cdot nH_2O$ (0.1 g). Aqueous phase: nitric acid containing 1×10^{-4} mol dm^{-3} uranyl nitrate at initial time (10 cm^3).

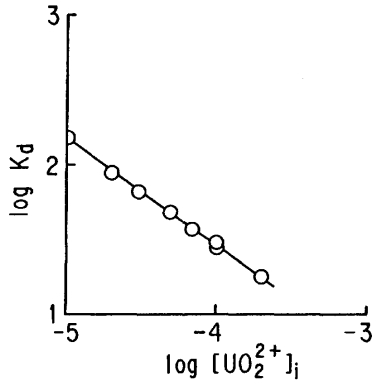

Fig. 3. The distribution coefficient of the uranium as a function of initial uranium concentration in the aqueous phase at 298 K. Ion exchanger: $H_2Ti_4O_9 \cdot nH_2O$ (0.1 g). Aqueous phase: uranyl nitrate solution of various concentrations (10 cm^3).

order with respect to pH value under the substantially constant concentration of the hydrogen ion in the solid. Furthermore, the rate of ion-exchange reaction for uranium is as fast as that for alkali metal ions.[5] These facts may indicate that uranium acts as a univalent metal complex ion on adsorption. The two kinds of univalent uranium complex ions exist in the solution as $[UO_2NO_3]^+$ [11] or $[UO_2OH]^+$.[12] However, since the stability constant for $[UO_2NO_3]^+$($\log K_{(UO_2NO_3^+)} = -0.3$)[11] is extremely larger than that for $[UO_2OH]^+$ ($\log K_{(UO_2OH^+)} = -5.0$)[12] in the aqueous solution, the adsorption reaction of uranium in this system can be written as

$$m[UO_2NO_3]^+ (aq) + H_2Ti_4O_9 \cdot nH_2O (s) \longrightarrow [UO_2NO_3]_mH_{(2-m)}Ti_4O_9 \cdot nH_2O (s) + mH^+ (aq) \quad (0<m<2), \qquad (2)$$

where the subscripts "aq" and "s" denote the aqueous and solid phase.

Figure 3 gives the log K_d values as a function of the initial uranium concentration in the aqueous solution. The K_d increases with a decrease of the uranium concentration. Accordingly, this result is to be expected for the recovery of uranium in seawater since these ions are contained only about 3 ppb in sea water.

The authors are very grateful to Professor Tatsuya Sekine and Mr.Kazuho Inaba of Science University of Tokyo for their valuable discussions during the work, and to Professor Mitsuo Abe of Tokyo Institute of Technology who encouraged us during this work.

References

1) N. J. Keen, *J. Br. Nucl. Energy Soc.*, **7**, 178 (1968).
2) N. Ogata, *Nippon Genshiryoku Gakkai Shi*, **13**, 121 (1971).
3) N. Ohta and Y. Fujiki, *Yogyo Kyokai Shi*, **89**, 134 (1981).
4) Y. Komatsu and Y. Fujiki, *Chem. Lett.*, **1980**, 1525.
5) Y. Komatsu, Y. Fujiki, and T. Sasaki, *Bunseki Kagaku*, **31**, E225 (1982).
6) T. Sasaki, Y. Komatsu, and Y. Fujiki, *Chem. Lett.*, **1981**, 957.
7) Y. Komatsu, Y. Fujiki, and T. Sasaki, *Bunseki Kagaku*, **32**, E33 (1983).
8) Y. Komatsu, Y. Fujiki, and T. Sasaki, *Bunseki Kagaku*, **33**, E159 (1984).
9) Y. Komatsu, Y. Fujiki, and T. Sasaki, *Yogyo Kyokai Shi*, **92**, 665 (1984).
10) T. Sasaki, Y. Komatsu, and Y. Fujiki, *Sep. Sci. Technol.*, **18**, 49 (1983).
11) L. G. Sillen and A. E. Martel, "Stability Constants," the Chemical Society, Spec, Pub. (1964), p. 17.
12) J. Stary, *Collect. Czech. Chem. Commun.*, **25**, 890 (1960).

The Magnetic Properties of the Copper(II) (Disubstituted Acetate) Adducts with Ammonium Chloride

Shuji EMORI,* Yayoi TOHYAMA, and Yoneichiro MUTO
Department of Chemistry, Faculty of Science and Engineering, Saga University, Honjo-machi, Saga 840
(Received June 16, 1987)

Synopsis. Various copper(II) (disubstituted acetate) adducts with ammonium chloride have been prepared and characterized by magnetic susceptibility and IR spectroscopy measurements. Factors affecting the magnetic moments of the dinuclear copper(II) alkanoates are discussed.

Previously, we have shown that in a series of dinuclear copper(II) (monosubstituted acetate)s with coordinated chloride ions in the axial positions their room-temperature magnetic moments tend to increase as the pK_a values of their parent carboxylic acids decrease,[1] being approximated well by a linear equation:

$$\mu_{eff} = -0.052(pK_a - 4.56) + 1.31_8. \quad (1)$$

This empirical relationship has been explained in terms of the inductive effect of the carboxylato substituents, and is supported by molecular orbital analyses,[2,3] However, it seems likely that other factors also contribute to the magnetic properties of copper(II) carboxylates, since several modes of interaction concern the spin-exchange coupling in these dinuclear compounds.[3] Actually, the magnetic moments of the copper(II) salts of acetic acid and fluoroacetic acid deviate from the above trend,[1,4] Thus, in order to obtain more information concerning α-substitution effects in dinuclear copper(II) alkanoates, we have studied copper(II) difluoroacetate, dichloroacetate, *dl*-2-chloropropionate, *dl*-2-bromopropionate, and isobutyrate adducts with the following ammonium chlorides: methylammonium, dimethylammonium, trimethylammonium, tetramethylammonium, *N*-ethylpiperidinium, and quinuclidinium chlorides.

All compounds, apart from the isobutyrates, were prepared by leaving the aqueous solution containing appropriate ammonium chloride and copper(II) carboxylate for a few days in a refrigerator at ca. 5 °C.[4] The isobutyrates were prepared by evaporating the ethanolic solutions under reduced pressure at room temperature.

The effective magnetic moments of these compounds (Table 1) were evaluated from the room-temperature magnetic susceptibilities, which were corrected for the diamagnetic contribution of the constituent atoms using Pascal constants,[6] and a value of $N\alpha = 60\times10^{-6}$ emu mol^{-1} (1 emu$=4\pi\times10^{-6}$ m^3) was used throughout the present study. For the dimethylammonium chloride adducts of copper(II) 2-chloropropionate and copper(II) isobutyrate, the temperature dependence of their magnetic susceptibilities was measured in the temperature range of 80—300 K in order to confirm their dinuclear structures. The results agreed well with the Bleaney-Bowers equation,[7] using the following parameters: $g=2.18$ and $2J=-309$ cm^{-1} for the 2-chloropropionate and $g=2.17$ and $2J=-331$ cm^{-1} for the isobutyrate, respectively. The IR spectra of the solid compounds show characteristic bands in the ranges of 1680—1595 and 1465—1460 cm^{-1} connected with symmetric and unsymmetric COO stretching vibrations of the carboxyl groups.[8] The magnetic and IR spectral data indicate that the

Table 1. Analytical Data and Effective Magnetic Moments at 20 °C

Compound		Found (Calcd)/%					μ_{eff}/BM
		Cu	Cl^-	C	H	N	
$Cu(F_2CHCOO)_2 \cdot CH_3NH_3Cl$	(1)	19.74 (19.79)	11.68 (11.04)	18.50 (18.70)	2.56 (2.51)	4.41 (4.36)	1.35
$Cu(F_2CHCOO)_2 \cdot (CH_3)_2NH_2Cl$	(2)	19.09 (18.96)	10.73 (10.58)	21.40 (21.50)	3.01 (3.01)	4.13 (4.18)	1.35
$Cu(F_2CHCOO)_2 \cdot (CH_3)_3NHCl$	(3)	18.18 (18.20)	10.19 (10.15)	23.88 (24.08)	3.44 (3.46)	3.91 (4.01)	1.37
$Cu(F_2CHCOO)_2 \cdot (CH_3)_4NCl$	(4)	17.62 (17.50)	9.72 (9.76)	26.41 (26.46)	3.89 (3.89)	3.83 (3.86)	1.39
$Cu(Cl_2CHCOO)_2 \cdot C_7H_{13}NHCl$	(6)	13.67 (13.61)	7.45 (7.59)	27.83 (28.29)	3.55 (3.45)	2.79 (3.00)	1.49
$Cu(Cl_2CHCOO)_2 \cdot C_7H_{15}NHCl$	(7)	13.46 (13.55)	7.40 (7.56)	28.16 (28.17)	3.86 (3.87)	2.93 (2.99)	1.50
$Cu(CH_3CHClCOO)_2 \cdot (CH_3)_2NH_2Cl$	(8)	17.25 (17.64)	9.88 (9.86)	26.86 (26.68)	4.39 (4.48)	3.70 (3.89)	1.39
$Cu(CH_3CHBrCOO)_2 \cdot (CH_3)_2NH_2Cl$	(9)	14.02 (14.13)	7.92 (7.89)	21.26 (21.40)	3.77 (3.59)	3.56 (3.12)	1.39
$Cu[(CH_3)_2CHCOO]_2 \cdot (CH_3)_2NH_2Cl$	(11)	20.22 (19.90)	11.08 (11.10)	37.47 (37.62)	6.96 (6.94)	4.31 (4.39)	1.31
$Cu[(CH_3)_2CHCOO]_2 \cdot CH_3NH_3Cl$	(12)	20.94 (20.81)	11.60 (11.61)	35.38 (35.41)	6.62 (6.60)	4.53 (4.59)	1.32

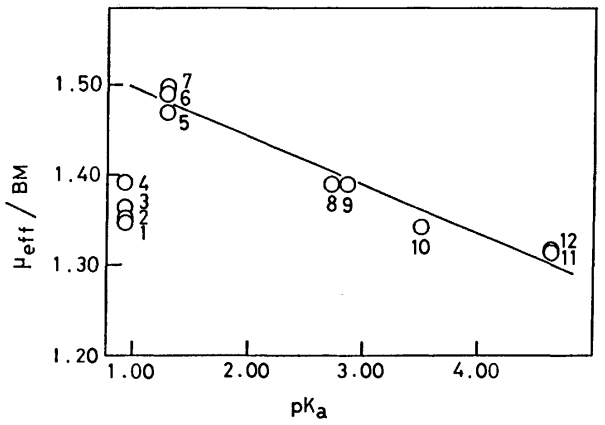

Fig. 1. The magnetic moment at 20°C plotted against the pK_a value of the parent carboxylic acid for the copper(II) salts of disubstituted acetic acids containing coordinated chloride ions in the axial positions; the difluoroacetates (**1—4**), the dichloroacetates (**5—7**), the 2-chloropropionate (**8**), the 2-bromopropionate (**9**), the (3-piperidinio)-formate (**10**),[11] and the isobutyrates (**11**, **12**).

present compounds have a bridged dinuclear structure similar to copper(II) acetate monohydrate,[9,10] The ammonium cations in these compounds may affect the dinuclear structure due to packing effects and the hydrogen bonds; however, no marked difference was observed in the magnetic moments for the respective copper(II) carboxylates.

A plot (Fig. 1) of the room-temperature magnetic moment vs. the pK_a value of the parent alkanoic acid for the present compounds, except difluoroacetates, confirms the correlation between these quantities,[1] with the best least-squares fit yielding

$$\mu_{eff} = -0.052\,(pK_a - 4.56) + 1.30_5. \quad (2)$$

The obtained slope agrees satisfactorily with that for the corresponding series of monosubstituted acetates. The variation of singlet-triplet separation values (e.g. $-2J$=271,[5] 309, and 331 cm^{-1} for the dimethylammonium chloride adducts of copper(II) dichloroacetate, 2-chloropropionate, and isobutyrate compounds, respectively) indicates that the smaller magnetic moment is accompanied by the strong magnetic interaction between copper(II) ions. On the other hand, the slight difference observed between the intercepts for the series of mono- and disubstituted acetates, indicates that some decrease in the magnetic moment (ca. −0.01 BM) is accompanied, probably due to an increase in the steric strain and a decrease of hyperconjugation by the substitution of the methyl group of acetic acid. However, the substantially small magnetic moments of the fluoro- and difluoroacetates can not be explained in terms of the inductive effect of the fluoro substituent. From a study of the ^{19}F NMR in the series of fluoromethanes, Gutowsky and Hoffman have suggested the use of higher energy orbitals in the hybridized orbitals of atoms attached to fluorine atoms.[12] On the other hand, Roberts and Carboni have pointed out that, in the transmission of the electrical influence of the dipolar substituents, the inductive and field effects are of comparable importance.[13] For an explanation of the magnetic moments for the fluoro- and difluoroacetates, it is necessary to consider these effects. The higher magnetic moments of the copper(II) salts of acetic acid[4] may also be explained by the mechanism described above.

References

1) S. Emori, N. Morishita, and Y. Muto, *Bull. Chem. Soc. Jpn.*, **60**, 1913 (1987).
2) P. J. Hay, J. C. Thibeaul, and R. Hoffmann, *J. Am. Chem. Soc.*, **97**, 4884 (1975).
3) P. de Loth, P. Cassoux, J. P. Daudey, and J. P. Malriew, *J. Am. Chem. Soc.*, **103**, 4007 (1981).
4) S. Emori and Y. Muto, *Bull. Chem. Soc. Jpn.*, **57**, 291 (1984).
5) S. Emori, N, Haramaki, and Y. Muto, *Bull. Chem. Soc. Jpn.*, **58**, 761 (1985).
6) G. Foex, "Constants Sélectionées, Diamagnétisme et Paramagnétisme," Masson, Paris (1957).
7) J. Lewis, Y. C. Lin, L. K. Royston, and R. C. Thomson, *J. Chem. Soc.*, **1965**, 428.
8) S. Yamada, H. R. Nakamura, and R. Tsuchida, *Bull. Chem. Soc. Jpn.*, **31**, 303 (1958).
9) J. N. van Niekerk and F. R. L. Schoening, *Acta Crystallogr.*, **6**, 227 (1953).
10) G. M. Brown and R. Chidambaram, *Acta Crystallogr., Sect. B*, **29**, 2393 (1973).
11) S. Emori, N. Morishita, and Y. Muto, *Bull. Chem. Soc. Jpn.*, **59**, 2893 (1986).
12) H. S. Gutowsky and C. J. Hoffman, *J. Chem. Phys.*, **19**, 1259 (1951).
13) J. D. Roberts and R. A. Carboni, *J. Am. Chem. Soc.*, **77**, 5554 (1955).

Reactions of Tropone Tosylhydrazone Sodium Salt with 2-Pyrone Derivatives: Nucleophilic Addition of 1,2,4,6-Cycloheptatetraene to 2-Pyrone Derivatives

Katsuhiro SAITO* and Hiraku ISHIHARA
Department of Chemistry, Nagoya Institute of Technology, Gokiso-cho, Showa-ku, Nagoya 466
(Received June 1, 1987)

Synopsis. The reaction of tropone tosylhydrazone sodium salt with 3- or 5-methoxycarbonyl-2-pyrones afforded benzotropilidene derivatives. These products are considered to be formed via addition reactions of the 2-pyrone derivatives with 1,2,4,6-cycloheptatetraene derived from cycloheptatrienylidene, which is the initial product of the decomposition of tropone tosylhydrazone sodium salt.

It has been reported that upon heating or irradiation tropone tosylhydrazone sodium salt (**1**) generates cycloheptatrienylidene (**2**), which is considered to be a nucleophilic singlet carbene because of a contribution of a 6π-electrons type aromatic structure (**2a**).[1] The possibility of a rearrangement of the carbene (**2**) to an allene, 1,2,4,6-cycloheptatetraene (**3**) has been pointed out by Unch et al.[2] The present authors[3] have documented some experimental examples of the rearrangement and Alder et al.[4] have reported a theoretical investigation of the rearrangement.

Recently, Waali et al. documented that **2** is actually a planar transition state for the interconversion of chiral, nonplanar allenes (**3**), which could have nucleophilicity because the strained cyclic allene, 1,2-cyclohexadiene, had a nucleophilicity.[5] As one part of our research on the reactivities of **2** and **3**,[3] we invesitigated the reactions of **1** with 3- (**4a**) or 5-methoxycarbonyl-2-pyrone (**4b**). Here, the results of these reactions will be discussed.

A mixture of **1** and three molar equivalents of **4a** in anhydrous diglyme was heated at 120 °C for 15 min. The separation and purification of the reaction mixture by chromatography afforded 2-methoxycar-

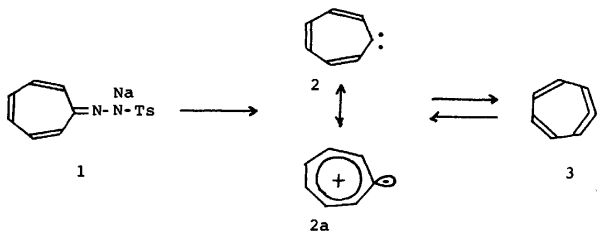

Fig. 1.

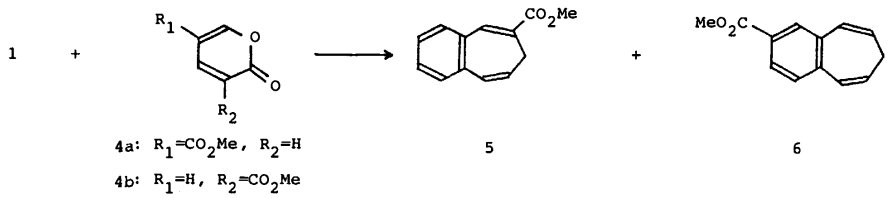

Fig. 2.

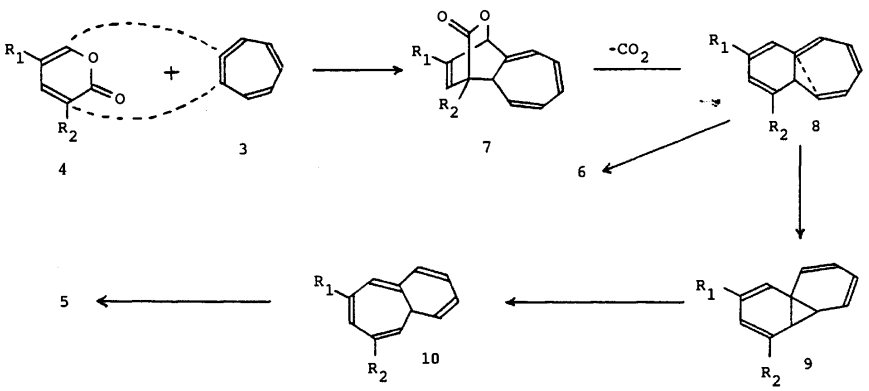

Fig. 3.

bonylbenzo[*f*]-1,4,5a-cycloheptatriene (**5**) and 8-methoxycarbonylbenzo[*f*]-1,4,5*a*-cycloheptatriene (**6**) in 8.1 and 15% yields, respectively. The same reaction, but using **4b**, gave **5** in 2.8% yield. The structures of **5** and **6** were deduced on the basis of their spectral properties, especially from their NMR spectral properties, and confirmed by comparisons of these spectral properties with those of analogous compounds.[3,6]

The products are considered to be formed via a reaction mechanism resembling that of the reaction of **1** with cyclopentadienone derivatives.[1e,3c] A [$4\pi + 2\pi$]-type cycloaddition of **3** with **4** gives **7**, which generates **8** via an elimenation of carbon dioxide. A hydrogen migration in **8** gives **6**. On the other hand, a valence tautomerization of **8** yields a norcaradiene form **9**,[7] which again undergoes a valence tautomerization to tropilidene form **10**. A hydrogen migration of **10** affords **5**. The reaction of **3** with **4b** proceeds via almost the same mechanism as above. The low product yield from the reaction of **4b** is due to a steric hindrance of the methoxycarbonyl group.

The electron densities on carbon atoms of **4a** and **4b** are known to be as shown in Fig. 3.[8] The 2-position carbons bear the smallest electron densities in both **4a** and **4b**. Considering the above fact, the experimental result that the allenic carbon atom of **3** attacks the 2-position carbon atoms of both **4a** and **4b**, seems to prove the nucleophilicity of the allene **3**.

Experimental

NMR spectra were measured with Varian XL 200 or Hitachi R 20B spectrometers with tetramethylsilane as an internal standard. IR spectra were measured with a DS 701G spectrometer. Mass spectra were measured with Hitachi M-52 or JMS DX300 spectrometers. Diglyme was dried over Molecular Sieves 3A, 1/16. Wako gel C 200 and Wako gel B5F were used for column and thin-layer chromatography, respectively.

Reaction of 1 with 4a. A mixture of **1** (8.40 g, 28.4 mmol), and **4a** (13.20 g, 85.7 mmol) in diglyme (100 ml) was heated at 120 °C for 15 min. The reaction mixture was poured into water, extracted with ethyl acetate, washed with water and brine, and dried over anhydrous sodium sulfate. After evaporation of the solvent, the oily residue was column chromatographed to give an oily mixture of **5** and **6** (1.10 g) by the use of pet. ether (bp 35—60 °C)-benzene 1 : 4 and crystals of tropone tosylhydrazone (2.63 g, 31%) by the use of benzene-ether 9 : 1. The NMR spectrum of the mixture of **5** and **6** showed that the mixture contained 35% of **5** (8.1% yield)[9] and 65% of **6** (15.0% yield).[9] Each compound was separated by thin-layer chromatgraphy using benzene-ether 3 : 1 as a developing solvent (**5**, R_f=0.60; **6**, R_f=0.55). 2-Methoxycarbonylbenzo[*f*]-1,4,5a-cycloheptatriene (**5**): Found: *m/z* 200.0819. Calcd for $C_{13}H_{12}O_2$: M, 200.0836. MS *m/z* (rel intensity): 200 (M^+, 29), 186 (25), 155 (57), 127,(100). IR (oil): 3030, 2950, 1720, 1440 cm^{-1}; ^1H NMR ($CDCl_3$) δ=2.80 (d, 2H, *J*=7 Hz), 3.90 (s, 3H), 5.6—6.8 (m, 3H), 7.1—8.0 (m, 4H).

8-Methoxycarbonylbenzo[*f*]-1,4,5a-cycloheptatriene (**6**): Found: *m/z* 200.0864. Calcd for $C_{13}H_{12}O_2$: M, 200.0836. MS *m/z* (rel intensity): 200 (M^+, 100), 169 (95), 139 (43), 127 (53). IR (oil): 3030, 2970, 1725, 1440 cm^{-1}. ^1H NMR ($CDCl_3$) δ=2.50 (t, 2H, *J*=7 Hz), 3.80 (s, 3H), 5.6—6.8 (m, 4H), 7.2—8.0 (m, 3H).

Reaction of 1 with 4b. A mixture of **1** (8.88 g, 30 mmol) and **4b** (13.86 g, 90 mmol) in diglyme (100 ml) was heated at 120 °C for 20 min. The same procedure as above using column chromatography gave an oil **5** (0.12 g, 2.8%,[9] benzene-ether 17 : 3) and crystals of tropone tosylhydrazone (2.28 g, 27.8%, benzene-ether 9 : 1).

The authors are indebeted to Professor Toshio Mukai of Tohoku University for his fruitfull suggestions. The present work was supported by a Grant-in-Aid for Science Research No. 61540367 from the Ministry of Education, Science and Culture.

References

1) a) T. Mukai, T. Nakazawa, and K. Isobe, *Tetrahedron Lett.*, **1968**, 565; b) W. M. Jones and C. L. Ennis, *J. Am. Chem. Soc.*, **91**, 6391 (1969); c) W. M. Jones, B. N. Hamon, R. C. Joines, and C. L. Ennis, *Tetarhedron Lett.*, **1969**, 3909; d) W. M. Jones, *Angew. Chem., Int. Ed. Engl.*, **11**, 325 (1972); e) T. Mitsuhashi and W. M. Jones, *J. Chem. Soc., Chem. Commun.*, **1974**, 103.

2) K. Untch, G. J. Mattheus, and T. Hylton, Abstract of International Symposium on the Chemistry of Non-Benzenoid Aromatic Compounds, Sendai, Japan (1970), p. 79; C. Mayor and W. M. Jones, *Tetrahedron Lett.*, **1977**, 3855.

3) a) K. Saito, Y. Omura, and T. Mukai, *Chem. Lett.*, **1980**, 349; b) *idem, Bull. Chem. Soc. Jpn.*, **58**, 1663 (1985); c) K. Saito and H. Ishihara, *ibid.*, **58**, 2664 (1985); d) *idem, ibid.*, **59**, 1095 (1986).

4) M. Z. Kassaee, M. R. Nimlos, K. E. Downie, and E. E. Waali, *Tetrahedron*, **41**, 1579 (1985); R. W. Alder, J. C. Petts, and T. Clark, *Tetrahedron Lett.*, **26**, 1585 (1985).

5) S. Harnos, S. Tivakornpannarai, and E. E. Waali, *Tetrahedron Lett.*, **27**, 3701 (1986).

6) C. H. Jutz, I. Rommel, I. Lengyel, and J. Feeney, *Tetrahedron*, **22**, 1809 (1966); A. S. Kende, *Tetrahedron Lett.*, **1967**, 2661; T. Toda, K. Saito, and T. Mukai, *ibid.*, **1972**, 1981; M. Yasuda, K. Harano, and K. Kanematsu, *J. Am. Chem. Soc.*, **103** (1981).

7) E. Ciganek, *J. Am. Chem. Soc.*, **87**, 1149 (1965); T. Mukai, H. Kubota, and T. Toda, *Tetarhedron Lett.*, **1967**, 3581; R. Hoffmann, *ibid.*, **1970**, 2907; H. Gunther, *ibid.*, **1970**, 5173.

8) J. A. Reed, C. L. Shilling, Jr., R. F. Jarrin, T. A. Rettig, and J. K. Stille, *J. Org. Chem.*, **34**, 2188 (1969).

9) The yields were calculated based on the amount of really consumed **1**.

Effect of Catalyst on the Oxygenation of Styrene with BH_4^- and Molecular Oxygen[1)]

Tadashi OKAMOTO,* Yoshihiro SASAKI, Ken SASAKI, and Shinzaburo OKA
Institute for Chemical Research, Kyoto University, Uji 611
(Received June 4, 1987)

Synopsis. The effects of equatorial ligands and central metals on the catalytic conversion of styrene to 1-phenylethanol were examined. Accompanying hydrogenation and hydrodimerization of the substrate to ethylbenzene and 2,3-diphenylbutane, respectively, was facilitated in the presence of a catalyst ligated with an electron-releasing ligand such as 1,4,8,11-tetraazacyclotetradecane or sulfur-containing ligands.

Previously we reported the catalytic conversion of aryl-conjugated olefins to the derivatives of benzyl alcohol by molecular oxygen and tetrahydroborate ion at room temperature.[2,3)] The reaction proceeded with high reio- and chemoselectivities affording the corresponding alcohols in high yields. A related reaction by using nitrogen monoxide in place of molecular oxygen also presented a new process for preparation of oximes under mild reaction conditions.[4)] As for the catalyst of these reactions, successful results were reported with cobalt complexes of the monoanion of 2,3-butanedione dioxime (DMG)[2)] and tetraphenylporphyrin (TPP).[3)] The catalytic effects of some other transition metal complexes in the oxygenation of styrene was examined in the present study to reveal a distinctive effects of equatorial ligands and the central metals on the distribution of the products.

Results and Discussion

In the transition metal-catalyzed oxygenation of styrene with tetrahydroborate and molecular oxygen, the main product of 1-phenylethanol (**1**) was occasionally accompanied by three by-products. Two of them were ethylbenzene (**2**) and 2,3-diphenylbutane (**3**) which

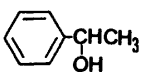

1

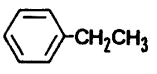

2

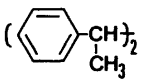

3

were produced by hydrogenation and hydrodimerization of styrene, respectively. The other was acetophenone, a compound formally produced by dehydrogenation of the alcohol **1**. The relative yields of these products were dependent on the various reaction conditions. Typically, the yields of products via hydrogenation, **2** and **3**, increased at the high concentration of tetrahydroborate ion. On the other hand, the yield of acetophenone increased when the low concentration of BH_4^- was used. At low reaction temperature the yield of acetophenone increased relative to the alcohol. The contribution of bimolecular process affording **3** was important at the high concentration of the catalyst.

Except for these general phenomena, the product distribution was dependent on the metal complex used as the catalyst. The effect of equatorial ligand was compared with eight cobalt complexes having the equatorial coordinating atoms of nitrogen, oxygen, and sulfur such as **4**—**11**. The effect of central metal ion was also examined for complexes with a nitrogen

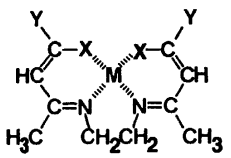

4 X=O, Y=Ph
5 X=S, Y=Ph
6 X=S, Y=CH3

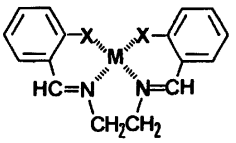

7 X=O
8 X=N

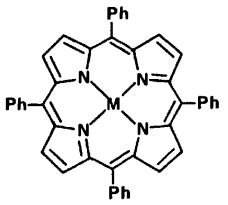

9

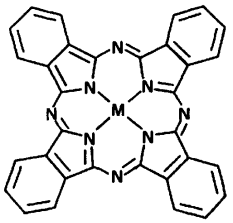
10

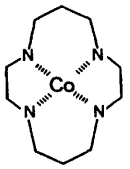

11

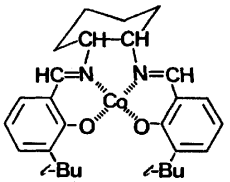

12

Table 1. The Effect of Catalyst on the Oxygenation of Styrene[a)]

Catalyst	Conversion/%	Product yield/%[b)]			
		1	**2**	**3**	$PhCOCH_3$
$Co(DMG)_2$[c)]	92	80	7	9	—
4	100	80	7	10	—
5	98	41	16	18	—
6	93	53	18	19	—
7	50	30	9	4	—
8	69	56	6	25	—
9 (M=Co)	100	83	9	1	—
10 (M=Co)	96	86	0	0	—
11	79	3	33	29	—
9 (M=FeCl)	100	91	3	1	1
10 (M=Fe)	100	97	0	0	0
$Fe(DMG)_2$	27	75	0	Trace	—
9 (M=MnOAc)	100	42	0	0	51
12[d)]	100	57	16	—	7

a) Reaction conditions: styrene/catalyst=10, in 50% 1,2-dimethoxyethane/isopropyl alcohol at room temperature, 25 h. b) Yields were calculated on the basis of the amounts of consumed substrate. c) DMG: monoanion of 2,3-butanedione dioxime. d) At −60 °C; optical yield, 2%.

ligand such as DMG (Co and Fe complexes) or TPP (Co, Fe, and Mn complexes). The results are summarized in Table 1.

The effect of metal ion is characterized by the tendency that the activity for hydrogenation increases in the order of the periodic table, Mn(III)<Fe(III)< Co(II). In the case of TPP complex, nearly one tenth of the total products was converted to hydrogenation and hydrodimerization products, **2** and **3** by using Co(tpp), while the corresponding value by the use of Fe(tpp)Cl was less than 5%. For the catalysis by Mn(tpp)(OAc), no hydrogenation to **2** and **3** proceeded and the main product was acetophenone instead of **1**. Thus hydrogenation is not a favorable process by the use of Mn(tpp)(OAc) as the catalyst. The related tendency was observed in the catalysis by DMG complexes; the relative amount of hydrogenation product increased in the order, Fe<Co.

The effect of equatorial ligand also showed a distinct tendency. A cobalt complex of a chelating ligand bearing four coordination sites with two nitrogen and two oxygen atoms **4** gave quite similar results with the DMG complex. The change of carbon framework of the ligand has minor importance. The results show that the oxygen and nitrogen atoms have similar effect on the catalytic reaction. However, when two coordinating oxygen atoms of the ligand were substituted by sulfur atoms such as **5** and **6**, the yields of **2** and **3** increased significantly at the expense of oxygenation product **1**. Again, the change of organic substituents, Y, from phenyl to methyl group had little effect compared with the ligating atoms. Related result was obtained with the complex of saturated cyclic ligand **11**. In the reaction by the catalysis of this electron-rich complex, the formation of the oxygenation product **1** was almost inhibited. The results of Schiff base complexes **7** and **8** were not straightfoward. The low conversion and low yields of products as well as its distribution should be accounted for by the instability of the Schiff bases under the reaction conditions. In fact, almost quantitative amount of salicylaldehyde was found after the reaction by the catalysis of **7**. The effect of equatorial ligand are thus interpreted that the cobalt complex ligiated with an electron-releasing ligand promotes hydrogenation and hydrodimerization relative to oxygenation. Electron-releasing ligand increases the electron density of the central cobalt ion and stabilizes the alkyl-cobalt bond against homolytic dissociation to cobalt(Il) and alkyl radical.[5] In this context the observed tendency supports the mechanism of a free radical combination process for the oxygenation step. As the catalyst of oxygenation, rigid cyclic tetraaza ligands such as porphyrin and phthalocyanine gave the best results with respect to both stability of the catalyst and the selectivity of the product alcohol. An attempt for the asymmmetric catalysis by using complex (1*R*,2*R*)-**12** at −60 °C resulted in only the isolation of **1** with optical yield of 2% (S) in 50% 1,2-dimethoxyethane-isopropyl alcohol. Intermediate formation of π-type free radical might be a possible explanation of the low optical yield.

Experimental

Complexes **4**—**11** were prepared according to the methods in literature.[6-10] Styrene was distilled before use. Other chemicals were commercial products and used as received. Experimental procedure of catalytic oxygenation was similar as the previous study. Reaction conditions were; Catalyst, 0.05 mmol; styrene, 0.5 mmol; tetraethylammonium tetrahydroborate, 1 mmol; in 5 ml of 50% 1,2-dimethoxyethane-isopropyl alcohol under atmospheric pressure of oxygen at room temperature. The yields of the reaction products were determined by Yanaco G2800 gas chromatography fitted with OV 101 packed column and calculated on the basis of the consumed amounts of the substrate.

The authors acknowledge Prof. Masafumi Goto of Nagoya City University for a gift of complex 12.

References

1) Presented at the 45th National Meeting of the Chemical Society of Japan, Tokyo, April 1982, Abstr. No. 1C18.
2) T. Okamoto and S. Oka, *Tetrahedron Lett.*, **22**, 2191 (1981).
3) T. Okamoto and S. Oka, *J. Org. Chem.*, **49**, 1589 (1984).
4) T. Okamoto and S. Oka, *J. Chem. Soc., Chem. Commun.*, **1984**, 289.
5) J. Halpern, *Acc. Chem. Res.*, **15**, 238 (1982).
6) A. E. Martell, R. L. Belford, and M. Calvin, *J. Inorg. Nucl. Chem.*, **5**, 170 (1958).
7) P. R. Blum, R. M. C. Wei, and S. G. Cummings, *Inorg. Chem.*, **13**, 450 (1974).
8) R. H. Bailes and M. Calvin, *J. Am. Chem. Soc.*, **69**, 1886 (1947).
9) M. Sakurada, *Bull. Inst. Chem. Res., Kyoto Univ.*, **58**, 140 (1980).
10) E. K. Barefield, F. Wagner, A. W. Herlinger, and A. R. Dahl, *Inorg. Chem.* **16**, 223 (1976).

Formation of Chlorosulfonium Salt of 1,5-Dithiacyclooctane and Transannular Sulfur-Sulfur Interaction in Hydrolysis of Its Salt

Hisashi FUJIHARA, Ryouichi AKAISHI, and Naomichi FURUKAWA*
Department of Chemistry, University of Tsukuba, Sakura-mura, Niihari-gun, Ibaraki 305
(Received June 11, 1987)

Synopsis. The reaction of 1,5-dithiacyclooctane 1-oxide (**2**) with thionyl chloride afforded the corresponding chlorosulfonium chloride as a stable salt and an evidence for the intermediary formation of the bis-sulfide dication with an equilibrium mixture of the chlorosulfonium salt was found. In contrast to **2**, 1,4-dithiacyclohexane 1-oxide (**6**) reacts with thionyl chloride like a simple sulfoxide.

Normally, the sulfoxides bearing α-protons react with thionyl chloride ($SOCl_2$) to form initially a (chlorosulfinyloxy)sulfonium cation (**A**) which then decomposes to give a chlorosulfonium chloride (**B**) and sulfur dioxide.[1a,b] Finally chlorosulfonium salts generated are easily converted to α-chloro sulfides[1c] as shown below.

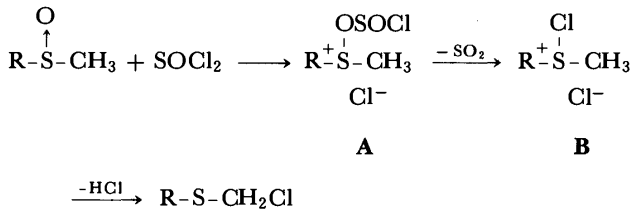

An intermediacy of the bis-sulfide dication of 1,5-dithiacyclooctane (**1**) has been confirmed kinetically by Musker et al. in the reduction of the corresponding sulfoxide with HI.[2] Recently, we reported that the bis-sulfide dication of **1** is formed in either the reaction of the corresponding sulfoxide with concd H_2SO_4 or the Pummerer reaction with acetic anhydride.[3,4] These results indicate that when a positive charge is induced on the one sulfur atom in the cyclic bis-sulfide, the remote second sulfur atom participates transannularly to stabilize the charge via formation of the S-S bond. We present here the formation of chlorosulfonium salt of **1** and the transannular sulfur-sulfur interaction in the hydrolysis of its salt, and the distinct difference between **1** and 1,4-dithiacyclohexane (**5**) in the reaction mode of the corresponding sulfoxides with thionyl chloride.

The reaction of 1,5-dithiacyclooctane 1-oxide (**2**) with thionyl chloride in anhydrous dichloromethane at 0°C gave the corresponding chlorosulfonium chloride **3** as a stable salt in 74% isolated yield. Secondary ion mass spectrum (SIMS) of **3** indicates the peaks at *m/z* 185 and 183 (base peak) which correspond to $C_6H_{12}S_2Cl^+$. This salt could be stabilized by transannular interaction of the second sulfur atom even in the absence of antimony pentachloride ($SbCl_5$). Treatment of **3** with H_2O and work-up led to sulfoxide **2** in 70% yield and sulfide **1** in 15% yield (Scheme 1). The sulfide was presumably formed by reduction of the halosulfonium ion by the second halide ion as a counterpart of the cation. 2,2,8,8-Tetradeuterated 1,5-dithiacyclooctane 1-oxide (**2a**) was treated similarly with thionyl chloride to afford the chlorosulfonium salt [$^2H_4$]-**3** in 75% yield. Hydrolysis of the salt [$^2H_4$]-**3** led to the sulfoxide in 69% yield and the tetradeuterated sulfide **1a** in 17% yield. The ^1H NMR spectra of the recovered sulfoxide indicate that it is a 1:1 mixture of 2,2,8,8- and 4,4,6,6-tetradeuterated sulfoxides (**2a**) and (**2b**) (Scheme 2). Furthermore, sulfoxide **2** was treated with thionyl chloride in the presence of antimony pentachloride in anhydrous dichloromethane to give 1-chloro-5-thia-1-thioniacyclooctane hexachloroantimonate (**4**) in 75% yield. The ^1H NMR spectrum of salt **4** in CD_3CN showed signals at δ 4.16—3.58 [m, 4H, $S(Cl)CH_2$], 3.52—2.71 (m, 4H, SCH_2), and 2.60—2.32 (m, 4H, CH_2). Hydrolysis of salt **4** gave only sulfoxide **2** in 67% yield. The tetradeuterated hexachloroantimonate salt [$^2H_4$]-**4**[5] gave a similar result to [$^2H_4$]-**3**. These results suggest the intermediary formation of bis-sulfide dication **8** with an equilibrium mixture of the chlorosulfonium salt ([$^2H_4$]-**3** or **4**) (Scheme 2).

Meanwhile, 1,4-dithiacyclohexane 1-oxide (**6**) in which transannular interaction of the sulfur atoms is

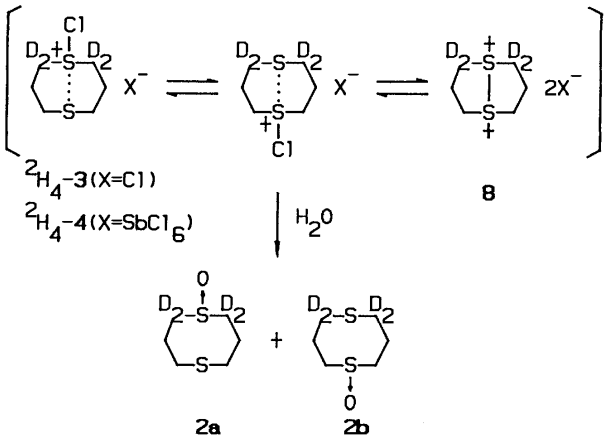

Scheme 2.

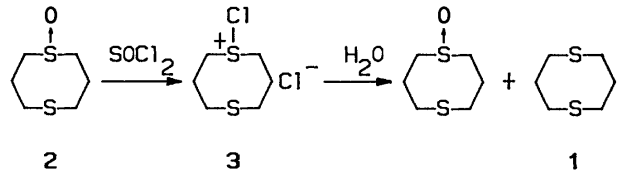

Scheme 1.

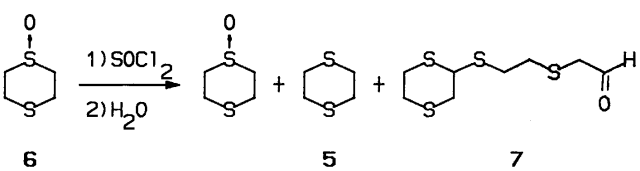

Scheme 3.

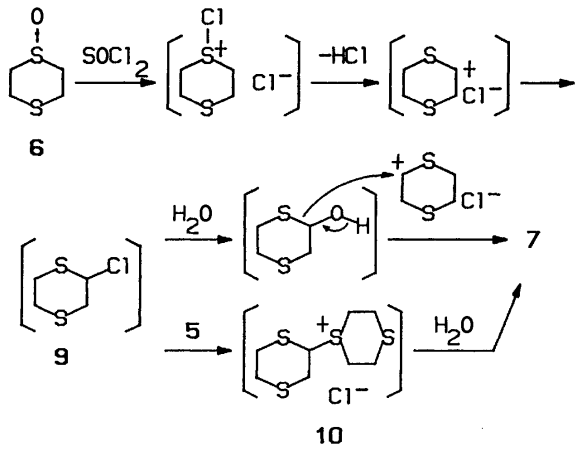

Scheme 4.

minimal, was treated similarly with thionyl chloride as described in **2**. The chlorosulfonium chloride of **5** could not be isolated as a salt in the reaction of **6** with thionyl chloride in the absence of antimony pentachloride. Hydrolysis of the reaction mixture in situ gave sulfoxide **6** in 9%, sulfide **5** in 20%, and aldehyde **7** in 41% yields (Scheme 3). This reaction may have proceeded through the formation of the Pummerer product such as α-chloro sulfide **9** which subsequently is converted into **7** by hydrolysis of **9** as illustrated in Scheme 4. However, an alternative process involving the formation of the sulfonium salt **10** by the reaction of **9** with **5** cannot be excluded (Scheme 4). The structure of **7** was confirmed by the formation of 2,4-dinitrophenyl hydrazone **11**. Thus, this distinct difference of reactivity between **2** and **6** should depend on the degree of the transannular S-S interaction in the six- and eight-membered rings.

Experimental

^{1}H NMR spectra were measured on a Hitachi R-600 FT-NMR spectrometer. The IR spectra were obtained on JASCO A-3 spectrometer. Secondary ion mass spectra were taken by Hitachi M-80B mass spectrometer. Elemental analyses were carried out by the Chemical Analytical Center at this University.

1,5-Dithiacyclooctane was synthesized by a modification of the method of Meadow and Reid.[6] 1,4-Dithiacyclohexane was obtained from Wako Pure Chemical Industries, Ltd.

Cyclic Bis-Sulfide Monosulfoxides. The monosulfoxides were obtained by general oxidation using *m*-chloroperbenzoic acid.

1,5-Dithiacyclooctane 1-Oxide (2): Yield 76%; mp 27—29 °C; IR (neat) 1010 cm^{-1} (S=O); ^{1}H NMR ($CDCl_3$) δ=2.18—2.43 (m, 4H, CH_2), 2.54—2.76 (m, 4H, SCH_2), and 3.04—3.23 [m, 4H, $S(O)CH_2$].

1,4-Dithiacyclohexane 1-Oxide (6): Yield 36%; mp 125.5—127.0 °C; IR (KBr) 1020 cm^{-1} (S=O); ^{1}H NMR ($CDCl_3$) δ=2.40—2.70 (m, 2H, SCH_2-*e*), 2.91—3.22 [m, 4H, $S(O)CH_2$], and 3.43—3.77 (m, 2H, SCH_2-*a*).

Preparation of 2,2,8,8-Tetradeuterated 1,5-Dithiacyclooctane 1-Oxide (2a). Deuteration of sulfoixde **2** was carried out in NaOD-D_2O under nitrogen atmosphere at 100 °C for 24 h. After usual work-up the tetradeuterated sulfoxide **2a** was obtained in 91% yield; the deuterium content of **2a** was more than 95 atom% by ^{1}H NMR spectroscopy.

Isolation of Chlorosulfonium Chloride 3. Addition of pure thionyl chloride (1 mmol) in anhydrous dichloromethane (1 ml) to a solution of 1,5-dithiacyclooctane 1-oxide (**2**) (1 mmol) in anhydrous dichloromethane (1 ml) under N_2 atmosphere at 0 °C resulted in a white crystalline precipitate. Upon filtration in a dry box under rigorously anhydrous conditions, 1-chloro-5-thia-1-thioniacyclooctane chloride (**3**) was obtained in 74% yield as stable hygroscopic crystalline salt: Mp 80°C; SIMS *m/z* (rel intensity) 185(42), 183(100) 151(17), 107(44), and 73(23).

Reactions of Sulfoxide 2 with Thionyl Chloride in the Presence of Antimony Pentachloride. To a stirred solution of sulfoxide **2** (1 mmol) and antimony pentachloride (1 mmol) in anhydrous dichloromethane (1 ml) was added thionyl chloride (1 mmol) in anhydrous dichloromethane under nitrogen at 0 °C. 1-Chloro-5-thia-1-thioniacyclooctane hexachloroantimonate (**4**) was obtained in 75% yield as stable hygroscopic crystalline salt: Mp 106—107 °C (decomp); ^{1}H NMR (CD_3CN) δ=2.32—2.60 (m, 4H, CH_2), 2.71—3.52 (m, 4H, SCH_2), and 3.58—4.16 [m, 4H, $S(Cl)CH_2$]; MS *m/z* 183 (M^+-SbCl_6).

Hydrolysis of Chlorosulfonium Salt 3. The salt **3** was treated with aqueous $NaHCO_3$ on ice bath. The mixture was extracted with dichloromethane. The combined organic phase was dried over $MgSO_4$, filtered, and concentrated under vacuum to give sulfoxide **2** in 70% and sulfide **1** in 15% yields. The salt **4** was hydrolyzed by the same procedure as **3**.

Reaction of Sulfoxide 6 with Thionyl Chloride. To a stirred solution of 1,4-dithiacyclohexane 1-oxide (**6**) (1 mmol) in anhydrous dichloromethane (1 ml) was added thionyl chloride (1 mmol) in anhydrous dichloromethane (1 ml) under nitrogen at 0 °C. Then the reaction mixture was treated with aqueous $NaHCO_3$ to afford sulfide **5** in 20%, sulfoxide **6** in 9%, and aldehyde **7** in 41% yields. The hydrazone of **7** was prepared as follows. To a solution of aldehyde **7** (19 mg) in ethanol (3 ml) was added 2,4-dinitrophenylhydrazine (50 mg, 0.1%-HCl solution). The reaction mixture was stirred at room temperature for 2 h. The solution was extracted with carbon tetrachloride, and the extract was dried over Na_2SO_4. After removal of the solvent, hydrazone **11** was purified by silica-gel column chromatography. **11**: Mp 125—126 °C; IR (KBr) 1610 (C=N), 1504 and 1321 cm^{-1} (NO_2); ^{1}H NMR ($CDCl_3$) δ=2.70—3.19 (m, 10H), 3.47 (d, *J*=6Hz, 2H, SCH_2CH=N), 4.10 (m, 1H, SCHS), 7.47 (t, *J*=6 Hz, 1H, CH=N), 7.92 (d, *J*=9 Hz, 1H, ArH), 8.36 (dd, *J*=9, 3 Hz, 1H, ArH), 9.13 (d, *J*=3 Hz, 1H, ArH), and 11.11 (br s, 1H, NH). Found: C, 38.69; H, 4.17; N, 12.89%. Calcd for $C_{14}H_{18}N_4O_4S_4$: C, 38.38; H, 4.14; N, 12.85%.

References

1) a) F. G. Bordwell and B. M. Pitt, *J. Am. Chem. Soc.*, **77**, 572 (1955); b) W. E. Truce, G. Birum, and E. T. McBee, *J. Am. Chem. Soc.*, **74**, 3594 (1952); c) H. Böhme and H. J. Gran, *Justus Liebigs Ann. Chem.*, **577**, 68 (1952).

2) J. T. Doi and W. K. Musker, *J. Am. Chem. Soc.*, **100**, 3533 (1978); W. K. Musker, *Acc. Chem. Res.*, **13**, 200 (1980).

3) N. Furukawa, A. Kawada, and T. Kawai, *J. Chem. Soc., Chem. Commun.*, **1984**, 1151.

4) N. Furukawa, A. Kawada, T. Kawai, and H. Fujihara, *J. Chem. Soc., Chem. Commun.*, **1985**, 1266.

5) In the ^{1}H NMR spectrum of [$^2H_4$]-**4** in CD_3CN, the splitting pattern is complicated and could not be resolved.

6) J. R. Meadow and E. E. Reid, *J. Am. Chem. Soc.*, **56**, 2177 (1934).

Terpenoids. X.[1] Natural Autoxidation of Thujopsene

Shizuo NAGAHAMA* and Masato TAZAKI
The Kumamoto Institute of Technology, Ikeda 4-22-1, Kumamoto 860
(Received June 22, 1987)

Synopsis. The natural autoxidation of thujopsene **1** afforded three dimeric peroxides (**14**, **15**, and **16**) as the major products. 9α,10-Epoxy-8α-thujopsanol **17** was separated as a minor product besides other known compounds, allylic alcohols **2** and **3**, mayurone **7**, thujopsane-8α,9α-diol **11**, and thujopsan-9-ones **19** and **20**.

Kawamura[2] described in his first report the instability of thujopsene **1** towards exposure to air or sunlight; i.e., **1** suffers autoxidation very easily. The photosensitized[3,4] and catalytic[5] autoxidations were examined extensively; however, the oxidation occuring naturally with atmospheric oxygen has not been studied so far, in which the reaction can proceed under extremely mild conditions. In this paper, we will show the products from the natural autoxidation of **1**, as analyzed by chromatographic separation.

Results and Discussion

Three crystalline bis(Δ^9-thujopsen-8-yl) peroxides were separated by repeated alumina chromatography in the order of elution: **14** mp 100—102 °C, **15** mp 62—68 °C, and **16** mp 136—138 °C. Upon the reduction by $LiAlH_4$, the peroxide **14** gave only Δ^9-thujopsen-8β-ol[1] **2**, whearas the peroxide **16** gave Δ^9-thujopsen-8α-ol[1] **3**. The peroxide **15** gave a 1 : 1 mixture of **2** and **3**. The gas chromatography of peroxides showed a broad peak accompanied with the peaks of thujopsadiene[1] **6** and mayurone[1] **7** as decomposition products.

A crystalline compound **17** mp 106—107 °C was isolated as a minor product. The IR spectrum of **17** showed the presence of an OH group. The ^1H NMR spectrum showed two protons on an epoxy ring, one of which showed a long-range coupling constant of 1.8 Hz. The reductive cleavage of the epoxy ring in **17** with $LiAlH_4$ resulted in the formation of thujopsane-8α,9α-diol[1] **11** as a minor product. Thus, 9α,10-epoxy-8α-thujopsanol was assigned to **17**. The major reduction product was 8α,10α-diol **18**.

As the known compounds, **2**, **3**, thujopsan-9-ones[6] **19** and **20**, **7** and **11** were also separated from the natural autoxidation products.

Experimental

A thujopsene fraction (23.8 g) obtained by spinning band column distillation of Hiba wood neutral oil was allowed to stand for 6 years. The viscous oil afforded by repeated chromatography on alumina following fractions: hydrocarbons 24%, peroxides (**14**—**16**) 25%, a 1 : 1 mixture of thujopsan-9-ones (**19** and **20**) 6%, allylic alcohols **2** and **3**, 2%, mayurone **7**, 6%, epoxy alcohol **17**, 5% and 8α,9α-diol **11**, 0.6%. The structures of the known compounds, **2**, **3**, **7**, **11**, **19**, and **20**, were confirmed by the comparison of their ^1H NMR and IR spectra with those reported earlier.[1,6] **17**: Mp 106—107 °C. IR (KBr) 3500 (OH), 3050, 2970, 2930, 1459, 1378, 1306, 1177, 1159, 1129, 1074, 1040, 1022, 1004, 922, 919, 910, 864, 830, and 809 cm^{-1}. ^1H NMR ($CDCl_3$) δ=0.18 (1H, dd, J=8.8, 4.0 Hz), 0.54 (3H, s), 1.00 (3H, s), 1.34 (3H, s), 1.41 (3H, s), 0.93—1.81 (8H, m), 2.05 (1H, broad), 2.74 (1H, d, J=4.0 Hz), and 3.02 (1H, dd, J=4.0, 1.8 Hz).

Separation of 14, 15, and 16: A later part of the peroxide fraction obtained above crystallized. Recrystallization from hexane gave peroxide **16** (1.05 g) mp 136—138 °C. Found: C, 81.73; H, 10.51%. Calcd for $C_{30}H_{46}O_2$: C, 81.63; H, 10.87%. IR (KBr) 3080, 2950, 1389, 1371, 1360, 1159, 1103, 1082, 770, 756,

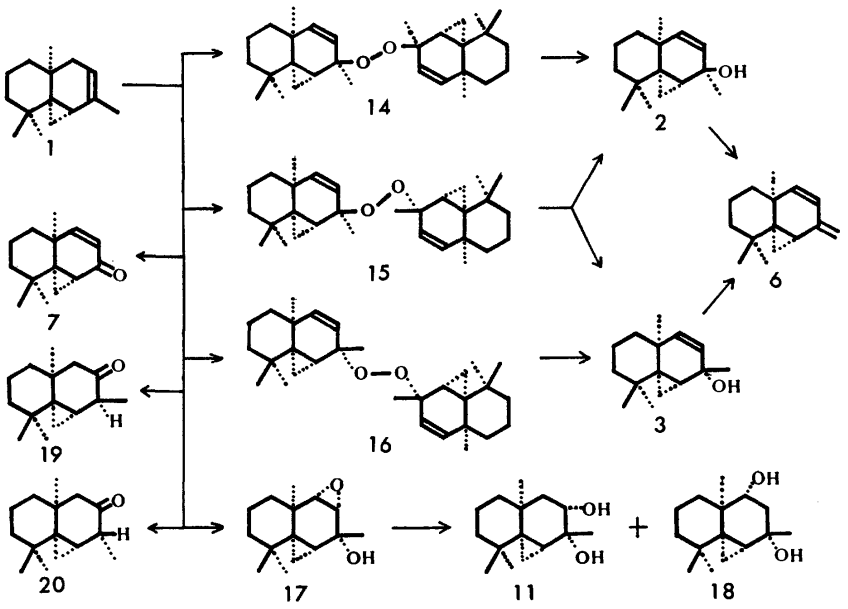

Scheme 1.

and 740 cm^{-1}. ^1H NMR ($CDCl_3$) δ=0.33—0.72 (4H, m), 0.65 (6H, s), 1.06 (6H, s), 1.15 (6H, s), 1.44 (6H, s), 1.0—1.7 (14H, m), 5.02 (2H, d, J=10.4 Hz), and 5.42 (2H, dd, J=10.4, 1.8 Hz).

The intermediate fraction between hydrocarbons and **16** was re-chromatographed. The fast-running fraction crystallized and afforded peroxide **14** (0.15 g) mp 100—102 °C (from hexane). IR (KBr) 3055, 3010, 1466, 1381, 1371, 1160, 1100, 1091, 1080, 901, 882, 764, and 741 cm^{-1}. ^1H NMR ($CDCl_3$) δ=−0.03 (2H, dd, J=5.6, 4.6 Hz), 0.39 (2H, dd, J=9.6, 4.6 Hz), 0.63 (6H, s), 1.04 (6H, s), 1.13 (6H, s), 1.28 (6H, s), 1.1—1.7 (14H, m), and 4.93—5.38 (4H, m).

Repeated chromatography of the middle fractions of **14** and **16** finally gave crystalline peroxide **15** (0.11 g) mp 62—68 °C. IR (neat) 3060, 2920, 1386, 1371, 1360, 1158, 1171, 1132, 1083, 1032, 952, 903, 881, 770, 751, and 740 cm^{-1}. ^1H NMR ($CDCl_3$) δ=0.00 (1H, dd, J=5.4, 4.6 Hz), 0.29—0.70 (3H, m), 0.64 (6H, s), 1.05 (6H, s), 1.14 (6H, s), 1.31 (3H, s), 1.44 (3H, s), 1.0—1.7 (14H, m), 5.08 (1H, d, J=10.4 Hz), 5.16 (2H, s), and 5.52 (1H, dd, J=10.4, 1.8 Hz).

Reduction of Peroxides 14—16: Peroxide **14** (120 mg) dissolved in 2 ml of dioxane was refluxed for 10 hrs with excess $LiAlH_4$. The usual work-up gave an oil (85.7 mg), identical to **2**, obtained by $KMnO_4$ oxidation of thujopsene.[1] Peroxide **16** (157 mg) was reduced as above, and gave 128 mg of **3**. The similar reduction product of peroxide **15** was a 1 : 1 mixture of **2** and **3** by gas chromatography.

Reductive Cleavage of Epoxy Ring in 17: Epoxy alcohol **17** (283 mg) in 10 ml dioxane was refluxed with $LiAlH_4$ for 1 day. The product (290 mg) was recrystallized from ether-hexane gave diol **18** mp 128—129.5 °C (98 mg). The residue from the mother liquor (160 mg) was chromatographed on an alumina column (6 g) and eluted with ether. **18** (54 mg) was recovered and 8α,9α-diol **11** (28 mg) was obtained. **18**: IR (KBr) 3260(broad, OH), 3010, 1370, 1252, 1141, 1091, 1048, 1002, 911, 888, 859, 838, and 741 cm^{-1}. ^1H NMR ($CDCl_3$) δ=0.43 (1H, dd, J=10.6, 5.0 Hz), 0.57 (3H, s), 1.01 (3H, s), 1.26 (3H, s), 1.42 (3H, s), 0.80—1.8 (8H, m), 1.69 (2H, d, J=3.4 Hz), 2.79 (1H, broad), 2.96 (1H, d, J=5.2 Hz), and 3.30 (1H, dt, J=5.2, 3.4 Hz).

References

1) Part IX, S. Nagahama and M. Tazaki, *Bull. Chem. Soc. Jpn.*, **60**, 4175 (1987).

2) J. Kawamura, *Bull. Govt. Forest Expt. Station*, **30**, 59 (1930).

3) S. Ito, H. Takeshita, T. Muroi, M. Ito, and K. Abe, *Tetrahedron Lett.*, **1969**, 3091; H. Takeshita, T. Sato, T. Muroi, and S. Ito, *ibid.*, **1969**, 3095; S. Ito, H. Takeshita, and M. Hirama, **1971**, 1181.

4) G. Ohloff, H. Strickler, B. Willhalm, C. Borer, and M. Hinder, *Helv. Chim. Acta*, **53**, 623 (1970).

5) M. Ito, T. Nishimura, and K. Abe, *Bull. Chem. Soc. Jpn.*, **45**, 1914 (1972); K. Abe and M. Ito, *ibid.*, **52**, 261 (1979).

6) S. P. Acharya and H. C. Brown, *J. Org. Chem.*, **35**, 3874 (1970).

Reaction between Copper(II) Chloride and Active Carbon for the Formation of Solid Carbon Monoxide Adsorbent

Makoto KOMIYAMA,*,† Hiroaki ANDO, and Hidefumi HIRAI††
Department of Industrial Chemistry, Faculty of Engineering, The University of Tokyo, 7-3-1, Hongo, Bunkyo-ku, Tokyo 113
(Received April 24, 1987)

Synopsis Evolution of hydrochloric acid on the preparation of carbon monoxide adsorbents from copper(II) chloride and active carbon has been experimentally confirmed. Relationship between the amount of hydrochloric acid evolved and the adsorbing capacity shows that the efficient adsorption by the adsorbents is attributable to the function of the copper(I) chloride, which is formed during the preparation by the reaction between copper(II) chloride and active carbon.

In industry, carbon monoxide is usually obtained as gas mixtures with nitrogen, hydrogen, methane, and carbon dioxide. Thus carbon monoxide must be separated from gas mixtures for the effective utilization.[1)]

Previously,[2)] the present authors have reported that solid adsorbents, prepared from copper(II) chloride and active carbon, adsorb carbon monoxide efficiently and reversibly under mild conditions. These adsorbents have an advantage from the viewpoint of practical application that both of the starting materials are stable against oxygen and thus the preparations are successfully achieved even under air. The adsorbing capacities of the adsorbents are much larger than the sum of the values for copper(II) chloride and active carbon. Thus it has been proposed that copper(II) chloride ($CuCl_2$) and active carbon (AC-H) react during the preparation as shown by Eq. 1, resulting in the formation of copper(I) chloride (CuCl).[2)] The resultant copper(I) chloride supported on the active carbon effectively adsorbs carbon monoxide.[3)]

$$\text{AC-H} + 2\,CuCl_2 \rightarrow \text{AC-Cl} + 2\,CuCl + HCl \qquad (1)$$

In this article, evolution of hydrogen chloride during the preparation of the adsorbents from copper(II) chloride and active carbon are quantitatively analyzed. The relationship between the amounts of hydrogen chloride evolved and the adsorbing capacities of the adsorbents is described.

Experimental

Active carbon (Kureha Chemical Industry Co., BAC G-70R, Lot. No. 810117) was subjected to a reduced pressure (5 mmHg (1 mmHg=133.322 Pa)) at 200 °C for 5 h prior to use.

The adsorbents were prepared by refluxing 20 g of the active carbon and 30 mmol of copper(II) chloride in 30 cm^3 of water, followed by removal of the liquid phase under 5 mmHg. Here, hydrogen chloride evolved was trapped with the use of liquid nitrogen traps, and was titrated with 1.0 mol dm^{-3} aqueous solution of sodium hydroxide. The amount of copper atoms, which were supported onto the active carbon, was 28.2 g-atoms as determined by atomic absorption spectroscopy.

Results and Discussion

When aqueous solution of silver nitrate was added to the contents obtained in the liquid nitrogen traps on the preparation of the adsorbents from copper(II) chloride and the active carbon, white precipitates (AgCl) were immediately formed. This result definitely shows that the reaction of Eq. 1 in fact takes place, yielding hydrogen chloride.

No hydrogen chloride was trapped, when only water-active carbon mixtures were evaporated at 180 °C under 2.5 mmHg. On evaporation of 30 cm^3 of aqueous solution of copper(II) chloride (1.0 mol dm^{-3}), the amount of hydrogen chloride was only 0.2 mmol.

Table 1 shows the amounts of hydrogen chloride trapped in the liquid nitrogen traps under various preparation conditions, together with the carbon monoxide adsorbing capacities of the resultant adsorbents. When the adsorbent is prepared by refluxing copper(II) chloride and the active carbon in water for 6 h, followed by the evaporation of the liquid phase at 180 °C, the amount of hydrogen chloride trapped is 13.5 mmol. The adsorbing capacity of the adsorbent is 19.3 mmol. On increase of the evaporation temperature from 180 to 200 °C, the amount of hydrogen chloride trapped is slightly increased to 14.1 mmol.

According to Eq. 1, 28.2 mmol of copper(I) chloride should be formed during the preparation of the adsorbent, when 14.1 mmol of hydrogen chloride is evolved. The molar ratio (0.68) of the adsorbing capacity (19.3

Table 1. Carbon Monoxide Adsorbing Capacities of the Adsorbents Prepared from the Active Carbon and Copper(II) Chloride as well as the Amounts of Hydrogen Chloride Trapped on Their Preparation

Preparation condition		Adsorbing capacity/ mmol	Amount of HCl/ mmol[c)]
Refluxing[a)] period/h	Evaporation[b)] temp/°C		
6	180	19.3	13.5
6	200	19.3	14.1
0	180	16.5	9.5

a) The period in which the active carbon and copper(II) chloride are refluxed in water. b) The temperature of the removal of the liquid phase under 2.5 mmHg. c) The amount of hydrogen chloride trapped in the liquid nitrogen traps on the preparation of the adsorbents.

†Institute of Materials Science, University of Tsukuba, Sakura-mura, Ibaraki 305.
††Department of Industrial Chemistry, Faculty of Engineering, Science University of Tokyo, 1-3 Kagurazaka, Shinjuku-ku, Tokyo 162.

mmol) of the adsorbent to the estimated amount (28.2 mmol) of copper(I) chloride formed is almost identical with the corresponding value (0.64)[3] for the adsorbent, which is prepared directly from copper(I) chloride and active carbon in water. Thus the carbon monoxide adsorbing activity of the present adsorbent is ascribed to the function of the copper(I) chloride, which is formed during the preparation and is supported on the active carbon.

The adsorbent, prepared by the removal of the liquid phase at 180 °C without refluxing the mixture in water, shows a smaller adsorbing capacity (16.5 mmol). The amount (9.5 mmol) of hydrogen chloride trapped during the preparation is about 2/3 of the value (13.5 mmol) for the adsorbent obtained by the evaporation at 180 °C after refluxing.

These results indicate that the reaction of Eq. 1 occurs both during the refluxing and during the evaporation of the liquid phase. Refluxing of the reaction mixture in water probably facilitates the dissolution of hydrogen chloride, which is formed in the micropores of the active carbon and is adsorbed there, into aqueous phase.

The reaction of Eq. 1 proceeds in a similar way as electrophilic chlorination of anthracene by copper(II) chloride,[4] in which 9,10-dichloroanthracene and copper(I) chloride are formed. Active carbons have many reaction sites for this reaction, since they are composed of conjugated aromatic rings.

In conclusion, it has been experimentally established that the reaction of Eq. 1 occurs during the preparation of carbon monoxide adsorbents from copper(II) chloride and active carbon. The resultant copper(I) chloride supported on the active carbon is responsible for the efficient adsorption of carbon monoxide by the adsorbents.

This work was partially supported by a Grant-in-Aid for Scientific Research from the Ministry of Education, Science and Culture.

References

1) A. L. Kohl and F. C. Riesenfeld, "Gas Purification," 3rd ed, Gulf Publishing Co., Houston (1979).

2) H. Hirai, K. Wada, and M. Komiyama, *Chem. Lett.*, **1986**, 943.

3) H. Hirai, K. Wada, and M. Komiyama, *Bull. Chem. Soc. Jpn.*, **59**, 2217 (1986).

4) J. C. Ware and E. E. Borchert, *J. Org. Chem.*, **26**, 2263 (1961).

Low Temperature Synthesis of Dispersed Fine Particle of Cobalt Aluminate—A New Application of Zeolite

Tatsuo OHGUSHI* and Shigeru UMENO
School of Materials Science, Toyohashi University of Technology, Tempaku-cho, Toyohashi 440
(Received May 11, 1987)

Synopsis. $CoAl_2O_4$, with the spinel structure in a dispersed form, was synthesized at 400 °C by using zeolite A as a starting material. A specific surface area of the products was measured by adsorption of $(CH_3)_2CHCH_3$ gas at −110 °C and the mean size of the product particles was estimated to be about 14 nm.

Zeolites have been used as catalysts, adsorbent or ion exchangers owing to their porous structure. In these applications, the zeolitic structure is, of course, preserved. In the present work, zeolite A was used as a source of aluminium for the synthesis of cobalt aluminate. The methods of synthesis and characterization of the product are described in the following.

Experimental

The starting material, Na-A zeolite, was treated several times with 0.1 mol dm^{-3} $CaCl_2$ solution, and $Ca_{5.7}Na_{0.2}H_{0.3}(AlO_2)_{11.9}(SiO_2)_{12.1}$ was obtained. This zeolite (abbreviated as Ca_6-A) was further ion-exchanged, at 80±1 °C for 3 days, with solutions of $CoCl_2$ or mixed solutions of $CoCl_2$ and $CaCl_2$ of 0.1 (or 0.01) mol dm^{-3}. The pH value of the solution was not strictly controlled during the ion exchange, and the values before and after the ion exchange were in a range of 6.5—5.5 at room temperature, irrespective of the concentration of the solution (0.1 or 0.01 mol dm^{-3}). The composition Co_xCa_{6-x}-A was calculated from the composition of the solution and the material balance. The composition of the solution was determined by spectrophotometry. All chemical reagents used were S.P. grade, and the adsorbate gases used, oxygen and $(CH_3)_2CHCH_3$, had nominal purities better than 99.99 and 99.9%, respectively.

The amount of gas adsorbed was measured by the volumetric method in a clean vacuum system. A vacuum of 10^{-5} Pa was easily attained. Prior to adsorption experiments, the adsorbents were dehydrated at room temperature for 5 h and carefully baked out by raising the temperature stepwise. The samples were finally kept at 400 °C for 6 h in a vacuum of 10^{-5} Pa.

Results and Discussion

$Co_{5.5}Ca_{0.5}$-A zeolite (prepared in 0.1 mol dm^{-3} solution) was heated under various conditions (specified as (a), (b), ···) and rehydrated at 20 °C. Its color changed as follows (P denotes pink and B blue),

$Co_{5.5}Ca_{0.5}$-A (P)
- →(a) 20 °C in vac.(B)→20 °C rehy.(P)
- →(b) 20 °C in vac.(B)→400 °C in vac.(B)→20 °C rehy.(B)
- →(c) 400 °C in vac.(B)→20 °C rehy.(B)
- →(d) 400 °C in Ar(B)→20 °C rehy.(B)
- →(e) 1000 °C in Ar(deep B)→20 °C rehy.(deep B)
- →(f) 1000 °C in air(deep B)→20 °C rehy.(deep B)
- →(g) 400 °C in air(gray-brown)→20 °C rehy.(gray-brown).

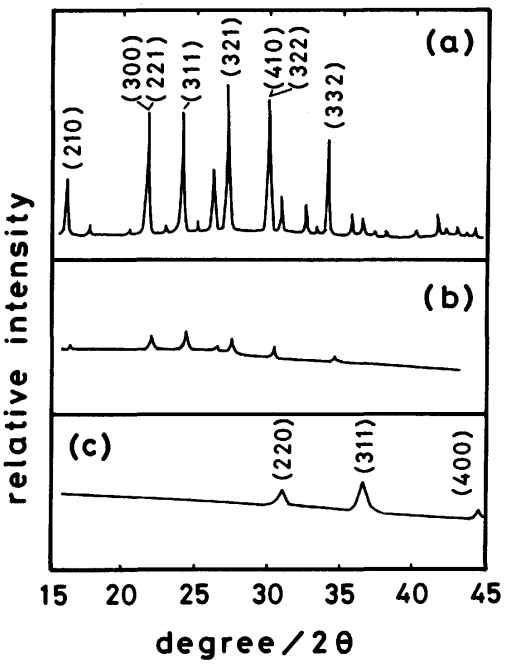

Fig. 1. X-Ray diffraction patterns of Co_xCa_{6-x}-A zeolites heat-treated. Copper radiation ($K\alpha$, λ=0.154 nm) was used. The patterns in (a) and (c) are characteristic to zeolite A and $CoAl_2O_4$, respectively. The pattern in (b) is characteristic to zeolite A but each peak is much weaker than that in (a). Representative indices of planes are shown in parenthesis. (a) x=0, heated at 400 °C in vacuum (b) x=4.1, heated at 400 °C in vacuum (c) x=5.5, heated at 1000 °C in air.

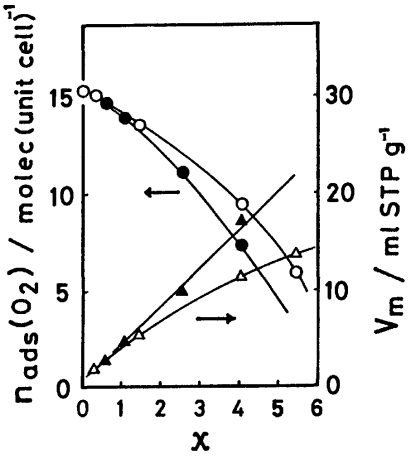

Fig. 2. Adsorptive capacities of Co_xCa_{6-x}-A zeolite heat-treated at 400 °C in vacuum. $n_{ads}(O_2)$; amount of O_2 adsorbed at −196 °C and 2000 Pa, v_m; monolayer capacity of $(CH_3)_2CHCH_3$ at −110 °C. ○△; zeolite prepared in 0.1 mol dm^{-3} solution, ●▲; zeolite prepared in 0.01 mol dm^{-3} solution.

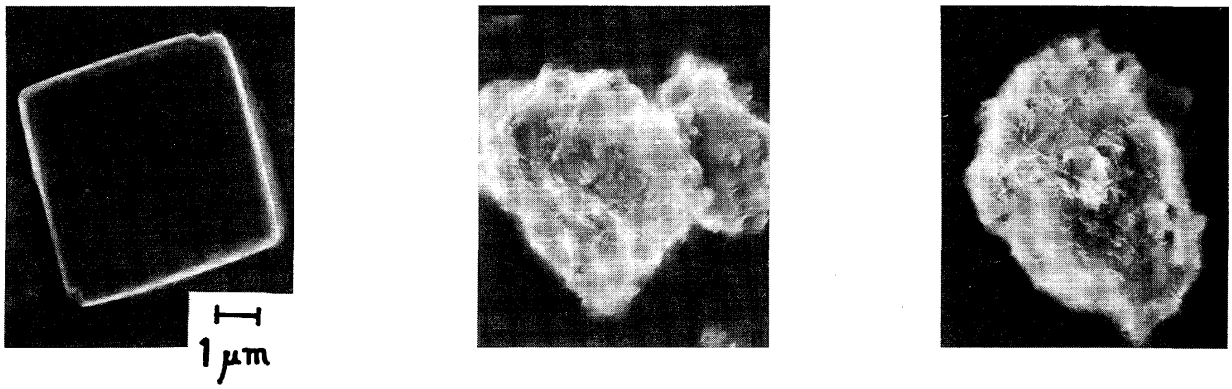

Fig. 3. Electron micrographs of Co_xCa_{6-x}-A zeolite, ion-exchanged with 0.1 mol dm^{-3} solution and then heat-treated at 400 °C in vacuum. (a) x=0, (b) x=4.1, (c) x=5.5.

With samples of $x<5.5$, the same changes were observed, though the color became thin with decreasing x-values. In $Co_{5.5}Ca_{0.5}$-A, heat treatments at 400 °C or higher always caused irreversible changes. All substances produced in treatments (b)—(g) were dipped in water, but did not return to the original color, pink. X-Ray diffractions of heat-treated zeolites were measured, and representative patterns are shown in Fig. 1. All peaks in the diffraction pattern of $Co_{4.1}Ca_{1.9}$-A, in Fig. 1(b), are assigned to zeolite A.[1] The same is the case with zeolites containing less Co than this. The peaks became weak with increasing x and vanished at x=5.5. The products in the treatments (e) and (f) contained $CoAl_2O_4$ as judged from their X-ray diffraction patterns[2] (Fig. 1(c)). The products in the treatment (g) gave no X-ray diffraction peaks but gave electron diffraction spots, which could not be assigned to any crystal. Products obtained in the treatments (b)—(d) contained $CoAl_2O_4$ as judged from electron diffraction patterns. The fraction of zeolite decomposed was estimated from the decrease in the adsorption capacity of O_2 which can penetrate into the zeolite cavity.[3,4] The amount of O_2 adsorbed was measured at −196 °C, and is given in Fig. 2. Representative scanning electron micrographs are shown in Fig. 3. In Fig. 3(c), the products are fine flakes. It was observed with the scanning electron microscope that the surface of Co_x. Ca_{6-x}-A became increasingly rough with the increasing x-value. Their surface became much rougher on heating. From the above results, it is concluded that the fraction of Co_xCa_{6-x}-A decomposed, by heating at 400 °C in vacuum or Ar atmosphere, increases with increasing x and becomes 0.7—0.8† at x=5.5, and the degradation products contain $CoAl_2O_4$.

The outer-surface area (BET area) of the degradation products was measured by the adsorption of $(CH_3)_2CHCH_3$ at −110 °C, which cannot penetrate into the zeolite cage.[4,5] Monolayer capacities of the products are shown in Fig. 2. The surface area of $CoAl_2O_4$ powder can not be deduced with confidence from this BET area. Now, let us roughly estimate the mean particle size of the products by assuming that the products contain $CoAl_2O_4$, SiO_2, Al_2O_3, and Ca_2SiO_4, all components have a cubic form of the same size, and the cross sectional area of $(CH_3)_2CHCH_3$ molecule at −110 °C is 0.29 nm^2. The edge of the products obtained from $Co_{5.5}Ca_{0.5}$-A was about 14 nm. The size, however, depended upon the ion-exchange condition, as shown in Fig. 2.

$CoAl_2O_4$ with the spinel structure is usually synthesized from CoO and Al_2O_3 at temperatures higher than 1000 °C.[6] In the present work, $CoAl_2O_4$ was obtained at such a low temperature as 400 °C by using (Co,Ca)-A zeolite as a precursor. The precursor method has frequently been used in the synthesis of some spinel compounds.[7-9] The use of zeolite material as a precursor is a new development and further investigations may open a new way of techniques for the synthesis.

The present authors wish to thank Prof. Tetsuo Takaishi of Toyohashi University of Technology, for useful discussions and language correction, and Mr. Keiji Itabashi of Toyo Soda Co., who kindly supplied zeolite materials.

†Oxygen gas adsorbs into the zeolite cage, and onto the outer surface of the zeolite and degradation products. In three kinds of adsorptions, the amount of O_2 adsorbed onto the zeolite outer surface is negligible at all x-values. Hence, the fraction of zeolite decomposed is obtained by correcting for the amount adsorbed on the degradation products.

References

1) L. Broussard and D. P. Shoemaker, *J. Am. Chem. Soc.*, **82**, 1041 (1960).
2) A. S. T. M. Diffraction Data File, No. 10—458.
3) A. Yusa, T. Ohgushi, and T. Takaishi, *J. Phys. Chem. Solids*, **38**, 1233 (1977).
4) D. W. Breck, W. G. Eversole, R. M. Milton, T. B. Reed, and T. L. Thomas, *J. Am. Chem. Soc.*, **78**, 5963 (1956).
5) R. M. Barrer, "Zeolites and Clay Minerals," Academic Press, London (1978), p. 287.
6) G. Grauer, "Handbuch der Praparation Anorganischen Chemie," Ferdinand Enke Verlag, Stuttgart, 1. Aulflage (1954) s. 1139.
7) D. G. Wickham, E. R. Whipple, and E. G. Larson, *J. Inorg. Nucl. Chem.*, **14**, 217 (1960).
8) E. Whipple and A. Wold, *J. Inorg. Nucl. Chem.*, **24**, 23 (1962).
9) A. Wold, *J. Chem. Ed.*, **57**, 531 (1980).

Hydrates of Organic Compounds. XIV. The Formation of Clathrate-Like Hydrates of Tetrabutylammonium Amino Carboxylates

Haruo NAKAYAMA,* Hideyuki USUI, and Hiroshi MATSUI†
Department of Chemistry, Faculty of Engineering, Yokohama National University, Tokiwadai, Hodogaya-ku, Yokohama 240
†The Radio Isotope Center, Yokohama National University, Tokiwadai, Hodogaya-ku, Yokohama 240
(Received March 24, 1987)

Synopsis. The solid-liquid phase diagrams of binary mixtures of water with a series of tetrabutylammonium α-amino carboxylates, $(n\text{-}C_4H_9)_4NOOCCH(NH_2)R$ (R=H, CH_3, C_2H_5, $n\text{-}C_3H_7$, and $(CH_3)_2CH$), were examined. It was found that all the salts examined could form hydrates with hydration numbers either around 30 or around 39.

A series of tetrabutylammonium carboxylates has been known to form a clathrate-like hydrate[1] similar to the so-called gas hydrate.[2] According to a crystal structural analysis by Jeffrey et al. on a tetrabutylammonium benzoate hydrate,[3] oxygen atoms of the benzoate anion are incorporated into the water lattice, making an anionic host structure. The characteristics found for the tetrabutylammonium carboxylate hydrates are summarized as follows: (1) Two types of hydrates exist; group I which has fairly high melting points and hydration numbers around 30 and group II which has relatively low melting points and hydration numbers around 39; and (2) a methyl group attached to the carbon atom of the α-position of the carboxylate anion pronouncely lowers the stability of the hydrate due to a deformation effect imposed on the host structure.[1]

In this study, the solid-liquid phase diagrams for binary mixtures of a series of tetrabutylammonium α-amino carboxylates with water were examined in order to determine (1) whether these amino carboxylates can form similar types of clathrate-like hydrates and (2) the degree of distortion effect of a NH_2 group attached to the carbon atom of α-position on the stability of the hydrate.

Experimental

An aqueous solution of tetrabutylammonium amino carboxylates was prepared by the neutralization of a tetrabutylammonium hydroxide solution with each amino acid. The hydroxide solution was prepared by the same procedure as described in previous papers.[1,4] All amino acids were purchased from Tokyo Kasei Kogyo Co. Ltd., and were purified by a conventional method: A hot aqueous solution of an amino acid was added dropwise to 95 v/v% ethyl alcohol with stirring, followed by filtration of a solid phase and by washing the solid with 95 v/v% ethyl alcohol.

Solid-liquid phase diagrams for the binary systems of water-tetrabutylammonium amino carboxylates were determined in the same manner as described in the previous papers[1,4] (an ampoule method).

Results and Discussion

The solid-liquid phase diagrams for binary systems of tetrabutylammonium aminoacetate (glycine salt)-water and of tetrabutylammonium DL-α-aminopropionate (alanine salt)-water are shown in Fig. 1. Similar phase diagrams for binary systems of tetrabutylammonium DL-α-aminoisobutyrate (valine salt)-water and of tetrabutylammonium DL-α-aminopentanoate (norvaline salt)-water are shown in Fig. 2. In these figures the logarithm of the concentration expressed in the mole fraction, X, is plotted against the reciprocal of the absolute temperature. The temperature, expressed in ordinary Celcius units, is shown on the upper side of the figure. Because of the similarity of the phase diagram of tetrabutylammonium DL-α-aminobutyrate-water system with that of the tetrabutylammonium DL-α-aminopropionate-water system, the phase diagram of the former system is excluded from Fig. 1.

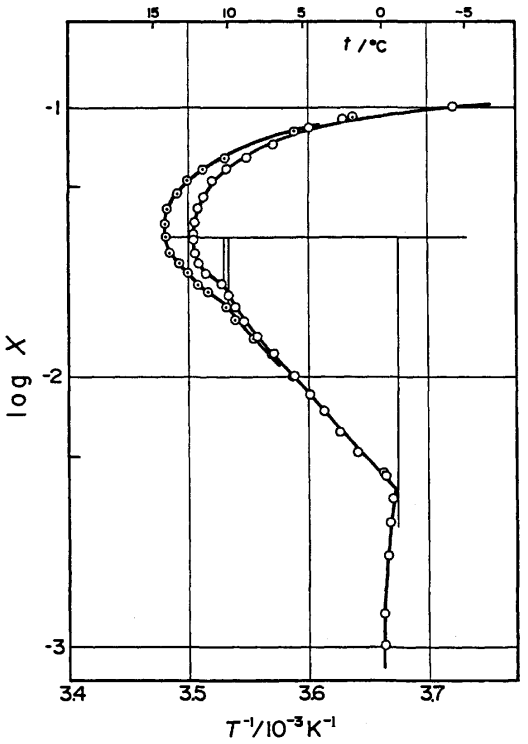

Fig. 1. Solid-liquid phase diagrams for the tetrabutylammonium aminoacetate-water system (◉) and for the tetrabutylammonium DL-α-aminopropionate-water system (○).

The existence of congruent melting points at $X\simeq0.032$ in Fig. 1 and at $X\simeq0.025$ in Fig. 2 clearly indicates that these salts form a hydrate which has large hydration numbers: the congruent composition of $X\simeq0.032$ corresponds to a hydrate whose hydration numbers are around 30 and of $X\simeq0.025$ to the one with hydration numbers around 39. Judging from such large hydration numbers, these hydrates seem to be

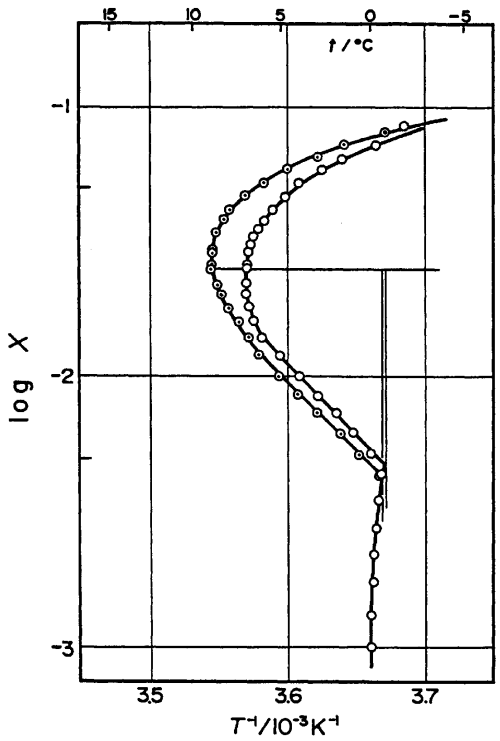

Fig. 2. Solid-liquid phase diagrams for the tetrabutylammonium DL-α-aminoisobutyrate-water system (○) and for the tetrabutylammonium DL-α-aminopentanoate-water system (◉).

clathrate-like hydrates, similar to $(n\text{-}C_4H_9)_4NF \cdot 30H_2O$[5] and $(n\text{-}C_4H_9)_4NOOCC_6H_5 \cdot 39.5H_2O$[3] hydrates. The presence of tetrabutylammonium amino carboxylate hydrates has never been known before. As can be seen in Fig. 1, phase diagrams of the tetrabutylammonium aminoacetate-water system and the tetrabutylammonium DL-α-aminopropionate-water system show an incongruent melting point of 10.1 °C at $X \simeq 0.018$ and of 10.4 °C at $X \simeq 0.022$, respectively. The exact hydration numbers of the hydrates formed in the concentration range between eutectic composition ($X \simeq 0.004$) and the concentration corresponding to the incongruent point are not obvious at present.

All the melting points and hydration numbers, determined from each congruent melting point and congruent composition are summarized in Table 1. From these results the clathrate-like hydrates of tetrabutylammonium DL-α-amino carboxylates can be classified into two groups, group I and group II, just as in the case of tetrabutylammonium carboxylate hydrates.[1] The classification of group I and II is also given in Table 1. The group I hydrate, whose hydration numbers are around 30, has fairly high melting points and is formed by amino carboxylates with small alkyl groups. The group II hydrate, whose hydration numbers are around 39, has relatively low melting points and is formed by amino carboxylates with relatively large alkyl groups.

In previous studies[1,4,6] it became clear that the melting point of tetrabutylammonium salt hydrate is largely dependent upon the molar volume of the anion

Table 1. Melting Points and Hydration Numbers of Clathrate-Like Hydrates of Tetrabutylammonium DL-α-Amino Carboxylates $(n\text{-}C_4H_9)_4NOOCCH(NH_2)R$

R	Mp θ_m/°C	Hydration number	Group
H	14.2	30±1	I
CH_3	12.3	30±2	I
CH_3CH_2	12.2	30±2	I
$(CH_3)_2CH$	6.9	39±2	II
$CH_3(CH_2)_2$	8.9	38±2	II

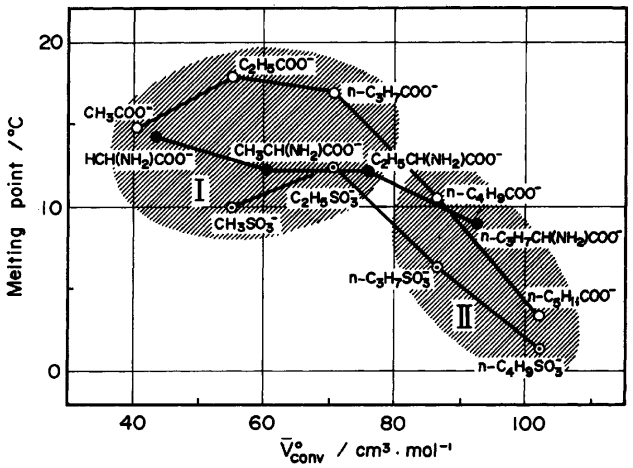

Fig. 3. Relationship between the melting points of the tetrabutylammonium DL-α-amino carboxylate hydrates and the conventional partial molar volumes of DL-α-amino carboxylate anions. The same relationships for tetrabutylammonium carboxylate hydrates[1] and tetrabutylammonium alkanesulfonate hydrates[4] are also shown.

of the salt. This relation is represented in Fig. 3, in which the melting point of each hydrate is plotted against the conventional partial molar anionic volume at 25 °C as an indication of the effective volume of the anion within the hydrate solid.[6] The conventional partial molar volume of each amino carboxylate anion was obtained from the literature.[7] In Fig. 3 the same relationships for a series of tetrabutylammonium carboxylate hydrates[1] and of tetrabutylammonium alkanesulfonate hydrates[4] are also shown. Although the dependence of the melting point of the amino carboxylate hydrates upon the anionic volume is not so marked as compared with the other two series of hydrates, the region in which either the group I hydrate or the group II hydrate is formed is essentially identical for the three types of hydrates. For this reason, concerning the crystal structure of the amino carboxylate hydrates, the same speculation as was done regarding both the carboxylate hydrates and the alkanesulfonate hydrates may be made: The group I hydrate is iso-structural with $(n\text{-}C_4H_9)_4NF$ hydrate[5] and a vacant pentagonal dodecahedron is occupied by a small alkyl group, such as CH_3 and C_2H_5, of the amino carboxylate anion; and the group II hydrate is iso-structural with $(n\text{-}C_4H_9)_4NOOCC_6H_5$ hydrate[3] and the amino carboxylate anion like $CH_3(CH_2)_2CH(NH_2)$-

Table 2. Melting Points of Clathrate-Like Hydrates of Three Types of Tetrabutylammonium Carboxylates

R	Mp θ_m/°C Carboxylate anion		
	RCH_2-COO^- a)	$RCH(NH_2)$-COO^- b)	$RCH(CH_3)$-COO^- a)
H	14.8(I)c)	14.2(I)	18.0(I)
CH_3	18.0(I)	12.3(I)	9.8(I)
CH_3CH_2	17.0(I)	12.2(I)	7.7(II)
$(CH_3)_2CH_2$	11.3(II)	6.9(II)	—
$CH_3(CH_2)_2$	10.6(II)	8.9(II)	5.1(II)

a) Taken from the Ref. 1. b) DL except for the R=H salt. c) I and II in parentheses indicate the group of the hydrates.

COO^- and $(CH_3)_2CHCH(NH_2)COO^-$ is enclathrated within a large polyhedron, such as tetrakaidecahedron and pentakaidecahedron.

In Table 2 the melting points of the hydrates of three types of tetrabutylammonium carboxylates (ordinary carboxylates,[1] DL-α-amino carboxylates and α-methyl carboxylates[1]) are compared with each other. This table clearly indicates that the effect of a NH_2 group upon the melting points of the hydrate is generally intermediate between that of a H group and of a CH_3 group. However, it is interesting to note that (1) the melting point of the tetrabutylammonium aminoacetate hydrate (14.2 °C) is almost the same as that (14.8 °C) of the tetrabutylammonium acetate hydrate, in spite of the situation that a slightly bulky $CH_2(NH_2)$ group is expected to be more suitable for being intercalated within a pentagonal dodecahedron than a CH_3 group; and (2) the melting point of the valine salt hydrate (6.9 °C) is lower than that of the norvaline salt hydrate (8.9 °C), in contrast to the slightly higher melting point (11.3 °C) of tetrabutylammonium isovalerate hydrate as compared with that of tetrabutylammonium pentanoate hydrate (10.6 °C). These phenomena may be explained by the formation of hydrogen bonding between the NH_2 group and water lattice since the configuration of the group attached to the carbon atom of α-position is restricted if both the COO^- group and the NH_2 group make hydrogen bonding with water lattice at the same time. Though the effect of the formation of a hydrogen bonding between the NH_2 group and water lattice upon the stability of the hydrates is not so eminent, this effect will lead to the anticipation that there will be some difference in the melting points of the hydrates between a D-amino carboxylate and of a L-amino carboxylate. Preliminary experiments for α-aminopropionate and α-aminoisobutyrate hydrates showed that the melting points of the hydrates were slightly different between the D and the L isomers. Precise investigations are now in progress.

The present work was supported by a Grant-in-Aid for Scientific Research No.60470006 from the Ministry of Education, Science and Culture.

References

1) H. Nakayama and S. Torigata, *Bull. Chem. Soc. Jpn.*, **57**, 171 (1984).
2) W. F. Claussen, *J. Chem. Phys.*, **19**, 259, 662 (1951). M. von Stackelberg and H. R. Muller, *ibid.*, **19**, 1319 (1951). L. Pauling and R. E. Marsh, *Proc. Natl. Acad. Sci. U.S.A.*, **38**, 112 (1952).
3) M. Bonamico, G. A. Jeffrey, and R. K. McMullan, *J. Chem. Phys.*, **37**, 2219 (1962).
4) H. Nakayama and H. Usui, *Bull. Chem. Soc. Jpn.*, **59**, 833 (1986).
5) D. Feil and G. A. Jeffrey, *J. Chem. Phys.*, **35**, 1863 (1961).
6) H. Nakayama, *Bull. Chem. Soc. Jpn.*, **56**, 877 (1983).
7) S. Cabani, G. Conti, E. Matteoli, and M.R. Tiné, *J. Chem. Soc., Faraday Trans. 1*, **77**, 2377 (1981).

Excited-State Reactions of Coumarins in Aqueous Solutions. V. Fluorescence Lifetimes of 7-Ethoxycoumarin in Acidic Solutions

Tetsuo MORIYA
Electrotechnical Laboratory, 1-1-4 Umezono, Sakura-mura, Niihari-gun, Ibaraki 305
(Received May 11,1987)

Synopsis. The fluorescence lifetime of 7-ethoxycoumarin (7EC) was measured in acidic aqueous solutions while varying the concentration of Cl^- as a fluorescence quencher. The subsequent analysis of the two-component fluorescence decay curves indicated that the protonated species in the excited state led to the fluorescence quenching; this result was quantitatively consistent with the fluorescence-yield study under steady-state conditions.

Since the extensive study of the photophysics of aromatic compounds was carried out by Ware and his co-workers,[1] it has been confirmed that steady-state and time-dependent analyses provide complementary information on various reaction processes and kinetic rate constants. The main concern of this report is to clarify the relation between the fluorescence lifetime and the steady-state quenching measurements of 7-ethoxycoumarin (7EC), which exhibits very interesting excited-state reactions, as has been extensively studied in previous papers.[2,3] Coumarin derivatives are heterocyclic compounds with a ring oxygen and a carbonyl group. Usually they have a very efficient fluorescing ability and show a variety of protonation or deprotonation reactions in the excited state, depending on the solvent conditions. To know the detailed mechanisms of such reactions, we must determine several rate constants which correspond to phenomena in a nanosecond region.

The transient spectroscopy of aqueous 7EC solutions has been conducted as a function of the quencher concentration, and the results have been compared with those of the steady state measurement. Assuming that two reacting species exist in the excited state, only one of which can cause a fluorescence-quenching reaction, the dependence of the lifetimes on the quencher concentration has been analyzed. The proposed model can consistently explain the results of both steady-state and transient studies.

Experimental

The high-purity-grade reagent of 7-ethoxycoumarin (7EC) was obtained from Molecular Probes, Inc., and was used without further purification; mp 84.8 °C. The hydrochloric acid and perchloric acid were of a pure quality and were obtained from Wako Pure Chemical Ind. The water was permeated and distilled.

The usual UV absorption and fluorescence spectra of the aqueous 7EC solution of $\approx 5\times10^{-5}$ mol dm^{-3} were measured at 20 °C. The pH of the solution was controlled with HCl and $HClO_4$, the chloride-ion concentration being adjusted by changing their ratio. The fluorescence lifetime measurements were performed by means of a time-correlated single-photon-counting fluorometer similar to the one described in Ref. 4. Since the lifetime of the fluorescer was close to the decay time of a repetitive short-pulsed light at 337 nm from an air-flash lamp, the result was deconvoluted in order to ascertain the true decay character, unaffected by the response function of the measurement system; the typical accuracy of this procedure was ±0.05 ns.

Results

The fluorescence quenching phenomenon of 7EC by chloride ions in acidic aqueous solutions has already been investigated under steady-state light illumination.[3] When $[H^+]$ was set at 0.5 mol dm^{-3} by the addition of HCl or $HClO_4$, the absorption maximum was at 324 nm, which corresponded to the neutral form (N) of 7EC. On the other hand, the fluorescence spectrum was composed of the emission from the neutral form of excited molecules ($\overset{*}{N}$), peaking at 390 nm, and the weak component from the protonated form ($\overset{*}{C}^+$), peaking at 423 nm. The general scheme of the excited state reaction and the fluorescence quenching process was given by:[3]

$$\begin{array}{ccccc} & & \overset{*}{N} & + H^+ \underset{k_2}{\overset{k_1}{\rightleftharpoons}} & \overset{*}{C}^+ \\ G \nearrow & & \searrow \tau^{-1} & & \downarrow \tau'^{-1} \\ h\nu_A & & h\nu_F & & h\nu_F' \end{array} \qquad (1)$$

$$\overset{*}{C}^+ + Cl^- \xrightarrow{k_q} C^+ + Cl^- \qquad (2)$$

The excited neutral species ($\overset{*}{N}$) is generated by a continuous UV-light illumination at the rate of G, and it is rapidly equilibrated with the excited protonated species ($\overset{*}{C}^+$) in the acidic solution. Then, $\overset{*}{C}^+$ interacts with the chloride ions and is deactivated to the ground state (C^+). k_1 and k_2 are the forward and backward rate constants for equilibration; τ and τ' are the fluorescence lifetimes of the neutral and protonated species respectively. k_q is the quenching rate constant caused by the collisional interaction between $\overset{*}{C}^+$ and Cl^-. By the analysis of the relative fluorescence intensity, I_0/I, depending on $[Cl^-]$ (I_0 and I are the fluorescence intensities in the absence and in the presence of chloride ions), the various rate constants in Eqs. 1 and 2 have already been determined, as cited in Table 1.[3] The ClO_4^- ion showed no observable quenching ability.

Under the pulsed-light excitation at 337 nm which

Table 1. Lifetimes of the Neutral and Protonated 7EC, τ and τ', and Rate Constants Obtained for the Excited State Equilibration, k_1 and k_2, and for the Collisional Quenching Process, k_q[3]

τ	τ'	$k_1\times10^{-9}$	$k_2\times10^{-9}$	$k_q\times10^{-9}$
ns	ns	mol^{-1} dm^3 s^{-1}	s^{-1}	mol^{-1} dm^3 s^{-1}
2.0_0	4.9_0	1.2_5	1.2_4	5.8_0

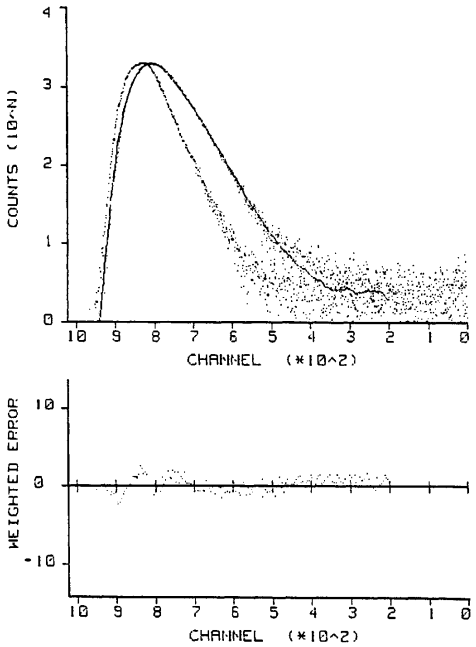

Fig. 1. Decay profiles of a light source and a fluorescence response (dots delayed to the right-hand side) of the aqueous 7EC solution with $[HClO_4]=0.4\,mol\,dm^{-3}$ and $[HCl]=0.1\,mol\,dm^{-3}$. 23.6 channels/ns; the channel number is reversed to the time progress. The solid line shows the fitted theoretical curve for the fluorescence decay; $\tau_+=1.85$ ns, $\tau_-=0.35$ ns, $C=0.3$. The weighted residual, $(f_i^{obs}-f_i^{calc})/(f_i^{obs})^{1/2}$, is also shown.

Table 2. Experimental Values for the Fluorescence Lifetime Parameters (τ_+, τ_-, and C) of the Neutral Form of 7EC at 20 °C and Those Calculated by Using the Constants in Table 1

$[Cl^-]$ / mol dm^{-3}	τ_+ / ns	τ_- / ns	C	τ_+^{cal} / ns	τ_-^{cal} / ns	C^{cal}
0	2.7_0	0.4_0	0.4_0	2.56	0.46	0.70
0.1	1.8_5	0.3_5	0.3_0	1.71	0.39	0.38
0.2	1.5_0	0.3_0	0.2_5	1.40	0.33	0.22
0.3	1.3_0	0.2_5	0.2_0	1.25	0.29	0.14
0.4	1.2_0	0.2_0	0.1_5	1.16	0.25	0.09
0.5	1.1_5	0.1_5	0.1_0	1.11	0.22	0.07

generates $\overset{*}{N}$, the decay characteristic of fluorescence from the neutral fluorescer has been measured at 390 nm in the acidic aqueous solution while varying the concentration of Cl^-. The pH is kept constant by satisfying $[HClO_4]+[HCl]=0.5\,mol\,dm^{-3}$, and $[Cl^-]$ is controlled by the amount of the HCl component added. The time-dependent light intesity, $i^N(t)$, of $\overset{*}{N}$ could be analysed by means of a decay curve of a double exponential character:

$$i^N(t) \propto \exp(-t/\tau_+) + C\cdot\exp(-t/\tau_-) \quad (3)$$

The best-fitted values for τ_+, τ_-, and C are shown in Table 2. The typical decay profiles of a light source, a fluorescence response, and the fitted curve are shown in Fig. 1. The total fluorescence spectrum of 7EC at $[H^+]\approx0.5\,mol\,dm^{-3}$ includes two components which

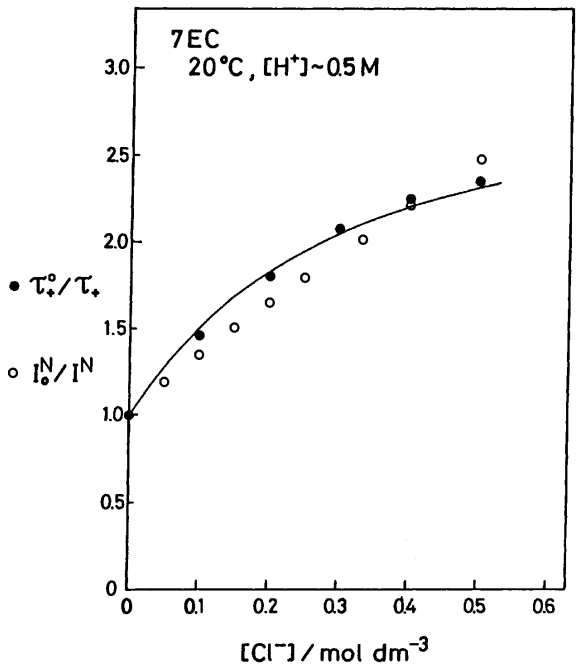

Fig. 2. Dependences of the relative fluorescence intensity, I_0^N/I^N (○), and the relative lifetime, τ_+^0/τ_+ (●), of 7EC on $[Cl^-]$ in the acidic aqueous solution at 20 °C. The solid line shows the theoretical prediction for τ_+^0/τ_+ vs. $[Cl^-]$ presented in the text.

result from the $\overset{*}{N}$ and $\overset{*}{C}^+$ in the solution. Since the concentration of $\overset{*}{C}^+$ is lower than that of $\overset{*}{N}$ by about one order of magnitude at $[H^+]\approx0.5\,mol\,dm^{-3}$, the fluorescence contribution of $\overset{*}{C}^+$ at 390 nm is negligible in the lifetime measurement. Equation 2 describes how the fluorescence quenching by Cl^- is operative only for $\overset{*}{C}^+$, as was proved previously.[3] This has been reaffirmed by the fact that the time-variation in the $\overset{*}{N}$ fluorescence in a simple neutral solution, where no $\overset{*}{C}^+$ is formed, is not changed by the further addition of 0.5 mol dm^{-3} NaCl.

In Fig. 2, the dependences of the relative fluorescence intensity, I_0^N/I^N, and the relative lifetime, τ_+^0/τ_+, on $[Cl^-]$ are shown, where τ_+^0 is a slow-decay component of the fluorescence lifetime of $\overset{*}{N}$ in the absence of Cl^-. These plots do not obey the linear Stern-Volmer relationship. The nonlinear dependency of the steady state result (I_0^N/I^N vs. $[Cl^-]$) was clearly explained in a previous paper.[3]

Discussion

Based on the scheme described by Eqs. 1 and 2, the time-dependent rate equation of the excited species can be derived. Subsequently, the response of $i^N(t)$ for a light pulse with an ideal δ-function is easily obtained:

$$\tau_\pm^{-1} = \frac{1}{2}\left[\tau^{-1} + \tau'^{-1} + k_1[H^+] + k_2 + k_q[Cl^-] \mp \sqrt{\{(\tau^{-1}+k_1[H^+]) - (\tau'^{-1}+k_2+k_q[Cl^-])\}^2 + 4k_1[H^+]k_2}\right] \quad (4)$$

$$C = -\frac{\tau'^{-1} + k_2 + k_q[Cl^-] - \tau_-^{-1}}{\tau'^{-1} + k_2 + k_q[Cl^-] - \tau_+^{-1}} \quad (5)$$

From Eqs. 4 and 5, τ_+, τ_-, and C are theoretically predictable using the constants given in Table 1. The calculated values are shown in the last three columns of Table 2; the dependence of $\tau_\Phi^{cal}/\tau_+^{cal}$ on $[Cl^-]$ is drawn in Fig. 2 with a solid line. The quencher-concentration dependence of τ_Φ/τ_+ agrees very well with the theoretical prediction. It is possible in principle to determine the rate constants, k_1, k_2, and k_q, from the obtained set of τ_+, τ_-, and C values by using $1/\tau_+ + 1/\tau_- \propto$ const.$+k_q[Cl^-]$, etc. Because of the relatively low accuracy of deconvolution for the fast-decay component (τ_- and C, ±10—30%) compared with that of τ_+ (±2—5%), the rate constants to be determined are less reliable than those given by steady-state measurements (±1%). The lifetime analysis based on observing the fluorescence component from $\overset{*}{N}$ of 7EC is analogous to the lifetime measurement of a monomer form in aromatic compound-quencher molecule systems, where an exciplex is generated to result in fluorescence quenching.[1] The excited-state reaction of coumarin derivatives is classified essentially as an acid-base reaction and has time constants of a nanosecond order because of the very high mobilties of the participating species, such as H^+ and Cl^-, whereas the exciplex-formation reaction is a usually slower phenomenon by one or more orders.

The fluorescence-lifetime study of the aqueous solution of 7EC is characteristic in that the instantaneous or 'static' quenching process, which makes the steady state analysis complex, does not appear in the first approximation if the quencher concentration is not very high. A similar example has been presented by Efftink and Ghiron,[5] who have shown experimentally, in an indole-quencher system, that τ^0/τ is independent of the $W=\exp(-V[Q])$ factor, in contrast to I_0/I, where V is the static quenching constant. After pulsed-light illumination, the fraction, W, of the generated excited state, $\overset{*}{C}^+$, is actually quenched by the collisional mechanism corresponding to the rate constant, k_q. The remaining fraction, $1-W$, is deactivated almost instantaneously after being formed because the quencher, Cl^-, is accidentally positioned in the proximity of $\overset{*}{C}^+$ and interacts directly with it. Including such a static quenching mechanism, the fluorescence-yield decrease of 7-ethoxycoumarins by Cl^- in acidic solutions under steady state conditions has been successfully explained.[3] In the rate equations for the time-variations of $[\overset{*}{N}]$ and $[\overset{*}{C}^+]$ under pulsed excitation, the fraction of excited species that never give fluorescence over an observing interval of, typically, 50 nanoseconds and which result in the static quenching must be treated separately from a reaction system described with time-independent rate constants. That is, the generation rate, G, of $\overset{*}{N}$ should be reduced effectively to $G\cdot\{(\tau^{-1}+Wk_1[H^+])/(\tau^{-1}+k_1[H^+])\}$, maintaining the same equational form as $W=1$.[3] Such an approximation is valid for a weak static quenching case ($V \ll k_q\tau'$) and for rapid protonation and deprotonation reactions. A more rigorous treatment has appeared in the serial works of Ware et al.[1] and Weller,[6] who formulate the transient nature of the diffusing reactants by introducing a time-dependent rate constant into the rate equation and who show that the static quenching mentioned here is essentially equivalent to the transient effect. The replacement of the quenching-reaction term with $k_q(t)[Cl^-][\overset{*}{C}^+]$ will be required in the present problem, where $k_q(t)$ decreases to the usual constant k_q at a large t. However, except for a very short interval after pulsed excitation, the two different ways of analysis which utilize W and $k_q(t)$ as the key parameters give approximately the same results for the case of a weak transient effect.[1,5,6] It may be concluded that, under appropriately chosen conditions, the normalized intensity for $i^N(t)$ is given by Eq. 3—5, even if $W \neq 1$, whereas the integrated yield of the fluorescence is not correctly derived without taking account of the static quenching effect.

It has been made clear that, in the steady state study, the static quenching parameter, W, is a very important factor in analyzing the nonlinear behavior of I_0/I vs. $[Cl^-]$, but, in the transient study, W is less important for the time variation in the fluorescence from $\overset{*}{N}$. Experimentally, the quencher dependence of τ_Φ/τ_+ behaves very differently from I_0^N/I^N, as is shown in Fig. 2. The parameters determined by the steady state measurement could consistently reproduce the data from the transient spectroscopy, although these two methods differ in the treatment of the static quenching factor, W. Therefore, the validity of the fundamental scheme of Eqs. 1 and 2 for the excited state reactions of 7EC has been well confirmed by independent experiments.

The author gratefully acknowledges support for this work by the "Sunshine Project" and by the special research on "Molecular Electronics" of the Ministry of International Trade and Industry, Agency of Industrial Science and Technology.

References

1) D. V. O'Connor and W. R. Ware, *J. Am. Chem. Soc.*, **101**, 121 (1979) and the references cited therein.
2) T. Moriya, *Bull. Chem. Soc. Jpn.*, **57**, 1723 (1984).
3) T. Moriya, *Bull. Chem. Soc. Jpn.*, **59**, 962 (1986).
4) C. Lewis, W. R. Ware, L. J. Doemeny, and T. L. Nemzek, *Rev. Sci. Instrum.*, **44**, 107 (1973).
5) M. R. Efftink and C. A. Ghiron, *J. Phys. Chem.*, **80**, 486 (1976).
6) A. Weller, *Z. Phys. Chem. N. F.*, **15**, 438 (1958).

Preparation of Noble Metal Organosols Containing Polyethylene Glycol Mono-*p*-nonylphenyl Ether

Yukimichi NAKAO* and Kyoji KAERIYAMA
Research Institute for Polymers and Textiles, Yatabe-Higashi, Tsukuba, Ibaraki 305
(Received June 26, 1987)

Synopsis. Stable organosols of ruthenium, rhodium, palladium, and platinum were prepared by evaporating the corresponding noble metal hydrosols containing nonionic surfactant, polyethylene glycol mono-*p*-nonylphenyl ether, followed by dissolving the resulting residues in organic solvents such as chloroform. The organosol of the noble metals was exclusively yielded at a definite range of the surfactant concentration. A mechanism for the formation of the organosols is proposed.

There are fewer reports on the organosols of metals than those on their hydrosols. Svedberg's method is known to be applicable to the preparation of a variety of metal organosols which are somewhat unstable and polydispersed.[1] Thomas[2] reported that the pyrolytic decomposition of organometallic compounds such as dicobaltoctacarbonyl in organic media gave monodispersed organosols of the corresponding metals. Hirai et al.[3] prepared extremely fine colloidal rhodium dispersed in methanol by reducing $RhCl_3 \cdot 3H_2O$ with the methanol in the presence of NaOH. More recently, Boutonnet et al.[4] proposed a preparative method for colloidal metals in organic solvents from microemulsion. On the other hand, Meguro and Kondo[5] found that colloidal Fe_2O_3 having positive charge coagulated on addition of sodium dodecylbenzenesulfonate and that the resulting coagulum was redispersed in organic solvents to give an organosol.

In the preceding paper[6] are reported a variety of noble metal hydrosols stabilized by cationic, anionic, or nonionic surfactant. We have succeeded in converting the hydrosols of noble metals stabilized by nonionic surfactant, polyethylene glycol mono-*p*-nonylphenyl ether, into their organosols. In this paper, preparative procedures and adaptable noble metals and dispersion media are described.

Experimental

Materials. Noble metal salts used as starting materials were reagent grade $RuCl_3 \cdot 3H_2O$, $RhCl_3 \cdot 3H_2O$, $PdCl_2$, and $H_2PtCl_6 \cdot 6H_2O$. Polyethylene glycol mono-*p*-nonylphenyl ether (degree of polymerization=10, PN) as a protecting agent and sodium borohydride ($NaBH_4$) as a reductant were also of reagent grade. Water was deionized and distilled before use.

Preparation of Noble Metal Organosols. Noble metal organosols were prepared via the corresponding hydrosols previously reported.[5]

A typical procedure for the preparation of a rhodium organosol is as follows. $RhCl_3 \cdot 3H_2O$ (0.05 mmol) and PN (10 mg) were dissolved in water (95 cm^3). Then, an aqueous solution (5 cm^3) of $NaBH_4$ (0.2 mmol) was poured into the mixture with vigorous stirring. At that time, rhodium ion was rapidly reduced to result in the formation of a clear dark-brown hydrosol of rhodium. The hydrosol was then placed into a Petri dish and heated to evaporate to dryness on a hot plate of a temperature of about 150 °C. A tarry residue left after evaporation was redissolved in chloroform (100

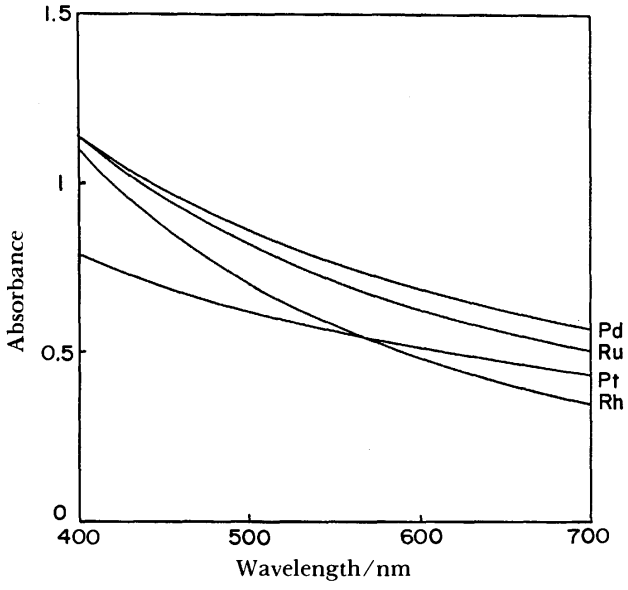

Fig. 1. Visible absorption spectra of noble metal organosols in chloroform (PN conc. in starting hydrosols; 0.01% for Ru and Rh, 0.05% for Pd and Pt).

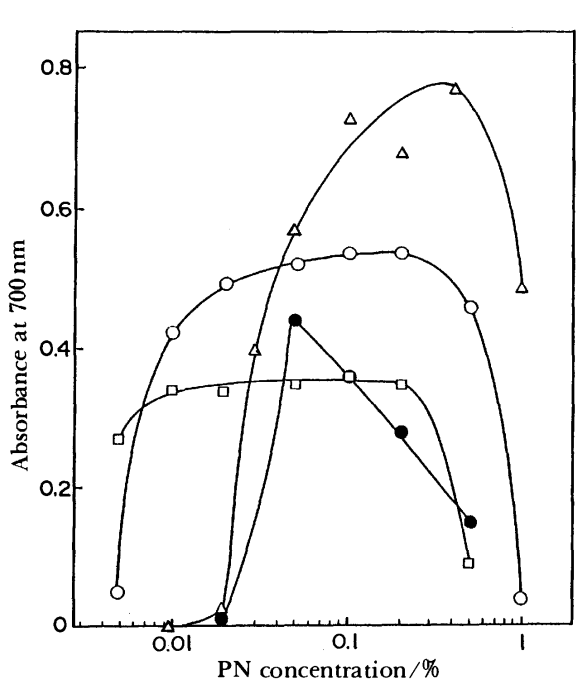

Fig. 2. Absorbance at 700 nm by noble metal organosols in chloroform (○: Ru, □: Rh, △: Pd, ●: Pt).

cm^3) to yield a clear dark-brown sol of rhodium. A small amount of insolble colorless part of the residue was then removed by decantation.

According to a similar precedure, ruthenium, palladium, and platinum sols dispersed in chloroform were obtained. In the case of palladium, NaCl (0.25 mmol) was added to dissolve $PdCl_2$.

Visible Spectroscopy. The visible spectra of the noble metal sols in chloroform were measured on a Shimadzu Model UV-240 spectrophotometer using a cell of a light-path length of 1 cm.

Electron Microscopy. A very small amount of a noble metal sol in chloroform was evaporated to dryness on a thin carbon film supported by Cu-mesh and observed with a Hitachi Model H-800 electron microscope at a magnification of 200000.

Results and Discussion

Hydrosols of ruthenium, rhodium, palladium, and platinum were prepared with varying amounts of PN, and the formation of noble metal organosols from the hydrosols was examined. Thus, the hydrosols were evaporated to dryness and chloroform was added to the residues to dissolve them. In Fig. 1 are shown the typical visible absorption spectra of the supernatant solutions, that is, noble metal organosols. Figure 2 shows the absorbance at 700 nm of the organosols.

Table 1. Solubility of Residues from Noble Metal Hydrosols Left after Evaporation

Solvent	Noble metal, PN(%)			
	Ru 0.01	Rh 0.01	Pd 0.05	Pt 0.05
Chloroform	++	++	++	++
Toluene	++	++	++	−
Ethyl acetate	+	++	++	−
Hexane	−	++	−	−
Acetone	−	−	+	−
Methanol	−	−	−	−

++ Completely soluble, + partly soluble, − insoluble.

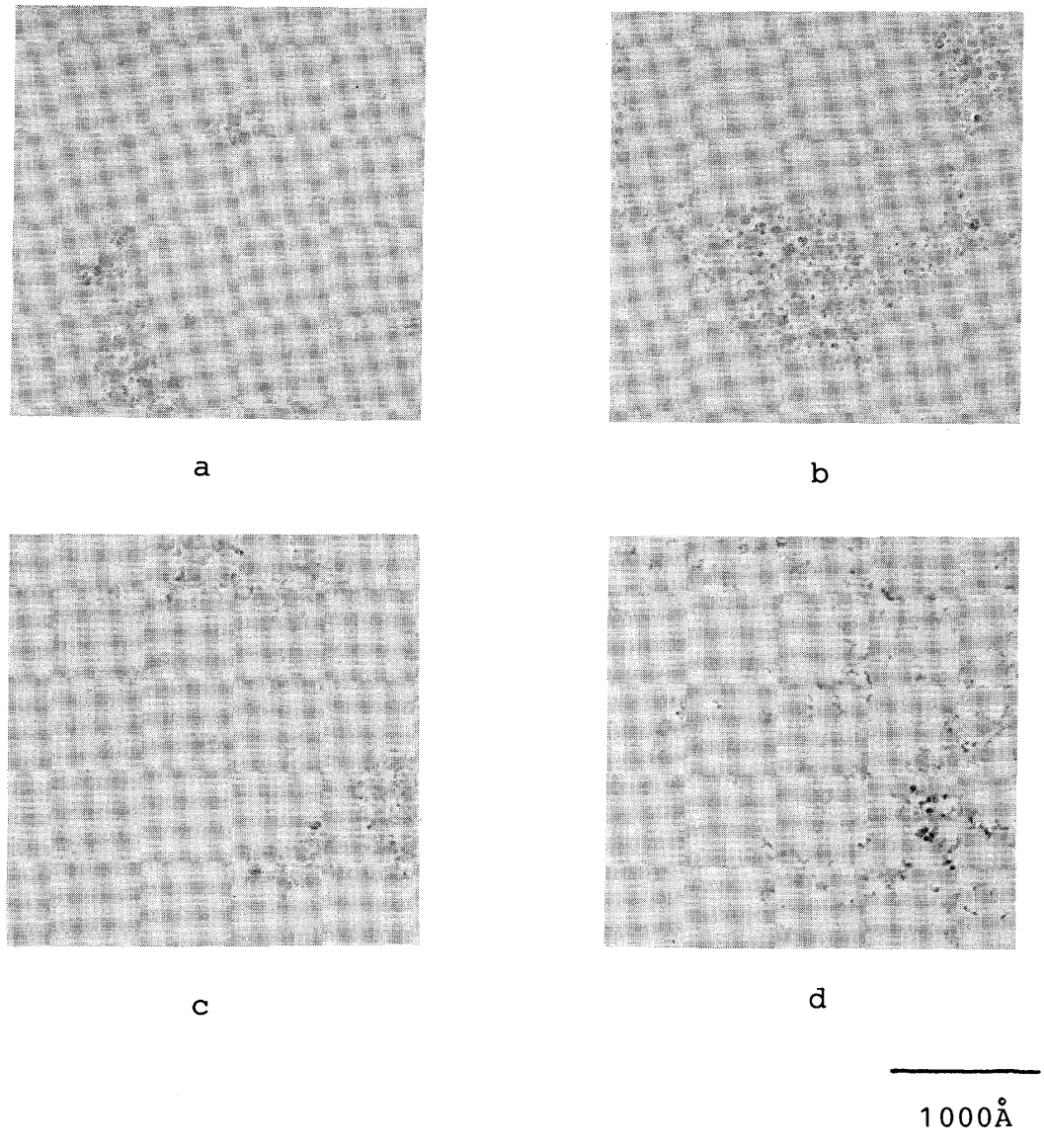

Fig. 3. Electron micrographs of colloidal ruthenium (a), rhodium (b), palladium (c), and platinum (d) from the organosols in chloroform.

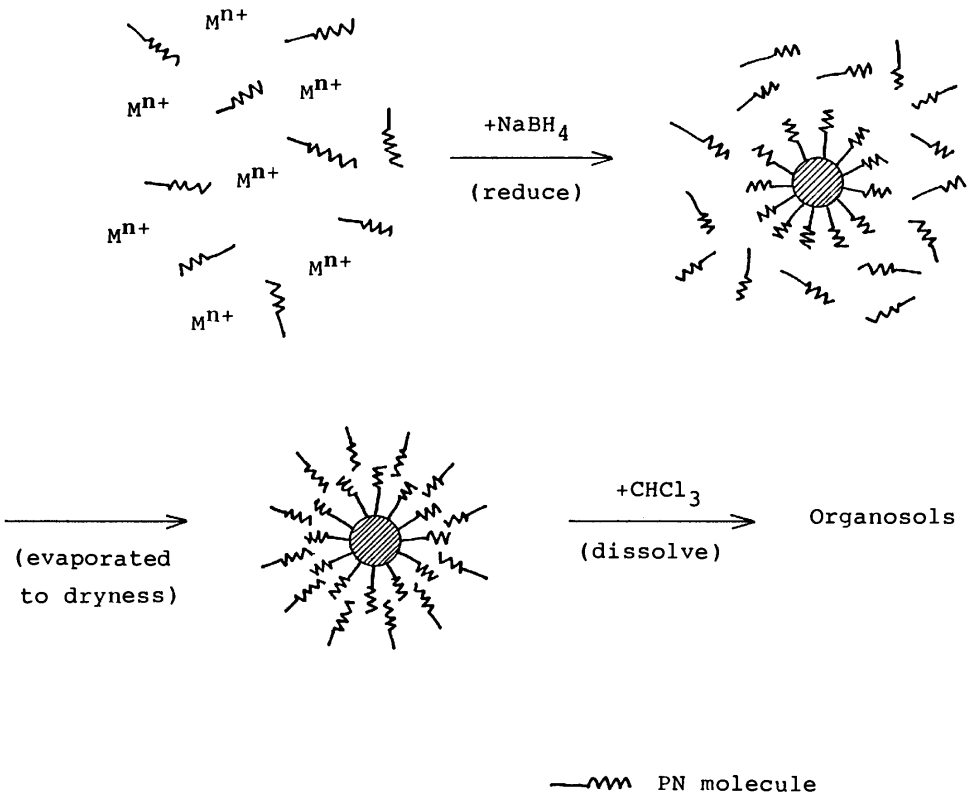

Fig. 4. Mechanism for the formation of noble metal organosols in the presence of PN (∧∧∧∨ and —— designate the hydrophilic and hydrophobic moieties of PN molecules, respectively).

The absorbance is presumed to be an indication of the amounts of colloidal noble metals in the organosols.[7] This figure indicates that noble metal organosols in chloroform were successfully yielded at a definite range of PN concentration. In other cases, all or a part of colloidal noble metal particles remained in the insoluble residues. Rhodium organosols were obtained at PN concentration of 0.01—0.2% with good reproducibility and were quite similar in color to each other. Ruthenium organosols were also yielded at a wide range of PN concentration. In the case of palladium, larger amounts of PN were required for organosol formation. Among residues from platinum hydrosols, only that from a sol containing 0.05% PN was completely dissolved in chloroform to give an organosol.

In Table 1 are shown the solubilities of the residues from the noble metal hydrosols in a variety of organic solvents. This indicates that chloroform was the most useful dispersion medium for organosols.

Colloidal noble metal particles in the organosols observed by an electron microscope are shown in Fig. 3. Two-dimensional aggregation of the colloidal particles appeared in the electron micrographs might be occurred in the course of evaporation. Such two-dimensional aggregations were also observed in the electron micrographs of the noble metal hydrosols,[6] and the colloidal particles had almost equal dimensions as those in the precursor hydrosols. Narrow spaces lain between the colloidal particles in the aggregates are presumed to correspond to PN layers on the surface of the particles.

A possible mechanism for the formation of noble metal organosols is shown in Fig. 4. At the first step, noble metal ions are reduced with $NaBH_4$ to yield colloidal metal particles. Then the surface of the particles may be immediately covered with PN molecules, of which the hydrophobic moiety orients to the surface. At the second step, excess PN molecules, which exist apart from the surface of the particles, are forced to be attached on the first-adsorbed layers of PN as the evaporation proceeds, and form themselves into the second layer with hydrophobic outer surface. Thus, the colloidal particles could be dispersed in organic solvents.

References

1) B. Jirgensons, M. E. Straumanis,"Short Textbook of Colloid Chemistry," 2nd ed, Pergamon Press (1962).

2) J. R. Thomas, Ger. Patent 1154442 (1963); *Chem. Abstr.*, **60**, P 1143 g; *J. Appl. Phys.*, **37**, 2914 (1966).

3) H. Hirai, Y. Nakao, and N. Toshima, *Chem. Lett.*, **1978**, 545.

4) M. Boutonnet, J. Kizling, P. Stenius, and M. Gilbert, *Colloid Surf.*, **5**, 209 (1982).

5) K. Meguro and T. Kondo, *Nippon Kagaku Zasshi*, **76**, 642 (1955).

6) Y. Nakao and K. Kaeriyama, *J. Colloid Interface Sci.*, **110**, 82 (1986).

7) H. Hirai, Y. Nakao, and N. Toshima, *J. Macromol. Sci. Chem.*, **A13**, 727 (1979).

Ortho Substituent Effect of the Side-Chain Phenyl Group on the Dehydrogenation of Flavanones with 2,3-Dichloro-5,6-dicyano-*p*-benzoquinone

Yukio HOSHINO* and Noboru TAKENO†

Department of Natural Science, Muroran Institute of Technology, Mizumoto-cho, Muroran 050

†Department of Industrial Chemistry, Muroran Institute of Technology, Mizumoto-cho, Muroran 050

(Received April 6, 1987)

Synopsis. Rates of the dehydrogenation of 2′-substituted flavanones with 2,3-dichloro-5,6-dicyano-*p*-benzoquinone were measured by means of HPLC analyses. All substituents at the ortho position of the side-chain phenyl group of flavanones showed a retarding effect on the reaction. A correlation analysis for the ortho effect using the linear combination model has led to a conclusion that the inductive effect is much more important than the steric and the resonance effect, and that the steric effect is slightly greater than the resonance effect.

We previously examined the rate of dehydrogenation of flavanones (**1**) with 2,3-dichloro-5,6-dicyano-*p*-benzoquinone (DDQ) in dry benzene in the presence of acetic acid.[1] The following conclusions were drawn: (1) the reaction is first-order in both concentrations of substrate and DDQ; (2) the reaction proceeds along a path of the two-step ionic mechanism and its rate-determining step is a hydride abstraction by quinol cation of DDQ (Scheme 2); (3) the rate is increased by introduction of an electron-donating group at the meta or para position of the side-chain phenyl group, and decreased by introduction an electron-withdrawing one; (4) the apparent second order rate constant, $k_{2,a}$, is proportional directly to the square root of the initial concentration of acetic acid.

On the other hand, it is generally considered that the ortho substituent effect on the reactivity results in various kinds of influences depending upon the sort and condition of reaction. Namely, the steric and proximity effects may participate complicatedly in addition to the normal inductive and resonance ones. Thus, it is general to analyse the ortho substituent effect independently of the meta and/or para substituent ones.

Now, for the purpose of examination of the ortho substituent effect on the dehydrogenation of flavanones, reactions of 2′-substituted flavanones (**1b—f**) with DDQ were conducted under the same reaction conditions as those in the previous work.[1] All analyses of rates of reaction were continued for ten hours after the beginning of reaction (percentages of reaction were ca. 15—33%) by means of HPLC analyses. In this series also, all reactions for five flavanone derivatives followed the second rate law (Eq. 1):

$$dx/dt = k_{2,a}(a-x)(b-x) \quad (1)$$

where a and b are the initial concentrations of substrate and DDQ, respectively, and x is the concentration of product. Rates were determined by the calibration method from the peak area ratio vs. the concentration ratio. Values of $k_{2,a}$, which are the mean of three runs for each sample, are summarized in Table

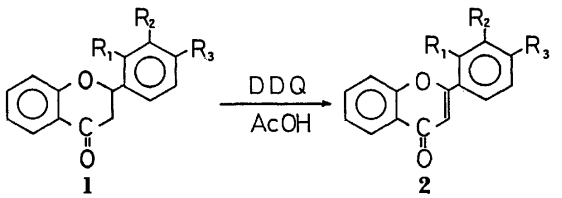

1 **2**

a $R_1=R_2=R_3=H$ **d** $R_1=OCH_3$, $R_2=R_3=H$
b $R_1=Cl$, $R_2=R_3=H$ **e** $R_1=R_3=CH_3$, $R_2=H$
c $R_1=CH_3$, $R_2=R_3=H$ **f** $R_1=R_2=OCH_3$, $R_3=H$

Scheme 1.

Table 1. Apparent Second Order Rate Constants and Relative Rates of Dehydrogenation of 2′-Substituted Flavanones with DDQ[a] at 80.0±0.2 °C

Substrate	Product	$k_{2,a}\times10^3$ / 1 mol^{-1} s^{-1}	k_{rel}[b]
1a	**2a**	1.43[c]	1.00
1b	**2b**	0.472	0.330
1c	**2c**	1.18	0.825
1d	**2d**	0.706	0.494
1e	**2e**	1.49	1.04
1f	**2f**	0.881	0.616

a) Initial concentrations: $[Substrate]_0=[DDQ]_0=1.0\times10^{-2}$ mol l^{-1}; $[CH_3COOH]_0=0.920$ mol l^{-1}. b) k_{rel} relative to $k_{2,a}$ for **1a**. c) From Ref. 1.

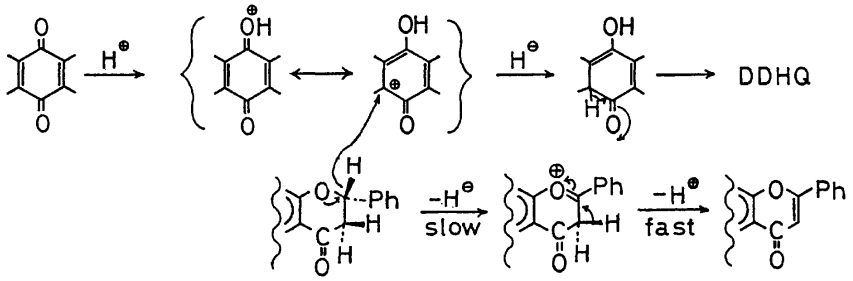

Scheme 2.

1. In the table, k_{rel} is the value relative to $k_{2,a}$ of **1a**. When the reaction proceeded above ca. 50%, correct analysis of the rate was no longer possible because of the precipitation of 2,3-dichloro-5,6-dicyanohydroquinone (DDHQ).

From the results in Table 1, it is clear that all the reaction rates decrease as compared with **1a**, except for **1e**. In contrast with the previous results (conclusion (3)), it is suggested that all the ortho substituents function with a retarding effect on this reaction regardless of their electronic properties. Although the reaction rate of **1e** is slightly greater than that of **1a**, it should be considered that an acceleration effect of the para-methyl group on the rate is comparatively canceled by the ortho-methyl group, because the relative rate of dehydrogenation of 4'-methylflavanone is 1.10.[1)]

A transition state of this reaction is a carbonium cation having a positive charge on the C_2-atom (conclusion (2) and Scheme 3). This carbocation corresponds to a flavylium cation (Scheme 3). In our work

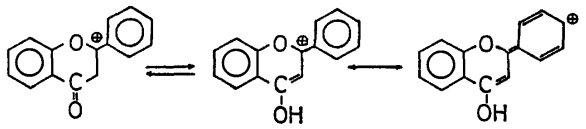

Scheme 3.

on the basicity of flavones,[2)] it has been revealed that the side-chain phenyl group would be planar with the benzopyrylium ring in the state where the proton is added at the carbonyl oxygen atom. When a substituent is present at the ortho position of the side-chain phenyl group, the above-mentioned coplanarity seems to be prohibited in the transition state of this reaction. Thus the resonance effect of the substituent on the phenyl group is inhibited for such a steric reason. Furthermore, the reaction center, the C_2-position, might be blocked by the ortho substituent for the approach of an attacking species, and the rate of reaction decreases consequently. The values of **1b** and **1d** suggest that the inductive effect appears more eminent than the resonance one, because the former effect of the chlorine atom and methoxyl group functions in a retarding way for this reaction; the relative rates of the corresponding para-isomers are 0.923 and 1.37, respectively.[1)]

Taft[3)] and Charton[4)] represented the ortho effect as a linear combination of the inductive, resonance, and steric effects as Eq. 2:

$$\log (k_{rel})_{ortho} = \rho_I \sigma_I + \rho_R \sigma_R + \delta E_s \quad (2)$$

where σ_I, σ_R, and E_s are the inductive, resonance, and steric substituent constants, and ρ_I, ρ_R, and δ are the inductive, resonance, and steric reaction constants, respectively. In the present work, **1e** and **1f** have a meta or para substituent in addition to the ortho one. Then the relation obtained in the previous work[1)] for the meta or para substituted derivatives is added to both sides of Eq. 2 to give Eq. 3:

$$\log (k_{rel})_{o,m,p} = \rho_I \sigma_I + \rho_R \sigma_R^+ + \delta E_s - 0.190 \sigma_{(m,p)}^+ \quad (3)$$

where σ_R^+ is used instead of σ_R because of the introduction of Brown-Okamoto's electrophilic substituent constants, $\sigma_{(m,p)}^+$. According to Eq. 3, ρ_I, ρ_R, and δ were calculated by means of multiple least squares, where the values proposed by Ehrenson et al.[5)] were used for σ_I and σ_R^+ and those by Taft[3)] and Kutter and Hansch[6,7)] were used for E_s (Table 2). The reason for the adoption of these values is their popularity. Particularly, values of constant E_s were derived for heteroatom substituents and for symmetrical-top groups such as H and CX_3 (X=H, halogen, or CH_3). Consequently Eq. 4 was obtained as a linear free energy relationship for the substituent effect on the side-chain phenyl group in this reaction:

$$\log (k_{rel})_{o,m,p} = -0.893\sigma_I - 0.042\sigma_R^+ + 0.088E_s - 0.190\sigma_{(m,p)}^+ \quad (4)$$

The correlation coefficient of Eq. 4, 0.999, was obtained on the basis of a slope of the relation between the observed and the calculated values of the logarithmic relative rate (Fig. 1).

Table 2. Ortho Substituent Parameters for the Correlation Using the Linear Combination Model

Substituent	ρ_I[a)]	σ_R^+[b)]	E_S[c)]
H	0	0	0
Cl	0.46	−0.36	−0.97
CH_3	−0.04	−0.25	−1.24
OCH_3	0.27	−1.02	−0.55

a) Inductive substituent constant cited from Ref. 5.
b) Resonance substituent constant cited from Ref. 5.
c) Steric substituent constant cited from Refs. 3, 6, and 7.

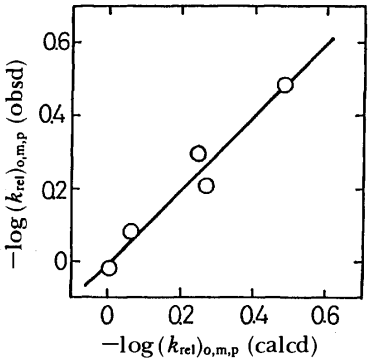

Fig. 1. Correlation between the calculated and the observed logarithmic relative rate.

From the results in Table 1 and Eq. 4, it can be concluded that, in the ortho substituent effect on the side-chain phenyl group for the dehydrogenation of flavanones with DDQ, the inductive effect (ρ_I= −0.893±0.05) is much more important than the steric and resonance effects, of which the steric one is somewhat influential, whereas the latter one is negligibly small. This conclusion is in accord with our recently proposed stepwise mechanism[1)] via the benzopyrylium type cationic intermediate for the DDQ dehydrogenation.

Experimental

All melting points were uncorrected. ^{1}H NMR spectra

were obtained with a Hitachi R-22 (90 MHz) spectrometer by using tetramethylsilane as an internal standard. HPLC analyses were conducted with a Yanagimoto High Speed Liquid Chromatograph L-2000 under the following conditions:

Stationary phase: Yanapak-SA-1

Mobile phase: Hexane-EtOH=10/1 (v/v) for **1d** and **1f**, and 40/1 (v/v) for **1b**, **1c**, and **1e**.

Detector: Yanagimoto U-212 Spectrometer (240 and 300 nm) Estimation: Yanagimoto Computing Integrator-SYSTEM 1000.

Materials. Benzene, acetic acid, and DDQ were of the same grade as those used in the previous work.[1] Flavanones were synthesized from the corresponding 2'-hydroxychalcones by the known procedures,[8] and identified by melting points, ^{1}H NMR, and elemental analyses.

2'-Chloroflavanone (1b): Mp 100—101 °C: ^{1}H NMR (CCl_4) δ=2.52—3.72 (2H, m, C_3-H_{ax}, H_{eq}), 5.75 (1H, d·d, C_2-H_{ax}, $J_{ax\cdot ax}$=12.0 Hz, $J_{ax\cdot eq}$=3.5Hz), 6.89—7.55 (7H, m, Aromatic), and 7.83 (1H, d·d, C_5-H, J_{ortho}=7.5Hz, J_{meta}=2.4 Hz). Found: C, 69.65; H, 4.13; Cl, 13.72%. Calcd for $C_{15}H_{11}O_2Cl$: C, 69.64; H, 4.29; Cl, 13.70%.

2'-Methylflavanone (1c): Mp 68.5—70.0 °C; ^{1}H NMR (CCl_4) δ=2.39 (3H, s, 2'-CH_3), 2.58—3.11 (2H, m, C_3-H_{ax}, H_{eq}), 5.58 (1H, d·d, C_2-H_{ax}, $J_{ax\cdot ax}$=12.2 Hz, $J_{ax\cdot eq}$=5.0 Hz), 6.89—7.56 (7H, m, Aromatic), and 7.85 (1H, d·d, C_5-H, J_{ortho}=8.4 Hz, J_{meta}=2.3 Hz). Found: C, 80.61; H, 6.03%. Calcd for $C_{16}H_{14}O_2$: C, 80.65; H, 6.03%.

2'-Methoxyflavanone (1d): Mp 61.0—62.0 °C; ^{1}H NMR (CCl_4) δ=2.53—3.11 (2H, m, C_3-H_{ax}, H_{eq}), 3.83 (3H, s, 2'-OCH_3), 5.76 (1H, d·d, C_2-H_{ax}, $J_{ax\cdot ax}$=11.0 Hz, $J_{ax\cdot eq}$=6.4 Hz), 6.78—7.60 (7H, m, Aromatic), and 7.85 (1H, d·d, C_5-H, J_{ortho}=8.0 Hz, J_{meta}=1.6 Hz). Found: C, 75.50; H, 5.62%. Calcd for $C_{16}H_{14}O_3$: C, 75.57; H, 5.55%.

2',4'-Dimethylflavanone (1e): Mp 88—89 °C; ^{1}H NMR (CCl_4) δ=2.33 and 2.36 (3H, 3H, s, s, 2' and 4'-CH_3), 2.56—3.12 (2H, m, C_3-H_{ax}, H_{eq}), 5.56 (1H, d·d, C_2-H_{ax}, $J_{ax\cdot ax}$=12.5 Hz, $J_{ax\cdot eq}$=4.6 Hz), 6.92—7.53 (6H, m, Aromatic), and 7.88 (1H, d·d, C_5-H, J_{ortho}=7.8 Hz, J_{meta}=2.2 Hz). Found: C, 81.31; H, 6.55%. Calcd for $C_{17}H_{16}O_2$: C, 81.25; H, 6.42%.

2',3'-Dimethoxyflavanone (1f): Mp 96.0—96.5 °C; ^{1}H NMR (CCl_4) δ=2.64—3.08 (2H, m, C_3-H_{ax}, H_{eq}), 3.87 (6H, s, 2' and 3'-OCH_3), 5.74 (1H, d·d, C_2-H_{ax}, $J_{ax\cdot ax}$=10.5 Hz, $J_{ax\cdot eq}$=6.8 Hz), 6.79—7.52 (6H, m, Aromatic), and 7.88 (1H, d·d, C_5-H, J_{ortho}=8.5 Hz, J_{meta}=2.0 Hz). Found: C, 72.20; H, 5.74%. Calcd for $C_{17}H_{16}O_4$: C, 71.82; H, 5.67%.

Flavones as authentic samples for HPLC analyses were prepared by the same reaction as carried out in the kinetic experiment, and were isolated and purified by the known procedures.[9] Their physical data are as follows, except for **2c** which was identified by the value in literature.[10]

2'-Chloroflavone (2b): Mp 117.0—117.5 °C; ^{1}H NMR (CCl_4) δ=6.48 (1H, s, C_3-H), 7.27—7.75 (7H, m, Aromatic), and 8.14 (1H, d·d, C_5-H, J_{ortho}=8.3 Hz, J_{meta}=2.3 Hz). Found: C, 70.40; H, 3.47; Cl, 13.71%. Calcd for $C_{15}H_9O_2Cl$: C, 70.19; H, 3.53; Cl, 13.76%.

2'-Methylflavone (2c): Mp 46.0—47.5 °C (lit, 47.5 °C[10]).

2'-Methoxyflavone (2d): Mp 98.5—100 °C; ^{1}H NMR (CCl_4) δ=3.93 (3H, s, 2'-OCH_3), 6.84 (1H, s, C_3-H), 6.92—7.83 (7H, m, Aromatic), and 8.11 (1H, d·d, C_5-H, J_{ortho}=8.2 Hz, J_{meta}=2.0 Hz). Found: C, 76.09; H, 4.80%. Calcd for $C_{16}H_{12}O_3$: C, 76.18; H, 4.79%.

2',4'-Dimethylflavone (2e): Mp 64.5—66.0 °C; ^{1}H NMR (CCl_4) δ=2.34 (3H, s, 4'-CH_3), 2.43 (3H, s, 2'-CH_3), 6.24 (1H, s, C_3-H), 6.96—7.66 (6H, m, Aromatic), and 8.12 (1H, d·d, C_5-H, J_{ortho}=8.5 Hz, J_{meta}=2.0 Hz). Found: C, 81.50: H, 5.71%. Calcd for $C_{17}H_{14}O_2$: C, 81.58; H, 5.64%.

2',3'-Dimethoxyflavone (2f): Mp 85.5—87.5 °C; ^{1}H NMR (CCl_4) δ=3.91 and 3.94 (3H, 3H, s, s, 2' and 3'-OCH_3), 6.98 (1H, s, C_3-H), 7.05—7.80 (6H, m, Aromatic), and 8.25 (1H, d·d, C_5-H, J_{ortho}=7.6 Hz, J_{meta}=1.5 Hz). Found: C, 67.64; H, 4.77%. Calcd for $C_{17}H_{14}O_4$: C, 67.55; H, 4.67%.

Procedures. Reactions and kinetic analyses were carried out in almost the same conditions and procedures as in the previous work.[1] Some comments are given in the footnote of Table 1.

References

1) Y. Hoshino and N. Takeno, *Nippon Kagaku Kaishi*, **1986**, 157.

2) Y. Hoshino, S. Takeda, M. Hamada, and N. Takeno, *Nippon Kagaku Kaishi*, **1982**, 1564.

3) R. W. Taft, "Steric Effects in Organic Chemistry," ed by M. S. Newman, John Wiley & Sons, New York (1956), p. 556.

4) M. Charton, *Prog. Phys. Org. Chem.*, **8**, 235 (1971).

5) S. Ehrenson, R. T. C. Brownlee and R. W. Taft, *Prog. Phys. Org. Chem.*, **10**, 1 (1973).

6) E. Kutter and C. Hansch, *J. Med. Chem.*, **12**, 674 (1969).

7) R. W. Taft, T. Fujita, and T. Nishioka, "Progress in Physical Organic Chemistry," Vol. 12, John Wiley & Sons, New York (1976), p. 49.

8) T. Oyamada, *Nippon Kagaku Zasshi*, **55**, 1256 (1934); S. Fujise, Y. Fujii, H. Maeda, K. Takagi, and S. Nakamura, *Nippon Kagaku Zasshi*, **74**, 827 (1953); B. Sen, *J. Am. Chem. Soc.*, **74**, 3446 (1952).

9) P. T. Kropp, *J. Org. Chem.*, **29**, 3110 (1930).

10) F. Cramer and G. H. Elschnig, *Chem. Ber.*, **89**, 1 (1956).

Fluorinated Tertiary Thio- and Selenoethers from the Reaction of Sulfenyl or Selenenyl Chloride with Perfluoropropene Dimers in the Presence of Alkali Fluoride

Hitomi SUZUKI,* Hiroshi SATAKE, Hidemitsu UNO, and Hiroaki SHIMIZU†
Department of Chemistry, Faculty of Science; Advanced Instrumentation Centre for Chemical Analysis, Ehime University, Bunkyo-cho, Matsuyama 790
†Central Research Laboratory, NEOS Company Ltd., Oike-machi, Kosei-cho, Koga-gun, Shiga 520-32
(Received April 13, 1987)

Synopsis. Perfluoro(1,1-dimethylbutanide) anion generated from hexafluoropropene dimers and alkali fluorides in dry *N,N*-dimethylformamide, reacts with arenesulfenyl or areneselenenyl chloride to give the corresponding aryl perfluoro(1,1-dimethylbutyl) sulfides or selenides in low to good yields.

Fluorinated organic sulfides find uses as fungicides, insecticides, and surface-active agents. The usual procedures for the preparation of aryl perfluoroalkyl sulfides involve the alkylation of arenethiolates with perfluoroalkyl iodides,[1] reaction of aryl iodides[2] or arenediazonium salts[3] with metal perfluoroalkanethiolates, and photochemical reaction of arenethiols[4] or diaryl disulfides[5] with perfluoroalkyl iodides. Thermal decomposition of trifluoromethylazosulfonylarenes in the presence of diaryl disulfides[6] and reaction of aryl perfluoroalkyliodonium compounds with sodium arenethiolates[7] also lead to aryl perfluoroalkyl sulfides. In most of these cases, however, reactions are limited to the synthesis of fluorinated sulfides of short or straight alkyl chains. The synthesis of tertiary perfluoroalkyl sulfides is quite difficult, because the nucleophilic displacement of halogen atom from tertiary carbon is not feasible with perfluoro compounds.

In the present paper, we wish to report that aryl perfluoroalkyl sulfides of branched side chains can be easily obtained by the reaction of arenesulfenyl chlorides with perfluoroalkenes in the presence of alkali fluorides.[8] We used perfluoro(2-methyl-2-pentene) (**1a**) and perfluoro(4-methyl-2-pentene) (**1b**) as perfluoroalkenes, since these are inexpensive commercial products obtained by the dimerization of hexafluoropropene.[9]

When alkene **1a** or **1b** is stirred with potassium fluoride in dry *N,N*-dimethylformamide (DMF) at 50—60 °C, perfluoro(1,1-dimethylbutanide) anion is generated and smoothly reacts with arenesulfenyl chloride (**2**) to afford the corresponding aryl perfluoro (1,1-dimethylbutyl) sulfides (**3**) in 58—86% yields, which are of interest as additives to some organic fluids.[10]

Although **1a** appears to react more smoothly than **1b**, the yields of the common product **3** do not differ appreciably after appropriate duration of time. Tertiary structures of perfluoroalkyl chains are confirmed by ^{19}F NMR spectrum ($CFCl_3$) of **3a**, which exhibits absorptions due to CF_3 groups at δ 61.1 and 80.2 and those due to CF_2 groups at δ 104.3 and 121.3 with an intensity ratio of 6:3:2:2. Cesium fluoride is excellent as a source of fluoride ion, but it can be replaced by cheaper potassium fluoride without significant decrease in yields. Perfluoroalkene **1b** is known to isomerize into the thermodynamically more stable isomer **1a** in the presence of fluoride ion.[11] Both **1a** and **1b** are known to react with arenethiolates to give a complicated mixture of fluorinated vinylic sulfides.[12]

The present procedure is extended to the preparation of phenyl perfluoro(1,1-dimethylbutyl) selenide (**5**). Benzeneselenenyl chloride (**4**), generated in situ by the chlorinolysis of diphenyl diselenide with sulfuryl chloride, reacted with perfluoro(1,1-dimethylbutanide) anion in DMF at room temperature to give the expected selenide **5** in a low yield. The conversion is

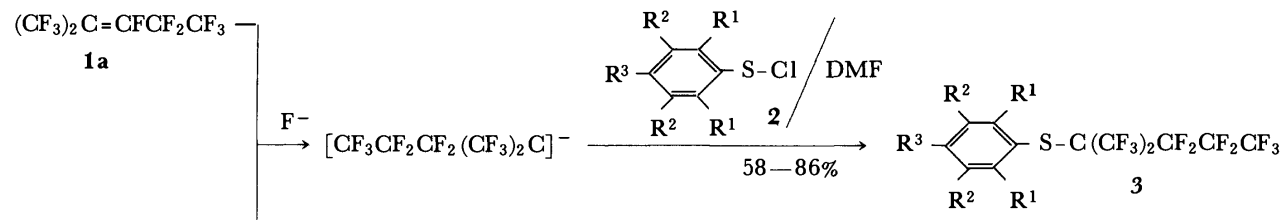

	R^1	R^2	R^3
a	H	H	H
b	H	H	CH_3
c	CH_3	H	CH_3
d	CH_3	CH_3	H
e	CH_3	CH_3	CH_3
f	H	H	Cl

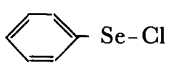

4

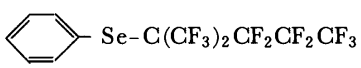

5

Table 1. Aryl Perfluoro(1,1-dimethylbutyl) Sulfides Obtained

Sulfide 3	Bp (θ_b/°C)/ mmHg[a]	Yield[b] %	IR (KBr)[c] cm^{-1}	^{1}H NMR (CCl_4/TMS)[d] δ(ppm)	MS (20 eV)[e] m/z (%)	Elementary analysis/% Found	Calcd
3a	108/27	75	1335, 1210—1225, 1115, 965, 755, 710	7.33—7.50 (m, 3H), 7.68—7.80 (m, 2H)	428 (M^+, 48), 109 (100)	C: 33.56 H: 1.08	33.66 1.18
3b	132/28	60	1335, 1210—1250, 1115, 965, 820, 735, 710	2.41 (s, 3H), 7.16 (d, 2H; J=8.4 Hz), 7.60 (d, 2H; J=8.4 Hz)	442 (M+, 32), 123 (100)	C: 35.55 H: 1.63	35.31 1.60
3c	155/27	86	1335, 1210—1245, 1115, 950, 820, 730, 710	2.27 (s, 3H), 2.54 (s, 6H), 6.92 (s, 2H)	470 (M+, 12), 151 (100)	C: 38.14 H: 2.39	38.31 2.36
3d	96/0.22	80	1335, 1210—1245, 1115, 820, 735, 710	2.24 (s, 6H), 2.52 (s, 6H), 7.03 (s, 1H)	484 (M+, 29), 165 (100)	C: 39.85 H: 2.70	39.68 2.71
3e	115/0.2 (51—53)[f]	59	1335, 1205—1260, 1115, 960, 820, 730, 710	2.22 (s, 9H), 2.58 (s, 6H)	498 (M^+, 17), 179 (100)	C: 40.88 H: 3.05	40.97 3.03
3f	132/34	58	1480, 1335, 1210—1250, 1115, 1095, 965, 830	7.37 (d, 2H; J=8.4 Hz), 7.68 (d, 2H; J=8.4 Hz)	462 (M^+, 25), 143 (100)	C: 30.88 H: 0.80	31.15 0.87

a) Bulb-to-bulb distillation (1 mmHg=133.322 Pa). b) Isolated yields based on **2** are not optimized. c) Measured on a Hitachi 260-10 spectrophotometer and only prominent peaks indicated. d) Recorded at 60 MHz using a Hitachi R-600 spectrometer. e) Obtained on a Hitachi M-80B spectrometer. f) Melting point.

incomplete even after prolonged reaction time. The product **5** is a photo-labile oil, which slowly decomposes on storage, even in a refrigerator, to form diphenyl diselenide. Reaction of **1a** with 2,4,6-trimethylbenzeneselenenyl chloride in the presence of an alkali fluoride also affords the corresponding selenide in a similar yield, but the product is unstable and soon begins to decompose on standing at room temperature. Introduction of methyl groups into aromatic rings appears to lower the stability of fluorinated tertiary selenoethers. Literature so far contains only few descriptions on the preparation of aryl perfluoroalkyl selenides; they are obtained either by photochemical reaction of areneselenols with trifluoromethyl iodide[13] or by treatment of trifluoromethaneselenenyl chloride with arylmagnesium bromides.[14]

In summary, the present method is a simple, efficient, and straightforward procedure for the preparation of various ring-substituted aryl tertiary perfluoroalkyl sulfides from readily accessible diaryl disulfides and commercially available perfluoroolefins.

Experimental

Perfluoro(2-methyl-2-pentene) (**1a**) and perfluoro(4-methyl-2-pentene) (**1b**) are commercial products available from NEOS Co. Ltd. (Kano-cho, Chuo-ku, Kobe 650, Japan). Diaryl disulfides are prepared by heating aryl iodides with copper(I) thiocyanate in hexamethylphosphoric triamide.[15] Diaryl diselenides are obtained by the alkaline decomposition of aryl selenocyanates.[16] Potassium fluoride is dried over phosphorus pentaoxide under reduced pressure at 100—120 °C prior to use.

Arenesulfenyl Chloride (2); General Procedure: To a stirred solution of diaryl disulfide (1 mmol) in dichloromethane (1 ml) is added dropwise sulfuryl chloride (1 mmol) at room temperature. Stirring is continued for 30 min to afford arenesulfenyl chloride **2** as a red solution, which is immediately used for the following reaction.

Aryl Perfluoro(1,1-dimethylbutyl) Sulfide (3); General Procedure: A mixture of perfluoro(2-methyl-2-pentene) **1a** (3.0 g; 10 mmol) and potassium fluoride (0.23 g; 4 mmol) in dry DMF (5 ml) is stirred at 50—60 °C for 3 h under nitrogen. Color gradually turns deep yellow. Then arenesulfenyl chloride **2** (2 mmol) is added dropwise and stirring is continued at this temperature for 1—2 h. After cooling the mixture is diluted with water and extracted with ether (3×10 ml). The organic extract is washed with brine, dried with sodium sulfate, and evaporated. The residual oil is chromatographed on silica gel (Wako Gel C-200) using hexane as eluent to give **3** in the yields given in the Table.

Perfluoro(1,1-dimethylbutyl) Phenyl Selenide (5): A mixture of perfluoroalkene **1a** (3.0 g; 10 mmol), potassium fluoride (0.23 g; 4 mmol) and DMF (5 ml) is stirred at 50—60 °C for 3 h under nitrogen. The resulting yellow liquid is cooled to room temperature and diphenyl diselenide (0.31 g; 1 mmol) followed by sulfuryl chloride (0.134 g; 1 mmol) is added with vigorous stirring. After stirring for 1 h, the reaction is quenched by the addition of water and the product is extracted with ether (3×10 ml). The combined extract is washed with brine, dried with sodium sulfate, and evaporated to leave an oily residue, which is chromatographed on silica gel (Wako Gel C-200) using hexane as eluent to give **5** as a pale yellow oil; yield, 0.195 g (21%). MS (20 eV) m/z (rel intensity) 476 (M^+, 3), 281 (8), 181 (46), and 157 (100); ^{1}H NMR (CCl_4): δ 7.33—7.50 (m, 3H) and 7.76—7.89 (m, 2H); IR (KBr) 3070, 1250—1210 (vs), 1150, 1100, 960, 820, 750, 730, and 710 cm^{-1}. Found: C, 30.12; H, 0.98%. Calcd for $C_{12}H_5F_{13}Se$: C, 30.34; H, 1.06%.

On standing, **5** gradually decomposes to separate diphenyl diselenide as yellow needles, mp 60—61 °C (lit,[17] mp 63 °C).

References

1) C. Wakselman and M. Tordeux, *J. Chem. Soc., Chem. Commun.*, **1984**, 793; *J. Org. Chem.*, **50**, 4047 (1985); A. E. Feiring, *J. Fluorine Chem.*, **24**, 191 (1984).

2) N. Ishikawa, T. Kitazume, and T. Mizuno, Jpn. Patent 75123609 (1974); *Chem. Abstr.*, **85**, 20593 (1976); L. M. Yagupol'skii, N. V. Kondoratenko, and V. P. Sambur, *Synthesis*, **1975**, 721.

3) N. V. Kondoratenko and V. P. Sambur, *Ukr. Khim. Zh.* (Russ. Ed.), **41**, 516 (1975); *Chem. Abstr.*, **83**, 58321 (1975).

4) V. I. Popov, N. V. Boiko, and L. M. Yagupol'skii, *J. Fluorine Chem.*, **21**, 365 (1982); N. V. Boiko, G. M. Shchupak, and L. M. Yagupol'skii, *Zh. Org. Khim.*, **13**, 1057 (1977).
5) L. Z. Gandel'sman and V. N. Boiko, *Ukr. Khim. Zh.* (Russ. Ed.), **43**, 1224 (1977); *Chem. Abstr.*, **88**, 89253 (1977).
6) A. Sekiya and T. Umemoto, *Chem. Lett.*, **1982**, 1519.
7) L. M. Yagupol'skii, I. I. Maletina, N. V. Kondoratenko, and V. V. Orda, *Synthesis*, **1978**, 835.
8) I. V. Popov, N. V. Kondoratenko, and A. Haas, *Ukr. Khim. Zh.* (Russ. Ed.), **49**, 861 (1983); *Chem. Abstr.*, **99**, 194535 (1983). Trifluoromethanesulfenyl chloride reacts with arylmercury(II) chlorides to give low to moderate yields of aryl trifluoromethyl sulfides among other products.
9) Since the commercial product contains isomeric impurity, it is purified by fractional distillation prior to use.
10) H. Suzuki, H. Uno, H. Shimizu, and F. Nemoto, Jpn. Patent applied for.
11) N. Ishikawa and A. Nagashima, *Nippon Kagaku Kaishi*, **1975**, 1439.
12) M. Maruta and N. Ishikawa, *J. Fluorine Chem.*, **13**, 111 (1979).
13) V. G. Voloshchuk, V. N. Voiko, and L. M. Yagupol'skii, *Zh. Org. Khim.*, **13**, 2008 (1977).
14) L. M. Yagupol'skii and V. G. Voloshchuk, *Zh. Obshch. Khim.*, **37**, 1543 (1967).
15) H. Suzuki and M. Shinoda, *Bull. Chem. Soc. Jpn.*, **50**, 321 (1977).
16) H. Suzuki and M. Shinoda, *Synthesis*, **1977**, 640.
17) K. B. Sharpless and R. F. Lauer, *J. Am. Chem. Soc.*, **95**, 2697 (1973).

Studies on 5-8 Fused Ring Compounds. IV. The Syntheses of 5-8-5 Fused Ring Compounds and the Conformations of Their Eight-Membered Rings

Misao UMEHARA,* Shinzaburo HISHIDA,† Satoshi OKUMOTO,†† Shigeru OHBA,††
Masatoki ITO,†† and Yoshihiko SAITO††
Department of Chemistry, Keio University, Hiyoshi 4-1-1, Kohoku-ku, Yokohama 223
†Naka Works, Hitachi Ltd., Ichige, Katsuta, Ibaraki 312
††Department of Chemistry, Faculty of Science and Technology, Keio University, Hiyoshi 3-14-1, Kohoku-ku, Yokohama 223
(Received July 1, 1987)

Synopsis. The isomers, *cis-cisoid-cis-* and *cis-transoid-cis*-tricyclo[9.3.0.0^{4,8}]tetradecane-2,9-dione (**2** and **3**) and *cis-cisoid-cis*-tricyclo[9.3.0.0^{3,7}]tetradecane-2,9-dione (**4**) were synthesized by the photocycloaddition of bicyclo[4.3.0]nonane-2,4-dione (**1**) to cyclopentene. X-Ray analyses of those compounds revealed that the conformations of the eight-membered rings are twist-boat in **2**, chair in **3**, and boat-chair form in **4**.

The 5-8-5 fused tricyclic systems have been found as the carbon skeletons of ophiobolin[1] sesterterpenes, and fusicoccin[2] and basmane[3] diterpenes. Although several reports[4] have appeared concerning the syntheses of 5-8-5 fused ring compounds, the synthetic and conformational studies on such compounds are still insufficient. In this paper we report the syntheses of some 5-8-5 fused ring compounds via the photocycloaddition of bicyclo[4.3.0]nonane-2,4-dione (**1**) to cyclopentene and their molecular structures and conformations.

The starting material, bicyclo[4.3.0]nonane-2,4-dione (**1**), was synthesized by Michael condensation between 1-acetylcyclopentene and diethyl malonate, accompanied by intramolecular cyclization and followed by decarboxylation, in an analogous synthetic procedure of dimedone.[5] The enolization of β-diketone (**1**) is feasible in two forms, **1a** and **1b**. For the photoadducts, therefore, two structural isomers (**C** and **D**) are possible.

The photocycloaddition was carried out in a methanol solution of **1** and cyclopentene by high-pressure mercury lamp, and yielded directly 5-8-5 fused ring compounds; *cis-cisoid-cis-* and *cis-transoid-cis*-tricyclo[9.3.0.0^{4,8}]tetradecane-2,9-dione (**2** and **3**) and *cis-cisoid-cis*-tricyclo[9.3.0.0^{3,7}]tetradecane-2,9-dione (**4**). The latter compound (**4**) has the same carbon ring skeleton as that of ophiobolin and fusicoccin. The ratio of **2**, **3**, and **4** was approximately 4 : 1 : 2.

The molecular structures of **2**, **3**, and **4** were determined by X-ray analyses.[6] Figure 1 shows perspective views of the molecules and Fig. 2 shows the side views of eight-membered rings. Molecules **3** has a center of symmetry. In these compounds, two five-membered rings are fused to eight-membered ring in a *cis-*

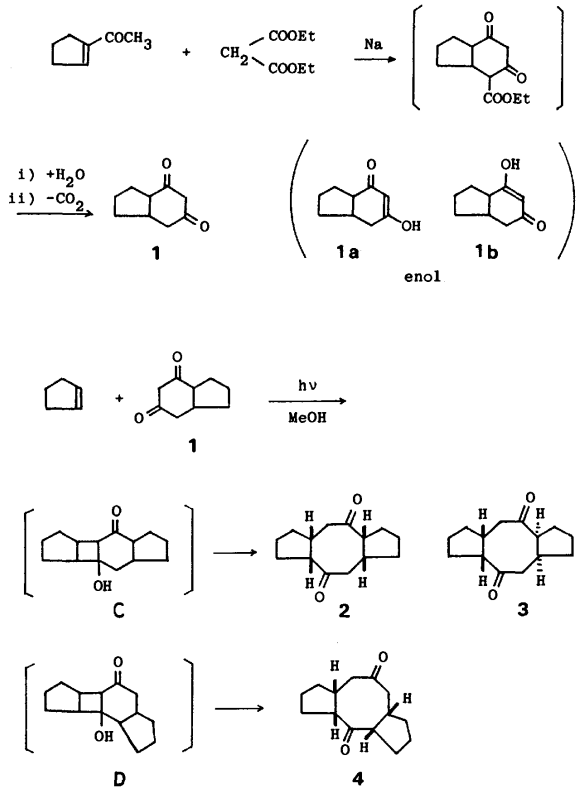

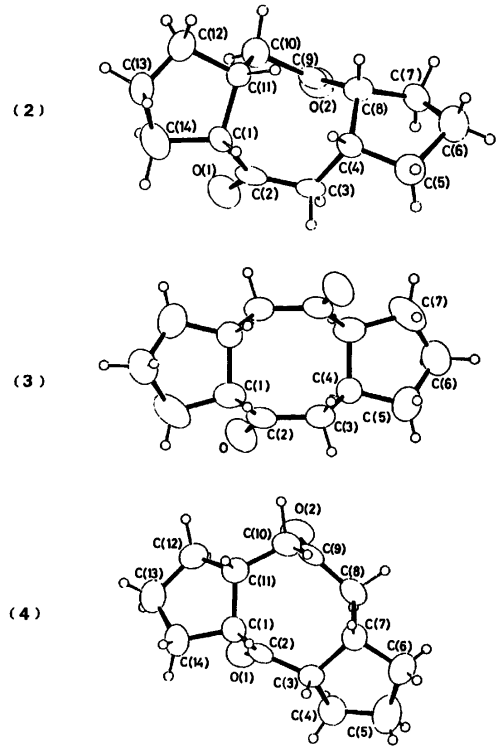

Fig. 1. Perspective views of the molecules **2**, **3**, and **4**.

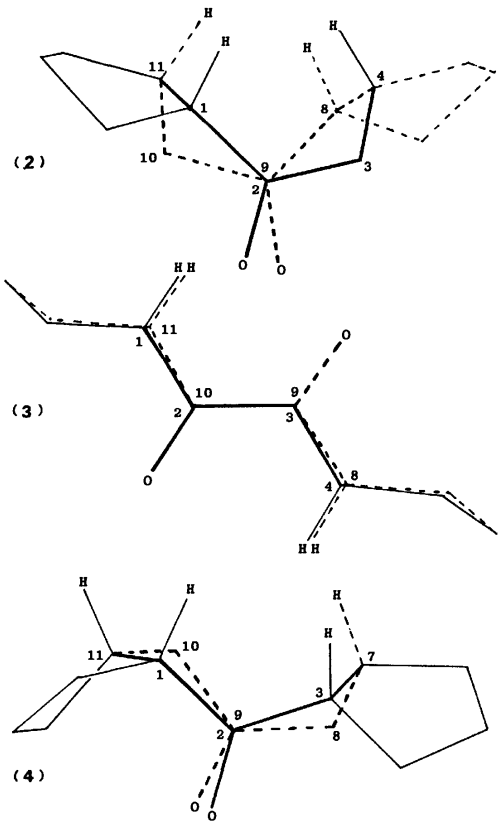

Fig. 2. The side views of the molecules **2**, **3**, and **4**. **2** and **4**: Projections along the C(2)···C(9) vectors. **3**: Projection along the C(2)···C(10) and C(3)···C(9) vectors.

configuration. Consequently, **2** and **4** have a *cis-cisoid-cis* configuration and **3** has a *cis-transoid-cis* configuration. Broadly speaking, two carbonyl groups in **2** and **4** are arranged in parallel orientation, whereas those in **3** take antiparallel orientation.

Cyclooctane, its simple derivatives, and 1,5-cyclooctanedione have been shown to exist predominantly in boat-chair(BC) form,[7] which is the most stable conformation predicted by the molecular mechanics calculations.[8] The X-ray analysis of *trans*-7-bromo-4,4-dimethylbicyclo[6.3.0]undecane-2,6-dione[9] and *trans*-5-bromobicyclo[6.3.0]undecane-2,6-dione[10] revealed that their eight-membered rings in the molecules are BC form. In this study the central eight-membered ring of **4** takes considerably distorted BC form. In contrast the conformations in **2** and **3** are a twist-boat and a chair forms, respectively, and these two conformations are quite unique in 5-8-5 fused ring systems.

Experimental

The IR spectra were recorded on a JASCO IR-G spectrometer. The mass spectra were measured with a Hitachi M-80B mass spectrometer. The GC-analyses were carried out on a 263-50 Hitach gas chromatograph.

Bicyclo[4.3.0]nonane-2,4-dione (1). Sodium (5 g) was dissolved in absolute ethanol (85 ml) with stirring under reflux. To the solution diethyl malonate (36 g) was added; then 1-acetylcyclopentene (22 g) was added dropwise. After being refluxed with stirring for 2 h., a solution of KOH (25 g) in water (140 ml) was added to the reaction mixture, which was refluxed with stirring for 8 h. The hot mixture was acidified with dilute HCl (4 M (1M=1 mol dm^{-3})), and then ethanol was evaporated. The residue was boiled with charcoal (3 g) until no more carbon dioxide was evolved, then again acidified with dil. HCl, and again boiled with charcoal (3 g). The hot mixture was finally acidified (pH<3) with dil. HCl, and boiled for a few minutes. In order to dissolve the resulting oily phase, acetone was added to the mixture, and then boiled and filtered. The filtrate was evaporated under reduced pressure and the residue was crystallized from carbon tetrachloride to give **1** (66% yield): Mp 95—96 °C (from CCl_4); IR (Nujol) 2600 (broad, enol OH), 1610 cm^{-1} (β-diketone C=O); MS *m/z* (rel intensity) 152 (M^+, 64), 124 (19), 111 (30), 95 (28), 83 (45), 82 (42), 67 (100), 54 (22), 43 (30). HRMS; Found: *m/z* 152.0845. Calcd for $C_9H_{12}O_2$: M, 152.0837.

Table 1. Mp, IR, and Mass Spectra of **2**, **3**, and **4**

	2	**3**	**4**
Mp θ_m/°C	204—204.5	142—143	96—97
IR (Nujol) $\nu_{C=O}$/cm^{-1}	1690	1690	1685 1700 (sh)
MS (*m/z*)		(rel intensity %)	
220 (M^+)	18	39	13
192 (M−28)	3	7	2
178 (M−42)	7	10	2
165 (M−55)	25	28	7
153 (M−67)	100	58	100
152 (M−68)	23	15	55
137 (M−83)	20	19	10
124	80	57	42
111	17	16	37
95	28	28	29
83	44	46	20
81	24	30	25
67	68	100	75
55	35	65	23
41	29	68	26
HRMS (*m/z*)			
Found	220.1461	220.1472	220.1457
Calcd for $C_{14}H_{20}O_2$: M, 220.1464			

***cis-cisoid-cis*- and *cis-transoid-cis*-Tricyclo[9.3.0.0^{4,8}]-tetradecane-2,9-dione (2 and 3) and *cis-cisoid-cis*-Tricyclo-[9.3.0.0^{3,7}]tetradecane-2,9-dione (4).** A solution of **1** (1 g) in methanol (150 ml) and cyclopentene (20 ml) was irradiated for 10 h.[11] through quartz filter[11] with a 100 W high-pressure mercury lamp at 5 °C in a nitrogen atmosphere. After the irradiation, the solvent was removed under reduced pressure, and a small amount of ether was added in the residue. Immediately, the photoadduct (**2**) was isolated as a crystalline solid, sparingly soluble in ether. **2** was recrystallized from ether-acetone. Subjecting to silica-gel column chromatography of the residual ether solution (eluted with hexane-ether), **3**, **4**, additional amount of **2** and also unreacted starting material (**1**) were obtained. Compounds of **3** and **4** were crystallized from ether-hexane. In a GC-analysis of the reaction mixture the ratio of **2**, **3**, **4**, and **1** was approximately 4:1:2:6. The yield of the photoadducts mixture (**2**, **3**, and **4**) was 40%, based on the starting material consumed. Mp, IR, and MS; (see Table 1).

References

1) S. Nozoe, M. Morisaki, K. Tsuda, Y. Iitaka, N. Takahashi, S. Tamura, K. Ishibashi, and M. Shirasaka, *J. Am. Chem. Soc.*, **87**, 4968 (1965).

2) K. D. Barrow, D. H. R. Rarton, E. Chain, U. F. W. Ohnsorge, and R. Thomas, *J. Chem. Soc. C*, **1971**, 1265.

3) I. Wahlberg, A. Eklund, T. Nishida, and C. R. Enzell, *Tetrahedron Lett.*, **24**, 843 (1983).

4) R. K. Boeckman, J. J. P. Bershas, J. Clardy, and B. Solheim, *J. Org. Chem.*, **42**, 3630 (1977); W. G. Dauben and D. S. Hart, *ibid.*, **42**, 922 (1977); T. K. Das and P. C. Dutta, *J. Chem. Soc., Perkin Trans. 1*, **1977**, 1287; R. M. Coates, P. D. Senter, and W. R. Baker, *J. Org. Chem.*, **47**, 3597 (1982); L. A. Paquette, D. R. Andrews, and J. P. Springer, *ibid.*, **48**, 1147 (1983); H. Takeshita, N. Kato, K. Nakanishi, H. Tagoshi, and T. Hatsui, *Chem. Lett.*, **1984**, 1495; L. A. Paquete, J. A. Colapret, and D. R. Andrews, *J. Org. Chem.*, **50**, 201 (1985).

5) R. L. Shriner and H. R. Todd, *Org. Synth.*, Coll. Vol. 2, 200 (1943).

6) A full report will be published by S. Okumoto elsewhere. The crystal data and R values are as follows: (**2**) monoclinic, Cc, a=11.994(2), b=5.451(1), c=18.306(2) Å, β=91.49(2)°, V=1196.5(3) Å^3, Z=4, D_x=1.22, D_m=1.21(2) Mg m^{-3}, Mo $K\alpha$, λ=0.71073 Å, μ=0.07 mm^{-1}, R=0.033 for 745 observed unique reflections. (**3**) monoclinic, $P2_1/n$, a=11.761(3), b=9.208(1), c=5.594(1) Å, β=98.02(2)°, V=599.8(2) Å^3, Z=2, D_x=1.22, D_m=1.19(2) Mg m^{-3}, μ=0.07 mm^{-1}, R=0.048 for 603 reflections. (**4**) monoclinic, $P2_1/n$, a=12.316(2), b=17.833(3), c=5.390(1) Å, β=90.06(2)°, V=1183.9(4) Å^3, Z=4, D_x=1.24, D_m=1.23(2) Mg m^{-3}, μ=0.08 mm^{-1}, R=0.052 for 1293 reflections.

7) M. Dobler, J. D. Dunitz, and A. Mugnoli, *Helv. Chim. Acta*, **49**, 2492 (1966); H. B. Bürgi and J. D. Dunitz, *ibid.*, **51**, 1514 (1968); J. E. Anderson, E. S. Glazer, D. L. Griffith, R. Knorr, and J. D. Roberts, *J. Am. Chem. Soc.*, **91**, 1386 (1969); F. A. L. Anet and J. Krane, *Tetrahedron Lett.*, **1973**, 5029; F. A. L. Anet, M. St. Jacques, D. M. Henrichs, A. K. Cheng. J. Krane, and L. Wong, *Tetrahedron*, **30**, 1629, (1974); R. W. Miller and A. T. McPhail, *J. Chem. Soc., Perkin Trans. 2*, **1979**, 1527.

8) J. B. Hendrickson, *J. Am. Chem. Soc.*, **86**, 4854 (1964), *ibid.*, **89**, 7036, 7043 (1967); M. Bixon and S. Lifson, *Tetrahedron*, **23**, 769 (1967); N. L. Allinger, J. A. Hirsch, M. Miller, J. J. Tyminski, and F. A. Van Catledge, *J. Am. Chem. Soc.*, **90**, 1199 (1968); E. Engler, J. D. Andose, and P. von R. Schleyer, *ibid.*, **95**, 8005 (1973); N. L. Allinger. M. T. Tribble, and M. A. Miller, *Tetrahedron*, **28**, 1173 (1972).

9) M. Umehara, H. Takayanagi, H. Ogura, and S. Hishida, *Bull. Chem. Soc. Jpn.*, **51**, 3277 (1978).

10) S. Okumoto, S. Ohba, Y. Saito, T. Ishii, M. Umehara, and S. Hishida, *Acta Crystallogr., Sect. C*, **43**, 1584 (1987).

11) Although in this period a considerable amount of starting material remained, the irradiation was discontinued because prolonged irradiation reduced the yield of **4**. In this photocycloaddition the rate of reaction through Pyrex filter is very slow, therefore quartz filter was used.

X-Ray Structure and Magnetism of μ-Bromo-μ-pyrazolatobis-(diethylenetriaminecopper(II)) Perchlorate Monohydrate

Keiji MATSUMOTO,* Shun'ichiro OOI, Wasuke MORI,† and Yasuo NAKAO††
Department of Chemistry, Faculty of Science, Osaka City University, Sumiyoshi-ku, Osaka 558
†Institute of Chemistry, College of General Education, Osaka University, Toyonaka, Osaka 560
††Chemical Laboratory, Faculty of Education, Okayama University, Okayama 700
(Received June 1, 1987)

Synopsis. The structure of the title compound has been determined by an X-ray method. The dinuclear complex is composed of two Cu(dien) units which are bridged by pyrazolate and Br^- anions. The geometry around each copper(II) may be described as a square pyramid. The antiferromagnetic interaction within the dinuclear complex has been observed ($J=-14\,cm^{-1}$, $H=-2JS_1\cdot S_2$).

A number of studies have been conducted on magneto-structural correlation of dinuclear copper(II) complexes bridged by imidazolate anion (im), in view of their importance as structural models for the active site of bovine erythrocyte superoxide dismutase.[1] On the other hand, there has been continuing interest in the magnetic properties of dinuclear copper(II) complexes bridged by pyrazolate anion (pz) which is similar to im.[2-4] Few such studies, however, have been appeared. We report here on the structure and magnetism of $[Cu_2(dien)_2(pz)(Br)](ClO_4)_2\cdot H_2O$ (**1**) (dien= diethylenetriamine).

Experimental

Preparation of $[Cu_2(dien)_2(pz)(Br)](ClO_4)_2\cdot H_2O$ (1). An aqueous solution of $AgClO_4$ (0.38 g, 1.8 mmol) was added to an aqueous solution of $[Cu_2(dien)_2(pz)]Br_3\cdot H_2O$[4] (0.60 g, 0.92 mmol), and the mixture was stirred for 15 min. After removing precipitated AgBr, the filtrate was evaporated to dryness. The violet-blue solids obtained were recrystallized from ethanol containing a small quantity of water. Found: C, 18.86; H, 4.38; N, 16.03%. Calcd for $C_{11}H_{29}O_8N_8Cl_2Cu_2Br\cdot H_2O$: C, 18.94; H, 4.49; N, 16.07%.

Crystal Data. $C_{11}H_{31}O_9N_8Cl_2Cu_2Br$, $F.W.=697.4$, triclinic, space group $P\bar{1}$, $a=23.294(10)$ Å, $b=14.084(5)$ Å, $c=7.750(2)$ Å, $\alpha=92.50(2)°$, $\beta=92.07(2)°$, $\gamma=90.98(2)°$, $Z=4$, $D_m=1.80\,g\,cm^{-3}$, $D_c=1.82$, $\mu(MoK\alpha)=36.8\,cm^{-1}$, $\lambda(MoK\alpha)=0.71069$ Å, $U=2538.1(15)$ Å^3.

X-Ray Data Collection. The crystal chosen for data collection and lattice constants determination had dimensions of $0.12\times0.30\times0.38$ mm^3. It was mounted in an arbitrary orientation on a Philips PW1100 automated diffractometer. The PW1100 program obtained 23 centered reflections and an orientation matrix, and then identified the triclinic cell. The space group $P\bar{1}$ was assumed throughout the structure analysis and confirmed by the successful refinement of the structure. The unit cell dimensions with standard deviations were derived from a least-squares fit from the angular positions of 25 centered reflections. The intensity data ($4°\leqq2\theta\leqq50°$) were collected at room temperature by the use of graphite monochromated Mo$K\alpha$ radiation. The ω-scan method was employed. The scan range was $(1.0+0.3\,\tan\theta)°$ and the scan speed $0.05°\,s^{-1}$; the background was counted for 10 s at each side of the scan range. During the data collection, intensities of 3 standard reflections were monitored every 4 h in order to check the orientation and stability of the crystal. The compound remained quite stable. A total of 3635 reflections [$F_o^2\geqq3\sigma(F_o^2)$] were considered as observed. The intensities were corrected for Lorenz-polarization effects,[5] but not for absorption.

Structure Solution and Refinement. MULTAN 78[6] provided the positions of the copper and bromine atoms. Subsequent least-squares refinement followed by difference Fourier syntheses revealed the positions of all non-hydrogen atoms. The least-squares refinement with anisotropic temperature factors for the non-hydrogen atoms gave $R=0.068$ and $R'=(\sum w\Delta F^2/\sum wF_o^2)^{1/2}=0.092$. The hydrogen atoms were located on calculated positions (N-H, C-H= 1.0 Å). In the final cycles of refinement, the hydrogen atoms, except for the water hydrogen atoms, were included with a common isotropic temperature factor $B=5.0$ Å^2, but their parameters were not refined. The function minimized was $\sum w(F_o-|F_c|)^2$, where $w=1/(\sigma^2(F_o)+0.005\,F_o^2)$ was used. All the parameter shifts were less than 0.5σ. The atomic scattering factors for Cu, Br, O, N, C, and H atoms were taken from Ref. 7, with corrections for anomalous scattering for the Cu and Br atoms. The final difference Fourier map was featureless and showed no peaks greater than 0.8 e Å^{-3}. Observed and calculated structure factors, thermal parameters, and hydrogen atom coordinates are preserved by the Chemical Society of Japan (Document No. 8763). Final atomic coordinates for non-hydrogen atoms are given in Table 1. The computer programs used in the calculations were a local version of the UNICS.[8] Figure 1 was drawn by the use of ORTEP.[9] Calculations were performed on a FACOM M 180II AD computer at Osaka City University.

Measurement. The Faraday method was applied for the measurement of magnetic susceptibility over the range from liquid helium temperature to room temperature.

Results and Discussion

Figure 1 gives a perspective view of the complex cation of **1**. There are two crystallographically independent complexes in a cell and their structures are similar to each other. Each complex is composed of two Cu(dien) units which are bridged by pyrazolate and bromine anions, forming a dimeric $[Cu_2(dien)_2(pz)(Br)]^{2-}$. The complexes are described as an intermediate between a trigonal bipyramid and a square pyramid. From the trigonal bipyramidal view point, N(1)[N(9)], N(3)[N(11)], and Br(1)[Br(2)] atoms, and N(4)[N(12)], N(6)[N(14)], and Br(1)[Br(2)] atoms form the equitorial planes and, N(2)[N(10)] and N(7)[N(15)], and N(5)[N(13)] and N(8)[N(16)] atoms occupy the apical positions. In the square pyramidal approximation, Br(1) and Br(2) occupy the apical positions. N(1)[N(9)], N(2)[N(10)], N(3)[N(11)], and N(7)[N(15)] atoms, and N(4)[N(12)], N(5)[N(13)], N(6)[N(14)] and N(8)[N(16)] atoms form the basal planes. The intermediate coordination geometry has been characterized by the structural index parameter $\tau=(\beta-\alpha)/60$,[10] where α and β are the two largest metal ligand bond angles in the complex. Application of the formula to the present complex gives the τ values of 0.33, 0.31, 0.29, and 0.35, indicating that the complex lies closer

Table 1. Fractional Coordinates and Temperature Factors for **1**

Atom	x	y	z	U_{eq}[a)]	Atom	x	y	z	U_{eq}[a)]
Cu(1)	0.3342(1)	0.2690(1)	0.4010(2)	0.0345(6)	C(12)	−0.0057(8)	0.910(1)	0.297(3)	0.11(1)
Cu(2)	0.4922(1)	0.2293(1)	0.4651(2)	0.0333(6)	C(13)	−0.0608(7)	0.872(1)	0.194(3)	0.11(1)
Br(1)	0.4272(1)	0.3421(1)	0.2553(2)	0.0528(6)	C(14)	−0.0959(7)	0.775(1)	−0.049(3)	0.079(8)
N(1)	0.3213(5)	0.3642(9)	0.602(1)	0.049(5)	C(15)	−0.0696(8)	0.717(2)	−0.189(3)	0.093(9)
N(2)	0.2843(4)	0.3576(8)	0.264(1)	0.036(4)	C(16)	0.191(1)	0.707(1)	−0.495(3)	0.10(1)
N(3)	0.3065(5)	0.1690(9)	0.219(2)	0.059(5)	C(17)	0.2362(7)	0.774(1)	−0.440(2)	0.072(7)
N(4)	0.4951(4)	0.1137(8)	0.302(2)	0.045(4)	C(18)	0.2592(7)	0.889(1)	−0.212(2)	0.069(7)
N(5)	0.5618(4)	0.2727(7)	0.338(1)	0.037(4)	C(19)	0.2368(8)	0.921(1)	−0.041(3)	0.090(9)
N(6)	0.5225(4)	0.3254(9)	0.648(1)	0.044(4)	C(20)	0.0832(6)	0.594(1)	0.202(2)	0.056(6)
N(7)	0.3731(4)	0.1793(7)	0.551(1)	0.034(4)	C(21)	0.1292(7)	0.538(1)	0.182(2)	0.061(7)
N(8)	0.4299(4)	0.1788(7)	0.598(1)	0.035(4)	C(22)	0.1631(6)	0.584(1)	0.065(2)	0.062(7)
C(1)	0.2979(7)	0.452(1)	0.525(2)	0.060(6)	Cl(1)	0.3811(2)	0.9174(3)	0.2736(5)	0.045(1)
C(2)	0.2548(6)	0.423(1)	0.382(2)	0.054(6)	O(11)	0.3314(5)	0.918(1)	0.358(2)	0.126(8)
C(3)	0.2452(7)	0.299(1)	0.146(2)	0.058(6)	O(12)	0.3866(5)	0.9959(8)	0.165(1)	0.068(5)
C(4)	0.2780(7)	0.218(1)	0.072(2)	0.064(7)	O(13)	0.4286(6)	0.920(1)	0.388(2)	0.119(7)
C(5)	0.5329(7)	0.135(1)	0.157(2)	0.051(6)	O(14)	0.386(1)	0.834(1)	0.178(2)	0.19(1)
C(6)	0.5846(6)	0.192(1)	0.237(2)	0.043(5)	Cl(2)	0.3242(2)	0.5972(3)	0.0062(5)	0.051(1)
C(7)	0.6016(5)	0.324(1)	0.460(2)	0.041(5)	O(21)	0.2943(5)	0.653(1)	−0.113(2)	0.093(6)
C(8)	0.5649(6)	0.385(1)	0.575(2)	0.052(6)	O(22)	0.3113(6)	0.627(1)	0.177(2)	0.108(7)
C(9)	0.3429(6)	0.123(1)	0.663(2)	0.049(6)	O(23)	0.3846(4)	0.6087(8)	−0.018(2)	0.067(5)
C(10)	0.3827(6)	0.087(1)	0.780(2)	0.053(6)	O(24)	0.3068(6)	0.4996(8)	−0.019(2)	0.087(6)
C(11)	0.4352(6)	0.123(1)	0.733(2)	0.039(5)	Cl(3)	0.1592(2)	0.0331(3)	0.3887(6)	0.068(2)
Cu(3)	0.0231(1)	0.7552(1)	0.0512(3)	0.0534(7)	O(31)	0.1036(6)	0.069(1)	0.377(2)	0.117(7)
Cu(4)	0.1694(1)	0.7535(1)	−0.1413(2)	0.0425(6)	O(32)	0.1939(6)	0.069(1)	0.269(2)	0.125(8)
Br(2)	0.0751(1)	0.8562(2)	−0.1891(3)	0.095(1)	O(33)	0.1859(8)	0.051(1)	0.556(2)	0.143(9)
N(9)	0.0341(6)	0.832(1)	0.280(2)	0.080(6)	O(34)	0.1548(6)	−0.0691(9)	0.364(2)	0.095(6)
N(10)	−0.0488(5)	0.8318(9)	0.030(2)	0.068(6)	Cl(4)	0.0827(2)	0.4253(3)	0.6615(6)	0.074(2)
N(11)	−0.0192(6)	0.665(1)	−0.119(2)	0.069(6)	O(41)	0.0494(9)	0.350(1)	0.630(4)	0.23(2)
N(12)	0.1688(7)	0.655(1)	−0.347(2)	0.081(7)	O(42)	0.1392(7)	0.418(1)	0.659(4)	0.23(2)
N(13)	0.2126(5)	0.8353(8)	−0.305(2)	0.049(5)	O(43)	0.070(1)	0.498(2)	0.583(4)	0.34(2)
N(14)	0.2125(5)	0.836(1)	0.044(2)	0.057(5)	O(44)	0.065(1)	0.451(3)	0.803(3)	0.33(3)
N(15)	0.0870(5)	0.6708(8)	0.097(2)	0.052(5)	O(1)	0.2105(5)	0.253(1)	0.669(2)	0.106(7)
N(16)	0.1369(5)	0.6630(8)	0.015(2)	0.049(5)	O(2)	0.4271(6)	0.418(1)	0.845(1)	0.092(6)

Standard deviations of the least significant figures are given in parentheses.
a) $U_{eq}=1/3(U_{11}+U_{22}+U_{33}+2U_{12}\cos\gamma+2U_{13}\cos\beta+2U_{23}\cos\alpha)$.

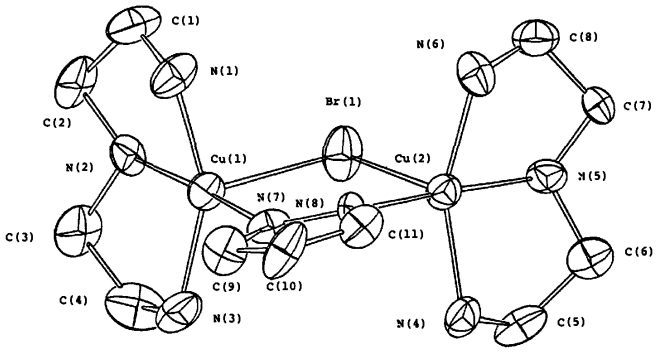

Fig. 1. A perspective view of one of the two crystallographically independent complex cations. Similar numbering scheme is used in the other complex.

to the idealized square pyramidal limit (τ=0) than the trigonal bipyramidal limit (τ=1.0). Selected bond lengths and angles are given in Tables 2 and 3. The five-membered rings in the bridges are nearly planar; deviations of the atoms from the respective best planes are: 0.029(4) [0.020(4)], −0.055(4) [0.067(4)], 0.012(3)-[−0.039(3)], −0.11(1)[0.04(1)], and 0.12(1)[−0.09(1)]Å for Cu(1)[Cu(3)], Cu(2)[Cu(4)], Br(1)[Br(2)], N(7)[N-(15)], and N(8)[N(16)].

Table 2. Bond Distances (l/Å) of **1**

Cu(1)-Br(1)	2.690(2) Å	Cu(3)-Br(2)	2.702(3) Å
Cu(2)-Br(1)	2.756(2)	Cu(4)-Br(2)	2.673(3)
Cu(1)-N(1)	2.042(12)	Cu(3)-N(9)	2.044(16)
Cu(1)-N(2)	2.028(11)	Cu(3)-N(10)	2.014(12)
Cu(1)-N(3)	2.031(13)	Cu(3)-N(11)	2.010(14)
Cu(1)-N(7)	1.966(10)	Cu(3)-N(15)	1.953(12)
Cu(2)-N(4)	2.021(11)	Cu(4)-N(12)	2.064(14)
Cu(2)-N(5)	2.027(11)	Cu(4)-N(13)	2.032(12)
Cu(2)-N(6)	2.018(11)	Cu(4)-N(14)	2.034(12)
Cu(2)-N(8)	1.954(10)	Cu(4)-N(16)	1.959(12)

Cu···Cu distance (l/Å) for **1**

Cu(1)···Cu(2)	3.752(2) Å
Cu(3)···Cu(4)	3.769(3)

Short contact (l/Å) less than 3.10 Å

Cu(2)···O(13)(1−x, 1−y, 1−z)	3.05(2) Å
N(1)···O(1)(x, y, z)	3.07(2)
N(2)···O(24)(x, y, z)	3.09(2)
N(3)···O(32)(x, y, z)	3.00(2)
N(4)···O(13)(1−x, 1−y, 1−z)	3.00(2)
N(6)···O(2)(x, y, z)	3.02(2)
O(1)···O(33)(x, y, z)	2.97(2)
O(1)···O(42)(x, y, z)	2.89(2)
O(2)···O(23)(x, y, 1+z)	3.04(2)

The standard deviation of the least significant figure of each distance is given in parenthesis.

Table 3. Bond Angles (ϕ/°) of **1**

Br(1)-Cu(1)-N(1)	102.7(3)°
Br(1)-Cu(1)-N(2)	89.1(3)
Br(1)-Cu(1)-N(3)	101.7(4)
Br(1)-Cu(1)-N(7)	98.6(3)
N(1)-Cu(1)-N(2)	84.1(5)
N(1)-Cu(1)-N(3)	152.7(5)
N(1)-Cu(1)-N(7)	92.9(5)
N(2)-Cu(1)-N(3)	84.3(5)
N(2)-Cu(1)-N(7)	172.2(4)
N(3)-Cu(1)-N(7)	95.3(5)
Br(1)-Cu(2)-N(4)	97.9(3)
Br(1)-Cu(2)-N(5)	87.5(3)
Br(1)-Cu(2)-N(6)	101.3(3)
Br(1)-Cu(2)-N(8)	97.9(3)
N(4)-Cu(2)-N(5)	83.7(4)
N(4)-Cu(2)-N(6)	156.1(4)
N(4)-Cu(2)-N(8)	94.7(4)
N(5)-Cu(2)-N(6)	83.2(4)
N(5)-Cu(2)-N(8)	174.5(4)
N(6)-Cu(2)-N(8)	96.5(4)
Cu(1)-Br(1)-Cu(2)	87.1(1)
Br(2)-Cu(3)-N(9)	106.6(4)
Br(2)-Cu(3)-N(10)	91.8(4)
Br(2)-Cu(3)-N(11)	95.6(4)
Br(2)-Cu(3)-N(15)	96.4(4)
N(9)-Cu(3)-N(10)	83.1(6)
N(9)-Cu(3)-N(11)	154.5(6)
N(9)-Cu(3)-N(15)	94.5(5)
N(10)-Cu(3)-N(11)	83.7(6)
N(10)-Cu(3)-N(15)	171.7(6)
N(11)-Cu(3)-N(15)	95.5(5)
Br(2)-Cu(4)-N(12)	105.5(5)
Br(2)-Cu(4)-N(13)	90.5(3)
Br(2)-Cu(4)-N(14)	100.3(4)
Br(2)-Cu(4)-N(16)	97.4(3)
N(12)-Cu(4)-N(13)	83.1(5)
N(12)-Cu(4)-N(14)	150.8(6)
N(12)-Cu(4)-N(16)	93.4(5)
N(13)-Cu(4)-N(14)	83.3(5)
N(13)-Cu(4)-N(16)	172.0(5)
N(14)-Cu(4)-N(16)	96.6(5)
Cu(3)-Br(2)-Cu(4)	89.0(1)

The standard deviation of the least significant figure of each angle is given in parenthesis.

The magnetic moment(μ_{eff} value) for **1** was found to be 1.83 B.M. at 291.5 K using a Gouy magnetic apparatus. Figure 2 gives the temperature-dependence of the magnetic susceptibility for **1**. The magnetic data show a peak near 25 K and a rapid decrease to zero at lower temperatures, indicating an antiferromagnetic interaction within the dinuclear complex. The magnetic parameters are estimated as g=2.15, $N\alpha$=60×10^{-6} cgs emu mol^{-1}, and J=−14 cm^{-1} from the best fit of the χ_a values to the Bleaney-Bowers equation.[11] In 1, the pyrazolate anion bridges two basal planes of the two square pyramids, while the bridging Br atom shares the common apical position of the two square pyramids. It appears that the present complex has the $d_{x^2-y^2}$ ground state. The coordination geometries around the two copper(II) ions in **1** are unfavorable for exchanging two unpaired electrons through the bridging Br$^-$ ion. Accordingly, the antiferromagnetic exchange interaction of the two magnetic orbitals through pz seems to be more important than that through Br

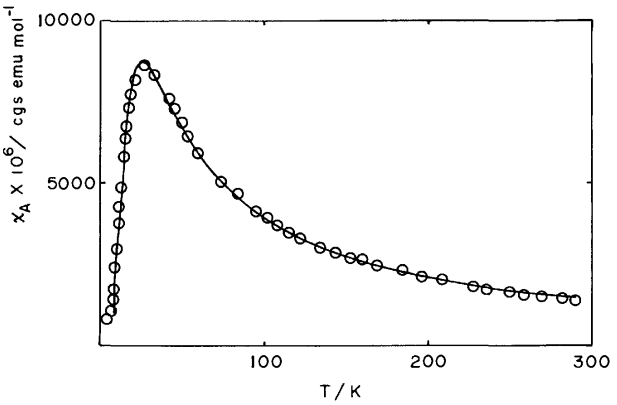

Fig. 2. Temperature dependence of the magnetic susceptibility of **1**. The open circles indicate observed susceptibility. The solid line shows the theoretical susceptibility calculated by the Bleaney-Bowers equation.

atom. The antiferromagnetic interaction is also observed in some complexes which are bridged by pz and J values range from −35.0 to −12.3 cm^{-1}.[2,4,12,13] Since no detailed stereochemistry around copper(II) in other pz-bridged copper(II) complexes[2,4,12,13] except **1** is available, a discussion concerning the relationship between the structure and the magnetism in these compounds is difficult at present. The exchange interaction in pz-bridged complexes, however, seems to be weaker than those in the dinuclear copper(II) complexes connected by imidazolate anion.[1]

We wish to thank Mr. Junichi Gohda for elemental analyses.

References

1) A. Bencini, C. Benelli, D. Gatteschi, and C. Zanchini, *Inorg. Chem.*, **25**, 398 (1986), and references cited therein.
2) W. Mori, T. Sakurai, A. Nakahara, and Y. Nakao, *Inorg. Chim. Acta*, **88**, L17 (1984), and references cited therein.
3) W. Mazurek, A. M. Bond, M, J, O'Connor, and A. G. Wedd, *Inorg. Chem.*, **25**, 906 (1986).
4) W. Mori, T. Sakurai, A. Nakahara, and Y. Nakao, *Inorg. Chim. Acta*, **132**, 247 (1987).
5) J. Hornstra and B. Stubbe, PW1100 Data Processing Programs, Philips Research Labolatories, Eindhoven, Holland, 1972.
6) G. Germain, P. Main, and M. M. Woolfson, *Acta Crystallogr., Sect. B*, **26**, 274 (1970).
7) "International Tables for X-Ray Crystallography," Kynoch Press, Birmingham (1974), Vol. IV, pp. 71, 148.
8) "The Universal Crystallographic Computation Program System," The Crystallographic Society of Japan, Tokyo (1969).
9) C. K. Johnson, "ORTEP II," Report ORNL-5138, Oak Ridge National Laboratory, Oak Ridge, TN (1976).
10) A. W. Addison, T. N. Rao, J. Reedijk, J van Rijn, and G. C. Verschoor, *J. Chem. Soc., Dalton Trans.*, **1984**, 1349.
11) B. Bleaney and K. D. Bowers, *Proc. R. Soc. London, Ser. A*, **214**, 451 (1952).
12) C. G. Barraclough, R. W. Brookes, and R. L. Martin, *Aust. J. Chem.*, **27**, 1843 (1974).
13) W. Mori, T. Sakurai, A. Nakahara, and Y. Nakao, *Inorg. Chim. Acta*, **65**, L51 (1982).

An Unusual Cyclization of Trifluoroacetohydroximoyl and -hydrazonoyl Bromides with Malononitrile[1)]

Kiyoshi TANAKA,* Takashi SUZUKI, Seiji MAENO, and Keiryo MITSUHASHI
Department of Industrial Chemistry, College of Technology, Seikei University, Musashino, Tokyo 180
(Received June 23, 1987)

Synopsis. Trifluoroacetohydroximoyl bromide etherate (**1**) reacted with an excess of malononitrile in the presence of sodium methoxide, giving a fused isoxazolopyridine **3**, participated by two molecules of malononitrile, along with the conventional isoxazole **2**. Similar concomitant formation of **7** and the fused pyrazolopyridines **8** was also recognized from the hydrazonoyl bromides **6** and their product ratio was found to depend on the reaction conditions, particularly on the concentration of malononitrile used.

It has been well explored that nitrile oxides and nitrilimines offer a wide variey of isoxazoles and pyrazoles, respectively, through the reaction with the doubly activated methylene compounds.[2-4)] So far, we have demonstrated the successful synthetic routes to 3-trifluoromethylisoxazoles and -pyrazoles by the reactions of trifluoroacetohydroximoyl bromide etherate (**1**) and *N*-aryltrifluoroacetohydrazonoyl bromides (**6**), respectively, with various active methylene compounds such as β-keto esters,[5)] β-diketones, and cyanoacetates.[6)] As an extension of this study, we now wish to describe an unusual cyclization of **1** and **6** with two molecules of malononitrile other than the conventional cyclization giving 5-amino-4-cyanoazole derivatives.

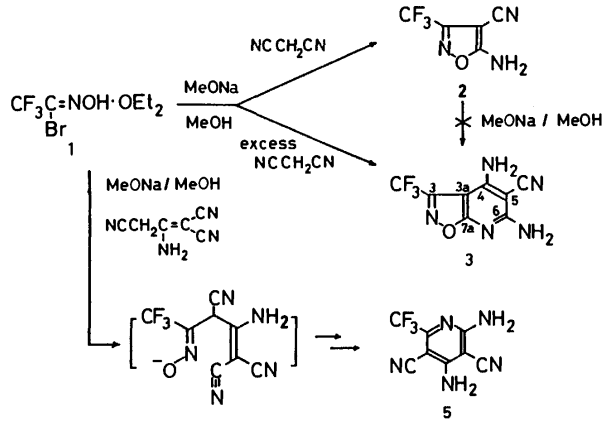

Scheme 1.

The bromide **1** reacted with an equimolar malononitrile in the presence of sodium methoxide to give 5-amino-4-cyano-3-trifluoromethylisoxazole (**2**) in 45% yield (Table 1). The orientation of the cycloaddition was deduced by the chemical shifts of its 4-and 5-carbons compared with those of 4-methoxycarbonyl analogue **2'**[6)] (Table 2). However, the treatment with an excess of malononitrile resulted in the formation of brown tarry matter, from which 4,6-diamino-5-cyano-3-trifluoromethylisoxazolo[5,4-*b*]pyridine (**3**) could be isolated in 18% yield. Thus obtained bicyclic product **3** was converted into the 6-chloro analogue, 4-amino-6-chloro-5-cyano-3-trifluoromethylisoxazolo[5,4-*b*]pyridine (**4**), by diazotization followed by chlorination with hydrochloric acid. The structure of **3** and **4** was supported by their elemental analysis and spectral data, particularly by ^{13}C NMR analysis (Table 2). The similar behavior producing the fused pyridine was also recognized in case of the hydrazonoyl bromides **6**. Thus, the reaction of **6a** with three times of malononitrile afforded a mixture of 5-amino-4-cyano-1-phenyl-3-trifluoromethylpyrazole (**7a**) (38%) and 4,6-diamino-

Table 1. Analytical and Spectral Data of Products

Compound	Formula	Calcd (Found)/% C	H	N	IR ν/cm^{-1}	^1H NMR δ
2	$C_5H_2F_3N_3O$	33.91	1.14	23.73	3340, 3250, 3200, 3160 (NH_2)	7.5 (br. s)
		(33.70)	(1.12)	(23.83)	2240 (C≡N), 1660 (C=N)	
3	$C_8H_4F_3N_5O$	39.52	1.66	28.80	3442, 3330, 3220 (NH_2)	6.7 (br. s, 2H)
		(39.70)	(1.57)	(28.71)	2199 (C≡N), 1638 (C=N)	7.1 (br. s, 2H)
4	$C_8H_2F_3N_4OCl$	36.59	0.77	21.34	3475, 3330, 3225 (NH_2)	3.2 (br. s)
		(36.77)	(0.68)	(21.38)	2230 (C≡N), 1655 (C=N)	
7a	$C_{11}H_7F_3N_4$	52.39	2.80	22.22	3458, 3368, 3312, 3212, 3190	5.65 (br. s, 2H)
		(52.05)	(2.74)	(22.56)	(NH_2), 2224 (C≡N), 1642 (C=N)	7.5 (s, 5H)[a)]
7b	$C_{11}H_6F_3N_5O_2$	44.46	2.03	23.56	3405, 3309, 3219, 3195 (NH_2)	7.5 (br. s, 2H)
		(44.69)	(1.99)	(23.76)	2205 (C≡N), 1640 (C=N)	8.15 (A_2X_2, 4H)
8a	$C_{14}H_9F_3N_6$	52.84	2.85	26.41	3505, 3461, 3323, 3231, 3209	6.6 (br. s, 2H), 6.85 (br. s, 2H)
		(52.90)	(2.76)	(26.70)	(NH_2), 2200 (C≡N), 1661, 1640 (C=N)	7.1—8.3 (m, 5H)
8b	$C_{14}H_8F_3N_7O_2$	46.29	2.22	26.99	3464, 3372, 3332, 3239 (NH_2)	6.8 (br. s, 2H), 7.1 (br. s, 2H)
		(46.08)	(2.18)	(26.84)	2199 (C≡N), 1661 (C=N)	8.5 (A_2X_2, 4H)
10	$C_{14}H_7F_3N_5OCl$	49.80	2.09	20.74	3480, 3325, 3220 (NH_2)	3.3 (br. s, 2H)
		(50.29)	(2.07)	(20.27)	2230 (C≡N), 1660 (C=N)	7.4—8.0 (m, 5H)

a) Measured in deuteriochloroform.

Table 2. ^{13}C NMR Data of Products

Isoxazole and pyrazole Compound	^{13}C chemical shifts (coupling constants with fluorine)							
	3-C	4-C	5-C	CF_3	C≡N	C=O	CH_3	Ar
2	152.8 (37.2)	61.3	172.6	117.3 (271.9)	108.9			
2′	151.9 (37.2)	82.5	172.6	118.5 (271.9)		160.9	50.7	
7a	142.7 (39.1)	74.0	151.2	119.7 (270.9)	111.4			135.9, 130.2 129.9, 124.6[a]
7a′	141.0 (38.2)	92.5	151.0	120.4 (270.0)		163.6	51.4	136.4, 129.9 129.2, 124.4[a]
7b	141.0 (38.1)	70.5	151.7	118.1 (270.0)	109.9			145.0, 140.0 123.4, 123.2

Fused isoxazolo- and pyrazolopyridine Compound	^{13}C chemical shifts (coupling constants with fluorine)								
	3-C	3a-C	4-C	5-C	6-C	7a-C	CF_3	C≡N	Ar
3	146.3 (39.1)	70.2	151.1	86.0	161.4	172.5	118.0 (270.9)	113.7	
4	147.6 (39.1)	89.3	151.8	93.7	156.1	170.4	118.1 (271.9)	112.3	
8a	131.9 (38.1)	69.9	150.4 or 151.7	93.7	159.4	151.7 or 150.4	124.7 (269.0)	114.6	136.8, 127.2 125.3, 120.7
10	132.2 (39.1)	85.4	150.7 or 148.8	98.5	152.1	148.8 or 150.7	119.2 (270.9)	112.8	135.8, 127.7 126.6, 121.1

a) Measured in deuteriochloroform.

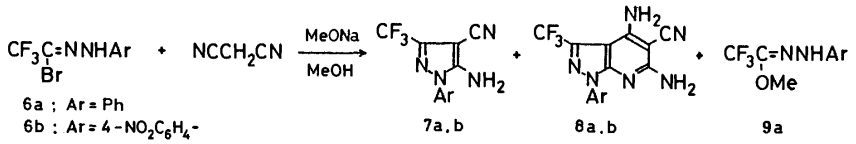

Scheme 2.

5-cyano-1-phenyl-3-trifluoromethylpyrazolo[5,4-*b*]-pyridine (**8a**) (3%) along with 20% of methyl *N*-phenyltrifluoroacetohydrazonate (**9a**).[7] The structure of **7a** was confirmed by a comparison of its ^{13}C NMR spectra with those of 4-methoxycarbonyl analogue **7a′**[6] (Table 2). The pyrazolopyridine **8a** was similarly converted into 4-amino-6-chloro-5-cyano-1-phenyl-3-trifluoromethylpyrazolo[5,4-*b*]pyridine (**10**). *N*-(4-Nitrophenyl)hydrazonoyl bromide **6b** also afforded a mixture of **7b** and **8b** in 64 and 7% yields, respectively, with no appreciable formation of the corresponding hydrazonate **9b**. It should be noted that the product ratio of **8a** increased remarkably with increase in malononitrile used.

The formation of the fused pyridines **3** and **8** is characteristic of the trifluoromethylated bromides **1** and **6** and three plausible reaction paths could be considered. These paths involve 1) the process where the initially formed **2** and **7** cyclized subsequently with another molecule of malononitrile, 2) the reaction of **1** and **6** with dimeric malononitrile, formed under the used reaction conditions, as reported in the literature on the formation of an isoxazolopyridine analogue from benzohydroximoyl chloride and dimeric malononitrile,[8] or 3) the cycloaddition of a certain reactive intermediate with another molecule of malononitrile. Out of these, the paths 1) and 2) can be both ruled out from the following results. First, the isolated **2** and **7** were subjected to the further reaction with malononitrile under similar conditions, the former giving a tarry matter with no appreciable amount of **3** and the latter being recovered almost. Second, the treatment of **6a** with the commercially available dimeric malononitrile did not give **8a**, resulting in substitution into **9a**, whereas that of **1** afforded an unexpected product, 2,4-diamino-3,5-dicyano-6-trifluoromethylpyridine (**5**) in 9% yield. Elemental analysis and MS spectra of **5** strongly support the absence of oxygen, and ^1H NMR and IR spectra features the characteristic pattern of diaminodicyanopyridine.[9] From the fact that the product ratio of **8a** depends on the reaction conditions, particularly on the concentration of malononitrile, the intervention of the reactive anions **3′** and **8′** seems to be reasonable, where the anions attack another molecule of malononitrile to give **3** and **8**, respectively.

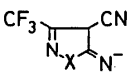

3′ : X = O
8′ : X = NAr

Experimental

The IR spectra were recorded on a JASCO A-100 spectrometer. Samples were run as potassium bromide pellets. The ^1H and ^{13}C NMR spectra were measured with a JEOL

JNM-GX270 spectrometer using tetramethylsilane as an internal standard, the chemical shifts being given in δ ppm downfield. Samples were prepared by dissolving in deuteriochloroform-bis(deuteriomethyl) sulfoxide unless otherwise noted. The UV spectra were observed with a Hitachi 340 spectrometer. The MS spectra were obtained on a Finnigan 4023 GC-MS DS spectrometer. The bromides **1** and **6** were prepared by the methods reported in our previous paper.[6]

Reaction of 1 with Malononitrile. (A) A solution of **1** (3.65 g, 13.7 mmol) in 20 cm^3 of methanol was rapidly added dropwise to a solution of malononitrile (0.91 g, 13.8 mmol) and sodium methoxide (0.75 g, 13.9 mmol) in 25 cm^3 of methanol. After stirring at room temperature for 2 h, the solvent was removed to leave a residue which was extracted with diethyl ether. The extracts were washed with water and brine, dried over magnesium sulfate, and evaporated. The resulting residue was chromatographed on silica gel with chloroform to give 1.10 g (45%) of the isoxazole **2**, mp 149—150 °C (recrystallized from hexane-chloroform).

(B) Three times of malononitrile was reacted on a similar procedure to the above and the solvent was removed. The resulting mixture was washed with chloroform and extracted with acetone. The extracts were evaporated and the residual solid was sublimed, giving 0.60 g (18%) of **3** which was further purified by recrystallization from chloroform-acetone (sublimed at around 200 °C).

Reaction of 6a with Malononitrile. (A) To a solution of malononitrile (0.89 g, 13.5 mmol) and sodium methoxide (0.73 g, 13.5 mmol) in 20 cm^3 of methanol was added a solution of **6a** (1.20 g, 4.5 mmol) in 10 cm^3 of methanol. After the mixture was refluxed for 2 h, the solvent was removed to leave a residue which was extracted with diethyl ether. The extracts were dried over magnesium sulfate and evaporated under reduced pressure. To the residue was added excess hexane and the deposited solid was collected on a filter to give 0.05 g (3%) of **8a** which was recrystallized from acetone-methanol, mp 249.5—250.5 °C. On the other hand, hexane-extracts were evaporated and the resulting mixture was chromatographed (silica gel, hexane-chloroform, 4:1) to give 0.43 g (38%) of **7a**, which was further purified by recrystallization from hexane-chloroform, mp 115—116 °C, along with 0.20 g (20%) of oily **9a**. The spectral data of **9a** are consistent with those of our authentic sample.[7]

(B) A solution of **6a** (4.80 g, 18.0 mmol) in 20 cm^3 of methanol was added to a solution of malononitrile (3.56 g, 53.9 mmol) and sodium methoxide (2.92 g, 54.1 mmol) in 40 cm^3 of methanol and the mixture was heated under reflux for 2 h. Usual work-up yielded 1.01 g (22%) of **7a** and 2.27 g (40%) of **8a**.

Reaction of 6b with Malononitrile. A mixture of malononitrile (0.76 g, 11.5 mmol), sodium methoxide (0.62 g, 11.5 mmol), and **6b** (1.20 g, 3.8 mmol) in 30 cm^3 of methanol was stirred at room temperature for 15 h. The formed solid was collected on a filter, washed with water, and dried at the pump to give 0.10 g (7%) of **8b** which was recrystallized from chloroform-ethyl acetate, mp 309 °C (decomp). On the other hand, the filtrate was concentrated and chromatographed (silica gel, hexane-ethyl acetate, 1:1) to give 0.72 g (64%) of **7b** which was further purified by recrystallization from chloroform-ethyl acetate, mp 213—214 °C.

Chlorination of 3 into 4. Isoxazolopyridine **3** (0.40 g, 1.6 mmol) was dissolved in 50 cm^3 of 6 mol dm^{-3} hydrochloric acid under reflux. To this solution was added dropwise a solution of 0.40 g of sodium nitrite in 5 cm^3 of water at the same temperature. The mixture was refluxed for 2 h and cooled overnight in a refrigerator. The deposited solid was collected on a filter and passed through a short column (silica gel, hexane-ethyl acetate, 3:1) to give 0.09 g (21%) of **4**, which was recrystallized from hexane-diethyl ether, mp 165—166 °C.

Chlorination of 8a into 10. In a similar manner to the above, diazotization of 0.25 g of **8a** was carried out at the same temperature for 10 min, giving 0.13 g (49%) of **10**, mp 221—222 °C (recrystallized from hexane-ethanol).

Reaction of 1 with Dimeric Malononitrile. A mixture of 2.40 g (18.2 mmol) of dimeric malononitrile and 1.00 g (18.5 mmol) of sodium methoxide in 30 cm^3 of methanol was stirred for 40 min. And to this mixture was added dropwise a solution of 4.00 g (15.0 mmol) of **1** in 10 cm^3 of methanol over a period of 30 min. After stirring at room temperature for 25 h, the solvent was removed to leave a residue which was extracted with acetone and evaporated under reduced pressure. The resulting mixture was chromatographed (silica gel, hexane-ethyl acetate, 4:1) to give 0.32 g (9%) of **5** which was further purified by recrystallization from hexane-ethanol, mp 290—291.5 °C (decomp), IR 3460, 3330, 3230, 3160 (NH_2), 2210 (C≡N), 1630 cm^{-1} (C=N, C=C), ^{1}H NMR δ=7.1 (br.s, 2H), 7.4 (br.s, 2H), ^{13}C NMR δ=159.6, 157.3, 150.8 (J_{CCF}=33.3 Hz), 118.5 (J_{CF}=277.8 Hz), 112.4, 111.4, 78.5, 72.2, MS (CI, *m/z*) 228 $(M+H)^+$, 208 $(M+H-HF)^+$, UV λ_{max}^{EtOH} (ε) 238 (4.143×10^4), 324 (5.516×10^3), 328 (5.600×10^3).

Found: C, 42.19; H, 1.49; N, 30.64%. Calcd for $C_8H_4F_3N_5$: C, 42.30; H, 1.77; N, 30.83%.

References

1) Part XIII in "Applications of the fluorinated 1,3-dipolar compounds as the building blocks of the heterocycles with fluorine groups." Part XII: K. Tanaka, M. Ohsuga, Y. Sugimoto, Y. Okafuji, and K. Mitsuhashi, J. Fluorine Chem., in press.

2) S. A. Lang, Jr. and Y. -i Lin, "Isoxazoles and their Benzo Derivatives," in "Comprehensive Heterocyclic Chemistry," ed by A. Katritzky and C. W. Rees, Pergamon Press, Oxford (1984); A. S. Shawali and C. Párkányi, *J. Heterocyclic Chem.*, **17**, 833 (1980).

3) C. Grundmann and S. K. Datta, *J. Org. Chem.*, **34**, 2016 (1969).

4) A. O. Abdehamid, C. Párkányi, A. S. Shawali, and M. A. Abdalla, *J. Heterocyclic Chem.*, **21**, 1049 (1984).

5) K. Tanaka, M. Kishida, S. Maeno, and K. Mitsuhashi, *Bull. Chem. Soc. Jpn.*, **59**, 2631 (1986).

6) K. Tanaka, T. Suzuki, S. Maeno, and K. Mitsuhashi, *J. Heterocyclic Chem.*, **23**, 1535 (1986).

7) For the formation of **9a** in the reaction of **6a** with sodium methoxide in methanol, see K. Tanaka, S. Maeno, and K. Mitsuhashi, *Bull. Chem. Soc. Jpn.*, **58**, 1841 (1985).

8) H. Junek, B. Thierrichter, and G. Lukas, *Chem. Ber.*, **113**, 1195 (1980).

9) H. Junek, M. Mittelbach, and B. Thierrichter, *Monatsh. Chem.*, **110**, 1279 (1979); A. Sakurai and H. Midorikawa, *Bull. Chem. Soc. Jpn.*, **41**, 430 (1968).

Some Applications of Thermodynamic Equations on the Pressure Effect of the Chemical Reactions

Jong-Gi JEE
Department of Chemistry, Teacher's College, Kyungpook National University, Taegu 635, Korea
(Received August 24, 1985)

Synopsis. This paper is concerned with the theoretical derivation of the linear relationship between enthalpy and entropy for pressure change in chemical equilibria, and its application to the dissociation equilibria of some 4-substituted 1-methylpyridinium iodides in water-ethanol mixture. The isoequilibrium temperature, $\bar{\beta}$, for this system was derived to be 322 K.

In the studies of chemical equilibria and reaction kinetics in gas and liquid phases, it is better to measure the pressure effect on the system, because pressure is the conjugated thermodynamic variable of the volume which is more direct parameter than entropy conjugated to temperature. We have found experimentally the interesting fact that a linearity between enthalpy and entropy for pressure change exists in chemical equilibria and reaction rates.[1,2] B. S. El'yanov and E. M. Vasylvistskaya[3] have proved the same relationship theoretically and defined the isoequilibrium temperature, $\bar{\beta}$, under high pressure.

Theory

From the Maxwell relation of thermodynamic, we get the following equation;

$$(\partial S/\partial P)_T = -(\partial V/\partial T)_P = -V\alpha, \tag{1}$$

where α is the isobaric volume expansivity.

From the first and second laws of thermodynamics, $dH = TdS + VdP$, we obtain directly Eq. 2,

$$V = (\partial H/\partial P)_T - T(\partial S/\partial P)_T. \tag{2}$$

Substituting V in Eq. 2 into Eq. 1, we get Eq. 3,

$$(\partial H/\partial P)_T = \frac{T\alpha - 1}{\alpha}(\partial S/\partial P)_T. \tag{3}$$

On the other hand, we can define volume as

$$V = -\frac{1}{\beta}(\partial V/\partial P)_T, \tag{4}$$

where β is the isothermal compressibility. Inserting Eq. 4 into Eq. 1 leads to

$$(\partial V/\partial P)_T = \frac{\beta}{\alpha}(\partial S/\partial P)_T. \tag{5}$$

From Eqs. 3 and 5, we obtain the following result.

$$(\partial H/\partial P)_T = \frac{T\alpha - 1}{\beta}(\partial V/\partial P)_T \tag{6}$$

Experimental

The experiments were performed in the 5 ml conductance cell which had been made to use under high pressure. A detailed explanation of the equipment and the procedures has been given in the previous papers.[4-7]

The equilibria of several 4-substituted 1-methylpyridinium iodides in ehanol-water mixture (95/5 vol%) were measured by monitoring the conductance in the range over 25—40 °C (±0.01 °C) and 1—20000 bar (±10 bar), and also by monitoring UV absorbance at the wavelength of the absorption maximum in the same range of temperature.[8,9] Purified 4-substituted 1-methylpyridinium iodides were diluted to

Table 1. Association Constants ($K \times 10^{-3}$ dm^3 mol^{-1}) of 4-Substituted 1-Methylpyridiniumiodides in Ethanol-Water Mixture (95/5 vol%)

Substituent	T/°C	P/bar				
		1	500	1000	1500	2000
-H	25	3.94±0.10	4.08±0.12	4.16±0.11	4.34±0.12	4.60±0.11
	30	3.26±0.08	3.35±0.09	3.45±0.10	3.57±0.09	3.79±0.10
	35	2.70±0.07	2.74±0.06	2.89±0.07	3.04±0.08	3.23±0.08
	40	2.50±0.08	2.55±0.07	2.65±0.06	2.78±0.07	2.87±0.07
$-CH_3$	25	2.64±0.07	2.80±0.07	3.01±0.08	3.26±0.08	3.56±0.09
	30	2.37±0.06	2.46±0.07	2.66±0.06	2.97±0.09	3.09±0.08
	35	2.18±0.05	2.29±0.06	2.44±0.06	2.61±0.07	2.84±0.09
	40	2.04±0.06	2.16±0.05	2.27±0.06	2.37±0.08	2.54±0.10
-CN	25	9.61±0.24	10.5±0.26	11.6±0.29	12.8±0.25	13.9±0.32
	30	7.32±0.18	8.20±0.21	9.07±0.22	9.99±0.19	10.9±0.31
	35	6.63±0.16	7.26±0.18	7.84±0.20	8.46±0.21	9.12±0.28
	40	5.45±0.14	6.18±0.15	6.78±0.21	7.38±0.18	7.89±0.19
$-NH_2$	25	3.67±0.09	4.15±0.12	4.58±0.11	4.96±0.12	5.41±0.16
	30	2.98±0.07	3.32±0.08	3.65±0.09	4.10±0.11	4.46±0.11
	35	2.61±0.07	2.86±0.08	3.23±0.08	3.56±0.09	3.74±0.12
	40	2.14±0.05	2.37±0.07	2.61±0.07	2.86±0.08	3.11±0.11

Table 2. Thermodynamic Parameters of 4-Substituted Pyridinium Iodides in Ethanol-Water Mixture (95/5%) at 30°C and Various Pressures

Substituent	Parameter	P/bar					Error
		1	500	1000	1500	2000	
-H	ΔH/kcal mol^{-1}	−4.66	−4.93	−5.13	−5.27	−5.46	±0.15
	ΔS/e.u.	0.69	−0.39	−0.79	−1.12	−1.65	±0.04
	ΔV/cm^3 mol^{-1}	4.46	4.42	4.38	4.34	4.32	±0.13
$-CH_3$	ΔH	−3.12	−3.18	−3.32	−3.48	−3.97	±0.12
	ΔS	5.24	5.01	4.71	4.38	2.87	±0.15
	ΔV	4.44	4.42	4.41	4.40	4.39	±0.13
-CN	ΔH	−5.86	−5.92	−6.04	−6.18	−6.26	±0.18
	ΔS	−1.35	−1.62	−1.85	−2.08	−2.39	±0.06
	ΔV	6.43	6.36	6.28	6.20	6.13	±0.19
$-NH_2$	ΔH	−6.10	−6.14	−6.16	−6.28	−6.36	±0.18
	ΔS	−3.98	−4.02	−4.06	−4.12	−4.19	±0.13
	ΔV	5.71	5.65	5.59	5.53	5.47	±0.17

about 9.10×10^{-5}—5.10×10^{-4} mol dm^{-3} by the use of the water-ethanol mixture.

The association constants (K) of the sample determined in this way are shown in Table 1. The values of K were evaluated as the average value obtained from four measurements. Their absolute errors were about ±3%.

The values of ΔH, ΔS, and ΔV were calculated from the following equations;

$$\Delta H = -R(\partial \ln K/\partial(\frac{1}{T}))_P, \quad (7)$$

$$\Delta S = (\Delta H - \Delta G)/T, \quad (8)$$

$$\Delta V = -RT(\partial \ln K/\partial P)_T. \quad (9)$$

The values of these thermodynamic parameters were shown in Table 2.

Results and Discussion

A form of $\delta\Delta H=\bar{\beta}\delta\Delta S$ with $\bar{\beta}\geqq 0$ is called an isoequilibrium relationship. A corresponding expression between the kinetcic quantities is called an isokinetic relationship.[10-12] The reason for this nomenclature is clear from the following equation;

$$\delta\Delta G = \delta\Delta H - T\delta\Delta S,$$
$$= (\bar{\beta}-T)\delta\Delta S \quad (10)$$

where the parameter, $\bar{\beta}$, has the unit of absolute temperature. If the value of $\bar{\beta}$ approaches to the experimental temperature (T), all the differences in the rate or equilibrium constants will vanish;

$$\lim_{T\to\beta}(\partial\Delta G) = 0 \quad (11)$$

To illustrate the pressure dependence of $\delta\Delta H=\bar{\beta}\delta\Delta S$, we integrated Eq. 3 in the range from 1 to P bars assuming that the pressure dependence of $(T\alpha-1)/\alpha$ is negligible as shown in Fig. 1, although α is slightly dependent on pressure in the liquid phase reaction;

$$(\Delta H_P-\Delta H_0) = \frac{T\alpha-1}{\alpha}(\Delta S_P-\Delta S_0), \quad (12)$$

where subscripts 0 and P represent 1 and P bars respectively. Its slope is defined as the isokinetic (isoequilibrium) temperature, $\bar{\beta}$, which is independent of pressure. This equation is consistent with the B. S. El'yanov and E. M. Vasylvitskaya's result;[3]

$$(\Delta H_P-\Delta H_0) = (\Delta S_P-\Delta S_0) = -(n/m)(\Delta S_P-\Delta S_0), \quad (13)$$

where m and n represent R ln $10(\partial V_0/\partial T)$ and R ln $10(\Delta V_0-T\cdot\partial V_0/\partial T)$, respectively. The method of derivation in this paper is simpler than their method because this method derives the equation from the basic thermodynamic equation whereas their derivation required a complicated procedure by the use of a linear free energy relationship.[13]

Similarly, integrating Eqs. 5 and 6, we have the following two equations;

$$(\Delta V_P-\Delta V_0) = \frac{\beta}{\alpha}(\Delta S_P-\Delta S_0) \quad (14)$$

$$(\Delta H_P-\Delta H_0) = \frac{T\alpha-1}{\beta}(\Delta V_P-\Delta V_0) \quad (15)$$

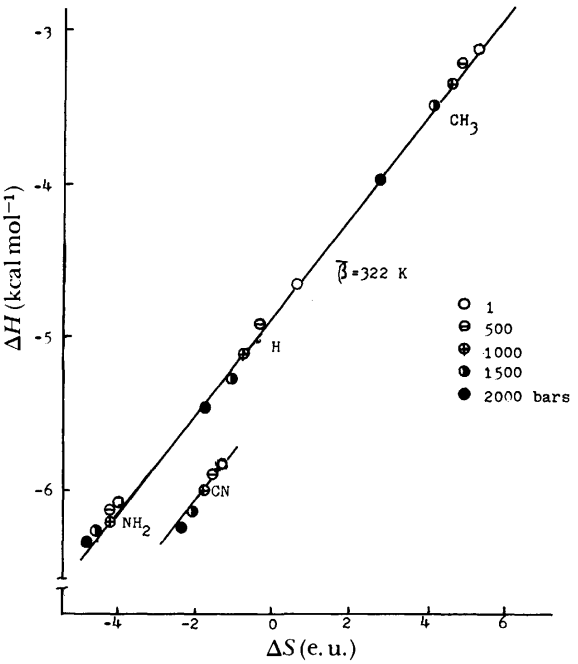

Fig. 1. The plot of ΔH vs. ΔS for changing pressure.

From Eq. 12 and either one of these two equations, the values of α and β can be obtained.

Replacing Eq. 12, on the other hand, with the values of ΔH and ΔS listed in Table 2, we obtained the iso-equilibrium relationship of the following reaction as shown Fig. 1.

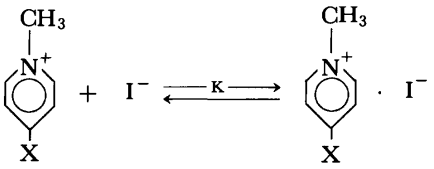

The figure shows a satisfactory linearity as expected from Eq. 12. The slope, $\bar{\beta}$, is 322 K. The value of $\bar{\beta}$ deduced from Fig. 1 is independent of both substituent change and pressure change. It is very interesting and important for us to determine the mechanism of chemical reaction under high pressure. The $\bar{\beta}$ value is larger than the experimental temperature, 303.15 K, and hence the contribution to ΔG from ΔH is larger than that from ΔS. Accordingly, we could suggest the equilibrium of the above raction is enthalpy-controlled.

The present study was supported by the Basic Science Research Institute Program, Ministry of Education, Korea, 1985.

References

1) J. U. Hwang, S. D. Yoh, and J.-G. Jee, *J. Korean Chem. Soc.*, **24**, 405 (1980).
2) J.-G. Jee, Y. H. Lee, and Y. J. Kwak, *Bull. Korean Chem. Soc.*, **6**, 266 (1985).
3) B. S. El'yanov and E. M. Vasylvitskaya, "Modern Aspects of Physical Chemistry at High Pressure," ed by J. Osugi, The Physico-Chemical Society of Japan, Kyoto (1980), p. 180.
4) J.-G. Jee, J. J. Chung, and J. U. Hwang, *J. Korean Chem. Soc.*, **18**, 320 (1974).
5) J. U. Hwang, S. D. Yoh, and J.-G. Jee, *J. Korean Chem. Soc.*, **24**, 150 (1980).
6) J.-G. Jee, Ph. D. Thesis, University of Han Yang, 1981.
7) J. U. Hwang, J. J. Chung, S. D. Yoh, and J.-G. Jee, *Bull. Korean Chem. Soc.*, **4**, 237 (1983).
8) P. Hemmes, J. N. Costanzo, and F. Jordan, *J. Phys. Chem.*, **82**, 387 (1978).
9) J.-G. Jee, Y. H. Lee, E. H. Woo, and K. H. Lee, *Bull. Korean Chem. Soc.*, **4**, 115 (1983).
10) J. E. Leffler, *J. Org. Chem.*, **20**, 1202 (1955).
11) W. M. Schubert and R. G. Minton, *J. Am. Chem. Soc.*, **82**, 6188 (1960).
12) Y. Yukawa and Y. Tsno, *J. Am. Chem. Soc.*, **79**, 5530 (1959).
13) B. S. El'yanov, *Aust. J. Chem.*, **28**, 933 (1975).

Nitriles in Heterocyclic Synthesis. Novel Synthesis of Pyridazine Derivatives

Nadia Sobhy IBRAHIM,* Fathy Mohamed ABDEL-GALIL, Ramadan Maawad ABDEL-MOTALEB, and Mohamed Hilmy ELNAGDI*

Department of Chemistry, Faculty of Science, Cairo University, Giza, A. R. Egypt

(Received February 3, 1986)

Synopsis. The crotononitriles **1a—c** coupled with arenediazonium salts to yield either the acyclic mono- or dihydrazones depending on coupling reaction conditions. Both mono- and dihydrazones could be cyclized to the corresponding pyridazine derivatives. Direct formation of pyridazines on coupling **1b** and **1c** with arenediazonium salts was observed. Structures of reaction products are confirmed by spectral and analytical data.

Nitriles are versatile reagents and their utility in organic synthesis is now receiving considerable interest.[1-3] In the last few years we have been involved in a program aiming to develop new efficient procedures for the synthesis of polyfunctionally substituted heterocycles utilizing simple laboratory available functionally substituted nitriles as starting materials.[4-6] As a part of this work we have investigated the possible utility of crotononitrile derivatives **1a—c** for synthesis of pyridazines. The methyl function in 1-phenylethylidenemalononitrile (**1a**) and isopropylidenemalononitrile (**1c**) has been reported to react readily with a variety of nucleophiles.[7] However, it has been reported[8] that this function does not couple with aromatic diazonium salts. Reaction of **1a**, c with arenediazonium salts afforded arylhydrazonomesoxalonitrile through a suggested complicated mechanism. Inspection of the literature experimental procedure indicated that the author has utilized methanolic sodium hydroxide as a medium for the coupling reaction. We have recently provided evidence that ylidenemalononitrile decomposes in basic medium into its constituents. Thus it was believed that in Coenen experiment malononitrile was the realy reacting species. We have thus investigated the behavior of **1a, b** towards arenediazonium salts under conditions that do not allow hydrolysis of the ylidenemalononitriles. The nature of the coupling products was found to be dependent on the applied coupling reaction conditions and the nature of the substituents on **1**. Acetic acid-sodium acetate and ethanolic sodium acetate were selected as media that fulfil requirements. The first medium affords weak basic conditions while the second allows more basic medium. Thus, **1a** coupled with arenediazonium salts in ethanolic sodium acetate solution to yield brown coupling products. ^{13}CNMR of these products revealed that they are the acyclic hydrazones **2a, b** and not the isomeric **3a, b** as they revealed signals for two C=N carbons. When **2a, b** were refluxed for 2 h in aqueous acetic acid the 3(2*H*)-pyridazinones **4a, b** were obtained in almost quantitative yields. Compounds **4a, b** are assumed to be formed via intermediacy of the imines **3a, b**. Attempted isolation of the imines **3a, b** were unsuccessfull. Compounds **4a, b** were also

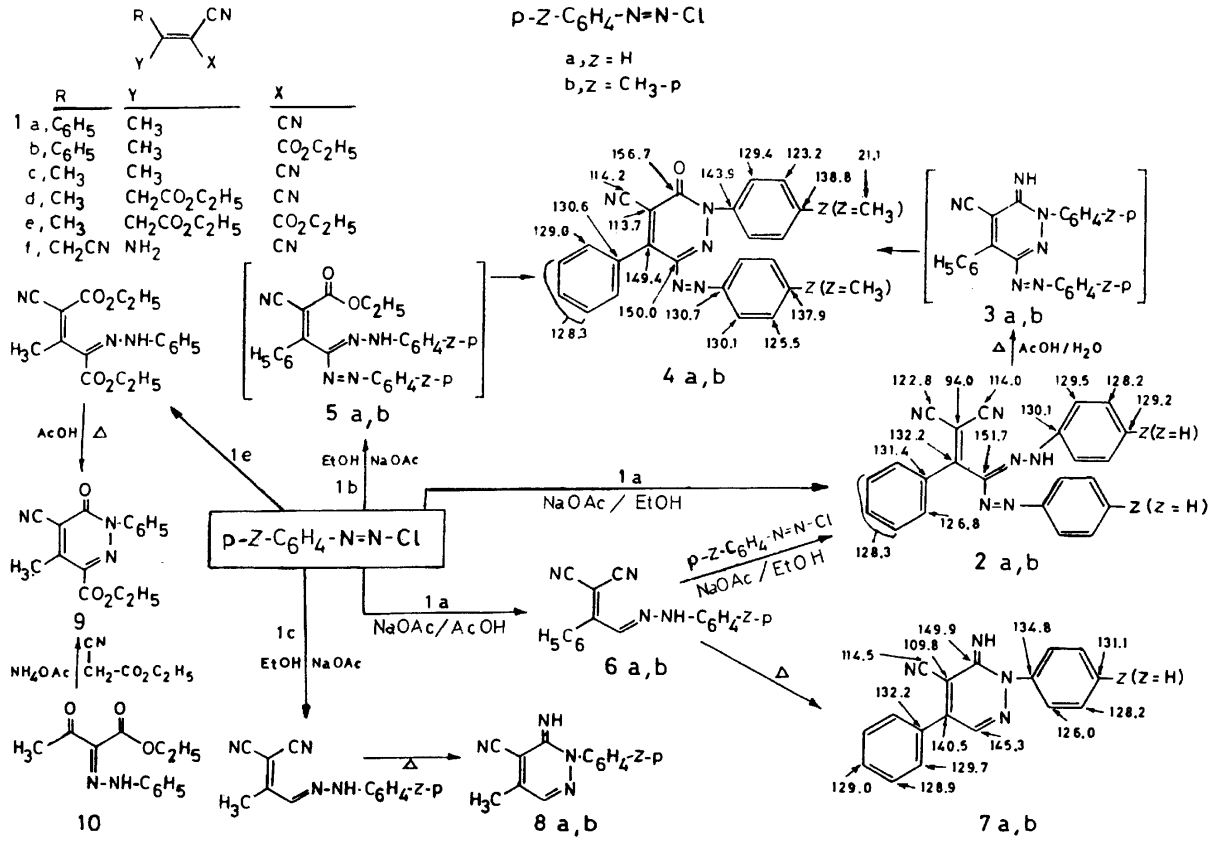

formed on coupling **1b** with arenediazonium salts. Again the arenehydrazones **5a, b** are the assumed reaction intermediates. Trials to obtain a pure form of **5a, b** were unsuccessful, and they were converted to **4a, b** even on attempted chromatographing. However the crude product showed MS and IR in accordance with proposed structure but ^{13}C NMR revealed a pattern for a mixture. In contrast to the behavior of **1a** towards arenediazonium salts in ethanolic sodium acetate solutions, **1a** coupled with arenediazonium salts in acetic acid in the presence of sodium acetate to yield the hydrazones **6a, b**, which afforded the 3(2*H*)-pyridazinimines

Table 1. List of Synthesized Compounds

Compound (Color)	Crystalization solvent	Mp θ_m/°C	Yield %	Mol. formula (Mol. weight)	Analysis/% Found (Calcd)		
					C	H	N
2a (Brown)	EtOH	205	70[a] 60[b]	$C_{23}H_{16}N_6$ (M^+=376)	73.1 (73.4)	4.2 (4.2)	22.0 (22.3)
2b (Brown)	EtOH	197	78[a] 65[b]	$C_{25}H_{20}N_6$ (404)	73.9 (74.2)	4.7 (4.9)	20.8 (20.7)
4a (Red)	AcOH	240	80[a] 72[b]	$C_{23}H_{15}N_5O$ (M^+=377)	73.4 (73.2)	4.2 (3.9)	18.3 (18.5)
4b (Red)	AcOH	230	82[a] 75[b]	$C_{25}H_{19}H_5O$ (M^+=405)	74.2 (74.0)	4.5 (4.6)	17.0 (17.2)
6a (Red)	AcOH	135	50	$C_{17}H_{12}N_4$ (272)	75.2 (75.0)	4.2 (4.4)	20.3 (20.5)
6b (Red)	AcOH	155	55	$C_{18}H_{14}N_4$ (286)	75.6 (75.5)	5.0 (4.8)	19.4 (19.5)
7a (Orange)	EtOH	173	80	$C_{17}H_{12}N_4$ (M^+=272)	75.3 (75.0)	4.4 (4.4)	20.6 (20.5)
7b (Orange)	EtOH	150	80	$C_{18}H_{14}N_4$ (286)	75.4 (75.5)	4.8 (4.8)	19.4 (19.5)
8a (Red)	AcOH	117	60	$C_{12}H_{10}N_4$ (210)	68.3 (68.5)	4.5 (4.7)	26.4 (26.6)
8b (Red)	AcOH	120	70	$C_{13}H_{12}N_4$ (224)	69.6 (69.6)	5.6 (5.3)	24.8 (25.0)
9 (Colorless)	AcOH	150	65[a] 80[b]	$C_{15}H_{13}N_3O_3$ (283)	63.5 (63.6)	4.4 (4.5)	14.8 (14.8)

a) Method A. b) Method B.

Table 2. Spectroscopic Data of Some Products Listed in Table 1

Compound	IR/cm^{-1} (selected band)	^1H NMR/δ
2a	3200 (NH); 2220, 2200 (CN)	7.4—7.7 (m, 16H, aromatic protons and NH)
2b	3100 (NH); 2200, 2190 (CN)	
4a	2200 (CN)	7.4—7.8 (m, 15H, aromatic protons)
4b	2200 (CN)	2.3 (m, 6H, $2CH_3$); 7.4—7.8 (m, 13H, aromatic protons)
6a	3200 (NH); 2225, 2215 (CN)	
6b	3250 (NH); 2220, 2220 (CN)	2.3 (s, 3H, CH_3); 6.7—7.9 (m, 11H, aromatic, ylidenic CH and NH protons)
7a	3300 (NH); 2200 (CN)	7.3—7.9 (m, 12H, aromatic and NH protons)
8b	3350 (NH); 2200 (CN)	2.2 (s, 3H, CH_3); 2.4 (s, 3H, CH_3); 7.3—7.6 (m, 5H, aromatic protons); 8.2 (s, 1H, NH)

7a, b on heating above their melting points. No trial was made to convert **7a, b** into the corrresponding pyridazinones. Compounds **6a, b** could be converted into **2a, b** on coupling with arenediazonium salts in ethanolic sodium acetate solutions. Compound **1c** also coupled with arenediazonium salts to yield hydrazones which could not be isolated in pure form but the 3(2*H*)-pyridazinimines **8a, b** were isolated on short reflux of the hydrazones in acetic acid. Compounds **1b, c** failed to couple with arenediazonium salts in acetic acid-sodium acetate. The formation of hydrazones on coupling of **1a, b** with arenediazonium salts finds a parallism to the reported[9-11] coupling of **1d—f** with arenediazonium salts and the cyclization of the formed coupling products. The results, however, reveal that the presence of electron-withdrawing substituent on the methyl group in **1** is not necessary for coupling reaction to take place. The methyl group adjacent to activated double bond with two cyano or cyano and ester function on the β-carbon is sufficiently acidic to react with arenediazonium salts.

Although **1e** was reported[12] to afford **9** on coupling with benzene-diazonium salt and cyclization of the formed hydrazone, trials to repeat these results in our laboratories revealed that this synthetic route is highly inefficient as **1e** is obtainable only in low yield and polymerizes quickly on storage. Thus we developed more efficient synthesis of **9** via condensation of the readily obtainable hydrazone **10** with ethyl cyanoacetate in the presence of ammonium acetate.

Experimental

All melting points are uncorrected. IR spectra (KBr) were recorded on a Pye Unicam SP-1100 spectrophotometer. ^1H and ^{13}C NMR spectra were obtained in $(CD_3)_2SO$ with a Varian EM 390 and Bruker Wm 300 spectrometer with $SiMe_4$ as internal standard and chemical shifts are expressed as δ values. Mass spectra were recorded on mass spectrometer MS 30 and MS 9 (AEI) 70 eV. Microanalytical data were performed by the microanalytical centre at Cairo University.

(2-Arylazo-2-arylhydrazono-1-phenylethylidene)malononitriles 2a, b. Method A: A solution of **1a** (0.01 mol) in ethanol (30 ml) containing sodium acetate (6.0 g) was cooled to 0 °C, stirred and treated gradually with a cooled solution of the appropriate diazonium salt (prepared from 0.02 mol of the aromatic amine and the appropriate quantities of hydrochloric acid and sodium nitrite). The solid products formed on standing were collected by filtration and crystallized from the proper solvent.

Method B: A solution of either **6a** or **6b** (0.01 mol) in ethanol (30 ml) containing sodium acetate (6.0 g) was cooled to 0 °C, stirred and treated gradually with a cooled diazonium salt (prepared as described above). The solid product formed was collected by filtration and crystallized from the proper solvent.

2-Arly-6-arylazo-4-cyano-5-phenyl-3(2*H*)-pyridazinones 4a, b. Method A: A solution of either **2a** or **2b** (0.01 mol) in aqueous acetic acid (30 ml; 70%) was refluxed for 2 h and then left to cool. The solid products so formed were collected by filtration and crystallized from the proper solvent.

Method B: An ice-cold solution of arenediazonium solid prepared from 0.02 mol of the aromatic amine and the appropriate amounts of sodium nitrite and hydrochloric acid was added to a solution of 0.01 mol of **1b** in ethanol (30 ml) containing sodium acetate (6.0 g). The products formed on standing were refluxed in acetic acid (20 ml) for 15 min and the reaction mixture was left to cool. The solid products formed were collected by filtration and crystallized from the proper solvent.

(2-Arylhydrazono-1-phenylethylidene)malononitriles 6a, b. A solution of **1a** (0.01 mol) in glacial acetic acid (50 ml) was treated with anhydrous sodium acetate (3.0 g), then with a solution of the appropriate diazonium salt (prepared as described above). The reaction mixture was left in a refrigerator for 24 h, then left to warm to room temperature. The solid products so formed were collected by filtration and crystallized from the proper solvent.

2-Aryl-4-cyano-5-phenyl-3(2*H*)-pyridazinimines 7a, b. Compounds **6a, b** (0.01 mol) were heated at 160 °C (bath temperature) for 30 min, then left to cool to room temperature. The products so formed were triturated with ethanol, collected by filtration and crystallized from the ptoper solvent.

2-Aryl-4-cyano-5-methyl-3(2*H*)-pyridazinimines 8a, b. A solution of **1c** (0.01 mol) in ethanol (30 ml) containing sodium acetate (6.0 g) was coupled with an ice-cold solution of the appropriate arenediazonium salt (prepared as described above). The products formed on standing were separated and refluxed in acetic acid (30 ml) for 15 min, then poured onto water. The solid products formed were filtered off and crystallized from glacial acetic acid.

4-Cyano-6-ethoxycarbonyl-5-methyl-2-phenyl-3(2*H*)-pyridazinone 9. Method A: Compound **9** was prepared in 65% yield from coupling **1e** with an ice-cold benzenediazonium salt using the procedure recently described by Gewald and Hain.[12] The product reveals analytical and spectral data consistent with those reported in literature.

Method B: Equimolecular amounts of **10** and ethyl cyanoacetate (0.01 mol) were heated in presence of ammonium acetate at 160 °C (bath temperature) for 1 h. The formed solid product was crystallized from acetic acid. Compound **9** was identical with authentic speciment (identity was made by mp and mixed mp).

We are deeply indebted to Prof. Dr. W. Steglich, Institut fur Organische Chemie und Biochemie, Universitat Bonn, F.R.G. for facilities that enabled measurements of MS and ^{13}C NMR.

References

1) S. Kambe, K. Saito, M. Hirose, A. Sakarai, and H. Midorikawa, *Synthesis*, **1984**, 860.
2) F. J. Cuadrado, M. A. Pérez, and J. L. Soto, *J. Chem. Soc., Perkin Trans. 1*, **1984**, 2447.
3) M. H. Elnagdi, H. A. Elfahham, and G. E. H. Elgemeie, *Heterocycles*, **1983**, 519.
4) M. H. Elnagdi, H. A. Elfahham, S. A. S. Ghozlan, and G. E. H. Elgemeie, *J. Chem. Soc., Perkin Trans. 1*, **1982**, 1667.
5) H. A. Elfahham, F. M. Abdel-Galil, Y. R. Ibrahim, and M. H. Elnagdi, *J. Heterocycl. Chem.*, **20**, 667 (1983).
6) M. H. Elnagdi, M. R. H. Elmoghayer, and G. E. H. Elgemeie, *Synthesis*, **1984**, 1.
7) F. Freeman, *Chem. Rev.*, **1980**, 329.
8) M. Coenen, *Justus Liebigs Ann. Chem.*, **640**, 85 (1961).
9) S. M. Fahmy, N. M. Abed, R. M. Mohareb, and M. H. Elnagdi, *Synthesis*, **1982**, 490.
10) N. M. Abed, N. S. Ibrahim, S. M. Fahmy, and M. H. Elnagdi, *Org. Prep. Proced. Int.*, **17**, 107 (1985).
11) E. A. A. Hafez, M. A. Khalifa, S. K. A. Guda, and M. H. Elnagdi, *Z. Naturforsch.*, **B 35**, 485 (1980).
12) K. Gewald and U. Hain, *Synthesis*, **1984**, 62.

The Effect of the Carbonyl Group, Phenyl Ring, and Ring Size of α-Iodo Cycloketones on the Nature of the Photochemical Carbon-Iodine Bond Cleavage

Boris Šket* and Marko Zupan
Department of Chemistry and Jožef Stefan Institute, Edvard Kardelj University, Ljubljana, Yugoslavia
(Received October 7, 1986)

Synopsis. UV irradiation of 2-iodo-3,4-dihydro-1(2*H*)-naphthalenone and 2-iodo-1-indanone has been found to involve competing radical and ionic photoprocesses. The carbonyl group, phenyl ring and ring size of cycloketones have an influence on the nature of the photochemical carbon-iodine bond cleavage.

The photochemistry of alkyl halides[1] and cycloalkanones[2] has been extensively studied, but little attention has been paid to the study of α-halo cycloalkanones. There are a few reports on the study of the photochemistry of α-halo cycloalkanones which include different types of photoprocesses, such as α-cleavage,[3] photoelimination,[4] hydrogen abstraction by α-keto radicals,[5] and rearrangement.[6] The nature of the photochemical carbon-halogen bond cleavage mainly depends on the hybridization of the carbon atom, on the type of the halogen bonded, the solvent polarity and the used wavelength. It has been generally observed that by the irradiation of alkyl halides, the ratio of ionic to radical products is substantially larger for iodides than for bromides,[1] while this tendency becomes reversed when the halogen atom is bonded to an olefinic carbon.[7,8]

It is known from literature that the irradiation of iodocyclohexane[9] in nonpolar solvents, or even in methanol, resulted in the formation of cyclohexene as the product derived from the carbocationic intermediate and only a low percentage of cyclohexane as the radical product was observed. On the other hand, the irradiation of 2-iodocyclohexanone[5] undergoes both ionic and radical photoprocesses, with the ratio between radical to ionic products 3.16:1. The mentioned results show that the photochemistry of carbon-iodine bond is greatly influenced by the α-keto group.

As the formation of α-keto carbonium ions depends on the α-halogen atom, the ring size of the ketone and the other functional groups present in the molecule, we found it reasonable to study the influence of another chromophore (phenyl ring), which is in conjugate position with the carbonyl group as also the

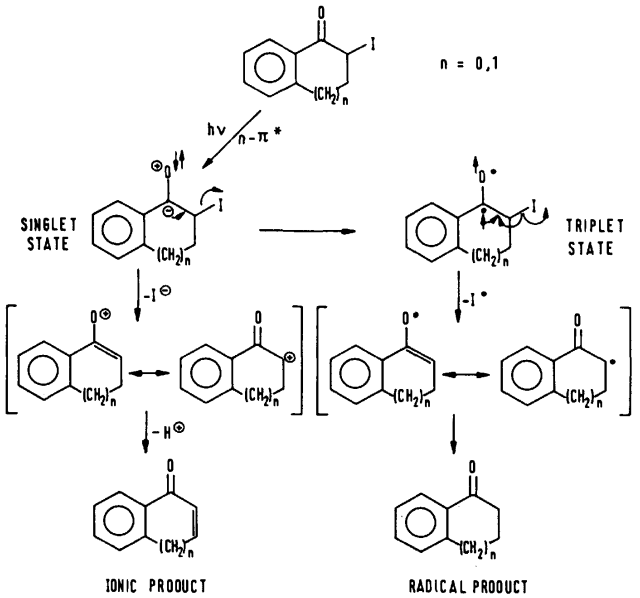

n	Solvent	λ/nm	% Conversion	Radical : Ionic Product
0	*c*-C_6H_{12}	253.7	83	68 : 32 = 2.1 : 1
1	*c*-C_6H_{12}	253.7	100	43 : 57 = 1 : 1.32
0	CH_3COCH_3	253.7	100	100 : 0
1	CH_3COCH_3	253.7	100	81 : 19 = 4.26 : 1
1	*c*-C_6H_{12}	300	100	48 : 52 = 1 : 1.08
1	CH_3COCH_3	300	68	73 : 27 = 2.7 : 1
1	*c*-C_6H_{12} Saturated with oxygen	253.7	72	36 : 64 = 1 : 1.78

Scheme 1. The effect of the ring size on the nature of the carbon-iodine bond cleavage.

influence of the ring size of cycloketone on the behavior of excited states of α-iodo cycloalkanones.

Irradiation of 2-iodo-3,4-dihydro-1(2*H*)-naphthalenone[10] in cyclohexane solution resulted in two products: 3,4-Dihydro-1(2*H*)-naphthalenone and 1-naphthol in the ratio 1 : 1.32 (Scheme 1). The formation of the reduction product corresponds to the radical reaction pathway, while 1-naphthol formation can be explained as a tautomer of the initially formed ionic product. On irradiation, iodine atom liberated on homolytic fission of C-I bond prefers to combine with another iodine atom than to undergo hydrogen abstraction, which is known to be extremely slow.[11] The quantity of liberated iodine corresponds to the quantity of the radical products formed, which was determined by iodine titration. 3,4-Dihydro-1(2*H*)-naphthalenone is, in the presence of iodine, under the same reaction conditions photostable and does not undergo phototransformation to 1-naphthol. Irradiation at λ=300 nm only slightly influenced the ratio of the products formed (Scheme 1). A comparison of the ratio of the radical to the ionic products formed by irradiation of 2-iodocyclohexanone (3.1 : 1) and 2-iodo-3,4-dihydro-1(2*H*)-naphthalenone (1.32 : 1) in cyclohexane solution shows that the conjugation of the carbonyl group with the phenyl ring lowers this ratio.

To understand the nature of the excited states involved, we carried out the reaction in acetone, which is a triplet sensitizer, and noted a significant change in the ratio of the radical to the ionic products (4.26 : 1). This result indicates that the solvent acetone strongly favoured the formation of the radical product. The quenching studies carried out, using oxygen as the triplet quencher, show a slight decrease in the radical product formation and a lower conversion of the starting α-iodo ketone was observed (Scheme 1).

In order to compare the influence of the phenyl group and the ring size of the cycloketone, we carried out the photoreaction of 2-iodo-1-indanone. Fifteen-hours irradiation of the indanone at λ=253.7 nm in cyclohexane resulted in a crude reaction mixture containing two products: 1-Indanone as the radical product and 2-inden-1-one[12] as the ionic product in a ratio of 2.1 : 1, while irradiation of the acetone solution under the same reaction conditions led to a complete conversion of the starting material with only 1-indanone formation (Scheme 1). On the other hand, irradiation of 2-iodo-1-indanone in methanol at λ=300 nm resulted in the formation of 2-methoxy-1-indanone (27%)[13] as ionic and 1-indanone (73%) as the radical product. The photoprocess in cyclohexane using triethylamine resulted in a marked decrease of conversion of the starting α-iodo ketone (26% conversion).

From the above results several conclusions can be derived: (i) The photochemistry of the carbon-iodine bond is greatly influenced by the α-keto group. (ii) The phenyl ring in a conjugate position with the carbonyl group has an influence on the excited states of the α-iodo cycloalkanones. (iii) The ratio between the radical and the ionic products depends on the ring size of cycloketone; the five-membered ring favours the expulsion of the iodine atom, while in the six-membered ring the expulsion of the halide anion is preferential, which can be explained by the geometry of the excited state, being, by its partially negative charge on the carbonyl carbon atom, more stabilized in the conformation of the six-membered ring[14] than in the nearly planar five-membered[15] system in α-indanone. (iv) Reaction rate of the six-membered cycloalkanone in a cyclohexane solution is larger than that of the five-membered compound. (v) The results of the quenching and sensitizing experiments indicate that the radical processes may occurr mostly through n-π^* triplet states and the ionic through singlet states, which clearly supports the Wagner model.[16]

Experimental

Irradiation was carried out in a Rayonet Photochemical Chamber, Reactor Model RPR-100 with RPR 253.7 nm and RPR 300 nm lamps. IR spectra (KBr disc) were recorded by using a Perkin-Elmer 257 spectrometer, ^{1}H NMR spectra were determined by a JEOL JNM-PS-100 in CCl_4 solution with Me_4Si as an internal standard and mass spectra were recorded on a CEC 21-110 spectrometer. Gas liquid chromatography was carried out on a Varian Aerograph Model 1800 and preparative TLC on Merck-PSC-Fertigplatten Kieselgel F 254. Melting points were determined on a Kofler apparatus and are uncorrected.

2-Iodo-1-indanone and 2-iodo-3,4-dihydro-1(2*H*)-naphthalenone[10] were prepared by iodination of the 1-indanone and 3,4-dihydro-1(2*H*)-naphthalenone in acetic acid using poly[styrene-co-4-vinylpyridinium dichloroiodate (I)].

2-Iodo-1-indanone: IR 710, 1260, 1600, 1710 cm^{-1}, ^{1}H NMR (CCl_4) δ=3.45 (1H, dd, J_{AB}=18 Hz, $J_{2,3A}$=3 Hz, H-3A), 3.90 (1H, dd, J_{AB}=18 Hz, $J_{2,3B}$=7.5 Hz, H-3B), 4.92 (1H, dd, $J_{2,3B}$=7.5 Hz, $J_{2,3A}$=3 Hz, H-2), 7.50 (4H, m, aromatic H's), mass spectra *m/z* (relative intensity): M^+ 258 (100), 131 (88), 127 (23), 103 (84), 102 (35), 77 (61). Found: *m/z* 257.9550, Calcd for C_9H_7IO: M, 257.9544. Mp 68—70 °C (from ethanol).

General Procedures: An 18-ml, 0.028 M (1M=1 mol dm^{-3}) solution of the 2-iodo-1-indanone or 2-iodo-3,4-dihydro-1(2*H*)-naphthalenone was irradiated in a quartz tube for 15 h, the solvent was evaporated in vacuo, the crude reaction mixture was analyzed by ^{1}H NMR and the products from irradiations outlined in Scheme 1 were isolated by preparative gas chromatography (FFAP 30% on Chromosorb AW) or preparative TLC (SiO_2, benzene), whose spectral properties agreed with those of authentic samples.

To measure the reactivity difference, 18 ml of 0.028 M cyclohexane solution of the 2-iodo-1-indanone or 2-iodo-3,4-dihydro-1(2*H*)-naphthalenone was irradiated at λ=253.7 nm and 25 °C in a quartz tube for 3 and 5 h and the degree of conversion of the starting α-halo ketone determined from the ^{1}H NMR spectrum of the crude reaction mixture.

References

1) P. J. Kropp, *Acc. Chem. Res.*, **17**, 131 (1984).

2) a) J. C. Dalton and N. J. Turro, *Ann. Rev. Phys. Chem.*, **21**, 499 (1970); b) N. J. Turro, J. C. Dalton, K. Dawes, G. Farrington, R. Hautala, D. Morton, M. Niemczyk, and N. Schores, *Acc. Chem. Res.*, **5**, 92 (1972).

3) H. G. Ferguson, P. De Mayo, F. L. M. Pattison, and T. Tabata, *Can. J. Chem.*, **41**, 2099 (1963).

4) G. Hüppi, F. G. Eggart, S. Iwasaki, H. Wehrli, K. Schaffner, and O. Jeger, *Helv. Chim. Acta*, **49**, 1986 (1966); G. Jones II and L. P. Mc Donnell, *J. Am. Chem. Soc.*, **98**, 6203 (1976).

5) P. C. Purohit and H. R. Sonowane, *Tetrahedron*, **37**,

873 (1981).
6) B. E. Kaplan and A. L. Hartwig, *Tetrahedron Lett.* **1970**, 4855.
7) B. Šket and M. Zupan, *J. Chem. Soc., Perkin Trans. 1*, **1979**, 752.
8) T. Kitamura, S. Kobayashi, and H. Taniguchi, *J. Org. Chem.*, **47**, 2323 (1982).
9) P. J. Kropp, J. A. Sawyer, and J. J. Snyder, *J. Org. Chem.*, **49**, 1583 (1984).
10) C. L. Stevens, J. J. Beereboom, and K. G. Rutherford, *J. Am. Chem. Soc.*, **77**, 4592 (1955).
11) W. V. Sherman, *Adv. Free Radical Chem.*, **3**, 50 (1969).
12) P. H. Lacy and D. C. C. Smith, *J. Chem. Soc. C*, **1971**, 41.
13) J. C. Arnould and J. P. Pete, *Tetrahedron*, **31**, 815 (1975).
14) K. Gatto, J. D. Reinheimer, K. Shafer, and J. T. Gerig, *Org. Magn. Reson.*, **6**, 577 (1974).
15) J. B. Lambert and F. R. Koeng, *Org. Magn. Reson.*, **3**, 389 (1971).
16) P. J. Wagner, *Topics in Current Chemistry*, **66**, 1 (1976).

Reduction of Nitrostyrenes to Nitroalkanes with a NADH Grafted Model

Thierry TRÉFOUEL, Patrik TINTILLIER, Georges DUPAS,
Jean BOURGUIGNON,* and Guy QUÉGUINER
Laboratoire de Chimie Organique Fine et Hétérocyclique-INSA-BP 08, Mont Saint Aignan 76130, France
(Received December 1, 1986)

Synopsis. Grafting of the 1,4-dihydronicotinamide structure on a Merrifield type resin is described. With this reagent, arylnitroethanes have been obtained by regioselective reduction of β-nitrostyrenes. The yields are good and no dimeric compounds are formed. The role of magnesium ions in these reductions is different from that observed with classical NADH models.

Arylnitroethanes are compounds of special interest since they are useful synthetic intermediates. The nitro group can be converted to other functional groups such as carbonyl, nitrile oxides, or amino group.

A widely used method to obtain 2-aryl-1-nitroethanes involves reduction of nitrostyrenes. Selective reduction of the ethylene double bound is rather difficult: borohydride reduction under various conditions often leads to contamination of the desired product by side reactions: for example a dimeric compound can be formed by Michael addition of the nitronate intermediate to the starting nitroalkene.[1]

$$ArCH{=}CH\text{-}NO_2 \xrightarrow{NaBH_4} ArCH_2CH_2NO_2 + Ar\text{-}CH_2\text{-}\underset{\displaystyle Ar\text{-}CH\text{-}CH_2\text{-}NO_2}{\underset{|}{CH}}\text{-}NO_2$$

Recently some improvements to the usual procedure led the authors to better results.[2]

Other reagents have been used to ensure selective reduction of the ethylenic double bond of nitrostyrenes, for example NADH models such as 1,4-dihydronicotinamide derivatives or Hantzsch ester. With this last reagent good results in the reduction of various nitroolefins in the presence or silica gel have been reported.[3]

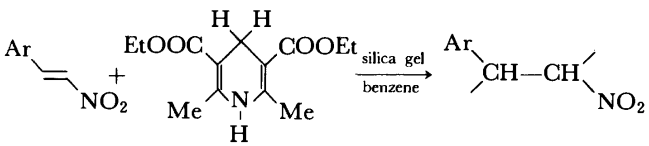

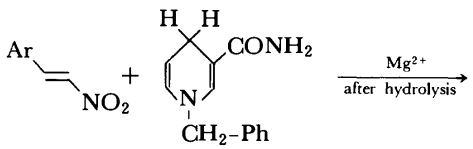

BNAH

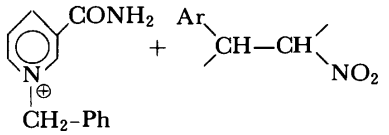

$BNA^{\oplus}$

With 1,4-dihydronicotinamide derivatives there are few examples of such reductions[4] and the yields are rather poor. Moreover it was established that β-nitrostyrene is not reduced in the absence of magnesium ions.[4a]

The work-up of reactions performed with BNAH is not easy. It is rather difficult to isolate the desired product from starting reagents or other products formed during the reduction.

Grafting reagents on to an insoluble matrix can constitute an elegant way of resolving the practical problems encountered with free reagents.[5] A few NADH grafted models have been studied.[6] In our laboratory we have synthesized the first truly reactive polymer-bound NADH model.[7] With this reagent excellent results are obtained in the reduction of activated carbonyl compounds.[7]

In this publication we describe the optimisation of the synthesis of the grafted reagent on a Merrifield type resin and its use in the reduction of aryl nitro olefins.

Preparation of Grafted Reagent. The reagent is obtained by reaction of the halomethylated copolymer styrene and divinylbenzene resin with nicotinamide (Scheme 1). The pyridinium salt is just filtered, not dried, before being subjected to regioselective 1,4-reduction with $Na_2S_2O_4$. If the polymer-bonded pyridinium salt **1** is quite free of the solvent used during the quaternarization (CH_3CN), wetting of the polymer does not occur and reaction of $Na_2S_2O_4$ becomes impossible.

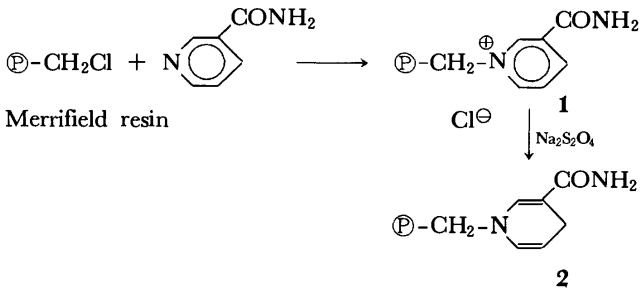

The reduction of **1** is complete as shown by the absence of chlorine in the analysis of **2**.

Reduction of Nitrostyrenes. With BNAH, reduction of a substrate in the presence of magnesium ions usually occurs in acetonitrile as solvent. With the reagent **2** we observed that in this solvent the polymer matrix did not swell and consequently no reduction occured. The access to the active site of the polymer bonded reagent is probably impossible. A swelling cosolvent is needed which also ensures the solubility of Mg^{2+} ions. Finally the best results were obtained in a benzene-acetonitrile (1/1) mixture. In typical conditions [grafted NADH model 1.2 milliequivalent, $Mg(ClO_4)_2$ 1 mmol, nitrostyrene 1 mmol, solvents 14 ml, 5 d, 80 °C] the results were as follows:

$$\underset{\mathbf{3}}{ArCH{=}CHNO_2} + \mathbf{2} \longrightarrow \underset{\mathbf{4}}{ArCH_2CH_2NO_2} + \mathbf{1}$$

Table 1. Reduction of β-Nitrostyrenes

Ar in starting nitrostyrene **3**		Yield in **4**	Ar in starting nitrostyrene **3**		Yield in **4**
Phenyl	**3a**	100	3,4-(Methylenedioxy)phenyl	**3e**	72
2-Naphtyl	**3b**	98	3-Pyridyl	**3f**	60
p-Methoxyphenyl	**3c**	77	2-Thienyl	**3g**	70
3,4-Dichlorophenyl	**3d**	90			

$ArCH_2\text{-}CH_2\text{-}NO_2$ **4**
β α

Ar=			NMR (Chemical shift)
4a	Phenyl	Oil (2b)	3.17 (t) $CH_2\beta$; 4.45 (t) $CH_2\alpha$; 6.93—7.4 (m) H arom.
4b	2-Naphthyl	Oil $C_{12}H_{11}NO_2$	3.42 (t) $CH_2\beta$; 4.65 (t) $CH_2\alpha$; 7.50 (m) H arom.
4c	*p*-Methoxyphenyl	Oil (2b)	3.21 (t) $CH_2\beta$; 4.53 (t) $CH_2\alpha$; 3.75 (s) CH_3O; 6.84 and 7.12 H arom.
4d	3,4-Dichlorophenyl	Oil $C_8H_7Cl_2NO_2$	3.30 (t) $CH_2\beta$; 4.60 (t) $CH_2\alpha$; 7.30 (m) H arom.
4e	3,4-(Methylenedioxy)phenyl	F=55 (2b)	3.20 (t) $CH_2\beta$; 4.52 (t) $CH_2\alpha$; 6.56—6.80 (m) H arom.
4f	3-Pyridyl	Oil $C_7H_8N_2O_2$	3.30 (t) $CH_2\beta$; 4.60 (t) $CH_2\alpha$; 7.10—7.60 (m) H_4 and H_5 arom.; 8.43 (m) H_2 and H_6 arom.
4g	2-Thienyl	Oil (3)	3.43 (t) $CH_2\beta$; 4.50 (t) $CH_2\alpha$; 6.70—7.20 (m) H arom.

The most interesting features of these reductions are: (i) Yields are good to quantitative. (ii) The work-up is easy; filtration followed by evaporation of the solvents gives the pure arylnitroethanes. Some of them (**3b**, **3d**, and **3f**) are new compounds. They have been identified by the usual spectroscopic methods. (iii) No dimeric compound was detected in the final product [absence of signals near δ 5.0 in the ^1H NMR spectra[1]].

Role of Magnesium Ions. The role of magnesium ions in BNAH reduction is to ensure an interaction between the substrate and the model through a ternary complex.[8] In the case of free models in the absence of Mg^{2+}, generally no reaction occurs. However the reduction of (α-methylbenzylidene)malonitrile with a BNAH derivative affords different product depending upon the presence or not of Mg^{2+} (9). We have performed the reduction of **3a** in the typical conditions described above but without the magnesium ion. A large quantity of polymeric compounds is obtained but after chromatographic purification we could isolate 10% of **4a**. To our knowledge it is the first partial reduction of 1-phenyl-2-nitroethene observed with a 1,4-dihydronicotinamide reagent in the absence of magnesium ions. We think that a "polymer effect" occurs: the redox potential of the reactants are changed and the transition state becomes different to that ocurring with a free model. The medium used (CH_3CN-C_6H_6) is less polar and the polymeric matrix contains numerous phenyl rings. The micro environment in the neighbourhood of the active site is less favorable to solvatation of the dihydronicotinamide by CH_3CN. So the interaction between the reagent and the substrate is forced. This phenomenon could be sufficient to induce a partial reduction.

Experimental

Nitrostyrenes derivatives were prepared according to the literature.[10] Merrifield resin was purchased from Merck (Art. 818178). NMR spectra were recorded with a Varian EM 360 L spectrometer (solvent $CDCl_3$, internal reference HMDS). Analyses have been performed with a Carlo Erba 1106 apparatus).

Grafted Reagent. Merrifield resin (50 g) nicotinamide (20 g) in 300 ml of dry acetonitrile were stirred at 90 °C during 6 d. The pyridinium derivative **1** was filtered, washed with acetonitrile then with hot water. The product was suitable for the next step.

Analysis of a dried sample gave the following typical values. C: 79.9; H: 7.0; N: 3.6; Cl: 5.0%.

The wet quaternarized resin (about 20 g) was treated with a mixture of $Na_2CO_3 \cdot 10H_2O$ (20 g) and $Na_2S_2O_4$ (40 g) in 200 ml of water. The mixture was stirred for 6 h at room temperature. The color of the resin turned from red-orange to yellow. After filtration the resin was dried for 2 d (40 °C/0.5 Torr (1 Torr=133.322 Pa)). The grafted NADH model was storred under argon in the refrigerator.

Typical analysis is as follows. C: 83.5; H: 3.5; N: 3.8% (absence of chlorine).

This corresponds to 1.3 meq of the 1,4-dihydronicotinamide moiety pergram (based on N percentage).

Reduction of Nitrostyrenes. In a dry glass tube 1.2 meq of grafted reagent **2**, 250 mg of $Mg(ClO_4)_2$ (1 mmol), 1 mmol of nitrostyrene, 7 ml of hyperdry benzene and 7 ml of hyperdry acetonitrile were introduced under an argon

atmosphere. The tube was sealed, then heated at 80 °C for 5 d. After cooling the tube was broken. The resin is discarded, washed with acetonitrile, and water (1 ml) was added. The solvents were evaporated. The residue was extracted with water, then extrated with chloroform. After evaporation of the solvent the pure arylnitroethanes were recovered.

The aryl-2-nitroalkanes have the characteristics given on the precedent page.

References

1) A. I. Meyers and J. C. Sircar, *J. Org. Chem.*, **32**, 4134 (1967).

2) A. K. Sinhababu and R. T. Borchardt, *Tetrahedron Lett.*, **24**, 227 (1983); A. Bhattacharjya, R. Mulhopadhyay, and S. C. Pakrashi, *Synthesis*, **1985**, 886.

3) K. Nakamura, M. Fujii, S. Oka, and A. Ohno, *Chem. Lett.*, **1985**, 523.

4) S. Shinkai, Y. Kusano, T. Ide, T. Sone, and O. Manabe, *Bull. Chem. Soc. Jpn.* **51**, 3544 (1978); K. Wallenfels, W. Ertel, A. Hockendorf, J. Rieser, and K. H. Uberschar, *Naturwissenschaften*, **62**, 459 (1975); *Chem. Abstr.*, **84**, 84708g.

5) A. Akelah, *Synthesis*, **1981**, 413; A. Akelah and D. C. Sherrington, *Chem. Rev.*, **81**, 557 (1981).

6) A. S. Lindsey, S. E. Hunt, and N. G. Savill, *Polymer*, **7**, 479 (1966); B. Eling, G. Challa, and U. K. Pandit, *J. Polym. Sci., Polym. Chem. Ed.*, **23**, 2165 (1985).

7) R. Mathis, G. Dupas, A. Decormeille, and G. Quéguiner, *Tetrahedron Lett.*, **22**, 59 (1981); G. Dupas, J. Bourguignon, C. Ruffin, and G. Quéguiner, *Tetrahedron Lett.*, **23**, 5141 (1982).

8) R. A. Gase, G. Boxhoorn, and U. K. Pandit, *Tetrahedron Lett.*, **1976**, 2889; M. Hughes and R. H. Prince, *J. Inorg. Nucl. Chem.*, **40**, 703 (1978); A. Ohno, T. Kimura, A. Yamamoto, S. G. Kim, S. Oka, and Y. Ohnishi, *Bull. Chem. Soc. Jpn.*, **50**, 1535 (1977).

9) Y. Ohnishi, M. Kagami, T. Numakunai, and A. Ohno, *Chem. Lett.*, **1976**, 915.

10) J. Bourguignon, G. Le Nard, and G. Quéguiner, *Can. J. Chem.*, **63**, 2354 (1985).